Stress metabolites of *Solanum melongena*:[1,2] biosynthetic studies and isolation of auberganol and α- and β-eudesmol

ALBERT STOESSL AND J.B. STOTHERS

London Research Centre, Agriculture Canada and the Department of Chemistry, University of Western Ontario, London, Ont. Canada N6A 5B7

Received May 8, 1985

ALBERT STOESSL and J. B. STOTHERS. Can. J. Chem. **64**, 1 (1986).

Attempts to clarify the biosynthetic origin of the eggplant stress metabolite aubergenone (**1**) by incorporation of label from sodium [2-$^2H_3$,1-^{13}C]acetate were frustrated by low yields and enrichment levels. However, the presence of deuterium in the biosynthetically significant 5-position was demonstrated by ^{2}Hmr for the closely related auberganol (**5**) and α- and β-eudesmol (**10** and **11**), suggesting that these compounds, and hence also **1**, are normal eudesmanes and not the products of a possible double rearrangement. Deuterium was also incorporated into the expected positions of 9-oxonerolidol (**12**), 9-oxynerolidol (**13**), and lubimin (**4**). Incorporation of label from [1,2-$^{13}C_2$]acetate could be determined satisfactorily only for **13** and its allylic isomer **14**, corresponding with expectations. This is the first report of **5** as a natural product and of **10**, **11**, and the 10-epimer of **4** as eggplant stress metabolites.

ALBERT STOESSL et J. B. STOTHERS. Can. J. Chem. **64**, 1 (1986).

Dans le but de déterminer l'origine biosynthétique de l'auberginone (**1**), un métabolite de stress de l'aubergine, on a effectué des essais d'incorporation de l'acétate-[$^2H_3$-2,^{13}C-1] de sodium qui n'ont pas réussi à cause des faibles rendements et des faibles niveaux d'enrichissement. Toutefois, on a pu démontrer la présence de deutérium dans la position 5, qui est significative d'un point de vue biosynthétique, en faisant appel à la rmn du ^{2}H de l'auberganol (**5**) et des α- et β-eudesmol (**10** et **11**) qui lui sont très apparentés; ces résultats suggèrent que ces composés et, par conséquent, le composé **1** sont des eudesmanes normaux et non pas des produits provenant d'une double transposition. Il y a aussi incorporation de deutérium dans les positions prévues du oxo-9 nérolidol (**12**), du oxo-9 nérolidol (**13**) et de la lubimine (**4**). Ce n'est qu'avec le composé **13** et son isomère allylique **14** que l'on a pu déterminer d'une façon satisfaisante l'incorporation d'un marqueur de l'acétate-[$^{13}C_2$-1,2] qui corresponde aux expectatives. Les résultats obtenus dans ce travail correspondent à une première concernant l'existence du composé **5** comme produit naturel et des produits **10**, **11** et de l'épimère en position 10 du composé **4** comme métabolites de stress de l'aubergine.

[Traduit par le journal]

Aubergenone (**1**), a metabolite of *Solanum melongena*, has until now been unique among the carbocyclic stress metabolites of the Solanaceae in that its structure is that of a normal eudesmane whereas the many other compounds of the group are derived from hypothetical eudesmane precursors by carbon and hydrogen migrations (1, 2). However, it has been shown recently (3) that the biosynthesis of rishitin (**2**), a member of the group, involves a remarkable second rearrangement of the vetispirane, hydroxylubimin (**3**) (Scheme 1). The possibility therefore arises that **1** may also be formed through a similar sequence. In principle, this question might be answered through the biosynthesis of **1** with [2-$^2H_3$,1-^{13}C]acetate incorporation. If a vetispirane is an intermediate, its formation may be accompanied by hydrogen (deuterium) migration from C-5 to C-4, as has been unambiguously demonstrated for **2**, **3**, and lubimin (**4**) (4). In the present case this could give rise to an observable signal in an uncluttered region of the ^{2}Hmr spectrum provided, of course, that the incorporation level is sufficiently high and that the C-4 hydrogen (deuterium) does not itself participate in the hypothetical second rearrangement. On the other hand, if **1** arises from an acyclic precursor without carbon–carbon rearrangement, the salient deuterium atom will remain bonded to C-5 and, therefore, be observable either directly or through the β-isotope shift in the C-6 absorption pattern.

To test these notions, eggplant fruit was treated with a suspension of *Monolinia fructicola*, as stress compound inducer, and, after 18 h, with [2-$^2H_3$,1-^{13}C]acetate (1.86×10^{-3} *M* effective concentration). A small amount of **1** was isolated after 2 days but the incorporation level was so low that only the deuterium signals for the methyl groups were observed in the ^{2}Hmr spectrum. The ^{13}C spectrum was similarly uninformative, revealing neither signal enhancements nor β-shifts for C-2, -4, -6, -8, -10, or -11. Fortunately, the situation was saved in part by the isolation of a new compound that was identified as a tetrahydroaubergenone, auberganol (**5**), by its ^{1}H, ^{13}Cmr, and mass spectra. Although this compound was not previously

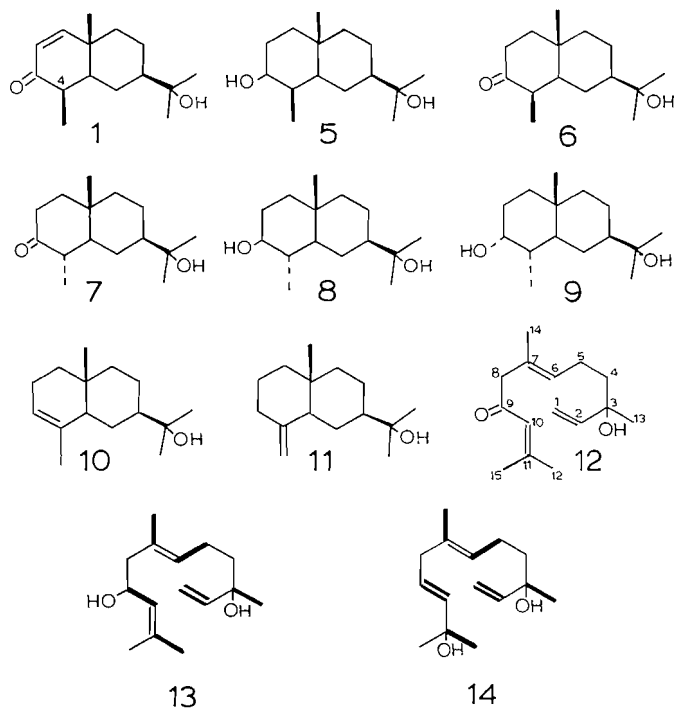

[1]Part 121 of ^{13}Cmr studies; for Part 120 see ref. 12.

[2]Communication No. 1010 from the Research Centre; Part 47 of "Postinfectional inhibitors from plants"; for Part 46 see ref. 13; for Part 45 see ref. 14; for Part 44 see ref. 15.

known from eggplant or other natural sources, it has been described as one of the intermediates in the laboratory synthesis of **1** from α-cyperone (5). The ^{1}Hmr and ms data for the eggplant metabolite are in excellent agreement with the literature values and the mp is satisfactorily close. To confirm the identity of **5**, however, the compound was oxidized to **6**, which was completely transformed to **7** on refluxing with ethanolic potassium hydroxide. Ketol **7** was obtained earlier as an intermediate in the synthesis of 4-*epi*-aubergenone (6). A sample of the latter compound[3] was hydrogenated to furnish authentic **7**, which was found to be identical to that obtained from **5**. As an aid for the assignment of the ^{13}Cmr spectrum of **5**, a portion of ketol **7** was reduced with sodium borohydride to furnish a mixture of two diols **8** and **9**. The major product **8** was isolated by fractional crystallization and exhibited the properties reported earlier for **8** as a precursor of **7** in the aforementioned synthesis of 4-*epi*-aubergenone (6). The minor diol **9** was therefore the 3α isomer. The ^{13}C data for **5**–**9** are collected in Table 1.

As in the case of **1**, the incorporation levels in **5** were too low to be detected by ^{13}Cmr. On the other hand, however, the ^{2}Hmr spectrum clearly showed the presence of deuterium in the methyl groups, with well-defined signals at δ 0.84, 0.86, and 1.18 for the 4-, 10-, and 11-methyl groups, respectively (^{2}H enrichment ca. 0.5%), and for some of the skeletal positions (broad absorptions ca. δ 1.05, 1.25, 1.4, 1.6). Most significantly, a sharp signal at δ 3.70 established the presence of deuterium at C-3 (enrichment ca. 0.15%) and the absence of absorption near δ 1.88 showed there was little or no deuterium at C-4. The absorption positions for the 3- and 4-deuterons were known from analysis of the proton spectrum in which irradiation at δ 1.88 collapsed the 4-methyl doublet, δ 0.84, to a singlet and eliminated a 5.5-Hz coupling in the carbinyl pattern at δ 3.70, thereby reducing the latter to a doublet of doublets, J = 5.5, 10.5 Hz. Some alteration in the spectrum near δ 1.25 indicated this to be the position of the 5-proton, thereby tentatively identifying an additional ^{2}H signal. From these observations it can be concluded that **5** was probably formed without deuterium migration from C-5 to C-4.[4] A definitive conclusion follows from the presence of deuterium at C-3, since this establishes that **5** is not formed by reduction of **1** but, rather, is either in a precursor or shunt relationship to **1**.

Another crystalline substance, m.p. 81–83°C, was isolated from the product and from its ^{13}C spectrum, found to be a 2:3 mixture of α- and β-eudesmols, **10** and **11**, respectively. These could not be separated by either column or preparative thin-layer chromatography but corresponded in all respects to the like mixture of the two compounds obtained by Cordano *et al.* (7) from *Balanites roxburghii*. The ^{13}Cmr spectrum of our product once again showed no discernible enrichment or β-shifts; the data are listed in Table 1. The ^{2}Hmr spectrum contained distinctive methyl signals at δ 0.71, 0.75, and 1.18 arising from the 4-, 10-, and 11-methyl groups, respectively, with broadened skeletal deuterium signals centred at δ 1.36, 1.44, 1.50, 1.60, and 2.30. The δ 2.30 signal corresponded to a multiplet in the proton spectrum containing one large coupling, ~12 Hz, which could be attributed to the 5-proton.

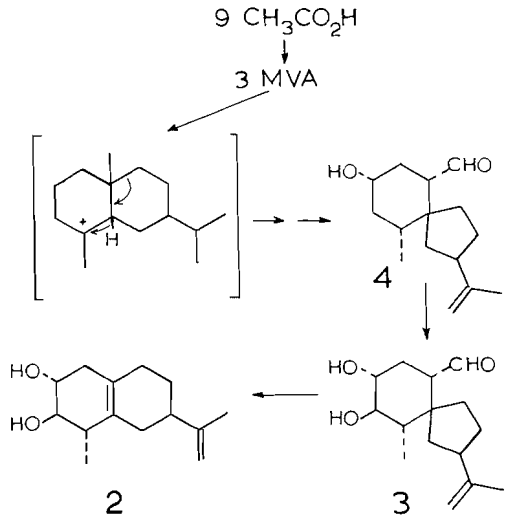

SCHEME 1

To evaluate the situation more fully, the major eggplant phytoalexins lubimin (**4**), 9-oxonerolidol (**12**), and 9-oxynerolidol (**13**) were also isolated for examination of their spectra. The ^{1}Hmr spectrum of the lubimin sample revealed the presence of ca. 10% of the 10-*epi* isomer which had been found previously in potato (8) but not eggplant. The ^{2}H spectrum of this sample was essentially the same as that recorded earlier for **4** isolated in the course of analogous incorporation experiments with potatoes (4), exhibiting readily assigned signals for deuterium at the aldehydic (δ 9.78), *exo*-methylene (δ 4.65), allylic (δ 1.60), and secondary methyl (δ 0.93) positions. In addition, broad signals centred at δ 1.0, 1.4, 1.8, and 2.3 arising from skeletal deuterons were evident, that at 1.4 corresponding to 1-^{2}H and (or) 4-^{2}H. The ^{2}Hmr spectrum of **12** contained prominent signals for each of the four methyl groups, δ 1.20, 1.50, 1.80, and 2.05, with that at δ 1.50 superimposed on absorption for skeletal methylene deuterons. In addition, a signal at δ 3.00 arising from the 8-methylene deuterons and weaker signals at δ 5.25, 5.95, and 6.10 confirmed the presence of deuterium at C-2, -6, and -10. These assignments followed from the proton spectra obtained in an earlier study (9) and reported previously by Hiroi and Takaoka (10). The major metabolite isolated in the experiment was 9-oxynerolidol (13) for which the ^{2}H spectrum readily revealed incorporation at the four methyl sites, δ 1.20 and 1.54, the latter signal arising from the three unresolved allylic methyl groups and more than three times as intense as the δ 1.20 signal. In addition, methylene absorption at δ 2.05 and olefinic signals at δ 5.95 and 5.22 were apparent. The lack of absorption in the range δ 2.1–5.1 confirmed the absence of incorporation at C-9. The ^{13}C spectrum of **13** revealed the presence of two diastereomers, as found previously (9, 10) in a ratio of ca. 2:1. In contrast to our earlier report, slightly different shieldings were found for 12 of the 15 carbons owing to the increased shift dispersion produced by the 3-fold increase of the observing frequency (300 vs. 100 MHz). The data are listed in Table 1. It may be noted that the original assignments for C-6 and -10 have been reversed (see below). The effects of deuterium incorporation were just apparent in the patterns observed for each of the enriched centres, C-1, -3, -5, -7, -9, and -11, with distinctive β-isotope shifts for C-1 (Δ =

[3]Professor R. B. Kelly kindly provided a generous sample of 4-*epi*-aubergenone.

[4]An unambiguous conclusion on this point is elusive because of the possibility of two consecutive deuterium migrations, i.e. an eudesmane → a vetispirane → an eudesmane with C-5 → C-4 → C-5 deuterium migration, although it is known that the second migration does not occur in the rearrangement of **3** → **2** (4). It would appear that the only approach to a solution of this question would involve testing of suitable vetispiranes for incorporation into **1**, experiments which are beyond the scope of the present study.

137 ppb), C-5 (110 ppb), C-7 (55 ppb), and C-9 (64 ppb) while the C-3 and -11 signals were broadened.

In a preliminary experiment, similarly inoculated aubergines were treated with sodium [1,2-$^{13}C_2$]acetate. Although aubergenone (**1**) was present in trace amounts, insufficient material could be isolated for spectroscopic examination. However, **13** and its allylic isomer **14** were isolated from tissue extracts by chromatography and their ^{13}C spectra recorded to determine the pattern of intact acetate units in each compound as indicated by the bold linkages in **13** and **14**. For each unit, the ^{13}C–^{13}C coupling constants could be measured and these data are included in Table 1. The relative intensities of the ^{13}C satellites and the central signal for the coupled carbons indicated that the ^{13}C enrichments were low, 0.25 and 0.15 ± 0.05% for **13** and **14**, respectively. The very low incorporation levels and the minimal yield of **1** dictated a change in tactics, leading to the experiment with [2-$^{2}H_3$,1-^{13}C]acetate described above.

Auberganol (**5**) and the eudesmols **8** and **9** were not present in readily detectable amounts in extracts from uninoculated aubergines. The experiments described above suggest that these, together with aubergenone (**1**), are normal, i.e. non-rearranged eudesmanoids. No eudesmanes have as yet been reported as stress metabolites of other species of the Solanaceae. It is at present unknown whether auberganol is antifungally active but at least one report describes (+)-β-eudesmol, isolated from *Hymenoclea monogyra*, as active against *Alternaria* spp. (11).

Experimental

General experimental procedures and instrumentation utilized were as described in earlier papers (8, 9) unless otherwise indicated. The ^{13}C and ^{2}Hmr spectra were recorded with a Varian XL-300 system using $CDCl_3$ (^{13}C) and $CHCl_3$ (^{2}H) solutions in 5-mm tubes.

Aubergines (imported from Florida) were purchased in the local market in November and were of unknown storage age and variety. The fruits (25) were cut longitudinally into equal halves, seeds and pith were scooped out, and the resulting shells were charged with a suspension of *Monilinia fructicola* (2×10^5 spores/mL, 40 mL/shell) and, after 22 h, with sodium [2-$^{2}H_3$,1-^{13}C]acetate (Merck Isotopes Inc., 98% ^{2}H, 90% ^{13}C, 8 mg (0.093 mmol in 10 mL of H_2O/shell). Two days after inoculation, the liquid diffusate was collected, combined with water rinsings, and extracted with ether. Necrotic tissue was scraped from the shells and extracted by steeping overnight in MeOH/EtOAc (1:1), concentrating the filtered extract until mainly aqueous, and reextracting with ether. On column chromatography over SiO_2 (Camag DFO; 300 g) in *sec*-BuOH/EtOAc (5:95), the diffusate extract afforded fractions (20 mL each) that consisted predominantly of 9-oxonerolidol (**12**) together with **10** and **11** (fractions 26–28, 53 mg), 9-oxynerolidol (**13**) and its allyl isomer **14** (fractions 29–34, 140 mg), a mixture of **4** and **1** (fractions 38–44, 41 mg), and crude crystalline **5** (fractions 50–61; 14.9 mg).

Rechromatography of fractions 26–28 gave 9-oxonerolidol (**12**) (18 mg, no discernible enhancement or shifts in the ^{13}C spectrum) and compounds **10** and **11** as a crystalline mixture (13.5 mg); mp 81–83°C after two recrystallizations (light petrol, −10°C); ^{1}Hmr ($CDCl_3$) δ (**10**): 0.75 (s, 3H, 10-Me), 1.18 (s, 6H, isopropyl Me's), 1.60 (bs, 3H, 4-Me), 5.30 (m, 1H, H-3); δ (**11**): 0.66 (s, 3H, 10-Me), 1.18 (s, 6H, isopropyl Me's), 4.42 (m, 1H), and 4.70 (m, 1H) *exo*-methylene protons; ^{13}Cmr (see Table 1); ^{2}Hmr indicated low enrichment of ca. 0.016 atoms D/molecule; *m/e*: 222, 204, 189, 164, 161, 149, 93, and 59 (100%). *Exact Mass* calcd. for $C_{15}H_{26}O$: 222.19835; found: 222.19805.

9-Oxynerolidol (**13**) was obtained nearly pure (97 mg) by rechromatography of fractions 29–34 ($MeOH/CHCl_3$ 5:95). The small amount of its allylic isomer that was also obtained was not further examined.

Aubergenone (**1**) (5 mg) was obtained from fractions 38–44 by column chromatography ($MeOH/CHCl_3$ 1:99) followed by multiple

TABLE 1. ^{13}C shielding data[a] for **5–11**, **13**, and **14**

Compound	C-1	C-2	C-3	C-4	C-5	C-6	C-7	C-8	C-9	C-10	C-11	C-12	C-13	C-14	C-15
5	44.0	27.9	74.2	46.0	40.2	26.4	49.8	22.8	39.7	33.1	8.4	72.8	27.0	27.4	19.8
8	39.5	31.0	76.9	48.7	39.5	25.0	49.4	22.2	41.5	33.2	15.0	73.0	26.9	27.5	16.9
9	35.2	29.2	72.3	42.8	35.7	24.8	49.6	22.3	41.6	33.5	16.0	73.0	27.0	27.4	16.1
6	43.1	35.1	216.2	46.4	49.3	26.7	49.4	22.7	40.5	33.2	13.5	72.8	27.0	27.6	18.8
7	41.2	38.1	213.2	45.4	51.0	26.4	48.7	22.1	40.7	33.4	11.3	72.8	26.9	27.6	16.4
10	37.9	23.0	121.0	135.1	46.7	24.4	50.0	22.5	40.2	32.2	21.3	73.1	26.8	27.8	15.6
11	(41.9)	23.5	36.9	151.1	49.5	25.1	49.8	22.4	(41.2)	35.9	105.3	73.0	27.2_1	27.1_6	16.3
13[b,c]	111.6_4	144.8_3	73.3	41.7	22.9_0	128.4_1	134.3_8	48.0_0	65.8_6	127.6_4	131.5_0	25.6	28.0_4	16.1_2	18.1
		[70.0]	[39.4]		[43.5]		[42.5]		[72.3]	[50.0]			[39.4]	[42.5]	[41.8]
	111.5_6	144.9_7	73.2_1		22.8_0	128.3_2	134.4_9	47.9_7	65.9_0	127.5_7	131.6_2		27.7_6	16.1_4	
14[c]	111.6	144.8	73.4	42.3	27.7	125.0	134.1	41.9	125.0	139.2	70.6	29.8	27.9	16.1	29.8
		[70.0]	[39.8]		[43.5]		[42.8]		[72.3]		[39.4]		[39.8]	[42.8]	[39.4]

[a]In ppm from internal TMS for $CDCl_3$ solutions.
[b]Upper data set for the major diastereomer (see text).
[c]One-bond ^{13}C–^{13}C coupling constants in Hz listed in square brackets; samples obtained from [1,2-$^{13}C_2$]acetate experiment.

preparative tlc (high performance precoated plates, Whatman Multi-K type CS5KC$_{18}$F/K5F; EtOAc/toluene/HOAc 30:60:1) and was combined for spectroscopy with another 3.2 mg similarly obtained from the tissue extract.

Lubimin (15 mg) was obtained in the above purification of **1**. It consisted of **4** accompanied by a small amount of its 10-epimer as judged from the ^{1}Hmr spectrum.

Auberganol (**5**) was purified by recrystallization from EtOAc (5 mg), mp 155–158°C; after a further recrystallization (EtOAc/hexane) it had mp 173.0–173.5°C (lit. (5) mp 166–166.5°C); ir ($CHCl_3$): 3605 (s), 3460 (br), 2935, 2870, 2855, 1450 (d), 1382, 1370, 1130, 1080, 1008, 903 cm^{-1}; too little sample was available for determination of the small rotation (lit. (5), $[\alpha]_D$ −2.7°); ^{1}Hmr ($CDCl_3$) δ: 0.86 (s, 3H, 10-Me), 0.84 (d, 3H, J = 7.4 Hz, 4-Me), 1.18 (s, 6H, isopropyl Me's), 1.92 (m, 1H, H-4), 3.71 (dt, J = 10.4 and 5.5 Hz, 1H, H-3); ^{13}Cmr (see Table 1). *Exact Mass* calcd for $C_{15}H_{28}O$: 240.20891; found: 240.20879.

The very complex tissue extract was used only for the isolation of **1** by similar chromatographic techniques.

In another experiment, similarly inoculated aubergines (20) were treated with sodium [1,2-$^{13}C_2$]acetate (1.68 mg) in 1 mL of H_2O added to 10 mL of spore suspension/shell. Aubergenone (**1**) was present only in trace amounts and could not be studied. 9-Oxynerolidol (**13**) (15 mg) and its isomer **14** (16 mg) were isolated from the tissue extract by chromatography over SiO_2 in EtOAc/CH_2Cl_2 1:4.

Reduction–epimerization of **5**

Auberganol (2.5 mg) in acetone (1 mL) at 0°C was treated at increasingly long intervals with small drops of the Jones' reagent (59 mg CrO_3, 2 mL H_2SO_4, H_2O to 15 mL) until a yellow colour persisted for 30 min. Excess reagent was destroyed with MeOH (few drops) and the solution extracted with Et_2O (2 × 10 mL); the extract was washed with 5% Na_2CO_3 (2 mL) and water (2 × 4 mL) and evaporated to give **6** (1.9 mg), homogeneous by tlc and ^{1}H and ^{13}Cmr spectra. This product was refluxed in 0.1 *M* KOH in EtOH (2 mL) at 74°C for 1 h, poured into H_2O (10 mL), acidified (2 *M* HCl, 0.11 mL), and extracted into $CHCl_3$ (2 × 5 mL) to give **7** as a syrup (~1 mg) identical (except for the presence of trace amounts of different impurities) with the sample prepared from synthetic 4-*epi*-aubergenone by tlc, ir, ^{1}H, and ^{13}Cmr spectra.

Reduction of 4-epi-*aubergenone*

The synthetic ketol (**6**) (15 mg) was hydrogenated over 5% Pd/C (25 mg, prereduced) in EtOH (15 mL) for 6 h. Essentially pure *trans*-dihydrocarissone (**7**) was obtained as a syrup on evaporation of the filtered solution.

4-epi-*Auberganols*

Synthetic **7** (12 mg) in MeOH (2 mL) was reduced with $NaBH_4$ (few grains) at 0°C. Extraction ($CHCl_3$) from ice-water gave a mixture of diols **8** and **9** (^{13}Cmr, see Table 1) as a syrup (11.5 mg). Crystallization from CH_2Cl_2 at −10°C gave **8** (3.2 mg), mp 136–140°C, raised to 138–140°C by a further crystallization; ^{1}Hmr ($CDCl_3$) δ: 0.83 (s, 3H, 10-Me), 0.97 (d, 3H, J = 6.8 Hz, 4-Me), 1.19 (s, 6H, $(CH_3)_2C(OH)$—), 3.14 (ddd, 1H, J = 5.0, 9.8, 11.0 Hz, H-3).

Acknowledgements

Thanks are due to G. Rock for general experimental assistance, S. Wilson and D. Hairsine for recording ^{1}Hmr and mass spectra, respectively; and to the Natural Sciences and Engineering Research Council of Canada for financial support. We thank Professor R. B. Kelly for the sample of 4-*epi*-aubergenone.

1. J. B. STOTHERS. Pure Appl. Chem. **53**, 1241 (1981).
2. A. STOESSL. *In* Phytoalexins. *Edited by* J. A. Bailey and J. W. Mansfield, Blackie, Glasgow and London. 1982. p. 133.
3. A. MURAI, S. SATO, A. OSADA, N. KATSUI, and T. MASAMUNE. J. Chem. Soc. Chem. Commun. 32 (1982).
4. A. STOESSL and J. B. STOTHERS. Can. J. Chem. **61**, 1766 (1983).
5. A. MURAI, A. ABIKO, M. ONO, and T. MASAMUNE. Bull. Chem. Soc. Jpn. **55**, 1191 (1982).
6. R. B. KELLY, S. ALWARD, K. S. MURTY, and J. B. STOTHERS. Can. J. Chem. **56**, 2508 (1978).
7. G. CORDANO, M. A. MERRIEN, M. ANNICK, J. POLONSKY, R. M. RABANAL, and P. VARENNE. J. Ind. Chem. Soc. **55**, 1148 (1978).
8. A. STOESSL, J. B. STOTHERS, and E. W. B. WARD. Can. J. Chem. **56**, 645 (1978).
9. A. STOESSL, J. B. STOTHERS, and E. W. B. WARD. Can. J. Chem. **53**, 3351 (1975).
10. M. HIROI and D. TAKAOKA. Chem. Lett. 1213 (1972).
11. M. MIYAKADO, T. KATO, N. OHNO, and T. J. MABRY. Phytochemistry, **15**, 846 (1976).
12. A. J. RAGAUSKAS and J. B. STOTHERS. Can. J. Chem. **63**, 2969 (1985).
13. M. ESSENBERG, A. STOESSL, and J. B. STOTHERS. J. Chem. Soc. Chem. Commun. 556 (1985).
14. K. A. HILLS, A. STOESSL, A. P. OLIVA, and J. ARDITTI. Bot. Gazz. **145**, 298 (1984).
15. A. STOESSL and J. B. STOTHERS. Can. J. Chem. **61**, 1766 (1983).

Influence de nitrates métalliques sur l'équilibre de dissociation ionique: $N_2O_4 \rightleftarrows NO^+ + NO_3^-$ dans le sulfolane

ABDELLATIF BOUGHRIET, MICHEL WARTEL[1] ET JEAN-CLAUDE FISCHER

Laboratoire de chimie analytique et marine, bâtiment C8, Université de Lille, 59655 Villeneuve D'Ascq Cédex, France

Reçu le 1er avril 1985

ABDELLATIF BOUGHRIET, MICHEL WARTEL et JEAN-CLAUDE FISCHER. Can. J. Chem. **64**, 5 (1986).

Au cours de la nitration des noyaux aromatiques par le N_2O_4 en milieu aprotonique, la présence d'un nitrate métallique tel que $Zn(NO_3)_2$, $Cu(NO_3)_2$ ou $UO_2(NO_3)_2$, génère l'espèce catalytique NO^+ selon la réaction $N_2O_4 + M(NO_3)_2 \rightleftarrows NO^+ + M(NO_3)_3^-$ [1]. L'étude voltampérométrique de la réduction de N_2O_4 en présence de nitrates métalliques $M(NO_3)_2$ sur électrode de platine a permis d'atteindre la valeur de la constante de l'équilibre [1] et celle de la constante de stabilité du complexe trinitrato formé selon $M(NO_3)_2 + NO_3^- \rightleftarrows M(NO_3)_3^-$ [2] dans le sulfolane (M = Zn, Cu, UO_2). La forte stabilité des complexes trinitrato $M(NO_3)_3^-$ est due aux propriétés peu solvatantes du solvant. Les comportements des ligands Cl^- et NO_3^- étant très voisins, cette hypothèse est vérifiée par l'étude de la stabilité des complexes chlorozincates[II] ($ZnCl_i^{2-i}$ (i = 1, 2, 3, 4)) dans le sulfolane, par voltampérométrie à courant nul sur électrode d'argent.

ABDELLATIF BOUGHRIET, MICHEL WARTEL, and JEAN-CLAUDE FISCHER. Can. J. Chem. **64**, 5 (1986).

The addition of a metallic nitrate such as $Zn(NO_3)_2$, $Cu(NO_3)_2$, or $UO_2(NO_3)_2$ to N_2O_4 solutions in aprotic media leads to the reclaiming of the NO^+ species (which is considered as a catalyst for the nitration of aromatics by N_2O_4) as follows: $N_2O_4 + M(NO_3)_2 \rightleftarrows NO^+ + M(NO_3)_3^-$ [1]. Using linear voltammetry, the study of the N_2O_4 reduction in the presence of metallic nitrates with a platinum electrode has allowed us to derive the equilibrium constant for reaction [1] and that corresponding to the formation of the trinitrato complexes in sulfolane according to: $M(NO_3)_2 + NO_3^- \rightleftarrows M(NO_3)_3^-$ [2] (M = Zn, Cu, UO_2). The strong stability of the $M(NO_3)_3^-$ complexes is due to the weak solvating character of the sulfolane. This hypothesis is also confirmed by the stability constants of zinc[II] chloride complexes: $ZnCl_i^{2-i} \rightleftarrows ZnCl_{i-1}^{3-i} + Cl^-$ (i = 1, 2, 3, 4) in sulfolane from a potentiometric study by means of a silver chloride – silver electrode.

Introduction

La nitration du naphtalène par N_2O_4 en milieu aprotonique a lieu selon un mécanisme faisant intervenir l'espèce catalytique NO^+ (1) provenant de la dissociation ionique de N_2O_4 selon $N_2O_4 \rightleftarrows NO^+ + NO_3^-$. Cependant, la constante de dissociation de N_2O_4 dans différents solvants aprotoniques est faible ($K^i_{N_2O_4} = 7{,}1 \times 10^{-8}$ mol dm^{-3} à 303 K dans le sulfolane (2), et $K^i_{N_2O_4} = 6{,}3 \times 10^{-10}$ mol dm^{-3} à 298 K dans le nitrométhane (3*a*)). Des composés tels que les nitrates métalliques ($UO_2(NO_3)_2$, $Cu(NO_3)_2$ et $Zn(NO_3)_2$) dans des solvants peu solvatants (favorisant les homoconjugaisons ou hétéroconjugaisons) favorisent la dissociation ionique de N_2O_4 par formation de complexes nitrato $M(NO_3)_i^{2-i}$ (i = 1, 2, 3, 4 et M = UO_2, Cu et Zn). Afin de mieux connaître le phénomène d'interaction entre N_2O_4 et ces nitrates métalliques, nous avons étudié les constantes de stabilité de ces complexes nitrato-métalliques:

[1] $M(NO_3)_{i-1}^{3-i} + NO_3^- \rightleftarrows M(NO_3)_i^{2-i}$

N'ayant pu intégrer ces différentes entités chimiques dans un couple électrochimique, mais également en raison de la faible concentration des espèces $M(NO_3)^+$, M^{2+} et NO_3^- en solution, les constantes de stabilité des complexes $M(NO_3)_2$ et $M(NO_3)^+$ n'ont pas pu être déterminées. Néanmoins, une étude voltampérométrique sur électrode de platine poli des solutions des dérivés oxygénés de l'azote (3) a montré que le système NO^+/NO est rapide dans le sulfolane, ce qui nous a permis d'entreprendre l'étude de la réaction entre N_2O_4 et $M(NO_3)_2$ selon

[2] $N_2O_4 + M(NO_3)_2 \rightleftarrows NO^+ + M(NO_3)_3^-$

La formation de NO^+ au cours de cette réaction a été suivie par ampérométrie.

Il est à noter que si les nitrates de cuivre et d'uranyle conduisent à des complexes trinitrato ($M(NO_3)_3^-$) (4), Addison *et al.* (4) soulignent, dans le cas du zinc, l'existence d'un complexe tétranitrato ($(NO^+)_2Zn(NO_3)_4^{2-}$). Ce complexe, formé lors d'un mélange $Zn(NO_3)_2$ et N_2O_4 en excès, est peu stable et se décompose à température ordinaire. Peu d'informations n'ont pu être relevées dans la bibliographie quant à sa stabilité en solvant aprotonique dipolaire. Les ions nitrate et chlorure ayant des propriétés solvatantes très proches dans le sulfolane, la transposition de l'étude des complexes $ZnCl_i^{2-i}$ (i = 1, 2, 3, 4), par potentiométrie à courant nul sur électrode d'argent, au complexe $Zn(NO_3)_4^{2-}$ devrait permettre de justifier la non-stabilité du tétranitratozincate[II] de dinitrosyle dans notre solvant.

Partie expérimentale

Le sulfolane (Prolabo) est purifié selon la méthode déjà décrite (5). Les perchlorates d'argent (Fluka) et de tétraéthylammonium (Carlo Erba) sont séchés à 333 K sous pression réduite durant 1 mois. Les chlorures de tétraéthylammonium (Eastman Kodak) et de zinc (Merck) sont séchés respectivement à 353 et 423 K sous pression réduite durant 8 jours.

Le $UO_2(NO_3)_2$ anhydre est obtenu par déshydratation à 373 K de $UO_2(NO_3)_2,6H_2O$ (Merck) sous pression réduite. Une telle technique n'est pas applicable aux nitrates de zinc et de cuivre qui se décomposent en conditions de déshydratation. Les nitrates $Zn(NO_3)_2$ et $Cu(NO_3)_2$ rigoureusement exempts d'eau sont donc préparés "*in situ*" par réaction dans le sulfolane entre de la poudre de métal (Cu, Zn) et un excès de N_2O_4. Quand la réaction est terminée, le mélange réactionnel est placé sous pression réduite, ce qui permet l'élimination de N_2O_4 en excès et des oxydes d'azote NO et N_2O_3 formés au cours de la réaction.

Le perchlorate de nitrosyle est préparé dans le nitrométhane par addition d'un excès de N_2O_3 à une solution de $HClO_4,H_2O$. Le solide recueilli après filtration est lavé au tétrachlorure de carbone.

Un millivoltmètre Isis 20000 Tacussel est utilisé pour la potentiométrie. La stabilité des mesures est contrôlée sur un enregistreur Tacussel EPL 2, relié au millivoltmètre. Toutes les préparations de solutions sont effectuées en boîte à gants. Les manipulations sont réalisées à 303 ± 0,1 K. L'électrode d'argent est recouverte d'un dépôt de AgCl, avant chaque manipulation, selon la méthode déjà décrite (2).

[1]Auteur à qui adresser la correspondance.

Les courbes intensité–potentiel, en régime stationnaire, sont tracées à 303 ± 0,1 K à l'aide d'un ensemble voltampérométrique Tacussel. La vitesse de rotation de l'électrode indicatrice de platine (diamètre, 0,8 mm) est de 10 tours/s. La vitesse de balayage des potentiels est de 5 mV/s. La voltammétrie cyclique est réalisée soit à l'aide de la même électrode soit avec une électrode de diamètre ≃ 2 mm.

L'électrode de référence a déjà été décrite (2). Le potentiel de demi-vague du système ferrocène–ferricinium est pris comme origine de l'échelle de potentiel.

Le dosage de l'eau est effectué par la méthode de Karl–Fischer (réactif généré par coulométrie (6)).

Les spectres Raman de solutions équimoléculaires des mélanges de N_2O_4 et nitrate métallique dans le sulfolane ont été obtenus à l'aide d'un spectromètre Raman Dilor R.T. 30. Pour cela, nous avons utilisé des tubes scellés contenant des solutions de 0,2 mol dm^{-3} en nitrate métallique et 0,2 mol dm^{-3} en N_2O_4. La radiation excitatrice est la raie à 488,0 nm d'un laser à argon ionisé, avec une puissance de 150 mW.

Résultats et discussion

Les courbes voltampérométriques sur électrode de platine poli de solutions de nitrate métallique ($UO_2(NO_3)_2$, $Cu(NO_3)_2$ ou $Zn(NO_3)_2$), en présence de perchlorate de tétraéthylammonium comme électrolyte indifférent, ne révèlent pas dans le sulfolane la vague d'oxydation caractéristique de l'ion nitrate ($E_{\frac{1}{2}}$ = +1,57 V (3)). Ce résultat suggère donc que ces nitrates métalliques sont peu dissociés dans notre solvant. L'addition de N_2O_4 à ces solutions fait apparaître sur les courbes $i = f(E)$ une vague cathodique différente de celle correspondant à la réduction de N_2O_4, et qui croît avec le rapport de concentration $[N_2O_4]/[M(NO_3)_2]$. De même, si l'on ajoute une solution de nitrate métallique à une solution de N_2O_4, il apparaît une nouvelle vague dont le potentiel, $E_{\frac{1}{2}} \simeq +0{,}74$ V, correspond à celui du système $NO^+ + e^- \rightleftarrows NO$ en présence de N_2O_4 (3*b*) (fig. 1, cas du nitrate d'uranyle). La présence de l'entité NO^+ en solution est confirmée par l'étude en spectroscopie Raman des mélanges équimoléculaires N_2O_4–$Cu(NO_3)_2$, N_2O_4–$UO_2(NO_3)_2$ et N_2O_4–$Zn(NO_3)_2$ dans le sulfolane. En effet, les spectres présentent une bande intense à 2285 cm^{-1}, caractéristique de la vibration d'élongation ν_{NO} de NO^+ (fig. 2) (7). Nous représentons en figure 3 l'évolution du courant limite de diffusion de la vague cathodique attribuée à NO^+ lors de l'addition de nitrate métallique à une solution de N_2O_4. La hauteur de cette vague tend vers une limite, ce qui laisse supposer l'existence d'un équilibre partiellement déplacé. Addison (4) signale, pour le cuivre et l'uranium, la formation des complexes $Cu(NO_3)_3^-$ NO^+ et $UO_2(NO_3)_3^-$ NO^+, et pour le zinc, la formation des complexes $Zn(NO_3)_3^-$ NO^+ et $Zn(NO_3)_4^{2-}$ $2NO^+$, lors de l'addition de nitrate métallique à N_2O_4 liquide. La réaction peut donc s'écrire, dans le cas des ions cuivrique et uranyle,

$$[2] \quad M(NO_3)_2 + N_2O_4 \rightleftarrows M(NO_3)_3^- + NO^+$$

Cette réaction laisse présager que la dissociation de $M(NO_3)_3^-$ en $M(NO_3)_2$ et NO_3^- est plus faible que celle de N_2O_4 selon $N_2O_4 \rightleftarrows NO^+ + NO_3^-$. Il est à noter que le complexe $[Zn(NO_3)_4][NO]_2$ se décompose à température ambiante (4). Des travaux récents (8) confirment, dans le cas de l'uranium, que seul le complexe $[UO_2(NO_3)_3^-][NO^+]$ existe. Notre étude portera, dans une première étape, sur les sels de cuivre et d'uranyle.

I. *Constantes d'équilibre de la réaction de N_2O_4 avec les nitrates de cuivre et d'uranyle dans le sulfolane*

L'étude électrochimique des mélanges N_2O_4–$M(NO_3)_2$ (avec $M^{2+} = Cu^{2+}$ et UO_2^{2+} et $[M(NO_3)_2]/[N_2O_4] \simeq 1$) montre que: (*i*) en voltammétrie cyclique, l'intensité du courant du pic cathodique i_c^p est proportionnelle à la racine carrée de la vitesse de balayage de potentiel; (*ii*) par voltammétrie linéaire, le courant limite i_l est proportionnel à la racine carrée de la vitesse de rotation de l'électrode. Le processus électrochimique n'est donc pas contrôlé par la cinétique de la réaction chimique [2]. La réduction de N_2O_4 en présence de nitrate métallique peut s'interpréter selon le processus

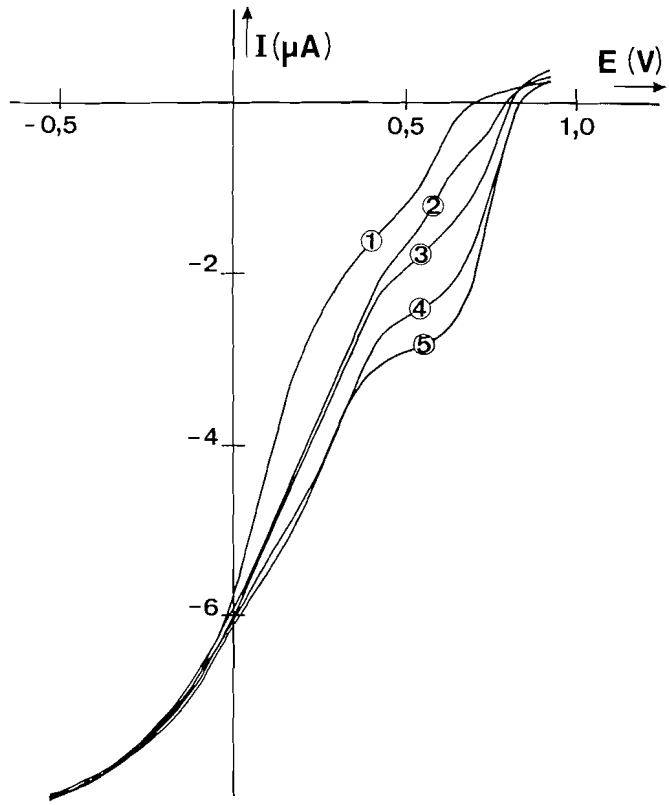

FIG. 1. Courbes intensité–potentiel obtenues dans le sulfolane à 303 K (électrode de platine poli) lors de l'addition de nitrate d'uranyle à une solution de N_2O_4. Électrolyte indifférent: $[(C_2H_5)_4NClO_4]$ = 0,1 mol dm^{-3}. $[N_2O_4]$ = 6,83 × 10^{-3} mol dm^{-3}; $[UO_2(NO_3)_2]$ = 0 (1), 1,01 × 10^{-3} (2), 2,47 × 10^{-3} (3), 4,90 × 10^{-3} (4), 6,87 × 10^{-3} mol dm^{-3} (5).

$$[2] \quad N_2O_4 + M(NO_3)_2 \rightleftarrows NO^+ + M(NO_3)_3^-$$

$$NO^+ + e^- \rightleftarrows NO$$

Le courant limite de diffusion étant proportionnel à la concentration de NO^+, soit $i_l(NO^+) = k_{NO^+}[NO^+]$, il est possible, connaissant le coefficient de proportionnalité $i_l(NO^+)/[NO^+]$ de la réduction de NO^+ (obtenue lors de l'étude d'une solution de $NOClO_4$) pour une même électrode tournante (surface: 0,50 mm^2) animée d'une vitesse de rotation identique (ω = 62,8 rad s^{-1}): k_{NO^+} = 770 ± 15 μA dm^3 mol^{-1}, d'atteindre la concentration en NO^+ libre. Nous pouvons ensuite déduire la constante d'équilibre $K_M^* = [NO^+][M(NO_3)_3^-]/[N_2O_4] \times [M(NO_3)_2]$, relative à la réaction [2]. À 303 K, les constantes K_M^* sont égales à 2,5 ± 0,4 et 1,7 ± 0,2, respectivement, pour $M^{2+} = Cu^{2+}$ et UO_2^{2+}. Ces constantes sont en accord avec une réaction [2] non totalement déplacée. En utilisant la valeur de la constante de formation de N_2O_4 selon $NO^+ + NO_3^- \rightleftarrows N_2O_4$, soit $K_{N_2O_4}^* = 1{,}6 \times 10^{+7}$ mol^{-1} dm^3 (2), nous pouvons atteindre les constantes de stabilité des complexes métalliques trinitrato à partir de la relation

$$K_3^*(M) = [M(NO_3)_3^-]/[M(NO_3)_2][NO_3^-] = K_M^* K_{N_2O_4}^*$$

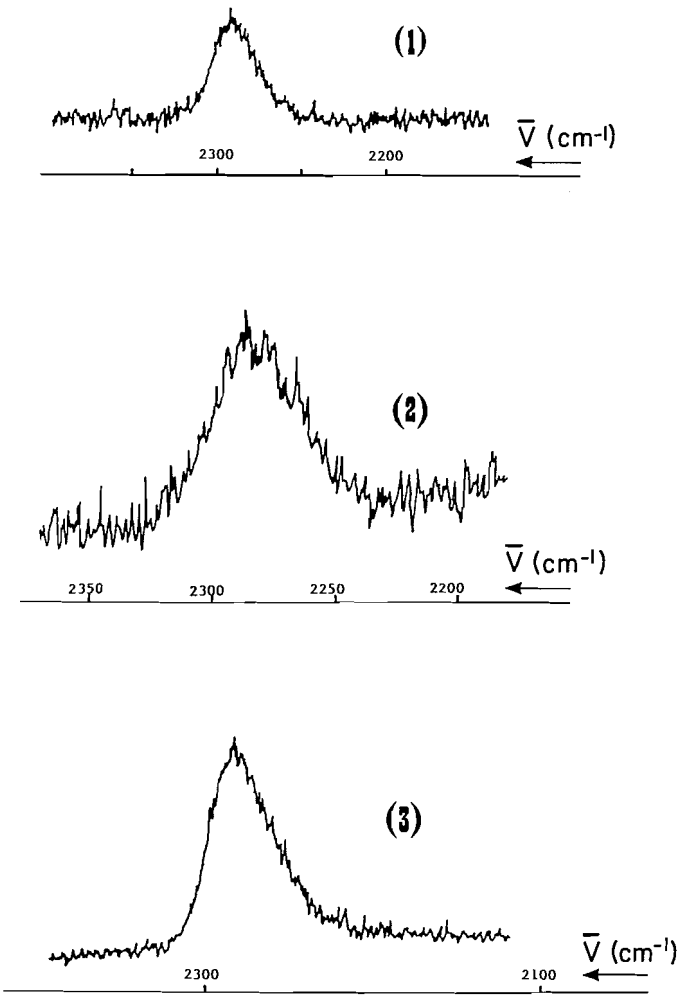

FIG. 2. Spectres Raman de mélanges N_2O_4 + $M(NO_3)_2$ dans le sulfolane. $[N_2O_4] = [M(NO_3)_2] = 0{,}2$ mol dm^{-3}. $\nu_0 = 488{,}0$ nm; puissance, 150 mW. N_2O_4 + $UO_2(NO_3)_2$ (1); N_2O_4 + $Zn(NO_3)_2$ (2); N_2O_4 + $Cu(NO_3)_2$ (3).

À 303 K, la constante $K_3^*(M)$ est égale à $4{,}0 \times 10^{+7}$ et $2{,}7 \times 10^{+7}$ mol^{-1} dm^3 respectivement pour le cuivre[II] et l'ion uranyle.

Les valeurs des constantes de dissociation des complexes trinitrato $M(NO_3)_3^-$ ($1/K_3^*(M)$) sont donc très proches de celle relative à la constante de dissociation ionique de N_2O_4 ($K^i_{N_2O_4} = 1/K^*_{N_2O_4}$), ce qui confirme la présence d'une réaction [2] équilibrée entre les nitrates métalliques et N_2O_4. Généralement les constantes de stabilité des complexes tétracoordonnés sont plus faibles que celles des complexes tricoordonnés; c'est le cas du cuivre[II] en présence du ligand Cl^- dans les solvants eau (9–11), acétonitrile (12), diméthylsulfoxyde (13, 14). Il était intéressant de confirmer cette hypothèse dans le cas du zinc[II] afin de montrer que le complexe $Zn(NO_3)_4(NO)_2$ n'existe pas dans le sulfolane. Ne pouvant déterminer la constante de stabilité du complexe $Zn(NO_3)_4^{2-}$, nous nous sommes intéressés à la complexation du zinc[II] avec le ligand Cl^- de comportement voisin de celui de l'ion NO_3^-.

II. *Constantes de stabilité des complexes chlorozincates[II] dans le sulfolane*

Il existe peu de travaux relatifs à la stabilité des complexes du zinc[II] en milieu aprotonique. Citons pour exemple ceux réalisés dans le solvant DMSO (16).

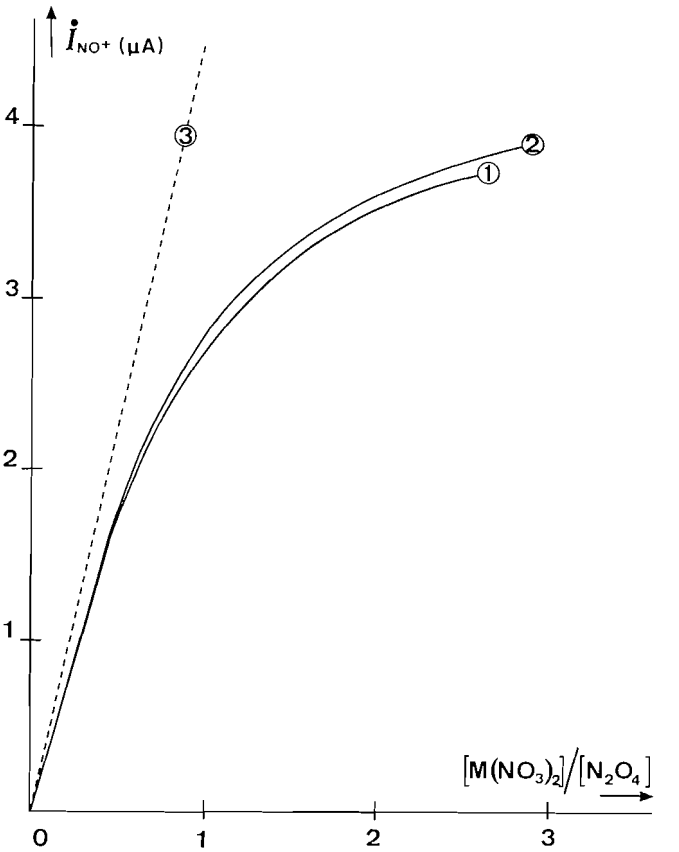

FIG. 3. Variation du courant limite ($i_l(NO^+)$) obtenu lors de l'addition de nitrate métallique à une solution $5{,}96 \times 10^{-3}$ mol dm^{-3} de N_2O_4 dans le sulfolane à 303 K (électrode de platine poli). Électrolyte indifférent: $[(C_2H_5)_4NClO_4] = 0{,}1$ mol dm^{-3}. $UO_2(NO_3)_2$ ou $Zn(NO_3)_2$ (1); $Cu(NO_3)_2$ (2); courant limite de diffusion pour une solution de NO^+ (3).

Afin d'accéder aux valeurs des constantes de stabilité K_i^* des complexes chlorozincates[II] relatives aux équilibres

[3] $\quad ZnCl_{i-1}^{3-i} + Cl^- \rightleftarrows ZnCl_i^{2-i}$

avec $i = 1, 2, 3, 4$

$$K_i^* = \frac{[ZnCl_i^{2-i}]}{[ZnCl_{i-1}^{3-i}][Cl^-]}$$

nous avons cherché à intégrer chacun de ces équilibres dans un couple électrochimique. Les complexes $ZnCl_4^{2-}$, $ZnCl_3^-$, $ZnCl_2$ et $ZnCl^+$ étant meilleurs donneurs de Cl^- que AgCl, nous avons pensé atteindre les constantes de stabilité de ces espèces grâce à l'utilisation de l'électrode d'argent recouverte de chlorure d'argent. En effet, cette électrode est indicatrice de la concentration de chlorure dans le sulfolane (2).

Nous avons suivi la neutralisation d'une solution de $ZnCl_4^{2-}$ (obtenue en mélangeant $ZnCl_2$ et $(C_2H_5)_4NCl$ dans un rapport de concentrations égal à 1/2) par une solution de perchlorate d'argent, par potentiométrie à courant nul. La courbe de titrage fait apparaître trois sauts de potentiel pour les rapports $[Ag^+]/[Cl^-]$: 0,25; 0,5; 1 (fig. 4). Ces sauts sont caractéristiques respectivement des réactions suivantes:

[4] $\quad ZnCl_4^{2-} + Ag^+ \rightarrow AgCl\downarrow + ZnCl_3^-$

[5] $\quad ZnCl_3^- + Ag^+ \rightarrow AgCl\downarrow + ZnCl_2$

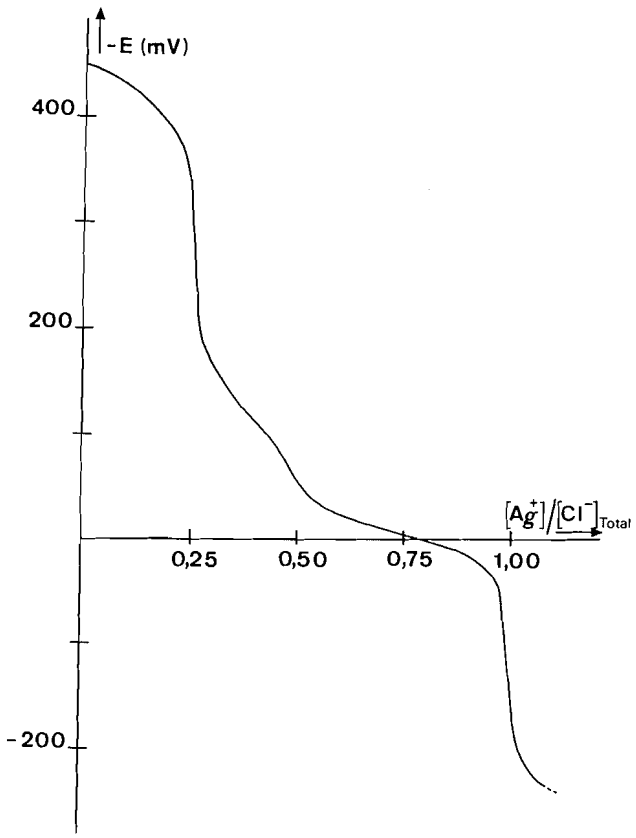

FIG. 4. Courbe potentiométrique (électrode Ag/AgCl) de dosage d'une solution de $ZnCl_4^{2-}$ ($0,5 \times 10^{-2}$ mol dm^{-3}) par une solution de $AgClO_4$ (0,2 mol dm^{-3}) dans le sulfolane. Électrolyte indifférent: $[(C_2H_5)_4NClO_4] = 0,1$ mol dm^{-3}.

et des deux réactions non discernables

[6] $ZnCl_2 + Ag^+ \rightarrow AgCl_\downarrow + ZnCl^+$

[7] $ZnCl^+ + Ag^+ \rightarrow AgCl_\downarrow + Zn^{2+}$

qui peuvent s'écrire globalement

$$ZnCl_2 + 2Ag^+ \rightarrow 2AgCl_\downarrow + Zn^{2+}$$

L'équation de Nernst appliquée au système électrochimique ([4]–[7])

[8] $ZnCl_i^{2-i} + Ag_\downarrow \rightleftarrows AgCl_\downarrow + ZnCl_{i-1}^{3-i} + e^-$

avec $i = 1, 2, 3, 4$, donne

$$E = E_0^i + 2{,}303 \frac{RT}{nF} \log \frac{[ZnCl_{i-1}^{3-i}]}{[ZnCl_i^{2-i}]}$$

L'analyse mathématique de la courbe de titrage montre que les réactions [4] et [5] sont rapides. Les coefficients de la loi de Nernst expérimentaux sont très proches de la valeur théorique (59 mV par unité logarithmique pour le couple [4] et 61 mV par unité logarithmique pour le couple [5]). Les potentiels normaux E_0^2 et E_0^3 ont été déterminés et ont pour valeurs respectives -420 mV et -124 mV (± 3 mV). Ces valeurs jointes aux valeurs du potentiel normal du système Ag^+/Ag (+373 mV (5)) et du produit de solubilité de AgCl ($3,7 \times 10^{-19}$ mol^2 dm^{-6} (5)), dans le sulfolane, permettent de calculer les constantes log K_4^* et log K_3^*, qui ont respectivement pour valeurs $+5,2 \pm 0,2$ et $+10,1 \pm 0,2$.

En ce qui concerne la variation de potentiel relative aux deux réactions simultanées [6] et [7], nous avons effectué un traitement mathématique des données par affinement selon la méthode des moindres carrés. Les résultats obtenus sont: coefficient expérimental de la loi de Nernst, $60 \pm 0,5$ mV; log $K_1^* = 12,1 \pm 0,2$; log $K_2^* = 13,4 \pm 0,2$; potentiels normaux $E_0^1 = +71 \pm 3$ mV et $E_0^2 = -7 \pm 2$ mV. Nous constatons que la constante K_2^* est supérieure à K_1^* comme le laissait présager la courbe potentiométrique où les neutralisations de $ZnCl_2$ et $ZnCl^+$ ne sont pas séparées. Ce phénomène a déjà été observé dans des solvants autres que le sulfolane: DMSO (16), méthanol (17), avec les ligands Cl^-, Br^-, I^- et SCN^-.

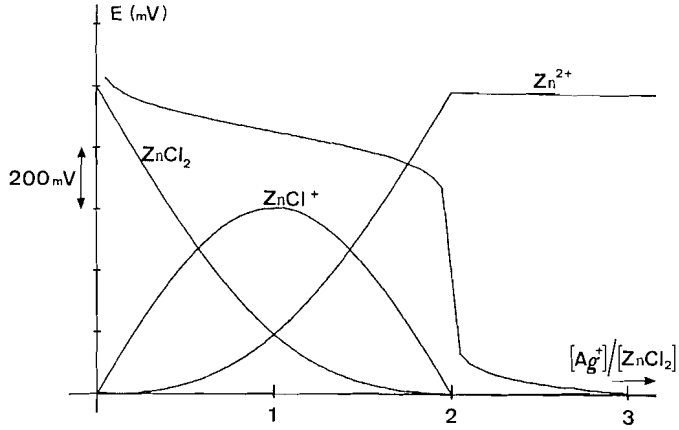

FIG. 5. Simulation de la neutralisation d'une solution de $ZnCl_2$ par $AgClO_4$. Évolution de la concentration des espèces $ZnCl_2$, $ZnCl^+$ et Zn^{2+} au cours du dosage.

À l'aide des valeurs des constantes K_1^* et K_2^*, nous avons effectué la simulation d'un dosage d'une solution de $ZnCl_2$ par $AgClO_4$ (fig. 5). Nous avons également reporté sur cette figure l'évolution de la concentration des différentes espèces au cours du dosage. Les deux réactions [6] et [7] donnent naissance a une seule vague, comme nous l'avons constaté expérimentalement.

Les complexes $ZnCl_4^{2-}$, $ZnCl_3^-$ sont plus stables dans le sulfolane et le diméthylsulfoxyde (16) (solvants aprotoniques) que dans le méthanol (17) et l'eau (18), en raison des propriétés peu solvatantes du sulfolane et du DMSO (tableau 1). Ces résultats sont en accord avec les hypothèses formulées par Ahrland (19), relatives à la solvatation des complexes métalliques en milieux protoniques et aprotoniques. En effet, les ligands susceptibles de former des liaisons hydrogènes sont fortement solvatés par les solvants protoniques, ce qui diminue la stabilité des complexes.

III. *Constante de stabilité du complexe trinitratozincate[II] dans le sulfolane*

Nous avons vu que la stabilité du complexe tétrachlorozincate[II] est plus faible que celle du trichlorozincate[II] (log $K_3^* = +10,1 \pm 0,2$ et log $K_4^* = 5,2 \pm 0,2$ à 303 K), ce qui est en accord avec les résultats relevés, dans le cas du cuivre, pour un solvant à propriété physique voisine du sulfolane (pouvoir donneur (DN) = 14,8), l'acétonitrile (DN = 14,1) (12). Cet écart de stabilité doit être retrouvé avec les complexes du nitrate tri- et tétra-coordonnés puisque les ligands Cl^- et NO_3^- ont, dans notre solvant, des solvatations très voisines: (*i*) les constantes d'acidité de HNO_3 et HCl sont proches, soit 16 (3*a*) et 14,5 (20), respectivement; (*ii*) les constantes d'homoconjugaison de HNO_3 et HCl ($AH + A^- \rightleftarrows A_2H^-$) sont toutes deux égales à 3,1 (2, 3*a*).

La réaction de N_2O_4 avec le complexe trinitrato selon

[9] $N_2O_4 + Zn(NO_3)_3^- \rightleftarrows NO^+ + Zn(NO_3)_4^{2-}$

doit être peu déplacée vers la formation du complexe nitrosyle,

TABLEAU 1. Constantes de stabilité des complexes chlorozincates[II]: $Zn(Cl)_i^{2-i}$ (i = 1, 2, 3, 4), en milieux protoniques et aprotoniques, relatives aux équilibres

$$Zn(Cl)_{i+1}^{3-i} + Cl^- \rightleftarrows Zn(Cl)_i^{2-i} \; (K_i^*)$$

Solvant (DN[a])	log K_1^*	log K_2^*	log K_3^*	log K_4^*	Réf.
Eau (DN = 18,0)	−0,19	−0,40	0,75	—	18
Méthanol	3,9	4,3	—	—	17
Diméthylsulfoxyde (DN = 29,8)	1,94	3,89	2,26	—	16
Sulfolane (DN = 14,8)	12,1±0,2	13,4±0,2	10,1±0,2	5,2±0,2	[b]

[a]Pouvoir donneur du solvant selon l'échelle de basicité de Gutmann et coll. (15).
[b]Nos valeurs.

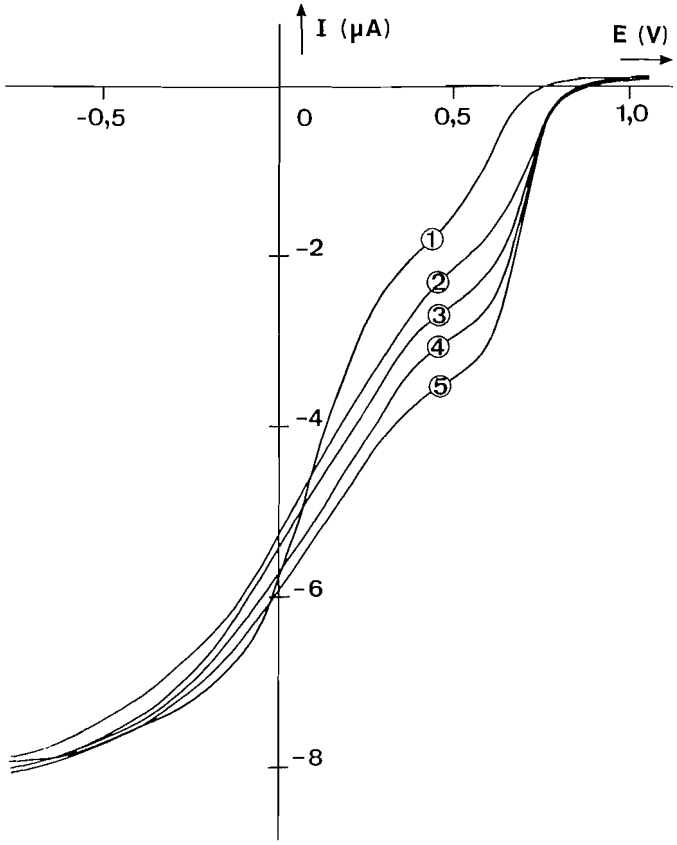

FIG. 6. Courbes intensité–potentiel obtenues dans le sulfolane à 303 K (électrode de platine poli) lors de l'addition de nitrate de zinc à une solution de N_2O_4. Électrolyte indifférent: $[(C_2H_5)_4NClO_4]$ = 0,1 mol dm^{-3}. $[N_2O_4] = 5{,}96 \times 10^{-3}$ mol dm^{-3}; $[Zn(NO_3)_2] = 0$ (1), $3{,}10 \times 10^{-3}$ (2), $5{,}30 \times 10^{-3}$ (3), $7{,}20 \times 10^{-3}$ (4), $11{,}40 \times 10^{-3}$ mol dm^{-3} (5).

et donc négligeable. Cette hypothèse est d'ailleurs confirmée par l'allure des courbes $i = f(E)$ obtenues au cours de l'addition de nitrate de zinc à une solution de N_2O_4 (fig. 6), allure très semblable à celle des courbes relatives aux mélanges N_2O_4 + $UO_2(NO_3)_2$ (fig. 1) donnant lieu uniquement à la formation d'un complexe $[(UO_2(NO_3)_3][NO]$.

De plus, la courbe représentant l'évolution du courant limite ($i_l(NO^+)$) de réduction de NO^+ (formé au cours de la réaction [2]) en fonction du rapport $[Zn(NO_3)_2]/[N_2O_4]$ (fig. 3), coïncide bien avec celle exprimant $i_l(NO^+)$ en fonction de $[UO_2(NO_3)_2]/[N_2O_4]$. Il est alors possible de déterminer la constante de la réaction

[10] $N_2O_4 + Zn(NO_3)_2 \rightleftarrows NO^+ + Zn(NO_3)_3^-$

par une étude similaire à celle réalisée avec les nitrates de cuivre et d'uranyle. La constante de la réaction [10] est égale à 1,8 ± 0,3, et la constante de stabilité du complexe trinitratozincate[II] est égale à $2{,}9 \times 10^{+7}$ mol^{-1} dm^3 à 303 K. Cette valeur, proche de celle de la constante de dissociation ionique de N_2O_4, empêche, dans le sulfolane, la formation par N_2O_4 de complexes plus coordonnés. La spectroscopie Raman apporte une preuve directe de la formation d'un sel de nitrosyle, lors de l'étude d'une solution équimoléculaire N_2O_4–$Zn(NO_3)_2$ (fig. 2), mais ne permet pas de conclure sur l'absence en solution du complexe $Zn(NO_3)_4^{2-}$; les bandes caractéristiques des vibrations de NO_3^- libre ou complexé sont masquées par les raies intenses et larges du sulfolane. Notons que la stabilité du complexe $Zn(NO_3)_3^-$ ($K_3^*(Zn) = 2{,}9 \times 10^{+7}$ dm^3 mol^{-1} à 303 K) est légèrement plus faible que celle du complexe $Cu(NO_3)_3^-$ ($K_3^*(Cu) = 4{,}0 \times 10^{+7}$ dm^3 mol^{-1} à 303 K), ce qui est en accord avec la classification des métaux en fonction de leur pouvoir complexant proposée par Irving et Williams (21).

En résumé, la présence de l'acide de Lewis $Zn(NO_3)_2$, dans une solution de N_2O_4, conduit dans le sulfolane à la formation de NO^+ et du complexe trinitratozincate[II]. Cette réaction est observée dans notre solvant grâce à une stabilité du complexe $Zn(NO_3)_3^-$ ($K_3^*(Zn) = 2{,}9 \times 10^{+7}$ dm^3 mol^{-1} à 303 K) voisine de celle de N_2O_4 selon $NO^+ + NO_3^- \rightleftarrows N_2O_4$ ($K_{N_2O_4}^* = +1{,}6 \times 10^{+7}$ dm^3 mol^{-1} à 303 K).

Conclusion

L'utilisation de la voltampérométrie a permis d'élucider le mécanisme de la réduction de N_2O_4 en présence des nitrates métalliques $Zn(NO_3)_2$, $Cu(NO_3)_2$ et $UO_2(NO_3)_2$ en milieu aprotonique:

[C] $N_2O_4 + M(NO_3)_2 \rightleftarrows NO^+ + M(NO_3)_3^-$

[E] $NO^+ + e^- \rightleftarrows NO$

Le processus électrochimique est contrôlé par le transfert monoélectronique réversible mis en jeu lors de la réduction de NO^+ en NO (système [E]). Ce résultat a rendu possible la détermination de la constante d'équilibre de la réaction [C], (K_M^*), et celle relative à la formation du complexe métallique trinitrato, $K_3^*(M)$, selon $M(NO_3)_2 + NO_3^- \rightleftarrows M(NO_3)_3^-$. À 303 K, les valeurs trouvées sont: $K_{Zn}^* = 1{,}8 \pm 0{,}3$; $K_{Cu}^* = 2{,}5 \pm 0{,}4$; $K_{UO_2}^* = 1{,}7 \pm 0{,}2$; $K_3^*(M) = 2{,}9 \times 10^{+7}$, $4{,}0 \times 10^{+7}$ et $2{,}7 \times 10^{+7}$ mol^{-1} dm^3, respectivement pour M = Zn, Cu et UO_2. Nous

avons négligé l'intervention des entités $M(NO_3)_4^{2-}$, $M(NO_3)^+$ et M^{2+}, dans les réactions précédentes, en raison de leur concentration trop faible dans la solution. Cette hypothèse a été confirmée par des travaux sur les mélanges N_2O_4–$M(NO_3)_2$ signalés dans la littérature, et par nos résultats obtenus dans la série des complexes chlorozincates[II] où la base Cl^- a un comportement vis-à-vis du métal Zn^{2+} très semblable à celui de NO_3^-.

L'addition de ces nitrates métalliques dans une solution de N_2O_4 permet donc, en milieu aprotonique, le déplacement de la base nitrate dans l'équilibre de dissociation ionique $N_2O_4 \rightleftarrows NO^+ + NO_3^-$, en libérant l'espèce NO^+. L'emploi facile de ces sels minéraux ainsi que leur grande solubilité dans le sulfolane, nous ont conduits à les utiliser comme agent catalytique dans les réactions de nitration par N_2O_4 des noyaux aromatiques (en générant en solution l'espèce catalytique NO^+) (1).

Remerciements

Nous tenons à remercier Monsieur le professeur M. Wozniak (Université de Lille I) pour les discussions fructueuses.

1. A. Boughriet, C. Bremard, J. C. Fischer et M. Wartel. Nouv. J. Chim. Sous presse.
2. M. Wartel, A. Boughriet et J. C. Fischer. Anal. Chim. Acta, **110**, 211 (1979).
3. (*a*) A. Boughriet. Thèse, Lille (1984); (*b*) A. Boughriet, M. Wartel, J. C. Fischer, et Y. Auger. J. Electroanal. Chem. **186**, 201 (1985); (*c*) A. Boughriet, J. C. Fischer, G. Leman et M. Wartel. Bull. Soc. Chim. Fr. **1**, 8 (1985); (*d*) A. Boughriet, C. Bremard, J. C. Fischer et M. Wartel. J. Electroanal. Chem. Sous presse.
4. C. C. Addison, W. Karcher et H. Hecht. Chemie in Flüssigem Distickstofftetrioxid und Schwefeldioxid. Vol. 3. Friedr. Vieweg & Sohn, Pergamon Press, Braunschweig, W. Germany. 1967.
5. P. Pierens, Y. Auger, J. C. Fischer et M. Wartel. Can. J. Chem. **53**, 2989 (1975).
6. J. Bizot. Bull. Soc. Chim. Fr. **1**, 151 (1967).
7. K. Nakamoto. Infrared and Raman spectra of inorganic and coordination compounds. 2 éd. Wiley–Interscience, John Wiley & Sons, New York. 1970. p. 78.
8. (*a*) L. V. Kobets, G. N. Klavsut et D. S. Umreiko. Zh. Neorg. Khim. **26**, 173 (1981); Chem. Abstr. **94**, 681 (1981); (*b*) L. V. Kobets, G. N. Klavsut, V. M. Dolgov et D. S. Umreiko. Radiokhimiya, **25**, 48 (1983); Chem. Abstr. **98**, 483 (1983); (*c*) G. N. Klavsut et L. V. Kobets. Zh. Neorg. Khim. **28**, 1542 (1983); Chem. Abstr. **99**, 357 (1983); (*d*) L. V. Kobets, G. N. Klavsut et V. M. Dolgov. Radiokhimiya, **25**, 661 (1983); Chem. Abstr. **99**, 443 (1983).
9. M. J. Schwing-Weill. Bull. Soc. Chim. Fr. 823 (1973).
10. M. A. Khan et M. J. Schwing-Weill. Inorg. Chem. **15**, 2202 (1976).
11. J. Bjerrum et L. H. Skibsted. Acta Chem. Scand. Ser. A, **31**, 673 (1977).
12. S. E. Manahan et R. T. Iwamoto. Inorg. Chem. **4**, 1409 (1965).
13. A. Foll, M. Le Demezet et J. Courtot-Coupez. J. Electroanal. Chem. **35**, 41 (1972).
14. T. E. Suarez, R. T. Iwamoto et J. Kleinberg. Inorg. Chim. Acta, **7**, 292 (1973).
15. (*a*) V. Gutmann. Chem. Technol. 255 (1977); (*b*) U. Mayer et V. Gutmann. Struct. Bonding (Berlin), **12**, 113 (1973).
16. S. Ahrland et N.-O. Björk. Acta Chem. Scand. Ser. A, **30**, 270 (1976).
17. H. Hoffmann, G. Platz et M. Franke. Proc. 16th Int. Conf. Coord. Chem. Paper 3.35. (1974).
18. P. Gerding. Acta Chem. Scand. **23**, 1695 (1968).
19. S. Ahrland. Pure Appl. Chem. **54**, 1451 (1982).
20. J. F. Coetzee et R. J. Bertozzi. Anal. Chem. **43**, 961 (1971).
21. H. Irving et R. J. P. Williams. J. Chem. Soc. 3192 (1953).

The electrochemical oxidation of 2,5-dihydroxybenzoic acid on a mercury electrode in aqueous solutions

D. SAZOU AND N. PAPADOPOULOS

Laboratory of Physical Chemistry, Department of Chemistry, University of Thessaloniki, Thessaloniki, Greece

Received August 29, 1984[1]

D. SAZOU and N. PAPADOPOULOS. Can. J. Chem. **64**, 11 (1986).

The electrochemical behaviour of 2,5-dihydroxybenzoic acid (2,5-DHBA) has been studied in the pH range 5.5–12.7 at a hanging mercury drop electrode (HMDE). Voltammograms show the existence of one reversible wave of 2,5-DHBA governed by diffusion conditions. In the oxidation process a two-electron transfer takes place, as shown by the controlled potential electrolysis. From the calculation of the voltammetric parameters (peak width $E_p - E_{p/2}$, peak current function $i_p/\sqrt{v}$) and from the other experimental data, a mechanism for the overall reaction in two different pH ranges, 5.5–9.5 and 9.5–12, is proposed.

D. SAZOU et N. PAPADOPOULOS. Can. J. Chem. **64**, 11 (1986).

Le comportement électrochimique de l'acide dihydroxy-2,5 benzoïque a été étudié à des pH allant de 5,5 à 12,7, à l'aide d'une électrode de mercure à goutte tombante. La vague réversible cyclovoltammétrique de l'acide dihydroxy-2,5 benzoïque est contrôlée par la diffusion. Le processus d'oxydation implique un transfert de deux électrons. Sur la base de calculs des paramètres voltammétriques (largeur du pic à mi-hauteur, $E_p - E_{p/2}$, et la fonction du courant du pic) ainsi que sur la base des autres données expérimentales, on propose un mécanisme concernant la réaction globale dans deux régions différentes de pH (5,5–9,5 et 9,5–12,0).

[Traduit par le journal]

Introduction

Several studies have been carried out on the electrochemical behaviour of the hydroquinone–quinone system in aqueous as well as in nonaqueous solutions at different electrodes (1–9).

The oxidation–reduction potentials of a number of quinones have been studied to determine the aromatic character, particularly in the fused ring systems (10, 11). Ring substituents have a significant effect on these potentials, and the course of many reactions is regulated by them. Methyl substituted quinones have also been studied (12, 13).

The hydroxy-derivatives of salicylic acid, classical reagents in inorganic analytical chemistry, belong to the group of substituted hydroquinones. Very few papers have been reported on their complex formation and on the determination of their protonation constants (14–16). The monosubstituted hydroquinones with strong electron-withdrawing substituents such as —COOH, —CHO, and —NO_2 undergo anodic hydroxylation at low potentials in aqueous solutions. The evidence for this anodic hydroxylation has been provided by electrochemical techniques with carbon – Nujol paste electrodes for voltammetric studies and carbon cloth for preparative scale electrolysis (17, 18).

In this paper, we investigate the electrochemical behaviour of 2,5-dihydroxybenzoic acid (DHBA) in the pH range 5.5–12.7 phosphate buffer, at a hanging mercury drop electrode (HMDE). We attempted to investigate, under the same conditions, the electrochemical behaviour of 2,6- and 2,4-dihydroxybenzoic acids, but an oxidation wave was not obtained at the potential range available on mercury.

Experimental

2,5-Dihydroxybenzoic acid (2,5-DHBA), from Fluka A. G. "puriss p.a.", was purified by recrystallization from water and dried under vacuum.

As a supporting electrolyte solution, a solution buffered with phosphates was used. The ionic strength was 0.3 *M*. All reagents used were Fluka A. G. "puriss p.a.". The solutions of 2,5-DHBA were freshly prepared, after the deaeration of the supporting electrolyte. High purity argon was used for oxygen removal and all measurements were carried out in an argon atmosphere and at a temperature of 25 ± 0.1°C.

Cyclic voltammetric measurements were carried out on a HMDE (PAR 9323) of surface area 3.51×10^{-2} cm^2. A Pt sheet and a calomel electrode were used as counter and reference electrodes, respectively, and they were separated from the working electrode compartment by glassy diaphragms.

Electrolysis was carried out using a mercury pool working electrode.

The experimental setup included a G. Bank Electronic PCA-72L potentiostat, a G. Bank Electronic VSG-72L function generator, and a Hewlett Packard 7045A X–Y recorder.

Results

Cyclic voltammetric behaviour

The electrochemical behaviour of 2,5-DHBA was studied as a function of increasing pH. In acid solution, pH range 2–5, the 2,5-DHBA does not give any oxidation wave at a HMDE, in contrast to the hydroquinone, which under the same conditions gives a regular reversible wave from pH = 2.

At pH 5–6 one poorly-defined oxidation–reduction wave appears, while at pH 6 a well-defined wave is obtained. 2,5-DHBA oxidizes to the corresponding quinoid form, which, on the cathodic scan, reduces to the initial substance.

The peak separation, $E_{pa} - E_{pc}$, is equal to about 35 mV over the whole pH range studied.

In Fig. 1, the cyclic voltammogram of 2,5-DHBA in neutral solution at different sweep rates, v, is shown as an example. The peak current, i_p, at these scan rates is directly proportional to the 2,5-DHBA concentration, C, over the whole pH range, and, at the same sweep rates and pH values, the slope of the log i_p – log C line is equal to unity.

The peak potential, E_p, corresponding to the oxidation wave, does not vary with scan rate (Fig. 2). It can be seen that the plot is a straight line almost parallel to the x-axis over the whole scan rate range studied.

At pH about 9.5 the anodic wave of 2,5-DHBA appears to be distorted (split into two poorly-defined waves). This suggests that the depolarizer exists under two different forms. At this pH value the ionization of the first phenolic group begins, as the pK_2 of 2,5-DHBA has been found to be equal to about 10 (16).

[1]Revision received July 4, 1985.

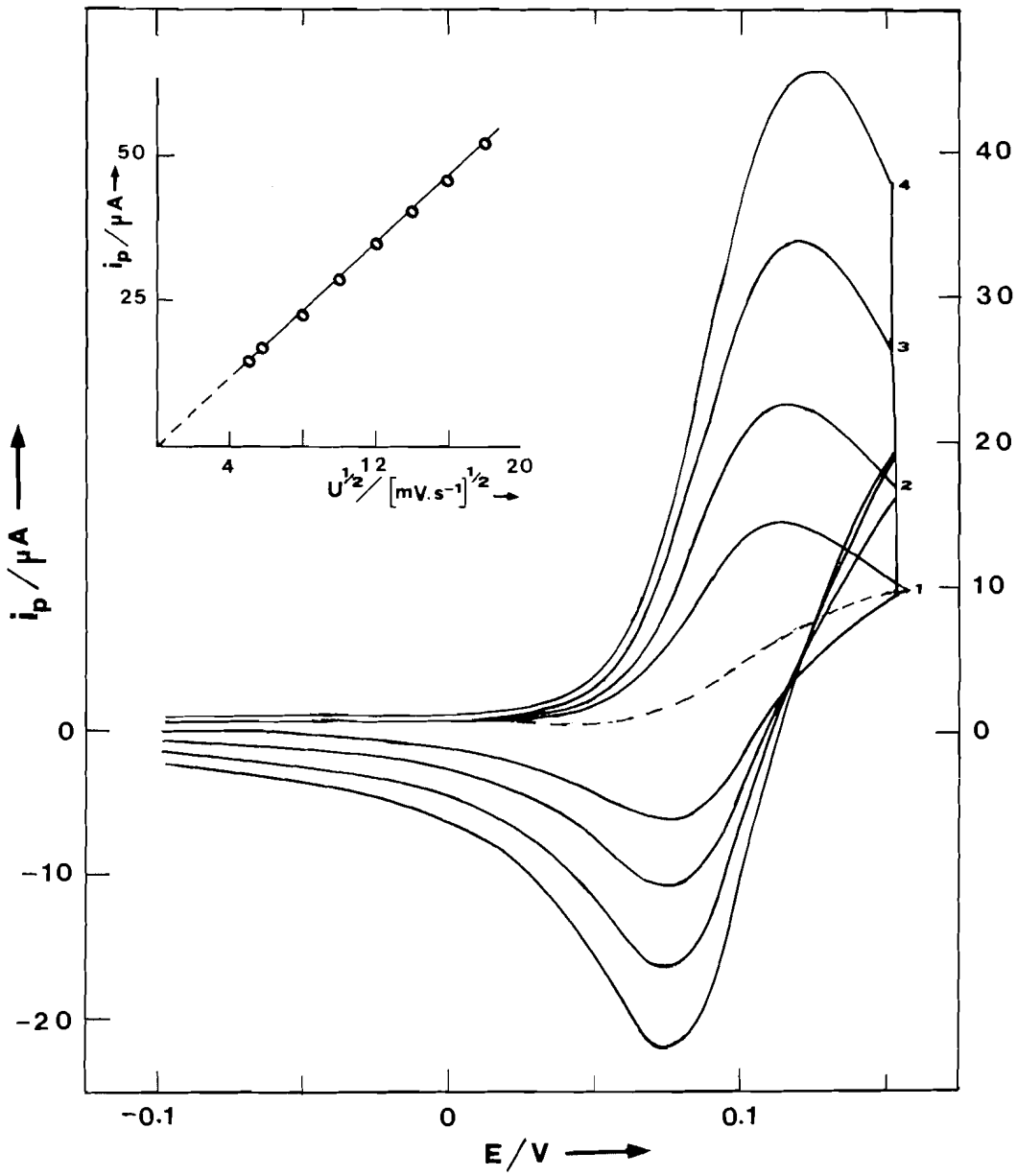

FIG. 1. Cyclic voltammogram of 2,5-DHBA ($C = 10^{-3}$ M) in phosphate buffer pH = 7.4 at different scan rates in mV s^{-1}: (1) 25, (2) 64, (3) 144, (4) 256. Inset: plot of i_p vs. $v^{1/2}$ for the anodic wave at different scan rates in mV s^{-1}: 25, 36, 64, 100, 144, 196, 256, 324.

In the pH range 5.5–9.5, the height of the anodic wave decreases with increasing pH and at pH 9.5 is split into two waves. Above this pH value only one wave appears, and its height decreases again as the pH increases. The peak potential shifts to more negative potentials with an increase in pH. The relationship between E_p and pH is shown in Fig. 3 where the values of the slopes of the linear segments are approximately −60 and −30 mV/pH unit.

At pH >12.7 the mechanism of the overall reaction changes. The cyclic voltammogram (Fig. 4), at this pH, illustrates an anodic wave and a corresponding reduction wave, owing to the oxidation product. At more negative potentials a second cathodic wave with a corresponding oxidation wave on a second scan appears. The first reduction wave, B, is not observed at low sweep rates, but as the scan rate increases, its height increases also. Moreover, when the mercury drop remains for several seconds at −0.15 V, both waves C and D increase. These results are explained by an ece (electrochemical chemical electrochemical) mechanism, in which the products of the chemical reaction are electroactive as well (19, 20). The oxidation product is probably a substituted quinone that, according to the bibliographic data for the behaviour of quinones in alkaline media, forms the intermediate substituted semiquinone resulting from one-electron reduction (17, 18, 21, 22). The radical anion may undergo radical dimerization or may disproportionate (waves C and D) (23).

A detailed study at pH >12.3 will be the subject of other work.

Protons involved in the overall process

As mentioned above, the variation of peak potential, E_p, of the anodic wave with pH is shown in Fig. 3.

The slope $(\partial E_p/\partial \text{pH})_C = (-0.059/n)\cdot p$ gives the number of protons, p, involved in the overall process.

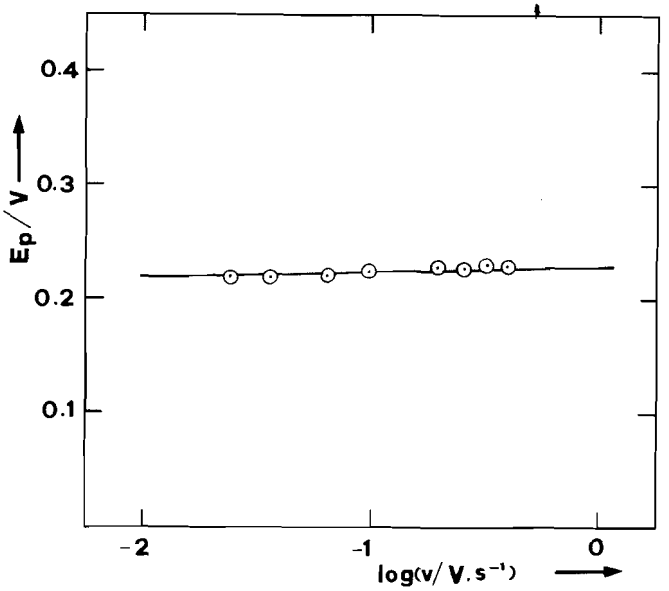

FIG. 2. Dependence of the peak potential, E_p, of the cyclic voltammogram of 2,5-DHBA ($C = 10^{-3}$ M) in phosphate buffer pH = 7.4 on the sweep rate, v.

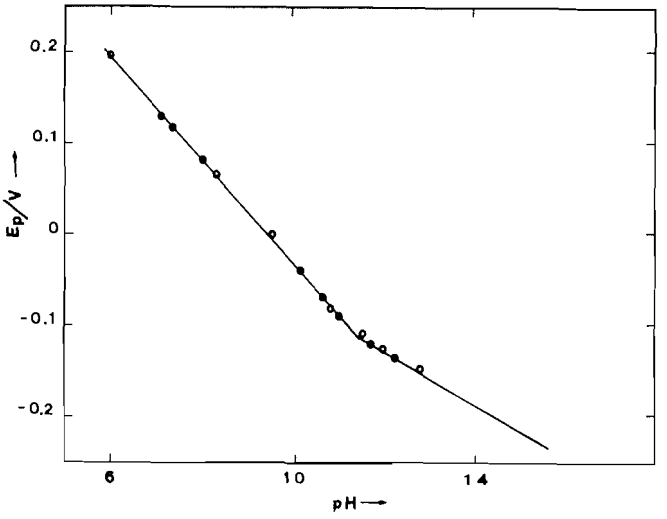

FIG. 3. Peak potential variation with pH for the anodic wave of 2,5-DHBA ($C = 10^{-3}$ M) at the scan rate of 100 mV s^{-1}.

Two linear segments with slopes −60 and −30 mV/pH unit are observed in the pH ranges 5–9.5 and 9.5–12, respectively. These slope values indicate that, in the overall reaction, two protons intervene in the pH range 5–9.5 and one proton intervenes in the pH range 9.5–12.

Discussion

The data obtained indicate that the oxidation of 2,5-DHBA corresponds to a two-electron reversible diffusion controlled charge transfer process.

The slope values of the E_p vs. pH plot indicate that in the overall reaction two protons intervene in the pH range 5.0–9.5, because of the existence of both undissociated phenolic groups, and one proton in the pH range 9.5–12, where the first phenolic group is dissociated. The change in the slope of the plot E_p–pH, at pH about 9.5, is attributed to the second dissociation constant of the 2,5-DHBA ($pK_2 = 10$). These data, together with the pH dependence of the peak current, indicate the occurrence of a chemical reaction involving H^+ ions prior to the electron transfer taking place at the surface of the electrode.

The overall reaction in the two pH ranges can be expressed as follows:

pH = 5.5–9.5

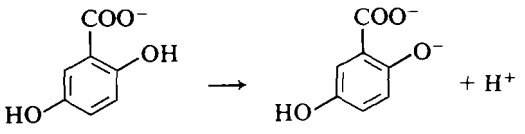

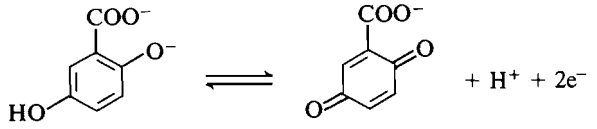

pH = 9.5–12

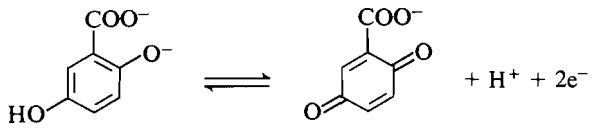

Finally, the oxidation of 2,5-DHBA seems to be a typical uncomplicated multistep reaction in which both charge transfers are reversible. Both, the initial form and the form that results after the transfer of the first electron, seem to be oxidized at the same potential and the wave observed has a peak height between a one-electron and two-electron reversible wave. These statements are supported by the following experimental results: The peak width, $E_p - E_{p/2}$, has an average value of 40 mV. This means that there is a small difference between the E_0 values for the two individual one-electron transfers (24, 25). The quantity $i_p/\sqrt{v}$ was constant over the wide range of scan rates used. The E_p was not shifted by increasing the scan rate. The ratio i_{pa}/i_{pc} was approximately unity when the base line was properly taken (24–26).

It has been reported by other authors (17, 18) that, in the case of 2-substituted hydroquinones, if the 2-substituent is electron withdrawing, such as —COOH, —CHO, —NO_2, hydroxylation occurs in an overall process, with a total of four electrons being found using controlled potential coulometry.

This hydroxylation was studied using carbon – Nujol paste electrodes and Pt electrodes modified by adsorbed metals and it was found that the M_{ads} promotes the reaction of hydroxylation (17, 18, 27).

However, in our case, in the pH range 5–12 on a mercury electrode, the reaction involves only a two-electron oxidation to the substituted benzoquinone. No evidence for anodic hydroxylation appeared under the voltammetric conditions used in this study.

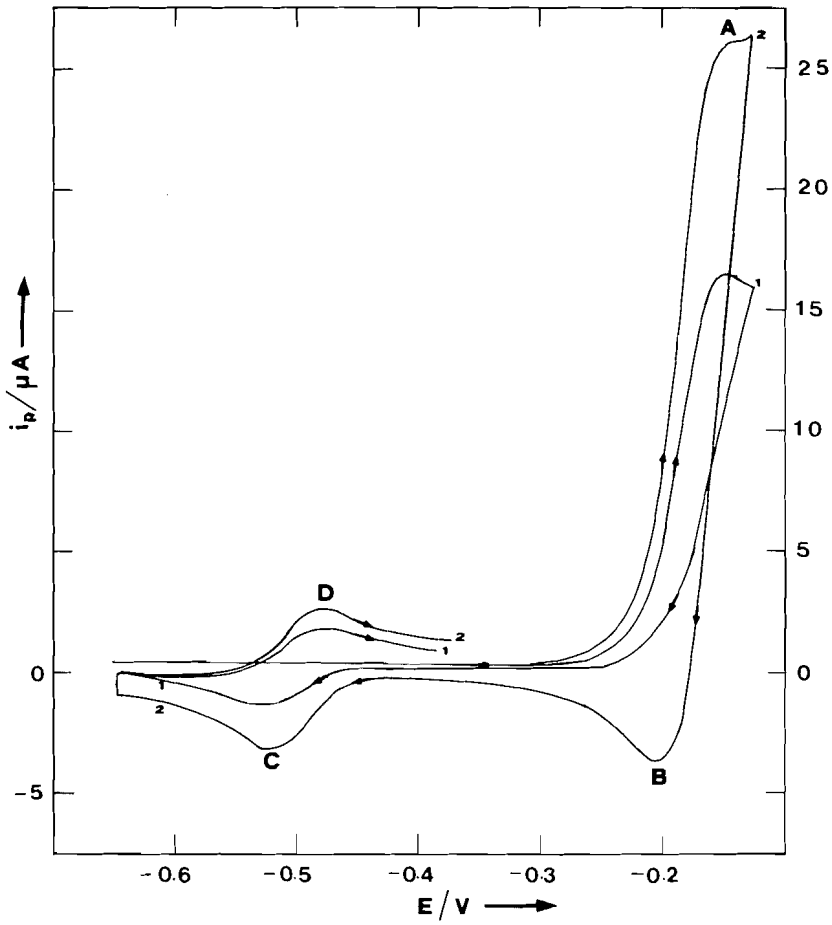

FIG. 4. Cyclic voltammogram of 2,5-DHBA ($C = 10^{-3} M$) at HMDE in phosphate buffer pH = 12.7 at two different scan rates: (1) 25 mV s^{-1}, (2) 100 mV s^{-1}.

1. K. J. VETTER. Z. Electrochem. **56**, 797 (1982).
2. J. M. HALE and R. PARSONS. Trans. Faraday Soc. **59**, 1429 (1963).
3. K. S. V. SANTHANAM and V. R. KRISHNAN. Z. Physik. Chem. **39**, 137 (1963).
4. K. M. C. DAVIS, P. R. HAMMOND, and M. E. PEOVER. Trans. Faraday Soc. **61**, 1516 (1965).
5. M. PEOVER. J. Chem. Soc. 4540 (1962).
6. M. E. PEOVER and J. D. DAVIES. J. Electroanal. Chem. **6**, 46 (1963).
7. P. J. ELVING and A. F. KRIVIS. Anal. Chem. **30**, 1645 (1968).
8. V. D. PARKER. Electrochim. Acta, **18**, 519 (1973).
9. L. A. KAMEL and A. M. SHAMS EL DIN. J. Electroanal. Chem. **24**, 229 (1970).
10. L. F. FIESER. Theory of the structure and reactions of organic compounds. *In* Organic chemistry. Vol. 1. 2nd ed. *Edited by* H. Gilman. John Wiley and Sons, Inc., New York. 1943. pp. 117–213.
11. L. F. FIESER and M. FIESER. Organic chemistry. 3rd ed. Reinhold Publishing Corp., New York. 1956. pp. 710–731.
12. R. D. RIEKE, T. SAZI, and N. KUZUNDZIC. J. Electroanal. Chem. **102**, 397 (1979).
13. K. TAKAMURA and J. HAYAKAWA. J. Electroanal. Chem. **31**, 219 (1971).
14. L. G. SILLEN and A. E. MARTEILL. Stability constants of metal ion complexes. Spec. Publ. No. 25, The Chemical Society, London. 1971.
15. L. H. J. LAJUNEN and M. KARVA. Anal. Chim. Acta, **97**, 423 (1978).
16. L. H. J. LAJUNEN, J. SAARINEN, and S. PARHI. Talanta **27**, 71 (1980).
17. L. PAPOUCHADO, G. PETRIE, J. H. SHARP, and R. N. ADAMS. J. Am. Chem. Soc. **90**, 5620 (1968).
18. L. PAPOUCHADO, G. PETRIE, and R. N. ADAMS. J. Electroanal. Chem. **38**, 389 (1972).
19. R. S. NICHOLSON and I. SHAIN. Anal. Chem. **37**, 178 (1965).
20. R. S. NICHOLSON and I. SHAIN. Anal. Chem. **37**, 190 (1965).
21. I. M. KOLTHOFF and J. J. LINGANE. Polarography. 2nd ed. Vol. I. Wiley–Interscience, New York. 1952. p. 153.
22. J. Q. CHAMBERS. *In* The chemistry of the quinoid compounds. *Edited by* S. Patai. J. Wiley, New York. 1974. p. 737.
23. M. M. BAIZER. Organic electrochemistry. Marcel Dekker, Inc., New York. 1973. p. 408.
24. D. S. POLCYN and I. SHAIN. Anal. Chem. **38**, 370 (1966).
25. R. L. MYERS and I. SHAIN. Anal. Chem. **41**, 980 (1969).
26. R. S. NICHOLSON and I. SHAIN. Anal. Chem. **36**, 706 (1964).
27. M. SAKAMOTO and K. TAKAMURA. Bioelectrochem. Bioenerg. **10**, 251 (1983).

Study of the main extracted species of cobalt(II) ion with dodecylthioglycolic acid as extractor

P. BENEITEZ,[1] S. J. ORTIZ, AND J. ORTEGA

Departamento de Electroquímica, Facultad de Ciencias, Universidad Autónoma, Cantoblanco, 28049 Madrid, España

Received November 6, 1984[2]

P. BENEITEZ, S. J. ORTIZ, and J. ORTEGA. Can. J. Chem. **64**, 15 (1986).

The distribution of cobalt(II) between water and an organic extractant (dodecylthioglycolic acid) dissolved in kerosene has been studied using a tracer of ^{60}Co. The aqueous media were always constituted by buffer solutions (acetic acid – sodium acetate) and the ionic strength was adjusted with sodium nitrate to 1 mol dm^{-3}. The main species of cobalt(II) originating in the organic phase has been isolated and characterized on the basis of elemental analysis, thermal gravimetric analysis, and ir spectra.

P. BENEITEZ, S. J. ORTIZ et J. ORTEGA. Can. J. Chem. **64**, 15 (1986).

Utilisant du ^{60}Co comme marqueur, on a étudié la distribution du cobalt(II) entre l'eau et l'acide dodécylthioglycolique, dissous dans du kérosène. Tous les milieux organiques étaient constitués de solutions tampons (acide acétique/acétate de sodium) et, dans chaque cas, on a ajusté la force ionique à 1 mol/dm^3, à l'aide de nitrate de sodium. On a isolé les principales espèces de cobalt(II) qui se retrouvent dans la phase organique et on les a caractérisées en se basant sur l'analyse élémentaire, l'analyse thermogravimétrique et sur les spectres ir.

[Traduit par le journal]

Introduction

Many papers have shown the utility of carboxylic acids in the extraction of metal ions but only some of them have involved a study of the stoichiometry of the extracted species (1–12). The cobalt extraction characteristic has attracted attention over a period of time. The early works of Jaycock and Jones, Schweitzer and Howe (13, 14) postulated that, for the extraction of that metal, the major species in the organic phase was CoR_2, but later works of Jaycock, Gindin, and co-workers (15–17) proposed that a dimeric species is present to a major extent in the organic phase. For the moment the situation concerning the structure of the extracted cobalt species does not appear to be resolved and the purpose of the present work is to report on some new studies. Thus the present paper is concerned with the extraction of cobalt(II) by dodecylthioglycolic acid in kerosene and the characterization of a solid compound isolated from the extract on the basis of elemental analysis, thermal gravimetric analysis, and ir spectra. A carboxylic acid containing a sulphide group in the β position with respect to the carboxylic group has been chosen, since the presence of the sulphur atom emphasizing the acid character of the compound enhances the cobalt ion extraction and allows their separation from stronger acid media.

Experimental

Reagents

The principal solution of ^{60}Co tracer was obtained from the Radiochemical Center of Amersham containing 10 μg Co/mL in the chloride state with an activity of 1 mCi/mL. HDTG acid (dodecylthioglycolic) was obtained from Phillips Petroleum Company with the general structure of:

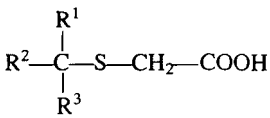

where $R^1 + R^2 + R^3 = C_{11}H_{25}$, boiling point 220°C, and was used as received. Solutions of this organic acid were prepared in kerosene (S.S.T.) from Sociedad Petrolífera Española, Shell S.A., with dielectric constant 2.03. All the other reagents were of A.R. grade and were used without further purification. The solutions of these chemicals were freshly prepared just prior to use.

Extraction procedure

An aqueous solution (2 cm^3) containing ^{60}Co, buffer reagents (mixtures of acetic acid – sodium acetate 0.1 *M* with different pH), the metal salt (2×10^{-4} *M*), and with the ionic strength adjusted to unity with sodium nitrate was mixed in a glass tube with the same volume of organic solution containing the desired concentration of HDTG, and the tube was shaken for 50 min at constant temperature (25 ± 0.1°C). After equilibration, each sample was centrifuged, a 1-cm^3 portion of each phase was pipetted into a counting tube, and the γ-activity was measured in a well-type scintillation counter (Tracerlab Model 132 MA scaler). The remaining part of the aqueous phase was used for pH measurement with a pH meter (Metrohm Herisau E500) equipped with a glass combination electrode.

Preparation of the metal carboxylate

The metal carboxylate was prepared by extraction of cobalt(II) from an aqueous solution containing this metal (3×10^{-1} *M*) and the ionic strength adjusted to 1 *M* (sodium nitrate) with a solution of HDTG acid (1 *M*) in S.S.T. After equilibration the phases were separated and the organic phase was equilibrated once again with new aqueous solutions of metal. This organic phase, saturated with the metal carboxylate, was mixed with acetone (1:5) and a pink precipitate formed. It was removed, washed with two portions of acetone, recrystallized from ethanol, and dried at 90°C during 2 days.

Analyses

Elemental analysis was carried out by the Microanalytical Unit of the Consejo Superior de Investigaciones Cientificas (C.S.I.C.). The metal and sulphur contents were measured by standard methods (18, 19). The thermal gravimetric analysis was carried out by the Unit of the Instituto del Cemento (Eduardo Torroja).

Physical measurements

The ir spectra were measured between KBr discs and recorded in a Perkin–Elmer 557 spectrophotometer in the 200–4000 cm^{-1} region. The uv and vis spectra were obtained by a Beckman Acta 3-C spectrophotometer. The melting point was determined by a Yanagimoto MP-1 melting point apparatus. The water molecules in the cobalt species were determined by titration with Karl–Fischer reagent and free from a wet atmosphere. Molar conductance measurements were obtained with a Beckman type RC16B2 conductivity bridge using 5×10^{-4} *M* solution in chloroform at 25°C. Magnetic susceptibility measurement was carried out at room temperature by the Gouy method and was corrected for the diamagnetism of the component atoms using Pascal's constants (24).

[1]Author to whom correspondence may be addressed.

[2]Revision received July 2, 1985.

Results and discussion

The plot of the experimental data, as log D against equilibrium pH, for the extraction of cobalt(II) from nitrate and buffer (HAc–NaAc) solutions with dodecylthioglycolic acid in kerosene leads to a similar curve in both cases, hence the nature of the extracted species is unaffected by acetate ions. Accordingly, and since the use of buffer solutions may contribute certain advantages to the extraction process, we have always used these buffer solutions in the extraction of Co(II).

The most general equilibrium for the extraction of cobalt(II) with a carboxylic acid can be written as follows (13).

$$[1]\quad j\mathrm{Co}^{2+} + 1/2(2j+x)\overline{(\mathrm{HDTG})_2} \rightleftarrows \overline{(\mathrm{Co(DTG)_2})_j(\mathrm{HDTG})_x} + 2j\mathrm{H}^+$$

for which

$$[2]\quad \log D = \log j + \log Kex + 1/2(2j+x)\log(\overline{C_{\mathrm{HDTG}}}) + (j-1)\log C_{\mathrm{Co}} - j\log\alpha_{\mathrm{Me}} + 2j\mathrm{pH} - 1/2(2j+x)\log 2$$

where α_{Me} denotes the side-reaction coefficient of the metal ion in the aqueous phase. Considering that under the experimental conditions of this work the hydrolysis of the metal ion may be assumed insignificant, then $\alpha_{Me} = 1$.

The data obtained in the extraction of cobalt(II) by dodecylthioglycolic acid in S.S.T. are shown in Fig. 1 as log D against equilibrium pH, and it can be seen that the slopes of the least-squares best-line fits range from about 2.6 to 3.4 and therefore j is not unity. The linearity of the plots falls off at high values of pH; it may suggest that at low hydrogen ion concentrations Co^{2+} exists as a mixture of hydrolysed forms. Using the data given in Fig. 1 the plot of log D − log C_{Co} against equilibrium pH leads to straight lines with slopes approximately 4.0 (Fig. 2); then, under the experimental conditions of this study the species of cobalt(II) extracted is dimeric ($j = 2$). From a plot of log D − log C_{Co} − 4 pH against log $(\overline{C_{\mathrm{HDTG}}})$ may be determined the number of acid molecules involving the extracted species. The plot for the experimental data (Fig. 3) leads to a straight line with slope = 2.5 and therefore $x = 1$. Thus, the graphical analysis of the data indicated a complex $(Co(DTG)_2)_2(HDTG)$ as the main extracted species and the extraction equilibrium [1] becomes:

$$[5]\quad 2\mathrm{Co}^{2+} + 5/2\overline{(\mathrm{HDTG})_2} \rightleftarrows \overline{(\mathrm{Co(DTG)_2})_2(\mathrm{HDTG})} + 4\mathrm{H}^+$$

The elemental analysis data of the isolated metal species (found: C 58.28, H 9.80, S 11.25, Co 10.05%) indicate the general formula $C_{28}H_{54}O_4S_2Co$ (*Anal.* calcd.: C 58.21, H 9.42, S 11.09, Co 10.20%). This species in the solid state is slightly soluble in the nonpolar solvents toluene, methanol, and diethyl ether; insoluble in solvents with high dipole moment, such as acetone, DMF, and DMS; and quite soluble in chloroform. The molar conductance in chloroform at 25°C was $\Lambda_m = 35.5\,\Omega^{-1}\,\mathrm{cm}^2\,\mathrm{mol}^{-1}$. It showed low melting point (192–195°C), and it decomposed at a temperature near the melting point showing colour change from pink to black.

The thermal gravimetric analysis study showed that the species was stable up to 200°C. At this temperature decomposition of the organic matter took place and the thermolysis curve showed a weight loss of about 80% of the whole weight (weight of sample 283.1 mg), all of which suggested that the isolated cobalt(II) species was not hydrated. The destruction of organic matter continued up to 310°C; at this point a perfectly horizontal stretch began, corresponding to the carbonate $CoCO_3$, and which continued up to 850°C. A new weight loss began at this temperature, to give finally a horizontal line due to the oxide Co_3O_4, which extended above 950°C. The titration with Karl–Fischer reagent for determination of water molecules likewise showed that the isolated cobalt species was anhydrous.

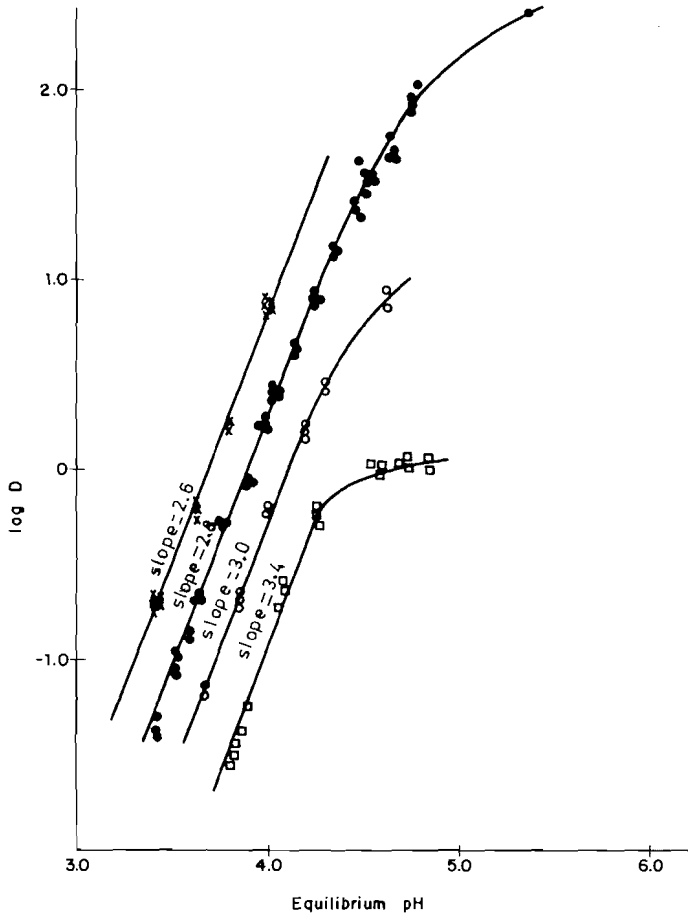

FIG. 1. Extraction of Co(II) with dodecylthioglycolic acid in kerosene. Acid concentration: ×, 1.0 *M*; ●, 0.5 *M*; ○, 0.25 *M*; □, 0.1 *M*.

The ir spectrum of the organic solution with the metallic species indicates the presence of the metal carboxylate; it shows two bands at 1590 cm^{-1} and 1385 cm^{-1}, which correspond to the antisymmetrical and symmetrical vibrations of the COO^- structure, respectively (21). Two strong bands at 1710 cm^{-1} and 1290 cm^{-1}, arising from the stretching vibration of the C=O and C—O in the COOH group, respectively, denote the presence of acid molecules in excess. One absorption band at 1645 cm^{-1} suggests an internal association (21), which is supported by the appearance of another band at 300 cm^{-1} attributed to ν(Me-S) (22). The ir spectrum of the pink precipitate formed exhibits almost the same pattern as that of the species in solution (bands at 1590 cm^{-1}, 1385 cm^{-1}, 1645 cm^{-1}, and 300 cm^{-1}). The absence of absorption bands at 1710 cm^{-1} and 1290 cm^{-1} suggests the absence of acid molecules in excess and therefore involving the complex. Likewise, the absence of a C=O stretching vibration band (1725–1690 cm^{-1}) shows the absence of an addition complex between the acetone and the extracted species, which was expected since the acetone rarely forms stable complexes. The magnetic moment of the compound is

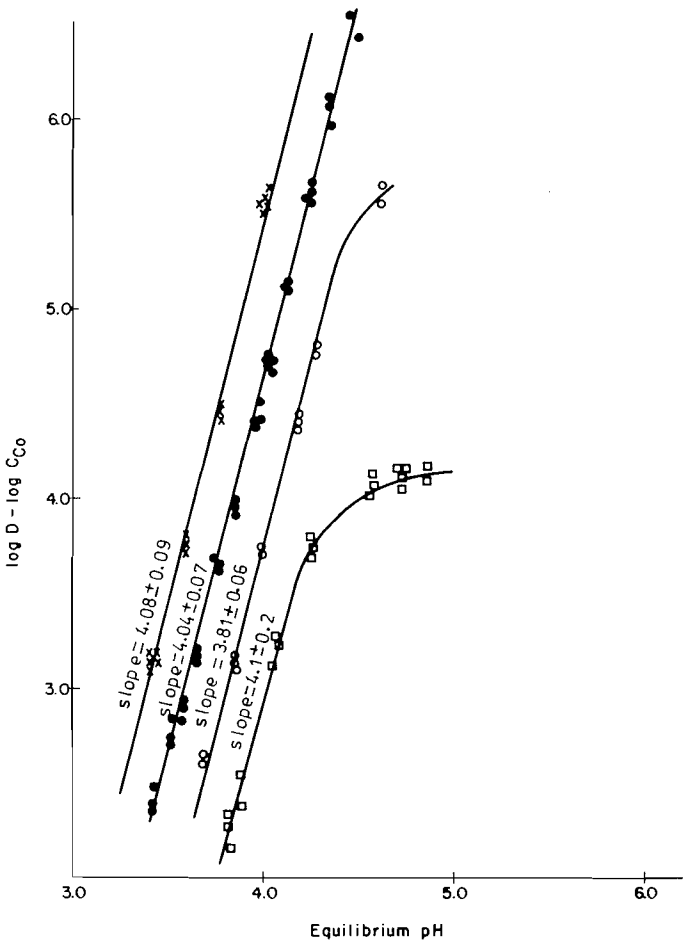

FIG. 2. Variation of log D − log C_{Co} against equilibrium pH in the extraction of cobalt(II) with dodecylthioglycolic acid in kerosene. Acid concentration: ×, 1.0 M; ●, 0.5 M; ○, 0.25 M; □, 0.1 M.

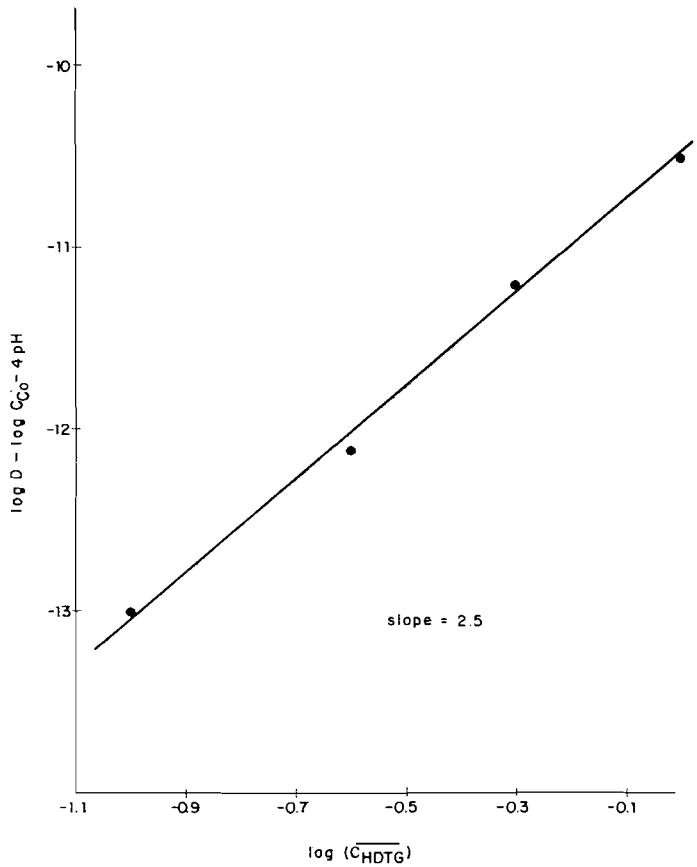

FIG. 3. Variation of log D − log C_{Co} − 4pH against equilibrium pH in the extraction of cobalt(II) with dodecylthioglycolic acid in kerosene.

found to be 4.65 BM, which is acceptable for tetrahedral structure.

In summary, all these observations together with the elemental analysis indicate the species $Co(R—S—CH_2—COO)_2$ with a feasible tetrahedral structure (**1**):

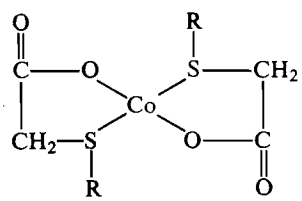

1

Studies of mixed complex formation between metal carboxylates and amines, in the case of copper, have shown that an interaction takes place between the copper and free base amine. Ultraviolet spectra suggested that the amine interaction had destroyed the dimeric bridged structure of the copper carboxylate, as seen by the disappearance of a shoulder in the region 300–400 nm on addition of an amine to a copper carboxylate solution in chloroform (23). These studies, in the case of our cobalt carboxylate, have shown no band in that region and no effect on the uv spectrum of the metal carboxylate by the addition of trilaurylamine, all of which could suggest that the isolated cobalt species is not dimeric.

1. A. I. MIKHAILICHENKO, M. A. KLIMENCO, and T. V. FEDULOVA. ZH. NEORG. KHIM. **19**, 3344 (1974).
2. H. YAMADA and M. TANAKA. J. Inorg. Nucl. Chem. **35**, 3307 (1973).
3. R. W. CATTRALL and M. J. WALSH. J. Inorg. Nucl. Chem. **36**, 1643 (1974).
4. A. BOLD and S. FISEL. An. Stiint. Univ. "Al. I. Cuza" Iasi, Sect. Ic, **17**, 19 (1971).
5. A. W. ASHBROOK. J. Inorg. Nucl. Chem. **34**, 3523 (1972).
6. N. NAKASUKA, Y. MITSUOKA, and M. TANAKA. J. Inorg. Nucl. Chem. **36**, 431 (1974).
7. J. ORTEGA and J. GUTIÉRREZ. International Solvent Extraction Conference. Vol. 2. Liege, Belgium. 1980. pp. 80–103.
8. D. S. FLETT and M. J. JAYCOCK. Ion exchange and solvent extraction. Marcel Dekker Inc., New York. 1973.
9. I. KOJIMA, M. YOSHIDA, and M. TANAKA. J. Inorg. Nucl. Chem. **32**, 987 (1970).
10. G. F. KOKOSZKA, M. LINZER, and G. GORDON. Inorg. Chem. **7**, 1730 (1968).
11. J. C. LEYTE, L. H. ZUIDERWEG, and M. VAN REISEN. J. Phys. Chem. **72**, 1127 (1968).
12. K. INOUE, H. AMMANO, and I. KAKAMORI. International Solvent Extraction Conference. Vol. 3. Liege, Belgium. 1980. pp. 80–135.
13. M. J. JAYCOCK and A. D. JONES. *In* Solvent extraction chemistry. *Edited by* D. Dyrssen, J. O. Liljenzin, and J. Rydberg. North Holland, Amsterdam. 1967. p. 160.

14. G. K. SCHWEITZER and L. H. HOWE. J. Inorg. Nucl. Chem. **29**, 2027 (1967).
15. A. I. KHOL'KIN and L. M. GINDIN. Izv. Sib. Otdel. Akad. Nauk SSSR, Ser. Khim. Nauk, 70 (1969).
16. V. I. BELOVA, A. I. KHOL'KIN, and L. M. GINDIN. Izv. Sib. Otdel. Akad. Nauk SSSR, Ser. Khim. Nauk, 1943 (1969).
17. M. J. JAYCOCK, A. D. JONES, and C. ROBINSON. J. Inorg. Nucl. Chem. **36**, 887 (1974).
18. Z. MARCZENKO. Spectrophotometric determination of elements. John Wiley and Sons Inc., England. 1976. p. 229.
19. R. N. WALTER. Anal. Chem. **22**, 1332 (1950).
20. W. J. GEARY. Coord. Chem. Rev. **7**, 81 (1971).
21. L. J. BELLAMY. The infrared spectra of complex molecules. Lowe and Brydone Ltd., Thetford, Norfolk. 1975.
22. J. R. FERRARO. Low frequency vibrations of inorganic and coordination compounds. Plenum Press, New York. 1971.
23. D. S. FLETT. Trans. Natl. Res. Inst. Met. (Jpn) **9**, 215 (1967).
24. J. LEWIS and R. G. WILKINS. Modern coordination chemistry. Interscience, New York. 1960.

Kinetics and mechanisms of oxidations by metal ions. Part VI.[1] Oxidation of α-hydroxy acids by cerium(IV) in aqueous nitric acid

NARAIN DATT,[2] RATAN R. NAGORI,[3] AND RAJ N. MEHROTRA[3,4]
Department of Chemistry, Kumaun University, Naini Tal 263 002, India

Received November 22, 1984[5]

NARAIN DATT, RATAN R. NAGORI, and RAJ N. MEHROTRA. Can. J. Chem. **64**, 19 (1986).

The kinetics of oxidation of glycolic, malic, tartaric, and citric acids by cerium(IV) ammonium nitrate were investigated in 0.006 mol dm^{-3} nitric acid. The reaction was catalysed by H^+ in the range 0.006–0.016 mol dm^{-3} at constant [NO_3^-] (0.02 mol dm^{-3}). The pseudo first-order rate constant k_{obs} was independent of [Ce^{III}] (0.0004–0.002 mol dm^{-3}). The proposed mechanism is based on the assumption that the formation of the precursor Ce(IV) – α-hydroxy acid complex precedes its rate controlling disproportionation, which is assisted by a proton, possibly due to the formation of the activated state [H^+—Ce^{IV} – HA]‡ (where Ce^{IV} is the reactive cerium(IV) species and HA is the α-hydroxy acid). The free radical $R^1R^2\dot{C}OH$ produced in the rate controlling step further reacts with a number of Ce(IV) molecules in the fast step to yield the final oxidation product. The activation parameters for the rate controlling step could be evaluated only in the oxidation of tartaric acid.

NARAIN DATT, RATAN R. NAGORI et RAJ N. MEHROTRA. Can. J. Chem. **64**, 19 (1986).

Opérant dans des solutions 0,006 mol/dm^3 en acide nitrique, on a étudié la cinétique des réactions d'oxydation des acides glycolique, malique, tartrique et citrique par le nitrate d'ammonium cérique(IV). À des concentrations en acide allant de 0,006 à 0,016 mol/dm^3 et à des [NO_3^-] constantes (0,02 mol/dm^3), la réaction est catalysée par les ions H^+. La constante de vitesse de pseudo-premier ordre, k_{obs}, est indépendante de la [Ce^{III}] (0,0004–0,002 mol/dm^3). Le mécanisme proposé repose sur l'hypothèse que la formation du complexe précurseur, Ce(IV) – acide α-hydroxylé, précède sa disproportionation dans l'étape qui détermine la vitesse et qui est assistée par un proton; cette assistance pourrait provenir de la formation de l'état activé [H^+—Ce^{IV} – HA]‡ (dans lequel Ce^{IV} est une espèce réactive du Ce(IV) et HA est un acide α-hydroxylé). Le radical libre $R^1R^2\dot{C}OH$, qui est formé dans l'étape qui détermine la vitesse, réagit ensuite avec un certain nombre de molécules de Ce(IV) dans l'étape rapide pour conduire au produit final d'oxydation. On n'a pu évaluer les paramètres d'activation de l'étape déterminante que dans le cas de l'oxydation de l'acide tartrique.

[Traduit par le journal]

Introduction

Since Krishna and Tewari (2) studied the kinetics of oxidation of α-hydroxy acids (lactic, malic, and mandelic acids) by cerium(IV) in aqueous sulphuric acid, there have been numerous investigations on the subject. These studies (3) dealt with one aspect or another, such as emphasizing a particular cerium(IV) species or suggesting a different one as the reactive species, supporting or contesting the formation of an intermediate cerium(IV) – α-hydroxy acid complex, reporting on the thermodynamic parameters, or investigating the effect of substituents on the benzene ring of mandelic acid, etc.

The oxidation in perchloric acid proceeded through an inner-sphere mechanism (4, 5). The complex $[CeA]^{3+}$, where A is the anion of the α-hydroxy acid HA, is thermodynamically more stable than its protonated form $[CeHA]^{4+}$ and is kinetically more reactive. One of these papers (5) also compared the results of the oxidation in sulphuric and perchloric acids.

However, the study of the reaction in nitric acid medium has not attracted much attention, the only report available being on the oxidation of substituted mandelic acids (6). This study drew our attention because the second-order rate constant (= k_{obs}/[mandelic acid]) was reported as 7.42×10^{-4} dm^3 mol^{-1} s^{-1} at 25°C and [HNO_3] = 1 mol dm^{-3}, in comparison to the value 3.39 dm^3 mol^{-1} s^{-1} at 20°C and [H_2SO_4] = 1 mol dm^{-3} (2). This seemed most unlikely in view of the various considerations related to the solution chemistry of cerium (IV) in nitric and sulphuric acid solutions.

Yet another reason for investigating this reaction was our interest in examining the dependence of the pseudo first-order rate constant k_{obs} on the initial [Ce^{IV}], for we had noted that k_{obs} decreased with increasing [Ce^{IV}] in the oxidation of diols (7) and carboxylic acids (8) in nitrate medium, though the disappearance of [Ce^{IV}] was always first order in any kinetic run corresponding to any initial [Ce^{IV}]. This phenomenon was ascribed to the reactivity of the dimeric cerium(IV) species, the existence of which has been demonstrated (9, 10) and questioned (11), in addition to monomeric species.

The preliminary investigations indicated that the rate of oxidation of mandelic acid was too fast to measure conveniently by the method adopted by us for following the kinetics. Strictly speaking, the rates are such that a clear picture of the study could be best provided by stopped flow technique, a facility presently not available to us.

Experimental

AnalaR (BDH) or Puriss (Fluka) grade α-hydroxy acids were used as received. The solutions were freshly prepared and standardized against a standard alkali. The solution of Ce(IV) ammonium nitrate (Loba, GR) was also freshly prepared and standardized against a standard Fe(II) solution. Ce(III) ammonium nitrate solution was prepared by the reduction of a standard cerium(IV) solution by hydrogen peroxide (Sarabhai-M.). The solution was heated, after the reduction of Ce(IV), to decompose the unreacted hydrogen peroxide. Sodium nitrate (E. Merck) solution of the desired strength was prepared by weighing of the sample. Nitric acid (BDH, AnalaR) solution was standardized against a standard alkali. The nitroferroin (G. F. Smith) solution was suitably diluted.

Stoichiometry

The stoichiometry in the oxidations of malic and tartaric acids was determined under conditions similar to those in the kinetic runs ([α-hydroxy acid] > 10 [Ce^{IV}]). The method adopted was the same as that described in the oxidation of malic acid in perchloric acid (4),

[1]For part V, see ref. 1.

[2]Present address: Kumaun University, Almora Campus, Almora 263 601, India.

[3]Present address: Department of Chemistry, University of Jodhpur, Jodhpur 342 001, India.

[4]Author to whom correspondence may be addressed.

[5]Revision received July 12, 1985.

and involved the determination of formic acid by using mercury(II) chloride. The mercury(I) chloride was determined using an iodine–thiosulphate titration. Taking into account the blank corrections, it was found that $\Delta[HCO_2H]/\Delta[Ce^{IV}]$, from three determinations, was 0.097 ± 0.004 and 0.123 ± 0.008 respectively for malic and tartaric acids. Hence the stoichiometric equations for the oxidation of these acids are:

[1] $HO_2C.CH_2CHOH.CO_2H + 3H_2O + 10Ce^{IV} \rightarrow HCO_2H + 3CO_2 + 10Ce^{III} + 10H^+$

[2] $HO_2C.CHOHCHOH.CO_2H + 2H_2O + 8Ce^{IV} \rightarrow HCO_2H + 3CO_2 + 8Ce^{III} + 8H^+$

The oxidized reaction mixtures of glycolic, 2-methyl-2-hydroxypropanoic, and citric acids were treated with 2,4-dinitrophenylhydrazine. The precipitated hydrazones were purified and their melting points determined. The mps of the hydrazones from glycolic and 2-methyl-2-hydroxypropanoic acid were 165°C and 130°C, respectively, which correspond to the mps of the hydrazones of formaldehyde (lit. (12*a*) mp 163.5–164.5°C) and acetone (lit. (12*b*) mp 128°C). The hydrazone from citric acid decomposed on heating. Considering that citric acid and 2-methyl-2-hydroxypropanoic acid are structurally similar, it is concluded that citric acid is oxidized to acetone dicarboxylic acid. The stoichiometric equation in the oxidation of each of these acids is expressed as:

[3] $CH_2OH.CO_2H + 2Ce^{IV} \rightarrow HCHO + CO_2 + 2Ce^{III} + 2H^+$

[4] $HO_2C.CH_2.C(OH)CO_2H.CH_2CO_2H + 2Ce^{IV} \rightarrow HO_2C.CH_2.CO.CH_2CO_2H + 2Ce^{III} + CO_2 + 2H^+$

[5] $CH_3.C(OH)CO_2H.CH_3 + 2Ce^{IV} \rightarrow CH_3COCH_3 + CO_2 + 2Ce^{III} + 2H^+$

Test for free radicals

Reaction mixtures were degassed with nitrogen before the reaction was initiated. Acrylonitrile was added to partially oxidized reaction mixtures. The monomer was polymerized within a few minutes, indicating the presence of free radical in the reaction mixtures. The monomer was not polymerized when it was added separately to the solution of α-hydroxy acids and cerium(IV) ammonium nitrate.

Rate measurements

The kinetics were followed under pseudo first-order conditions, i.e. α-hydroxy acid was present in excess. The ionic strength of the reaction mixture was maintained with sodium nitrate. The pseudo first-order rate constant k_{obs} was calculated from the gradients of the linear plots between ln $(a - x)$ and time, where $(a - x)$ is the change in the titre value. Five milliliters of the reaction mixture was quenched in the same volume of Fe(II) solution, which was titrated against cerium(IV) sulphate solution of the same strength as that of the Fe(II) solution, using nitroferroin as the indicator. The microburette reading therefore directly gave the value of x. The microburette was graduated to 0.02 mL. Before adopting this method, it was ensured that the presence of α-hydroxy acid in concentrations present in the reaction mixtures did not alter the titre value of Fe(II) against cerium(IV) sulphate solution. This was achieved by using approximately 3 mol dm^{-3} sulphuric acid in the preparation of Fe(II) and Ce(IV) solutions. The reaction was invariably followed up to 80% completion, and the k_{obs} values were reproducible within ±5% from the replicate runs. The average values are reported in the tables.

Results

Dependence on [Ce^{IV}]

The first-order dependence on $[Ce^{IV}]$, indicated by the linearity of the plots between ln $(a - x)$ and time, was further confirmed by the fact that k_{obs} was independent of the initial $[Ce^{IV}]$ when varied in the range 0.002–0.012 mol dm^{-3} at constant $[NO_3^-]$, $[H^+]$, and [α-hydroxy acid].

TABLE 1. Dependence of k_{obs} on [α-hydroxy acid] at 12°C; $[Ce(NO_3)_6^{2-}] = 0.002$ mol dm^{-3}, $[HNO_3] = 0.006$ mol dm^{-3}

	$10^3 k_{obs}$ (s^{-1})			
[α-Hydroxy acid] (mol dm^{-3})	Glycolic acid	Malic acid	Tartaric acid*	Citric acid
0.02	2.56	1.56	0.25	3.07
0.08	2.48	1.62	0.23	3.12
0.14	2.52	1.58	0.25	3.08
0.20	2.46	1.70	0.30	3.15

*$[HNO_3] = 0.02$ mol dm^{-3}.

TABLE 2. Dependence of k_{obs} on [nitric acid] at constant ionic strength at 9°C. $[Ce(NO_3)_6^{2-}] = 0.002$ mol dm^{-3}, [α-hydroxy acid] = 0.02 mol dm^{-3}, and $I = 0.02$ mol dm^{-3}

	$10^3 k_{obs}$ (s^{-1})			
[Nitric acid] (mol dm^{-3})	Glycolic acid	Malic acid	Citric acid	Tartaric acid*
0.006	1.70	1.27	2.15	—
0.008	1.80	1.75	2.45	—
0.010	—	1.87	3.09	—
0.012	2.41	2.45	4.02	—
0.016	3.42	3.45	5.16	—
0.020	—	—	—	0.42
0.024	—	—	—	0.57
0.028	—	—	—	0.64
0.032	—	—	—	0.78

*$I = 0.044$ mol dm^{-3} at 16°C.

Dependence on [Ce^{III}]

The effect of $[Ce^{III}]$ on the k_{obs} was investigated in the oxidation of malic acid only. The k_{obs} was independent of the initial $[Ce^{III}]$ over a tenfold variation (0.0002–0.002 mol dm^{-3}). It was found that $10^3 k_{obs} = 2.30 \pm 0.12$ s^{-1} at $[H^+] = 0.006$ mol dm^{-3}, [malic acid] = 0.02 mol dm^{-3}, $[Ce^{IV}] = 0.002$ mol dm^{-3} at 15°C.

Dependence on [α-hydroxy acid]

This was investigated for all the α-hydroxy acids. The results, Table 1, indicated an apparent zero-order dependence on [α-hydroxy acid]. However, a later analysis of the results indicated that these k_{obs} values were in fact the limiting values.

Dependence on [nitric acid]

These measurements were carried out at constant $[NO_3^-]$. The results in Table 2 indicated that k_{obs} increased with $[H^+]$. This observation is in disagreement with the one recorded in the oxidation of mandelic acid (6). This observation also distinguishes this study from the one in perchloric acid (5), in which k_{obs} decreased with increasing $[H^+]$.

The plot between k_{obs} and $[H^+]$ was linear and passed through the origin, indicating that the presence of H^+ is essential for the reaction, which is understandable because cerium(IV) salts hydrolyze in the absence of hydrogen ions. The representative plots for the oxidation of malic and citric acids are shown in Fig. 1.

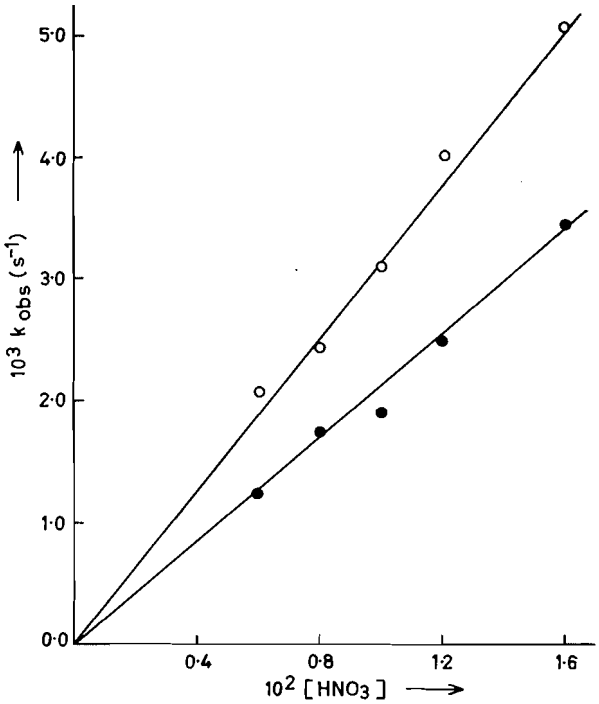

FIG. 1. Dependence of k_{obs} (s^{-1}) on [HNO_3] at constant ionic strength for the oxidation of malic (○) and citric (●) acids. Similar plots were also obtained in the oxidations of glycolic and tartaric acids. The experimental conditions are given in Table 2.

Dependence on [NO_3^-]

No systematic study was made to measure k_{obs} at different [NO_3^-] because of the well-known retarding effect of nitrate ions in oxidations in nitrate medium. However, a few experiments carried out at randomly varied [NO_3^-] confirmed that k_{obs} decreased with increasing [NO_3^-]. The reason for avoiding this study was that such measurements do not help in establishing the exact nature of the reactive cerium(IV) species, which could be any one of the various nitrate complexes of cerium(IV) (see reaction [8]).

Discussion

Cerium(IV) species

The chemistry of cerium(IV) in aqueous nitric acid is complicated. Several complexes represented by $[Ce(NO_3)_n]^{(4-n)}$, where n has an integral value between 1 and 6, are known (13). The mixed hydroxy–nitrate complexes represented by $[CeOH(NO_3)_n]^{(3-n)}$ (14–17), the hydroxy species $CeOH^{3+}$ (6, 18–21), and the equilibrium between monomeric and dimeric cerium(IV) (7–11), have all been postulated to explain the observed kinetics.

Since we used [HNO_3] < 0.06 mol dm^{-3}, both Ce^{4+} and $CeOH^{3+}$ could be present in the system (15). However, $CeOH^{3+}$ is not favoured as the reactive species because k_{obs} did not decrease with increasing [H^+], as expected in view of equilibrium [6]. A mixed hydroxy–nitrate complex, formed as a result of equilibrium [7], is also not favoured for the same reason. The possibility of the Ce^{4+} as oxidant is also excluded because of its extensive complexation with nitrate ions (22). This thus leaves the possibility that one of the several nitrate complexes may be reactive. The identification of a particular cerium(IV)–nitrate complex as the reactive one is not easy and this is perhaps one reason why several workers (23) have consistently avoided being specific about the reactive cerium(IV) species in nitrate medium.

$$[6]\quad Ce^{4+} + H_2O \overset{K_h}{\rightleftarrows} CeOH^{3+} + H^+$$

$$[7]\quad Ce(NO_3)_n^{(4-n)} + H_2O \overset{K_h'}{\rightleftarrows} [CeOH(NO_3)_n]^{(3-n)} + H^+$$

Mechanism

The formation of a Ce(IV) – α-hydroxy acid complex is evident from the deepening of the colour of Ce(IV) solution upon addition of α-hydroxy acids. Since the deepening of the colour is instantaneous, the formation of the precursor complex is considered to precede the slow rate controlling step. Measurements such as the wavelength of maximum absorbance, and determination of the formation constants of the precursor complexes, required the application of a high speed microprocessor controlled uv–visible recording spectrophotometer with a thermostatic compartment, a facility presently not available to us. The formation of the precursor complex is considered essential and is supported by the study in sulphuric (2) and perchloric acid (4, 5) solutions. The fact that k_{obs} was independent of [Ce^{III}] precluded the possibility of participation of Ce(III) in any step preceding the rate controlling step.

The consideration of the pK_a values of the α-hydroxy acids and the [H^+] used implied that both the dissociated and the undissociated forms of the α-hydroxy acid existed in the system. However, in view of the dependence of k_{obs} on [H^+], the possibility of A^-, the dissociated hydroxy acid, becoming the reactive entity is ruled out. Hence it is proposed that the undissociated hydroxy acid, HA, formed the precursor complex with the reactive cerium(IV) species.

The hydrolytic (22) and spectral studies (24, 25) have confirmed that cerium(IV) exists as a nitrate complex, and the X-ray crystallographic study (26) indicated that six bidentate nitrates are present around the cerium(IV) ion. Now, if it is assumed that a bidentate complex is formed between reactive cerium(IV) species and the α-hydroxy acid, then a nitrate ion will be lost in order to maintain the coordination number of 12. The situation is illustrated in equilibrium [8], which is consistent with the observed retarding effect of nitrate ions.

$$[8]\quad Ce(NO_3)_n^{(4-n)} + HA \overset{K}{\rightleftarrows} \left[\begin{array}{l} R^1\text{-}C(H)(O\text{-}Ce(NO_3)_{n-1})\text{-}R^2 \\ \quad\quad\quad\quad C(=O)\text{-}O\text{-}H \end{array}\right]^{(5-n)} + NO_3^-$$

[9] 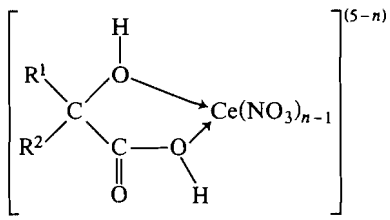 $+ H^+ \xrightarrow{k} R^1R^2\dot{C}OH + Ce(III) + 2H^+$

[10] $(m-1)Ce^{IV} + R^1R^2\dot{C}OH \xrightarrow{\text{fast}}$ 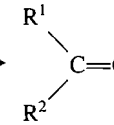 $+ (m-1)Ce^{III} + (m-1)H^+$

In equation [10], m is the number of Ce(IV) equivalents used in the oxidation of α-hydroxy acid according to the stoichiometric equations [1–5], and n has any integer value between 1 and 6. The rate of disappearance of $[Ce^{IV}]$ in terms of reactions [8]–[10] is given by eq. [11] where K_n is defined in the equilibrium [12].

$$[11]\quad \frac{-d[Ce^{IV}]}{dt} = \frac{mkK[Ce^{IV}][HA]\dfrac{K_n[NO_3^-]^n}{[NO_3^-]}[H^+]}{1 + K_n[NO_3^-] + \dfrac{KK_n[HA][NO_3^-]^n}{[NO_3^-]}}$$

$$[12]\quad Ce^{4+} + nNO_3^- \rightleftarrows [Ce(NO_3)_n]^{(4-n)}$$

The rate law deduced in eq. [11] is further simplified by dividing the numerator and denominator by $K_n[NO_3^-]^n/[NO_3^-]$, whence eq. [11] is reduced to eq. [13].

$$[13]\quad \frac{-d[Ce^{IV}]}{dt} = \frac{mkK[Ce^{IV}][HA][H^+]}{\dfrac{[NO_3^-]}{K_n[NO_3^-]^n} + [NO_3^-] + K[HA]}$$

Since $[NO_3^-] = 0.02$ mol dm^{-3} (the total ionic strength of the medium), it is easily seen that

$$K[HA] \gg \left(\frac{[NO_3^-]}{K_n[NO_3^-]^n} + [NO_3^-]\right)$$

Equation [13] is therefore further simplified to eq. [14], which is the observed rate law. Again, at constant $[H^+]$, $mk[H^+]$ can be replaced by the constant k_{lim} where k_{lim} is the limiting rate constant, and eq. [14] is reduced to eq. [15].

$$[14]\quad k_{obs} = mk[H^+]$$

$$[15]\quad k_{obs} = k_{lim}$$

The value of k ($= k_{lim}/8[H^+]$, $m = 8$ for tartaric acid) at different temperatures in the oxidation of tartaric acid is given in Table 3. The values of $\Delta H^{\ddagger}$ and $\Delta S^{\ddagger}$ are also reported there. The corresponding values for the other hydroxy acids could not be obtained because the rate measurements in these systems were too fast.

The inclusion of a proton in the activated state, which could be visualized as $[H^+—Ce^{IV} - HA]^{\ddagger}$ formed in reaction [9], could help the delocalization of the electron and the formation of the free radical $R^1R^2\dot{C}OH$. The formation of the activated state $[H^+—Ce^{IV} - HA]^{\ddagger}$ as a result of reaction between a protonated Ce(IV) species and HA is not favoured because of the fact that the Ce(IV) species extracted by ether from a solution having 5.5 mol dm^{-3} nitric acid contained no ionizable proton (9*a*). The equilibrium between the monomeric and dimeric cerium(IV) species has no mechanistic significance in the present reaction because k_{obs} is independent of the initial $[Ce^{IV}]$. This will always be the case in all those reactions in which either the monomeric or dimeric species are singularly reactive.

The attempt to characterize the free radical by flow–esr technique proved unsuccessful (5). However, the formation of $R^1R^2\dot{C}OH$ (27) is favoured because its fast oxidation by a second Ce(IV) molecule explains the formation of HCHO in the oxidation of glycolic acid ($R^1 = R^2 = H$), and acetone dicarboxylic acid in the oxidation of citric acid ($R^1 = R^2 = CH_2CO_2H$), which is akin to the formation of acetone in the oxidation of 2-methyl-2-hydroxypropanoic acid ($R^1 = R^2 =$ Me).

The values of k decreased in the order: citric > glycolic > malic > tartaric acid, which is consistent with the reactivity: mandelic > 2-methyl-2-hydroxypropanoic > lactic > glycolic > malic acid in perchloric acid medium (4, 5). It is noted that the mechanism of the oxidation in nitric acid is different from that in perchloric acid because (*i*) k_{obs} decreased with increasing $[HClO_4]$ (4, 5), whereas it increased with increasing $[HNO_3]$, and (*ii*) k_{obs} was independent of $[NO_3^-]$ in perchloric acid (5), whereas nitrate ions retarded the k_{obs} in nitric acid. The latter needs an explanation. In perchloric acid, $CeOH^{3+}$(aq.) is the major reactive species because the contribution from Ce^{4+}(aq.) to k_{obs} is considered negligible (5). The k_{obs} will remain unaffected if $[CeOH^{3+}$(aq.)] is not adversely affected by the nitrate ions, and this is exactly the case because the hydrolytic studies in nitric acid (11) have suggested that the complexing of $CeOH^{3+}$(aq.) by NO_3^- is not appreciable in comparison to complexation of Ce^{4+}(aq.) by NO_3^-.

Although this study could not provide a value of k_{obs} for the oxidation of mandelic acid because the rate was too fast to handle with the method adopted, it has been established that the oxidation is not as slow as claimed by Banerji (6).

TABLE 3. The values of the rate limiting constant k in the oxidation of tartaric acid at different temperatures, and the values of $\Delta H^{\ddagger}$, and $\Delta S^{\ddagger}$

T (°C)	12	15	20	25
10^3k (dm^3 mol^{-1} s^{-1})	1.57	2.68	4.50	8.32

$\Delta H^{\ddagger} = 90 \pm 2$ kJ mol^{-1}, $\Delta S^{\ddagger} = 17 \pm 3$ J K^{-1} mol^{-1}

Acknowledgements

N.D. thanks Dr. K. N. Mathpal, Head of the Department in the Constituent College of Kumaun University at Almora for the laboratory facilities, and R.R.N. thanks UGC for the award of a Research Associateship at the University of Jodhpur, Jodhpur.

1. RAJ N. MEHROTRA. Bull. Chem. Soc. Jpn. (1985). In press.
2. B. KRISHNA and K. C. TEWARI. J. Chem. Soc. 3097 (1961).
3. RAJ N. MEHROTRA and S. GHOSH. Z. Phys. Chem. (Leipzig), **224**, 57 (1963); K. P. BHARGAVA, R. SHANKAR, and S. N. JOSHI.

J. Sci. Ind. Res. **21B**, 573 (1962); K. K. SENGUPTA, S. ADITYA, and B. N. GHOSH. J. Indian Chem. Soc. **40**, 823 (1963); RAJ N. MEHROTRA and S. GHOSH. Z. Phys. Chem. (Leipzig), **230**, 231 (1965); A. MCAULEY. J. Chem. Soc. 4053 (1965); A. MCAULEY and C. H. BRUBAKER, JR. J. Chem. Soc. (A), 960 (1966); K. K. SENGUPTA. Bull. Chem. Soc. Jpn. **42**, 298 (1969); V. K. GROVER, S. K. MISRA, and Y. K. GUPTA. Indian J. Chem. **8**, 247 (1970); V. K. GROVER and Y. K. GUPTA. Aust. J. Chem. **23**, 757 (1970); R. DAYAL and G. V. BAKORE. J. Indian Chem. Soc. **49**, 657 (1972); Indian J. Chem. **10**, 1165 (1972); S. B. HANNA and S. A. SARAI. J. Org. Chem. **42**, 2063 (1977); **42**, 2069 (1977); G. R. ARCOLEO, G. CALVARUSO, F. P. CAVASINO, and C. SBRIZIOLO. Inorg. Chim. Acta, **23**, 227 (1977); S. PRASHAD and J. CHAUDHARY. Indian J. Chem. **17A**, 167 (1979).
4. Z. AMJAD and A. MCAULEY. J. Chem. Soc. Dalton Trans. 2521 (1974).
5. Z. AMJAD, A. MCAULEY, and U. D. GOMWALK. J. Chem. Soc. Dalton Trans. 82 (1977).
6. K. K. BANERJI. J. Indian Chem. Soc. **52**, 573 (1975).
7. R. R. NAGORI, MAHENDRA MEHTA, and RAJ N. MEHROTRA. Indian J. Chem. **21A**, 41 (1982).
8. R. R. NAGORI, MAHENDRA MEHTA, and RAJ N. MEHROTRA. J. Inorg. Nucl. Chem. **43**, 2899 (1981).
9. (*a*) B. D. BLAUSTEIN and J. W. GRYDER. J. Am. Chem. Soc. **79**, 540 (1957); (*b*) M. K. DORFMAN and J. W. GRYDER. Inorg. Chem. **1**, 799 (1962).
10. I. M. BATYAEV, M. S. ZAKHARIVSKII, and B. V. PATCHEVSKII. Chem. Abstr. **63**, 1258h (1965).
11. C. F. BAES, JR. and R. E. MESMER. The hydrolysis of cations. Wiley-Interscience, New York. 1976. p. 43.
12. J. BUCKINGHAM (*Editor*). Dictionary of organic compounds. Chapman and Hall, London. 1982. (*a*) p. 2676, (*b*) p. 17.
13. V. S. SMELOV and YU. I. VERESHCHAGIN. Zh. Neorg. Khim. **9**, 2775 (1964).
14. D. M. YOST, H. RUSSEL, and C. S. GARNER. The rare earth elements and their compounds. Wiley, New York. 1947. p. 61.
15. A. A. NOYES and C. S. GARNER. J. Am. Chem. Soc. **58**, 1265 (1936).
16. R. J. MEYER and R. JACOBY. Ber. Dtsch. Chem. Ges. **33**, 2136 (1900).
17. A. A. FORIST and F. R. DUKE. J. Am. Chem. Soc. **71**, 2790 (1949).
18. J. SHORTER. J. Chem. Soc. 1863 (1962).
19. D. L. MATHUR and G. V. BAKORE. Bull. Chem. Soc. Jpn. **44**, 2600 (1971).
20. D. L. MATHUR and G. V. BAKORE. J. Indian Chem. Soc. **48**, 363 (1971).
21. A. KUMAR, P. S. SANKHLA, and RAJ N. MEHROTRA. Indian J. Chem. **11**, 567 (1973).
22. P. R. DANESI. Acta Chem. Scand. **21**, 143 (1967).
23. W. S. TRAHANOVSKY and L. B. YOUNG. J. Am. Chem. Soc. **91**, 5060 (1969); W. S. TRAHANOVSKY, P. J. FLASH, and L. W. SMITH. J. Am. Chem. Soc. **91**, 5068 (1969); W. S. TRAHANOVSKY, L. B. YOUNG, and M. D. ROBINS. J. Am. Chem. Soc. 91, 7084 (1969); P. M. NAVE and W. S. TRAHANOVSKY. J. Am. Chem. Soc. **93**, 4536 (1971); W. S. TRAHANOVSKY and J. CRAMMER. J. Org. Chem. **36**, 1890 (1971); W. S. TRAHANOVSKY and D. B. MACAULEY. J. Org. Chem. **38**, 1497 (1973); W. S. TRAHANOVSKY, J. CRAMMER, and D. W. BRIXIUS. J. Am. Chem. Soc. **96**, 1077 (1974); M. K. DORFMAN and J. W. GRYDER. Inorg. Chem. **4**, 791 (1962); T. J. KEMP, P. MOORE, and G. R. QUICK. J. Chem. Soc. Perkin Trans. 2, 291 (1980).
24. J. T. MILLER and D. E. IRISH. Can. J. Chem. **45**, 147 (1967).
25. D. G. KARRAKER. Inorg. Nucl. Chem. Lett. **4**, 309 (1968).
26. T. A. BEINKE and J. DELGAUDIO. Inorg. Chem. **7**, 715 (1968).
27. T. J. KEMP. *In* Comprehensive chemical kinetics. Vol. 7, 1972. p. 274. *Edited by* C. H. Bamford and C. F. H. Tipper. Elsevier, Amsterdam.

Study of interaction of polymeric aluminium hydroxide with fluoride

N. PARTHASARATHY, J. BUFFLE,[1] AND W. HAERDI

Department of Inorganic, Analytical, and Applied Chemistry, University of Geneva, 1211 Geneva 4, Switzerland

Received January 10, 1985

N. PARTHASARATHY, J. BUFFLE, and W. HAERDI. Can. J. Chem. **64**, 24 (1986).

The interaction between polymeric aluminium hydroxide, Al_p, and fluoride has been investigated to optimize the conditions for removal of fluoride from waste waters of aluminium manufacturing plants using Al_p. The results of these studies have shown that the nature of products formed between Al_p and fluoride depends on the molar concentration ratio of fluoride to aluminium (r_F), pH, and initial fluoride concentration. In the absence of interfering ions, fluoride can be effectively precipitated as $Al_{13}(OH)_{29}F_{10}$ with Al_p, using $r_F \simeq 0.7$ and $4 < pH \leq 7$. At $r_F > 1$, Al_p dissociates and fluoride is precipitated as cryolite, and the residual fluoride concentration is controlled by its high solubility.

N. PARTHASARATHY, J. BUFFLE et W. HAERDI. Can. J. Chem. **64**, 24 (1986).

Dans le but d'optimiser les conditions permettant d'éliminer les ions fluorures des eaux usées des usines produisant de l'aluminium à partir de l'hydroxyde d'aluminium sous forme de polymère (Al_p), on a étudié l'interaction entre Al_p et les ions fluorures. Les résultats de ces études démontrent que la nature des produits formés entre Al_p et les ions fluorures dépend du pH, de la concentration initiale des fluorures et du rapport des concentrations molaires des ions fluorures/aluminium (r_F). Sous l'influence de Al_p et en l'absence d'ions pouvant créer des interférences, les ions fluorures peuvent être précipités d'une façon efficace sous forme de $Al_{13}(OH)_{29}F_{10}$, en utilisant un $r_F \simeq 0{,}7$ et $4 < pH \leq 7$. Lorsque $r_F > 1$, le Al_p se dissocie et les ions fluorures précipitent sous forme de cryolite; la concentration des ions fluorures résiduels est contrôlée par sa grande solubilité.

[Traduit par le journal]

Introduction

In the past few years there has been a growing interest in the small, highly charged cationic polymeric aluminium hydroxide, Al_p, because it seems to be a promising substitute for conventional aluminium salts as a coagulant in water treatment (1–3). The preparation and characteristics of Al_p have been reported in the literature (1, 3–15). We showed (15) that hydrolysed aluminium solutions having $r_{OH} = 2.5$ consist mainly (ca. 80%) of active polymeric aluminium hydroxide, Al_p. With increasing r_{OH} values, the proportion of Al_p formed decreases and increasing amounts of Al are found to be associated with the inert form of aluminium hydroxide. In addition, small amounts (5–10%) of monomeric aluminium are present in all the hydrolysed solutions. Al_p prepared by slow addition of base to aluminium nitrate solution to an OH/Al ratio of 2.5 showed (15) that its size is 10–20 Å, its average net positive charge is +7 (i.e. 0.5 per aluminium atom), and it consists probably of $Al_{13}O_4(OH)_{24}^{7+}$. Since Al_p is highly positively charged, it is expected to be very reactive towards dissolved species, particularly towards inorganic anions such as fluoride and phosphate, but the reactions between Al_p and dissolved inorganic pollutants have received very little attention (16, 17). In this paper the interaction of Al_p and fluoride has been investigated in order to get some insight into the reactivity of Al_p and to find optimal conditions for treatment of fluoride-containing waste waters, in particular those produced in the aluminium industry.

II. Experimental

II.1 *Reagents*

Reagent grade chemicals and demineralized water purified on Millipore – Milli Q systems were used throughout. All fluoride standards were prepared by serial dilution of stock 0.2 *M* sodium fluoride solution. Stock solutions of aluminium hydroxide were prepared as described in our previous paper (15) by hydrolysing aluminium nitrate solutions with a base (NaOH) to the desired hydrolysis ratio, r_{OH}, where $r_{OH} = [OH]_t/[Al]_t$; $[OH]_t$ is the total concentration of hydroxide ions, and $[Al]_t$ is the total aluminium ion concentration. r_{OH} was varied in the range 2.5–3.0. The total initial aluminium ion concentrations $[Al]_t$ were varied in the range $5 \times 10^{-3} - 2 \times 10^{-1}$ *M*, and the initial base concentrations were varied between 0.1 and 1 *M*. The hydrolysed solutions were characterized by ultrafiltration, aluminium-27 nmr, and Ferron methods as described elsewhere (15). The hydrolysed solutions were left to stand for 6 days before use, as the variations in pH of these solutions were found to be small (0.01 pH/day) after this period. Ionic strengths of the solutions were adjusted to the desired values with sodium nitrate solution.

II.2 *Apparatus*

Fluoride titrations were carried out using the titration assembly described in ref. 18. A fluoride ion selective electrode (ISE) coupled to a Metrohm (EA 441/5) Ag/AgCl reference electrode with saturated KCl salt bridge was used for making fluoride measurements. A Metrohm combination pH glass electrode (EA 120) was calibrated with pH 7 and 4 Merck standard buffers. Metrohm digital pH meters (E500) coupled to a Metrohm chart recorder (E478) were used for pH and potential measurements. A Tacussel PHIT NUM pH stat was used to maintain the pH constant.

The pH and emf were read to within ±0.01 pH unit and ± 0.1 mV, respectively, and the potentials were noted only after checking that the drift was less than 0.004 mV/min.

Unless otherwise stated, all measurements were made in polyethylene titration cells (or beakers) thermostated at 25 ± 0.1°C, with stirring and under an atmosphere of nitrogen.

II.3 *Methods*

II.3.1 *Analytical methods*

All analytical methods used were the same as those described elsewhere (18). However, the salient features are reiterated here. The free and the total fluoride concentrations in the samples were determined by means of a fluoride ISE. The total fluoride concentration was determined by using TISAB III containing CDTA as decomplexing agent for the aluminium fluoride complexes. The total aluminium concentrations in the samples were determined by flame atomic absorption spectrometry (faas) using a Pye Unicam SP1900 atomic absorption spectrometer. Size fractionation of the samples was performed by filtering samples successively through Schleicher and Schull filters of porosities: 8 μm, 0.45 μm, and 0.2 μm and Amicon membranes XM300, PM10, and UM 05 in an Amicon ultrafiltration (uf) cell (model 52). A 0.2-μm filter instead of the conventional 0.45-μm filter was chosen to distinguish between the particulate and dissolved components, because colloidal forms of aluminium have been found to pass through 0.45-μm filters (5) but to be retained by 0.2-μm filters (5, 15).

[1]Author to whom correspondence should be addressed.

II.3.2 *Interaction of fluoride with Al_p*

For the sake of convenience the symbols r_F and r_F^b are designated for $[F]_t/[Al]_t$ and $[F]_b/[Al]_b$ respectively. r_F is a useful parameter for practical purposes, whereas r_F^b is indicative of the stoichiometry of the species formed. $[F]_b$ and $[Al]_b$ are the concentrations of fluoride bound to aluminium and aluminium initially bound to hydroxide as Al_p, respectively. Three forms of aluminium, denoted by Al_a, Al_p, and Al_c, have been shown to exist in partially hydrolysed aluminium solution (12, 13, 15). Al_a consists of monomeric species such as Al^{3+}, $AlOH^{2+}$, $Al(OH)_2^+$. Al_p is the polymeric aluminium hydroxide species. Al_c, the inert form of aluminium hydroxide, is composed of microcrystalline particles of solid aluminium hydroxide. For the sake of clarity the symbol r_{OH}^b will be used for the ratio $[OH]_b/[Al]_b$, where $[OH]_b$ is the concentration of hydroxide ions bound to aluminium as polymer.

II.3.2.1 *Potentiometric titration of Al_p with F*

Aliquots of a 0.1 *M* sodium fluoride solution were added to a solution of Al_p at the same pH (5.0) and ionic strength (0.1 *M*) as Al_p solution ($Al_t = 6 \times 10^{-3}$ *M*). The titrant was added at 30-min intervals and the pH was kept constant at 5.0 by means of a pH stat. The total concentration of fluoride was varied in the range $10^{-6} - 10^{-2}$ *M*. The potential, *E*, was measured with F^- ISE 10–15 min after each addition of the titrant and the corresponding free fluoride concentration was evaluated from the previously constructed calibration curve. As in the present system, the equilibrium was reached slowly. The attainment of equilibrium was checked by performing other titrations using longer equilibration times (24 h). The titrant in this case was added manually.

These experiments were run with solutions having various r_{OH} ratios ($2.5 \leqslant r_{OH} \leqslant 3$).

II.3.2.2 *Batch method*

To determine the nature of products formed during various stages of the titration, a batch technique was used. Aliquots of Al_p ($[Al]_t = 0.12\,M$; $r_{OH} = 2.5$; pH = 5.0) were added to known volumes of sodium fluoride solutions (pH = 5.0) contained in a series of polyethylene beakers under constant stirring. The ionic strengths of these solutions were adjusted to 0.1 *M* with sodium nitrate solution. The total aluminium concentration was kept constant ($[Al]_t = 6 \times 10^{-3}$ *M*) and $[F]_t$ was varied such that $0.1 \leqslant r_F \leqslant 3$ in one set of experiments. All solutions were kept at constant pH for 30 min, then filtered in cascade successively through membranes of porosity: 8 μm, 0.45 μm, 0.2 μm, XM300 (130 Å), PM10 (20 Å), and UM-05 (10 Å). $[Al]_t$, $[F]_t$, and the free fluoride concentrations, [F], were determined in each filtrate. The precipitate formed (if any) was washed with ethanol (70% v/v), dried over silica gel in a desiccator, and analysed by using chemical methods, ir, and photoelectron spectroscopy (ESCA).

II.3.3 *Effect of pH*

The Al_p–fluoride interaction was studied in two systems: (a) excess of aluminium and (b) excess of fluoride.

(a) $r_F \geqslant 3$ *(excess fluoride) (using a batch method)*

The batch method described above was used; r_F was kept constant and the pH was varied over the range $3 < pH \leqslant 7$. [F], $[F]_t$, and $[Al]_t$ in the 0.2-μm filtrates were determined.

(b) $r_F \geqslant 0.1$ *(using a titration procedure)*

Aliquots of fluoride solutions were added to hydrolysed aluminium solutions having varying r_{OH} immediately after performing the hydrolysis, and left to stand overnight under stirring conditions. These solutions were then back titrated with 0.1 *M* nitric acid, and the pH and [F] were measured after each addition. It must be pointed out that the titrant was added at intervals of 24 h in the pH range 4.5–5.5 as the attainment of equilibrium was slow under these conditions. These titrations were performed over the pH range $3 < pH \leqslant 8.5$. The aluminium concentrations studied were in the range $5.0 \times 10^{-3} - 10^{-4}$ *M* and the $[F]_t$ was 10^{-4} *M* in all cases except for $[Al]_t = 1.5 \times 10^{-4}$ *M*, where $[F]_t$ used was 10^{-5} *M*. The ionic strengths of these solutions were adjusted to 0.1 *M* with $NaNO_3$.

III. Results

III.1 *Fluoride bound and hydroxide released*

A typical plot of the potential, *E*, of F^- ISE against log $[F]_t$ for the titration of Al_p with fluoride is shown in Fig. 1. The solution appeared clear in zone 1, became turbid in zone 2, and finally a precipitate was observed (indicated by an arrow in Fig. 1). Hydroxide was released during the titration. The corresponding amounts of hydroxide released were calculated from the amount of acid required to maintain the pH constant.

The maximum amount of bound fluoride per aluminium(III) ion in the polymer is given by:

$$[1] \quad r_F^b = r_F^{eq}$$

and is found at the end point of the titration, i.e. when $[F]_t = [F]_{eq}$ (Fig. 1). Then:

$$[2] \quad r_F^{eq} = [F]_t^{eq}/[Al]_b = ([F]_t - [AlF] - [F])/[Al]_b$$

[AlF] is the concentration of the dissolved AlF^{2+} species. [AlF] was calculated by using the mass balance for monomeric aluminium species, Al_a, the free fluoride concentration obtained from F^- ISE measurement, and the stability constant of AlF,

$$[3] \quad \beta_1^F = [AlF]/[Al][F]$$

(Log $\beta_1^F = 6.03$ at $I = 0.1\,M$; ref. 19):

$$[4] \quad [Al]_a = [Al] + [AlF]$$

By combining eqs. [3] and [4] one obtains:

$$[5] \quad [AlF] = \frac{[Al]_a.\beta_1^F.[F]}{(1 + \beta_1^F.[F])}$$

r_F^{eq} in Fig. 1 was found to be 0.8. Similar titration curves were obtained for hydrolysed solutions having various r_{OH}. The corresponding r_F^{eq} are plotted against r_{OH}^b (Fig. 2). These results indicate that as r_{OH}^b increases, the amount of fluoride incorporated in the precipitate decreases.

The amount of OH^- released during the titration shown in Fig. 1 is replotted as a function of r_F (Fig. 3, curve (a)). Also shown are the results obtained from a batch method and by manual titration (curves (b) and (c)). This figure allows comparison of the results at three different time scales. For instance, at $r_F = 1$ the total equilibration time was 30 min for curve (c), 9 h for curve (a), and 240 h for curve (b). In all cases $[OH]_{rel}$ increases with r_F^b, but the comparison of these experiments shows that a relatively long time (hours) is required for the completion of reaction.

III.2 *Nature of the species formed in the Al_p–F system*

III.2.1 *$[Al]_t$ constant*

The size fractionation results for solutions with r_F ranging from 0.1 to 3.3 are summarized in Table 1. The percentages of Al and F in each fraction were calculated with respect to the total initial aluminium and fluoride concentrations, respectively. The proportion of aluminium and fluoride in the UM 05 filtrate is small regardless of the r_F value. Knowing that UM 05 filters retain Al_p and let through monomeric aluminium species Al^{3+} and AlF_n (15), the fraction of fluoride bound to aluminium as soluble Al_pF_n and AlF_n may be evaluated from the measured free and total fluoride concentrations in the UM 05 retentate and filtrates, respectively. For $r_F = 0.1$, the soluble fluoride was mainly present as Al_pF_n (found: 0.7% as F^-, 9.4% as AlF, 26% in Al_pF_n, and 64% in the solid with respect to $[F]_t$), whereas with r_F values greater than 0.5, the predominant form of soluble fluoride was AlF^+ (found: 0.7–2.3%, as F^-, 6.4–9.4% as AlF, 1.9–4.0% in Al_pF_n, and ≃70–90% in the solid).

The fluoride associated with the particulate form (0.2 μm)

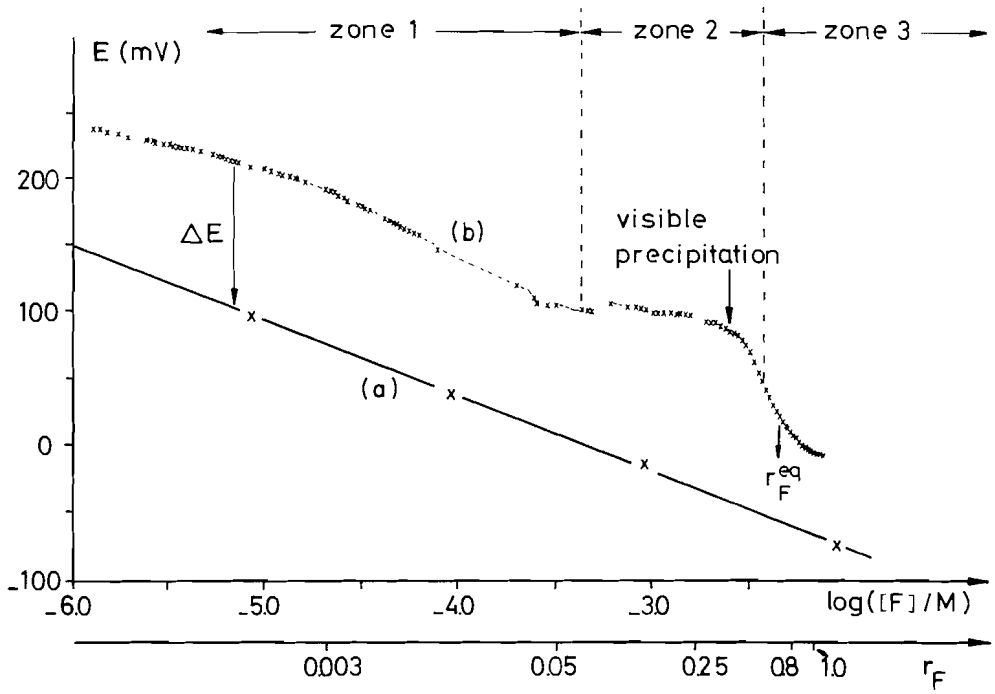

FIG. 1. A typical plot of E vs. log $[F]_t$ for the titration of Al_p with fluoride, monitored with fluoride ion selective electrode. Reference electrode used: Ag/AgCl/saturated KCl. Conditions used: curve (b), $[Al]_t = 6 \times 10^{-3}$ M; $r_{OH} = 2.5$; $I = 0.1$ M; pH = 5.0; $T = 25°C$. Curve (a), $[Al]_t = 0$; the other conditions were the same as for curve (b).

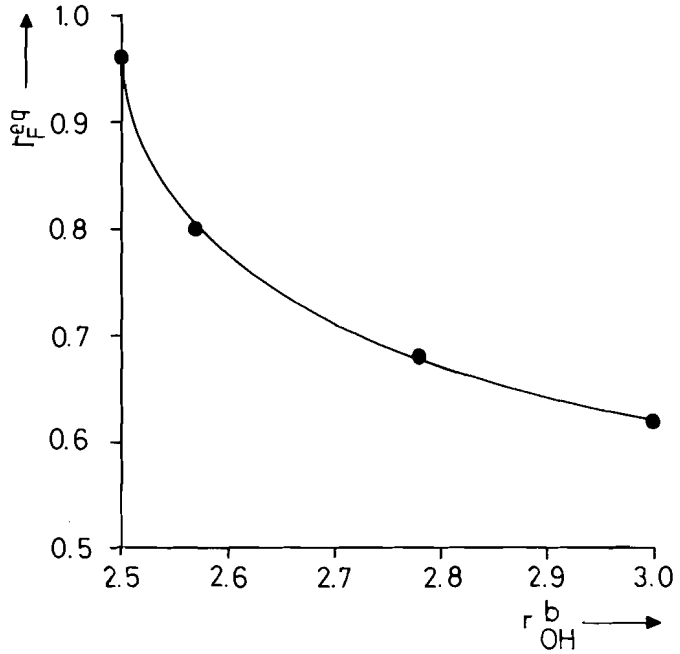

FIG. 2. A plot of r_F^{eq} vs. r_{OH}^b. Conditions used: $[Al]_t = 6 \times 10^{-3}$ M; $I = 0.1$ M $NaNO_3$.

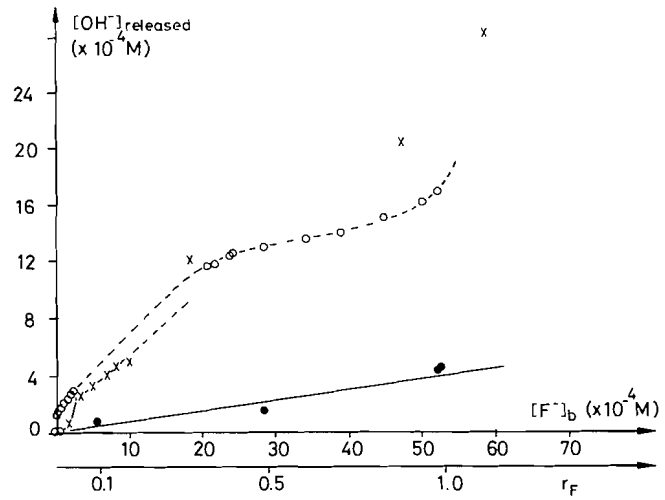

FIG. 3. Amount of hydroxide released ($[OH]_{rel}$) vs. fluoride bound to the polymer $Al_p([F]_b)$. Conditions used: $r_{OH} = 2.5$; $[Al]_t = 6 \times 10^{-3}$; $I = 0.1$ M $NaNO_3$. Curve (a) (○), automatic titration with the titrant added at 30-min intervals; curve (b) (×), manual titration, the interval between each addition being 24 h; curve (c) (●), batch method: each point in the curve was obtained after 30-min contact time.

increases with increase in the r_F ratio (64% of $[F]_t$ at $r_F = 0.1$; 90% at $r_F \geq 0.5$), which is consistent with the observation of turbidity followed by precipitation in zone 2 of the titration curve in Fig. 1. The ir, ESCA, and chemical analysis revealed that the nature of the solid formed depends on the r_F value. At r_F ratios of 0.1–1.0, the solid includes: 13% Al, 6.6% F, 20% OH, 0.1% Na, 59.6% H_2O, and the molar F/Al ratio = 0.69. This corresponds to a basic aluminium hydroxide of composition: $Al(OH)_{2.32}F_{0.68}Na_{0.01}$. With r_F ratio > 1, ESCA, chemical, and ir analysis of the solid yielded: 21% Al, 14.1% F, 6.7% Na, 43% H_2O, molar ratios of F/Al = 1.0 and Na/Al = 0.2, and characteristic ir bands for cryolite and alumina. These data correspond to a mixture of cryolite (Na_3AlF_6) and alumina (Al_2O_3) in a mole ratio of 1:3. These results suggest that Al_p decomposes into these products in the presence of excess of fluoride.

III.3 *Effect of pH on the nature of species formed*

III.3.1. *Excess of fluoride: zone 3 (Fig. 1)*

The distribution of various forms of fluoride are shown in Fig. 4 as a function of pH. These results were obtained with $[Al]_t =$

TABLE 1. Effect of r_F on the composition of Al_p–F system

Initial solution				0.2-μm Filtrate*				Filtrate of UM-05			
r_F	r_F^b	$[Al]_t$ (mM)	$[F]_t$ (mM)	$[Al]_f$ (mM)	$[Al]_f$ (%)	$[F]_f$ (mM)	$[F]_f$ (%)	$[Al]_f$ (mM)	$[Al]_f$ (%)	$[F]_f$ (mM)	$[F]_f$ (%)
0.1	0.11	5.8	0.57	5.3	91.4	0.21	36.2	0.67	11.6	0.06	9.8
0.5	0.56	5.8	2.9	0.43	7.4	0.35	12.1	0.57	9.9	0.23	7.9
1.0	1.13	5.9	5.9	0.63	10.7	0.71	12.0	0.60	10.1	0.53	9.0
3.16	3.58	6.0	19.0	0.13	2.2	2.3	12.1			1.91	10.1

*The results obtained with XM300 and PM10 filtrates were similar to those obtained with 0.2-μm filtrates. $I = 0.1\,M$ $NaNO_3$ M; pH = 5.5; $[X]_f$ = total concentration of X in a given filtrate.

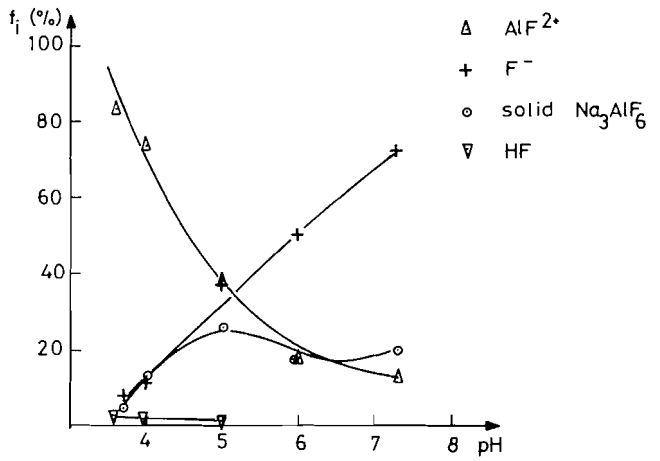

FIG. 4. Distribution of various forms of fluoride as a function of pH. f_i = fraction of each species with respect to total fluoride concentration. Conditions used: $[Al]_t = 1.7 \times 10^{-3}\,M$; $[F]_t = 5.1 \times 10^{-3}\,M$; $r_F = 3$, $r_{OH} = 2.5$.

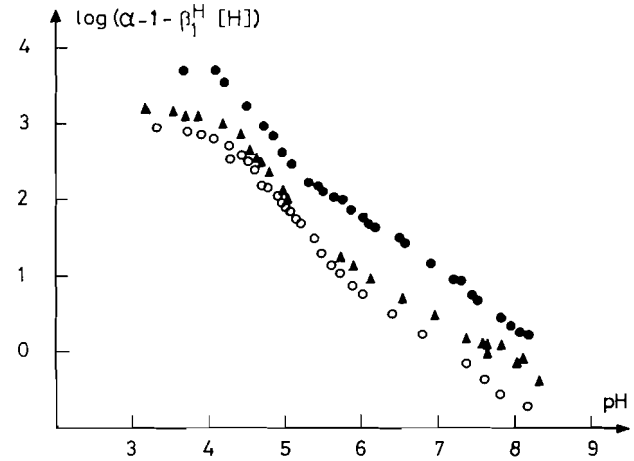

FIG. 5. Typical plots of log ($\alpha - 1 - \beta_1^H.[H]$) vs. pH. Conditions used: M; $[F]_t = 10^{-4}\,M$; $I = 0.1\,M$; $T = 25 \pm 0.1$°C; curve (●), $[Al]_t = 4.4 \times 10^{-3}\,M$; curve (▼), $[Al]_t = 2.2 \times 10^{-3}\,M$; curve (○), $[Al]_t = 7.7 \times 10^{-4}\,M$.

1.7×10^{-3} and $[F]_t = 5.1 \times 10^{-3}\,M$ using a batch method. The distribution of different forms of fluoride was computed from the measurements of the total and free fluoride concentrations in the 0.2-μm filtrates and retentates. It can be seen that the fraction of fluoride present as insoluble species is more or less independent of pH in the range 4.5–6.0, whereas the proportion of free and complexed fluoride varies with pH under the same conditions.

III.3.2. *Excess aluminium: zone 1 (Fig. 1)*

From the free fluoride concentrations measured at various pH during the back titration of Al_p plus F solutions with acid (sect. II.3.3 b), the degree of complexation of F, α, defined as (20):

[6] $\alpha = [F]_t/[F]$

was evaluated. For pH < 4.5, fluoride forms HF with hydrogen ions. Thus the mass balance equation for $[F]_t$ is:

[7] $[F]_t = [F] + [HF] + \Sigma\,[\text{All forms of F bound to Al}]$

Combining eqs. [6] and [7] with eq. [4] and the formation constants of HF, $\beta_1^H = [HF]/[H][F]$, and eq. [4] one obtains:

[8] $(\alpha - 1 - \beta_1^H.[H]) = \Sigma\,[\text{All forms of F bound to Al}]/[F]$

A value of $\beta_1^H = 3.01$ at $I = 0.1\,M$, independently evaluated, was used to compute the left hand side of eq. [8]. Typical plots of log ($\alpha - 1 - \beta_1^H[H]$) vs. pH for various $[Al]_t$ are shown in Fig. 5. The main feature of this titration curve is that it can be divided into three pH zones corresponding to the changes in its slopes:

(*i*) 5.5 < pH < 8. In this pH domain, the reactions proceed rapidly and the slopes of plots such as those shown in Fig. 5 can be evaluated for various aluminium concentrations. An average value of 0.65 ± 0.05 for the slope was obtained from titration curves performed at six different aluminium concentrations in the range $10^{-4} - 5 \times 10^{-3}\,M$.

(*ii*) 4.5 < pH < 5.5. In this pH range, the reactions were found to be very slow, taking up to 24 h to attain equilibrium. This may be due to depolymerization of polynuclear hydrolysed species. No attempt was made to interpret these results quantitatively as reactions were too sluggish.

(*iii*) pH < 4. The results in Fig. 5 show that log ($\alpha - 1 - \beta_1^H.[H]$) becomes independent of pH. The reactions in this case were found to be rapid.

IV. Discussion

In our previous paper (15) we showed that under mild hydrolysing conditions, hydrolysed aluminium solution is predominantly made up of polymeric aluminium hydroxide species which closely resembles $Al_{13}O_4(OH)_{24}^{7+}$. In particular, our results showed that the polydispersity of Al_p is small, more than 80% of the polymeric species being in the size range 10–20 Å. Consequently, in the subsequent discussions Al_p will be represented by $Al_{13}O_4(OH)_{24}^{7+}$ or $[Al(OH)_{2.48}]_n$ (n = 13), the two being stoichiometrically equivalent. It was also shown that the remainder of $[Al]_t$, which represents only ca. 10–20%, consists

of finely divided nonreactive aluminium oxi-hydroxide in equilibrium with traces of monomeric aluminium species.

IV.1. *Zone 1:*

IV.1.1. $r_F \leq 0.1$; *pH* < 4 *(Figs. 1 and 5)*

Hem and Roberson (5) showed that at pH < 4 aluminium exists mainly as monomeric species. Hence it may be assumed that for pH < 4, Al_p will dissociate completely into monomeric aluminium hydroxo species, provided equilibrium is attained. Since Al is present in excess, the predominant fluoro complex of aluminium would be AlF, whereas a major part of the total aluminium is present as Al^{3+} and $AlOH^{2+}$. Thus eq. [8] can be written as:

$$[8a] \quad (\alpha - 1 - \beta_1[H]) = [AlF]/[F] = \beta_1^F.[Al]$$

and the mass balance for the total aluminium concentration is given by:

$$[9] \quad [Al]_t = [Al] + [AlF] + [AlOH]$$

Since aluminium ions are present in excess, the approximation:

$$[10] \quad [Al]_t = [Al] + [AlOH]$$

holds. Combining eq. [10] with the formation constant given in eq. [11]:

$$[11] \quad \beta_1^{OH} = [AlOH]/[Al][OH]$$

one obtains:

$$[12] \quad [Al] = [Al]_t/(1 + \beta_1^{OH}.[OH])$$

β_1^F was evaluated from eqs. [8] and [12] using $\log \beta_1^{OH} = 9.0$ at 0.1 *M* ionic strength (19) and the experimental value of 3.01 for $\log \beta_1^H$. From all the titration data (Fig. 5), the mean value of $\log \beta_1^F$ was found to be 6.13 ± 0.04 (for 95% confidence limit). Considering the complexity of the system used, this value is in reasonable agreement with the value of 6.32 at 0.1 *M* ionic strength reported in the literature (19). Thus these results confirm that at pH values below 4.0, Al_p dissociates completely into monomeric aluminium species provided sufficient time is allowed to reach equilibrium (ca. 1 week).

IV.1.2. $r_F \leq 0.1$; $5 < pH < 8$

In this case a soluble complex is formed between the polymer and fluoride (Table 1, Fig. 1). As aluminium ions are present in excess, the fixation of one fluoride per molecule of polymer has been assumed for the reaction of Al_p with fluoride. This reaction may be written as:

$$[13] \quad Al_{13}O_4(OH)_{24} + F \rightleftharpoons Al_{13}O_4(OH)_{24-z}F + zOH$$

where z is the number of hydroxide ions released per fluoride bound. Let K_p be the ligand exchange constant:

$$[14] \quad K_p = \frac{[Al_{13}O_4(OH)_{24-z}F][OH]^z}{[Al_{13}O_4(OH)_{24}][F]}$$

The total fluoride concentration, $[F]_t$ is given by:

$$[15] \quad [F]_t = [F] + [Al_{13}O_4(OH)_{24-z}F]$$

or

$$[16] \quad \alpha = [F]_t/[F] = 1 + K_p[Al_{13}O_4(OH)_{24}]/[OH]^z$$

The concentrations of all forms of aluminium except Al_p are negligible compared to $[Al]_t$ under these conditions. As a first approximation, it is reasonable to assume:

$$[17] \quad [Al_{13}O_4(OH)_{24}] \simeq [Al]_t/13$$

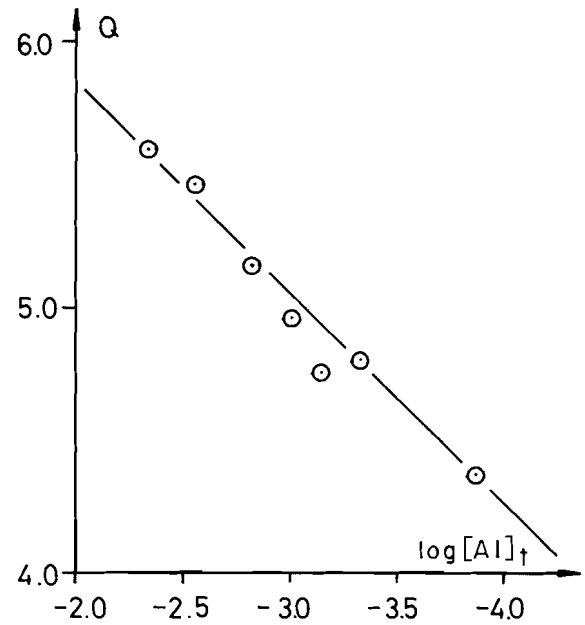

FIG. 6. A plot of Q vs. $[Al]_t$ (see eq. [19]).

Equation [16] can be written as:

$$[18] \quad (\alpha - 1) = \log (K_p/K_w^z.13) + \log [Al]_t + z\,pH$$

where K_w is the ionic product of water.

The value of z *was found* to be 0.65 ± 0.05 (for 95% confidence limits) (see sect. III.1.2). An average value of 0.6 OH released per fluoride fixed was also found experimentally for $r_F \leq 0.1$ (Fig. 3, curves (a) and (b)). Thus if sufficiently long equilibration times are used, then the observed stoichiometry for fluoride bound per hydroxide ion released is independent of the titration mode and is close to 0.6.

The value of K_p *can* be found from Fig. 5 and eq. [18]. Indeed the intercepts on the ordinate, Q, of the straight line plots (Fig. 5) in the pH region of interest should be dependent on $[Al]_t$:

$$[19] \quad Q = \log (K_p/K_w^z) + \log [Al]_t$$

The slope of such a plot (Fig. 6) was found to be 0.97, which is close to the theoretically predicted value of 1. K_p can be evaluated from the intercept of this plot and was found to be 1.03 ± 0.01, which is in agreement with a value of 1 expected for ligand exchange reaction between OH and F (5).

IV.2 *Zone 2:* $0.5 < r_F \leq 1$

Fluoride precipitates in this region. Under similar conditions Hsu (16) also observed the precipitation of phosphates and silicates with polymeric aluminium hydroxide species and has proposed a model for these precipitation reactions. According to this model, the phosphate and silicate ions reduce the charge of Al_p, inducing precipitation when its charge is completely neutralized. Analogous reaction schemes can be used for interpreting the fluoride–aluminium interactions. However, in this case, in addition to the neutralization of charge, the fluoride ions can replace some of the hydroxide ions incorporated in the polymer since it has a stronger affinity than phosphate for aluminium and is similar in size to hydroxide ions. This would then explain the release of hydroxide ions observed during the reaction between Al_p and fluoride. Since r_F^b represents the number of fluoride ions bound per aluminium, the reaction between Al_p and F can be represented in the general form:

[20] $1/n[Al(OH)_{2.46}]_n + r.F \rightleftharpoons 1/n[Al(OH)_{(2.46)}F_r]_n + mOH$

where $r = r_F^b$ in eq. [20].

In order to get an uncharged reaction product one must have:

[21] $0.54 + m = r_F^b$

By substituting the experimental value of r_F^b (= 0.8) in eq. [21], the value of m was found to be 0.26. The ratio $m/r_F^b = [OH]_{rel}/[F]_b$ is then found to be 0.32, which is in agreement with the experimental value of 0.35 obtained from Fig. 3, curves (a), (b), at $r_F = 0.8$.

The results of analysis of the solid phase also support the formation of mixed fluoro-aluminium compound. Thus all these results favour eq. [20], and by substituting $n = 13$ and $r_F^b = 0.8$, it becomes:

[22] $Al_{13}O_4(OH)_{24}^{7+} + 10\,F^- \rightleftharpoons Al_{13}O_4(OH)_{21}F_{10}(s) + 3\,OH^-$

As mentioned above, the formation of a mixed phosphato-aluminium complex in the reaction between phosphate and hydroxy aluminium species has also been reported (16, 17, 21). The H_2PO_4/Al mole ratio of the precipitate calculated from the results reported for $r_{OH} = 2.5$ and similar pH conditions yielded a value of 0.46, which would be comparable with the F/Al mole ratio (0.54) if no hydroxide ions were replaced by fluoride ions, as is the case for H_2PO_4. These findings therefore tend to suggest that the reaction mechanisms for the reaction of Al_p with both fluoride and phosphate follow similar pathways. It must be pointed out that the nature of the solid formed under these conditions is markedly different from the one formed where excess of fluoride is present (see sect. III.3.1).

IV.3. *Zone 3:* $r_F \geq 3$

In this case two observations were made: (a) formation of precipitate, and (b) existence of dissolved complexed fluoride (Fig. 1).

The results of analysis of the solid suggest that Al_pF_n depolymerizes into cryolite and alumina under these conditions. The formation of cryolite in the presence of excess of fluoride has also been reported by Hem and Roberson (5). A comparison of these results with those of Fig. 4 shows that the solubility of the fluoride is dependent on the total aluminium concentration and pH when $r_F > 3$. The solubility decreased with increased aluminium concentrations, whereas it increased with increased acidity below pH 4 and remains unaffected in the pH range 4.5–8.

The nature of the various forms of fluoride at $r_F \geq 3$ is shown in Fig. 4. It is apparent that the concentrations of free and bound fluoride are dependent on pH and the total aluminium concentration initially present.

Conclusions

The results of this study show that the interaction between fluoride and aluminium hydroxide polymer, Al_p, leads to the formation of several soluble and insoluble products depending on r_F, pH, and total applied fluoride and aluminium concentrations. The types of products formed as a function of r_F are summarized in Table 2. For $r_F \leq 0.1$, a significant portion of the total fluoride is present as soluble fluoride. At $r_F = 0.7$, $r_{OH} = 2.5$, and pH between 4 and 7, a major proportion of total fluoride is precipitated as $Al_{13}(OH)_{29}F_{10}$. Under these conditions about 7 mg/L of fluoride remains in the solution owing to the intrinsic solubility of this compound. At $r_F > 1$, Al_p dissociates and the reaction products under these conditions consist of a mixture of hydrated alumina and cryolite. The amount of dissolved fluoride present in these solutions was found to vary with the applied aluminium concentration and it is controlled by the high solubility of cryolite (0.042 g/L) (22).

TABLE 2. Summary of the main species formed between Al_p and F under the experimental conditions used in this work

	r_F		
pH	≤0.1	0.5–1.0	>1.0
4	HF, AlF	HF, AlF	HF, AlF
4–5.5	AlF		AlF
		Al_pF_{10} (s)	Na_3AlF_6
5.5–7	Al_pF_n	Al_pF_n	Al_2O_3, Na_3AlF_6
7–8		F adsorbed on Al $(OH)_3$	F

Thus if Al_p is used for precipitating fluoride, then the optimal conditions are as follows: $r_{OH} = 2.5$, $r_F = 0.7$, and $4 < pH < 7$, provided no interfering components are present. The removal of fluoride by Al_p from waste waters of aluminium manufacturing plants where interfering components are present is discussed elsewhere (23).

1. F. FIESSINGER and J. L. BERSILLON. CEBEDEAU–BECEWA. No. 399. 1979. p. 52.
2. B. A. DEMPSEY, R. M. GANHO, and C. R. O'MELIA. J. Am. Water Works Assoc. **76**, 141 (1984).
3. C. R. O'MELIA and B. A. DEMPSEY. Proc. 24th Annual Public Water Supply Engineers Conf., Champaign, Illinois. No. 4. 1982. p. 5.
4. P. H. HSU and T. F. BATES. Mineral. Mag. **33**, 749 (1965).
5. J. D. HEM and C. E. ROBERSON. U.S. Geol. Surv. Water-Supply Pap. 1827A. 1967.
6. J. W. AKITT and A. L. FARTHING. J. Magn. Reson. **44**, 584 (1981).
7. J. W. AKITT and A. L. FARTHING. J. Chem. Soc. Dalton Trans. 1606 (1981).
8. J. W. AKITT and A. L. FARTHING. J. Chem. Soc. Dalton Trans. 1617 (1981).
9. J. W. AKITT and A. L. FARTHING. J. Chem. Soc. Dalton Trans. 1624 (1981).
10. C. F. BAES and R. E. MESMER. Hydrolysis of cations. J. Wiley Interscience Publications, New York. 1976.
11. VON. H. SCHONHHERR and P. FREY. Z. Anorg. Allg. Chem. **476**, 195 (1981).
12. R. C. TURNER. Can. J. Chem. **54**, 1910 (1976).
13. R. W. SMITH. U.S. Geol. Surv. Water Supply Paper, 1827D. 1972.
14. R. J. STOL, A. K. VAN HELDEN, and P. L. DE BRUYN. J. Colloid. Interface Sci. **57**, 115 (1976).
15. N. PARTHASARATHY, J. BUFFLE, and W. HAERDI. Water Res. **19**, 25 (1985).
16. P. H. HSU. Soil Sci., 219 (1979).
17. P. H. HSU. Water Res. **9**, 1155 (1975).
18. J. BUFFLE, N. PARTHASARATHY, and W. HAERDI. Water Res. **19**, 7 (1985).
19. L. G. SILLEN and A. E. MARTELL. Special Publication No. 17. The Chemical Society, London. 1964.
20. A. RINGBOM. Complexation in analytical chemistry, Wiley, New York. 1963.
21. W. L. YUAN and P. H. HSU. Proc. 5th Int. Water Pollut. Res. Conf. I-16, San Francisco. 1971.
22. I. TANANAEV and SH. TALIPOV. J. Gen. Chem. USSR, **9**, 1155 (1939).
23. N. PARTHASARATHY, J. BUFFLE, and W. HAERDI. J. Fr. Hydrol. In press.

Layered metal uranyl phosphates. Retention of divalent ions by amine intercalates of uranyl phosphates

R. POZAS-TORMO, L. MORENO-REAL,[1] M. MARTÍNEZ-LARA, AND S. BRUQUE-GAMEZ
Departamento de Química Inorgánica, Universidad de Málaga, Apartado 59, 29080 Málaga, Spain

Received April 12, 1985

R. POZAS-TORMO, L. MORENO-REAL, M. MARTÍNEZ-LARA, and S. BRUQUE-GAMEZ. Can. J. Chem. **64**, 30 (1986).

$HUO_2PO_4 \cdot 4H_2O$ (HUP) forms a laminar intercalate with butylamine, c = 29.30(5) Å, which accepts cationic metals in exchange for the n-butylammonium ions. Hydrated uranyl metal phosphates $M(UO_2PO_4)_2 \cdot nH_2O$ (M = Mn, Co, Ni, Cu, Zn, Cd) are obtained by ionic exchange and were studied by thermal analysis and X-ray diffraction. The tetragonal structures of all these product compounds are derived from HUP. The diffuse electronic reflectance spectra of every sample show characteristic UO_2^{2+} absorption bands. In the spectra of the Co, Ni, and Cu phosphates there are other bands in the 500–800 nm zone compatible with their observed aquocation transitions.

R. POZAS-TORMO, L. MORENO-REAL, M. MARTÍNEZ-LARA et S. BRUQUE-GAMEZ. Can. J. Chem. **64**, 30 (1986).

Le $HUO_2PO_4 \cdot 4H_2O$ (HUP) et la butylamine forment un composé laminaire intercalé (c = 29,30(5) Å) qui accepte des métaux cationiques en échange pour les ions n-butylammonium. On obtient les phosphates métalliques d'uranyle hydratés [$M(UO_2PO_4)_2 \cdot nH_2O$ dans lesquels M = Mn, Co, Ni, Cu, Zn et Cd] grâce à un échange ionique et on les a étudiés par analyse thermique et par diffraction des rayons-X. En se basant sur le HUP, on en déduit que tous ces composés existent dans des structures tétragonales. Les spectres de réflectance électronique diffuse de chacun de ces échantillons présentent des bandes d'absorption caractéristiques du UO_2^{2+}. Dans les spectres des phosphates de Co, Ni ou Cu, on trouve aussi d'autres bandes, dans la région de 500 à 800 nm, qui sont compatibles avec les transitions observées pour leurs aquocations.

[Traduit par le journal]

Introduction

The intercalation chemistry of the inorganic layered compounds is becoming increasingly important; in particular, the ionic exchange and adsorption characteristics and the host–guest relationships of the layered phosphates have been intensively studied in: $Zr(HPO_4)_2 \cdot H_2O$ (1); $Sn(HPO_4)_2 \cdot H_2O$ (2); $VOPO_4 \cdot 2H_2O$ (3), and $HUO_2PO_4 \cdot 4H_2O$ (HUP) (4, 5).

HUP belongs to the large family of uranium mica compounds with the general formula $M(UO_2PO_4)_2 \cdot nH_2O$ where M may be a mono or divalent cation. These compounds have a typical structure of negatively charged layers of $(UO_2PO_4)_n^{n-}$ separated by staggered layers of water molecules and compensating cations (6). In HUP, the latter are H^+, but these may be substituted by almost any other cations.

Pekarek and Vesely (7) have studied some thermodynamic phenomena of the ionic uptake by HUP/M (M^I to M^{IV}). Other authors investigated the proton conductivity of HUP and the HUAs (8, 9). The photoluminescent properties of these phosphates are reported in detail by Olken *et al.* (5).

A large number of synthetic compounds of the uranium mica type have been prepared. Uranyl phosphates of alkali metals, alkaline earth cations, and some transition metal ions were isolated by precipitating their respective ionic solutions (10–13) and also by ion exchange in HUP (5, 14).

The present work studies the uptake of divalent transition metal ions by the expanded intercalate $(C_4H_9NH_3)UO_2PO_4 \cdot 3H_2O$ and characterizes the final homoionic products, which all show good crystallinity and high degrees of hydration. The concept of using butylamine to facilitate exchange in layered hydrogen phosphates was first demonstrated by Clearfield and Tindwa (15), although Weiss *et al.* had prepared n-alkylammonium derivatives of hydrogen uranyl phosphate (16).

[1]Author to whom correspondence may be addressed.

Experimental

Synthesis

The uranyl hydrogen phosphate tetrahydrate $HUO_2PO_4 \cdot 4H_2O$ (HUP) was prepared from uranyl nitrate and orthophosphoric acid in aqueous solution with the proportion U/P 1:1.1, according to the method of Schreyer and Baes (17). The resulting product was air dried and kept in a controlled humidity atmosphere (P_{H_2O} = 9.12 Torr; 1 Torr = 133.3 Pa). It was identified by chemical analysis, X-ray diffraction, and thermal analysis.

The intercalate $(C_4H_9NH_3)UO_2PO_4 \cdot 3H_2O$ (BAUP) was prepared by exposing HUP to a saturated atmosphere of n-butylamine vapour (NBA) for 2 days in a desiccator. The product was evacuated at room temperature and was left in a controlled humidity atmosphere (H_2SO_4 40% w/w). The composition of the intercalate, BAUP, was determined by spectrophotometry of P and U and Kjeldahl microanalysis of N; water content was measured by thermal analysis.

X-ray diffraction and infrared spectroscopy were used for structural arrangement determination.

Ionic uptake process

The $M^{2+}/C_4H_9NH_3^+$ uptake process was studied by bringing into contact aqueous suspensions of the BAUP intercalate with aqueous metal acetate solutions (up to final concentrations of 10^{-2} M) for 48 h at 25°C. Experiments were made with different equivalent amounts of metallic ions ranging from 0.4056 mequiv./g, or 20% of theoretical maximum uptake capacity (2.028 mequiv./g), to 4.056 mequiv./g, a 100% excess over capacity. The suspensions were then centrifuged and the solids washed until acetate removal was complete. These were then air dried and stored in an environment controlled at 50% humidity. The uptake of metallic ions in the exchange process was determined by analysis of the solid phase and its equilibrium solutions. Analytical data for the butylammonium and the various cation intercalates are available as supplementary material.[2]

[2]A table of analytical data (Table 1, supplementary material) may be purchased from the Depository of Unpublished Data, CISTI, National Research Council of Canada, Ottawa, Ont., Canada K1A 0S2.

Instrumental

The instrumental techniques employed to characterize the new materials were infrared spectroscopy (Perkin Elmer 580), X-ray diffraction (Philips PW 1710), differential thermal and thermogravimetric analysis (Rigaku Thermoflex), diffuse reflectance and visible–ultraviolet spectroscopy (Kontron Uvikon 810), and atomic absorption spectroscopy (Varian AA 475 ABD).

Results and discussion

Characterization and structural determination of BAUP intercalate

The product powder X-ray diffraction pattern (Table 2) can be indexed on a tetragonal unit cell with $a = 6.968(7)$ and $c = 29.30(5)$ Å, though the basal spacing observed is 14.65 Å, which corresponds to the 002 reflection.[3] All the starting product *hk*0 lines were present in the intercalate with systematic absences when $h + k \neq 2n$. These data (Table 2)[3] show the persistence of the HUP framework *ab* plane and, in addition, clearly indicate that the tetragonal layer structure was preserved although the *c* axis was expanded. The most probable space group is $P4_2/n$.

Botto *et al.* (18) found 9.05 Å for the basal spacing (d_{002}) of the isostructural compound $NH_4UO_2PO_4 \cdot 3H_2O$. The perpendicular arrangement of an alkyl chain with four atoms of carbon between the layers would originate from 14.85 Å layer spacing, very close to that obtained here (14.65 Å). The existence of a monolayer in the *n*-butylamine intercalate (BAUP) contrasts with the bilayer found in the hydrogen phosphate of zirconium (19). This compound has an available layer surface area around the hydrogen atoms that is smaller than the HUP (24 $Å^2$ against 48.8 $Å^2$).

In the intercalate infrared spectrum, as well as the bands of the phosphate, water, and UO_2^{2+} vibrations, there are others which correspond to the following groups: $\nu_{CH_3\,sym.}$ (2970 cm^{-1}); $\nu_{CH_2\,sym.\,and\,asym.}$ (2940 cm^{-1}); $\nu_{CH_3\,sym.}$ (2880 cm^{-1}); $\delta_{NH_3^+\,asym.}$ (1620 cm^{-1}); $\delta_{NH_3^+\,sym.}$ (1530 cm^{-1} and 1510 cm^{-1}); δ_{CH_2,CH_3} (1470 cm^{-1}).

These data show that protonation of the guest amine has occurred to give rise to the butylammonium ions between the layers.

The thermogravimetric curve (Fig. 1) exhibits three stages of weight loss. The first corresponds to the initial dehydratation and is associated with two endothermic effects, which may be seen on the DTA curve, and are centred on 90 and 130°C. In the two following stages (150–200°C and 300–400°C), the organic cation is removed; this process occurs in two endothermic effects (at 240 and 315°C). The last of these immediately precedes a DTA exothermic effect (340°C), the result of the combustion of organic residues. These processes are comparable to the observed by Clearfield and Tindwa (19).

Ionic uptake

When the intercalate BAUP is placed in contact with metallic acetate solutions (M = Mn, Co, Ni, Cu, Zn, Cd), the following reaction takes place:

$$[1]\quad M^{2+}(aq) + 2(C_4H_9NH_3)UO_2PO_4 \cdot 3H_2O \rightarrow M(UO_2PO_4)_2 \cdot nH_2O + 2C_4H_9NH_3^+(aq)$$

[3]A table of crystal and X-ray powder diffraction data $(C_4H_9NH_3)UO_2PO_4 \cdot 3H_2O$ (Table 3, supplementary material) may be purchased from the Depository of Unpublished Data, CISTI, National Research Council of Canada, Ottawa, Ont., Canada K1A 0S2.

TABLE 2. X-ray crystallographic data of $(C_4H_9NH_3)UO_2PO_4 \cdot 3H_2O$

fw = 493.09	tetragonal,	$a = 6.968(7)$ Å $c = 29.30(5)$ Å
$V = 1422.6\,Å^3$,	$d_o = 2.31(1)$,	$d_o = 2.30$, $Z = 4$
Cu $K\alpha_1$, α_2, $\lambda = 1.54184$ Å, 20°C		

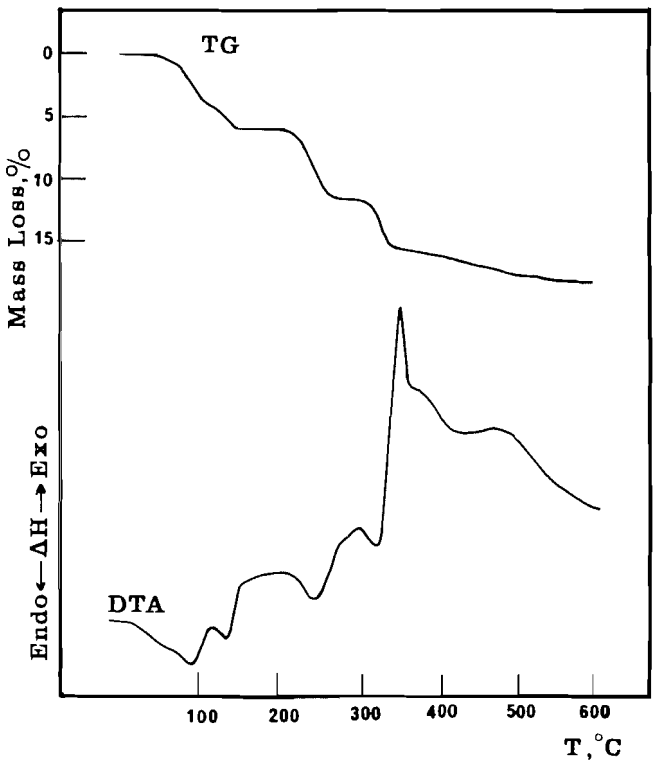

FIG. 1. TG and DTA curves of the $(C_4H_9NH_3)UO_2PO_4 \cdot 3H_2O$.

The ionic exchange reaction $M^{2+}/C_4H_9NH_3^+$ took place without hydrolysis of the ion-exchange solid. This was confirmed by determining P and U in the equilibrium solutions. In all cases the hydrolysis of P and U detected was below 0.6 and 1%, respectively. Greater percentages of hydrolysis were obtained when nitrate, chloride, or sulphate salts were involved in the ionic uptake reactions because of the higher acidity of these solutions.

The ionic exchange described in eq. [1] is quite fast and may be followed by measuring the equivalent values of the butylammonium liberated (Kjeldahl N analysis), and of the metallic ions that remain in the solution, to determine the quantity removed; both values coincide. The apparent velocity of the uptake process was studied for each metallic ion and, by way of example, we shall consider the exchange $Co^{2+}/C_4H_9NH_3^+$, taking place with an initial molar ratio of 0.65:1 (1.3 equivalents for each *n*-butylammonium equivalent at 25°C). Figure 2 shows that after an hour, 90% of the intercalated butylammonium ions have been substituted by cobalt. After 12 h, all the exchange positions are occupied. The exchange sites are now saturated by cobalt and the reaction is complete.

The curves obtained for the other ions are similar; their equilibrium times are between 10 and 12 h, and the molar ratios are 0.6–0.8 (M^{2+}): 1 (NBA).

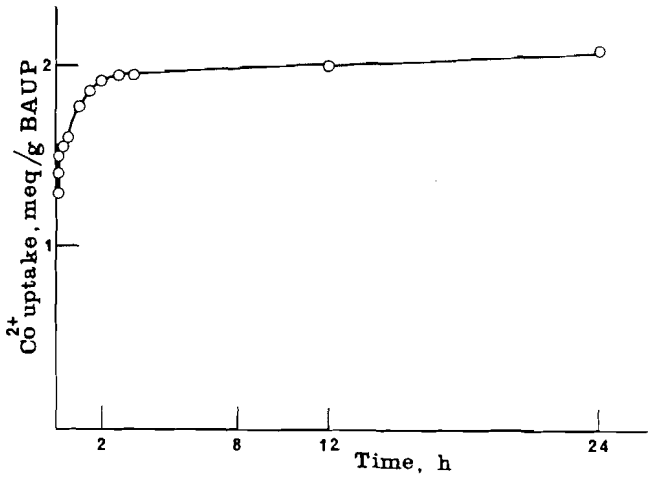

FIG. 2. Uptake of Co^{2+} by butylammonium uranylphosphate as function of time.

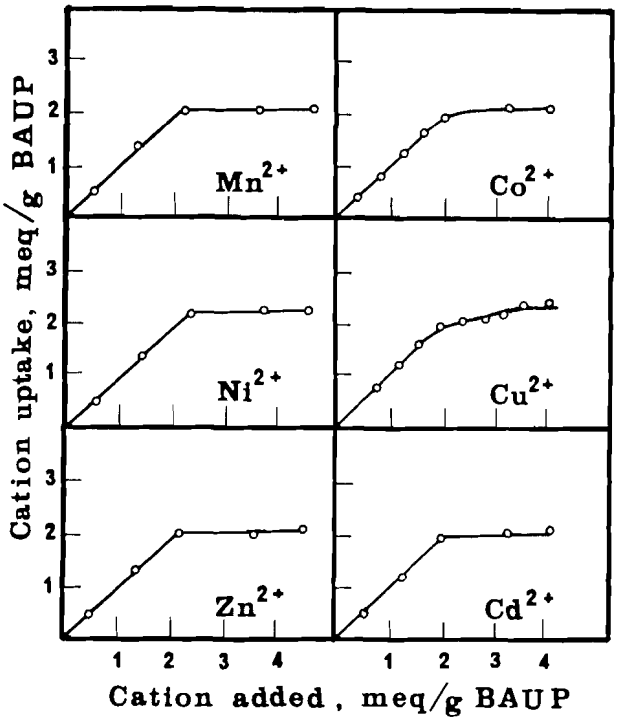

FIG. 3. Retention isotherms of cations by butylammonium uranylphosphate (BAUP).

In order to ensure equilibrium conditions, each isotherm point was obtained with 48 h contact time.

The exchange isotherms show that the BAUP ion exchanger has great affinity for metallic ions and that 1–1.6 equivalents of metallic ion for each equivalent of *n*-butylammonium are quite sufficient to give fully exchanged phases. All the isotherms (Fig. 3) show similar behaviour and may be fitted to a straight line using the equation of Langmuir's isotherm.

Following the exchange process, the product was examined by X-ray diffraction and, in comparison with starting product, the basal spacing was changed; in particular, there was a decrease in the *d*(001). As the exchange sites become saturated, the *hk*0 reflections persist; they are not affected by the ionic uptake. Figure 4 shows the changes in the X-ray diffraction patterns when the butylammonium is exchanged by Cu^{2+}. This indicates that the layered structure *ab* plane is unaltered.

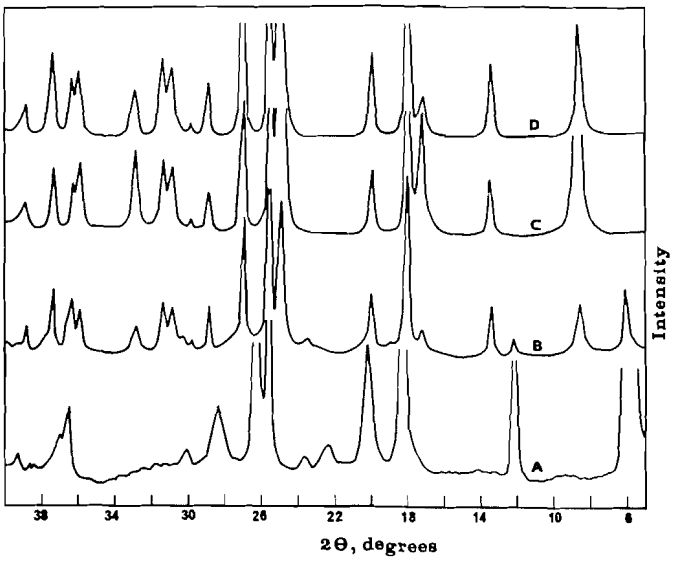

FIG. 4. X-ray diffraction patterns of Cu^{2+} exchanged $(C_4H_9NH_3)$-$UO_2PO_4 \cdot 3H_2O$ at various loadings: (A) BAUP; (B) BAUP + 0.6 symmetries of Cu^{2+}; (C) BAUP + 1.0 symmetries of Cu^{2+}; (D) BAUP + 1.6 symmetries of Cu^{2+}.

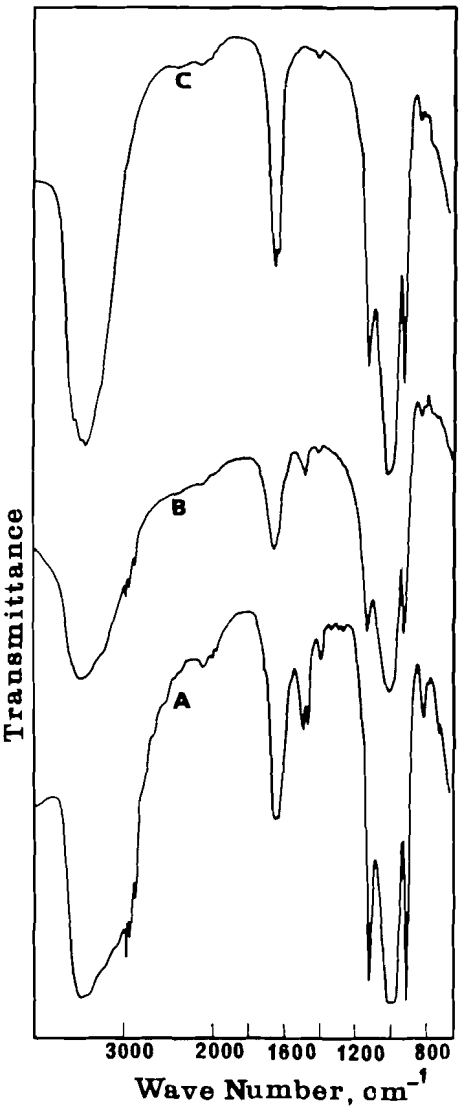

FIG. 5. Infrared spectra of Co^{2+} exchanged $(C_4H_9NH_3)UO_2PO_4 \cdot 3H_2O$: (A) 20% exchanged; (B) 50% exchanged; (C) fully exchanged.

TABLE 4. Thermal data of $M(UO_2PO_4)_2 \cdot nH_2O$

Compound	Step I (25–80°C)		Step II (80–150°C)		Step III (150–300°C)	
	TG (x)	DTA (peak)	TG (y)	DTA (peak)	TG (z)	DTA (peak)
$Co(UO_2PO_4)_2 \cdot 9H_2O$	3	60°C	4	127°C	2	250°C
$Ni(UO_2PO_4)_2 \cdot 9H_2O$	4	55°C, 77°C	3	135°C	2	295°C
$Cu(UO_2PO_4)_2 \cdot 10H_2O$	3	75°C	5	110, 143°C	2	237°C
$Mn(UO_2PO_4)_2 \cdot 9.5H_2O$	3	60°C, 74°C	4.5	115°C	2	215, 260°C
$Zn(UO_2PO_4)_2 \cdot 9.5H_2O$	3	56°C, 68°C	5.5	106°C	1	163, 300°C
$Cd(UO_2PO_4)_2 \cdot 8.5H_2O$*	3	50°C, 63°C	3.5	100°C	2	160, 193°C

*Two mixed phases.

Significant changes in the infrared spectra are produced by the substitution of *n*-butylamine by the metallic ions. In Fig. 5 a progressive decrease may be seen in the vibration bands corresponding to the CH_3, CH_2, and NH_3^+ groups as the uptake process of Co^{2+} ions proceeds. In the fully exchanged phases these bands have disappeared.

The P/U/M molar ratios of the solid compounds in which uptake is complete are 2:2:1; they correspond to hydrates with the general formula $M(UO_2PO_4)_2 \cdot nH_2O$, where $n = 8–10$.

Thermal analysis of the MUP hydrates shows that the water molecules are lost in a succession of endothermic effects (from 3 to 5) which occur between 50 and 300°C. In general, the successive stages of weight loss may be summarized by the following formulae:

$$M(UO_2PO_4)_2 \cdot nH_2O \xrightarrow[-xH_2O]{\text{I}} M(UO_2PO_4)_2 \cdot (n-x)H_2O$$

$$\xrightarrow[-yH_2O]{\text{II}} M(UO_2PO_4)_2 \cdot zH_2O \xrightarrow[-zH_2O]{\text{III}} M(UO_2PO_4)_2$$

Table 4 gives the values of x, y, and z and also the ranges of temperatures in which weight loss occurs. The DTA curves exhibit similar behaviour in all the solids studied. There are sharp, clear endothermic peaks associated with the initial effects of weight loss. The peaks of the third stages are more diffuse. In Fig. 6 may be seen the DTA and TG curves of NiUP.

The metal uranyl phosphates reported here correspond to fully hydrated phases that are structurally related to the naturally occurring minerals autunite and torbernite (13, 20, 21).

The diffractogram of hydrated UCdP shows a mixture of two phases: one, the fully hydrated compound with basal spacing of 11 Å, and the other, possibly a metaphase, whose basal spacing is close to 9 Å. When the cadmium compound was heated to 50°C, only one phase was seen; its composition was $Cd(UO_2PO_4)_2 \cdot 7H_2O$.

The crystalline compounds obtained by cation exchange showed very well-defined X-ray powder diffraction patterns that were indexed on the basis of a tetragonal unit cell.[4] Other authors (10, 11) obtained amorphous, or only slightly crystalline, phases when the transition metal uranyl phosphates are synthesized by precipitation from aqueous solutions of the appropriate ion.

Table 7 shows the lattice constants and X-ray powder pattern data obtained for the exchanged compounds. The a values compatible with the indexing of the recorded reflections are within limits of ± 0.008 Å of the a value obtained for the BAUP

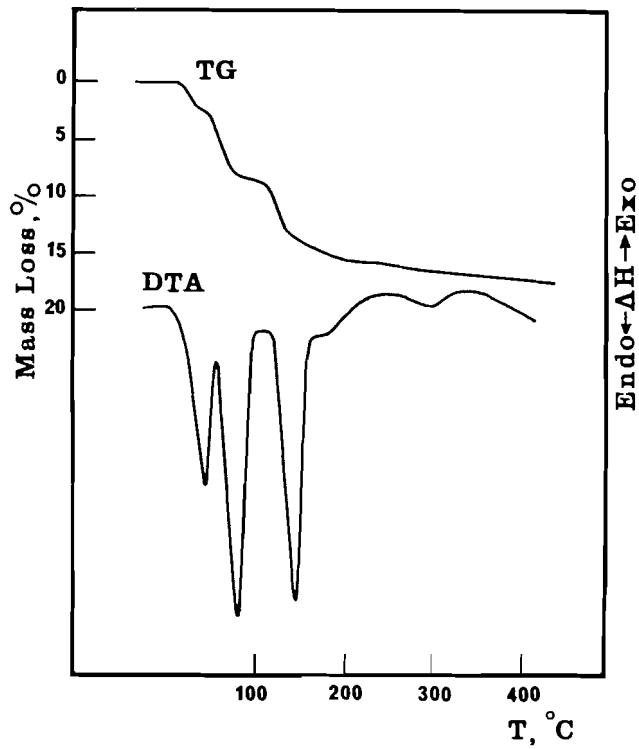

FIG. 6. TG and DTA curves of the $Ni(UO_2PO_4)_2 \cdot 9H_2O$.

intercalate. On the other hand, the c spacing values were double the values of the interlamellar spacings. This is in agreement with the literature (5, 14) for isostructural compounds.

Heated overnight at 50–60°C, the uranyl metal phosphates lose 1–3 water molecules and the basal spacing decreases to 8.5 or 9 Å. Some structural modification may be detected in the diffractograms, although their crystallinity persists and they may be indexed on a tetragonal system. Consequently $Cu(UO_2PO_4)_2 \cdot 10H_2O$, which is found naturally as the mineral torbernite, evolves into a very crystalline compound whose diffractogram and composition (7 hydrate) is identical to metatorbernite (21). In the case of $Mn(UO_2PO_4)_2 \cdot 9.5H_2O$, the partial dehydration leads to a non-tetragonal compound with lower symmetry. None of the 7-hydrate and 8-hydrate compounds subjected to heating will rehydrate in atmospheres of 50 to 60% relative humidity.

The uranyl metal phosphates (UMP) are yellow when the cation electron shell is complete or semi-complete (closed shell ions) (M = Zn, Cd, or Mn) and its electronic diffuse reflectance spectrum only shows the uranyl group vibronic transition bands in the region of 350–500 nm (22). The remaining UMP compounds (M = Co, Ni, and Cu) give a spectral pattern which contains

[4]Tables of crystal data and X-ray powder diffraction patterns of $M(UO_2PO_4)_2 \cdot nH_2O$ (Tables 5 and 6, supplementary material) may be purchased from the Depository of Unpublished Data, CISTI, National Research Council of Canada, Ottawa, Ont., Canada K1A 0S2.

TABLE 7. X-ray crystallographic data of $M(UO_2PO_4)_2 \cdot nH_2O$ (Cu $K\alpha_1$, α_2; λ = 1.5418 Å, 20°C)

Compound*	Formula weight	a (Å)	c (Å)	Z	V (Å^3)	d_c	d_o
$Co(UO_2PO_4)_2 \cdot 9H_2O$	950.93	6.962(9)	20.10(6)	2	974.2	3.24	3.27(1)
$Ni(UO_2PO_4)_2 \cdot 9H_2O$	950.71	6.907(9)	22.07(7)	2	1052.9	3.00	3.08(1)
$Cu(UO_2PO_4)_2 \cdot 10H_2O$	973.54	7.005(8)	20.67(6)	2	1014.3	3.19	3.26(1)
$Mn(UO_2PO_4)_2 \cdot 9.5H_2O$	955.94	6.968(6)	20.92(6)	2	1015.7	3.12	3.18(1)
$Zn(UO_2PO_4)_2 \cdot 9.5H_2O$	966.37	7.050(7)	20.08(7)	2	998.0	3.21	3.29(1)
$Cd(UO_2PO_4)_2 \cdot 7H_2O$†	968.40	6.966(8)	18.08(5)	2	877.3	3.66	3.68(1)

*All compounds belong to the tetragonal system.
†Heated to 50°C

TABLE 8. Electronic absorption bands of $M(UO_2PO_4)_2 \cdot nH_2O$ in the region 500–800 nm (diffuse reflectance)

Compound	Colour	λ (nm)
$Co(UO_2PO_4)_2 \cdot 9H_2O$	Pale orange	520
$Ni(UO_2PO_4)_2 \cdot 9H_2O$	Pale green	655, 700
$Cu(UO_2PO_4)_2 \cdot 10H_2O$	Blue green	655

other bands in the 500–800 nm zone (Table 8) in addition to those mentioned previously. The values of λ_{max} of these 500–800 nm bands are compatible with the observed transitions in the respective aqueous cations with different degrees of distorted octahedral symmetry.

Concluding remarks

In this work we have shown that the layered intercalate BAUP, which was obtained from the HUP(s) + n-$BuNH_2$(v) reaction by ion exchange, gives very crystalline and highly hydrated uranyl metal phosphates. The layered material structures resulting from this process maintain the *ab* plane of the tetragonal lattice of the starting product; the basal spacing of each species is dependent on its degree of hydration. The water molecules serve an important structural function as they are found coordinated with the metallic cations in the form of labile octahedral aqueous complexes. Ongoing studies in these laboratories suggest that the intercalate ligand-substitution reactions might be occurring in the host compounds.

Acknowledgements

We thank the Comisión Asesora de Investigación Científica y Técnica (Ministry of Education and Science, Spain) for financial support. We are grateful to Mr. David W. Schofield for reviewing the English version.

1. A. CLEARFIELD. *In* Inorganic ion exchange materials. *Edited by* A. Clearfield. CRC Press, Boca Raton, FL. 1982. Chapt. 1.
2. E. RODRIGUEZ-CASTELLÓN, S. BRUQUE, and A. RODRIGUEZ GARCÍA. J. Chem. Soc. Dalton Trans. 213 (1985).
3. J. W. JOHNSON, A. J. JACOBSON, J. F. BRODY, and S. M. RICH. Inorg. Chem. **21**, 3820 (1982).
4. A. T. HOWE. *In* Inorganic ion exchange materials. *Edited by* A. Clearfield, CRC Press, Boca Raton, FL. 1982. Chapt. 4.
5. M. M. OLKEN, R. N. BIAGIONI, and A. B. ELLIS. Inorg. Chem. **22**, 4128 (1983).
6. B. MOROSIN. Acta Crystallogr. Sect. B, **34**, 3733 (1978).
7. V. PEKAREK and V. VESELY. J. Inorg. Nucl. Chem. **27**, 1151 (1965).
8. A. T. HOWE and M. G. SHILTON. J. Solid State Chem. **28**, 345 (1979).
9. A. T. HOWE and M. G. SHILTON. J. Solid State Chem. **31**, 393 (1980).
10. V. PEKAREK, V. VESELY, and J. ULLRICH. Bull. Soc. Chim. Fr. Spec. Publ. 1844 (1968).
11. R. BERMAN. Am. Mineral. **42**, 905 (1957).
12. R. F. VOCHTEN. Geol. Soc. S. Afr. Spec. Publ. **7**, 287 (1983).
13. F. GONZÁLEZ-GARCIA and R. R. DÍAZ. An. Quim. **55B**, 383 (1959).
14. F. WEIGEL and G. HOFFMANN. J. Less-Common Met. **44**, 99 (1976).
15. A. CLEARFIELD and R. M. TINDWA. Inorg. Nucl. Chem. Lett. **15**, 251 (1979).
16. V. A. WEISS, K. HARTL, und U. HOFMANN. Z. Naturforsch. Teil B, **12**, 351 (1957).
17. J. M. SCHREYER and C. F. BAES. J. Am. Chem. Soc. **76**, 354 (1954).
18. I. L. BOTTO, E. J. BARAN, and P. J. AYNONINO. Z. Chem. **16**, 163 (1976).
19. A. CLEARFIELD and R. TINDWA. J. Inorg. Nucl. Chem. **41**, 871 (1979).
20. M. Ross and H. T. EVANS. Am. Mineral. **49**, 1578 (1964).
21. M. ROSS, H. T. EVANS, and D. E. APPLEMAN. Am. Mineral. **49**, 1603 (1964).
22. C. GÖRLLER-WALRAND and S. DE JAEGERE. Spectrochim. Acta Part A, **28**, 257 (1972).

Ion exchange reactions of *n*-butylamine intercalates of tin(IV) hydrogen phosphate and hydrogen uranyl phosphate with cobalt(III) complexes

RAFAELA POZAS-TORMO, LAUREANO MORENO-REAL, MARÍA MARTÍNEZ-LARA, AND ENRIQUE RODRÍGUEZ-CASTELLÓN[1]

Departamento de Química Inorgánica, Facultad de Ciencias, Universidad de Málaga, 29080 Málaga, Spain

Received May 1, 1985

RAFAELA POZAS-TORMO, LAUREANO MORENO-REAL, MARÍA MARTÍNEZ-LARA, and ENRIQUE RODRÍGUEZ-CASTELLÓN. Can. J. Chem. **64**, 35 (1986).

The ion exchange reactions of *n*-butylamine intercalates of tin(IV) hydrogen phosphate and hydrogen uranyl phosphate towards carbonatotetraamminecobalt(III), chloropentaamminecobalt(III), and hexaamminecobalt(III) have been investigated. Independent of the complex cation charges, the amounts of Co(III) complex exchanged by the *n*-butylamine intercalate of tin(IV) hydrogen phosphate are practically the same. With the *n*-butylamine intercalate of hydrogen uranyl phosphate, the ionic exchange was completed and the composition was fixed by the exchanged Co(III) complex. The layer charge densities of these phosphates justify the different ionic exchange behaviour observed towards the large complex cations. All the products were characterized by chemical analysis, X-ray diffractometry, infrared spectroscopy, diffuse reflectance spectroscopy, and thermal analysis.

RAFAELA POZAS-TORMO, LAUREANO MORENO-REAL, MARÍA MARTÍNEZ-LARA et ENRIQUE RODRÍGUEZ-CASTELLÓN. Can. J. Chem. **64**, 35 (1986).

On a étudié les réactions d'échange d'ions des composés d'intercalation entre la butylamine et l'hydrogenophosphate d'étain(IV) et l'hydrogénophosphate d'uranyle avec le carbonatotétraamminecobalt(III), le chloropentaamminecobalt(III) et l'hexaamminecobalt(III). La charge des complexes cationiques n'influence pas le taux d'ions complexes de Co(III) échangés par les composés d'intercalation entre la butylamine et l'hydrogénophosphate d'étain. Dans le cas du composé d'interaction entre la butylamine et l'hydrogénophosphate d'uranyle, l'échange ionique est totale et le complexe d'ion Co(III) échangé en détermine la composition. Les densités de charge de la couche de ces phosphates justifient le comportement des différents échanges ioniques observés avec les grands complexes cationiques. On a caractérisé tous les produits obtenus par l'analyse chimique, la diffraction de rayons X, la spectroscopie infrarouge, la spectroscopie de reflexion diffuse et par l'analyse thermique.

[Traduit par le journal]

Introduction

Tin(IV) hydrogen phosphate monohydrate, $Sn(HPO_4)_2 \cdot H_2O$ (α-SnP), and hydrogen uranyl phosphate tetrahydrate, $HUO_2PO_4 \cdot 4H_2O$ (HUP), are layered inorganic ion exchangers (1, 2). α-SnP crystallizes in the monoclinic system; the interlayer distance is 7.8 Å. On the other hand, HUP crystallizes in the tetragonal system, with an interlayer distance of 8.8 Å. The ion exchange behaviour with alkali metals, alkaline earths, and first row transition metals of these phosphates was investigated (3–8). However, very little is known about ion exchange with large complexes on these exchangers. α-SnP is isostructural to α-zirconium hydrogen phosphate (α-ZrP) (1). Complex ions like $[Co(NH_3)_6]^{3+}$ and $[Cu(NH_3)_4]^{2+}$ were exchanged using the monohydrogen form, or the wider-spaced *n*-butylamine – α-ZrP intercalate (9, 10). Cr(III) Werner complexes have also been exchanged into HUP (11, 12).

The *n*-butylamine intercalated forms of α-SnP (BASnP) and HUP (BAUP) were chosen because of their large interlayer distances (19.5 and 14.4 Å, respectively), with wide passageways leading to the exchange site that would permit the interlayer penetration of large complexes. The characterization of the exchanged behaviour of BAUP will be reported.

Experimental

Preparation

All the chemicals were of reagent grade and were used without further purification. α-SnP and BASnP were prepared as described elsewhere (13, 14). HUP was prepared according to the method proposed by Schreyer and Baes (15). The BAUP was obtained by the same method used for BASnP. The complexes $[Co(NH_3)_4CO_3]NO_3$, $[Co(NH_3)_5Cl]Cl_2$, and $[Co(NH_3)_6]Cl_3$ were synthesized as reported in the literature (16).

Weighed amounts of $Sn(C_4H_{11}N)_2(HPO_4)_2 \cdot H_2O$ and $(C_4H_9NH_3)UO_2PO_4 \cdot 3H_2O$ were suspended for one day, at 25°C, in aqueous solutions of $[Co(NH_3)_4CO_3]NO_3$, $[Co(NH_3)_5Cl]Cl_2$, and $[Co(NH_3)_6]Cl_3$, which represented 300% of the exchange capacity. This operation was repeated once. The mixtures were filtered, and the solids were analyzed for their metal, water, and nitrogen contents.

Instrumentation

Metal content was determined using a Varian Techtron 475 ABD atomic spectrophotometer. The nitrogen content was determined by a micro-Kjeldahl method. X-ray films were obtained in Huber Debye–Scherrer cameras with diameters of 11.46 cm using a Siemens X-ray generator. A Siemens D-500 diffractometer was used for the X-ray diagrams. The radiation was nickel-filtered CuKα in each case. TG and DTA analyses were carried out using a Rigaku Thermoflex thermoanalyzer, at a heating rate of 10°C min^{-1}. Diffuse reflectance spectra were recorded on a Kontron–Uvikon 810 spectrophotometer with an integrating sphere attachment, which used $BaSO_4$ as the reference. Infrared studies were performed on a Beckman 4260 spectrophotometer by the KBr disc method.

Anal. calcd. for $Sn[Co(NH_3)_4CO_3]_{0.49}H_{1.51}(PO_4)_2 \cdot 1.5H_2O$: Co 6.74, N 6.40; % loss on ignition (TGA to 900°C) (LOI) 22.27; found: Co 6.72, N 6.56, LOI 22.29. *Anal.* calcd. for $Sn[Co(NH_3)_5Cl]_{0.5}H(PO_4)_2 \cdot 1.5H_2O$: Co 6.91, N 8.20, LOI 18.43; found: Co 6.98, N 8.00, LOI 18.36. *Anal.* calcd. for $Sn[Co(NH_3)_6]_{0.5}H_{0.5}(PO_4)_2 \cdot 3H_2O$: Co 6.69, N 9.54, LOI 24.75; found: Co 6.66, N 9.83, LOI 24.68. *Anal.* calcd. for $[Co(NH_3)_4CO_3]UO_2PO_4 \cdot H_2O$: Co 10.34, N 9.82, LOI 22.83; found: Co 10.76, N 9.40, LOI 23.14. *Anal.* calcd. for $[Co(NH_3)_5Cl]_{0.5}UO_2PO_4 \cdot 2.5H_2O$: Co 5.89, N 7.00, LOI 17.52; found: Co 5.5, N 6.90, LOI 17.51. *Anal.* calcd. for $[Co(NH_3)_6]_{0.33}UO_2PO_4 \cdot 2.21H_2O$: Co 4.31, N 6.12, LOI 16.75; found: Co 4.40, N 6.28, LOI 16.74.

[1]Author to whom correspondence may be addressed.

TABLE 1. Composition and interlayer distances of the exchanged phases at 25°C

Composition	Interlayer distance (Å)
$Sn[Co(NH_3)_4CO_3]_{0.49}H_{1.51}(PO_4)_2 \cdot 1.5H_2O$	11.90
$Sn[Co(NH_3)_5Cl]_{0.5}H(PO_4)_2 \cdot 1.51H_2O$	12.40
$Sn[Co(NH_3)_6]_{0.5}H_{0.5}(PO_4)_2 \cdot 3H_2O$	11.60
$[Co(NH_3)_4CO_3]UO_2PO_4 \cdot H_2O$	13.60
$[Co(NH_3)_5Cl]_{0.5}UO_2PO_4 \cdot 2.5H_2O$	9.64
$[Co(NH_3)_6]_{0.33}UO_2PO_4 \cdot 2.21H_2O$	9.88

Results and discussion

Composition and X-ray data

Table 1 shows the composition and the interlayer distance of the exchanged phases at 25°C. The amount of cobalt(III) complex exchanged by BASnP is independent of the charge of the complex. Although the interlayer distances of these compounds are different, a reflection line at 9.1 Å was observed in the powder patterns of all the complex exchanged compounds. Because of the crystal distortion suffered in the intercalation process, the X-ray diffraction data of the BASnP derivatives show few reflection lines, and thus the calculation of unit cell constants based on the powder patterns is not possible.[2] The observed composition results from the "covering effect" of the guest molecule; that is to say, the complex ion bonded to phosphate groups impedes bonding at an adjacent site, as this site is now covered. A similar composition was seen when BAZrP was ion exchanged with tetraamminecopper(II) (9). With BAUP there was a complete ionic exchange with the complex cations. In this case, the composition is a function of the complex cation charge. This different behaviour between HUP and α-SnP is due to the different layer charge densities. HUP has a smaller layer density than α-SnP and consequently a bigger free area around the active site (48.8 $Å^2$ for HUP and 21.5 $Å^2$ for α-SnP (14)). Thus, total saturation with large complex cations can be attained. The hydration stoichiometry of these compounds shows a wide range.

Table 3 shows the X-ray crystallographic data for the HUP exchanged phases. All samples could be indexed to tetragonal unit cells. The reflection lines corresponding to the original *hk*0 planes were maintained.[3] The absence of *hk*0 lines when $h + k \neq 2n$ demonstrates the retention of the *n* glide plane of uranyl phosphate. The layer structure has been preserved, while the *c* axis has varied.

Infrared spectra

The ir spectra of the exchanged compounds of BASnP are shown in Fig. 1. The $Sn[Co(NH_3)_4CO_3]_{0.49}H_{1.51}(PO_4)_2 \cdot 1.51H_2O$ spectrum (curve A) shows bands, due to zeolitic water, occurring at 3570, 3490, and 1640 cm^{-1}; they can be superimposed upon those reported previously for α-SnP (17).

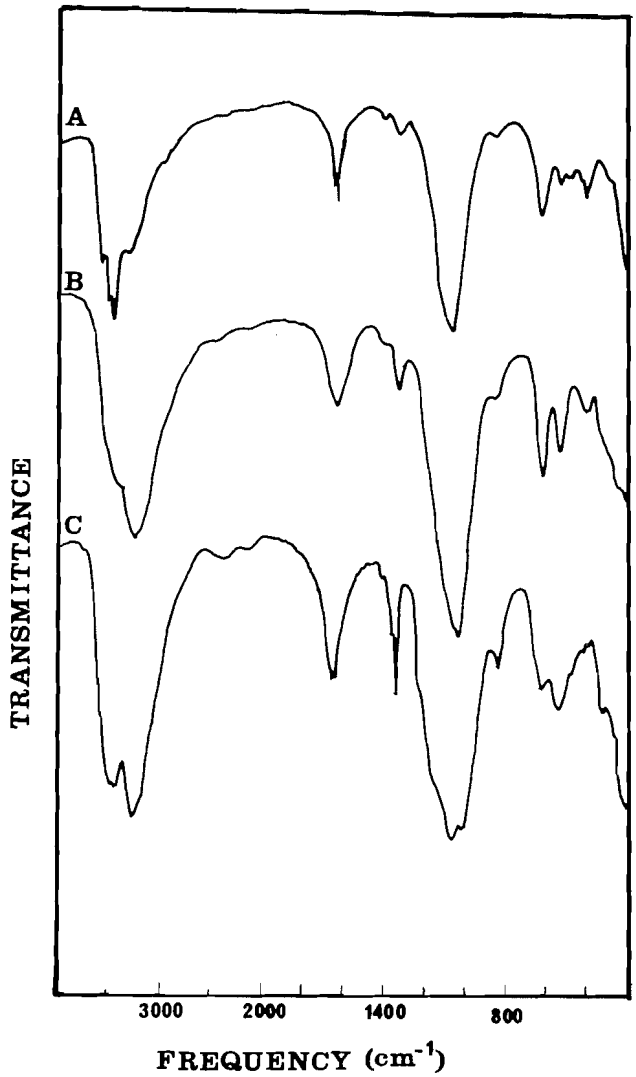

FIG. 1. Infrared spectra of (A), $Sn[Co(NH_3)_4CO_3]_{0.49}H_{1.51}(PO_4)_2 \cdot 1.5H_2O$; (B), $Sn[Co(NH_3)_5Cl]_{0.5}H(PO_4)_2 \cdot 1.5H_2O$; (C), $Sn[Co(NH_3)_6]_{0.5}H_{0.5}(PO_4)_2 \cdot 3H_2O$.

The water stretching in the $Sn[Co(NH_3)_5Cl]_{0.5}H(PO_4)_2 \cdot 1.5H_2O$ (curve B) and $Sn[Co(NH_3)_6]_{0.5}H_{0.5}(PO_4)_2 \cdot 3H_2O$ (curve C) are not so sharply defined and they are overlapped by the NH_3 stretching bands. Generally, the NH_3 stretching bands occur at higher frequencies (3300–3200 cm^{-1}) because these frequencies are sensitive to changes in the anion. (The anion of the complex salts (Cl^-) is substituted by the layer O_3PO^-.) The broadening of these bands is the result of hydrogen bonding as well as the overlapping of the individual N—H stretching bands of the complex (18). The NH_3 scissoring bands at 1330 cm^{-1} (curve B), and 1335 cm^{-1} (curve C), are sharp and practically superimposable on those of the original complexes (18). In all cases, the NH_3 rocking vibrations shift to higher frequencies and overlap the absorption bands of the phosphate group, as this rocking mode is very sensitive to the outer ions and the hydrogen bonding (19). The absence of characteristic bands in the region of 1500–1400 cm^{-1} and the higher frequency shift of the rocking mode indicate that the cobalt complex ion is now present as an amine complex and that the ammonia is hydrogen-bonded with the layer phosphate (20). The cobalt–nitrogen stretching bands are very weak and occur near 500 cm^{-1}.

[2]A table of X-ray powder diffraction data of $Sn[Co(NH_3)_4CO_3]_{0.49}H_{1.51}(PO_4)_2 \cdot 1.51H_2O$, $Sn[Co(NH_3)_5Cl]_{0.5}H(PO_4)_2 \cdot 1.51H_2O$, and $Sn[Co(NH_3)_6]_{0.5}H_{0.5}(PO_4)_2 \cdot 3H_2O$ (Table 2, supplementary material) may be purchased from the Depository of Unpublished Data, National Research Council of Canada, Ottawa, Ont., Canada K1A 0S2.

[3]Tables of X-ray powder diffraction data of $[Co(NH_3)_4CO_3]UO_2PO_4 \cdot H_2O$, $[Co(NH_3)_5Cl]_{0.5}UO_2PO_4 \cdot 2.5H_2O$, and $[Co(NH_3)_6]_{0.33}UO_2PO_4 \cdot 2.21H_2O$ (Tables 4, 5, and 6, supplementary material) may be purchased from the Depository of Unpublished Data, National Research Council of Canada, Ottawa, Ont., Canada K1A 0S2.

TABLE 3. X-ray crystallographic data of cobalt(III) complex uranyl phosphates (Cu $K_{\alpha_1\alpha_2}$; λ = 1.5418 Å, 20°C)

Compound*	Formula weight	a (Å)	c (Å)	Z	V (Å^3)	d_c	d_o
$[Co(NH_3)_4CO_3]UO_2PO_4 \cdot H_2O$	566.89	6.94(3)	27.42(42)	4	1321.41	2.85	2.83(1)
$[Co(NH_3)_5Cl]_{0.5}UO_2PO_4 \cdot 2.5H_2O$	499.79	6.94(2)	19.38(60)	4	932.33	3.56	3.55(1)
$[Co(NH_3)_6]_{0.33}UO_2PO_4 \cdot 2.21H_2O$	446.32	6.98(3)	19.84(16)	4	967.72	3.06	3.09(1)

*All compounds belong to the tetragonal system.

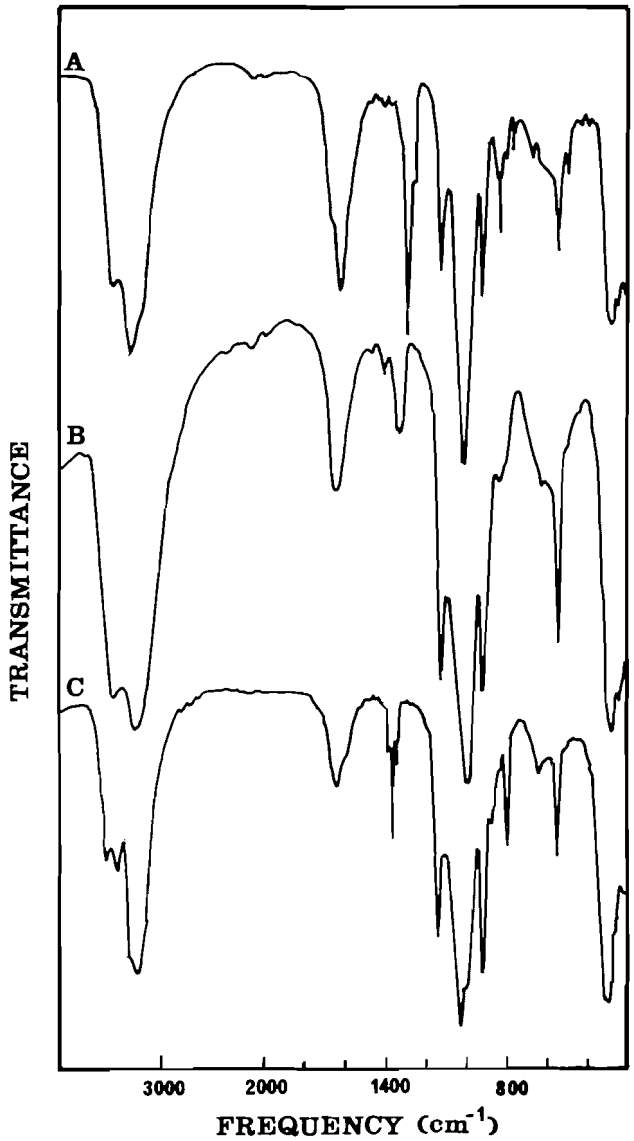

FIG. 2. Infrared spectra of (A), $[Co(NH_3)_4CO_3]UO_2PO_4 \cdot H_2O$; (B), $[Co(NH_3)_5Cl]_{0.5}UO_2PO_4 \cdot 2.5H_2O$; (C), $[Co(NH_3)_6]_{0.33}UO_2PO_4 \cdot 2.21H_2O$.

Phosphate vibration bands centered at 1000 cm^{-1} dominate all the spectra of Fig. 1.

Figure 2 shows the ir spectra of the exchanged phases of BAUP: $[Co(NH_3)_4CO_3]UO_2PO_4 \cdot H_2O$ (curve A), $[Co(NH_3)_5Cl]_{0.5}UO_2PO_4 \cdot 2.5H_2O$ (curve B), and $[Co(NH_3)_6]_{0.33}UO_2PO_4 \cdot 2.21H_2O$ (curve C). These spectra are well defined; there is a strong absorption band centered at 1000 cm^{-1} assigned to phosphate stretching (21), and a sharp band at 925 cm^{-1} assigned to the UO_2^{2+} asymmetric stretching vibration; the two dominate

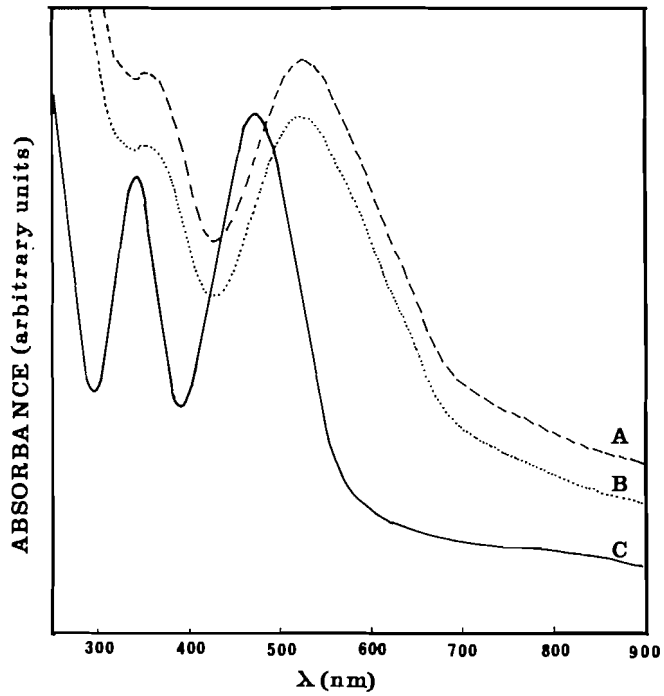

FIG. 3. Diffuse reflectance spectra of (A), $Sn[Co(NH_3)_4CO_3]_{0.49}H_{1.51}(PO_4)_2 \cdot 1.5H_2O$; (B), $Sn[Co(NH_3)_5Cl]_{0.5}H(PO_4)_2 \cdot 1.5H_2O$; (C), $Sn[Co(NH_3)_6]_{0.5}H_{0.5}(PO_4)_2 \cdot 3H_2O$.

all the spectra. Water bands occur at 3500 and 1630 cm^{-1}. The ammonia stretching vibration bands of these exchanged phases appear at 3300–3200 cm^{-1}. These values are near those previously observed in the α-SnP derivatives. This is to be expected, because the anions in the layered phosphate are similar. The NH_3 scissoring bands at 1270–1370 cm^{-1} are very sharp and similar to those of the cobalt(III) α-SnP complex. The metal–nitrogen stretching bands are better defined than those of α-SnP derivatives, and occur near 500 cm^{-1}. Sometimes these bands are overlapped by the phosphate group bending vibration band.

In a comparative study, the spectra of α-SnP and HUP derivatives are seen to be composites of those of the phosphate layer and the corresponding cobalt(III) ammonia complex ion. In both series the NH_3 stretching, bending, and rocking modes shift to higher frequencies due to hydrogen bonding phosphate. The NH_3 bending bands at 1620–1640 cm^{-1} overlap the water bending mode.

In all cases, the *n*-butylammonium ion absorption bands of the starting material disappeared.

Diffuse reflectance ultraviolet–visible spectra

The diffuse reflectance spectra of the α-SnP derivatives (Fig. 3) and the HUP derivatives (Fig. 4) are very different. In the

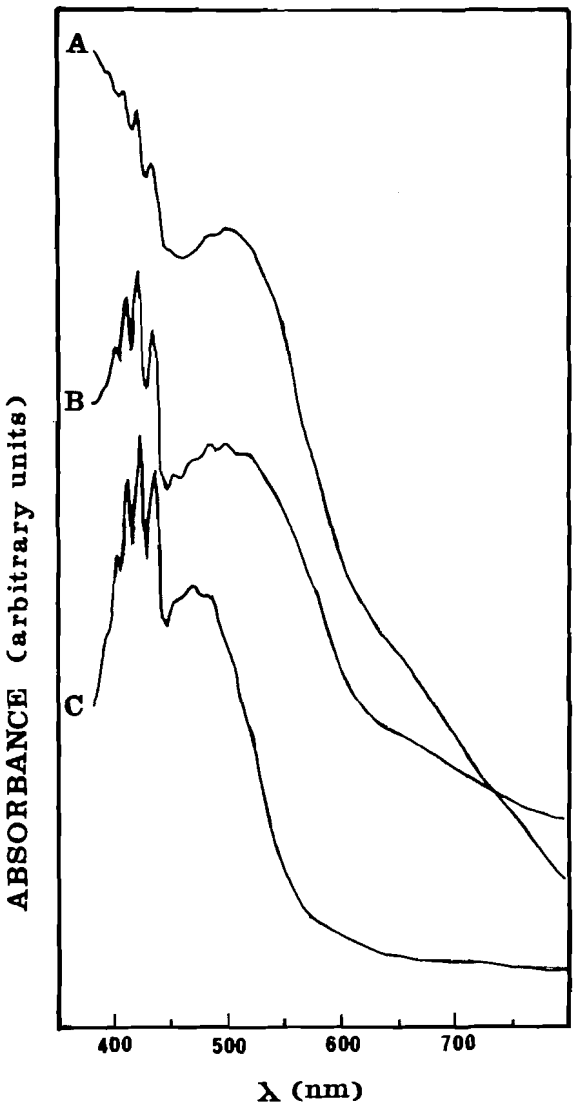

FIG. 4. Diffuse reflectance spectra of (A), $[Co(NH_3)_4CO_3]UO_2PO_4 \cdot H_2O$; (B), $[Co(NH_3)_5Cl]_{0.5}UO_2PO_4 \cdot 2.5H_2O$; (C), $[Co(NH_3)_6]_{0.33}UO_2PO_4 \cdot 2.21H_2O$.

former, the layered phosphate is inactive in the 300–900 nm region. However, the HUP diffuse reflectance spectrum shows many sharp peaks in the 340–500 nm region; these are derived from the spectrum of the uranyl moiety (22).

The spectra of the α-SnP derivatives correspond to the following ions exchanged: carbonatotetraamminecobalt(III), with maxima at 515 and 350 nm (curve A); chloropentaamminecobalt(III), with maxima at 520 and 350 nm (curve B); and hexaamminecobalt(III), with maxima at 470 and 340 nm (curve C). These spectra are practically superimposable on those of the salt complex employed (23, 24).

The spectra of the HUP derivatives (Fig. 4) are composed of those of HUP and the cobalt(III) complex ions. All the samples exhibit similar spectra in the 370–500 nm region. The absorption bands that correspond to the Co(III) complex ions overlap; it is only possible to distinguish them at 510 nm for $[Co(NH_3)_4CO_3]$-UP and $[Co(NH_3)_5Cl]$-UP, and at 470 nm for $[Co(NH_3)_6]$-UP. These values observed in the visible region coincide closely with those reported for the complex ions. However, the high absorption of the HUP layer in the ultraviolet

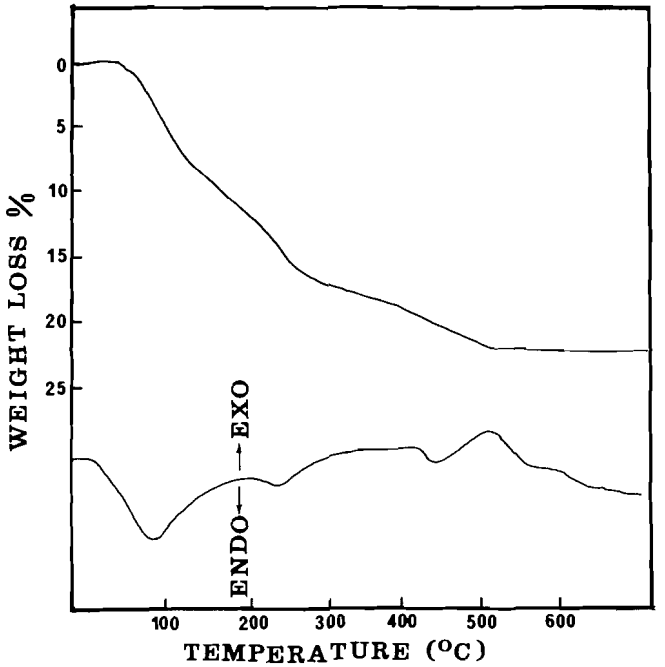

FIG. 5. DTA–TG curves of $Sn[Co(NH_3)_4CO_3]_{0.49}H_{1.51}(PO_4)_2 \cdot 1.5H_2O$.

region impedes the detection of the corresponding bands assigned to the $^1T_{2g} \leftarrow {}^1A_{1g}$ transition.

From these data we conclude that the Co(III) complex ions are present in the exchangers.

Thermal data

The thermal behaviour of the α-SnP derivatives and HUP derivatives was investigated. As representative examples, we show the decomposition processes of $Sn[Co(NH_3)_4CO_3]_{0.49}H_{1.51}(PO_4)_2 \cdot 1.5H_2O$ and $[Co(NH_3)_6]_{0.33}UO_2PO_4 \cdot 2.21H_2O$. In the DTA–TG curves of the former compound (Fig. 5), three different stages can be seen. The first (DTA peak at 84°C) corresponds to the removal of the water of crystallization. The second corresponds to the evolution of ammonia and carbon dioxide. Finally, the condensation of orthophosphate to pyrophosphate takes place between 400 and 500°C. In the X-ray powder diffraction patterns of the sample heated at 900°C, SnP_2O_7 could be identified[4] (25). This confirms the presence of the proton in the exchanged compound. However, the expected Co_3O_4 could not be detected. This spinel is the final product when $[Co(NH_3)_4CO_3]_2SO_4 \cdot 3H_2O$ is heated at 800°C (26).

The thermogravimetric curve of $[Co(NH_3)_6]_{0.33}UO_2PO_4 \cdot 2.21H_2O$ (Fig. 7) indicates that the decomposition of this compound occurs in three stages. The first corresponds to the removal of water. In the second, the ammonia and nitrogen liberation are almost overlapped; the cobalt(III) ion is reduced, as in the case of the hexaamminecobalt(III) halides (27). The third corresponds to the condensation of orthophosphate to pyrophosphate. The DTA curve supports this mode of decomposition. The experimental per cent weight loss on ignition agrees with the calculated value if the Co(III) reduction and the condensation to pyrophosphate are considered. A significant increment of the magnetic susceptibility was observed in the compound

[4]Figure 6, X-ray powder diffraction patterns of $Sn[Co(NH_3)_4CO_3]_{0.49}H_{1.51}(PO_4)_2 \cdot 1.5H_2O$ heated at 900°C, (Fig. 6, supplementary material) may be purchased from the Depository of Unpublished Data, National Research Council of Canada, Ottawa, Ont., Canada K1A 0S2.

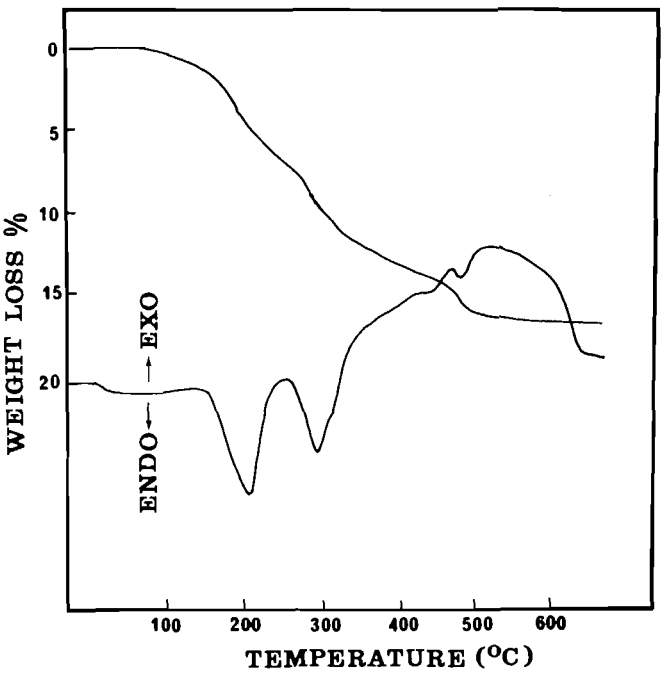

FIG. 7. DTA–TG curves of $[Co(NH_3)_6]_{0.33}UO_2PO_4 \cdot 2.21H_2O$.

heated at 600°C. This also supports the Co(III) reduction to Co(II).

Acknowledgement

We thank the "Comisión Asesora de Investigación Científica y Técnica" for financial support of the work carried out at the University of Málaga.

1. N. G. CHERNORUKOV, I. R. MOCHALOVA, E. P. MOSCUICHEV, and G. B. SIBRINA. Zh. Prikl. Khim. **50**, 1618 (1977).
2. A. T. HOWE. *In* Inorganic ion exchange materials. *Edited by* A. Clearfield. CRC Press, Boca Raton, FL. 1982. Chapt. 4.
3. U. COSTANTINO and A. GASPERONI. J. Chromatogr. **51**, 289 (1970).
4. M. J. FULLER. J. Inorg. Nucl. Chem. **33**, 559 (1971).
5. N. G. CHERNORUKOV and G. S. SIBRINA. Zh. Prikl. Khim. **53**, 939 (1980).
6. E. RODRÍGUEZ-CASTELLÓN, A. RODRÍGUEZ-GARCÍA, and S. BRUQUE. Mater. Res. Bull. **20**, 115 (1985); Anal. Quim. In press.
7. F. WEIGEL and G. J. HOFFMANN. J. Less Common Met. **44**, 99 (1976).
8. M. M. OLKEN, R. N. BIAGIONI, and B. ELLIS. Inorg. Chem. **22**, 4128 (1983).
9. A. CLEARFIELD and R. M. TINDWA. Inorg. Nucl. Chem. Lett. **15**, 251 (1979).
10. Y. HASEGAWA and S. KISAKI. Chem. Lett. Jpn. 241 (1980).
11. M. M. OLKEN and A. B. ELLIS. J. Am. Chem. Soc. **106**, 7468 (1984).
12. M. M. OLKEN, C. M. VERSSCHOOR, and A. B. ELLIS. J. Lumin. **31/32**, 552 (1984).
13. E. RODRÍGUEZ-CASTELLÓN, A. RODRÍGUEZ-GARCÍA, and S. BRUQUE. Inorg. Chem. **24**, 1187 (1985).
14. E. RODRÍGUEZ-CASTELLÓN, S. BRUQUE, and A. RODRÍGUEZ-GARCÍA. J. Chem. Soc. Dalton Trans. 213 (1985).
15. J. M. SCHREYER and C. F. BAES. J. Am. Chem. Soc. **76**, 354 (1954).
16. G. SCHLESSINGER. Inorg. Synth. **6**, 173 (1960); T. MOELLER and G. L. KING. Inorg. Synth. **5**, 185 (1957); J. BJERRUM and J. P. MCREYNOLDS. Inorg. Synth. **2**, 216 (1946).
17. N. G. CHERNORUKOV. Zh. Neorg. Khim. **26**, 535 (1981).
18. K. NAKAMOTO. The infrared spectra of inorganic and coordination compounds. Wiley–Interscience. New York. 1963.
19. J. FUJITA, K. NAKAMOTO, and M. KOBAYASHI. J. Am. Chem. Soc. **78**, 3295 (1965).
20. Y. HASEGAWA, S. KIZAKI, and H. AMEKURA. Bull. Chem. Soc. Jpn. **56**, 734 (1983).
21. V. PEKAREK and V. VESELY. J. Inorg. Nucl. Chem. **27**, 1151 (1965).
22. H. D. BURROWS and T. KEMP. J. Chem. Soc. Rev. **3**, 139 (1974).
23. D. SUTTON. Electronic spectra of transition metal complexes. McGraw-Hill, London. 1972.
24. W. WENDLANDT and H. G. HECHT. Reflectance Spectroscopy. Wiley–Interscience, New York. 1962.
25. JCPDS Powder Diffraction File 3-278.
26. J. M. AMIGÓ, J. GARCÍA GONZÁLEZ, and C. MIRAVITLLES. J. therm. Anal. **3**, 169 (1971).
27. T. FLORA. Acta Chim. Acad. Scien. Hung. **52**, 133 (1967).

Flow calorimetry of viscous liquids. Volumes and heat capacities of mixtures of *N*,*N*-dimethylformamide with *N*-alkylacetamides

H. C. ZEGERS, R. BOEGSCHOTEN, W. MELS, AND G. SOMSEN[1]

Department of Chemistry, Free University, De Boelelaan 1083, 1081 HV Amsterdam, The Netherlands

Received May 2, 1985

H. C. ZEGERS, R. BOEGSCHOTEN, W. MELS, and G. SOMSEN. Can. J. Chem. **64**, 40 (1986).

A sampling device is described which enables the Picker flow heat capacity calorimeter to handle viscous liquids. The necessary constant liquid flow through the calorimetric cell is achieved by an overpressure on the entering liquids, and can be maintained by pressure control. In addition, the device permits automatic measurement of a number of samples. The approach is applied to densities and heat capacities of binary mixtures of dimethylformamide and the viscous liquids *N*-ethylacetamide, *N*-n-propylacetamide, and *N*-n-butylacetamide. The results appear to be accurate enough to establish excess molar heat capacities as well as apparent molar heat capacities.

H. C. ZEGERS, R. BOEGSCHOTEN, W. MELS et G. SOMSEN. Can. J. Chem. **64**, 40 (1986).

On décrit un dispositif déchantillonnage qui permet d'examiner des liquides visqueux à l'aide du calorimètre à écoulement de Picker. L'écoulement constant du liquide à travers la cellule calorimétrique, qui est nécessaire avec cette méthode, est réalisé en appliquant une surpression sur les liquides introduits et en maintenant un contrôle sur la pression. De plus, ce dispositif permet de réaliser une mesure automatique de plusieurs échantillons. On a appliqué cette approche à la détermination des densités et des capacités calorifiques de mélanges binaires de diméthylformamide avec des liquides visqueux comme les *N*-éthyl-, *N*-n-propyl- et *N*-n-butylacétamides. Les résultats semblent être assez fiables pour permettre de déterminer les capacités calorifiques molaires en excès ainsi que les capacités calorifiques molaires apparentes.

[Traduit par le journal]

Introduction

Heat capacities at constant pressure are useful quantities in the study of mixtures and solutions. They can be used to predict the temperature dependence of enthalpies of different processes in mixtures or solutions (dilution, reaction, etc.) and to relate adiabatic and isothermal compressibilities. Another use of heat capacities is to derive from them the apparent or partial molar heat capacities $C_{p,B,\phi}$ or $C_{p,B}$ of a component B, since these functions reflect the heat capacity of that component itself together with all changes in heat capacity caused by the different environments of a component particle in mixtures. Being related to the second derivative of the chemical potential with respect to the temperature, these functions are very sensitive to structural changes in the mixtures, especially in aqueous media. Although the importance of values of $C_{p,B,\phi}$ and $C_{p,B}$ to solution chemistry is obvious, their accurate experimental determination is difficult.

Since its introduction in 1971, the Picker flow microcalorimeter (1) has been used successfully to obtain volumetric heat capacities (C_p/V) of pure liquids, liquid mixtures, and solutions in such an accurate way that reliable apparent and partial molar heat capacities can be calculated. In essence, the microcalorimeter is a very sensitive heat balance that is able to detect differences in the volumetric heat capacities of two liquid samples down to $7 \times 10^{-5}\,J\,K^{-1}\,cm^{-3}$. To achieve this high accuracy, the flow rate of the liquid through the calorimetric cell must have a value of about $0.010\,cm^3\,s^{-1}$. In addition it must be very stable (±0.1%). Often this is hard to achieve, especially with organic liquids which may cause damage to pumps. In that case a popular alternative is to obtain the liquid flow supply by gravity. However, many organic liquids are too viscous to apply the gravity method and (or) may be so hygroscopic or sensitive to oxygen that contact with air should be avoided, making the flow-by-gravity method cumbersome. In order to overcome these problems we have developed a device that maintains a constant liquid flow through the calorimetric cell by a controlled overpressure on the entering liquids. Use of nitrogen as pressurizing gas at the same time provides protection of the liquid samples against contact with air. In addition, the device is able to handle a number of liquid samples automatically.

[1]Author to whom correspondence may be addressed.

Experimental

Apparatus

A scheme of the sampling device is given in Fig. 1. The central unit is a programmable timer which activates simultaneously two nitrogen valves (a), an hplc valve (b), two sample changers (carrousels, (c)), and two pistons (d) to which a lid (e), a descending tube (f), and a nitrogen inlet (g) are attached. The device operates in the following way. Vials containing the liquid samples (h) and sealed by means of aluminum foil are installed in sample holders (i) mounted on a carrousel. Activated by the timer, a sample holder moves to a position below a piston. Subsequently the piston moves down, closing the sample holder by the lid (e). At the same time the descending tube pierces the aluminum foil and plunges into the liquid sample. After that, a slight overpressure of nitrogen gas is applied to the closed sample holder and the sample liquid starts to rinse the tubing between vial and valve (b). After some time valve (b) switches the liquid flow into the calorimeter. This situation is maintained until a measurement is finished. Then the same procedure is applied to a second sample by means of the other piston. The instrument is able to accommodate a total of 24 samples.

In this way the device can follow automatically a stepwise procedure as described by Grolier *et al.* (2) and Fortier and Benson (3), to measure the volumetric heat capacities of liquid mixtures with gradually changing compositions. Only the flow rate of the liquids through the calorimetric cell has to be watched, which can be performed by means of a flow meter or simple inspection of the electric output signal of the calorimeter. Changing viscosities of the mixtures may make it necessary to adjust the nitrogen overpressure in the sample holders, to maintain a constant flow of liquid. To achieve an optimal flow rate we never needed pressures higher than 1.7 bar (1 bar = 100 kPa).

Measurements

As a test, we carried out measurements with mixtures fed to the calorimeter both by our pressure device and by gravity. The results appeared to be identical, provided that the flow rates in both methods are comparable (4). This is due to the fact that heat loss to the environment of the calorimetric cell is dependent on the flow rate (see ref. 5).

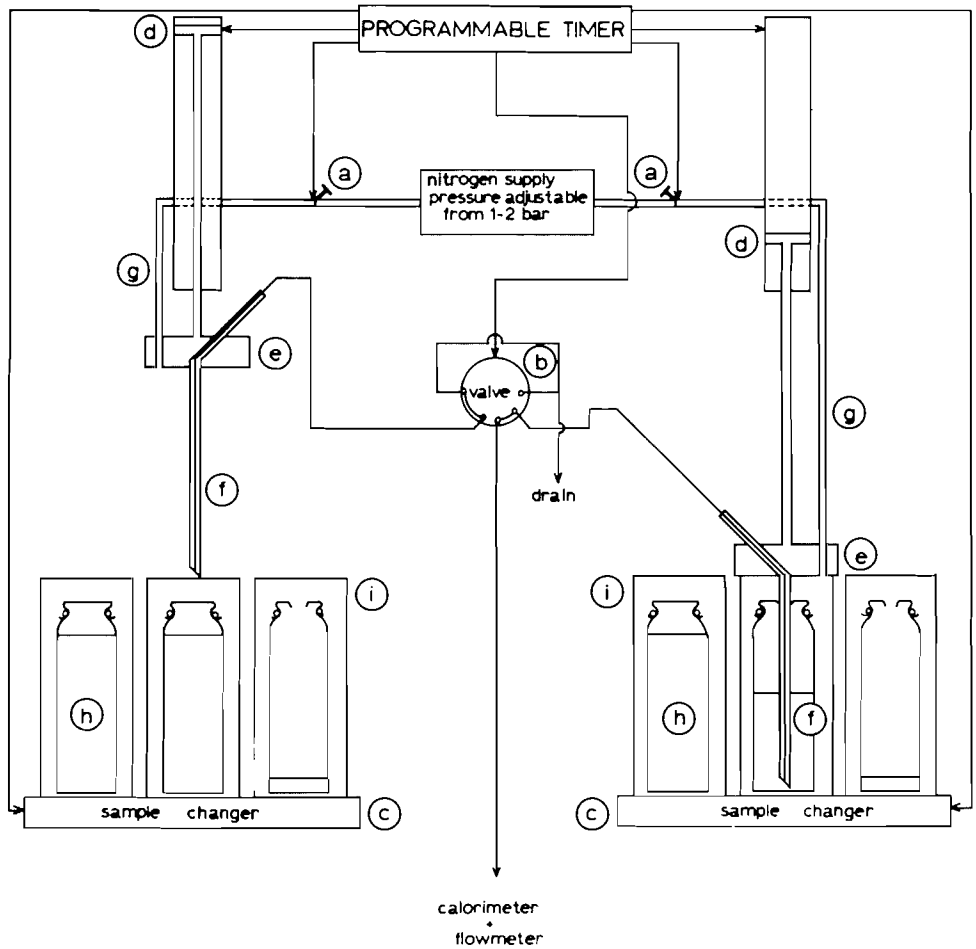

FIG. 1. Scheme of the sampling device for the Picker flow microcalorimeter; (a) nitrogen valve; (b) hplc valve; (c) sample changer (carrousel); (d) piston; (e) lid; (f) descending tube; (g) nitrogen inlet; (h) vial containing the liquid sample; and (i) sample holder.

In addition, a low flow rate must be avoided. In that case not only does the heat loss become very high but also the zones in which some mixing occurs between subsequent samples may become very large. Both influences reduce the reliability of the method. Our pressure device eliminates these undesirable effects and renders the calorimeter suitable for viscous liquids. We will illustrate this by presenting results of measurements on mixtures of *N*,*N*-dimethylformamide (DMF) with *N*-ethylacetamide (NEA), *N*-n-propylacetamide (NPrA), and *N*-n-butylacetamide (NBuA) over the complete mole fraction range. The latter three compounds constitute a series of liquids with increasing viscosity, 6.01, 10.7, and 14.0 cP, respectively (6).

Materials

DMF (Baker Analyzed Reagent) was stored over molecular sieves 4A for at least one week and used without further purification. NEA (Fluka, purum) was taken from stock. NPrA and NBuA were synthesized according to the reaction:

$$CH_3COOH + RNH_2 \rightarrow CH_3CONHR + H_2O$$

where R denotes an alkyl group (7, 8). This reaction was made quantitative by adding acetic anhydride to the reacting mixture. Acetic acid and acetic anhydride were removed by azeotropic distillation with methylcyclohexane (9). NEA, NPrA, and NBuA were purified by azeotropic distillation with benzene (to remove last traces of water and acetic acid) followed by fractional distillation under reduced pressure. The middle fraction was taken and stored over molecular sieves 4A.

The water contents of all compounds were determined by the modified Karl Fischer procedure of Verhoef and Barendrecht (10). In all cases the volume fraction of water was less than 0.0001. Gas–liquid chromatography showed a mole fraction purity of 0.995 or higher for each compound.

Procedure

Liquid mixtures of DMF with the various *N*-alkylacetamides were prepared by mass. Details of the procedure have been described before (11). The densities of the mixtures relative to the density of pure DMF were measured by a digital flow densimeter (Sodev, model 03D, Sherbrooke, Quebec). Heat capacities were obtained from volumetric heat capacities (C_p/V) measured with a Picker flow microcalorimeter (Setaram, model "chaleur specifique", Lyon, France), equipped with the automatic pressure device described above.

Results

Volumes

Densities d of the binary mixtures relative to the density of pure DMF (d_1^*) are presented in Table 1 as function of the mole fraction x_1 of DMF. The density of pure DMF measured with respect to that of pure water (12) is 0.943289 g cm^{-3} at 298.15 K, corresponding to a molar volume $V_1^* = 77.489$ cm^3 mol^{-1}. The molar volumes of the pure *N*-alkylacetamides NEA, NPrA, and NBuA are $V_2^* = 94.734$, 111.641, and 128.697 cm^3 mol^{-1} respectively, and compare very well with the values $V_2^* =$

TABLE 1. Experimental relative densities $d - d_1^*$ and changes in heat capacity per unit volume $\Delta(C_p/V)$ at 298.15 K.

x_1	$10^3(d - d_1^*)$ (g cm^{-3})	$10^3\Delta(C_p/V)$ (J K^{-1} cm^{-3})	x_1	$10^3(d - d_1^*)$ (g cm^{-3})	$10^3\Delta(C_p/V)$ (J K^{-1} cm^{-3})
Dimethylformamide (1) + ethylacetamide (2)					
0.000000	−23.642	−11.614	0.547163	−10.135	2.123
0.029594	−22.888	−11.132	0.600022	−8.881	2.895
0.054080	−22.260	−10.684	0.653073	−7.659	3.548
0.077114	−21.675	−10.180	0.698129	−6.606	3.714
0.103742	−20.998	−9.496	0.749572	−5.415	3.751
0.125044	−20.448	−8.918	0.810031	−4.072	3.509
0.170595	−19.301	−7.599	0.844937	−3.297	3.184
0.208943	−18.347	−6.477	0.864074	−2.878	2.941
0.250458	−17.329	−5.363	0.903622	−2.023	2.374
0.299090	−16.095	−3.839	0.924511	−1.573	1.970
0.351258	−14.834	−2.276	0.950019	−1.032	1.388
0.398358	−13.694	−1.089	0.975559	−0.501	0.724
0.451123	−12.408	0.201	1.000000	0.000	0.000
0.499517	−11.247	1.306			
Dimethylformamide (1) + n-propylacetamide (2)					
0.000000	−37.258	−52.047	0.547575	−18.604	−14.509
0.027373	−36.389	−50.339	0.607416	−16.351	−11.411
0.053724	−35.551	−48.587	0.643876	−14.924	−9.608
0.076294	−34.830	−47.006	0.701153	−12.654	−7.195
0.099668	−34.084	−45.313	0.750558	−10.652	−5.261
0.129936	−33.098	−43.188	0.795686	−8.819	−3.718
0.157905	−32.195	−40.992	0.837565	−7.065	−2.546
0.178497	−31.516	−39.518	0.864162	−5.922	−1.899
0.249724	−29.149	−34.084	0.891480	−4.764	−1.352
0.298528	−27.494	−30.467	0.925180	−3.305	−0.785
0.350203	−25.737	−26.761	0.949794	−2.227	−0.456
0.406878	−23.729	−22.891	0.976593	−1.044	−0.180
0.453348	−22.105	−19.853	1.000000	0.000	0.000
0.502137	−20.290	−17.027			
Dimethylformamide (1) + n-butylacetamide (2)					
0.000000	−48.342	−73.952	0.501666	−29.008	−29.334
0.023965	−47.552	−71.949	0.549373	−26.749	−25.684
0.048481	−46.737	−69.833	0.600930	−24.208	−21.819
0.077184	−45.765	−67.224	0.651353	−21.623	−18.074
0.102860	−44.890	−64.907	0.698473	−19.080	−14.739
0.139064	−43.620	−61.537	0.751076	−16.127	−11.375
0.162370	−42.786	−59.393	0.790938	−13.787	−9.154
0.195946	−41.565	−56.274	0.842881	−10.614	−6.483
0.239937	−39.931	−52.232	0.864032	−9.288	−5.296
0.264105	−39.003	−50.048	0.898194	−7.059	−3.686
0.301794	−37.533	−46.559	0.925305	−5.259	−2.587
0.335177	−36.192	−43.626	0.947877	−3.700	−1.742
0.367435	−34.867	−40.848	0.977950	−1.594	−0.714
0.402147	−33.400	−37.486	1.000000	0.000	0.000
0.450073	−31.341	−33.414			

94.66, 111.57, and 128.53 cm^3 mol^{-1} obtained by Vaughn and Sears (6).

Excess molar volumes of the mixtures were calculated from

$$[1] \quad V_m^E = V_m + x_1(V_2^* - V_1^*) - V_2^*$$

and are represented in Fig. 2. Apparent molar volumes $V_{i,\phi}$ of component i with mole fraction x_i are obtained from

$$[2] \quad V_{i,\phi} = V_i^* + V_m^E/x_i$$

with $i = 1, 2$. They are given graphically in Figs. 3 and 4.

Heat capacities

Volumetric heat capacities relative to DMF, $\Delta(C_p/V) = C_p/V - C_{p,1}^*/V_1^*$, were measured corresponding to a mean temperature of (298.15 ± 0.1) K. Using $C_{p,1}^*/V_1^* = 1.9146$ J K^{-1} cm^{-3} we obtained the molar heat capacities of the pure compounds NEA, NPrA, and NBuA. The values $C_{p,2}^* = 180.28$, 207.94, and 236.89 J K^{-1} mol^{-1}, respectively, agree very well with $C_{p,2} = 180$, 207, and 236 J K^{-1} mol^{-1} determined by Konicek, Suurkuusk, and Wadsö with a drop calorimeter (13, 14).

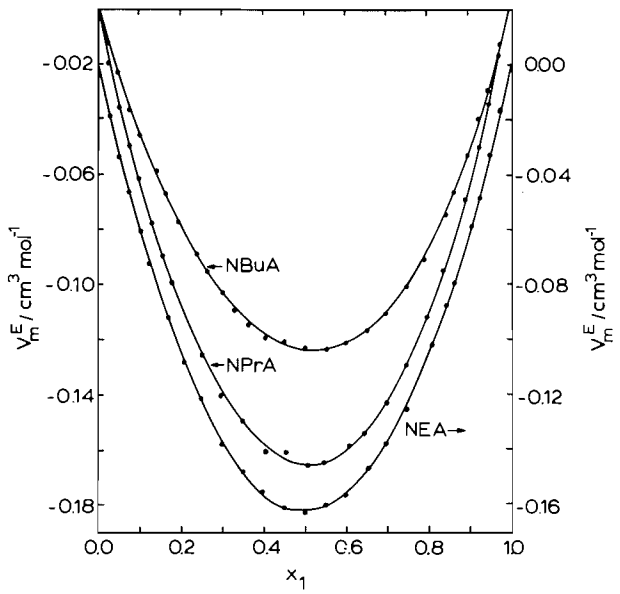

FIG. 2. Excess molar volumes for mixtures of dimethylformamide with some *N*-alkylacetamides.

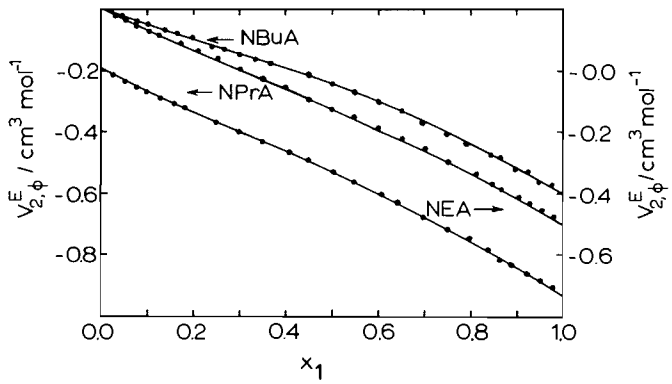

FIG. 3. Excess apparent molar volumes of *N*-alkylacetamides in mixtures with dimethylformamide.

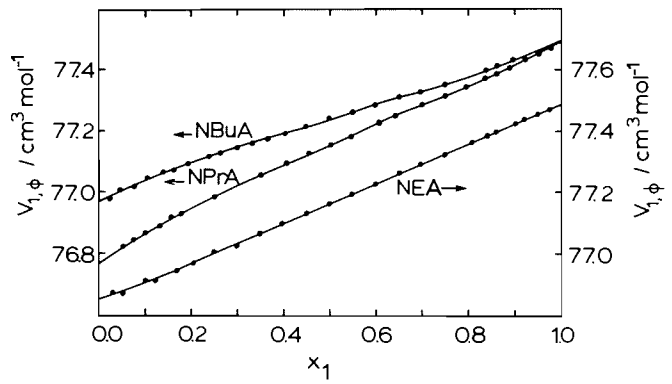

FIG. 4. Apparent molar volumes of dimethylformamide in mixtures with several *N*-alkylacetamides.

Excess molar heat capacities were calculated according to

[3] $$C^{E}_{p,m} = \{C^*_{p,1}/V^*_1 + \Delta(C_p/V)\}V_m - x_1C^*_{p,1} - x_2C^*_{p,2}$$

where the subscript 2 refers to NEA, NPrA, and NBuA. They are represented in Fig. 5. The apparent molar heat capacities $C_{p,i,\phi}$ of component i were calculated by

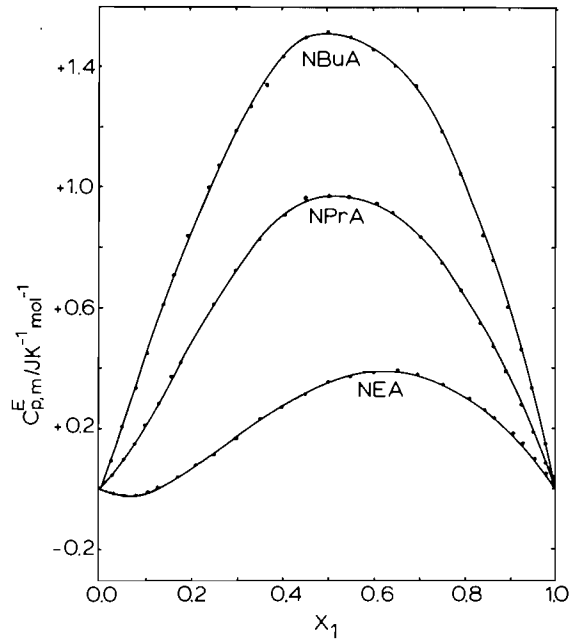

FIG. 5. Excess molar heat capacities for mixtures of dimethylformamide with several *N*-alkylacetamides.

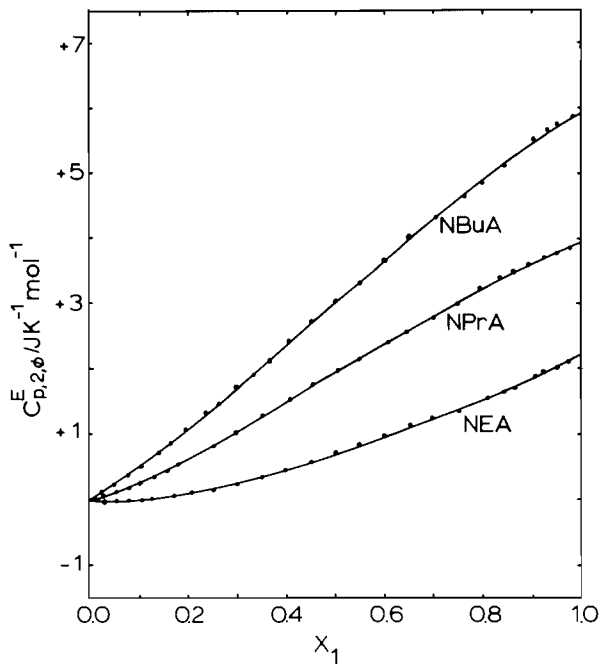

FIG. 6. Excess apparent molar heat capacities of *N*-alkylacetamides in mixtures with dimethylformamide.

[4] $$C_{p,i,\phi} = C^*_{p,i} + C^{E}_{p,m}/x_i$$

and are shown in Figs. 6 and 7.

Discussion

The molar excess volumes and heat capacities of the mixtures considered here can be described by the polynomial:

[5] $$Y^{E}_{m} = x_1x_2 \sum_{i=0}^{n-1} a_i(x_1 - x_2)^i$$

The coefficients a_i were obtained by a least-squares analysis and

TABLE 2. Coefficients of eq. [5] and standard deviations of fit for excess molar volumes and excess molar heat capacities of mixtures of DMF with some monosubstituted acetamides at 298.15 K

Acetamide	a_0 ($cm^3\,mol^{-1}$)	a_1 ($cm^3\,mol^{-1}$)	a_2 ($cm^3\,mol^{-1}$)	a_3 ($cm^3\,mol^{-1}$)	a_4 ($cm^3\,mol^{-1}$)	a_5 ($cm^3\,mol^{-1}$)	a_6 ($cm^3\,mol^{-1}$)	a_7 ($cm^3\,mol^{-1}$)	δ ($cm^3\,mol^{-1}$)
NEA	−0.64950	−0.04076	−0.04078	−0.03316	0.02136				7.8×10^{-4}
NPrA	−0.66179	−0.02391	−0.07016	0.01537	0.01220				1.0×10^{-3}
NBuA	−0.49511	−0.03348	−0.10304	−0.07631	0.10695	0.08143	−0.07238		6.4×10^{-4}
Acetamide	a_0 ($J\,K^{-1}\,mol^{-1}$)	a_1 ($J\,K^{-1}\,mol^{-1}$)	a_2 ($J\,K^{-1}\,mol^{-1}$)	a_3 ($J\,K^{-1}\,mol^{-1}$)	a_4 ($J\,K^{-1}\,mol^{-1}$)	a_5 ($J\,K^{-1}\,mol^{-1}$)	a_6 ($J\,K^{-1}\,mol^{-1}$)	a_7 ($J\,K^{-1}\,mol^{-1}$)	δ ($J\,K^{-1}\,mol^{-1}$)
NEA	1.3988	1.1511	−0.7052	0.3502					3.8×10^{-3}
NPrA	3.8912	0.3917	−1.1076	2.0789	0.2725	−2.4854	−0.4645	1.3516	4.6×10^{-3}
NBuA	5.9514	0.5731	−0.9299	0.2157	1.0414	0.3141	−1.2368		9.8×10^{-3}

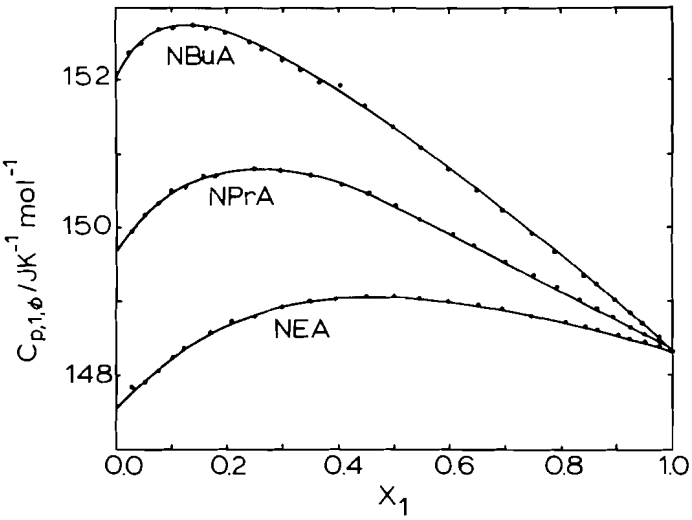

FIG. 7. Apparent molar heat capacities of dimethylformamide in mixtures with some *N*-alkylacetamides.

are presented in Table 2. Each experimental value was assigned unit weight. Table 2 gives also the standard deviation of the fit δ defined by

$$[6] \quad \delta^2 = \Sigma_N[Y_m^E(\text{exp}) - Y_m^E(\text{calc})]^2/(N - n)$$

where N and n denote the number of experimental points and coefficients, respectively.

As observed earlier (4), apparent molar quantities of compounds in binary mixtures of this type are largely determined by the molar quantities of the pure compounds and the apparent molar quantities of each compound at infinite dilution. Therefore a compilation of these data is presented in Table 3.

Apparent molar volumes

The functions $V_{2,\phi} - V_2^*$ $(= V_{2,\phi}^E)$ for the *N*-alkylacetamides are represented in Fig. 3. They are all negative and depend on x_1 almost linearly. Values of $V_{2,\phi}^E$ at infinite dilution, $V_{2,\phi}^{E,\infty}$, are −0.70, −0.73, and −0.60 $cm^3\,mol^{-1}$ for NEA, NPrA, and NBuA, respectively.

The apparent molar volumes of DMF in the mixtures (see Fig. 4) are smaller than its molar volume $V_1^* = 77.49\,cm^3\,mol^{-1}$. At infinite dilution in NEA, NPrA, and NBuA they amount to 76.85, 76.77, and 76.97 $cm^3\,mol^{-1}$, respectively.

According to the general equation

$$[7] \quad x_1(V_{1,\phi} - V_1^*) = x_2(V_{2,\phi} - V_2^*)$$

an observed linearity in the curves relating $(V_{2,\phi} - V_2^*)$ and x_1 means that also $V_{1,\phi}$ should depend on x_1 in a linear way. Hence, the approximately straight lines in Fig. 4 are in accordance with the almost linear relationships in Fig. 3.

The apparent molar volumes of DMF at infinite dilution, $V_{1,\phi}^{\infty}$, in the solvents NEA, NPrA, and NBuA do not show a systematic trend. In a series of dialkyl-substituted amidic solvents (CH_3CONR_2), we found earlier (4) that $V_{1,\phi}^{\infty}$ of DMF increases with the size of the alkyl group from R = ethyl. $V_{1,\phi}^{\infty}$ of DMF dissolved in dimethylacetamide does not fit the relation. This might indicate that in the present case the value of $V_{1,\phi}^{\infty}$ in NEA is the deviating one. Similar reasoning leads to the conclusion that the value of $V_{2,\phi}^{E,\infty}$ for NEA dissolved in DMF lies outside a general trend (see ref. 4).

Apparent molar heat capacities

Generally the values of $C_{p,2,\phi} - C_{p,2}^*$ $(= C_{p,2,\phi}^E)$ for NEA,

TABLE 3. Apparent molar volumes and heat capacities in the limiting regions of mixtures of DMF with several monosubstituted acetamides

Acetamide	$V^{\infty}_{1,\phi}$ ($cm^3\,mol^{-1}$)	$V^{*\,a}_{2}$ ($cm^3\,mol^{-1}$)	$V^{\infty}_{2,\phi}$ ($cm^3\,mol^{-1}$)	$C^{\infty}_{p,1,\phi}$ ($J\,K^{-1}\,mol^{-1}$)	$C^{*\,b}_{p,2}$ ($J\,K^{-1}\,mol^{-1}$)	$C^{\infty}_{p,2,\phi}$ ($J\,K^{-1}\,mol^{-1}$)
NEA	76.85	94.73	94.03	147.56	180.28	182.44
NPrA	76.77	111.64	110.91	149.69	207.94	211.85
NBuA	76.97	128.70	128.10	152.15	236.89	242.81

[a] $V^*_1 = 77.49\,cm^3\,mol^{-1}$.
[b] $C^*_{p,1} = 148.36\,J\,K^{-1}\,mol^{-1}$.

TABLE 4. Values of $C^{E,\infty}_{p,i,\phi}/V_i$ for mixtures of DMF with monosubstituted acetamides

Acetamide	$C^{E,\infty}_{p,1,\phi}/V_1$ ($J\,K^{-1}\,cm^{-3}$)	$C^{E,\infty}_{p,2,\phi}/V_2$ ($J\,K^{-1}\,cm^{-3}$)
NEA	−0.0103	0.0228
NPrA	0.0172	0.0350
NBuA	0.0489	0.0460

NPrA, and NBuA are positive over the complete mole fraction range. Only those for NEA at $0 < x_1 < 0.15$ are slightly negative. As Fig. 6 shows, there is a steady increase with the mole fraction of DMF towards a maximal value at infinite dilution. Here $C^{E,\infty}_{p,2,\phi}$ ranges from $2.2\,J\,K^{-1}\,mol^{-1}$ for NEA to $5.9\,J\,K^{-1}\,mol^{-1}$ for NBuA. The mean CH_2 increment in $C^{E,\infty}_{p,2,\phi}$ of $1.9\,J\,K^{-1}\,mol^{-1}$ is in good agreement with the same increment found for dialkylacetamides in DMF (4).

The apparent molar heat capacities $C_{p,1,\phi}$ of DMF in the three solvents NEA, NPrA, and NBuA (see Fig. 7) do not depend on x_1 in a monotonic way, but show maxima at $x_1 = 0.46$, $x_1 = 0.26$, and $x_1 = 0.13$, respectively. At infinite dilution, $C^{\infty}_{p,1,\phi}$ is 147.6, 149.7, and $152.2\,J\,K^{-1}\,mol^{-1}$, respectively. Only $C^{\infty}_{p,1,\phi}$ in NEA is smaller than the molar heat capacity of pure DMF. The mean CH_2 increment in the values is $+2.3\,J\,K^{-1}\,mol^{-1}$.

In previous work (4) we observed that heat capacities of binary mixtures of DMF and dialkylacetamides can be adequately described by equations of the type derived by Hildebrand and Wood (15), Scatchard (16), and Redlich *et al.* (17), like:

$$[8] \quad C^{E}_{p,m} = x_i(1 - \phi_i)V^*_i\sigma$$

$$[9] \quad C_{p,i,\phi} = C^*_{p,i} + (1 - \phi_i)V^*_i\sigma$$

$$[10] \quad C_{p,1} = C^*_{p,i} + (1 - \phi_i)^2V^*_i\sigma$$

where ϕ_i is the volume fraction of compound i in the mixture, $C_{p,i}$ is the partial molar heat capacity of compound i, and σ is an adjustable parameter. In order to describe the experimental data with the eqs. [8]–[10] it is necessary that

$$[11] \quad C^{E,\infty}_{p,1,\phi}/V^*_1 = C^{E,\infty}_{p,2,\phi}/V^*_2\ (= \sigma)$$

Within experimental error this is the case for mixtures of DMF and dialkylacetamides. Values of $C^{E,\infty}_{p,1,\phi}/V^*_1$ and $C^{E,\infty}_{p,2,\phi}/V^*_2$ for the compounds in this paper are presented in Table 4. They differ substantially. In our opinion this is due to a larger short range interaction in the present mixtures, caused by hydrogen bonding. Indeed a recent computer simulation study (18) indicates marked differences in short range ordering of the molecules between aprotic disubstituted amides and protic mono- or unsubstituted amides. Consequently, application of the eqs. [8]–[10] will be restricted to mixtures of related compounds where strong and directional short range interactions are absent.

1. P. PICKER, P.-A. LEDUC, P. R. PHILIP, and J. E. DESNOYERS. J. Chem. Thermodyn. **3**, 631 (1971).
2. J.-P. E. GROLIER, G. C. BENSON, and P. PICKER. J. Chem. Eng. Data, **20**, 243 (1975).
3. J.-L. FORTIER and G. C. BENSON. J. Chem. Thermodyn. **8**, 411 (1976).
4. H. C. ZEGERS and G. SOMSEN. Fluid Phase Equil. **18**, 299 (1984).
5. J.-L. FORTIER, G. C. BENSON, and P. PICKER. J. Chem. Thermodyn. **8**, 289 (1976).
6. J. W. VAUGHN and P. G. SEARS. J. Phys. Chem. **62**, 183 (1958).
7. W. J. CHUTE, G. E. NUNN, J. C. MACKENZIE, G. S. MYERS, G. N. R. SMART, J. W. SUGGIT, and G. F. WRIGHT. Can. J. Res. B, **26**, 114 (1948).
8. J. H. ROBSON and J. J. REINHART. J. Am. Chem. Soc. **77**, 498 (1955).
9. M. L. FEIN and C. H. FISHER. Ind. Eng. Chem. **36**, 235 (1944).
10. J. C. VERHOEF and E. BARENDRECHT. Anal. Chim. Acta, **94**, 395 (1977).
11. H. C. ZEGERS and G. SOMSEN. J. Chem. Thermodyn. **16**, 225 (1984).
12. G. S. KELL. J. Chem. Eng. Data, **12**, 66 (1967).
13. J. KONICEK and I. WADSÖ. Acta Chem. Scand. **25**, 1541 (1971).
14. J. KONICEK, J. SUURKUUSK, and I. WADSÖ. Chem. Scr. **1**, 217 (1971).
15. J. H. HILDEBRAND and S. E. WOOD. J. Chem. Phys. **1**, 817 (1933).
16. G. SCATCHARD. Chem. Rev. **44**, 7 (1949).
17. O. REDLICH, E. L. DERR, and G. J. PIEROTTI. J. Am. Chem. Soc. **81**, 2283 (1959).
18. W. L. JORGENSEN and C. J. SWENSON. J. Am. Chem. Soc. **107**, 569 (1985).

Thermodynamics of solvent mixtures. I. Density and viscosity of binary mixtures of *N*-methylpyrrolidinone – tetrahydrofuran and propylene carbonate – acetonitrile

A. V. ANANTARAMAN
Defence Research Establishment Ottawa, Ottawa, Ont., Canada K1A 0Z4

Received April 25, 1985

A. V. ANANTARAMAN. Can. J. Chem. **64**, 46 (1986).

Excess volumes and viscosities of binary liquid mixtures of *N*-methylpyrrolidinone – tetrahydrofuran and propylene carbonate – acetonitrile are measured and examined in the light of empirical theories such as absolute rate, free volume, and regular solution theories. It is shown that non-ideality arises due to (a) shape factors, (b) molecular interaction, and that the two properties, excess volume and viscosity, illustrate these two aspects of non-ideality.

A. V. ANANTARAMAN. Can. J. Chem. **64**, 46 (1986).

On a mesuré les volumes en excès et les viscosités de mélanges liquides binaires de *N*-méthylpyrrolidinone – tétrahydrofuranne et de carbonate de propylène – acétonitrile et on les a étudiés en faisant appel à des théories empiriques comme celle de la vitesse absolue, et les théories du volume libre et de la solution régulière. On montre que le comportement non-idéal est dû aux facteurs de forme et à l'interaction moléculaire. On montre également que ces deux propriétés, à savoir le volume en excès et la viscosité, illustrent les deux aspects de ce comportement non-idéal.

[Traduit par le journal]

Introduction

During the past decade, significant advances have taken place in the commercial development of batteries using nonaqueous electrolytes. Such remarkable progress could not have been achieved without fundamental understanding of the thermodynamic and electrochemical behaviour of the active components in a battery. Mixed solvents of propylene carbonate (PC) with 1,2-dimethoxyethane (DME) or with tetrahydrofuran (THF) have been reported to give good cell performance (1, 2). Since organic mixed solvents offer a wide range of variations in electrolyte properties, their use in the development of high energy – density batteries is relevant and attractive.

The electrochemical behaviour of a nonaqueous battery can depend critically on the properties of the electrolyte. Among the properties of solvent mixtures, viscosity has an important role, because a low viscosity implies a low resistance to ionic transport within the medium. As part of a continuing investigation of the thermodynamic and other properties of solvent mixtures for nonaqueous battery systems, this paper reports the measurements of density and viscosity of mixtures of propylene carbonate – acetonitrile (AN) and *N*-methylpyrrolidinone (NMP) – tetrahydrofuran in the complete range of composition.

Experimental

Starting from high purity grade, the solvents were agitated with calcium hydride for 24 h in an argon atmosphere. Subsequently they were distilled under reduced pressure, and only the middle fractions were collected and stored in a dry argon atmosphere. The relevant properties of the pure solvents are listed in Table 1.

The solvent mixtures were prepared gravimetrically in an argon atmosphere and the measurements were done completely isolated from atmospheric contact.

The densities of pure solvents and their mixtures were measured at 5.0 ± 0.05°C, using a long-stem pyknometer which was calibrated with mercury. The experimental reproducibility, in general, is better than 1 part in 10^4.

Kinematic viscosities were measured in a specially designed capillary viscometer that allows measurements to be made without contact with air (3). A schematic diagram of the viscometer is shown in Fig. 1.

A gas-tight syringe of about 20-mL capacity is connected through a short silicon rubber tubing to the outlet at stopcock S_1. The ground glass stopcocks S_1 and S_2 are slightly greased and the clean dry viscometer is weighed. The apparatus is taken into an argon glove box and the required volume of high purity solvent is carefully introduced into the pear-shaped reservoir R. All the stopcocks and the rotoflo are tightly closed, and the unit is carefully taken out of the box and connected to a vacuum line at the ground joint G. The solvent in the reservoir is degassed by alternate freezing and thawing. The viscometer is set up in a suitable thermostat bath and, after attaining temperature equilibrium, the liquid is slowly drawn above the mark, M_1, by means of the syringe with the stopcocks S_1 open and S_2 closed. Any vapour drawn into the syringe is slowly pushed back into the viscometer with the pressure equalizer stopcock S_2 open. The stopcock S_1 is now closed and the time for flow between the two marks M_1 and M_2 is recorded. The procedure can be repeated for consistency.

The viscometer was calibrated using triple-distilled water and pure solvents. All measurements were done in a thermostat maintained at 5.0 ± 0.05°C. The accuracy of the measurement of viscosity is estimated to be better than 1%.

TABLE 1. Properties of pure components at 5.0°C.

Solvent	Density ρ (g cm^{-3})	Kinematic viscosity ν (CS)	Vapour pressure (Torr)[a]
N-methylpyrrolidinone	1.0447	2.168	≈0.2
Tetrahydrofuran	0.9035	0.635	62.7
Propylene carbonate	1.2203	3.128	0.5
Acetonitrile	0.7984	0.541	34.5

1 Torr = 133.3 Pa.

Results

The experimental values of densities and viscosities of the two binary systems are shown in Tables 2 and 3.

Excess volume

The excess volume V^E is calculated from densities, according to the relations

$$[1] \quad V^E = X_1 M_1 \left(\frac{1}{\rho} - \frac{1}{\rho_1}\right) + X_2 M_2 \left(\frac{1}{\rho} - \frac{1}{\rho_2}\right)$$

where X_i, M_i, and ρ_i are the mole fraction, molar mass, and density of component i and ρ denotes the density of the mixture. The results are shown in Figs. 2 and 3. The data can be fitted into

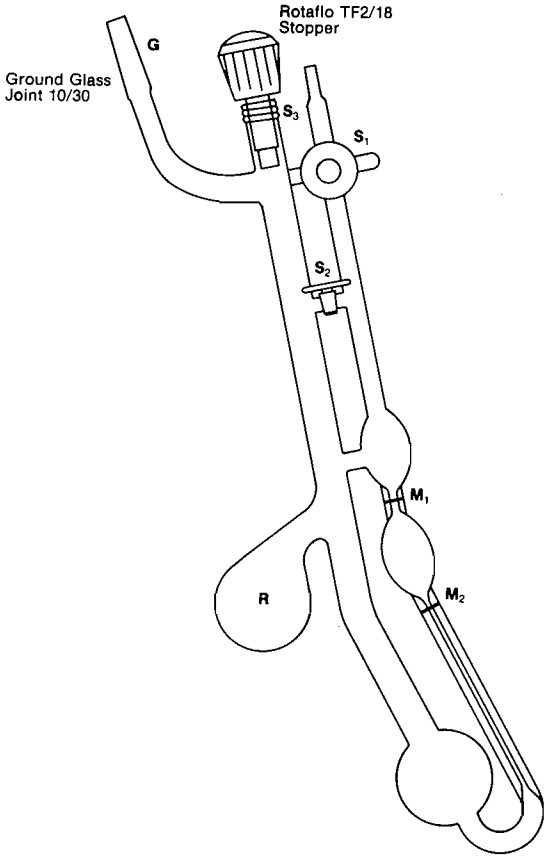

FIG. 1. Viscometer.

TABLE 2. Experimental densities and kinematic viscosities of mixtures of the system. PC–AN at 5.0 ± 0.05°C (X_1 = mole fraction of component 1 (PC))

X_1	ρ (g cm^{-3})	ν (CS)
0.0	0.7984	0.541
0.0920	0.8616	0.594
0.1675	0.9069	0.683
0.3043	0.9808	0.871
0.3763	1.0149	0.992
0.4910	1.0636	1.234
0.6293	1.1137	1.622
0.7795	1.1615	2.058
0.7953	1.1667	2.151
0.9537	1.2093	2.910
1.0000	1.2203	3.128

an equation of the form

$$[2] \quad V^E = X_1 X_2 \sum_{i=0}^{n} A_i (X_1 - X_2)^i$$

The optimum number of coefficients A_i is determined by the magnitude of the standard deviation σ. These coefficients are given in Table 4.

Viscosity

The dynamical viscosity η is calculated from the measured kinematic viscosity ν, and the corresponding density ρ, using the relation $\eta = \nu/\rho$. For ideal binary mixtures, viscosity is given by the Arrhenius equation,

TABLE 3. Experimental densities and kinematic viscosities of mixtures of the system. NMP–THF at 5.0 ± 0.05°C (X_1 = mole fraction of component 1 (NMP))

X_1	ρ (g cm^{-3})	ν (CS)
0.0	0.9035	0.635
0.1004	0.9217	0.721
0.2369	0.9445	0.825
0.3418	0.9608	0.948
0.4511	0.9782	1.110
0.5601	0.9926	1.318
0.7055	1.0119	1.544
0.8122	1.0239	1.814
0.8685	1.0304	1.953
0.9625	1.0405	2.102
1.0000	1.0447	2.168

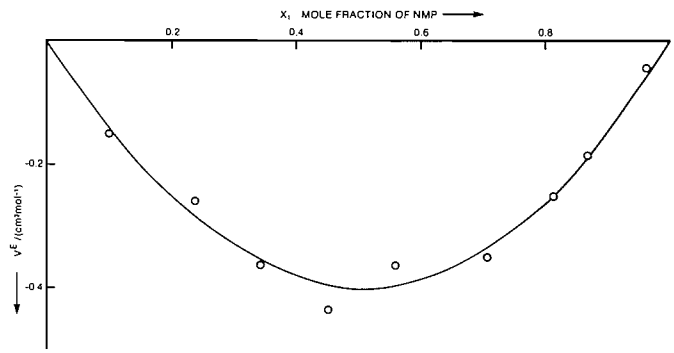

FIG. 2. Excess volume as a function of composition. System: NMP–THF. Temperature: 5.0 ± 0.05°C.

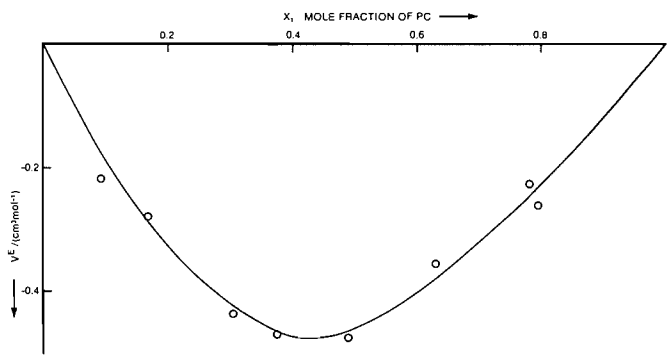

FIG. 3. Excess volume as a function of composition. System: PC–AN. Temperature: 5.0 ± 0.05°C.

TABLE 4. Coefficients A_i of eq. [2] fitted to experimental V^E at 5.0°C

Mixture	A_0	A_1	A_2	A_3	σ
PC–AN	−1.834	0.6414	0.5496	0.1396	0.013
NMP–THF	−1.596	−0.1575	0.0101	0.2623	0.036

$$[3] \quad \ln \eta_{id} = X_1 \ln \eta_1 + X_2 \ln \eta_2$$

where X_i and η_i are the mole fraction and viscosity of the pure components. Ideal viscosities calculated on the basis of eq. [3] for the two systems, along with the corresponding experimental data, are shown in Figs. 4 and 5.

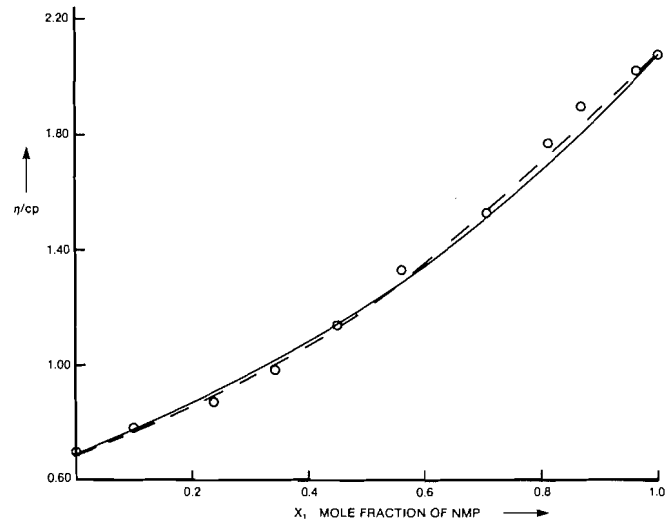

FIG. 4. Dynamic viscosity as a function of composition. System: NMP–THF. Temperature: 5.0 ± 0.05°C. --- Measured, — Ideal eq. [3].

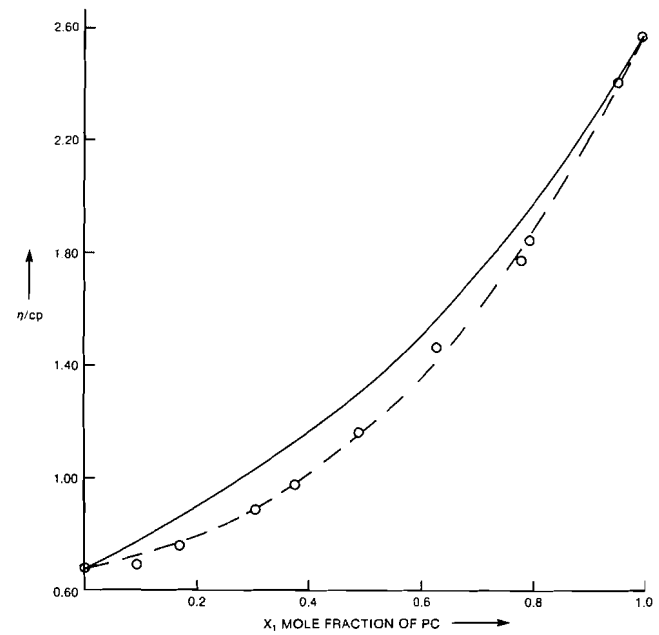

FIG. 5. Dynamic viscosity as a function of composition. System: PC–AN. Temperature: 5.0 ± 0.05°C. --- Measured, — Ideal eq. [3].

Discussion

The excess volumes for both the binary mixtures NMP–THF and PC–AN are negative over the entire range of composition. This implies that geometrical factors allowing the molecular species to form a more dense structure within the mixture may be important in both cases. The dense packing may be due to (a) different molecular sizes leading to interstitial accommodation in the mixture and (b) differences in free volume between the components.

On the basis of such geometrical arguments, the excess volume is expressed in terms of a reduced interaction energy parameter Λ_{ij}^* (4).

$$[4]\quad \frac{V^E}{V^*} = \frac{2.03}{Z}\left(\frac{kT}{\Lambda_{ij}^*} - X_i\frac{kT}{\Lambda_{ii}^*} - X_j\frac{kT}{\Lambda_{jj}^*}\right)$$

The reduced volume V^* is defined as $V^* = r^*/\gamma$, where γ is a numerical factor which depends on the geometrical arrangement of the molecules. r^* is the distance corresponding to the minimum of $\Lambda(r)$ and Z is the number of first neighbours in the quasi-lattice.

In this simple model, the solution behaves as a pure component characterized by the average value of the interaction parameter Λ_{ij}^*. The negative excess volumes of the two systems over the entire composition range suggest that the potential energy minimum of the unlike molecules is lower than the potential energy minima of either or both the like molecules.

Viscosity is a complex property and existing theories cannot adequately explain the viscosity behaviour of even simple fluid mixtures. Empirical theories such as the absolute rate theory and the free volume theory have been used in predicting the viscosity of liquid mixtures (5–7). Macedo and Litovitz (8) have combined the two theories so that the probability for viscous flow is taken as the product of probabilities for acquiring sufficient activation energy and the occurrence of an empty site. However, the validity and physical justification for the use of such theories in predicting viscosities of complex liquid mixtures is in doubt.

Based on the ideas of regular solution theory (9, 10), Grunberg and Nissan (11) have proposed an empirical expression for viscosities of real liquid mixtures,

$$[5]\quad \ln\eta = X_1\ln\eta_1 + X_2\ln\eta_2 + X_1X_2\epsilon$$

where ϵ denotes the extent of non-ideality of the system. The parameter ϵ is interpreted as a constant proportional to W/RT where W is the interchange energy arising from the increase in lattice energy due to juxtaposition of molecule 1 into the lattice of molecule 2. Grunberg (12) has derived an expression for the viscosity contribution to the interchange energy,

$$[6]\quad \ln\frac{\eta_{obs}}{\eta_{id}} = \frac{W}{RT}\alpha_1X_1X_2\left[X_2 + \frac{\alpha_2}{\alpha_1}X_1\right]$$

where η_{obs} represents the measured viscosity of the mixture; the constants α_1 and α_2 are calculated from the vapour pressures p_0 of pure components 1 and 2 according to

$$[7]\quad \frac{d(\ln\eta)}{d(\ln p_0)} = \alpha$$

Following Grunberg's procedure, we have calculated the interchange energy W as defined by eq. [6]. The results are shown in Tables 5 and 6 where the measured viscosities and the deviation, ϵ, are also included.

$$[8]\quad \epsilon = (\ln\eta_{obs} - \ln\eta_{id})/X_1X_2$$

It should be pointed out that the results shown in Tables 5 and 6 depend on the assumed parallelism between viscosity and vapour pressure, as given by eq. [7]. Also, accurate experimental data for viscosity and vapour pressure of pure components are required for evaluating reliable values of the constants α_1 and α_2. This is particularly so where the pure components have low vapour pressures, as in the case NMP and PC. The molar volumes of NMP and THF at 5.0°C are 94.86 cm^3 and 79.81 cm^3, respectively, and the viscosities of the two substances at 5.0°C are 2.075 cp and 0.703 cp, respectively. This suggests that the mixture NMP–THF would be expected to show considerable deviation from ideal behaviour. Furthermore, the constants α_1 and α_2 for NMP and THF, respectively, are significantly different, indicating that the two liquids are geometrically different.

Based on formal ideas of statistical mechanics, Bearman and

TABLE 5. System: propylene carbonate – acetonitrile; deviation of viscosity from ideal behaviour

Mole fraction X_{PC}	η_{obs} (cp)	$\epsilon = \left(\frac{\ln \eta_{obs} - \ln \eta_{id}}{X_1 X_2}\right)$	W/RT (eq. [6])	η_{12} (cp) (eq. [9])
0.0920	0.689	−1.263	5.35	0.649
0.1675	0.753	−0.844	3.69	0.757
0.3043	0.888	−0.637	2.97	0.764
0.3763	0.977	−0.576	2.77	0.746
0.4910	1.160	−0.462	2.36	0.732
0.6293	1.456	−0.310	1.69	0.745
0.7795	1.772	−0.442	2.65	0.529
0.7953	1.843	−0.354	2.15	0.597
0.9537	2.406	−0.046	0.30	0.832

TABLE 6. System: NMP–THF; deviation of viscosity from ideal behaviour

Mole fraction X_{NMP}	η_{obs} (cp)	$\epsilon = \left(\frac{\ln \eta_{obs} - \ln \eta_{id}}{X_1 X_2}\right)$	W/RT (eq. [6])	η_{12} (cp) (eq. [9])
0.1004	0.782	−0.03	0.26	1.061
0.2369	0.873	−0.22	1.48	0.961
0.3418	0.987	−0.14	0.82	0.978
0.4511	1.135	−0.04	0.19	1.012
0.5601	1.328	+0.12	−0.54	1.097
0.7055	1.526	+0.06	−0.24	1.038
0.8122	1.772	+0.29	−1.12	1.239
0.8685	1.895	+0.45	−1.59	1.395
0.9625	2.020	+0.39	−1.27	1.347

Jones (13) have derived an expression where the viscosity coefficient of a binary mixture is given as the sum of three integrals representing the interactions of like and unlike pairs of molecules. Using the simplifying assumptions of regular solution theory, the authors express the viscosity of a binary mixture in terms of the viscosities of pure components η_1 and η_2

$$[9] \quad \eta = X_1^2\eta_1 + 2X_1X_2\eta_{12} + X_2^2\eta_2$$

where η_{12} is a parameter attributed to unlike pair interactions. An identical equation was proposed earlier by Hind *et al.* (14) from purely empirical arguments.

Values of the parameter η_{12} calculated from experimental results for the two systems NMP–THF and PC–AN are shown in Tables 5 and 6. The interaction parameter η_{12} appears to give a constant value, particularly at low concentrations of the denser component in both systems. The arithmetic mean approximation, $\eta_{12} \sim (\eta_1 + \eta_2)/2$, and the geometric mean approximation, $\eta_{12} \simeq \sqrt{\eta_1\eta_2}$, are in poor agreement with the value of η_{12} calculated from eq. [9]. One of the major difficulties of fundamental theories such as that of Bearman and Jones is that η_{12} can only be obtained from experimental measurements and cannot be calculated a priori from η_1 and η_2.

Viscosity and excess volume are properties that exemplify different aspects of solution non-ideality. While excess volume reflects molecular dissimilarity among the components, viscosity, on the other hand, expresses the strength of intermolecular interaction. The system NMP–THF clearly illustrates this aspect. It shows a large excess volume of mixing, indicating the geometrical dissimilarity between NMP and THF. On the other hand, the viscosity of the system conforms closely to the Arrhenius expression for binary liquid mixtures, clearly pointing out the absence of specific intermolecular interactions between the components.

Our studies suggest that, contrary to the observations of Prolongo *et al.* (15), negative volume changes of mixing (denoting strong geometrical rearrangements between the components) do not result in a positive value for ϵ of eq. [5] and vice versa. General correlations between V^E and ϵ are difficult to make; the two properties are fundamentally different.

Jambon and Delmas (16) have measured the solution viscosities of binary systems involving globular molecules such as SnR_4 compounds (R = CH_3, C_2H_5, C_4H_9). Their analysis, based on free volume theories, suggests that no significant correlation exists between excess viscosity and free volume and that such empirical theories are fundamentally inadequate to explain the origin of excess viscosity.

Finally, our results show that viscosity behaviour of binary liquid mixtures cannot be explained in terms of interchange energy, as defined by eq. [6]. This equation is derived on the basis of the assumptions of regular solution theory, which ignores specific intermolecular interactions. It is believed that molecular shapes resulting from packing and intermolecular interaction energies are both important in accounting for viscosity behaviour.

Acknowledgement

The author wishes to thank Dr. C. L. Gardner for advice and encouragement.

1. H. IKEDA, T. SAITO, and H. TAMURA. Denki Kagaku, **45**, 314 (1977).
2. R. JASINSKI. Adv. Electrochem. Electrochem. Eng. **8**, 253 (1971).

3. A. V. ANANTARAMAN. Canadian Patent Pending. 1983.
4. I. PRIGOGINE. Molecular theory of solutions. North-Holland, Amsterdam. 1957.
5. S. GLASSTONE, K. J. LAIDLER, and H. EYRING. The theory of rate processes. McGraw–Hill, New York. 1941.
6. M. H. COHEN and D. TURNBULL. J. Chem. Phys. **31**, 1164 (1959).
7. M. L. WILLIAMS, R. F. LANDEL, and J. D. FERRY. J. Am. Chem. Soc. **77**, 3701 (1955).
8. P. B. MACEDO and T. A. LITOVITZ. J. Chem. Phys. **31**, 1164 (1965).
9. E. A. GUGGENHEIM. Mixtures. Clarendon Press, Oxford. 1952.
10. J. H. HILDEBRAND, J. M. PRAUSNITZ, and R. L. SCOTT. Regular and related solutions. Van Nostrand Reinhold Company, New York. 1970.
11. L. GRUNBERG and A. H. NISSAN. Nature, **164**, 799 (1949).
12. L. GRUNBERG. Trans. Faraday Soc. **50**, 1293 (1954).
13. R. J. BEARMAN and P. F. JONES. J. Chem. Phys. **33**, 1432 (1960).
14. P. K. HIND, E. MCLAUGHLIN, and A. R. UBBELOHDE. Trans. Faraday Soc. **56**, 328 (1960).
15. M. G. PROLONGO, R. M. MASEGOSA, I. HERNANDEZ-FUENTES, and A. HORTA. J. Phys. Chem. **88**, 2163 (1984).
16. C. JAMBON and G. DELMAS. Can. J. Chem. **55**, 1360 (1977).

The synthesis and X-ray structural characterization of bis[(2*S*,3*S*)-2,3-bis(diphenylphosphino)butane]rhodium(I) chloride and its reactivity towards small gas molecules

CHARLES G. YOUNG, STEVEN J. RETTIG,[1] AND BRIAN R. JAMES[2]

Department of Chemistry, University of British Columbia, Vancouver, B.C., Canada V6T 1Y6

Received April 9, 1985

CHARLES G. YOUNG, STEVEN J. RETTIG, and BRIAN R. JAMES. Can. J. Chem. **64**, 51 (1986).

The Rh(*S*,*S*-chiraphos)$_2^+$ cation, where chiraphos is 2,3-bis(diphenylphosphino)butane, has been synthesized and fully characterized by spectroscopy and single crystal data on the chloride salt (**1**). Crystals are monoclinic, a = 23.106(3), b = 12.4987(8), c = 21.455(3) Å, β = 128.539(5)°, Z = 4, space group $C2$. The structure was solved by conventional heavy atom methods and was refined by full-matrix least-squares procedures to R = 0.046 and R_w = 0.032 for 4509 reflections with $I > \sigma(I)$. The coordination about Rh is square planar distorted toward tetrahedral within the five-membered chelate rings, similar to that in Rh(dpe)$_2^+$, where dpe is 1,2-bis(diphenylphosphino)ethane, but the distortion toward tetrahedral is significantly greater in **1**; the methyl substituents further restrict rotational freedom about the P—Ph bonds, which leads to some blocking of the axial ligand sites by the four H atoms of the chelate-ring carbon atoms. In solution, **1** is unreactive towards O_2, CO, and H_2, but oxidatively adds HX (X = Cl, Br) to give *trans*-RhHX(*S*,*S*-chiraphos)$_2^+$ species.

CHARLES G. YOUNG, STEVEN J. RETTIG et BRIAN R. JAMES. Can. J. Chem. **64**, 51 (1986).

On a synthétisé le cation Rh(*S*,*S*-chiraphos)$_2^+$, où le groupe chiraphos est le bis(diphénylphosphino)-2,3 butane, et on l'a caractérisé par la spectroscopie de rayons X sur un monocristal de son chlorure (**1**). Les cristaux appartiennent au groupe d'espace monoclinique C_2 avec a = 23,106(3), b = 12,4987(8), c = 21,455(3) Å, β = 128,539(5)°, Z = 4. On a résolu la structure par la méthode conventionnelle de l'atome lourd et on l'a affinée par la méthode des moindres carrés (matrice complète) jusqu'à des valeurs de R = 0,046 et de R_w = 0,032 pour 4509 réflexions avec $I > \sigma(I)$. La coordination autour du Rh est un plan carré déformé de façon tétraédrique à l'intérieur du cycle à 5 chaînons du chélate, comme celle du Rh(dpe)$_2^+$, où le groupe dpe est le bis(diphénylphosphino)-1,2 éthane, mais la déformation tétraédrique est beaucoup plus accentuée dans le cas du composé **1**. De plus, les substituants méthyles restreignent la rotation libre autour des liaisons P—Ph, ce qui conduit à un certain blocage des sites axiaux du ligand par les 4 atomes d'hydrogène des atomes de carbone du cycle du chélate. Le composé **1**, en solution, ne réagit pas avec le O_2, le CO et le H_2 mais les halogénures HX (X = Cl, Br) s'additionnent de façon oxydante pour donner des espèces RhHX(*S*,*S*-chiraphos)$_2^+$ *trans*.

[Traduit par le journal]

Introduction

Earlier work from this laboratory has reported on the synthesis and characterization of Rh(P—P)$_2$X complexes, and their reactivity towards the small gas molecules H_2, O_2, CO, and HCl, with a view to exploring catalytic reactivity: X = Cl, BF_4, PF_6, SbF_6; P—P = dpm, dpe, dpp, dpb, and diop[3] (1, 2). The Rh(P—P)$_2^+$ cations, for example, were active for catalytic hydrogenation of olefins, including asymmetric hydrogenation with the chiral diop ligand system; even in cases where coordinatively saturated dihydrides, RhH$_2$(P—P)$_2^+$, are present, catalytic activity can result when one of the ditertiary phosphine ligands becomes monodentate (3). Reversible binding of CO by some of the Rh(P—P)$_2^+$ cations, particularly with P—P = dpp, led to studies revealing their efficiency for catalytic decarbonylation of aldehydes (4, 5), these systems being discovered independently by Pignolet and co-workers (6, 7). Attempts to then effect asymmetric decarbonylation of racemic aldehydes required the use of Rh(P—P$_2$)$^+$ complexes with P—P chiral; the known rigidity of the five-membered chiraphos ring (8, 9) prompted us to synthesize the Rh(chiraphos)$_2^+$ cation, and test its activity for decarbonylation, and for reactivity generally towards small gas molecules. We have reported on the attempted decarbonylation of racemic olefinic aldehydes, studies that led to a kinetic resolution of the aldehyde, one enantiomer preferentially undergoing intramolecular hydroacylation to a chiral disubstituted cyclopentanone, eq. [1].

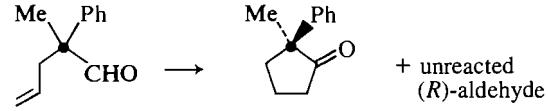

[1]

(*R*,*S*)-aldehyde (*S*)-cyclopentanone

We report here the details and full characterization of the Rh(chiraphos)$_2^+$ Cl$^-$ complex (**1**) that catalyzes reaction [1] (10, 11) and also note its nonreactivity towards CO, O_2, and H_2; however, **1** oxidatively adds HCl to give *trans*-RhHCl(chiraphos)$_2^+$ Cl$^-$.

The well-known Rh(dpe)$_2^+$ cation, containing the corresponding unsubstituted, non-chiral, five-membered rings, was the earliest of the bis(ditertiaryphosphine)rhodium(I) cations to be studied regarding reactivity towards H_2 (12) amd O_2 (13). Since that time, as well as studies reported from this laboratory (1–5, 10, 11), several other groups have reported on Rh(P—P)$_2^+$ systems and their reactivity towards small gas molecules and related catalysis: hydrogenation, decarbonylation, hydroformylation, and hydroacylation (6, 7, 14–21).

[1]Experimental Officer, University of British Columbia Crystal Structure Service.

[2]Author to whom correspondence should be addressed.

[3]Abbreviations used: (+)-diop = 4*S*,5*S*-bis((diphenylphosphino)-methyl)-2,2-dimethyl-1,3-dioxolane; dpm = bis(diphenylphosphino)-methane; dpe = 1,2-bis(diphenylphosphino)ethane; dpp = 1,3-bis(diphenylphosphino)propane; dpb = 1,4-bis(diphenylphosphino)butane; (−)-chiraphos = 2*S*,3*S*-bis(diphenylphosphine)butane; *cis*(2=phos) = 1,2-bis(diphenylphosphino)ethylene.

Experimental

The cyclooctene dimer $[RhCl(C_8H_{14})_2]_2$ was prepared by a literature method (22). (2*S*,3*S*)-Chiraphos was purchased from Strem Chemicals Inc. and was used without further purification. Unless otherwise stated, all synthetic procedures were performed under argon using dry, deoxygenated solvents.

Conductivity measurements employed a Thomas Serfass bridge and cell using 10^{-3} *M* nitromethane solutions. Infrared spectra were recorded on a Perkin–Elmer 598 instrument as Nujol mulls. Ultraviolet–visible spectra were recorded on a Perkin–Elmer 552A spectrophotometer and optical rotation measurements employed a Perkin–Elmer 141 polarimeter. Proton (δ_{TMS} = 0 ppm) and ^{31}P-{^1H} nmr spectra were recorded on Bruker WH 400 MHz and Varian XL 100 (40.4 MHz for ^{31}P) spectrometers, respectively, at ambient temperatures. The ^{31}P nmr experiments employed an external PPh_3 reference but δ values are reported in ppm (upfield negative) from 85% H_3PO_4. Microanalyses were performed by Mr. P. Borda of this Department.

Rh(S,S-*chiraphos*)$_2^+$ *Cl*$^-$, **1**

A solution of *S*,*S*-chiraphos (0.94 g, 2.2 mmol) in benzene (10 mL) was added to a stirred solution of $[RhCl(C_8H_{14})_2]_2$ (0.36 g, 0.5 mmol) in benzene (20 mL); the resulting suspension was stirred for 1.5 h, whereupon the yellow solid was filtered, washed with warm benzene (30 mL), and vacuum-dried. The yield was 0.92 g (90%). At this stage the compound retains a half molecule of benzene of crystallization. *Anal.* calcd. for $C_{59}H_{59}ClP_4Rh$: C 68.80, H 5.77; found: C68.9, H 5.8. The unsolvated compound was obtained upon recrystallization (in air) from CH_2Cl_2/diethyl ether. *Anal.* calcd. for $C_{56}H_{56}ClP_4Rh$: C 67.88, H 5.70; found: C 67.8, H 5.7. Decomposition point in air = 275°C. Conductivity $\Lambda_M = 59\ \Omega^{-1}\,cm^2\,mol^{-1}$; $[\alpha]_D^{25°}$ +23.6° (*c* 2.5, ethanol); ir: strongest bands at 1420, 1090, 990, 735, 685, 520, 500, 470 cm^{-1}; uv–vis (CH_3OH): 410 (4130), 345 (sh. 4620), 313 (7040), 265 (29 400), 237 nm (ε 44 700 $M^{-1}\,cm^{-1}$); (CH_3NO_2): 410 nm (ε 4080); ^1H nmr ($CDCl_3$) δ: 0.53 (m, br, 12H, C*H*$_3$), 1.87 (m, br, 4H, C*H*), 7.0–7.5 (m, 40H, Ph); ^{31}P-{^1H} nmr (2:1 CH_2Cl_2/C_6D_6) δ: 60.6 (d, J_{Rh-P} = 130.8 Hz).

Yellow needles of **1** for a crystal structure analysis were grown in air by diffusing ether into a CH_2Cl_2 solution of the compound.

Rh(S,S-*chiraphos*)$_2^+$ *BF*$_4^-$, **2**

A solution of **1** (0.46 g, 0.46 mmol) in CH_2Cl_2 (10 mL) was treated with a solution of $AgBF_4$ (0.092 g, 0.47 mmol) in MeOH (10 mL). The resulting mixture was stirred for 1 h, then reduced to dryness under vacuum. The residue was extracted with CH_2Cl_2 (5–10 mL) and, after filtration, the compound was precipitated with diethyl ether. The yield was 0.43 g (90%). The compound was recrystallized in air from CH_2Cl_2/diethyl ether. *Anal.* calcd. for $C_{56}H_{56}BF_4P_4Rh$: C 64.54, H 5.42; found: C 64.2, H 5.5. Decomposition point in air = 305°C. Conductivity $\Lambda_M = 68\ \Omega^{-1}\,cm^2\,mol^{-1}$; ir: strongest bands at 1420, 1090–1010, 745, 690, 520, 500, 470 cm^{-1}; uv–vis and ^1H nmr as for **1**; ^{31}P-{^1H} nmr (2:1 CH_2Cl_2/C_6D_6) δ: 60.4 (d, J_{Rh-P} = 132.0 Hz). The PF_6^- and SbF_6^- salts are prepared similarly using the appropriate silver compound.

Reactivity of ***1*** *with gases*

The complex, either in the solid state or solution (MeOH or CH_2Cl_2), was completely unreactive toward CO, O_2, and H_2 at 1 atm (101.3 kPa) pressure and ambient temperatures. Hydrogen halides added oxidatively, however, to give the halogeno(hydrido)rhodium(III) derivative.

A solution of **1** (0.1 g, 0.1 mmol) in EtOH or CH_2Cl_2 (10 mL) was treated with HCl gas for ~10 min. The volume of the bleached solution was then reduced *in vacuo* to ca. 1 mL, when diethyl ether (20 mL) was added. Cooling produced white crystals that were filtered, washed with ether, and vacuum dried. The yield of *trans*-RhHCl(*S*,*S*-chiraphos)$_2^+$ Cl$^-$, **3**, was 0.09 g (90%). *Anal.* calcd. for $C_{56}H_{57}Cl_2P_4Rh$: C 65.48, H 5.50; found: C 62.5, H 6.0. Decomposition point in air = 90°C. Conductivity $\Lambda_M = 57\ \Omega^{-1}\,cm^2\,mol^{-1}$; $[\alpha]_D^{25°}$ +220.4° (*c* 2.6, ethanol); ir ν(Rh–H): 2130 cm^{-1}; uv–vis (CH_3OH): 288 (28 600), 275 (30 400), 268 (31 000), 265 nm (ε 30 700 $M^{-1}\,cm^{-1}$); ^1H nmr ($CDCl_3$) δ: −16.23 (9 lines, J_{Rh-H} = 16.0 Hz, $^2J_{H-P_A}$ = 16.0 Hz, $^2J_{H-P_B}$ = 8.0 Hz, 1H, Rh=*H*), 0.46 (virtual quartet, $^3J_{HH}$ = 7.5 Hz, $^{3,5}J_{HP}$ (apparent) = 7.5 Hz, 6H, 2 × C*H*$_3$), 0.96 (virtual quartet, $^3J_{HH}$ = 7.5 Hz, $^{3,5}J_{HP}$ (apparent) = 7.5 Hz, 6H, 2 × C*H*$_3$), 2.0 (m, 2H, 2 × C*H*), 3.4 (m, 2H, 2 × C*H*), 6.8–7.8 (m, 40H, Ph); ^{31}P-{^1H} nmr ($CDCl_3$) δ: 38.4 (dt, J_{P_A-Rh} = 94 Hz, J_{AB} = 27 Hz, 2P), 62.7 (dt, J_{P_B-Rh} = 94 Hz, J_{AB} = 27 Hz, 2P). The nmr spectra are essentially identical in acetone-d^6.

The complex *trans*-RhHBr(*S*,*S*-chiraphos)$_2^+$ Cl$^-$, **4**, was characterized by ^1H nmr after its formation *in situ* ($CDCl_3$) from the reaction of **1** and gaseous HBr; ^1H nmr ($CDCl_3$) δ: −15.12 (9 lines, J_{Rh-H} = 16.0 Hz, $^2J_{H-P_A}$ = 16.0 Hz, $^2J_{H-P_B}$ = 8.0 Hz, 1H, Rh—*H*), 0.53 and 1.00 (virtual quartets, as for **2**), 1.95 (m, 2H, 2 × C*H*), 3.72 (m, 2H, 2 × C*H*), 6.8–7.6 (m, 40H, Ph).

*X-ray crystallographic analysis of bis[2(*S*),3(*S*)-2,3-bis(diphenylphosphino)butane]rhodium(I) chloride*

A crystal bounded by the 8 faces (followed by their distances in mm from a common origin): {−1 1 1}, 0.07, {1 − 1 − 1}, 0.07, {1 0 − 1}, 0.08, {3 0 1}, 0.26 was mounted in a general orientation. Unit-cell parameters were refined by least squares on 2 sin θ/λ values for 25 reflections (2θ = 30–38°) measured on a diffractometer with Mo-*K*α radiation ($\lambda(K\alpha_1)$ = 0.70930, $\lambda(K\alpha_2)$ = 0.71359 Å). Crystal data at 22°C are:

$C_{56}H_{56}ClP_4Rh$ f.w. = 991.3

Monoclinic, a = 23.106(3), b = 12.4987(8), c = 21.455(3) Å, β = 128.539(5)°, V = 4847(1) Å^3, Z = 4, ρ_c = 1.359 g cm^{-3}, $F(000)$ = 2056, μ(Mo-*K*α) = 5.68 cm^{-1}. Absent reflections: *hkl*, $h + k$ odd, space group $C2$ (C_2^3, No. 5) required by molecular chirality.

Intensities were measured with graphite-monochromated Mo-*K*α radiation on an Enraf–Nonius CAD4-F diffractometer. An ω–2θ scan at 1.06–10.06° min^{-1} over a range of (0.70 + 0.35 tan θ) degree in ω (extended by 25% on both sides for background measurement) was employed. Data were measured to 2θ = 55°. The intensities of 3 check reflections, measured every 3600 s throughout the data collection, showed only small random fluctuations. After data reduction,[4] an absorption correction was applied using the Gaussian integration method (23, 24). Transmission factors ranged from 0.915 to 0.933 for 100 integration points. Of the 5793 independent reflections measured, 4509 (77.8%) had intensities greater than or equal to $\sigma(I)$ above background where $\sigma^2(I) = S + 2B + (0.04(S - B))^2$ with S = scan count and B = normalized background count.

The structure was solved by conventional heavy-atom methods, the Rh and P coordinates being determined from the Patterson function and those of the remaining non-hydrogen atoms from a subsequent difference map. Refinement of the non-hydrogen atoms with anisotropic thermal parameters resulted in R = 0.054. In the final stages of refinement the hydrogen atoms were included as fixed contributors in idealized positions (methyl groups staggered in accordance with positions observed on a difference map, C(sp^2)—H = 0.97 and C(sp^3)—H = 0.98 Å, recalculated after each cycle). The absolute configuration is determined by that known for the chiral phosphine ligands. The scattering factors of ref. 25 were used for non-hydrogen atoms and those of ref. 26 for hydrogen atoms. Anomalous scattering factors from ref. 27 were used for the Rh, Cl, and P atoms. The weighting scheme $w = 1/\sigma^2(F)$, where $\sigma^2(F)$ is derived from the previously defined $\sigma^2(I)$, gave uniform average values of $w(|F_o| - |F_c|)^2$ over ranges of both $|F_o|$ and sin θ/λ and was employed in the final stages of full-matrix refinement of 559 variables. Reflections with $I < \sigma(I)$ were not included in the refinement. Convergence was reached at R = 0.046 and R_w = 0.032 for 4509 reflections with $I \geq \sigma(I)$. For all 5793 reflections, R = 0.069. The function minimized was $\Sigma w(|F_o| - |F_c|)^2$, $R = \Sigma||F_o| - |F_c||/\Sigma|F_o|$ and $R_w = (\Sigma w(|F_o| - |F_c|)^2/\Sigma w|F_o|^2)^{1/2}$.

On the final cycle of refinement the mean and maximum parameter shifts corresponded to 0.04 and 0.19σ, respectively. The mean error in an observation of unit weight was 1.676. A final difference map

[4]The computer programs used include locally written programs for data processing and locally modified versions of the following: ORFLS, full-matrix least-squares, and ORFFE, function and errors, by W. R. Busing, K. O. Martin and H. A. Levy; FORDAP, Patterson and Fourier syntheses, by A. Zalkin; ORTEP II, illustrations, by C. K. Johnson.

TABLE 1. Final positional (fractional × 10^4; Rh, Cl, P × 10^5) and isotropic thermal parameters ($U \times 10^3$ Å^2) with estimated standard deviations in parentheses

Atom	x	y	z	U^*_{eq}
Rh	25337(3)	50000	25174(4)	29
Cl(1)	0	51596(35)	0	68
Cl(2)	50000	47860(29)	50000	75
P(1)	24725(9)	34742(18)	18785(10)	34
P(2)	25637(9)	58308(19)	15853(11)	33
P(3)	27058(8)	64949(18)	32390(10)	33
P(4)	23575(9)	42093(20)	33602(11)	37
C(1)	2261(3)	3837(5)	898(3)	39
C(2)	1983(3)	4993(7)	672(3)	40
C(3)	3129(3)	6028(5)	4259(3)	39
C(4)	2686(3)	5109(7)	4228(3)	46
C(5)	1751(4)	3037(8)	197(4)	69
C(6)	1914(4)	5376(7)	−55(4)	53
C(7)	3301(4)	6887(6)	4849(4)	46
C(8)	3100(5)	4551(7)	5032(5)	78
C(9)	3356(3)	2784(6)	2367(4)	41
C(10)	3976(4)	3115(7)	3085(5)	59
C(11)	4635(5)	2682(9)	3384(6)	83
C(12)	4743(4)	1858(8)	3110(5)	74
C(13)	4133(5)	1509(8)	2359(6)	75
C(14)	3451(4)	1964(6)	2020(4)	56
C(15)	1814(3)	2435(6)	1658(4)	37
C(16)	2020(3)	1430(6)	1963(4)	49
C(17)	1516(4)	683(7)	1822(6)	66
C(18)	768(4)	906(7)	1325(5)	62
C(19)	556(4)	1885(8)	1006(5)	66
C(20)	1063(3)	2671(7)	1135(4)	47
C(21)	3483(3)	5888(6)	1879(4)	38
C(22)	4077(4)	5585(7)	2646(4)	52
C(23)	4796(4)	5605(7)	2887(4)	70
C(24)	4937(4)	5894(7)	2433(7)	90
C(25)	4349(4)	6222(7)	1609(4)	64
C(26)	3643(3)	6215(7)	1375(5)	56
C(27)	2194(4)	7160(6)	1208(4)	39
C(28)	2659(4)	8013(6)	1433(5)	52
C(29)	2369(5)	9021(7)	1103(6)	67
C(30)	1611(6)	9189(9)	543(7)	96
C(31)	1158(5)	8333(10)	340(6)	96
C(32)	1422(4)	7321(7)	676(5)	57
C(33)	1842(3)	7202(6)	2850(4)	39
C(34)	1224(4)	6886(7)	2091(4)	53
C(35)	528(4)	7369(8)	1731(6)	83
C(36)	472(4)	8120(7)	2205(5)	61
C(37)	1097(4)	8452(8)	2920(5)	64
C(38)	1776(3)	7998(6)	3258(4)	49
C(39)	3351(3)	7551(5)	3439(4)	36
C(40)	3134(4)	8564(7)	3119(6)	66
C(41)	3643(4)	9333(6)	3277(5)	63
C(42)	4349(4)	9082(8)	3717(5)	64
C(43)	4593(4)	8058(7)	4038(5)	60
C(44)	4095(3)	7306(7)	3866(4)	50
C(45)	1373(4)	4067(6)	2924(5)	49
C(46)	839(3)	4311(6)	2101(5)	56
C(47)	80(4)	4260(7)	1735(5)	72
C(48)	−104(5)	3914(7)	2247(9)	113
C(49)	400(5)	3702(8)	2984(6)	75
C(50)	1148(5)	3764(7)	3362(6)	74
C(51)	2750(3)	2885(7)	3820(4)	44
C(52)	2320(4)	1985(8)	3675(5)	59
C(53)	2647(6)	990(9)	3993(7)	87
C(54)	3384(6)	897(8)	4443(6)	77
C(55)	3833(4)	1765(8)	4590(5)	71
C(56)	3493(4)	2747(8)	4270(5)	63

*U_{eq} = 1/3 trace of diagonalized U; coordinates with esd's are fixed parameters.

TABLE 2. Bond lengths (Å) with estimated standard deviations in parentheses

Bond	Length (Å)	Bond	Length (Å)
Rh—P(1)	2.301(2)	P(3)—C(33)	1.839(6)
Rh—P(2)	2.292(2)	P(3)—C(39)	1.832(6)
Rh—P(3)	2.298(2)	P(4)—C(4)	1.882(7)
Rh—P(4)	2.308(2)	P(4)—C(45)	1.852(6)
P(1)—C(1)	1.894(6)	P(4)—C(51)	1.850(9)
P(1)—C(9)	1.829(6)	C(1)—C(2)	1.532(10)
P(1)—C(15)	1.825(7)	C(1)—C(5)	1.563(10)
P(2)—C(2)	1.860(6)	C(2)—C(6)	1.543(9)
P(2)—C(21)	1.801(6)	C(3)—C(4)	1.512(9)
P(2)—C(27)	1.812(8)	C(3)—C(7)	1.512(9)
P(3)—C(3)	1.849(6)	C(4)—C(8)	1.524(11)

TABLE 3. Bond angles (deg) with estimated standard deviations in parentheses

Bonds	Angle (deg)	Bonds	Angle (deg)
P(1)—Rh—P(2)	83.09(8)	C(3)—P(3)—C(33)	108.2(3)
P(1)—Rh—P(3)	174.89(7)	C(3)—P(3)—C(39)	101.4(3)
P(1)—Rh—P(4)	97.85(8)	C(33)—P(3)—C(39)	104.8(3)
P(2)—Rh—P(3)	97.64(8)	Rh—P(4)—C(4)	111.1(3)
P(2)—Rh—P(4)	173.29(7)	Rh—P(4)—C(45)	113.9(3)
P(3)—Rh—P(4)	82.03(7)	Rh—P(4)—C(51)	122.3(2)
Rh—P(1)—C(1)	109.9(2)	C(4)—P(4)—C(45)	99.7(3)
Rh—P(1)—C(9)	114.7(2)	C(4)—P(4)—C(51)	104.2(3)
Rh—P(1)—C(15)	118.4(2)	C(45)—P(4)—C(51)	102.9(4)
C(1)—P(1)—C(9)	99.9(3)	P(1)—C(1)—C(2)	110.1(3)
C(1)—P(1)—C(15)	106.7(3)	P(1)—C(1)—C(5)	115.7(5)
C(9)—P(1)—C(15)	105.4(3)	C(2)—C(1)—C(5)	112.5(5)
Rh—P(2)—C(2)	105.7(2)	P(2)—C(2)—C(1)	108.2(4)
Rh—P(2)—C(21)	112.5(2)	P(2)—C(2)—C(6)	116.3(5)
Rh—P(2)—C(27)	122.9(2)	C(1)—C(2)—C(6)	111.8(6)
C(2)—P(2)—C(21)	108.1(3)	P(3)—C(3)—C(4)	110.1(4)
C(2)—P(2)—C(27)	102.5(3)	P(3)—C(3)—C(7)	115.9(4)
C(21)—P(2)—C(27)	104.1(3)	C(4)—C(3)—C(7)	113.2(5)
Rh—P(3)—C(3)	106.4(2)	P(4)—C(4)—C(3)	110.0(4)
Rh—P(3)—C(33)	113.7(2)	P(4)—C(4)—C(8)	115.4(6)
Rh—P(3)—C(39)	121.2(2)	C(3)—C(4)—C(8)	111.6(6)

showed maximum fluctuations of −0.63 to +0.55 e Å^3 near Rh and was essentially featureless elsewhere. The final positional and thermal parameters appear in Tables 1 and 6,[5] respectively. Measured and calculated structure factors have been placed in the Depository of Unpublished Data.[5] Selected bond lengths, bond angles, and intra-annular torsion angles for the two chelate rings appear in Tables 2–4, respectively. Bond lengths and angles involving phenyl carbon atoms (Tables 2a and 3a), calculated hydrogen atom parameters (Table 5), and additional torsion angles (Table 7) are included as deposited material.

Discussion

Synthesis and characterization of the complexes

The yellow complex Rh(S,S-chiraphos)$_2^+$ Cl$^-$, **1**, is readily prepared from the rhodium(I) cyclooctene precursor as a benzene hemisolvate according to eq. [2]. The unsolvated complex is obtained by recrystallization from CH_2Cl_2/ether, or by sub-

[5]The structure factor table, Table 6 (anisotropic thermal parameters), and other material mentioned in the text may be purchased from the Depository of Unpublished Data, CISTI, National Research Council of Canada, Ottawa, Ont., Canada K1A 0S2.

[2] $RhCl(C_8H_{14})_2]_2 + 4$ chiraphos $\xrightarrow{C_6H_6}$ $2Rh(chiraphos)_2^+ Cl^- + 4C_8H_{14}$

jecting a finely ground sample of the hemisolvate to high vacuum. Treatment of **1** with Ag^+X^- ($X = BF_4$, PF_6, SbF_6) yields the corresponding X^- salt. The syntheses parallel those used earlier (1) for the analogous dpm, dpe, dpp, dpb, and diop complexes, although, in contrast to these (2), the chiraphos salts are completely air stable in the solid state and solution.

The conductivity data (28), identical uv–visible spectra of **1** and **2**, the absence of ν(Rh—Cl) bands in the 400–200 cm^{-1} region, and the crystallographic data for **1** are consistent with the presence of discrete cations and counter-anions in solution as well as the solid state. A solid state visible spectrum of **1** also shows an absorption maximum at 410 nm, the same as the solution value. The electronic absorption and emission spectral data for square planar $Rh(P—P)_2^+$ complexes have been analyzed in some detail (29–31). It should be noted that the $Rh(P—P)_2Cl$ complexes with P—P = dpm, dpb, and diop are five-coordinate in the solid state and in nonpolar solvents, while the dpe (diphos) and dpp analogues contain ionic chloride (1). Crystallographic data are now available for the ionic $Rh(dpe)_2^+ ClO_4^-$ (32), $Rh(dpp)_2^+ BF_4^-$ (33), $Rh(dpb)_2^+ BF_4^-$ (19), and $Rh(chiraphos)_2^+ Cl^-$ complexes (see below).

The ^{31}P-$\{^1H\}$ nmr spectrum of $Rh(chiraphos)_2^+$ at ambient temperatures displays a simple doublet produced by equivalent P atoms coupled to Rh; the large downfield shift, typical of five-membered ring systems, and coupling constant are very similar to the data for $Rh(dpe)_2^+$ (1). The ^1H nmr data are uninformative.

The nonreactivity of $Rh(chiraphos)_2^+$ towards H_2 or CO parallels that of $Rh(dpe)_2^+$ (2), while the inertness towards O_2 is surprising considering that the dpe analogue forms an isolable peroxorhodium(III) complex (2, 13, 34). In solution under Ar, however, the $Rh(dpe)_2O_2^+$ species readily loses O_2, and the process has been monitored spectrophotometrically to yield the following data at 30°C in methanol: $k_{on} \approx 0.25\ M^{-1}\ s^{-1}$, $k_{off} = 2.6 \times 10^{-3}\ s^{-1}$, and equilibrium constant K, measured by an independent static method, $= 60\ M^{-1}$, or $P_{1/2}$ (the pressure for 50% formation of the dioxygen complex) = 2.3 atm (2, 4). Steric factors within the chiraphos system must either decrease the k_{on}, or increase the k_{off} values, respectively, compared to the dpe system (see below).

Oxidative addition of HCl yields the *trans*-chlorohydrido derivative, **3**; the low carbon analysis is considered to result from contamination with lattice-held HCl, a feature observed with other $RhHCl(P—P)_2^+$ complexes (2) and the iridium analogues (35). The spectroscopy (ir and nmr) is consistent with the presence of a single metal complex. The high-field hydride resonance (Fig. 1) is an overlapping doublet of triplets of triplets (9 lines) produced by coupling to ^{103}Rh (16.0 Hz) and two sets of ^{31}P nuclei (16.0 and 8.0 Hz). A molecular two-fold symmetry in the $RhHCl(chiraphos)_2^+$ cation is indicated also by the pairs of well-separated resonances of two sets of $—CH_3$ (δ 0.46 and 0.96) and —CH groups (δ 2.0 and 3.4) in the ^1H nmr. Of interest, both $—CH_3$ resonances are quartets due to coupling to the neighbouring —CH proton and P nuclei, as well as virtual coupling to another P atom. This pattern implies strong $^2J_{PP}$ coupling, indicative of *trans*-P nuclei (36); decoupling of the —CH protons gives the expected virtual triplet due to coupling to two equivalent P nuclei (36).

The $^{31}P\{^1H\}$ nmr of **3** (Fig. 1) exhibits an A_2B_2X pattern, the two sets of P nuclei (δ 62.7, 38.4) being coupled to Rh and P.

TABLE 4. Intra-annular torsion angles (deg) with standard deviations in parentheses

Atoms	Value (deg)
P(2)—Rh—P(1)—C(1)	−13.1(2)
Rh—P(1)—C(1)—C(2)	−15.1(4)
P(1)—C(1)—C(2)—P(2)	42.2(4)
Rh—P(2)—C(2)—C(1)	−52.8(4)
P(1)—Rh—P(2)—C(2)	33.4(2)
P(4)—Rh—P(3)—C(3)	32.4(2)
Rh—P(3)—C(3)—C(4)	−50.5(4)
P(3)—C(3)—C(4)—P(4)	38.6(5)
Rh—P(4)—C(4)—C(3)	−11.7(5)
P(3)—Rh—P(4)—C(4)	−14.2(2)

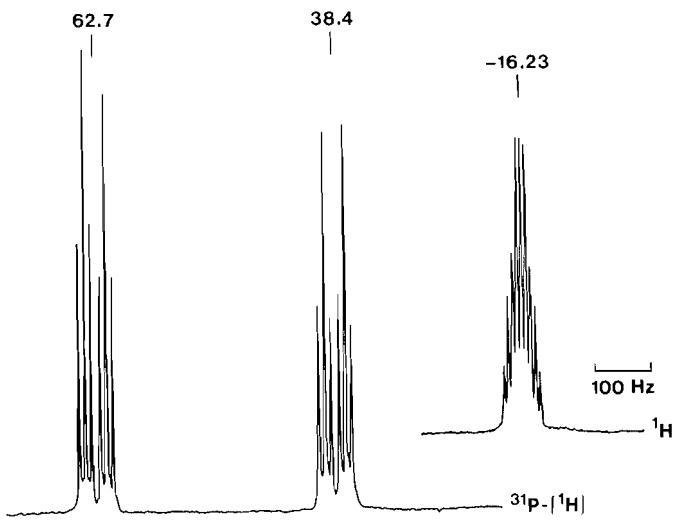

FIG. 1. The ^1H and $^{31}P\{^1H\}$ nmr spectra of *trans*-RhHBr(*S*,*S*-chiraphos)$_2^+$ Cl^- in $CDCl_3$ at ambient temperature.

Such A_2B_2 spectra have been used more commonly as diagnostic of *cis* geometry within $MHCl(P—P)_2$ complexes, with the required assumption of rapid exchange between H and Cl (17, 34, 37). However, distortion from C_{4v} (*trans*) symmetry, such that the pairs of P atoms become nonequivalent, can also give rise to A_2B_2 spectra; this is exemplified by the *trans*-$RuHCl((+)diop)_2$ complex, that distorts to minimize phenyl–phenyl interactions such that the P atom pairs subtend respective H—Ru—P angles of about 75° and 96°, a difference of >20° (37, 38). Such a structural feature in **3**, resulting from the preferred conformations of equatorial chiraphos ligands, would account for the two $^2J_{HP}$ values observed. The *trans* structure is strongly supported by: (a) the ^1H nmr virtual coupling data which require two sets of P nuclei, the members of which are mutually *trans*, i.e. near square-planar P donors; (b) the $^2J_{HP}$ couplings are typical of *cis*-disposed nuclei; the characteristically large *trans* J_{HP} values (39) are not observed; (c) the relatively high value of 2130 cm^{-1} for ν(Rh—H) is consistent with hydride *trans* to chloride (2, 39, 40); (d) the essential features of the metal–hydride resonance in the nmr are maintained at −60°C, which argues against a fluxional *cis*-HCl structure. Of other $RhHCl(P—P)_2^+$ cations (2), the only crystallographic data

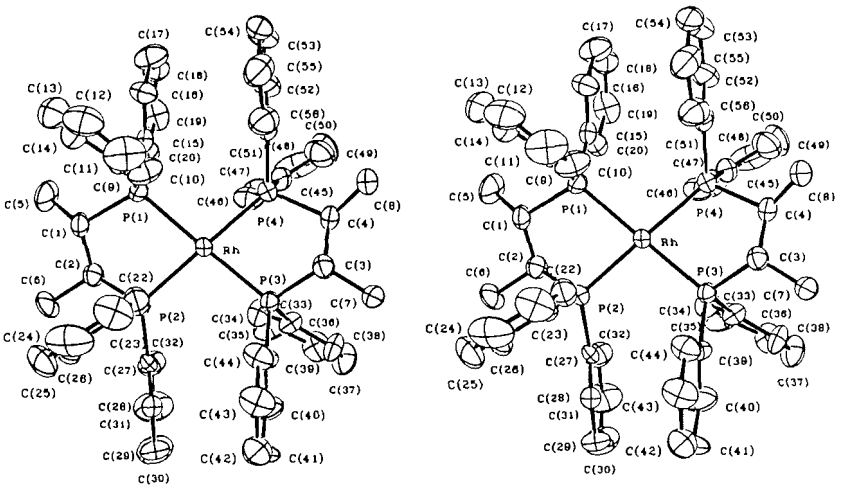

FIG. 2. A stereoscopic view of the Rh(S,S-chiraphos)$_2^+$ cation, and the numbering scheme used. Thermal ellipsoids enclose 50% probability levels. Hydrogen atoms have been deleted for clarity.

available are those for the P—P = dpm system, which has *trans* geometry (41).

The RhHBr(chiraphos)$_2^+$ complex was formed *in situ* from **1** using HBr; the nmr data correspond closely to those for **3**, and a *trans* geometry is again favoured. Unfortunately, **1** did not react with HF, which prevented a probing of the geometry via a $^2J_{HF}$ measurement.

*Structure description of Rh(*S,S*-chiraphos)$_2^+$ Cl$^-$*

The structure consists of discrete Rh(S,S-chiraphos)$_2^+$ cations and Cl$^-$ anions, the latter situated along the twofold axes $(0, y, 0)$ and $(\frac{1}{2}, y, \frac{1}{2})$. The nearest neighbours of each of the two crystallographically independent Cl$^-$ anions are six hydrogen atoms at distances of 2.79–2.90 Å. All cation–cation distances correspond to normal van der Waals interactions. Figure 2 shows a stereoscopic view of the rhodium cation, including the atom numbering scheme.

The Rh(S,S-chiraphos)$_2^+$ cation, as a whole, possesses approximate C_2 symmetry and, ignoring the carbon atoms of the chelate rings (and their methyl substituents), the symmetry is close to C_{2h}. The coordination about Rh is square planar, distorted toward tetrahedral. The Rh atom lies essentially in the P_4 mean plane (displacement −0.008(1) Å), while the phosphorus atoms lie alternately above and below the P_4 mean plane (displacements: −0.112(2), 0.120(2), −0.108(2), and 0.132(2) Å, respectively for P(1)–P(4)). The distortion of the coordination group in the closely related Rh(dpe)$_2^+$ cation is similar, but displacements of the P atoms from the coordination plane are significantly smaller (0.04 Å) (32).

The Rh—P distances in Rh(S,S-chiraphos)$_2^+$ (2.291(2)–2.308(2), mean 2.300 Å) are slightly longer than the values of 2.232(2)–2.289(2) Å reported for other square-planar S,S-chiraphos complexes of Rh(I) (9, 42) and similar to values of 2.289(6)–2.313(6), mean 2.306 Å, observed for Rh(dpe)$_2^+$ (32). The conformations of the two chelate rings are nearly identical (see Table 4) and are very similar to those observed in other complexes of S,S-chiraphos (9, 42, 43) and in the Rh(dpe)$_2^+$ cation (32).

One of the most unusual features of the Rh(S,S-chiraphos)$_2^+$ structure is the highly symmetric disposition of the phenyl rings. It is this feature that represents the major structural difference between this cation and the Rh(dpe)$_2^+$ cation, as well as nearly all structurally characterized complexes of bidentate bis(diphenylphosphine) ligands forming five-membered chelate rings. In addition to the steric interactions between the phenyl rings noted earlier for the Rh(dpe)$_2^+$ cation (32), the methyl substituents on the chelate rings further restrict rotational freedom about the P—Ph bonds. The C(5) and C(8) methyl groups make contact with carbon atoms of adjacent pseudoequatorial phenyl rings, while the C(6) and C(7) methyl groups are in contact with both adjacent phenyl rings (C(Me)···C(Ph) = 3.02(1)–3.37(9) Å, H(Me)···C(Ph) = 2.66–2.80 Å). As a result, the pseudoaxial phenyl rings are oriented more nearly perpendicular to the RhP_4 plane than in Rh(dpe)$_2^+$ and are oriented such that the hydrogen atoms attached to C(10), C(22), C(34), and C(46) effectively block any axial approach to the metal (Rh···H = 3.05, 2.87, 2.84, and 2.92 Å, respectively). These "blocking" hydrogen atoms, two from each ligand situated on opposite sides of the coordination plane, are in close contact with one another (H···H = 2.28, 2.36 Å) and with a phenyl hydrogen atom associated with a pseudoequatorial phenyl ring of the other ligand (H···H = 2.38–2.46 Å). This steric factor must certainly contribute to the lack of reactivity toward O_2 (compared with Rh(dpe)$_2^+$), even in solution.

Bond lengths and angles are generally as expected although some distances, particularly in the phenyl rings, are shortened as a result of relatively high thermal motion. The phenyl rings containing C(9), C(15), C(27), C(33), and C(39) are all significantly nonplanar (maximum deviation from the mean plane = 0.055(12) Å). This nonplanarity is most probably an artifact arising from the uncertainties in the positions of some of the peripheral ring atoms having higher thermal amplitudes, although some small deviations from planarity may arise from steric effects.

Acknowledgements

This work was supported by a grant from the Natural Sciences and Engineering Research Council of Canada. We thank J. Trotter for use of X-ray facilities, and Johnson, Matthey Ltd. for the loan of rhodium.

1. B. R. JAMES and D. MAHAJAN. Can. J. Chem. **57**, 180 (1979).
2. B. R. JAMES and D. MAHAJAN. Can. J. Chem. **58**, 996 (1980).
3. B. R. JAMES and D. MAHAJAN. J. Organomet. Chem. **279**, 31 (1985).
4. B. R. JAMES and D. MAHAJAN. 7th Canadian Symposium on Catalysis. Preprints, Vol. 1. 1980. p. 58.

5. B. R. JAMES, D. MAHAJAN, and C. G. YOUNG. Proc. 1st Intern. Symp. Inorg. Chem. Transition Metal Chemistry; Coordination and Molecular Activation. Santiago, Chile. 1985. p. 32.
6. L. H. PIGNOLET, D. H. DOUGHTY, S. C. NOWICKI, M. P. ANDERSON, and A. L. CASALNUOVO. J. Organomet. Chem. **202**, 211 (1980).
7. D. H. DOUGHTY, M. P. ANDERSON, A. L. CASALNUOVO, M. F. MCGUIGGAN, C. C. TSO, H. H. WANG, and L. H. PIGNOLET. Adv. Chem. Ser. **196**, 65 (1982).
8. M. D. FRYZUK and B. BOSNICH. J. Am. Chem. Soc. **99**, 6262 (1977).
9. R. G. BALL and N. C. PAYNE. Inorg. Chem. **16**, 1187 (1977).
10. B. R. JAMES and C. G. YOUNG. J. Chem. Soc. Chem. Commun. 1215 (1983).
11. B. R. JAMES and C. G. YOUNG. J. Organomet. Chem. **285**, 321 (1985).
12. K. A. TAYLOR. Adv. Chem. Ser. **70**, 195 (1968).
13. J. A. MCGINNETY, N. C. PAYNE, and J. A. IBERS. J. Am. Chem. Soc. **91**, 6301 (1969).
14. L. VASKA, L. S. CHEN, and W. V. MILLER. J. Am. Chem. Soc. **93**, 6671 (1971).
15. D. SINUO and H. B. KAGAN. J. Organomet. Chem. **114**, 325 (1976).
16. A. R. SANGER. J. Chem. Soc. Dalton Trans. 120 (1977).
17. (*a*) D. A. SLACK, I. GREVELING, and M. C. BAIRD. Inorg. Chem. **18**, 3125 (1979); (*b*) D. A. SLACK and M. C. BAIRD. J. Organomet. Chem. **142**, C69 (1977).
18. L. H. PIGNOLET, D. H. DOUGHTY, S. C. NOWICKI, and A. L. CASALNUOVO. Inorg. Chem. **19**, 2172 (1980).
19. M. P. ANDERSON and L. H. PIGNOLET. Inorg. Chem. **20**, 4101 (1981).
20. R. V. KASTRUP, J. S. MERDA, and A. A. OSWALD. Adv. Chem. Ser. **196**, 43 (1982).
21. R. C. LAROCK, K. OERTLE, and G. F. POTTER. J. Am. Chem. Soc. **102**, 190 (1980).
22. A. VAN DER ENT and A. L. ONDERDELINDEN. Inorg. Synth. **14**, 92 (1973).
23. P. COPPENS, L. LEISEROWITZ, and D. RABINOVICH. Acta Crystallogr. **18**, 1035 (1965).
24. W. R. BUSING and H. A. LEVY. Acta Crystallogr. **22**, 457 (1967).
25. D. T. CROMER and J. B. MANN. Acta Crystallogr. Sect. A, **24**, 321 (1968).
26. R. F. STEWART, E. R. DAVIDSON, and W. T. SIMPSON. J. Chem. Phys. **42**, 3175 (1965).
27. D. T. CROMER and D. LIBERMAN. J. Chem. Phys. **53**, 1891 (1970).
28. W. J. GEARY. Coord. Chem. Rev. **7**, 81 (1971).
29. R. BRADY, W. V. MILLER, and L. VASKA. J. Chem. Soc. Chem. Commun. 393 (1974).
30. G. L. GEOFFROY, M. S. WRIGHTON, G. S. HAMMOND, and H. B. GRAY. J. Am. Chem. Soc. **96**, 3105 (1974).
31. G. L. GEOFFROY, H. ISCI, J. LITRENTI, and W. R. MASON. Inorg. Chem. **16**, 1950 (1977).
32. M. C. HALL, B. T. KILBOURN, and K. A. TAYLOR. J. Chem. Soc. A, 2539 (1970).
33. R. G. BALL, D. MAHAJAN, and B. R. JAMES. To be published.
34. J. S. MILLER and K. G. CAULTON. J. Am. Chem. Soc. **97**, 1067 (1975).
35. L. VASKA and D. L. CATONE. J. Am. Chem. Soc. **88**, 5324 (1966).
36. (*a*) J. M. JENKINS, and B. L. SHAW. Proc. R. Soc. London, 279 (1963); (*b*) R. K. HARRIS. Can. J. Chem. **42**, 2275 (1964); (*c*) F. B. OGILVIE, J. M. JENKINS, and J. G. VERKADE. J. Am. Chem. Soc. **92**, 1916 (1970); (*d*) D. A. REDFIELD, L. W. CARY, and J. M. NELSON. Inorg. Chem. **14**, 50 (1975), and references therein.
37. R. G. BALL, B. R. JAMES, J. TROTTER, D. K. W. WANG, and K. R. DIXON. J. Chem. Soc. Chem. Commun. 460 (1979).
38. R. G. BALL and J. TROTTER. Inorg. Chem. **20**, 261 (1981).
39. J. P. JESSON. *In* Transition metal hydrides. *Edited by* E. L. Muetterties. Marcel Dekker, New York. 1971. p. 110.
40. G. L. GEOFFROY and J. R. LEHMAN. Adv. Inorg. Chem. Radiochem. **20**, 189 (1977).
41. M. COWIE and S. K. DWIGHT. Inorg. Chem. **18**, 1209 (1979).
42. A. S. C. CHAN, J. J. PLUTH, and J. HALPERN. J. Am. Chem. Soc. **102**, 5952 (1980).
43. P. A. AGASKAR, F. A. COTTON, I. F. FRASER, and R. D. PEACOCK, J. Am. Chem. Soc. **106**, 1851 (1984).

The hot atom chemistry of muonium in alkane vapors

DONALD G. FLEMING,[1] MASAYOSHI SENBA, DONALD J. ARSENEAU, IVAN D. REID, AND DAVID M. GARNER
Department of Chemistry and TRIUMF, University of British Columbia, Vancouver, B.C., Canada V6T 1Y6

Received June 13, 1985

DONALD G. FLEMING, MASAYOSHI SENBA, DONALD J. ARSENEAU, IVAN D. REID, and DAVID M. GARNER. Can. J. Chem. **64**, 57 (1986).

Energetic positive muons thermalizing in alkane vapors are observed in either diamagnetic environments, with relative fraction f_D, or as the polarized muonium atom (Mu = μ^+e^-), with fraction f_{Mu}. The fraction f_D is found to vary from ~0.12 in CH_4 to ~0.24 in n-C_6H_{14} at pressures near 1 atm (300 K); some pressure dependence in yield is also observed, notably for the heavier alkanes. The diamagnetic fraction (yield) is interpreted as due to hot atom reactions (Mu*) in complete analogy with past studies in hot tritium (T*) chemistry. The data have been interpreted within the Wolfgang–Estrup formalism and compared with similar analyses of T* reactions for (unmoderated) alkane systems. It is concluded that the energy loss parameter (α) is determined largely by inelastic scattering effects. If these are assumed to be the same for both Mu* and T* moderation, then the resulting reactivity integrals (I) for the noncyclic alkanes are found to exhibit the same trend with mass as in hot tritium chemistry, giving, on average, ~6:1 for the ratio I(T*)/I(Mu*).

DONALD G. FLEMING, MASAYOSHI SENBA, DONALD J. ARSENEAU, IVAN D. REID et DAVID M. GARNER. Can. J. Chem. **64**, 57 (1986).

On a observé que des muons positifs, qui sont chargés d'énergie et qui se rechauffent dans des vapeurs d'alcane, existent soit dans un environnement diamagnétique avec une fraction relative f_D soit sous forme d'atome de muomum polarisé (Mu = μ^+e^-) avec une fraction f_{Mu}. À des pressions voisines de 1 atm (300 K), on a trouvé que la fraction f_D varie d'environ 0,12 dans le CH_4 à environ 0,24 dans le n-C_6H_{14}; on a aussi observé une relation entre la pression et le rendement, notamment dans le cas des alcanes plus lourds. On pense que la fraction diamagnétique (rendement) est due à des réactions d'atomes chauds (Mu*) et ceci est en accord complet avec les études antérieures réalisées dans la chimie du tritium chaud (T*). On a fait appel au formalisme de Wolfgang–Estrup pour interpréter les données et on les a comparées à des analyses identiques de réactions du T* dans des systèmes d'alcanes (non-modérés). On en conclut que le paramètre de perte d'énergie (α) est déterminé en grande partie par des effets de dispersion non élastiques. Si on admet que ces effets sont les mêmes pour les modérations tant du Mu* que du T*, on trouve alors que les intégrales résultantes d'activité (I) des alcanes non-cycliques exhibent la même tendance en ce qui a trait à la masse que dans la chimie du tritium chaud; on obtient ainsi un rapport moyen de I(T*)/I(Mu*) qui est d'environ 6:1.
[Traduit par le journal]

1. Introduction

1.1 General remarks

The realm of studies in chemical reaction dynamics can be broadly divided into "hot" and "thermal" reactions, distinguished roughly by the translational energy of reacting species. In hot (atom or ion) reactions this energy is large compared to the value of k_BT characterizing thermal reactions, with the result that certain reaction channels which are energetically forbidden in the thermal energy regime become accessible at higher energies. The most direct knowledge about energetic reactions comes from atomic and molecular beam studies, where the capability of systematically varying the reaction energy (and angle) exists. The goal of such experiments is the measurement of true state-to-state cross sections, and while this goal is often not fully realized, molecular beam studies do provide the means by which theories of reaction dynamics can be most effectively tested on a microscopic level (1, 2). However, particularly in the case of *atom*–molecule reactions, these studies are limited to beam energies that are typically $\lesssim$1 eV so that the excitation function describing the energy dependence of the reactive cross section ($\sigma(E)$) cannot be extended to higher energies. The role of probing $\sigma(E)$ at energies $\gtrsim$1 eV has traditionally fallen to "hot atom" reactions, particularly recoil tritium experiments, in which the upper energy for significant reactivity is $\lesssim$30 eV (3–6). Although the excitation function in such studies emerges only indirectly as an integral result, defined by the hot atom "yield," these continue to be of interest (3). Photochemically generated hot H atoms (H*, D*, T*) have also been utilized and the much lower (few eV) incident energies characteristic of these atoms (7–9) provides some overlap with atomic beam work.

The importance of isotopic substitution, notably of the hydrogen atom, to the study of chemical reaction dynamics is well known, exemplified by the seminal work of Polanyi and co-workers on mass effects in chemical reactivity (10). In this respect there has recently been considerable interest in exploring the isotopic similarity between the muonium (Mu = μ^+e^-) and hydrogen (H) atoms, in both gases (11–14)[2] and liquids (15), motivated by the fact that the mass of the positive muon is only 1/9th the proton mass.

The effects of a change in isotopic mass on reaction dynamics can be quite different in hot versus thermal reactions. In the case of thermal reactions it is the threshold region of the excitation function that is of paramount importance, a region that is poorly explored by either hot atom or molecular beam studies. Both classical and quantum mechanical effects are important in thermal reactions (10), with marked changes seen upon the substitution of Mu for H (11–15); in particular, Mu is a very sensitive probe of quantum tunneling. In contrast, at the much higher energies characteristic of hot reactions, tunneling is relatively unimportant and mass effects on reaction dynamics should be almost entirely classical in nature (3, 4, 16–18). Indeed, atomic beam results at energies of ~1 eV are often very well described by classical calculations (1), even in the case of the H(D) + H_2 reaction (16, 19, 20).

Traditionally, recoil hot T chemistry has been the mainstay of

[1]1983–1984 John Simon Guggenheim Fellow. Author to whom correspondence may be addressed.

[2]Also, J. N. L. Connor and J. C. Whitehead, private communication.

studies in (light) hot atom chemistry (3–6), in which the incident triton is produced with kinetic energies ~ 100 keV, orders of magnitude larger than those of chemical interest. This is also the situation in Mu formation and hence the hot Mu (Mu*) chemistry in alkane vapors discussed here should be directly comparable with similar studies of T* reactivity (21–27).

The alkane vapors have been chosen for this comparison because the hot tritium yields seem to have been most reliably and systematically determined for these systems. From such a study one can hope to learn about the sensitivity of hot atom reaction dynamics to changes in isotopic mass, as in previous work on thermal reactions (11–14); indeed, a factor of *27* between the masses of Mu and T is the widest possible isotopic variation at the most sensitive end of the mass scale. The present paper is the first time that the subject of hot Mu reactivity has been addressed directly, although it has often been referred to (15, 28–30). It is hoped that comparison with the analogous hot tritium studies will help to sharpen the criteria for different theoretical models of hot atom reaction dynamics.

1.2. Muonium (tritium) formation and thermalization in gases

Positive muons (μ^+) enter the (gas) target of interest with kinetic energies $\gtrsim$ 3 MeV. The energy loss processes that the muon then undergoes can be divided into three stages (28–30), in analogy with related studies of proton charge exchange (31). Most of the incident energy is lost in the first stage, where Bethe–Bloch ionization dominates until a kinetic energy of ~30 keV is reached. At this energy, the muon velocity is comparable to that of electrons bound in atoms of the moderator and the μ^+ enters a regime of *cyclic* charge exchange, in which Mu is formed in one collision (with cross section σ_{10}) and lost in a subsequent collision (with cross section σ_{01}). There are ~100 of these charge exchange cycles, following which the muon emerges either in the Mu atom or as a bare μ^+ at a kinetic energy of ~30 eV.

In the third and final stage of thermalization a further factor of ~1000 loss in energy to k_BT occurs. It is during this third stage when hot atom (or ion) chemistry will be important, since reactive processes will compete with elastic and inelastic scattering in thermalizing the muon. In the present study of low ionization potential moderators (all lower than the 13.6-eV value of Mu itself), any muons that survive the charge exchange regime as bare muons are expected to rapidly produce Mu in subsequent collisions, since σ_{10} for exothermic charge exchange is large at such low energies (28, 31). Hence in hydrocarbon vapors charge exchange alone implies 100% Mu formation ($f_{Mu} = 1.0$), while observations of $f_{Mu} < 1.0$ are taken as evidence for the presence of Mu* reactions. In general these differences are small, manifest in the fraction of muons appearing in *diamagnetic* environments (f_D). In contrast to the present study of alkane vapors, it is noted that, in other gases, only in Kr and Xe is $f_{Mu} = 1.0$ observed (28), cases in which hot atom chemical reactions are not possible.

The concept that muonium is formed as a result of cyclic charge exchange is also believed to be the case in recoil tritium atom chemistry (3, 4, 6, 32). In the gas phase, tritons are produced from thermal neutrons via the ^{3}He(n, p)T reaction, endowing the recoil triton with 191 keV of kinetic energy. While this is much lower than the incident μ^+ energy of ~3 MeV, it is still much larger than chemical bond energies. The triton is likely also produced as an ion but, unlike the μ^+, at 191 keV its initial velocity is already comparable to those of the bound electrons in the moderator and hence it can be expected to undergo cyclic charge exchange as part of the initial thermalization stage. However, because of its mass, the triton (T atom) will emerge from the charge exchange regime at much higher energies than the muon, ~900 eV. At such energies, the electron loss cross section σ_{01} is appreciably larger than is the case for Mu at ~30 eV (31), and thus one might expect hot ion chemistry to be relatively more important in the case of the triton. The contribution of hot ions in determining measured yields in recoil tritium studies is, however, still thought to be small (3, 4, 32, 33).

2. The Wolfgang–Estrup theory of hot (T*) atom reactivity

In the Wolfgang–Estrup (WE) formalism (3–5), the fundamental expression for the total probability P of a hot (T*) atom reaction (often referred to as the "yield") is defined by

$$[1] \quad P = \sum_j \int_{E_1}^{E_2} f_j p_j(E) n(E) \mathrm{d}E$$

where $p_j(E)$ is the probability per collision for formation of product j at energy E, f_j is the relative chance of collision with component j, and $n(E)$ is the density of collisions between E and $E + \mathrm{d}E$. Collisions at energies above E_2 are too energetic to result in stable molecules, while E_1 is the minimum (threshold) energy for reaction. The central hypothesis of the WE theory is that the collisional density is given in terms of a *constant* fractional energy loss α, defined in the *absence* of reaction by

$$[2] \quad n(E)\mathrm{d}E = -\frac{1}{\alpha E}\mathrm{d}E$$

where, in the case of *elastic* scattering from *rigid spheres* (rs), α is given by

$$[3] \quad \alpha_{rs} = 1 - \frac{(M-m)^2}{2mM}\ln\frac{M+m}{M-m} \approx \frac{2m}{M}$$

with m and M being the masses of the incident hot atom and the moderator molecule, respectively. It is also assumed that the initial energy of the hot atom $E_0 \gg E_2$, ensuring a sufficient number of collisions so that a statistically well-defined energy distribution of hot atoms exists in the region $E_2 > E > E_1$. This assumption should be well justified for recoil T* ($E_0 \lesssim 900$ eV) and for the present Mu* study ($E_0 \lesssim 30$ eV), but may well be suspect for photochemically induced (epithermal) reactions (34). A further assumption is that $E_1 \gg k_BT$ so that any contribution from thermal reactions can be ignored (this is accomplished experimentally by the use of scavengers).

If $p_j(E)$ is finite at high energies, eq. [2] must be modified to take account of the fact that the hot atom may have already undergone reaction in the energy region of interest,

$$[4] \quad n(E)\mathrm{d}E = \frac{\mathrm{d}E}{\alpha E}\left[1 - \int_E^{E_2} fp(E')n(E')\mathrm{d}E'\right.$$

where here a single reactive component is assumed (hence the label "j" is no longer necessary). If $p(E)$ in this region is small, eq. [4] can be written as an exponential ($e^{-x} \sim 1 - x$) which, upon substitution into eq. [1] and re-expanding, yields the basic result of WE theory,

$$[5] \quad P = \frac{fI}{\alpha} - \frac{1}{2}\left(\frac{fI}{\alpha}\right)^2 + \frac{1}{6}\left(\frac{fI}{\alpha}\right)^3 + \ldots = 1 - \exp\left(\frac{-fI}{\alpha}\right)$$

Here I is the "reactivity integral," defined by

$$[6] \quad I = \int_{E_1}^{E_2}\frac{p(E)\mathrm{d}E}{E} = \frac{1}{\sigma_{max}}\int_{E_1}^{E_2}\frac{\sigma(E)\mathrm{d}E}{E}$$

where σ_{max} gives the total "geometrical" cross section. For a binary mixture of one reactant (R) and *inert* moderator (M), the collisional energy loss parameter can be written as $\alpha = f\alpha_R + (1 - f)\alpha_M$, which upon substitution into eq. [6] yields the result

$$[7] \quad \frac{-1}{\ln(1-P)} = \frac{\alpha_R}{I} + \frac{\alpha_M}{I}\frac{(1-f)}{f}$$

Hence, if the *total* reaction probability P can be found as a function of moderator mole fraction, then a kinetic plot of eq. [7] yields a straight line of slope α_M/I and intercept α_R/I. In practice, this may not be nearly so easy as it sounds. In hot tritium chemistry there can be several products formed from even a single reactant and the individual reaction probabilities P_i must be found for each product ($P = \Sigma_i P_i$).

Although the WE formalism has little *predictive* capability, since there is no a priori way to determine I and hence the cross section $\sigma(E)$, it has been very successful over the years in providing an easily understandable framework for the interpretation of experimental yields. From eq. [5] it can be seen that there are two competitive processes that determine these yields: the reactivity I and the collisional energy loss α; if I is large or α is small (or both), then the hot atom yield will be high. A large value for I clearly implies a large reaction cross section, while a small α means a large number of collisions during the slowing-down process, enhancing the probability for reaction. It is worth noting that the WE development can be "exact" only in the limit $p(E) \rightarrow 0$ (eq. [4]), a condition more likely to be met in Mu* than in T* chemistry.

Of the approximations noted above that form the basis of the WE theory, the most suspect is that of a constant fractional energy loss (α) with its implication of a time-independent (steady state) collision density $n(E)$. In recent years this assumption has been questioned, and alternative methods for the theoretical interpretation of hot atom reactions based on Monte Carlo methods (33, 35, 36) or on explicit time-dependent solutions of the Boltzmann equation (37–39) have been developed. See also refs. 16–18. These theoretical treatments demonstrate, however, that the WE formalism still provides a reasonable framework for the interpretation of experimental hot atom yields. In the discussion to follow we apply this formalism to a comparison of the yields of Mu* and T* reactions in alkane vapors.

3. Experimental technique and results

3.1 The μSR signals

The experiments were carried out at the TRIUMF cyclotron, a meson facility adjacent to the campus of the University of British Columbia. Surface (4.1 MeV) muons (40) were brought to rest in a gas target positioned between a pair of Helmholtz coils of 1.5-m diameter, which provided a magnetic field transverse to the muon spin in the range ~1 G to ~300 G. As a result of charge exchange and hot atom (or possibly hot ion) reactions, one can expect to observe thermalized muons in two environments: diamagnetic, with fraction f_D, and paramagnetic (Mu), with fraction f_{Mu}. A third possibility, the formation of muonium radicals (41), is regarded as extremely unlikely in the saturated bond systems under consideration and will not be discussed further here (see also ref. 30).

Regardless of its environment, the μ^+ ultimately decays in the parity violating process $\mu^+ \rightarrow e^+\bar{\nu}_\mu\nu_e$, emitting the positron preferentially along the muon spin axis. The decay positron is detected in coincidence with a data gate that is triggered by a stopped muon; the time difference between muon and positron is, on average, just the mean life of the muon, $\tau_\mu = 2.2\,\mu s$. This time-differential process is repeated many times until a histogram of ~10^6 events has been accumulated. In a transverse magnetic field, muons bound in the paramagnetic Mu atom and those in diamagnetic environments precess with distinctly different Larmor frequencies ($\nu_{Mu} = 103 \times \nu_D = 1.39\,MHz\,G^{-1}$), manifest as modulations of the decay histograms, and referred to as μSR (Muon Spin Rotation) "signals" $S(t)$. Examples are shown in Fig. 1 for room-temperature ethane gas at 1 atm pressure, at 7.6 G (top), and at 195 G (bottom). These can be thought of in analogy with free induction decay signals in magnetic resonance. The curves are χ^2 fits to the data, defined in the case of the top spectrum in Fig. 1 by

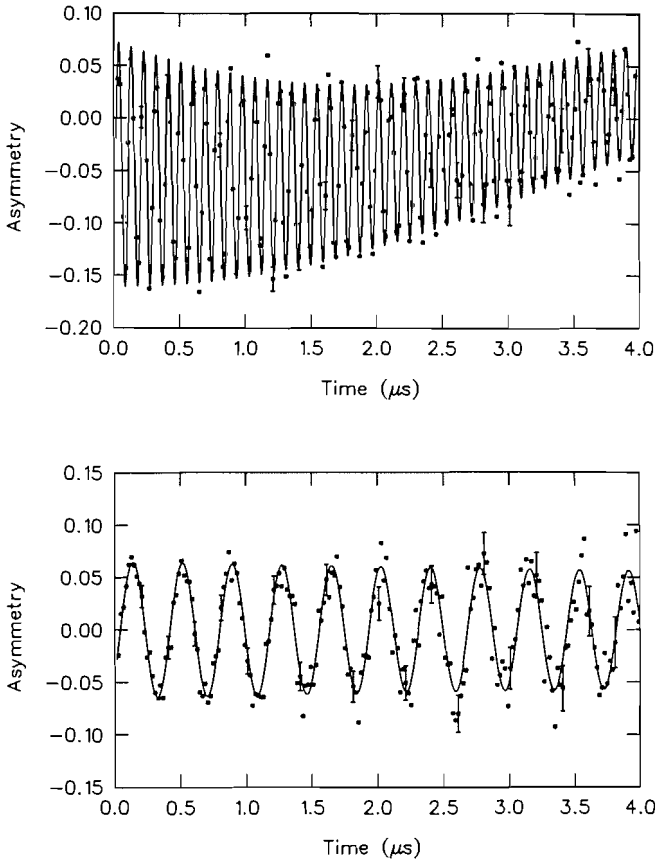

FIG. 1. μSR signals at room temperature in 1 atm ethane gas at 7.6 G (top) and 195 G (bottom). The solid line is a χ^2 fit to the data, as discussed in the text.

$$[8] \quad S(t) = A_{Mu}e^{-\lambda_{Mu}t}\cos(\omega_{Mu}t + \phi_{Mu}) + A_D e^{-\lambda_D t}\cos(\omega_D t - \phi_D)$$

where A_{Mu}, ω_{Mu}, ϕ_{Mu} and A_D, ω_D, ϕ_D are the initial amplitudes, precession frequencies, and phases for paramagnetic Mu and diamagnetic muons, respectively, while λ_M, λ_D are transverse relaxation times ($\lambda = 1/T_2$) accounting for the interaction of these species with their environments. In the weak (7.6 G) field of Fig. 1 (top), the signal is dominated by fast Mu precession; the signal from slowly precessing diamagnetic muons appearing only as an underlying curvature in the data. This is in contrast to the bottom spectrum at 195 G, where Mu precession is averaged out, both by the experimental time resolution (~3 ns) and by the coarse binning used, so that only the second term of eq. [8] is relevant. For further details of the technique, the reader is referred to refs. 28–30.

Of the parameters in eq. [8], we are concerned in this paper only with the amplitudes A_{Mu} and A_D of muons in paramagnetic muonium and in diamagnetic environments, since these indirectly reveal the hot process occurring during the muon's slowing down process. In particular, the polarizations (P_{Mu} and P_D) and relative fractions (f_{Mu} and f_D) are defined by

$$[9a] \quad P_{Mu} = 2A_{Mu}/A_{max} \qquad P_D = A_D/A_{max}$$

$$[9b] \quad f_{Mu} = P_{Mu}/(P_{Mu} + P_D), \qquad f_D = P_D/(P_{Mu} + P_D)$$

where A_{max} is the maximum possible amplitude for the experimental conditions (typically ~0.3); the factor of two accounts for the loss of observable Mu due to the μ^+–e^- hyperfine interaction (28–30, 42). The sum $P_D + P_{Mu}$ may be less than unity, the difference reflecting a "lost" or "missing" fraction of polarization, P_L.

Since we are interested in the signal amplitudes from muons stopping in the gas, any muons that actually stop in the walls of the target vessel must be corrected for. The source of this "wall effect" is the initial defining counter (3/8-mm thickness) and thin (1/8-mm) entrance window, which scatter some fractions of the more energetic muons into the Al walls, where they precess as diamagnetic muons (with amplitude A_W) and hence contribute to f_D. This can be corrected for experimentally, as discussed elsewhere (28–30) and can also be modeled from a Monte Carlo calculation of the muon stopping distribution. In the tables below (and in eqs. [9] above) A_D is defined by $A_D = A_D(obs) - A_W$, where $A_D(obs)$ is the experimentally observed total signal (e.g., Fig. 1, bottom).

3.2. *Procedure and results*

The alkanes employed as vapors in this study were all obtained commercially and were generally of high purity (total impurity content typically ≲0.5%, including other hydrocarbons). Two different gas target vessels were used. The gaseous alkanes (up to propane) were taken directly from the bottle without further purification and were used to fill a large vessel of ~180-L capacity. The heavier liquid alkanes (up to hexane, $n = 6$) were degassed by several freeze–pump–thaw cycles prior to usage in order to remove any dissolved oxygen. For these cases a different target design of smaller capacity (~30 L) was used (29, 30).

For each run the target vessel was filled with *neat* alkane vapor at a given pressure and μSR histogram spectra were recorded by detecting positron events in two independent "counter telescopes" at each of two different magnetic fields; ~200 G to measure A_D (Fig. 1, bottom) and ~8 G to measure A_{Mu} (Fig. 1, top). Usually at least two total pressures were employed in the range ~0.2 – ~1 atm, depending on the gas density. The polarizations P_D and P_{Mu} and the lost fraction P_L, as well as the relative fractions f_D and f_{Mu} (eqs. [9]), are recorded as a function of pressure in Table 1; the values given are weighted averages from the two independent histograms. Those for n-hexane and c-hexane are taken from ref. 30. The values for CH_4 are in good agreement with those previously reported (28).

It is noted, in agreement with previous studies (28–30, 42), that the lost fraction $P_L \rightarrow 0$ as the pressure increases to even moderate values (≲1 atm) at the relatively high densities of the present study. The missing fraction in gases is due to muon depolarization from the μ^+–e^- hyperfine interaction (ν_0 = 4463 MHz) *during* the charge exchange regime, an effect that is rapidly suppressed in the limit of "high" pressures when the time between collisions becomes short compared to $1/\nu_0$ (0.22 ns). This situation is in marked contrast to complementary studies of Mu formation in condensed media, where relatively large missing fractions (P_L ~ 20%) are routinely observed (15). In some cases the data in Table 1 also reveal a pressure dependence in the fraction f_D, notably in c-pentane (although curiously not in n-pentane), c-hexane, and n-hexane. Figure 2 presents a plot of f_D versus pressure for c-hexane; the solid curve shown is a fit to a simple three-body model which is discussed further in ref. 30.

TABLE 1. Muon polarizations and relative fractions in alkane vapors[a]

Vapor	Pressure (Torr)[b]	P_D	P_{Mu}	P_L	f_{Mu}	f_D
CH_4	800	9±1	76±2	15±2	89±2	12±2
C_2H_6	350	19±2	69±4	12±4	78±2	22±2
	500	16±2	71±1	13±1	82±2	18±1
	760[c]				81±2	19±2
C_3H_8	490[c]				79±2	21±2
n-C_4H_{10}	380[c]				79±2	21±2
i-C_4H_{10}	215	13±2	51±4	36±4	80±2	20±2
	295	13±1	65±2	22±2	83±2	17±2
	430	15±1	69±2	16±2	82±2	18±2
c-C_5H_{10}	175	4±2	50±2	46±3	92±2	8±3
	250	15±1	63±1	23±2	81±2	19±2
n-C_5H_{12}	165	17±2	42±2	51±3	86±3	14±3
	240	11±1	67±1	22±2	86±2	14±2
	290	12±1	68±2	20±2	85±2	15±2
c-C_6H_{12}[d]	175	11±1	64±3	25±3	86±1	14±1
	500	23±2	71±2	5±3	75±2	25±2
	760	27±1	72±2	1±3	73±1	27±1
n-C_6H_{14}[d]	225	13±2	78±2	9±3	86±2	14±2
	500	22±1	73±2	5±2	76±1	24±1
	1010	25±1	75±2	0±2	75±1	25±1

[a]Average values from two independent histograms, given as per cent. The diamagnetic amplitude has been corrected for μ^+ scattered into the walls of the target vessel.

[b]1 Torr = 133.3 Pa.

[c]Maximum amplitude not determined and thus only relative fractions can be found from the measured μSR amplitudes A_D and A_{Mu}.

[d]Selected values from ref. 30.

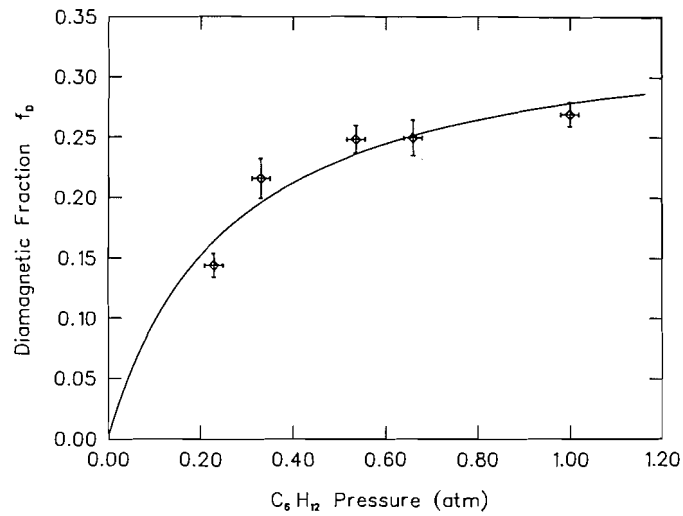

FIG. 2. The muon diamagnetic yield (f_D) in cyclohexane vapor as a function of total pressure. The solid line is a fit to a three-body model, as discussed in ref. 30.

4. Discussion

4.1 *Comparison of Mu* and T* yields in the alkanes*

In general, the extraction of reliable *absolute* total reaction yields from experimental data in hot tritium chemistry ($P = \Sigma_i P_i$) is not easily done since it is the *primary* reaction yield that is of interest, but the experimental (radiochromatographic) yields are obtained long after the reaction has ceased and complicated exchange processes may have occurred. Moreover, scavengers (e.g., Br_2, O_2) are invariably required in order to minimize the competition between hot and thermal tritons for specific reaction channels. As a result, often the yield of only one product (e.g. HT) is reliably determined and this is frequently given *relative* to some other yield, notably HT/RT yields in hydrocarbons. As a consequence, it is difficult to compare results from different laboratories and, in some cases, even to extract total yields from a given publication. Nevertheless, by examining a number of representative reports of both absolute yields and HT/RT ratios (21–27) one can hope to arrive at a reasonably reliable set of absolute T* yields with which the f_D values found in Mu* chemistry (Table 1) can be compared.

It is worth pointing out that two distinct advantages are

brought to the field of hot atom reactions by Mu chemistry: the μSR technique allows a *direct* interpretation of hot atom (ion) reactivity as manifest in the initial ($t = 0$) diamagnetic amplitudes A_D (and hence f_D, eq. [9]); and, moreover, truly thermal reactions can be distinguished from hot ones occurring at early times by the long (μs) time scale for *relaxation* of the μSR signal (eq. [8]), obviating the need for thermal scavengers. On the other hand, there is no possibility of clearly identifying individual diamagnetic product yields in muonium chemistry.

In analogy with hot tritium studies (7–9, 21–27), hot Mu atom reactivity with saturated hydrocarbon vapors (RH) can be described principally in terms of two reactions: abstraction ([10*a*]) and substitution (or displacement) ([10*b*])

$$\text{Mu}^* + \text{RH} \rightarrow \begin{cases} [10a] & (\text{MuH})^* + \text{R} \\ [10b] & (\text{MuR})^* + \text{H} \end{cases}$$

where the * indicates the possibility of forming translationally or rovibrationally excited product molecules, for which third-body collisions may be required to form a stable product. In hot tritium studies, the ratio of HT/RT yields exhibits a rather marked sensitivity to incident energy, pressure, moderator type, and to the nature of the hydrocarbon being attacked. Such a variation in reaction parameters can be expected to similarly affect the corresponding HMu/RMu yields.

There are two sources of moderator and (or) total pressure effects influencing the HT/RT yields in T* (Mu*) chemistry: translational excitation of (HT)* as a result of a high energy abstraction, and rovibrational excitation of (RT)* resulting from substitution reactions. In the case of translational excitation, light moderators (He) are very efficient at cooling, and hence result in a relative increase in HT yield, whereas heavy moderators (Xe) have the opposite effect, promoting dissociation of HT* and hence a reduction in yield (26, 35, 43). On the other hand, in those same studies it has been shown that for a range of moderators of mass comparable to that of the CH_3 group, such as Ne, there is little change in the HT/RT ratio; in addition, these ratios and the *total* yields are found to be essentially pressure independent for the alkanes up to $n = 4$ (21–26, 35). This is important for the present comparison of Mu* and T* reactivity in *pure* alkanes, since differences in measured yields can be construed as largely reflecting differences in hot atom reactivity rather than in moderation. Such a conclusion is consistent with recent studies of photochemically induced reactions in which only minor differences in the energy loss parameter α are found for different alkanes (7, 9). Moreover, these studies strongly indicate that *inelastic* effects dominate the energy loss process, as seen also in recoil tritium work in a variety of polyatomic moderators (26, 35, 43).

Although there is ample evidence that neither Mu* (Table 1 and refs. 28–30) nor T* (21–26, 44) yields are dramatically dependent on *total* pressure, in general some pressure dependence is expected, particularly for substitution reactions (eq. [10*b*]), depending on the level of residual excitation in the RT* (RMu*) product formed. In the hot tritium work there is a steady but modest increase in tritiated product yields related to (RT)* formation; typically ~30% increase for a factor of ~20 change in pressure up to ~3 atm (see, however, ref. 25). Analysis of these data in terms of RRK(M) theory indicates a broad distribution of excitation energies with a mean value of ~5 eV (23, 25, 26, 45, 46). A more dramatic change in yield with pressure is seen in the f_D values in Mu* chemistry in the heavier alkanes, which reach a constant yield asymptote at lower pressures (≲1 atm) than is typically seen in the T* data (Fig. 2 and ref. 30). This dependence suggests that the average excitation energy in the corresponding MuR* complex is lower (and also sharper) than in RT*, consistent with an expected reduced average energy for (substitution) reactions of hot muonium, since the initial (E_0) energy is so much less than in the case of hot tritium. The lack of any total pressure dependence in Mu* reactivity with the lighter alkanes (Table 1, ref. 30) suggests either relatively lower RMu* excitation energy, possibly due to their somewhat higher C—H bond energies (22, 47), or that H abstraction dominates for Mu*, unlike T* reactivity.

TABLE 2. Comparison of Mu* and T* hot atom yields in (primarily) alkane vapors

RH	$T^*(P)^{a,b}$	$T^*_{RH}/T^*_{CH_4}{}^c$	$Mu^*(f_D)^d$	$Mu^*_{RH}/Mu^*_{CH_4}{}^c$
N_2	—	—	0.16±0.03	1.3±0.3
CH_4	0.50	1.0	0.12±0.02	1.0±0.2
C_2H_6	0.65	1.3	0.19±0.02	1.6±0.2
C_3H_8	0.66	1.3	0.21±0.02	1.7±0.3
n-C_4H_{10}	0.68	1.4	0.21±0.02	1.8±0.3
i-C_4H_{10}	0.62	1.3	0.18±0.02	1.5±0.3
n-C_5H_{12}	0.69	1.4	0.15±0.02	1.3±0.2
n-C_6H_{14}	0.72	1.4	0.24±0.02	2.0±0.3
c-C_3H_8	0.84	1.7	—	—
c-C_5H_{10}	1.1	2.2	0.19±0.02	1.6±0.3
neo-C_5H_{12}	0.51	1.0	—	—
c-C_6H_{12}	1.2	2.4	0.25±0.02	2.1±0.3
TMS	—	—	0.20±0.02	1.7±0.3

[a]Absolute reaction probability (total yield) of T* reactions, determined from several sources, as discussed in the text.

[b]Estimated errors ±10% (or more) for the noncyclic alkanes and ±20% (or more) for the cyclanes, as discussed in the text.

[c]Ratio of measured yield to that found for CH_4.

[d]The experimental hot atom Mu* yields, from Table 1 this paper and from refs. 28–30.

Table 2 compares our best estimates of absolute T* yields (i.e., total reaction probabilities, P) for *unmoderated* alkane (RH) vapors (21–27) with the corresponding f_D values seen in Mu* chemistry. The Mu values for N_2 and tetramethylsilane (TMS) are also included. In all cases, the values given are meant to be *pressure-independent* yields, taken from average values of "high" (~1 atm) pressure asymptotes from the original references and the present study. The hot atom yields in Table 2 likely represent upper bounds. In T* chemistry there could be contributions from thermal reactions, although the data were invariably obtained in the presence of scavengers. In addition, some of the earlier T* yields may have been obtained using slightly incorrect recoil tritium ranges, which could result in reported yields being about 10% too large (48). An indication of the absolute error expected in the T* data can be seen from the values for the cyclanes given in the lower half of Table 2; since P should be ≤1, ±20% is probably a conservative overall error, although ±10% is often quoted in some of the original papers. In the subsequent comparison with the WE formalism we consider only the noncyclic alkanes.

In both T* and Mu* chemistry, the role played by hot *ion* reactions is not clear; any such contributions would tend to raise the observed hot (atom) yield. In μSR studies, the importance of molecular ions is established to date only in the rare gases (49) and they can be expected to be of some importance in molecular

gases as well. However, it is unlikely that a significant number of molecular ions could be stably formed at energies much above a few eV (where hot atom reactivity dominates). Moreover, in the case of the alkanes, which all have ionization potentials lower than that of Mu (or T), molecular ion formation has to compete with exothermic Mu (or T) formation by low energy charge exchange. Hence, it is probably reasonable to ignore the role of hot ions in both the Mu* and T* yields of Table 2. This conjecture is supported by recent theoretical calculations on hot tritium ions in CH_4 (33), where it is concluded that their effect on both the collision density (eq. [4]) and on the integrated yield is relatively minor (except at very high energies), and also by earlier work in He-moderated hot tritium reactions in hydrocarbon vapors (21, 26, 48). See also discussion in refs. 3, 4, and 32.

The results for diamagnetic (hot atom) yields given in Table 2 for both Mu* and T* reactions should also be examined in light of results on the failure of the "additivity rule" in proton electron capture cross sections (σ_{10}) in the alkanes (50). At proton energies of ~800 keV (which would correspond to ~90 keV μ^+) significant loss of neutral atom formation in the larger alkanes is seen, due to a concomitant increase in the electron stripping cross section (σ_{01}) as the H (or Mu) atom traverses a large alkane molecule. By extrapolating the trend in ref. 50 to the data in Tables 1 and 2, however, one would expect about 50% less Mu formation in hexane than in methane, implying a corresponding increase of about a factor of five in the diamagnetic fraction, f_D. Although the present data do exhibit this trend, what is observed is not nearly so dramatic a change. Moreover, it must be remembered that the Mu (or T) atom actually *stops* in the gas and so the effects reported in ref. 50 need to be averaged over a wide energy interval, particularly down to energies near k_BT, where electron loss cross sections are much smaller than at higher energies. It can also be assumed that any loss of Mu in the larger alkanes will affect T in the same way and hence the ratios of T*/Mu* yields discussed below will not be affected.

Despite the above uncertainties, it appears that the following general conclusions can be drawn from the original references, the data in Table 1 and the comparisons in Table 2: (*1*) For the noncyclic alkanes the trends relative to CH_4 are essentially the same for both Mu* and T* reactions; in particular, both reactions exhibit an essentially constant yield beyond ethane. (*2*) Both Mu* and T* reactions exhibit pressure-dependent yields in many of the hydrocarbons, notably in the case of c-pentane, c-hexane, hexane (and TMS) in the case of Mu* (see also ref. 30) and in ethane (25), c-butane (23, 45), and ethyl fluoride (44) in T* chemistry. (*3*) In all cases, the absolute Mu* (f_D) yields are smaller than the corresponding yields for T* (*P*) reactions. In the case of the noncyclic alkanes in particular, the Mu* yields are lower on average than the corresponding T* yields by a factor of about 3.5.

We conclude then that Mu* and T* reactions behave rather similarly in the *gas phase*, although this situation is in contrast to that seen in the *liquid* phase. As noted, in hot tritium chemistry, the yields seen in liquids are usually the same as those found from high pressure (~3 atm) values in the corresponding gas phase studies (22–24), whereas in Mu chemistry, diamagnetic fractions seen in liquids are typically 3–5 times larger than in the gas phase (15). As we have remarked in earlier publications (29, 30), this dramatic difference is strongly supportive of the contention that radiation-induced "spur effects" dominate the determination of observed muon fractions in condensed media (15). However, it should be kept in mind tha many-body effects can also play an important role; indeed significant changes are known to occur in charge changing cros sections between the gas and condensed phases (51), effect which may be related to the loss of neutral atoms referred t above in the case of proton charge exchange in the larger alkane (50).

TABLE 3. T*(Mu*) energy loss parameters, α_M[b]

RH	$\alpha_{rs}(Mu^*)$[b]	$\alpha_{rs}(T^*)$[b]	$\alpha_{ss}(T^*)$[c]
CH_4	0.0141	0.332	0.090
C_2H_6	0.0075	0.187	0.046
C_3H_8	0.0051	0.130	0.031
C_4H_{10}	0.0039	0.100	0.024
C_5H_{12}	0.0031	0.0811	0.020
C_6H_{14}	0.0026	0.0682	0.017
Ne	0.0112	0.272	0.035
Ar	0.0056	0.142	0.036

[a] α_M refers to the different (pure) moderators M in the table, for either T* or Mu*.
[b] Calculated from the rigid sphere approximation, eq. [3] in text.
[c] Calculated at 10 eV from intermolecular potentials using procedure of Estrup (52) and Belyaev *et al.* (53) as described in text.

4.2 *Reactivity integrals for Mu* and T* reactions in the alkanes*

In the WE theory of hot atom reactions the reactivity integral *I*, and the collisional energy loss parameter, α, are related to th measured hot atom yield by eq. [5]. For the comparison to b made here of Mu* and T* reactivity in *pure* alkanes, $f = 1$ (w also refer to these single component alkanes as "moderators") The experimental values for the reaction probabilities (yields are found in Table 2 for both T*(*P*) and Mu*(f_D) reactions. W now interpret these yields, for the noncyclic alkanes, in terms o the WE formalism.

Because the reaction yield in this formalism is given in term of the *ratio* I/α, some functional form of α must be assumed i order to arrive at a value for *I*, which is the more fundamenta quantity since it contains the reaction cross section of interes (eq. [6]). A common choice over the years has been to assum the rigid sphere values, α_{rs} (eq. [3]), for the energy los parameter. These values are given in Table 3 for both Mu* an T* colliding with the alkane moderators of Table 2; for refer ence, the corresponding values for Ne and Ar moderators ar also given. Table 3 also presents the value of α calculated fro "soft-sphere" intermolecular potentials (α_{ss}) at 10 eV from th calculations of Estrup (52) and Belyaev *et al.* (53) for moderator M = Ne, Ar, $H_2(D_2)$, and CH_4. For the other alkanes, the sam functional form as that used for CH_4 in ref. 52 is assumed. In th calculation of α (Table 3), the ss values depend on energy wit the rs (energy independent) limit being obtained at the lowes energies. However, at $\gtrsim$1 eV, the energy dependence in α_{ss} i relatively weak (52, 53), suggesting that photochemical an recoil T* studies and the present Mu* studies can be compare on the same basis.

From the α_M values (i.e., for moderator "M") given in Tabl 3, it is clear that considerable differences between different RH moderators should be expected. However, as previously referre to, this is decidedly not the case in hot tritium chemistry, where for example, beyond CH_4, the ratio α_M/α_{Ar} for M = C_2H_6 C_3H_8, and C_4H_{10} is essentially constant in both the ~1-e

TABLE 4. Calculated Mu* reactivity integrals in alkanes from the Wolfgang–Estrup formalism

RH	$I(T^*)^a$	$\alpha_M(T^*)^b$	$\alpha_M(Mu^*)^c$	$I(Mu^*)^d$	$I(T^*)/I(Mu^*)^e$
CH_4	0.70	1.0	0.70	0.089	7.9
C_2H_6	1.5	1.3	1.2	0.25	6.0
C_3H_8	2.1	1.9	1.8	0.42	5.0
n-C_4H_{10}	2.3	2.0	1.9	0.45	5.1
n-C_5H_{12}	~2.4[f]	2.1	2.0	0.33	~7.3[f]
n-C_6H_{14}	~2.5[f]	2.0	2.0	0.55	~4.5[f]

[a]Reactivity integrals for T* reactions obtained in a Ne moderator, taken from values given in ref. 21.
[b]Empirical value of α from eq. [5] for each alkane moderator M, using the T* reactivity integrals in column 2 and the experimental yields of Table 2.
[c]Determined from values of $\alpha_M(T^*)$ in column 3 and the definition $\alpha = \alpha_{rs} + \alpha_{inel}$, where α_{rs} is given in Table 3.
[d]Calculated reactivity integrals for Mu* from eq. [5] using the α_M values from column 4 and the experimental yields of Table 2. Estimated errors are ±30%.
[e]Ratio of reactivity integrals for T* (column 2)/Mu* (column 5).
[f]Extrapolated from trends in the lower mass alkanes.

photochemical T* study of ref. 7 and in the recoil T* study of ref. 21. This large discrepancy between the experimentally determined values for α_M and those expected from elastic scattering models are strongly supportive of the earlier suggestion that *inelastic* cross sections play a dominant role in determining the energy loss process in T* chemistry and, by extension, in Mu* chemistry as well.

Indeed, if one assumes pure elastic scattering, then $\alpha(Mu^*)/\alpha(T^*) \simeq m_{Mu}/m_T$ for both rigid sphere and soft sphere moderation, which means that the factor of 3.5 in the ratio of T*/Mu* yields in the pure alkanes of Table 2 would translate into a factor of $\gtrsim$100 enhancement in the reactivity integrals $I(T^*)/I(Mu^*)$. This does not seem reasonable. Not only do we expect T* and Mu* to undergo appreciable hot atom reactivity in the same energy region ($\lesssim$20 eV), but extrapolation of isotope effects on reactive cross sections in the eV range from classical trajectory studies on a variety of molecules (12, 16, 17) indicates that a ratio $I(T^*)/I(Mu^*) \lesssim 10$ should be expected. In the absence of any detailed dynamical studies of hot atom Mu reactivity, we propose here to use the WE model to empirically determine $\alpha_M(T^*)$ in each *pure* alkane M from the experimental hot tritium yields (Table 2) and the published reactivity integrals $I(T^*)$ determined in different inert moderators. These $\alpha_M(T^*)$ values are then used to calculate $\alpha_M(Mu^*)$ for each M, recognizing the importance of inelastic contributions. Since the largest elastic contribution comes from the rigid sphere value, we adopt the definition

[11] $$\alpha = \alpha_{rs} + \alpha_{inel}$$

and determine α_{inel} from the T* data.

In general, $I(T^*)$ is obtained from kinetic plots of reaction yields vs. moderator mole fraction (eq. [7]) and thus its value depends on the choice of moderator. The most complete data have been obtained for CH_4, C_2H_6, C_3H_8, and C_4H_{10} (21) in different noble gas moderators, from which the extracted reactivity integrals for each alkane are found to differ by $\approx \pm 30\%$, on average. This can be taken as a measure of error in the procedure to extract $I(Mu^*)$ in comparison with the $I(T^*)$ values for each alkane. For the purposes of comparison, though, we adopt the value of $I(T^*)$ determined in a Neon moderator from ref. 21 since, as previously noted, the moderating efficiency of Ne is comparable to that of the CH_3 group in each alkane (26, 35, 43). The values for $I(T^*)$ are given in Table 4; those for pentane and hexane have not been reported, to our knowledge, so the values given are extrapolated from the lower mass alkanes. Using these values and those for the pure alkane yields from Table 2 in eq. [5] gives the results shown in the 3rd column of Table 4 for $\alpha_M(T^*)$. As expected, these show little variation with mass compared to the rigid sphere values (7, 9, 26, 35) and, moreover, exhibit the opposite trend; the value for CH_4 is also consistent with that determined by Seewald and Wolfgang in unmoderated methane (21). Correcting for $\alpha_{rs}(T^*)$ using the values in Table 3 in eq. [11] yields the corresponding values for $\alpha_{inel}(T^*)$.

A question now of considerable importance is: how different is α_{inel} likely to be for Mu* and T* slowing down in the alkane moderators? In general, one expects nonresonant vibrational relaxation of at least small molecules to be enhanced by light atoms (Mu), but relaxation of rotational levels to be enhanced for heavier atoms (T) (54); on the other hand, vibrational excitation due to strongly attractive potentials is expected to depend directly on the mass (1, 55). In addition, the transfer of incident translational energy to translational–rotational energy in the exit channel can depend both on the incident energy and the target molecule (10). We will simply assume here that α_{inel} is the *same* for both Mu* and T*, averaged over their respective energy intervals. In practice, then, from eq. [11], $\alpha_M(Mu^*) = \alpha_{inel}(T^*)$ for the RH moderators of Table 4 since $\alpha_{rs}(Mu^*)$ is too small (Table 3) in every case. The values for $\alpha_M(Mu^*)$ determined in this way for each of the alkane moderators M are given in column 4 of Table 4. These values are then used in conjunction with the experimental Mu* yields (Table 2) to find the corresponding reactivity integrals $I(Mu^*)$ from eq. [5], as given in column 5.

The reactivity integrals determined in this way for Mu* reactions mirror the trend seen to increasing reactivity with increasing numbers of C—H bonds in the corresponding $I(T^*)$ values, both exhibiting the saturation apparent in the yields themselves beyond ethane. It is apparent that beyond ethane (or even methane) the excitation functions for T*(Mu*) reactions in the alkanes do not display any pronounced intrinsic dependence on structure and (or) on the number of carbon atoms, consistent with model calculations (35, 46, 56) of hot tritium reactivity.

The last column in Table 4 gives the ratio of $I(T^*)/I(Mu^*)$, the overall average of which is ~6:1. If the reactive cross sections are assumed constant over a common energy interval, then $\sigma(T^*)$ would be larger than $\sigma(Mu^*)$ by this same factor (eq. [6], ref. 37). It should be kept in mind, however, that the data

have been viewed within the framework of the WE theory, a formalism that is constantly being called into question (37, 43). In addition, several simplifying assumptions have been made, the most suspect of which is likely the assumption that the dominant *inelastic* contributions to the slowing-down processes are the same for both hot muonium and hot tritium. The calculated ratios are certainly sensitive to this assumption, as can be seen by arbitrarily weighting the inelastic (or elastic) contribution differently for Mu* and T* moderation. For example, if we define $\alpha_{inel}(Mu^*) = 2\alpha_{inel}(T^*)$, then the ratio $I(T^*)/I(Mu^*)$ is simply reduced by approximately this same factor; conversely, if the opposite weighting is assumed, the ratio is correspondingly increased by a factor of two. Differences of a factor of five or so in the number of collisions required to moderate Mu* vs. T* atoms are probably reasonable. Clearly one cannot state with any confidence what the absolute reactivity integrals (or cross sections) are for hot muonium (or hot tritium) reactivity in the absence of more detailed theoretical guidance.

The present comparison of Mu* and T* reactivity in the alkanes represents, in fact, the first time that there has been a wide enough variation in isotopic mass to "test", in principle, dynamical models of hot atom reactivity. Unfortunately, the record to date on the success of direct theoretical calculations of $I(T^*)$ from specific excitation functions generated on a particular potential energy surface, in comparison with hot tritium results, is poor (18, 43). In Raff's calculation on methane (18), for example, the theoretical value for $I(T^*)$ is about a factor of 10 too low, although the ratio of HT/RT yields is well predicted. In general, this lack of success likely reflects a combination of poorly known potential surfaces at high energies and errors in the calculation of the collisional density $n(E)dE$, rather than in the dynamics themselves, which can presumably be accurately treated classically. It may be, moreover, that inaccuracies in the nature of the potential surface for a given reaction would cancel in the *ratio* of $I(T^*)/I(Mu^*)$, thus allowing a theoretical calculation of the corresponding collisional density and hence the reaction cross section. No calculation of this nature has yet been reported.

The only calculation to date of an excitation function comparing Mu* and T* over a wide enough energy range is the current work of Connor *et al.* on the $Mu^*(T^*) + F_2$ reaction (12), in which the same potential surface that was successfully utilized in calculations of *thermal* reaction rates (13) is employed. Although this surface is likely quite incorrect at high energies for the HF_2 system, and, moreover, cannot be expected to mirror the alkane systems of Table 4, it is interesting to note that an evaluation of eq. [6] with their excitation function gives ~2.5 for the ratio $I(T^*)/I(Mu^*)$, suggesting that the slowing down processes for Mu* are more efficient than for T*. It is hoped that the present results comparing hot Mu chemistry with hot tritium chemistry in the alkanes will stimulate further theoretical calculations.

5. Summary

In this paper we have compared the hot atom reactions of muonium (Mu*) on the alkane vapors, C_nH_{2n+2} (n = 1–6), with those determined elsewhere (7–9, 21–27) for hot tritium (T*) reactivity on these same alkanes. The corresponding experimental yields (Table 2) are found to be in the ratio $T^*(P)/Mu^*(f_D) \sim 3.5{:}1$, essentially independent of n; moreover, within experimental error (~±30%), they exhibit the same trend with increasing n, both showing a saturation effect in total yield beyond ethane. This kind of similarity and consistency in hot muonium and hot tritium yields in alkane vapors strongly supports our contention that the same reactions (eq. [10]), over comparable energy intervals are being seen by both Mu* and T*, and the factor of ~3.5 difference in their yields is a manifestation of dynamical mass effects on hot atom reactivity. Although it may seem surprising that the marked difference of a factor of 27 in isotopic mass between muonium and tritium should be reflected in only a factor of ~3.5 in total yields (indeed, differences in *thermal* rate constants between H and Mu are frequently much greater than this (11–15)), it must be remembered that the hot atom yield reflects a competition between moderating collisions, which are primarily nonreactive, and reactive (hot atom) collisions, during the slowing down process.

The measured yields of both Mu* and T* reactions in the alkanes have been interpreted within the framework of the Wolfgang–Estrup (WE) theory (3–5), in which the hot atom yield (P) of eq. [5] is defined in terms of two quantities: the reactivity integral "I" (eq. [6]) and the energy-loss parameter "α" (f = 1 in the present study of pure alkane moderators). Despite the continuing questions about the validity of this formalism (37, 43) recently brought into focus by current theories in which the explicit time dependence of the rate equations for the slowing down process is considered (37–39), the WE theory still remains the only easily tractable procedure for the interpretation of experimental hot atom yields, a role it has played for over 20 years now. In our analysis, we have observed that α is dominated by inelastic scattering effects, and moreover we have assumed that $\alpha_{inel}(Mu^*) = \alpha_{inel}(T^*)$, the latter determined from experimental hot tritium yields (eq. [11] and Table 4). With this assumption, the ratio of reactivity integrals $I(T^*)/I(Mu^*)$ is ~6:1 for the alkanes, from methane to n-hexane (Table 4). As emphasized in the text, the WE formalism makes no a priori prediction of either I (or equivalently, the excitation function, $\sigma(E)$) or of α, both being essentially model-dependent parameters in the theory; indeed, if we assume that inelastic moderation is more (or less) efficient for Mu* compared to T* (e.g., by a factor of 2), then the ratio $I(T^*)/I(Mu^*)$ changes accordingly.

Nevertheless, despite the uncertainties inherent in the WE formalism used and hence in our analyses of the T* and Mu* data carried out, the present study of these reactions represents the *first* time that the hot atom yields of two isotopes of such enormously differing masses have been carried out on the same (alkane) systems. It is hoped that the results will stimulate more detailed calculations of dynamical mass effects for hot atom reactivity, on the alkanes or on related systems (16–18). Some progress along these lines is currently underway (12).

Acknowledgements

One of us (D.G.F.) would like to thank Dr. Ian W. M. Smith and the Physical Chemistry Laboratory at Cambridge University for their hospitality during a three-month stay in 1984. D.G.F. would also like to thank the John Simon Guggenheim Foundation and the Scientific Council of NATO for their financial support during a sabbatical year abroad. The continuing research support of NSERC (Canada) is also gratefully acknowledged. Finally, we would like to thank Professors B. Shizgal, University of British Columbia, E. Mason, Brown University, and B. Rabinovitch, University of Washington, for their helpful comments concerning the theory of hot atom reactivity.

1. R. B. BERNSTEIN (*Editor*). Atom molecule collision theory, a guide for the experimentalist. Plenum Press, New York. 1979. p. 1; R. D. LEVINE and R. B. BERNSTEIN. Molecular reaction dynamics. Oxford Press, U.K. 1974.
2. M. FAUBEL. Adv. At. Mol. Phys. **19**, 345 (1983); M. FAUBEL, K. H. KOHL, J. P. TOENNIES, and F. A. GIANTURCO. J. Chem. Phys. **78**, 5629 (1983); G. O. ESTE, G. KNIGHT, and G. SCOLES. Chem. Phys. **35**, 421 (1978).
3. T. MATSUURA (*Editor*). Hot atom chemistry, recent trends and applications in the physical and life sciences. Kodansha Ltd. Elsevier, Tokyo. 1984.
4. D. S. URCH. MTP Int. Rev. Sci. Inorg. Chem. Series 1, **8**, 149 (1972); R. WOLFGANG. Prog. React. Kinet. **3**, 97 (1965); R. WOLFGANG. Ann. Rev. Phys. Chem. **16**, 15 (1965); R. WOLFGANG. J. Chem. Phys. **39**, 2983 (1963); P. J. ESTRUP and R. WOLFGANG. J. Am. Chem. Soc. **82**, 2661 (1960); **82**, 2665 (1960).
5. D. J. MALCOME-LAWES. J. Chem. Phys. **57**, 2476 (1972); **57**, 2481 (1972).
6. F. S. ROWLAND. *In* Molecular beams and reaction kinetics; hot atom chemistry. Vols. I, II. Academic Press, New York. 1970. pp. 108–138.
7. G. A. OLDERSHAW and A. SMITH. J. Chem. Soc. Faraday Trans. 1, **74**, 1687 (1978); D. GRIEF and G. OLDERSHAW. J. Chem. Soc. Faraday Trans. 2, **78**, 1211 (1982); G. A. OLDERSHAW. Gas kinetics and energy transfer. Spec. Period. Rep. Chem. Soc. London, Vol. 2. 1977. p. 96.
8. C. C. CHOU, T. SMAIL, and F. S. ROWLAND. J. Am. Chem. Soc. **91**, 3104 (1969); C. C. CHOU and F. S. ROWLAND. J. Am. Chem. Soc. **88**, 2612 (1966).
9. P. VIDAUD, R. D. FINK, and J. E. NICHOLAS. J. Chem. Soc. Faraday Trans. 1, **75**, 1619 (1979).
10. J. C. POLANYI and N. SATHYAMURTHY. Chem. Phys. **37**, 259 (1979), and references therein; J. C. POLANYI. Acc. Chem. Res. **5**, 161 (1972).
11. D. M. GARNER, D. G. FLEMING, and R. J. MIKULA. Chem. Phys. Lett. In press; D. G. FLEMING. Proc. of XII Int. Conf. on Physics of Electronic and At. Collision (ICPEAC). *Edited by* S. Datz. North Holland, Amsterdam. 1982. p. 297; D. G. FLEMING, D. M. GARNER, and R. J. MIKULA. Hyperfine Interact. **8**, 337 (1981).
12. J. N. L. CONNOR, C. J. EDGE, and A. LAGANA. Mol. Phys. **46**, 1231 (1982).
13. J. N. L. CONNOR, W. JAKUBETZ, A. LAGANA, J. MANZ, and J. C. WHITEHEAD. Chem. Phys. **65**, 29 (1982); J. N. L. CONNOR. Hyperfine Interact. **8**, 423 (1981); J. N. L. CONNOR, W. JAKUBETZ, and J. MANZ. Chem. Phys. **28**, 219 (1978).
14. B. C. GARRETT and D. G. TRUHLAR. J. Chem. Phys. **81**, 309 (1984); N. C. BLAIS, D. G. TRUHLAR, and B. C. GARRETT. J. Chem. Phys. **78**, 2363 (1983).
15. P. W. PERCIVAL. Radiochim. Acta, **26**, 1 (1979); D. C. WALKER. J. Phys. Chem. **85**, 3960 (1981); Y. C. JEAN, B. W. NG, J. H. BREWER, D. G. FLEMING, and D. C. WALKER. J. Phys. Chem. **85**, 451 (1981); D. C. WALKER. *In* Muon and muonium chemistry. Cambridge Univ. Press, U.K. 1983; P. W. PERCIVAL, J. C. BRODOVITCH, and K. E. NEWMAN. Hyperfine Interact. **17–19**, 721 (1984).
16. R. N. PORTER. J. Chem. Phys. **45**, 2284 (1966); R. WOLFGANG. Acc. Chem. Res. **2**, 248 (1969); R. N. PORTER and S. KUNT. J. Chem. Phys. **52**, 3240 (1970); D. J. MALCOME-LAWES. J. Chem. Soc. Faraday Trans. 2, **71**, 1183 (1975); J. S. WRIGHT, S. K. GRAY, and R. N. PORTER. J. Phys. Chem. **83**, 1033 (1979).
17. D. J. MALCOME-LAWES. J. Chem. Soc. Faraday Trans. 2, **74**, 182 (1977).
18. L. M. RAFF. J. Chem. Phys. **60**, 2220 (1973); D. L. BUNKER and D. PATTENGILL. J. Chem. Phys. **53**, 3041 (1970).
19. N. C. BLAIS and D. G. TRUHLAR. Chem. Phys. Lett. **102**, 120 (1983); H. R. MAYNE and J. P. TOENNIES. J. Chem. Phys. **75**, 1794 (1981); N. C. BLAIS, D. G. TRUHLAR, and B. C. GARRETT. J. Chem. Phys. **76**, 2768 (1982).
20. R. GÖTTING, H. R. MAYNE, and J. P. TOENNIES. J. Chem. Phys. **80**, 2230 (1984); G. KWEI and V. W. S. LO. J. Chem. Phys. **72**, 6265 (1980); R. GEGENBACH, CH. HAHN, and J. P. TOENNIES. J. Chem. Phys. **62**, 3620 (1975).
21. R. T. K. BAKER, M. SILBERT, and R. WOLFGANG. J. Chem. Phys. **52**, 1120 (1970); D. SEEWALD and R. WOLFGANG. J. Chem. Phys. **47**, 145 (1967).
22. E. TASCHIKAWA and F. S. ROWLAND. J. Am. Chem. Soc. **90**, 4767 (1968); E. K. C. LEE and F. S. ROWLAND. J. Am. Chem. Soc. **84**, 3085 (1962).
23. E. K. C. LEE and F. S. ROWLAND. J. Am. Chem. Soc. **85**, 897 (1963).
24. J. W. ROOT, W. BRECKENRIDGE, and F. S. ROWLAND. J. Chem. Phys. **43**, 3694 (1965).
25. D. J. MALCOME-LAWES. J. Chem. Soc. Chem. Commun. 146 (1973); A. J. JOHNSTON, D. J. MALCOME-LAWES, D. S. URCH, and M. J. WELCH. J. Chem. Soc. Chem. Commun. 187 (1966).
26. T. K. BAKER and D. J. MALCOME-LAWES. J. Chem. Soc. Faraday Trans. 1, **69**, 928 (1973); **69**, 1858 (1973); D. J. MALCOME-LAWES. J. Chem. Soc. Chem. Commun. 1285 (1972).
27. R. B. HALL and D. J. MALCOME-LAWES. J. Chem. Soc. Faraday Trans. 1, **70**, 648 (1974).
28. D. G. FLEMING, R. J. MIKULA, and D. M. GARNER. Phys. Rev. A, **26**, 2527 (1982); R. J. MIKULA. Ph.D. Thesis, University of B.C. 1980.
29. D. G. FLEMING, D. J. ARSENEAU, D. M. GARNER, M. SENBA, and R. J. MIKULA. Hyperfine Interact. **17–19**, 655 (1984).
30. D. J. ARSENEAU, D. M. GARNER, M. SENBA, and D. G. FLEMING. J. Phys. Chem. **88**, 3688 (1984); D. J. ARSENEAU. M.Sc. Thesis, Univ. of B.C. 1984.
31. H. TAWARA. At. Data Nucl. Data Tables, **22**, 491 (1978); L. H. TOBUREN, M. Y. NAKAI, and R. A. LANGLY. Phys. Rev. **171**, 114 (1968).
32. M. MENZINGER, R. L. LEROY, and A. J. XENCHA. J. Phys. Chem. **76**, 2937 (1972); E. TACHIKAWA and D. S. URCH. *In* Hot atom chemistry, recent trends and applications in the physical and life sciences. *Edited by* T. Matsuura. Elsevier, Tokyo. 1984. p. 33; M. MENZINGER and R. WOLFGANG. J. Chem. Phys. **50**, 2991 (1969); D. S. URCH and R. L. WOLFGANG. J. Am. Chem. Soc. **83**, 2982 (1961).
33. T. VALENCICH. Chem. Phys. Lett. **104**, 620 (1984).
34. S. ARONOWITZ, S. CHANG, and T. SCATTERGOOD. J. Phys. Chem. **85**, 360 (1981).
35. D. J. MALCOME-LAWES. J. Chem. Soc. Faraday Trans. 2, **68**, 1613 (1972); **68**, 2051 (1972); P. J. KUNTZ, E. M. NEMETH, J. C. POLYANI, and W. H. WONG. J. Chem. Phys. **52**, 4654 (1970).
36. D. J. MALCOME-LAWES. J. Chem. Soc. Faraday Trans. 2, **73**, 1222 (1977); J. Chem. Phys. **56**, 3442 (1972).
37. B. SHIZGAL. J. Chem. Phys. **74**, 1401 (1981).
38. B. SHIZGAL and J. M. FITZPATRICK. J. Chem. Phys. **72**, 3143 (1980); B. SHIZGAL. J. Chem. Phys. **72**, 3156 (1980).
39. K. D. KNIERIM, S. L. LIN, and E. A. MASON. J. Chem. Phys. **75**, 1159 (1981); M. G. PRISANT, W. M. OLLISEN, and R. J. CROSS. J. Chem. Phys. **69**, 4797 (1978); K. KOURA. J. Chem. Phys. **65**, 3883 (1976); J. KEIZER. J. Chem. Phys. **56**, 5958 (1972); **58**, 4524 (1973).
40. A. E. PIFER, T. BOWEN, and K. R. KENDALL. Nucl. Instrum. Methods, **135**, 39 (1976).
41. E. RODUNER, P. W. PERCIVAL, D. G. FLEMING, J. HOCHMANN, and H. FISCHER. Chem. Phys. Lett. **57**, 37 (1978); E. RODUNER. *In* Exotic atoms 79: fundamental interaction and structure of matter. *Edited by* K. Crowe, J. Duclos, G. Forentini, and G. Tovelli. Plenum Press, New York. 1980. p. 379; E. RODUNER. Hyperfine Interact. **8**, 561 (1981).
42. R. E. TURNER and M. SENBA. Hyperfine Interact. **17–19**, 697 (1984); R. E. TURNER and M. SENBA. Phys. Rev. A, **29**, 2541 (1984).
43. D. J. MALCOME-LAWES. *In* Hot atom chemistry, recent trends and

applications in the physical and life sciences. *Edited by* T. Matsuura. Elsevier, Tokyo. 1984. p. 39.
44. Y. N. TANG, E. C. WU, J. W. ANDERTON, and R. R. CLARK. J. Chem. Phys. **79**, 2181 (1983).
45. L. J. FERRO and L. D. SPICER. J. Chem. Phys. **69**, 4335 (1978).
46. L. D. SPICER. J. Chem. Soc. Faraday Trans. 2, **74**, 527 (1977); L. D. SPICER and B. S. RABINOVITCH. Ann. Rev. Phys. Chem. **21**, 349 (1970).
47. R. C. WEAST (*Editor*). CRC Handbook of Chemistry and Physics. 55th ed. CRC Press, Cleveland, OH. 1975. p. F-213.
48. D. J. MALCOME-LAWES. J. Chem. Soc. Faraday Trans. 1, **76**, 860 (1980).
49. D. G. FLEMING, R. J. MIKULA, M. SENBA, D. M. GARNER, and D. J. ARSENEAU. Chem. Phys. **82**, 75 (1983).
50. G. BISSINGER, J. M. JOYCE, G. LAPICKI, R. LAMBERT, and S. L. VARGHEJE. Phys. Rev. Lett. **49**, 318 (1982).
51. C. J. WOODS, C. J. SOFIELD, M. E. B. COWAN, M. MURRELL, and J. DRAPERT. J. Phys. B, **17**, 867 (1984).
52. P. J. ESTRUP. J. Chem. Phys. **41**, 164 (1964); R. M. FELDER and M. D. KOSTIN. J. Chem. Phys. **43**, 3082 (1965).
53. YU. N. BELYAEV, N. V. KAMYSHOV, and V. B. LEONAS. Khim. Vys. Energ. **4** (1970); Engl. Transl., High Energy Chem. USSR, **4**, 224 (1970).
54. G. XIAO and X. ZHU-DE. Chem. Phys. Lett. **98**, 563 (1983); G. D. BILLING and D. C. CLARY. Chem. Phys. **80**, 213 (1983); D. C. CLARY. Chem. Phys. **65**, 247 (1982); G. D. BILLING and D. C. CLARY. Chem. Phys. Lett. **90**, 27 (1982); M. HUETZ-AUBERT, G. LOUIS, and J. TAINE. Physica C, **93**, 237 (1978).
55. C. R. QUICK, JR., R. E. WESTON, JR., and G. W. FLYNN. Chem. Phys. Lett. **83**, 15 (1981); S. DATTA, R. E. WESTON, JR., and G. W. FLYNN. J. Chem. Phys. **80**, 4071 (1984).
56. R. L. LEROY, A. J. YENCHA, M. MENZINGER, and R. WOLFGANG. J. Chem. Phys. **58**, 1741 (1973).

The one- and two-electron reduction of 2-thioriboflavin by radical anions of CO_2 and dithiothreitol

PARMINDER S. SURDHAR AND DAVID A. ARMSTRONG
Department of Chemistry, University of Calgary, Calgary, Alta., Canada T2N 1N4
AND
VINCENT MASSEY
Department of Biological Chemistry, University of Michigan, Ann Arbor, Michigan, U.S.A

Received June 25, 1985

PARMINDER S. SURDHAR, DAVID A. ARMSTRONG, and VINCENT MASSEY. Can. J. Chem. **64**, 67 (1986).

The one- and two-electron reductions of 2-thioriboflavin with $\cdot CO_2^-$ and cyclic disulphide anion of dithiothreitol ($DS_2^-\cdot$) have been studied by the steady state γ and pulse radiolysis techniques. The $\cdot CO_2^-$ radical reacted with 2-thioriboflavin to give the neutral semiquinone ($\cdot$FlH) and the radical anion ($\cdot Fl^-$) at pH 5 and 10 respectively. The pK of the $\cdot$FlH radical was determined to be 7.4. In the case of the anion, the 2-thioriboflavin spectrum is similar in shape to that of FAD radical anion, but red shifted by 40–50 nm. Red shifts are also seen in the neutral $\cdot$FlH form for the 370-nm peak and 580-nm shoulder. However, in addition, there is strong enhancement of the absorbance at 500 nm. The spectrum of 2-thioriboflavin semiquinone produced in the presence of 2–5 mM dithiothreitol was perturbed, as was observed previously for unsubstituted flavin semiquinones in the presence of sulphydryls. The rate constants for the initial one-electron reduction step viz: [5] $Fl + \cdot CO_2^- \rightarrow \cdot Fl^- + CO_2$ were $4.0 \pm 0.5 \times 10^9\ M^{-1}\ s^{-1}$ and $1.3 \pm 0.2 \times 10^9\ M^{-1}\ s^{-1}$ at pH 7 and 10 respectively. The corresponding rate for the reaction of $DS_2^-\cdot$ with 2-thioriboflavin at pH 7 was determined to be $2.4 \pm 0.2 \times 10^9\ M^{-1}\ s^{-1}$. The continuous production of $DS_2^-\cdot$ radicals by γ radiolysis reduced 2-thioriboflavin to the dihydro form, and the flavin was regenerated on the addition of air. The $\cdot CO_2^-$ radical also effected a two-electron reduction. However, in this case, if the process was taken beyond the equivalence point, the dihydroflavin spectrum was bleached and the oxidized flavin could not be recovered.

PARMINDER S. SURDHAR, DAVID A. ARMSTRONG et VINCENT MASSEY. Can. J. Chem. **64**, 67 (1986).

Faisant appel aux techniques de la radiolyse γ de l'état stationnaire et de la radiolyse pulsée, on a étudié les réductions à 1 et à 2 électrons de la thio-2 riboflavine avec le $\cdot CO_2^-$ et l'anion cyclique disulfuré du dithiothréitol ($DS_2^-\cdot$). Le radical $\cdot CO_2^-$ réagit avec la thio-2 riboflavine pour donner la semiquinone neutre ($\cdot$FlH) et l'anion radicalaire ($\cdot Fl^-$) à des pH respectifs de 5 et de 10. Le pK du radical $\cdot$FlH est égal à 7,4. Dans le cas de l'anion, la forme du spectre de la thio-2 riboflavine est semblable à celle de l'anion radicalaire du FAD mais les bandes sont déplacées vers le rouge par environ 40–50 nm. Dans le cas de la forme neutre du $\cdot$FlH, on observe également un déplacement vers le rouge du pic à 370 et de l'épaulement à 580 nm. Mais, il y a de plus une forte augmentation de l'absorption à 500 nm. Le spectre de la semiquinone de la thio-2 riboflavine produite en présence de 2–5 mM dithiothréitol est perturbé par rapport à ce qui a été observé précédemment dans le cas des semiquinones de la flavine non substituée en présence de sulphydryles. Les constantes de vitesse de l'étape initiale de la réduction à l'électron [5] $Fl + \cdot CO_2^- \rightarrow \cdot Fl^- + CO_2$ sont respectivement de $4,0 \pm 0,5 \times 10^9\ M^{-1}\ s^{-1}$ et de $1,3 \pm 0,2 \times 10^9\ M^{-1}\ s^{-1}$ à des pH respectifs de 7 et de 10. La vitesse correspondante de la réaction $DS_2^-\cdot$ avec la thio-2 riboflavine à un pH de 7 est de $2,4 \pm 0,2 \times 10^9\ M^{-1}\ s^{-1}$. La production continue de radicaux $DS_2^-\cdot$ par radiolyse γ réduit la thio-2 riboflavine en la forme dihydro et l'addition d'air permet de regénérer la flavine. Le radical $\cdot CO_2^-$ permet également une réduction à 2 électrons. Mais dans ce cas, si on considère la réaction en déça du point d'équivalence, la coloration du spectre de la dihydroflavine disparaît et il n'est pas possible de récupérer la flavine oxydée.

[Traduit par le journal]

Introduction

Chemically modified flavins (Fl)[1] have been used successfully in recent years as probes of reaction mechanisms and of the protein environment around the bound flavin in a number of flavoproteins (1–4). In most cases the modified flavins have quite different absorption spectra, pKs, and redox potentials from their normal counterparts FAD or FMN. This also applies to the one-electron reduced semiquinone forms: $\cdot FlH/\cdot Fl^-$. Studies of the spectra of these semiquinone forms in the protein is an additional source of information on the immediate environment of the flavin and on the interactions with protein residues that may serve to stabilize it. For these reasons it is important to have as a reference the spectrum of the uncomplexed semiquinone forms of the modified flavins in aqueous solution.

This investigation is concerned with the formation and spectra of the semiquinone forms of 2-thioriboflavin, which has found use in several recent studies (1, 4). The experiments were performed by the pulse radiolysis technique (5), which was also utilized in earlier examinations of flavin semiquinones (6–9). The reducing radicals $\cdot CO_2^-$ and $DS_2^-\cdot$ (the radical of dithiothreitol, see reaction [4] below and footnote 1), were produced by the well-established sequence of reactions (5, 10):

[1] $4.2H_2O \rightsquigarrow 2.7e_{aq}^- + 0.6\cdot H + 2.8\cdot OH + 2.7H^+ + 0.5H_2 + 0.7H_2O_2$

[2] $e_{aq}^- + N_2O + H_2O \rightarrow OH^- + \cdot OH + N_2$

[3] $\cdot OH\ (\text{or}\ \cdot H) + HCO_2^- \rightarrow H_2O\ (\text{or}\ H_2) + \cdot CO_2^-$

[4] $\cdot OH\ (\text{or}\ \cdot H) + D(SH)_2 \rightarrow DS_2^-\cdot + H_2O\ (\text{or}\ H_2) + H^+$

Suitable concentrations of $D(SH)_2$ and formate were chosen so that the time scale of reactions [1]–[4] was much shorter ($\leqq 10^{-7}$ s) than that for the reaction of Fl with primary radicals e_{aq}^-, $\cdot H$, and $\cdot OH$. The Secondary radicals, $\cdot CO_2^-$ and $DS_2^-\cdot$,

[1]Abbreviations: Fl, flavin; $\cdot$FlH, flavin semiquinone; $\cdot Fl^-$, flavin semiquinone anion; FlH_2, dihydroflavin; FlH^-, dihydroflavin anion; LFl, lumiflavin; FAD, flavin adenine dinucleotide; FMN, flavin mononucleotide; $D(SH)_2$, reduced dithiothreitol; DS_2, oxidized dithiothreitol; $DS_2^-\cdot$, radical anion of dithiothreitol.

reacted with Fl on a ~10-μs time scale:

[5] $Fl + \cdot CO_2^- \rightarrow \cdot Fl^- + CO_2$

[6]/[−6] $\cdot FlH \rightleftarrows \cdot Fl^- + H^+$

[7] $Fl + DS_2^- \cdot \rightarrow \cdot Fl^- + DS_2$

Low dose rate "steady state" radiolysis experiments were also conducted with a Co^{60} γ source to establish that the final product formed by these reductions was the dihydroflavin FlH_2 (11).

Experimental

Materials

Dithiothreitol was from the Sigma Chemical Co. All other chemicals were the purest available grade and were used as supplied. The water for preparing solutions was redistilled, first from alkaline permanganate and then from acid dichromate (10).

Apparatus and procedures

All experiments were conducted at room temperature (24 ± 2°C) with solutions containing 10 m*M* phosphate buffer. In order to prevent its oxidation by air, solutions requiring dithiothreitol $D(SH)_2$ were prebubbled with nitrous oxide, which had been passed through a column of Ridox (Fisher Scientific Co.). The pH was finally adjusted by adding $HClO_4$ or NaOH.

The γ irradiations were performed in an A.E.C.L. ^{60}Co "gamma cell" with a steady dose rate of ~10 Gy/min. The precise dose rate was checked with a Fricke dosimeter (10) and corrections were made routinely for the natural decay of the isotope. The procedures were as described by Ahmad and Armstrong (11).

The pulse radiolysis experiments were performed by utilizing 2-μs pulses of electrons with a dose of 2–4 Gy/pulse from the 1.5-MeV Van de Graaff generator. Details of the generator and dosimetry have been described earlier (12).

Values of ΔA, the change in absorption per unit dose observed at a given time after the radiation pulse, were converted to [ε(Fl Radical) − ε(Fl)] at each wavelength by dividing ΔA by the concentration of radicals produced per kilogray. Values of ε(Fl Radical) at different pHs were then obtained by adding the appropriate values of ε(Fl). The values of ε(Fl, 490 nm) were taken to be 21 000 and 19 100 at pH 7 and 10 respectively (1).

Results and discussion

Pulse radiolysis

The changes in absorption produced by the reaction of $\cdot CO_2^-$ with 10–14 μ*M* 2-thioriboflavin at pH 5 at 80 μs after the irradiation pulse are plotted as a function of wavelength in Fig. 1. A typical oscilloscope trace illustrating the loss of absorbance at 490 nm with time can be seen in the top inset. The absolute spectra of the radicals at pH 5 and 10 were calculated from the changes in absorbance as described above. They have been presented in Figs. 2(a) and (b) (solid lines). Each spectrum has been based on at least two sets of experimental points.

The main features of the spectrum at pH 5 were a minimum at 420 nm, maxima at 360 and 500 nm, and a broad shoulder at about 620 nm. The spectrum at pH 10 showed a much stronger peak at 400 nm and a maximum at 510 nm. Above 540 nm the absorption tailed off and the shoulder at 620 nm was absent. The inset in Fig. 2(a) shows the absorbance coefficient of the radical at 580 nm as a function of pH. The curve through the points has been calculated for a p*K* of 7.4. This p*K* is attributed to the ionization of the radical in reaction [6], and may be compared to the p*K* of the radical of riboflavin, which is 8.3 (6). The lower value observed for 2-thioriboflavin is in accord with a similar lowering of the p*K* of the fully reduced form to 5.2,[2] which can be compared with the value of 6.5 for riboflavin (14).

The spectra of the neutral form of lumiflavin semiquinone and

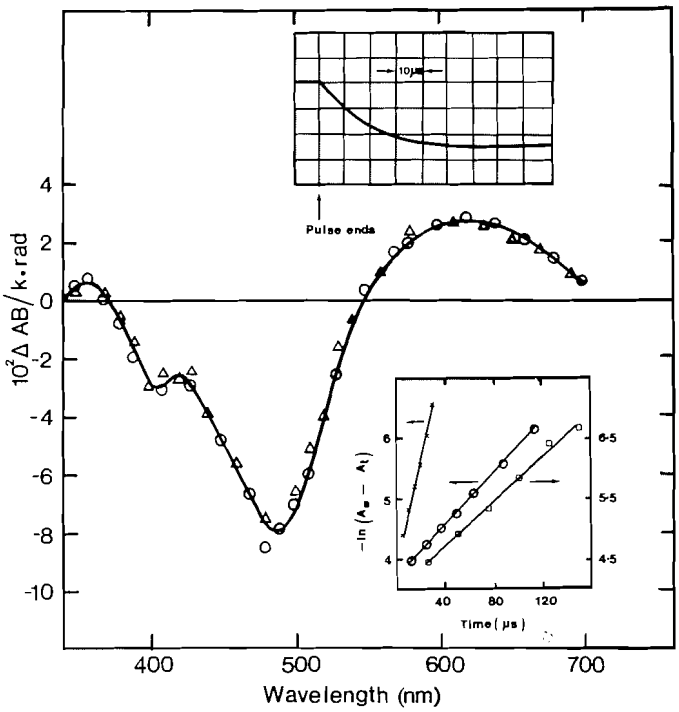

FIG. 1. Circles and triangles: change in absorbance (ΔAB) at pH 5 of 10–14 μ*M* 2-thioriboflavin in N_2O saturated 10 m*M* phosphate buffer containing 20 m*M* sodium formate. Dose 4 Gy/pulse. Top inset: oscilloscope trace illustrating the loss of absorbance with time at 490 nm. Bottom inset: plot of $-\ln(A_\infty - A_t)$ versus time for reaction of $\cdot CO_2^-$ with 15 μ*M* Fl (×), 7.7 μ*M* Fl (□) at pH 7, and 16.89 μ*M* Fl (○) at pH 10.

the FAD radical anion obtained under similar conditions (15, 16) are shown as dashed lines in Figs. 2(a) and (b). In the case of the anion the 2-thioriboflavin spectrum is similar in shape but red shifted by 40–50 nm. Red shifts are also seen in the neutral $\cdot FlH$ form for the 370-nm peak and 580-nm shoulder of lumiflavin. In addition there is strong enhancement of the absorbance at 500 nm.

The dash–dot lines in Figs. 2(a) and (b) are, respectively, the neutral semiquinone form of 2-thio-FMN flavodoxin and the anionic form of 2-thio-FMN lactate oxidase obtained by photoreduction (4). The anion spectrum in the flavoprotein is similar in shape to the free anion spectrum but the peaks are red shifted by 20–30 nm. In the flavodoxin, the 370-nm peak is similar in intensity and position. However, the 490-nm peak is drastically reduced and there is a much enhanced absorbance at 670 nm. These features must be attributed to interactions with amino acid residues in the flavin binding site.

The changes in absorbance during the period of reaction of Fl with $\cdot CO_2^-$ (top inset in Fig. 1) can be treated in terms of a pseudo first-order integrated rate equation. Plots of $\ln(A_\infty - A_t)$ versus time at two different flavin concentrations at pH 7 and a third plot at pH 10 have been presented in Fig. 1 (bottom inset). The pseudo first-order rate constants at pH 7 were plotted against [Fl] to obtain the value of k_5. This rate constant was $4.0 \pm 0.5 \times 10^9 M^{-1} s^{-1}$ in 20 m*M* formate and can be compared with $3.6 \pm 0.4 \times 10^9 M^{-1} s^{-1}$ for the corresponding reaction with riboflavin (6) and lumiflavin (15). As the pH increased above 8.5 the value of k_5 fell, reaching $1.3 \pm 0.2 \times 10^9 M^{-1} s^{-1}$ at pH 10. It may be noted that this corresponds to the pH region for ionization of thioriboflavin (p*K* = 9.8, Claiborne *et al.* (1)). Thus above pH 10 the dominant form of thioriboflavin, $Fl(-H)^-$, bears a negative charge, which would reduce the rate of reaction with $\cdot CO_2^-$. A similar reduction in

[2]Al. Claiborne and V. Massey, unpublished data.

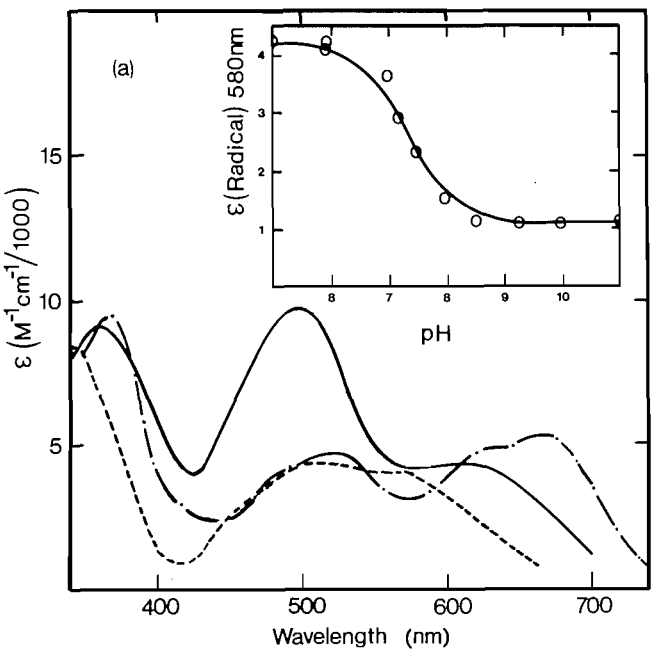

FIG. 2(a). Absorption spectra, at pH 5, of the neutral semiquinone produced from 10–14 μ*M* 2-thioriboflavin in N_2O-saturated 20 m*M* formate solutions by $\cdot CO_2$ (—). Absorption spectra, at pH 7, of lumiflavin radical produced under similar conditions (---). Absorption spectra of 2-thio-FMN flavodoxin radical produced by photoirradiation in 0.1 *M* potassium phosphate, pH 7.0, containing 30 m*M* EDTA and 1 μ*M* 5-deazaflavin (-·-). Inset: plot of ε(Radical) at 580 nm versus pH.

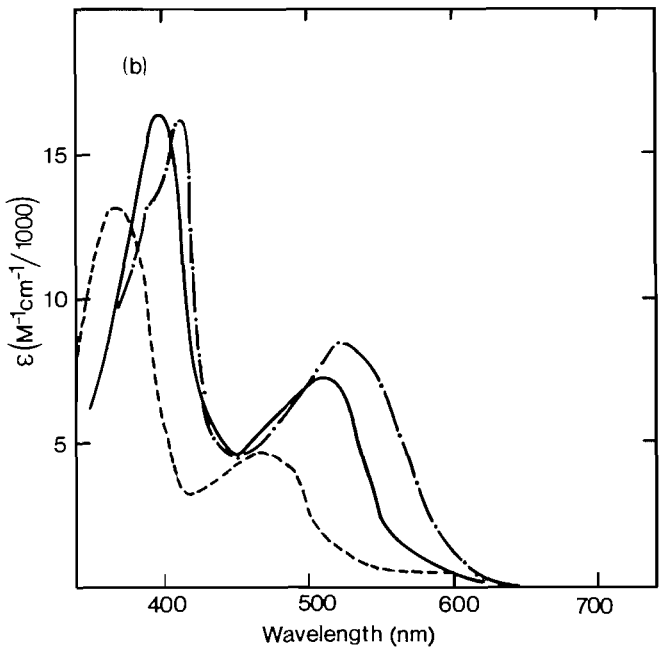

FIG. 2(b). Absorption spectra, at pH 10, of the radical anion produced from 16–18 μ*M* 2-thioriboflavin (—) and 10–40 μ*M* FAD (---) in N_2O-saturated 20 m*M* formate solutions at pH 10 by $\cdot CO_2^-$. Absorption spectra of 2-thio-FMN lactate oxidase at pH 7 produced under anaerobic conditions in the presence of 0.1 *M* glycine, 6 μ*M* 5-deazaflavin, and 0.01 *M* imidazole (-·-). Ordinate scale for (-·-) is in arbitrary units.

rate has been observed with unsubstituted flavins (6, 16). It may be noted that step [6] is too fast to be seen in our buffered solutions (17).

A number of pulse experiments were also performed in

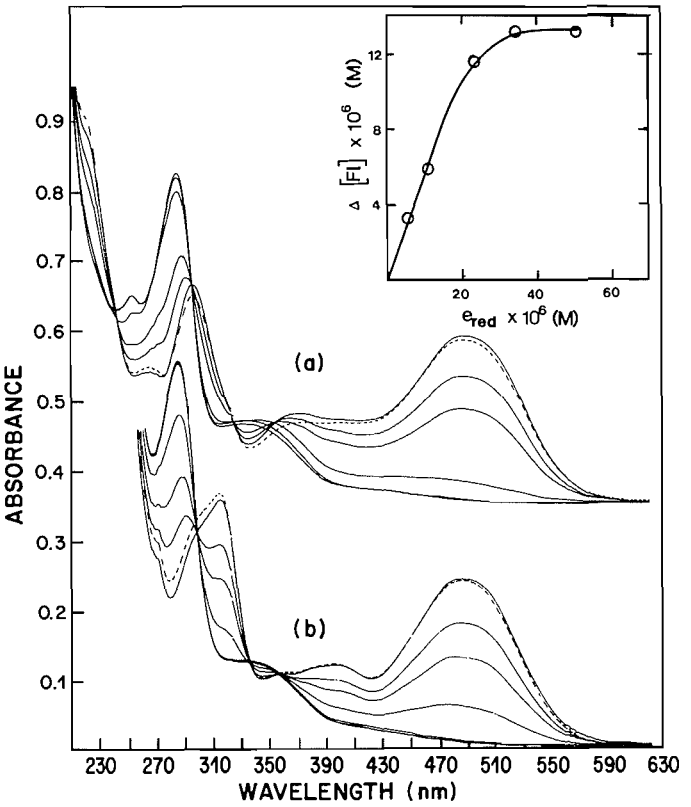

FIG. 3. (a) Spectra obtained from an N_2O-saturated solution of 13.43 μ*M* 2-thioriboflavin at pH 10 in 40 m*M* formate and 10 m*M* phosphate buffer before irradiation and after 1, 2, 4, 6, and 8 min of γ irradiation at 10 Gy min^{-1}. The absorbance scale has been displaced by 0.35 from zero for clarity. (b) Spectra obtained from an N_2O-saturated solution of 12.98 μ*M* 2-thioriboflavin at pH 9 in 2 m*M* dithiothreitol and 10 m*M* phosphate buffer before irradiation and after 1, 2, 4, 8, 12, and 15 min of γ irradiation at 10 Gy min^{-1}. The spectra after aeration of the irradiated solutions are shown by the dashed lines. Inset: change in [Fl], Δ[Fl], versus number of reducing equivalents of reducing species reacted for Fl + $\cdot CO_2^-$ at pH 10.

2–5 m*M* $D(SH)_2$ solutions at pH 7, using the $DS_2^- \cdot$ radical as the reducing species. As in the case of lumiflavin semiquinone, formed in sulphydryl-containing solutions (16, 18), the spectrum of the 2-thioriboflavin radical was somewhat perturbed, exhibiting increased absorption in the 400–500 nm region and lesser absorbance above 540 nm.

The slopes of pseudo first-order rate constants versus [Fl] for the reaction of $DS_2^- \cdot$ with 2-thioriboflavin at pH 7 gave $k_7 = 2.4 \pm 0.2 \times 10^9 M^{-1} s^{-1}$, which is a bit larger than $1.6 \pm 0.2 \times 10^9 M^{-1} s^{-1}$ for the corresponding reaction with lumiflavin (18).

Co^{60} γ-radiolysis

Spectral changes resulting from the reduction of 2-thioriboflavin with $\cdot CO_2^-$ and $DS_2^- \cdot$ radicals are shown in Figs. 3(a) and (b), respectively. In both cases the absorbance of Fl was suppressed by each successive dose of irradiation. For the $DS_2^- \cdot$ radicals there was no further change after 12 min of irradiation. Also, apart from the increase in absorbance below 310 nm due to the formation of DS_2 in reaction [7], the initial flavin absorption was completely restored on the addition of air. These observations are consistent with dihydroflavin as the only major product, formed via reactions [7], [6], and [8*a*–*c*] or [9].

[8*a*] $2FlH\cdot \rightarrow FlH_2 + Fl$

[8*b*] $\cdot Fl^- + FlH\cdot \rightarrow FlH^- + Fl$

[8c] $2\cdot FlH^- + H^+ \rightarrow FlH^- + Fl$

[9] $\cdot FlH + DS_2^-\cdot \rightarrow FlH^- + DS_2$

The flavin species present would vary with pH because of the ionizations of $\cdot FlH$ and FlH_2 (see above).

In the case of the $\cdot CO_2^-$ radicals, reference to the isobestic point at 354 in Fig. 3(a) and (b) shows that up to 2 min of radiation there was only one product formed. This is again attributed to dihydroflavin formation by the above reactions. Further treatment with $\cdot CO_2^-$ caused an apparent shift in the isobestic point and a continuing reduction in the absorption between 310 and 410 nm. On admission of air, the initial absorption of the flavin was completely restored only if the reduction was stopped at or before the equivalence point. If the reduction proceeded beyond this, the absorbance on reoxidation with air followed the pattern illustrated by the dashed line in Fig. 3(a). This type of behaviour has been seen in reactions of e_{aq}^-, and certain amine radicals with lumiflavin (15, 19). It is attributed to a further and irreversible reduction of FlH_2 by these species. It is interesting that in the case of 2-thioriboflavin it occurs with $\cdot CO_2^-$, which does not react with the dihydro forms of lumiflavin or FAD at this pH.

The spectra at the equivalence points for $\cdot CO_2^-$ reductions were taken to be those of 2-thiodihydroriboflavin. Values of $\epsilon(FlH_2)$ at 490 nm calculated from these agreed within ±2% for different flavin and formate concentrations at the pHs used. From these and the known value of ϵ(Fl) at 490 nm, the change in flavin concentration Δ[Fl] could be calculated. The inset in Fig. 3 is a plot of $\Delta[Fl] \times 10^6 M$ versus the equivalents of $\cdot CO_2^-$ radicals produced, $e_{red} \times 10^6 M$ (cf. Ahmad and Armstrong (15)). The values of η, the moles of reducing equivalents taken up per mole of flavin, were calculated from the initial slopes of such plots. As shown in Table 1, they lie in the range 1.8–2.2 with an average value of $1.9_3 \pm 0.1_1$, independent of $[HCO_2^-]$ and [Fl]. This indicates a two-electron reduction of the thioriboflavin in accord with eq. [10] at both pH 7 and 10.

[10] $2\cdot CO_2^- + Fl^- + 2H^+ \rightarrow FlH_2$ (or $FlH^- + H^+$)

Similar experiments were performed with $DS_2^-\cdot$ radicals from dithiothreitol except that in these cases a correction had to be made for the thermal reaction (13, 20):

[11] $D(SH)_2 + Fl \rightarrow DS_2 + FlH_2$ (or $FlH^- + H^+$)

At pH 10 the initial rate calculated from the slope of the absorbance versus time plot observed with an unirradiated 2 mM $D(SH)_2$ solution was $2.02 \times 10^{-7} M$ min^{-1}. Changes in flavin concentration calculated from this rate were subtracted from the initial changes observed in irradiated solutions to obtain the true change due to $DS_2^-\cdot$ radicals. A similar procedure was used at pH 9. However, below this pH the rate of the thermal reaction was negligible and no correction was necessary. The values of η for 10–20 μM Fl and 2 mM $D(SH)_2$ solutions were 2.24 ± 0.10, independent of pH in the range 5–10. This confirms the two-electron reduction of thioriboflavin by the $DS_2^-\cdot$ radicals.

TABLE 1. Summary of η for $\cdot CO_2^-$ radicals

[2-Thioriboflavin], μM	$[HCO_2^-]$, mM	pH	η
11.04	10	7	1.99
5.3	20	7	2.18
14.63	20	7	1.90
11.22	10	10	1.93
5.83	20	10	1.90
13.68	20	10	1.86
20.21	20	10	1.91
13.43	40	10	1.80

Summary

The present study has demonstrated that, as with unsubstituted flavins, the $\cdot CO_2^-$ and $DS_2^-\cdot$ anion radicals can effect the two-electron reduction of 2-thioriboflavin to the dihydroflavin. The rate constants for the initial one-electron step, reactions [5] and [7], are close to the "diffusion control limit" at pH 7 and are slightly reduced at pH 10 due to charge repulsion. These results are quite similar to those obtained with FAD, lumiflavin, and riboflavin. The spectrum of the radical anion of 2-thioriboflavin in free solution is similar to that of the normal flavin, but slightly red shifted. However, the spectrum of the neutral $\cdot FlH$ form is significantly different. This feature should certainly be taken into account in interpreting spectral data of the semiquinone spectrum in flavoproteins.

Acknowledgements

This work was supported by NSERCC grant A3571. The 2-thioriboflavin was kindly supplied by the late Dr. P. Hemmerich.

1. AL. CLAIBORNE, V. MASSEY, P. F. FITZPATRICK, and L. M. SCHOPFER. J. Biol. Chem. **257**, 174 (1982), and references cited therein.
2. AL. CLAIBORNE, P. HEMMERICH, V. MASSEY, and R. LAWTON. J. Biol. Chem. **258**, 5433 (1983).
3. AL. CLAIBORNE and V. MASSEY. J. Biol. Chem. **258**, 4919 (1983).
4. Y. S. CHOONG and V. MASSEY. Eur. J. Biochem. **131**, 501 (1983).
5. G. E. ADAMS and P. WARDMAN. Free radicals in biology. Vol. 3. *Edited by* W. A. Pryor. Academic Press, New York. 1977. Chapt. 2.
6. E. L. LAND and A. J. SWALLOW. Biochemistry, **8**, 2117 (1969).
7. R. F. ANDERSON. Ber. Bunsenges. Phys. Chem. **80**, 969 (1976).
8. R. F. ANDERSON. *In* Oxygen and oxy-radicals in chemistry and biology. *Edited by* E. L. Powers and M. J. Rodgers. Academic Press, New York. 1981.
9. M. GOLDBERG, I. PECHT, H. E. A. KRAMER, R. TRABER, and P. HEMMERICH. Biochim. Biophys. Acta, **673**, 570 (1981).
10. I. G. DRAGANIĆ and Z. D. DRAGANIĆ. The radiation chemistry of water. Academic Press, New York. 1971.
11. R. AHMAD and D. A. ARMSTRONG. Biochemistry, **21**, 5445 (1982).
12. A. J. ELLIOT, F. WILKINSON, and D. A. ARMSTRONG. Int. J. Radiat. Biol. **38**, 1 (1980).
13. E. L. LOECHLER and T. C. HOLLOCHER. J. Am. Chem. Soc. **97**, 3235 (1975).
14. K. H. DUDLEY, A. EHRENBERG, P. HEMMERICH, and F. MULLER. Helv. Chim. Acta, 1354 (1964).
15. R. AHMAD, WU ZHENNAN, and D. A. ARMSTRONG. Biochemistry, **22**, 1806 (1983).
16. P. S. SURDHAR, R. AHMAD, and D. A. ARMSTRONG. Can. J. Chem. **62**, 580 (1984).
17. P. F. HEELIS, B. J. PARSONS, and G. O. PHILLIPS. Biochim. Biophys. Acta, **587**, 455 (1979).
18. P. S. SURDHAR and D. A. ARMSTRONG. *In* Flavins and flavoproteins. *Edited by* R. C. Bray, P. C. Engel, and S. G. Mayhew. Walter de Gruyter and Co., Berlin. 1984; and unpublished data.
19. P. S. SURDHAR, D. E. BADER, and D. A. ARMSTRONG. Can. J. Chem. **63**, 1357 (1985).
20. M. GASCOIGNE and G. X. RADDA. Biochim. Biophys. Acta, **131**, 498 (1967).

Direct observation of low spin – high spin electronic ground states and cross-over exchange in manganocene derivatives, $(\eta^5\text{-}C_5H_4R)_2Mn$, R = H, CH_3, C_2H_5 by paramagnetic nuclear magnetic resonance[1]

DANIEL COZAK,[2] FRANÇOIS GAUVIN, AND JACQUES DEMERS

Département de chimie, faculté des sciences et de génie, Université Laval, Québec (Qué.), Canada G1K 7P4

Received May 28, 1985

DANIEL COZAK, FRANÇOIS GAUVIN, and JACQUES DEMERS. Can. J. Chem. **64**, 71 (1986).

The paramagnetic ^1H nmr spectra for manganocene (**1**) and 1,1′-dimethylmanganocene (**2**), and the ^{13}C nmr spectra for 1,1′-diethylmanganocene (**3**) have been recorded in toluene solvent over a −90 to 90°C temperature range. **1** shows a low field and a high field ring proton resonance in its spectrum near −59°C. At higher temperatures the low field resonance is prevalent and becomes gradually averaged due to a fast spin exchange process that dominates the spectrum at 90°C. For the ring substituted derivatives **2** and **3**, resonances due to only one paramagnetic species were detected in the low temperature range. Above ambient temperature a new spectrum due to rapid spin exchange averaging is observed for these complexes. Results are readily interpreted in terms of ground state molecular cross-over exchanges between the $^2E_{2g}$, $^6A_{1g}$, and $^2A_{1g}$ spin states of the complexes.

DANIEL COZAK, FRANÇOIS GAUVIN et JACQUES DEMERS. Can. J. Chem. **64**, 71 (1986).

Nous avons enregistré les spectres de la rmn ^1H du manganocène (**1**), du diméthyl-1,1′ manganocène (**2**) ainsi que les spectres de résonance du ^{13}C pour le diéthyl-1,1′ manganocène à différentes températures entre −90 et 90°C. Le spectre du composé **1**, déterminé à −59°C, présente deux résonances paramagnétiques dues aux protons annulaires. La résonance se trouvant à champs faible domine les spectres déterminés à plus hautes températures. À 90°C, ce signal est dû à un spectre moyen causé par un échange rapide entre plusieurs états paramagnétiques de la molécule. Les spectres des composés **2** et **3**, déterminés à basse température, présentent un seul état paramagnétique. Aux températures supérieures à celles de la pièce, un nouveau spectre, dû aussi à un échange rapide entre plusieurs états paramagnétiques, remplace graduellement le premier. Les résultats expérimentaux sont interprétés en fonction de la dynamique des états électroniques fondamentaux $^2E_{2g}$, $^6A_{1g}$ et $^2A_{1g}$ connus pour ces molécules.

Introduction

Several paramagnetic transition metal compounds are known to exist in an equilibrium ground state between their low spin (ls) and high spin (hs) electronic configurations (1). However, the d^5 manganocene compounds are the only sandwich complexes known to have such an equilibrium (2). Also, magnetic susceptibility, epr (electron paramagnetic resonance), and photoelectronic studies have shown that both the electronic ls $a_{1g}^2 e_{2g}^3$ configuration, or $^2E_{2g}$ state, and the hs $a_{1g}^1 e_{2g}^2 e_{1g}^2$ configuration, or $^6A_{1g}$ state, are possible structures for the molecular ground states of $(\eta^5\text{-}C_5H_5)_2Mn$ (**1**) and its 1,1′-dimethyl substituted derivative $(\eta^5\text{-}C_5H_4CH_3)_2Mn$ (**2**) (3–5). Moreover, the electronic state associated with the other possible ls configuration, $e_{2g}^4 a_{1g}^1$, or $^2A_{1g}$ state, is generally considered too far above the ground state energy level to be significantly populated or involved in a multiple ground state cross-over exchange process (6). However, the $^2A_{1g}$ doublet state has been used to interpret the gas phase photoelectronic spectrum (7) of **1** and it has been suggested as a contributing factor to the larger isotropic paramagnetic nmr proton shifts (6) observed at room temperature for **2** compared to **1**. Thus, spectroscopic data point to the possible existence of these three ground states for manganocene compounds but direct spectroscopic detection and characterization of only the ls $^2E_{2g}$ and the hs $^6A_{1g}$ states have so far been reported (2, 6, 8).[3]

We wish to report here the paramagnetic ^1H nmr behavior for the unsubstituted manganocene complex **1** and its methylcyclopentadienyl derivative **2**, together with ^{13}C nmr data for the ethyl analogue, $(\eta^5\text{-}C_5H_4C_2H_5)_2Mn$ (**3**).

Experimental

Chemical reactions and manipulation of the compounds were carried out under a blanket of purified nitrogen in Schlenk-type vessels. Oxygen and water impurities from the nitrogen gas were controlled by passing the gas first over supported copper catalyst (BASF-R3-11) heated at 200°C, which was purchased from Badische Anilin and Soda-Fabrik AG, W. Germany, followed by 4A molecular sieve beds. The solvents used were refluxed for 1 h in a nitrogen atmosphere and passed over a drying agent before being distilled and stored.

Melting points were measured, in a nitrogen atmosphere, in sealed glass capillaries on a Thomas Hoover oil immersion type apparatus and are reported uncorrected. Mass spectra (ms) of the complexes studied were recorded on a Hewlett Packard 5995A mass spectrometer. Samples were placed in capillary glass tubes and introduced into the apparatus by means of a steel rod; they were then heated at a temperature rate of 64°C/min to 200°C under 10^{-6} Torr pressure (1 Torr = 133.3 Pa). Background subtracted spectra were regularly recorded for 15 min. A Varian EM 360A and a Bruker HX90 CW instrument were used to record the proton nuclear magnetic resonance (nmr) spectra of the diamagnetic compounds. The nmr spectra for the manganocenes were recorded on a Bruker WH-400 instrument from toluene-d_8 saturated solutions in 5-mm nmr tubes filled with nitrogen gas. For the liquid complex **3**, 1:10 (^1H) or 2:5 (^{13}C) (v/v) complex – toluene-d_8 mixtures were used to run the spectra. The temperature range from −90 to 90°C was covered in this study. The experimental chemical shifts were measured against the internal methyl carbon or proton resonance of the non-perdeuterated toluene solvent (<1%) and are reported in the text in δ units with positive values increasing downfield from TMS. Internal reference chemical shift values used: $\delta(C^1HD_2C_6D_5)$, 2.3 ppm and $\delta(^{13}CD_3C_6D_5)$, 21.3 ppm. Band widths at half-height, $H_{1/2}$, are given in parentheses following each chemical paramagnetic shift value in the text. Elemental C, H, and N analyses were done in duplicate by Schwarzkopf Microanalytical Laboratory, New York.

Anhydrous manganese bromide, $MnBr_2$, and sodium hydride, NaH,

[1]Taken in part from the M.Sc. Thesis of F.G., Laval University, Québec (Qué.), Canada, 1985.

[2]Author to whom correspondence may be addressed.

[3]Some controversy seems to exist on the necessity of involving the $^2A_{1g}$ ground state to explain the photoelectronic spectra of gaseous complex **1**, see refs. 4 and 7. Subsequently it was shown by epr that the ground states for **1** and **2** depend on the molecular environment. The epr spectroscopic data are available at low temperature. However, the main drawback of this spectroscopic method in the study of the dynamic spin process is the line broadening caused by rapid electron relaxation, which makes observation of the hyperfine structure impossible above −229°C; see refs. 2 and 8 for more details.

were purchased from Aldrich Chemical Co. Ethyl bromide was used as received from Fisher Scientific Co.

Synthesis

The sodium cyclopentadienides used in the preparations given here were prepared by deprotonating the corresponding dienes with sodium hydride (10).

Manganocene (1) and 1,1'-dimethylmanganocene (2)

Complexes **1** and **2** were prepared following the procedure described in the literature (11, 12). The following analytical data were obtained for the synthesized products. **1**: yield 46%; mp 167–169°C (lit. (11) mp 172–173°C). *Anal.* calcd. for $C_{10}H_{10}Mn$: C 64.88, H 5.45%; *Mol. Wt.*: 185.13 g; found: C 64.36, H 5.34%; *Mol. Wt.* (ms): 185. **2**: yield 57%; mp 60–62°C (lit. (12) mp 61–63°C). *Anal.* calcd. for $C_{12}H_{14}Mn$: C 67.61, H 6.62%; *Mol. Wt.*: 213.18 g; found: C 67.29, H 6.15%; *Mol. Wt.* (ms): 213.

1,1'-Diethylmanganocene (3)

First, ethylcyclopentadiene ligand was prepared in the following manner. Ethyl bromide, 32.9 g (302 mmol), diluted in an equal volume of tetrahydrofuran (THF) was added dropwise from a dropping funnel over a period of 1 hour to a 200-mL solution of sodium cyclopentadienide 1.50 *M* (300 mmol) in THF maintained at −10°C. The mixture was magnetically stirred for the next 15 h. The solution temperature was then raised to room temperature and the solution filtered on a glass frit to remove a white solid (NaBr). The filtrate was then extracted with 100 mL distilled water and the aqueous fraction further washed with 3 × 100 mL pentane. The THF and pentane fractions were then combined and dried over magnesium sulfate. The bulk of the pale yellow organic solution was then fraction distilled under normal pressure. Following the distillation of the pentane (35–36°C) and THF (66–67°C) fractions, a colorless liquid (11.4 g, 40%) passing at 53°C was collected by increasing the heating rate of the distillation. The expected mixture of structural isomers for the monomeric ethylcyclopentadiene gave the following proton chemical shifts and peak intensities: ^{1}H nmr ($CDCl_3$) δ: 1.14 (t, 9H), 2.38 (m, 6H), 2.90 (m, 4H), 6.23 (m, 6H) ppm. The product was then stored in a Schlenk tube over Dry Ice.

The sodium ethylcyclopentadienide salt was prepared by adding, dropwise, ethylcyclopentadiene, 13.4 g (142 mmol), to 3.50 g (146 mmol) sodium hydride in suspension in ca. 200 mL THF. The reaction mixture was left under magnetic agitation overnight, then filtered over a glass frit to remove any unreacted hydride. The reaction yield was determined by volumetric titration (0.471 *M*, 66%) of the organic sodium. This value was then used to determine the quantity of reactants used in the following step. Proton nmr spectra of the reaction product were recorded after evaporating the THF solvent under vacuum from an aliquot placed in an nmr tube, and replacing it by a deuterated solvent: ^{1}H nmr (toluene-d_8) δ: 1.02 (t, 3H), 2.33 (q, 2H), 5.38 (s, 4H) ppm.

In a typical experiment 11.30 g (52.6 mmol) manganese bromide was suspended in 10 mL THF in a 500-mL Schlenk flask and 200 mL sodium ethylcyclopentadienide (110 mmol) solution, 0.55 *M* in THF, was slowly added at 0°C while stirring. Once the addition was completed, the mixture was magnetically stirred at room temperature for 15 h. The insoluble NaBr formed during the reaction was removed from the solution by filtration and the solvent was pulled off on a vacuum line. This left an oily brown residue, which was washed with 3 × 200 mL hexane, leaving behind an insoluble solid. The hexane was then vacuum distilled until a thick red-brown oil (ca. 5 g) was left in the flask. The residue was then distilled under 13 Torr pressure. The middle distillate (107°C) gave 1.92 g (15%) of a highly air-sensitive red liquid corresponding to the pure product. *Anal.* calcd. for $C_{14}H_{18}Mn$: C 69.69, H 7.54, Mn 22.78%. *Mol. Wt.*: 241.24 g; found: C 69.82, H 7.56, Mn 21.43%; *Mol. Wt.* (ms): 241.

Results

Selected variable temperature proton nmr spectra showing the ring proton isotropic shifts for **1** over the full temperature range examined are shown in Fig. 1. These spectra can be regrouped in three temperature regions each having their spectral features. Starting at high temperatures (90°C), a single resonance at δ 27.9 ppm (800 Hz), due to the ring protons, is present at low field from the usual proton resonance region where π-bonded cyclopentadienyl rings are generally observed. This resonance showed two distinct temperature dependences. For the first, between 90 and 41°C, the ring protons moved upfield as the temperature was lowered. For the second, below 41°C, the same resonance shifted downfield, as predicted by the Curie Law, until the temperature reached −76°C. A third temperature region appeared at low temperatures, near −59°C, where a new resonance grew in at high field with concomitant decrease in intensity of the other low-field resonance, see Fig. 1. For example, at −59°C, the new signal is present at δ −25.8 ppm (1800 Hz) while the former is now at δ 28.3 ppm (4300 Hz). As the temperature is further lowered to −90°C the new signal moved upfield, following once more the Curie Law normally observed for the temperature-dependent isotropic shifts for most paramagnetic metallocene complexes (13, 14). The total shift variation observed is quite small for a given series of related spectra (ca. 2 ppm), considering the resonance band widths (probable error). Nevertheless, the spectra are quite reproducible and therefore the observed experimental errors fall well within the shift variations discussed or graphically represented below.

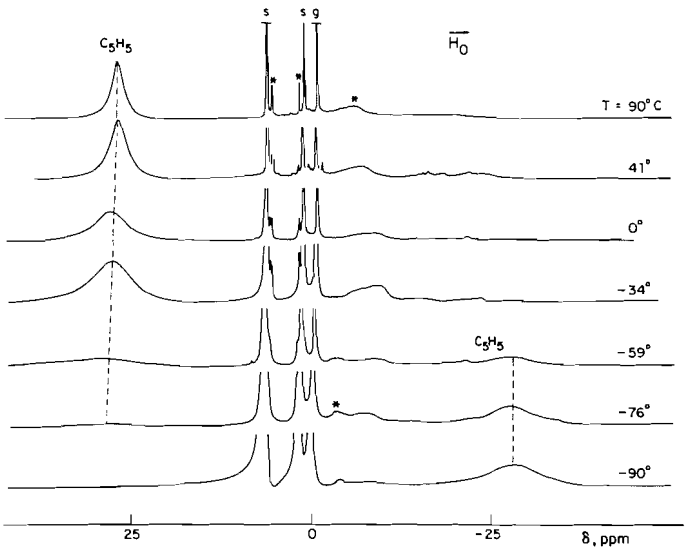

FIG. 1. Proton nmr spectra of **1** in toluene-d_8 at various temperatures. The C_5H_5 resonance at low temperatures is more evident at stronger recording amplitudes. The spectra *Y* scale is not constant in the figure: s, solvent; g, silicon grease; *, impurities.

The variable temperature proton nmr spectra for substituted complexes **2** and **3** were also recorded. In both cases two main temperature-dependent spectra were observed, one at high temperatures and the other at low temperatures. The high temperature limit spectrum, taken at 90°C, for the 1,1'-dimethyl substituted complex **2** is given in Fig. 2A and shows two broad resonances and a narrow signal at low field from the nmr region where the complexed diamagnetic ligand resonances are usually found. The low-field δ 131.8 (7700 Hz) and 78.3 ppm (3800 Hz) resonances observed at this temperature are assigned to the resolved ring protons and the δ 12.9 ppm (920 Hz) signal to the remaining methyl protons of **2**. At 41°C extensive line broadening in the spectrum made detection of paramagnetic nmr resonances impossible. Further lowering of the temperature yielded an exchange broadened spectrum discernible at 2°C and fully

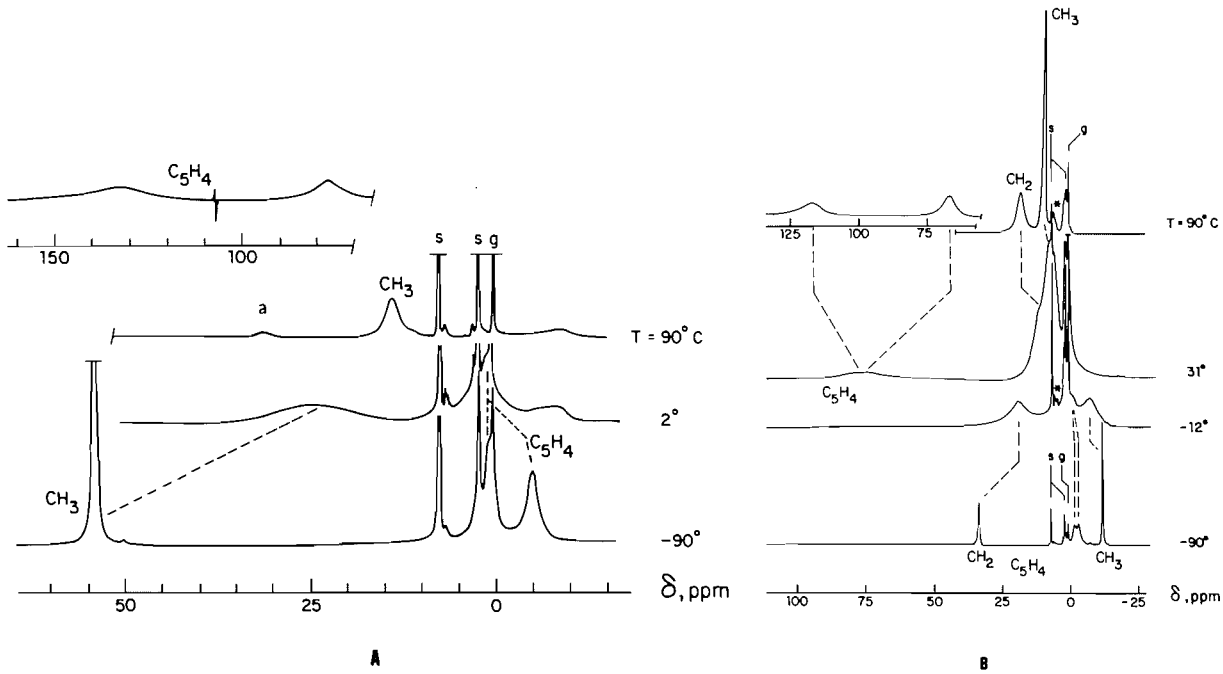

FIG. 2. Proton nmr spectra of **2** (A) and **3** (B) in toluene-d_8 at various temperatures. Only the "limit" spectra are shown: a, complex **1** as impurity; s, solvent; g, silicon grease; *, impurities.

grown-in at −90°C, as shown in Fig. 2A. The higher-field signals in the −90°C spectrum are assigned to the nonequivalent cyclopentadienyl protons δ 0.5 (540 Hz) and −4.5 ppm (650 Hz), and the low-field resonance at δ 50.6 ppm (270 Hz) is attributed to the methyl protons.

Similarly, the variable temperature proton nmr spectra for the 1,1′-diethyl substituted complex **3** are analogous to the dimethyl derivative discussed above and mutually confirm the chemical assignments made here for the resonances. The main temperature-dependent spectra are depicted in Fig. 2B. Hence at 90°C the spectrum showed two broad ring resonances present at δ 114.5 (3500 Hz) and 64.2 ppm (2300 Hz), together with two narrow signals at δ 18.5 (1200 Hz) and 10.3 ppm (340 Hz) assigned to the CH_2 and CH_3 protons, respectively. The isotropic chemical shifts observed did not follow the Curie Law. All four isotropic shifts moved upfield instead of downfield as the temperature was lowered from 90°C to approximately 31°C. Moreover, at 31°C the former two low-field ring resonances were fully collapsed into one signal at δ 77.8 ppm (8000 Hz) and the latter CH_2 and CH_3 signals were overlapping at δ 11.7 (ca. 2300 Hz) and 8.1 ppm (ca. 2000 Hz), respectively (see Fig. 2B). This spectrum gradually disappeared as the temperature was lowered and a new set of resonances was present at −12°C. This new spectrum evolved as the temperature was further lowered and was fully resolved at −90°C, with relatively narrow peaks at δ 33.6 (230 Hz) and −11.5 (110 Hz) ppm, due to CH_2 and CH_3 respectively, and a doublet resonance at δ −1.4 (570 Hz) and −2.8 ppm (570 Hz), due to nonequivalent ring protons.

Because of their poor solubility in toluene we were unable to record the corresponding ^{13}C nmr spectra for **1** and **2**. In THF-d_8 both ^1H and ^{13}C nmr results indicated a strong paramagnetic exchange interaction between the complexes and the solvent. Moreover, the proton spectra bear no resemblance to those taken in toluene. This result is not unexpected since THF and other Lewis bases are known to associate with manganocene to form addition compounds (15, 16). More details on this will be given elsewhere. However, **3** is miscible in toluene and its variable temperature ^{13}C nmr spectra were recorded. The spectra recorded above 44°C show non-Curie Law temperature-dependent isotropic carbon shifts as for the proton spectra. Though no other manganocene spectrum in toluene is available for comparison, we tentatively assign the two paramagnetic resonances in the spectrum, δ 471.1 ppm (480 Hz) and −126.0 ppm (210 Hz), to the ethyl CH_2 and CH_3 groups, respectively. The ring carbon resonance was not observed. At −9°C, no paramagnetic signals were detected in the spectrum due to line broadening caused by spin exchange. Below this temperature, near −43°C, a new spectrum appeared with a broad low-field peak at δ 271.8 ppm (650 Hz), followed by a doublet at δ 57.7 (270 Hz) and 43.7 ppm (220 Hz) located in the middle-field range, and at higher field a sharp signal was present at δ −104.0 ppm (220 Hz). At −28°C a single resonance at δ 52.4 ppm (480 Hz) is observed due to the collapsed middle-field signals, which are assigned to the nonequivalent ring carbons. The remaining low- and high-field resonances are due to the CH_2 and CH_3 carbons, respectively.

Figure 3 shows the dependence upon temperature of the observed proton chemical shifts (δ versus T^{-1}) for **1** and **3**. Once more, the plots represented in this graph underline the distinct magnetic behavior of these compounds. Hence at low temperatures ($T^{-1} \geq$ ca. 0.004 K^{-1}) the resonances have a linear Curie-type dependence on temperature and the extrapolation of this portion of the plots intercepts the ordinate axis within a reasonable value for the diamagnetic ligand chemical shifts. The other distinct region of these curves is at high temperature where the isotropic chemical shift variations do not obey the Curie Law. This is depicted in Fig. 3 by the departure from linearity in the curves, and increased paramagnetism is observed as the temperature increases ($T^{-1} <$ ca. 0.004 K^{-1}). A similar type of isotropic shift behavior has also been reported to be caused by metal-ring non-rigidity in cobaltocene derivatives (17). According to the Curie Law, the paramagnetic isotropic shift is inversely proportional to the temperature. Hence, at infinite temperature or $T^{-1} = 0\ K^{-1}$ the paramagnetic isotropic

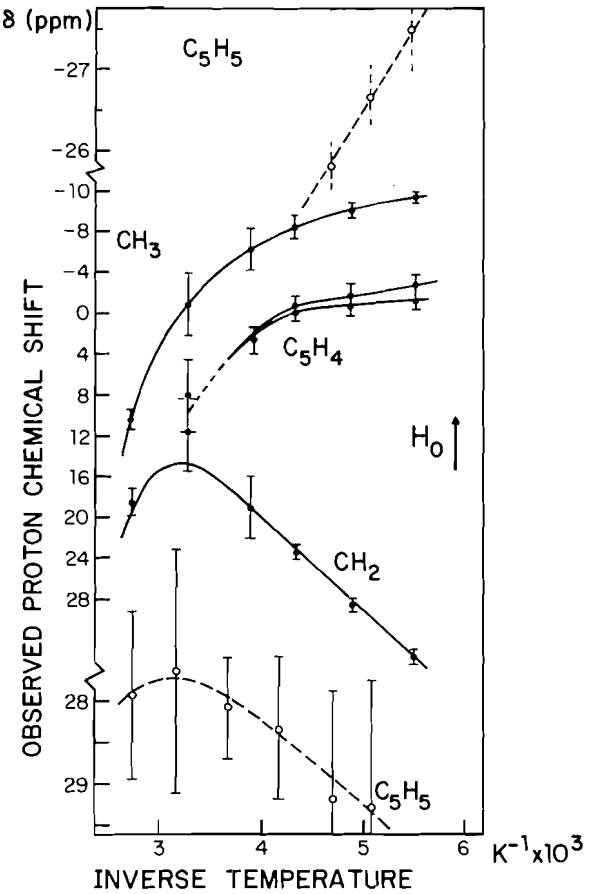

FIG. 3. The observed chemical shifts versus the inverse temperature plots for **1** (---○---) between −90 and 90°C and for **3** (—●—) between −90 and 30°C. The vertical bars on the curves are the probable errors for the observed chemical shifts, based on the band width at half-height, and are equal to $0.287 \times H_{1/2}$.

shifts should ideally be nil and the observed nmr chemical shifts would then be those of the diamagnetic ligand. In practice, extrapolation of the observed chemical shifts often falls in the δ 0–10 ppm region because of some error in the measured frequencies reported; $H_{1/2} = 10^2$–10^3 Hz.

The room temperature isotropic proton resonance for the solid complex **1** was first reported to be far upfield of the diamagnetic nmr region (−120 ppm from H_2O) (18). Our room temperature solution results coincide more closely with those of a subsequent communication where, in benzene solution, the ring protons for **1** are reported at δ 25.8 ppm and, for **2**, an unresolved doublet centered at δ 141 ppm is assigned to the ring protons with the methyl resonance reported to be at δ 81 ppm (117 and 70 ppm, respectively, in cyclohexane-d_{12}).[4] The differences in the shift positions quoted here and our results are due to the strong temperature and solvent dependence observed for the paramagnetism in these manganocenes.

Discussion

The low- and high-field proton resonances detected in the spectra of **1** can be interpreted as being due to two slow or non-exchanging molecular states of the manganocene molecule (exchange rate $< 10^3\ s^{-1}$). Slow exchange on the epr time scale between hs and ls configurations of **1** in host lattices has been observed previously (8). Departure of the chemical shifts from the Curie Law, evident in Fig. 3 by the inflection in the curve at high temperature ($T^{-1} < 0.004\ K^{-1}$), suggests that above ca. 40°C the resonances are time averaged by rapid spin exchange over two or more paramagnetic molecules, of which at least one has a strongly deshielding effect on the ring.

The nmr properties for **2** and **3** in toluene solution are better related to each other than with **1**. For the former complexes the resonances are at much lower fields at a given temperature (especially above room temperature) and there is a total absence of Curie Law behavior at elevated temperatures (low-field ring proton resonances). The linear relationship for the low temperature resonances (see Fig. 3 for **3**, for example) is indicative that spin exchange is not significant below ca. −46°C for the substituted manganocene complexes in solution. This contrasts with the two resonances observed for **1** in the same temperature range (see Fig. 3). Above this temperature there is, for both substituted complexes, an inflection in the curves towards low magnetic fields as the temperature is increased. Data for the high temperature region (30–90°C) are not shown on Fig. 3 for scaling reasons, i.e. $T^{-1} < 0.003\ K^{-1}$, but it can be seen that there is reversal of the slope below this point. Hence, the observed resonances for **2** and **3** can not be accounted for by the Curie Law in this temperature range and must be due to a rapid spin exchange similar to that mentioned for **1**.

The large low-field proton shift observed at 37°C for **2** relative to **1** has been interpreted by Switzer *et al.* as due to the presence of a rapid equilibrium involving a doublet $^2A_{1g}$ ground state (6). Moreover, variable temperature epr studies have shown that **1** and **2** have thermally populated $^2E_{2g}$ and $^6A_{1g}$ ground states exchanging in hydrocarbon solutions (2, 8). Based on the known electronic equilibria mentioned above, our variable temperature solution nmr results for the complexes studied can be interpreted in the following manner. For **1** at low temperatures in toluene, the ls $^2E_{2g}$ molecular ground state gives way to a hs $^6A_{1g}$ spin state as the temperature is raised. At higher temperatures a second spin exchange process is observed, presumably due to the rapid equilibrium between mainly $^6A_{1g}/^2A_{1g}$ spin states of the molecule. Similarly, at low temperatures, the substituted manganocenes show spectra for one main populated electronic state, which can be either the $^2E_{2g}$ or the $^6A_{1g}$ state, or possibly the time-averaged spectra of these rapidly exchanging states. At higher temperatures a rapid three-way $^2E_{2g}/^6A_{1g}/^2A_{1g}$ or a two-way $^6A_{1g}/^2A_{1g}$ spin exchange sets in, depending respectively on the preceding attribution.

Acknowledgments

We are grateful to the "programme de formation de chercheur et d'action concertée du Québec" (FCAC, No. EQ2094) and to the Natural Sciences and Engineering Research Council of Canada (NSERC, No. A1527) for their financial assistance. A scholarship to F.G. from the "institut de recherche en santé et sécurité du travail du Québec" (IRSST) is greatly appreciated.

1. A. T. CASEY. Theory and applications of molecular paramagnetism. *Edited by* E. A. Boudreaux and L. N. Mulay. John Wiley, New York. 1976. p. 67.
2. J. H. AMMETER. J. Magn. Reson. **30**, 299 (1978).
3. G. WILKINSON, F. A. COTTON, and J. M. BIRMINGHAM. J. Inorg. Nucl. Chem. **2**, 95 (1956); L. T. REYNOLDS and G. WILKINSON. J. Inorg. Nucl. Chem. **9**, 86 (1959).
4. S. EVANS, M. L. H. GREEN, B. JEWITT, G. H. KING, and A. F. ORCHARD. J. Chem. Soc. Faraday Trans. 2, **70**, 356 (1974).

[4]Values taken from ref. 6 discussed here are transposed in δ units using: $(C_2H_5)_2Fe$, δ = 4.0 ppm; $(C_5H_4CH_3)_2Fe$, δ = 4.0 and 1.8 ppm, taken from ref. 9.

5. G. WILKINSON, F. G. A. STONE, and E. W. ABEL (*Editors*). Comprehensive organometallic chemistry. Vol. 3. Pergamon Press, New York. 1982. p. 28.
6. M. E. SWITZER, R. WANG, M. F. RETTIG, and A. H. MAKI. J. Am. Chem. Soc. **96**, 7669 (1974).
7. J. W. RABALAIS, L. O. WERME, T. BERGMARK, L. KARLSSON, M. HUSSAIN, and K. SIEGBAHN. J. Chem. Phys. **57**, 1185 (1972).
8. J. H. AMMETER, R. BUCHER, and N. OSWALD. J. Am. Chem. Soc. **96**, 7833 (1974).
9. F. H. KÖHLER. J. Organomet. Chem. **110**, 235 (1976).
10. M. F. RETTIG and R. S. DRAGO. J. Am. Chem. Soc. **91**, 1361 (1969).
11. G. WILKINSON, F. A. COTTON, and J. M. BIRMINGHAM. J. Inorg. Nucl. Chem. **2**, 95 (1956).
12. L. T. REYNOLDS and G. WILKINSON. J. Inorg. Nucl. Chem. **9**, 86 (1959).
13. A. CARRINGTON and A. D. MCLACHLAN. Introduction to magnetic resonance. Harper and Row, Publishers, New York. 1967. p. 221; F. H. KÖHLER and W. PRÖßDORF. Chem. Ber. **111**, 3464 (1978).
14. H. J. KELLER and K. E. SCHWARZHANS. Angew. Chem. Int. Ed. Engl. **9**, 196 (1970); K. E. SCHWARZHANS. Angew. Chem. Int. Ed. Engl. **9**, 946 (1970).
15. J. T. WEED, M. F. RETTIG, and R. M. WING. J. Am. Chem. Soc. **105**, 6510 (1983); J. T. WEED. Ph.D. Thesis. University of California, Riverside, CA., U.S.A. 1983.
16. C. G. HOWARD, G. S. GIROLAMI, G. WILKINSON, M. THORNTON-PETT, and M. B. HURSTHOUSE. J. Am. Chem. Soc. **106**, 2033 (1984).
17. F. H. KÖHLER. J. Organomet. Chem. **160**, 299 (1978).
18. H. M. MCCONNELL and C. H. HOLM. J. Chem. Phys. **28**, 749 (1958).

Electrically conducting polymers: a review of the electropolymerization reaction, of the effects of chemical structure on polymer film properties, and of applications towards technology

R. J. WALTMAN[1]
IBM Almaden Research Center, 650 Harry Road, San Jose, CA, U.S.A. 95120-6099
AND
J. BARGON
Institut für Physikalische Chemie, Universität Bonn, West Germany

Received November 14, 1984[2]

R. J. WALTMAN and J. BARGON. Can. J. Chem. **64**, 76 (1986).

The electrochemical oxidation of aromatic heterocyclic compounds thiophene, pyrrole, and indole and benzenoid and nonbenzenoid polycyclic hydrocarbons azulene, fluorene, and pyrene yield electrically conducting polymers with conductivities of 10^{-5}–10 S/cm. The presence of substituents affects the electrical conductivity of these films and also their electroactive properties. Furthermore, substituents determine whether electropolymerization of these compounds can occur or whether soluble products are formed. The relative importance of these pathways is dependent on the stability of the intermediate radical cation. These effects are investigated by INDO molecular orbital calculations.

R. J. WALTMAN et J. BARGON. Can. J. Chem. **64**, 76 (1986).

L'oxydation électrochimique de composés hétérocycliques aromatiques comme le thiophène, le pyrrole et l'indole et des hydrocarbures polycycliques de type benzénique et nonbenzénique comme l'azulène, le fluorène et le pyrène donne des polymères conducteurs d'électricité avec des conductivités de 10^{-5} à 10 S/cm. La présence de substituants affecte la conductivité électrique de ces films ainsi que leur activité électrique. De plus, selon les substituants, on obtient soit une électropolymérisation de ces composés, soit la formation de produits solubles. L'importance relative de ces mécanismes dépend de la stabilité du cation radicalaire intermédiaire. On étudie ces effets à l'aide de calculs INDO d'orbitales moléculaires.

[Traduit par le journal]

I. Introduction

The electrochemical oxidation of aromatic heterocyclic, benzenoid, or nonbenzenoid molecules frequently leads to the formation of an electrically conducting organic polymer film at the electrode surface (1–5). These films typically have good adhesion and electrical contact to the electrode surface. Thin films, when supported by an electrode surface, can be electrochemically cycled between the oxidized, conducting state, and the neutral, insulating state. Thicker films can be produced in the oxidized, conducting state and can be peeled off from the electrode surface to yield free-standing, electrically conducting films. Because these films are in the oxidized state, they represent polymeric cations, whereby their overall charge balance is achieved by the incorporation of counteranions which stem from the electrolyte of the "electroplating" solution.

According to this approach, conducting films have now been prepared from a wide variety of organic molecules. These include heterocyclic compounds such as pyrrole (1), thiophene (2), furan (3), indole (4), thianaphthene (4), and carbazole (5). Conducting polymeric films have also been prepared from polycyclic benzenoid and nonbenzenoid hydrocarbons such as azulene (5), fluorene (6), fluoranthene (6), triphenylene (6), and pyrene (6). Thus, the set of organic molecules which undergo electrochemical stoichiometry of the film-forming reactions; (*b*) opportunity to investigate the generality of the electropolymerization reaction. This can be achieved by studying: (*a*) the electrochemical stoichiometry of the film-forming reactions; (*b*) the parameters which determine the aptitude of a molecule to electropolymerize; and (*c*) how the aptitude for electropolymerization, i.e., reactivity, responds to the presence of substituents. The substituent effects can be further categorized into: (*i*) *electronic* effects, i.e., by its effect on the distribution of electrons at the reactive site; and (*ii*) *steric* effects, i.e., by its effect due to crowding at or near the reactive site. These considerations should provide a qualitative picture of the electropolymerization reaction.

Additional parameters, such as the properties of the resulting polymer films, are important in that the eventual technological application of these polymer films will require some versatility of their properties. This will most likely include the ability to vary the electrical conductivity of the films and the ability to improve the mechanical properties thereof. These goals can be met by chemical modification of: (*a*) the polymer film; (*b*) the electroplating solution; and (*c*) the structure of the starting molecule. This latter category falls into the domain of substituent effects and will be considered in some detail below. With respect to chemical modification of the polymer film itself (7) or of the electroplating solution (8), these topics have been the subject of recent reviews (7, 8). Recently also, the electrochemical preparation of conductive composites (such as from polyvinylchloride and polypyrrole) have provided polymer composite films which have the advantageous mechanical properties of the host polymer, yet retain the high electrical conductivity of the conductive polymer (9). In this report, we will describe the effect of substituents on the electropolymerization reaction and how substituents affect polymer film properties, i.e., their electrical conductivity. These aspects will be considered utilizing the following molecules as illustrative examples: pyrrole, thiophene, indole, azulene, fluorene, and pyrene. Finally, we will summarize some technological applications for which the high electrical conductivity and stability of these electrically conducting polymers have been exploited.

II. The electropolymerization reaction

Electrochemical stoichiometry

One of the important features found with the electropolymerization reaction is that it proceeds with electrochemical stoichi-

[1]Author to whom correspondence should be addressed.
[2]Revision received August 13, 1985.

TABLE 1. Electrochemical data, elemental composition, and electrical conductivity of some electrically conducting polymers

Compound	E_{pa} monomer (V)	Voltammogram n value	Elemental composition of polymer	σ ($ohm^{-1}\,cm^{-1}$)	Reference
Pyrrole (C_4H_5N)	1.2	2.2–2.4	$C_{4.0}H_{3.5}N_{0.9}\,(BF_4)_{0.19}$	100	2, 11
Thiophene (C_4H_4S)	2.06	2.7	$C_{4.0}H_{3.3}S_{0.9}\,(BF_4)_{0.07}$	0.02	12, 13
2,2′-Bithiophene (C_8H_6S)	1.32	—	$C_{4.0}H_{2.1}S_{1.0}(HSO_4)_{0.17}$	0.1	12, 13
Indole (C_8H_7N)	1.26	2.1	$C_{8.0}H_{6.1}N_{1.0}(ClO_4)_{0.34}$	0.02	4
Thianaphthene (C_8H_6S)	1.75	2.4	$C_{8.0}S_{5.4}S_{1.0}(ClO_4)_{0.16}$	0.008	4
Carbazole ($C_{12}H_9N$)	1.30	2.5	$C_{12}H_{13}N(ClO_4)_{0.45}$	10^{-3}	5, 14
Azulene ($C_{10}H_8$)	0.96	2.1	$C_{10}H_{6.5}(ClO_4)_{0.25}$	10^{-2}–1	5
Fluorene ($C_{13}H_{10}$)	1.82	2.5	$C_{13.0}H_{9.5}(BF_4)_{0.23}$	10^{-4}	6
Fluoranthene ($C_{16}H_{10}$)	1.68	2.0	$C_{16.0}H_{9.6}(BF_4)_{0.18}$	10^{-5}–10^{-3}	6
Triphenylene ($C_{18}H_{12}$)	1.83	2.7	$C_{18.0}H_{11.4}(BF_4)_{0.20}$	10^{-4}	6
Pyrene ($C_{16}H_{10}$)	1.33	1.7	$C_{16.0}H_{12.0}(ClO_4)_{0.31}$	10^{-1}–1	6

ometry (2). This allows characterization of the film-forming reactions, which typically proceed with n values which are slightly in excess of 2.0 (2, 4–6). The n values can be measured in several ways. One of the most convenient is from voltammograms, utilizing the Nicholson and Shain (10) treatment for a totally irreversible reaction. For most of the film-forming reactions discussed here, the n values are usually in the range between 2.0 and 2.7 (Table 1), whereby 2 electrons/molecule are involved in the film-forming reaction, and the charge in excess of 2.0 is consumed in the concomitant electrooxidation of the polymer film. However, the n values derived from voltammograms really represent the total reaction at the electrode surface and can include secondary chemical reactions that accompany the electropolymerization reaction, such as dimerization reactions to form soluble products. This has been observed in the electropolymerization reaction of pyrene (6), and will be discussed below (Sect. III*f*) in more detail. For the moment, these data at least establish the fact that the electropolymerization reaction does involve approximately 2 electrons/molecule (Table 1).

A more quantitative estimate of the degree of oxidation in the polymer films comes from their elemental composition data (Table 1). These data reveal that all of the polymers of Table 1 are oxidized to the extent of 0.07 to 0.45. These data are, in general, consistent with the n values obtained from voltammetry.

Electrochemical aspects

Cyclic voltammetric studies of the molecules listed in Table 1 reveal that they all electrooxidize irreversibly. These data suggest that the intermediate radical cations are unstable and rather reactive. As an illustrative example, a typical cyclic voltammogram using pyrene is shown in Fig. 1. The first oxidation wave of pyrene occurs at an anodic potential of +1.33 V. Upon reversing the direction of sweep from the first oxidation wave, a corresponding cathodic wave owing to the reduction of the oxidized polymer film is observed in the region from ≃+1.0 to +0.6 V. Subsequent anodic sweeps reveal the growth of the polymer film at a lower oxidation potential, where the peak potential (E_{pa}) occurs at ca. +1.1 V. Thus, the cyclic voltammogram of pyrene has all the characteristics of an ECE reaction (15, 16), i.e., a sequence of steps whereby an electron transfer event (E) is followed by a chemical reaction (C) and a subsequent electron transfer reaction (E). Since the film-forming reaction can be described as a cascade of ECE reactions, the general term $E(CE)_n$ has been recently forwarded to describe the film-forming reactions (5).

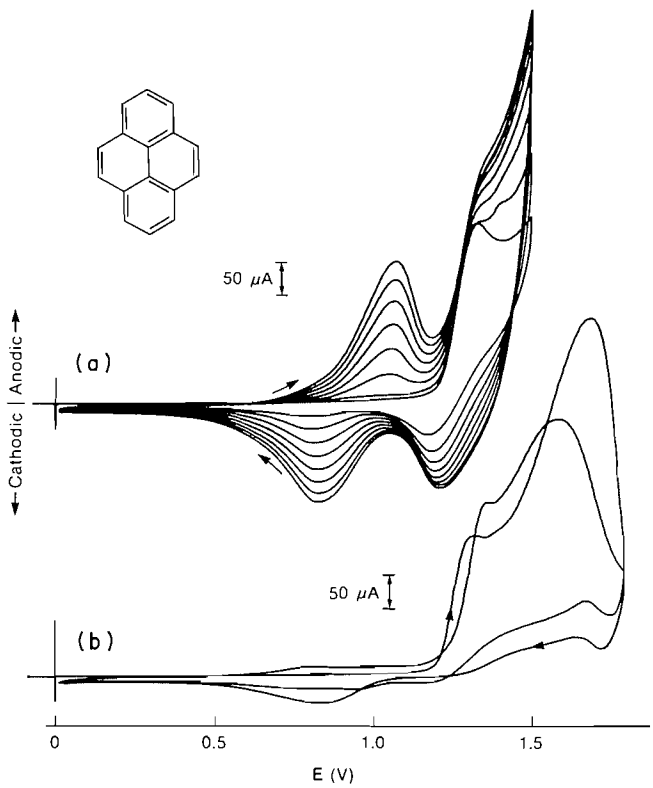

FIG. 1. Cyclic voltammogram of ≃5 μmol/cm³ pyrene in 0.1 *M* TEAFB/CH_3CN; (*a*) successive sweeps (200 mV/s) revealing growth of polymer and (*b*) two consecutive sweeps of pyrene from 0 to +1.80 V. The trace marked by the arrows is the first sweep. TEAFB is tetraethylammonium fluoroborate, an electrolyte.

Radical-cation coupling

When a molecule (R) is electrooxidized to its radical cation ($R^{+\bullet}$) at the electrode surface, the electron transfer reaction is much faster than the diffusion of R from the bulk solution to the electrode surface. Accordingly, at the applied voltage, molecules close to the electrode surface region will occur only in their oxidized state $R^{+\bullet}$. This insures a high concentration of $R^{+\bullet}$ at the electrode surface, which is continuously maintained by the steady state diffusion of R from the bulk. These monomeric radical cations can undergo a variety of follow-up reactions depending upon their intrinsic stability (4). When $R^{+\bullet}$ is relatively stable, it can diffuse away from the electrode surface and undergo reactions to form low molecular weight soluble products. If $R^{+\bullet}$ is very unstable, it can rapidly undergo indis-

criminate reactions with either the solvent or anions to form low molecular weight, and thus soluble, products equally well. Between these two stability ranges (which vary depending on the nature of $R^{+\bullet}$), $R^{+\bullet}$ can undergo dimerization reactions or "electropolymerization." These reactions are thought to proceed by the coupling of two radical cations. The concept of radical-cation coupling as a consequence of electrooxidation is not new, and has been applied before to explain the ECE reactions of many irreversible systems in which a monomer dimerizes to form a coupled product (14, 16). We wish to point out that electropolymerization reactions can be regarded as an extension of the dimerization reaction, i.e., they represent a sequence of dimerization reactions involving radical-cation coupling of $R^{+\bullet}$ with its oligomeric radical cations. Evidence for such a reaction pathway, in which chain propagation is dependent on the presence of $R^{+\bullet}$ (as opposed to R), is reflected in the following: (*a*) the cyclic voltammograms reveal an $E(CE)_n$ process, consistent with radical-cation coupling reactions; (*b*) the finding that in order to sustain film growth at the electrode surface the electrode potential (voltage) has to be maintained at the electrochemical oxidation potential of R, where R is not limited to a monomer, as evidenced by the facile electropolymerization of 2,2′-bithiophene) (17); (*c*) the film-forming reaction is surface localized, and no evidence of polymerization in the bulk of the solution has yet been observed (where for the concentrations the relation $[R] \ggg [R^{+\bullet}]$ holds); and (*d*) chronoabsorptometric studies (for R = pyrrole) reveal that polypyrrole films grow linearly with time t, and not $\sqrt{t}$. This latter finding implies that the rate-limiting step during film growth is the radical coupling process itself, and not the diffusion of monomer to the electrode surface (18). Thus, the evidence favoring the radical-cation coupling reaction is strong. In general then, the electropolymerization reaction for a molecule can be summarized by eqs. [1]–[4]. Equations [1]–[3] describe the step by step electropolymerization reaction of a monomer RH_2, while eq. [4] represents the overall electropolymerization reaction. Note that the electropolymerization reaction proceeds via an intermediate dihydro-oligomer dication, which then loses two protons to form the neutral oligomer.

$$[1]\quad RH_2 \xrightarrow[E_{pa}]{-e^-} RH_2^{+\bullet}$$

$$[2]\quad 2RH_2^{+\bullet} \rightarrow [H_2R{-}RH_2]^{2+} \xrightarrow{-2H^+} HR{-}RH$$

$$[3]\quad HR{-}RH \xrightarrow[E_{pa}]{-e^-} [HR{-}RH]^{+\bullet}$$

$$\xrightarrow{RH_2^{+\bullet}} [HR{-}RH{-}RH_2]^{2+} \xrightarrow{-2H^+} HR{-}R{-}RH$$

$$[4]\quad (X+2)RH_2 \xrightarrow[E_{pa}]{} HR{-}(R)_X{-}RH + (2X+2)H^+ + (2X+2)e^-$$

Street *et al.* (21) have observed that during the electropolymerization reaction, the pH of the solution becomes increasingly acidic, consistent with the elimination of protons during electropolymerization. The actual value of X is unknown, although recent tritium labelling studies (19) of poly-3,4-dimethylpyrrole-ClO_4 indicate that $X \simeq 750$, which corresponds to a molecular weight of $\simeq$100 000. However, Street *et al.* (19) have concluded that polypyrrole has a wide range of chain lengths, including some short-chained oligomers; therefore, such conversions may not be applicable in the usual way.

Structure–reactivity correlation

Due to the insolubility and the poorly crystalline nature of conducting polymers, characterization of their structure and physical properties has represented a considerable challenge. For example, solid state CMAS (^{13}C magic angle spinning) nmr studies of polyazulene-BF_4 films give rise to a single, broad-line resonance in the aromatic region, which only provides evidence for its ring integrity but no evidence for the linkage pattern of the monomer units in the polymer film (20). Much progress in the structural characterization of polypyrroles has been made, but the body of evidence comes primarily from a variety of indirect measurements, again due to its poorly crystalline structure (21). However, since vastly different aromatic molecules (Table 1) representing different classes of compounds have been found to electropolymerize and, moreover, since their anodic oxidation pathways are remarkably consistent, it would not be surprising if the polymer films were formed by a universal polymerization mechanism. Knowledge of this mechanism would decidedly assist characterization efforts, since a hypothetical polymer structure could be predicted. Accordingly, we have studied (13, 23) the electropolymerization reaction pathway by investigating: (*a*) the electronic structures of radical cations; and (*b*) the effect of substituents on the electropolymerization reaction. For this purpose, we will take advantage of a known (16) correlation between reactivity and the unpaired electron density of $R^{+\bullet}$, in particular with its degree of localization at a specific site. The electropolymerization reaction of pyrrole will be used as an illustrative example; however, all of the molecules listed in Table 1 follow an analogous reaction pathway.

The electrooxidation of pyrrole gives rise to polypyrrole in which the monomer units are linked primarily via their α,α′-positions (2). This hypothesis has been supported primarily by the failure of 2-substituted pyrroles to electropolymerize (2). Furthermore, oxidative degradation studies of chemically synthesized polypyrrole (25) yielded primarily 2,5-disubstituted products. Nuclear magnetic resonance studies (26) also suggest primarily α,α′-linked polypyrrole, although more recent XPS (X-ray photoemission spectroscopy) studies (27) show that as many as one out of three pyrrole rings is affected by structural disorder, part of which may be attributed to non-α,α′-linkages. Nevertheless, for a "simple" structure such as pyrrole, the gross structural features of its polymer can be predicted from the symmetry and reactivity of the pyrrole monomer. In fact, it has been suggested that the susceptibility of a given molecule towards electrophilic substitution is a valid reactivity index in determining the overall polymer linkage sites (22). Thus, polypyrrole can be expected to be (ideally) α,α′ linked, based upon the high selectivity of pyrrole to undergo electrophilic substitution at the α-positions. However, because electropolymerization proceeds via radical-cation coupling reactions, $R^{+\bullet}$ is the key intermediate species and, accordingly, its reactivity parameters are the pertinent ones. Moreover, as the electropolymerization reaction proceeds, *oligomeric* radical cations, which undergo radical coupling with other $R^{+\bullet}$ molecules, are produced at the electrode surface. As the oligomeric radical cations become larger in chain length, they become easier to electrooxidize (16, 17), and they become less reactive (23). However, electropolymerization is sustained because reactive monomer radical cations, which react with the oligomeric radical cations, are continuously produced. The site of radical coupling of $R^{+\bullet}$ to the oligomeric radical cation will depend upon the unpaired electron distribution in the oligomeric radical cation, which could be different from that of the monomeric $R^{+\bullet}$. Depending upon the unpaired electron distribution, nonregular linkages may occur. Thus, consideration of only the

TABLE 2. The π-electron density and the unpaired electron density of neutral and radical cation monomers, respectively, and their idealized polymer structures

Compound	π-Electron Density	Primary Electrophilic Reactive Site(s)	Unpaired Electron Density of Radical Cation	Ideal Polymer Structure
	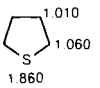 Reference 28	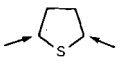 Reference 28		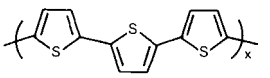 Reference 2, 12
	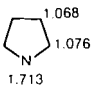 Reference 29	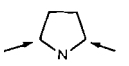 Reference 30	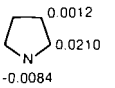 Reference 23	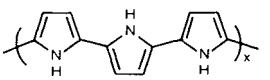 Reference 2
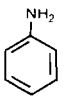	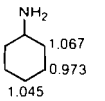 Reference 31	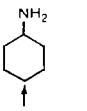 Reference 32	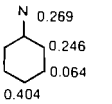 Reference 33	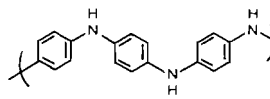 Reference 41
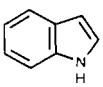	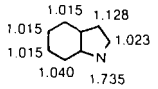 Reference 29	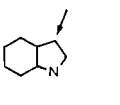 Reference 34	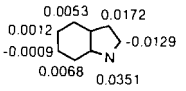 Reference 4	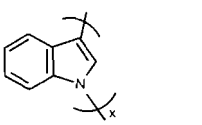 Reference 4
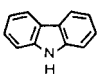	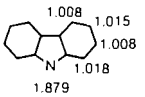 Reference 35	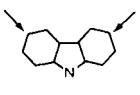 Reference 36, 37	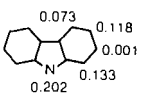 Reference 14	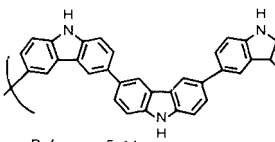 Reference 5, 14
	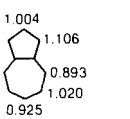 Reference 38	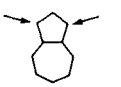 Reference 39	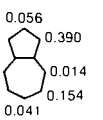 Reference 40	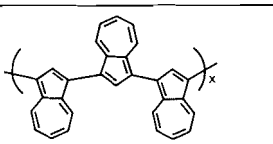 Reference 20

unpaired electron distribution of monomeric $R^{+\bullet}$ would allow, at best, extrapolation to a polymer structure whose linkage sites are the same as the reactive sites of the monomer radical cation $R^{+\bullet}$, i.e., an *idealized* polymer structure. These considerations are summarized in Table 2. Again, focussing on pyrrole as the illustrative example, it can be seen from Table 2 that the α-positions of the neutral monomer have the highest π-electron density, and accordingly, would be reactive in these positions. Thus, the primary electrophilic reactive sites are the α-positions (30). Consideration of the pyrrole radical cation also reveals that the positions of highest unpaired electron distribution are the very same α-positions, and thus, point to α,α′-linked polypyrrole. The other molecules shown in Table 2 reveal similar behavior. Thus, in general, the ideal polymer structure can be gleaned from either of the above considerations. However, because chain propagation does in fact depend upon $R^{+\bullet}$ and its oligomeric radical cations, departure from such an ideal structure based on the reactivity pattern of the monomer would not be unexpected. Thus, again utilizing the electropolymerization reaction of pyrrole as an illustrative example, we have applied INDO (intermediate neglect of differential overlap) (24) molecular orbital calculations to its various oligomeric radical cations, which occur intermediately in the electropolymerization reaction of pyrrole, to determine the trends in their reactivities and any differences which may occur in the reactivity pattern of oligomeric radical cations from their monomer radical cations. Therefore, we may determine the most probable linkage sites of the monomer units in the polymer.

The electrooxidation of monomeric pyrrole at an electrode surface gives rise to a delocalized radical cation. Our (23) INDO molecular orbital calculations reveal that, as expected, the delocalized pyrrole monomer radical cation **1** has the highest unpaired electron density at its equivalent α-positions (Fig. 2). Thus, among the resonance forms **2**–**4** shown, **3** is the most

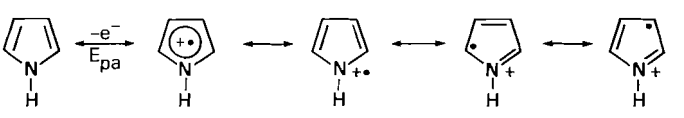

1 **2** **3** **4**

important. Accordingly, when two monomeric pyrrole radical cations dimerize, radical coupling can be expected to occur at the α-positions. Indeed, dimerization to the dihydrodimer dication **5** proceeds with great facility, followed by loss of two protons to yield the neutral 2,2′ dimer **6**. The driving force for deprotonation among other things is stabilization by return to aromaticity.

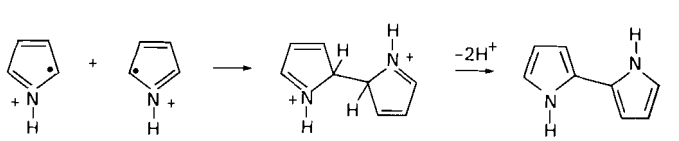

5 **6**

The $E(CE)_n$ reaction at the anode surface continues with the electrooxidation of the dimer **6** to its radical cation **7**. Since the

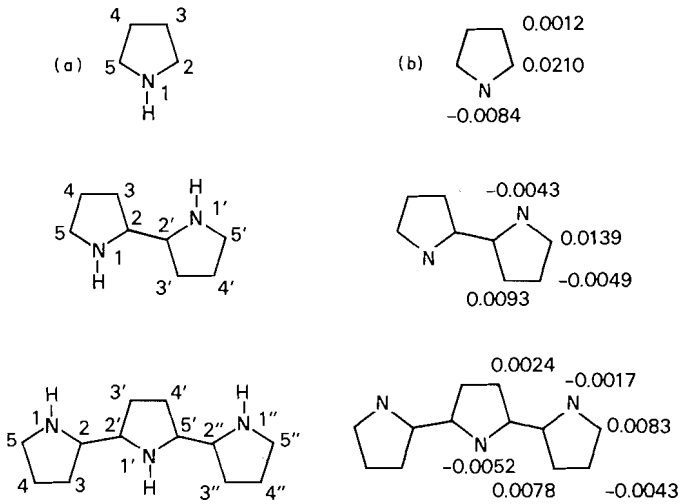

FIG. 2. (*a*) The numbering scheme for pyrrole oligomers and (*b*) open shell INDO molecular orbital calculations of the unpaired electron distribution of pyrrole, coplanar *anti* 2,2′-bipyrrole, and 2,2′:5′,2″-terpyrrole radical cations.

loss of an electron is now accommodated by two monomer units, the oxidation potential of **6** is lower than that of the monomer and should therefore be readily electrooxidized at the applied voltage (i.e., the voltage needed to electrooxidize the monomer), provided that it is not severely twisted (16). An example is given in Fig. 1. The unpaired electron distribution of the coplanar *anti* form **7** is given in Fig. 2. As was the case with the monomer radical cation, the highest unpaired electron density remains at the α-positions, namely the 5,5′-positions. However, because the unpaired electron is now distributed over two monomer units, delocalization dilutes the unpaired electron density (i.e., reactivity) of the α-positions in the dimer. Conversely, the β-positions have acquired more unpaired electron density, indicative of a different type of spin distribution in the dimer radical cation. A resulting consequence is stabilization and thus decreased reactivity of **7** in comparison with **1**. This may well account for the difficulty found in producing thick, continuous, free-standing polypyrrole films from the electrooxidation of either 2,2′-bipyrrole or 2,2′:5′,2″-terpyrrole (17), although it is reported to be possible (21).

Among the resonance forms shown for the dimer radical cation, INDO calculations (Fig. 2) predict **9** to be the predominant structure. The dimer radical cation can, therefore, be expected to continue to react primarily via the α-positions.

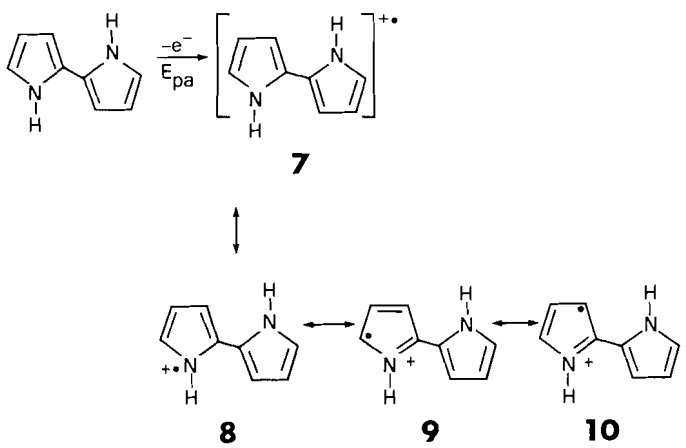

7 ↔ **8** ↔ **9** ↔ **10**

Thus, at this stage of the electropolymerization reaction, the surplus of monomer radical cations **3** at the electrode surface assures further predominance of α,α′-coupling, to yield the dihydrotrimer dication **11** that, upon deprotonation, forms the neutral trimer, i.e., 2,2′:5′,2″-terpyrrole **12**. Subsequent electrooxidation yields the radical cation **13**, for which the unpaired

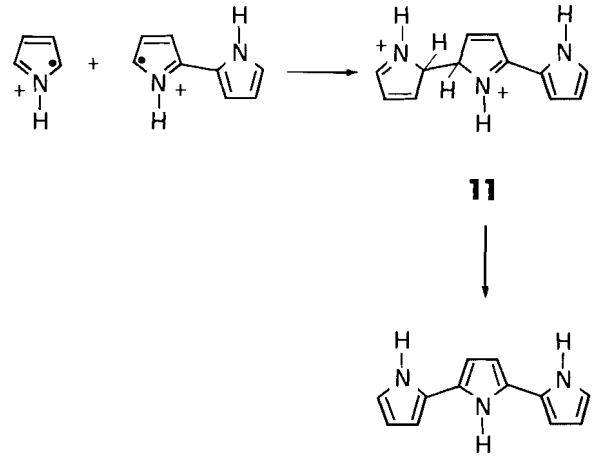

11

12

electron distribution predicted by the INDO calculations is given in Fig. 2. The radical cation **13** in its coplanar *anti* configuration is predicted to be well delocalized, with much of the unpaired electron density residing at the 2′,5′-,5,5″-, and 3,3″-positions. It is interesting to note that here the α-positions, namely the 5,5″-positions, are no longer the positions with the highest unpaired electron density. They are comparable in the magnitude of their unpaired electron densities to those predicted for the 2′,5′- and 3,3″-positions. The 2′,5′-positions should be sterically inaccessible to monomer radical-cation attack. Conversely, the 5,5″-positions can be easily attacked by the monomer radical cations, thereby propagating α,α′ linkages still further. The 3- or 3″-positions, i.e., the β-positions, are somewhat sterically hindered and, therefore, a monomer radical cation would have to couple with the trimer radical cation in a nonplanar configuration. Thus, our INDO calculations predict that monomer radical cations could in principle undergo radical coupling reactions at either the 5,5″-positions (i.e., α-positions) or the 3,3″-positions (i.e., β-positions) of these oligomeric radical cations. The above conclusion is valid only if the criterion for reaction is the unpaired electron density. However, because the β-position is somewhat sterically inaccessible, α coupling should continue to predominate. Nevertheless, the INDO calculations reveal an important trend, namely, that as oligomerization proceeds from monomer to dimer to trimer radical cations, the unpaired electron distribution pattern does indeed differ from that of the monomer radical cation. Extrapolation of this trend suggests that as the oligomer progressively increases in chain length, the extensive π delocalization which sets in will delocalize the unpaired electron over the entire oligomer, such that further radical coupling would not be overwhelmingly favored at any single position. If the INDO results are taken literally, nonregular linkages would be much more prevalent in polypyrrole than previously appreciated, and the simple picture of a regularly α,α′-bonded polypyrrole would thus be grossly incomplete. Indeed, XPS studies of polypyrrole by Street *et al.* (27) reveal that as many as one in three pyrrole rings is affected by some kind of structural

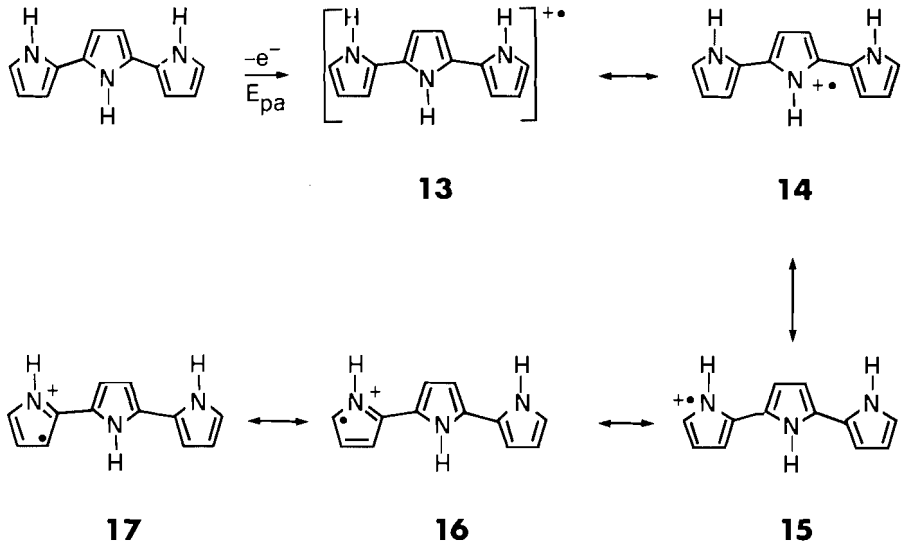

13 14

17 16 15

disorder. This may include nonregular linkages. For example, the poor crystallinity of polypyrrole (27) could in part be explained in terms of β linkages. Thus, β,β′-dimethylpyrrole, which has both β-positions blocked with methyl groups, should contain none or few β linkages, and indeed yields a much more crystalline polymer (27).

If this concept is extrapolated to a more "complex" monomer such as pyrene (see below), which has potentially many more reactive positions, then nonregular bonding can be expected to occur more frequently.

III. Substituent effects

The stoichiometric electropolymerization reaction described above is not limited to the unsubstituted parent molecules (R). Rather, some substituted forms thereof undergo electropolymerization, provided that the substituent does not dramatically affect the reactivity of the molecule. As stated previously in the introduction, substituents can influence the electropolymerization reaction by either a *steric effect* or an *electronic effect*. They can also cause changes in the overall properties of the polymer film. These aspects will now be considered for a group of monomers that electropolymerize, and which exhibit such a substituent effect.

a. Polythiophene

1. Electrochemical data

Cyclic voltammetric data for thiophene and some 3-substituted thiophenes are summarized in Table 3. In general, the reactions which produce polymer films have n values between 2 and 2.7. These include thiophene, 3-methyl-, 3-bromo-, 3-iodothiophene, and thiophene-3-acetonitrile (Table 3). Among these, the best polymer films are prepared from thiophene, 2,2′-bithiophene, and 3-methylthiophene. These thin films, when supported by an electrode surface, display electroactive and electrochromic properties (12, 13). The peak oxidation potential (E_{pa}) of polythiophene-BF_4 occurs at +1.0 V. The cyclic voltammogram of a 1-μm thick film has a peak width at half height (PWHH) of ≃300–350 mV. Polythiophene films derived from 2,2-bithiophene also have an E_{pa} of +1.0 V, as may be expected. However, its cyclic voltammogram reveals a much sharper oxidation peak with a PWHH of ≃90 mV for a 1-μm thick film. This is most probably due to the more regularly α,α′-linked monomer units in the dimer derived polymer film, and the much lower degree of hydrogen saturation of the dimer derived film (Table 4), which may preserve the regularity of the polymer film to a higher degree than the monomer derived film. This hypothesis is consistent with a more homogeneous, i.e., more regularly α,α′-linked polymer film. A more uniform distribution of polymer chains can be expected to yield a much sharper peak.

With the introduction of a β-methyl substituent, the polymer film is much more easily oxidized. A cyclic voltammogram of poly-3-methylthiophene shows similar features (Fig. 3): The presence of β-methyl substituent shifts the E_{pa} by ca. 300 mV cathodic of the E_{pa} of the unsubstituted polymer film, and is therefore electroactive in a region considerably less anodic than polythiophene. Also, the PWHH for a 1-μm thick film of poly-3-methylthiophene is ≃200 mV, considerably sharper than the parent polythiophene, although still not as sharp as the film derived from the 2,2′ dimer. Thus, we find that polythiophene films, when appropriately substituted, are electroactive in different regions of the electrochemical voltage scale.

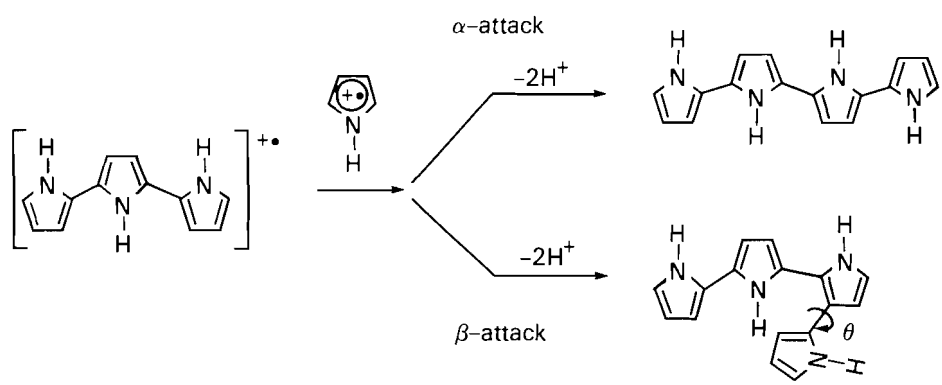

TABLE 3. Cyclic voltammetric data for thiophenes: monomer concentration 8.9–23.0 μmol cm^{-3} in 0.1 *M* TEAFB/CH_3CN with sweep rate 40 mV s^{-1} (ref. 13)

Compound	Monomer E_{pa} (V)	Monomer ($A\ cm\ s^{1/2}\ mol^{-1}\ V^{-1/2}$)	Monomer n	Polymer E_{pa} (V)
Thiophene	2.06	3791	2.7	0.96
3-Methylthiophene	1.86	3203	2.4	0.72
3-Iodothiophene	2.03	2362	2.0	
3-Bromothiophene	2.10	3085	2.3	1.06
3-Thiopheneacetonitrile	2.22	2725	2.2	1.12
3-Thiophenecarboxylic acid	2.28	1031	1.2	
3-Cyanothiophene	2.46	2260	1.9	
3-Nitrothiophene	2.69	2476	2.0	

TABLE 4. The elemental composition and electrical conductivity of some polythiophene films: f = film; p = pressed polymer

Compound	Elemental composition	σ (S/cm)	Reference
Thiophene	$C_{4.0}H_{3.3}S_{0.9}(BF_4)_{0.07}$	0.02(f)	12, 13
	$C_4H_2S(ClO_4)_{0.30}$	10–20(p)	45
	$C_4H_2S(BF_4)_{0.30}$	10–20(p)	45
	$C_4H_2S(CF_3SO_3)_{0.30}$	10–20(p)	45
	$C_{4.0}H_{2.0}S_{0.98}(BF_4)_{0.05}$	$\sim 10^{-1}$(f)	46
	$C_{4.0}H_{2.0}S_{0.92}(ClO_4)_{0.13}$	$\sim 10^{-1}$–1(f)	46
2,2′-Bithiophene	$C_{4.0}H_{2.1}S_{1.0}(HSO_4)_{0.17}$	0.1(f)	12,13
3-Methylthiophene	—	1(f)	12
	$C_5H_4S(ClO_4)_{0.25}$	10–30(p)	45
	$C_5H_4S(CF_3SO_3)_{0.30}$	30–100(p)	45
	$C_{5.0}H_{4.4}S_{0.98}(ClO_4)_{0.18}$	~100(f)	46
3,4-Dimethylthiophene	$C_6H_6S(CF_3SO_3)_{0.30}$	10–50(p)	45
	—	10^{-3}(f)	27

The electropolymerization of 3-thiopheneacetonitrile, and of 3-bromo- and 3,4-dibromothiophene is accompanied by much discoloration of the acetonitrile solution. This suggests that significant amounts of soluble products are produced simultaneously with the film-forming reaction. Polymer films are not obtained from 3-thiophene carboxylic acid and 3-cyano- and 3-nitrothiophenes. Thus, not all of the thiophene monomers electrooxidize to produce films. However, for those that do, a plot of the E_{pa} monomer versus E_{pa} polymer yields a structure–property correlation between thiophene monomers and their respective polymers (12). In particular, a linear correlation is obtained (Fig. 4), suggesting that the β-substituted monomers and their respective polymers are made up of a related system of π electrons, consistent with the fact that polythiophenes ought to consist primarily of α,α′-linked monomer units.

2. Hammett correlation and electropolymerization

In Fig. 5, the E_{pa} of some 3-substituted thiophenes are plotted against their respective Hammett substituent constants (σ^{+i}, according to Brown and Okamoto, see ref. 42). While E^0 should be used for this treatment, only the E_{pa} values are available for these irreversible reactions. However, we have shown (43) recently that the E_{pa} values are close to the E^0 values within a regular series of substituted fluorenes which electropolymerize. Thus, by analogy, the E_{pa} values of irreversible systems such as thiophenes must be close to, or linearly related to E^0 within a regular series. Accordingly, the shift in the E_{pa} values of the series of β-substituted thiophenes is dependent on three parameters, namely their polar, steric, and mesomeric effects (44). This behavior can be described by the usual Hammett–Taft equation:

$$[5] \quad E = \rho_\pi \sigma^{+i} + S$$

where $\rho_\pi \sigma^{+i}$ describes the polar-mesomeric effects, and S accounts for the steric factor (44). From these considerations, Fig. 5 allows three conclusions to be drawn. First of all, the straight line fit with a slope of $m = 0.80$ indicates that all of the monomers electrooxidize by the removal of a π electron from the thiophene ring. Secondly, the positive sign for the substituent constant ρ_π reveals that as the substituents take on more electrophilic character, the oxidation of the corresponding thiophene monomers proceeds with more difficulty. Finally, the steric term S appears to be minimal for the electrooxidation reaction of the thiophene monomers. Therefore, the primary effect exerted by the β-substituents is *electronic* and described by the $\rho_\pi \sigma^{+i}$ term. Thus, it appears that there is an optimum reactivity of the radical-cation intermediate which favors radical-cation coupling in the follow-up reaction to yield polymeric films. In this case, polymer films are obtained from thiophene, 3-methyl-, 3-bromo-, and 3-iodothiophenes. However, thick, free-standing conducting films are obtained only from the parent and methyl-substituted thiophene monomers (13). 3-Bromo- and 3-iodothiophene yield poorly conducting thin films. 3-Thiophenecarboxylic acid and 3-cyano- and 3-nitrothiophene yield no polymer films. Several reasons may be attributed to this

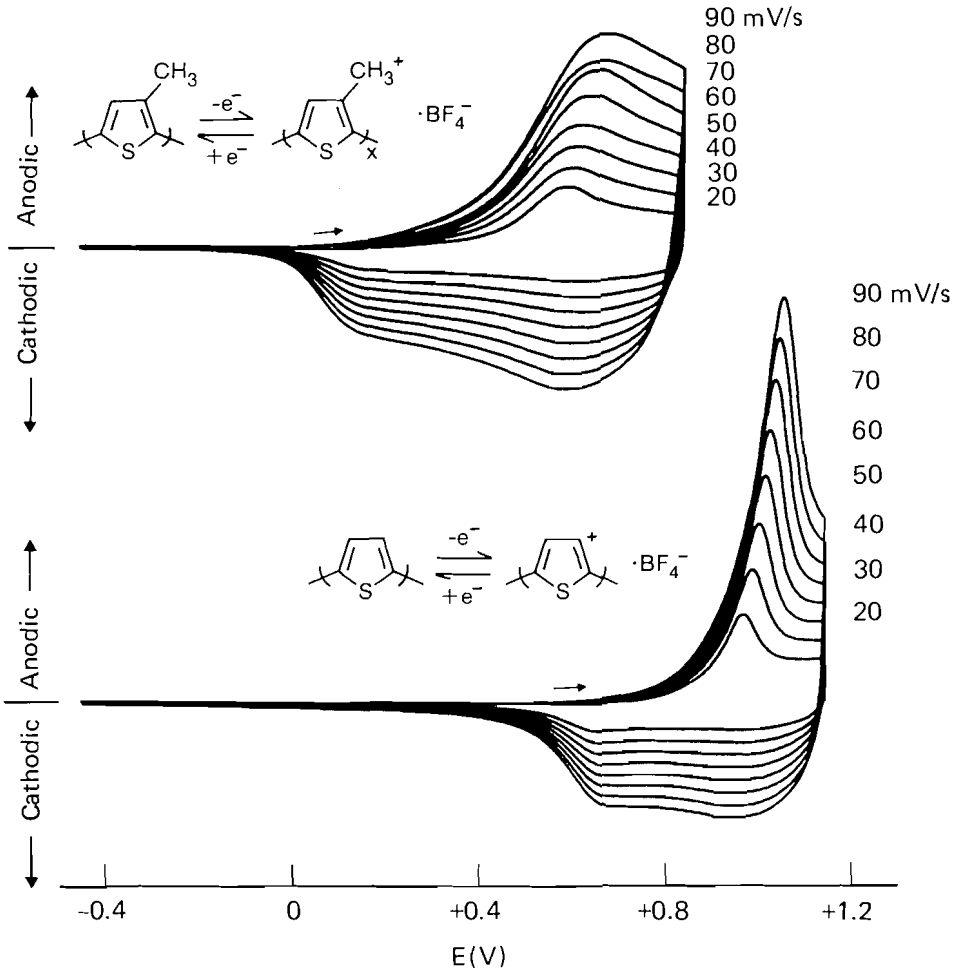

FIG. 3. Cyclic voltammograms of poly-1-methylthiophene-BF_4 (top figure) and polythiophene-BF_4 (bottom figure), in 0.1 *M* TEAFB/CH_3CN containing no other electroactive species.

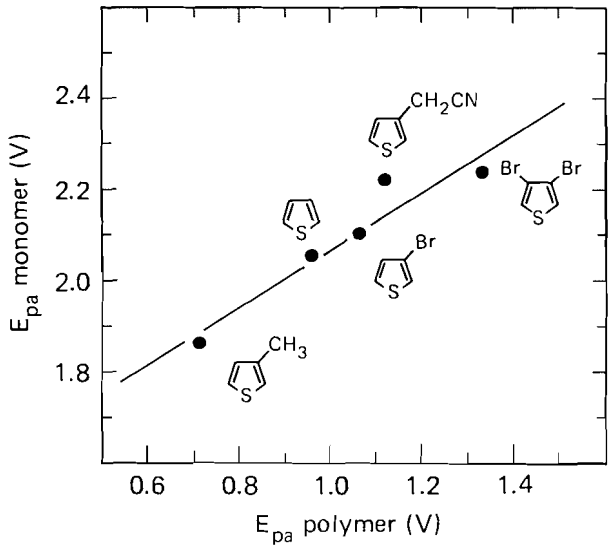

FIG. 4. Peak oxidation potential of thiophene monomers versus their respective polymers in 0.1 *M* TEAFB/CH_3CN.

finding. One interpretation postulates that the stability (or reactivity) of these monomers is affected by the β-substituents. As the reactivity of the radical cation increases, as reflected in their increasing oxidation potentials (Fig. 5), the more reactive they become. Thus, strongly electron-withdrawing groups destabilize the radical-cation intermediate such that its decreased lifetime favors rapid reaction with solvent or anions to form soluble products, rather than to electropolymerize.

While steric effects do not appear to play any significant role in the electrooxidation of the monomer, their subsequent follow-up reactions (such as electropolymerization) may be more susceptible to steric effects that, therefore, may well play a role in deciding whether the electropolymerization reaction can compete favorably with other accessible follow-up reactions, such as dimerization or capture by solvent. This may explain the overall inferior quality of the polymer films derived from 3-bromo- and 3-iodothiophenes, since their oxidation potential is not much different from the parent, and since halogens do not usually exert a strong electronic substituent effect. It is, however, interesting to note that while a 3-methyl substituent allows facile electropolymerization, a less bulky 3-cyano substituent altogether suppresses electropolymerization. Again, this is consistent with the interpretation of electronically induced substituent effects.

Thiophenes in which the 2-position is substituted do not electropolymerize, presumably due to blockage of the reactive α-position.

3. Polymer composition and electrical conductivity

The electrical conductivities of variously substituted polythiophene films are summarized in Table 4. Their elemental analyses reveal that the basic monomer units are preserved in the polymer films, and that their level of oxidation varies from ≈0.05 to 0.30. In general, polythiophenes have electrical

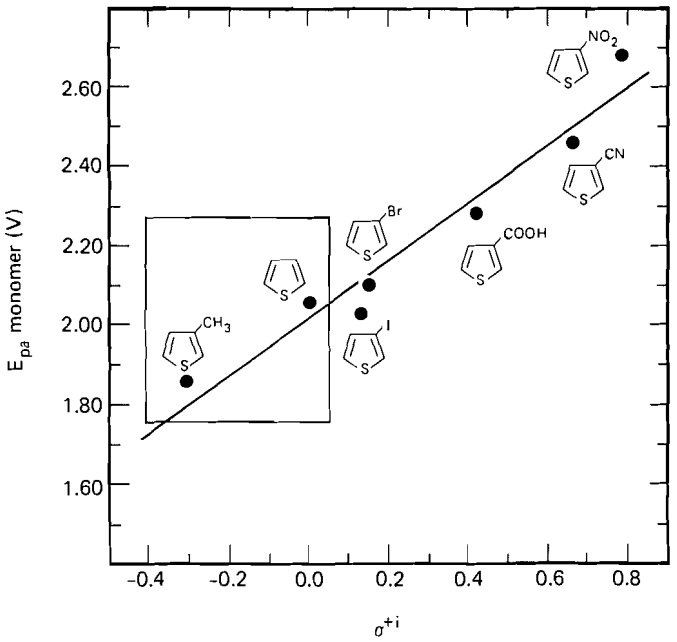

FIG. 5. Electrochemical peak oxidation potential of thiophene monomers versus their respective Hammett substituent constants. The monomers enclosed within the square electropolymerize.

conductivities between 10^{-2} and 20 S/cm, depending on the growth conditions (Table 4) and the counteranion that is incorporated into the polymer film. These values strongly depend on the exact nature of the polymerization conditions, which explains the variances that are observed in the electrical conductivity and film quality of polythiophene films (Table 4). Despite these shortcomings, the agreement is generally good. Comparisons with derivatized polythiophene films reveal that, in general, the addition of a 3-methyl substituent enhances the electrical conductivity of polythiophene by a factor of ≈10–1000 (Table 4). Thus, we see a case in which the electrical conductivity of a parent polymer is actually improved by the addition of a substituent. For polymer films derived from 3,4-dimethylthiophene (27, 45), the results are less definitive. In one case, pressed films of poly-3,4-dimethylthiophene-CF_3SO_3 exhibit conductivities as high as 50 S/cm (45). On the other hand, free-standing films derived from perchlorate anions (27) exhibit conductivities of 10^{-3} S/cm.

Hotta *et al.* (46) have shown that the preparation temperature of polythiophene films has a significant effect on the polymer film properties. In particular, films that were prepared at lower temperatures were consistently higher in their electrical conductivity than those prepared at room temperature. This was especially prominent for polythiophene-SO_4 films, whose electrical conductivity was higher by a factor of $\sim 10^3$ when prepared at 5°C compared with room temperature (46). Films prepared at the lower temperatures were also found to be more dense and tougher than their room temperature counterparts (46).

b. Poly-1-substituted pyrroles

*1. Poly-*n*-alkylpyrroles*

Another example in which substituents give rise to modifications in polymer film properties comes from 1-alkyl-substituted pyrroles (48). These data are summarized in Table 5. In particular, the electrical conductivity of the 1-alkyl-substituted pyrroles decreases with increasing size of the alkyl substituent (48). Thus, while polypyrrole films have an electrical conductivity of 100 S/cm, poly-1-methylpyrrole has a conductivity of 10^{-3} S/cm, and poly-1-isobutylpyrrole 10^{-5} S/cm. Also, the level of oxidation in the polymer films shows a decreasing trend with increasing size of the substituent (Table 5). The quality and yield of the polymer films also become poor with the larger alkyl substituents. From these results, it was concluded that the alkyl substituents alter the polymer film properties solely via a steric effect (48).

TABLE 5. The oxidation potential, oxidation level, and electrical conductivity of *N*-alkyl substituted pyrroles and polypyrroles. Data taken from Diaz *et al.* (48)

N-alkyl Group	E_{pa} (monomer) (V)	Oxidation level of polymer	σ (S/cm)
H	1.20	0.25–0.30	100
CH_3	1.12	0.23–0.29	10^{-3}
CH_2CH_3	1.22	0.20	10^{-3}
$CH_2CH_2CH_3$	1.26	0.20	10^{-3}
$CH_2CH_2CH_2CH_3$	1.22	0.11	10^{-4}
$CH_2CH(CH_3)_2$	1.24	0.08	10^{-5}

*2. Poly-*p*-substituted* n*-phenylpyrrole*

The substituent effects exerted by *p*-substituted *n*-phenylpyrroles are much more subtle than 1-substituted pyrroles since the electronic substituent effect is first transmitted through a phenyl ring before the pyrrole structure is affected. Furthermore, if the phenyl ring is twisted relative to the pyrrole moiety, the substituent effect is further diluted. Thus, the substituent effect is expected to be rather modest, and this is indeed the case (49). Salmon *et al.* (49) have plotted the E_{pa} of a variety of *p*-substituted *n*-phenylpyrroles versus their respective substituent constants, and obtained a straight line of slope $m = 0.16$, much less than that obtained for the 3-substituted thiophenes ($m = 0.80$) discussed previously. They have also obtained a straight line plot ($m = 0.18$) from a plot of the E_{pa} of poly-*p*-substituted *n*-phenylpyrroles as a function of σ^{+i}. From these data, they have concluded that substituents affect the *p*-substituted *n*-phenylpyrroles and their respective polymers similarly (49).

The assertion may be further verified if a plot of the E_{pa} values of the monomers against their respective polymers yields a linear correlation. Such a plot has been constructed in Fig. 6, utilizing the data of Salmon *et al.* (49). A least-squares fit yields approximately a straight-line fit, albeit a correlation coefficient of only 0.77. However, this serves to substantiate the structure–property correlation between monomers and their respective polymers, as discussed previously with poly-3-substituted thiophenes.

c. Polyindole

1. Electrochemical data

Cyclic voltammetric data for indole and some 5-substituted indoles are summarized in Table 6 (4). In general, the film-forming reactions have *n* values of approximately 2, as do the thiophenes (Sect. III*a*). These values are consistent with the *n* values obtained from elemental analysis (see below) and constant potential electrolysis. The constant potential electrooxidation of indole itself produces a light-green colored solution, and a green-black polymer film is deposited at the electrode surface. Among the substituted indoles that electropolymerize (Table 6), 5-cyanoindole and indole-5-carboxylic acid produce the best

TABLE 6. Cyclic voltammetric data of 0.5–2.0 μmol/cm^3 of indole and 5-substituted indole monomers in 0.1 *M* tetrabutylammonium perchlorate – acetonitrile versus NaSCE

Compound	E_{pa} (V)	$i/AC\nu^{1/2}$ (A cm s$^{1/2}$ mol^{-1} V$^{-1/2}$)	n	Polymer film formation
Indole	1.26	2867	2.1	+
5-Aminoindole	0.64	746	0.9	−
5-Hydroxyindole	0.90	—	—	−
5-Methoxylindole	1.12	2378	1.9	−
5-Methylindole	1.14	2617	2.0	−
5-Bromoindole	1.30	2804	2.1	+
5-Chloroindole	1.31	2651	2.0	+
5-Fluoroindole	1.52	2254	1.8	+
5-Indole carboxylic acid	1.40	2512	1.9	+
5-Cyanoindole	1.59	2782	2.1	+
5-Nitroindole	1.70	3419	2.4	−

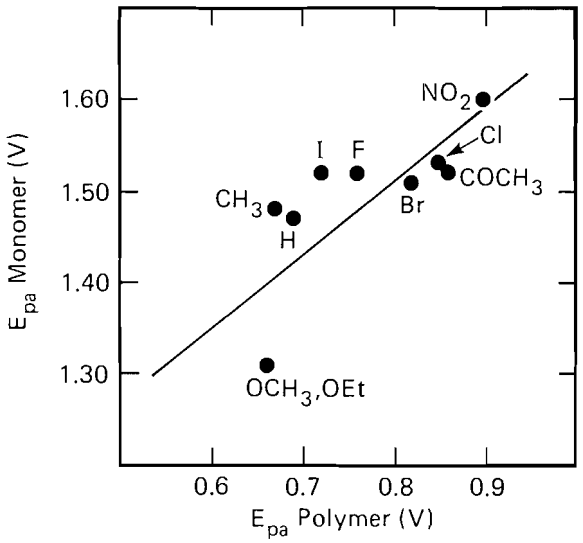

FIG. 6. Peak oxidation potential of *p*-substituted *N*-phenylpyrrole monomers versus their respective polymers, constructed from the data of Salmon *et al.* (49).

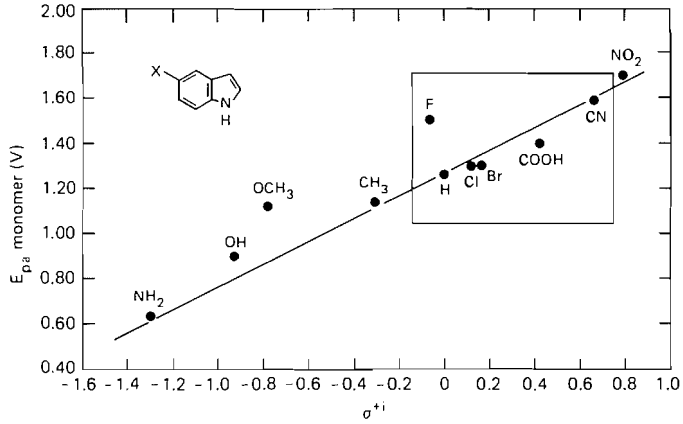

FIG. 7. Electrochemical peak oxidation potential of indole monomers versus their respective Hammett substituent constants. The monomers enclosed within the square electropolymerize.

films. The relative yields are 0.6, 0.5, and 0.4 mol/F (F = faraday) for indole-5-carboxylic acid, 5-cyanoindole, and indole, respectively.

From the electrooxidation of a wide variety of substituted indoles, it was found (4) that polymers can be obtained when substituents are present on the benzene ring, but not when they are present on the five-membered ring of indole. These included bulky substituents, such as with 5-chloro- or 5-bromoindole. Thus, these data suggested that the linkage sites of the monomer units in polyindole occur away from the benzene ring, namely at the five-membered ring of indole. Therefore, substituents on the benzene ring should have only an electronic but not a steric influence on the reactive radical cation.

2. Hammett correlation and electropolymerization

In Fig. 7, the E_{pa} of some 5-substituted indoles plotted against their respective Hammett substituent constants are shown. As observed previously for the thiophenes (Sect. III*a*), a linear correlation is obtained. Thus, electrooxidation of 5-substituted indoles results in a π-delocalized radical cation. The linear correlation also suggests that steric effects (see eq. [5]) are not important in the electrooxidation step. The slope obtained for the indole series is $m = 0.56$, smaller than that found previously for the thiophene series ($m = 0.80$). This indicates a less-pronounced substituent effect for the indole series, which can be accounted for in terms of its much larger π-structure, as well as to the fact that the substituents are further removed from the reactive sites, i.e., on an adjacent benzene ring.

Among the 5-substituted indoles, electropolymerization is observed when they are substituted with electron-withdrawing groups, and not with electron-donating groups (Fig. 7). The exceptions are the strongly destabilizing nitro substituent, and the weakly donating fluorene substituent. Since the 5-substituents exert only an electronic effect, inspection of Fig. 7 suggests that there is an optimum region in which the reactivity of the indole radical cation is well suited for the radical-cation coupling reaction, i.e., electropolymerization. Appropriate substituents can push indole in or out of this optimum region. Thus, with the more strongly electron-donating substituents such as a methyl or methoxy, the indole radical-cation intermediate becomes sufficiently stabilized to diffuse away from the electrode surface during its increased lifetime. The previously postulated tendency of the radical cations to undergo coupling reactions (Sect. II) would thus become reduced in favor of reactions in which the radical-cation intermediates would be captured by nucleophiles or solvent outside of the electrode surface region. Conversely, electron-withdrawing substituents up to the cyano group do not push the indole radical cation out of its optimum reactivity range (with respect to radical-cation coupling), and

TABLE 7. Open shell INDO molecular orbital calculations of the unpaired electron densities of some 5-substituted indole monomer radical cations (ref. 4)

	X						
Position[a]	NH_2	OH	CH_3	F	H	CN	NO_2
1	0.0074	0.0331	0.0353	0.0357	0.0351	0.0352	0.0349
2	−0.0039	−0.0123	−0.0130	−0.0132	−0.0129	−0.0130	−0.0130
3	0.0035	0.0138	0.0161	0.0159	0.0172	0.0169	0.0161
4	0.0097	0.0062	0.0053	0.0049	0.0053	0.0051	0.0052
5	−0.0022	0.0042	0.0030	0.0034	0.0012	0.0020	0.0030
6	0.0030	−0.0055	−0.0031	−0.0039	−0.0009	−0.0018	−0.0035
7	−0.0022	0.0081	0.0078	0.0076	0.0068	0.0071	0.0075
8	0.0049	−0.0069	−0.0067	−0.0070	−0.0057	−0.0062	−0.0069
9	−0.0051	−0.0031	−0.0037	−0.0033	−0.0046	−0.0042	−0.0036
(X)	0.0299(N)	0.0024(O)	−0.0018(C)	0.0004(F)		−0.0019(C) 0.0008(N)	−0.0002(N)

[a] 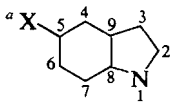

thus electropolymerization is still possible. This behavior is opposite to that observed with the thiophenes (Sect. III*a*), whereby electropolymerization is suppressed by electron-withdrawing substituents, but not with a donating methyl group. This comparison serves to illustrate that, because the intrinsic stability of radical cations varies according to their structure, substituent effects need not follow the same pattern.

3. *Electronic structure of 5-substituted indoles: an INDO study*

In order to qualitatively investigate the "push–pull" effect of substituents on the indole moiety, open-shell INDO (24) calculations were performed. These results are summarized in Table 7. The indole radical cation is characterized by high unpaired electron densities at the 1- and 3-positions of the five-membered ring. The unpaired electron densities in the adjacent benzene ring are comparatively low. Thus, delocalization into the benzo-moiety of indole does not seem to be attractive, possibly because such resonance structures would require a loss of aromaticity of the six-membered ring. The indole radical cation can accordingly be represented via the resonance structures as shown below. The high unpaired electron density at the 1- and 3-positions identify these as the reactive sites, and also suggest that the monomer linkages in the polymer do occur in these same

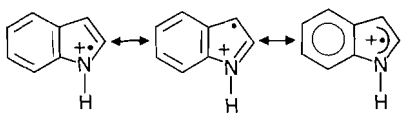

positions, at least in an idealized structure for polyindole (Sect. II, Table 2).

Since the INDO calculations (Table 7) reveal that the unpaired electron density in indole is primarily localized in the five-membered ring, the electronic push–pull effects exerted by the 5-substituents can be expected to be mild. This appears to be the case indeed. The electronic structure of indole with a strongly destabilizing group such as cyano is similar to the parent. 5-Cyanoindole would therefore be expected to electropolymerize, and does so (4). The exception is 5-nitroindole, which does not electropolymerize even though its unpaired electron distribution is not too different from indole itself. It is important to emphasize here that the value of the INDO calculations comes from evaluating the *trends* which result from substitution, rather than from evaluating the data in any quantitative manner. In this way, some insights into the aptitude of any given molecule to electropolymerize, and its reactive sites, may be ascertained.

The *trend*, which is observed in the indole radical cation when substituted with increasingly electron-donating substituents, is one of decreasing unpaired electron density in the five-membered ring, concomitant with an increase in the unpaired electron density in the benzene ring. With 5-aminoindole, most of the unpaired electron is localized on the substituent nitrogen atom. Because of the decreasing reactivity at the 1- and 3-positions, radical-cation coupling becomes less likely as the substituent becomes more electron donating. This is indeed observed experimentally, where 5-methyl-, 5-methoxy-, 5-hydroxy-, and 5-aminoindole are found not to electropolymerize (Fig. 7). These findings establish two very important results: First, $R^{+\bullet}$ can undergo a variety of reaction pathways, depending upon its intrinsic stability. When $R^{+\bullet}$ is relatively stable, it can diffuse away from the electrode surface and undergo reactions to form soluble products. If $R^{+\bullet}$ is a highly unstable radical-cationic species, it can rapidly undergo indiscriminate reactions with either the solvent or anions to yield soluble products. In between these two stability extremes, $R^{+\bullet}$ can undergo electropolymerization. These findings also imply the possibility of electropolymerization of a substituted monomer that would otherwise not have electropolymerized in its unsubstituted form. Secondly, these data indicate that substituents, even when removed from the reactive position such that *steric effects* are unimportant, nevertheless can suppress the electropolymerization reaction by *electronic effects*.

TABLE 8. Elemental composition and electrical conductivity of pressed films of polyindole and polythianaphthene

Compound	Elemental composition	(ohm cm)$^{-}$
Indole	$C_{8.0}H_{6.13}N_{0.98}(ClO_4)_{0.34}$	0.020
Indole-5-carboxylic acid	$C_{9.0}H_{6.60}N_{1.02}(ClO_4)_{0.25}$	0.024
5-Cyanoindole	$C_{9.0}H_{5.21}N_{1.94}(ClO_4)_{0.23}$	0.014
Thianaphthene	$C_{8.0}H_{5.35}S_{0.99}(ClO_4)_{0.16}$	0.008

TABLE 9. Cyclic voltammetric data for azulene and some azulene derivatives

Compound	E_{pa} (V)	$i/AC\nu^{1/2}$ (A cm s$^{1/2}$ mol^{-1} V$^{-1/2}$)	n	Polymer film
Azulene	0.96	2855	2.1	+
4,6,8-Trimethylazulene	0.90	1048	1.1	+
Guaiazulene	0.73	949	1.0	−
1-*tert*-Butylazulene	0.91	1644	1.5	−
1,3-di-*tert*-Butylazulene	0.85	1112	1.1	−
4,6,8-Trimethyl-1-azulenealdehyde	1.26	880	1.0	−

NOTE: + indicates polymer formation.

4. Polymer composition and electrical composition

The elemental analyses and electrical conductivities of some substituted polyindoles are summarized in Table 8. Their elemental analysis reveals that the basic monomer unit and substituent are preserved in the polymer films. Their level of oxidation varies from 0.23 to 0.34. Polyindoles are poorly electrically conducting, as seen in Table 8. Their conductivities are between 10^{-5} and 10^{-4} S/cm. These data establish that a high uptake of counteranions does not necessarily give rise to highly conducting polymers (Table 1).

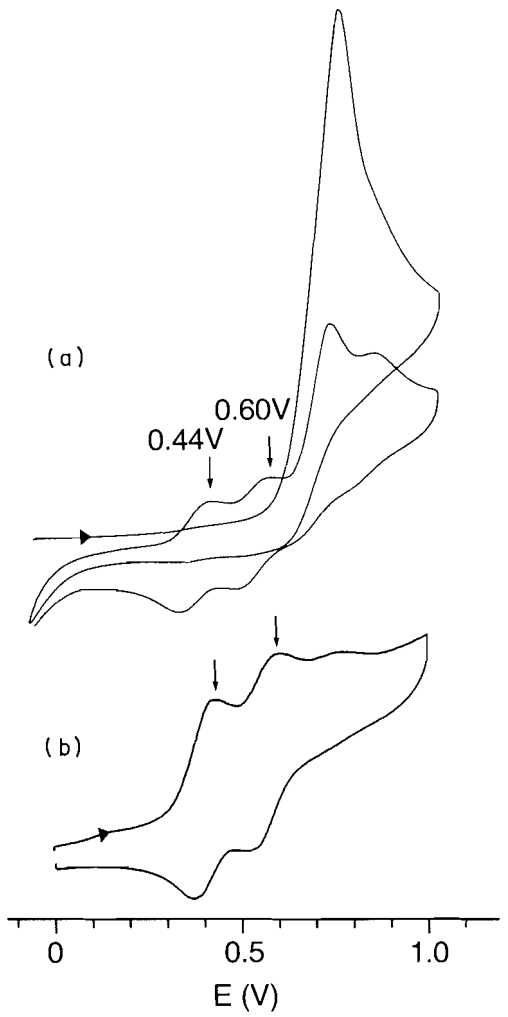

FIG. 8. Cyclic voltammogram in 0.1 *M* TEAFB/CH_3CN of: (*a*) guaiazulene, showing formation of the 3,3′ dimer on the second sweep (500 mV/s), and (*b*) the authentic 3,3′-biguaiazulene dimer.

d. Polyazulene

1. Electrochemical data

Cyclic voltammetric data for azulene and some 1-substituted azulenes are summarized in Table 9. All of the monomers electrooxidize irreversibly, except for 1,3-di-*tert*-butylazulene, which exhibits a reversible redox reaction. Among the monomers shown in Table 9, electropolymerization is observed only for azulene and 4,6,8-trimethylazulene. 1-Substituted azulenes do not electropolymerize, but instead form soluble products. These reactions are characterized by n values of $\simeq 1$, which is indicative of the formation of dimeric products (50). The formation of these dimers can be observed via cyclic voltammetry utilizing rapid sweep rates. For example, successive sweeps in the cyclic voltammogram of monomeric guaiazulene (Fig. 8) reveal the formation of 3,3′-biguaiazulene, which exhibits a two-wave reversible redox couple. These new peaks are in good agreement with the cyclic voltammogram of authentic 3,3′-biguaiazulene (Fig. 8). These data suggest that the equivalent 1- and 3-positions of azulene are important for electropolymerization. When the 1-position of azulene is blocked with a substituent, only dimerization occurs upon electrooxidation. This finding is consistent with the electronic structure of the azulene radical cation (40), which reveals that the positions of highest unpaired electron density occur at the equivalent 1- and 3-positions. These data identify them as the reactive positions, and also suggest that, in the idealized structure of polyazulene (Table 2), the monomer linkages in the polymer do occur in these same positions (Fig. 9). Thus, 1-substituents on azulene sterically hinder the electropolymerization reaction, much as 2-substituents block the electropolymerization reaction of pyrrole (2) or thiophene (12).

e. Polyfluorene

1. Electrochemical data

Cyclic voltammetric data for fluorene and some 1-substituted fluorenes are summarized in Table 10. As shown, the monomers that electropolymerize have n values in excess of 2.0. These include fluorene, and 1-methyl- and 1-methoxyfluorene.

2. Hammett correlation and electropolymerization

The E_{pa} values of some 1-substituted fluorenes plotted against their respective Hammett substituent constants are shown in Fig. 10. As seen previously with the thiophene series (Sect. III*a*) and the indole series (Sect. III*c*), a linear correlation is obtained (Fig. 10). Thus, the electrooxidation of 1-substituted fluorenes produces a delocalized radical cation whose substituents exert an electronic push–pull effect in a predictable manner. The slope of the line is $m = 0.18$, which does not indicate a pronounced substituent effect, at least when compared with the thiophenes series ($m = 0.80$) or the indole series ($m =$

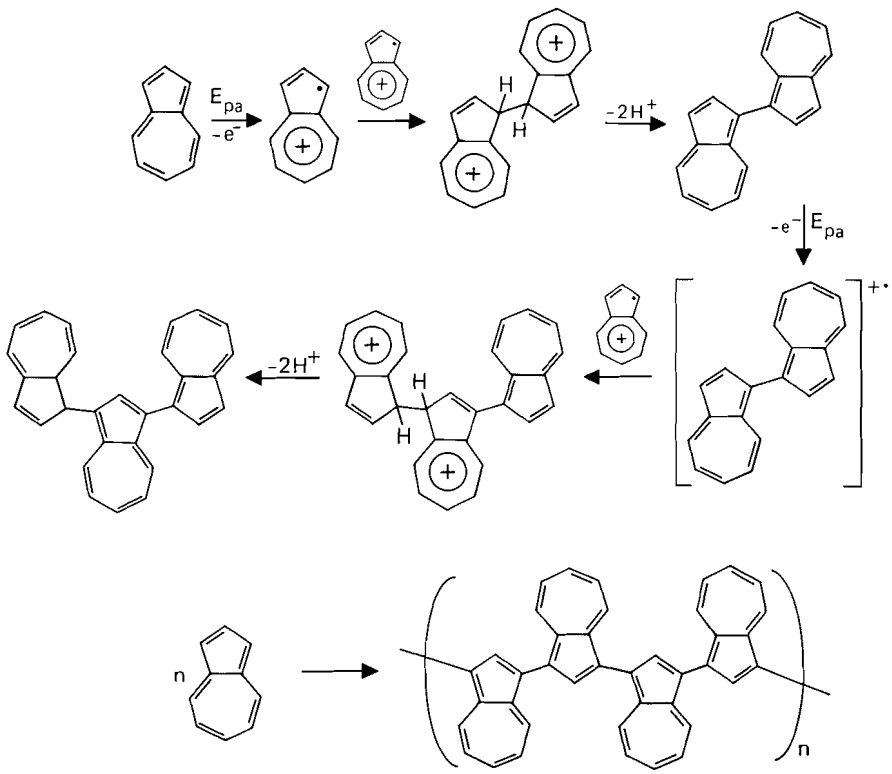

FIG. 9. A possible electropolymerization pathway for azulene.

TABLE 10. Cyclic voltammetric data for 2–5 μmol/cm^3 of fluorene and 1-substituted fluorenes in 0.1 *M* TEAFB/CH_3CN

Compound	E_{pa} (monomer) (V)	$i/AC\nu^{1/2}$ (A cm s$^{1/2}$ mol^{-1} V$^{-1/2}$)	n	Polymer film
Fluorene	1.86	3683	2.5	+
1-Hydroxyfluorene	1.63	1931	1.6	−
1-Methoxyfluorene	1.66	3791	2.5	+
1-Methylfluorene	1.78	3925	2.6	+
Fluorene-1-carboxylic acid	1.87	—	—	−

0.56). This may be attributed to the larger π structure of fluorene over thiophene or indole, which dilutes the substituent effect to a greater degree.

Among the 1-substituted fluorenes, electropolymerization is observed with the fluorenes that are substituted with electron-donating groups. These include the 1-methoxy- and 1-methylfluorenes. No electropolymerization is observed with the more strongly electron-donating hydroxy substituent, which stabilizes the delocalized fluorene radical cation such that electropolymerization is no longer a favorable follow-up reaction. Instead, its increased lifetime allows it to diffuse away from the electrode, and react to form soluble products. With the electron-withdrawing carboxylic acid group, the failure to electropolymerize indicates that the fluorene radical cation is sufficiently destabilized, and therefore very reactive. The unstable intermediate is rapidly captured by solvent or anion to produce soluble products.

3. Electronic structure of fluorene: an INDO study

INDO (24) molecular orbital calculations of the fluorene radical cation (51, 52) indicate that the positions of highest unpaired electron density occur at the equivalent 2- and 7-positions (Fig. 11). Thus, in the idealized structure of polyfluorene, the monomer units can be expected to be primarily 2,7 linked. The addition of substituents at the 1-position alters the distribution of the unpaired electron density and the stability of the fluorene radical cation, which in turn affects its aptitude to electropolymerize. With increasingly electron-donating substituents (methyl, methoxy, hydroxy), the unpaired electron-density distribution is increasingly localized within the substituted benzene ring, and the reactive 7-position becomes increasingly unreactive. As shown in Fig. 10, the electropolymerization cut-off point is reached at the methoxy substituent, and no electropolymerization is observed with fluorene substituted with a more electron-donating substituent such as a hydroxy.

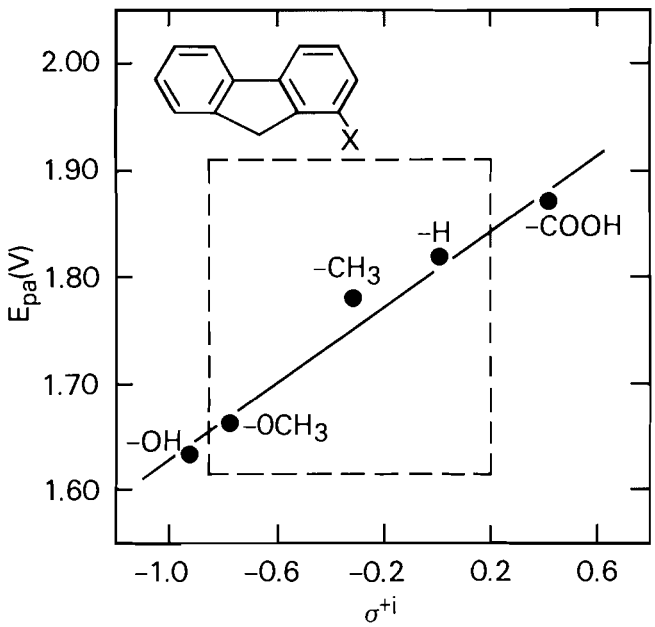

FIG. 10. Electrochemical peak oxidation potential of fluorene monomers versus their respective Hammett substituent constants. The 1-substituted fluorenes enclosed within the square electropolymerize.

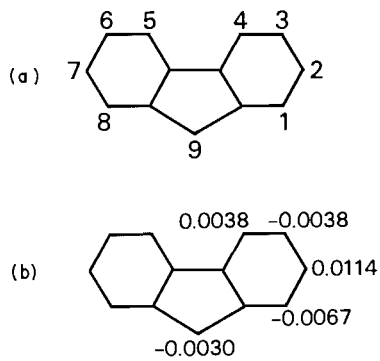

FIG. 11. (*a*) The numbering scheme for fluorene, and (*b*) open shell INDO molecular orbital calculation of the unpaired electron density of the fluorene radical cation.

TABLE 11. Elemental composition and electrical conductivity of some polyfluorenes (pressed polymers)

Compound	Elemental composition	σ (S/cm)
Fluorene ($C_{13}H_{10}$)	$C_{13.0}H_{9.5}(BF_4)_{0.23}$	10^{-4}
1-Methylfluorene ($C_{14}H_{12}$)	$C_{14.0}H_{10.9}(BF_4)_{0.12}$	10^{-5}
1-Methoxyfluorene ($C_{14}H_{12}O$)	$C_{14.0}H_{12.4}O_{1.9}(BF_4)_{0.16}$	10^{-5}

This result stems from the decreased unpaired electron density at the 7-position, which prevents a 2,7 linkage of the monomer units to form a polymer.

4. Polymer composition and electrical conductivity

The elemental analyses and electrical conductivities of some 1-substituted polyfluorenes are summarized in Table 11. Elemental analysis data indicate that the basic monomer units and

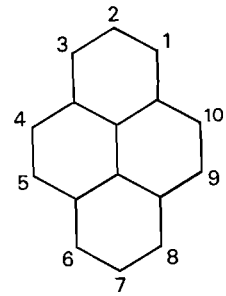

FIG. 12. The numbering scheme for pyrene.

substituents are preserved in the polymers and that the polymers are oxidized to the extent of 0.12 to 0.23 per monomer unit. The electrical conductivity of polyfluorenes is between 10^{-5} and 10^{-4} S/cm.

f. Polypyrene

1. Electrochemical data

Cyclic voltammetric data for pyrene (Fig. 12) and some of its 1-substituted derivatives are summarized in Table 12. As mentioned previously in Sect. II, the electrochemically estimated n value for pyrene (n = 1.7) is lower than would ordinarily be expected for these film-forming reactions, i.e., less than 2.0. This may result from the presence of competitive reaction pathways which have different electrochemical stoichiometries and different products, e.g., polymer versus soluble products (6). Thus, the n value of 1.7 is an apparent n value (n_{app}) for the *total* reaction. The n value for the film-forming reaction (n_p) is provided by the elemental composition of the polymer. Since n_{app} and n_p are both known (Table 1), the fraction of pyrene monomer which leads to polymer can be estimated. This assumes that the competing reaction is a dimerization reaction with n = 1, and that it is the only competing reaction (6). Thus, if f is the fraction of monomer which electropolymerizes, then $(1 - f)$ is the fraction that forms soluble species. From eq. [6],

$$[6] \quad n_{app} = n_p f + n_s(1 + f)$$

where n_p is 2.31 and is the n value of polypyrene determined from elemental analysis, and n_s is 1.0 and is the n value for dimerization. Thus, the fraction of pyrene monomers that gives rise to polymers is 0.54; i.e., approximately half of the monomers are used in the film-forming reaction.

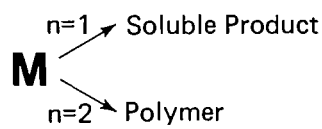

2. Hammett correlation and electropolymerization

The E_{pa} values of pyrene and some 1-substituted derivatives plotted against their respective substituent constants are shown in Fig. 13. As previously observed with the thiophenes (Sect. III*a*), indoles (Sect. III*c*), and fluorenes (Sect. III*e*), a linear correlation is obtained. Thus, the electrooxidation of pyrene results in the removal of a π electron, yielding a delocalized radical cation. The slope of the line is m = 0.26, which, like 1-substituted fluorenes (m = 0.18), indicates a mild substituent effect. Of the monomers shown in Fig. 13, all give rise to

TABLE 12. Cyclic voltammetric data for 2–4 μmol/cm^3 of pyrenes in 0.1 *M* TEAFB/CH_3CN

Compound	E_{pa} (monomer) (V)	$i/AC\nu^{1/2}$ (A cm s$^{1/2}$ mol^{-1} V$^{-1/2}$)	n	Polymer formation
Pyrene	1.33	2033	1.7	+
1-Chloropyrene	1.42	1900	1.6	+
1-Bromopyrene	1.41	1973	1.6	+
1-Methylpyrene	1.27	1528	1.4	+
Pyrene-1-carboxylic acid	1.45	1790	1.5	+
Pyrene-1-sulfonic acid	1.82	—	—	−

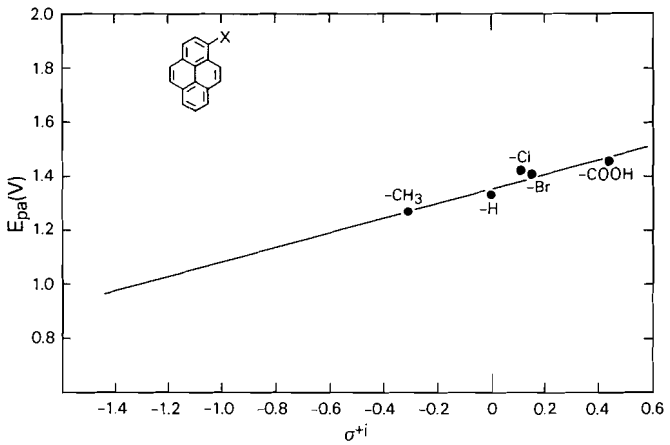

FIG. 13. Electrochemical peak oxidation potential of pyrene monomers versus their respective Hammett substituent constants.

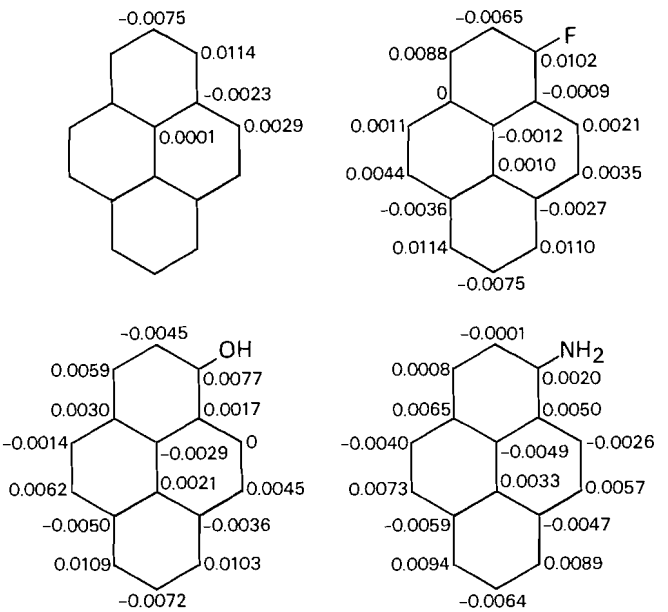

FIG. 14. Open shell INDO molecular orbital calculations of the unpaired electron density of some pyrene radical cations.

conducting polymer films. This includes the range from the electron-donating methyl group to the electron-withdrawing carboxylic acid group. Substituents outside of this range, i.e., those substituents which are either more electron donating than methyl, or more electron withdrawing than carboxylic acid, were not tested.

3. Electronic structure of pyrenes: an INDO study

The electronic structure of the pyrene radical cation (53) is summarized in Fig. 14. An INDO (24) molecular orbital calculation reveals that the positions of highest unpaired electron density occur at the equivalent 1-, 3-, 6-, and 8-positions. The high unpaired electron densities also identify these positions as the reactive sites, suggesting that the monomer linkages in an idealized polymer structure do occur in these same positions. Thus, the first step in the electropolymerization reaction sequence (Sect. II), i.e., dimerization, produces 1,1′-bipyrene (Fig. 15). As with the monomer pyrene radical cation, the positions of highest unpaired electron density in the 1,1′-dimer occur at the 1-, 3-, 6-, and 8-positions, according to esr data (54, 55) for the 1,1′-bipyrene radical cation (Fig. 16). Thus, when 1,1′-bipyrene is electrooxidized to its radical cation, a monomer radical cation will attack the 1,1′-dimer radical cation at its unblocked 3-, 6-, or 8-positions, to produce a 1,1′:8′,1″-, 1,1′:6′,1″- and (or) 1,1′:3′,1″-trimer (Fig. 15). Extrapolation of the reactivity pattern suggests a polymer that is linked primarily via these positions, or some combination thereof.

4. Polymer composition and electrical conductivity

The elemental compositions and electrical conductivities of polypyrene and some 1-substituted polypyrenes are summarized in Table 13. These data reveal that the polymers are oxidized to the extent of 0.06–0.31 per monomer unit. Their electrical conductivities are in the range of 10^{-2}–1 S/cm, similar to the polyazulenes and polythiophenes.

IV. Substituent effects on the electropolymerization reaction: competitive kinetics

As outlined in the previous section, substituents decidedly influence the follow-up reaction, and therefore, the aptitude for the electropolymerization reaction of a molecule upon electrooxidation. They occur via a steric effect, or an electronic effect. In the latter case, the stability of the radical-cation intermediate is affected, and as shown in the scheme below, the fate of $R^{+\bullet}$ at

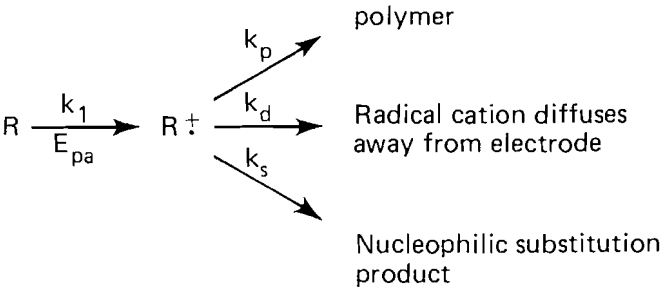

steady state is either to react with the polymer electrode, i.e., electropolymerization (k_p), to diffuse away from the electrode

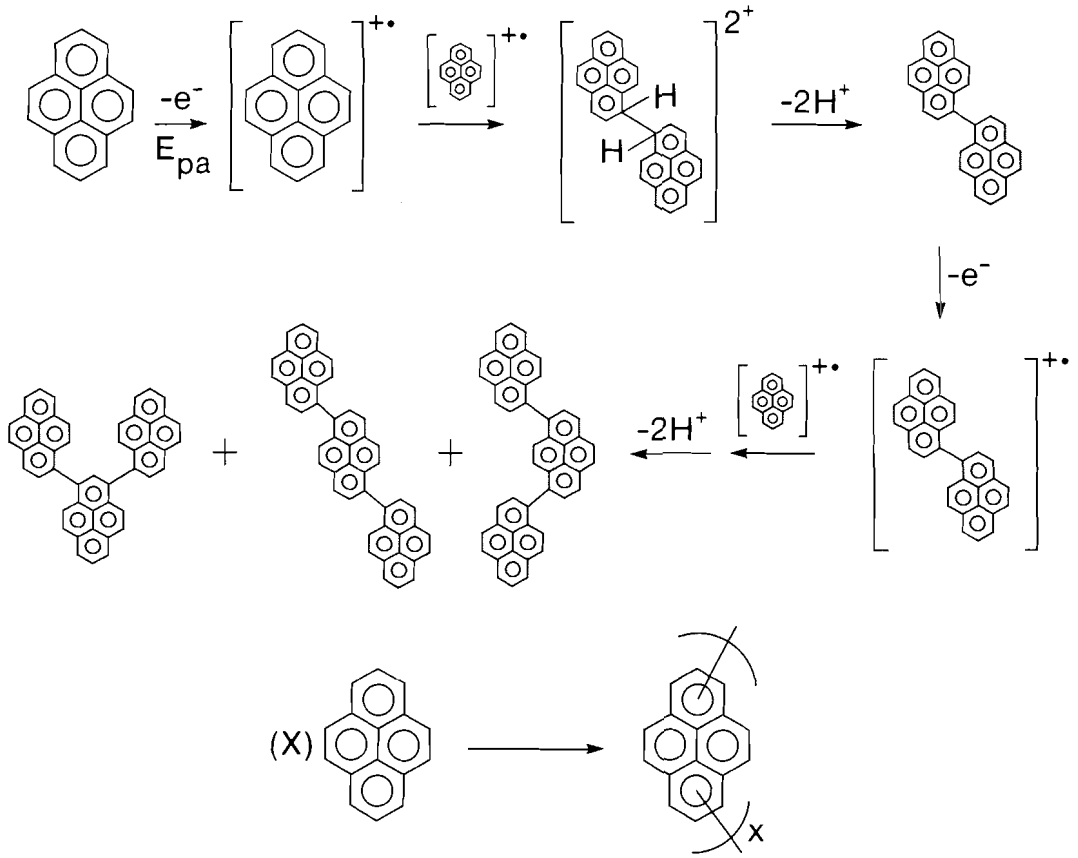

FIG. 15. A possible electropolymerization pathway for pyrene.

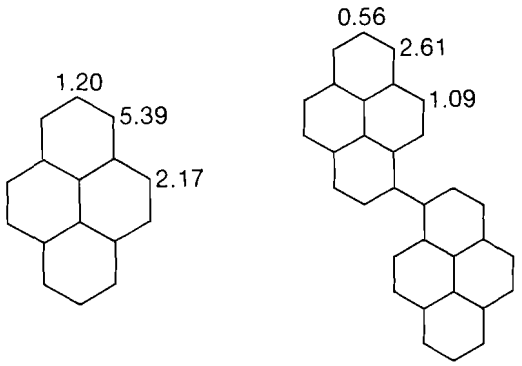

FIG. 16. Hyperfine splitting constants of pyrene and 1,1′-bipyrene radical cations according to the data of Cooper and Forbes (54).

(k_d), or to react with solvent (S) or anions (X^-) in the vicinity of the electrode surface (k_s) (4). Therefore, the fraction f_p of $R^{+\bullet}$ which undergoes electropolymerization is given by

$$[7] \quad f_p = \frac{k_p}{k_p + k_d + k_s([s] + [X^-])}$$

From eq. [7], we see that electropolymerization will occur when the stability of $R^{+\bullet}$ is such that $k_p \gg k_d + k_s([S] + [X^-])$. When the stability of $R^{+\bullet}$ is enhanced, for example by a substituent, then k_d becomes greater than $k_p + k_s([S] + [X^-])$. Under these conditions, $R^{+\bullet}$ will diffuse away from the electrode to produce soluble products. The proclivity of $R^{+\bullet}$ to undergo the electropolymerization reaction becomes reduced in favor of capture by nucleophiles or solvent. When $R^{+\bullet}$ becomes sufficiently unstable, it reacts indiscriminately with either solvent or anions and electropolymerization is suppressed. In this case, $k_s([S] + [X^-]) \gg (k_p + k_d)$. These considerations were vividly illustrated by the E_{pa}–Hammett plots of the various compounds discussed above.

TABLE 13. Elemental composition and electrical conductivity of some polypyrenes (pressed polymers)

Compound	Elemental composition	σ (S/cm)
Pyrene ($C_{16}H_{10}$)	$C_{16.0}H_{12.0}(ClO_4)_{0.31}$	10^{-1}–1^a
1-Methylpyrene ($C_{17}H_{12}$)	$C_{17.0}H_{12.0}(BF_4)_{0.06}$	10^{-3}
1-Chloropyrene ($C_{16}H_9Cl$)	$C_{16.0}H_{10.2}Cl_{0.4}(BF_4)_{0.07}$	10^{-2}

[a]Either tetrafluoroborate or perchlorate pressed polymers.

V. Technological applications

a. Polymer electrodes

In the oxidized state, conducting polymer films such as polypyrrole (56), when supported by a Pt anode, are electrically conducting and therefore may be used as an anode to drive oxidation reactions. In particular, polypyrrole films coated onto Pt anodes, i.e., [Pt] polypyrrole electrodes, were used to investigate the redox reactions of various electroactive species dissolved in aprotic electrolyte solutions (7). Diaz *et al.* (7) found that the electrochemical data obtained from [Pt] polypyrrole electrodes compared favorably with bare Pt electrodes: the redox reactions occurred only at the electrode surface, electron transfer was rapid, and no absorption, adsorption, or reaction of the polymer electrode with the dissolved species occurred. Furthermore, modification of the polymer electrode surface by

TABLE 14. Some typical electrochromic data for a variety of polyheterocycles. Data taken from Garnier *et al.* (47)

Polymer	Anion	Oxidized form λ (nm)	Reduced form λ (nm)	Frequency response time (ms)
Pyrrole	ClO_4^-	660	420	20
Thiophene	BF_4^-, ClO_4^-	730	470	40–50
3-Methylthiophene	BF_4^-	750	480	12
3,4-Dimethylthiophene	ClO_4^-	750	620	60
2,2′-Bithiophene	$CF_3SO_3^-$	680	460	40

TABLE 15. A comparison of the "all-polymer" battery cell characteristics of polyazulene, polythiophene, and polyacetylene with the polyacetylene/Li battery

	Polyazulene[a]	Polythiophene[a]	Polyacetylene[b]	Polyacetylene/Li[b]
I_{sc} (mA/cm^2)	0.4–2.2	0.02	3	15–200
V_{oc} (V)	0.5–2.3	0.5	1	3.7

[a]Reference 13.
[b]Reference 61*c*.
[c]Reference 61*a*.

the attachment of electroactive species is facile. For example, polypyrrole films can be easily nitrated, then electrochemically reduced, followed by acylation to attach a desired group (57).

b. Electro-optical display devices

The color changes that accompany the electrochemical switching reaction, i.e., the reversible cycling between the oxidized conducting state and the neutral insulating state, suggest the applicability of electroactive polymers in passive display devices (58). In this regard, Garnier *et al.* (47, 59) have investigated the electrochromic behavior of a variety of polythiophene thin films supported by a Pt anode. Their data (59) are summarized in Table 14. The colors that are obtained depend upon both the chemical structure of the polymer and the counteranion that is incorporated into the film. The switching response times are typically 10–50 ms and are dependent on film thickness. They have concluded that a 0.1-μm film would represent the minimum thickness required to yield a sufficient color contrast on a Pt surface (59). Druy and Seymour (60) have also investigated the electrochromic behavior of polythiophene electropolymerized from the 2,2′ dimer. They report a switching response time of ~500 ms for a 0.42-μm thick film.

c. Battery applications

To our knowledge, *electrochemically* produced conducting polymers as battery electrodes have not yet been exploited to the same degree as has the chemically synthesized conducting polymer polyacetylene (61). However, polyacetylene batteries remain the prototype among batteries that are constructed using electrically conducting polymers, so the interested reader is referred to the pertinent references (61). As for electrochemically produced polymers, a preliminary account (13) utilizing polyazulene and polythiophene films, supported by a Pt surface as electrode, will be dilineated briefly and compared to the polyacetylene standard.

A simple "all-polymer" battery cell design consists of a neutral and an oxidized film of polyazulene (or of polythiophene) supported by a Pt surface, in an electrolytic solution (13). Such a cell in a closed circuit loop yields a maximum open-circuit voltage of ~2.3 V, and a maximum initial short-circuit current of ~4 mA. These data are summarized and compared with an all-polymer polyacetylene battery (61*c*) in Table 15. A typical voltage change during a constant current discharge of a polyazulene battery is shown in Fig. 17. The polyazulene batteries tested could be recharged to yield similar values in the regenerated cells, at least in the short term (13).

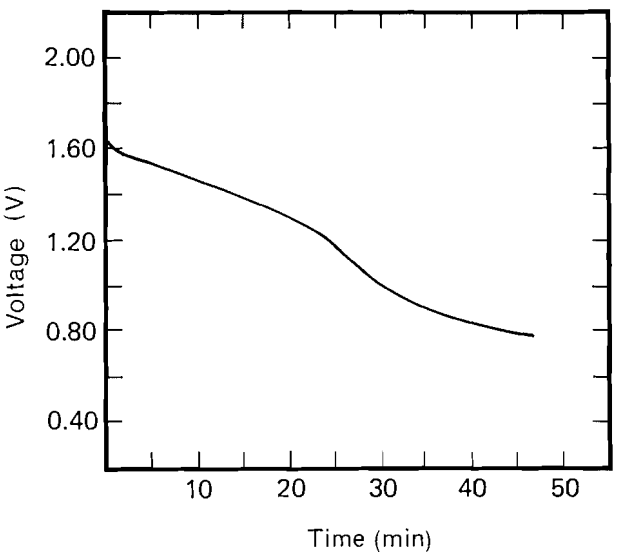

FIG. 17. A typical voltage change during 0.15-mA constant current discharge of a polyazulene battery cell.

d. Protection of semiconductor photoanodes

The proclivity of small-band-gap semiconductor photoanodes to photocorrosion in aqueous media has thwarted the development of inexpensive yet efficient photoelectrochemical cells for the conversion and storage of solar energy. Various approaches have now been undertaken in an effort to stabilize the semiconductor–electrolyte interface. They include, for example, (*a*) coating the semiconductor with thin metal films (62) or with semiconductors (63); (*b*) using nonaqueous electrolytes (64); (*c*) derivatizing the semiconductor surface itself with electroactive species (65); and (*d*) coating the semiconductor surface

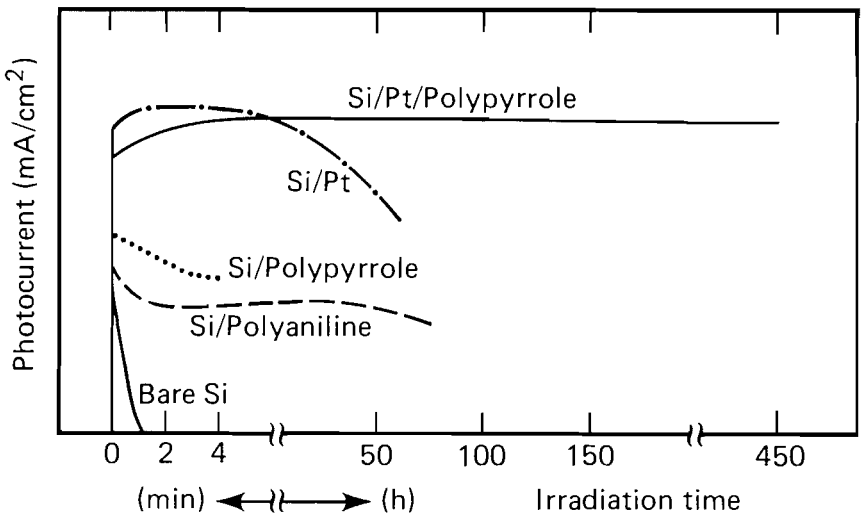

FIG. 18. A comparison of the relative stability of variously coated photoanodes. The bare Si, Si/Pt, and Si/Pt/polypyrrole photoanodes are in I^-/I_3^- electrolyte; taken from Skotheim *et al.* (66*b*). The Si/polyaniline photoanode is in a pH = 1 solution of 0.15 *M* $Fe^{2+/3+}$ and 0.1 *M* Na_2SO_4 in H_2SO_4; taken from Noufi *et al.* (68).

with electrically conducting polymers (66–71). The salient features of the latter will be summarized briefly.

The driving force for utilizing electrically conducting polymers as protective thin-film coatings on photoanodes stems from their high electrical conductivity and chemical stability (58). Thin films also have good adhesion to the Pt surface (72), although peeling off of the polymer films from the photoanodes continues to be a problem. More recently, poly-3-methylthiophene has been shown to yield improved adhesion to semiconductor photoanodes (71). Nevertheless, an electrically conducting polymer film acts as a barrier to ion/solvent transport to the photoanode surface and effectively minimizes photocorrosion for up to approximately several hundred hours, depending upon the system (66–71). Accordingly, redox reactions may be utilized to yield optimum open-circuit voltages with improved stability of the photoelectrochemical cell (68). Thus far, polypyrrole has been the film of choice primarily because of its high electrical conductivity, and because other electrochemically generated conducting polymers have not been available until more recently (Table 1). The stabilization to corrosion imparted by a polypyrrole (PP) film on n-Si is shown as an illustrative example in Fig. 18, taken from the data of Skotheim *et al.* (66*b*), and from Noufi *et al.* (68). The lifetime and photocurrent output of a Si/PP photoelectrode is improved over a bare Si photoelectrode; however, a Si/Pt/PP photoelectrode shows the greatest longevity with a lifetime of ~450 h and with no loss in photocurrent output. A thin metal-coated photoelectrode (Si/Pt) and a polyaniline-coated Si photoelectrode (68) are also shown for comparison (Fig. 18). It is also noteworthy that the performance characteristics of the polymer-coated photoanodes are comparable to those of the bare photoelectrodes (66–71).

e. Information storage

In a novel application exploiting the high electrical conductivity of polypyrrole, Meyer *et al.* (73) have explored the possibility of its use for high-density information storage (74). As shown in the scheme below, adapted from Meyer *et al.* (73), polypyrrole is electrochemically grown onto an anode with a surface relief pattern. Polypyrrole is then peeled off and made to adhere to a solid substrate, leaving exposed the inverse surface relief pattern of the anode. The high electrical conductivity of polypyrrole may then be utilized for information storage as long as the information is stored as a relief pattern on the polymer film surface. The information is accessed by reading it capacitively with an electrode (73). Subsequent testing of this material in a video disk machine, as a disk of 210-mm diameter and supported by a substrate, revealed a virtually defect-free material of constant signal-to-noise ratio over the entire information containing disk; i.e., a high degree of surface relief replication with no distortion of information was achieved. Furthermore, because the decrease in conductivity of polypyrrole occurs over long periods (i.e., years), Meyer *et al.* (73) anticipate no problems associated with the readability of the information even after years of storage.

f. Other applications

The increasing usage of home-electronics products, coupled with an increasing density of electronic circuitry on chips, has presented problems with electromagnetic interference (EMI) previously unforeseen (75). In this regard, conductive plastics (9) may find use as shielding materials to prevent the passing of electromagnetic signals into the airwaves (75).

When polypyrrole is exposed to ammonia, its resistivity

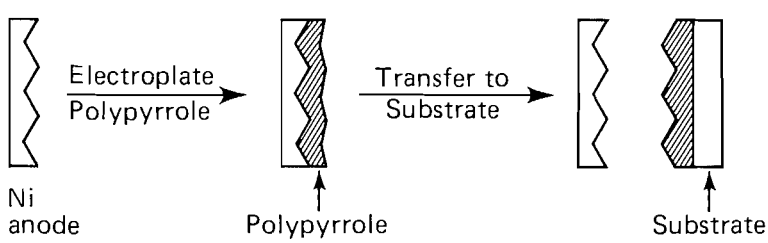

increases. Lundström and co-workers (76) have prepared polypyrrole–paper composites, which can be used as sensitive ammonia detectors. When exposed to ammonia, the change in electrical conductivity of polypyrrole is related to the concentration of ammonia in air.

The search for electrode materials that extract metallic cations from solutions and interfaces has prompted Le Berre *et al.* (77, 78) to electrochemically synthesize electrically conducting polymers from macrocyclic ligands such as crown ethers. For example, thin films of poly(dibenzo-24-crown-8)-BF_4 supported by a Pt anode can be cycled reversibly from its oxidized, conducting state to its neutral, insulating state with no apparent loss of electroactivity, as long as the polymer is not electrochemically driven beyond its first oxidation state. The dicationic state is reported to be rather sensitive to the presence of nucleophiles, such that electroactivity becomes lost (77).

1. A. F. DIAZ, K. K. KANAZAWA, and G. P. GARDINI. J. Chem. Soc. Chem. Commun. 635, (1979).
2. A. F. DIAZ. Chem. Scr. **17**, 145 (1981).
3. G. TOURILLON and F. GARNIER. J. Electroanal. Chem. **135**, 173 (1982).
4. R. J. WALTMAN, A. F. DIAZ, and J. BARGON. J. Phys. Chem. **88**, 4343 (1984).
5. J. BARGON, S. MOHMAND, and R. J. WALTMAN. IBM J. Res. Dev. **27**, 330 (1983).
6. R. J. WALTMAN, A. F. DIAZ, and J. BARGON. J. Electrochem. Soc. **132**, 632 (1985).
7. A. F. DIAZ, J. M. VASQUEZ VALLEJO, and A. MARTINEZ DURAN. IBM J. Res. Dev. **25**, 42 (1981).
8. A. F. DIAZ and J. BARGON. Electrochemical synthesis of conducting polymers. *In* Handbook of conducting polymers. *Edited by* T. A. Skotheim. Marcel Dekker Inc., New York. In press.
9. (*a*) M.-A. DEPAOLI, R. J. WALTMAN, A. F. DIAZ, and J. BARGON. J. Chem. Soc. Chem. Commun. 1015 (1984); (*b*) O. NIWA and T. TAMAMURA. J. Chem. Soc. Chem. Commun. 817 (1984); (*c*) M.-A. DEPAOLI, R. J. WALTMAN, A. F. DIAZ, and J. BARGON. J. Polym. Sci. Polym. Chem. Ed. **26**, 1687 (1985); (*d*) S. F. LINDSEY and G. B. STREET. Synth. Met. **10**, 67 (1984/85).
10. R. S. NICHOLSON and I. SHAIN. Anal. Chem. **36**, 706 (1964).
11. A. F. DIAZ, J. J. CASTILLO, J. A. LOGAN, and W.-Y. LEE. J. Electroanal. Chem. **129**, 115 (1981).
12. R. J. WALTMAN, J. BARGON, and A. F. DIAZ. J. Phys. Chem. **87**, 1459 (1983).
13. R. J. WALTMAN, A. F. DIAZ, and J. BARGON. J. Electrochem. Soc. **131**, 1452 (1984).
14. J. F. AMBROSE and R. F. NELSON. J. Electrochem. Soc. **115**, 1159 (1968).
15. R. N. ADAMS. Electrochemistry at solid electrodes. Marcel Dekker Inc., New York. 1969.
16. R. N. ADAMS. Acc. Chem. Res. **2**, 175 (1969).
17. A. F. DIAZ, J. CROWLEY, J. BARGON, G. P. GARDINI, and J. B. TORRANCE. J. Electroanal. Chem. **121**, 355 (1981).
18. E. M. GENIES, G. BIDAN, and A. F. DIAZ. J. Electroanal. Chem. **149**, 101 (1983).
19. A. NAZZAL and G. B. STREET. J. Chem. Soc. Chem. Commun. 83 (1984).
20. J. BARGON, S. MOHMAND, and R. J. WALTMAN. Mol. Cryst. Liq. Cryst. **93**, 279 (1983).
21. G. B. STREET. Polypyrrole — from powders to plastics. *In* Handbook of conducting polymers. *Edited by* T. A. Skotheim. Marcel Dekker Inc., New York. In press.
22. A. F. DIAZ, J. BARGON, and R. J. WALTMAN. Proceedings of the symposium on membranes and ionic and electronic conducting polymers, **83**, 332 (1982).
23. R. J. WALTMAN and J. BARGON. Tetrahedron, **40**, 3963 (1984).
24. (*a*) J. A. POPLE and D. L. BEVERIDGE. Approximate molecular orbital theory. McGraw-Hill, New York, 1970; (*b*) Quantum Chemistry Program Exchange, No. 141.
25. G. P. GARDINI. Adv. Heterocycl. Chem. **15**, 95 (1973).
26. G. B. STREET, T. C. CLARKE, M. KROUNBI, K. KANAZAWA, V. LEE, P. PFLUGER, J. C. SCOTT, and G. WEISER. Mol. Cryst. Liq. Cryst. **83**, 253 (1982).
27. G. B. STREET, T. C. CLARKE, R. H. GEISS, V. Y. LEE, P. PFLUGER, and J. C. SCOTT. J. Phys. Colloq. **C3**(6), 599 (1983).
28. A. J. H. WACHTERS and D. W. DAVIES. Tetrahedron, **20**, 2841 (1964).
29. R. L. FLURRY, E. W. STOUT, and J. J. BELL. Theoret. Chim. Acta, **8**, 203 (1967).
30. A. R. COOKSEY, K. J. MORGAN, and D. P. MORREY. Tetrahedron, **26**, 5101 (1970).
31. A. MILLEFIORI, G. FAVINI, and S. MILLEFIORI. Z. Phys. Chem. (Munich), **94**, 167 (1975).
32. E. D. HUGHES and G. T. JONES. J. Chem. Soc. 2678 (1950).
33. F. A. NEUGEBAUER, S. BAMBERGER, and W. R. GROH. Tetrahedron Lett. 2247 (1973).
34. M. H. PALMER. The structure and reactions of heterocyclic compounds. St. Martin's Press, New York. 1967.
35. K. HATTORI and Y. WADA. J. Polym. Sci. **13**, 1863 (1975).
36. J. PIELICHOWSKI and A. PUSZYNSKI. Monatsh. Chem. **105**, 772 (1974).
37. R. D. BROWN and B. A. W. COLLER. Aust. J. Chem. **12**, 152 (1959).
38. R. Zahradnik. Nonalternant hydrocarbons, radical ions, and their heteroanalogs; characteristics of ground and excited states. *In* Nonbenzenoid aromatics. *Edited by* J. P. Snyder. Academic Press Inc., New York. 1971.
39. A. G. ANDERSON, J. A. NELSON, and J. J. TAZUMA. J. Am. Chem. Soc. **75**, 4980 (1953).
40. R. M. DESSAU and S. SHIH. J. Chem. Phys. **53**, 3169 (1970).
41. A. F. DIAZ and J. A. LOGAN. J. Electroanal. Chem. **111**, 111 (1980).
42. H. C. BROWN and Y. OKAMOTO. J. Am. Chem. Soc. **80**, 4979 (1958).
43. R. J. WALTMAN and J. BARGON. J. Electroanal. Chem. **194**, 49 (1985).
44. P. ZUMAN. Substituent effects in organic polarography. Plenum Press, New York. 1967.
45. G. TOURILLON and F. GARNIER. J. Phys. Chem. **87**, 2289 (1983).
46. (*a*) S. HOTTA, T. HOSAKA, and W. SHIMOTSUMA. Synth. Met. **6**, 69 (1983); (*b*) S. HOTTA, T. HOSAKA, and W. SHIMOTSUMA. Synth. Met. **6**, 317 (1983).
47. F. GARNIER, G. TOURILLON, M. GAZARD, and J. C. DUBOIS. J. Electroanal. Chem. **148**, 299 (1983).
48. A. F. DIAZ, J. CASTILLO, K. K. KANAZAWA, J. A. LOGAN, M. SALMON, and O. FAJARDO. J. Electroanal. Chem. **133**, 233 (1982).
49. M. SALMON, M. E. CARBAJAL, J. C. JUAREZ, A. F. DIAZ, and M. C. ROCK. J. Electrochem. Soc. **131**, 1802 (1984).
50. A. F. DIAZ, A. MARTINEZ, K. K. KANAZAWA, and M. SALMON. J. Electroanal. Chem. **130**, 181 (1981).
51. G. M. BROWN and M. H. BORTNER. Acta Crystallogr. **7**, 139 (1954).
52. J. A. POPLE and M. GORDON. J. Am. Chem. Soc. **89**, 4253 (1967).
53. A. CAMERMAN and J. TROTTER. Acta Crystallogr. **18**, 636 (1965).
54. J. T. COOPER and W. F. FORBES. Can. J. Chem. **46**, 1158 (1968).
55. J. T. COOPER. Can. J. Chem. **48**, 1996 (1970).
56. A. F. DIAZ and J. J. CASTILLO. J. Chem. Soc. Chem. Commun., 397 (1980).
57. A. F. DIAZ, W.-Y. LEE, A. LOGAN and D. C. GREEN. J. Electroanal. Chem. **108**, 377 (1980).
58. A. F. DIAZ and K. K. KANAZAWA. *In* Extended linear chain compounds. *Edited by* J. S. Miller. Plenum Press, New York. 1982. p. 417.
59. M. GAZARD, J. C. DUBOIS, M. CHAMPAGNE, F. GARNIER, and G. TOURILLON. J. Phys. Colloq. **C3**(6), 537 (1983).

60. M. A. DRUY and R. J. SEYMOUR. J. Phys. Colloq. **C3**(6), 595 (1983).
61. (*a*) P. J. NIGREY, A. G. MACDIARMID, and A. J. HEEGER. Mol. Cryst. Liq. Cryst. **83**, 309 (1982); (*b*) A. G. MACDIARMID, R. B. KANER, R. J. MAMMONE, and A. J. HEEGER. J. Phys. Colloq. **C3**(6), 543 (1983); (*c*) A. G. MACDIARMID, M. ALDISSI, R. B. KANER, M. MAXFIELD, and R. J. MAMMONE. Abstract 557. Proc. Electrochem. Soc. Extended Abstracts, **83-1** (1983).
62. (*a*) Y. NAKATO, T. OHNISHI, and H. TSUBOMURA. Chem. Lett. 883 (1975); (*b*) L. A. HARRIS, M. E. GERSTNER, and R. H. WILSON. J. Electrochem. Soc. **124**, 1511 (1977); (*c*) S. MENEZES, A. HELLER, and B. MILLER. J. Electrochem. Soc. **127**, 1268 (1980).
63. P. A. KOHL, S. N. FRANK, and A. J. BARD. J. Electrochem. Soc. **124**, 225 (1977).
64. (*a*) S. N. FRANK and A. J. BARD. J. Am. Chem. Soc. **97**, 7427 (1975); (*b*) M. MIYAKE, H. YONEYAMA, and H. TAMURA. Electrochim. Acta, **22**, 319 (1977); (*c*) K. NAKATANI and H. TSUBOMURA. Bull. Chem. Soc. Jpn. **50**, 783 (1977).
65. (*a*) J. M. BOLTS, A. B. BOCARSLY, M. C. PALAZATTO, E. G. WALTON, N. S. LEWIS, and M. S. WRIGHTON. J. Am. Chem. Soc. **101**, 1378 (1979); (*b*) A. B. BOCARSLY, E. G. WALTON, M. G. BRADLEY, and M. S. WRIGHTON. J. Electroanal. Chem. **100**, 283 (1979).
66. (*a*) T. SKOTHEIM, I. LUNDSTRÖM, and J. PREJZA. J. Electrochem. Soc. **128**, 1625 (1981); (*b*) T. SKOTHEIM, L.-G. PETERSSON, O. INGANAS, and I. LUNDSTRÖM. J. Electrochem. Soc. **129**, 1737 (1982).
67. R. NOUFI, D. TENCH, and L. F. WARREN. J. Electrochem. Soc. **128**, 2596 (1981).
68. R. NOUFI, A. J. NOZIK, J. WHITE, and L. F. WARREN. J. Electrochem. Soc. **129**, 2261 (1982).
69. R. NOUFI, A. J. FRANK, and A. J. NOVIK. J. Am. Chem. Soc. **103**, 1849 (1981).
70. F. F. FAN, B. L. WHEELER, A. J. BARD, and R. F. NOUFI. J. Electrochem. Soc. **128**, 2042 (1981).
71. G. HOROWITZ and F. GARNIER. J. Electrochem. Soc. **132**, 634 (1985).
72. K. K. KANAZAWA, A. F. DIAZ, W. D. GILL, P. M. GRANT, G. B. STREET, G. P. GARDINI, and J. F. KWAK. Synth. Met. **1**, 329 (1979/80).
73. W. H. MEYER, H. KIESS, B. BINGGELI, E. MEIER, and G. HARBEKE. Synth. Met. **10**, 255 (1985).
74. J. P. HUIGNARD, F. MICHERON, and E. SPITZ. *In* Optical properties of solids: new developments. *Edited by* B. O. Seraphin. North-Holland Publishing Company, Amsterdam. 1976. p. 851.
75. Chemical Week. July 20, 1983. p. 38.
76. R. B. BJORKLUND and I. LUNDSTRÖM. J. Electron. Mat. **13**, 211 (1984).
77. V. LEBERRE, R. CARLIER, A. TALLEC, and J. SIMONET. J. Electroanal. Chem. **143**, 425 (1982).
78. V. LEBERRE, R. CARLIER, J. SIMONET, and A. TALLEC. J. Phys. Colloq. **C3**(6), 1269 (1983).

Intrinsic selectivity and its geometric significance in S_N2 reactions

SASON S. SHAIK
Department of Chemistry, Ben Gurion University, Beer Sheva 84105, Israel
Received July 8, 1985

SASON S. SHAIK. Can. J. Chem. **64**, 96 (1986).

An intrinsic selectivity is defined for identity S_N2 reactions ($X^- + RX \rightarrow XR + X^-$). This selectivity parameter is shown to yield information about: (*a*) the average looseness of the TS geometry in a reaction series; and (*b*) the sensitivity of the reaction series to geometric loosening.

SASON S. SHAIK. Can. J. Chem. **64**, 96 (1986).

On définit une sélectivité intrinsèque pour les réactions S_N2 d'identité ($X^- + RX \rightarrow XR + X^-$). On démontre que ce paramètre de sélectivité fournit de l'information concernant: (*a*) l'état de relachement de la géométrie de l'ET dans une série de réactions; et (*b*) la sensibilité des séries de réactions à des relachements géométriques.

[Traduit par le journal]

Ever since Leffler's proposal (1) that the Brønsted parameter can serve as a measure of transition state (TS) structure, there has existed an ongoing debate regarding the significance of selectivity parameters (2). The key question is, what kind of TS information is provided by selectivity measurements? To begin answering that, one must start with the fundamental reaction, *the identity exchange*. This work defines the *intrinsic selectivity* of identity S_N2 reactions (eq. [1]) and shows that such selectivity experiments may lead to geometric information about the *looseness* of the TS and the "flexibility" of its C···X bonds.

[1] $X:^- + R—X \rightarrow X—R + :X^-$

The reaction profile for an identity S_N2 reaction (3) is shown in Fig. 1. The reaction barrier follows eq. [2] where f is a

[2] $\Delta E^{\ddagger} = f(I_{X:} - A_{RX}) - B$

steepness variable that derives from the curvature of the intersecting curves. Whenever the curves descend steeply from the upper states towards the crossing point, the f-factor will be *small*, and vice versa when the descent is shallow (3, 4). The $I_{X:} - A_{RX}$ term is the vertical electron transfer energy from $X:^-$ to RX under the reaction conditions (gas phase (3*a*,*c*) or solution (3*b*)). The B factor is the crossing avoidance interaction which appears to be approximately constant for various X's (3*b*,*c*, 5).

Figure 2 shows a structure–reactivity plot using eq. [2]. The ensemble of reactions is predicted to fall into families such that the members ($X:^-/RX$) of each family share a common f-factor (6). In each family line the barriers increase in proportion to $I_{X:} - A_{RX}$ and the line slope is the characteristic f of the reaction family. The f-factor defines then the intrinsic selectivity (IS) of a reaction family as specified in eq. [3]:

[3] $$\text{IS} = f = \frac{\partial(\Delta E^{\ddagger})}{\partial(I_{X:} - A_{RX})}$$

The physical property that determines f has been shown (3*a*,*b*, 4) to derive from the delocalization properties of the substrate's radical anion $(R\text{—}\dot{X})^-$, which is described in eq. [4] in valence bond terms:

[4] $(R\text{—}\dot{X})^- = W_{X:}(R\cdot\ :X^-) + W_{R:}(R:^-\ \cdot X);\ W_{R:} + W_{X:} = 1$

Whenever the weight ($W_{R:}$) of $R:^-\cdot X$ is large, the odd electron of $(R\text{—}\dot{X})^-$ is delocalized away from the R union center. In such a case, the bond coupling interaction between X· and $(R\text{—}\dot{X})^-$ will become weak and the $X\cdot/(R\text{—}\dot{X})^-$ ⇝ $(X\text{—}R)/:X^-$ correlation lines will possess a shallow descent towards the crossing point in Fig. 1 (4). This will result in a large f, in eqs. [2] and [3], and hence also in a large intrinsic selectivity (IS). The IS of an identity-reaction family can then be reexpressed as in eq. [5] in terms of the $W_{R:}$ property.

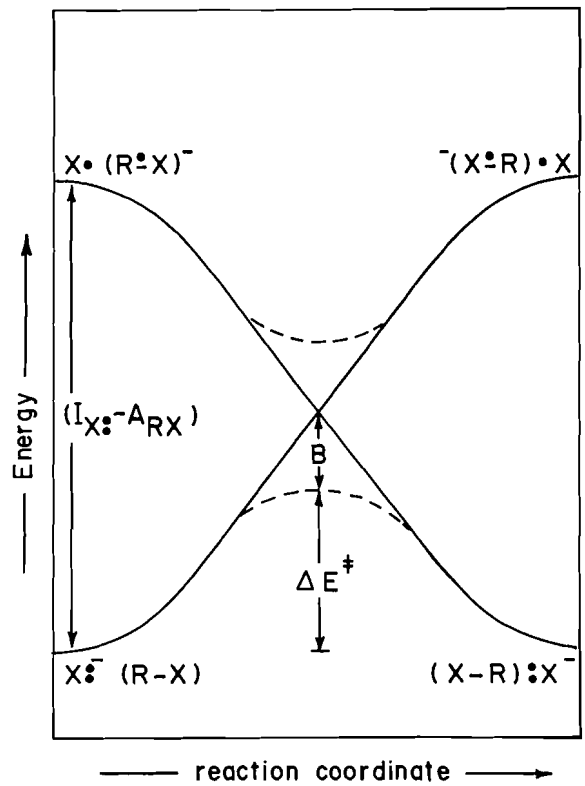

FIG. 1. State correlation diagram for identity S_N2 reactions. The two ends of the reaction coordinate represent the geometries of the encounter ion–molecule complexes. In reactions in solutions all the states are solvated (ref. 3*b*). The avoided crossing is shown by dashes near the intersection point. $\Delta E^{\ddagger}$ is the resulting reaction barrier.

[5] $$\text{IS} = f = \frac{\partial(\Delta E^{\ddagger})}{\partial(I_{X:} - A_{RX})} \propto W_{R:}$$

Collected in Table 1 are $W_{R:}$ indices and barriers for a few identity reactions that have been investigated experimentally and computationally (7, 8). As may be seen, the halide exchange reactions in entries 1–4 have smaller $W_{R:}$ values than

TABLE 1. $W_{R:}$ indices and barriers ($\Delta E^{\ddagger}$) for identity reactions $X^- + CH_3X \rightarrow XCH_3 + X^-$ in the gas phase and in solutions

		$W_{R:}$[a,b]			$\Delta E^{\ddagger}$ (kcal/mol)		
	X	Gas phase	H_2O	DMF	Gas phase[d]	H_2O[e]	DMF[e]
(1)	F	0.242	0.204	0.209	11.7	31.8	—
(2)	Cl	0.253	0.242	0.245	5.5	26.5	22.7
(3)	Br	0.246	0.241	0.244	—	23.7	18.4
(4)	I	0.240	0.244	0.242	—	22.0[f]	16.0
(5)	HS	0.340	0.326	0.328	15.6	—	—
(6)	PhS	0.331[c]	0.326[c]	0.328[c]	—	~34[g]	—
(7)	HO	0.357	0.307	0.313	21.2	41.8	—
(8)	NC	0.309	0.304	0.306	43.8	50.9	—

[a] $W_{R:}$ is defined in eq. [4].
[b] The values are taken from ref. 3*b*. Note that in ref. 3*b* the symbol (b^2) is used for the $W_{R:}$ index.
[c] Calculated as described in refs. 3*b*,*c*, 4, 6*b*.
[d] Data from ref. 8.
[e] $\Delta G^{\ddagger}$ data from ref. 7*a*.
[f] $\Delta G^{\ddagger}$ datum from ref. 7*b*.
[g] $\Delta G^{\ddagger}$ datum from ref. 7*c* for ethanol as a solvent.

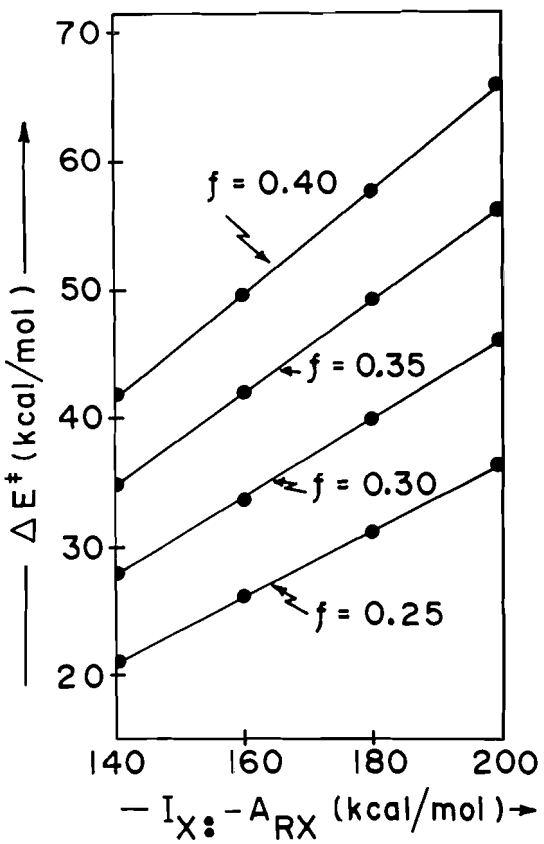

FIG. 2. Structure–reactivity plots of barriers ($\Delta E^{\ddagger}$) vs. vertical electron transfer energies ($I_{X:} - A_{RX}$) using eq. [2] (B = 14 kcal/mol, see ref. 3). Note that the slopes of the family lines are equal to the corresponding *f*-factors.

the exchange reactions of PhS^-, HS^-, HO^-, and NC^-. In accord with eq. [5], the halide exchange series is predicted to possess *a lower intrinsic selectivity* than the exchange series of PhS^-, HS^-, HO^-, and NC^-, in either the gas phase or in solution. Figure 3 is a plot of the experimental $\Delta G^{\ddagger}$ values (7) against the corresponding vertical electron transfer energies (3*b*) for the aqueous solution identity reactions that are collected in Table 1. The experimental data set is seen to obey the above prediction and to behave as the theoretical plots in Fig. 2. While it is clear from Fig. 3 that the two families exhibit different intrinsic selectivities, the question remains whether one can associate any property of the TS with such experimental IS parameters?

Consider then the geometric looseness (L) of the TS as defined (5), in eq. [6], by the fraction of C—X bond stretching

$$[6] \quad \Delta d^{\ddagger}/d^0 = L = (d^{\ddagger}_{CX} - d^0_{CX})/d^0_{CX}$$

in the TS relative to the bond length in the R—X molecule (d^0_{CX}). In previous publications (5, 6*b*) it was demonstrated that TS looseness correlates with the height of the barrier since both properties derive primarily from the C—X stretching deformation (5) that is required to achieve the crossing in Fig. 1.[1] Thus, looseness in a series of identity reactions is a result of the extent of C—X stretching that overcomes the $I_{X:} - A_{RX}$ energy gap and achieves a transition state at the crossing point of $X:^-/(R—X)$ and $X\cdot/(R\cdot\!\!-X)^-$ in Fig. 1. Large $I_{X:} - A_{RX}$ gaps and delocalization indices ($W_{R:}$) will require a greater C—X deformation and will thereby lead to looser transition state geometries (5). Since barriers and transition state geometries behave alike, it follows then that the intrinsic selectivity that derives from plots of barriers $\Delta E^{\ddagger}$ vs. ($I_{X:} - A_{RX}$) may serve as an indicator of transition state geometry.

Reliable geometric data for the identity reactions of X^- = NC^-, HO^-, HS^-, F^-, Cl^- is available from the *ab initio* studies of Wolfe *et al.* (8). These data are plotted in Fig. 4 against the natural logarithm of the gas phase electron transfer energies, $I_{X:} - A_{RX}$ (3*b*).[2] The looseness of the transition state is seen to

[1] This means that high barriers are associated with a high R—X stretching deformation and, hence, also loose TS geometries. See ref. 5 for a detailed treatment of this correlation. Such a correlation exists because the energy requried to dissociate the TS into three fragments ($X:^- + \dot{C}H_3 + X$) is given by $\Delta E_{dis} = D_{C—X} - \Delta E^{\ddagger}$ where D is the C—X bond energy (ref. 6*b*). Thus, the larger the $\Delta E^{\ddagger}$, the closer the TS to its dissociation limit.

[2] A line for the halide exchange transition states of X^- = F^-, Cl^-, and Br^- can be generated from MNDO geometries (ref. 9). The looseness varies in the order $F^- > Cl^- > Br^-$. The slope of the line, $\Delta d^{\ddagger}/d^0$ vs. ($I_{X:} - A_{RX}$), is 0.127 with 0.995 correlation coefficient. The looseness varies in proportion to the calculated barrier heights.

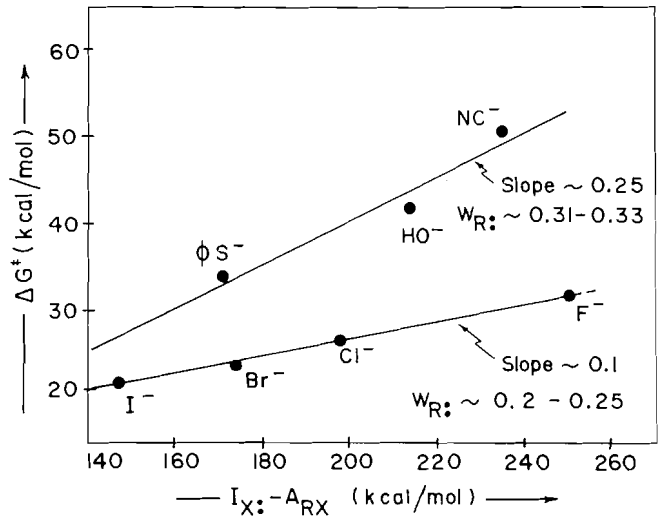

FIG. 3. Plots of experimental free energies of activation (ref. 7) against vertical electron transfer energies (ref. 3*b*) for aqueous solution identity reactions $X^- + CH_3X \rightarrow XCH_3 + X^-$. The X's are indicated alongside the family lines.

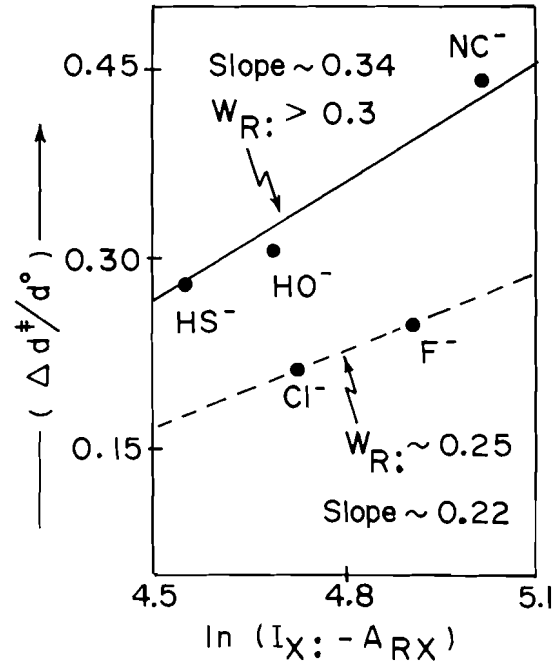

FIG. 4. Plots of the computed $\Delta d^{\ddagger}/d^0$ indices (ref. 5) against the vertical electron transfer energies (ref. 3*b*) for gas phase identity reactions $X^- + CH_3X \rightarrow XCH_3 + X^-$. The d^0 value refers to the C—X bond length of CH_3X in the ion–dipole encounter complex. The correlation coefficient for the upper solid line is 0.992. The lower dashed line is a two-point straight line that is used to indicate the separation of the two families (see, however, footnote 2).

increase in the following order of $X^- = NC^- > HO^- > HS^- > F^- > Cl^-$.[2] This is also the order of the corresponding barriers in the gas phase (or in solution), so that the loosest transition state, $(CN\cdots CH_3\cdots CN)^-$, belongs to the reaction with the highest barrier (see Table 1).[2] This correlation (5, 6*b*, 10) provides a basis for attaching a geometric significance to the intrinsic selectivity parameter (IS) that derives from plots of barriers $\Delta E^{\ddagger}$ vs. $(I_{X:} - A_{RX})$. Such a significance is projected in Fig. 4, which shows that the identity reactions fall into two families that differ in their $W_{R:}$ indices. The larger the $W_{R:}$ index of the reaction series, the looser the *average* transition state of the series. Thus, the exchange reactions of HS^-, HO^-, and NC^-, which are characterized by a large $W_{R:}$ index, possess on the average looser transition state geometries than the halide exchange reactions, which are characterized by a smaller $W_{R:}$ index. Since the IS parameter varies in proportion to $W_{R:}$ (eq. [5], Fig. 3), the intrinsic selectivity of a reaction series is associated then with the average transition state looseness in the series: *the higher the IS parameter, the looser, on the average, the transition states in the reaction series.*

A solvent is expected to effect only small changes in the looseness of transition states (6*b*, 10, 11) of the type $(X\cdots CH_3\cdots X)^-$.[3] Therefore the foregoing conclusion will carry over to the corresponding reactions in solutions. In general then, the curve-crossing model predicts that *an identity reaction series that possesses high intrinsic selectivity, IS, will exhibit, on the average, high intrinsic barriers and loose transition state geometries.* It follows that, both in the gas phase and in solution (Fig. 3), the *less* selective series of the halide exchange reactions will possess, on the average, *tighter* transition states than the more selective series of $X^- = NC^-$, HO^-, PhS^- (and (or) HS^-). Furthermore, both the intrinsic selectivity and the average transition state looseness will correlate with the average height of the intrinsic barriers in the corresponding series. These conclusions regarding the looseness of the transition states and the correlation of barriers and looseness in the two reaction series are in disagreement with previous conclusions of Albery and Kreevoy (7*a*).[4]

The geometric significance of the intrinsic selectivity (IS) parameter may be somewhat refined by inspecting Fig. 4. Having different slopes, the two lines[2] in the figure will theoretically intersect at $I_{X:} - A_{RX} \approx 41$ kcal/mol. This means that, *theoretically*, two reactions that belong to families having different IS parameters *may* possess the same degree of transition state looseness. This is the reason why the IS parameter can be strictly associated *only* with the *average* degree of looseness in a reaction series. There may then exist a more basic transition state property that is probed by the IS parameter. As shown in the following discussion, this property is the sensitivity of the reaction series to bond loosening in the transition state, $(X\cdots CH_3\cdots X)^-$, as a result of varying X.

The looseness of the transition state is a result of the C—X

[3]An extreme hydration (solvation by H_2O) is a complete proton transfer by the solvent (stabilization relative to the unprotonated TS by >100 kcal/mol). But even such extreme "solvation" does not seem to change the looseness of the TS significantly. Thus, $(H_2N\cdots CH_3\cdots NH_2)^-$ (supplementary material of ref. 8) differs by 4.5% in looseness in comparison with the doubly protonated TS $(H_3N\cdots CH_3\cdots NH_3)^+$ (ref. 12). The same difference is observed for the free molecules $CH_3—NH_2$ vs. $CH_3—NH_3^+$ (refs. 8, 12). Similar data exist for $(HO\cdots CH_3\cdots OH)^-$ vs. $(H_2O\cdots CH_3\cdots OH_2)^+$ (ref. 8 vs. ref. 13) and $CH_3—OH$ vs. $CH_3—OH_2^+$ (ref. 8 vs. ref. 14). Thus the $(X\cdots CH_3\cdots X)^-$ transition states appear to possess strong covalent bonds much like $CH_3—X$ molecules. The solvent will not change significantly the looseness of such transition states. For detailed thermochemical arguments, see refs. 6*b* and 10, while for isotope effect evidence see ref. 11.

[4]See refs. 5 and 6*b* for comparisons with the conclusions of the three-dimensional potential energy surface diagram model.

stretching deformation that is required to achieve a transition state (5) at the crossing point of Fig. 1. In accord, the looseness has been shown (10) to fit the approximate expression in eq. [7] where G is a constant, in energy units, for a reaction series (X^-/RX) that is typified by a constant $W_{R:}$. This equation is

$$[7] \quad (\Delta d^{\ddagger}/d^0) = L \approx {}_{/R:} \ln\left(\frac{I_{X:} - A_{RX}}{G}\right)$$

seen to mimic the trends in Fig. 4 such that in each series the looseness of the transition state increases as the electron transfer energy gap $I_{X:} - A_{RX}$ increases.[2] The change in TS looseness, which is brought about by varying X in the series, is proportional then to $W_{R:}$ as expressed in eq. [8].

$$[8] \quad \frac{\partial L}{\partial[\ln (I_{X:} - A_{RX})]} \approx W_{R:}$$

Thus a reaction series that possesses large $W_{R:}$ will experience great TS loosening or tightening effects as X is varied. In accord, the exchange series of $X^- = NC^-, HO^-, HS^-$ (and (or) PhS^-) is expected to exhibit a greater rate of variation in transition state looseness in comparison with the exchange series of $X^- = F^-, Cl^-, Br^-$, and I^-.

As can be seen from eqs. [5] and [8], both the barriers and the looseness of the transition state vary in proportion to $W_{R:}$ and, therefore, a somewhat stricter definition of IS can be formulated. Thus, intrinsic selectivity parameters, which derive from plots of $\Delta E^{\ddagger}$ vs. $(I_{X:} - A_{RX})$, measure not only the average looseness of the transition state, but also the sensitivity of the reaction series to geometric loosening as X is varied. It follows that a series of identity reactions that possesses a high IS parameter will then be characterized, *on the average*, by high intrinsic barriers and loose transition states. The looseness in such a series will be more sensitive to changes of X than a series that is characterized by low IS. This correlation of transition state properties derives from the notion (5, 6*b*, 10) that both barriers and transition state geometries result from the C—X stretching deformation required to overcome the $I_{X:} - A_{RX}$ gap and to achieve a transition state, $(X\cdots CH_3\cdots X)^-$, at the crossing point of Fig. 1.

Other identity reaction series can be generated by varying X. Intrinsic selectivity parameters can then be measured and coupled with isotope effect[5] measurements to test the predictions of this work. Once the physical significance of the intrinsic selectivity is unravelled, there may then exist a basis from which to understand the physical nature of selectivity parameters in nonidentity reactions.

Acknowledgement

The author is grateful to Professor S. Wolfe for support, hospitality, and discussions during the sabbatical leave at Queen's University, where the research was carried out.

1. J. E. Leffler. Science, **117**, 340 (1953).
2. A. Pross. J. Org. Chem. **49**, 1811 (1984), and references therein.
3. (*a*) S. S. Shaik. Nouv. J. Chim. **6**, 159 (1982); (*b*) J. Am. Chem. Soc. **106**, 1227 (1984); (*c*) S. S. Shaik and A. Pross. J. Am. Chem. Soc. **104**, 2708 (1982).
4. S. S. Shaik. J. Am. Chem. Soc. **105**, 4359 (1983).
5. D. J. Mitchell, H. B. Schlegel, S. S. Shaik, and S. Wolfe. Can. J. Chem. **63**, 1642 (1985).
6. (*a*) S. S. Shaik. Nouv. J. Chim. **7**, 201 (1983); (*b*) Prog. Phys. Org. Chem. **15**, 197 (1985).
7. (*a*) W. J. Albery and M. M. Kreevoy. Adv. Phys. Org. Chem. **16**, 87 (1978); (*b*) D. J. McLennan. Aust. J. Chem. **31**, 1897 (1978); (*c*) E. S. Lewis and S. Kukes. J. Am. Chem. Soc. **101**, 417 (1979).
8. S. Wolfe, D. J. Mitchell, and H. B. Schlegel. J. Am. Chem. Soc. **103**, 7674 (1981).
9. M. J. S. Dewar and E. Healy. Organometallics, **1**, 1705 (1982).
10. S. S. Shaik. Isr. J. Chem. In press.
11. K. C. Westaway. Can. J. Chem. **56**, 2691 (1978).
12. I. H. Williams. J. Am. Chem. Soc. **106**, 7206 (1984).
13. S. Yamabe, E. Yamabe, and T. Minato. J. Chem. Soc. Perkin Trans. 2, 1881 (1983).
14. K. Raghavachari, J. Chandrasekhar, and R. Burnier. J. Am. Chem. Soc. **106**, 3124 (1984).
15. J. Hayami, N. Hihara, N. Tanaka, and A. Kaji. Bull. Chem. Soc. Jpn. **52**, 831 (1979).
16. K. C. Westaway, Z. Waszczylo, P. J. Smith, and K. S. Rangappa. Tetrahedron Lett. **26**, 25 (1985).

[5]Some caution is warranted regarding isotope effect mesurements, since ion–dipole complexes $X^-\cdots CH_3X$ may exist in aprotic solvents (ref. 15). The observed isotope effect will consist then of an equilibrium isotope effect for complex formation and a kinetic contribution (ref. 15). See also concentration dependence of isotope effects in ref. 16.

The effect of substituents on the electrochemical oxidation potentials of 1,1,2,2-tetraphenylcyclopropane and 1,1,3,3-tetraphenylpropenyl radical

DANIAL D. M. WAYNER[1] AND DONALD R. ARNOLD[2]
Department of Chemistry, Dalhousie University, Halifax, N.S., Canada B3H 4J3

Received January 11, 1985[3]

DANIAL D. M. WAYNER and DONALD R. ARNOLD. Can. J. Chem. **64**, 100 (1986).

The effects of multiple substitution by methoxy and cyano in the 4-position(s) of 1,1,2,2-tetraphenylcyclopropane (**1**) and 1,1,3,3-tetraphenylpropenyl radical (**2**$^{\bullet}$) on the oxidation potentials have been measured. The results indicate that the oxidation process for the cyclopropanes (**1***a–m*) is irreversible. Nevertheless, the substituent effect on the potential is essentially additive and correlates reasonably well with $\Sigma\sigma^+$. A slow electron transfer process (an overall conversion of **1** to $\mathbf{2}^+$), with a transition state resembling the ring-opened radical cation, is consistent with these observations. The oxidation of the radical **2**$^{\bullet}$ is quasi-reversible in dichloromethane. In this case also, the substituent effect on the oxidation potential is additive and correlates with $\Sigma\sigma^+$. Any deviation from planarity of **2**$^{\bullet}$ is not sufficient to prevent substituents from exerting normal (additive) behaviour.

DANIAL D. M. WAYNER et DONALD R. ARNOLD. Can. J. Chem. **64**, 100 (1986).

On a mesuré les variations des potentiels d'oxydation du tétraphényl-1,1,2,2 cyclopropane (**1**) et du radical tétraphényl-1,1,3,3 propényle (**2**$^{\bullet}$) portant des substituants méthoxy et cyano en position 4. Les résultats indiquent que l'oxydation est irréversible dans le cas des cyclopropanes (**1***a–m*). Cependant, l'effet du substituant sur l'oxydation est essentiellement additif et cet effet est en bonne corrélation avec la valeur de $\Sigma\sigma^+$. Ces observations suggèrent un processus de transfert d'électron (une transformation globale de **1** en $\mathbf{2}^+$), qui est lent et qui implique un état de transition s'apparentant au cation radicalaire à chaîne ouverte. Dans le cas du radical **2**$^{\bullet}$, l'oxydation est quasi réversible dans le dichlorométhane. Dans ce cas, également, le substituant a un effet additif sur l'oxydation et cet effet est en accord avec la valeur de $\Sigma\sigma^+$. Les déviations de la planéité du composé **2**$^{\bullet}$ ne suffisent pas à contrecarrer l'effet normal (additif) des substituants.

[Traduit par le journal]

Introduction

The electrochemical oxidation of 1,1,2,2-tetraphenylcyclopropane (**1***a*) has been shown to lead to the formation of the 1,1,3,3-tetraphenylpropenyl cation ($\mathbf{2}a^+$) in acetonitrile and dichloromethane (1). This carbocation subsequently cyclizes to form 1,3,3-triphenylindene (**3**) or deprotonates to give tetraphenylallene (**4**), depending on the basicity of the medium (Scheme 1). The photosensitized (electron transfer) reactions of **1***a* involve the same intermediate ($\mathbf{2}a^+$). In this case, the ratio of **3** to **4** depends on the choice of sensitizer for the reaction (2).

Both of these reactions undoubtedly involve the 1,3-radical cation as the first intermediate. 1,3-Radical cations have not been well characterized. Because of the stabilizing effect of the tetraphenyl substitution, we had hoped to obtain some direct evidence for the involvement of this species during the electrochemical oxidation of **1***a*. Radical cations are generally more stable in dichloromethane than in acetonitrile (3), but even in this solvent, at sweep rates as high as 20 V s^{-1}, no evidence for a single one-electron transfer was obtained (2).

The homologous 1,2-radical cations are more easily studied. The effect of substitution on the electrochemical oxidation of tetraphenylethylene (**5**) is particularly interesting in this regard. It has been observed, by Bard and Phelps, that tetrakis(4-*N*,*N*-dimethylaminophenyl)ethylene undergoes a two-electron reversible oxidation while tetraanisylethylene is oxidized in two closely spaced one-electron steps (4). Furthermore, the anodic oxidation of the unsubstituted tetraphenylethylene occurs in two one-electron steps that are even further apart (5). Presumably, electron-donating substituents on the tetraphenylethylene decrease the potential of the second electron transfer step so that only one two-electron wave is observed in these cases. By analogy, it was anticipated that substitution with electron-withdrawing substituents on **1** would separate the two one-electron transfer steps. It was found, in fact, that the cyclic voltammogram of 1,1,2,2-tetra(4-cyanophenyl)cyclopropane (**1***i*) does exhibit two closely spaced waves of approximately equal peak currents (1).

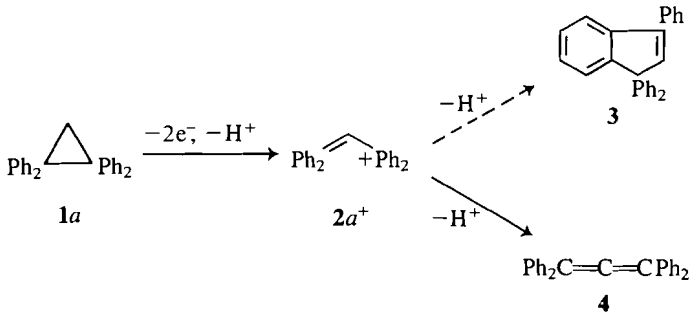

SCHEME 1

The purpose of this paper is to report the details of the effect of substitution on the electrochemical oxidation potential of **1**. Combinations of cyano and methoxy substitutions were used in order to study the additivity of the substituent effects in these species. The preparation (and thermal isomerization) of these compounds has already been described (6).

The consequent formation of the allylic cation $\mathbf{2}^+$ from the oxidation of **1** provides a convenient opportunity to study the substituent effects on the reduction potentials of these intermediates. This potential, of course, corresponds to the oxida-

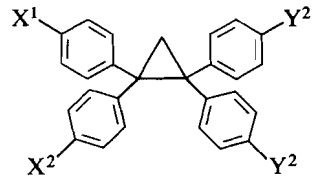

[1]Present address: National Research Council of Canada, Ottawa, Ont., Canada, K1A 0R6.

[2]Author to whom correspondence should be addressed.

[3]Revision received August 12, 1985.

TABLE 1. Oxidation potentials of **1** in dichloromethane (0.1*M* TBAP)[a]

1	X^1	X^2	Y^1	Y^2	E_p (V)[b]	$E_p - E_p/2$ (mV)	αn_a[c]
a	H	H	H	H	1.36	130	0.37
b	OMe	H	H	H	1.30	160	0.30
c	OMe	OMe	H	H	1.10	130	0.37
d-cis	OMe	H	OMe	H	1.10	140	0.34
d-trans	OMe	H	H	OMe	1.10	140	0.34
e	OMe	OMe	OMe	OMe	1.03	150	0.32
f	CN	H	H	H	1.54	140	0.34
g	CN	CN	H	H	1.70	180	0.27
h-cis	CN	H	CN	H	1.75	220	0.22
h-trans	CN	H	CN	H	1.75	220	0.22
i	CN	CN	CN	CN	1.95[d]	150	0.32
j	CN	OMe	H	H	1.28	160	0.30
k-cis	CN	H	OMe	H	1.25	140	0.34
k-trans	CN	H	H	OMe	1.25	140	0.34
l	CN	CN	OMe	OMe	1.36	220	0.22
m-cis	CN	OMe	CN	OMe	1.22	120	0.40
m-trans	CN	OMe	OMe	CN	1.22	120	0.40

[a]Measured by cyclic voltammetry at a sweep rate of 400 mV s^{-1}.
[b]Versus SCE.
[c]Calculated from $E_p - E_p/2 = 0.0483/\alpha n_a$.
[d]First wave.

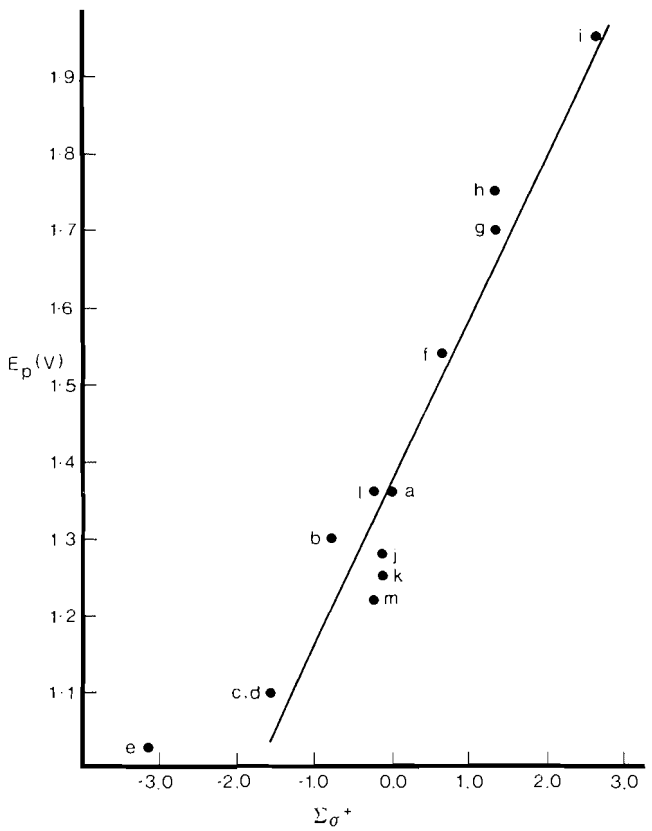

FIG. 1. The oxidation potentials (E_p) of the 1,1,2,2-tetraphenylcyclopropanes (**1***a–m*) versus $\Sigma\sigma^+$. (σ^+: OCH_3, −0.78; CN, 0.66).

tion potential of the radical **2**·. Possible mechanistic implications also are considered.

Results

The oxidation potentials of **1***a–m* are listed in Table 1. All of the oxidations are irreversible with $E_p - E_{p/2}$ ranging from 130 to 230 mV. A plot of E_p versus $\Sigma\sigma^+$ gives a linear correlation with a slope of 217 ± 17 mV, an intercept of 1.38 ± 0.02 V, and a correlation coefficient of 0.956 (Fig. 1).

TABLE 2. Reduction potentials of $\mathbf{2}^+$ in dichloromethane (0.1*M* TBAP)[a]

$\mathbf{2}^+$	$E_{1/2}$ (V)[c,d]	$E_{p_c} - E_{p_a}$
a	0.37	90
b	0.22	90
c	0.07	90
d-cis[b]	0.12	90
d-trans[b]	0.12	70
e	−0.04	70
f	0.48	70
g	0.65	80
h-cis[b]	0.66	80
h-trans[b]	0.66	80
i	Not observed	
j	0.30	80
k-cis[b]	0.28	90
k-trans[b]	0.28	90
l	0.31	80
m-cis[a]	0.32	80
m-trans[a]	0.32	80

[a]Measured by cyclic voltammetry at a sweep rate of 400 mV s^{-1}.
[b]The stereochemical designation represents that of the tetraphenylcyclopropane precursor.
[c]Versus SCE.
[d]$E_{1/2} \approx E^0$ (ref. 14).

The reduction potentials of **2***a–m*$^+$ are given in Table 2. All of these reductions are quasi-reversible with a separation of $E_{p_a} - E_{p_c}$ between 70 and 90 mV. The plot of $E_{1/2}$ versus $\Sigma\sigma^+$ has a slope of 193 ± 12 mV and an intercept of 0.37 ± 0.01 V with a correlation coefficient of 0.982 (Fig. 2).

Discussion

The Hammett equation for electrochemical reactions (ref. 7, eq. [1]) is often used to describe the effect of varying electron

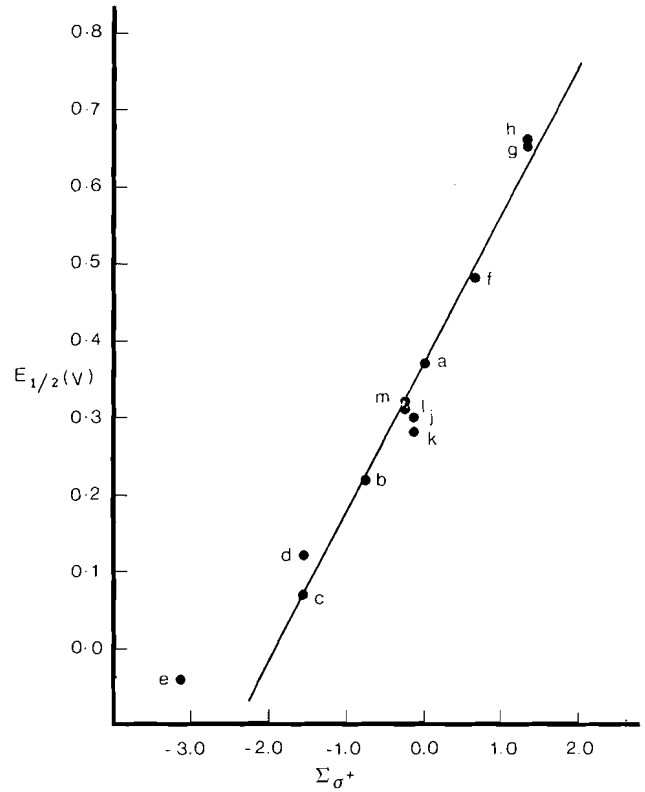

FIG. 2. The oxidation potentials ($E_{1/2}$) of the 1,1,3,3-tetraphenylpropenyl radicals (**2***a–m*$^{\bullet}$) versus $\Sigma\sigma^+$. (σ^+: OCH_3, −0.78; CN, 0.66).

demand at the reactive centre on the equilibrium constants (E^0) for a series of structurally related compounds. In general, these plots have slopes in the range 0.1–0.8 V (8). While this relationship is thermodynamically significant for reversible electrode processes, for irreversible processes the analysis is not straightforward.

[1] $E_{1/2} = (RT/nF)\rho\sigma$

Analysis of the oxidation of **1***a–m* by the Hammett approach gives a best-fit line with a slope of 217 mV and with a correlation coefficient of 0.956 (Fig. 1). The oxidation potential of **1***e*, which falls well off the line, was not included in this correlation. Including this point has a significant effect on the correlation coefficient (0.927 in this case) and the slope of the best-fit line decreases markedly, to 185 mV. The reason why the oxidation potential of this derivative falls off the line is not obvious but it may represent a saturation in terms of the substituent effect on the oxidation of **1**, or a change in the mechanism for the anodic process. In all cases only one anodic wave is observed.

There has been some controversy over the ability of a cyclopropyl ring to transmit electronic effects (9). It is in fact surprising to find that the oxidation potentials of **1***a–m* correlate as well as they do with $\Sigma\sigma^+$. If the electron is removed from a molecular orbital that is essentially localized on an aromatic ring, then substitution at another ring should not have a large effect on the oxidation potential, and certainly not an additive effect. The oxidation of **1***c*, however, is the same as that of **1***d*; similarly, the oxidation potentials of **1***h* and **1***g* are close. It is interesting that the oxidation potential of **1***j* is close to that of **1***k*. However, **1***m* is significantly easier to oxidize than **1***l*. In the latter case, the difference may be attributed to merostabilization in the radical ion. This effect has been used to explain the observed variation in reduction potentials of 4,4′-disubstituted benzophenones (10) and the oxidation (and reduction) potentials of tetraarylethylenes (11). However, the effect of merostabilization in the 4-methoxy, 4′-cyano substituted diphenylmethyl moiety is not large (only 3 kcal mol^{-1}). Furthermore, the observed oxidation potential of **1***j* (and **2***j*$^+$ and **2***m*$^+$, Table 2) is not anomalous.

The cyclopropane ring will be distorted in the 1,3-radical cation. Theoretical estimates of the length of the 1,2-bond in the radical cation of 1,2-divinylcyclopropane give a value of more than 1.9 Å (12). Thermochemical estimates of the strength of the one-electron, two-centre bond in **1***a*$^{\bullet+}$ give a value of only 5–8 kcal mol^{-1} (2). For the oxidation of **1**, the additivity of the substituent effect is undoubtedly derived from the interaction of all of the aryl rings in this ring-opened species, which interact through the vacant and half-filled *p*-orbitals. The idea of this product-like transition state is compatible with a slow electron transfer step (i.e. the electrochemical irreversibility).

Shono and Matsumura have measured the half-wave oxidation potentials of some 4-substituted arylcyclopropanes (13). In their work, a slope of 730 mV was obtained from the Hammett plot of $E_{1/2}$ versus σ^+. The slope of the best-fit line from the Hammett plot for **1***a–m* would be expected to be about one-fourth of the slope obtained for these monoarylcyclopropanes if the transition states (i.e. α) are similar. One-fourth of the slope reported by Shono and Matsumura is 183 mV. The observed slope of 217 mV obtained from **1***a–m* is close to this value. However, the limited number of substituents used in both studies makes further comparison difficult.

There are some interesting comparisons to be made with the oxidation potentials reported for the homologous tetraarylethylenes (**5**) (11). In this previous report the variation in the oxidation potential of several 4-methyl, 4-cyano, and 4-methoxy derivatives of **5** were correlated with $\Sigma\sigma^+$. The deviation of 1,2-di(4-methoxyphenyl)-1,2-di(4-cyanophenyl)-ethylene (**5***m*) from the best-fit line was attributed to merostabilization of the intermediate radical cation. We notice now, however, that there are some inconsistencies with this interpretation. For the oxidation (and reduction) of **5**, those compounds that show reversible electrochemical behavior form one line while those that show irreversible behavior fall on another line; all of the irreversible potentials show a positive deviation from the line formed by plotting the reversible potentials. This is to be expected since the deviation represents an increasing activation energy or, in electrochemical terminology, an increasing overpotential for oxidation. (Similarly, a negative deviation is observed for the reduction potential, indicating that there is an overpotential associated with the irreversible reduction.) The correlation of the overpotentials with $\Sigma\sigma^+$ is not a surprise since the overpotentials are related to the activation energy for the heterogeneous electron transfer. The oxidation (and reduction) of **5***m* is reversible. This point, in fact, lies on the line defined by the reversible oxidation potentials. These electrode processes probably involve the transfer of two electrons; thus, the effect of merostabilization *should not be observed* since the radical cation will not exist as a discrete intermediate.

It is interesting that the slope of the best-fit line for the irreversible oxidation potentials of **5** is 190 mV, which compares well with the 217 mV found for the oxidation potentials of **1**. (The slope of the line through those points corresponding to the reversible oxidation of **5** is 110 mV.) In the case of **1***m* the deviation *may* be attributed to merostabilization since the irreversible oxidation represents the barrier to the transfer of the first electron. However, the scatter of the points near $\Sigma\sigma^+ = 0$ as

well as the absence of the effect on the oxidation of $\mathbf{2}^{\bullet}$ preclude definitive conclusions from being drawn.

The electrochemical oxidation of **1***a* leads to the formation of $\mathbf{2}a^{+}$ (1, 2). A quasi-reversible wave in dichloromethane for the reduction of $\mathbf{2}a$–m^{+} is observed from the cathodic sweep in the cyclic voltammogram. In all cases, the reduction of $\mathbf{2}a^{+}$ is chemically reversible. Therefore, although the system is not electrochemically reversible, the value of E^{0} must lie between E_{p_a} −30 mV and E_{p_c} +30 mV (14). Analysis of the reduction potentials of $\mathbf{2}a$–m^{+} by the Hammett approach gives a slope of 193 mV with a correlation coefficient of 0.982 (Fig. 2). As was the case with **1***e*, the reduction potential of $\mathbf{2}e^{+}$ does not fall on the line. If this point is included in the correlation, the slope of the Hammett plot decreases to 163 mV, and the correlation coefficient decreases significantly (r = 0.966). The esr spectrum of $\mathbf{2}a^{\bullet}$ has been observed; it is a well-resolved spectrum of over 200 lines (15). In this study the radical (as well as the corresponding anion) was assumed to have a conformation in which two of the phenyl rings were in the plane of the propenyl π-system and the other two phenyl rings were parallel to each other but perpendicular to the propenyl π-system. If this were the case, additivity of the substituent effects would be unlikely since the heterogenous electron transfer process is fast and therefore cannot be preceded by, or concurrent with, aryl ring rotation. The additivity of substituent effects in, for example, the reduction of $\mathbf{2}c^{+}$ and $\mathbf{2}d^{+}$, $\mathbf{2}g^{+}$ and $\mathbf{2}h^{+}$, and the other pairs that have the same number and type of substituents indicates that a more reasonable conformation is one in which all of the rings are twisted in a propeller-like conformation. Otherwise, the effect of preferential rotation of, for example, the 4-cyanophenyl rings in $\mathbf{2}g^{+}$ out of the plane should be observed. A similar propeller-like conformation was reported for the tetraanisylethylene radical cation ($5e^{\bullet+}$) in which the rings were estimated to be twisted by about 30° (16).

It is interesting that the slope of the Hammett plot of the oxidation potentials of $\mathbf{2}a$–$m^{\bullet}$ is about the same as the slope from the plot of the oxidation potentials of **1***a*–*m*. In fact, a plot of E_p of **1** versus $E_{1/2}$ of **2** gives a slope of 1.09 ± 0.15, an intercept of 0.98 ± 0.06 V, and a correlation coefficient of 0.967. This, again, supports the suggestion that at the transition state for oxidation of **1**, all four aryl rings can interact with the developing charge.

Experimental

The synthesis and spectral characterization of **1***a*–*m* have been described previously (6, 17). Tetrabutylammonium perchlorate (TBAP) was obtained from Fisher Scientific Company, recrystallized three times from 95% ethanol, and dried in a vacuum oven (12 h at 80°C, 10 Torr (1 Torr = 133.3 Pa)). Dichloromethane (Fisher) was distilled from P_2O_5 and stored over 4A molecular sieves. The electrochemical cell and apparatus have been described previously (2). Typically, concentrations of 0.001 *M* (**1**) were used in a total cell volume of 10 mL. A sweep rate of 400 mV s^{-1} was used for all measurements.

Acknowledgments

This work was supported by a grant from the Natural Sciences and Engineering Research Council of Canada (including a scholarship to D.D.M.W.).

1. D. D. M. Wayner and D. R. Arnold. J. Chem. Soc. Chem. Commun. 1087 (1982).
2. D. D. M. Wayner and D. R. Arnold. Can. J. Chem. **63**, 871 (1985).
3. J. Phelps, K. S. V. Santhanam, and A. J. Bard. J. Am. Chem. Soc. **89**, 1752 (1967).
4. A. J. Bard and J. Phelps. J. Electroanal. Chem. **25**, App. 2 (1970).
5. J. D. Stuart and W. E. Ohnsorge. J. Am. Chem. Soc. **93**, 4531 (1971).
6. D. R. Arnold, D. D. M. Wayner, and M. Yoshida. Can. J. Chem. **60**, 2313 (1982).
7. A. J. Fry. Synthetic organic electrochemistry. Harper and Row, Publishers, New York. 1972.
8. V. D. Parker. Colloq. Int. CNRS, **278**, 217 (1977); Chem. Abstr. **91**, 148269 (1979).
9. (*a*) E. M. Kosower and M. Ho. Proc. Chem. Soc. 25 (1962); (*b*) A. C. Goodman and R. H. Eastman. J. Am. Chem. Soc. **86**, 908 (1964); (*c*) I. Prins, J. W. Verhoefen, Th. J. DeBoer, and C. Worrell. Tetrahedron, **33**, 127 (1977); (*d*) H. H. Jaffe and M. Orchin. Theory and applications of ultraviolet spectroscopy. John Wiley and Sons Inc., New York. 1962; (*e*) S. Winstein and R. Baird. J. Am. Chem. Soc. **79**, 756 (1957); (*f*) C. F. Wilcox, L. M. Loew, and R. Hoffman. J. Am. Chem. Soc. **95**, 8192 (1973); (*g*) A. de Meijere. Angew. Chem. Int. Ed. Engl. **18**, 809 (1979).
10. W. J. Leigh, D. R. Arnold, W. R. W. Humphreys, and P. C. Wong. Can. J. Chem. **58**, 2537 (1980).
11. W. J. Leigh and D. R. Arnold. Can. J. Chem. **59**, 3061 (1981).
12. D. D. M. Wayner, R. J. Boyd, and D. R. Arnold. Can. J. Chem. **61**, 2310 (1983).
13. T. Shono and Y. Matsumura. J. Org. Chem. **35**, 4157 (1970).
14. J. O. Howell, J. M. Goncalves, C. Amatore, L. Klasine, R. M. Wightman, and J. K. Kochi. J. Am. Chem. Soc. **106**, 3968 (1984), footnote 6.
15. R. Dietz, M. E. Peover, and R. Wilson. J. Chem. Soc. B, 75 (1968).
16. J. A. Valenzuela and A. J. Bard. J. Phys. Chem. **72**, 286 (1968).
17. J. E. Hodgkins and M. P. Hughes. J. Org. Chem. **27**, 4187 (1962).

Regioselectivity control in metal hydride reductions of substituted maleic anhydrides

MARGARET M. KAYSER[1] AND LIVAIN BREAU
Department of Chemistry, Mount Allison University, Sackville, N.B., Canada E0A 3C0
AND
SONIA ELIEV,[2] PETER MORAND, AND H. S. IP[2]
Department of Chemistry, University of Ottawa, Ottawa, Ont., Canada K1N 9B4

Received February 8, 1985[3]

MARGARET M. KAYSER, LIVAIN BREAU, SONIA ELIEV, PETER MORAND, and H. S. IP. Can. J. Chem. **64**, 104 (1986).

A systematic study of reductions of unsymmetrically substituted maleic anhydrides by a variety of metal hydride reagents indicates that the high regioselectivity observed in these reactions is controlled chiefly by electronic factors.

MARGARET M. KAYSER, LIVAIN BREAU, SONIA ELIEV, PETER MORAND et H. S. IP. Can. J. Chem. **64**, 104 (1986).

Une étude systématique de la réduction d'anhydrides maléiques substitués d'une façon non symétrique, par divers hydrures métalliques, indique que la régiosélectivité observée au cours de ces réactions est contrôlée principalement par des facteurs électroniques.

[Traduit par le journal]

There is continuing interest in reductions of unsymmetrical cyclic anhydrides to the corresponding lactones (1), and much effort has gone into the study of the mechanism of these reactions and into the development of methods permitting the selective reduction of one or the other carbonyl group to obtain the desired lactone (2).

The reductions of unsymmetrically substituted succinic anhydride **1** by simple metal hydrides ($NaBH_4$ and $LiAlH_4$) yield as the principal product lactone **2**, resulting from reduction of the more hindered carbonyl function (1). However, when selectrides (Aldrich Catalog No. 19, 987-7, 21-340-3, 22-076-0) are used as reducing agents, the major product of the reaction is lactone **3** (3).

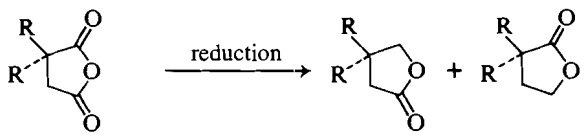

1 **2** **3**

R = CH_3 or C_6H_5

These results have been rationalized in terms of steric effects in the following manner (4). The interaction between the substituent R, protruding above the plane of the carbonyl function, and the highly hindered selectride reagent is strong enough to offset other effects usually implicated in the regioselectivity control (5).

In the case of planar, unsymmetrical anhydrides such as phthalic **4** or maleic anhydride **7**, the substituent is located in the plane of the carbonyl function; thus, the steric interaction between the incoming reagent and the substituent should be minimal.

However, a recent study (6) on reductions of 3-methoxyphthalic anhydride **4** has shown that, while $NaBH_4$ reduction yields a mixture of two lactones in approximately 1:1 ratio, the selectride reduction produces mostly lactone **6**.

Knight and Pattenden (7) examined the regioselectivity of reductions of 2-methoxy-3-methyl and 2-methoxy-3-phenyl maleic anhydrides, *7a* and *7b*, by $LiAlH_4$ and lithium tri-*tert*-butoxyaluminum hydride (LITBAL). The only products obtained in these reductions resulted from hydride attack at the carbonyl function adjacent to the methoxy group (**8** and **9**).

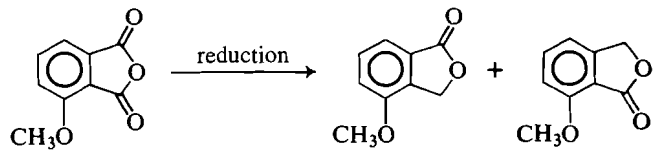

4 **5** **6**

On the basis of (*i*) *ab initio* calculations for the complexation of methoxymaleic anhydride *7c* with a counterion (5), and (*ii*) the fact that the activation of a carbonyl function by a cation appears necessary for the reaction to occur (8), we have concluded that the regioselectivity observed in reductions of methoxymaleic anhydrides is due principally to the chelation of the methoxy group and the adjacent carbonyl function by the counterion (5).

In view of the above results, the methoxy substituent appears to be a key element in directing reduction to the adjacent carbonyl function in methoxymaleic anhydrides, but sterically prevents reduction of the neighbouring carbonyl function in 3-methoxyphthalic anhydride **4**. Such puzzling results and conflicting interpretations have prompted us to undertake a systematic study of the relative importance of chelating versus steric effects in reductions of planar cyclic anhydrides. The substituted methoxymaleic anhydrides were chosen as suitable models for this investigation, since chelating and electronic

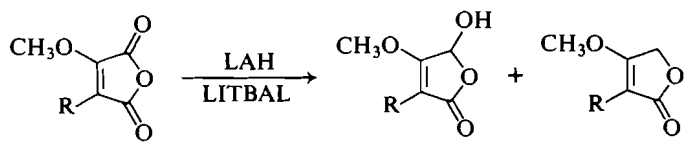

7
a R = C_6H_5
b R = CH_3
c R = H

8 **9**

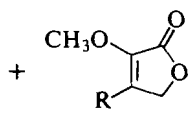

10

[1]Author to whom correspondence may be addressed.
[2]Undergraduate participants in research.
[3]Revision received August 28, 1985.

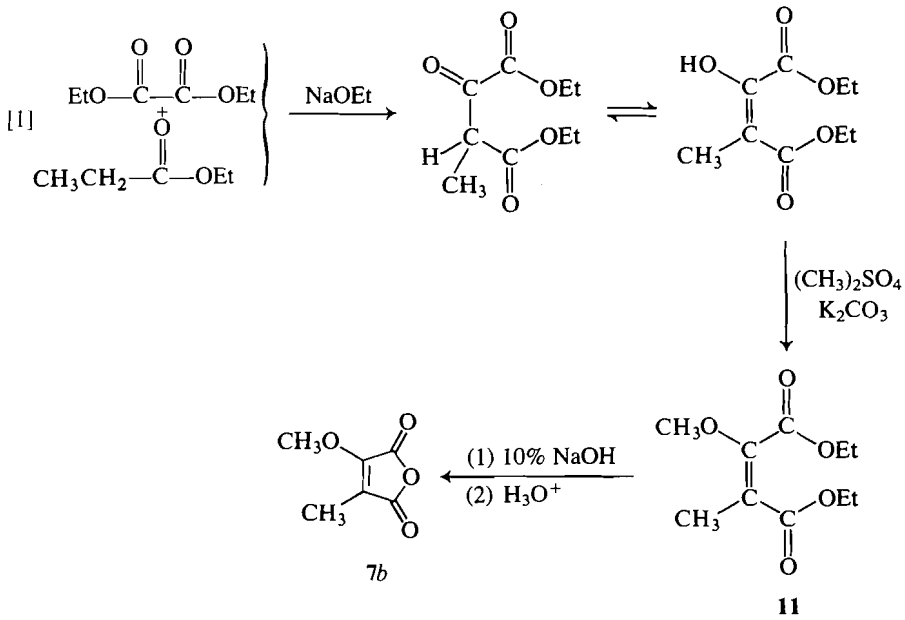

effects of the methoxy substituent in position 2 could be consistently confronted with the steric effect of the substituent in position 3 of methoxymaleic anhydride molecule **7**. At the same time an insight into the steric influence of methyl (and phenyl) substituent(s) could be gained from a parallel study of reductions of methyl (and phenyl) maleic anhydrides.

Results

All model compounds were prepared via short synthetic routes. 2-Methoxy-3-phenylmaleic anhydride *7a* was synthesized by condensation of phenylacetonitrile with diethyloxalate, followed by methylation and acid hydrolysis (7). 2-Methoxy-3-methylmaleic anhydride *7b* was prepared by a slightly modified synthetic sequence first reported by Schreiber (9). The condensation between ethylpropionate and diethyloxalate in the presence of sodium ethoxide, generated *in situ*, gave ethyl β-methyloxalacetate, which was subsequently methylated with dimethylsulfate–K_2CO_3 to the diester **11**. Basic hydrolysis of **11** gave 2-methoxy-3-methylmaleic anhydride *7b* (eq. [1]).

Methyoxymaleic anhydride *7c* was prepared from tartaric acid **12** in a three-step synthetic sequence. In the first step tartaric acid **12**, on treatment with acetic anhydride and sulfuric acid, was converted to diacetyltartaric anhydride **13** (10). The anhydride **13** reacted with pyridine and glacial acetic acid to give the pyridinium salt of hydroxymaleic anhydride **14** (11), which was subsequently methylated with diazomethane to methoxymaleic anhydride *7c* (eq. [2]). This sequence gives an excellent overall yield of methoxymaleic anhydride.

The three substrates *7a*, *7b*, and *7c* were reduced with simple metal hydrides ($LiAlH_4$) and ($NaBH_4$) and with bulky selectride reagents (L-, Na-, and K-selectrides). The crude products were analyzed by proton nmr and gc/ms before purification. The results are listed in Table 1.

TABLE 1. Metal hydride reductions of methoxymaleic anhydrides

Compound	Reducing agent	Product ratio* 8 : 9
7a	$NaBH_4$	83 17
	LAH	25 75
	L-sel	17 83
	K-sel	30 70
7b	$NaBH_4$	80 20
	LAH	30 70
	L-sel	10 90
	K-sel	10 90
7c	$NaBH_4$	100
	LAH	100
	L-sel	100
	K-sel	100

*Product ratios were obtained from the analysis of nmr spectra of crude reaction products.

In all reactions, regardless of counterion present (Li^+, Na^+, K^+) or the nature of the nucleophile (compact or bulky), the products obtained were the result of hydride transfer to the carbonyl function adjacent to the methoxy substituent. We could not detect the isomeric lactone **10**, or the corresponding lactol, in either crude or purified products.

Citraconic (methylmaleic) anhydride **20** was reduced with several reducing agents under various conditions of concentration and temperature. The results are shown in Table 2. Several attempts to reduce phenylmaleic anhydride with selectride reagents gave no indication as to selectivity of this compound since the first step in the reduction appears to be hydride transfer

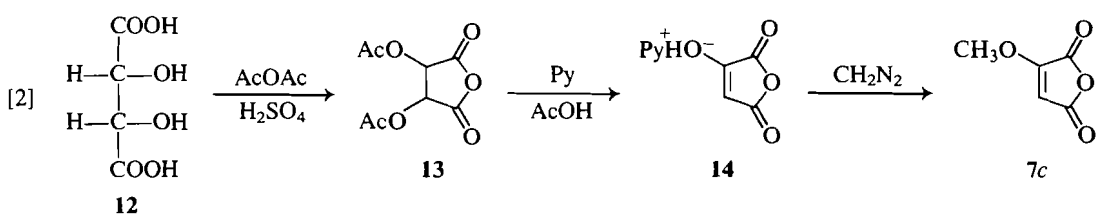

TABLE 2. Reductions of methylmaleic anyhydride **20**

Reducing agent	Temperature (°C)	Time (h)	Yield (%) Crude	Yield (%) Isolated	Reduction (%)*	Lactonic products Ratio† **21** : **22**
1 mol $NaBH_4$	0 → +22	2	100	85–90	100	92 —
1 mol KBH_4	−10 → 0	2	—‡	—	Trace	Trace —
2 mol KBH_4	−10 → 0	2	—‡	—	Trace	Trace —
1 mol KBH_4	−22 → 22	2	—‡	—	Trace	Trace —
2 mol KBH_4	22	2	100‡	50–60	70	91 9
1 mol $LiAlH_4$	−78 → −30	2	100	85–90	100	88 12
L-sel	−78 → −30	2	100	85–90	96	83 17
L-sel	−78 → +22	48	100	85–90	100	70 30
L-sel	22	2	100	85–90	100	75 25
Na-sel	−78 → −30	2	100	85–90	100	91 9
K-sel	−78 → −30	2	90–100	78–85	93	88 12
K-sel	−30 → +22	2	100	75–80	100	83 17

*Reduction 100% means that no starting anhydride or diacid could be detected in the nmr spectrum of the crude product.

†Lactonic ratio α:β was established from the nmr spectra of the crude reduction products by comparing the signals for hydrogen attached to a double bond, δ 5.85 (α) vs. 7.15 (β), and methyl groups CH_3, δ 2.10 (α) vs. 1.95 (β).

‡Diacid recovered.

to a carbon–carbon double bond. The subsequent reduction of phenyl succinic anhydride gives a mixture of two phenyl butyrolactones.

Discussion

The role of a methoxy substituent in controlling regioselectivity of hydride transfer can be double in nature: (*1*) the formation of chelate (5), which activates the implicated carbonyl group α toward hydride transfer; (*2*) the promotion of enolization, which deactivates the carbonyl group β (13). Since both effects were discussed elsewhere (5, 13), we shall present here only a brief resumé.

The *ab initio* calculations for methoxymaleic anhydride – Li^+ complex have shown that the preferred binding site for the cation is the "bridged position", **15**, corresponding to the strong overlap between the cation and the lone pairs on the two oxygen atoms (5).

Chelate **15** is energetically favoured over the alternate structure **16** by 6 kcal mol^{-1} and over **17** by 10 kcal mol^{-1}.

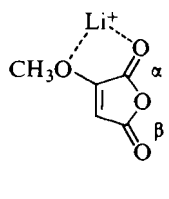

15

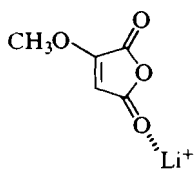

16

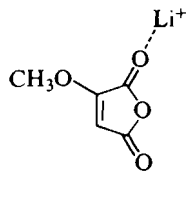

17

E (kcal mol^{-1}) −10 −4 0

Since association with a cation activates carbonyl function toward nucleophilic addition, the preferentially formed complex **15** is reduced selectively at the α-carbonyl group. Of the two remaining isomeric complexes, **16** is more stable than **17** by 4 kcal mol^{-1}. From the energy viewpoint **16** is the more likely candidate for reduction. However, the same effect that stabilizes complex **16** also diminishes reactivity of the carbonyl function β.

It is apparent from examination of the canonical forms of the complexes **16** and **17** that the stabilization of **16** is due to the π-electron donating capacity of the methoxy substituent **18**. For the same reason, **16** possesses a higher degree of enolate

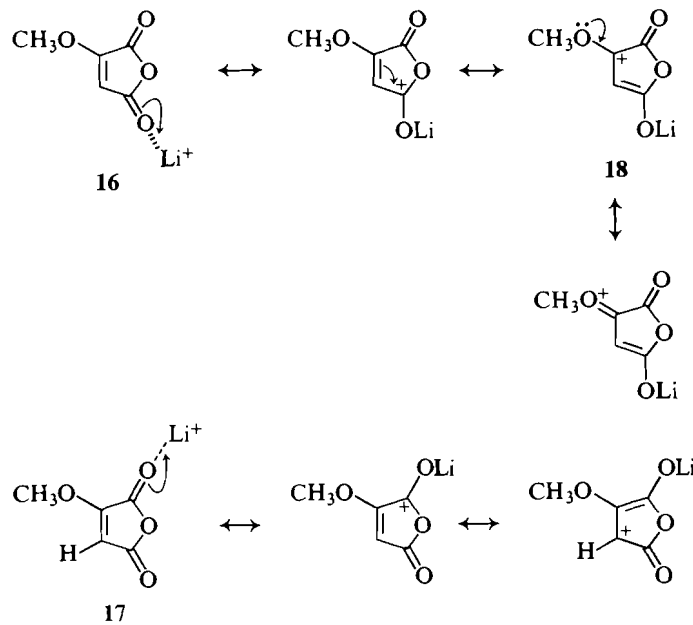

16 **18** **17**

character and, since enolized carbonyl groups resist reduction by metal hydrides (14), the complex **15** is reduced in preference to **16**. The observed selectivity is a net result of these two effects.

Steric effects, if any, are clearly less important. Evidently, the results of reductions of **7***a* and **7***b* could be interpreted in terms of steric control in the follow manner. The methyl substituent occupies "more space" in the immediate vicinity of the carbonyl function (β) than the methoxy group occupies in the immediate vicinity of the carbonyl function (α). Similarly, the phenyl group, which may assume a position perpendicular to the plane of the anhydride ring as shown in **19**, is more sterically important than the methoxy substituent. Thus, both the methyl and phenyl groups could, in theory, hinder the approach of a nucleophile, particularly a bulky selectride, toward the neighbouring carbonyl function more effectively than the methoxy group. However, if steric effects alone were involved, we would expect reversed regioselectivity in reductions of the unsubstituted methoxymaleic anhydride **7***c*, where steric com-

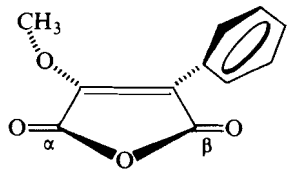

19

petition is between the methoxy group and the hydrogen atom. This, of course, is not the case; the regioselectivity in the reduction of **7***c* follows the pattern observed in reductions of other methoxymaleic anhydrides. In all the reductions studied only the lactone **9***c* was obtained and we were unable to detect any evidence of the isomeric lactone **10***c* in the crude reaction product.

The results obtained from reductions of methylmaleic anhydride suggest that the steric effect of a methyl substituent situated in the plane of the anhydride ring is only marginal (see Table 2). In a preliminary communication (4) on selectride reductions we have reported that, while $NaBH_4$ reduction of methylmaleic anhydride **20** gave mostly lactone **21**, the reduction with K-selectride yielded lactone **22** as the principal product. Systematic study of methylmaleic anhydride reductions with a variety of metal hydrides, under different reaction conditions (Table 2), has shown that the preliminary results were incorrect. The error was most likely due to the selective loss of the lactone **21** during work-up and distillation. In the present study we have examined, by proton nmr and gc/ms, the crude reaction products before attempting isolation and purification of the lactones. The results show that in all cases preferential reduction occurs at the carbonyl function next to the methyl group. The highest proportion (25–30%) of the alternate lactone **22** was obtained in the reduction of **20** by L-selectride, carried out at room temperature.

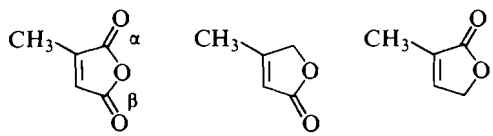

20 **21** **22**

Under the usual reaction conditions (temperature $-78°C \rightarrow -30°C$) the product distribution ratio is only marginally affected by the size of the nucleophile, which suggests that the steric effect is feeble.

What does affect regioselectivity of these reductions, if the steric effect is ruled out, chelation is not applicable, and the stabilization of the enolate **23** is weak in comparison to the stabilization of enol **18**?

The *ab initio* calculations performed for the "naked" methylmaleic anhydride (**24**) show a small difference in the magnitude of the LUMO coefficients on the carbon atoms of the two carbonyl groups. We should point out that this difference is

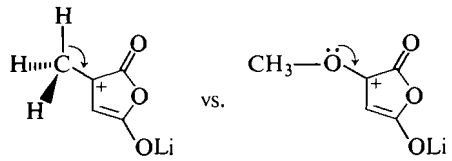

23 **18**

considerably larger in methoxymaleic anhydride, **25**. Since the size of the LUMO coefficient correlates well with the reactivity of a carbonyl function toward a nucleophile, these results indicate that the carbonyl group adjacent to the methyl substituent is intrinsically more reactive than the β-carbonyl group and is attacked preferentially even by a sterically demanding selectride reagent. These considerations are supported by the *ab initio* calculations (Gaussian 70 program with a minimal STO-3G basis set) (16). The study of protonation of methylmaleic anhydride[4] indicates that the association of H^+ with the β

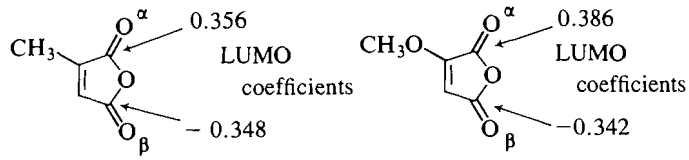

24 **25**

carbonyl group is favoured by 3.0 kcal mol^{-1} (**26**, **27**) which confirms the slight stabilizing effect of methyl substituent as illustrated in **23**. The calculations also show that the H^- attack should occur preferentially at the α-carbonyl group, **28** and **29**.

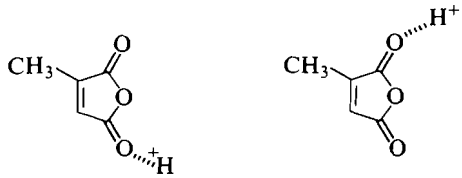

26 **27**

E (kcal mol^{-1}) −3 0

For both structures **28** and **29**, the optimal position for hydride attack, at the distance of 2 Å, was found to be above the double bond and at the angle of 110° to the plane of the carbonyl group. We did not optimize the position of H^- attacking the carbonyl group – H^+ complex. The calculations carried out for perpendicular attack showed slight, but consistent, preference

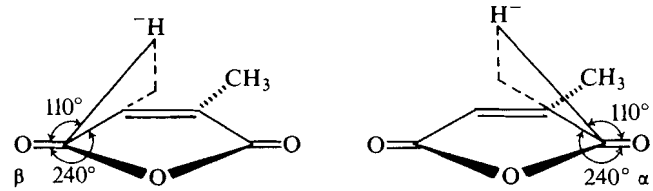

28 **29**

E (kcal mol^{-1}) 0 −7.5

for the α-attack. Hence, the intuitive interpretation of the experimental results in terms of electronic effects is supported by *ab initio* calculation.

Conclusion

The present studies indicate that the regioselectivity of metal hydride reductions of substituted maleic anhydrides is only marginally affected by steric congestion. The principal factors controlling regioselectivity of these reactions appear to be electronic in nature. These effects seem to be the following: (*1*) intrinsic reactivity of the carbonyl group adjacent to phenyl, methyl, or methoxy substituent; (*2*) activation of the carbonyl function next to the methoxy substituent by chelation with a counterion; (*3*) deactivation of the carbonyl function capable of forming (by electron-releasing substituent) stabilized enolate.

[4]The geometry for the parent maleic anhydride was obtained from the crystallographic data (17*a*). For the methyl substituted maleic anhydride, standard bond lengths and bond angles were used (17*b*).

Experimental

Proton and ^{13}C nmr spectra were recorded on a Varian HA-100 spectrometer in $CDCl_3$ or $(CD_3)_2CO$ as solvent and TMS as internal standard. The gc/ms spectra were obtained on a VG mass spectrometer with a DANI 7070 gas chromatograph, and infrared spectra on a Beckman TR-20 instrument.

The general procedure for the reactions with $LiAlH_4$ and $NaBH_4$ is described in ref. 15. The selectride reductions were carried out as follows: an anhydride (0.003 mol) was dissolved in dry, freshly distilled THF (100 mL). The mixture, flushed with a constant slow stream of dry N_2, was cooled in a Dry Ice – acetone bath. Li-, Na- or K-selectride (1 *M* in THF, 10 mL) was injected slowly into the reaction flask. The reaction was stirred for 2 h while the temperature was allowed to rise slowly to −30 or −20°C. At that time NaOH (4 *N*, 2 mL) and 30% H_2O_2 (3 mL) were added and stirring was continued overnight. The reaction mixture was acidified with 6 *N* HCl, reduced on a rotatory evaporator, and extracted several times with chloroform and diethyl ether. The combined organic layers were evaporated to dryness.

2-Methoxy-3-phenylmaleic anhydride, 7a

Condensation of phenylacetonitrile with diethyloxalate in the presence of sodium hydride (50% oil dispersion) gave ethyl (3-cyano-3-phenyl) pyruvate: mp 129–130°C (18); proton nmr δ ($CDCl_3$): 1.40 (t, 3H), 4.40 (q, 2H), 7.25–7.50 (m, 3H), 7.60–7.80 (m, 2H). Methylation of the pyruvate with dimethyl sulfate – K_2CO_3 gave ethyl (3-cyano-2-methoxy) cinnamate; proton nmr δ ($CDCl_3$): 1.40 (t, 3H), 3.8 (s, 3H), 4.43 (q, 2H), 7.30–7.50 (m, 3H), 7.60–7.80 (m, 2H). The hydrolysis in concentrated HCl/glacial acetic acid gave anhydride **7***a* as pale needles (yield 80%); ν_{max} (KBr): 1835, 1765, and 1635 cm^{-1}; proton nmr δ ($CDCl_3$): 4.30 (s, 3H), 7.35–7.50 (m, 3H), 7.85–8.00 (m, 2H). These results are in agreement with the data reported in the literature (7).

Reductions of 2-methoxy-3-phenylmaleic anhydride, 7a

Reductions carried out according to the general procedures gave 80–90% isolated yields of reduced products (**8***a* and **9***a*). Crude products were analyzed by proton nmr. Separation by chromatography in hexane–ether (1:4) gave 4-hydroxy-3-methoxy-2-phenylbut-2-enolide **8***a*: mp 132–134°C; ν_{mas} (KBr): 3280, 1715, and 1650 cm^{-1}; proton nmr δ ($(CD_3)_2CO$): 4.16 (s, 3H), 6.35 (s, 1H), 7.20–7.55 (m, 3H), 7.80–8.05 (m, 2H); and 3-methoxy-2-phenylbut-2-enolide **9***a*: mp 123–124°C; ν_{max} (KBr): 1745, 1645 cm^{-1}; proton nmr δ ($(CD_3)_2CO$): 4.15 (s, 3H), 5.15 (s, 2H), 7.26–7.45 (m, 3H), 7.85–8.12 (m, 2H).

2-Methoxy-3-methylmaleic anhydride, 7b

Under the continuous flow of N_2, sodium hydride (60% suspension in oil, 61.0 g) was washed with two portions of hexane and one of dry diethyl ether. After decanting solvents, a fresh diethyl ether (800 mL) was added. Absolute ethanol was added dropwise until evolution of H_2 ceased. The reaction mixture was cooled on an ice bath. Diethyl oxalate (209.0 g) followed by ethyl propionate (130.0 g) wre added to the stirred mixture. The reaction mixture was refluxed for 2 h 45 min, then cooled, diluted with ice water, and acidified with 6 *N* HCl to pH 2. The mixture was extracted with three 500-mL portions of ether. The combined organic layers were dried over $CaCl_2$ and reduced on a rotatory evaporator. Vacuum distillation of the residue gave β-methyl-oxalacetic ester (1.0 Torr (133.3 Pa), 85–95°C, 157 g, 63% yield). The ester was methylated with dimethyl sulfate – K_2CO_3 according to the procedure described by Knight and Pattenden (7). The resulting diethyl ether **11** (20.0 g) was refluxed for 2 h with 4 *N* KOH (100 mL). After cooling, the mixture was acidified with 6 *N* HCl and extracted with five 100-mL portions of ether. Ethereal extracts were dried over anhydrous $MgSO_4$ and the solvent was removed. The product obtained gave ir and nmr spectra identical to those described in the literature (8): mp 40–42°C; ν_{max} ($CHCl_3$): 1875, 1775, and 1675 cm^{-1}; proton nmr δ ($CDCl_3$): 4.25 (OCH_3), 2.10 (CH_3). The yield was 71%.

Reduction of 2-methoxy-3-methylmaleic anhydride, 7b

The reductions of **7***b* according to the general procedures gave 75–80% yields of isolated reduced products. Crude products were analyzed by proton nmr. Separation on thick-layer chromatography gave 5-hydroxy-4-methoxy-3-methyl-furan-2(5*H*)-one, **8***b*: mp 93°C (crystallized from benzene); ν_{max}: 3315, 1750, 1733, 1686 cm^{-1}; proton nmr δ ($CDCl_3$): 1.79 (s, 3H), 4.07 (s, 3H), 5.96 (C*H*OH), 6.2 (OH); and 4-methoxy-3-methyl-furan-2(5*H*)-one, **9***a*: ν_{max} (KBr): 1740 and 1665 cm^{-1}; proton nmr δ ($CDCl_3$): 1.75 (m, 3H), 3.97 (s, 3H), 4.67 (m, CH_2). The spectral data are identical with those described in the literature (19).

Methoxymaleic anhydride, 7c

Tartaric acid (103 g) was placed in a round-bottom flask, to which freshly distilled acetic anhydride (220 mL) and concentrated H_2SO_4 (6 mL) were added slowly. The mixture was stirred until all solid was dissolved. The solution was warmed and refluxed briefly (20 min). White crystalline diacetyltartaric anhydride precipitated on cooling. It was filtered, washed with cold dry ether, and dried. The yield of pure product was 118 g. Diacetyltartaric anhydride (26.0 g) was placed in a flask containing dry acetone (40 mL) and heated gently until dissolved. The solution was cooled in an ice bath to 10°C and dry pyridine (18 mL) was added with stirring. After a few minutes the colour of the reaction mixure changed from colourless to yellow-green. Glacial acetic acid (14 mL) was added in one portion with vigorous stirring to the mixture cooled below 10°C. The mixture was left overnight in a refrigerator. Pyridinium salt crystallized as fine, brown needles. It was filtered and washed with ice-cold *dry* diethylether (yield 15.2 g). The alcohol-free diazomethane (2.0 mg in 150 mL of dry ether) was added to a dry THF (200 mL) solution of the pyridinium salt (3.69 g). The solution was allowed to react for 30 min at 0°C. Then $AlCl_3$ (0.95 g) dissolved in dry ether (30 mL) was added. The reaction mixture was stirred for 1 h at room temperature. The white, flaky precipitate was removed by filtration. The organic solvents were removed and the product distilled at reduced pressure (0.5 Torr, 111°C) (ref. 12). The yield of **7***c* was 2.45 g, 100%; ν_{max} ($CHCl_3$): 1860, 1775, and 1645 cm^{-1}; proton nmr δ ($CDCl_3$): 4.05 (s, 3H), 5.75 (s, H); ms: M^+ 128, $M^+ - 44$, 84.

Reductions of methoxymaleic anhydride, 7c

Reductions carried out according to the general procedures gave only the lactonic product **9***c*. The isolated yields varied between 60 and 94%. In general the best yields were obtained with $LiAlH_4$, the poorest with $NaBH_4$. The selectride reductions produced **9***c* in 70–85% yields; **9***c*: ν_{max} ($CHCl_3$): 1785, 1745, and 1640 cm^{-1}; proton nmr δ ($CDCl_3$): 3.92 (s, 3H), 4.55 (s, 2H), 5.05 (s, 1H), ms: M^+ 114, 85, 69, 56.

Reductions of methylmaleic anhydride, 15

Reductions were carried out according to the general procedures. The variations in time and temperature as well as the yields and ratios of lactonic products obtained are shown in Table 2. Lactone **15***a*: proton nmr δ ($CDCl_3$): 2.14 (CH_3), 4.73 (d, CH_2—O), 5.87 (m, 1H); ms: M^+ 98. Lactone **15***b*: proton nmr δ ($CDCl_3$): 1.95 (CH_3), 4.77 (1, CH_2O), 7.15 (q, 1H); ms: M^+ 98.

1. M. M. KAYSER and P. MORAND. Can. J. Chem. **56**, 1524 (1978), and references cited therein; B. BAYEIL and M. WAHREN. Z. Chem. **21**, 149 (1981).
2. P. MORAND and M. M. KAYSER. J. Chem. Soc. Chem. Commun. 314 (1976); A. J. MCALEES, R. MCCRINDLE, and D. W. SNEDDON. J. Chem. Soc. Perkin Trans. 1, 2030 (1977); 2037 (1977); J. DREPELKA and J. HOLUBEK. Collect. Czech. Chem. Commun. **46**, 2123 (1981).
3. M. M. KAYSER and P. MORAND. J. Chem. Soc. Chem. Commun. 458 (1982).
4. M. M. KAYSER, J. SALVADOR, and P. MORAND. Can. J. Chem. **61**, 439 (1983).
5. M. M. KAYSER and G. WIPFF. Can. J. Chem. **60**, 1192 (1982).
6. M. A. MAKHLOUF and B. RICKBORN. J. Org. Chem. **46**, 4810 (1981).
7. D. W. KNIGHT and G. PATTENDEN. J. Chem. Soc. Perkin Trans. 1, 62 (1979).
8. J. L. PIERRE and H. HANDEL. Tetrahedron Lett. 2317 (1974); J. L. PIERRE, H. HANDEL, and R. PERRAND. Tetrahedron, **31**, 2795

(1975); H. HANDEL and J. L. PIERRE. Tetrahedron, **31**, 2799 (1975).
9. J. SCHREIBER. C. R. Acad. Sci. **242**, 139 (1956).
10. A. WOHL and C. OESTERLIN. Chem. Ber. **34**, 1139 (1901).
11. D. A. VAN DROPS and J. F. ARENS. Recl. Trav. Chim. Pays-Bas, **67**, 459 (1948).
12. R. K. RALPH, G. SHAW, and R. N. NAYLOR. J. Chem. Soc. 1169 (1959).
13. M. M. KAYSER and P. MORAND. Can. J. Chem. **58**, 2484 (1980).
14. D. H. R. BARTON, R. H. HESSE, C. WILSHIRE, and M. PECHET. J. Chem. Soc. Perkin Trans. 1, 1075 (1977).
15. M. M. KAYSER, J. SALVADOR, P. MORAND, and H. G. KRISHNAMURTY. Can. J. Chem. **60**, 1199 (1982).
16. W. J. HEHRE, W. A. LATHAN, R. DITCHFILED, M. D. NEWTON, and J. A. POPLE. Gaussian 70, Q.C.P.E. No. 236, Bloomington, Indiana.
17. (*a*) R. DESTRO, G. FILIPPINI, C. M. GRAMACIOLI, and M. SIMONETTA. Acta. Crystallogr. Sect. B, **27**, 2023 (1971); (*b*) J. A. POPLE and D. L. BEVERIDGE. Approximate molecular orbital theory. McGraw–Hill, New York. 1970. p. 111.
18. R. L. EDWARDS and M. GILL. J. Chem. Soc. Perkin Trans. 1, 1538 (1973).
19. D. W. KNIGHT and G. PATTENDEN. J. Chem. Soc. Perkin Trans. 1, 635 (1975); 641 (1975).

Thionium analogs of the opiates levorphanol and isolevorphanol: synthesis of the 17-deaza-17-thia isosteres (sulforphanol and isosulforphanol)

B. Belleau, U. Gulini,[1] R. Camicioli, B. J. Gour-Salin, and G. Sauvé
Department of Chemistry, McGill University, Montreal, P.Q., Canada H3A 2K6
Received May 1, 1985

B. Belleau, U. Gulini, R. Camicioli, B. J. Gour-Salin, and G. Sauvé. Can. J. Chem. **64**, 110 (1986).

The total synthesis of the position-17 sulfur analogs of the perchlorate salts of the morphinans, (±)-levorphanol and (±)-isolevorphanol via 4a-(2-aminoethyl)-1,2,3,4,4a,9-hexahydro-6-methoxyphenanthrene, a key intermediate in the synthesis of butorphanol (**4**), is described. 2D-Correlation and heterocorrelation nuclear magnetic resonance spectroscopy confirmed the configurational relationship of the isosteres.

B. Belleau, U. Gulini, R. Camicioli, B. J. Gour-Salin et G. Sauvé. Can. J. Chem. **64**, 110 (1986).

On décrit la synthèse totale des analogues portant un atome de soufre en position 17 des perchlorates des morphinanes, (±)-lévorphanol et (±)-isolévorphanol; ces synthèses se font par l'intermédiaire du (amino-2 éthyl)-4a hexahydro-1,2,3,4,4a,9 méthoxy-6 phénanthrène, un intermédiaire clé dans la synthèse du butorphanol (**4**). La rmn, corrélation 2D et hétérocorrélation, a permis de confirmer les relations configurationnelles des isostères.

[Traduit par le journal]

Introduction

In a previous publication (1) a rationale was presented that ascribes a fundamental role to the directionality of the nitrogen lone pair of morphinan-like structures in a stereocontrolled proton transfer process at the opiate receptor level. Structure–activity relationship studies (2) led to the conclusion that sulfonium salt analogs of well-known opiates like levorphanol and isolevorphanol **1***a,b* would help clarify the separate roles of ion pairing and hydrogen bond complex formation (as in a proton transfer complex) at the key counter anionic site level of the receptor. The key structural feature deserving exploitation here centers on the fact that the sulfonium ion cannot carry a proton-like tertiary amine, so that its incorporation as a substitute for the basic nitrogen of an opiate such as levorphanol should yield useful information about the role of the nitrogen lone pair (and its attached proton) in productive interactions with the receptors. In order that an unambiguous answer to this question may be secured, it is essential that the receptor probe engages in a unique mode of binding, as is the case for morphinan-like structures whose enantiomers are discriminated against in an absolute manner by the receptor binding sites, hence our choice of the levorphanol and isolevorphanol geometries as the patterns for the generation of sulfonium isosteres. In a preceding article (1), we described the synthesis of the sulfonium analog of isolevorphanol (isosulforphanol **3***a*) using a strategy patterned after that of Grewe and Mondon for the generation of morphinans (3). As it turned out, this strategy as applied to analogous sulphur-containing, non-nitrogenous intermediates led exclusively to the isomorphinan geometry (*trans* B/C fusion **3***a*) rather than the morphinan stereochemistry **2***a*, the usual well-known outcome of the Grewe process. The structure of the isosulforphanol **3***a* thus obtained (as well as that of an unexpected by-product) was established by single crystal X-ray analysis (1). It became obvious then that a different synthetic strategy had to be conceived in order to generate the isomeric sulforphanol analog **2***a* (*cis* B/C fusion). It is the purpose of this communication to describe such a selective but bifurcate strategy, allowing as well for an alternative and efficient synthesis of the already described isosulforphanol analog **3***a*.

[1]Permanent address: Department of Chemical Sciences, University of Camerino, Camerino, Italy.

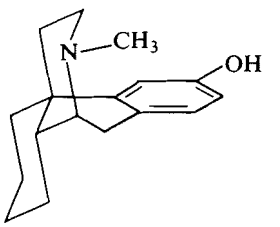

1*a*

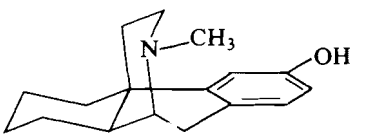

1*b*

The synthetic strategies leading to **2** and **3** are outlined in Scheme 1. The starting material **4** is the key intermediate in the commercial synthesis of butorphanol (4), and we endeavored to replace its amine function by a hydroxyl group that could then be transformed into a thiol group. In principle, a more direct approach to this transformation would involve reaction with a pyridinium intermediate with a suitable thiolate anion, a sequence based on Katritzky's method (5). Although the requisite 2,4,6-triphenylpyridinium intermediate could be easily obtained from **4**, all attempts at reacting it with a variety of relevant nucleophiles (thioacetate, thioxanthate, thiourea, acetate, iodide) failed to give any of the desired products (aromatization of ring B being the major event). In a parallel fashion all attempts at diazotization of **4** and its *N*-acetyl or 3,5-dinitrodibenzoyl derivatives (6) failed to yield any of the corresponding alcohol **6** or its esters. We thus turned our attention to a transamination process, with the hope of generating aldehyde intermediate **5**. Attempts to extrapolate the recently developed method of Buckley and Rapoport (7) to amine **4** using a 4-formyl-1-methyl pyridinium salt led to disappointing results, only very small yields of aldehyde **5** being formed. However, the use of excess ninhydrin under controlled conditions led to the desired aldehyde **5** in acceptable yields. Its structure was readily confirmed by spectroscopic methods and by borohydride reduction in high yield to the corresponding alcohol intermediate **6**. Access to this key intermediate provided an opportunity to develop an im-

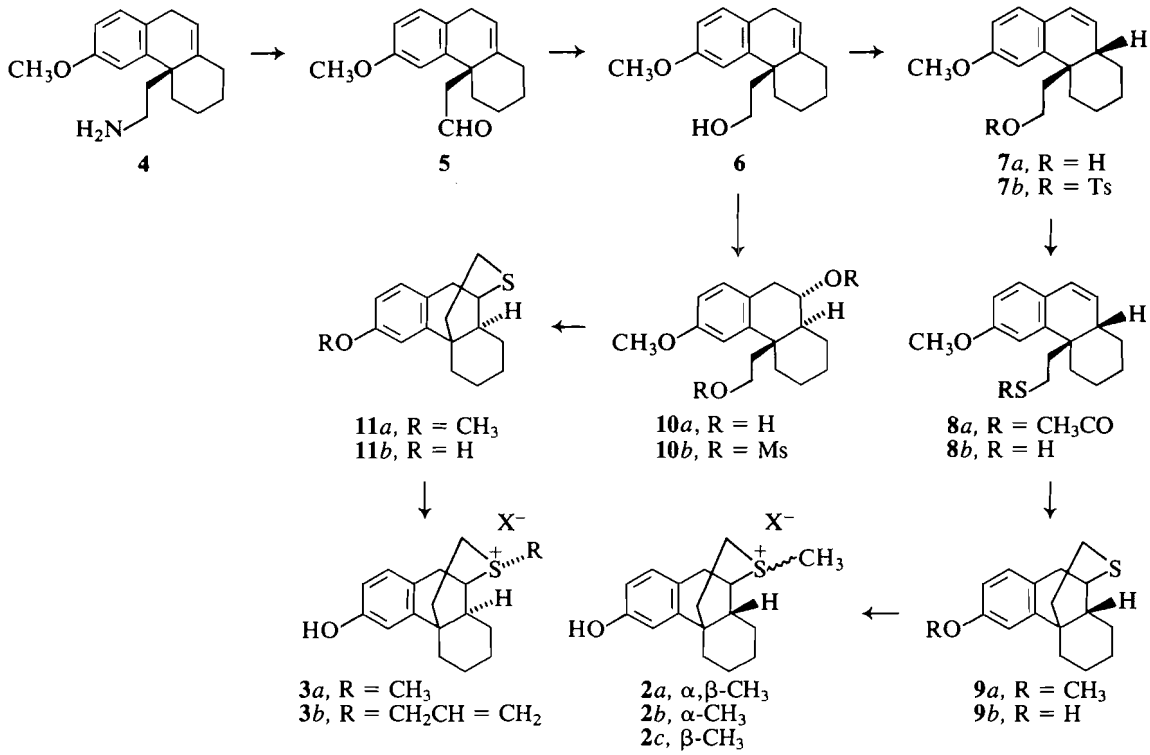

SCHEME 1

proved process for the production of the isosulforphanol **3** previously synthesized (1). Thus hydroboration of **6** in the expected *anti*-Markovnikov fashion (8), followed by peroxide oxidation, produced diol **10***a* exclusively, as judged by nmr spectroscopy. The corresponding bis-mesylate **10***b* was readily obtained; this, upon treatment with sodium sulfide, led in good yield to the isosulforphan derivative **11***a*, which was identical in every respect with an authentic specimen. It was transformed into the isosulforphanol **3***a* as previously reported (1), and into **3***b* by reaction with allyl bromide (the structure of **3***a* having been established by single crystal X-ray analysis). Attention was then turned to the generation of the sulforphanol stereochemistry as in **9** (*cis* B/C fusion). We have previously shown (9) that angularly substituted hexahydrophenanthrenes analogous to **6** can be isomerized stereospecifically to conjugated forms like **7** to yield exclusively the product of β-face protonation at the B/C ring junction, thus allowing for the smooth generation of the desired *cis* fusion of the two rings. Intermediate **6** was therefore treated with potassium *tert*-butoxide in DMSO (9), whereupon **7***a* was obtained in good yield as judged on the basis of its nmr characteristics (distinct olefinic protons and expected coupling constant for a bridgehead proton). It was converted to the tosylate, which upon treatment with potassium thioacetate yielded thioacetate **8***a* readily and then thiol **8***b* after base-catalyzed deacetylation. After extensive experimentation, this air-sensitive thiol could be induced to undergo photochemical cyclization in 25–35% yields to the sulforphan derivative **9***a*. Conclusive evidence that **9***a* is the B/C-*cis* isomer of the established structure **11***a* was adduced by correlated homo- and heteronuclear nmr spectroscopy (Figs. 1–4) (10). The ^1H and ^{13}C nmr chemical shifts are given in Tables 1 and 2 respectively. The structure of **3***a*, as noted previously, was established from an analysis of its X-ray crystal structure.

Because the X-ray crystal structure of **2** is not yet available, evidence for its morphinan-like structure rests in part on the obvious presence in **9***a* of the benzylic $CH_{10A,B}$—CH_9—CH_{14} system, which in the nmr spectrum displays absorption characteristics closely similar to those of **11***a* (**9***a*, 3.15 (H_{10A}, ArCH), 3.47 (H_{10B}, ArCH) (AB portion of ABX pattern, $J_{H_{10A},H_{10B}} = 16$ Hz, $J_{H_{10A},H_9} = 6$ Hz); **11***a*, 3.24 (H_{10A}, ArCH), 3.56 (H_{10B}, ArCH) (AB portion of ABX pattern, $J_{H_{10A},H_{10B}} = 16$ Hz, $J_{H_{10A},H_9} = 6$ Hz). The configurational relationship between **2** and **3***a* was deduced from an analysis of the variations in ^1H and ^{13}C nmr chemical shifts in compounds **11***a* and **9***a*.

The H-15_{ax} appears at 2.53 ppm in **11***a* and at 1.84 ppm in **9***a*. The downfield shift experienced by this axial hydrogen in **11***a* is similar to that of the hydrogen of an axial methyl group on a cyclohexane ring (11). In the case of **9***a*, this interaction is removed and, as a consequence, the signal representing H-15_{ax} has shifted upfield by 0.69 ppm. The most dramatic change was observed with H-8_{ax}. This proton experiences two steric interactions, downfield shifting, paramagnetic in nature, with C-15_{ax} and S-17. When rings B and C are *cis* fused as in **9***a*, these two interactions are removed and the observed shift difference of −0.99 ppm (an average of 1.3 δ was used for H-$8_{ax,eq}$ in **9***a*) may be viewed as a reflection of this change. It is also interesting to note that the H-6_{ax} and H-6_{eq} protons in **11***a* appear at the same place (1.66 ppm) in spite of the anticipated shift difference between them (0.55 ppm: cyclohexane (12)). This is obviously due to its proximity to the H-15_{ax}, which imparts a downfield shifting effect on H-6_{ax}, thus offsetting the expected shift difference between H-6_{ax} and H-6_{eq} protons.

The diastereomeric relationship between **11***a* and **9***a* is also evident from their relative C-13 nmr chemical shifts. The most characteristic change is seen at C-15. This carbon has two γ-*gauche* interactions with C-6 and C-8 in **11***a* and therefore is expected to be shifted upfield. In **9***a*, the C-15 carbon has an *anti*-relationship with these two carbons and hence should be shifted downfield, as compared to **11***a*. The observed 12.89-ppm downfield shift of C-15 from **11***a* to **9***a* confirms this change in geometric relationship. Also consistent is the upfield

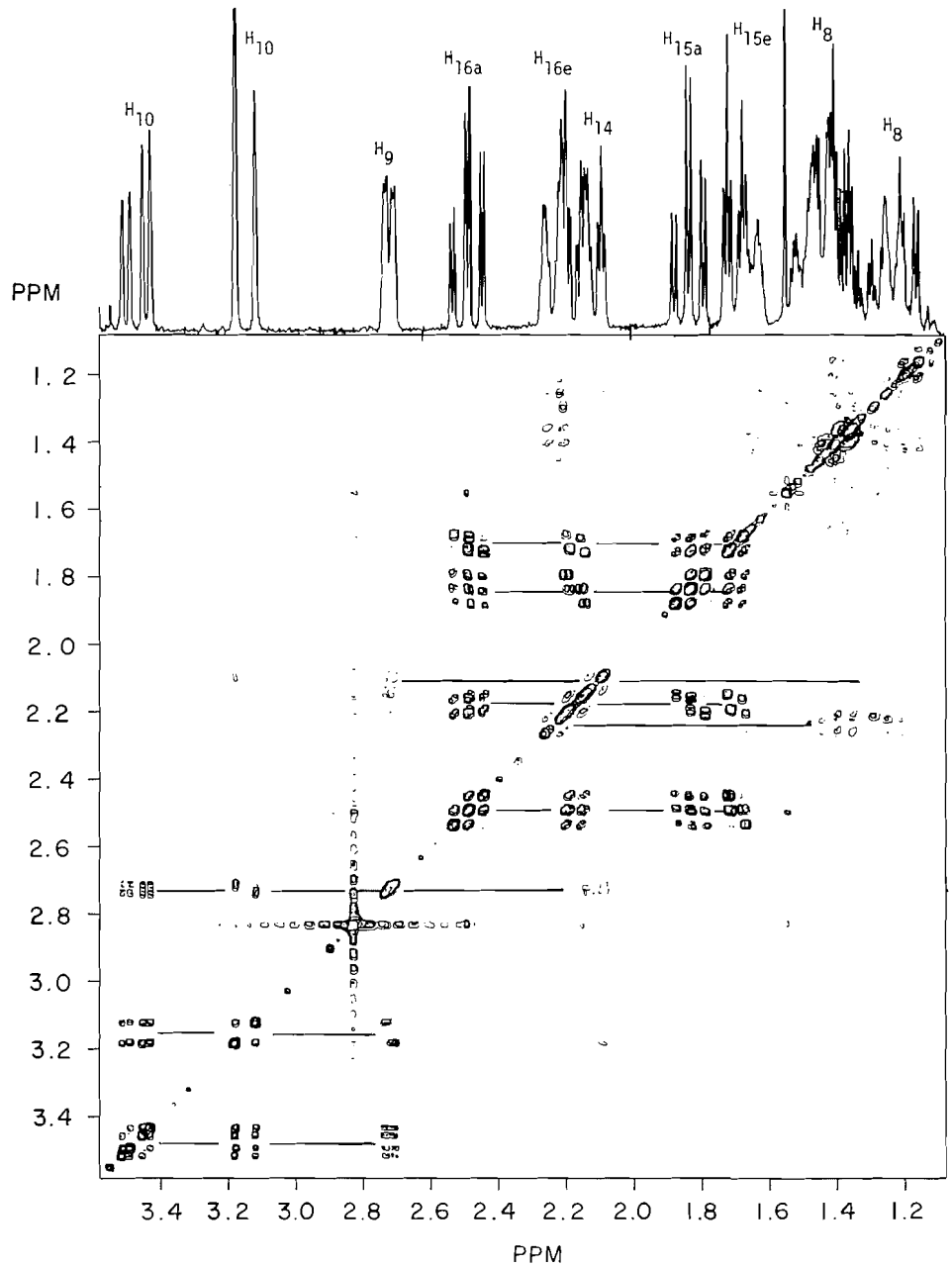

FIG. 1. Contour plot of the COSY 45 map of the aliphatic region of 3-methoxy-17-deaza-17-thiamorphinan (**9***a*); 256 were recorded (4 scans/spectrum). The matrix was 1024 × 1024 data points. The data were processed with a sine bell function.

shift (−5.07 ppm) of the C-12 carbon. In **11***a* this carbon is *anti* to both C-6 and C-8, whereas in **9***a* these are *gauche* to it. The reduced upfield shift, as compared to C-15, may be due to the absence of attached protons on the C-12 atom. The upfield shift (−5.2 ppm) experienced by C-10 in **9***a* is also in accordance with the geometric changes required when **11***a* is formally converted into **9***a*, namely an additional γ-*gauche* interaction with the C-8 atom. The downfield shift (5.02 ppm) of C-14 (from **11***a* to **9***a*) may have its origin in the reversal of the relative orientations of the C-15 and C-12 atoms which are β to the C-14 atom.

The ^{1}H and ^{13}C nmr shift differences therefore corroborate each other and support the geometric changes required in the formal conversion of **11***a* into **9***a*, thus establishing the diastereomeric relationship between **11***a* and **9***a*.

Sulforphan intermediate **9***a* was *O*-demethylated using boron tribromide to give **9***b*, which was *S*-methylated with methyl iodide to yield a mixture of the two possible methyl sulfonium iodide salts **2***a* (ratio of 55:45 as estimated by nmr). This result is in marked contrast to that observed with isosulforphan **11***b*, which gives a single sulfonium salt, that in which the *S*-methyl assumes the equatorial configuration (1). This different behaviour of **9***b* can only be ascribed to the absence of steric interference by ring C to an axial approach of the methylating reagent. However, the *trans*-B/C geometry of the isosulforphan isomer **11***b* effectively prevents such an axial approach. Separation of the two geometrical isomers **2***a* by chromatographic methods could not be achieved in a practical manner. Fractional crystallization of the iodide, perchlorate, or hexafluorophosphate salts was also unproductive. However, separation into the α-(equatorial) and β-(axial) (**2***b* and **2***c*) isomers could be achieved using the picrate salts.

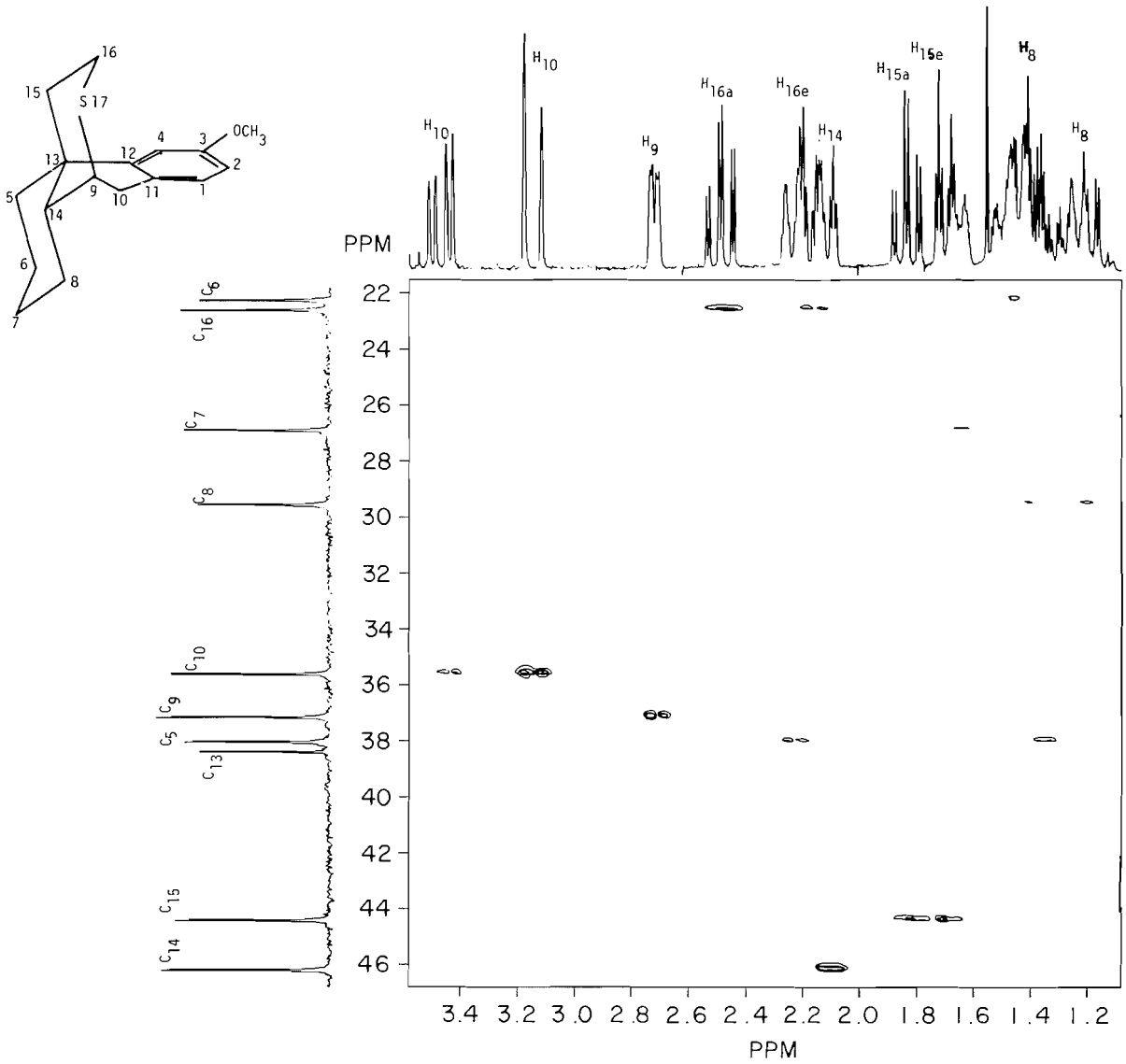

FIG. 2. Contour plot of the 2D heterocorrelation map of the aliphatic region of 3-methoxy-17-deaza-17-thiamorphinan (**9***a*) in $CDCl_3$; 256 spectra were recorded (16 scans/spectrum). The matrix was 1024 × 512 data points. The data were processed with line broadening in the detection domain and with a pseudo echo shape function in the evolution domain.

The configuration of the *S*-methyl groups of the two sulfonium salts was assigned unambiguously by ^{13}C nmr spectroscopy as based on well-known precedents (13). The relevant chemical shift assignments were made by 2D-homocorrelation and 2D-heterocorrelation nmr and the results compared with those previously reported for the case of 2*H*-tetrahydrothiapyran and the corresponding isomeric *S*-methyl salts (13). An axial *S*-methyl induces a smaller downfield shift (β-interaction) at the β-carbons than an equatorial *S*-methyl. The relevant ^1H and ^{13}C nmr data for epimers **2***b* and **2***c* are assembled in Tables 1 and 2, from which it can be deduced that the former has its *S*-methyl equatorially oriented and the latter has the same group axially oriented. Noteworthy are the C-14, C-15, and C-18 of **2***c*, which resonate upfield relative to those of **2***b*, whereas C-10 of the latter appears upfield relative to the same atom in **2***c*. These differences originate from γ-*gauche* interactions as well as a β-interaction with C-16 of the *S*-methyl group, as quantitatively specified in Table 2.

Supporting evidence for the assignment of configurations **2***b* and **2***c* was obtained from the geminal $^2J(H,H)$ values for the H-$16_{ax,eq}$ protons. These amounted to 12.2 and 14.0 Hz for **2***b* and **2***c*, respectively, in agreement with the experimental evidence of Fava and co-workers for relevant *S*-methylthionium cations (14).

The question of the relative thermodynamic stabilities of the equatorial (**2***b*) and the axial (**2***c*) epimers was answered by submitting each isomer to conditions of equilibration in acetonitrile-d_3 at 110°C for 1 week according to a previously established protocol (13). The ratio of epimers was monitored by nmr, using the relative peak intensities of the *S*-methyl groups at 2.86 (axial) and 2.76 ppm (equatorial) as the reference peaks. At equilibrium, both epimers yielded an identical K_{eq} value of 2.33, which translates in a ΔG°_{383} value of −0.66 kcal/mol in favor of the axial configuration. An examination of CPK models revealed that in the equatorial orientation (**2***b*), the *S*-methyl is in very close contact with C-10 (hindering free rotation of the methyl) whereas in **2***c*, the axial methyl does not suffer serious repulsions or rotational restrictions. This reversed

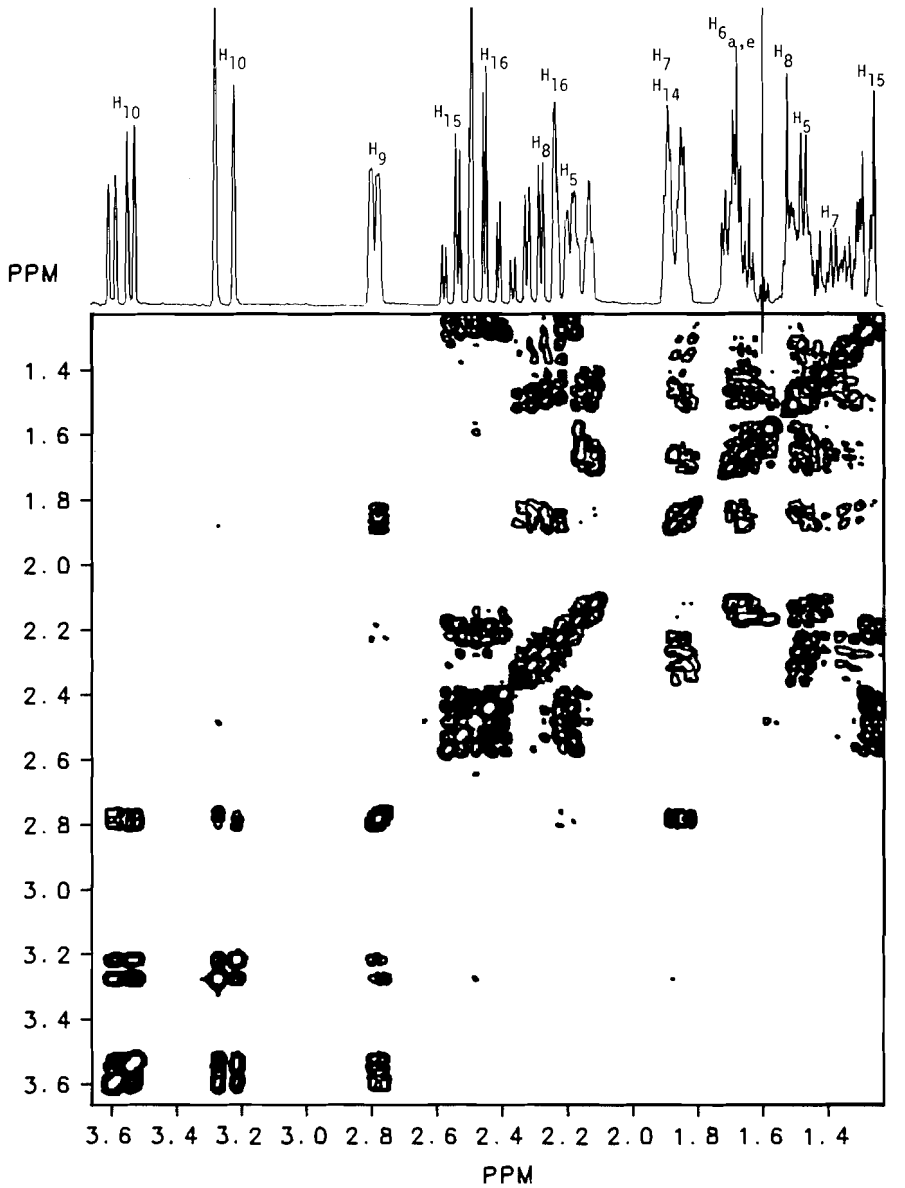

FIG. 3. Contour plot of the COSY 45 map of the aliphatic region of 3-methoxy-17-deaza-17-isothiamorphinan (**11***a*); 256 were recorded (4 scans/spectrum). The matrix was 1024 × 1024 data points. The data were processed with a sine bell function.

order of configurational stabilities for a methyl substituent relative to cyclohexane models has its origin in the relief of 1,3-diaxial compressions associated with the longer C—S bonds (≥1.8 Å). This result parallels those of Eliel and Willer (13) who also observed substantial destabilizing *gauche* interactions (ΔG^0_{373} = 1.2 kcal/mol) for an equatorial *S*-methyl in the *cis*-1-thiadecalin series. With **2***b*, the analogous destabilizing interaction is estimated to approach a similar value.

Preliminary pharmacological testing, using the experimental protocol already defined (1), indicated that the isomer mixture **2***a* is significantly more active than isosulforphanol **3***a*.

Experimental

General

Melting points and distillation temperatures are uncorrected. Infrared spectra were recorded on a Perkin–Elmer model 297 spectrometer. Proton nuclear magnetic resonance (^{1}H nmr) spectra were measured using a Varian XL-200 spectrometer. The 2D nuclear magnetic resonance experiments were carried out using a Varian XL-300 spectrometer. Tetramethylsilane was employed as the internal standard for all compounds. Mass spectrometric measurements were recorded on a Dupont 21-492B or LKB 9000 mass spectrometer.

1,2,3,4,4a,9-Hexahydro-6-methoxy-4a-phenanthrylacetaldehyde **5**

The hydrochloride salt of 4a-(2′-aminoethyl)-1,2,3,4,4a,9-hexahydro-6-methoxyphenanthrene **4** (2.5 g, 8.5 mmol) was dissolved in saturated aqueous $NaHCO_3$ solution (50 mL) and extracted with chloroform (3 × 50 mL). The organic extracts were dried and the solvent removed *in vacuo*. To the residue was added ethanol/water (1:1 v/v) (100 mL), followed by ninhydrin (6.0 g, 33.7 mmol) also dissolved in ethanol/water (1:1 v/v) (100 mL). If the reaction mixture became gummy an additional 100 mL of ethanol was added. The reaction flask was wrapped in aluminum foil and stirred under nitrogen for 30 min, after which time solid $NaHCO_3$ (7.5 g, 0.09 mol) was added. Stirring under nitrogen was continued for an additional 14 h and the ethanol evaporated *in vacuo*. The aqueous layer was extracted several times with ethyl acetate and the combined extracts washed with water, dried, and the solvent evaporated. The blue residue was purified by flash chromatography (8 in. × 1 in. silica gel 60 (230–400 mesh)), using hexane/ethyl acetate (9:1 v/v) as the eluent, to give a colourless oil that crystallized from hexane to yield 1.36 g (5.3 mmol, 62% yield) of white crystals; mp 72–74°C; ir ($CHCl_3$): 2815, 2715, 1712, 1610,

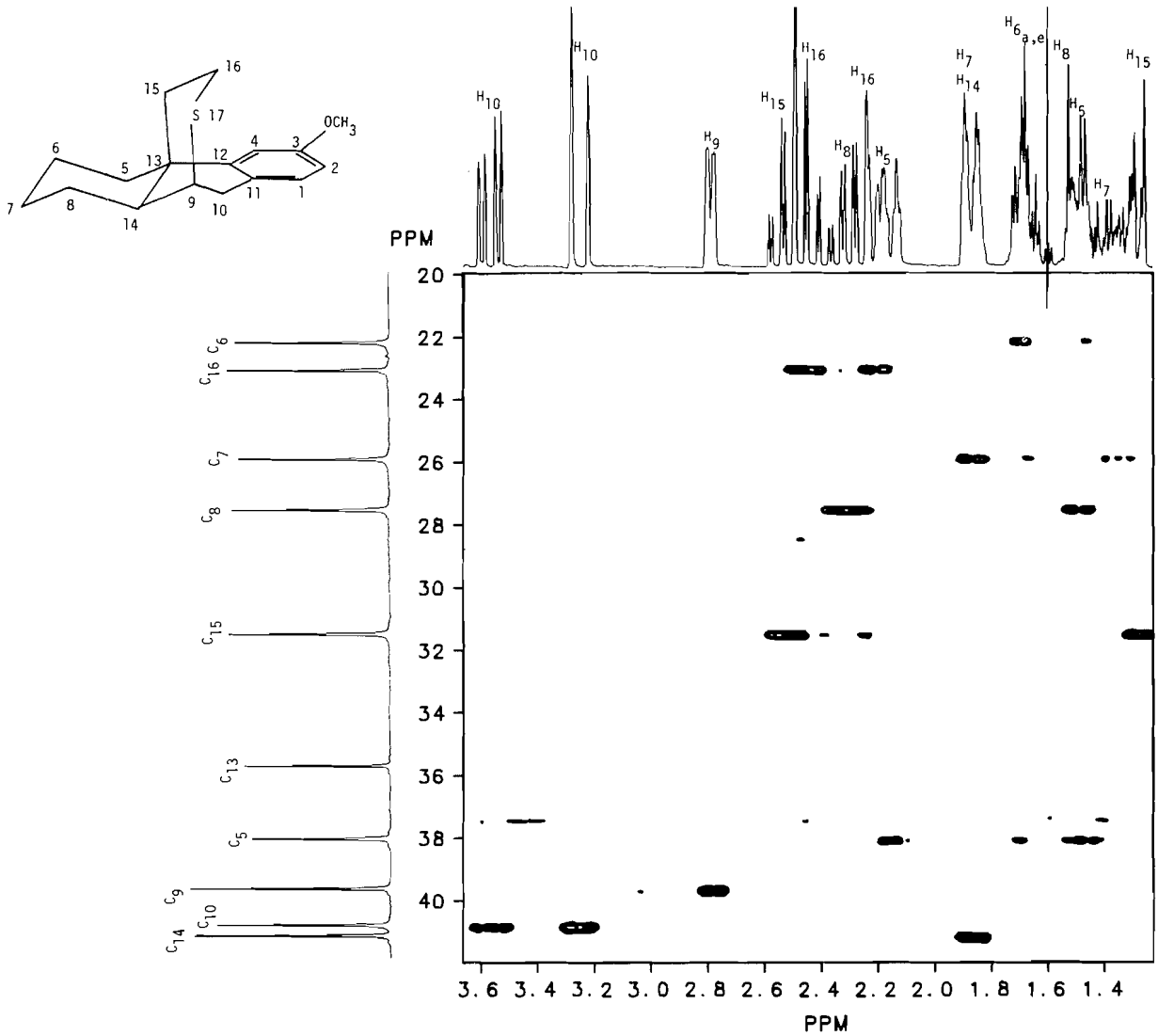

FIG. 4. Contour plot of the 2D heterocorrelation map of the aliphatic region of 3-methoxy-17-deaza-17-isothiamorphinan (**11***a*) in $CDCl_3$; 256 spectra were recorded (16 scans/spectrum). The matrix was 1024 × 512 data points. The data were processed with line broadening in the detection domain and with a pseudo echo shape function in the evolution domain.

TABLE 1. ^1H chemical shifts (ppm) in the nmr spectra of sulforphan pairs of analogs **11***a*/**9***a* and **2***b*/**2***c* respectively

	Position of hydrogen																	
	1	2	3	4	5	6	7	8	9	10	11	12	13	14	15	16	18	19
11*a*[a]					2.15_e 1.48_a	1.66	1.87_e 1.35_a	2.29_a 1.50_e	2.79	3.56_a 3.25_e				1.87	2.53_a 1.26_e	2.45_a 2.21_e		
9*a*[a]	7.06	6.72	—	6.77	2.24_e 1.35_a	1.46_e 1.20_a	1.64	1.42_a 1.21_e	2.73	3.47_a 3.15_e				2.12	1.84_a 1.71_e	2.49_a 2.18_e		
$\Delta(^1H)$[b]							−0.21	−0.99							-0.69_a 0.45_e			
2*b*[c]	7.11	6.74	—	6.77	2.37_e 1.42_a	1.54_e 1.19_a	1.67_e 1.41_a	1.58_a 1.30_e	3.75	3.42_a 3.22_e				2.20	~1.90	3.23_e 2.61_a	2.76	6.95
2*c*[c]	7.06	6.74	—	6.79	2.32_e 1.50_a	1.54_e 1.14_a	1.72_e 1.41_a	1.50_a ~1.22_e	3.55	3.58_a 3.10_e				2.32	2.13_a 1.75_e	2.96_e 2.63_a	2.86	6.95

[a]Solvent for nmr, $CDCl_3$.
[b]Negative and positive values represent upfield and downfield shifts, respectively, for the change from **11***a* to **9***a*.
[c]Solvent for nmr, CD_3CN.

TABLE 2. ^{13}C chemical shifts (ppm) in the nmr spectra of sulforphan pairs of analogs **11***a*/**9***a*, **9***a*/**2***b*, and **9***a*/**2***c*, respectively, and the relevant shift differences (Δ)

	Position of carbon																
	1	2	3	4	5	6	7	8	9	10	11	12	13	14	15	16	18
11*a*[a]	129.25	111.13 or 110.19	158.30	110.19 or 111.13	37.94	22.12	25.82	27.52	39.55	40.82	129.25	145.66	35.64	41.15	31.52	22.97	
9*a*[a]	129.30	111.18 or 110.87	158.45	110.87 or 111.18	38.05	22.31	26.94	29.60	37.17	35.62	129.51	140.59	38.40	46.17	44.41	22.67	
$\Delta^{13}C^{b,c}$								2.08	−2.38	−5.2				5.02	12.89		
2*b*[d]	130.90	115.43 or 112.92	157.78	112.92 or 115.43	36.94	22.71	26.76	29.91	46.90	24.50	125.24	139.16	37.95	43.02	40.66	34.14	22.21
$\Delta^{13}C^{b,e}$									9.73[i]	−11.12[g]				−3.15[h]	−3.75[h]	11.47[i]	
2*c*[d]	131.28	115.59 or 112.92	157.81	112.92 or 115.59	37.18	22.85	27.04	28.23	46.95	30.03	124.85	139.00	37.32	36.20	34.55	30.94	19.31
$\Delta^{13}C^{b,f}$									9.78[i]	−5.59[h]				−9.97[g]	−9.86[g]	8.27[i]	

[a]Solvent for nmr, $CDCl_3$.
[b]Negative and positive values represent upfield and downfield shifts respectively.
[c]Change from **11***a* to **9***a*.
[d]Solvent for nmr, CD_3CN.
[e]Change from **9***a* to **2***b*.
[f]Change from **9***a* to **2***c*.
[g]γ-*gauche* interactions; based on ref. 13, the expected value is −10.
[h]γ-*anti* interactions; expected value (13) is −4.
[i]β-interactions; expected value (13) is 11 (an axial *S*-methyl may accordingly be expected to be deshielded more weakly by about 6 ppm; however, the trend is in the correct direction).

1574, 1500, 1460, 1444 cm^{-1}; ^1H nmr ($CDCl_3$) δ: 1.2–2.5 (m, 8H), 2.55, 3.12 (d of ABq, $CH_2C(O)$, J = 4 Hz, J = 16 Hz), 3.25–3.4 (m, CH_2Ar), 3.8 (s, OCH_3), 5.75 (s, $CH{=}C(R_2)$), 6.7–7.1 (m, 3H, ArH), and 9.25 (m, C(O)H); *m/e*: 212 ($M^{+\cdot}$ − $CH_3C(O)H$), base peak). *Anal.* calcd. for $C_{17}H_{20}O_2$: C 79.65, H 7.86; found: C 79.64, H 7.88.

4a-(2'-Hydroxyethyl)-1,2,3,4,4a,9-hexahydro-6-methoxy-phenanthrene **6**a

The preceding aldehyde **5** (0.50 g, 1.95 mmol) was dissolved in chloroform (20 mL) under nitrogen and the solution cooled to 0°C. A slurry of sodium borohydride (0.08 g, 2 mmol) in dry ethanol was added and the mixture stirred at 0°C for 30 min, followed by the addition of enough 10% aqueous HCl to produce a clear solution (10 mL). The aqueous layer was extracted with $CHCl_3$ (4 × 50 mL) and the combined extracts washed with saturated aqueous NaCl, dried, and the solvent evaporated *in vacuo*, leaving a pale yellow oil that crystallized from hexane to yield 0.47 g (1.82 mmol, 93.4% yield) of the alcohol **6** as white crystals; mp 78–79°C; ir (neat, oil): 3385, 1607, 1571, 1495, 1458, 1440 cm^{-1}; ^1H nmr ($CDCl_3$) δ: 1.02–2.6 (m, 12H), 3.2–3.5 (m, 3H, CH_2OH), 3.77 (s, 3H, OCH_3), 5.63 (br s, 1H, $R_2C{=}C(H)$), 6.52–7.05 (m, 3H, ArH); *m/e*: 258 ($M^{+\cdot}$), 213 (base peak).

4a-(2'-Hydroxyethyl)-1,2,3,4,4a,10a-hexahydro-6-methoxy-phenanthrene 7a

The preceding alcohol **6** (1.0 g, 3.87 mmol) was dissolved in dry DMSO (20 mL) under nitrogen, the solution cooled to 5°C, and potassium *tert*-butoxide (1.0 g, 9.0 mmol) added. After stirring at room temperature for 48 h the mixture was cooled again, an additional quantity of potassium *tert*-butoxide (1.0 g, 9.0 mmol) added, and stirring continued for an additional 48 h. The mixture was poured onto water (50 mL), extracted with methylene chloride (3 × 50 mL), and the combined extracts washed several times with water (in order to remove all of the DMSO), then dried and decolourized with charcoal. Evaporation of the solvent left 0.9 g (3.49 mmol, 90.1% yield) of a colourless oil, which formed white crystals from hexane; mp 73.5–75°C; ir (neat, oil): 3380, 1602, 1563, 1487, 1470, 1430, 1420 cm^{-1}; ^1H nmr ($CDCl_3$) δ: 0.9–2.6 (m, 12H), 3.2–3.6 (m, 3H, CH_2OH) 3.8 (s, 3H, OCH_3), 5.8 (H_{10_A}), 6.25 (H_{10_B}) (AB portion of ABX pattern, $J_{H_9H_{10A}}$ = 8 Hz, $J_{H_{10A}H_{10B}}$ = 16 Hz), 7.6–8.1 (m, 3H, ArH); *m/e*: 258 ($M^{+\cdot}$), 213 (base peak).

4a-(2'-Tosyloxyethyl)-1,2,3,4,4a,10a-hexahydro-6-methoxy-phenanthrene 7b

The above alcohol **7***a* (2.93 g, 11.34 mmol) was treated at 0°C in dry pyridine (18 mL) with a solution of *p*-toluenesulfonyl chloride (2.59 g, 13.58 mmol) in dry pyridine (5 mL). After stirring at 0°C for 20 h, the mixture was gradually diluted with cold water, causing separation of a light yellow solid, which was collected, washed with water, and dried *in vacuo* to yield 4.305 g (10.44 mmol, 92.0% yield) of the tosylate **7***b*; mp 86–88°C. It was used as such in the next step. An analytical sample was prepared by recrystallization from ether–hexane to give white crystals; mp 90.5–92°C; ir (neat, oil): 1170, 1355 cm^{-1}; ^1H nmr ($CDCl_3$) δ: 0.7–2.5 (m, 10H), 3.7–4.05 (m, CH_2O), 3.8 (s, OCH_3), 5.75 (H_{10_A}), 6.25 (H_{10_B}) (AB portion of ABX pattern, $J_{H_9H_{10A}}$ = 8 Hz, $J_{H_{10A}H_{10B}}$ = 16 Hz)), 6.6–7.0 (m, 3H, ArH), 7.3, 7.6 (AB q, 4H, J_{AB} = 4 Hz, ArTs); *m/e*: 257 ($M^{+\cdot}$ − Ts), 91 (base peak). *Anal.* calcd. for $C_{24}H_{28}O_4S$: C 69.87, H 6.84; found: C 69.64, H 6.60.

4a-(2'-Acetylthioethyl)-1,2,3,4,4a,10a-hexahydro-6-methoxy-phenanthrene 8a

The preceding tosylate **7***b* (1.38 g, 3.33 mmol) was treated under N_2 with potassium thioacetate (0.42 g, 3.7 mmol) in refluxing dry THF (50 mL) for 12 h. The solvent was removed *in vacuo*, the residue taken up in $CHCl_3$ (74 mL), the solution washed with H_2O (4 × 50 mL), and the organic layer dried and evaporated *in vacuo*, leaving a yellowish oil. This oil was purified by flash chromatography (8 in. × 1 in. silica gel 60 (230–400 mesh)) using hexane/ethyl acetate (9:1 v/v) as the

eluent to give 0.7 g (2.2 mmol, 66.5% yield) of a colourless oil (homogeneous by tlc); ir (neat): 1688 cm^{-1}; nmr ($CDCl_3$) δ: 0.9–2.9 (m, 12H), 2.2 (s, 3H, C(O)CH_3), 3.8 (s, 3H, OCH_3), 5.8 (H_{10_A}), 6.25 (H_{10_B}), (AB portion of ABX pattern, $J_{H_9H_{10A}}$ = 6 Hz, $J_{H_{10A}H_{10B}}$ = 16 Hz)); *m/e*: 316 ($M^{+\cdot}$), 213 (base peak).

3-Methoxy-17-deaza-17-thiamorphinan **9**a

The above thioacetate **8***a* (9.08 g, 28.7 mmol) was treated under N_2 in dry deoxygenated THF (100 mL) with a solution of sodium methoxide (1.86 g, 34.42 mmol) in deoxygenated methanol. The mixture was stirred for 3 h, the pH adjusted to 4 with 5% deoxygenated aqueous citric acid, and the aqueous layer extracted with deoxygenated chloroform. The combined extracts were dried, the solvent removed *in vacuo* under N_2, and the resulting air-sensitive thiol **8***b* (colourless oil) irradiated under nitrogen in deaerated benzene (air cooling) with two GE sunlamps 136 (275 W, 110–125 VAC, 60 cyc) for 54 h. The solvent was removed *in vacuo* and the residue purified by flash chromatography (12 in. × 3 in. silica gel 60 (230–400 mesh)) using hexanes/toluene (3:1, v/v) as the eluent to yield a light yellow solid that was crystallized from hexane to give **9***a* as white crystals (1.93 g, 25.2% yield); mp 106.5–108°C; ir **9***a* (CH_2Cl_2): 2925, 1610, 1490, 1230 cm^{-1}; ^1H nmr **9***a* ($CDCl_3$) δ: 1–2.7 (m, 14H), 3.15 (H_{10A}, ArCH), 3.47 (H_{10B}, ArCH) (AB portion of ABX pattern, $J_{H_9H_{10B}}$ = 6 Hz, $J_{H_{10A}H_{10B}}$ = 16 Hz)), 3.8 (s, 3H, OCH_3), 6.6–7.1 (m, 3H, ArH); *m/e* (15): 274 ($M^{+\cdot}$), 213 (base peak). *Anal.* calcd. for $C_{17}H_{22}OS$: C 74.40, H 8.08; found: C 74.22, H 7.96; ^1H nmr **8***b* ($CDCl_3$) δ: 1.07–2.7 (m, 14H), 3.8 (s, 3H, OCH_3), 5.8 (H_{10_A}), 6.25 (H_{10_B}) (AB portion of ABX pattern $J_{H_9H_{10A}}$ = 6 Hz, $J_{H_{10A}H_{10B}}$ = 16 Hz)), 6.6–7.1 (m, 3H, ArH).

3-Hydroxy-17-deaza-17-thiamorphinan **9**b

The preceding 3-methoxy-17-deaza-17-thiamorphinan **9***a* (0.5 g, 1.82 mmol) was dissolved under N_2 in dry methylene chloride (10 mL) at −78°C followed by the addition of a solution (5 mL) of BBr_3 in CH_2Cl_2 (0.5 *M*) at −78°C. The reaction mixture was allowed to warm slowly to room temperature and, after 18 h, it was poured onto H_2O and the aqueous layer washed with CH_2Cl_2 (4 × 20 mL). The combined extracts were dried, the solvent removed *in vacuo*, and the residue purified by flash chromatography (6 in. × 1 in. silica gel 60 (230–400 mesh)) using $CHCl_3$ as the eluent to give a colourless oil that was crystallized from methylene chloride to yield 0.317 g (1.3 mmol, 67% yield) of white crystals; mp 134–136°C; ir (KBr disc): 3300, 2920, 2840, 1615, 1490, 1450, 1290, 1220 cm^{-1}; ^1H nmr ($CDCl_3$) δ: 0.9–2.8 (m, 14H), 3.1 (H_{10A}), 3.5 (H_{10B}) (AB portion of ABX pattern $J_{H_9H_{10B}}$ = 6 Hz, $J_{H_{10A}H_{10B}}$ = 16 Hz)), 4.75 (br s, 1H, OH), 6.7–7.1 (m, 3H, ArH); *m/e*: 260 ($M^{+\cdot}$), 199 (base peak).

α *and* β *sulforphanol isomers* **2**a

The above 3-hydroxy-17-deaza-17-thiamorphinan **9***b* (0.60 g, 2.32 mmol) was treated with CH_3I (4 mL) in CH_3CN (22 mL) and, after standing for 14 h, dry ether was added to the solution, whereupon white crystals separated. These were washed with dry ether and dried *in vacuo* to yield 0.90 g (2.24 mmol, 96.4% yield) of white crystals; no definite mp; ^1H nmr ($CDCl_3$ + CF_3COOD) δ: 1.2–4.0 (complex m, 20H), 2.98 (s, SCH_3), 3.1 (s, SCH_3), 6.8–7.3 (ArH); *m/e*: 260 ($M^{+\cdot}$ − CH_3I), 199 (base peak). *Anal.* calcd. for $C_{17}H_{23}IOS$: C 50.75, H 5.76; found: C 50.53, H 5.62.

The iodide salt (761 mg, 1.89 mmol) was dissolved without delay in methanol and the solution passed through an anion exchange column in the perchlorate form prepared as described previously (1) to yield a methanol solution of the perchlorate salt of sulforphanol **2***a*; the salt was obtained as a white solid after evaporation of the solvent. It was recrystallized from CH_3CN/hexane to give 671 mg (1.79 mmol, 94.6% yield) of long white needles incorporating the two *S*-methyl stereoisomers, as judged by nmr analysis; ^1H nmr ($CDCl_3/CF_3COOD$) δ: 1.1–3.8 (m, 20H), 2.8 (s, 3H, SCH_3), 3.0 (s, 3H, SCH_3), 6.7–7.2 (m, 3H, ArH); *m/e*: 260 ($M^{+\cdot}$ − CH_3ClO_4), 199. *Anal.* calcd. for $C_{17}H_{23}ClO_5S$: C 54.47, H 6.18; found: C 54.49, H 6.33.

The α-(equatorial CH_3) and β-(axial CH_3) isomers (**2***b* and **2***c*) could not be separated efficiently by hplc or as their perchlorate or hexafluorophosphate salts, but could be separated as their picrate salts. Thus treatment of the perchlorate or iodide salts mixture with sodium picrate in aqueous ethanol gave crude yellow crystals that, after three recrystallizations from warm ethanol, yielded **2***c* picrate as yellow needles; mp 176–178°C. The mother liquor, upon concentration followed by several recrystallizations of the solid from CH_3CN/Et_2O, yielded pure **2***b* picrate as yellow needles; mp 120–122°C. The two isomers were converted into their corresponding perchlorate salts by the anion exchange method previously described (1) to give, after recrystallization from CH_3CN/hexane, white crystals of pure α-sulforphanol perchlorate (**2***b*, mp 200°C (dec.)) and its isomer **2***c* (mp 208°C (dec.)).

4a-(2'-Hydroxyethyl)-10-hydroxy-1,2,3,4,4a,9,10,10a-octahydro-6-methoxyphenanthrene **10**a

The alcohol **6** (0.224 g, 0.95 mmol) was dissolved in CH_2Cl_2 (10 mL) under nitrogen and 10 *M* borane–dimethylsulfide (1 mL) was added. After 1 hour, 15% aqueous sodium hydroxide (20 mL) was added, followed by 30% aqueous hydrogen peroxide (20 mL), and the mixture was allowed to stand an additional 24 h. The solution was extracted with ether, which was washed with 15% aqueous sodium tartrate (3 × 40 mL) and H_2O (2 × 50 mL). The organic phase was dried and the solvent removed *in vacuo* to yield 0.26 g (0.95 mmol, 100% yield) of the crude diol. The diol was purified by flash chromatography (4 in. × 1 in. silica gel 60 (230–400 mesh)) using hexane/ethyl acetate (1:2 v/v) as an eluent to give 0.22 g (0.81 mmol, 85% yield) of white crystals; mp 138–139°C; ir (Kbr disc): 3300, 1600, 1570, 1490, 1400 cm^{-1}; ^1H nmr ($CDCl_3$) δ: 1.1–4.3 (m, 18H), 3.78 (s, 3H, OCH_3), 6.57–7.13 (m, 3H, ArH); *m/e*: 258 ($M^{+\cdot}$ − H_2O), 83 (base peak). *Anal.* calcd. for $C_{17}H_{24}O_2$: C 73.88, H 8.75; found: C 73.86, H 8.76.

4a-(2'-Mesyloxyethyl)-10-mesyloxy-1,2,3,4,4a,9,10,10a-octahydro-6-methoxyphenanthrene **10**b

The preceding diol **10***a* (1.97 g, 7.1 mmol) was dissolved in dry pyridine (100 mL) at 0°C, methane sulfonylchloride (3 mL) added, and, after 24 h at 0°C, the mixture was poured onto water (400 mL) and extracted with CH_2Cl_2 (3 × 50 mL). The combined extracts were washed several times with 10% aqueous HCl (5 × 50 mL), once with H_2O (50 mL), dried, and evaporated *in vacuo* to yield 2.77 g (6.42 mmol, 90.4% yield) of a yellow oil. This was purified by flash chromatography using ethyl acetate/hexane (2:1) as the eluent to yield 2.60 g (6.02 mmol, 84.8% yield) of a white solid, which was recrystallized from absolute ethanol to give 2.55 g (5.90 mmol, 83.1% yield) of white crystals; mp 115–116°C; ir (CH_2Cl_2): 1350, 1330, 1170 cm^{-1}; ^1H nmr ($CDCl_3$) δ: 0.7–2.6 (m, 13H), 2.83 (s, 3H, CH_3SO_2), 3.00 (s, 3H, CH_3SO_2), 3.72 (s, 3H, OCH_3), 3.82–4.3 (m, 2H, CH_2OSO_2R), 4.63–5.18 (m, 1H, $CHOSO_2R$), 6.53–7.17 (m, 3H, ArH); *m/e*: 337 ($M^{+\cdot}$ − CH_3SO_3H, 213 (base peak). *Anal.* calcd. for $C_{19}H_{28}O_7S_2$: C 52.75, H 6.52; S 14.67; found: C 52.68, H 6.63, S 14.56.

3-Methoxy-17-deaza-17-isothiamorphinan **11**a

The above dimesylate **10***b* (2.4 g, 5.5 mmol) was treated in absolute ethanol (300 mL) with sodium sulfide nonanhydrate (14.5 g, 60.4 mmol) under N_2 and the mixture heated under reflux for 20 h. After cooling, the solvent was removed *in vacuo*, methylene chloride added to the residue, the suspended sulfur filtered off, the filtrate dried, and the solvent removed *in vacuo* to leave a yellow oil. This was purified by flash chromatography (6 in. × 1 in. silica gel 60 (230–400 mesh)) using hexane/ethyl acetate (25:1 v/v) as the eluent to give 1.02 g (3.72 mmol, 66.9% yield) of white crystals; mp 73–74°C; ir (neat, oil): 3300, 1600, 1570, 1490, 1400 cm^{-1}; ^1H nmr ($CDCl_3$) δ: 1.1–2.8 (m, 14H), 3.24 (H_{10_A}, ArCH), 3.61 (H_{10_B}, ArCH), (AB portion of ABX pattern, $J_{H_{10A},H_{10B}}$ = 16 Hz, $J_{H_9,H_{10A}}$ = 6 Hz)), 3.8 (s, 3H, OCH_3), 6.7–7.0 (m, 4H, ArH); *m/e*: 274 ($M^{+\cdot}$), 213 (base peak). *Anal.* calcd. for $C_{17}H_{22}OS$: C 74.40, H 8.08; found: C 74.61, H 8.17.

3-Hydroxy-17-deaza-17-allylthionium-17-isothiamorphinan bromide **3**b

3-Hydroxy-17-deaza-17-isothiamorphinan (0.222 g, 0.853 mmol)

was prepared by *O*-demethylation of **11***a* as previously described (1) and treated in dry acetonitrile (3 mL) with allylbromide (4.1 mL) under N_2. After 42 h, the solution was poured onto dry ether and the solid collected, washed with dry ether, and recrystallized from acetonitrile/ether to yield 273 mg (0.72 mmol, 84.0% yield) of white crystals; mp 131–133°C (dec.). *Anal.* calcd. for $C_{19}H_{25}BrOS$: C 59.84, H 6.61; found: C 59.93, H 6.55.

Acknowledgements

We are grateful to the Natural Sciences and Engineering Research Council of Canada and the Government of Quebec (Fonds F.C.A.C.) for their financial support. We are indebted to Dr. Francoise Sauriol for carrying out the 2D nmr experiments.

1. B. Belleau, U. Gulini, B. Gour-Salin, and F. Ahmed. Can. J. Chem. **63**, 1268 (1985).
2. (*a*) K. Opheim and B. M. Cox. J. Med. Chem. **19**, 857 (1976); (*b*) R. J. Kobylecki, A. C. Lane, C. F. C. Smith, L. P. G. Wakelin, W. B. T. Cruse, E. Egert, and O. Kennard. J. Med. Chem. **25**, 1278 (1982).
3. R. Grewe and A. Mondon. Chem. Ber. **81**, 279 (1948).
4. (*a*) B. Belleau, T. T. Conway, T. W. Doyle, L. Morris, and W. Verbestel. Can. J. Chem. **53**, 237 (1975); (*b*) I. Monkovic, T. T. Conway, H. Wong, Y. G. Perron, I. J. Pachter, and B. Belleau. J. Am. Chem. Soc. **95**, 7910 (1973); (*c*) I. Monkovic, H. Wong, B. Belleau, I. J. Pachter, and Y. G. Perron. Can. J. Chem. **53**, 2515 (1975).
5. A. R. Katritzky. Tetrahedron, **36**, 679 (1980).
6. (*a*) A. Streitwieser, Jr. and W. D. Schaeffer. J. Am. Chem. Soc. **79**, 2888 (1957); (*b*) E. H. White and D. J. Woodcock. *In* The chemisty of the amino group. *Edited by* S. Patai. Interscience, New York. 1968. Chapt. 8. p. 407.
7. T. H. Buckley and H. Rapoport. J. Am. Chem. Soc. **104**, 4446 (1982).
8. I. Monkovic and H. Wong. Can. J. Chem. **54**, 883 (1976).
9. T. T. Conway, T. W. Doyle, Y. G. Perron, J. Chapius, and B. Belleau. Can. J. Chem. **53**, 295 (1975).
10. (*a*) A. Bax, R. Freeman, and G. A. Morris. J. Magn. Reson. **42**, 169 (1981); (*b*) K. Nagayama, A. Kumar, K. Wuthrich, and R. R. Ernst. J. Magn. Reson. **40**, 321 (1980); (*c*) W. P. Aue, E. Bartholdi, and R. R. Ernst. J. Chem. Phys. **64**, 2229 (1976); (*d*) A. Bax and G. A. Morris. J. Magn. Reson. **45**, 501 (1981); (*e*) A. A. Mandsley, L. Mullen, and R. R. Ernst. J. Magn. Reson. **28**, 463 (1977); (*f*) A. A. Mandsley and R. R. Ernst. Chem. Phys. Lett. **50**, 368 (1977).
11. F. W. Vierhapper and E. L. Eliel. J. Org. Chem. **40**, 2734 (1975).
12. G. Binsch. Top. Stereochem. **3**, 97 (1968).
13. E. L. Eliel and R. L. Willer. J. Am. Chem. Soc. **99**, 1925 (1977); R. L. Willer and E. L. Eliel. Org. Magn. Reson. **9**, 285 (1977); G. Barbarella, P. Dembech, A. Garbesi, and A. Fava. Org. Magn. Reson. **8**, 469 (1976).
14. G. Barbarella, P. Dembech, A. Garbesi, and A. Fava. Tetrahedron, **32**, 1045 (1976).

Characterization and elimination of cationic interferences on platinum

M. A. MOSTAFA AND M. A. KABIL
Chemistry Department, Faculty of Science, Mansoura University, Mansoura, A.R. Egypt

Received April 9, 1984[1]

M. A. MOSTAFA and M. A. KABIL. Can. J. Chem. **64**, 119 (1986).

Interfering effects of different cations on the atomic absorption signal of platinum can be completely eliminated by adding *n*-butylamine. The releasing action of *n*-butylamine comes through the formation of a volatile, platinum–amine complex, so the platinum species reaching the flame will normally be independent of the original composition of the solution. The inhibition release titration method has been used in studying the interfering effects to achieve a determinate characterization of compound formation.

M. A. MOSTAFA et M. A. KABIL. Can. J. Chem. **64**, 119 (1986).

Les interférences de divers cations sur l'absorption atomique des signaux du platine peuvent être complètement éliminés par l'addition de *n*-butylamine. L'effet de relargage de la *n*-butylamine provient de la formation d'un complexe volatil platine–amine qui fait que les espèces platiniques qui atteignent la flamme seront normalement indépendantes de la composition originale de la solution. On a fait appel à la méthode de titration avec élimination de l'inhibition pour étudier les effets d'interférence et obtenir une caractérisation déterminée de la formation du composé.

[Traduit par le journal]

Introduction

The determination of platinum by atomic absorption spectroscopy (AAS) has been reported in the literature (1–3). Lockyer and Hames (4) observed serious interferences from several metal ions. Addition of copper sulphate with a concentration above 20 000 μg/mL overcame the interferences encountered from noble metals and sodium. Although copper sulphate was added in a large excess, the interferences were not completely eliminated. Another study (5) showed that the serious depressive inter-element interferences of Ag, Al, Au, Bi, Ca, Co, Cr, Fe, Hg, K, Mg, Mn, Mo, and Ni were removed by buffering the solution with a mixture of cadmium and copper sulphates, each at 0.5%.

The disadvantage of the above method is the limitation of the buffer capacity in controlling interferences when some of the offending ions are present in concentration levels exceeding 200 μg/mL. Extraction procedures (6) have been presented to avoid interferences from a variety of matrices. The standard releasing agent for platinum is 1% lanthanum chloride (7). However, such methods hinder a better understanding of the phenomena during aspiration and atomization of the sample in the flame.

Experimental

Solutions

All solutions were prepared from B.D.H. chemicals and Analar grades. Stock solutions of the metals were prepared as chlorides; aliquots were suitably diluted to give the desired metal ion concentration used for the experiments. The stock solution of platinum (7×10^{-3} *M* chloroplatinic acid) was standardized using thiophenol (8).

Equipment

The atomic absorption spectrophotometer, Unicam SP 90A series 2, was fitted with a new HTA phototube, No. R 270 from EMI. Air was supplied through a PU 9003 air compressor. Acetylene was obtained from cylinders after passing through concentrated sulphuric acid and glass wool for purification. A continuous titration device (9) was attached to the instrument and the results were analyzed on a CASIO FX-502P type programmable pocket calculator. Absorbance values were recorded with a Philips PM 8251 single-pen recorder at chart speed of 30 cm min^{-1}.

The instrumental parameters were: lamp current, 12 mA; wavelength, 265.9 nm; slit width, 0.15 mm; obervation height, 1.0 cm; air flow rate, 5.0 L min^{-1}; fuel flow rate, 1.0 L min^{-1}.

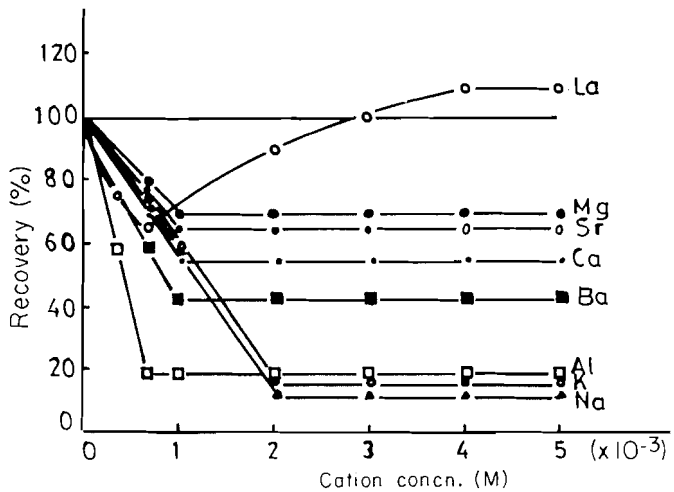

FIG. 1. Effect of some cations on the recovery of 1.025×10^{-3} *M* chloroplatinic acid.

Results and discussion

Interference of cations

Metal–metal interactions in a flame present a very complicated problem. Analysts can be puzzled from data reported by many workers in which no general observation can be concluded because any proposed mechanism for an inter-element interaction cannot be applied in general for others.

The initial study concerning the effect of different cations (as chlorides) on the absorbance of the standard platinum solution in an air–acetylene flame are represented in Figs. 1 and 2. It is evident that the absorbance is changed considerably by the foreign cations and that at a definite concentration of the interferent a pronounced inflection is observed. The graphs obtained when the time axis of the titration plot was converted to molar ratio between the interfering ion and platinum showed that the distinct breakpoints corresponded to $[M^+]/[Pt]$ at a ratio of 1:2, $[M^{2+}]/[Pt]$ at a ratio of 1:1, and $[M^{3+}]/[Pt]$ at a ratio of 2:3 (where M^+, M^{2+}, and M^{3+} are the mono, bi, and trivalent cations). The ratios are directly related to the formation of

[1]Revision received September 2, 1985.

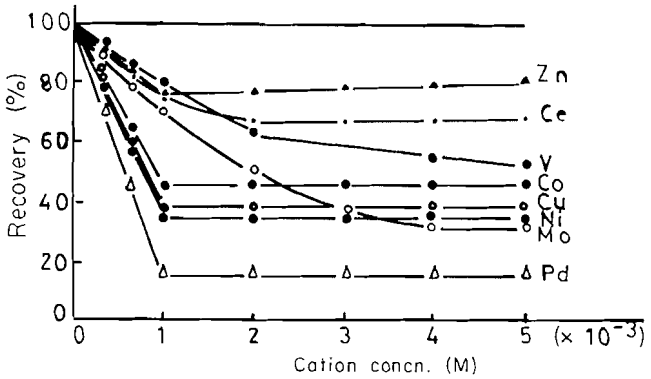

FIG. 2. Effect of some other cations on the recovery of 1.025×10^{-3} *M* chloroplatinic acid.

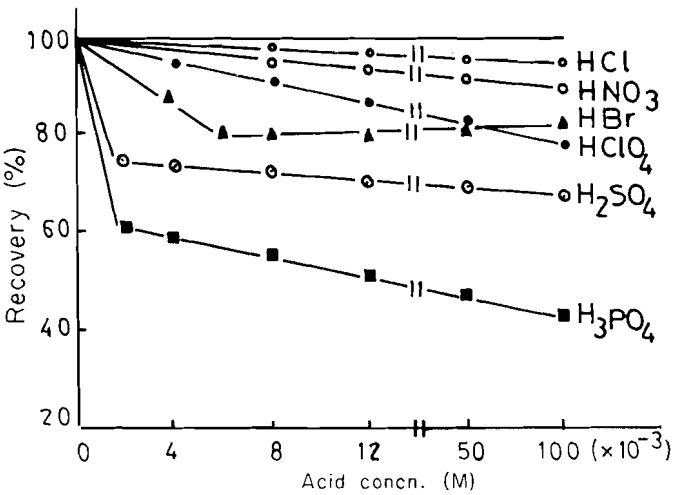

FIG. 3. Changes in the absorption signal of 200 μg/mL (1.025×10^{-3} *M*) platinum in the presence of inorganic acids.

$M_{2/n}[PtCl_6]$ and $M_2[PtCl_6]_3$, according to the following equations:

$$[1] \quad \frac{2}{n} M^{n+} + H_2[PtCl_6] \rightleftharpoons M_{2/n}[PtCl_6] + 2H^+, \qquad (n = 1 \text{ or } 2)$$

and

$$[2] \quad 2M^{3+} + 3H_2[PtCl_6] \rightleftharpoons M_2[PtCl_6]_3 + 6H^+$$

Thus the data suggests a condensed phase chemical interference in which a less volatile platinum salt is formed (10). The general trend of the graphs indicates that the absorbance decreases at the first stage of the titration, and after the stoichiometry is attained the graphs plateau, except for lanthanum. In the case of La the absorbance of platinum was restored to about 110 recovery percentage at a concentration of 4×10^{-3} *M* of lanthanum.

Effect of anions

It is difficult to independently investigate the influence of anions on the absorption signal of platinum because essentially all cations cause serious interferences on platinum. Inorganic acids are used for the decomposition of most samples, and the hydrogen ion has little effect on the dissociation of chloroplatinic acid. Thus anion interferences are best investigated using inorganic acids. The data in Fig. 3 show that the absorption signal of platinum is affected by the nature of the acid added. Hydrochloric and nitric acids have little influence. The decrease in the absorption signal was pronounced for other acids when the acid concentration became greater than 0.2 *M*. These acids decrease the signal even at low concentration. This may be due to some condensed phase interferences, i.e., crystallization of mixed salts with different thermal stabilities during evaporation and disintegration of aerosol. Evaporation of chloroplatinic acid solutions in the presence of sulphuric acid gives platinum sulphate (11). Curves 3, 5, and 6 of Fig. 3 indicate distinct breakpoints corresponding to $[PO_4^{3-}]/[Pt]$ and $[SO_4^{2-}]/[Pt]$ at ratios of 2:1 and $[Br^-]/[Pt]$ at a ratio of 6:1. Such ratios are directly related to the formation of $H_2[Pt(SO_4)_2(OH)_2]$, PtP_2O_7, and $H_2[PtBr_6]$ which are known as less volatile compounds in the flame (11).

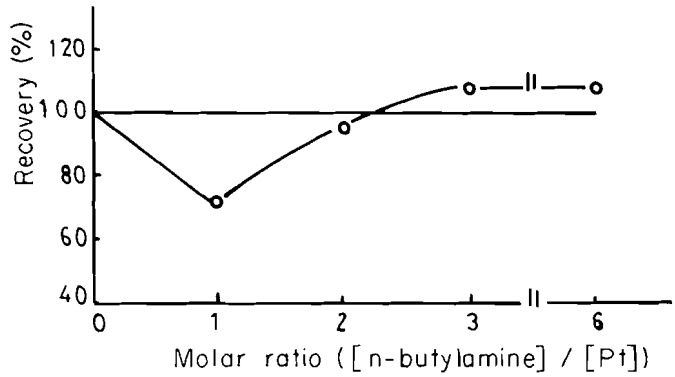

FIG. 4. Changes of the absorption signal of platinum as a function of the *n*-butylamine/Pt ratio.

Elimination of interferences

Platinum is known to form stable complexes with different amine compounds (12). A continuous AAS titration method was used to study the effect of *n*-butylamine on the chemical interferences affecting the Pt absorbance signal. Changes in the absorption signal of Pt were monitored continuously and recorded as a function of amine concentration and the data are shown in Fig. 4. A feature of the data shown in Fig. 4 is that the absorbance decreases and reaches a minimum at an [*n*-butylamine]/[platinum] ratio of 1:1. After reaching this ratio an enhancement occurs, reaching a maximum at about 108 recovery percentage. The behaviour of *n*-butylamine can be discussed according to three main steps which take place during the process of atomization. (*i*) Vaporization of the solid Pt–amine complex, followed by its decomposition in the flame produces platinum atoms, which instantaneously react with the oxidizing species already present in the flame. Such reaction yields PtO leading to the deficiency of platinum atoms, followed by a depression in the absorption signal. (*ii*) After a particular stoichiometric ratio was attained at 1:1 for Pt/*n*-butylamine, the decomposition of the complex may form a reducing species in the flame, such as, CN, NH, or CH, which may react with PtO according to the following equations:

$$[3] \quad PtO + NH \rightleftharpoons Pt + N + OH$$

$$[4] \quad PtO + CN \rightleftharpoons Pt + N + CO$$

(*iii*) The excess of *n*-butylamine leads to the formation of more reducing radicals in the flame which balance the excess of oxidizing species and restores the absorption signal to its normal value.

In support for the previous mechanism, Fig. 5 shows the relatively steady decrease in the emission intensity of the OH radical with the continuous increase in NH emission intensity as

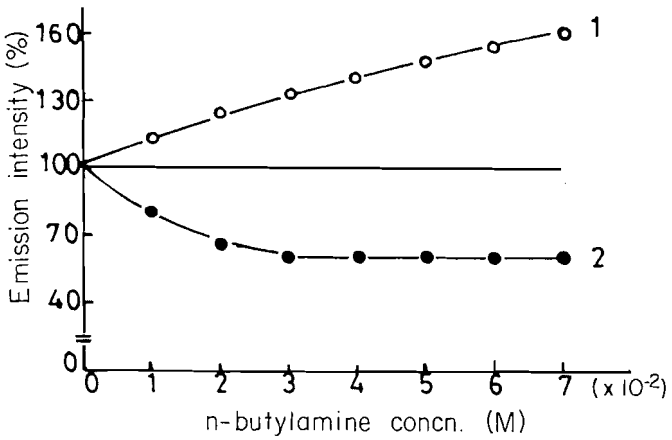

FIG. 5. Effet of *n*-butylamine on preclusion of the formation of oxidizing species OH and facility of the formation of reducing species NH. Emission intensity of NH or OH already present in the flame is assumed to be 100. All other results are normalized against this value. (○) NH emission intensity at 337 nm; (●) OH emission intensity at 281.1 nm.

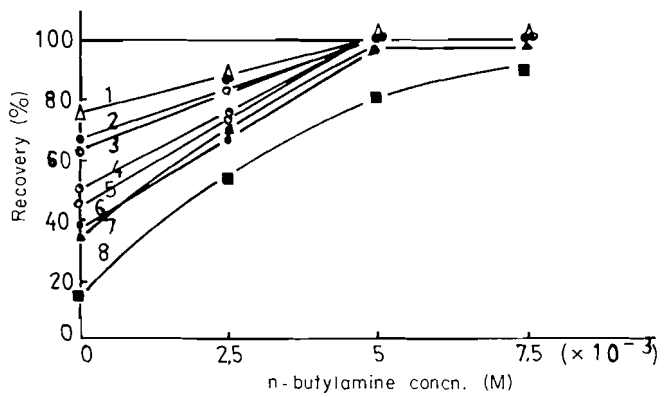

FIG. 6. Use of *n*-butylamine in eliminating interferences on 1.025×10^{-3} *M* Pt encountered from 2×10^{-3} *M* of some cations. Curves: 1, Zn; 2, Ce; 3, V; 4, Mo; 5, Co; 6, Cu; 7, Ni; 8, Pd.

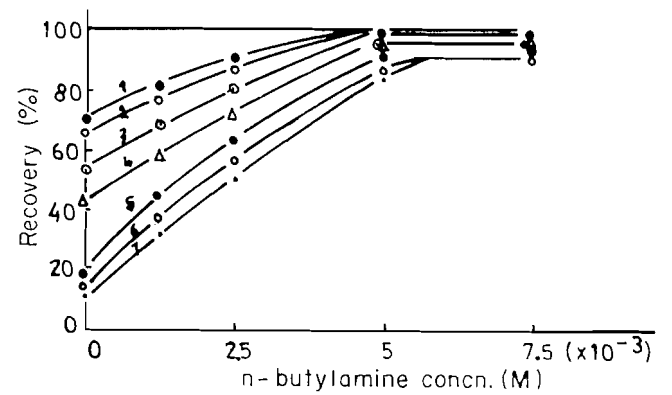

FIG. 7. Use of *n*-butylamine in eliminating interferences on 1.025×10^{-3} *M* platinum encountered from 2×10^{-3} *M* of some other cations. Curves: 1, Mg; 2, Sr; 3, Ca; 4, Ba; 5, Al; 6, K; 7, Na.

the *n*-butylamine solution is added. In such a case the decomposition of *n*-butylamine gives reducing fragments (CN and NH). Accordingly an enhancement in NH band emission intensity has occurred (Fig. 5, graph 1). Also, such fgragments scavenge OH radicals in the flame giving a suppression in OH band emission intensity (Fig. 5, graph 2). Such foundations can

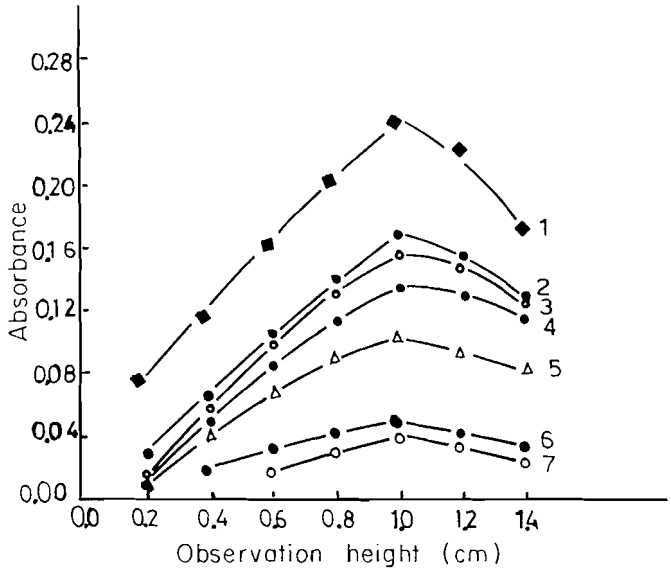

FIG. 8. Distribution of platinum atoms (1.025×10^{-3} *M*) as a function of observation height for different interferents, each in 2×10^{-3} *M*: 1, Pt only, the others having Pt and 2, Mg; 3, Sr; 4, Ca; 5, Ba; 6, Al; and 7, K.

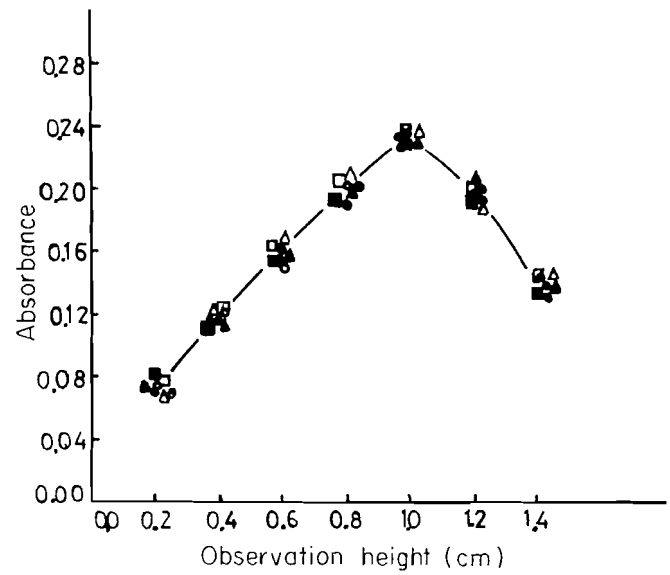

FIG. 9. Distribution of platinum atoms (1.025×10^{-3} *M*) as a function of observation height in 5×10^{-3} *M* of *n*-butylamine for different interferents, each in 2×10^{-3} *M* (○) Pt only, the others having Pt, *n*-butylamine, and (▲) Mg, (●) Sr, (⊙) Ca, (□) Ba, (△) Al, and (■) K.

be represented by the following equations:

[5] $CN + NH \rightleftharpoons N_2 + CH$

[6] $CN + OH \rightleftharpoons CO + NH$

When *n*-butylamine is added in sufficient concentration to samples containing interfering cations, the suppression is gradually eliminated (Figs. 6 and 7). The data are encouraging, except for Na, K, and Pd, where the recovery percentages are 84, 87, and 80.

The data in Fig. 8 illustrate the distribution of platinum atoms in the presence of different cations as a function of observation height. The effect of different concomitants were examined as a

function of observation height in the presence of 5×10^{-3} *M* *n*-butylamine. The data were completely coincident (Fig. 9) indicating that the formation of platinum–amine complex is attained in solution, protecting platinum from offending species. These data clearly illustrate the possibility of applying *n*-butylamine as a good masking agent for AAS determination of platinum.

1. P. B. ZEEMAN and J. A. BRINK. Analyst (London), **93**, 388 (1968).
2. J. G. SEN GUPTA. Anal. Chim. Acta, **63**, 19 (1973).
3. R. BARBARA and S. ZOFIA. Chem. Anal. (Warsaw), **25**(2), 295 (1980).
4. R. LOCKYER and G. E. HAMES. Analyst (London), **84**, 385 (1959).
5. M. M. SCHNEPFE and F. S. GRIMALDI. Talanta, **16**, 591 (1959).
6. A. DIAMANTATOS. Anal. Chim. Acta, **131**, 53 (1981).
7. J. C. VAN LOON. Anal. Chem. **246**, 122 (1969).
8. F. E. BEAMISH. The analytical chemistry of the noble metals. Pergamon Press, Oxford. 1966.
9. J. POSTA and J. LAKATOS. Magy. Kem. Foly. **86**, 284 (1980).
10. H. URBAIN and M. CATTENOT. Analysis, **7**(4), 196 (1979).
11. A. E. PITTS, G. C. VAN LOON, and F. E. BEAMISH. Anal. Chim. Acta, **50**, 181 (1970).
12. N. N. ZHELIGOVSKAYA, E. P. KRASOVSKAYA, and N. KAMALOV. Koord. Khim. **5**, 1527 (1979).

Étude des Hernandiacées. XII.[1] Dimères aporphine–benzylisoquinoléine originaux isolés de *Hernandia peltata*

M. C. CHALANDRE ET J. BRUNETON[2]

Centre d'études des plantes médicinales, Unité d'enseignement et de recherche des sciences médicales et pharmaceutiques, 49000 Angers, France

P. CABALION

Office de la recherche scientifique et technique d'outre-mer, B.P. 76, Port-Vila, Vanuatu

ET

H. GUINAUDEAU

Faculté de médecine et de pharmacie, 87032 Limoges Cédex, France

Reçu le 17 juin 1985

M. C. CHALANDRE, J. BRUNETON, P. CABALION et H. GUINAUDEAU. Can. J. Chem. **64**, 123 (1986).

En plus d'une aporphine, les écorces de *Hernandia peltata* Meissner (Hernandiacées) ont fourni deux nouvelles bisréticulines et 10 dimères aporphine–benzylisoquinoléine. Quatre d'entre eux sont nouveaux: la (+) northalicarpine-6 **6**, la (+) *N*-oxythalicarpine-2′ **10**, la (+) hébridamine **11** et la (+) vilaportine **12**. L'hébridamine est le premier exemple de benzylisoquinoléine–phénanthrène et la vilaportine est un dimère comportant une moitié zwitterionique. La déhydrothalmélatine-6a,7 **9** est isolée ici pour la première fois à l'état naturel. La possibilité d'une relation biogénétique entre la (+) vanuatine et la (+) thalicarpine est envisagée.

M. C. CHALANDRE, J. BRUNETON, P. CABALION, and H. GUINAUDEAU. Can. J. Chem. **64**, 123 (1986).

The bark of *Hernandia peltata* Meissner (Hernandiaceae) has yielded four new dimeric alkaloids, namely (+)-6-northalicarpine **6**, (+)-thalicarpine 2′-*N*-oxide **10**, (+)-hebridamine **11**, and (+)-vilaportine **12**. Hebridamine is the first example of a benzylisoquinoline–phenanthrene dimer and (+)-vilaportine is a dimer with an oxoaporphinium zwitterionic moiety. The 6a,7-dehydrothalmelatine **9**, previously known as a synthetic compound, has been isolated from a natural source for the first time. The possibility of a biogenetic relationship between (+)-vanuatine and (+)-thalicarpine **7** is considered.

Il est connu que la (+) réticuline conduit, via un couplage oxydatif intramoléculaire, à de nombreuses structures monomériques (2, 3). Or récemment nous avons pu isoler de *Hernandia peltata* Meissner trois alcaloïdes dimères qui constituent le premier exemple connu d'un couplage oxydatif intermoléculaire de deux unités dérivées de la (+) réticuline (4). L'un d'entre eux, la (+) vanuatine **1** pourrait s'inscrire dans un schéma biogénétique conduisant à la (+) thalicarpine **7**, alcaloïde aporphine–benzylisoquinoléine dimère cytostatique présent en particulier chez *Hernandia ovigera* (**5**) et dont la présente note rapporte l'isolement en quantité notable dans *H. peltata*. Avant d'envisager une étude spécifique de cette biosynthèse, il importait d'approfondir la connaissance de la composition en alcaloïdes dimères de cette espèce. Nous rapportons ici l'isolement et l'identification de 13 alcaloïdes, 1 aporphine et 12 dimères, obtenus lors d'une étude sur un nouvel échantillon de cette plante. Six des molécules isolées sont originales: deux bisbenzylisoquinoléines de type bisréticuline et quatre dimères aporphine–benzylisoquinoléine.

L'extraction est conduite selon le procédé déjà décrit (4): une séparation préliminaire des monomères et des dimères est réalisée par filtration moléculaire sur gel de Sephadex LH 20; la fraction des alcaloïdes dimères est scindée en bases phénoliques et non phénoliques par partage entre une solution aqueuse d'hydroxyde de sodium diluée et du chlorure de méthylène.

Le fractionnement des bases phénoliques conduit à l'isolement de la (+) malékulatine **2** (0,2%) (4) et de deux nouveaux alcaloïdes bisbenzylisoquinoléiques de type bisréticuline, la (+) ambrimine **3** et la (+) éfatine **4**; la structure de ces deux dimères diphénoliques monopontés "tête à queue" a fait l'objet d'une autre note (1). Une suite de chromatographies sur colonnes de silice et de chromatographies sur couche mince préparatives a permis d'isoler neuf alcaloïdes à partir du mélange de bases non phénoliques. Un seul monomère, la (−) laetine a été isolé (6*c*); les autres alcaloïdes obtenus sont des dimères: la (+) thalicarpine **7** qui représente l'acaloïde majoritaire de cette fraction (0,1%), accompagnée de (+) vanuatine **1** (4), de (+) northalicarpine-2′ **5** et de (+) thalmélatine **8**.[3] Le cinquième alcaloïde isolé est la (+) déhydrothalmélatine-6a,7 **9** qui n'était jusqu'alors connue qu'à l'état de produit synthétique (5, 7).

La (+) northalicarpine **6**, $C_{40}H_{46}N_2O_8$, est un isomère structural de la (+) northalicarpine-2′ **5** (5). Le spectre de masse de **6** est très proche de celui de **5**, mais il présente un pic de base à m/z 206 au lieu de 192 comme dans le spectre de **5**. Le spectre de rmn du proton de **6** présentant un seul singulet dû à un *N*-méthyle est également très proche de celui de **5**, avec cependant deux différences sensibles; le singulet dû au méthoxyle en 7′ apparaît à δ 3,54 ppm comme dans le cas de la (+) thalicarpine (3,58 ppm) ou de la (+) pennsylvanine (3,56 ppm) (15), au lieu de 3,72 ppm comme dans le spectre de **5**, ce qui permet de dire que l'azote 2′ de **6** est engagé dans une amine tertiaire. La substitution de N-2′ par un méthyle est confirmée par la deuxième particularité du spectre de rmn de **6**, c'est-à-dire par la position relativement blindée du singulet dû au proton 8′ à 6,14 ppm. De même, le pic de base présenté par le spectre de masse de **6** à m/z 206, résultant de la coupure de la liaison

[1]Pour la partie XI de la série, voir la référence 1.

[2]Auteur à qui adresser la correspondance.

[3]Pour une liste complète des aporphines–benzylisoquinoléines dimères, voir la référence 5. Pour une liste complète des alcaloïdes aporphiniques, voir la référence 6.

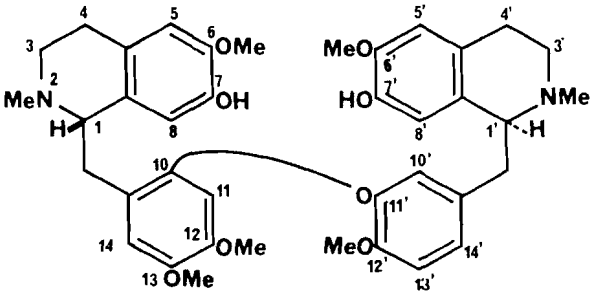

1

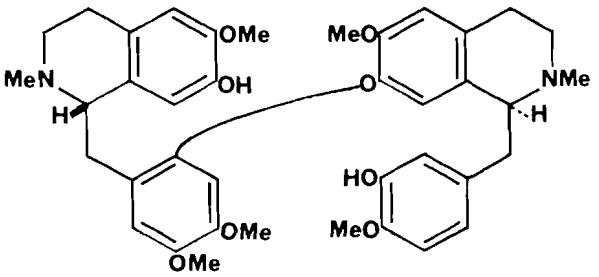

2

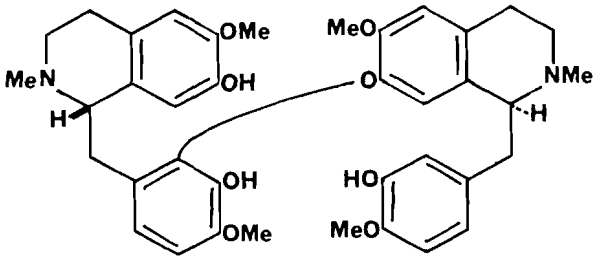

3

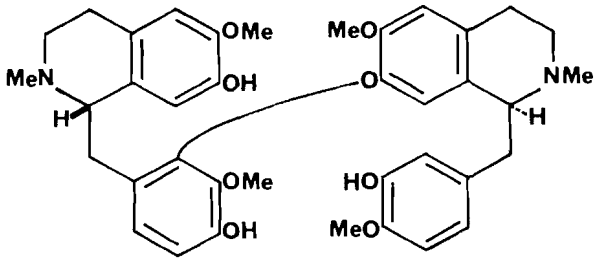

4

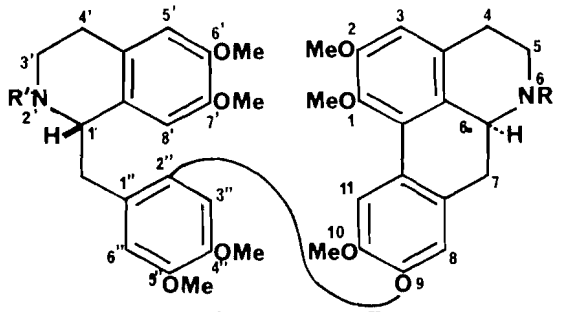

5 R :Me R':H 6 R :H R':Me 7 R : Me R': Me

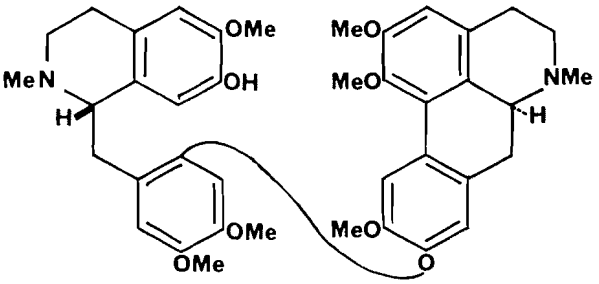

8

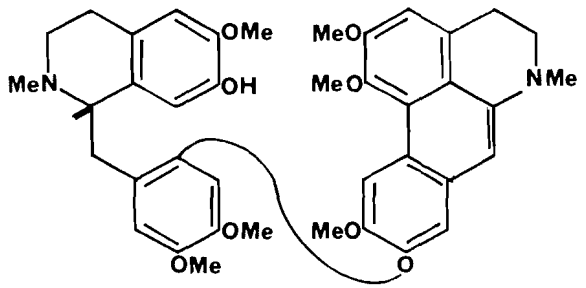

9

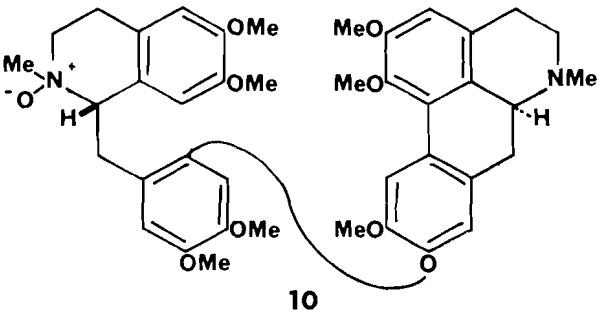

10

benzylique 1′-α, est en faveur d'une amine tertiaire en 2′ et d'une amine secondaire en 6, c'est-à-dire du côté aporphinique de la molécule. La (+) northalicarpine-6 est le premier exemple connu d'aporphine–benzylisoquinoléine déméthylée sur l'azote aporphinique, les seuls dimères"nor" connus dans cette série portant l'amine secondaire du côté de la partie benzylisoquinoléine ((+) northalicarpine-2′ et (+) noradiantifoline-2′) (5).

La (+) thalicarpine *N*′-oxide **10**, $C_{41}H_{48}N_2O_9$, présente dans son spectre de masse un très faible pic moléculaire à *m/z* 712 (0,1), traduisant l'incorporation d'un oxygène supplémentaire par rapport à la (+) thalicarpine **7** (5). Les spectres de rmn du proton de **7** et de **10** sont voisins bien que un des singulets dû à un *N*-méthyle de **10** soit déplacé vers les champs faibles à δ 3,39 ppm au lieu de 2,50 ppm, ainsi que le signal donné par le proton 1′ (4,87 au lieu de vers 3,80 ppm). L'ensemble de ces données et le fait que la réduction de **10** par le zinc chlorhydrique conduit à la (+) thalicarpine **7**, indiquent que **10** est la *N*-oxythalicarpine-2′.

Les positions respectives des signaux du proton 1′ et du *N*-méthyle-2′ (δ 4,81 et 3,39 ppm, respectivement) laissent penser qu'ils sont en position *trans* l'un par rapport à l'autre et donc que **10** serait la (+) β-*N*-oxythalicarpine-2′; cependant, une étude plus approfondie serait nécessaire pour confirmer la configuration de la fonction *N*-oxyde (8).

Peu de dimères porteurs d'une fonction *N*-oxyde ont été décrits jusqu'alors; 11 bisbenzylisoquinoléines de ce type ont

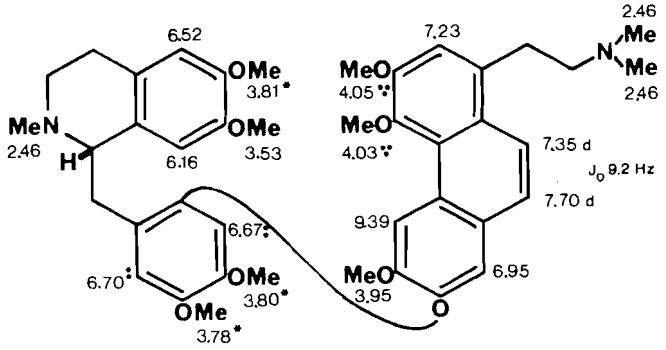

11

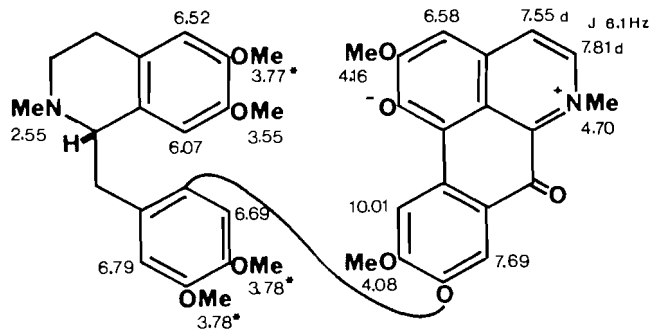

12

été rapportées (8), mais il semble que la (+) *N*-oxythalicarpine-2′ soit la première aporphine–benzylisoquinoléine *N*-oxyde à être isolée.

La (+) hébridamine **11**, $C_{42}H_{50}N_2O_8$, est un dimère dont le spectre de masse présente un pic moléculaire à m/z 710 (0,1%). Son spectre de masse présente les caractéristiques d'un groupement phénanthrène, en particulier un pic de forte intensité à m/z 58. Le pic de base à m/z 206 et le pic moléculaire très faible à m/z 710 indiquent que **11** est un dimère avec une moitié benzylisoquinoléique.

Le spectre de rmn du proton de **11** est également en faveur d'une structure de ce type présentant, à 2,46 ppm, un singulet de 9 protons résultant de la superposition d'un signal dû à un *N*-méthyle et d'un signal dû à un groupement diméthylamino d'un phénanthrène. Le système AB de deux protons à 7,35 (d) et 7,70 (d) ppm (J = 9,2 Hz), dû aux protons 6a et 7, ainsi que la présence d'un singulet fortement déblindé à 9,39 ppm, dû au proton en 11, sont des indications caractéristiques dans la série des phénanthrènes dérivés d'une moitié aporphinique (6). Les autres signaux présentés par le spectre de rmn sont identiques à ceux observés pour la (+) thalicarpine **7**, permettant donc d'attribuer à la (+) hébridamine la structure **11**.

Le dernier alcaloïde, la (+) vilaportine **12**, $C_{40}H_{44}N_2O_9$, est fortement coloré en vert. Son spectre uv (EtOH, λ_{max}: 227, 257, 320 et 392) est proche de celui des oxoaporphines et pratiquement superposable à celui des zwitterions type bétaïne des oxoaporphiniums comme l'alcaloïde PO-3, la corunnine, la nandazurine ou l'arosinine (6); pour ces derniers comme pour **12**, le spectre uv est fortement modifié en milieu acide (pour **12**; λ_{max}: 227, 255, 187 et 379), ce qui résulte de la tautomérie possible pour ces molécules (9). Le spectre de masse de la (+) vilaportine **12** indique qu'il s'agit d'une molécule dimère, présentant un pic moléculaire à m/z 692 (10%) et un pic de base à m/z 206, caractéristique d'une moitié benzylisoquinoléine. Le spectre de rmn du proton, résumé autour de la formule **12**, est en accord avec cette hypothèse; il est à noter tout particulièrement la position, dans les champs faibles à 4,70 ppm, du singulet de trois protons donnés par le *N*-méthyle de la moitié oxoaporphinium ainsi que la présence de six singulets dus à des méthoxyles; la présence de neuf oxygènes dans la molécule et de seulement six méthoxyles montre l'existence d'une fonction phénolique, ce qui confirme le type bétaïne de la (+) vilaportine et non d'un sel d'ammonium quaternaire comme dans la thaïlandine ou l'uthongine (6). La coloration verte et la position normale du signal correspondant au proton en 3 impliquent que l'hydroxyle soit en 1 (10). La comparaison des spectres de rmn de la (+) thalicarpine **7**, de la (+) thalmélatine **8** et de la (+) vilaportine **12** montre que la substitution sur la moitié benzylisoquinoléine reste la même.

Il n'existe qu'une seule structure dimère possédant une moitié oxoaporphinium vrai, le beccapolinium, un bisaporphinoïde isolé de l'Annonacée *Polyalthia cauliflora* (5). La (+) vilaportine constitue donc le premier exemple de dimère possèdant une structure benzylisoquinoléine–oxoaporphine.

Au terme de cette étude, il convient de procéder à un certain nombre de remarques. La première concerne la différence de composition alcaloïdique observée entre notre première étude réalisée sur un lot récolté en juillet et cette présente analyse effectuée sur un échantillon récolté en novembre. Il apparaît alors que si la (+) malékulatine **2** est présente dans les deux échantillons, la vanuatine **1**, qui représentait environ 2,5% des alcaloïdes de l'échantillon précédent, n'est présente ici qu'à l'état de traces; au contraire, la (+) thalicarpine **7** que nous n'avions pas pu mettre en évidence lors de la première étude, représente ici 4% des alcaloïdes totaux. En première approximation, tout semble se passer comme si une "balance biogénétique" existait entre la (+) thalicarpine **7** et la (+) vanuatine **1**. Une telle affirmation, cependant, doit être vérifiée par l'étude des variations saisonnières et par élimination, à la suite de prélèvements multiples, des possibilités de variations liées à des conditions édaphiques, écologiques ou climatiques. De plus, si une telle balance existe, on peut s'interroger sur la disparition, dans le lot de novembre, de la (+) vatéamine sans qu'apparaissent pour autant des dimères du type (+) foetidine. Il conviendrait enfin d'étudier les variations éventuelles de la composition en monomères; *H. peltata* est en effet riche en aporphines monomères (11) et donc rien n'exclut l'hypothèse que la (+) thalicarpine soit formée par couplage de la (+) réticuline avec une aporphine-1,2,9,10 tétrasubstituée (12).

Une autre remarque souligne l'homogénéité des structures décrites ici, toutes dimères de la (+) réticuline, ne variant que par leur état d'oxydation. Bien que les quantités isolées soient souvent faibles (quelques milligrammes ou dizaines de milligrammes par kilogramme de plante sèche), l'absence de stockage ainsi que les conditions de dessiccation et d'extraction permettent d'exclure l'hypothèse que ces composés soient des artéfacts. De plus, des dérivés oxydés comme la (+) oxothalicarpine et la (+) déhydrothalicarpine-6a,7 (5) ont déjà été mis en évidence dans des *Hernandia*. Enfin, il est intéressant de remarquer que *Hernandia peltata* livre presque tous les intermédiaires postulés pour le passage des aporphines aux oxoaporphines (13).

Partie expérimentale

Les pouvoirs rotatoires sont mesurés dans le $CHCl_3$ à l'aide d'un polarimètre Schmidt Haensch; les spectres uv sont enregistrés sur un appareil Beckman 530 et les spectres ir sur Perkin Elmer 580. Les spectres de rmn ont été réalisés sur des appareils Varian EM 360 et

Bruker WB 360 ($CDCl_3$, TMS = 0 ppm); les spectres de masse, sur AEI-MS 902.

Extraction des alcaloïdes totaux, purification

L'échantillon étudié (3,5 kg) a été récolté en novembre 1982 (réf PCNH-1079) et l'extraction est conduite selon le procédé déjà décrit (4). Les alcaloïdes totaux (105 g) sont filtrés sur Sephadex LH-20 ($CHCl_3$–MeOH, 30:70) ce qui conduit à recueillir une fraction enrichie en dimères de 31 g. La fraction d'alcaloïdes dimères est dissoute dans $CHCl_3$–Et_2O et la solution organique extraite par une solution diluée de NaOH (5%) pour séparer les bases phénoliques (17 g) et non phénoliques (11 g).

Fractionnement des alcaloïdes

Les bases phénoliques sont chromatographiées sur alumine désactivée par addition de 6% d'eau. L'élution par des solvants de polarité croissante permet d'isoler la (+) malékulatine **2** (3,2 g) (éluée par $CHCl_3$–C_6H_6, 50:50) et un mélange de **2**, **3**, **4** et de produits polaires (élué par $CHCl_3$–MeOH, 95:1, 95:5, 90:10); 1,8 g du mélange est rechromatographié sur colonne de gel de silice pour ccm (chromatographie en conche mince) ($CHCl_3$–MeOH, 88:12) et fournit **2** (306 mg) ainsi que la (+) ambrimine **3** (172 g) et la (+) éfatine **4** (298 mg).

Les bases non phénoliques sont séparées par chromatographie sur silice. L'élution est conduite avec un gradient de MeOH (de 0,5 à 20%) dans $CHCl_3$. Sont successivement isolés: 780 mg d'épimagnoline, lignane déjà décrit chez *H. peltata* (14), 3,5 g de (+) thalicarpine **7**, 1,3 g d'un mélange complexe, 1,1 g de **2** et 0,78 g de produits non identifiés. Le mélange élué après **7** est purifié par passage sur colonne de silice pour ccm ($CHCl_3$–MeOH, 95:5) et séparé en quatre groupes. Les groupes 1 (350 mg), 2 (165 mg) et 3 (105 mg) sont rechromatographiés sur colonne de silice pour ccm (pour 1, $CHCl_3$–C_6H_{12}–DEA, 40:55:5; pour 2 et 3, $CHCl_3$–AcOEt–MeOH–NH_4OH, 79:10:10:1). Le groupe 4 est traité en ccm préparative (CH_3CN–C_6H_6–EtOAc–MeOH–NH_4OH, 40:30:20:5:5). Le groupe 1 fournit la (+) hébridamine **11** (7 mg), les northalicarpine **5** (1,4 mg) et **6** (6,5 mg) ainsi que la (+) thalmélatine **8** (17 mg) et son dérivé déhydro-6a,7 **9** (2,2 mg). Le groupe 2 livre la laetine (1,1 mg), la (+) vanuatine **1** (3,2 mg) et la (+) vilaportine **12** (6 mg). Du groupe 3 sont isolés des produits en cours d'étude et le groupe 4 fournit 4,4 mg de (+) *N*-oxythalicarpine **10**.

Les produits **1**, **2** (4), **3**, **4** (1), **5**, **7**, **8**, **9** (5) ayant déjà été décrits, leurs constantes ne seront pas reprises ici. Pour **1**, **2** et **7**, ils sont identiques à des échantillons authentiques (f, ir, rmn, R_f en ccm); pour **5** et **9**, les constantes et données spectrales sont en bon accord avec les valeurs publiées.

(+) *Northalicarpine-6* ***6***: rmn (240 MHz (FT), $CDCl_3$): 2,45 (2′-NMe), 3,55 (7-OMe), 3,71 (1-OMe), 3,77 (6′-OMe), 3,78 et 3,83 (12′-OMe et 13′-OMe), 3,90 (2-OMe), 3,92 (10-OMe), 6,16 (H-8′), 6,47, 6,55, 6,58, 6,60, 6,62 (H-5′, H-3, H-11′, H-14′ et H-8), 8,21 (H-11); *m/z*: 680 (1), 490 (8), 324 (20), 322 (27), 206 (49), 192 (100).

(+) N-*Oxythalicarpine-2′* ***10***: $[\alpha]_D$ +15°, (0,14, $CHCl_3$); uv (MeOH) λ_{max}: 215, 280, 300 sh (log ε 4,36, 3,98, 3,86); rmn (200 MHz (FT), $CDCl_3$): 2,53 (6-NMe), 3,39 (2′-NMe), 3,70, 3,73, 3,74, 3,77, 3,85, 3,86, 3,90 (7-OMe), 4,81 (m, H-1′), 6,50, 6,51, 6,54, 6,58, 6,62, 6,64 (6H), 8,18 (H-11); *m/z*: 712 (0,1), 696 (0,3), 695 (0,8), 505 (1,5), 490 (4), 340 (7,3), 206 (100).

(+) *Hébridamine* ***11***: $[\alpha]_D$ positif; uv (MeOH) λ_{max}: 220, 260, 315; rmn (200 MHz (FT), $CDCl_3$); *m/z*: 710 (0,2), 708 (0,8), 504 (0,1), 503 (0,2), 206 (100), 58 (65).

(+) *Vilaportine* ***12***: uv (MeOH) λ_{max}: 297 sh, 257 sh, 320, 392 (log ε 4,57, 4,30, 4,45, 3,67); dc Δε (nm): +0,25 (286), +2 (257 sh), +11 (246), 0 (220), fin de courbe positive; *m/z*: 692 (40), 648 (20), 647 (40), 632 (12), 487 (6), 486 (4), 324 (13), 206 (100).

Remerciements

Les auteurs remercient Monsieur A. J. Freyer et Monsieur le professeur M. Shamma (The Pennsylvania State University) pour l'enregistrement des spectres de rmn à 360 MHz (FT) ainsi que pour l'échantillon de (+) thalicarpine.

1. M. C. Chalandre, H. Guinaudeau et J. Bruneton. C.R. Acad. Sci. **301**, 1185 (1985).
2. M. Shamma. The isoquinoline alkaloids. Academic Press, New York. 1972, et références citées.
3. M. Shamma et J. L. Moniot. Isoquinoline alkaloids research 1972–1977. Plenum Press, New York. 1978, et références citées.
4. J. Bruneton, M. Shamma, R. D. Minard, A. J. Freyer et H. Guinaudeau. J. Org. Chem. **48**, 3957 (1983).
5. H. Guinaudeau, M. Leboeuf et A. Cavé. J. Nat. Prod. **42**, 133 (1979); **47**, 565 (1984).
6. H. Guinaudeau, M. Leboeuf et A. Cavé. (*a*) Lloydia, **38**, 275, 1975; (*b*) J. Nat. Prod. **42**, 325 (1979); (*c*) **46**, 761 (1983).
7. H. B. Dutschewska et N. M. Mollov. Chem. Ber. **100**, 3135 (1967).
8. M. Lavault, A. Fournet, H. Guinaudeau et J. Bruneton. J. Chem. Res. (S), 248 (1985).
9. I. Ribas, J. Sueras et L. Castedo. Tetrahedron Lett. 3093 (1971).
10. V. Preininger, J. Hrbekjun, Z. Samek et F. Santavy. Arch. Pharm. (Paris), **302**, 808 (1969).
11. M. Lavault, P. Cabalion et J. Bruneton. Planta Med. **46**, 119 (1980).
12. A. T. Sidjimov et N. L. Marekov. Phytochemistry, **21**, 871 (1982).
13. M. Shamma et H. Guinaudeau. Tetrahedron, **40**, 4795 (1984).
14. P. Richomme, P. Cabalion, M. M. Debray et J. Bruneton. J. Nat Prod. **47**, 879 (1984).
15. M. Shamma et L. Moniot. Tetrahedron Lett. 2291 (1974).

The influence of pH in the tautomerism of 9,10-anthracenediols and 1,3-diketones

JOHN C. ANDERSON AND A. DOUGLAS BROADBENT[1]

Department of Chemistry, Mount Allison University, Sackville, N.B., Canada E0A 3C0

Received July 2, 1985

JOHN C. ANDERSON and A. DOUGLAS BROADBENT. Can. J. Chem. **64**, 127 (1986).

Equations have been derived to describe how the ratio of the total concentration of all keto forms to that of all enolic forms (K') varies with changing pH, for a tautomeric system in which the enol and ketone are polyprotic acids. The influence of pH on the tautomerism of 2-amino-9,10-anthracenediol, 2,9,10-anthracenetriol, 2,4-pentanedione, and 1-(3-pyridyl)-1,3-butanedione was examined. The equilibrium constants for all the acid–base equilibria involved were calculated from the dependence of K' on pH.

JOHN C. ANDERSON et A. DOUGLAS BROADBENT. Can. J. Chem. **64**, 127 (1986).

On a dérivé des équations qui décrivent les variations du rapport (K') de la concentration totale de toutes les formes cétoniques sur celle de toutes les formes énoliques en fonction du pH d'un système tautomère dans lequel l'énol et la cétone sont des acides polyprotiques. On a étudié l'influence du pH sur la tautomérie de l'amino-2 anthracènediol-9,10, de l'anthracènetriol-2,9,10, de la pentanedione-2,4 et de la (pyridyl-3)-1 butanedione-1,3. À partir de l'effet du pH sur K', on a calculé les constantes d'équilibre de tous les équilibres acide–base impliqués dans cette étude.

[Traduit par le journal]

Introduction

A simple prototropic tautomerism, of the keto–enol type, consists of four coupled acid–base equilibria, as shown in Scheme 1. This represents the accepted pathways for interconversion of an enol (EH) and a ketone (KH). A clear distinction between the acidic dissociation reactions and the overall tautomerism is essential (1, 2). The tautomerism equilibrium constant, K_T, is a function of the acidic dissociation constants and is independent of pH (3).

$$EH \underset{}{\overset{K_1}{\rightleftharpoons}} E^- + H^+ \overset{K_2}{\rightleftharpoons} KH$$

$$H^+ + EH \underset{K_3}{\rightleftharpoons} HKH^+ \underset{K_4}{\rightleftharpoons} KH + H^+$$

$$K_T = [KH]/[EH] = K_1/K_2 = K_4/K_3$$

SCHEME 1

The influence of pH on the coupled acid–base reactions, constituting a tautomeric equilibrium, has not been widely studied, despite the significance of keto–enol and nitrogen heterocycle tautomerism in organic chemistry. The paucity of data on this aspect of tautomerism is not surprising on consideration of the criteria for optimum analysis of this problem. Firstly, the solution must have measurable amounts of the tautomeric species, and the analytical technique used must determine the concentrations of these without disturbing the equilibrium. Since the influence of pH is being considered, an aqueous or semi-aqueous solution is needed. This should not introduce any competing reactions, such as hydration, or result in inadequate solubility. Finally, the effect of the acid–base equilibra of the tautomers will be most obvious when at least one of them has an acidic dissociation constant in the normal aqueous pH range.

In this paper, the overall tautomerism equilibrium constant, K', is defined as the ratio of the total concentration of all ketonic to that of all enolic species. For Scheme 1,

$$K' = ([HKH^+] + [KH])/([EH] + [E^-])$$

An equation for the dependence of K' on the concentration of hydrogen ion has been derived for a tautomeric system where both the ketone and enol are polyprotic acids. The tautomerism of 2-amino-9,10-anthracenediol, 2,9,10-anthracenetriol, 2,4-pentanedione, and 1-(3-pyridyl)-1,3-butanedione has been examined and the dependence of K' on pH has been used to determine the acidic dissociation constants of the various keto and enol forms and their influence on K_T.

Results and discussion

Reaction scheme

In a system where the enol and keto forms are polyfunctional acids and bases, Scheme 2 is applicable. Enolic species are represented by the symbol E and ketonic species by K.

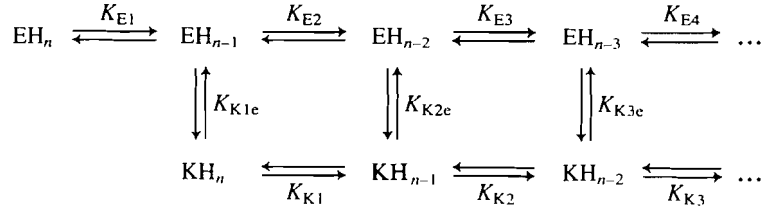

SCHEME 2

Scheme 2 clearly illustrates that the overall tautomerism is a series of coupled acid–base equilibria. Hydrogen ions and ionic charges have been omitted from the scheme for clarity. The acidic dissociation constants are given for each step. These are apparent constants, which would be experimentally determined, so that no distinction between isomeric conjugate bases from ionization of a polyprotic acid is considered (4).

The overall tautomerism equilibrium constant, K', will have a form dependent upon the analytical technique that is used to measure the concentrations of the various species present in the

[1]Author to whom correspondence should be addressed. Present address: Département de génie chimique, Faculté des sciences appliquées, Université de Sherbrooke, Sherbrooke (Qué.), Canada J1K 2R1.

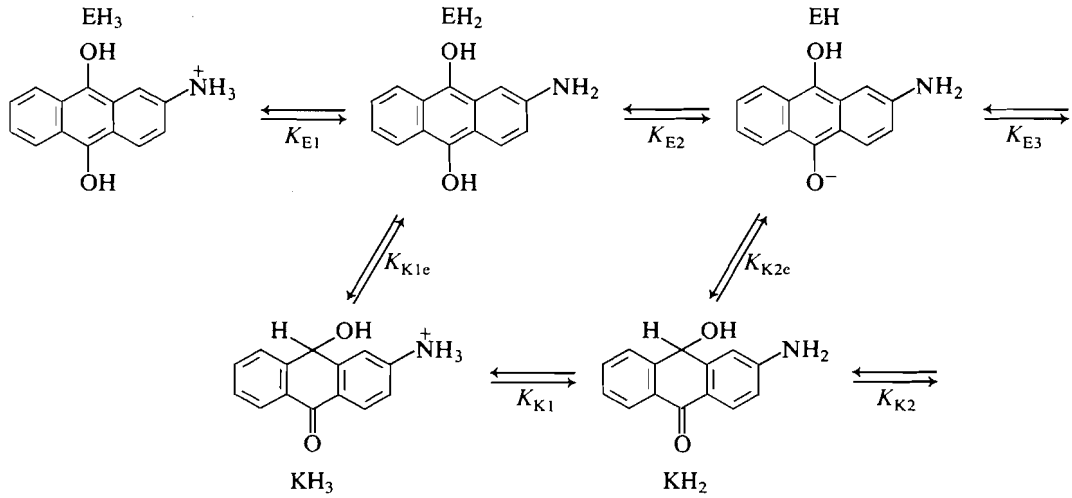

SCHEME 3

solution. If ideal solution behaviour is assumed, so that molarities are valid for activities, K' may be defined by

$$K' = \sum_0^n [KH_n] / \sum_0^n [EH_n]$$

Simple equilibrium considerations give

$$[1] \quad K' = \frac{K_{T1}\cdot(1 + K_{K1}/[H^+] + K_{K1}\cdot K_{K2}/[H^+]^2 + K_{K1}\cdot K_{K2}\cdot K_{K3}/[H^+]^3\cdots)}{(1 + K_{E1}/[H^+] + K_{E1}\cdot K_{E2}/[H^+]^2 + K_{E1}\cdot K_{E2}\cdot K_{E3}/[H^+]^3\cdots)}$$

$$[2] \quad = \frac{K_{T2}\cdot(1 + [H^+]/K_{K1} + K_{K2}/[H^+] + K_{K2}\cdot K_{K3}/[H^+]^2\cdots)}{(1 + [H^+]/K_{E1} + K_{E2}/[H^+] + K_{E2}\cdot K_{E3}/[H^+]^2\cdots)}$$

$$[3] \quad K_{T1} = [KH_n]/[EH_n] = K_{E1}/K_{K1e}$$

$$[4] \quad K_{T2} = [KH_{n-1}]/[EH_{n-1}] = K_{E2}/K_{K2e}$$

Both K_{T1} and K_{T2} are independent of pH and are related by

$$[5] \quad K_{T1}/K_{T2} = K_{E1}/K_{K1}$$

The above equations represent a more general situation than has been considered previously (3, 5) and are applicable over any range of pH.

2-Amino-9,10-anthracenediol

Bredereck *et al.* have studied the tautomerism of 2-amino-9,10-anthracenediol (2-amino-HOAOH) in aqueous ethanol solutions of varying pH (6). Although the keto form can be isolated by precipitation from a solution of the two tautomers (6), we were unable to confirm the structure by FT ^{1}Hmr, because of the very low solubility of the compound in the usual solvents. By analogy with the corresponding hydroxy-substituted derivatives (7), the keto form is considered to be 3-amino-10-hydroxy-9(10*H*)anthracenone, in which conjugation of the carbonyl and amino groups results in a low frequency ir carbonyl absorption band (6).

An interpretation of Bredereck's data on the variation of K' with changing pH, in terms of eq. [2], would require that the decrease in K', with decrease in pH from 8 to 6, as illustrated in Fig. 1, be related to protonation of the amino group in 2-amino-HOAOH ($EH_2 \rightarrow EH_3$ in Scheme 3). The ammonium ion would, therefore, have to have a pK_a of about 7. This is less acidic than typical phenylammonium ions, e.g., the conjugate acid of 2-aminoanthracene has a pK_a of 3.40 in 50% aqueous ethanol at 25°C (8).

Because of this unusual discrepancy, we re-investigated the tautomerism of 2-amino-HOAOH in buffered, aqueous ethanol solutions, over a wide range of pH, using polarography as described earlier (6, 7). The value of K' was determined from the ratio of the limiting, diffusion-controlled, cathodic current for the reduction of the anthracenone to the anodic current for the oxidation of the 2-amino-HOAOH. It was assumed that all the species had identical diffusion coefficients and that the influence of the applied potential on the drop-time did not affect the ratio of the recorded currents. The sum of the limiting currents for the 2-amino-HOAOH and its keto form was always within ±5% of the initial limiting current for the parent quinone, from which the 2-amino-HOAOH was generated by reduction using sodium dithionite, in neutral and basic solutions, or hydrogen and colloidal palladium in acidic solutions. The data are shown in Fig. 1.

Above pH 9, equilibrium between the two tautomers was attained within 1–2 min. In this pH region, there is reasonable correspondence between the previous and present K'–pH data, considering that all our pH values were 0.3–0.5 units higher than reported in the former study (6, 9). Below pH 9, the rate of ketonization of the 2-amino-HOAOH decreased significantly with decreasing pH. This is a consequence of the general base-catalysed mechanism, typical of tautomerism of an enol via the enolate ion, which is formed in a rapid pre-equilibrium. At pH <7, equilibration required 2–3 days and it became apparent that the values of K', previously reported for the pH range 6–9, were too low and were not equilibrium values. In addition, because of the confusion between acid–base and tautomeric equilibria, the published linear free energy relationship (6, 10) does not describe the influence of substituents on the

TABLE 1. Acidic dissociation constants for various tautomers according to Scheme 2

Enol or ketone	K_{T1}	K_{T2}	pK_{E1}	pK_{E2}	pK_{K1}	pK_{K1e}	pK_{K2e}
2-Amino-9,10-anthracenediol	0.08 ±0.03	2.71 ±0.07	4.34 ±0.06	10.57 ±0.05	2.9 ±0.2	3.3 ±0.2	11.0 ±0.1
2,9,10-Anthracenetriol	3.9 ±1.1	30 *	8.70 ±0.16	9.67 ±0.09	7.90 ±0.27	9.3 ±0.2	11.1 *
1,3-Pentanedione	~0.45 ±0.06	5.03 ±0.16	−5.12 ±0.07	8.19 ±0.04	−6.2 ±0.1	−5.5 ±0.1	8.9 ±0.1
1-(3-Pyridyl)-1,3-butanedione	0.21 ±0.02	0.38 ±0.18	5.51 ±0.75	9.18 ±0.26	5.2 *	4.8 *	8.7 *

*Large standard error caused by scatter or paucity of data points.

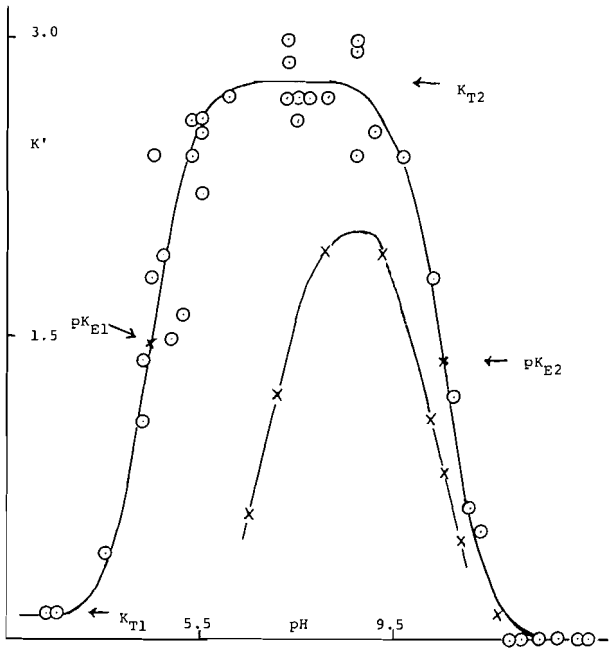

FIG. 1. The dependence of K' on pH for 50% aqueous ethanolic solutions of 2-amino-9,10-anthracenediol at 25°C. Circles represent experimental values and the line is based on the appropriate form of eq. [2], given below, using the values $K_{T1} = 0.08$, $K_{T2} = 2.71$, $pK_{E1} = 4.34$, and $pK_{E2} = 10.57$, which were derived from the K' data. Crosses represent previously published data (6).

$$K' = \frac{K_{T2} + K_{T1}\cdot[H^+]/K_{E1}}{1 + [H^+]/K_{E1} + K_{E2}/[H^+]}$$

equilibrium constant for tautomerism of anthracenediols, but rather their effect on the acidity of the C—H bond in the keto forms.

The redetermined values of K' are plotted as a function of pH in Fig. 1, which also shows the dependence based on the plateau values K_{T1} and K_{T2} and the two acidic dissociation constants, K_{E1} and K_{E2}, whose values were confirmed independently. The weighted least-squares estimates of these parameters were derived from the experimental data using a nonlinear regression procedure. Only these four constants are needed to define the curve, since the value of K_{E3} is so small that the term involving it in eq. [2] only becomes significant after K' is essentially zero. In addition, K_{K2} and K_{K3} are negligibly small and KH_3 and KH_2 (Scheme 3) are the only keto species present in the solution. Values of the constants are listed in Table 1.

The graph of $E_{1/2}$ versus pH, for the diffusion-controlled anodic wave for polarographic oxidation of the 2-amino-HOAOH, consisted of three linear sections with slopes close to −90, −60, and −30 mV/pH unit. These lines intersected at pH values of 3.9 ± 0.2 and 10.4 ± 0.1, which correspond to the values of pK_{E1} and pK_{E2} (11). The value of pK_{E3} was inaccessible since no evidence was found that $E_{1/2}$ became independent of pH in alkaline solution, as reported earlier (6).

Freshly prepared solutions of 2-amino-HOAOH at pH 1 exhibited maximum absorbance at 381 nm in the uv spectrum, which decreased on increasing the pH of the solution. A graph of absorbance at 381 nm versus pH gave a typical neutralization curve, for which regression analysis of the usual plot of pH versus $\log (A_1 - A)/(A - A_2)$ gave an intercept of 4.15 ± 0.05, corresponding to pK_{E1}. In the acidic solutions examined, the 2-amino-HOAOH was generated by reduction of the parent quinone using hydrogen and colloidal palladium. The absorbance at 381 nm was determined as soon as reduction was complete, but it remained constant over 5–10 min since the rate of ketonization was too low to influence the reading.

The spectrophotometrically determined value of pK_{E1} of 4.15 is the most reliable. The determination of pK_a values from the dependence of $E_{1/2}$ on pH is inferior because the potentials cannot be measured with a precision better than ±5 mV and errors occur if the polarographic process is irreversible, or variations of diffusion coefficients occur over the pH range examined. Derivation of pK_a values from the dependence of K' on pH, in the case of 2-amino-HOAOH, was limited by the considerable scatter of the K' values. This was a consequence of the errors inherent in measuring limiting currents and the long equilibration time necessary for the volatile, air-sensitive, neutral and acidic solutions. Despite this, the constants K_{T1}, K_{T2}, pK_{E1}, and pK_{E2} uniquely describe the dependence of K' on pH and could be calculated from the experimental data. The other equilibrium constants in Scheme 3 were then calculated using eqs. [3], [4], and [5] (see Table 1).

2,9,10-Anthracenetriol

Equation [1] was applied to the published data on the tautomerism of 2,9,10-anthracenetriol in aqueous solution, where extensive ketonization occurs over only a narrow range of pH (7). The keto form KH_3 is considered to be 3,10-dihydroxy-9(10*H*)anthracenone, based on the structures of the 3,6,10- and 3,7,10-trihydroxy derivatives, which were established by ^{1}Hmr (7). The various species present are illustrated in Scheme 4.

Figure 2 shows how the polarographically determined values of K' for 2,9,10-anthracenetriol depend on pH and includes a matching plot of the appropriate form of eq. [1]. Only two keto

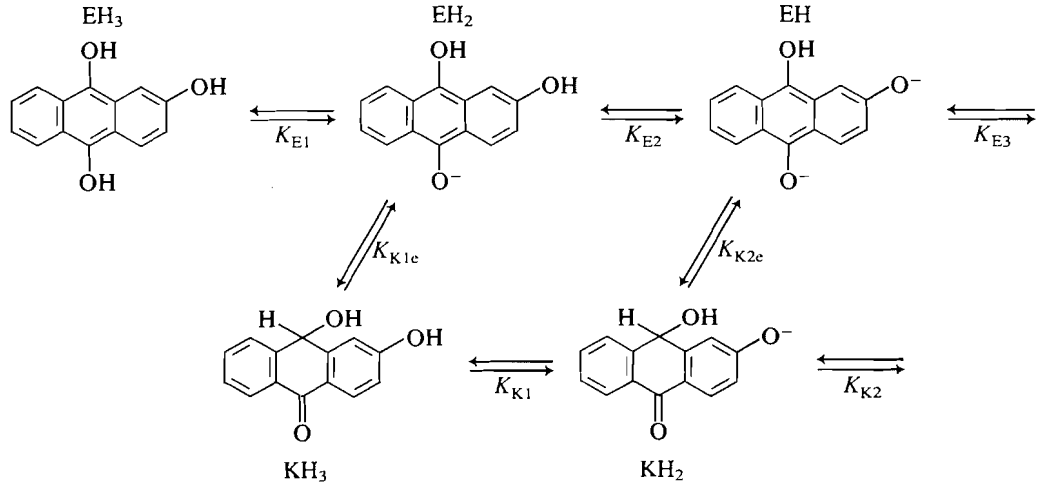

SCHEME 4

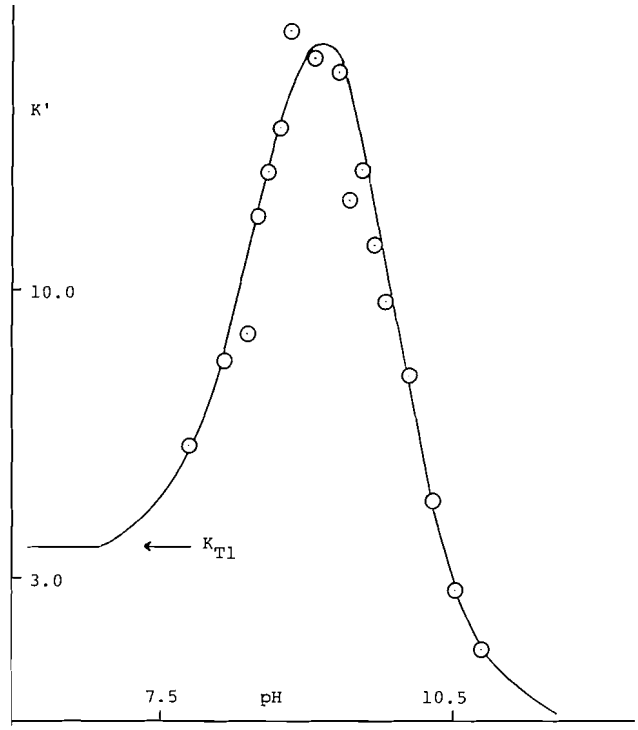

FIG. 2. The dependence of K' on pH for aqueous solutions of 2,9,10-anthracenetriol. Circles represent the published experimental data (7) and the line is the plot of the appropriate form of eq. [1], given below, using $K_{T1} = 3.9$, $pK_{E1} = 8.70$, $pK_{E2} = 9.67$, and $pK_{K1} = 7.90$.

$$K' = \frac{K_{T1}\cdot(1 + K_{K1}/[H^+])}{1 + K_{E1}/[H^+] + K_{E1}\cdot K_{E2}/[H^+]^2}$$

forms (KH_3 and KH_2) exist in the solution, because $K_{E2} > K_{E2e} > K_{K2}$, and K_{K3} is essentially zero, corresponding to the dissociation of an aromatic C—H bond. In addition, the value of K_{E3} is too small (2.5×10^{-13}) to be of influence (7).

The experimental data for K' did not show any plateau because of the proximity of the values of K_{E1} and K_{E2}. In this case, therefore, these acidity constants and K_{T2} cannot be derived from direct examination of Fig. 2. The values of K' above 10 could not be measured with great precision (±10%), so initially the analysis of the experimental data was achieved by adjustment of the values of K_{T1}, K_{E1}, K_{E2}, and K_{K1} to give the best visual fit to the K' – pH data points using the appropriate form of eq. [1]. Subsequently, better estimates of these equilibrium constants were derived by a nonlinear regression

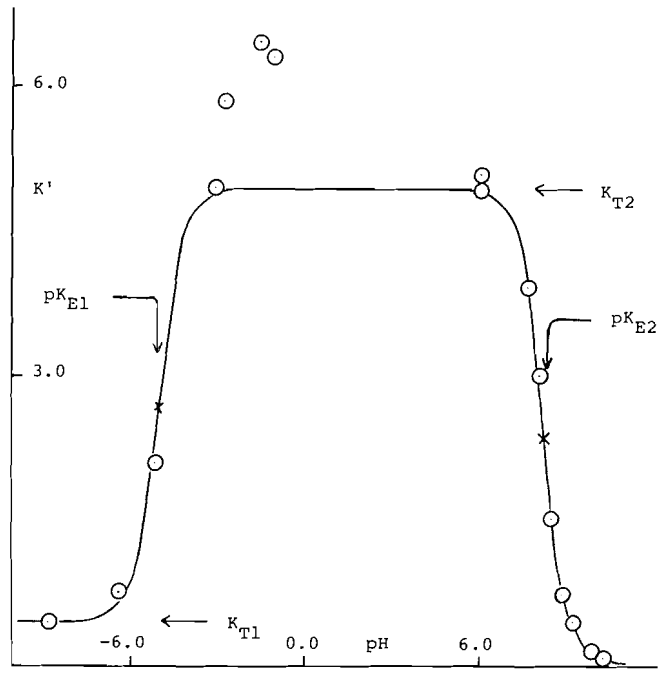

FIG. 3. The dependence of K' on pH for aqueous and sulfuric acid solutions of 2,4-pentanedione. The points represent published experimental data (5, 13) and the line is the plot of the appropriate form of eq. [2] with $K_{T2} = 5.03$, $pK_{E1} = -5.12$, $pK_{E2} = 8.19$, and $K_{T1} = 0.45$.

$$K' = \frac{K_{T2} + K_{T1}\cdot[H^+]/K_{E1}}{1 + [H^+]/K_{E1} + K_{E2}/[H^+]}$$

procedure. Their values are given in Table 1. This analysis demonstrated that the values of the four parameters uniquely define the dependence of K' on pH.

2,4-Pentanedione

There is little published data on the influence of pH in keto–enol systems. Zuman and co-workers (12) have studied the tautomerism of 1,3-dicarbonyl and related compounds, in the basic pH range, using spectrophotometric, polarographic, and bromine titration methods. Their results allowed the calculation of acidic dissociation constants for the enol and keto forms. Because of the limited pH range involved, the solutions contained only the enol and keto forms, and the enolate anion. A more detailed description is required when a wider pH range is considered.

The enol content of aqueous sulfuric acid and basic solutions

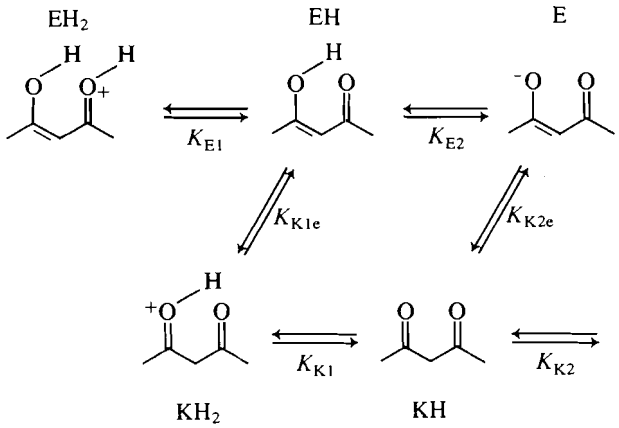

SCHEME 5

of 2,4-pentanedione has been determined (5, 13) and we chose to examine these data in relation to eq. [2] because of the range of acidity of the aqueous solutions studied. Values of K', calculated from the published data, are plotted as a function of pH in Fig. 3. The various species present are illustrated in Scheme 5.

The protonated enol EH_2 behaves as a diprotic acid (K_{E1}, K_{E2}), but for the keto form KH, K_{K2} is negligibly small since it corresponds to acidic dissociation of a C—H bond in a methyl group of the 2,4-pentanedione. This also applies to K_{E3}. The solution contains up to 5 species (Scheme 5) and there are 5 acidic dissociation constants neglecting K_{K2}. The appropriate form of eq. [2], given in Fig. 3, involves four constants, which can be read from the diagram. Nonlinear least-squares regression gave the values of the constants listed in Table 1, which differ slightly from those previously calculated (5, 13).

The K_{T2} plateau is not well defined, primarily because K' increases as the pH (Hammett acidity function) decreases from 0 to −3, prior to the large decrease in K' associated with the formation of the resonance-stabilized, protonated enol in strongly acidic solutions (pH < −3). This anomalous behaviour is a consequence of the large changes in sulfuric acid concentration resulting in variations of activity coefficient ratios (5).

To confirm the value of K' in weakly acidic aqueous solutions, we investigated the proton nmr spectrum of 2,4-pentanedione in such solutions. Integration of the ^{1}Hmr signals at 154 Hz (CH_3—CO group in enol and ketone) and 166 Hz (CH_3—C= group in enol) upfield from the water resonance of a 1.0 *M* aqueous 2,4-pentanedione solution, adjusted to pH 4.1 with dilute HCl, gave a value of $K_T = 4.68 \pm 0.16$ at 25°C. That this is lower than the anticipated plateau value is a consequence of the effect of the high concentration of the diketone decreasing K_T (14).

Various groups have established that the apparent acidic dissociation constant pK_{app} of 2,4-pentanedione in aqueous solution at 25°C is 9.05 ± 0.03 (15–17).

$$K_{app} = \frac{[H^+]\cdot[E^-]}{[K] + [E]} = \frac{K_{E2}}{1 + K_{T2}}$$

From the above equation, a value of $pK_{app} = 9.05$ and $K_{T2} = 5.0$ gives $pK_{E2} = 8.27$, which is in good agreement, considering differences in concentraton and ionic strength, with the value of 8.19 derived from the K' – pH data. The dependence of K' on pH thus provides a useful method for the determination of the acidic dissociation constants. In the case of K_{E1}, however, the value derived is not the true acidic dissociation constant because ketones follow a different acidity function than the amine indicators used to establish the Hammett acidity function used in Fig. 3 (18).

1-(3-Pyridyl)-1,3-butanedione

Scheme 6 describes the tautomerism of 1-(3-pyridyl)-1,3-butanedione. For this sytem, $n = 2$, but K_{K2} is negligibly small.

K' was determined by ^{1}Hmr spectroscopy in aqueous buffered dioxan solutions, by integration of the signal areas for the resolved methyl resonances of the enol and keto forms (enol CH_3, 2.04 ppm; keto CH_3, 2.20 ppm) and for the enol alkene and aromatic H-5 proton resonances (enol =C—H, 6.20 ppm; enol and keto aromatic H-5, 7.3 ppm).

$$K' = (\text{keto } CH_3)/(\text{enol } CH_3)$$

$$K' + 1 = (\text{aromatic H-5})/(\text{enol} =C—H)$$

Both methods gave consistent results but, in basic solutions of pH >8, the resolution of the enol and keto methyl resonances was unsatisfactory because of peak broadening, resulting from the enhanced rate of base-catalysed tautomer interconversion. In addition, because of the concentrated solutions required to obtain reliable signal integrations, and also because of the need to maintain a constant ionic strength, precise K' values could not be obtained at pH >8.7.

The experimental data are illustrated in Fig. 4, along with a plot of the appropriate form of eq. [2]. Approximate values for K_{T1}, K_{T2}, K_{E1}, and K_{E2} could be read from the points plotted in Fig. 4. Nonlinear least-squares regression gave the values in Table 1.

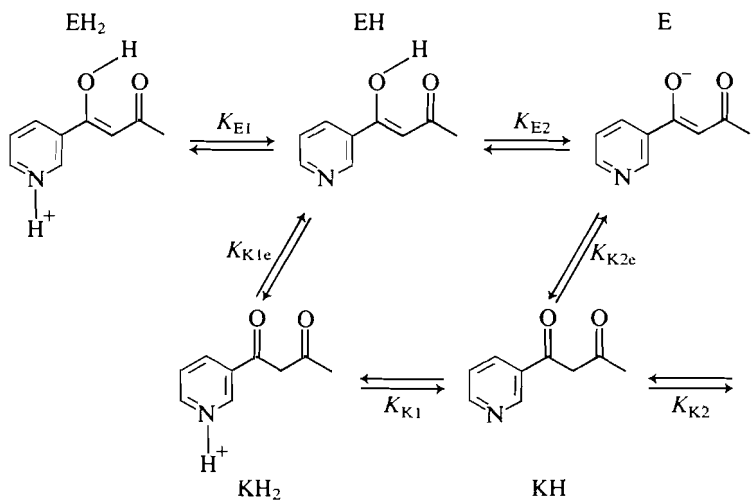

SCHEME 6

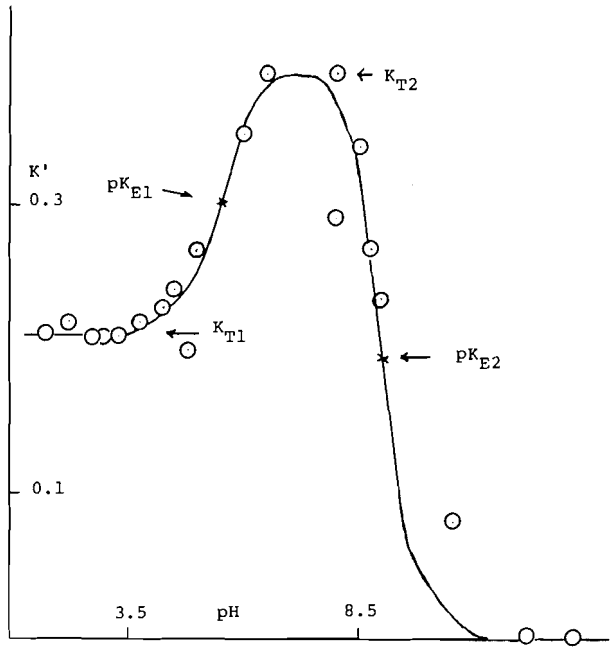

FIG. 4. The dependence of K' on pH for 30% v/v dioxan/water solutions of 1-(3-pyridyl)-1,3-butanedione at 35°C. The points represent experimental values and the line is the plot of the appropriate form of eq. [2] using $K_{T1} = 0.21$, $K_{T2} = 0.38$, $pK_{E1} = 5.51$, and $pK_{E2} = 9.18$.

$$K' = \frac{K_{T2} + K_{T1}\cdot[H^+]/K_{E1}}{1 + [H^+]/K_{E1} + K_{E2}/[H^+]}$$

Conclusion

The reaction scheme and equations used in this study describe the tautomeric and acid–base equilibria linking polyprotic enols and ketones. The experimental dependence of K' on pH provides sufficient data to calculate all the relevant acidic dissociation constants for both tautomers (see Table 1). In several cases, good estimates of both equilibrium and acidic dissociation constants could be read directly from the graph of K' vs. pH. The nonlinear regression provided the best values of the constants and also clearly established that the set of equilibrium and acidic dissociation constants uniquely describes the pH dependence of K'.

When the enol is the predominant tautomer, the acidic dissociation of the enol O—H bond, to give the enolate ion, is less favourable than that of the keto C—H bond, which gives the common conjugate base; i.e., $K_{En} < K_{Kne}$, a reversal of the usual order of O—H and C—H acidities.

Experimental

Materials

Commercial 2-amino-9,10-anthracenedione was purified by column chromatography ($SiO_2/HCCl_3$) and recrystallized from ethanol, mp 301°C.

1-(3-Pyridyl)-1,3-butanedione was synthesized from ethyl nicotinate by reported methods and recrystallized from ethanol/water, mp 81–82°C (19); ^{1}Hmr ($DCCl_3$) δ: 2.15 (s, 3H, enol CH_3), 6.15 (s, 1H, enol =C—H), 7.36 (m, $J_{4,5} = 8$ Hz, $J_{5,6} = 5$ Hz, $J_{2,5} = 1$ Hz, 1H, H-5), 8.14 (m, $J_{4,5} = 8$ Hz, $J_{4,6} = J_{2,4} = 2$ Hz, 1H, H-4), 8.72 (m, $J_{5,6} = 5$ Hz, $J_{4,6} = 2$ Hz, 1H, H-6), 9.05 (m, $J_{2,4} = 2$ Hz, $J_{2,5} = 1$ Hz, 1H, H-2), 16 (s, b, 1H, enol O—H).

Polarography

All polarographic measurements were performed using a Metrohm Polarecord E261. The polarographic cell has been described (20). The solutions of 2-amino-HOAOH were prepared by diluting 50.0 cm^3 of 8×10^{-4} M solution of 2-amino-9-10-anthracenedione in absolute ethanol with aqueous buffer solution and water to a final volume of 100 cm^3. Stoichiometric reduction of the quinone was achieved by amperometric titration with alkaline 0.05 M sodium dithionite solution under nitrogen, for solutions with pH >6.5, or by using hydrogen and colloidal palladium, and subsequent displacement of hydrogen by nitrogen, for acidic solutions. All solutions had an ionic strength of 0.1 M and were maintained at 25°C. The polarographic behaviour and the evaluation of K' (precision ±7%) have been described (9). For pH measurements with the Beckman Research pH Meter, the glass electrode was calibrated with aqueous standard solutions and the pH of the ethanolic solutions was recorded after adequate equilibration (~15 min).

Nuclear magnetic resonance

The ^{1}Hmr spectra of 1.0 M 1-(3-pyridyl)-1,3-butanedione solutions in 30% v/v dioxan/water were recorded using a Varian EM 360-L spectrometer at 35°C. Multiple integration of the appropriate signals gave K' with a precision of ±8%. The pH of the solutions was adjusted by including aqueous HCl, NaOH, or aqueous buffer solutions, so that the ionic strength was always 0.5 M. Two solutions with pH >9 had higher ionic strengths.

Nonlinear regression

Values of the equilibrium and acidic dissociation constants were derived from the K'–pH data using the weighted nonlinear least-squares regression procedure of the SAS Institute (SAS-ELIN).

Acknowledgements

This study was supported by grants from the Natural Sciences and Engineering Research Council of Canada. The authors also wish to thank Mr. Ken Morrison, Département de génie chimique, Université de Sherbrooke for the SAS-ELIN analysis.

1. A. R. KATRITZKY and J. M. LAGOWSKI. Adv. Heterocycl. Chem. **1**, 339 (1963).
2. J. C. ANDERSON and A. D. BROADBENT. Chem. Ber. **116**, 1252 (1983).
3. D. BARNES and P. ZUMAN. Talanta, **16**, 975 (1969).
4. R. A. ROBINSON and R. H. STOKES. Electrolyte solutions. 2nd ed. Butterworths, London. 1959. p. 348 ff.
5. G. SCHWARZENBACH and C. WITTWER. Helv. Chim. Acta, **30**, 659 (1947).
6. K. BREDERECK, F. SOMMERMANN, and M. DIAMONTOGLOU. Chem. Ber. **102**, 1053 (1969).
7. A. D. BROADBENT and E. F. SOMMERMANN. J. Chem. Soc. B, 1144 (1968).
8. J. J. ELLIOTT and S. F. MASON. J. Chem. Soc. 2352 (1959).
9. F. SOMMERMANN. Dr. rer. nat. dissertation, Technische Hochschule, Stuttgart. 1967.
10. K. BREDERECK and F. SOMMERMANN. Tetrahedron Lett. 5009 (1966).
11. W. M. CLARK. Oxidation–reduction potentials of organic systems. Williams and Wilkins, Baltimore. 1960.
12. G. MISLI, D. BARNES, and P. ZUMAN. J. Chem. Soc. B, 764 (1970); 771 (1970); 778 (1970); S. SINGER and P. ZUMAN. J. Org. Chem. **39**, 836 (1974).
13. M. L. EIDINOFF. J. Am. Chem. Soc. **67**, 2073 (1945).
14. G. ALLEN and R. DWEK. J. Chem. Soc. B, 161 (1966).
15. J. P. SHULKA and M. S. SUBRAMANIAN. Thermochim Acta, **35**, 293 (1980).
16. K. I. PASHKEVICH, V. I. SALOUTIN, and L. G. EGOROVA. J. Gen. Chem. USSR, **49**, 188 (1979).
17. E. BOTTARI and R. MONTALI. Monatsh. Chem. **108**, 1033 (1977).
18. C. H. ROCHESTER. Acidity functions. Academic Press, London. 1970.
19. L. F. KUICK and H. ADKINS. J. Am. Chem. Soc. **57**, 143 (1935).
20. A. D. BROADBENT and E. F. SOMMERMANN. J. Chem. Soc. B, 376 (1967).

Kinetics of acid and nucleophile catalysis of the diazotization of 1-naphthylamine

JULIO CASADO,[1] ALBINO CASTRO, EMILIA IGLESIAS,[2] M. ELENA PEÑA, AND JOSÉ VÁZQUEZ TATO
Departamento de Química Física, Facultad de Química, Universidad, E-Santiago de Compostela, España
Received June 24, 1985

JULIO CASADO, ALBINO CASTRO, EMILIA IGLESIAS, M. ELENA PEÑA, and JOSÉ VÁZQUEZ TATO. Can. J. Chem. **64**, 133 (1986).

The diazotization of 1-naphthylamine has been studied at acidities ranging from 10^{-2} to 1.5 *M*. At low acidities nitrosation takes place via the unprotonated form of the amine, and the rate-controlling step is either the interaction with the nitrosating agent or, if high concentrations of a nucleophile are present, the loss of a proton from the protonated nitrosamine (the nucleophiles studied were Cl^-, Br^-, SCN^-, and thiourea). At high acidities the protonated and free amines also react, the former of these reactions involving proton transfer to the solvent. In each case the proposed mechanism was supported by studying the reaction in D_2O, which also allowed the isotopic effect of the solvent on the formation equilibria of the various nitrosating agents to be obtained.

JULIO CASADO, ALBINO CASTRO, EMILIA IGLESIAS, M. ELENA PEÑA, et JOSÉ VÁZQUEZ TATO. Can. J. Chem. **64**, 133 (1986).

On a étudié la diazotation de la naphtylamine-1 dans un intervalle d'acidités allant de 10^{-2} à 1,5 *M*. À faible acidité, la nitrosation se produit via la forme non protonée de l'amine; l'étape déterminante de la réaction est soit l'interaction avec l'agent de nitrosation ou, s'il y a une forte concentration de nucléophiles, la perte d'un proton à partir de la forme protonée de la nitrosamine (les nucléophiles étudiés sont les ions Cl^-, Br^-, SCN^- et la thiourée). À des acidités élevées, les amines protonées et libres réagissent également. Dans le cas des amines protonées, la réaction implique un transfert de proton au solvant. Dans chaque cas, le mécanisme proposé repose sur une étude de la réaction dans le D_2O, qui permet également d'obtenir l'effet isotopique du solvant sur la formation à l'équilibre des divers agents de nitrosation.

[Traduit par le journal]

Introduction

The rate equations of diazotization reactions are heavily dependent on the experimental conditions, whose modification may change both the nitrosating agent (nitrosation being a preliminary step towards diazotization) and the slow step of the reaction, and at one time this behaviour gave rise to considerable controversy, the general validity of conflicting rate equations being claimed by their authors (1). Most research in this area has involved aromatic amines such as anilines and pyridines, whose diazonium ions are relatively stable and for which the effect of substitution has been analysed in some detail, but rather less is known about compounds with multiple rings. These considerations have led us to carry out a detailed study of the diazotization of 1-naphthylamine (1-NA) in water and in D_2O, at acidities ranging from 10^{-2} to 1.5 *M* and in the presence of various nucleophiles. 1-NA was chosen for its simplicity and the value of its pK_a, and because the only published study of its diazotization (2), in which ClNO was used as nitrosating agent, yielded a value of $1.9 \times 10^{10} M^{-1} s^{-1}$ for the attack constant at 0°C, which is surprisingly high compared with the values of $(1.0–5.9) \times 10^9 M^{-1} s^{-1}$ obtained at 25°C for anilines and their derivatives (3), and which are widely accepted as evidence of these reactions being diffusion controlled. It was expected that varying the experimental conditions might result in 1-NA exhibiting nucleophile catalysis, rate-limiting proton transfer to the solvent, and reactions via its free and protonate forms.

Experimental

All the reagents employed were Merck p.a. products and were used directly after drying. D_2O was supplied by the Spanish Nuclear Energy Board (Junta de Energía Nuclear) and contained 99.77% D. 1-NA and its solutions were protected from light to prevent their photodecomposition, but fresh solutions were in any case prepared at short intervals. The stability of the diazonium salt produced by the reaction and that of the 1-NA were verified experimentally under the various working conditions used. The decomposition of nitrite was also observed to be negligible during the course of the reaction, even under the most unfavourable conditions.

Kinetic measurements were carried out in a UVIKON 820 spectrophotometer, the temperature of the cell carrier being kept constant by a HETO 03T623 thermostat. A Radiometer 82 pH-meter with a GK 2401C combined electrode was used to measure pH.

The formation of the diazonium salt was monitored spectrophotometrically at 362 nm, a wavelength at which this salt is the only component of the reaction mixture to exhibit any appreciable absorption ($\epsilon = 6400\ M^{-1}\ cm^{-1}$). The integration method was used for kinetic analysis. When equal concentrations of nitrite and 1-NA were employed, the equation fitted to the experimental absorbance–time data was

$$[1] \qquad \frac{1}{A_\infty - A_t} = \frac{1}{A_\infty - A_0} - (k_2/\epsilon)t$$

A_t, A_∞, and A_0 being the absorbances at times t, infinity, and 0 respectively. When the reaction was slow enough for more than a 20-fold excess of amine to be used, the method of Davies, Swann, and Campey (4, 5) was used to fit the equation

$$[2] \qquad \ln (A_\infty - A_t) = \ln (A_\infty - A_0) - k_1 t$$

In either case the corresponding graphs (respectively $1/(A_\infty - A_t)$ against t and $\ln (A_\infty - A_t)$ against t) were linear for at least 85% of the reaction (Fig. 1) with standard deviations of less than 2%. When eq. [1] was used the values of A_∞ and A_0 were obtained experimentally. The values of k_1 and k_2 were reproducible to within ±3%. All experiments were carried out at 25°C.

Results and discussion

At acidities in the range 0.085–1.62 *M* $HClO_4$ the diazotization of 1-NA was found, using excess amine, to be of first order with respect to both reagents (Table 1). First-order behaviour with respect to HNO_2 was confirmed by the agreement between the experimental A_t–t data and eq. [2]. Thus,

$$[3] \qquad v = k_1[HNO_2] = k_2[1\text{-NA}]\,[HNO_2]$$

[1]Present address: Departamento de Química Física, Facultad de Química, Universidad, Salamanca, España.

[2]Author to whom correspondence may be addressed.

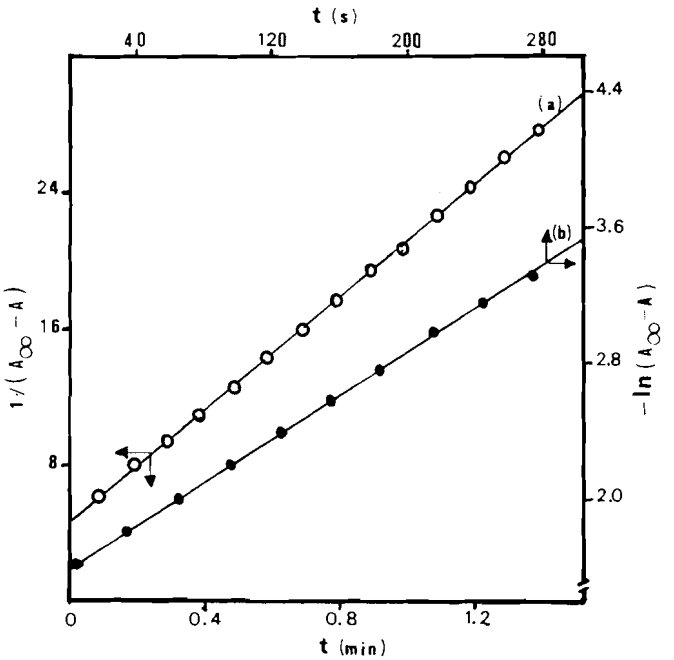

FIG. 1. (a) Typical pseudo-second-order plot of the diazotization of 1-NA at 25°C, $I = 0.35$ *M*, $[HNO_2] = [1\text{-NA}] = 3.27 \times 10^{-5}$ *M*, $[NaSCN] = 2 \times 10^{-3}$ *M*, $[H^+] = 0.1$ *M*. (b) Typical pseudo-first-order plot of the diazotization of 1-NA at 25°C, $I = 0.35$ *M*, $[1\text{-NA}] = 1.05 \times 10^{-3}$ *M*, $[HNO_2] = 3.27 \times 10^{-5}$ *M*, [NaCl] = 0.0266 *M*, $[H^+] = 0.1$ *M*.

Catalysis by nucleophiles

The influence of the nucleophiles Cl^-, Br^-, SCN^-, and $(NH_2)_2CS$ was studied at 25°C in 0.1 *M* $HClO_4$ using constant concentrations of nitrous acid and 1-NA ($I = 0.35$ *M*). Cl^-, Br^-, and SCN^- were used in the form of their sodium salts. The concentrations of NaCl and NaBr employed varied from 0.017 *M* to 0.25 *M*, those of NaSCN from 0.001 *M* to 0.015 *M*, and those of thiourea from 1.48×10^{-4} *M* to 2.23×10^{-4} *M*. The concentrations of HNO_2 and 1-NA were 3.3×10^{-5} *M* except in the experiments with Cl^-, which were slow enough to allow the use of excess amine (1.06×10^{-3} *M*).

Under the above conditions the halide ions and thiourea all catalysed the reaction. The graphs of k_2 against [Nucleophile] are curves in which k_2 tends with increasing [Nucleophile] to a limit that is the same for all nucleophiles employed (Fig. 2). This limiting value may be evaluated from the intercepts of the plots $1/k_2$ vs. $1/[X^-]$ (the average value is 4500 M^{-1} s^{-1} for all of them). This suggests the reaction mechanism to be of the kind put forward by Woppmann (2), in which the nitrosating agent is the nitrosyl salt of the nucleophile (Scheme 1). No evidence of nitrosation by any other agent ($NO^+(H_2NO_2^+)$ or N_2O_3) was observed.

Assuming the steady-state condition to be applicable to the intermediate I in Scheme 1,

$$[4] \qquad k_2 = \frac{k_2 K_{XNO} K_a [X^-]}{1 + (k_{-3}/k_4)[X^-]}$$

where $K_{XNO} = K_1 K_2$ is the equilibrium constant of the formation of the nitrosyl salt of the nucleophile, and K_a is the dissociation constant of the protonated amine (the value of 3.96 obtained spectrophotometrically by the present authors for the pK_a at 25°C and an ionic strength of 0.2 *M* agrees well with the value published by Hall and Sprinkle (6). Except for thiourea,[3] the values of k_2 were unchanged on working at pH 1.5.

TABLE 1. Values of the first-order pseudo-constant k_1 and A_∞ under various conditions

$[HClO_4]$ (*M*)	[1-NA] (*M*)	[Nitrite] (*M*)	A_∞	k_1 (s^{-1})
1.62	1.35×10^{-3}	1.65×10^{-5}	0.100	2.00×10^{-2}
1.62	1.01×10^{-3}	6.60×10^{-5}	0.415	1.49×10^{-2}
1.62	6.77×10^{-4}	3.30×10^{-5}	0.213	9.98×10^{-3}
1.08	1.35×10^{-3}	1.65×10^{-5}	0.097	1.68×10^{-2}
1.08	6.77×10^{-4}	6.60×10^{-5}	0.426	8.40×10^{-3}
0.085*	1.35×10^{-3}	1.65×10^{-5}	0.114	3.02×10^{-3}
0.085	1.01×10^{-3}	6.60×10^{-5}	0.427	2.29×10^{-3}
0.085	6.77×10^{-4}	3.30×10^{-5}	0.217	1.52×10^{-3}

*Calculated from the pH.

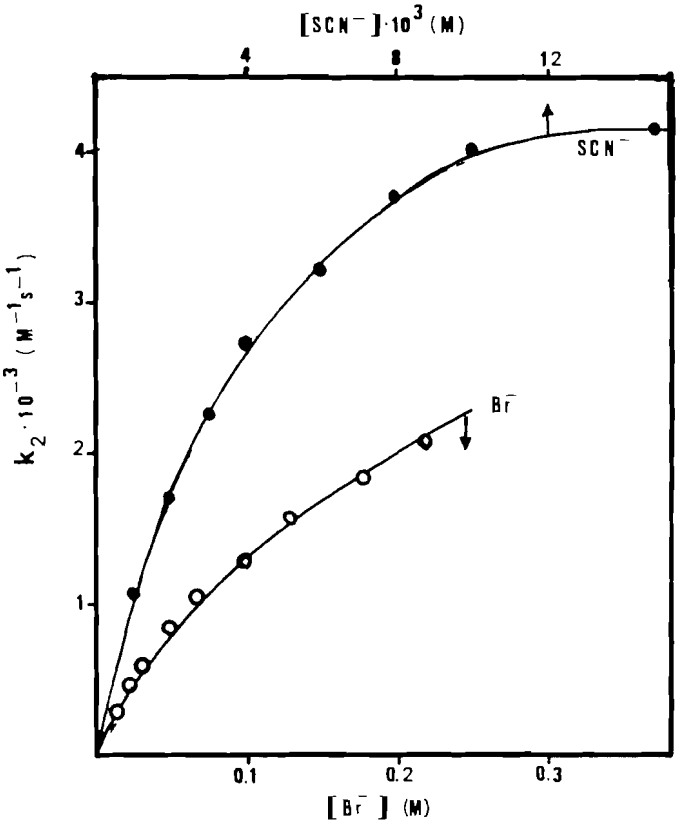

FIG. 2. Influence of the concentration of SCN^- (●) and Br^- (○) on the second-order rate coefficient, k_2 (eq. [4]) at 25°C, $I = 0.35$ *M*.

The values of k_3 and k_{-3}/k_4 obtained by plotting k_2^{-1} against $[\text{Nucleophile}]^{-1}$ are listed in Table 2. The values thus found for k_3(ClNO) and k_3(BrNO) indicate diffusion-controlled processes and are compatible with those reported by Williams and co-workers (3) and Schmid and Fouad (11) (Table 2). The much lower values of k_3 for SCNNO and nitrosothiourea are in keeping with the lower reactivity of these latter nitrosating agents, their greater catalytic effect being due to their large K_{XNO}. Figure 3 shows that the values of log (k_{-3}/k_4) are satisfactorily correlated with Pearson's nucleophilicity param-

[3]In this case it is necessary to take into account that the initial stoichiometric concentration of nitrous acid is equal to $[HNO_2]$ + [Nitrosothiourea]. Thus, $k_2 = k_3 K_{XNO} K_a [TU]/\{1 + (k_{-3}/k_4)[TU]\}(1 + K_{XNO}[H^+][TU])$.

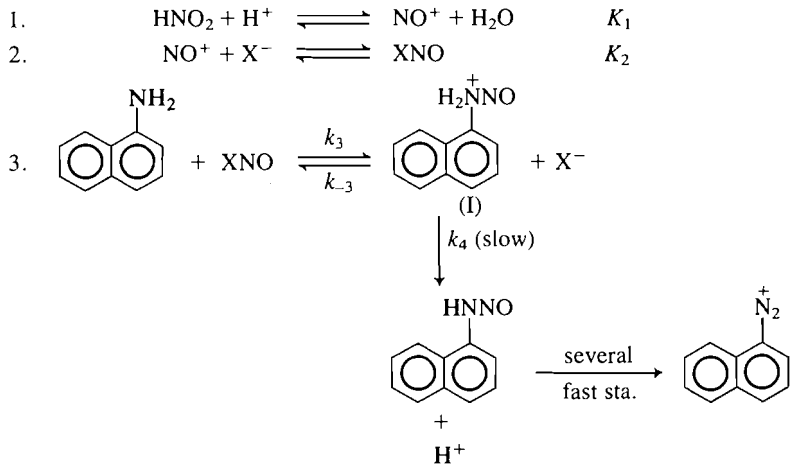

(X^- = Cl^-, Br^-, SCN^-, thiourea)

SCHEME 1

TABLE 2. Values of k_3 and k_{-3}/k_4 (eq. [4]) at 25°C and $I = 0.35$ M, together with some published values

X^-	K_{XNO}	$k_3 \times 10^{-9}$ * (M^{-1} s^{-1})	k_{-3}/k_4*	$k_3 \times 10^{-9}$(M^{-1} s^{-1}) A	*p*-ClA	*p*-MeA
Cl^-	1.14×10^{-3}(7)[a] 5.50×10^{-4}(7)[b]	2.22	0.359	2.2[d] 2.5[e]	1.8[d] 2.3[e]	
Br^-	5.10×10^{-2}(8)[a]	3.70	5.80	1.7[e] 3.2[f]		2.8[e] 3.2[d]
SCN^-	32 (9)[c]	0.382	248			
TU	5000 (10)[a]	0.00245	548			

*This paper; A = aniline; *p*-ClA = *p*-chloroaniline; *p*-MeA = *p*-methoxyaniline; TU = thiourea.
[a]25°C (ref. in parentheses).
[b]0°C.
[c]20°C.
[d]Acidity 0.2 M, cf. ref. 3.
[e]Acidity 1–5 M, cf. ref. 3.
[f]Reference 11.

eter, n (12), the value of 1.1 for the slope of the line being similar to those usually found for typical S_N2 substitutions on the carbon atom. The present results are thus in keeping with the usual order of nucleophilicity, $Cl^- < Br^- < SCN^- < (NH_2)_2CS$.

Support for the proposed k_4 step was sought by repeating the Br^- and SCN^- experiments in heavy water. The constants obtained in water and D_2O are shown in Table 3. If, as is reasonable, the isotopic effect on the k_3 process is assumed to be negligible, then a value of 3.11 may be calculated for the isotopic effect on the k_4 step. Since this value is that of a primary isotopic effect, the slow k_4 step must involve proton transfer.

The D_2O experiments also allow the isotopic effect on the K_1 equilibrium to be calculated from the values of $k_3K_{XNO}K_a$. If the effects on the K_2 equilibrium constant and the diffusion-controlled k_3 step are assumed negligible, then when the nucleophile employed is SCN^- or Br^- the values of pK_a obtained in water and D_2O and listed in Table 3 imply isotopic effects of 2.19 and 2.96, respectively, on the formation of NO^+. These values agree well with each other and with those reported by Challis *et al.* (13) for the nitrosation reaction

$$I^- + H_2NO_2^+ \rightarrow INO + H_2O$$

which supports the assumptions made in their derivation.

Experiments carried out to determine the influence of temperature on the diazotization of 1-NA by ClNO yielded the value of 79.67 kJ/mol for the Arrhenius activation energy and the values $\Delta H^{\ddagger} = 13.89$ kJ/mol and $\Delta S^{\ddagger} = -19.45$ J/(mol K) for the k_3 step.[4] The enthalpy of activation is within the accepted limits for a diffusion-controlled step (10–20 kJ/mol), and thus agrees with the value obtained for the constant k_3.

Catalysis by $HClO_4$ and $NaClO_4$

The influence of ionic strength on the diazotization of 1-NA was studied by varying the concentration of $NaClO_4$ in a series of experiments carried out at 25°C in 0.5 M $HClO_4$, using constant concentrations of nitrite and 1-NA of 2.75×10^{-5} M

[4]These quantities were calculated from the values at different temperatures of $k_3K_{ClNO}K_a$ (the slope of the graph of k_2^{-1} against $[Cl^-]^{-1}$) together with published values for K_{ClNO} at 0 and 25°C (7) and the values of K_a at 14 (5.55×10^{-5} M, $I = 0.2$ M) and 25°C (Table 3). The latter were obtained spectrophotometrically at 310 nm by the present authors because the values found in the literature for K_a at 15°C (14) and 25°C (6) afford a value of 136.6 kJ/mol for the enthalpy of ionization of the 1-naphthylammonium ion, which is enormously high compared with the values of 20–53 kJ/mol found for anilines (15) and would imply a negative enthalpy of activation.

TABLE 3. Values of the kinetic and thermodynamic parameters of eq. [4] in water and D_2O, $t = 25°C$

	H_2O		D_2O			
	k_{-3}/k_4	$k_3K_{XNO}K_a$	k_{-3}/k_4	$k_3K_{XNO}K_a$	$\frac{(k_4)_H}{(k_4)_D}$	$\frac{(K_{XNO})_D}{(K_{XNO})_H}$
SCN^-	248	1.346×10^6	778	9.13×10^5	3.14	2.19
Br^-	5.80	2.08×10^4	17.91	1.91×10^4	3.09	2.96
	$k_a = 1.09 \times 10^{-4}$ M ($I = 0.2$ M)		$K_a = 3.39 \times 10^{-5}$ M[a] ($I = 0.35$ M)			

H = H_2O; D = D_2O.
[a]Determined by us.

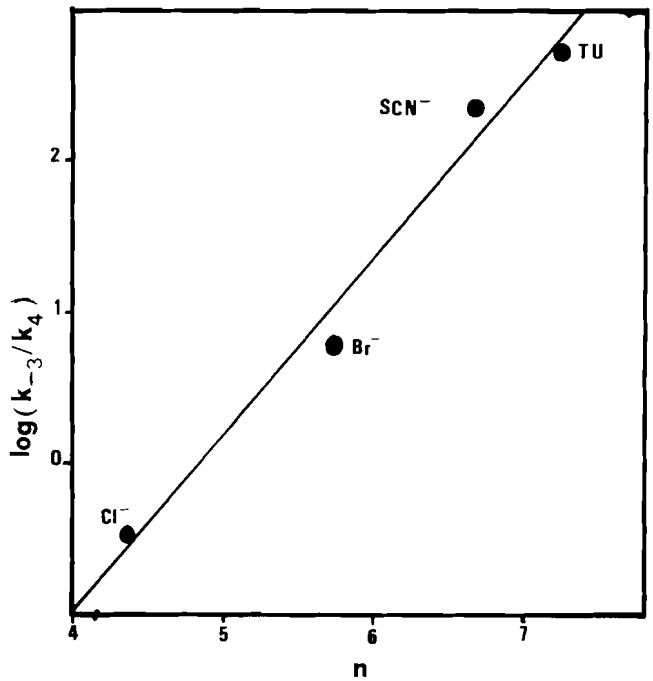

FIG. 3. Variation of log (k_{-3}/k_4) with Pearson nucleophilicity, n.

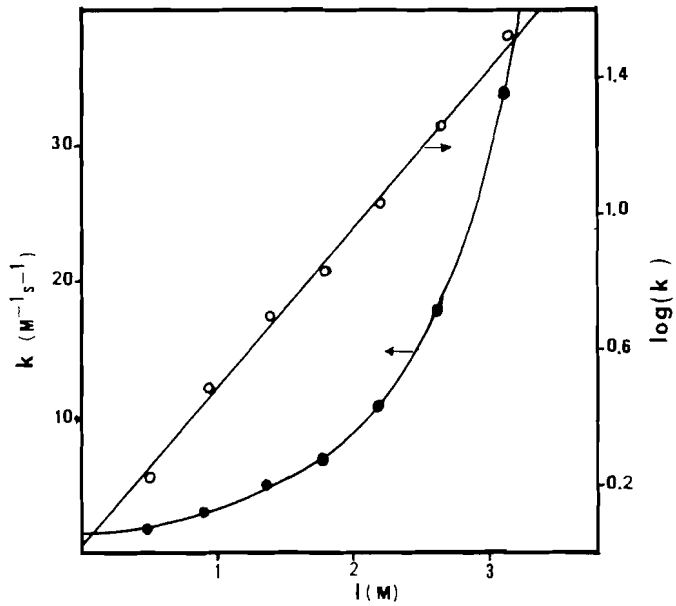

FIG. 4. Influence of the ionic strength on the second-order rate constant, k, at 25°C, $[HClO_4] = 0.5$ M, $[NaNO_2] = 2.75 \times 10^{-5}$ M, $[1\text{-NA}] = 1.32 \times 10^{-3}$ M.

and 1.32×10^{-3} M, respectively. The observed reaction rates reveal increasing catalysis as the concentration of salt rises, the dependence of the logarithm of the second-order experimental rate constant k on the ionic strength of the medium being linear, with a slope of 0.485 ± 0.017 (Fig. 4). These findings are similar to those obtained for other substrates (15), and may be considered as evidence of a secondary saline effect acting to increase the equilibrium concentration of the nitrosating agent (NO^+ or $H_2NO_2^+$).

The influence of acidity was studied by varying the concentration of $HClO_4$ from 0.15 to 1.5 M at 25°C and an ionic strength of 1.5 M controlled by $NaClO_4$, the concentrations of nitrous acid and 1-NA being those mentioned in the previous paragraph. In these conditions the rate equation is (16, 17)

$$[5] \qquad v = k[\text{Amine}][HNO_2]$$

Figure 5 shows that the slope of the graph of log k against $-H_0$ varies with acidity, H_0 being the Hammett acidity function, whose values for concentrations of $HClO_4$ corrected for an ionic strength of 1.5 M were taken from ref. 17. The experimental constant k itself, however, is a linear function of h_0. These results are in keeping with there being interaction between the nitrosating agent (NO^+ or $H_2NO_2^+$) and the free and protonated forms of the amine, as in the diazotization of *o*-chloroaniline (17) and 2- and 4-aminopyridine-1-oxides (16*a*), for then

$$[6] \qquad v = k_5[\text{1-NA}][HNO_2]h_0 + k_6[\text{1-NAH}^+][HNO_2]h_0$$

which, since $[\text{1-NA}]h_0 = [\text{1-NAH}^+]K_a$, implies the linear relationship

$$[7] \qquad k = k_5K_a + k_6h_0$$

between k and h_0. If this hypothesis is accepted, comparison of eq. [7] with Fig. 5 implies values of 2.17 ± 0.09 and 2.44 ± 0.04 for k_5K_a and k_6, respectively, and the former of these in turn implies a value of 1.97×10^4 for $k_5 = k_{attack}K_{NO^+}$, (k_{attack} being the rate constant for the elementary process of reaction between NO^+ and the free amine), which is extremely high compared with the values of 2000–6000 found for the nitrosation of other amines by NO^+, and accepted as indicating a diffusion-controlled process (18). One reason for the high value of k_5 may lie in the exponential influence of ionic strength on the reaction (see above). If this effect is allowed for by using the data of Fig. 4 to obtain an equivalent value for zero ionic

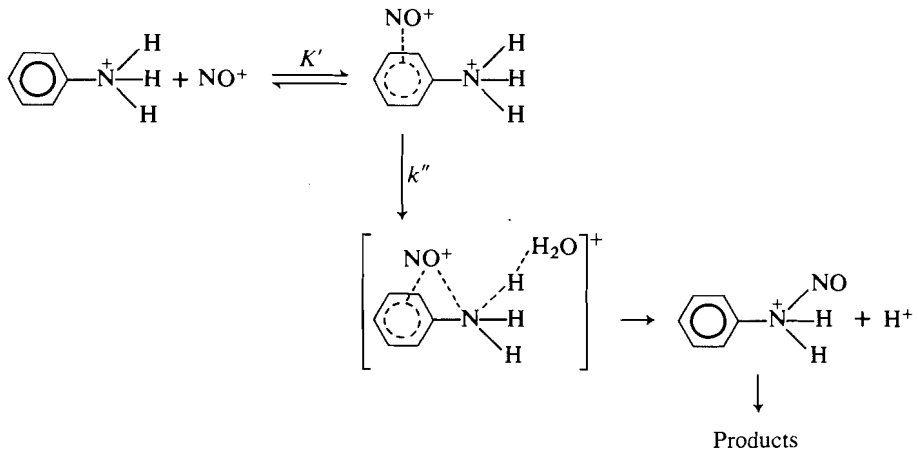

SCHEME 2

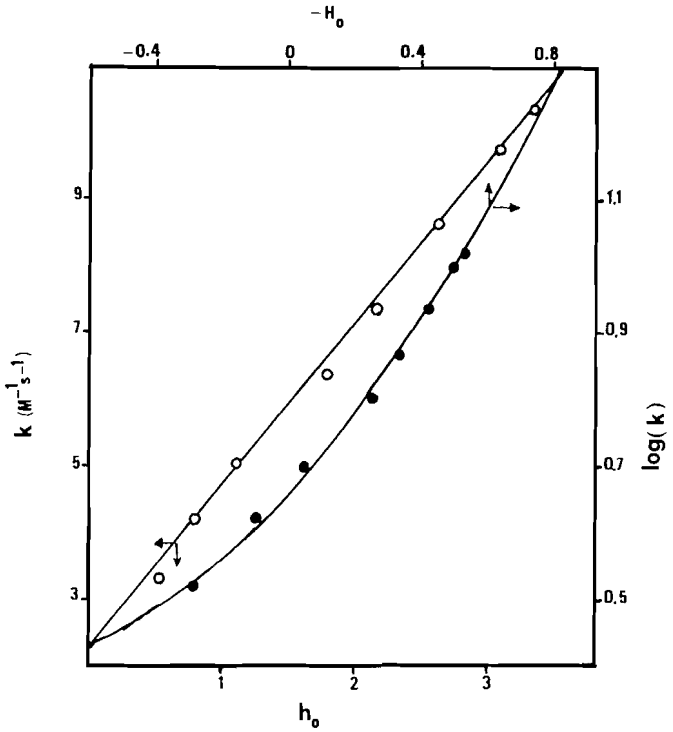

FIG. 5. Dependence of k (eq. [7]) on H_0 (●) and h_0 (○) at 25°C, $I = 1.5$ M, $[NaNO_2] = 2.75 \times 10^{-5}$ M, [1-NA] = 1.32×10^{-3} M.

strength according to the equation

$$[8] \qquad \log k_5 = \log k_5^0 + 0.485\, I$$

the result is a value of 3690 for k_5 that is fully compatible with published values for other substrates.

For the k_6 interaction between the nitrosating agent and the protonated form of the amine, a mechanism analogous to that shown in Scheme 2 for aniline is proposed, involving the association of the NO^+ ion and the aromatic ring in a complex that, upon losing a proton, rearranges to yield the nitroso compound. Naphthylamine's possession of two condensed rings increases the number of possible positions for NO^+ in the initial complex and hence the importance of nitrosation *via* the protonated form and, indeed, the value of k_6 for 1-NA is greater by a factor of 10 than for anilines and pyridines (16*c*), making this pathway significant at intermediate acidities.

Since the above scheme involves proton transfer to the solvent in the rate-controlling step of the reaction, a primary isotopic effect ought to be detectable. Measurements of k_6 in D_2O yielded the value of 1.59 for $(k_6)_{H_2O}/(k_6)_{D_2O}$ and, since $k_6 = k''K'K_{NO^+}$, the value of $(K_{NO^+})_{H_2O}/(K_{NO^+})_{D_2O}$ obtained earlier implies an isotopic effect of 3.50 for $K'k''$, which is indeed a primary isotopic effect and thus supports the validity of Scheme 2.

Acknowledgements

The authors wish to thank the Spanish Comisión Asesora de Investigación Científica y Técnica for subsidizing the research reported in this article as part of an investigation into the mechanisms of formation of nitroso compounds. E.I. likewise wishes to thank the Spanish Ministry of Education and Science for the grant (Formación de Personal Investigador) allowing her to take part in this research.

1. J. H. RIDD. Q. Rev. **15**, 418 (1961).
2. A. WOPPMANN. Monatsh. Chem. **111**, 1125 (1980).
3. M. R. CRAMPTON, J. T. THOMPSON, and D. L. H. WILLIAMS. J. Chem. Soc. Perkin Trans. **2**, 18 (1979).
4. P. R. ADBY and M. A. H. DEMPSTER. Introduction to optimization methods. Chapman and Hall, London. 1974.
5. J. CASADO, M. MOSQUERA, A. RIVAS, M. F. RODRIGUEZ, and J. A. SANTABALLA. Comput. Chem. **7**, 209 (1983).
6. N. F. HALL and M. R. SPRINKLE. J. Am. Chem. Soc. **54**, 3472 (1932).
7. H. SCHMID and A. MASCHKA. Z. Phys. Chem. **49**, 171 (1941).
8. H. SCHMID. Chem. Ztg. **78**, 571 (1954).
9. G. STEDMAN and P. A. E. WHINCUP. J. Chem. Soc. 5796 (1963).
10. P. COLLINGS, K. AL-MALLAH, and G. STEDMAN. J. Chem. Soc. Perkin Trans. **2**, 1734 (1975).
11. H. SCHMID and M. G. FOUAD. Monatsh. Chem. **88**, 631 (1957).
12. R. C. PEARSON, H. SOBEL, and J. SONGSTAD. J. Am. Chem. Soc. **90**, 319 (1968).
13. B. C. CHALLIS, L. F. LARKWORTHY, and J. H. RIDD. J. Chem. Soc. 5203 (1962).
14. V. H. VELEY. J. Chem. Soc. **93**, 2132 (1908).
15. (*a*) J. J. CHRISTENSEN, R. M. IZATT, D. P. WRATHALL, and L. D. HANSEN. J. Chem. Soc. (A), 1212 (1969); (*b*) N. F. HALL and M. R. SPRINKLE. J. Chem. Soc. **54**, 3469 (1932); (*c*) A. C. BACARELLA, E. GRUNWALD, H. P. MARSHALL, and E. L. PURLEE. J. Org. Chem. **20**, 747 (1955).
16. (*a*) E. KALATZIS and C. MASTROKALOS. J. Chem. Soc. Perkin Trans. 2, 499 (1974); (*b*) 1830 (1977); (*c*) E. KALATZIS and P. PAPADOPOULOS. J. Chem. Soc. Perkin Trans. 2, 239 (1981); (*d*) E. KALATZIS and C. MASTROKALOS. J. Chem. Soc. Perkin Trans. 2, 53 (1983).
17. B. C. CHALLIS and J. H. RIDD. J. Chem. Soc. 5208 (1962).
18. J. H. RIDD. Adv. Phys. Org. Chem. **16**, 1 (1978).

Replacement of the carboxylic acid function with fluorine[1]

TIMOTHY B. PATRICK,[2] KAMALESH K. JOHRI, DAVID H. WHITE,[3] WILLIAM S. BERTRAND, RODZIAH MOKHTAR, MICHAEL R. KILBOURN,[4] AND MICHAEL J. WELCH[4]

Department of Chemistry, Southern Illinois University at Edwardsville, Edwardsville, IL 62026, U.S.A.

Received May 14, 1985

TIMOTHY B. PATRICK, KAMALESH K. JOHRI, DAVID H. WHITE, WILLIAM S. BERTRAND, RODZIAH MOKHTAR, MICHAEL R. KILBOURN, and MICHAEL J. WELCH. Can. J. Chem. **64**, 138 (1986).

Replacement of a carboxyl function by fluorine, fluorodecarboxylation, is a new process that can be accomplished by the reaction of alkanoic acids with xenon difluoride. Primary, tertiary, and benzylic acids perform best in the reaction, which is conducted at room temperature in methylene chloride or chloroform solution. A reaction mechanism is proposed in which the acid is initially converted to a fluoroxenon ester, RCO_2XeF. The esters of the primary and secondary acids react by nucleophilic displacement by fluoride, as evidenced by incorporation of $^{18}F^-$ and no reactions common to free radicals or carbocations. The esters of the tertiary and benzylic acids react by converting to free radicals that can be further oxidized to carbocations. Thus incorporation of $^{18}F^-$ and racemization are observed with α-methoxy-α-trifluoromethylphenylacetic acid. Hydroxyl and amino functions inhibit the reaction. Aromatic and vinylic acids do not react.

TIMOTHY B. PATRICK, KAMALESH K. JOHRI, DAVID H. WHITE, WILLIAM S. BERTRAND, RODZIAH MOKHTAR, MICHAEL R. KILBOURN et MICHAEL J. WELCH. Can. J. Chem. **64**, 138 (1986).

Le remplacement d'une fonction carboxyle par un fluor, la fluorodécarboxylation, est une nouvelle réaction que l'on peut réaliser en faisant réagir les acides alcanoïques avec le diflorure de xénon. Les acides primaires, tertiaires et benzyliques sont les meilleurs acides pour cette réaction qui s'effectue à la température ambiante, dans du chlorure de méthylène ou du chloroforme. On propose un mécanisme réactionnel dans lequel l'acide conduit initialement à un ester fluoroxénonique RCO_2XeF. Les esters des acides primaires et secondaires réagissent par le biais d'un déplacement nucléophile par les ions fluorures tel que mis en évidence par l'incorporation du $^{18}F^-$, et non pas par les réactions mettant en jeu les radicaux libres ou les carbocations. Les esters des acides benzyliques et tertiaires réagissent en se transformant en radicaux libres qui peuvent être oxydés par la suite en carbocation. Ainsi, on observe l'incorporation de l'ion $^{18}F^-$ et la racémisation avec l'acide α-méthoxy α-trifluorométhylphényl acétique. Les fonctions hydroxy et amino inhibent la réaction. Les acides aromatiques et vinyliques ne réagissent pas.

[Traduit par le journal]

The decarboxylation of carboxylic acids with replacement of halogen, halodecarboxylation, has proven both synthetically useful and mechanistically intriguing. The Hunsdiecker (1) or Kochi (2) reactions, which employ the use of silver, mercury, or lead salts, are the normal procedures for accomplishing halodecarboxylation. However, in current halodecarboxylation methodology the replacement halogen is restricted to chlorine, bromine, or iodine, and methodology for replacement by fluorine is unknown (3). In this paper we report our details on the reaction of xenon difluoride with alkanoic acids, the first general method for fluorodecarboxylation (4). In addition, the mechanistic aspects of the reaction are presented.

Results and discussion

Aliphatic carboxylic acids react with one equivalent of xenon difluoride (5) in methylene chloride or chloroform solution, according to eq. [1]. The reaction may be performed at room temperature and usually requires 8–16 h for completion. The yields of pure product reported in Table 1 are obtained simply by washing the reaction mixture with sodium carbonate solution followed by removal of the solvent.

[1] $RCOOH + XeF_2 \rightarrow R{-}F + Xe + HF + CO_2$

Alkanoic acids (entries 4, 5, 7, 9), arylalkanoic acids (entries 1–3, 6), and aryloxyacetic acids (entries 10,11) are examples of primary carboxylic acids that readily undergo fluorodecarboxylation. Although aromatic fluorination is known to occur with xenon difluoride (5), aromatic fluorination does not compete with the reaction at the carboxyl group by the xenon difluoride. Two dicarboxylic acids (entries 18, 19) are converted smoothly into the difluoro products with two equivalents of xenon difluoride. Also, the ketone function of levulinic acid (entry 8) is unaffected in the reaction and the carboxyl group is smoothly fluorodecarboxylated. Several secondary carboxylic acids tested for fluorodecarboxylation (entries 12, 13) give only small amounts of fluoro products, while norbornane-2-carboxylic and *trans*-2-phenylcyclopropanoic acids give no reaction.

Tertiary carboxylic acids, similar to the primary aids, are smoothly fluorodecarboxylated as seen in entries 15 and 16. However, the bicyclic acid, 3-phenylbicyclo[1.1.1]pentan-1-oic acid (entry 17)[5] displays decarboxylation with formation of its dimer; no fluoro product is obtained.

Carboxylic acids containing other protic functions, such as amino acids and cholic acid, give only unreacted starting material, as does cinnamic acid. Benzoic acid (entry 20) gives small amounts of benzoyl fluoride (6).

Our studies on fluorodecarboxylation show that both primary and tertiary acids react very well, but secondary acids react less readily. Mechanistic studies have allowed us to explain this behavior. Our mechanism, summarized in Scheme 1, begins with the formation of a xenon ester. We have not detected the ester, but its formation is based on experiments by DesMarteau and co-workers (7), who have shown that a xenon ester can be isolated from the reaction of trifluoroacetic acid with xenon difluoride at −24°C ($CF_3COOH + XeF_2 \rightarrow CF_3COOXeF +$

[1]Presented at the 7th Winter Fluorine Conference, Orlando, Florida. 1985.

[2]Author to whom correspondence may be addressed.

[3]Mallinckrodt, Inc., St. Louis, MO 63134, U.S.A.

[4]Division of Radiation Sciences, Washington University School of Medicine, St. Louis, MO 63110, U.S.A.

[5]We thank Professor W. Adcock, the Flinders University of South Australia, for a sample of this acid.

TABLE 1. Yields and properties of fluorinated compounds

Entry	Acid	Product[a]	Yield[b]	^{19}F nmr[c]	^{1}H nmr[c]	Mass spectrum (m/e)
1	$PhCH_2COOH$	$PhCH_2F$	76	−207.0 (t, $^2J_{HF}$ = 48.4)	4.25 (d, CH_2), 7.15 (Ph)	110
2	$Ph(CH_2)_2COOH$	$Ph(CH_2)_2F$	76	−215.3 (2t, $^2J_{HF}$ = 47.0, $^3J_{HF}$ = 22.3)	2.8 (d, t), 4.4 (d, t), 7.13 (Ph)	124
3	$Ph(CH_2)_3COOH$	$Ph(CH_2)_3F$	60	−220.2 (2t, $^2J_{HF}$ = 47.0, $^3J_{HF}$ = 25.0)	1–3 (CH_2, m), 7.13 (Ph)	138
4	$CH_3(CH_2)_8COOH$	$CH_3(CH_2)_8F$	54	−218.2 (septet, $^2J_{HF}$ = 46.4) $^3J_{HF}$ = 23.1)	1.6 (m), 5.5 (d, t, J = 50)	146
5	$CH_3(CH_2)_{14}COOH$	$CH_3(CH_2)_{14}COOH$	62	−218.3 (septet, $^2J_{HF}$ = 47.0, $^3J_{HF}$ = 24.0)	1.2–2 (m, CH_2), 5.5 (m, CH_2)	236
6	Ph_2CHCH_2COOH	Ph_2CHCH_2F	63	−214.9 (d, t, $^2J_{HF}$ = 47.1, $^3J_{HF}$ = 17.3)	4.9 (d, d, CH_2, J_{FF} = 47, J_{HE} = 7), 6.9 (m, Ch), 7.0–7.5 (m, Ph)	200
7	Cholanic acid	23-Fluoro-23-norcholane*	71	−218.13 (m)	0.7–2.2 (m, ring), 5.4 (m)	310
8	$CH_3C(O)CH_2CH_2COOH$	$CH_3C(O)CH_2CH_2F$*	82	−221.3 (m, $^2J_{HF}$ = 46,4, $^3J_{HF}$ = 22.0)	2.1 (s, CH_3), 2.7 (t, d, CH_2, J_{HF} = 12.1, J_{HH} = 4.7), 4.67 (t, d, CH_2F, J_{FF} = 46.9, J_{HH} = 5.4)	90
9	2-Norbornane acetic acid	2-Fluoromethyl norbornane*	74	−213.97 (t, d, $^2J_{HF}$ = 46.4, $^3J_{HF}$ = 14.6)	1.1–2.3 (CH_2, ring) 4.2 d, d, J_{HF} = 48, J_{HH} = 6)	128
10	$PhOCH_2COOH$	$PhOCH_2F$	64	−148.7 (t, $^2J_{HF}$ = 53.7)	5.1 (d, CH_2), 7.15 (Ph)	126
11	$2,4\text{-}Cl_2PhOCH_2COOH$	$2,4\text{-}Cl_2PhOCH_2F$*	84	−149.8 (t, $^2J_{HF}$ = 53.7)	5.7 (d, CH_2), 7.15 (Ph)	195
12	$(CH_3)_2CHCOOH$	$(CH_3)_2CHF$*	10	−149.5 (m)	1.4 (d, d J_{HF} = 30,6, J_{HH} = 9), 4.83 (d, sept J_{HF} = 72.9, J_{HH} = 9)	[e]
13	$(CH_2)_5CHCOOH$	$(CH_2)_5CHF$	3	−172.9 (m, $^2J_{HF}$ = 46.4)	1.35–1.7 (m, CH_2), 4.5 (d, m, CH, J_{HF} = 46)	[e]
14	1-adamantanoic acid	1-F-adamantane	82	−128.7 (s)	1.1–2.1 (m, CH, CH_2)	[e]
15	Ph_3CCOOH	Ph_3CF	65	−126.1 (s)	7.21 (Ph)	212
16	$PhC(OCH_3)(CF_3)(COOH)$	$PhC(F)(OCH_3)(CF_3)$*	95	−83.8 (d, J_{FF} = 3.52), −134.3 (q, F, J_{FF} = 3.52)	3.83 (s, CH_3), 7.51 (s, Ph)	208
17	3-Phenylbicyclo[1.1.1]pentanoic	Bis(3-phenylbicyclo[1.1.1]-1-pentanyl)*	35	[d]	1.25 (CH_2) 7.2–7.4 (Ph)	262
18	$PhCH(CH_2COOH)_2$	$PhCH(CH_2F)_2$	60	−225.4 (d, t, $^2J_{HF}$ = 49.4) $^3J_{HF}$ = 20.8)	2.4–3 (m, CH_2) 6.9–7.4 (m, Ph)	156
19	$PhCH_2CH(COOH)_2$	$PhCH_2CHF_2$	68	−115.1 (t, d, $^2J_{HF}$ = 56.2, $^3J_{HF}$ = 17.1)	3.2 (CH_2, m) 5.5 (m), 7.2 (Ph)	142
20	PhCOOH	PhCOF	20	[e]	[e]	
21	$BrCH_2CH_2CH_2COOH$	$BrCH_2CH_2CH_2F$*	91	−228.8 (m)	2.4 (m, $BrCH_2CH_2$), 4.0 (d of t, J_{HF} = 45, J_{HH} = 6, CH_2—F	140

[a]New compounds are marked with an asterisk and gave satisfactory elemental analyses. These analyses have been deposited and may be purchased from the Depository of Unpublished Data, CISTI, National Research Council of Canada, Ottawa, Ont., Canada K1A 0S2. Other compounds are reported in refs. 4 or 16.

[b]Isolated yields (%) based on the quantity of starting acid.

[c]Multiplicities are as follows: s = (singlet), d = (doublet), t = (triplet), m = (multiplet).

[d]^{13}C nmr ($CDCl_3$) δ: 29.7 (C-1), 41.8 (C-3), 53.3 (CH_2), 125.9, 126.9, 128,2, 133.4 (aromatic), no elemental analysis.

[e]Not obtained.

$$RCOOH + XeF_2 \longrightarrow RCOOXeF + HF$$
$$\text{A}$$
$$RCOOXeF + F^- \longrightarrow RF + CO_2 + Xe + F^- \quad (a)$$
$$RCOOXeF \longrightarrow R\cdot + CO_2 + XeF \quad (b)$$
$$\downarrow \cdot XeF$$
$$R^+ Xe + F^-$$
$$R\cdot + \cdot XeF \longrightarrow RF + Xe$$
$$R^+ + F^- \longrightarrow RF$$

SCHEME 1

$(CF_3COO)_2$ Xe + HF). DesMarteau further showed that the xenon esters decarboxylated on warming to 23°C. Xenon esters have also been suggested as reaction intermediates in the works of Gregorcic and Zupan (8), Nikolenko and co-workers (6), and Musher (9). Thus our postulation of the formation of fluoroxenon ester A is strongly backed by literature precedent and supported by our observation of a required 1:1 acid–XeF_2 reaction stoichiometry.

For the case of primary and secondary carboxylic acids, the fluoro product is derived from nucleophilic displacement of CO_2 and Xe by F^-, mechanism (a). Evidence for this process comes from radiolabeling experiments performed with $(n\text{-}Bu)_4{}^+N\ {}^{18}F^-$. Thus when 3-phenylpropanoic acid is allowed to react with xenon difluoride in the presence of $^{18}F^-$ for 30 min at room temperature, a 40% radiochemical yield of 1-[^{18}F]-fluoro-2-phenylethane is obtained. Similarly, reaction of 4-bromobutanoic acid with $^{18}F^-/XeF_2$ leads to a 78% radiochemical yield of 1-[^{18}F]-fluoro-3-bromopropane. The ^{18}F could be incorporated into the products either as fluoride-18 ion or as a ^{18}F-exchanged xenon difluoride species such as $^{18}FXe^{19}F$. A complete exchange of $^{18}F^-$ with XeF_2 to produce $^{18}FXe^{19}F$ would permit statistically a maximum radiochemical yield of 50%, as only one of the two fluorine atoms of the $^{18}FXe^{19}F$ is radioactive. The 78% radiochemical yield of 1-[^{18}F]-fluoro-3-bromopropane could not be attained through involvement of an exchanged species. Furthermore, we have conducted an experiment in which $^{18}F^-$ and XeF_2 were allowed to react in methylene chloride solution under our radiochemical reaction conditions but in the absence of substrate acid. After evaporation of the methylene chloride with helium, the xenon difluoride was recovered quantitatively by vacuum sublimation at room temperature. The xenon difluoride recovered contained no radioactivity, and thus further shows that exchange of $^{18}F^-$ with XeF_2 did not occur. Literature precedent also exists to show that $^{18}F^-/XeF_2$ exchange would not occur under our reaction conditions (10). Thus in the major portion of the reaction the $^{18}F^-$ is incorporated into the product by the nucleophilic process shown in mechanism (a) in Scheme 1. Nucleophilic displacement also explains the higher reactivity of primary acids over secondary acids. Minor reaction processes may also be in operation, such as S_Ni substitution in ester A which has undergone exchange with radioactive fluoride.

$$PhCH_2CH_2COOH + XeF_2 + {}^{18}F^- \rightarrow PhCH_2CH_2{}^{18}F\ (40\%)$$

$$BrCH_2CH_2CH_2COOH + XeF_2 + {}^{18}F^- \rightarrow BrCH_2CH_2CH_2{-}{}^{18}F\ (78\%)$$

Several experiments showed that free radicals were not involved with primary acids. Thus 3-phenylpropanoic acid does not produce styrene by elimination nor does it react with benzene to produce bibenzyl. Also, 4-phenylbutanoic acid showed no internal cyclization similar to that observed when a primary radical is generated from lead tetraacetate reaction as described by Davies and Waring (11). In addition, rearrangement is not observed from reaction of 3,3-diphenylpropanoic acid (entry 6) with xenon difluoride. One would anticipate the formation of a 1,2-diphenylethane derivative if a primary radical were formed, because rearrangement is a well-known process in the 2-phenylethyl radical systems (12). In an interesting comparison with other halodecarboxylation methods, one observes that in the Hunsdiecker Cristol–Firth reactions of primary acids (1), a questionable free-radical process (13), rearrangement is rarely found. But in the Kochi lead tetraacetate – chloride chlorodecarboxylation, a known radical reaction (2), rearrangement and elimination both are common. Thus our experiments show that free radicals are not observed with primary acids, but that $^{18}F^-$ is incorporated in a nucleophilic process (mechanism (a)).

Evidence for mechanism (b) is obtained for systems which produce relatively stable free radicals and carbocations, the tertiary and benzylic systems. Thus when phenylacetic acid and xenon difluoride react in benzene solution, a mixture of diphenylmethane and benzyl fluoride is obtained. Control experiments show that the diphenylmethane did not arise from reaction of benzyl fluoride with benzene. The formation of diphenylmethane shows that a reactive intermediate is generated, and the absence of bibenzyl from radical coupling indicates that the intermediate is a carbocation.

$$PhCH_2COOH + XeF_2 + C_6H_6 \rightarrow PhCH_2Ph + PhCH_2F$$

The reaction of optically active α-trifluoromethyl-α-methoxyphenylacetic acid (**1**) gives α-fluoro-α-trifluoromethyl-α-methoxytoluene (**2**) in 95% yield with complete loss of optical activity, showing that a trivalent intermedite is involved in the mechanism. Furthermore, when the reaction is conducted in the presence of $(n\text{-}Bu)_4{}^+N\ {}^{18}F^-$ for 30 min at room temperature, the $^{18}F^-$ is incorporated into **2** in 65% radiochemical yield. The $^{18}F^-/XeF_2$ exchange experiments cited above and the 65% radiochemical yield show that a ^{18}F-exchanged species is not involved. Thus $^{18}F^-$ is incorporated as free fluoride ion in a reaction with a cationic intermediate. These results support mechanism (b) shown in Scheme 1 for tertiary and benzylic acids.

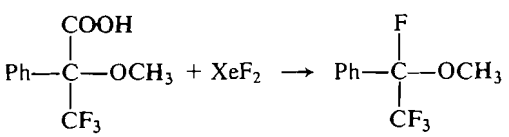

1 (optically active) **2** (racemic)

Finally, when 3-phenylbicyclo[1.1.1.]pentanoic-1-acid, a substrate which can produce a free radical but not a planar carbocation (13, 14), reacts with xenon difluoride, only radical dimerization is observed (entry 17). Thus each component of mechanism (b) has been observed experimentally.

In conclusion, we have shown that fluorodecarboxylation with xenon difluoride is an effective process for the conversion of carboxylic acids to alkyl fluorides. The mechanism of the

reaction involves nucleophilic displacement by fluoride for the primary and secondary acids, while free radicals and carbocations are involved for tertiary and benzylic systems. The reaction also holds promise as an important new method for the preparation of fluorine-18 labeled radiopharmaceuticals.

Experimental

Nuclear magnetic resonance spectra were obtained in deuteriochloroform solution on a JEOL FX-90 Q at 89.75 MHz for proton spectra with internal tetramethylsilane (δ 0.0) as a standard and at 84.26 MHz for fluorine spectra with external Freon-11 (fluorotrichloromethane, δ 0.0) as a standard. Mass spectra were obtained at 70 eV on a Varian MAT-111 direct inlet system or at the University of Illinois Mass Spectrometry Center. Xenon difluoride was purchased from PCR, Inc., Gainesville, Florida and used as obtained. Solvents CH_2Cl_2, $CHCl_3$, $CDCl_3$, and benzene were dried before use.

General procedure. 1-Fluoro-2-phenylethane (entry 2)

To a solution of 3-phenylpropanoic acid (150 mg, 1 mmol) in 15 mL of methylene chloride contained in a polyethylene bottle was added crystalline xenon difluoride (170 mg, 1 mmol).

The solution was stirred magnetically at 22°C for 10 h during which the colorless solution becomes slightly yellow. The resulting mixture was washed with 3% sodium bicarbonate (50 mL) solution. The organic solution was dried ($MgSO_4$) and concentated to yield analytically pure 1-fluoro-2-phenylethane (76% yield).

1-[^{18}F]-fluoro-2-phenylethane

A solution containing 2 mg 3-phenylpropanoic acid, 2 mmol of tetra-*n*-butylammonium fluoride, 2 mCi of $^{18}F^-$, and 0.3 mL of methylene chloride was treated with 2 mg of xenon difluoride. After standing for 30 min the solution was analyzed on a Waters high pressure liquid chromatograph equipped with a Magnum Parisil M9 10/50 silica gel column. Elution with CH_2Cl_2–CH_3CN (3:1) at a flow rate of 2.4 mL/min showed simultaneous ultraviolet detection (254 nm) and radioactive detection (NaI(Tl) detector) for the product at 16 min. Thin-layer chromatography on silica gel with 3:1 CH_2Cl_2–CH_3CN showed that 40% of the total radioactivity of the crude product was present as 1-[^{18}F]-fluoro-2-phenylethane. 1-[^{18}F]-fluoro-3-propane was prepared from 4-bromobutanoic acid in 78% radiochemical yield, and α-[^{18}F]-fluoro-α-trifluoromethyl-α-methoxytoluene **2** was prepared in 65% radiochemical yield from **1**. These reactions were conducted under identical conditions to those described for the preparation of 1-[^{18}F]-fluoro-2-phenylethane.

Preparation of tetrabutylammonium [^{18}F]fluoride: general procedure

Fluorine-18[6] was prepared from [^{18}O]H_2O by the $^{18}O(p, n)^{18}F$ reaction in a 2-mL metal cyclotron target (15). Approximately 3–5 mCi of the activity produced was mixed with 5 mmol of tetra-*n*-butylammonium fluoride (Aldrich) in a platinum crucible and taken to dryness at 100°C under a stream of nitrogen. The residue was further dried azeotropically by the addition and evaporation of two 0.1-mL portions of acetonitrile. The mixture was redissolved in 0.4 mL of methylene chloride to give approximately 1.5–3 mCi of radioactivity, which was added to the substrate contained in a small glass vial.

Bis(3-phenylbicyclo[1.1.1]-1-pentanyl)

3-Phenylbicyclo[1.1.1]pentan-1-oic acid (96 mg, 0.5 mmol) in 8 mL of $CDCl_3$ was treated with 90 mg (0.55 mmol) of xenon difluoride. After 8 h, gas evolution ceased and the yellow solution was analyzed by nmr. The analysis showed the complete absence of starting material and the complete absence of fluorinated products. Preparative hplc (Whatman Magnum Silica Gel, 50 mm × 10 mm, hexane–CH_2Cl_2, 9:1) gave pure product, 39 mg (35%).

α-Trifluoromethyl-α-methoxy-α-fluorotoluene

A solution containing 230 mg (1 mmol) of (+)-α-methoxy-+-trifluoromethyl-phenylacetic acid (α_D^{23} +69°, c = 1.6, CH_3OH) and 170 mg (1 mmol) of xenon difluoride in 15 mL of $CDCl_3$ was allowed to react until gas evolution ceased (4 h). Both nmr and hplc analyses showed the presence of only a single product, and the solution showed no optical activity at the sodium D line. Isolation by preparative hplc (Whatman Magnum Silica Gel, 50 mm + 10 mm, hexane–CH_2Cl_2, 3:1) gave 197 mg (95%) of pure product. The product showed no optical activity in either methanol or chloroform solvents.

[6]Fluorine-18 has a half-life of 110 min and its radioactivity may be counted conveniently in a gamma counter at 511 keV.

Acknowledgements

This research was supported by the donors of the Petroleum Research Fund, administered by the American Chemical Society, and by the National Institutes of Health (Washington University), grant HL13851.

1. C. V. WILSON. Org. React. **9**, 332 (1957).
2. J. K. KOCHI. J. Am. Chem. Soc. **87**, 2500 (1965); R. A. SHELDON and J. K. KOCHI. Org. React. **19**, 179 (1972).
3. V. GRAUKASKAS. J. Org. Chem. **34**, 2446 (1969).
4. T. B. PATRICK, K. K. JOHRI, and D. H. WHITE. J. Org. Chem. **48**, 4159 (1983).
5. R. FILLER. Isr. J. Chem. **17**, 71 (1978).
6. M. ZUPAN. Chimia, **30**, 305 (1976); L. D. SHUSTOV, T. D. TEL'KOVKAYA, and L. N. NIKOLENKO. Zh. Org. Khim. **11**, 2137 (1975); Chem. Abstr. **84**, 30028s (1976).
7. M. EISENBERG and D. DESMARTEAU. Inorg. Nucl. Chem. Lett. **6**, 29 (1970); D. DESMARTEAU, R. D. LEBLOND, S. F. HASSAIN, and D. NOTHE. J. Am. Chem. Soc. **103**, 7734 (1981).
8. A. GREGORCIC and M. ZUPAN. J. Org. Chem. **44**, 4120 (1979).
9. J. I. MUSHER. J. Am. Chem. Soc. **90**, 7371 (1968).
10. G. SCHROBILGEN, G. FIRNAU, and R. CHIRAKEL. J. Chem. Soc. Chem. Commun. 198 (1981).
11. D. E. DAVIES and C. WARING. J. Chem. Soc. C, 1865 (1968).
12. J. W. WILT. *In* Free radicals. Vol. 1. *Edited by* J. K. Kochi. John Wiley and Sons, New York, NY. 1973. p. 333.
13. L. KAPLAN. *In* Free radicals. Vol. 2. *Edited by* J. K. Kochi. John Wiley and Sons, New York, NY. 1973. p. 372.
14. D. C. NORABEL and J. C. WALTON. Free radical chemistry. Structure and mechanism. Cambridge Univ. Press, Great Britain. 1974. pp. 84–106; J. P. LORAND, S. D. CHODROFF, and R. W. WALLACE. J. Am. Chem. Soc. **90**, 5266 (1960).
15. M. R. KILBOURN, P. A. JERABEK, and M. J. WELCH. Int. J. Appl. Radiat. Isot. **36**, 327 (1985).
16. F. L. WEIGERT. J. Org. Chem. **45**, 3476 (1980).

Synthesis, crystal and molecular structure, and vibrational spectra of the complex $(COOH)_2 \cdot 2H_2O \cdot 18$-crown-6

SUZANNE DEGUIRE AND FRANÇOIS BRISSE[1]
Département de chimie, Université de Montréal, C.P. 6210, Succ. A, Montréal (Qué.), Canada H3C 3V1

AND

JACQUES OUELLET AND RODRIGUE SAVOIE[1]
Département de chimie, Université Laval, Cité universitaire, Québec (Qué.), Canada G1K 7P4

Received July 8, 1985

SUZANNE DEGUIRE, FRANÇOIS BRISSE, JACQUES OUELLET, and RODRIGUE SAVOIE. Can. J. Chem. **64**, 142 (1986).

A stoichiometric complex of formula $(COOH)_2 \cdot 2H_2O \cdot 18$-crown-6 has been obtained from oxalic acid and the macrocyclic polyether 18-crown-6. The crystals of the complex have a monoclinic unit cell and belong to the $P2_1/c$ space group. The components in the adduct are linked through hydrogen bonds in a polymer-like fashion: –crown–H_2O–HOOCCOOH–OH_2–crown–, where the oxalic acid molecules are present in two distinct disordered orientations. The infrared and Raman spectra of the complex are also reported and interpreted.

SUZANNE DEGUIRE, FRANÇOIS BRISSE, JACQUES OUELLET et RODRIGUE SAVOIE. Can. J. Chem. **64**, 142 (1986).

Un complexe de formule $(COOH)_2 \cdot 2H_2O \cdot 18$-couronne-6 a été obtenu à partir de l'acide oxalique et l'éther macrocyclique 18-couronne-6. Les cristaux du complexe ont une maille monoclinique et appartiennent au groupe d'espace $P2_1/c$. Le cristal est constitué d'un enchaînement –couronne–H_2O–HOOCCOH–OH_2–couronne–, où les différentes unités structurales sont reliées par ponts hydrogène. Les molécules d'acide oxalique sont alignées, de façon désordonnée, dans deux orientations différentes. Les spectres infrarouge et Raman du complexe sont rapportés et interprétés.

Introduction

Many neutral molecules with hydrogen bonding capacity form complexes with macrocyclic polyethers, such as 18-crown-6 (henceforth called 18C6), in which a water molecule serves as a linker between the proton donor and the crown (1). Carboxylic acids generally follow this trend, forming complexes with 18C6 of 2:2:1 or 1:1:1 (acid/water/18C6) stoichiometry, in which the acid is more or less firmly bound to water, depending on its acid strength, and the water molecules are themselves weakly hydrogen bonded to oxygen atoms of the crown (2). A particularly good example of this is found in the $CH_2(CN)COOH \cdot H_2O \cdot 18C6$ adduct, whose crystal and molecular structures have been determined by X-ray diffraction (3). Also of interest is the corresponding compound of 2:2:1 stoichiometry obtained from dichloropicric acid, in which proton transfer seems to occur from the acid to water, giving a charged-component complex involving the hydronium ion (4).

From the mode of complexation of carboxylic acids with the 18C6 crown, it was expected that dicarboxylic acids would simultaneously interact with two crown molecules in adducts of this type. This hypothesis has been verified by the synthesis of the $(COOH)_2 \cdot 2H_2O \cdot 18C6$ complex, whose crystal structure and vibrational spectra are reported in this paper.

Experimental

The complex (mp 90–94°C) was prepared by adding anhydrous oxalic acid (0.68 g) to a solution of 18C6 (2 g) in tetrahydrofuran (10 mL). Crystallization occurred at room temperature after addition of a small amount (0.3 mL) of water. The deuterated complex (~90% d_4) was obtained in a similar way, using a proportionally larger amount of D_2O. The stoichiometry of the complex was determined by elemental analysis, titration by NaOH, and from the integrated intensities of the peaks in the ^1H nmr spectrum ((CD_3COCD_3) δ:5.5 ($H_2C_2O_4$ and H_2O) and 3.6 (18C6)).

The infrared spectra, obtained from Nujol and hexachlorobutadiene mulls, were recorded on a Beckman IR4250 spectrophotometer and on a Bomem DA3.02 interferometer. The Raman spectra of solid samples sealed in capillary tubes were excited by the 514.5-nm line from a Spectra Physics Model 165 argon ion laser, and recorded on a microcomputer-controlled Spex Model 1400 spectrometer. The spectra were typically obtained at 400 mW laser power at the sample, 2 cm^{-1} spectral slit width, with an integration time of 2 s for each frequency increment of 1 cm^{-1}. The low-temperature measurements in both the infrared and the Raman spectra were made using conventional liquid nitrogen cryostats.

For this X-ray study, a well-developed single crystal of the complex, obtained by slow evaporation of a THF solution, was mounted on a Nonius-CAD4 diffractometer. The unit-cell dimensions and the orientation matrix have been obtained by a least-squares refinement of the angular settings of 25 well-centered reflections in the range $10 < 2\theta < 38°$. The diffracted intensities of 1747 reflections were measured within the sphere of reflection limited by $2\theta \leq 50°$ and $0 \leq h \leq 11$, $0 \leq k \leq 9$, $-17 \leq l \leq 17$, using the graphite monochromatized molybdenum radiation. The $\omega/2\theta$ scan technique was used with a scan width calculated by $\omega = (1.00 + 0.35 \tan\theta)°$. The intensities of three reference reflections, measured every hour, did not vary by more than 2% over the duration of the data collection. The centering of the crystal was verified every 100 measurements, and readjustment was made when needed. The diffracted intensities were corrected for Lorentz and polarization effects, but since the absorption coefficient for the Mo radiation was small, no absorption correction was applied.[2]

The 1206 reflections (69%) that satisfied the criterion $I \geq 1.96\sigma(I)$ were retained for the structure determination and refinement. $\sigma(I)$ was derived from the counting statistics. The scattering curves for O and C were taken from ref. 9 and those for H atoms from ref. 10. The $P2_1/c$ space group was assigned unambiguously from the systematic absence $0k0$, $k \neq 2n$ and $h0l$, $l \neq 2n$. Since there are only two formulas per asymmetric unit, the center of the 18-crown-6 as well as that of the oxalic acid molecules must coincide with crystallographic centers of symmetry of the unit cell. The structure was solved using the multisolution program MULTAN. All the atoms constituting the 18C6

[1]Authors to whom correspondence may be addressed.

[2]The programs used here are locally modified versions of NRC-2, data reduction; NRC-10, bond distances and angles; NRC-22, mean planes; FORDAP, Fourier and Patterson syntheses (A. Zalkin); MULTAN, multisolution program; NUCLS, least-squares refinement; and ORTEP, stereo drawings (ref. 5–8).

TABLE 1. Crystal data for the $(COOH)_2 \cdot 2H_2O \cdot 18$-crown-6 complex

$(COOH)_2 2H_2O \cdot C_{12}H_{24}O_6$	FW = 390	$F(000) = 210$ e
Monoclinic	$P2_1/c$	$Z = 2$
$a = 9.322(4)$	$b = 7.779(3)$	$c = 14.666(3)$ Å
$\beta = 111.41(2)°$	$V = 990.1$ Å^3	$d_c = 1.309$ g cm^{-3}
$\mu = (MoK\alpha) = 1.08$ cm^{-1}	$\lambda(MoK\bar{\alpha}) = 0.71069$ Å	$T = 22°C$
Crystal size 0.30 × 0.36 × 0.40 mm		

part were found on the first E-map. The others, including all the H atoms, were located on subsequent difference Fourier syntheses. The weighted least-squares refinement, minimizing $\Sigma w(|F_o| - |F_c|)^2$, was carried out with anisotropic temperature factors for O and C and isotropic temperature factors for H atoms. As the refinement proceeded, it was discovered that the oxalic acid, situated at $(0\,0\,\frac{1}{2})$, was present in two distinct orientations. A 50:50 distribution between the two orientations led to very different values of the corresponding isotropic thermal parameters. They were held at their averaged values and only the occupation factor of each atom was refined. For three of the atoms the occupation factors reached a value of 0.6, while at the same time they tended towards 0.4 for the other three atoms. This unequal convergence coincided for the three pairs of atoms, namely C(11), C(21); O(11), O(21); and O(12), O(22). Since the C—C distances of the two molecules of oxalic acid were unequal, the positions of these C atoms (C(11) and C(21)), were adjusted so that the two C—C distances remain equal to 1.540 Å. The least-squares process was resumed, but only the coordinates and thermal parameters of the oxygen and hydrogen atoms of both oxalic acids were refined. After convergence, R and wR had not changed while S was slightly lowered.[3] Since both refinements did converge in the same way whether the C coordinates were refined or set so that d(C—C) = 1.540 Å, the final coordinates and structure factor tables given here reflect the chemically more meaningful situation. The refinement was concluded when $R = 0.033$, $wR = 0.039$, and $S = 1.454$. At that time, the mean and highest values of the displacement-to-sigma ratio were 0.05 and 0.4, respectively. A final difference Fourier synthesis revealed only small fluctuations of the electron density, with extreme values of −0.13 and 0.11 e Å^{-3}.

Results and discussion

The unit-cell dimensions and other crystal data of interest determined from the X-ray diffraction study are given in Table 1. The atomic numbering is given on the diagram in Fig. 1. The bond distances and angles, calculated from the final atomic coordinates (Table 2),[4] are given in Table 3. The various structural units (18C6, oxalic acid, water) that are part of the complex are shown by the stereopair of Fig. 2. The structural units are H-bonded to one another to form a columnar arrangement in which the following sequence, crown ether–water–oxalic acid–water, repeats itself.

The 18-crown-6 molecule

The center of this molecule coincides with a crystallographic center of symmetry at $(\frac{1}{2}\,\frac{1}{2}\,0)$. The conformation of the ring is described by the $t\,t\,g$ sequence repeated six times (t = *trans*, g = *gauche*). The actual values of the ring torsion angles are given in Table 4. The C—O bond distances (average value 1.484 Å) are normal. However, the CH_2—CH_2 bond distances are all significantly shorter (average 1.484 Å) than the accepted distance of 1.535(5) Å for a C(sp^3)—C(sp^3) bond. Such a shortening of a CH_2—CH_2 bond in a —O—CH_2—CH_2—O— moiety has also been reported in noncyclic situations (11, 12) and does not depend upon the value of the —O—CH_2—CH_2—O torsion angle. Concurrently with a short C—C bond, it was noted that the O—C—C angles tended to be smaller than

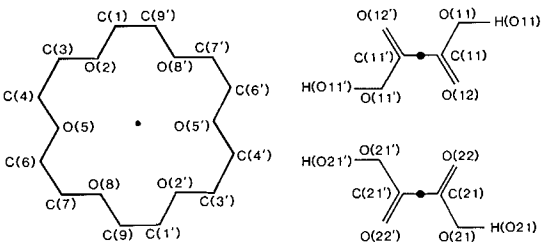

FIG. 1. Atomic numbering adopted for the $(COOH)_2 \cdot 2H_2O \cdot 18C6$ complex.

TABLE 2. Fractional atomic coordinates and their esd's (× 10^4 for O and C, × 10^3 for H atoms), U_{eq} (× 10^4 for O and C) and U_{iso} (× 10^3 for H atoms)

Atom	x	y	z	U_{eq}/U_{iso}
C(1)	3438(2)	1201(2)	766(2)	601
O(2)	4881(1)	2047(1)	1005(1)	526
C(3)	5654(2)	2283(2)	2031(1)	602
C(4)	7161(2)	3136(2)	2235(1)	590
O(5)	6935(1)	4885(1)	1944(1)	506
C(6)	8354(2)	5803(2)	2213(1)	575
C(7)	8057(2)	7566(2)	1795(1)	566
O(8)	7662(1)	7459(1)	771(1)	517
C(9)	7262(2)	9073(2)	298(1)	605
O(11)	1426(2)	6288(2)	−171(1)	437
O(12)	1486(2)	4691(3)	1131(1)	522
C(11)	843	5223	309	304
O(21)	1878(3)	5253(4)	751(2)	530
O(22)	519(4)	6585(4)	−653(2)	712
C(21)	649	5595	−18	408
O(W)	4345(1)	6694(2)	582(1)	576
H(11)	358(2)	7(2)	111(1)	61
H(12)	273(2)	189(2)	102(1)	72
H(31)	490(2)	303(2)	228(1)	73
H(32)	583(2)	121(2)	237(1)	73
H(41)	778(2)	311(2)	294(1)	64
H(42)	776(2)	259(2)	187(1)	71
H(61)	878(2)	584(2)	290(1)	65
H(62)	906(2)	516(2)	197(1)	59
H(71)	719(2)	816(2)	195(1)	65
H(72)	896(2)	826(2)	207(1)	72
H(91)	817(2)	974(2)	46(1)	74
H(92)	655(2)	973(2)	57(1)	72
H(O11)	269(4)	639(4)	30(2)	102
H(O21)	196(6)	581(7)	32(4)	110
H(W1)	459(2)	694(2)	7(1)	86
H(W2)	491(3)	599(3)	88(2)	119

[3] $R = \Sigma||F_o| - |F_c||/\Sigma|F_o|$; $wR = [\Sigma w(|F_o| - |F_c|)^2/\Sigma w|F_o|^2]^{1/2}$; $S = [\Sigma w(|F_o| - |F_c|)^2/(m - n)]^{1/2}$.

[4] The tables of anisotropic temperature factors, least-squares planes, and structure factors have been deposited and may be purchased from the Depository of Unpublished Data, CISTI, National Research Council of Canada, Ottawa, Ont., Canada K1A 0S2.

TABLE 3. Bond distances and angles for the $(COOH)_2 \cdot 2H_2O \cdot 18$-crown-6 complex

Bond	Distances (esd's), Å	Bonds	Angles (esd's), deg
18-Crown-6			
C(1)—O(2)	1.423(2)	C(9′)—C(1)—O(2)	109.2(2)
O(2)—C(3)	1.423(2)	C(1)—O(2)—C(3)	112.3(1)
C(3)—C(4)	1.482(3)	O(2)—C(3)—C(4)	110.4(2)
C(4)—O(5)	1.418(2)	C(3)—C(4)—O(5)	110.1(2)
O(5)—C(6)	1.426(2)	C(4)—O(5)—C(6)	112.1(1)
C(6)—C(7)	1.486(3)	O(5)—C(6)—C(7)	109.5(1)
C(7)—O(8)	1.412(2)	C(6)—C(7)—C(8)	108.7(1)
O(8)—C(9)	1.417(2)	C(7)—O(8)—C(9)	112.9(1)
C(9)—C(1′)	1.484(3)	O(8)—C(9)—C(1′)	109.1(2)
Oxalic acid			
C(11)—O(11)	1.325(3)	O(11)—C(11)—O(12)	126.5(2)
C(11)—O(12)	1.207(3)	O(11)—C(11)—C(11′)	110.9(2)
C(11)—C(11′)	1.540	O(12)—C(11)—C(11′)	122.6(2)
C(21)—O(21)	1.308(5)	O(21)—C(21)—O(22)	128.2(4)
C(21)—O(22)	1.180(5)	O(21)—C(21)—C(21′)	107.5(4)
C(21)—C(21′)	1.540	O(22)—C(21)—C(21′)	124.3(4)

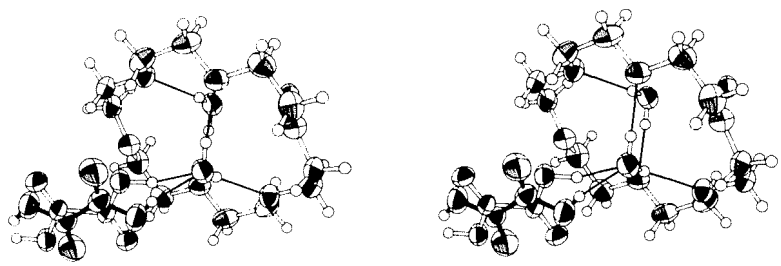

FIG. 2. Stereopair showing the various structural units and their linkage through hydrogen bonding. In order to differentiate between the two molecules of oxalic acid, the bonds of one of them have been blackened.

TABLE 4. Torsion angles (°) in the 18-crown-6 molecule

Bonds	Angle
C(9′)—C(1)—O(2)—C(3)	−117.3(2)
C(1)—O(2)—C(3)—C(4)	178.9(2)
O(2)—C(3)—C(4)—O(5)	71.7(2)
C(3)—C(4)—O(5)—C(6)	174.3(1)
C(4)—O(5)—C(6)—C(7)	173.9(1)
O(5)—C(6)—C(7)—O(8)	−71.3(2)
C(6)—C(7)—O(8)—C(9)	176.3(1)
C(7)—O(8)—C(9)—C(1′)	−168.5(1)
O(8)—C(9)—C(1′)—O(2′)	67.3(2)

109.5°. In the present case, where the —O—C—C—O sequence is included in a ring, the average of the six O—C—C angles is 109.5° while the average C—O—C angle is 112.4°.

The oxalic acid

As mentioned in the experimental section, the molecule of oxalic acid is present in the crystal form under two distinct orientations in a 40:60 ratio. However, when the C coordinates were refined, the C—C distances took the unusually different values of 1.569(4) and 1.504(6) Å. To remedy this anomaly, both C—C distances were kept at the fixed value of 1.540 Å. This choice took into account the C—C distance of oxalic acid in the gas phase, 1.548 Å (21), and 1.537 Å in both its α and β crystalline forms (22), as well as the value of 1.538 Å in the α-modification of the dihydrate (23).

The bond distances and angles (Table 3) of the two oxalic acid molecules agree very well. The two molecules are planar but for the H atoms, which deviate by 0.10(3) and 0.23(6) Å from their respective least-squares planes. These deviations favor the H bonds formed with the oxygen atom of the water molecule. The dihedral angle formed between the planes of the two molecules is close to 180°.

Hydrogen bonding

The water molecule, O(W), is the link between the crown ether and the oxalic acid. This disposition is identical to that observed with cyanoacetic acid (3). Since, however, oxalic acid is a diacid, instead of forming a complex of limited dimensions as in ref. 3, the structural units are arranged here in a polymer-like fashion.

O(W) forms two relatively long hydrogen bonds with the atoms O(2) and O(5) of the 18C6 molecule. At the same time, O(W) is an acceptor vis-à-vis the oxalic acid. The molecule of oxalic acid is present in two distinct orientations such that each hydrogen atom is H-bonded to O(W). These H bonds are significantly shorter than those between O(W) and the crown ether. The characteristics of these hydrogen bonds are presented in Table 5. All these H-bond distances compare well with those reported for the 18C·cyanoacetic acid·water complex of ref. 3.

TABLE 5. Characteristics of the hydrogen bonding in the $(COOH)_2 \cdot 2H_2O \cdot 18$-crown-6 complex

O(W)—H(W1)	0.88(2) Å	H(W1)···O(2)	1.98(2) Å	O(W)···O(2)	2.850(2) Å	O(W)—H(W1)···O(2)	169(2)°
O(W)—H(W2)	0.78(2)	H(W2)···O(5)	2.14(2)	O(W)···O(5)	2.877(2)	O(W)—H(W2)···O(5)	159(2)
O(11)—H(O11)	0.98(3)	H(O11)···O(W)	1.60(4)	O(11)···O(W)	2.555(2)	O(11)—H(O11)···O(W)	166(3)
O(21)—H(O21)	0.81(6)	H(O21)···O(W)	1.86(6)	O(21)···O(W)	2.650(4)	O(21)—H(O21)···O(W)	166(6)

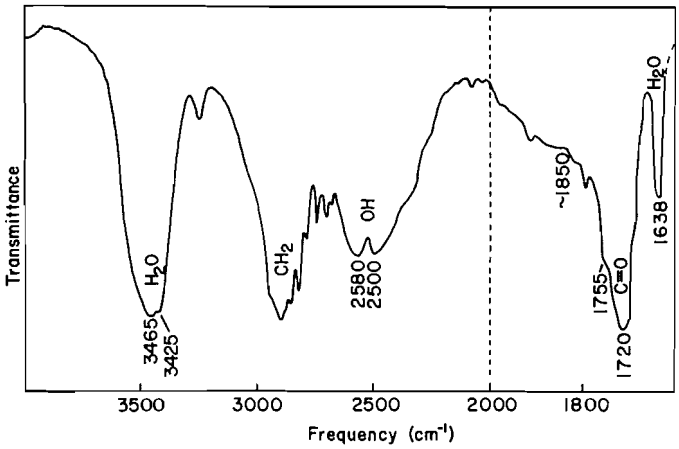

FIG. 3. Room temperature infrared spectrum of the $(COOH)_2 \cdot 2H_2O \cdot 18C6$ complex (hexachlorobutadiene mull) in the region 1500–4000 cm^{-1}.

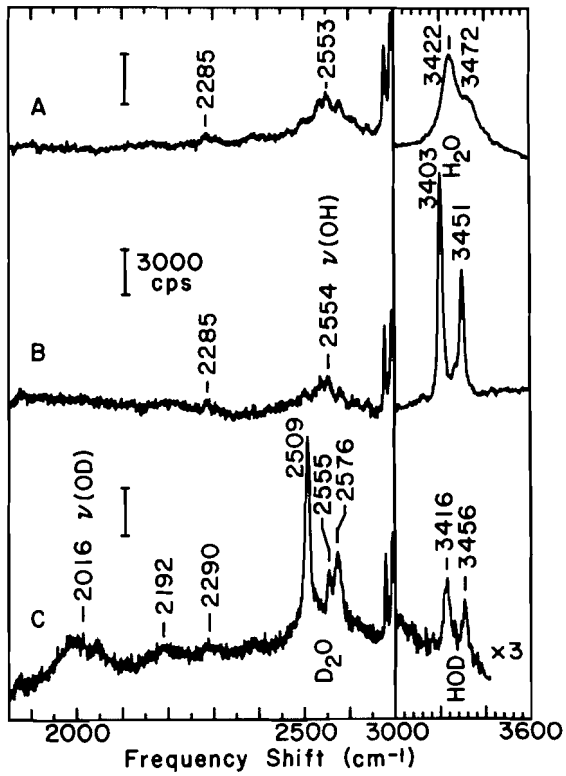

FIG. 4. High-frequency region of the Raman spectrum of the $(COOH)_2 \cdot 2H_2O \cdot 18C6$ complex at (A) 20°C and (B) −180°C. (C) Corresponding spectrum of a ~90% deuterated (acid and water) sample.

Vibrational spectra

The O—H stretching vibrations of the weakly bound water molecules give a strong doublet at 3425/3465 cm^{-1} in the infrared spectrum (Fig. 3). The two components are more easily seen in the Raman spectrum (3422/3472 cm^{-1}) (Fig. 4) even though their overall intensity is relatively much lower than in the infrared. At liquid nitrogen temperature, the doublet is completely resolved at 3403/3451 cm^{-1}. The observed splitting, 48 cm^{-1}, is very nearly equal to that expected for the ν_1 and ν_3 vibrations of intermolecularly uncoupled and symmetrically bound water molecules (13). However, as shown by X-ray diffraction, the two HOH···crown bonds in the complex are not exactly similar (O···O: 2.850 and 2.877 Å), and this is indicated in the spectrum of an incompletely deuterated sample by the appearance of a doublet, at 3431/3455 cm^{-1} (3417/3457 cm^{-1} at −180°C), due to the O—H stretching vibration of the HOD molecules (Fig. 4). The D_2O ν_1/ν_3 vibrations are shifted by a factor of 1.35 in the spectra of the deutero compound, where they give a doublet near 2550 cm^{-1}.

From the centrosymmetric structure of the oxalic acid molecules in the complex and the two different orientations that they can take, the O—H stretching modes of these units are expected to give doublets in both the infrared and Raman spectra. Furthermore, the two components of these doublets should have frequencies of ~2100 and 1900 cm^{-1} (14), based on the acid···water distances of 2.555 and 2.650 Å that characterize the two nonequivalent types of acid molecules in the crystal. However, both the infrared and Raman spectra (Figs. 3 and 4) fail to show any band of appreciable intensity in the 2100 cm^{-1} region. Neither can the absorption at ~1850 cm^{-1} in the infrared spectrum be attributed to a ν(OH) vibration, as this same band is present in the spectra of other similar complexes where the ν(OH) vibration is clearly identified at a much higher frequency (2). The 1850 cm^{-1} infrared band is most likely due to the overtone of the out-of-plane γ(OH) vibration of the acid, and to combination modes of the ether, such as those responsible for the very strong bands in the 800–1100 cm^{-1} region of the vibrational spectra.

The assignment of the acid ν(OH) vibrations in the spectra of the complex can be made in two different ways. Firstly, the two expected vibrations could be taken as having nearly equal frequencies, and thus explain the infrared doublet at 2500/2580 cm^{-1} and the scattering in the corresponding region of the Raman spectrum. This frequency range is characteristic of O···O distances of ~2.60 Å (14), which is the average of the water···crown distances (2.555 and 2.650 Å) determined above by X-ray diffraction. Alternatively, one of the expected vibrations could occur at ~2500 cm^{-1}, the second one being overshadowed by the CH stretching modes in the 2900 cm^{-1} region. This explanation is preferred, as the Raman spectrum of the deuterated complex shows two bands, at 2020 and 2195 cm^{-1}, with isotopic frequency shifts (1.26 and ~1.32 respectively) equal to those expected from the assumed frequencies of the corresponding ν(OH) vibrations (14). Note that both interpretations point to O···O distances that are not exactly equal to those determined by X-ray diffraction. The infrared spectrum of the deuterated complex (not shown) is similar to the Raman, with two absorption bands at 1985 and 2175 cm^{-1}, that at lower

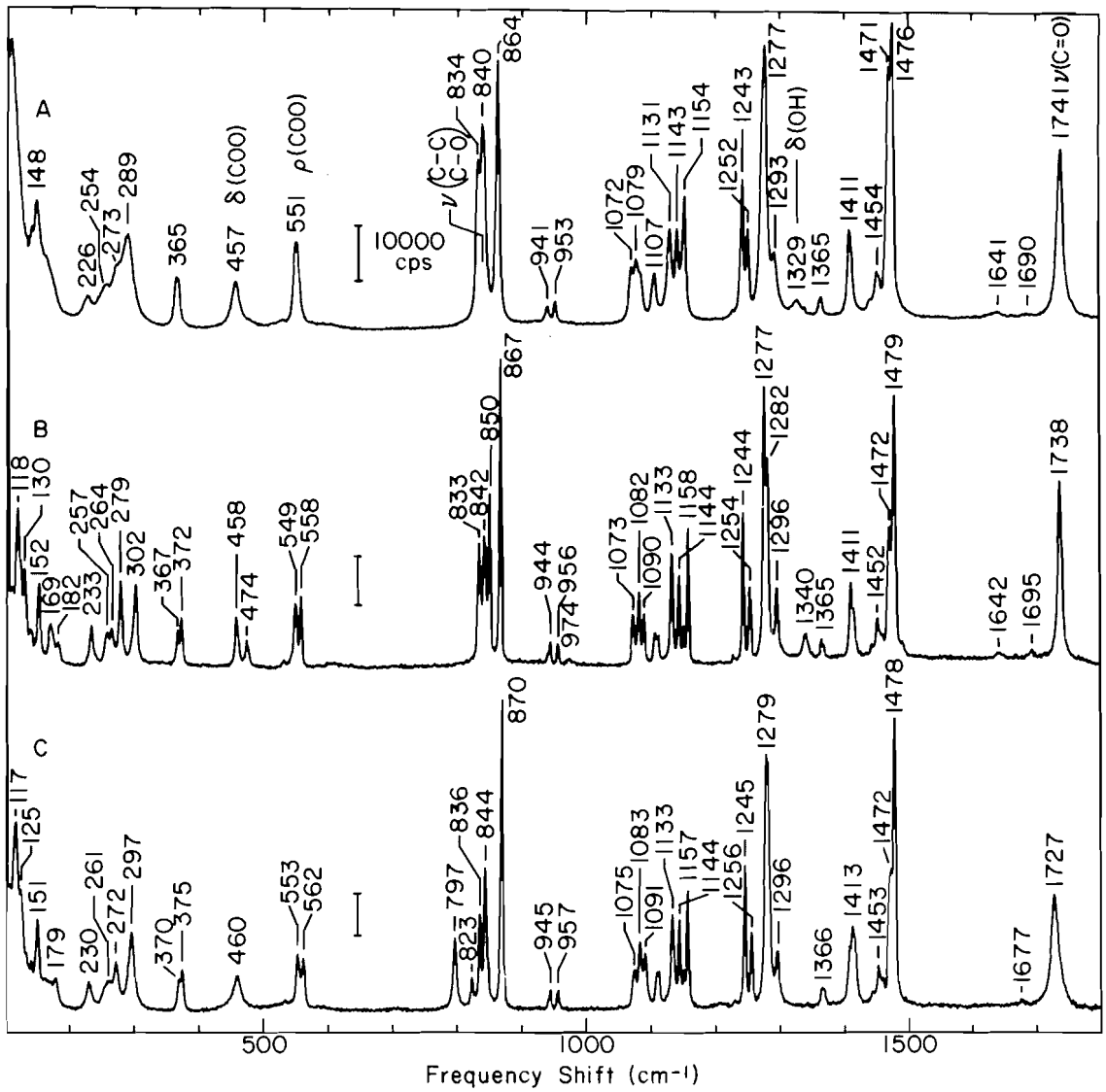

FIG. 5. Low-frequency region of the Raman spectrum of the $(COOH)_2 \cdot 2H_2O \cdot 18C6$ complex at (A) 20°C and (B) ~180°C. (C) Corresponding spectrum of a ~90% deuterated (acid and water) sample.

frequency being about twice as intense as the other one. If these two bands are assigned to the ν(OD) vibrations of the two types of acid molecules identified by X-ray diffraction, then their relative intensities should reflect the different occupational factors (0.6 and 0.4) associated with the two species.

The Raman spectrum of the crown moiety in the complex (Fig. 5) is almost identical to that obtained with metal complexes in which the crown adopts its highly symmetric D_{3d} conformation (15). This is in complete agreement with the X-ray results.

The bands attributable to the oxalic acid molecules can be readily identified in the Raman spectra, as this species has been thoroughly investigated by vibrational spectroscopy, in the gas phase (16), in rare gas matrices (17), and in both its α and β crystalline modifications (18–20). The room temperature Raman spectrum of the hydrogenated complex (Fig. 5A) is consistent with the centrosymmetric structure of these molecules, deduced from the X-ray measurements. This type of local symmetry results in a frequency non-coincidence of the infrared and Raman-active bands. For example, the C=O stretching modes give a symmetric vibration (A_g species in the C_{2h} space group), which is Raman active only, and an antisymmetric mode (B_u species), which is infrared active only. These two bands occur at 1738 cm^{-1} in the Raman and 1720 cm^{-1} in the infrared spectra. The shoulders at ~1755 and 1700 cm^{-1} alongside the main infrared band are probably due to combination modes, as they are also present in the infrared spectra of the uncomplexed acid (17, 19). The CO_2 rocking and bending modes at 551 and 457 cm^{-1} are also observed as singlets in the room temperature spectrum of the nondeuterated complex.

The structural parameters for the two types of acid molecules in the adduct (Fig. 2 and Table 3) are very similar. There is a general agreement between these findings and the Raman results, as many of the bands of the oxalic acid molecules are split in the low-temperature spectrum, which is consistent with a slight nonequivalence of the two types of acid molecules.

The C—C bond should give rise, for the mixed C—C/C—O stretching mode, to a band occurring near 840 cm^{-1}. Although there are several bands due to the ether in this region of the Raman spectrum (834, 840(?), and 864 cm^{-1}), the oxalic acid vibration appears to occur as a singlet, at 850 and 797 cm^{-1} in the spectra of the normal and deuterated complex respectively,

the weak band at 823 cm^{-1} in the spectrum of the deutero compound being attributable to the HOOCCOOD mixed isotopic species.

Acknowledgements

The financial assistance of the Natural Science and Engineering Research Council of Canada is gratefully acknowledged. We also thank Mr. M. J. Olivier for the collection of the X-ray intensities.

1. W. H. Watson, J. Galloy, D. A. Crosbie, F. Vogtle, and W. M. Müller. J. Org. Chem. **49**, 347 (1984).
2. R. Savoie, A. Rodrigue, M. Pigeon-Gosselin, and R. Chênevert. Can. J. Chem. **63**, 1457 (1985).
3. A. Elbasyouny, H. J. Brügge, K. Von Deuten, M. Dickel, A. Knöchel, K. U. Koch, J. Kopf, D. Melzer, and G. Rudolph. J. Am. Chem. Soc. **105**, 6568 (1983).
4. D. Britton, M. K. Chantooni Jr., W.-J. Wang, and I. M. Kolthoff. Acta Crystallogr Sect. C, **40**, 1584 (1984).
5. F. R. Ahmed, S. R. Hall, M. E. Pippy, and C. P. Huber. J. Appl. Crystallogr. **6**, 309 (1973). Accession Nos. 133–147.
6. P. Main, S. E. Hull, L. Lessinger, G. Germain, J. Declercq, and M. M. Woolfson. Multan. A system of computer programs for the automatic solution of crystal structures from X-ray diffraction data. Univs. of York, England and Louvain, Belgium. 1978.
7. R. J. Doedens and J. A. Ibers. Inorg. Chem. **6**, 204 (1967).
8. C. K. Johnson. Ortep. Report ORNL-3794. Oak Ridge National Laboratory, Tennessee. 1965.
9. D. T. Cromer and J. B. Mann. Acta Crystallogr. Sect. A, **24**, 321 (1968).
10. R. F. Stewart, E. R. Davidson, and W. T. Simpson. J. Chem. Phys. **53**, 1891 (1970).
11. S. Pérez and F. Brisse. Can. J. Chem. **53**, 3551 (1975).
12. F. Brisse, N. Molhant, and S. Pérez. Acta Crystallogr Sect. B, **35**, 1825 (1979).
13. J. Schiffer, M. Intenzo, P. Hayward, and C. Calabrese. J. Chem. Phys. **64**, 3014 (1976).
14. A. Novak. Struct. Bonding (Berlin), **18**, 177 (1974).
15. M. Fouassier and J.-C. Lassegues. J. Chim. Phys. Phys.-Chim. Biol. **75**, 865 (1978).
16. B. C. Stace and C. Oralratmanee. J. Mol. Struct. **18**, 339 (1973).
17. R. L. Redington and T. E. Redington. J. Mol. Struct. **48**, 165 (1978).
18. J. De Villepin and A. Novak. Spectrochim. Acta Part A, **34**, 1019 (1978).
19. J. De Villepin and A. Novak. Spectrochim Acta Part A, **34**, 1009 (1978).
20. J. De Villepin, A. Novak, and D. Bougeard. Chem. Phys. **73**, 291 (1982).
21. Z. Náhlovská, B. Náhlovský, and T. G. Strand. Acta Chem. Scand. **24**, 2617 (1970).
22. J. L. Derissen and P. H. Smit. Acta Crystallogr. Sect. B, **30**, 2240 (1974).
23. R. G. Delaplane and J. A. Ibers. Acta Crystallogr. Sect. B, **25**, 2423 (1969).

Complexation of glycylglycine by the methylmercury cation: a vibrational spectroscopy and X-ray diffraction study

SERGE ALEX AND RODRIGUE SAVOIE[1]
Département de chimie, Université Laval, Cité universitaire, Québec (Qué.), Canada G1K 7P4

AND

MARIE-CLAUDE CORBEIL AND ANDRÉ L. BEAUCHAMP[1]
Département de chimie, Université de Montréal, C.P. 6210, Succ. A, Montréal (Qué.), Canada H3C 3V1

Received June 13, 1985

SERGE ALEX, RODRIGUE SAVOIE, MARIE-CLAUDE CORBEIL, and ANDRÉ L. BEAUCHAMP. Can. J. Chem. **64**, 148 (1986).

Two different crystalline complexes have been obtained from aqueous mixtures of glycylglycine (GlyGly) and methylmercury(II), and they were studied by vibrational spectroscopy and X-ray diffraction. In the first compound, a hydrogen atom of the protonated amino group of GlyGly is substituted by the CH_3Hg^+ cation, giving (CH$_3$Hg)GlyGly: orthorhombic, $Pna2_1$, a = 7.920(6) Å, b = 13.473(5) Å, c = 8.059(3) Å, and Z = 4. Further complexation on the carboxylate group yielded the complex [(CH$_3$Hg)$_2$GlyGly]ClO$_4$: monoclinic, $P2_1/c$, a = 6.407(4) Å, b = 24.439(6) Å, c = 8.461(2) Å, β = 93.82(4)°, and Z = 4. The sites of complexation and the conformations of these solid complexes are well reflected in their vibrational spectra. Raman spectra indicate that complexation in aqueous solutions is limited to substitution on the $-NH_3^+$ group of GlyGly.

SERGE ALEX, RODRIGUE SAVOIE, MARIE-CLAUDE CORBEIL et ANDRÉ L. BEAUCHAMP. Can. J. Chem. **64**, 148 (1986).

Deux complexes cristallins différents ont été isolés à partir de solutions aqueuses de glycylglycine (GlyGly) et de méthylmercure(II), et ils ont été étudiés par spectroscopie de vibration et par diffraction des rayons X. Le premier composé a été obtenu par la substitution d'un hydrogène de la fonction amino protonée de la GlyGly par le cation CH_3Hg^+, pour donner la (CH$_3$Hg)GlyGly: orthorhombique, $Pna2_1$, a = 7,920(6) Å, b = 13,473(5) Å, c = 8,059(3) Å et Z = 4. Une complexation plus poussée, sur la fonction carboxylate, a permis d'obtenir le complexe [(CH$_3$Hg)$_2$GlyGly]ClO$_4$: monoclinique, $P2_1/c$, a = 6,407(4) Å, b = 24,439(6) Å, c = 8,461(2) Å, β = 93,82(4)° et Z = 4. Les spectres de vibration réflètent bien les sites de complexation de ces espèces, ainsi que leurs conformations propres. Les spectres Raman ont permis d'établir que la complexation en milieu aqueux était limitée à la substitution sur la fonction $-NH_3^+$ de la glycylglycine.

Introduction

The methylmercury cation CH_3Hg^+ has been used in our (1–4) and other laboratories (5) as a convenient probe for the coordination sites in nucleic acid constituents. This cation can also bind to proteins (6), and various organomercury compounds are currently used as heavy-atom labeling agents for structural studies by electron microscopy and X-ray diffraction (7).

Although the thiol groups appear to be the primary targets for mercury in proteins (6), coordination is likely to take place with other groups as well. The model complexes with monomeric amino acids considered so far involved mainly the sulfur-containing acids (8–13). Selenium analogs have also been examined (14). Relying mainly on ^{1}H nmr spectroscopy, Rabenstein *et al.* (15, 16) have investigated the equilibrium reactions between the CH_3Hg^+ cation and various amino acids in aqueous solutions. The only available crystal structure with a non-sulfur-containing amino acid is the tyrosine complex, in which one CH_3Hg^+ group is bonded to the NH_2 end of the molecule (17).

As part of our research program aimed at determining (via model systems) the mode of attachment of the CH_3Hg^+ cation to proteins and peptides, our initial effort is being directed to sulfur-free model ligands. Raman spectroscopy, applicable to both solids and aqueous solutions, is used to transfer the detailed structural information obtained by X-ray diffraction on solids to the species present in water. This technique also presents the advantage of providing an "instant" picture of the species in solution, since its time scale makes it less sensitive to exchange equilibria leading to signal averaging in ^{1}H nmr.

The present paper deals with glycylglycine (GlyGly), a dipeptide devoid of a side chain

$$^+H_3N—C(\alpha)H_2—CO—NH—C(\beta)H_2—COO^-$$

It can be regarded as a model for interactions of CH_3Hg^+ with the $-NH_3^+$ and $-COO^-$ ends of a protein chain.

Experimental

Reagents and techniques

Glycylglycine (BDH Chemicals) was used without further purification. The sources of CH_3Hg^+ ions were the hydroxide CH_3HgOH (1 *M* aqueous solution from Alfa Inorganics), the perchlorate CH_3HgClO_4, and the nitrate CH_3HgNO_3 (1 *M* aqueous solutions prepared as described earlier (2)). The CH_3Hg^+ ion was analysed potentiometrically by titration with KCl in ethanol (Ag/AgCl indicator electrode) (18). The various solutions studied by Raman spectroscopy were prepared at a concentration of 0.33 *M*, their pH being adjusted in each case with either NaOH or HNO_3 (4 *N*).

Raman spectroscopy

The Raman spectra, excited by the 514.5-nm line from a Spectra Physics Model 165 argon ion laser, were recorded on a Spex Model 1400 microcomputer-controlled spectrometer. The samples were contained in capillary tubes that, in the case of the highly light-sensitive solid complexes, were mounted on a motor shaft and rotated at high speed in the laser beam. Even so, the laser power at the sample had to be kept very low (~25 mW) in order to prevent sample decomposition. Solid glycylglycine and the various solutions, contained in cells mounted in a copper block maintained at 10°C, were studied at a laser power of 200 mW at the sample. The spectra were typically recorded at 5 cm^{-1} spectral slit width, with a 2-s integration time at each 2 cm^{-1} frequency increment.

Infrared spectroscopy

The ir spectra were recorded as KBr pellets with a Digilab FTS-15 C/D Fourier-transform spectrophotometer equipped with a Globar source and wide-band mercury cadmium telluride detector (Infrared

[1]Authors to whom correspondence may be addressed.

Associates, New Brunswick, NJ). Typically, 100 interferograms of 4096 points, recorded at an optical velocity of 1.2 cm/s and a maximal optical retardation of 0.5 cm, were co-added, apodized with a boxcar function, and Fourier transformed with 4 levels of zero filling, resulting in a spectral resolution of 2 cm^{-1}. The apparatus was purged with dry nitrogen during the experiments.

Nuclear magnetic resonance spectroscopy

The ^1H nmr spectra were obtained with a Bruker WH-90 spectrometer and they were referenced to TMS for DMSO-d_6 solutions or to DSS for D_2O solutions. The solvents were Silanor DMSO-d_6 (Merck, Sharp & Dohme Canada, 99.5% isotopic purity) and D_2O (Cambridge Isotope Lab., 99.8% isotopic purity).

Preparations

$(CH_3Hg)GlyGly$

One mmole (132 mg) of glycylglycine was dissolved in 1.0 mL of 1 *M* aqueous CH_3HgOH. On addition of absolute ethanol (10 mL), a colorless powder was immediately obtained. It was filtered off, washed with ethanol, and dried *in vacuo* for 24 h; yield 0.29 g, 82%; ^1H nmr (D_2O) δ: 3.97 (2H, s, α-CH_2), 3.81 (2H, s, β-CH_2), 0.90 (3H, s, CH_3Hg), $^2J(^1H-^{199}Hg)$ = 219 Hz. Crystals were grown by vapor diffusion of ethanol into a concentrated aqueous solution of the complex. The composition was confirmed by X-ray work (*vide infra*).

$[(CH_3Hg)_2GlyGly]ClO_4$

One mmole (132 mg) of glycylglycine was dissolved in a mixture of 1.0 mL of 1.0 *M* CH_3HgOH and 1.0 mL of CH_3HgClO_4. Ethanol was then added (~10 mL). After a few days at room temperature and in open air (hood), colorless rectangular platelets were obtained; yield: 0.21 g, 31%; ^1H nmr (D_2O) δ: 3.90 (2H, s, α-CH_2), 3.94 (2H, s, β-CH_2), 0.96 (6H, s, CH_3Hg), $^2J(^1H-^{199}Hg)$ = 228 Hz; (in DMSO-d_6) δ: 3.77 (2H, s, CH_2), 3.80 (2H, d, CH_2), 5.26 (2H, s, br, NH_2), 8.74 (1H, t, NH), 0.73 (6H, s, CH_3Hg), $^2J(^1H-^{199}Hg)$ = 220 Hz. The singlet at high field corresponds to both CH_3Hg groups in fast exchange. A crystal from the homogeneous samples was used for X-ray work.

The same compound was obtained by mixing $(CH_3Hg)GlyGly$ with an equal number of moles of CH_3HgClO_4 (from a 1.0 *M* aqueous solution), and adding ethanol. Precipitation occurred instantly, yielding very thin plates. The sample obtained this way had the same ir and ^1H nmr spectra as those prepared by the first method.

Crystal structure of $[(CH_3Hg)_2GlyGly]ClO_4$

$C_6H_{13}ClHg_2N_2O_7$ fw = 661.81

Monoclinic, $P2_1/c$, a = 6.407(4), b = 24.439(6), c = 8.461(2) Å, β = 93.82(4)°, V = 1321.9 $Å^3$, Z = 4, D_c = 3.324 g cm^{-3}, λ(MoKα̃) = 0.71069 Å (graphite monochromator), μ(MoKα) = 234.2 cm^{-1}, T = 293 K.

A crystal of dimensions (mm) 0.025 (between $0\bar{1}0$ and 010) × 0.115 ($001-00\bar{1}$) × 0.30 (irregular faces) was used for X-ray work. Initial cell parameters and monoclinic Laue symmetry were observed from precession and cone axis photographs. The systematic absences ($h0l$, $l \neq 2n$ and $0k0$, $k \neq 2n$), noted on the precession films and subsequently confirmed from the full data set, unambiguously defined the $P2_1/c$ space group. The cell parameters obtained from films were accurately determined by least-squares refinement on the setting angles of 25 randomly distributed reflections centered on an Enraf–Nonius CAD-4 diffractometer. The Niggli coefficients clearly indicated that no symmetry higher than monoclinic was present.

The intensity data were collected with the CAD-4 diffractometer as reported earlier (19). Three standard reflections monitored during the experiment indicated that the crystal slowly decomposed in the beam: their intensities had regularly decreased by 20% at the end of the data collection. This decay was taken into account at the data reduction stage. A total of 1763 independent $\bar{h}kl$ and hkl reflections ($2\theta < 45°$) were collected. After eliminating the systematically absent reflections, the data set consisted of 1705 unique reflections, of which 957 were retained as significantly above background ($I > 3\sigma(I)$) for structure determination. These data were corrected for the Lorentz effect, polarization, and absorption (Gaussian integration, grid 8 × 8 × 8, transmission range: 0.064–0.564).

The structure was solved by the heavy-atom method and refined on $|F_o|$ by standard least-squares procedures. Both Hg atoms were located from a Patterson synthesis and the remaining non-hydrogen atoms were located from a difference Fourier (ΔF) map phased on Hg. Isotropic refinement by full-matrix least squares converged to $R = \Sigma||F_o| - |F_c||/\Sigma|F_o| = 0.116$ and $R_w = [\Sigma w(|F_o| - |F_c|)^2/\Sigma w|F_o|^2]^{1/2} = 0.134$. The subsequent steps were carried out by block-diagonal least squares. The non-hydrogen atoms were refined anisotropically. The hydrogens whose positions were determined by those of the non-hydrogen atoms were fixed at idealized positions (C—H = 0.95 Å, N—H = 0.87 Å, B_{iso} = 5.0 $Å^2$). The methyl hydrogens were not visible in the ΔF map. The hydrogen parameters were not refined, but their coordinates were recalculated after each least-squares cycle. Anisotropic refinement of all non-hydrogen atoms converged to R = 0.043, R_w = 0.052, and a goodness-of-fit ratio of 1.78. The final ΔF map contained peaks in the range ±(1.2 − 2.2) e/$Å^3$ near Hg, and the general background was below ±0.9 e/$Å^3$ elsewhere.

Crystal structure of $(CH_3Hg)GlyGly$

$C_5H_{10}HgN_2O_3$ fw = 346.74

Orthorhombic, $Pna2_1$, a = 7.920(6), b = 13.473(5), c = 8.059(3) Å, V = 859.9 $Å^3$, Z = 4, D_c = 2.677 g cm^{-3}, λ(Mokα) = 0.71069 Å, μ(MoKα) = 178.5 cm^{-1}, T = 293 K.

The specimen used had the following distances (mm) between the indicated pairs of faces: 0.040 ($01\bar{1}-0\bar{1}1$) × 0.048 ($011-0\bar{1}\bar{1}$) × 0.490 ($100-\bar{1}00$). It was mounted on an Enraf–Nonius CAD-4 diffractometer and a set of 25 randomly distributed reflections were created by the search routine of the system. These reflections were centered and the indexing routine yielded a reduced cell of dimensions a = 7.920, b = 8.059, c = 13.473 Å with three 90° angles. This cell was checked with long-exposure oscillation photographs taken along the axes. These three films showed the expected layer line spacings and contained mirror planes consistent with the orthorhombic *mmm* Laue symmetry. The Niggli parameters unambiguously indicated that the lattice had no higher symmetry. Crystal density and fast scans on the $hk0$, $h0l$, and $0kl$ reflections pointed to $Pn2_1a$ (alternate orientation for $Pna2_1$) as the most likely space group. Prior to data collection, the b and c axes of the reduced cell were interchanged in order to define the cell in the standard $Pna2_1$ orientation.

The intensity data were collected as above. The three standards monitored during the experiment showed random fluctuation within ±3.4%. A set of 923 independent hkl reflections ($2\theta < 50°$) was collected. After removal of the systematic absences, a total of 819 unique reflections remained, of which 596 were retained ($I > 3\sigma(I)$) for structure determination. The data were corrected for the Lorentz effect, polarization, and absorption (Gaussian integration, grid 8 × 8 × 8, transmission range: 0.33–0.54).

The conditions of systematic absence ($0kl$, $k + l \neq 2n$; $h0l$, $h \neq 2n$) for space group $Pna2_1$ were confirmed by inspection of the full data set. These conditions were also consistent with the centric *Pnam* space group (alternate definition for *Pnma*), but this group was rejected at the end of the refinement. The structure was solved by the heavy-atom method and refined by full-matrix least-squares procedures. The x and y coordinates of Hg were determined from the Patterson synthesis. The z coordinate was arbitrarily set to 0.25 to define the origin along c. The ΔF map phased on Hg contained an artificial inversion center and two overlapping images as expected. However, all the non-hydrogen atoms belonging to one of the images could be assembled. Isotropic refinement converged to R = 0.094 and R_w = 0.101. The hydrogen atoms were treated as in the previous case. Anisotropic refinement converged to R = 0.023, R_w = 0.028, and a goodness-of-fit ratio of 1.08. The final ΔF map showed peaks of ±(0.7 − 1.0) e/$Å^3$ near Hg and a general background below ±0.54 e/$Å^3$ elsewhere. Refinement of the enantiomorphic structure led to R = 0.026 and R_w = 0.032. Therefore the results from the first refinement were retained. The absence of a mirror plane perpendicular to the c axis ruled out the possibility that the unit cell belongs to the *Pnam* space group.

TABLE 1. Refined coordinates ($\times 10^3$, Hg, Cl $\times$ 10^4) and equivalent temperature factors ($\times 10^3$)

Atom	x	y	z	U_{eq}
		$[(CH_3Hg)_2GlyGly]ClO_4$		
Hg(1)	6756(2)	1728(1)	4703(2)	60
Hg(8)	7710(2)	−1367(1)	−1357(2)	53
Cl(1)	1936(12)	1275(3)	6934(9)	47
O(4)	695(3)	117(1)	180(3)	67
O(8)	763(3)	−57(1)	−54(3)	80
O(9)	702(3)	−15(1)	−293(3)	56
O(11)	23(4)	146(1)	759(4)	138
O(12)	384(4)	141(1)	759(4)	133
O(13)	186(3)	147(1)	535(2)	62
O(14)	177(5)	71(1)	679(3)	126
N(1)	643(3)	86(1)	496(3)	66
N(5)	757(3)	31(1)	115(3)	42
C(1)	702(5)	258(1)	463(5)	83
C(2)	774(4)	56(1)	388(4)	65
C(3)	737(4)	69(2)	213(4)	54
C(6)	738(4)	38(1)	−51(3)	43
C(7)	730(4)	−17(2)	−146(4)	55
C(8)	788(5)	−218(1)	−209(4)	74
		$(CH_3Hg)GlyGly$		
Hg(1)	4303(7)	19318(3)	25000	47
O(4)	−262(1)	121(1)	344(1)	59
O(8)	−649(1)	127(1)	583(1)	40
O(9)	−751(1)	38(1)	374(1)	56
N(1)	19(2)	193)1)	510(3)	35
N(5)	−339(1)	26(1)	560(2)	43
C(1)	81(3)	200(2)	−12(5)	68
C(2)	−78(2)	111(1)	582(2)	54
C(3)	−237(2)	87(1)	483(2)	42
C(6)	−480(3)	−7(2)	481(2)	37
C(7)	−645(2)	58(1)	483(2)	36

The scattering curves were from standard sources (20). The f' and f'' contributions of Hg and Cl to anomalous dispersion were included in structure factor calculations (20). The programs used are listed elsewhere (21). The refined coordinates and equivalent isotropic temperature factors are listed in Table 1.[2]

Discussion

Description of the structures

The crystal of $(CH_3Hg)GlyGly$ contains discrete molecules (Fig. 1) in which one of the ammonium protons of the zwitterionic glycylglycine molecule has been substituted by a CH_3Hg^+ group. In view of the very soft character of mercury, preference for this nitrogen site over the harder carboxylate or amide oxygens was anticipated. In the $[(CH_3Hg)_2GlyGly]^+$ cation (Fig. 2) present in the perchlorate, one of the CH_3Hg^+ ions is similarly attached to the $-NH_2$ end, whereas a second CH_3Hg^+ ion is bonded to the carboxylate acting as a monodentate group.

The interatomic distances and bond angles are listed in Table 2. In all cases, the coordination of mercury is linear within 4(1)°. The Hg—N(1) distances found here (2.10(3) and 2.14(3) Å) are similar to those reported for complexes with simple amino acids (8, 17). Mercury binds less readily to harder oxygen sites, but the Hg—O(8) distance (2.07(2) Å) indicates a normal single bond (22) in the $[(CH_3Hg)_2GlyGly]^+$ ion. Linearly coordinated CH_3Hg^+ groups usually retain some electrophilic character in the equatorial region (assuming that the H_3C—Hg—N(O) direction is axial), where the metal is accessible. In the solid state this commonly leads to clustering around mercury of negatively charged groups, forming loose coordination bonds. In both of our compounds, one such secondary bond with Hg(1) is intramolecular and involves the amide oxygen O(4) at 2.82(2) Å in $[(CH_3Hg)_2GlyGly]^+$ and 2.71(1) Å in $(CH_3Hg)GlyGly$ (Table 3). Although weaker than the contact with a free carboxylate oxygen in the tyrosine complex (Hg···O = 2.62(2) Å) (17), this interaction is strong enough to control the conformation at this end of the complexes.

Light-atom positions cannot be determined with high accuracy in the presence of Hg (and Cl) atoms. Considering the large esd's, the bond lengths and angles of glycylglycine (23, 24) are not significantly affected by complexation. However, chain conformation is appreciably changed in the complexes. Glycylglycine should ideally contain two planar fragments: the carboxylate group (C(6), C(7), O(8), O(9)) and the amide group (C(2), C(3), O(4), N(5), C(6)). Therefore molecular conformation depends on the torsion angles about the C(2)—C(3), N(5)—C(6), and C(6)—C(7) bonds. In a strictly planar elongated chain, the angles about C(2)—C(3) and N(5)—C(6) should be 180°. For C(6)—C(7) the value would be 0° or 180°, depending on the carboxylate oxygen used to define it; the O(8) atom (leading to the torsion angle nearer 0°) is used here. In crystalline glycylglycine, departure from these ideal angles and

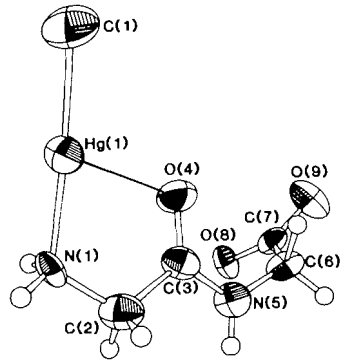

FIG. 1. ORTEP drawing of the $(CH_3Hg)GlyGly$ molecule. The ellipsoids correspond to 50% probability. The long Hg···O contact is shown as a thin line.

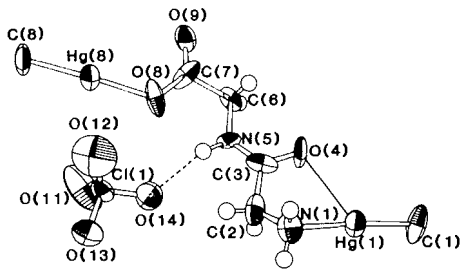

FIG. 2. ORTEP drawing of the asymmetric unit in $[(CH_3Hg)_2GlyGly]ClO_4$. The ellipsoids correspond to 50% probability. The dashed line indicates hydrogen bonding. The long Hg···O contact is shown as a thin line.

[2]The supplementary material includes lists of refined temperature factors, the coordinates of the hydrogen atoms, details on least-squares plane calculations, and tables of observed and calculated structure factor amplitudes for both compounds. This material may be purchased from the Depository of Unpublished Data, CISTI, National Research Council of Canada, Ottawa, Ont., Canada K1A 0S2.

TABLE 2. Interatomic distances and bond angles

Bond	Distance (Å)		Bonds	Angle (deg)	
	$[(CH_3Hg)_2GlyGly]ClO_4$	$(CH_3Hg)GlyGly$		$[(CH_3Hg)_2GlyGly]ClO_4$	$(CH_3Hg)GlyGly$
Hg(1)—N(1)	2.14(3)	2.10(3)	C(1)—Hg(1)—N(1)	176(1)	176(1)
Hg(1)—C(1)	2.09(3)	2.13(4)	C(8)—Hg(8)—O(8)	177(1)	
Hg(8)—O(8)	2.07(2)		Hg(1)—N(1)—C(2)	111(2)	116(1)
Hg(8)—C(8)	2.09(3)		N(1)—C(2)—C(3)	116(3)	113(1)
N(1)—C(2)	1.48(4)	1.46(3)	C(2)—C(3)—N(5)	118(3)	113(1)
C(2)—C(3)	1.52(5)	1.52(2)	C(2)—C(3)—O(4)	116(3)	122)1)
C(3)—O(4)	1.23(5)	1.23(2)	O(4)—C(3)—N(5)	126(3)	125(1)
C(3)—N(5)	1.26(5)	1.31(2)	C(3)—N(5)—C(6)	124(3)	119(2)
N(5)—C(6)	1.41(4)	1.36(3)	N(5)—C(6)—C(7)	114(2)	120(2)
C(6)—C(7)	1.56(5)	1.57(3)	C(6)—C(7)—O(9)	118(3)	116(1)
C(7)—O(8)	1.26(4)	1.23(2)	C(6)—C(7)—O(8)	111(3)	117(1)
C(7)—O(9)	1.25(4)	1.24(2)	O(8)—C(7)—O(9)	131(3)	127(1)
Cl(1)—O(11)	1.34(3)		C(7)—O(8)—Hg(8)	122(2)	
Cl(1)—O(12)	1.35(3)		O(11)—Cl(1)—O(12)	119(2)	
Cl(1)—O(13)	1.42(2)		O(11)—Cl(1)—O(13)	108(2)	
Cl(1)—O(14)	1.39(3)		O(11)—Cl(1)—O(14)	108(2)	
			O(12)—Cl(1)—O(13)	106(2)	
			O(12)—Cl(1)—O(14)	110(2)	
			O(13)—Cl(1)—O(14)	105(2)	

TABLE 3. Distances in hydrogen bonds and Hg···O contacts

Bond	Distance (Å)
$[(CH_3Hg)_2GlyGly]ClO_4$	
N(5)···O(14)[a]	3.06(4)
N(1)···O(9)[b]	3.05(3)
N(1)···O(9)[c]	3.22(3)
N(1)···O(12)	3.16(4)
Hg(1)···O(4)	2.82(2)
Hg(1)···O(12)	3.27(3)
Hg(1)···O(13)	3.28(2)
Hg(1)···O(11)[d]	3.26(3)
Hg(8)···O(4)[c]	3.02(2)
$(CH_3Hg)GlyGly$	
N(5)···O(9)[e]	2.77(2)
N(1)···O(8)[d]	2.84(2)
N(1)···O(8)[f]	2.83(2)
Hg(1)···O(4)	2.71(1)
Hg(1)···O(4)[f]	3.04(1)
Hg(1)···O(9)[d]	2.83(1)

[a] $1 - x, -y, 1 - z$.
[b] $x, y, 1 + z$.
[c] $1 - x, -y, -z$.
[d] $1 + x, y, z$.
[e] $-1 - x, -y, \frac{1}{2} + z$.
[d] $\frac{1}{2} + x, \frac{1}{2} - y, z$.

displacement of 0.15 Å of C(6) from the amide plane result in a dihedral angle of 24.9° between the carboxylate and the amide planes. In the $[(CH_3Hg)_2GlyGly]^+$ ion, the deviations are differently distributed and C(6) is not significantly displaced from the amide plane, so that the dihedral angle is only 8.6°. It is noteworthy that the O(8)-bonded CH_3Hg^+ group lies in the carboxylate plane, in spite of the absence of electronic constraint to force this orientation. Therefore, the roughly planar portion in the complex extends from the H_3C—Hg(8) group to the C(2) methylene group. In $(CH_3Hg)GlyGly$, the C(3)—N(5)—C(6)—C(7) angle differs by ~90° from those of glycylglycine and the 2:1 complex (Table 4). This is reflected by the bent conformation shown in Fig. 1. The conformation at the NH_2 end of the molecules is undoubtedly dictated by the Hg(1)···O(4) bonding contact mentioned earlier, which stabilizes the *cisoid* arrangement of N(1) and O(4).

The packing diagram of $[(CH_3Hg)_2GlyGly]ClO_4$ shows that the complex cations are organized in pairs in the unit cell (upper part of Fig. 3). The "dimer" consists of two centrosymmetrically-related $[(CH_3Hg)_2GlyGly]^+$ cations forming a pair of complementary N(1)—H(11)···O(9) hydrogen bonds of 3.05(3) Å. This N···O distance is typical of this type of hydrogen bonds (25). Two long complementary contacts of 3.02(2) Å are also found between Hg(8) and the amide oxygen O(4), but the binding effect is probably very small, because the O(8)—Hg(8) and C(3)=O(4) bonds are roughly parallel. In each molecule, the amide proton forms a N(5)—H(5)···O(14) hydrogen bond with a ClO_4^- oxygen (N(5)···O(14) = 3.06(4) Å). Besides these two moderately strong interactions, cohesion between the various structural subunits in the cell does not involve strong individual interactions. Dimers roughly oriented along the *c* axis are repeated along this direction, thereby defining infinite ribons at $y \sim 0$ and ~1/2. Successive dimers along *c* form two weak centrosymmetrically related hydrogen bonds, in which the remaining amino proton H(12) acts as a donor to the free oxygen O(9) of the next molecule. The N(1)···O(9) distance (3.22(3) Å) lies at the upper limit of the range proposed for such hydrogen bonds (25). As mentioned above, the ClO_4^- ion forms a strong hydrogen bond to the amide N—H proton. However, in contrast with most other CH_3Hg^+ comnplexes containing this anion (26), the Hg···O contacts are very long (Table 3). The shortest contact observed here is 3.26 Å for Hg···O(11), whereas distances just above 3.0 Å are common.

In the $(CH_3Hg)GlyGly$ neutral complex, the intermolecular interactions are on the average much stronger. They are shown in the packing diagram of Fig. 4. Besides the intramolecular

TABLE 4. Torsion angles

Bonds	GlyGly (refs. 23, 24)	$[(CH_3Hg)_2GlyGly]ClO_4$	$(CH_3Hg)GlyGly$
Hg(1)—N(1)—C(2)—C(3)	—	−57(3)	−42(2)
N(1)—C(2)—C(3)—N(5)	152.7	−146(3)	−169(2)
C(3)—N(5)—C(6)—C(7)	155.0	−170(3)	−84(2)
N(5)—C(6)—C(7)—O(8)	11.3	−6(3)	−14(3)
C(6)—C(7)—O(8)—Hg(8)	—	−179(2)	

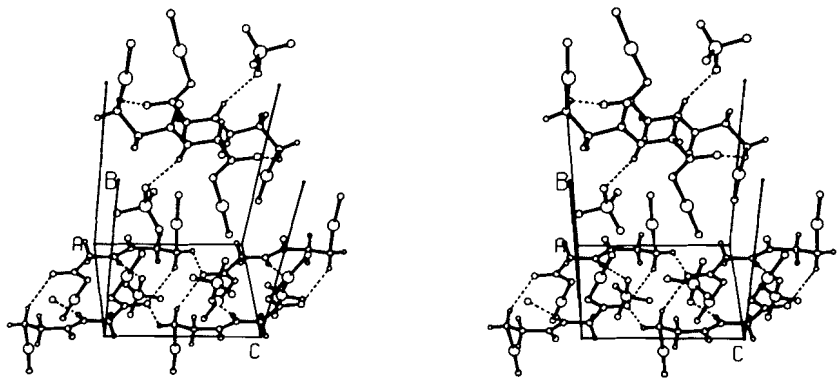

FIG. 3. Stereoview of the molecule packing for $[(CH_3Hg)_2GlyGly]ClO_4$. Dashed lines correspond to hydrogen bonding. The Hg···O contacts are shown as thin bonds. The atoms are represented by spheres of arbitrary size, with Hg and Cl being larger than the remaining non-hydrogen atoms. The atoms can be identified by comparison with Fig. 2. Only the O-1/2 portion of the *b* axis is shown.

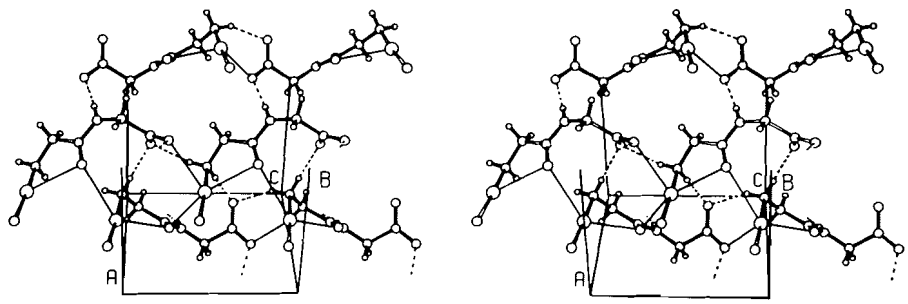

FIG. 4. Packing diagram for $(CH_3Hg)GlyGly$. Dashed lines represent hydrogen bonds. The Hg···O contacts are shown as thin bonds. The atoms can be identified by comparison with Fig. 1. Only the O-1/2 portion of the *b* axis is shown.

Hg···O(4) contact of 2.71(1) Å with the amide oxygen, any given Hg atom forms a strong intermolecular secondary bond with a carboxylate oxygen O(9) at 2.83(1) Å, and a weaker one with an amide oxygen at 3.04(1) Å. In addition, the $-NH_2$ groups establish moderately strong hydrogen bonds with O(8) oxygens belonging to two different molecules related by the *a* glide plane (N···O = 2.84 Å). These infinite chains extending along *a* are held to adjacent chains by strong interactions of 2.77(2) Å taking place at each monomer between the amide N(5)—H bond and carboxylate oxygen O(9).

Vibrational spectra

The Raman spectra of glycylglycine and of its two complexes with CH_3Hg(II) are shown in Figs. 5 and 6. The infrared spectra (Fig. 9, supplementary material) have also been obtained in the course of the present study. As they bring little information on these systems compared to the Raman data, they will not be discussed in detail.

The vibrational spectra of glycylglycine are well documented (27–31) and the interpretation of the spectra presented here is based on these earlier results.

CH_3Hg

The most characteristic spectral changes associated with the formation of the complexes are found in the 500 and 1200 cm^{-1} regions, where new strong bands due to methylmercury appear. A characteristic broad absorption is also observed in the infrared spectrum at ~810 cm^{-1}. The presence of methylmercury(II) in both the $[(CH_3Hg)_2GlyGly]ClO_4$ and $(CH_3Hg)GlyGly$ compounds can be clearly established from the very strong Raman bands at ~560 cm^{-1}, attributable to the Hg—CH_3 stretching vibration (ν(Hg—CH_3)) (refs. 32–34). The strong peak at 466 cm^{-1} in the spectrum of the *N*-substituted $CH_3HgGlyGly$ complex can also be unambiguously assigned to the Hg—N stretching vibration (ν(N—$HgCH_3$)), by comparison with other similar compounds, such as NH_2-substituted 9-methyladenine

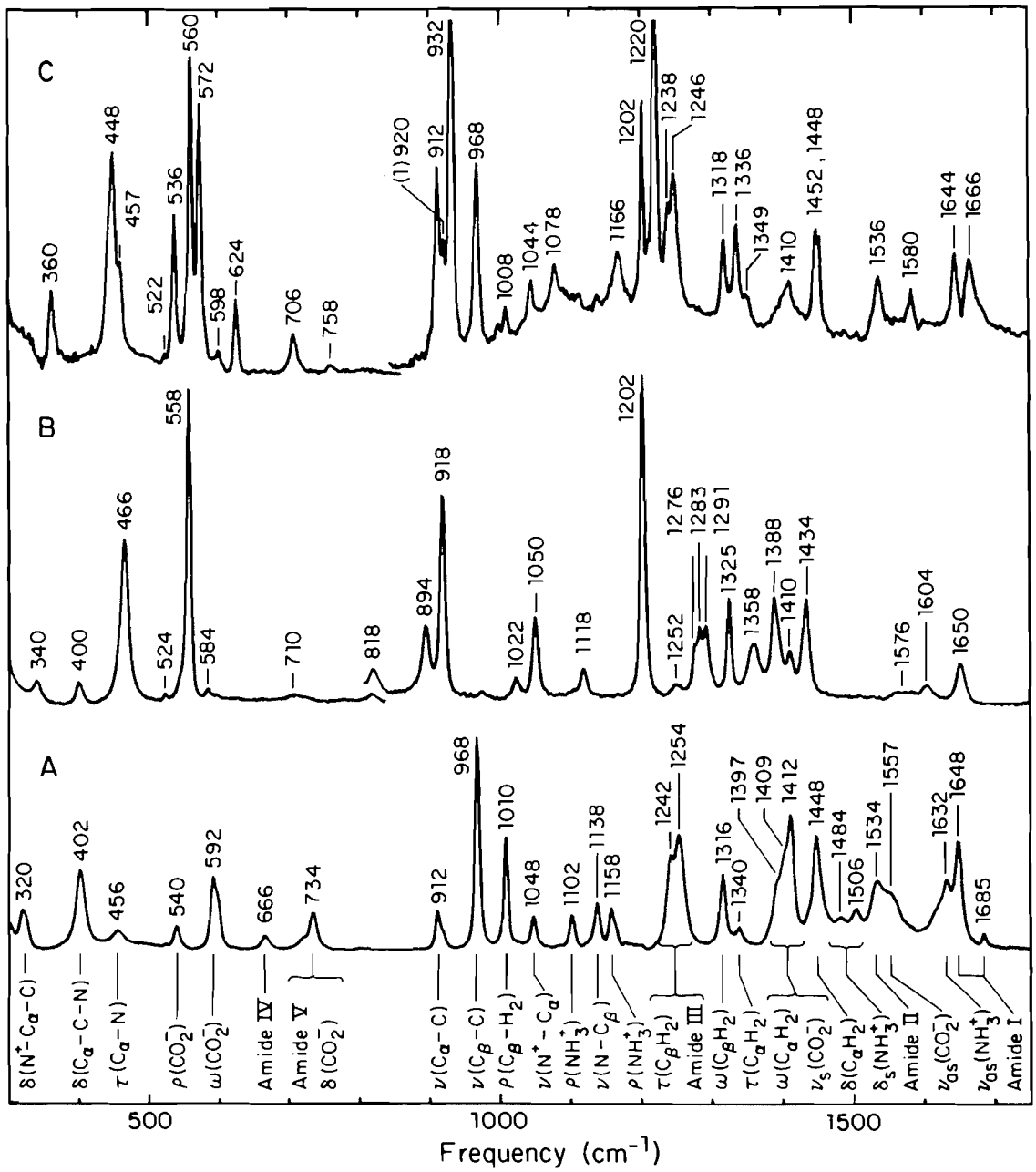

FIG. 5. Raman spectra of solid (A) glycylglycine (GlyGly), (B) $(CH_3Hg)GlyGly$, and (C) $[(CH_3Hg)_2GlyGly]ClO_4$ in the region 300–1750 cm^{-1}.

(482 cm^{-1}) (4) and adenine (470 cm^{-1}) (3), (methioninato)mercury(II) complex (481 and 518 cm^{-1}) (35), and the mercury–glycine complex (36).

In the $[(CH_3Hg)_2GlyGly]^+$ ion, the vibrations of the CH_3Hg group fixed on the NH_2-terminal section of the molecule have frequencies which are almost identical to those of (CH_3Hg)-GlyGly: the symmetric CH_3 bending mode ($\delta(CH_3)$) and $\nu(Hg—CH_3)$ vibrations occur at ~1200 and ~560 cm^{-1} respectively in both cases, whereas the $\nu(Hg—N)$ mode is shifted to ~450 cm^{-1} in the 2:1 compound, where it overlaps the ν_2 band of the perchlorate ion. This leaves the 536 cm^{-1}, 572 cm^{-1}, and 1220 cm^{-1} bands in the spectrum of the latter for the corresponding vibrations of the CH_3Hg unit linked to the carboxylate group. The assignment of the 536 cm^{-1} band to the Hg—O stretching mode is questionable, as this vibration has been given much lower frequencies in the compounds CH_3HgNO_3 (292 cm^{-1}) (32), and $CH_3HgSO_3CH_3$ (246 cm^{-1}) and $CH_3HgSO_4^-$ (273 cm^{-1}) (37). On the other hand, Green (33) has concluded from his extensive vibrational study of alkyl and aryl compounds of mercury(II) that absorptions due to Hg—O vibrations occur in the region 500–650 cm^{-1}. The antisymmetric $\nu_{as}(Hg—O)$ stretching mode of the $(CH_3Hg)_3O^+$ oxonium ion has also been given a relatively high frequency of 549 cm^{-1} (38). The $\nu(Hg—O)$ vibration of the methylmercury unit linked to the carboxylate group in $[(CH_3Hg)_2GlyGly]ClO_4$ should have a frequency somewhat lower than the corresponding $\nu(Hg—N)$ vibration of the *N*-substituted unit (466 cm^{-1} in $(CH_3Hg)GlyGly$), from the relative masses involved. However, the assignment of the 536 cm^{-1} peak to this vibration is consistent with the shorter Hg—O distance (2.09 Å vs. *r*(Hg—

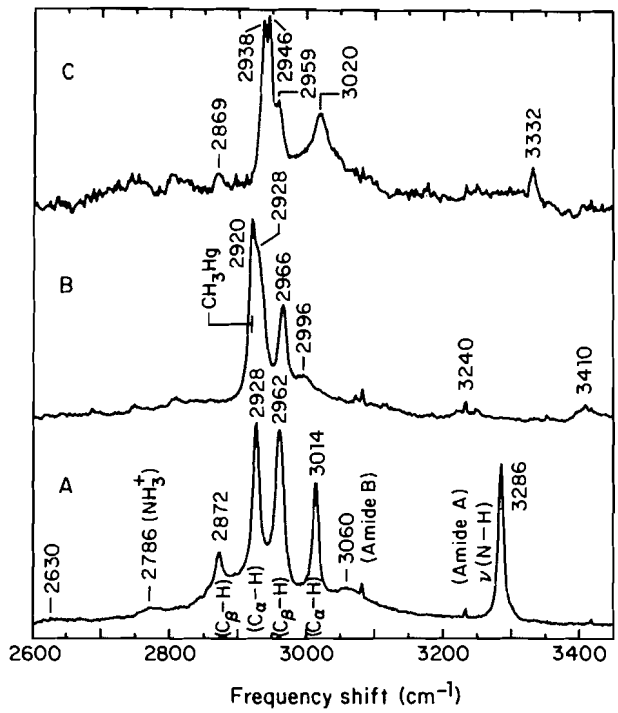

FIG. 6. High-frequency region of the Raman spectra of solid (A) glycylglycine (GlyGly), (B) (CH_3Hg)GlyGly, and (C) $[(CH_3Hg)_2$-GlyGly$]ClO_4$.

N): 2.14 Å) indicated from the X-ray study, although these values are highly uncertain. The local geometry could also be responsible for this increase of the ν(Hg—O) frequency: ∠ Hg—O—C: 121° vs. ∠ Hg—N—C: 114° and r(C—OHg): 1.31 Å vs. r(C—NHg): 1.51 Å.

—NH_3^+

The substitution of a proton of the NH_3^+ group by a CH_3Hg^+ ion in both complexes causes a disappearance of a number of bands attributable to vibrations of the protonated amino end of glycylglycine. These include the bands due to the symmetric and antisymmetric bending modes of this group near 1500 and 1630 cm^{-1} respectively, and those near 1100 and 1160 cm^{-1}, due to rocking modes. The absence of these bands in the spectra of the complexes is particularly meaningful, as they are not expected to be sensitive to other effects, such as conformational and environmental changes. The stretching modes of the NH_3^+ group are of little help in characterizing amino substitution, as they give weak and broad bands in the 3200–3250 cm^{-1} (ν_{as}) (27) and 2600–2800 cm^{-1} (ν_s) (39) regions of both the infrared and Raman spectra. Similarly, the vibrations of the NH_2 group resulting from the substitution of a proton by CH_3Hg^+ are weak, and they cannot be unambiguously identified in the spectra.

COO^-

The spectral changes associated with the neutralization of a carboxyl group and the formation of a Hg—O bond, such as in the $[(CH_3Hg)_2$GlyGly$]ClO_4$ complex, are not very characteristic when only the vibrational bands of the COO^- group are considered. The ν_{as} vibration at 1557 cm^{-1} in the Raman spectrum of GlyGly (1554/1576 cm^{-1} in the infrared) is shifted to 1580 cm^{-1} upon formation of the Hg—O bond, while the band at 1412 cm^{-1}, due to the corresponding symmetric stretching mode, loses most of its intensity. We have observed the same phenomenon with the $CH_3COOHgCH_3$ complex, where the band due to the $\nu_{as}(COO^-)$ mode of the CH_3COO^- ion shifted from 1564 to 1578 cm^{-1}, with a large intensity increase, and the band due to the $\nu_s(COO^-)$ mode at 1418 cm^{-1} showed a large decrease in intensity upon complex formation.[3] It has already been noted by Nakamoto *et al.* (41) that the shifts in frequency of the ν(CO) stretching vibrations of the COO^- group of carboxylic and amino acids are mostly confined to the asymmetric mode in such cases.

Conformation

The spectra of (CH_3Hg)GlyGly differ markedly from those of GlyGly, much more so than does that of the 2:1 complex. For example, the very strong infrared and Raman peak due to the amide N—H stretching vibration (amide A) at 3286 cm^{-1} in the spectra of GlyGly, and which is shifted to higher frequency (3332 cm^{-1}) with reduction in intensity in the Raman spectrum of the 2:1 complex, practically disappears in the spectra of (CH_3Hg)GlyGly. In fact, this band is shifted to 3240 cm^{-1} in the latter, with drastically reduced intensity. This behaviour is not directly related to the presence of CH_3Hg(II) in the complex and it must be interpreted in terms of the change in the backbone conformation of the dipeptide (see Table 4). Similar effects have been observed in the spectra of polypeptides (23, 42), a strong peak near 3290 cm^{-1} being characteristic of β-sheet structure, whereas a weak one near 3245 cm^{-1} is indicative of a non-ordered secondary structure. In the present case, both GlyGly and the 2:1 complex exist as extended molecular units, with crystal structures related to the β-sheet arrangement found in some polypeptides and proteins. On the other hand, the monosubstituted complex has a different conformation. The N(1)—C(2)—C(3)—N(5) and C(3)—N(5)—C(6)—C(7) torsion angles in this compound (−169° and −84° respectively) are better related to the ψ (= −145.3°) and φ (= −76.9°) angles measured in 3_1 helical polyglycine II (44).

A change of conformation of (CH_3Hg)GlyGly with respect to GlyGly is also indicated in other conformation-sensitive regions of the spectra (43). In the unsubstituted dipeptide, the amide III and amide I Raman bands are found at 1254 and 1665 cm^{-1} (average of the two factor-group components at 1644 and 1682 cm^{-1} (27)), whereas these vibrations occur at 1283/1291 and 1650 cm^{-1} in (CH_3Hg)GlyGly. The values for the complex are very similar to the frequencies of crystalline polyglycine II (1283 and 1654 cm^{-1}), which exists as a 3_1 helix (44). On the other hand, the frequencies of both GlyGly and the 2:1 complex are closer to those of polyglycine I (1255 and 1674 cm^{-1} (45)) which has an antiparallel rippled-sheet structure. Other conformation-related differences are evident when the Raman spectrum of (CH_3Hg)GlyGly is compared to that of GlyGly: (*i*) The very strong peak at 968 cm^{-1} in the Raman spectrum of GlyGly, assigned to the $\nu(C_\beta—C)$ stretching mode, is hardly detectable in the spectrum of (CH_3Hg)GlyGly. This region of the Raman spectrum is known to be conformation sensitive (46). (*ii*) The relative intensity of the C_α—N and C_β—N stretching modes at 1048 and 1138 cm^{-1} in the spectrum of GlyGly is strongly modified in that of (CH_3Hg)GlyGly, the peak at 1138 cm^{-1} being also shifted to 1118 cm^{-1}. (*iii*) The CH_2 bending mode at 1448 cm^{-1} in GlyGly is shifted to 1434 cm^{-1} in the *N*-substituted complex. This change parallels that observed in the spectrum of polyglycine II (3_1 helix), where this mode is shifted to a lower frequency by 12 cm^{-1}, from 1432 to 1420 cm^{-1}, with respect to polyglycine I (rippled-sheet structure) (30, 46). (*iv*) The C_β—H stretching more at 2872 cm^{-1} and the C_α—H vibration at 3014 cm^{-1} in the spectrum of

[3] S. Alex and R. Savoie, unpublished results.

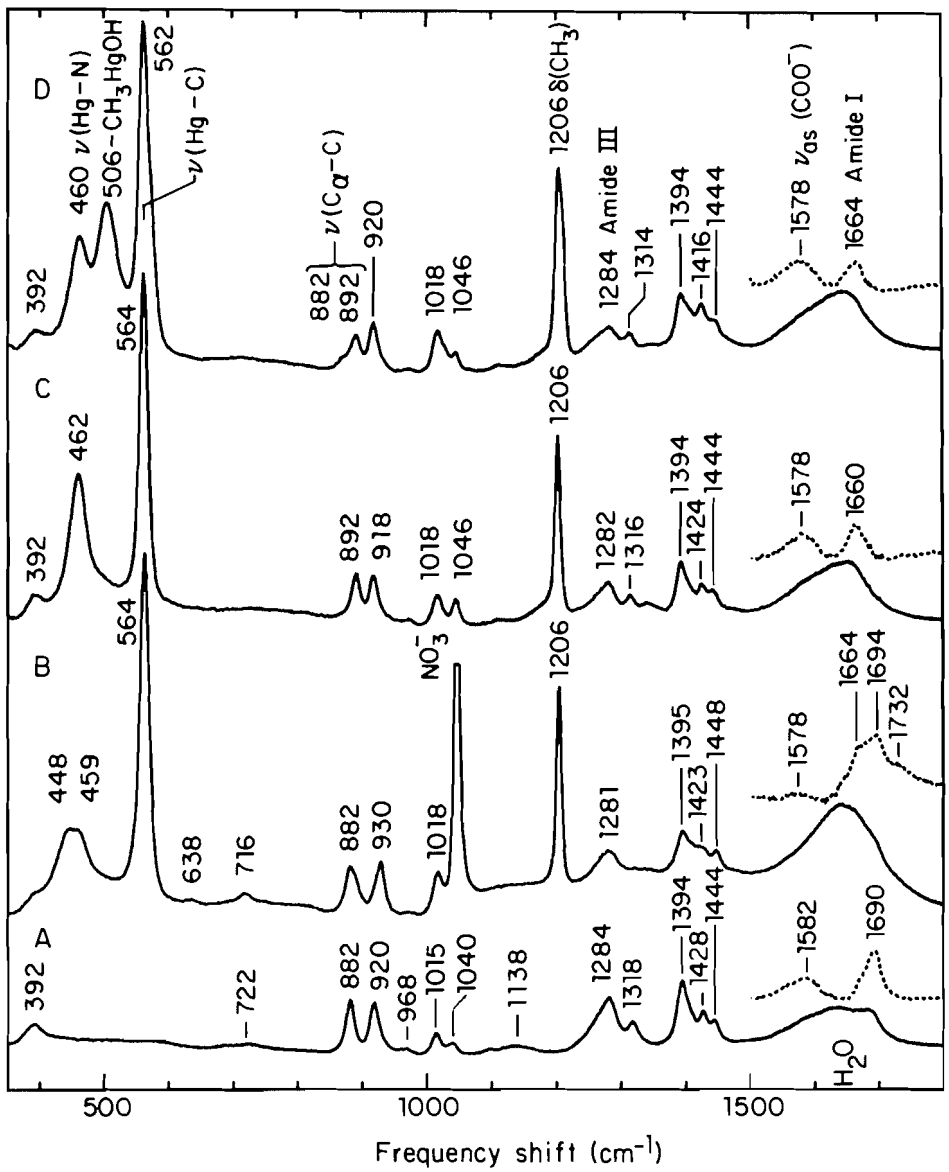

FIG. 7. Raman spectra of aqueous solutions of (A) glycylglycine (0.33 *M*) at pH = 7, and (B–D) equimolar mixtures (0.25 *M*) of glycylglycine and CH_3Hg(II) at (B) pH = 3, (C) pH = 7, and (D) pH = 9.

GlyGly merge into the central 2900–3000 cm^{-1} region of the spectrum of (CH_3Hg)GlyGly. It is noteworthy that these spectral changes, which are associated with a change in the conformation of the ligand, are more important than those expected on the basis of a mere substitution of a proton by a CH_3Hg^+ group.

Aqueous solutions

The Raman spectra of aqueous GlyGly in the presence of CH_3Hg(II) at various pH are shown in Fig. 7. The spectrum of the free species at pH 7 is also given for comparison. It shows that the dipeptide in aqueous solution has a structure that differs from that in the solid. In fact, the spectrum of aqueous GlyGly is quite similar to that of solid $CH_3HgGlyGly$, for which a bent rather than an extended structure is indicated from the spectra. The Raman spectrum of aqueous GlyGly varies little with the pH, the main changes being associated with the protonation of the carboxylic group (pK_a = 3.1) at low pH, which results in a decrease of the $\nu_{as}(COO^-)$ band at 1578 cm^{-1} and a corresponding increase in the band due to the C=O stretching mode of the COOH group at ~1730 cm^{-1}. Changes are also noted in the 900 cm^{-1} region at low pH, presumably for the same reason.

The disappearance of the 506 cm^{-1} band of CH_3HgOH from the spectrum of an equimolar aqueous mixture of GlyGly and CH_3Hg(II) at pH 7 shows that quantitative complexation of the methylmercury occurs. Furthermore, the 462 cm^{-1} band in the spectrum indicates that this occurs through substitution of a proton of the NH_3^+ group by a methylmercury ion. The presence of this sole type of complex is suggested by the sharpness of the peaks at 564 and 1206 cm^{-1}. At pH 9, the complex is partly dissociated, as evidenced by the band at 506 cm^{-1} and the shoulders present on the high-frequency side of the 562 and 1206 cm^{-1} bands. These secondary features, which are not present in the spectrum at pH 7, are attributable to CH_3HgOH (32). Note that the intensity of the 506 cm^{-1} band is misleading with regard to the actual amount of uncomplexed methylmercury in the solution, as this peak is basically much more intense than that at 462 cm^{-1}. (Full dissociation would

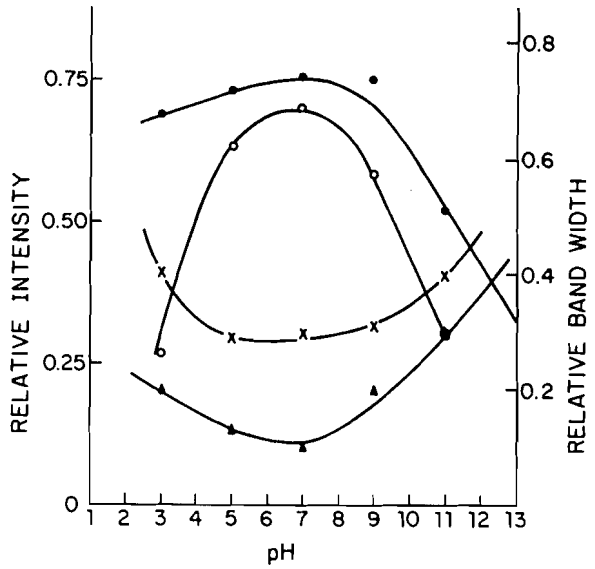

FIG. 8. Peak-height intensities of the (●) 564 (ν(Hg—C)) and (○) 462 cm^{-1} (ν(Hg—N)) Raman bands relative to the 1206 cm^{-1} ($\delta(CH_3)$) peak, and widths at half-intensity of the (×) 1206 ($\delta(CH_3)$) and (△) 564 cm^{-1} (ν(Hg—C)) bands, as a function of pH, in a 1:1 GlyGly/CH_3Hg(II) aqueous mixture.

cause the 506 cm^{-1} band to be twice as intense as that at 562 cm^{-1}, the latter being shifted to 572 cm^{-1}.)

The spectrum at pH 3 differs little from that at pH 7, except for the splitting of the 462 cm^{-1} band into an unresolved doublet at 448/459 cm^{-1}. The presence of the ~453 cm^{-1} component is quite significant, as it corresponds to the ν(Hg—O) vibration of the oxonium $CH_3HgOH_2^+$ ion (32), which also contributes to the 564 and 1206 cm^{-1} peaks.

Although it is not possible to determine accurately from the spectra the extent of complexation of GlyGly and CH_3Hg^+ in aqueous solutions at various pH, spectral changes in the bands associated with free and complexed CH_3Hg(II) clearly indicate that complexation is maximum near pH 7 (Fig. 8). The variation in intensity of the ν(N—$HgCH_3$) band at 462 cm^{-1} is particularly revealing in this respect, as it is not perturbed by other bands. The widths of the $\delta(CH_3)$ and ν(Hg—CH_3) bands are also indicative of the extent of the complexation, as these peaks become sharper when the concentration of the complexed species increases. This occurs because neighboring bands due to free methylmercury vanish upon complexation.

Methylmercury has been shown by ^1H nmr to react with the COO^- group of selected carboxylic and amino-carboxylic acids at low pH (15, 16, 40). In the present study, we have had no indication from the Raman spectra that this type of complexation occurs to any appreciable extent in aqueous solutions of GlyGly and CH_3Hg(II) at any pH between 1 and 6, even for a [CH_3Hg(II)]/[GlyGly] molar ratio of 2.

Subtraction of the spectrum of the solvent from those of the solutions permits the direct observation of the amide I band of the ligand in the 1650 cm^{-1} region (Fig. 7). This band surprisingly occurs at 1690 cm^{-1} in the spectrum of an aqueous solution of GlyGly at neutral pH, a value which is much higher than in solid GlyGly (1648/1682 cm^{-1}) and in crystalline (CH_3Hg)GlyGly (1650 cm^{-1}). This could mean that the conformation of GG changes upon dissolution in water. However, this hypothesis is not corroborated by the rest of the spectrum, particularly from the frequency of the amide III band, which remains unchanged at ~1280 cm^{-1}. More likely, the observed change in the amide I region is caused by a disruption of the hydrogen bonding network around the protonated amino group.

Substitution of a proton of the NH_3^+ group by a CH_3Hg^+ ion also shifts the amide I band from 1690 to 1660 cm^{-1}, the same effect being observed when the pH of an aqueous solution of free GlyGly is raised to high values (≧9), possibly as a result of the deprotonation of the NH_3^+ group. This emphasizes the fact that the spectral modifications associated with protonation, hydrogen bond formation, and conformational changes can be just as important as those resulting from the formation of a complex. However, the changes in the regions of the Raman spectra where vibrations involving the highly polarizable mercury atom occur are very characteristic, and they do reflect quite accurately the state, as well as the nature, of the sites involved in the complexation of peptides.

Acknowledgements

Financial support of this work by the Natural Sciences and Engineering Research Council of Canada and by the Ministère de l'Education du Québec is gratefully acknowledged. We also wish to thank M. J. Olivier for the collection of the X-ray data.

1. L. PRIZANT, M. J. OLIVIER, R. RIVEST, and A. L. BEAUCHAMP. J. Am. Chem. Soc. **101**, 2765 (1979); L. PRIZANT, M. J. OLIVIER, R. RIVEST, and A. L. BEAUCHAMP. Can. J. Chem. **59**, 1311 (1981); J. P. CHARLAND, M. SIMARD, and A. L. BEAUCHAMP. Inorg. Chim. Acta, **80**, L57 (1983); F. GUAY, A. L. BEAUCHAMP, C. GILBERT, and R. SAVOIE. Can. J. Spectrosc. **28**, 13 (1983).
2. L. PRIZANT, R. RIVEST, and A. L. BEAUCHAMP. Can. J. Chem. **59**, 2290 (1981).
3. R. SAVOIE, J.-J. JUTIER, L. PRIZANT, and A. L. BEAUCHAMP. Spectrochim. Acta, Part A, **38**, 561 (1982).
4. R. SAVOIE, D. POIRIER, L. PRIZANT, and A. L. BEAUCHAMP. J. Raman Spectrosc. **11**, 481 (1981).
5. E. BUNCEL, B. K. HUNTER, R. KUMAR, and A. R. NORRIS. J. Inorg. Biochem. **20**, 171 (1984); A. J. CANTY, R. S. TOBIAS, N. CHAICHIT, and B. M. GATEHOUSE. J. Chem. Soc. Dalton Trans. 1693 (1980); S. MANSY and R. S. TOBIAS. Biochemistry, **14**, 2952 (1975); R. B. SIMPSON. J. Am. Chem. Soc. **86**, 2059 (1964).
6. J. T. MACGREGOR and T. W. CLARKSON. Protein metal interactions, *Edited by* M. L. Friedman. Plenum Press, New York. 1974. p. 463; A. J. CARTY and S. F. MALONE. The biogeochemistry of mercury in the environment. *Edited by* J. O. Nriager. Elsevier, Amsterdam. 1979. Chapt. 17.
7. D. J. ABRAHAM, S. E. V. PHILLIPS, and P. E. KENNEDY. J. Mol. Biol. **170**, 249 (1983); S. L. MOWBRAY and G. A. PETSKO. J. Biol. Chem. **258**, 5634 (1983); V. Z. PLETNEV, I. N. TSYGANNIK, and V. A. POPOVICH. Kristallografiya, **28**, 708 (1983).
8. Y. S. WONG, A. J. CARTY, and C. CHIEH. J. Chem. Soc. Dalton Trans. 1801 (1977); Y. S. WONG, N. J. TAYLOR, P. C. CHIEH, and A. J. CARTY. J. Chem. Soc. Chem. Commun. 625 (1974); Y. S. WONG, P. C. CHIEH, and A. J. CARTY. Can. J. Chem. **51**, 2597 (1973).
9. Y. HOJO, Y. SUGIURA, and H. TANAKA. J. Inorg. Nucl. Chem. **38**, 641 (1976).
10. R. S. REID and D. L. RABENSTEIN. Can. J. Chem. **59**, 1505 (1981).
11. N. J. TAYLOR, Y. S. WONG, P. C. CHIEH, and A. J. CARTY. J. Chem. Soc. Dalton Trans. 438 (1975)
12. D. L. RABENSTEIN and R. S. REID. Inorg. Chem. **23**, 1246 (1984).
13. C. PERCHARD, M. H. BARON, and C. DE LOZE. J. Mol. Struct. **112**, 247 (1984).

14. A. J. CANTY, A. J. CARTY, and S. F. MALONE. J. Inorg. Biochem. **19**, 133 (1983).
15. D. L. RABENSTEIN, R. OZUBKO, S. LIBICH, C. A. EVANS, M. T. FAIRHURST, and C. SUVANPRAKORN. J. Coord. Chem. **3**, 263 (1974).
16. D. L. RABENSTEIN. Acc. Chem. Res. **11**, 100 (1978).
17. N. W. ALCOCK, P. A. LAMPE, and P. MOORE. J. Chem. Soc. Dalton Trans. 1324 (1978).
18. F. ALLAIRE and A. L. BEAUCHAMP. Can. J. Chem. **62**, 2249 (1984).
19. F. BÉLANGER-GARIÉPY and A. L. BEAUCHAMP. J. Am. Chem. Soc. **102**, 3461 (1980).
20. D. T. CROMER and J. T. WABER. Acta Crystallogr. **18**, 104 (1965); R. F. STEWART, E. R. DAVIDSON, and W. T. SIMPSON. J. Chem. Phys. **42**, 3175 (1965); D. T. CROMER. Acta Crystallogr. **18**, 17 (1965).
21. M. AUTHIER-MARTIN and A. L. BEAUCHAMP. Can. J. Chem. **55**, 1213 (1977).
22. D. GRDENIC and M. SIKIRICA. Z. Kristallogr. **150**, 107 (1979); R. D. BACH, R. A. WOODWARD, J. T. ANDERSON, and M. D. GLICK. J. Org. Chem. **47**, 3707 (1982); D. GRDENIC, B. KAMENAR, B. KORPAR-COLIG, M. SIKIRICA, and G. JOVANOVSKI. Cryst. Struct. Commun. **11**, 565 (1982); B. KAMENAR and M. PENAVIC. Inorg. Chim. Acta, **6**, 191 (1972); R. ALLMAN and H. MUSSO. Chem. Ber. **106**, 3001 (1973).
23. A. B. BISWAS, E. W. HUGHES, B. D. SHARMA, and J. N. WILSON. Acta Crystallogr. Sect. B, **24**, 40 (1968).
24. E. W. HUGHES. Acta Crystallogr. Sect. B, **24**, 1128 (1968).
25. G. H. STOUT and L. H. JENSEN. X-ray structure determination, a practical guide. Macmillan, London. 1968. p. 303.
26. M. J. OLIVIER and A. L. BEAUCHAMP. Acta Crystallogr. Sect. B, **38**, 2159 (1982); A. L. BEAUCHAMP. J. Cryst. Mol. Struct. **10**, 149 (1980).
27. P. LAGANT, G. VERGOTEN, M. H. LOUCHEUX-LEFEBVRE, and G. FLEURY. Biopolymers, **22**, 1267 (1983).
28. C. DESTRADE, E. DUPART, M. JOUSSOT-DUBIEN, and C. GARRIGOU-LAGRANGE. Can. J. Chem. **52**, 2590 (1974).
29. A. M. DWIVEDI and V. D. GUPTA. Biopolymers, **11**, 2091 (1972).
30. M. SMITH, A. G. WALTON, and J. L. KOENIG. Biopolymers, **8**, 29 (1969).
31. J. F. PEARSON and M. A. SLIFKIN. Spectrochim. Acta, Part A, **28**, 2403 (1972).
32. J. H. R. CLARKE and L. A. WOODWARD. Trans. Faraday Soc. **62**, 3022 (1966).
33. J. H. S. GREEN. Spectrochim. Acta, Part A, **24**, 863 (1968).
34. D. L. RABENSTEIN, M. C. TOURANGEAU, and C. A. EVANS. Can. J. Chem. **54**, 2517 (1976).
35. Y. K. SZE, A. R. DAVIS, and G. A. NEVILLE. Inorg. Chem. **14**, 1969 (1975); Y. S. WONG, A. J. CARTY, and P. C. CHIEH. J. Chem. Soc. Dalton Trans. 1157 (1977).
36. T. V. LONG II and C. M. YOSHIDA. Inorg. Chem. **7**, 1754 (1967).
37. J. H. R. CLARKE and L. A. WOODWARD. Trans. Faraday Soc. **64**, 1041 (1968).
38. J. H. R. CLARKE and L. A. WOODWARD. Spectrochim. Acta, Part A, **23**, 2077 (1967).
39. C. BRISSETTE and C. SANDORFY. Can. J. Chem. **38**, 34 (1960).
40. S. LIBICH and D. L. RABENSTEIN. Anal. Chem. **45**, 118 (1973).
41. K. NAKAMOTO, Y. MORIMOTO, and A. E. MARTELL. J. Am. Chem. Soc. **83**, 4528 (1961); Y. INOMATA, T. KAKEUCHI, and T. MARIKAWI. Spectrochim. Acta, Part A, **40**, 179 (1984).
42. R. LINDEMANN and G. ZUNDEL. Biopolymers, **17**, 1285 (1978).
43. A. T. TU. Raman spectroscopy in biology: principles and applications. John Wiley and Sons, New York. (1982).
44. A. M. DWIVEDI and S. KRIMM. Biopolymers, **21**, 2377 (1982).
45. A. M. DWIVEDI and S. KRIMM. Macromolecules, **15**, 177 (1982).
46. J. L. KOENIG. Macromol. Rev. **6**, 59 (1972).

Long-range proton coupling constants and molecular orbital calculations as indicators of conformational populations of benzene-1,2- and -1,3-dicarbaldehydes

TED SCHAEFER, GLENN H. PENNER, RUDY SEBASTIAN, AND CRAIG S. TAKEUCHI[1]
Department of Chemistry, University of Manitoba, Winnipeg, Man., Canada R3T 2N2

Received June 19, 1985

TED SCHAEFER, GLENN H. PENNER, RUDY SEBASTIAN, and CRAIG S. TAKEUCHI. Can. J. Chem. **64**, 158 (1986).

The ^{1}H nmr spectra of the benzene-1,2- and -1,3-dicarbaldehydes in carbon tetrachloride, benzene-d_6, and acetone-d_6 solutions at 300 K are analyzed. The stereospecific long-range couplings over five formal bonds between the sidechain and ring protons show that the 1,2 isomer exists as an 87:13 mixture of the *cis–trans* and *trans–trans* conformers in carbon tetrachloride. These populations are insensitive to solvent. Molecular orbital calculations utilizing extensive geometry optimization procedures imply that the *cis–cis* form, with proximate C=O bonds, is indeed of negligible significance as assumed in obtaining the populations of the other forms. Further calculations define a pathway of relatively low energy for interconversion of the two abundant forms, in agreement with dynamic nmr studies. For the 1,3 isomer the long-range couplings provide a check of the conformer populations deduced from dipole moment and ^{13}C nmr studies. For example, if the *cis–trans* form is 70% abundant, as deduced from the dipole moment in benzene solution, then the long-range couplings imply that the population of the *cis–cis* conformer is insignificant.

TED SCHAEFER, GLENN H. PENNER, RUDY SEBASTIAN et CRAIG S. TAKEUCHI. Can. J. Chem. **64**, 158 (1986).

On analyse les spectres rmn du ^{1}H des benzène dicarbaldehydes-1,2 et -1,3 qui ont été mesurés à 300 K et dans des solutions dans le tétrachlorure de carbone, le benzène-d_6 et l'acétone-d_6. Le couplage stéréospécifique à longue distance à travers cinq liaisons normales entre les protons du cycle et ceux de la chaîne latérale indique que dans le tétrachlorure de carbone l'isomère 1,2 existe sous la forme d'un mélange à 87:13 des conformères *cis–trans* et *trans–trans*. Le solvant n'a aucune influence sur cette répartition. Les calculs d'orbitales moléculaires, faisant appel à des procédés extensifs d'optimisation géométrique, suggèrent que la forme *cis–cis* ayant des liaisons s'approchant de C=O n'a pratiquement aucune importance dans la détermination des populations des autres formes. Des calculs plus poussés définissent un chemin réactionnel de faible énergie pour l'interconversion des deux formes abondantes et ceci est en accord avec les études de la rmn dynamique. Dans le cas de l'isomère-1,3, les couplages à longue distance constituent une vérification des populations des conformères qui ont été déduites à partir des études du moment dipolaire et de la rmn du ^{13}C. Par exemple, si la forme *cis–trans* est à 70%, tel que déduit à partir du moment dipolaire en solution dans le benzène, alors le couplage à longue distance implique que la population de la forme *cis–cis* n'est pas significative.

[Traduit par le journal]

Introduction

The conformational preferences of the benzenedicarbaldehydes in solution have been investigated by a variety of techniques. The 1,2 isomer is often discussed in terms of three planar forms, for which the *ct* conformer has a statistical weight of two. Because the barrier to internal rotation in benzaldehyde is at least 19.5 kJ/mol in the gas phase (1–3) and about 30 kJ/mol in solution (4, 5), at ambient temperatures this approach seems reasonable, except perhaps for the *cc* form in which steric or electrostatic repulsions between the carbonyl bonds compete with the conjugation energy favoring planarity.

Indeed, based on extensive STO 3G MO computations that, however, did not utilize geometry optimization procedures, it was argued that the 1,2 isomer has three nonplanar stable conformers (6). The calculated populations gave a net dipole moment in good agreement with that measured in dioxane solution at 298 K (6). Alternatively, if only the planar *tt* and *ct* forms existed in dioxane, then the *ct* form was 60% abundant at this temperature (6). The same assumption, applied to the dipole moment in benzene solution, led to 64% as the abundance of the *ct* conformer (7). In the latter study, the dipole moment did not change significantly between 287 and 327 K.

The ^{13}C nmr spectrum of the 1,2 isomer in a 0.5 *M* Freon solution gave no indication of restricted rotation at the lowest attainable temperatures (8). Force field calculations suggested that the barrier to internal rotation in this isomer is rather lower than for the other two isomers, for which spectra arising from

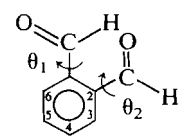

ct

$\theta_1 = \theta_2 = 0°$

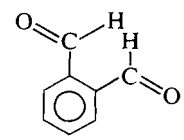

tt

$\theta_1 = 0°, \theta_2 = 180°$

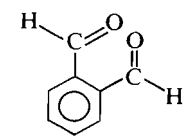

cc

$\theta_1 = 180°, \theta_2 = 0°$

the individual conformers could be observed (8). It also appeared that ^{1}H,^{13}C couplings could not be used as indicators of conformer populations (8).

Turning to the 1,3 isomer, dipole moments in benzene solution imply the presence of all three conformers (7), the double weighted *ct* form being 70% abundant near room temperature. In dioxane solution, the observed dipole moment was considered to be in reasonable agreement with a 0.18:0.56:0.26 ratio of *cc*/*ct*/*tt* forms, as was the Kerr constant (6). At 132 K in 0.5 *M* Freon solution, the ^{13}C nmr peak intensities yielded a ratio of 0.15:0.58:0.27 (8).

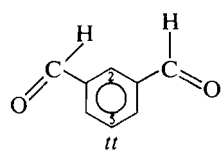

tt

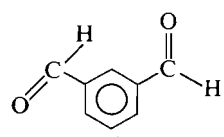

ct

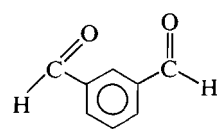

cc

Now, it is known that $^5J(H, CHO) \equiv {}^5J$, in benzaldehyde and its derivatives, is stereospecific (9–12).

In **1**, ^5J(H-3, CHO) $\equiv {}^5J_t$ is 0.76 Hz and ^5J(H-5, CHO) $\equiv {}^5J_c$ is 0.00 Hz to within experimental error. That is, if the aldehyde group is held in one orientation, say by an intramolecular

[1]Undergraduate research participant, 1984–1985.

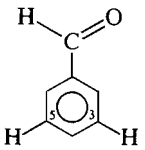

1

hydrogen bond, no ^5J_c is observable under conditions of very high resolution (13). The magnitude of ^5J_t changes slightly in the presence of an electronegative *ortho* substituent. This perturbation can be incorporated into conformational deductions.

For the 1,2 isomer, two ^5J values are in principle available from spectral analysis and can be used for conformational assessments. For the 1,3 isomer, only one ^5J is present, yet its value is useful as a check of possible conformer distributions. For example, the *tt* conformer has a large ^5J while the *cc* conformer should display no ^5J at all. The 1,4 isomer has degenerate chemical shifts for the ring protons and is not amenable to this approach. In any event, the ^{13}C nmr and dipole moment studies agree that it exists in equal proportions of the *ct* and *cc* conformers (6–8, 14).

Accordingly, the ^1H nmr spectra were analyzed for CCl_4, C_6D_6, and $(CD_3)_2C{=}O$ solutions of the 1,2 and 1,3 isomers. Furthermore, extensive geometry optimizations at the STO 3G level of molecular orbital theory were performed, particularly for the 1,2 isomer in which considerable bond angle deformations are likely to exist. This paper reports on the conformational deductions reached in this manner.

Experimental

The benzene-1,2- and -1,3-dicarbaldehydes (Aldrich) were prepared as 4.0 mol% solutions in CCl_4, C_6D_6, and $(CD_3)_2C{=}O$, which also contained a few drops of tetramethylsilane. The CCl_4 solutions had 10 mol% of C_6D_{12} as an internal lock material. These solutions were transferred to 5-mm od nmr sample tubes, were degassed by a number of freeze–pump–thaw cycles, and the tubes were then flame sealed.

The ^1H nmr spectra were accumulated on a Bruker AM 300 spectrometer at a probe temperature of 300 K. A wide sweepwidth survey spectrum was obtained in order to reference the spectrum with respect to TMS, and to locate the aromatic and sidechain regions. Each region was examined in detail, with sweepwidth and data size adjusted to give acquisition times of approximately 40 s. Four to sixteen scans were acquired. Zero filling to twice the original data size was done before transforming the FIDs using an exponential broadening of −0.1 and a gaussian multiplication of 0.6. Line widths at half height were approximately 0.05 Hz after this resolution enhancement (see Fig. 1).

The STO 3G MO (15) computations utilized the program Monstergauss (16). INDO MO (17) and INDO MO FPT (18, 19) calculations were also performed on an Amdahl 470/V8 system.

Results and discussion

Spectral analyses

These were done with the computer program NUMARIT (20), as modified in this laboratory. The ^1H nmr spectra of the 1,2 isomer arise from AA′BB′XX′ spin systems. Even though most calculated transitions were assigned and the root mean square deviations were ≤0.01 Hz, some significant correlations existed among the spectral parameters. These are given in Table 1.

Table 2 contains the ^1H nmr spectral parameters for the 1,3 isomer in three solvents. The spectra correspond to ABCC′XX′ spin systems, but in C_6D_6 solution the iterations diverged for such an approach. This occurred because of the particular magnitudes of the coupling constants and chemical shift differences. Therefore the spectrum was analyzed as if it arose from an ABC_2X_2 spin system. For the other two solutions, the spectra were analyzed in both ways. It turned out that the parameter of interest, $^5J(H,CHO)$, had the same value in both analyses for a given solution. $^4J_{46}$, the coupling between H-4 and H-6, could not be established.

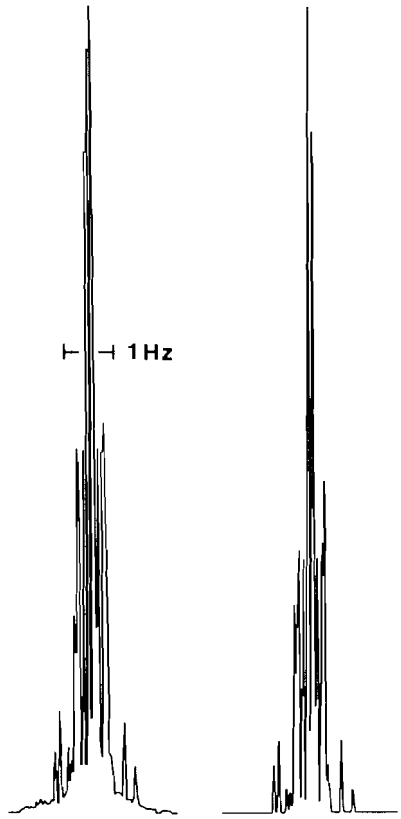

FIG. 1. The observed and calculated ^1H nmr spectra, at 300 MHz and 300 K, of the aldehyde protons in benzene-1,3-dicarbaldehyde as a 4.0 mol% solution in C_6D_6. The spectrum was accumulated as described in the text. The line width at half height is about 0.05 Hz. The computed spectrum assumed a lorentzian line shape and the plotter had some difficulty in reproducing the closely spaced peaks.

STO 3G MO computations

Previous computations of conformational energies (6, 7) did not use geometry optimization procedures, which should be particularly important for the 1,2 isomer. Because previous computations implied stable nonplanar conformers for the 1,2 isomer and because their abundant presence would complicate the conformational analysis, the present calculations used extensive geometry optimizations in an attempt at establishing the presence of nonplanar minima in the energy.

Calculations on benzaldehyde, in which the benzene moiety was held as a regular hexagon but all other bond angles and lengths were allowed to vary, gave eq. [1] as the potential function for rotation about the exocyclic C—C bond. Here $\theta = 0$ corresponds to the planar conformer and the fit uses seven angular values (15° intervals). At the 95% confidence level, the barrier is calculated as predominantly twofold with a small fourfold component. Full geometry optimization, allowing *all* angles and lengths to vary, yields an energy difference of 24.1 kJ/mol between the planar and perpendicular conformers. Microwave and far infrared spectra give an assumed twofold barrier of 19.5–20.5 kJ/mol (1, 3), so that the present calcula-

TABLE 1. ^{1}H nmr spectral parameters at 300 MHz and 300 K for benzene-1,2-dicarbaldehyde in CCl_4, C_6D_6, and $(CD_3)_2C{=}O$ solutions

Parameter	Value		
	CCl_4	C_6D_6	$(CD_3)_2CO$
ν(CHO)[a]	3141.666(1)[b]	3054.902(2)[c]	3166.113(1)[d]
$\nu_3 = \nu_6$	2376.863(1)	2217.036(1)	2410.802(1)
$\nu_4 = \nu_5$	2316.908(1)	2089.088(1)	2365.742(1)
$^3J_{34} = {}^3J_{56}$	7.653(1)[e]	7.659(2)	7.662(1)
$^3J_{45}$	7.493(2)	7.500(2)	7.517(2)
$^4J_{35} = {}^4J_{46}$	1.295(2)	1.286(2)	1.279(2)
^4J(H, CHO)	−0.228(1)	−0.236(2)	−0.231(1)
$^5J_{36}$	0.504(1)	0.507(2)	0.513(2)
^5J(H-4, CHO)	0.439(1)	0.439(2)	0.445(1)
^5J(H-3, CHO)	0.339(1)	0.329(2)	0.324(2)
^5J(CHO, CHO)	−0.000(1)	−0.000(2)	−0.000(2)
^6J(H, CHO)	−0.036(2)[f]	−0.040(3)[f]	−0.051(3)[f]
Calculated transitions	180	182	180
Assigned transitions	165	165	164
Peaks observed	82	90	78
Largest difference	0.022	0.024	0.025
RMS deviation	0.007	0.010	0.009
^5J(H-3, CHO)/$^5J_{36}$	0.43[g]	0.53	0.46
^5J(H-3, CHO)/^6J(H, CHO)	0.53	0.68	0.68
$^4J_{35}/{}^3J_{45}$	−0.63	−0.63	−0.63

[a]Chemical shifts in Hz at 300.135 MHz to high frequency of internal TMS.
[b]4.0 mol% in CCl_4 containing 10 mol% of C_6D_{12} and 0.5 mol% TMS.
[c]4.0 mol% in C_6D_6 with 0.5 mol% TMS.
[d]4.0 mol% in $(CD_3)_2C{=}O$ with 0.5 mol% TMS.
[e]Numbers in parentheses are standard deviations in the last significant figure.
[f]No splittings actually observed.
[g]Correlations between the indicated parameters.

TABLE 2. ^{1}H nmr spectral parameters at 300 MHz for benzene-1,3-dicarbaldehyde in CCl_4, C_6D_6, and $(CD_3)_2C{=}O$ solutions

Parameter	Value				
	CCl_4		C_6D_6	$(CD_3)CO$	
ν(CHO)[a]	3024.262(1)[b]		2856.934(1)[c]	3054.942(1)[d]	
ν_2	2494.159(1)[e]		2333.326(1)	2534.962(1)	
$\nu_4 = \nu_6$	2429.884(1)		2261.911(1)	2472.021(1)	
ν_5	2307.315(1)		2063.489(1)	2354.529(1)	
$^3J_{45} = {}^3J_{56}$	7.613(1)[f]	7.613(1)[g]	7.625(1)[h]	7.636(1)[f]	7.636(1)[g]
$^4J_{24} = {}^4J_{26}$	1.662(1)	1.662(1)	1.674(1)	1.681(1)	1.681(1)
$^4J_{46}$	2.052(402)[i]	—	—	0.987(217)[i]	—
^4J(H-2, CHO)	−0.101(1)	−0.100(1)	−0.103(1)	−0.106(1)	−0.106(1)
^4J(H-4, CHO)	−0.151(1)[i]	−0.064(1)[i]	−0.071(1)	−0.135(1)[i]	−0.068(1)[i]
$^5J_{25}$	0.605(1)	0.605(1)	0.602(1)	0.614(1)	0.616(2)
^5J(H-5, CHO)	0.483(1)	0.482(1)	0.496(1)	0.438(1)	0.438(1)
^6J(H-4, CHO)	0.023(17)[i]	—	—	0.001(14)[i]	—
^6J(C*H*O, C*H*O)	0.032(98)[i]	—	—	0.013(59)[i]	—
Calculated transitions	128	128	128	128	128
Assigned transitions	113	111	119	105	106
Peaks observed	69	69	74	69	69
Largest difference	0.010	0.017	0.015	0.017	0.026
RMS deviation	0.003	0.004	0.005	0.005	0.006

[a]Chemical shifts in Hz at 300.135 MHz to high frequency of internal TMS.
[b]4.0 mol% in CCl_4 containing 10 mol% C_6D_{12} and 0.5 mol% TMS.
[c]4.0 mol% in C_6D_6 containing 0.5 mol% TMS.
[d]4.0 mol% in $(CD_3)_2C{=}O$ containing 0.5 mol% TMS.
[e]Numbers in parentheses are the standard deviations in last significant figure, but see footnote [i].
[f]Analyzed as an ABCC′XX′ spin system. See text.
[g]Analyzed as an ABC_2X_2 spin system. See text.
[h]Parameters from an ABC_2X_2 analysis; iterations diverged for an ABCC′XX′ analysis.
[i]Due to the magnitudes of the couplings and the chemical shift differences, these parameters are not known; that is, the spectrum is insensitive to their values. ^6J(H-4, CHO) and $^4J_{46}$ are almost completely correlated, at 0.97.

TABLE 3. Relative energies of the conformers[a] of benzene-1,2-dicarbaldehyde calculated by geometry optimized STO 3G MO methods

θ_1 (deg)[b]	θ_2 (deg)	Energy (kJ/mol)	θ_1 (deg)	θ_2 (deg)	Energy (kJ/mol)
0	0	0.00[c]	0	30[d]	3.27
0	180	4.45[c]	0	60	11.95
180	0	20.32[c]	0	90	13.59
0	90	16.81	0	120	13.05
90	90	39.55	0	150	6.73
90	270	37.65	0	180	4.45

[a]The energies are given for structures in which the carbon framework of the benzene moiety is held as a regular hexagon but all other bond angles and lengths are optimized. The energy of the 0,0 conformer is −450.345 054 au.

[b]$\theta_1 = \theta_2 = 0$ defines the *cis–trans* or *ct* conformer, see structure in text.

[c]When *all* bond angles and lengths are optimized, the 0,0 conformer has an energy of −450.345 590 au and the 0,180 (*tt*) form is less stable by 4.50 kJ/mol while the 180,0 (*cc*) form is 18.81 kJ/mol less stable.

[d]The angles in this column identify one low-energy pathway of interconversion between the *ct* and *tt* conformers, the *cc* conformer having an insignificant population at 300 K.

tions somewhat overestimate the barrier. In the liquid or in solution, however, the internal barrier is nearer 30 kJ/mol.

[1] $V(\theta) = (24.26 + 0.05) \sin^2 \theta - (0.53 \pm 0.06) \sin^2 2\theta$

Perhaps, therefore, STO 3G MO computations on the 1,2 and 1,3 isomers will yield useful information on the stability of nonplanar conformers, in the sense that, although the calculations overestimate the energy necessary to break the π electron conjugation by a few kJ/mol in the gas phase, the presence of solvent will tend to compensate for the overestimation.

In fact, for the 1,3 isomer it is highly unlikely that nonplanar conformers are abundant at 300 K in solution, since the free energy of activation for interconversion of the planar conformers is 31.0 ± 0.5 kJ/mol at 163 K, the entropy of activation being small (8). Optimization of the geometry, with the constraint of a regular hexagon for the carbon network of the benzene entity, gave the *tt* form as 0.35 kJ/mol higher in energy than the *ct* form. The latter had an energy of −450.349907 au.

Some STO 3G MO results for the 1,2 isomer appear in Table 2. As expected, the *ct* form is most stable, followed by the *tt* form at 4.45 kJ/mol. The *cc* form is computed as 20.32 kJ/mol less stable than the *ct* form. This is up to 600 kJ/mol lower than that computed (6, 7) without bond angle and bond length relaxation. Nevertheless, the population of the *cc* form is expected to contribute negligibly to the conformational equilibrium at ambient temperatures, at least in the absence of substantial solvent perturbations of the conformer stabilities.

To test the possibility of relatively low rotational barriers in the 1,2 isomer, as indicated by the force field calculations and by the ^{13}C nmr data, one low-energy pathway between the *ct* and *tt* conformers is given in Table 3. The barrier to interconversion is only 13.6 kJ/mol. If 5 kJ/mol is added to this value to account for the overestimate expected on the basis of the computations for benzaldehyde above, but partially compensated by the solvent effect on the barrier of benzaldehyde, then the failure to observe ^{13}C nmr spectra of the *cc* and *tt* forms at the lowest temperatures attained (8) is rationalized. To trace out a complete rotational surface computationally would be very expensive.

To test, in a relatively inexpensive manner, whether the planar 1,2 conformers can lower their energy by out-of-plane rotations (6), *complete* optimizations were done in which the rotational angles θ_1 and θ_2 were also allowed to change and in which the benzene framework was allowed to distort from a hexagon. The conformers remained planar during these calculations, the energy of the *ct* form decreased to −450.345590 au, and the *tt* and *cc* forms lay 4.50 and 18.81 kJ/mol above *ct* in energy. Figure 2 displays the calculated geometry of the *cc* form, showing large angle distortions.

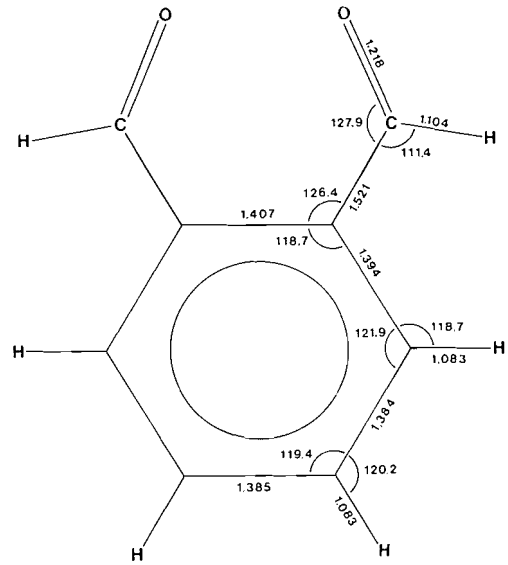

FIG. 2. The geometry of the planar *cis–cis* conformer of benzene-1,2-dicarbaldehyde as computed by STO 3G MO methods. Note the large deviations from a standard geometry, accounting for the fact that the relative energy of this structure is more than an order of magnitude lower than the computed energies in the literature (6, 7).

$^5J(H, CHO) \equiv {}^5J$ *and the conformational populations*

(i) The 1,2 isomer

According to the immediately preceding relative energies, the fractional populations in the gas phase are 0.92, 0.08, and 0.00 for the *ct*, *tt*, and *cc* forms, respectively, at 300 K.

In terms of the stereospecific properties of ^5J discussed in the introduction, namely that ^5J_t is large and ^5J_c vanishes, one has eqs. [2]–[4]. However, these equations are not linearly independent. If it is assumed that p_{cc} is zero, as seems likely form the computations above, then p_{ct} and p_{tt} follow from eqs. [2]–[4]. Note that $^5J_t = {}^5J_{26} + {}^5J_{24}$ is 0.778(2), 0.768(4), and 0.768(3) Hz in CCl_4, C_6D_6, and $(CD_3)_2C{=}O$ solutions, respectively. These numbers are very near the 0.76 Hz reported for benzaldehyde (21), implying a negligible intrinsic perturbation of ^5J by

the second substituent. The ratios of p_{ct}/p_{tt} follow as 0.87: 0.13, 0.86: 0.14, and 0.84:0.16 in CCl_4, C_6D_6, and $(CD_3)_2C{=}O$, respectively.

$$[2] \quad {}^5J_{24} = p_{ct}{}^5J_t/2 + p_{tt}{}^5J_t + 0p_{cc}$$

$$[3] \quad {}^5J_{26} = p_{ct}{}^5J_t/2 + 0p_{tt} + {}^5J_t p_{cc}$$

$$[4] \quad 1 = p_{ct} + p_{tt} + p_{cc}$$

These ratios are much larger than 0.64:0.36 in benzene and 0.60:0.40 in dioxane, as deduced from dipole moment measurements under the assumption that p_{cc} vanishes. Furthermore, on the basis of dipole moments computed by INDO MO methods, 1.44, 4.23, and 5.23 D for *tt*, *ct*, and *cc*, respectively, the simplest reaction field model (22) predicts an increase in this ratio on passing from CCl_4 to $(CD_3)_2C{=}O$ solutions. It may be noted, however, that for the pyridinecarbaldehydes (23) the conformer stabilities in solution depend significantly on the quadrupolar terms in this model (22). The measured moments are 4.42 D in benzene (7) and 4.27 D in dioxane (6). We see no reason to doubt the population ratios obtained from ^5J. Perhaps the additivity of group dipole moments assumed for the 1,2 isomer is somewhat less reliable than for the 1,3 isomer.

If some *cc* conformer is present, then the ratios above will change, of course. Suppose that p_{cc} is as large as 0.05. Then p_{ct}/p_{tt} becomes 0.76:0.19 in C_6D_6 solution, for example; the ratio decreases from 6.1 to 4.0. Naturally, this approach will not bring the ^5J results into agreement with the dipole results because the latter were interpreted on the basis of a vanishing p_{cc}.

Curiously, the gas phase populations based on STO 3G MO energies are in closer agreement with those deduced from ^5J in solution than the latter are with the populations deduced from dipole moments in solution. It is interesting that the populations appear to be insensitive to solvent polarity.

Substantial populations of nonplanar conformers would entail (24) a significant magnitude for $^6J(H,CHO)$. In benzaldehyde itself, ^6J is reported as 0.03 Hz (21) and, as a $\sigma{-}\pi$ coupling depending on $\sin^2\theta$, becomes -0.21 Hz in 2,6-dinitrobenzaldehyde (24). In the latter substantial out-of-plane conformations occur. In $(CD_3)_2C{=}O$ solution, ^6J for the 1,2 isomer is given as $-0.051(3)$ Hz by the iterative analysis. If this were a reliable number and the low-energy pathway computed above were correct also in solution, therefore implying significant out-of-plane torsional amplitudes, then one would conclude that both the *ct* and *tt* conformers represent only parts, albeit the major parts, of the conformational distribution. However, the -0.05 Hz was *not* observed as a splitting and in solution the potentials hindering torsions of aldehyde groups are usually larger than given by STO 3G MO methods, so that countable nonplanar forms cannot be substantiated in this manner.

Large populations of the *cc* conformer might well be reflected by an observable $^5J(CHO,CHO)$ because the INDO MO FPT computations yield 0.18 Hz for this conformer and only 0.06 Hz for the *ct* form, while the *tt* form is calculated to have a coupling of -0.05 Hz. The data in Table 1 imply a vanishing coupling in the three solutions.

It appears that the long-range coupling constants in the 1,2 isomer yield conformational information additional to that obtained from dipole moments and ^{13}C nmr spectra. For the 1,3 isomer these couplings are less informative.

(ii) The 1,3 isomer

The computed energies for optimized geometries yield gas phase fractional populations at 300 K of 0.57, 0.25, and 0.18 for the planar *ct*, *tt*, and *cc* conformers, respectively. In Freon solution, estimated to have a dielectric constant of about 10 at the temperature of measurement (8), the ^{13}C nmr spectra yield 0.56, 0.26, and 0.18 for these populations.

There is only one $^5J(H, CHO)$ value for the 1,3 isomer and eqs. [4] and [5] hold. Taking ^5J_c as zero as before and ^5J_t as 0.771 Hz (the mean of the values for the 1,2 isomer and very near the 0.76 Hz for benzaldehyde) yields eq. [6]. That the populations of *ct* and *tt* are somewhat solvent dependent can be seem from the data in Table 2, where ^5J is 0.482(1), 0.496(1), and 0.438(1) Hz in CCl_4, C_6D_6, and $(CD_3)_2C{=}O$ solutions, respectively.

$$[5] \quad {}^5J = p_{ct}{}^5J_t/2 + p_{tt}{}^5J_t + p_{cc}{}^5J_c$$

$$[6] \quad {}^5J = 0.38_6\, p_{ct} + 0.771\, p_{tt}$$

From the dipole moment in benzene solution it was concluded only that $p_{ct} = 0.70$. If this number is correct, then p_{tt} follows as 0.29 from eq. [6], leaving p_{cc} effectively zero at 300 K. In dioxane solution the dipole moment is apparently in reasonable agreement with the STO 3G MO energies above and with those computed in ref. 6. Such a distribution yields 0.413 Hz for ^5J, not in agreement with any of the numbers in Table 3 but closest to the value of 0.438 Hz in $(CD_3)_2C{=}O$ solution. The *cc* conformer of high dipole moment may be favored in this polar solvent, yet contributes nothing to ^5J. Its increased population in this solvent may well be the cause of the smaller ^5J observed.

Some limits on the populations of the various conformers can be established on the basis of ^5J. Thus, from eq. [6], one has ^5J as 0.386 Hz for $p_{ct} = 1$, 0.771 Hz for $p_{tt} = 1$, and 0.00 Hz for $p_{cc} = 1$. Reproduction of 0.482 Hz, as measured in CCl_4 solution at 300 K, is successful for $p_{ct}/p_{tt}/p_{cc}$ values of 0.75:0.25:0.00, 0.70:0.275:0.025, 0.60:0.33:0.07, 0.50:0.39: 0.11, 0.40:0.42:0.18, and so forth. In other words, p_{ct} cannot be more than 0.75 and then only if p_{cc} vanishes. Similarly, for the $(CD_3)_2C{=}O$ solution, p_{ct} can be as large as 0.86 if p_{cc} vanishes. However, this situation is unlikely and it is probable, as stated above, that p_{cc} increases in this solution.

Acknowledgements

We are grateful to the Natural Sciences and Engineering Research Council of Canada for financial assistance and to a referee for helpful scientific and grammatical criticism. Grants towards the purchase of the AM300 spectrometer from NSERC and the Manitoba Health Research Council are gratefully acknowledged.

1. K. KAKAR, E. E. RINEHART, C. R. QUADE, and T. KOJIMA. J. Chem. Phys. **52**, 3803 (1970).
2. F. A. L. ANET and M. GHIACI. Chem. Commun. 588 (1979).
3. F. A. MILLER, W. G. FATELEY, and R. E. WITOWSKI. Spectrochim. Acta Part A, **23**, 891 (1967).
4. F. A. L. ANET and M. AHMAD. J. Am. Chem. Soc. **86**, 119 (1964).
5. T. DRAKENBERG, J. SOMMER, and R. JOST. J. Chem. Soc. Perkin Trans. **2**, 363 (1980).
6. D. MIRARCHI, L. PHILLIPS, H. LUMBROSO, and G. L. D. RITCHIE. Aust. J. Chem. **37**, 465 (1984).
7. H. LUMBROSO, C. LIEGEOIS, G. C. PAPPALARDO, and V. LIBRANDO. J. Mol. Struct. **62**, 195 (1980).
8. J.-M. BERNASSAU, T. DRAKENBERG, and T. Liljefors. Acta Chem. Scand. Part B, **31**, 836 (1977).
9. G. J. KARABATSOS and F. M. VANE. J. Am. Chem. Soc. **85**, 3886 (1963).

10. R. WASYLISHEN and T. SCHAEFER. Can. J. Chem. **49**, 3216 (1971).
11. D. G. KOWALEWSKI and S. CASTELLANO. Mol. Phys. **16**, 567 (1969).
12. T. SCHAEFER, G. H. PENNER, K. J. DAVIE, and R. SEBASTIAN. Can. J. Chem. **63**, 777 (1985).
13. T. SCHAEFER, R. SEBASTIAN, R. LAATIKAINEN, and S. R. SALMAN. Can. J. Chem. **62**, 326 (1984).
14. L. LUNAZZI, A. TICCA, D. MACCIANTELLI, and G. SPUNTA. J. Chem. Soc. Perkin Trans. **2**, 1121 (1976).
15. W. J. HEHRE, R. DITCHFIELD, R. F. STEWART, and J. A. POPLE. J. Chem. Phys. **52**, 2769 (1970).
16. M. R. PETERSEN and R. A. POIRIER. MONSTERGAUSS. Department of Chemistry, University of Toronto, Toronto, Ontario, 1981.
17. J. A. POPLE, D. L. BEVERIDGE, and P. A. DOBOSH. J. Chem. Phys. **47**, 2026 (1967).
18. J. A. POPLE, J. W. MCIVER, and N. S. OSTLUND. J. Chem. Phys. **49**, 2965 (1968).
19. P. DOBOSH and N. S OSTLUND. QCPE, **11**, 281 (1975).
20. A. R. QUIRT and J. S. MARTIN. J. Magn. Reson. **5**, 318 (1971); J. S. Martin, A. R. Quirt, and K. E. Worvill. The nmr program library. Daresbury Laboratory, Darebury, U.K.
21. R. J. KOSTELNIK, M. P. WILLIAMSON, D. E. WISNOSKY, and S. M. CASTELLANO. Can. J. Chem. **47**, 3313 (1969).
22. R. J. ABRAHAM and E. BRETSCHNEIDER. *In* Internal rotation in molecules. *Edited by* W. J. Orville-Thomas. J. Wiley and Sons, New York. 1974. Chapt. 13.
23. W. DANCHURA, T. SCHAEFER, J. B. ROWBOTHAM, and D. J. WOOD. Can. J. Chem. **52**, 3986 (1974).
24. C. L. BELL, S. S. DANYLUK, and T. SCHAEFER. Can. J. Chem. **47**, 3529 (1969).

The chemistry of peptides related to metabolites of *Trichoderma* spp. 2. An improved method of characterization of peptides of 2-methylalanine[1]

I. M. SHAW AND A. TAYLOR[2]

National Research Council of Canada, Atlantic Research Laboratory, Halifax, N.S., Canada B3H 3Z1

Received February 19, 1985[3]

I. M. SHAW and A. TAYLOR. Can. J. Chem. **64**, 164 (1986).

4-Chlorobenzoylazide reacts with amino acid and peptide esters to give the 4-chlorobenzoyl derivatives in 60–90% yield, at room temperature, without measurable racemization. The reaction also proceeds smoothly with hindered amines such as methyl 2-methylalaninate and with secondary amines, e.g. methyl L-prolyl-L-valinate. Ten examples of the reaction are reported with peptides, synthesized for the purpose, that might be accessible from hydrolysates of the numerous fungal metabolites now known, which contain a high proportion of 2-methylalanine. The derivatives of di-, tri-, tetra-, and pentapeptides were highly crystalline, with sharp melting points, and could be detected and integrated in the effluent from chromatography columns at about the 10-ng level. This simple method of derivatization might be usefully applied to the resolution of discrepancies in the physical properties of ostensibly the same 2-methylalanyl peptide prepared in different laboratories.

I. M. SHAW et A. TAYLOR. Can. J. Chem. **64**, 164 (1986).

L'azoture du chloro-4 benzoyle réagit avec les esters d'acides aminés et de peptides, à la température ambiante, pour conduire aux dérivés chloro-4 benzoylés avec des rendements de 60 à 90% et sans racémisation mesurable. La réaction se produit aussi facilement avec des amines encombrées, comme le méthyl-2 alaninate de méthyle, et avec des amines secondaires, comme le L-prolyl-L-valinate de méthyle. On rapporte dix exemples de la réaction avec des peptides, synthétisés à cette fin, qui peuvent se retrouver dans les hydrolysats de plusieurs métabolites de champignons qui sont maintenant connus pour contenir une grande proportion de méthyl-2 alanine. Les dérivés des di-, tri-, tétra- et pentapeptides sont très cristallins, ils ont des points de fusion bien définis et ils peuvent être détectés et intégrés en chromatographie à des niveaux de 10 ng. Cette simple méthode de préparer un dérivé peut être appliquée utilement à la résolution des différences dans les propriétés physiques de peptides de la méthyl-2 alanine qui semblent les mêmes, mais qui ont été préparés dans des laboratoires différents.

[Traduit par le journal]

In 1952 C. T. Calam and A. D. Ainley, working in the laboratories of the Dyestuffs Division of Imperial Chemical Industries, isolated a trypanocidal group of metabolites from a culture of a *Paecilomyces* sp.[4] The toxicity of the material led to its being abandoned as a therapeutic agent and further investigation of its chemistry was undertaken by Kenner and his colleagues. Kenner's work (2–4) on M13959 (= trypanocidin[4]) showed that its hydrolysis provided a number of unknown amino acids but that, among known compounds, there was a high proportion of 2-methylalanine. Since this work was published a large number of other fungal metabolites, which on acid hydrolysis provide 2-methylalanine in high yield, have been discovered. A list of these materials is given in Table 1 and it will be seen that a wide range of fungal genera are represented therein. In addition to the metabolites given in Table 1, stilbellin (8), elvapeptin (9), lilacinin (10), and CC1014 (1) may also belong to this group. The proportion of 2-methylalanine isolated from these materials is given in Table 2 and if (as is likely) the amino acid moieties are linked as peptides, then either the 2-methylalanine residues form an abnormal continuous segment or they are to be found in more or less alternate fashion. The resistance of these compounds to peptidases suggests that the latter supposition is true and this has found considerable support from fast atom bombardment (FAB) mass spectroscopy of some of the mixed natural products.

It has been shown that the zervamicins (Table 2 and ref. 11), the suzukacillins (6), and the alamethicins (12) are very complex mixtures and that the proportions of the individual components of the mixture depend on the conditions of growth of the producing fungus. These facts and the worldwide interest in the physiological properties of these materials have led to extraordinary synthetic efforts to obtain a single entity by synthesis (13–17). The results of these efforts in the alamethicin field have been symmarized by Schmidt and Jung (16), who show that the measurements of the physical properties of the synthetic products by the different groups fall outside normally accepted ranges of error. The structures of many of the intermediates in the syntheses have been established by detailed assignment of ^1H and ^{13}C nmr spectra (see e.g., ref. 18), by elemental analysis, and, in some cases, by X-ray crystallographic studies. However, the structures of several other intermediates are open to doubt. Seven examples are given in Table 3; these compounds have been synthesized by two or more groups of workers and there are few examples of duplicated experimental results lying within the normally accepted range of error (included in Table 3 are two examples where the results from different workers are in agreement). An explanation for the discrepancies in Table 3 may be the known abnormal behaviour of 2-methylalanyl peptides under various reaction conditions, including those commonly used in peptide synthesis (19–21). Whatever the explanation, it is clear that better methods of characterizing these peptides, either obtained by degradation of natural products or by synthesis, are required. We have attempted during the past decade to devise improvements in the characterization of these materials; some progress has been made and is reported in this and a following paper.

[1]NRCC No. 24958.

[2]Author to whom correspondence may be addressed.

[3]Revision received August 26, 1985.

[4]We are indebted to Dr. W. B. Turner for a sample of M13959 and for the communication from our colleagues in the Laboratories of Imperial Chemical Industries of the decision to call this material "trypanocidin." In view of the fact (see Table 1) that two completely different groups of mould metabolites are now called "leucinostatin" it might be useful to reserve this term for the material described by Arai and his colleagues (48) and to call leucinostatin = M13959 = P168 = A20688 = 1907, metabolites of *Paecilomyces lilacinus*, trypanocidins. This would avoid confusion and would honour traditional prerogatives.

TABLE 1. Fungal peptide metabolites containing 2-methylalanine residues

Trivial name of metabolite	Producing fungus	Melting point (°C)	Specific optical rotation $[\alpha]_D$ (°)	T (°C)	Solvent	Conc. (g/100 mL)	pK_a	Ultraviolet spectrum λ_{max} (nm)	References[a]
Alamethicin = U22324	*Trichoderma viride*	275–279	−5	25	Alcohol	0.86	6.04	257	12,* 25, 40,* 41
Antiamebin	*Emericellopsis synnematicola*	219–220	+10	25	MeOH	1.02			42
	E. poonensis								
	Cephalosporium pimprina	194–196	+17.8	25	MeOH	2.1			43
Efrapeptin = A23871	*Tolypocladium inflatum*		+6.8	25	MeOH	1.0			[b]
Emerimicin II	*Emericellopsis microspora*	261	+5	25	MeOH	1.0		273, 281, 289	45
III		257	+12					253, 257, 264, 267	
IV		240	+13.5					252, 257, 264, 267	
Gliodeliquescin A	*Gliocladium deliquescens*	260							62
Hypelcin I	*Hypocrea peltata*		−17	21	MeOH	1.0			46
II			−16	21	MeOH	1.0			
Leucinostatin	*Penicillium lilacinum*	131–136	+644	22	MeOH	0.5			47
Leucinostatin A = M13959 = P168 = A20688 = 1907	*Paecilomyces lilacinus*	98–101	−11	20	MeOH	0.1		202, 220 (sh)	48, 49
Leucinostatin B = 1907-II		132–140	−31	20	MeOH	0.091		204, 213	
	Paecilomyces marquandii								50
Paracelsin(s)	*Trichoderma reesei*	253–255	−19.5	21	MeOH	2.0			7
Samarosporin	*Samarospora sp.*	255–256	+16.5	20	MeOH	1.0		260	51
Suzukacillin A	*Trichoderma viride*	259–261	−85.7	20	MeOH	0.07	5.5	258, 264, 268	5, 6
Trichopolyn A = I = Tricholides	*Trichoderma polysporun*								52
Trichopolyn B = II		114–116							
Trichorzianine	*Trichoderma hartzianum*						4.9	197	56*
Trichotoxin A	*Trichoderma viride*	187					4.8	191	53, 54
B									
A40		158–160					5.4		
Zervamicins I	*Emericellopsis salmosynnemata*	220	+16	25	MeOH	1.0	5.5	217, 273, 282, 289 315	55
II		257	+4.5	25	MeOH	1.0			

[a]An asterisk (*) indicates that X-ray crystallographic data can be obtained from the reference.
[b]The physical properties of efrapeptin(s) were kindly sent to us by Dr. R. L. Hamill, Lilly Research Laboratories, before publication.

In our hands peptides containing 2-methylalanine residues are easily and quantitatively esterified by treatment of the peptide, in solution in tetrahydrofuran (THF) containing 1% water, with ethereal diazomethane. We therefore sought an N-terminal group that, to serve our purpose, would have most of the following characteristics. It should enhance the ease of crystallization of the peptide and should confer absorption in the ultraviolet. Additionally, it should introduce an element not normally found in peptides, e.g. Cl, Br, or P, and which for mass spectroscopic reasons, discussed in a following paper, should exist as two or more stable isotopes whose natural abundance is known with high precision. Finally, the derivative should be formed under very mild conditions with minimum racemization of the terminal amino acid residue, but when formed should be sufficiently stable to withstand vigorous reaction conditions such as those encountered in the permethylation reaction (22).

It has been found that *N*-4-chlorobenzoyl derivatives satisfy many of the criteria given in the previous paragraph. Advocation of the use of this N-terminal group is not new (23), but we have found that such derivatives can be made at room temperature in THF by reaction of the peptide methyl esters with

TABLE 2. Proportions of common α-amino acids present in fungal peptide metabolites containing 2-methylalanine

Metabolite	Aib	Iva	Gly	Ala	Val	Leu	Ileu	Phe	Pro	3-OH Pro	3-Me Pro	Glu	Gln	Reference
Alamethicin I	8		1	2	2	1			2			1	2	57, 58, 59
II	9		1	1	2	1			2			1	2	
Antiamebin	6	2	1			1		1	1	2			1	42, 43
Efrapeptin	7	1	2			2								60
Emerimicin IIA	5					1	2		1	2			2	45
IIB	4	1				1	2		1	2			2	
III	5	1	1	1	1	1		1		2			1	
IV	6	1	1		1	1		1		2			1	
Hypelicin A	10			1	1	1			2				3	46
Leucinostatin(s)	3					2					1			2, 3, 4, 48
Paracelsin A	9		1	3	2				1				3	
B	9		1	3	1	1			1				3	
C	10		1	2	2				1				3	
D	10		1	2	1	1			1				3	7
Samarosporin	6		1		1	1		1		2		1		51
Suzukacillin	10		1	2	3	2			2			1	2	5, 6
Trichopolyn	4			2		1								61
Trichorzianine	8			2	1	1	1		1				3	56
Trichotoxin A	9	1	1	1		2			1			1	1	53, 54
B	9			3		2			1			1	1	
Zervamicin IA	4	1			1	1	1		1	2			2	11
IB	4	1			1	1	1		1	2			2	
IB′	5					2	1		1	2			2	
IC	4	1				2	1		1	2			2	
II-1	5				1	1	1		1	2			2	
II-2	5				1	2			1	2			2	
II-3	5				1	1	1		1	2			2	
II-4	4	1			1	1	1		1	2			2	
II-5	4	1			1	2			1	2			2	

Abbreviations used: Aib = 2-methylalanine; Iva = 2-amino-2-methylbutyric acid; Gly = glycine; Ala = alanine; Val = valine; Leu = leucine; Ileu = 2-amino-3-methylvaleric acid; Phe = phenylalanine; Pro = proline; 3-OHpro = 3-hydroxyproline; 3-Mepro = 3-methylproline; Glu = glutamic acid; Gln = glutamine. Unless stated otherwise all asymmetric centers are assumed to be L.

4-chlorobenzoylazide. As reported in the literature (24), this compound is a relatively stable crystalline solid and an improved preparation is given in the experimental section. It melts without decomposition at 42°C and shows no sign of decomposition at 80°C. We have kept 10-g samples at −15°C (it is volatile) for 2–3 years without measurable change in the melting point. The reaction of this reagent with a number of peptides is summarized in Table 4. The choice of peptides was dictated by their potential formation during degradation of the metabolites listed in Table 1. Thus proline is the N-terminus of most of these examples, because of the several methods available of preferential hydrolysis at proline peptide bonds (25–27). Details of the syntheses of the parent peptides are given in the experimental section; they usually followed the methods previously reported (28) and are summarized in Fig. 1. Whilst it is obvious that the compounds in Table 4 could be prepared by shorter and more simple routes than shown in Fig. 1, the object of the work was to use common preparative reactions in peptide chemistry to secure crystalline products and then to determine if analysis of the *N*-4-chlorobenzoyl derivatives would reveal the presence of unexpected impurities.

Figure 2 shows a chromatogram of the compounds in Table 4 on a commercially available reversed phase partition chromatography column; all components can be distinguished. The yields obtained in the chlorobenzoylation reaction are given in Table 4, and were calculated for analytically pure material without corrections for losses due to recrystallization, etc. Crude yields, i.e. material after removal of excess 4-chlorobenzoylazide and acidic and basic impurities, lay in the range of 65–90%. Mass spectroscopic evidence was obtained for the presence of hydrazine derivatives of the type $ClC_6H_4CO{\cdot}NH{\cdot}NR_2$ (where R_2 is the peptide chain) among the basic impurities, thus accounting, in part, for the low yields. A further possibility, that the low yields were due to reacemization of the N-terminal residue, was investigated by studying the reaction of the azide with the diastereoisomeric pair, methyl *N*-4-chlorobenzoyl-L(and D)-alanyl-2-methylalanyl-L-alaninates. The optical rotations of the intermediates made during the syntheses of these diastereoisomers are given in Table 5. Their separation by partition chromatography was difficult, but a partial separation (Fig. 3) was achieved and the conditions given in Fig. 3 were critical in the sense that very small changes led to apparently identical partition coefficients. About 40 ng of the D-alanine derivative was detected and integrated in the presence of about 0.4 μg of the L-alanine isomer. Similarly, about 70 ng of the latter was detected and integrated in the presence of 0.4 μg of the D-alanine isomer. Quantities in the range 10–15 ng were detected, but the peaks were not integrated, or the integration error was very great, due to incomplete separation. A linear least-mean-squares fit of all the data (weight of compound in ng vs. integrated area) gave a line of index of fit (= r^2) of 0.989 with a standard error of estimation of ±27 ng. Hence one can reliably estimate about 7% of one diastereoisomer in a mixture. When the analysis was carried out on the crude reaction products of 4-chlorobenzoylazide and methyl (L(or D)-alanyl-2-methylalanyl-

TABLE 3. Comparison of melting points and specific optical rotations of 2-methylalanine peptides prepared in different laboratories

Compound[a]	Melting point (°C)	$[\alpha]_D$ (°)	Concentration (in methyl alcohol)	Reference
BOC-L-Pro.AibOH	163–165	−64	1.0	15
	161	−60.2	1.0	16
BOC-L-Ala.Aib-L-AlaOMe	158	−2.5	0.2	13
	171	−32	0.1	29
Cbz-L-Ala.Aib-L-AlaOMe	161–162	−35	2.0	This work
	148	−48.8	0.4	44
BOC-L-Glu-L-Gln-L-Phol | OBzl	145	−36.2	1.0	15
	145–148	−26.7	1.0	14
	165	−52.5	0.2	13
	135–137	−36.6	1.0	16
BOC-L-Gln.AibOH	183–184	−17	1.0	15
	176	−27.5	0.2	13
	184	−14.6	1.0	16
BOC-L-Gln.AibOBzl	101	+22.5	0.2	13
	121–122	−17.6	1.0	15
BOC-L-Val.AibOMe	115–118	−27.5	0.2	13
	151	−28	1.1	28
	140	Not given	—	16
BOC-L-Pro.Aib-L-Ala.Aib-L-Ala-L-Gln.Aib-L-Val.-Aib.Gly = A	150	−28.2	1.0	16
	156–158	−17.5	1.0	15
A-L-Leu.Aib-L-Pro-L-Val.-$(Aib)_2$-L-Glu-L-Gln-L-Phol | OBzl	145	−22.2	1.0	16
	155.8	−11.6	1.0	15

[a]Abbreviations as in Table 2 with the following additions: BOC = *tert*-butyloxycarbonyl; Cbz = phenylmethoxycarbonyl; Phol = L-phenylalaninol; Bzl = benzyl.

TABLE 4. Physical properties of some *N*-4-chlorobenzoyl peptides containing 2-methylalanine residues

Peptide[a]	Mol. Wt.[b]	Yield (%)	Melting point (°C)	$[\alpha]_D^{24}$ (°)	λ_{max} (nm)	ϵ	R_V[c] (mL) (T = 24°C)
R-AibOMe	255	63	134	—	236	13 200	11.1
R-L-Pro-L-ValOMe	366	43	124	−126	225	13 500	17.2
R-L-Ala.Aib-L-AlaOMe	397	78	194	−9.5	236	17 800	11.8
R-L-Ala.Aib-L-AlaOMe	397	78	160	−24	236	17 800	11.8
R-L-Pro-L-Val.AibOMe	451	79	168	−137	222	13 900	19.5
R-L-Pro-L-Val.AibOMe	451	35	171	−2	224	11 211	22.4
R-L-Pro-L-Val.Aib.AibOMe	536	30	153	−87	218	13 300	26.4
R-L-Pro.Aib-L-Ala.Aib-L-AlaOMe	579	64	194	−40	225	13 100	20.0
R-L-Pro-L-Val.Aib.Aib-L-GluOMe | OMe	679	47	162	−99	224	14 400	34.2
R-L-Pro-L-Val.Aib.Aib-L-GluO-*t*-Bu | OMe	721	60	(93)178	−86	223	13 400	49.1

[a]R = 4-chlorobenzoyl, other abbreviations as in Table 2. Ciphers written below glutamic acid residues are γ-esters.
[b]Molecular weights calculated for the ^{35}Cl isotope.
[c]R_v = retention volume, i.e. time of elution × flow rate.

L-alaninate, only one isomer was detected (either L or D according to the starting material) and hence the extent of racemization was less than 7% in either case.

In agreement with other workers (29), we were unable to obtain satisfactory elemental analyses for crystalline methyl L-alanyl-2-methylalanyl-L-alaninate, possibly because of its deliquescent nature and (or) the presence of dioxopiperazines (19) formed during hydrogenolysis of its carbobenzyloxy derivative. However, methyl *N*-4-chlorobenzoyl-L-alanyl-2-methylalanyl-L-alaninate could be fully characterized (see experimental section and Fig. 2). In addition, the basic tripeptide methyl ester could be converted into the pentapeptide derivative (**1**), which also provided elemental analyses within acceptable error, though only one of the two proline conformers was detected in its ^{13}C nmr spectrum (30). An X-ray crystallographic structure determination (31) of this pentapeptide (**1**) established its structure and conformation and in particular the N-terminal acylproline residue.

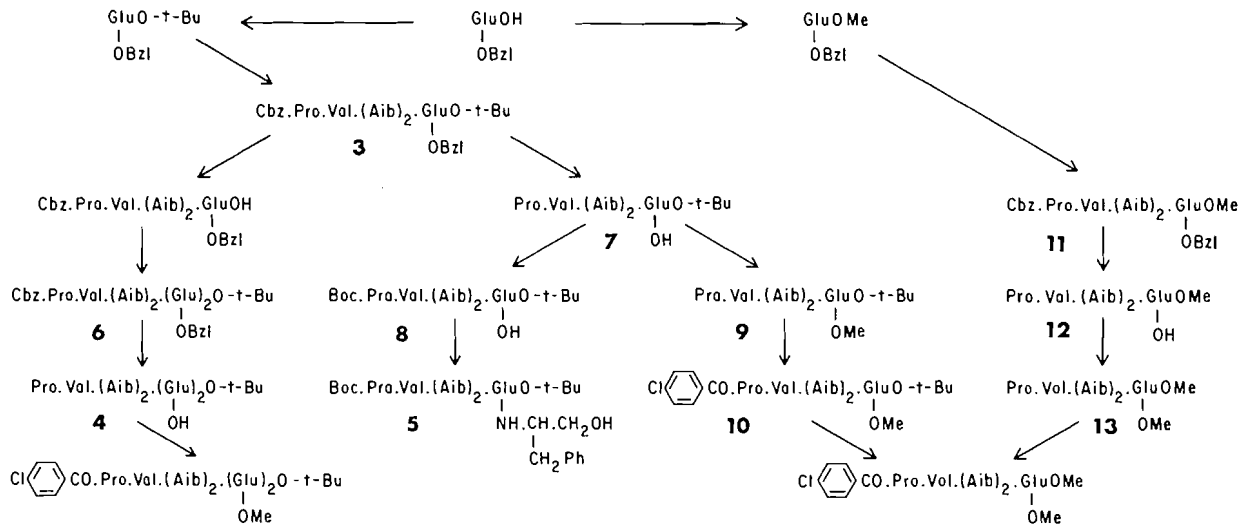

FIG. 1. Synthetic steps reported in the preparation of penta- and hexapeptides of 2-methylalanine. Abbreviations are the same as those defined in Tables 2, 4, and 5.

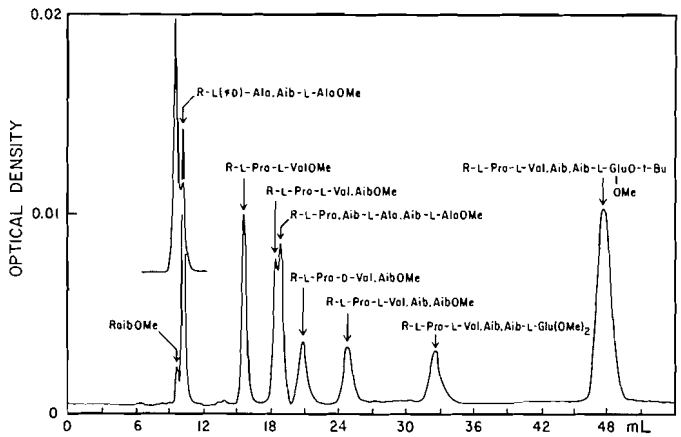

FIG. 2. Reversed phase partition chromatogram of the 4-chlorobenzoyl peptides found in Table 4. The column was a Dupont C_8 "Zorbax" 6 μm of dimensions 0.46 × 25 cm, of dead volume ca. 3 mL, and the solvent was 46% ammonium acetate buffer (0.01 *M*, pH 4.2) in methyl alcohol. The column was run at 22°C and the flow rate was 1.5 mL min^{-1}.

These encouraging results led us to investigate the elaboration of the tetrapeptide (**2**, R′ = H), the preparation of which on the 100-g scale has been reported (28), into the various structures postulated for the C-terminal moieties thought to be present in many of the natural products listed in Table 1. The reactions investigated are summarized in Fig. 1. Condensation of the tetrapeptide (**2**, R′ = H) with glutamyl diesters (α,γ-dimethyl; α-methyl-γ-benzyl; α-*tert*-butyl-γ-benzyl) gave reproducible yields on the 10-g scale in the range 50–60%, and conversion of these products to the *N*-4-chlorobenzoyl dimethyl ester derivative gave crystalline material in all cases. However, partition chromatography of the 3 products showed them to be mixtures of 4 components eluted at 29, 49, 61, and 72 mL. The 2 components of higher R_f were not detected after one recrystallization; the proportions of the 2 components of lower R_f depended on the nature of the glutamyl diester used in the condensation reaction and were (in the order given above) 100:100, 100:44, 100:10. It was possible in the 2 latter cases to purify the major component to the point where it represented

TABLE 5. Specific optical rotations of intermediates in the syntheses of methyl 4-chlorobenzoyl-L (and D)-alanyl-2-methylalanyl-L-alaninates

Compound[a]	Specific optical rotation L	$[\alpha]_D^{24}$ (*c* 1, MeOH) D
Cbz.AlaOH	−6.9°	+7.0°
Cbz.Ala.AibOH	−31°	+25°
Cbz.Ala.Aib-L-AlaOMe	−35°	−21°

[a]Abbreviations as in Table 3.

>99% of the mixture. The material from the 2 preparations shown in Fig. 1 had closely similar melting points, mass spectra, optical rotations, and ^1H and ^{13}C nmr spectra. However, the X-ray diffraction patterns of the crystals from different preparations were not always identical and the crystals were, physically, insufficiently stable for data collection. Like the 4-chlorobenzoylpentapeptide (**1**), only one acylproline conformer was detected in the ^{13}C nmr spectrum.

As shown in Fig. 1, the pentapeptide derivative (**3**) was converted into the crystalline *tert*-butyl ester (**4**). Correct elemental analytical data were obtained for this compound and many of the chemical shifts and C—H couplings in its ^{13}C nmr spectrum could be assigned (see experimental section). It was treated with diazomethane and the gummy product with 4-chlorobenzoylazide, but we were unable to induce the 4-chlorobenzoyl derivative to crystallize. It was obtained as a

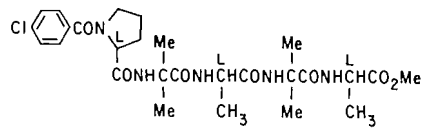

1

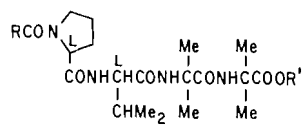

2

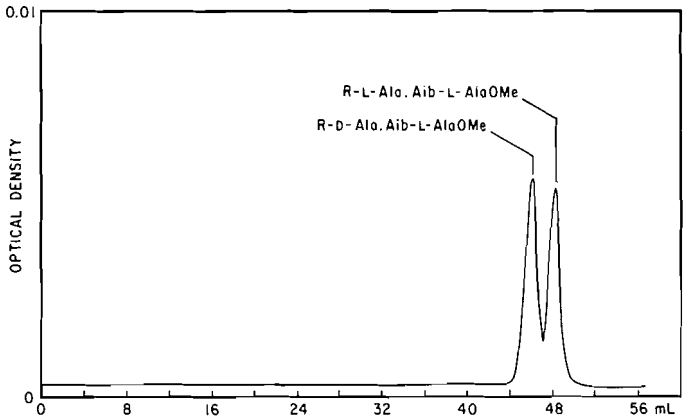

FIG. 3. Separation of methyl 4-chlorobenzoyl-L(and D)-alanyl-2-methylalanyl-L-alaninates. The column was the same as that used for the separations in Fig. 2, the solvent 62% ammonium acetate buffer (pH 4.2) in methyl alcohol, the flow rate 2 mL min^{-1}, and the separation was run at 22 ± 0.2°C. The peptides (0.2 μg of each) were applied to the column in 0.1 μL of methyl alcohol. The standard deviations of the retention volumes were 1.5 mL, $n = 11$, in the case of the L isomer and 1.4 mL, $n = 11$ for the D.

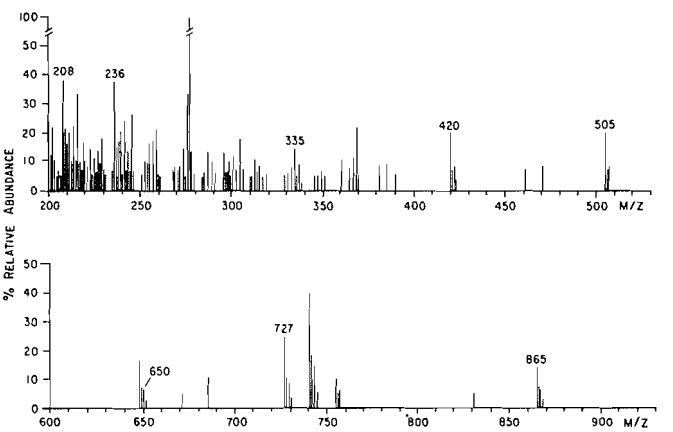

FIG. 4. Fast atom bombardment mass spectrum of ? di-γ-methyl α-*tert*-butyl *N*-4′-chlorobenzoyl-L-prolyl-L-valyl-2-methylalanyl-2-methylalanyl-L-glutamyl-L-glutamate.

colorless amorphous solid that, however, gave a FAB mass spectrum (Fig. 4) in complete accord with its supposed structure. The crystalline L-phenylalaninolhexapeptide (**5**) was also obtained, and much of its ^{13}C nmr spectrum assigned (see experimental section), but we were unable to convert it into a crystalline *N*-4-chlorobenzoyl derivative.

Experimental

Melting points are corrected, and infrared spectra were measured on a Perkin–Elmer 283 spectrometer. Ultraviolet spectra and optical rotations were determined on solutions of peptides in methyl alcohol on a Cary 14 spectrometer and a Rudolph polarimeter, respectively. The greatest error in optical rotation measurements was ±2%. The ^1H nmr spectra were obtained on a Varian 220-MHz instrument at the Canadian NMR Center at Toronto University Medical School; ^{13}C nmr data were collected on a Varian XL-100 instrument except those marked *, which were recorded on a Nicolet 360 NB spectrometer of the Atlantic Region Magnetic Resonance Center, Halifax, Nova Scotia. All nmr data are presented in the format used by Shaw and Taylor (28); all chemical shifts are reported in ppm downfield from the signal of Me_4Si. The equipment used for high pressure liquid chromatography has been described in detail (32); analytical chromatography was performed on Dupont C_8 "Zorbax" 6-μm columns of dimensions 0.46 × 25 cm; two Waters μBondapak C_{18} columns (0.78 × 30 cm) in series were used for preparative chromatography. The solvent used in all cases was methyl alcohol mixed with ammonium acetate buffer (0.01 *M*, pH 4.2, water of resistance >10 Mohms), the composition of the mixture being controlled by a solvent programming device (Waters Model No. 660). Mass spectra were measured on Kratos MS-50 and Dupont 21-110B instruments. Full experimental details of mass spectroscopic measurements are given in a following paper.

4-Chlorobenzoylazide

4-Chlorobenzoyl hydrazide (33) (10 g) was dissolved in acetic acid (150 mL) and the solution treated with hydrochloric acid (2 *N*, 250 mL). Light petroleum (bp 30–60°C, 400 mL) was added and the stirred mixture cooled to <5°C, when a solution (40 mL) of sodium nitrite (4.4 g) in water was added below the surface of the liquid. After 30 min at 5°C, the colorless precipitate had dissolved, the petroleum layer was separated, the aqueous raffinate extracted with light petroleum, and the dried (Na_2SO_4) combined extracts evaporated at 10°C/30 Torr (1 Torr = 133.3 Pa) to 100 mL. The mixture was kept at −15°C for 18 h, when the colorless crystals, mp 42°C, 8.3 g, 80%, were collected on a filter precooled to −15°C. This material was stored at −15°C in a screw-capped bottle kept inside a wide-mouth screw-capped jar that contained calcium chloride.

Methyl N-4-chlorobenzoyl-2-methylalaninate

Methyl 2-methylalaninate (0.5 g) (28) was dissolved in tetrahydrofuran (THF, 10 mL) and the solution treated with 4-chlorobenzoylazide (1 g). After 3 days at room temperature, the reaction solution was evaporated and the residue digested 3 times with light petroleum, the digest being decanted from the sticky residue each time. The final crystalline residue was collected (0.75 g, mp 115–125°C, 69%) and recrystallized from *n*-butyl acetate as plates, mp 134°C (subliming >115°C), 0.69 g, 63%. *Anal.* calcd. for $C_{12}H_{14}ClNO_3$: C 56.4, H 5.5, Cl 13.9, N 5.5%; found: C 56.3, H 5.5, Cl 14.1, N 4.6%.

N-Phenylmethoxycarbonyl-L-prolyl-2-methylalanine

N-Phenylmethoxycarbonyl-L-proline (34) (64.6 g), methyl 2-methylalaninate (30.5 g), and 1-ethoxycarbonyl-2-ethoxy-1,2-dihydroquinoline (EEDQ, 64 g) were dissolved in toluene (1.75 L) and the solution stirred at 55°C for 72 h. The toluene was evaporated, the residue dissolved in ethyl acetate (0.9 L), and the solution washed with dilute sodium bicarbonate (2%, 500 mL), dilute hydrochloric acid (2 *N*, 500 mL), and water. The dry (Na_2SO_4) solution was filtered and evaporated, the residue (100 g) dissolved in methyl alcohol (1 L), and the solution treated with sodium hydroxide (*N*, 416 mL) at 0°C. The reaction mixture was kept at room temperature and aliquots (5 mL) titrated with standard acid to determine when the reaction was complete. The solution was then evaporated to half volume, diluted with water (250 mL), extracted with ethyl acetate, and the raffinate acidified. The precipitated oil was taken up in ethyl acetate (500 mL), and the solution dried (Na_2SO_4), filtered, and evaporated. The residual oil usually crystallized spontaneously but crystallization can be induced by seeding. *N-Phenylmethoxycarbonyl-L-prolyl-2-methylalanine* (52 g, 60%) separated from tetrahydropyran as prisms, mp 137°C, $[\alpha]_D^{23}$ −65° (*c* 2, MeOH), δ_C ($C^2H_3O^2H$): 177.4; 174.0, 173.9; 156.5, 156.3; 137.8; 129.3; 128.9; 128.7; 68.0; 61.2; 61.0; 56.9; 48.3, 48.1; 32.1, 30.9; 25.6; 24.8; 25.1, 24.4. *Anal.* calcd. for $C_{17}H_{22}N_2O_5$: C 61.1, H 6.6, N 8.4, O 23.9%; found: C 61.2, H 6.7, N 8.4, O 24.1%.

Methyl 4-chlorobenzoyl-L-alanyl-2-methylalanyl-L-alaninate

N-Phenylmethoxycarbonyl-L-alanyl-2-methylalanine (77 g) (35) was suspended in toluene (500 mL), and freshly distilled methyl L-alaninate (26 g) and EEDQ (83 g) were added. The reaction mixture became a viscous paste and required a stirrer with adequate torque to keep it in suspension. The reaction mixture was heated to 45°C and was stirred for 42 h, after which the crystalline precipitate (83 g, 84%, mp 158–162°C) was collected. *Methyl N-phenylmethoxycarbonyl-L-alanyl-2-methylalanyl-L-alaninate* separated from tetrahydrofuran –

isopropyl ether (1:1) as needles, mp 164–165°C; $[\alpha]_D^{24}$ −35° (*c* 2, MeOH). *Anal.* calcd. for $C_{19}H_{27}N_3O_6$: C 58.0, H 6.9, N 10.7, O 24.4%; found: C 58.05, H 6.65, N 10.75, O 24.5%. The crude ester (77 g) was suspended in methyl alcohol (0.6 L), palladium on carbon (5%, 5 g) added, and the mixture agitated with hydrogen at 18°C and 70 atm (1 atm = 101.3 kPa). After 48 h, the reaction mixture was filtered through a bed of Celite, the filtrate evaporated at 40°C/12 Torr, and the residual oily solid stirred with ethyl acetate (0.5 L). The crystalline precipitate (44 g, 83%, mp 140–147°C, δ_C: 176.2; 174.8; 171.2; 57.7; 52.8 ($^1J_{CH_3}$ 147 Hz); 50.9 ($^1J_{CH}$ 145 Hz, $^2J_{CH_3}$ 4 Hz); 49.7 ($^1J_{CH}$ 139 Hz, $^2J_{CH_3}$ 5 Hz); 25.7 ($^1J_{CH_3}$ 129 Hz, $^3J_{CH_3}$ 4.5 Hz); 24.8 ($^1J_{CH_3}$ 127 Hz, $^3J_{CH_3}$ ~ 3 Hz); 17.8 ($^1J_{CH_3}$ 130 Hz, $^2J_{CH}$ ~ 1 Hz); 17.2 ($^1J_{CH_3}$ 130 Hz, $^2J_{CH}$ 5 Hz)) was collected. This ester was deliquescent and we were unable to obtain a satisfactory elemental analysis; it (0.5 g) was suspended in THF (15 mL) and the stirred suspension treated with 4-chlorobenzoylazide (0.37 g), when the precipitate gradually dissolved during 24 h. The reaction mixture was filtered through a bed of Celite 535 and the filtrate evaporated. The residue was digested with light petroleum, and the insoluble residue recrystallized from *n*-butyl acetate as needles, mp 190°C. *Anal.* calcd. for $C_{18}H_{24}ClN_3O_5$: C 54.3, H 6.1, Cl 8.9, N 10.6%; found: C 54.3, H 6.1, Cl 9.1, N 10.4%.

Methyl N-*4-chlorobenzoyl-*D*-alanyl-2-methylalanyl-*L*-alaninate*

Phenylmethoxycarbonyl-D-alanine (36) (5.6 g), methyl 2-methylalaninate (2.9 g), EEDQ (6.2 g), and toluene (100 mL) were stirred together at room temperature for 5 days. The reaction solution was evaporated, the residue dissolved in ethyl acetate (250 mL), and the solution washed successively with hydrochloric acid (*N*, ×2), water, sodium bicarbonate solution (2%, ×2), and finally water. The dry (Na_2SO_4) ethyl acetate solution was evaporated and the residual gum (7.3 g) dissolved in methyl alcohol (80 mL) and sodium hydroxide solution (10%, 20 mL). After 2 h at room temperature the solution was concentrated to 20 mL, acidified, and the precipitate collected (6.45 g, mp 168–170°C). N-*Phenylmethoxycarbonyl-*D*-alanyl-2-methylalanine* separated from ethyl acetate as prisms, mp 171–172°C, (*Anal.* calcd. for $C_{15}H_{20}N_2O_5$: C 58.4, H 6.5, N 9.1%; found: C 58.4, H 6.5, N 9.1%.) This acid (3.08 g) was suspended in toluene (70 mL), methyl L-alaninate (1.05 g) added, and then EEDQ (2.5 g). The mixture was stirred at 44°C for 72 h, when the solution was evaporated, the residue taken up in ethyl acetate (250 mL), and the acidic and basic by-products removed as usual. The dry (Na_2SO_4), filtered ethyl acetate solution was evaporated and the crystalline residue (mp 127°C, 3.32 g) collected. This protected tripeptide (3 g) in methyl alcohol (50 mL) was shaken with hydrogen (3.5 kg cm^{-2}) and palladium on carbon (5%, 0.2 g) for 18 h. The reaction mixture was filtered through a bed of Celite 535, the filtrate evaporated, the residue (1.8 g, mp 226–228°C) in THF (50 mL) treated with 4-chlorobenzoylazide (1.5 g), and the mixture stirred at room temperature for 48 h. The reaction mixture was filtered, the filtrate evaporated, and the residual gum taken up in ethyl acetate (25 mL). The solution was washed with dilute hydrochloric acid (*N*, 2 × 10 mL), water, sodium bicarbonate solution (2%, 2 × 10 mL), then dried, filtered, and evaporated. The resulting gum spontaneously crystallized after standing on the bench for 6 months (crystals are available for those in need). *Methyl* N-*4-chlorobenzoyl-*D*-alanyl-2-methylalanyl-*L*-alaninate* separated from *n*-butyl acetate as rectangular plates, mp 160°C, 2.1 g (*Anal.* found: C 54.5, H 6.1, Cl 8.45, N 10.7%).

Methyl N-*(4-chlorobenzoyl)-*L*-prolyl-2-methylalanyl-*L*-alanyl-2-methylalanyl-*L*-alaninate*

N-Phenylmethoxycarbonyl-L-prolyl-2-methylalanine (15.7 g), methyl L-alanyl-2-methylalanyl-L-alaninate (12.95 g), and EEDQ (13 g) in tetrahydrofuran (THF, 0.5 L) were stirred together at 20°C for 72 h, when all the insoluble tripeptide had dissolved. The solution was evaporated and the residue dissolved in a mixture of ethyl acetate (0.7 L) and hydrochloric acid (*N*, 250 mL). The ethyl acetate phase was washed successively with hydrochloric acid (*N*, 250 mL), sodium bicarbonate solution (2%, 250 mL), and water (100 mL). The ethyl acetate solution was dried (Na_2SO_4), filtered, evaporated, and the crystalline residue (10.5 g, 39%, mp 178–179°C) taken up in hot *n*-butyl acetate (100 mL). The N-*phenylmethoxycarbonylpentapeptide* (**2**, R = C_7H_7O, R′ = Me) separated from *n*-butyl acetate as prisms, mp 180°C (blue in transmitted light just prior to melting); $[\alpha]_D^{22}$ −53° (*c* 1, MeOH). *Anal.* calcd. for $C_{28}H_{41}N_5O_8$: C 58.4, H 7.2, N 12.2, O 22.2%; found: C 58.3, H 7.3, N 12.2, O 22.3%. This ester (7.7 g) was dissolved in methyl alcohol (100 mL), palladium on carbon (5%, 0.5 g) added, and the mixture shaken with hydrogen at 3.5 kg cm^{-2} for 24 h, at which time the mixture was filtered through a pad of Celite and the filtrate evaporated. The residue was taken up in the minimum volume of hot THF, cooled, kept at 4°C for 18 h, and the crystalline precipitate (5.3 g, mp 157°C, 90%) collected. The *base* (pK_a 7.6) separated from tetrahydropyran as prisms, mp 157–159°C; $[\alpha]_D^{25}$ −81° (*c* 0.59, $CHCl_3$). *Anal.* calcd. for $C_{20}H_{35}N_5O_6$: C 54.4, H 7.9, N 15.9%; found: C 54.3, H 8.0, N 15.7%. This base (4.4 g) was stirred with THF (50 mL) and the mixture treated at 20°C with a solution of 4-chlorobenzoylazide (1.9 g) in THF (34 mL). The mixture was stirred for 24 h, when a clear solution was obtained, and after a further 24 h the solution was evaporated and the residue digested with petroleum ether (3 × 50 mL). The residue was taken up in ethyl acetate (250 mL) and the solution washed successively with hydrochloric acid (2*N*, 3 × 100 mL), water (100 mL), sodium bicarbonate solution (2%, 100 mL), and water (100 mL). The ethyl acetate solution was dried (Na_2SO_4), filtered, and evaporated and, to prepare a crystal for X-ray crystallography, the crystalline residue (3.7 g, 64%, mp 193–194°C) was taken up in hot *n*-butyl acetate (50 mL). The flask containing the hot (100°C) solution was placed in a water bath (capacity 12 L) at 55°C for 4 h, when the bath heater was switched off and it and the butyl acetate solution allowed to cool overnight. *Methyl* N-*(4′-chlorobenzoyl)-*L*-prolyl-2-methylalanyl-*L*-alanyl-2-methylalanyl-*L*-alaninate* (31) (**1**) separated from *n*-butyl acetate, mp 194°C; $[\alpha]_D^{24}$ −40° (*c* 1, $CHCl_3$); δ_C ($C^2H_3O^2H$): 177.0; 176.9; 174.7 (2C, resolved in $C_6{}^2H_6$–$C^2H_3O^2H$, 1:1), 174.25; 170.7; 137.75; 135.7; 130.1 (2C); 129.7 (2C); 62.8 (J_{CH} 146 Hz); 57.9; 57.6 (2C); 52.6 (J_{CH_3} 148 Hz); 51.8; 51.6 (J_{CH} 144 Hz, $^2J_{CH}$ 5 Hz); 49.7 (J_{CH} 142 Hz, $^2J_{CH}$ ~ 5 Hz); 30.5 (J_{CH_2} 135 Hz; 27.2; 26.55; 26.35; 24.5; 24.2; 17.4 (J_{CH_3} 129 Hz, $^2J_{CH}$ 5 Hz); 16.55 (J_{CH_3} 128 Hz, $^2J_{CH}$ 5 Hz). *Anal.* calcd. for $C_{27}H_{38}ClN_5O_7$: C 55.9, H 6.6, Cl 6.1, N 12.1, O 19.3%; found: C 56.1, H 6.6, Cl 6.0, N 12.0, O 19.4%.

*Methyl 4-chlorobenzoyl-*L*-prolyl-*L*-valinate*

L-Prolyl-L-valine (Sigma, 0.2 g) was suspended in THF (25 mL) and the stirred suspension treated with a solution (10 mL) of diazomethane (50 mg) in diethyl ether. After 18 h at room temperature a clear pale yellow solution was obtained. The solution was concentrated to 20 mL to remove ether and excess diazomethane and the concentrate was treated with 4-chlorobenzoylazide (0.18 g) in THF (10 mL). The solution was kept at room temperature for 24 h and was then filtered and evaporated. The residue was digested with light petroleum (bp 30–60°C, 3 × 20 mL) and the insoluble crystalline product recrystallized from cyclohexane as rosettes of very fine needles, mp 124–127°C. *Anal.* calcd. for $C_{18}H_{23}ClN_2O_4$: C 58.9, H 6.3, Cl 9.7, N 7.6%; found: C 58.6, H 6.4, Cl 9.8, N 7.6%.

Methyl N-*4-chlorobenzoyl-*L*-prolyl-*L*(and* D*)-valyl-2-methylalaninates*

These two compounds were prepared in exactly the same way and on the same scale as described for methyl *N*-4-chlorobenzoyl-L-prolyl-L-valinate, starting with L-prolyl-L(and D)-valyl-2-methylalanines (28). *Methyl* N-*4-chlorobenzoyl-*L*-prolyl-*L*-valyl-2-methylalaninate* separated from THF – isopropyl ether (1:1.5) as needles, mp 168°C. *Anal.* calcd. for $C_{22}H_{30}ClN_3O_5$: C 58.5, H 6.7, Cl 7.8, N 9.3%; found: C 58.4, H 6.7, Cl 7.8 N 9.3%. Its D-*valine isomer* separated from ethyl acetate as prisms, mp 171–172°C. *Anal.* found: C 58.5, H 6.5, Cl 7.9, N 9.6%.

*γ-Benzyl α-*tert*-butyl* N-*phenylmethoxycarbonyl-*L*-prolyl-*L*-valyl-2-methylalanyl-2-methylalanyl-*L*-glutamate*

γ-Benzyl L-glutamic acid (37) (30 g) suspended in dioxan (dried over Linde 4A molecular sieve, 60 mL) was cooled to −40°C, treated

with concentrated sulphuric acid (9 mL), and then with isobutylene (40 mL). The mixture was shaken in a glass pressure vessel at 20°C for 4 days, after which the pressure was released, ethyl acetate (200 mL) added, and the solution washed with sodium bicarbonate solution (5%, 3 × 100 mL). The bicarbonate washings were extracted with ethyl acetate (100 mL) and the combined organic phases washed with water, dried, and evaporated. The residue was taken up in ether and the theoretical quantity of hydrogen chloride in ether added at −10°C. The hydrochloride (23 g, mp 107–109°C; $[\alpha]_D^{22}$ +15° (*c* 2, MeOH)) was collected after storage at −15°C for 48 h. This hydrochloride (6.6 g) was suspended in toluene (200 mL), and the mixture treated with triethylamine (2.02 g) and shaken at 20°C for 15 min. *N*-Phenylmethoxycarbonyl-L-prolyl-L-valyl-2-methylalanyl-2-methylalanine (28) (**2**, R = C_7H_7O, R′ = H, 10.4 g) was added and, when it had dissolved, EEDQ (5.06 g). The mixture was stirred at 50°C for 72 h, when it was evaporated to ca. 50 mL, ethyl acetate (0.5 L) added, and the solution washed with citric acid (2*N*, 3 × 100 mL), brine (2%, 100 mL), sodium bicarbonate solution (2%, 2 × 150 mL), and finally water. The solution was dried (Na_2SO_4), filtered, and evaporated. The residue was taken up in THF (50 mL) and isopropyl ether (50 mL) added when the product (9.1 g, 57%, mp 160°C) separated. The N-*phenylmethoxycarbonylpentapeptide diester* (**3**) separated from ethyl acetate as needles, mp 165–166°C; $[\alpha]_D^{22}$ −58° (*c* 2, MeOH); δ_H (C^2HCl_3): 7.37 (5H), 7.34 (H, e), 7.34 (5H), 7.07 (H, e, J = 6 Hz), 6.83 (H, e), 6.75 (H, e), 5.31, 5.13 (2H, q, J = 13.3 Hz), 5.11 (2H), 4.41 (2H, m), 3.80 (H, t, J = 6 Hz), 3.54 (2H, t, J = 7 Hz), 2.57 (2H, m), 2.14 (5H, m), 1.93 (2H, m), 1.54 (3H), 1.48 (3H), 1.45 (15H), 0.88 (3H, d, J = 7 Hz), 0.83 (3H, d, J = 7 Hz); δ_C ($C^2H_3O^2H$): 177.2; 175.5 (bs); 175.2, 174.9, 174.4; 173.4; 172.4; 156.8, 156.2; 137.9 (bs); 137.5; 129.4; 129.0; 128.7; 82.4; 68.1; 67.0; 61.3; 60.3; 60.6; 57.7; 54.0; 48.4; 32.8; 31.5; 31.8; 31.0; 28.3; 27.7; 27.4; 26.7; 23.8; 19.6; 19.5; 19.2. *Anal.* calcd. for $C_{42}H_{59}N_5O_{10}$: C 63.5, H 7.5, N 8.8, O 20.2%; found: C 63.5, H 7.5, N 8.8, O 20.3%.

α-tert-*Butyl* L-*prolyl*-L-*valyl*-2-*methylalanyl*-2-*methylalanyl*-L-*glutamyl*-L-*glutamate*

The fully protected pentapeptide (**3**, 3 g) in deuteriochloroform (15 mL) was treated with a solution (30 mL) of trifluoroacetic acid (15 mL) in deuteriochloroform. The course of the reaction was determined by taking the ^1H nmr spectra of aliquots. After ca. 1.5 h there was no further decrease in intensity of the signal at δ_H 1.45. The reaction mixture was evaporated, the residue treated with diisopropyl ether, the amorphous solid collected, and the *acid* (2.7 g, $[\alpha]_D^{22}$ −58° (*c* 1.5, MeOH), δ_H (C^2HCl_3): 7.73 (H), 7.51 (H), 7.32 (5H), 7.30 (5H), 7.30 (H, e), 7.00 (H), 5.14 (2H), 5.08 (2H), 4.27 (2H, m), 3.81 (H, m), 3.55 (2H, m), 2.56 (2H, m), 2.00 (7H, bm), 1.46 (6H), 1.42 (6H), 0.82 (3H, d, $^3J_{HH}$ 6.5 Hz), 0.79 (3H, d, $^3J_{HH}$ 6.5 Hz). *Anal.* calcd. for $C_{38}H_{51}N_5O_{10}\cdot H_2O$: C 60.4, H 7.1, N 9.3 O 23.3%; found: C 60.4, H 7.1, N 9.3; O 23.1%, precipitated from dioxan solution (5 mL) with diisopropyl ether (50 mL). This acid (7 g), EEDQ (2.6 g), α-*tert*-butyl-γ-benzyl L-glutamate (from 3 g of hydrochloride, see above), and toluene (500 mL) were stirred together at room temperature for 72 h. The reaction mixture was evaporated, the residue taken up in ethyl acetate (500 mL), and acidic and basic by-products removed as described. The residue (= A, 35 mg) obtained after evaporation of the dry (Na_2SO_4) extract was purified by high pressure liquid chromatography, using methyl alcohol – ammonium acetate buffer (pH 4.2) 4:1. The main band eluting at ca. 48 mL was collected, the solution evaporated, and the residue taken up in *tert*-butyl alcohol. Lyophilization of the solution gave the N-*phenylmethoxycarbonylhexapeptide* (**6**) as a colorless solid, mp 50–55°C; $[\alpha]_D^{22}$ −43° (*c* 0.6, MeOH), δ_H (C^2HCl_3): 7.63 (H, e, d, $^3J_{HH}$ 8 Hz), 7.59 (H, e, d, $^3J_{HH}$ 8 Hz), 7.36 (5H), 7.34 (5H), 7.31 (5H), 7.05 (H, e), 6.95 (H, e), 6.46 (H, d, $^3J_{HH}$ 6 Hz), 5.24, 5.10 (2H, $^3J_{HH}$ 14.3 Hz), 5.09 (2H), 5.06 (2H), 4.40 (2H, m), 4.24 (H, m), 3.79 (H, t, $^3J_{HH}$ 7.5 Hz), 3.61 (2H, m), 2.50 (4H, m), 2.14 (9H), 1.55 (3H), 1.45 (12H), 1.38 (3H), 1.36 (3H), 0.75 (3H, d, $^3J_{HH}$ 7 Hz), 0.69 (3H, d, $^3J_{HH}$ 7 Hz). *Anal.* calcd. for $C_{54}H_{72}N_6O_{13}\cdot 0.5H_2O$: C 63.4, H 7.2, N 8.2, O 21.1%; found: C 63.2, H 6.95, N 8.1, O 21.2%. This triester (**9**, 10 g) in methyl alcohol (30 mL) was shaken with palladium on carbon (5%, 5 g) and hydrogen (3.5 kg cm^{-2}) at room temperature for 18 h. The reaction mixture was filtered through a bed of Celite (1 cm) and the filtrate evaporated. The residue (5.5 g) was taken up in hot methyl alcohol (15 mL) and the solution kept at 4°C for 48 h. The precipitated crystalline solid (3.85 g, mp 153–155°C) was collected. α-*tert-Butyl* L-*prolyl*-L-*valyl*-2-*methylalanyl*-2-*methylalanyl*-L-*glutamyl*-L-*glutamate* (**4**) separated from methyl alcohol as triclinic blades, mp 154–155°C; $[\alpha]_D^{21}$ −40.5° (*c* 0.8, MeOH); δ_C^* ($C^2H_3O^2H$): 179.4; 178.0; 177.1; 176.4; 174.5; 173.6; 172.2; 170.6; 82.7 (C, *t*-Bu); 60.94 ($^1J_{CH}$ 150.3 Hz); 60.0 ($^1J_{CH}$ 141 Hz); 58.1 (α-C aib); 58.0 (α-C aib); 55.0 ($^1J_{CH}$ 143 Hz); 54.25 ($^1J_{CH}$ 142 Hz); 47.5 ($^1J_{CH_2}$ 146 Hz); 34.2 ($^1J_{CH_2}$ 131 Hz); 32.7 ($^1J_{CH_2}$ ~ 125 Hz); 32.4 ($^1J_{CH}$ 129.7 Hz, β-val); 31.3 ($^1J_{CH_2}$ 136 Hz); 29.2 (?CH_2); 28.2 ($^1J_{CH_2}$ ~ 133 Hz); 28.3 (3C, $^1J_{CH_3}$ 127.9 Hz), 26.5 (?CH_3); 25.1 (3C, $^1J_{CH_3}$ 128 Hz); 19.9 ($^1J_{CH_3}$ 125 Hz); 18.5 ($^1J_{CH_3}$ ~ 123 Hz). *Anal.* calcd. for $C_{32}H_{54}N_6O_{11}$: C 55.0, H 7.8, N 12.0, O 25.2%; found: C 54.7, H 7.8, N 12.0, O 25.3%.

α-tert-*Butyl* L-*prolyl*-L-*valyl*-2-*methylalanyl*-2-*methylalanyl*-L-*glutamate*

The protected pentapeptide (**3**, 9 g) in methyl alcohol (120 mL) was shaken with palladium on carbon (5%, 0.6 g) and hydrogen (3.5 kg cm^{-2}) for 40 h at 20°C. The reaction mixture was filtered through a bed of Celite, the filtrate evaporated, and the crystalline residue (mp 115–117°C, 6.3 g) recrystallized from prop-2-ol-isopropyl ether (1:1) gave the α-*tert-butyl* L-*prolyl*-L-*valyl*-2-*methylalanyl*-2-*methylalanyl*-L-*glutamate* (**7**) as rosettes, mp 117–119°C; $[\alpha]_D^{22}$ −41° (*c* 0.87, MeOH); δ_C ($C^2H_3O^2H$): 180.2; 177.2; 175.5; 173.3; 172.9; 172.0; 82.2; 69.9; 60.6; 57.9; 57.7; 54.9; 47.6; 34.2; 31.7; 28.4; 27.5; 26.6; 25.8; 24.0; 23.1; 19.7; 19.1. *Anal.* calcd. for $C_{27}H_{47}N_5O_8$: C 56.9, H 8.3, N 12.3; O 22.5%; found: C 57.0, H 8.6, N 11.9, O 23.0%.

α-tert-*Butyl* tert-*butyloxycarbonyl*-L-*prolyl*-L-*valyl*-2-*methylalanyl*-2-*methylalanyl*-L-*glutamyl*(γ)-L-*phenylalaninol*

The *tert*-butyl ester described in the previous paragraph (**7**, 6 g) and magnesium oxide (0.9 g) were stirred with a solution (150 mL) of dioxan (75 mL) in water for 1 h at room temperature, when *tert*-butyloxycarbonylazide (3 g) was added and the mixture stirred at 35°C for 72 h. The reaction mixture was diluted with sodium bicarbonate solution (5%), cooled to 0°C, filtered, and extracted (pH 7.0) with ethyl acetate. The cold (0°C) raffinate was acidified to pH 3.0 with citric acid solution (2%), sodium chloride added to saturation, and the solution extracted (3 × 50 mL) with ethyl acetate. The extract was washed with water, dried (Na_2SO_4), filtered, and evaporated. The residue recrystallized from ethyl acetate – methyl alcohol (100:1) gave the N-*tert-butyloxycarbonyl derivative* (**8**) as prisms, mp 200–202°C; $[\alpha]_D^{22}$ −57° (*c* 1.15, MeOH). *Anal.* calcd. for $C_{32}H_{55}N_5O_{10}$: C 57.4, H 8.3, N 10.5%; found: C 57.2, H 8.3, N 10.4%. This product (**8**, 2.4 g), L-phenylalaninol (Aldrich, 0.54 g), and 2-isobutoxy-1-isobutyloxycarbonyl-1,2-dihydroquinoline (38) (1.2 g) were dissolved in ethyl alcohol (dried over Linde molecular sieve 3A and redistilled, 100 mL) and the reaction mixture was stirred at 35°C for 4 days. The resulting solution was evaporated, the residue (3.3 g) taken up in ethyl acetate (100 mL), and the solution washed successively with water (50 mL), sodium bicarbonate solution (2 × 50 mL), and water. The dry solution was evaporated, the residue dissolved in hot ethyl acetate (5 mL), and light petroleum added to turbidity. The mixture was kept at 4°C for 36 h, when the crystalline mass that had separated was collected. The *hexapeptide* (**5**) separated from ethyl acetate – light petroleum (bp 30–60°C, 1:1) as prisms, mp 110–112°C; $[\alpha]_D^{22}$ −83.6°; δ_C^* ($C^2H_3O^2H$): 177.2, 177.1; 176.1, 175.9; 175.6; 175.3; 174.9; 173.9, 173.8; 172.4, 172.3; 139.9 (quat. C); 130.5 (2C, $^1J_{CH}$ ~ 157 Hz); 129.4 (2C, $^1J_{CH}$ 158.8 Hz, $^2J_{CH}$ ~ 5 Hz); 127.2 ($^1J_{CH}$ 157.7 Hz, $^2J_{CH}$ ~ 8 Hz); 82.6 (quat. Bu ester); 81.25, 81.2 (quat. Bu urethane); 64.0 ($^1J_{CH_2}$ 144.7 Hz, CH_2OH); 60.8, 60.6 ($^1J_{CH}$ ~ 145 Hz, α-pro); 60.85 ($^1J_{CH}$ 142.6, αval); 57.9 (aib α-C); 57.85 (aib α-C); 54.55 ($^1J_{CH}$ 140 Hz); 53.8 ($^1J_{CH}$ 139.5 Hz); 48.4, 48.0 ($^1J_{CH_2}$ 142 Hz, α-pro); 38.1 ($^1J_{CH_2}$ 129 Hz, PhCH_2); 33.7, 33.0 ($^1J_{CH_2}$ 133 Hz, pro); 32.2, 30.8 (? pro); 31.85 ($^1J_{CH}$ 130 Hz, β-val (39)); 28.8 ($^1J_{CH_3}$ 127 Hz, Bu(3)); 28.4 ($^1J_{CH_3}$ 128 Hz, Bu(3)); 27.8 ($^1J_{CH_3}$ 128 Hz); 26.8 (? CH_3); 25.6 (? CH_2); 24.8 (? CH_2), 23.9 ($^1J_{CH_3}$ 128 Hz); 23.7 ($^1J_{CH_3}$ 128 Hz);

19.2, 19.3 ($^1J_{CH_3}$ 128 Hz, val). *Anal.* calcd. for $C_{41}H_{66}N_6O_{10}\cdot H_2O$: C 60.0, H 8.4, N 10.2, O 21.4%; found: C 60.3, H 8.4, N 10.2, O 21.2%.

Dimethyl N-*(4-chlorobenzoyl)-L-prolyl-L-valyl-2-methylalanyl-2-methylalanyl-L-glutamate*

(a) The α-*tert*-butyl ester (**7**, 1.7 g) was suspended in THF (100 mL) and the stirred mixture treated with diazomethane (70 mg) in ether (20 mL). After 0.5 h at 20°C the excess diazomethane was blown off with a stream of nitrogen, the solution evaporated, and the residue taken up in hot tetrahydropyran (15 mL). The solution was kept at 4°C for 18 h, when the crystals that separated were collected (1.7 g). The *α-tert-butyl-γ-methyl ester* (**9**) separated from tetrahydropyran as blades, mp 178–179°C; $[\alpha]_D^{24}$ −51° (*c* 1.38, $CHCl_3$). *Anal.* calcd. for $C_{28}H_{49}N_5O_8$: C 57.6, H 8.5, N 12.0%; found: C 57.4, H 8.4, N 12.0%. This diester (3 g) was dissolved in THF (150 mL) and the solution treated with *p*-chlorobenzoylazide (1.1 g) in THF (10 mL). The solution was stirred at 20°C for 72 h, then was evaporated and the residue digested with petroleum ether (bp 30–60°C, 3 × 50 mL). The crystalline residue was collected and the N-(*4-chlorobenzoyl*) derivative (**10**) separated from *n*-butyl acetate as prisms, mp 90–95°C, recrystallizing at 125–130°C and finally melting sharply at 178–179°C; $[\alpha]_D^{24}$ −86° (*c* 0.66, $CHCl_3$). *Anal.* calcd. for $C_{35}H_{52}ClN_5O_9$: C 58.2, H 7.2, Cl 4.9, N 9.7%; found: C 57.8, H 7.3, Cl 4.9, N 9.9%. This *tert*-butyl ester (**10**, 1 g) was dissolved in methyl alcohol (100 mL) and hydrogen chloride passed into the solution for 15 min. The temperature of the reaction mixture increased to 55°C, when it was cooled to 20°C and kept at this latter temperature for 72 h. The solution was evaporated, the residue taken up in ethyl acetate (100 mL), and the solution washed with sodium bicarbonate solution (2%, 3 × 50 mL), with ice-cold sodium carbonate solution (1%, 50 mL), and finally with water (2 × 50 mL). The dry (Na_2SO_4) ethyl acetate solution was filtered, evaporated, and the residue (0.72 g, 76%, mp 162°C; $[\alpha]_D^{24}$ −90°, containing 3.5% of a byproduct of lower R_f) was recrystallized by dissolving in *n*-butyl acetate (8 mL) and adding diethyl ether (12 mL). The precipitate was collected after storage at 4°C for 96 h. After 6 recrystallizations in this manner, *dimethyl* N-*(4'-chlorobenzoyl)-L-prolyl-L-valyl-2-methyalanyl-2-methylalanyl-L-glutamate* was obtained, containing 0.15% of the impurity, mp 168–169°C; $[\alpha]_D^{24}$ −99° (*c* 0.57, $CHCl_3$); crystal data: $P2_12_12_1$; orthorhombic; a = 16.60, b = 25.16, c = 10.23 Å; δ_H (C^2HCl_3): 7.48 (2H, J = 8.6 Hz), 7.42 (2H, J = 8.6 Hz), 7.39 (H, e, J = 6.2 Hz), 6.80 (H, e, aib NH), 6.55 (H, e, aib NH), 4.78 (H, $J_{H_\alpha H_\beta}$ = 7.8 Hz, $J_{H_\alpha H_{(N)}}$ = 6.2 Hz, val α-C*H*), 4.5 (H, m, glu α-CH), 3.76 (H, t, J = 6.1 Hz, pro α-CH), 3.70 (3H), 3.64 (3H), ~3.5 (H, m, val β-CH), ~2.5 (2H, m, pro δ-CH_2), 2.32 (H, m, pro β-CH_2), ~2.2 (2H, m, glu γ-CH_2), 2.1–2.3 (3H, m, pro), 1.91 (2H, glu β-CH_2), 2.04 (H, m, glu CH_2), 1.55 (3H, aib), 1.49 (3H, aib), 1.47 (3H, aib), 1.46 (3H, aib), 0.98 (3H, J = 6.3 Hz, val), 0.98 (3H, J = 6.3 Hz, val); δ_C^* ($C^2H_3O^2H$): 177.6; 175.7; 175.1; 174.5; 173.9; 173.8; 170.8; 137.5 (quat. arom.); 136.0 (quat. arom., $^2J_{CH}$ ~ 7 Hz); 130.0 (2C, $^1J_{CH}$ 164 Hz, $^2J_{CH}$ ~ 7 Hz); 129.7 (2C, $^1J_{CH}$ 167.5 Hz); 61.6 ($^1J_{CH}$ 148 Hz); 60.8 ($^1J_{CH}$ 141 Hz); 57.9 (aib α-C); 53.5 ($^1J_{CH}$ 138 Hz); 52.65 ($^1J_{CH_3}$ 147 Hz, ester Me); 52.0 ($^1J_{CH_3}$ 147 Hz, ester Me); 51.9 (aib α-C); 31.9 ($^1J_{CH}$ 138 Hz, β-val (39)); 31.3 ($^1J_{CH_2}$ ~ 130 Hz), 31.1 (? CH_2); 27.7 (? CH_3); 27.2 ($^1J_{CH_2}$ ~ 130 Hz); 26.9 ($^1J_{CH_3}$ 132 Hz); 26.6 ($^1J_{CH_2}$ 134 Hz); 23.7 ($^1J_{CH_3}$ 128 Hz); 23.6 ($^1J_{CH_3}$ 128 Hz); 19.6 ($^1J_{CH_3}$ 127 Hz); 19.3 ($^1J_{CH_3}$ 127 Hz). *Anal.* calcd. for $C_{32}H_{46}ClN_5O_9$: C 56.5, H 6.8, Cl 5.2, N 10.3, O 21.2%; found: C 56.4, H 6.9, Cl 5.2, N 10.1, O 21.1%.

(b) γ-Benzyl-L-glutamic acid (10.5 g) was suspended in THF (150 mL) and water (1.5 mL) was added. The mixture was stirred with a solution (100 mL) of diazomethane (2 g) in ether for 3 days at room temperature, after which the solution was evaporated, the residue taken up in ether (100 mL), the ether solution washed with sodium bicarbonate solution (2%, 100 mL), dried (Na_2SO_4), filtered, and the filtrate treated with hydrogen chloride. The precipitated hydrochloride (mp 133–134°C, 79%, 6 g), suspended in toluene (400 mL), was treated with triethylamine (2.04 g) and, after shaking the mixture for 5 min, with the *N*-phenylmethoxycarbonyl tetrapeptide (**2**, R = C_7H_7O, R′ = H, 10 g) (28) and EEDQ (5.2 g). The reaction mixture was treated as described for the analogous *tert*-butyl ester (**6**) and gave the *pentapeptide* (**11**) as prisms from *n*-butyl acetate, mp 144–146°C, 6 g, 41%; $[\alpha]_D^{24}$ −67° (*c* 4, MeOH). *Anal.* calcd. for $C_{39}H_{53}N_5O_{10}\cdot 0.25H_2O$: C 61.9, H 7.1, N 9.3, O 21.7%; found: C 61.9, H 7.2, N 9.5; O 21.2%. This ester (5 g) in methyl alcohol (120 mL) was shaken with hydrogen (4.2 kg cm^{-2}) and palladium on carbon (5%, 1 g). The reaction mixture was worked up as described for the ester (**10**) and gave the *pentapeptide methyl ester* (**12**) as prisms from methyl alcohol (70 mg mL^{-1}), mp 132–134°C. *Anal.* calcd. for $C_{24}H_{41}N_5O_8\cdot 1.5H_2O$: C 52.0, H 7.9, N 12.6, O 27.4%; found: C 51.9, H 8.0, N 12.5; O 27.0%. This iminoester (**12**, 1.5 g) was suspended in THF (75 mL) and a solution of diazomethane (0.12 g) in ether added. The peptide dissolved just as the color of the diazomethane disappeared. The *dimethyl ester* (**13**) separated from THF – isopropyl ether (1:3) as plates of characteristic trapezoid shape, mp 201–202°C, 1.5 g; δ_C: 177.5; 177.2; 175.3; 174.7; 173.7; 173.7; 61.4 ($^1J_{CH}$ 142 Hz); 60.1 ($^1J_{CH}$ 143 Hz); 57.7 ($^2J_{CH_3}$ 4.5 Hz); 57.7 (aib α-C); 53.3 ($^1J_{CH}$ ~ 145 Hz); 52.5 ($^1J_{CH_3}$ 147 Hz); 51.8 ($^1J_{CH_3}$ 147 Hz); 47.9 ($^1J_{CH_2}$ 144 Hz); 31.8 ($^1J_{CH_2}$ 134 Hz); 31.1 ($^1J_{CH}$ 131 Hz, val β-CH (39)); 27.1; 26.4 ($^1J_{CH_2}$ ~ 140 Hz); 27.8 ($^1J_{CH_3}$ 129 Hz, $^3J_{CH_3}$ 4 Hz); 26.8 ($^1J_{CH_3}$ 129 Hz, $^3J_{CH_3}$ 4 Hz); 23.5 (2C, $^1J_{CH_3}$ 129 Hz, $^3J_{CH_3}$ 4 Hz); 19.5 ($^1J_{CH_3}$ 130 Hz); 19.0 ($^1J_{CH_3}$ 130 Hz). *Anal.* calcd. for $C_{25}H_{43}N_5O_8$: C 55.5, H 7.9, N 12.9, O 23.7%; found: C 55.4, H 8.0, N 12.6; O 23.4%. This dimethyl ester (0.11 g) was suspended in THF (5 mL) and the mixture treated with 4-chlorobenzoylazide (40 mg). The reaction mixture was stirred at room temperature for 96 h, was evaporated, the residue titurated with light petroleum (3 × 20 mL), and the residue (0.12 g) then taken up in butyl acetate (3 mL) and diethyl ether (3 mL) added. The solution was kept for 18 h at 4°C, when the crystalline precipitate (0.1 g, mp 165–167°C; $[\alpha]_D^{24}$ −91° (*c* 1, $CHCl_3$)) was collected. The ^1H broadband-decoupled ^{13}C nmr spectrum of this material was identical to that of the material prepared by method (a); recrystallization as described in method (a) gave material with identical mp and specific optical rotation.

Acknowledgements

One of us (A.T.) thanks Dr. B. C. Das and Sir Ewart Jones F.R.S. in whose laboratories some of this work was done. Part of the work was carried out under the auspices of the joint France–Canada scientific agreement. We thank Dr. R. Greenhalgh for the FAB mass spectrum shown in Fig. 4, Dr. A. W. Hanson for crystallographic data, and Dr. A. W. McCulloch for helpful suggestions and comments on the typescript.

1. P. F. Wiley, J. M. Koert, and L. J. Hanka. J. Antibiot. **35**, 1231 (1982).
2. G. W. Kenner, and R. C. Sheppard. Nature (London), **181**, 48 (1958).
3. S. Dalby, G. W. Kenner, and R. C. Sheppard. J. Chem. Soc. 968 (1960).
4. J. S. Dalby, G. W. Kenner, and R. C. Sheppard. J. Chem. Soc. 4387 (1962).
5. Asahi Chemical Industry Co., Japan 13, 795 ('65); T. Ooka, Y. Shimojima, T. Akimoto, I. Takeda, S. Senoh, and J. Abe. Agric. Biol. Chem. **30**, 700; T. Ooka, and I. Takeda. Agric. Biol. Chem. **36**, 112 (1972).
6. G. Jung, W. A. Konig, D. Leibfritz, T. Ooka, K. Janko, and G. Boheim. Biochim. Biophys. Acta, **433**, 164 (1976); E. Katz, M. Aydin, N. Lucht, W. A. Konig, T. Ooka, and G. Jung. Annalen, 1041 (1985).
7. H. Brückner, and H. Graf. Experientia, **39**, 528 (1983); H. Brückner, H. Graf, and M. Bokel. Experientia, **40**, 1189 (1984).
8. K. Sasaki, H. Minato, K. Katagiri, S. Hayakawa, and T. Matsushima. J. Antibiot. **24**, 67 (1971); C. W. Gehrke, R. W. Zumwalt, and K. Kuo. J. Agric. Food Chem. **19**, 605 (1971).

9. D. A. BULLOUGH, C. G. JACKSON, P. F. J. HENDERSON, R. B. BEECHEY, and P. E. LINNETT. FEBS Lett. **145**, 258 (1982).
10. T. YAMANO. Jpn. Patent No. 7122522 (1971).
11. K. L. RINEHART, L. A. GAUDIOSO, M. L. MOORE, R. C. PANDEY, J. C. COOK, M. BARBER, R. D. SEDGWICK, R. S. BORDOLI, A. N. TYLER, and B. N. GREEN. J. Am. Chem. Soc. **103**, 6517 (1981).
12. D. BREWER, A. W. HANSON, I. M. SHAW, A. TAYLOR, and G. A. JONES. Experientia, **35**, 294 (1979).
13. R. NAGARAJ and P. BALARAN. Tetrahedron, **37**, 1263 (1981).
14. B. F. GISIN, D. G. DAVIS, Z. K. BOROWSKA, J. E. HALL, and S. KOBAYASHI. J. Am. Chem. Soc. **103**, 6373 (1981).
15. T. M. BALASUBRAMANIAN, N. C. E. KENDRICK, M. TAYLOR, G. R. MARSHALL, J. E. HALL, I. VODYANOY, and F. REUSSER. J. Am. Chem. Soc. **103**, 6127 (1981).
16. H. SCHMITT and G. JUNG. Annalen, 321 (1985).
17. E. KATZ, H. SCHMITT, M. AYDIN, W. A. KONIG, and G. JUNG. Annalen, 365 (1985).
18. H. SCHMITT and G. JUNG. Annalen, 345 (1985).
19. J. T. GERIG and R. S. MCLEOD. J. Org. Chem. **41**, 1653 (1976).
20. S. T. KIRKSEY, T. A. NEUBECKER, and D. A. MARGERUM. J. Am. Chem. Soc. **101**, 1631 (1979).
21. M. Y. ALI, A. J. DALE, and K. TITLESTAD. Acta Chem. Scand. **27**, 1509 (1973); M. Y. ALI and A. KHATUN. Tetrahedron, **41**, 451 (1985).
22. D. W. RUSSELL, W. D. JAMIESON, A. TAYLOR, and B. C. DAS. Can. J. Chem. **54**, 1355 (1976).
23. E. ABDERHALDEN, L. DINERSTEIN, and S. GENES. Fermentforschung. **10**, 532 (1929).
24. CHEN-HENG KAO, HSIN-YUAN FANG, and P. P. T. SAH. J. Chin. Chem. Soc. **3**, 137 (1935); Y. YUKAWA and Y. TSUNO. J. Am. Chem. Soc. **79**, 5530 (1957).
25. R. C. PANDEY, J. C. COOK, and K. L. RINEHART. J. Am. Chem. Soc. **99**, 8469 (1977).
26. H. BRUCKNER, W. A. KÖNIG, M. GREINER, and G. JUNG. Angew. Chem. Int. Ed. Engl. **18**, 476 (1979).
27. T. KAUFFMANN and J. SOBEL. Annalen, **698**, 235 (1966); M. A. RUTTENBERG, TE PIAO KING, and L. C. CRAIG. Biochemistry, **3**, 758 (1964); A. PATCHORNIK, M. WILCHEK, and S. SARID. J. Am. Chem. Soc. **86**, 1457 (1964); P. G. GASSMAN, P. K. G. HODGSON, and R. J. BALCHUNIS. J. Am. Chem. Soc. **98**, 1275 (1976).
28. I. M. SHAW and A. TAYLOR. J. Chem. Soc. Perkin Trans. 1, 1866 (1979).
29. R. OEKONOMOPULOS and G. JUNG. Annalen, 1151 (1979).
30. W. K. THOMAS and M. K. WILLIAMS. J. Chem. Soc. Chem. Commun. 994 (1972); W. VOELTER and O. OSTER. Org. Magn. Reson. **5**, 547 (1973); R. OEKONOMOPULOS, G. JUNG, and D. LEIBFRITZ. Tetrahedron, **38**, 2157 (1982).
31. T. S. CAMERON, A. W. HANSON, and A. TAYLOR. Cryst. Struct. Commun. **11**, 321 (1982).
32. A. FEICHT and A. TAYLOR. Proc. N. S. Inst. Sci. **32**, 313 (1982).
33. E. HOGGARTH. J. Chem. Soc. 1160 (1949).
34. R. L. M. SYNGE. Biochem. J. **42**, 99 (1948).
35. M. BERGMAN, L. ZERVAS, J. S. FRUTON, F. SCHNEIDER, and H. SCHLEICH. J. Biol. Chem. **109**, 338 (1935).
36. M. BERGMAN and L. ZERVAS. Chem Ber. **65**, 1192 (1932).
37. ST. GUTTMANN and R. A. BOISSONNAS. Helv. Chim. Acta, **41**, 1864 (1958).
38. Y. KISO, Y. KAI, and H. YAJIMA. Chem. Pharm. Bull. **21**, 2507 (1973).
39. W. VOELTER, G. JUNG, E. BREITMAIER, and E. BAYER. Z. Naturforsch. Teil B, **26**, 213 (1971).
40. The Upjohn Co., U. K. Patent No. 1152659 (1969).
41. R. O. FOX and F. M. RICHARDS. Nature (London), **300**, 325 (1982).
42. M. J. THIRUMALACHAR. Hind. Antibiot. Bull. **10**, 287 (1968); M. G. VAIDYA, P. V. DESHMUKH, and S. N. CHARI. Hind. Antibiot. Bull. **11**, 81 (1968).
43. R. C. PANDEY, HSI MENG, J. C. COOK, and K. L. RINEHART. J. Am. Chem. Soc. **99**, 5205 (1977).
44. R. NAGARAJ, N. SHAMALA, and P. BALARAM. J. Am. Chem. Soc. **101**, 16 (1979).
45. A. D. ARGOUDELIS and L. E. JOHNSON. J. Antibiot. **27**, 274 (1974).
46. T. FUJITA, Y. TAKAISHI, K. MATSUURA, Y. TAKEDA, Y. YOSHOKA, and H. BRUCKNER. Chem. Pharm. Bull. **32**, 2870 (1984).
47. T. ARAI, Y. MIKAMI, K. FUKUSHIMA, T. UTSUMI, and K. YAZAWA. J. Antibiot. **26**, 157 (1973).
48. T. FUJITA, Y. TAKAISHI, A. OKAMURA, E. FUJITA, K. FUJI, N. HIRATSUKA, M. KOMATSU, and I. ARITA. J. Chem. Soc. Chem. Commun. 585 (1981); K. FUKUSHIMA, T. ARAI, Y. MORI, M. TSUBOI, and M. SUZUKI. J. Antibiot. **36**, 1613 (1983).
49. M. SATO, T. BEPPU, and K. ARIMA. Agric. Biol. Chem. **44**, 3037 (1980); A. ISOGAI, A. SUZUKI, S. TAMURA, S. HIGASHIKAWA, and S. KUYAMA. J. Chem. Soc. Perkin Trans 1, 1405 (1984); A. ISOGAI, A. SUZUKI, S. HIGASHIKAWA, S. KUYAMA, and S. TAMURA. Agric. Biol. Chem. **44**, 3029 (1980).
50. C. ROSSI, Z. BENCIARI, C. G. CASINOVI, and L. TUTTOBELLO. Phytopathol. Mediterr. **22**, 209 (1983).
51. N. INOUE, A. INOUE, M. FURUKAWA, and N. KANDA. J. Antibiot. **29**, 618 (1976).
52. K. FUJI, E. FUJITA, Y. TAKAISHI, T. FUJITA, I. ARITA, M. KOMATSU, and N. HIRATSUKA. Experientia, **34**, 237 (1978).
53. C. T. HOU, A. CIEGLER, and C. W. HESSELTINE. Appl. Microbiol. **23**, 183 (1972).
54. G. IRMSCHER, G. BOVERMANN, G. BOHEIM, and G. JUNG. Biochim. Biophys. Acta, **507**, 470 (1978).
55. A. D. ARGOUDELIS, A. DIETZ, and L. E. JOHNSON. J. Antibiot. **27**, 321 (1974).
56. B. BACHET, C. BRASSY, I. MORIZE, E. SURCOUF, J. P. MORNON, B. BODO, and S. REBUFFAT. J. Mol. Biol. **170**, 795 (1983).
57. J. W. PAYNE, R. JAKES, and B. S. HARTLEY. Biochem. J. **117**, 757 (1970).
58. YU. A. OVCHINNIKOV, A. A. KIRYUSHKIN, and I. V. KOZHEVNIKOVA. Zh. Obshch. Khim. **41**, 2085 (1971).
59. D. A. MARTIN and R. J. P. WILLIAMS. Biochem. J. **153**, 181 (1976).
60. D. A. BULLOUGH, C. G. JACKSON, P. J. F. HENDERSON, F. H. COTTEE, R. B. BEECHEY, and P. E. LINNETT. Biochem. Int. **4**, 543 (1982).
61. T. FUJITA, Y. TAKAISHI, A. OKAMURA, K. FUJI, E. FUJITA, N. HIRATSUKA, M. KOMATSU, and I. ARITA. Koen Yoshishu-Tennen Yuki Kagobutsu Toronkai 22nd, 424 (1979).
62. H. BRUECKNER and M. PRZYBYLSKI. Chromatographia, **19**, 188 (1984).

Reactivity of electron-rich binuclear hydrides. Synthesis, structure, and reactions of $[\{(i\text{-Pr})_2PCH_2CH_2P(i\text{-Pr})_2\}Rh]_2(\mu\text{-H})(\mu\text{-OC}_6H_5)$

MICHAEL D. FRYZUK[1] AND MAY-LING JANG[2]
Department of Chemistry, University of British Columbia, 2036 Main Mall, Vancouver, B.C., Canada V6T 1Y6
AND
TERRY JONES AND FREDERICK W. B. EINSTEIN
Department of Chemistry, Simon Fraser University, Burnaby, B.C., Canada V5A 1S6
Received June 27 , 1985

MICHAEL D. FRYZUK, MAY-LING JANG, TERRY JONES and FREDERICK W. B. EINSTEIN. Can. J. Chem. **64**, 174 (1986).

The reaction of phenol with the binuclear rhodium hydride $[\{(i\text{-Pr})_2PCH_2CH_2P(i\text{-Pr})_2\}Rh]_2(\mu\text{-H})_2$ generates $[\{(i\text{-Pr})_2PCH_2CH_2P(i\text{-Pr})_2\}Rh]_2(\mu\text{-H})(\mu\text{-OC}_6H_5)$, **2**, which was characterized by both solution spectroscopic techniques and a single crystal X-ray diffraction study. The structure was solved using Patterson and Fourier methods and refined to $R = 0.019$ ($R_w = 0.027$) for 6062 reflections; crystals of the compound are triclinic, space group $P\bar{1}$, with $a = 9.018(2)$, $b = 12.988(2)$, $c = 17.558(3)$ Å, $\alpha = 99.42(1)$, $\beta = 92.62(2)$, $\gamma = 91.85(2)°$, and $Z = 2$. Further reaction with excess phenol leads to the mononuclear complex $(\eta^5\text{-}C_6H_5O)Rh\{(i\text{-Pr})_2PCH_2CH_2P(i\text{-Pr})_2\}\cdot 2C_6H_5OH$, which contains two phenol units hydrogen bonded to the oxygen of the η^5-cyclohexyldienylone ligand. The presence of the bridging phenoxide ligand in **2** results in reduced reactivity as compared to the starting binuclear hydride dimer.

MICHAEL D. FRYZUK, MAY-LING JANG, TERRY JONES et FREDERICK W. B. EINSTEIN. Can. J. Chem. **64**, 174 (1986).

La réaction du phénol avec l'hydrure binucléaire du rhodium $[\{(i\text{-Pr})_2PCH_2CH_2P(i\text{-Pr})_2\}Rh]_2(\mu\text{-H})_2$ génère le composé **2**, $[\{(i\text{-Pr})_2PCH_2CH_2P(i\text{-Pr})_2\}Rh]_2(\mu\text{-H})(\mu\text{-OC}_6H_5)$, qui a été caractérisé à la fois par des techniques spectroscopiques et par une étude de diffraction des rayons-X sur un monocristal. On a résolu la structure par les méthodes de Patterson et de Fourier et on l'a affinée jusqu'à une valeur de $R = 0{,}019$ ($R_w = 0{,}027$) pour 6062 réflexions; les cristaux sont tricliniques, groupe d'espace $P\bar{1}$, avec $a = 9{,}018(2)$, $b = 12{,}988(2)$, $c = 17{,}558(3)$ Å, $\alpha = 99{,}42(1)$, $\beta = 92{,}62(2)$, $\gamma = 91{,}85(2)°$ et $Z = 2$. Une réaction subséquente avec un excès de phénol conduit à la formation d'un complexe mononucléaire, $(\eta^5\text{-}C_6H_5O)Rh\{(i\text{-Pr})_2PCH_2CH_2P(i\text{-Pr})_2\}\cdot 2C_6H_5OH$, qui contient deux unités de phénol qui sont liées par des ponts hydrogène à l'oxygène du ligand η-cyclohexyldiènylone. La présence du ligand phénolate comme pont dans le composé **2** réduit sa réactivité par comparaison avec celle de l'hydrure dimère binucléaire de départ.

[Traduit par le journal]

Introduction

In attempts to design polynuclear metal complexes that are resistant to fragmentation, a variety of bridging ligands have been employed to secure two or more transition metals together. Some typical but not exhaustive examples of bridging ligands are phosphides (PR^{2-}, PR_2^-) (see ref. 1 for leading references), arsenides (AsR^{2-}, AsR_2^-) (see ref. 2 for leading references), sulfides (S^{2-}, SR^-) (see ref. 3 for leading references), and oxides (O^{2-}, OR^-) (see ref. 4 for leading references). Synthetic strategies in the construction of homonuclear and heteronuclear clusters with bridging ligands have been impressive; numerous methodologies now exist for the convergent synthesis of remarkably complex metal clusters (5). However, little mention has been given to the feasibility of these purported fragmentation-resistant clusters to act as catalysts (or even catalyst precursors) for a particular transformation. Indeed, many of these impressive syntheses lead to rather inert metal clusters, albeit with the bridging ligands appropriately in place (see ref. 6 for some exceptions).

For some time we have been investigating the synthesis and reactivity of coordinatively unsaturated rhodium-hydride clusters with chelating bidentate phosphine donors as the ancillary ligands (7–10). The binuclear members of this family of clusters **1** are especially active in the hydrogenation and isomerization of terminal olefins, apparently without fragmentation of the binuclear unit (8, 11, 12). Our strategy for the preparation of catalytically-active metal clusters that contain bridging ligands

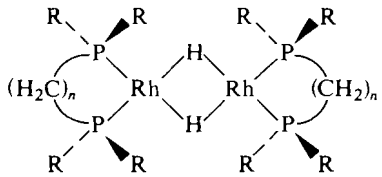

1*a*, $n = 2$, R = *i*-Pr
1*b*, $n = 3$, R = *i*-Pr
1*c*, $n = 2$, R = *i*-OPr

involves modification of existing catalytically-active systems such as **1** to generate potentially fragmentation-resistant clusters of the type **2**. This approach is not only complementary to the strategies mentioned previously, but it also allows one to examine the effects, beneficial or otherwise, of the presence of a bridging ligand.

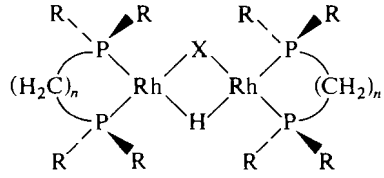

2, $n = 2$, $R = i$-Pr, X = OC_6H_5

In this paper we report some of our initial findings on the synthesis, structure and reactions of a complex of the type **2**, where the bridging ligand is a phenoxide (X = OC_6H_5).

Experimental section

General procedures and precautions were identical to those previously described (8, 13). The syntheses of $[(dippe)Rh]_2(\mu\text{-H})_2$ and

[1]Fellow of the Alfred P. Sloan Foundation (1984–1986).
[2]Recipient of an NSERC Summer Undergraduate Award (1983 and 1984).

(η^3-C_3H_5)Rh(dippe) (dippe = 1,2-bis(diisopropylphosphino)ethane) are described in ref. 9.

[(dippe)Rh]$_2$(μ-H)(μ-O—Ph)

To a solution of [(dippe)Rh]$_2$(μ-H)$_2$ (0.162 g, 0.22 mmol) in hexanes (4 mL) was added sublimed phenol (0.052 g, 0.55 mmol) in ~0.2 mL of toluene; the solution immediately turned from deep green to bright orange. The solution was allowed to sit undisturbed at room temperature for 12 h then at −30°C for 4 h to generate orange prisms. The solution was decanted away from the crystals, and the crystals washed with 3–4 mL of cold (−30°C) hexanes, and dried under vacuum. Yield: 0.151 g (83%), mp 182–184°C. ^{1}H nmr (C_6D_6, ppm): H_{ortho}, 7.38 (dd, $^3J_{meta}$ = 8.3 Hz, $^4J_{para}$ = 0.9 Hz); H_{meta}, 7.13 (dd, $^3J_{para}$ = 7.3 Hz); H_{para}, 6.73 (tt); PC*H*Me$_2$, 2.06, 1.76 (octets, ^2J_P = $^3J_{Me}$ = 7.1 Hz); PCH(C*H*$_3$)$_2$, 1.46, 1.17, 1.05, 0.94 (dd, ^3J_P = 15.3 Hz); PC*H*$_2$C*H*$_2$P, ~1.1 (complex multiplet obscured by PCH(C*H*$_3$)$_2$ resonances); Rh*H*Rh, −8.6 (ttt, $^2J_{Ptrans}$ = 61.5 Hz, $^2J_{Pcis}$ = 24.4 Hz, $^1J_{Rh}$ = 13.1). ^{1}P{^{1}H} nmr (C_6D_6, ppm relative to P(OMe)$_3$ at + 141.0): AA′MM′XX′ = P_A, 112.7 (m); P_B, 86.0 (m). IR (toluene, cm^{-1}): 1240 (C—O, s). *Anal.* calcd. for $C_{34}H_{70}OP_4Rh_2$: C 49.52; H 8.56; found: C 49.78; H 8.48.

[(dippe)Rh(η^5-C_6H_5O)]·2PhOH

Method 1: To a solution of [(dippe)Rh]$_2$(μ-H)$_2$ (0.162 g, 0.22 mmol) in toluene (5 mL) was added excess sublimed PhOH (~0.10 g, ~5 equiv.) in toluene (~0.5 mL) dropwise, then the resulting orange solution allowed to sit at room temperature for 18 h. The volatiles were removed under vacuum to give a red–orange solid. ^{1}H nmr analysis indicated a mixture of [(dippe)Rh]$_2$(μ-H)(μ-OPh) and [(dippe)Rh(η^5-C_6H_5O)]·2PhOH. Careful fractional crystallization from minimum toluene by the addition of hexanes yielded [(dippe)Rh(η^5-C_6H_5O)]·2PhOH as the more soluble component in approximately 50% yield.

Method 2: To a solution of (η^3-C_3H_5)Rh(dippe) (0.161 g, 0.40 mmol) in toluene (5 mL) was added sublimed PhOH (0.112 g, 1.19 mmol) in toluene (~0.5 mL) and the mixture allowed to stir for 24 h. The resulting deep orange solution was reduced in volume to ~0.5 mL and hexanes (1 mL) added. Cooling to −30°C gave orange crystals. Yield: 0.210 g (two fractions: 82%); mp 89–91°C. ^{1}H nmr (C_6D_6, ppm): PhO*H*...O, ~9–12 (br s); H_{ortho} (PhOH), 7.28 (dd, $^3J_{meta}$ = 8.0 Hz, $^5J_{para}$ = 0.9 Hz); H_{meta} (PhOH), 7.18 (dd, $^3J_{para}$ = 7.8 Hz); H_{para} (PhOH), 6.80 (tt); H_{ortho} (η^5-C_6H_5O), 6.25 (dd, $^3J_{meta}$ = 7.3 Hz; $^5J_{para}$ = 1.0 Hz); H_{meta} (η^5-C_6H_5O), 5.65 (dd, $^3J_{para}$ = 6.0 Hz); H_{para} (η^5-C_6H_5O), 4.70 (br t); PC*H*Me$_2$, 1.58 (br octet, ^2J_P = $^3J_{Me}$ = 7.0 Hz); PCH(C*H*$_3$)$_2$, 0.88 (dd, ^3J_P = 15.5 Hz); PC*H*$_2$C*H*$_2$P, 0.84 (m); PCH(C*H*$_3$)$_2$, 0.65 (dd, ^3J_P = 13.5 Hz). ^{31}P{^{1}H} nmr (C_6D_6, ppm relative to P(OMe)$_3$ at + 141.0); 105.5 (d, $^1J_{Rh}$ = 208 Hz). *Anal.* calcd. for $C_{32}H_{49}O_3P_2Rh$: C 59.44, H 7.64, found: C 59.66, H 7.57. IR (toluene, cm^{-1}): 2800 (OH, br); 1540 (C=O, s); 1271, 1246 (C—O, s).

Attempted preparation of (dippe)Rh(η^5-C_6H_5O)

To a solution of (η^3-C_3H_5)Rh(dippe) (0.032 g, 0.079 mmol) in toluene (2 mL) was added PhOH (0.79 mL of 0.1 *M* solution in toluene, 1 equiv.) and the mixture stirred at room temperature for 24 h. The volatiles were then removed and the mixture analyzed by ^{1}H nmr spectroscopy. Integration indicate that a ~2:1 mixture (η^3-C_3H_5)Rh-(dippe) and [(dippe)Rh(η^5-C_6H_5O)]·2PhOH was present.

Reactions of [(dippe)Rh]$_2$(μ-H)(μ-OPh)

Typically 10–20 mg of the complex was dissolved in C_6D_6 (0.4 mL) and placed in a 5 mm nmr tube sealed to a ground glass joint and fitted with a Teflon needle valve adapter. The nmr tube assembly was attached to the vacuum line and the solution degassed. Addition of the gaseous reactants (see below) was performed at −196°C and the tube sealed with a torch.

With H_2: by ^{1}H nmr, only the phenoxy-hydride dimer was detected even after long reaction times and heating to 75°C for 1 h.

With CH_2=CH_2: by ^{1}H nmr, only the phenoxy-hydride dimer was detected even after long reaction times.

With CO: As soon as the solution reached room temperature, an orange to yellow colour change was observed; by ^{1}H nmr, the solution contained PhOH and [(dippe)Rh(CO)]$_2$(μ-CO)$_2$ (12).

TABLE 1. Crystallographic data[a]

Formula	$C_{34}H_{70}OP_4Rh_2$
fw	824.64
Crystal system	Triclinic
Space group	$P\bar{1}$
a, Å	9.018(2)
b, Å	12.988(2)
c, Å	17.558(3)
α, deg	99.42(1)
β, deg	92.62(2)
γ, deg	91.85(2)
V, Å	2024.97
Z	2
D_{calcd}, g cm^{-3}	1.353
Crystal dimensions, mm	0.14 × 0.19 × 0.40
μ (Mo-K$_\alpha$), cm^{-1}	9.81
Transmission coefficients	0.807–0.895
Scan type	ω–2θ
w scan speed, deg min^{-1}	0.80–4.00
Scan range (deg in ω)	0.55 + 0.35 tan θ
Background fraction	0.25
Data collected	h, $\pm k$, $\pm l$
$2\theta_{max}$, deg	50
Take-off angle, deg	3
Crystal decay	Negligible
Unique reflections	7110
Observed reflections	6062
Number of variables	581
R	0.019
R_w	0.027

[a]Temperature 21 ± 1°C; Mo-K$_\alpha$ radiation, graphite monochromator, λ = 0.70930 Å (α$_1$), 0.71359 Å (α$_2$); function minimized was $\Sigma\omega(|F_o| - |F_c|)^2$, $R = \Sigma||F_o| - |F_c||/\Sigma|F_o|$, $R_w = (\Sigma\omega(|F_o| - |F_c|)^2/\Sigma\omega|F_o|^2)^{1/2}$, $\omega = 1/(\sigma^2(F) + 0.0006F^2)$.

Hydrogenation of 1-hexene

An identical procedure to that previously described (8) was utilized except that the catalyst precursor was [(dippe)Rh]$_2$(μ-H)(μ-OPh).

Deuterium labelling studies

[(dippe)Rh]$_2$(μ-D)$_2$ + PhOH. To a solution of [(dippe)Rh]$_2$(μ-D)$_2$ (0.039 g, 0.053 mmol) in C_6D_6 was added PhOH (0.009 g, 0.096 mmol) to generate an orange solution. Integration of the residual hydride resonance versus the proton resonances of the phenoxy ligand indicated an approx. 1:1 mixture of [(dippe)Rh]$_2$(μ-D)(μ-OPh) and [(dippe)Rh]$_2$(μ-H)(μ-OPh). The addition of excess PhOH does not change this ratio.

[(dippe)Rh]$_2$(μ-H) + d_5-PhOD. To a solution of [(dippe)Rh]$_2$-(μ-H)$_2$ (0.080 g, 0.107 mmol) in C_6D_6 (1 mL) was added C_6D_5OD (Aldrich; 0.012 g, 0.120 mmol); the resultant orange solution was analyzed by ^{1}H nmr. Integration of the hydride resonance indicated an approximately 50% (±5%) loss of the hydride intensity which corresponds to a ~1:1 mixture of [(dippe)Rh]$_2$(μ-H)(μ-OC$_6$D$_5$) and [(dippe)Rh]$_2$(μ-OC$_6$D$_5$) as found above.

Crystallographic analysis: Crystal data are given in Table 1. Precession and Weissenberg photographs (CuKα, λ = 1.5418 Å) were used to determine approximate cell dimensions and to assign the space group as *P*1 or $P\bar{1}$ (subsequent structure solution proved $P\bar{1}$ to be the correct space group). Accurate cell dimensions were determined by least squares refinement of 25 accurately centred reflections (2ρ = 15–20°) chosen from a variety of points in reciprocal space and measured with Mo-Kα radiation (λ = 0.71069 Å). Data were collected using an Enraf-Nonius CAD4-F diffractometer. Scan information is given in Table 1; background measurements were made by extending the scan range by 25% at each side of the scan. Measurement of 2 standard reflections every hour allowed monitoring of crystal decay and stability of the detection chain. Lorentz, polarization and absorption

TABLE 2. Final positional and thermal (Å^2) parameters for $C_{34}H_{70}OP_4Rh_2$

Atom	X	Y	Z	B_{iso}[a]
Rh(1)	0.19841(2)	0.31797(1)	0.19615(1)	2.169(8)
Rh(2)	0.20345(2)	0.19277(1)	0.31050(1)	2.355(8)
P(1)	0.21673(6)	0.32555(4)	0.07146(3)	2.54(2)
P(2)	0.13595(6)	0.47980(4)	0.20934(3)	2.45(2)
P(3)	0.22697(7)	0.03439(4)	0.34068(3)	2.96(3)
P(4)	0.16992(6)	0.24565(5)	0.43176(3)	2.75(2)
O	0.2546(2)	0.1603(1)	0.19286(8)	3.02(7)
C(11)	0.3915(3)	0.2870(2)	0.0247(1)	3.7(1)
C(111)	0.5243(3)	0.3487(3)	0.0691(2)	5.2(2)
C(112)	0.3926(4)	0.2935(3)	−0.0611(2)	5.8(2)
C(12)	0.0728(3)	0.2487(2)	0.0050(1)	3.3(1)
C(121)	−0.0829(3)	0.2790(2)	0.0269(2)	4.2(1)
C(122)	0.0899(4)	0.1329(2)	0.0044(2)	4.7(2)
C(13)	0.1986(3)	0.4612(2)	0.0532(1)	3.4(1)
C(21)	−0.0415(3)	0.5179(2)	0.2541(2)	3.4(1)
C(211)	−0.1677(3)	0.4400(3)	0.2222(2)	5.3(2)
C(212)	−0.832(4)	0.6306(3)	0.2510(2)	5.6(2)
C(22)	0.2696(3)	0.5806(2)	0.2635(1)	3.3(1)
C(221)	0.2796(4)	0.5754(3)	0.3489(2)	5.2(2)
C(222)	0.4208(4)	0.5721(3)	0.2304(2)	5.7(2)
C(23)	0.1096(3)	0.5248(2)	0.1148(1)	3.6(1)
C(31)	0.0990(3)	−0.0726(2)	0.2893(2)	4.6(2)
C(311)	0.1354(5)	−0.0991(3)	0.2056(2)	6.3(2)
C(312)	−0.0628(4)	−0.0437(3)	0.2976(3)	6.6(3)
C(32)	0.4121(3)	−0.0237(2)	0.3310(2)	3.7(1)
C(321)	0.4218(4)	−0.1355(2)	0.3468(2)	5.7(2)
C(322)	0.5294(3)	0.0466(2)	0.3816(2)	4.4(2)
C(33)	0.1878(3)	0.0349(2)	0.4434(2)	4.0(1)
C(41)	0.2938(3)	0.3572(2)	0.4794(1)	3.4(1)
C(411)	0.4519(3)	0.3493(3)	0.4547(2)	4.6(1)
C(412)	0.2908(4)	0.3806(3)	0.5678(2)	4.7(2)
C(42)	−0.0154(3)	0.2875(2)	0.4648(2)	4.1(1)
C(421)	−0.1300(4)	0.1986(4)	0.4486(4)	8.6(4)
C(422)	−0.0684(4)	0.3763(3)	0.4267(2)	5.8(2)
C(43)	0.2159(3)	0.1437(2)	0.4909(1)	3.8(1)
C(51)	0.3954(3)	0.1317(2)	0.1771(1)	3.4(1)
C(52)	0.5196(3)	0.1834(2)	0.2159(2)	4.3(1)
C(53)	0.6635(4)	0.1516(3)	0.1995(2)	5.9(2)
C(54)	0.6813(5)	0.0672(3)	0.1425(2)	6.8(2)
C(55)	0.5585(5)	0.0159(3)	0.1034(2)	6.5(2)
C(56)	0.4155(4)	0.0465(2)	0.1194(2)	4.9(2)
H(1)	0.175(3)	0.319(2)	0.294(2)	5.0(0)

[a] $B_{iso} = 8\Pi^2[(U_{11}^2 + U_{22}^2 + U_{33}^2)/3]^{1/2}$.

corrections have been made (see Table 1 for range of transmission coefficients).

The structure was solved by conventional Patterson and Fourier methods. All atoms were located by successive difference-maps. The final cycles of full-matrix least-squares refinement were performed by varying the coordinates of all atoms, with anisotropic temperature factors for all non-hydrogen atoms and fixed isotropic temperature factors for hydrogen atoms (the U values used for hydrogen atoms were determined during earlier refinement when hydrogen coordinates were fixed). A weighting scheme was derived on the basis of trends in $w\Delta^2$ as a function of $|F_0|$ and sin ρ/λ (Table 1). An extinction correction (14) was also applied. The final difference map was essentially clean apart from a couple of weak peaks [0.24–0.30(5) e/Å^3] in the vicinity of Rh atoms. The maximum parameter shift during the last cycle of refinement was 0.1σ for a hydrogen atom and 0.03σ for a non-hydrogen atom. Atomic scattering factors including anomalous dispersion were taken from Tables for X-ray crystallography (15). Final positional and thermal parameters for non-hydrogen atoms were given in Table 2. Anisotropic thermal parameters, final positional, and thermal parameters for hydrogen atoms and structure factor listings are available as supplementary material (Tables 81–83).[3] The computer programs used here are those belonging to "The VAX 750/780 crystal structure system" (16).

Results and discussion

The reaction of deep green solutions of $[(dippe)Rh]_2(\mu\text{-}H)_2$ **1***a* (dippe = 1,2-bis)diisopropylphosphino)ethane) with phenol (C_6H_5OH) leads to an immediate colour change to orange and the formation of **2** in excellent yields. Monitoring the reaction shown in reaction [1] by $^{31}P\{^1H\}$ nmr spectroscopy indicates that one equivalent of phenol is enough to completely convert **1***a* to **2** in quantitative yield; in practice, between one and two

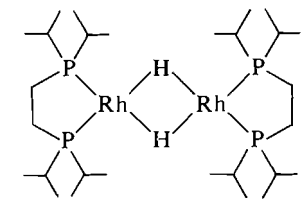

1*a*

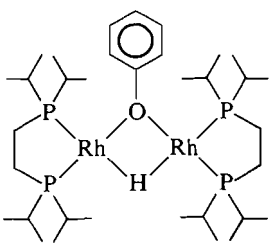

2

equivalents are used. Addition of excess phenol does not affect the $^{31}P\{^1H\}$ nmr spectrum initially, however, a new species does begin to grow in with time (*vide infra*). The ^1H nmr spectrum of **2** is characterized by a symmetrical multiplet (triplet of triplet of triplets due to coupling with two ^{103}Rh, two *trans* ^{31}P and two *cis* ^{31}P nuclei) for the bridging hydride at −8.9 ppm and an AA′BB′C pattern for the protons on the bridging phenoxide; the dippe ligand resonances are appropriate for the symmetry of the complex. The $^{31}P\{^1H\}$ nmr spectrum consists of two sets of symmetrical resonances due to the AA′MM′XX′ spin system. The ir spectrum shows a strong C—O absorption at 1240 cm^{-1}.

The single crystal X-ray structure of **2** shown in Fig. 1 confirms the above basic structure (reaction [1]). The four phosphorus, two rhodium, the bridging hydrogen, and the bridging oxygen atoms are essentially coplanar. Selected bond distances and angles are contained in Table 3. The molecule is quite symmetrical with both Rh(1)—H(1) and Rh(2)—H(1) bond distances equal to 1.74(3) Å; similarly, the respective Rh(1)—O and Rh(2)—O bond distances of 2.117(1) and 2.114(2) Å are almost identical. The Rh—P bonds *trans* to the bridging hydride are approximately 0.05 Å longer than the Rh—P bonds *trans* to the bridging phenoxide group (compare Rh(1)—P)1) and Rh(2)—P(3) at 2.2209(7) Å to Rh(1)—P(2) at 2.1720(7) Å and Rh(2)—P(4) at 2.1657(7) Å). Although the Rh—P bond distances correlate with the stronger *trans* influence (17) of a hydride versus an oxygen donor, non-bonding

[3] Anisotropic thermal parameters, final positional and thermal parameters for hydrogen atoms and calculated structure amplitudes are available at a nominal charge from the Depository of Unpublished Data, CISTI, National Research Council of Canada, Ottawa, Ont., Canada K1A 0S2.

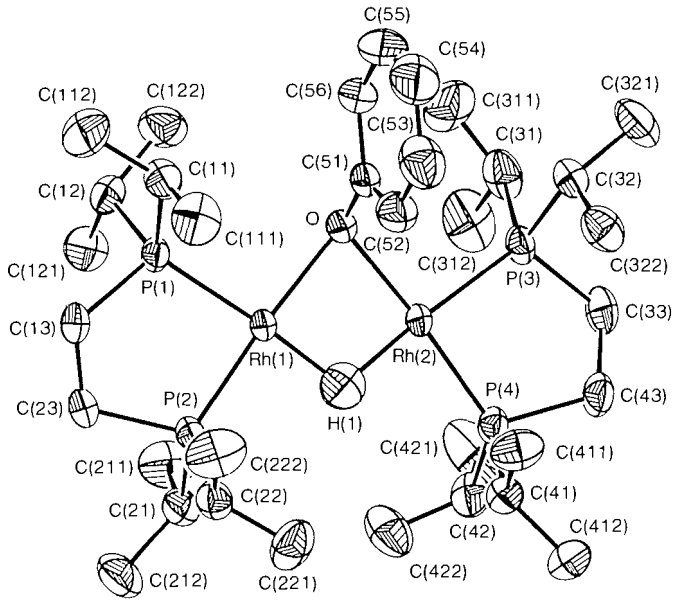

FIG. 1. ORTEP view and numbering and labelling scheme for $[(dippe)Rh]_2(\mu\text{-}H)(\mu\text{-}OC_6H_5)$. Thermal ellipsoids are drawn at the 50% probability level.

repulsions between the phenyl and the isopropyl groups may also be operative. The geometry around the oxygen atom is pyramidal with the following bond angles: Rh(1)—O—Rh(2), 88.22(5)°; Rh(1)—O—C(51), 119.6(2)°; Rh(2)—O—C(51), 117.2(2)°. The bite angles of the dippe ligands of 86.57(2)° and 86.77(3)° are only slightly larger than the previously observed angles of 85.89(4)° and 86.44(4)° in $[(dippe)Rh]_2(\mu\text{-}H)(\mu\text{-}\eta^2\text{-}CH{=}CH_2)$ (19). The Rh—Rh distance of 2.7825(4) Å is similar to the observed distance of 2.8655(5) Å found in $[(dippe)Rh]_2(\mu\text{-}H)(\mu\text{-}\eta^2\text{-}CH{=}CH_2)$.

The source of the bridging-hydride in the μ-phenoxide derivative **2** was investigated by analysis of the reaction of the dideuteride **1***a*′ with unlabelled phenol (reaction [2]) and the complementary reaction of the dihydride **1***a* with deuterated phenol reaction [3] (Rh* = Rh(dippe)).

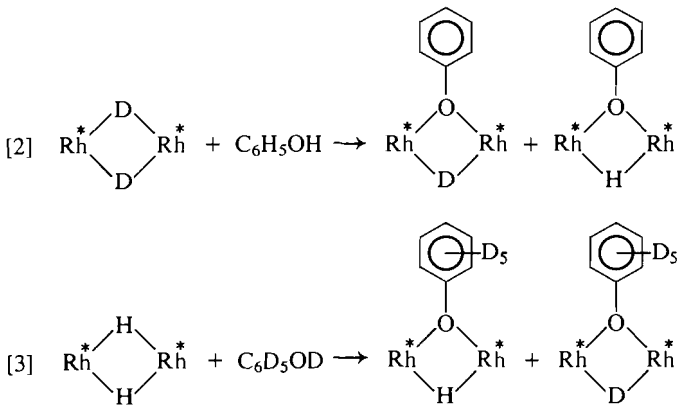

In both reactions, ^1H nmr spectral analysis of the products showed that the phenoxy-deuteride and the phenoxy-hydride were formed in approximately equal amounts, regardless of the experimental conditions. These experiments establish that protonation by phenol, or more accurately oxidative adition of HX (X = OC_6H_5) proceeds through an intermediate which scrambles the hydrides and deuterides before the reductive elimination step.

The phenoxy-hydride **2** is much less reactive than the starting binuclear dihydride **1***a*. For example, the addition of either H_2 (4 atm) or ethylene (1 atm) to **2** does not result in any observable change in the ^1H nmr spectrum. However, the addition of carbon monoxide to **2** results in an immediate colour change from orange to yellow; ^1H nmr spectral analysis indicates the presence of free phenol (equiv.) and the formation of $[(dippe)Rh(CO)]_2(\mu\text{-}CO)_2$ (12). Insertion of CO into the bridging-phenoxide was not observed (Scheme 1).

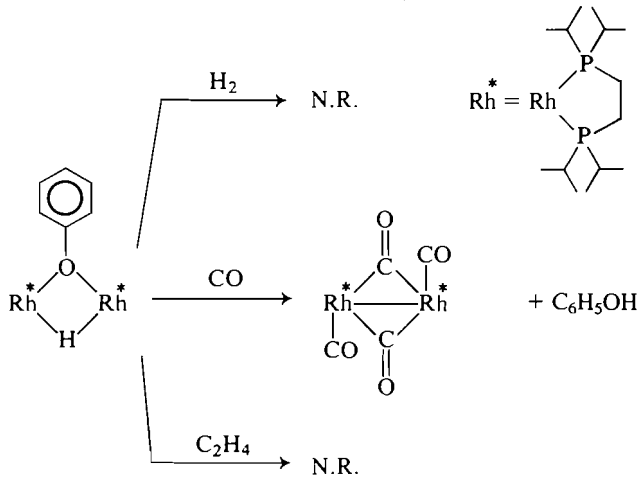

SCHEME 1

Under typical hydrogenation conditions, the phenoxy-hydride **2** does act as a catalyst precursor for the reduction (and isomerization) of 1-hexene; however, the rate is an order of magnitude slower than the starting dihydride **1***a* (see Experimental section (12)).

As mentioned above, when the formation of the phenoxy-hydride **2** from the binuclear dihydride **1***a* is monitored by $^{31}P\{^1H\}$ nmr spectroscopy, another product grows in with time in the presence of excess phenol, as evidenced by the appearance of a sharp doublet ($^1J_{Rh}$ = 208 Hz). This new material is formulated as the mononuclear complex $(dippe)Rh(\eta^5\text{-}C_6H_5O)\cdot 2C_6H_5OH$, **3**.

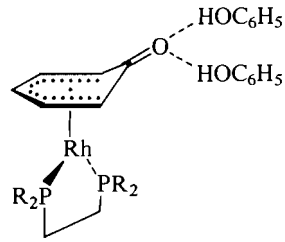

3, R = *i*-Pr

Characteristic of the cyclohexadienylone ligand is the upfield shift of the protons of the coordinated $\eta^5\text{-}C_6H_5O$ group in the ^1H nmr spectrum, and the presence of a strong band in the ir at 1545 cm^{-1} for the carbonyl stretch. The presence of the additional phenol units hydrogen-bonded to the carbonyl is apparent both from the broad singlet downfield (~9–11 ppm) in the ^1H nmr spectrum and the broad OH stretch in the ir; the analytical figures also support this formulation.

This type of structural unit contained in **3** is not unique. A number of ruthenium(II) derivatives of the general formula $(Ph_3P)_2HRu(\eta^5\text{-}C_6H_5O)\cdot S_X$ (where S = PhOH or MeOH), as well as the rhodium analogues of formula $(Ph_3P)_2Rh(\eta^5\text{-}C_6H_5O)\cdot(PhOH)_n$ (n = 2 or 3) have been isolated (18). The single crystal X-ray structure of $(Ph_3P)_2HRu(\eta^5\text{-}$

TABLE 3. Selected bond parameters for $C_{34}H_{70}OP_4Rh_2$

Bond	Distance (Å)	Bond	Distance (Å)
Rh(1)—Rh(2)	2.7825(4)		
Rh(1)—P(1)	2.2209(7)	Rh(2)—P(3)	2.2209(7)
Rh(1)—P(2)	2.1720(7)	Rh(2)—P(4)	2.1657(7)
Rh(1)—H(1)	1.74(3)	Rh(2)—H(1)	1.74(3)
Rh(1)—O	2.117(1)	Rh(2)—O	2.114(2)
P(1)—C(11)	1.856(2)	P(3)—C(31)	1.862(3)
P(1)—C(12)	1.855(2)	P(3)—C(32)	1.858(3)
P(1)—C(13)	1.853(2)	P(3)—C(33)	1.852(3)
P(2)—C(21)	1.861(3)	P(4)—C(41)	1.860(3)
P(2)—C(22)	1.859(2)	P(4)—C(42)	1.863(3)
P(2)—C(23)	1.856(2)	P(4)—C(43)	1.857(2)
C(13)—C(23)	1.524(4)	C(33)—C(43)	1.525(4)

Bonds	Angle (deg)	Bonds	Angle (deg)
P(1)—Rh(1)—P(2)	86.57(2)	P(3)—Rh(2)—P(4)	86.77(3)
P(1)—Rh(1)—O	98.12(4)	P(3)—Rh(2)—O	99.14(4)
P(1)—Rh(1)—H(1)	176(1)	P(3)—Rh(2)—H(1)	175(1)
P(2)—Rh(1)—O	175.26(4)	P(4)—Rh(2)—O	172.06(5)
P(2)—Rh(1)—H(2)	90(1)	P(4)—Rh(2)—H(1)	89(1)
O—Rh(1)—H(1)	85(1)	O—Rh(2)—H(1)	86(1)
Rh(1)—O—Rh(2)	82.22(5)	Rh(1)—H(1)—Rh(2)	106(2)
Rh(1)—O—O(51)	119.6(2)	Rh(2)—O—C(51)	117.2(2)
Rh(1)—P(1)—C(11)	119.07(9)	Rh(2)—P(3)—C(31)	117.69(9)
Rh(1)—P(1)—C(12)	115.08(8)	Rh(2)—P(3)—C(32)	117.46(9)
Rh(1)—P(1)—C(13)	110.80(8)	Rh(2)—P(3)—C(32)	110.50(9)
C(11)—P(1)—C(12)	102.7(1)	C(31)—P(3)—C(32)	102.8(1)
C(11)—P(1)—C(13)	102.5(1)	C(31)—P(3)—C(33)	102.6(1)
C(12)—P(1)—C(13)	104.3(1)	C(32)—P(3)—C(33)	103.9(1)
Rh(1)—P(2)—C(21)	119.48(8)	Rh(2)—P(4)—C(41)	115.48(8)
Rh(1)—P(2)—C(22)	117.59(8)	Rh(2)—P(4)—C(42)	120.91(9)
Rh(1)—P(2)—C(23)	112.04(8)	Rh(2)—P(4)—C(43)	111.46(9)
C(21)—P(2)—C(22)	101.8(1)	C(41)—P(4)—C(42)	101.9(1)
C(21)—P(2)—C(23)	101.0(1)	C(41)—P(4)—C(43)	101.6(1)
C(22)—P(2)—C(23)	102.5(1)	C(42)—P(4)—C(43)	103.2(1)
P(1)—C(13)—C(23)	111.1(2)	P(3)—C(33)—C(43)	111.1(2)
P(2)—C(23)—C(13)	111.3(2)	P(4)—C(43)—C(33)	110.6(2)

$C_6H_5O)\cdot 2PhOH$ is reported[4] to show the pentahapto mode of ligation of the cyclohexadienylone ligand and the presence of the two hydrogen-bonded phenol units. A more recent (19) crystal structure of $(Ph_3P)_2Rh(\eta^5\text{-ArO})$ (where ArO = 2,6-di-*tert*-butyl-4-methylphenoxy) also shows the interaction of just five carbons of the aromatic fragment with the rhodium centre.

The synthesis of **3** can also be achieved by the addition of excess phenol to the (dippe)rhodium allyl derivative **4** as shown in reaction [4].

Interestingly, attempts to generate **3** *without* the hydrogen-bonded phenol units by the direct addition of exactly *one equivalent* of phenol to the allyl complex **4** only resulted in the isolation of the starting allyl **4** and **3** in a 2:1 ratio, respectively: it would appear that in the presence of phenol the hydrogen-bonded adduct **3** is the preferred product. No further attempt

[4] 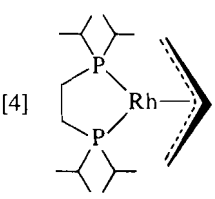

+ $3C_6H_5OH$ $\xrightarrow{-C_3H_6}$ 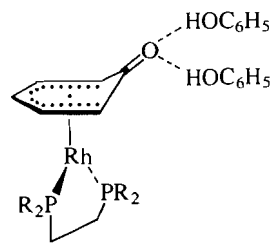

3, R = *i*-Pr

[4] J. C. McConway and A. C. Skapski. Cited in ref. 18.

was made to generate the analogous cyclohexadienylone complex free of hydrogen-bonded phenol.

Conclusions

The results of this study show that the incorporation of a bridging ligand such as phenoxide to replace the bridging hydride diminishes the reactivity of the binuclear rhodium fragment; this is evidenced by both a complete lack of reactivity in stoichiometric reactions with dihydrogen and ethylene, as well as an order of magnitude reduced reactivity in the catalytic mode in the hydrogenation of 1-hexene, when compared to the very reactive $[(dippe)Rh]_2(\mu\text{-}H)_2$, **1***a*. Given that the typical bridging ligands are four- or six-electron donors (two electrons to each metal), coordinative saturation in polynuclear systems incorporating these bridging ligands is more easily achieved, ultimately generating less reactive or inert metal clusters.

Acknowledgements

Financial support for this research was provided by the Natural Sciences and Engineering Research Council of Canada. The generous loan of rhodium trichloride to M.D.F. from Johnson-Matthey Inc. is gratefully acknowledged.

1. (*a*) A. J. Carty. Adv. Chem. Ser. **196**, 163 (1982); Pure Appl. Chem. **54**, 113 (1982); (*b*) Y-F. Yu, C-N. Chau, A. Wojcicki, M. Calligaris, G. Nardin, and G. Balducci. J. Am. Chem. Soc. **106**, 3704 (1984); (*c*) D. A. Roberts, G. R. Steinmetz, M. J. Breen, P. M. Shulman, E. D. Morrison, M. R. Duttera, C. W. DeBrosse, R. R. Whittle, and G. L. Geoffroy. Organometallics, **2**, 246 (1983); (*d*) R. G. Finke, G. Gaughan, C. G. Pierpont, and M. E. Cass. J. Am. Chem. Soc. **103**, 1394 (1981); (*e*) J. G. Gaudiello, T. C. Wright, R. A. Jones, and A. J. Bard. J. Am. Chem. Soc. **107**, 888 (1985); (*f*) R. Glaser, D. J. Kountz, R. D. Waid, J. C. Galluci, and D. W. Meek. J. Am. Chem. Soc. **106**, 6324 (1984); (*g*) P. Braunstein, D. Matt, O. Bars, M. Louer, D. Grandjean, J. Fischer, and A. Mitschler. J. Organomet. Chem. **213**, 79 (1981); (*h*) E. P. Kyba, J. D. Mather, K. L. Hassett, J. S. McKennis, and R. E. Davis. J. Am. Chem. Soc. **106**, 5371 (1984); (*i*) H. Werner and R. Zolk. Organometallics, **4**, 601 (1985); (*j*) L. Chen, D. J. Kountz, and D. W. Meek. Organometallics, **4**, 598 (1985); (*k*) R. T. Baker, P. J. Krusic, T. H. Tulip, J. C. Calabrese, and S. S. Wreford. J. Am. Chem. Soc. **105**, 6763 (1983); (*l*) M. M. Olmstead and P. P. Power. J. Am. Chem. Soc. **106**, 1495 (1984).
2. (*a*) R. A. Jones and B. R. Whittlesey. J. Am. Chem. Soc. **107**, 1078 (1985); (*b*) G. Huttner, B. Wigwarth, J. von Seyerl, and L. Zsolnai. Chem. Ber. **115**, 2035 (1982); (*c*) K. M. Flynn, B. D. Murray, M. M. Olmstead, and P. P. Power. J. Am. Chem. Soc. **105**, 7460 (1983); (*d*) H. Vahrenkamp and E. Keller. Chem. Ber. **112**, 1991 (1979).
3. (*a*) F. A. Cotton and G. L. Powell. J. Am. Chem. Soc. **106**, 3371 (1984); (*b*) J. Sola, Y. Do, J. M. Berg, and R. H. Holm. J. Am. Chem. Soc. **105**, 7784 (1983); (*c*) D. Coucouvanis, M. G. Kanatzidis, W. R. Dunham, and W. R. Hagen. J. Am. Chem. Soc. **106**, 7998 (1984); (*d*) T. R. Halbert, K. McGauley, W-H. Pan, R. S. Czernuszewicz, and E. I. Stiefel. J. Am. Chem. Soc. **106**, 1849 (1984); (*e*) R. D. Adams and I. T. Horvath. J. Am. Chem. Soc. **106**, 1869 (1984); (*f*) R. D. Adams, I. T. Horvath, and P. Mathur. J. Am. Chem. Soc. **106**, 6296 (1984); (*g*) W. E. Cleland, D. A. Holtman, M. Sabat, J. A. Ibers, G. C. DeFotis, and B. A. Averill. J. Am. Chem. Soc. **105**, 6021 (1983); (*h*) T. B. Rauchfuss, T. D. Weatherill, S. R. Wilson, and J. P. Zebrowski. J. Am. Chem. Soc. **105**, 6508 (1983); (*i*) B. Zhuang, J. W. McDonald, F. A. Shultz, and W. E. Newton. Organometallics, **3**, 943 (1984); (*j*) M. Rakowski-DuBois, D. L. DuBois, M. C. VanDerveer, and R. C. Haltiwanger. Inor. Chem. **20**, 3064 (1981) (*k*) D. Seyferth, R. S. Henderson and L-C. Song. Organometallics, **1**, 125 (1982); (*l*) A. Agresti, M. Bacci, F. Cecconi, C. A. Ghilardi, and S. Midollini. Inorg. Chem. **24**, 689 (1985); (*m*) P. Braunstein, E. Sappa, A. Tiripicchio, M. Tiripicchio-Camellini. Inorg. Chim. Acta, **45**, L191 (1980); (*n*) P. M. Boorman, J. M. Ball, K. J. Moynihan, V. D. Patel, and J. F. Richardson. Can. J. Chem. **61**, 2809 (1983).
4. (*a*) D. C. Bradley, R. C. Mehrotra, and D. P. Gaur. Metal alkoxides Academic Press, London 1978; (*b*) M. H. Chisholm, K. Folting, J. C. Huffman, and C. C. Kirkpatrick. Inorg. Chem. **23**, 1021 (1984); (*c*) R. C. Mehrotra and J. Singh. Inorg. Chem. **23**, 1046 (1984); (*d*) F. A. Cotton, D. O. Marler, and W. Schwotzer. Inorg. Chem. **23**, 4211 (1984); (*e*) A. Bencini, D. Gatteschi, and C. Zanchini. Inorg. Chem. **24**, 700 (1985); (*f*) M. H. Chisholm, D. M. Hoffman, and J. C. Huffman. Inorg. Chem. **24**, 797 (1985); (*g*) W. A. Herrman, R. Serrano, M. L. Ziegler, H. Pfisterer, and B. Nuber. Angew. Chem. Int. Ed. Engl. **24**, 50 (1982).
5. (*a*) H. Vahrenkamp. Adv. Organomet. Chem. **22**, 169 (1983); (*b*) W. L. Gladfelter and G. L. Geoffroy. Adv. Organomet. Chem. **18**, 207 (1980); (*c*) E. L. Muetterties. Chem. Eng. News, Aug. 30, 28 (1982).
6. (*a*) C. U. Pittman, Jr., G. M. Wilemon, W. D. Wilson, and R. C. Ryan. Angew. Chem. Int. Ed. Engl. **19**, 478 (1980); (*b*) P. E. Kreter and D. W. Meek. Inorg. Chem. **22**, 319 (1983); (*c*) R. A. Jones, T. C. Wright, J. L. Atwood, and W. E. Hunter. Organometallics, **2**, 470 (1983); (*d*) G. L. Geoffroy, S. Rosenberg, P. M. Shulman, and R. R. Whittle. J. Am. Chem. Soc. **106**, 1519 (1984).
7. M. D. Fryzuk. Organometallics, **1**, 408 (1982).
8. M. D. Fryzuk. Can. J. Chem. **61**, 1347 (1983).
9. M. D. Fryzuk, T. Jones, and F. W. B. Einstein. Organometallics, **3**, 185 (1984).
10. M. D. Fryzuk, T. Jones, and F. W. B. Einstein. J. Chem. Soc. Chem. Commun. 1556 (1984).
11. A. J. Sivak and E. L. Muetterties. J. Am. Chem. Soc. **101**, 4878 (1979).
12. M. D. Fryzuk and W. E. Piers. To be published.
13. M. D. Fryzuk. Inorg. Chem. **21**, 2134 (1982).
14. A. C. Larson. Crystallographic computing. Munksgaard, Copenhagen. 1970. p. 291.
15. International tables for X-ray crystallography, Vol. IV. Kynoch Press, Birmingham, England. 1974.
16. E. J. Gabe, A. C. Larson, F. L. Lee, and Y. Wang. The NRC VAX 750/780 Crystal Structure System Chemistry Division, NRC, Ottawa, Ontario. 1983.
17. T. G. Appleton, H. C. Clark, and L. W. Manzer. Coord. Chem. Rev. **10**, 335 (1973).
18. D. J. Cole-Hamilton, R. J. Young, and G. Wilkinson. J. Chem. Soc. Dalton, 1995 (1976).
19. B. Cetinkaya, P. B. Hitchcock, M. F. Lappert, S. Torroni, J. L. Atwood, W. E. Hunter, and M. J. Zaworotko. J. Organomet. Chem. **188**, C31 (1980).

Thermal rearrangement of functionalized 1,2-divinylcyclopropane systems. A convenient synthesis of substituted 4-cyclohepten-1-ones

EDWARD PIERS, MAX S. BURMEISTER, AND HANS-ULRICH REISSIG

Department of Chemistry, University of British Columbia, 2036 Main Mall, University Campus, Vancouver, B.C., Canada V6T 1Y6

Received July 12, 1985

EDWARD PIERS, MAX S. BURMEISTER, and HANS-ULRICH REISSIG. Can. J. Chem. **64**, 180 (1986).

Reaction of the acyl chlorides **14–21** with lithium (phenylthio)(*cis*-2-vinylcyclopropyl)cuprate (**2**) provided the ketones **22–29**. Compounds **22–25**, upon treatment with i-Pr_2NLi–Me_3SiCl, were converted cleanly into the enol silyl ethers **30–33**, which gave the 1,4-cycloheptadienes **34–37** upon thermolysis (100–110°C). Acid hydrolysis of the latter materials produced the corresponding 4-cyclohepten-1-ones **38–41**. However, subjection of the *cis*-2-vinylcyclopropyl ketones **26–29** to i-Pr_2NLi–*t*-$BuMe_2SiCl$ afforded, in each case, a mixture of isomeric enol ethers (**26** → **42** + **44** (1:1); **27** → **43** + **45** (1:9); **28** → **56** + **58** (1:1); **29** → **57** + **59** (4:1)). Thermolysis (150–175°C) of these mixtures, followed by acid hydrolysis of the resultant products, gave the 4-cyclohepten-1-ones **54**, **55**, **64**, and **65**, admixed with the corresponding 3-methylenecyclopentenes **52**, **53**, **62**, and **63**. On the other hand, treatment of the *trans*-2-vinylcyclopropyl ketones **70–74** with i-Pr_2NLi–*t*-$BuMe_2SiCl$ provided exclusively or predominantly the enol ethers **75–79**. Thermolysis (230°C) of the latter materials and subsequent acid hydrolysis of the resultant products **80**, **50**, **51**, **60**, and **61** afforded the 4-cyclopenten-1-ones **38**, **54**, **55**, **64**, and **65**.

EDWARD PIERS, MAX S. BURMEISTER, et HANS-ULRICH REISSIG. Can. J. Chem. **64**, 180 (1986).

La réaction des chlorures d'acyle **14–21** avec le (phénylthio)(vinyl-2 cyclopropyle-*cis*) cuprate de lithium (**2**) conduit aux cétones **22–29**. Les composés **22–25**, traités par le i-Pr_2NLi–Me_3SiCl, se transforment proprement en éthers énoliques silylés **30–33** qui, par thermolyse (100–110°C), donnent les cycloheptadiènes-1,4 **34–37**. L'hydrolyse acide des composés **34–37** conduit aux cyclo-4 heptène-4 ones-1 **38–41**. Cependant, si on traite les vinyl-2 cyclopropylcétones-*cis* **26–29** avec le i-Pr_2NLi–*t*-$BuMe_2SiCl$ on obtient, dans chaque cas, un mélange d'éthers énoliques isomères (**26** → **42** + **44** (1:1); **27** → **43** + **45** (1:9); **98** → **56** + **58** (1:1); **29** → **57** (4:1)). La thermolyse (150–175°C) de ces mélanges, suivie d'une hydrolyse acide, donne les cycloheptène-4 ones-1 **54**, **55**, **64** et **65** mélangés avec les méthylènes-3 cyclopentènes correspondants **52**, **53**, **62** et **63**. Par ailleurs, si on traite les vinyl-2 cyclopropylcétones-*trans* **70–74** avec le i-Pr_2NLi–*t*-$BuMe_2SiCl$, on obtient exclusivement ou d'une façon majoritaire les éthers énoliques **75–79**. La thermolyse (230°C) de ces derniers, suivie d'une hydrolyse acide des produits résultants **80**, **50**, **51**, **60** et **61**, conduit aux cyclopentène-4 ones-1 **38**, **54**, **55**, **64** et **65**.

[Traduit par le journal]

Introduction

Recent reports (1, 2) from this laboratory described, *inter alia*, the development and utilization of a new seven-membered ring annulation method which can be summarized in general terms by eq. [1]. Thus, reaction of cyclic β-iodo α,β-unsaturated ketones **1** (3) with a mixture of the lithium

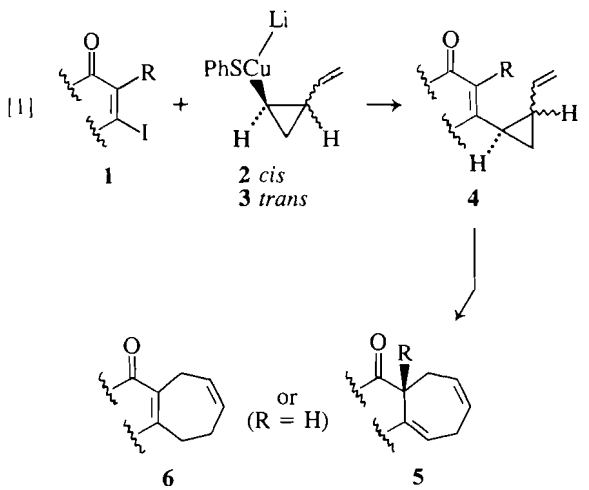

(phenylthio)(2-vinylcyclopropyl)cuprates **2** and **3**, followed by thermal (Cope) rearrangement of the resultant mixture of β-(2-vinylcyclopropyl)enones **4**, provides the annulation products **5**, or, if R = H, **6**.

From a structural point of view, β-iodo enones **1** are vinylogous acyl iodides and, therefore, it is not surprising that these substances react smoothly and efficiently with cuprate reagents such as **2** and **3**. However, on the basis of this line of reasoning, it appeared appropriate to investigate whether or not this type of chemistry could be extended to include a new synthesis of 4-cyclohepten-1-ones **11** via a route outlined in eq. [2]. Explicitly, reaction of a suitable acyl derivative **7** with the cuprate reagents **2** and (or) **3** should provide the ketones **8**. Conversion of the latter materials into appropriate enol derivatives **9** and subsequent thermal rearrangement of the latter materials would, if successfully executed, lead to the cycloheptadienes **10**. Hydrolysis of the enol ether function of **10** would provide the substituted 4-cyclohepten-1-ones **11**. We report herein the results of our studies in this area.[1]

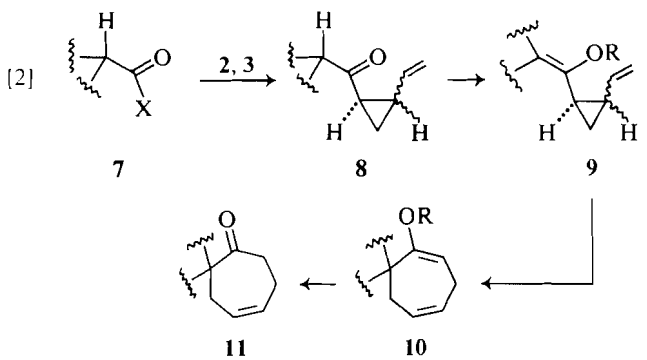

[1]For a preliminary report regarding some of the work outlined herein, see ref. 4. It should be noted that Wender and Filosa (5) have reported the preparation of 2,2,5-trimethyl-4-cyclohepten-1-one (karahanaenone) via a route similar to that outlined in eq. [2], although they did not prepare the requisite 2-vinylcyclopropyl ketone by reaction of an acyl derivative with an appropriate cuprate (cf. **7** + **2**, **3** → **8**).

Results and discussion

(a) *Preparation of the alkyl and cycloalkyl* cis-*2-vinylcyclopropylketones 22–29* (see Chart 1)

The thermal Cope rearrangement of compounds containing a *trans*-divinylcyclopropane system can normally be carried out efficiently by heating these substances at elevated temperatures (usually >160°C). However, it is well known (refs. 6, 7; see also citations given in ref. 1) that the corresponding rearrangement of *cis*-divinylcyclopropane substrates ordinarily occurs under much milder conditions, often at or slightly above ambient temperatures. Because of this fact, and because we wished to be able to characterize synthetic intermediates without resorting to tedious separations of isomeric substances, our initial work was carried out on isomerically pure alkyl and cycloalkyl *cis*-2-vinylcyclopropyl ketones.

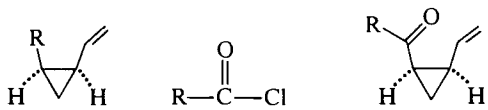

12 R=Br
13 R=Li
2 R=Cu(SPh)Li

14–21 **22–29**

14, 22 R=*n*-C_5H_{11}
15, 23 R=CH_2Ph
16, 24 R=*c*-C_4H_7
17, 25 R=*c*-C_5H_9
18, 26 R=*c*-C_6H_{11}
19, 27 R=3,3-dimethylcyclohexyl
20, 28 R=CH_2CMe_3
21, 29 R=*c*-C_7H_{13}

CHART 1

The *cis* ketones **22–29** that were used in this work were prepared conveniently by reaction of the cuprate reagent **2** with the corresponding acyl chlorides **14–21**.[2] Thus, treatment of *cis*-1-bromo-2-vinylcyclopropane (**12**)[3] with 1.1–1.4 equivalents of *tert*-butyllithium in dry ether or tetrahydrofuran at −78°C, followed by reaction of the resultant cyclopropyllithium reagent **13** with phenylthiocopper (10) at −20°C, afforded a brown solution of the cuprate **2**. When the latter species was allowed to react (−78°C to room temperature) with each of the acyl chlorides **14–21**, the required ketones **22–29**, respectively, were formed smoothly and, in 7 out of the 8 cases, efficiently. Only the yield (41%) of the benzyl ketone **15** was below 80%. In each case, the ketone could be obtained in high purity (>95%) by simple distillation of the crude product.

(b) *Conversion of the ketones 22–29 into enol silyl ethers and thermal rearrangement of the latter substances* (see Chart 2)

Treatment of the ketone **22** with 1.2 equiv. of lithium diisopropylamide (tetrahydrofuran, −78°C), followed by trapping of the resultant enolate anion with Me_3SiCl, provided the crude enol ether **30**[4] in essentially quantitative yield. In similar fashion, the ketones **23–25** could be transformed smoothly into the ethers **31–33**, respectively. Enol trimethylsilyl ethers are not noted for their stability and, in addition, it was found that substances **30** and **31** rearranged slowly at or slightly above ambient temperatures. Therefore, compounds **30–33** were not purified but were subjected directly to thermolysis (neat, 100–110°C, 30 min). The resultant products **34–37**, respectively, were produced in excellent yields (>85%), could be purified by simple distillation, and were individually characterized. Acid hydrolysis of each of the Cope rearrangement products provided (>84%) the substituted 4-cyclohepten-1-ones **38–41**. Thus, at least with the substrates **22–25**, the initially proposed conversion (see **8** → **11**, eq. [2]) can be effected conveniently and efficiently.

Consecutive treatment of the cyclohexyl ketone **26** with i-Pr_2NLi and *t*-$BuMe_2SiCl$ under conditions similar to those outlined above did not produce cleanly the expected enol ether **42**. Instead, a mixture (~1:1) of **42** and the positional isomer **44**[5] was obtained. Thus, in contrast to the cyclobutyl (**24**) and cyclopentyl (**25**) ketones, kinetic deprotonation of **26** with lithium diisopropylamide resulted in competitive removal of protons H_A and H_B. This unusual result may be due at least partially to the fact that the (axial) proton H_A in **26** is sterically more hindered than the corresponding protons in **24** and **25**. Indeed, it appears that steric factors are of some importance in these reactions since deprotonation of **26** with lithium 2,2,6,6-tetramethylpiperidide (a more hindered base than i-Pr_2NLi) gave, after addition of *t*-$BuMe_2SiCl$, the enol ethers **42** and **44** in a ratio of ~3:7, respectively. Furthermore, when the 3,3-dimethylcyclohexyl ketone **27** (H_A hindered further by an axial methyl group) was subjected to the i-Pr_2NLi–*t*-$BuMe_2SiCl$ sequence, the products **43** and **45** were produced in a ratio of ~1:9, respectively.

It appears, however, that steric influences are not exclusively operative in these deprotonations, since subjection of cyclohexyl cyclopropyl ketone (**46**) to kinetic deprotonation (i-Pr_2NLi) and silylation gave exclusively (81% isolated yield) the enol ether **47**. Thus, the kinetic acidity of H_B in **26** is significantly greater than that of the corresponding proton H_C in **46**, even though the steric environments of these protons are similar. It is known (12) that the kinetic acidity of proton H_D in *cis*-1-acetyl-2-phenylcyclopropane (**48**) is 100 times that of H_E in the corresponding *trans* isomer **49**, a phenomenon which has been attributed to an electronic effect involving conjugation between the phenyl and acetyl groups in the *cis* isomer **48**. Perhaps the vinyl group in **26** exerts an electronic effect similar to that of the phenyl group in **48**, resulting in a relative increase in acidity of H_B (in **26**) compared to that of H_C in **46**.

Thermolysis (150°C, 1 h) of the mixture of **42** and **44** (~1:1) provided, in 81% yield, a mixture of substances consisting mainly of **50** (the product of Cope rearrangement of **42**) and **52** (the product of a "2-vinylmethylenecyclopropane rearrange-

[2]Other functional derivatives of carboxylic acids (e.g. RCOSPh, RCOSePh) can be employed in these reactions. However, in some of the cases in which comparisons were made, superior yields were obtained with acyl chlorides.

[3]Reduction of 1,1-dibromo-2-vinylcyclopropane (8) with tri-*n*-butylstannane (9) or with zinc metal in ether – acetic acid (1) provides mixtures of *cis*- and *trans*-1-bromo-2-vinylcyclopropane (ratios ~7:3 and 4–5:1, respectively). The monobromides can be separated by a combination of fractional distillation and column chromatography (180 g of silica gel/g of mixture, elution with pentane). See also ref. 5.

[4]This material was quite unstable and, therefore, its homogeneity and stereochemistry could not be established. However, it seems likely (ref. 11 and papers cited therein) that this enol ether consisted largely of the *Z* isomer, as shown in the structural formula.

[5]The presence of **44** in the isolated product mixture was indicated by an ir absorption at 1765 cm^{-1}, attributable to the stretching vibration of the exocyclic double bond in **44**, and by the subsequent acquisition of the rearrangement product **52**.

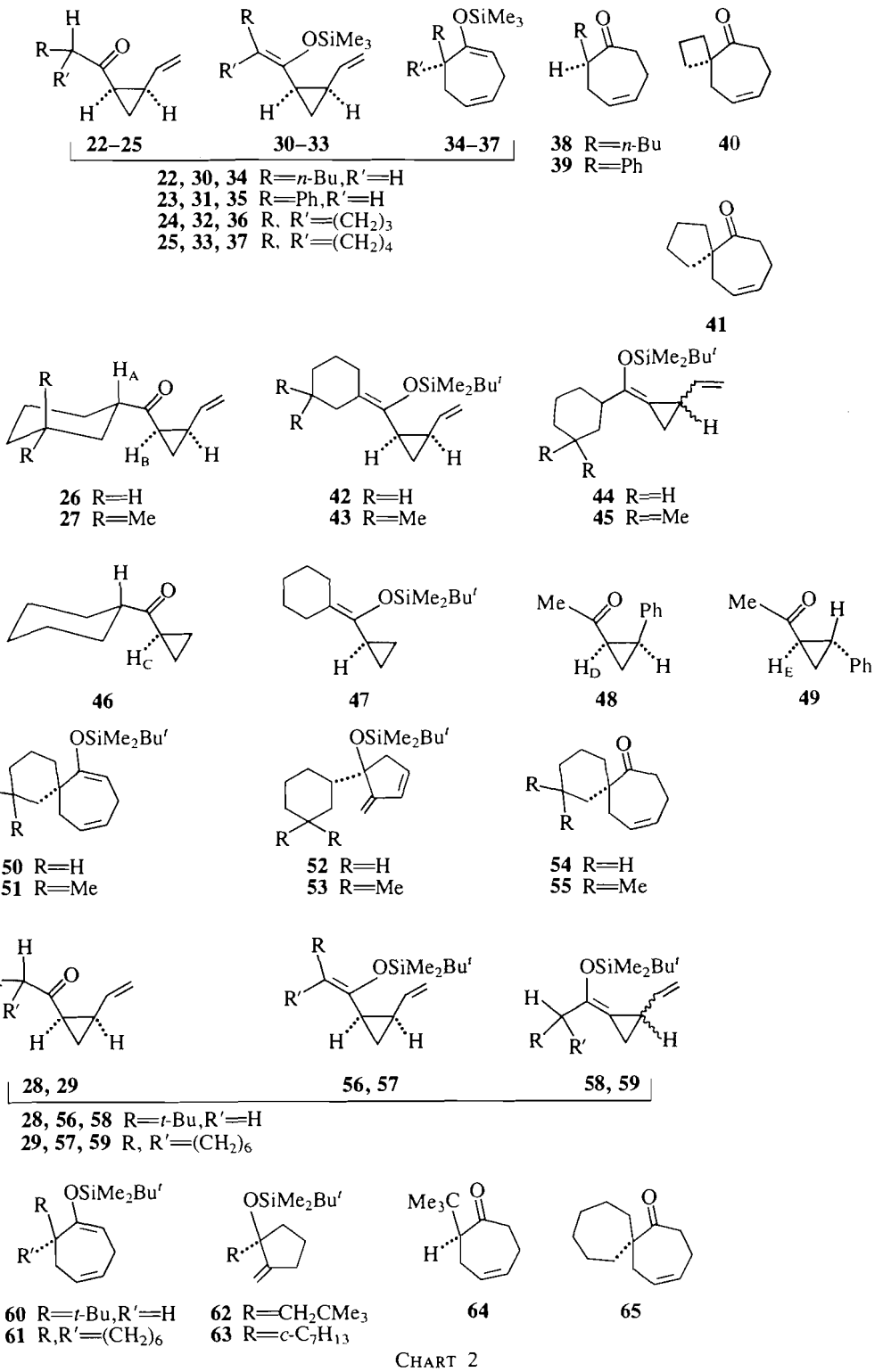

CHART 2

ment"[6] of **44**), in a ratio of about 1:1. When the thermolysis products were treated with 1 *N* hydrochloric acid in tetrahydrofuran, the enol ether **50** was hydrolyzed to the spiro ketone **54**, while **52** remained unchanged. Separation of **54** and **52** was achieved by chromatography and these materials were individually characterized. In similar fashion, thermolysis of the 1:9 mixture of **43** and **45**, followed by acid treatment of the resultant products **51** and **53**, gave a 1:9 mixture of compounds **55** and **53**, from which the latter substance could be isolated in pure form.

Use of the *cis* ketones **28** and **29** as substrates produced results similar to those obtained with **26** and **27**. Thus **28**, upon treatment with i-Pr_2NLi–*t*-$BuMe_2SiCl$, gave the positionally isomeric enol ethers **56** and **58** (ratio ~1:1), while **29** afforded a 4:1 mixture of **57** and **59**, respectively. Thermolysis of these mixtures and treatment of the resultant products (**60**, **62**; **61**, **63**) with aqueous acid produced, in each case, a mixture of the corresponding 4-cyclohepten-1-one (**64**, **65**) and the methyl-

[6]For examples and a discussion of this type of thermal rearrangement, see ref. 13 and papers cited therein.

enecyclopentene (**62**, **63**). The latter mixtures were separated and the substances were individually identified.

The results summarized above make it clear that some alkyl and cycloalkyl *cis*-2-vinylcyclopropyl ketones (e.g. **22–25**) serve as excellent substrates for the synthesis of functionalized 4-cyclohepten-1-ones (e.g. **38–41**) via the reaction sequence originally proposed (eq. [2]). However, other structurally similar ketones (e.g. **26–29**) did not give clean-cut results. Obviously, the difficulties associated with these substrates (general structure **66**) can be traced to the fact that when H_F is quite hindered, kinetically controlled deprotonation results in competitive removal of H_F and H_G. A possible solution to this problem would be to employ pure *trans* ketones (general structure **67**) in the place of the *cis* isomers **66**. In substrates **67**, the cyclopropyl proton H_I is sterically more hindered than H_G in **66** and, in addition, the (possible) acidity-enhancing electronic effect of the vinyl group (*vide supra*) on H_G in **66** would, presumably, be absent in **67**. Therefore, one might expect kinetic deprotonation of **67** to result in clean removal of H_H even in those cases in which this proton is quite hindered. Silylation of the enolate anion thus formed would give the enol ethers **68**.

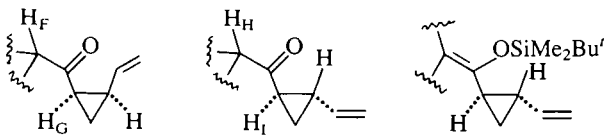

66 **67** **68**

If the (high temperature) Cope rearrangement of the latter substances were to be clean and efficient, the problem of ultimately producing 4-cyclohepten-1-ones admixed with varying amounts of "unwanted" methylenecyclopentenes (e.g. **52**, **53**, **62**, **63**) will have been eliminated. The results of our experiments with *trans*-2-vinylcyclopropyl ketones are described below.

(c) *Preparation of the alkyl and cycloalkyl* trans*-2-vinylcyclopropyl ketones* ***70–74*** (see Chart 3)

The *trans* ketones **70**, **71**, and **74** were prepared efficiently by reaction of the corresponding acyl chlorides **14**, **18**, and **21** with the isomerically homogeneous cuprate reagent **3**. The latter

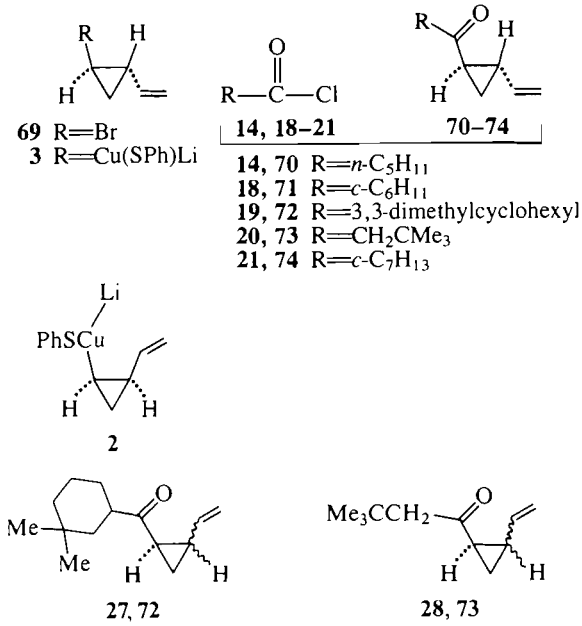

69 R=Br
3 R=Cu(SPh)Li

14, 18–21 **70–74**

14, 70 R=*n*-C_5H_{11}
18, 71 R=*c*-C_6H_{11}
19, 72 R=3,3-dimethylcyclohexyl
20, 73 R=CH_2CMe_3
21, 74 R=*c*-C_7H_{13}

2

27, 72 **28, 73**

CHART 3

species was obtained from *trans*-1-bromo-2-vinylclopropane (**69**).[3] Alternatively, in order to avoid the rather tedious separation of the isomeric 1-bromo-2-vinylcyclopropanes **12** and **69**, the *trans* ketones could be derived by base-catalyzed equilibration of mixtures of *cis* and *trans* ketones. For example, reaction of the chlorides **19** and **20** with mixtures of the cuprate reagents **2** and **3**, followed by treatment of the resultant product mixtures (**27**, **72**; **28**, **73**) with potassium *tert*-butoxide in *tert*-butyl alcohol – tetrahydrofuran provided the *trans* ketones **72** and **73**, respectively. These materials were contaminated with small amounts (~6–7%) of the corresponding *cis* isomers but, from a preparative point of view, this lack of purity did not cause significant difficulties.

(d) *Conversion of the ketones* ***70–74*** *into enol silyl ethers and thermal rearrangement of the latter substances* (see Chart 4)

Treatment of the ketone **70** with i-Pr_2NLi–*t*-$BuMe_2SiCl$ produced, in high yield, the expected enol ether **75**. More importantly, similar reactions involving the substrates **71–74** gave, in each case, exclusively or predominantly the enol ether (**76–79**) resulting from initial removal of the proton H_J. Only in the case of the 3,3-dimethylcyclohexyl ketone **72**, in which removal of H_J is hindered by an axial methyl group, was any of the isomeric enol ether (**45**) formed (~12%).[7] Thus, use of the *trans* ketones as substrates did indeed eliminate largely or completely the problem of competitive deprotonation and the eventual production of mixtures of products.

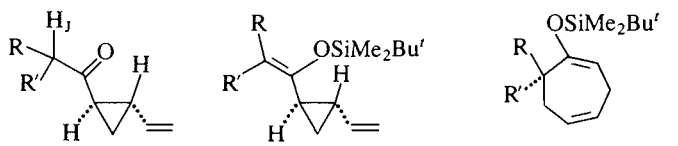

70–74 **75–79** **80, 50, 51, 60, 61**

70, 75, 80 R=*n*-Bu,R'=H
71, 76, 50 R, R'=$(CH_2)_5$
72, 77, 51 R, R'=$CH_2CMe_2(CH_2)_3$
73, 78, 60 R=*t*-Bu, R'=H
74, 79, 61 R, R'=$(CH_2)_6$

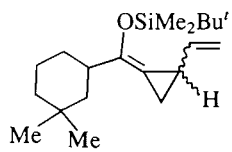

45

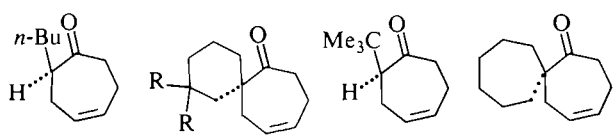

38 **54** R=H **64** **65**
55 R=Me

CHART 4

As expected, Cope rearrangement of the *trans* divinylcyclopropanes **75–79** required temperatures (~230°C) considerably higher than those employed for the thermolysis of the *cis* compounds **30–33**, **42**, **43**, **56**, and **57**. However, in each case, it was gratifying to find that the corresponding cycloheptadiene

[7]Probably about one-half of this amount of **45** was formed from the *cis* ketone **27**, which was a contaminant (~7%) in the sample of **72** employed.

(**80**, **50**, **51**, **60**, **61**) was formed cleanly and efficiently. Acid hydrolysis of the enol ether function of each of these thermolysis products gave the 4-cyclohepten-1-ones **38**, **54**, **55**, **64**, and **65**, respectively.

Conclusion

The overall conversion of the acid chlorides **14–21** into the structurally diverse 4-cyclohepten-1-ones **38–41**, **54**, **55**, **64**, and **65**, respectively, reveals that the initially proposed scheme (eq. [2]) represents a viable method in organic synthesis. The study outlined above showed, however, that the method is more generally successful using alkyl and cycloalkyl *trans*-2-vinylcyclopropyl ketones (e.g. **70–74**) as intermediates rather than the corresponding *cis* ketones.

Experimental

General information

Melting points and distillation temperatures are uncorrected. Ultraviolet (uv) spectra were obtained on methanol solutions using a Cary 15 spectrophotometer. Infrared (ir) spectra were recorded on a Perkin–Elmer model 710B spectrophotometer. Proton nuclear magnetic resonance (^{1}H nmr) spectra were measured on deuterochloroform solutions using a Bruker WP-80 spectrometer or Varian Associates HA-100 or XL-100 spectrometers. Signal positions are given in δ units, with tetramethylsilane as the internal standard. For compounds containing one or more *tert*-butyldimethylsilyl groups, the chemical shifts were measured relative to that of the chloroform proton (δ 7.25). High resolution mass spectra were measured with a Kratos MS-50 mass spectrometer. Gas–liquid chromatography (glc) was carried out with a Hewlett–Packard HP-5832 A gas chromatograph. Microanalyses were performed in the Microanalytical Laboratory at the University of British Columbia.

General procedure A. Preparation of the alkyl and cycloalkyl cis-*(22–29) and* trans-*2-vinylcyclopropyl ketones (70, 71, 74)*

To a cold (−78°C), stirred solution of *cis*- (**12**) or *trans*-1-bromo-2-vinylcyclopropane (**69**) in dry ether or dry tetrahydrofuran (3–4 mL/mmol of **12** or **69**), under an atmosphere of argon, was added, dropwise (syringe), a solution (~1.6 *M*) of *tert*-butyllithium (1.1–1.4 equiv.) in pentane, and the resulting solution was stirred at −78°C for 2 h. Solid phenylthiocopper (1 equiv.) was added, the resulting slurry was diluted with dry tetrahydrofuran (~5 mL/mmol of **12** or **69**), was allowed to warm to −20°C, was stirred at this temperature for 30 min, and was then recooled to −78°C. To the resulting clear, brown solution was added the appropriate acyl chloride (0.66 equiv.) and the reaction mixture was stirred at −78°C for 10 min, at −20°C for 1 h, and at room temperature for 1 h. The solution was treated with saturated aqueous ammonium chloride and ether (~0.25 mL and 10 mL/mmol of **12** or **69**, respectively). The mixture (a precipitate formed) was stirred for 20 min, was treated with anhydrous magnesium sulfate, and was then filtered through a column of Florisil (3 cm) layered over anhydrous magnesium sulfate (3 cm). The column was washed thoroughly with ether. Removal of the solvent from the combined filtrate gave an oil, which, upon distillation under reduced pressure, afforded the *cis*- or *trans*-2-vinylcyclopropyl ketone.

The following compounds were prepared by means of this procedure.

n-*Pentyl* cis-*2-vinylcyclopropyl ketone (22)*

From 73 mg (0.54 mmol) of hexanoyl chloride (**14**) there was obtained 78.5 mg (87%) of **22**; distillation temperaature 90–100°C/12 Torr (1 Torr = 133.3 Pa); ir(film): 3090, 3020, 1700, 1620 cm^{-1}; ^{1}H nmr δ: 0.75–2.4 (diffuse m, 13H), 2.50 (t, 2H, J = 7 Hz), 4.9–5.3 (8-line m, 2H), 5.48–5.9 (8-line m, 1H). *Anal.* calcd. for $C_{11}H_{18}O$: C 79.46, H 10.91; found: C 79.60, H 11.00.

Benzyl cis-*2-vinylcyclopropyl ketone (23)*

From 169 mg (1.09 mmol) of phenylethanoyl chloride (**15**) there was obtained 84 mg (41%) of **23**; distillation temperature 70–80°C/0.1 Torr; ir(film): 1695, 1640, 1605, 1500 cm^{-1}; ^{1}H nmr δ: 0.98–1.48 (m, 2H), 1.70–2.36 (m, 2H), 3.68 (s, 2H), 4.82–5.18 (6-line m, 2H), 5.4–5.8 (8-line m, 1H), 7.02–7.46 (m, 5H), *Anal.* calcd. for $C_{13}H_{14}O$: C 83.83, H 7.58; found: C 83.66, H 7.77.

Cyclobutyl cis-*2-vinylcyclopropyl ketone (24)*

From 155 mg (1.31 mmol) of the acyl chloride **16** there was obtained 182 mg (93%) of **24**; distillation temperature 100–110°C/12 Torr; ir(film): 3100, 1690, 1635 cm^{-1}; ^{1}H nmr δ: 0.8–1.5 (m, 2H), 1.55–2.4 (m, 8H), 3.12–3.5 (m, 1H), 4.82–5.26 (8-line m, 2H), 5.44–5.86 (8-line m, 1H). *Anal.* calcd. for $C_{10}H_{14}O$: C 80.01, H 9.40; found: C 79.70, H 9.33.

Cyclopentyl cis-*2-vinylcyclopropyl ketone (25)*

From 60 mg (0.45 mmol) of the acyl chloride **17** there was obtained 62.4 mg (85%) of **25**; distillation temperature 110–120°C/12 Torr; ir(film): 3100, 1695, 1635 cm^{-1}; ^{1}H nmr δ: 1.02–2.42 (m, 12H), 2.78–3.12 (m, 1H), 4.82–5.24 (8-line m, 2H), 5.40–5.82 (8-line m, 1H). *Exact Mass* calcd. for $C_{11}H_{16}O$: 164.1201; found: 164.1204.

Cyclohexyl cis-*2-vinylcyclopropyl ketone (26)*

From 233 mg (1.59 mmol) of the acyl chloride **18** there was obtained 231 mg (82%) of **26**; distillation temperature 120–140°C/12 Torr; ir(film): 3090, 3020, 1690, 1640 cm^{-1}; ^{1}H nmr δ: 0.84–2.64 (m, 15H), 4.84–5.26 (8-line m, 2H), 5.42–5.84 (8-line m, 1H). *Anal.* calcd. for $C_{12}H_{18}O$: C 80.85, H 10.18; found: C 80.76, H 10.19.

3,3-Dimethylcyclohexyl cis-*2-vinylcyclopropyl ketone (27)*

From 895 mg (5.51 mmol) of the acyl chloride **19** there was obtained 922 mg (87%) of **27**; distillation temperature 90–95°C/0.25 Torr; ir(film): 3060, 2990, 1690, 1630 cm^{-1}; ^{1}H nmr δ: 0.94 (s, 6H), 1.0–2.82 (m, 13H), 4.9–5.3 (m, 8 lines, 2H), 5.45–5.87 (m, 1H). *Exact Mass* calcd. for $C_{14}H_{22}O$: 206.1670; found: 206.1669.

Neopentyl cis-*2-vinylcyclopropyl ketone (28)*

From 179 mg (1.33 mmol) of 3,3-dimethylbutanoyl chloride (**20**) there was obtained 218 mg (88%) of **28**; distillation temperature 80–90°C/12 Torr; ir(film): 3075, 1695, 1640 cm^{-1}; ^{1}H nmr δ: 0.95–1.5 (m, 2H), 1.03 (s, 9H), 1.82–2.4 (m, 2H), 2.44 (s, 2H), 4.92–5.32 (8-line m, 2H), 5.56–5.96 (8-line m, 1H). *Exact Mass* calcd. for $C_{11}H_{18}O$: 166.1357; found: 166.1359.

Cycloheptyl cis-*2-vinylcyclopropyl ketone (29)*

From 75 mg (0.47 mmol) of the acyl chloride **21** there was obtained 73 mg (81%) of **29**; distillation temperature 70–80°C/0.1 Torr; ir(film): 3075, 3005, 1695, 1635 cm^{-1}; ^{1}H nmr δ: 0.82–2.4 (m, 16H), 2.42–2.76 (broad unresolved m, 1H), 4.84–5.24 (8-line m, 2H), 5.44–5.86 (8-line m, 1H). *Exact Mass* calcd. for $C_{13}H_{20}O$: 192.1515; found. 192.1518.

n-*Pentyl* trans-*2-vinylcyclopropyl ketone (70)*

From 99 mg (0.74 mmol) of hexanoyl chloride (**14**) there was obtained 105 mg (86%) of **70**; distillation temperature 100–110°C/12 Torr; ir(film): 3080, 3000, 1695, 1640 cm^{-1}; ^{1}H nmr δ: 0.8–2.1 (diffuse m, 13H), 2.55 (t, 2H, J = 7 Hz), 4.9–5.66 (m, 3H). *Exact Mass* calcd. for $C_{11}H_{18}O$: 166.1357; found: 166.1355.

Cyclohexyl trans-*2-vinylcyclopropyl ketone (71)*

From 76 mg (0.52 mmol) of the acyl chloride **18** there was obtained 84 mg (91%) of **71**; distillation temperature 110–120°C/12 Torr; ir(film): 3080, 3000, 1695, 1640 cm^{-1}; ^{1}H nmr δ: 0.8–21. (diffuse m, 14H), 2.3–2.65 (m, 1H), 4.84–5.64 (m, 3H). *Anal.* calcd. for $C_{12}H_{18}O$: C 80.85, H 10.18; found: C 80.99, H 10.24.

Cycloheptyl trans-*2-vinylcyclopropyl ketone (74)*

From 278 mg (1.74 mmol) of the acyl chloride **21** there was obtained 236 mg (71%) of **74**; distillation temperature 65–75°C/0.1 Torr; ir(film): 3080, 3000, 1690, 1640 cm^{-1}; ^{1}H nmr δ: 0.84–1.08 (m, 1H), 1.32–2.10 (m, 15H), 2.50–2.84 (m, 1H), 4.90–5.68 (m, 3H). *Exact Mass* calcd. for $C_{13}H_{20}O$: 192.1515; found: 192.1520.

Preparation of 3,3-dimethylcyclohexyl (72) and neopentyl trans-*2-vinylcyclopropyl ketone (73)*

Reaction of the acyl chloride **19** (200 mg, 1.15 mmol) with 1.5 equiv. of a 1:1 mixture of the cuprate reagents **2** and **3**, via a procedure very similar to that described above, gave 174 mg (73%) of a mixture of the ketones **27** and **72** (~1:1). Similarly, treatment of 3,3-dimethyl-

butanoyl chloride (**20**) (430 mg, 3.19 mmol) with 1.5 equiv. of a mixture of **2** and **3** (~4.2:1, respectively) afforded 469 mg (90%) of a mixture of the ketones **28** and **73** (~3:1, respectively).

A solution of the 1:1 mixture of **27** and **72** (87 mg, 0.42 mmol) and potassium *tert*-butoxide (71 mg, 0.63 mmol) in 3 mL of dry tetrahydrofuran and 3 mL of dry *tert*-butyl alcohol was stirred at room temperature, under an atmosphere of argon, for 3 h. The reaction mixture was acidified by addition of dilute hydrochloric acid and the resultant mixture was extracted thoroughly with hexanes. The combined extract was washed with dilute aqueous sodium bicarbonate and brine, dried ($MgSO_4$), and concentrated. Distillation (90–100°C/0.25 Torr) of the residual oil gave 80 mg (92%) of a colorless oil that consisted of a mixture of the ketones **27** and **72** in a ratio of ~7:93, respectively. This material exhibited ir(film): 3060, 2990, 1690, 1630 cm^{-1}; ^1H nmr δ: 0.94 (s, 6H), 1.0–2.14 (complex m, 12H), 2.48–2.86 (m, 1H), 4.90–5.70 (m, 3H). *Exact Mass* calcd. for $C_{14}H_{22}O$: 206.1670; found: 206.1667.

A solution of the 3:1 mixture of **28** and **73** (380 mg, 2.32 mmol) and potassium *tert*-butoxide (104 mg, 0.93 mmol) in 3 mL of dry tetrahydrofuran and 0.5 mL of dry *tert*-butyl alcohol was stirred at room temperature, under an atmosphere of argon, for 23 h. Work-up as described above and distillation (80–90°C/12 Torr) of the crude product gave 197 mg (52%) of a colorless oil that consisted of a 6:94 mixture of the ketones **28** and **73**, respectively. This material exhibited ir(film): 3080, 1690, 1640 cm^{-1}; ^1H nmr δ: 0.9–1.55 (m, 2H), 1.05 (s, 9H), 1.86–2.12 (m, 2H), 2.48 (s, 2H), 4.90–5.68 (m, 3H). *Exact Mass* calcd. for $C_{11}H_{18}O$: 166.1357; found: 166.1356.

General procedure B. Conversion of the cis*-2-vinylcyclopropyl ketones 22–25 into the cycloheptadienes 34–37*

To a cold (−78°C), stirred solution of lithium diisopropylamide (1.3–1.5 mmol/mmol of ketone) in dry tetrahydrofuran (3 mL/mmol of base), under an atmosphere of argon, was added slowly a solution of the ketone (**22–25**) in dry tetrahydrofuran (2 mL/mmol of ketone), and the resultant solution was stirred at −78°C for 1 h.

A quenching solution was prepared as follows. To a solution of trimethylsilyl chloride (~0.3 mL) in dry tetrahydrofuran (~1 mL) was added dry triethylamine (~0.2 mL). The mixture was stirred (argon atmosphere) for a few minutes and then was centrifuged. The solution above the solid material was used to trap the enolate anions.

Freshly prepared quenching solution (~1.2 mL/mmol of ketone) was added to the cold (−78°C) enolate anion solution and the mixture was stirred at −78°C for 15 min and then at room temperature for ~1 h. The mixture was partitioned between saturated aqueous sodium bicarbonate and pentane (~10 mL and 20 mL/mmol of ketone, respectively) and the aqueous phase was washed twice with pentane. The combined extract was washed with brine, dried (Na_2SO_4), and concentrated. The enol silyl ethers **30–33** thus obtained as yellow oils in essentially quantitative yields exhibited no ir carbonyl absorption and, since they were quite unstable, these substances were not purified further.

Thermolysis (neat, argon atmosphere, 100–110°C, 30 min) of the yellow oils, followed by bulb-to-bulb distillation of the resultant materials, provided the cycloheptadienes **34–37** as colorless oils.

*7-*n*-Butyl-1-trimethylsiloxy-1,4-cycloheptadiene (34)*

From 94 mg (0.57 mmol) of the ketone **22** there was obtained 119 mg (88%) of **34**; distillation temperature 120–130°C/12 Torr; ir(film): 1660, 1260, 840 cm^{-1}; ^1H nmr δ: 0.13 (s, 9H), 0.74–2.94 (diffuse multiplets, 14H), 4.81 (t, 1H, J = 5.5 Hz), 5.5–5.9 (m, 2H). *Exact Mass* calcd. for $C_{14}H_{26}OSi$: 238.1753; found: 238.1747.

7-Phenyl-1-trimethylsiloxy-1,4-cycloheptadiene (35)

From 92 mg (0.49 mmol) of the ketone **23** there was obtained 107 mg (85%) of **35**; distillation temperature 85–95°C/0.1 Torr; ir(film): 1655, 1600, 1495, 1250, 840 cm^{-1}; ^1H nmr δ: ~0 (s, 9H), 2.2–3.0 (m, 4H), 3.1–3.7 (m, 1H), 5.0 (t, 1H, J = 5.5 Hz), 5.3–6.2 (m, 2H), 7.1–7.5 (m, 5H). *Exact Mass* calcd. for $C_{16}H_{22}OSi$: 258.1440; found: 258.1448.

5-(Trimethylsiloxy)spiro[3.6]deca-5,8-diene (36)

From 120 mg (0.8 mmol) of the ketone **24** there was obtained 155 mg (87%) of **36**; distillation temperature 95–105°C/12 Torr; ir(film): 1660, 1645, 1250, 840 cm^{-1}; ^1H nmr δ: 0.19 (s, 9H), 1.54–2.74 (m, 10H), 4.82 (t, 1H, J = 6 Hz), 5.7–5.9 (m, 2H). *Exact Mass* calcd. for $C_{13}H_{22}OSi$: 222.1434; found: 222.1442.

6-(Trimethylsiloxy)spiro[4.6]undeca-6,9-diene (37)

From 68 mg (0.42 mmol) of the ketone **25** there was obtained 94 mg (96%) of **37**; distillation temperature 110–120°C/12 Torr; ir(film): 1650, 1250, 840 cm^{-1}; ^1H nmr δ: 0.17 (s, 6H), 1.1–2.1 (m, 8H), 2.22 (d, 2H, J = 6 Hz), 2.70 (t, 2H, J = 6 Hz), 4.84 (t, 1H, J = 6 Hz), 5.6–6.25 (m, 2H). *Exact Mass* calcd. for $C_{14}H_{24}OSi$: 236.1597; found: 236.1590.

General procedure C. Conversion of the trans*-2-vinylcyclopropyl ketones 70–74 into the cycloheptadienes 80, 50, 51, 60, 61*

To a cold (−78°C), stirred solution of lithium diisopropylamide (1.4–1.5 mmol/mmol of ketone) in dry tetrahydrofuran (4 mL/mmol of base), under an atmosphere of argon, was added slowly a solution of the ketone (**70–74**) in dry tetrahydrofuran (1 mL/mmol of ketone), and the resultant solution was stirred at −78°C for 45 min. A solution of freshly sublimed *tert*-butyldimethylsilyl chloride (1.6 mmol/mmol of ketone) in dry tetrahydrofuran (1 mL/mmol of chloride) was added, followed by dry hexamethylphosphoramide (0.5 mL/mmol of ketone). After the solution had been stirred at −78°C for 15 min and at room temperature for 2–3 h, it was partitioned between saturated aqueous sodium bicarbonate and pentane (~10 mL and 20 mL/mmol of ketone, respectively). The aqueous phase was washed twice with pentane. The combined extract was washed four times with saturated aqueous sodium bicarbonate, twice with brine, and dried ($MgSO_4$). Removal of the solvent, followed by bulb-to-bulb distillation of the remaining oil, gave the corresponding enol silyl ether (**75–79**)[8] as a colorless oil that exhibited no ir carbonyl stretching absorption.

Thermolysis of **75–79** was accomplished by heating (neat, argon atmosphere) these substances at 230°C (air-bath temperature) for 30–60 min. Direct distillation of the resultant materials provided the cycloheptadienes **80**, **50**, **51**, **60**, and **61**, respectively, as clear colorless oils.

*7-*n*-Butyl-1-*tert*-butyldimethylsiloxy-1,4-cycloheptadiene (80)*

From 197 mg (1.19 mmol) of the ketone **70** there was obtained 282 mg (85%) of **80**; distillation temperature 140–150°C/12 Torr; ir(film): 1660, 1260, 840 cm^{-1}; ^1H nmr δ: 0.09, (s, 6H), 0.88 (s, 9H), 0.70–2.95 (series of m, 14H), 4.80 (t, 1H, J = 5.5 Hz), 5.5–5.9 (m, 2H). *Exact Mass* calcd. for $C_{17}H_{32}OSi$: 280.2222; found: 280.2228.

7-(tert-Butyldimethylsiloxy)spiro[5.6]dodeca-7,10-diene (50)

From 176 mg (0.99 mmol) of the ketone **71** there was obtained 210 mg (74%) of **50**; distillation temperature 100–110°C/0.1 Torr; ir(film): 1640, 1250, 840 cm^{-1}; ^1H nmr δ: 0.12 (s, 6H) 0.94 (s, 9H), 1.15–1.95 (m, 10H), 2.30 (d, 2H, J = 6.5 Hz), 2.64 (t, 2H, J = 6.0 Hz), 4.76 (t, 1H, J = 6.0 Hz), 5.6–6.1 (m, 2H). *Anal.* calcd. for $C_{18}H_{32}OSi$: C 73.90, H 11.03; found: C 74.21, H 11.30. *Exact Mass* calcd.: 292.2222; found: 292.2226.

2,2-Dimethyl-7-(tert-butyldimethylsiloxy)spiro[5.6]dodeca-7,10-diene (51)

From 84 mg (0.41 mmol) of the ketone **72** (this material contained ~7% of the *cis* ketone **27**) there was obtained 78 mg (60%) of **51**, which contained ~12% of the methylenecyclopentene **53**; distillation temperature 110–120°C/0.35 Torr; ir(film): 1630, 1255, 850 cm^{-1}; ^1H nmr δ: 0.17, 0.19 (s, s), 0.75–1.00 (series of s), 1.01–2.75 (series of m), 4.72 (t, 1H), 5.60–5.86 (m, 2H).

*7-*tert*-Butyl-1-*tert*-butyldimethylsiloxy-1,4-cycloheptadiene (60)*

From 188 mg (1.15 mmol) of the ketone **73** (this material contained ~6% of the *cis* ketone **28**) there was obtained 267 mg (83%) of **60**; distillation temperature 140–150°C/12 Torr; ir(film): 1670, 1250, 840 cm^{-1}; ^1H nmr δ: 0.10, 0.12 (s, s, 3H each), 0.89, 0.99 (s, s, 9H each), 2.16–2.54 (m, 3H), 2.6–2.9 (m, 2H), 4.89 (t, 1H, J = 5.5 Hz), 5.36–5.82 (m, 2H). *Exact Mass* calcd. for $C_{17}H_{32}OSi$; 280.2222; found: 280.2226.

[8]The enol silyl ether **77** was accompanied by a small amount (~12%) of the isomeric enol ether **45**.

*1-(*tert*-Butyldimethylsiloxy)spiro[6.6]trideca-1,4-diene (**61**)*

From 186 mg (0.97 mmol) of the ketone **74** there was obtained 272 mg (91%) of **61**; distillation temperature 100–110°C/0.1 Torr; ir(film): 1665, 1260, 840 cm^{-1}; ^1H nmr δ: 0.10 (s, 6H), 0.90 (s, 9H), 1.22–2.08 (m, 12H), 2.29 (d, 2H, J = 6.5 Hz), 2.59 (t, 2H, J = 5.5 Hz), 4.62 (t, 1H, J = 5.5 Hz), 5.6–6.1 (m, 2H). *Exact Mass* calcd. for $C_{19}H_{34}OSi$: 306.2379; found: 306.2372.

*General procedure D. Hydrolysis of the enol silyl ethers **34** (**80**), **35–37**, **50**, **51**, **60**, **61** to the 4-cyclohepten-1-ones **38–41**, **54**, **55**, **64**, **65***

To a solution of the enol silyl ether in methanol or tetrahydrofuran (~10 mL/mmol of substrate) was added 1 *N* hydrochloric acid (~3 mL/mmol of substrate) and the resultant mixture was stirred, under an atmosphere of argon, at room temperature for 1–3 h. The reaction mixture was made basic by careful addition of cold saturated aqueous sodium bicarbonate and then was extracted thoroughly with pentane. The combined extract was washed with brine and dried ($MgSO_4$). Removal of the solvent, followed by bulb-to-bulb distillation of the residual material, provided the corresponding 4-cyclohepten-1-one as a colorless oil.

*2-*n*-Butyl-4-cyclohepten-1-one (**38**)*

From 97 mg (0.41 mmol) of the trimethylsilyl enol ether **34** there was obtained 58 mg (85%) of the ketone **38**. Alternatively, acid hydrolysis of the *tert*-butyldimethylsilyl enol ether **80** (87 mg, 0.31 mmol) gave 41 mg (80%) of **38**; distillation temperature 100–110°C/12 Torr; ir(film): 1705, 1660 cm^{-1}; ^1H nmr δ: 0.89 (br t, 3H, J = 6 Hz), 1.08–2.0 (m, 6H), 2.0–3.0 (m, 7H), 5.6–5.86 (m, 2H). *Exact Mass* calcd. for $C_{11}H_{18}O$: 166.1358; found: 166.1366.

*2-Phenyl-4-cyclohepten-1-one (**39**)*

From 85 mg (0.33 mmol) of compound **35** there was obtained 51 mg (84%) of the ketone **39**; distillation temperature 95–105°C/0.1 Torr; ir(film): 1695, 1660, 1605, 1500 cm^{-1}; ^1H nmr δ: 2.2–3.1 (m, 6H, 4.00 (d of d, 1H, J =4.5, 10.5 Hz), 5.72–5.88 (m, 2H), 7.08–7.44 (m, 5H). *Anal.* calcd. for $C_{13}H_{14}O$: C 83.83, H 7.58; found: C 84.00, H 7.58.

*Spiro[3.6]dec-8-en-5-one (**40**)*

From 55 mg (0.25 mmol) of the enol ether **36** there was obtained 34 mg (91%) of the ketone **40**; distillation temperature 100–110°C/12 Torr; ir(film): 1700, 1660 cm^{-1}; ^1H nmr δ; 0.82–2.84 (series of m, 12H), 5.7–5.94 (m, 2H). *Anal.* calcd. for $C_{10}H_{14}O$: C 80.01, H 9.40; found: C 79.75, H 9.30.

*Spiro[4.6]undec-9-en-6-one (**41**)*

From 36 mg (0.15 mmol) of the trimethylsilyl enol ether **37** there was obtained 21 mg (85%) of the ketone **41**; distillation temperature 100–110°C/12 Torr; ir(film): 1695 cm^{-1}; ^1H nmr δ: 1.3–2.84 (series of m, 14H), 5.48–5.84 (m, 2H). *Anal.* calcd. for $C_{11}H_{16}O$: C 80.44, H 9.82; found: C 80.10, H 9.83.

*Spiro[5.6]dodec-10-en-7-one (**54**)*

From 92 mg (0.31 mmol) of the enol silyl ether **50** there was obtained 46 mg (84%) of the ketone **54**; distillation temperature 70–80°C/ 0.1 Torr; ir(film): 1700, 1650 cm^{-1}; ^1H nmr δ: 1.16–1.74 (series of m, 14H), 5.64–5.80 (m, 2H). *Anal.* calcd. for $C_{12}H_{18}O$: C 80.85, H 10.18; found: C 81.10, H 10.30.

*2,2-Dimethylspiro[5.6]dodec-10-en-7-one (**55**)*

From 70 mg (0.22 mmol) of the enol silyl ether **51** (this material contained ~12% of **53**) there was obtained 33 mg (73%) of an oil (distillation temperature 95–105°C/0.25 Torr) that consisted of the ketone **55** and the methylenecyclopentene **53** (ratio ~87:13). A sample of **55**, obtained from this mixture by column chromatography on silica gel (elution with 1:7 ether – petroleum ether), exhibited ir(film): 1690, 1640 cm^{-1}; ^1H nmr δ: 0.76 (s, 3H), 0.91 (s, 3H), 0.9–2.45 (series of m, 13H), 2.78–2.88 (m, 1H), 5.72–5.84 (m, 1H), 5.86–5.97 (m, 1H). *Exact Mass* calcd. for $C_{14}H_{22}O$: 206.1670; found: 206.1683.

*2-*tert*-Butyl-4-cyclohepten-1-one (**64**)*

From 206 mg (0.74 mmol) of the *tert*-butyldimethylsilyl enol ether **60** there was obtained 108 mg (88%) of the ketone **64**; distillation temperature 110–120°C/12 Torr; ir(film): 1705, 1660 cm^{-1}; ^1H nmr δ: 0.94 (s, 9H), 2.1–3.14 (m, 7H), 5.4–5.86 (m, 2H). *Exact Mass* calcd. for $C_{11}H_{18}O$: 166.1358; found: 166.1362.

*Spiro[6.6]tridec-4-en-1-one (**65**)*

From 75 mg (0.24 mmol) of compound **61** there was obtained 34 mg (73%) of the ketone **65**; distillation temperature 80–90°C/0.1 Torr; ir(film): 1700, 1650 cm^{-1}; ^1H nmr δ: 1.1–2.9 (series of m, 18H), 5.44–5.84 (m, 2H). *Exact Mass* calcd. for $C_{13}H_{20}O$: 192.1514; found: 192.1505.

Subjection of the cis*-2-vinylcyclopropyl ketones **26–29** to the sequence (a) LiN(i-Pr)$_2$–t-BuMe$_2$SiCl, (b) thermolysis, and (c) 1 N hydrochloric acid in tetrahydrofuran. Characterization of the dienes **52**, **53**, **62**, **63***

Deprotonation of each of the ketones **26–29** with lithium diisopropylamide, followed by reaction of the resultant mixtures of enolate anions with *tert*-butyldimethylsilyl chloride, was accomplished as described in general procedure C. From **26** there was obtained a mixture consisting mainly of the enol silyl ethers **42** and **44** (ratio ~1:1); **27** produced primarily compounds **43** and **45** (ratio ~1:9); **28** gave **56** and **58** (ratio ~1:1); **29** afforded **57** and **59** (ratio ~4:1). The yields were >85%. In each case, the product mixture exhibited an ir absorption at ~1765 cm^{-1}, attributable to the stretching vibration of the exocyclic double bond in compounds **44**, **45**, **58**, and **59**.

Thermolysis (**42**, **44**: neat, 150°C, 1 h; **43**, **45**: neat, 160°C, 45 min; **56**, **58**: neat, 175°C, 1 h; **57**, **59**: neat, 150°C, 1 h) of each of these mixtures, followed by bulb-to-bulb distillation of the resultant oils, provided (>80%) the corresponding rearrangement products **50**, **52**; **51**, **53**; **60**, **62**; **61**, **63**. In each case, the product ratio was close to that of the starting materials. Treatment of the mixtures of rearrangement products with 1 *N* hydrochloric acid in tetrahydrofuran as described in general prodedure D gave, in each case, a mixture of the corresponding 4-cyclohepten-1-one (**54**, **55**, **64**, **65**) and the unchanged methylenecyclopentene (**52**, **53**, **62**, **63**).

Compounds **54** (which showed spectra identical with those summarized previously) and **52** were separated by preparative tlc. The latter substance (distillation temperature 100–110°C/0.1 Torr) exhibited ir(film): 1635, 1250, 840 cm^{-1}; uv(MeOH): 231 nm (log ε 4.12); ^1H nmr δ: −0.05 (s, 6H), 0.84 (s, 9H), 0.9–2.15 (m, 11H), 2.36 (d of t, 1H, J = 18, 2 Hz), 2.65 (d of t, 1H, J = 18, 2 Hz), 4.90 (br s, 1H), 5.04 (s, 1H), 5.85–6.03 (m, 1H), 6.06–6.20 (m, 1H). *Exact Mass* calcd. for $C_{18}H_{32}OSi$: 292.2222; found: 292.2226.

Column chromatography (silica gel) of the 9:1 mixture of **53** and **55** gave a sample of the diene **53** (distillation temperature 95–105°C/0.1 Torr) which exhibited ir(film): 1630, 1250, 840 cm^{-1}; uv (MeOH): 232 nm (log ε 4.07); ^1H nmr δ: −0.07 (s, 6H), 0.80 (s, 3H), 0.82 (s, 9H), 0.88 (s, 3H), 1.05–2.75 (m, 11H), 4.88 (br s, 1H), 5.02 (s, 1H), 5.84–5.98 (m, 1H), 6.02–6.20 (m, 1H). *Exact Mass* calcd. for $C_{20}H_{36}OSi$: 320.2535; found: 320.2514.

Compounds **64** (spectral data identical with those given above) and **62** were separated by column chromatography on Florisil. The diene **62** (distillation temperature 120–130°C/12 Torr) exhibited ir(film): 1640, 1260, 840 cm^{-1}; uv (MeOH): 237 nm (log ε 4.05); ^1H nmr δ: −0.07, −0.05 (s, s, 3H each), 0.83, 1.01 (s, s, 9H each), 1.31 (d, 1H, J = 15 Hz), 1.75 (d, 1H, J = 15 Hz), 2.54 (d of t, 1H, J = 19, 2 Hz), 2.90 (d of t, J = 19, 2 Hz), 4.93 (br s, 1H), 4.99 (s, 1H), 5.84–6.02 (m, 1H), 6.06–6.22 (m, 1H). *Exact Mass* calcd. for $C_{17}H_{32}OSi$: 280.2222; found: 278.2225.

Compounds **65** (spectra identical with those given above) and **63** were separated by column chromatography on Florisil. The diene **63** (distillation temperature 100–110°C/0.1 Torr) exhibited ir(film): 1640, 1250, 830 cm^{-1}; uv (MeOH): 233 nm (log ε 3.95); ^1H nmr δ: −0.06 (s, 6H), 0.84 (s, 9H), 1.12–2.14 (m, 13H), 2.33 (d of t, 1H, J = 18, 2 Hz), 2.59 (d of t, 1H, J = 18, 2 Hz), 4.90 (br s, 1H), 5.03 (s, 1H), 5.88–6.06 (m, 1H), 6.08–6.26 (m, 1H). *Exact Mass* calcd. for $C_{19}H_{34}OSi$: 306.2378; found: 306.2382.

Acknowledgements

We gratefully acknowledge the financial support of the Natural Sciences and Engineering Research Council of Canada

and thank the Deutscher Akademischer Autauschdienst for a NATO Postdoctoral Fellowship (to H.-U.R.).

1. E. PIERS, H. E. MORTON, I. NAGAKURA, and R. W. THIES. Can. J.Chem. **61**, 1226 (1983).
2. E. PIERS and E. H. RUEDIGER. Can. J. Chem. **61**, 1239 (1983).
3. E. PIERS, J. R. GRIERSON, C. K. LAU, and I. NAGAKURA. Can. J. Chem. **60**, 210 (1982).
4. E. PIERS and H.-U. REISSIG. Angew. Chem. Int. Ed. Engl. **18**, 791 (1979).
5. P. A. WENDER and M. P. FILOSA. J. Org. Chem. **41**, 3490 (1976).
6. S. J. RHOADS and N. R. RAULINS. Org. React. **22**, 1 (1975).
7. E. M. MIL'VITSKAYA, A. V. TARAKANOVA, and A. V. PLATE. Russ. Chem. Rev. **45**, 469 (1976).
8. R. C. WOODWORTH and P. S. SKELL. J. Am. Chem. Soc. **79**, 2542 (1957); L. SKATTEBOL. J. Org. Chem. **29**, 2951 (1964).
9. D. SEYFERTH, J. YAMAZAKI, and D. L. ALLESTON. J. Org. Chem. **28**, 703 (1963); J. A. LANDGREBE and L. W. BECKER. J. Org. Chem. **33**, 1173 (1968).
10. G. H. POSNER, C. E. WHITTEN, and J. J. STERLING. J. Am. Chem. Soc. **95**, 7788 (1973); G. H. POSNER, D. J. BRUNELLE, and L. SINOWAY. Synthesis, 662 (1974).
11. A. S. NARULA. Tetrahedron Lett. **22**, 4119 (1981).
12. O. ITOH, N. YAMAMOTO, H. FUJIMOTO, and K. ICHIKAWA. J. Chem. Soc. Chem. Commun. 101 (1979).
13. J. J. GAJEWSKI. Hydrocarbon thermal isomerizations. Academic Press, Inc., New York, NY. 1981. pp. 155–158.

Zero-field optical detection of magnetic resonance of chlorophyll *b* in n-octane

S. HOTCHANDANI[1]

Centre de recherche en photobiophysique, Université du Québec à Trois-Rivières, Trois-Rivières (Qué.), Canada G9A 5H7

R. H. CLARKE

Department of Chemistry, Boston University, Boston, MA 02215, U.S.A.

AND

R. M. LEBLANC

Centre de recherche en photobiophysique, Université du Québec à Trois-Rivières, Trois-Rivières (Qué.), Canada G9A 5H7

Received April 15, 1985

S. HOTCHANDANI, R. H. CLARKE, and R. M. LEBLANC. Can. J. Chem. **64**, 188 (1986).

The zero-field ODMR of triplet state of chlorophyll *b* in n-octane has been carried out. The ODMR parameters measured at various fluorescence wavelengths suggest that Chl *b* is probably present in more than two ligated species in which water serves as the ligand.

S. HOTCHANDANI, R. H. CLARKE et R. M. LEBLANC. Can. J. Chem. **64**, 188 (1986).

Les études de ODMR au champ zéro d'état triplet de Chl *b* dans le n-octane ont été faites. Les paramètres ODMR mesurés à différentes longueurs d'ondes de fluorescence suggèrent que la Chl *b* existe sous la forme de plus de deux types de complexes où l'eau agit comme ligand.

Introduction

Recently, we reported the ligand effects on chlorophyll *a* (Chl *a*) in n-octane by zero-field optical detection of magnetic resonance (ODMR) of its triplet state (1). From the ODMR parameters, namely the zero-field splitting (ZFS) parameters and rate constants for the decay of first triplet to ground state measured at various fluorescence detection wavelengths (excited with 457.9 nm and 514.5 nm argon-ion laser lines), we showed that Chl *a* exists in two distinct monomeric species. These species were assigned to the mono- and biligated chlorophyll monomer in which water served as the ligand coordinated to the magnesium metal center. The molecule chlorophyll *b* (Chl *b*) also plays an important role in photosynthesis and possesses an aldehyde group instead of a methyl group in Chl *a* (2). The ligand effects on Chl *b* are thus worth examining.

The Chl *b* – ligand (water) interaction has been studied by Ballschmiter and Katz (3) and by Cotton *et al.* (4) by ir and electronic spectroscopic methods. Recently, Chapados and Leblanc (5) using ir technique have discussed the effect of water on Chl *a* and Chl *b* mono- and multilayer arrays. The presence of various ligated species was, however, not discussed in the above studies. Since the ZFS parameters of the triplet state are quite sensitive to the local interactions, the ODMR technique provides a suitable means for probing particularly the subtle ligand substitution differences in triplet state. Preliminary results on the zero-field ODMR of Chl *b* in n-octane have been reported by Clarke and Hofeldt (6); the ODMR experiments were carried out at only one wavelength (fluorescence maximum) and excited only with 457.9 nm argon-ion laser line. We present in this article the zero-field ODMR study of Chl *b* in n-octane at 2 K carried out at various fluorescence detection wavelengths and excited with 457.9 nm and 514.5 nm laser lines to examine the ligand effect on Chl *b* triplet state.

Materials and methods

Chlorophyll *b* was obtained from Sigma Chemical Co. and was used without further purification. The solvent n-octane (Gold Label, Aldrich Chemical Co.) was distilled once and did not show any emission in the region of Chl *b* fluorescence. The concentration of solutions used in these experiments were kept in the range of $\sim 10^{-6}$ *M*.

The zero-field ODMR experiments at 2 K were performed as described by Clarke and Hofeldt (6). The overall intersystem crossing rate constants (k_{dT}) for decay from the lowest triplet state to ground state were measured at 77 K by method of Avarmaa (7). The excitation of samples was achieved by irradiation with 457.9 or 514.5 nm lines of an argon-ion laser (Spectra Physics Model 164).

Results

(a) Fluorescence

When light from an argon-ion laser is used to excite a frozen solution of Chl *b* (not rigorously dried) in n-octane, fluorescence maximum is found to be dependent upon wavelength of excitation. For example, as shown in Fig. 1, the 514.5 nm excitation line produces fluorescence maximum at 659 nm whereas the 457.9 nm laser line produces maximum at 649 nm with a shoulder at 659 nm. The fluorescence maximum at 649 nm ($\lambda_{exc} = 457.9$ nm) is in agreement with the results of Clarke and Hofeldt (6) and is characteristic of Chl *b* monomers. All fluorescence spectra also show a band at ~710 nm, the origin of which is not yet well established but could be due to the water-linked Chl *b* dimer.

(b) ODMR frequencies

Figures 2 and 3 show the zero-field fluorescence detected ODMR spectra of Chl *b* in n-octane at 2 K recorded at various fluorescence detection wavelengths when excited with 457.9 and 514.5 nm laser lines.

It is seen from Fig. 2 ($\lambda_{exc} = 457.9$ nm) that at detection wavelengths 640 and 649 nm, two quite intense and well-resolved transitions, namely $|D| - |E|$ and $|D| + |E|$, both corresponding to microwave-induced decrease in fluorescence intensity, are clearly visible at 870 ± 10 and 1080 ± 10 MHz. These frequencies are consistent with the earlier results of Clarke and Hofeldt (6). As one moves to longer detection wavelengths, these ODMR transitions become less intense but appear at the same frequencies.

For excitation with 514.5 nm (Fig. 3), similar to $\lambda_{exc} =$ 457.9 nm, two transitions, leading to microwave-induced decrease in fluorescence intensity, at 870 and 1080 MHz are

[1]Author to whom all correspondence should be addressed.

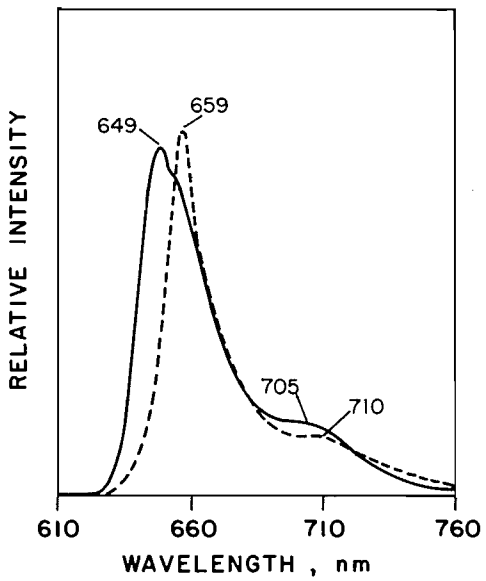

FIG. 1. The fluorescence spectra of Chl *b* in n-octane at 77 K. (—) λ_{exc} = 457.9 nm, (---) λ_{exc} = 514.5 nm.

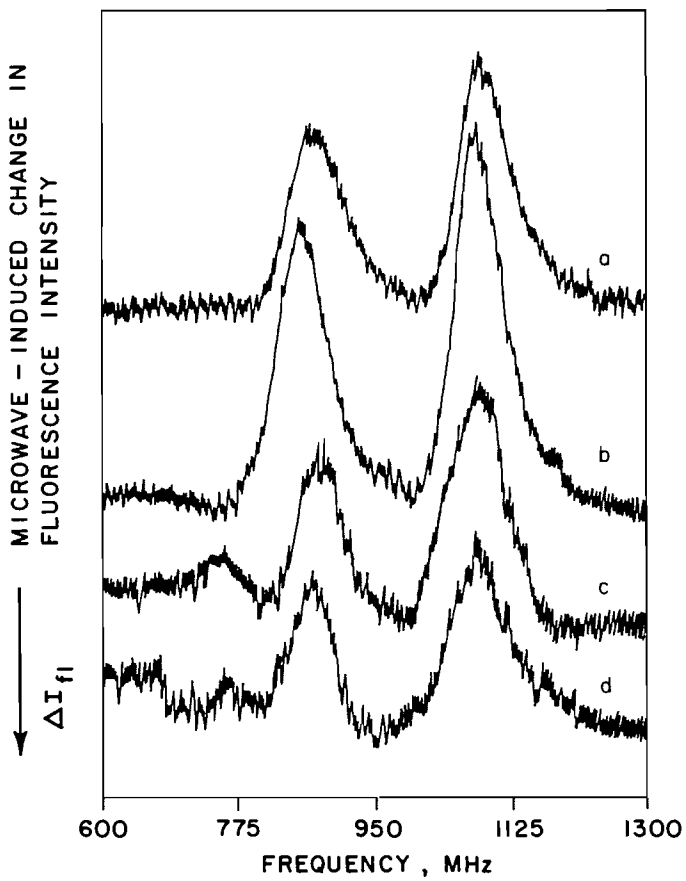

FIG. 2. Fluorescence detected zero-field ODMR spectra of Chl *b* in n-octane at 2 K. The sample is excited with a 457.9 nm line from argon-ion laser and spectra recorded at (*a*) 640 nm, (*b*) 649 nm, (*c*) 659 nm, and (*d*) 682 nm.

observed for 640 and 649 nm detection wavelengths although not as intense and not as well resolved. As one goes to longer wavelengths, one starts to notice the distortion of these (870 and 1080 MHz) transitions and growing in of the other transitions. At the detection wavelength of 659 nm the spectrum is already

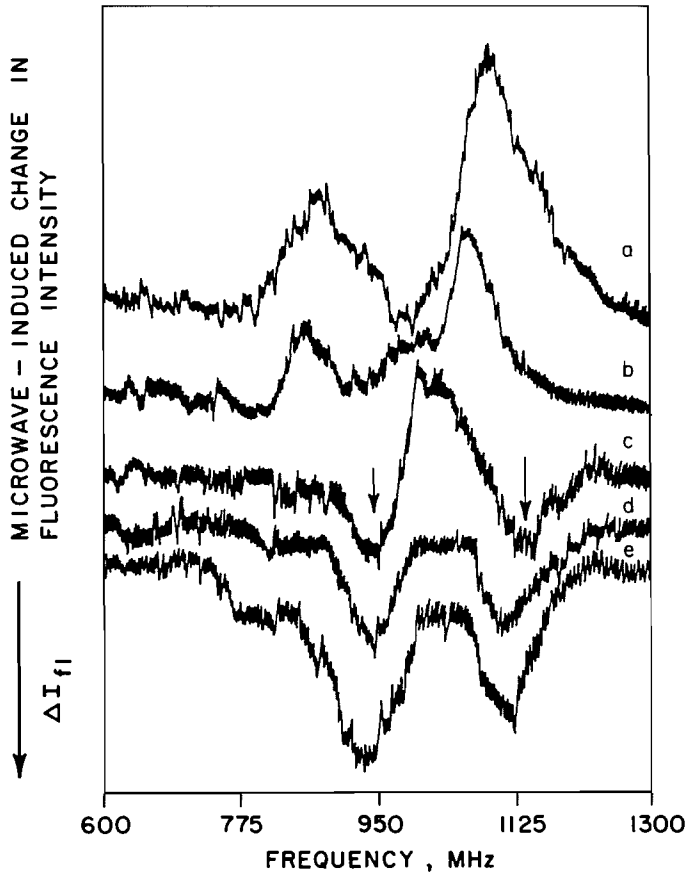

FIG. 3. Fluorescence detected zero-field ODMR spectra of Chl *b* in n-octane at 2 K; λ_{exc} = 514.5 nm laser line. The detection wavelengths are (*a*) 640 nm, (*b*) 649 nm, (*c*) 659 nm, (*d*) 672 nm, and (*e*) 682 nm.

complex. The transition at 870 MHz has completely disappeared and that at 1080 MHz has been replaced by transition at 1011 MHz. Furthermore, one can see feeble transitions (marked by arrows) at ~920 and 1120 MHz, both leading to microwave-induced increase in fluorescence intensity. At 672 nm a very interesting feature appears. There are now only two well-resolved and intense transitions at 923 and 1125 MHz leading to microwave-induced increase in fluorescence intensity. At 682 nm, the same transitions as observed at 672 nm are predominant.

It thus seems that excitation wavelength 457.9 nm predominantly excites the species with ODMR transitions at ~870 and 1080 MHz (leading to decrease in fluorescence intensity), while 514.5 nm is able to excite the species with ODMR transitions 920 and 1126 MHz (leading to an increase in fluorescence intensity) and also the species with ODMR transitions at ~870 and 1080 MHz (leading to decrease in fluorescence intensity). The complex shape of ODMR spectrum at 659 nm is probably due to simultaneous excitation of both species and thereby mixing the ODMR transitions. However, at wavelength 672 nm, far removed from 649 nm (fluorescence maximum due to one species) one can see only two well-resolved transitions at 920 and 1125 MHz due to another species. It should be mentioned that we have limited our ODMR discussion to Chl *b* monomers only (i.e. fluorescence wavelengths from 640 to 690 nm).

(c) Intersystem crossing rate constants (k_{dT})

The overall decay constants k_{dT} have been measured at various detection wavelengths (λ_{exc} = 457.9 nm and 514.5 nm)

TABLE 1. Triplet ODMR data of Chl *b* in n-octance

λ_{exc} (nm)	$\lambda_{fluorescence}$ (nm)	$\lambda_{detection}$ (nm)	Transition frequencies (MHz)	k_{dT}† (s^{-1})
457.9	649	640	866 (d)*, 1084 (d)	340
		649	857 (d), 1072 (d)	410
		659	750 (d), 885 (d), 1085 (d)	428
		682	878 (d), 1088 (d)	380
514.5	659	640	870 (d), 1087 (d)	160
		645	858 (d), 1062 (d)	175
		659	924 (i)*, 1011 (d), 1125 (i)	370
		672	923 (i), 1125 (i)	400
		682	739 (i), 919 (i), 1109 (i)	420

*(d) and (i) = microwave — induced decrease or increase in fluorescence intensity, respectively.
†k_{dT} = overall triplet decay constant.

and are presented in Table 1. A value of 380 ± 40 for k_{dT} is obtained when Chl *b* is excited with 457.9 nm. However, when excited with 514.5 nm laser line the rate constants seem to fall into two groups: (*1*) slower ($170 \pm 10\ s^{-1}$) rates for lower wavelengths 640–645 nm, and (*2*) faster (approximately double, $360 \pm 40\ s^{-1}$) rates for higher wavelengths 659, 672, etc.

Discussion

From fluorescence spectra it seems fairly reasonable to assign the two maxima at 649 and 659 nm to two distinct species, one being preferentially excited with 457.9 nm and the other by 514.5 nm laser line.

The two sets of ODMR frequencies, i.e., 870 and 1070 MHz, and 920 and 1125 MHz seem to support this assignment, and similar to the case of Chl *a* in n-octane, the higher frequencies can be assigned to monoligated and the lower frequencies to biligated species of Chl *b* (1). The analysis of rate constants, however, is not straightforward. These rate constants are known to be quite sensitive to local chlorophyll environment, particularly with respect to ligands attached to the central magnesium atom. Unless rigourously dried, water is always available for complexing with chlorophylls (via magnesium atom). Furthermore, there is also an aldehyde group available for binding with water in Chl *b*.

Comparing the results with Chl *a* in n-octane, where the assignment of rate constants to two species was a clear cut case, Chl *b* poses a problem. In Chl *a*, the rates for biligated species measured at its fluorescence maximum (excited with 457.9 nm) were found to be approximately double the rates for monoligated species detected at its fluorescence maximum (λ_{exc} = 514.5 nm). In Chl *b* too, we do see the slow ($160 \pm 10\ s^{-1}$) and fast ($340\ s^{-1}$, approximately double) rates, but the rates detected at 649 nm (fluorescence maximum of one species, λ_{exc} = 457.9 nm) and those at 659 nm (fluorescence maximum of other species, λ_{exc} = 514.5 nm) are almost the same $\sim 360 \pm 40\ s^{-1}$. This makes the assignment of fluorescence maxima as due to mono- and biligated species rather difficult. However, one can invoke the presence of the following species: (*1*) species excited preferentially with 457.9 nm laser line with fluorescence maximum at 649 nm, with ODMR frequencies at ~870 and 1080 MHz, and decay constants k_{dT} equal to $380 \pm 40\ s^{-1}$; (*2*) species preferentially excited with 514.5 nm and has fluorescence maximum at 659 nm, ODMR frequencies at 920 and 1125 MHz, and rates k_{dT} equal to $360 \pm 40\ s^{-1}$; and (*3*) species which emits fluorescence in short wavelength region 635–640 nm, (excited with 514.5 nm laser line) and has rates k_{dT} equal to $160 \pm 10\ s^{-1}$. Its ODMR transitions are probably very feeble, so much so that they are completely masked by 870 and 1080 MHz transitions belonging to the first species. The rate constants of first species ($380 \pm 40\ s^{-1}$) will, however, be dominated by the slower rates ($160 \pm 10\ s^{-1}$) of the third species.

It is at present difficult to pin point which one of the above three species is mono- or biligated (at the central magnesium atom), or ligated at aldehyde group, or ligated at ring V-keto group or ligated at all groups. However, following the arguments of Clarke and Frank (8) regarding the sensitivity of rate constants with respect to the ligand attachment; the first and the third species could be assigned, as in case of Chl *a*, to biligated and monoligated Chl *b* monomer, respectively, in which water is coordinated to magnesium metal center.

The assignment of the second species with fluorescence maximum at 659 nm, ODMR frequencies at 920 and 1125 MHz, and rate constants equal to $360 \pm 40\ s^{-1}$, is even harder. The higher ODMR frequencies suggest a monoligated (at Mg) species while higher rate constants suggest a biligated species. At present, we are unable to say much about its origin except to speculate that (in this species) the central magnesium atom is probably mono- or biligated with aldehyde or ring V-keto group or ligated with both the water on one side and the aldehyde or the ring V-keto group on the other side.

It should be pointed out that in all the species mentioned above, ring V-keto and aldehyde groups are probably always hydrogen bonded with water (if not ligated to magnesium atom). However, it is the ligation at the magnesium atom that produces the pronounced changes in the triplet state ODMR parameters (9) and other properties of chlorophylls (5, 10).

It thus seems that, substitution of an aldehyde group in Chl *b* for a methyl group in Chl *a* brings in quite dramatic changes: (*i*) contrary to Chl *a*, 457.9 nm laser line yields fluorescence of Chl *b* at shorter wavelength (i.e. 649 nm) relative to excitation with 514.5 nm (λ_{fl} = 659 nm); (*ii*) the detection and assignment of various species is much easier in Chl *a* than in Chl *b*; (*iii*) the rate constants k_{dT} for Chl *b* are approximately half those for Chl *a*. This can be explained due to more nonplanar structure of Chl *a* relative to Chl *b* (with —CHO group) leading to efficient spin–orbit coupling (6); (*iv*) the respective ODMR frequencies are higher in Chl *b* compared to those for Chl *a*, which is again due to the increased conjugation of π-electron network in Chl *b* due to —CHO group than in Chl *a* which has a methyl group.

In conclusion, the ODMR experiments suggest that Chl *b* in n-octane is probably present in more than two species though a definitive assignment of mono- or biligated species or species ligated at aldehyde group is not easy. The ligand is most probably water, however, the present results do not point out to the exact nature of the ligand, i.e., whether it is water or the aldehyde group.

Acknowledgement

We would like to acknowledge the financial support from Natural Sciences and Engineering Research Council of Canada.

1. R. H. CLARKE, S. HOTCHANDANI, S. P. JAGANNATHAN, and R. M. LEBLANC. Chem. Phys. Lett. **89**, 37 (1982).
2. J. J. KATZ and J. R. NORRIS. *In* Current topics in bioenergetics. *Edited by* D. R. Sanadi and L. Packer. Vol. 5. Academic Press, New York. 1973. pp. 41–75.
3. K. BALLSCHMITER and J. J. KATZ. J. Am. Chem. Soc. **91**, 2661 (1969).
4. T. M. COTTON, P. A. LOACH, J. J. KATZ, and K. BALLSCHMITER. Photochem. Photobiol. **27**, 735 (1978).
5. C. CHAPADOS and R. M. LEBLANC. Biophys. Chem. **17**, 211 (1983).
6. R. H. CLARKE and R. H. HOFELDT. J. Chem. Phys. **61**, 4582 (1974).
7. R. AVARMAA. Chem. Phys. Lett. **46**, 279 (1977).
8. R. H. CLARKE and H. H. FRANK. Chem. Phys. Lett. **51**, 13 (1977).
9. R. P. H. KOOYMAN, T. J. SCHAAFMA, and J. F. KLEIBEUKER. Photochem. Photobiol. **26**, 235 (1978).
10. T. A. EVANS and J. J. KATZ. Biochim. Biophys. Acta, **396**, 414 (1975).

Ion/molecule reactions in allene. III. Reactions of the parent ion with neutral alkanes

KENZO NAGASE[1] AND JAN A. HERMAN

Centre de Recherches sur les Atomes et les Molécules et le Département de Chimie, Université Laval, Québec (Qué.), Canada G1K 7P4

Received March 19, 1985

KENZO NAGASE and JAN A. HERMAN. Can. J. Chem. **64**, 192 (1986).

Ion/molecule reactions between the ion $C_3H_4^{+\cdot}$ ion, from allene and neutral alkanes were investigated by mass spectrometry. There are four $H^{\cdot}/CH_3^{\cdot}/H^-/H_2^-$ transfer reactions and relative rate constants were calculated. The overall rates increased in the order $CH_4 < C_2H_6 < C_3H_8 <$ i-$C_4H_{10} <$ n-C_4H_{10}. There is also a stabilization process by alkanes of $C_6H_8^{+\cdot}$ ion species, but its importance is lower than the above transfer processes.

KENZO NAGASE et JAN A. HERMAN. Can. J. Chem. **64**, 192 (1986).

Faisant appel à la spectrométrie de masse, on a étudié les réactions ion/molécule entre l'ion radical $C_3H_4^{+\cdot}$, obtenu à partir de l'allène, et des alcanes neutres. Il se produit quatre réactions de transfert $H^{\cdot}/CH_3^{\cdot}/H^-/H_2^-$ et on en a calculé les constantes relatives de vitesse. Les vitesses globales augmentent suivant l'ordre suivant: $CH_4 < C_2H_6 < C_3H_6 <$ i-$C_4H_{10} <$ n-C_4H_{10}. Il existe aussi un processus de stabilisation par les alcanes des espèces ioniques $C_6H_8^{+\cdot}$; toutefois, son importance est plus faible que celle provenant des processus de transferts mentionnés plus haut.

[Traduit par le journal]

Introduction

In allene–alkane systems (alkanes: CH_4, C_2H_6, C_3H_8, n-C_4H_{10}, and iso-C_4H_{10}) photoionized at 10.0–10.6 eV (krypton resonance lines) only allene parent ions are formed. It was verified experimentally that the $\lambda = 116.5$ nm resonance line of krypton (10.6 eV) does not ionize to a measurable extent the n-butane and the methylpropane molecules, the ionization potentials (IP) of these compounds being near this threshold (10.55 and 10.57 eV, respectively). At 10 eV the parent ion, $C_3H_4^{+\cdot}$ (IP 9.6 eV), has some internal energy (<0.5 eV) but not enough to lead to fragmentation. It reacts with neutral allene in some characteristic ion/molecule reactions, which have been extensively studied (1–9). However, there is no report on the reactions of allene ions with neutral alkanes.

In the $C_3H_4 + RH_2$ systems where R is C_nH_{2n} one should expect the $H^-/H_2^-/H^{\cdot}$ transfers to be important ion/molecule processes (10, 11). The H^- transfer occurs efficiently in those cases where production of RH_2 represents a reasonable exothermic reaction channel for the ground state reactants. Transfer of H_2^- is always favoured thermodynamically in any $C_nH_{2n}^{+\cdot} + RH_2$ combination, which accounts for the observation that $k(H^-)/k(H_2^-) < 1.0$ even when hydride transfer is highly exothermic. It was also reported that thermoneutral or slightly endothermic H^-/H_2^- transfer processes with low cross-sections occur in the C_3H_6 + n-C_4D_{10} system and in this case it was assumed that a long-lived collision complex is formed favouring these reactions (12).

One can expect that since allene is a highly unsaturated hydrocarbon, its parent ions might form a long-lived collision complex with alkanes and undergo hydride and hydrogen atom transfer reactions, beside stabilization processes of excited ion species formed during ionization of allene. The present experiments describe the ion/molecule processes found in allene + alkane systems and an attempt is made to rationalize the results obtained.

Experimental

The experimental procedure and the high-pressure photoionization mass spectrometer have already been described (13). The measurements were made under field-free conditions inside the collision chamber with an electric field of low intensity (~5 V cm^{-1}) applied in the ionic optics. The distance between the plane of formation of the parent ions by photon impact and the exit slit was 2.2 mm. The experiments were done at room temperature, 25 ± 2°C, as indicated by a thermocouple connected to the collision chamber.

The allene from Matheson of 99.5% purity was used without further purification. Methane, ethane, propane, n-butane, and methylpropane, also from Matheson were of instrumental grade purity. Mixtures of known concentrations (usually around 10% of C_3H_4) were prepared in a conventional high vacuum manifold.

Results

The mass spectrum of the allene–methane mixture was, essentially, similar to that of the allene – rare gas system (9). On the other hand, the spectrum of the allene–ethane system was somewhat different, and those of propane, butane, and methylpropane systems were much different from that of allene – rare gas mixture. The pressure range employed in the present experiments is relatively high, favouring cluster formation of neutral allene. In all these $C_3H_4 + RH_2$ systems only neutral allene molecules form the solvation shell of the ion species. Therefore, the real abundance of each daughter-ion starting a family of solvated species can be represented by the total intensities of each family (e.g. $\Sigma I[C_6H_9^+(C_3H_4)_n]$ with $n = 0, 1, 2, \ldots$). The pressure dependence of the fractional intensities of the families of solvated ions species is shown in Figs. 1–5. In general there appear to be eight solvated ion families: $(C_6H_7^+)_f$, $(C_6H_8^{+\cdot})_f$, $(C_6H_9^+)_f$, $(C_6H_{11}^+)_f$, $(C_7H_7^+)_f$, $(C_7H_{11}^+)_f$, $(C_7H_{12}^{+\cdot})_f$, and $(C_7H_{13}^+)_f$, where the f subscript indicates the corresponding family of solvated ion species by neutral allene molecules. Their fractional intensities are pressure dependent and varied also with the nature of the alkane molecule.

In the case of allene–methane mixtures, four families of ion species were present: $(C_6H_7^+)_f$, $(C_6H_8^{+\cdot})_f$, $(C_6H_9^+)_f$, and $(C_7H_7^+)_f$. There was no evidence for ion/molecule reactions between the parent ion and methane.

On the other hand, the allene–ethane system showed an additional family of ions, $(C_7H_{11}^+)_f$. When perdeuterated ethane was used instead of C_2H_6, the intensity of the $(C_7H_{11}^+)_f$ family decreased and a mass peak corresponding to $C_7H_8D_3^+$ appeared, suggesting a neutral methyl group transfer. Furthermore, the fractional intensity of the $C_6H_9^+$ family increased, while in the case of allene + rare gas systems the abundance of

[1]Visiting Professor 1982. Present address: College of General Education, Tohoku University, Sendai 980, Japan.

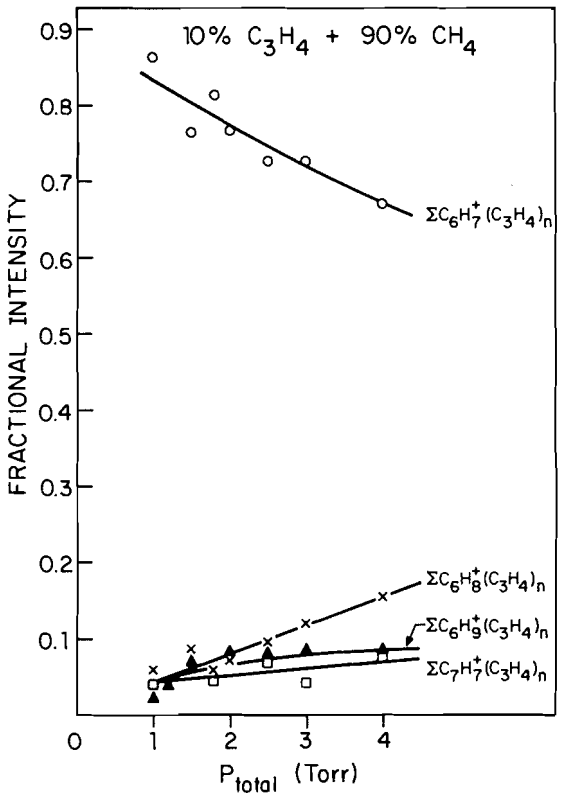

FIG. 1. Pressure dependence of the fractional intensities for the major ion families in the allene–methane mixture.

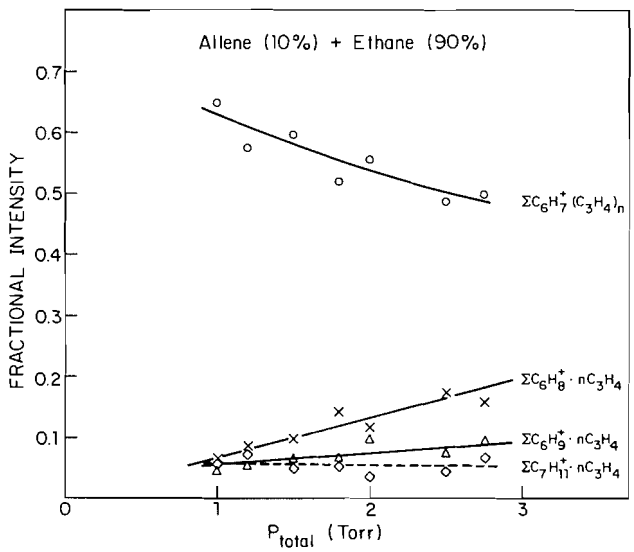

FIG. 2. Pressure dependence of the fractional intensities for the major ion families with allene–ethane mixture.

$(C_6H_9^+)_f$ was almost independent of the presence of the non-reacting gas (9).

In the case of allene + propane mixtures, a new family of ions appeared, $(C_6H_{11}^+)_f$, and the fractional intensities of the $(C_6H_{11}^+)_f$, $(C_6H_9^+)_f$, and $(C_7H_{11}^+)_f$ were strongly enhanced compared to allene + ethane system, indicating the occurrence of reactions between $C_3H_4^+$ and C_3H_8. A $H^\cdot$ transfer process explains the formation of the $C_6H_{11}^+$ species.

The butane + allene system gave two further additional families of ions species: $C_7H_{12}^{+\cdot}$ and $C_7H_{13}^+$. The ion species,

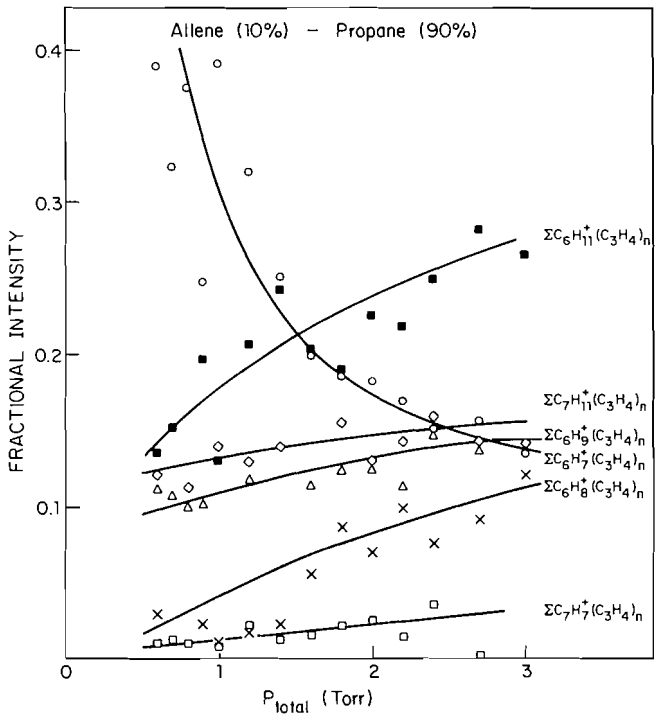

FIG. 3. Pressure dependence of the fractional intensities for the major ion families in the allene–propane mixture.

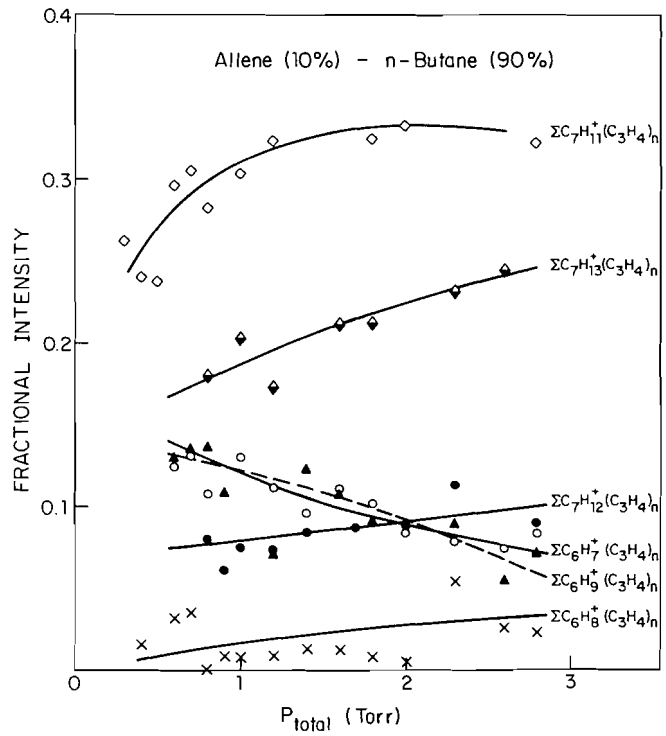

FIG. 4. Pressure dependence of the fractional intensities for the major ion families in the allene–n-butane mixture.

$C_7H_{13}^+$, is formed in a H^- transfer process, while the $C_7H_{12}^{+\cdot}$ results from a H_2^- transfer.

The families of ions formed in methylpropane + allene mixtures were the same as in the n-butane + allene mixtures, but important differences in fractional intensities were observed between the two isomers (Figs. 4, 5).

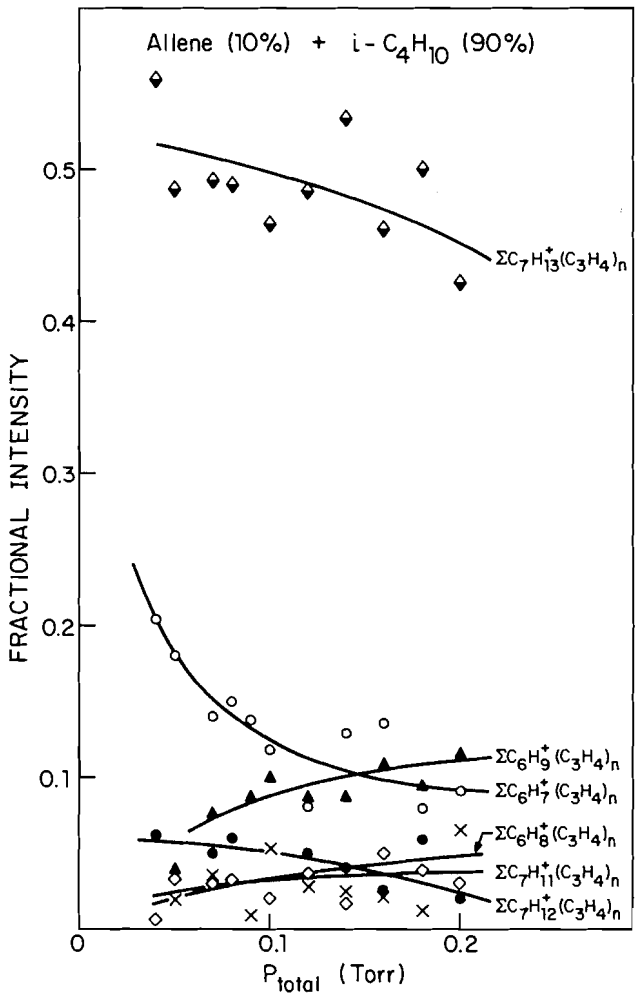

FIG. 5. Pressure dependence of the fractional intensities for the major ion families in the allene–i-butane mixture.

Discussion

In Part II we have proposed the following reaction scheme for allene-chemically "inert" gas systems in the relatively high pressure range ($0.2 < P(C_3H_4) < 1$ Torr) (9)

[1] $C_3H_4^+ + C_3H_4 \rightarrow (C_3H_4^{+\cdot}\cdot C_3H_4)^* \longrightarrow C_6H_7^+ + H^\cdot$

[2] $A^{+*} + C_3H_4 \longrightarrow C_6H_9^+ + C_3H_3^\cdot$

[3] $A^{+*} + C_3H_4 \xrightarrow[k_s(\text{or } k_s')]{} C_7H_7^+ + C_2H_5^\cdot$

[4] $A^{+*} + M\ (\text{or } C_3H_4) \longrightarrow C_6H_8 + M\ (\text{or } C_3H_4)$

where A^{+*} stands for the excited ion complex $(C_3H_4^{+\cdot}\cdot C_3H_4)^*$, M stands for a "chemically inert" third body molecule and k_s and k_s' are the collision stabilization or deactivation rate constants of the excited dimer-ion by M or neutral allene, respectively.

The $H^\cdot/CH_3^\cdot/H^-/H_2^-$ transfer processes might in principle take place either in reactive encounters between allene parent ions, $C_3H_4^{+\cdot}$, and the alkane neutrals, or between the complex dimer-ion, $(C_3H_4)_2^{+\cdot}$ and the alkane molecules. It is found experimentally that the formation of $C_6H_9^+$, $C_7H_{11}^+$, $(C_nH_{2n+1}\cdot C_3H_4)^+$, and $(C_nH_{2n}\cdot C_3H_4)^{+\cdot}$ species resulting from the above transfer processes, obeys a *second order* rate kinetics. This is easily explained assuming long-lived intermediate species, $(C_nH_{2n+2}\cdot C_3H_4)^{+\cdot *}$ and $(C_3H_4)_2^{+\cdot *}$, which on collision with neutrals can either dissociate in a backward reaction into reactants, or form the species under consideration.[2] In our experimental conditions the much higher concentration of alkane neutrals over the allene molecules suggests that the following reactions are favoured over the reaction involving the allene dimer-ion, $(C_3H_4)_2^{+*}$:

[5] $(C_3H_4^{+\cdot}\cdot C_nH_{2n+2})^* + C_3H_4 \rightarrow C_6H_9^+ + C_nH_{2n+1}^\cdot$

[6] $+ C_3H_4 \rightarrow C_7H_{11}^+ + C_{n-1}H_{2n+1}^\cdot$

[7] $+ C_3H_4 \rightarrow (C_nH_{2n+1}\cdot C_3H_4)^+ + C_3H_5^\cdot$

[8] $+ C_3H_4 \rightarrow (C_nH_{2n}\cdot C_3H_4)^{+\cdot} + C_3H_6$

where the $(C_3H_4^{+\cdot}\cdot C_nH_{2n+2})^*$ stands for the excited ion complex between the parent ion and the neutral alkane undergoing a $H^\cdot$ transfer (reaction [5]), $CH_3^\cdot$ transfer (reaction [6]), H^- transfer (reaction [7]), and H_2^- transfer (reaction [8]).

Reactions [1]–[8] yield the following kinetic expressions:

[9] $d[C_6H_7^+] = k_1[A^{+*}]$

[10] $d[C_6H_8^{+\cdot}] = k_s'[A^{+*}][C_3H_4] + k_s[A^{+*}][C_nH_{2n+2}]$

[11] $d[C_6H_9^+] = k_2[A^{+*}][C_3H_4] + k_5[C_3H_4^{+\cdot}\cdot C_nH_{2n+2}][C_3H_4]$

[12] $d[C_7H_{11}^+] = k_6[C_3H_4^{+\cdot}\cdot C_nH_{2n+2}][C_3H_4]$

[13] $d[(C_nH_{2n+1}\cdot C_3H_4)^{+\cdot}] = k_7[C_3H_4^{+\cdot}\cdot C_nH_{2n+2}][C_3H_4]$

[14] $d[(C_nH_{2n}\cdot C_3H_4)^{+\cdot}] = k_8[C_3H_4^{+\cdot}\cdot C_nH_{2n+2}][C_3H_4]$

For the convenience of the kinetic analysis, relative rates can be introduced. They are defined by the ratio of the rate of formation of the ion under consideration to the rate of formation of $C_6H_7^+$ species:

[15] $d[C_6H_9^+]/d[C_6H_7^+] = R/(R+1)\{k_2/k_1 + k_5/R'k_1\}P_t$

[16] $d[C_7H_{11}^+]/d]C_6H_7^+] = \{k_6/k_1(R+1)\}P_t$

[17] $d[C_nH_{2n+1}\cdot C_3H_4)^{+\cdot}]/d[C_6H_7^+] = \{k_7/k_1(R+1)\}P_t$

[18] $d[C_nH_{2n}\cdot C_3H_4)^{+\cdot}]/d[C_6H_7^+] = \{k_8/k_1(R+1)\}P_t$

[19] $d[C_6H_8^{+\cdot}]/d[C_6H_7^+] = R/(R+1)\{k_s'/k_1 + k_s/R'k_1\}P_t$

where R stands for the experimental mixing ratio $[C_3H_4]/[C_nH_{2n+2}]$ and $P_t = P(C_3H_4) + P(C_nH_{2n+2})$. In all experiments $R = 0.11$.

We will assume that the ratio $R' = [C_3H_4^{+\cdot}\cdot C_3H_4]/[C_3H_4^{+\cdot}\cdot C_nH_{2n+2}]$ of the concentrations of the ion complexes is proportional to the concentrations of reactants from which they are formed and therefore is equal or very close to the experimental mixing ratio, R. This is justified, because the life-time of collisional complexes formed from similar species is not very sensitive to their nature.

The left-hand side terms of the eqs. [15]–[19] correspond to the experimental ratio of fractional intensities of corresponding families of ion species.

The plots of expressions [15]–[18] are presented in Figs. 6–10, and the ratios of rate constants obtained from the corresponding slopes are given in Table 1. Some additional information about each plot are given below.

(*i*) The plots for expression [15] gave almost straight lines for all alkanes, Figs. 6, 7. From the slopes the values k_5/k_1 can be obtained, since the ratio k_2/k_1 is already known to be constant and its mean value is 0.25 $Torr^{-1}$ (9). The value k_5/k_1 for ethane is very small, but $H^\cdot$ transfer is certainly occurring, since a clear difference is observed in the slopes of $(C_3H_4 + C_2H_6)$ and

[2]Unpublished results from this laboratory.

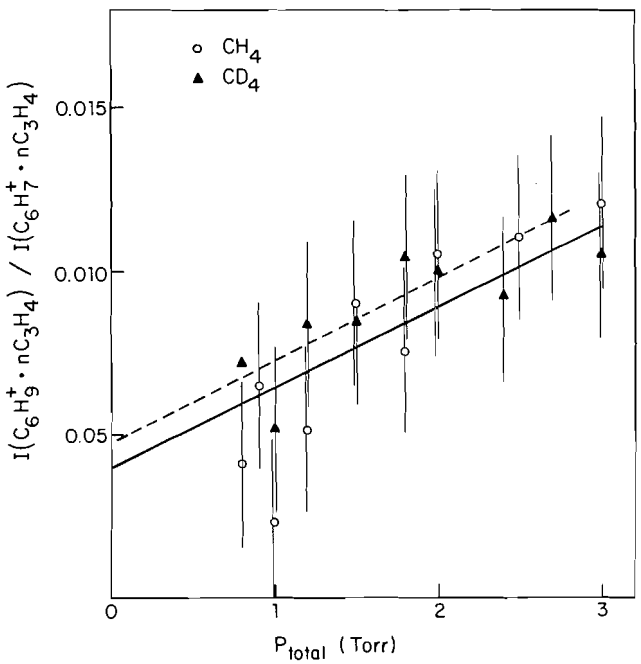

FIG. 6. Plot of expression [15] for the H• transfer process in the C_3H_4–CH_4 and C_3H_4–CD_4 mixtures.

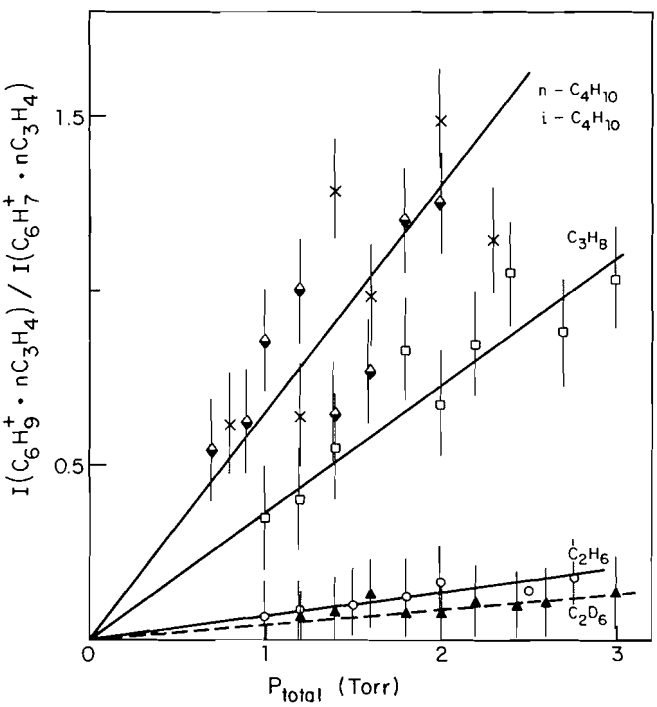

FIG. 7. Plot of expression [15] for the H• transfer process in the allene–alkane mixtures.

$(C_3H_4 + C_2D_6)$ systems and the difference could be accounted for by the formation of $C_6H_8D^+$.

(*ii*) The plots for expression [16] gave also straight lines for all alkanes, although the slope for n-butane changed and became small above 1 Torr, as shown in Fig. 8. The values k_6/k_1 obtained from the corresponding slopes which represent the relative CH_3• rate transfer are tabulated in the fourth column in Table 1.

(*iii*) In Fig. 9 are shown the plots for expression [17] for propane and butane isomers. In the case of ethane the fractional intensity was too weak to be plotted.

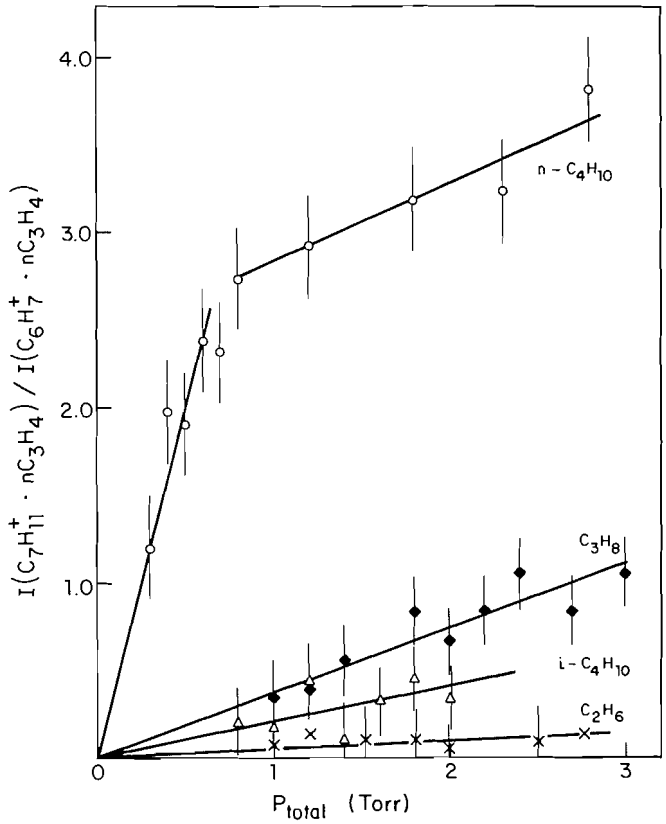

FIG. 8. Plot of expression [16] for the CH_3• transfer process in the allene–alkane mixtures.

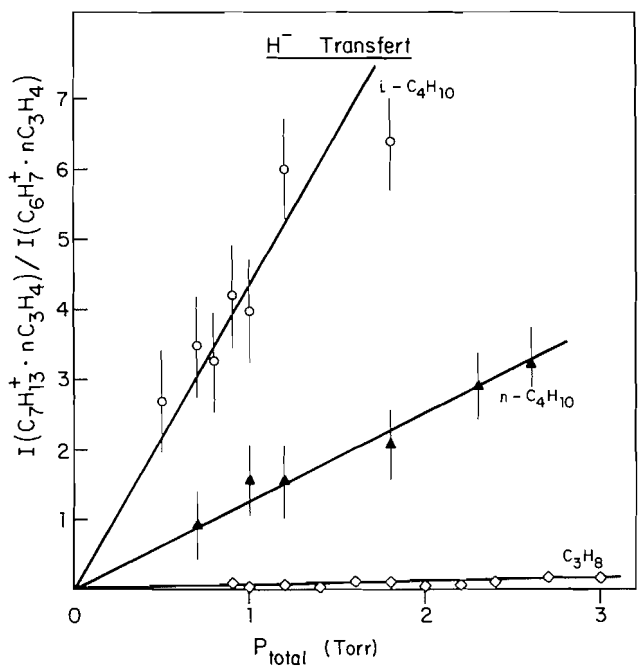

FIG. 9. Plot of expression [17] for the H^- transfer process in the allene–alkane mixtures.

(*iv*) In Fig. 10 the plots for expression [18] are shown. The corresponding ratios k_8/k_1 are given in the sixth column in Table 1.

TABLE 1. Relative rate constants for the ion/molecule reactions between the parent ion $C_3H_4^{+\cdot}$ and the alkanes

Alkane	$(k_5 + k_6 + k_7 + k_8)/k_1$, $Torr^{-1}$ (overall reaction)	k_5/k_1, $Torr^{-1}$ ($H^\cdot$ transfer)	k_6/k_1, $Torr^{-1}$ ($CH_3^\cdot$ transfer)	k_7/k_1, $Torr^{-1}$ (H^- transfer)	k_8/k_1, $Torr^{-1}$ (H_2^- transfer)	k_s/k_1, $Torr^{-1}$ (stabilization of $C_6H_8^{+\cdot}$)
CH_4	~0	~0	~0	~0	~0	0.048 ± 0.02
C_2H_6	0.13	0.07	0.06	~0	~0	0.11 ± 0.03
C_3H_8	1.06	0.38	0.42	0.07	0.19	n.m.[a]
n-C_4H_{10}	7.4	~0.7	4.6	1.4	0.70	n.m.
i-C_4H_{10}	6.3	~0.7	0.23	4.8	0.54	n.m.

[a]n.m. = not measured.

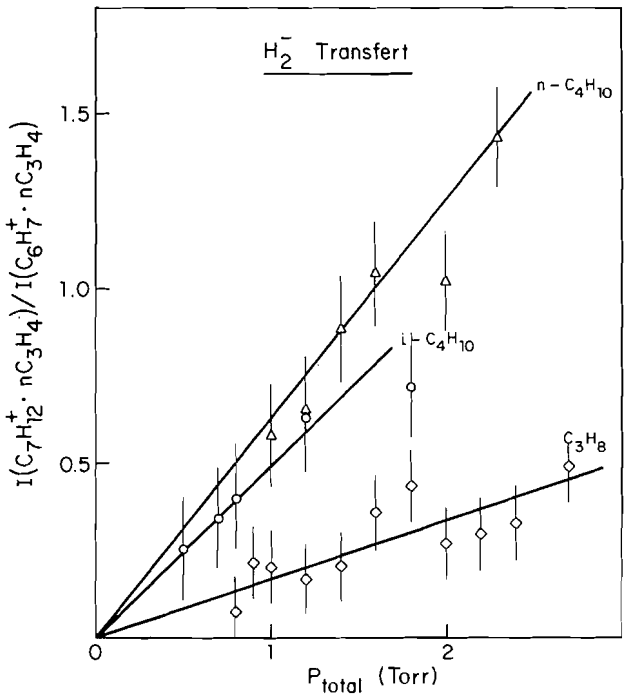

FIG. 10. Plot of expression [18] for the H_2^- transfer process in the allene–alkane mixtures.

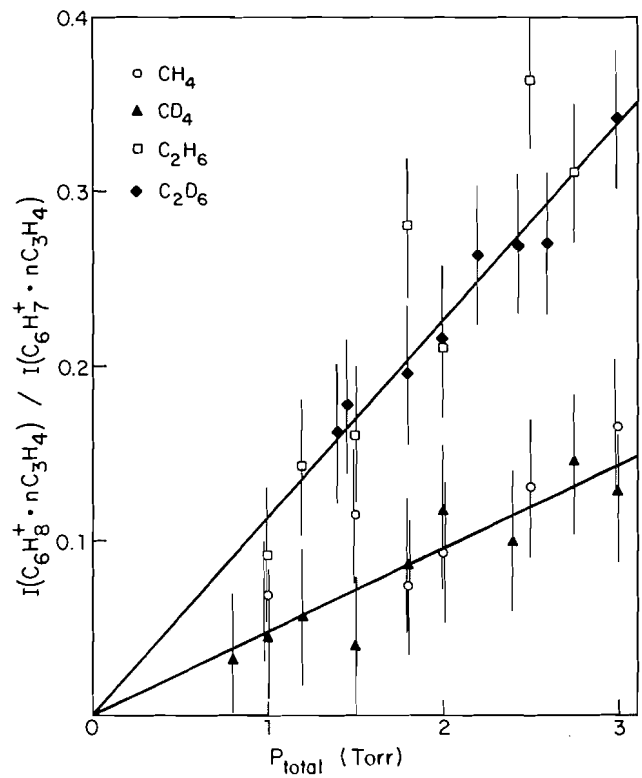

FIG. 11. Plot of expression [19] for the stabilization process of $C_6H_8^{+\cdot}$ in methane and ethane mixtures with allene.

(*v*) The energy transfer in stabilization processes from the parent ions to the alkanes acting as a bath gas was examined by plotting expression [19]. As shown in Fig. 11 methane and ethane gave straight lines and from the corresponding slopes the values of the ratio k_s/k_1 were calculated. They are 0.048 ± 0.02 for methane and 0.11 ± 0.03 $Torr^{-1}$ for ethane, when k_s'/k_1 is assumed to be 0.11 $Torr^{-1}$ (9). For the C_3–C_4 alkanes the fluctuations were too big to allow calculation of k_s/k_1 from the slopes and therefore their values are not given in Table 1.

Thus the kinetic treatment based on expressions [15] to [19] support the reaction scheme described by reactions [1] to [8]. The total relative reactivity for the four channels of ion/molecule reactions involving parent ions of allene, $C_3H_4^{+\cdot}$, and neutral alkanes is given by the sum of the relative rate constants for each channel and is presented in the first column of Table 1. It can be seen that the total relative reactivity increases with the size of the neutral alkane.

Although the reactivities might depend on the IP's other molecular factors will influence the specific reaction channels. In Table 2 are presented the heats of reactions of $CH_3^\cdot$/$H^\cdot$/H^-/H_2^- transfer processes for some systems involved in this study. The enthalpies of formation were taken from refs. 15 and 16.

In each case, with the exception of methane, the $CH_3^\cdot$ transfer is exothermic and, indeed, occurs in the $C_3H_4 + RH_2$ systems. It is also more favorable for propane and butane compared to $H^\cdot$ transfer (Table 2). One possible reason is that the C—C bond is weaker than the C—H bond by 35 kJ mol^{-1} in RH_2. On the other hand, in allene + methylpropane system the $H^\cdot$ transfer is more important compared to $CH_3^\cdot$ tansfer. This anomaly appears not to relate to thermochemistry (Table 2) and so presumably is kinetic in origin.

The differences in H^-/H_2^- transfer for the two butanes can be also accounted for on kinetic grounds. Although the H^- transfer is more favorable by ~8 and ~25 kJ mol^{-1} in butane and methylpropane, respectively, relative to H_2^- transfer, one also has to take into account the relative probability that the reaction complex does or does not fall apart after the transfer of the H^- entity. It was shown that the H_2^- transfer reaction proceeds through a two-steps stereospecific mechanism, refs. 14, 17–19. The reactive encounter between species initially involves the transfer of a singly H^- ion in the reaction complex in an exothermic process. This complex may then fall apart, resulting in a single particle transfer process, or a second H atom may be

TABLE 2. Enthalpies of some $H^{\cdot}/CH_3^{\cdot}/H^-/H_2^-$ transfer reactions for the $C_3H_4 + RH_2$ systems

Transfer process	Reaction	$\Delta H_r^{a,b}$ (kJ mol^{-1})
$H^{\cdot}$	$C_3H_4^{+\cdot}(C_3H_8, C_3H_7^{\cdot})C_3H_5^+$	+2
	$C_3H_4^{+\cdot}(n\text{-}C_4H_{10}, sec\text{-}C_4H_9^{\cdot})C_3H_5^{+\cdot}$	−2
	$C_3H_4^{+\cdot}(i\text{-}C_4H_{10}, tert\text{-}C_4H_9^{\cdot})C_3H_5^+$	−7
$CH_3^{\cdot}$	$C_3H_4^{+\cdot}(CH_4, H^{\cdot})C_4H_7^+$	32
	$C_3H_4^{+\cdot}(C_2H_6, CH_3^{\cdot})C_4H_7^+$	−30
	$C_3H_4^{+\cdot}(C_3H_8, C_2H_5^{\cdot})C_4H_7^+$	−59
	$C_3H_4^{+\cdot}(n\text{-}C_4H_{10}, n\text{-}C_3H_7^{\cdot})C_4H_7^+$	−47
	$C_3H_4^{+\cdot}(i\text{-}C_4H_{10}, i\text{-}C_3H_7^{\cdot})C_4H_7^+$	−50
H^-	$C_3H_4^{+\cdot}(n\text{-}C_4H_{10}, C_3H_5^{\cdot})sec\text{-}C_4H_9^+$	−60
	$C_3H_4^{+\cdot}(i\text{-}C_4H_{10}, C_3H_5^{\cdot})tert\text{-}C_4H_9^+$	−123
H_2^-	$C_3H_4^{+\cdot}(n\text{-}C_4H_{10}, C_3H_6)$ 1-$C_4H_8^{+\cdot}$	−52
	$C_3H_4^{+\cdot}(i\text{-}C_4H_{10}, C_3H_6)$ i-$C_4H_8^{+\cdot}$	−98

[a]Heats of formation are taken from refs. 15 and 16.

[b]Due to the approximate value of the heat of formation of the allene ion (15), the estimated values of the heats of reactions are assumed to have an uncertainty of ±12 kJ.

transferred on an adjacent carbon atom while the reactants remain in the "loose" complex. Because the H_2^- transfer process is always in competition with H^- transfer reaction, both the total rate of reaction and the relative rates of the competing H^- and H_2^- reactions must be considered. It was already observed that the importance of H_2^- transfer relative to H^- transfer decreases with increasing branching (18). In methylpropane, the presence of a weakly bonded tertiary hydrogen atom in the reactant molecule apparently favors the occurrence of the H^- transfer reaction over the H_2^- transfer process as shown by the value of the ratio $k(1)/k(2) = 8.9$, compared to $k(1)/k(2) = 2$ for n-butane (Table 1). Here $k(1)$ and $k(2)$ stand for one- and two-particle transfer.

Acknowledgements

The authors are indebted to the Natural Sciences and Engineering Research Council of Canada for financial support. They are also indebted to Drs. Forst and P. Burgers for valuable discussions.

1. J. J. MYHER and A. G. HARRISON. J. Phys. Chem. **72**, 1905 (1968).
2. M. T. BOWERS, D. D. ELLEMAN, R. M. O'MALLEY, and K. R. JENNINGS. J. Phys. Chem. **74**, 2583 (1970).
3. P. R. LEBRETON, A. D. WILLIAMSON, J. L. BEAUCHAMP, and W. T. HUNTRESS. J. Chem. Phys. **62**, 1623 (1975).
4. A. NATO, M. NIWA, H. HOMMA, I. TANAKA, and I. KOYANO. Int. J. Mass Spectrom. Ion Phys. **34**, 2871 (1980).
5. C. LIFSHITZ, Y. GLEITMAN, S. GEFEN, U. SHAINOK, and I. DOTAN. Int. J. Mass Spectrom. Ion Phys. **40**, 1 (1981).
6. C. LIFSHITZ and Y. GLEITMAN. Int. J. Mass Spectrom. Ion Phys. **40**, 17 (1981).
7. V. G. ANICICH, G. A. BLAKE, J. K. KIM, M. J. MCEVAN, and W. T. HUNTRESS. J. Phys. Chem. **88**, 4608 (1984).
8. D. CARRIER and J. A. HERMAN. Int. J. Mass Spectrom Ion Proc. **44**, 183 (1984).
9. K. NAGASE and J. A. HERMAN. Can. J. Chem. **62**, 2364 (1984).
10. L. W. SIECK and S. K. SEARLES. J. Am. Chem. Soc. **92**, 2937 (1970).
11. S. LIAS and P. AUSLOOS. *In* Ion–molecule reactions. Am. Chem. Soc. Washington, DC. 1975. p. 120.
12. I. KOYANO, N. NAKAYAMA, and I. TANAKA. J. Chem. Phys. **54**, 2384 (1971).
13. Z. ŁUCZYNSKI and J. A. HERMAN. Int. J. Mass Spectrosc. Ion Phys. **31**, 237 (1979).
14. F. P. ABRAMSON and J. H. FUTRELL. J. Phys. Chem. **71**, 1233 (1967).
15. H. M. ROSENSTOCK, K. DRAXL, B. W. STEINER, and J. T. HERRON. J. Phys. Chem. Ref. Data, vol. 6, Suppl. 1, 1977.
16. D. F. MCMILLAN and D. M. GOLDEN. Ann. Rev. Phys. Chem. **33**, 493 (1982).
17. P. AUSLOOS. *In* Progress in reaction kinetics. vol. 5. Pergamon Press, London. 1970. p. 142.
18. S. G. LIAS and P. AUSLOOS. J. Chem. Phys. **43**, 127 (1965).
19. R. D. DOEPKER and P. AUSLOOS. J. Chem. Phys. **44**, 1951 (1966).

Limiting activity coefficients in dilute solutions of nonelectrolytes. II. Determination for polar–nonpolar and polar–polar binary mixtures, and the application of some solubility-parameter treatments

SHAPOUR AFRASHTEHFAR AND GENILLE C. B. CAVE
Department of Chemistry, McGill University, Montreal, P.Q., Canada H3A 2K6

Received April 2, 1985

SHAPOUR AFRASHTEHFAR and GENILLE C. B. CAVE. Can. J. Chem. **64**, 198 (1986).

Activity coefficients were determined at 293.15 K for the more dilute component in 24 binary solutions of nonelectrolytes, by gas-chromatographic analysis of the equilibrium vapor phase. One component of the binary mixture was either nitromethane, nitroethane, 1-nitropropane, 2-nitropropane, ethanenitrile, propanenitrile, ethyl ethanoate, or butyl ethanoate; and the other component was either heptane, 1-heptene, or 1,6-heptadiene.

From the limiting activity coefficients of these components, some factors that affected their magnitude were identified. The values were also used to test the modifications of Prausnitz, Blanks, and Weimer, of Helpinstill and Van Winkle, and of Keller, Karger, and Snyder to the Scatchard–Hildebrand equation modified to accommodate polar components. In addition, the degree of constancy of the ratio of the dipole – induced dipole interaction parameter for a series of solutes in one solvent to that in another was considered.

SHAPOUR AFRASHTEHFAR et GENILLE C. B. CAVE. Can. J. Chem. **64**, 198 (1986).

Les coefficients d'activité ont été déterminés à 293.15 K pour la composante la plus diluée de 24 solutions binaires de non-électrolytes, par chromatographie en phase gazeuse de la phase vapeur à l'équilibre. L'une des composantes du mélange provenait de chacun des composés suivants: le nitromethane, le nitroéthane, le nitro-1 propane, le nitro-2 propane, l'éthanenitrile, le propanenitrile, l'éthanoate d'éthyle et l'éthanoate de butyle, tandis que l'autre composante provenait de chacun des composés suivants: l'heptane, l'heptène-1 et l'heptadiène-1,6.

L'utilisation des coefficients limites de l'activité de ces composantes ont permis l'identification de quelques facteurs qui affectent leur intensité. Ces valeurs ont également été utilisées pour vérifier la validité des modifications de Prausnitz, Blanks et Weimer, de Helpinstill et Van Winkle, et, de Keller, Karger et Snyder, à l'équation de Scatchard–Hildebrand, modifiée de façon à devenir applicable aux composantes polaires. De plus, le degré de constance du rapport du paramètre de l'interaction dipôle – dipôle induit pour une série de solutés dans un solvant, sur ce même paramètre évalué dans le cas d'un autre solvant, a été examiné.

Introduction

A previous study (1, 2*a*) described a static equilibration apparatus having a novel gas-chromatographic headspace sampler, which was used to evaluate the limiting activity coefficients of eight polar compounds in heptane and in benzene. In the present work, this study has been extended to include the same polar compounds in 1-heptene and 1,6-heptadiene as solvents, as well as heptane, 1-heptene, and 1,6-heptadiene as solutes in each of the eight polar compounds as solvents.

From the resulting limiting activity coefficients, some factors that affected their magnitude were identified, namely: (*i*) the chain length and the polarity of the solute, and (*ii*) the effect of one or more double bonds in the solvent, on the limiting activity coefficients of the polar compounds. The data may also be used for testing extended solubility-parameter models. In the present paper three such extended-solution treatments (3–8) are considered. In addition, the degree of constancy of the ratio of the dipole – induced dipole interaction parameters of a solute in two given solvents, first reported by Milanova and Cave (1), was tested.

Experimental

Static equilibration apparatus

The equilibration apparatus was the same one previously designed and used by Milanova (1, 2*a*). However, for the present work it was improved by enclosing the metal headspace sampler in an air thermostat, which led to better precision, and by adding a sidearm near the base of the cell to facilitate adding and removing the solutions. The improved version of the entire equilibration apparatus has been described in detail elsewhere (9).

The metal headspace sampler was housed in a double-walled air bath which fitted snugly over the sampler and its copper loops. Water at 295.15 K from a water thermostat was pumped continuously through the double-walled jacket of the air bath. A 2 K differential was thereby ensured between the sampling loops and the equilibration cell, in order to prevent any possibility of some condensation of equilibrated vapor in the loops.

When ethanenitrile was the solvent in the binary systems, somewhat high and non-reproducible results were obtained for the concentration of the hydrocarbon solute in the copper sampling loops. In this connection, Putnam *et al.* (10) have reported that liquid and solid ethanenitrile reacted with copper. Therefore, an all-glass headspace sampler was constructed and used for systems having ethanenitrile as solvent. It provided exactly the same function as the metal sampler of Milanova, and has been described in detail elsewhere (9*a*). It is illustrated in Fig. 1. This unit was custom-made including fabrication of the stopcock barrel and stopcock plug, from borosilicate thick-walled tubing to permit tapering. Briefly, a large six-way stopcock had a tapered hollow plug, inside which three hollow tubes had been blown (Fig. 1). These three tubes formed the actual sampling containers for the samples of equilibrium vapor. Six short hollow glass tubes were blown onto the stopcock barrel. Four of them ended in 10/19 outer joints, of which two (A and B, Fig. 1) were connected to the carrier-gas line, one (C) was connected to the vacuum, and one (D) was plugged. A fifth tube (E) ended in a 19/26 inner joint. Sixty-degree rotation of the stopcock brought each of the three sampling tubes in the plug in turn into juxtaposition with the barrel end of tube E; and the 19/26 joint could be connected directly to the equilibration cell so that the sampling tube in the stopcock became part of the cell space. The sixth tube (S_1) was to permit evacuation of the cell when necessary. The three sampling tubes were calibrated by filling them with water from a preweighed syringe which was then reweighed. Their volumes and standard deviations were found to be 2.9671 ± 0.00095 cm^3, 3.2811 ± 0.0121 cm^3, and 3.9285 ± 0.0108 cm^3 for 12 replicates.

Materials

The purification procedures are described in detail elsewhere (9*b*).

TABLE 1. Purity and physical properties at 293.15 K of the purified reagents

Reagents	Source	Final purity %	Refractive index(n_D) Exptl.[b]	Refractive index(n_D) Lit. (11)	Density[a] × 10^{-3} Exptl.[c]	Density[a] × 10^{-3} Lit. (11)
Nitromethane	Aldrich	99.972	1.3804	1.3812	1.1370	1.1382
Nitroethane	Aldrich	99.950	1.3924	1.3919	1.0510	1.0506
1-Nitropropane	Aldrich	99.985	1.4011	1.4016	1.0035	1.0014
2-Nitropropane	Eastman	99.945	1.3947	1.3944	0.9876	0.9884
Ethanenitrile	B.D.H.	99.998	1.3440	1.3441	0.7840	0.7822
Propanenitrile	Aldrich	99.925	1.3648	1.3658	0.7842	0.7818
Ethyl ethanoate	B.D.H.	99.927	1.3725	1.3724	0.9004	0.9006
Butyl ethanoate	B.D.H.	99.990	1.3936	1.3941[d]	0.8815	0.8825[d]
Heptane	Aldrich	99.995	1.3862	1.3876	0.6834	0.6838
1-Heptene	Aldrich	99.971	1.3987	1.3998	0.6976	0.6970
1,6-Heptadiene	I.C.N.	99.850	1.4136	1.4142[e]	0.7135	0.7142[e]

[a]Unit kg m^{-3}.
[b]Typical standard deviation for triplicate experimental readings was 0.0008.
[c]Typical standard deviation for triplicate experimental measurements was 0.00115.
[d]Taken from CRC Handbook of Chemistry and Physics (12).
[e]Taken from Egloff (13).

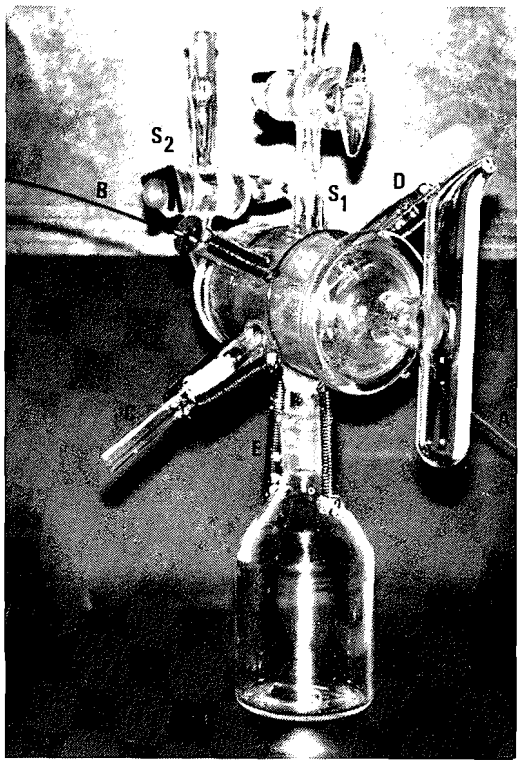

FIG. 1. Six-way all-glass headspace sampler attached to equilibration cell.

The final purities are in Table 1, together with the sources of the reagents, and the refractive indices and densities of the purified products. Final purities were determined by gas chromatographic analysis for impurities.

Except for a few variations noted below, the fractional distillations were carried out under reduced pressure after flushing the still with nitrogen, at an output rate of ca. 20 $cm^3 h^{-1}$ and a reflux ratio of ca. 50:1. The middle cuts were retained, stored in the dark over molecular sieves 3A, and used no later than a week after their purification.

The nitrocompounds were dried over P_2O_5, then fractionally distilled. The nitriles were fractionally distilled over molecular sieves 3A, at an output rate of 10 $cm^3 h^{-1}$. The esters were fractionally distilled without initial drying.

Heptane was purified by four fractional crystallizations followed by fractional distillation under nitrogen at atmospheric pressure.

1-Heptene was distilled from sodium in a spinning-band still and a nitrogen atmosphere, at a rate of 10 $cm^3 h^{-1}$ and a reflux ratio of 65:1.

1,6-Heptadiene was purified by preparative gas chromatography in a Varian Aerograph 705 in manual mode, on a column packed with 10% Carbowax 20M on 80/100 Chromosorb W at 255 K. The lots were processed 1 mL at a time.

Benzene was purified by six fractional crystallizations. Tetrachloromethane was fractionally distilled at atmospheric pressure. Cyclohexane was fractionally distilled over sodium at atmospheric pressure.

Procedure

The procedure used for equilibration and gas chromatographic analysis of the binary solutions and their vapors was essentially the one developed and used earlier by Milanova (2*b*), and reported in outline form in ref. 1. However, for the present work some precautionary refinements were added. The complete modified procedure is given elsewhere (9*c*). The refinements were (*i*) the equilibration apparatus was flushed with nitrogen before use; (*ii*) the solute and solvent were introduced into the equilibration cell via the sidearm that had been added to it, by two syringes weighed before and after dispensing the pure solute and solvent, respectively; (*iii*) the apparatus was degassed twice instead of once; (*iv*) not only was the equilibration cell immersed in a water thermostat set at 293.15 K as previously (2*b*), but also the metal headspace sampler was enclosed in the above-described air thermostat set at 295.15 K; (*v*) although liquid–vapor equilibrium was reached in 30 min; 2 h were allowed before the first sampling; (*vi*) after two to four vapor samples had been taken and analyzed, four samples of the liquid phase remaining in the cell were removed by syringe via the sidearm and analyzed by gas chromatography.

It was necessary to know the solubility parameter of 1,6-heptadiene, previously unreported. The value of $\Delta H^v_{298.15}$ was measured for us by Majer. He used our above-described product, with molecular sieves 3A added to prevent contamination by atmospheric humidity, and an adiabatic vaporization calorimeter described by Majer *et al.* (14). The mean of three runs was $\Delta H^v_{298.15} = 35.00$ kJ mol^{-1}. Then from their empirical relationship $\Delta H^v = K\,[(1 - T_r)e^{-T_r}]^{0.275}$, where T_r is the reduced temperature, 0.275 is a parameter from ΔH^v data on alkenes, K is obtained from the value of $\Delta H^v_{298.15}$, and using as the critical temperature 532.6 K, Majer calculated $\Delta H^v_{293.15} = 35.20$ kJ mol^{-1}, with an estimated uncertainty of 0.3%. We then calculated the

TABLE 2. Experimetnal values of activity coefficients of components at infinite dilution, for binary liquid mixtures at 293.15 K[a]

	Component 1					
	Heptane		1-Heptene		1,6-Heptadiene	
Component 2	γ_1^∞	γ_2^∞	γ_1^∞	γ_2^∞	γ_1^∞	γ_2^∞
Nitromethane	78.31 ± 0.13	49.28 ± 0.13	30.22 ± 0.16	23.87 ± 0.07	17.39 ± 0.06	13.53 ± 0.08
Nitroethane	19.85 ± 0.06	25.27 ± 0.48[b]	10.61 ± 0.06	11.86 ± 0.03	5.443 ± 0.068	7.677 ± 0.034
1-Nitropropane	8.259 ± 0.026	16.31 ± 0.21[b]	5.192 ± 0.04	8.606 ± 0.023	3.107 ± 0.018	5.426 ± 0.039
2-Nitropropane	7.610 ± 0.043	12.71 ± 0.22[b]	4.446 ± 0.026	6.874 ± 0.019	2.961 ± 0.076	4.784 ± 0.102
Ethanenitrile	51.71 ± 0.20	40.17 ± 0.12	19.55 ± 0.04	20.92 ± 0.05	10.77 ± 0.08	13.29 ± 0.05
Propanenitrile	15.12 ± 0.09	23.93 ± 0.38[b]	7.736 ± 0.041	12.04 ± 0.03	4.342 ± 0.022	6.523 ± 0.040
Ethyl ethanoate	4.303 ± 0.023	3.679 ± 0.031[b]	3.500 ± 0.019	2.458 ± 0.016	1.888 ± 0.013	1.837 ± 0.033
Butyl ethanoate	2.408 ± 0.009	2.812 ± 0.028[b]	1.807 ± 0.011	2.005 ± 0.006	1.351 ± 0.007	1.317 ± 0.008

[a]Note: Subscript 1 refers to the C_7 component, and subscript 2 to the polar component listed in column 1. Thus, the notation γ_1^∞ means that, for example, the values in column 2 are for heptane at infinite dilution in each of the polar liquids in column 1; γ_2^∞ means that, for example, the values in column 3 are for each of the polar compounds at infinite dilution in heptane.

[b]Values calculated from data by Milanova (2*c*), but using Tsonopoulos method (15) for calculating values of mixed virial coefficients.

TABLE 3. Dispersion $^d\delta$, polar $^p\delta$, dipole–dipole $^o\delta$, and induced dipole $^{in}\delta$ contributions to the total solubility parameter δ of some compounds at 293.15 K, in $MPa^{1/2}$ units[a]

				$^{in}\delta$		$^o\delta$	
Compound	δ	$^d\delta$	$^p\delta$	This work	Lit.	This work	Lit.
Nitromethane	25.9	16.2	20.3	7.0	6.1	13.6	17.0
Nitroethane	23.53	16.3	17.0	5.5	4.5	10.2	12.3
1-Nitropropane	21.54	16.4	13.9	3.8	8.4		
2-Nitropropane	20.86	16.2	13.1	3.3		8.0	
Ethanenitrile	24.30	14.5	19.5	6.3	5.7	14.1	16.8
Propanenitrile	21.93	15.0	16.0	4.5	3.7	10.9	13.5
Ethyl ethanoate	18.39	15.3	10.2	2.3	2.0	5.8	8.2
Butyl ethanoate	17.77	16.0	7.73	1.4	4.1		
Heptane	15.32	15.3	Nil				
1-Heptene	15.42	15.2	2.65	0.09 ± 0.07		1.41 ± 0.11	
1,6-Heptadiene	15.57	15.1	3.84	0.25 ± 0.13		2.44 ± 0.20	

[a]Literature values of $^o\delta$ and $^{in}\delta$ are from ref. 7, converted to $MPa^{1/2}$ units. δ values were calculated from molal enthalpies of vaporization, reported in (1), except for 1-heptene which was from (11), and 1,6-heptadiene which was calculated from $\Delta 3H^v_{298.15}$, specially measured for the present study. Values of $^d\delta$, $^p\delta$, $^o\delta$, and $^{in}\delta$ have been rounded to three and two figures, as shown.

solubility parameter of 1,6-heptadiene to be 15.57 $MPa^{1/2}$ units at 293.15 K, using a molar volume of 135.6 $cm^3\ mol^{-1}$ (13).

Results

The method used to calculate limiting activity coefficients (γ_i^∞) from measured vapor concentrations of the solute is described in detail elsewhere (9*d*), and follows that used in an earlier study (1, 2). Briefly, an uncorrected activity coefficient (γ_i') was calculated for a solute in a given solvent at 293.15 K at each of its several concentrations, by assuming an ideal vapor and using the usual formula $\gamma_i' = C_i/C_i^0 x_i$. Here C_i is the molar concentration of solute in the equilibrium vapor over a solution of mole fraction x_i, and C_i^0 is the molar concentration of vapor over the pure liquid solute. The pure liquid at 293.15 K is taken as the standard state. The values obtained for γ_i' were then corrected for the non-ideality of the vapor by using second virial coefficients, to give the corrected values of γ_i. The values used for the pure (B_{ii}) and mixed (B_{ij}) virial coefficients were estimated by using the empirical method of Tsonopoulos (15).

For each binary system the vapor concentration of solute had been measured for 5 or 6 solutions over a range of mole fractions x_i of solute. The value of γ_i^∞ for the solute was then found by a linear least-squares fit of the (x_i, γ_i) data, i.e. $\gamma_i = \gamma_i^\infty + bx_i$. Application of the statistical F-test showed that at the 95% confidence level, terms higher than x_i were not significant in the concentration range used ($x_i < 0.01$).

The values for the limiting activity coefficients and their standard deviations are in Table 2, where subscript 1 refers to the C_7 component of the binary solution, and subscript 2 refers to the polar component listed in column 1.

The solubility parameter δ of each polar liquid was considered to consist as usual of a dispersion $^d\delta$ and a polar $^p\delta$ contribution, where $\delta^2 = {}^d\delta^2 + {}^p\delta^2$. These values for the eight polar compounds and the three hydrocarbons are in Table 3. For 1-heptene, δ was calculated from the molal heat of vaporization (11), and for 1,6-heptadiene from Majer's value of the molal heat of vaporization. The values of $^d\delta$ for 1-heptene and 1,6-heptadiene were calculated by the procedure already reported (1) for the eight polar compounds, namely, from a plot of $\bar{R}_0^{3/4} n^{1/4}/V^{1/4}$ vs. δ for the appropriate homologous series, where $\bar{R}_0$

TABLE 4. The values of the interaction parameter ψ_{12} and ψ_{21}, for the systems hydrocarbon + polar compound, in $MPa^{1/2}$ units[a]

	Component 1					
	Heptane		1-Heptene		1,6-Heptadiene	
Component 2	ψ_{21}	ψ_{12}	ψ_{21}	ψ_{12}	ψ_{21}	ψ_{12}
Nitromethane	163	108	174	129	182	147
Nitroethane	116	84.9	125	103	134	114
1-Nitropropane	78.9	58.0	86.9	71.5	95.1	81.9
2-Nitropropane	68.5	50.8	77.1	63.8	84.3	72.8
Ethanenitrile	152	96.4	164	116	172	131
Propanenitrile	102	69.1	112	85.7	120	100
Ethyl ethanoate	38.8	34.6	44.6	44.2	53.6	51.7
Butyl ethanoate	22.9	20.7	29.6	28.3	35.9	36.1

[a]The values of ψ_{21} are for component 1 at infinite dilution, and those of ψ_{12} are for component 2 at infinite dilution.

TABLE 5. Ratios of ψ for a solute at infinite dilution in one solvent to its value in another solvent, for several polar–polar and polar–nonpolar binary mixtures at 293.15 K

System (solute in solvent)*	$\psi_{12}(A)/\psi_{12}(B)$†	s.d.
A: The 8 polar components in 1-C_7 B: The 8 polar components in n-C_7	1.23	0.040
A: The 8 polar components in 1,6-C_7 B: The 8 polar components in n-C_7	1.47	0.15
A: The 8 polar components in benzene B: The 8 polar components in n-C_7	1.34	0.061
System (solute in solvent)*	**$\psi_{21}(A)/\psi_{21}(B)$†**	**s.d.**
A: 1-C_7 in the 8 polar components B: n-C_7 in the 8 polar components	1.11	0.061
A: 1,6-C_7 in the 8 polar components B: n-C_7 in the 8 polar components	1.27	0.17
A: CCl_4 in the 8 polar components B: n-C_7 in the 8 polar components	1.16‡	0.097

*1-Heptene and 1,6-heptadiene are treated as polar in [1].

†$\psi_{12}(A)$ and $\psi_{12}(B)$ refer to ψ_{12}, and $\psi_{21}(A)$ and $\psi_{21}(B)$ refer to ψ_{21} from Table 4, for systems A and B respectively, named in column 1 of Table 5. The ratios in column 2 are in each case the means of eight systems; and s.d. is the standard deviation.

‡From ref. 1.

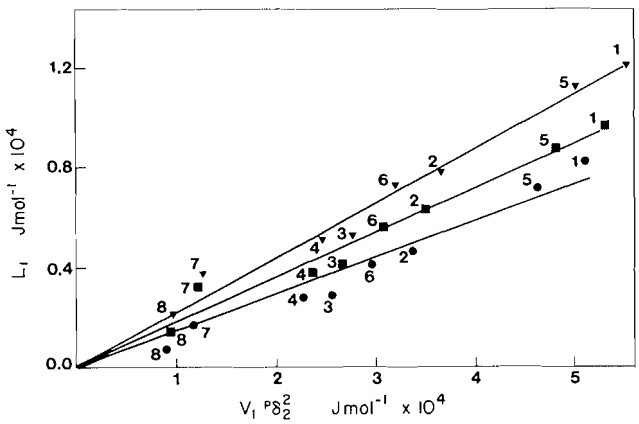

FIG. 2. Correlation between L_1 in [2] and $V_1{}^p\delta_2{}^2$ for hydrocarbons at infinite dilution in polar solvents. ▼, Heptane; ■, 1-heptene; ●, 1,6-heptadiene; *1*, nitromethane; *2*, nitroethane; *3*, 1-nitropropane; *4*, 2-nitropropane; *5*, ethanenitrile; *6*, propanenitrile; *7*, ethyl ethanoate; *8*, butyl ethanoate.

is the molar refractivity at zero frequency, n is the number of valence electrons in the constituent atoms, and V is the molar volume of the compound.

Discussion

Each value γ_2^∞ in Table 2 was used to compute a parameter ψ_{12} from

$$[1]\quad RT \ln \gamma_2^\infty = V_2[({}^d\delta_1 - {}^d\delta_2)^2 + {}^p\delta_1{}^2 + {}^p\delta_2{}^2 - 2\psi_{12}] + RT[1 - (V_2/V_1) + \ln (V_2/V_1)]$$

which is a combination of relationships proposed and used by Prausnitz and co-workers (3, 4). Similarly, each value of γ_1^∞ was used to compute a corresponding parameter ψ_{21} by using [1] with subscripts 1 and 2 replaced by 2 and 1, respectively. The second subscript in ψ_{ij} will henceforth denote the component which is at infinite dilution. The results are in Table 4. The values used for ${}^d\delta$ and ${}^p\delta$ were from Table 3, and those of molar volume V from ref. 11.

Milanova and Cave (1) evaluated ψ_{12} when each of the eight polar compounds in column 1 of Table 2 was the solute at infinite dilution in heptane and in benzene. The ratio of ψ_{12} when benzene was sovlent, to its value when heptane was solvent was nearly constant for the eight polar solutes, namely 1.34 ± 0.061. The values of ψ_{12} and ψ_{21} in Table 4 were used to test more extensively the degree of constancy of this ratio. The results are shown in Table 5.

The values in Tables 2 and 3 were also used to test the empirical correlation $\psi_{21} = k{}^p\delta_2{}^2$ of Weimer and Prausnitz (3), for binary mixtures of hydrocarbons (subscript 1) at infinite dilution in polar solvents (subscript 2). They evaluated k from plots of $V_1{}^p\delta_2{}^2$ vs. L_1, where

$$[2]\quad L_1 = RT \ln \gamma_1^\infty - V_1(\delta_1 - {}^d\delta_2)^2 - RT[1 - (V_1/V_2) + \ln (V_1/V_2)]$$

To be comparable, we also used this method. Figure 2 shows our linear plots forced through the origin for heptane, 1-heptene, and 1,6-heptadiene each infinitely dilute in our eight polar solvents. The resulting least-square values of k are given in Table 6. Thus, these systems obeyed the Weimer–Prausnitz

TABLE 6. Correlation constants in $\psi_{21} = k^{p}\delta_2^2$ and $\psi_{21} = k_1(^{p}\delta_1 - {}^{p}\delta_2)^2$ for hydrocarbons at infinite dilution in polar solvents

Class of hydrocarbon	k	k_1'	k_1''
Saturated (C_7)	0.390 ± 0.003	0.390 ± 0.003	0.399 ± 0.004
Saturated (C_5–C_{16})	0.396[a]	0.399[b]	
Mono-olefinic (1-C_7)	0.410 ± 0.003	0.388 ± 0.004	0.387 ± 0.005
Mono-olefinic (1-C_5)	0.415[a]	0.388[b]	
Di-olefinic (1,6-C_7)	0.426 ± 0.003	0.428 ± 0.004	0.383 ± 0.003

NOTE: The values of $^{d}\delta$ used for the calculation of k were from homomorph plots, to permit comparison with the k values of (3); k_1' refers to k_1 when $^{d}\delta$ values were found from homomorph plots, and k_1'' when $^{d}\delta$ values were found from refractivity data.

[a]Taken from ref. 3.

[b]Taken from ref. 4.

correaltion, even though only heptane was nonpolar. Moreover, as the number of double bonds was increased, so was k. However, this Weimer–Prausnitz correlation failed for those systems that consisted of the eight polar compounds at infinite dilution, in each of the three hydrocarbons. That is, linear plot through the origin, of L_2 vs. $V_2{}^{p}\delta_2{}^2$, were not reasonable ones (9*e*). Milanova and Cave (2) and Blanks and Prausnitz (4) reported the same failure.

Helpinstill and Van Winkle (5) carried out similar studies for saturated and unsaturated hydrocarbons at infinite dilution in polar solvents, but they took the small polarity of the olefins into account. Thus they wrote

$$[3]\quad RT \ln \gamma_1^{\infty} = V_1[(^{d}\delta_1 - {}^{d}\delta_2)^2 + (^{p}\delta_1 - {}^{p}\delta_2)^2 - 2\psi_{21}{}^*] + RT[1 - (V_1/V_2) + \ln (V_1/V_2)]$$

and they plotted $L_1{}^*$ vs. $V_1(^{p}\delta_1 - {}^{p}\delta_2)^2$, where

$$[4]\quad L_1{}^* = RT \ln \gamma_1^{\infty} - V_1(^{d}\delta_1 - {}^{d}\delta_2)^2 - RT[1 - (V_1/V_2) + \ln (V_1/V_2)]$$

and obtained a straight line through the origin, with $\psi_{21}{}^* = k_1(^{p}\delta_1 - {}^{p}\delta_2)^2$. From the data in Tables 2 and 3 for our hydrocarbons at infinite dilution in the eight polar solvents, values were found for k_1 and are given in Table 6. When the Helpinstill – Van Winkle correlation was tried by using the eight polar compounds at infinite dilution in each of the three hydrocarbons it failed. It is to be noted that in [3], dipole – induced dipole interactions are included in two terms, namely $(^{p}\delta_1 - {}^{p}\delta_2)^2$ and also $\psi_{21}{}^*$.

Keller *et al.* (6) proposed a solubility-parameter model for polar–polar and for polar–nonpolar binary systems, in which the solubility parameter δ of a non-hydrogen-bonding polar substance was derived to be

$$[5]\quad \delta^2 = {}^{d}\delta^2 + {}^{p}\delta^2 = {}^{d}\delta^2 + {}^{o}\delta^2 + 2^{in}\delta^{d}\delta$$

where $^{o}\delta$ is the contribution due to dipole–dipole interactions, and $2^{in}\delta^{d}\delta$ is that due to dipole – induced dipole interactions. Here, for a compound possessing a single polar substituent of dipole moment μ, $^{in}\delta = C\mu^2/V$ by definition, where C is a constant. Karger *et al.* (7, 8) applied the equations of Keller *et al.* (6) to evaluate $^{o}\delta$ and $^{in}\delta$ for many compounds.

In terms of relationships described by Keller *et al.* (6), the parameter ψ_{12} of [1] for a binary mixture would be given by

$$[6]\quad \psi_{12} = {}^{in}\delta_1{}^{d}\delta_2 + {}^{in}\delta_2{}^{d}\delta_1 + {}^{o}\delta_1{}^{o}\delta_2$$

for a polar–polar mixture. For a polar component 2 at infinite dilution in a nonpolar solvent 1, [6] becomes

$$[7]\quad {}^{in}\delta_2 = \psi_{12}/\delta_1$$

For each of the eight polar compounds in column 1 of Table 4, at infinite dilution in the solvent heptane, $^{in}\delta_2$ was calculated by using in [7] the data in column 3 of Table 4, and $\delta_1 = 15.32$. The resulting values of $^{in}\delta_2$ along with those of $^{o}\delta_2$ found from [5] are in Table 3. Values reported by Karger *et al.* (7) for some of these polar compounds are also in Table 3.

For heptane at infinite dilution in each of the eight polar compounds as solvents, inspection of columns 2 and 3 of Table 4 shows that a different set of $^{in}\delta_2$ values would be obtained. This suggests a limitation to the right-hand side of [6]; but the use of only the Flory–Huggins term for the entropy in [1] may also be a contributing factor. Hildebrand *et al.* (16) have already suggested that ψ_{12} would not expected to be the same as ψ_{21}.

It was noted above, and illustrated in Table 5, that for a given pair of hydrocarbon solvents, the ratio of ψ_{12} for a polar compound in one of these solvents, to its value ψ_{12}' in the other was reasonably constant for all eight polar compounds tested. Equation [6] may be used to describe this ratio. Thus, for polar–nonpolar mixtures

$$[8]\quad \frac{\psi_{12}}{\psi_{12}'} = \frac{^{in}\delta_2\delta_1}{^{in}\delta_2'\delta_1'}$$

where component 2 is the polar compound, and 1 the solvent.

Thus, ψ_{12}/ψ_{12}' becomes simply the ratio of the solubility parameters of the two solvents, which in the case of benzene and heptane reported by Milanova and Cave (2), is 1.23. Their experimental value was 1.34 ± 0.063.

For a polar–polar mixture, rearrangement of [6] gives

$$[9]\quad {}^{in}\delta_1 + \frac{^{o}\delta_2}{^{d}\delta_2}{}^{o}\delta_1 = \frac{\psi_{12} - {}^{d}\delta_1{}^{in}\delta_2}{^{d}\delta_2}$$

Therefore plots of the right hand side vs. $^{o}\delta_2/{}^{d}\delta_2$ for the polar solutes in 1-heptene and 1,6-heptadiene as solvents should be linear. By using [9], $^{in}\delta_1$ and $^{o}\delta_1$ for these solvents were calculated by least-squares fits of the relevant data in Table 3 and columns 5 and 7 of Table 4. The results with the standard deviations are in columns 5 and 7 of Table 3.

Finally, inspection of Table 4 shows that the values of ψ_{12} and ψ_{21} decrease when (*i*) the chain length in a homologous series of a component increases, in the case of each of the three C_7 hydrocarbon components in turn; (*ii*) the number of the double bonds in the C_7 component is decreased. The values of γ_1^{∞} and γ_2^{∞} in Table 3 obey trend (*i*) above. In that connection, Gerster *et al.* (17) found that γ_1^{∞} for pentane and 1-pentene decreased in several polar solvents as the chain length of those solvents increased.

These trends and values, and some others of $^{in}\delta$ in Table 3 are

useful as empirical guides when partial molal free energies alone are being considered. However, the values given for ψ have depended on the use of the Flory–Huggins entropy term in [1], and the use of that term alone for entropies of polar systems is suspect. Experimental values for the partial molal enthalpy would provide a better basis; and in conjunction with those of the partial molal free energy would provide values directly for the partial molal entropy. Such evaluations will be the subject of a subsequent report.

Acknowledgments

We are grateful to Dr. Vladimir Majer of the Institute of Chemical Technology in Prague for his generosity in measuring the enthalpy of vaporization of 1,6-heptadiene for us, and to Mr. George Kopp of McGill University for the fabrication of the six-way glass stopcock.

1. E. MILANOVA and G. C. B. CAVE. Can. J. Chem. **60**, 2697 (1982).
2. E. MILANOVA. Ph.D. Thesis. McGill University, Montreal, Quebec. 1975. (*a*) pp. 45–52; (*b*) pp. 55–58, 75–78.
3. R. F. WEIMER and J. M. PRAUSNITZ. Hydrocarbon Processing, **44**, (9), 237 (1966).
4. R. F. BLANKS and J. M. PRAUSNITZ. I & EC, Fundamentals, **3**, 2 (1964).
5. J. C. HELPINSTILL and M. VAN WINKLE. I & EC Process Des. Develop. **7**, 213 (1968).
6. R. A. KELLER, B. L. KARGER, and L. R. SNYDER. *In* Gas chromatography. 1970 Proceedings of the 8th International Symposium. *Edited by* R. Stock and S. G. Perry. The Institute of Petroleum, London. 1971. p. 125.
7. B. L. KARGER, L. R. SNYDER, and C. EON. J. Chromatogr. **125**, 71 (1976).
8. B. L. KARGER, L. R. SNYDER, and C. EON. Anal. Chem. **50**, 2126 (1978).
9. S. AFRASHTEHFAR. Ph.D. Thesis. McGill University, Montreal, Quebec. 1981. (*a*) pp. 14–17, 21, 163–167; (*b*) pp. 27, 25, 170–173; (*c*) pp. 25, 27–32, 168, 169; (*d*) pp. 32–37, 179–181; (*e*) p. 106.
10. W. E. PUTNAM, D. M. MCEACHERN JR., and J. E. KILPATRICK. J. Chem. Phys. **42**, 794 (1965).
11. J. A. RIDDICK and W. B. BUNGER. Techniques of chemistry. Vol. II. Organic solvents. 3rd ed. John Wiley, New York, Interscience. 1970.
12. R. C. WEAST and N. J. ASTLE. CRC Handbook of chemistry and physics. 59th ed. CRC Press, Inc., FL. 1979.
13. G. EGLOFF. Physical constants of hydrocarbons. Vol. V. Paraffins, olefins, acetylenes, and other aliphatic hydrocarbons. ACS monograph series. Reinhold Publishing Co. New York, NY. 1953.
14. V. MAJER, V. SVOBODA, V. HYNEK, and J. PICK. Collect. Czech. Chem. Commun. **43**, 1313 (1978).
15. C. TSONOPOULOS. Am. Inst. Chem. Eng. J. **20**, 263 (1974).
16. J. H. HILDEBRAND, J. M. PRAUSNITZ, and R. L. SCOTT. Regular and related solutions. Van Nostrand Reinhold Company, New York, NY. 1970. p. 107.
17. J. A. GERSTER, J. A. GORTON, and R. B. EKLUND. J. Chem. Eng. Data, **5**, 423 (1960).

The reaction of 3-methyltricarballylic acid with acetic anhydride. Addendum: On Fittig's product from acylative decarboxylation of camphoronic acid

GEORGE M. STRUNZ AND PIERRE GIGUÈRE

Maritimes Forest Research Centre, Canadian Forestry Service, P.O. Box 4000, Fredericton, N.B., Canada E3B 5P7

Received September 6, 1985

GEORGE M. STRUNZ and PIERRE GIGUÈRE. Can. J. Chem. **64**, 204 (1986).

Two products, 2,7-dioxa-1,4,4,5-tetramethylbicyclo[3.2.1]octane-3,6-dione (**5**), and 2-acetonyl-2,3,3-trimethylsuccinic anhydride (**4**) were identified from the base-catalysed reaction of camphoronic acid, **2** (R′, R″ = CH_3), with acetic anhydride. The former (**5**) is believed to be identical with the product described by Fittig and assigned an isomeric formulation.

GEORGE M. STRUNZ et PIERRE GIGUÈRE. Can. J. Chem. **64**, 204 (1986).

On a identifié deux produits de la réaction de l'acide camphoronique avec l'anhydride acétique sous catalyse basique: le bicyclo[3.2.1] octane dioxa-2,7 dicéto-3,6 tetraméthyl-1,4,4,5 (**5**) et l'anhydride succinique acétonyl-2- triméthyl-2,3,3 (**4**). On croit que le premier composé (**5**) est le produit décrit par Fittig, qui lui a assigné une formulation isomerique.

In studying the mechanism by which bislactones of structure **1** are produced on reaction of the sodium salt of tricarballylic acid, **2** (R′, R″ = H), with carboxylic acid anhydrides, Fittig (1) extended his investigations to the more highly substituted homologue, camphoronic acid, **2** (R′, R″ = CH_3). The sodium salt of camphoronic acid, when heated with acetic anhydride, afforded some 3% of a crystalline product that Fittig considered to be the bislactone **3**. From this he concluded that formation of the bislactones **1** involves a mechanistic sequence other than the expected initial acylation at C-3 of tricarballylic acid with decarboxylation of the resulting β-ketoacid.

Our recent investigation of products derived from acylative decarboxylation of 3-methyltricarballylic acid, **2** (R′ = H, R″ = CH_3), led us to speculate that Fittig's product may in fact have been **4** or **5**, which can arise by a mechanism involving acylation at C-4 of a suitable derivative of camphoronic acid (2).

In this communication we report that acylative decarboxylation of camphoronic acid[1] through the agency of acetic anhydride in the presence of 4-dimethylaminopyridine affords the products **4** and **5** in yields of 24% and 37% respectively (crude crystalline products). These compounds were interconvertible through the ketodiacid, and their structures were readily assigned by comparison of their spectra with those of the analogous bisdemethyl products (2). The bislactone **5** is believed, by virtue of its melting point, to be identical with the product described by Fittig and assigned the isomeric structure **3** (1).

While the substituted succinic anhydride product predominated over the bislactone in the 3-methyltricarballylic acid experiment (2), the reverse is found here, presumably as a consequence of unfavorable steric interactions of the eclipsed groups in **4** (cf. Ref. 6).

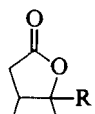

1

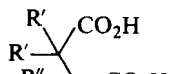

2

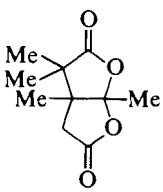

3

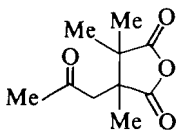

4

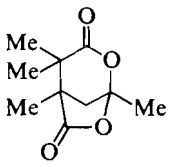

5

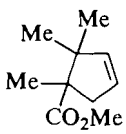

6

Experimental

See ref. 2 for general description of instrumentation, etc.

Reaction of camphoronic acid with acetic anhydride

To freshly distilled acetic anhydride (10 mL) containing 4-dimethylaminopyridine (100 mg, 0.82 mmol) was added camphoronic acid (1.0 g, 4.58 mmol). The solution was heated under reflux for 32 h. During this period very slow evolution of carbon dioxide, indicative of the desired reaction, could be detected by the precipitation of carbonate from a solution of barium hydroxide. This had not completely ceased when the reaction was terminated by distillation of the volatile material under reduced pressure (water pump; bath temperature, ambient to 95°C). The dark brown residue was dissolved in ethyl acetate and treated with activated charcoal. After removal of the charcoal by filtration, the volume of the filtrate was reduced *in vacuo*, and the resulting solution deposited crystals of **5** (105 mg), mp 147–149°C, on standing in the refrigerator.

The mother liquor, after successive flash chromatography ($CHCl_3$–EtOAc, 99:1) and preparative layer chromatography ($CHCl_3$–EtOAc, 97:3), afforded additional crude crystalline **5** (234 mg; total yield 37%) as well as crude crystalline **4** (220 mg; 24%).

[1]The camphoronic acid used in this experiment was obtained by stepwise oxidation of (+) camphoric acid. The sequence, which involved oxidative decarboxylation (3) of the monomethyl ester of camphoric acid (4), and ozonolysis of the resulting methyl 3-dehydrocamphonanate, **6**, gave in our hands a more satisfactory yield (overall 36%) of camphoronic acid than the classical nitric acid oxidation of camphor (5).

Recrystallization of **5** from toluene gave fine colorless needles (289 mg), mp 146–149°C (lit. (1) mp 147.5–148°C); $[\alpha]_D^{27}$ +118° (*c* 0.525, $CHCl_3$); ir (KBr): 3000, 2955, 2890, 1803, 1747, 1467, 1454, 1397, 1379, 1373, 1344, 1298, 1264, 1247, 1195, 1173, 1135, 1108, 1073, 1033, 1013, 981, 939, 908, and 880 cm^{-1}; nmr ($CDCl_3$, 60 MHz) δ: 1.28 (3H, s), 1.34 (3H, s), 1.39 (3H, s), 1.77 (3H, s), 2.33 (2H, q, $|J_{AB}| \sim 12.5$ Hz; $\Delta\nu_{AB} \sim 20.5$ Hz); mass spectrum (*inter alia*) *m/z*: 199 $(MH)^+$, 198 $(M^{\ddagger})$, 141 $(M - C_3H_5O)^+$, 126 (M − CO and $CO_2)^{\ddagger}$, 111 $(C_6H_7O_2)^+$, 83 $(C_6H_{11})^+$, 43 $(CH_3\ CO)^+$ (base peak). *Anal.* calcd. for $C_{10}H_{14}O_4$: C 60.59, H 7.12; found: C 60.80, H 7.14.

Recrystallization of **4** (toluene–CCl_4) gave colorless needles (89 mg), mp 91–96°C; $[\alpha]_D^{27}$ +8.3° (*c* 0.53, $CHCl_3$); ir (KBr): 2990, 2955, 2915, 2890, 1845, 1772, 1708, 1485, 1470, 1455, 1406, 1385, 1372, 1364, 1283, 1255, 1196, 1166, 1122, 985, 958, and 935 cm^{-1}; nmr ($CDCl_3$, 200 MHz) δ: 1.22 (3H, s), 1.36 (3H, s), 1.40 (3H, s), 2.19 (3H, s), 2.94 (2H, q, $|J_{AB}|$ 18.7 Hz; $\Delta\nu_{AB}$ 27.6 Hz); mass spectrum (*inter alia*) *m/z*: 198 $(M^{\ddagger})$, 141 $(M - C_3H_5O)^+$, 126 (M − CO and $CO_2)^{\ddagger}$, 111 $(C_6H_7O_2)^+$, 83 $(C_6H_{11})^+$ (M − CO and CO_2 − $CH_3CO)^+$, 43 $(CH_3CO)^+$ (base peak).

An analytical sample, recrystallized from toluene–CCl_4, melted at 95–97°C. *Anal.* calcd. for $C_{10}H_{14}O_4$: C 60.59, H 7.12; found: C 60.60, H 7.13.

Acknowledgement

The authors are indebted to Valerie Hansen, University of New Brunswick, for providing the 200-MHz nmr spectrum and the mass spectra. We thank Carol McCoy for typing this manuscript.

1. R. FITTIG. Justus Liebigs Ann. Chem. **314**, 1 (1901).
2. G. M. STRUNZ, G. BRISARD, and P. GIGUÈRE. Can. J. Chem. **63**, 2123 (1985).
3. J. D. BACHA and J. K. KOCHI. Tetrahedron, **24**, 2215 (1968).
4. C. ENZELL and H. ERDTMAN. Tetrahedron, **4**, 361 (1958).
5. J. BREDT. Justus Liebigs Ann. Chem. **292**, 55 (1896).
6. L. EBERSON and L. LANDSTRÖM. Acta Chem. Scand. **26**, 239 (1972).

COMMUNICATIONS

Differential heats of dilution of *tert*-butanol into water–*tert*-butanol mixtures at 26.90°C

YOSHIKATA KOGA
Department of Chemistry, University of British Columbia, Vancouver, B.C., Canada V6T 1Y6
Received August 27, 1985

YOSHIKATA KOGA. Can. J. Chem. **64**, 206 (1986).

The differential heats of dilution of *tert*-butanol into water–*tert*-butanol mixtures were measured at 26.90°C. The results in the range where the mole fraction of *tert*-butanol, x, is less than 0.05 indicate that the hydrophobic interaction is repulsive and of long range; the interaction appears to extend its tail as far as six molecular distances or longer. Above the threshold concentration $x \simeq 0.06$, the differential heats of dilution were close to zero and approximately independent of concentration and temperature.

YOSHIKATA KOGA. Can. J. Chem. **64**, 206 (1986).

On a mesuré à 26,90°C, les chaleurs différentielles de dilution du *tert*-butanol dans des mélanges *tert*-butanol–eau. Les résultats pour le *tert*-butanol dans la zone de fraction molaire $x < 0{,}05$ indiquent que l'interaction hydrophobe est répulsive et de grande portée; l'interaction semble prolonger son influence jusqu'à au moins six molécules de distance. Au-dessus de la concentration limite de $x \simeq 0{,}06$, les chaleurs différentielles de dilution se rapprochent de zéro et sont approximativement indépendantes de la concentration et de la température.

[Traduit par le journal]

The anomalous physical properties of *tert*-butanol (TBA) – H_2O mixtures at low concentrations of TBA have attracted much attention, and there are numerous thermodynamic data available in the literature (1–14). Of these, the quantities proportional to the second derivatives of the free energy with respect to appropriate variables appear to show more pronounced features. Examples include the concentration fluctuations (5–7), the compressibility (8, 9, 11), the expansibility (10, 12), the heat capacity (10, 12), and the partial molar volume (10, 13). While the integral heats of mixing have been determined and compiled (14), it is surprising that there appears to be no actual measurement of the differential heats of dilution in the literature.

In view of the fact that the differential heats of dilution could provide direct information about the energetics of the solute–solute interaction, or the hydrophobic interaction (2), such measurements were made in the present work at 26.90°C. The results suggest clearly that the solute–solute interaction is repulsive and of long range. It seems that this repulsive interaction is already operative at the mole ratio of TBA to H_2O of 1:1000. This is consistent with the concept of cooperative hydrogen bonding in H_2O (15); namely, the structure reinforcement of H_2O due to TBA molecules, or the hydrophobic hydration (1–4), extends a long distance via cooperative hydrogen bonding. Recent computer experiments (16, 17), while providing a deeper insight into the structure of the TBA–H_2O mixture, may be improved if the number of molecules is increased and the cooperativeness of the hydrogen bonds in H_2O is somehow included.

tert-Butanol was purified by refluxing for 24 h with CaH_2, followed by distillation. The normal boiling point was 82.42 ± 0.02°C. Freshly distilled water was used. The differential heats of dilution were measured by means of a LKB Bromma 8700 precision calorimetry system. A glass capsule containing about 0.7 g (≃0.01 mol) of TBA was broken in about 90 g of TBA–H_2O mixture. A small temperature change was followed by means of a thermister. The calibration of the system and the calculation of the differential heats of dilution, Δh, is standard (18). A small, almost negligible, correction was applied to the measured value of Δh to obtain the value at the unified temperature, 26.90 ± 0.02°C, the temperature of the bath, using $\Delta C_p (= \partial \Delta h / \partial T)$. The latter was obtained by performing the calibration runs before and after the capsule of TBA was broken (18). The error limit in Δh was estimated to be ±0.05 kJ mol^{-1}. The uncertainty in ΔC_p is inevitably large due to the fact that the method is not designed for measuring ΔC_p. It was estimated to be about ±100 J mol^{-1} K^{-1}, except for the range $0.07 < x < 0.13$, where it became enormous since the value of ΔC_p was calculated in effect as a quotient of zero over zero.

The results are plotted against the mole fraction of TBA, x, in Fig. 1 for Δh and in Fig. 2 for ΔC_p. In Fig. 2, the points in the range $0.07 < x < 0.13$ are omitted. The values at infinite dilution of TBA are those of Arnett, Kover, and Carter (19) and are shown by an arrow in each graph. Their value of Δh was corrected to that at 26.90°C. While they observed that Δh was constant for the range of x less than 2×10^{-4}, at the lowest mole fraction of the present measurement, $x \simeq 1 \times 10^{-3}$, the slope of the curve Δh vs. x already appears to be non-zero and positive. This means that at about this or a lower concentration, a solute molecule starts to feel the presence of the others in a repulsive manner. In other words, the structure reinforcement of H_2O due to TBA tails as far as $\sqrt[3]{(3/4\pi \times 1 \times 10^{-3})} \simeq 6$ molecular distance or longer. This repulsive interaction increases as the separation between solutes becomes shorter, as shown in Fig. 1 by the fact that the positive slope increases along with x for small x. When x reaches about 0.06, Δh becomes close to zero and approximately independent of x thereafter. This implies that in this region an additional TBA molecule feels as if it is within the bulk of pure TBA. The postulate that a clathrate of the type TBA $(H_2O)_n$, with $n \simeq 20$, forms at room temperature (6, 7) is not inconsistent. Thus, up to this threshold value of concentration, an additional TBA molecule has to force itself into an already somewhat reinforced network of H_2O and finds the least reinforced area, i.e. far enough from the existing TBA molecules to settle in. Then, it reorganizes the surrounding H_2O

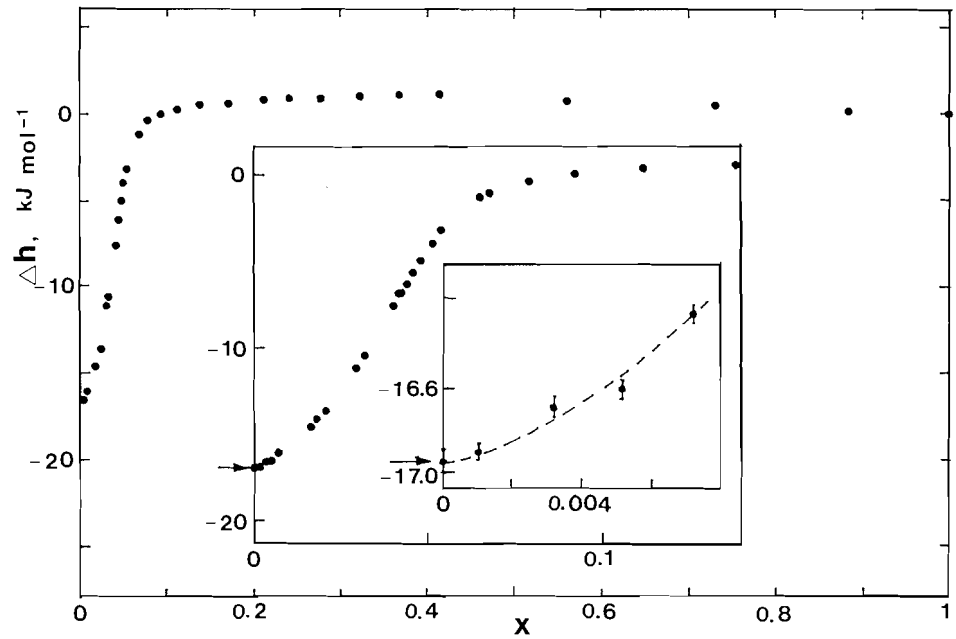

FIG. 1. The differential heats of dilution of *tert*-butanol into water–*tert*-butanol mixtures, Δh, against mole fraction, x, at 26.90°C.

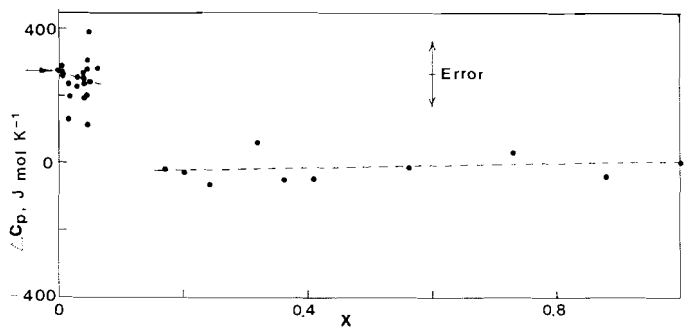

FIG. 2. The differential heat capacity changes, ΔC_p, against mole fraction, x, at 26.90°C.

molecules. As a result, the next TBA has more difficulty with a less exothermic differential heat of dilution. Beyond the threshold concentration, there is no more room for hydrophobic hydration, and the mixture consists of clathrates and TBA.

As shown in Fig. 2, ΔC_p is positive for x less than 0.06 and is small and negative, if not zero, for higher concentrations. It follows that the threshold occurs at a smaller value of x at higher temperature, which is consistent with the interpretation of the light scattering data (7).

Acknowledgements

The author thanks Drs. D. H. Dolphin and L. G. Harrison for the use of their facilities.

1. F. FRANKS and D. J. G. IVES. Q. Rev., **20**, 1 (1966).
2. F. FRANKS. *In* Water, a comprehensive treatise. Vol. 4. *Edited by* F. Franks. Plenum Press, New York. 1975. Chapt. 1.
3. F. FRANKS. *In* Water, a comprehensive treatise. Vol. 2. *Edited by* F. Franks. Plenum Press, New York. 1973. Chapt. 1.
4. F. FRANKS and D. S. REID. *In* Water, a comprehensive treatise. Vol. 2. *Edited by* F. Franks. Plenum Press, New York. 1973. Chapt. 5.
5. Y. KOGA. Chem. Phys. Lett. **111**, 176 (1984).
6. K. IWASAKI and T. FUJIYAMA. J. Phys. Chem. **81**, 1908 (1977).
7. K. IWASAKI and T. FUJIYAMA. J. Phys. Chem. **83**, 463 (1979).
8. T. MORIYOSHI, Y. MORISHITA, and H. INUBUSHI. J. Chem. Thermodyn. **9**, 577 (1977).
9. M. NAKAGAWA, H. INUBUSHI, and T. MORIYOSHI. J. Chem. Thermodyn. **13**, 171 (1981).
10. C. DEVISSER, G. PERRON, and J. E. DESNOYERS. Can. J. Chem. **55**, 856 (1977).
11. J. LARA and J. E. DESNOYERS. J. Solution Chem. **10**, 465 (1981).
12. J. F. ALARY, M. A. SIMARD, J. DUMONT, and C. JOLICOEUR. J. Solution Chem. **11**, 755 (1982).
13. F. FRANKS and H. T. SMITH. Trans. Faraday Soc. **64**, 2962 (1968).
14. S. WESTMEOER. Chem. Technol. **29**, 218 (1977).
15. H. S. FRANK. Proc. R. Soc. (London), Ser. A, **247**, 481 (1958).
16. K. NAKANISHI, K. IKARI, S. OKAZAKI, and H. TOUHARA. J. Chem. Phys. **80**, 1656 (1984).
17. H. TANAKA, K. NAKANISHI, and H. TOUHARA. J. Chem. Phys. **81**, 4065 (1984).
18. I. WADSO. Sci. Tools, **13**, 33 (1966).
19. E. M. ARNETT, W. B. KOVER, and J. V. CARTER. J. Am. Chem. Soc. **91**, 4028 (1969).

Synthesis and characterization of durene-capped porphyrins and the crystal structure of a hemin derivative

SHANTHA DAVID, DAVID DOLPHIN, BRIAN R. JAMES, JOHN B. PAINE III, AND TILAK P. WIJESEKERA
Department of Chemistry, University of British Columbia, 2036 Main Mall, Vancouver, B.C., Canada V6T 1Y6

AND

FREDERICK W. B. EINSTEIN AND TERRY JONES
Department of Chemistry, Simon Fraser University, Burnaby, B.C., Canada V5A 1S6

Received July 16, 1985

SHANTHA DAVID, DAVID DOLPHIN, BRIAN R. JAMES, JOHN B. PAINE III, TILAK P. WIJESEKERA, FREDERICK W. B. EINSTEIN, and TERRY JONES. Can. J. Chem. **64**, 208 (1986).

Sterically hindered porphyrins having a fully hydrophobic cavity have been prepared. The cavity is capped with a 2,3,5,6-tetramethylbenzene moiety containing at the 1,4-positions methylene —$(CH_2)_n$— chains (n = 4, 5, 7) bonded at *trans* pyrrole rings of a porphyrin that is alkylated with methyl or ethyl groups at the other β-pyrrolic positions. The iron(III) chloride derivative of the 4,4-durene-capped base has been obtained as single crystals, and subjected to X-ray structural analysis. The typical high spin, square pyramidal geometry of five-coordinate hemin chlorides is maintained; the porphyrin core is strongly distorted and there is no interaction between the phenyl group of the strap and the iron.

SHANTHA DAVID, DAVID DOLPHIN, BRIAN R. JAMES, JOHN B. PAINE III, TILAK P. WIJESEKERA, FREDERICK W. B. EINSTEIN et TERRY JONES. Can. J. Chem. **64**, 208 (1986).

On a préparé des porphyrines stériquement empêchées et possédant une cavité hydrophobe complète. La cavité est cappée par un tétraméthyl-2,3,5,6 benzène portant, dans les positions 1 et 4, des chaines méthylènes (—$(CH_2)_n$— où n = 4, 5, 7) liés aux cycles pyrroliques *trans* d'une porphyrine qui est alkylée par des groupements méthyle ou éthyle dans les autres positions β du pyrrole. On a obtenu un cristal unique du dérivé du chlorure de fer(III) de la base cappée par le durène-4,4 et on l'a soumis à une analyse par diffraction des rayons-X. La géométrie de pyramide carrée et à spin élevée qui est typique des chlorures d'hémines pentacoordonnées est maintenue; le noyau de la porphyrine est fortement déformé et il n'y a acune interaction entre le groupement phényle et le fer.

[Traduit par le journal]

There have been numerous attempts to prepare simple iron(II) porphyrin complexes which will reversibly bind oxygen in a manner analogous to hemoglobin and myoglobin (1–3). A major problem with the "readily available" protein-free model systems is that, in the presence of oxygen, an irreversible oxidation to μ-oxo-iron(III) dimers occurs; this autooxidation proceeds via the formation of a monomeric iron-dioxygen adduct, which subsequently reacts with a second iron(II) porphyrin unit (4). The synthesis of porphyrins with protective structures covering one face of the macrocycle has proved to be an effective way of inhibiting this "dimerization." Several such porphyrins have been synthesized, the best-known systems being the "picket-fence" (5) and "pocket" (6) porphyrins of Collman *et al.*, the "capped" (7) porphyrins of Baldwin and co-workers, and the "cyclophane hemes" (8) of Traylor *et al.* In addition, model systems with steric hindrances on both faces of the porphyrin (the "basket-handle" porphyrins (9) of Momenteau *et al.*), as well as those with protective structures on one and appended imidazole ligand on the other side, have been prepared (10, 11).

Two fundamentally different approaches have been adopted for the synthesis of hindered porphyrins. The first is an extension of single-step coupling of benzaldehyde and pyrrole to produce *meso*-tetraphenylporphyrin (12). Aromatic aldehydes with potential amino groups as *ortho*-substituents are condensed with pyrrole and the protective structures are linked to the amino groups via amide linkages using appropriate acyl chlorides (5, 6). In a modification of this method, the protective structures are linked to the aromatic aldehydes at their *ortho* positions via ester or ether functions, prior to the coupling with pyrrole (7, 9, 10). The most widely used approach to the synthesis of hindered porphyrins has been to condense, via ester or amide linkages, a diagonally β-substituted preformed porphyrin with a terminally bifunctional molecule carrying appropriate functional groups (8, 11, 13–15).

Porphyrins produced by such methods are limited, however, in the size of the cavity produced. In addition, truly hydrophobic cavities cannot be produced since the protective structures are linked to the porphyrin by polar amide, ester, or ether linkages. An early attempt at the preparation of such a hydrophobic system using rigid dipyrromethene precursors resulted in very low yields during the cyclization step (16).

The synthetic route originally developed in this department to construct permanently deformed porphyrins (17, 18) appeared to be ideally suited for the synthesis of a sterically hindered porphyrin having a fully hydrophobic cavity.

Commercially available 1,4-bis(chloromethyl)-2,3,5,6-tetramethylbenzene (**1**) was converted into the diacid chlorides (**2**) using standard malonate chemistry. The incorporation of the durene strap into the porphyrin[1] was initially carried out with the bis-pentanoic and heptanoic acid derivatives (**2**, n = 5 and 7), as outlined in the scheme. 2-Ethoxycarbonyl-3,5-dimethylpyrrole (**3**), prepared by the reductive condensation (19) of diethyloximinomalonate with 2,4-pentanedione, was condensed with **2** to give the diketo bispyrrole (**4**), using a method previously employed for the preparation of covalently linked porphyrins (20). Diborane reduction, in THF, of **4** gave the bispyrrole ethyl ester (**5**, R = CO_2Et), which was transbenzylated (21) in refluxing benzyl alcohol and catalytic sodium benzyloxide. The benzyl ester (**5**, R = CO_2CH_2Ph) was converted to the dicyanovinyl protected derivative (**6**, R = CH_3) using standard

[1]All new compounds were characterized by satisfactory elemental analysis, and mass and nmr spectroscopy.

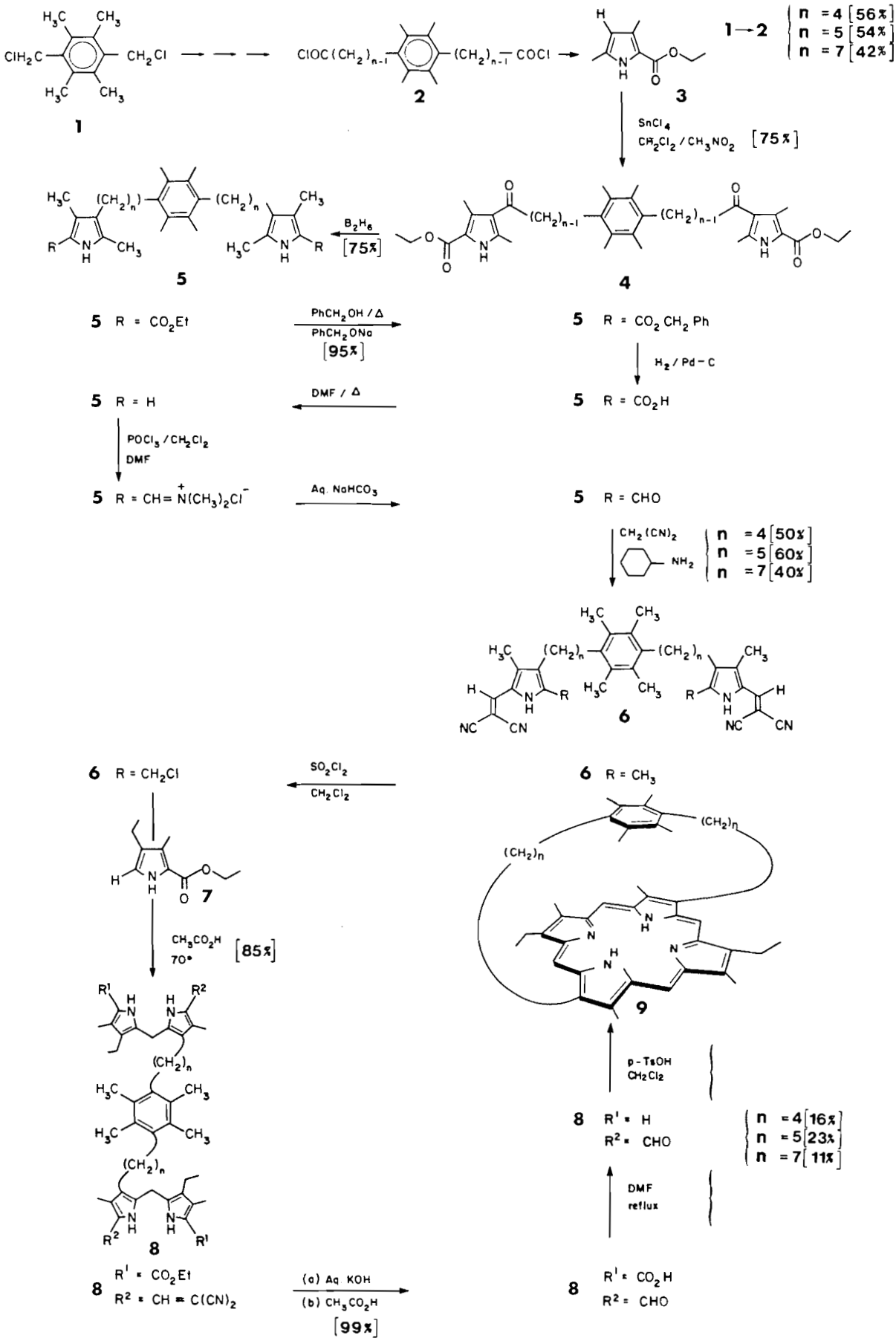

SCHEME I

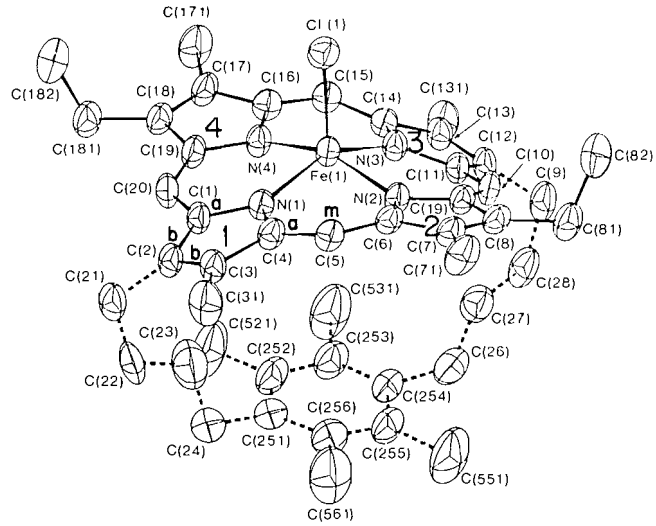

FIG. 1. A SNOOPI (32) diagram of the hemin **10** (50% probability contours for all atoms; hydrogen atoms have been omitted for clarity; the dashed bonds are used to distinguish between the "strap" and the porphyrin skeleton).

techniques (21–23). The intermediates in this sequence were unstable and neither isolated nor characterized. However, the dicyanovinyl group both protects the aldehyde function and provides a compound suitable for chromatographic purification.

The conversion of **6** (R = CH_3) to the chloromethyl derivative **6** (R = CH_2Cl) was carried out under conditions favourable for an electrophilic, rather than a radical, reaction to prevent competitive chlorination of the benzene substituents (24–28); chlorination in the dark using two equivalents of sulfuryl chloride in methylene dichloride at room temperature gave **6** (R = CH_2Cl), which was isolated and immediately condensed with the pyrrole **7** (17) to give **8** (R^1 = CO_2Et; R^2 = $CH{=}C(CN)_2$ in consistently greater than 90% yield, attesting to the high regioselectivity of the preceding chlorination step.

Deprotection of the formyl group and saponification of the esters was achieved using KOH in refluxing aqueous *n*-propanol. The reaction was followed by the disappearance and appearance of bands at 407 and 320 nm, respectively. Removal of the *n*-propanol followed by acidification gave the 5-carboxy-5′-formyldipyrromethane dimer **8** (R^1 = CO_2H; R^2 = CHO). Decarboxylation in refluxing DMF (followed by the disappearance of a 280-nm band) gave **8** (R^1 = H; R^2 = CHO), which was not isolated. Instead, most of the DMF was removed *in vacuo*, the residue dissolved in dichloromethane, and the remaining DMF removed by extraction with water. The dried dichloromethane containing the 5-unsubstituted-5′-formyldipyrromethane was added to a solution of *p*-toluenesulfonic acid in methanol/dichloromethane over a period of 5–6 days using a syringe pump.

The capped porphyrins **9** (*n* = 4 or 5 or 7) were the only porphyrins present in the reaction mixture and were readily isolated and purified by chromatography. The overall yields of the decarboxylation and cyclization steps were 11–16% (**9**, *n* = 4), 22–31% (**9**, *n* =5), and 9–13% (**9**, *n* = 7) and ~100 mg of porphyrin was readily available from one such reaction sequence.

The free base **9** (*n* = 4), in THF, was treated with an excess of $FeCl_2$, in methanol. The mixture was refluxed, under N_2, for 1 h. The solvent was removed and the residue washed with water and then chromatographed on alumina (activity V). Elution with CH_2Cl_2 gave the green μ-oxo dimer. Treatment of the eluate with 0.2 *M* HCl gave the hemin chloride **10**, which was recrystallized from CH_2Cl_2/hexane (85% yield). Crystals of the hemin **10** were prepared by the addition of methanol to a dichloromethane solution (~0.1 *M*) to a ratio of 3:7 (v/v). Standing at room temperature for ~5 days yielded single crystals for X-ray structural analysis.[2]

The molecular structure of the hemin **10** shown in Fig. 1 (32) indicates a very distorted porphyrin core, which results directly from the carbon "strap." Nevertheless, the square pyramidal coordination environment found about the Fe atom is typical of

[2]A crystal suitable for data collection was mounted in a thin-walled glass tube and centred on an Enraf–Nonius CAD4-F diffractometer. Accurate cell dimensions were determined by least-squares refinement of the setting angles of 25 accurately centred reflections (with $15° < 2\theta < 20°$) chosen from a variety of points in reciprocal space. The crystal system was found to be triclinic and consequently the space group was P1 or $P\bar{1}$ (subsequent structure solution uniquely defined the space group as $P\bar{1}$). A total of 5795 independent reflections were measured, of which 3271 were classed observed ($F/\sigma(F) > 5\sigma(F)$) and used in structure refinement. Lorentz and polarization corrections have been made. The Fe atom was located from the Patterson map, while all other non-hydrogen atoms were found from subsequent difference-Fourier maps. At this stage, the presence of a crystallization molecule of dichloromethane was detected in the unit cell, disordered in at least two different arrangements. The exact mode of this disorder is complicated and, although a number of chemically reasonable models were investigated, no satisfactory description of this volume could be made. We were able to minimize the electron density in this volume by fixing the "porphyrin" parameters and performing full-matrix least-squares refinement of the occupancies, coordinates, and temperature factors of two fractional dichloromethane molecules that overlapped at a common C site. Subsequent difference maps revealed clearly the positions of the hydrogen atoms of the porphyrin molecule (solvent hydrogens were not located). Refinement was continued by separation of the structure into three batches: batch 1 contained Fe(1), Cl(1), and the porphinato skeleton (248 variables); batch 2 consisted of the "strap" and peripheral methyl and ethyl groups (369 variables); and batch 3 was made up of the disordered solvent molecule (31 variables). A number of full-matrix least-squares cycles were performed on each batch alternately until the refinement had converged. During these cycles, hydrogen atoms were constrained with respect to their parent carbon atoms (C—H = 0.95(2) Å; H—C—H = 110(2)°; C—C—H = 110(2)°) and an overall isotropic temperature factor was refined for (*i*) methyl hydrogens, (*ii*) methylene hydrogens, and (*iii*) "C_m" hydrogens. The final cycle of refinement, with all hydrogen and solvent parameters fixed and the coordinates and anisotropic thermal parameters of the non-hydrogen atoms allowed to vary, produced essentially no shifts ($\Sigma(\text{shift/e.s.d.})^2 = 2.52$) and gave final agreement factors of $R = 0.038$ and $R_w = 0.048$ for 470 variables. The final difference map contained a number of residual peaks (0.18–0.40 A^{-3}) in the solvent region and two peaks (0.28 and 0.31 e A^{-3}) close to Fe(1). Weights were derived on the basis of trends in $w\Delta^2$ as a function of $\sin\theta/\lambda$ and F_0 (Table 1).[3] Atomic scattering factors including anomalous dispersion were taken from Tables for X-ray Crystallography (29). Final positional and U_{iso} temperature factors are given in Table 2.[3] Anisotropic, thermal parameters, hydrogen parameters, bond parameters, mean-planes data, and structure factor listings have also been deposited (Tables 3–7).[3] Data reduction and initial structure solution were performed using "The NRC VAX crystal structure system" (30), whereas the latter stages of structure solution and refinement were carried out using "CRYSTALS, Oxford University" (31). All calculations were performed using an "in-house" VAX750 computer.

other high spin Fe(III) porphyrins that do not contain a "strap" (33) (Table 8).[3] The Fe(1)—Cl(1) distance of 2.232(1) Å is close to the value of 2.218(6) Å found for [Fe(proto)(Cl)] (34) and the distance from Fe(1) to the centre of the phenyl ring of 5.613 Å indicates no interaction between the phenyl group of the "strap" and Fe(1).

The distortion of the porphinato skeleton found here is not as marked as found in the related deformed free-base porphyrin with short-strap bridging reported earlier (18, 35). The angle between the best planes of pyrrole rings 1 and 3 is 43.0° compared with 68.5° in the earlier example, while the corresponding angle between rings 2 and 4 is 17.2° compared to 13.5° in the more deformed case (18, 35). Atom pyramidalization (χ_{pyr}) and bond twist (τ_{twist}) parameters (36) for the porphinato skeleton (Table 9) suggest that strain induced by the strap is distributed throughout the entire molecule rather than being localized within the two "strapped" pyrrole rings. Mean-plane data determined for each pyrrole ring further support distribution of strain throughout the molecule, viz. the "strapped" C atoms C(2) and C(12) within rings 1 and 3, respectively, lie well out (0.06–0.10 Å) of the plane defined by the other atoms in their rings. Also, C_a atoms in pyrrole rings 2 and 4 lie out of plane with respect to the other ring members, in a direction towards the "strap."

Bond distances and angles around the porphinato skeleton are remarkably similar to those found in other "undistorted" nonstrapped XFe(III) porphyrins (Table 10) (37, 38). The bond parameters for the "strap" and alkyl substituents do not appear unusual. Transannular parameters indicate that the central porphyrin cavity has contracted as a result of binding to Fe(1), e.g. N(1)—N(3) and N(2)—N(4) are 3.965(5) and 4.016(5) Å, respectively, cf. 4.003(4) and 4.241(4) Å in a severely distorted porphyrin (35).

Acknowledgements

This work was supported by the U.S. National Institutes of Health (AM 17989) and the Natural Sciences and Engineering Research Council of Canada.

1. E. C. Niederhoffer, J. H. Timmons, and A. E. Martell. Chem. Rev. **84**, 137 (1984).
2. B. R. James. *In* The porphyrins. Vol. V. *Edited by* D. Dolphin. Academic Press, New York. 1978.
3. T. G. Traylor. Acc. Chem. Res. **14**, 102 (1981).
4. A. L. Balch, Y-W. Chan, R-J. Cheng, G. N. La Mar, L. Latos-Grazynski, and M. W. Renner. J. Am. Chem. Soc. **106**, 7779 (1984).
5. J. P. Collman, R. R. Gagné, T. R. Halbert, J. C. Marchon, and C. A. Reed. J. Am. Chem. Soc. **95**, 7868 (1973); J. P. Collman, R. R. Gagné, C. A. Reed, T. R. Halbert, G. Lang, and W. T. Robinson. J. Am. Chem. Soc. **97**, 1427 (1975).
6. J. P. Collman, J. I. Brauman, T. J. Collins, B. L. Iverson, G. Lang, R. B. Pettman, J. L. Sessler, and M. A. Walters. J. Am. Chem. Soc. **105**, 3038 (1983); J. P. Collman, J. I. Brauman, B. L. Iverson, J. L. Sessler, R. M. Morris, and Q. H. Gibson. J. Am. Chem. Soc. **105**, 3052 (1983).
7. J. Almog, J. E. Baldwin, R. L. Dyer, and M. K. Peters. J. Am. Chem. Soc. **97**, 226 (1975); J. Almog, J. E. Baldwin, M. J. Crossley, J. F. Debernaedis, R. L. Dyer, J. R. Huff, and M. K. Peters. Tetrahedron, **37**, 3589 (1981); T. Hashimoto, R. L. Dyer, M. J. Crossley, J. E. Baldwin, and F. Basolo. J. Am. Chem. Soc. **104**, 2101 (1982).
8. T. G. Traylor, D. Campbell, S. Tsuchiya, M. Mitchell, and D. V. Stynes. J. Am. Chem. Soc. **102**, 5939 (1980); T. G. Traylor, M. J. Mitchell, S. Tsuchiya, D. H. Campbell, D. V. Stynes, and N. Koga. J. Am. Chem. Soc. **103**, 5234 (1981); T. G. Traylor, S. Tsuchiya, D. H. Campbell, M. Mitchell, D. Stynes, and N. Koga. J. Am. Chem. Soc. **107**, 604 (1985).
9. M. Momenteau, B. Loock, J. Mispelter, and E. Bisagni. Nouv. J. Chim. **3**, 77 (1979); M. Momenteau, J. Mispelter, B. Loock, and E. Biasagni. J. Chem. Soc. Perkin Trans. 1, 189 (1983).
10. M. Momenteau, B. Loock, D. Lavalette, C. Tétneau, and J. Mispelter. J. Chem. Soc. Chem. Commun. 962 (1983); M. Momenteau and D. Lavalette. J. Chem. Soc. Chem. Commun. 341 (1982).
11. A. R. Battersby, A. J. Bartholomew, and T. Nitta. J. Chem. Soc. Chem. Commun. 1291 (1983).
12. A. D. Adler, F. R. Longo, J. D. Finarelli, J. Goldmatcher, J. Assow, and L. Korsakoff. J. Org. Chem. **32**, 476 (1967); A. D. Adler, F. R. Longo, and W. Shergalis. J. Am. Chem. Soc. **86**, 3145 (1964).
13. A. R. Battersby, D. G. Buckley, S. G. Hartley, and M. D. Turnbull. J. Chem. Soc. Chem. Commun. 879 (1976).
14. H. Ogoshi, H. Sigimoto, and Z. Yoshida. Tetrahedron Lett. 4477 (1976).
15. C. K. Chang. J. Am. Chem. Soc. **99**, 2819 (1977).
16. H. Dieckmann, C. K. Chang, and T. G. Traylor. J. Am. Chem. Soc. **93**, 4068 (1971).
17. T. P. Wijesekera, J. B. Paine III, and D. Dolphin. J. Org. Chem. **50**, 3832 (1985).
18. T. P. Wijesekera, J. B. Paine III, D. Dolphin, F. W. B. Einstein, and T. Jones. J. Am. Chem. Soc. **105**, 6747 (1983).
19. G. G. Kleinspehn. J. Am. Chem. Soc. **77**, 1546 (1955).
20. J. B. Paine III, and D. Dolphin. Can. J. Chem. **56**, 1710 (1978).
21. J. B. Paine III, R. B. Woodward, and D. Dolphin. J. Org. Chem. **41**, 2826 (1976).
22. H. Fischer and M. Neber. Justus Liebigs Ann. Chem. **496**, 1 (1932); H. Fischer and H. Wasenegger. Justus Liebigs Ann. Chem. **461**, 277 (1928).
23. R. B. Woodward. Angew. Chem. **72**, 651 (1960).
24. G. Angelini, G. Illuminati, A. Monaci, G. Sleiter, and M. Speranza. J. Am. Chem. Soc. **102**, 1377 (1980).
25. C. Walling. Free radicals in solution. Wiley, New York. 1957.
26. K. H. Lee. Tetrahedron, **25**, 4363 (1969).
27. E. Baciocchi and G. Illuminati. Tetrahedron Lett. **15**, 637 (1962).
28. E. Baciocchi, A. Ciana, G. Illuminati, and C. Pasini. J. Am. Chem. Soc. **87**, 3953 (1965).
29. D. T. Cromer and J. T. Waber. International tables for X-ray crystallography. Vol. IV. Kynoch Press, Birmingham, England. 1974.
30. A. C. Larson, F. L. Lee, Y. LePage, and E. J. Gabe. The N.R.C. VAX crystal structure system. Chemistry Division, NRC, Ottawa, Ontario, Canada.
31. D. Watkin. CRYSTALS, Crystallographic Suite. Chemical

[3]The following tables of crystallographic data have been deposited as supplementary material and may be purchased from the Depository of Unpublished Data, CISTI, National Research Council of Canada, Ottawa, Ont., Canada K1A 0S2. Table 1. Crystallographic data; Table 2. Final positional and U_{iso} thermal parameters for the non-hydrogen atoms of **10**; Table 3. Final anisotropic thermal parameters for **10**; Table 4. Final positional parameters for the hydrogen atoms of **10**; Table 5. Bond parameters for **10**; Table 6. Mean-plane calculations for atoms within the pyrrole rings of **10**; Table 7. Structure factors listings; Table 8. Comparison of the square pyramidal coordination sphere in **10** with other high spin iron(III) porphyrins; Table 9. Atom pyramidalization (χ_{pyr}) and bond twist (τ_{twist}) angles for **10**; Table 10. Average bond distance and bond angles for some high spin Fe(III) porphyrins.

Crystallography Laboratory. Oxford University, 9 Parks Road, Oxford, England.
32. E. K. DAVIES. SNOOPI, plotting routine. 1984, Chemical Crystallography Laboratory, 9 Parks Road, Oxford, England.
33. W. R. SCHEIDT and C. A. REED. Chem. Rev. **81**, 543 (1981).
34. D. F. KOENIG. Acta Crystallogr. **18**, 663 (1965).
35. F. W. B. EINSTEIN and T. JONES. Acta Crystallogr. Sect. C, **10**, 696 (1984).
36. F. K. WINKLER and J. D. DUNITZ. J. Mol. Biol. **59**, 169 (1971).
37. S. C. TANG, S. KOCH, G. C. PAPAEFTHYMIOU, S. FONER, R. B. FRANKEL, J. A. IBERS, and R. H. HOLM. J. Am. Chem. Soc. **98**, 2414 (1976).
38. K. ANZAI, K. HATANO, Y. T. LEE, and W. R. SCHEIDT. Inorg. Chem. **20**, 2337 (1981).

The aminolysis of phosphinates; the kinetics and mechanism of the aminolysis of phosphinate esters in acetonitrile[1]

ROBERT D. COOK[2]
Department of Chemistry, Erindale College, University of Toronto, Mississauga, Ont., Canada L5L 1C6
AND
WAFA A. DAOUK, ASAAD N. HAJJ, AHMAD KABBANI, ANWAR KURKU, MUNA SAMAHA, FUAD SHAYBAN, AND OHANNES V. TANIELIAN
Department of Chemistry, American University of Beirut, Beirut, Lebanon

Received May 8, 1985

ROBERT D. COOK, WAFA A. DAOUK, ASAAD N. HAJJ, AHMAD KABBANI, ANWAR KURKU, MUNA SAMAHA, FUAD SHAYBAN, and OHANNES V. TANIELIAN. Can. J. Chem. **64**, 213 (1986).

The aminolysis of aryl diphenylphosphinates, *p*-nitrophenyl diphenylphosphinothionate, -phosphinothioate, and -phosphinodithioate by *n*-butylamine, by the secondary amines piperidine, pyrrolidine, morpholine, and dipropylamine, as well as by a series of diamines, has been studied in acetonitrile. The general reactivity order is diamines > butylamine > *sec*-amines. Butylaminolysis follows a two-term rate law, one first order in amine and the other second order in amine. The second order in amine term predominates. *sec*-Amines and diamines follow a rate law which is first order in amine only. Leaving group effects, solvent effects, and activation parameters support a pathway which involves rate-determining collapse of a zwitterionic pentacoordinate intermediate. In the case of butylamine this collapse is general base catalyzed and for the diamines the reaction is intramolecularly general base catalyzed.

ROBERT D. COOK, WAFA A. DAOUK, ASAAD N. HAJJ, AHMAD KABBANI, ANWAR KURKU, MUNA SAMAHA, FUAD SHAYBAN et OHANNES V. TANIELIAN. Can. J. Chem. **64**, 213 (1986).

Opérant dans l'acétonitrile, on a étudié l'aminolyse des diphénylphosphinates d'aryles et des diphényl-phosphinothionate, -phosphinothioate et -phosphinodithioate de *p*-nitro-phényle par la *n*-butylamine, par les amines secondaires comme la pipéridine, la pyrrolidine, la morpholine et la dipropylamine ainsi que par une série de diamines. L'ordre de réactivité générale est le suivant: diamines, butylamine, amines secondaires. La butylaminolyse obéit à une équation de vitesse impliquant deux termes, un du premier ordre en amine et un autre du deuxième ordre en amine. Le terme du deuxième ordre en amine prédomine. Les réactions avec les amines secondaires et avec les diamines obéissent à une équation du premier ordre en amine seulement. Les effets de groupements nucléofuges et de solvants ainsi que les paramètres d'activation sont en accord avec un mécanisme réactionnel impliquant une étape déterminante au cours de laquelle il y a décomposition d'un intermédiaire zwitterionique pentacoordonné. Dans le cas de la butylamine, cette décomposition est soumise à une catalyse générale des bases et, pour les diamines, la réaction est soumise à une catalyse générale des bases qui est intramoléculaire.

[Traduit par le journal]

Introduction

Aminolysis reactions of carboxylic esters in aprotic solvents have been the subject of several reports starting with the work of Menger in 1966 (1). Menger found that the butylaminolysis of *p*-nitrophenyl acetate (*p*-NPA) in chlorobenzene is second order in amine and that tertiary amines only mildly catalyze the reaction. A mechanism involving concerted bifunctional catalysis was proposed, with a transition state similar to **1**.

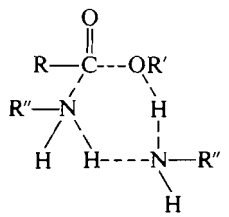

1

Shawali and Biechler (2) reported that the butylaminolysis of both phenyl dichloroacetate and difluoroacetate in *p*-dioxane follows a mixed rate law (eq. [1]) and that tertiary amines do catalyze the reaction. On the other hand, for secondary amine aminolysis, only the term which is first order in amine appears. For butylaminolysis the authors suggest that the reaction proceeds via a neutral tetrahedral intermediate, with the second amine molecule catalyzing the breakdown of this intermediate by proton removal. The bifunctional cyclic mechanism was proposed by Satchell and Secemski (3) as the pathway of the aminolysis of *p*-NPA in diethyl ether. These authors also report that [2.2.2]diazobicyclooctane catalyzes the reaction; a pathway involving nucleophilic catalysis was proposed (4). Later papers by the groups of Menger (5) and Watson (6) clearly show the presence of catalysis by tertiary amines in several systems and concluded that a two-step general base mechanism is preferable over the concerted pathway. Menger and Smith (5*a*) also reported linear free energy relationship data that strongly support the collapse of the intermediate as the rate-determining step, with the second amine molecule catalyzing the reaction by removing a proton from the zwitterionic form of the intermediate (**2**).

[1] Rate = k_2[ester][amine] + k_3[ester][amine]^2

There have been several other reports on the aminolysis of carboxylic esters in aprotic media showing catalysis by proton

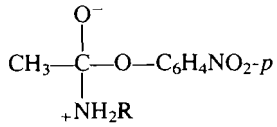

2

[1]Taken in part from the M.S. Theses of W.A.D., A.H., Ah.K., A.K., F.S., and O.T., American University of Beirut, Beirut, Lebanon.

[2]Author to whom correspondence may be addressed. Address for the academic years 1984–1986 at the University of Toronto.

acceptors (7), ionophones (8), as well as intramolecular effects by groups in the acid part (9) and the phenol part (10) of the ester. Aminolysis reactions by imidazole (11) and by aminopyridines (12) as well as catalysis of the imidazole reaction by lithium perchlorate (13) have also been studied.

In this paper we report our results on the aminolysis of three phosphinate esters (**3**–**5**) as well as on *p*-nitrophenyl diphenylphosphinothionate (**6**), -phosphinothioate (**7**), and -phosphinodithioate (**8**). Compounds **4**–**8** were studied with butylamine

$(C_6H_5)_2P(O)OC_6H_4X$	**3**	X = *p*-NO_2
	4	X = *p*-CN
	5	X = *m*-NO_2
$(C_6H_5)_2P(S)OC_6H_4NO_2$-*p*	**6**	
$(C_6H_5)_2P(O)SC_6H_4NO_2$-*p*	**7**	
$(C_6H_5)_2P(S)SC_6H_4NO_2$-*p*	**8**	

only but ester **3** was studied with butylamine, a series of secondary amines, and diamines. There is one previous report on the aminolysis of a phosphinate ester and a comparison will be made with this work (14).

Results

Rate data

The observed rate constants as well as the calculated second-order rate constants ($k_2 = k_{obs}/[amine]$) for the butylaminolysis of **3**–**8** are given in Table 1. A plot of the k_2 for the butylaminolysis of **3** versus amine concentration is given in Fig. 1. The slope, k_3, is $5.31 \times 10^{-2}\ M^{-2}\ s^{-1}$ ($r = 0.987$) and the intercept, k_2, is $8.02 \times 10^{-4}\ M^{-1}\ s^{-1}$ or approximately 1.4% of the k_3. Therefore within the range of amine concentrations used in our experiments the butylaminolysis of **3** follows the rate law of eq. [1] with the third-order term predominating. The other esters in Table 1 give similar results and their k_2 and k_3 values are reported in Table 2.

The k_{obs} and k_2 values for the aminolysis of **3** with *sec*-amines and diamines are given in Tables 3 and 4, respectively. Figure 2 gives the plot of k_{obs} versus amine concentration for the piperidinolysis of **3**. Table 5 gives the data collected on the aminolysis reactions in chlorobenzene and Table 6 reports the results of the experiments carried out in the presence of tertiary amines.

Activation parameters

The activation parameters for the butylaminolysis of **3** and **8** as well as for the piperidinolysis, and the aminolysis with 1,3-diaminopropane of **3** are given in Table 7.

Limitations on the rate data

The reproducibility of the rate data for a given amine concentration was good. The major source of fluctuation was due to the difficulty of reproducing identical amine concentrations. The best results were obtained when the amine was delivered using a Gilmont microsyringe (for all primary amines and diamines). For the secondary amines, stock solutions were prepared and delivered by pipet. In the latter case the third figure in the observed rate constants is unlikely to be significant.

The values of k_2 and k_3 for most systems are determined graphically. The errors in this determination, especially when less than 5 data points are used, are going to be large (±10%). This will be particularly true for k_2, which is determined from the intercept. These errors in the rate constants will carry over to the calculations of the activation parameters. A reasonable error limit for the second-order reaction would be ±3 kcal/mol for the $E_a(\Delta H^{\neq})$ and ±10–15 eu for the $\Delta S^{\neq}$.

TABLE 1. Rate constants[a] for the butylaminolysis of **3**–**8** in acetonitrile

Compound	[Amine]	$k_{obs} \times 10^3$ (s^{-1})	$k_2 \times 10^3$ ($M^{-1}\ s^{-1}$)
3	0.08[c]	0.39	4.86
	0.10[c]	0.63	6.31
	0.12[c]	0.85	7.05
	0.14[c]	1.20	8.60
	0.16[c]	1.44	9.02
	0.16[b]	1.65	10.31
	0.16[d]	1.16	7.25
	0.16[e]	0.80	5.00
	0.30[d]	4.78	15.9
	0.40[d]	8.45	21.1
	0.50[d]	13.1	26.2
4	0.30[d]	0.399	1.34
	0.40[d]	0.711	1.78
	0.50[d]	1.11	2.22
5	0.30[d]	0.230	0.767
	0.40[d]	0.404	1.01
	0.50[d]	0.635	1.27
6	0.16[d]	0.0321	0.201
	0.20[d]	0.0485	0.243
	0.24[d]	0.0646	0.269
	0.28[d]	0.0939	0.335
	0.32[d]	0.131	0.409
	0.36[d]	0.154	0.428
7	0.10[b]	21.9	219
	0.12[b]	26.9	224
	0.14[b]	34.4	246
	0.16[b]	45.0	281
	0.18[b]	51.6	287
8	0.36[b]	3.58	9.94
	0.50[b]	6.06	12.1
	0.60[b]	7.94	13.2
	0.70[b]	10.2	14.6
	0.85[b]	14.1	16.6
	0.36[d]	4.62	12.8
	0.50[d]	7.08	14.2
	0.60[d]	9.32	15.5
	0.70[d]	11.8	16.9
	0.85[d]	15.5	18.2

[a]Average of 2–3 runs; [ester] = $1.3 \times 10^{-5}\ M$.
[b]T = 25°C.
[c]T = 30°C.
[d]T = 40°C.
[e]T = 50°C.

TABLE 2. Graphically determined[a] k_2 and k_3 values for the butylaminolysis of esters **3**–**8** in acetonitrile

Compound[b]	T (°C)	$k_2 \times 10^3$ ($M^{-1}\ s^{-1}$)	$k_3 \times 10^3$ ($M^{-2}\ s^{-1}$)	r[c]
3	30	0.802	53.1	0.986
	40	0.467	51.5	0.998
4	40	0.0133	4.45	0.999
5	40	0.0097	2.52	0.996
6	40	—	1.24	0.987
7	25	116	965	0.965
8	25	5.20	13.4	0.999
	40	8.67	11.4	0.996

[a]Determined from a plot of $k_{obs}/[amine]$ vs. [amine]; slope = k_3 and the intercept = k_2.
[b][Ester] = $1.3 \times 10^{-5}\ M$.
[c]r = correlation coefficient of the least-squares plot.

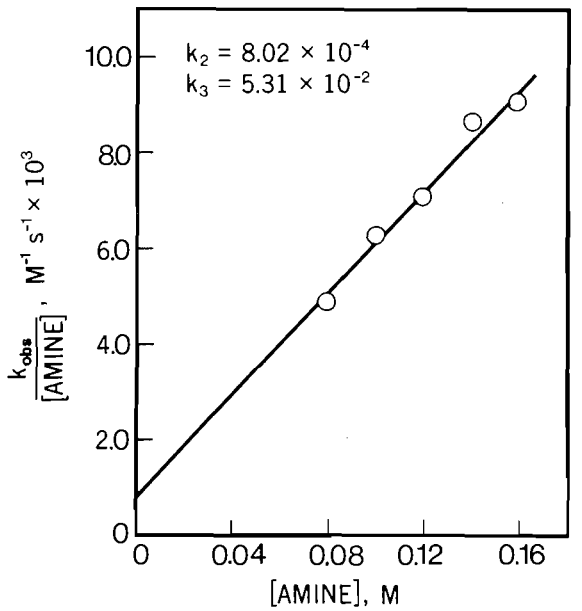

FIG. 1. Plot of k_{obs}/[amine] vs. [amine] for the butylaminolysis of **3** in acetonitrile; T = 30°C.

TABLE 3. Rate constants[a] for the secondary amine aminolysis of **3** in acetonitrile at 50°C

Amine	[Amine]	$k_{obs} \times 10^5$ (s^{-1})	$k_2 \times 10^5$ ($M^{-1}\,s^{-1}$)
Piperidine	1.00	34.3	34.3
	0.75	24.5	32.7
	0.50	17.2	34.4
	0.25	9.10	36.4
	1.00[b]	27.7	27.7
	1.00[c]	48.0	48.0
			$k_2 = 3.32 \times 10^{-4}$[d]
Morpholine	1.00	2.69	2.69
	1.40	3.55	2.54
	1.75	5.11	2.91
	2.00	5.54	2.77
	2.50	6.19	2.47
			$k_2 = 2.46 \times 10^{-5}$[d]
Pyrrolidine	1.00	215	215
	0.75	166	220
	0.50	115	220
	0.25	46.3	185
			$k_2 = 2.23 \times 10^{-3}$[d]
Dipropylamine	1.00	4.76	4.76
	1.25	6.68	5.34
	1.50	7.64	5.09
	1.80	8.25	4.71
	2.00	9.71	4.85
			$k_2 = 4.46 \times 10^{-5}$[d]
Methylbutylamine	0.16[e]	5.90	37.0

[a]Average of 2–3 runs; [ester] = 1.3×10^{-5} M.
[b]T = 40°C.
[c]T = 60°C.
[d]k_2 determined from the slope of the plot of k_{obs} vs. [amine].
[e]T = 30°C.

TABLE 4. Rate constants[a] for the diaminolysis of **3** in acetonitrile at 30°C

Amine	[Amine] (M)	$k_{obs} \times 10^3$ (s^{-1})	$k_2 \times 10^3$ (s^{-1})
1,2-Diaminoethane	0.08	1.69	21.2
1,3-Diaminopropane	0.04	2.13	53.1
	0.06	3.43	57.2
	0.08	4.40	56.2
	0.08[b]	2.88	36.0
	0.08[c]	1.92	24.0
1,4-Diaminobutane	0.08	5.21	65.1
1,5-Diaminopentane	0.04	1.31	32.8
	0.06	2.10	34.9
	0.08	2.45	30.6
1,6-Diaminohexane	0.08	0.96	12.0
N-methyl-1,2-diaminoethane	0.08	1.78	22.2
N,*N*′-dimethyl-1,2-diaminoethane	0.08	0.109	1.36
	0.16	0.228	1.43
N,*N*-dimethyl-1,2-diaminoethane	0.08	0.781	9.76
N-methyl-1,3-diaminopropane	0.08	3.53	44.1
N,*N*-dimethyl-1,3-diaminopropane	0.08	2.59	32.4

[a]Average of 2–3 runs; [ester] = 1.3×10^{-5} M.
[b]T = 40°C.
[c]T = 50°C.

TABLE 5. Rate constants[a] for the butylaminolysis of **3** in chlorobenzene at 30°C

[Amine] (M)	$k_{obs} \times 10^5$ (s^{-1})	$k_2 \times 10^5$ ($M^{-1}\,s^{-1}$)
1.00	3.33	3.33
2.00	12.8	6.40
3.00	26.3	8.77
	$k_2 = 7.27 \times 10^{-6}$[b] $M^{-1}\,s^{-1}$	
	$k_3 = 2.72 \times 10^{-5}$[b] $M^{-2}\,s^{-1}$	

[a]Average of 2–3 runs; [ester] = 1.3×10^{-5}.
[b]Determined from a plot of k_{obs}/[amine] vs. [amine].

TABLE 6. Rate constants[a] for the aminolysis of **3** in the presence of tertiary amines

Amine	M	*tert*-Amine	M	$k_{obs} \times 10^5$ (s^{-1})
Butylamine[b]	0.08	—	—	38.9
	0.08	Imidazole	0.08	66.7
	0.08	Pyridine	0.08	62.4
	0.08	Triethylamine	0.08	77.7
1,3-Diaminopropane[b]	0.08	—	—	450
	0.08	Imidazole	0.08	256
	0.08	Pyridine	0.08	409
	0.08	Triethylamine	0.08	414
Piperidine[c]	0.50	—	—	17.2
	0.50	Pyridine	0.50	20.0
	0.50	Triethylamine	0.50	21.0

[a]Average in 2–3 runs; [ester] = 1.3×10^{-5} M.
[b]T = 30°C in acetonitrile.
[c]T = 50°C in acetonitrile.

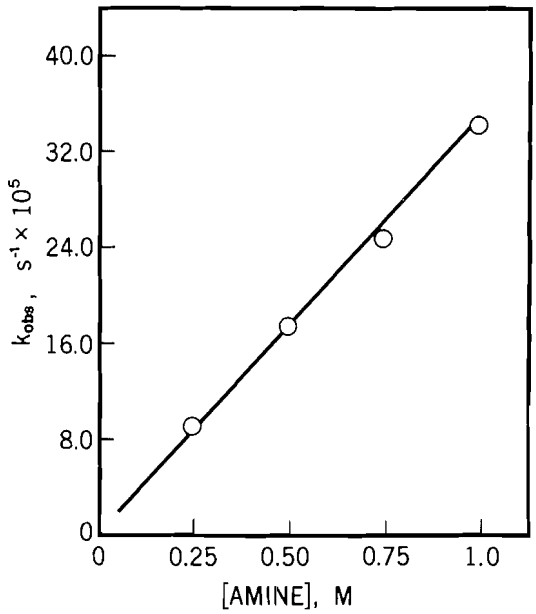

FIG. 2. Plot of k_{obs} vs. [amine] for the piperidinolysis of **3** in acetonitrile; T = 50°C.

TABLE 7. Activation parameters for the aminolysis of phosphinates in acetonitrile

Ester	Amine	E_a	ΔG^*	ΔH^*	ΔS^*
		kcal/mol			eu
3	Butylamine[a]	−0.5	20.0	−1.2	−68
8	Butylamine[b]	−3.2	20.0	−3.8	−80
8	Butylamine[c]	3.3	20.6	2.7	−60
3	Piperidine[d]	5.75	24.1	5.1	−59
3	1,3-Diaminopropane[e]	−8.1	19.5	−8.4	−92

[a] T = 30°C in acetonitrile; k_3 component.
[b] T = 25°C in acetonitrile; k_3 component.
[c] T = 25°C in acetonitrile; k_2 component.
[d] T = 50°C in acetonitrile.
[e] T = 30°C in acetonitrile.

Discussion

Butylaminolysis

The butylaminolysis of all the esters studied follows the two-term rate law represented in eq. [1] with the exception of ester **6**, which has only a k_3 component. With all the esters k_3 is larger than k_2 (Table 2), and the k_3/k_2 ratio is larger; that is, catalysis is more important for the esters with the more basic leaving groups (**3**, **4**, **5**, and **6** versus **7** and **8**). The aminolysis of **3** is catalyzed by the tertiary amines imidazole, pyridine, and triethylamine (Table 6) and therefore a cyclic concerted mechanism is ruled out. There are two reasonable pathways: (*i*) a general base-catalyzed direct displacement and (*ii*) a rate-determining general base-catalyzed breakdown of a pentacoordinate zwitterionic intermediate (eq. [2]).

In the rate-determining step of both of these pathways, negative charge is generated on the leaving group in the transition state. Although only three compounds with *para* substituents have been studied (**3**–**5**), their rates of aminolysis (k_3) correlate with the σ^- values of the substituents and not with the σ values. The calculated ρ value using σ^- is 2.55 (r = 0.983). The significance of such a correlation with only three points is limited; however, what is clear is that the *p*-CN ester (**4**) is more reactive than the *m*-NO_2 ester (**5**), in line with the σ^- values and not with the σ values of the substituents. In support of rate-determining loss of the leaving group are the reactivity ratios for the phenol versus thiophenol leaving groups. The ratios of the k_3 values for **7**/**3** and **8**/**6** are 18.2 and 9.4, respectively. For the uncatalyzed reaction (k_2), where the basicity of the leaving group might be expected to be more important, the ratio for esters **7**/**3** is 143. The large drop in rate when the butylaminolysis of **3** is studied in chlorobenzene also supports a pathway with a highly charged transition state (Table 5). These data have led to the suggestion of a transition state with negative charge on the leaving group and, for the case of the pathway involving intermediate formation, rate-determining collapse of the intermediate will only be possible if the intermediate is the dipolar ion represented in structure **9** (5).

The question of whether or not there is an intermediate along the reaction path in displacement at phosphorus in acyclic phosphorus esters is the difficult one to answer. Kirby and Warren (15) and Emsley and Hall (16) have summarized the evidence and argue for a direct displacement in these acyclic systems. On the other hand, there is ample evidence for intermediates in the reactions of cyclic phosphorus esters (17) and in two acyclic systems involving the acid-catalyzed hydrolysis of a phosphinothionate (18*a*) and a phosphonate (18*b*). In our report on the alkaline hydrolysis of a series of alkyl dialkylphosphinates and their sulfur analogs we were unable to eliminate either possibility, i.e., direct displacement versus intermediate formation (19). However, in the hydrolysis of aryl esters, with one exception (20), the rates correlate with Hammett's σ values, and not with the σ^- values, supporting a mechanism where no charge is generated on the leaving group in the rate-determining step and therefore, by implication, supporting rate-determining formation of an intermediate (21). The ratio of reactivity under conditions of alkaline hydrolysis for aryl diphenylphosphinothioates and aryl diphenylphosphinates is only 4, which is considerably less than is observed in the aminolysis reactions and is in line with the above statements.

The atom doubly bonded to phosphorus influences the reactivity of the esters significantly. For example, the ratios of k_3's for **3**/**6** and **7**/**8** are 22.8 and 72, respectively. The greater reactivity of the P=O esters is generally rationalized in terms of the differences in polarizability and solvation of the two groups (22). In acetonitrile the latter may not be very important. A summary of P=O/P=S reactivity ratios is presented in ref. 19 for several different systems and it is suggested that the values of these ratios cannot lead to significant mechanistic conclusions.

[2] $R_2P(O)OR' + R''NH_2 \underset{k_{-1}}{\overset{k_1}{\rightleftharpoons}} \underset{\underset{+NH_2R''}{|}}{\overset{O^-}{\overset{|}{R_2P-O-R'}}} \xrightarrow[H_2NR'']{k_2} R_2P(O)NHR'' + R'OH$

9

The butylaminolysis reactions give highly negative entropies of activation (Table 7). The values obtained are quite small for both the k_2 and k_3 components (23) (the entropies of activation for the second-order reaction have larger errors incorporated into the calculation because of the fact that the values of k_2 are intercepts). Negative activation energies have been obtained for the third-order components, which, although unusual, have been observed in other systems and are suggested as being support for intermediate formation along the reaction pathway in contrast to a direct displacement (24). The transition from tetrahedral phosphorus to a charged pentacoordinate intermediate, coupled with the incorporation of a second amine molecule in the transition state, should lead to very negative entropies of activation. As well as being a termolecular reaction, there should also be considerable restriction of rotation in the transition state as well as some electrorestriction of solvent.

Therefore, for the mechanism, a process similar to eq. [2] is likely. The transition from intermediate (**10**) to transition state (**11**) can be pictured as in eq. [3], where a zwitterion is going

[3]

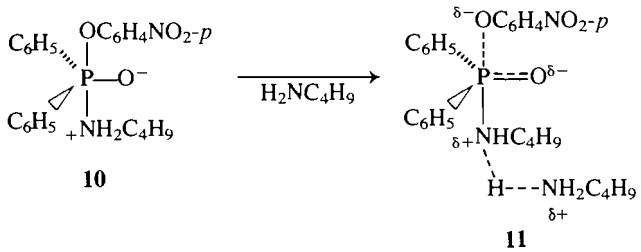

10 **11**

towards two separated ions; that is, there is greater charge separation in the transition state, which is reached late on the reaction coordinate, than there is in the intermediate. Under the reaction conditions it is the *p*-nitrophenoxide anion that is being observed at 423 nm (25). The slower reaction in the less polar chlorobenzene would be expected for this process.

The bimolecular reaction pathway can be thought of as the slow dissociation of the zwitterionic intermediate, with subsequent loss of a proton to a second amine molecule, or as slow simultaneous intramolecular proton transfer to O^- and loss of phenoxide followed by proton loss to a second amine molecule.

Bel'skii *et al.* (14) have reported their results on the aminolysis of the very reactive phosphinate *p*-nitrophenyl bis(chloromethyl)phosphinate by a series of primary and secondary amines in benzene. They have also suggested, in line with Menger's original suggestion for carboxylates, that a zwitterionic intermediate exists along the reaction pathway.

Secondary amine aminolysis

The aminolysis reactions of **3** with the secondary amines piperidine, morpholine, pyrrolidine, and di-*n*-propylamine all follow a rate law where only the k_2 term appears. This result is supported by the lack of significant catalysis with tertiary amines (Table 6). The observed rate of aminolysis by these amines is slower than that observed for butylamine and this rate order is the opposite of that observed for carboxylate esters (5). The overall slower rate is due to the absence of a general base-catalyzed pathway for the *sec*-amine aminolysis. Both for most carboxylic ester systems (5) and for the phosphinate studied by Bel'skii's group (14), a mixed rate law was obtained for the reactions with secondary amines. The reactivity order observed in the aminolysis reactions of *p*-nitrophenyl bis-(chloromethyl)phosphinate is piperidine > butylamine > diethylamine (14).

There is a good correlation between the rates of aminolysis of **3** and the pK_a of the amines as measured in acetonitrile (26) with the exception of morpholine, which is considerably more reactive than its basicity would predict. The entropy of activation of the piperidinolysis of **3** is −59 eu, which is very small for a bimolecular reaction and suggests a restricted transition state.

TABLE 8. Relative rates for the diaminolysis of **3** in acetonitrile at 30°C; $[H_2N(CH_2)_nNH_2]$ = 0.08 *M*

n	Relative rate	pK_a[a]	ΔpK_a[b]
2	1.75	18.46	5.45
3	4.66	18.70	4.72
4	5.42	20.12	4.78
5	2.58	19.14	2.17
6	1.00	—	—

[a] pK_a in acetonitrile; ref. 26.
[b] $\Delta pK_a = pK_a^2 - pK_a^1$; ref. 26.

The reason for the lack of a third-order term is most likely steric in origin, inasmuch as the larger secondary amines prevent a second amine molecule from being involved in the rate-determining step. The observation of general base catalysis with Bel'skii's ester reflects the smaller size of the $ClCH_2$ substituent.

Once again this bimolecular pathway can be rationalized as either rate-determining dissociation of the zwitterionic intermediate, followed by loss of a proton, or as a rate-determining intramolecular proton transfer to the O^-, coinciding with loss of the leaving group.

Diaminolysis

The diaminolysis reactions of **3** follow a rate law which is first order in amine only; their reaction rates, however, are greater than those observed for either butylamine (7 times faster per amino group) or for the secondary amines. Anderson, Su, and Watson (6) observed a similar rate enhancement for 1,3-diaminopropane over butylamine in the aminolysis of *p*-NPA in chlorobenzene. A mechanism identical to the other systems but with intramolecular general base catalysis would appear to best fit these results. Of the unsubstituted diamines, the 1,4-diaminobutane is the most reactive (Table 8), in accord with its having the highest basicity of the diamines studied (26). Table 8 also gives the ΔpK_a ($pK_a^2 - pK_a^1$) values for the diamines, which show a break at the point at which intramolecular hydrogen bonding, and subsequently catalysis, becomes less important. The diamine that gives the maximum rate would go through a transition state (**13**) involving proton transfer in a seven-membered ring, one atom of which is the sterically small hydrogen.

The entropy of activation calculated for the 1,3-diaminopropane reaction is −92 eu. This is an extremely small value for

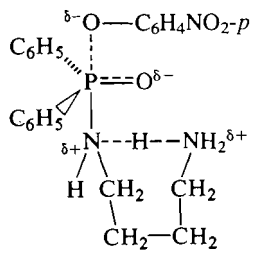

13

TABLE 9. Relative rates for the aminolysis of **3** by *N*-substituted diamines in acetonitrile at 30°C

Diamine	Relative rate
$H_2NCH_2CH_2NH_2$	1.08[a]
$CH_3NHCH_2CH_2NH_2$	2.28
$(CH_3)_2NCH_2CH_2NH_2$	1.00
$H_2N(CH_2)_3NH_2$	0.87[a]
$CH_3NH(CH_2)_3NH_2$	1.36
$(CH_3)_2N(CH_2)_3NH_2$	1.00
$CH_3NHCH_2CH_2NHCH_3$	1.84[a]
$CH_3NHCH_2CH_2CH_2CH_3$	1.00

[a]Rate/2 to account for two reactive sites.

a bimolecular reaction and reflects a large degree of freezing of rotation of the molecules in the transition state. This same system has also been studied in chlorobenzene, where the reaction followed a mixed rate law (eq. [1]) and the overall rate is considerably decreased ($k_2 = 6.12 \times 10^{-4} M^{-2} s^{-1}$). Such a solvent effect supports a highly charged transition state.

A most interesting observation is the inhibition of reaction observed when tertiary amines are present. Table 6 shows that the rate of aminolysis with 1,3-diaminopropane is retarded in the presence of imidazole, pyridine, and triethylamine. A possible explanation for this result would involve the inhibition of catalysis because of intermolecular hydrogen bonding between the "free" end of the diamine and the tertiary amine. There is no spectral evidence, in this case or in any other in this study, of imidazole acting as a nucleophile.

Table 9 summarizes the data for the *N*-substituted diamines. In the case of the monosubstituted diamines it is assumed that the reaction proceeds via nucleophilic attack of the primary amine and catalysis by the secondary amine, a conclusion reached because of the differences in reactivity between the two amine systems. The order of catalytic ability parallels the basicity of the amine end that is acting as a catalyst ($1° < 2° > 3°$) (26). Although a third-order term is not observed in the reactions with secondary amines, it appears that there is some intramolecular catalysis of a secondary amine reaction by another secondary amine in the case of *N*,*N*′-dimethylethylene diamine, where it is 4 times more reactive than methylbutylamine (2 times per amino group) (Table 9).

Experimental

Synthesis of the esters

The *p*-nitrophenyl diphenylphosphinate, **3**, *p*-cyanophenyl diphenylphosphinate, **4**, and *m*-nitrophenyl diphenylphosphinate, **5**, were prepared according to the method of Haake and Hurst (27). The *p*-nitrophenyl diphenylphosphinothioate, **7**, and diphenylphosphinodithioate, **8**, were prepared by the method of Spense, Swan, and Wright (28) while the *p*-nitrophenyl diphenylphosphinothionate, **6**, was synthesized by the procedure of Williams, Douglas, and Loran (29). Table 10 gives the physical constants for the esters, as well as their literature values. The highly reactive ester **7** could never be purified completely; small amounts of diphenylphosphinic acid always remained in the sample. The ester was used as is in the kinetic determinations and it was shown that adding diphenylphosphinic acid had no effect on the reaction.

Kinetics

The reaction rates were followed by measuring the increase in absorbance due to the production of phenol or thiophenol using Pye–Unicam model SP6-550, model SP8-250, and the Perkin–Elmer model 450 spectrophotometers. Reactions were carried out in thermostatted cells and the temperatures reported are within ±0.1°C. The kinetic wavelengths used for the different esters are reported in Table 10.

TABLE 10. Melting points and kinetic wavelengths for the esters **3**–**8**

	Melting point (°C)		Kinetic wavelength (nm)	
Ester	Observed	Literature	CH_3CN	C_6H_5Cl
3	149–150	149–150[a]	423	336
4	110–112[b]	—	290	—
5	120–123	124[c]	350	—
6	84–86	88–90[d]	423	—
7	121–123[e]	—	490	—
8	165–167	168–169[f]	490	—

[a]Reference 27.
[b]Elemental analysis, found (calcd.): C 71.47 (71.69), H 4.57 (4.39), P 10.3 (9.72), N 4.07 (4.39).
[c]Reference 30.
[d]Reference 29.
[e]Elemental analysis and tlc indicated that the ester was contaminated with a small amount of diphenylphosphinic acid (see text).
[f]Reference 28.

Most reactions were initiated by adding the required amount of amine with a Gilmont microsyringe to a 25-mL volumetric flask containing $1.3 \times 10^{-5} M$ ester in acetonitrile or chlorobenzene. For the very fast reactions the amine was added directly to the thermostatted cuvette. In all runs the amine was in large excess over the ester so that pseudo-first-order conditions prevailed. Reactions were followed to completion, except for ester **8**, and all plots gave excellent straight lines to well over 95% reaction, with correlation coefficients of the least-squares analyses of the data greater than 0.99. The data reported in the tables are the average of 2–3 runs in each case; reproducibility of the kinetic determinations was excellent. For ester **8** the rates were determined from Guggenheim plots because the thiophenol product undergoes slow oxidation. This oxidation was not a problem in the aminolysis of **7** because of its much faster rate. Second-order rate constants were determined by dividing the k_{obs} by the amine concentration and third-order rate constants were obtained from the plot of k_{obs}/[amine] vs. [amine]. The reactions with 1,6-diaminohexane, a solid, as well as with some of the secondary amines, were carried out by making a stock solution of the amine in acetonitrile and adding an appropriate volume to a stock solution of ester. The amide product with 1,6-diaminohexane precipitated from solution; however, because of the relative slowness of the reaction the solution could be filtered before absorbance readings were taken.

The amides formed with three of the amines were isolated from the reaction mixtures and identified by comparison with authentic samples.

Acknowledgement

The authors thank the Arts and Sciences Research Committee of the American University of Beirut for financial support.

1. F. M. MENGER. J. Am. Chem. Soc. **88**, 3081 (1966).
2. A. SAMI A. S. SHAWALI and S. S. BIECHLER. J. Am. Chem. Soc. **89**, 3020 (1967).
3. D. P. N. SATCHELL and I. I. SECEMSKI. J. Chem. Soc. B, 130 (1969).
4. D. P. N. SATCHELL and I. I. SECEMSKI. J. Chem. Soc. B, 1013 (1970).
5. (*a*) F. M. MENGER and J. H. SMITH. Tetrahedron Lett. 4163 (1970); (*b*) J. Am. Chem. Soc. **94**, 3824 (1972); (*c*) F. M. MENGER and A. C. VITALE. J. Am. Chem. Soc. **95**, 1854 (1974).
6. (*a*) H. ANDERSON, C. W. SU, and J. W. WATSON. J. Am. Chem. Soc. **91**, 482 (1969); (*b*) C. W. SU and J. W. WATSON. J. Am. Chem. Soc. **96**, 1854 (1974).

7. T. D. SINGH and R. W. TAFT. J. Am. Chem. Soc. **97**, 3867 (1975).
8. R. D. GANDOUR, D. A. WALKER, A. NAYAK, and G. R. NEWKOME. J. Am. Chem. Soc. **100**, 3608 (1978).
9. (*a*) L. SENATORE, E. CIUFFARIN, M. ISOLA, and M. VICHI. J. Am. Chem. Soc. **98**, 5306 (1976); (*b*) A. J. KIRBY and K. L. LIN. Tetrahedron Lett. 4079 (1978); (*c*) G. GUANTI, S. THEA, C. DELL'ERBA, and F. PERO. J. Chem. Soc. Chem. Commun. 886 (1978).
10. E. CIUFFARIN and A. LOI. J. Org. Chem. **48**, 1047 (1983).
11. F. RIVETTI and U. TONELLATO. J. Chem. Soc. Perkin Trans. **2**, 1176 (1977).
12. Y. POCKER and D. L. ELLSWORTH. J. Am. Chem. Soc. **99**, 2284 (1977).
13. L. W. DEADY and W. L. FINLAYSON. Aust. J. Chem. **33**, 2441 (1980).
14. V. E. BEL'SKII, L. S. NOVIKOVA, L. A. KUDRYAVTSEVA, and B. E. IVANOV. Izv. Akad. Nauk SSSR Ser. Khim. 1292 (1977); Engl. trans. p. 1188.
15. A. J. KIRBY and S. G. WARREN. The organic chemistry of phosphorus. Elsevier, Amsterdam. 1967. Chapt. 10
16. J. EMSLEY and D. HALL. The chemistry of phosphorus. J. Wiley, New York. 1976. Chapt. 8.
17. (*a*) F. H. WESTHEIMER. Acc. Chem. Res. **1**, 70 (1968); (*b*) K. MISLOW. Acc. Chem. Res. **3**, 321 (1970); (*c*) D. MARQUARDING, H. KLUSACEK, P. GILLESPIE, and F. RAMIREZ. Acc. Chem. Res. **4**, 288 (1971).
18. (*a*) R. D. COOK and M. METNI. Can. J. Chem. **63**, 3155 (1985). (*b*) I. SIGAL and F. H. WESTHEIMER. J. Am. Chem. Soc. **101**, 752 (1979).
19. R. D. COOK, S. FARAH, L. GHAWI, A. ITANI, and J. RAHIL. To be published.
20. K. T. DOUGLAS and A. WILLIAMS. J. Chem. Soc. Perkin Trans. **2**, 515 (1976).
21. R. D. COOK and L. RAHHAL-ARABI. Tetrahedron Lett. 3147 (1985).
22. (*a*) A. A. NEIMYSHEVA and I. L. KNUNYANTS. Dokl. Acad. Nauk SSSR, **181**, 888 (1968); Engl. trans. p. 697; (*b*) A. A. NEIMYSHEVA, V. I. SAVSHUK, M. V. ERMOLAEVA, and I. L. KNUNYANTS. Izv. Akad. Nauk SSSR Ser. Khim 2222 (1968); Engl. trans. p. 2104.
23. L. L. SCHALEGER and F. A. LONG. Adv. Phys. Org. Chem. **1**, 1 (1963).
24. (*a*) N. J. TURRO, G. F. LEHR, J. A. BUTCHER, JR., R. A. MOSS, and W. GUO. J. Am. Chem. Soc. **104**, 1754 (1982); (*b*) J. JAHME and C. RUCHARDT. Tetrahedron Lett. 4011 (1982).
25. J.-L. M. ABBOUD, R. W. TAFT, and M. J. KAMLET. Bull. Chem. Soc. Jpn. **55**, 603 (1982).
26. J. F. COETZEE. Prog. Phys. Org. Chem. **4**, 75 (1967).
27. P. HAAKE and G. HURST. J. Am. Chem. Soc. **88**, 2544 (1966).
28. R. SPENSE, J. SWAN, and S. WRIGHT. Aust. J. Chem. **22**, 2359 (1969).
29. A. WILLIAMS, K. DOUGLAS, and J. LORAN. J. Chem. Soc. Perkin Trans. **2**, 1010 (1975).
30. A. WILLIAMS and R. A. NAYLOR. J. Chem. Soc. B, 1968 (1971).

Polymérisation de l'acide molybdique induite par l'acide métatungstique

P. COURTIN ET J. LEFEBVRE[1]

Laboratoire de chimie des polymères inorganiques, Université Pierre et Marie Curie, 4, place Jussieu, 75230 Paris Cédex 05, France

Reçu le 17 janvier, 1985[2]

P. COURTIN et J. LEFEBVRE. Can. J. Chem. **64**, 220 (1986).

En solution aqueuse, l'acide métatungstique se décompose très lentement en oxyde tungstique, haut polymère insoluble, et la polymérisation de l'acide molybdique préparé par échange d'ions à partir du molybdate, Na_2MoO_4, est limitée ($n = 24$). L'addition d'acide métatungstique à l'acide molybdique entraîne la formation relativement rapide de hauts polymères solubles. Ce sont des acides mixtes molybdotungstiques dont la composition dépend de la fraction molaire $f = [Mo]/[Mo + W]$ du mélange. En particulier si $0{,}80 \leqslant f \leqslant 0{,}95$, la réaction des acides est totale; c'est une méthode pour obtenir des sols très riches en molybdène, puisque le rendement en haut polymère est égal à 80%. La formation de l'acide mixte peut résulter soit de l'interaction directe des deux acides, soit de la décomposition de l'acide métatungstique substitué par le molybdène, formé transitoirement. Durant la polymérisation suivie par ultracentrifugation et échange d'ions, la teneur en Mo et W des acides mixtes ne varie pas.

P. COURTIN and J. LEFEBVRE. Can. J. Chem. **64**, 220 (1986).

In acid media, metatungstic acid very slowly decomposes into tungstic oxide, an insoluble high polymer; under the same conditions, the polymerization of molybdic acid, prepared by ion exchange from the molybdate, Na_2MoO_4, is limited ($n = 24$). The addition of metatungstic acid to molybdic acid involves the relatively rapid formation of soluble high polymers. These are mixed molybdotungstic acids whose compositions vary according to the molar fraction, $f = [Mo]/[Mo + W]$, of the reaction mixture. When $0.80 \leqslant f \leqslant 0.95$, this reaction is complete: this is a method of obtaining colloids very rich in molybdenum since the yield in high polymer is equal to 80%. The formation of the mixed acid can be due either to the direct interaction of the two acids or to the decomposition of the metatungstic acid, substituted by the molybdenum, which would be formed transiently. As determined by ultracentrifugation and by ion exchanges, the relative proportions of Mo and W in the mixed acids do not vary during the course of the polymerization.

[Journal translation]

Introduction

Beaucoup d'oxydes de métaux de transition (WO_3, V_2O_5) peuvent être obtenus à l'état colloïdal ou de gel; ce sont alors des matériaux aux propriétés intéressantes, qui se prêtent à de nombreuses applications: réalisation de cellules électrochromiques ou de dispositif d'affichage, emploi comme semi-conducteur (1). Les gels tungstiques ou vanadiques sont facilement obtenus suivant une méthode développée au laboratoire (2): préparation d'un acide à partir d'un sel passé sur une résine échangeuse de protons, suivie de la polymérisation de cet acide par élimination de H_2O entre deux groupements M—OH voisins. Les gels molybdiques, par contre, ne sont pas obtenus par cette voie parce que la polymérisation de l'acide molybdique formé est limitée. Il est donc nécessaire d'utiliser la préparation de Graham–Murgier (3) qui part de solutions très concentrées.

Cependant, un autre moyen d'accéder aux gels molybdiques dans des conditions moins restrictives de concentration pourrait consister à incorporer à l'acide molybdique peu condensé un autre acide pouvant évoluer spontanément vers une forme hautement condensée, par exemple, l'acide tungstique, afin d'induire la formation d'un haut polymère mixte. En effet, des composés mixtes à base de tungstène et de molybdène sont aisément obtenus aussi bien dans le domaine des faibles condensations (hexa- et dodéca-métallates (4)) que dans celui des condensations élevées caractéristiques des gels (5). Le problème est donc de savoir si la texture hautement condensée de l'acide tungstique est susceptible de se maintenir dans le polymère mixte, même lorsqu'il y est présent en faible proportion.

Dans ce travail, le tungstène a été introduit dans la solution aqueuse molybdique sous forme d'hétéropolyacide possédant la structure de Keggin (6) de formule générale $H_{(8-n)}[X\,W_{12}O_{40}]$ où n est le degré d'oxydation de l'hétéro-élément X (X = Si, H_2). En effet, nous avons observé qu'en solution aqueuse pure, l'un de ces composés faiblement condensés, l'acide métatungstique ($X = H_2$), avait la propriété de se transformer très lentement en acide tungstique très condensé.[3] C'est donc sous cette forme que le tungstène a principalement été introduit dans la solution aqueuse molybdique, avec l'avantage de ne pas apporter d'autre élément étranger que le tungstène. D'autres hétéropolyacides du type précédent (X = Si) ou mixtes lui ont été ensuite comparés pour tenter de préciser le mécanisme de formation des acides mixtes molybdotungstiques polymérisés.

Partie expérimentale

1. *Réactifs*

1.1 *Acide molybdique*

Il est préparé par échange d'ions sur une résine cationique de type Dowex 50 W X-2, 100–200 mesh, sous forme H^+, à partir d'une solution de molybdate de sodium $Na_2MoO_4 \cdot 2H_2O$ à 20°C.

1.2 *Hétéropolyacides tungstiques*

Ils sont préparés suivant les méthodes classiques (8), par extraction ou par échange d'ions.

1.3 *Hétéropolyacides substitués molybdotungstiques*

Les sels sont d'abord préparés (4, 9), puis les acides, par échange d'ions.

Le système mixte à étudier est préparé soit par mélange des réactifs 1.1 et 1.2, soit par dissolution de 1.3. Il est défini par sa fraction molaire $f = [Mo]/[Mo + W]$. Les réactions sont lentes; elles sont suivies pour la plupart à température constante de 20°C.

2. *Techniques et méthodes analytiques*

2.1 *Ultracentrifugation préparative*

Réalisée dans un appareil Beckman Spinco, modèle E équipé d'un rotor à godets SW65E, à 36 000 r/min pendant 100 min, elle permet la séparation des hauts polymères qui sont rassemblés au fond du tube sous forme d'un gel. En surface, on dispose d'une solution pure de composés légers.

[1]Auteur à qui adresser la correspondance.

[2]Révision reçue le 19 septembre 1985.

[3]P. Courtin, résultats non publiés.

2.2 *Échange d'ions*

Par passage sur une résine Amberlite CG-400, 100–200 mesh, sous forme Cl^-, les ions polymolybdiques sont fixés. En utilisant 2 méquiv. de résine pour 0,10 méquiv. de molybdène, l'échange est complet quelle que soit la concentration.

2.3 *Hydrolyse rapide à pH contrôlé*

Réalisée sous azote, à pH constant égal à 8, par addition de soude pendant 1 min à l'aide d'un combititreur Methrohm E 415, elle permet la dégradation alcaline en ions MoO_4^{2-} et WO_4^{2-} des formes labiles du mélange exclusivement.

2.4 *Hydrolyse totale*

Réalisée par un excès de soude à l'ébullition, elle permet la décomposition totale du système à l'état d'ions MoO_4^{2-} et WO_4^{2-}.

2.5 *Analyse*

Les hétéropolyanions substitués $[XMoW_{11}O_{40}]^{(8-n)-}$ sont dosés par polarographie en milieu acide chlorhydrique $1{,}0 \times 10^{-1}$ *M* (X = H_2) et par spectrophotométrie d'absorption à 500 nm, après réduction, à pH 2, du molybdène par le chlorure stanneux en solution dans le glycérol (10) (X = Si). Les autres dosages sont effectués après hydrolyse des mélanges:

Hydrolyse rapide: la somme $[MoO_4^{2-} + WO_4^{2-}]$ labile est titrée par dosage protométrique avec l'acide chlorhydrique en présence de mannitol (11), et MoO_4^{2-} est déterminé, à 475 nm, par spectrophotométrie d'absorption du complexe coloré formé avec le pyrocatéchol en tampon phosphate (pH 7,50) (12); le métatungstate est dosé par polarographie en tampon phosphate de pH 7,50 (13).

Hydrolyse totale: MoO_4^{2-} et WO_4^{2-} sont dosés simultanément, à 475 et 350 nm, par spectrophotométrie d'absorption du complexe formé avec le pyrocatéchol en tampon phosphate de pH 7,50, ou par polarographie en milieu acide chlorhydrique 8 *M* (14).

3. *Masse molaire*

La condensation est mesurée par ultracentrifugation analytique à l'aide d'un appareil Beckman équipé de l'optique Schlieren.

3.1 *Les coefficients de sédimentation apparents*, $(s_p)_{app}$, sont déterminés en cellule de 12 mm d'épaisseur, à double secteur, à différentes vitesses de rotation ($14\,000 < v < 26\,000$ r/min), dans des solutions suffisamment diluées pour éliminer les effets dus aux interactions moléculaires ($1{,}0 \times 10^{-2}\ M < \text{Mo} < 5{,}0 \times 10^{-2}\ M$). Le solvant ajouté au moment de la mesure est constitué de chlorure de lithium à la concentration $5{,}0 \times 10^{-2}$ *M*. La distribution des coefficients $(s)_{app}$ est obtenue au moyen de la fonction de distribution normalisée $g(s) = 1/C(dC/ds)$ où *C* est la concentration du soluté (15).

3.2 *Les coefficients de diffusion*, D_w, sont obtenus par centrifugation à basse vitesse, $v = 10\,000$ r/min, en cellule à frontière synthétique à capillaire, selon la méthode de Fujita – Van Holde (16).

3.3 *La masse molaire* des composés lourds est calculée à l'aide de la relation de Svedberg (17); celle des composés légers est obtenue par construction du diagramme d'Archibald après centrifugation en transition vers l'équilibre de sédimentation (18), à différentes vitesses ($15\,000 < v < 42\,000$ r/min), avec cellule à double secteur, à remplissage homogène.

Résultats expérimentaux

I. *État du système à l'équilibre*

Il est déterminé lorsque les concentrations des constituants ne varient plus avec l'âge, c'est-à-dire au bout de 30 jours à 20°C. Le système est toujours homogène.

1. *Polymérisation du système*

Le coefficient de sédimentation apparent est supérieur à 50 svedbergs pour tous les mélanges dont la fraction molaire $f = [Mo]/[Mo + W]$ est comprise entre 0,08 et 0,94. Il se forme donc des hauts polymères dans un domaine étendu de compositions. Le système est assez polydispersé (fig. 1) mais ne renferme qu'une famille de composés lourds de coefficient de sédimentation moyen de l'ordre de 100 svedbergs quelle que soit la valeur de *f* entre 0 et 1, la concentration en molybdène

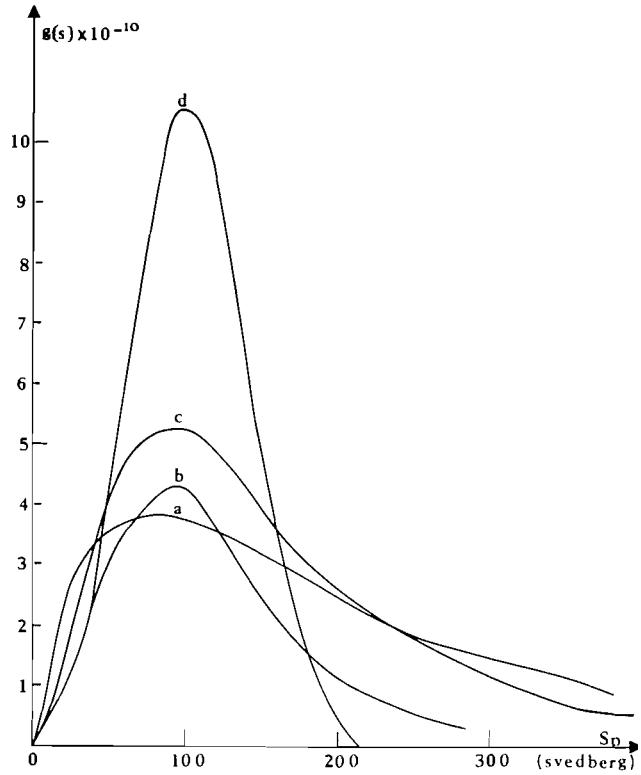

FIG. 1. Distribution du coefficient de sédimentation apparent $(s_p)_{app}$ mesuré dans les mélanges de fraction molaire $f = 0{,}50$ (a); 0,66 (b); 0,75 (c) et 0,80 (d).

dans le haut polymère étant voisine de $1{,}0 \times 10^{-2}\ M$. La distribution des coefficients de sédimentation tend à se resserrer lorsque *f* augmente.

2. *Composés lourds formés dans le système*

Ils sont recueillis après ultracentrifugation préparative, sous forme d'un gel amorphe aux rayons X. La proportion de molybdène et de tungstène polymérisé peut être importante—80% de ce qui a été introduit. Elle est atteinte dans un domaine de compositions qui est plus large pour le molybdène, $0{,}14 < f < 0{,}94$ (fig. 2, courbe a), que pour le tungstène, $0{,}80 < f < 0{,}94$ (fig. 2, courbe b), en raison de la persistance de la forme métatungstique dans les mélanges de $f < 0{,}80$ (fig. 2, courbe c). À partir des résultats de l'analyse élémentaire (tableau 1), on peut exprimer la composition des acides mixtes dans le haut polymère (H.P.), en fraction molaire $f_{H.P.} = [Mo]_{H.P.}/[Mo + W]_{H.P.}$. Elle dépend de la composition initiale du mélange (fig. 3): d'abord constante et égale à 0,50 pour les faibles valeurs de *f* ($0 < f < 0{,}30$), elle croît ensuite jusqu'en $f = 0{,}90$ de façon pratiquement linéaire. Au-delà de $f = 0{,}95$, la précision des analyses n'est plus suffisante pour préciser le mode de variation de $f_{H.P.}$, en particulier l'existence éventuelle d'une limite vers $f_{H.P.} = 0{,}95$.

La masse molaire des composés lourds calculée à partir des mesures de coefficients de sédimentation et de diffusion du gel remis en solution est de l'ordre de $1{,}0 \times 10^5$ pour une concentration moyenne de $(1{,}0\text{–}4{,}0) \times 10^{-2}\ M$ en molybdène (tableau 2).

II. *Évolution des mélanges avec l'âge*

1. *Masse molaire*

Durant les trois premiers jours d'évolution, la masse molaire apparente des mélanges reste égale à la masse moyenne des

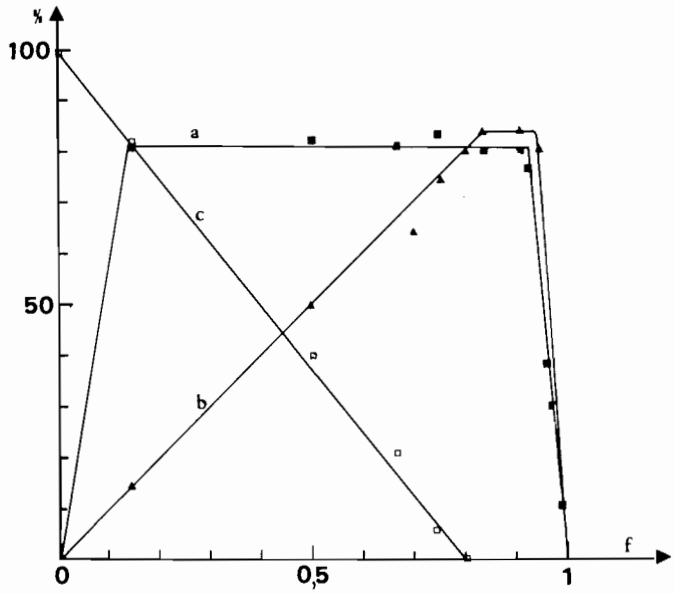

FIG. 2. Répartition du molybdène et du tungstène dans les mélanges à l'équilibre, en fonction de leur fraction molaire f: Mo (a) et W (b) dans le haut polymère; W(c) sous forme métatungstique.

TABLEAU 1. Analyse élémentaire des gels en fonction de la fraction molaire f du mélange

	%			
f	Mo	W	Mo/W	Charge par mole (Mo + W)
0,08	19,80	36,50	1	0,16
0,17	20,50	39,25	1	0,15
0,50	25,00	32,80	1,46	0,10
0,66	25,50	22,00	2,25	0,17
0,80	25,83	12,63	3,92	0,18

constituants ($M \simeq 3000$). Puis un composé lourd sédimente en ultracentrifugation. Au fur et à mesure que progresse la formation de ce composé lourd, on observe que son coefficient de sédimentation, mesuré dans le milieu même de formation, augmente (tableau 3). Ceci pourrait signifier que le composé lourd tend à se polymériser davantage, mais il est également possible que la variation du coefficient de sédimentation soit due simplement aux changements de concentration du milieu réactionnel. Pour le vérifier, le composé lourd a été isolé par ultracentrifugation, puis redissous dans du LiCl $5{,}0 \times 10^{-2}$ M: son coefficient de sédimentation prend alors une valeur approximativement constante (40–50 svedbergs), quels que soient son âge et le rapport f (tableau 4). Il ne semble donc se former qu'une seule famille de hauts polymères.

2. *Composition des acides mixtes légers*

Les mélanges en cours d'évolution sont constitués de formes labile et inerte. La forme inerte ne renferme que du métatungstate; la forme labile contient des acides mixtes, lourds et légers et éventuellement l'acide molybdique n'ayant pas réagi. Les composés légers peuvent être isolés durant les premiers jours d'évolution avant que le haut polymère ne se forme: les ions polymolybdiques sont d'abord éliminés par échange d'ions, puis le composé mixte est séparé du métatungstate par précipitation de son sel de césium à 25°C. Le rapport $[Mo/W]_{léger}$ des composés légers ainsi isolés (tableau 5) est égal à celui

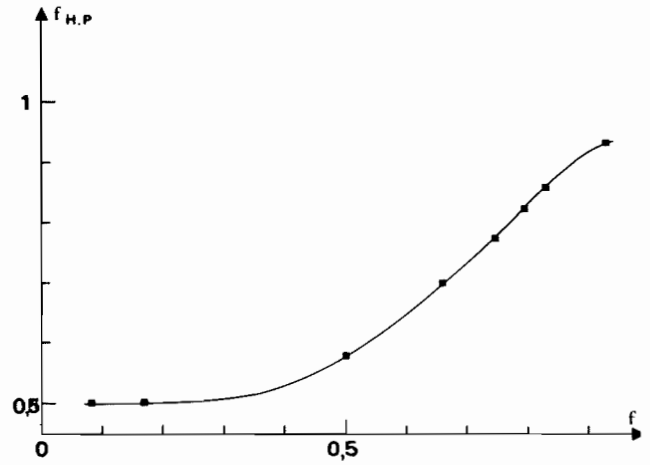

FIG. 3. Fraction molaire $f_{H.P.}$ du haut polymère en fonction de la fraction molaire f du mélange.

TABLEAU 2. Masse molaire des gels en fonction de la fraction molaire f du mélange

f	$[Mo]_{H.P.}$ $(10^{-2} M)$	$(s_p)_{app}$ (svedberg)	D_w (10^{-6})	$(M_{ww})_{app}$
0,08	0,50	52	0,95	$1{,}6 \times 10^5$
0,17	1	50	0,90	$1{,}7 \times 10^5$
0,50	3,75	48	1,02	$1{,}5 \times 10^5$
0,66	4	40	1,27	$1{,}0 \times 10^5$

déterminé dans les composés lourds à l'équilibre (tableau 1), la charge, par contre, est plus élevée. D'après la masse molaire mesurée ($M \simeq 3400$), le degré de condensation moyen des acides mixtes formés initialement est égal à 18. La polymérisation a donc lieu par simple diminution de la charge, sans modification de la composition en molybdène et tungstène. Ceci est vérifié par les dosages des constituants dans les composés lourds et légers, en cours d'évolution des mélanges. Ils indiquent en effet que le rapport [Mo/W] y est le même et que sa valeur demeure constante durant l'évolution (tableau 6). De plus, ils indiquent que l'acide molybdique finit par réagir totalement (fig. 4, courbe a), contrairement à l'acide métatungstique (fig. 2). La vitesse de réaction peut être mise sous la forme d'une loi du premier ordre par rapport à la concentration en acide molybdique, $v = k_1[Mo]$, avec $k_1 = 0{,}115$ d^{-1} à 20°C.

3. *Comparaison avec d'autres hétéropolyacides*

3.1 *Acide silico-12 tungstique (X = Si).* En fin d'évolution, après 20 jours à 40°C, un composé lourd sédimente en ultracentrifugation et tout l'acide molybdique a réagi. En cours d'évolution, les dosages par la soude, à pH 8, des acides débarassés des ions polymolybdiques par échange d'ions, indiquent que le molybdène se répartit sous une forme labile constituée d'un acide mixte molybdotungstique, de composition constante, en grande partie polymérisé, et sous une forme inerte, constituée de l'acide substitué $H_4[SiMoW_{11}O_{40}]$. Cette dernière réaction n'était pas observée avec l'acide métatungstique.

3.2 *Acides substitués* $H_{(8-n)}[XMoW_{11}O_{40}]$. Aucune évolution n'est observée par polarographie et ultracentrifugation dans la solution d'acide $H_4[SiMoW_{11}O_{40}]$, même en présence d'acide molybdique, au contraire de la solution d'acide $H_6[H_2MoW_{11}O_{40}]$. Dans celle-ci, le pourcentage d'acide

TABLEAU 3. Valeurs du coefficient de sédimentation apparent $(s_p)_{app}$ dans le mélange $f = 0,17$ en fonction de l'âge

$(s_p)_{app}$	(svedberg)	25	40	48	65	74	80	85	95	110	125
Âge	(jours)	6	7	8	9	11	12	15	18	22	35
$[Mo]_{H.P.}$	$(10^{-2}\ M)$	0,15	0,17	0,22	0,275	0,35	0,40	0,54	0,64	0,75	0,80

TABLEAU 4. Valeurs des coefficients de sédimentation apparents $(s_p)_{app}$ des gels isolés à des âges différents (en jours) des mélanges de fraction molaire f

f	$(s_p)_{app}$ (6 d)	$(s_p)_{app}$ (13 d)	$(s_p)_{app}$ (20 d)	[Mo] $(10^{-2}\ M)$
0,17	32	42	42	4,36
0,50	39	40	45	3,40
0,66	49	35	38	4,06
0,75	41	37	45	3,95
0,80	39	40	39	0,80

TABLEAU 5. Analyse élémentaire des composés légers en fonction de la fraction molaire f du mélange

	%			
f	Mo	W	Mo/W	Charge par mole (Mo + W)
0,08	15,00	30,90	1	0,50
0,17	19,00	39,00	0,94	0,50
0,50	1,30	1,70	1,43	0,50
0,80	7,00	3,25	4,00	0,50

TABLEAU 6. Valeurs du rapport $[Mo/W]_{combiné}$ à des âges différents (en jours), dans les mélanges de fraction molaire f

f	[Mo/W] (6 d)	[Mo/W] (13 d)	[Mo/W] (20 d)	[Mo/W] (30 d)
0,50	1,35	1,32	1,40	1,40
0,66	2,83	2,20	2,20	2.32
0,75	3,30	3,30	3,55	3,50
0,80	4,00	3,90	3,80	4,07

s'annule au bout de 30 jours à 20°C (fig. 4, courbe b): sa vitesse de réaction peut se mettre sous la forme $v = k_3$[acide substitué], avec $k_3 = 0,123\ d^{-1}$ à 20°C; elle ne dépend pas de la concentration en acide molybdique éventuellement présent. Au terme de l'évolution, le coefficient de sédimentation vaut 57 svedbergs et le molybdène est totalement dosé sous une forme labile à pH 8, tandis que le tungstène se répartit sous formes labile (en quantité égale au molybdène) et inerte (seul, à l'état de métatungstate). Les produits de la réaction sont donc l'acide métatungstique et un acide mixte, de rapport Mo/W = 1, qui se polymérise.

Discussion

1. Les résultats montrent qu'il est possible d'obtenir des acides mixtes hautement polymérisés en solution, par interaction des acides molybdique et métatungstique, dans un grand intervalle de fraction molaire $f = [Mo]/[Mo + W]$ des mélanges. En particulier si $0,80 < f < 0,95$, la réaction est totale; ce sont les conditions de préparation de sols riches en molybdène.

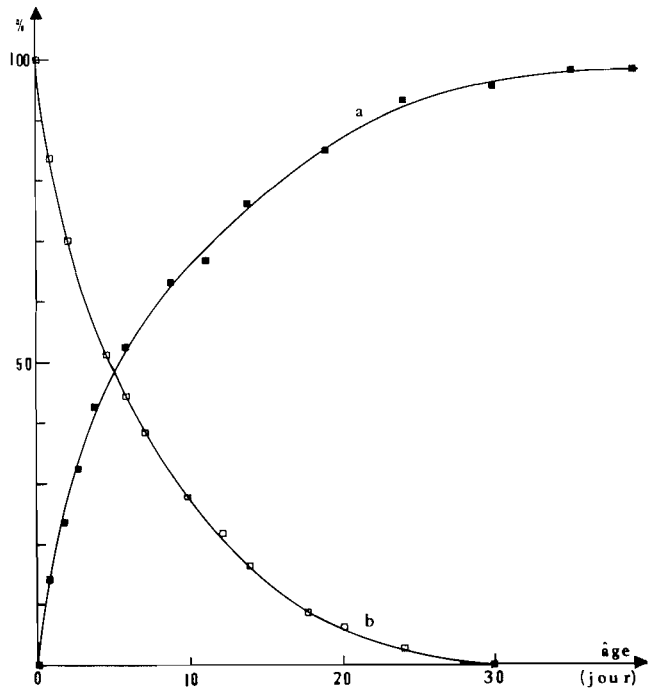

FIG. 4. Évolution du système avec l'âge: (a) solution d'acides métatungstique et molybdique de fraction molaire $f = 0,17$: pourcentage de Mo combiné; (b) solution d'acide métatungstique substitué par du molybdène ($H_6[H_2MoW_{11}O_{40}]$): pourcentage d'acide restant.

La fraction molaire du haut polymère $f_{H.P.}$ est alors égale à celle du mélange. Toutefois au-delà de $f = 0,90$, sa détermination précise devient vite difficile, en raison justement du pourcentage très élevé de Mo par rapport à celui de W. La fraction molaire $f_{H.P.}$ devrait tendre vers une limite correspondant à celle de l'espèce légère formée. Expérimentalement, elle se situe au-dessus de $f_{H.P.} = 0,94$, ce qui correspond à l'introduction d'un tungstène dans une molécule de 18 ou 24 centres métalliques ($f_{H.P.} = 0,944$ ou $0,958$).

Les sols sont constitués de deux familles de composés de même rapport Mo/W, mais de masses très différentes. La répartition entre les deux s'établit en général ainsi: 80% d'espèces lourdes et 20% de légères. Du point de vue polymérisation, le système étudié ici se comporte comme les autres systèmes mixtes, à base d'acide antimonique en particulier, étudiés au laboratoire. Tous ces systèmes sont constitués de plusieurs familles d'espèces de masse molaire différente en équilibre. Si les deux acides en présence peuvent évoluer spontanément vers une forme hautement condensée, les familles d'espèces en présence diffèrent à la fois par leur masse molaire et leur composition. Ceci a été vérifié sur le système acide antimonique – acide tungstique (19). Par contre, si l'un des éléments en présence n'évolue pas spontanément vers une forme hautement condensée, les familles d'espèces en présence ne diffèrent que par leur masse molaire. Cette conclusion valable dans le cas des composés de l'acide antimonique et des acides phosphorique, arsénique et arsénieux (20) est aussi

vérifiée dans le cas des composés molybdovanadiques (7) et dans le cas présent des composés molybdotungstiques.

2. La fraction molaire $f_{H.P.}$ ne varie pas de façon continue comme la fraction molaire f du mélange, puisqu'elle est constante dans l'intervalle $0 < f < 0{,}30$. Cette particularité est le signe d'un comportement différent des mélanges selon la valeur de leur fraction molaire. C'est probablement au niveau de la formation de l'espèce légère que se situe cette différence, puisque la polymérisation ne modifie pas la fraction molaire de l'espèce mixte.

À partir des résultats obtenus avec les deux hétéropolyacides tungstiques ($X = H_2$ et Si) d'une part, et avec les acides substitués correspondants d'autre part, nous proposons le schéma suivant pour rendre compte de la formation des acides mixtes.

(*i*) L'action de l'acide molybdique sur l'hétéropolyacide est double:

[1] formation d'espèce légère mixte

[2] formation d'espèce substituée $[XMoW_{11}O_{40}]^{8-n}$

(*ii*) Suivant la nature de X, une troisième réaction peut avoir lieu:

[3] formation d'espèce légère mixte à partir de l'espèce substituée.

L'influence de la valeur de la fraction molaire f du mélange intervient au niveau de la compétition entre les réactions 1 et 2: aux faibles valeurs de f, la réaction 1 est négligeable devant l'autre, dans le cas des mélanges avec l'acide métatungstique. Les réactions 1 et 2 sont bien mises en évidence dans le cas de l'acide silico-12 tungstique; elles sont simultanées, puisque la polymérisation ne se fait pas à partir de l'acide substitué, même en présence d'acide molybdique. Dans le cas de l'acide métatungstique, nous pouvons penser que la réaction se déroule suivant le même processus, bien qu'aucun résultat ne montre la présence de l'espèce substituée correspondante (en particulier, la présence de molybdène sous une forme inerte à pH 8). Pour que la réaction 2 ne soit pas observée expérimentalement, il suffit que sa vitesse soit égale à celle de la réaction 3 qui a lieu obligatoirement dans ce cas. C'est ce qui est vérifié expérimentalement: les deux constantes de vitesse k_1 et k_3 sont voisines et k_1 est bien la constante de vitesse de la réaction 2 si la réaction 1 est négligeable en $f = 0{,}17$. Dans ces conditions ($0 < f < 0{,}30$), l'acide mixte ne se forme que suivant [3] et sa composition est constante. Aux plus fortes valeurs de f, la réaction 1 n'est plus négligeble, et la composition varie.

1. J. Livage et J. Lemerle. Annu. Rev. Mater. Sci. **12**, 103 (1982).
2. J. Lemerle, L. Nejem et J. Lefebvre. J. Inorg. Nucl. Chem. **42**, 17 (1980).
3. P. Pascal. Nouveau traité de chimie minérale. Vol. XIV. Masson, Paris. 1958. pp. 666–667.
4. P. Courtin. Bull. Soc. Chim. Fr. 2747 (1974); 2751 (1974); P. Courtin et J. Lefebvre. Bull. Soc. Chim. Fr. 1983 (1975); C. Sanchez, J. Livage, J. P. Launay, M. Fournier et Y. Jeannin. J. Am. Chem. Soc. **104**, 3194 (1982).
5. P. Courtin et J. Lefebvre. Bull. Soc. Chim. Fr. 1727 (1976).
6. J. F. Keggin. Nature, **131**, 908 (1933).
7. J. Mandavo. Thèse de 3e cycle, Paris (1983).
8. M. Margueritte. Ann. Chim. Phys. **17**, 477 (1946); H. Copeaux. Ann. Chim. Phys. **17**, 217 (1909); E. F. Smith. Chem. News, **136**, 129 (1927).
9. T. J. R. Weakley. Struct. Bonding (Berlin), **18**, 131 (1974).
10. S. Arribas, R. Rincon, R. Moro et M. L. Alvarez. Anal. Chim. Acta, **33**, 205 (1965).
11. P. Souchay. Polyanions et polycations. Gauthiers–Villars, Paris. 1963. p. 93.
12. S. Seifter et B. Novic. Anal. Chem. **23**, 188 (1951).
13. P. Souchay et J. P. Launay. C. R. Acad. Sci. **268**, 1354 (1969).
14. I. M. Kolthoff et J. Lingane. Polarography. Vol. 2. Interscience, New York. 1952. pp. 457–461.
15. V. N. Schumaker et H. K. Schachman. Biochim. Biophys. Acta, **23**, 268 (1957).
16. K. E. Van Holde. J. Phys. Chem. **64**, 1582 (1960).
17. T. Svedberg et K. O. Pedersen. The ultracentrifuge. Johnson Reprint Co., New York. 1940. p. 39.
18. W. J. Archibald. J. Phys. Colloid Chem. **51**, 1204 (1947).
19. J. Lemerle et J. Lefebvre. Bull. Soc. Chim. Fr. 409 (1976).
20. J. P. Jolivet, J. Lemerle et J. Lefebvre. Bull. Soc. Chim. Fr. 2415 (1975).

Synthetic applications of chromium(VI) reagents in combination with chlorotrimethylsilane[1]

FERNANDO P. COSSÍO, JESÚS M. AIZPURUA, AND CLAUDIO PALOMO[2]
Kimika Organikako Departamendua, Kimika Fakultatea, Euskal Herriko Unibertsitatea, Altza, Donostia, Spain
Received May 13, 1985

FERNANDO P. COSSÍO, JESÚS M. AIZPURUA, and CLAUDIO PALOMO. Can. J. Chem. **64**, 225 (1986).

The synthetic utility of chromium(VI) reagents together with chlorotrimethylsilane, as new oxidizing systems, is described. Pyridinium dichromate (PDC) in combination with chlorotrimethylsilane oxidizes *tert*-butyldimethylsilyl ethers in good to excellent yields. Trimethylsilyl chlorochromate, a new chromium(VI) reagent, also was found efficient for this oxidative-deprotection method. These reagents were applied to the oxidation of some *N*-(2-phenyl-2-hydroxyethyl)azetidin-2-ones as well as *N*-(2-phenyl-2-trialkylsiloxy)azetidin-2-ones into their corresponding carbonyl compounds, key intermediates for *N*-unsubstituted β-lactams. Oxidation of hydroquinones and protected trialkylsilyl hydroquinones was also described. Protection of hydroquinones by means of the *tert*-butyldimethylsilyl group was achieved by using the readily available *tert*-butyldimethylchlorosilane (TBDMCS) and 1,8-diazabicyclo[5.4.0]undec-7-ene (DBU) as base, which avoids the use of sophisticated and (or) sensitive reagents.

FERNANDO P. COSSÍO, JESÚS M. AIZPURUA et CLAUDIO PALOMO. Can. J. Chem. **64**, 225 (1986).

On décrit l'utilité en synthèse des réactifs du chrome(VI), utilisés de concert avec le chlorotriméthylsilane, comme nouveaux systèmes oxydants. Le dichromate de pyridinium (DCP), utilisé de concert avec le chlorotriméthylsilane, oxyde les éthers *tert*-butyldiméthylesilylés avec des rendements qui vont de bons à excellents. On a aussi trouvé que le chlorochromate de triméthylsilyle, un nouveau réactif du chrome(VI), est un réactif utile pour la méthode de déprotection oxydative. On a appliqué ces réactifs à l'oxydation, en dérivés carbonylés correspondants, de quelques *N*-(phényl-2 hydroxy-2 éthyl) azétidinones-2 ainsi que de *N*-(phényl-2 trialkylsiloxy-2) azétidinones-2, des intermédiaires clés dans la préparation de β-lactames qui ne sont pas substitués sur l'azote. On décrit aussi l'oxydation d'hydroquinones et d'hydroquinones protégées par des groupements trialkylsilyles. On a réalisé la protection des hydroquinones par le groupement *tert*-butyl-diméthylesilyle en les faisant réagir avec le *tert*-butyl-diméthylchlorosilane (TBDMCS), qui est facilement disponible, en présence du diaza-1,8 bicyclo[5.4.0] undécène-7 (DBU) comme base; cette méthode évite l'utilisation de réactifs sophistiqués ou sensibles.

[Traduit par le journal]

Oxidation is a fundamental process in organic synthesis and several reagents have been developed for a wide variety of transformations (1). Among the reagents available for the oxidation of organic compounds, the chromium(VI) derivatives have received growing attention in the past years (2). However, there is still considerable interest in the development of new methods for oxidation reactions. Since the appearance of pyridinium dichromate **1** (PDC) (3) and pyridinium chlorochromate **2** (PCC) (4), other similar oxidizing reagents have been developed by varying the amine ligand associated with the dichromate and chlorochromate anions. Recently, we have reported (5) a new class of chromium(VI) reagent, trimethylsilyl chlorochromate **3**, which was an efficient reagent in the

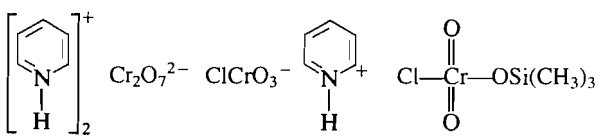

(PDC) **1** (PCC) **2** **3**

oxidation of alcohols into the corresponding aldehydes and ketones.

This communication reports new synthetic applications of this heretofore unknown reagent **3** and some quite fruitful investigations on a new oxidizing system involving pyridinium dichromate (PDC) in combination with trimethylchlorosilane.

Oxidation of alcohols and trialkylsilyl esters

In connection with our objectives in carbacephem antibiotics, we required an efficient synthesis of β-lactams of type **11** as model key intermediates. A synthetic route of this kind is based on the transformations outlined in Scheme 1, in which we need an effective mild oxidizing reagent.

The key to the first step of our approach is that protection of the hydroxyl group as its trialkylsilyl ether in the starting imine **6** seems to be critical in order to obtain the desired precursors **10**. Without protection of the hydroxyl group the product obtained was an oxazolidine **9** instead of the expected β-lactam **10**. Thus, treatment of an acetic acid **8** with an appropriate trimethylsilyl protected imine **7** (R^3: TMS) in equimolar amounts with phenyl dichlorophosphate in the presence of triethylamine gave, after work-up, the free hydroxy β-lactam **10** (R^3: H) (6).

However, we now have found that when the *tert*-butyldimethylsilyl group was used in place of the trimethylsilyl moiety for the protection of the hydroxyl group in the starting imine **6**, the *tert*-butyldimethylsiloxy β-lactam **10** (R^3: TBDMS) was obtained instead of the corresponding unprotected β-lactam **10** (R^3: H). An unexpected result was found on attempting to prepare the β-lactam **10***d* from phenoxyacetic acid and the trimethylsilyl protected imine **7***d* by means of our recently reported reagent, thionyl chloride/*N*,*N*-dimethylformamide (7). In such a case, the trimethylsiloxy β-lactam **10***e* was obtained instead of the expected unprotected β-lactam **10***d*.

The second step of the method involves the use of an efficient reagent for oxidation of protected as well as unprotected β-lactam **10**. Although the direct conversion of trimethylsilyl ethers of secondary alcohols to ketones has been reported (8), there is no report concerning the oxidation of TBDMS ethers of alcohols.[3] Among many oxidizing reagents available, the general utility of pyridinium dichromate (PDC) in nonaqueous media is well recognized; this reagent allows mild and large-

[1]Considered as Reagents and Synthetic Methods 45.
[2]Author to whom correspondence may be addressed.

[3]After this work was submitted, a paper appeared concerning the conversion of silyl ethers into carbonyl compounds with Jones reagent in the presence of potassium fluoride. See ref. 17.

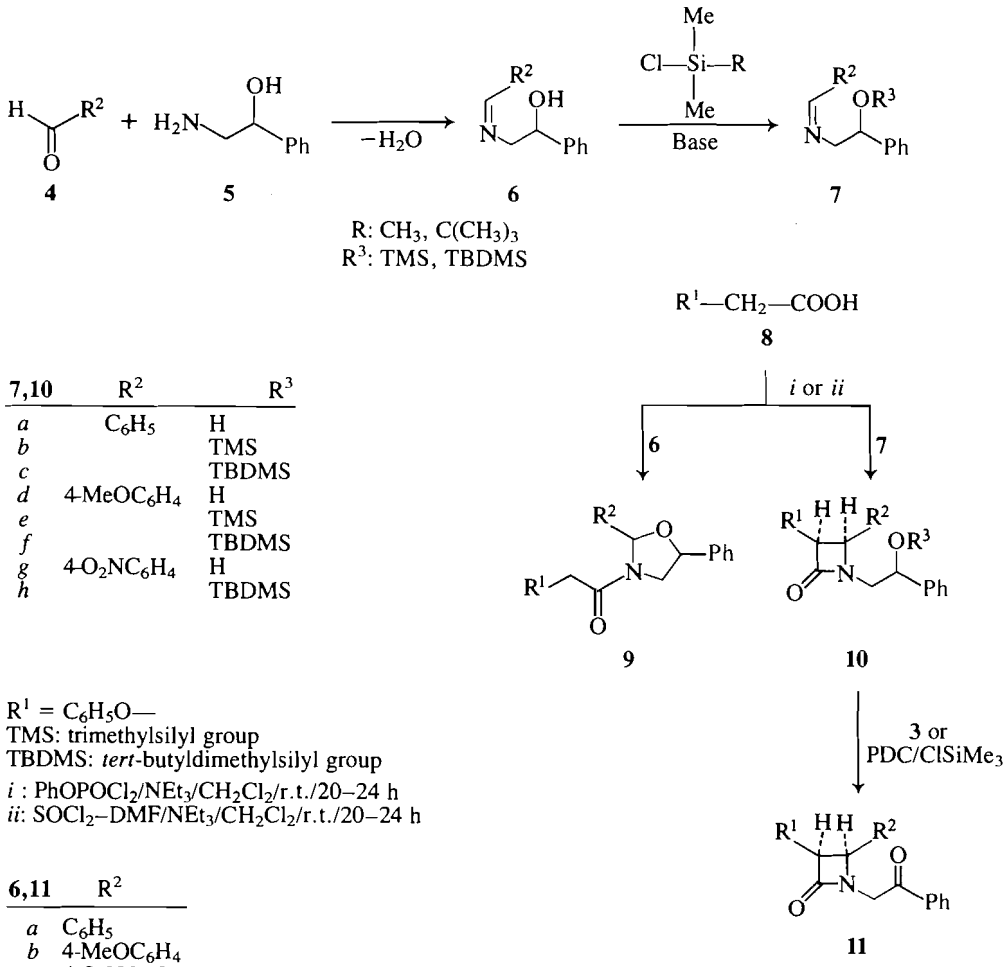

7,10	R^2	R^3
a	C_6H_5	H
b		TMS
c		TBDMS
d	4-$MeOC_6H_4$	H
e		TMS
f		TBDMS
g	4-$O_2NC_6H_4$	H
h		TBDMS

R^1 = C_6H_5O—
TMS: trimethylsilyl group
TBDMS: *tert*-butyldimethylsilyl group
i : $PhOPOCl_2/NEt_3/CH_2Cl_2$/r.t./20–24 h
ii: $SOCl_2$–DMF/NEt_3/CH_2Cl_2/r.t./20–24 h

6,11	R^2
a	C_6H_5
b	4-$MeOC_6H_4$
c	4-$O_2NC_6H_4$

SCHEME 1

scale oxidation of a wide range of alcohols to carbonyl compounds in dichloromethane at room temperature. Unfortunately, in the case of free hydroxy β-lactam **10** (R^3: H) these conditions lead to a very long and incomplete reaction and in some cases undesired products are obtained. For instance, we have found that when β-lactam **10***d* was subjected to PDC oxidation in dichloromethane at room temperature for 30 h, the corresponding β-lactam **11***b* was isolated in 60% yield along with the starting material **10***d* (as directed by tlc analysis of the crude product). In this case, 4-methoxybenzaldehyde was also detected, probably by oxidative cleavage of the C-4 bond. When the method was tested with the β-lactam **10***g*, the corresponding oxidized β-lactam **11***c* was obtained in 66% yield, but the starting β-lactam **10***g* was also recovered. Attempts to apply this procedure for the oxidative deprotection of *tert*-butyldimethylsiloxy β-lactams **10** was unsuccessful: no oxidation takes place between PDC or PCC reagents and **10***c* or **10***f* in dichloromethane as solvent.

Our new finding is that reaction of protected as well as unprotected β-lactams **10** with PDC reagent in combination with trimethylchlorosilane leads to a rapid and mild efficient method for oxidation of these β-lactams to their corresponding carbonyl compounds **11**. Thus, treatment of β-lactam **10***f*, prepared from the β-lactam **10***d* by means of *tert*-butyldimethylchlorosilane (TBDMCS) and 1,8-diazabicyclo[5.4.0]undec-7-ene (DBU) (9), with PDC reagent and trimethylchlorosilane (molar ratio, substrate/reagent/$ClSiMe_3$ 1:1.5:3.5) in dichloromethane as solvent, gave after 60 min of reaction at room temperature the corresponding oxidized β-lactam **11***b* in 95% isolated yield. The utility of this method is exemplified by the direct oxidative deprotection of *tert*-butyldimethylsiloxy β-lactam **10** prepared by reaction of phenoxyacetic acid **8** with the corresponding *tert*-butyldimethylsilylated Schiff bases **7** (R^3: TBDMS) promoted by phenyl dichlorophosphate reagent. In these cases, the oxidized β-lactams **11** were obtained in overall yields in the range of 40%. From the examples listed in Table 1, the reagent **3** as well as the PDC/$ClSiMe_3$ system is general in scope, since various hydroxy compounds, trimethylsilyl ethers, and *tert*-butyldimethylsilyl ethers are readily oxidized into their corresponding carbonyl compounds in good to excellent yields.

It is noteworthy that our procedure represents the first oxidative-deprotection method for *tert*-butyldimethylsilyl ether.[3] These compounds are stable towards Jones reagent (10) and towards PDC reagent, as we have demonstrated here; however, they are readily oxidized by reagent **3** or by the PDC/$ClSiMe_3$ system. A key feature of these β-lactams **11** is shown by their use as potential precursors of *N*-unsubstituted β-lactam antibiotics (Scheme 3). Thus, we have found that treatment of **11***b* with 4-*N*,*N*-dimethylaminopyridinium bromide perbromide ($DMAPHBr_3$) (11) affords the corresponding α-bromoketone **14**, which was easily converted into the *N*-unsubstituted β-lactam **15** by means of sodium hydrogen carbonate and water in acetone as solvent. Better results can be obtained following Barluenga's method (12) for the bromine substitution. Treat-

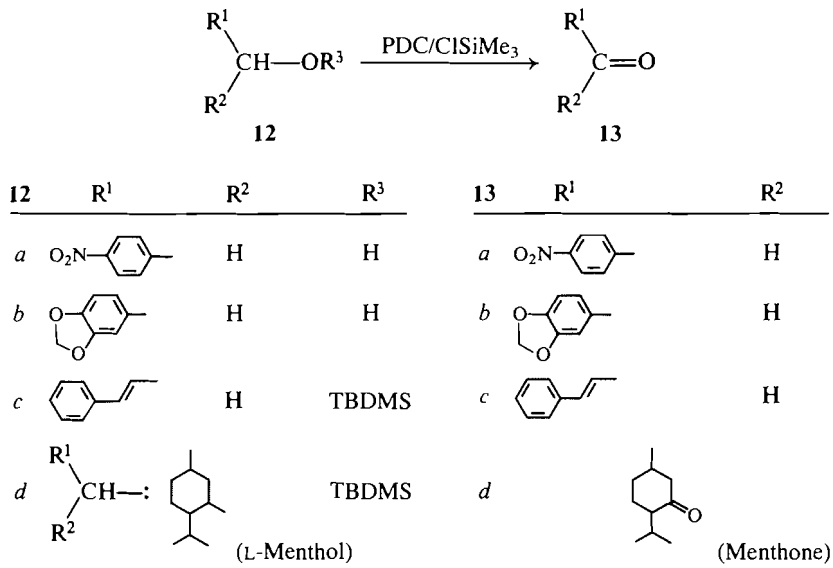

SCHEME 2

TABLE 1. Oxidation of hydroxy compounds and trialkylsilyl ethers

Substrate	Reagent[a]	Time	Product	Yield (%)[b]
10*a*	**1**/TMCS	25 min	**11***a*	88
10*b*	**1**/TMCS	25 min		90
10*c*	**1**/TMCS	1 h		85
	3	35 min		40[c]
10*d*	**1**/TMCS	30 min	**11***b*	85
10*e*	**1**/TMCS	30 min		85
10*f*	**1**/TMCS	1 h		95
10*g*	**1**/TMCS	30 min	**11***c*	80
10*h*	**1**/TMCS	4 h		40[c]
12*a*	**1**/TMCS	2 h	**13***a*	90
12*b*	**1**/TMCS	15 min	**13***b*	100
12*c*	**3**	1 h	**13***c*	95
12*d*	**1**/TMCS	1 h	**13***d*	95

[a]TMCS: $ClSi(CH_3)_3$.
[b]Yield of isolated pure products.
[c]Overall yield from imine **6**.

ment of the resulting amidocarbinol with triethylamine for a few hours gives the *N*-unsubstituted β-lactam **15** in moderate yield.

Oxidation of hydroquinones and trialkylsilyl protected hydroquinones

In view of the results obtained, we also extended our studies to the oxidation of the silyl ethers of hydroquinones. Although Miller and co-workers (13) have demonstrated the utility of silylation–oxidation as a method for the protection and deprotection of the hydroquinone function, in some cases the oxidative deprotection failed to provide the expected quinone. Now we have found that oxidation of trimethylsilyl hydroquinones and *tert*-butyldimethylsilyl hydroquinones by means of trimethylsilyl chlorochromate **3** or by the PDC/$ClSiMe_3$ system proceeds quickly at room temperature, giving the corresponding quinones in excellent yields.

The reaction was carried out in dichloromethane as solvent by addition of a dichloromethane solution of the silyl ether to a solution of the reagent **3** in the same solvent. The solution was initially homogeneous, but within a few minutes the reaction mixture darkened and a black residue appeared. The progress of the reaction can be followed by tlc analysis and the reaction was found complete in 10–15 min in all the cases tested. After work-up, the isolated crude products are almost pure as judged by their physical properties. As can be seen from the results listed in Table 4, the oxidation reaction is more rapid than the oxidation of unprotected hydroquinones (Table 2), but this is probably due to the low solubility of these last compounds in the reaction solvent. It is interesting to note that, whereas the PCC oxidation (13) was unsuccessful for compounds containing electron-withdrawing groups such as **16***d* in the aromatic ring, as well as the nonactivated bis(*tert*-butyldimethylsilyl) ether **16***a*, our procedure gives the corresponding quinones in good yields. Similarly, we have found that PDC reagent also was found unsuitable for carrying out this transformation. However, PDC reagent in combination with trimethylchlorosilane provides another efficient route to quinones from trialkylsilyl protected hydroquinones.

TABLE 2. Oxidation of hydroquinones **16** into quinones **17** by means of reagent **3**

16 (R^3: H)	Time (h)	Yield (%)[a]
a	1.5	90
b	0.5	97
d	0.5	95
e	1.0	90

[a]Isolated yield of **17** by column chromatography (silica gel 70–230 mesh. Eluent: ether/hexane 1:1).

On the other hand, the *tert*-butyldimethylsilyl ethers were prepared by treatment of hydroquinones **16** with *tert*-butyldimethylchlorosilane (TBDMCS) and 1,8-diazabicyclo-[5.4.0]undec-7-ene (DBU) as base in dichloromethane. The reaction was slightly exothermic and, after 5–10 min of stirring at room temperature, a single spot was detected by tlc analysis (silica gel plates, eluent: EtOAc/hexane 1:3), which indicated a complete transformation. These compounds were isolated by vacuum distillation and used in the next step without further purification. In comparison, the TBDMCS/pyridine system was unsuccessful for *tert*-butyldimethylsilylation of hydroquinones, and the

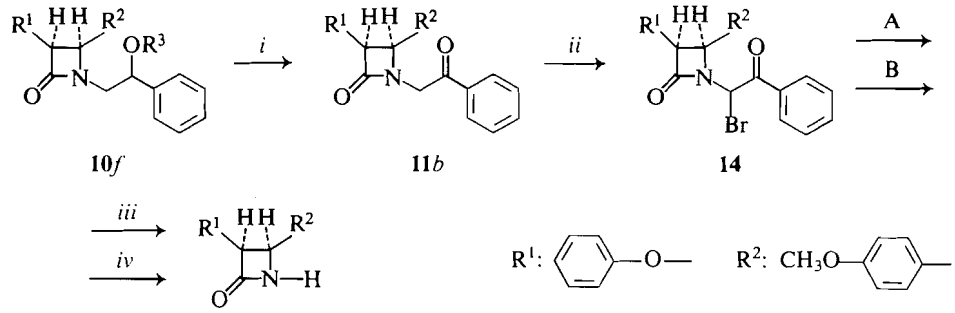

i: $PDC/ClSiMe_3/CH_2Cl_2$/r.t.
ii: $DMAPHBr_3/AcOH$
iii: $H_2O/Me_2CO/NaHCO_3$
iv: HgO/TFBA/THF, then $NaHCO_3$/NaOH

SCHEME 3

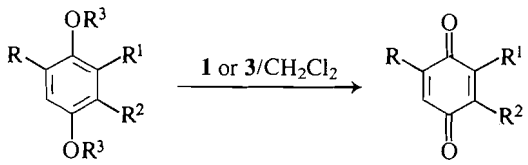

	R	R^1	R^2
a	H	H	H
b	OCH_3	H	H
c	CH_3	CH_3	CH_3
d	Cl	H	H
e	CH_3	H	H
f	$C(CH_3)_3$	H	$C(CH_3)_3$

SCHEME 4

use of triethylamine instead of DBU provided the expected silyl hydroquinones, but in lower yields and with longer reaction times. Particularly, in the case of 1,4-bis(*tert*-butyldimethylsiloxy)-2,5-di-(*tert*-butyl)benzene, reaction of TBDMCS and 2,5-di-(*tert*-butyl)-1,4-hydroquinone in the presence of triethylamine does not take place and the starting hydroquinone was recovered unchanged. Our procedure would appear to be an attractive alternative to the perchlorate (14*a*) or *tert*-butyldimethylsilyltriflate (13) methods, and avoids the use of other sophisticated or sensitive reagents such as allyl-*tert*-butyldimethylsilane (14*b*), *tert*-butyldimethylsilyl enol ethers of 2,4-pentanedione (14*c*,*d*), *tert*-butyldimethyliodosilane (14*e*), and *N*-*tert*-butyldimethylsilylamides (10).

Although the causes of differences in reactivity of PDC and $PDC/ClSiMe_3$ towards TBDMS ethers are not clear at present, the easy preparation and the synthetic versatility of the reagents reported, as good oxidizing agents, is obviously, as demonstrated by these limited number of examples, and may be readily extended to further applications.

Experimental

Melting points were determined on a Büchi SMP-20 melting point apparatus and are uncorrected. Proton nmr spectra were measured on a Varian EM-360 Espectrometer and are reported in parts per million downfield from internal tetramethylsilane. All the starting materials used in this work were either commercially available in generally 98% or higher purity, and used without further purification, or prepared by standard literature procedures.

TABLE 3. Silylation of hydroquinones **16**

16	Reagent[a]	Time (min)	Yield (%)[b]
a	TMCS	30	60
	TBDMCS	30	95
b	TMCS	25	90
	TBDMCS	25	94
c	TBDMCS	20	91
d	TMCS	40	81
	TBDMCS	25	94
e	TBDMCS	25	94
f	TBDMCS	20	84

[a]TMCS: trimethylchlorosilane. TBDMCS: *tert*-butyldimethylchlorosilane.
[b]Yields of isolated pure products; a single spot was observed in tlc analysis.

TABLE 4. Oxidative deprotection of silyl ethers of hydroquinones **16**

16	Protecting group;[a] R^3	Method	Reagent	Time[b] (min)	Yield (%)[c]
a	TMS	A	$ClCrO_3SiMe_3$	20	97
		B	$PDC/ClSiMe_3$	15	96
		—	PDC	—	No reaction
	TBDMS	A	$ClCrO_3SiMe_3$	30	70[d]
		B	$PDC/ClSiMe_3$	15	74[d]
		—	PDC	—	No reaction
b	TMS	A	$ClCrO_3SiMe_3$	30	70
	TBDMS	A	$ClCrO_3SiMe_3$	35	70[d]
c	TBDMS	A	$ClCrO_3SiMe_3$	30	68[d]
d	TMS	A	$ClCrO_3SiMe_3$	50	95
		B	$PDC/ClSiMe_3$	20	90
		—	PDC	—	No reaction
	TBDMS	A	$ClCrO_3SiMe_3$	25	60[d]
		B	$PDC/ClSiMe_3$	15	70[d]
		—	PDC	—	No reaction
e	TBDMS	A	$ClCrO_3SiMe_3$	25	70[d]
f	TBDMS	A	$ClCrO_3SiMe_3$	30	84[d]

[a]TMS: trimethylsilyl group; TBDMS: *tert*-butyldimethylsilyl group.
[b]Conditions: molar ratio substrate/reagent, 1:3; solvent: CH_2Cl_2, room temperature.
[c]Yield of isolated pure products by comparison with authentic samples. A single spot in tlc analysis.
[d]Isolated by column chromatography (eluent: diethyl ether/hexane 1:1).

Preparation of trimethylsilyl chlorochromate ***3***

Finely powdered chromium trioxide (1.0 g, 10 mmol) was exposed to atmospheric moisture for 5–10 min and then chlorotrimethylsilane (1.30 mL, 10 mmol) was added. The mixture was stirred at 30–35°C until the formation of an homogeneous orange-red solution (5–10 min), which was diluted with 20 mL of the appropriate solvent (CH_2Cl_2, CCl_4, or $ClCH_2CH_2Cl$). Finally, dry nitrogen was bubbled through the solution to eliminate the traces of hydrogen chloride formed.

General procedure for the preparation of Schiff bases ***6***

All the Schiff bases were prepared in a similar manner and used without purification. The following are representative of general procedures.

Method A

The liquid aldehyde (10 mmol) was added to the finely powdered 2-amino-1-phenylethanolamine (1.4 g, 10 mmol) and the mixture was heated until total solution was obtained and was then allowed to stand at room temperature. The precipitated product was dissolved in dichloromethane and dried with magnesium sulphate. Filtration and evaporation of the solvent gave the imine in sufficient purity for use in the next step.

Method B

A mixture of the aldehyde (10 mmol), 2-amino-1-phenylethanolamine (10 mmol), and magnesium sulphate in dichloromethane (30 mL) was stirred at room temperature for 2 h. The work-up, as described in method A, gave the corresponding Schiff base **6**.

Preparation of trialkylsilyl ethers of Schiff bases ***6***

General procedure for trimethylsilylation of Schiff bases ***6***

To a solution of an imine **6** (10 mmol) and triethylamine (1.4 mL, 10 mmol) in dry dichloromethane (25 mL) cooled at 0°C was added trimethylchlorosilane (1.2 mL, 10 mmol). The resulting mixture was stirred at room temperature for 60 min, and the resulting solution of the Schiff base **7** (R^3: TMS) was used as such for the next step.

General procedure for tert*-butyldimethylsilylation of Schiff bases* ***6***

To a suspension of the Schiff base **6** (2.5 mmol) in dichloromethane (10 mL), DBU (0.52 mL, 3.5 mmol) was added. When the imine was dissolved, *tert*-butyldimethylchlorosilane (0.53 g, 3.5 mmol) was added and the mixture was stirred at room temperature for a certain time (30–60 min, the reaction can be monitored by tlc analysis; eluent: EtOAc/hexane 1:1). The *tert*-butyldimethylsilyl ether of the Schiff base **7** (R^3: TBDMS) was used as such for the next step.

Preparation of β-lactams ***10*** *(R^3: H). General procedure from phenyl dichlorophosphate reagent* ***(6)***

To a solution of an imine **6** (10 mmol) and triethylamine (1.4 mL, 10 mmol) in dry dichloromethane (25 mL) cooled at 0°C, trimethylchlorosilane (1.2 mL, 10 mmol) was added. The resulting mixture was stirred at room temperature for 60 min. A substituted acetic acid **8** (10 mmol), triethylamine (4.2 mL, 30 mmol), and phenyl dichlorophosphate (1.5 mL, 10 mmol) were consecutively added at 0°C. The resulting mixture was stirred for 24 h at room temperature. Water (20 mL) was added and stirring was continued for a further 15 min. This washing was repeated and finally the organic layer was separated and dried (Na_2SO_4). Evaporation of the solvent gave a waxy residue that was treated with ethanol–water to give the β-lactams **10** (R^3: H): **10***a*, mp 185–190°C; **10***d*, mp 175–177°C; **10***g*, mp 175–178°C (lit. (6) mps 185–190, 175–177, 175–178°C, respectively).

Preparation of tert*-butyldimethylsilyl ethers of β-lactams* ***10*** *(R^3: TBDMS). General procedure*

To a suspension of the β-lactam **10** (R^3: H) in benzene (10 mL), and DBU (0.48 mL, 3.2 mmol), was added *tert*-butyldimethylchlorosilane (0.45 mL, 3 mmol) at room temperature and the reaction mixture was refluxed for 5 h (the reaction can be monitored by tlc; silica gel plates, eluent: AcOEt/hexane 1:1); then, the resulting suspension was diluted with dichloromethane and washed with water (10 mL) and 0.2 *N* hydrochloric acid (10 mL). The organic layer was dried (Na_2SO_4) and the solvent evaporated under reduced pressure to give the nearly pure β-lactam **10** (R^3: TBDMS), which was recrystallized from hexane or ethanol/hexane to give a fairly pure product in 90–95% yield.

cis*-3-Phenoxy-4-phenyl-1-(2′-phenyl-2′-*tert*-butyldimethylsiloxyethyl)azetidin-2-one* ***10***c

From β-lactam **10***a* (0.36 g, 1.0 mmol), yield: 90%, mp 111–114°C; ir ($CHCl_3$) ν (cm^{-1}): 1780 (C=O); nmr ($CDCl_3$) δ (ppm): 7.3–6.4 (m, 15H, arom.), 5.1 (d, J = 5 Hz, 1H, CH), 4.8 (t, J = 6 Hz, 1H, CH—OSi), 4.3 (d, J = 5 Hz, 1H, CH), 3.9 (d, d, J = 6 Hz, J' = −14 Hz, 1H, N—CH—COSi), 2.8 (d, d, J = 6 Hz, J' = −14 Hz, 1H, N—CH—COSi), 0.8 (s, 9H, C—CH_3), 0.0 (s, 3H, Si—CH_3), −0.2 (s, 3H, Si—CH_3). *Anal.* calcd. for $C_{29}H_{35}NO_3Si$: C 73.52, N 2.96, H 7.46; found: C 73.53, N 3.18, H 7.37.

cis*-3-Phenoxy-4-phenyl-4-(4′-methoxyphenyl)-1-(2′-phenyl-2′-*tert*-butyldimethylsiloxyethyl)azetidin-2-one* ***10***f

From β-lactam **10***d* (0.39 g, 1 mmol), yield: 92%, mp 131–134°C; ir ($CHCl_3$) ν (cm^{-1}): 1770 (C=O); nmr ($CDCl_3$) δ (ppm): 7.3–6.4 (m, 14H, arom.), 5.0 (d, J = 5 Hz, 1H, CH), 4.7 (t, J = 6 Hz, 1H, CH—OSi), 4.2 (d, J = 5 Hz, 1H, CH), 3.9 (d, d, J = 6 Hz, J' = −14 Hz, 1H, N—CH—COSi), 3.6 (s, 3H, OCH_3), 2.8 (d, d, J = 6 Hz, J' = −14 Hz, 1H, N—CH—COSi), 0.8 (s, 9H, C—CH_3), 0.0 (s, 3H, $SiCH_3$), −0.2 (s, 3H, $SiCH_3$). *Anal.* calcd. for $C_{30}H_{37}NO_4Si$: C 71.52, N 2.78, H 7.42; found: C 71.43, N 2.97, H 7.52.

cis*-4-(4′-Methoxyphenyl)-3-phenoxy-1-(2′-phenyl-2′-trimethylsiloxyethyl)azetidin-2-one* ***10***e*. Typical procedure from thionyl chloride – dimethylformamide reagent*

In a 25-mL dropping funnel, benzene (5 mL), *N,N*-dimethylformamide (1 mL, 10.2 mmol), and thionyl chloride (0.8 mL, 11 mmol) were added consecutively. After 3–5 min, two phases were separated and the reagent (lower layer) was added to a suspension of phenoxyacetic acid (1.52 g, 10 mmol) in dichloromethane (10 mL) at 0°C. After stirring at 5–10°C for 10 min, the resulting solution was added dropwise to a solution of the Schiff base **7***d* (2.55 g, 10 mmol) and triethylamine (4.7 mL, 33.6 mmol) in dichloromethane (25 mL) at 0–5°C. The resulting mixture was stirred overnight at room temperature, and washed with water (25 mL) and saturated sodium hydrogen carbonate solution (25 mL). The organic layer was dried (Na_2SO_4) and the solvent evaporated under reduced pressure. The resulting oil was crystallized from ethanol–water to give **10***e* (1.4 g, 30%), mp 135–136°C; ir ($CHCl_3$) ν (cm^{-1}): 1790 (C=O); nmr ($CDCl_3$) δ (ppm): 6.4–7.4 (m, 14H, arom.), 5.3 (d, J = 5 Hz, 1H, CH), 5.0 (t, J = 6 Hz, 1H, CH), 4.5 (d, J = 5 Hz, 1H, CH), 4.1 (d, d, J = 6 Hz, J' = −14 Hz, 1H, N—CH—COSi), 3.9 (s, 3H, OCH_3), 3.0 (d, d, J = 6 Hz, J' = −14 Hz, N—CH—COSi), 0.2 (bs, 9H, CH_3). *Anal.* calcd. for $C_{27}H_{31}NO_4Si$: C 70.25, N 3.03, H 6.77; found: C 70.11, N 3.06, H 6.74.

Oxidation of β-lactams ***10***

cis*-3-Phenoxy-4-phenyl-1-(2′-phenyl-2′-oxoethyl)azetidin-2-one* ***11***a

Method A: To a suspension of PDC (1.13 g, 3 mmol) in dichloromethane (20 mL), trimethylchlorosilane (0.9 mL, 7.09 mmol) was added and the dark red-brown mixture was stirred for 3 min. Then *cis*-3-phenoxy-4-phenyl-1-(2′-phenyl-2′-hydroxyethyl)azetidin-2-one **10***a* (0.72 g, 2 mmol) was added and the mixture was stirred for 30 min. Next, moist silica gel was added and the suspension was filtered off through a pad of silica gel to give a dark solution, which was concentrated under reduced pressure. The product was isolated by column chromatography (silica gel 70–230 mesh, eluent: AcOEt/hexane 1:1) to give **11***a* (0.60 g, 85%), mp 175–176°C; ir ($CHCl_3$) ν (cm^{-1}): 1760, 1690 (C=O); nmr ($CDCl_3$) δ (ppm): 7.7–6.4 (m, 15H, arom.), 5.5 (d, J = 5 Hz, 1H, CH), 5.2 (t, J = 5 Hz, 1H, —CH—), 5.0 (d, J = −18 Hz, 1H, N—CH—CO), 4.0 (d, J = −18 Hz, 1H, N—CH—CO). *Anal.* calcd. for $C_{23}H_{19}NO_3$: C 77.28, H 5.37, N 3.92; found: C 77.83, H 5.11, N 3.70.

Method B: To a solution of *N*-(2′-phenyl-2′-*tert*-butyldimethylsiloxyethyl)-2-phenylimine **7***c* prepared as above in dichloro-

methane (20 mL) was consecutively added, at 0°C, phenoxyacetic acid (1.52 g, 10 mmol), triethylamine (4.2 mL, 30 mmol), and phenyl dichlorophosphate (1.5 mL, 10 mmol) and the mixture was stirred at room temperature for 20 h. After this time, the reaction product was worked up by washing with water (20 mL), 0.1 *N* hydrochloric acid (15 mL × 2), and water (20 mL) again, and by drying over sodium sulphate to give a solution of the crude *cis*-1-(2′-phenyl-2′-*tert*-butyldimethylsiloxyethyl)-3-phenoxy-4-phenyl-azetidin-2-one, which was added dropwise to a solution of the trimethylsilyl chlorochromate **3** (20 mmol) prepared as above. The resulting dark suspension was stirred at 0°C for 35 min. When the reaction was complete, moist silica gel was added to hydrolyze the remaining oxidizing agent. Filtration of the mixture through a pad of silica gel and evaporation of the solvents yielded a crude solid that was heated under vacuum (60°C/1 Torr; 1 Torr = 133.3 Pa) to eliminate siloxane by-products, affording *cis*-3-phenoxy-4-phenyl-1-(2′-phenyl-2′-oxoethyl)azetidin-2-one **11***a* (1.42 g, 40% overall yield), mp 175–176°C, from ethanol.

cis-*4-(4′-Methoxyphenyl)-3-phenoxy-1-(2′-phenyl-2′-oxoethyl)-azetidin-2-one* ***11***b

To a suspension of PDC (0.82 g, 2.18 mmol) in dichloromethane (20 mL), trimethylchlorosilane (0.96 mL, 7.56 mmol) was added at 0°C. After 3 min, *cis*-4-(4′-methoxyphenyl)-3-phenoxy-1-(2′-phenyl-2′-*tert*-butyldimethylsiloxyethyl)azetidin-2-one **10***f* (0.48 g, 0.96 mmol) was added and the dark-brown reaction mixture was stirred at room temperature for 60 min. Moist silica gel was then added and the resulting suspension was filtered off through a pad of silica gel, the solvent being evaporated under reduced pressure. The product was purified by column chromatography (silica gel 70–230 mesh; eluent: AcOEt/hexane 1:1) to give **11***b* (0.34 g, 95%), mp 97–99°C; ir ($CHCl_3$) ν (cm^{-1}): 1790, 1730 (C=O); nmr ($CDCl_3$) δ (ppm): 7.7–6.1 (m, 14H, arom.), 5.4 (d, J = 5 Hz, 1H, —CH—), 5.1 (d, J = 5 Hz, 1H, —CH—), 4.9 (d, J = −18 Hz, 1H, N—CH—CO), 3.9 (d, J = −18 Hz, 1H, N—CH—CO), 3.5 (s, 3H, OCH_3). *Anal.* calcd. for $C_{24}H_{21}NO_4$: C 74.39, H 5.47, N 3.62; found: C 75.03, H 5.91, N 4.10.

cis-*4-(4′-Nitrophenyl)-3-phenoxy-1-(2′-phenyl-2′-oxoethyl)-azetidin-2-one* ***11***c

To a suspension of the crude *N*-(2′-phenyl-2′-*tert*-butyldimethylsiloxyethyl)-1-(4′-nitrophenyl)imine **7***h* (10 mmol) prepared from 4-nitrobenzaldehyde (1.51 g, 10 mmol) and 2-amino-1-phenylethanolamine (1.4 g, 10 mmol), followed by *tert*-butyldimethylsilylation as described above, was added consecutively, at 0°C, phenoxyacetic acid (1.52 g, 10 mmol), triethylamine (4.2 mL, 30 mmol), and phenyldichlorophosphate (1.5 mL, 10 mmol) and the mixture was stirred at room temperature for 20 h. After general work-up, the crude β-lactam **10***h* was dissolved in dichloromethane (30 mL) and PDC (11.3 g, 10 mmol) was added. Then, trimethylchlorosilane (9 mL, 70 mmol) was added dropwise at 0–5°C and the resulting mixture was stirred at room temperature for 4 h. After general work-up, the pure product was isolated by column chromatography (eluent: AcOEt/hexane 1:3) to give *cis*-4-(4′-nitrophenyl)-3-phenoxy-1-(2′-phenyl-2′-oxoethyl)azetidin-2-one **11***c* (1.6 g, 40%), mp 160–165°C (from ethanol); ir ($CHCl_3$) ν (cm^{-1}): 1800, 1720 (C=O); nmr ($CDCl_3$) δ (ppm): 8.1–6.5 (m, 14H, arom.), 5.6 (d, J = 5 Hz, 1H, CH), 5.3 (d, J = 5 Hz, 1H, CH), 5.1 (d, J = −18 Hz, 1H, N—CH—CO), 4.1 (d, J = −18 Hz, 1H, N—CH—CO). *Anal.* calcd. for $C_{23}H_{18}N_2O_5$: C 68.64, H 4.52, N 6.96; found: C 69.15, H 4.07, N 7.32.

cis-*4-(4′-Methoxyphenyl)-3-phenoxy-1-(1′-bromo-2′-phenyl-2′-oxoethyl)azetidin-2-one* ***14***

cis-4-(4′-Methoxyphenyl)-3-phenoxy-1-(2′-phenyl-2′-oxoethyl)-azetidin-2-one (0.97 g, 2.5 mmol) was dissolved in acetic acid (10 mL), 4-*N*,*N*-dimethylaminopyridinium bromide perbromide (0.91 g, 2.5 mmol) was added, and the mixture stirred for 15 min. The precipitate was then filtered off and washed with water and ethanol, giving the product **14** (1.0 g, 86%), mp 110–112°C (dec.); ir ($CHCl_3$) ν (cm^{-1}): 1780, 1700 (C=O); nmr ($DCCl_3$) *erythro* and *threo* compound δ (ppm): 3.2 and 3.3 (s, 3H, OCH_3), 4.8 (d, J = 5 Hz, 1H, CH), 4.9 and 5.0 (d, J = 2 Hz, 1H, Br—CH—CO), 5.3 (d, J = 5 Hz, 1H, CH), 6.0–7.5 (m, 14H, arom.). *Mol. wt.* calcd. for $C_{24}H_{20}BrNO_4$: 466.36; found: M^+, 466.

cis-*4-(4′-Methoxyphenyl)-3-phenoxyazetidin-2-one* ***15***

Method A: cis-4-(4′-Methoxyphenyl)-3-phenoxy-1-(1′-bromo-2′-phenyl-2′-oxoethyl)azetidin-2-one **14** (1.4 g, 3 mmol) was dissolved in acetone (30 mL) and water (10 mL). Sodium hydrogen carbonate (0.51 g, 6 mmol) was then added and the mixture was stirred at room temperature for 15 h. After this time, the solid was filtered off and washed with water and ethanol and the product was recrystallized from ethanol to give the title product **15** (0.61 g, 20%), mp 166–170°C (lit. (15) mp 166–167°C).

Method B: To s stirred solution of HgO (0.28 g, 1.25 mmol) and 35% aqueous tetrafluoroboric acid (0.62 g, 2.5 mmol) in tetrahydrofuran (5 mL) was added *cis*-4-(4′-methoxyphenyl)-3-phenoxy-1-(1′-bromo-2′-phenyl-2′-oxoethyl)azetidin-2-one **14** (1.16 g, 2.5 mmol). The mixture was stirred at room temperature for 2 h and then treated successively with saturated sodium hydrogen carbonate solution and 2 *N* sodium hydroxide until basic. The precipitated HgO was filtered off (0.23 g, 80%) and the filtrate was extracted with dichloromethane (20 mL × 2). The organic extracts were dried and the solvent evaporated under reduced pressure giving an oil, which was dissolved in dichloromethane (5 mL); then triethylamine (0.28 mL, 2 mmol) was added and the mixture was stirred for 3 h. Next, the mixture was washed successively with 2 *N* hydrochloric acid (5 mL) and water (5 mL). The organic layer was separated and dried over sodium sulfate and the solvent evaporated under reduced pressure to give **15**, which was crystallized from ethanol (0.24 g, 35%), mp 167–170°C (lit. (16) mp 167–170°C; lit. (15) mp 166–167°C).

General procedure for the oxidation of hydroquinones ***16***

A solution of reagent **3** (30 mmol) prepared as above was added dropwise to a suspension of the hydroquinone **16** (10 mmol) in the same solvent (10 mmol). The resulting dark-brown mixture was stirred at room temperature for the time indicated in Table 2. The progress of the reaction was monitored by tlc analysis at regular intervals. Soon after completion of the reaction moist silica gel was added and the mixture was filtered off through a pad of silica gel to give a yellow solution that was concentrated under reduced pressure to afford crude product. Isolation by column chromatography (silica gel; eluent: diethyl ether/hexane 1:1) gave a pure 1,4-benzoquinne **17**.

*Preparation of 1,4-bis(*tert*-butyldimethylsiloxy)benzenes*

A solution of *tert*-butyldimethylchlorosilane (0.660 g, 4.4 mmol), in CH_2Cl_2, the hydroquinone **16** (2.0 mmol), and 1,8-diazabicyclo[5.4.0]undec-7-ene (DBU) (0.760 g, 5.0 mmol), was stirred at room temperature for 30 min. The mixture was washed with water (5 mL), 0.1 *N* hydrochloric acid (10 mL), and saturated $NaHCO_3$ solution (5 mL), then dried (Na_2SO_4) and evaporated to yield crude 1,4-bis-(*tert*-butyldimethylsiloxy)benzenes, which were purified by reduced pressure distillation.

For 1,4-bis(trimethylsiloxy)benzenes, the same procedure was followed, using trimethylchlorosilane instead of *tert*-butyldimethylchlorosilane.

General procedure for the oxidation of 1,4-bis(trimethylsiloxy)-benzenes

Method A

To a stirred ice-cold solution of trimethylsilyl chlorochromate **3** (6.0 mmol) prepared as above in dichloromethane (10 mmol), a solution of the corresponding 1,4-bis(trimethylsiloxy)benzene (2.0 mmol) in the same solvent (5 mL) was added dropwise over a 5-min period, and stirred for 30 min. The reaction was monitored by tlc analysis (silica gel plates; eluent: AcOEt/hexane 1:2). On completion, moist silica gel (5.0 g) was added and the mixture was shaken for 5 min, decolorized, and filtered off through a pad of silica gel to give a solution that was concentrated and purified by reduced pressure distillation to afford a fairly pure quinone **17**.

Method B

To a suspension of PDC (5.64 g, 15 mmol) in dichloromethane (15 mL), trimethylchlorosilane (4.5 mL, 35.4 mmol) was added at 0°C and then the corresponding 1,4-bis(trimethylsiloxy)benzene (5 mmol) was added to the resulting red-brown mixture. The reaction was stirred at room temperature for 15 min, then filtered off through a pad of silica gel (230–400 mesh) and washed with dichloromethane. The resulting yellow solution was treated with water (15 mL × 2). The organic layer was dried (Na_2SO_4) and the solvent evaporated under reduced pressure to give the corresponding quinone **17**.

*General procedure for the oxidation of 1,4-bis(*tert*-butyldimethylsiloxy)benzene*

Method A

To a cooled (0°) solutions of trimethylsilyl chlorochromate **3** (15 mmol), prepared as above in dichloromethane (15 mmol) was added and the reaction mixture was stirred at the same temperature for 20–30 min. On completion, wet silica gel (10 g) was added to hydrolyze the remaining oxidizing species and the mixture was filtered through a pad of silica gel. The organic solution was dried and the crude quinone purified by column chromatography (silica gel; eluent: hexane/ether 1:1).

Method B

To a suspension of PDC (1.97 g, 5.23 mmol) in dichloromethane (10 mL), trimethylchlorosilane (1.59 mL, 12.52 mmol) was added at 0°C and the corresponding 1,4-bis(*tert*-butyldimethylsiloxy)benzene (5.0 mmol) was then added to the resulting red-brown mixture. The reaction was stirred for 15 min, then filtered off through a pad of silica gel (230–400 mesh) and washed with dichloromethane. The resulting yelow solution was treated with water (15 mL × 2) and the organic layer was dried (Na_2SO_4). The solvent was evaporated under reduced pressure and the resulting product was purified (elution of silanol) by column chromatography (silica gel; eluent: diethyl ether/hexane 1:1) to give the corresponding pure benzoquinone **17**.

Acknowledgements

A grant from the Ministerio de Educación y Ciencia to F. P. Cossío is gratefully acknowledged. We thank J. M. Castillo, B. Lecea, and A. Arrieta for their collaboration in this work. This work was in part supported by Gema-Liesa A. S. (Spanish) and Lonza A. G. (Swiss).

1. (*a*) K. B. WIBERG. Oxidation in organic chemistry. Academic Press, New York. 1965; (*b*) H. O. HOUSE. *In* Modern synthetic reactions. *Edited by* W. A. Benjamin, London. 1972. p. 257; (*c*) C. A. BUHELER and D. E. PEARSON. Survey of organic synthesis. Vol. I. Wiley – Interscience, New York. 1970.
2. (*a*) G. CAINELLI and G. CARDILLO. *In* Chromium oxidations in organic chemistry. Springer Verlag, Berlin. 1984; (*b*) M. FIESER. Reagents for organic synthesis. Vol. 11. Wiley–Interscience, New York. 1984. p. 450, and references cited therein.
3. E. J. COREY and G. SCHMIDT. Tetrahedron Lett. 399 (1979).
4. E. J. COREY and J. W. SUGGS. Tetrahedron Lett. 2647 (1975).
5. (*a*) J. M. AIZPURUA and C. PALOMO. Tetrahedron Lett. **24**, 4367 (1983); (*b*) J. M. AIZPURUA, B. LECEA, M. JUARISTI, and C. PALOMO. Tetrahedron, **41**, 2903 (1985).
6. (*a*) J. M. AIZPURUA, I. GANBOA, F. P. Cossío, A. GONZÁLEZ, A. ARRIETA, and C. PALOMO. Tetrahedron Lett. **25**, 3905 (1984); (*b*) A. ARRIETA, F. P. Cossío, and C. PALOMO. Tetrahedron, **41**, 1703 (1985).
7. A. ARRIETA, J. M. AIZPURUA, and C. PALOMO. Tetrahedron Lett. **25**, 3365 (1984).
8. (*a*) G. A. OLAH and T. L. HO. Synthesis, 609 (1976); (*b*) M. E. JUNG. J. Org. Chem. **41**, 1479 (1976); (*c*) H. W. PINNICK and N. H. LAJIS. J. Org. Chem. **43**, 371 (1978); (*d*) R. BAKER, V. B. RAO, P. D. RAVENSCROFF, and C. J. SWAIN. Synthesis, 572 (1983).
9. J. M. AIZPURUA and C. PALOMO. Tetrahedron Lett. 475 (1985).
10. TH. P. MAWHINNEY and M. A. MADSON. J. Org. Chem. **47**, 3336 (1982).
11. A. ARRIETA, I. GANBOA, and C. PALOMO. Synth. Commun. **14**, 939 (1984).
12. J. BARLUENGA, L. ALONSO CIRES, P. J. CAMPS, and G. ASENSIO. Synthesis, 53 (1983).
13. J. P. WILLIS, K. A. Z. GOPINS, and L. L. MILLER. J. Org. Chem. **46**, 3215 (1981).
14. (*a*) T. J. BARTON and C. R. TULLY. J. Org. Chem. **43**, 3649 (1978); (*b*) T. MORITA, Y. OKAMOTO, and H. SAKURAI. Tetrahedron Lett. 99 (1979); (*c*) T. VEYSOGLU and L. A. MITSCHER. Tetrahedron Lett. **22**, 1299 (1981); **22**, 1303 (1981); (*d*) C. F. BUGGE and M. P. MERTES. J. Org. Chem. **46**, 1984 (1981); (*e*) M. R. DETTY. J. Org. Chem. **45**, 924 (1980).
15. A. K. BOSE, H. TSAI, S. D. SHARMA, and M. S. MANHAS. Tetrahedron Lett. 3851 (1973).
16. I. GANBOA, F. P. Cossío, and C. PALOMO. Tetrahedron Lett. **26**, 3041 (1985).
17. H-J. LIU and I-S. HAN. Synth. Commun. **15**, 759 (1985).

The preferred conformation of 2-fluoro-2-deoxy β-D-mannopyranosyl fluoride. An X-ray crystallographic and 2-dimensional proton nuclear magnetic resonance study

STEPHEN G. WITHERS,[1] IAN P. STREET, AND STEVEN J. RETTIG[2]
Department of Chemistry, University of British Columbia, Vancouver, B.C., Canada V6T 1Y6
Received July 3, 1985

STEPHEN G. WITHERS, IAN P. STREET, and STEVEN J. RETTIG. Can. J. Chem. **64**, 232 (1986).

The preferred conformation of 2-fluoro-2-deoxy β-D-mannopyranosyl fluoride has been determined in the solid state by X-ray crystallography and in aqueous solution by 2-dimensional *J*-resolved proton nuclear magnetic resonance. Crystals of 2-fluoro-2-deoxy β-D-mannopyranosyl fluoride are monoclinic, *a* 4 10.9150(8), *b* 4 4.9079(4), *c* 4 6.9902(6) Å, β = 105.158(4)°, $Z = 2$, space group $P2_1$. The structure was solved by direct methods and was refined by full-matrix least-squares procedures to $R = 0.028$ and $R_w = 0.031$ for 797 reflections with $I \geq 3\sigma(I)$. The sugar ring was present in an essentially undistorted $^4C_1$ chair conformation. Weak, but significant interactions, presumably hydrogen bonding of the type OH ... F and CH ... F, are observed within the crystal lattice. Coupling constants observed in the proton nmr were consistent only with a $^4C_1$ chair conformation in solution. These observations are briefly discussed in terms of recent findings concerning the interaction of fluorodeoxy sugars with enzymic binding sites.

STEPHEN G. WITHERS, IAN P. STREET et STEVEN J. RETTIG. Can. J. Chem. **64**, 232 (1986).

On a déterminé la conformation privilégiée du fluorure du fluoro-2 déoxy-2 β-D-mannopyrannosyle tant à l'état solide en faisant appel à diffraction des rayons-X qu'en solution aqueuse en faisant appel à la rmn du ^1H bidimensionnelle résolue pour *J*. Les cristaux du fluorure du fluoro-2 déoxy-2 β-D-mannopyrannosyle sont monocliniques avec $a=10,9150(8)$, $b=4,9079(4)$, $c=6,9902(6)$ Å, β=105,158(4)°, $Z=2$ et groupe d'espace $P2_1$. On a résolu la structure par des méthodes directes et on l'a affinée par la méthode des moindres carrés (matrice entière) jusqu'à des valeurs de $R=0,028$ et $R_w = 0,031$ pour 797 réflexions avec $I \geq 3\sigma(I)$. Le cycle du sucre existe essentiellement dans une conformation chaise $^4C_1$ qui n'est pas déformée. Dans la maille du cristal, on observe des interactions faibles, mais significatives, qui sont probablement dues à des liaisons hydrogènes du type OH . . . F et CH . . . F. Les constantes de couplage observées dans le spectre rmn du ^1H en solution ne peuvent être expliquées que par une conformation chaise $^4C_1$. On discute brièvement de ces résultats par rapport aux résultats obtenus récemment concernant l'interaction des sucres fluoro-déoxy avec les sites de liaison enzymatique.

[Traduit par le journal]

Introduction

The mode of interaction of carbohydrates and proteins has been attracting considerable interest of late, particularly since the antigenic determinants of red blood cells are oligosaccharides and it is their interaction with receptor proteins that is central to blood type recognition (1). In order to probe the intermolecular forces dominating such interactions, deoxy- and fluorodeoxy-saccharide analogues have been employed in several specificity studies (2–5). Such analogues are useful since the hydroxyl moiety is replaced by a smaller, and therefore sterically compatible, substituent, but one of different electronic properties. Systematic studies of mono-substituted derivatives can therefore provide information on the factors contributing to binding at each position. The enzyme glycogen phosphorylase provides a useful model system for a study of carbohydrate/protein interactions since the three-dimensional structure of the glycogen phosphorylase/glucose complex has been determined by X-ray crystallography (4). Studies currently in progress involve a systematic study of the specificity of this enzyme for glucose as an inhibitor and for its substrate glucose-1-phosphate, using a series of deoxy and fluorodeoxy analogues. However, since the enzyme is known to bind glucose in its $^4C_1$ conformation (4, 6) it was considered important to establish that substitution of one or more fluorine atoms into the ring did not distort the sugar away from this preferred $^4C_1$ conformation. Such concerns were based upon the previous observation (7) that 2,3,4-tri-*O*-acetyl β-D-xylopyranosyl fluoride adopts the $^1C_4$ conformation in solution, as a result of interactions between the dipole associated with the C—F bond and that associated with the ring oxygen atom. This provided a convincing demonstration of the strength of the anomeric effect associated with a fluorine substituent at the anomeric centre, since in its preferred conformation the acetoxy substituents at C(2), C(3), and C(4) are forced into unfavourable axial orientations. In the case under consideration a complete inversion to a $^1C_4$ conformation is considerably less likely, primarily as a result of the requirement for the bulky hydroxymethyl group at C(5) to then adopt an axial configuration with consequent repulsive interaction. However, since any significant distortion in the molecule could affect its ability to bind to the enzyme, it was deemed important to investigate this possibility.

2-Fluoro-2-deoxy-β-D-mannopyranosyl fluoride was selected as the most likely compound, in the series being texted, to be distorted, on the basis of dipolar repulsions between the two fluorine substituents and the ring oxygen atom, in the $^4C_1$ conformation. Its solid state structure was thus determined by X-ray crystallography and its conformation in solution ascertained by proton nmr. The X-ray crystal structure has also provided some insight into the involvement of the fluorine atom in hydrogen bonding within the crystal lattice.

Experimental

2-Fluoro-2-deoxy β-D-mannopyranosyl fluoride was obtained by Zemplen deacetylation (8) of its tri-*O*-acetate. The protected sugar, obtained by the addition of trifluoromethyl hypofluorite to D-glucal tri-*O*-acetate (9), was kindly provided by Dr. D. Dolphin.

The ^1H nmr spectra were determined in D_2O at ambient temperature on a Bruker WH-400 spectrometer. The ^1H nmr chemical shifts are referenced to external DSS at 0 ppm. The ^{19}F nmr chemical shifts are referenced to external trifluoroacetic acid in D_2O at 0 ppm. The

[1]Author to whom correspondence may be addressed.
[2]Experimental Officer, University of British Columbia Crystallographic Service Laboratory.

homonuclear 2-dimensional *J*-resolved spectrum was obtained using the standard pulse sequence shown below, at 256 different values of t_1. 256 spectra of 1K data points requiring 48 acquisitions each were thus obtained and the resultant matrix then transformed in the t_1 and t_2 dimensions.

Single crystals of 2-fluoro-2-deoxy β-D-mannopyranosyl fluoride were obtained by vapour diffusion of petroleum ether into a solution of the title compound in diethyl ether/methanol.

X-ray crystallographic analysis

A crystal bounded by the 10 faces (followed by their distances in mm from a common origin): ±(1 0 0), 0.12, ±(1 0 −1), 0.09, ±(1 0 1), 0.14, ±(1 1 −2), 0.19, ±(−1 1 2), 0.23 was mounted in a general orientation. Unit-cell parameters were refined by least squares on 2 sin θ/λ values for 25 reflections (2θ = 35–42°) measured on a diffractometer with Mo-*K*α radiation (λ(*K*α$_1$) = 0.70930 Å, λ(*K*α$_2$) = 0.71359 Å). Crystal data at 22°C are:

$C_6H_{10}F_2O_4$ fw = 184.14

Monoclinic, a = 10.9150(8), b = 4.9079(4), c = 6.9902(6) Å, β = 105.158(4)°, V = 361.43(5) Å^3, Z = 2, ρ_c = 1.692 Mg m^{-3}, $F(000)$ = 192, μ(Mo-*K*α) = 1.62 cm^{-1}. Absent reflections: 0*k* 0, *k* odd, space group $P2_1$ (C_2^2, No. 4).

Intensities were measured with graphite-monochromated Mo-*K*α radiation on an Enraf–Nonius CAD4-F diffractometer. An ω–2θ scan at 0.80–10.06° min^{-1} over a range of (0.60 + 0.35 tan θ) degrees in ω (extended by 25% on both sides for background measurement) was employed. Data were measured by 2θ = 55°. The intensities of 3 check reflections, measured every 3600 s throughout the data collection, showed only small random variations. Of the 919 independent reflections measured and processed,[3] 797 (86.7%) had intensities greater than or equal to 3σ(I) above background, where $\sigma^2(I) = S + 2B + (0.04(S-B))^2$ with S = scan count and B = normalized background count.

The structure was solved by direct methods, the coordinates of all non-hydrogen atoms being determined from an *E*-map and those of the hydrogen atoms from a subsequent difference map. Hydrogen atoms were refined with isotropic and non-hydrogen atoms with anisotropic thermal parameters. The scattering factors of ref. 10 were used for non-hydrogen atoms and those of ref. 11 for hydrogen atoms. The weighting scheme $w = 1/\sigma^2(F)$, where $\sigma^2(F)$ is derived from the previously defined $\sigma^2(I)$, gave uniform average values of $w(|F_o| - |F_c|)^2$ over ranges of both $|F_o|$ and sin θ/λ and was employed in the final stages of full-matrix refinement of variables. Reflections with $I < 3\sigma(I)$ were not included in the refinement. Convergence was reached at R = 0.028 and R_w = 0.031 for 797 reflections with $I \geq 3\sigma(I)$. For all 919 reflections, R = 0.041. The function minimized was $\Sigma w(|F_o| - |F_c|)^2$, $R = \Sigma \| F_o| - |F_c\| / \Sigma |F_o|$ and $R_w = (\Sigma w(|F_o| - |F_c|)^2 / \Sigma w|F_o|^2)^{1/2}$.

On the final cycle of refinement the mean and maximum parameter shifts corresponded to 0.001 and 0.014σ respectively. The mean error in an observation of unit weight was 1.648. A final difference map showed no unusual features, maximum fluctuations being −0.26 and +0.18 e Å^{-3}. The final positional and thermal parameters appear in Tables 1 and 6[4] respectively. Measured and calculated structure factors have been placed in the Depository of Unpublished Data.[4]

The ellipsoids of thermal motion for the non-hydrogen atoms are shown in Fig. 1 and the packing diagram in Fig. 2. The thermal motion has been analysed in terms of the rigid-body modes of translation, libration, and screw motion (12). The rms standard error in the temperature factors σU_{ij} (derived from the least-squares analysis) is 0.0007 Å^2. Analysis of the six-membered ring gave rms ΔU_{ij} = 0.0009 Å^2 and physically reasonable rigid-body parameters. The appropriate bond distances have been corrected for libration (12, 13), using shape parameters q^2 of 0.08 for all atoms involved. Corrected bond lengths appear in Table 2 along with the uncorrected values; corrected bond angles do not differ by more than 1σ from the uncorrected values given in Table 3. Intra-annular torsion angles defining the conformation of the six-membered ring are listed in Table 4, and hydrogen bond and weak C—H . . . (F/O) interaction data in Table 5. Bond lengths and angles involving hydrogen and a complete listing of torsion angles (Tables 7–9) are included as supplementary material.

TABLE 1. Final positional (fractional × 10^4, H × 10^3) and isotropic thermal parameters (U × 10^3 Å^2) with estimated standard deviations in parentheses*

Atom	x	y	z	U_{eq}/U_{iso}
F(1)	−345(1)	5109	7178(2)	48
F(2)	1588(1)	4938(5)	10472(2)	44
O(3)	3406(1)	9172(5)	11317(2)	32
O(4)	4609(1)	7772(5)	8300(2)	28
O(5)	1459(1)	4702(5)	6369(2)	28
O(6)	4123(1)	5281(5)	4306(2)	34
C(1)	743(1)	6504(7)	7197(3)	31
C(2)	1424(2)	7287(6)	9296(3)	30
C(3)	2714(2)	8483(6)	9355(2)	25
C(4)	3435(2)	6543(6)	8340(2)	21
C(5)	2637(1)	5918(6)	6241(2)	23
C(6)	3237(2)	3873(6)	5133(3)	29
H(O3)	345(2)	783(6)	1198(3)	29(6)
H(O4)	513(3)	663(8)	849(4)	51(9)
H(O6)	464(3)	426(11)	404(5)	72(10)
H(1)	47(2)	820(6)	639(3)	39(7)
H(2)	98(2)	848(6)	988(3)	26(5)
H(3)	259(2)	1018(6)	866(3)	24(5)
H(4)	360(2)	483(5)	907(3)	20(5)
H(5)	247(2)	748(6)	546(3)	28(5)
H(6a)	257(2)	287(7)	415(4)	45(7)
H(6b)	366(2)	248(7)	605(3)	35(6)

*U_{eq} = 1/3 trace $U_{diagonalized}$.

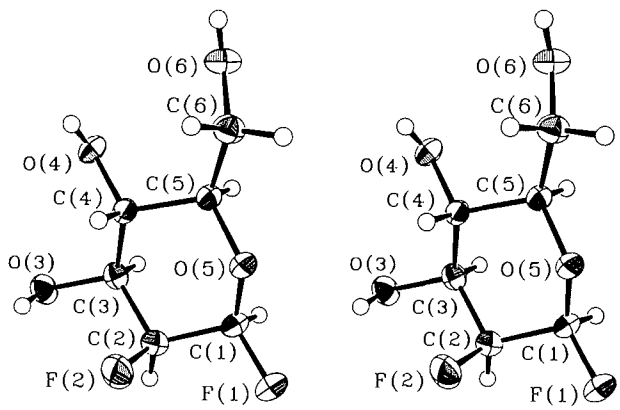

FIG. 1. Stereoview of the 2-fluoro-2-deoxy β-D-mannopyranosyl fluoride molecule. 50% probability thermal ellipsoids are shown for the non-hydrogen atoms. Hydrogen atoms were assigned arbitrarily small thermal parameters for the sake of clarity.

Results and discussion

The one-dimensional ^{1}H nmr spectrum of the title compound is presented in Fig. 3(a). Attempts to unequivocally assign all

[3]The computer progams used include locally written programs for data processing and locally modified versions of the following: MULTAN 80, multisolution program by P. Main, S.J. Fiske, S.E. Hull, L. Lessinger, G. Germain, J.P. Declercq, and M.M. Woolfson; ORFLS, full-matrix least squares, and ORFFE, function and errors, by W.R. Busing, K.O. Martin, and H.A. Levy; FORDAP, Patterson and Fourier syntheses, by A. Zalkin; ORTEP II, illustrations, by C.K. Johnson.

[4]The structure factor table, Table 6 (anisotropic thermal parameters) and other material mentioned in the text may be purchased from the Depository of Unpublished Data, CISTI, National Research Council of Canada, Ottawa, Ont., Canada K1A 0S2.

TABLE 2. Bond lengths (Å) with estimated standard deviations in parentheses

Bond	Length		Bond	Length	
	Uncorr.	Corr.		Uncorr.	Corr.
F(1)—C(1)	1.368(2)	1.372	O(6)—C(6)	1.429(2)	1.432
F(2)—C(2)	1.400(3)	1.405	C(1)—C(2)	1.511(3)	1.516
O(5)—C(1)	1.401(2)	1.406	C(2)—C(3)	1.515(3)	1.520
O(5)—C(5)	1.442(2)	1.446	C(3)—C(4)	1.524(3)	1.529
O(3)—C(3)	1.423(2)	1.426	C(4)—C(5)	1.529(2)	1.534
O(4)—C(4)	1.424(2)	1.427	C(5)—C(6)	1.517(3)	1.521

TABLE 3. Bond angles (deg) with estimated standard deviations in parentheses

Bonds	Angle(deg)	Bonds	Angle(deg)
C(1)—O(5)—C(5)	111.53(14)	C(2)—C(3)—C(4)	109.53(15)
F(1)—C(1)—O(5)	104.9(2)	O(4)—C(4)—C(3)	108.8(2)
F(1)—C(1)—C(2)	109.98(14)	O(4)—C(4)—C(5)	110.84(13)
O(5)—O(1)—C(2)	112.08(14)	C(3)—C(4)—C(5)	109.79(13)
F(2)—C(2)—C(1)	108.4(2)	O(5)—C(5)—C(4)	108.47(12)
F(2)—C(2)—C(3)	109.15(15)	O(5)—C(5)—C(6)	105.47(12)
C(1)—C(2)—C(3)	110.03(14)	C(4)—C(5)—C(6)	114.18(15)
O(3)—C(3)—C(2)	111.95(14)	O(6)—C(6)—C(5)	108.3(2)
O(3)—C(3)—C(4)	112.86(14)		

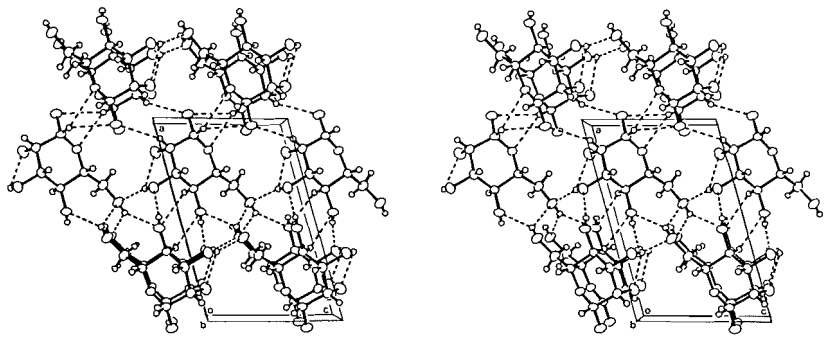

FIG. 2. Stereoview of the packing of 2-fluoro-2-deoxy β-D-mannopyranosyl fluoride. Broken lines represent hydrogen bond and H...(F/O) interactions with H...F ≤ 2.47 Å and H...O ≤ 2.56 Å.

TABLE 4. Intra-annular torsion angles (deg) with standard deviations in parentheses

Atoms	Value(deg)
C(5)—O(5)—C(1)—C(2)	−62.1(2)
O(5)—C(1)—C(2)—C(3)	56.0(2)
C(1)—C(2)—C(3)—C(4)	−52.2(2)
C(2)—C(3)—C(4)—C(5)	55.0(2)
C(3)—C(4)—C(5)—O(5)	−59.3(2)
C(1)—O(5)—C(5)—C(4)	63.0(2)

resonances and couplings in this spectrum as a means of determining its solution conformation were unsuccessful. Rather than embark on a lengthy series of decoupling experiments to permit assignment, a homonuclear (^{1}H) two-dimensional *J*-resolved spectrum was obtained and is presented as a contour plot in Fig. 3(b). In such a presentation the coupling constant axis contains ^{1}H–^{1}H coupling constant information only, while the projection onto the chemical shift axis produces the proton-decoupled, but still fully fluorine-coupled ^{1}H spectrum, thus enormously simplifying assignment. The assignment achieved is presented in Table 10. The coupling constants observed are consistent only with a $^4C_1$ conformation for the sugar, as follows. Large coupling constants (approximately 10 Hz) between H(5) and H(4) and between H(4) and H(3) are uniquely consistent with a *trans*-diaxial arrangement of these protons, while large vicinal proton–fluorine coupling constants of 30 Hz and 17.8 Hz between H(3) and F(2) and between H(1) and F(2) respectively are indicative of a *trans*-diaxial arrangement of these substitutents (14, 15). In fact, all the *trans*-diaxial coupling constants are slightly larger than those determined for the fully acetylated sugar (15). This could be due to differences in electronegativity of acetate (16) versus hydroxyl substituents or to a solvent effect, but is more likely due to the deprotected sugar adopting a more rigid $^4C_1$ conformation in D_2O than the protected sugar adopts in $CDCl_3$. The possibility of some degree of distortion of the protected sugar (based upon nmr data) was discussed in this earlier paper (15). The value of 2-dimensional nmr in such a spectral

TABLE 5. Hydrogen bonds and weak C—H...(F/O) interactions*

Atoms	Length		Angle
	H...A(Å)	D...A (Å)	D—H...A(deg)
O(3)—H(03)...O(6)[1]	2.03(3)	2.787(2)	158(2)
O(3)—H(03)...F(2)[2]	2.47(2)	2.827(2)	108(2)
O(4)—H(04)...O(3)[3]	1.98(3)	2.754(2)	170(3)
O(6)—H(06)...O(4)[4]	2.14(4)	2.841(2)	144(3)
O(6)—H(06)...O(6)[4]	2.48(5)	3.108(2)	134(3)
C(1)—H(1)...O(5)[5]	2.56(2)	3.365(2)	136(2)
C(2)—H(2)...F(1)[6]	2.46(2)	3.301(2)	151(2)
C(4)—H(4)...O(4)[3]	2.52(2)	3.298(2)	137(2)

*Superscripts refer to symmetry operations: $x, y, 1+z$; x, y, z; $1-x, y-1/2, 2-z$; $1-x, y-1/2, 1-z$; $-x, 1/2+y, 1-z$; and $-x, 1/2+y, 2-z$, respectively.

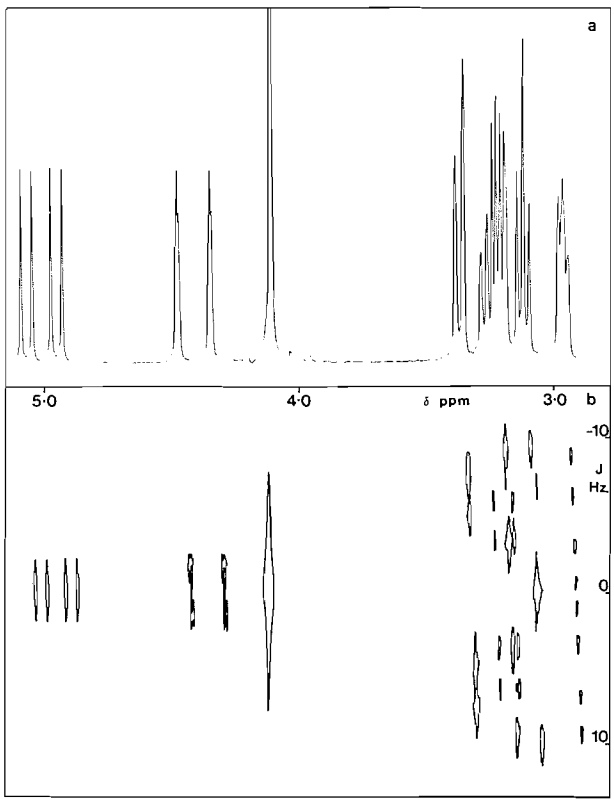

FIG. 3. The ^1H nmr spectra of 2-fluoro-2-deoxy β-D-manno-pryanosyl fluoride in D_2O at 400 MHz and ambient temperature. (a) 1-Dimensional spectrum; (b) 2-dimensional *J*-resolved spectrum.

assignment is best illustrated by a couple of examples from Fig. 3. The multiplet due to H(5) ($\delta = 2.95$ ppm) is well resolved in the two-dimensional nmr, and all couplings are seen to be proton–proton couplings, with no proton–fluorine coupling. The multiplets between $\delta = 3.14$ ppm and $\delta = 3.30$ ppm are well resolved in the two-dimensional nmr as resonances from two protons, one of which (H(6′), $\delta = 3.21$ ppm) is a proton coupled double doublet ($J(6–6') = 12.4$ Hz, $J(6' -5) = 5.9$ Hz) with a small long-range fluorine coupling that manifests itself as a broadened contour. The other resonance (H(3), $\delta = 3.23$ ppm) contains both fluorine–proton and proton–proton coupling and thus appears as two double doublets separated along the chemical shift axis by the fluorine coupling constant. Similarly the resonance due to H(1) is seen to contain only fluorine–proton couplings and no proton–proton coupling, and thus appears as a multiplet along the chemical shift axis. A $^4C_1$ conformation is therefore unequivocally assigned for this compound under these conditions.

The bond lengths and bond angles for the title compound, as determined by X-ray crystallography, are presented in Tables 2 and 3. The three-dimensional structure with carbon, oxygen, and fluorine atoms represented as thermal ellipsoids is presented in stereo format in Fig. 1. The compound is clearly in the normal $^4C_1$ conformation with one axial fluorine (F(2) and one equatorial fluorine (F(1). The distance C(2)—F(2) is very similar to the average C—F value of 1.40 Å observed for several other deoxyfluoro sugar derivatives (17–21), but slightly greater than the average value for the paraffinic C—F bond (22) (1.38 Å), whereas the C(1)—F(1) bond is slightly shorter (1.368 Å). This shorter C(1)—F(1) bond length is interesting, as similar observations have been made previously on the relative shortening of the C(1)—O(1)H bond length in many structure determinations of pyranose sugars (23). The pyranose ring is essentially unstrained since very little distortion is observed based upon the intra-annular torsion angles (23) (Table 4) and upon the calculated puckering parameters as defined by Cremer and Pople (24). Comparison of the intra-annular torsion angles with a set of average torsion angles for mannose calculated previously (23), based upon 12 mannose structures, reveals that some small differences (5° or less) in angle, centred around C(5) and O(5), are observed. The puckering parameters reveal the same minor distortions. Parameters calculated are $Q = 0.582$ Å, $\theta = 4.2°$, $q_2 = 0.043$ Å, $q_3 = 0.580$ Å. Comparable values for mannose calculated from the average mannose coordinates (25) are $Q = 0.5505$ Å, $\theta = 2.56°$, $q_2 = 0.0245$ Å, $q_3 = 0.5499$ Å. The deviation from an ideal chair conformation ($\theta = 0°$) is proportional to θ and is small, although slightly greater than that of the average mannose structure. The above average total puckering amplitude, Q, arises from larger than normal (by about 0.03 Å) displacements of atom O(5) and C(5) from the mean plane of the ring. As a consequence, the intracyclic bond angles at O(5) and C(5) are smaller than the average values of 113.4° and 110.2°, respectively (25).

There is a considerable amount of hydrogen bonding in the crystal, both between adjacent molecules and also within the molecule (Fig. 2). All the hydroxyls are involved in hydrogen bonding both as donors and as acceptors, and are often multiply involved. The ring oxygen also acts as a hydrogen bond acceptor. Several weak interactions involving the fluorine atoms are observed. F(2) is involved in a weak intramolecular interaction with OH(3), as evidenced by the relatively short

TABLE 10. ^1H nuclear magnetic resonance assignment

Chemical Shift δ (ppm)	^1H–^1H coupling constants (Hz)	^{19}F–^1H coupling constants (Hz)
H(1) = 5.01	H(1)–H(2) = 0	F(1)–H(1) = 47.4
H(2) = 4.41	H(2)–H(3) = 2.71	F(1)–H(2) = 2.8
H(3) = 3.23	H(3)–H(4) = 9.7	F(2)–H(2) = 51.8
H(4) = 3.11	H(4)–H(5) = 9.9	F(2)–H(1) = 17.8
H(5) = 2.95	H(5)–H(6) = 2.4	F(2)–H(3) = 30.0
H(6) = 3.36	H(5)–H(6′) = 5.9	F–H(4) ≈ 1
H(6′) = 3.21	H(6)–H(6′) = 12.4	F–H(69) ≈ 1
F(1) = 31.37 (Φ* = 147.53)		F(1)–F(2) = 12.7
F(2) = − 43.50 (Φ* = 222.40)		

F...H distance. This results in OH(3) being rotated slightly away from its other stronger hydrogen bonding partner, OH(6) of an adjacent molecule. F(1) is involved in a weak interaction with the CH proton of C(2), which is presumably activated towards such interaction by virtue of its two electronegative substituents. Such involvement of fluorine atoms in hydrogen bonding interactions is relatively unusual but not unprecedented, and Glusker and co-workers (26) have recently summarized their status. A more recent structure (27) in which a short intermolecular C—F---H—O bond is observed has also been published and an earlier study (28) has established the existence of weak C—H---F hydrogen bonds. While such interactions are weak, they are doubtless significant, as evidenced in this case by the high density and low temperature factors observed despite the removal of two hydroxyl groups.

Direct observation of such interactions is important in the light of the many recent studies regarding interaction of fluorinated substrate analogues with biological systems (2–5, 29, 30), and particularly with regard to studies of fluorocarbohydrate/protein interactions where such hydrogen bonding has been invoked (4, 30) to explain the high affinity for the protein of fluorodeoxy derivatives as compared to deoxy derivatives.

Acknowledgments

We thank the Natural Sciences and Engineering Research Council of Canada, the Research Corporation, and the British Columbia Health Care Research Foundation for financial support and the University of British Columbia Computing Centre for assistance. We are also indebted to Professor James Trotter, Supervisor, University of British Columbia Crystallographic Service, for the use of equipment and computer programs.

1. R. U. LEMIEUX. Chem. Soc. Rev. **7**, 423 (1978).
2. I. J. GOLDSTEIN, C. M. REICHERT, and A. MISAKI. Ann. N.Y. Acad. Sci. **234**, 283 (1974).
3. E. M. BESSELL, A. B. FOSTER, and J. H. WESTWOOD. Biochem. J. **128**, 199 (1972).
4. S. R. SPRANG, E. J. GOLDSMITH, R. J. FLETTERICK, S. G. WITHERS, and N. B. MADSEN. Biochemistry, **21**, 5364 (1982).
5. A. MARADUFU and A. S. PERLIN. Carbohydr. Res. **32**, 93 (1974).
6. P. J. KASVINSKY. J. Biol. Chem. **257**, 10805 (1982).
7. L. D. HALL and J. F. MANVILLE. Can. J. Chem. **47**, 19 (1969).
8. A. THOMPSON and M. L. WOLFROM. Methods Carbohydr. Chem. **2**, 215 (1963).
9. J. ADAMSON, A. B. FOSTER, L. D. HALL, R. N. JOHNSON, and R. H. HESSE. Carbohydr. Res. **15**, 351 (1970).
10. D. T. CROMER and J. B. MANN. Acta Crystallogr. Sect. A, **24**, 321 (1968).
11. R. F. STEWART, E. R. DAVIDSON, and W. T. SIMPSON. J. Chem. Phys. **42**, 3175 (1965).
12. V. SCHOMAKER and K. M. TRUEBLOOD. Acta Crystallogr. Sect. B, **24**, 63 (1968).
13. D. W. J. CRUICKSHANK. Acta Crystallogr. **9**, 747 (1956); **9**, 754 (1956); **14**, 896 (1961).
14. L. PHILLIPS and V. WRAY. J. Chem. Soc. (B), 1618 (1971).
15. L. D. HALL, R. N. JOHNSON, J. ADAMSON, and A. B. FOSTER. Can. J. Chem. **49**, 118 (1971).
16. C. A. G. HASNOOT, F. A. A. M. DE LEUW, and C. ALTONA. Tetrahedron, **36**, 2783 (1980).
17. J. C. CAMPBELL, R. A. DWEK, P. W. KENT, and C. K. PROUT. Carbohydr. Res. **10**, 71 (1969)
18. G. KOTHE, P. LUGER, and J. PAULSEN. Acta Crystallogr. Sect. B, **32**, 2710 (1976).
19. G. KOTHE, P. LUGER, and H. PAULSEN. Acta Crystallogr. Sect. B, **35**, 2079 (1979).
20. J. PODLAHOVA and J. LOUB. Acta Crystallogr. Sect. C, **40**, 1284 (1984).
21. T. HAKOSHIMA, H. OMORI, K. TOMITA, H. MIKI, and M. IKEHARA. Nucleic Acids Res. **9**, 711 (1981).
22. L. E. SUTTON *et al.* Tables of interatomic distances. Chem. Soc. London. 1959.
23. S. H. KIM and G. A. JEFFREY. Acta Crystallogr. **22**, 537 (1967)
24. D. CREMER and J. A. POPLE. J. Am. Chem. Soc. **97**, 1354 (1975).
25. B. SHELDRICK and D. AKRIGG. Acta Crystallogr. Sect. B, **36**, 1615 (1980).
26. P. MURRAY-RUST, W. G. STALLINGS, C. T. MONTI, R. K. PRESTON, and J. P. GLUSKER. J. Am. Chem. Soc. **105**, 3206 (1983).
27. A. KARIPIDES and C. MILLER. J. Am. Chem. Soc. **106**, 1494 (1984).
28. S. J. RETTIG and J. TROTTER. Acta Crystallogr. Sect. B, **30**, 2139 (1974).
29. C. WALSH. Adv. Enzymol. Relat. Areas Mol. Biol. **55**, 197 (1983).
30. Y. ITTAH and C. P. J. GLAUDEMANS. Carbohydr. Res. **95**, 189 (1981).

The photochemistry of 6- and 7-cyano-2,3-benzobicyclo[4.2.0]octa-2,4,7-triene

CHRISTOPHER OWEN BENDER, DONALD LAVERNE BENGTSON, DOUGLAS DOLMAN, AND SEAMUS FRANCIS O'SHEA
Department of Chemistry, University of Lethbridge, Lethbridge, Alta., Canada T1K 3M4
Received September 23, 1985

CHRISTOPHER OWEN BENDER, DONALD LAVERNE BENGTSON, DOUGLAS DOLMAN, and SEAMUS FRANCIS O'SHEA. Can. J. Chem. **64**, 237 (1986).

The direct irradiation of 7-cyanobenzocyclooctatetraene (**5**) led to 6- and 7-cyano-2,3-benzobicyclo[4.2.0]octa-2,4,7-triene (**7** and **8**; $\Phi_7 = \Phi_8 < 0.0001$). On direct irradiation, **7** gave 1-cyanobenzosemibullvalene (**6**; $\Phi = 0.19$), **5** ($\Phi = 0.022$), and 2-cyanonaphthalene ($\Phi = 0.04$), whereas **8** gave 7-cyanobenzosemibullvalene (**16**; $\Phi = 0.03$), **5** ($\Phi = 0.22$), naphthalene ($\Phi = 0.12$), and 4-cyano-7,8-benzotetracyclo[3.3.0.$0^{2,4}$.$0^{3,6}$]oct-7-ene (**17**, $\Phi = 0.03$). Upon sensitized irradiation, **7** gave **6** ($\Phi = 0.68$) and 2-cyanonaphthalene ($\Phi = 0.007$), while **8** gave **16** ($\Phi = 0.01$) and naphthalene ($\Phi = 0.52$). Deuterium labelling studies suggest that **6** and **16** derive from Zimmerman di-π-methane rearrangements.

CHRISTOPHER OWEN BENDER, DONALD LAVERNE BENGTSON, DOUGLAS DOLMAN et SEAMUS FRANCIS O'SHEA. Can. J. Chem. **64**, 237 (1986).

La photolyse directe du cyano-7 benzocyclooctatetraène (**5**) conduit aux cyano-6 et -7 benzo-2,3 bicyclo[4.2.0]octatriènes-2,4,7 (**7** et **8**; $\Phi_7 = \Phi_8 < 0{,}0001$). Par irradiation directe, **7** conduit au cyano-1 benzo semi-bullvalène (**6**; $\Phi = 0{,}19$), à **5** ($\Phi = 0{,}022$) et au cyano-2 naphtalène ($\Phi = 0{,}04$), tandis que **8** conduit au cyano-7 benzo semi-bullvalène (**16**; $\Phi = 0{,}03$), à **5** ($\Phi = 0{,}22$), au naphtalène ($\Phi = 0{,}12$), et au cyano-4 benzo-7,8 tetracyclo[3.3.0.$0^{2,4}$$0^{3,6}$]octène-7 (**17**; $\Phi = 0{,}03$). Par irradiation sensibilisée, **7** conduit à **6** ($\Phi = 0{,}68$) et au cyano-2 naphtalène ($\Phi = 0{,}007$), alors que **8** conduit à **16** ($\Phi = 0{,}01$) et au naphtalène ($\Phi = 0{,}52$). Des études de marquages au deuterium suggèrent que **6** et **16** dérivent des transpositions di-π-méthanes de Zimmerman.

Introduction

On the basis of deuterium labelling studies we reported that the photoformation of 6,7-dimethylbenzosemibullvalene (i.e., 6,7-Me_2-BSB (**4**)) from 6,7-dimethylbenzocyclooctatetraene (i.e., 6,7-Me_2-BCOT (**1**)) can be accounted for in terms of a Zimmerman di-π-methane (DPM) rearrangement of the initially formed diene **2** (1). In the light of this observation we suggested that the known (2) conversion of 7-CN-BCOT (**5**) to 1-CN-BSB (**6**) on direct irradiation might follow a similar reaction sequence, and hence involve the intermediate formation of 6-cyano-2,3-benzobicyclo[4.2.0]octa-2,4,7-triene (i.e., diene **7**). We now present evidence to support this view, and other results which demonstrate that the extent of DPM rearrangement in such dienes is strongly dependent on substituent location.

Results

The direct irradiation of COT **5** at wavelengths > 340 nm led cleanly not only to the anticipated diene **7** but also to the alternate $2\pi + 2\pi$ ring closure product **8**. The two products were formed in equal amounts, in high chemical yield, but in very low quantum efficiency ($\Phi_7 = \Phi_8 < 0.0001$).

The structures of **7** and **8** were deduced from nmr data (see Experimental) and chemical evidence. Thus, treatment of **7** with diimide led to the selective reduction of the nonconjugated (cyclobutene) double bond to give 7,8-dihydro-6-cyano-2,3-benzobicyclo[4.2.0]octa-2,4-diene (**9**). The nmr data for **9** agree well with those reported for the corresponding protons of **10** (3) (see Scheme 3). In the case of diene **8**, reduction with diimide was ineffective. However, catalytic hydrogenation with 10% Pd on C gave **11**, a tetrahydro derivative of **8**. The same

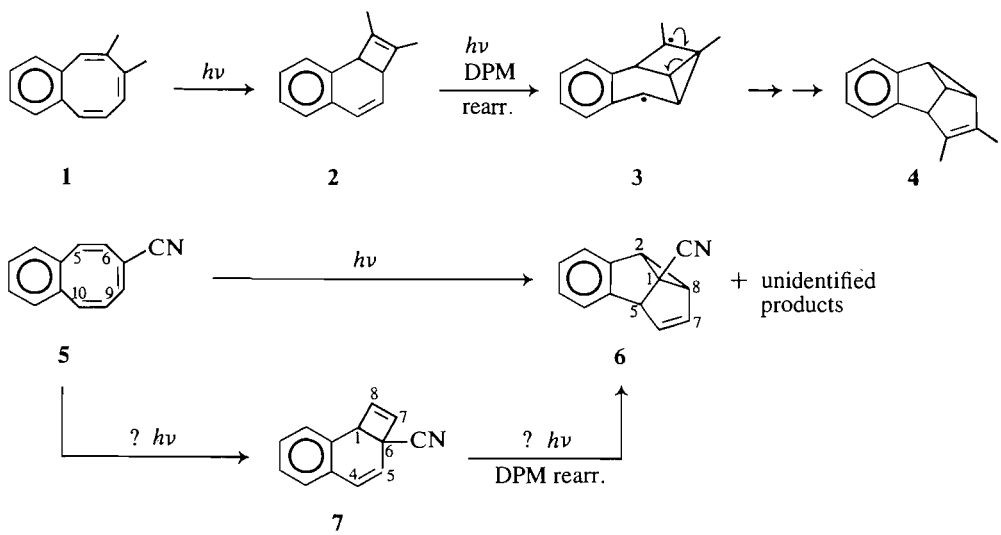

SCHEME 1

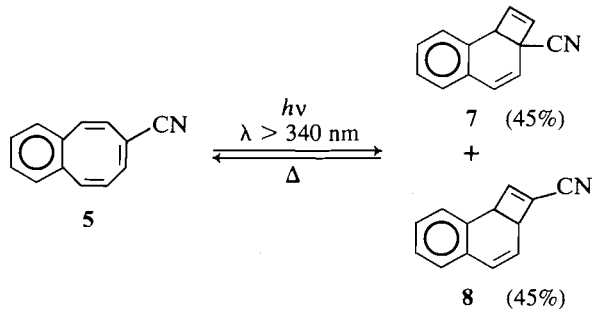

SCHEME 2

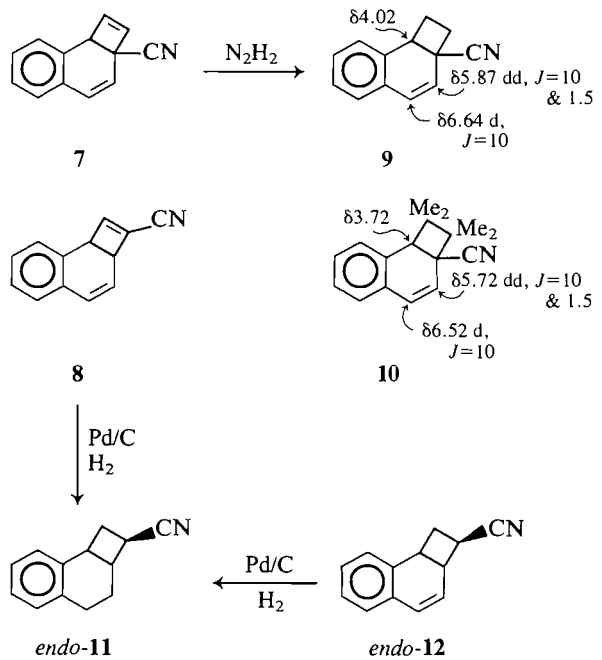

SCHEME 3

material was the only significant product from the hydrogenation of the known compound **12** (4).[1]

Further support for structures **7** and **8** derives from their facile thermal conversion to COT **5** (cf. the thermolysis of **13** to **14**, Scheme 4 (5)). The rearrangements were detectable on the gc at column temperatures >100°C for **7**, and >135°C for **8**, and are essentially quantitative upon flash gas phase thermolysis at 350°C.

Photochemically, dienes **7** and **8** are also labile. The product formations from the direct and sensitized irradiations are depicted in Scheme 5; the yields given are based on consumed starting materials.

The formation of 4-cyano-7,8-benzotetracyclo-[3.3.0.$0^{2,4}$.$0^{3,6}$]oct-7-ene (**17**) in the direct irradiation of **8** is analogous to the photoisomerization of **13** to **15** reported by Collin and Sasse (5). The structure of **17** was assigned on spectroscopic grounds alone. The mass spectrum shows a strong molecular peak at *m/e* 179 and, like **15**, contains a major fragmentation peak at *m/e* 128, corresponding to naphthalene ion. The C_2 symmetry of **17** is reflected by the ^{1}H nmr spectrum, which shows only five sets of resonance signals: three in the aliphatic region centred at δ 4.36 (H-1, 6), δ 3.28 (H-5), and at δ 2.96 (H-2, 3) (cf. δ 4.24 (H-1, 6), and δ 2.52 (H-2, 3) for **15**

[1]We thank Professor McCullough of McMaster University for a comparison sample of authentic **12**.

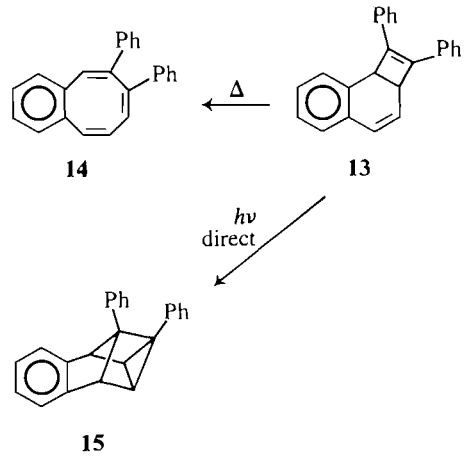

SCHEME 4

(6)), and two in the aromatic region. The aliphatic signals approximate an AA'MXX' spin system, with H-5 appearing as a quintet ($J_{5,1(6)} = J_{5,2(3)} = 4.5$ Hz), as does the corresponding proton in the related derivative **18** ($J_{5,1(6)} = 4.5$ Hz and $J_{5,2(3)} = 5$ Hz (7)).[2]

Structural assignment in the case of photoproduct **16** was less straightforward since the compound undergoes rapid polymerization upon solvent removal, thus limiting the physical characterization. Nevertheless, the mass spectrum, nmr data, and hydrogenation results provide strong support for the proposed benzosemibullvalene structure.

The mass spectrum (via gc/ms) established the molecular weight as 179 and the ^{1}H nmr spectrum revealed the uniquely characteristic coupling constants of the rigid benzosemibullvalene framework. The nmr data for **16** are compared with those of **6** and parent benzosemibullvalene **19** (8) in Table 1. Note that the protons of **16** appear within the expected chemical shift regions; the 0.7-ppm downfield shift of H-6 relative to H-6 in **19** agrees well with the reported chemical shift substituent constant of 0.8 ppm for the *cis* proton of acrylonitrile (9). Chemical evidence in favour of the structure was obtained from the brief exposure of **16** to catalytic hydrogenation (10% Pd on C; 3 min). Two major components were formed, but only one (**20**, 31%) was isolated. 7-Cyano-2,3-benzobicyclo[3.3.0]octa-2,6-diene (**20**) is a stable crystalline dihydro derivative of **16** and can be viewed as a product of 1,4-addition of hydrogen to C-2 and C-6 of **16**. Other 1,4-addition reactions of semibullvalenes are well known (7, 10).

In addition to aromatic signals, the nmr spectrum of **20** shows one vinylic proton at δ 6.52 and six distinctly separated one-proton multiplets, corresponding to four allylic or benzylic methylene protons between δ 2.76 and δ 3.27, and two benzylic or allylic bridgehead methine protons at δ 3.75 (H-5) and δ 3.98 (H-1), which are strongly coupled ($J_{1,5} = 8.5$ Hz). This large coupling between the methine protons is incompatible with bicyclo[3.2.1]octadiene structures that could conceivably arise from alternative cyclopropyl ring cleavages of **16**. Furthermore, the high-field methine at δ 3.75 is coupled to the vinylic proton ($J = 2.5$ Hz), and this observation, along with other features of the nmr, permits us to exclude **21** as a contending structure.

Lastly, in connection with the photoproducts **16** and **17**, control experiments were carried out to examine if either

[2]We are grateful to Professor Klumpp of Vrije Universiteit, The Netherlands, for communicating to us nmr spin decoupling results for **18**.

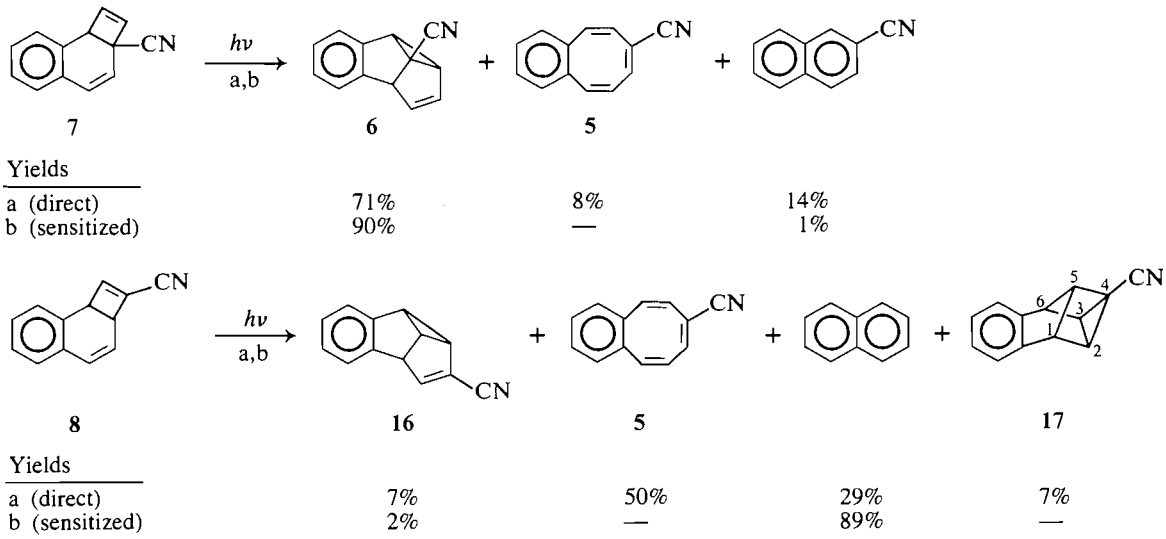

SCHEME 5

TABLE 1. The ^{1}H nmr data of SB's **6**, **16**, and **19**

Assignment	Description and signal positions, $\delta^{a,b}$		
	16	**19**	**6**
Aromatics	6.97–7.45 m	6.80–7.33 m	7.00–7.44 m
H-1	3.36 q	3.14 q	—
H-2	3.15 t	2.86 t	3.66 d
H-5	4.02 dd	3.81 dd	4.22 d
H-6	6.24 d	5.47 dd	5.70 dd
H-7	—	5.08 dd	5.20 dd
H-8	2.90 t	2.60 dt	3.33 dd

[a]Run in $CDCl_3$ (**6**) or CCl_4 (**16** and **19**) solvent with TMS as internal standard.
[b]Corresponding coupling constants, where applicable, are within 0.5 Hz; typically, $J_{1,2} = J_{1,5} = J_{2,8} = 6.5$, $J_{5,6} = J_{7,8} = 2.5$, and $J_{6,7} = 5.0$ Hz.

converted to the other under the conditions used for the photolyses of diene **8**. Tetracyclic **17** was found to be stable to direct (Pyrex filter) and sensitized (benzophenone) photolyses, but SB **16** slowly disappeared under both irradiation conditions to give polymeric mterial. Thus **16** is not a secondary photoproduct arising from **17**, and vice versa.

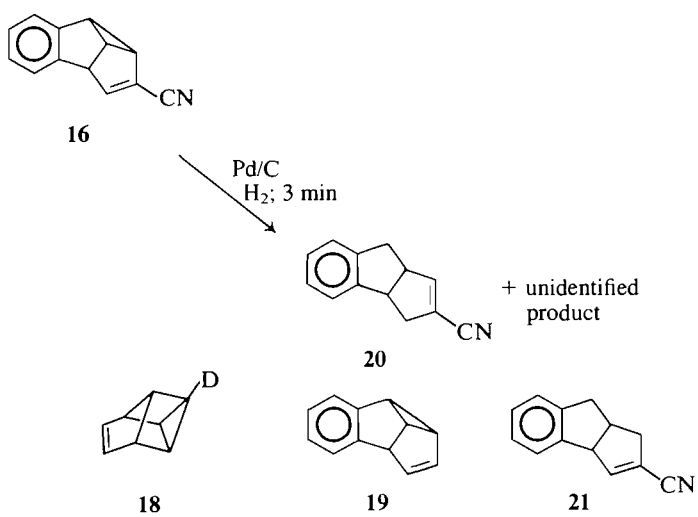

SCHEME 6

Mechanistic considerations

Whereas the formation of SB **6** from diene **7** can be most reasonably accounted for in terms of a single mechanism, a DPM rearrangement involving initial bridging between C-5 and C-7 (Scheme 7, route *i*), there are at least two plausible pathways that can rationalize the formation of SB **16** from diene **8**, i.e., route *ii* (Scheme 7), a DPM rearrangement which commences with C-5–C-7 bridging, and route *iii*, which involves initial C-4–C-8 bridging. Routes *ii* and *iii* are skeletally nonequivalent and deuterium labelling studies were therefore undertaken to determine which operates.

The labelled dienes **7***a* and **8***a* were conveniently obtained from the photolysis of the known (2) deuterated COT **5***a* (ca. 86%-d_1 at C-9). The observation that SB **16***a* is produced on either direct or sensitized photolysis of **8***a*, as determined by ^{1}H nmr analysis, can be seen to be in accord with the DPM mechanism depicted as route *ii*.

In the case of diene **7***a*, the direct and sensitized irradiations led to SB product containing the deuterium label at C-6, as required by the DPM rearrangement shown (Scheme 7, route *i*). The results complement those obtained from a previous labelling study of the conversion of COT **5** to SB **6** on direct irradiation, where COT **5** was deuterated at C-6 and C-10 (1, 2).

Singlet and triplet energies of 7 and 8 and quantum yields

Diene **7** showed strong fluorescence in cyclohexane at room temperature, and a singlet energy of 95 kcal/mol was assigned from intersection of the absorption and fluorescence spectra. No fluorescence could be detected for diene **8**, but a value of $92 \leq E_s \leq 95$ kcal/mol was estimated from the uv long-wavelength band.

"Effective" triplet energies of ca. 59 kcal/mol for both **7** and **8** (cf. E_T 61 kcal/mol for styrene, and $61 \leq E_T \leq 59$ kcal/mol for Me_2-diene **2** (1)) were obtained from triplet sensitization experiments. Thus the diene triplet reactions were efficiently sensitized by benzophenone (E_T 69 kcal/mol) and Michler's ketone (E_T 62 kcal/mol), modestly by 2-acetonaphthone (E_T 59 kcal/mol), but not effectively by 1-acetonaphthone (E_T 56 kcal/mol). These data are included with other quantum yield information in Table 2.

A remaining aspect is the sensitized photolysis of COT **5**. Attempts to sensitize **5** with thioxanthone or with *p*-dimethylaminobenzophenone, using filters transmitting light between

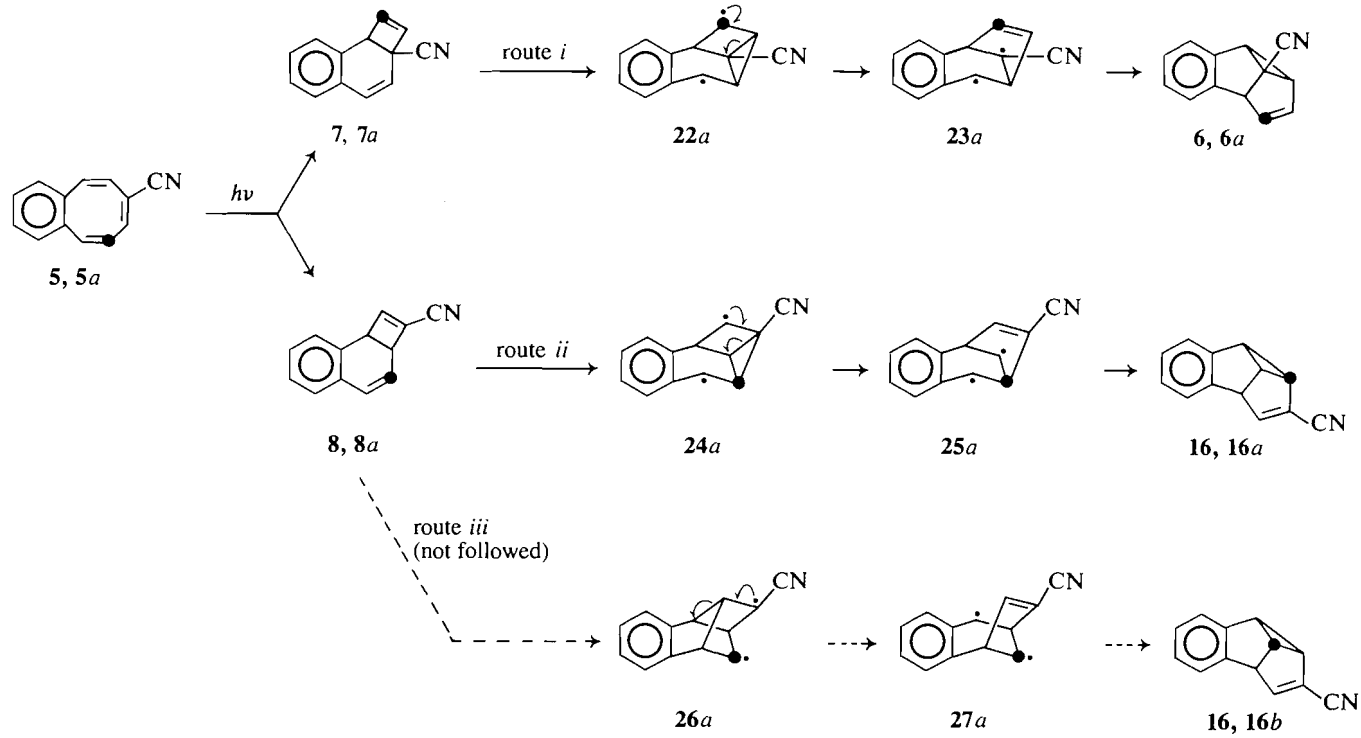

SCHEME 7

TABLE 2. Quantum yield data for COT **5** and dienes **7** and **8**[a]

Compound	Light wavelength (nm)	Sensitizer (E_T, kcal/mol)	Φ (Product appearance)						
			COT **5**	SB **6**	SB **16**	**17**	Nap[b]	2-CN-Nap[b]	Other
7(**8**)	280	None	0.022 (0.22)	0.19	(0.03)	(0.03)	(0.12)	0.04	—
7(**8**)	334	Benzophenone (69)	—	0.68	(0.01)	—	(0.52)	0.007	—
7(**8**)	334	Michler's ketone (61)	—	0.63	(0.01)	—	(0.51)	0.007	—
7(**8**)	334	2-Acetonaphthone (59)	—	0.26	(0.003)	—	(0.16)	<0.007	—
7(**8**)	334	1-Acetonaphthone (56)	—	0.026	(<0.003)	—	(0.01)	<0.007	—
5	313	None	—	—	—	—	—	—	<0.0001 (**7**, **8**)

[a]Ferrioxalate actinometry; runs for **7** and **8** were done in cyclohexane, and those for **5** were done in both cyclohexane and benzene. Φ's given are extrapolated to zero conversion; product analyses (internal hydrocarbon standard) by gc (and nmr for **7**) at several conversions <10%. Experimental error of Φ's is ±10%. For sensitized runs, sensitizers absorb <95% of incident light.

[b]Nap = naphthalene.

wavelengths 315 and 383 nm (the absorption tail of **5** at $3 \times 10^{-3} M$ extends beyond 440 nm, hence the need for a window, rather than a cut-off filter), led to no observable formation of **7** or **8** (i.e., Φ_7, $\Phi_8 < 0.0001$) or any other product. Here the triplet energy of COT **5** (**5** is not phosphorescent) is assumed to be close to that of COT **1** ($E_T \leq 56$ kcal/mol (1)), and it is assumed that energy transfer from thioxanthone (E_T 65.5 kcal/mol) at $1.4 \times 10^{-3} M$ (11) and *p*-dimethylaminobenzophenone (E_T 62 kcal/mol) at $3.1 \times 10^{-3} M$ is efficient. These sensitization results, coupled with only "upper-limit" quantum yields for the formation of dienes **7** and **8** upon direct irradiation, caution us about speculating as to the excited state(s) involved in the photochemistry of COT **5**.

Discussion

Excited state multiplicities

Sensitization of **7** and **8** led to naphthalene and semibullvalene products (i.e., SB **6** plus 2-cyanonaphthalene from **7**, and SB **16** plus naphthalene from **8**) and are attributed to triplet (T_1) processes. For the direct irradiations, multiplicity assignments cannot be made for all the photoproducts. Clearly, however, COT **5** is a singlet product of both **7** and **8**, and tetracyclic **17** is a singlet product of **8**, since they are not formed in sensitized runs. For the remaining products from direct irradiations, straightforward application of the Zimmerman "ratio bracketing rule" (12) suggests that 2-cyanonaphthalene (from **7**) and SB **16** (from **8**) are mainly (>90%) singlet derived, but SB **6** (from **7**) and naphthalene (from **8**) may arise from singlet or triplet states (via intersystem crossing from S_1), or some composite of the two. The singlet (mostly) origin of SB **16** is noteworthy, since DPM rearrangements in rigid systems are generally triplet initiated (13).

Product dependency on substituent location

The singlet products of **7** and **8** are similar to those reported for the benzobicyclo[4.2.0]octa-2,4,7-trienes **2** (1) and **13** (5),

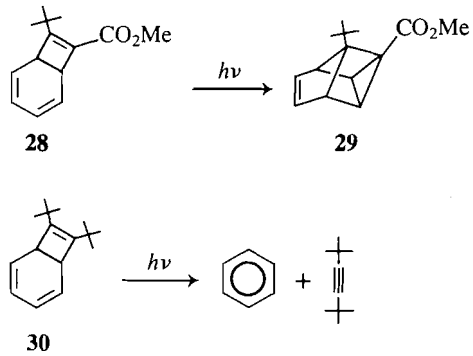

SCHEME 8

and here we comment only on the failure of **7** to give a tetracyclic isomer of the type observed for **8** (→ **17**) and **13** (→ **15**). That **7** does not undergo the cycloaddition (nor does diene **2** (1)) is attributed to the lack of sufficient donor–acceptor interactions between the potential $2\pi + 2\pi$ partners (14, 15). This situation resembles that found for the dienes **28** (16) and **30** (17), where only polar substituted **28** undergoes the ring closure process (→ **29**, Scheme 8).

For the diene triplets, a striking divergence of behaviour has been encountered. As was found for diene **2**, the triplet reactivities of **7** and **8** involve competition between two reaction types: a DPM rearrangement to a semibullvalene, and a cyclobutene ring cleavage to a naphthalene (and presumably an acetylene). Extremes of the competition are observed for the cyano derivatives, where the DPM rearrangement is of synthetic proportions in **7**, but is almost totally suppressed in the case of **8**.

The meager production of SB **16** may reflect a general reluctance of di-π-methanes to rearrange via initial bridging to the α-carbon of an acrylonitrile moiety. Note the avoidance of such a liaison in the sensitized rearrangements of the related compounds, 2-cyanobenzobarrelene (2), 5,6-dihydro-2-cyanobenzobarrelene (18), and 2-cyanobenzonorbornadiene (19), where bridging to the β-carbon of the acrylonitrile moiety occurs. Contrastingly, the high efficiency of the DPM rearrangement in bridgehead[3] substituted **7** accords with the enhanced DPM reactivity noted by Zimmerman for systems in which the methane carbon is substituted by delocalizing groups (20).

However, the importance of the above correlations on the triplet product bifurcation is difficult to assess since factors promoting the cleavage process may also be significant and working in tandem with those favoring SB formation. One observation to be made in this regard is that the proportion of naphthalene product increases as the stability (in terms of π-bond energy) of the acetylene unit expelled increases, i.e., the SB/naphthalene product ratios are 99:1 for **7**, 37:63 for **2** (1), and 2:98 for **8**, and the order of acetylene stability is HC≡CCN > MeC≡CMe > HC≡CH.

Finally, CNDO/S-Cl calculations of changes of atom–atom interaction energies in excited states of **2**, **7**, and **8** were carried out to examine for possible correlations between initial distributions of electronic excitation and the observed triplet product competitions.[4] Selected atom–atom energies for the dienes are given in Table 3 (see Experimental). Inspection of the data

TABLE 3. Changes[a] in atom–atom interaction energies (eV) resulting from electronic excitation to the lowest triplet (T_1) state of dienes **2**, **7**, and **8**

	Change in interaction energy (eV)		
Atom–atom	**2**	**7**	**8**
1–2	−0.55	−0.64	1.34
2–3	3.61	3.64	−0.01
3–4	−3.76	−3.85	0.17
4–5	6.82	6.93	−0.06
5–6	−1.06	−0.97	0.56
1–6	−0.27	−0.30	0.39
6–7	1.11	1.08	−1.03
7–8	−0.18	−0.45	9.77
1–8	0.74	0.88	−1.85
2–8	−0.04	−0.07	−0.35
4–8	−0.02	−0.02	0.02
5–7	−0.08	0.04	−0.08

[a]Calculated by the CNDO/S-CI method using the theoretical parameterization (26). Negative values are interpreted as "forces" tending to bring atoms together, while positive values cause the atoms to move further apart. Calculations on the full molecules were performed; only selected values are given here.

reveals no convincing correspondence to the product preferences. In part this is due to the near-degeneracy of the T_1 and T_2 states of **2**, and the sensitivity of the T_1 and T_2 states of **8** to the different parameterization forms employed (see Experimental). Further studies aimed at delineating the product-controlling feature(s) in 2,3-benzobicyclo[4.2.0]octa-2,4,7-trienes are in progress.

Experimental

The nmr spectra were recorded on either Bruker 400-MHz, Varian 200-MHz or 60-MHz instruments, with TMS as internal standard. The chemical shifts are in δ units and the coupling constants (J) in Hz. The abbreviations br, s, d, t, q, and m refer to broad, singlet, doublet, triplet, quartet, and multiplet, respectively. The ir spectra were recorded on a Perkin–Elmer 337 spectrometer and are given in cm^{-1}. The uv spectra (run in cyclohexane solvent) were measured on a Cary 15 spectrometer; maxima are given in nm, with ϵ_{max} values in parentheses; sh = shoulder. The gc/ms was recorded on an HP 5985 B instrument fitted with an SPB-1 glass capillary column, 30 m × 0.32 mm. All other mass spectra were recorded on an MS 9 (A.E.I.) instrument. Melting points are uncorrected. Elemental analyses were performed by Galbraith Labs, Inc., Knoxville, TN. Fluorescence and phosphorescence studies were carried out on an Aminco–Bowman spectrometer. Column chromatography was performed with Silica Gel 60 (230–400 mesh; Merck) mixed with Sylvania 2282 phosphor and slurry packed into quartz columns permitting monitoring by a hand uv lamp. The gc analyses were made on a Varian 3700 instrument (FID), coupled to a Varian CDS 111 computing integrator, and fitted with an SE-30 glass capillary column, 30 m × 0.32 mm. Cyclohexane solvent for photolyses was prepared by scrubbing with 20% fuming sulfuric acid, followed by washing with 10% aqueous sodium hydroxide, drying ($MgSO_4$), and finally distilling from calcium hydride. Sensitizers were distilled or recrystallized prior to use.

General procedures for preparative photolyses

The apparatus consisted of a 450-W Hanovia medium pressure mercury arc surrounded by a water-cooled quartz immersion well. For direct irradiations, the light was filtered through a cylindrical Pyrex sleeve, unless otherwise stated. For irradiations at wavelengths > 340 nm the light was passed through an aqueous filter (Pyrex) jacket (10-mm path length) containing a solution prepared from 750 g NaBr and 8 g $Pb(NO_3)_2$ in 1 L of water. Three types of sample cell were used.

[3]For a discussion of the influence of bridgehead substituents in DPM photochemistry, note the recent publications of Paquette *et al.* (21).

[4]This approach is similar to the "ΔP" method originally suggested by Zimmerman (22, and references cited therein).

Cell A (200-mL sample volume) consisted of a cylindrical collar (Pyrex), which surrounded the aqueous filter jacket. The cell was fitted with gas inlet and exit ports, and sample solutions were purged with argon prior to, and during irradiations. Cells B (35 mL volume) and C (3.5 mL volume) were test-tube-like vessels (quartz) and sample solutions contained therein were deoxygenated by flushing with argon and sealed under a positive pressure; the solutions were magnetically stirred throughout the course of the irradiations.

Direct irradiation of COT 5

A solution of 228.5 mg (1.28 mmol) of **5** (2) in 200 mL of benzene was photolyzed at >340 nm for 55 h in cell A. The photolysate composition analysed for 113.9 mg (50%) of COT **5**, 51.0 mg (22%) of **7**, and 51.2 mg (22%) of **8**, as determined by a combination of gc and nmr analyses, after the addition of a known amount of standardized tetradecane. (Note: due to the facile thermal conversion of **7** (but not **8**) to COT **5** on the column (at 120°C), gc analysis alone is inadequate.) The photolysate was concentrated and the residue chromatographed on Silica Gel 60 (2 cm × 60 cm) with 2% ether–cyclohexane solvent. The first band contained a mixture of **5** and **8**, and the second band gave 48.5 mg (21%) of **7**, mp 57–59°C (from hexane); ir (Nujol): 2230, C≡N; uv: 258 sh (5 800), 266 (7 700), 276 (7 500), 285 sh (4 700), 287 sh (3 600), and 293 sh (1 000): nmr (400 MHz; $CDCl_3$): 7.19–7.28 (m, 2H, aromatics), 7.11–7.17 (m, 2H, aromatics), 6.46 (d, 1H, H-4, $J_{4,5} = 10$), 6.19 (dd, 1H, H-7, $J_{7,8} = 2.8$, $J_{7,1} = 1$), 6.07 (dd, 1H, H-8, $J_{8,7} = 2.8$, $J_{8,1} = 1$), 5.85 (d, 1H, H-5, $J_{5,4} = 10$), and 4.46 (br s, 1H, H-1); spin decoupling experiments: irradiation of H-4 collapsed H-5 to an s; irradiation of H-1 collapsed H-7 and H-8 to doublets ($J_{7,8} = 2.8$). Mass spectrum showed molecular ion at *m/e* = 179.0724 (100%); $C_{13}H_9N$ requires 179.0734. *Anal.* calcd. for $C_{13}H_9N$: C 87.12, H 5.06, N 7.82; found: C 86.86, H 5.21, N 7.75.

The first band from chromatography was concentrated and the residue dissolved in 4 mL of hexane. Storage of the solution at 2°C led to crystallization of COT **5**. Filtration gave 72.1 mg (32%) of recovered COT **5**; the filtrate (90.6 mg) contained 54% **8** and 46% **5** by gc analysis. The filtrate was rechromatographed as above; early fractions contained mixtures of **8** and **5**, and later fractions gave 30.2 mg (13%) of pure **8** (from hexane), mp 68–70°C; ir (Nujol): 2220, C≡N; uv: 262 sh (6 600), 268 (7 600), 278 sh (6 600), 291 sh (3 200), and 302 sh (650); nmr (400 MHz; $CDCl_3$): 7.16–7.22 (m, 2H, aromatics, 7.06–7.13 (m, 2H, aromatics), 6.71 (d, 1H, H-8, $J_{8,1} = 1$), 6.42 (d, 1H, H-4, $J_{4,5} = 10$), 5.93 (dd, 1H, H-5, $J_{5,4} = 10$, $J_{5,6} = 4.5$), 4.22 (br d, 1H, H-1, $J_{1,6} = 4.5$), and 4.00 (t, 1H, H-6, $J_{6,1} = J_{6,5} = 4.5$); spin decoupling experiments: irradiation of H-8 sharpened the H-1 d ($J_{1,6} = 4.5$); irradiation of H-5 collapsed H-6 to a d ($J_{6,1} = 4.5$) and H-4 to an s: irradiation of H-1 collapsed H-8 to an s and H-6 to a d ($J_{6,5} = 4.5$); irradiation of H-6 collapsed H-1 to a br s and H-5 to a d ($J_{5,4} = 10$). Mass spectrum showed molecular ion at *m/e* = 179.0734 (33%), 128 (base peak). *Anal.* found: C 87.32, H 5.08, N 7.78.

Diimide reduction of diene 7

To a stirred mixture of 50.6 mg (0.28 mmol) of **7** and 1.0 g (5.2 mmol) of potassium azodicarboxylate in 25 mL of dioxane at room temperature, a total of 2 mL of acetic acid was added during a 5-h period. The mixture was stirred overnight, then treated with a second portion of 1.0 g (5.2 mmol) of potassium azodicarboxylate and 2 mL of acetic acid. The resulting mixture was then added to 100 mL of toluene, and washed with 10% sodium carbonate solution (100 mL), followed by water (2 × 50 mL). The toluene solution was dried ($MgSO_4$), concentrated, and the residue was passed through Silica Gel 60 (0.7 cm × 12 cm) with 4% ether–cyclohexane solvent, to give 33.6 mg (66%) of colourless **9**, mp 46–48°C, after two recrystallizations from hexane; ir (Nujol): 2200, C≡N; uv: 257 sh (6 380), 265 (7 900), 269 sh (7 500), 273 sh (7 400), 281 sh (4 900), and 286 sh (3 570); nmr (400 MHz; $CDCl_3$): 6.97–7.26 (m, 4H, aromatics), 6.64 (d, 1H, H-4, $J_{4,5} = 10$), 5.77 (dd, 1H, H-5, $J_{5,4} = 10$, $J_{5,1} = 1.5$), 4.02 (br, t, 1H, H-1, $J_{1,8} = J_{1,8'} = 9$, $J_{1,5} = 1.5$), 2.93 (m, 1H, H-7), and 2.36 (m, 3H remaining methylenes); spin decoupling experiments: irradiation of H-4 collapsed H-5 to a d ($J_{5,1} = 1.5$); irradiation of H-5 collapsed H-4 to an s and sharpened the H-1 t; irradiation of H-1 collapsed H-5 to a d ($J_{5,4} = 10$) and modified to δ 2.36 m; irradiation of the δ 2.36 m collapsed H-1 and H-7 to singlets. Mass spectrum showed molecular ion at *m/e* = 181.0889 (10%), 153 (base peak); $C_{13}H_{11}N$ requires 181.0892. *Anal.* calcd. for $C_{13}H_{11}N$; C 86.15, H 6.12, N 7.73; found: C 86.21, H 6.21, N 7.73.

Catalytic reduction of endo*-7-cyano-2,3-benzobicyclo[4.2.0]octa-2,4-diene (12)*

A stirred mixture of 110.0 mg (0.61 mmol) of **12** (4) and 23 mg of 10% Pd on C in 10 mL of ethyl acetate was hydrogenated at room temperature and pressure during 10 min. The catalyst was removed (centrifuge) and the solution concentrated. The residue was chromatographed on Silica Gel 60 (1 cm × 55 cm) with 5% ether–cyclohexane. Short-path distillation (75°C/0.1 Torr; 1 Torr = 133.3 Pa) of the main band gave 102 mg (92%) of *endo*-7-cyano-2,3-benzobicyclo[4.2.0]-oct-2-ene (**11**) (gc purity >99%) as a colourless oil; ir (neat liquid): 2230, C≡N; uv: 247 sh (105), 253 sh (190), 260 sh (290), 265 sh (360), 266 (380), and 272 (385); nmr (400 MHz; $CDCl_3$): 7.14–7.20 (m, 3H, aromatics), 6.98–7.03 (m, 1H, aromatic), 3.63 (q, 1H, H-1, $J_{1,6} = J_{1,8} = J_{1,8'} = 9$), 3.40 (br q, 1H, H-7, $J_{7,6} \simeq J_{7,8} \simeq J_{7,8'} \simeq 9$), 2.83–3.05 (m, 3H, H-4, H-6, H-8), 2.78 (ddd, 1H, H-4′, $J_{4',4} = 15.5$, $J_{4',5(5')} = 9$, $J_{4',5'(5)} = 4$), 2.34 (m, 1H, H-8′, $J_{8',7} \simeq J_{8',1} \simeq 9$, $J_{8',8} = 11$, $J_{8',x} \simeq 1.0$), 2.10–2.20 and 1.99–2.08 (m, 2H, C-5 methylenes) spin decoupling experiments: irradiation of H-1 modified H-8′ (incomplete decoupling) and the 2.83–3.05 m; irradiation of H-8′ collapsed H-1 and H-7 to br triplets ($J = 9$). Mass spectrum showed molecular ion at *m/e* = 183.1048 (23%), 130 (base peak); $C_{13}H_{13}N$ requires 183.1048. *Anal.* calcd. for $C_{13}H_{13}N$: C 85.21, H 7.15, N 7.64; found: C 85.47, H 7.09, N 7.62.

Catalytic reduction of diene 8

A stirred mixture of 14.5 mg (0.08 mmol) of **8** and 9.0 mg of 10% Pd on C in 10 mL of ethyl acetate was hydrogenated at room temperature and pressure during 15 min. The reaction mixture was worked up as in the hydrogenation of **12** (above) to give 12.9 mg (87%) of colourless oil identical (gc, ir, nmr) to **11**.

Gas phase thermolysis of diene 7

Over a 30-min period, 18.0 mg (0.10 mmol) of **7** was distilled into a Pyrex tube (2 cm × 30 cm) packed with glass beads (0.5-cm diameter) maintained at 350°C. The pressure in the system was kept at 8 Torr by the passage of nitrogen. The thermolysis product (no 2-cyanonaphthalene by gc), collected in a cooled U-trap (ice-water), was chromatographed on Silica Gel 60 (1 cm × 40 cm) with 2% ether–cyclohexane. Crystallization of the main band from hexane gave 16.5 mg (92%) of COT **5**, mp 101–103°C (lit. (2) mp 102–103°C).

Gas phase thermolysis of diene 8

The above apparatus and same conditions were used to convert 12.1 mg (0.07 mmol) of diene **8** to 11.6 mg (96%) of COT **5**, mp 101–103°C. No naphthalene was detected (gc) in the thermolysis product.

Direct irradiation of diene 7

A solution of 88.6 mg (0.50 mmol) of **7** in 30 mL of cyclohexane was photolyzed (Pyrex filter) for 3.5 h in cell B. The photolysate composition analysed for 7.5 mg (10%) 2-cyanonaphthalene, 44.3 mg (50%) SB **6**, 26.2 mg (30%) diene **7**, and 5.1 mg (6%) COT **5**, as determined by gc and nmr after addition of a known amount of standardized tetradecane. The photolysate was concentrated and the residue chromatographed on Silica Gel 60 (1.5 cm × 55 cm) with 2% ether–cyclohexane solvent. The first band gave 4.9 mg (6%) of COT **5**, mp 101–103°C (from hexane). The second band gave 6.2 mg (8%) of 2-cyanonaphthalene, mp 62–64°C (from hexane). The third band gave 23.4 mg (26%) of unreacted diene **7**. The fourth band gave 41.7 mg (47%) of material, mp 94–96°C (from hexane), identical (mixture mp, nmr, gc) to the known (2) 1-cyanobenzotricyclo-[3.3.0.$0^{2,8}$]octa-3,6-diene (**6**).

Direct irradiation of diene 8

A solution of 92.6 mg (0.52 mmol) of **8** in 30 mL of cyclohexane was photolyzed (Pyrex filter) for 4.5 h in cell B. The photolysate composi-

tion analysed for 15.9 mg (24%) naphthalene, 38.1 mg (41%) COT **5**, 16.6 mg (18%) diene **8**, 5.3 mg (6%) tetracyclic **17**, and 5.1 mg (6%) SB **16**, as determined by gc and nmr after the addition of a known amount of standardized tetradecane. The photolysate was concentrated to 10 mL and chromatographed in Silica Gel 60 (1.5 cm × 45 cm) with 3% ether–cyclohexane. The first band gave 9.3 mg (14%) of naphthalene, mp 78–80°C (from ethanol). The second band gave 40.8 mg of a mixture of COT **5** and diene **8**; crystallization of the mixture from hexane gave 17.2 mg (19%) of COT **5**, mp 101–103°C (from hexane), and the filtrate when rechromatographed gave 7.5 mg (8%) of recovered **8** and 15.6 mg of a mixture of COT **5** and diene **8**. The third band, containing SB **16**, was concentrated to ca. 5 mL (note: SB **16** rapidly polymerizes when solvent free), then diluted with 30 mL of CCl_4, and concentrated to ca. 5 mL. Subsequent repetitions of the CCl_4 addition (30 mL each) and concentration cycle led to essentially complete removal of the original ether–cyclohexane solvent system to give a solution of **16** (gc purity >99%) in CCl_4: nmr (200 MHz; CCl_4), see Table 1; nmr (400 MHz; 1:1 ratio of $CCl_4/CDCl_3$): 7.36–7.42 (m, 1H, aromatic), 7.03–7.23 (m, 3H, aromatics), 6.30 (d, 1H, H-6, $J_{6,5} = 2.5$), 4.05 (dd, 1H, H-5, $J_{5,1} = 6.5$, $J_{5,6} = 2.5$), 3.38 (q, 1H, H-1, $J_{1,5} = J_{1,2} = J_{1,8} = 6.5$), 3.20 (t, 1H, H-2, $J_{2,1} = J_{2,8} = 6.5$), and 2.95 (t, 1H, H-8, $J_{8,1} = J_{8,2} = 6.5$); spin decoupling experiments: irradiation of H-6 collapsed H-5 to a d ($J_{5,1} = 6.5$): iradiation of H-5 collapsed H-6 to an s, and H-1 to a t ($J_{1,8} = J_{1,2} = 6.5$); irradiation of H-1 collapsed H-5 to a d ($J_{5,6} = 2.5$), H-2 to a d ($J_{2,8} = 6.5$), and H-8 to a d ($J_{8,2} = 6.5$); irradiation of H-2 collapsed H-1 to a t ($J_{1,8} = J_{1,5} = 6.5$) and H-8 to a d ($J_{8,2} = 6.5$); irradiation of H-8 collapsed H-1 to a t ($J_{1,2} = J_{1,5} = 6.5$) and H-2 to a d ($J_{2,1} = 6.5$); gc/ms showed molecular ion at *m/e* = 179 (67%), 178 (base peak).

The fourth and last band gave 4.1 mg (4%) of **17**, mp 130–132°C (from hexane); ir (Nujol): 2225, C≡N; uv: 249 sh (120), 254 sh (200), 260 (320), 265 sh (440), 266 (480), and 273 (560); nmr (400 MHz; $CDCl_3$): 7.22–7.28 (m, 2H, aromatics), 7.16–7.22 (m, 2H, aromatics), 4.33–4.38 (m, 2H, H-1 and H-6), 3.28 (quintet, 1H, H-5, $J_{5,1(6)} = J_{5,2(3)} = 4.5$), and 2.91–2.98 (m, 2H, H-2 and H-3); spin decoupling experiments: irradiation of H-1,6 collapsed H-5 to a t ($J_{5,2} = J_{5,3} = 4.5$) and H-2,3 to a d ($J_{2(3),5} = 4.5$); irradiation of H-5 modified both H-1,6 and H-2,3; irradiation of H-2,3 collapsed H-5 to a t ($J_{5,1} = J_{5,6} = 4.5$) and H-1,6 to a d ($J_{1(6),5} = 4.5$). Mass spectrum showed molecular ion at *m/e* = 179.0723 (72%), 178 (base peak), 128 (51%).

Sensitized irradiation of diene 7

A solution of 34.8 mg (0.19 mmol) of **7** and 4.7 mg (0.02 mmol) of Michler's ketone in 35 mL of cyclohexane was photolyzed at >340 nm for 1 h in cell B (100% conversion by gc). The photolysate composition analysed for 31.2 mg (90%) SB **6** and 0.3 mg (1%) 2-cyanonaphthalene, as determined by gc after the addition of a known amount of standardized tetradecane. The photolysate was concentrated and the residue chromatographed on Silica Gel 60 (1.5 cm × 25 cm) with 2% ether–cyclohexane solvent. The first band gave a trace of 2-cyanonaphthalene (identified by tlc and gc comparisons with authentic sample), and the second band gave 30.4 mg (87%) of SB **6**, mp 94–96°C (from hexane).

Sensitized irradiation of diene 8

A solution of 46.0 mg (0.26 mmol) of **8** and 4.7 mg (0.02 mmol) of Michler's ketone in 35 mL of cyclohexane was photolyzed at >340 nm for 1 h in cell B (100% conversion by gc). The photolysate composition analysed for 29.3 mg (89%) naphthalene and 1.1 mg (2%) SB **16**, as determined by gc after the addition of a known amount of standardized tetradecane. The photolysate was concentrated (to 10 mL), and chromatographed on Silica Gel 60 (1.5 cm × 30 cm) with 3% ether–cyclohexane. The first band gave 16.8 mg (51%) naphthalene, mp 78–80°C (from ethanol). The second band was concentrated to ca. 5 mL and the solvent was exchanged for CCl_4. The nmr spectrum of the resulting solution was identical to that of SB **16**.

Catalytic reduction of SB 16

A stirred mixture of ca. 28 mg (ca. 0.16 mmol) of **16** and 6.4 mg of 10% Pd on C in 5 mL of ethyl acetate was hydrogenated at room temperature and pressure during 3 min. The catalyst was removed (centrifuge) and the resulting solution, when analysed by gc, showed three major peaks of relative area 1 (**16**): 2 (**20**): 3 (unknown). The solution was diluted with 30 mL of cyclohexane and concentrated to 5 mL. Repetition of the cyclohexane addition (30 mL) and concentration to 5 mL was followed by chromatography on Silica Gel 60 (1.5 cm × 60 cm) with 3% ether–cyclohexane solvent; 10-mL fractions were collected. Fractions 1–47 contained nothing. Fractions 48–51 gave 8.7 mg (31%) of colourless **20**, mp 99–101°C (from hexane); ir (Nujol): 2225, C≡N; uv: 248 sh (20), 253 sh (340), 259 (600), 263 sh (740), 266 (980), and 272 (1 200); nmr (400 MHz; $CDCl_3$): 7.20–7.32 (m, 4H, aromatics), 6.52 (dt, 1H, H-6, $J_{6,5} = J_{6,8} = 2.5$, $J_{6,8'} = 1.5$), 3.98 (br t, 1H, H-1, $J_{1,5} = J_{1,8} = 8.5$, $J_{1,8'} \simeq 1.0$), 3.75 (m, 1H, H-5), 3.27 (dd, 1H, H-4, $J_{4,5} = 9$, $J_{4,4'} = 16.5$), 3.16 (m, 1H, H-8, $J_{8,8'} = 16$, $J_{8,1} = 8.5$, $J_{8,6} = 2.5$, and $J_{8,5} = 2.7$ (homo-allylic coupling)), 2.96 (dd, 1H, H-4′, $J_{4',4} = 16.5$, $J_{4',5} = 2$), 2.76 (dm, 1H, H-8′, $J_{8',8} = 16$, $J_{8',1} \sim 1.0$, $J_{8',5} = 2$, $J_{6',8} = 1.5$); spin decoupling experiments: irradiation of H-6 modified H-5 and collapsed H-8 to a ddd ($J_{8,8'} = 16$, $J_{8,1} = 8.5$, $J_{8,5} = 2.7$), and H-8′ to a ddd ($J_{8',8} = 16$, $J_{8',1} = 1$, $J_{8',5} = 2$); irradiation of H-1 collapsed H-5 to a dm ($J_{5,4} = 9$), H-8 to a dt ($J_{8,8'} = 16$, $J_{8,5} = 2.7$, $J_{8,6} = 2.5$), and modified H-8′; irradiation of H-5 modified H-6 to a br s, and collapsed H-1 to a br d ($J_{1,8} = 8.5$), H-4 to a d ($J_{4,4'} = 16.5$), H-8 to a ddd ($J_{8,8'} = 16$, $J_{8,1} = 8.5$, $J_{8,6} = 2.5$), H-4′ to a d ($J_{4,4'} = 16.5$), and H-8′ to a br d ($J_{8',8} = 16$); irradiation of H-4 modified H-5 and H-4′ (incomplete decoupling) irradiation of H-8 modified H-5 and H-1 (incomplete decoupling),and collapsed H-6 to a br s and H-8′ to a single m; irradiation of H-4′ modified H-5 and collapsed H-4 to a d ($J_{4,5} = 9$); irradiation of H-8′ modified H-5 and H-8, and collapsed H-6 to a t ($J_{6,5} = J_{6,8} = 2.5$) and H-1 to a sharp t ($J_{1,5} = J_{1,8} = 8.5$). Mass spectrum showed molecular ion at *m/e* = 181.0894 (100%); $C_{13}H_{11}N$ requires 181.0892.

Fractions 52–59 contained 4.2 mg (15%) of recovered **16** as determined by gc after the addition of a known amount of standardized tetradecane. Fractions 60–120 contained essentially nothing. Further elution with 0.5 L of 5% ether–cyclohexane also gave no product material. Thus the major reduction product (unknown) adheres strongly to the silica gel.

*Labelled COT 5*a

Deuterated COT **5***a* (86%-d_1 at C-9) was prepared as previously described (2); nmr (400 MHz; $CDCl_3$): 7.21–7.31 (m, 2.88H, 2 aromatics + residual C*H*Cl_3), 6.95–7.05 (m, 2.00H, 2 aromatics), 6.75 and 6.73 (d and s, 1.95H, H-5 and H-10, $J_{5,6} = 11.5$), 6.67 (s, 0.95H, H-8), 6.07 (dd, 0.14H, H-9, $J_{9,10} = 11.5$, $J_{9,8} = 4$), and 5.95 (d, 0.96H, H-6, $J_{6,5} = 11.5$); errors from nmr signal integrations are within ±0.05H for **5***a*, and for all subsequent integrations of deuterated compounds.

*Labelled dienes 7*a *and 8*a *from COT 5*a

A solution of 219.3 mg (1.22 mmol) of COT **5***a* (86%–d_1 at C-9) (2) in 200 mL of benzene was photolyzed at >340 nm for 40 h in cell A. The photolysate was worked up as in the case of the direct irradiation of COT **5** to give 38.7 mg (18%) of **7***a* and 23.3 mg (11%) of **8***a*. For **7***a*, nmr (400 MHz; $CDCl_3$): 7.19–7.28 (m, 3.17H, 2 aromatics + residual C*H*Cl_3), 7.11–7.17 (m, 2.00H, 2 aromatics), 6.46 (d, 0.98H, H-4, $J_{4,5} = 10$), 6.19 (s, 0.96H, H-7), 6.07 (dd, 0.12H, H-8, $J_{8,7} = 2.8$, $J_{8,1} = 1$), 5.85 (d, 1.00H, H-5, $J_{5,4} = 10$), and 4.46 (s, 0.95H, H-1). For **8***a*, nmr (400 MHz; $CDCl_3$): 7.16–7.22 (m, 1.97H, 2 aromatics), 7.06–7.13 (m, 2.00H, 2 aromatics), 6.71 (d, 0.97H, H-8, $J_{8,1} = 1$), 6.42 (s, 0.98H, H-4), 5.93 (dd, 0.14H, H-5, $J_{5,4} = 10$, $J_{5,6} = 4.5$), 4.22 (br d, 1.03H, H-1, $J_{1,6} = 4.5$), and 4.00 (d, 1.00H, H-6, $J_{6,1} = 4.5$).

*Direct irradiation of labelled diene 7*a

A solution of 21.6 mg (0.12 mmol) of **7***a* in 30 mL of cyclohexane was photolyzed (Pyrex filter) for 6 h in cell B. The photolysate, when worked up as in the case of the direct irradiation of unlabelled **7**, gave 11.6 mg (54%) of SB **6***a*; nmr (60 MHz; CCl_4): 6.90–7.40 (m, 4.00H, aromatics), 5.60 (dd, 0.14H, H-6, $J_{6,5} = 2.5$, $J_{6,7} = 5$), 5.12 (d, 0.94H, H-7, $J_{7,8} = 2.5$), 4.12 (s, 1.01H, H-5), 3.60 (d, 1.02H, H-2, $J_{2,8} = 7$), and 3.27 (dd, 0.99H, H-8, $J_{8,2} = 7$, $J_{8,7} = 2.5$).

*Sensitized irradiation of labelled diene 7*a

A solution of 16.1 mg (0.09 mmol) of **7***a* and 4.7 mg (0.02 mmol) of Michler's ketone in 35 mL of cyclohexane was photolyzed at >340 nm for 20 min in cell B. The photolysate, when worked up as in the case of the sensitized irradiation of unlabelled **7**, gave 13.5 mg (84%) of SB **6***a*; nmr (60 MHz; CCl_4): 6.90–7.40 (m, 4.00H, aromatics), 5.60 (dd, 0.14H, H-6, $J_{6,5} = 2.5$, $J_{6,7} = 5$), 5.12 (d, 0.95H, H-7, $J_{7,8} = 2.5$), 4.12 (s, 0.94H, H-5), 3.60 (d, 0.95H, H-2, $J_{2,8} = 7$), and 3.27 (dd, 0.95H, H-8, $J_{8,2} = 7$, $J_{8,7} = 2.5$).

*Direct irradiation of labelled diene 8*a

A solution of 39.9 mg (0.22 mmol) of **8***a* in 35 mL of cyclohexane was photolyzed (Pyrex filter) for 9 h in cell B. The photolysate, when worked up as in the case of the direct irradiation of unlabelled **8**, gave ca. 1.7 mg (4%) of SB **16***a*; nmr (400 MHz: 1:1 ratio of $CCl_4/CDCl_3$): 7.36–7.42 (m, 1.00H, 1 aromatic), 7.03–7.23 (m, 3.12H, 3 aromatics), 6.30 (d, 0.99H, H-6, $J_{6,5} = 2.5$), 4.05 (dd, 1.00H, H-5, $J_{5,1} = 6.5$, $J_{5,6} = 2.5$), 3.38 (t, 0.97H, H-1, $J_{1,2} = J_{1,5} = 6.5$), 3.20 (d, 0.96H, H-2, $J_{2,1} = 6.5$), and 2.95 (t, 0.14H, H-8, $J_{8,1} = J_{8,2} = 6.5$).

*Sensitized irradiation of labelled diene 8*a

A solution of 35.9 mg (0.20 mmol) of **8***a* and 4.7 mg (0.02 mmol) of Michler's ketone in 35 mL of cyclohexane was photolyzed at >340 nm for 38 min in cell B. The photolysate, when worked up as in the case of the sensitized irradiation of unlabelled **8**, gave ca. 0.5 mg (ca. 1%) of SB **16***a*; nmr (400 MHz; 1:1 ratio of $CCl_4/CDCl_3$): 7.36–7.42 (m, 1.00H, 1 aromatic), 7.03–7.23 (m, 3.06H, 3 aromatics), 6.30 (d, 1.01H, H-6), 4.05 (dd, 0.97H, H-5), 3.38 (t, 0.98H, H-1), 3.20 (d, 1.00H, H-2), and 2.95 (t, 0.13H, H-8).

Phosphorescence and fluorescence of COT 5 and dienes 7 and 8

Compounds **5**, **7**, and **8** showed no phosphorescence spectra at 77 K in 1:1 isopentane/methylcyclohexane glass, and only **7** showed fluorescence in cyclohexane at room temperature (maxima at 330 nm). Intersection of emission and absorption spectra for **7** occurred at 300 nm, corresponding to a singlet energy of 95 kcal/mol. The singlet energy of **8** was estimated to be $92 \leq E_s \leq 95$ kcal/mol from the uv spectrum, which showed onset of absorption at ca. 310 nm and the lowest energy peak (a shoulder) at 302 nm.

Quantum yield determinations

Quantum yields were performed on an apparatus previously described (23), which includes an optical bench arranged for beam splitting into a ferrioxalate actinometer (24). Sample solutions (3 mL) of reactants (ca. $3–10 \times 10^{-3}$ *M*) and sensitizer, if any (benzophenone, 2×10^{-2} *M*; Michler's ketone, 0.57×10^{-3} *M*; 1- and 2-acetonaphthone, 3×10^{-2} *M*), were dexoygented prior to irradiation by flushing with argon. A positive pressure of argon was maintained over the stirred solutions throughout the course of the irradiations. For Φ's and further experimental details, see Table 2. Note that Φ's for sensitized irradiations of COT **5** with thioxanthone (E_T 65.5 kcal/mol; 1.4×10^{-3} *M*) or with *p*-dimethylaminobenzophenone (E_T 62 kcal/mol (25); 3.1×10^{-3} *M*) in benzene solvent are not included in Table 2 since we were unable to show that photoproduct(s) formed in these runs (see below). However, actinometer experiments carried out on the optical bench, with 366 nm light, permit us to place an upper value of $\Phi < 0.0001$ for the formation of **7** or **8**, if either were a photoproduct; gc together with nmr analyses would have detected >1% presence of the dienes, if formed.

Sensitized irradiations of COT 5

(a) With thioxanthone

A solution of 1.8 mg (0.01 mmol) of COT **5** and 1.0 mg (0.005 mmol) of thioxanthone in 3 mL of benzene was irradiated for 24 h in cell C with 315–385 nm light (obtained from a cylindrical uranium glass (Ace) sleeve (2 mm) and a UG-11 (Schott) glass filter (3 mm); transmission maximum was 42% at 357 nm; transmittance at 366 nm was 35%). The photolysate composition showed no loss of starting material or sensitizer, as indicated by a combination of gc and nmr analyses after the addition of a known amount of standardized tetradecane. No photoproducts were observed. Note that with the same apparatus and filter system, a solution of 1.6 mg (0.009 mmol) of diene **7** and 1.0 mg (0.005 mmol) of thioxanthone in 3 mL of benzene was 30% converted to SB **6** within 2 min.

(b) With p*-dimethylaminobenzophenone*

A solution of 5.7 mg (0.03 mmol) of COT **5** and 6.3 mg (0.03 mmol) of *p*-dimethylaminobenzophenone in 90 mL of benzene was divided into three equal portions. Each portion was separately irradiated for 12 h in cell C with 315–385 nm light. The three photolysates were combined and chromatographed on Silica Gel 60 (0.9 cm × 15 cm). Elution with 2% ether–cyclohexane gave 5.0 mg (88%) of recovered COT **5**, mp 101–103°C (from hexane); further elution with 6% ether–cyclohexane gave 6.4 mg (102%) of recovered sensitizer, mp 83–87°C.

Calculations

All calculations were made within the general framework of the CNDO semi-empircal molecular orbital method as previously described (2, 18). With the exception of the bridgehead C5—C6—C7 angle (23), the ground state geometries were determined using the CNDO-2 parameterization (26). By repeating the calculations for a range of values (105–120°), the bridgehead angles were shown to have negligible effects on the results; the values given in Table 3 were obtained for a fixed angle of 115°.

The vertical excitation energies were determined by configuration interaction with the CNDO/S parameterization (27), using a modified version of the program QCPE #315, originally written by Del Bene and Jaffé (28). The number of configurations included was found not to importantly influence the results, and the values given in Table 3 were obtained from 90 states. The CI expansion coefficients were employed to partition the excitation energy into single atom and atom–atom interaction energies (2).

Previously, we had interpreted the changes in atom–atom energies to indicate the initial nuclear motions resulting from excitation, and the approach proved useful for rationalizing product distributions in the DPM rearrangements of several benzobarrelene derivatives (2, 18). In the present examples this approach clearly does not work, e.g., note the entries for C5–C7; the changes in atom–atom energies are not only small, but in the case of **7**, where SB formation is the observed major product, predict repulsion between the initial bridging atoms of the DPM rearrangement.

Additionally, it should be pointed out that even the competition between localization of the excitation in the cyclobutenyl (C7—C8) versus the styrenyl (C4—C5) vinyl moieties is not clear-cut, since for **2**, T_1 and T_2 are near-degenerate ($T_1 - T_2 \simeq 0.1$ eV), with T_2 being more heavily weighted with excitation energy in the cyclobutenyl vinyl. Also, changing from the theoretical to the Pariser form of the repulsion integrals, usully held to be better for calculating triplet excitation energies, leads to a reversal in the order of the two lowest triplets for **8**, and results in a heavier weighting of excitation energy in the styrenyl vinyl of T_1. This combination of circumstances leads us to conclude that the calculations are unreliable in product prediction in the systems at hand.

Acknowledgements

The authors thank the Spectroscopic Services Laboratory of the University of Alberta for the 400-MHz nmr and mass spectra, the University of Calgary for the 200-MHz nmr spectrum, the Agriculture Canada Research Station at Lethbridge for the gc/ms spectrum, and the University of Lethbridge Computing Centre for the use of the DEC-20 system computer. Financial support from the Natural Sciences and Engineering Research Council of Canada is gratefully acknowledged.

1. C. O. Bender, I. M. Cassis, D. Dolman, L. D. Heerze, and F. L. Schultz. Can. J. Chem. **62**, 2769 (1984).
2. C. O. Bender, D. W. Brooks, W. Cheng, D. Dolman, S. F. O'Shea, and S. S. Shugarman. Can. J. Chem. **56**, 3027 (1978).
3. (*a*) J. J. McCullough, R. C. Miller, and W.-S. Wu. Can. J. Chem. **55**, 2909 (1977); (*b*) T. S. Cantrell. J. Am. Chem. Soc. **94**, 5929 (1972).

4. R. M. BOWMAN, C. CALVO, J. J. MCCULLOUGH, R. C. MILLER, and I. SINGH. Can. J. Chem. **51**, 1060 (1973).
5. P. J. COLLIN and W. H. F. SASSE. Tetrahedron Lett. 1689 (1968).
6. W. H. F. SASSE, P. J. COLLIN, and G. SUGOWDZ. Tetrahedron Lett. 3373 (1965).
7. J. STAPERSMA, I. D. C. ROOD, and G. W. KLUMPP. Tetrahedron, **38**, 191 (1982).
8. H. E. ZIMMERMAN, R. S. GIVENS, and R. M. PAGNI. J. Am. Chem Soc. **90**, 6096 (1968).
9. C. PASCUAL, J. MEIR, and W. SIMON. Helv. Chim. Acta, **49**, 164 (1966).
10. (*a*) L. A. PAQUETTE, G. H. BIRNBERG, J. CLARDY, and B. PARKINSON. J. Chem. Soc. Chem. Commun. 129 (1973); (*b*) R. M. MORIARTY and C.-L. YEH. Tetrahedron Lett. 383 (1972); (*c*) R. ASKANI and H. SÖMNEZ. Tetrahedron Lett. 1751 (1973).
11. O. L. CHAPMAN and G. WAMPFLER. J. Am. Chem. Soc. **91**, 5390 (1969).
12. H. E. ZIMMERMAN and R. A. BUNCE. J. Org. Chem. **47**, 3377 (1982).
13. S. S. HIXSON, P. S. MARIANO, and H. E. ZIMMERMAN. Chem. Rev. **73**, 531 (1973).
14. D. BRYCE-SMITH, A. GILBERT, B. ORGER, and H. TYRREL. J. Chem. Soc. Chem. Commun. 334 (1974).
15. C. O. BENDER and D. W. BROOKS. Can. J. Chem. **53**, 1684 (1975).
16. Y. HANZAWA and L. A. PAQUETTE. Synthesis, 661 (1982).
17. Y. HANZAWA and L. A. PAQUETTE. J. Am. Chem. Soc. **103**, 2269 (1981).
18. C. O. BENDER and S. F. O'SHEA. Can. J. Chem. **57**, 2804 (1979).
19. L. A. PAQUETTE, A. Y. KU, C. SANTIAGO, M. D. ROZENBOOM, and K. N. HOUK. J. Am. Chem. Soc. **101**, 5972 (1979).
20. (*a*) H. E. ZIMMERMAN and R. L. SWAFFORD. J. Org. Chem. **49**, 3069 (1984); (*b*) H. E. ZIMMERMAN and R. E. FACTOR. Tetrahedron, **37**, 125 (1981); (*c*) H. E. ZIMMERMAN, D. ARMESTO, M. G. AMEZUA, T. P. GANNETT, and R. P. JOHNSON. J. Am. Chem. Soc. **101**, 6367 (1979); (*d*) H. E. ZIMMERMAN, R. J. BOETTCHER, and W. BRAIG. J. Am. Chem. Soc. **95**, 2155 (1973).
21. (*a*) L. A. PAQUETTE and E. BAY. J. Am. Chem. Soc. **106**, 6693 (1984); (*b*) L. A. PAQUETTE, A. VARADARAJAN, and E. BAY. J. Am. Chem. Soc. **106**, 6702 (1984).
22. H. E. ZIMMERMAN. Acc. Chem. Res. **10**, 312 (1982).
23. C. O. BENDER, D. L. BENGTSON, D. DOLMAN, C. E. L. HERLE, and S. F. O'SHEA. Can. J. Chem. **60**, 1942 (1982).
24. (*a*) C. G. HATCHARD and C. A. PARKER. Proc. R. Soc. London, Ser. A, **235**, 518 (1956); (*b*) W. D. BOWMAN and J. N. DEMAS. J. Phys. Chem. **80**, 2434 (1976).
25. H. E. ZIMMERMAN and W. D. RAMSDEN. Can. J. Chem. **62**, 2592 (1984).
26. (*a*) J. A. POPLE, D. P. SANTRY, and G. A. SEGAL. J. Chem. Phys. **43**, S130 (1965); (*b*) J. A. POPLE and G. A. SEGAL. J. Chem. Phys. **43**, S136 (1965).
27. J. DEL BENE and H. H. JAFFE. J. Chem. Phys. **50**, 1126 (1969).
28. J. DEL BENE and H. H. JAFFE. J. Chem. Phys. **48**, 1807 (1968); **48**, 4050 (1968); **49**, 1221 (1968); **50**, 1126 (1969).

Reactions of 1-hydroxy-1,3-dihydrobenzo[*c*]thiophen-2,2-dioxides. Preparation of benz-fused δ-sultines

TONY DURST, JAMES L. CHARLTON, AND DAVID B. MOUNT

Ottawa–Carleton Chemistry Institute, Department of Chemistry, University of Ottawa, Ottawa, Ont., Canada K1N 9B4

Received April 29, 1985

TONY DURST, JAMES L. CHARLTON, and DAVID B. MOUNT. Can. J. Chem. **64**, 246 (1986).

4,5-Benzo-3,6-dihydro-1,2-oxathiin-2-oxides (benz-fused δ-sultines) **1**, were prepared by reaction of 1-hydroxy-1,3-dihydrobenzo[*c*]thiophen-2,2-dioxides **6** with $NaBH_4$. Derivatives of **1** bearing alkyl substituents at position 6 are accessible from **1** upon reaction of **6** with 2RLi. 3-Aryl substituted derivatives were prepared by converting 2-benzylbenzylalcohols into their O, C dianion followed by quenching with SO_2 and acidification. Benz-fused δ-sultines such as **15–17** were also prepared via the dianion route.

TONY DURST, JAMES L. CHARLTON et DAVID B. MOUNT. Can. J. Chem. **64**, 246 (1986).

On a préparé les benzo-4,5 dihydro-3,6 oxathiine-1,2 oxydes-2 (δ-sultines fusionnées avec des benzènes (**1**) en faisant réagir les hydroxy-1 dihydro-1,3 benzo[*c*]thiophène-dioxydes-2,2 (**6**) avec le $NaBH_4$. On peut obtenir les dérivés de **1** portant des substituants alkyles en position 6 en faisant réagir les composés **6** avec 2 RLi. On a préparé les dérivés portant des groupements aryles en position 3 en transformant les benzyl-2 benzylalcools en leurs dianions O et C qui sont ensuite piégés par le SO_2 avant d'être acidifiés. On a aussi préparé les δ-sultines **15–17** par le biais de la voie impliquant les dianions.

[Traduit par le journal]

A number of years ago we developed a route to cyclic sulfinate esters that we applied to the synthesis of several benz-fused sultines such as **1** (1). These 6-membered ring sultines showed considerable promise as sources of *o*-quinodimethanes since they readily lost SO_2 at about 80°C (1), or approximately 100–150° lower than the corresponding 1,3-dihydrobenzo[*c*]thiophene-1,1-dioxide, **3** (2).[1,2] The ortho-quinodimethane **2**, generated from **1**, was trapped efficiently with dienophiles such as dimethyl fumarate and maleic anhydride (1). When less reactive trapping agents were used the diene was recaptured by sulfur dioxide to afford the sulfone **3** (1, 2).

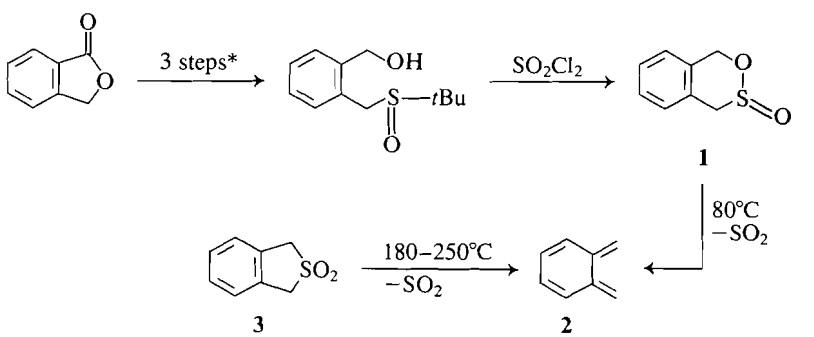

*Reagents: *t*BuSK, Δ; $LiAlH_4$; MCPBA, −20°C, EtOAc

SCHEME 1

Because of problems associated with the preparation of the derivatives of **1** via the route shown in Scheme 1, the full potential of these compounds as precursors of **2** has not been realized.

Very recently we showed that **1** and a number of derivatives are easily synthesized via a two or three-step sequence commencing with the readily available *ortho*-substituted benzaldehydes, **4***a*, *b*, or the related ketons such as **4***c* (3).

Thus photolysis of **4** in benzene, containing sulfur dioxide, generated the dienols **5**, which were trapped by the SO_2 to afford the α-hydroxysulfones **6** in acceptable yields (4, 5). The photolysis reaction can be carried out on multigram quantities. The desired compounds were easily separated from neutral organic by-products, based on their reversible conversion to the aldehyde sulfinates **7** (Scheme 2).

The hydroxy sulfones **6** can be converted to a variety of substituted δ-sultines in several ways. Reaction of **6***a* with sodium borohydride in methanol followed by acidification afforded the sultine **1** in 70% yield. The sequence obviously involves the reduction of the *in situ* generated **7***a* to the benzylic alcohol **8**. Two possible mechanisms could account for the formation of sultine **1** (Scheme 3). The function of the acid could be to protonate either the sulfinic acid function of **8**, to generate **8***a*, or the benzylic alcohol, giving **8***b*. Cyclization occurs in the case of **8***a* by a displacement at sulfinyl sulfur, while loss of H_2O from **8***b* could generate a benzylic cation that is trapped by the sulfinate oxygen rather than at sulfur to form **1**.

We had initially suggested the mechanism passing through **8***b*, since the benzylic cation generated from **8***b* by loss of H_2O should represent a hard electrophilic centre and Meeks and

[1]In our earlier publications (3, 5) this compound was inadvertently named as the [*b*] isomer.

[2]For a review on the generation of *o*-quinodimethanes from a variety of sources including 1,3-dihydrobenzothiophene-2,2-dioxides see ref. 2*a*.

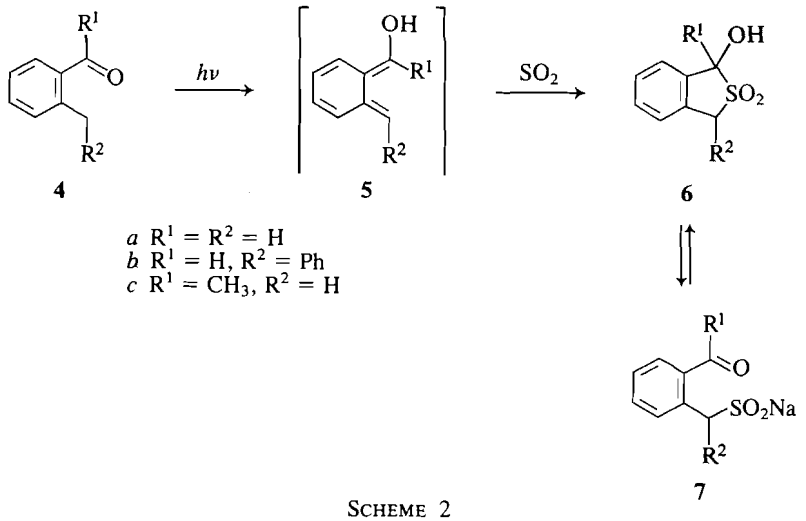

SCHEME 2

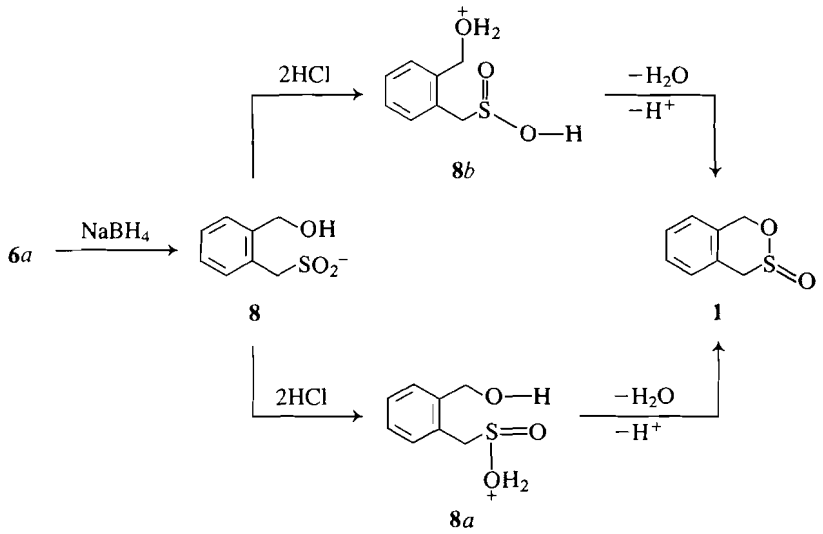

SCHEME 3

Fowler (6) had shown that sulfinates are alkylated preferentially at oxygen with hard, very reactive, alkylating agents and at sulfur by soft reagents. The alternative route involving displacement of H_2O from the protonated sulfinic acid **8***a* is now considered more reasonable, since Bunton and Hendy (7) have shown via ^{18}O labelling that methyl *p*-toluenesulfinate undergoes hydrolysis in acidic media with S—O bond cleavage.[3]

$$C_7H_7—\overset{\overset{O}{\|}}{S}—OCH_3 + H_2O^{18} \xrightarrow{H^+} C_7H_7—\overset{\overset{^{18}O}{\|}}{S}OH + CH_3OH$$

None of the isomeric sulfone **3** was detectable in the nmr spectrum of the crude product, an observation which gives additional support to the latter mechanism.

Similar treatment of the hydroxysulfones **6***b* and **6***c* gave **9** (79%) and **10** (55%), respectively. In these cases isomeric mixtures were obtained. The structures were assigned on the basis of the nmr and infrared spectra, and analytical data (see experimental section). All sultines showed the expected S=O stretching frequency in the 1100–1140 cm^{-1} range. The δ-sultines reported herein failed to show the molecular ion peaks in their mass spectra, with the base peaks generally occurring at $M^{+\cdot} - 64$.

Non-hydrogen substituents can be introduced α to the sultine oxygen by reaction of **6** with alkyllithiums, such as methyllithium: i.e., **6***c* → **11**. Functionalized lithocarbanions should react likewise, thus suggesting the possibility of preparing a wide variety of sultines by this route. Grignard reagents, unfortunately, do not react cleanly with the hydroxy sulfones **6** and we have as yet been unable to isolate and identify products from these attempts.

The fact that the hydroxy sulfinate **8** is an intermediate in the conversion of **6***a* to **1** suggested that other routes to **8** should be investigated. An obvious method was the generation of the dilithio species **12** followed by treatment with sulfur dioxide. Thus, raction of *ortho*-benzylbenzyl alcohol with 2 equivalents

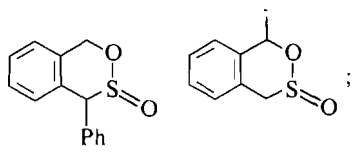

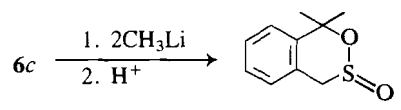

[3]We are indebted to a referee for pointing out this reference.

of *n*Buli in THF at 20°C for 1 h gave a dark-colored solution containing **12**, which was quenched with excess SO_2. The solvent was evaporated and the residue warmed with concentrated HCl. The nmr yield of sultine **9** was 50–70% (several experiments), with the remainder being recovered starting material. Similar treatment of *ortho*-benzyl-α,α′-dimethylbenzyl alcohol afforded the sultine **13**, mp 104°C, in 38% isolated yield. An attempted conversion of *ortho*-methylbenzyl alcohol into sultine **1** was unsuccessful, presumably due to the difficulty of forming the required dianion. The dianion route to these interesting δ-sultines is apparently restricted to cases in which the intermediate is accessible, as in the case for **12**.

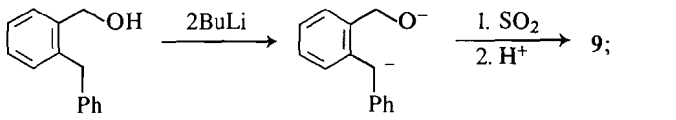

12

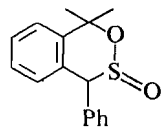

13

The dianion route is also applicable to the formation of 5-membered benz-fused sultines. Thus the dianions of **14***a–c*, generated from the appropriate bromoalcohols by treatment with 2 equivalents of *n*Buli in THF at 0°C, reacted with sulfur dioxide at −78°C to form the intermediate sulfinates, which on acidification gave the expected sultines **15***a–c* in 60–70% isolated yield. Similar metallation of 6-bromo-3,4-methylenedioxybenzyl alcohol followed by SO_2 treatment gave a variable ratio of the sultines **16** and **17** in up to 70% yield. The mixture resulted from the isomerization of the initially formed 6-lithio derivative to the more stable 2-lithio anion. A similar isomeriza-

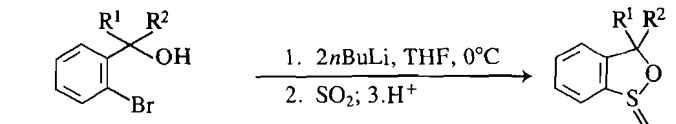

14*a* $R^1 = R^2 = H$
14*b* $R^1 = H, R^2 = CH_3$
14*c* $R^1 = R^2 = CH_3$

15*a–c*

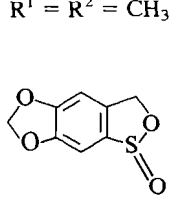

16

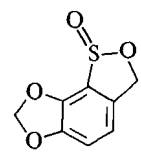

17

tion has been observed during the halogen–metal exchange of the cyclohexylimine of 6-bromopiperonal (9). Pure **17** was produced upon treatment of 3,4-methylenedioxybenzyl alcohol with 2*n*Buli, SO_2, and acidification as above. These sultine-forming reactions mirror the formation of γ-lactones via the reaction of the same dianion intermediates with carbon dioxide and suggest that, in general, this parallel should continue to be expected (10).

We are currently studying the preparation of δ-sultines fused to heterocyclic systems such as the furan, thiophene, and indole rings and the use of such compounds for the generation of the corresponding orthoquinodimethanes. The latter have received considerable attention in the indole series as key intermediates in the synthesis of some indole alkaloids (11).

Experimental

"Work-up" indicates that the reaction mixture was poured into a saturated NH_4Cl solution and extracted with CH_2Cl. The organic extracts were dried over anhydrous $MgSO_4$ and the solvent evaporated to yield the crude product. The nmr spectra were taken on a Varian XL-300 or Varian T-60 instrument in $CDCl_3$ solution.

*Conversion of the hydroxy sulfones **6** to sultines. General procedure using $NaBH_4$*

The hydroxy sulfone (**6***a*, *b*, or *c*), 100 mg, was dissolved in 5 mL of methanol at 0°C. $NaBH_4$ (70 mg) was added, the reaction was stirred for 30 min, and then the solvent was evaporated. To the crude product was added 5 mL of concentrated HCl, the mixture was stirred at 50°C for 3 min, cooled, diluted with H_2O, and extracted with CH_2Cl_2. Further work-up afforded the crude sultines, which were purified by silica gel chromatography.

*Sultine **1***

Yield 70%; ir: 1130 cm^{-1}; ^1H nmr: 3.55 (d, J = 15.5 Hz, 1H), 4.42 (d, J = 15.5 Hz, 1H), 4.96 (d, J = 13.7 Hz, 1H), 5.30 (d, J = 13.7 Hz, 1H), 7.2–7.4 (m. 4H); ms *m/e* (rel. %): 168 (0.2), 105 (10), 104 (100), 103 (42). *Anal.* calcd. for $C_8H_8O_2S$: C 68.82, H 4.95, S 13.13; found: C 68.70, H 4.67, S 12.94.

*Sultine **9***

Yield 79%; ir: 1130 cm^{-1}; ^1H nmr: 4.71 (s, 1H), 5.06 (d, J = 14.4 Hz, 1H), 5.43 (d, J = 14.4 Hz, 1H), 7.06 (d, J = 6 Hz, 1H), 7.2–7.7 (m, 8H): ms *m/e* (rel. %): 181 (14), 180 (93), 179 (100), 178 (46). *Anal.* calcd. for $C_{14}H_{12}SO_2$: C 68.82, H 4.95, S 13.13; found: C 68.70, H 4.67, S 12.94.

*Sultine **10***

Yield 55%, 1:1 mixture of diastereomers, separable on silica gel chromatography using ethyl acetate – hexane 1:3. The less polar isomer had ir: 1110, 1140 cm^{-1}; ^1H nmr: 1.82 (d, J = 6.6 Hz, 3H), 3.51 (d, J = 15.2 Hz, 1H), 4.57 (d, J = 15.2 Hz, 1H), 5.40 (q, J = 7.6 Hz, 1H), 7.25–7.5 (m, 4H); ms *m/e* (rel. %): 119 (10), 118 (100), 117 (85), 116 (16), 91 (22). *Anal.* calcd. for $C_9H_{10}O_2S$: C 59.31, H 5.53, S 17.60; found: C 59.63, H 5.20, S 17.20.

The less polar isomer had ir: 1110, 1140 cm^{-1}; ^1H nmr: 1.85 (d, J = 6.6 Hz, 3H), 3.82 (d, J = 14.2 Hz, 1H), 4.01 (d, J = 14.2 Hz, 1H), 5.06 (q, 1H, J = 6.6 Hz), 7.3–7.5 (m); ms *m/e* (rel. %): 119 (10), 118 (100), 117 (87), 115 (21) 91 (25). *Anal.* calcd. for $C_2H_{10}SO_2$: C 59.31, H 5.53, S 17.60; found: C 59.55, H 5.23, S 17.86.

*Sultine **11***

Sulfone **6***c* (50 mg) was dissolved 15 mL of dry THF under N_2 at 20°C and treated with 3.0 mL of 1.6 *M* CH_3Li (large excess). After 1 h the reaction mixture was quenched with 2 mL of methanol. The solvents were evaporated, and the residue was warmed to 40°C with 5 mL concentrated HCl for 5 min, cooled, and diluted with 20 mL of H_2O. Extraction with CH_2Cl_2 afforded 39 mg (80%) of **11**; ir: 1120 cm^{-1}; ^1H nmr: 1.60 (s, 3H), 1.83 (s, 3H), 3.79 (d, J = 15 Hz, 1H), 4.03 (d, J = 15 Hz, 1H), 7.2–7.6 (m, 4H): *Anal.* calcd. for $C_{10}H_{12}O_2S$: C 61.19, H 6.16, S 16.34; found: C 60.92, H 6.02, S 16.55.

*Sultine **9** via the dianion route*

o-Benzylbenzyl alcohol (1.0 g) was dissolved in 25 mL of THF containing 0.4 mL of tetramethylethylenediamine. The solution was cooled to −78°C and *n*Buli (2.2 *M* in hexane) was added slowly. The solution was warmed to 20°C and left for 1 h. Sulfur dioxide was introduced until the deep red colour was quenched. The reaction mixture was evaporated and the residue stirred with 10 mL of concentrated HCl for 15 min. The reaction was worked up by diluting with 40 mL of H_2O, extracting with CH_2Cl_2, and washing the extracts with 5% $NaHCO_3$ solution. The yield of crude product was 1.19 g, which appeared to be a 70:30 mixture of **9** and starting alcohol by nmr. Recrystallization from ethanol afforded 494 mg (40%) of **9** with properties identical to those described above.

Sultine ***13***

ortho-Benzyl-α,α′-dimethylbenzyl alcohol (470 mg) and 0.2 mL of tetramethylpiperidine were dissolved in 25 mL of THF at 0°C under N_2. *n*Buli (2.3 mL of 2.5 *M*, 2.2 equiv.) was added dropwise via syringe and the solution was stored for 3 h at 20°C during which time a deep red colour developed. The flask was recooled to 0°C and SO_2 was introduced until the colour changed to yellow. The solvent was evaporated and the residue treated with concentration HCl as above. Work-up gave 465 mg of an orange oil, which contained 65% of the sultine **13** in addition to the starting alcohol. Chromatography on silica using 9:1 hexane – ethyl acetate afforded 206 mg (38%) of **13**, mp 104°C; ^{1}H nmr: 1.67 (s, 3H), 1.90 (s, 3H), 5.04 (s, 1H), 7.1–7.5 (m, 9H); ms *m/e* (rel. %): 209 (37), 193 (100), 178 (56), 165 (17). *Anal.* calcd. for $C_{16}H_{16}O_2S$: C 70.55, H 5.92, S 11.77; found: C 70.28, H 6.09, S 11.97.

Preparation of sultines ***15*** *and* ***16****. General procedure*

The appropriate *o*-bromobenzyl alcohol, ~1 g, was dissolved in THF at −78°C, reacted with 2.2 equiv. of *n*Buli for 15 min, warmed to 0°C for 15 min, and then recooled to −78°C. Excess SO_2 was introduced. The THF was evaporated and the residue stirred with 1 mL H_2O and 5 mL of concentrated HCl for 10 min. Extraction with CH_2Cl_2, followed by washing with saturated $NaHCO_3$ solution, furnished a crude product that was purified by silica gel chromatography.

Sultine ***15***a: isolated yield (61%) (8).

Sultine ***15***b: isolated yield 78% (mixture of diastereomers) (8).

Sultine ***15***c: isolated yield (56%) (8).

Sultine ***16***

Isolated yield 70%, mp 130–132°C; ^{1}H nmr: 5.43 (d, J = 13.3 Hz, 1H), 5.87 (d, J = 13.3 Hz, 1H), 6.10 (d, J = 1.2 Hz, 1H), 6.12 (d, J = 1.2 Hz, 1H), 6.82 (s, 1H), 7.10 (s, 1H); ms *m/e* (rel. %): 198 (75), 181 (10), 150 (100), 134 (28), 121 (21), 104 (16), 76 (31). *Exact Mass* calcd. for $C_8H_6O_4S$: 197.9985; found: 197.9978.

Sultine ***17***

To 1.00 g of 3,4-methylenedioxybenzyl alcohol, disolved in 15 mL of dry THF at 0°C, was added 5.8 ml of 2.5 *M* *n*Buli (2.2 equiv.). The solution was stirred for 2 h during which time a red colour developed. Sulfur dioxide was introduced until the red colour disappeared. Work-up, identical to that described for **15**, yielded 925 mg of crude product, which was judged to be 70% product **17** by nmr. Silica gel chromatography using hexane – ethyl acetate (4:1) afforded 56% of **17**, mp 120–121°C; ^{1}H nmr: 5.48 (d, J = 13.0 Hz, 1H), 5.91 (d, J = 13.0 Hz, 1H), 6.13 (d, J = 1.4 Hz, 1H), 6.15 (d, J = 1.4 Hz, 1H), 6.87 (d, J = 7.8 Hz, 1H), 6.99 (d, J = 7.8 Hz, 1H); ms *m/e* (rel. %): 198 (100), 150 (20), 134 (94), 121 (11), 105 (12), 104 (10), 92 (12), 78 (22). *Exact Mass* calcd. for $C_8H_6O_4S$: 197.9985; found: 197.9997.

Acknowledgement

The continued financial support of the NSERC (Canada) is gratefully acknowledged.

1. F. Jung, M. Molin, R. Vanden Elzen, and T. Durst. J. Am. Chem. Soc. **96**, 935 (1974).
2. (*a*) W. Oppolzer. Heterocycles, **14**, 1615 (1980); (*b*) W. Oppolzer, D. A. Roberts, and T. G. C. Bird. Helv. Chim. Acta, **62**, 2017 (1979); (*c*) K. C. Nicolaou, W. B. Barnette, and P. Ma. J. Org. Chem. **45**, 1463 (1980).
3. J. L. Charlton and T. Durst. Tetrahedron Lett. **25**, 5287 (1984).
4. P. G. Sammes. Tetrahedron Lett. **32**, 405 (1976).
5. J. L. Charlton and T. Durst. Tetrahedron Lett. **25**, 2663 (1984).
6. J. S. Meeks and J. S. Fowler. J. Org. Chem. **33**, 3422 (1968).
7. C. A. Bunton and B. N. Hendy. J. Chem. Soc. 2562 (1962).
8. T. Durst, J. C. Huang, M. K. Sharma, and D. J. H. Smith. Can. J. Chem. **56**, 512 (1978).
9. F. E. Ziegler and K. W. Fowler. J. Org. Chem. **41**, 1564 (1976).
10. R. Marsden and D. B. MacLean. Can. J. Chem. **62**, 306 (1984).
11. P. Magnus, T. Gallagher, P. Brown, and P. Pappalardo. Acc. Chem. Res. **17**, 35 (1984).

Open-chain nitrogen compounds. Part IX.[1] 1,2,3-Triazolo[1,5-*a*]quinazoline and its 5-alkyl and 5-aryl derivatives from alumina-catalysed cyclization of 1-(2′-acylphenyl)-3-cyanomethyltriazene

DONALD L. HOOPER
Department of Chemistry, Dalhousie University, Halifax, N.S., Canada B3H 4J3
AND
HARTFORD W. MANNING, RONALD J. LAFRANCE, AND KEITH VAUGHAN[2]
Department of Chemistry, Saint Mary's University, Halifax, N.S., Canada B3H 3C3

Received July 5, 1985

DONALD L. HOOPER, HARTFORD W. MANNING, RONALD J. LAFRANCE, and KEITH VAUGHAN. Can. J. Chem. **64**, 250 (1986).
Alumina-catalysed cyclization of a series of 1-(2′-acylphenyl)-3-cyanomethyltriazenes (**5**) affords good yields of the previously unreported 5-alkyl- and 5-aryl-1,2,3-triazolo[1,5-*a*]quinazolines (**8**). The parent heterocycle, 1,2,3-triazolo[1,5-*a*]quinazoline, has been observed for the first time as the product of cyclization of 1-(2′-formylphenyl)-3-cyanomethyltriazene.

DONALD L. HOOPER, HARTFORD W. MANNING, RONALD J. LAFRANCE et KEITH VAUGHAN. Can. J. Chem. **64**, 250 (1986).
La cyclisation, catalysée par l'alumine, d'une série de (acyl-2 phényl)-1 cyanométhyl-3 triazènes (**5**) conduit, avec de bons rendements, aux alkyl-5 et aryl-5 triazolo-1,2,3[1,2-*a*]quinazolines (**8**) qui n'avaient pas été décrites antérieurement. L'hétérocycle de base, la triazolo-1,2,3[1,5-*a*]quinazoline a été observée pour la première fois comme produit de la cyclisation du (formyl-2 phényl)-1 cyanométhyl-3 triazène.

[Traduit par le journal]

1,2,3-Triazolo[1,5-*a*] pyrimidines undergo thermal equilibrium between two isomeric structures **1** and **3** via the intermediacy of an open-chain diazo compound **2** (1). The diazo form (**2**) can become the predominant isomer of the equilibrium mixture when the pyrimidine ring is fused at R^1 and R^2 to a π-deficient aromatic heterocycle, such as a *v*-triazole (2). On the other hand, ring fusion at R^1/R^2 with a π-excessive thiophene ring (3) results in preference for the tricyclic angular structure (**1**), as is also the case for benzene ring fusion in the 1,2,3-triazolo[1,5-*a*]quinazolines. The first examples of this comparatively rare heterocycle were reported as products of the base-catalysed condensation of reactive methylene compounds with *o*-azidobenzoic acids (4), which affords 1,2,3-triazolo[1,5-*a*]quinazolines invariably substituted with 5-oxo or 5-amino groups and with a substituent at position C-3. In this communication, we report that alumina-catalysed cyclization of a series of 1-(2′-acylphenyl)-3-cyanomethyltriazenes (**5**) provides a convenient synthesis of the previously unreported 1,2,3-triazolo[1,5-*a*]quinazoline **8***a* and of its 5-alkyl[3] and 5-aryl derivatives **8***b*–*g*.

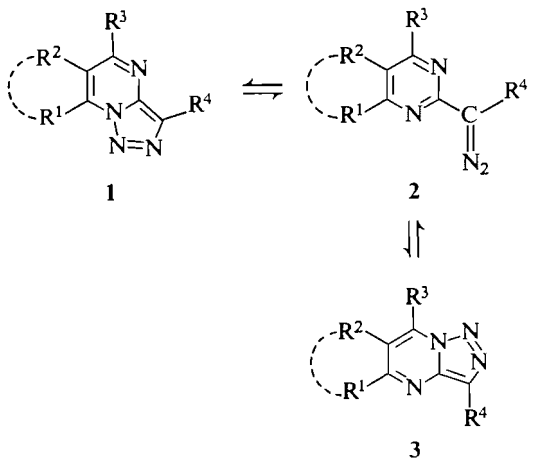

Diazotization of the arylamine **4** and coupling with α-aminoacetonitrile, followed by neutralization with aqueous sodium carbonate to pH 8, affords the triazene **5**, which exists in the solid state and in DMSO solution as the cyclic isomer, the 1,2,3-benzotriazinol (**6**). In chloroform solution, the equilibrium **5** ⇌ **6** lies in favour of the open-chain triazene form, so that when a chloroform solution of a triazinol ⇌ triazine is treated with solid, neutral alumina over a 24- to 48-h period, cyclization of the triazene occurs readily. The intermediate 1-aryl-5-amino-1,2,3-triazole (1) is not isolated, and further cyclization, with dehydration, affords the novel 1,2,3-triazolo[1,5-*a*]quinazoline **8**. Presumably the initial cyclization step **5** → **7** is the rate-determining step in the overall process; the subsequent cyclization of **7**, by nucleophilic attack of the 5-amino group of the intermediate triazole at the 2′-acyl carbonyl group, must be relatively fast.

Yields and physical data of the intermediate 3-cyanomethyl-1,2,3-benzotriazin-4-ols (**6***a*–*g*) are given in Table 1. The ir spectrum in Nujol of, typically, **6***b* shows the absence of carbonyl and the presence of a broad hydroxyl band at 3170 cm^{-1} anticipated for the cyclic structure (5). The ^1H nmr spectra of the triazinols in DMSO-d_6 (Table 2) demonstrate clearly the exclusive adoption of the cyclic form (**6**) with no trace of the ring-open form (**5**) in this medium; all the spectra show a characteristic AB quartet, J_{AB} ~ 17.8 Hz, as expected for the diastereotopic N—CH_2—CN protons adjacent to the chiral centre at C-4 of the triazine. The spectrum of **6***c* also shows multiplicity of the diastereotopic methylene protons of the ethyl substituent at C-4. All compounds in this series exhibit a low-field singlet at ca. δ 8 arising from the hydroxylic proton at C-4. The aromatic patterns all show a characteristic high-field signal, corresponding to a proton on the α-carbon of the benzene

[1]For Part VIII, see ref. 6.
[2]Author to whom all correspondence should be addressed.
[3]A preliminary account of the synthesis of **8***b* has been described in a recent article, which describes the general cyclization of 1-(2′-acetylphenyl)3-alkyltriazenes (6).

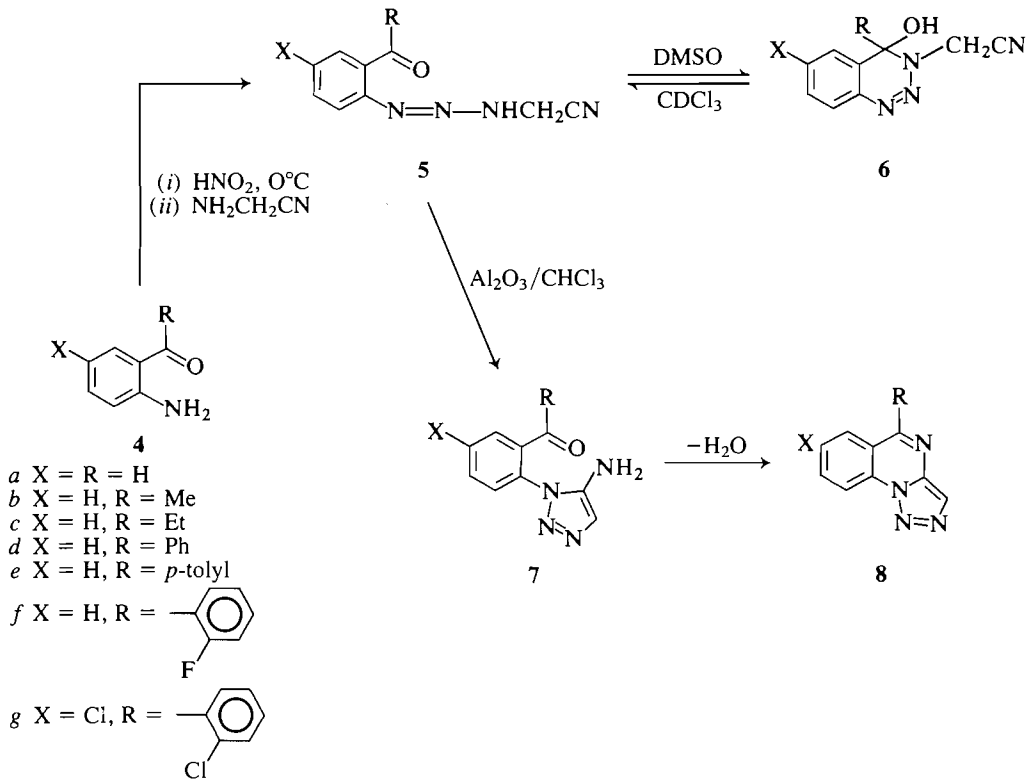

ring (adjacent to the CR(OH)N moiety); this signal is an 8-Hz doublet with fine structure arising from long-range coupling, except in the case of **6***g*, in which only the long-range coupling is observed.

The ring-open forms of these triazinols, the triazenes (**5**), are clearly evident in nmr and ir spectra run in chloroform solution. For example, the ir spectrum of the phenyl derivative (**5***d*) in $CHCl_3$ shows a strong carbonyl band at 1710 cm^{-1} and a weak, broad NH absorption band at 3250 cm^{-1}; the strong OH absorption band observed at 3150 cm^{-1} in the Nujol mull spectrum is absent in the chloroform solution spectrum. The ^1H nmr spectrum of **5***d* in $CDCl_3$ shows a strong two-proton singlet for the methylene protons at δ 4.7 ppm; only a trace of the AB system of **6***d* is evident in the $CDCl_3$ spectrum. The ^{13}C nmr spectrum of this solution (Table 3) confirms the dominance of the open-chain form (**5***d*), as indicated by the low-field carbonyl signal at δ 198.7 and a single observable N—CH_2 signal at δ 47.4. The ^{13}C nmr spectrum of the ethyl analogue (**5***c*) in deuteriochloroform also shows a carbonyl signal at δ 204.0, the N—CH_2 signal at δ 47.4, and C-ethyl group signals at δ 32.8 (CH_2) and 8.3 (CH_3).

The conversion of the triazene (**5**) in chloroform to the triazoloquinazoline (**8**) over alumina is a general high-yield reaction for all of the *o*-acylarylamines that we have investigated (see Table 4 for physical data). The ^1H nmr spectra of the triazoloquinazolines are listed in Table 5 and are totally consistent with the assigned structures. The common characteristic of these spectra is the one-proton singlet at ca. δ 8.2–8.3, arising from the isolated proton at C-3 of the triazoloquinazoline. Other features of the spectra are readily assigned to the 5-alkyl and 5-aryl group protons or to the protons of the pyrimidine-fused benzene ring. The parent heterocycle, 1,2,3-triazolo[1,5-*a*]quinazoline (**8***a*), has the additional feature in the ^1H nmr spectrum of a one-proton singlet at δ 9.00, assigned

TABLE 1. Yields and physical data for the 3-cyanomethyl-1,2,3-benzotriazin-4-ols (**6**)

Compound	X	R	Yield (%)	Melting point (°C)	Solvent
6*a**	H	H	58	123–125	$CHCl_3$
6*b*	H	CH_3	82	85	CH_2Cl_2/hexane
6*c**	H	Et	81	83–86	Ether/pet. ether
6*d**	H	Ph	95	103–105	CH_2Cl_2/hexane
6*e*	H	*p*-Tolyl	56	92	CH_2Cl_2/hexane
6*f*	H	2′-Fluorophenyl	32	103	CH_2Cl_2/hexane
6*g*	Cl	2′-Chlorophenyl	8	60	—

*Representative compounds of this series were analysed for elemental composition (Table 7).

TABLE 2. ^{1}H nuclear magnetic resonance characteristics of the 3-cyanomethyl-3,4-dihydro-1,2,3-benzotriazin-4-ols (**6**)

			δ (DMSO-d_6), ppm			
Compound	X	R	R	N—CH_2 (AB quartet) (δ_A, δ_B, J)	Aromatic	OH
6*a*	H	H	5.85 (1H, d, *J* 8 Hz)	4.97, 5.08, 17.6 Hz	7.37–7.39, 7.53–7.66 (4H, m)	6.96 (d, *J* 8 Hz)
6*c*	H	Et	0.51 (3H, t, *J* 7.4 Hz) 2.87–2.51 (2H, q of AB quartets)	4.89, 5.04, 17.9 Hz	7.50–7.55 (4H, m)	7.22(s)
6*d*	H	Ph	(aromatic)	4.45, 4.66, 17.9 Hz	6.91 (1H, dd, *J* 7.8 Hz) 7.35–7.65 (m)	7.89(s)
6*e*	H	*p*-Tolyl	2.50 (3H, t, *J* 1.7 Hz)	4.44, 4.63, 17.7 Hz	6.90 (1H, d, *J* 7.8 Hz) 7.21–7.30 (4H, AA′BB′, *J* 8.2 Hz) 7.37–7.62 (3H, m)	7.80(s)
6*f*	H	2′-Fluorophenyl	(aromatic)	4.59, 4.70, 18.0 Hz	6.96 (1H, dd, *J* 7.76, 0.84 Hz) 7.10 (1H, ddd, *J* 11.7, 8.2, 1.0 Hz) 7.34–7.39 (2H, m) 7.45–7.53 (2H, m) 7.61 (1H, dd, *J* 7.9, 0.9 Hz) 7.97 (1H, dt, *J* 8.0, 1.8 Hz)	8.07(s)
6*g*	Cl	2′-Chlorophenyl	(aromatic)	4.53, 4.67, 18.0 Hz	6.76 (1H, d, *J* 2.1 Hz) 7.48–7.66 (5H, m) 8.20 (1H, dd, *J* 7.7, 1.3 Hz)	8.33(s)

TABLE 3. ^{13}C nuclear magnetic resonance characteristics of 1-(2′-acylphenyl)-3-cyanomethyltriazenes* (**5**) in $CDCl_3$

Compound	X	R	δ ($CDCl_3$), ppm
5*c*	H	Et	8.3 (q, *J* 128 Hz, CH_3), 32.8 (t, *J* 126 Hz, CH_2—CO), 47.4 (t, *J* 146 Hz, N—CH_2), 114.7 (dd, *J* 166 and 7.4 Hz), 115.0 (t, *J* 8.7 Hz, C≡N), 118.4 (s), 121.4 (dd, *J* 164 and 8 Hz), 130.6 (dd, *J* 158 and 8 Hz), 134.6 (dd, *J* 160 and 8.6 Hz), 142.8 (s) and 204.0 (s, *C*=O)
5*d*	H	Ph	47.4 (N—CH_2), 115.0 (*C*≡N), 119.4, 121.1, 128.2, 129.4, 132.0, 133.8, 134.4, 138.6, 143.0, 198.7 (*C*=O)

*Solutions obtained by dissolving the corresponding triazinol (**6***c* or **6***d*) in deuteriochloroform.

TABLE 4. Yields and physical data of the 1,2,3-triazolo[1,5-*a*]quinazolines (**8**)

Compound	X	R	Yield (%)	Melting point (°C)	Solvent
8*a*	H	H	62	143–144	$CHCl_3$
8*b**	H	Me	83	142–145	CH_2Cl_2/hexane
8*c**	H	Et	95	164–165.5	CH_2Cl_2/hexane
8*d**	H	Ph	64	169	CH_2Cl_2/hexane
8*e*	H	*p*-Tolyl	84	194	Ether/$CHCl_3$
8*f**	H	2′-Fluorophenyl	62	212–214	CH_2Cl_2/hexane
8*g*	Cl	2′-Chlorophenyl	69	194–196	$CHCl_3$

*Representative compounds of this series were analysed for elemental composition (Table 7).

TABLE 5. ^{1}H nuclear magnetic resonance characteristics of the 1,2,3-triazolo[1,5-*a*]-quinazolines (**8**)

Compound	X	R	δ ($CDCl_3$), ppm
8*a*	H	H	7.76 (H-8, ddd, *J* 7.98, 7.35, 1.07 Hz), 8.02 (H-7, ddd, *J* 7.98, 1.37 Hz), 8.30 (H-3, s), 8.69 (H-6, dddd, *J* 8.38, 1.07, 0.77, 0.63 Hz), 9.00 (H-5, *J* 0.77 Hz)
8*b*	H	Me	2.95 (3H, s, CH_3), 7.73 (H-8, ddd, *J* 8.22, 7.28, 1.08 Hz), 7.99 (H-7, ddd, *J* 8.39, 7.28, 1.20 Hz), 8.13 (H-9, dd, *J* 8.22, 1.20 Hz), 8.18 (H-3, s), 8.72 (H-6, ddd, *J* 8.39, 1.08, 0.51 Hz)
8*c*	H	Et	1.49 (3H, t, *J* 7.5 Hz, CH_3), 3.31 (2H, q, *J* 7.5 Hz, CH_2), 7.72 (1H, t), 7.97 (1H, t), 8.17 (1H, d, *J* 8 Hz), 8.22 (1H, s), 8.73 (1H, d, *J* 8 Hz)
8*d*	H	Ph	7.59–7.61 (3H, m), 7.68 (1H, dt), 7.73–7.76 (2H, m), 8.02 (1H, t), 8.12 (1H, d), 8.33 (1H, s), 8.81 (1H, d)
8*e*	H	*p*-Tolyl	2.49 (3H, s, CH_3), 7.38–7.65 (4H, AA′BB′, *J* 7.9 Hz), 7.65 (1H, t), 8.00 (1H, dt, *J* 8.1 and 1.1 Hz), 8.14 (1H, d, *J* 8.3 Hz), 8.29 (1H, s), 8.77 (1H, d, *J* 8.2 Hz)
8*f*	H	2′-Fluorophenyl	7.30 (1H, dt), 7.39 (1H, dt), 7.57–7.65 (2H, m), 7.67 (1H, dt), 7.83–7.86 (1H, m), 8.02 (1H, dt), 8.35 (1H, s), 8.80 (1H, dd)
8*g*	Cl	2′-Chlorophenyl	7.49–7.62 (5H, m), 7.96 (1H, dd, *J* 8.8 and 2.2 Hz), 8.35 (1H, s), 8.75 (1H, d, *J* 8.9 Hz)

TABLE 6. ^{13}C nuclear magnetic resonance characteristics of the 1,2,3-triazolo[1,5-*a*]-quinazolines (**8**)

Compound	X	R	δ ($CDCl_3$), ppm
8*a*	H	H	115.6 (d), 118.7 (s), 127.8 (d, two coincident carbons), 128.6 (d), 133.2 (s), 134.8 (d), 140.8 (s), 154.1 (d)
8*b**	H	Me	22.7 (q), 115.8 (d), 118.4 (s), 126.6 (d), 127.0 (d), 127.5 (d), 132.8 (s), 134.3 (d), 139.9 (d), 161.3 (q)
8*c*	H	Et	11.8 (q, *J* 128 Hz, CH_3), 28.3 (t, *J* 125 Hz, CH_2), 116.0 (d, *J* 168 Hz), 117.8 (s), 126.8 (d, *J* 198 Hz), 127.3 (s), 127.5 (d, *J* 155 Hz), 134.0 (d, *J* 163 Hz), 140.1 (s), 157.5 (s), 165.1 (s)
8*d*	H	Ph	115.8, 117.6, 127.4, 127.7, 128.6, 129.4 (two coincident carbons), 130.0, 133.8, 134.3, 136.7, 140.0, 162.3
8*e*	H	*p*-Tolyl	21.5 (CH_3), 116.0, 117.9, 127.4, 127.7, 129.4, 129.5, 133.9, 134.0, 134.3, 140.3, 140.4, 162.5

*See ref. 6.

to the isolated proton at C-5 in the pyrimidine moiety. The structures of representative triazoloquinazolines (**8***a*, **8***c*, **8***d*, and **8***e*) were corroborated by ^{13}C nmr spectroscopy (Table 6).

Experimental

Melting points were recorded with a Kofler hot-stage apparatus and are uncorrected. The ir spectra were recorded with Perkin–Elmer Series 299 and 1300 spectrometers, and the nmr spectra with Varian EM360 and Nicolet 360 NB spectrophotometers. Microanalyses were carried out by the Canadian Microanalytical Laboratory, Vancouver, B.C., for representative compounds of types **6** and **8**; the non-analyzed compounds gave ^{1}H nmr, ^{13}C nmr and ir spectra exactly analogous to those of the compounds analyzed.

*3-Cyanomethyl-1,2,3-benzotriazin-4-ols (**6**). General procedure*

The 2-amino-ketone or -aldehyde (**4**) (0.01 mol) was diazotized in hydrochloric acid with 1 equivalent of sodium nitrite. The resulting diazonium salt solution was coupled with α-aminoacetonitrile bisulfate (0.02 mol) over a period of 0.5 h, and the mixture neutralized with aqueous sodium carbonate to pH 8. After stirring until precipitation was complete (1–1.5 h), the product was filtered, dried, and recrystal-

TABLE 7. Elemental composition of representative compounds of types **6** and **8**

Compound	Formula	Calculated (%)			Found (%)		
		C	H	N	C	H	N
6*a*	$C_9H_8N_4O$	57.44	4.28	29.77	57.46	4.28	29.84
6*c*	$C_{11}H_{12}N_4O$	61.10	5.59	25.91	61.21	5.58	25.83
6*d*	$C_{15}H_{12}N_4O$	68.17	4.58	21.20	68.22	4.64	21.30
8*b*	$C_{10}H_8N_4$	65.21	4.38	30.42	64.65	4.42	30.06
8*c*	$C_{11}H_{10}N_4$	66.65	5.08	28.26	66.36	5.10	28.22
8*d*	$C_{15}H_{10}N_4$	73.16	4.09	22.75	73.05	4.17	22.94
8*f*	$C_{15}H_9N_4F$	68.18	3.43	21.20	68.11	3.49	21.13

lized to afford the triazinol (**6**). Yields, and physical and spectroscopic data of these products are given in Tables 1 and 2. Table 3 gives the nmr characteristics of two of these products in deuteriochloroform, in which the triazinols revert to the open-chain triazene form (**5**).

1,2,3-triazolo[1,5-a]quinazolines (8). General procedure

The appropriate triazinol (0.40 g) was dissolved in chloroform (25 mL) and the solution poured over anhydrous neutral alumina (14 g). The mixture was stirred at room temperature and the progress of reaction followed by tlc until complete disappearance of the reactant had taken place (usually within 24 h, but sometimes requiring 48 h). The mixture was filtered and the alumina washed with several aliquots of chloroform. The combined chloroform solutions were evaporated and the residual product recrystallized from a suitable solvent to afford the 1,2,3-triazolo[1,5-*a*]quinazoline (**8**). Yields, and physical and spectroscopic characteristics of these products are given in Tables 4, 5, and 6. The proton spectra measured for compounds **8***a* and **8***b* were iteratively fitted using the ITRCAL program supplied by Nicolet Instrument Corporation as part of the software package for the NIC-360 NB spectrometer.

Acknowledgements

The authors are grateful to the Natural Sciences and Engineering Research Council of Canada for research funding (to K.V.) and to the Atlantic Regional Magnetic Resonance Centre at Dalhousie University for the 360-MHz nmr spectra.

1. G. TENNANT and R. J. S. VEVERS. J. Chem. Soc. Chem. Commun. 671 (1974).
2. G. L'ABBÉ, F. GODTS, and S. TOPPET. J. Chem. Soc. Chem. Commun. 589 (1985).
3. C. WESTERLUND. J. Heterocycl. Chem. **17**, 1765 (1980).
4. G. TENNANT. J. Chem. Soc. C, 2290 (1966); J. Chem. Soc. Perkin Trans. 1, 534 (1974).
5. P. L. FAYE, D. L. HOOPER, and K. VAUGHAN. Can. J. Chem. **61**, 179 (1983).
6. K. VAUGHAN, R. J. LAFRANCE, Y. TANG, and D. L. HOOPER. Can. J. Chem. **63**, 2455 (1985).

Two-dimensional nuclear magnetic resonance at 500 MHz: the structural elucidation of a *Salmonella* serogroup N polysaccharide antigen[1]

DAVID R. BUNDLE, MANFRED GERKEN,[2] AND MALCOLM B. PERRY
Division of Biological Sciences, National Research Council of Canada, Ottawa, Ont., Canada K1A 0R6

Received August 8, 1985

DAVID R. BUNDLE, MANFRED GERKEN, and MALCOLM B. PERRY. Can. J. Chem. **64**, 255 (1986).

High resolution ^1H and ^{13}C nmr spectroscopy at 500 MHz and 125 MHz was used for the structural analysis of the *O*-antigen of *Salmonella landau*, which belongs to the Kauffmann–White serogroup N. This bacterial lipopolysaccharide was extracted from whole cells and hydrolyzed by mild acid to give lipid-free *O*-polysaccharide. Conventional one-dimensional ^1H and ^{13}C nmr data showed the polysaccharide to contain four monosaccharides in each repeating unit and, in addition, to carry an average of one *O*-acetyl group for every two repeating units. Two-dimensional nmr experiments aided the unambiguous assignment of the ^1H and ^{13}C resonances and thereby permitted the structural analysis of this polysaccharide by nmr techniques alone. The structure of the de-*O*-acetylated repeating unit was established as→2)-α-D-PerNAc*p*-(1 → 3)-α-L-Fuc*p*-(1 → 4)-β-D-Glc*p*-(1 →3)-α-D-GalNAc*p*(1→$_n$ through the use of methods which included homonuclear shift correlated (COSY and NOESY) experiments. The interpretation of this data was supported and simplified by consideration of firmly established ^{13}C chemical shift assignments obtained from a heteronuclear $^1H/^{13}C$ shift correlated experiment. A three-dimensional model of the *O*-antigen obtained by semi-empirical calculations is shown to be consistent with interatomic distance constraints imposed by data from 2-D NOESY and one-dimensional nOe difference spectroscopy.

DAVID R. BUNDLE, MANFRED GERKEN et MALCOLM B. PERRY. Can. J. Chem. **64**, 255 (1986).

On a utilisé le rmn du ^1H et du ^{13}C à 500 et à 125 MHz pour déterminer la structure du *O*-antigène de la *Salmonella landau* qui appartient au groupe sérique N de Kauffmann et White. On a extrait ce lipopolysaccharide bactérien des cellules complètes et on l'a hydrolysé en milieu légèrement acide pour obtenir le *O*-polysaccharide sans lipides. Les données conventionnelles en une dimension de la rmn du ^1H et du ^{13}C montrent que le polysaccharide contient quatre monosaccharides dans chaque unité de base et que, de plus, il porte une moyenne d'un groupement *O*-acétyle par deux unités de base. Sur la base d'expériences de rmn en deux dimensions on a pu faire des attributions non-ambiguës des résonances ^1H et ^{13}C qui ont ainsi permis de faire une analyse structurale de ce polysaccharide uniquement par des techniques de rmn. On a établi que la structure de l'unité de base déacétylée est→2)-α-D-PerNAc*p*-(1 → 3)-α-L-Fuc*p*-(1 → 4)-β-D-Glc*p*-(1 → 3)-α-D-GalNAc*p*(1→$_n$ en faisant appel à des méthodes qui incluent des expériences de corrélations de déplacements homonucléaires (COSY et NOESY). L'interprétation de ces données est en accord avec et a été simplifiée par la considération d'attributions de déplacements chimiques de ^{13}C qui sont bien établies et qui ont été obtenues à partir d'une expérience de corrélation hétéronucléaire de déplacements $^1H/^{13}C$. On démontre qu'un modèle tridimensionnel du *O*-antigène, obtenu par des calculs semi-empiriques, est en accord avec les contraintes de distances interatomiques imposées par les données de NOESY en 2-D et par la spectroscopie différentielle unidimensionnelle de l'effet Overhauser nucléaire.

[Traduit par le journal]

Introduction

The lipopolysaccharides (LPS) of gram-negative bacteria assigned in the Kauffmann–White scheme (1) to serogroup N, have been shown to be serologically cross-reactive with *Yersinia enterocolitica* 0:9, *Brucella abortus*, and *E. coli* 0:157 (2–4). This observation gained structural significance when the O-antigens of the first two bacteria were shown to be homopolymers of 1,2-linked 4,6-dideoxy-4-formamido-α-D-mannopyranosyl (perosamine) units (5, 6). Compositional analysis showed that the O-antigens of *S. landau* and *E. coli* 0:157 also contained the sugar, perosamine (7), and structural analysis of these O-antigens became necessary in order to further understanding of these important cross-serological relationships.

Bacterial LPS contains three structurally distinct portions, each covalently linked to the other in a contiguous structure. The polymeric O-chain is linked to the core oligosaccharide, which in turn is linked via the acid-labile, 3-deoxyoctulosonic acid (KDO), ketosidic bond to lipid A, the hydrophobic anchor that secures the whole "molecule" in the outer membrane of the gram-negative cell wall (11). Mild acid hydrolysis severs the KDO – lipid A linkage, liberating the O-chain still linked to core oligosaccharide and chloroform-soluble lipid A.

The success of two-dimensional nmr experiments at 500 MHz, when applied to low molecular weight proteins (8, 9), indicated that such techniques should be particularly useful for the analysis of O-antigen structure. Since these polymers, unlike much larger capsular polysaccharides, have an average molecular weight around 10 000 daltons, the limitations to the successful execution of certain two-dimensional experiments, such as $^1H/^{13}C$ shift correlation, imposed by short transverse relaxation times (T_2) (10), should not apply. This communication reports the application of homo- and heteronuclear shift correlated spectroscopy to the delineation of a complex heteroglycan structure, without recourse to other structural methods except for the initial identification of the component monosaccharides.

Results and discussion

In order to perform a complete structural analysis of a polysaccharide, the following questions must be answered unambiguously: (*1*) the identity of the component monosaccharides present and their absolute configuration; (*2*) the ring size and anomeric configuration of each monosaccharide; (*3*) the position of linkages between sugar units; (*4*) sequence and arrangement of sugar residues in linear or branched structures; (*5*) the nature, position, and quantity of non-carbohydrate substituents. With the exception of absolute configuration, nmr methods can in principle satisfy all aspects of these requirements. Indeed, an unstated objective, the elucidation of

[1]NRCC No. 25101.
[2]NRCC Research Associate 1983–1985.

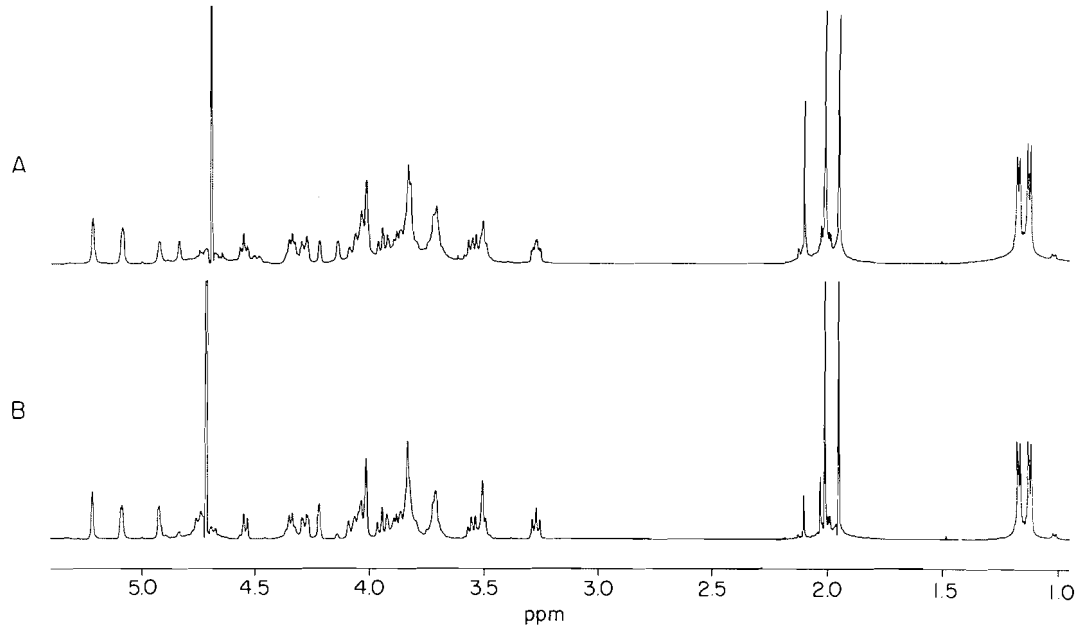

FIG. 1. Resolution enhanced ^{1}H nmr spectra of: A, the native *O*-polysaccharide liberated from LPS by mild acid hydrolysis and recorded at 303 K; B, the *O*-deacetylated polysaccharide recorded at 300 K.

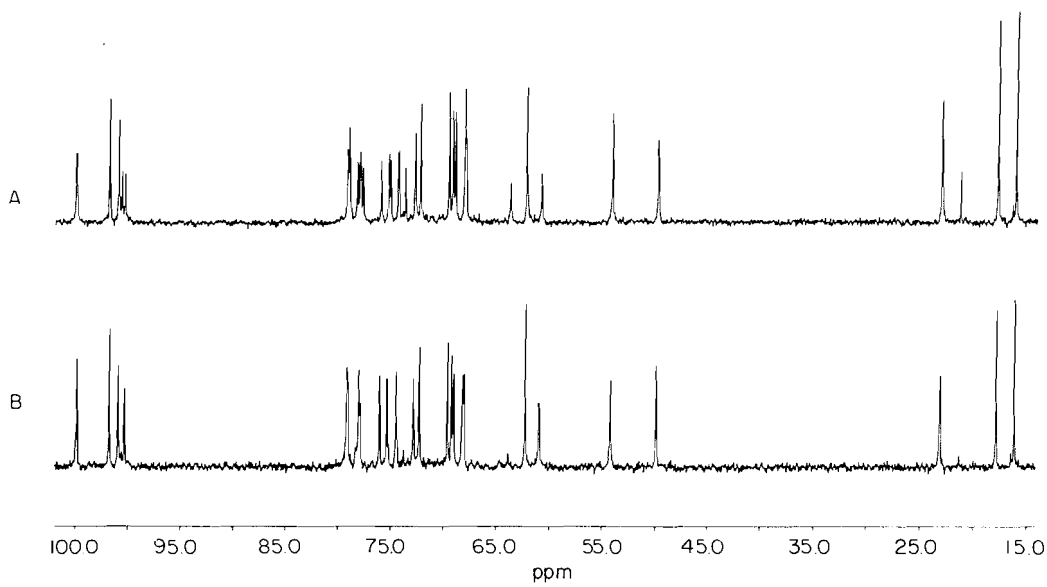

FIG. 2. The ^{13}C nmr spectra of A, native, and B, *O*-deacetylated polysaccharides recorded at 310 K. Simplification of the spectrum follows the removal of the *O*-acetyl residue.

three-dimensional structure, may also be approached by the nmr technique.

The lipid-free O-polysaccharide was prepared from the LPS of *S. landau* by conventional methods, which involved mild acid hydrolysis and gel filtration on Sephadex G-50 to obtain polymeric material. This O-polysaccharide was subjected to total acid hydrolysis, reduction, acetylation, and gc – mass spectrometry of alditol acetates. In this way the component sugars were identified and the absolute configuration was determined after conversion of the monosaccharides to the corresponding (−)-2-butyl glycosides (12). The component sugars were shown to be 2-amino-2-deoxy-D-galactose, D-glucose, L-fucose, and 4-amino-4,6-dideoxy-D-mannose (perosamine, PerN), present in equimolar proportions. Examination of the ^{1}H nmr spectrum of the O-polysaccharide (Fig. 1) also showed the presence of ester-linked acetate, 0.5 mol relative to the two *N*-acetyl groups, which indicated that both amino sugars were present as their acetamido derivatives. Complex spectral patterns were simplified by saponification of ester-bound acetate (Figs. 1 and 2), and the resultant spectra were consistent with a repeating unit structure containing four sugars and one *O*-acetyl group for every two repeating units. The limited complexity of the ^{13}C spectrum of the native polysaccharide (Fig. 2A) suggested that *O*-acetylation occurred at only one site in the tetrasaccharide repeat. Analysis of typical ^{1}H and ^{13}C features supports the analytical data for sugar composition, in that two amino sugars, present as acetamido derivatives, and two 6-deoxy sugars are component monosaccharides. Proton

TABLE 1. First-order proton chemical shifts (δ) and coupling constants (Hz) of the *Salmonella landau O*-polysaccharide*

	Hexopyranosyl unit			
Proton	Residue A α-D-PerNAc	Residue B α-D-GalNAc	Residue C α-L-Fuc	Residue D β-D-Glc
H-1	5.21 (~1)	5.08 (3.6)	4.84† 4.92 (2.4)	4.50† 4.55 (7.9)
H-2	4.02 (4.8)	4.29† 4.29 (10.7)	3.86 m‡	3.72† 3.27 (8.9)
H-3	4.02 (10.3)	4.06 (~3.0)	3.83 m‡	3.57† 3.56 (8.5)
H-4	3.94 (10.0)	4.14† 4.22 (~1.0)	3.83 (1.0)	3.54† 3.51 (8.5)
H-5	3.85 (6.2)	4.04	4.34 (6.4)	3.50† 3.51
H-6	1.17	3.72 (6.6)	1.12	4.28† 3.82 (2.5, 11.1)
H-6′		3.72 (6.6)		4.55† 3.89 (6.1)
CH_3CONH	1.95	2.01		
CH_3COO				2.10†

*Chemical shifts determined at 300 K relative to internal acetone (δ 2.225 ppm).
†Shifted resonances in the O-6d acetylated repeating unit.
‡Unresolved multiplet.

TABLE 2. Carbon-13 chemical shifts (δ) of the *Salmonella landau O*-polysaccharide* and anomeric $^1J_{C,H}$ coupling constants (Hz)

	Hexopyranosyl unit			
Carbon atom	Residue A α-D-PerNAc	Residue B α-D-GalNAc	Residue C α-L-Fuc	Residue D β-D-Glc
C-1	101.7 (172 Hz)	100.8 (174 Hz)	100.5† 100.2 (170 Hz)	104.8† 104.7 (163 Hz)
C-2	78.9	49.7† 49.8	69.1	74.2† 74.3
C-3	68.8	78.1† 78.0	79.1	75.0† 75.1
C-4	54.0	69.4	72.6	77.6† 75.9
C-5	67.9† 68.0	72.1	67.9† 67.8	73.6† 77.9
C-6	17.7	62.1	16.0	63.1† 60.7
CH_3CONH	175.5[a]	175.7[a]		
CH_3CONH	22.9[b]	23.0[b]		
CH_3COO				174.8
CH_3COO				21.2

*Chemical shift measured at 310 K and expressed relative to 1% internal dioxane (δ = 67.4 ppm).
†Resonances shifted by the presence of an acetyl at O-6d.
[a,b]Resonance whose assignment may be reversed.

and ^{13}C chemical shift and heteronuclear coupling constant data (13) (Tables 1 and 2) also indicated the presence of three α- and one β-linked monosaccharide in each repeating unit.

Considerable information was obtained even from such cursory examination of the one-dimensional spectra. However, to deduce the sequence and position of interglycosidic linkages by nmr methods, to a degree of certainty comparable with that reached by classical methylation analysis and chemical degradation, requires unambiguous assignment of all the ^1H and ^{13}C resonances. When this is done for proton signals, nOe (nuclear Overhauser effect) difference spectra (14) provide a reliable method for determination of both the sequence and linkage between contiguous residues (15–17), provided serious overlap of the resonances of interest do not occur. Conclusions from proton nOe measurements may be supported by ^{13}C data for the aglyconic carbon atoms, which are known to experience considerable deshielding (18). The approach adopted here was to make as complete an assignment as possible of the proton resonances via COSY experiments and, since the quantities of polysaccharide permitted it, to support this analysis by assigning the ^{13}C spectrum through a $^1H/^{13}C$ shift correlated experiment. Following these, proton nOe experiments to establish the sequence and postion of glycosidic linkages were envisioned.

Homonuclear shift correlated spectra were recorded with and without suppression of the HOD signal. At one temperature, 300 K, this signal could be positioned between the two highest field anomeric resonances, a position in which no resonances were obscured by solvent peaks. Two windows, the anomeric and 6-deoxy resonances, are available as starting points for the analysis of the COSY spectra (Fig. 3). The first of these signals led to the identification (via cross-peaks) of H-2 ring protons, whilst the H-5 signals of the deoxy residues are located from cross-peaks to the methyl resonances at ca. 1.20 ppm. The anomeric resonances in order of decreasing chemical shift were arbitrarily assigned the notation H-1a, H-1b, H-1c, and H-1d; then, following the cross-peaks, resonances H-1b to H-4b and H-1d to H-4d were assigned. In the case of residue, d, coincident resonances occurred, H-3d/H-4d, with an apparent absence of cross-peaks. This introduced a degree of uncertainty into the assignments, which were, nevertheless, substantiated via a $^1H/^{13}C$ shift correlation map. Overlapping signals due to

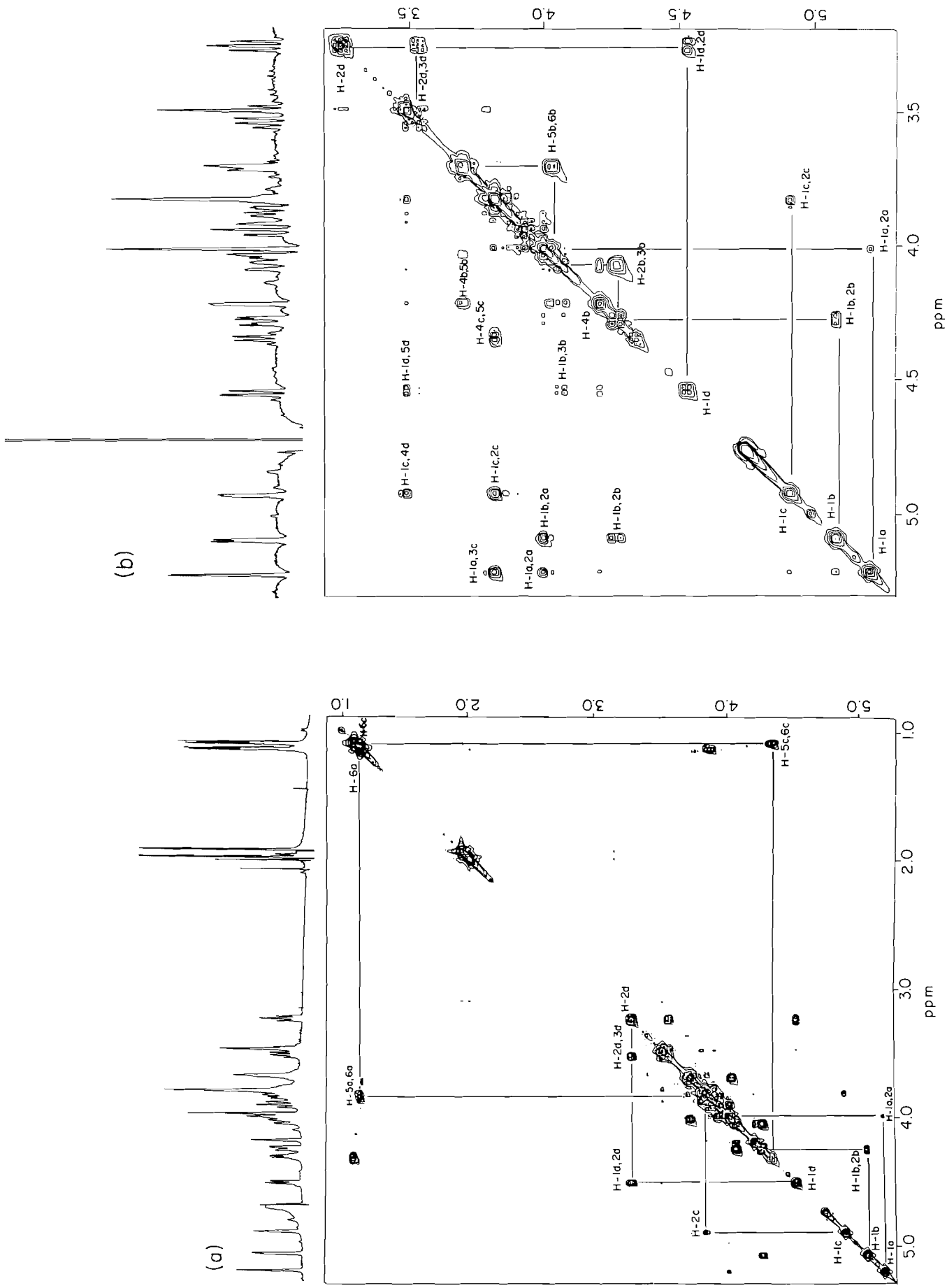

FIG. 3. (a) COSY contour plot of the full spectrum of the de-*O*-acetylated polysaccharide 5.30–1.00 ppm recorded at 300 K. (b) COSY (lower half) and NOESY (upper half) contour plots of the ^{1}H spectral region 5.30–3.20 ppm. The NOESY experiment was conducted with a 200-ms mixing time. Some spin diffusion is apparent. The one-dimensional projection is depicted along the F_2 axis.

H-2a and H-3a prevented the unambiguous location of H-4a, which may be assigned via H-6a and H-5a. The identity of the 6-deoxy signals as originating from either unit a or c was clearly evident since H-5a, a pseudo quartet in the one-dimensional spectrum, is typical of a pyranoside possessing the *galacto* configuration with small $J_{4,5} \sim 1$ Hz and $J_{5,6} \approx 6$ Hz. Although a low-intensity cross-peak identifies H-4c via H-5c (Fig. 3(a)), proximity or overlap of H-2c, H-3c, and H-4c prevents the unambiguous assignment of the former two resonances. Thus via the COSY experiment, 70% of the ring proton resonances were identified without assumptions of the identity or configuration of the component saccharides. Based on the monosaccharide composition and the partial ^{1}H assignments, residues a and c were identified as the 6-deoxy sugars. Comparison of chemical shift data (Table 1) with that compiled from the literature (18) enabled residue d to be identified as a β-D-glucopyranosyl unit and residue b as a 2-acetamido-2-deoxy-α-D-galactopyranosyl unit. Residue c, on the basis of the chemical shift and $J_{1,2}$ value (2.4 Hz), was assigned as an α-L-fucopyranosyl unit, which required residue a to be a 4-acetamido-4,6-dideoxy-α-D-mannopyranosyl unit.

Numerous variants of the COSY experiment continue to be introduced and a relayed COSY (19) could in principle be used to identify the missing assignments H-3a, H-5b, H-6b, H-3c, H-4d, H-5d, and H-6d, although in this modification attention to J tuning becomes important (20). Since the quantity of polysaccharide available allowed it, an alternate approach was adopted, the construction of a ^{1}H/^{13}C correlation map (Fig. 5). This identified the ^{1}H chemical shifts of the H-6b and H-6d protons via their respective C-6 resonances, in agreement with partially relaxed ^{1}H spectra (18). The assignment of H-6 resonances led directly to the assignment of H-5b and H-5d, leaving only H-3a, H-3c, and H-4d as the ambiguous ^{1}H signals. It should be recalled that in each of these cases the evidence from the COSY experiment suggested that coincident signals were responsible for the absent cross-peaks, H-3a with H-2a, H-3c with H-2c, and H-4d with H-3d. Correlation of most ^{1}H signals with the corresponding ^{13}C resonances via the ^{1}H/^{13}C shift correlated experiment was straightforward, although for certain ring protons coincident resonances in F_1 complicated assignment of the ^{13}C spectrum. This problem was partially resolved by examination of F_1 cross sections through each ^{13}C signal, as the ^{13}C resonances were well resolved. However, since resolution in F_1 permitted only those proton multiplets with large ^3J values to be observed, this approach was limited to the identification of H-4d, H-3c, and H-3a.

Examination of ^{13}C chemical shifts (Table 2) and a comparison of these with literature values (21, 22) indicated which pyranose ring atoms were involved in glycosidic linkages. Thus those ^{13}C atoms that experienced significant deshielding, C-2a, C-3b, C-3c, and C-4d, were the putative linkage sites. Although ^{13}C chemical shifts are strongly indicative of the position of glycosidic linkages, the sequence of monosaccharides in the polymer chain together with the position of the linkages were most readily determined by measurement of inter-residue nOe's. This may be accomplished by one-dimensional nOe difference spectra (Fig. 4) (15, 17) or via the two-dimensional nmr equivalent, a NOESY experiment (Fig. 3(b)) (16, 23). Interpretation of the sequence via such dipolar coupling is strongly dependent upon conformation; however, substantial experimental evidence supports the *exo*-anomeric effect (24), which requires anomeric and aglyconic protons to be in virtual van der Waals contact (25), thereby forming the basis of this

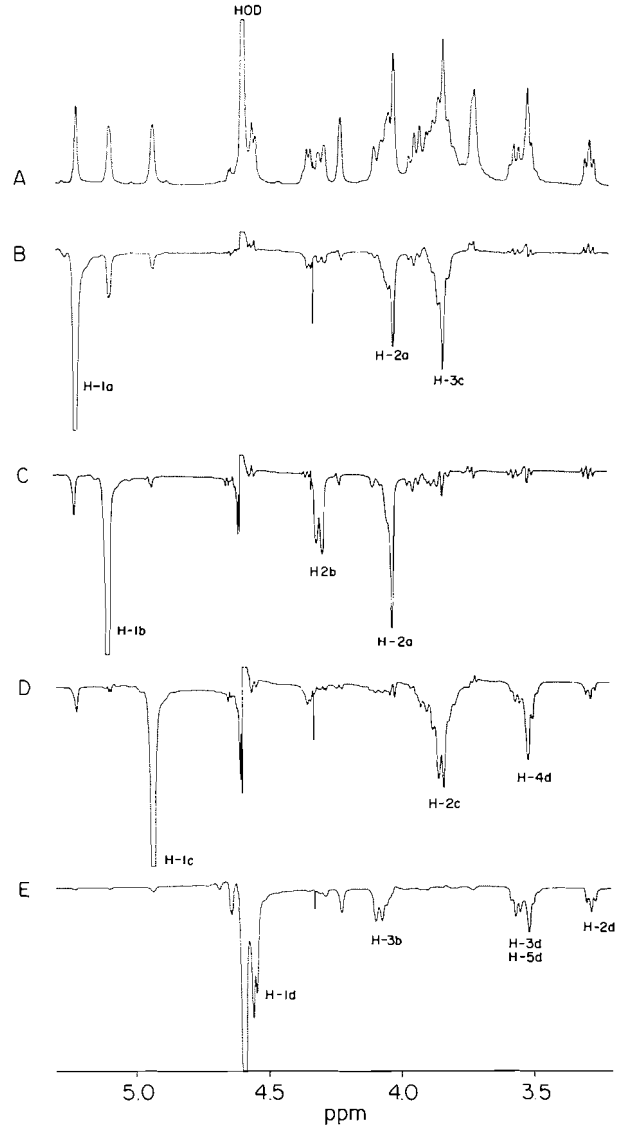

FIG. 4. One-dimensional nOe difference spectra for irradiation of the respective anomeric protons H-1a – H-1d, measured at 310 K. A, off-resonance control spectrum. B, difference spectrum obtained by irradiation of H-1a. C, difference spectrum obtained by irradiation of H-1b. D, difference spectrum obtained by irradiation of H-1c. E, difference spectrum obtained by irradiation of H-1d.

method of sequence and linkage determination. Thus nOe difference spectra permitted the proton attached to the aglyconic carbon atom to be identified, and in the NOESY contour plot the same resonance is correlated via a cross-peak to the anomeric proton involved in each glycosidic linkage. The results of the nOe difference and NOESY experiments (Figs. 4 and 3(b)) require that residue a (α-D-PerNAc) is linked α-1,3 to α-L-Fuc (residue c), since irradiation of H-1a resulted in nOe's for H-2a and, in addition, for a proton which may only be one of H-2c, H-3c, or H-4c. Thus residue a must be glycosidically linked to residue c and the ^{13}C data (Table 2) require that the position of this linkage be C-3c. The α-L-Fuc unit is linked to the 4 position of the β-D-Glc residue since the dipolar coupling across the glycosidic bond is to either H-3d or H-4d, and ^{13}C data (Table 2) indicated that the aglyconic carbon atom was C-4d. The β-D-glucopyranosyl unit exhibited significant intra-ring nOe's between H-1d, H-3d, and H-5d, which was consistent with the

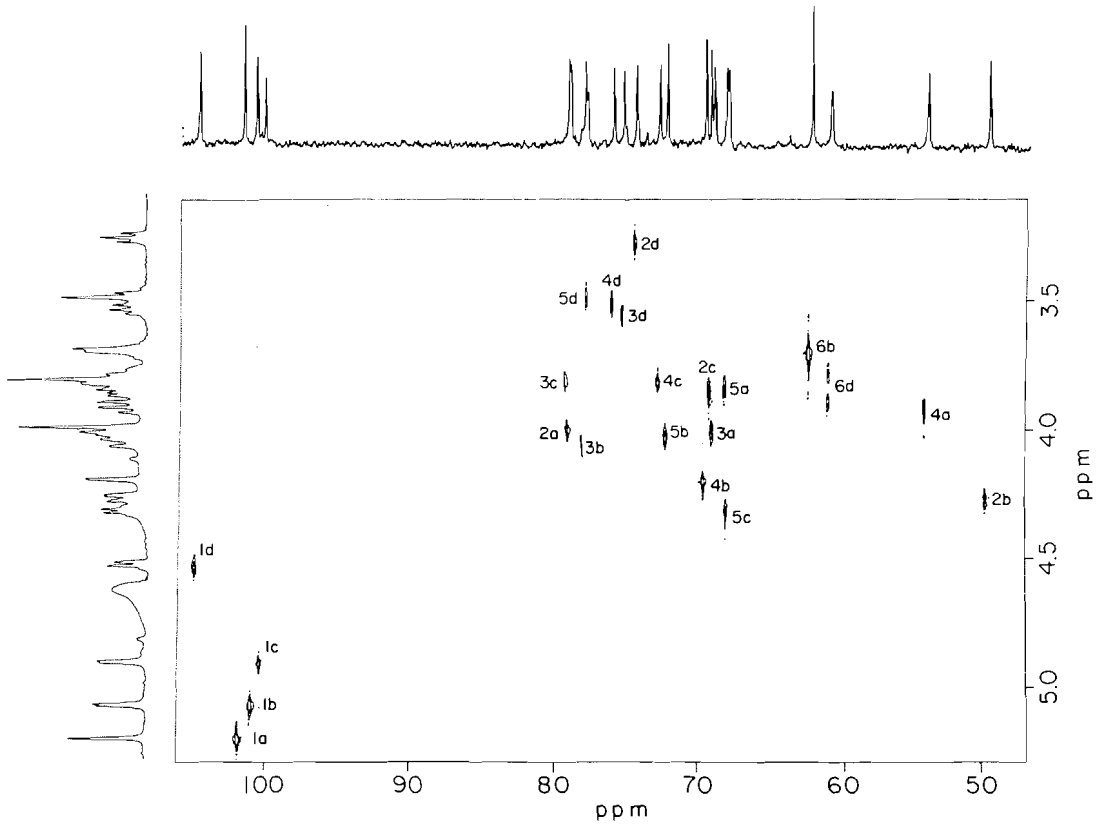

FIG. 5. Heteronuclear $^1H/^{13}C$ shift correlation map for the spectral regions of F_2, δ 106.0–47.0 ppm and F_1, δ 5.30–3.10 ppm. The sample, 60 mg of de-*O*-acetylated polysaccharide dissolved in 500 μL of D_2O, gave acceptable S/N after 800 scans, permitting data to be acquired at 310 K during 62.5 h of instrument time. The respective ^{13}C and ^1H one-dimensional projections are displayed along the F_2 and F_1 axes.

1,3 diaxial orientation of the protons of this pyranosyl moiety. The largest inter-ring nOe was observed between H-1d and H-3b, in agreement with the downfield shifted C-3b resonance. Thus the β-D-Glc, residue d, was linked 1,3 to α-D-GalNAc, unit b. Lastly, nOe's observed from H-1b to H-2b and either H-2a or H-3a established the sequence b–a, but again overlap of crucial proton resonances failed to distinguish between the two possible sites of the inter-ring linkage. However, the one-dimensional nOe difference spectrum showed a narrow multiplet at δ 4.02 suggesting a 1,2 linkage, which was supported by the ^{13}C shift of C-2a. Although overlap of proton resonances H-2a/H-3a, H-2c, H-3c/H-4c, and H-3d/H-4d complicated identification of linkage position in three out of four cases, the proton nOe experiments did permit the repeating unit sequence a–c–d–b to be established. In combination with the $^1H/^{13}C$ correlation map, linkage positions were clearly and unambiguously determined. In this connection the assignment of ^{13}C resonances made possible by the extensive homo- and heteronuclear shift correlations was an essential element of this approach.

The chemical repeating unit of the *Salmonella landau* O-antigen determined by nmr methods was

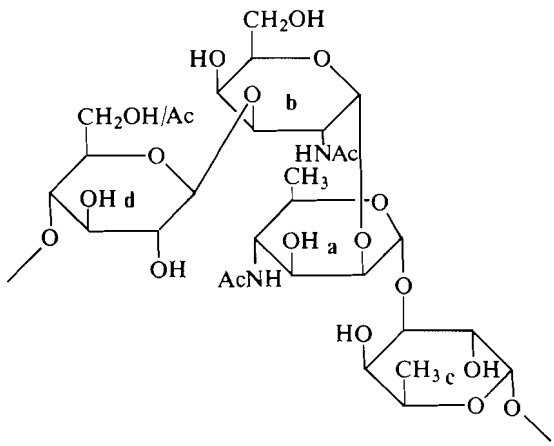

→4)-β-D-Glc*p*-(1→3)-α-D-GalNAc*p*-(1→2)-α-D-PerNAc*p*-(1→3)-α-L-Fuc*p*-(1—

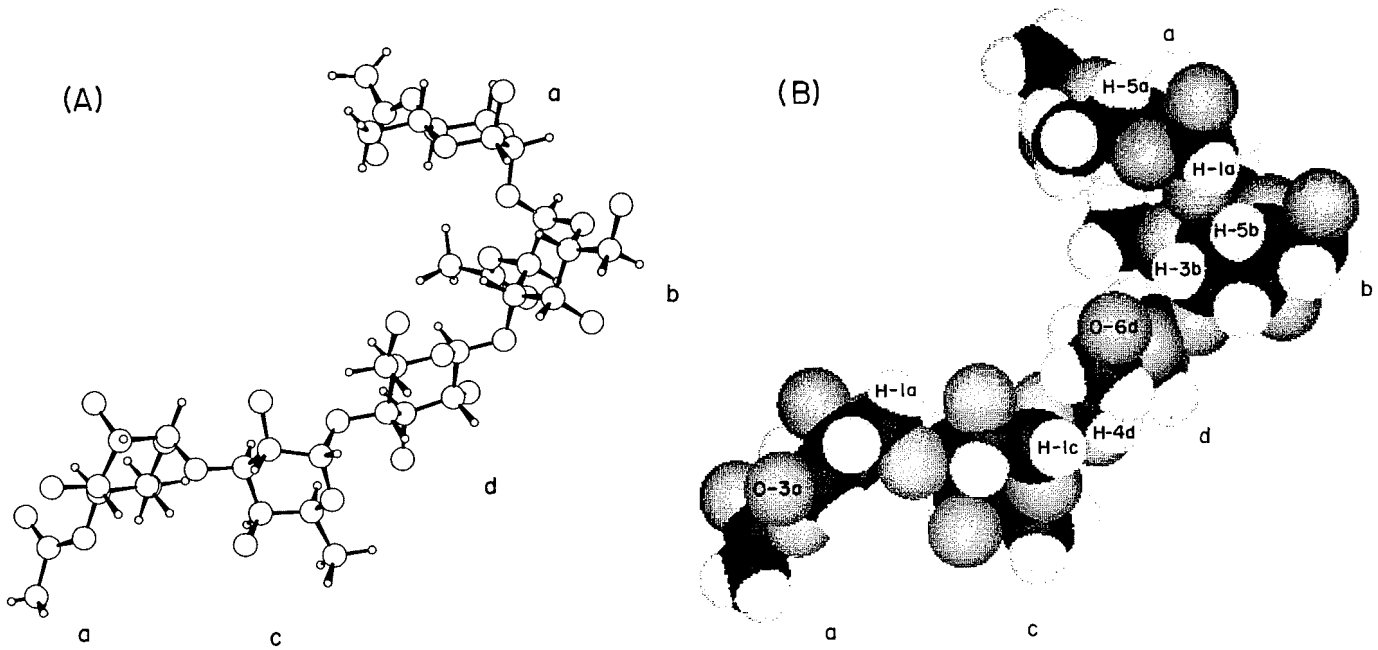

FIG. 6. Ball and stick (A) and CPK (B) models of a hypothetical minimum energy conformation of the pentasaccharide of *S. landau* *O*-antigen, unit sequence PerNAc→Fuc→Glc→GalNac→PerNAc (designated a→c→d→b→a). The ϕ/ψ values for each of the consecutive glycosidic linkages are presented in Table 3. The torsional angles H-5—C-5—C-6—O-6 depicted for the Glc and GalNAc residues are −60° and −60°. Hydrogen atoms of hydroxyl groups are omitted from the calculation and the model plots.

As previously mentioned, the native polysaccharide carried one *O*-acetyl group for every two repeating units and the location of this group remained the outstanding feature to be determined. The chemical shifts of the ^{13}C resonances affected by the occurrence of an ester-linked acetate are recorded in Table 2. Proton and ^{13}C data indicated that one in two repeating units carried an *O*-acetate group, which complicated assignment since resonances due to acetylated and non-acetylated structural elements exhibited similar intensities. It was immediately obvious from a ^{13}C DEPT experiment (26), which distinguishes methine and methylene carbons, that the C-6d resonance at 60.74 ppm was reduced in intensity and a new signal, downfield shifted by 2.39 ppm and also due to C-6d, had appeared in this spectrum of the native polysaccharide. Similarly, new resonances occurred corresponding to other carbon atoms in immediate proximity to the site of acetylation; thus the C-5d resonance was upfield shifted by 4.30 ppm, whilst C-4d exhibited a downfield shift of 1.76 ppm, a pattern of shift changes consistent with C-6d as the site of acetylation, and with literature values for the sign and magnitude of these shifts (27). In agreement with this, C-1c experienced a small but significant 0.3-ppm shift, which could be expected since the α-L-Fuc, unit c, was linked 1,4 to the β-D-Glc residue. The H-1c signal was shielded by ca. 0.1 ppm (Fig. 1) and both these effects could be anticipated, since a 1,4 linkage places the anomeric centre of residue c in close proximity to the hydroxymethyl group of unit d (Fig. 6) (28). Examination of a resolution enhanced proton spectrum of the native polysaccharide revealed that the multiplets due to the acetylated H-6d resonances were located at ca. 4.30 and 4.55 ppm. Minor shift differences throughout the ring protons of residue d were observed but, with the exception of the H-1c signal, barely perceptible shifts were seen for other ring protons. Finally, nOe difference spectra performed by irradiation of each H-1c signal, due to acetylated and non-acetylated components, showed that an nOe to a multiplet centred at 4.30 ppm, a downfield shifted H-6d resonance, could be detected only for irradiation of the shifted H-1c resonance. The native *Salmonella* serogroup N O-chain, therefore, possesses the tetrasaccharide sequence shown above, which may be acetylated at O-6d and, in the case of *Salmonella landau*, carries one such *O*-acetyl per two repeating units.

Finally, drawing on the network of inter-ring nOe's in combination with semi-empirical calculations, it was possible to propose a three-dimensional model of the O-antigenic polysaccharide. The minimum energy molecule calculated by the HSEA method (24, 29) and by application of the related but more sophisticated GESA programme (30) gave ϕ and ψ values for each glycosidic linkage that differed in each ϕ,ψ pair (calculated by either method) by less than 5 degrees (Table 3). The distance matrix for this molecule without the *O*-acetyl group at O-6d was consistent with the nOe data from the one-dimensional experiments and the semi-quantitative data obtained from NOESY experiments carried out with different mixing times. In addition to the short interproton distances corroborated by the pattern of observed nOe's, specific deshielding effects may be correlated with short, ca. 2.5 Å, oxygen-to-proton distances (Table 3). One such case is the H-5c resonance that, compared to the chemical shift observed in the corresponding glycoside (18), is deshielded by 0.4 ppm. This correlates with a H-5c to O-3d separation of 2.5 Å in the minimum energy conformation. These results are in agreement with similar observations made for other O-antigens, in that the HSEA-calculated conformation for the repeating unit also satisfies the observable nmr parameters for the polymeric structure (31, 32). Ball and stick and CPK projections of the repeating unit without the *O*-acetyl group are presented (Figs. 6A and 6B).

In this study we have used the COSY, NOESY, and heteronuclear shift correlated experiments for the structural analysis of a polysaccharide. The most powerful of the three is the COSY

TABLE 3. Glycosidic torsion angles and selected interatomic distances for the *S. landau* repeating unit in the minimum energy conformation

Parameter	Glycosidic torsional angles			
	α-D-PerNac-(1 → 3)-α-L-Fuc-(1 → 4)-β-D-Glc-(1 → 3)-α-D-GalNac-(1 → 2)-α-D-PerNac			
ϕ^H/ψ^H	−50.0°/−11.5°	43.0°/7.0°	53.5°/15.0°	−42.5°/−23.0°
Selected inter-atomic distances (in Å) across glycosidic bonds	H-1a, H-3c 2.47; H-5a, H-4c 2.31; O-5a, H-3c 2.64;	H-1c, H-4d 2.33; H-5c, O-3d 2.62; O-5c, H-4d 2.79;	H-1d, H-3b 2.49; O-5d, H-3b 2.50;	H-1b, H-2a 2.44 O-5b, H-2a 2.70 H-5b, H-1a 2.39

experiment, which through the rigorous assignment of the proton spectrum provides the key to the assignment of the ^{13}C spectrum and, finally, the interpretation of the nOe's in terms of linkage and sequence. Although the quantity of polysaccharide or spectrometer time available does not always allow the $^{13}C/^{1}H$ shift correlation experiment to be performed, it is clear that the assignment of linkage position can often only be unambiguously decided by reference to the chemical shifts of the aglyconic carbon atoms, which are most readily obtained from this experiment. Less time demanding experiments (33, 34) to identify the aglyconic carbon atoms are available but the unambiguous identification of these is then dependent upon correct assignment of the remaining ring carbon atoms. Although these may often be assigned by inspection or comparison with extensive literature data (21, 22), a rigorous treatment requires a $^{1}H/^{13}C$ correlation map. Elaborate nmr experiments to establish polysaccharide structure, although possible, are not necessarily the most practical approach to structural analysis. Recent publications from this laboratory illustrate the effective combination of classical methods with high resolution nmr at high field strength for the analysis of complex bacterial polysaccharides (35, 36). Conventional methylation analysis can most effectively establish linkage positions, leaving the nOe experiment to determine the sequence of saccharide units either in the polymer itself or within fragments readily obtained by particular degradation techniques suited to the structure under study. Such an approach combats the problem encountered even at 500 MHz (37), overlapping and poorly separated ring proton multiplets.

Experimental

Bacterial strain and growth

Salmonella landau (LCDC S-1358; NRCC 4124) a Kauffman–White serogroup N organism, was obtained from Dr. H. Lior, Laboratory for Disease Control, National Health and Welfare Canada, Tunney's Pasture, Ottawa, Ontario. Bacteria were grown in a 28-L fermentor on brain heart infusion media in submerged culture for 18 h (7) and cells were killed by addition of phenol to 0.75% (w/v) final concentration. After 2 h at 6°C, cells were collected by centrifugation in a Sharples continuous centrifuge, and the twice-saline-washed cells were digested with lysozyme, ribonuclease, deoxyribonuclease, and trypsin (38), followed by phenol–water extraction (39). Purified LPS (250 mg) from the phenol phase was heated in 1.5% acetic acid (200 mL) for 2 h at 100°C. Precipitated "lipid A" was removed by centrifugation and the supernatant was lyophilized and chromatographed on a Sephadex G-50 column (2.5 × 60 cm) eluted with 0.05% pyridinium acetate pH 4.7 buffer. The column effluent was monitored for refractive index changes and the peak eluting at the void volume was collected and lyophilized (100 mg), once from water and twice from deuterium oxide.

Gas chromatographic analysis

Glycoses were determined by glc of their alditol acetates (40) using inositol as an internal standard. Polysaccharide samples (0.5 mg) were hydrolyzed in sealed glass tubes with 1 *M* sulphuric acid (500 μL) for 15 h at 100°C followed by barium carbonate neutralization. Aminoglycose estimation was performed following hydrolysis with anhydrous hydrofluoric acid (500 μL) for 4 h at 20°C, HF was evaporated by a stream of dry nitrogen, and the amino-hexose was converted to either an alditol acetate or TMS derivative. The configuration of the individual hexoses was determined by glc analysis of their trimethylsilylated (−)-2-butyl glycosides (12).

Alditol acetates were separated on a column of 3% (w/w) SP2340 on 80–100 mesh Supelcoport, and trimethylsilylated derivatives were separated on a column of 10% neopentylglycol sebacate polyester on 80–100 mesh Chromosorb W, both as previously described (7).

Gas–liquid chromatography – mass spectra were done using a Hewlett–Packard 5985B glc–ms system employing the 3% (w/v) SP2340 column above and an ionization potential of 70 eV. Identification of each hexose was based upon comparison of retention time and mass spectrum with those of authentic laboratory reference specimens.

Nuclear magnetic resonance measurements

Two solutions of the polysaccharide in deuterium oxide (5 mg/400 μL and 80 mg/mL) were prepared for ^{1}H and ^{13}C measurements respectively. All spectra were recorded in the pulsed Fourier transform mode, with quadrature detection on a Bruker AM-500 spectrometer using either selective or dual $^{1}H/^{13}C$ 5-mm probeheads and a 10-mm broadband probehead.

Proton spectra, 500 MHz, were recorded at 300 and 310 K using spectral widths of 2.5 kHz, a $\pi/2$ pulse (9 μs for selective and 28 μs for the dual probehead), a 16 K data set for a digital resolution of 0.3 Hz/point, an acquisition time of 3.2 s, and a relaxation delay of 3.0 s during which an r.f. field, 22 dB below 0.2 W, was applied at the resonance frequency of the HOD signal. Resolution enhancement prior to Fourier transformation was achieved in one of two ways; either the Lorentz-to-Gauss line shape transformation (41) was used with typical values for line broadening of −1.0 Hz and a Gaussian broadening factor of 0.4, or a non-shifted sine bell filtering function was used for maximum resolution enhancement with good S/N (signal-to-noise). Chemical shifts are expressed relative to internal acetone (1%) (δ = 2.225 ppm). In order to optimize delay periods for 2-D experiments, proton T_1 values were determined by the nonselective inversion recovery method (42) and were ca. 1.5 s for the hexose ring protons. Heteronuclear $^{1}J_{C,H}$ coupling constants for the anomeric positions were measured by gated decoupling (18).

Carbon-13 spectra, 125 MHz, were recorded at 310 K for a 25-kHz spectral width using a $\pi/2$ pulse (8.5 μs for the 5-mm and 22 μs for the 10-mm probeheads) and a 32 K data set. In order to minimize heating effects, gated broadband decoupling of 1 W was used to establish nOe buildup during a delay period of 0.7 s, followed by ca. 1-W composite pulse decoupling (WALTZ) (43) during a 0.65 s acquisition time. Coupled and decoupled DEPT experiments (26) were performed for a 12.5-kHz spectral width, using a $3\pi/2$ proton pulse to distinguish CH and CH_2 resonance and for enhanced S/N during measurement of the anomeric $^{1}J_{C,H}$ coupling constants. The delay between pulses $(2J)^{-1}$ was set at 3.4 ms. Chemical shifts are expressed relative to internal 1,4-dioxane (1% v/v) (δ = 67.4 ppm).

Two-dimensional nmr experiments were recorded by means of the

Bruker DISNMRP software. Homonuclear shift correlated COSY (44) and NOESY (45) experiments were performed with and without suppression of the HOD resonance. Selective and continuous irradiation at the frequency of the HOD signal using decoupler power 40 dB below 0.2 W, except during acquisition, provided optimal suppression of this solvent peak. The COSY and NOESY data were obtained using a matrix ($t_1 \times t_2$) of 256 × 1024 points that was zero filled to either 512 × 1024 or 1024 × 2048 points and, following resolution enhancement in both dimensions by a non-shifted sine-bell window function, the doubly-transformed data were processed to give magnitude spectra. The spectral width of the matrix was 2500 Hz in both dimensions (a digital resolution of either 4.88 Hz/pt or 2.44 Hz/pt depending on the level of zero filling employed). The $\pi/2$ pulse was 9.0 μs and a minimum delay of 1.5 s was used between transients for each value of the incrementable delay t_1. The number of transients per FID was 64 for the COSY and 128 for the NOESY experiments.

Heteronuclear shift correlated spectra (46) were recorded on a 500-μL sample (containing 60 mg of polysaccharide) in a 5-mm tube using a spectral width in F_2 of 7800 Hz (62 ppm) covering the anomeric and ring carbon atoms, and 1140 Hz (2.24 ppm) in F_1 for the corresponding protons. The data were obtained using a matrix ($t_1 \times t_2$) of 256 × 2048 points that were zero filled to 1024 × 4096 points and doubly transformed to give a power spectrum. The $\pi/2$ pulse widths were 8.5 μs for ^{13}C and 30.0 μs for ^1H, while the fixed delays τ_1 and τ_2 were selected for all multiplicities ($\tau_1 = (2J)^{-1}$ 3.4 ms, $\tau_2 = (4J)^{-1}$ 1.7 ms). Digital resolution in F_2 was 3.8 Hz/pt and in F_1, 1.1 Hz/pt. A recycle delay of ca. one proton T_1 was employed, and 800 transients/FID were collected and composite decoupling of ca. 1 W was applied during acquisition in order to minimize heating effects. Gaussian window functions were used in both dimensions, a line broadening of 5 Hz was employed for the F_2 domain, whilst the F_1 domain was optimized by the Lorentz-to-Gauss transformation employing a line broadening of −4.0 Hz and a Gaussian broadening factor of 0.3. The total acquisition time was 62.5 h.

Semi-empirical calculations

Semi-empirical potential energy calculations, HSEA method (29, 30), were used to compute the minimum energy for a pentasaccharide corresponding to the repeating unit of *S. landau* O-polysaccharide. Calculations were performed in 5-degree steps of the φ and ψ angles, for each disaccharide segment of the polysaccharide, and the glycosidic valence angle was set at 117°. The same structure was also modelled using the GESA (29) programme, which uses an algorithm that allows all the glycosidic torsion angles to be simultaneously relaxed together with the H5—C5—C6—O6 torsion angles. The atomic coordinates for heavy atoms of α-L-fucopyranose (47), β-D-glucopyranose (48), and 2-acetamido-2-deoxy-α-D-galactopyranose (49) were taken from X-ray data and the coordinates of the hydrogen atoms were generated as previously described (30) using a C—H bond length of 11.0 nm. Coordinates for 4-acetamido-4,6-dideoxy-α-D-mannopyranose were generated by bond modification of α-D-mannopyranose neutron diffraction data (50). The *N*-acetyl group was positioned such that the carbonyl bond eclipsed the C-4 to H-4 bond. An *O*-acetyl group was also positioned on the O-6d atom of β-D-Glc and the minimum energy recalculated for incorporation of this feature.

The ball and stick drawings and shaded CPK plots were produced by the PLUTO and VERSFAN (51) programmes. All programmes were run on the NRC IBM 3080 computer.

Acknowledgements

The authors wish to thank Dr. K. Bock, Dr. C. Roger, and Dr. J.-R. Brisson for advice and valuable discussions. The assistance of D. W. Griffith and L. MacLean for the bacterial cultures and purification of polysaccharides used in this work is gratefully acknowledged.

1. F. KAUFFMANN. The bacteriology of Enterobacteriaceae. 2nd ed. Munksgaard, Copenhagen. 1966.
2. M. J. CORBEL. J. Hyg. (Cambridge), **75**, 151 (1975).
3. F. A. STUART and M. J. CORBEL. Vet. Rec. **110**, 202 (1982).
4. M. J. CORBEL, F. A. STUART, and R. A. BREWER. Dev. Biol. Stand. **56**, 341 (1984).
5. M. CAROFF, D. R. BUNDLE, and M. B. PERRY. Eur. J. Biochem. **139**, 195 (1984).
6. M. CAROFF, D. R. BUNDLE, M. B. PERRY, J. W. CHERWONOGRODZKY, and J. R. DUNCAN. Infect. Immun. **46**, 384 (1984).
7. M. B. PERRY, L. MACLEAN, and D. W. GRIFFITH. Can. J. Biochem. In press.
8. G. WIDER, K. H. LEE, and K. WÜTHRICH. J. Mol. Biol. **155**, 367 (1981).
9. P. STROP, G. WIDER, and K. WÜTHRICH. J. Mol. Biol. **166**, 641 (1983).
10. K. D. BARROW, J. G. COLLINS, P. L. ROGERS, and G. M. SMILT. Eur. J. Biochem. **145**, 173 (1984).
11. O. LÜDERITZ. Angew. Chem. Int. Ed. Engl. **9**, 649 (1970).
12. G. J. GERWIG, J. P. KAMMERLING, and J. F. G. VLIEGENTHART. Carbohydr. Res. **62**, 349 (1978).
13. K. BOCK and C. PEDERSEN. J. Chem. Soc. Perkin Trans. 2, 293 (1974).
14. R. RICHARZ and K. WÜTHRICH. J. Magn. Reson. **30**, 147 (1978).
15. A. A. GREY, S. NARSIMHAN, J.-R. BRISSON, H. SCHACHTER, and J. P. CARVER. Can. J. Biochem. **60**, 1123 (1982).
16. J. H. PRESTEGARD, T. A. W. KOERNER, JR., P. C. DEMOU, and R. K. YU. J. Am. Chem. Soc. **104**, 4993 (1982).
17. J.-R. BRISSON and J. P. CARVER. J. Biol. Chem. **258**, 1431 (1983).
18. K. BOCK and H. THØGERSEN. Annu. Rep. NMR Spectrosc. **13**, 1 (1982).
19. G. WAGNER. J. Magn. Reson. **55**, 151 (1983).
20. A. BAX and G. DROBNY. J. Magn. Reson. **61**, 306 (1985).
21. K. BOCK and C. PEDERSEN. Adv. Carbohydr. Chem. Biochem. **41**, 27 (1983).
22. K. BOCK, C. PEDERSEN, and H. PEDERSEN. Adv. Carbohydr. Chem. Biochem. **42**, 193 (1984).
23. B. H. MEIER and R. R. ERNST. J. Am. Chem. Soc. **101**, 6441 (1979).
24. H. THØGERSEN, R. U. LEMIEUX, K. BOCK, and B. MEYER. Can. J. Chem. **60**, 44 (1982).
25. R. U. LEMIEUX and S. KOTO. Tetrahedron, **30**, 1933 (1974).
26. D. M. DODDRELL, D. T. PEGG, and M. R. BENDALL. J. Magn. Reson. **48**, 323 (1982).
27. D. R. BUNDLE, H. J. JENNINGS, and I. C. P. SMITH. Can. J. Chem. **51**, 3812 (1973).
28. R. U. LEMIEUX and K. BOCK. Arch. Biochem. Biophys. **221**, 125 (1983).
29. K. BOCK. Pure Appl. Chem. **55**, 605 (1983).
30. H. PAULSEN, T. PETERS, V. SINNWELL, R. LEBUHN, and B. MEYER. Liebigs Ann. Chem. 489 (1985).
31. K. BOCK, S. JOSEPHSON, and D. R. BUNDLE. J. Chem. Soc. Perkin Trans. 2, 59 (1982).
32. K. BOCK, M. MELDAL, D. R. BUNDLE, T. IVERSEN, B. M. PINTO, P. J. GAREGG, I. KVANSTRÖM, T. NORBERG, A. A. LINDBERG, and S. B. SVENSON. Carbohydr. Res. **130**, 35 (1984).
33. A. BAX, W. EAGAN, and P. KOVÁC. J. Carbohydr. Chem. **3**, 593 (1984).
34. M. J. GIDLEY and S. M. BOCIEK. J. Chem. Soc. Chem. Commun. 220 (1985).
35. J. RICHARDS, M. B. PERRY, and P. J. KNISKERN. Can. J. Biochem. Cell Biol. **63**, 953 (1985).
36. J. RICHARDS and M. B. PERRY. Abstr. Int. Symp. on Molecular Immunology of Complex Carbohydrates. Texas A and M University. Sept. 1985.
37. D. R. BUNDLE and M. B. PERRY. Biochem. Soc. Trans. In press.
38. K. G. JOHNSON and M. B. PERRY. Can. J. Microbiol. **22**, 29 (1976).
39. O. WESTPHAL, O. LÜDERITZ, and F. BISTER. Z. Naturforsch. Teil B, **7**, (1952).
40. S. W. GUNNER, J. K. N. JONES, and M. B. PERRY. Can. J. Chem. **39**, 1892 (1961).

41. R. R. ERNST. Adv. Magn. Reson. **2**, 1 (1966).
42. R. L. VOLD, J. S. WAUGH, M. P. KLEIN, and D. E. PHELPS. J. Chem. Phys. **48**, 3831 (1968).
43. A. J. SHAKA, J. KEELER, T. FRENKIEL, and R. FREEMAN. J. Magn. Reson. **52**, 335 (1983).
44. A. BAX, R. FREEMAN, and G. MORRIS. J. Magn. Res. **42**, 164 (1981).
45. A. KUMAR, R. R. ERNST, and K. WÜTHRICH. Biochem. Biophys. Res. Commun. **95**, 1 (1980).
46. A. BAX and G. A. MORRIS. J. Magn. Reson. **42**, 501 (1981).
47. W. J. COOK and C. E. BUGG. Biochem. Biophys. Acta, **389**, 428 (1975).
48. F. ARÈNE, A. NEUMAN, and F. LONGCHAMBON. C. R. Acad. Sci. Ser. C, **288**, 331 (1979).
49. W. T. WINTER, S. ARNOTT, D. H. ISAAC, and E. D. T. ATKINS. J. Mol. Biol. **125**, 1 (1978).
50. G. A. JEFFREY, R. K. MCMULLAN, and S. TAKAGI. Acta Crystallogr. Sect. B **33**, 728 (1977).
51. R. NORRESTAM. In press.

Ternary charge transfer complexes. II.[1] Complexes with Group III and IV elements in the anion[2]

SYDNEY BROWNSTEIN,[3] ANNE MORRISON, AND LIANG K. TAN
Division of Chemistry, National Research Council of Canada, Ottawa, Ont., Canada K1A 0R9
Received August 15, 1985

SYDNEY BROWNSTEIN, ANNE MORRISON, and LIANG K. TAN. Can. J. Chem. **64**, 265 (1986).

Intensely colored charge transfer complexes are formed from $NOMX_4$ (M = B,Al,Ga,Tl; X = Cl,F) and benzene or methyl substituted benzenes. $(NO)_2MX_6$ (M = Si,Ge,Sn,Ti; X = Cl,F) also form complexes with methyl substituted benzenes. Magnetic resonance and optical spectroscopic parameters are presented. $NOMX_4$ forms stronger complexes than $(NO)_2MX_6$ and complexes containing fluorine are stronger than those with chlorine.

SYDNEY BROWNSTEIN, ANNE MORRISON et LIANG K. TAN. Can. J. Chem. **64**, 265 (1986).

Il se forme des complexes de transfert de charge très colorés lors des réactions du benzène ou de benzènes substitués par des groupements méthyles avec des dérivés $NOMX_4$, dans lesquels M = B, Al, Ga et Tl alors que X = Cl et F. Les dérivés $(NO)_2MX_6$, dans lesquels M = Si, Ge, Sn et Ti alors que X = Cl et F, forment aussi des complexes avec les benzènes substitués par des groupements méthyles. On rapporte les paramètres de rmn et de spectroscopie optique des complexes. Les $NOMX_4$ forment des complexes qui sont plus forts que ceux provenant des $(NO)_2MX_6$ et les complexes contenant du fluor sont plus forts que ceux contenant du chlore.

[Traduit par le journal]

Introduction

The preparation of stable charge transfer complexes of NOCl, MCl_n, and an aromatic hydrocarbon has been reported (1). In this article the properties of such complexes will be discussed as a function of the aromatic compound and the counterion to the NO group, where the central element of the counterion is from Group III or IV of the periodic table and the halogen is chlorine or fluorine.

Following is a brief description of the nitrosyl salts that were used in this study. A reproducible synthesis of $NOBCl_4$ has been reported (2). From an analysis of its Raman spectrum (3) and the temperature dependence of its dissociation it is concluded that the compound should be formulated as $NO^+BCl_4^-$ (4). $NOBF_4$ is also a well-known ionic solid (5). Both Raman (6) and X-ray (7) studies of $NOAlCl_4$ support its formulation as an ionic solid. There is no definitive evidence for $NOAlF_4$ nor $(NO)_3AlF_6$. $NOGaCl_4$ may be readily synthesized from excess NOCl and the metal (8). An apparently definitive study has been made on the synthesis of $NOTlCl_4$ (9). $(NO)_2SiF_6$ (10), $(NO)_2GeF_6$ (11), $(NO)_2SnF_6$ (10), and $(NO)_2TiF_6$ (10) are known, but the mixed chloride fluoride has only been reported with tin as central atom (12). There is no report of $(NO)_2MCl_6$; M = Si, Ge. The compound $(NO)_2SnCl_6$ is an ionic compound insoluble in liquid nitrosyl chloride (13). Both it and $(NO)_2TiCl_6$ can be readily prepared by reaction of NOCl with the metal chloride dissolved in CCl_4 (14)

The existence of charge transfer complexes was first established with iodine/aromatic complexes, where equilibrium constants of 1 and 6 were found for their formation with benzene and mesitylene (15). The appearance of a new, intense ultraviolet absorption maximum, which is definitive for these complexes, was explained as arising from the partial transfer of a Π electron from the donor to the acceptor species (16). Strong complexes were found with tetracyanoethylene as acceptor, giving equilibrium constants of 2 and 17 for benzene and mesitylene (17).

Complexation of the nitrosyl cation with aromatic compounds was first reported in 1963 (18), and has been studied in solution and in the gas phase by optical and ion cyclotron resonance spectroscopy (19, 20). Solid charge transfer complexes between the nitrosyl cation and aromatic compounds were only recently reported and have much greater stability towards dissociation than those with iodine and tetracyanoethylene (1). Complexes of similar stoichiometry but with NO^+ replaced by Ga^+ have been reported (21, 22). They are not charge transfer complexes since they are colorless and dissociate very readily.

Experimental

Magnetic resonance spectra were obtained on a Varian Associates XL-100 spectrometer equipped with a Nicolet Fourier transform attachment operating at 100 MHz for protons, or on a Bruker AM-400 operating at 400 MHz for protons. All chemical shifts, except for ^{19}F, are reported with respect to tetramethylsilane, although neopentane was used as an internal reference since it is inert under these conditions. A correction of 0.92 ppm was applied for protons and 31.4 ppm for ^{13}C. Fluorine chemical shifts are reported with respect to internal $CFCl_3$ as zero. Visible spectra were obtained on a Cary 210 spectrometer in CH_2Cl_2 as solvent.

Chemicals

Nitrosyl chloride, nitrosyl fluoride, boron trichloride, boron trifluoride, aluminum trifluoride, silicon tetrafluoride, germanium tetrafluoride, stannic fluoride, and bromine trifluoride were used without further purification. Benzene, toluene, *p*-xylene, mesitylene, sulfur dioxide, neopentane, and methylene chloride were purified and used as previously described (23, 24).

Aluminum chloride, purified by repeated vacuum sublimation, was transferred in a dry box under dried nitrogen, via a sidearm, to a glass tube closed by a stainless steel valve. The sidearm was then sealed under vacuum. An excess of nitrosyl chloride was condensed into the reactor and the reaction was allowed to proceed to completion in excess NOCl as solvent. All volatile materials were removed by pumping under vacuum to give $NOAlCl_4$, which was stored under vacuum. $NOGaCl_4$ was prepared in a similar manner except that the pure metal, rather than the chloride, was used as starting material. $NOTlCl_4$ was prepared directly in the spectral cell by reaction of NOCl with the appropriate amount of anhydrous thallic chloride. Both $SnCl_4$ and $TiCl_4$ were vacuum distilled into containers closed with Teflon high

[1]The preceding article in this series is ref. 1.
[2]Issued as NRCC No. 25103.
[3]Author to whom correspondence may be addressed.

TABLE 1. Chemical shifts of some boron, aluminum, and gallium chloro and fluoro species

Sample	$\Xi^{11}B$[a]	$\Xi^{27}Al$[b]	$\Xi^{71}Ga$	$\delta^{19}F$
MCl_3	32 085 475	26 058 956[c]	30 514 807[c]	
MCl_3·NOCl + NOCl	32 084 235	25 059 535	30 504 434	
MCl_3·NOCl + MCl_3	32 084 897	26 059 538		
Tetramethylammonium MCl_4	32 084 185[c]	26 059 270	30 514 359[c]	
MCl_3·NOCl + benzene		26 059 583	30 504 503	
MCl_3·NOCl + toluene	32 084 206			
BF_3	32 084 244			−127.64
Tetramethylammonium BF_4	32 083 932			−139.77
BF_3·NOF + *p*-xylene	32 083 932			−143.10
MF_3·NOF + mesitylene	32 083 931	26 058 642		−142.04(B) 39.82(Al)
MF_3·NOF + hexamethylbenzene	32 083 926	26 058 753		−140.42(B) 40.43(Al)

[a] Ξ for $(CH_3O)_3B$ is 32 084 591.
[b] Ξ for $(CH_3CH_2)_3Al$ is 26 060 416 and for Al^{3+} aq. is 26 056 874.
[c] Reference 25.

vacuum stopcocks. $(NO)_2MCl_6$; M = Sn, Ti, were prepared in the reaction vessels by vacuum transfer of weighed quantities of NOCl and MCl_4. A similar procedure was followed with $(NO)_2GeF_4Cl_2$. An excess of NOF was added to $SnCl_4$ or $TiCl_4$ dissolved in SO_2 and all volatile materials were removed under vacuum to give white, solid $(NO)_2MCl_4F_2$; M = Sn,Ti, in good yield. Some attack of the NOF upon the glass reaction vessel was observed. $(NO)_2MF_6$; M = Sn,Ti, were prepared by reaction of MF_4 with neat BrF_3 and NOCl, followed by evaporation of the volatile species under vacuum. Attack on the reaction vessel was observed. $(NO)_2MF_6$; M = Si, Ge was prepared directly from NOF and MF_4 in SO_2 solution.

Sample preparation

An appropriate weighed quantity of $NOMCl_4$ was transferred in a dry box into either an nmr tube equipped with a straight-line, high vacuum Teflon stopcock or a similarly equipped sidearm to a quartz curette containing a magnetically controlled spacer to vary the optical path length. The other reagents were then transferred as vapors, via a vacuum line system, to the container. The quantity of solvent was weighed in a precalibrated container before transfer to the spectral cell so that accurate equilibrium constants or extinction coefficients could be calculated. Aromatic compounds of low volatility were weighed and added, in the dry box, to $NOMCl_4$ before addition of the volatile species. Similar procedures were followed with $(NO)_2MCl_6$ except that its transfer, as such, was unnecessary.

Results and discussion

The reaction of NOCl and BCl_3 in anhydrous methylene chloride as solvent does not immediately lead to the formation of solid insoluble $NO^+BCl_4^-$. From the boron chemical shift values listed in Table 1 for freshly prepared samples containing NOCl and BCl_3 it appears that there is immediate complex formation and rapid exchange between complexed BCl_3 and an excess of free BCl_3. After several hours there is extensive precipitation and the samples set to a semi-solid mass. The boron chemical shifts agree with those observed for the dimethyl sulfide complex (25). Although the characteristic deep color of a ternary charge transfer complex was observed for solutions containing toluene, *p*-xylene, and hexamethylbenzene, the erratic onset of precipitation of $NOBCl_4$ prevented a detailed study of these systems.

The reaction of NOF and BF_3 in sulfur dioxide as solvent immediately produces white, solid, insoluble $NOBF_4$. A pale yellow solution with an excess of benzene, and orange with an excess of toluene, are formed in SO_2 with negligible solubilization of the $NOBF_4$. Most of the $NOBF_4$ is brought into solution with an excess of *p*-xylene to give an intense red color. From the boron and fluorine chemical shifts, listed in Table 1 for the complexes with *p*-xylene, mesitylene, and hexamethylbenzene, one can conclude that in these soluble complexes the ion BF_4^- is in a similar environment to that of tetramethylammonium fluoroborate dissolved in SO_2. The proton resonance and uv spectra of the $NOBF_4$·hexamethylbenzene complex are listed in Table 2.

$NOAlCl_4$ is quite soluble in liquid sulfur dioxide. There is rapid exchange between the complexed $AlCl_3$ and an excess of free $AlCl_3$, but little change in chemical shift of ^{27}Al from that of $NOAlCl_4$ upon formation of a ternary charge transfer complex. The chemical shift values for some representative samples are listed in Table 1. The chemical shift values are consistent with those observed for the $AlCl_3$·dimethyl ether complex (25). The dependence of the proton and carbon chemical shifts of benzene upon the relative concentrations of the free and complexed species is shown in Table 3. It is assumed that all the benzene is complexed in the presence of excess $NOAlCl_4$. From the chemical shifts thus obtained for pure complex and that of benzene alone, it is possible to calculate the equilibrium constant for complex formation from the chemical shifts observed with an excess of benzene. The large values found in this way confirm the assumption of complete complex formation with excess $NOAlCl_4$. The accuracy of the calculations is quite poor since it depends upon a small difference between two large numbers. The calculated values are listed in Table 3.

Proton and carbon chemical shifts in SO_2 solution and uv–visible spectral data in CH_2Cl_2 solution for many complexes with $NOAlCl_4$ are listed in Table 2. For comparison, the uv parameters are listed for the uncomplexed hydrocarbons and for the tetracyanoethylene (TCNE) complexes.

The reaction of AlF_3 with NOF in SO_2 as solvent requires a few minutes at room temperature. Under these conditions the Pyrex glass also reacts, so that upon addition of the aromatic hydrocarbon one gets a mixture of the charge transfer complexes with $NOBF_4$, $(NO)_2SiF_6$, and nitrosyl aluminum fluoride. The relative proportions can be inferred from the intensities of the fluorine resonance signals, which confirms the reaction between NOF and AlF_3. Proton chemical shifts and visible absorption parameters will be average values and not definitive but the ^{19}F and ^{27}Al chemical shifts of some complexes are listed

TABLE 2. Magnetic resonance and ultraviolet spectral parameters for some aromatic hydrocarbons and their $NOMX_4$ and $(NO)_2MX_6$ complexes

Compound	δ^1H		$\delta^{13}C$		λ_{max}(Å)	ϵ	λ_{max} TCNE[a]	ϵ
	CH_3	H	CH_3	CH				
Benzene		7.41		129.2	2680		3840	3570
$NOAlCl_4$·Benzene		8.03		137.1	3350			
$NOGaCl_4$·Benzene		7.75		134.8	3350			
$NOTlCl_4$·Benzene		7.60		132.2				
Toluene	2.30	7.20	20.8	126.1	2680	310	4060	3330
				129.1				
				129.8				
				138.8				
$NOAlCl_4$·Toluene	2.67	7.92			3380	11000		
$(NO)_2SnCl_4F_2$·Toluene	2.56	7.65	21.3	132.6				
		7.74		135.1				
				136.0				
tert-Butylbenzene	1.30	7.11	31.1	126.2	2670			
		7.24		128.8				
		7.39		152.2				
$(NO)_2SnCl_6$·*tert*-butylbenzene					3600 (weak)			
p-Xylene	2.28	7.11	22.9	132.6	2750		4600	2650
$NOAlCl_4$·*p*-xylene	2.63	7.81			3400			
$(NO)_2SnCl_4F_2$·*p*-xylene	2.67	7.83	21.1	139.9				
				151.1				
$(NO)_2TiCl_6$·*p*-xylene	2.38	7.30						
Mesitylene	2.23	6.81	20.6	130.5	2820		4610	3120
$NOAlCl_4$·mesitylene	2.58	7.58		139.1	3430			
$(NO)_2SiF_6$·mesitylene					3900			
$(NO)_2SnCl_6$·mesitylene	2.42	7.21						
$(NO)_2SnCl_4F_2$·mesitylene	2.60	7.57			3910			
$(NO)_2TiCl_6$·mesitylene	2.52	7.41	20.9	135.2	2850			
$(NO)_2TiCl_4F_2$·mesitylene *cis*	2.41	7.21	20.1	137.9				
and *trans*	2.56	7.50	20.9	152.1				
Hexamethylbenzene	2.15		15.7	131.0	2710	4100	5450	4390
$NOBF_4$·hexamethylbenzene	2.42				3250	7300		
$NOAlCl_4$·hexamethylbenzene	2.48		17.3	149.9	3340	10000		
$(NO)_2SiF_6$·hexamethylbenzene	2.42		16.9	144.6	3380			
$(NO)_2Ge\ Cl_2F_4$·hexamethylbenzene	2.45		16.7					
$(NO)_2GeF_6$·hexamethylbenzene	2.32		16.7	142.1	3380	7100		
$(NO)_2SnCl_6$·hexamethylbenzene	2.49				3360			
$(NO)_2SnCl_4F_2$·hexamethylbenzene	2.50		17.3	150.2	3360			
$(NO)_2Ti\ Cl_6$·hexamethylbenzene	2.50		17.3	150.2	3100			
$(NO)_2TiCl_4F_2$·hexamethylbenzene					3400			
$(NO)_2TiF_6$·hexamethylbenzene	2.48		17.1	148.8	3260			
Chlorobenzene		7.28			2720			
		7.32						
		7.34						
$NOGaCl_4$·chlorobenzene		7.38			2900 (shoulders)			

[a] Data from ref. 17.

in Table 1. These were confirmed for the hexamethylbenzene complex by a synthesis using BrF_3 and NOCl (26).

Evidence from uv, and from proton, fluorine, and carbon resonance spectroscopy shows that $(NO)_2SiF_6$ is brought into solution and forms charge transfer complexes with mesitylene and hexamethylbenzene but not with less highly methyl substituted benzenes. The data are presented in Table 2. Similar reactivity was observed with $(NO)_2GeF_6$. The fluorine chemical shifts for these species are listed in Table 4. The mixed chlorofluoride $(NO)_2GeF_4Cl_2$ also forms a complex with hexamethylbenzene and spectral parameters are listed in Tables 2 and 4.

$(NO)_2SnCl_6$ forms complexes of reasonable stability with hexamethylbenzene and mesitylene. The mixed chloride fluoride $(NO)_2SnCl_4F_2$ is brought into SO_2 solution and forms complexes with *p*-xylene, toluene, and benzene as well. Spectral data are listed in Tables 2 and 4. Where complex formation is not essentially complete, proton and carbon chemical shifts are not listed since these would be average values for the mixture of free and complexed hydrocarbon. Neither SnF_2 nor SnF_4 react with NOF or NOCl in SO_2 suspension. $(NO)_2SnF_6$, prepared from SnF_4, BrF_3, and NOCl (26), appears to react, at least partially, with benzene and the other aromatic hydrocarbons. Spectral data are listed in Tables 2 and 4. Reactions with TiX_4 are essentially similar to those with SnX_4 and their spectral parameters are also listed in Tables 2 and 4.

Complexes with fluorine in the anions appear to form more

TABLE 3. Chemical shifts and equilibrium constants for ternary complex formation

$[AlCl_3]_0$[a]	$[NOCl]_0$	$[Benzene]_0$	δ^1H[b]	$\delta^{13}C$[b]	[Complex]	[Benzene]	$[NOAlCl_4]$	K
0	0.0095	0.0119	7.408		0	0.0119	0	
0.0104	0.0131	0.0050	8.030		0.0050	0	0.0054	
0.00876	0.0177	0.0091	7.948		0.00809	0.00096	0.00067	12 600
0.00871	0.00878	0.0249	7.620		0.00849	0.0164	0.0029	1 970
0.00878	0.0148	0.0183	7.687		0.00822	0.0100	0.0056	1 470
0.0117	0.00847	0.00883	7.963		0.00788	0.00059	0.00095	14 052
0	0.0541	0.0333		129.23	0	0.0333	0	
0.0488	0.0489	0.0243		137.14	0.0243	0	0.0245	
0.0261	0.0278	0.0525		133.64	0.0293	0.0232	—	—
0.218	0.0236	0.0655		132.00	0.0229	0.0426	—	—

[a] Concentrations are given as mole fractions. The subscript indicates initial concentrations.
[b] In ppm to low field of TMS.

TABLE 4. Fluorine resonance shifts of some charge transfer complexes

Compound	$\delta^{19}F$
SiF_4	−162.2
$(NO)_2SiF_6$·hexamethylbenzene	−138.6
GeF_4	−168.1
$(NO)_2GeF_4Cl_2$·hexamethylbenzene	−161.9
$(NO)_2GeF_6$·hexamethylbenzene	−129.1
$(NO)_2SnCl_4F_2$ *cis* and *trans*	−62.1 and −67.8
$(NO)_2SnCl_4F_2$·hexamethylbenzene	−62.4
$(NO)_2SnCl_4F_2$·mesitylene	−62.9
$(NO)_2SnCl_4F_2$·*p*-xylene *cis* and *trans*	−63.3 and −68.2
$(NO)_2SnCl_4F_2$·toluene	−63.4
$(NO)_2SnCl_4F_2$·benzene	−63.2
$(NO)_2TiCl_4F_2$·mesitylene *cis* and *trans*	−18.4 and −121.9
$(NO)_2TiCl_4F_2$·hexamethylbenzene *cis* and *trans*	−20.6 and −110.7
$(NO)_2TiF_6$·hexamethylbenzene	47.0

readily than those which only contain chlorine ligands. Thus $NOBF_4$ is brought into solution by *p*-xylene, mesitylene, and hexamethylbenzene to form a complex, but $NOBCl_4$ is not. Reasonably complete complex formation is observed with $(NO)_2SnCl_4F_2$ and toluene, but with $(NO)_2SnCl_6$ mesitylene is required for a complex of similar strength.

It is reasonable to assume that the displacement to lower field of the chemical shift for the ring protons and carbon atoms in the charge transfer complexes, compared to the uncomplexed hydrocarbon, is probably larger when there is greater electron transfer. This displacement increases from 0.62 for the aromatic protons of benzene to 0.72 for toluene, 0.70 for *p*-xylene, and 0.77 for mesitylene. A similar trend is found in the 7.9-ppm displacement of the aromatic carbons in $NOAlCl_4$·benzene to 18.9 ppm for $NOAlCl_4$·hexamethylbenzene. For a given hydrocarbon the extent of the shift of λ_{max} to longer wavelength is taken as an indication of the strength of complex formation within this series. Although the equilibrium constant for complex formation of an aromatic hydrocarbon is much greater with $NOMCl_4$ than with tetracyanoethylene, the long wavelength shift of the absorption maximum is greater with the tetracyanoethylene complexes. The difference in the maxima between free and complexed hydrocarbon decreases for the $NOMCl_4$ complexes from benzene at 670 Å to hexamethylbenzene at 560 Å, while for the tetracyanoethylene complexes it increases from 1.160 Å for benzene to 2.670 Å for hexamethylbenzene. These results suggest a slightly different origin for the charge transfer band in the two series of complexes.

From these considerations one may conclude that within Group III the order of complex formation is $NOAlCl_4$>$NOGaCl_4$>$NOTlCl_4$>$NOBF_4$. It appears that the species $NOMCl_4$; M = Al,Ga,Tl, form stronger complexes than $(NO)_2MX_6$; M = Si, Ge, Sn, Ti, X = Cl,F, since only the former have strong complexes with benzene. Within Group IV, titanium and tin complexes are of approximately equal strength, with those of germanium being weaker, and those of silicon still weaker. There is therefore a very significant effect of the anion upon the extent of charge transfer complexation in solution for this type of compound.

There is a slight decrease in nuclear magnetic resonance frequency on going from MCl_3 to MCl_4^- where M is boron or gallium, and a slight increase for aluminum. Similar shifts are observed upon reaction of BCl_3 or $AlCl_3$ with NOCl, but there is a very large gallium resonance change from $GaCl_3$ to $NOGaCl_4$ and its complex with benzene. There is no obvious explanation for the different behaviour of the gallium resonance since the proton and carbon resonances and uv spectra of its benzene complex are similar to those with aluminum and thallium.

The moisture sensitivity of all of these complexes was such that meaningful infrared spectra could not be obtained. We were also unable to grow adequate quality crystals of these compounds for single crystal X-ray structure determinations. No

ternary complexes were observed with hexamethylbenzene, $TiCl_4$ and NO, NO_2, $SOCl_2$, $POCl_3$, ICl_3, and SCl_4.

1. S. BROWNSTEIN, E. GABE, F. LEE, and L. TAN. J. Chem. Soc. Chem. Commun. 1566 (1984).
2. J. R. PARTINGTON and A. L. WHYNES. J. Chem. Soc. 3135 (1949).
3. M. C. DHAMELINCOURT and M. MIGEON. Rev. Chim. Miner. **15**, 464 (1978)
4. A. FINCH, P. N. GATES, and T. H. PAGE. J. Inorg. Nucl. Chem. **42**, 292 (1980).
5. G. BALZ and E. MAILANDER. Z. Anorg. Allgem. Chem. **217**, 161 (1934).
6. H. GERDING. Recl. Trav. Chim. Pays-Bas, **75**, 589 (1956).
7. P. BARBIER, G. MAIRESSE, J. P. WIGNACOURT, and F. BAERT. Cryst. Struct. Commun. **5**, 633 (1976).
8. H. GERDING and J. C. DUINKER. Rev. Chim. Miner. **3**, 815 (1966).
9. K. C. MALHOTRA. Indian J. Chem. **14A**, 869 (1976).
10. F. SEEL and H. MASSAT. Z. Anorg. Allgem. Chem. **280**, 186 (1955).
11. P. BOUY. Ann. Chim. **4**, 853 (1959).
12. A. A. WOOLF. J. Inorg. Nucl. Chem. **3**, 285 (1956).
13. A. B. BURG and G. W. CAMPBELL. J. Am. Chem. Soc. **70**, 1964 (1948).
14. H. RHEINHOLDT and R. W. WASSERFUHR. Ber. **60B**, 732 (1927).
15. H. A. BENESI and J. H. HILDEBRAND. J. Am. Chem. Soc. **71**, 2703 (1949).
16. R. S. MULLIKEN. J. Am. Chem. Soc. **74**, 811 (1952).
17. R. E. MERRIFIELD and W. D. PHILLIPS. J. Am. Chem. Soc. **80**, 2778 (1958).
18. D. DIMITROV and F. FRATEV. C. R. Acad. Bulg. Sci. **16**, 825 (1963).
19. W. D. REENTS, JR. and B. S. F. FREISER. J. Am. Chem. Soc. **102**, 271 (1980).
20. W. D. REENTS, JR. and B. S. F. FREISER. J. Am. Chem. Soc. **103**, 2791 (1981).
21. H. SCHMIDBAUR, U. THEWALT, and T. ZAFIROPOULOS. Organometallics, **2**, 1550 (1983).
22. U. THEWALT, T. ZAFIROPOULOS, and H. SCHMIDBAUR. Z. Naturforsch, Teil B, **39**, 1642 (1984).
23. L. K. TAN and S. BROWNSTEIN. J. Org. Chem. **48**, 302 (1983).
24. A. M. EASTHAM. J. Am. Chem. Soc. **78**, 6040 (1956).
25. B. GLAVINCEVSKI and S. BROWNSTEIN. Can. J. Chem. **59**, 3012 (1981).
26. S. A. WOOLF. J. Chem. Soc. 1053 (1950).

Substituent effects on benzyl radical hydrogen hyperfine coupling constants (hfc's). Part 5. The comparison of electron spin resonance hfc's and the stabilization energy of π-radicals due to spin delocalization

A. Martin de P. Nicholas and Donald R. Arnold[1]

Department of Chemistry, Dalhousie University, Halifax, N.S., Canada B3H 4J3

Received June 27, 1985

A. Martin de P. Nicholas and Donald R. Arnold. Can. J. Chem. **64**, 270 (1986).

Electron spin resonance (esr) hfc values of π-radicals are found to be linearly related to the stabilization energy due to spin delocalization. Application of this relationship to benzyl radicals permits the representation of $\sigma^{\cdot}_{\alpha}$ values on an energy scale. Mulliken charges in the α- and β-spin systems are found to provide valuable information about factors governing the effects of substituents on spin delocalization in benzyl radicals. These effects can be rationalized by considering four types of spin–spin interactions involving σ- and π-electrons in the α- and β-spin systems. The Mulliken analysis shows that all substituents are stronger π α-acceptors (or weaker π α-donors) at the *para* position relative to the *meta* position. Similarly, in the β system the *meta* derivatives are the better acceptors. This may be understood in terms of the excess of π α-spin at the *para*-carbon and the excess of π β-spin at the *meta*-carbon. Similar effects are observed in the σ framework.

A. Martin de P. Nicholas et Donald R. Arnold. Can. J. Chem. **64**, 270 (1986).

On a trouvé que les valeurs de chf de la rpe des radicaux π sont reliés d'une façon linéaire avec l'énergie de stabilisation due à la délocalisation du spin. L'application de cette relation aux radicaux benzyles permet de représenter les valeurs $\sigma^{\cdot}_{\alpha}$ sur une échelle d'énergie. On à trouvé que les charges de Mulliken des systèmes de spin α et β fournissent des informations utiles concernant les facteurs gouvernant les effets des substituants sur la délocalisation des spin dans les radicaux benzyles. On peut rationaliser ces effets en considérant quatre types d'interactions spin–spin impliquant des électrons σ et π dans les systèmes de spin α et β. L'analyse de Mulliken montre que, par rapport aux substituants en position *méta*, tous ceux qui sont en position *para* sont des accepteurs -απ plus forts (ou des donneurs -απ plus faibles). De la même manière, dans les systèmes substitués en β, les dérivés substitués en *méta* sont de meilleurs accepteurs. On peut comprendre ceci en fonction d'un excès de spin-α π sur le carbone en *para* et d'un excès de spin-β π sur le carbone *méta*. On observe des effets similaires dans le cadre des électrons σ.

[Traduit par le journal]

Introduction

The dominant interaction of the unpaired electron in a π-radical is with the electrons paired in the π-bonds. Such interactions are characterized by the delocalization of the spin throughout the π system. The resulting spin density distribution is apparent from the electron spin resonance (esr) spectrum of these species. The esr hyperfine coupling constants (hfc's) reflect this delocalization of the unpaired electron and, intuitively, should be related to the stabilization energy of these radicals. Thus, we proposed the $\sigma^{\cdot}_{\alpha}$ scale, based on esr hfc's of the benzylic hydrogens, which should indicate the effect of ring substituents on the delocalization, and therefore the stabilization, of benzyl radicals (1, 2). This substituent parameter scale is defined by eq. [1].

$$[1] \quad (\sigma^{\cdot}_{\alpha})_X = 1 - (\alpha\text{-hfc}_X) / (\alpha\text{-hfc}_H)$$

where α-hfc is the hfc due to the hydrogens at the benzylic position and the subscript indicates the substituent.

Values of $\sigma^{\cdot}_{\alpha}$ can be used in Hammett type linear free-energy relationships to assess the relative importance of variation in spin density on reaction rates and equilibrium. Although correlation of the rate of reaction, for example, with $\sigma^{\cdot}_{\alpha}$ indicates benzyl radicals are involved, and the magnitude of the reaction constant, $\rho^{\cdot}$, assesses the relative importance of the variation in benzyl radical stabilization on the rate of reaction, it has not been possible, up to now, to quantitatively evaluate $\rho^{\cdot}$ values on an absolute energy scale (1).

In this paper, we describe how esr hfc's and experimentally determined rotational barriers (V_2) can be used to quantitatively assess the effects of substituents on the π-stabilization of benzyl radicals due to spin delocalization (SE(R$^{\cdot}$)). Accordingly, we will not include contributions from other stabilizing interactions in our assessment of radical stability. Hence, these SE(R$^{\cdot}$) values will differ significantly from other SE values based on the total stabilization of the open-shell species, R$^{\cdot}$. For example, in polyenyl radicals SE(R$^{\cdot}$) will be, by our definition, the *additional* stabilization conferred on the radical on account of spin delocalization.

In closed-shell species, a Mulliken population analysis (3, 4) permits an understanding of the charge interactions present in the molecule. We have found such an analysis to be useful in rationalizing interaction energies in benzenoid systems (5). Here, we apply such an approach to substituted benzyl radicals. Mulliken charges in the α- and β-spin systems are used to make a semiquantitative analysis of the interactions governing the stability of a radical.

Details of calculations

Standard single determinant MO theory was used. The *ab initio* MO calculations described were obtained by the use of the GAUSSIAN 76 program (6) on a Control Data CYBER 170-730 system. The open-shell, spin-unrestricted (UHF) procedure was employed (7) to compute the energies of the benzyl radicals with the benzyl group coplanar with the phenyl ring. The minimal STO-3G basis set (8) was used. Partial geometry optimizations, subject to imposed symmetry constraints, were performed. A standard phenyl ring (optimized values for benzene) with hexagonal symmetry was assumed in every case (9). The parameters used for the STO-3G calculation were r_{CC} = 1.38669 Å and r_{CH} = 1.08258 Å (9).

Geometry optimizations were carried out at the STO-3G level (10). The r_{CH} of the CH_2 group for X=H was assumed for all the substituted radicals because the optimization of this parameter for the substituents, X = H, *meta*-F, *para*-F, *meta*-CN,

[1]Author to whom correspondence should be addressed.

TABLE 1. The total UHF energies of substituted benzyl radicals at the STO-3G level (E_{UHF})

Substituent	$-E_{UHF}$(au)
H	265.87735[a]
3-Me	304.46068
4-Me	304.46064
3-CN	356.43598
4-CN	356.43646
2-F	363.33550
3-F	363.33581
4-F	363.33574
3-OMe	378.29038
4-OMe	378.29031

[a]Reference 10.

and *para*-CN, in the coplanar form of $XC_6H_4CH_2$ affected the total energy by less than 0.03 kJ mol^{-1}. Model CH_3 groups (r_{CH} = 1.09 Å and <HCH = 109.47°) were used for the methyl and methoxy substituents. For the methoxy radicals, the orientation of the OMe group with the C—O bond perpendicular to the ring was found to be more stable than when it was coplanar with the ring.

Except in the cases mentioned above, all other geometrical parameters of the substituent and the CH_2 group were optimized. The STO-3G total energies are listed in Table 1.

Results and discussion

Relationship between π-stabilization energy and esr hfc's of π-radicals

The π-stabilization energy of a π-radical, SE(R$^\cdot$), is given by eq. [2]:

$$[2] \quad SE(R^\cdot) = V_2(CH_2) - V_2^* \qquad \text{(1)}$$

where $V_2(CH_2)$ and V_2^* are the rotational barriers of the $CH_2^\cdot$ group of the radical $R^\cdot = ZCH_2^\cdot$, in the presence and absence of spin delocalization, respectively (11, 12). In this section, we investigate the relationship between SE(R$^\cdot$) and the α-hfc of the methylene hydrogens for a series of π-radicals. The relevant data are listed in Table 2; the radicals are arranged in the order of decreasing α-hfc's.

The first radical considered is a hypothetical π-radical with a SE(R$^\cdot$) of zero. The α-hfc of this species is equal to the Q value given by the McConnell relationship (13).

$$[3] \quad \alpha\text{-hfc} = Q\rho \qquad \text{(2)}$$

where ρ is the π spin density, unity in this case. This Q value is obtained conveniently as the algebraic sum of the hyperfine coupling constants of the allyl radical (13*b*). It is interesting to note that the Q value derived in this way is in excellent agreement with the α-hfc of the methyl radical, in a planar conformation, corrected for vibrational effects (14).

The α-hfc and SE(R$^\cdot$) values for the acetylmethyl (15) and allyl (11) radicals were available in the literature. The SE(R$^\cdot$) for the benzyl radical was assumed to be equal to that of the phenethyl radical (16). Such an assumption is reasonable because the hfc for the benzylic (α) and *para*-hydrogens are approximately the same in the two radicals (17).

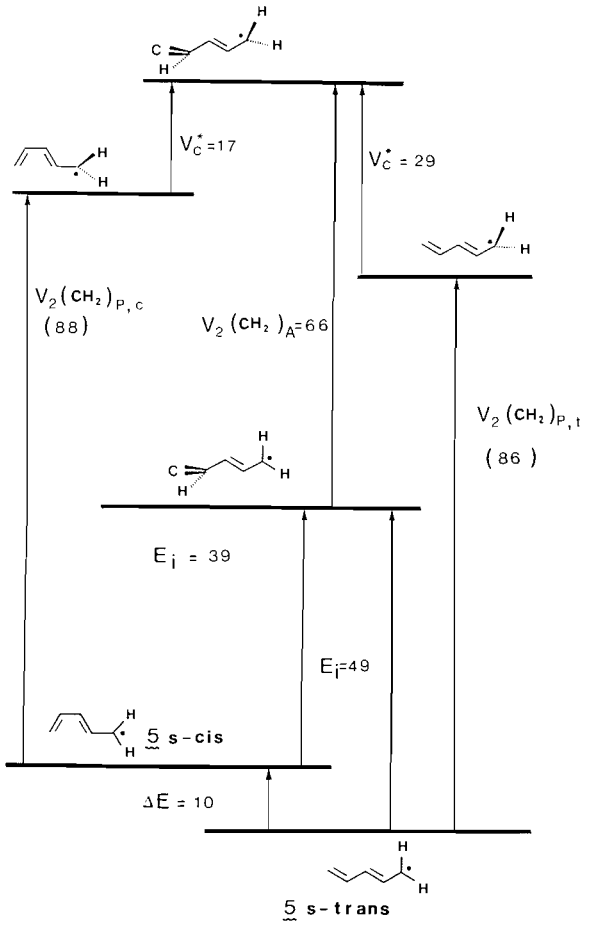

FIG. 1. A schematic representation of the relationship between the π-stabilization energy due to spin delocalization (SE(R$^\cdot$)) and the activation barrier for the terminal s-*cis* s-*trans* isomerization in the pentadienyl radical. Values are given in units of kJ mol^{-1}.

In the pentadienyl and heptatrienyl radicals a direct determination of SE(R$^\cdot$) from eq. [2] is at present not feasible. Here we will show how these SE values may be estimated using the thermochemical cycle illustrated in Fig. 1 for the pentadienyl radical.

From Fig. 1 we get:

$$[4a] \quad V_2(CH_2^\cdot)_{P(t)} = E_i(t \rightarrow c)_P + V_2(CH_2^\cdot)_A - V_c^*(t \rightarrow c)_P \qquad \text{(3)}$$

$$[4b] \quad V_2(CH_2^\cdot)_{P(c)} = E_i(c \rightarrow t)_P + V_2(CH_2^\cdot)_A - V_c^*(c \rightarrow t)_P \qquad \text{(4)}$$

Substitution of eq. [2] in eq. [4] gives:

$$[5a] \quad SE(R^\cdot)_{P(t)} = E_i(t \rightarrow c)_P + SE(R^\cdot)_A - V_c^*(t \rightarrow c)_P \qquad \text{(5)}$$

$$[5b] \quad SE(R^\cdot)_{P(c)} = E_i(c \rightarrow t)_P + SE(R^\cdot)_A - V_c^*(c \rightarrow t)_P \qquad \text{(6)}$$

where the subscripts P and A denote the pentadienyl and allyl radicals, respectively, and *c* and *t* correspond to the s-*cis* and s-*trans* forms of the pentadienyl radical, respectively. Values of E_1, the barrier to rotation of the terminal double bond about the C_2—C_3 bond, have been determined by esr spectroscopy (12). V_c^* corresponds to the E_i value in the perpendicular form of the radical. Since the $CH_2^\cdot$ group is orthogonal to the π system in this conformation, the V_c^* barrier is analogous to the E_i^* barrier in the following isomerization of closed-shell polyenes.

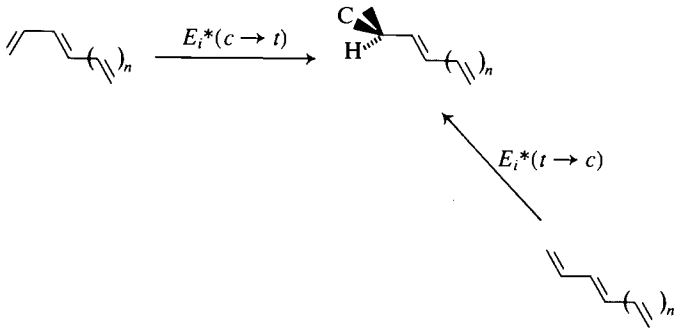

Hence,

[6a] $E_i^*(c \rightarrow t)_n = V_c^*(c \rightarrow t)_n$

[6b] $E_i^*(t \rightarrow c)_n = V_c^*(t \rightarrow c)_n$

where the pentadienyl and heptatrienyl radicals correspond to $n = 0$ and 1, respectively. For $n = 0,1$ and 2, values of $E_i^*(c \rightarrow t)$ and $E_i^*(t \rightarrow c)$ of 17 and 29 kJ mol^{-1} have been reported (18).

From eqs. [5] and [6], we get values of 82 and 84 kJ mol^{-1} for the $SE(R^{\cdot})_{P(t)}$ and $SE(R^{\cdot})_{P(c)}$, respectively. The difference of 10 kJ mol^{-1} in the heat of formation for the two forms of this radical is approximately equal to the corresponding difference of 12 kJ mol^{-1} in the closed-shell polyenes. That is, while the π-stabilization due to spin delocalization is the same for the two forms of the pentadienyl radical, the ΔH^0_f values differ on account of greater steric interaction in the *cis* form. Accordingly, we may assume that in general, for a polyenyl radical (X),

[7] $SE(R^{\cdot})_{X(c)} = SE(R^{\cdot})_{X(t)} = SE(R^{\cdot})_X$

In the heptatrienyl radical, using arguments discussed above, we can write equations similar to eqs. [5*a*] and [5*b*]:

[8] $SE(R^{\cdot})_{H(t)} = E_i(t \rightarrow c)_H + SE(R^{\cdot})_{P(t)} - V_c^*(t \rightarrow c)_H$

[9] $SE(R^{\cdot})_{H(c)} = E_i(t \rightarrow c)_H + SE(R^{\cdot})_{P(c)} - V_c^*(c \rightarrow t)_H$

where the subscript H denotes the heptatrienyl radical. An upper limit of 35 kJ mol^{-1} has been evaluated for $E_i(c \rightarrow t)_H$ using the esr method and, since $SE(R^{\cdot})_{P(c)}$ and $V_c^*(c \rightarrow t)_H$ are known, a $SE(R\cdot)_H$ value of 102 kJ mol^{-1} is obtained from eqs. [7] and [9].

The *linear* relationship between the α-hfc of the methylene hydrogen and the π-stabilization energy, plotted in Fig. 2, is represented well ($r = 0.997$) by:

[10] $SE(R^{\cdot})$ (kJ mol^{-1}) $= 145 \pm 3 - (5.75 \pm 0.20)$ α-hfc (G)

It is interesting to note that the magnitude of the intercept in Fig. 2 is equal to half the π-bond energy in ethylene. We can rationalize this observation in the following way: spin delocalization is in essence the interaction of α-spin with β-spin. This interaction is at a maximum for the formation of the π-bond of ethylene from two $CH_2^{\cdot}$ moieties, with unit spin density on each of the carbons. The intrinsic energy of this π-bond is equal to twice the stabilization resulting from the complete "delocalization" (that is, bonding, in this case) of an unpaired electron in a π framework. Consequently, such "delocalization" results in zero residual spin on the carbons. Hence the $SE(R^{\cdot})$ value of a hypothetical π-radical with a zero α-hfc should be equal to half the intrinsic energy of the π-bond in ethylene, as is observed.

Green and Walton have alternatively suggested that $SE(R^{\cdot})$ is dependent upon the *logarithm* of α-hfc (12). We favour the inverse linear relationship for several reasons. The correlation coefficient for the linear plot in Fig. 2 is excellent ($r = 0.997$), significantly better than for the alternative logarithmic relationship ($r = 0.97$). Furthermore, there is a fundamental inconsistency in the SE values derived by Green and Walton that causes us to question the validity of their analysis. For the pentadienyl and heptatrienyl radicals they have derived a total π-stabilization energy, SE(total), that includes contributions from factors other than spin delocalization. Consequently, this leads to an artificial increase in the SE values in these two species relative to the other radicals. For example, the SE(total) for the benzyl radical corresponds to the sum of $SE(R^{\cdot})$ and the intrinsic aromatic stabilization present in the benzyl radical with the $CH_2^{\cdot}$ group perpendicular to the ring. While such SE(total) values may be of

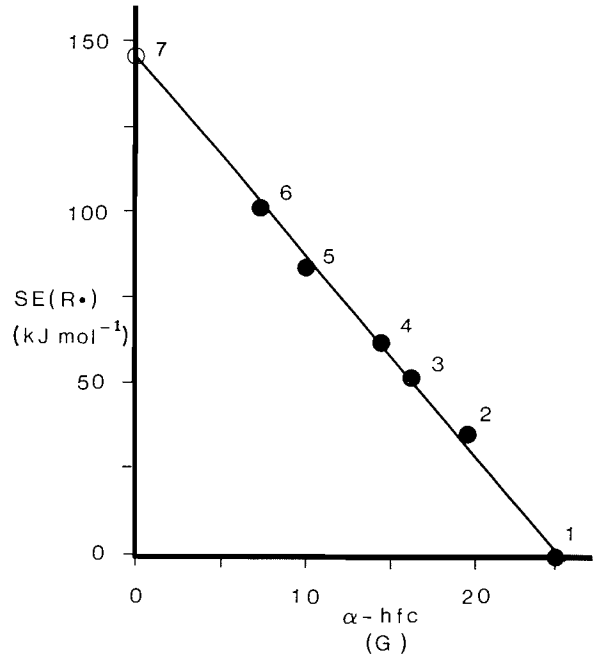

FIG. 2. A plot of the π-stabilization energy ($SE(R^{\cdot})$) versus the esr hfc of α-H of the CH_2 group (α-hfc) in π-radicals of the form $ZCH_2^{\cdot}$. Points are numbered according to Table 2. The correlation coefficient for the line, including points 1–6, is $r = 0.997$.

TABLE 2. Electron spin resonance hyperfine coupling constants of the methylene hydrogens (α-hfc) and π-stabilization energies of π-radicals due to spin delocalization ($SE(R^{\cdot})$)

Radical	α-hfc (G)	$SE(R^{\cdot})^a$ (kJ mol^{-1})
1. *Pseudo*-methyl	24.65[b]	0
2. Acetylmethyl	19.7[c]	35[c]
3. Benzyl	16.25[d]	52[e]
4. Allyl	14.40[f]	62[f]
5. Pentadienyl	10.0[g]	84[h]
6. Heptatrienyl	7.55[g]	102[h]
7. 1/2 (CH_2—CH_2)[i]	0	146[j]

[a]Unless stated otherwise, SE values were calculated from eq. [2], assuming a V_2^* value of 4 kJ mol^{-1}

[b]For a hypothetical radical with a zero SE value.

[c]Reference 15.

[d]Reference 1.

[e]V_2 value assumed to be equal to that of the phenethyl radical and obtained from ref. 16.

[f]Reference 11.

[g]Reference 12*a*.

[h]Obtained after correction of value in ref. 12, as indicated in the text (eqs. [5] and [9]).

[i]A hypothetical radical with a zero α-hfc value (see text).

[j]π-Bond energy from ref. 4.

TABLE 3. Total σ and π Mulliken group charges in monosubstituted toluenes[a,b]

Substituent (X)	$10^3\ q_\sigma$(Y)	$10^3\ q_\sigma$(X)	$10^3\ q_\pi$(Y)	$10^3\ q_\pi$(X)
3-H	−6.9	−62.0	−7.7	0
4-H	−6.9	−60.9	−7.7	0
3-Me	−5.7	−5.7	−7.7	−7.7
4-Me	−4.6	−4.6	−7.2	−7.2
3-CN	−19.6	107.3	−8.6	21.0
4-CN	−19.7	107.5	−9.8	23.3
3-F	−13.7	204.4	−8.5	−70.0
4-F	− 8.9	203.5	−7.3	−68.0

[a]Reference 5.

[b]q_σ(Y), q_σ(X), q_π(Y), and q_π(X) are the total σ and π charges respectively donated (withdrawn) by a substituent, Y or X, to (from) the ring; Y = CH_3 and X = *meta* or *para* substituent. Negative (positive) q values indicate donation (withdrawal).

TABLE 4. Total σ and π Mulliken group charges in monosubstituted benzyl radicals[a]

Substituent (X)	$10^3\ q_\sigma$(Y)	$10^3\ q_\sigma$(X)	$10^3\ q_\pi$(Y)	$10^3\ q_\pi$(X)
3-H	−2.4	−61.1	−1.3	0
4-H	−2.4	−61.1	−1.3	0
3-Me	−1.5	−3.5	−0.5	−6.1
4-Me	−1.7	−3.5	0.1	−6.0
3-CN	−9.8	96.2	−7.1	13.9
4-CN	−8.2	95.9	−7.5	14.2
2-F	−12.6	202.0	−3.6	−65.9
3-F	−6.9	202.4	−3.5	−65.5
4-F	−5.1	202.5	−1.9	−65.9
3-OMe	−5.4	178.7	−2.4	−79.4
4-OMe	−3.1	178.9	0.1	−80.1

[a]Y = CH_2 and X = *meta* or *para* substituent.

interest, we believe that attempting to relate these energy quantities to hfc's is unwarranted, and can lead to erroneous conclusions. This is so because SE(total) values include stabilizing interactions not dependent on the unpaired spin distribution, which can vary significantly from one system to another without a concomitant change in the hfc.

It is also significant that the result for the acetylmethyl radical is in agreement. The apparent discrepancy between the SE value for this radical (15) and the bond dissociation enthalpy value (DH^0) for acetone (19) is not surprising, since the stability of the radical is only one factor affecting DH^0 (20).

Application to benzyl radicals

Applications of eqs. [1] and [10] to benzyl radicals gives:

$$[11]\quad \delta SE(R^\cdot) = K\,\sigma^\cdot_\alpha$$

where δSE(R˙) is the substituent effect, relative to hydrogen, on the π-stabilization energy of a benzyl radical, and K is a constant. This definition of benzyl radical stability, eq. [11], focuses only on substituent effects involved directly with variations in spin density at the benzylic position. This approach has been adopted because we are primarily interested in correlating relative stability to reactivity involving the benzylic radical, and in assessing ρ˙ values on an energy scale.

A reduction of the α-hfc of a benzyl radical by 1.0 G corresponds to an increase in stabilization of ca. 6 kJ mol^{-1}, or, one $\sigma^\cdot_\alpha$ unit is equivalent to 93 kJ mol^{-1}. The range of known $\sigma^\cdot_\alpha$ values (1), from *para*-thiomethyl (0.063) to *meta*-cyano (−0.026) represents a variation in benzyl radical stability of 8 kJ mol^{-1}.

This analysis now allows a more quantitative evaluation of the significance of ρ˙ values. For example, the ρ˙ for the thermal isomerization of 2-aryl-3,3-dimethylmethylenecyclopropane (1,21) indicates that this rearrangement is only about half as sensitive to substituent effects as is the benzyl radical. This, of course, assumes that the entropy of the reaction is unaffected by substitution.

Relationship between Mulliken charges and $\sigma^\cdot_\alpha$ values

Table 3 lists σ and π charges donated (or withdrawn) by the substituent and the CH_3 group of monosubstituted toluenes. Table 4 lists σ and π charges donated (or withdrawn) by the substituent and the CH_2 group of the analogous benzyl radicals in the coplanar conformation. These calculated charge effects reflect interactions resulting only from charge redistribution (5); spin redistribution is not taken into account. For example, the group charges for the benzyl radicals (Table 4) are smaller than those observed for he corresponding toluenes (Table 3), but the isodesmic interaction energies are generally larger in the benzyl radicals (Table 5). This is because spin related effects are not included in the charge analysis in Table 4.

Table 4 shows that the net charge effect on the radical is similar to that in closed-shell systems, for all substituents. For example, the net charge effect of both *meta*- and *para*-cyano

TABLE 5. Substituent effects on isodesmic interaction energies (ΔE) in benzyl radicals and toluenes

Substituent (X)	$\Delta E^{a,b,c}$ Y=CH_2 Benzyl radical	Y=CH_3 Toluene	$\delta DE^{0\,d}$
H	0	0	0
3-Me	0.9	−0.1	1.1
4-Me	1.0	0.5	0.3
3-CN	−15.0	−5.1	−9.9
4-CN	−16.3	−6.2	−10.1
3-F	3.2	−1.0	4.2
4-F	3.4	0.5	2.9
3-OMe	5.8	−0.9	6.7
4-OMe	6.0	1.3	4.7

[a]All values in kJ mol^{-1}.
[b]ΔE values for the isodesmic reaction: $C_6H_5Y + C_6H_5X \rightarrow YC_6H_4X + C_6H_6$, where X = substituent and Y = fixed group.
[c]Negative (positive) value indicates a stabilizing (destabilizing) interaction.
[d]Relative bond dissociation energies.

substituents is strong π and σ withdrawal. However, the ability of these substituents to delocalize spin from the benzylic position is very different in nature (1). It is useful, therefore, to examine whether a better understanding of the effects of spin delocalization in benzyl radicals can be obtained by separating the total charge effect into the individual contributions from the α- and β-spin systems.

Table 6 shows the effects of substituents on interactions involving Mulliken α-charges. These charges are essentially estimates of α-spin donation (or withdrawal) by a group attached to the phenyl ring. The benzylic group is shown to be a strong π α-spin donor and σ α-spin acceptor. Thus, substituents that are strong π α-spin acceptors and σ α-spin donors favourably interact with the benzyl group and stabilize the radical.

Table 7 shows the effects of substituents on interactions involving Mulliken β-charges. The benzylic group is shown to be a strong π β-spin acceptor and σ β-spin donor. Consequently, substituents that are strong π β-spin donors and σ β-spin acceptors should favourably interact with the benzyl group and stabilize the radical.

Next, we compare this Mulliken population analysis of the α- and β-spin systems with the relevant $\sigma^{\cdot}_{\alpha}$ values for several substituents.

Cyano substituent

The $\sigma^{\cdot}_{\alpha}$ values indicate that this substituent very effectively delocalizes spin when in the *para* position and localizes spin (relative to hydrogen) when in the *meta* position (1). This behaviour is described well by the Mulliken analysis; while *para*-cyano shows stabilizng interactions, *meta*-cyano displays destabilizing interactions with the benzylic groups in both spin systems.

Depending on the electron demand of the benzylic group, the nature of the substituent can vary significantly from that observed in closed-shell systems. Thus, while the cyano substituent is usually considered a strong π acceptor, reflected by a large positive σ-value, in a benzyl radical this group acts as a π α-donor in the *meta* position and a π β-donor in the *para* position. Furthermore, the calculated dipole moments of the cyano substituted benzyl radical and toluene, listed in Table 8, also indicate that the nature of the cyano substituent is very different in the two systems.

Methoxy substituent

This group strongly delocalizes spin in the *para* position (1). From Tables 6 and 7 it is apparent that *para*-methoxy has a positive $\sigma^{\cdot}_{\alpha}$ value because of stabilizing interactions in the β-spin system. This substituent has similar types of interactions at the *meta* position, but, now the destabilizing interactions in the α-spin system dominate to make this radical slightly destabilized relative to the unsubstituted benzyl radical (1). All π effects involving the lone pair of electrons require rehybridization of the electronegative oxygen atom and consequently will be susceptible to effects caused by σ interactions. In fact, in comparison to the cyano substituent, the methoxy derivatives show larger σ effects. The calculations show that the most stable orientation of the methoxy group is with the C—O bond perpendicular to the phenyl ring. Thus, C—O type hyperconjugative spin delocalization is possible. It is clear that the effect of this substituent, although usually regarded simply as a two-centre–three-electron interaction, is actually the net result of both σ and π effects in the α- and β-spin systems.

Fluoro substituent

Fluoro is one of the few substituents with a destabilizing interaction at all positions (Table 9). The population analysis

TABLE 6. Total σ and π Mulliken group α-charges in monosubstituted benzyl radicals[a]

Substituent (X)	α-Charges $10^3\,q_\sigma$(Y)	$10^3\,q_\sigma$(X)	$10^3\,q_\pi$(Y)	$10^3\,q_\pi$(X)
3-H	54.7	−1.9	−72.4	0
4-H	54.7	−60.1	−72.4	0
3-Me	55.1	26.1	−72.0	−9.1
4-Me	55.0	−30.5	−71.8	3.4
3-CN	51.1	103.6	−75.7	−27.1
4-CN	51.9	−8.4	−76.6	42.7
2-F	49.3	78.6	−74.0	−11.9
3-F	52.4	121.1	−73.3	−52.4
4-F	53.3	80.5	−72.7	−12.3
3-OMe	53.1	108.6	−72.3	−63.4
4-OMe	54.3	69.4	−71.4	−15.0

[a]Y = CH_2 and X = *meta* or *para* substituent. Charges obtained by considering only the electrons with α-spin.

TABLE 7. Total σ and π Mulliken group β-charges in monosubstituted benzyl radicals[a]

Substituent (X)	β-Charges			
	$10^3\ q_\sigma$(Y)	$10^3\ q_\sigma$(X)	$10^3\ q_\pi$(Y)	$10^3\ q_\pi$(X)
3-H	−57.1	−59.2	71.1	0
4-H	−57.1	−0.9	71.1	0
3-Me	−56.6	−29.6	71.5	3.1
4-Me	−56.7	26.9	71.8	−9.4
3-CN	−60.9	−7.4	68.6	40.9
4-CN	−60.1	103.9	69.1	−28.4
2-F	−61.9	123.4	70.4	−54.1
3-F	−59.3	81.3	69.7	−13.1
4-F	−58.4	122.0	70.7	−53.6
3-OMe	−58.5	70.1	70.2	−16.0
4-OMe	−57.3	109.4	72.0	−65.2

[a]Y = CH_2 and X = *meta* or *para* substituent. Charges obtained by considering only the electrons with β-spin.

TABLE 8. Comparison of calculated dipole moments (D) in toluenes and benzyl radicals

Substituent	Dipole moment	
	Toluene[a]	Benzyl radical
H	0.25	0.00
3-Me	0.21	0.18
4-Me	0.04	0.18
3-CN	3.85	3.21
4-CN	4.02	3.25
3-F	1.17	1.10
4-F	1.27	1.09
3-OMe	0.97	1.18
4-OMe	1.22	1.18

[a]Reference 5.

TABLE 9. Electron spin resonance hyperfine coupling constants (hfc) and $\sigma^{\cdot}_\alpha$ values of fluorobenzyl radicals

Position	Hyperfine coupling constant[a,b]		
	Type of derivative		
	ortho-F[c]	*meta*-F[d]	*para*-F[d]
ortho (i)	5.28	5.15	5.30
(ii)	8.18[e]	4.95	5.30
meta (i)	1.75	1.80	1.75
(ii)	1.70	4.72[e]	1.75
para	6.32	6.19	14.43[e]
benzylic (i)	16.42	16.39	16.42
(ii)	16.32	16.39	16.42
$\sigma^{\cdot}_\alpha$ value[f]	−0.007[g]	−0.009[d]	−0.011[d]

[a]Unless stated otherwise, hfc's are due to hydrogen and are in G.
[b]Uncertainty in hfc's ca. ±0.03 G.
[c]This work. Determined by the procedure described in refs. 1 and 2.
[d]Reference 1.
[e]^{19}F.
[f]Uncertainty ±0.003.
[g]Calculated from eq. [1] using the average of the two benzylic hfc's.

suggests that this is due to the destabilizing interaction in the α-spin system, which more than compensates for the stabilizing effects in the β-spin system. Although both fluoro and methoxyl act as β donors in closed-shell species, their behaviour in the benzylic radical is very different. This results from weaker π and stronger σ effects in the fluoro substituted radicals.

The charge/spin analysis predicts that the behaviour of this substituent should be similar at the *para* and *ortho* positions, as observed in their esr spectra.

Methyl substituent

The $\sigma^{\cdot}_\alpha$ value is positive for this group at both the *para* and *meta* positions, although, at the *meta* position the stabilizing effect is very small (0.002 ± 0.003). The Mulliken analysis correctly predicts that the methyl group will delocalize spin strongly at the *para* position, but the *meta*-methyl group is shown as destabilizing in both spin systems. However, *meta*-methyl is a weaker σ β-donor than *meta*-hydrogen. Thus, the σ β-interaction in *meta*-methyl will be stabilizing relative to the unsubstituted benzyl radical; this may account for the mild stabilizing power of this substituent. The magnitude of the π-charge effects of this substituent are relatively small, and hence may change in sign on small perturbations. Furthermore, the assumption of equal partitioning, intrinsic to the Mulliken scheme, may cause incorrect assignments of charges to be made in this case.

Acknowledgments

This work was supported by a grant from the Natural Sciences and Engineering Research Council of Canada. We are grateful to R. J. Boyd for his continuing interest in this program. A. M. N. is grateful for the award of an Izaak Walton Killam Memorial Scholarship. The authors also thank the Dalhousie University Computer Centre for generous amounts of computer time.

1. J. M. DUST and D. R. ARNOLD. J. Am. Chem. Soc. **105**, 1221, (1983); **105**, 6531 (1983).
2. D. D. M. WAYNER and D. R. ARNOLD. Can. J. Chem. **62**, 1164 (1984).
3. R. S. MULLIKEN. J. Chem. Phys. **23**, 1833 (1955); **23**, 1841 (1955); **23**, 2338 (1955); **23**, 2343 (1955)
4. S. FLISZAR. J. Am. Chem. Soc. **102**, 6946 (1980).
5. A. M. DE P. NICHOLAS and D. R. ARNOLD. Can. J. Chem. **62**. 1860 (1984).
6. J. S. BINKLEY, R. A. WHITESIDE, P. C. HARIHARAN, R. SEEGER, J. A. POPLE, W. J. HEHRE, and M. D. NEWTON. QCPE, **11**, 368 (1978).

7. J. A. POPLE and R. K. NESBET. J. Chem. Phys. **22**, 571 (1954).
8. W. J. HEHRE, R. F. STEWART, and J. A. POPLE. J. Chem. Phys. **51**, 2657 (1969).
9. R. A. WHITESIDE, J. S. BINKLEY, R. KRISHNAN, D. J. DEFREES, H. B. SCHLEGEL, and J. A. POPLE. Carnegie–Mellon Quantum Chemistry Archive (1981). Carnegie–Mellon University, Pittsburgh, PA 15213, U.S.A.
10. A. M. DE P. NICHOLAS, R. J. BOYD, and D. R. ARNOLD. Can. J. Chem. **60**, 3011 (1982).
11. H. G. KORTH, H. TRILL, and R. SUSTMANN. J. Am. Chem. Soc. **103**, 4483 (1981).
12. (*a*) I. G. GREEN and J. C. WALTON. J. Chem. Soc. Perkin Trans. 2, 1253 (1984); (*b*) I. MACINNES and J. C. WALTON. J. Chem. Soc. Perkin Trans. 2, 1073 (1985).
13. (*a*) H. M. MCCONNELL. J. Chem. Phys. **24**, 764 (1956); (*b*) J. E. WERTZ and J. R. BOLTON. Electron spin resonance. McGraw–Hill, New York. 1972. Chapt. 6.
14. D. M. CHIPMAN. J. Chem. Phys. **78**, 3112 (1983).
15. J. K. KOCHI. Adv. Free-Radical Chem. **5**, 189 (1975).
16. M. S. CONDRADI, H. ZELDES, and R. LIVINGSTON. J. Phys. Chem. **83**, 2160 (1979).
17. D. R. ARNOLD, A. M. DE P. NICHOLAS and M. S. SNOW. Can. J. Chem. **63**, 1150 (1985); D. R. ARNOLD, A. M. DE P. NICHOLAS, and K. M. YOUNG. Can. J. Chem. In press.
18. J. R. ACKERMAN and B. E. KOHLER. J. Chem. Phys. **80**, 45 (1984).
19. D. F. MCMILLEN and D. M. GOLDEN. Ann. Rev. Phys. Chem. **33**, 493 (1982).
20. A. M. DE P. NICHOLAS and D. R. ARNOLD. Can. J. Chem. **62**, 1850 (1984).
21. X. CREARY. J. Org. Chem. **45**, 280 (1980).

The chemistry of peptides related to metabolites of *Trichoderma* Spp. 3. An unusual dehydration reaction of 2-methylalanine peptides after electron impact ionization[1]

W. D. JAMIESON AND A. TAYLOR[2]

National Research Council of Canada, Atlantic Research Laboratory, Halifax, N.S., Canada B3H 3Z1

Received June 27, 1985

W. D. JAMIESON and A. TAYLOR. Can. J. Chem. **64**, 277 (1986).

Peptides of 2-methylalanine, where this residue is not the C-terminus, give molecular ions of low abundance on electron impact ionization, but abundant ions are formed by loss of the elements of water from the molecular ion. The dehydration reaction does not occur in permethylated derivatives, nor under the milder ionization conditions in the chemical ionization source. The reaction does not appear to be time or temperature dependent, but depends on the steric hindrance of the NH group of the 2-methylalanine residue. The reaction occurs at sites where 2-methylalanine is not the C-terminal amino acid. In the cases of two pentapeptides where the dehydration reaction was of high probability, the correct sequence was found by semi-quantitative measurements of reaction rates in the first field-free region of a double focussing mass spectrometer.

W. D. JAMIESON et A. TAYLOR. Can. J. Chem. **64**, 277 (1986).

Lors de la spectrométrie de masse par ionisation sous impact électronique, les peptides de la méthyl-2 alanine, dans lesquels ce résidu n'est pas C-terminal, donnent des ions moléculaires dont l'abondance relative est faible; toutefois, il se forme des ions abondants par la perte des éléments de l'eau à partir de l'ion moléculaire. La réaction de déshydratation ne se produit pas ni avec les dérivés perméthylés ni avec les conditions d'ionisation plus douces prévalentes lors d'ionisations chimiques. Il ne semble pas que la réaction dépende du temps ou de la température; toutefois, elle dépend de l'empêchement stérique du groupement NH du résidu de la méthyl-2 alanine. La réaction se produit à des sites où la méthyl-2 alanine n'est pas l'acide aminé C-terminal. Dans les cas de deux pentapeptides pour lesquels la réaction de déshydratation était très probable, on a pu établir la séquence correcte en effectuant des mesures semi-quantitatives de vitesses de réactions dans la première région sans champ d'un spectromètre de masse à double focalisation.

[Traduit par le journal]

Some aspects of the chemistry of the complex fungal metabolites containing 2-methylalanine moieties have been reviewed in a recent paper (1). Although these metabolites are resistant to catalytic hydrolysis by peptidases (2), there is a considerable body of evidence which can best be interpreted by assuming that they are polypeptides (3). Foremost among this evidence are mass spectroscopic studies on degradation products obtained by acid hydrolysis of metabolites (4). More recently, use of fast atom bombardment (FAB) sources has provided impressive mass spectroscopic data, which has thrown light on the structure of several of the natural products (5). By contrast, mass spectroscopy of some *N*-acyl derivatives of synthetic peptides of 2-methylalanine gave anomalous results in the sense that molecular ions were not observed (6). For example, methyl L-prolyl-L-valyl-2-methylalanyl-2-methylalaninate (6), examined directly or as its *N*-chloroacetyl, *N*-trifluoroacetyl, *N*-deuterioacetyl, or phenylmethoxycarbonyl derivative, did not provide a detectable molecular ion, nor fragment ions of high molecular weight that could be attributed to well-known ion reactions, e.g. $(R.COX.R')^+ \rightarrow R.CO^+$ or R^+ (X=O, NH). Examination of these spectra suggested that ionization preferentially occurred at the N-terminal acyl group and resulted in loss of the marker group, thus making the spectra complex. A further disadvantage of these N-terminal groups emerged when it was found that they were either unstable under permethylation conditions (7), or underwent *C*-methylation.

In an attempt to overcome these problems we investigated the mass spectroscopy of *N*-4-bromobenzoyl and *N*-4-chlorobenzoyl derivatives of the tetrapeptide mentioned in the previous paragraph. These groups were chosen because the natural abundances of the bromine and chlorine isotopes are well established (8), thus making them eminently suitable as markers. In addition, it seemed likely that they would survive permethylation without elaboration or degradation. Part of the electron impact mass spectrum of the tetrapeptide (**4**, R = 4-Br.C_6H_4CO) is shown in Fig. 1A. If one disregards the presence of protonated species, there are only 5 pairs of isotopic pairs, each of the 5 pairs being separated by 28 (31) mass units. Going down the mass scale, they represent the sequential loss of $NH.CMe_2CO_2Me$; $NH.CMe_2CO$; $NH.CH(C_3H_7).CO$; and $N(C_4H_7)CO$. The ions of m/z 538, 540 probably arise by loss of the valine side chain by the mechanism previously proposed (9); clearly this reaction is of low probability in this case. Omitted from Fig. 1A are prominent doublet metastable ions corresponding to the fragmentations (only ^{79}Br species given): $581^+ \rightarrow 549^+ + 31$; $549^+ \rightarrow 464^+ + 85$; $464^+ \rightarrow 436^+ + 28$; $436^+ \rightarrow 379^+ + 57$; $379^+ \rightarrow 280^+ + 99$; $280^+ \rightarrow 252^+ + 28$; and $252^+ \rightarrow 183^+ + 79$. However, as can be seen in Fig. 1A, the spectrum is complicated by the presence of protonated species of all the major ions, leading to uncertainty as to the molecular weight and difficulty in interpretation of ion reactions in the first field-free region of the mass spectrometer (see below). Though such protonated ions are present in published spectra of many aromatic bromo compounds (10), they (as far as we know) have excited little comment, despite the presence in our MS-50 spectra of prominent metastable species indicating the reactions: $(R+H)^+ \rightarrow R^+ + H$.

The mass spectrum of the tetrapeptide (**4**, R = 4-Cl.C_6H_4.CO) is shown in Fig. 1B for comparison. The spectrum is clearly very similar, but it is complicated by the presence of protonated species only in the cases of the M^+ and $(M-31)^+$ ions, where they are of relatively low abundance. This result, together with the known (11) greater stability of aromatic chloro groups in the electron impact ionization source, led us to restrict our studies to this marker group.

The pentapeptide **9** (6) has an abnormal ^{13}C nmr spectrum, because ^{13}C signals due to only one conformer of the proline ring are observed. We thought, based on the promising results

[1]NRCC No. 25104.

[2]Author to whom correspondence should be addressed.

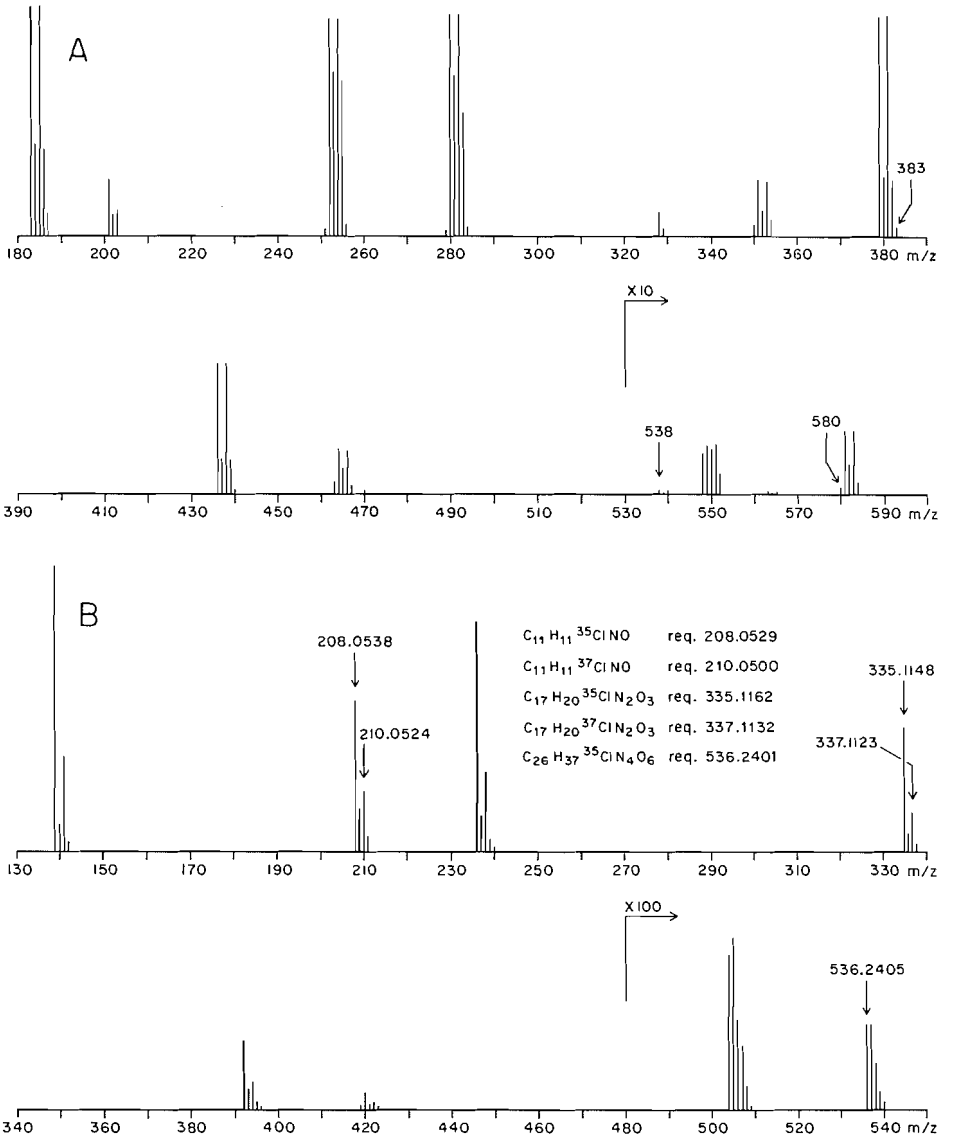

FIG. 1. Electron impact ionization mass spectrum of methyl *N*-4-bromobenzoyl-L-prolyl-L-valyl-2-methylalanyl-2-methylalaninate. Ions of lower abundance than those at m/z 538 and all metastable ions have been omitted. B. Mass spectrum of methyl *N*-4-chlorobenzoyl-L-prolyl-L-valyl-2-methylalanyl-2-methylalaninate (**4**, R = ClC_6H_4CO).

described in the previous paragraph, that this structural uncertainty might be resolved by an examination of its mass spectrum. To our surprise, the mass spectrum shown in Fig. 2A was obtained. The abundances of the group of ions at m/z 561, 562, 563, 564, and 565 were consistent with the view that m/z 561 was a molecular ion instead of that expected at m/z 579^+. No ion reaction $579^+ \rightarrow 561^+ + 18$ could be demonstrated in the first field-free region of the mass spectrometer, and although an ion of m/z 579 could be detected at high gain its intensity was, on average, only about 2% of the ion at m/z 561. Further, the ratio of abundances of ions at m/z 579 and 581 did not correspond to that expected for ions of the elemental compositions $C_{27}H_{38}{}^{35}ClN_5O_7$ and $C_{27}H_{38}{}^{37}ClN_5O_7$. Permethylation of this compound gave a single product as determined by chromatography, but the expected ions at m/z 635, 637 were not observed (Fig. 2B). The question of the structure of the peptide **9** was unequivocally solved by X-ray crystallographic analysis (12), thus demonstrating that the mass spectrum of **9** (Fig. 2A) was anomalous.

Mass measurement of the ions at m/z 561, 563 revealed that they differed from that expected for the peptide **9** in elemental composition by the elements of water. Dehydration of peptides containing serine, threonine, asparagine, and (or) glutamine residues in the electron impact ionization source of the mass spectrometer is common (13), but we know of no precedent for the experimental results given in Fig. 2A.

It was decided, therefore, to investigate the question of whether this dehydration reaction was an anomaly characteristic only of **9** or whether it was an example of a more general phenomenon.

To this end a number of compounds have been synthesized; the syntheses have either been reported or are to be found in the experimental section. All of the compounds were crystalline, had sharp melting points, and on elemental analysis gave results within experimental error. All were homogeneous on reverse phase partition chromatography and the retention volumes measured are given in Table 1. The protected glutaminyl di- and tripeptides (e.g. **7**) were appreciably soluble in water and the

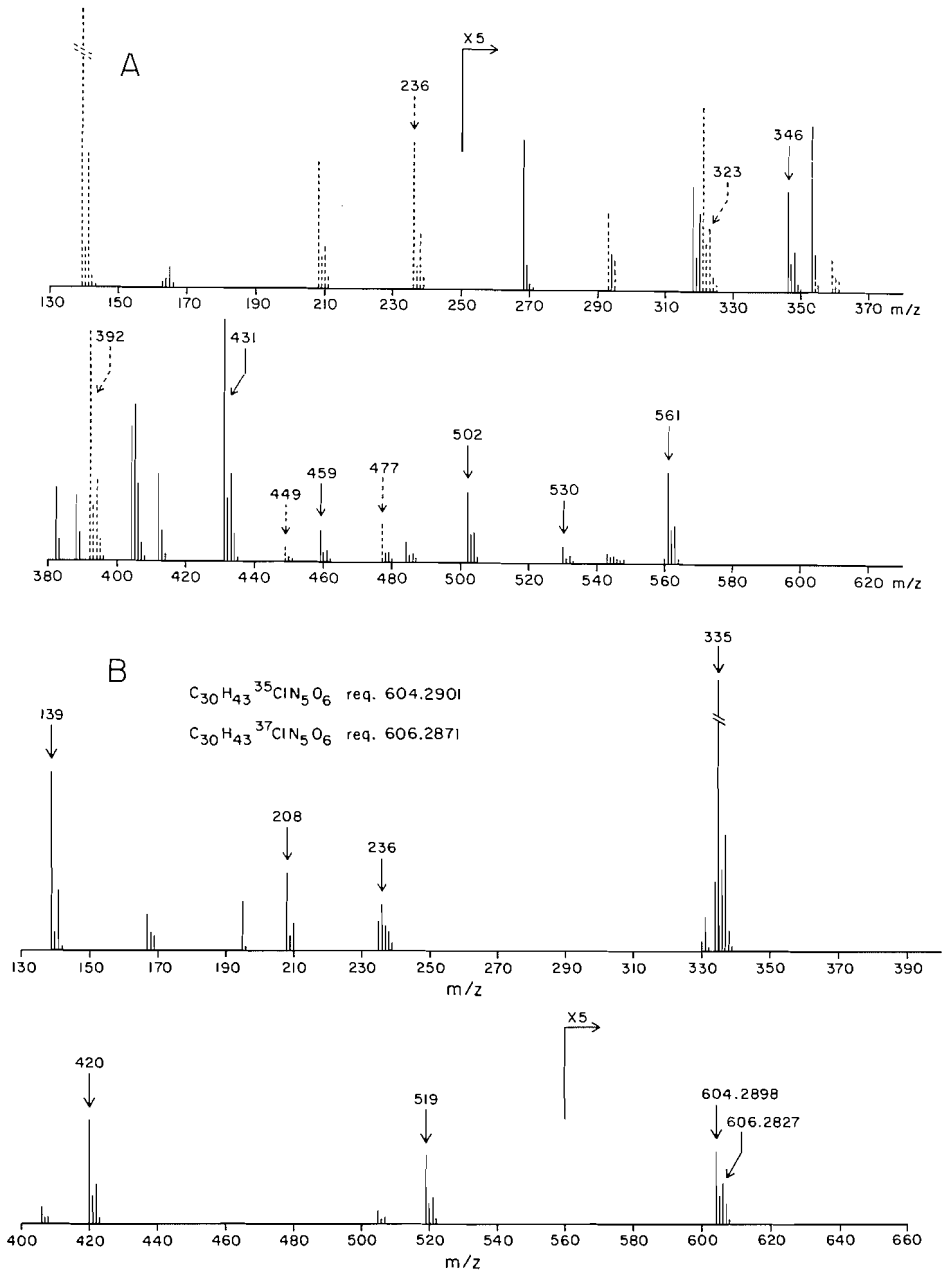

FIG. 2. A. Electron impact ionization mass spectrum of methyl *N*-4-chlorobenzoyl-L-prolyl-2-methylalanyl-L-alanyl-2-methylalanyl-L-alaninate (**9**, R = ClC_6H_4CO). Ions represented by dotted lines are expected fragments from normal C=O fissions in peptide chains; solid lines represent fragments derived from $(M - 18)^+$ or $(M - 36)^+$. B. Mass spectrum of methyl *N*-4-chlorobenzoyl-L-prolyl-*N*-2-dimethylalanyl-L-*N*-methylalanyl-*N*-2-dimethylalanyl-L-*N*-methylalaninate. Ions of <1% of the ion at *m/z* 604 have been omitted.

crystalline peptides were hydrated, the water of hydration being tenaciously held. This unexpected phenomenon was reported recently for an analogous compound (14).

The following conclusions may be drawn from the data given in Tables 1 and 2. The dehydration reaction does not occur when the C-terminal amino acid is 2-methylalanine but does occur when the C-terminal sequence is *N*-2-methylalanylglycine, *N*-2-methylalanylalanine, *N*-2-methylalanylvaline, or *N*-2-methylalanylglutamic acid. The abundances of some of the fragment ions seen in the spectra are given in Table 2. In those cases where the dehydration reaction was probable, the reaction which resulted in fission of the ester alkoxy group was always attended by the corresponding dehydrated ion. When the C-terminal group was a glutamyl diester (e.g. **6**, **7**), dehydrated ions were observed corresponding to the sequential loss of alkoxyl, carbonyl, and the two methylene moieties of the side chain.

Several of the peptides were permethylated; these are indicated in Table 1 by an entry indicating their retention volumes on partition chromatography. None of the permethylated compounds underwent the dehydration reaction and this is illustrated by a comparison of Figs. 2A and 2B. It follows that at least one of the hydrogen atoms eliminated as water in the dehydration reaction is a nitrogen substituent. The data in Tables 1 and 2 suggest that the nature of the side chain of the amino acid that *N*-acylated the 2-methylalanine residue is important in the dehydration reaction. Thus the abundance ratio $(M-18)^+/M^+$ in the case of α-methyl-γ-benzyl *N*-

TABLE 1. Molecular ion data and partition coefficients of 4-chlorobenzoyl peptides containing 2-methylalanine residues

Compound	M^+ (^{35}Cl) Found	M^+ (^{35}Cl) Theory	Ratio (^{35}Cl) $(M-18)^+/M^+$	T °C	R_V	R_V(P)	Ref.
1 R.Aib.OMe	255.0659	255.0662	0.004*	66	10.0		1
2 R.Gly.Aib.OMe	312.0867	312.0874	0.2	123	8.47	9.93	A
3 R.Pro.Val.Aib.OMe (L L)	451.1887	451.1874	0.04*	110	16.62	27.15	1
4 R.Pro.Val.Aib.Aib.OMe (L L)	536.2405	536.2401	0.09*	217	21.98		1
5 R.Pro.Val.Aib.Gly.OEt (L L)	522.2257	522.2245	2	185			A
6 R.Pro.Val.Aib.Aib.Glu.OMe (L L, L, OMe)	679.3009	679.2984	3	261	27.46		1
7 R.Gln.Aib.Val.OMe (L L, L)	482.1918	482.1932	5	203			A
8 R.Gly.Aib.Glu.OMe (OC_7H_7)			23	190	38.1		A
9 R.Pro.Aib.Ala.Aib.Ala.OMe (L, L, L)			42	253	17.15		1
10 R.Ala.Aib.Ala.OMe (L, L)			70*	167	10.42		1
11 R.Gly.Aib.Gly.OEt			89*	120	8.47	7.97	A

Abbreviations: Aib = 2-methylalanyl; Ala = alanyl; Gly = glycyl; Glu = glutamyl; Gln = glutaminyl; Pro = prolyl; Val = valyl; R_V = retention volume; R_V(P) = retention volume of permethylated peptide; M = molecular ion; T = temperature; * indicates that the $^{35}Cl/^{37}Cl$ ratio calculated for either $M^+/(M+2)^+$ or $(M-18)^+/(M-16)^+$ was incorrect; A = synthesis in experimental section.

TABLE 2. Relative abundances of ions resulting from fragmentation reactions of the C-terminal amino acid ester functionality in *N*-4-chlorobenzoyl peptides containing 2-methylalanine residues.

Compound	Fragmentation ions $(M-31(45))^+$	$(M-18-31(45))^+$	$(M-NH.CHR.CO_2R')^+$	$(M-18-NH.CHR.CO_2R')^+$
11	19	20	84	2*
8	39	116	310	17*
10	73	45	205	1.5*
7	56	27*	630	(?)190*
5	390	55	950	4*
9	24	111	395	325
6	13	22	395	8*

Compound numerals refer to Table 1; * indicates relative intensities of the $^{35}Cl/^{37}Cl$ pairs, not natural abundance.

4-chlorobenzoylglycyl-2-methylalanylglutamate (**8**) is 23, but for the pentapeptide with the C-terminus 2-methylalanyl-2-methylalanylglutamate (**6**), the ratio is 3. The NH group between two 2-methylalanine residues is not readily exchanged (14), and in our hands cannot be methylated except under forcing conditions when C-methylation also occurs. The data in Table 1 therefore support the hypothesis that the probability of dehydration depends on the steric hindrance of the 2-methylalanyl NH group. Thus all the 6 peptide-chain atoms $^1NH.^2C(ME)_2.^3CO.^4NH.^5CH(R).^6CO$ are involved in the dehydration process.

Reference to Fig. 2A shows that the same functionality can be involved in a dehydration reaction when it is embedded in a peptide chain; for this peptide, chlorine-containing ions that have lost 2 mols of water (Fig. 2A, m/z 543) are observed, and also ions that have lost the terminal $CO.NH.CH(Me).CO_2Me$ (m/z 431) group and yet are still 18 mass units less than expected (Fig. 2A, m/z 449).

The dehydration reaction was not observed in the chemical ionization source when methane was used as the reagent gas, and the $(M-1)^+$, $(M+1)^+$, $(M+29)^+$, and $(M+41)^+$ abundance ratios ($(M+1)^+ = 100$) for a representative group of compounds are give in Table 3. Except for the glutamic acid derivative (**8**), these ratios are those expected for ionization at an ester functionality (15), but ions providing sequence information were scarce and loss of chlorine was an important competing reaction.

Thus there are difficulties in unambiguously determining the molecular weights and the sequence of amino acid residues in peptides of unknown structure containing 2-methylalanine. A possible method of surmounting these difficulties lies in using the ion fragmentation reactions that occur in the first field-free region of the CEC 21-110B mass spectrometer. In Figs. 3A and 3B are shown the results of such parent ion fragmentation experiments for the daughter ions m/z 236, 238 and m/z 280, 282, recorded in the spectra reproduced in Figs. 1B and 1A respectively.

When the curves representing the ^{35}Cl and ^{37}Cl species and

TABLE 3. Normalized abundances of $(M - 1)^+$, $(M + 1)^+$, $(M + 29)^+$, and $(M + 41)^+$ ions in chemical ionization mass spectra of peptides containing 2-methylalanine residues using methane as the reagent

	Molecular ions			
Compound	$(M-1)^+$	$(M+1)^+$	$(M+29)^+$	$(M+41)^+$
5	2.6	100	32	10
10	1.2	100	30	11
11	1.7	100	32	11
13	0.4	100	17	6

Compound numerals refer to Table 1.

the ^{79}Br and ^{81}Br analogues are compared, it is apparent that the areas under the peaks (in Figs. 3A and 3B) are in the same ratio as the ratio of the natural abundances of the isotopes. In the case of the Cl species, similar experiments (see below) to determine the parents of other prominent pairs of daughter ions in Fig. 1A also revealed that the ratio of the areas under the peaks was the same as the ratio of the natural abundance of the isotopes. In all, 10 determinations of the ratios of the areas were made and the mean value found was 2.81 ± 0.30, which compares well with the generally accepted value of 3.08 (8). Thus an estimate of the precision of the measurements can be made.

Figure 3 shows that the analogous pairs of daughter ions m/z 236, 238 and m/z 280, 282 are formed by decomposition of pairs of parent ions and that both pairs of 4 reactions are: $R.NH.CH(C_3H_7).CO^+ \rightarrow R^+ + NH.CH(C_3H_7).CO$ and $R.NH.CH(C_3H_7)^+ \rightarrow R^+ + NH.CH(C_3H_7)$. Similar unimolecular decomposition reactions were observed when the peptide **9** (R = ClC_6H_4CO) was examined. Thus the ions at 139, 141 were the daughters of parents of m/z 208, 210 and 236, 238, and the latter, in turn, were the daughters of parents $R.NH.CMe_2CO^+$ (m/z 321, 323) and $R.NH.CMe_2^+$ (m/z 293, 295). The experiments were continued, using the parents as daughter ions until no further parents could be found. In all cases it was found that the daughter ions arose preeminently from only two parent ions. The pair m/z 579, 581 had no detectable parents. The experiments, therefore, provided unambiguous sequence information.

An estimate of the probability of the reactions with respect to one another may be made by normalizing the signals of the daughter ions (e.g. see Fig. 3A) to their relative abundances in the mass spectrum (Fig. 2A). These calculations give the relative rates, in arbitary units, of the various reactions and these are summarized for the sequence $579^+ \rightarrow 548^+ \rightarrow 477^+ \rightarrow 392^+ \rightarrow 321^+ \rightarrow 236^+$ in Table 4. Also in Table 4 is given the reaction rate for the fragmentation $346^+ \rightarrow 236^+ + 110$ and it is clear that the probability of this reaction is much lower than that of the alternative: $321^+ \rightarrow 236^+ + 85$. A similar analysis applied to the pentapeptide **6** also gave the correct sequence of amino acids and demonstrated that the ions of m/z 505, 507 (= $Cl.C_6H_5CO—N(C_4H_7)CO—NH.CH(CHMe_2).CO.NH.C(Me_2).CO.NH.C(Me_2).CO^+$) were not daughters of parents of m/z 630, 632, or 661, but were derived from m/z 648, 650 and 679, 681. The method, which requires about 50 μg of sample, therefore has some promise but requires automation and application to many other examples.

N-4-Chlorobenzoylation of peptides of 2-methylalanine is a useful procedure for their characterization, since these derivatives are easy to crystallize, can be detected in the effluent from chromatograms in quantities of a few ng, and can be prepared without detectable racemization at the N-terminal amino acid residue (1). The mass spectroscopic results reported here add to the value of these derivatives, for although the spectra are complicated by dehydration reactions and by protonation, reliable sequence information can be obtained.

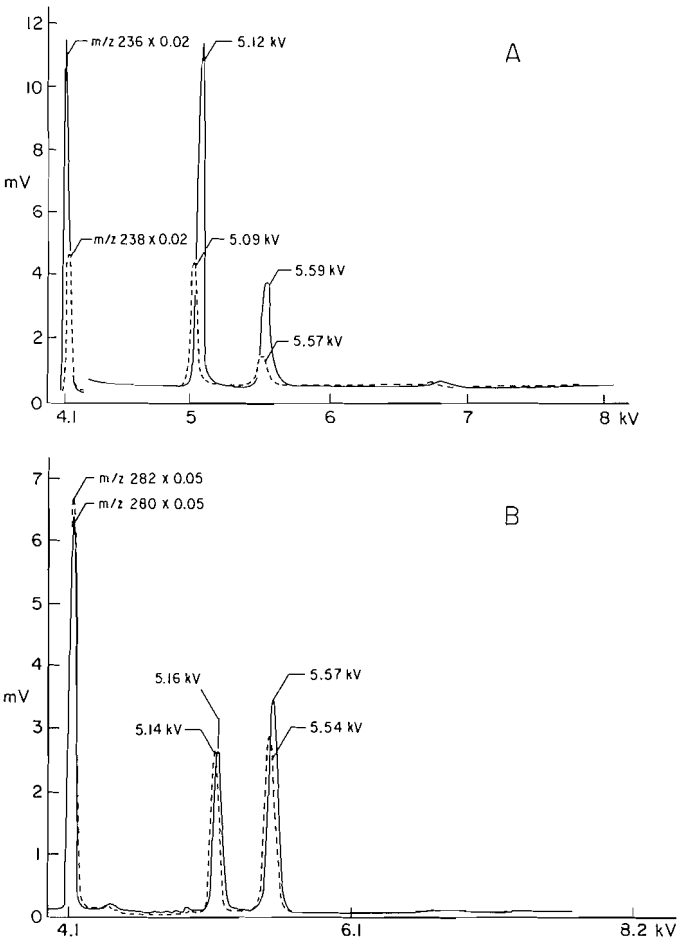

FIG. 3. A. Unimolecular ion decomposition of $Cl.C_6H_4.CO.N(C_4H_7).CO.NH.CH(C_3H_7)CO^+$ (5.59 kV) and $Cl.C_6H_4.CO.N(C_4H_7).CO.NH.CH(C_3H_7)^+$ (5.12 kV); solid line represents ^{35}Cl species and the dotted line ^{37}Cl. B. Ion decompositions of $Br.C_6H_4.CO.N(C_4H_7).CO.NH.CH(C_3H_7).CO^+$ (5.57 kV) and $Br.C_6H_4.CO.N(C_4H_7.CO.NH.CH(C_3H_7)^+$ (5.16 kV); solid line ^{79}Br, dotted line ^{81}Br. In all cases the abscissa are the accelerating voltages and the mass of the parent ions can be calculated from the formula: m/z daughter ion × p/q, where p is the acceleration voltage (kV) at which the parent ions appear and q is the voltage at which the daughter ion is observed.

Experimental

Melting points are not corrected. Infrared spectra were measured on a Perkin Elmer 238B spectrometer; samples were dispersed in potassium bromide discs. The ^1H and ^{13}C nmr spectra were measured on solutions in $C^2H_3O^2H$ using a Varian XL-100 spectrometer and the facilities at the Atlantic Region Magnetic Resonance Center, Halifax, N.S. Ultraviolet spectra were determined on solutions in methyl alcohol using a Cary 14 spectrometer. The purity of all peptides was assessed by high pressure reversed phase partition chromatography on a Dupont "Zorbax" C_8 column of dimensions 0.46 × 25 cm. All other instrumentation used for chromatography has been described in detail (16). Electron impact mass spectra were recorded on Kratos MS-50 and C.E.C. 21-110B instruments. The sensitivity of the latter instrument was enhanced[3] by using an Hamamatsu (Model R595)

[3]We are indebted to Dr. S. E. Scheppele for details of these modifications before publication.

TABLE 4. Relative rates, in arbitrary units, of ion reactions that indicate the sequence of amino acid residues in the pentapeptide **9** (R = 4-chlorobenzoyl)

Ion reaction	Relative rate
$\rightarrow 579^+$	ND
$579^+ \rightarrow 548^+ + 31$	150
$548^+ \rightarrow 477^+ + 71$	470
$477^+ \rightarrow 392^+ + 85$	1200
$392^+ \rightarrow 321^+ + 71$	8600
$321^+ \rightarrow 236^+ + 85$	3100
$(346^+ \rightarrow 236^+ + 110)$	4

electron multiplier (20 stage, modified to have 300 kΩ stage resistors), the output of which was amplified by a Keithley (Model 427) current amplifier. Samples were introduced directly into the source of both instruments, in the case of the C.E.C. mass spectrometer by means of a temperature-controlled quartz probe.[4] All mass measurements were made by the peak matching method using an ion in the spectrum of perfluorokerosene as a standard. The relative rates of ion decomposition reactions in the first field-free zone of the ionic flight path of the CEC instrument were measured by tuning the magnetic field to detect a particular daughter ion when the accelerating voltage was 4 kV (defining the average kinetic energy of the ion beam). The accelerating voltage was then scanned to higher values, keeping the setting of the magnetic field and the electric sector voltage constant. Ionic decompositions were detected and recorded by using the ion current as the *y*-axis signal on an *x*/*y* recorder and the accelerating voltage (suitably attenuated) as the *x*-axis signal. The intensities of the peaks obtained (see Fig. 3) were measured by making several Xerox copies of the graphs, excising the peaks, and weighing the excised paper. Chemical ionization mass spectra were obtained using a Finnigan 4000 quadrupole mass spectrometer equipped with a modified (17) INCOS data system and using methane or deuteriomethane as the reagent gas. Some CI spectra were measured on a modified (18) MS-9 instrument using the same ionization gases. Peptides were permethylated by the method described in an earlier paper (7).

N-*4-Chlorobenzoylglycyl-2-methylalanine*

Ethyl 4-chlorobenzoylglycinate (19) (18 g) was dissolved in methyl alcohol (250 mL) and a solution (50 mL) of sodium hydroxide (5 g) in water added. After 2 h, titration of an aliquot showed that the ester had been completely hydrolysed and the remainder of the reaction mixture was concentrated to 40 mL, cooled to 0°C, and acidified. The precipitate (mp 133–137°C (sublimes above 120°C), 15.5 g, 97%) was taken up in boiling water (700 mL), the mixture filtered, the filtrate kept at 4°C for 18 h, and the crystalline precipitate (14.7 g, lit. (20) mp 143–145°C) collected. This acid (6.4 g) was suspended in toluene (300 mL) and the stirred mixture treated with a solution (100 mL) of 1-ethoxycarbonyl-2-ethoxy-1,2-dihydroquinoline (EEDQ, 7.5 g). The mixture was stirred at room temperature for 10 min, when methyl 2-methylalaninate (6) (4.5 g) was added. The reaction mixture was heated to 50°C and maintained at this temperature for 60 h, when it was cooled and evaporated. The residue was taken up in ethyl acetate (300 mL), acidic and basic impurities removed in the usual way (6), and the dried (Na_2SO_4), filtered solution evaporated. The colorless solid residue (7 g) was taken up in hot toluene (50 mL), and the filtered solution kept at room temperature for 50 h, at which time the crystals that had separated were collected. *Methyl 4-chlorobenzoylglycyl-2-methylalanine* (**2**) separated from toluene as needles, mp 150–151°C; λ_{max}: 236 nm (ϵ = 17 400). *Anal.* calcd. for $C_{14}H_{17}ClN_2O_4$: C 53.8, H 5.4, Cl 11.4, N 8.95%; found; C 53.7, H 5.5, Cl 11.3, N, 8.5%. This ester (5 g) was dissolved in methyl alcohol (50 mL) at 55°C and the warm solution treated with a solution (25 mL) of sodium hydroxide (1.2 g) in water. The reaction mixture was immediately cooled to room temperature and aliquots of the solution titrated to follow the extent of the hydrolysis. When the hydrolysis was complete (ca. 1 h) the solution was evaporated to 20 mL, then diluted with water (50 mL) and acidified. N-*4-Chlorobenzoylglycyl-2-methylalanine* separated from ethyl alcohol as needles mp 247–249°C; 4.3 g, 90%. *Anal.* calcd. for $C_{13}H_{15}ClN_2O_4 \cdot 0.5H_2O$: C 50.7, H 5.2, N 9.1%; found: C 50.5, H 4.7, N 9.6%.

Ethyl N-*4-chlorobenzoylglycyl-2-methylalanyglycinate* (***11***)

Ethyl glycinate hydrochloride (Mann Laboratories, 0.7 g) was suspended in toluene (40 mL) and the mixture treated with triethylamine (0.51 g). The mixture was shaken for 10 min, when *N*-4-chlorobenzoylglycyl-2-methylalanine (1.5 g) and EEDQ (1.25 g) were added. The mixture was heated to 50°C and was stirred at that temperature for 60 h, at which time it was evaporated, the residue taken up in ethyl acetate (150 mL), and acidic and basic impurities removed as usual (6). The dry (Na_2SO_4) ethyl acetate solution was filtered and the filtrate evaporated to give a colorless gum (2.1 g). This gum crystallized spontaneously after standing on the bench for several days; the crystals were readily recrystallized from either toluene or *n*-butyl acetate. *Ethyl* N-*chlorobenzoylglycyl-2-methylalanylglycinate* (***11***) separated from *n*-butyl acetate as needles, mp 125–126°C; λ_{max}: 236 nm (ϵ 16 800). *Anal.* calcd. for $C_{17}H_{22}ClN_3O_5$: C 53.2, H 5.7, Cl 9.3, N 10.95, O 20.9%; found C 53.1, H 6.0, Cl 9.3, N 10.8, O 21.0%.

α-*Methyl* γ-*benzyl* N-*4-chlorobenzoylglycyl-2-methylalanyl-*L-*glutamate*

α-Methyl γ-benzyl L-glutamate hydrochloride (21) (1.43 g) was suspended in toluene (100 mL) and the mixture shaken with triethylamine (0.55 g) for 10 min. *N*-4-chlorobenzoylglycyl-2-methylalanine (1.5 g) and EEDQ (1.25 g) were added to the stirred mixture, which was kept at 45–50°C for 7 days, when it was evaporated and the residue dispersed in ethyl acetate (200 mL). The precipitate (0.32 g) dissolved when the mixture was shaken with sodium bicarbonate solution (5%, 100 mL). The ethyl acetate phase was washed successively with ice-cold hydrochloric acid (2 *N*, 4 × 100 mL), water, sodium bicarbonate solution (5%, 2 × 50 mL), and water. The dry (Na_2SO_4), filtered ethyl acetate solution was evaporated and the crystalline residue collected. The *tripeptide diester* (**8**) separated from *n*-butyl acetate (2 g in 15 mL) as long fine needles, mp 144°C; $[\alpha]_D^{24}$ −13.7° (*c* 0.84, MeOH); λ_{max}: 236 nm (ϵ 15 400). *Anal.* calcd. for $C_{26}H_{30}ClN_3O_7$: C 58.7, H 5.6, Cl 6.7, N 7.9%; found: C 58.6, H 5.6, Cl 6.8, N 8.1%.

Ethyl N-*4-chlorobenzoyl-*L-*prolyl-*L-*valyl-2-methylalanylglycinate*

Ethyl glycinate hydrochloride (2.8 g) was suspended in toluene (20 mL), triethylamine (2 g) added, and the mixture shaken for 10 min at room temperature. The stirred reaction mixture was treated with a solution of *N*-phenylmethoxycarbonyl-L-prolyl-L-valyl-2-methylalanine (6) (8.7 g) and EEDQ (5 g) in toluene (200 mL). After 70 h at 45°C the reaction mixture was evaporated, the residue taken up in ethyl acetate (300 mL), and acidic and basic by-products removed in the usual way. The dry (Na_2SO_4) ethyl acetate solution was filtered and the filtrate evaporated to provide a gum (9 g), which has resisted all attempts at crystallization. This gum (8 g) in methyl alcohol (100 mL) was shaken with palladium on carbon (5%, 0.25 g) and hydrogen (3.5 kg cm^{-2}) for 24 h when the reaction mixture was filtered through a bed of Celite 545 (0.5 cm) and the filtrate evaporated. When the gummy residue was titurated with THF or tetrahydropyran, crystals were obtained that could be recrystallized as hexagonal plates, mp 89–91°C, from either solvent. However, on standing at room temperature they changed to a clear resin, which readily crystallized when treated with one of these solvents. The crystalline material (1 g) in THF (15 mL) was treated with 4-chlorobenzoylazide (1) (0.5 g) and the colorless solution kept for 3 days at room temperature. The reaction mixture was evaporated and the residue digested several times with petroleum ether (bp 30–60°C, 3 × 50 ml), when the residual gum was taken up in ethyl acetate (50 mL), and the solution washed with ice-cold hydrochloric acid (2 *N*, 4 × 10 mL) and water (2 × 50 mL). The dry (Na_2SO_4), filtered solution was evaporated to give a gum (0.32 g,

[4]Available from Masspec Inc., P.O. Box 9314, College Station, Texas 77840, U.S.A.

24%). This gum, which appeared to be homogeneous chromatographically, was found to contain a few crystals after standing for several months. It was found that treatment of the mixture of gum and crystals with a few drops of *n*-butyl acetate (but not with any of some 20 other solvents tried) resulted in very slow crystallization and a crop of needles (0.18 g, mp 112–118°C) could be collected after 2–3 weeks. These needles exhibited the same characteristics as the gum, i.e. they could be taken up in about 5 mL of *n*-butyl acetate at 100°C, and the solution over a period of 3–4 weeks, in a sealed container, deposited fine needles of **5** (*R* = *4-chlorobenzoyl*), mp 113–116°C; $[\alpha]_D^{24}$ −93 (*c* 0.46, MeOH); λ_{max}: 225 nm (ε 12 900). *Exact Mass* (ms), *m/z*: 524.2284 ($C_{25}H_{35}{}^{37}ClN_4O_6$ requires 524.2215), 522 (Table 1), 506.2124 ($C_{25}H_{33}{}^{37}ClN_2O_5$ requires 506.2110), 504.2103 ($C_{25}H_{33}{}^{35}ClN_2O_5$ requires 504.2139). *Anal.* calcd. for $C_{25}H_{35}ClN_4O_6$: C 57.4, H 6.7, Cl 6.8, N, 10.7%; found: C 57.3, H 6.7, Cl 7.1, N 10.7%.

Methyl N-*4-chlorobenzoyl-*L*-glutaminyl-2-methylalanine-*L*-valinate*

N-Phenylmethoxycarbonyl-L-glutamine (22) (15 g) and EEDQ (14.5 g) were dissolved in THF (200 mL). After 5 min methyl 2-methylalaninate (6.2 g) was added to the solution and a voluminous precipitate was obtained. The reaction mixture needed a stirrer of adequate torque to keep the precipitate in suspension while it slowly went into solution over a period of 18 h. After 44 h at 35°C, the solution was evaporated, the residue dissolved in ethyl acetate (100 mL), and acidic and basic by-products removed. The ethyl acetate solution was evaporated and the residue (19.9 g) taken up in methyl alcohol (200 mL). The solution was treated with sodium hydroxide (*N*, 70 mL), the reaction mixture kept for 2 h at room temperature, then concentrated at 40°C under reduced pressure to 50 mL, diluted with brine (10%, 50 mL), and extracted with ethyl acetate (2 × 50 mL). The raffinate was acidified and extracted with ethyl acetate (3 × 100 mL). The combined acid extracts were washed with brine (10%, 2 × 50 mL) and with ice-cold water (10 mL). The dry (Na_2SO_4) solution was filtered and evaporated to give a gum (11.9 g), which solidified on trituration with petroleum ether (bp 30–60°C) N-*Phenylmethoxycarbonyl-*L*-glutaminyl-2-methylalanine* separated from ethyl acetate as very fine needles, mp 142°C; $[\alpha]_D^{22}$ −24.1° (*c* 1.4, MeOH), δ_H (THF($^2H_8$)): 7.73 (H, e), 7.30 (5H), 6.90 (H, e), 6.76 (H, e), 6.61 (H, e), 5.05 (2H), 4.17 (H, m), 2.23 (2H, m), 1.97 (2H, m), 1.47 (3H), 1.46 (3H). *Anal.* calcd. for $C_{17}H_{22}N_3O_6$: C 56.0, H 6.1, N 11.5%); found: C 55.8, H 6.3, N 11.2%. This acid (7.3 g) was suspended in toluene (200 mL) and EEDQ (5 g) added. The stirred mixture was treated with methyl valinate (2.6 g; methyl valinate hydrochloride (23) (10 g) was dissolved in chloroform (700 mL) and the solution cooled to 5°C when it was saturated with ammonia. The precipitated ammonium chloride was collected by filtration and the filtrate evaporated at −5°C, 15 Torr (1 Torr = 133.3 Pa), to about 50 mL. The residue was fractionally distilled through a Fenski column (15 × 1 cm), the ester (8.5 g) collected at 35°C, 20 Torr, and the mixture stirred at 45°C for 60 h. The crystalline precipitate (7.5 g) was collected and was recrystallized from ethyl acetate as fine needles of *methyl* N-*phenylmethoxycarbonyl-*L*-glutaminyl-2-methylalanyl-*L*-valinate* (**7**, R = C_7H_7OCO), mp 138–140°C; $[\alpha]_D^{24}$ −28° (*c*, 0.311, MeOH), δ_H ($C^2H_3O^2H$): 7.33 (5H, m), 5.08 (2H), 4.24 (H, *J* = 6.9 Hz), 4.05 (H, m), 3.69 (3H), 2.32 (2H, m), ca. 2.0 (3H, m), 1.49 (3H), 1.44 (3H), 0.90 (3H, *J* = 6.9 Hz), 0.87 (3H, *J* = 6.9 Hz). *Anal.* calcd. for $C_{23}H_{34}N_4O_7 \cdot 0.25H_2O$: C 57.2, H 7.2%; found: C 57.1, H 6.8%. The *ethyl ester* was similarly prepared and was recrystallized as needles from water, mp 87–91°C. *Anal.* calcd. for $C_{24}H_{36}N_4O_7 \cdot H_2O$: C 56.5, H 7.5, N 11.0%; found: C 56.4, H 7.5, N 10.9%. The urethane methyl ester (2 g) in methyl alcohol (100 mL) was treated with dilute hydrochloric acid (0.2 *N*, 20 mL) and palladium on carbon (0.25 g, 5%). The mixture was shaken with hydrogen (1.76 kg cm^{-2}) for 48 h. The colorless precipitate that separated was dissolved by adding water (30 mL). The catalyst was filtered, and most of the methyl alcohol evaporated from the filtrate. The residual aqueous solution was lyophilized, the residue suspended in chloroform, and the stirred suspension saturated with ammonia. The precipitated ammonium chloride was collected by filtration, the filtrate evaporated, the residue taken up in THF (75 mL), and the solution treated with 4-chlorobenzoylazide (0.9 g). After 3 days at room temperature the reaction was evaporated, the residue stirred with petroleum ether (100 mL) for 6 h, and the amorphous solid (1.8 g) thoroughly washed with petroleum ether. The product was taken up in hot water (125 mL), a small quantity of insoluble material removed by filtration, and the filtrate kept at 4°C for 18 h. *Methyl 4-chlorobenzoyl-*L*-glutaminyl-2-methylalanyl-*L*-valinate* (**7**, R = ClC_6H_4CO) separated from water as needles, mp 91–92°C; $[\alpha]_D^{24}$ +1 ± 5° (*c*, 0.4 MeOH); λ_{max}(MeOH); 238 nm (ε 15 100); δ_H: 7.87 (2H), 7.46 (2H, *J* = 8.5 Hz), 4.41 (gluαCH, *J* = 7 Hz), 4.22 (valαCH, *J* = 6.5 Hz), 3.7 (3H), ca. 2.4 (gluαCH_2, m), ca. 2.1 (gluβCH_2, valβCH, m, assigned by double resonance experiments), 1.52 (3H), 1.46 (3H), 0.85 (valMe, *J* = 6.8 Hz), 0.77 (valMe, *J* = 6.8 Hz); δ_C: 177.8; 176.7; 173.6 (2, C=O); 168.9, 139.0; 133.4; 130.3; (2C, $^1J_{CH}$ = 164 Hz); 129.6 (2C, $^1J_{CH}$ = 167 Hz); 58.1; 55.7 ($^1J_{CH}$ = 143.5 Hz); 52.39 ($^1J_{CH_3}$ = 148.5 Hz); 32.49 ($^1J_{CH_2}$ = 127.5 Hz); 31.63 ($^1J_{CH}$ = 134.5 Hz); 27.95 ($^1J_{CH_2}$ = 131 Hz); 26.68 ($^1J_{CH_3}$ = 129.7 Hz); 24.38 ($^1J_{CH_3}$ = 128.6 Hz); 19.49 ($^1J_{CH_3}$ = 127 Hz); 19.03 ($^1J_{CH_3}$ = 125 Hz). *Anal.* calcd. for $C_{22}H_{31}ClN_4O_6 \cdot H_2O$: C 52.75, H 6.6, Cl 7.2, N 11.2%; found: C 52.4, H 6.7, Cl 7.2, N 11.5%. The ether ester was prepared in the same way and separated from water as needles, mp 85°C.

Methyl N-*4-bromobenzoyl-*L*-prolyl-*L*-valyl-2-methylalanyl-2-methylalaninate*

A solution (50 mL) of methyl L-prolyl-L-valyl-2-methylalanyl-2-methylalaninate (6) (**4**, R = H, 1 g) in THF (75 mL) was treated with 4-bromobenzoylazide (24) (mp 46°C, prepared from 4-bromobenzoylhydrazide (24) in the same way as has been described (1) for 4-chlorobenzoylazide, 0.7 g) and the reaction mixture stirred at room temperature for 3 days. The reaction mixture was filtered, the filtrate evaporated, and the residue digested with cold toluene (3 × 20 mL). The residual 4-bromobenzoyltetrapeptide (**4**, R = 4-bromobenzoyl) separated from THF–diisopropyl ether (1:2) as prisms, mp 144–146°C; $[\alpha]_D^{23}$ −85° (*c* 0.37, MeOH); λ_{max}: 229 nm (ε 13 000). *Anal.* calcd. for $C_{26}H_{37}BrN_4O_6$: C 53.7, H 6.4, Br 13.8, N 9.6%; found: C 53.65, H 6.4, Br 13.6, N 9.7%.

Acknowledgements

We thank Dr. B. C. Das in whose laboratory this work was initiated under the Canada–France scientific agreement. We thank Dr. I. M. Shaw for the preparation of some intermediates and Mr. D. Embree for technical assistance.

1. I. M. Shaw and A. Taylor. Can. J. Chem. **64**, 164 (1986).
2. J. W. Payne, R. Jakes, and B. S. Hartley. Biochem. J. **117**, 757 (1970).
3. B. F. Gisin, D. G. Davies, Z. K. Borowska, J. E. Hall, and S. Kobayashi. J. Am. Chem. Soc. **103**, 6373 (1981).
4. R. C. Pandy, J. C. Cook, and K. L. Rinehart. J. Am. Chem. Soc. **99**, 8469 (1977).
5. K. L. Rinehart, L. A. Gaudioso, M. L. Moore, R. C. Pandy, J. C. Cook, M. Barber, R. D. Sedgwick, R. S. Bordoli, A. N. Tyler, and B. N. Green. J. Am. Chem. Soc. **103**, 6517 (1981).
6. I. M. Shaw and A. Taylor. J. Chem. Soc. Perkin Trans. 1, 1866 (1979).
7. D. W. Russell, W. D. Jamieson, A. Taylor, and B. C. Das. Can. J. Chem. **54**, 1355 (1976).
8. R. L. Heath. Handbook of chemistry and physics. CRC Press, Boca Raton, Florida. 1979. pp. B-241, B-252.
9. C. G. MacDonald, J. S. Shannon, and A. Taylor. Tetrahedron Lett. 2087 (1964).
10. J. Momigny. Bull. Soc. Chim. Belg. **64**, 144 (1955).
11. J. H. Beynon. Mass spectroscopy and its applications to organic chemistry. Elsevier, Amsterdam. 1960. p. 417.
12. T. S. Cameron, A. W. Hanson, and A. Taylor. Cryst. Struct. Commun. **11**, 321 (1982).

13. K. BIEMANN, C. CONE, B. R. WEBSTER, and G. P. ARSENAULT. J. Am. Chem. Soc. **88**, 5598 (1966).
14. H. SCHMITT and G. JUNG. Ann. 321 (1985).
15. A. A. KIRYUSHKIN, H. M. FALES, T. AXELROD, E. J. GILBERT, and G. W. A. MILNE. Org. Mass Spectrosc. **5**, 19 (1971).
16. A. FEICHT and A. TAYLOR. Proc. N. S. Inst. Sci. **32**, 313 (1982).
17. W. D. JAMIESON, E. LEWIS, and F. G. MASON. J. Mass Spectrom. Ion Phys. **46**, 103 (1983).
18. P. VARENNE, B. BARDEY, P. LONGEVIALLE, and B. C. DAS. Bull. Soc. Chim. Fr. 886 (1977).
19. R. N. JOHNSON and J. A. ANDERSON. U. K. Patent 1335363 (1972).
20. N. J. NOVELLO, S. R. MIRIAM, and C. P. SHERWIN. J. Biol. Chem. **67**, 555 (1926).
21. B. HARGITAY, A. J. HUBERT, and R. BUYLE. Makromol. Chem. **56**, 104 (1962).
22. T. WIELAND and H. L. WIEDENMULLER. Ann. **597**, 111 (1955).
23. R. L. M. SYNGE. Biochem. J. **42**, 99 (1948).
24. T. CURTIS and E. PORTNER. J. Prakt. Chem. **58**(2), 190 (1898).

The Raman spectrum of kaolinite #9 at 21°C

K. H. MICHAELIAN

Energy, Mines & Resources Canada, CANMET, Edmonton Coal Research Laboratory, P.O. Bag 1280, Devon, Alta., Canada T0C 1E0

Received August 8, 1985

K. H. MICHAELIAN. Can. J. Chem. **64**, 285 (1986).

The Raman spectrum of kaolinite #9, a layer silicate of composition $Al_2Si_2O_5(OH)_4$ from Mesa Alta, New Mexico, USA, is reported and compared to previously published Raman and infrared spectra, as well as calculated lattice vibration frequencies, of other kaolinite samples. In the OH stretching region, a Raman band is observed at 3684 cm^{-1}, a frequency which is generally unknown in infrared spectra of kaolinite. The two most likely origins of this band are (*a*) uncoupled inner-surface hydroxyl stretching, and (*b*) transverse/longitudinal splitting involving the 3695 cm^{-1} band, which occurs in both Raman and infrared spectra of kaolinite. The existing data do not conclusively show which of these explanations is correct. In the lattice vibration region, most of the observed Raman bands of kaolinite #9 have been tentatively assigned by comparison with published frequency calculations and existing assignments of infrared spectra of various kaolinites. The descriptions of many of the vibrational modes are approximate, partly because extensive mixing of vibrations makes a simple description of them impossible.

K. H. MICHAELIAN. Can. J. Chem. **64**, 285 (1986).

On rapporte les spectres Raman de la kaolinite #9, une couche de silicate de composition $Al_2Si_2O_5(OH)_4$ provenant de Mesa Alta, New Mexico, USA, et on les compare aux spectres Raman et infrarouges rapportés antérieurement ainsi qu'aux fréquences de vibration calculées pous des réseaux d'autres échantillons de kaolinite. Dans la région d'élongation OH, on observe une bande de vibration à 3684 cm^{-1}, une fréquence qui est généralement inconnue dans les spectres infrarouges de la kaolinite. Les deux origines le plus probables pour cette bands sont (*a*) une élongation qui n'est pas couplée d'un hydroxyle de la surface interne, ou (*b*) un déboublement transversal/longitudinal impliquant la bande à 3695 cm^{-1} qui se retrouve tant dans les spectres Raman qu'infrarouges de la kaolinite. Les données existentes ne démontrent pas d'une façon concluante laquelle de ces explications serait correcte. Dans la région de vibration du réseau, on a attribué la plupart des bandes Raman observées pour la kaolinite #9 en faisant une comparaison avec les fréquences calculées qui ont été publiées et avec les attributions existantes des spectres infrarouges de diverses kaolinites. Les descriptions de plusieurs modes vibrationnels ne sont qu'approximatifs; ceci est dû au fait que des recouvrements importants de vibrations font qu'il est impossible de les décrire simplement.

[Traduit par le journal]

Introduction

The scarcity of Raman spectra of clay minerals in the literature means that important structural information is lacking in many cases. For example, interpretation of the OH stretching vibrations of the layer silicates in terms of known structures has, in most cases, been based only on infrared absorption spectra. This situation is largely caused by two factors: first, infrared spectrometers tend to be more readily available and simpler to operate than Raman instrumentation; secondly, clays such as layer silicates yield weak Raman spectra, making it difficult to obtain research-quality results.

Several years ago, Wiewiora, Wieckowski, and Sokolowska (1) published what is believed to be the first successful Raman study of kaolinite sub-group minerals, which are made up of layers consisting of a single silica tetrahedral sheet and a single alumina octahedral sheet, and have the formula $Al_2Si_2O_5(OH)_4$. For Keokuk kaolinite the authors observed, but did not assign, a a number of bands between 100 and 1100 cm^{-1}; in the OH stretching region, they found bands at 3620, 3650, 3667, 3682, and 3692 cm^{-1}. The known (2) infrared-active OH stretching vibrations of kaolinite occur at 3620, 3652, 3669, and 3697 cm^{-1}; hence 3682 cm^{-1} can be regarded as a new OH stretching frequency.

The assignment of the OH stretching bands of kaolinite to particular types of hydroxyl groups has been a subject of interest for many years, and the observation of another OH vibrational frequency has important implications regarding previous spectra–structure correlations for kaolinite. Wiewiora *et al.* (1) attributed the 3682 cm^{-1} band to a "coupling vibration in phase" involving inner-surface hydroxyl groups. As is discussed below, assignment of this band to an uncoupled inner-surface hydroxyl vibration and, alternatively, to longitudinal/transverse splitting has also been considered in the present investigation. The available evidence suggests that the 3682 cm^{-1} band arises from uncoupled inner-surface hydroxyl stretching.

The present study of the Raman spectrum of kaolinite #9 was undertaken with the following goals: (*1*) comparison with previously published Raman spectra of kaolinite, to determine whether differences due to particle size, origin of the kaolinite, or other factors, are observed; (*2*) assignment of the Raman spectrum of kaolinite in terms of hydroxyl group vibrations, the vibrations of the silica layer, and those of the alumina layer; (*3*) comparison with infrared specta of kaolinite; (*4*) establishment of priorities for further Raman investigations of kaolinite.

Experimental

Kaolinite #9, from Mesa Alta, New Mexico, USA, was obtained from Ward's Natural Science Establishment, Inc. Its purity was checked using X-ray diffraction and an inductively coupled argon plasma spectrometer. The only impurity detectable in the X-ray analysis was a small amount of quartz. The ICAP showed trace quantities of Ca, Fe, Mg, and Na, in decreasing order of abundance. Potassium was not included in this analysis.

Raman spectra were excited using the 476.5-, 488.0-, and 514.5-nm lines of a Coherent Radiation CR6 argon ion laser; power levels at the sample were between 40 and 300 mW. A small monochromator eliminated argon plasma lines from the laser beam before it was allowed to strike the sample. All of the bands reported in this paper were observed using at least two different excitation lines.

Scattered light was analysed with a 0.85-m Spex model 1403 double monochromator equipped with 1800 groove/mm holographic gratings,

and detected with a thermoelectrically cooled RCA C31034 photomultiplier tube and photon counting electronics. The monochromator and the electronics were controlled by a Spex Datamate. The strongest Raman bands gave intensities of about 3.5×10^4 counts/s at a laser power of 40 mW and a spectral slit width of 5 cm^{-1}. Spectra were calibrated using neon emission lines; accuracies of the band positions are about ± 1 cm^{-1} for the stronger bands, decreasing to about ± 3 cm^{-1} for weaker bands. No correction was made for the slight frequency dependence of the sensitivity of the optical system.

The best spectra were obtained for large (~25 mm) lumps of kaolinite, the form in which it was supplied. Powdered samples and films on microscope slides were also briefly examined. In all three cases, the spectra showed the same Raman bands. However, the scattering from finely ground kaolinite is very weak, giving Raman spectra with poor signal/noise ratios. Because of this, spectra of lumps of kaolinite #9 are the only ones presented in this paper.

Results and discussion

Each of the laser lines used to excite the Raman spectra of kaolinite caused fluorescence that subsides with time, reaching a minimum in about 1–2 h. Further irradiation does not totally eliminate the fluorescence, however, and Raman spectra of kaolinite #9 contain a broad fluorescence band that extends from about $\Delta\nu = 200$ to 6000 cm^{-1} with respect to the 488.0-nm laser line. A similar background is visible in the spectra of Wiewiora *et al.* (1) and in Raman spectra of other layer silicates (3). Ideally, the effect of this fluorescenee could be eliminated by utilizing the difference in the times required for the fluorescence and scattering processes. For simplicity, in the present work the fluorescence background was reduced in the 300–1000 cm^{-1} and 3600–3720 cm^{-1} regions with a baseline linearization program.

The vibrations of layer silicates are conveniently discussed in terms of their constituent units. Hence, for kaolinite, Raman and infrared spectra can be interpreted by considering vibrations of the hydroxyl groups, the silica tetrahedra, and the alumina octahedra. With regard to the latter two structures, Ishii *et al.* (4,5) have published results of detailed calculations of lattice vibration frequencies of a series of layer silicates, which facilitates assignment of some of the Raman bands of kaolinite. Therefore the Raman spectrum of kaolinite is discussed below in terms of hydroxyl vibrations and lattice vibrations. The different regions of the spectrum are shown in Figs. 1–4; band positions and relative intensities are given in Table 1.

1. *Hydroxyl vibrations*

1.1 *Kaolinite #9*

The OH stretching region of the Raman spectrum of kaolinite #9 is shown in Fig. 1. Five bands are identifiable, the two at highest frequency being incompletely resolved. Four of the bands (3695, 3669, 3651, and 3620 cm^{-1}) occur at the same frequencies as the well-known infrared absorption bands designated (6) A, B, C, D, respectively. The fifth band, at 3684 cm^{-1}, is not found in published infrared spectra of kaolinite; this band will be denoted A′ in this paper. As indicated in the Introduction, all five bands were observed in the Raman spectrum of Keokuk kaolinite by Wiewiora *et al.* (1); however, band A′ is more prominent in their spectra than is the case in Fig. 1.

Figure 2 shows resolution enhancement of the inner-surface hydroxyl stretching region of the Raman spectrum of kaolinite #9. The sharpened spectrum was obtained using the frequency domain deconvolution method of Jones and Shimokoshi (7). In this example, a Lorentzian band shape and a half width of 10 cm^{-1} were used; the effective range of the triangle-squared apodization function was 0.2 cm. Improved resolution of bands A and A′ permits determination of their frequencies as 3695 ± 1 cm^{-1} and 3684 ± 1 cm^{-1}, respectively. The use of other apodization functions is not expected to affect these conclusions significantly.

In addition to the OH stretching vibrations, the in-plane bending of inner hydroxyls and of surface hydroxyls (both of which include some motion of aluminum ions (8)) also yields

TABLE 1. Raman spectrum of kaolinite #9 from 100 to 3700 cm^{-1}

ν (cm^{-1})	Intensity[a]
130	sh
143	m
197	vw
245	w
270	m
336	m
394	w
418	sh
431	m
463	m
516	w
638	m
710	vw
751	w
790	w
915	w
938	sh
3620	s
3651	w
3669	w
3684	s
3695	m

[a]vw = very weak; w = weak; m = medium; s = strong; sh = shoulder.

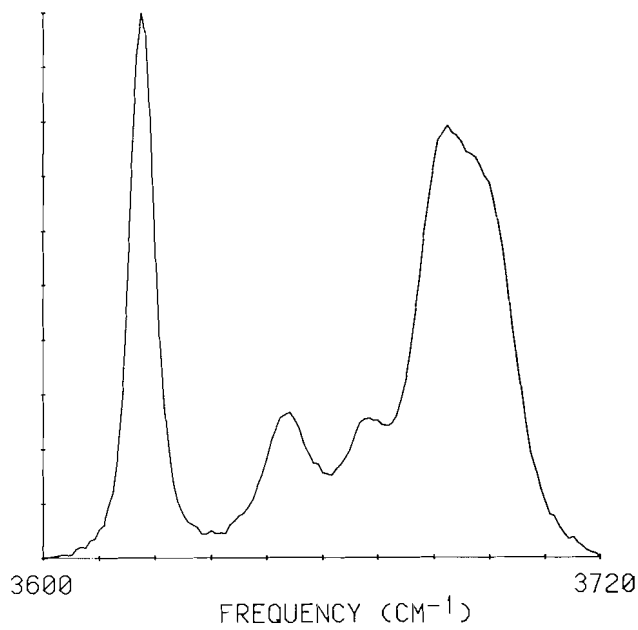

FIG. 1. Raman spectrum of kaolinite #9: OH stretching region. Bands at 3669, 3651, and 3620 cm^{-1} are designated B, C, and D, respectively (see text).

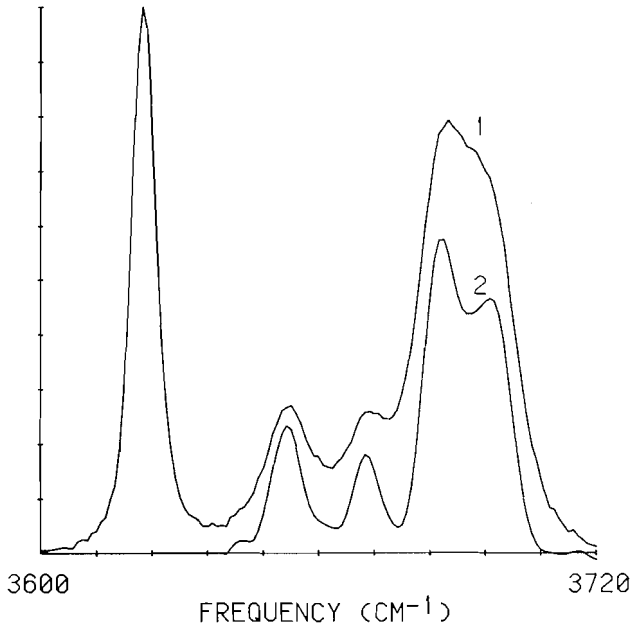

FIG. 2. Curve 1: observed spectrum, OH stretching region; Curve 2: deconvolution of inner surface hydroxyl stretching bands. Bands at 3695 and 3684 cm^{-1} are designated A and A′, respectively (see text).

Raman bands. The inner hydroxyls give rise to the band at 915 cm^{-1} (Fig. 4), while the surface hydroxyls cause the shoulder at ~938 cm^{-1} (9).

1.2 *Assignment of OH stretching vibrations*

Although A′ was regarded as a newly-found OH stretching band by Wiewiora *et al.* (1), it should be noted that several authors have proposed the existence of a second band within the envelope of band A, which is asymmetric in infrared spectra of kaolinite. Serratosa, Hidalgo, and Vinas (10) suggested that band A originates from two types of hydroxyls with a slight difference in energy. The comparatively high frequency of this band implies that the OH groups involved do not participate in hydrogen bonding, whereas the band width indicates the opposite. These conflicting viewpoints can be rationalized by postulating that the observed envelope contains two bands (10,11). More recently, Rouxhet, Samudacheata, Jacobs, and Anton (12) studied infrared spectra of synthetic kaolinites with varying degrees of deuteration, which permitted conclusions regarding coupling of OH or OD stretching vibrations. They found that band fitting of the OH stretching region assuming the presence of four bands was unsuccessful, and concluded that "five components are necessary to account for the spectrum of a kaolinite in which both coupled and uncoupled OH or OD groups are present." Hence even before Raman spectra were available, five OH stretching bands were expected for kaolinite.[1]

Before discussing the assignment of these OH stretching bands, it should be recalled that there are three types of hydroxyl groups in kaolinite (13): (*a*) "outer hydroxyls" at the surface of microcrystals, including both hydroxyls at broken edges and hydroxyls of the octahedral sheet at the upper surface; (*b*) "inner-surface" hydroxyls at the surface of the octahedral sheet opposite tetrahedral oxygens of the next layer; and (*c*) "inner hydroxyls" which are common to the octahedral and tetrahedral sheets. Assignments of the infrared OH stretching bands of kaolinite, which have been reviewed by Farmer (14), generally invoke only the latter two types of hydroxyl groups. Intercalation studies (15,16) show that bands A, B, and C arise from inner-surface hydroxyls, while D is due to inner hydroxyls. Some authors associate each of A, B, and C with particular hydroxyls in the kaolinite structure, while others attribute these bands to coupling of the inner-surface hydroxyl stretching vibrations. Possible confusion may arise from the fact that the relative intensities of the bands are somewhat dependent on the source of the kaolinite (2,17); e.g., band B is observable only in the spectra of well-crystallized samples (18).

The assignment by Rouxhet *et al.* (12) combines features of both of the just-mentioned interpretations regarding coupling of inner-surface stretches. These authors attributed bands A and B to, respectively, in-phase and out-of-phase stretching of the two inner-surface hydroxyls perpendicular to the kaolinite layers; band C was assigned to the third inner-surface hydroxyl, which, on the basis of electrostatic energy calculations (19) and transition moments of A, B, and C (11,12), was believed to be nearly parallel to the layers. A recent infrared study of kaolinite crystallinity (20) concluded that this assignment was consistent with the calculated (19) structure. However, this attribution of band C may now have to be revised, since very recent theoretical (21) and crystal structure (22, 23) investigations of kaolinite have shown that the third inner-surface hydroxyl group has a more vertical orientation than was previously thought to be the case.

Infrared spectra obtained by Rouxhet *et al.* (12) show that weakly deuterated kaolinite (in which the OD oscillators are uncoupled) has an OD stretching band at 2714 cm^{-1} that is replaced by bands at 2723 and 2708 cm^{-1} in spectra of fully deuterated samples. The isotope shifts of the latter two bands with respect to bands A and B of undeuterated kaolinite are 1.357 and 1.355, respectively. Using an average isotope shift of 1.356[2] and 2714 cm^{-1} as the frequency of an uncoupled OD stretching vibration leads to a calculation of $1.356 \times 2714\ cm^{-1} = 3680\ cm^{-1}$ for the frequency of an uncoupled inner-surface hydroxyl vibration. This prediction is supported by the observed shift of band A to lower frequency, caused by growing-in of the ~3680 cm^{-1} band at a high degree of deuteration, when the OH oscillators are not coupled. Moreover, it is consistent with the conclusion that a fifth band, at about 3680 cm^{-1}, is necessary to fit the observed infrared spectrum of kaolinite. In fact, a frequency of about 3680 cm^{-1} for uncoupled inner-surface hydroxyl stretching has been proposed previously by other authors (24, 25). In contrast, the stretching frequency of "free" OH groups (24) is about 3750 cm^{-1}, as has been observed for kaolinite by reflection spectroscopy (26).

Wiewiora *et al.* (1) rejected the conclusion that A′ arises from uncoupled OH groups, largely because the kaolinite that they examined was well crystallized. These authors emphasized the general tendency of symmetrical vibrations to yield strong Raman bands, and therefore attributed A′ to the "the coupling vibrations in phase" of the OH groups that give rise to bands B and C. However, the appearance of a strong OH stretching band in the Raman spectrum does not necessarily indicate that it arises from in-phase coupling; as Wiewiora *et al.* (1) noted, the symmetrical OH stretching vibrations of dickite, which involves three hydroxyl groups, does not yield a strong Raman band.

[1]We have observed an intensity differential at the frequency of band A′ when subtracting diffuse reflectance FTIR spectra of kaolinite #9, and a shoulder on band A near 3684 cm^{-1} in photoacoustic FTIR spectra of other kaolinites.

[2]This value is erroneously given as 1.366 in ref. 12.

Moreover, Raman spectra of two different kaolinite samples that have been examined in the present investigation show band A′ with relative intensity significantly less than observed by Wiewiora *et al.* (1), bringing further uncertainty to an interpretation based on the high intensity of A′ in their spectra.

An alternative assignment of band A′ can be suggested using the reasoning of Farmer and Russell (27), who showed that transverse and longitudinal frequencies need to be considered when analysing spectra of layer silicates. Vibrations perpendicular to the layers occur at the longitudinal frequency ν_l, while those parallel to the layers occur at the transverse frequency ν_t. Hence a particular vibration can give rise to two bands: the characteristic splitting of the ~1100 cm^{-1} infrared absorption band of kaolinite (2), which is observed only for larger particle sizes (18), is due to this effect. Similar reasoning suggests that band A′ could be the transverse mode equivalent to band A, which falls near the longitudinal frequency. If this explanation is correct, A′ would appear with reduced intensity in the Raman spectrum of kaolinite in which the particle size is smaller than that of kaolinite #9. This was investigated by recording the OH region of the Raman spectrum of international kaolinite,[3] which was shown to have an average particle size significantly less than that of kaolinite #9 by comparing FTIR spectra of the two samples. Raman spectra of international kaolinite showed an A′/A intensity ratio which is equal, within experimental uncertainty, to that of kaolinite #9. These results suggest that transverse/longitudinal splitting is not responsible for the occurrence of band A′ in the Raman spectrum of kaolinite.

The interpretations of band A′ that have been outlined show that the data presently available do not permit a definite conclusion with regard to its assignment. If one considers coupling of OH vibrations to be the likely origin of A′, then the assignment of Wiewiora *et al.* (1) seems less satisfactory than that of Rouxhet *et al.* (12), since a qualitative observation regarding Raman intensities is not as definitive as the results of deuteration experiments, which are a common means for analysing coupling of OH vibrations. Furthermore, the present investigation has shown that band A′ is probably not due to transverse/longitudinal splitting, but further Raman studies of other kaolinite samples having a range of particle sizes are required before this explanation can be fully evaluated.

2. *Lattice vibrations*

2.1 *The 100 – 300 cm^{-1} region*

The 100 – 300 cm^{-1} region of the Raman spectrum of kaolinite #9 is shown in Fig. 3. Bands are identifiable at 143, 197, 245, and 270 cm^{-1}; a shoulder occurs on the low frequency side of the 143 cm^{-1} band at about 130 cm^{-1}. Because the low frequency vibrations of kaolinite have not been studied very thoroughly, the assignments of these bands, which are presented below, must be regarded as tentative.

Ishii *et al.* (4,5) calculated vibrational frequencis of 127, 130 and 285 cm^{-1} for the ideal hexagonal C_{6v} Si_2O_5 lattice; for the less symmetrical C_{3v} lattice, the predicted frequencies were 113, 209, and ~290 cm^{-1}. The symmetry of the Si_2O_5 lattice is certainly less than C_{6v} in kaolinite; however, if the effect of deviation from C_{6v} symmetry on the vibrational modes is not very great, the calculated 127 and 130 cm^{-1} bands could still be invoked to account for the 130 and 143 cm^{-1} Raman bands, respectively. The corresponding frequencies reported for Keokuk kaolinite[4] (1) are 120 and 132 cm^{-1}; a very recent spectrum of Georgia kaolinite (28) shows a single band at 141 cm^{-1}. Far infrared diffuse reflectance spectra of kaolinite obtained in our laboratory (29) show, among others, bands at 120, 132, and 141 cm^{-1}, which may be analogous to the observed Raman bands.

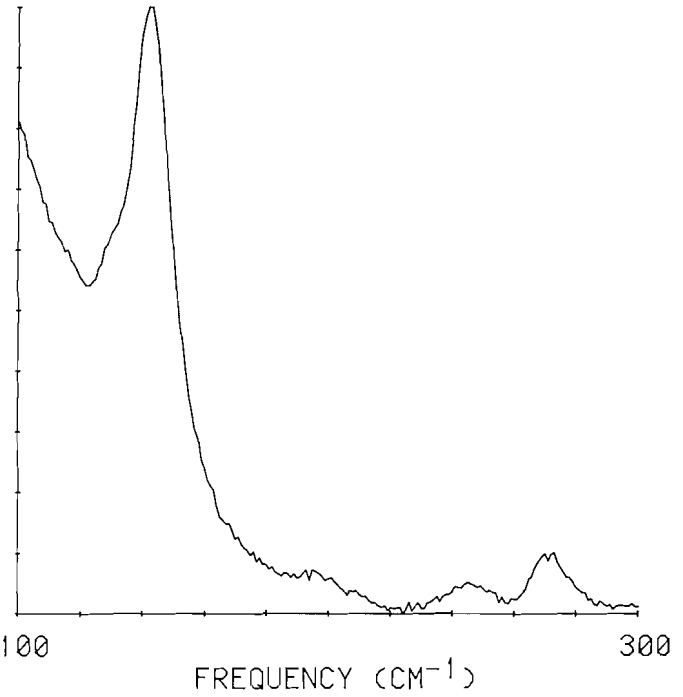

FIG. 3. Raman spectrum of kaolinite #9: 100 – 300 cm^{-1} region.

The 197 cm^{-1} Raman band, whose infrared counterpart is at 196 cm^{-1} (29), can be attributed to vibrations (probably translations) of hydroxyl ions (4). An alternative assignment is to the 209 cm^{-1} mode calculated for the C_{3v} Si_2O_5 lattice. The 245 cm^{-1} Raman band, which corresponds to a shoulder in the infrared spectrum (29) at 248 cm^{-1}, is assigned to a mixture of silicon–oxygen deformation and hydroxyl libration (4). The final Raman band in this region, at 270 cm^{-1}, is observed in infrared spectra at 273 cm^{-1} in transmission (18) and at 279 cm^{-1} by diffuse reflectance (29); this band is assigned (18) to mixed silicon–oxygen deformations and octahedral sheet vibrations.

2.2 *The 300 – 900 cm^{-1} region*

The remainder of the lattice vibration region is shown in Fig. 4. The Raman spectrum of kaolinite #9 between 300 and 900 cm^{-1} contains bands at 336, 394, 418, 431, 463, 516, 638, 710, 751, and 790 cm^{-1}. Comparison of these frequencies with those in infrared spectra of kaolinite shows that several Raman bands occur at lower frequencies than their nearest infrared counterparts: recent ir data for kaolinite (18) include bands at 348, 432, 472, 542, 650, 755, and 797 cm^{-1}. The only infrared frequencies near 394 and 418 cm^{-1} are shoulders at 383, 411, and 421 cm^{-1} recently observed (29) using diffuse reflectance. The 710 cm^{-1} Raman band does not have an obvious infrared analogue. The origin of the differences between Raman and infrared frequencies may be transverse/longitudinal splitting, or simply

[3]The author is grateful to Dr. V. C. Farmer for providing this sample.

[4]Identical frequencies of 120 and 132 cm^{-1} are given in Table 1 of ref. 1 for kaolinite, dickite, and nacrite, although the spectra in that paper suggest that the frequencies are not the same for each mineral.

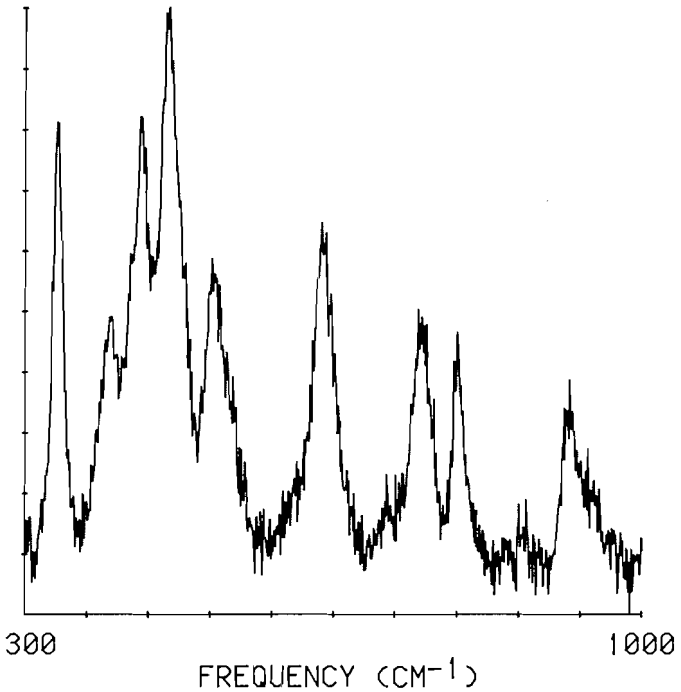

FIG. 4. Raman spectrum of kaolinite #9: 300 – 1000 cm^{-1} region.

that different vibrations are active in the Raman and infrared spectra; further work is required before the comparison of infrared and Raman spectra of kaolinite can be more thoroughly understood. This will permit more detailed conclusions regarding the structure of this mineral.

The Raman frequencies (except 394 and 710 cm^{-1}) can be assigned in a straightforward manner if it is assumed that the respective Raman and infrared frequencies have common origins. Bands at 336, 418, 431, 463, 516, and 638 cm^{-1} are attributed to mixed SiO deformations and octahedral sheet vibrations (18); the 516 cm^{-1} vibration involves an Si—O—Al linkage (8). The 751 cm^{-1} band is due to vibrations of SiOAl groups (8) and surface hydroxyls (14). SiOAl vibrations also give rise to the 790 cm^{-1} band (8).

The bands at 516 and 638 cm^{-1}, which are prominent in the Raman spectrum of kaolinite #9 (Fig. 4), are also present in the spectrum of Georgia kaolinite recently published by Johnston *et al.* (28); however, these bands were not observed for Keokuk kaolinite (1). Several attempts to observe these two bands in the spectrum of international kaolinite were inconclusive because of the extremely weak scattering in the lattice vibration region for this finely ground sample. Thus the data available so far suggest that the 516 and 638 cm^{-1} bands are sample dependent, although investigation of the Raman spectra of other kaolinite samples is required before these results can be fully explained.

Conclusions

The above discussion has shown that a significant amount of work must be carried out before the Raman spectrum of kaolinite is fully understood. The following experiments are proposed in order to elucidate some of the ambiguous points which have already been mentioned.

(*a*) Raman spectra of a number of different kaolinite samples should be obtained in order to determine whether differences in relative intensities of band A′ (3684 cm^{-1}) are attributable to sample origin.

(*b*) Raman spectra of a particular kaolinite sample ground to different particle sizes are required to establish whether transverse/longitudinal splitting accounts for the appearance of band A′.

(*c*) The samples mentioned in (*a*) should be examined with respect to possible occurrence of Raman bands at 516 and 638 cm^{-1}.

(*d*) As a final point, the experiment mentioned under (*a*) could be repeated at low temperature, where reduced band widths might facilitate the characterization of the OH stretching bands.

1. A. WIEWIORA, T. WIECKOWSKI, and A. SOKOLOWSKA. Arch. Mineral. **35**, 5 (1979)
2. V. C. FARMER and J. D. RUSSELL. Spectrochim. Acta, **20**, 1149 (1964).
3. P. MARTINEC, Z. WEISS, V. SKODA, and R. STRAUCH. Eighth Conference on Clay Mineralogy and Petrology, Teplice, Czechoslovakia. 1979. p. 91.
4. M. ISHII, T. SHIMANOUCHI, and M. NAKAHIRA. Inorg. Chim. Acta, **1**, 387 (1976).
5. M. ISHII, M. NAKAHIRA, and H. TAKEDA. Proc. Int. Clay Conf. (Tokyo), 247 (1969).
6. J. G. MILLER and T. D. OULTON. Clays Clay Miner. **18**, 313 (1970).
7. R. N. JONES and K. SHIMOKOSHI. Appl. Spectrosc. **37**, 59 (1983).
8. V. STUBICAN and R. ROY. Z. Kristallogr. **115**, 200 (1961).
9. K. WADA. Clay Miner. **7**, 51 (1967).
10. J. M. SERRATOSA, A. HIDALGO, and J. M. VINAS. Proc. Int. Clay Conf. (Sweden), 17 (1963).
11. J. M. SERRATOSA, A. HIDALGO, and J. M. VINAS. Nature, **195**, 486 (1962).
12. P. G. ROUXHET, N. SAMUDACHEATA, H. JACOBS, and O. ANTON. Clay Miner. **12**, 171 (1977).
13. R. L. LEDOUX and J. L. WHITE. Proc. Int. Clay Conf. (Jerusalem), 361 (1966).
14. V. C. FARMER. The infrared spectra of minerals. *Edited by* V. C. Farmer. Mineralogical Society, London. 1974. Chapt. 15.
15. R. L. LEDOUX and J. L. WHITE. Science, **145**, 47 (1964).
16. R. L. LEDOUX and J. L. WHITE. Clays Clay Miner. **13**, 289 (1965).
17. H. W. VAN DER MAREL and P. KROHMER. Contrib. Mineral. Petrol. **22**, 73 (1969).
18. V. C. FARMER. Data handbook for clay materials and other nonmetallic minerals. *Edited by* H. van Olphen and J. J. Fripiat. Pergamon Press, London, 1979. p. 285.
19. R. F. GIESE and P. DATTA. Am. Mineral. **58**, 471 (1973).
20. M. CRUZ-CUMPLIDO, C. SOW, and J. J. FRIPIAT. Bull. Mineral. **105**, 493 (1982).
21. R. F. GIESE. Bull. Mineral. **105**, 417 (1982).
22. J. M. ADAMS. Clays Clay Miner. **31**, 352 (1983).
23. P. R. SUITCH and R. A. YOUNG. Clays Clay Miner. **31**, 357 (1983).
24. M. CRUZ, H. JACOBS, and J. J. FRIPIAT. Proc. Int. Clay Conf. (Madrid), 35 (1973).
25. H. JACOBS and M. STERCKX. Reun. Hisp.-Belga Miner. Arcilla, An. 154 (1970).
26. T. WIECKOWSKI. Arch. Mineral. **33**, 79 (1977).
27. V. C. FARMER and J. D. RUSSELL. Spectrochim. Acta, **22**, 389 (1966).
28. C. T. JOHNSTON, G. SPOSITO, D. F. BOCIAN, and R. R. BIRGE. J. Phys. Chem. **88**, 5959 (1984).
29. J. C. ZWINKELS and K. H. MICHAELIAN. Infrared Phys. **25**, 629 (1985).

Stability of bismuth oxyiodides in aqueous solutions at 25°C [1]

PETER TAYLOR AND VINCENT J. LOPATA
Research Chemistry Branch, Atomic Energy of Canada Limited, Whiteshell Nuclear Research Establishment, Pinawa, Man., Canada R0E 1L0

Received June 25, 1985

PETER TAYLOR and VINCENT J. LOPATA. Can. J. Chem. **64**, 290 (1986).

Equilibrium iodide activities have been measured as a function of pH for the phase assemblages α-Bi_2O_3 + Bi_5O_7I + aqueous solution and Bi_5O_7I + BiOI + aqueous solution, yielding the following Gibbs energies of formation for the bismuth oxyiodides: $\Delta_fG^0(Bi_5O_7I, s, 298\ K) = -1266.1 \pm 5.8\ kJ\ mol^{-1}$; and $\Delta_fG^0(BiOI, s, 298\ K) = -247.8 \pm 2.8\ kJ\ mol^{-1}$. Using published data for the assemblage BiOI + BiI_3 + aqueous solution, we estimate that $\Delta_fG^0(BiI_3, s, 298\ K) = -160.0 \pm 16.2\ kJ\ mol^{-1}$ and $\log K_{sp}(BiI_3) = -15.3 \pm 3.4$.

PETER TAYLOR et VINCENT J. LOPATA. Can. J. Chem. **64**, 290 (1986).

On a mesuré les activités des iodures à l'équilibre en fonction du pH des assemblages de phase α-Bi_2O_3 + Bi_5O_7I + solution aqueuse et Bi_5O_7I + BiOI + solution aqueuse et l'on en a déduit les énergies de Gibbs suivantes pour la formation des oxyiodures: $\Delta_fG^0(Bi_5O_7I, s, 298\ K) = -1266{,}1 \pm 5{,}8\ kJ\ mol^{-1}$; et $\Delta_fG^0(BiOI, s, 298\ K) = -247{,}8 \pm 2{,}8\ kJ\ mol^{-1}$. En se basant sur des données connues relatives à l'assemblage de phase BiOI + BiI_3 + solution aqueuse, nous avons évalué les paramètres suivants: $\Delta_fG^0(BiI_3, s, 298\ K) = -160{,}0 \pm 16{,}2\ kJ\ mol^{-1}$ et $\log K_{sp}(BiI_3) = -15{,}3 \pm 3{,}4$.

[Traduit par le journal]

Introduction

Many metal halides undergo hydrolysis to one or more basic halides, and ultimately to the metal oxide or hydroxide. In 1934, Montignie (1) reported the sequential hydrolysis of BiI_3 by KOH to BiOI and Bi_5O_7I. Dyrssen and Yen (2) have described equilibria between BiI_3 and BiOI in acidic iodide solutions. Rulmont (3) and Ketterer and Krämer (4) have recently described the preparation and characterization of Bi_5O_7I, while Klimakov *et al.* (5) have determined phase relationships involving BiOI, $Bi_7O_9I_3$, and Bi_5O_7I in the condensed anhydrous system BiI_3–Bi_2O_3.

Here we report the stability limits of Bi_5O_7I with respect to interconversion with BiOI and α-Bi_2O_3 in aqueous solutions at 25°C, and estimate the Gibbs energies of formation of solid Bi_5O_7I, BiOI, and BiI_3. This work was prompted by the possibility of using Bi_5O_7I to immobilize radioactive isotopes of iodine. In this regard, Kharbanda *et al.* (6), Ramani *et al.* (7), and Mel'nikov *et al.* (8) have described the sorption of ^{131}I on "bismuth hydroxide." Basic iodides have received little attention as hosts for ^{129}I, according to recent reviews by Vance *et al.* (9) and Burger *et al.* (10).

Experimental methods

Starting materials were reagent-grade $Bi(NO_3)_3 \cdot 5H_2O$, α-Bi_2O_3, KI, and carbonate-free aqueous solutions of NaOH and KOH. Solutions of desired iodide and hydroxide molarities were prepared using deionized water. The pH was adjusted and measured using automatic titration equipment (Metrohm E526 titrator and E535 dosimat, or Mettler DV/DK modular system). This system was calibrated with standard buffer solutions at pH = 7.00 and 9.18. This provided an adequate basis for measurements of pH up to about 11.5, above which the electrode showed discernible deviation from Nernstian response, as discussed below. Iodide activities were measured using an Orion Model 94-53 specific ion electrode and a Model 90-02 double-junction reference electrode, calibrated using standard solutions with iodide activities ranging from 10^{-2} to 10^{-7} mol dm^{-3}. Nernstian response was sustained over this range so long as solutions were carefully purged with nitrogen.

Solution compositions were computed on a molar activity basis. Since the equilibrium constants determined from this work (K_9 and K_{10}) are dimensionless, it is not necessary to distinguish between molarity and molality in subsequent calculations. In any case, most of the solutions used in the final equilibrium determinations were too dilute for this distinction to be significant.

Solids were identified by X-ray powder diffraction (XRD), using CuKα radiation and a Philips PW-1150 diffractometer with a diffracted-beam monochromator. Solid iodides were also characterized by thermogravimetric analysis, done manually on 1-g samples because of damage by evolved iodine to components of a recording microbalance in preliminary experiments with lead and bismuth iodides. Samples were heated in fireclay boats in a horizontal tube furnace, for periods of ~0.5 h at increasing temperatures (~25 K intervals), until constant weight indicated complete conversion to Bi_2O_3.

Preparation and characterization of bismuth oxyiodides

(a) BiOI

About 10 g of BiOI was prepared by mixing solutions of $Bi(NO_3)_3 \cdot 5H_2O$ and a small excess of KI over that required by eq. [1].

$$[1] \quad Bi(NO_3)_3 + H_2O + I^- \rightarrow BiOI + 2H^+ + 3NO_3^-$$

A deep orange-red precipitate of BiOI formed rapidly, together with some dark gray material, probably BiI_3 formed by reaction [2].

$$[2] \quad BiOI + 2H^+ + 2I^- \rightarrow BiI_3 + H_2O$$

The solids were isolated by filtration, and the BiI_3 was rapidly hydrolyzed back to BiOI upon washing with water (reverse of reaction [2]). The solid was identified as pure BiOI by XRD, based on the published diffraction pattern (11). Thermal decomposition of the BiOI in air occurred in two stages. In the first stage, between 250 and 480°C, the observed weight loss of 26.4% agreed well with the value of 27.03%, calculated for the formation of Bi_5O_7I, according to eq. [3].

$$[3] \quad 5BiOI + O_2 \rightarrow Bi_5O_7I + 2I_2$$

In the second stage, between 600 and 700°C, the remaining

[1]Issued as AECL No. 8736.

iodine was removed, in accordance with eq. [4].

[4] $4Bi_5O_7I + O_2 \rightarrow 10Bi_2O_3 + 2I_2$

The overall weight loss of 33.9% agreed well with the calculated value of 33.79%, based on eq. [5].

[5] $4BiOI + O_2 \rightarrow 2Bi_2O_3 + 2I_2$

This decomposition behaviour is similar to that reported by Rulmont (3). Krämer (12) determined a different route for the decomposition of BiOI in a nitrogen atmosphere, with successive losses of BiI_3 to form progressively more oxygen-rich phases: $Bi_4O_5I_2$, $Bi_7O_9I_3$, Bi_5O_7I, and finally, Bi_2O_3.

(b) Bi_5O_7I

This iodide was prepared in 10-g quantities, both by hydrolysis of BiOI with excess aqueous KOH, and by the reaction of α-Bi_2O_3 powder with excess aqueous KI, in accordance with eqs. [6] and [7], respectively.

[6] $5BiOI + 4OH^- \rightarrow Bi_5O_7I + 4I^- + 2H_2O$

[7] $5Bi_2O_3 + 2I^- + H_2O \rightarrow 2Bi_5O_7I + 2OH^-$

Each reaction proceeded to completion overnight in a stirred reaction vessel at room temperature. The XRD patterns of the filtered, washed solids were identical with each other and with the pattern obtained from the intermediate product of thermal decomposition of BiOI, described above (eq. [3]). These patterns are similar to those previously reported for Bi_5O_7I (3–5), except for additional weak features, as shown in Table 1. These features are reproducible, and the entire pattern can be indexed on the basis of the orthorhombic unit cell reported by Ketterer and Krämer (4), as shown in Table 1. The tetragonal and orthorhombic unit cells proposed by Rulmont (3) cannot account for all the lines. All the diffraction peaks we observed can be assigned Miller indices, *hkl*, with *l* even, suggesting a cell with *c* equal to one half of the value reported by Ketterer and Krämer (4). We presume that they observed some weak features in their single-crystal diffraction data that necessitated the larger cell. The general agreement between our intensity data and theirs is poor, perhaps because our 00*l* intensities are increased by preferred orientation. There was no indication that our solids contained any structurally essential water or other components, and thermogravimetric data agreed well with eq. [4]. All the samples decomposed between 500 and 700°C, with total weight losses of 9.35, 9.7, and 9.0%, respectively, from solids prepared from Bi_2O_3 and iodide, BiOI and hydroxide, and partial thermal decomposition of BiOI. The calculated weight loss for eq. [4] is 9.26%.

The crystal structure of a second form of Bi_5O_7I, designated β-Bi_5O_7I, was recently reported by Ketterer *et al.* (14); we have not observed this solid in any of our experiments.

Determination of stability limits

The stability limits of bismuth oxide – iodide solids in contact with aqueous solutions can be expressed by equilibria [8]–[10].

[8] $\frac{1}{2}BiI_3(s) + OH^-(aq) \overset{K_8}{\rightleftharpoons} \frac{1}{2}BiOI(s) + I^-(aq) + \frac{1}{2}H_2O(l)$

[9] $\frac{5}{4}BiOI(s) + OH^-(aq) \overset{K_9}{\rightleftharpoons} \frac{1}{4}Bi_5O_7I(s) + I^-(aq) + \frac{1}{2}H_2O(l)$

[10] $Bi_5O_7I(s) + OH^-(aq) \overset{K_{10}}{\rightleftharpoons} \frac{5}{2}Bi_2O_3(s) + I^-(aq) + \frac{1}{2}H_2O(l)$

These are variants of eqs. [2], [6], and [7], respectively, chosen

TABLE 1. X-ray powder diffraction data for Bi_5O_7I (*d* in Å)

			This work[1]			Ref. 4		Ref. 3
h	*k*	*l*	d_{calc}	d_{obs}	I/I_1	d_{obs}	I/I_1	d_{obs}
0	0	1	11.503	11.457	19	11.5110	2	11.392
2	0	0	8.134	8.125	4	8.1087	5	—
2	0	1	6.641	6.642	3	6.6439	3	—
0	0	2	5.751	5.753	2	—	—	5.731
0	0	3	3.834	3.832	4	3.8273	2	3.824
4	0	1*	3.834					
2	0	3	3.468	3.467	2	—	—	—
3	1	2	3.177	3.175	85	3.1720	100	3.168
1	1	3	3.062	3.060	5	3.0551	4	3.058
0	0	4	2.876	2.874	100	2.8737	15	2.872
2	0	4	2.711	2.710	30	2.7094	28	2.705
6	0	0*	2.711					
0	2	0	2.678	2.678	7	2.6717	22	—
1	1	4	2.503	2.502	2	2.5020	3	—
5	1	2*	2.503					
0	0	5	2.301	2.302	2	—	—	2.298
2	0	5	2.214	2.214	7	—	—	2.212
6	0	3	2.214					
1	1	5	2.096	2.095	1	—	—	—
7	1	1	2.096					
3	2	3	2.035	2.034	1	—	—	—
5	2	1	2.035					
8	0	0	2.033					
4	0	5	2.002	2.002	3	—	—	—
8	0	1	2.002					
6	0	4	1.9726	1.9722	17	1.9719	16	1.968
0	2	4	1.9598	1.9601	10	1.9570	14	—
2	2	4	1.9053	1.9054	6	1.9019	18	1.903
6	2	0*	1.9053					
7	1	3	1.8632	1.8635	2	1.8620	3	—
1	1	6	1.7940	1.7938	4	—	—	1.793
		(many)		~1.75	1	—	—	—
3	1	6*	1.7126	1.7128	23	1.7128	13	1.712
7	1	4	1.7126					
9	1	0	1.7126					
		(many)		~1.66	1	—	—	—
9	1	2	1.6414	1.6415	10	1.6392	19	1.638
10	0	0	1.6267	1.6269	4	1.6228	16	—
3	3	2*	1.6266					
		(many)		~1.61	6	—	—	—
6	2	4*	1.5883	1.5883	3	1.5858	10	—
2	3	3	1.5874					
5	1	6	1.5783	1.5784	3	—	—	—
1	1	7	1.5637	1.5635	2	—	—	1.564
7	1	5	1.5637					
9	1	3	1.5637					
3	1	7	1.5089	1.5092	1	—	—	1.509
0	0	8	1.4378	1.4378	4	—	—	—

[1]Orthorhombic unit cell, a = 16.267(4) Å (1 Å = 0.1 nm), b = 5.356(2) Å, c = 11.503(2) Å, obtained by least-squares refinement of the cell reported by Ketterer and Krämer (4), but with the value of c halved. The 18 uniquely indexed lines were used in the refinement. For the 30 lines listed, the maximum difference between observed and calculated 2θ is 0.031°, and only three values exceed 0.02°. Observed d spacings were calibrated using a BaF_2 internal standard (a = 6.1971 Å, according to the unpublished data of D. A. Hewitt (13)). Computations were done using a program written by D. E. Appleman and H. T. Evans, Jr., U.S. Geological Survey, Geological Division, Washington, DC, U.S.A. 20244. The large number of near coincidences of d_{calc} values arise because $a \simeq \sqrt{2}c$, hence $d(hkl) \simeq d(h'kl')$ when $h^2 + 2l^2 = h'^2 + 2l'^2$. Asterisks indicate the *hkl* values favoured in ref. 4.

because each equilibrium constant, in a dilute aqueous system, is simply expressed as the quotient of iodide and hydroxide activities.

[11] $K_{eq} = \{I^-\}/\{OH^-\}$

whence

[12] $-\log K_{eq} = \log K_w + pH + pI$

where $pI = -\log \{I^-\}$. In other words, each pair of adjacent solids in the sequence $BiI_3 \rightarrow BiOI \rightarrow Bi_5O_7I \rightarrow Bi_2O_3$ should buffer the iodide activity at a particular value at a given pH. Dyrssen and Yen (2) observed such behaviour with BiI_3 + BiOI in acidic solutions with an ionic strength of 3.0 mol dm^{-3}. Their data correspond to a value of about 10.0 for log K_8, as discussed below. We have measured equilibrium iodide activities as a function of pH for each of the solid pairs, BiOI + Bi_5O_7I and Bi_5O_7I + α-Bi_2O_3 and hence estimated K_9 and K_{10}, respectively.

A third bismuth(III) oxyiodide, $Bi_7O_9I_3$, was reported by Klimakov *et al.* (5) as an equilibrium phase in the system BiI_3–Bi_2O_3. We have not positively identified it in this study, but have evidence that it occurred in some experiments at 100°C. This suggests that it is metastable with respect to the disproportionation reaction [13] near ambient temperature.

[13] $Bi_7O_9I_3 \rightleftharpoons Bi_5O_7I + 2BiOI$

However, it is more likely that it is a stable solid, but is difficult to nucleate in ambient-temperature aqueous solutions.

Equilibrium between α-Bi_2O_3, Bi_5O_7I and solution

Preliminary attempts to determine the equilibrium constant K_{10}, by allowing mixtures of α-Bi_2O_3 and Bi_5O_7I powders to equilibrate with various solutions of KOH and (or) KI, met with limited success because of slow kinetics. However, one series of experiments, in which 0.3 g of each solid was shaken for a week in 20 cm^3 of KI solution (0.001 to 1.0 mol dm^{-3}) in stoppered Teflon bottles, gave results consistent with the expected equilibrium behaviour, with log $K_{10} \simeq -3$. Similar results were obtained when successive aliquots of KOH and (or) KI were added to stirred suspensions of the mixed solids, while the pH and pI were monitored. A deviation towards less negative values of log K_{10} occurred at pI values above about 6; this deviation was reduced by continuously purging the reaction vessel with nitrogen. Dissolved oxygen is known to interfere with iodide-selective electrodes at such low iodide activities (15); displacement of iodide from the solid phase by traces of carbonate may also have contributed to the deviation.

Some preliminary kinetic experiments showed that the rate of uptake of iodide by Bi_2O_3 powder is enhanced by pretreating the oxide with aqueous iodide, presumably because a layer of Bi_5O_7I is formed on the oxide surface. We therefore ran a series of equilibration experiments with iodide-treated Bi_2O_3. About 5 g of α-Bi_2O_3 was stirred overnight with sufficient aqueous KI to achieve about 20% conversion to Bi_5O_7I (eq. [7]). Measurements of iodide activity and pH confirmed that iodide uptake was almost quantitative. The solution was filtered, and the solid was washed repeatedly with water and immediately resuspended in 40 cm^3 of deionized water purged with nitrogen. The solution chemistry stabilized at pH $\simeq$ 9.5 and pI $\simeq$ 8. Aliquots of KOH or KI were then added, and the pH and pI were monitored continuously. After addition of each aliquot, equilibrium was re-established at successively higher pH and lower pI values, with pH + pI remaining constant at about 17.6, which corresponds to log $K_{10} \simeq -3.6$, at ambient temperature (23 ± 2°C). Although equilibrium could be approached from either direction, it was attained more quickly after addition of KI than KOH (ca. 10 min, rather than ca. 100 min). Therefore, in the definitive series of equilibrium measurements, aliquots of KI only were added to the solution, to minimize the total duration of the experiments.

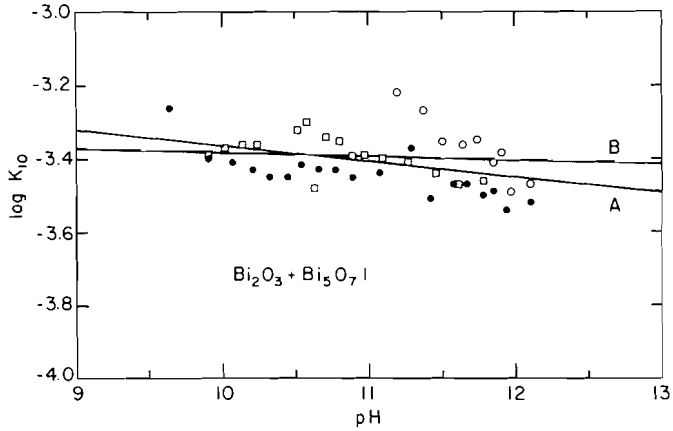

FIG. 1. Measurements of log K_{10} (14.00 − pH − pI) as a function of pH, from three series of experiments with α-Bi_2O_3 + Bi_5O_7I at 25°C. Lines A and B represent linear regressions of all data and data at pH < 11.5, respectively.

In this final series of experiments, the above procedure was repeated in a vessel thermostatted at 25°C, at least 30 min being allowed for equilibration between addition of aliquots of iodide. No significant changes were observed on standing for a further 16 h. Results are presented in Fig. 1.

Linear regression analysis of all 44 data yielded line A, with a slope, $d(\log K_{10})/d(pH) = -0.042$. The main cause for this nonzero slope appeared to be a small deviation of the pH-sensing electrode from linear behaviour at pH > 11.5. The existence of such a deviation was confirmed by pH measurements on freshly diluted standard hydroxide solutions, but no correction was attempted. When the analysis was limited to the 30 data at pH ≤ 11.5, the slope was reduced to −0.011 (line B). Based on these data, we obtained log $K_{10} = -3.39 \pm 0.13$ (2σ). However, some systematic differences are apparent between the three experiments, probably because of minor calibration errors. A value of log $K_{10} = -3.39 \pm 0.20$ probably represents the total experimental uncertainty more accurately.

Equilibria between Bi_5O_7I, BiOI, and solution

Although Bi_5O_7I was converted to BiOI by acidic iodide solutions, and BiOI was hydrolyzed to Bi_5O_7I by basic solutions, our intitial attempts to measure equilibrium behaviour between these two solids in near-neutral solutions (eq. [10]) were unsuccessful, because of the very slow interconversion kinetics. However, our success in obtaining equilibrium data from iodide-treated Bi_2O_3, as opposed to simple mixtures of Bi_2O_3 and Bi_5O_7I (preceding section), prompted us to attempt equilibrium measurements on partially hydrolyzed BiOI, rather than on a mixture of BiOI and Bi_5O_7I.

About 5 g of BiOI was stirred overnight with sufficient aqueous KOH to achieve about 20% conversion to Bi_5O_7I. The solid was isolated by filtration, washed, and then submitted to an experimental procedure similar to that for the Bi_2O_3–Bi_5O_7I equilibrium measurements, described above. In these experiments, equilibrium was usually re-attained within a few seconds

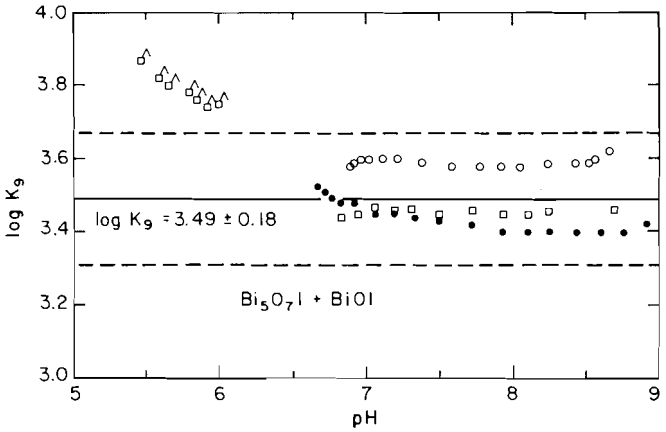

FIG. 2. Measurements of log K_9 (14.00 − pH − pI) as a function of pH, from three series of experiments with Bi_5O_7I + BiOI at 25°C. Flagged squares are measurements recorded while the pH was slowly drifting up and represent upper limits of log K_9 (see text).

of addition of aliquots of hydroxide, but only after several hours following addition of iodide. Most equilibrium measurements were therefore made by successive additions of hydroxide.

Results of three series of experiments with BiOI and Bi_5O_7I in a solution thermostatted at 25°C are shown in Fig. 2. The data at pH < 7 represent upper limits of K_9, since both pH and pI continued to drift for several hours, perhaps because of slow equilibration of the polymeric species that dominate the solution chemistry of bismuth in this pH range (16). Both pH and pI remained stable in experiments at pH values between 7 and 9; they were normally recorded about 15 min after addition of hydroxide. Analysis of the data obtained at 7 < pH < 9 in these three runs yielded values for log K_9 of 3.42 ± 0.04 (2σ), 3.59 ± 0.02, and 3.46 ± 0.01. Clearly, systematic errors between the series outweigh the random errors within each series. Based on these three separate measurements, we estimate that log K_9 = 3.49 ± 0.18.

Gibbs energies of formation of Bi_5O_7I, BiOI, and BiI_3

The Gibbs energies of formation of the bismuth iodides can be calculated from those of α-Bi_2O_3(s), $H_2O(l)$, OH^-(aq), and I^-(aq), together with K_8, K_9, and K_{10}, using eqs. [14]–[16]:

$$[14]\quad \Delta_fG^0(Bi_5O_7I, s) = \tfrac{5}{2}\Delta_fG^0(\alpha\text{-}Bi_2O_3, s) + \Delta_fG^0(I^-, aq) + \tfrac{1}{2}\Delta_fG^0(H_2O, l) - \Delta_fG^0(OH^-, aq) + RT \ln K_{10}$$

$$[15]\quad \Delta_fG^0(BiOI, s) = \tfrac{4}{5}\{\tfrac{1}{4}\Delta_fG^0(Bi_5O_7I, s) + \Delta_fG^0(I^-, aq) + \tfrac{1}{2}\Delta_fG^0(H_2O, l) - \Delta_fG^0(OH^-, aq) + RT \ln K_9\}$$

$$= \tfrac{1}{2}\Delta_fG^0(\alpha\text{-}Bi_2O_3, s) + \Delta_fG^0(I^-, aq) + \tfrac{1}{2}\Delta_fG^0(H_2O, l) - \Delta_fG^0(OH^-, aq) + RT(0.2 \ln K_{10} + 0.8 \ln K_9)$$

$$[16]\quad \Delta_fG^0(BiI_3, s) = 2\{\tfrac{1}{2}\Delta_fG^0(BiOI, s) + \Delta_fG^0(I^-, aq) + \tfrac{1}{2}\Delta_fG^0(H_2O, l) - \Delta_fG^0(OH^-, aq) + RT \ln K_8\}$$

$$= \tfrac{1}{2}\Delta_fG^0(\alpha\text{-}Bi_2O_3, s) + 3\Delta_fG^0(I^-, aq) + \tfrac{3}{2}\Delta_fG^0(H_2O, l) - 3\Delta_fG^0(OH^-, aq) + RT(0.2 \ln K_{10} + 0.8 \ln K_9 + 2 \ln K_8)$$

Robie *et al.* (17) list the following Gibbs energies of formation at 298.15 K and 100 kPa, with aqueous species referring to a standard state of 1 mol kg^{-1}: Bi_2O_3(s), −493.453 ± 1.464 (2σ) kJ mol^{-1}; $H_2O(l)$, −237.141 ± 0.084 kJ mol^{-1}; OH^-(aq), −157.328 ± 0.090 kJ mol^{-1}; I^-(aq), −51.915 ± 0.860 kJ mol^{-1}. (These error limits are stated in ref. 17 as twice the estimated standard deviations.) Substituting in eqs. [14]–[16], we obtain expressions [17]–[19].

$$[17]\quad \Delta_fG^0(Bi_5O_7I, s, 298\ K) = [(-1246.79 \pm 4.65) + RT \ln K_{10}]\ kJ\ mol^{-1}$$

$$[18]\quad \Delta_fG^0(BiOI, s, 298\ K) = [(-259.88 \pm 1.72) + RT(0.2 \ln K_{10} + 0.8 \ln K_9]\ kJ\ mol^{-1}$$

$$[19]\quad \Delta_fG^0(BiI_3, s, 298\ K) = [(-286.20 \pm 3.70) + RT(0.2 \ln K_{10} + 0.8 \ln K_9 + 2 \ln K_8)]\ kJ\ mol^{-1}$$

Using the values for K_9 and K_{10} derived here, we obtain

$$\Delta_fG^0(Bi_5O_7I, s, 298\ K) = -1266.1 \pm 5.8\ kJ\ mol^{-1}$$

$$\Delta_fG^0(BiOI, s, 298\ K) = -247.8 \pm 2.8\ kJ\ mol^{-1}$$

Dyrssen and Yen (2) obtained log K_{20} (= 2 log [H^+] + 2 log [I^-] (their log K_s)) = −8.50 for equilibrium [20] in 3 mol dm^{-3} aqueous sodium perchlorate solution.

$$[20]\quad BiI_3(s) + H_2O \rightleftharpoons BiOI(s) + 2H^+ + 2I^-$$

Equilibrium constants K_{20} and K_8 are related by eq. [21].

$$[21]\quad \log K_{20} = 2 \log K_8 + 2 \log K_w$$

Using the value log K_w = −14.22 ± 0.02 in 3 mol dm^{-3} aqueous sodium perchlorate, as reported by Ingri *et al.* (18), but without attempting to correct K_{20} for ionic strength effects, we estimate log K_8 = 10.0 ± 1.0. Application of this value to eq. [19] yields $\Delta_fG^0(BiI_3, s, 298\ K)$ = −160.0 ± 16.2 kJ mol^{-1}. Combining this value with data for Bi^{3+}(aq) and I^-(aq) from ref. 17 (Δ_fG^0 = 82.80 ± 0.85 and −51.915 ± 0.860 kJ mol^{-1}, respectively), we calculated the solubility product of BiI_3: log $K_{sp}(BiI_3, 298\ K)$ = −15.3 ± 3.4.

This solubility product is in better agreement with the value of −15.6 reported by Dyrssen and Yen (2) than −18.1, as reported by Ahrland and Grenthe (19), although both literature values lie within our estimated error limits. A value near −15 also appears to be more consistent with observations on BiI_3 precipitation, as summarized by Eve and Hume (20). However, since the Dyrssen–Yen data again refer to 3 mol dm^{-3} perchlorate media, direct comparisons are not strictly valid.

Conclusions

From the viewpoint of radioactive iodine immobilization, the most important conclusion is that Bi_5O_7I is seven orders of magnitude more stable than BiOI, and about fourteen orders of magnitude more stable than BiI_3, towards hydrolysis, if "stability" is expressed as the minimum iodide activity at a given pH, at which the solid can exist at equilibrium. Expressed another way, the lowest controlled iodide activities that can be achieved in this system are those buffered by the solid phase assemblage, Bi_2O_3 + Bi_5O_7I, and are expressed by the relationship, pH + pI = 17.39 ± 0.20 at 25°C. However, considerable care is necessary in the pretreatment of solids in order to achieve this equilibrium in a reasonably short time. A full understanding of the behaviour of a bismuth oxyiodide waste form for radioactive iodine also requires some knowledge of redox chemistry, iodine speciation, and interactions with other anions. We have previously reported data on the stability

of basic bismuth carbonates (21), and are presently investigating reactions of Bi_2O_3 with other common anions in aqueous systems. The Gibbs energy data presented here permit calculation of stability at 25°C with respect to redox reactions involving any other species for which Gibbs energies of formation are known.

Acknowledgements

We are grateful to J. M. Snider for the XRD data and to R. J. Lemire and J. Paquette for helpful discussions.

1. E. MONTIGNIE. Bull. Soc. Chim. Fr. [5], **1**, 692 (1934).
2. D. DYRSSEN and A.-C. YEN. *In* Solvent extraction chemistry: Proceedings of international conference, Gothenburg, Sweden, 1966. *Edited by* D. Dyrssen, J.-O. Liljenzin and J. Rydberg. North-Holland, Amsterdam and Wiley–Interscience, New York. 1967. pp. 470–476.
3. A. RULMONT. Rev. Chim. Miner. **14**, 277 (1977).
4. J. KETTERER and V. KRÄMER. Z. Naturforsch. B: Anorg. Chem. Org. Chem. Biochem. Biophys. Biol. **39**, 105 (1984).
5. A. M. KLIMAKOV, B. A. POPOVKIN, and A. V. NOVOSELOVA. Zh. Neorg. Khim. **19**, 2553 (1974); Russ. J. Inorg. Chem. Engl. Transl. **19**, 1394 (1974).
6. J. L. KHARBANDA, I. J. SINGH, and R. V. AMALRAJ. Indian J. Chem. Sect. A, **14**, 340 (1976).
7. M. P. S. RAMANI, P. K. PANICKER, A. L. MOHAN, M. V. RAJAN, and J. L. KHARBANDA. Manage. Radioact. Wastes Nucl. Fuel Cycle, Proc. Symp. **1**, 153 (1976).
8. V. A. MEL'NIKOV, L. N. MOSKVIN, and V. V. CHETVERIKOV. Radiokhimiya, **25**, 675 (1983); Sov. Radiochem. Engl. Transl. **25**, 636 (1984).
9. E. R. VANCE, D. K. AGRAWAL, B. E. SCHEETZ, J. G. PEPIN, S. D. ATKINSON, and W. B. WHITE. Ceramic phases for immobilization of ^{129}I. Report No. DOE/ET/41900-9, Rockwell International, Canoga Park, CA 91304, U.S.A.
10. L. L. BURGER, R. D. SCHELLE, and K. D. WIEMERS. Selection of a form for fixation of iodine-129. Report No. PNL-4045, Battelle Pacific Northwest Laboratory, Richland, WA 99352, U.S.A. 1981.
11. H. E. SWANSON, M. I. COOK, T. ISAACS, and E. H. EVANS. Natl. Bur. Stand. Circ. (U.S.), 539, **9**, 16 (1960).
12. V. KRÄMER. J. Therm. Anal. **16**, 295 (1979).
13. J. B. HIGGINS and P. H. RIBBE. Am. Mineral. **61**, 878 (1976).
14. J. KETTERER, E. KELLER, and V. KRÄMER. Z. Kristallogr. In press.
15. J. KONTOYANNAKOS, G. J. MOODY, and J. D. R. THOMAS. Anal. Chim. Acta, **85**, 47 (1976).
16. C. F. BAES and R. E. MESMER. The hydrolysis of cations. Wiley-Interscience, New York. 1976. p. 382.
17. R. A. ROBIE, B. S. HEMINGWAY, and J. R. FISHER. U.S. Geol. Surv. Bull. 1452 (reprinted with corrections, 1979).
18. N. INGRI, G. LAGERSTRÖM, M. FRYDMAN, and L. G. SILLÉN. Acta Chem. Scand. **11**, 1034 (1957).
19. S. AHRLAND and I. GRENTHE. Acta Chem. Scand. **11**, 1111 (1957).
20. A. J. EVE and D. N. HUME. Inorg. Chem. **3**, 276 (1964).
21. P. TAYLOR, S. SUNDER, and V. J. LOPATA. Can. J. Chem. **62**, 2863 (1984).

Structure de l'opigénine: triterpène pentacyclique isolé d'Opilia celtidifolia

DANIÈLE DRUET ET LOUIS COMEAU[1]
Laboratoire de chimie biologique appliquée, Place Victor Hugo, 13331 Marseille Cédex 3, France

ET

JEAN-PIERRE ZAHRA
Laboratoire de stéréochimie, rue Henri Poincaré, 13397 Marseille Cédex 13, France

Reçu le 29 mai 1985

DANIÈLE DRUET, LOUIS COMEAU et JEAN-PIERRE ZAHRA.Can. J. Chem. **64**, 295 (1986).

La structure de l'opigénine, une aglycone issue de la fraction glycosidique d'*Opilia celtidifolia*, a été établie grâce aux données spectroscopiques (ir, rmn du ^1H et du ^{13}C, masse) de l'opigénine et des ses dérivés. Il s'agit d'un triterpène nouveau, de structure voisine de celle du 3β-hydroxy lupane, mais avec un isopropyle en position 20 et un pont oxyméthylène en position 20–28.

DANIÈLE DRUET, LOUIS COMEAU, and JEAN-PIERRE ZAHRA. Can. J. Chem. **64**, 295 (1986).

The structure of opigenin, an aglycone from the glycosidic fraction of *Opilia celtidifolia*, has been established by study of the genin and its derivatives by means of ir, mass spectroscopy, and ^1H and ^{13}C nmr spectroscopy. This is a new triterpene whose skeleton resembles that of 3β-hydroxy lupane but with an isopropyl group in position 20 and an oxymethylene bridge in position 20–28.

[Traduit par le journal]

Introduction

Dans le cadre d'une étude sur les plantes médicinales d'Afrique de l'Ouest, une Opiliacée de Côte d'Ivoire, *Opilia celtidifolia*, a retenu notre intérêt. Il s'agit d'une liane que l'on trouve le plus souvent dans la zone des savanes et dont la pharmacopée locale fait de multiples usages (1–3).

Dans un premier temps, l'étude structurale des aglycones issues de la fraction glycosidique de la plante nous a permis, d'identifier les composés majeurs (4). Il s'agit de l'acide oléanolique de son acétate et de l'hédéragénine, des triterpènes pentacycliques.

Dans un second temps, l'étude des composés mineurs a permis la mise en évidence de plusieurs substances comprenant, entre autres, un alcool terpénique présent en très faible quantité (moins de 0,7%, en poids, de la totalité des aglycones), dont nous avons tenté d'établir la structure. Une étude analytique préliminaire n'a pas permis d'identifier ce composé à un triterpène de structure connue. Il nous a donc fallu, afin de compléter l'étude structurale, préparer quelques uns de ses dérivés. Les résultats obtenus lors de l'étude de ces dérivés ont révélé un squelette hydrocarboné assez inhabituel dans la série des triterpènes pentacycliques. Nous avons donc dénommé cette aglycone "opigénine". Une étude ultérieure, conduite sur les autres composés mineurs, devrait nous permettre d'établir les relations existant entre l'opigénine et les autres triterpènes présents dans la plante. S'il s'avère que cette aglycone ne résulte pas d'un réarrangement subi par une aglycone de structure classique, il sera alors nécessaire d'établir le processus biosynthétique qui est à l'origine de sa formation.

Résultats et discussion

L'opigénine a été isolée plusieurs fois à partir d'extraits provenant de lots différents d'*Opilia celtidifolia*, selon les conditions décrites dans la partie expérimentale. Obtenue par chromatographie sur colonne à partir du mélange des aglycones acétylées, sa pureté est contrôlée par ccm (chromatographie sur couche mince) et clhp (chromatographie liquide à haute pression). Les traces d'acide oléanolique résiduel sont éliminées par cristallisation du chlorure de méthylène. Les cristaux obtenus (F = 275–280°C) présentent une structure en feuillet qui ne convient pas pour la diffraction des rayons X. Ils répondent positivement au test de Liebermann–Burchard et négativement à celui du tétranitrométhane.

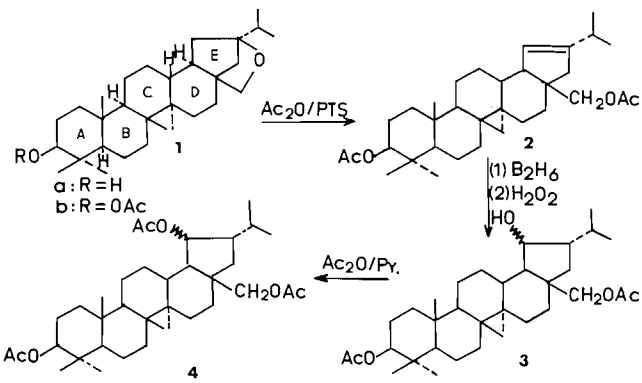

FIG. 1. Structure de l'opigénine et de ses dérivés.

Une partie des cristaux est désacétylée par hydrolyse en milieu basique afin d'établir les constantes physico-chimiques de l'opigénine **1***a*, Recristallisée du dichlorométhane, l'opigénine présente un point de fusion de 265–267°C. Le résultat de l'analyse centésimale et la présence en spectrométrie de masse d'un pic d'ion moléculaire à m/z = 442 conduisent à la formule brute $C_{30}H_{50}O_2$. La spectrométrie infrarouge montre qu'il s'agit d'un alcool (νOH à 3500 cm^{-1}) *gem*-diméthylé (νCH à 1360 et 1380 cm^{-1}). L'absence d'absorption dans le domaine 850–870 cm^{-1} laisse supposer que l'opigénine ne présente pas de liaison éthylénique, ce qui confirme le test au tétranitrométhane. En spectrométrie de masse, l'opigénine donne la fragmentation caractéristique des triterpènes pentacycliques hydroxylés en 3: on remarque, en effet, à m/z = 189, 203 et 207, les pics résultant d'une scission au niveau du cycle C, déjà décrite par ailleurs (5–8). Deux autres fragments permettent de préciser la structure de l'aglycone: l'un, à m/z = 411, doit résulter de la perte de CH_2O et H• et suggère la présence d'un

[1]Auteur à qui toute correspondance doit être adressée.

TABLEAU 1. En rmn du ^1H, glissements chimiques comparés de l'opigénine et de ses dérivés et de composés de référence

Composé (réf.)	Me 23–24–25	Me 26	Me 27	Me 28	Me 29–30	—CH_2O—	3H
Acétate d'opigénine **1***b* (ce travail	0,84 (×2)–0,87	1,03	0,98	—	0,86(t), ^3J = 6,5 Hz	3,35(dd) et 4,16(dd) ^2J = −7,5 Hz	4,5(q)
3β-Acétoxy 19β,28β-époxy lupa-20,29-ène (11)	0,83–0,85–0,86	1,02	0,92	—	—	3,36(d) et 4,0(dd) ^2J = −7 Hz	—
Composé **2** (ce travail)	0,84 (×2)–0,88	1,04	0,97	—	0,87(d)–1,0(d) ^3J = 6,5 Hz	3,83(d) et 4,30(d) ^2J = −10 Hz	4,5(q)
3β,28β-Diacétoxy lupa-20,30-ène (12)	0,85–0,87 (×2)	1,05	0,98	—	—	3,86(d) et 4,27(d)	4,48(m)
Composé **3** (ce travail)	0,83–0,84–0,85	1,05	0,96	—	0,86(d)–1,11(d) ^3J = 6,5 Hz	3,79(d) et 4,42(d) ^2J = −11 Hz	4,49(m)
Composé **4** (ce travail)	0,83–0,84–0,86	1,04	0,96	—	0,96(d) –1,09(d) ^3J = 6,5 Hz	3,98(d) et 4,27(d) ^2J = −11 Hz	4,49(m)

NOTA: Les valeurs des déplacements chimiques sont données en parties par million avec le TMS comme référence (d = doublet, dd = doublet dédoublé, t = triplet, q = quadruplet, m = multiplet).

pont oxyméthylène; l'autre, à m/z = 381, provient de la perte d'une molécule d'eau et d'un groupement isopropyle. La présence de ce groupement sur la molécule est confirmée par le pic de base à m/z = 43 (5). La rmn du ^1H à 200 MHz est effectuée, pour des raisons de commodité, sur l'opigénine acétylée **1***b*. Les signaux obtenus pour les groupements méthyles (tableau 1) correspondent à la présence de cinq groupements angulaires et d'un groupement isopropyle. À δ = 2,04 ppm, un singulet (3H dû au méthyle d'un groupement acétyle montre que l'opigénine ne possède qu'un hydroxyle acétylable. La position de ce groupement est donnée à δ = 4,5 ppm (^3J = 10 Hz, ^3J = 6 Hz) par le quadruplet caractéristique, dans les systèmes triterpéniques pentacycliques, du couplage $^3J_{aa}$ et $^3J_{ae}$ du proton en 3 axial, lorsque celui-ci se trouve en α d'un acétyle (10). On en déduit que l'hydroxyle acétylable occupe la position 3 équatoriale. Les doublets dédoublés observés à δ = 3,35 et 4,16 ppm ($^2J_{AB}$ = −7 Hz, $^4J_{AA'}$ = 2 Hz, $^4J_{BB'}$ = 1,5 Hz) correspondent à deux hydrogènes situés sur un carbone porteur d'une fonction éther-oxyde, en l'occurrence un groupement oxyméthylène. On peut considérer qu'ils constituent les deux parties A et B d'un système AB dont chaque branche est dédoublée par la présence d'un couplage à longue distance du type ^4J. Il s'avère, d'après les observations effectuées par certains auteurs (9) sur des dérivés de triterpènes possédant un pont oxyméthylène, que de tels couplages ne sont possibles que si les têtes de pont sont des carbones quaternaires (fig. 2). La valeur relativement faible trouvée pour la constante de couplage J_{AB} des protons du groupement oxyméthylène indique que ce pont se trouve inclus dans un cycle tendu à quatre ou cinq atomes. On note en effet, dans la littérature, des valeurs de J_{AB} de cet ordre pour des composés dont le groupement —CH_2O— appartient à un cycle à cinq atomes: 6 et 7 Hz pour des dérivés du 3β-hydroxy 13β,28β-époxy oléan-11,12-ène (11), 7 et 7,5 Hz pour des dérivés du 3β-acétoxy 19β,28β-époxy lupane (12). Cette constante est comprise entre 10 et 12 Hz lorsque le groupement —CH_2O— fait partie d'un cycle à six atomes: 11 Hz pour le 3β-acétoxy 20β,28β-époxy lupane (13). Le spectre de rmn du ^{13}C, enregistré sur l'acétate **1***b* en utilisant toutes les techniques appropriées à la détermination de la nature des différents types de carbones présents dans la molécule (APT, INEPT, ADEPT), fait apparaître: 8 carbones primaires (CH_3—) à δ = 27,9; 24,8; 21,3; 20,1; 16,4; 16,4; 15,8; 14,2 ppm; 11 carbones secondaires (—CH_2—) à δ = 69,0; 38,5; 34,9; 33,8; 29,8; 27,9; 26,5; 25,4; 23,7; 22,7; 18,1 ppm; 6 carbones tertiaires (—CH—) à δ 80,9; 55,5; 50,7; 47,1; 42,4; 39,7 ppm; 7 carbones quaternaires (—C—) dont aucun n'est éthylénique à δ = 170,9; 72,2; 41,5; 40,7; 37,8; 37,1; 31,7 ppm.

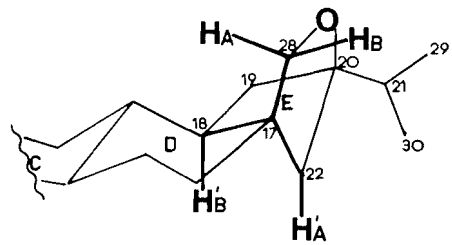

FIG. 2. Structure du cycle D de l'opigénine.

L'attribution de ces différents glissements chimiques figure dans le tableau 2 établi après détermination de la structure de l'opigénine.

Le test de Liebermann–Burchard, la fragmentation caractéristique en spectrométrie de masse et la présence de méthyles angulaires en rmn du ^1H suggèrent un squelette hydrocarboné de type triterpène pentacyclique.

La présence d'un groupement isopropyle, caractérisé aussi bien en spectrométrie de masse qu'en rmn du ^1H, nous a amené à effectuer une étude comparative des constantes de rmn du ^1H et du ^{13}C obtenues pour l'acétate d'opigénine **1***b*, avec celles données par la littérature (9, 12–20). En rmn du ^1H, on constate que l'opigénine présente une certaine similitude avec les dérivés du lupane et du hopane et plus particulièrement avec ceux du 3β-acétoxy lupène (tableau 1). On note l'absence de signal pour le méthyle en 17, ce qui peut être l'indice d'une "fonctionnalisation" du carbone en 28. En rmn du ^{13}C, on constate une identité presque parfaite entre les glissements chimiques des carbones des cycles A, B, C et d'une partie du cycle D ($C_{(1)}$–$C_{(16)}$ et $C_{(23)}$) de l'acétate d'opigénine et du 3β-acétoxy lupane (tableau 2), les différences constatées au niveau des cycles D et E étant vraisemblablement dues à la présence du pont oxyméthylène et du groupement isopropyle sur ces cycles. L'ouverture du pont oxyméthylène est effectuée par action de l'acide paratoluène sulfonique dans l'anhydride acétique sur l'acétate d'opigénine

TABLEAU 2. En rmn du ^{13}C, glissements chimiques comparés du 3β-acétoxy lupane et de l'opigénine et de ses dérivés

C	3β-Acétoxy lupane	**1***b*	**2**	**4**	C	3β-Acétoxy lupane	**1***b*	**2**	**4**
1	38,3	38,5	38,6	38,0	16	35,5	34,9	35,3	32,1
2	23,6	23,7	23,7	23,4	17	43,1	31,7	37,0	40,5
3	80,7	80,9	80,9	80,7	18	47,5	47,1	48,6	49,4
4	37,7	37,8	37,8	38,2	19	44,6	25,4	117,9	73,6
5	55,3	55,5	55,4	55,0	20	29,3	72,2	140,1	45,3
6	18,2	18,1	18,2	18,0	21	21,9	42,4	36,1	37,6
7	34,1	33,8	34,1	34,2	22	40,4	29,8	30,5	29,4
8	40,7	40,7	41,1	40,8	23	27,9	27,9	27,9	27,7
9	50,2	50,7	50,3	50,2	24	16,5	16,4	16,3	16,5
10	37,0	37,1	37,2	36,8	25	16,1	16,4	16,3	16,5
11	20,9	22,7	22,8	21,3	26	15,9	15,8	16,1	16,0
12	25,0	26,5	26,8	25,7	27	14,4	14,2	14,9	14,7
13	37,9	39,7	38,4	37,5	28	18,0	69,0	61,0	61,9
14	42,7	41,5	42,2	44,0	29	15,1	20,1	21,1	20,8
15	27,4	27,9	27,6	28,8	30	23,0	24,8	22,9	21,2

NOTA: Les valeurs de δ sont données en parties par million avec le TMS comme référence. Pour **1***b*: δ(*C*=O) = 170,9 ppm et δ(CO*C*H$_3$) = 21,3 ppm. Pour **2**: δ(*C*=O) = 171,0 ppm et 171,5 ppm et δ(CO*C*H$_3$) = 21,3 et 21,5 ppm. Pour **4**: δ(*C*=O) = 177,8; 171,8; 170,3 ppm et δ(CO*C*H$_3$) = 21,1; 21,3; 21,5 ppm.

1*b* (21). On obtient ainsi le composé **2** qui présente, en spectrographie infrarouge, l'absorption caractéristique des liaisons éthyléniques à 800 cm^{-1}. En spectrométrie de masse, le pic de l'ion moléculaire situé à m/z = 526 permet, avec l'analyse centésimale, de déterminer la formule brute: $C_{34}H_{54}O_4$. À côté des fragments 189 et 203 caractéristiques des triterpènes, on remarque trois fragments intéressants: Le premier à m/z = 423 ($M^{+\cdot}$ − CH_3CO_2H−$CH(CH_3)_2$) confirme la présence d'un groupement isopropyle. Le second à m/z = 406 ($M^{+\cdot}$ − 2 CH_3CO_2H) montre que la molécule est diacétylée et le troisième nous apprend que l'un des acétyles est porté par un carbone primaire: m/z = 453 ($M^{+\cdot}$ − CH_2OCOCH_3). La rmn du ^1H apporte quelques précisions sur la conformation de la molécule (tableau 1). Ainsi pour les méthyles de l'isopropyle on observe deux doublets. L'un est centré sur δ = 0,86 ppm (^3J = 6,5 Hz), et ses composantes sortent dans les signaux des méthyles du cycle A à δ =0,84 et 0,88 ppm; l'autre doublet, centré sur δ = 1,00 ppm, (^3J = 6,5 Hz) apparaît nettement. La courbe d'intégration est en accord avec cette analyse. La présence de ces deux doublets traduit la nonéquivalence des méthyles du groupement isopropyle (22). Deux singulets, à δ = 2,04 et 2,08 ppm (2 × 3H), dus aux méthyles de deux acétyles confirment la diacétylation. La présence d'une fonction alcool primaire est marquée par deux doublets centrés respectivement sur δ = 3,83 et 4,30 ppm (2 × 1H, $^2J_{AB}$ = −11 Hz) et attribuables aux protons non équivalents d'un groupement —CH_2OAc porté par un carbone quaternaire. Enfin, centré sur δ = 5,23 ppm, un doublet (1H, ^3J = 7 Hz) indique la présence d'une liaison éthylénique trisubstituée dont le proton n'est couplé qu'avec un seul proton vicinal, donc en α d'un carbone tertiaire: $(R)_2$—CH—CH=C—$(R)_2$. La rmn du ^{13}C confirme cette disposition avec deux pics dus respectivement à un carbone éthylénique quaternaire à δ = 140,1 ppm et à un carbone éthylénique tertiaire à = 117,9 ppm.

Le composé **2** se présente donc comme un diol triterpénique pentacyclique insaturé. L'ouverture du pont oxyméthylène a conduit à l'apparition d'une fonction alcool primaire et d'une liaison éthylénique trisubstituée. L'absence du méthyle angulaire sur le carbone 17 et les valeurs des glissements chimiques des protons du groupement —CH_2OAc, très voisines de celles données dans la littérature (12) pour le 3β,28β-diacétoxy lupa-20,30-ène, nous amènent à positionner ce groupement sur le carbone en 17. L'emplacement de la double liaison, vraisemblablement sur les cycles D ou E, ne peut être déterminé avec précision que si l'on additionne sur celle-ci un groupement chimique convenable. L'hydroboration oxydative de **2** conduit, après purification, au composé d'addition hydroxylé **3**. En rmn du ^1H, on constate que les doublets attribués aux protons non équivalents du —CH_2OAc ont subi un déplacement (δ = 3,79 et 4,42 pm, 2 × 1H, $^2J_{AB}$ = −11 Hz) par rapport au composé **2**, ce qui indique un changement dans l'environnement chimique de ces protons. On remarque également deux quadruplets (1H au total), situés à δ = 5,29 et 5,45 ppm, et présentant des constantes de couplage voisines et égales respectivement à ^3J = 12 Hz, ^3J = 6 Hz et ^3J = 10 Hz, ^3J = 6 Hz. Ces deux quadruplets sont dans le rapport de 1:4, si l'on compare les intégrations respectives. Comme cela a déjà été signalé par ailleurs (23), la réaction d'hydroboration a conduit aux deux stéréoisomères α et β. La présence, dans le spectre, de deux singulets situés à δ = 8,55 et 9,15 ppm (1H au total), et disparaissant par échange avec D_2O, donc attribuables aux protons des OH, confirme l'isomérie. Les valeurs relativement importantes des glissements chimiques observées ici, et que l'on peut attribuer en première approximation aux protons situés en α des groupements hydroxyles apparus après hydroboration oxydative, montrent que ceux-ci sont situés dans le cône de blindage d'un groupement chimique voisin. En fait, si l'on considère les étapes qui ont conduit au composé **3**, il ne peut s'agir que du groupement —CH_2OAc. L'acétylation de **3** donne le triacétate **4** que l'on recristallise facilement dans l'hexane. La masse de l'ion moléculaire, 586, obtenue en spectrométrie de masse, jointe à l'analyse centésimale, conduit à la formule $C_{36}H_{58}O_6$. On retrouve à nouveau les fragments 203 et 189 caractéristiques des triterpènes pentacycliqus et quelques fragments qui montrent que la molécule est triacétylée (m/z = 526, 466 et 406), que l'une des fonctions alcools acétylées est primaire (m/z = 453, $M^{+\cdot}$—CH_3CO_2H – CH_2OCOCH_3; m/z = 393. $M^{+\cdot}$ −(2 × CH_3CO_2H) − CH_2OCOCH_3) et qu'il existe un groupement isopropyle (m/z = 483, $M^{+\cdot}$ − CH_3CO_2H − $CH(CH_3)_2$). La rmn du ^1H confirme la présence des trois

groupements acétyles (trois singulets 3 × 1H à δ = 2,02; 2,05; 2,13 ppm) et montre que les protons non équivalents du —CH_2OAc en 17 ont subi à nouveau une variation de glissement chimique (δ = 3,98 et 4,28 ppm, $^2J_{AB} = -11$ Hz). Ceci est en faveur de l'hypothèse que nous avons faite concernant la présence, dans l'environnement immédiat de ce groupement, d'un autre groupement, en l'occurrence l'hydroxyle acétylé provenant de l'hydroboration oxydative. La rmn du ^{13}C permet, au moyen de l'APT d'attribuer tous les glissements chimiques observés aux différents carbones de la molécule (tableau 1). On note que le carbone porteur de l'hydroxyle provenant de l'hydroboration oxydative est un carbone secondaire.

En résumé, l'étude du dérivé résultant de l'ouverture du pont oxyméthylène nous a permis de fixer la position de ce groupement entre le carbone en 17 et un autre carbone tétrasubstitué en tête de pont. En tenant compte du fait qu'il existe un groupement isopropyle, vraisemblablement situé sur le cycle E, et que l'hétérocycle formé par le pont oxyméthylène ne comporte pas plus de cinq atomes, il est alors possible de proposer la structure **1***a* pour l'opigénine.

Deux faits expérimentaux justifient le choix de cette structure. En premier lieu, l'examen du modèle moléculaire correspondant à la structure **1***a* montre qu'après ouverture du pont oxyméthylène, le proton de la liaison éthylénique présente un angle dièdre d'environ 100° avec le proton en 18α. Cet angle correspond à une constante de couplage en rmn du ^1H d'environ 7 Hz. C'est bien ce que l'on observe expérimentalement. En second lieu, si notre hypothèse structurale est exacte, le composé résultant de l'hydroboration oxydative doit présenter un proton en position 19, qui par couplage avec les protons 18α et 20β donnera un quadruplet en rmn du ^1H. Nous observons en effet une telle figure de couplage avec, toutefois, la particularité d'un dédoublement dû à l'isomérie α–β du proton en 19.

La structure **1***a* est donc cohérente avec les résultats expérimentaux obtenus et peut donc être raisonnablement proposée pour l'opigénine.

Partie expérimentale

Les points de fusion ont été pris sur microscope à platine chauffante de Reichert. Les spectres ir ont été effectués sur un appareil Leitz. Les pouvoirs rotatoires ont été mesurés dans le chloroforme au moyen d'un micropolarimètre Perkin–Elmer. Les spectres de rmn du ^1H ont été enregistrés indifféremment sur Varian XL 100, Varian XL 200 et Brucker AM 200, en solution dans le deutérochloroforme avec le TMS comme référence interne. Les spectres de rmn du ^{13}C ont été déterminés sur Varian XL 200 et les spectres de masse, sur Thompson ou L. K. B.

1. *Isolement de l'acétate d'opigénine 1b*

L'opigénine est extraite à partir des aglycones brutes obtenues par hydrolyse acide de la fraction glycosidique d'*Opilia celtidifolia* (4). Celles-ci (79 g), placées dans un Soxhlet, sont lavées à l'oxyde d'éthyle durant 72 h. L'évaporation du solvant permet de récupérer 40 g de résidu que l'on acétyle à 25°C à l'aide de 80 mL d'anhydride acétique en présence de 400 mL de pyridine anhydre. La réaction dure 48 h. Après élimination des réactifs sous pression réduite la phase organique est reprise au dichlorométhane, lavée successivement au Na_2CO_3, à l'eau, à l'HCl 2 *N*, puis à nouveau à l'eau jusqu'à neutralité. Après séchage sur Na_2SO_4 et élimination du solvant, on obtient 41,2 g d'acétates d'aglycones.

Ces acétates sont ensuite fractionnés par chromotographie sur colonne de silice (50 g de silice par gramme d'aglycones), avec comme éluant le mélange hexane–oxyde d'éthyle (90:10 en volume). À partir de 5 g d'aglycones acétylées, on isole en moyenne 35 mg d'acétate d'opigénine **1***b*, soit 0,7% en poids des aglycones brutes. Après cristallisation du mélange dichlorométhane–hexane, l'acétate d'opigénine présente les caractéristiques suivantes: *F* 275–280°C; α_D^{45} +25,6°, (*c* 26,6×10^{-3}, $CHCl_3$); ir cm^{-1} (KBr); 1724, 1389, 1380, 1250, 1142, 1117, 869; rmn ^1H et ^{13}C ($CDCl_3$): tableaux 1 et 2; masse *m/z*: 484(49), 424(100), 409(38), 381(47), 355(35), 342(24), 219(19), 205(35), 203(37), 189(94). *Anal.* calc. pour $C_{32}H_{52}O_3$: C 79,33; H 10,74; O 9,92; tr.: C 79,17; H 11,09; O 9,74%.

2. *Obtention de l'opigénine*

On saponifie durant 3 h au reflux, 21 mg d'acétate d'opigénine **1***b* à l'aide de 8 mL de potasse 2 *N* méthanolique. Après dilution, la fraction hydro-alcoolique est extraite à l'oxyde de éthyle, l'extraite éthéré est lavé à l'eau, séché sur Na_2SO_4, et le solvant est éliminé. Le résidu (18 mg) est recristallisé dans le dichlorométhane et l'on observe les caracteristiques suivantes: *F* 265–267°C; ir cm^{-1}(KBr): 3500, 1380, 1360, 1142, 1117, 865; rmn ^1H et ^{13}C ($CDCl_3$): tableaux 1 et 2; masse *m/z*: 442(45), 424(20), 411(6), 409(8), 381(3), 207(33), 203(15), 189(45), 43(100). *Anal.* calc. pour $C_{30}H_{50}O_2$: C 81,45; H 11,31; O 7,24; tr.: C 81,16; H 11,44; O 7,40%.

3. *Ouverture du pont oxyméthylène*

On additionne 53 mg d'acide paratoluène sulfonique à 64 mg d'opigénine **1***a* dans 10 mL d'anhydride acétique et porte le tout à 117–120°C durant 30 min (21). Après ce temps, on dilue à l'eau et extrait au dichlorométhane. La solution organique est lavée au $NaHCO_3$ aqueux, puis à l'eau jusqu'à neutralité. Après séchage sur Na_2SO_4 et élimination du solvant, on récupère 74 mg de résidu. Le composé **2** est séparé des produits secondaires par chromatographie sur colonne de silice avec le mélange hexane – oxyde d'éthyle (90:10 en volume) comme éluant. On isole ainsi 14 mg de produit pur que l'on recristallise à partir du mélange hexane–dichlorométhane et qui présente les caractéristiques suivantes: *F* 237–240°C; α_D^{25} +13,6° (*c* 21×10^{-3}, $CHCl_3$); ir cm^{-1}(KBr): 1725, 1355, 1232, 1025, 975, 800; rmn ^1H et ^{13}C ($CDCl_3$): tableaux 1 et 2; masse *m/z*: 526(9), 466(42), 423(10), 406(16), 393(10), 363(5), 203(39), 189(72), 43(100). *Anal.* calc. pour $C_{34}H_{54}O_4$: C 77,56; H 10,26; O 12,17; tr.: C 77,43; H 10,34; O 12,23%.

4. *Hydroboration oxydative du composé 2*

Une solution de 20 mg de produit **2** dans 2 mL de THF anhydre est portée à 0°C, puis saturée successivement à l'aide d'azote désoxygéné et de diborane. On maintient la solution sous agitation à 20°C durant 3 h et alcalinise à l'aide de 3,2 mL de soude 3 *N*. On ajoute alors goutte à goutte, sous agitation, 3,2 mL de peroxyde d'hydrogène à 30%. Le mélange est abandonné 1 h à 20°C, puis la fraction organique est extraite à l'oxyde d'éthyle. Après lavage à l'eau jusqu'à neutralité et séchage sur Na_2SO_4, le solvant est éliminé. Le résidu pèse 19,3 mg. L'analyse par ccm montre que ce résidu est essentiellement constitué de deux produits pondéralement majoritaires, accompagnés de trois produits secondaires. L'un des produits majoritaires est identifié à **2**, l'autre est isolé en ccm préparative sur plaque Merck 60 GF_{254}. Après élution à l'aide du mélange hexane – oxyde d'éthyle (25:75 en volume), on obtient 9,2 mg de produit **3**.

L'acétylation de **3** est effectuée à 25°C durant 48 h à l'aide de 1 mL d'anhydride acétique et 2 mL de pyridine anhydre. L'acétate est récupéré de la manière habituelle et recristallisé à partir de l'hexane. On obtient 7 mg de composé **4** que l'on identifie par rmn du ^1H et du ^{13}C ainsi que par spectrométrie de masse, et qui présente les caractéristiques suivantes: *F* 240–245°C; ir cm^{-1}(CS_2): 2925, 1740, 1475, 1370, 1250; rmn du ^1H et du ^{13}C ($CDCl_3$): tableaux 1 et 2; masse *m/z*: 586(35), 526(20), 483(15), 466(45), 453(33), 406(10), 393(9), 203(20), 189(50), 43(100). *Anal.* calc. pour $C_{36}H_{58}O_6$: C 73,72; H 9,90; O 16,38; tr.: C 73,63; H 9,91; O 16,45%.

1. A. Bouquet et M. Debray. Plantes médicinales de la Côte d'Ivoire. Trav. ORSTOM **32**, 133 (1974).
2. J. Kerharo et J. G. Adam. La pharmacopée sénégalaise traditionnelle. Vigot et Frères, Paris. 1974. p. 617.
3. E. Adjanohoun et L. Ake Assi. Plantes pharmaceutiques de Côte d'Ivoire. Rapport au Ministère du Plan de Côte d'Ivoire, Abidjan. 1973. p. 210

4. D. DRUET et L. C. COMEAU. Ann. Univ. Abidjan, **XIV**, 57 (1978).
5. H. BUDZIKIEWICZ, J. M. WILSON et C. DJERASSI. J. Am. Chem. Soc. **85**, 3688 (1963).
6. J. L. COURTNEY et J. S. SHANNON. Tetrahedron Lett. 13 (1963).
7. C. G. MACDONALD et J. S. SHANNON. Tétrahédron Lett. 173 (1963).
8. J. S. SHANNON. Aust. J. Chem. **16**, 683 (1963).
9. J. M. LEHN et A. VYSTRCIL. Tétrahédron, **19**, 1733 (1963).
10. M. SHAMMA, R. E. GLICK et R. O. MUMMA. J. Org. Chem. **27**, 4512 (1962).
11. I. KITAGAWA, K. KITAZANA et I. YIOSOKA. Tétrahédron, **28**, 907 (1972).
12. A. VYSTRCIL et Z. BLECHA. Collect. Czech. Chem. Commun. **37**, 610 (1972).
13. A. VYSTRCIL et M. BUDEZINSKY. Collect. Czech. Chem. Commun. **35**, 312 (1970).
14. J. C. MANI. Ann. Chim. **10**, 533 (1965).
15. R. SAVOIR, R. OTTINGER, B. TURSCH et G. CHIURDOGLU. Bull. Soc. Chim. Belgs. **76**, 335 (1967).
16. E. WENKERT, G. V. BADDELEY, I. R. BURFITT et L. N. MORENO. Org. Magn. Reson. **11**, 337 (1978).
17. S. A. KNIGHT. Org. Magn. Reson. **6**, 603 (1974).
18. S. HUNECK et J. M. LEHN. Bull. Soc. Chim. Fr. 1702 (1963).
19. W. J. CHIN, R. E. CORBETT et L. K. HENG. J. Chem. Soc. Perkin Trans. 1, **14**, 1437 (1973).
20. J. M. LEHN et G. OURISSON. Bull Soc. Chim. Fr. 1137 (1962).
21. L. RUZICKA, W. BAUMGARTNER et V.PRELOG. Helv. Chim. Acta, **32**, 2069 (1949).
22. J. M. LEHN. Bull. Soc. Chim. Fr. 1832 (1962).
23. A. VYSTRCIL et J. PROTIVA. Collect. Czech. Chem. Commun. **39**, 1382 (1974).
24. E. KLINOTOVA, S. BOSAK et A. VYSTRCIL. Collect. Czech. Chem. Commun. **43**, 2204 (1978).

Kinetic solvent effects on alkaline decolorization of crystal violet in some aquo-organic solvents

URMILA MANDAL, SUMITA SEN, KAUSHIK DAS, AND KIRON KUMAR KUNDU[1]
Physical Chemistry Laboratories, Jadavpur University, Calcutta 700 032, India
Received April 25, 1985

URMILA MANDAL, SUMITA SEN, KAUSHIK DAS, and KIRON KUMAR KUNDU. Can. J. Chem. **64**, 300 (1986).

Rate constants (k_s) of alkaline fading of crystal violet (CV^+) have been determined at 25°C by spectrophotometric measurements in aqueous mixtures of some protic, aprotic, and dipolar aprotic cosolvents. Transfer free energies of the substrate (CV^+), $\Delta G_t^0(CV^+)$, were also determined in some of the solvent systems from solubility measurements of the chloride salt, and by subtracting $\Delta G_t^0(Cl^-)$ obtained earlier by use of the tetraphenylarsonium tetraphenylboron (TATB) extrathermodynamic assumption. This helped determine transfer free energies of the transition state ($X^{\neq}$), $\Delta G_t^0(X^{\neq})$, as ΔG_t^0 values of lyate ion (S^-) based on the TATB assumption are already known for all of these solvent systems. The observed log (k_s/k_w) – composition profiles reveal that the relative solvation of the reacting species rather than the dielectric constant of the solvents dictates the complex variation of the rates of the reaction in these solvent systems. Correlation of $-\Delta G_t^{\neq}(= RT \ln k_s/k_w)$ with $\Delta G_t^0(S^-)$ indicates that the reaction is largely controlled by the relative solvation of S^- in most of the cases. But analysis of $\Delta G_t^0(CV^+)$ and $\Delta G_t^0(X^{\neq})$ – composition profiles for some of the solvent systems reveals that the non-compensation of the ΔG_t^0 contributions of initial-state substrate and of the transition-state complex, which may be considered to be an outer-sphere complex $[CV^+](S^-)$, is also in accord with what is expected from the relative solvating characteristics of the cosolvents as guided by their respective physico-chemical properties.

URMILA MANDAL, SUMITA SEN, KAUSHIK DAS et KIRON KUMAR KUNDU. Can. J. Chem. **64**, 300 (1986).

On a déterminé les constantes de vitesse (k_s) de la décoloration alcaline du cristal violet (CV^+), opérant à 25°C, dans des mélanges aqueux de cosolvants protiques, aprotiques et aprotiques dipolaires et faisant appel à des mesures spectrophotométriques. On a aussi déterminé les énergies libres de transfert du substrat (CV^+), $\Delta G_t^0(CV^+)$, dans quelques systèmes de solvants en se basant sur des mesures de solubilité du chlorure et en soustrayant les valeurs de $\Delta G_t^0(Cl^-)$ qui ont été obtenues antérieurement en faisant l'hypothèse extrathermodynamique du tétraphénylbore tétraphénylarsinium (TBTA). On a ainsi pu déterminé les énergies libres de transfert de l'état de transition ($X^{\neq}$), $\Delta G_t^0(X^{\neq})$, sous la forme de valeurs de ΔG_t^0 de l'ion lyate (S^-) qui sont basées sur l'hypothèse du TBTA et qui sont déjà connues pour tous ces systèmes de solvants. Les profils composition – log (k_s/k_w) observés révèlent que c'est la solvatation relative des espèces plutôt que la constante diélectrique des solvants qui régit la variation complexe des vitesses de réaction dans ces systèmes. Une corrélation entre le $-\Delta G_t^{\neq}(=RT \ln k_s/k_w)$ et le $\Delta G_t^0(S^-)$ indique que, dans la plupart des cas, la réaction est principalement contrôlée par la solvatation relative de S^-. Une analyse des profils composition $-\Delta G_t^0(CV^+)$ et $\Delta G_t^0(X^{\neq})$ pour quelques solvants révèle que l'on peut considérer que le fait qu'il n'y a pas de compensation des contributions du substrat de l'état initial et du complexe de l'état de transition, qui peut être considéré comme un complexe périphérique $[CV^+](S^-)$, est aussi en accord avec ce que l'on peut attendre à partir de caractéristiques de solvatations relatives des cosolvants, tels que prescrites par leurs propriétés physico-chimiques.

[Traduit par le journal]

Introduction

Kinetic solvent effects on reactions in different media are often rationalized in the light of general parameters such as "solvent polarity," which sum up all the specific and non-specific interactions of the media with initial and transition states (1). Unfortunately, a quantitative measure of this property is always empirical and the values obtained are of best use only for reactions having reactants similar in nature to those employed as model probes. Consequently a large number of solvent polarity scales are available (1). Moreover, such data for mixed solvents are scanty and are quite difficult to assess on the basis of the values for the pure components.

Since the pioneering work of Leffler and Grunwald (2), Arnett *et al.* (3), and Parker and co-workers (4), increasing efforts (5–11) to rationalize kinetic solvent effects on various reactions from a thermodynamic approach have recently been noted. These essentially entail determining the kinetic solvent effects by splitting the activation parameters into contributions from initial and transition states, and hence attempting to correlate (12) and to understand (8) their behaviour in light of the relevant physico-chemical properties of the solvents.

Recent evaluation of free energies of transfer, $\Delta G_t^0(i)$, of individual ions in various pure and mixed solvents provides a useful means to study the solvent effect on rates of reactions involving charged particles in solution from the viewpoint of short-range interactions between the ions and the solvent media. Thus the kinetic characteristics of a chemical reaction can be correlated with, or even predicted from, the thermodynamic properties of the reacting species. The present paper aims to study kinetic solvent effects for the alkaline decolorization reaction of the dye crystal violet (CV^+), which is actually the process of carbinol base formation as shown below (13). In fact, the contribution of (**2**) to the resonance hybrid suggests an electron deficiency at the *tert*-carbon position and hence lyate ion (S^-) is likely to attack this position to form the colorless carbinol base (13).

Notably, nucleophilic substitution reaction involving tertiary centres of CV^+ or malachite green (MG) as the substrates and various nucleophiles including OH^-, H_2O, etc. have been extensively studied (14). In fact, on the basis of these studies using water as the standard nucleophile and MG as the standard substrate, Ritchie (14) proposed his well-known linear free energy relation (LFER): $\log (k/k_0) = N^+$, where the terms have the usual significance. This relation accommodates the unusual and interesting situation that cation–anion combination reactions involving tertiary centres show no change in selectivity with change of substrate. Later Scott and co-workers (15) proposed a general form of the Ritchie equation, $\log (k/k_0) = S^+N^+$ (S^+ = constant), to accommodate further data of a similar nature.

[1]Author to whom all correspondence should be addressed.

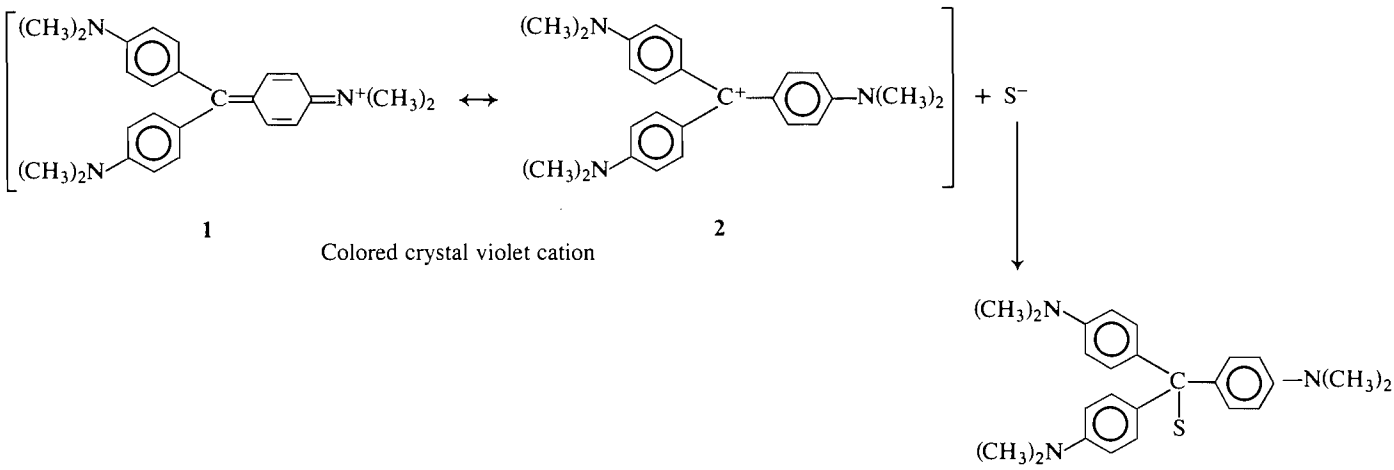

1 2

Colored crystal violet cation

Colorless carbinol base

In the present study the rate of the reaction has been followed spectrophotometrically in aqueous mixtures of dimethyl sulphoxide (DMSO), *N,N*-dimethyl formamide (DMF), acetonitrile (ACN), tetrahydrofuran (THF), dioxane (D), 1,2-dimethoxyethane (DME), 2-methoxyethanol (ME), urea (UH), ethylene glycol (EG), and glycerol (GL). The solubilities of crystal violet chloride (CV^+Cl^-) in some of these mixed solvents (aqueous DMSO, UH, EG, and GL) have also been determined with a view to evaluating standard free energies of transfer of the initial-state substrate $\Delta G_t^0(CV^+)$ and hence that of the transition state $\Delta G_t^0(X^{\neq})$, as $\Delta G_t^0(S^-)$ values are obtainable from earlier work (16). Here S^- denotes the lyate ion, which is purely OH^- in the case of aqueous aprotic or dipolar aprotic solvents but comprises OH^- and possibly some conjugate base ion OR^- in amphiprotic cosolvants (ROH) like ME, EG, or GL. These are based on the widely used tetraphenylarsonium tetraphenylboron "reference electrolyte" extrathermodynamic assumption (17):

$$\Delta G_t^0(PH_4B^-) = \Delta G_t^0(Ph_4As^+) = \tfrac{1}{2}\Delta G_t^0(Ph_4AsBPh_4)$$

Experimental

The organic cosolvents were purified by following usual methods (16). Crystal violet chloride (CV^+Cl^-) (E. Merck) was used as received. The absorption maximum was found to be at 590 nm (13, 18), the molar extinction coefficient at this wavelength being 9.27×10^4 (18). All the experiments were carried out at 25°C. The mixed solvents were prepared by mass dilution.

The reaction under study can be considered to be pseudo-first order if the concentration of the lyate ion is maintained at a much higher level than that of crystal violet. This was precisely the experimental condition, the concentrations of S^- and crystal violet being ~ 1.5–5.0×10^{-3} *M* and 7.0–7.5×10^{-6} *M* respectively. Under these conditions

$$-\frac{d[dye]}{dt} = k'[dye]$$

where $k' = k[S^-]$. k' was obtained by following the reaction with the help of a Perkin Elmer D2000 spectrophotometer and k was calculated to eliminate the effect of differing concentrations of S^-. These rate constant k (L mol^{-1} min^{-1}) values have been presented in Table 1 along with $\Delta G_t^{\neq}$ values (see Discussion) obtained therefrom. $\Delta G_t^0(S^-)$ values are taken from the literature as cited in the footnotes to Table 1.

Table 2 gives the solubilities of crystal violet chloride. ΔG_t^0 values for the dye have been calculated by the usual relation (19) computing the required activity coefficient data by the extended Debye–Hückel equation, tentatively assuming the ion size parameters for crystal violet cation and the chloride ion to be 5 Å and 3 Å, respectively. $\Delta G_t^0(CV^+)$ has been obtained by subtracting the literature values (as cited in footnote to Table 2) of $\Delta G_t^0(Cl^-)$ from the total ΔG_t^0 for the dye.

Discussion

As indicated in the Introduction, the usual approach of correlating the kinetic solvent effects with some of the widely used solvent polarity scales (1), though feasible and useful for pure nonaqueous solvents, is difficult in most of the aquo-organic solvents because of scanty "solvent polarity" data. It was therefore considered useful to analyze the present data on the basis of solute–solvent interactions of the involved species and the relevant physico-chemical properties of the mixed solvents.

Thus turning to the results of the present study, it is found that in general the rate constant increases with addition of organic cosolvent to water, as shown by a plot of log (k_s/k_w) vs. mol% organic cosolvents (Fig. 1). This may be expected, as in most of the cases the mixed solvents have a lower dielectric constant than water and the reaction under study involves charge annihilation. Accordingly, in the only case where the dielectric constant progressively increases, i.e. UH–water mixtures (20), the rate constant has been found to decrease. However, that the dielectric constant is not the only parameter involved is clearly demonstrated by the log (k_s/k_w) – composition profiles in some other media, e.g., aqueous mixtures of GL, EG, ACN, and DMF. In the first case, the rate constant decreases in spite of decreasing dielectric constant while in the latter three cases the rate constant profiles pass through extrema, whereas the dielectric constants are known to decrease almost monotonically with cosolvent compositions (21–23). Furthermore, no reflection of the initial maxima in dielectric constant in aqueous DME (24) has been observed in the variation of rate constant in the mixtures.

A closer look at Fig. 1 reveals that the log (k_s/k_w) – composition profiles are similar in pattern for aqueous GL, EG, ME, and THF. It is interesting to note that the number of OH groups in the hydroxylic cosolvent molecules decreases in the order GL > EG > ME, and this is just the reverse of the order of the rate constant values. Apparently, this shows that the presence of hydroxylic cosolvents renders the nucleophile OH^-

TABLE 1. Kinetic and thermodynamic data for the reaction under study and the reacting species involved at 25°C

Organic cosolvent	Wt.%	Mol%	log k	log k_s/k_w	$\Delta G_t^{\ddagger}$ (kJ mol^{-1})	$\Delta G_t^0(S^-)$ (kJ mol^{-1})[a–f]
			1.06 (= log k_w)			
DMSO[a]	10.8	2.7	1.02	−0.04	0.2	3.3
	21.4	5.7	1.15	0.09	−0.5	6.8
	31.9	9.7	1.30	0.23	−1.3	10.8
	41.9	14.2	1.47	0.40	−2.3	14.9
	53.6	21.0	1.88	0.81	−4.6	21.4
	61.7	27.0	2.23	1.17	−6.6	—
	70.7	35.6	2.96	1.90	−10.8	—
ACN[b]	7.8	3.6	1.04	−0.02	0.1	1.6
	24.5	12.4	0.85	−0.21	1.2	5.4
	44.5	26.0	0.78	−0.29	1.6	11.2
	53.9	33.9	0.93	−0.14	0.8	15.0
	59.8	39.5	1.03	−0.04	0.2	18.4
	65.1	45.0	1.16	0.10	−0.6	—
	70.6	51.2	1.30	0.24	−1.4	—
DMF[b]	9.4	2.4	0.88	−0.18	1.0	−3.0
	18.9	5.4	0.86	−0.21	1.2	−3.8
	25.5	7.8	0.95	−0.12	0.7	−2.7
	38.4	13.3	1.18	0.11	−0.7	1.9
	48.8	19.0	1.50	0.44	−2.5	5.4
	58.3	25.6	1.77	0.71	−4.1	8.3
THF[c]	9.2	2.5	1.60	0.53	−3.0	5.0
	17.9	5.1	1.73	0.66	−3.8	8.4
	27.4	8.6	1.84	0.78	−4.4	11.5
	37.6	13.1	2.26	1.20	−6.8	14.2
	47.6	18.5	2.44	1.37	−7.8	17.6
D[c]	10.2	2.3	1.10	0.03	−0.2	3.1
	20.3	5.0	1.10	0.03	−0.2	6.6
	30.4	8.2	1.22	0.16	−0.9	9.7
	40.9	12.4	1.47	0.41	−2.3	12.2
	50.7	17.3	1.79	0.72	−4.1	13.8
	60.6	23.9	2.22	1.16	−6.6	—
	70.6	32.9	2.74	1.67	−9.5	—
DME[c]	8.7	1.9	1.07	0.00	0.0	3.0
	17.6	4.1	1.06	0.00	0.0	5.9
	27.2	6.9	1.13	0.06	−0.4	9.5
	36.6	10.3	1.29	0.23	−1.3	13.2
	46.1	14.6	1.50	0.44	−2.5	17.6
	56.8	20.8	1.83	0.77	−4.4	—
	67.4	29.2	2.21	1.14	−6.5	—
ME[d]	9.6	2.4	1.41	0.34	−2.0	1.0
	19.4	5.4	1.45	0.39	−2.2	2.6
	28.8	8.7	1.50	0.44	−2.5	4.3
	59.1	25.5	1.82	0.76	−4.3	8.5
	69.5	35.1	2.03	0.97	−5.5	9.5
	79.6	48.0	2.43	1.37	−7.8	—
UH[a]	11.5	3.8	0.77	−0.30	1.7	−1.7
	20.3	7.1	0.70	−0.36	2.1	−2.1
	25.0	9.1	0.64	−0.43	2.4	−1.7
	29.6	11.2	0.59	−0.48	2.7	−1.3
	32.5	12.6	0.55	−0.52	2.9	—
GL[e]	18.8	4.3	1.00	−0.07	0.4	−3.0
	27.7	7.0	0.91	−0.15	0.9	−4.3
	36.4	10.1	0.83	−0.24	1.3	−5.3
	44.8	13.7	0.59	−0.47	2.7	−6.2
	52.9	18.0	0.58	−0.48	2.7	−7.0
	60.8	23.3	0.56	−0.51	2.9	—
	68.4	29.7	0.51	−0.56	3.2	—

TABLE 1. (*concluded*)

Organic cosolvent	Wt.%	Mol%	log k	log k_s/k_w	$\Delta G_t^{\ddagger}$ (kJ mol^{-1})	$\Delta G_t^0(S^-)$ (kJ mol^{-1})[a–f]
EG[f]	10.8	3.4	1.31	0.25	−1.4	0.5
	14.6	4.7	1.34	0.28	−1.6	0.0
	32.3	12.2	1.26	0.20	−1.1	−0.5
	42.0	17.4	1.26	0.19	−1.1	−1.0
	53.1	24.7	1.19	0.13	−0.7	−1.1
	62.4	32.6	1.12	0.06	−0.3	−0.7
	72.1	42.9	1.29	0.22	−1.3	0.0
	82.4	57.7	1.40	0.34	−1.9	—

[a]Reference 27.
[b]Reference 30.
[c]Reference 25*a*.
[d]Reference 40.
[e]Reference 38.
[f]Computed from the autoionization data published in ref. 16 and $\Delta G_t^0(H^+)$ data published in ref. 39; ΔG_t^0(i) values are on molar scale.

TABLE 2. Solubility data of the dye crystal violet chloride and its constituent ions

Organic cosolvent	Wt.%	Mol%	Solubility (mol kg^{-1})	$\Delta G_t^0(CV^+Cl^-)$ (kJ mol^{-1})	$\Delta G_t^0(Cl^-)$[a–c] (kJ mol^{-1})	$\Delta G_t^0(CV^+)$ (kJ mol^{-1})
			0.041 (in water)			
DMSO[a]	10.0	2.5	0.089	−4.0	1.7	−5.2
	20.0	5.5	0.154	−6.8	3.3	−9.8
	30.0	9.0	0.207	−8.5	5.1	−13.0
EG[b]	10.0	3.1	0.048	−1.1	0.8	−1.8
	20.0	6.8	0.089	−4.3	1.4	−5.3
	30.0	11.1	0.144	−6.7	1.9	−8.1
GL[c]	20.0	4.7	0.051	−1.8	−0.6	−0.9
	40.0	11.5	0.083	−4.8	−0.9	−3.2
	50.0	16.4	0.087	−5.5	−1.1	−3.5
UH[a]	10.0	3.2	0.060	−2.2	−2.0	0.3
	20.0	7.0	0.078	−3.9	−3.5	−0.2
	30.0	11.4	0.150	−5.7	−3.7	−1.6

[a]Reference 27.
[b]Reference 39.
[c]Reference 19; ΔG_t values of (CV^+Cl^-) and Cl^- are on a mole fraction scale and that of CV^+ on a molar scale.

or OR^- less reactive than in the presence of aprotic cosolvents. On the other hand THF, being an aprotic solvent, makes OH^- increasingly desolvated (25, 26) and hence more and more active than for reactions in water, provided initial and transition states are more or less equally solvated in the respective solvent systems.

However, for other aqueous aprotic mixtures, e.g. aqueous DMSO, DMF, ACN, and DME, an initial minimum or such a trend can be observed in the respective log (k_s/k_w) – composition profiles. Clearly, something occurs at lower organic compositions in these mixtures which opposes the effect of the well-known "anion desolvating" affinity of these aprotic cosolvents (26–30). This might be the effect of initial- and transition-state solvation and (or) the effect of the release of water monomers by possible breakdown of three-dimensional (3D) hydrogen-bonded water structure on addition of these cosolvents (6*b*, 23, 28, 29, 31–34). This sometimes influences the relative solvation of certain ionic and non-ionic solutes (25–30, 34), especially large-sized hydrophobic ones, and is referred to as structural interactions (35). Once this compensating effect is overcome, the log (k_s/k_w) – composition profiles rise sharply at higher composition of these dipolar aprotic cosolvents.

In the case of aqueous UH, another factor may be operative to some extent. The zwitterionic forms of UH molecules may stabilize the positive charge of crystal violet cations on the peripheral N atoms of its quinonoid forms, thus hindering the formation of carbinol base. This would then contribute to the decrease of k_s values in aqueous UH, in addition to the effects of dielectric constant referred to earlier, and to the observed increased solvation of OH^- through positive charge centres of zwitterionic forms of UH (27).

The above discussion suggests that the change in rate of a reaction upon solvent transfer is primarily determined by the solvation of reacting species. To test the validity of this hypothesis, plots of $-\Delta G_t^{\ddagger}$, which is the negative of change in free energy of activation upon solvent transfer, and of $\Delta G_t^0(S^-)$ vs. mol% cosolvent have been shown in Fig. 2 for a few

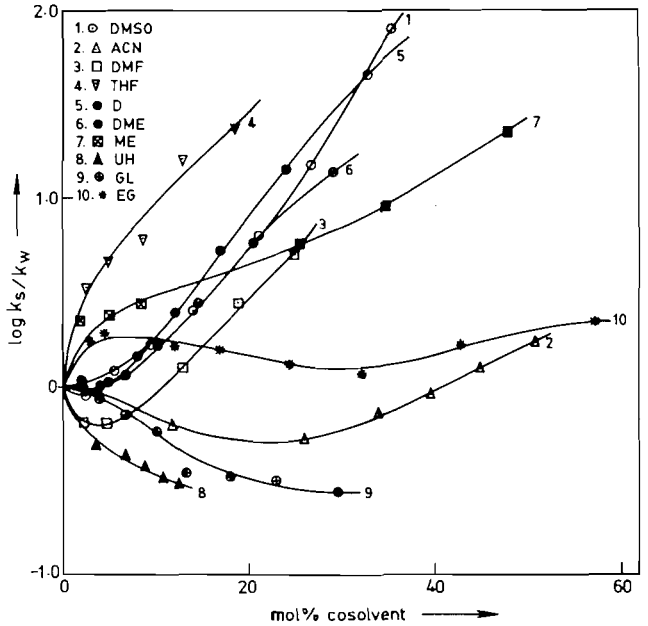

FIG. 1. Variation of log k_s/k_w with mol% cosolvent for alkaline decolorization of crystal violet at 25°C.

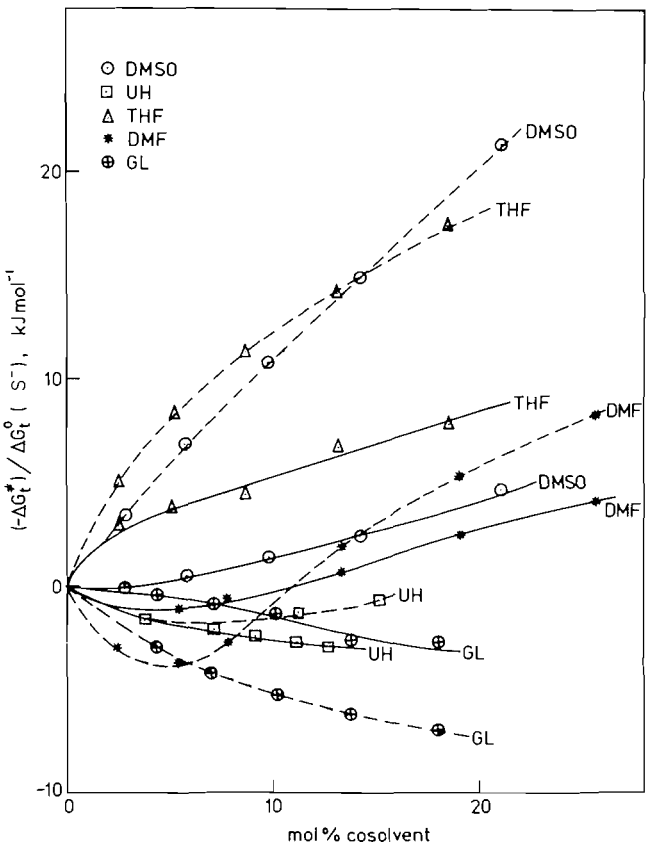

FIG. 2. Variation of $\Delta G_t^{\ddagger}$ (solid lines) and $\Delta G_t^0(S^-)$ (dotted lines) with mol% cosolvent.

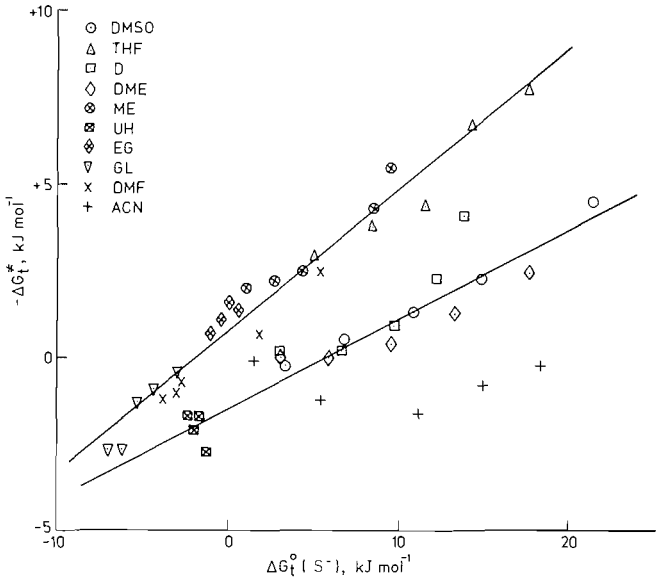

FIG. 3. Plots of $-\Delta G_t^{\ddagger}$ vs. $\Delta G_t^0(S^-)$ for alkaline decolorization of crystal violet in different aquo-organic solvent mixtures.

representative mixed solvents. $\Delta G_t^{\ddagger}$ can be obtained by applying Eyring's equation

$$k = (RT/Nh) \exp(-\Delta G^{\ddagger}/RT)$$

the symbols having their usual significance, and defining

$$\Delta G_t^{\ddagger} = \Delta G_s^{\ddagger} - \Delta G_w^{\ddagger} = 2.303\, RT \log(k_w/k_s)$$

In all the cases the two profiles are found to be qualitatively similar, which implies that the kinetics of the chosen reaction is seemingly largely controlled by the solvation of S^-. Inspired by this observation, a plot of $-\Delta G_t^{\ddagger}$ vs. $\Delta G_t^0(S^-)$ has been constructed for all the solvent systems studied (Fig. 3). Despite a small amount of scatter, the data are largely found to lie on two straight lines of differing slopes, one consisting of the results from aqueous mixtures of DMSO, D, DME, and UH and the other of results from aqueous THF, ME, DMF, EG, and GL. Data from ACN–water mixtures seem to fit neither line. However, the slopes of both lines are far from unity, which indicates that there is a large difference between the solvation of the initial state (substrate, CV^+) and its transition state.

Evidently, analysis of the relative contributions of initial and transition states should be rewarding. Four solvent mixtures, two from each group, viz., aqueous DMSO, UH, EG, and GL, have been therefore selected to study the effect of solvation of the substrate crystal violet cation (CV^+) and its transition state $X^{\ddagger}$. Figure 4 compares the values of $\Delta G_t^0(CV^+)$ and $\Delta G_t^0(X^{\ddagger})$ with solvent composition. $\Delta G_t^0(X^{\ddagger})$ has been obtained from the relation

$$\Delta G_t^{\ddagger} = \Delta G_t^0(X^{\ddagger}) - \Delta G_t^0(CV^+) - \Delta G_t^0(S^-)$$

From Fig. 4 it appears that CV^+ and its transition state $X^{\ddagger}$ are increasingly more solvated in aqueous mixtures of the cosolvents DMSO, EG, and GL, but less so in UH; their relative order is DMSO > EG > GL $\gg$ UH.

In view of the fact that CV^+ is a triphenyl methyl dye with three $(CH_3)_2N$-substituted phenyl groups attached to the positively charged *tert*-carbon atom at the centre and has quinonoid resonating forms, its solvation in aqueous mixtures of different

TABLE 3. Dipole moment and polarizability of some cosolvents at 25°C

Parameter	Water	DMSO	UH	GL	EG
Dipole moment ($\mu \times 10^{18}$ esu)	1.85	3.96[b]	4.56[a]	2.68[c]	2.28[d]
Polarizability ($\alpha \times 10^{24}$ cm^{-3})[c]	1.44	7.99	5.55	8.16	5.76

[a]Reference 41.
[b]Reference 8.
[c]Reference 42.
[d]Reference 43.

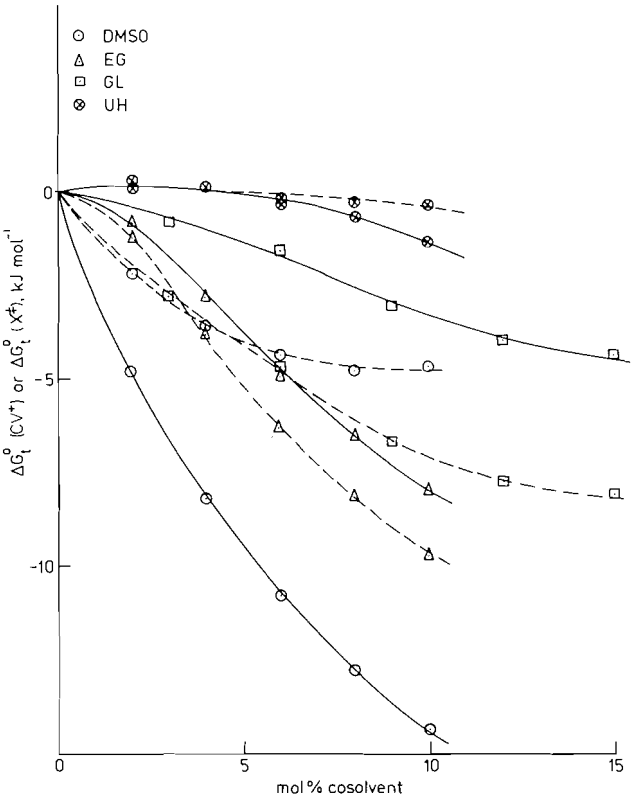

FIG. 4. Variation of $\Delta G_t^0(CV^+)$ (solid lines) and $\Delta G_t^0(X^*)$ (dotted lines) with mol% cosolvents.

cosolvents with varying physico-chemical properties is likely to be an involved process. Firstly, because of its large size, Born-type (36) electrostatic interactions seem negligibly small. This is also borne out by the fact that, despite increased dielectric constant of aqueous urea solution, the $\Delta G_t^0(CV^+)$ – composition profile grazes the abscissa instead of becoming increasingly negative due to this effect, while the reverse would have been true in the other cases because of decreased dielectric constant. Evidently other factors are more important. Of the various other possible factors, such as ion–dipole, ion – induced dipole, ion–quadrupole, and dispersion interactions, which are likely to affect its solvation, the last factor is seemingly most effective. Just as the Born-type electrostatic interactions are negligibly small, because of low surface charge density around this large-sized ion, so are the other types of ion–dipole/quadrupole interactions. This is also borne out by the observation that CV^+ is much more strongly solvated in aqueous DMSO than in aqueous UH, which follows the order of polarizabilities and not the dipole moments (vide Table 3). Of course the effective polarizability, which contributes directly to the magnitude of the dispersion interaction, is rather difficult to assess in the mixed solvents. However, the extent of hydrogen-bonding interactions in aquo-organic mixtures is likely to determine the accessibility of the hydrophobic portion of the organic cosolvent molecule for dispersion interaction. Thus the presence of increased number of H-bonding centres is likely to decrease the hydrophobicity of an organic cosolvent molecule in aqueous mixtures and thus reduce the magnitude of dispersion interaction with an organic solute, as expected on the basis of polarizability of the pure cosolvents, alone. Thus for urea, though not most polar among these cosolvents (vide Table 3), its possible pronounced ion–dipole interaction effect is seemingly hindered by its capability of forming urea–water clusters (37) due to three possible H-bonding centres in its zwitterionic forms. Despite the possible formation of hydrates of DMSO (6*b*), the larger polarizability and unhindered hydrophobicity of two CH_3 groups of the DMSO molecule possibly cause larger dispersion interactions in DMSO–water mixtures than in urea–water mixtures. The observed larger solvation of Ph_4As^+/Ph_4B^- in DMSO – water mixtures as compared to that in urea–water mixtures (27) also substantiates this contention. Notably, that the possibility of increased stabilization of the quinonoid forms of CV^+ by the zwitterionic forms of UH might partly contribute to the decreased k_s values in UH–water mixtures, as referred to earlier, is not seemingly correct.

Again, the above consideration regarding the effect of H-bonding on hydrophobicity of the cosolvents and on dispersion interactions is also true for aqueous protic cosolvents and accounts for the observation that CV^+ is more strongly solvated in aqueous EG than in aqueous GL in spite of the higher polarizability of GL compared to that of EG (vide Table 3). Moreover, the dispersion interaction, being of short range, requires close proximity of the interaction centres. The approach of the large CV^+ towards the hydrophobic methylene chains in the cosolvents is sterically more hindered in aqueous GL than in aqueous EG owing to H-bonding interactions between H_2O and OH groups, and can be expected from the conformational structures of EG (**1***a* and **1***b*) and GL (**2***a* and

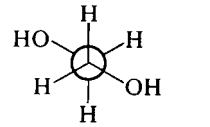

1*a*

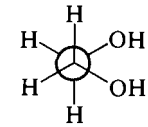

1*b*

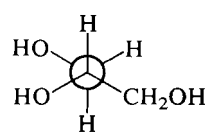

2*a*

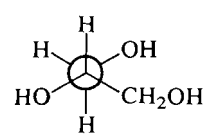

2*b*

2*b*) molecules. The presence of three H-bond donating centres in GL, compared to two in EG, thus decreases the hydrophobicity of the former to a greater extent. ΔG_t^0 of another larger hydrophobic organic ion, viz. Ph_4As^+/Ph_4B^-, was found earlier to follow the same order as the number of H-bond donating centres in the organic cosolvent molecule, for aqueous mixtures of ethanol, EG, and GL (38). Evidently, despite the larger polarizability of the cosolvent GL compared to DMSO (Table 3), the larger H-bonding propensity of GL with water molecules through three OH groups of GL seemingly hinders the hydrophobic CH_2 chain from approaching CV^+ to impart a large dispersion interaction, as compared to that in DMSO–water mixtures.

The observed qualitative similarity between the composition profiles of $\Delta G_t^0(CV^+)$ and $\Delta G_t^0(X^+)$ indicates that the solvation of the transition state is dictated by the factor involved in solvation of the substrate, i.e. by dispersion interactions. Consequently, the $\Delta G_t^0(X^+)$ values are found to be nearly zero in UH–water mixtures, as are the $\Delta G_t^0(CV^+)$ values, whereas both these values are highly negative in DMSO–water mixtures. It is interesting to note that while in aqueous DMSO $\Delta G_t^0(X^+) > \Delta G_t^0(CV^+)$, the order is just the reverse in aqueous EG or GL. In other words, the transition state becomes less solvated in the presence of DMSO, an aprotic cosolvent, compared to the substrate, contrary to what is observed in mixtures of water with hydroxylic cosolvents EG or GL. This is compatible with the expectation that for effective solvation the transition state, which may be considered as a quasi-stable outer-sphere union of CV^+ and OH^- or OR^-, requires molecules having good hydrogen bond donating ability, besides being capable of undergoing dispersion interactions. So, relative to the substrate, the transition state is found to be solvated to a greater extent in GL, which contains three OH groups, than in EG, which has only two of them.

Thus it appears that in DMSO–water mixtures the effect of larger stabilization of CV^+ over its transition state opposes the effect of pronounced stabilization of OH^- (37) and results in a slight minimum in the log (k_s/k_w) – composition profile at the initial composition. The same may also be more or less true for other aqueous dipolar aprotic cosolvents. In urea–water mixtures, the opposing effects of initial- and transition-state solvation being relatively small, the observed decreased rates of the reaction are chiefly guided by the effect of increased stabilization of OH^- (27) as referred to earlier. On the other hand, in the cases of aqueous EG and GL mixtures, larger stabilization of the transition state over its initial state opposes the effect of increased stabilization OH^-/S^- (38, 39) in the respective cases. And while the former effect nearly nullifies the other in the case of EG, the retarding effect of the pronounced solvation of OH^-/S^- in GL–water mixtures (38) overcomes the accelerating effect of larger stabilization of the transition state over its initial state, thus imparting smaller k_s than k_w values.

Thus, the results of the present study clearly demonstrate that correlation of the relative solvation of the reactants and the transition state with the relative physico-chemical properties of the solvents offers better insight into the kinetic solvent effect. It is hoped that the same will be true for other reactions as well.

Acknowledgements

The authors wish to record their thanks to the CSIR, New Delhi for financial assistance and a Junior Research Fellowship to U. Mandal, and to the UGC, New Delhi for a Junior Research Fellowship to S. Sen.

1. C. Reichardt. Angew. Chem. **18**, 9 (1974); C. Reichardt. *In* Organic liquids–structure, dynamics and chemical properties. *Edited by* E. Leppert and S. Bratos, Wiley–Interscience, New York, 1978.
2. J. E. Leffler and E. Grunwald. Rates and equilibria of organic reactions. Wiley, New York. 1963.
3. E. M. Arnett, W. G. Bentrude, J. J. Burke, and P. McDuggleby. J. Am. Chem. Soc. **87**, 1541 (1965).
4. A. J. Parker. Adv. Phys. Org. Chem. **5**, 173 (1967); R. Alexander, E. C. Ko, A. J. Parker, and T. Broxton. J. Am. Chem. Soc. **90**, 5049 (1968); A. J. Parker. Chem. Rev. **69**, 1 (1969).
5. M. H. Abraham. J. Chem. Soc. Perkin Trans. 1, 1343 (1972); Prog. Phys. Org. Chem. **11**, 1 (1974).
6. (*a*) M. J. Blandamer and J. Burgess. Chem. Soc. Rev. **4**, 55 (1975); (*b*) M. J. Blandamer. Adv. Phys. Org. Chem. **14**, 203 (1977), and references therein.
7. E. Buncel and H. Wilson. Adv. Phys. Org. Chem. **14**, 144 (1977); Acc. Chem. Res. **12**, 42 (1979).
8. J. B. F. N. Engberts. *In* Water: a comprehensive treatise. Vol. 6. *Edited by* F. Franks. Plenum Press, New York. 1976. p. 139, references therein; Pure Appl. Chem. **54**, 1947 (1982).
9. Y. Kondo, M. Ittoh, and S. Susabayashi. J. Chem. Soc. Faraday Trans. 1, **78**, 3793 (1982), references therein.
10. C. F. Wells. J. Chem. Soc. Dalton Trans. 1494 (1980).
11. A. J. Parker, D. Mayer, R. Schmid, and U. Gutman. J. Org. Chem. **43**, 1843 (1978), and references therein.
12. C. D. Ritchie. J. Am. Chem. Soc. **105**, 3573 (1983), references therein.
13. G. Carbora. J. Chem. Educ. **41**, 48 (1964).
14. C. D. Ritchie. J. Am. Chem. Soc. **97**, 1163 (1975); **97**, 1970 (1975) and references therein.
15. K. Hillier, J. M. W. Scott, D. J. Barnes, and F. J. P. Steele. Can. J. Chem. **54**, 3312 (1977).
16. S. K. Banerjee, K. K. Kundu, and M. N. Das. J. Chem. Soc. **70**, 247 (1966).
17. B. G. Cox, G. R. Hedwig, A. J. Parker, and D. W. Watts. Aust. J. Chem. **27**, 477 (1974), and references therein.
18. International critical tables. Vol VII. McGraw–Hill, New York.
19. I. N. Basu-Mullick and K. K. Kundu. Can. J. Chem. **58**, 79 (1980).
20. J. Wymen, Jr. J. Am. Chem. Soc. **55**, 4416 (1933).
21. G. Akeriof. J. Am. Chem. Soc. **54**, 4125 (1932).
22. G. Moreau and C. Douheret. J. Chem. Thermodyn. **8**, 403 (1976).
23. P. Rohdewald and M. Moldner. J. Phys. Chem. **72**, 2718 (1968).
24. R. N. Roy, E. E. Swensson, G. Lacross, Jr., and C. W. Krueger. *In* Adv. Chem. Ser. No. 155. *Edited by* W. F. Furter. Am. Chem. Soc., Washington, DC. 1976. p. 220.
25. J. Datta and K. K. Kundu. (*a*) Can. J. Chem. **59**, 3141 (1981); (*b*) **61**, 625 (1983); (*c*) J. Phys. Chem. **86**, 4055 (1982).
26. A. Bhattacharya, J. Datta, K. Das, and K. K. Kundu. Indian J. Chem. **21A**, 9 (1981).
27. A. K. Das and K. K. Kundu. J. Solution Chem. **8**, 259 (1979).
28. K. Das, A. K. Das, and K. K. Kundu. Electrochim. Acta, **26**, 479 (1981).
29. K. Das, K. Bose, and K. K. Kundu. Electrochim. Acta, **26**, 479 (1981).
30. U. Mandal, S. Bhattacharya, and K. K. Kundu. Indian J. Chem. **24A**, 191 (1985).
31. F. Frank and D. S. Reid. *In* Water: a comprehensive treatise. Vol. 2. *Edited by* F. Franks. Plenum Press, New York. 1976. p. 323.
32. C. De Visser and S. Somsen. Z. Phys. Chem. **92**, 159 (1074); J.

BOUGARD and R. JADOT. J. Chem. Thermodyn. **7**, 1185 (1975); M. SAITO. Anal. Chem. **47**, 1784 (1975).
33. R. E. ROBERTSON and S. E. SUGUMARI. Can. J. Chem. **50**, 1353 (1972), and references therein.
34. R. G. BATES. *In* Hydrogen bended solvent systems. *Edited by* A. K. Covington and P. Jones. Taylor and Francis, London. 1968. p. 45.
35. J. E. DESNOYERS and C. JOLICOEUR. *In* Modern aspects of electrochemistry. *Edited by* J. O'M. Bockris and B. E. Conway. Plenum Press, New York. 1969. p. 125.
36. M. BORN. Z. Physik. **1**, 45 (1920).
37. A. K. DAS and K. K. KUNDU. J. Phys. Chem. **79**, 2604 (1975), and references therein.
38. I. N. BASU-MULLICK and K. K. KUNDU. Can. J. Chem. **58**, 79 (1980); Indian J. Chem. **18A**, 1 (1979).
39. A. K. DAS and K. K. KUNDU. Indian J. Chem. **17A**, 467 (1978).
40. A. BHATTACHARYA, A. K. DAS, and K. K. KUNDU. Can. J. Chem. **59**, 1153 (1981).
41. R. C. WEAST (*Editor*). Handbook of chemistry and physics. 52nd ed. The Chemical Rubber Co., Cleveland, Ohio. 1971–1972.
42. H. A. RIZK and I. M. ELANWAR. Can. J. Chem. **46**, 507 (1968).
43. J. I. KIM. J. Phys. Chem. **82**, 191 (1978).

The metathesis of *N*-silylamines and benzeneselenenyl chloride. An efficient selenenamide synthesis

THOMAS G. BACK[1] AND RUSSELL G. KERR
Department of Chemistry, University of Calgary, Calgary, Alta., Canada T2N 1N4
Received July 23, 1985

THOMAS G. BACK and RUSSELL G. KERR. Can. J. Chem. **64**, 308 (1986).

The metathesis reactions of *N*-(trimethylsilyl)dialkylamines with benzeneselenenyl chloride afford high yields of *N*,*N*-dialkylselenenamides **1***a*–**1***f*. Similarly, *N*-(trimethylsilyl)acetamide produces the unstable *N*-(phenylseleno)amide **2** *in situ* while *N*-(trimethylsilyl)imidazole and *N*-(trimethylsilyl)benzimidazole undergo selenenylation at the 4- and 2-position, respectively, to provide the selenides **3** and **4**. *N*-(Trimethylsilyl)phthalimide failed to react under these conditions.

THOMAS G. BACK et RUSSELL G. KERR. Can. J. Chem. **64**, 308 (1986).

Les réactions de métathèse des *N*-(triméthylsilyl)dialkyl-amines avec le chlorure de benzènesélénényle conduisent aux *N*,*N*-dialkyl-sélénénamides **1***a*–**1***f*. De la même manière, la *N*-triméthylsilyl)acétamide conduit, *in situ* à la *N*-(phénylséléno) amide **2** instable alors que le *N*-(triméthylsilyl)imidazole et le *N*-(triméthylsilyl)benzimidazole subissent respectivement des sélénénylations dans les positions 4 et 2 pour conduire aux sélénides **3** et **4**. La *N*-(triméthylsilyl)phtalimide ne réagit pas dans ces conditions.

[Traduit par le journal]

Introduction

N,*N*-Dialkylbenzeneselenenamides (**1**) (1) comprise a relatively unexplored class of compounds that have recently been shown to possess some synthetically useful properties. They transform aldehydes to their α-selenenylated derivatives (1–3) and convert olefins such as cyclohexene to β-acetoxy selenides in the presence of acetic anyhydride (1). They are also sufficiently nucleophilic to perform Michael additions upon acceptors such as enones (1) and dimethyl acetylenedicarboxylate (4) to afford β-amino-α-phenylseleno carbonyl compounds after intramolecular selenenylation.

Unfortunately, the preparation of selenenamides **1** is hampered by their hydrolytic instability, and their direct synthesis via eq. [1] often provides but modest yields, particularly in the case of more hindered amines (1).

[1] $$PhSeX + 2R_2NH \rightarrow \underset{\mathbf{1}}{PhSeNR_2} + R_2NH_2^+X^-$$
X = Cl, Br, OH

Recently the metathesis reactions of benzeneselenenyl chloride with trimethylsilyl cyanide (5) (eq. [2]) and trimethylsilyl isothiocyanate (6) (eq. [3]) have proven convenient methods for the synthesis of phenyl selenocyanate and benzeneselenenyl thiocyanate, respectively. These reactions are rapid and quantitative and the volatile by-product chlorotrimethylsilane is easily removed with the solvent.

[2] $$PhSeCl + Me_3SiCN \rightarrow PhSeCN + Me_3SiCl$$

[3] $$PhSeCl + Me_3SiNCS \rightarrow PhSeSCN + Me_3SiCl$$

It therefore seemed a reasonable extension of these processes to prepare selenenamides by the similar metathesis of the selenenyl chloride with *N*-(trimethylsilyl)amines (eq. [4]). We now report that this approach provides an efficient and simple synthesis of both cyclic and acyclic selenenamides. The results are summarized in Table 1, which indicates the yields of distilled products. The crude products obtained after removal of volatile material, but prior to distillation, are formed essentially quantitatively and are of sufficient purity for most purposes, providing that strictly anhydrous conditions are maintained.[2]

[4] $$PhSeCl + Me_3SiNR_2 \rightarrow \underset{\mathbf{1}}{PhSeNR_2} + Me_3SiCl$$

TABLE 1. Preparation of selenenamides $PhSeNR_2$ (**1**)

Selenenamide	$-NR_2$	Isolated yield, %	bp, °C (Torr)[a]
1*a*	$-NMe_2$	83	40 (0.10)[b]
1*b*	$-NEt_2$	81	70 (0.10)
1*c*	$-N\text{-}iPr_2$	80	75 (0.10)
1*d*	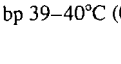	82	75 (0.12)
1*e*	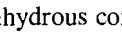	77	80 (0.10)
1*f*	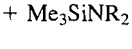	79	80 (0.10)

[a]All products were distilled in a Kugelrohr apparatus.
[b]Literature (1) bp 39–40°C (0.1 Torr).

Several related systems were also investigated. *N*-(Trimethylsilyl)acetamide reacted rapidly with the selenenyl chloride in an nmr experiment to provide a new product with a methyl singlet at δ 1.98, attributed to the expected *N*-(phenylseleno)-acetamide (**2**) (eq. [5]). An impurity signal was also observed at δ 1.76. Attempts to purify the desired product resulted in decomposition.

[5] $$PhSeCl + Me_3SiNHC(=O)Me \rightarrow \underset{\mathbf{2}}{PhSeNHC(=O)Me} + Me_3SiCl$$

N-(Trimethylsilyl)imidazole and *N*-(trimethylsilyl)benzimidazole underwent selenenylation at carbon instead of at nitrogen to afford the products **3** and **4** (eqs. [6] and [7]), respectively. It is not known whether *C*-selenenylation occurs directly in the first

[1]Author to whom correspondence should be addressed.

[2]While this work was in progress, Tomoda *et al.* reported the generation of **1***b* *in situ* by a similar procedure and employed it to selenenylate butanal (7). The selenenamide was characterized by nmr spectroscopy but was not isolated.

step of these processes, or whether the *N*-phenylseleno derivatives are the initial products but rearrange rapidly to the more stable compounds **3** and **4**. By analogy, it has been suggested that anilines undergo similar initial *N*-selenenylation followed by rearrangement of the phenylseleno group to the aromatic ring (8).

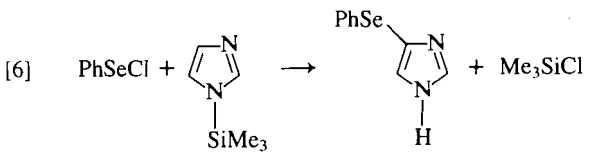

3

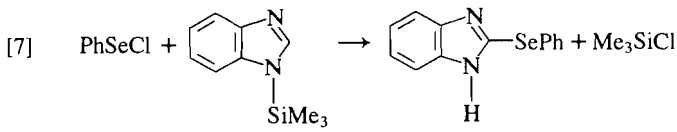

4

An attempt to prepare the useful reagent *N*-(phenylseleno)-phthalimide (**5**) (9) from *N*-(trimethylsilyl)phthalimide and the selenenyl chloride failed as no reaction occurred. It is interesting to note that, in contrast to the latter processs, *N*-(trimethylsilyl)amides, -azoles, and -imides are known to react with various sulfur chlorides to afford generally high yields of stable *N*-thioamides (10), *N*-thioazoles (11), and *N*-thioimides (12).

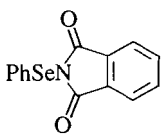

5

It is evident that the above method provides a convenient route to *N*,*N*-dialkylselenenamides. Similar methodology may furnish access to other selenium-nitrogen compounds in the future.

Experimental

The nmr spectra were recorded on a Hitachi Perkin Elmer R24B or on a Varian XL200 spectrometer in deuteriochloroform solution unless otherwise noted. Chemical shifts are reported in ppm downfield from tetramethylsilane. Infrared spectra were obtained on a Nicolet 5DX FTIR spectrometer and mass spectra were recorded on a Kratos MS80 instrument. Elemental analyses were performed by Dr. W. S. Lin at the University of Calgary.

All *N*-silylamines and *N*-silylazoles were obtained from commercial sources or were prepared by standard literature methods (13). All other reagents were commercially available.

A typical procedure for the preparation of selenenamide **1***a* follows. All other products in Table 1 were prepared in the same manner. Known compounds **1***a*–**1***c* (1) and **1***f* (3) were identified by their ir and nmr spectra, while complete spectral and analytical details are provided for new compounds **1***d*, **1***e*, **3**, and **4**.

N,N-*Dimethylbenzeneselenenamide (**1**a)*

Benzeneselenenyl chloride (960 mg, 5.00 mmol) in 8 mL of dichloromethane was added to a solution of *N*-(trimethylsilyl)dimethylamine (585 mg, 5.00 mmol) in 2 mL of the same solvent. The red colour of the selenenyl chloride was immediately discharged. The resulting pale yellow solution was concentrated under a stream of nitrogen and distilled in a Kugelrohr apparatus at ca. 40°C (0.10 Torr; 1 Torr = 133.3 Pa) to afford 831 mg (83%) of the title compound, with nmr spectrum as reported previously (1).

N-*(Phenylseleno)pyrrolidine (**1**d)*: ir (film): 1574, 1176, 1022, 937, 739, 693 cm^{-1}; nmr: 7.7–7.1 (complex, 5H), 3.1 (m, 4H), 1.8 (m, 4H); mass spectrum, *m/e* (relative intensity, %): 227 (M^+, ^{80}Se, 38), 225 (M^+, ^{78}Se, 24), 70 (M^+ − PhSe, 100). *Anal.* calcd. for $C_{10}H_{13}NSe$: C 53.09, H 5.80, N 6.19; found: C 52.88, H 5.91, N 6.50.

N-*(Phenylseleno) piperidine (**1**e)*: ir (film): 1578, 1211, 1022, 897. 735, 691 cm^{-1}; nmr: 7.7–7.1 (complex, 5H), 2.96 (m, 4H), 1.5 (complex, 6H); mass spectrum, *m/e* (relative intensity, %): 241 (M^+, ^{80}Se, 45), 239 (M^+, ^{78}Se, 23), 84 (M^+ − PhSe, 100). *Anal.* calcd. for $C_{11}H_{15}NSe$: C 54.99, H 6.31, N 5.83; found: C 54.89, H 6.08, N 6.12.

N-*(Phenyseleno)acetamide (**2**)*

The product **2** was prepared in $CDCl_3$ solution in the usual manner; nmr: 7.5–6.9 (complex, 5H, Ph), 1.98 (s, 3H, MeC=O of **2**), 0.37 (s, 9H, Me_3SiCl). An impurity was observed at 1.76 (s), integrating at 1.2H. Attempts to isolate the product resulted in decomposition.

*4-(Phenylseleno)imidazole (**3**)*[3]

Benzeneselenenyl chloride (192 mg, 1.00 mmol) in 2 mL of dichloromethane was added to *N*-(trimethylsilyl)imidazole (140 mg, 1.00 mmol) in 2 mL of the same solvent. After stirring for 5 min at ambient temperature, the colour of the reaction mixture changed from red to orange and a white precipitate formed. This was filtered and washed with 2 mL of dichloromethane to afford 205 mg (92%) of compound **3**, mp 191–195°C (from methanol–ether); ir (Nujol); 3390–2200 (very broad) 1654, 1567, 1542, 1055, 937, 734, 661 cm^{-1}; nmr ($CDCl_3$ – DMSO-d_6): 7.65 (s, 1H), 7.20 (shoulder) and 7.1 (br s, total 6H); ^{13}C nmr: 140.0, 131.8, 129.5, 129.3, 128.7, 126.0, 118.8; mass spectrum, *m/e* (relative intensity, %): 224 (M^+, ^{80}Se, 47), 222 (M^+, ^{78}Se, 28), 144 (M^+ − Se, 100). *Anal.* calcd. for $C_9H_8N_2Se$: C 48.44, H 3.62, N 12.56; found: C 48.52, H 3.60, N 12.74.

*2-(Phenylseleno)benzimidazole (**4**)*[4]

Benzeneselenenyl chloride (192 mg, 1.00 mmol) in 2 mL of dichloromethane was added to N-(trimethylsilyl)benzimidazole (190 mg, 1.00 mmol) in 2 mL of the same solvent. The colour of the reaction mixture immediately changed from red to yellow. Concentration *in vacuo* afforded product **4** as a solid foam (254 mg, 93%), mp 131–135°C (from dichloromethane–hexane); ir (Nujol): 3300–2100 (very broad), 1769, 1619, 1586, 1571, 1273, 1246, 752, 745, 735 cm^{-1}; nmr ($CDCl_3$ – DMSO-d_6): 8.74 (br s, 1H, exchanged with D_2O), 8.0–7.1 (complex, 9H); ^{13}C nmr: 141.2, 135.1, 131.2, 129.1, 127.7, 122.1, 121.7, 115.4; mass spectrum, *m/e* (relative intensity, %): 274 (M^+, ^{80}Se, 8), 272 (M^+, ^{78}Se, 5), 118 (M^+ − C_6H_4Se, 100). *Anal.* calcd. for $C_{13}H_{10}N_2Se$: C 57.15, H 3.70, N 10.26; found: C 57.28, H 3.43, N 10.04.

Acknowledgment

We thank the Natural Sciences and Engineering Research Council of Canada for financial support.

1. H. J. Reich and J. M. Renga. J. Org. Chem. **40**, 3313 (1975).
2. M. Jefson and J. Meinwald. Tetrahedron Lett. **22**, 3561 (1981).
3. C. Paulmier and P. Lerouge. Tetrahedron Lett. **23**, 1557 (1982);

[3]The isomeric 2-(phenylseleno)imidazole structure can be ruled out on the basis of the ^1H and ^{13}C nmr spectra. The low field proton singlet at 7.65 ppm is consistent with a hydrogen atom at C-2. Furthermore, since 2-substituted imidazoles have tautomerically equivalent C-4 and C-5 positions, the appearance of three ^{13}C nmr signals at 140.0, 126.0, and 118.8 ppm from the imidazole moiety (the remaining signals are assigned to the PhSe group) confirms the 4-(phenylseleno) structure.

[4]In contrast to **3**, the lack of a low field proton signal from the hydrogen atom at C-2 (ca. 8.4 in benzimidazole) indicates that **4** is the 2-(phenylseleno) isomer. This is confirmed by the ^{13}C nmr spectrum, which contains only four benzimidazole signals in addition to the resonances from the PhSe group. This is consistent only with the symmetrical 2-substituted system where tautomerization renders C-4, C-7 and C-5, C-6 equivalent (14).

P. LEROUGE and C. PAULMIER. Tetrahedron Lett. **25**, 1983; 1987 (1984).
4. H. J. REICH, J. M. RENGA, and J. E. TREND. Tetrahedron Lett. 2217 (1976).
5. S. TOMODA, Y. TAKEUCHI, and Y. NOMURA. Chem. Lett. 1069 (1981).
6. T G. BACK and R. G. KERR. J. Organomet. Chem. **286**, 171 (1985).
7. S. TOMODA, Y. TAKEUCHI and Y. NOMURA. Synthesis, 212 (1985).
8. P. T. SOUTHWELL-KEELY, I. L. JOHNSTONE, and E. R. COLE. Phosphorus Sulfur, **1**, 261 (1976).
9. P. A. GRIECO, J. Y. JAW, D. A. CLAREMON, and K. C. NICOLAOU. J. Org. Chem. **46**, 1215 (1981); S. V. LEY, D. NEUHAUS; N. S. SIMPKINS, and A. J. WHITTLE. J. Chem. Soc. Perkin Trans. 1, 2157 (1982); S. V. LEY, N. S. SIMKINS, and A. J. WHITTLE. J. Chem. Soc. Chem. Commun. 503 (1983).
10. D. N. HARPP, D. F. MULLINS, K. STELIOU, and I. TRIASSI. J. Org. Chem. **44**, 4196 (1979).
11. D. N. HARPP, K. STELIOU, and T. H. CHAN. J. Am. Chem. Soc. **100**, 1222 (1978).
12. D. N. HARPP, B. FRIEDLANDER, D. MULLINS, and S. M. VINES. Tetrahedron Lett. 963 (1977).
13. L. BIRKOFER, P. RICHTER, and A. RITTER. Chem. Ber. **93**, 2804 (1960).
14. P. N. PRESTON. *In* The chemistry of heterocyclic compounds. Vol. 40. Part 1. *Edited by* A. WEISSBERGER and E. C. TAYLOR. Wiley, New York. 1981. pp. 67–75.

Kinetics and mechanism of the thermal decomposition of the thiosulphatopentaamminecobalt(III) ion in dilute aqueous acid

ANTHONY MARTIN NEWTON

Department of Chemistry, University of the West Indies, Cave Hill, St. Michael, Barbados

Received May 14, 1985

ANTHONY MARTIN NEWTON. Can. J. Chem. **64**, 311 (1986).

In acetic acid – sodium acetate buffer of pH 5.6 (25°C) the $Co(NH_3)_5S_2O_3^+$ ion undergoes redox decomposition rather than aquation. First-order kinetic are observed and the reaction products Co^{2+}, NH_3, and $S_4O_6^{2-}$ are due to internal reduction of Co(III) by coordinated $S_2O_3^{2-}$. In dilute perchloric acid of pH <4 the rate is retarded, first-order plots are not linear, and $S_4O_6^{2-}$ is not a major product of the reaction. It is proposed that, in dilute $HClO_4$, protonation of $Co(NH_3)_5S_2O_3^+$ depletes the concentration of the reactive complex and that decomposition of coordinated $HS_2O_3^-$ occurs. Conversion of O-bonded $S_2O_3^{2-}$ to S-bonded $S_2O_3^{2-}$ in the reactive complex is also considered.

ANTHONY MARTIN NEWTON. Can. J. Chem. **64**, 311 (1986).

Dans un tampon d'acide acétique – acétate de sodium, à pH 5,6 et à 25°C, l'ion $Co(NH_3)_5S_2O_3^+$ subit plutôt une réaction d'oxydo-réduction qu'une réaction d'aquation. On observe une cinétique du premier ordre et les produits de la réaction, soit le Co^{2+}, le NH_3 et le $S_4O_6^{2-}$, proviennent de la réduction interne du Co(III) par l'ion $S_2O_3^{2-}$ coordonné. L'acide perchlorique dilué, pH <4, retarde la vitesse alors que les courbes d'ordre un ne sont pas linéaires et que l'ion $S_4O_6^{2-}$ n'est pas un produit majoritaire de la réaction. On pense que, en présence de $HClO_4$ dilué, la protonation de l'ion $Co(NH_3)_5S_2O_3^+$ diminue la concentration du complexe réactif et que l'ion coordonée $HS_2O_3^-$ se décompose. On considère également la transformation de l'ion $S_2O_3^{2-}$ lié par l'oxygène en l'ion $S_2O_3^{2-}$ lié par le soufre dans le complexe réactif.

[Traduit par le journal]

Introduction

In dilute aqueous acid the majority of acidopentaammine complexes of cobalt(III) undergo the aquation reaction and pseudo-first-order kinetics are observed (1, 2). However, redox decomposition is reported to complicate the aquation of $Co(NH_3)_5I^{2+}$ (3) and of $Co(NH_3)_5NO_2^{2+}$ (4). The results reported here show that in dilute aqueous acid the $Co(NH_3)_5S_2O_3^+$ ion undergoes redox decomposition rather than aquation.

Experimental

Analytical grade reagents and deionized water were used throughout. Thiosulphatopentaamminecobalt(III) nitrate was prepared by Ray's method (5). It was analysed for content of ammonia and the relative formula mass was measured by ion exchange chromatography. (Calculated for $[Co(NH_3)_5S_2O_3]NO_3$: NH_3 = 26.8%; M_r = 318; found: NH_3 = 26.6%; M_r = 318.)

Sodium tetrathionate dihydrate was prepared by slowly adding, with shaking, a suspension of iodine in absolute ethanol to solid sodium thiosulphate pentahydrate until the iodine colour persisted in the reaction mixture. The crude product was rapidly filtered and washed with ethanol to remove excess iodine. It was then dissolved in the minimum volume of water, ethanol was added, and the mixture was cooled in an ice–salt bath overnight. The crystals which formed were filtered off, washed with ethanol, ether, and stored over calcium chloride. Analyses for tetrathionate ion (6), water of crystallization, and relative formula mass were done. (Calculated for $Na_2S_4O_6 \cdot 2H_2O$: $S_4O_6^{2-}$ = 73.2%; H_2O = 11.7%; M_r = 306; found: $S_4O_6^{2-}$ = 73.2%; H_2O = 11.7%; M_r = 308. The absorption spectrum in dilute $HClO_4$ showed a maximum at 216 nm with $\epsilon = 9.20 \times 10^3\ M^{-1}\ cm^{-1}$, while in acetic acid–sodium acetate buffer at pH 5.6 (25°C) the maximum was at 219 nm with $\epsilon = 8.53 \times 10^3\ M^{-1}\ cm^{-1}$.

Spectrophotometric measurements were carried out using a Zeiss PMQ-II and a Pye Unicam SP8-400 spectrophotometer. The absorption maximum of $Co(NH_3)_5S_2O_3^+$ at 290 nm ($\epsilon = 1.37 \times 10^4\ M^{-1}\ cm^{-1}$) was used to follow the kinetic runs and the concentration of $Co(NH_3)_5S_2O_3^+$ was about $4 \times 10^{-5}\ M$. In those cases where the appearance of Co^{2+} was followed, the Co^{2+} was measured by Kitsen's method (7) and the HCl method (8).

The reaction mixtures were protected from light. Kinetic studies in acetic acid–sodium acetate buffer at pH 5.6 (25°C) were done in the temperature range 45–60°C and at least 80% of each run was followed. Kinetic studies were also done in dilute $HClO_4$ ($10^{-3} - 10^{-1}\ M$) at 59°C.

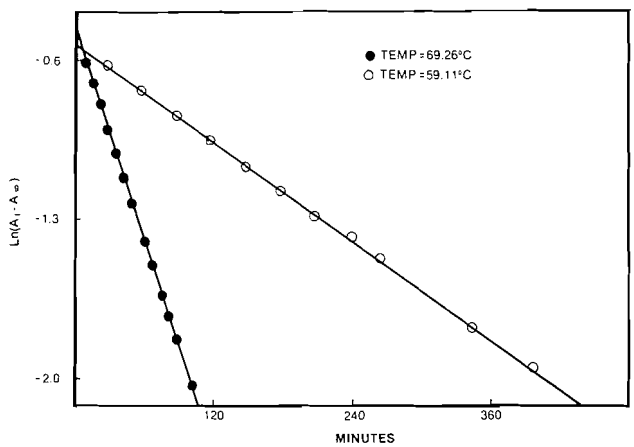

FIG. 1. Semilog plot for the decomposition of $Co(NH_3)_5S_2O_3^+$ in acetic acid – sodium acetate buffer of pH 5.6.

Results

Decomposition at pH 5.6

As shown in Fig. 1, the reaction at pH 5.6 is first order and the rate constants, k, were obtained from the equation

$$[1] \quad \ln [(A_0 - A_\infty) / (A_t - A_\infty)] = kt$$

and are summarized in Table 1. These rate constants fit an Arrhenius equation

$$[2] \quad k = 5.82 \times 10^{16} \exp(-E_a/RT)$$

k being in the units s^{-1} and E_a being 133 kJ mol^{-1}. The results from Table 2 show the stoichiometry of the reaction to be that given by eq. [3].

$$[3] \quad Co(NH_3)_5S_2O_3^+ \rightarrow Co^{2+} + 5NH_3 + \tfrac{1}{2}S_4O_6^{2-}$$

The addition of sodium thiosulphate to the reaction mixture

TABLE 1. First-order rate constants for the decomposition of $Co(NH_3)_5S_2O_3^+$ at pH 5.6

Temperature (°C)	10^5k (s^{-1})
69.26	28.6 ± 0.10
59.11	6.70 ± 0.06
	7.29 ± 0.06[a]
	7.34 ± 0.09[b]
44.58	0.82 ± 0.01

[a]$[Co(NH_3)_5S_2O_3]^+ = 4 \times 10^{-4} M$; measuring rate of appearance of Co^{2+}.
[b]$[Co(NH_3)_5S_2O_3]^+ = 4 \times 10^{-4} M$; measuring rate of disappearance of complex ion.

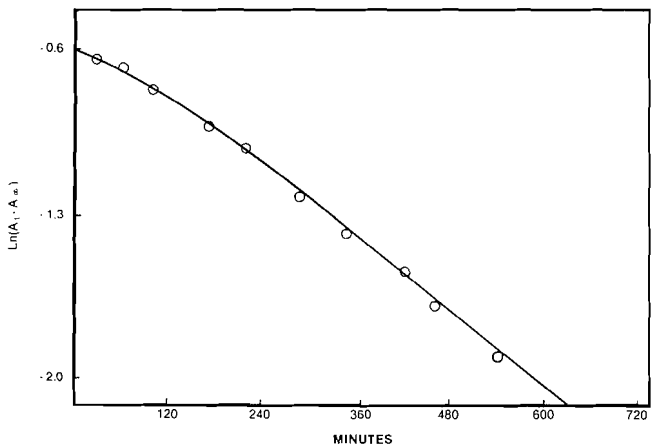

FIG. 2. Time dependence of the optical absorbance, A (290 nm), of a solution of $[Co(NH_3)_5S_2O_3]NO_3$ in 0.1 M $HClO_4$ at 59°C.

had no appreciable effect on the rate in the concentration range (1.0–5.0) × 10^{-3} M, and free $S_2O_3^{2-}$ is therefore not a reactant at any stage of the reaction.

Decomposition in dilute $HClO_4$

In dilute perchloric acid at pH 4 or lower, the kinetics of the redox decomposition of $Co(NH_3)_5S_2O_3^+$ are more complicated than at pH 5.6, and semilog lots are concave downwards with the latter part of these plots being almost linear (Fig. 2). There was no evidence from the spectra of partially reacted solutions or from ion exchange chromatography on such solutions of any cobalt-containing species other than the starting material and $Co(H_2O)_6^{2+}$. Analysis of the product solutions under these conditions showed a complete conversion of Co(III) to Co(II). The absorbance of the solutions at 216 nm (the wavelength of maximum absorbance of the tetrathionate ion in dilute perchloric acid) suggested a concentration of tetrathionate that was much higher than was possible from the mass of the starting material and assuming the stoichiometry to be that of eq. [3].

It seems clear therefore that in dilute perchloric acid (pH < 4) $Co(NH_3)_5S_2O_3^+$ either does not decompose according to eq. [3] or, if it does, the tetrathionate ion produced decomposes partially or completely, giving one or more products of molar absorbance index greater than that of $S_4O_6^{2-}$ and which may also have a catalytic effect on the redox process, thus causing curvature of the semilog plots.

To test the latter interpretation, the effect of added tetrathionate on the rate was studied at 59°C and $[S_4O_6^{2-}] = 1.9 \times 10^{-3}$ M. Under these conditions the semilog plots (Fig. 3) were similar to those for the reaction in dilute perchloric acid only.

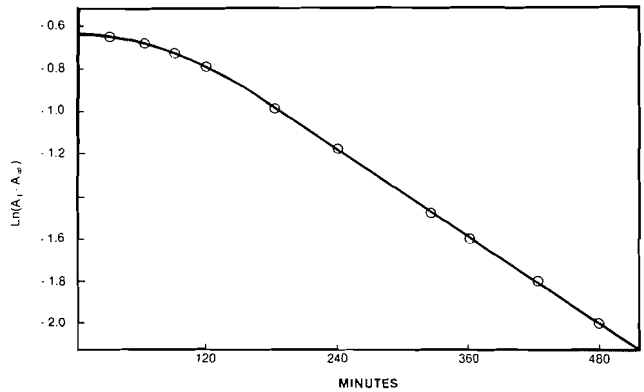

FIG. 3. Semilog plot for the decomposition of $Co(NH_3)_5S_2O_3^+$ in 0.1 M $HClO_4$ − 1.9 × 10^{-3} M $Na_2S_4O_6$ at 59°C.

TABLE 2. Analysis of the products of the decomposition of $Co(NH_3)_5S_2O_3^+$ at 59.11°C in acetic acid – sodium acetate buffer of pH 5.6.

10^4 [Complex] (M)	Product	Found	Expected by reaction [3]
1.00	$10^4[Co^{2+}]$ M	1.01[a]	1.00
1.03		1.01[a]	1.03
90.0		88.5[a]	90.0
0.448		0.430[b]	0.448
43.2	$10^3[NH_3]$ M	20.9[c]	21.6
35.0		17.1[c]	17.5
0.652	$10^5[S_4O_6^{2-}]$ M	3.57[d]	3.26
6.628		3.38[d]	3.14

[a]$[Co^{2+}]$ determined by Kitsen's method (7).
[b]Reaction in 0.1 M $HClO_4$ and $[Co^{2+}]$ determined by the HCl method (8).
[c]$[NH_3]$ determined by micro-Kjeldahl distillation.
[d]$[S_4O_6^{2-}]$ determined spectrophotometrically.

Furthermore, a 1.9 × 10^{-3} M solution of $Na_2S_4O_6$ in 0.1 M perchloric acid and at a temperature of 59°C showed no change in optical absorbance over a period of 72 h, and added Na_2SO_4 (1.9 × 10^{-3} M) and added $Na_2S_2O_8$ (1.9 × $10^{-3}M$) had the same effect on the rate as did the $Na_2S_4O_6$. It is therefore safe to conclude that the decomposition of $S_4O_6^{2-}$ is not important in the redox decomposition of $Co(NH_3)_5S_2O_3^+$ in dilute perchloric acid.

The product Co^{2+} is reported to catalyse the radiolytic decompositions of $Co(NH_3)_5H_2O^{3+}$ and $Co(NH_3)_6^{3+}$ (9). The effect of added $CoSO_4$ (1.9 × 10^{-3} M at 59°C) was therefore studied, but no change in the rate of the redox decomposition was detected. This observation therefore rules out the participation of $Co(H_2O)_6^{2+}$ in the reduction of the Co(III) centre by either an inner sphere or outer sphere mechanism.

Discussion

That the ammine ligand in $Co(NH_3)_5S_2O_3^+$ is involved in the redox process is unlikely, since coordination deactivates NH_3 towards oxidation (10). Furthermore, in the redox decomposition of $Co(NH_3)_5OH_2^{3+}$, a slow process at 59°C (k_{obs} at 70°C = 1 × 10^{-8} s^{-1}) (11), oxidation of an aquo ligand rather than an ammine ligand is the initial redox step (12).

Since $S_2O_3^{2-}$ is readily oxidized by a number of oxidising agents, including Fe^{3+}, it is almost certain that the redox decomposition of $Co(NH_3)_5S_2O_3^+$ involves a single electron transfer from the thiosulphato ligand to Co(III). The mechanism which seems to be operative when $Co(NH_3)_5S_2O_3^+$ decomposes at pH 5.6 is that given in eqs. [4] and [5].

[4] $Co(NH_3)_5S_2O_3^+ \rightarrow Co^{2+} + 5NH_3 + S_2O_3^-$

[5] $2S_2O_3^- \rightarrow S_4O_6^{2-}$

The existence of the $S_2O_3^-$ radical ion has been postulated for other systems (13,14) and an intramolecular electron transfer mechanism has been suggested for the redox decomposition of $Co(NH_3)_5NO_2^{2+}$ (4).

An alternative mechanism is one in which the $Co(NH_3)_5S_2O_3^+$ undergoes aquation, followed by a redox reaction between the products $Co(NH_3)_5OH_2^{3+}$ and $S_2O_3^{2-}$. This mechanism was, however, rejected for the following reasons:

1. The rate of disappearance of the complex was always the same as the rate of appearance of Co^{2+}, whereas the rate at which Co^{2+} is produced by the reaction of $Co(NH_3)_5H_2O^{3+}$ with $S_2O_3^{2-}$ is much too slow to account for the rate of production of Co^{2+} in the reaction of interest.

2. This alternative mechanism would require the rate of Co^{2+} production to be dependent on the concentration of added $S_2O_3^{2-}$, a requirement which has not been met.

An acid-catalysed pathway contributes to the aquation of $Co(NH_3)_5SO_4^+$ (15). Since the $S_2O_3^{2-}$ and SO_4^- ions are of similar basicity (pK_a for dilute $HS_2O_3^-$ and HSO_4^- being ~1.74 and 2.0, respectively, at 25°C (16)), protonation of the starting complex at pH 4 and lower seems a reasonable suggestion in the present case.

[6] $Co(NH_3)_5S_2O_3^+ + H^+ \rightleftharpoons Co(NH_3)_5S_2O_3H^{2+}$

The protonated species should be relatively inactive in internal redox since the electron transfer process should now be more difficult. Protonation of some of the $Co(NH_3)_5S_2O_3^+$ would deplete the concentration of reactive complex, resulting in a reduction in the rate of the redox process. This latter suggestion is supported by the fact that at 59°C, at pH 5.6, the rate is $6.7 \times 10^{-5}\ s^{-1}$, whereas at the same temperature but in $4.02 \times 10^{-3}\ M$ $HClO_4$ it is $5.4 \times 10^{-5}\ s^{-1}$ and in $1.05 \times 10^{-1}\ M$ $HClO_4$ it is $5.1 \times 10^{-5}\ s^{-1}$. The latter two rate constants were determined from the linear portions of the semilog plots. Since $S_2O_3^{2-}$ disproportionates in acid, it may be that a similar process occurs involving coordinated $HS_2O_3^-$ and this may account for the optical absorbance at 216 nm of the final product solutions of the redox decomposition of $Co(NH_3)_5S_2O_3^+$ at pH $\leq$ 4.

No reaction is known to occur between SO_4^{2-} and I_2, whereas iodine is readily reduced by $S_2O_3^{2-}$, which is structurally similar to SO_4^{2-}. On this basis it has been suggested that a species **a** rather than **b** is an intermediate in the $I_2/S_2O_3^{2-}$ reaction (17).

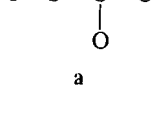

a

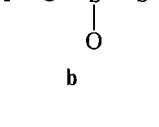

b

Similarly a species containing an I—S bond rather than an I—O bond has been suggested as an intermediate in the oxidation of the tetrathionate ion to SO_4^{2-} by iodine (18).

The available evidence shows the O-bonded isomer to comprise at least 90% of the $Co(NH_3)_5S_2O_3^+$ ion (19). Since an intermediate having an I—S bond is believed to be involved in the $I_2/S_2O_3^{2-}$ redox reaction, it therefore seems that the O-bonded $Co(NH_3)_5S_2O_3^+$ must convert to the S-bonded isomer before the redox reaction occurs. Rates of isomerization are known to be retarded by the presence of acid (20) and hence such a mechanism may be important in depleting the concentration of the reactive complex. Additionally, the relative rates of such an isomerization at pH $\leq$ 4, and the redox process, may be responsible for, or at least contribute to, the curvature of the first-order plots.

Acknowledgment

The author thanks Dr. T. W. Swaddle for helpful discussions.

1. F. Basolo and R. G. Pearson. Mechanisms of inorganic reactions. 2nd ed. John Wiley and Sons, Inc., New York. 1968.
2. T. W. Swaddle. Coord. Chem. Rev. **14**, 217 (1974).
3. R. G. Yalman. J. Am. Chem. Soc. **75**, 1842 (1953).
4. D. Banerjea. J. Inorg. Nucl. Chem. **29**, 2795 (1967).
5. P. R. Ray. J. Ind. Chem. Soc. **4**, 64 (1927).
6. R. Jay. Anal. Chem. **25**, 288 (1953).
7. R. E. Kitsen. Anal. Chem. **22**, 664 (1950).
8. R. J. Mureinik, A. M. Feltham, and M. Spiro. J. Chem. Soc. Dalton Trans. 1981 (1972).
9. D. Katakis and A. O. Allen. J. Phys. Chem. **71**, 3121 (1967).
10. D. Thusius and H. Taube. J. Phys. Chem. **71**, 3845 (1967). J. Am. Chem. Soc. **88**, 850 (1966).
11. A. M. Newton. Ph.D. Thesis, University of Calgary (1974).
12. A. M. Newton and T. W. Swaddle. Can. J. Chem. **52**, 2571 (1974).
13. M. S. Evans and J. H. Baxendale. Trans. Faraday Soc. **42**, 197 (1946).
14. G. Dodd and R. O. Griffith. Trans. Faraday Soc. **45**, 461 (1949).
15. F. Monacelli. Inorg. Chim. Acta, **7**, 65 (1973).
16. R. M. Smith and A. E. Martell. Critical stability constants. Vol. 4. Plenum Press, New York. 1976.
17. A. D. Awtrey and R. E. Connick. J. Am. Chem. Soc. **73**, 1341 (1951).
18. A. D. Awtrey and R. E. Connick. J. Am. Chem. Soc. **73**, 4546 (1951).
19. D. E. Peters and R. T. M. Fraser. J. Am. Chem. Soc. **87**, 2758 (1965).
20. B. Adell. Svensk Kem. Tidskr. **56**, 318 (1944); Z. Anorg. Chem. **252**, 272 (1944); Svensk Kem. Tidskr, **57**, 260 (1945); Chem. Abstr. **40**, 4281[6] (1946).

Free-radical redox reactions of uranium ions in sulphuric acid solutions[1]

A. JOHN ELLIOT,[2] SHAHSULTAN PADAMSHI, AND JANA PIKA[3]

Physical Chemistry Branch, Atomic Energy of Canada Limited, Research Company, Chalk River Nuclear Laboratories, Chalk River, Ont., Canada K0J 1J0

Received August 12, 1985

A. JOHN ELLIOT, SHAHSULTAN PADAMSHI, and JANA PIKA. Can. J. Chem. **64**, 314 (1986).

The radiolytic reduction of uranyl ions in degassed sulphuric acid solutions containing various organic solutes was studied. It was shown that while ĊOOH, CO_2^-, and α-hydroxy-alkyl radicals reduced uranyl ions, the β-hydroxy-alkyl radicals and those derived from gluconic acid could not affect the reduction. The oxidation of uranium(IV) by hydrogen peroxide at pH 0.7 involves hydroxyl radicals in a chain mechanism but at pH 2.0 the oxidation proceeds by a non-radical reaction pathway. From the enhancement of the rate of oxidation of uranium(IV) by oxygen in the presence of 2-propanol, a mechanism involving the perhydroxyl radical, which reconciles earlier published data on kinetics and oxygen tracer studies, is proposed for the oxygen–uranium(IV) reactions.

A. JOHN ELLIOT, SHAHSULTAN PADAMSHI et JANA PIKA. Can. J. Chem. **64**, 314 (1986).

On étudie la réduction radiolytique des ions uranyles dans des solutions dégazées d'acide sulfurique contenant divers solutés organiques. On montre que, contrairement aux radicaux ĊOOH, CO_2^- et α-hydroxy-alkyles qui réduisent les ions uranyles, les radicaux β-hydroxy-alkyles et ceux provenant de l'acide gluconique ne peuvent effectuer la réduction. L'oxydation de l'uranium(IV) par le peroxyde d'hydrogène à un pH de 0,7 fait intervenir des radicaux hydroxyles dans un mécanisme en chaîne; toutefois, à un pH de 2,0, la réaction d'oxydation s'effectue par une voie non-radicalaire. En se basant sur le fait que la vitesse d'oxydation de l'uranium(IV) par l'oxygène est plus grande en présence de propanol-2, on propose pour cette réaction un mécanisme qui implique le radical perhydroxyle. Ce mécanisme permet de concilier les données publiées antérieurement tant sur la cinétique que sur les études par marqueurs d'oxygène.

[Traduit par le journal]

Introduction

Contamination of pipework with UO_2 will occur following the rupture of a nuclear fuel bundle either in test or in accident conditions. One strategy to decontaminate this pipework is to oxidize the insoluble UO_2 (a uranium(IV) compound) in the presence of suitable complexing agents and corrosion inhibitors to the more soluble uranyl ion (a uranium(VI) species). One mixture reported to be effective for this decontamination is a solution containing hydrogen peroxide, oxalic acid, gluconic acid, and 8-hydroxyquinoline (1). During the decontamination many free-radical reactions will be initiated both from the radiation fields and from the chemistry involved in the oxidation of uranium ions. However, in the open literature only limited information is available on free-radical reactions involving uranium. In this paper we report on the reduction of uranyl ions by organic radicals, and the oxidation of soluble uranium(IV) ions by both hydrogen peroxide and oxygen with and without organic solutes present.

Experimental

Materials

The chemicals used were purchased from the following companies: Fisher Scientific (uranyl sulphate, 2-propanol, sodium formate, sodium oxalate), Anachemia (sulphuric acid), Aldrich (sodium gluconate ($HOCH_2[CHOH]_4CO_2Na$)), J. T. Baker (hydrogen peroxide, 2-methyl-2-propanol (*tert*-butanol)). All were used as supplied except *tert*-butanol, which was multiply recrystallized. Triply distilled water was used for solution preparation. Uranium(IV) ions were prepared by electrolytically reducing uranyl ions at a platinum electrode under a nitrogen atmosphere.

Methods

Samples for steady-state radiolysis studies were degassed on a vacuum line (freeze–pump–thaw cycles) in a round-bottom flask and then poured under vacuum into a 10-cm pathlength Spectrosil optical cell. The above procedures were carried out in semi-darkness to prevent photolytic reduction of the uranyl ion. The samples were irradiated in an AECL Gammacell at a dose rate of about 1.7×10^{19} eV $L^{-1} s^{-1}$. In experiments where the sample was photolyzed, a high pressure xenon arc lamp was used. The uv–vis spectra of these solutions were recorded on a Cary 17 spectrophotometer.

A limited number of pulse radiolysis experiments were also performed and in these studies the solutions were degassed by the syringe-bubbler technique. The 2.25-MeV electron accelerator and detection system has been described elsewhere (2).

To study the reaction of uranium(IV) ions with hydrogen peroxide, the solution containing the uranium(IV) ions and the solution containing the hydrogen peroxide were deoxygenated separately by stripping with nitrogen gas, rapidly mixed, and then transferred to a 10-cm cell under a nitrogen atmosphere. For experiments where organic solutes were present, the solute was added to the uranium(IV) solution before deoxygenation. The change in concentration of uranium(IV) during the experiment was monitored by its absorption near 650 nm using either a Cary-17 or Cary-118 uv–vis spectrometer. Hydrogen peroxide was assayed by the tri-iodide method of Ghormley and co-workers (3).

For the autoxidation of uranium(IV), the reaction is slow enough for the solution to be saturated with oxygen. When this oxidation was carried out with an alcohol present, the alcohol was added after the solutions were oxygen saturated.

Results and discussion

Radiolysis of uranyl sulphate solutions

Experimental observations

The yields of uranium(IV) have been measured in γ-irradiated degassed sulphuric acid solutions containing 10^{-3} mol L^{-1} uranyl sulphate and one of the following organic solutes: 0.1 mol L^{-1} 2-propanol, 0.1 mol L^{-1} sodium formate, 0.1 mol L^{-1} sodium gluconate, 1.0 mol L^{-1} *tert*-butanol. The yield of uranium(IV) was monitored (see Fig. 1) by its absorption near 650–670 nm (the absorption maxima varied depending on the degree of complexation with the organic solute). In general, the procedure was to give the solution an irradiation dose of

[1]AECL No. 8971.

[2]Author to whom all correspondence should be addressed.

[3]Concordia University Co-operative Program Student.

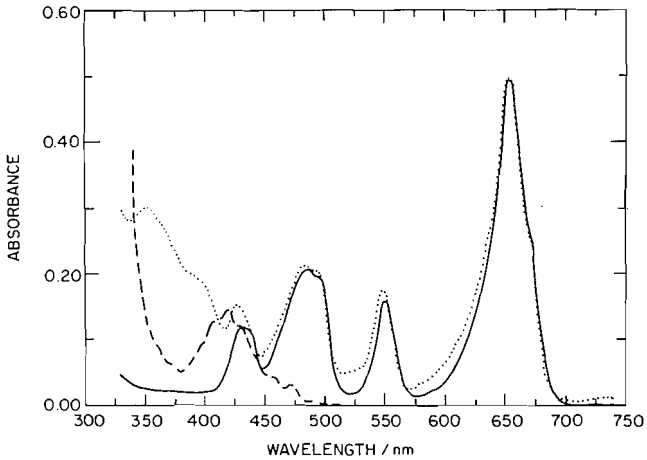

FIG. 1. Spectra of a degassed 10^{-3} mol L^{-1} UO_2SO_4 solution containing 0.1 mol L^{-1} 2-propanol at pH 1.1; before irradiation (---); after 22.5×10^{21} eV L^{-1} radiation, where complete conversion to U(IV) has occurred (—); after 30×10^{21} eV L^{-1} radiation where some U(III) has been formed (...).

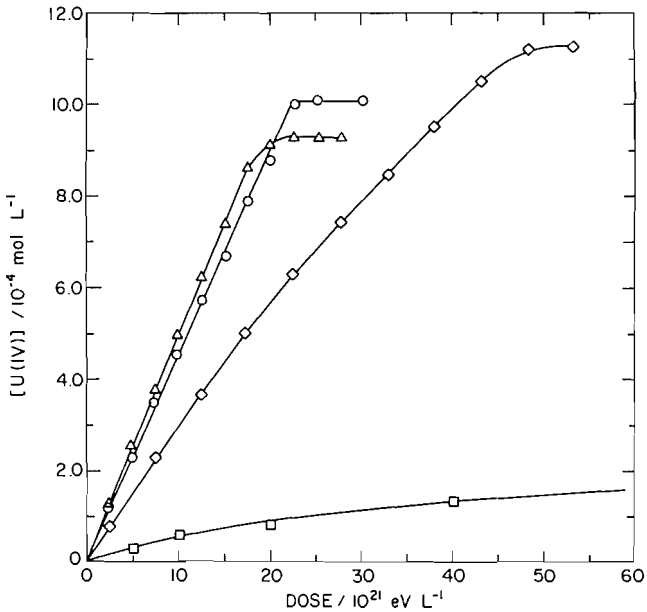

FIG. 2. Yield of uranium(IV) as a function of dose for degassed 10^{-3} mol L^{-1} uranyl sulphate solutions containing: 0.1 mol L^{-1} 2-propanol at pH 1.1 (○); 0.11 mol L^{-1} oxalate at pH 2.0 (△) and pH 5.0 (◇); 1.0 mol L^{-1} *tert*-butanol at pH 1.4 (□).

$2-5 \times 10^{21}$ eV L^{-1} and then record the spectrum; this cycle was repeated until such time as all the uranyl ions were converted to uranium(IV), as illustrated in Fig. 2. For solutions containing 2-propanol, formate, or oxalate, the yield of uranium(IV) was calculated assuming 100% conversion. As a check, the maximum yield of uranium(IV) was confirmed by photolytically reducing the uranyl ions. This was not possible when oxalate was present, as photolysis of these solutions forms CO and CO_2 but very little uranium(IV) (4). In the cases where *tert*-butanol or gluconate were present, complete reduction by radiolysis was not always possible; however, the extinction coefficient of uranium(IV) was determined by the complete photolytic reduction of uranyl ions in these solutions.

With the 2-propanol and formate solutions, after complete conversion of the uranyl ions to uranium(IV) (either radiolytically or photolytically), a small steady-state concentration of uranium(III) was formed (see Fig. 1) on continued radiation. Both from the published extinction coefficient at 350 nm (1200 L mol^{-1} cm^{-1} (5)) and from oxidizing the uranium(III) back to uranium(IV) (by air or the slower reaction with water), it is estimated that uranium(III) constituted less than 2% of the uranium ions under these conditions.

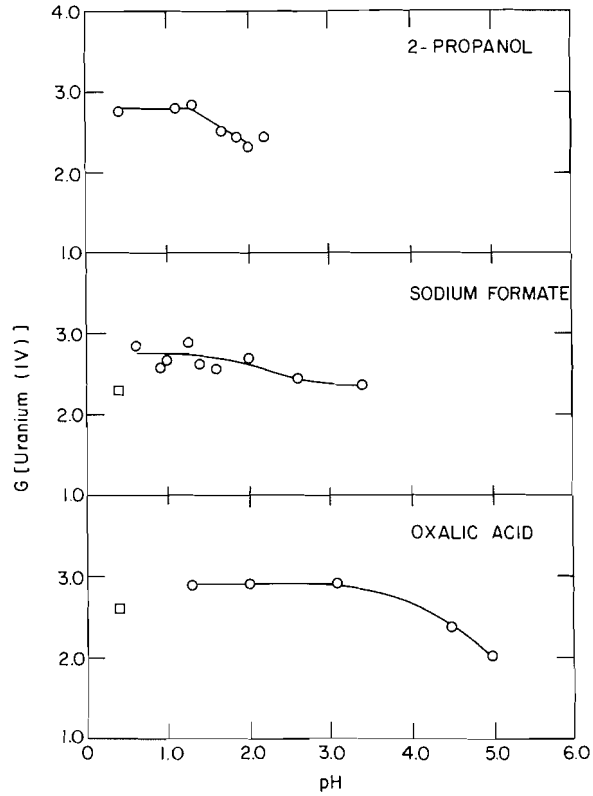

FIG. 3. The *G*-value for uranium(IV) as a function of pH from degassed 10^{-3} mol L^{-1} uranyl sulphate and 0.1 mol L^{-1} organic solute (○). The symbols (□) are the data reported by Hyder.

The dependence of the *G*-value (i.e. number formed per 100 eV of energy absorbed) of uranium(IV) on pH for solutions containing 2-propanol, sodium formate, and oxalic acid is shown in Fig. 3. The pH was adjusted using sulphuric acid. Also shown by the squares in Fig. 3 are the *G*-values reported by Hyder (6). For solutions containing 2-propanol and sodium formate, the uranium(IV) formed precipitated above pH 2.1 and 3.5, respectively. For solutions containing 0.1 mol L^{-1} sodium gluconate, at pH 4.4 the *G*-value for uranium(IV) was 1.4 as calculated from the initial slope of the yield versus dose plot, while at pH 2.0, the *G*-value was zero. The uranium(IV) ion can exist in this solution as it was formed by photolytic reduction. For 1.0 mol L^{-1} *tert*-butanol solutions, the initial *G*-value for uranium(IV) was 0.35 ± 0.10 for the pH range 0.7–2.0. An example of the data is shown in Fig. 2. The uranyl ion could be totally reduced to uranium(IV) photolytically in these solutions.

Some further radiolysis experiments were performed using deoxygenated 10^{-3} mol L^{-1} uranium(IV) sulphuric aid solutions containing 0.5 mol L^{-1} *tert*-butanol. The *G*-value for uranium-(IV) loss was less than 0.3 for pH 0.7–2.1. This small yield can be attributed to oxidation by radiolytic hydrogen peroxide (see later).

Proposed mechanism

For the solutions studied here, most of the ionizing radiation is absorbed by the water to form the species shown in reaction [1].

[1] $H_2O \rightarrow e^-_{aq}(2.7), OH(2.7), H(0.55), H_2(0.45), H_2O_2(0.7)$

The yields for dilute aqueous solutions are given in parentheses and are expressed in G-values. These values will be up to 10% higher for $G(e^-_{aq} + H)$ and $G(OH)$ at some of the solute concentrations used in these experiments (8).

Depending on the pH of the solution, the organic solute (S) present, and how far the reduction of the uranyl ions has proceeded, the solvated electrons will be scavenged either by the uranyl ions or the organic solute to form uranium(V) (reactions [2]–[4]),

[2] $UO_2^{2+} + e^-_{aq} \rightarrow U(V) \qquad k_2 = 1\text{–}3 \times 10^{10}\,L\,mol^{-1}\,s^{-1}$ (8)

[3] $S + e^-_{aq} \rightarrow S^- \qquad k_3 < 10^8\,L\,mol^{-1}\,s^{-1}$ (9)

[4] $S^- + UO_2^{2+} \rightarrow U(V)$

or will be scavenged by the protons to form hydrogen atoms (reaction [5]).

[5] $H^+ + e^-_{aq} \rightarrow H \qquad k_5 = 2 \times 10^{10}\,L\,mol^{-1}\,s^{-1}$ (9)

These hydrogen atoms formed through [1] and [5] will either reduce the uranyl ions,

[6] $UO_2^{2+} + H \rightarrow U(V) \qquad k_6 = 4.5 \times 10^7\,L\,mol^{-1}\,s^{-1}$ (10)

or react with the organic solute present. For all solutes except oxalic acid, the radical produced from the reaction of the hydrogen atom will be the same as that formed from the hydroxyl radical. With oxalic acid it is thought that the product from hydrogen atom reaction is similar to the electron adduct of oxalic acid (11).

In the discussion so far, all reactions involving uranyl ions (reactions [2], [3], and [6]) lead to the formation of uranium(V). Uranium(V) is not long lived in aqueous solution as it disproportionates as shown in reaction [7] (for solutions containing sulphate ions):

[7] $U(V) + U(V) \rightarrow UO_2^{2+} + U(IV) \qquad 2k_7 \sim 1.2 \times 10^4[H^+]\,L\,mol^{-1}\,s^{-1}$ (12, 13)

In general, where the degree of hydrolysis and complexation of the uranium ions is poorly defined, they will be referred to as U(IV), etc. However, in the present experiments the uranium-(VI) was always present as the uranyl ion UO_2^{2+} and will be referred to as such, although it will be complexed with anions in the solution, e.g. SO_4^{2-}.

Not all the radicals formed from the reaction of hydroxyl radicals and hydrogen atoms with the organic solute are capable of reducing uranyl ions. This is best illustrated with β-hydroxy-alkyl radical formed from *tert*-butanol.

[8] $(CH_3)_3COH + OH \rightarrow \dot{C}H_2\text{—}C(CH_3)_2OH + H_2O \qquad k_8 = 6.3 \times 10^8\,L\,mol^{-1}s^{-1}$ (14)

[9] $(CH_3)_3COH + H \rightarrow \dot{C}H_2\text{—}C(CH_3)_2OH + H_2 \qquad k_9 = 1.7 \times 10^5\,L\,mol^{-1}s^{-1}$ (15)

With *tert*-butanol present, the initial $G(U(IV))$ of 0.35 ± 0.10 (see Fig. 2) can be explained by the 25% of $G(e^-_{aq} + H)$ which are scavenged by the uranyl ions through reactions [5] and [6] followed by reaction [7]. This leads to a prediction of a G-value for uranium(IV) of ~0.4. It is obvious from these results that the β-hydroxy-alkyl radical does not reduce uranyl ions. Likewise the low G-value for uranyl ions (<0.3) when uranium(IV) solutions containing $0.5\,mol\,L^{-1}$ *tert*-butanol were irradiated indicates that this β-hydroxy-alkyl radical also cannot oxidize uranium(IV). The small G-value is consistent with the oxidation of uranium(IV) by radiolytically produced hydrogen peroxide and this reaction will be discussed later.

The radicals formed from gluconic acid by reaction with hydroxyl radicals and hydrogen atoms also cannot reduce uranyl ions to uranium(IV). At pH 4.4, where all the electrons were scavenged by the uranyl ion, $G(U(IV))$ was about half of $G(e^-_{aq})$, i.e. 1.5 (reactions [2] and [7]), while at pH 2, where $G(U(IV))$ was zero, greater than 90% of the solvated electrons were scavenged through reaction [5]. Assuming the rate constant for hydrogen atom reaction with gluconic acid is similar to that with glucose (i.e. $\sim 10^8\,L\,mol^{-1}\,s^{-1}$ (15)), all the hydrogen atoms were scavenged by the gluconic acid.

Over the pH range studied (pH 0.7–3.4) with formate added, the formate will exist essentially as formic acid ($pK = 3.75$). In these experiments all the radical species formed from water (reaction [1]) will lead to the reduction of uranyl ions. The hydrogen atoms and hydroxyl radicals that react with the formic acid will, depending on the pH, form either CO_2^- or COOH ($pK = 1.4$ (17)), both of which are strong one-electron reducing agents.

[10] $UO_2^{2+} + CO_2^-(COOH) \rightarrow U(V) + CO_2(+H^+)$

As can be seen in Fig. 3, the G-value for uranium(IV) drops as the pH increases, this in part can be attributed to the decrease in radical yield over this pH range (7). Also over this pH range, the mechanism for the reaction of the hydrogen peroxide (formed in [1]) with uranium(IV) changes, as will be described in detail in the next section. In summary, oxidation by hydrogen peroxide of uranium(IV) proceeds slowly at pH 0.7 and predominantly by a mechanism which produces hydroxyl radicals.

[11] $U(IV) + H_2O_2 \rightarrow U(V) + OH^- + OH$

In the presence of formic acid, the hydroxyl radicals are converted to COOH, which undergoes reaction [10], so that, overall, little uranium(IV) is lost. At pH 2, the oxidation of uranium(IV) is much faster and proceeds through a path that does not produce hydroxyl radicals. Under these conditions uranium(IV) will be oxidized directly to uranium(VI) by the radiolytically produced hydrogen peroxide. This is indicated in Fig. 3 by the decrease in the G-value of uranium(IV) with an increase of the pH from pH 0.7, where the G-value is given by [12],

[12] $G(U(IV)) \sim 0.5\,[G(e^-_{aq}) + G(H) + G(OH)]$

to a value approaching, at pH 3, that given by [13],

[13] $G(U(IV)) \sim 0.5\,[G(e^-_{aq}) + G(H) + G(OH)] - G(H_2O_2)$

The situation when 2-propanol was added is very similar to that of formate. In these experiments all the radicals formed in [1] and [5] react with 2-propanol.

[14] $(CH_3)_2CHOH + OH \rightarrow 0.86\,(CH_3)_2\dot{C}OH + 0.14\,\dot{C}H_2CH(CH_3)OH + H_2O \qquad k_{14} = 2.3 \times 10^9\,L\,mol^{-1}\,s^{-1}$ (14)

[15] $(CH_3)_2CHOH + H \rightarrow 0.86\,(CH_3)_2\dot{C}OH + 0.14\,\dot{C}H_2CH(CH_3)OH + H_2 \qquad k_{15} = 7.9 \times 10^7\,L\,mol^{-1}\,s^{-1}$ (15)

Of the radicals formed in reactions [14] and [15], only 86% of these are α-hydroxy-alkyl radicals (18) that are capable of reducing uranyl ions (reaction [16]). By analogy to the *tert*-butanol experiments described earlier, the 14% which are β-hydroxy-alkyl radicals will not reduce uranyl ions. The rate constant for reaction [16] was measured in pulse radiolysis experiments by following pseudo-first-order decay of the $(CH_3)_2\dot{C}OH$ radical at 340 nm in a pH 1 solution containing 2.7–5.2 × 10^{-3} mol L^{-1} uranyl sulphate and 1 mol L^{-1} 2-propanol. The value for k_{16} at 22°C was (4.1 ± 0.3) × 10^7 L mol^{-1} s^{-1}.

[16] $(CH_3)_2\dot{C}OH + UO_2^{2+} \rightarrow U(V) + (CH_3)_2CO$

$k_{16} = 4.1 \times 10^7$ L mol^{-1} s^{-1}

The situation when oxalate is the added solute is different in that oxalate complexes strongly with both the uranyl ion (19) and with uranium(IV). For the pH range 1.3–3.1 (Fig. 3), the *G*-value for uranium(IV) was constant at 2.9. This is consistent with the hydroxyl radical reacting with oxalate to form a radical that can reduce the uranyl ion.

[17] $\begin{matrix}COO^- \\ | \\ COOH\end{matrix} + OH \rightarrow \begin{matrix}CO\dot{O} \\ | \\ COOH\end{matrix}$ or $\dot{C}OOH + CO_2$

$k_{17} = 6 \times 10^7$ L mol^{-1} s^{-1} (16)

The drop in the *G*-value above pH 3 is probably a consequence of the competition for hydroxyl radicals between the oxalate and the radiolysis product uranium(IV) as the radiolysis proceeds. This is supported by the yield versus dose plot at pH, which is gently curved (Fig. 2).

[18] $\begin{matrix}COO^- \\ | \\ COO^-\end{matrix} + \dot{O}H \rightarrow \begin{matrix}CO\dot{O} \\ | \\ COO^-\end{matrix}$ (or $CO_2 + CO_2^-$)

$k_{18} = 1 \times 10^7$ L mol^{-1} s^{-1} (16)

[19] $U(IV) + OH \rightarrow U(V) + OH^-$ $k_{19} = 8 \times 10^8$ L mol^{-1} s^{-1} (10)

At pH 5, the oxalate exists essentially as the dianion, which has a lower rate constant (reaction [18]) than at lower pH's where the oxalic acid is in the mono-anion form (reaction [17]).

Reactions of uranium(IV) ions with hydrogen peroxide

Experimental observations

To understand the role of radiolytically produced hydrogen peroxide in the radiation chemistry of uranium ions, the reaction of uranium(IV) ions with hydrogen peroxide was studied in deoxygenated sulphuric acid solutions at pH 0.7, 1.5, and 2.0. These experiments were carried out with and without hydroxyl radical scavengers present. In the absence of scavengers, the uranium(IV) ions were oxidized to uranyl ions; the rate of this reaction increased with pH for a given uranium(IV) ion and hydrogen peroxide concentration, as shown in Figs. 4a and b. At pH 0.7 for 10^{-3} mol L^{-1} uranium(IV) ions, increasing the hydrogen peroxide concentration increased the reaction rate (compare open to filled circles in Fig. 4a). The addition of 0.12 mol L^{-1} 2-propanol to a solution containing 10^{-3} mol L^{-1} uranium(IV) and 10^{-3} mol L^{-1} hydrogen peroxide (Figs. 4a and b: triangles) inhibits the loss of uranium(IV) at pH 0.7, while at pH 2.0 the addition of 0.12 and 1.2 mol L^{-1} 2-propanol had only a minimal effect on uranium(IV) loss (Fig. 4: triangles and squares; note that 1.2 mol L^{-1} 2-propanol has a lower initial uranium(IV) concentration than the 0.12 mol L^{-1} 2-propanol solution). The effect of adding 0.08 mol L^{-1} formate to the reaction solution at pH 0.7 was similar to that of adding

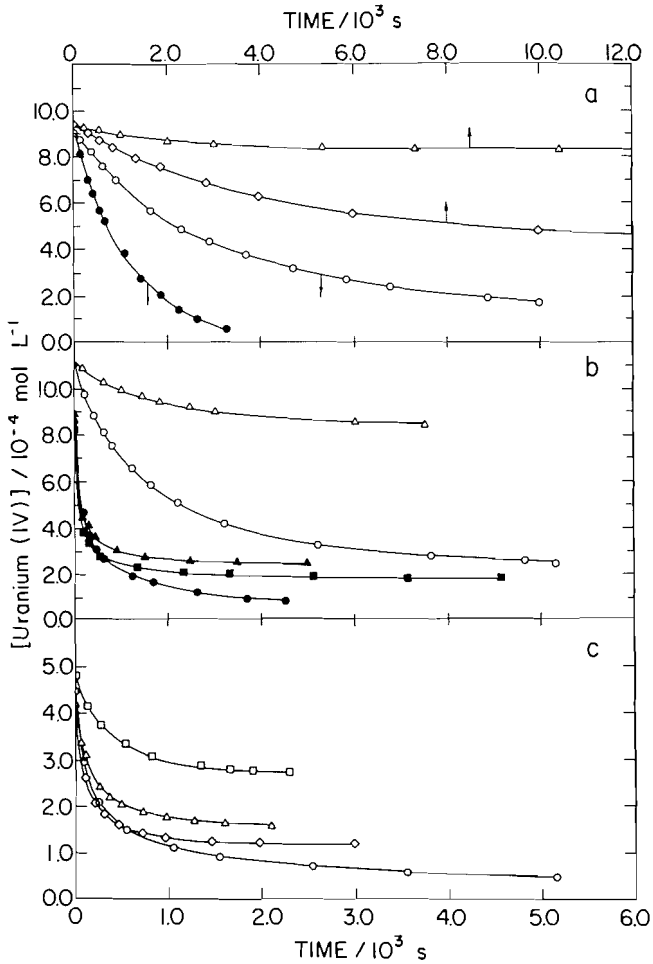

FIG. 4. The disappearance of uranium(IV) as a function of time. Graph (a): (○) ≡ $[U(IV)]_0 = 9.1 \times 10^{-4}$ mol L^{-1}; $[H_2O_2]_0 = 9.6 \times 10^{-4}$ mol L^{-1}; pH = 0.7; (●) ≡ $[U(IV)]_0 = 9.1 \times 10^{-4}$ mol L^{-1}; $[H_2O_2]_0 = 17.8 \times 10^{-4}$ mol L^{-1}; pH = 0.7; (△) ≡ $[U(IV)]_0 = 9.4 \times 10^{-4}$ mol L^{-1}; $[H_2O_2]_0 = 9.4 \times 10^{-4}$ mol L^{-1}; [2-propanol] = 0.12 mol L^{-1}; pH = 0.7; (◇) ≡ $[U(IV)]_0 = 9.4 \times 10^{-4}$ mol L^{-1}; $[H_2O_2]_0 = 9.4 \times 10^{-4}$ mol L^{-1}; [*tert*-butanol] = 0.46 mol L^{-1}; pH = 0.7. Graph (b): (○) ≡ $[U(IV)]_0 = 11.1 \times 10^{-4}$ mol L^{-1}; $[H_2O_2]_0 = 9.4 \times 10^{-4}$ mol L^{-1}; pH = 1.5; (△) ≡ $[U(IV)]_0 = 11.1 \times 10^{-4}$ mol L^{-1}; $[H_2O_2]_0 = 9.5 \times 10^{-4}$ mol L^{-1}; [2-propanol] = 0.12 mol L^{-1}; pH = 1.5; (●) ≡ $[U(IV)]_0 = 8.5 \times 10^{-4}$ mol L^{-1}; $[H_2O_2]_0 = 8.5 \times 10^{-4}$ mol L^{-1}; pH = 2.0; (▲) ≡ $[U(IV)]_0 = 8.9 \times 10^{-4}$ mol L^{-1}; $[H_2O_2]_0 = 9.5 \times 10^{-4}$ mol L^{-1}; [2-propanol] = 0.12 mol L^{-1}; pH = 2.0; (■) ≡ $[U(IV)]_0 = 8.0 \times 10^{-4}$ mol L^{-1}; $[H_2O_2]_0 = 8.7 \times 10^{-4}$ mol L^{-1}; [2-propanol] = 1.1 mol L^{-1}; pH = 2.0. Graph (c): (○) ≡ $[U(IV)]_0 = 4.5 \times 10^{-4}$ mol L^{-1}; $[H_2O_2]_0 = 4.8 \times 10^{-4}$ mol L^{-1}; pH = 2.0; (◇) ≡ $[U(IV)]_0 = 4.1 \times 10^{-4}$ mol L^{-1}; $[H_2O_2]_0 = 4.7 \times 10^{-4}$ mol L^{-1}; [2-propanol] = 0.12 mol L^{-1}; pH = 2.0; (△) ≡ $[U(IV)]_0 = 4.6 \times 10^{-4}$ mol L^{-1}; $[H_2O_2]_0 = 4.2 \times 10^{-4}$ mol L^{-1}; [formate] = 0.08 mol L^{-1}; pH = 2.0; (□) ≡ $[U(IV)]_0 = 4.8 \times 10^{-4}$ mol L^{-1}; $[H_2O_2]_0 = 4.6 \times 10^{-4}$ mol L^{-1}; [formate] = 0.45 mol L^{-1}; pH 2.0.

0.12 mol L^{-1} 2-propanol. However, in contrast to 2-propanol, at pH 2 the addition of higher concentrations of formate (0.45 mol L^{-1}) did inhibit the uranium(IV) loss to a limited extent over the addition of 0.08 mol L^{-1} formate. This is shown in Fig. 4c, along with the results for 0.12 mol L^{-1} 2-propanol. In this figure, the initial concentrations of uranium(IV) and hydrogen peroxide were halved to slow the initial rate.

Figure 5 summarizes the stoichiometry of the reaction in the absence of hydroxyl radical scavengers for the three pH values

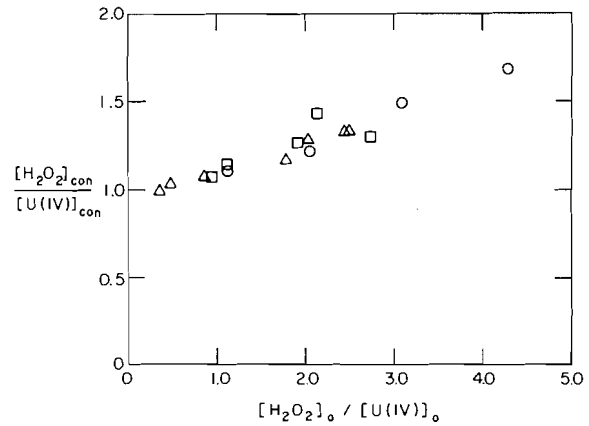

FIG. 5. A plot of the ratio of hydrogen peroxide consumed to uranium(IV) consumed as a function of the initial concentration ratio: pH 0.7 (○); pH 1.5 (△); and pH 2.0 (□).

where the ratio of hydrogen peroxide consumed to uranium(IV) consumed is plotted as a function of the initial concentration ratio. It should be noted that an earlier study by Baker and Newton (20) found that in deoxygenated 2 mol L^{-1} perchloric acid, the consumption ratio of $[H_2O_2]/[U(IV)]$ was constant at 1.024 ± 0.016 for the initial concentration ratio range of $[H_2O_2]/[U(IV)]$ of 0.54–18. This is quite different from our results in the less acidic sulphuric acid solutions studied here and may be associated with the ionic state of uranium(IV) ion. In 2 mol L^{-1} perchloric acid, the uranium(IV) will exist as U^{4+}.

[20] $U^{4+} + H_2O \rightleftharpoons UOH^{3+} + H^+ \qquad K_{20} = 0.1$ (21)

In the current experiments at pH 2, about 55% of the uranium(IV) will be UOH^{3+}, 5% as U^{4+}, and the remainder as the ion pair USO_4^{2+}.

[21] $U^{4+} + HSO_4^- \rightleftharpoons USO_4^{2+} + H^+ \qquad K_{21} = 3.3 \times 10^2$ (22)

At pH 1, the uranium(IV) will essentially all exist as the ion-pair USO_4^{2+}.

Proposed mechanism

Our results at pH 0.7 can be understood in terms of the free-radical chain sequence originally proposed by Baker and Newton (20) (reactions [11], [22], [19], [23], [7]) and the additional reactions [24]–[26]. In these reactions, U(VI) can either be the ion pair, USO_4^{2+}, or U^{4+} but not the hydrolysed form UOH^{3+}.

Initiation:

[11] $U(IV) + H_2O_2 \rightarrow U(V) + OH + OH^-$

Propagation:

[22] $U(V) + H_2O_2 \rightarrow UO_2^{2+} + OH + OH^-$

[19] $U(IV) + OH \rightarrow U(V) + OH^- \qquad k_{19} = 8 \times 10^8$ L mol^{-1} s^{-1} (10)

Termination:

[23] $U(V) + OH \rightarrow UO_2^{2+} + OH^-$

[7] $U(V) + U(V) \rightarrow U(IV) + UO_2^{2+}$

Side reactions:

[24] $OH + H_2O_2 \rightarrow OOH + H_2O \qquad k_{24} = 2.7 \times 10^7$ L mol^{-1} s^{-1} (23)

[25] $OOH + OOH \rightarrow H_2O_2 + O_2 \qquad 2k_{25} = 8.6 \times 10^5$ L mol^{-1} s^{-1} (24)

[26] $U(IV) + OOH \rightarrow UO_2^{2+} + OH$

Reactions [24]–[26] would explain the stoichiometry observed in Fig. 5. In these reactions, hydrogen peroxide (reaction [24]) competes with uranium(IV) (reaction [19]) for the hydroxyl radical. Provided reaction [25] can compete with [26], then more hydrogen peroxide will be consumed than uranium(IV). The reason for our choice of reaction [26] (25, 26) over reaction [27] (27) will be outlined in the next section.

[27] $U(IV) + OOH \rightarrow U(V) + H_2O_2$

The situation is even more complex than the above side reactions suggest. Studies on the disproportionation reaction [7] have indicated an effect of the product UO_2^{2+} on the rate due to a uranium(V)–uranyl complex (13). Other studies indicate that the uranyl ion will complex with both hydrogen peroxide (28) and the perhydroxyl radical, OOH (29). This also will affect the kinetics as the uranyl ion concentration builds up during the experiment.

The results for the addition of 2-propanol or formate at pH 0.7 basically conform with this mechanism, i.e. hydroxyl radicals formed in [11] and [22] are scavenged to form a reducing radical that can then reduce the uranyl ions back to a lower oxidation state by reactions [10] or [16] followed by [7]. Furthermore, the results when 0.46^{-1} mol L *tert*-butanol was added to 10^{-3} mol L^{-1} uranium(IV), 10^{-3} mol L^{-1} hydrogen peroxide solution at pH 0.7 are also consistent with the mechanisms [11], [22], [23], and [7]. In this case, approximately two molecules of peroxide were consumed for every uranium(IV) lost (Fig. 4a) since *tert*-butanol scavenges the hydroxyl radicals formed in reactions [11] and [22] but, as was seen in previous section, the β-hydroxy-radical formed (reaction [8]) cannot reduce the uranyl ion back to uranium(IV). These results indicate that in the presence of *tert*-butanol the reaction rate is controlled by reaction [11] because all the hydroxyl radicals formed in [11] and [22] are scavenged by the *tert*-butanol and cannot propagate the chain reaction. In the absence of *tert*-butanol, reactions [22] and [19] can propagate the chain reaction so that now reaction [22] is the rate-limiting step. Based on these last two statements and the data in Fig. 4a, estimates for k_{11} of 0.21 L mol^{-1} s^{-1} and for k_{22} or 55 L mol^{-1} s^{-1} have been made.

In pH 2 solutions in which the 0.12 and 1.2 mol L^{-1} 2-propanol added was more than sufficient to scavenge all the hydroxyl radicals generated (reaction [14]), the uranium(IV) was still consumed. This implies that hydroxyl radicals are not a major intermediate at this pH. An explanation is that the oxidation proceeds by two mechanisms: one involving U^{4+} and USO_4^{2+} in which hydroxyl radicals are formed as intermediates, and the other involving UOH^{3+} in which hydroxyl radicals are not generated. This second mechanism has a rate constant which is larger than that associated with the first mechanism. This would also explain the pH dependence of the rate. As mentioned earlier, at pH 1.0 the UOH^{3+} will constitute less than 5% of the uranium(IV) ions but that percentage rises to 55% at pH 2 for the solutions containing 2-propanol. The formic acid results are also consistent with the above proposal. The 0.08 mol L^{-1} formate solutions at pH 0.7 and 2.0 both behaved similarly to the 0.12 mol 2-propanol solutions. The probable reason that the 0.45 mol L^{-1} formate could inhibit the loss of uranium(IV) at pH 2 (Fig. 4c) was that the sulphate ion concentration was higher in this experimental solution because the pH of the sodium formate was adjusted by the addition of sulphuric acid. The higher sulphate concentration would decrease the UOH^{3+} concentration and raise the USO_4^{2+} concentration. It should be noted that no evidence exists for a complex between uranium(IV) ions and formate ions, as the wavelength of maximum absorption and the asociated extinction did not change in the presence of the 0.45 mol L^{-1} formic acid.

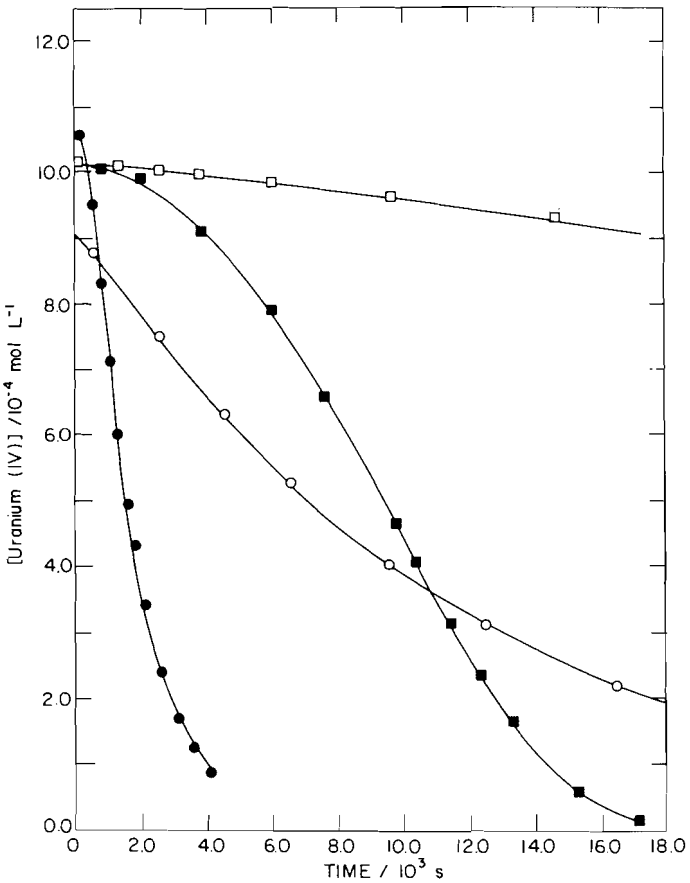

FIG. 6. The time dependence for the reaction of oxygen (initially 1.3 $\times$ 10^{-3} mol L^{-1}) with uranium(IV) without (○, □) and with 0.12 mol L^{-1} 2-propanol (●, ■) present. The circles are for pH = 2.0 and the squares are for pH = 0.8.

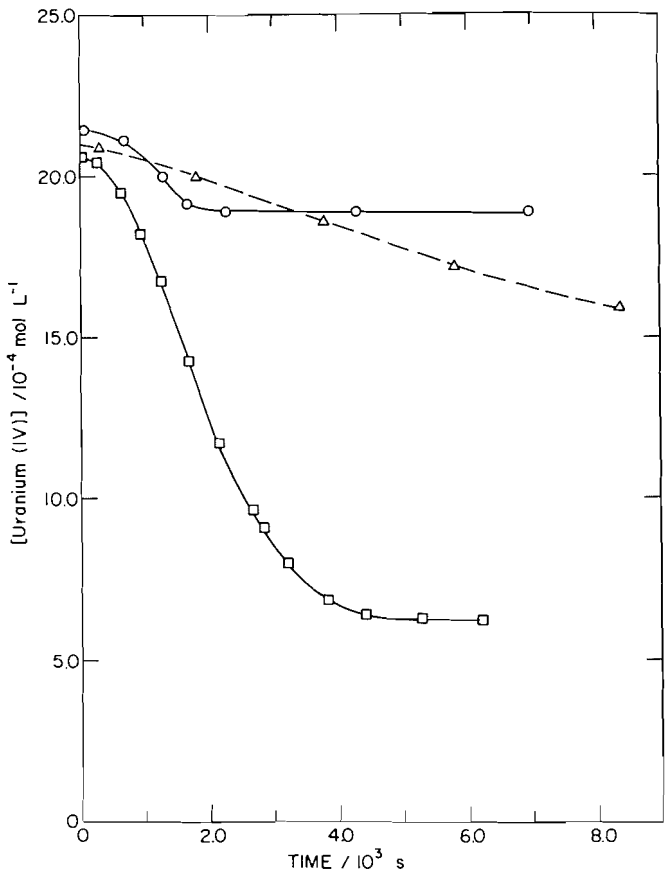

FIG. 7. The time dependence for the reaction of uranium(IV) (initially ~2.1 $\times$ 10^{-3} mol L^{-1}) with oxygen at pH 1.3: $[O_2]_0$ = 1.3 $\times$ 10^{-3} mol L^{-1} (△); $[O_2]_0$ = 1.3 $\times$ 10^{-3} mol L^{-1} oxygen and 0.12 mol L^{-1} 2-propanol (□); $[O_2]_0$ = 2.6 $\times$ 10^{-4} mol L^{-1} oxygen and 0.12 mol L^{-1} 2-propanol (○).

A possible mechanism for the reaction of UOH^{3+} with hydrogen peroxide could be the simpler bimolecular reaction [28].

[28] $UOH^{3+} + H_2O_2 \rightarrow UO_2^{2+} + H_2O$

However, this reaction does not explain the stoichiometry observed at this pH, as shown in Fig. 5. At the present we have been unable to propose a mechanism that satisfactorily explains these pH 2 results. The results obtained at pH 1.5 can be explained if both mechanisms are operating simultaneously.

The above results are consistent with the oxygen tracer experiments of Gordon and Taube (30) for the oxidation of uranium(IV) with hydrogen peroxide. They reported that as the pH rose from 0.35 to 1.5, the number of oxygen atoms transferred from the peroxide to the product uranyl ion increased from 1.0 to 1.18. This could be rationalized in terms of the mechanism change we observed in this study.

Reaction of uranium(IV) with molecular oxygen

Experimental observations

The effect of 2-propanol on the rate of oxidation of uranium(IV) by molecular oxygen was studied to determine if free radicals were involved. In general, the loss of uranium(IV) was followed (spectroscopically at 652 mn) in solutions that initially contained about 10^{-3} mol L^{-1} uranium(IV) ions and were oxygen saturated (1.3 $\times$ 10^{-3} mol L^{-1}). The pH (0.8–2.0) was adjusted with sulphuric acid. In agreement with earlier reports, the rate of uranium(IV) loss increases with pH (open symbols in Fig. 6); the effect of adding 0.12 mol L^{-1} 2-propanol was to increase the rate of oxidation (sigmoidal curves—solid points in Fig. 6). From Fig. 7 the overall stoichiometry of the reaction when 2-propanol was present shows that one oxygen molecule was consumed for every uranium(IV) ion oxidized. The increase in the rate of reaction on addition of 0.12 mol L^{-1} 2-propanol at all pH's studied implies that free radicals are involved and that at least some hydroxyl radicals are generated.

Proposed mechanism

Before speculating as to what these reactions are, it should be noted that little consensus exists in the literature as to the mechanism involved in the oxidation by molecular oxygen of uranium(IV) ions (27, 30, 31). A mechanism which accommodates the kinetic results of Halpern and Smith (27), the tracer study of Gordon and Taube (30), and the present results is given below. In these reactions the oxygen atoms derived from molecular oxygen are marked with an asterisk. The pH dependence of the reaction indicates that UOH^{3+} (equilibrium [20]) is the most reaction uranium(IV) ion.

Initiation:

[29] $UOH^{3+} + O^*O^* \rightarrow UO_2^{+} + O^*O^*H$

[30] $UO_2^{+} + O^*O^* + H^+ \rightarrow UO_2^{2+} + O^*O^*H$

Labelling propagation step:

[31] $UOH^{3+} + O^*O^*H \rightarrow UOO^{*2+} + O^*H + H^+$

[32] $UOH^{3+} + O^*H \rightarrow UOO^{*+} + 2H^+$

[33] $UOO^{*+} + O^*O^* + H^+ \rightarrow UOO^{*2+} + O^*O^*H$

The termination reactions are given by reactions [23] and [7]. Summing reactions [31]–[33], the overall equation [34] is arrived at,

[34] $2\,UOH^{3+} + O^*O^* \rightarrow 2\,UOO^{*2+} + 2H^+$

where both atoms in the molecular oxygen are incorporated into different uranyl ions. This satisfies the restrictions imposed by the tracer experiments (28). The pH dependence is satisfied by UOH^{3+} acting as the active species (equilibrium [20]). In fact, the reported (32) retardation of the reaction in sulphuric acid solutions (as compared to perchloric acid) could be the direct result of equilibrium [20] competing with equilibrium [21].

The effect of adding 2-propanol is to circumvent reaction [32] by scavenging the hydroxyl radical formed in reaction [31] through reaction [14]. The alkyl radicals (HR) formed in [14] react with oxygen to form a peroxy radical, which will dissociate to form the perhydroxyl radical (33).

[35] $H\dot{R} + O_2 \rightarrow HROO\dot{} \rightarrow R + HOO\dot{}$

The OOH radical recycles back to [31] so that the reactions [31], [14], and [35] become the propagating cycle. As the alcohol molecule is oxidized in this cycle also, this leads to the stoichiometry observed in our experiments where one uranium(IV) ion was oxidized per oxygen molecule consumed.

The choice for the mechanism of the reaction of OOH with uranium(IV) as being reaction [31] rather than reaction [27] was made for two reasons. Firstly, if hydrogen peroxide was the product (reaction [27]) then, at pH 2, based on the uranium(IV)/hydrogen peroxide/2-propanol results reported earlier, no hydroxyl radicals would be formed and hence 2-propanol should have had no effect on the reaction rate. Secondly, to meet the isotopic labelling requirements (30) over the pH range studied, reaction [31] has to be chosen rather than [30], followed by reactions [11], [22], [19], [23], [7].

Conclusion

In this study, some of the free-radical redox reactions involving uranium ions have been characterized. In particular, we have shown that for alkyl radicals derived from alcohols, only the α-hydroxy-alkyl radical can reduce uranyl ions and that the β-hydroxy-alkyl radicals can neither reduce uranyl ions nor oxidize uranium(IV) ions. The mechanism for the reaction of hydrogen peroxide with uranium(IV) was demonstrated to change from a free-radical chain reaction involving hydroxyl radicals (reactions [11], [22], [19], [23], [7]) at pH 0.7 to non-free-radical oxidation reaction at pH 2 (possibly reaction [27]). From studying the 2-propanol mediated oxidation of uranium(IV) by oxygen, the reaction of the perhydroxyl radical (OOH) with uranium(IV) has been shown to form hydroxyl radicals (reaction [26]) rather than hydrogen peroxide (reaction [27]). This has enabled us to propose a mechanism for the reaction of oxygen with uranium(IV) (reactions [29]–[33]) that satisfies both the kinetic (27) and tracer (30) experiments.

Acknowledgement

The authors wish to acknowledge discussions with Drs. J. W. Fletcher and J. Gulens during the course of this study.

1. L. F. Munson, C. J. Card, and J. R. Divine. Electric Power Research Institute Report EPRI NP-2866 (1983).
2. A. J. Elliot and F. C. Sopchyshyn. Int. J. Chem. Kinet. **16**, 1247 (1984).
3. A. O. Allen, C. J. Hochanadel, J. A. Ghormley, and T. W. Davis. J. Phys. Chem. **56**, 575 (1952).
4. L. J. Heidt, G. W. Tregay, and F. A. Middleton. J. Phys. Chem. **74**, 1877 (1970).
5. D. Cohen and W. T. Carnall. J. Phys. Chem. **64**, 1933 (1960).
6. M. L. Hyder. Radiat. Eff. **1**, 191 (1969).
7. J. W. T. Spinks and R. J. Woods. An introduction to radiation chemistry. John Wiley and Sons, New York. 1976.
8. K. Nash, W. Mulac, M. Noon, S. Fried, and J. C. Sullivan. J. Inorg. Nucl. Chem. **43**, 897 (1981).
9. M. Anbar, M. Bambenek, and A. B. Ross. National Bureau of Standards Report NSRDS-NBS 43 (1973).
10. A. K. Pikaev. High Energy Chem. **17**, 147 (1983).
11. V. Markovic, K. Sehested, and E. Bjergbakke. Int. J. Radiat. Phys. Chem. **5**, 15 (1973).
12. H. G. Heal and J. G. N. Thomas. Trans. Faraday Soc. **45**, 11 (1949).
13. A. Ekstrom. Inorg. Chem. **13**, 2237 (1974).
14. A. J. Elliot and A. S. Simson. Radiat. Phys. Chem. **24**, 229 (1984).
15. M. Anbar, Farhataziz, and A. B. Ross. National Bureau of Standards Report NSRDS-NBS 51 (1975).
16. Farhataziz and A. B. Ross. National Bureau of Standards Report NSRDS-NBS 59 (1977).
17. G. V. Buxton and R. M. Sellers. Trans. Faraday Soc. **69**, 555 (1973).
18. K.-D. Asums, H. Mockel and A. Henglein. J. Phys. Chem. **77**, 1218 (1973).
19. C. Miyae and H. W. Nurnberg. J. Inorg. Nucl. Chem. **29**, 2411 (1967).
20. F. B. Baker and T. W. Newton. J. Phys. Chem. **65**, 1897 (1961).
21. K. A. Klaus and F. Nelson. J. Am. Chem. Soc. **72**, 3901 (1950).
22. P. A. Day, R. N. Wilhite, and F. D. Hamilton. J. Am. Chem. Soc. **77**, 3180 (1955).
23. H. Christensen, K. Sehested, and H. Corfitzen. J. Phys. Chem. **86**, 1588 (1982).
24. B. H. J. Bielski. J. Photochem. Photobiol. **28**, 645 (1978).
25. M. Haissinsky and M. Duflo. J. Chem. Phys. **53**, 970 (1956).
26. P. K. Bhattacharyya and R. D. Sani. Radiat. Phys. Chem. **13**, 57 (1979).
27. J. Halpern and J. G. Smith. Can. J. Chem. **34**, 1419 (1956).
28. J. C. Sullivan, S. Gordon, D. Cohen, W. Mulac, and K. H. Schmit. J. Phys. Chem. **80**, 1684 (1976).
29. D. Meisel, Y. A. Ilan, and G. Czapski. J. Chem. Phys. **78**, 2330 (1974).
30. G. Gordon and H. Taube. Inorg. Chem. **1**, 69 (1962).
31. S. Fallab. Angew. Chem. Int. Ed. Engl. **6**, 496 (1967).
32. K. Juznic and S. Fedina. J. Inorg. Nucl. Chem. **36**, 2609 (1974).
33. Y. Ilan, J. Rabani, and A. Henglein. J. Phys. Chem. **80**, 1558 (1978).

Synthesis and characterization of molybdenum–tin complexes derived from the molybdenum tricarbonyl anion, $[MeGapz_3]Mo(CO)_3^-$, and organotin chlorides. X-ray crystal structure of $[MeGapz_3]Mo(CO)_3SnPh_3$ (where pz = pyrazolyl, $N_2C_3H_3$)

EMMANUEL C. ONYIRIUKA, STEVEN J. RETTIG, AND ALAN STORR[1]

Department of Chemistry, University of British Columbia, 2036 Main Mall, Vancouver, B.C., Canada V6T 1Y6

Received August 7, 1985

EMMANUEL C. ONYIRIUKA, STEVEN J. RETTIG, and ALAN STORR. Can. J. Chem. **64**, 321 (1986).

The reaction of the molybdenum tricarbonyl anion, $[MeGapz_3]Mo(CO)_3^-$, with the organotin chlorides, Ph_3SnCl, Me_3SnCl, and Me_2SnCl_2, has yielded a series of complexes in which direct Mo—Sn single bonds are featured. The $[MeGapz_3]Mo(CO)_3SnMe_2Cl$ complex shows an interesting solution behavior in which a transition from a 3:4, or piano stool structure, to a 3:3:1, or capped octahedral arrangement, is thought to occur. The 3:3:1 structure has been demonstrated in the solid state for the $[MeGapz_3]Mo(CO)_3SnPh_3$ compound by means of a crystal structure determination. Crystals of [methyltris(1-pyrazolyl)-gallato-*N*,*N*,*N*](triphenylstannyl)tricarbonylmolybdenum are monoclinic, a = 11.4439(8), b = 19.5116(8), c = 15.2686(12) Å β = 111.370(3)°, Z = 4, space group $P2_1/c$. The structure was solved by conventional heavy-atom methods and was refined by full-matrix least-squares procedures to R = 0.025 and R_w = 0.031 for 5259 reflections with $I \geq 3\sigma(I)$. Important bond lengths include: Mo—Sn = 2.8579(3), Mo—N = 2.239(2)–2.244(2), Mo—C = 1.967(3)–2.000(3), Sn—C = 2.151(3)–2.166(3), Ga—N = 1.920(3)–1.931(3), and Ga—C = 1.943(4)Å.

EMMANUEL C. ONYIRIUKA, STEVEN J. RETTIG et ALAN STORR. Can. J. Chem. **64**, 321 (1986).

L'anion molybdène tricarbonyle, $[MeGapz_3]Mo(CO)_3^-$, réagit avec les chlorures organo-stanniques, Ph_3SnCl, Me_3SnCl et Me_2SnCl_2, pour donner une série de complexes dans lesquels on remarque des liaisons simples directes Mo—Sn. Le complexe $[MeGapz_3]Mo(CO)_3SnMe_2Cl$ en solution présente un comportement intéressant; on croit qu'il se produit une transition d'une structure 3:4, arrangement en tabouret de piano, vers une structure 3:3:1, arrangement octaédrique cappé. En se basant sur une détermination de la structure cristalline, on démontre l'existence de la structure 3:3:1 dans le composé $[MeGapz_3]Mo(CO)_3SnPh_3$ à l'état solide. Les cristaux du [méthyltris(pyrazolyl-1)gallato-*N*,*N*,*N*](triphénylstannyl)tricarbonylmolybdène sont monocliniques et appartiennent au groupe d'espace $P2_1/c$ avec a = 11,4439(8), b = 19,5116(8), c = 15,2686(12) Å, β = 111,370(3)°, Z = 4. On a résolu la structure par les méthodes conventionnelles de l'atome lourd et on l'a affinée par la méthode des moindres carrés (matrice complète) jusqu'à des valeurs de R = 0,025 et de R_w = 0,031 pour 5259 réflexions avec $I \geq 3\sigma(I)$. Les longueurs importantes de liaison comprennent Mo—Sn = 2,8579(3), Mo—N = 2,239(2)–2,244(2), Mo—C = 1,967(3)–2,000(3), Sn—C = 2,151(3)–2,166(3), Ga—N = 1,920(3)–1,931(3) et Ga—C = 1,943(4) Å.

[Traduit par le journal]

Introduction

Some time ago Trofimenko (1) introduced the anionic symmetrical tridentate chelating tris(1-pyrazolyl)borate ligand systems, $[RBpz_3]^-$ (where R = H, alkyl, aryl, or pyrazolyl; pz = pyrazolyl, $N_2C_3H_3$). The analogous $[MeGapz_3]^-$ ligand was introduced later and its coordinating properties explored (2–5). Both the above ligand systems, being six-electron donors, have been likened to, and compared with, the cyclopentadienyl ion in many isoelectronic complexes (1–5). Recently we have exploited this similarity in investigations of the reactivity of the $[HBpz_3]Mo(CO)_3^-$ and $[MeGapz_3]Mo(CO)_3^-$ ions towards transition metal halide species to produce novel transition metal – transition metal bonded compounds (6). The present account details our findings on the reactivity of the $[MeGapz_3]Mo(CO)_3^-$ ion towards Ph_3SnCl, Me_3SnCl, and Me_2SnCl_2. Complexes containing direct Mo—Sn bonds have been isolated and the compound $[MeGapz_3]Mo(CO)_3SnPh_3$ has been characterized by an X-ray crystallographic analysis.

Experimental

Starting materials

Air-sensitive materials were handled in a nitrogen atmosphere. Tetrahydrofuran (THF), CH_2Cl_2, benzene, and *n*-hexane were dried by refluxing over Na/benzophenone, CaH_2, potassium, and $CaSO_4$ respectively, followed by distillation. Me_3SnCl (Aldrich Chemicals), Ph_3SnCl (Alpha Chemicals), and Me_2SnCl_2 (PCA Chemicals) were used as supplied. The sodium salt of the methyltris(1-pyrazolyl)gallate ligand, $Na^+[MeGapz_3]^-$, was prepared as a THF solution as described previously (2). Tris-acetonitrile molybdenum tricarbonyl, $(MeCN)_3Mo(CO)_3$, was prepared as described in the literature (7).

Synthesis of $[MeGapz_3]Mo(CO)_3SnMe_3$

To a stirred THF solution of $(MeCN)_3Mo(CO)_3$ (0.107 g, 0.353 mmol) an equimolar amount of the $Na^+[MeGapz_3]^-$ ligand solution (0.353 mmol in 10 mL THF) was added. An almost immediate color change from yellow to amber was observed upon mixing the reactants. The reaction mixture was stirred at room temperature for ~2 days and the ir spectrum of the resulting solution was recorded to ensure the complete formation of $Na^+[MeGapz_3]Mo(CO)_3^-$. The resulting solution was then reacted directly with an equimolar amount of Me_3SnCl (0.070 g, 0.353 mmol) in the same solvent. The cloudy, dark orange, reaction mixture produced was stirred for another 2 days after which the solvent was removed *in vacuo* to afford a dark orange-brown oily residue. This residue was extracted with *n*-hexane and filtered. Upon slow evaporation of the solvent from the filtrate, dark orange crystals of the desired product were recovered in ~68% yield. The compound is stable under nitrogen but decomposes slowly on exposure to air. Analytical, ir, and nmr data for the complex are presented in Table 1 and its ^1H nmr spectrum is shown in Fig. 1. The mass spectrum of the compound displayed signals due to the $[P-3CO]^+$ ion at ~544, but signals due to the parent ion, P^+, were not observed.

Synthesis of $[MeGapz_3]Mo(CO)_3SnPh_3$

A solution of the Na^+ $[MeGapz_3]Mo(CO)_3^-$ salt in THF was prepared as described above. An equimolar amount of Ph_3SnCl (0.136 g, 0.353 mmol) in THF was added to the salt solution. The resulting cloudy reaction mixture was stirred for ~2 days after which the solvent was removed *in vacuo*. The dark yellow residue remaining was extracted with CH_2Cl_2 and filtered. An equal amount of hexane was added to the filtrate and the mixed solvents were allowed to evaporate slowly. A chocolate-brown sticky solid with some visible tinge of yellow was left

[1]Author to whom correspondence may be addressed.

TABLE 1. Physical data for complexes $[MeGapz_3]Mo(CO)_3SnY$

Y	Analysis Calcd./found C	H	N	ν_{CO} (cm^{-1}) CH_2Cl_2 (Nujol)		^{1}H nmr GaMe	SnMe	pz-H^4	pz-H^5	pz-H^3	Ph_3
Me_3	30.51 31.13	3.34 3.45	13.35 13.65	2020w,1970w,1870vs		[a]9.86s	9.01s $J_{119_{Sn-Me}}$, $J_{117_{Sn-Me}} \simeq$ 50Hz	4.09t	2.91d	2.36d	
$ClMe_2$	27.70 27.72	2.77 2.74	12.93 13.00	2018w,1912s,1890s (1989w,1905s,1880s)	[a]A B	9.93s 10.00s	8.73s $J_{119_{Sn-Me}}$ = 52, $J_{117_{Sn-Me}}$ = 50 Hz 8.96s 9.11s	4.12t 4.19t	2.95d 3.07d	2.40d 2.17d	
Ph_3	45.62 44.98	3.31 3.32	10.50 10.42	(1990w,1900s,1875s)		[b]9.98s		4.14t	2.73d	2.12d	1.86d 2.65m 2.93m

[a]In toluene-d_8 solution (τ_{Me} = 7.91 ppm); $J_{HCCH} \simeq$ 2 Hz for pz protons.
[b]In C_6D_6 solution ($\tau_{C_6H_6}$ = 2.84 ppm); A, 3:3:1 structure, B, 3:4 structure (see Fig. 4).

behind. This mixture was washed with CH_2Cl_2 and the liquid decanted off slowly to leave behind bright-yellow air-stable crystals of the desired product $[MeGapz_3]Mo(CO)_3SnPh_3$ in approximately 40% yield. Pertinent physical data for this complex are presented in Table 1. The mass spectrum of the complex displayed the parent ion signal, P^+, at ~816, together with prominent signals due to the ions $[P\text{-}CO]^+$, $[P\text{-}2CO]^+$, $[P\text{-}3CO]^+$, and $[P\text{-}3CO\text{-}Me]^+$.

Synthesis of $[MeGapz_3]Mo(CO)_3SnMe_2Cl$

A THF solution of the Na^+ $[MeGapz_3]Mo(CO)_3^-$ salt was prepared as described above and an equimolar amount of Me_2SnCl_2 (0.1933 g, 0.880 mmol), in the same solvent, was added slowly. The initial yellow color of the starting molybdenum tricarbonyl anion darkened slightly during the reaction. The reaction mixture was stirred for ~1 day after which the solvent was removed *in vacuo*. The resulting orange residue was extracted with benzene and filtered. Slow evaporation of the solvent from the filtrate yielded yellow crystals of the desired product from concentrated solutions in ~50% yield. Pertinent physical data for this complex are included in Table 1. The mass spectrum of the complex displayed a strong parent ion, P^+, signal at ~650. In addition signals due to the $[P\text{-}CO]^+$, $[P\text{-}2CO]^+$, $[P\text{-}3CO\text{-}Me]^+$, and $[P\text{-}3CO]^+$ ions were also observed, the latter being the strongest in the spectrum. The relative intensities of the lines in these signals agreed well with a computer-generated profile, taking into account the relative abundances of the naturally occurring isotopes of Mo, Ga, Sn, and Cl (see Fig. 2).

Physical measurements

The ir spectra were recorded on a Perkin–Elmer 598 spectrometer, ^{1}H nmr spectra were recorded on a Bruker WP-80 instrument, and mass spectra on a Kratos AES M50 spectrometer at ~100°C and 70 eV. Elemental analyses were performed by Mr. P. Borda of the U. B. C. microanalytical laboratory.

X-ray crystallographic analysis of [methyltris(1-pyrazolyl)gallato-N,N,N](triphenylstannyl)tricarbonylmolybdenum

A crystal bounded by the 7 faces (followed by their distances in mm from a common origin: {0 1 0}, 0.21, {1 0 0}, 0.13, (0 −1 1), 0.29, (0 1 1), 0.22, (0 1 −2), 0.28 was mounted in a general orientation. Unit-cell parameters were refined by least squares on $2\sin\theta/\lambda$ values for 25 reflections (2θ = 40–47°) measured on a diffractometer with Mo-$K\alpha$ radiation ($\lambda(K\alpha_1)$ = 0.70930, ($\lambda(K\alpha_2)$ = 0.71359 Å. Crystal data at 22°C are:

$C_{31}H_{27}GaMoN_6O_3Sn$ fw = 815.94

Monoclinic, a = 11.4439(8), β = 19.5116(8), c = 15.2686(12) Å, β = 111.370(3)°, V = 3174.9(4) Å^3, Z = 4, ρ_c = 1.707 Mg m^{-3}, $F(000)$ = 1608, μ(Mo-$K\alpha$) = 20.4 cm^{-1}. Absent reflections: $h0l$, l odd, and $0k0$, k odd, uniquely indicate the space group $P2_1/c$ (C_{2h}^5, No. 14).

Intensities were measured with graphite-monochromated Mo-$K\alpha$ radiation on an Enraf–Nonius CAD4-F diffractometer. An ω–2θ scan at 1.26–10.06° min^{-1} over a range of (0.70 + 0.35tan θ) degrees in ω (extended by 25% on both sides for background measurement) was employed. Data were measured to 2θ = 55°. The intensities of 3 check reflections, measured every 3600 s throughout the data collection, remained constant to within 3%. After data reduction,[2] an absorption correction was applied using the Gaussian integration method (8,9). Transmission factors ranged from 0.469 to 0.610 for 96 integration points. Of the 7254 independent reflections measured, 5259 (72.5%) had intensities greater than or equal to $3\sigma(I)$ above background where $\sigma^2(I) = S + 2B + (0.04(S-B))^2$ with S = scan count and B = normalized background count.

The structure was solved by conventional heavy-atom methods, the coordinates of the Sn, Mo, and Ga atoms being determined from the Patterson function and those of the remaining non-hydrogen atoms from a subsequent difference map. In the final stages of refinement the non-hydrogen atoms were refined with anisotropic thermal parameters and the hydrogen atoms were fixed in idealized positions (C(sp^3)—H = 0.98, C(sp^2)—H = 0.97 Å, methyl groups staggered in accordance with observed peaks), recalculated after each cycle of refinement. The scattering factors of ref. 10 were used for non-hydrogen atoms and those of ref. 11 for hydrogen atoms. Anomalous scattering factors from ref. 12 were used for the Sn, Mo, and Ga atoms. The weighting scheme $w = 1/\sigma^2(F)$, where $\sigma^2(F)$ is derived from the previously defined $\sigma^2(I)$, gave uniform average values of $w(|F_o|-|F_c|)^2$ over ranges of both $|F_o|$ and $\sin\theta/\lambda$ and was employed in the final stages of full-matrix refinement of variables. Reflections with $I < 3\sigma(I)$ were not included in the refinement. Convergence was reached at R = 0.025 and R_w = 0.031 for 5259 reflections with $I \geq 3\sigma(I)$. For all 7254 reflections R = 0.050. The function minimized was $\Sigma w(|F_o| - |F_c|)^2$, $R = \Sigma||F_o|-|F_c||/\Sigma|F_o|$, and $R_w = (\Sigma w(|F_o|-|F_c|)^2/\Sigma w|F_o|^2)^{1/2}$.

On the final cycle of refinement the mean and maximum parameter shifts corresponded to 0.03 and 0.21σ respectively. The mean error in an observation of unit weight was 1.280. A final difference map showed maximum fluctuations of −1.3 to +0.61 e Å^{-3} within 1.0 Å of Mo and

[2]The computer programs used include locally written programs for data processing and locally modified versions of the following: ORFLS, full-matrix least-squares, and ORFFE, function and errors, by W. R. Busing, K. O. Martin and H. A. Levy; FORDAP, Patterson and Fourier syntheses, by A. Zalkin; ORTEP II, illustrations, by C. K. Johnson.

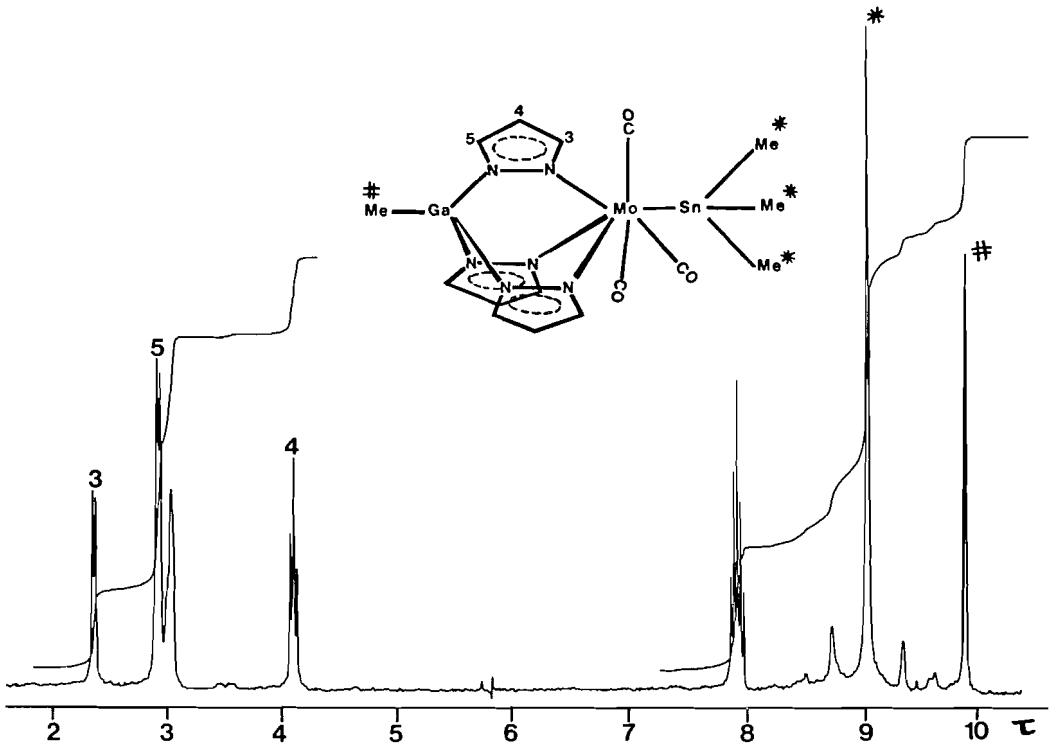

FIG. 1. Room temperature 80-MHz ^{1}H nmr spectrum of $[MeGapz_3]Mo(CO)_3SnMe_3$ in toluene-d_8.

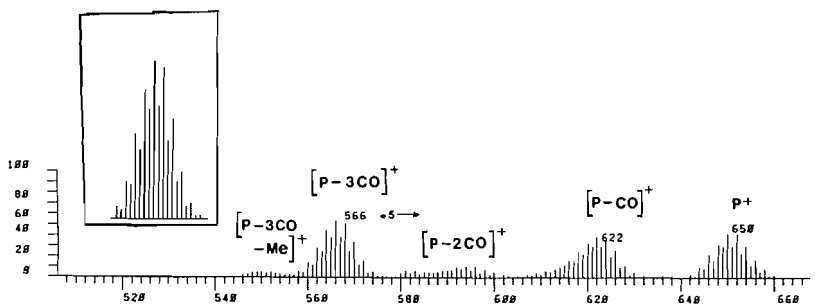

FIG. 2. Partial mass spectrum of $[MeGapz_3]Mo(CO)_3SnMe_2Cl$. Inset: computer-generated profile of signal for ions containing Ga, Mo, Sn, and Cl atoms.

Sn, respectively, and was essentially featureless away from the heavy atoms. The final positional and thermal parameters appear in Tables 2 and 6[3], respectively. Bond lengths and angles appear in Tables 3 and 4, respectively. Calculated hydrogen atom parameters (Table 5) and a complete listing of torsion angles (Table 7) are included as supplementary material.[3] Measured and calculated structure factors have been placed in the Depository of Unpublished Data.[3]

Results and discussion

A number of complexes of the type $[MeGapz_3]M(CO)_2X$ (where M = Mo or W, X = η^3-allyl or NO) have been reported and the compound $[MeGapz_3]M(CO)_2(\eta^3-C_3H_5)$ has been structurally characterized (2). Recently the tricarbonyl anion $[MeGapz_3]Mo(CO)_3^-$ has yielded complexes with Mo—Rh and Mo—Cu bonds by reaction with Wilkinson's catalyst, $Rh(PPh_3)_3Cl$, and the tetrameric copper species $[Cu(PPh_3)Cl]_4$ (6). As part of an ongoing investigation into the reactivity of the $[MeGapz_3]Mo(CO)_3^-$ ion, its behavior towards a number of organotin chlorides has been studied. Thus, 1:1 reactions with Ph_3SnCl, Me_3SnCl, and Me_2SnCl_2 yielded yellow-orange crystalline products of Mo—Sn bonded species, e.g.

$$[MeGapz_3]Mo(CO)_3^- + Ph_3SnCl \rightarrow [MeGapz_3]Mo(CO)_3SnPh_3 + Cl^-$$

The complexes are moderately air-stable in the solid state but solutions deteriorate on exposure to air. It is interesting to compare the compounds with those reported some time ago by Patil and Graham in which the $MeGapz_3^-$ ligand is replaced by the Cp^- group (13). In both series of compounds only terminal CO bands are displayed in their ir spectra, indicative of direct Mo–Sn interaction without accompanying bridging CO ligands. In the case of the cyclopentadienyl complexes three strong terminal CO bands were observed in each case, whereas the three compounds reported here show different patterns. Thus, both the "$SnPh_3$" and "$SnMe_2Cl$" complexes give one weak and two strong ν_{CO} vibrations, whereas the "$SnMe_3$" complex

[3]The structure factor table, Table 6 (anisotropic thermal parameters), and other material mentioned in the text may be purchased from the Depository of Unpublished Data, CISTI, National Research Council of Canada, Ottawa, Canada K1A 0S2.

TABLE 2. Final positional (fractional × 10^4; Sn, Mo, and Ga × 10^5) and isotropic thermal parameters ($U \times 10^3$ Å^2) with estimated standard deviations in parentheses[a]

Atom	x	y	z	U_{eq}
Sn	38401(2)	45855(1)	26802(1)	31
Mo	28691(2)	42524(1)	7230(2)	26
Ga	16030(3)	37846(2)	−17567(2)	45
O(1)	3498(3)	2903(1)	1886(2)	61
O(2)	881(2)	5110(1)	1220(2)	55
O(3)	5314(2)	5126(1)	1184(2)	53
N(1)	2216(2)	4953(1)	−528(2)	34
N(2)	1794(2)	4743(1)	−1445(2)	40
N(3)	3807(2)	3656(1)	−89(2)	33
N(4)	3249(2)	3462(1)	−1007(2)	40
N(5)	1149(2)	3630(1)	−41(2)	37
N(6)	687(2)	3501(1)	−978(2)	41
C(1)	3301(3)	3436(2)	1534(2)	38
C(2)	1658(3)	4800(2)	1108(2)	35
C(3)	4430(3)	4813(1)	1078(2)	34
C(4)	934(4)	3533(3)	−3079(3)	84
C(5)	2203(3)	5633(2)	−543(2)	46
C(6)	1775(4)	5877(2)	−1452(3)	55
C(7)	1532(3)	5300(2)	−2001(3)	54
C(8)	4971(3)	3409(2)	210(2)	43
C(9)	5188(3)	3053(2)	−497(3)	52
C(10)	4091(3)	3101(2)	−1242(2)	48
C(11)	328(3)	3360(2)	308(3)	50
C(12)	−657(3)	3056(2)	−402(3)	61
C(13)	−407(3)	3162(2)	−1197(3)	55
C(14)	3547(3)	5646(2)	2939(2)	37
C(15)	3912(3)	6175(2)	2490(3)	53
C(16)	3742(4)	6853(2)	2685(3)	60
C(17)	3218(4)	7014(2)	3330(3)	60
C(18)	2832(4)	6495(2)	3776(3)	63
C(19)	3011(4)	5818(2)	3589(2)	52
C(20)	5841(3)	4415(2)	3353(2)	37
C(21)	6404(3)	3809(2)	3277(3)	55
C(22)	7675(4)	3695(2)	3743(3)	69
C(23)	8397(3)	4203(3)	4326(3)	69
C(24)	7861(4)	4805(3)	4405(3)	69
C(25)	6587(3)	4917(2)	3923(3)	54
C(26)	2995(3)	3997(1)	3484(2)	35
C(27)	1723(3)	3866(2)	3179(2)	55
C(28)	1201(4)	3479(2)	3695(3)	63
C(29)	1952(4)	3207(2)	4553(3)	57
C(30)	3218(4)	3333(2)	4874(2)	57
C(31)	3736(3)	3720(2)	4345(2)	45

[a] U_{eq} = 1/3 trace (diagonalized U).

TABLE 3. Bond lengths (Å) with estimated standard deviations in parentheses

Bond	Length (Å)	Bond	Length (Å)
Sn—Mo	2.8579(3)	N(6)—C(13)	1.346(4)
Sn—C(14)	2.157(3)	C(5)—C(6)	1.377(5)
Sn—C(20)	2.166(3)	C(6)—C(7)	1.370(6)
Sn—C(26)	2.151(3)	C(8)—C(9)	1.380(5)
Mo—N(1)	2.244(2)	C(9)—C(10)	1.356(5)
Mo—N(3)	2.239(2)	C(11)—C(12)	1.380(5)
Mo—N(5)	2.244(2)	C(12)—C(13)	1.362(6)
Mo—C(1)	1.967(3)	C(14)—C(15)	1.384(5)
Mo—C(2)	2.000(3)	C(14)—C(19)	1.385(4)
Mo—C(3)	1.994(3)	C(15)—C(16)	1.386(5)
Ga—N(2)	1.923(3)	C(16)—C(17)	1.362(6)
Ga—N(4)	1.920(3)	C(17)—C(18)	1.379(6)
Ga—N(6)	1.931(3)	C(18)—C(19)	1.382(5)
Ga—C(4)	1.943(4)	C(20)—C(21)	1.372(5)
O(1)—C(1)	1.154(4)	C(20)—C(25)	1.380(5)
O(2)—C(2)	1.139(3)	C(21)—C(22)	1.384(5)
O(3)—C(3)	1.141(3)	C(22)—C(23)	1.386(6)
N(1)—N(2)	1.367(3)	C(23)—C(24)	1.351(6)
N(1)—C(5)	1.327(4)	C(24)—C(25)	1.390(5)
N(2)—C(7)	1.343(4)	C(26)—C(27)	1.380(5)
N(3)—N(4)	1.364(3)	C(26)—C(31)	1.388(4)
N(3)—C(8)	1.331(4)	C(27)—C(28)	1.376(5)
N(4)—C(10)	1.343(4)	C(28)—C(29)	1.384(5)
N(5)—N(6)	1.356(3)	C(29)—C(30)	1.372(5)
N(5)—C(11)	1.344(4)	C(30)—C(31)	1.386(5)

displays one strong and two weak ν_{CO} bands. Perhaps these variations reflect a difference in structure between the complexes (see below). The ^{1}H nmr data for the "$SnPh_3$" and "$SnMe_3$" complexes show all three pyrazolyl groupings to be equivalent in solution, indicating a symmetrical structure for the complexes. The spectrum for the $[MeGapz_3]Mo(CO)_3SnMe_3$ complex is shown in Fig. 1. The ^{1}H nmr spectrum of $[MeGapz_3]Mo(CO)_3SnMe_2Cl$ is interesting since it changes with time and solvent (Fig. 3 shows the change, with time, in the spectrum of the complex in toluene-d_8. A similar effect was observed using benzene-d_6 as solvent. Thus, initially the spectrum shows two "sets" of signals. The most intense set of signals is consistent with a symmetrical 3:3:1 or capped octahedral structure as shown in Fig. 4A, similar to that established for the "$SnPh_3$" derivative (see below). In this arrangement free rotation about the Mo—Sn bond in solution would give the observed pattern of equivalent pyrazolyl signals and a singlet for the "$SnMe_2$" grouping. In the second "set" of signals the two Sn—Me groups are nonequivalent and yet the pyrazolyl groups seemingly remain equivalent. This pattern is difficult to rationalize since even a static 3:4, or four-legged piano stool arrangement (Fig. 4B) would be expected to give inequivalent pyrazolyl groups as well as possibly distinguishing between the two Me groups on the Sn atom. A rotation of the $MeGapz_3$ moiety about the Ga···Mo axis might afford a rationale for the observed equivalence of the pyrazolyl groups in this second arrangement. A similar rotation of the $HBpz_3$ grouping in the complexes $[HBpz_3]Mo(CO)_2(\eta^3-C_3H_5)$ and $Cp_2MoH_2 \rightarrow Cu[HBpz_3]_2$ has been invoked to explain the equivalence of the pyrazolyl groups in the room temperature ^{1}H nmr spectra of these compounds (14). In any event, with time, the species responsible for the weaker set of signals gradually disappears and one is left with only one set of signals, explicable in terms of a 3:3:1 structure. Interestingly, Patil and Graham (13) report a singlet for the "$SnMe_2$" protons in their $CpMo(CO)_3SnMe_2Cl$ complex for which they speculate a 3:4 or piano stool structure similar to that demonstrated by Bennett and Mason (15) for the complex $(\eta\text{-}C_5H_5)Mo(CO)_3Et$.

The chemistry of M—M′ bonded derivatives (where M′ = Ge or Sn; M = Mo or W) has been studied quite extensively but, rather surprisingly, no X-ray structural data has been reported for complexes of the type $(\eta\text{-}C_5H_5)M(CO)_3M'R_3$ (where R = alkyl or aryl), the molecular arrangements proposed for these species being based primarily on ir and ^{1}H nmr data (16). The X-ray crystal structure of the complex $[MeGapz_3]Mo(CO)_3SnPh_3$ presented here represents what we believe to be the first reported structure of this type, in which the $[MeGapz_3]$ moiety replaces the $\eta\text{-}C_5H_5$ ligand in the general formulation given above. The

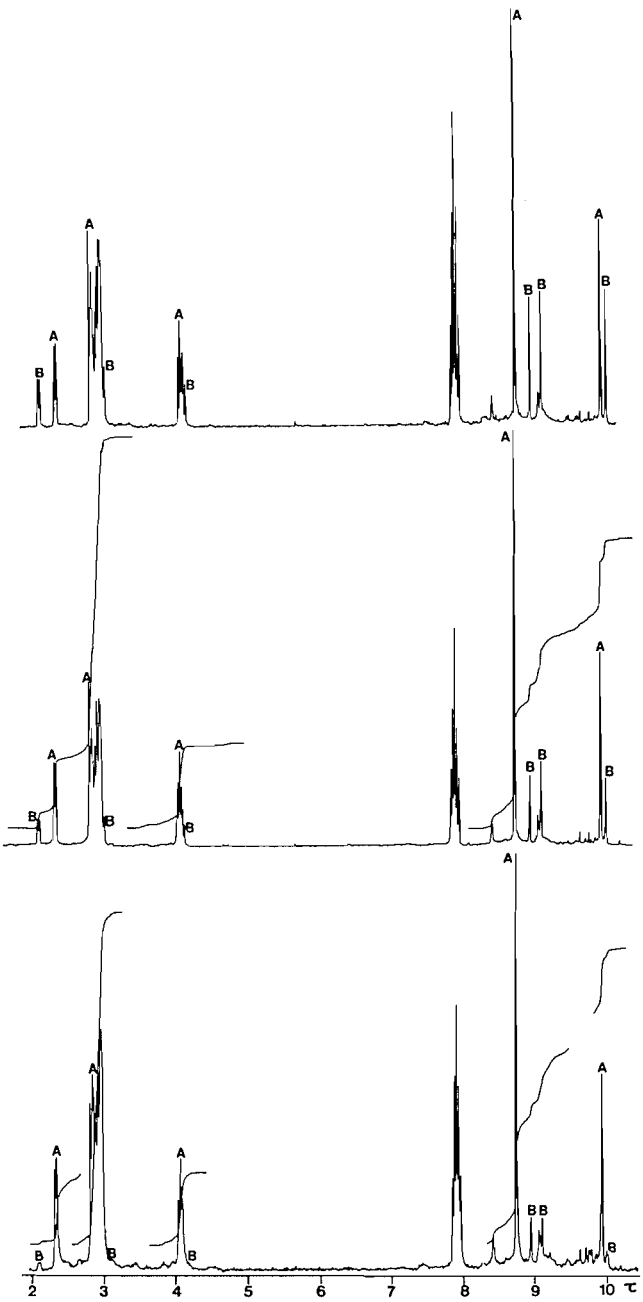

FIG. 3. Room temperature 80-MHz ^{1}H nmr spectra of [MeGapz$_3$]-Mo(CO)$_3$SnMe$_2$Cl in toluene-d_8, showing the change with time: initial spectrum (top), after 1 day (middle), and after 5 days (bottom). (A) 3:3:1 structure, (B) 3:4 structure.

X-ray structure analysis confirms the 3:3:1 arrangement predicted on the basis of the ^{1}H nmr and ir data. The molecule, which has approximate C_3 symmetry, is shown in Fig. 5. The structure is similar to that recently reported for the compound [MeGapz$_3$]Mo(CO)$_3$Cu(PPh$_3$) (6) but different from the 3:4 piano stool structures of the related molecules (η-C$_5$H$_5$)-Mo(CO)$_3$Sn(Cl)[η-C$_5$H$_5$)Fe(CO)$_2$]$_2$ (17), [HBpz$_3$]Mo(CO)$_3$Br (18), and (η-C$_5$H$_5$)Mo(CO)$_3$Et (15). The multi-metal species with η-C$_5$H$_5$ replacing MeGapz$_3$ on Mo and the [(η-C$_5$H$_5$)-Fe(CO)$_2$] groupings replacing the Me groups on Sn may well be incapable of adopting a 3:3:1 structure due to the bulky Fe-containing substituents. However, one of the interesting aspects that prompted Curtis and Shiu (18) to determine the structure of

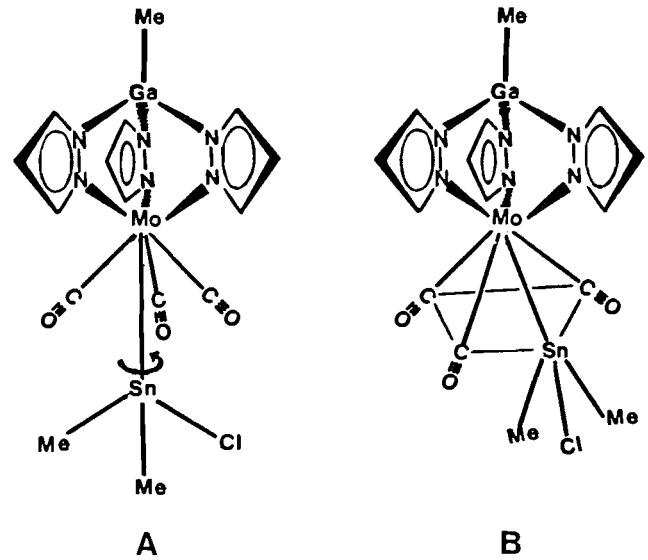

FIG 4. Possible molecular arrangements for the [MeGapz$_3$]Mo-(CO)$_3$SnMe$_2$Cl complex in solution: (A) 3:3:1 structure, (B) 3:4 structure.

the above bromo derivative was the possibility of observing a 3:3:1 capped octahedral structure. Thus calculations by Kubacek *et al.* (19) had shown that such an arrangement represents a minimum in the potential energy surface for (η-C$_5$H$_5$)ML$_4$ complexes where the global minimum (ground state) is always the 3:4 structure.

The structure of the [MeGapz$_3$]Mo(CO)$_3$SnPh$_3$ complex clearly shows the presence of three terminal carbonyl groups with bond angles of 169.7(3), 172.1(3), and 172.7(3)° for the Mo—C—O units, the slight deviations from linearity being directed away from the Sn centre and probably caused by the proximity of the phenyl groups on the Sn atom. The C—O bond distances of 1.154(4), 1.139(3), and 1.141(3) Å are also in the range expected for terminal carbonyl groups and the Mo—C distances of 1.967(3), 2.000(3), and 1.994(3) Å are consistent with a terminal CO bonding arrangement. The above parameters show that one of the carbonyl groups differs significantly from the other two. This represents the most significant departure from overall C_3 molecular symmetry and can be ascribed to a weak C—H···O hydrogen bond (C(10)—H(10)···O(1)(x, 1/2-y,z-1/2), H···O = 2.39, C···O = 2.326(4) Å, C—H···O = 162°, C—O···H = 156°) linking molecules in infinite chains extending along the b axis. All other intermolecular distances are greater than the sums of van der Waals radii.

The Ga···Mo—Sn unit with angle of 178.49(1)° is essentially linear and, as expected, the planar pyrazolyl groups (χ^2 = 0.2–6.9, maximum deviation from the mean plane 0.007(4) Å), whilst eclipsing the distant phenyl groups (planar to within 0.011(5) Å, χ^2 = 2.0–13.1) on Sn, are staggered with respect to the three CO ligands on the Mo centre. The Mo—Sn distance of 2.8579(3) Å observed for the present complex is considerably shorter than the expected distance of 3.00 Å based on the sum of covalent radii (1.39 + 1.61 Å) for the two atoms (15, 20–22). The distance is, however, comparable to the first Mo—Sn distance reported, 2.891(5) Å for the complex [(η-C$_5$H$_5$)Mo-(CO)$_3$]Sn(Cl)[(η-C$_5$H$_5$)Fe(CO)$_2$]$_2$ (17). As in the structure described herein, the Sn atom in this multi-metal complex is in a pseudotetrahedral environment. Cameron and Prout (23) have reported a Mo—Sn distance of 2.691(4) Å for the complex

TABLE 4. Bond angles (deg) with estimated standard deviations in parentheses

Bonds	Angle (deg)	Bonds	Angle (deg)
Mo—Sn—C(14)	112.50(8)	N(3)—N(4)—C(10)	107.9(3)
Mo—Sn—C(20)	113.69(8)	Mo—N(5)—N(6)	125.4(2)
Mo—Sn—C(26)	113.00(8)	Mo—N(5)—C(11)	127.9(2)
C(14)—Sn—C(20)	105.57(11)	N(6)—N(5)—C(11)	106.6(2)
C(14)—Sn—C(26)	106.01(11)	Ga—N(6)—N(5)	120.5(2)
C(20)—Sn—C(26)	105.38(11)	Ga—N(6)—C(13)	130.7(2)
Sn—Mo—N(1)	129.32(6)	N(5)—N(6)—C(13)	108.9(3)
Sn—Mo—N(3)	127.95(6)	Mo—C(1)—O(1)	169.7(3)
Sn—Mo—N(5)	126.83(7)	Mo—C(2)—O(2)	172.1(3)
Sn—Mo—C(1)	67.22(9)	Mo—C(3)—O(3)	172.7(3)
Sn—Mo—C(2)	67.57(8)	N(1)—C(5)—C(6)	111.1(3)
Sn—Mo—C(3)	67.82(8)	C(5)—C(6)—C(7)	104.6(3)
N(1)—Mo—N(3)	85.61(9)	N(2)—C(7)—C(6)	109.2(3)
N(1)—Mo—N(5)	86.02(9)	N(3)—C(8)—C(9)	110.9(3)
N(1)—Mo—C(1)	163.46(11)	C(8)—C(9)—C(10)	104.2(3)
N(1)—Mo—C(2)	82.72(10)	N(4)—C(10)—C(9)	110.3(3)
N(1)—Mo—C(3)	83.38(10)	N(5)—C(11)—C(12)	110.3(3)
N(3)—Mo—N(5)	86.42(9)	C(11)—C(12)—C(13)	104.9(3)
N(3)—Mo—C(1)	82.32(10)	N(6)—C(13)—C(12)	109.4(3)
N(3)—Mo—C(2)	164.47(10)	Sn—C(14)—C(15)	121.9(2)
N(3)—Mo—C(3)	82.72(10)	Sn—C(14)—C(19)	120.2(2)
N(5)—Mo—C(1)	81.98(11)	C(15)—C(14)—C(19)	117.8(3)
N(5)—Mo—C(2)	82.59(10)	C(14)—C(15)—C(16)	120.9(3)
N(5)—Mo—C(3)	165.35(10)	C(15)—C(16)—C(17)	120.5(4)
C(1)—Mo—C(2)	106.84(12)	C(16)—C(17)—C(18)	119.6(3)
C(1)—Mo—C(3)	106.15(12)	C(17)—C(18)—C(19)	120.0(3)
C(2)—Mo—C(3)	105.97(12)	C(14)—C(19)—C(18)	121.1(3)
N(2)—Ga—N(4)	99.99(11)	Sn—C(20)—C(21)	122.7(2)
N(2)—Ga—N(6)	99.47(11)	Sn—C(20)—C(25)	119.6(2)
N(2)—Ga—C(4)	117.9(2)	C(21)—C(20)—C(25)	117.6(3)
N(4)—Ga—N(6)	100.00(11)	C(20)—C(21)—C(22)	122.2(4)
N(4)—Ga—C(4)	117.8(2)	C(21)—C(22)—C(23)	119.0(4)
N(6)—Ga—C(4)	118.1(2)	C(22)—C(23)—C(24)	119.7(3)
Mo—N(1)—N(2)	125.0(2)	C(23)—C(24)—C(25)	120.8(4)
Mo—N(1)—C(5)	128.4(2)	C(20)—C(25)—C(24)	120.7(4)
N(2)—N(1)—C(5)	106.5(2)	Sn—C(26)—C(27)	123.0(2)
Ga—N(2)—N(1)	120.7(2)	Sn—C(26)—C(31)	120.1(2)
Ga—N(2)—C(7)	130.6(2)	C(27)—C(26)—C(31)	116.9(3)
N(1)—N(2)—C(7)	108.6(3)	C(26)—C(27)—C(28)	122.2(3)
Mo—N(3)—N(4)	125.2(2)	C(27)—C(28)—C(29)	120.2(3)
Mo—N(3)—C(8)	128.3(2)	C(28)—C(29)—C(30)	118.7(3)
N(4)—N(3)—C(8)	106.7(2)	C(29)—C(30)—C(31)	120.6(3)
Ga—N(4)—N(3)	120.8(2)	C(26)—C(31)—C(30)	121.4(3)
Ga—N(4)—C(10)	131.0(2)		

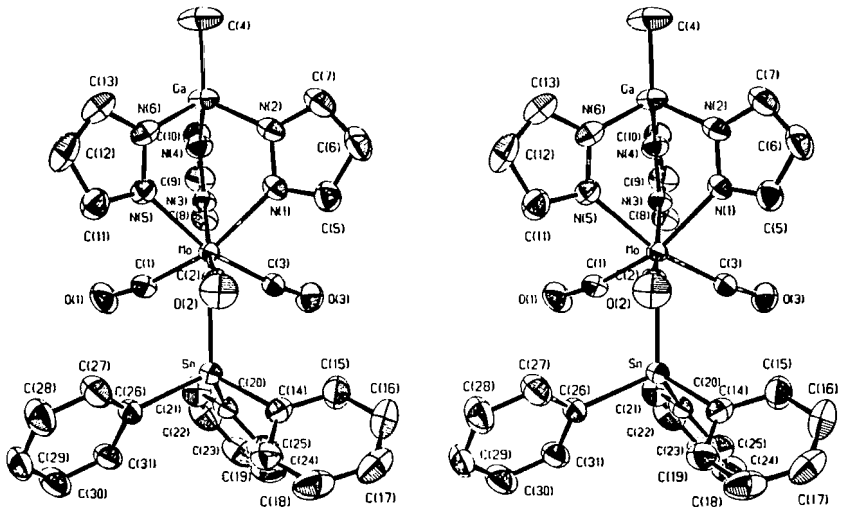

FIG. 5. Stereoscopic view of the $[MeGapz_3]Mo(CO)_3SnPh_3$ molecule; 50% probability thermal ellipsoids are shown.

$(\eta\text{-}C_5H_5)_2Mo(SnBr_3)Br$ in which the Sn atom is in a distorted trigonal bipyramidal environment with a fourth, long, Sn···Br interaction of 3.411 Å. A similar environment for the Sn atom has been reported for the complex (bipy)(Cl)$Mo(CO)_3$(SnMeCl_2), (bipy = 2,2′-bipyridyl), in which the Mo—Sn distance of 2.753(3) Å was interpreted as indicative of some multiple bond character (24). The same authors reported the structure of the tungsten–tin complex ($MeS(CH_2)_2SMe$)(Cl)$W(CO)_3$(SnMeCl_2) in which the W—Sn distance of 2.759(3) Å was argued to reflect the similarity of the W and Mo covalent radii (25). In both these structures there is a bridging Cl ligand between the metal centres, with a long Sn—Cl distance.

The present study has demonstrated the ability of the $[MeGapz_3]Mo(CO)_3^-$ anion to form complexes with organotin moieties in which the Mo and Sn metal centres are linked by a single covalent bond. We are presently extending our investigations into the reactivity of the $[MeGapz_3]Mo(CO)_3^-$ anion to include other main group compounds and will report on our findings in due course.

Acknowledgments

We thank the Natural Sciences and Engineering Research Council of Canada for financial support, Professor James Trotter (Supervisor, University of British Columbia Crystallographic Service) for the use of laboratory facilities and computer programs, and the University of British Columbia Computing Centre for assistance.

1. S. Trofimenko. Chem. Rev. **72**, 497 (1972).
2. K. R. Breakell, S. J. Rettig, D. L. Singbeil, A. Storr, and J. Trotter. Can. J. Chem. **56**, 2099 (1978).
3. K. R. Breakell, S. J. Rettig, A. Storr, and J. Trotter. Can. J. Chem. **57**, 139 (1979).
4. S. J. Rettig, A. Storr, and J. Trotter. Can. J. Chem. **57**, 1823 (1979).
5. B. M. Louie, S. J. Rettig, A. Storr, and J. Trotter. Can. J. Chem. **62**, 633 (1984).
6. G. A. Banta, B. M. Louie, E. Onyiriuka, S. J. Rettig, and A. Storr. Can. J. Chem. **64**, 373 (1986).
7. D. P. Tate, W. R. Knipple, and J. M. Augl. Inorg. Chem. **1**, 433 (1962).
8. P. Coppens, L. Leiserowitz, and D. Rabinovich. Acta Crystallogr. **18**, 1035 (1965).
9. W. R. Busing and H. A. Levy. Acta Crystallogr. **22**, 457 (1967).
10. D. T. Cromer and J. B. Mann. Acta Crystallogr. Sect. A, **24**, 321 (1968).
11. R. F. Stewart, E. R. Davidson, and W. T. Simpson. J. Chem. Phys. **42**, 3175 (1965).
12. D. T. Cromer and D. Liberman. J. Chem. Phys. **53**, 1891 (1970).
13. H. R. H. Patil and W. A. G. Graham. Inorg. Chem. **5**, 1401 (1966).
14. P. Meakin, S. Trofimenko, and J. P. Jesson. J. Am. Chem. Soc. **94**, 5677 (1972); O. M. A. Salah and M. I. Bruce. Aust. J. Chem. **30**, 2292 (1977).
15. M. J. Bennett and R. Mason. Proc. Chem. Soc. 273 (1963).
16. K. M. Mackay and B. K. Nicholson. *In* Comprehensive organometallic chemistry. Vol. 6. *Edited by* G. Wilkinson, F. G. A. Stone, and E. W. Abel. Pergamon Press, Oxford. 1982. p. 1043.
17. J. E. O'Connor and E. R. Corey. J. Am. Chem. Soc. **89**, 3930 (1967).
18. M. D. Curtis and K. Shiu. Inorg. Chem. **24**, 1213 (1985).
19. P. Kubacek, R. Hoffman, and Z. Halvas. Organometallics, **1**, 180 (1982).
20. R. J. Doedens and L. F. Dahl. J. Am. Chem. Soc. **87**, 2576 (1965).
21. F. C. Wilson and D. P. Shoemaker. J. Chem. Phys. **27**, 809 (1957).
22. D. H. Olsen and R. E. Rundle. Inorg. Chem. **2**, 1310 (1963).
23. T. S. Cameron and C. K. Prout. J. Chem. Soc. Dalton Trans. 1447 (1972).
24. M. Elder and D. Hall. Inorg. Chem. **8**, 1268 (1969).
25. M. Elder and D. Hall. Inorg. Chem. **8**, 1273 (1969).

Adsorption isotherms for coadsorption studies from solution

PANAGHIOTIS NIKITAS AND ADRIANI PAPPA-LOUISI
Laboratory of Physical Chemistry, University of Thessaloniki, Thessaloniki, Greece
Received April 11, 1985

PANAGHIOTIS NIKITAS and ADRIANI PAPPA-LOUISI. Can. J. Chem. **64**, 328 (1986).

The mixed adsorption of k adsorbates from solution on energetically homogeneous surfaces is studied by means of lattice statistical thermodynamics. The adsorption layer is considered to behave as a non-electrolyte bulk solution composed from k adsorbates and solvent. On the basis of this assumption the adsorption isotherms and their state equations are determined by means of the lattice theory of strictly regular solutions and Flory–Huggins statistics. The thermodynamic restrictions imposed when these models have to be applied to real systems are also determined and discussed.

PANAGHIOTIS NIKITAS et ADRIANI PAPPA-LOUISI. Can. J. Chem. **64**, 328 (1986).

Faisant appel à la thermodynamique statistique des résaux, on a étudié l'adsorption mixte des adsorbates de type k en solution sur des surfaces homogènes actives. On considère que la couche d'adsorption se comporte comme une solution non électrolytique formée par les adsorbates de type k et par le solvant. Cette hypothèse permet de déterminer les isothermes d'adsorption et leurs équations d'état en faisant appel à la théorie de réseau des solutions strictement régulières et aux statistiques de Flory–Huggins. On détermine également et on discute des restrictions thermodynamiques qui s'imposent lorsqu'on applique ces modèles à des systèmes réels.

[Traduit par le journal]

I. Introduction

When a substance is adsorbed on a solid surface from solution, then the adsorption process takes place by the displacement of the preadsorbed solvent molecules by the adsorbate ones. This adsorption process may be also considered to take place on the coadsorption of k substances, $A_1, A_2, \ldots, A_k$ from a solution of a solvent S, provided that there are not significant differences in the adsorption free energies of A_i. That is, we can accept that the adsorption of A_i may be described by the following chemical equations:

$$[1] \quad A_i(b) + r_i S(ads) \rightleftarrows A_i(ads) + r_i S(b)$$

where r_i is the number of solvent molecules displaced from the surface solution by one A_i molecule and the symbols (b), (ads) denote the bulk solution and the adsorption layer, respectively.

The number of the equilibrium equations [1] is equal to k and therefore the relation between the concentrations of the adsorbed particles and those in the bulk solution, i.e. the adsorption isotherm, will be expressed by a system of k equations. In the case of dilute solutions the general expression of these equations is

$$[2] \quad F_i(\vartheta_1, \vartheta_2, \ldots, \vartheta_k) = \beta_i c_i$$

where ϑ_i is the fraction of the surface covered by A_i, c_i the concentration of A_i in the bulk solution, and β_i is an adsorption equilibrium constant.

According to current views (1–5) we can consider that the adsorption layer on an electrode surface behaves as a non-electrolyte bulk solution of $k+1$ components, i.e. of the k adsorbates $A_1, A_2, \ldots, A_k$ and of the solvent S. The non-electrolyte solution theories which have already been used for the study of the adsorption of a single solute from a solution onto an energetically homogeneous surface are (*i*) the lattice theory of the strictly regular solutions (SRS) (6–9) and (*ii*) Flory–Huggins statistics (FH) (6, 8, 10). The isotherms developed on the basis of these theories give a realistic description of the adsorption layer features (4, 5, 11–14). For this reason, in the present work we shall apply the above theories to the general problem of the coadsorption of k adsorbates from solution on energetically homogeneous surfaces.

II. Adsorption from $k+1$ component solution

1. Model of SRS theory

In this model we accept the following:

a. The adsorption layer is a three-dimensional phase and behaves as a non-electrolyte bulk solution composed of N_1 molecules of adsorbate A_1, N_2 molecules of A_2, ..., N_k molecules of A_k, and $N_{k+1} \equiv N_S$ molecules of the solvent S. The molecules are spherical or effectively spherical and they are approximately of the same size.

b. The $N = \sum_{i=1}^{k+1} N_i$ molecules of the adsorption layer occupy sites of a regular lattice. Each molecule occupies a single site and there are no vacant sites in the lattice. All sites are energetically equivalent.

c. The interactions between the adsorbed molecules are weak so that interactions between non-nearest-neighbouring molecules are considered negligible.

The adsorbed molecules may vibrate about their lattice sites. If the vibration modes and, more generally, the internal degrees of freedom of a molecule are independent of the presence of other molecules in neighbouring sites, then the canonical ensemble partition function, Q, for the surface solution will be

$$[3] \quad Q = \prod_{i=1}^{k+1} q_{\text{in},i}^{N_i} \sum e^{-E/kT}$$

where E is the total interaction potential energy and $q_{\text{in},i}$ is the internal partition function of the A_i component. The sum is over all the possible distributions of the adsorbed molecules on the lattice sites.

If N_{ij} is the number of the nearest-neighbouring pairs of sites occupied by an A_i and an A_j molecule, W_{ij} the interaction energy between the molecules A_i, A_j in the pair, and E_i the residual energies due to interactions of the adsorbed particle A_i with the adsorbing surface and surrounding particles in the bulk solution including the dipole-field interactions, then the total energy E may be expressed as

Printed in Canada / Imprimé au Canada

[4] $$E = \sum_{i=1}^{k+1} N_i E_i + \sum_{i \leq j}^{k+1} N_{ij} W_{ij}$$

However, in an arbitrary lattice we generally have

[5] $$N_{ii} = \tfrac{1}{2} c N_i - \tfrac{1}{2}\{N_{i1} + N_{i2} + \ldots + N_{i(i-1)} + N_{i(i+1)} + \ldots + N_{ik+1}\}$$

where c is the coordination number of the lattice. Therefore

[6] $$E = \sum_{i=1}^{k+1} (N_i E_i + U_i) + \sum_{i<j}^{k+1} N_{ij} W^{ij}$$

where

[7] $$U_i = c N_i W_{ij}/2$$

and

[8] $$W^{ij} = W_{ij} - (W_{ii} + W_{jj})/2$$

Now, introducing eq. [6] into eq. [3] and using the zeroth approximation (6) for the evaluation of the sum we get

[9] $$\ln Q = \sum_{i=1}^{k+1} \{N_i \ln q_{\mathrm{in},i} - N_i \ln N_i - (U_i + N_i E_i)/kT\} + N \ln N - \sum_{i<j} (N_i N_j c W^{ij}/NkT)$$

since for random mixing the mean value of N_{ij} is equal to cN_iN_j/N.

The chemical potentials of the adsorbed molecules, $\mu_i(\mathrm{ads})$, are

[10] $$\frac{\mu_l(\mathrm{ads})}{kT} = -\left(\frac{\partial \ln Q}{\partial N_l}\right)_{N_{i \neq l}, T} = -\ln q_{\mathrm{in},l} + (cW_{ll}/2 + E_l)/kT + \ln X_l + \sum_{i \neq l} X_i(1 - X_l)\mathrm{A}_{il} - \sum_{\substack{i<j \\ i,j \neq l}} X_i X_j \mathrm{A}_{ij}$$

where

[11] $$X_i = N_i/N$$

and

[12] $$\mathrm{A}_{ij} = cW^{ij}/kT$$

The chemical potentials in the bulk solution, $\mu_i(\mathrm{b})$, can be expressed in terms of mole fractions. If we also accept the unsymmetrical system as the reference system (15, 16) then at the region where Henry's law is valid we have

[13] $$\mu_i(\mathrm{b}) = \mu^0{}_i + kT \ln (c_i/c_s) \qquad i \neq k+1$$

and

[14] $$\mu_s(\mathrm{b}) = \mu^0{}_s$$

where $\mu_i{}^0$ is the chemical potential of the ith component in its standard state.

At equilibrium the chemical potentials will fulfill the equations:

[15] $$\mu_l(\mathrm{ads}) - r_l \mu_s(\mathrm{ads}) = \mu_l(\mathrm{b}) - r_l \mu_s(\mathrm{b}) \qquad l \neq k+1$$

since we accept that the adsorption process takes place on the basis of eq. [1]. Introducing eqs. [10], [13], and [14] into eq. [15] we obtain:

[16] $$\ln \frac{X_l}{X_s{}^{rl}} + \{X_s(1 - X_l) - r_l X_l(1 - X_s)\}A_{lk+1} + \sum_{i \neq l,k+1} X_i(1 - X_l + r_l X_l)A_{il} - \sum_{i \neq l,k+1} \{X_s X_i + r_l X_i(1 - X_s)\}A_{ik+1} + \sum_{i<j} X_i X_j (r_l - 1)A_{ij} = \ln \frac{c_l}{c_s} + \ln \beta_l$$

where

[17] $$\ln \beta_l = \{\ln (q_{\mathrm{in},l}/q_{\mathrm{in},s}^{rl}) + c(r_l W_{ss} - W_{ll})/2kT + (E_l + \mu_l{}^0 - r_l \mu_s{}^0)/kT\}$$

Equations [16] compose the system of isotherms which describes the coadsorption of the substances A_i ($i = 1, \ldots, k$) from a solution of a solvent S on an energetically homogeneous surface under the assumption that the adsorption layer behaves as a strictly regular bulk solution. So isotherms [16] are strictly valid for $r_i = 1$ or for values of r_i very close to unity. Isotherms [16] may be also used for values of r_i appreciably different from unity (9, 14). However, in this case, the interaction parameters A_{ij} are not any longer given by eq. [12], since the faults resulting from the entropic terms, $\ln (X_l/X_s{}^{rl})$, are expected to contribute erroneously to the values of A_{ij}.

For isotherms [16] to be used in the interpretation of adsorption experimental data, the mole fraction X_i have to be expressed as a function of the surface coverages ϑ_i. If Γ_i is the number of moles per unit area of the adsorbate A_i, then we have:

[18] $$X_l = \Gamma_l / \sum_{i=1}^{k+1} \Gamma_i$$

But $\Gamma_i = \vartheta_i \Gamma_{i,\max}$ and $\Gamma_{s,\max} = r_i \Gamma_{i,\max}$. Therefore we have

[19] $$X_l = \frac{\vartheta_l / r_l}{1 - \sum_{i=1}^{k} \frac{r_i - 1}{r_i} \vartheta_i}$$

and

[20] $$X_s = 1 - \sum_{x=1}^{k} X_i$$

2. Models of FH statistics

In this model, as in the case of SRS model, the adsorbed molecules are arranged in space following the geometry of a regular lattice. However, in this model, the adsorption layer is a two-dimensional phase and each adsorbed molecule can occupy more than one site in the lattice.

In order to analyze the properties of this model we first examine the case of a surface solution having zero energy of mixing. If M is the total number of lattice sites and n_i the number of sites occupied by a single A_i molecule, then we have

[21] $$M = \sum_{i=1}^{k+1} n_i N_i$$

and

[22] $$\vartheta_i = n_i N_i / M$$

The total differential of the free energy of the adsorbed phase

can be expressed in the form:

$$[23]\quad \frac{dA}{MkT} = \sum_{i=1}^{k} \frac{1}{n_s n_i} \ln (\lambda_i^{n_s}/\lambda_s^{n_i}) d\vartheta_i$$

where λ_i is the absolute activity of A_i. However, the ratio $\lambda_i^{n_s}/\lambda_s^{n_i}$ is directly proportional to the ratio of the probability that a group of $n_i n_s$ sites are occupied entirely by n_s particles of A_i, $P(n_s$ particles $A_i)$, to the probability that this group is occupied by n_i particles of the solvent S, $P(n_i$ particles $S)$. That is (6, 7, 10)

$$[24]\quad \frac{\lambda_i^{n_s}}{\lambda_s^{n_i}} = \kappa_i \frac{P(n_s \text{ particles } A_i)}{P(n_i \text{ particles } S)} = \kappa_i \alpha_i$$

where κ_i is a constant independent of the composition of the adsorption layer. Now, if we accept that the probability of occupation of a lattice site is independent of the presence of particles in neighbouring sites, then we have

$$[25]\quad \alpha_i = (\vartheta_i/\rho_i)^{n_s}/(\vartheta_s/\rho_s)^{n_i}$$

where ρ_i is the number of distinguishable ways in which a particle A_i as a whole can be placed in the lattice after one of its elements has been placed.

Introducing eqs. [24], [25] into eq. [23] and integrating, we obtain

$$[26]\quad \frac{A}{MkT} = \sum_{i=1}^{k} \{\vartheta_i[\ln (\kappa_i \rho_s^{n_i/n_s}/\rho_i) + \ln \vartheta_i - 1]/n_i\} + (\vartheta_s \ln \vartheta_s - \vartheta_s)/n_s + \text{const.}$$

while the free energy of mixing will be given by

$$[27]\quad \frac{\Delta A_m}{MkT} = \sum_{i=1}^{k+1} (\vartheta_i \ln \vartheta_i)/n_i$$

Now, the chemical potentials of the adsorbed particles can be easily obtained from

$$[28]\quad \frac{\mu_l(\text{ads}) - \mu_l^0(\text{ads})}{kT} = \left(\frac{\partial \Delta A_m/kT}{\partial N_l}\right) N_{i \neq l} = \ln \vartheta_l + 1 - n_l \sum_{i=1}^{k+1} \vartheta_i/n_i \qquad l = 1, \ldots, k+1$$

where $\mu_l^0(\text{ads})$ is the chemical potential of the pure A_l substance at the adsorption layer.

The above equations hold for the ideal case where the energy of mixing is zero. Yet the field effect is not taken into consideration. In order to overcome these weaknesses we can introduce into eq. [28] appropriate activity coefficients, f_i, and internal partition functions, q_i, in which we formally include both the internal degrees of freedom and the field effect. Thus we have

$$[29]\quad \frac{\mu_l(\text{ads})}{kT} = \ln \vartheta_l + 1 - n_l \sum_{i=1}^{k+1} \vartheta_i/n_i + \mu_l^0(\text{ads})/kT + \ln f_l - \ln q_l$$

If the process of adsorption is again assumed to be represented by eq. [1], then we have $r_i = n_i/n_s$ and, introducing eq. [29] into eq. [15], we obtain the isotherms:

$$[30]\quad \ln \frac{\vartheta_l}{e^{(r_l-1)} \cdot \left(1 - \sum_{i=1}^{k} \vartheta_i\right)^{r_l}} + \ln \frac{f_l}{f_s^{r_l}} = \ln \frac{c_l}{c_s} + \ln \beta_l$$

where we have

$$[31]\quad \ln \beta_l = (\mu_l^0 - r_l \mu_s^0 - \mu_l^0(\text{ads}) + r_l \mu_s^0(\text{ads}))/kT + \ln (q_l/q_s^{r_l})$$

Isotherms [30] can be used only when the relation between f_i and ϑ_i or X_i is known. To a molecular level and for the adsorption of a single adsorbate from solution, this relation has been determined by means of the Bragg–Williams and the quasi-chemical approximation (13). However, these two approximations lead to remarkable deviations from the experimental data (13, 14), so that it is useless to extend them to the case of the joint adsorption. On the contrary, the determination of the relation between $f_i/f_s^{r_i}$ and X_i to a macroscopic level has led to isotherms with high applicability (13). This treatment can be easily extended to the joint adsorption from solution. The excess free energy, g^e, with respect to the free energy of an athermal mixture due to the non-zero energy of mixing, is related to the activity coefficients by the known relation (17)

$$[32]\quad g^e/kT = \sum_{i=1}^{k+1} X_i \ln f_i$$

Then

$$[33]\quad \frac{\partial g^e/kT}{\partial X_l} = \ln f_l - \ln f_s$$

and therefore

$$[34]\quad \ln f_l = \frac{g^e}{kT} + \frac{\partial g^e/kT}{\partial X_l} + \sum_{i \neq k+1} X_i \frac{\partial g^e/kT}{\partial X_i}$$

$$[35]\quad \ln f_s = \frac{g^e}{kT} - \sum_{i \neq k+1} X_i \frac{\partial g^e/kT}{\partial X_i}$$

Now, if we expand the excess free energy g^e to a power series

$$[36]\quad g^e = kT \sum_{i<j}^{k+1} \sum_{m=0}^{n} A_m^{ij} X_i X_j (X_i - X_j)^m$$

we obtain

$$[37]\quad \ln f_l = \sum_{i<j} \sum_m A_m^{ij} \{(\lambda X_p - X_i X_j)(X_i - X_j)^m - m X_i X_j (X_i - X_j + (-1)^{\mu}\lambda)(X_i - X_j)^{m-1}\}$$

$$[38]\quad \ln f_s = \sum_{i<j} \sum_m A_m^{ij} \{(\sigma X_i - X_i X_j)(X_i - X_j)^m - m X_i X_j (X_i - X_j + \sigma)(X_i - X_j)^{m-1}\}$$

where $\lambda = 1$ when i or $j = l$, $\lambda = 0$ when i and $j \neq l$; μ is an even number when $l = j$ and odd number when $l = i$; $p \neq l$ and $p = i$ or j; finally, $\sigma = 1$ when $j = k$ and $\sigma = 0$ when $j \neq k$. Also, m may depend upon the values of i, j.

III. Thermodynamic restrictions and equations of state

Isotherms [16] and [30] are of the general form

$$[39]\quad F_i(X_1, X_2, \ldots, X_k) = \beta_i c_i$$

If Φ is the surface pressure of the adsorbed phase, then

$$[40]\quad d\Phi = \sum_{i=1}^{k} \frac{\partial \Phi}{\partial \ln c_i} d \ln c_i$$

However,

$$[41]\quad d \ln c_i = \sum_{l=1}^{k} \frac{\partial \ln F_i}{\partial X_l} dX_l$$

and, in dilute solutions, from the Gibbs adsorption theorem we get

$$[42]\quad \vartheta_i = a_i \frac{\partial \Phi}{\partial \ln c_i}$$

where

$$[43]\quad a_i = 1/RT \cdot \Gamma_{i,\max}$$

Therefore

$$[44]\quad d\Phi = \sum_j \left(\sum_i \frac{\vartheta_i}{a_i} \frac{\partial \ln F_i}{\partial X_j} \right) dX_j$$

$d\Phi$ is an exact differential. So we must have

$$[45]\quad \frac{\partial}{\partial X_n}\left\{\sum_i \frac{\vartheta_i}{a_i}\frac{\partial \ln F_i}{\partial X_l}\right\} = \frac{\partial}{\partial X_l}\left\{\sum_i \frac{\vartheta_i}{a_i}\frac{\partial \ln F_i}{\partial X_n}\right\} \qquad n \neq l$$

The system of isotherms [39] should fulfill these equations in order to be compatible with thermodynamics. Substituting F_i from eq. [16] or [30] into eq. [45], we obtain that the condition [45] is fulfilled if and only if

$$[46]\quad r_i/a_i = \text{constant}$$

Parameter r_i is taken equal to the ratio of the molecular volumes of the adsorbate A_i and the solvent S, (V_i/V_s), or equal to the ratio of the areas covered by these substances on the electrode surface. These two choices depend upon the choice of the dimensions of the adsorbed phase. If this is considered as a two-dimensional layer, as it is used in the case of Flory–Huggins isotherms, then $r_i = S_i/S_s$ and

$$[47]\quad r_i/a_i = RT \cdot 10^{14}/S_s L = \text{const.}\ (S_i,\ S_s \text{ in nm}^2/\text{molecule})$$

where L is Avogadro's constant; i.e., in this case no thermodynamic restriction is imposed. However, if we consider the adsorption layer as a three-dimensional phase, then the restriction r_i/a_i = const. is not always fulfilled. Usually in this case the restriction [46] presupposes that the adsorbed substances have the same height in the adsorption layer.

Integrating [45] and following lengthy algebra, or alternatively from eq. [9], taking into account the restriction [46], the equations of state of the coadsorption isotherms developed here may be calculated. They are the following:

a. *Model of SRS theory*

$$[48]\quad \frac{\Phi}{b} = -\ln X_s + \sum_{i<j\neq k+1} X_i X_j A_{ij} - \sum_{i\neq k+1} X_i(1-X_s)A_{ik+1}$$

where

$$[49]\quad b = r_i/a_i$$

b. *Model of FH statistics*

$$[50]\quad \frac{\Phi}{b} = -\ln \vartheta_S - 1 + \sum_{i=1}^{k+1} \frac{\vartheta_i}{r_i} + \sum_{i<j}\sum_m A_m{}^{ij}\{mX_iX_j(X_i - X_j + \sigma) - (\sigma X_i - X_iX_j) \times (X_i - X_j)\}(X_i - X_j)^{m-1}$$

IV. Adsorption from three-component solution

The general relationships developed above can be used in practice only for coadsorption of two substances from solution. In this case, for the use of isotherms [16], [30] ca. 10^2 measurements are required, while an increase in the number of adsorbates increases the number of measurements exponentially.

For adsorption from three-component solution the above equations may be rewritten in the following form:

a. *Model of SRS theory*

Adsorption isotherms

$$[51]\quad \ln(X_A/X_s{}^{r_A}) + X_B\{1 + (r_A - 1)X_A\}A_{AB} + \{X_s(1-X_A) - X_A(1-X_s)r_A\}A_{AS} - X_B\{r_A - (r_A-1)X_s\}A_{BS} = \ln(c_A/c_S) + \ln\beta_A$$

$$[52]\quad \ln(X_B/X_S{}^{r_B}) + X_A\{1 + (r_B - 1)X_B\}A_{AB} - X_A\{r_B - (r_B-1)X_S\}A_{AS} + \{X_S(1-X_B) - X_B(1-X_S)r_B\}A_{BS} = \ln(c_B/c_S) + \ln\beta_B$$

Equation of state

$$[53]\quad \frac{\Phi}{b} = -\ln X_S + X_AX_BA_{AB} - (X_A{}^2 + X_AX_B)A_{AS} - (X_B{}^2 + X_AX_B)A_{BS}$$

b. *Model of FH statistics*

Adsorption isotherms

$$[54]\quad \ln\frac{\vartheta_A}{e^{(r_A-1)}(1-\vartheta_A-\vartheta_B)^{r_A}} + \ln\frac{f_A}{f_S{}^{r_A}} = \ln\frac{c_A}{c_S} + \ln\beta_A$$

$$[55]\quad \ln\frac{\vartheta_B}{e^{(r_B-1)}(1-\vartheta_A-\vartheta_B)^{r_B}} + \ln\frac{f_A}{f_S{}^{r_B}} = \ln\frac{c_B}{c_S} + \ln\beta_B$$

where

$$[56]\quad \ln\frac{f_A}{f_S{}^{r_A}} = \sum_{i=0}^{n}\{[X_B(1-X_A) + r_AX_AX_B](X_A - X_B) + iX_AX_B[1 - X_A + X_B - r_A(X_B - X_A)]\}A_i(X_A - X_B)^{i-1} + \sum_{i=0}^{n}\{[X_S(1-X_A) - r_AX_A(X_A + X_B)](X_A - X_S) + iX_AX_S[1 - X_A + X_S + r_A(2X_A + X_B)]\}B_i(X_A - X_S)^{i-1} - \sum_{i=0}^{n}\{[X_BS_S + r_AX_B(X_A + X_B)](X_B - X_S) - iX_BX_S[1 - X_A - 2X_B + r_A(X_A + 2X_B)]\}C_i(X_B - X_S)^{i-1}$$

$$[57]\quad \ln\frac{f_B}{f_S{}^{r_B}} = \sum_{i=0}^{n}\{[X_A(1-X_B) + r_BX_AX_B](X_A - X_B) - iX_AX_B[1 + X_A - X_B + r_B(X_B - X_A)]\}A_i(X_A - X_B)^{i-1} - \sum_{i=0}^{n}\{[X_AX_S + r_BX_A(X_A + X_B)](X_A - X_S) - iX_AX_S[1 - 2X_A - X_B + r_B(2X_A + X_B)]\}B_i(X_A - X_S)^{i-1} + \sum_{i=0}^{n}\{[X_S(1-X_B) - r_BX_B(X_A + X_B)](X_B - X_S) + iX_BX_S[1 - X_B + X_S + r_B(X_A + 2X_B)]\}C_i(X_B - X_S)^{i-1}$$

However, this form of isotherms is not also appropriate for an easy application to experimental data. The study of the individual adsorption on the basis of isotherms of this model showed that a satisfactory description of the experimental data is possible, even if $n = 0$ (13). If $n_i = 0$ then eqs. [56], [57] are reduced to

$$[58]\quad \ln(f_A/f_S^{r_A}) = X_B[1 + (r_A - 1)X_A]A_0 + [X_S(1 - X_A) - r_A X_A(1 - X_S)]B_0 - X_B[r_A - (r_A - 1)X_S]C_0$$

$$[59]\quad \ln(f_B/f_S^{r_B}) = X_A[1 + (r_B - 1)X_B]A_0 - X_A[r_B - (r_B - 1)X_S]B_0 + [X_S(1 - X_B) - r_B X_B(1 - X_S)]C_0$$

Note that eqs. [58], [59] are identical to the energetic terms of isotherms [51], [52].

Equation of state

$$[60]\quad \frac{\Phi}{b} = \frac{1 - \vartheta_A - \vartheta_B}{1 - X_A - X_B} - \ln(1 - \vartheta_A - \vartheta_B) - 1 + A_0 X_A X_B - B_0(X_A^2 + X_A X_B) - C_0(X_B^2 + X_A X_B)$$

In the above equations the interaction parameters A_{AS}, A_{BS}, B_0, and C_0 may be obtained from the individual adsorption of the substances A and B under the assumption that the presence of an adsorbate (say A) at the interface does not change significantly the intermolecular interactions of the other adsorbate (B) with the solvent and within its molecules. On the contrary, the parameters A_{AB} and A_0 can be calculated only from the interpretation of the coadsorption experimental data.

When $r_A = r_B = 1$, isotherms [51], [52] or [54], [55] are reduced to

$$[61]\quad \ln\frac{\vartheta_A}{1 - \vartheta_A - \vartheta_B} + \vartheta_B A_{12} + \vartheta_A A_1 = \ln\frac{c_A}{c_S} + \ln\beta_A$$

$$[62]\quad \ln\frac{\vartheta_B}{1 - \vartheta_A - \vartheta_B} + \vartheta_A A_{12} + \vartheta_B A_2 = \ln\frac{c_B}{c_S} + \ln\beta_B$$

i.e., the known isotherms of Frumkin for adsorption of two substances are obtained with parameters:

$$[63]\quad A_{12} = A_{AB} - A_{AS} - A_{BS},\ A_1 = -2A_{AS} \text{ and } A_2 = -2A_{BS}$$

The equation of state of these isotherms is

$$[64]\quad \frac{\Phi}{b} = \frac{A_1}{2}\vartheta_A^2 + \frac{A_2}{2}\vartheta_B^2 + A_{12}\vartheta_A\vartheta_B - \ln(1 - \vartheta_A - \vartheta_B)$$

The Frumkin isotherms are also obtained if we accept that $r_A = r_B = 1$ and that the solvent behaves as a continuous medium. In this case we obtain the isotherms [61], [62] with parameters:

$$[65]\quad A_{12} = cW_{AB}/kT,\ A_1 = cW_{AA}/kT, \text{ and } A_2 = cW_{BB}/kT$$

Note that there is a characteristic difference in the physical meaning of the interaction parameters between the two models of the Frumkin isotherms. Thus in the case of the continuous solvent model, parameters A_1 and A_2 are identical to those of the single adsorption. On the contrary, in the case of the discrete solvent model there is no identity in the interaction parameters of the individual and the joint adsorption. So we have to use eq. [63] for the calculation of A_1, A_2. Obviously, the values of A_{12}, obtained in the two cases, will be different. Finally the restriction [46] leads to the identity $S_A = S_B$. Therefore in the Frumkin isotherms the identity of the dimensions of the adsorbed molecules is not imposed simply from the model of the isotherm but also from thermodynamic reasoning.

1. J. E. Randles and B. Behr. J. Electroanal. Chem. **35**, 389 (1972).
2. H. Nakadomari, D. Mohilner, and P. Mohilner. J. Phys. Chem. **80**, 1761 (1976).
3. D. Mohilner, H. Nakadomari, and P. Mohilner. J. Phys. Chem. **81**, 244 (1977).
4. R. Bennes., J. Electroanal. Chem. **105**, 85 (1979).
5. A. Mazhar, R. Bennes, P. Vanel, and D. Schuhmann. J. Electroanal. Chem. **100**, 395 (1979).
6. E. Guggenheim. Mixtures. Oxford University Press, London. 1952.
7. I. Prigogine. The molecular theory of solutions. North-Holland Publishing Co, Amsterdam. 1957.
8. T. L. Hill. An introduction to statistical thermodynamics. Addison–Wesley, London. 1962.
9. A. Münster. Statistical thermodynamics. Vol. 2. Academic Press, New York. 1969.
10. E. Guggenheim and M. MacGlashan. Proc. R. Soc. Ser. A, **203**, 435 (1950).
11. M. Hamdi, P. Vanel, D. Schuhmann, and R. Bennes. J. Electroanal. Chem. **136**, 229 (1982).
12. P. Nikitas, A. Pappa-Louisi, and D. Jannakoudakis. J. Electroanal. Chem. **162**, 175 (1984).
13. P. Nikitas. J. Chem. Soc. Faraday Trans. 1, **80**, 3315 (1984).
14. P. Nikitas. J. Chem. Soc. Faraday Trans. 1, **81**, 1767 (1985).
15. A. Sanfeld. *In* Physical chemistry, an advanced treatise. Vol. I. *Edited by* H. Eyring, D. Henderson, and W. Jost. Academic Press, New York. 1971.
16. P. Nikitas. J. Electroanal. Chem. **170**, 333 (1984).
17. M. L. McGlashan. J. Chem. Educ. **10**, 516 (1963).

Coadsorption of triphenylphosphine – triphenylphosphine oxide, triphenylphosphine – dodecyldiphenylphosphine oxide, and dodecyldiphenylphosphine oxide – tri(*n*)octylphosphine oxide from methanolic solutions on a polarized mercury electrode

ADRIANI PAPPA-LOUISI AND PANAGHIOTIS NIKITAS
Laboratory of Physical Chemistry, University of Thessaloniki, Thessaloniki, Greece
Received August 11, 1985

ADRIANI PAPPA-LOUISI and PANAGHIOTIS NIKITAS. Can. J. Chem. **64**, 333 (1986).

The coadsorption of triphenylphosphine – triphenylphosphine oxide, triphenylphosphine – dodecyldiphenylphosphine oxide, and dodecyldiphenylphosphine oxide – tri(*n*)octylphosphine oxide on a polarized mercury electrode from methanolic solutions of LiCl is investigated by means of electrocapillary measurements. Results show that reorientation or other molecular modifications do not take place during the coadsorption process. The adsorbed molecules maintain their orientation with the phenyl and alkyl groups in contact with the electrode surface. Thus, the adsorption maxima of the substances in the mixed adsorption are located at the same polarization region as in the single adsorption, although their separation distance increases as the bulk concentration of adsorbates rises due to changes in the electrical characteristics of the interface. This shift is not observed when the two substances are adsorbed at the same, or nearly the same, potentials (charges). In all cases the adsorption of a substance leads to a decrease in the adsorption of the coadsorbate to an extent depending on the electric field. The influence of the field on the adsorption isotherms cannot be determined by means of the surface pressure method but by determining the type of adsorption isotherm. It was found that all the systems studied follow an isotherm based on the strictly regular solutions theory. The interaction parameters are independent of the field, while the standard free energy of adsorption of an adsorbate, within experimental error, is independent of the presence of the coadsorbate. This is due to the insignificant change in the bulk adsorbate solvent interactions caused by the presence of the coadsorbed substance in the solution.

ADRIANI PAPPA-LOUISI et PANAGHIOTIS NIKITAS. Can. J. Chem. **64**, 333 (1986).

On fait appel à des mesures électrocapillaires pour étudier la coadsorption des mélanges triphénylphosphine – oxyde de triphénylphosphine, triphénylphosphine – oxyde de dodécyldiphénylphosphine, oxyde de dodécylediphénylphosphine – oxyde de tri(*n*)octylphosphine, en solution de LiCl dans le méthanol, sur une électrode polarisée au mercure. Les résultats indiquent qu'il n'y a pas de réorientation ou d'autres modifications moléculaires lors de la coadsorption. Les molécules adsorbées maintiennent leur orientation avec les groupes phényles et alkyles, qui sont en contact avec la surface de l'électrode. Ainsi les maxima d'adsorption de ces substances dans l'adsorption mixte se situent dans la région de polarisation qui correspond à l'adsorption simple et ceci en dépit du fait que leur distance de séparation augmente avec l'augmentation de la concentration globale des adsorbates due aux variations des caractéristiques électriques de l'interface. On n'observe pas ce déplacement lorsque les deux substances sont adsorbées au même potentiel (charges) ou presque. Dans tous les cas, l'adsorption d'une substance provoque une diminution du taux d'adsorption de la molécule coadsorbée et cet effet dépend du champ électrique. On ne peut pas déterminer l'influence du champ sur les isothermes d'adsorption en faisant appel à la méthode de la pression de la surface; toutefois, il est possible de le faire en déterminant le type d'isotherme d'adsorption. On a trouvé que tous les systèmes étudiés obéissent à un isotherme basé sur la théorie des solutions rigoureusement régulières. Les paramètres d'interaction ne dépendent pas du champ alors que l'énergie libre normale d'adsorption d'une molécule adsorbée ne dépend pas, à l'intérieur des erreurs expérimentales, de la présence d'une molécule coadsorbée. Ceci est dû à des changements non significatifs dans les interactions entre la molécule adsorbée et le solvant que provoquent la présence de molécules coadsorbées en solution.

[Traduit par le journal]

I. Introduction

Although the investigation of the mixed adsorption of organic substances from solutions began in 1930, with the work of Ockrent and Butler (1–3), the literature on this subject is poor. The main reason must be attributed to the great number of measurements necessary for a detailed study of this phenomenon. If N, where $N > 10$, is the number of the necessary measurements for the study of the individual adsorption of a substance, then for the coadsorption of two substances ca. 10^2 measurements are required. Because of the experimental difficulties, but also due to the lack of a quantitative approach to the coadsorption phenomenon based on realistic models, a number of publications have a purely qualitative character (4–7). A strictly quantitative work is that of the Russian investigators, which exclusively involves the model of the three parallel condensers as a basis for the study of the mixed adsorption (8–13). However, this approach, being oriented towards a certain direction, leaves some aspects of the problem undefined.

In the present work we attempt a quantitative study of the coadsorption of organic compounds from solution without reference to a priori models, such as that of the three parallel capacitors. We check the possibility of extending the thermodynamic method, developed through the works of Parsons, Trasatti, and their co-workers (14–20) for the interpretation of adsorption data, to the mixed adsorption from solution as well as the applicability of the mixed adsorption isotherms developed in ref. 21. For this reason we studied the interfacial behaviour of the systems triphenylphosphine (TPP) – triphenylphosphine oxide (TPO), triphenylphosphine (TPP) – dodecyldiphenylphosphine oxide (DDPO), and dodecyldiphenylphosphine oxide (DDPO) – tri(*n*)octylphosphine oxide (TOPO) at the mercury – methanolic solution interface. The individual adsorption of these substances has already been studied in our laboratory (22–24). So by studying their mixed adsorption there is the possibility of a quantitative study of the adsorption characteristics of one substance in the presence of another at the interface.

II. Experimental

Description of the experimental apparatus and details on the origin and purity of the chemicals employed are given elsewhere (22–24). Measurements were carried out with a non-siliconized capillary. The

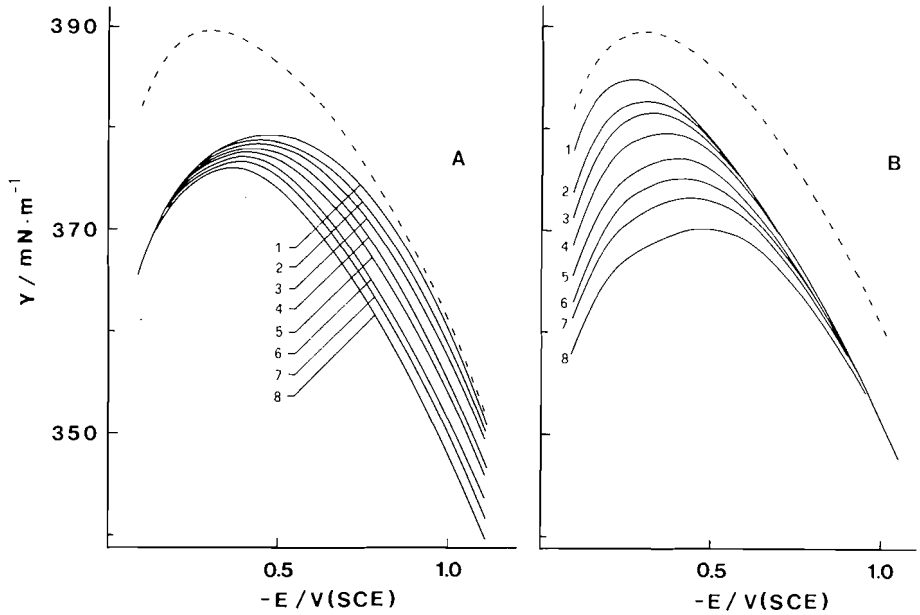

FIG. 1. Electrocapillary curves of Hg in methanolic 0.1 *M* LiCl + *xM* TPP + *yM* TPO solutions. (A) $x = 4 \times 10^{-3}$ and *y*: (1) 0, (2) 5×10^{-3}, (3) 1×10^{-2}, (4) 2×10^{-2}, (5) 3×10^{-2}, (6) 5×10^{-2}, (7) 7×10^{-2}, (8) 0.1. (B) $y = 5 \times 10^{-2}$ and *x*: (1) 0, (2) 4×10^{-4}, (3) 1×10^{-3}, (4) 2×10^{-3}, (5) 4×10^{-3}, (6) 7×10^{-3}, (7) 1×10^{-2}, (8) 2×10^{-2}. Broken line corresponds to the base electrolyte solution.

characteristics of the capillary, its calibration, and the procedure used for measuring the surface tension has also been described previously (25).

For the study of the coadsorption of the substances under investigation, the electrocapillary curves of Hg in the solutions 0.1 *M* LiCl + *xM* A + *yM* B/MeOH where A, B = TPP, TPO, DDPO, TOPO were determined. In the system TPP (A) – TPO (B) we used 12 values of *x* between 0 and 2×10^{-2} and 12 values of *y* in the range from 0 to 0.2. For every value of *x* (or *y*), *y* (or *x*) ranged through its values. In the system TPP (A) – DDPO (B) we used 12 values of *x* (or *y*) between 0 and 2×10^{-2} for *y* (or *x*) = 0 and *y* (or *x*) = 2×10^{-3}, while in the system TOPO (A) – DDPO (B) *x*, *y* took also 12 values, *x* between 0 and 2×10^{-2} for $y = 0$ and 1×10^{-3}, and *y* between 0 and 0.1 for $x = 0$, 1×10^{-3}. In addition, for a detailed study of the change in the adsorption maximum of a substance due to the presence of another adsorbate at the interface, we also took measurements, at an indicative level, in the systems TOPO–TPP and TOPO–TPO.

III. Results and discussion

1. Generalities

Figure 1 shows some of the electrocapillary curves of the system TPP–TPO. It is seen that the presence of a second adsorbate, in the bulk of the solution from which the adsorption of a substance takes place, causes depression of the surface tension (γ) values. This depression depends upon the electrical state of the electrode. In the system of constant TPP concentration (Fig. 1A), electrocapillary curves are strongly depressed in the negative region whereas they coincide with that of the base solution in the positive region. The opposite holds in a system of constant TPO concentration (Fig. 1B). Therefore TPP, in the presence of TPO, is not practically adsorbed on Hg at extreme negative potentials, whereas, on the contrary, the adsorption of TPP in the positive region prevails over TPO adsorption. An analogous behaviour is observed in the system TPP–DDPO (Fig. 2). On the contrary, in the system DDPO–TOPO (Fig. 3) a characteristic depression of the surface tension values over all the potential range examined is observed. Particularly for the system of constant TOPO concentration, the shape of the electrocapillary curves shows that, phenomenologically, the electric field of the interface does not affect the free energy of DDPO adsorption in the presence of TOPO.

The shift of the electrocapillary maximum (ecm) is positive as the concentration of phosphinoxides in the solution increases, and it is negative for the TPP adsorption. In all cases this is analogous to the shift of the ecm that is shown by the corresponding substances on their individual adsorption from the same base electrolyte solution (22–24). Therefore in the systems under investigation, the adsorption of a substance does not lead to reorientation of the coadsorbate, at least at the electrocapillary maximum region.

2. Potential and charge of maximum adsorption

According to the Gibbs adsorption theorem, the electrical coordinates of the maximum in adsorption of an adsorbate A_l in the presence of other adsorbates $A_{i \neq l}$, $i = 1, 2, \ldots k$ can be determined from the charge (σ^m) vs. potential (*E*) curves (18). As in the case of the individual adsorption of a substance from solution, of a given A_l concentration, c_{A_l}, the adsorption of A_l is at a maximum at the charge and potential of the intersection point of the relevant curve with that of the base solution.

The coordinates of the adsorption maximum can also be determined from the maximum in the curves of surface pressure (Φ) against potential (*E*) or charge (σ^m) at constant concentrations of $A_{i \neq l}$. However, we should note that in this case, the maximum in the Φ vs. *E* curve, which corresponds to the concentration c_{A_l}, is not always identified with the maximum adsorption of A_l at this concentration. In the limit of dilute solution, the Gibbs adsorption equation for constant potential and constant concentrations of all the substances in the solution, except from that of A_l, takes the form (26)

$$[1] \qquad -d\gamma = RT\Gamma^S_{A_l} d \ln c_{A_l}$$

where $\Gamma_{A_l}{}^S$ is the relative concentration of A_l. Intergrating eq. [1], we have

$$[2] \qquad \Phi = \gamma_0 - \gamma = RT \int_0^{c_{A_l}} \Gamma^S_{A_l} d \ln c_{A_l}$$

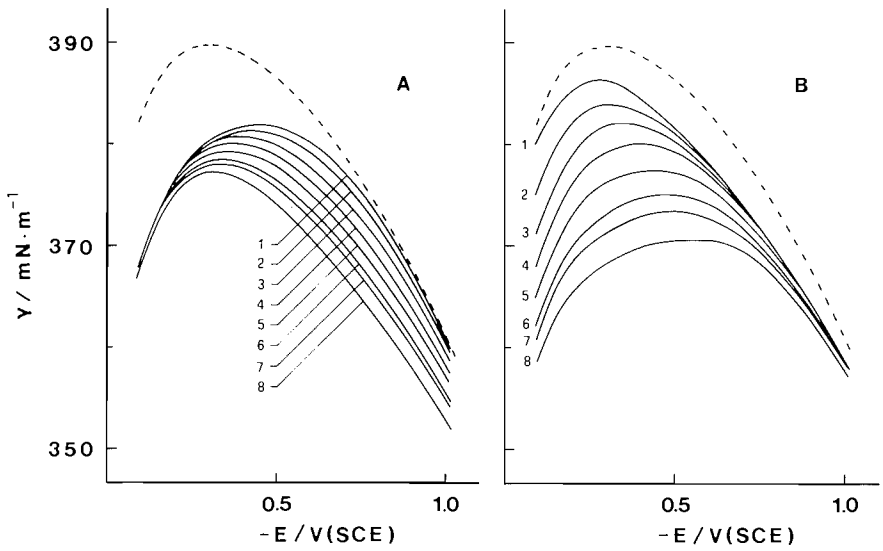

FIG. 2. Electrocapillary curves of Hg in methanolic 0.1 *M* LiCl + *xM* TPP + *yM* DDPO solutions. (A) $x = 2 \times 10^{-3}$ and *y*: (1) 0, (2) 4×10^{-4}, (3) 1×10^{-3}, (4) 2×10^{-3}, (5) 4×10^{-3}, (6) 7×10^{-3}, (7) 1×10^{-2}, (8) 2×10^{-2}. (B) $y = 2 \times 10^{-3}$ and *x* as the *y* values in (A). Broken line corresponds to the base electrolyte solution.

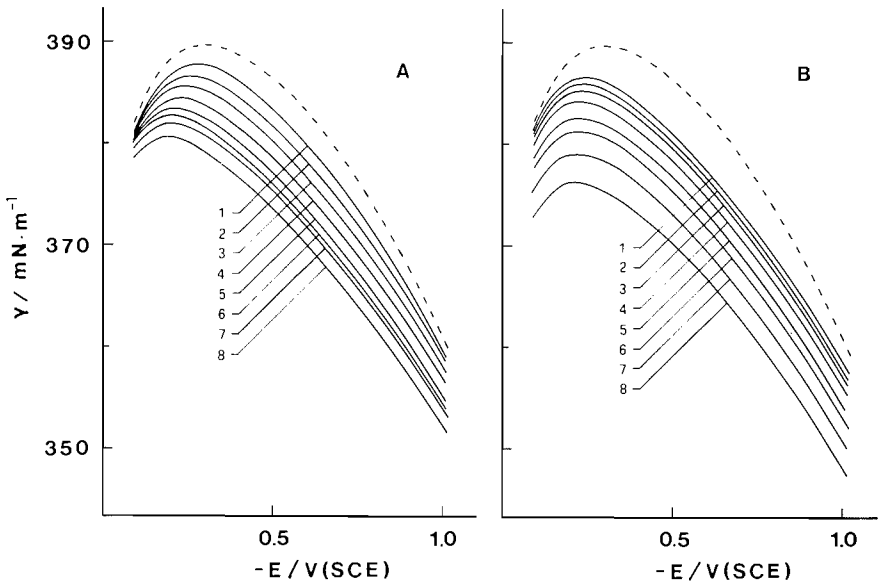

FIG. 3. Electrocapillary curves of Hg in methanolic 0.1 *M* LiCl + *xM* DDPO + *yM* TOPO. (A) $x = 1 \times 10^{-3}$, and *y*: (1) 0, (2) 4×10^{-4}, (3) 1×10^{-3}, (4) 2×10^{-3}, (5) 4×10^{-3}, (6) 7×10^{-3}, (7) 1×10^{-2}, (8) 2×10^{-2}. (B) $y = 1 \times 10^{-3}$ and *x*: (1) 0, (2) 1×10^{-3}, (3) 2×10^{-3}, (4) 4×10^{-3}, (5) 1×10^{-2}, (6) 2×10^{-2}, (7) 4×10^{-2}, (8) 0.1. Broken line corresponds to the base electrolyte solution.

where γ_0 is the surface tension of the base solution, that is, the electrolyte solution that contains the substances $A_{i \neq l}$ at constant concentrations. From eq. [2] and the first mean value theorem we obtain

$$[3] \quad \left(\frac{\partial \Phi}{\partial E}\right)_{c_{A_l}} = RT \int_0^{c_{A_l}} \left(\frac{\partial \Gamma^S_{A_l}}{\partial E}\right)_{c_{A_l}} \cdot \mathrm{d} \ln c_{A_l} = c_{A_l} \left(\frac{\partial \Gamma^S_{A_l}}{\partial E}\right)_{c'_{A_l} \leq c_{A_l}}$$

where c_{A_l}' denotes that the quantity $(\partial \Gamma^s_{A_l}/\partial E)$ refers to a concentration of A_l less than or equal to c_{A_l}. At the maximum of the Φ vs. *E* curve, which corresponds to c_{A_l}, we have

$$[4] \quad \left(\frac{\partial \Phi}{\partial E}\right)_{c_{A_l}} = 0 \quad \text{and} \quad \left(\frac{\partial^2 \Phi}{\partial E^2}\right)_{c_{A_l}} < 0$$

and therefore

$$[5] \quad \left(\frac{\partial \Gamma^S_{A_l}}{\partial E}\right)_{c'_{A_l}} = 0 \quad \text{and} \quad \left(\frac{\partial^2 \Gamma^S_{A_l}}{\partial E^2}\right)_{c'_{A_l}} < 0$$

That is, the maximum in the Φ vs. *E* curve at c_{A_l} corresponds to the adsorption maximum of A_l at a concentration c_{A_l}', which generally is smaller than c_{A_l}. The maximum in the Φ vs. *E* plots will give the adsorption maximum of A_l only when it is independent of the concentration of A_l.

If we now use Parson's function (27) $\xi (= \gamma + \sigma^m E)$, then at constant electrode charge, Gibbs eq. [1] takes the form

$$[6] \quad -\mathrm{d}\, \xi = RT \Gamma^S_{A_l} \mathrm{d} \ln c_{A_l}$$

and, therefore, whatever holds for Φ vs. *E* plots also holds for the plots of $\Phi (= \xi^0 - \xi)$ against σ^m.

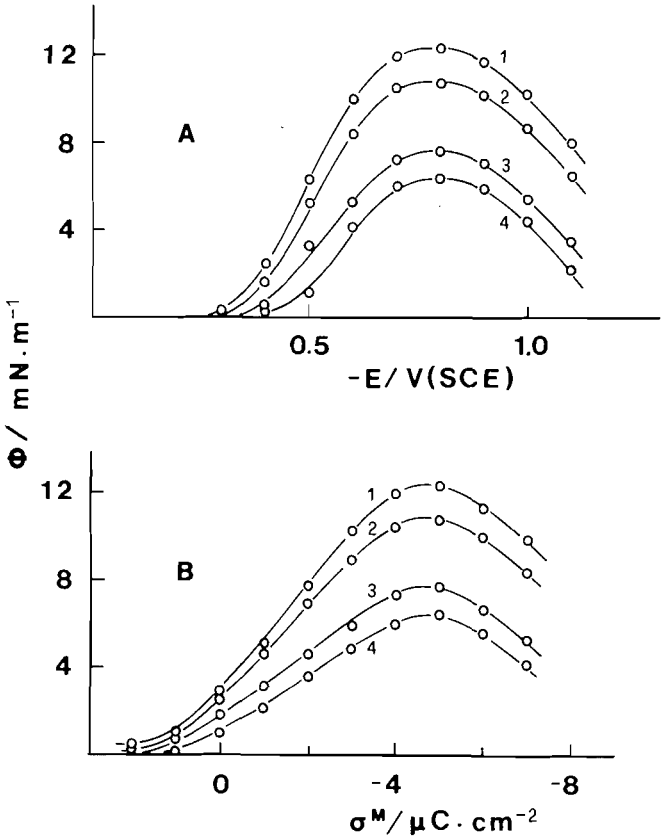

FIG. 4. Relative surface pressure curves as a function of potential (A), and charge (B), of methanolic 0.1 M LiCl + $1 \times 10^{-2} M$ TPP solutions in the presence of the following TOPO concentrations: (1) 6×10^{-2}, (2) 3×10^{-2}, (3) 1×10^{-2}, (4) 5×10^{-3} M.

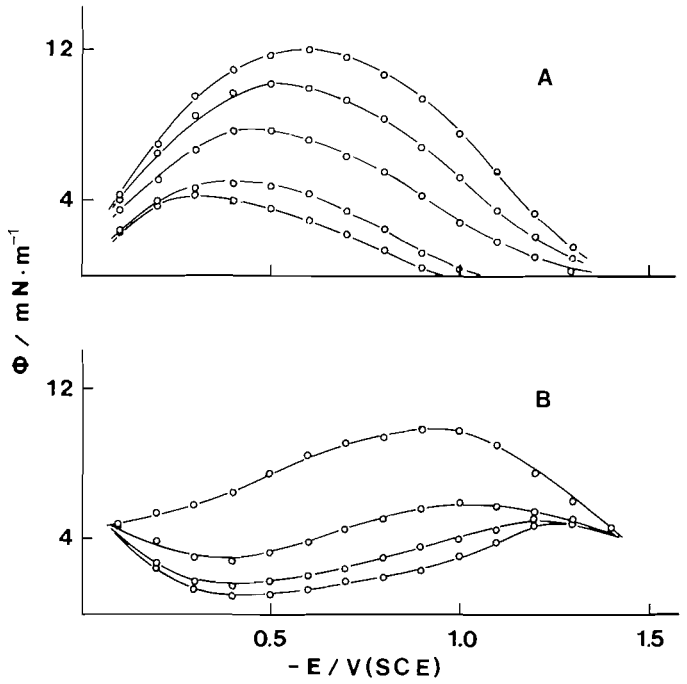

FIG. 5. Relative surface pressure curves as a function of potential (A) due to TOPO ($1 \times 10^{-2} M$) adsorption in methanolic 0.1 M LiCl + xM TPO solutions, where x: (1) 0, (2) 1×10^{-2}, (3) 2×10^{-2}, (4) 5×10^{-2}, (5) 0.1. and (B) due to TPO ($5 \times 10^{-2} M$) adsorption in methanolic 0.1 M LiCl + xM TOPO, where x: (1) 0, (2) 1×10^{-3}, (3) 5×10^{-3}, (4) 1×10^{-2}.

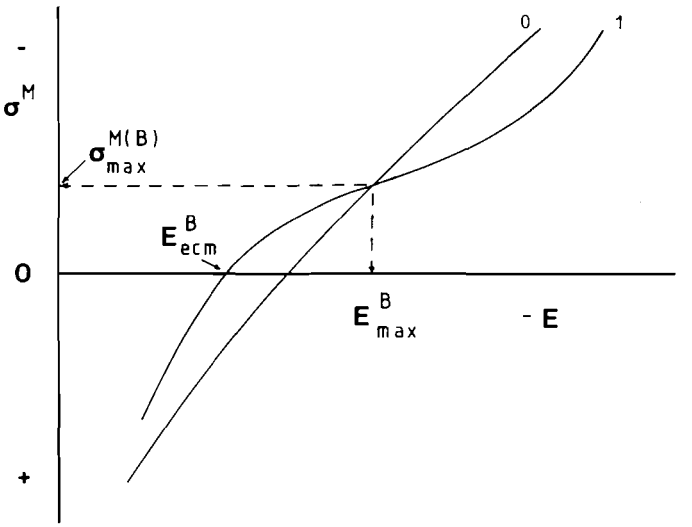

FIG. 6. Typical dependence of the electrode charge on potential in the absence (0) and in the presence (1) of a substance (B) adsorbed at the negative region.

In the systems studied the adsorption maxima were determined from the σ^m vs. E and Φ vs. E (or σ^m) plots, since in all cases they were concentration independent (Fig. 4). It was found that when two substances in their individual adsorption show adsorption maxima at different potentials and charges, then in their mixed adsorption, these maxima mutually separate further. This is shown in Fig. 5 where we give, as examples, some Φ vs. E plots of the system TPO–TOPO. The extent of the mutual separation depends on the position of the individual adsorption maxima and on the concentration of the adsorbates. The more remote the individual adsorption maxima of adsorbates, the weaker their mutual shift, while the bulk concentration of one absorbate affects only the adsorption maximum of the other adsorbate, shifting it with its increase. When the two substances are adsorbed at the same, or nearly the same, potentials (charges), as in the case of the system DDPO–TOPO, then there is no detectable shift in the adsorption maxima in the mixed adsorption of these substances.

Qualitatively, the interpretation of these experimental data can be achieved if we take into consideration the changes in the total dipole moment per unit area of the interface due to the adsorption process. Figure 6 displays typical σ^m vs. E curves for a substance (B) absorbed in the negative region. Note that at the adsorption maximum of B, the net dipole moment per unit area, introduced by the solvent, is equal to that introduced by the substance B. At potentials more negative than E^{B}_{max}, the solvent introduces greater dipole moment than B, due mainly to the reorientation process of its molecules (28–30), while at more positive potentials than E^{B}_{max}, the dipole moment introduced by the solvent is less than that of B. Now if we regard the system "solvent S + adsorbate B" as a new solvent S′, then the solvent S′ introduces into the interface smaller dipole moment (per unit area) than the solvent S at potentials more negative than E^{B}_{max}, but greater at the opposite potential region. So, if an adsorbate A has its adsorption maximum in S at a potential more negative than E^{B}_{max}, then, in the solvent S′, this maximum will be shifted to even more negative potentials until the dipole moment introduced by A into the interface becomes equal to that introduced by S′. The opposite will occur if A is adsorbed at more positive potentials than E^{B}_{max}.

This could also explain the shift of E_{max}, $\sigma^m{}_{max}$ of DDPO and TOPO to lower negative values with respect to that of TPO in their individual adsorption from methanolic solutions (23, 24).

The increase in the concentration of B causes the solvent S′ to be more differentiated than S. Consequently, the greater the surface concentration of B, the greater the effect on the adsorption maximum of A. An exception is the case of coadsorbed substances that have their adsorption maxima at about the same position. Then the dielectic characteristics of the new solvent S′ are differentiated only on both sides of their common maximum, and therefore there is no change in their adsorption maxima. Finally, the independence of the adsorption maximum of a substance A from its concentration, when it is coadsorbed with a substance B, can be explained if, at a certain potential, the ratio of the B molecules to those of S (which are displaced directly or indirectly from the surface solution by one A molecule) is independent of the concentration of A. This must hold, as the ratio of the displaced molecules of B and S depends mainly upon the bulk B–S interactions and the field -dipole interactions of the substances B and S.

The above interpretation of the shift of E_{max}, $\sigma^m{}_{max}$ holds in the case where the adsorbates A and B behave as simple dielectrics. If, during the coadsorption process, molecular modifications or reorientations of the adsorbed A and B molecules take place, then strong deviations from the expected behaviour are possible.

3. Experimental adsorption isotherms

The relative surface concentration of an adsorbed species A_l may be determined from eq. [1] and it is related to the real surface concentration Γ_{A_l} by means of

$$[7] \quad \Gamma^S_{A_l} = \frac{1}{RT}\left(\frac{\partial\gamma}{\partial \ln c_{A_l}}\right)_{c_{A_i\neq l}} = \Gamma_{A_l} - \frac{X^b_l}{X^b_S}\Gamma_s$$

where X_l^b, $X_s{}^b$ are the bulk mole fractions of the substance A_l and solvent S, respectively. When the adsorbed molecules are effectively spherical or cylindrical, we have:

$$[8] \quad 1 = \sum_{i=1}^{k} S_{A_i}\frac{\Gamma_{A_i}}{n_i}L\cdot 10^{-14} + S_s\frac{\Gamma_s}{n_s}L\cdot 10^{-14}$$

where n_i, n_s are the number of the adsorbed layers of the substance A_i and the solvent S; S_{A_i}, S_s are the areas covered by an adsorbed A_i and S molecule, respectively, at saturation, and L is the Avogadro constant. In eq. [8] Γ_{A_i}, Γ_s are expressed in mol/cm^2 and S_{A_i}, S_s in mm^2. Now, from eqs. [7] and [8] we obtain

$$[9] \quad \Gamma_{A_l} = \frac{\Gamma^S_{A_l}\dfrac{S_s}{n_s} + \left(\dfrac{10^{14}}{L} - \sum\limits_{i\neq l}^{k}\Gamma_{A_i}\dfrac{S_{A_i}}{n_i}\right)\dfrac{X^b_{A_l}}{X^b_s}}{\dfrac{S_s}{n_s} + \dfrac{S_{A_l}}{n_l}\dfrac{S^b_{A_l}}{X^b_s}}$$

The fraction of the electrode surface covered by the molecules of A_l may be calculated from

$$[10] \quad \vartheta_{A_l} = \Gamma_{A_l}/(\Gamma_{A_l})_{max} = \Gamma_{A_l}/(10^{14}/L\,S_{A_l})$$

Equation [10] was used for the calculation of the surface composition of the system TPP–TPO. In these calculations the following approximations were made: We assumed that the area covered by an adsorbed A (or B) molecule, S_A (or S_B) is independent of the presence of the other substance at the interface and equal to the corresponding value of S_A (or S_B) obtained from the individual adsorption of A (or B). This approximation is justified by the fact that the interpretation of the shifts of E_{ecm} and E_{max} shows that in the systems studied the presence of substance A (or B) in a solution of B (or A) does not cause, at the interface, reorientation or any other kind of molecular modification that would strongly affect the intermolecular interactions, and, consequently, the intermolecular distances of the adsorbed molecules. We also accepted that $n_A = n_B = 1$ and approximately $n_s = 2$.

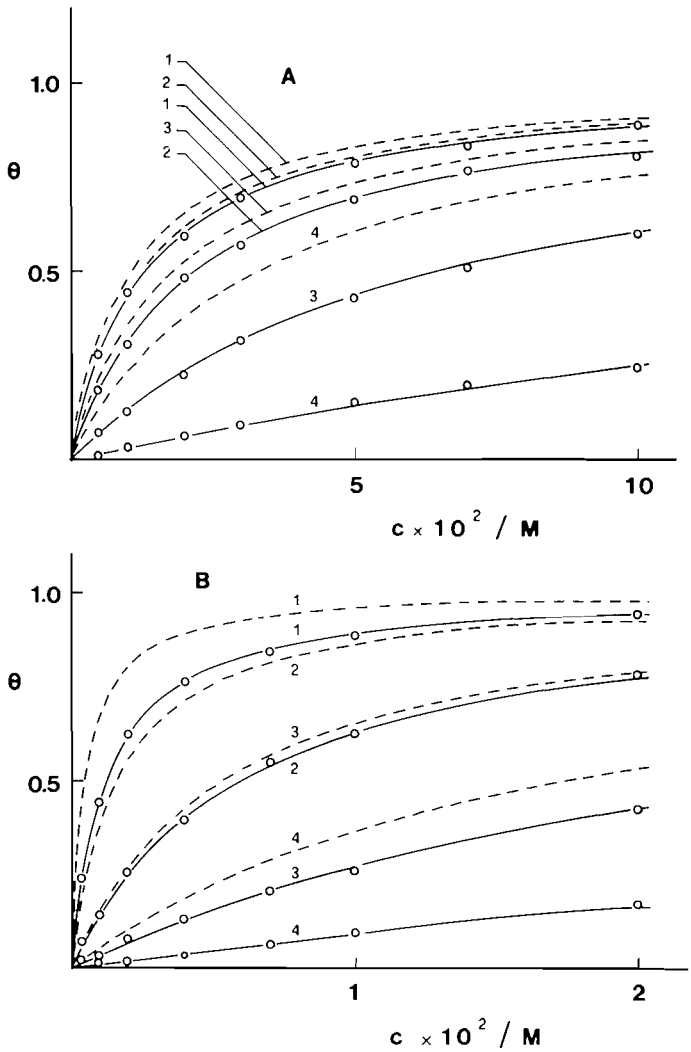

FIG. 7. Experimental adsorption isotherms (A) of TPO in methanolic 0.1 M LiCl + 4 × 10^{-3} M TPP solution at the following potentials: (1) −0.9, (2) −0.7, (3) −0.5, (4) −0.3 V (SCE) and (B) of TPP in methanolic 0.1 M LiCl + 5 × 10^{-2} M TPO at the following potentials: (1) −0.3, (2) −0.5, (3) −0.7, (4) −0.9 V (SCE). Broken lines are the corresponding individual experimental isotherms of (A) and (B).

In the systems TPP–DDPO and TOPO–DDPO there is no possibility of using eq. [10] because of the limited experimental data. However, the use of dilute solutions allows for calculations of the interfacial composition, with a good approximation, by means of

$$[11] \quad \vartheta_i = \vartheta_i^s = \Gamma_i^s/(\Gamma_i)_{max}, \qquad i = \text{A or B}$$

Some mixed–adsorption isotherms of TPP and TPO on Hg are provided in Fig. 7. In the same figure the isotherms of the individual adsorption of TPP, TPO are also provided for comparison purposes. As is expected, the amount adsorbed from each component in its mixed adsorption is lower than that

in its individual adsorption. Yet the adsorption of a component decreases to a greater extent at field values where the second component, which coexists at the interface, is more strongly adsorbed.

4. Influence of the electric field on the adsorption isotherms

In the individual adsorption of a substance from solution the field effect on the isotherms may be determined by means of the surface pressure method (14, 18). We shall show that this method does not provide information in the case of the mixed adsorption.

Let us consider two surface pressure curves, Φ^0 vs. ln c_A at constant c_B for two different potentials or, more correctly, for two different values of potential difference across the inner layer. Here Φ^0 is the surface pressure of A with respect to the solution of the base electrolyte. At not too high concentrations of A the slope of these curves is directly proportional to ϑ_A. The surface pressure Φ^0 may be generally expressed as

$$[12] \quad \Phi^0 = \Phi^0(\vartheta_A, \vartheta_B)$$

while from the adsorption isotherms we have

$$[13] \quad f(\vartheta_A, \vartheta_B) = \beta_B c_B$$

where β_B is the adsorption equilibrium constant of B. From eqs. [12] and [13], $\vartheta_A = g(\Phi^0, \beta_B)$; that is, the slope of Φ^0 vs. ln c_A at a constant value of Φ^0 depends on the electric field. Therefore, independent of whether or not the field changes the isotherm interaction parameters, the surface pressure curves (Φ^0 vs. ln c_A) are not superimposed by sliding parallel to the horizontal axis. The same is expected to hold for the relative surface pressure Φ, that is, the surface pressure with respect to the base electrolyte solution that also contains, in constant concentration, the substance B, because we have

$$[14] \quad \Phi = \Phi^0(\vartheta_A, \vartheta_B) - \Phi^0(\vartheta_A = 0, \vartheta_B{}^0)$$

$$[15] \quad f(\vartheta_A, \vartheta_B) = \beta_B c_B$$

$$[16] \quad f(\vartheta_A = 0, \vartheta_B{}^0) = \beta_B{}^0 c_B$$

which again lead to a field dependence relation for ϑ_A of the form: $\vartheta_A = g\,(\Phi, \beta_B, \beta_B{}^0)$.

In Figs. 8, 9, and 10 examples of surface pressure curves Φ^0, for the substances studied, are shown. Note that they cannot be superimposed.

On the contrary, in all systems studied and in the polarization range for which the individual adsorption isotherms are congruent with respect to potential (22–24), the relative surface pressure curves were superimposed, by sliding parallel to the horizontal axis, in opposition to the expected behaviour (Fig. 11). This disagreement will be analysed below.

The electric field of the interface affects the interaction parameters of the isotherm and its equilibrium constant, which is related to the free energy of adsorption.

The interaction parameters of the mixed-adsorption isotherms are determined from the A–B, A–A, B–B, A–S, and B–S interfacial interactions (21). If, in the coadsorption process, reorientation or any other molecular modification of the adsorbed molecules of A and B does not occur, then, with a good approximation, we can accept that the presence of a substance at the interface does not affect the interactions of the molecules of the other substance, between themselves and the solvent. Therefore the influence of the field on the isotherm interaction parameters, relate to the A–A, A–S, B–S interactions, may be calculated from the study of the individual adsorption of the substances A and B. For the isotherm

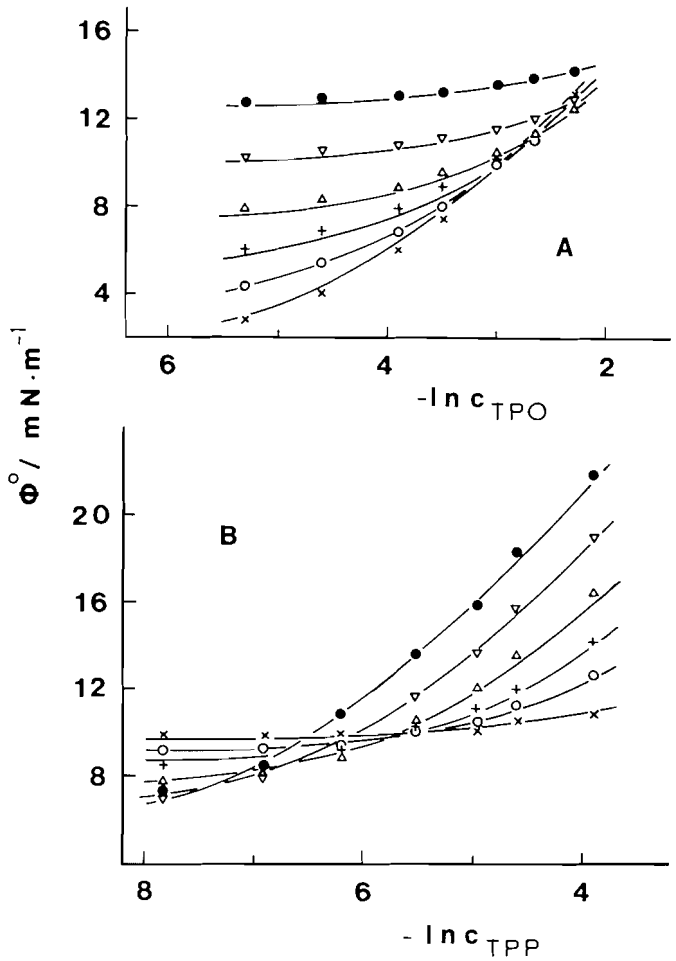

FIG. 8. Surface pressure curves (A) of TPO in methanolic 0.1 *M* LiCl + 4×10^{-3} *M* TPP solution and (B) of TPP in methanolic 0.1 *M* LiCl + 5×10^{-2} *M* TPO at the following potentials: (●) −0.3, (▽) −0.4, (△) −0.5, (+) −0.6, (○) −0.7, (×) −0.9 V (SCE). Solid lines are calculated according to SRS isotherms with parameters as indicated in Table 1.

parameter related to the A–B interactions, information may only be obtained from its determination at every potential (charge), as it is shown below.

In what concerns the free energy of adsorption ΔG_i^0, i = A or B, we can notice the following. The value of ΔG_i^0 is mainly determined from the bulk interactions of the species i with the solvent medium, its specific interactions with the electrode surface, and the electrostatic interactions of i with the electric field. Consequently, the change of ΔG_i^0 with the field is expected to be determined only from the electrostatic interactions of the molecules of species i with the electric field, provided again that there is no reorientation of the adsorbates A and B in the coadsorption process. Therefore, the change of ΔG_i^0 (say i = A), to a good approximation, is independent of the presence of the other substance (B) at the interface and may be determined from the study of the individual adsorption of the i component by the surface pressure method.

5. Isotherm parameters

The experimental data for the systems studied were analyzed by means of the isotherms of the SRS theory, of the Flory–Huggins statistics with $n_i = 0$, and the Frumkin isotherms, all in the form given in ref. 21. In order to test these isotherms, and for reasons mentioned above, we accepted that the parameters A_{AS}, A_{BS}, A_1, A_2 of the isotherms, related to the A–A, B–B, A–S,

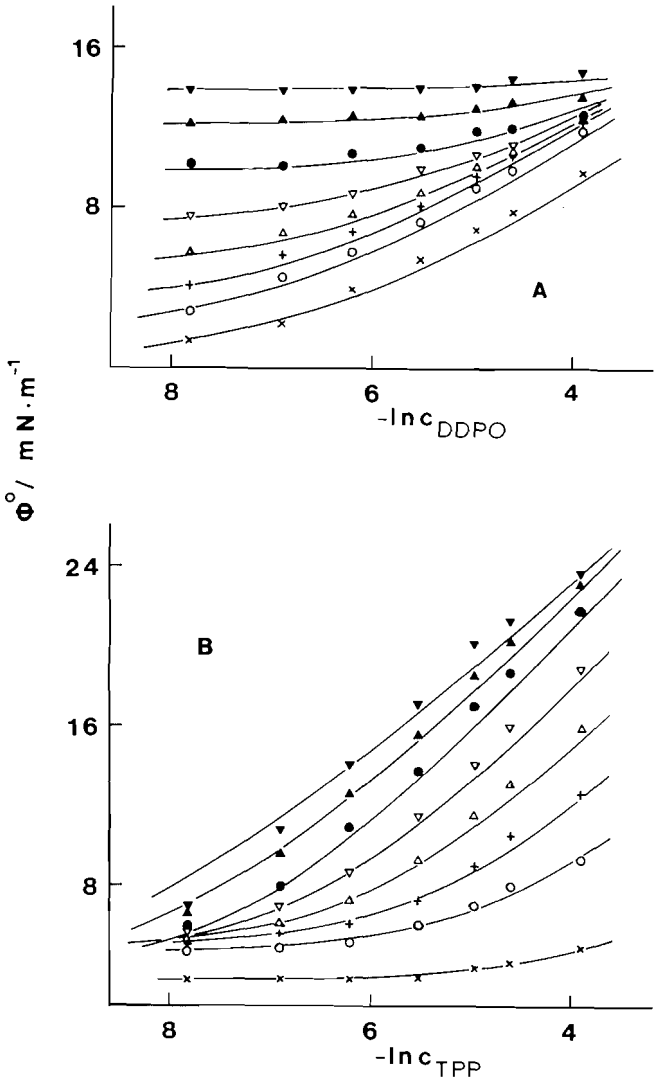

FIG. 9. Surface pressure curves (A) of DDPO in methanolic 0.1 *M* LiCl + 2×10^{-3} *M* TPP solution and (B) of TPP in methanolic 0.1 *M* LiCl + 2×10^{-3} *M* DDPO solution at various potentials. Symbols as in Fig. 8, plus (▼) for −0.1 and (▲) for −0.2 V (SCE). Solid lines are calculated according to SRS isotherms with parameters as indicated in Table 1.

and B–S interactions, may be calculated from the individual adsorption of the corresponding substance. In the present paper the values of these parameters were calculated from ϑ vs. c data by using the procedure described in ref. 31, with isotherms of individual adsorption obtained from eqs. [51], [54], and [61] of ref. 21. The surface pressure method was also used with state equations obtained from eqs. [53], [60], and [64] of ref. 21. The results obtained are provided in Table 1. These are in reasonable agreement with those obtained in refs. 22–24. Note that the isotherm of Flory–Huggins statistics does not describe the adsorption of DDPO and TOPO (32), and therefore the corresponding mixed-adsorption isotherms cannot be applied to the systems TPP–DDPO and TOPO–DDPO.

Now, before testing the mixed-adsorption isotherms in the systems studied, it is necessary to consider the thermodynamic restrictions imposed (21). As it has been shown (21), the Frumkin isotherms can be used when $S_A = S_B$, SRS isotherms when $b_A = b_B$ (where $b_i = r_i\ RT\ (\Gamma_i)_{max}$), while for the Flory–Huggins isotherms there is no restriction if we consider that the adsorption phase is a two-dimensional layer. Table 2

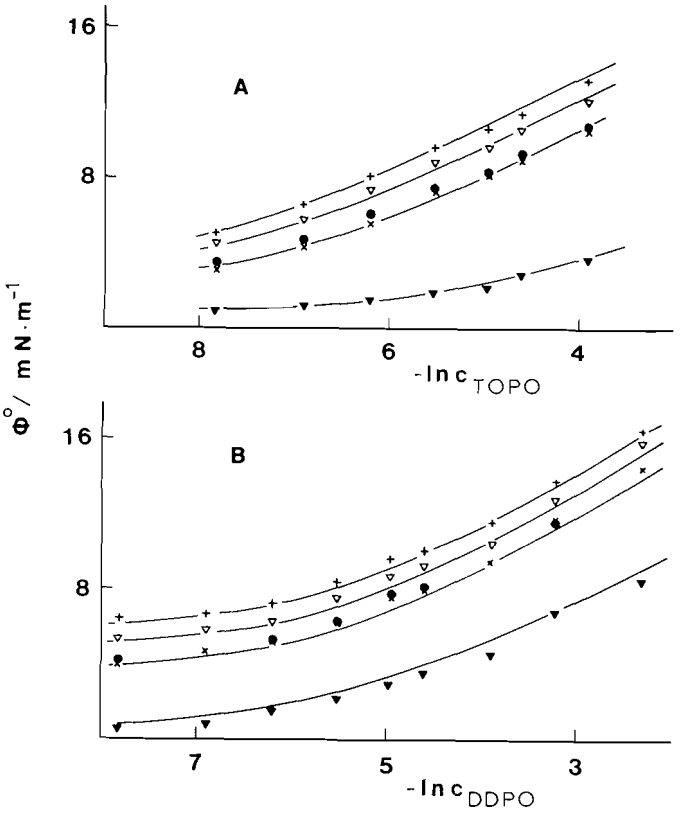

FIG. 10. Surface pressure curves (A) of TOPO in methanolic 0.1 *M* LiCl + 1×10^{-3} *M* DDPO solution and (B) of DDPO in methanolic 0.1 *M* LiCl + 1×10^{-3} *M* TOPO solutions at various potentials. Symbols as in Fig. 9. Solid lines are calculated according to SRS isotherms with parameters as indicated in Table 1.

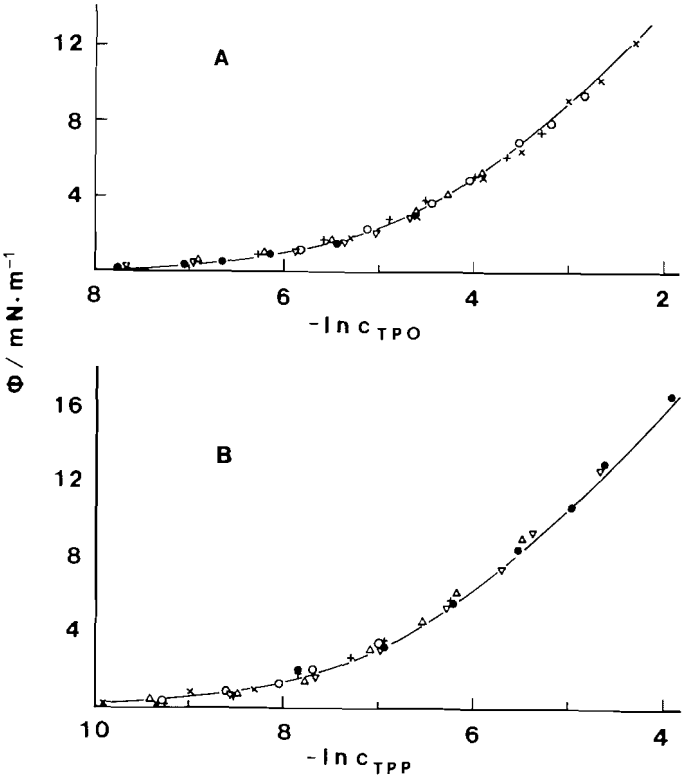

FIG. 11. Composite relative surface pressure curves corresponding to the surface pressure curves in Fig. 8. Solid lines are calculated according to SRS isotherms at potentials −0.9 V (SCE) (A) and −0.3 V (SCE) (B).

TABLE 1. Interaction parameters for TPP, TPO, DDPO, TOPO adsorption (individual and joint) on Hg from methanolic 0.1 *M* LiCl solutions

Isotherm Parameter	Frumkin A_1			Bennes (36) A_{AS}			Flory–Huggins A_{AS}		
E, V(SCE)	<−0.3	−0.2	−0.1	<−0.3	−0.2	−0.1	<−0.3	−0.2	−0.1
Adsorbate:									
TPP	0.00	2.00	5.00	1.47	0.60	−1.00	2.20	1.50	−0.30
TPO	0.00	0.00	0.00	1.42	1.42	1.42	2.20	2.20	2.20
DDPO	1.50	2.40	3.00	1.65	0.80	0.50	—	—	—
TOPO	−0.60	1.00	2.40	1.95	1.80	1.00	—	—	—

Isotherm Parameter	Frumkin A_{12}			SRS theory A_{AB}			Flory–Huggins A_{AB}		
E, V(SCE)	<−0.3	−0.2	−0.1	<−0.3	−0.2	−0.1	<−0.3	−0.2	−0.1
Adsorbate system:									
TPP–TPO	0.00	1.60	5.00	0.00	2.50	4.80	0.00	3.20	5.70
TPP–DDPO	—	—	—	−1.00	−2.00	−4.00			
DDPO–TOPO	—	—	—	0.00	0.00	0.00	—	—	—

TABLE 2. Adsorption parameters used in this work

Compound	*S*, nm^2 molecule^{-1}	$\Gamma_{max} \times 10^{10}$, mol cm^{-2}	*r*(Bennes)	*r*(Bennes)·$RT\Gamma_{max}$, mN m^{-1}	*r*(Flory–Huggins)
TTP	0.74	2.24	5.51	30.59	3.98
TPO	0.70	2.36	5.45	31.85	3.78
DDPO	1.26	1.32	8.96	29.30	6.76
TOPO	1.61	1.03	10.90	27.82	8.67

shows the values of the relevant parameters. Note that the Frumkin isotherms may be applied only to the TPP–TPO system, while the SRS isotherms, to a good approximation, may be applied to all systems we have studied, by using a mean value for $r_i\,RT\,(\Gamma_i)_{max}$.

The tests of the isotherms were carried out either by using ϑ vs. *c* data or the state equations of the isotherms from Φ vs. ln *c* data. In the first case the isotherms are rewritten in a linear form and the experimental data are plotted accordingly. For example, SRS isotherms may be expressed as

$$F = -A_{AB}\Theta_B + \ln \beta_A \quad [17]$$

$$G = -A_{AB}\Theta_A + \ln \beta_B \quad [18]$$

where

$$F = \ln (X_A/X_S^{r_A}) + [X_S(1 - X_A) - X_A(1 - X_S)r_A]A_A - X_B[r_A - (r_A - 1)X_S]A_{BS} - \ln (c_A/c_S) \quad [19]$$

$$G = \ln (X_B/X_S^{r_B}) - X_A[r_B - (r_B - 1)X_S]A_{AS} + [X_S(1 - X_B) - X_B(1 - X_S)r_B]A_{BS} - \ln (c_B/c_S) \quad [20]$$

$$\Theta_B = X_B[1 + (r_A - 1)X_A] \quad [21]$$

$$\Theta_A = X_A[1 + (r_B - 1)X_B] \quad [22]$$

$$X_i = (\vartheta_i/r_i) \Big/ \left(1 - \frac{r_A - 1}{r_A}\vartheta_A - \frac{r_B - 1}{r_B}\vartheta_B\right), \quad i = \text{A or B} \quad [23]$$

$$X_S = 1 - X_A - X_B \quad [24]$$

and the experimental data are plotted as *F* vs Θ_B at c_A = const. and *G* vs. Θ_A at c_B = const. Examples of some tests are given in Fig. 12.

The slopes of these plots yield the values of A_{AB} parameters and the intercepts of the graphs give the free energy of mixed adsorption of the substances studied. The values of the isotherm parameters calculated in this way were used as a first approximation for the calculation of the theoretical surface pressure curves from the corresponding equation. The calculated curves were compared with experimental points in plots of Φ against ln *c*. Usually, small changes in A_{AB}, β_A, β_B parameters were found to be necessary in order for the calculated curves to be fitted to the experimental points. Figures 8–11 show some of the tests of the isotherms under investigation on the basis of the state equations. The calculated values of the interaction parameters are provided in Table 1, while Fig. 13 shows the change in free energy of mixed adsorption of the substances studied, which is calculated from the SRS isotherms, as a function of potential.

In all cases we have studied, the free energy of mixed adsorption of a substance coincides with the corresponding value of the individual adsorption of this substance. On the basis of models, ΔG_i^0 (i = A or B) is given by eq. [17] or [31] of ref. 21. Note that the main influence of a substance B on the free energy of adsorption of A comes from the change in the chemical potential μ_A^0 caused by the presence of B in the bulk solution. μ_A^0 is the chemical potential of A in a hypothetical ideal solution of A, B, and S having $X_A^b = 1$ (33–35). Therefore μ_A^0 depends upon the solvent system and changes when B is added to the solution. However, in our systems, the bulk concentration of B is quite low, thus resulting in negligible influence of B on μ_A^0 and, consequently, on ΔG_A^0.

Having calculated the isotherm parameters, we can now check the superimposability of the relative surface pressure curves (Fig. 11). In the negative region, the coadsorption of TPP and TPO is described by the Langmuir isotherms. In this ideal case, we have

$$\Phi = -RT(\Gamma_A)_{max} \ln \frac{1 - \vartheta_A - \vartheta_B}{1 - \vartheta_B^0}$$

TABLE 3. Values of relative surface pressure due to the coadsorption of TPP–DDPO and DDPO–TOPO calculated according to the SRS isotherms

Adsorbate system	TPP–DDPO					
Constant molar concentration, c/M	2×10^{-3} TPP			2×10^{-3} DDPO		
	DDPO			TPP		
ϑ	0.3	0.5	0.8	0.3	0.5	0.8
Φ, mN m^{-1} ($E = -0.3$ V)	1.30	2.95	8.79	1.89	3.58	8.36
($E = -1.0$ V)	1.29	2.66	6.31	1.92	3.64	8.13
Adsorbate system	DDPO–TOPO					
Constant molar concentration, c/M	1×10^{-3} DDPO			1×10^{-3} TOPO		
	TOPO			DDPO		
ϑ	0.3	0.5	0.8	0.3	0.5	0.8
Φ, mN m^{-1} ($E = -0.3$ V)	0.98	1.95	3.95	1.13	2.18	4.89
($E = -1.0$ V)	0.99	1.98	4.03	1.15	2.26	5.04

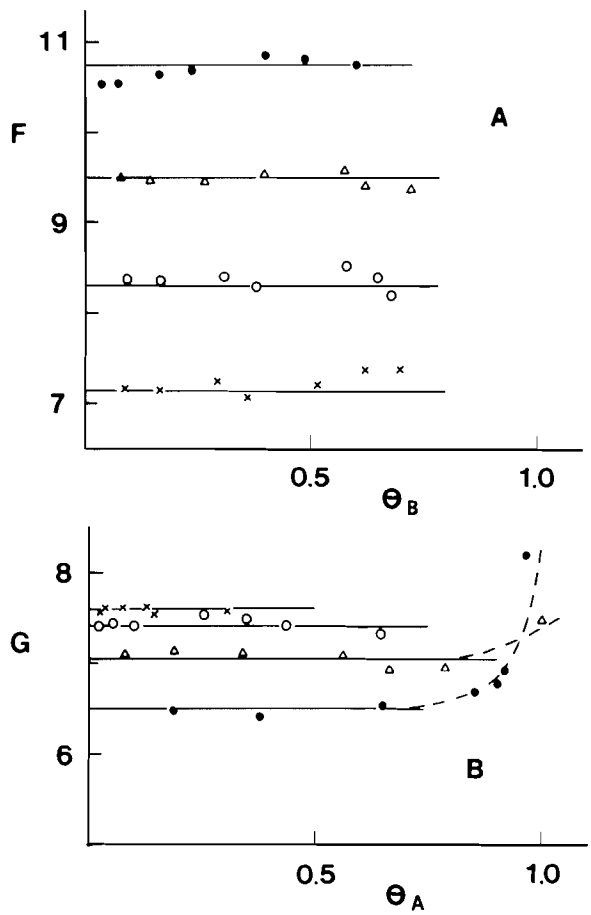

FIG. 12. Tests of SRS isotherms for the coadsorption of TPP–TPO on Hg. (A) Constant TPP concentration, 4×10^{-3} M and (B) constant TPO concentration, 5×10^{-2} M. Symbols as in Fig. 8.

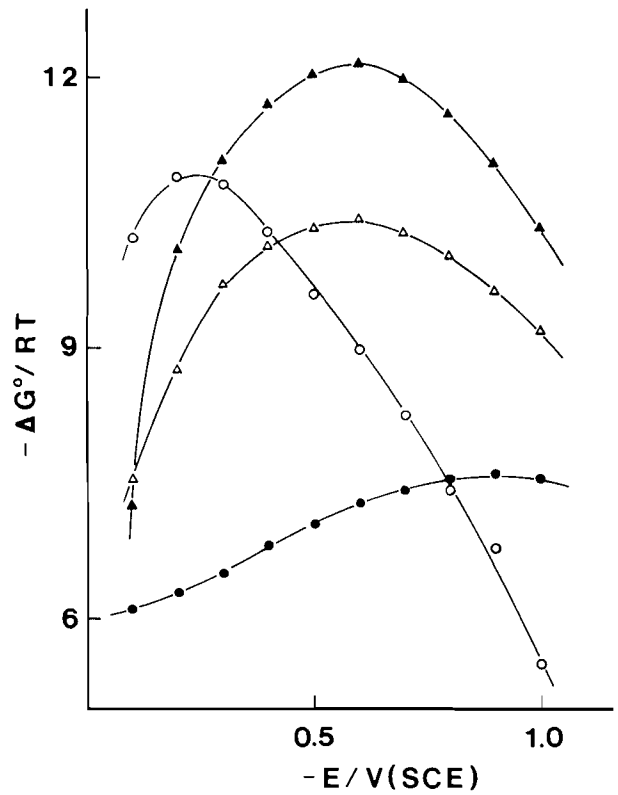

FIG. 13. Standard free energy of adsorption of TPP (○), TPO (●), DDPO (△), and TOPO (▲) at zero surface coverage of the coadsorbate, calculated according to the SRS isotherms.

where ϑ_B^0 is the value of ϑ_B at $\vartheta_A = 0$. However,

$$\frac{\vartheta_B}{1 - \vartheta_A - \vartheta_B} = \beta_B c_B, \frac{\vartheta_B^0}{1 - \vartheta_B^0} = \beta_B^0 c_B$$

and it is found experimentally that $\beta_B^0 = \beta_B$. Therefore

$$\Phi = -RT(\Gamma_A)_{max} \ln \frac{\vartheta_B}{\vartheta_B^0} = -RT(\Gamma_A)_{max} \ln (1 - \vartheta_A)$$

or

$$\vartheta_A = \frac{1}{RT(\Gamma_A)_{max}} \cdot \frac{\partial \Phi}{\partial \ln c_A}$$

$$= 1 - \exp\{-\Phi/RT(\Gamma_A)_{max}\} = f(\Phi)$$

That is, the curves in plots of Φ vs. ln c_A at c_B = const. (or Φ vs. ln c_B at c_A = const.) have the same slope for the same Φ value and, consequently, they are superimposed by sliding parallel to the ln c axis.

On the contrary, in the systems TPP–DDPO and TOPO–DDPO the superimposability of the relative surface pressure curves is due to the small change in their curvature at different

potentials. This is shown in Table 3, where values of Φ, calculated from the SRS isotherms at two different potentials and at different ϑ values are provided. Note that at the same ϑ_A value of different potentials, the corresponding Φ values are not identical but the difference is too small to be experimentally detected. The notable exception observed at $\vartheta_{DDPO} = 0.8$ is due to the fact that at -0.3 V (SCE) the value $\Phi = 8.79$ mN m^{-1} corresponds to a concentration of DDPO that is outside the limits of our study and possibly out of the region where the approximation [11] holds.

Conclusions

1. The coadsorption of TPP–TPO, TPP–DDPO, and DDPO–TOPO on a Hg electrode from methanolic solutions takes pace without reorientation of the adsorbed molecules or other molecular modifications. The adsorbed molecules have a constant orientation, with their phenyl and alkyl groups in contact with the electrode surface.

2. The main effect caused by the presence of a second substance at the interface is the decrease in the amount of the coadsorbate adsorption. This decrease is more pronounced in field values close to the adsorption maximum of the second adsorbate.

3. The presence of a second substance at the interface affects also the adsorption maximum of the first adsorbate. In their mixed adsorption the separation distance of their adsorption increases to an extent depending on the position of the individual adsorption maxima and on the concentration of the adsorbates.

4. The surface pressure method can not be used in obtaining information about the field effect on the isotherms. This can be obtained by determining the isotherm parameters at every field value.

5. The coadsorption of the systems studied follows satisfactorily an isotherm based on the strictly regular solutions theory. The free energy of adsorption follows the same variation pattern as in the case of the individual adsorption. The free energy of adsorption is also independent of the presence of the second adsorbate at the interface due to the insignificant changes in bulk intermolecular interactions caused by the presence of the second substance.

1. C. Ockrent and J. Av. Butler. J. Phys. Chem. **34**, 2297 (1930).
2. J. Av. Butler and C. Ockrent. J. Phys. Chem. **34**, 2841 (1930).
3. C. Ockrent. J. Phys. Chem. **35**, 3354 (1931).
4. F. N. Schapink, O. Oudeman, K. W. Leu, and J. N. Helle. Trans. Faraday Soc. **56**, 415 (1960).
5. B. Kastening and L. Holleck. Talanta, **12**, 1275 (1965).
6. K. M. Joshi and S. Rajagopalan. Electrochim. Acta, **17**, 473 (1972).
7. K. M. Joshi, S. R. Tendulkar, and M. R. Bapat. J. Electroanal. Chem. **68**, 303 (1976).
8. G. A. Dobren'kov and Tr. Kazan. Khim. Tekhnol. Inst. **34**, 196 (1965).
9. B. B. Damaskin, A. N. Frumkin, and S. L. Dyatkina. Izv. Akad. Nauk SSSR, Ser. Khim. 2171 (1967).
10. B. B. Damaskin. Elektrokhimiya, **5**, 346 (1969).
11. G. A. Dobren'kov and G. D. Shilotkach. Elektrokhimiya, **5**, 863 (1969).
12. G. A. Dobren'kov and G. D. Shilotkach. Elektrokhimiya, **6**, 1416 (1970).
13. A. F. Nesterenko, K. G. Balakhanov, and M. A. Loshkarev. Elektrokhimiya, **14**, 1852 (1979).
14. R. Parsons. Proc. R. Soc. Ser. M, **261**, 79 (1961).
15. R. Parsons and F. G. R. Zobel. Trans. Faraday Soc. **62**, 3511 (1966).
16. S. Trasatti. J. Electroanal. Chem. **28**, 257 (1970).
17. A. DeBattisi and S. Trasatti. J. Electroanal. Chem. **48**, 213 (1973).
18. S. Trasatti. J. Electroanal. Chem. **53**, 335 (1974).
19. B. A. Abd-el-Nabey and S. Trasatti. J. Chem. Soc. Faraday Trans. 1, **71**, 1230 (1975).
20. R. Parsons and R. Peat. J. Electroanal. Chem. **122**, 299 (1981).
21. P. Nikitas and A. Pappa-Louisi. Can. J. Chem. **64**, 328 (1986).
22. P. Nikitas, A. Anastopoulos, and D. Jannakoydakis. J. Electroanal. Chem. **145**, 407 (1983).
23. P. Nikitas, A. Pappa-Louisi, and D. Jannakoudakis. J. Electroanal. Chem. **162**, 175 (1984).
24. A. Pappa-Louisi, P. Nikitas, and D. Jannakoudakis. Electrochim. Acta, **29**, 515 (1984).
25. P. Nikitas, A. Pappa-Louisi, and D. Jannakoudakis. J. Electroanal. Chem. **171**, 369 (1984).
26. R. Parsons. *In* Modern aspects of electrochemistry. Vol. I. *Edited by* J. O'M. Bockris. Butterworths, London. 1954.
27. R. Parsons. Trans. Faraday Soc. **51**, 1518 (1955).
28. J. O'M. Bockris, M. A. V. Devanathan, and K. Müller. Proc. R. Soc. Ser. A, **274**, 55 (1963).
29. J. O'M. Bockris, E. Gileadi, and K. Müller. Electrochim. Acta, **12**, 1301 (1967).
30. W. R. Fawcett. J. Phys. Chem. **82**, 1385 (1978).
31. P. Nikitas. J. Chem. Soc. Faraday Trans. 1, **80**, 3315 (1984).
32. A. Pappa-Louisi, P. Nikitas, and D. Jannakoudakis. Chim. Chron. New Series. In press.
33. J. Kirkwood and I. Oppenheim. Chemical thermodynamics. McGraw–Hill, New York. 1961.
34. A. Sanfeld. *In* Physical chemistry, an advanced treatise. Vol. 1. *Edited by* H. Eyring, D. Henderson, and W. Jost. Academic Press, New York, London. 1971.
35. P. A. Pock. Chemical thermodynamics, principles and applications. McMillan, London. 1969.
36. R. Bennes. J. Electroanal. Chem. **105**, 85 (1979).

Hydrolysis and condensation of chlorophosphine and alkyl phosphite ligands on platinum and palladium. ^{31}P and ^{195}Pt nuclear magnetic resonance studies and the crystal and molecular structures of $[Pt_2Cl_4\{\mu\text{-}(EtO)_2POP(OEt)_2\}_2]$ and $[Cl_2Pt\{\mu\text{-}(P(OEt)_2O)_2P(O)\}PtCl(PEt_3)_2]$

DAVID ERIC BERRY, KATHRYN ANNE BEVERIDGE, GORDON WILLIAM BUSHNELL, KEITH ROGER DIXON,[1] AND ALAN PIDCOCK
Department of Chemistry, University of Victoria, Victoria, B.C., Canada V8W 2Y2
Received July 25, 1985

DAVID ERIC BERRY, KATHRYN ANNE BEVERIDGE, GORDON WILLIAM BUSHNELL, KEITH ROGER DIXON, and ALAN PIDCOCK. Can. J. Chem. **64**, 343 (1986).

Hydrolysis of *cis*-$[PtCl_2\text{-}\{P(OEt)_2Cl\}_2]$ results in condensation of the phosphite to form $[Pt_2Cl_4\{\mu\text{-}(EtO)_2POP(OEt)_2\}_2]$, which crystallizes in the monoclinic space group $P2_1/n$, with a = 13.814(7), b = 11.429(4), c = 10.726(5) Å, β = 106.30(5)°. Reactions of $P(OEt)_2Cl$ or $(EtO)_2POP(OEt)_2$ with $[Pt_2Cl_4(PEt_3)_2]$ also yield very easily hydrolyzed products but in these cases an even more complex condensation occurs to yield $[Cl_2Pt\{\mu\text{-}(P(OEt)_2O)_2P(O)\}PtCl(PEt_3)_2]$, which crystallizes in the monoclinic space group $P2_1/c$, a = 17.547(8), b = 19.775(6), c = 11.268(3) Å, β = 106.42(3)°. Complete X-ray diffraction studies are reported for both crystals, confirming the presence of double $(EtO)_2POP(OEt)_2$ bridges in $[Pt_2Cl_4\{\mu\text{-}(EtO)_2POP(OEt)_2\}_2]$ and a novel triphosphite bridge in $[Cl_2Pt\{\mu\text{-}(P(OEt)_2O)_2P(O)\}PtCl(PEt_3)_2]$. Detailed analyses and computer simulation of the $^{31}P\{^1H\}$ and $^{195}Pt\{^1H\}$ nmr spectra of these complexes are also described, together with studies of the related compounds, $[Pt_2Me_4\{\mu\text{-}(EtO)_2POP(OEt)_2\}_2]$ and $[Cl_2(Et_3P)Pt\{\mu\text{-}(EtO)_2POP(OEt)_2\}PtCl_2(PEt_3)]$. In conjunction with previous studies of $[Pt_2Cl_2(dppm)_2]$ and related complexes, these spectra provide examples of several types of *AA'XX'* spin systems and the analysis of these systems is discussed in detail.

DAVID ERIC BERRY, KATHRYN ANNE BEVERIDGE, GORDON WILLIAM BUSHNELL, KEITH ROGER DIXON et ALAN PIDCOCK. Can. J. Chem. **64**, 343 (1986).

L'hydrolyse du *cis*-$[PtCl_2\text{-}\{P(OEt)_2Cl\}_2]$ provoque la condensation du phosphite en donnant le $[Pt_2Cl_4\{\mu\text{-}(EtO)_2POP(OEt)_2\}_2]$ qui cristallise dans le groupe d'espace monoclinique $P2_1/n$ avec a = 13,814(7), b = 11,429(4), c = 10,726(5) Å, β = 106,30(5)°. Les réactions du $P(OEt)_2Cl$ ou du $(EtO)_2POP(OEt)_2$ avec le $[Pt_2Cl_4(PEt_3)_2]$ donnent également des produits que l'on peut hydrolyser très facilement. Mais, dans ces cas, on obtient des condensations beaucoup plus complexes qui conduisent au $[Cl_2Pt\{\mu\text{-}(P(OEt)_2O)_2P(O)\}PtCl(PEt_3)_2]$ qui cristallise dans le groupe d'espace monoclinique $P2_1/c$ avec a = 17,547(8), b = 19,775(6), c = 11,268(3) Å, β = 106,42(3)°. On rapporte les études complètes de diffractions par rayon X pour les deux cristaux. Ces études confirment la présence d'un pont double de $(EtO)_2POP(OEt)_2$ dans le composé $[Pt_2Cl_4\{\mu\text{-}(EtO)_2POP(OEt)_2\}_2]$ et d'un nouveau pont triphosphite dans le composé $[Cl_2Pt\{\mu\text{-}(P(OEt)_2O)_2P(O)\}PtCl(PEt_3)_2]$. On décrit également une analyse détaillée et une simulation par ordinateur des spectres de rmn du $^{31}P\{^1H\}$ et du $^{195}Pt\{^1H\}$ de ces complexes ainsi que l'étude des composés apparentés du type $[Pt_2Me_4\{\mu\text{-}(EtO)_2POP(OEt)_2\}_2]$ et $[Cl_2(Et_3P)Pt\{\mu\text{-}(EtO)_2POP(OEt)_2\}PtCl_2(PEt_3)]$. Conjointement avec les études antérieures sur le $[Pt_2Cl_2(dppm)_2]$ et des complexes apparentés, ces spectres fournissent des exemples de plusieurs types de systèmes de spin *AA'XX'* et on discute en détail de l'analyse de ces systèmes.

[Traduit par le journal]

Introduction

The coordination chemistry of chlorophosphines and organophosphites is often complicated by the reactivity of the P—Cl and P—OR bonds. For example the solvolytic degradation of triorganophosphite ligands, $P(OR)_3$, to metal phosphite or phosphonate derivatives, $MOP(OR)_2$ or $MP(O)(OR)_2$,[2] has been known for a long time (1). More recently, similar transformations have been demonstrated to occur by methyl transfer to a metal and by a metal-catalyzed Arbuzov rearrangement (2), and in other processes trimethylphosphites have been converted to the unusual $P(OMe)_2$ and P(OMe) ligands (2–5). Reactions in which phosphorus(III) compounds condense and coordinate are also known. The simplest example is the reaction of phosphorous acid with K_2PtCl_4, which results in a bidentate ligand, O_2POPO_2, bridging two platinum atoms by phosphorus coordination (6, 7). A related ligand, $(MeO)_2POP(OMe)O$, is formed in one of the pyrolysis products of $[Os_3(CO)_{11}\{P(OMe)_3\}]$ but it bridges three Os centres by phosphorus and oxygen coordination (4, 8). Clearly solvolysis of P—Cl bonds can lead to analogous reactive $P—O^-$ and P—OR linkages and the chemistry of P—Cl bonds is also of considerable interest because this group is the most usual choice of reactive function for the elaboration of phosphorus ligands. Reactions with alcohols to form phosphorus esters and with Grignard or organolithium reagents to form phosphorus–carbon bonds are particularly well-studied examples. Reactions of coordinated chlorophosphines are less well studied and their potential for the *in situ* elaboration of ligands or the formation of bridges to other metal centres has not in general been realized.

We have been particularly interested in the chemistry arising when two chlorophosphine ligands occupy mutually *cis* positions in a coordination shell, and have discussed the literature background in some detail in a previous paper (9). Briefly, the expected first hydrolysis product of a *cis*-$M(PR_2Cl)_2$ fragment is a simple *cis*-$M(PR_2OH)_2$ group but in practice such simple products are rarely isolated. The most usual outcome is a fragment such as structure **I**, derived from deprotonation of the initial hydrolysis product, and examples have been reported for several metals, notably Pd (10, 11), Pt (10), Mo (11, 12), Ir (13, 14), and Rh (13). A second possibility is illustrated by the ready conversation of *cis*-$[Mo(CO)_4\{(PPh_2O)_2H\}]^-$ to *cis*-

[1]Author to whom correspondence may be addressed.

[2]The majority of authors have referred to both tautomers as phosphonates although strict nomenclature (Chem Abstr **76**, Index Guide section IV, paragraph 197) would seem to require that $MOP(OR)_2$ or $MOP(OR)_2M'$ bonding arrangements be named as derivatives of phosphorous acid and $MP(O)(OR)_2$ as derivatives of phosphonic acid.

$[Mo(CO)_4(Ph_2POPPh_2)]$ by elimination of hydroxide in an acid medium (15, 16). Ligands of the type R_2POPR_2 are capable of chelation (structure **II**) but more usually occur as bridge ligands (structure **III**) (15).

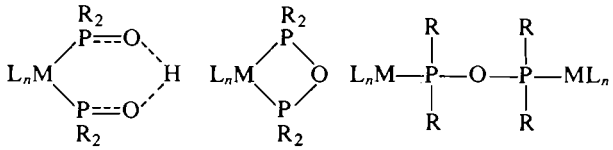

I **II** **III**

In our previous work (9), we describe X-ray diffraction studies of *cis*-$[PtCl_2(PPh_2OH)_2]$, the first well-characterized example of a *cis*-bis(hydroxyphosphine) complex, and of $[Pd_2(\mu\text{-}Cl)_2\{(P(OEt)_2O)_2H\}_2]$, an example of a type **I** complex. A primary objective of our work is to obtain good structural characterization for all possible hydrolysis products of chlorophosphine complexes, and in the present paper we describe two further structure determinations together with associated synthetic and spectroscopic results. Compound **IV**, $[Pt_2Cl_4\{\mu\text{-}(EtO)_2POP(OEt)_2\}_2]$, is readily obtained by hydrolysis of *cis*-$[PtCl_2\{P(OEt)_2Cl\}_2]$ in a reaction closely related to that mentioned above for molybdenum. In contrast to the chelate Ph_2POPPh_2 in the Mo case (15), the platinum complex is dinuclear with two bridging $(EtO)_2POP(OEt)_2$ ligands. Compound **VII**, $[Cl_2Pt\{\mu\text{-}(P(OEt)_2O)_2P(O)\}PtCl(PEt_3)_2]$, is a novel derivative of the unknown triphosphorous acid, $H_5P_3O_7$, and its formation is of especial interest since reactivity of both P—Cl and P—OR bonds is involved, leading to a ligand condensation to produce a more complex ligand than that initially present. This appears to be the first well-characterized complex involving condensation of more than two phosphorus units and we also note that tri- and polyphosphites are very rare even in simple phosphorus chemistry (17). A preliminary description of the structure and spectroscopy of **VII** has been published (18).

Results and discussion

(a) Synthesis

As we have described previously, complexes of the type *cis*-$[MCl_2(PR_2Cl)_2]$, M = Pt or Pd, are readily prepared by reactions of chlorophosphines with $[MCl_2(PhCN)_2]$ (9). However, the products are very easily hydrolyzed and the final outcome of the reactions under normal laboratory conditions is critically dependent on the nature of R and M. For example, for R = Ph and M = Pt we were able to isolate *cis*-$[PtCl_2(PPh_2OH)_2]$, the first well-characterized example of a *cis*-bis(hydroxyphosphine) complex, and to demonstrate its conversion to a type **I** complex, $[Pt_2Cl_2\{(PPh_2O)_2H\}_2]$ (9). When R = OEt and M = Pt the initial product, *cis*-$[PtCl_2\{P(OEt)_2Cl\}_2]$, is obtained as a colourless oil but, even when normal laboratory precautions against admission of moisture were taken, attempts at crystallization resulted in hydrolysis and condensation to a product whose initial spectroscopy suggested structure **IV**. Complex **IV** has been prepared previously by reaction of $(EtO)_2POP(OEt)_2$ with $[PtCl_2(SEt_2)_2]$ (19) and in the present work we have used $[PtCl_2(PhCN)_2]$ as the platinum substrate in an analogous reaction to confirm the nature of the above hydrolysis product.

The spectroscopy and structure of the bis(diphenylphosphino)methane (dppm) complexes **V** and **VI** have been extensively studied (20, 21). Complex **IV** is a close relative of these species except that the dppm derivatives normally have *trans* stereochemistry at the platinum centres (20), whereas previous work on **IV** had suggested that it has *cis* stereochemistry (19).

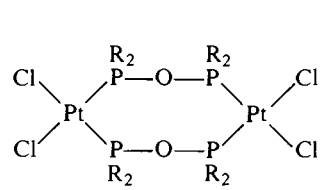

IV (R = OEt)

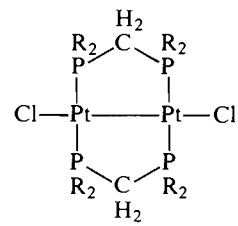

V (R = Ph)

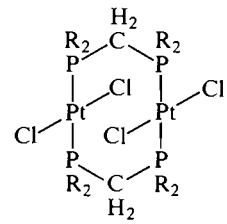

VI (R = Ph)

We therefore undertook a detailed study with the dual objectives of confirming the nature of our hydrolysis product and of establishing the structure and spectroscopy of these *cis* derivatives. In order to study variation of spectroscopic parameters with *trans* influence we also synthesized the tetramethyl analogue of **IV** by reaction of $(EtO)_2POP(OEt)_2$ with $[PtMe_2(COD)]$ and by reaction of $[Pt_2Cl_4\{\mu\text{-}(EtO)_2POP(OEt)_2\}_2]$ with methyl Grignard. Details of the spectroscopic and structure studies are reported below together with results on $[Cl_2(Et_3P)Pt\{\mu\text{-}(EtO)_2POP(OEt)_2\}PtCl_2(PEt_3)]$. This last complex is prepared by reaction of $(EtO)_2POP(OEt)_2$ with $[Pt_2Cl_4(PEt_3)_2]$ in benzene under carefully controlled anhydrous conditions. As discussed below, the reaction is more complex if traces of moisture are present.

The hydrolysis of the related monochlorophosphine complexes, *cis*-$[PtCl_2(PEt_3)(PR_2Cl)]$, is normally straightforward and results simply in *cis*-$[PtCl_2(PEt_3)(PR_2OH)]$ derivatives (9). However, the reaction of $P(OEt)_2Cl$ with $[Pt_2Cl_4(PEt_3)_2]$ provided a striking demonstration of the lability of P—Cl and P—OEt moities in these systems. Normally, *cis*-$[PtCl_2(PEt_3)\{P(OEt)_2Cl\}]$ was obtained from this reaction (9), but on one occasion colourless crystals of complex **VII** were obtained. Several attempts to repeat this preparation have failed, probably because the formation of **VII** depends critically on such factors as the moisture content and hydrogen chloride concentration. However, we were able to characterize **VII** completely by nmr

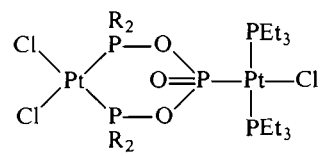

VII (R = OEt)

spectroscopy and by X-ray crystallography on the sample initially obtained, and we have found subsequently that **VII** can be obtained, apparently reproducibly, from reactions of $(EtO)_2POP(OEt)_2$ with $[Pt_2Cl_4(PEt_3)_2]$ in dichloromethane solution. Note that under rigorously anhydrous conditions in benzene this same reaction yields $[Cl_2(Et_3P)Pt\{\mu\text{-}(EtO)_2POP(OEt)_2\}PtCl_2(PEt_3)]$ as described above. Details of the ^{31}P and ^{195}Pt nmr spectra of **VII** have been published in a preliminary communication (18) and no further comment is necessary here. The data are included in Table 1.

TABLE 1. Phosphorus-31 and platinum-195 nuclear magnetic resonance parameters

Parameter	A	B	C	D
δ(P)	+120.15	+55.62	+55.12 $P(OEt)_2$ +14.68 PEt_3	+50.27 $P(OEt)_2$ +19.96 PEt_3 +37.02 P=O
^2J(P–Pt–P)	−23.1	−15	−22.2	25.6
^2J(P–O–P)	58.7	72	56.4	22.0
^4J(P–P)	+2.9	−5	~0	~0
^6J(P–P)			~0	
δ(Pt)	+32.64	+232.32	+106.33	+187.35 $PtCl_2P_2$ −99.49 $PtClP_3$
Ξ(Pt)	21.400699	21.404972	21.402275	21.404009 $PtCl_2P_2$ 21.397871 $PtClP_3$
^1J(Pt–P)	+3037.1	+5836.0	+6186.2 $P(OEt)_2$ +3287.4 PEt_3	5408.3 $P(OEt)_2$ 2322.4 PEt_3 6063.2 P=O
^3J(Pt–P)	+4.4	+54.0	~0	93.4 $P(OEt)_2$ ~0 P=O
^5J(Pt–P)			~0	
^4J(Pt–Pt)	<200	~270	<150	363

A = $[Pt_2Me_4(\mu\text{-}(EtO)_2POP(OEt)_2\}_2]$ in C_6D_6.
B = $[Pt_2Cl_4(\mu\text{-}(EtO)_2POP(OEt)_2\}_2]$, **IV**, in $CDCl_3$.
C = $[Cl_2(Et_3P)Pt\{\mu\text{-}(EtO)_2POP(OEt)_2\}PtCl_2(PEt_3)]$ in $CDCl_3$.
D = $[Cl_2Pt\{\mu\text{-}(P(OEt)_2O)_2P(O)\}PtCl_2(PEt_3)_2]$, **VII**, in $CDCl_3$.
NOTE: Chemical shifts (δ) are quoted in parts per million relative to 85% H_3PO_4 for phosphorus and relative to Ξ(^{195}Pt) = 21.4 MHz for platinum (see ref. 33). For the platinum resonances the absolute values of Ξ in MHz are also quoted. Coupling constants (J) are in Hz.

(b) Nuclear magnetic resonance

As we have pointed out above, the complexes **IV–VI**, are all closely related from the point of view of nmr spectroscopy, since each has the basic connectivity shown in **VIII**. To analyze the spectra it is necessary to recognize the existence of three distinct isotopomeric structures in each case, having respectively none, one, or two magnetically active ^{195}Pt atoms. Since platinum-195 is 33.8% abundant, these three isotopomers are respectively 43.9, 44.8, and 11.4% of the total sample. From the point of view of $^{31}P\{^1H\}$ spectroscopy the four chemically equivalent, but magnetically inequivalent, phosphorus atoms of the "no-^{195}Pt" isotopomer constitute an $AA'A''A'''$ spin system, as indicated in structure **VIII**, and contribute only a single central

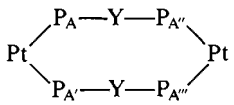

VIII

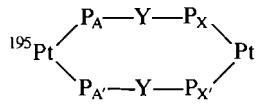

IX

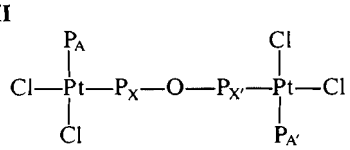

X

peak to the spectrum. The spectrum due to the "one-^{195}Pt" isotopomer is more interesting and analyses for the complexes of types **V** and **VI** have generally depended on a suggestion made by Sheppard and Turner in the early days of nmr (22). These authors were concerned with the ^{1}H spectra of ^{13}C enriched ethylene and pointed out that in an $H_2{}^{13}C{=}CH_2$ molecule the presence of the ^1J(C–H) coupling introduces an "effective chemical shift" difference between the two pairs of protons. Under these circumstances each ^{13}C satellite may be analyzed as half of an $AA'XX'$ spin system. The present complexes are clearly fundamentally similar spin systems and their ^{31}P spectra (see Fig. 2A for example) may be divided into three distinct regions: downfield and upfield satellites due to ^1J(Pt–P) and a central region containing the "no-^{195}Pt" singlet together with sidebands due to ^3J(Pt–P). Each of the satellite regions consists of one half of an $AA'XX'$ system as defined in structure **IX**, together with a single line contributed by the "two-^{195}Pt" isotopomer. The upfield and downfield lines of the "two-^{195}Pt" isotopomer are separated by ^1J(Pt–P) + ^3J(Pt–P) (21).

In their analysis of the $AA'XX'$ spin system, Pople *et al.* (23) define four secondary parameters:

$$K = J(AA') + J(XX')$$
$$M = J(AA') - J(XX')$$
$$N = J(AX) + J(AX')$$
$$L = J(AX) - J(AX')$$

Each half (A or X) of the spectrum then consists of a strong doublet separated by N and two symmetrical quartets. The line positions of the first quartet relative to the centre of the N doublet are given by:

$$\tfrac{1}{2}K + \tfrac{1}{2}(K^2 + L^2)^{1/2}$$
$$-\tfrac{1}{2}K + \tfrac{1}{2}(K^2 + L^2)^{1/2}$$
$$\tfrac{1}{2}K - \tfrac{1}{2}(K^2 + L^2)^{1/2}$$
$$-\tfrac{1}{2}K - \tfrac{1}{2}(K^2 + L^2)^{1/2}$$

and the other quartet is identical except that M replaces K.

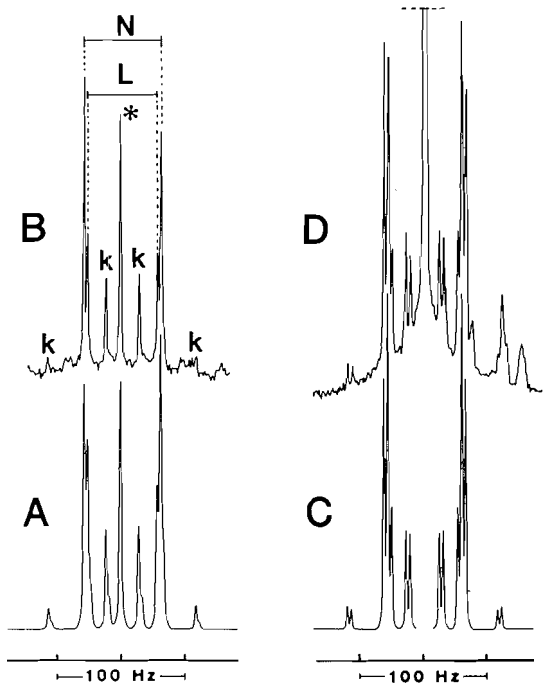

FIG. 1. $^{31}P\{^1H\}$ nuclear magnetic resonance spectrum of $[Pt_2Me_4\{\mu\text{-}(EtO)_2POP(OEt)_2\}_2]$ in C_6D_6 at 101.3 MHz. (A) Computer simulation of downfield ^{195}Pt satellite. (B) Observed downfield ^{195}Pt satellite. The peaks marked k are due to the K/L quartet and the meanings of K, L, N, and * are discussed in the text. (C) Computer simulation of central region. The very intense central peak has been omitted to facilitate plotting of the weaker components. (D) Observed spectrum of central region.

In the present examples, $J(AA') = J(XX')$, and it follows that $M = 0$ and the M/L quartet collapses to a doublet of separation L (21). Moreover, if the phosphorus atoms are mutually *trans* at the platinum centres then $J(AA')$ and $J(XX')$ are much larger than the other coupling constants and the K/L quartet collapses to a single central line (21). However, since the literature contains some apparent mis-assignments of spectra which depend on this point,[3] it is also important to realize that the inner (stronger) lines of the K/L quartet are always separated by the difference in magnitude of K and $(K^2 + L^2)^{1/2}$. This is easily demonstrated by reference to the line positions and especially the intensities (23) of the K/L quartet. Thus the *maximum* possible separation of the two strong lines is equal to L.

(i) $[Pt_2Me_4\{\mu\text{-}(EtO)_2POP(OEt)_2\}_2]$

The $^{31}P\{^1H\}$ spectrum of this complex is shown in Fig. 1. The overall spectrum is basically similar in form to the example shown in Fig. 2A, with downfield and upfield satellites and an intense central region but, in order to show the weaker features in detail, only the downfield satellite and the central region are illustrated in Fig. 1. The upfield satellite is a mirror image of the downfield satellite. This is perhaps the simplest of the current spectra to assign since all of the lines of the "half $AA'XX'$" pattern can be seen in the platinum satellites. The line marked with an asterisk is not symmetrical with respect to the other lines and cannot therefore be part of the $AA'XX'$ pattern. It is actually due to the "two-^{195}Pt" isotopomer. Remembering that the strong lines of the K/L quartet must be "inside" the L doublet, the assignment shown in Fig. 1B follows immediately and we can calculate all three P–P coupling constants. The separation between the "one-^{195}Pt" satellites gives $^1J(Pt–P)$ and the separation between the asterisked line and its upfield counterpart gives $^1J(Pt–P) + {}^3J(Pt–P)$ (21) so that all the parameters for a full computer simulation and refinement are available except for $^4J(Pt–Pt)$, which has little effect on the phosphorus spectrum. The results of this simulation with the contributions from all three isotopomers added together are shown in Figs. 1A and 1C and the final refined parameters are collected in Table 1. Also included in Table 1 are the parameters for the $^{195}Pt\{^1H\}$ spectrum, which was a simple triplet (J = 3039 Hz), confirming the value of $^1J(Pt–P)$. The line width in this ^{195}Pt spectrum did not allow resolution of $^4J(Pt–Pt)$ but the broadening at the base of the peaks suggested an upper limit of about 200 Hz for this parameter.

(ii) $[Pt_2Cl_4\{\mu\text{-}(EtO)_2POP(OEt)_2\}_2]$

This spectrum is more difficult to assign because of the lack of resolution in the satellite bands (Figs. 2B and 2D). The first problem was to decide which peak is due to the "two-^{195}Pt" isotopomer. This was accomplished using the ^{195}Pt spectrum, which showed two coupling constants (±5840 and ±50.5 Hz) whose sum was equal to the separation between the asterisked peaks in Fig. 2. Unfortunately, the L doublet and the inner lines of the K/L quartet are seen only as poorly defined shoulders on the N doublet, but the requirement that the K/L lines must be inside the L doublet identifies the K/L quartet as the lines marked k in Fig. 2B. The L doublet must then be the cause of the barely perceptible shoulders on the outside of the N doublet, implying that L is slightly greater than N. Refinement of this assignment presents a difficulty since the values for K and L are obviously very approximate because of the lack of resolution. However, using the parameters given in Table 1, a summation of the spectra of all three isotopomers gave a completely satisfactory computer simulation, which is shown in Figs. 2C and 2E. The broad, weak outer features of the satellite spectra are due to the "two-^{195}Pt" isotopomer and their position is very dependent on the value of $^4J(Pt–Pt)$. However, it is clear that the refined value of this parameter is rather approximate, as are all the P–P couplings. The choices given in Table 1 represent the centres of the acceptable ranges which are about ±3 Hz wide for the P–P couplings and perhaps ±20 Hz for the Pt–Pt coupling.

The $^{195}Pt\{^1H\}$ spectrum of $[Pt_2Cl_4\{\mu\text{-}(EtO)_2POP(OEt)_2\}_2]$ consisted of a triplet of triplets due to $^1J(Pt–P)$ and $^3J(Pt–P)$ with additional weak, poorly resolved sidebands due to $^4J(Pt–Pt)$.

(iii) $[Cl_2(Et_3P)Pt\{\mu\text{-}(EtO)_2POP(OEt)_2\}PtCl_2(PEt_3)]$

The analysis of the $^{31}P\{^1H\}$ spectrum of this complex is basically similar to those described above except that in this case the phosphorus atoms belong to an $AA'XX'$ spin system even in the absence of magnetically active platinum (structure **X**). Thus the overall spectrum consists of central A and X resonances (Figs. 3B and 3D), each with platinum satellites which are not shown in the figure. Also in this case $J(AA')$ and $J(XX')$ are no longer equal and the M/L quartet does not collapse to a doublet. Thus the central X region shown in Fig. 3B arises primarily from the "no-^{195}Pt" isotopomer and the strong pair of lines inside the N doublet can only be explained if the M/L and K/L

[3]For example, the complexes $[Pt_2R_4(\mu\text{-}Me_2PCH_2PMe_2)_2]$, R = Me or CCMe, both show only two rather weak lines inside an unusually intense N doublet. The two inner lines have been previously assigned to the L doublet (24, 25) but it seems more likely that the correct assignment has $L \simeq N$ and the inner lines are the inner components of the K/L quartet.

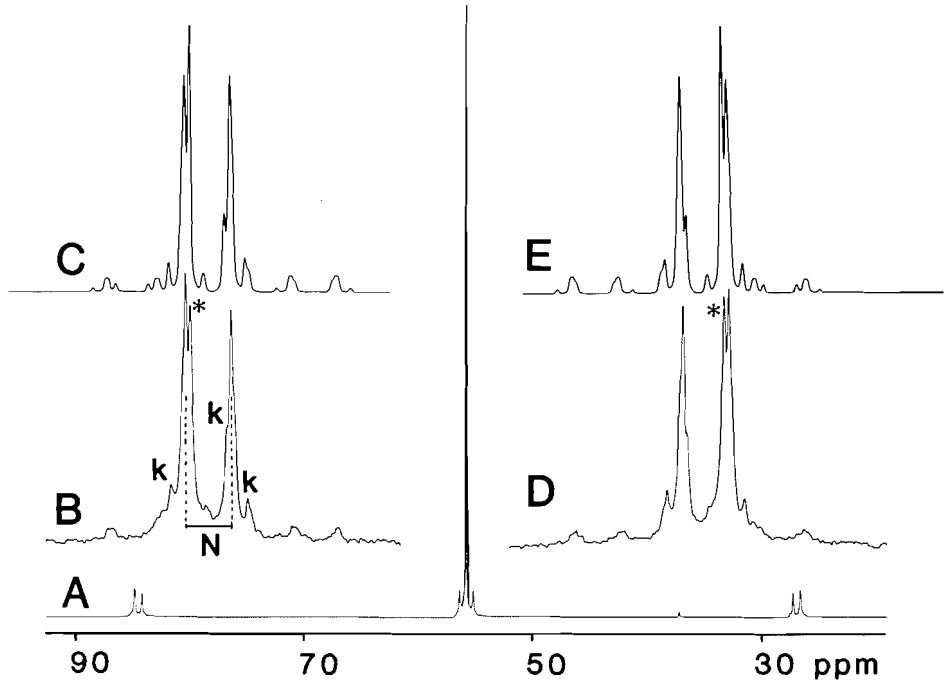

FIG. 2. $^{31}P\{^1H\}$ nuclear magnetic resonance spectrum of $[Pt_2Cl_4\{\mu\text{-}(EtO)_2POP(OEt)_2\}_2]$ in $CDCl_3$ at 101.3 MHz. (A) Complete spectrum showing the three regions; downfield and upfield ^{195}Pt satellites and the intense central region. (B) 20 Hz cm^{-1} expansion of the downfield ^{195}Pt satellite. The peaks marked k are due to the K/L quartet and the meanings of K, L, N, and * are discussed in the text. (C) Computer simulation of downfield ^{195}Pt satellite. (D) 20 Hz cm^{-1} expansion of the upfield ^{195}Pt satellite. The meaning of * is discussed in the text. (E) Computer simulation of upfield ^{195}Pt satellite.

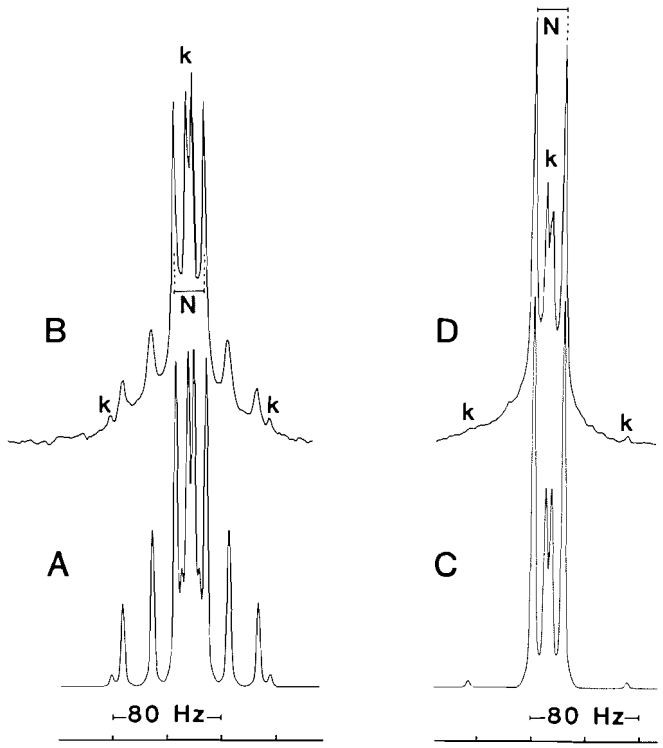

FIG. 3. $^{31}P\{^1H\}$ nuclear magnetic resonance spectrum of $[Cl_2(Et_3P)Pt\{\mu\text{-}(EtO)_2POP(OEt)_2\}PtCl_2(PEt_3)]$ in $CDCl_3$ at 101.3 MHz. Only the central $P(OEt)_2$ and PEt_3 resonances are shown. ^{195}Pt satellites are not illustrated. (A) Computer simulation of central $P(OEt)_2$ resonance. (B) Central $P(OEt)_2$ resonance at 55.12 ppm. The peaks marked k are due to the approximately coincident M/L and K/L quartets and the meanings of K, M, L, and N are discussed in the text. (C) Computer simulation of central PEt_3 resonance. (D) Central PEt_3 resonance at 14.68 ppm.

quartets are essentially coincident; i.e., $J(AA') \ll J(XX')$, which is entirely reasonable since the former is a six-bond and the latter a two-bond coupling. We also assumed that $^4J(AX') \ll {}^2J(AX)$, making N and L approximately equal. In order to calculate K ($= M$) it is necessary to identify the other components of the coincident quartets in Fig. 3B. These outer components should also occur in the central A resonance (Fig. 3D) but in fact no subsidiary peaks have significant intensity in Fig. 3D. This suggested that the weakest of the three pairs of subsidiary peaks in Fig. 3B was the correct choice for the outer components of the K/L quartet. On this basis we proceeded to calculate $^2J(AX)$ and $^2J(XX')$. The $^{195}Pt\{^1H\}$ spectrum consisted of a doublet of doublets due to the one-bond Pt–P couplings and a slight broadening of the peaks suggested that ^3J(Pt–P) is about 20 Hz. This gave all the parameters necessary to refine and simulate the contributions of the "no-^{195}Pt" and "one-^{195}Pt" isotopomers and essentially gave a complete explanation of the spectrum since the "two-^{195}Pt" isotopomer makes only a very small contribution. The final simulation (Figs. 3A and 3C) included this small contribution assuming that ^4J(Pt–Pt) is 0 Hz. The actual value of ^4J(Pt–Pt) is not critical for the interpretation of the ^{31}P spectrum but the line width in the ^{195}Pt spectrum suggested that it is <150 Hz.

(iv) Signs and magnitudes of coupling constants

The parameters listed in Table 1 present no particular surprises. The *cis* geometry at platinum in all four complexes is confirmed by the small magnitudes (15–23 Hz) found for ^1J(Pt–Pt) and, although the sign is not determined by the observed spectra, the values are probably negative in view of previous results (26). The magnitudes of ^1J(Pt–P) reflect the electronegativity of the groups attached to phosphorus and the known *trans* influences of the ligands occupying the *trans* position in the platinum coordination. Thus ^1J(Pt–P) for PEt_3 *trans* to Cl in $[Cl_2(Et_3P)Pt\{\mu\text{-}(EtO)_2POP(OEt)_2\}PtCl_2(PEt_3)]$ is

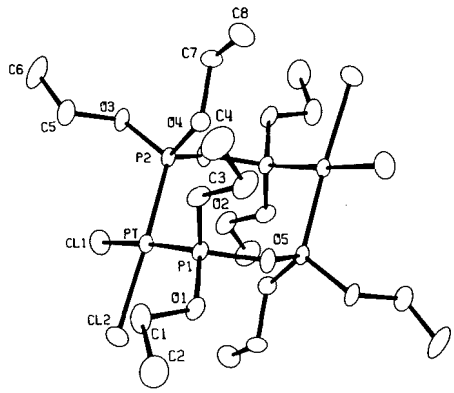

FIG. 4. ORTEP plot of **IV**, $[Pt_2Cl_4\{\mu\text{-}(EtO)_2POP(OEt)_2\}_2]$. The unlabelled half of the molecule is related to the labelled half by a crystallographic centre of symmetry.

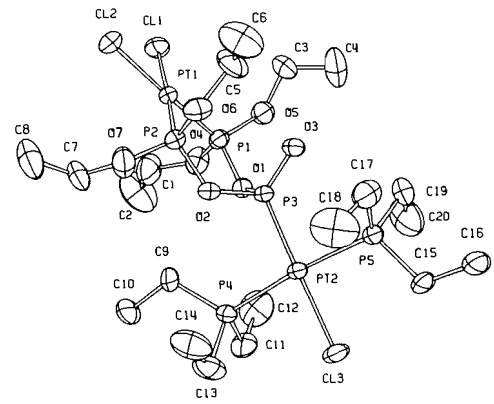

FIG. 5. ORTEP plot of **VII**, $[Cl_2Pt\{\mu\text{-}(P(OEt)_2O)_2P(O)\}PtCl(PEt_3)_2]$.

3287 Hz compared to 2322 Hz when PEt_3 is *trans* to phosphorus in $[Cl_2Pt\{\mu\text{-}(P(OEt)_2O)_2P(O)\}PtCl(PEt_3)_2]$. Corresponding values for the $P(OEt)_2$ groups are larger, reflecting the electronegativity of the ethoxy substituents, and range from 5408 to 6186 Hz when *trans* to Cl, to 3037 Hz *trans* to methyl. Interestingly, ^3J(Pt–P) also shows a very marked change with *trans* influence, decreasing from 54 Hz when *trans* to Cl in $[Pt_2Cl_4\{\mu\text{-}(EtO)_2POP(OEt)_2\}_2]$, to only 4.4 Hz *trans* to methyl in $[Pt_2Me_4\{\mu\text{-}(EtO)_2POP(OEt)_2\}_2]$. The sometimes very high sensitivity of long-range couplings to *trans*-influence effects has been noted previously (27). The observed spectra for $[Pt_2Cl_4\{\mu\text{-}(EtO)_2POP(OEt)_2\}_2]$ and its methyl analogue require that ^1J(Pt–P) and ^3J(Pt–P) have the same sign and, since directly bonded Pt–P couplings are known to be positive (28), it follows that the three-bond couplings are also positive. This is a difference between our analysis and a previous approximate interpretation of the ^{31}P spectrum of $[Pt_2Cl_4\{\mu\text{-}(EtO)_2POP(OEt)_2\}_2]$ (19) and it also leads to somewhat different P–P couplings from those suggested previously. The observed spectra also require that ^1J(P–O–P) and ^4J(P–P) have like signs in $[Pt_2Cl_4\{\mu\text{-}(EtO)_2POP(OEt)_2\}_2]$, and opposite signs in $[Pt_2Me_4\{\mu\text{-}(EtO)_2POP(OEt)_2\}_2]$, but the signs of these pairs relative to other couplings are not determined.

No sign information is available from the spectra of $[Cl_2(Et_3P)Pt\{\mu\text{-}(EtO)_2POP(OEt)_2\}PtCl_2(PEt_3)]$ and $[Cl_2Pt\{\mu\text{-}(P(OEt)_2O)_2P(O)\}PtCl(PEt_3)_2]$.

(c) Structures of $[Pt_2Cl_4\{\mu\text{-}(EtO)_2POP(OEt)_2\}_2]$, (IV), and $[Cl_2Pt\{\mu\text{-}(P(OEt)_2O)_2P(O)\}PtCl(PEt_3)_2]$, (VII)

The atomic labelling schemes and the structures of single molecules of the complexes **IV** and **VII** are shown in Figs. 4 and 5 respectively. Fractional atomic coordinates and isotropic temperature parameters, bond lengths, and bond angles are collected in Tables 2–4 and 5–7 respectively. Further tables of anisotropic temperature factors, structure factors, and selected intermolecular distances for both compounds have been deposited,[4] together with a table of mean plane information for **VII**.

The structure of **IV** consists of two square planar platinum centres linked by a pair of *cis* $(EtO)_2POP(OEt)_2$ bridges so as to form an eight-membered ring which lies in an extended chair conformation. There is a crystallographic centre of symmetry at the centre of the ring. The Pt—P bonds are relatively short (av. 2.20 Å; 1 Å = 0.1 nm) compared with many previous examples (29), but this is not unexpected in view of the low *trans* influence of the chloride ligand and the high electronegativity of the ethoxy substituents. It appears that this electronegativity also reduces the *trans* influence of the phosphorus ligand since the Pt—Cl bonds (av. 2.34 Å) are also somewhat shorter than is

TABLE 2. Fractional atomic coordinates and temperature parameters for compound **IV**

Atom	*x/a*	*y/b*	*z/c*	U_{eq}
Pt	−3636(2)	31524(2)	106352(3)	310(1)
Cl(1)	−1537(2)	3173(2)	11839(3)	600(11)
Cl(2)	−1280(2)	1610(2)	9422(3)	579(9)
P(1)	615(2)	3205(2)	9336(2)	317(7)
P(2)	363(2)	4611(2)	11898(2)	317(7)
O(1)	531(5)	2202(5)	8310(5)	43(2)
O(2)	1753(4)	3336(5)	10025(6)	42(2)
O(3)	500(5)	4496(5)	13384(5)	43(2)
O(4)	1392(4)	5008(5)	11731(5)	38(2)
O(5)	330(5)	4241(5)	8285(6)	40(2)
C(1)	927(10)	1010(8)	8727(11)	64(5)
C(2)	985(14)	338(10)	7558(13)	89(7)
C(3)	2502(8)	3647(12)	9336(10)	61(4)
C(4)	3519(10)	3183(12)	10072(15)	83(6)
C(5)	943(9)	3424(9)	14126(11)	59(4)
C(6)	1047(12)	3642(13)	15463(11)	84(5)
C(7)	2066(7)	5841(7)	12618(9)	48(3)
C(8)	3017(8)	5917(11)	12211(12)	69(5)

NOTE: Estimated standard deviations are given in parentheses. Coordinates $\times 10^n$ where $n = 5$ for Pt and $n = 4$ otherwise. Temperature parameters $\times 10^n$ where $n = 3$ for C and O and $n = 4$ otherwise. U_{eq} = the equivalent isotropic temperature parameter. $U_{eq} = \frac{1}{3}\Sigma_i\Sigma_u U_{ij}a_i^*a_j^*(a_i\cdot a_j)$.

TABLE 3. Interatomic distances for compound **IV**

Atoms	Distance (Å)	Atoms	Distance (Å)
Cl(1)—Pt	2.338(3)	P(1)—Pt	2.198(3)
Cl(2)—Pt	2.340(2)	P(2)—Pt	2.204(2)
O(1)—P(1)	1.570(6)	O(3)—P(2)	1.557(6)
O(2)—P(1)	1.545(6)	O(4)—P(2)	1.549(6)
O(5)—P(1)	1.605(6)	O(5)—P(2′)	1.604(6)
C(1)—O(1)	1.489(11)	C(5)—O(3)	1.495(11)
C(3)—O(2)	1.475(12)	C(7)—O(4)	1.476(9)
C(2)—C(1)	1.491(15)	C(6)—C(5)	1.422(16)
C(4)—C(3)	1.502(16)	C(8)—C(7)	1.498(16)

Estimated standard deviations are given in parentheses.

[4]Copies of these tables may be purchased from the Depository of Unpublished Data, CISTI, National Research Council of Canada, Ottawa, Ont., Canada, K1A 0S2.

TABLE 4. Bond angles for compound **IV**

Atoms	Angle (°)	Atoms	Angle (°)
Cl(2)—Pt—Cl(1)	87.9(1)	P(2)—Pt—P(1)	96.5(1)
P(2)—Pt—Cl(1)	85.4(1)	P(1)—Pt—Cl(2)	90.1(1)
P(1)—Pt—Cl(1)	174.1(1)	P(2)—Pt—Cl(2)	173.3(1)
O(1)—P(1)—Pt	119.1(3)	O(3)—P(2)—Pt	117.9(2)
O(2)—P(1)—Pt	115.0(3)	O(4)—P(2)—Pt	115.2(2)
O(5)—P(1)—Pt	113.0(2)	O(4)—P(2)—O(3)	106.9(4)
O(2)—P(1)—O(1)	105.8(4)	P(1)—O(5)—P(2′)	135.2(4)
O(5)—P(1)—O(1)	95.2(3)		
O(5)—P(1)—O(2)	106.3(4)		
C(1)—O(1)—P(1)	120.5(6)	C(5)—O(3)—P(2)	121.9(6)
C(3)—O(2)—P(1)	123.1(6)	C(7)—O(4)—P(2)	123.2(6)
C(2)—C(1)—O(1)	108.7(9)	C(6)—C(5)—O(3)	107.7(9)
C(4)—C(3)—O(2)	109.6(9)	C(8)—C(7)—O(4)	107.2(8)

Estimated standard deviations are given in parentheses.

TABLE 5. Fractional atomic coordinates and temperature parameters for compound **VII**

Atom	x/a	y/b	z/c	U_{eq}
Pt(1)	26201(3)	−11069(2)	151(4)	599(2)
Pt(2)	25296(4)	6654(3)	41434(4)	689(2)
Cl(1)	3612(3)	−1496(2)	−843(4)	93(2)
Cl(2)	1664(3)	−1651(2)	−1570(3)	94(2)
Cl(3)	2604(5)	1156(2)	6090(4)	158(4)
P(1)	3575(2)	−614(2)	1448(3)	63(1)
P(2)	1618(2)	−772(2)	696(3)	63(1)
P(3)	2523(2)	227(2)	2348(3)	60(1)
P(4)	2737(3)	−350(2)	5254(3)	74(1)
P(5)	2283(3)	1723(2)	3211(3)	79(2)
O(1)	3321(4)	−234(4)	2527(7)	63(3)
O(2)	1851(5)	−373(4)	1989(7)	63(3)
O(3)	2460(6)	651(4)	1253(8)	78(4)
O(4)	4252(6)	−1079(5)	2227(11)	98(5)
O(5)	4094(6)	−82(5)	1008(9)	93(4)
O(6)	967(6)	−316(6)	−212(8)	92(4)
O(7)	1080(7)	−1333(5)	994(12)	108(5)
C(1)	4194(16)	−1780(10)	2392(22)	150(12)
C(2)	4810(16)	−2103(15)	3202(32)	214(18)
C(3)	3800(12)	296(9)	−195(16)	113(9)
C(4)	4202(15)	952(10)	−35(30)	167(15)
C(5)	1162(12)	102(11)	−1143(17)	130(9)
C(6)	421(12)	374(14)	−1884(22)	173(13)
C(7)	1273(9)	−1994(8)	1354(16)	100(7)
C(8)	622(12)	−2449(11)	703(23)	155(11)
C(9)	2765(10)	−1144(7)	4455(14)	90(7)
C(10)	2928(12)	−1774(8)	5304(16)	110(8)
C(11)	3673(13)	−315(10)	6497(14)	113(8)
C(12)	4355(13)	−262(15)	5953(25)	171(14)
C(13)	2020(13)	−437(11)	6123(19)	122(10)
C(14)	1178(14)	−487(14)	5150(23)	160(14)
C(15)	2185(14)	2382(8)	4260(15)	127(10)
C(16)	1957(19)	3094(10)	3716(18)	169(15)
C(17)	1400(11)	1780(9)	1916(16)	110(8)
C(18)	671(14)	1481(18)	2330(28)	199(17)
C(19)	3062(12)	2024(8)	2560(17)	112(9)
C(20)	3895(16)	1958(15)	3523(27)	189(15)

NOTE: Estimated standard deviations are given in parentheses. Coordinates $\times 10^n$ where $n = 5$ for Pt and $n = 4$ for the other atoms. Temperature parameters $\times 10^n$ where $n = 4$ for Pt and 3 otherwise. U_{eq} = the equivalent isotropic temperature parameter. $U_{eq} = \frac{1}{3}\Sigma_i\Sigma_j U_{ij} a_i^* a_j^* (a_i \cdot a_j)$.

TABLE 6. Bond lengths for compound **VII**

Atoms	Length (Å)	Atoms	Length (Å)
	(a) Platinum coordination		
Cl(1)—Pt(1)	2.346(3)	Cl(2)—Pt(1)	2.338(4)
P(1)—Pt(1)	2.199(3)	P(2)—Pt(1)	2.209(3)
P(3)—Pt(2)	2.198(3)	Cl(3)—Pt(2)	2.368(4)
P(4)—Pt(2)	2.339(4)	P(5)—Pt(2)	2.325(4)
	(b) Phosphorus to oxygen bonds		
O(1)—P(1)	1.597(8)	O(2)—P(2)	1.605(8)
O(1)—P(3)	1.635(8)	O(2)—P(3)	1.640(9)
O(3)—P(3)	1.471(9)		
O(4)—P(1)	1.561(10)	O(6)—P(2)	1.584(10)
O(5)—P(1)	1.561(10)	O(7)—P(2)	1.554(11)
	The ethoxy groups		
C(1)—O(4)	1.406(21)	C(5)—O(6)	1.451(19)
C(3)—O(5)	1.506(19)	C(7)—O(7)	1.382(18)
C(2)—C(1)	1.360(30)	C(6)—C(5)	1.437(26)
C(4)—C(3)	1.462(26)	C(8)—C(7)	1.476(24)
	(d) The triethylphosphine ligands		
C(9)—P(4)	1.817(14)	C(15)—P(5)	1.799(14)
C(11)—P(4)	1.834(17)	C(17)—P(5)	1.807(17)
C(13)—P(4)	1.808(17)	C(19)—P(5)	1.824(19)
C(10)—C(9)	1.548(20)	C(16)—C(15)	1.542(24)
C(12)—C(11)	1.494(31)	C(18)—C(17)	1.594(32)
C(14)—C(13)	1.574(32)	C(20)—C(19)	1.560(30)

The estimated standard deviations are given in parentheses.

normal *trans* to phosphorus (30). Another point of interest concerns the question of a bridging versus a chelate role for the $(EtO)_2POP(OEt)_2$ ligand. Until recently, $R_2P—O—PR_2$ ligands were not known to function as chelates, a fact which was generally attributed to a requirement for a large POP angle (31). Undoubtedly this is an important factor in the predominance of bridged rather than chelate structures but two recent structural determinations, $[M(CO)_4(Ph_2POPPPh_2)]$, M = Cr, Mo, have shown chelate structures with the POP angle 100.3 and 103.3°, respectively (15). In the present complex this angle is 135°, so it is clearly a very flexible parameter.

The structure of **VII** consists of two square planar platinum units linked by a novel condensed phosphorus ligand. This ligand may be regarded as having two P(III) centres, P(1) and P(2), which act as two electron donors to Pt(1), and a P(V) centre, P(3), which acts as a one electron donor to Pt(2). The six-membered ring lies in a *chaise-longue* conformation with O(1) and O(2) held in the same plane as the Pt(1) coordination. P(3) is about 0.7 Å above this plane and the Pt(2) coordination is approximately perpendicular (93.6°) to that of Pt(1). The Pt—Cl bonds (av. 2.35 Å), which are all *trans* to phosphorus, and the Pt—P bonds (av. 2.20 Å) are closely similar to those found above in compound **IV** and do not appear to be affected by the formal oxidation state of the phosphorus. In contrast, there are four significantly different P—O lengths: P=O, 1.471(9); P(V)—OP, av. 1.637; P(III)—OP, av. 1.601; P(III)—OEt, av. 1.565 Å, all of which fall within the ranges found for similar bonds in tetrahedral phosphates (32): P=O, 1.38–1.56; P—OP, 1.48–1.66; P—OC, 1.56–1.64 Å.

TABLE 7. Bond angles for compound **VII**

Atoms	Angle (°)	Atoms	Angle (°)
		(a) The Pt angles	
Cl(2)—Pt(1)—Cl(1)	89.4(2)	P(3)—Pt(2)—Cl(3)	177.1(2)
P(1)—Pt(1)—Cl(1)	87.0(1)	P(4)—Pt(2)—Cl(3)	84.1(1)
P(1)—Pt(1)—Cl(2)	176.4(1)	P(4)—Pt(2)—P(3)	96.5(1)
P(2)—Pt(1)—Cl(1)	175.6(1)	P(5)—Pt(2)—Cl(3)	90.2(1)
P(2)—Pt(1)—Cl(2)	86.2(1)	P(5)—Pt(2)—P(3)	89.3(1)
P(2)—Pt(1)—P(1)	97.4(1)	P(5)—Pt(2)—P(4)	174.0(1)
		(b) The six membered ring P and O angles	
O(1)—P(1)—Pt(1)	116.7(3)	O(2)—P(2)—Pt(1)	116.1(3)
O(4)—P(1)—Pt(1)	116.9(4)	O(6)—P(2)—Pt(1)	116.5(4)
O(5)—P(1)—Pt(1)	117.3(4)	O(7)—P(2)—Pt(1)	116.9(4)
O(4)—P(1)—O(1)	100.4(5)	O(7)—P(2)—O(2)	99.8(6)
O(5)—P(1)—O(1)	103.8(5)	O(6)—P(2)—O(2)	104.9(5)
O(5)—P(1)—O(4)	99.0(6)	O(7)—P(2)—O(6)	100.0(6)
O(1)—P(3)—Pt(2)	108.9(3)	O(2)—P(3)—O(1)	99.2(4)
O(2)—P(3)—Pt(2)	109.2(3)	P(3)—O(1)—P(1)	125.6(5)
O(3)—P(3)—Pt(2)	121.8(4)	P(3)—O(2)—P(2)	124.0(5)
O(3)—P(3)—O(1)	106.3(5)	O(3)—P(3)—O(2)	109.1(5)
		(c) The ethoxy groups	
C(1)—O(4)—P(1)	125.7(12)	C(5)—O(6)—P(2)	121.1(10)
C(3)—O(5)—P(1)	122.6(10)	C(7)—O(7)—P(2)	128.7(10)
C(2)—C(1)—O(4)	118.6(24)	C(6)—C(5)—O(6)	105.8(18)
C(4)—C(3)—O(5)	107.3(18)	C(8)—C(7)—O(7)	109.8(14)
		(d) The triethylphosphine P angles	
C(9)—P(4)—Pt(2)	119.9(5)	C(15)—P(5)—Pt(2)	113.3(5)
C(11)—P(4)—Pt(2)	110.3(6)	C(17)—P(5)—Pt(2)	115.3(6)
C(11)—P(4)—C(9)	105.5(8)	C(17)—P(5)—C(15)	105.4(9)
C(13)—P(2)—Pt(2)	110.2(7)	C(19)—P(5)—Pt(2)	114.3(6)
C(13)—P(4)—C(9)	107.8(9)	C(19)—P(5)—C(15)	104.4(9)
C(13)—P(4)—C(11)	101.6(10)	C(19)—P(5)—C(17)	102.9(9)
		(e) The ethyl groups	
C(10)—C(9)—P(4)	114.6(11)	C(16)—C(15)—P(5)	117.5(12)
C(12)—C(11)—P(4)	109.7(13)	C(18)—C(17)—P(5)	108.5(14)
C(14)—C(13)—P(4)	106.8(13)	C(20)—C(19)—P(5)	110.7(14)

Estimated standard deviations are given in parentheses.

Experimental

(a) Synthetic and spectroscopic studies

Data relating to the characterization of the complexes are given in the tables, the Results section, and in the preparative descriptions below. Microanalysis was by the Canadian Microanalytical Service, Vancouver, B.C., Canada. Nuclear magnetic resonance spectra were recorded in appropriate solvents (Table 1) using a Bruker WP250 Fourier transform spectrometer locked to the solvent deuterium resonance. The spectrometer was operated at 101.3 MHz for ^{31}P and at 53.5 MHz for ^{195}Pt. For both nuclei, protons were decoupled by broad-band ("noise") irradiation at appropriate frequencies. ^{31}P chemical shifts were measured relative to external $P(OMe)_3$ and are reported in parts per million relative to 85% H_3PO_4 using a conversion factor of +141 ppm. ^{195}Pt chemical shifts are reported in ppm relative to $\Xi(^{195}Pt)$ = 21.4 MHz (33). Positive values are downfield of the references. Simulated nmr spectra were calculated on an IBM 3031 computer and plotted on a Calcomp 1039 plotter. The programs used were a locally constructed package based on the UEAITR and NMRPLOT programs from the literature (34, 35). In all cases the spectra of the different isotopomers were calculated separately and then summed to give the final simulation.

All operations were carried out at ambient temperature (ca. 25°C) under an atmosphere of dry nitrogen using standard Schlenk tube techniques. Solvents were dried by reflux over appropriate reagents (phosphorus pentoxide for dichloromethane and potassium/benzophenone for tetrahydrofuran, toluene, benzene, and hexane) and were distilled under nitrogen prior to use.

$P(OEt)_2Cl$ and $(EtO)_2POP(OEt)_2$ were commercially available from the Aldrich Chemical Co., and were used as received. $[PtCl_2(PhCN)_2]$ (36), $[Pt(CH_3)_2(COD)]$ (37), and $[Pt_2Cl_4(PEt_3)_2]$ (38), were prepared as previously described. Recrystallizations from solvent pairs were by dissolution of the complex in the first solvent (using about double the volume required for complete solution) followed by dropwise addition of sufficient second solvent to cause turbidity at ambient temperature. Crystallization was then completed either by continued very slow dropwise addition of the second solvent or, in those cases where a temperature is indicated in the detailed descriptions below, by setting the mixture aside at a reduced temperature.

$[Pt_2X_4\{\mu\text{-}(EtO)_2POP(OEt)_2\}_2]$

(i) X = Cl. $P(OEt)_3Cl$ (0.20 mL, 1.4 mmol) was added dropwise to a stirred solution of $[PtCl_2(PhCN)_2]$ (0.30 g, 0.64 mmol) in dichloromethane (10 mL). The initial yellow colour was slowly discharged during stirring for 6 h. The solvent was removed *in vacuo* and the resulting colourless oil characterized as *cis*-$[PtCl_2\{P(OEt)_2Cl\}_2]$ by ^{31}P nmr (9). Repeated attempts at crystallization caused apparent hydrolysis of the product to a compound whose spectroscopy suggested the known dimer $[Pt_2Cl_4\{\mu\text{-}(EtO)_2POP(OEt)_2\}_2]$ (19).

(ii) X = Cl. In order to confirm the above result we decided to synthesize an authentic sample of $[Pt_2Cl_4\{\mu\text{-}(EtO)_2POP(OEt)_2\}_2]$. This was achieved by a modification of the published method (19) using $[PtCl_2(PhCN)_2]$ as the starting material instead of $[PtCl_2(SEt_2)_2]$. Typically, $(EtO)_2POP(OEt)_2$ (0.15 mL, 0.61 mmol) was added dropwise to a stirred solution of $[PtCl_2(PhCN)_2]$ (0.30 g, 0.64 mmol) in dichloromethane (10 mL). Stirring was continued for 4 h before removal of the solvent *in vacuo*. Recrystallization of the residue from dichloromethane/diethyl ether at −20°C gave $[Pt_2Cl_4\{\mu\text{-}(EtO)_2POP(OEt)_2\}_2]$ (0.15 g, 0.14 mmol) as colourless crystals. *Anal.* calcd. for $C_{16}H_{40}Cl_4O_{10}P_4Pt_2$: C 18.3, H 3.85, Cl 13.5; found: C 18.4, H 4.00, Cl 13.6%.

(iii) X = Me. $(EtO)_2POP(OEt)_2$ (0.15 mL, 0.61 mmol) was added dropwise to a stirred solution of $[PtMe_2(COD)]$ (0.20 g, 0.53 mmol) in dichloromethane (20 mL). Stirring was continued for 3 h before removal of the solvent *in vacuo*. Recrystallization of the oily residue from dichloromethane/hexane gave $[Pt_2Me_4\{\mu\text{-}(EtO)_2POP(OEt)_2\}_2]$ (0.16 g, 0.17 mmol) as colourless crystals. *Anal.* calcd. for $C_{20}H_{52}O_{10}P_4Pt_2$: C 24.9, H 5.42; found: C 25.8, H 5.26%. The product was stable in the solid state and in deuterobenzene solution but decomposed over several hours in deuterochloroform solution.

A small-scale reaction carried out in an nmr tube by the addition of MeMgI (0.1 mmol in hexane) to a solution of $[Pt_2Cl_4\{\mu\text{-}(EtO)_2POP(OEt)_2\}_2]$ (0.03 g, 0.03 mmol) in dichloromethane (1 mL) showed essentially complete conversion (by ^{31}P nmr) to $[Pt_2Me_4\{\mu\text{-}(EtO)_2POP(OEt)_2\}_2]$ after 20 min.

$[Pt_2Cl_4(PEt_3)_2\{\mu\text{-}(EtO)_2POP(OEt)_2\}]$

$(EtO)_2POP(OEt)_2$ (0.07 mL, 0.29 mmol) was added dropwise to a stirred suspension of $[Pt_2Cl_4(PEt_3)_2]$ (0.20 g, 0.26 mmol) in carefully dried benzene (10 mL). Stirring was continued for 45 min, during which time the yellow colour of the suspension was gradually discharged. The solvent was removed *in vacuo* to leave an oily residue, which was eventually crystallized by precipitation from dry dichloromethane/hexane at −20°C followed by prolonged trituration with hexane. Final recrystallization from dichloromethane/hexane at −20°C gave $[Pt_2Cl_4(PEt_3)_2\{\mu\text{-}(EtO)_2POP(OEt)_2\}]$ as colourless crystals, mp 127–129°C. *Anal.* calcd. for $C_{20}H_{50}Cl_4O_5P_4Pt_2$: C 23.4, H 4.91; found: C 23.5, H 4.84%. Note that a similar reaction in dichloromethane without special precautions regarding drying of solvents resulted in the hydrolyzed product, **VII**.

$[Cl_2Pt\{\mu\text{-}(P(EtO)_2O)_2P(O)\}PtCl(PEt_3)_2]$

(i) $P(EtO)_2Cl$ (0.30 mL, 2.1 mmol) was added dropwise to a stirred

solution of $[Pt_2Cl_4(PEt_3)_2]$ (0.94 g, 1.22 mmol) in dichloromethane (30 mL). The yellow colour of the solution was quickly discharged but stirring was continued for 2 h before removal of the solvent *in vacuo*. The oily residue was crystallized from dichloromethane/hexane at −20°C to yield $[Cl_2Pt\{\mu\text{-}(P(OEt)_2O)_2P(O)\}PtCl(PEt_3)_2]$ as colourless crystals. Several attempts to repeat this reaction failed to give the same product and in consequence other routes were explored leading to the following synthesis.

(*ii*) $(EtO)_2POP(OEt)_2$ (0.10 mL, 0.41 mmol) was added dropwise to a stirred solution of $[Pt_2Cl_4(PEt_3)_2]$ (0.30 g, 0.39 mmol) in dichloromethane (15 mL). The yellow colour of the solution was almost immediately discharged and after 15 min the solvent was removed *in vacuo*. Recrystallization of the residue from dichloromethane/hexane at −20°C gave $[Cl_2Pt\{\mu\text{-}(P(OEt)_2O)_2P(O)\}PtCl(PEt_3)_2]$ as colourless crystals (0.10 g, 0.094 mmol), mp 130–133°C. *Anal.* calcd. for $C_{20}H_{50}Cl_3O_7P_5Pt_2$: C 22.8, H 4.78, Cl 10.1, P 14.7; found: C 22.7, H 4.83, Cl 10.8, P 15.2%. Note that a similar reaction in carefully dried benzene yielded a different product, $[Cl_2(Et_3P)Pt\{\mu\text{-}(EtO)_2POP(OEt)_2\}PtCl_2(PEt_3)]$ (see above).

(b) X-ray data collection

Compounds **IV**, $[Pt_2Cl_4\{\mu\text{-}(EtO)_2POP(OEt)_2\}_2]$, and **VII**, $[Cl_2Pt\{\mu\text{-}(P(EtO)_2O)_2P(O)\}PtCl(PEt_3)_2]$ were prepared as described above by reaction of $(EtO)_2POP(OEt)_2$ with $[PtCl_2(PhCN)_2]$ and by reaction of $P(OEt)_2Cl$ with $[Pt_2Cl_4(PEt_3)_2]$, and crystals suitable for study by X-ray diffraction were grown by vapour diffusion of hexane into solutions of the complexes in dichloromethane. Compound **IV** was mounted in a glass tube with a little solvent (dichloromethane/pentane) but no special precautions were necessary for compound **VII**. Preliminary photographic work on both compounds was carried out with Weissenberg and precession cameras using Cu K_α radiation. After establishment of symmetry and approximate unit cells the crystals were transferred to a Picker 4-circle diffractometer automated with a PDP11/10 computer and utilising Zr-filtered Mo K_α radiation (λ = 0.71069 Å). The unit cells were refined by least-squares methods employing respectively 28 and 22 pairs of centering measurements at $\pm 2\theta$ in the ranges $|2\theta| = 5$–47° (**IV**) and 17–44° (**VII**). The crystal of **IV** was mounted in the direction of −10, 8, −5 and crystal **VII** was approximately along the *c* axis. The crystal data at approximately 24°C were as follows. For *compound* **IV**:

$C_{16}H_{40}Cl_4O_{10}P_4Pt_2$

Monoclinic, space group $P2_1/n$, equivalent positions $x, y, z; \bar{x}, \bar{y}, \bar{z}; \frac{1}{2}+x, \frac{1}{2}-y, \frac{1}{2}+z; \frac{1}{2}-x, \frac{1}{2}+y, \frac{1}{2}-z$; a = 13.814(7), b = 11.429(4), c = 10.726(5) Å; β = 106.30(5)°; V(cell) = 1625(1) Å^3; D_m = 2.137 g cm^{-3} (flotation in $CCl_4/CHBr_3$), D_c = 2.142 g cm^{-3}; M_r = 1048.37; Z = 2; asymmetric unit = half molecule.

For *compound* **VII**:

$C_{20}H_{50}Cl_3O_7P_5Pt_2$

Monoclinic, space group $P2_1/c$, a = 17.547(8), b = 19.775(6), c = 11.268(3) Å; β = 106.42(3)°; V(cell) = 3750(2) Å^3; D_m = 1.896 g cm^{-3} (flotation in $CCl_4/CHBr_3$), D_c = 1.867 g cm^{-3}; M_r = 1054.02; Z = 4; asymmetric unit = one molecule.

Intensity measurements for both compounds were collected for two reciprocal space octants ($k, l \geq 0$) using a $\theta/2\theta$ scan with steps of 0.01° in 2θ, counting for 0.25 s per step, and with background measurements at each end of the scan. Measurements for **IV** extended to 2θ = 50° with 160 steps and background counts for 20 s, and for **VII** to 45° with 200 steps and 25 s counts. Each batch of 50 reflections was preceded by the measurement of three standard reflections (**IV**: 10, 0, 0; 0, 8, 0; 0, 0, 8; and **VII**: 6, 0, 0; 0, 6, 0; 0, 0, 2). The Lorentz and polarization factors were applied and each batch was scaled to maintain the sum of the standards constant. The standards for **IV** declined by about 10% during the data collection but there was no evidence of decomposition for **VII**. The initial files contained 3195 and 5271 reflections, respectively, and after systematically absent reflections, duplicate measurements, and those reflections with apparently negative net counts were eliminated, the final data sets contained 2855 and 4647 reflections.

For compound **IV**, the crystal faces were not identifiable and it was necessary to apply absorption corrections as a function of ϕ. Reflection −5, 4, 2 (near χ = 90°) was measured at 10° intervals in ϕ to construct an absorption correction curve. The intensity of −5, 4, 2 varied by a factor of 3.6 (μ = 96.09 cm^{-1} for MoK_α radiation). For compound **VII** absorption corrections were applied with a numerical integration procedure utilizing a 14 × 8 × 10 Gaussian grid. The crystal had pinakoidal forms {010} and {100} with the faces 0.112 and 0.257 mm, respectively, from a central origin; the faces at the tip were approximated by −1, 0, 1 at 0.404 mm, and a broken glued end by 1, 0, −2 at 0.327 mm. The absorption coefficient was 83.55 cm^{-1} and the range of transmission factors 0.04–0.18.

(c) Structure solution and refinement

The structures were found and refined using the SHELX-76 program package (39), and illustrations were drawn using ORTEP (40). The atomic scattering factors used were for neutral atoms, with corrections for anomalous dispersion (41). The structures were solved by direct methods, completed by standard Fourier synthesis procedures using difference maps, and refined by the method of least squares minimizing $\Sigma w\Delta^2$ where $\Delta = |F_o| - |F_c|$. The weights were obtained from counting statistics using $w = 1/(\sigma^2(F) + 0.001F^2)$. One intense low angle reflection, 2, 0, 0, was suppressed from the least-squares process for compound **VII**, but otherwise the refinements proceeded without incident with 163 and 334 parameters to be determined from 2855 and 4646 independent observations for **IV** and **VII**, respectively. Hydrogen atoms were not located. All other atoms were treated as vibrating anisotropically and convergence was obtained with maximum shift/esd ratios of 0.76 and 0.12, respectively. For compound **IV** the residuals were R = 0.0550 and $R_w = (\Sigma w\Delta^2/\Sigma wF_o^2)^{1/2}$ = 0.0688. The final difference map for compound **IV** had 5 peaks in the range 1.1–3.8 e Å^{-3} at distances of about 1 Å from heavy atoms. Other maxima were less than 1.1 e Å^{-3} and the minimum was −3.3 e Å^{-3}. Corresponding figures for **VII** were R = 0.0612, R_w = 0.0726, max = +1.83 e Å^{-3} (close to Pt(2)), min = −2.31 e Å^{-3}. Neither difference map gave any indication that any material had been overlooked. For compound **IV** the molecular symmetry was $\bar{1}$ and for the coordinates given in Table 2 the centre of inversion is located at (0, $\frac{1}{2}$, 1).

Acknowledgements

We thank the Natural Sciences and Engineering Research Council of Canada and the University of Victoria for research grants and Mrs C. Greenwood for recording nmr spectra.

1. D. M. Roundhill, R. P. Sperline, and W. B. Beaulieu. Coord. Chem. Rev. **26**, 263 (1978).
2. V. W. Day, I. Tavanaiepour, S. S. Abdel-Meguid, J. F. Kirner, L. Y. Goh, and E. L. Muetterties. Inorg. Chem. **21**, 657 (1982), and references therein.
3. H. W. Choi and E. L. Muetterties. J. Am. Chem. Soc. **104**, 153 (1982).
4. J. M. Fernandez, B. F. G. Johnson, J. Lewis, and P. R. Raithby. J. Chem. Soc. Dalton Trans. 2250 (1981).
5. J. M. Fernandez, B. F. G. Johnson, J. Lewis, P. R. Raithby, and G. M. Sheldrick. Acta Crystallogr. **35**, 1711 (1979).
6. R. Sperline, M. K. Dickson, and D. M. Roundhill. J. Chem. Soc. Chem. Commun. 62 (1977).
7. M. A. F. Dos Remedios Pinto, P. J. Sadler, S. Neidle, M. R. Sanderson, A. Subbiah, and R. Kuroda. J. Chem. Soc. Chem. Commun. 13 (1980).
8. A. G. Orpen and G. M. Sheldrick. Acta Crystallogr. **34**, 1992 (1978).
9. D. E. Berry, K. A. Beveridge, G. W. Bushnell, and K. R. Dixon. Can. J. Chem. **63**, 2949 (1985).
10. K. R. Dixon and A. D. Rattray. Can. J. Chem. **49**, 3997 (1971).
11. E. H. Wong and F. C. Bradley. Inorg. Chem. **20**, 2333 (1981).
12. G. M. Gray and C. S. Kraihanzel. J. Organomet. Chem. **146**, 23 (1978).
13. J. A. S. Duncan, D. Hedden, D. M. Roundhill, T. A.

STEPHENSON, and M. D. WALKINSHAW. Angew. Chem. Int. Ed. Engl. **21**, 452 (1982).
14. J. A. S. DUNCAN, T. A. STEPHENSON, W. B. BEAULIEU, and D. M. ROUNDHILL. J. Chem. Soc. Dalton Trans. 1755 (1983).
15. E. H. WONG, L. PRASAD, E. J. GABE, and F. C. BRADLEY. J. Organomet. Chem. **236**, 321 (1982).
16. G. M. GRAY and C. S. KRAIHANZEL. J. Organomet. Chem. **238**, 209 (1982).
17. A. D. F. TOY. *In* Comprehensive inorganic chemistry. Vol. 2. *Edited by* J. C. Bailar, H. J. Emeleus, R. Nyholm, and A. F. Trotman-Dickenson. Pergamon Press, Oxford. 1973. p. 475.
18. D. E. BERRY, G. W. BUSHNELL, K. R. DIXON, and A. PIDCOCK. Inorg. Chem. **22**, 1961 (1983).
19. R. J. HAINES, A. PIDCOCK, and M. SAFARI. J. Chem. Soc. Dalton Trans. 830 (1977).
20. R. J. PUDDEPHATT. Chem. Soc. Rev. **12**, 99 (1983).
21. M. P. BROWN, R. J. PUDDEPHATT, M. RASHIDI, and K. R. SEDDON. J. Chem. Soc. Dalton Trans. 951 (1977).
22. N. SHEPPARD and J. J. TURNER. Proc. R. Soc. **252**, 506 (1959).
23. J. A. POPLE, W. G. SCHNEIDER, and H. J. BERNSTEIN. High resolution nuclear magnetic resonance. McGraw–Hill, New York. 1959. p. 139.
24. L. MANOJLOVIC-MUIR, K. W. MUIR, A. A. FREW, S. S. M. LING, M. A. THOMSON, and R. J. PUDDEPHATT. Organometallics, **3**, 1637 (1984).
25. A. J. MCLENNAN and R. J. PUDDEPHATT. Organometallics, **4**, 485 (1985).
26. R. J. GOODFELLOW and B. F. TAYLOR. J. Chem. Soc. Dalton Trans. 1676 (1974).
27. M. A. CAIRNS, K. R. DIXON, and G. A. RIVETT. J. Organomet. Chem. **171**, 373 (1979).
28. W. MCFARLANE. J. Chem. Soc. A, 1922 (1967).
29. G. G. MATHER, A. PIDCOCK, and G. J. N. RAPSEY. J. Chem. Soc. Dalton Trans. 2095 (1973).
30. F. R. HARTLEY. Chem. Soc. Rev. **2**, 163 (1973).
31. A. L. DU PREEZ, I. L. MARAIS, R. J. HAINES, A. PIDCOCK, and M. SAFARI. J. Chem. Soc. Dalton Trans. 1918 (1981).
32. D. E. C. CORBRIDGE. The structural chemistry of phosphorus. Elsevier, Amsterdam. 1974. p. 262.
33. R. G. KIDD and R. J. GOODFELLOW. *In* NMR and the periodic table. *Edited by* R. K. Harris and B. E. Mann. Academic Press, London. 1978. p. 249.
34. R. B. JOHANNSEN, J. A. FERRETI, and R. K. HARRIS. J. Magn. Reson. **3**, 84 (1970).
35. J. D. SWALEN. *In* Computer programmes for chemistry. Vol. I. *Edited by* D. F. Detar. W. A. Benjamin, New York. 1968.
36. F. R. HARTLEY. The chemistry of platinum and palladium. Applied Science, London. 1973. p. 462.
37. C. R. KISTNER, J. H. HUTCHINSON, J. R. DOYLE, and J. C. STARLIE. Inorg. Chem. **2**, 1255 (1963).
38. R. J. GOODFELLOW and L. M. VENANZI. J. Chem. Soc. 7533 (1965).
39. G. M. SHELDRICK. SHELX-76: A computer program for crystal structure determination. University of Cambridge, Cambridge, England. 1976.
40. C. K. JOHNSON. ORTEP: A Fortran thermal ellipsoid plot program for crystal structure illustrations. ORNL-3794, Oak Ridge National Laboratory, Oak Ridge, TN. U.S.A. 1965.
41. D. T. CROMER and J. T. WABER. *In* International tables for X-ray crystallography. Vol. IV. *Edited by* J. A. Ibers and W. C. Hamilton. Kynoch Press, Birmingham, England. 1974. pp. 99, 148.

Densities and apparent molar volumes of aqueous aluminum chloride. Analysis of apparent molar volumes and heat capacities of aqueous aluminum salts in terms of the Pitzer and Helgeson theoretical models

LESLIE BARTA AND LOREN G. HEPLER
Department of Chemistry, University of Alberta, Edmonton, Alta., Canada T6G 2G2
Received July 3, 1985

LESLIE BARTA and LOREN G. HEPLER. Can. J. Chem. **64**, 353 (1986).

Densities of aqueous solutions of $AlCl_3$ (containing dilute HCl) have been measured at 10, 25, 40, and 55°C with results that have led to defined apparent molar volumes. We have used the Pitzer ion interaction model as the basis for analyzing these apparent molar volumes to obtain standard state (infinite dilution) partial molar volumes of $AlCl_3(aq)$ at each temperature. We have also made similar use of apparent molar heat capacities of aqueous solutions of $AlCl_3$–HCl and $Al(NO_3)_3$–HNO_3 from Hovey and Tremaine to obtain standard state partial molar heat capacities of $AlCl_3(aq)$ and $Al(NO_3)_3(aq)$ at these same temperatures. Finally, the standard state partial molar volumes and heat capacities have been used with the Helgeson–Kirkham semi-theoretical equation of state for aqueous ions to provide a basis for estimating the thermodynamic properties of $Al^{3+}(aq)$ at high temperatures and pressures.

LESLIE BARTA et LOREN G. HEPLER. Can. J. Chem. **64**, 353 (1986).

Opérant à 10, 25, 40 et 55°C, on a mesuré les densités de solutions aqueuses de $AlCl_3$ (contenant du HCl dilué) et l'on en a déduit les volumes molaires apparents. Comme point de départ, nous avons utilisés le modèle d'interaction ionique de Pitzer pour analyser ces volumes molaires apparents et pour obtenir les volumes molaires partiels apparents standards (dilution infinie) du $AlCl_3(aq)$ à chacune des températures. De la même façon, nous avons utilisé les capacités calorifiques molaires apparentes des solutions aqueuses de $AlCl_3$–HCl et de $Al(NO_3)_3$–HNO_3, déterminées par Hovey et Tremaine, pour obtenir les capacités calorifiques molaires partielles standard du $AlCl_3(aq)$ et du $Al(NO_3)_3(aq)$ à ces mêmes températures. Finalement, on a utilisé les capacités calorifiques et les volumes molaires partiels standard de concert avec l'équation d'état semi-théorique de Helgeson–Kirkham pour les ions aqueux pour avoir un point de départ dans l'évaluation des propriétés thermodynamiques des ions $Al^{3+}(aq)$ à des températures et à pressions élevées.

[Traduit par le journal]

Introduction

The thermodynamic properties of aqueous aluminum ion are needed in applying chemical equilibrium models to mineral–water interactions relevant to geothermal processes, to *in situ* bitumen recovery processes, and to soil and clay mineral chemistry. Specific examples include the precipitation of protective oxide or hydroxide on otherwise reactive surfaces and the enhanced solubility of aluminum-containing minerals due to complexation and hydrolysis equilibria.

Some standard state thermodynamic properties (Gibbs free energy of formation, enthalpy of formation, and entropy) of $Al^{3+}(aq)$ at 298.15 K and 1 bar (= 100 kPa) are already available (1). To use these properties for equilibrium calculations that apply to high temperature or high pressure systems, we also need the standard state partial molar heat capacity and volume of $Al^{3+}(aq)$, which are the principal subjects of this paper. In addition, the heat capacity and volume (temperature and pressure derivatives of the Gibbs free energy) are useful in connection with theoretical models of aqueous solutions (2–4) that are themselves applicable to the effective use of tabulated thermodynamic properties (298.15 K and 1 bar) for calculating properties at higher temperatures (5–8) and pressures (8–10).

Heat capacity data for aqueous solutions of aluminum chloride and nitrate have just recently become available (11), but have not yet been considered in relation to the Pitzer (2) and Helgeson (3, 4) models, which we do in this paper. Previously available volumetric data are limited to relative densities at 18°C of aqueous solutions of aluminum chloride and of aluminum nitrate (12) and of solutions of aluminum nitrate – nitric acid in the temperature range 0–60°C (12, 13). Calculation (14, 15) of the desired standard state partial molar volumes of the aluminum salts from these results (12, 13) is complicated in the first case by hydrolysis and in the second by substantial mixed electrolyte effects. Possibly because of these complications or possibly because of errors in the original experimental results, the standard state partial molar volumes of $Al^{3+}(aq)$ at 25°C derived from these earlier results differ by about 2 cm^3 mol^{-1}. We have therefore made new measurements of the densities of solutions of aluminum chloride – hydrochloric acid.

Results of our measurements of densities and the recently completed measurements of heat capacities by Hovey and Tremaine (11) have been used for the important extrapolation from finite concentration to the infinitely dilute reference state and in connection with theoretical models for the concentration, temperature, and pressure dependence of thermodynamic properties of aqueous electrolytes. More specifically, we have used the Pitzer (2) ion-interaction model and the Helgeson, Kirkham, and Flowers (4) extended Debye–Hückel model for extrapolation to infinite dilution, and the Helgeson and Kirkham (3) electrostatic model for the temperature dependence of the standard state thermodynamic properties.

Experimental

Densities of solutions at 10, 25, 40, and 55°C were measured relative to the density of pure water at the same temperature with a Sodev O3D vibrating tube densimeter (16) fitted with a platinum tube. A CT-L/PC-B temperature controller provided temperature stability of ±0.001 K. The densimeter was calibrated with distilled water and standard solutions of 1 *m* NaCl prepared by mass from Fisher ACS Certified crystals dried overnight at 110°C. Densities of 0.1 *m* NaCl solutions prepared from this standard were measured periodically to monitor reliability of the instrument's performance. Calibrations at 25°C were based on the density of water from Kell (17) and densities of solutions of NaCl from Fortier *et al.* (18). Densities of water and

TABLE 1. Compositions and densities of aqueous mixtures of aluminum chloride and hydrochloric acid

m_j (mol kg^{-1})	m_k (mol kg^{-1})	$(d - d_w) \times 10^2$ (g cm^{-3})	$\frac{(m_j + m_k)V_\phi(\text{mean})}{m_j}$ (cm^3 mol^{-1})	$V_\phi(AlCl_3)$ (cm^3 mol^{-1})
		10°C		
0.49617	0.01601	5.6811	18.91	18.35
0.34563	0.01132	4.0114	17.73	17.15
0.20150	0.00645	2.3764	16.16	15.59
0.14596	0.00526	1.7377	15.30	14.65
0.10733	0.00409	1.2855	14.74	14.06
0.07946	0.00324	0.9572	14.20	13.47
0.04813	0.00230	0.5858	13.26	12.41
0.02990	0.00174	0.3667	12.74	11.71
		25°C		
0.49617	0.01601	5.6065	20.11	19.55
0.34563	0.01132	3.9593	18.94	18.35
0.34563	0.01132	3.9586	18.96	18.37
0.20150	0.00645	2.3463	17.36	16.77
0.14596	0.00526	1.7154	16.54	15.87
0.10733	0.00409	1.2694	15.95	15.24
0.07946	0.00324	0.9453	15.40	14.64
0.04813	0.00230	0.5782	14.55	13.66
0.02990	0.00174	0.3631	13.65	12.57
0.02990	0.00174	0.3627	13.78	12.70
		40°C		
0.49617	0.01601	5.5745	20.30	19.74
0.34563	0.01132	3.9368	19.13	18.53
0.20150	0.00645	2.3360	17.39	16.78
0.14596	0.00526	1.7075	16.59	15.90
0.10733	0.00409	1.2648	15.88	15.15
0.07946	0.00324	0.9435	15.13	14.35
0.04813	0.00230	0.5806	13.53	12.62
0.02990	0.00174	0.3628	13.22	12.11
		55°C		
0.49617	0.01601	5.6666	17.89	17.34
0.34563	0.01132	3.9915	16.94	16.35
0.20150	0.00645	2.3623	15.42	14.81
0.14596	0.00526	1.7249	14.72	14.03
0.10733	0.00409	1.2793	13.81	13.08
0.07946	0.00324	0.9514	13.42	12.63
0.04813	0.00230	0.5854	11.78	10.86

solutions of NaCl at other temperatures were taken from Haar *et al.* (19) and Rogers and Pitzer (20), respectively.

A stock solution was prepared by dissolving approximately 90 g of Alfa Puratronic $AlCl_3 \cdot 6H_2O$ in 720 g of standard 0.015 *M* HCl. Aluminum was determined gravimetrically as the 8-hydroxyquinolate, with results that permitted us to calculate that the stock solution was 0.49617 ± 0.00057 molal in Al^{3+}. Preliminary pH measurements on a 0.5 *m* solution of $AlCl_3 \cdot 6H_2O$ in distilled water had indicated that the amount of HCl occluded in the solid was less than the estimated relative error of a gravimetric chloride determination. The HCl standard solution was therefore assumed to be the sole source of H^+ in our acidic solution of aluminum chloride, and the molality of chloride was calculated by difference.

A series of solutions of $AlCl_3$ in the composition range 0.03–0.5 *m* was obtained by diluting the stock solution by mass with standard 0.001 *M* HCl. Volumetric data for aqueous HCl (18) allowed calculation of solution compositions on a mass (molality, *m*) basis.

Water used as reference liquid and as solvent was singly distilled, deionized, filtered through activated carbon to remove organic contaminants, and boiled to remove dissolved gases.

Results and calculations

For treatment of densities of our mixed electrolyte ($AlCl_3$ and HCl) we follow principles summarized by Millero (21) in defining a mean apparent molar volume as

$$[1] \quad V_\phi(\text{mean}) = (V - 1000v_w)/\Sigma m_i$$

in which V is the total volume (cm^3) of a solution containing 1 kg of water, v_w is the volume of 1 g of water, and the m_i represent molalities of solutes i. Equation [1] leads to

$$[2] \quad V_\phi(\text{mean}) = [1000(d_w - d) + d_w\Sigma m_i W_i]/[dd_w\Sigma m_i]$$

in which d and d_w represent the densities of solution and pure water, respectively, and the W_i represent the molar masses of solutes i.

Compositions and densities of our solutions are given in the first three columns in Table 1, with mean apparent molar volumes calculated according to eq. [2] given in the fourth column.

TABLE 2. Smoothed Pitzer interaction model parameters for apparent molar volumes of HCl estimated from the fit to data from Akerlöf and Teare (23)

Temperature (°C)	V^0(HCl) ($cm^3\ mol^{-1}$)	σ* ($cm^3\ mol^{-1}$)	$\beta^{(1)V} \times 10^5$	$\beta^{(0)V} \times 10^5$	$2C^V \times 10^6$
10	17.15	0.04	3.60	−2.39	−1.63
25	17.95	0.06	4.96	−3.57	−2.11
40	18.35	0.07	5.99	−4.43	−2.49
55	18.34	0.10	6.85	−5.12	−2.83

*Standard error of the estimate at the 95% confidence level.

Because the fraction of the total ionic strength due to the aluminum chloride greatly exceeds that due to the hydrochloric acid in our solutions, we can attempt to isolate the defined apparent molar volume for each of our solutes by application of Young's rule (22), which we write as

$$[3] \quad (m_j + m_k)V_\phi(\text{mean}) = m_j V_\phi(AlCl_3) + m_k V_\phi(HCl)$$

where m_j and m_k refer to the molalities of aqueous $AlCl_3$ and HCl, respectively. Use of eq. [3] with our experimental results (Table 1) and the volumetric properties of aqueous HCl from Akerlöf and Teare (23) has led to the desired values of $V_\phi(AlCl_3)$ that are listed in the fifth column in Table 1. Although we can in principle use these calculated values of $V_\phi(AlCl_3)$ in an extended Debye–Hückel equation of the form

$$[4] \quad V_\phi = V_\phi^0 + A_V m^{1/2} + B_V m + \ldots \text{ (or } I \text{ instead of } m)$$

to obtain the desired standard state partial molar volume represented here by V_ϕ^0, there are ambiguities as to the appropriate use of the molality of $AlCl_3$ or the total ionic strength and also other difficulties. Similar problems arise in connection with application of the Helgeson, Kirkham, and Flowers model (4). It is therefore preferable to use the Pitzer model (2, 24), which explicitly deals with ionic interactions in mixed electrolyte solutions.

As the first step toward applying the Pitzer model to obtaining the standard state partial molar volume of the aqueous aluminum salt, $V^0(AlCl_3)$, from the experimentally based mean apparent molar volumes in Table 1, we define the excess volume of a solution as

$$[5] \quad V^{EX} = V - \Sigma n_i V^0(i)$$

in which the n_i and $V^0(i)$ are the numbers of moles and the standard state (infinitely dilute) partial molar volumes of solutes i, respectively. Combination of eqs. [4] and [5] leads to

$$[6] \quad V_\phi(\text{mean}) = (\Sigma m_i V^0(i) + V^{EX})/\Sigma m_i$$

We now go from the general eq. [6] to the corresponding specific equation for two electrolytes represented by j and k as in eq. [3]. Rearrangement of the resulting specific version of eq. [6] gives

$$[7] \quad [(m_j + m_k)V_\phi(\text{mean}) - m_k V^0(k)]/m_j = V^0(j) + (V^{EX}/m_j)$$

The excess volume, V^{EX}, may be represented directly as the pressure derivative of the excess Gibbs free energy as developed by Pitzer and others (2, 24, 25). For a ternary common ion system resulting from mixing electrolytes MX and NX of charge types 3:1 and 1:1, respectively, the interaction model representation, per kilogram of water, may be written

$$[8] \quad G^{EX}/RT = f^{GX}(I) + 2m_c(B_{MX}^{GX} + 2C_{MX}^{GX}m_c) + 2m_c(B_{NX}^{GX} + 2C_{NX}^{GX}m_c) + m_j m_k(2\theta_{MN} + m_c\psi_{MNX})$$

where m_j and m_k are molalities of electrolytes MX and NX in the mixture, and m_c is the molality of the common ion X. All other symbols are as previously defined (24). Because the pressure derivatives of the mixing coefficients, θ_{MN}^V and ψ_{MNX}^V, and also C_{MX}^V are too small to be important in our concentration range, we have assigned these parameters values of zero. Substituting the pressure derivative of eq. [8], modified as stated, into eq. [7] and rearranging gives

$$[9] \quad V_\phi(m_j + m_k)/m_j - (m_k/m_j)[V^0(HCl) + 2RTm_c(B_{HCl}^V + 2C_{HCl}^V m_c)] - \{A_V I \ln(1 + 1.2I^{1/2})\}/(1.2m_j) = V^0(AlCl_3) + 2RTm_c B_{AlCl_3}^V$$

The binary interaction coefficient, B^V, has an ionic strength dependence originally defined for the osmotic coefficient (2). For the excess Gibbs free energy the appropriate function is

$$[10] \quad B^{GX} = \beta^{(0)} + \beta^{(1)}[1 - (1 + 2I^{1/2})\exp(-2I^{1/2})]/(2I)$$

$V^0(AlCl_3)$, $\beta^{(1)V}$, and $\beta^{(0)V}$ were evaluated at each temperature by multiple linear regression analysis of our density data using eqs. [9] and [10] and values of B_{HCl}^V and C_{HCl}^V calculated from data (23) for aqueous HCl. The Debye–Hückel slope, A_V, is from Bradley and Pitzer (26). Values of the parameters for HCl are reported in Table 2. The desired resulting values of $V(AlCl_3)$ at the four temperatures of our measurements are listed in Table 3.

The values of $V^0(AlCl_3)$ were weighted statistically and then fit with an empirical function of temperature. Smoothed values calculated from this function were used to obtain final estimates of the parameters $\beta^{(1)V}$ and $\beta^{(0)V}$. The former was fit with an empirical function of temperature, and the latter was represented by a Lagrange polynomial. The result is that the temperature

TABLE 3. Standard partial molar volume of aqueous $AlCl_3$ obtained by extrapolation using the Pitzer interaction model

Temperature (°C)	$V^0(AlCl_3)$ ($cm^3\ mol^{-1}$)	σ* ($cm^3\ mol^{-1}$)
10	8.25	0.22
25	8.81	0.25
40	8.05	0.28
55	6.05	1.05

*Standard error of the estimate at the 95% confidence level.

dependence of the parameters for volumetric properties of $AlCl_3$ over the range 10–55°C may be represented by the following equations:

$$[11] \quad V^0(AlCl_3) = a_1 + a_2T + a_3T^2$$

$$[12] \quad \beta^{(1)V} = a_4 + a_5T + a_6/(T - 362)$$

$$[13] \quad \beta^{(0)V} = a_7T^3 + a_8T^2 + a_9T + a_{10}$$

Values of the coefficients $a_1 \ldots a_{10}$ are listed in Table 4. The temperature dependence of the interaction parameters is shown in Fig. 1.

A set of equations based on the Pitzer virial model can be developed similarly for analyzing and representing other apparent molar properties. In this work we have carried out such development for the apparent molar heat capacity and have applied the resulting equations to the recently available data of Hovey and Tremaine (11) for $AlCl_3$–HCl mixtures at temperatures of 10, 25, 40, and 55°C. As in the case of volumes, the mixing parameters may be neglected. The excess heat capacity is

$$[14] \quad C_p^{EX} = -T(\partial^2 G^{EX}/\partial T^2)_{p,X}$$

Combination of eqs. [14] and [8] with the general form of eq. [7] leads to a regression model for evaluating $C_p^0(AlCl_3)$ and the second temperature derivatives of the interaction parameters:

$$[15] \quad C_{p,\phi}(m_j + m_k)/m_j - (m_k/m_j)[C_p^0(HCl) - 2RT^2m_c(B^J_{HCl} + 2C^J_{HCl}m_c)] - [A_JI \ln (1 + 1.2I^{1/2})]/(1.2m_j) = C_p^0(AlCl_3) - 2RT^2m_c[B^J_{AlCl_3} + 2C^J_{AlCl_3}m_c]$$

Values of $C_p^0(HCl)$ and B^J_{HCl} were calculated from the equations of Tremaine *et al.* (8) and are listed in Table 5. Data for evaluating C^J_{HCl} are not yet available, and we have tentatively assigned this parameter a value of zero. Values of $C_{p,\phi}$(mean) were taken as reported (11). The Debye–Hückel slope, A_J, is from Bradley and Pitzer (26).

In addition to the intercept, $C_p^0(AlCl_3)$, which is the quantity that we want, only the $\beta^{(1)J}$ term was needed to fit the heat capacity data. The temperature dependence of this parameter and also that of $C_p^0(AlCl_3)$ were fit with the following empirical functions:

$$[16] \quad C_p^0(AlCl_3) = b_1 + b_2T + b_3/(T - 190)$$

$$[17] \quad \beta^{(1)J} = b_4 + b_5T + b_6/(T - 190)$$

Values of the coefficients $b_1 \ldots b_6$ are listed in Table 6. Figure 2 shows the temperature dependence of $\beta^{(1)J}$. Values of $C_p^0(AlCl_3)$ at the four temperatures of the measurements are listed in Table 7.

TABLE 4. Coefficients for apparent molar volume of $AlCl_3$ (eqs. [11]–[13])

Coefficient	Estimate
a_1	-2.30259×10^2
a_2	1.61255
a_3	-2.71925×10^{-3}
a_4	-9.85743×10^{-4}
a_5	4.63268×10^{-6}
a_6	2.43957×10^{-2}
a_7	$-4.63825175 \times 10^{-10}$
a_8	$4.30964174 \times 10^{-7}$
a_9	$-1.33541798 \times 10^{-4}$
a_{10}	$1.38003386 \times 10^{-2}$

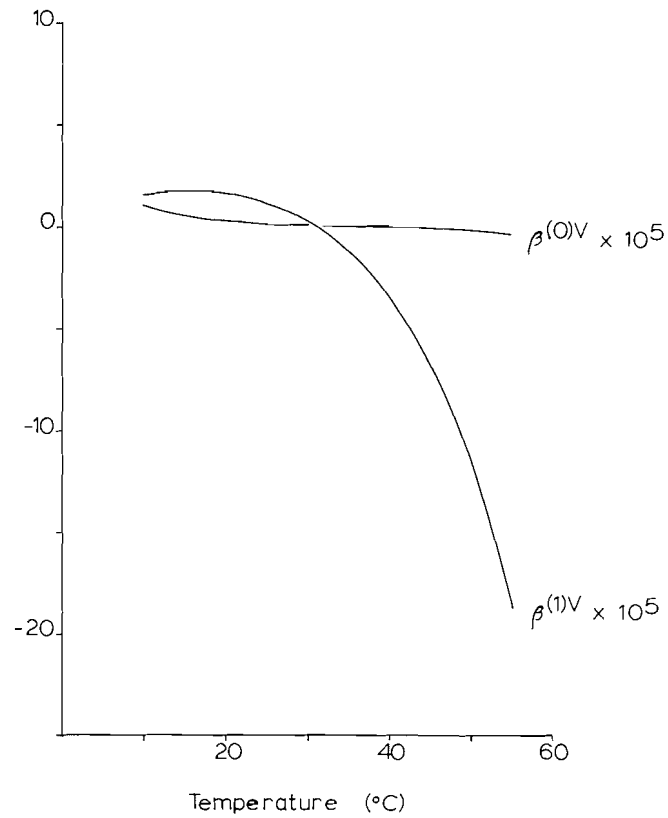

FIG. 1. Temperature dependence of binary interaction parameters for the apparent molar volume of aluminum chloride from 10–55°C.

TABLE 5. Smoothed Pitzer interaction model parameters for apparent molar heat capacities of HCl calculated from the equations given by Tremaine *et al.* (8)

Temperature (°C)	C_p^0(HCl) (J mol^{-1} K^{-1})	$\beta^{(0)J} \times 10^5$
10	−148.3	−8.48
25	−126.6	−1.35
40	−115.5	0.03
55	−111.7	0.19

TABLE 6. Coefficients for apparent molar heat capacity of $AlCl_3$ (eqs. [16]–[17])

Coefficient	Estimate
b_1	2.98006×10^3
b_2	−7.33879
b_3	-1.39146×10^5
b_4	4.31223×10^{-3}
b_5	-8.64283×10^{-6}
b_6	-1.74240×10^{-1}

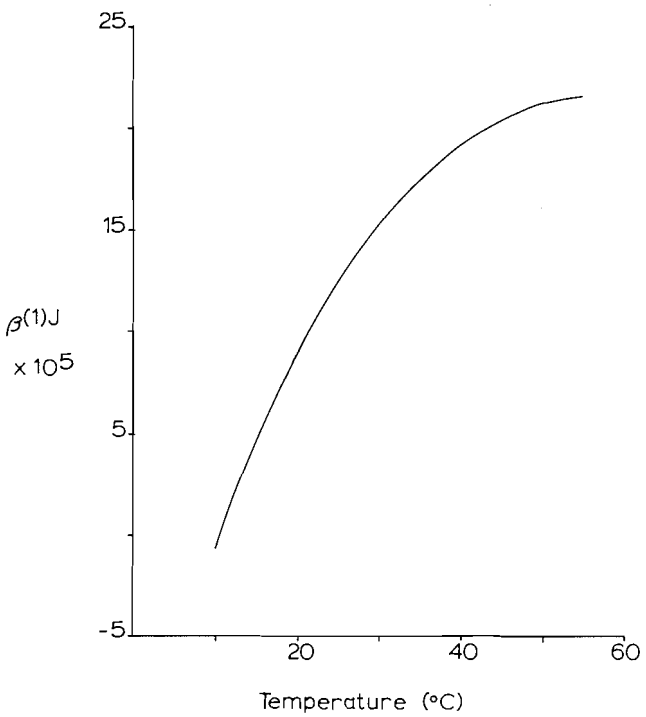

FIG. 2. Temperature dependence of binary interaction parameters for the apparent molar heat capacity of aluminum chloride from 10–55°C.

TABLE 7. Standard partial molar heat capacities of $AlCl_3$(aq) obtained by extrapolation using the Pitzer interaction model

Temperature (°C)	$C_p^0(AlCl_3)$ (J mol^{-1} K^{-1})	σ* (J mol^{-1} K^{-1})
10	−591.8	16.8
25	−493.8	6.3
40	−448.1	9.4
55	−433.3	18.8

*Standard error of the estimate at the 95% confidence level.

We turn now to the representation of the standard state properties of aluminum ion, $V^0(Al^{+3})$ and $C_p^0(Al^{+3})$, as semi-theoretical functions of temperature that can be combined with other data, as stated in the introduction, for use in equilibrium calculations at elevated pressures and temperatures. For this purpose we have chosen the equations of Helgeson and Kirkham (3), which express the standard state properties of ions as the sum of terms describing low-temperature electrostrictive collapse of the solvent structure and the change in hydration at high temperature due to rapid decrease in the dielectric constant of water. At constant pressure the appropriate relations are

$$[18]\quad V^0(Al^{3+}) = c_1 + c_2T/(T - \theta_{Al^{3+}}) - \omega_{Al^{3+}}Q$$

$$[19]\quad C_p^0(Al^{3+}) = d_1 + d_2T/(T - \theta_{Al^{3+}}) + \omega_{Al^{3+}}T\chi$$

in which c_1, c_2, d_1, and d_2 are adjustable parameters and $\theta_{Al^{3+}}$ is an adjustable "structural" temperature that allows a simple empirical description of the rapid decrease in the standard state properties, observed for many ions, with decreasing temperature in the low temperature region. The terms in $\omega_i(i = Al^{3+})$ are

TABLE 8. Coefficients for the Helgeson–Kirkham model for the standard state partial molar properties of Al^{3+} (aq) (eqs. [18] and [19])

Coefficient	Estimate
c_1	−43.984
c_2	1.160616196
d_1	135.543
d_2	−28.98818208
$\theta_{Al^{3+}}$	239.9 K

based on the Born hydration model and may be calculated from the following relations defined by Helgeson and Kirkham (3):

$$[20]\quad \omega_i = \eta z_i^2/(r_{xtl} + 0.94z_i) - 5.387 \times 10^4 z_i$$

$$[21]\quad Q = (1/D)(\partial \ln D/\partial p)_T$$

$$[22]\quad \chi = (1/D)[(\partial^2 \ln D/\partial T^2)_p - (\partial \ln D/\partial T)_p^2]$$

in which $\eta = 1.66027 \times 10^5$ Å cal mol^{-1}, r_{xtl} is the crystallographic radius of the ion, and D is the dielectric constant of pure water. Equations [18] and [19] in principle apply to ionic properties calculated on either the absolute or the conventional basis (assigning a value of zero to the corresponding property of hydrogen ion at each temperature). Because of the additional uncertainties involved in defining absolute thermodynamic properties of ions, we prefer to use conventional values and have chosen the corresponding form of ω_i (eq. [20]).

Combining the values of the standard state partial molar properties of $AlCl_3$ listed in Tables 3 and 7 with those for chloride ion based on the values for HCl listed in Tables 2 and 5, we have calculated conventional values of $V^0(Al^{3+})$ and $C_p^0(Al^{3+})$. Table 8 reports the results of the simultaneous optimization of eqs. [18] and [19] with respect to the common parameter, θ_i, using the Pauling radius of Al^{3+} and values of Q and χ calculated from the equations of Bradley and Pitzer (26). The temperature dependences of the standard state properties of aluminum ion are shown in Figs. 3*a* and 3*b*.

Discussion

The quantity on the right side of eq. [9] or [15] is equivalent to the difference between the apparent molar property of $AlCl_3$ as defined by Young's rule and that part of the Debye–Hückel term due to the aluminum salt. Values of this quantity calculated from the density and heat capacity data in combination with the information in Tables 2 and 5 and from the smoothed curves (eqs. [11]–[13] for volumes and eqs. [17] and [19] for heat capacities) are plotted against molality of aluminum in Figs. 4 and 5. The accuracy of the Pitzer interaction model correlation of the data as described in the preceding section is within the limit of the overall experimental uncertainties. The quality of fit of the Helgeson and Kirkham model to the standard state partial molar properties of aluminum ion is acceptable in the case of both volume (Fig. 3*a*) and heat capacity (Fig. 3*b*). Because no minimum relative sum of squares with respect to θ_i occurs in the objective function for the volume, the optimization is essentially governed by the heat capacity. The resulting value of $\theta_{Al^{3+}}$ (Table 8) leads to values of $V^0(Al^{3+})$ and $C_p^0(Al^{3+})$ within 0.6% (0.25 cm^3 mol^{-1}) and 0.9% (0.9 J mol^{-1} K^{-1}) of the respective calculated isothermal values. These differences are

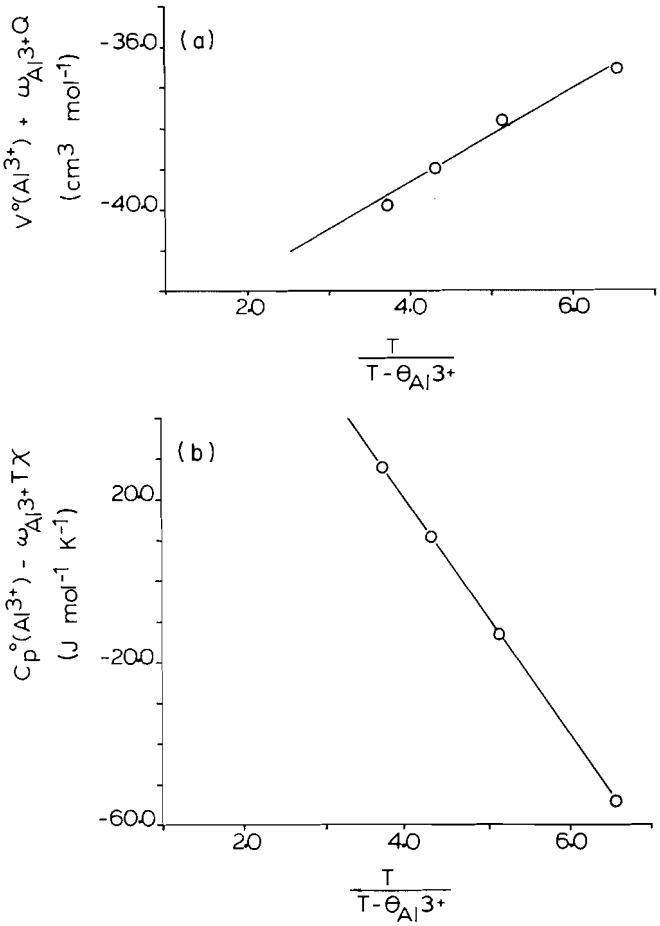

FIG. 3. Temperature dependence of the standard partial molar (*a*) volume and (*b*) heat capacity of Al^{3+}(aq). Helgeson–Kirkham model representation (solid lines) of the extrapolated values (circles), corrected for the Born hydration contribution.

TABLE 9. Pitzer interaction model parameters for apparent molar volumes and heat capacities of HNO_3 and $Al(NO_3)_3$ at 25°C: standard state partial molar properties of Al^{3+}(aq)

Electrolyte	Coefficient[a]	Estimate[a]	σ[a,b]	Source of data
HNO_3	$V^0(HNO_3)$	29.20	0.35	Ref. 27
	$\beta^{(1)V}$	6.50×10^{-5}		
	$\beta^{(0)V}$	0		
	$C_p^0(HNO_3)$	−72.4	0.5	Ref. 27
	$\beta^{(1)J}$	0		
	$\beta^{(0)J}$	-3.68×10^{-5}		
$Al(NO_3)_3$	$V^0(Al(NO_3)_3)$	43.47	0.77	Ref. 11
	$\beta^{(0)V}$	-1.48×10^{-4}		
	$\beta^{(1)V}$	0		
	$V^0(Al^{3+})$	−44.13	0.98	
	$C_p^0(Al(NO_3)_3)$	−327.2	4.4	Ref. 11
	$\beta^{(1)J}$	-1.91×10^{-4}		
	$\beta^{(0)J}$	2.11×10^{-5}		
	$C_p^0(Al^{3+})$	−110.0	4.5	
$AlCl_3$	$V^0(Al^{3+})$	−45.04	0.27	This work
	$C_p^0(Al^{3+})$	−114.2	6.3	Ref. 11

[a]Units are $cm^3\ mol^{-1}$ and $J\ mol^{-1}\ K^{-1}$.
[b]Standard error of the estimate at the 95% confidence level.

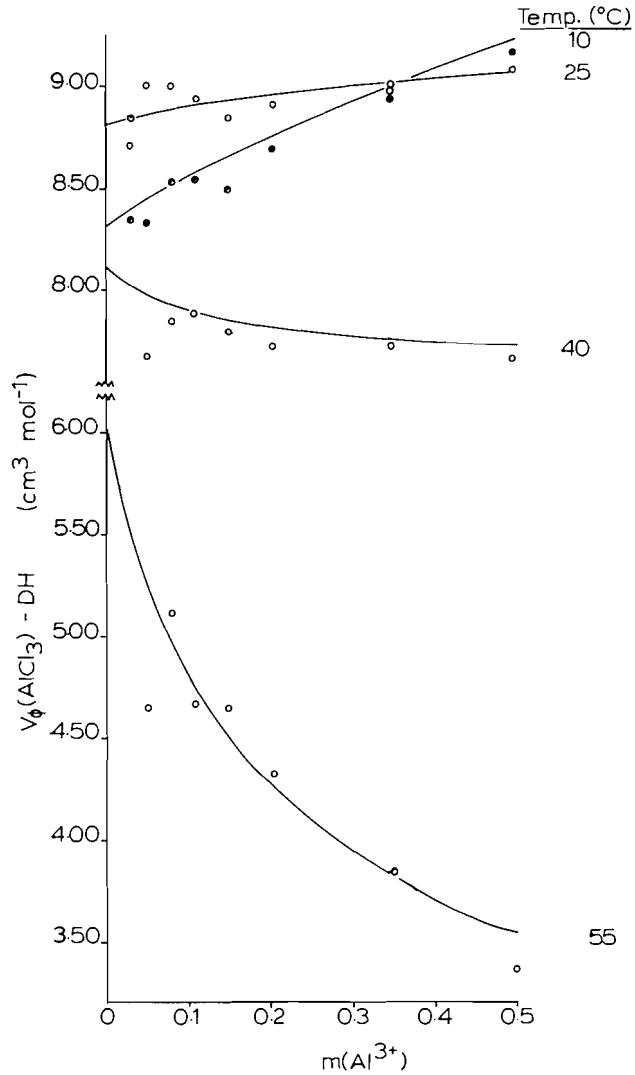

FIG. 4. Apparent molar volume of aluminum chloride from 10–55°C, corrected for the Debye–Hückel electrostatic contribution. Solid curves are calculated from the fit of the Pitzer virial model.

small enough that eqs. [18] and [19] may reasonably be used in estimating the pressure and temperature dependence of equilibria involving Al^{3+}(aq) to perhaps 1 kbar and 200°C. Equations [16] and [19] represent $C_p^0(AlCl_3)$ equally well; however, the empirical relation for $V^0(AlCl_3)$ (eq. [11]) is superior to the Helgeson–Kirkham model for the purpose of data representation.

Since only solute–solvent interactions contribute to the partial molar properties at infinite dilution, it is interesting to compare the values obtained in the preceding section for Al^{3+}(aq) calculated from the data for aluminum chloride with those that may be obtained from another aluminum salt. Using the equations developed in this paper, data for nitric acid from Enea *et al.* (27), and data for aluminum nitrate – nitric acid mixtures at 25°C from Hovey and Tremaine (11), we have compiled Table 9. Both $C_p^0(Al^{3+})$ and $V^0(Al^{3+})$ obtained from the chloride are slightly more negative than the corresponding properties obtained from the nitrate, but both sets of values are coincident within the limit of error at the 95% confidence level. The values of $V^0(Al^{3+})$ obtained by our analysis are in better

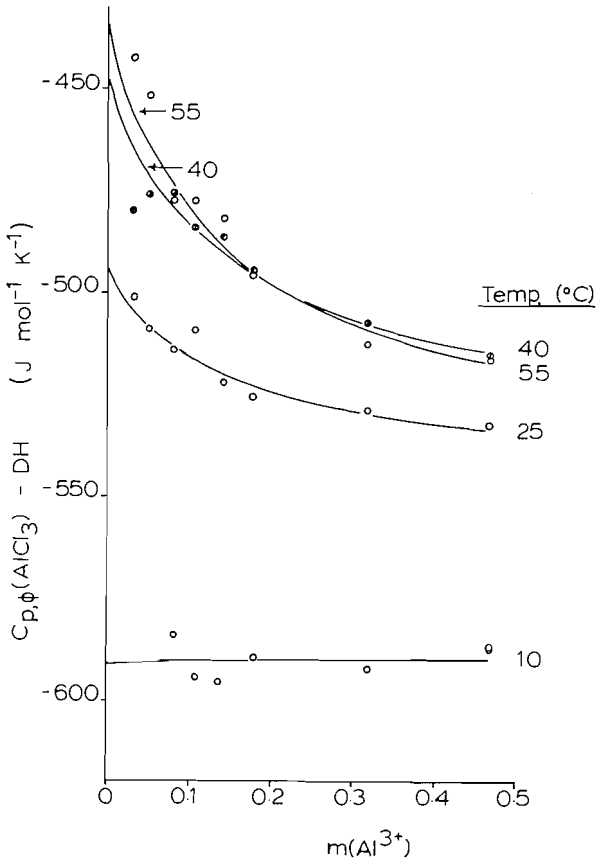

FIG. 5. Apparent molar heat capacity of aluminum chloride from 10–55°C, corrected for the Debye–Hückel electrostatic contribution. Solid curves are calculated from the fit of the Pitzer virial model. Data (circles) are from Hovey and Tremaine (11).

agreement than are those that may be calculated similarly from results listed in Millero's compilation (15).

ADDED NOTE: As a result of comments received from D. J. Bradley (Montana College of Mineral Science and Technology), it is appropriate to point out that there is a theoretical basis for including higher order electrostatic terms for unsymmetrical mixed electrolytes in the binary mixing coefficient that we have represented by θ_{MN}, as discussed in detail by Pitzer and others (25, 28, 29). These higher order terms, calculated according to theoretical principles described by Pitzer, contribute *less* than 0.02 cm^3 mol^{-1} and 0.05 J K^{-1} mol^{-1} to the objective functions represented in eqs. [9] and [15], respectively, with the result that the final values of the fitted parameters, including the standard partial molar properties, are not significantly affected by these terms. For our purposes, which include relative simplicity in mathematical representation of experimental results, it has therefore seemed appropriate to neglect these higher order terms.

Acknowledgements

We are grateful to J. K. Hovey and P. R. Tremaine for giving us the results of their measurements of heat capacities before publication (ref. 11), for allowing us to use the densimeter at the Alberta Research Council, and for helpful discussions. We also thank the Natural Sciences and Engineering Research Council of Canada for their support of this and related research.

1. D. D. WAGMAN, W. H. EVANS, V. B. PARKER, R. H. SCHUMM, I. HALOW, S. M. BAILEY, K. L. CHURNEY, and R. L. NUTTALL. J. Phys. Chem. Ref. Data **11**, Suppl. 2 (1982).
2. K. S. PITZER. J. Phys. Chem. **77**, 268 (1973).
3. H. C. HELGESON and D. H. KIRKHAM. Am. J. Sci. **276**, 97 (1976).
4. H. C. HELGESON, D. H. KIRKHAM, and G. C. FLOWERS. Am. J. Sci. **281**, 1249 (1981).
5. D. SMITH-MAGOWAN and R. H. WOOD. J. Chem. Thermodyn. **13**, 1047 (1981).
6. P. S. Z. ROGERS and K. S. PITZER. J. Phys. Chem. **85**, 2386 (1981).
7. J. A. BARBERO, L. G. HEPLER, K. G. MCCURDY, and P. R. TREMAINE. Can. J. Chem. **61**, 2509 (1983).
8. P. R. TREMAINE, K. SWAY, and J. A. BARBERO. J. Solution Chem. In press.
9. J. P. HERSHEY, S. SOTOLONGO, and F. J. MILLERO. J. Solution Chem. **12**, 233 (1983).
10. J. P. HERSHEY, R. DAMESCENO, and F. J. MILLERO. J. Solution Chem. **13**, 825 (1984).
11. J. K. HOVEY and P. R. TREMAINE. Geochim. Cosmochim. Acta. In press.
12. International Critical Tables. Vol. 3. McGraw–Hill Book Co., Inc., New York. 1928. pp. 70 and 97.
13. L. H. MILLIGAN. J. Am. Chem. Soc. **44**, 567 (1922).
14. K. FAJANS and O. JOHNSON. J. Am. Chem. Soc. **64**, 668 (1942).
15. F. J. MILLERO. *In* Water and aqueous solutions: structure, thermodynamics, and transport processes. *Edited by* R. A. Horne. Wiley–Interscience, New York. 1972. Chapt. 13.
16. P. PICKER, E. TREMBLAY, and C. JOLICOEUR. J. Solution Chem. **3**, 337 (1974).
17. G. S. KELL. *In* Water—a comprehensive treatise. *Edited by* F. Franks. Plenum, New York. 1972.
18. J. L. FORTIER, P.-A. LEDUC, and J. E. DESNOYERS. J. Solution Chem. **3**, 323 (1974).
19. L. HAAR, J. GALLAGHER, and G. S. KELL. NBS/NRC Steam Tables. Hemisphere, New York. 1984.
20. P. S. Z. ROGERS and K. S. PITZER. J. Phys. Chem. Ref. Data **11**, 15 (1982).
21. F. J. MILLERO. Chem. Rev. **71**, 147 (1971).
22. T. F. YOUNG and M. B. SMITH. J. Phys. Chem. **58**, 716 (1954).
23. G. AKERLÖF and J. TEARE. J. Am. Chem. Soc. **60**, 1226 (1938).
24. K. S. PITZER and J. J. KIM. J. Am. Chem. Soc. **96**, 5701 (1974).
25. K. S. PITZER. J. Solution Chem. **4**, 249 (1975).
26. D. J. BRADLEY and K. S. PITZER. J. Phys. Chem. **83**, 1599 (1979).
27. O. ENEA, P. P. SINGH, E. M. WOOLLEY, K. G. MCCURDY, and L. G. HEPLER. J. Chem. Thermodyn. **9**, 731 (1977).
28. K. S PITZER. J. Phys. Chem. **87**, 2360 (1983).
29. R. N. ROY, J. J. GIBBONS, J. C. PEIPER, and K. S. PITZER. J. Phys. Chem. **87**, 2365 (1983).

A theoretical study on the oxidation mechanism of triose reductone in reference to L-ascorbic acid

YASUO ABE,[1] HIDEO HORII, AND SETSUO TANIGUCHI
Radiation Center of Osaka Prefecture, Shinke-cho, Sakai 593, Japan
AND
SHINICHI YAMABE AND TSUTOMU MINATO[2]
Educational Technology Center, Nara University of Education, Takabatake-cho, Nara 630, Japan
Received May 30, 1985

YASUO ABE, HIDEO HORII, SETSUO TANIGUCHI, SHINICHI YAMABE, and TSUTOMU MINATO. Can. J. Chem. **64**, 360 (1986).

The oxidation of triose reductone H—CO—C(OH)=C(OH)—H (which has the same functional group as L-ascorbic acid) to dehydroreductone is investigated by *ab initio* molecular orbital computations. The geometries of the substrate, oxidized product, and of six possible intermediate species are optimized by gradient methods at the STO-3G basis set level. All the species are found to be planar and stable molecules by the vibrational analysis. The most possible oxidation route is shown to consist of four steps. The combination of the enediol and carbonyl groups in the deprotonated molecule **2** gives an effective π conjugation for the electron removal. The oxidation process of L-ascorbic acid is discussed on the basis of the results for triose reductone.

YASUO ABE, HIDEO HORII, SETSUO TANIGUCHI, SHINICHI YAMABE et TSUTOMU MINATO. Can. J. Chem. **64**, 360 (1986).

Faisant appel à des calculs *ab initio* d'orbitales moléculaires, on étudie l'oxydation de la triose réductone H—CO—C(OH)=C(OH)—H (qui a le même groupe fonctionnel que l'acide L-ascorbique) en déhydroréductone. On a optimisé les géométries du substrat, du produit oxydé et de six espèces intermédiaires possibles en utilisant les méthodes de gradient au niveau de l'ensemble de base STO-3G. L'analyse vibrationnelle indique que toutes ces espèces sont planaires et stables. On montre que la voie d'accès la plus probable aux produits d'oxydation comporte quatre étapes. La combinaison de l'ènediol et des groupes carbonyles dans la molécule déprotonée **2** donne une conjuguaison π qui facilite le départ de l'électron. On discute de l'oxydation de l'acide L-ascorbique à partir des résultats obtenus avec la triose réductone.

[Traduit par le journal]

I. Introduction

2,3-Dihydroxy-2-propenal is produced from dextrose by alkaline hydrolysis (1). It is called triose reductone (RH_2) because of its reducing power. The reductone is the simplest molecule having an enediol group. The physiologically important L-ascorbic acid (Vitamin C) is a typical compound with this structural moiety. Kinetic studies on the oxidation of RH_2 with oxygen (2), peroxodisulfate (3), and hexacyanoferrate(III) (4) have been reported. These data are comparable with those of L-ascorbic acid (5–7). Both of them are oxidized to dehydro forms with the successive one-electron removal. The probable reaction schemes from RH_2 to dehydroreductone (propantrione, DR) are given in Fig. 1 (4). In the overall process **1**→**8**, two protons and two electrons are lost.

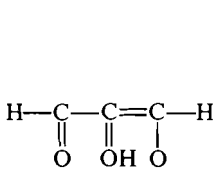

RH_2

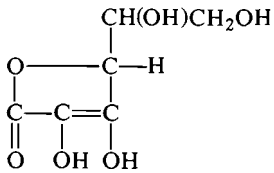

L-Ascorbic acid

It is of biochemical interest to examine the oxidation mechanism of RH_2, because its functional group is thought to operate in the same way as that of L-ascorbic acid. If some differences of the reactivity are found, those should be ascribed to the five-membered ring and (or) the attached substituent of the latter molecule. In this work, the oxidation mechanism of RH_2 to DR is examined by an *ab initio* molecular orbital (MO) calculation, and some transient species involved in Fig. 1 are also calculated.

[1]Author to whom correspondence may be addressed.

[2]Present address: Yuge Mercantile Marine College, Yuge-cho, Ochi-gun, Ehime 794-25, Japan.

The motive of the theoretical approach comes from the following mechanistic interest.

(1) In the equilibrium $RH_2 \rightleftarrows RH^- + H^+$, which proton of RH_2 is removed?
(2) Is the oxidation, $RH_2 \rightarrow DR$, the π electron removal or the loss of the lone-pair electron on the oxygen atom?
(3) How do the deprotonation and the electron loss work to convert RH_2 to DR?
(4) Are the intermediate species represented in Fig. 1 really stable?

When these questions are solved, the oxidation process of L-ascorbic acid as well as RH_2 will be clarified thoroughly.

II. Method of calculation and experimental background

The stable geometry and the electronic structure of each species in Fig. 1 are investigated. **1**, **2**, **3**, **7**, and **8** are calculated by the standard restricted Hartree–Fock (HF) method. For **4**, **5**, and **6**, the Pople–Nesbet unrestricted HF wavefunction is employed. Geometries are optimized with the STO-3G basis set by the use of the gradient technique implemented in the Gaussian 80 program (8). The one-point energy calculation is performed on the STO-3G geometry of each species with the 3-21G+p basis set (i.e., 3-21G+p//STO-3G). As the diffuse polarization functions, the p-type GTO's are added to 3-21G. The exponent on the carbon atom is 0.034, and that on the oxygen atom is 0.059 (9). To check whether the optimized geometries correspond to the stable states, vibrational analyses are carried out. The second energy derivatives are obtained by differentiating the analytical first derivatives numerically.

According to the kinetic data (4), the oxidation rate constant of **2**→**5** is 1000 times larger than that of **1**→**4**. The rate-determining step of the RH_2 oxidation has been shown to be **2**→**5** in the range of $5 > pH > 2$. This is because the second oxidation **5**→**7** is quite rapid. The route **1**→**2**→**5**→**7**→**8** is, therefore, most likely. An alternative route **1**→**2**→**5**→

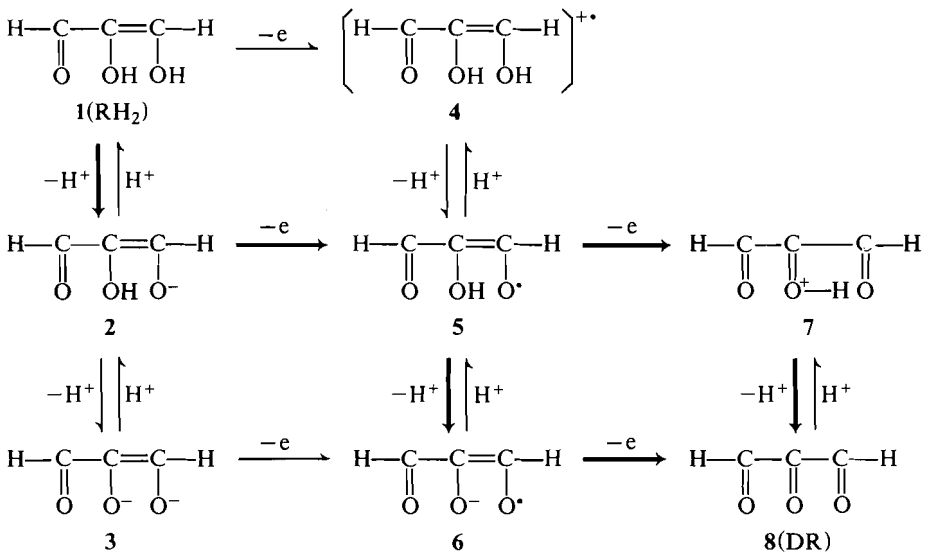

FIG. 1. The probable oxidation scheme ($RH_2 \rightarrow DR$) suggested from the kinetic measurements (4). Important routes are specified by bold lines.

6→ **8** is also probable. Radical species **5** and **6** coexist in the equilibrium state ($pK_a = 1.4$) (10). Since the oxidation rate constants of **5**→ **7** and **6**→ **8** are not available, we can hardly judge which route is more important. However, they differ only in the sequence of the deprotonation and the second oxidation. This is independent of the rate-determining step and is a minor difference. First, five species involved in the route **1**→ **2**→ **5**→ **7**→ **8** are analyzed in detail. Second, others including **6** are examined briefly.

III. Results of geometry determination

The geometry of each species in Fig. 1 is examined. In Fig. 2, the structure of RH_2 (planar) is given together with the observed X-ray data (11). The agreement of the covalent bond length between the two is satisfactory. Since it is the gas-phase data, two intramolecular hydrogen bonds are formed, $O_e \cdots H_g$ and $O_j \cdots H_f$. Encouraged by the similarity, we obtain the structures of the transient species and the product DR, which are shown in Fig. 3. The vibrational analysis demonstrates that they are all stable molecules (all the harmonic frequencies are real). In Fig. 4, their energy levels and zero-point vibration energies are drawn. Since these energies are for the gas phase, they do not correspond to the thermodynamic quantities in the aqueous media. Solvation to species will change the energy levels significantly. However, the solvation energy for each species is thought to be of a similar magnitude. A comparison of the reactivity by the use of the energy diagrams in Fig. 4 seems to be useful. For instance, the result of $k(\mathbf{2}\rightarrow\mathbf{5})/k(\mathbf{1}\rightarrow\mathbf{4}) = 1000$ mentioned in the previous section is explicable. The energy change along the oxidation **2**→ **5** is +30 kcal/mol(endothermic), while that along **1**→ **4** is +188 kcal/mol. Although qualitative, this energy difference corresponds to the large ratio of rate constants.

The effect of the diffuse *p*-type orbitals on total energies is examined. The largest stabilizing energy, +91.5 kcal/mol, relative to the 3-21G value is gained in the di-anion **3**. The anions **2** and **6** get the energy of ~ +50 kcal/mol. The stabilizing energy by 3-21G→ 3-21G+p of the neutral species is about +30 kcal/mol, and that of cations is +17 kcal/mol. Thus, the inclusion of diffuse orbitals is important to evaluate properly the energy of anions.

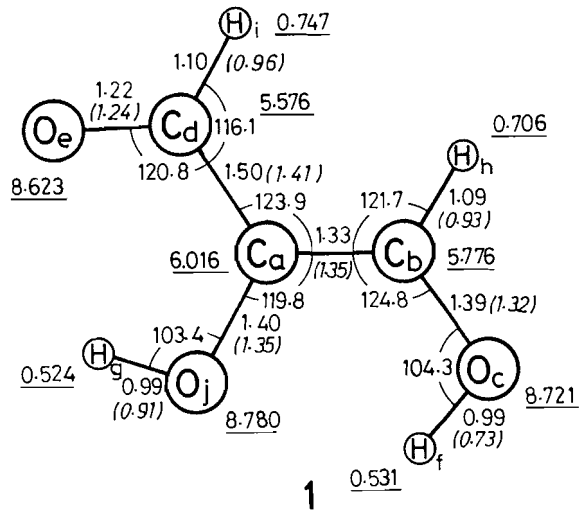

FIG. 2. The structure of triose reductone optimized with the MO calculation of the STO-3G basis set. The bond distance and angle are in Ångstroms and in degrees, respectively. The X-ray experimental data in parentheses (italic) are taken from ref. 11. The X-ray O_c—H_f bond length 0.73 Å is somewhat doubtful. The small letters (a, b, ..., and j) are used to specify atoms. Underlined numbers denote the atomic electron density calculated by 3-21G+p//STO-3G.

In the reversible deprotonation step **1** ⇄ **2**, H_f^+ is removed. An alternative model where H_g^+ is taken off is found to be 23.2 kcal/mol less stable than **2**. The problem of which proton, H_f^+ or H_g^+, is more removable may be solved by the frontier-electron theory of Fukui. The lowest σ* (in-plane) MO is antibonding for O_j—H_g and O_c—H_f bonds. The latter contribution to the MO is larger. This predicts the O_c—H_f bond cleavage for the nucleophilic attack and the deprotonation. In the step **1**→ **2**, some noticeable geometric changes take place. The single C_b—O_c bond in **1** is converted to the carbonyl group in **2**. Two C—C bonds of **2** are almost identical (1.42 and 1.41 Å), whereas they are distinguishable as single and double bonds in **1**. The anion species **2** is a conjugated system and its π electrons are readily ejected. When a π electron is abstracted from **2**, the neutral radical **5** (RH· is formed. The geometry of **5** is not so different from that of **2**.

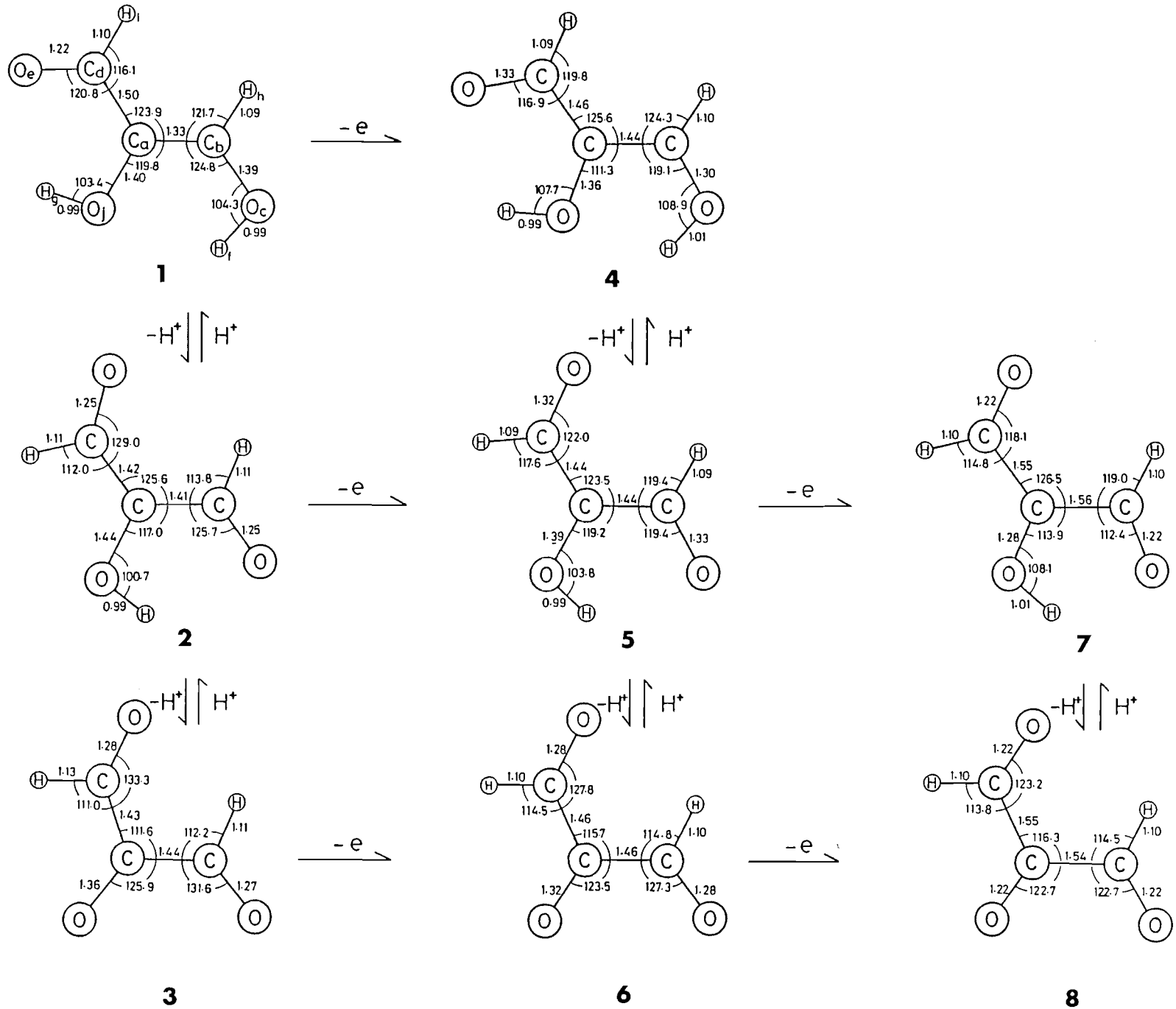

FIG. 3. Optimized geometries of the substrate, DR and transient species involved in the scheme of Fig. 1. All are calculated to be planar

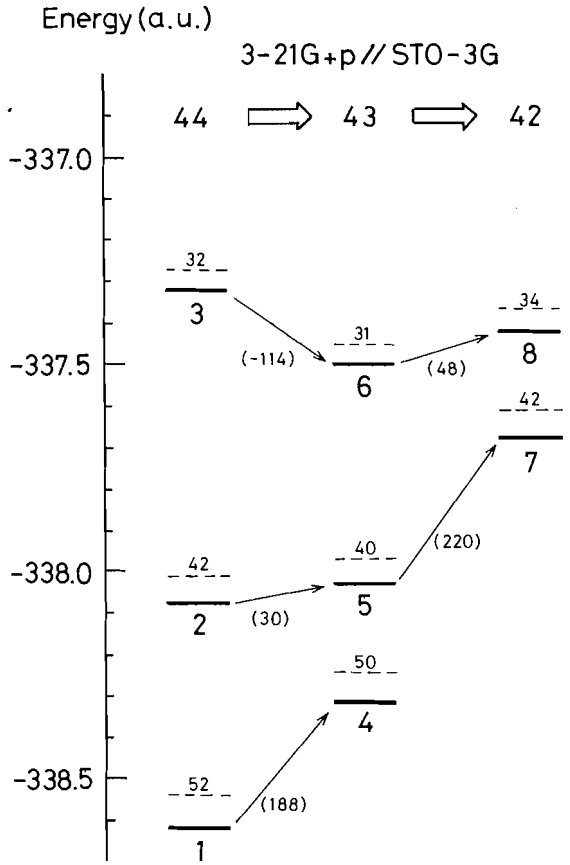

FIG. 4. The total electronic energies (bold lines) with the 3-21G+p basis set and zero-point vibration energies (broken lines with STO-3G, in kilocalories per mole relative to the bold lines) for eight species in Fig. 3. Values in parentheses denote the stabilizing (<0) and destabilizing (>0) energies in kcal/mol. From the left to the right, two electrons are lost (44 → 43 → 42).

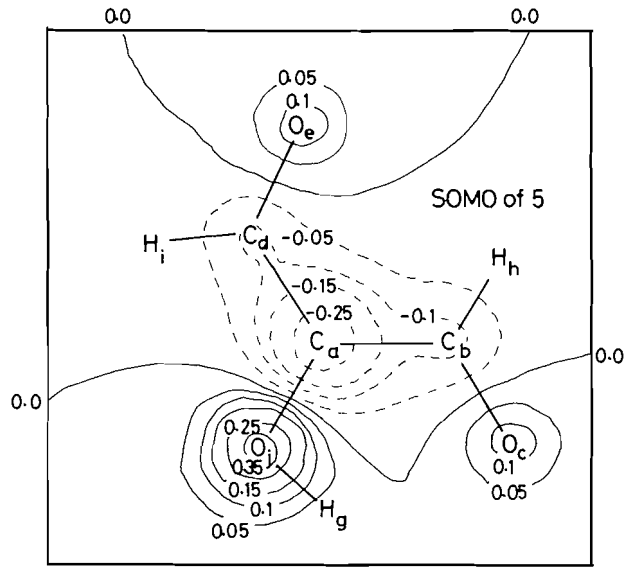

FIG. 5. Shape of the singly occupied molecular orbital (SOMO) of **5**. Contour lines are in Bohr$^{-3/2}$. When the sign of the lines is switched (broken line → full line and vice versa) along a covalent bond, SOMO is antibonding there. The cut plane for this density map is 1 Å above the molecular plane.

Next, the second oxidation **5** → **7** is considered. A large geometry distortion is caused by this electron loss. Two C—C bonds get the single bond character by **5** → **7**. The C_a—O_j—H_g site is the hydroxyl group in **5**, whereas it is the protonated carbonyl group in **7**. This change is shown by that of bond lengths (O—H = 0.99 → 1.01 Å and C—O = 1.39 → 1.28 Å). In the step **7** → **8**, the proton H_g^+ is removed and the molecular skeleton is kept almost constant during this deprotonation. The oxidized product **8** (DR) is a triketone in which the π conjugation is only about one third of that of **6**. In view of the process **1** → **2** → **5** → **7** → **8**, **1** → **2** and **5** → **7** involve significant geometric changes, i.e., the conversion of the C—C bond character and hydroxyl → protonated carbonyl.

Geometries of other species **3**, **4**, and **6** shown in Fig. 3 are discussed. Through the double deprotonation from **1**, **3** is formed. It is a conjugated π electron system. The presence of the dianion (R^{2-}) **3** was proposed by the uv spectra (2). The present vibrational analysis confirms the experimental result. After an electron removal from **3**, **6** is produced with a small geometric change. The anion radical **6** would be generated effectively by the deprotonation of **5** rather than by this oxidation of **3**. The difficulty of the latter route arises from the small concentration of **3** ($pK_{a(II)}$ = 13.0 of RH_2). The second π electron loss from **6** leads to **8** with a marked geometry variation.

The intermediates **4**, **5**, and **6** are all conjugated systems, because they are calculated to be planar. From them, π electrons are readily removed by oxidizing agents such as hexacyanoferrate(III). Radical species are detected both by pulse radiolysis (10, 12) and by esr (electron spin resonance) spectroscopy (13, 14). In the latter case, they are generated by the autoxidation of RH_2 with peroxidase catalyst. The present calculation confirms that odd-electron systems **5** and **6** are stable intermediates. We may therefore identify these as the esr measurable radical intermediates. In fact, the esr spectrum of **6** has been recorded by Yamazaki *et al.* (14).

IV. Discussion of the oxidation mechanism

From RH_2 to DR, various oxidation routes are illustrated in Fig. 1. Kinetic measurements have supported two routes **1** → **2** → **5** → **7** → **8** and **1** → **2** → **5** → **6** → **8** (5 > pH > 2). The electronic nature of molecules involved in the former is examined. In the step **1** → **2**, a proton removal raises the energy level of the highest occupied MO (HOMO). HOMO is of the π bond nature and an electron may be released readily in the step **2** → **5**. It is noted that this electron abstraction does not occur from the lone-pair (*n*) orbital on the O_c atom. Mobile π electrons in the conjugated system **2** are more easily removed. The radical species **5** is generated in the step **2** → **5**. The singly occupied MO (SOMO) is also a π orbital and its spatial extension is drawn in Fig. 5. An odd electron is delocalized over the molecular skeleton. At the C_b—C_a—C_d chain, it is bonding. In the second oxidation **5** → **7** (i.e., the loss of the SOMO electron), therefore, two C—C bonds are to be elongated. In fact, **7** has two C—C single bonds. SOMO is antibonding at three C—O bonds. This leads to their shortening for the second oxidation. In **7**, three C—O bonds attain the carbonyl character. Thus, the geometric change in **5** → **7** is understandable in terms of the nodal properties of SOMO. The loss of the SOMO electron naturally gives the geometry of the protonated triketone **7**. Once the protonated triketone **7** is produced, the proton H_g^+ may be removed in the aqueous solution. The hydration to the O_j—H_g bond causes the proton transfer, DRH^+ (**7**) + H_2O →

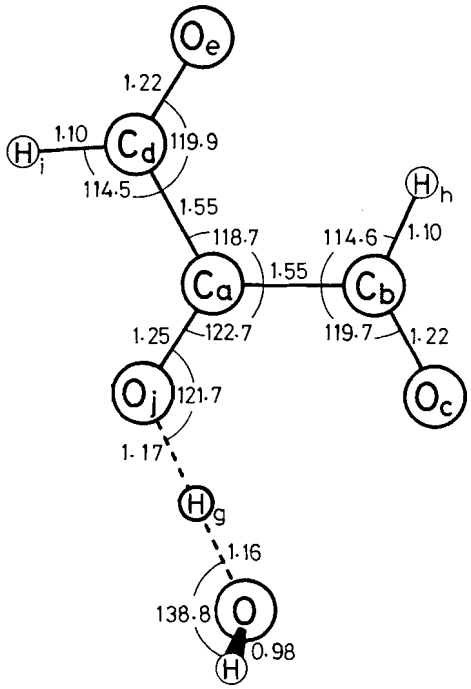

FIG. 6. The optimized structure of the protonated propantrione 7 (DRH^+)–water system. Through the hydrogen bond, the proton attached to DR may be moved readily to water.

DR (**8**) + H_3O^+. A model of this hydrogen-bond system is tested. The optimized geometry of $DR\cdots H^+\cdots OH_2$ is obtained and is exhibited in Fig. 6. An almost symmetric hydrogen-bond (1.16 ≃ 1.17 Å) is calculated, through which the proton transfer would take place readily in aqueous media. This leads to the product DR **8**. Thus, the second π-electron loss and the proton transfer are combined to carry on the reaction. The former takes place out of the molecular plane, while the latter occurs in the plane. The same discussion holds for the reversible step of the proton transfer **5** ⇄ **6**. This belongs to the second important route **1** → **2** → **5** → **6** → **8**. The proton H_g of **5** is readily removed. The σ* (in-plane) vacant MO of **5** is O_j—H_g antibonding and low-lying. The hydration to H_g^+ leads smoothly to the production of **6**. While the deprotonation **2** → **3** is difficult, **5** → **6** is easy. The difference is ascribed to that of the σ* MO energy levels (0.47 au of **2** vs. 0.25 au of **5**, whereas 0.23 au of **1**). A comparison of total energies shown in Fig. 4 also shows the difficulty or the ease of deprotonation. The energy gap between **2** and **3** is larger than that between **5** and **6**. This difference indicates that **5** → **6** is easier than **2** → **3**.

Two possible routes are related to the fact that the radical **5** has two functional sites. If the in-plane proton transfer from **5**

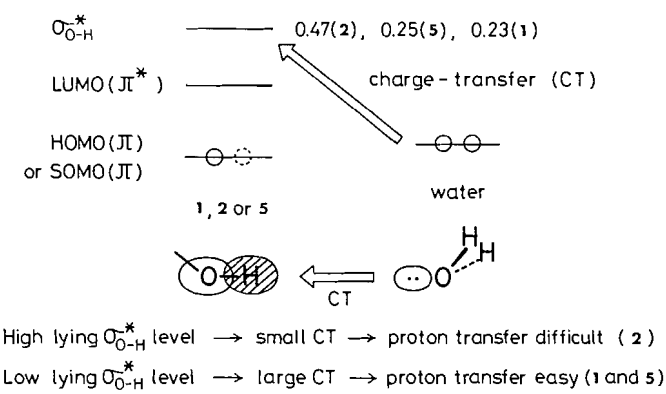

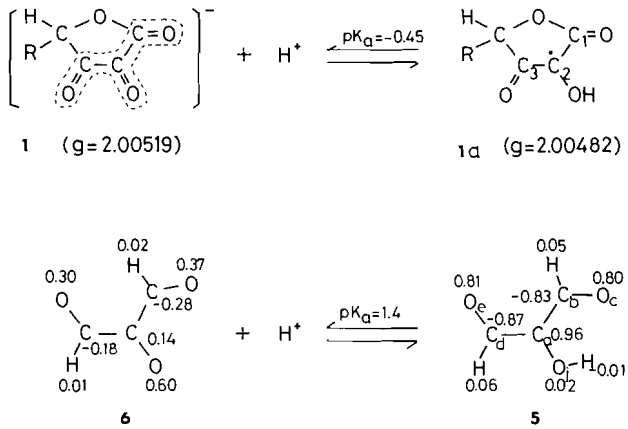

occurs, the route **1** → **2** → **5** → **6** → **8** predominates. If the out-of-plane π electron loss takes place primarily, the route **1** → **2** → **5** → **7** → **8** is operative.

The role of the carbonyl C_d—O_e bond (see Fig. 2) is discussed. First, the hydration to this group enhances the solubility of RH_2. Second, electronically this group is important to elongate the conjugate chain. In fact, it has a semi-single bond character (= 1.32 Å) in **5**. Thus, for the easier oxidation of the enediol group, the role of the carbonyl adjacent to it is indispensable.

V. The oxidation of L-ascorbic acid

The oxidation scheme of RH_2 seems to be applicable to that of L-ascorbic acid. According to the neutron-diffraction data (15), its five-membered ring is almost planar. Radical intermediates in the oxidation of the acid were reported by the radiolysis–esr study (16). This work has shown that the radical anion is produced by the oxidation in neutral and basic solutions and its odd electron is spread over a highly conjugated tricarbonyl system. The protonation to the C_2 position was assumed. In the present computational study, the assumption is shown to be valid, as far as the RH_2 – Vitamin C analogy is applicable. The figure of the protonation of the ascorbate radical is taken from the literature (16). In the equilibrium **6** ⇄ **5**, the spin densities calculated with 3-21G+p are exhibited. In both species, spin polarization takes place. In particular, the localization of the spin density of C_2 of $\mathbf{I}_a$ is well reproduced by the large density (0.96) on the C_a atom of **5**.

In view of the present result and the well-documented presence of the ascorbate radical, the oxidation mechanism of L-ascorbic acid may be deduced as shown in Fig. 7. The five-membered ring seems to increase the stability of the intermediate radical. Aside from this and the dependence of the kinetics on the pH, there weould be no reason to distinguish the oxidation mechanism of RH_2 from that of L-ascorbic acid.

VI. Concluding remarks

Although the solvent effect is not included, the oxidation process of triose reductone is clarified theoretically with the aid of kinetic information. The mehanism is partitioned into four steps, **1** → **2**, **2** → **5**, **5** → **7**, and **7** → **8**. After a proton is removed from the substrate through electrolytic dissociation equilibrium, two π electrons (not *n* electrons) are removed in a stepwise manner. At the second oxidation, the hydroxyl group is converted to the protonated ketone, followed by the proton transfer. An alternative route **1** → **2** → **5** → **6** → **8** is competitive with this route, because the radical intermediate **5** has two functional sites.

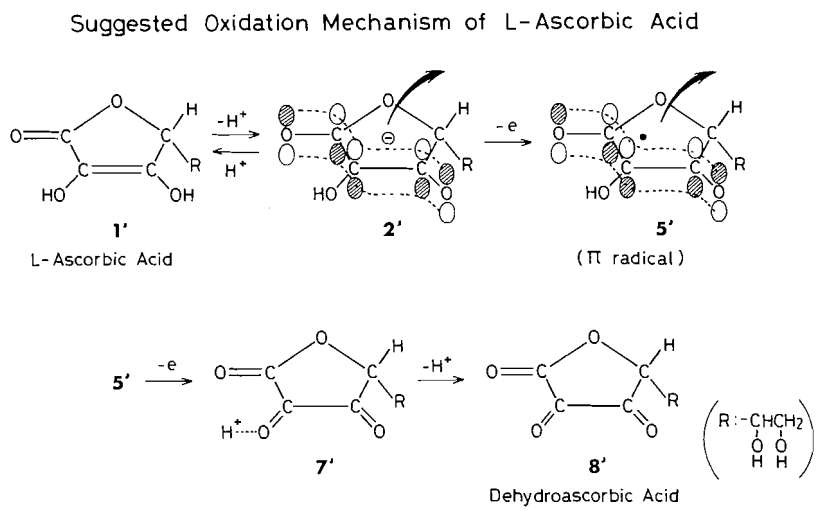

FIG. 7. Suggested oxidation mechanism of L-ascorbic acid (Vitamin C). The alternative route **1'** → **2'** → **5'** → **6'** → **8'** is omitted in the figure for simplicity.

Reviewing these results, we may answer four questions presented in the Introduction.

(1) In the equilibrium $RH_2 \rightleftarrows RH^- + H^+$, the leaving proton is H_f^+. The deprotonation from the right-side hydroxyl group in **1** is needed to elongate the π conjugated chain.

(2) In any oxidation step in Fig. 1, π electrons are taken off. The important intermediates **2**, **5**, and **6** have mobile π electrons which are readily removed.

(3) Deprotonation occurs through the hydrogen bond between the substrate and a water molecule. Deprotonation raises the HOMO energy levels for the easier oxidation. The in-plane proton transfer and the π electron loss work cooperatively.

(4) All the intermediate species suggested in Fig. 1 are found to be stable, according to the STO-3G optimization and vibrational analysis.

Acknowledgments

The authors thank the Institute for Molecular Science for the allotment of the CPU time on the HITAC M-200H computer. The authors also thank Dr. K. Yamashita who has coded the program package for the vibrational analysis.

1. H. V. EULER and C. MARTIUS. Justus Liebigs Ann. Chem. **505**, 73 (1933).
2. Y. ABE, H. HORII, S. TANIGUCHI, K. KAMAI, and M. TAKAGI. Bull. Chem. Soc. Jpn. **56**, 467 (1983).
3. Y. ABE, H. HORII, and S. TANIGUCHI. Bull. Chem. Soc. Jpn. **57**, 222 (1984).
4. Y. ABE, T. DOHMARU, H. HORII, and S. TANIGUCHI. Can. J. Chem. **63**, 1005 (1985).
5. A. WEISSBERGER, J. E. LUVALLE, and D. S. THOMAS, JR. J. Am. Chem. Soc. **65**, 1934 (1943).
6. M. KIMURA, A. KOBAYASHI, and K. BOKU. Bull. Chem. Soc. Jpn. **55**, 2068 (1982).
7. U. S. MEHROTRA, M. C. AGRAWAL, and S. P. MUSHRAN. J. Phys. Chem. **73**, 1996 (1969).
8. J. S. BINKLEY, R. A. WHITESIDE, R. KRISHNAN, R. SEEGER, D. J. DEFREES, H. B. SCHLEGEL, S. TOPIOL, L. R. KAHN, and J. A. POPLE. QCPE, **13**, 406 (1981).
9. T. H. DUNNING and P. J. HAY. *In* Modern theoretical chemistry. Vol. 3. Methods in electronic structure theory. *Edited by* H. F. Schaefer. Plenum, New York. 1977.
10. H. HORII, Y. ABE, and S. TANIGUCHI. Bull. Chem. Soc. Jpn. **58**, 2751 (1985).
11. D. SEMMINGSEN. Acta Chem. Scand. Ser. B, **28**, 141 (1974).
12. H. HORII, Y. ABE, S. TANIGUCHI, S. MAEDA, and T. WATANABE. Chem. Lett. 1313 (1983).
13. I. YAMAZAKI and L. H. PIETTE. Biochim. Biophys. Acta, **77**, 47 (1963).
14. L. H. PIETTE, I. YAMAZAKI, and H. S. MASON. *In* Free radicals in biological systems. *Edited by* M. S. Blois. Academic Press, New York. 1961. pp. 203–204.
15. J. HVOSLEF. Acta Crystallogr. Sect. B, **24**, 1431 (1968).
16. G. P. LAROFF, R. W. FESSENDEN, and R. H. SCHULER. J. Am. Chem. Soc. **94**, 9062 (1972).

Motional properties of spin labels in proteins: Effects of hydration

J. RUGGIERO

Instituto de Biociências, Letras e Ciências Exatas, Universidade Estadual Paulista, 15100 S. José do Rio Preto, São Paulo, Brazil

AND

R. SANCHES, M. TABAK,[1] AND O. R. NASCIMENTO

Instituto de Física e Química de São Carlos, Universidade de São Paulo, 13560 São Carlos, São Paulo, Brazil

Received November 26, 1984[2]

J. RUGGIERO, R. SANCHES, M. TABAK, and O. R. NASCIMENTO. Can. J. Chem. **64**, 366 (1986).

Conventional and saturation transfer (electron spin resonance) techniques are used to study the motional properties of several spin labels introduced in three proteins: lysozyme, sperm whale myoglobin and human hemoglobin. The mobilities of a maleimide spin label which binds covalently to the proteins, as well as of two small probes TEMPO and PD-TEMPOL were monitored in the temperature range from -10 to -150°C for samples in the dry and solution states. The three proteins show a similar temperature dependence as indicated by the parameters $2A_{zz}$ and ΔH. A small linear increase in $2A_{zz}$ with decrease in temperature is observed for the dry samples. For the proteins in solution, on the other hand, the $2A_{zz}$ temperature dependence shows a change of behaviour around -60°C that is related to the freezing of the water molecules in the hydration shell. The changes observed for the parameter ΔH are such that at temperatures below -60°C ΔH is greater for the solution sample, while at temperatures above -60°C ΔH is greater for the dry sample. Saturation transfer measurements show that the motion of the spin label is very restricted in all systems ($\tau_c > 10^{-5}$s) in the temperature range studied, so that the residual librational motion of the label is sensitive to the hydration, being responsible for the observed changes of the esr parameters with temperature.

J. RUGGIERO, R. SANCHES, M. TABAK et O. R. NASCIMENTO. Can. J. Chem. **64**, 366 (1986).

Faisant appel aux techniques de la rpe (résonance paramagnétique électronique) par transfert conventionnel et par transfert de saturation, on étudie le mouvement des marqueurs de spin introduits dans trois protéines, soit la lysozyme, la myoglobine du sperme de la baleine et l'hémoglobine humaine. Dans un intervalle de température allant de -10 à -150°C et opérant sur des échantillons secs ou en solution, on a mesuré les mobilités du marqueur de spin de la maléimide, qui se lie par covalence aux protéines, ainsi que les mobilités de deux petites sondes, TEMPO et PD-TEMPOL. En se basant sur les paramètres $2A_{zz}$ et sur le ΔH, on peut en déduire que les trois protéines subissent l'effet de la température de la même façon. Dans le cas des échantillons secs, on observe une faible augmentation linéaire du paramètre $2A_{zz}$ lorsque la température diminue. D'autre part, dans le cas des protéines en solution, l'effet de la température sur le paramètre $2A_{zz}$ change aux environs de -60°C et ceci qui correspond au point de congélation des molécules d'eau dans la sphère d'hydratation. Les changements observés sont tels qu'à des températures inférieures à -60°C, le ΔH de l'échantillon en solution est plus élevé tandis qu'au dessus de -60°C le ΔH de l'échantillon sec est plus élevé. Les mesures de rpe par transfert de saturation indiquent que dans l'intervalle de température étudié, le mouvement du marqueur de spin est très restreint dans tous les systèmes ($\tau_c > 10^{-5}$s). Par conséquent, le mouvement résiduel de libration du marqueur est sensible à l'hydratation et est responsable des changements des paramètres de la rpe en fonction de la température.

[Traduit par le journal]

Introduction

The hydration of biomolecules has been studied by several techniques such as calorimetry, absorption isotherms, infrared spectroscopy, nuclear magnetic relaxation (1,2), thermal stimulated depolarization (3), and computer simulation (4,5). Large discrepancies are observed when results obtained from different methods are compared. This is expected if one considers that different physical properties are probed in each case. Despite this difficulty in correlating new information with the known data, the hydration of macromolecules is an interesting subject for further studies.

The use of esr measurements to study the hydration of proteins was first proposed by Rupley *et al.* (6). They suggested that significant changes in the motional properties of a spin label (TEMPONE)[3] could be followed as a function of the sample hydration and interpreted as changes in the internal dynamics of the protein. The exclusion of possible structural changes induced in the protein by dehydration was crucial in the interpretation of these results. The absence of such structural changes was also suggested by Raman (7), infrared reflectance (8), and photoacoustic (9) spectroscopic studies.

The spin label motion as a function of temperature of hemoglobin–MAL-6 samples in the dry and solution states was studied by Johnson (10). For the lyophilized sample he observed spectral changes that were related to the librational motion of the spin label. A hydrogen bonding of the spin label to the protein or to a water molecule was the explanation given for the spectral changes observed for the solution sample.

These studies led us to consider the relevance of the spin label used and also the influence of the protein studied on the results obtained as a function of hydration. We propose to describe in this communication the esr studies in the dry and solution states of three different proteins: lysozyme, myoglobin, and hemoglobin using the spin labels: MAL-6, TEMPO, and PD-TEMPOL, as a function of temperature.

Experimental

Sample preparation

Hemoglobin solution was obtained from whole blood from healthy donors. The red blood cells were washed three times in phosphate buffered saline (135 m*M* NaCl, 5 m*M* phosphate, pH 7.4) and

[1]Author to whom correspondence may be addressed.

[2]Revision received September 13, 1985.

[3]Abbreviations: TEMPONE: 4-oxo-2,2,6,6-tetramethylpiperidine-1-oxyl; MAL-6: 4-maleimido-2,2,6,6-tetramethylpiperidine-1-oxyl; TEMPO: 2,2,6,6-tetramethylpiperidine-1-oxyl; PD-TEMPOL: 4-hydroxy-d_{17}-2,2,6,6-tetramethylpiperidine-1-oxyl; esr: electron spin resonance; st-esr: saturation transfer electron spin resonance.

hemolysis was achieved by dilution of equal volumes of packed cells and distilled water. The hemolyzed cells were centrifuged for 40 min at 20 000 rpm (Sorvall RC-5B refrigerated centrifuge) at 4°C, and the supernatant hemoglobin solution was maintained, discarding the pelleted membranes. The hemolyzate was then filtered in a Sephadex G-25 column (11) avoiding substantial dilution. This hemoglobin solution was used in our studies. Solutions of sperm whale myoglobin and egg-white lysozyme were obtained by dissolving the lyophilized commercial material (Sigma Chemical Co.) in phosphate buffer 0.05 *M*, pH 7.0 so that the protein concentration was approximately 10%. After dilution a centrifugation step was used to remove unsoluble material from the solution.

Spin labeling of the proteins

Hemoglobin solution was spin labeled with 2,2,6,6-tetramethylpiperidino-1-oxyl (TEMPO, Aldrich Chem. Co.) and 4-hydroxy-2,2,6,6-perdeuterotetramethylpiperidine-1-oxyl (PD-TEMPOL Merck Co.) in the following way: an aliquot of a stock solution of the label (approximately 10 m*M*) was introduced into the bottom of a test tube and dried under a N_2 flux. Then the hemoglobin solution was added on top in such volume as to make the final spin-label concentration 2×10^{-4} *M* for PD-TEMPOL and 5×10^{-4} *M* for TEMPO. In the case of the reaction of myoglobin and lysozyme with 4-maleimido-2,2,-6,6-tetramethylpiperidino-1-oxyl (MAL-6, Aldrich Chem. Co.) the procedure was similar: an aliquot of a stock solution of MAL-6 in acetone was introduced into the bottom of a test tube and dried under N_2. Then the protein solution was added in such a way as to make the following proportions: MAL-6/myoglobin 1:1 and MAL-6/lysozyme 1:1. The reaction mixture was left in the refrigerator at 4°C for 38 h. The excess spin label was removed by filtration of the reaction mixture in a small Sephadex G-25 column. All the labeled samples were lyophilized and dried over P_2O_5 in order to obtain the dry samples. In some experiments the sample was then exposed to a known water vapour pressure in a saturated salt solution container. The solution sample was used after the Sephadex G-25 filtration step.

Electron spin resonance measurements

Conventional esr and st-esr spectra were obtained using a Varian E-109 X-band spectrometer (9.14 GHz) equipped with a rectangular cavity E-248 and the temperature control accessory E-257. The temperature was monitored by a copper–constantan thermocouple attached to a Fluck potentiometer. The microwave power used was 2 mW and modulation amplitude 1.0 G. The st-esr spectra were obtained as the second harmonic out-of-phase signal. The self-null method was used in the adjustment of phase (12) with the sample in the cavity, modulation amplitude 5.0 G and 1-mW microwave power. After this adjustment the power was increased to 64 mW (measurements were also made at 30 mW at lower temperatures) and the second harmonic out-of-phase signal recorded. In the case of hemoglobin spin labeled with TEMPO or PD-TEMPOL, adjustments of phase were also made at the 0.1-mW power level, as at the lowest temperatures the sample is more readily saturated. The analysis of the st-esr spectra was made by comparison of the experimental spectra parameters L″/L and C′/C with calibrations obtained by Thomas (12).

Results and discussion

Covalent spin labels

In Fig. 1 the conventional esr spectra of spin labeled myoglobin are presented for different temperatures. In Fig. 1(a) the spectra were obtained for the solution sample while Fig. 1(b) is for the dry sample. The parameters used in our analysis are $2A_{zz}$, the splitting between the outer hyperfine lines, and ΔH, the linewidth at half height of the low field line. The spectra obtained with spin labeled lysozyme, in the temperature range -10 to -150°C, are similar to those of myoglobin, so that the spectra in Fig. 1 are characteristic of the two proteins. A careful inspection of the spectra shows clearly an increase in ΔH and $2A_{zz}$ as the temperature is lowered.

In Fig. 2(a) the parameter $2A_{zz}$ from the esr spectra is plotted

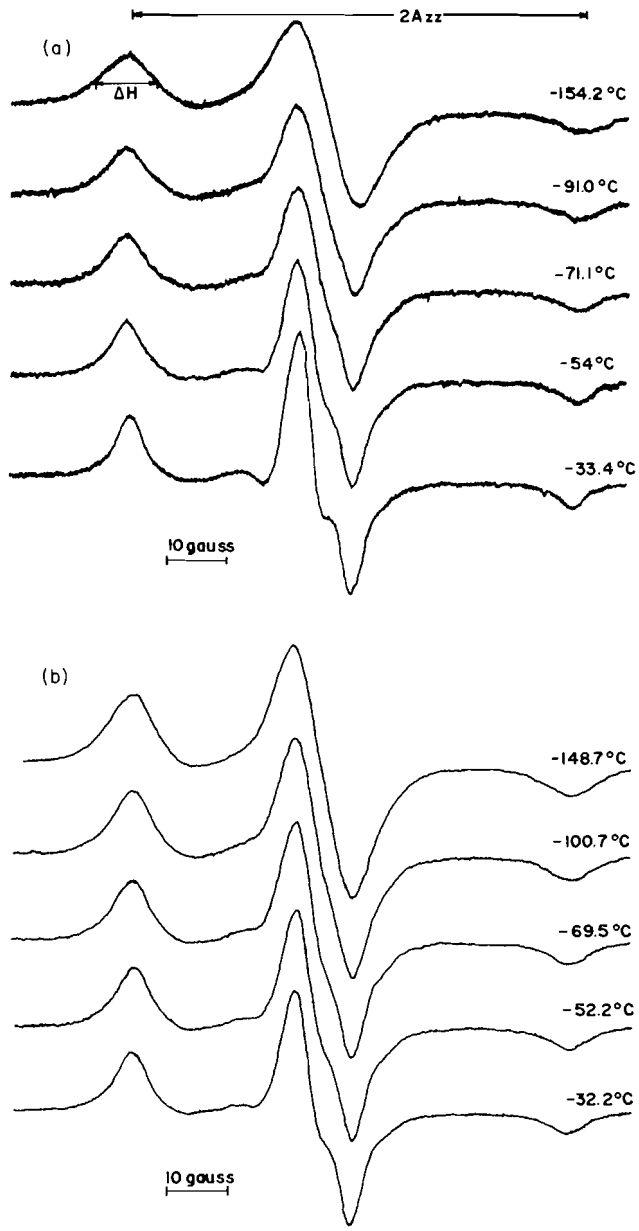

FIG. 1. (a) Conventional esr spectra of myoglobin–MAL-6 aqueous solution. The temperature is indicated in the spectrum as well as the esr parameters $2A_{zz}$ and ΔH. (b) Conventional esr spectra of myoglobin–MAL-6 dry powder sample. The temperature is indicated in the spectrum.

as a function of temperature for lyophilized and aqueous solution of myoglobin–MAL-6. For both samples a decrease is observed in $2A_{zz}$ with an increase in temperature, with the dry sample having a lower $2A_{zz}$ value over almost the whole temperature range studied. For the dry sample a single straight line could be fitted to the data as shown in Fig. 2(a). On the other hand, two straight lines were fitted to the data for the solution sample, one for temperatures below -60°C and another above this value. It is interesting to note that for the low temperature region the behavior of the two samples is similar, i.e., the straight lines fitted to the data are practically parallel, indicating that the rate of change of $2A_{zz}$ is the same. Above -60°C there is a faster decrease in $2A_{zz}$ for the solution sample, so that above ca. -10°C the value for the solution is smaller than the value for the dry sample.

In Fig. 2(b) the plot of the temperature dependence of the

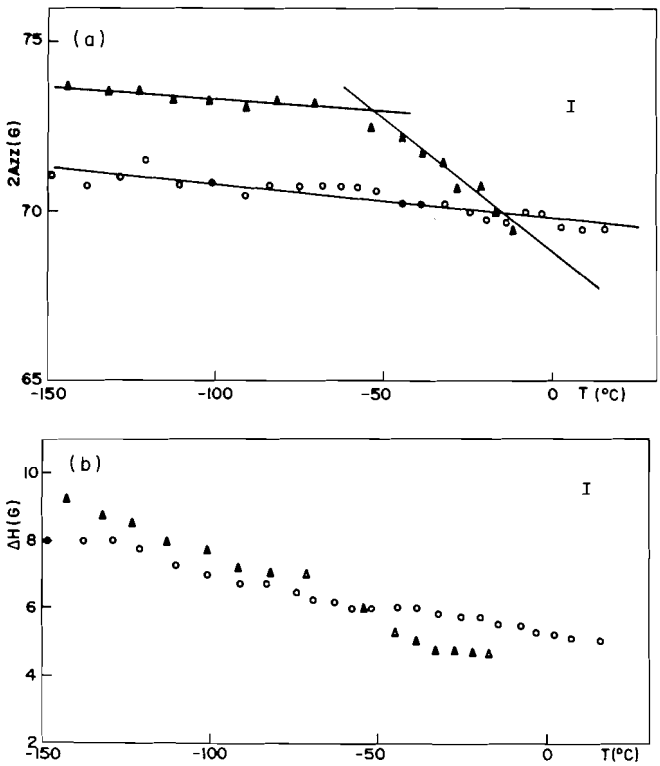

FIG. 2. (a) The parameter $2A_{zz}$ as a function of temperature for myoglobin–MAL-6 samples. The straight lines are least-square fits to the experimental points. Key: (Δ) aqueous solution; (o) lyophilized sample (water content: 0.12 g H_2O/g myoglobin). The error in the measurement above −100°C is 0.3 G; below −100°C it is increased to 0.5 G due to the broadening which introduces additional error especially in the high field. The bars in the figure correspond to the errors indicated above. (b) The linewidth of the low field line as a function of temperature for myoglobin–MAL-6 samples. Key: (Δ) aqueous solution; (o) lyophilized sample (water content: 0.12 g H_2O/g myoglobin). The error in ΔH is the same as in Fig. 2(a).

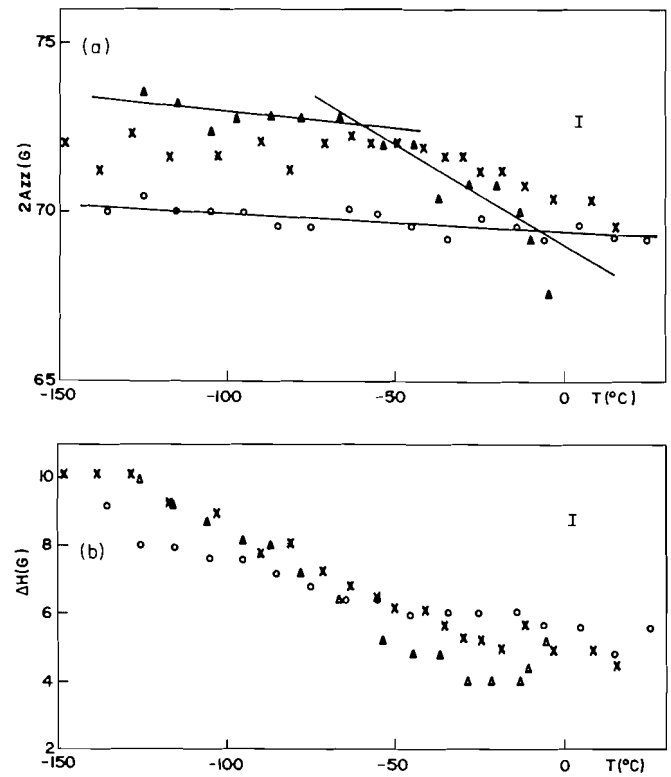

FIG. 3. (a) The parameter $2A_{zz}$ as a function of temperature for lysozyme–MAL-6 samples. The straight lines are least-square fits to the experimental points. Key: (Δ) aqueous solution; (o) lyophilized sample (water content: 0.07 g H_2O/g lysozyme); (x) intermediate water content sample (0.45 g H_2O/g lysozyme). The error is the same as in Fig. 2(a). (b) The linewidth of the low field line as a function of temperature for lysozyme–MAL-6 samples. Key: (Δ) aqueous solution; (o) lyophilized sample (water content: 0.07 g H_2O/g lysozyme); (x) intermediate water content (0.45 g H_2O/g lysozyme). The error is the same as in Fig. 2(a).

linewidth of the low field line is shown for the two samples of spin labeled myoglobin. A general decrease of ΔH is observed with an increase in temperature. In this case a different behavior can be noticed for the dry and solution samples below and above ca. −60°C. At lower temperatures (below −60°C) the linewidth for the dry sample is less than for the solution sample, while at temperatures above −60°C the linewidth for the solution sample is less than that for the dry sample. The variation of linewidth for the dry sample over the whole temperature range ($\Delta(\Delta H)$=3 G) is less than that for the solution sample ($\Delta(\Delta H)$ = 5 G). The error of the ΔH measurement is estimated to be 0.4 G.

In Figs. 3(a) and 3(b), respectively, the parameters $2A_{zz}$ and ΔH are presented as a function of temperature for lysozyme–MAL-6 with different water contents. The behavior of these parameters described for myoglobin is also valid in this case. The variation of $2A_{zz}$ for the dry sample is very small, while for the solution sample it is considerable. Again, for the dry sample a unique rate of decrease of $2A_{zz}$ with temperature is observed, while the solution sample shows this same rate below −60°C and a faster rate above −60°C. Over the whole temperature range, the variation of ΔH for the solution is greater than that for the dry sample. The two curves cross near −60°C, so that below this temperature the value for the solution is larger while above this temperature the value for the dry sample is larger. The experiment with lysozyme with an intermediate water content (0.45 g H_2O/g protein) resulted in a $2A_{zz}$ plot lying between the data for the dry and solution samples (Fig. 3(a)). Below ca. −45°C a straight line could be fitted to the data and it is parallel to the one fitted to the lyophilized sample data. Above ca. −45°C another straight line could be fitted to the data, with a slope between those obtained for the dry and solution samples. As shown in Fig. 3(b), −45°C is also the temperature at which the ΔH data obtained for this intermediate water content sample and for the lyophilized sample intersect.

The changes observed for the parameters $2A_{zz}$ and ΔH with temperature suggest that the spin label used is undergoing changes in motional properties (13,14). In order to verify this proposition the saturation transfer technique was used. In Fig. 4 the st-esr spectra obtained for myoglobin samples at different temperatures are shown. Fig. 4(a) is for the solution sample, while Fig. 4(b) is for the dry one. The parameters obtained from these spectra are L″/L and C′/C. They have different sensitivities to slow motion; L″/L is the most sensitive and for this reason was the parameter of our choice. The values of L″/L obtained for several samples studied in this work are presented in Table 1. Comparison of these values with the calibration curves of Thomas (16) shows that below −10°C the correlation times are greater than 10^{-5} s. The direct comparison of the lineshapes of our st-esr spectra with those reported in the literature (15,16) also shows that in our case the labels are very immobilized. In this way, st-esr indicates that the label is very

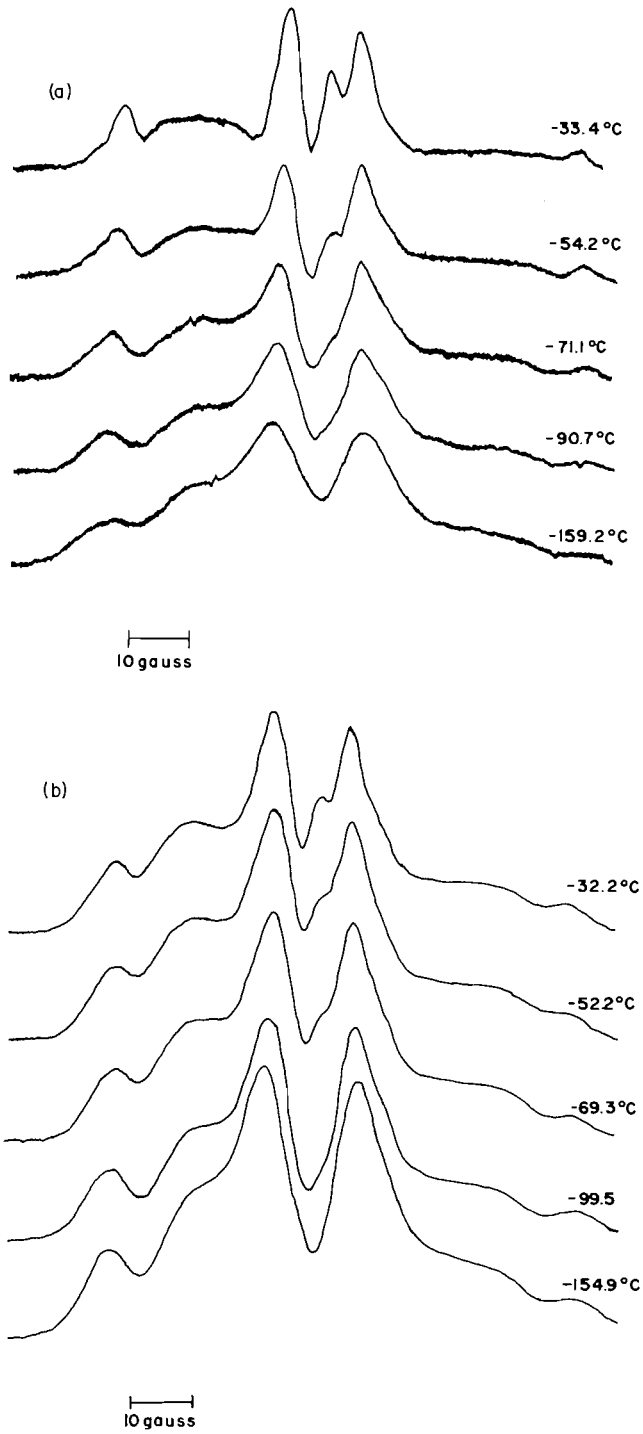

FIG. 4. (a) The st-esr spectra of myoglobin–MAL-6 aqueous solution. The temperature is indicated in the spectrum. The st-esr parameters measured are also indicated. (b) The st-esr spectra of myoglobin–MAL-6 dry powder sample at different temperatures.

immobilized so that the changes in $2A_{zz}$ and ΔH are not due to motional changes of the label.

The dependence of $2A_{zz}$ with temperature for the lyophilized samples can be interpreted in terms of the librational motion of the spin label, as proposed by Johnson (10). This model is based on the fluctuations of the $\diagdown$N—O$\diagup$ bond orientation with respect to the C—N—C plane of the nitroxide ring, which could produce torsional motion of the ring. This effect produces a temperature-dependent hyperfine separation of the form

$$2A_{zz}(T) = A^0_{zz}\,(1 + \cos\theta)$$

where $\theta = (RT/E_A)^{1/2}$, θ being the half angle of oscillation, E_A the torsional energy barrier, and $2A^0_{zz}$ the separation in absence of motion. For small oscillations it gives a linear dependence of $2A_{zz}$ with the temperature. This model was used to fit the experimental data for MAL-6 spin labeled lyophilized hemoglobin (10). For our lyophilized samples we observed this linear behavior over the whole temperature range studied. The solution samples at low temperatures also have this $2A_{zz}$ dependence, indicating that in the frozen solution the presence of the water does not affect the spin label motion. Its presence, however, increases the local polarity of the medium, causing an increase in the spin density on the nitrogen in the $\diagdown$N—O$\diagup$ group of the spin label, leading to an increase in $2A_{zz}$. The behavior of $2A_{zz}$ for the solution sample above -60°C can be explained as due to the thawing of the water of hydration, which will presumably facilitate the motion of the label. In the case of the lysozyme sample with intermediate hydration we found that the change in slope for the $2A_{zz}$ vs. T plot takes place at a higher temperature (-45°C) and the slope of this curve is less than that for the solution sample; in this way this temperature of slope change and the slope at this region are probably strongly dependent on the hydration of the protein. In the solution sample, as the temperature is raised above -10°C the free water also thaws and the spectra become typical of solutions. Therefore, below -10°C the same model, i.e., librational motion of the spin label, can be used for the dry and solution samples. Johnson (10) explained the dependence of $2A_{zz}$ upon temperature for hemoglobin–MAL solutions as due to the formation of a hydrogen bond between $\diagdown$N=O$\diagup$ group of the spin label and a proton that could be either in the protein (near the binding site of the label) or in a water molecule. The plots of the parameter $2A_{zz}$ as a function of temperature obtained for the proteins studied in the present work are similar to those described in ref. 10. The change of slope in the $2A_{zz}$ temperature dependence for the hemoglobin–MAL-6 solution sample in this reference also takes place around -60 to -70°C. This general behavior of $2A_{zz}$ suggests that the hydrogen bond is probably not due to the specific site of attachment of the label in the protein, as it is common to all three proteins, but that it involves a water molecule.

At a temperature near the transition between the first and second regions for $2A_{zz}$, considerable changes in ΔH are observed. Near -60°C the dependence of ΔH for the dry and solution samples cross one another so that at temperatures below -60°C ΔH is greater for the solution sample, while at temperatures above -60°C ΔH is greater for the dry sample. The increase in linewidth with a decrease in temperature comes from the inhomogeneous broadening due to the methyl protons of the spin label and the protons of water molecules near the label. Below -60°C the water in the solution sample is frozen and there is electron-nuclear interaction with the water protons and with the spin label methyl protons. For the dry sample, the interaction is mostly with the methyl protons since very few water molecules are present, hence the lower value of ΔH obtained. Above -60°C the water of hydration in the solution

TABLE 1. The st-esr parameter L″/L at different temperatures*

Temperature, °C	L″/L				
	Lyso–MAL-6 0.45 g H_2O/g lyso	Mb–MAL-6 solution	Mb–MAL-6 dry powder 0.12 g H_2O/g Hb	Hb–TEMPO dry powder 0.12 g H_2O/g Hb	Hb–PD-TEMPOL dry powder 0.12 g H_2O/ Hb
−156	—	—	1.29	—	1.64
−132	—	1.43	—	—	—
−114	—	1.31	—	—	1.60
−100	—	—	1.22	—	—
−90	2.05	1.31	—	—	—
−83	1.96	—	1.32	1.60	1.48
−70	—	1.10	1.45	—	—
−64	1.73	0.96	—	—	1.48
−52	1.64	0.93	1.45	1.57	—
−42	1.48	0.88	—	—	1.36
−33	1.30	0.79	1.35	—	—
−25	1.24	0.76	—	1.32	—
	The st-esr parameter C′/C in the temperature range −20 to −150°C				
	0.41–0.55	0.10–0.35	0.28–0.40	0.35–0.60	0.47–0.67

*From ref. 12 a value of L″/L of 0.98 corresponds to correlation times in the range 10^{-4} – 10^{-3} s; C′/C of 0.33 corresponds to correlation times in the range 10^{-5} – 10^{-4} s.

samples thaws, allowing the methyl groups and the water molecules to move more freely. This motion makes the electron-nuclear interaction less effective, and results in a smaller ΔH if compared to the value for the dry sample, where the methyl proton interaction is still effective. The temperature of −60°C, as noted above, also corresponds to the change in slope for $2A_{zz}$ vs. T plot. It is interesting that the linewidth changes described above can be observed directly from the esr spectra (Fig. 1): in the temperature range below −60°C, ΔH is increased in the solution sample to a greater extent than in the dry sample; the opposite occurs above −60°C. It is noticed that an improved resolution is obtained above −60°C for the solution sample in the central part of the esr spectra, consistent with the decrease in linewidth. Finally, it should be noted that the characteristic temperature for the lysozyme sample with intermediate hydration is the same both in the $2A_{zz}$ vs. T and ΔH vs. T plots (−45°C).

Noncovalent small spin probes

Since the results obtained with MAL-6 spin labeled samples suggest a general behavior of $2A_{zz}$ and ΔH for all proteins studied, an attempt was made to monitor the hydration of the samples with small noncovalent spin probes: human hemoglobin was labeled with two different small spin labels, TEMPO and PD-TEMPOL. In this second label the piperidine ring has deuterium instead of hydrogen, decreasing the inhomogeneuous broadening due to the electron-nuclear interaction. In Fig. 5(a) the parameter $2A_{zz}$ is presented for the spin labels TEMPO and PD-TEMPOL dissolved in hemoglobin solution and as dry powder samples. It can be seen that in the dry samples $2A_{zz}$ changes are quite small: a slight increase with lowering of the temperature is observed. The hemoglobin solution samples show a greater change of $2A_{zz}$ versus T: the slope of the curve becomes greater above ca. −60°C, and at low temperatures (below −60°C) the slope is similar to that in the dry sample. In fact, for PD-TEMPOL the slopes are the same. In this case, as the lines are relatively narrow and well resolved, $2A_{zz}$ is measured with good accuracy (0.2 G). In the case of TEMPO the lines are broader and the accuracy of measurement is not as good (around 0.4 G). For this reason the slopes are not exactly the same for this label. This behavior of $2A_{zz}$ vs. T is analogous to that obtained with the covalently labeled proteins. For the solution samples, again, a change of slope takes place around −60°C. On the other hand, the changes for the dry samples are quite small and linear over the whole temperature range. In Fig. 5(b) the linewidth ΔH for the samples described above is plotted as a function of temperature: it is clear that ΔH is much less for PD-TEMPOL than for TEMPO. As noted previously in the case of PD-TEMPOL, the inhomogenous broadening due to the protons in the piperidine ring is eliminated. This accounts for the difference of about 2 G in ΔH for TEMPO and PD-TEMPOL. The behavior of ΔH with temperature shows a very slight change over the whole temperature range. Furthermore, the differences in ΔH between the dry and solution samples are within experimental error. This result is different from that with the covalent spin label, where the changes in ΔH, although small, are significant. Perhaps this is related to the fact that the covalent label is tightly bound to the protein, while the small spin probes do not interact with the protein that remains dissolved in the solution (or powder). For this reason the linewidths for TEMPO and PD-TEMPOL represent a static distribution of orientations, which is the same both in the powder and in the frozen solution. The presence of water affects only the polarity of the label, making $2A_{zz}$ greater in the solution samples. In the case of the covalent label attached to the protein the linewidth is also affected by the restrictions imposed by the protein matrix. In this case the values of ΔH are not only given by a static distribution but also depend on the local state of the protein, which is a function of hydration. In this way the changes observed around −60°C can be correlated with the thawing of hydration water above this temperature: this will allow an increase in motion in the microenvironment of the spin label and a narrowing of the esr lines will take place for the solution sample (above −60°C, ΔH for the solution is smaller

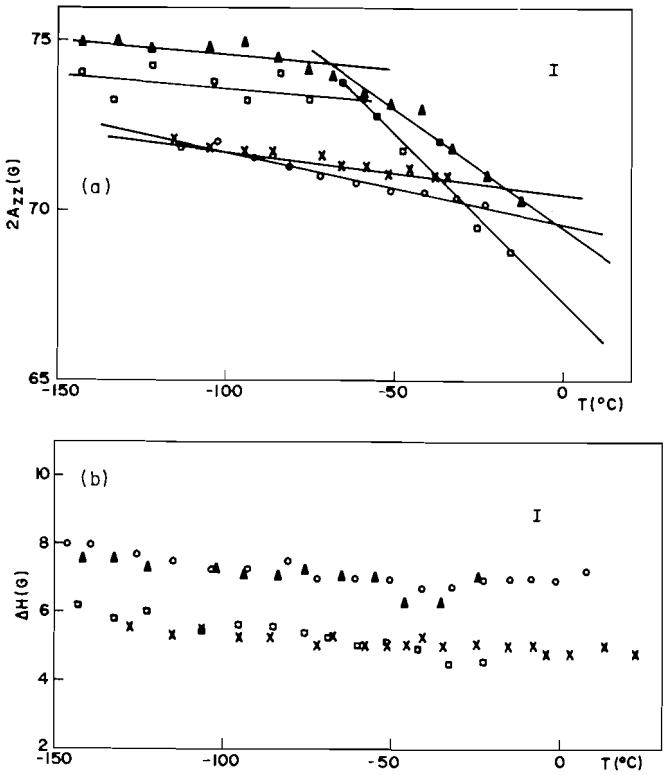

FIG. 5. (a) The parameter $2A_{zz}$ as a function of temperature for hemoglobin samples spin labeled with the small probes: TEMPO (Δ) aqueous solution and (o) dry powder sample (0.12 g H_2O/g hemoglobin), and PD-TEMPOL (o) aqueous solution and (x) dry powder sample (0.12 g H_2O/g hemoglobin). The error in the case of TEMPO is the same as in Fig. 2(a). For PD-TEMPOL it is reduced to 0.2 G due to the narrowing of the lines. (b) The linewidth of the low field as a function of temperature for hemoglobin samples. Key: (o) lyophilized hemoglobin–TEMPO (water content: 0.12 g H_2O/g hemoglobin; (Δ) hemoglobin–TEMPO aqueous solution; (x) lyophilized hemoglobin–PD-TEMPOL (water content: 0.12 g H_2O/g hemoglobin; (□) hemoglobin-PD-TEMPOL aqueous solution.

than ΔH for the dry sample). This would explain the ΔH changes for the covalent label. The $2A_{zz}$ changes are similar for all the labels used, as they reflect the polarity of the microenvironment. It is worth mentioning the results in refs. 17 and 18 on the dynamics of myoglobin at low temperature. These authors show that the mean-square displacements for most residues $\langle x^2 \rangle$ as a function of temperature show a discontinuity around 220 K (−53°C). It is suggested that these changes in the protein structure are correlated to the state of water in the protein. Studies of the absorption of microwaves in crystals of Met Mb also show a gradual thawing of water upon heating above −53°C (19). These results are in agreement with our data showing that a structural change takes place near −60°C.

Conclusions

Our conclusions can be summarized as follows.

(1) The behavior of the parameter $2A_{zz}$ with temperature is the same for the three proteins studied, hemoglobin, myoglobin, and lysozyme, as observed with the different spin labels, MAL-6, TEMPO, and PD-TEMPOL. This behavior must probably be common to all proteins and we believe reflects the sensitivity of the spin label to the polarity of its microenvironment.

(2) The lyophilized samples show a small linear increase in $2A_{zz}$ with decrease in temperature. Again, this is a feature common to proteins and spin labels used in this work. A restriction of the spin label librational motion could be responsible for this effect, as proposed by Johnson (10), although other possibilities are not excluded.

(3) The behavior of the protein in solution for temperatures below ca. −60°C is similar to the lyophilized protein ($2A_{zz}$ versus T). At this temperature the water present is already frozen and its presence does not affect the spin label motion. However, it changes the polarity of the medium and this explains the larger value of $2A_{zz}$ observed for the solution sample compared to the lyophilized sample. As the temperature is increased above −60°C the water of hydration starts to thaw. This facilitates the spin label motion and a larger rate of change of $2A_{zz}$ with temperature is observed. Around −10°C the thawing of the bulk water causes another change in the $2A_{zz}$ behavior.

(4) In the case of the parameter ΔH it is necessary to analyze separately the covalent spin label and the small probes. For the covalent maleimide label, the dependence of ΔH upon temperature also shows −60°C as a characteristic temperature. Below −60°C the sample in solution has a larger ΔH value than the lyophilized sample, while above −60°C the inverse is true. This can be interpreted as due to a motional narrowing effect in the solution sample due to the thawing of hydration water.

(5) The small probes TEMPO and PD-TEMPOL do not show differences in the behaviour of ΔH for solution and dry samples. This is explained as due to a similar static distribution of label orientations in both samples. As expected, the linewidth ΔH for the deuterated label PD-TEMPOL is 2 G less than ΔH for TEMPO. This is due to the elimination of inhomogenous broadening in PD-TEMPOL.

(6) The spectral changes observed as a function of temperature suggest that the parameter $2A_{zz}$ is quite sensitive to the hydration state of the sample. Since the sensitivity of ΔH depends on the spin label used and since its variation is small, it might be interesting to study in more detail the $2A_{zz}$ vs. T dependence as a function of protein hydration.

(7) Electron spin resonance measurements, as proposed by Rupley *et al.* (6) can be another method used to study protein hydration.

Acknowledgments

We appreciate the financial support of the Brazilian agencies FAPESP, CNPq, FINEP, and CAPES.

1. J. L. FINNEY, J. M. GOODFELLOW, and P. L. POOLE. Structural molecular biology. *Edited by* D. B. Davies, W. Saenger, and S. S. Danyluk. Plenum Press,New York. 1982. p. 387.
2. J. A. RUPLEY, E. GRATTON, and G. CARERI. Trends Biochem. Sci. **8**, 18 (1983).
3. S. MASCARENHAS. Top. Appl. Phys. **33**, 321 (1979).
4. K. S. KIM, G. CORONGIU, and E. CLEMENTI. J. Biomol. Struct. Dyn. **1**, 263 (1983).
5. J. A. MCGAMMON, B. R. GELIN, and M. KARPLUS. Nature (London), **267**, 585 (1977).
6. J. A. RUPLEY, P. H. YANG, and G. TOLLIN. Water in polymers. *Edited by* S. P. Rowland. Am. Chem. Soc., Washington. 1980. p. 111.
7. N. T. YU and B. H. JO. J. Am. Chem. Soc. **95**, 5033 (1973).
8. W. E. BROWN III, J. W. SUTCLIFFE, and P. D. PULSINELLI. Biochemistry, **22**, 2914 (1983).
9. V. RENUGOPALAKRISHNAN and R. S. BHATNAGAR. J. Am. Chem. Soc. **106**, 2217 (1984).
10. M. E. JOHNSON. Biochemistry, **20**, 3319 (1981).

11. M. W. NEAL and J. R. FLORINI. Anal. Biochem. **55**, 328 (1973).
12. D. D. THOMAS, L. R. DALTON, and J. S. HYDE. J. Chem. Phys. **55**, 3000 (1976).
13. S. A. GOLDMAN, G. V. BRUNO, and J. H. FREED. J. Phys. Chem. **76**, 1858 (1972).
14. R. P. MASON and J. H. FREED. J. Phys. Chem. **78**, 1321 (1974).
15. L. R. DALTON, B. H. ROBINSON, L. A. DALTON, and P. COFFEY. Adv. Magn. Reson. **8**, 149 (1976).
16. D. D. THOMAS. Ph. D. Thesis, Stanford University, 1975.
17. H. HARTMANN, F. PARAK, W. STEIGEMANN, G. A. PETSKO, D. R. PONZI, and H. FRAUENFELDER. Proc. Natl. Acad. Sci. USA, **79**, 4967 (1982).
18. E. R. BAUMINGER, S. G. COHEN, I. NOWIK, S. OFER, and J. YARIV. Proc. Natl. Acad. Sci. USA, **80**, 736 (1983).
19. G. P. SINGH, F. PARAK, S. HUNKLINGER, and K. DRANSFELD. Phys. Rev. Let. **47**, 685 (1981).

Synthesis and characterization of $LMo(CO)_3M(PPh_3)_x$ (where L = tridentate pyrazolyl-gallate or -borate ligand; M = Rh, x = 2; M = Cu, x = 1). X-ray crystal structures of $[MeGapz_3]Mo(CO)_3Rh(PPh_3)_2$ and $[MeGapz_3]Mo(CO)_3Cu(PPh_3)$ (where pz = pyrazolyl, $N_2C_3H_3$)

GREGORY A. BANTA, BRENDA M. LOUIE (IN PART), EMMANUEL ONYIRIUKA, STEVEN J. RETTIG, AND ALAN STORR[1]

Department of Chemistry, University of British Columbia, 2036 Main Mall, Vancouver, B.C., Canada V6T 1Y6

Received May 24, 1985

GREGORY A. BANTA, BRENDA M. LOUIE, EMMANUAL ONYIRIUKA, STEVEN J. RETTIG, and ALAN STORR. Can. J. Chem. **64**, 373 (1986).

The reactions of the $LMo(CO)_3^-$ ions (L = $MeGapz_3$, $HBpz_3$, $Me_2Gapz(OCH_2CH_2NMe_2)$) with $[Cu(PPh_3)Cl]_4$ and $Rh(PPh_3)_3Cl$ have yielded complexes with Mo—Cu and Mo—Rh bonds. The X-ray crystal structures of two such complexes have been determined. Crystals of $[MeGapz_3]Mo(CO)_3Cu(PPh_3)$ are monoclinic, a = 17.071(2), b = 16.738(1), c = 23.641(3) Å, β = 104.899(6)°, Z = 8, space group $P2_1/n$, and those of $[MeGapz_3]Mo(CO)_3Rh(PPh_3)_2$, are triclinic, a = 12.519(3), b = 17.182(4), c = 12.071(2) Å, α = 105.02(1), β = 109.87(1), γ = 97.10(2)°, Z = 2, space group $P\bar{1}$. Both structures were solved by conventional heavy atom methods and were refined by full-matrix least-squares procedures to R = 0.040 and R_w = 0.035 for 6296 reflections with $I \geq 2\sigma(I)$ and R = 0.036 and R_w = 0.037 for 5642 reflections with $I \geq 3\sigma(I)$, respectively. The former complex provides a rare example of a 3:3:1, or capped octahedral structure, with a short (mean) Mo—Cu distance of 2.513(9) Å. The latter compound displays one terminal and two bridging CO ligands and a Mo—Rh distance of 2.6066(5) Å.

GREGORY A. BANTA, BRENDA M. LOUIE, EMMANUEL ONYIRIUKA, STEVEN J. RETTIG et ALAN STORR. Can. J. Chem. **64**, 373 (1986).

Les réactions des ions $LMo(CO)_3^-$ (L = $MeGapz_3$, $HBpz_3$, $[Me_2Gapz(OCH_2Ch_2NMe_2)$) avec le $[Cu(PPh_3)Cl]_4$ et le $Rh(PPh_3)_3Cl$ conduisent à des complexes comportant des liaisons Mo—Cu et Mo—Rh. On a déterminé les structures cristallines de deux tels complexes par diffraction des rayons-X. Les cristaux de $[MeGapz_3]Mo(CO)_3Cu(PPh_3)$ sont monocliniques avec a = 17,071(2), b = 16,738(1), c = 23,641(3) Å, β = 104,899(6)°, Z = 8, groupe d'espace $P2_1/n$ alors que ceux du $[MeGapz_3]$-$Mo(CO)_3Rh(PPh_3)_2$ sont tricliniques avec a = 12,519(3), b = 17,182(4), c = 12,071(2) Å, α = 105,02(1), β = 109,87(1), γ = 97,10(2)°, Z = 2, groupe d'espace $P\bar{1}$. On a résolu les deux structures par les méthodes conventionnelles aux atomes lourds et on les a affinées par la méthode des moindres carrés (matrice entière) jusqu'à des valeurs respectives de R = 0,040 et R_w = 0,035 pour 6296 réflexions avec $I \geq 2\sigma(I)$ et R = 0,036 et R_w = 0,037 pour 5642 réflexions avec $I \geq 3\sigma(I)$. Le premier de ces complexes représente un rare exemple d'une structure 3:3:1, une structure octaédrique cappée, avec une distance Mo—Cu moyenne qui est courte, 2,513(9) Å. Dans le dernier composé, on observe la présence d'un ligand CO terminal avec deux agissant comme ponts; la distance Mo—Ph est de 2,6066(5) Å.

[Traduit par le journal]

Introduction

The anionic, symmetrical, tridentate chelating methyltris(1-pyrazolyl)gallate ligand $[MeGapz_3]^-$, was introduced some time ago (1) as an analogue of Trofimenko's $[RBpz_3]^-$ ligand systems, (R = H, alkyl, aryl or pyrazolyl) (2). In addition we have explored extensively the chelating properties of a number of unsymmetrical, uninegative, tridentate ligands having both the pyrazolyl group and an additional bifunctional donor entity attached to a "Me_2Ga" moiety (ref. 3 and references therein). The above ligand systems, being six-electron donors, have been likened to, and compared with, the cyclopentadienyl ion in many "isoelectronic" complexes (4–7). The present account details our recent findings on the reactivity of the $LMo(CO)_3^-$ ions (L = $MeGapz_3$, $HBpz_3$, $Me_2Gapz(OCH_2CH_2NMe_2)$) towards Wilkinson's catalyst, $Rh(PPh_3)_3Cl$, and also towards the $[Cu(PPh_3)Cl]_4$ tetrameric species. Complexes have been isolated containing direct Mo—Rh and Mo—Cu bonds, in addition to CO ligands in a number of bonding modes. X-ray structural data are presented for the two complexes $[MeGapz_3]$-$Mo(CO)_3Rh(PPh_3)_2$ and $[MeGapz_3]Mo(CO)_3Cu(PPh_3)$.

Experimental

Starting materials

Air-sensitive materials were handled in a nitrogen atmosphere. Tetrahydrofuran(THF), benzene, CH_2Cl_2, and hexane were dried by refluxing over Na/benzophenone, potassium, CaH_2 and $CaSO_4$, respectively, followed by distillation. $Rh(PPh_3)_3Cl$ (Strem Chemicals) was used as supplied. The sodium salt of the methyl tris(1-pyrazolyl)-gallate ligand, $Na^+[MeGapz_3]^-$, was prepared as a THF solution as described previously (1). The ligand $Na^+[Me_2Gapz(OCH_2CH_2NMe_2)]^-$ was also prepared as a THF solution as described in ref. 8. $K^+HBpz_3^-$ (9), $(MeCN)_3Mo(CO)_3$ (10), and $[Cu(PPh_3)Cl]_4$ (11) were prepared by literature methods.

Synthesis of $LMo(CO)_3Rh(PPh_3)_2$ (where L = $[MeGapz_3]$, $[HBpz_3]$, or $[Me_2Gapz(OCH_2CH_2NMe_2)]$)

The Na^+L^- ligand solution (~0.4 mmol in 100 mL) was added to a stirred solution of an equimolar amount of $(MeCN)_3Mo(CO)_3$ (~0.1 g) in the same solvent. The initial yellow coloration of the molybdenum complex in THF changed to an amber colour on addition of the ligand solution. The reaction mixture was stirred for ~2 days during which time the amber colour intensified. The resulting solution of Na^+LMo-$(CO)_3^-$ was reacted directly with $Rh(PPh_3)_3Cl$, added as a slurry in ~100 mL THF. The dark red reaction mixture was stirred for a further 2 days and then the solvent was removed *in vacuo* to afford dark red-black residues. The residue was extracted with benzene and filtered. Evaporation of the solvent from the filtrate gave an oily red-black material which was recrystallized from CH_2Cl_2/hexane to give air-stable dark-red crystals of the desired products in approximately 60% yield. Analytical, ir, nmr, and other data for the three complexes are collected in Table 1 and the ^1H nmr spectrum for the $[MeGapz_3]Mo$-$(CO)_3Rh(PPh_3)_2$ complex is shown in Fig. 1. The mass spectrum of this latter complex displayed signals due to the P—PPh_3^+ ion at ~890.

[1]Author to whom correspondence may be addressed.

TABLE 1. Physical data for the complexes $LMo(CO)_3M(PPh_3)_x$

L	M	x	Analysis (Calcd./found) C	H	N	ν_{CO}(cm^{-1}) CH_2Cl_2 (Nujol)	^{1}H nmr[a] GaMe	pz-H^3	pz-H^4	pz-H^5	PPh_3	Other
$MeGapz_3$	Rh	2	53.82	3.88	7.67	1873,1772,1758	[b]10.00s	2.70d	4.06t	2.89d	2.05m	—
			54.04	4.07	7.58	(1897,1763,1744)					3.04m	
$HBpz_3$[c]	Rh	2	53.23	3.80	7.60	1871,1772,1757	[b]—	2.71d	4.24t	2.96d	2.09m	5.71s CH_2Cl_2 solvate
			53.49	3.83	7.73	(1863,1772,1766)					3.04m	
$Me_2Gapz(OCH_2CH_2NMe_2)$	Rh	2	54.26	4.65	3.96	1852,1762,1737	[d]10.42s 10.29s	2.32d	3.69t	Obscured by PPh_3 signals	2.60m	8.07s 7.09s NMe_2
			54.52	4.72	3.83							
$MeGapz_3$	Cu	1	46.96	3.41	10.61	1898,1798	[d]9.42s	2.02d	3.69t	2.19d	2.45m	—
			46.91	3.43	10.54	(1890,1805,1780)						

[a]S = singlet, d = doublet, m = multiplet and t = triplet.
[b]C_6D_6 solution, $\tau_{C_6H_6}$ = 2.84 ppm, $J_{HCCH} \approx$ 2 Hz for pz protons.
[c]Crystallized as CH_2Cl_2 monosolvate, ν_{BH} = 2483 cm^{-1}.
[d]$(CD_3)_2CO$ solution, $\tau_{(CD_3)_2CO}$ = 7.89 ppm, $J_{HCCH} \approx$ 2 Hz for pz protons.

In the preparation of $[HBpz_3]Mo(CO)_3Rh(PPh_3)_2$ a yellow crystalline sample of the complex $(Ph_3P)_2Rh(CO)Cl$ *Anal.* calcd.: C 64.31, H 4.34; found: C 63.73, H 4.27; ν_{CO} 1980 cm^{-1} (CH_2Cl_2)) was also isolated in low yield.

Synthesis of [MeGapz$_3$]Mo(CO)$_3$CuPPh$_3$

A solution of the $Na^+[MeGapz_3]Mo(CO)_3^-$ salt in THF was prepared as described above. A one-quarter molar amount of $[Cu(PPh_3)Cl]_4$ was added to the reaction mixture and produced an immediate rusty-orange colour. This reaction mixture was stirred for approximately 1 day before the removal of solvent *in vacuo*. The resulting orange residue was extracted with CH_2Cl_2 and the mixture filtered. Hexane was added to the filtrate and the mixed solvents allowed to evaporate slowly. Golden-yellow air-stable crystals of the product, $[MeGapz_3]Mo(CO)_3CuPPh_3$, were produced from the concentrated solutions in approximately 60% yield. Pertinent physical data are included in Table 1 for the complex.

X-ray crystallographic analyses

*[Methyltris(1-pyrazolyl)gallato(*N,N,N*)]tricarbonylmolybdenum-(triphenylphosphine)copper (*Mo—Cu*)*

A crystal bounded by the 8 faces (followed by their distances in millimeters from a common origin): ±(0 0 1), 0.075, ±(1 0 1), 0.100 ±(−1 0 1), 0.113, ±(0 1 0), 0.219 was mounted in a general orientation. Unit-cell parameters were refined by least-squares on 2 sin θ/λ values for 25 reflections (2θ = 26–32°) measured on a diffractometer with Mo-$K\alpha$ radiation ($\lambda(K\alpha_1)$ = 0.70930, $\lambda(K\alpha_2)$ = 0.71359 Å). Crystal data at 22°C are:

$C_{31}H_{27}CuGaMoN_6O_3P$ fw = 791.8

Monoclinic, a = 17.071(1), b = 16.738(1), c = 23.641(3) Å, β = 104.899(6)°, V = 6528(1) Å^3, Z = 8, ρ_c = 1.611 Mg m^{-3}, $F(000)$ = 3168, μ(Mo-$K\alpha$) = 19.2 cm^{-1}. Absent reflections: $h0l$, $h+l$ odd, and $0k0$, k odd, uniquely indicate the space group $P2_1/n$ [non-standard setting of $P2_1/c$, C_{2h}^5, No. 14, equivalent positions: ±(x, y, z; ½−x, ½+y, ½−z)].

Intensities were measured with graphite-monochromated Mo-$K\alpha$ radiation on an Enraf–Nonius CAD4-F diffractometer. An ω–2θ scan at 1.01–10.06° min^{-1} over a range of (0.57 + 0.35 tan θ) degrees in ω (extending by 25% on both sides for background measurement) was employed. Data were measured to 2θ = 55°. The intensities of three check reflections, measured every 3600 s throughout the data collection, remained constant to within 1.5%. After data reduction,[2] an absorption correction was applied using the Gaussian integration method (12,13). Transmission factors ranged from 0.661 to 0.764 for 64 integration points. Of the 14 929 independent reflections measured, 6296 (42.2%) had intensities greater than or equal to 2σ(I) above background where $\sigma^2(I) = S + 2B + (0.04(S - B))^2$ with S = scan count and B = normalized background count.

The structure was solved by conventional heavy-atom methods, the coordinates of the Mo, Ga, Cu, and P atoms of each of the two independent molecules being determined from the Patterson function. The remaining non-hydrogen atoms were positioned from a subsequent difference map. In the final stages of refinement all non-hydrogen atoms were refined with anisotropic thermal parameters. Hydrogen atoms were included as fixed contributors in idealized positions (methyl hydrogens based on observed positions, C(sp^3)—H = 0.98, C(sp^2)—H = 0.97 Å), recalculated after each cycle of refinement. The scattering factors of ref. 14 were used for non-hydrogen atoms and those of ref. 15 for hydrogen atoms. Anomalous scattering factors from ref. 16 were used for the Mo, Ga, Cu, and P atoms. The weighting scheme $w = 1/\sigma^2(F)$, where $\sigma^2(F)$ is derived from the previously defined $\sigma^2(I)$, gave uniform average values of $w(|F_o| - |F_c|)^2$ over ranges of both $|F_o|$ and sin θ/λ and was employed in the final stages of full-matrix refinement of 793 variables. Reflections with $I < 2\sigma(I)$

[2]The computer programs used include locally written programs for data processing and locally modified versions of the following: ORFLS, full-matrix least-squares, and ORFFE, function and errors, by W. R. Busing, K. O. Martin, and H. A. Levy; FORDAP, Patterson and Fourier syntheses, by A. Zalkin; ORTEP II, illustrations, by C. K. Johnson.

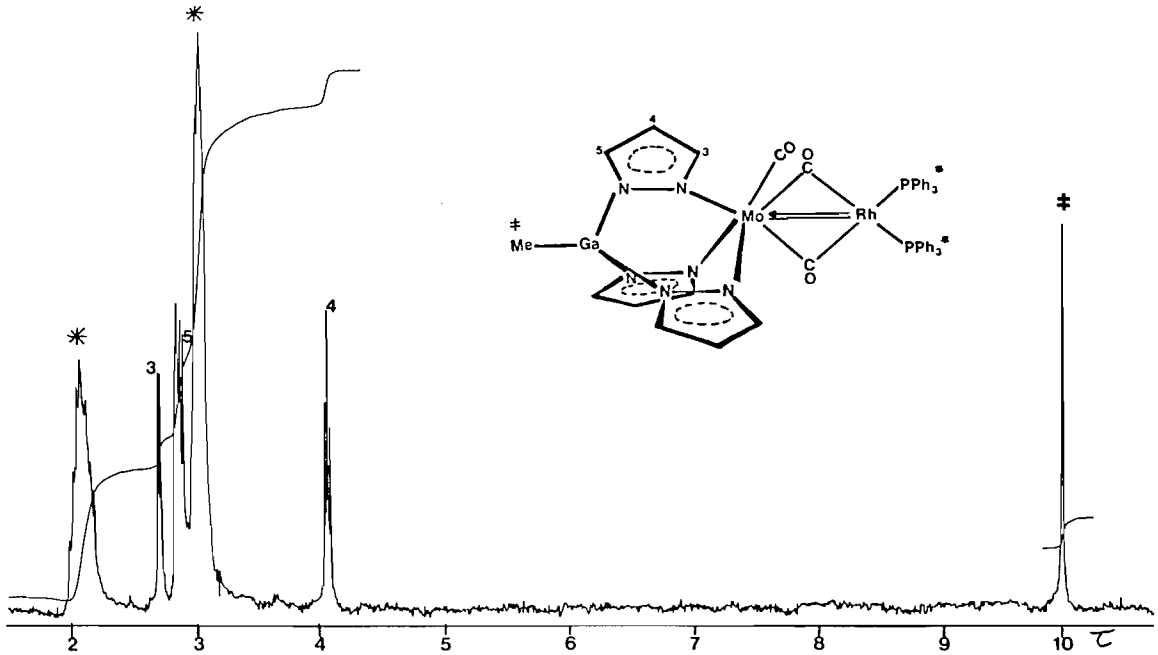

FIG. 1. Room temperature 100-MHz ^{1}H nmr spectrum of $[MeGapz_3]Mo(CO)_3Rh(PPh_3)_2$ in C_6D_6.

were not included in the refinement. Convergence was reached at $R = 0.040$ and $R_w = 0.035$ for 6296 reflections with $I \geq 2\sigma(I)$. For all 14 929 reflections $R = 0.216$. The function minimized was $\Sigma w(|F_o|-|F_c|)^2$, $R = \Sigma||F_o|-|F_c||/\Sigma|F_o|$ and $R_w = (\Sigma w(|F_o|-|F_c|)^2/\Sigma w|F_o|^2)^{1/2}$.

On the final cycle of refinement the mean and maximum parameter shifts correspond to 0.03 and 0.29σ, respectively. The mean error in an observation of unit weight was 1.220. A final difference map showed maximum fluctuations of -1.31 to $+0.61$ e Å^{-3} near the heavy atoms and was essentially featureless elsewhere. The final positional and thermal parameters appear in Tables 2 and 7[3] respectively. Bond lengths, bond angles, and intra-annular torsion angles appear in Tables 3–5, respectively. Calculated hydrogen parameters (Table 6) and a complete listing of torsion angles (Table 8) are included as deposited material.[3] Measured and calculated strucure factors have been placed in the Depository of Unpublished Data.[3]

*[Methyltris(1-pyrazolyl)gallato-(*N,N,N*)tricarbonylmolybdenum-bis(triphenylphosphine)rhodium* (Mo—Rh)

Experimental details are as above except where noted. The bounding planes of the crystal used for data collection were: (0 0 −1), 0.200, ±(1 −1 0), 0.050, ±(0 1 0), 0.125, (−1 −1 1), 0.200 mm. Reflections employed in the refinement of the unit-cell parameters had 2θ = 30–36°. Crystal data:

$C_{49}H_{42}GaMoN_6O_3P_2Rh$ fw = 1093.4

Triclinic, a = 12.519(3), b = 17.182(4), c = 12.071(2) Å, α = 105.02(1), β = 109.87(1), γ = 97.10(2)°, V = 2294(1) Å^3, Z = 2, ρ_c = 1.583 Mg m^{-3}, $F(000)$ = 1100, μ(Mo-$K\alpha$) = 13.1 cm^{-1}. Absent reflections: none, space group $P\bar{1}$ (C_i^1, No. 2, reduced cell, conventional orientation) from structure analysis.

An ω–2θ scan at 1.26–10.06° min^{-1} over a range of (0.75 + 0.35 tan θ)° in ω was employed. Of 10 493 independent reflections measured (to 2θ = 55°), 5642 had $I \geq 3\sigma(I)$ above background. The intensities of the standard reflections remained constant to within 3%. The data were corrected for absorption, transmission factors ranging from 0.578 to 0.913 for 72 sampling points.

The coordinates of the Mo, Rh, Ga, and P atoms were determined from the Patterson function (which suggested the centrosymmetric space group $P\bar{1}$) and those of the remaining non-hydrogen atoms from a subsequent difference map. Hydrogen atoms were fixed in idealized positions. Convergence was reached at $R = 0.036$ and $R_w = 0.037$ for 5642 reflections with $I \geq 3\sigma(I)$ and 568 variables. For all 10 493 reflections $R = 0.102$. The mean and maximum parameter shifts were 0.04 and 0.28σ respectively and the mean error in an observation of unit weight was 1.328. Anomalous scattering corrections were made for Mo, Rh, Ga, and P atoms. The final difference map showed maximum fluctuations of -1.76 to $+0.96$ e Å^{-3} near the Rh atom.

Spectra

The ir spectra were recorded on a Perkin–Elmer 598 spectrometer. The ^{1}H nmr spectra were recorded on a Varian XL-100 or a Bruker WP-80 instrument.

Results and discussion

The reactivity of the $[MeGapz_3]M(CO)_3^-$ ions (M = Mo or W) towards a number of three-electron donor ligands has been well documented and the complex $[MeGapz_3]Mo(CO)_2(\eta^3\text{-}C_3H_5)$ has been characterized structurally (1). The reactivity of the related species $[Me_2Gapz(OCH_2CH_2NR_2)]M(CO)_3^-$ (where R = H or Me) towards similar ligands has also been extensively investigated (17–22). Presently, we are probing the reactions of these tricarbonyl anions, $LM(CO)_3^-$ with a variety of transition metal complexes. The present account details reactions of the ligands (M = Mo) with $Rh(PPh_3)_3Cl$ and $[Cu(PPh_3)Cl]_4$. In all cases crystalline products were obtained and representative examples of these have been characterized structurally by X-ray analysis. These analyses confirm the presence of direct Mo—Rh and Mo—Cu bonds in these compounds in addition to carbonyl groups in a number of different bonding environments (23–26).

Much current research has been directed towards heterobimetallic complexes with transition metal – transition metal bonds, partly since it is reasoned that cooperative effects between the different metal centres may influence the reactivity of such complexes (27–36). It is also argued that studies of simple binuclear species may well provide useful clues into the design and synthesis of larger heterometallic cluster species with potential catalytic applications (ref. 27 and references therein).

[3]The structure factor table, Table 7 (anisotropic thermal parameters) and other material mentioned in the text may be purchased from the Depository of Unpublished Data, CISTI, National Research Council of Canada, Ottawa, Canada K1A 0S2.

TABLE 2. Final positional (fractional × 10^4; Mo, Rh, Ga, Cu, and P × 10^5) and isotropic thermal parameters ($U \times 10^3$ Å^2)[a] with estimated standard deviations in parentheses

Atom	x	y	z	U_{eq}
		$(MeGapz_3)Mo(CO)_3Cu(PPh_3)$		
Mo	31916(3)	9533(3)	39163(2)	37
Mo′	82590(3)	10906(3)	13912(2)	37
Ga	35991(4)	21723(4)	27436(3)	46
Ga′	91041(4)	20912(4)	27965(3)	50
Cu	27783(5)	1045(5)	46627(3)	57
Cu′	76804(4)	5016(5)	3890(3)	47
P	23574(10)	−6035(9)	53075(7)	43
P′	71624(9)	−1070(9)	−4482(6)	39
O(1)	2860(4)	−849(3)	3619(2)	93
O(2)	1675(3)	1514(3)	4317(2)	87
O(3)	4519(3)	850(3)	5102(2)	82
O(1′)	7152(3)	−390(3)	1399(2)	61
O(2′)	9503(3)	252(3)	821(2)	82
O(3′)	7239(3)	2200(3)	413(2)	77
N(1)	3542(3)	2254(3)	3942(2)	39
N(2)	3705(3)	2679(3)	3489(2)	44
N(3)	4179(3)	799(3)	3448(2)	38
N(4)	4271(3)	1243(3)	2984(2)	44
N(5)	2382(3)	1208(3)	3024(2)	40
N(6)	2544(3)	1700(3)	2604(2)	41
N(1′)	9128(3)	2128(3)	1591(2)	41
N(2′)	9405(3)	2495(3)	2120(2)	45
N(3′)	7597(3)	1748(3)	1971(2)	41
N(4′)	7942(3)	2078(3)	2501(2)	43
N(5′)	9015(3)	570(3)	2237(2)	44
N(6′)	9328(3)	968(3)	2750(2)	47
C(1)	2956(4)	−189(4)	3771(3)	57
C(2)	2257(4)	1255(4)	4206(3)	55
C(3)	3998(4)	849(4)	4677(3)	52
C(4)	3860(4)	2817(4)	2133(3)	84
C(5)	3685(4)	2753(4)	4396(3)	55
C(6)	3948(4)	3486(4)	4257(3)	65
C(7)	3845(4)	3420(4)	3680(3)	58
C(8)	4755(4)	231(4)	3537(3)	49
C(9)	5211(4)	299(4)	3141(3)	61
C(10)	4895(4)	937(4)	2802(3)	60
C(11)	1626(4)	947(4)	2803(3)	57
C(12)	1289(4)	1260(4)	2252(3)	63
C(13)	1886(4)	1725(4)	2148(2)	51
C(14)	2448(3)	−77(3)	5994(2)	40
C(15)	2537(4)	745(4)	6009(3)	57
C(16)	2636(5)	1141(4)	6535(4)	79
C(17)	2648(4)	731(4)	7042(3)	69
C(18)	2561(4)	−77(4)	7028(3)	59
C(19)	2464(4)	−474(3)	6505(3)	54
C(20)	2927(3)	−1521(3)	5542(2)	36
C(21)	2578(3)	−2221(4)	5665(2)	45
C(22)	3047(5)	−2884(4)	5858(3)	55
C(23)	3873(5)	−2843(4)	5945(3)	64
C(24)	4229(4)	−2143(5)	5825(3)	69
C(25)	3754(4)	−1483(4)	5619(3)	52
C(26)	1301(3)	−929(4)	5045(3)	45
C(27)	1061(4)	−1297(5)	4504(3)	70
C(28)	293(5)	−1598(5)	4306(3)	90
C(29)	−265(4)	−1510(5)	4628(4)	84
C(30)	−35(5)	−1129(6)	5143(4)	96
C(31)	742(4)	−845(4)	5362(3)	69
C(1′)	7538(4)	170(4)	1350(3)	47
C(2′)	8991(4)	557(4)	988(3)	51
C(3′)	7609(4)	1734(4)	734(3)	46
C(4′)	9529(5)	2648(5)	3528(3)	85
C(5′)	9459(4)	2525(4)	1227(2)	53
C(6′)	9938(4)	3136(4)	1497(3)	66
C(7′)	9881(4)	3092(4)	2066(3)	57
C(8′)	6808(4)	1882(4)	1866(3)	57
C(9′)	6624(4)	2295(4)	2328(3)	66
C(10′)	7352(5)	2409(4)	2709(3)	58
C(11′)	9253(4)	−188(4)	2342(3)	64
C(12′)	9711(5)	−284(4)	2905(3)	73
C(13′)	9743(4)	449(5)	3146(3)	64
C(14′)	7065(3)	438(3)	−1124(2)	40
C(15′)	6889(3)	1249(4)	−1144(3)	47
C(16′)	6774(4)	1667(4)	−1662(3)	56
C(17′)	6842(4)	1277(4)	−2160(3)	56
C(18′)	7020(4)	485(4)	−2147(3)	59
C(19′)	7125(4)	62(4)	−1628(3)	54
C(20′)	6147(3)	−467(3)	−492(3)	41
C(21′)	6006(4)	−879(4)	−26(3)	63
C(22′)	5234(5)	−1154(4)	−31(3)	69
C(23′)	4614(4)	−979(5)	−500(4)	74
C(24′)	4728(5)	−567(5)	−969(3)	85
C(25′)	5502(4)	−308(4)	−969(4)	63
C(26′)	7748(3)	−989(3)	−523(2)	38
C(27′)	7410(4)	−1735(4)	−679(3)	45
C(28′)	7899(5)	−2382(4)	−716(3)	52
C(29′)	8715(4)	−2291(4)	−601(3)	56
C(30′)	9056(4)	−1555(5)	−478(3)	66
C(31′)	8580(4)	−905(4)	−424(3)	53
		$(MeGapz_3)Mo(CO)_3Rh(PPh_3)_2$		
Rh	29551(3)	22664(2)	53790(3)	29
Mo	42958(4)	24771(3)	76743(4)	32
Ga	59902(5)	34331(3)	110112(5)	40
P(1)	14406(11)	27617(8)	44310(11)	34
P(2)	31138(11)	15462(8)	35870(11)	32
O(1)	4872(4)	923(3)	6168(3)	67
O(2)	1784(3)	1356(2)	6690(3)	58
O(3)	4791(3)	3827(2)	6472(3)	50
N(1)	4015(4)	3530(2)	9021(3)	37
N(2)	4706(4)	3879(2)	10258(4)	39
N(3)	6238(3)	3071(2)	8685(3)	37
N(4)	6838(3)	3397(2)	9942(3)	36
N(5)	4608(3)	1876(2)	9166(3)	36
N(6)	5237(3)	2273(2)	10411(3)	36
C(1)	4654(5)	1513(3)	6669(4)	46
C(2)	2676(5)	1812(3)	6944(4)	43
C(3)	4371(4)	3228(3)	6636(4)	36
C(4)	6882(6)	3972(4)	12771(5)	70
C(5)	3168(5)	3933(3)	8798(5)	47
C(6)	3295(6)	4534(3)	9870(6)	54
C(7)	4269(5)	4487(3)	10766(5)	49
C(8)	7026(5)	3143(4)	8186(5)	49
C(9)	8129(5)	3501(4)	9106(6)	56
C(10)	7972(5)	3648(3)	10185(5)	45
C(11)	4222(5)	1094(3)	9054(5)	47
C(12)	4578(5)	969(3)	10199(5)	48
C(13)	5214(4)	1723(3)	11023(5)	43
C(14)	1784(4)	3508(3)	3679(5)	38
C(15)	2698(5)	4187(3)	4437(5)	54
C(16)	3071(5)	4778(4)	3943(7)	64
C(17)	2519(6)	4692(4)	2724(7)	67
C(18)	1619(6)	4010(4)	1962(6)	66
C(19)	1264(5)	3410(4)	2434(5)	52
C(20)	73(4)	2027(3)	3307(4)	40
C(21)	−56(5)	1209(4)	3270(6)	58

TABLE 2. (*Concluded*)

Atom	*x*	*y*	*z*	U_{eq}
C(22)	−1094(7)	631(4)	2451(8)	82
C(23)	−1963(6)	865(6)	1687(7)	89
C(24)	−1847(6)	1675(6)	1738(7)	87
C(25)	−838(5)	2264(4)	2575(6)	60
C(26)	839(4)	3336(3)	5498(4)	38
C(27)	681(6)	4128(4)	5622(5)	60
C(28)	170(7)	4500(4)	6425(6)	74
C(29)	−181(6)	4092(4)	7097(6)	69
C(30)	−25(6)	3306(4)	6992(6)	70
C(31)	473(5)	2924(3)	6205(6)	57
C(32)	2618(4)	420(3)	3184(5)	41
C(33)	2170(5)	102(3)	3916(5)	47
C(34)	1756(5)	−745(4)	3593(6)	66
C(35)	1810(6)	−1273(3)	2575(7)	71
C(36)	2273(6)	−974(4)	1843(6)	70
C(37)	2645(5)	−132(3)	2117(5)	51
C(38)	2466(4)	1683(3)	2060(4)	37
C(39)	3018(4)	2268(3)	1705(4)	42
C(40)	2508(5)	2342(4)	536(5)	55
C(41)	1436(6)	1851(5)	−283(5)	66
C(42)	857(6)	1290(4)	66(5)	67
C(43)	1357(5)	1208(3)	1229(5)	54
C(44)	4685(4)	1716(3)	3878(4)	35
C(45)	5345(5)	2523(3)	4365(4)	43
C(46)	6535(5)	2676(4)	4632(5)	54
C(47)	7063(5)	2022(5)	4414(5)	61
C(48)	6416(5)	1226(4)	3948(5)	59
C(49)	5228(5)	1068(3)	3696(5)	46

[a] U_{eq} = ⅓ trace diagonalized *U*.

The reactions of the anionic ligands $[MeGapz_3]Mo(CO)_3^-$, $[HBpz_3]Mo(CO)_3^-$, and $[MeGa(pz)(OCH_2CH_2NMe_2)]Mo(CO)_3^-$ with Wilkinson's catalyst, $Rh(PPh_3)_3Cl$, in THF resulted in the displacement of the chloro ligand, the formation of molybdenum–rhodium bonds, and the loss of triphenylphosphine from the rhodium coordination sphere. The crystalline products are air stable but solutions of the complexes decompose on exposure to the air. In one experiment (using the $[HBpz_3]Mo(CO)_3^-$ anion) a small amount of the yellow crystalline material $Rh(PPh_3)_2(CO)Cl$ was isolated, presumably being produced via displacement of a phosphine from $Rh(PPh_3)_3Cl$ by a CO ligand emanating from the molybdenum tricarbonyl anion starting material.

The reaction of the $[MeGapz_3]Mo(CO)_3^-$ anion with the tetramer $[Cu(PPh_3)Cl]_4$ in the THF led to the isolation of a yellow crystalline product which resulted from displacement of the chloro ligand by the tricarbonyl anion. The solid material is air stable but solutions of the complex decompose rapidly on air exposure.

Physical data for the complexes are listed in Table 1. The ν_{CO} frequencies indicate the presence of both terminal and bridging carbonyl groups in the compounds. The room temperature ^1H nmr data of the complexes containing the "$MeGapz_3$" and "$HBpz_3$" ligands suggest equivalence of the three pyrazolyl rings since only one set of signals is observed for the pyrazolyl ring protons (e.g. Fig. 1). Low temperature spectra, although broadening these proton signals, did not distinguish clearly any difference between the three pyrazolyl rings. The room temperature ^1H nmr of the $[Me_2Ga(pz)(OCH_2CH_2NMe_2)]Mo(CO)_3Rh(PPh_3)_2$ complex is consistent with a facial coordination of the unsymmetric gallate ligand about the molybdenum centre, with two *Ga—Me* and two *N—Me* signals being recorded.

The crystal structure of the $[MeGapz_3]Mo(CO)_3Rh(PPh_3)_2$ complex is shown in Fig. 2, and consists of discrete molecules separated by normal van der Waals distances. The structure clearly shows the presence of a terminal Mo—C(1)—O(1) unit, which, although significantly nonlinear (173.9(5) Å) is too far removed from the Rh centre (Rh···C(1), 2.845(5) Å) to suggest any bridging interaction. This CO ligand presumably accounts for the highest ν_{CO} value recorded at 1879 cm^{-1} (Nujol). The two remaining Mo—CO units, although different, are both clearly in bridging range of the Rh centre with Mo—C—O angles of 167.4(4) and 153.2(4)° and Rh···C distances of 2.334(5) and 2.079(5) Å respectively (ν_{CO} values 1758, 1772 cm^{-1}). It is also evident that the pyrazolyl rings are nonequivalent in the solid state and to explain the solution ^1H nmr data it is necessary to postulate that a rapid fluxional process is taking place in solution. Two such processes may be envisaged, one in which there is a rapid rotation of the "$MeGapz_3$" ligand about the Ga···Mo axis, and another, perhaps more likely, in which there is a rapid interchange of the different roles of the three CO ligands, with concomitant equalization of the environments of the three pyrazolyl rings. The Ga···Mo—Rh unit is significantly nonlinear in this structure with an angle of 161.59(3)° at Mo. The pyrazolyl rings, here, and in the structure of the copper complex described below, are planar within experimental error (maximum deviation from N_2C_3 plane = 0.007(7) Å). The phenyl rings are either planar or, slightly, but significantly nonplanar (χ^2 = 0.2–20.7, mean 8.0, maximum deviation 0.018(7) Å for Cu; χ^2 = 0.3–37.0, mean 19.6, maximum deviation 0.025(6) Å for Rh). The rhodium complex reported here is very similar to one reported earlier by Carlton *et al.* (27). These authors reported the structure of the compound $(\eta\text{-}C_5H_5)Mo(CO)_3Rh(PPh_3)_2$, in which a "$\eta\text{-}C_5H_5$" ligand substitutes the "$MeGapz_3$" ligand of the present complex. The similarity of the two complexes illustrates once more the interchangeability of the "$\eta\text{-}C_5H_5$" and "$MeGapz_3$" ligand systems (1). The Mo—Rh bond distance of 2.6066(5) Å (cf. 2.588(1) Å in the $\eta\text{-}C_5H_5$ complex) in the present compound is well below the estimated single bond distance of 2.8–3.0 Å and suggests some multiple bond character between the two transition metals. A bonding scheme similar to that proposed by Carlton *et al.* would give an 18-electron count to the Mo atom and a 16-electron count to the Rh centre. In this picture, in addition to two bridging CO groups, a double bond between the two transition metals, with one component being a Rh → Mo dative link, constitutes an integral part of the overall molecular framework. In keeping with the different roles of the carbonyl ligands the C—O bond lengths involving the "bridging" ligands (1.190(5) and 1.175(6) Å) are significantly longer than that of

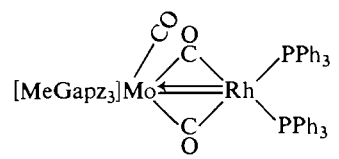

the unique terminal CO ligand (1.154(6) Å). The Rh $(\mu\text{-}CO)_2Mo$ framework possesses a butterfly arrangement as seen in the analogous $\eta\text{-}C_5H_5$ complex (27) with the Rh—C—Mo dihedral angle of 156° compared with 161° in the $\eta\text{-}C_5H_5$ compound.

The crystal structure of the $[MeGapz_3]Mo(CO)_3Cu(PPh_3)$

TABLE 3. Bond lengths (Å) with estimated standard deviations in parentheses

Bond	Length (Å)	Bond	Length (Å)
	$(MeGapz_3)Mo(CO)_3Cu(PPh_3)$		
Mo—Cu	2.5041(8)	N(3′)—N(4′)	1.358(6)
Mo—N(1)	2.254(5)	N(3′)—C(8′)	1.323(7)
Mo—N(3)	2.257(4)	N(4′)—C(10′)	1.348(7)
Mo—N(5)	2.246(4)	N(5′)—N(6′)	1.366(6)
Mo—C(1)	1.966(7)	N(5′)—C(11′)	1.336(7)
Mo—C(2)	1.958(7)	N(6′)—C(13′)	1.339(7)
Mo—C(3)	1.971(7)	C(5)—C(6)	1.375(9)
Mo′—Cu′	2.5216(8)	C(6)—C(7)	1.366(9)
Mo′—N(1′)	2.253(5)	C(8)—C(9)	1.367(8)
Mo′—N(3′)	2.273(5)	C(9)—C(10)	1.361(8)
Mo′—N(5′)	2.257(5)	C(11)—C(12)	1.385(8)
Mo′—C(1′)	1.958(7)	C(12)—C(13)	1.353(8)
Mo′—C(2′)	1.970(7)	C(14)—C(15)	1.383(7)
Mo′—C(3′)	1.980(7)	C(14)—C(19)	1.372(7)
Ga—N(2)	1.922(5)	C(15)—C(16)	1.379(8)
Ga—N(4)	1.929(5)	C(16)—C(17)	1.378(9)
Ga—N(6)	1.917(5)	C(17)—C(18)	1.361(8)
Ga—C(4)	1.943(6)	C(18)—C(19)	1.376(8)
Ga′—N(2′)	1.924(5)	C(20)—C(21)	1.378(7)
Ga′—N(4′)	1.926(5)	C(20)—C(25)	1.378(7)
Ga′—N(6′)	1.928(5)	C(21)—C(22)	1.375(8)
Ga′—C(4′)	1.935(6)	C(22)—C(23)	1.374(9)
Cu—P	2.193(2)	C(23)—C(24)	1.383(9)
Cu—C(1)	2.259(6)	C(24)—C(25)	1.383(9)
Cu—C(2)	2.274(7)	C(26)—C(27)	1.383(8)
Cu—C(3)	2.419(6)	C(26)—C(31)	1.365(8)
Cu′—P′	2.199(2)	C(27)—C(28)	1.371(9)
Cu′—C(1′)	2.410(6)	C(28)—C(29)	1.371(10)
Cu′—C(2′)	2.322(6)	C(29)—C(30)	1.341(10)
Cu′—C(3′)	2.234(6)	C(30)—C(31)	1.378(9)
P—C(14)	1.819(6)	C(5′)—C(6′)	1.361(8)
P—C(20)	1.826(6)	C(6′)—C(7′)	1.375(8)
P—C(26)	1.833(6)	C(8′)—C(9′)	1.395(8)
P′—C(14′)	1.811(6)	C(9′)—C(10′)	1.347(8)
P′—C(20′)	1.812(6)	C(11′)—C(12′)	1.368(9)
P′—C(26′)	1.817(6)	C(12′)—C(13′)	1.348(9)
O(1)—C(1)	1.160(7)	C(14′)—C(15′)	1.388(8)
O(2)—C(2)	1.174(7)	C(14′)—C(19′)	1.374(7)
O(3)—C(3)	1.159(6)	C(15′)—C(16′)	1.381(8)
O(1′)—C(1′)	1.169(6)	C(16′)—C(17′)	1.375(8)
O(2′)—C(2′)	1.164(7)	C(17′)—C(18′)	1.359(8)
O(3′)—C(3′)	1.155(6)	C(18′)—C(19′)	1.386(8)
N(1)—N(2)	1.373(6)	C(20′)—C(21′)	1.374(8)
N(1)—C(5)	1.332(7)	C(20′)—C(25′)	1.384(8)
N(2)—C(7)	1.347(7)	C(21′)—C(22′)	1.392(8)
N(3)—N(4)	1.367(6)	C(22′)—C(23′)	1.354(9)
N(3)—C(8)	1.345(7)	C(23′)—C(24′)	1.361(10)
N(4)—C(10)	1.347(7)	C(24′)—C(25′)	1.391(9)
N(5)—N(6)	1.371(6)	C(26′)—C(27′)	1.385(7)
N(5)—C(11)	1.334(7)	C(26′)—C(31′)	1.385(8)
N(6)—C(13)	1.343(7)	C(27′)—C(28′)	1.384(8)
N(1′)—N(2′)	1.364(6)	C(28′)—C(29′)	1.358(8)
N(1′)—C(5′)	1.323(7)	C(29′)—C(30′)	1.365(9)
N(2′)—C(7′)	1.316(7)	C(30′)—C(31′)	1.384(8)
	$(MeGapz_3)Mo(CO)_3Rh(PPh_3)_2$		
Rh—Mo	2.6066(5)	C(11)—C(12)	1.383(7)
Rh—P(1)	2.2491(13)	C(12)—C(13)	1.357(7)
Rh—P(2)	2.2836(12)	C(14)—C(15)	1.383(7)
Rh—C(1)	2.845(5)	C(14)—C(19)	1.374(7)
Rh—C(2)	2.334(5)	C(15)—C(16)	1.411(8)
Rh—C(3)	2.079(5)	C(16)—C(17)	1.355(9)
Mo—N(1)	2.249(4)	C(17)—C(18)	1.377(9)

TABLE 3. (*Concluded*)

Bond	Length (Å)	Bond	Length (Å)
Mo—N(3)	2.273(4)	C(18)—C(19)	1.396(8)
Mo—N(5)	2.247(4)	C(20)—C(21)	1.383(7)
Mo—C(1)	1.982(5)	C(20)—C(25)	1.366(7)
Mo—C(2)	1.971(6)	C(21)—C(22)	1.397(8)
Mo—C(3)	2.034(5)	C(22)—C(23)	1.348(10)
Ga—N(2)	1.915(4)	C(23)—C(24)	1.364(11)
Ga—N(4)	1.924(4)	C(24)—C(25)	1.388(9)
Ga—N(6)	1.927(4)	C(26)—C(27)	1.377(7)
Ga—C(4)	1.931(5)	C(26)—C(31)	1.393(7)
P(1)—C(14)	1.840(5)	C(27)—C(28)	1.399(8)
P(1)—C(20)	1.834(5)	C(28)—C(29)	1.344(9)
P(1)—C(26)	1.839(5)	C(29)—C(30)	1.368(9)
P(2)—C(32)	1.837(5)	C(30)—C(31)	1.380(8)
P(2)—C(38)	1.836(5)	C(32)—C(33)	1.381(7)
P(2)—C(44)	1.848(5)	C(32)—C(37)	1.400(7)
O(1)—C(1)	1.154(6)	C(33)—C(34)	1.385(7)
O(2)—C(2)	1.175(6)	C(34)—C(35)	1.353(9)
O(3)—C(3)	1.190(5)	C(35)—C(36)	1.376(9)
N(1)—N(2)	1.367(5)	C(36)—C(37)	1.378(8)
N(1)—C(5)	1.327(6)	C(38)—C(39)	1.386(7)
N(2)—C(7)	1.344(6)	C(38)—C(43)	1.396(7)
N(3)—N(4)	1.364(5)	C(39)—C(40)	1.385(7)
N(3)—C(8)	1.328(6)	C(40)—C(41)	1.369(8)
N(4)—C(10)	1.337(6)	C(41)—C(42)	1.369(9)
N(5)—N(6)	1.369(5)	C(42)—C(43)	1.382(8)
N(5)—C(11)	1.326(6)	C(44)—C(45)	1.383(7)
N(6)—C(13)	1.344(6)	C(44)—C(49)	1.383(7)
C(5)—C(6)	1.376(7)	C(45)—C(46)	1.387(7)
C(6)—C(7)	1.355(8)	C(46)—C(47)	1.385(9)
C(8)—C(9)	1.383(7)	C(47)—C(48)	1.364(8)
C(9)—C(10)	1.347(7)	C(48)—C(49)	1.390(8)

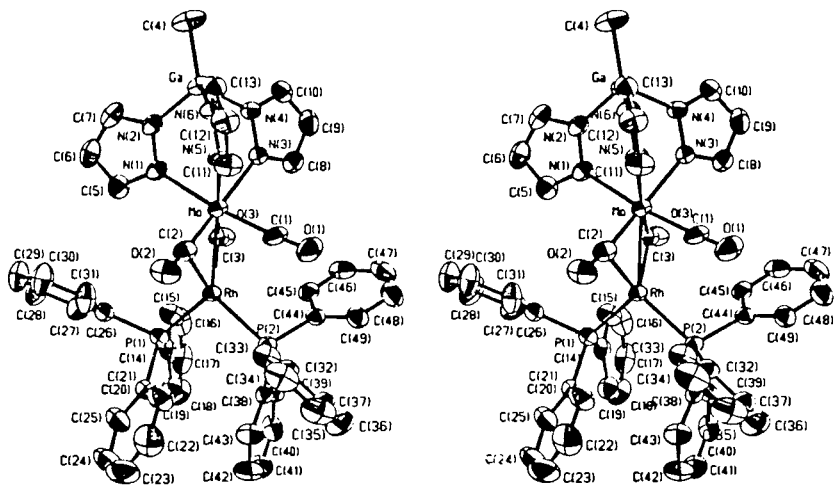

FIG. 2. Stereoscopic view of the [methyltris(1-pyrazolyl)gallato-(*N*,*N*,*N*)]tricarbonylmolybdenumbis(triphenylphosphine)rhodium(*Mo-Rh*) molecule; 50% probability thermal ellipsoids are shown. Hydrogen atoms are omitted for clarity.

complex is shown in Fig. 3 and again consists of discrete molecules separated by normal van der Waals distances. The only intermolecular contact of any possible significance is a C—H···O interaction associating pairs of unprimed molecules about the inversion centre at (0,0,1/2) (C(30)—H(30)···O(2) ($-x,-y,1-z$), C···O = 3.424(9), H···O = 2.55 Å, C—H···O = 151°). Apart from several small but statistically significant differences between the corresponding bond lengths and angles (Tables 3 and 4), the most notable difference between the two crystallographically independent molecules of [MeGapz$_3$]-Mo(CO)$_3$Cu(PPh$_3$) is in the orientation of the PPh$_3$ ligand. The conformation about the Cu—P bond in the molecule denoted by unprimed atom labels is about 4° from staggered compared with a value of 26° in the second molecule. A unit cell view of the structure is shown in Fig. 4. The complex [MeGapz$_3$]Mo(CO)$_3$Cu(PPh$_3$) is valence isoelectronic with the above Rh compound, [MeGapz$_3$]Mo(CO)$_3$Rh(PPh$_3$)$_2$. However, the Cu complex is of much higher symmetry, possessing an

TABLE 4. Bond angles (deg) with estimated standard deviations in parentheses

Bonds	Angle (deg)	Bonds	Angle (deg)
	$(MeGapz_3)Mo(CO)_3Cu(PPh_3)$		
Cu—Mo—N(1)	130.52(12)	N(5)—N(6)—C(13)	108.5(5)
Cu—Mo—N(3)	131.46(12)	Mo′—N(1′)—N(2′)	126.4(3)
Cu—Mo—N(5)	123.55(12)	Mo′—N(1′)—C(5′)	128.3(4)
Cu—Mo—C(1)	59.3(2)	N(2′)—N(1′)—N(5′)	105.3(5)
Cu—Mo—C(2)	59.8(2)	Ga′—N(2′)—N(1′)	120.0(4)
Cu—Mo—C(3)	64.1(2)	Ga′—N(2′)—C(7′)	130.7(4)
N(1)—Mo—N(3)	84.1(2)	N(1′)—N(2′)—C(7′)	109.3(5)
N(1)—Mo—N(5)	86.4(2)	Mo′—N(3′)—N(4′)	126.0(4)
N(1)—Mo—C(1)	170.0(2)	Mo′—N(3′)—C(8′)	127.4(4)
N(1)—Mo—C(2)	88.6(2)	N(4′)—N(3′)—C(8′)	106.5(5)
N(1)—Mo—C(3)	86.7(2)	Ga′—N(4′)—N(3′)	120.1(4)
N(3)—Mo—N(5)	85.3(2)	Ga′—N(4′)—C(10′)	131.3(5)
N(3)—Mo—C(1)	87.0(2)	N(3′)—N(4′)—C(10′)	108.3(5)
N(3)—Mo—C(2)	168.5(2)	Mo′—N(5′)—N(6′)	127.0(4)
N(3)—Mo—C(3)	90.2(2)	Mo′—N(5′)—C(11′)	127.6(4)
N(5)—Mo—C(1)	88.4(2)	N(6′)—N(5′)—C(11′)	105.4(5)
N(5)—Mo—C(2)	85.4(2)	Ga′—N(6′)—N(5′)	119.2(4)
N(5)—Mo—C(3)	172.1(2)	Ga′—N(6′)—C(13′)	132.0(5)
C(1)—Mo—C(2)	99.4(3)	N(5′)—N(6′)—C(13′)	108.7(5)
C(1)—Mo—C(3)	97.8(3)	Mo—C(1)—Cu	72.3(2)
C(2)—Mo—C(3)	98.3(3)	Mo—C(1)—O(1)	170.6(5)
Cu′—Mo′—N(1′)	125.14(11)	Cu—C(1)—O(1)	116.9(4)
Cu′—Mo′—N(3′)	128.36(12)	Mo—C(2)—Cu	72.1(2)
Cu′—Mo′—N(5′)	132.68(13)	Mo—C(2)—O(2)	170.6(6)
Cu′—Mo′—C(1′)	63.7(2)	Cu—C(2)—O(2)	117.2(5)
Cu′—Mo′—C(2′)	60.8(2)	Mo—C(3)—Cu	68.7(2)
Cu′—Mo′—C(3′)	58.0(2)	Mo—C(3)—O(3)	172.6(6)
N(1′)—Mo′—N(3′)	84.5(2)	Cu—C(3)—O(3)	118.6(5)
N(1′)—Mo′—N(5′)	85.2(2)	N(1)—C(5)—C(6)	111.8(6)
N(1′)—Mo′—C(1′)	171.1(2)	C(5)—C(6)—C(7)	104.4(6)
N(1′)—Mo′—C(2′)	89.1(2)	N(2)—C(7)—C(6)	109.4(6)
N(1′)—Mo′—C(3′)	87.2(2)	N(3)—C(8)—C(9)	110.9(6)
N(3′)—Mo′—N(5′)	85.0(2)	C(8)—C(9)—C(10)	104.9(5)
N(3′)—Mo′—C(1′)	90.4(2)	N(4)—C(10)—C(9)	109.8(5)
N(3′)—Mo′—C(2′)	170.8(2)	N(5)—C(11)—C(12)	111.7(6)
N(3′)—Mo′—C(3′)	86.8(2)	C(11)—C(12)—C(13)	103.7(5)
N(5′)—Mo′—C(1′)	87.1(2)	N(6)—C(13)—C(12)	110.5(5)
N(5′)—Mo′—C(2′)	88.0(2)	P—C(14)—C(15)	119.2(5)
N(5′)—Mo′—C(3′)	169.3(2)	P—C(14)—C(19)	121.9(4)
C(1′)—Mo′—C(2′)	95.1(2)	C(15)—C(14)—C(19)	118.9(6)
C(1′)—Mo′—C(3′)	99.8(2)	C(14)—C(15)—C(16)	119.1(6)
C(2′)—Mo′—C(3′)	99.4(2)	C(15)—C(16)—C(17)	121.1(6)
N(2)—Ga—N(4)	100.2(2)	C(16)—C(17)—C(18)	119.7(6)
N(2)—Ga—N(6)	101.7(2)	C(17)—C(18)—C(19)	119.4(6)
N(2)—Ga—C(4)	116.7(3)	C(14)—C(19)—C(18)	121.8(6)
N(4)—Ga—N(6)	100.3(2)	P—C(20)—C(21)	123.6(4)
N(4)—Ga—C(4)	115.7(3)	P—C(20)—C(25)	116.7(5)
N(6)—Ga—C(4)	119.1(3)	C(21)—C(20)—C(25)	119.6(6)
N(2′)—Ga′—N(4′)	100.0(2)	C(20)—C(21)—C(22)	120.6(6)
N(2′)—Ga′—N(6′)	101.3(2)	C(21)—C(22)—C(23)	119.8(6)
N(2′)—Ga′—C(4′)	117.1(3)	C(22)—C(23)—C(24)	120.0(6)
N(4′)—Ga′—N(6′)	99.7(2)	C(23)—C(24)—C(25)	120.0(6)
N(4′)—Ga′—C(4′)	116.4(3)	C(20)—C(25)—C(24)	119.9(6)
N(6′)—Ga′—C(4′)	119.1(3)	P—C(26)—C(27)	118.5(5)
Mo—Cu—P	177.02(6)	P—C(26)—C(31)	123.3(5)
Mo—Cu—C(1)	48.4(2)	C(27)—C(26)—C(31)	118.2(6)
Mo—Cu—C(2)	48.1(2)	C(26)—C(27)—C(28)	120.6(6)
Mo—Cu—C(3)	47.2(2)	C(27)—C(28)—C(29)	120.7(7)
P—Cu—C(1)	132.7(2)	C(28)—C(29)—C(30)	118.2(7)
P—Cu—C(2)	129.0(2)	C(29)—C(30)—C(31)	122.3(7)
P—Cu—C(3)	134.7(2)	C(26)—C(31)—C(30)	119.9(6)
C(1)—Cu—C(2)	82.6(2)	Mo′—C(1′)—Cu′	69.6(2)
C(1)—Cu—C(3)	78.6(2)	Mo′—C(1′)—O(1′)	171.5(5)

TABLE 4. (*Continued*)

Bonds	Angle (deg)	Bonds	Angle (deg)
C(2)—Cu—C(3)	78.5(2)	Cu′—C(1′)—O(1′)	118.4(4)
Mo′—Cu′—P′	175.17(6)	Mo′—C(2′)—Cu′	71.4(2)
Mo′—Cu′—C(1′)	46.72(15)	Mo′—C(2′)—O(2′)	170.7(5)
Mo′—Cu′—C(2′)	47.8(2)	Cu′—C(2′)—O(2′)	117.8(5)
Mo′—Cu′—C(3′)	48.8(2)	Mo′—C(3′)—Cu′	73.2(2)
P′—Cu′—C(1′)	128.8(2)	Mo′—C(3′)—O(3′)	169.6(5)
P′—Cu′—C(2′)	132.0(2)	Cu′—C(3′)—O(3′)	117.1(4)
P′—Cu′—C(3′)	135.2(2)	N(1′)—C(5′)—C(6′)	112.3(5)
C(1′)—Cu′—C(2′)	75.5(2)	C(5′)—C(6′)—C(7′)	103.5(5)
C(1′)—Cu′—C(3′)	80.8(2)	N(2′)—C(7′)—C(6′)	109.7(6)
C(2′)—Cu′—C(3′)	82.8(2)	N(3′)—C(8′)—C(9′)	111.0(6)
Cu—P—C(14)	113.0(8)	C(8′)—C(9′)—C(10′)	103.8(5)
Cu—P—C(20)	114.9(2)	N(4′)—C(10′)—C(9′)	110.2(6)
Cu—P—C(26)	113.3(2)	N(5′)—C(11′)—C(12′)	111.4(6)
C(14)—P—C(20)	102.7(2)	C(11′)—C(12′)—C(13′)	104.7(6)
C(14)—P—C(26)	107.3(3)	N(6′)—C(13′)—C(12′)	109.8(6)
C(20)—P—C(26)	104.7(3)	P′—C(14′)—C(15′)	119.4(5)
Cu′—P′—C(14′)	119.1(2)	P′—C(14′)—C(19′)	121.7(5)
Cu′—P′—C(20′)	111.3(2)	C(15′)—C(14′)—C(19′)	118.9(5)
Cu′—P′—C(26′)	111.1(2)	C(14′)—C(15′)—C(16′)	120.3(6)
C(14′)—P′—C(20′)	104.3(3)	C(15′)—C(16′)—C(17′)	119.7(6)
C(14′)—P′—C(26′)	104.6(3)	C(16′)—C(17′)—C(18′)	120.7(6)
C(20′)—P′—C(26′)	105.5(3)	C(17′)—C(18′)—C(19′)	119.7(6)
Mo—N(1)—N(2)	125.9(3)	C(14′)—C(19′)—C(18′)	120.7(6)
Mo—N(1)—C(5)	128.3(4)	P′—C(20′)—C(21′)	119.0(5)
N(2)—N(1)—C(5)	105.7(5)	P′—C(20′)—C(25′)	122.1(5)
Ga—N(2)—N(1)	119.7(4)	C(21′)—C(20′)—C(25′)	118.9(6)
Ga—N(2)—C(7)	131.5(5)	C(20′)—C(21′)—C(22′)	121.3(6)
N(1)—N(2)—C(7)	108.7(5)	C(21′)—C(22′)—C(23′)	118.4(6)
Mo—N(3)—N(4)	125.9(3)	C(22′)—C(23′)—C(24′)	122.0(7)
Mo—N(3)—C(8)	127.8(4)	C(23′)—C(24′)—C(25′)	119.5(7)
N(4)—N(3)—C(8)	106.2(4)	C(20′)—C(25′)—C(24′)	119.8(6)
Ga—N(4)—N(3)	119.5(3)	P′—C(26′)—C(27′)	123.8(5)
Ga—N(4)—C(10)	132.2(4)	P′—C(26′)—C(31′)	117.8(5)
N(3)—N(4)—C(10)	108.2(5)	C(27′)—C(26′)—C(31′)	118.4(5)
Mo—N(5)—N(6)	127.1(3)	C(26′)—C(27′)—C(28′)	120.4(5)
Mo—N(5)—C(11)	127.2(4)	C(27′)—C(28′)—C(29′)	120.5(6)
N(6)—N(5)—C(11)	105.6(4)	C(28′)—C(29′)—C(30′)	120.0(6)
Ga—N(6)—N(5)	118.6(3)	C(29′)—C(30′)—C(31′)	120.3(6)
Ga—N(6)—C(13)	132.9(4)	C(26′)—C(31′)—C(30′)	120.3(6)
	$(MeGapz_3)Mo(CO)_3Rh(PPh_3)_2$		
Mo—Rh—P(1)	135.80(4)	Ga—N(6)—N(5)	120.5(3)
Mo—Rh—P(2)	128.70(4)	Ga—N(6)—C(13)	130.8(3)
Mo—Rh—C(1)	42.35(10)	N(5)—N(6)—C(13)	108.8(4)
Mo—Rh—C(2)	46.61(13)	Rh—C(1)—Mo	62.37(15)
Mo—Rh—C(3)	49.91(14)	Rh—C(1)—O(1)	122.5(4)
P(1)—Rh—P(2)	95.27(5)	Mo—C(1)—O(1)	173.9(5)
P(1)—Rh—C(1)	172.17(12)	Rh—C(2)—Mo	74.0(2)
P(1)—Rh—C(2)	110.97(14)	Rh—C(2)—O(2)	117.9(4)
P(1)—Rh—C(3)	110.90(14)	Mo—C(2)—O(2)	167.4(4)
P(2)—Rh—C(1)	87.84(11)	Rh—C(3)—Mo	78.6(2)
P(2)—Rh—C(2)	130.20(13)	Rh—C(3)—O(3)	128.1(4)
P(2)—Rh—C(3)	116.64(14)	Mo—C(3)—O(3)	153.2(4)
C(1)—Rh—C(2)	61.9(2)	N(1)—C(5)—C(6)	110.6(5)
C(1)—Rh—C(3)	73.8(2)	C(5)—C(6)—C(7)	105.5(5)
C(2)—Rh—C(3)	93.1(2)	N(2)—C(7)—C(6)	108.8(5)
Rh—Mo—N(1)	111.64(11)	N(3)—C(8)—C(9)	110.6(5)
Rh—Mo—N(3)	128.38(10)	C(8)—C(9)—C(10)	105.1(5)
Rh—Mo—N(5)	142.50(10)	N(4)—C(10)—C(9)	109.3(5)
Rh—Mo—C(1)	75.27(14)	N(5)—C(11)—C(12)	111.4(4)
Rh—Mo—C(2)	59.40(14)	C(11)—C(12)—C(13)	104.4(4)
Rh—Mo—C(3)	51.45(13)	N(6)—C(13)—C(12)	109.5(4)
N(1)—Mo—N(3)	86.92(14)	P(1)—C(14)—C(15)	115.7(4)

TABLE 4. (*Concluded*)

Bonds	Angle (deg)	Bonds	Angle (deg)
N(1)—Mo—N(5)	85.69(14)	P(1)—C(14)—C(19)	125.3(4)
N(1)—Mo—C(1)	172.9(2)	C(15)—C(14)—C(19)	118.8(5)
N(1)—Mo—C(2)	96.1(2)	C(14)—C(15)—C(16)	120.5(5)
N(1)—Mo—C(3)	88.2(2)	C(15)—C(16)—C(17)	120.0(6)
N(3)—Mo—N(5)	83.74(14)	C(16)—C(17)—C(18)	119.7(6)
N(3)—Mo—C(1)	89.7(2)	C(17)—C(18)—C(19)	120.7(6)
N(3)—Mo—C(2)	169.7(2)	C(14)—C(19)—C(18)	120.2(5)
N(3)—Mo—C(3)	83.3(2)	P(1)—C(20)—C(21)	117.7(4)
N(5)—Mo—C(1)	87.8(2)	P(1)—C(20)—C(25)	122.9(4)
N(5)—Mo—C(2)	86.7(2)	C(21)—C(20)—C(25)	119.2(5)
N(5)—Mo—C(3)	166.0(2)	C(20)—C(21)—C(22)	119.8(6)
C(1)—Mo—C(2)	86.1(2)	C(21)—C(22)—C(23)	120.3(7)
C(1)—Mo—C(3)	97.5(2)	C(22)—C(23)—C(24)	120.0(6)
C(2)—Mo—C(3)	106.5(2)	C(23)—C(24)—C(25)	120.5(7)
N(2)—Ga—N(4)	103.0(2)	C(20)—C(25)—C(24)	120.0(6)
N(2)—Ga—N(6)	100.5(2)	P(1)—C(26)—C(27)	125.4(4)
N(2)—Ga—C(4)	116.3(2)	P(1)—C(26)—C(31)	117.3(4)
N(4)—Ga—N(6)	98.0(2)	C(27)—C(26)—C(31)	117.3(5)
N(4)—Ga—C(4)	116.5(2)	C(26)—C(27)—C(28)	121.1(6)
N(6)—Ga—C(4)	119.4(2)	C(27)—C(28)—C(29)	120.8(6)
Rh—P(1)—C(14)	114.8(2)	C(28)—C(29)—C(30)	119.0(6)
Rh—P(1)—C(20)	118.9(2)	C(29)—C(30)—C(31)	121.4(6)
Rh—P(1)—C(26)	113.5(2)	C(26)—C(31)—C(30)	120.4(5)
C(14)—P(1)—C(20)	106.5(2)	P(2)—C(32)—C(33)	120.0(4)
C(14)—P(1)—C(26)	103.3(2)	P(2)—C(32)—C(37)	121.5(4)
C(20)—P(1)—C(26)	97.5(2)	C(33)—C(32)—C(37)	118.5(5)
Rh—P(2)—C(32)	112.6(2)	C(32)—C(33)—C(34)	120.3(5)
Rh—P(2)—C(38)	126.2(2)	C(33)—C(34)—C(35)	120.7(6)
Rh—P(2)—C(44)	107.41(15)	C(34)—C(35)—C(36)	120.3(5)
C(32)—P(2)—C(38)	101.1(2)	C(35)—C(36)—C(37)	120.0(6)
C(32)—P(2)—C(44)	104.5(2)	C(32)—C(37)—C(36)	120.2(6)
C(38)—P(2)—C(44)	102.9(2)	P(2)—C(38)—C(39)	122.5(6)
Mo—N(1)—N(2)	125.6(3)	P(2)—C(38)—C(43)	119.6(4)
Mo—N(1)—C(5)	128.1(3)	C(39)—C(38)—C(43)	117.8(4)
N(2)—N(1)—C(5)	106.3(4)	C(38)—C(39)—C(40)	120.7(5)
Ga—N(2)—N(1)	120.4(3)	C(39)—C(40)—C(41)	120.6(5)
Ga—N(2)—C(7)	130.6(4)	C(40)—C(41)—C(42)	119.6(5)
N(1)—N(2)—C(7)	108.9(4)	C(41)—C(42)—C(43)	120.4(6)
Mo—N(3)—N(4)	126.5(3)	C(38)—C(43)—C(42)	120.7(5)
Mo—N(3)—C(8)	127.5(3)	P(2)—C(44)—C(45)	118.2(4)
N(4)—N(3)—C(8)	106.0(4)	P(2)—C(44)—C(49)	122.2(4)
Ga—N(4)—N(3)	118.9(3)	C(45)—C(44)—C(49)	119.5(5)
Ga—N(4)—C(10)	132.0(3)	C(44)—C(45)—C(46)	120.0(5)
N(3)—N(4)—C(10)	109.1(4)	C(45)—C(46)—C(47)	120.0(5)
Mo—N(5)—N(6)	125.3(3)	C(46)—C(47)—C(48)	120.1(5)
Mo—N(5)—C(11)	128.7(3)	C(47)—C(48)—C(49)	120.2(6)
N(6)—N(5)—C(11)	105.9(4)	C(44)—C(49)—C(48)	120.2(5)

approximate 3-fold axis along the near-linear C(4)—Ga...Mo—Cu—P atomic arrangement (mean angles: C—Ga...Mo = 178.0(3), Ga...Mo—Cu = 175.2(6), and Mo—Cu—P = 176.1(9)°). In this solid state structure the three pyrazolyl rings are in equivalent environments. If a similar arrangement pertains in solution, the ^{1}H nmr results, mentioned above, are satisfactorily explained. The three CO ligands are essentially symmetrically placed with mean bond angles Mo—C—O of 170.1(5), 170.7(1), and 172.1(6)°, Cu—C—O of 117.0(1), 117.5(3), and 118.5(1)°, and mean bond lengths Mo—C of 1.973(7), 1.964(6), and 1.966 (6) Å, Cu...C of 2.247(13), 2.298(23), and 2.415(5) Å,

The solution ir spectrum for the Cu complex shows two ν_{CO} bands (a and e modes) and is consistent with the approximate C_3 symmetry for the complex observed in the solid state, with nearly linear Mo—C—O units. The positions of these ν_{CO} bands (1898 and 1798 cm^{-1}, CH_2Cl_2 solution) are slightly higher than those observed for the uncomplexed anion [MeGapz$_3$]Mo(CO)$_3^-$ (Et_4N^+ salt) (1890 and 1760 cm^{-1}, CH_2Cl_2 solution) which in turn are close in value to the ν_{CO} vibrations, recorded some time earlier by Trofimenko (37), for the corresponding [HBpz$_3$]Mo(CO)$_3^-$ anion (Et_4N^+ salt) (1897 and 1761 cm^{-1}, MeCN solution). In the solid state the Cu complex displays three bands in the ν_{CO} region of the spectrum (1890, 1805, and 1780 cm^{-1}, Nujol mull). These could arise either from a splitting of the e mode observed in the solution spectrum, or from slightly different packing environments for the two independent molecules. As already noted above, one of the carbonyl groups of the unprimed molecules is involved in a possible C—H...O interaction. The solid state ir spectrum of the uncomplexed carbonyl anion in the salt [Et_4N^+][(MeGapz$_3$)-Mo(CO)$_3^-$] displayed two ν_{CO} bands (1885 and 1730 cm^{-1},

TABLE 5. Intra-annular torsion angles (deg) with standard deviations in parentheses

Atoms	Value (deg)
$(MeGapz_3)Mo(CO)_3Cu(PPh_3)$	
N(3)—Mo—N(1)—N(2)	42.9(4)
Mo—N(1)—N(2)—Ga	2.6(5)
N(4)—Ga—N(2)—N(1)	−53.3(4)
N(2)—Ga—N(4)—N(3)	47.5(4)
Mo—N(3)—N(4)—Ga	7.9(6)
N(1)—Mo—N(3)—N(4)	−49.1(4)
N(5)—Mo—N(1)—N(2)	−42.7(4)
Mo—N(1)—N(2)—Ga	2.6(5)
N(6)—Ga—N(2)—N(1)	49.6(4)
N(2)—Ga—N(6)—N(5)	−53.9(4)
Mo—N(5)—N(6)—Ga	5.4(5)
N(1)—Mo—N(5)—N(6)	38.4(4)
N(5)—Mo—N(3)—N(4)	37.7(4)
Mo—N(5)—N(6)—Ga	5.4(5)
N(6)—Ga—N(4)—N(3)	−56.6(4)
N(4)—Ga—N(6)—N(5)	48.9(4)
Mo—N(3)—N(4)—Ga	7.9(6)
N(3)—Mo—N(5)—N(6)	−46.0(4)
N(3′)—Mo′—N(1′)—N(2′)	41.0(4)
Mo′—N(3′)—N(4′)—Ga′	5.3(6)
N(4′)—Ga′—N(2′)—N(1′)	−53.6(4)
N(2′)—Ga′—N(4′)—N(3′)	48.3(4)
Mo′—N(1′)—N(2′)—Ga′	3.8(6)
N(1′)—Mo′—N(3′)—N(4′)	−46.3(4)
N(5′)—Mo′—N(1′)—N(2′)	−44.4(4)
Mo′—N(5′)—N(6′)—Ga′	1.7(6)
N(6′)—Ga′—N(2′)—N(1′)	48.5(4)
N(2′)—Ga′—N(6′)—N(5′)	−51.3(4)
Mo′—N(1′)—N(2′)—Ga′	3.8(6)
N(1′)—Mo′—N(5′)—N(6′)	41.4(4)
N(5′)—Mo′—N(3′)—N(4′)	39.3(4)
Mo′—N(5′)—N(6′)—Ga′	1.7(6)
N(6′)—Ga′—N(4′)—N(3′)	−55.1(4)
N(4′)—Ga′—N(6′)—N(5′)	51.0(4)
Mo′—N(3′)—N(4′)—Ga′	5.3(6)
N(3′)—Mo′—N(5′)—N(6′)	−43.5(4)
$(MeGapz_3)Mo(CO)_3Rh(PPh_3)_2$	
N(3)—Mo—N(1)—N(2)	−38.5(4)
Mo—N(1)—N(2)—Ga	−3.9(5)
N(4)—Ga—N(2)—N(1)	52.3(4)
N(2)—Ga—N(4)—N(3)	−47.4(4)
Mo—N(3)—N(4)—Ga	−3.8(5)
N(1)—Mo—N(3)—N(4)	43.3(4)
N(5)—Mo—N(1)—N(2)	45.4(4)
Mo—N(1)—N(2)—Ga	−3.9(5)
N(6)—Ga—N(2)—N(1)	−48.6(4)
N(2)—Ga—N(6)—N(5)	52.1(4)
Mo—N(5)—N(6)—Ga	−2.2(5)
N(1)—Mo—N(5)—N(6)	−41.7(4)
N(5)—Mo—N(3)—N(4)	−42.7(4)
Mo—N(3)—N(4)—Ga	−3.8(5)
N(6)—Ga—N(4)—N(3)	55.4(4)
N(4)—Ga—N(6)—N(5)	−52.8(4)
Mo—N(5)—N(6)—Ga	−2.2(5)
N(3)—Mo—N(5)—N(6)	45.7(4)

Nujol mull) as expected from its C_{3v} symmetry. These values again compare closely with those reported for the analogous boron species in the salt $[Et_4N^+][(HBpz_3)Mo(CO)_3^-]$ (1890 and 1750 cm^{-1}, KBr disc) (38).[4]

In the scheme presented below the Mo centre retains an 18-electron count if it is assumed that the CO groups of the molybdenum tricarbonyl anion retain their terminal character to

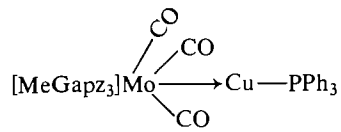

the Mo atom. The single donor bond, Mo → Cu, between the two transition metals gives the Cu of the $Cu^I(PPh_3)^+$ moiety a 14-electron count. The X-ray data however, do suggest some interaction between the Cu centre and the carbonyl groups, although the exact nature of this interaction is not clear. Obviously the interaction is of a semi-bridging type since the Mo—C—O angles are not far removed from linear. Numerous recent publications have documented and discussed different types of bridging CO interactions in heterobimetallic transition metal complexes (23–31,34,36). The present Cu compound does not appear to fit into the category of a distal electron-rich metal centre (the Cu centre has a 14-electron count) donating excessive charge into the CO π* orbitals (25), although, if $d\pi$–$d\pi$ bonding occurs between the Cu and the Mo centres, then an interaction with the CO groups similar to that postulated for the complex $(\eta\text{-}C_5H_5)_2Mo_2(CO)_4$ (26,39) may be possible. Such an interaction between a Mo—Cu π-bond and the π* orbital of a CO ligand is shown schematically below. This type of interaction would, of course, tend to lengthen the C—O bond, and, with a mean C—O distance of 1.164 Å, the carbonyl ligands do display slightly longer bonds than usually found for

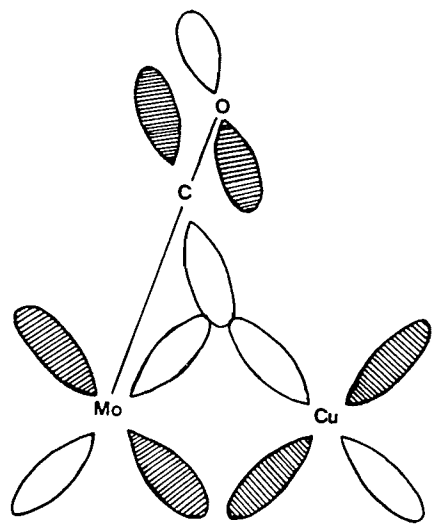

terminal CO ligands. The present structure does not meet the requirements for Π-CO type bonding. These were recently reviewed by Horwitz and Shriver (26). Thus the Cu—O distances (2.945(5)–3.143(5) Å) are much longer than the Cu—C distances (2.234(6)–2.419(6) Å) leading to Ω values of approximately 2.14–2.16 (Ω = exp [D(Cu—C)/D(Cu—O)]), a value much lower than expected for a Π-CO type interaction.

[4]The constructive comments of a referee regarding the ir data of the Cu complex are gratefully acknowledged.

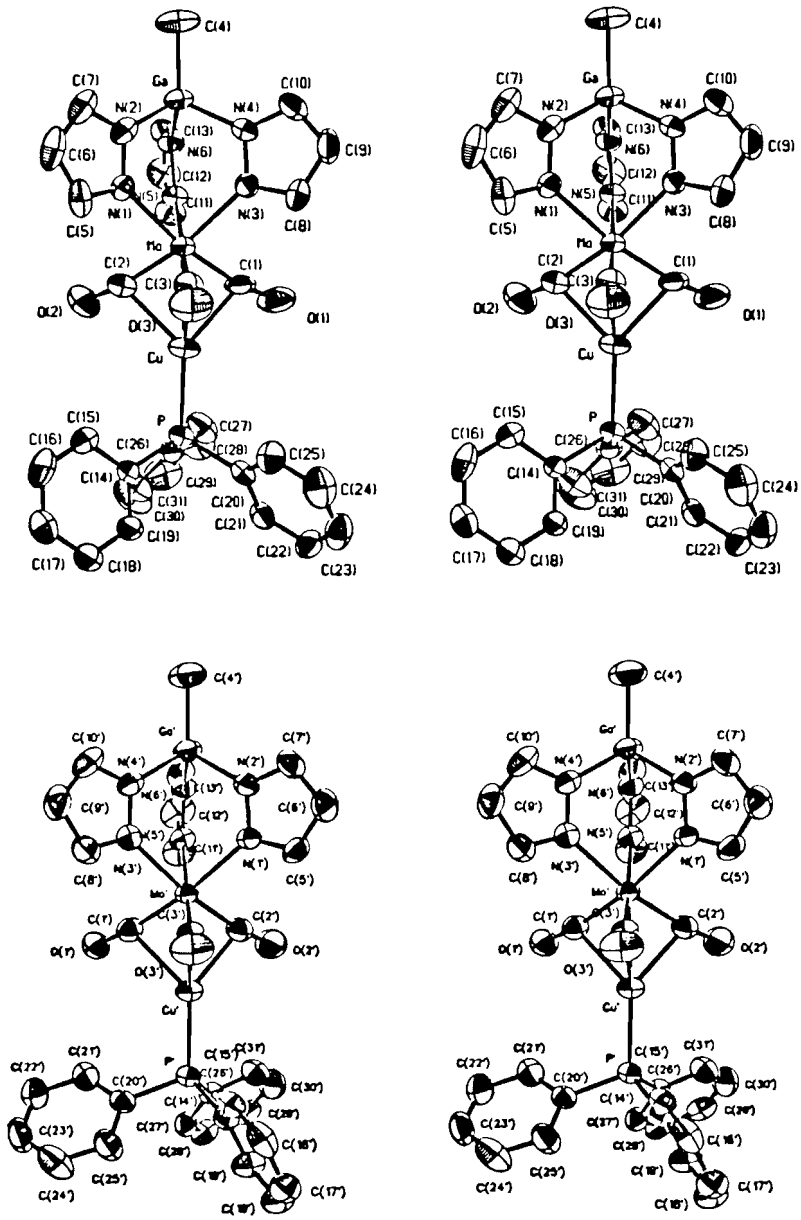

FIG. 3. Stereoscopic views of the two independent molecules of [methyltris(1-pyrazolyl)gallato-(*N*,*N*,*N*)]tricarbonylmolybdenum(triphenylphosphine)copper (*Mo-Cu*); 50% probability thermal ellipsoids are shown. Hydrogen atoms are omitted for clarity. The mirror image of the primed molecule is shown for direct comparison.

In addition, the ν_{CO} frequencies observed for the complex are all much higher than the expected value of $\sim 1650\ cm^{-1}$ for a Π-CO group.

Perhaps the bonding in the present complex is more subtle. In this regard recent MO calculations (28) on the complex $(\eta\text{-}C_6H_6)(CO)Cr(\mu\text{-}CO)_2Rh(CO)(\eta\text{-}C_5H_5)$, a complex originally postulated to contain a Cr → Rh donor bond in addition to semi-bridging CO interactions (30), suggest a strong interaction between the distal Rh centre and the bridging CO ligands (Cr—CO (bridge), 1.902(7) Å, Rh—CO (bridge), 2.200(7) Å) with a net bond order close to zero between the metal atoms (Rh···Cr, 2.757(2) Å). Similar calculations on the present system may well be invaluable in determining the major bonding interactions responsible for the short Mo—Cu separation.

It is again interesting to compare similar complexes in this area. Carlton *et al.* (27) have provided structural data on two different forms of the complex $(\eta\text{-}C_5H_5)W(CO)_3Cu(PPh_3)_2$, and suggest some semi-bridging interactions involving the two metals and two of the CO ligands. Three important differences occur with the $[MeGapz_3]Mo(CO)_3Cu(PPh_3)$ complex. First, only one PPh_3 ligand is attached to the Cu centre, making the molecule valence isoelectronic with the $[MeGapz_3]Mo(CO)_3$-$Rh(PPh_3)_2$ compound. Second, the present structure has three roughly equivalent CO groups whereas in Carlton's tungsten compounds one of the three CO groups is clearly terminal to tungsten. Third, the mean Mo—Cu distance of 2.513(9) Å is considerably shorter than either of the W—Cu distances of 2.771(1) and 2.721(1) Å reported by Carlton *et al.* Given that the radii for Mo and W are very similar at ~1.61 Å (the M—M distances in $(\eta\text{-}C_5H_5)(CO)_3M—M(CO)_3(\eta\text{-}C_5H_5)$ are 3.222(5) Å for M=Mo (40) and 3.24(1) Å for M=W (41),

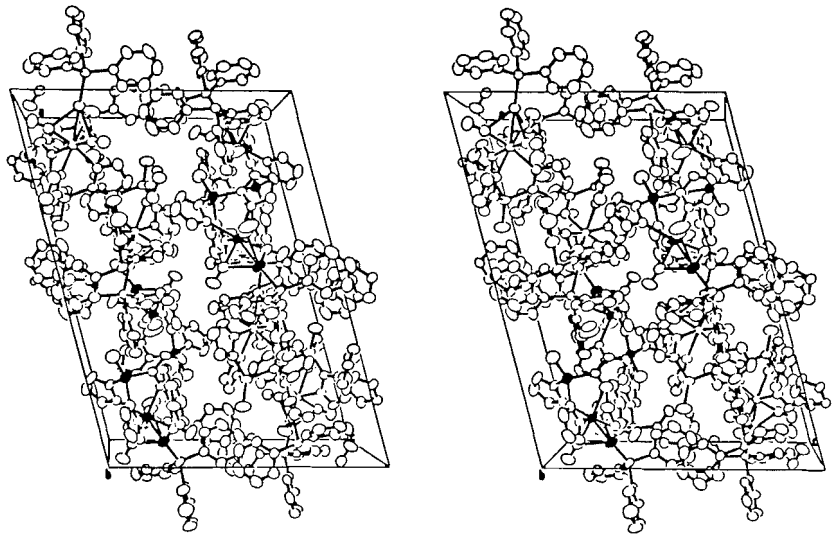

FIG. 4. Stereoscopic view of the [methyltris(1-pyrazolyl)gallato-(*N*,*N*,*N*)]tricarbonylmolybdenum(triphenylphosphine)copper (*Mo-Cu*) structure; metal atoms of the umprimed molecules are shaded for identification.

these differences in bond lengths suggest a much stronger Mo—Cu interaction in the present complex. Indeed, the observed Mo—Cu distance is significantly shorter than the estimated single Mo—Cu bond length of ~2.7–2.8 Å. Another noticeable difference occurs in the Cu—P distances in the two complexes. Thus the compound reported here displays a mean Cu—P distance of 2.196(3) Å, somewhat shorter than the corresponding mean distance of 2.299(12) Å reported for the two crystalline forms of $(\eta\text{-}C_5H_5)W(CO)_3Cu(PPh_3)_2$.

The structures of the $(\eta\text{-}C_5H_5)W(CO)_3Au(PPh_3)$ (42) and $[HBpz_3]Mo(CO)_3Br$ (38) complexes are worthy of comparison with the $[MeGapz_3]Mo(CO)_3Cu(PPh_3)$ structure. The W—Au compound displays an arrangement very different from that found for Mo—Cu complex. Thus, instead of a symmetrical structure analogous to that depicted in Fig. 3, with the $\eta\text{-}C_5H_5$ ligand replacing the $MeGapz_3$ ligand and the Au atom replacing the Cu atom, the arrangement adopted is that of a "four-legged" piano stool, or a distorted square pyramid with the $(\eta\text{-}C_5H_5)W$ unit at the apex and the three CO ligands and the $Au(PPh_3)$ grouping occupying the basal positions. A similar structure, described as a 3:4 piano stool, has been reported recently by Curtis and Shiu (38) for $[HBpz_3]Mo(CO)_3Br$. These authors mentioned that one of the interesting aspects which prompted their study was the possibility of observing a capped octahedral (3:3:1) structure, since calculations by Kubacek *et al.* (43) had shown that this arrangement represents a minimum in the potential energy surface for analogous $(\eta\text{-}C_5H_5)ML_4$ complexes whose global minimum (ground state) is always the four-legged piano stool, or 3:4 structure. It appears that the present copper complex $[MeGapz_3]Mo(CO)_3Cu(PPh_3)$ closely approaches this 3:3:1 capped octahedral arrangement.

Finally, the structure of the complex, $(\eta\text{-}C_3H_5)Fe(CO)_3\text{-}AuPPh_3$ (44) has many features similar to the Mo–Cu complex presented here. It has been proposed that the bonding in this iron complex results from the Lewis base $(\eta\text{-}C_3H_5)Fe(CO)_3^-$ donating a pair of electrons to the Lewis acid $Au(PPh_3)^+$ and does not necessarily involve any direct interaction between the Au atom and the CO ligands, the geometry of the complex being dictated by transition metal basicity. If this reasoning is correct then the Au centre attains a 14-electron count and the Fe—Au separation of 2.519(1) Å results entirely from the Fe → Au dative bond.

The present study has again shown the versatility of the "$MeGapz_3$" ligand in that it can, on the one hand, successfully mimic the behaviour of the "$\eta\text{-}C_5H_5$" ligand system (1) but, more importantly, on the other hand it can display significantly different behaviour (7). This versatility is being further exploited in the area of heterometallic complexes.

Acknowledgments

We thank the Natural Sciences and Engineering Research Council of Canada for financial support, Professor James Trotter (Academic Supervisor, University of British Columbia Crystallographic Service) for the use of laboratory facilities, and the University of British Columbia Computing Centre for assistance.

1. K. R. BREAKELL, S. J. RETTIG, D. L. SINGBEIL, A. STORR, and J. TROTTER. Can. J. Chem. **56**, 2099 (1978).
2. S. TROFIMENKO. Chem. Rev. **72**, 497 (1972).
3. S. J. RETTIG, A. STORR, J. TROTTER, and K. UHRICH. Can. J. Chem. **62**, 2783 (1984).
4. K. S. CHONG and A. STORR. Can. J. Chem. **57**, 167 (1979).
5. K. S. CHONG, S. J. RETTIG, A. STORR, and J. TROTTER. Can. J. Chem. **57**, 3107 (1979).
6. K. S. CHONG, S. J. RETTIG, A. STORR, and J. TROTTER. Can. J. Chem. **57**, 3113 (1979).
7. B. M. LOUIE, S. J. RETTIG, A. STORR, and J. TROTTER. Can. J. Chem. **62**, 633 (1984).
8. K. S. CHONG, S. J. RETTIG, A. STORR, and J. TROTTER. Can. J. Chem. **55**, 4166 (1977).
9. S. TROFIMENKO. Inorg. Synth. **XII**, 102 (1970).
10. D. P. TATE, W. R. KNIPPLE, and J. M. AUGL. Inorg. Chem. **1**, 433 (1962).
11. G. COSTA, E. REISENHOFER, and L. STEFANI. J. Inorg. Nucl. Chem. **27**, 2581 (1965).
12. P. COPPENS, L. LEISEROWITZ, and D. RABINOVICH. Acta Crystallogr. **18**, 1035 (1965).
13. W. R. BUSING and H. A. LEVY. Acta Crystallogr. **22**, 457 (1967).
14. D. T. CROMER and J. B. MANN. Acta Crystallogr. Sect. A, **24**, 321 (1968).

15. R. F. STEWART, E. R. DAVIDSON, and W. T. SIMPSON. J. Chem. Phys. **42**, 3175 (1965).
16. D. T. CROMER and D. LIBERMAN. J. Chem. Phys. **53**, 1891 (1970).
17. K. S. CHONG, S. J. RETTIG, A. STORR, and J. TROTTER. Can. J. Chem. **57**, 1335 (1979).
18. K. S. CHONG, S. J. RETTIG, A. STORR, and J. TROTTER. Can. J. Chem. **58**, 1080 (1980).
19. K. S. CHONG and A. STORR. Can. J. Chem. **58**, 2278 (1980).
20. K. S. CHONG and A. STORR. Can. J. Chem. **59**, 1331 (1981).
21. K. S. CHONG, S. J. RETTIG, A. STORR, and J. TROTTER. Can. J. Chem. **59**, 1665 (1981).
22. K. S. CHONG, S. J. RETTIG, A. STORR, and J. TROTTER. Can. J. Chem. **59**, 2391 (1981).
23. F. A. COTTON. Prog. Inorg. Chem. **21**, 1 (1976).
24. R. COLTON and M. J. MCCORMICK. Coord. Chem. Rev. **31**, 1 (1980).
25. A. BINO, F. A. COTTON, P. LAHUERTA, P. PUEBLA, and R. USON. Inorg. Chem. **19**, 2357 (1980).
26. C. P. HORWITZ and D. F. SHRIVER. Adv. Organomet. Chem. **23**, 219 (1984).
27. L. CARLTON, W. E. LINDSELL, K. J. MCCULLOUGH, and P. N. PRESTON. J. Chem. Soc. Dalton Trans. 1693 (1984).
28. R. D. BARR, T. B. MARDER, A. G. ORPEN, and I. D. WILLIAMS. J. Chem. Soc. Chem. Commun. 112 (1984).
29. M. GREEN, J. A. K. HOWARD, A. P. JAMES, C. M. NUNN, and F. G. A. STONE. J. Chem. Soc. Chem. Commun. 1113 (1984).
30. R. D. BARR, M. GREEN, K. MARSDEN, F. G. A. STONE, and P. WOODWARD. J. Chem. Soc. Dalton Trans. 507 (1983).
31. L. J. FARRAGUIA, A. D. MILES, and F. G. A. STONE. J. Chem. Soc. Dalton Trans. 2415 (1984).
32. R. D. BARR, M. GREEN, J. A. K. HOWARD, T. B. MARDER, A. G. ORPEN, and F. G. A. STONE. J. Chem. Soc. Dalton Trans. 2757 (1984).
33. C. P. CASEY, R. M. BULLOCK, and F. NIEF. J. Am. Chem. Soc. **105**, 7574 (1983).
34. R. F. FINKE, G. GAUGHAN, C. PIERPONT, and M. E. CASS. J. Am. Chem. Soc. **103**, 1394 (1981).
35. O. BARS and P. BRAUNSTEIN. Angew. Chem. Int. Ed. Engl. **21**, 308 (1982).
36. D. A. ROBERTS, W. C. MERCER, S. M. ZAHURAK, G. L. GEOFFROY, C. W. DEBROSSE, M. E. CASS, and C. G. PIERPONT. J. Am. Chem. Soc. **104**, 910 (1982).
37. S. TROFIMENKO. J. Am. Chem. Soc. **91**, 588 (1969).
38. M. D. CURTIS and K. B. SHIU. Inorg. Chem. **24**, 1213 (1985).
39. R. J. KLINGER, W. M. BUTLER, and M. D. CURTIS. J. Am. Chem. Soc. **100**, 5034 (1978).
40. F. C. WILSON and D. P. SHOEMAKER. J. Chem. Phys. **27**, 809 (1957).
41. F. C. WILSON and D. P. SHOEMAKER. Naturwiss. **43**, 57 (1956).
42. J. B. WILFORD and H. M. POWELL. J. Chem. Soc. Sect. A, 8 (1969).
43. P. KUBACEK, R. HOFFMAN, and Z. HALVAS. Organometallics, **1**, 180 (1982).
44. F. E. SIMON and J. W. LAUHER. Inorg. Chem. **19**, 2338 (1980).

Partial molal volumes of amines in benzene. Specific interactions[1]

ESTER F. G. BARBOSA AND ISABEL M. S. LAMPREIA

Centro de Electroquímica e Cinética da Universidade de Lisboa, Faculdade de Ciências, Rua da Escola Politécnica, 58, 1294 Lisboa Codex, Portugal

Received July 15, 1985

ESTER F. G. BARBOSA and ISABEL M. S. LAMPREIA. Can. J. Chem. **64**, 387 (1986).

Apparent molal volumes, V_ϕ, of secondary and tertiary amines and linear hydrocarbons were determined in benzene at 25°C, using a vibrating tube densimeter. These quantities have been extrapolated to infinite dilution to obtain partial molal volumes. The contribution to partial molal volume of the amine groups, calculated using a simple additive scheme, $\bar{V}^0 = \sum_k N_k \bar{V}_k^0$, were interpreted in terms of conformational effects present in these molecules. A first attempt to find a measure of the contribution to the partial molal volume of the specific interaction amine–benzene in tertiary and secondary amines was made. The results agree well in the two different approaches used.

ESTER F. G. BARBOSA et ISABEL M. S. LAMPREIA. Can. J. Chem. **64**, 387 (1986).

Faisant appel à un densimètre à tube vibrant et opérant dans le benzène à 25°C, on a mesuré les volumes molales apparents, V_ϕ, d'amines secondaires et tertiaires et d'hydrocarbures linéaires. On a extrapolé ces quantités à dilution infinie afin d'obtenir les volumes molales partiels. On a interprété la contribution au volume molale partiel des groupements amines, calculés en utilisant un schéma additif simple, $\bar{V}^0 = \sum_k N_k \bar{V}_k^0$, en fonction d'effets conformationnels présents dans ces molécules. On a tenté un premier essai dans le but de trouver une mesure de la contribution au volume molale partiel de l'interaction spécifique amine–benzène dans les amines secondaires et tertiaires. Les résultats obtenus avec l'une ou l'autre approche concordent bien.

[Traduit par le journal]

Introduction

The volumetric behaviour of solutes has proved to be of great importance in the understanding of interactions in solution. Much work has been published on $\bar{V}^0$ additive schemes in which every group contribution is assumed to be independent of the molecule under study, depending solely on the solvent (1–4). However, experience has shown that the position of the group in the molecule, size of the molecule, and specific solute–solvent interactions produce deviations from the simple additive behaviour. To get a deeper understanding of these factors, different kinds of reference volumes with respect to which volume changes could be calculated and interpreted have been used in the past (5–7). Molar volume of the solute V^0, Bondi's van der Waals volume V_W (8), and cavity volume $\bar{V}_{cav}$ as given by the scaled particle theory (SPT) have been used for the above purpose.

In this study we have tried to find a measure of the contribution of the specific interactions to the partial molal volumes of secondary and tertiary amines in benzene. Comparative values of these contributions were found using two different approaches, one based on the model of Terasawa *et al.* (6) and the other on SPT (7). In both cases linear hydrocarbons were used as reference materials, to separate the two types of interactions present in these molecules.

Experimental

Materials

All substances employed were guaranteed commercial reagents obtained from Merck, B.D.H., Eastman Kodak, Aldrich, and Fluka.

The three tertiary amines, triethylamine, tri-*n*-butylamine, and tri-*n*-octylamine, were first heated with an appropriate quantity of acetic anhydride and fractionally distilled, then refluxed with KOH for several hours and again fractionally distilled from BaO through a column packed with Pyrex glass rings. The two last amines mentioned were distilled in a vacuum jacketed column at 70 and 0.4 Torr (1 Torr = 133.3 Pa) respectively. Tri-*n*-propylamine, after having been heated with acetic anhydride, was shaken with KOH several times until all acetic anhydride has been extracted. Then it was allowed to stand over sodium hydroxide pellets for several days and fractionally distilled as previously described.

The secondary amines, diethylamine, di-*n*-butylamine, di-*n*-hexylamine, and di-*n*-octylamine, were refluxed with KOH pellets for several hours and fractionally distilled as described for the tertiary amines. Di-*n*-dodecylamine was fractionally recrystallized three times from a mixture of ethanol–benzene in a dry nitrogen atmosphere.

The two linear hydrocarbons, *n*-octane and *n*-decane, were refluxed for several hours over sodium thread and fractionally distilled from CaH_2 in a vacuum jacketed column.

The purity of the solutes was tested by density measurements. Values obtained are compared with the ones found in the literature (see Table 1).

Benzene was refluxed for several hours over CaH_2 and fractionally distilled in a column packed with Pyrex glass rings, under dry nitrogen.

The purity of benzene was also tested by density measurements. The average densities of the different samples used in the $\bar{V}^0$ determinations of each solute are shown in Table 2. Selected literature values at 25°C are 0.87365 (9), 0.87367 (10).

Measurements

Densities were measured using an Anton Paar DMA 02D vibrating tube densimeter. The temperature of the bath was kept constant at 25 ∓ 0.001°C with a Tronac PTC 40 temperature controller. The temperature of the bath was set with a Hewlett–Packard quartz crystal thermometer. The oscillator of the thermometer was kept at constant temperature in a distilled water–ice bath. The densimeter and the water bath were both enclosed in an air box thermostated to ∓0.1°C. The densimeter was calibrated using water and dry air. This calibration was repeated several times in each set of measurements.

Solutions were all prepared by weight in volumetric flasks of appropriate volume according to the expected error in each solute. Design to prevent evaporation was introduced into the flasks. The densities were precise to $\pm 2 \times 10^{-6}$ g cm^{-3}.

Results and discussion

Densities

Experimental density values for various amine and linear

[1]Portions of this work have been presented to the 2nd International Conference on Thermodynamics of Solutions of Non-Electrolytes, Lisbon, Portugal, 1982, and to the 6th International Symposium on Solute–Solute–Solvent Interactions, Osaka, Japan, 1982.

Printed in Canada / Imprimé au Canada

TABLE 1. Densities and molar volume of amines and linear hydrocarbons at 25°C

Compound	d (g cm^{-3})	V^0 (cm^3 mol^{-1})	Reference
Diethylamine	0.6990	104.63	This work
	0.69894	104.64	Swift (11)
	0.69948	104.56	Letcher (12)
Di-*n*-butylamine	0.75540	171.10	This work
	0.75572	171.02	Letcher (12)
	0.7577	170.58	17
Di-*n*-hexylamine	0.7825	236.88	This work
Di-*n*-octylamine	0.79717	302.90	This work
Triethylamine	0.72301	139.96	This work
	0.72318	139.93	Letcher (12)
	0.72345	139.88	Krichevskii *et al.* (13)
Tri-*n*-propylamine	0.75186	190.56	This work
	0.75234	190.44	Letcher (12)
Tri-*n*-butylamine	0.77306	239.77	This work
	0.77378	239.54	Letcher (12)
Tri-*n*-hexylamine	0.7937	339.57	Klofutar *et al.* (14)
Tri-*n*-octylamine	0.80823	437.60	This work
	0.8068	438.37	Klofutar *et al.* (14)
	0.8086	437.40	Kertes and Grauer (15)
Tri-*n*-decylamine	0.8155	536.90	Klofutar *et al.* (14)
Tri-*n*-dodecylamine	0,8207	636.05	Klofutar *et al.* (14)
	0.8217	635.27	Grauer and Kertes (16)
Pentane	0.62139	116.11	17
Hexane	0.65481	131.61	17
Heptane	0.67951	147.47	17
Octane	0.69873	163.49	This work
	0.69849	163.54	17
Nonane	0.71381	179.68	17
Decane	0.72627	195.91	This work
	0.72625	195.92	17

hydrocarbon solutions, in the molality ranges studied, obey equations of the type

$$[1] \quad d = A + Bm + Cm^2$$

where A, B, and C are empirical coefficients as shown in Table 2. As can be seen, the A values compare well with the average density of benzene, $\bar{d}_{C_6H_6}$, calculated from the different experimental determinations of benzene density when $\bar{V}^0$ values were obtained for each solute.

Partial molal volumes

The apparent molal volumes of all solutes were calculated in the usual way

$$[2] \quad V_\phi = \frac{MPd^0 - MPd}{pdd^0} + \frac{M}{d}$$

where M is the solute molecular weight; P the solvent weight; p the solute weight; and d^0 and d the densities of pure solvent and solution, respectively.

The V_ϕ values for the range of molalities studied are given in Table 3.

The partial molal volumes $\bar{V}^0$ of solute were obtained by linear extrapolation of the V_ϕ's to infinite dilution by a least-squares fitting method.

Table 4 summarizes the values at infinite dilution of the partial molal volumes $\bar{V}^0$, along with the excess $\Delta\bar{V}$ volumes calculated as $\Delta\bar{V} = \bar{V}^0 - V^0$.

In all the solutes investigated, positive values of $\Delta\bar{V}$ were obtained. This fact leads to the conclusion that the prevailing intermolecular interaction of any of the amines with benzene is due to the aliphatic part of the molecule. This is an indication of inappropriate geometrical fitting of the solutes in this solvent. A more careful look at the results, in particular for solutes of the same size, shows that for the amines the increase in volume is never as big as for the hydrocarbons, meaning that the amine group – benzene interaction produces a decrease in volume. This is in agreement with the findings of the previous workers: C_6H_6 – tertiary amines n–Π interactions and C_6H_6 – secondary amines n–Π and NH $\cdots\Pi$ interactions (19–21).

$\bar{V}^0$ group contributions

The linear dependence of partial molal volumes on the number of carbon atoms, n_C, found for the three homologous series studied allows us to identify the slopes, b, of eq. [3] with the contribution of the methylene group, and the intercepts, a, with the combination of group contributions as shown in eqs. [4]–[6].

$$[3] \quad \bar{V}^0 = a + bn_C$$

$$[4] \quad a_{HC} = 2\bar{V}^0_{CH_2} + 2\bar{V}^0_{CH_3}$$

$$[5] \quad a_{sec.amines} = -2\bar{V}^0_{CH_2} + 2\bar{V}^0_{CH_3} + \bar{V}^0_{>\ddot{N}H}$$

$$[6] \quad a_{tert.amines} = -3\bar{V}^0_{CH_2} + 3\bar{V}^0_{CH_3} + \bar{V}^0_{\geq N:}$$

The group contributions as presented in Table 5 were derived by a least-squares fitting of experimental $\bar{V}^0$ values to eq. [3] and using expressions [4]–[6]. In this statistical method we have taken into account the non-constancy of the standard deviation of the different $\bar{V}^0$ determinations.[2] Intercepts along with their standard deviations are $a_{HC} = 32.8_5 \pm 0.1_5$, $a_{sec.amines} = 37.4_5 \pm 0.2_0$, and $a_{tert.amines} = 41.0_1 \pm 0.2_1$ cm^3 mol^{-1}. The slopes $b \equiv \bar{V}^0_{CH_2}$ can be seen in Table 5, as referred to above. The $\bar{V}^0_{CH_2}$ used in eqs. [4]–[6] is the average of the values obtained from the three sets of compounds. Table 5 also shows the CH_2-group contribution to the pure solutes as well as their excess volume $\Delta\bar{V}_{CH_2} = \bar{V}^0_{CH_2} - V^0_{CH_2}$.

In this same table one can see that the methylene-group contribution is always bigger in C_6H_6 than in pure solutes. As already pointed out for the global solute molecules, this fact can be explained by the perturbation of benzene structure caused by the aliphatic part of these molecules, when they are introduced in this solvent. This result is in opposition to what can be observed in water, where hydrophobic bonding interactions are present. Another observation concerning this group contribution, in the three sets of compounds, is that their values are almost constant, although differences greater than the experimental error are present.

[2]Algebraic equations for first-order ($y = a + bx$) weighted least-squares fitting:

$a = (\Sigma w_i y_i \Sigma w_i x_i^2 - \Sigma w_i x_i \Sigma w_i x_i y_i)/D$

$b = (\Sigma w_i \Sigma w_i x_i y_i - \Sigma w_i x_i \Sigma w_i y_i)/D$

$D = \Sigma w_i \Sigma w_i x_i^2 - (\Sigma w_i x_i)^2$

$\sigma_a = \sigma(\Sigma w_i x_i^2/D)^{1/2}$

$\sigma_b = \sigma(\Sigma w_i/D)^{1/2}$

$w_i = C^2/\sigma_i^2$

with C equal to the smaller σ.

TABLE 2. Empirical parameters of the equation $d = A + Bm + Cm^2$, for amines and linear hydrocarbons in benzene at 25°C

Compound	A (g cm^{-3})	$B \times 10^2$ (g cm^{-3} mol^{-1} kg)	$C \times 10^3$ (g cm^{-3} mol^{-2} kg^2)	$\sigma \times 10^5$[a]	$\bar{d}_{C_6H_6}$[b]	C_6H_6 purified from
Diethylamine	0.873628	−1.6299	1.557	0.31	0.873619	Fluka puriss p.a.
Di-*n*-butylamine	0.873675	−1.9527	3.921	1.1	0.873672	B.D.H. Analar
Di-*n*-hexylamine	0.873633	−2.1797	4.177	0.36	0.873637	Merck p.a.
Di-*n*-octylamine	0.873623	−2.4997	7.912	1.9	0.873617	Merck p.a.
Di-*n*-dodecylamine	0.873592	−2.9430	11.625	1.1	0.873620	Merck p.a.
Triethylamine	0.873639	−1.8938	3.075	1.2	0.873630	Fluka puriss p.a.
Tri-*n*-propylamine	0.873604	−2.2852	4.869	0.91	0.873585	Merck p.a.
Tri-*n*-butylamine	0.873632	−2.4257	5.165	0.49	0.873632	Merck p.a.
Tri-*n*-octylamine	0.873569	−3.2005	13.376	0.47	0.873575	Merck p.a.
Octane	0.873697	−2.7877	4.011	0.70	0.873696	Fluka puriss p.a.
Decane	0.873623	−2.9082	4.946	2.1	0.873632	Merck p.a.

[a]Standard error of solution density estimation.
[b]$\bar{d}_{C_6H_6}$ is the average value of benzene density in the $\bar{V}_0$ determination of each solute. The average standard deviation was 2×10^{-6} g cm^{-3}.

TABLE 3. Apparent molal volume of amines and linear hydrocarbons in benzene at 25°C

m (mol^{-1} kg^{-1})	V_ϕ (cm^3 mol^{-1})	m (mol kg^{-1})	V_ϕ (cm^3 mol^{-1})	m (mol kg^{-1})	V_ϕ (cm^3 mol^{-1})
Diethylamine		Di-*n*-dodecylamine		Tri-*n*-butylamine (cont.)	
0.0322	105.08	0.0195	444.36	0.1235	243.91
0.0485	105.00	0.0466	443.99	0.1658	243.83
0.0761	104.89	0.0629	443.96	0.2210	243.87
0.1177	104.86	0.0827	444.00	0.2593	243.91
0.1476	104.99	0.1101	443.86	0.3009	243.80
0.1795	104.93	0.1298	443.73	Tri-*n*-octylamine	
0.2554	104.98	0.1653	443.46	0.0323	447.05
0.2998	104.98	0.1857	443.29	0.0417	446.84
0.3307	104.93	0.2559	443.00	0.0490	446.95
0.3598	104.97	0.2924	442.95	0.0604	446.89
Di-*n*-butylamine		0.3863	442.51	0.0699	446.79
0.0526	173.08	Tri-*n*-ethylamine		0.0834	446.78
0.0740	173.16	0.0283	140.24	0.0904	446.73
0.2011	173.17	0.0427	140.35	0.1015	446.80
0.2649	173.16	0.0505	140.25	*n*-Octane	
0.3341	173.08	0.0613	140.34	0.0187	167.47
Di-*n*-hexylamine		0.0773	140.18	0.0353	167.26
0.0198	240.80	0.1243	140.32	0.0503	167.11
0.0300	240.92	0.1634	140.31	0.0704	167.24
0.0501	240.79	0.2306	140.31	0.0954	167.19
0.0741	240.83	0.2629	140.29	0.1161	167.42
0.1185	240.86	0.3052	140.36	0.1502	167.31
0.2189	240.79	Tri-*n*-propylamine		0.1746	167.28
0.2597	240.80	0.0408	193.47	0.2220	167.18
Di-*n*-octylamine		0.0755	193.49	0.2543	167.23
0.0199	308.87	0.0846	193.50	0.3012	167.21
0.0244	308.86	0.1008	193.53	*n*-Decane	
0.0503	309.00	0.1227	193.57	0.0198	201.05
0.0857	308.84	0.1702	193.47	0.0347	200.87
0.0969	308.80	0.2048	193.56	0.0504	201.15
0.1355	308.82	0.2554	193.45	0.0759	200.87
0.1672	308.78	Tri-*n*-butylamine		0.0965	201.18
0.1884	308.68	0.0187	243.81	0.1212	201.08
0.2293	307.58	0.0351	243.90	0.1688	201.11
0.2594	308.50	0.0502	243.98	0.2234	201.08
0.2890	308.50	0.0746	243.99	0.2626	200.98
0.3026	308.44	0.0950	243.90	0.3104	201.02

TABLE 4. Partial molal volumes of amines and linear hydrocarbons at infinite dilution in benzene at 25°C

Compound	$\bar{V}^0$ ($cm^3\ mol^{-1}$)	$\Delta\bar{V}$ ($cm^3\ mol^{-1}$)
Diethylamine	104.97 ± 0.04[a]	0.33
Di-*n*-butylamine	173.13 ± 0.04[a]	2.01
Di-*n*-hexylamine	240.85 ± 0.03[a]	3.98
Di-*n*-octylamine	308.92 ± 0.03[a]	6.02
Di-*n*-dodecylamine	444.33 ± 0.05[a]	—
Triethylamine	140.27 ± 0.03[a]	0.37
Tri-*n*-propylamine	193.51 ± 0.07[a]	3.0
Tri-*n*-butylamine	243.92 ± 0.03[a]	4.15
Tri-*n*-hexylamine	344.8 ± 0.7[b]	5.0
Tri-*n*-octylamine	447.08 ± 0.07[a]	9.5
	441.9 ± 0.7[b]	3.5
Tri-*n*-decylamine	547.6 ± 0.5[b]	10.7
Tri-*n*-dodecylamine	645.9 ± 1.3[b]	10.0
Pentane	117.0 ± 0.1[c]	0.9
Hexane	133.8 ± 0.5[c]	2.2
Heptane	150.3 ± 0.3[c]	2.8
Octane	167.31 ± 0.06[a]	3.8
	167.6 ± 0.3[c]	3.8
Nonane	184.4 ± 0.3[c]	4.7
Decane	201.03 ± 0.06[a]	5.1
	201.8 ± 0.3[c]	5.9

[a]This work.
[b]Reference 14.
[c]Reference 18.

In relation to the tertiary amine group (≥N:), the introduction of Et_3N in the linear fit $\bar{V}^0$ vs. n_C changes considerably the intercept a. Therefore this compound was not included in the calculations of the average group contributions. The $\bar{V}^0_{\geq N:}$ for this amine was calculated and is $\bar{V}^0_{\geq N:}(Et_3N) = -10.4\ cm^3\ mol^{-1}$. This lower value may be justified by a noticeable difference of conformational effects in this amine as compared to the other amines of this series, in which a regular behaviour is observed (23). In respect to the higher amines, if one assumes that the CH_2-group contribution is the same as in linear hydrocarbons, the slightly different slope of the curve $\bar{V}^0$ vs. V_W would correspond to a small variation of the amine-group interaction along the series. This conclusion agrees with the observation made by Kertes and Grauer (15) and is related to the effect of chain length on excess enthalpies of mixing of these amines in C_6H_6. Kertes and Grauer explained this fact by the existence of a shielding effect to the lone-pair nitrogen electrons, due to the long aliphatic chains. In spite of this knowledge, the average of this amine-group contribution was calculated, as was the one for the secondary amines, assuming its constancy and using a simple additive scheme. The average values obtained, $V_{\geq N:} = -8.3\ cm^3\ mol^{-1}$ and $V_{\geq NH} = 4.6\ cm^3\ mol^{-1}$, both much smaller than their Bondi's van der Waals volumes, suggest the presence of another factor leading to a significant decrease in volume, in addition to the one caused by the specific interaction amine–benzene.

Conformational effects such as *gauche* interactions have been proven to influence physical properties of organic molecules (22). Terms containing those effects have already been introduced in additive schemes for $\bar{V}^0$ by Edward *et al.* (4). These authors refer to many cases in which decreases in volume were associated with *gauche* interactions. Similar results were obtained by ourselves as a result of a conformational study of some of these amines in benzene (23).

These conclusions gave us great incentive to obtain more detailed information about the effects on volume, corresponding to these specific interactions on the one hand and to conformational effects on the other hand. The continuation of these studies is important, to make possible the introduction of these contributions to more exact additive schemes.

Partial molal volumes of the specific interactions

As already pointed out, in the amine–benzene systems one may assume that the interactions present are composed of two different contributions. One is due to the aliphatic part of the molecule, leading to an increase in volume, and the other is due to the amine groups, producing the opposite effect.

To clarify the contribution to the partial molal volumes of the amine–benzene specific interactions, we have tried to separate the aliphatic from the amine contributions using two different approaches. One of these approaches, (*i*), is based on the model of Terasawa *et al.* (6) and the other, (*ii*), on SPT (7), considering V_W and $\bar{V}_{cav}$ respectively as reference volumes.

(*i*) According to Terasawa *et al.*, the partial molal volume of a solute A is composed of two contributions, i.e., the van der Waals volume, $V_{W,A}$, and the void partial molal volume, $\bar{V}_{void,A}$ (the actual void space created by addition of one mol of solute A to the solvent).

$$[7] \quad \bar{V}^0_A = V_{W,A} + \bar{V}_{void,A}$$

To estimate the contribution of specific solute–solvent interactions to the partial molal volume, the same authors had the idea of comparing $\bar{V}_{void,A}$ (or $\bar{V}^0_A$) with that of a reference material with the same van der Waals volume as the solute A. As hydrocarbons do not interact strongly with many organic solvents and all organic molecules are derived from them, these compounds were considered to be an appropriate standard material for this purpose. Then, applying eq. [7] to the hydrocarbon molecule having the same van der Waals volume as the solute A, we obtain

$$[8] \quad \bar{V}^0_{HC} = V_{W,A} + \bar{V}_{void,HC}$$

and, from eqs. [7] and [8],

$$[9] \quad \bar{V}_{S-S} = \bar{V}^0_A - \bar{V}^0_{HC} = \bar{V}_{void,A} - \bar{V}_{void,HC}$$

where $\bar{V}_{S-S}$ is the partial molal volume of the specific interactions.

To obtain $\bar{V}_{S-S}$ it is thus necessary to have values of the partial molal volumes of linear hydrocarbons with the same van der Waals volumes as the solutes studied. Since in general there are not real hydrocarbons with the requirement just stated, a weighted least-squares fitting linear relation $\bar{V}^0$ vs. V_W was obtained for these compounds and from it the suitable $\bar{V}^0_{HC}$ values were taken. Also, weighted linear regressions were done for the amines. This procedure is particularly important for the tertiary amines, as very different errors are associated with the experimental results. Table 6 shows the slopes and intercepts obtained.

The $\bar{V}_{S-S}$ parameter values calculated as explained above are listed in Table 9, and will be discussed jointly with the corresponding parameters presented in the next section.

(*ii*) Using now the statistical mechanical scaled particle theory (7, 24), we can derive in a similar way to (*i*) a comparative measure of the specific interactions from a different conception of the separation of the various contributions to $\bar{V}^0$.

The SPT expression for $\bar{V}^0$ is

TABLE 5. Average group contribution to the partial molal volumes in pure solutes and benzene at 25°C

Compounds	$V^0_{CH_2}$ (cm^3 mol^{-1})	$\bar{V}^0_{CH_2}$ (cm^3 mol^{-1})	$\Delta\bar{V}^0_{CH_2}$[a] (cm^3 mol^{-1})	$\bar{V}^0_{CH_3}$ (cm^3 mol^{-1})	$\bar{V}^0_{>\ddot{N}H}$ (cm^3 mol^{-1})	$\bar{V}^0_{\geqslant N:}$ (cm^3 mol^{-1})
Secondary amines	16.51	16.96 ± 0.01	0.45	—	4.6 ± 0.3	—
Tertiary amines	16.48[b]	16.91 ± 0.02[b]	0.43	—	—	−8.3 ± 0.3
Linear hydrocarbons	15.98	16.82 ± 0.02	0.84	33.3 ± 0.2	—	—

[a] $\Delta\bar{V}^0_{CH_2} = \bar{V}^0_{CH_2} - V^0_{CH_2}$.
[b] Et_3N was excluded from the least-squares fitting as this amine showed a different behaviour from their homologues.

TABLE 6. Empirical parameters of the weighted linear regressions $\bar{V}^0 = a + b\,V_W$ for linear hydrocarbons and amines in benzene at 25°C

Compounds	a (cm^3 mol^{-1})	b
Secondary amines	12.4 ± 0.2	1.659 ± 0.001
Tertiary amines	16.8 ± 0.2[a]	1.653 ± 0.002
Hydrocarbons	21.6 ± 0.2	1.644 ± 0.002

[a] Et_3N was excluded from the fit as this amine was shown to have a different behaviour from its homologues.

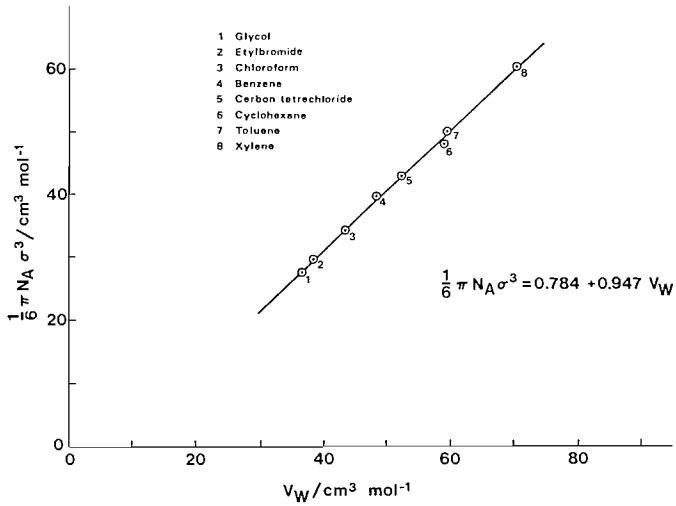

FIG. 1. Correlation of Mayer σ values with van der Waals volumes calculated after Bondi.

[10] $\bar{V}^0 = \bar{V}_{cav} + \Delta\bar{V}_i + k_T RT$

where $\bar{V}_{cav}$ is the partial molal volume associated with cavity formation, $\Delta\bar{V}_i$ is the partial molal volume contribution from solute–solvent interactions, and $k_T RT$ accounts for the change of standard state between the gas and solution. Application of [10] to amines and hydrocarbons with the same $\bar{V}_{cav}$, and subsequent subtraction leads to

[11] $\bar{I}_{S-S} = \bar{V}^0_A - \bar{V}^0_{HC} = \Delta\bar{V}_{i,A} - \Delta\bar{V}_{i,HC}$

$\bar{I}_{S-S}$ is a new parameter which will be compared with $\bar{V}_{S-S}$ calculated previously. In order to obtain this interaction contribution it is necessary to calculate $\bar{V}_{cav}$ for the amine and hydrocarbon molecules under consideration.

From SPT, $\bar{V}_{cav}$ is a known function of temperature, molar volume, isothermal compressibility, hard-sphere diameter of the solvent σ_1, and hard-sphere diameter of the solute σ_2

[12] $\bar{V}_{cav} = 0.3153\,\sigma_2^3 + A\sigma_2^2 + B\sigma_2 + C$

where

[13] $A = 3k_T RT\,(y + 2y^2)/(1 - y)^3\,\sigma_1^2$

[14] $B = 3k_T RT\,y/(1 - y)^2\,\sigma_1$

[15] $C = k_T RT\,y/(1 - y)$

and y as defined by:

[16] $y = N_A\,\Pi\,\sigma_1^3/6V$

is the ratio of the volume occupied by one mole of hard-sphere solvent molecules to the molar volume of the solvent. As can be seen from the above expressions, $\bar{V}_{cav}$ is extremely sensitive to the choice of σ_1; in fact, it appears as the 6th power of this parameter. On the other hand, $\bar{V}_{cav}$ varies much less with the solute diameter σ_2. The appropriate choice of these σ values, especially σ_1, is the first difficulty to be overcome.

As the theory claims, σ has a very precise physical meaning and can be determined from independent measurements such as viscosities, 2nd virial coefficients, compressibilities, surface tension, and solubilities. The SPT theoretical relationships for isothermal compressibilities, k_T, and surface tension, γ, as a function of σ have been established. Mayer (25) presents a series of σ values taken from k_T and γ experimental results. Another set of σ based on gas solubility technique (26) and compiled by Wilhelm and Battino (27) were used by French and Criss (28) in volumetric studies.

The two sets of molecular diameters are not in agreement, thus leading to very different $\bar{V}_{cav}$ and $\Delta\bar{V}_i$. Hence we decided to calculate these quantities for the process of introducing a molecule of a particular substance into a solution of itself, expecting to obtain $\Delta\bar{V}_i \simeq 0$. In Table 7 the results of these two parallel calculations for five organic molecules can be observed. As $\Delta\bar{V}_i$ corresponding to σ values based on the solubility approach are in all cases very negative and those derived from SPT are approximately zero, we have used these latter values to carry on our calculations. Consequently, $\sigma_1 = 5.01$ Å for benzene has been adopted.

Concerning the solutes, as we did not have the hard-sphere diameter for the amines and some linear hydrocarbons, we tried a linear relationship (29) between the volume of one mole of molecules of the Mayer diameter and the Bondi van der Waals volumes for molecules of nature and shape in best agreement with the model adopted. In Fig. 1 we present the plot and analytical expression for the relation, based on the assumptions we have made.

$\bar{V}_{cav}$ for the secondary and tertiary amines and linear hydrocarbons were then calculated and $\Delta\bar{V}_i$ derived. Table 8 shows σ_2, $\bar{V}_{cav}$, and $\Delta\bar{V}_i$ for the amines under study.

The curves $\Delta\bar{V}_i$ vs. $\bar{V}_{cav}$ for each class of compounds were then constructed (Fig. 2). As expected, three smooth curves were obtained, which approach each other towards the long-

TABLE 7. The SPT parameters for the process of introducing a particular substance in itself

Solvent and solute	V^0 ($cm^3\ mol^{-1}$)	k_T ($10^{-10}\ N^{-1}\ m^2$)	$\sigma_1 = \sigma_2$ (Å)	$\bar{V}_{cav}$ ($cm^3\ mol^{-1}$)	$\Delta\bar{V}_i$ ($cm^3\ mol^{-1}$)
C_6H_6	89.41	9.66[a]	5.01[d]	86.9	0.2
			5.26[e]	128.8	−41.8
n-Hexane	131.62	16.69[a]	5.65[d]	127.3	0.2
			5.92[e]	190.6	−63.1
n-Heptane	147.46	14.38[a]	5.97[d]	143.9	0.0
			6.25[e]	209.9	−66.0
n-Octane	163.54	11.98[b]	6.32[d]	161.2	−0.6
			6.54[e]	216.5	−56.0
CCl_4	97.09	10.77[c]	5.15[d]	95.6	−1.0
			5.37[e]	133.6	−39.2

[a]Reference 30.
[b]Reference 31.
[c]Reference 32.
[d]Reference 25.
[e]Reference 27.

TABLE 8. The SPT cavity and interaction contribution to partial molal volumes of secondary and tertiary amines in benzene at 25°C

Compound	σ_2 (Å)	$\bar{V}_{cav}$ ($cm^3\ mol^{-1}$)	$\Delta\bar{V}_{i,A}$[a] ($cm^3\ mol^{-1}$)	$\Delta\bar{V}_{i,HC}$[b] ($cm^3\ mol^{-1}$)
Diethylamine	5.27	97.48	5.26	13.8
Di-*n*-butylamine	6.46	158.18	12.45	20.2
Di-*n*-hexylamine	7.32	215.08	23.40	30.8
Di-*n*-octylamine	8.02	270.43	35.97	43.0
Di-*n*-dodecylamine	9.13	376.48	65.70	70.7
Triethylamine	5.91	127.68	10.20[c]	16.2
Tri-*n*-propylamine	6.69	172.26	18.57	22.5
Tri-*n*-butylamine	7.31	214.35	27.19	30.5
Tri-*n*-hexylamine	8.32	296.80	46.22	49.5
Tri-*n*-octylamine	9.13	376.48	68.00	70.7
Tri-*n*-decylamine	9.81	453.48	92.46	94.2
Tri-*n*-dodecylamine	10.41	529.60	117.80	118.7

[a]$\Delta\bar{V}_{i,A}$ calculated using smoothed values obtained from the weighted fit $\bar{V}^0_{exp}$ vs. V_W.
[b]$\Delta\bar{V}_{i,HC}$ for the hydrocarbons with the same cavity volume as that of the amines taken from the curve $\Delta\bar{V}_{i,HC}$ vs. $\bar{V}_{cav}$ (Fig. 2).
[c]$\Delta\bar{V}_{i,A}$ calculated from the experimental V^0 value.

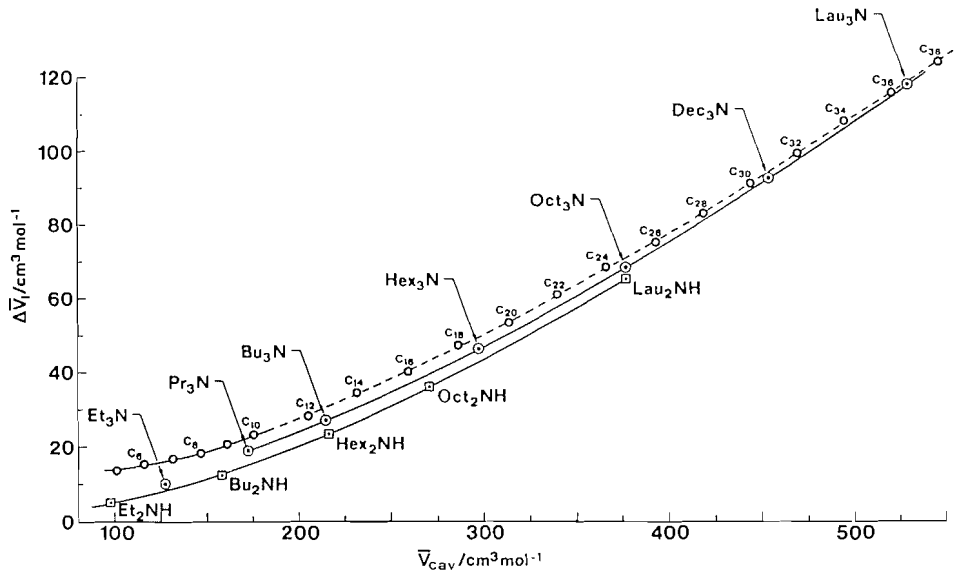

FIG. 2. Correlation of SPT interaction volume $\Delta\bar{V}_i$ with the cavity volume $\bar{V}_{cav}$ for secondary ⊡ and tertiary amines ⊙ and linear hydrocarbons ○ in benzene at 25°C.

TABLE 9. Contribution to the partial molal volume of the specific interaction amine–benzene at 25°C

Compound	$\bar{V}_{S-S}$	$\bar{I}_{S-S}$
Diethylamine	-8.3	-8.5
Di-*n*-butylamine	-7.7	-7.7
Di-*n*-hexylamine	-7.1	-7.4
Di-*n*-octylamine	-6.4	-7.0
Di-*n*-dodecylamine	-5.2	-5.0
Triethylamine	-6.3^a	-6.0^a
Tri-*n*-propylamine	-3.8	-3.9
Tri-*n*-butylamine	-3.5	-3.3
Tri-*n*-hexylamine	-3.0	-3.3
Tri-*n*-octylamine	-2.4	-2.7
Tri-*n*-decylamine	-1.9	-1.7
Tri-*n*-dodecylamine	-1.3	-0.9

[a]Calculated from the experimental $\bar{V}^0$ value.

chain compounds. Similar behaviour was detected when the straight lines $\bar{V}^0$ vs. V_W were drawn. The relative position of the curves is in agreement with the fact mentioned previously, that the amine group produces a decrease in volume; i.e. for the same cavity size, $\Delta\bar{V}_i$ for the amines is always smaller than for the hydrocarbons. Again, a stronger interaction for the secondary amines than for the tertiary ones is reflected in the same curves. Et_3N once more seems to be a special case lying outside the curve.

Finally, to calculate $\bar{I}_{S-S}$, eq. [11], the $\Delta\bar{V}_{i,HC}$ values required were taken from the respective curve and are also reported in Table 8. $\bar{I}_{S-S}$ and $\bar{V}_{S-S}$ values are listed in Table 9. As can be seen in this table, the two sets of results are in good agreement. The fact that these numbers were obtained from such different approaches gives support to both of them. The negative values observed for all the amines mean that the contribution to $\bar{V}^0$ of the amine-group interaction is always smaller than the corresponding contribution of the hydrocarbons, in benzene. However, we think that less negative values can be calculated if one takes into account the conformational differences between these two classes of compounds (23). Another striking feature concerning the results contained in Table 9 is the regular variation (with the exception of Et_3N) of both measures of partial molal volume of the specific interaction along the series. In the case of Et_3N, we think that the conformational difference already referred to is responsible for its particular behaviour and, once considered, would make this amine conform to the regularities observed for the higher ones. These regularities encourage the investigation of suitable expressions to account for the variation of amine-group contribution along these series, when applying additive schemes to these systems.

Acknowledgements

The authors wish to thank the Instituto Nacional de Investigação Científica of Portugal for financial support and to Associate Professor Francisca M. Viegas for collaboration in part of the experimental work.

1. S. CABANI, G. CONTI, and L. LEPORI. J. Phys. Chem. **78**, 1030 (1974).
2. F. J. MILLERO, A. L. SURDO, and C. SHIN. J. Phys. Chem. **82**, 784 (1978).
3. G. PERRON and J. E. DESNOYERS. Fluid Phase Equilib. **2**, 239 (1979).
4. J. T. EDWARD, P. G. FARRELL, and F. SHAHIDI. J. Phys. Chem. **82**, 2310 (1978).
5. H. HØILAND. J. Solution Chem. **5**, 773 (1976).
6. S. TERASAWA, H. ITSUKI, and S. ARAKAWA. J. Phys. Chem. **79**, 2345 (1975).
7. F. HIRATA and K. ARAKAWA. Bull. Chem. Soc. Jpn. **46**, 3367 (1973).
8. A. BONDI. J. Phys. Chem. **68**, 441 (1964).
9. R. TANAKA. J. Chem. Thermodyn. **14**, 259 (1982).
10. T. M. LETCHER and J. W. BAYLES. J. Chem. Eng. Data, **16**, 266 (1971).
11. E. SWIFT, JR. J. Am. Chem. Soc. **64**, 115 (1942).
12. T. M. LETCHER. J. Chem. Thermodyn. **4**, 159 (1972).
13. I. R. KRICHEVSKII, N. E. KHAZANOVA, G. M. SVETLOVA, and R. S. PANINA. Zh. Fiz. Khim. **34**, 2160 (1960). *From* J. Timmermans. Physicochemical constants of pure organic compounds. Elsevier, London. 1965.
14. C. KLOFUTAR, Š. PALJK, and D. KREMSER. J. Inorg. Nucl. Chem. **37**, 1729 (1975).
15. A. S. KERTES and F. GRAUER. J. Phys. Chem. **77**, 2107 (1973).
16. F. GRAUER and A. S. KERTES. J. Chem. Eng. Data, **18**, 405 (1973).
17. J. A. RIDDICK and W. B. BUNGER. Techniques of chemistry. Vol. II. *Edited by* A. Weissberger. Wiley–Interscience, New York. 1970.
18. J. T. EDWARD, P. G. FARRELL, and F. SHAHIDI. Can. J. Chem. **57**, 2887 (1979).
19. R. SIEDLER, L. GROTE, E. KAUER, U. WERNER, and H.-J. BITTRICH. Z. Phys. Chem. **241**, 203 (1969).
20. H. V. KEHIAIAN. Bull. Acad. Pol. Sci. Ser. Sci. Chim. **14**, 703 (1966).
21. T. M. LETCHER and J. W. BAYLES. J. Chem. Eng. Data, **16**, 266 (1971).
22. G. MANN. Tetrahedron, **23**, 3375 (1967).
23. A. M. AMORIM DA COSTA, L. A. E. BATISTA DE CARVALHO, J. J. C. TEIXEIRA-DIAS, E. F. G. BARBOSA, and I. M. S. LAMPREIA. Spectrochim. Acta. In press.
24. H. REISS. Adv. Chem. Phys. **9**, 1 (1965).
25. S. W. MAYER. J. Phys. Chem. **67**, 2160 (1963).
26. R. A. PIEROTTI. J. Phys. Chem. **69**, 281 (1965).
27. E. WILHELM and R. BATTINO. J. Chem. Phys. **55**, 4012 (1971).
28. R. N. FRENCH and C. M. CRISS. J. Solution Chem. **10**, 713 (1981).
29. C. L. LIGNY and N. G. VAN DER VEEN. J. Solution Chem. **4**, 841 (1975).
30. M. DIAZ PEÑA and G. TARDAJOS. J. Chem. Thermodyn. **4**, 637 (1972).
31. H. E. EDULJEE, D. M. NEWITT, and K. E. WEALE. J. Chem. Soc. 3086 (1951).
32. G. A. HOLDER and E. WHALLEY. Trans. Faraday Soc. **58**, 2095 (1982).

Apparent molar heat capacities and volumes of alkylbenzenesulfonate salts in water: substituent group additivity

K. SWAY, JAMEY K. HOVEY, AND PETER R. TREMAINE[1]

Oil Sands Research Department, Alberta Research Council, 1021 Hayter Rd., P.O.Box 8330, Station F, Edmonton, Alta., Canada T6H 5X2

Received May 23, 1985

K. SWAY, JAMEY K. HOVEY, and PETER R. TREMAINE. Can. J. Chem. **64**, 394 (1986).

Densities and specific heats were measured for the aqueous sodium salts of benzenesulfonate, *p*-toluenesulfonate, 2,4- and 2,5-dimethylbenzenesulfonate, mesitylenesulfonate, and *p*-ethylbenzenesulfonate. The limiting partial molar volumes, $\bar{V}^0$ and heat capacities, $\bar{C}_p^0$, lead to revised values in the group contributions for aromatic —CH_2— and —CH_3 groups in the additivity scheme proposed by Perron and Desnoyers. The heat capacities of substituted alkylbenzenes can deviate from group additivity by as much as 70 and 40 J K^{-1} mol, $^{-1}$, respectively, when polar groups are located on the α and β positions of the alkyl chain.

K. SWAY, JAMEY K. HOVEY, et PETER R. TREMAINE. Can. J. Chem. **64**, 394 (1986).

On a mesuré les densités et les chaleurs spécifiques de solutions aqueuses du benzènesulfonate, du *p*-toluènesulfonate, des diméthyl-2,4 et diméthyl-2,5 benzènesulfonates, du mésitylènesulfonate et du *p*-éthylbenzènesulfonate de sodium. Les volumes molaires partiels et les capacités calorifiques limites $\bar{V}^0$ et $\bar{C}_p^0$ conduisent à des valeurs corrigées des contributions de groupe pour les groupements CH_2 et CH_3 aromatiques dans le schéma d'additivité proposé par Perron et Desnoyers. Lorsqu'il y a des groupes polaires dans les positions α et β de la chaîne alkylée, les capacités calorifiques des alkylbenzènes substitués peuvent présenter des déviations de l'additivité du groupe qui peuvent aller respectivement jusqu'à 70 et 40 J K^{-1} mol^{-1}.

[Traduit par le journal]

Introduction

The temperature dependence of surfactant micellization equilibria is of increasing interest, both as a tool for developing fundamental insights and because surfactants can be used as steam additives in heavy oil recovery. Partial molar heat capacities and volumes are key parameters in describing the temperature and pressure dependence of such equilibria (1–3). The critical micelle concentrations of industrially important surfactants lie below the practical limit of modern calorimeters and densimeters. As a result, the properties of surfactant monomers at pre-micellar concentrations must be estimated from functional group additivity schemes.

At the low concentrations of interest in this context, it is often sufficient to know the standard state functions in water or dilute brines. Perron and Desnoyers (4) recently developed a comprehensive group additivity scheme for predicting the standard partial molar properties of benzene derivatives in water at 25°C. The parameters for benzene sulfonates were derived from heat capacity and volume measurements on sodium benzenesulfonates that included chloro, carboxylate, and sulfonate groups as substituents, but not simple alkyl groups. Here, we report heat capacity and volume measurements on *p*-ethylbenzenesulfonate, and on mono, di-, and tri-methylbenzene sulfonates, in order to better define the effects of alkyl substituents and isomerization.

Experimental

The sodium salts of benzenesulfonic acid and mesitylenesulfonic acid were prepared by neutralizing aqueous solutions of the acid (Pfaltz and Bauer, "Source 1"). Those of *p*-ethylbenzenesulfonic acid (Tokyo Kasei Kogyo Ltd.), *p*-toluenesulfonic acid (Eastman Kodak), 2,4- and 2,5-dimethylbenzenesulfonic acid (Pfaltz and Bauer), and a second sample of benzenesulfonic acid (Pfaltz and Bauer, "Source 2") were purchased as the salt.

Each salt was recrystallized at least twice from saturated hot aqueous solutions, then dried to constant weight in a vacuum desiccator, typically for two to five days. A faint orange coloration persisted in the sodium benzenesulfonate from Source 1, even after three recrystallizations. All water was distilled once and passed through a Milli-Q reagent grade mixed-bed ion exchange and activated carbon system before use. Stock solutions were prepared by weight. The molality of each was checked by passing three aliquots through strong cation exchange columns (Rexyn 101, acid form) and titrating the eluted acid with standard sodium hydroxide solution to a phenolphthalein end point. The results agreed to within 0.5%.

The heat capacity and density of each solution were measured relative to water at 25.0°C using a commercial Picker flow microcalorimeter (5) and vibrating tube densimeter (6). Values for the specific heat capacity and density of pure water at 25°C and 100 kPa were taken to be $c_{pw}{}^0 = 4.1793$ J K^{-1} g^{-1} and $d_w{}^0 = 0.997062$ g cm^{-3} (7,8). The average of the apparent molar heat capacities from the two calorimeter cells was multiplied by the mean heat leak corection factor, $f = 1.01 \pm 0.005$, which was obtained daily by calibration with aqueous NaCl (9).

Results

Apparent molar heat capacities, ${}^\Phi C_p$, and volumes, ${}^\Phi V$, are defined by the expression

$$[1] \quad {}^\Phi Y = (Y - n_w Y_w{}^0)/n$$

where Y is the heat capacity or volume of the solution, n_w and n are the number of moles of water and solute respectively (if $n_w = 55.509$, n = molality, m) and $Y^0{}_w$ is the property for 1 mole of pure solvent.

To obtain apparent molar heat capacities and volumes at infinite dilution, the experimental results were fitted to an extended Debye–Hückel equation of the form (9,10).

$$[2] \quad {}^\Phi Y = {}^\Phi Y^0 + A_Y m^{1/2} + B_Y m$$

using the method of least squares. The limiting slopes on the molal scale, $A_C = 32.51$ J K^{-1} $kg^{1/2}$ $mol^{-3/2}$ and $A_V = 1.865$ cm^3 $kg^{1/2}$ $mol^{-3/2}$, were taken from Bradley and Pitzer (11). At infinite dilution, the apparent molar properties become identical with partial molar (standard state) heat capacities and volumes so that ${}^\Phi C_p^0 \bar{C}_p^0$ and ${}^\Phi V^0 = \bar{V}^0$.

The experimental data and apparent molar properties are listed in Appendix 1. The derived values of $\bar{C}_p^0$, $\bar{V}^0$, and B_C, and B_V are listed in Table 1, along with the standard deviations obtained from the least-squares fit.

[1]Author to whom correspondence may be addressed.

TABLE 1. Standard state heat capacity, volume, and ionic strength parameters

Solute	Formula	$\overline{C}_p^0$ ($J K^{-1} mol^{-1}$)	B_C ($J K^{-1} kg mol^{-2}$)	$\overline{V}^0$ ($cm^3 mol^{-1}$)	B_V ($cm^3 kg mol^{-2}$)
Sodium benzenesulfonate (Source 1)	$\phi SO_3Na(aq)$	247.8 ± 0.2	−16.7 ± 0.6	101.73 ± 0.13	−0.58 ± 0.29
Sodium benzenesulfonate (Source 2)	$\phi SO_3Na(aq)$	259.0 ± 0.4	−8.4 ± 0.9	103.96 ± 0.08	0.03 ± 0.16
Sodium *p*-toluenesulfonate	$p\text{-}CH_3\phi SO_3Na(aq)$	333.6 ± 0.4	−32.4 ± 0.8	120.94 ± 0.04	−0.37 ± 0.07
Sodium 2,4-dimethylbenzenesulfonate	$2,4\text{-}(CH_3)_2\phi SO_3Na(aq)$	400.3 ± 2.0	−56.9 ± 6.5	132.4 ± 0.02	−1.00 ± 0.08
Sodium 2,5-dimethylbenzenesulfonate	$2,5\text{-}(CH_3)_2\phi SO_3Na(aq)$	416.4 ± 0.5	−28.9 ± 1.2	135.74 ± 0.08	−0.33 ± 0.17
Sodium mesitylenesulfonate	$2,4,6\text{-}(CH_3)_3\phi SO_3Na(aq)$	488.1 ± 0.9	−94.4 ± 2.0	148.03 ± 0.24	−1.37 ± 0.51
Sodium *p*-ethylbenzenesulfonate	$p\text{-}CH_3CH_2\phi SO_3Na(aq)$	392.1 ± 0.7	−61.0 ± 1.7	134.42 ± 0.10	−0.02 ± 0.02

Error limits are standard deviations (precision) from the least-squares fits of eq. [2] to data below 0.8 *m*. The accuracy is estimated to be ±6 $J K^{-1} mol^{-1}$ and ±1 $cm^3 mol^{-1}$.

TABLE 2. Group contribution to $\overline{V}^0$ and $\overline{C}_p^0$ in water at 25°C from Perron and Desnoyers (4). Contributions for —CH_2— and —CH_3(arom) are revised from this work

	$\overline{V}^0$ ($cm^3 mol^{-1}$)		$\overline{C}_p^0$ ($J K^{-1} mol^{-1}$)	
Group	Aromatic	Aliphatic	Aromatic	Aliphatic
Benzene	83.2		372	
—H	10.1	10.7	84	90
—CH_3	25.3*	26.7	156*	178
—OH	12.6	12.0	27	−4
—OH (*ortho* to COONa)	18.1		67	
—Cl	22.4		163	
—Br	26.2		176	
—I	35.6		204	
—NO_2	25.8		137	
—NH_2	14.9	15.1	37	−19
—COONa	12.6	10.5	−40	−109
—SO_3Na	30.2		−34	
—OCH_2COONa	33.4		24	
—CH_2—	14.6	16.0	54†	88
—O—	6.9	4.1	−9	−57
—COOH	25.7	25.5		−13
—CHO	23.0			

*23.2 $cm^3 mol^{-1}$, 145 $J K^{-1} mol^{-1}$, in ref. 4.
†85 $J K^{-1} mol^{-1}$ in ref. 4.

Discussion

Standard state heat capacities and volumes for a large number of benzene derivatives have been compiled by Perron and Desnoyers (4). These were used to derive the contribution of each group to the standard state properties of the solute, as tabulated in Table 2. The scheme is based on the assumption that the relative positions of the aromatic substituents about the ring do not affect the group contribution, and that all H atoms are equivalent.

In Table 3, we have compared our values of $\overline{C}_p^0$ and $\overline{V}^0$ for the sodium aryl sulfonates with experimental values reported by other workers, and with values calculated from the group additivity scheme. The experimental data cited by Perron and Desnoyers for aqueous neutral arenes, and for simple phenols, benzoates, phenylalkanols, and phenylcarboxylates are also included, for use in the discussion below. The absolute accuracy of measurements on organic electrolytes is somewhat lower than that for simple inorganic systems because purification is more difficult. Error limits of ±6 $J K^{-1} mol^{-1}$ and ±1 $cm^3 mol^{-1}$ are probably reasonable estimates. Our data for $\phi SO_3Na(aq)$ and $p\text{-}CH_3\phi SO_3Na(aq)$ agree with earlier results (4, 12) to within these limits. Data for the other sulfonates have not been reported previously.

The experimental heat capacities for the methyl substituted benzenesulfonates are systematically higher than those calculated from the group contributions by about 16 $J K^{-1} mol^{-1}$ per —CH_3(arom). The experimental value for *p*-ethylbenzenesulfonate is lower than the group contribution calculation by 41 $J K^{-1} mol^{-1}$. Constant discrepancies in the group assignments for —CH_3(arom) and —CH_2—(arom) also occur for all the other solutes in Table 3 *except* the phenylalkanols and phenylcarboxylates ($\phi(CH_2)_nOH$ and $\phi(CH_2)_nCOONa$).

Perron and Desnoyer's additivity scheme was based on rather limited results for alkylbenzene derivatives, a subset of the data in Table 3. We chose to recalculate the values for the aromatic methyl and methylene groups, using both the new and old data in Table 3. However, we omitted the values for all the phenylalkanols and phenylcarboxylates because the polar substituents might be expected to interact strongly with the aromatic ring. This treatment yields the values 156 $J K^{-1} mol^{-1}$ and 54 $J K^{-1}$

TABLE 3. Experimental standard state heat capacities and volumes compared to values calculated from group additivity

	$\bar{C}_p^0$ (J K^{-1} mol^{-1})			$\bar{V}^0$ (cm^3 mol^{-1})		
		Calculation			Calculation	
	Experiment	Perron and Desnoyers	This work	Experiment	Perron and Desnoyers	This work
Sulfonates						
ϕSO_3Na (Source 1)	248			101.7		
ϕSO_3Na (Source 2)	259	254	254	104.0	103.3	103.3
ϕSO_3Na (4)	253			105.2		
p-$CH_3\phi SO_3Na$	334	315	326	120.9	116.4	118.5
p-$CH_3\phi SO_3Na$ (12)	—			118.4		
2,4-$(CH_3)_2\phi SO_3Na$	400	376	398	132.4	129.5	113.7
2,5-$(CH_3)_2\phi SO_3Na$	416	376	398	135.8	129.5	133.7
2,4,6-$(CH_3)_3\phi SO_3Na$	488	437	470	148.0	142.6	148.9
p-$CH_3CH_2\phi SO_3Na$	392	433	402	134.4	134.5	134.5
Arenes						
Benzene (13)	372	372	372	83.2	83.2	83.2
Benzene (14)	361±5*					
$CH_3\phi$ (14)	430±13*	433	444	97.71	96.3	98.4
$CH_3CH_2\phi$ (14)	504±13*	551	520	—	114.4	114.4
$CH_3(CH_2)_2\phi$ (14)	606±25*	639	608	—	130.4	130.4
Benzoates and phenols						
p-$CH_3\phi COONa$ (4)	312	309	319	99.01	98.8	100.9
p-$CH_3\phi OH$ (15)	384	376	387	—	98.8	100.9
p-$CH_3CH_2\phi OH$ (15)	465	494	463	—	116.9	116.9
Phenylalkanols and Phenylcarboxylates						
ϕCH_2OH (15)	396	369	338	—	99.7	99.7
$\phi(CH_2)_2OH$ (15)	462	457	426	—	115.7	115.7
$\phi(CH_2)_3OH$ (15)	530	545	514	—	131.7	131.7
$\phi(CH_2COONa$ (16)	305	264	233	100.6	98.2	98.2
$\phi(CH_2)_2COONa$ (16)	362	352	321	116.8	114.2	114.2
$\phi(CH_2)_3COONa$ (16)	423	440	409	132.4	130.2	130.2
$\phi(CH_2)_4COONa$ (16)	504	528	497	148.5	146.2	146.2

*Error limits reported by the original authors.

mol^{-1} for the —CH_3(arom) and —CH_2—(arom) group contributions, respectively. A similar comparison for volumes leads to the value 25.3 cm^3 mol^{-1} for —CH_3(arom).

Values for $\bar{C}_p^0$ and $\bar{V}^0$ calculated from the original and revised group additivity schemes are compared in Table 3. The revised scheme yields much better agreement with experimental data for all systems listed except the phenylalkanols and phenylcarboxylates, which are treated in detail below. All other compounds that contain a single alkyl group deviate from additivity by no more than 14 J K^{-1} mol^{-1}. The dimethyl benzenesulfonates and mesitylenesulfonate deviate by no more than 18 J K^{-1} mol^{-1}. We note that the experimental data for the dimethylbenzene isomers in Table 1 differ from each other by 20 J K^{-1} mol^{-1} and 3.4 cm^3 mol^{-1}, just outside the combined estimate of accuracy. The revised group additivity scheme agrees best with the value for the 2,4 rather than the 2,5 isomer but, in fact, the difference between the two isomers is surprisingly small.

The deviations between experimental heat capacities for the phenylalkanols and phenylcarboxylates and values calculated from the revised group additivity scheme are plotted in Fig. 1, as a function of alkyl chain length. The additivity scheme underestimates $\bar{C}_p^0$ for the α-substituted solutes by about 70 J K^{-1} mol^{-1}. However, the discrepancy decreases dramatically with increasing chain length, and is nearly within experimental error at $n = 3$. It appears that substituted phenylalkanes have anomalous standard state heat capacities when polar groups occupy α or β positions ($n = 1$ or 2) on the alkyl chain. There is no evidence for a similar effect on volumes.

Finally, Perron and Desnoyers noted an approximately linear relationship between the contributions for aromatic and alkyl substituent groups. The revised values for —CH_3 and —CH_2— heat capacity contributions in Table 2 deviate much more from linearity than the original assignments of Perron and Desnoyers. The volumes are little affected.

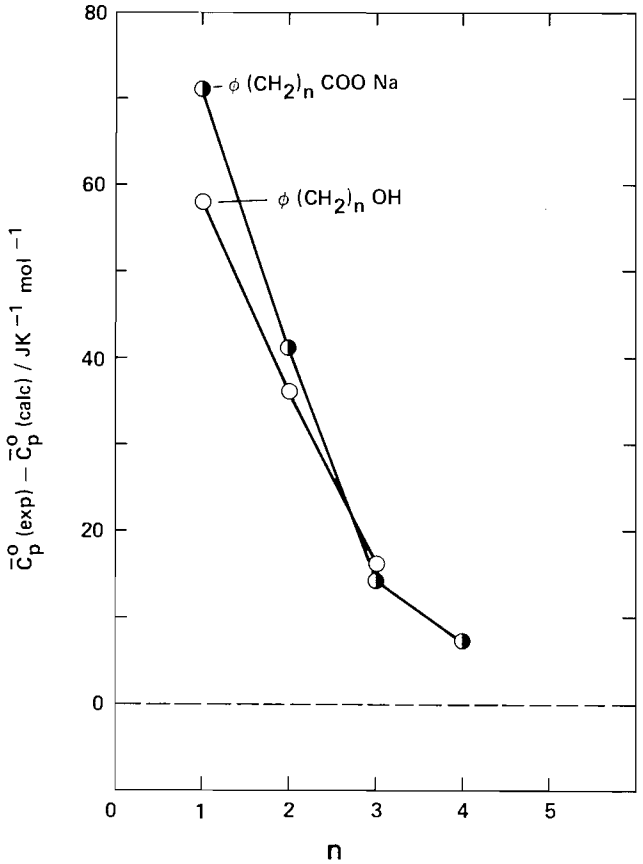

FIG. 1. The discrepancy between the experimental heat capacities and those calculated from group additivity (Table 2) for phenylalkanols and phenylcarboxylates. ○ = $\phi(CH_2)_nOH$; ◑ = ϕ $(CH_2)_nCOONa$. For $n \geq 4$, the discrepancy is presumably negligible.

Acknowledgments

We are grateful to Dr. K. G. McCurdy and Dr. Ian Tasker for valuable discussions and suggestions. This project was carried out as part of the Alberta Oil Sands Technology and Research Authority – Alberta Research Council Joint Oil Sands Research Program, ARC contribution no. 1367.

1. (*a*) T. E. BURCHFIELD and E. M. WOOLLEY. J. Phys. Chem. **88**, 2149 (1984). (*b*) E. M. WOOLLEY and T. E. BURCHFIELD. J. Phys. Chem. **88**, 2155 (1984).
2. J. E. DESNOYERS, G. CARON, R. DELISI, D. ROBERTS, A. ROUX, and G. PERRON. J. Phys. Chem. **87**, 1397 (1983).
3. J.B. ROSENHOLM, T. E. BURCHFIELD, and L. G. HEPLER. J. Colloid Interface Sci. **78**, 191 (1980).
4. G. PERRON and J. E. DESNOYERS. Fluid Phase Equilib. **2**, 239 (1979).
5. P. PICKER, P. A. LEDUC, P. R. PHILLIPS, and J. E. DESNOYERS. J. Chem. Thermodyn. **3**, 631 (1971).
6. P. PICKER, E. TREMBLAY, and C. JOLICOEUR. J. Solution Chem. **3**, 377 (1974).
7. G. S. KELL. *In* Water—a comprehensive treatise. Vol. 1. *Edited by* F. Franks. Plenum Press, New York. 1972.
8. L.HAAR, J. S. GALLAGHER, and G. S. KELL. NBS/NRC steam tables, thermodynamic and transport properties and computer programs for vapor and liquid states of water in SI units. Hemisphere Publishing, Washington. 1984.
9. J. E. DESNOYERS, C. DEVISSER, G. PERRON, and P. PICKER. J. Solution Chem. **5**, 605 (1976).
10. A. ROUX, G. M. MUSBALLY, G. PERRON, J. E. DESNOYERS, P. P. SINGH, E. M. WOOLLEY, and L. G. HEPLER. Can. J. Chem. **56**, 24 (1978).
11. D. J. BRADLEY and K. S. PITZER. J. Phys. Chem. **83**, 1599 (1979).
12. O. D. BONNER and R. W. GABLE. J. Chem. Eng. Data, **15**, 499 (1970).
13. C. JOLICOEUR, P. PICKER, and G. PERRON. Can. J. Chem. **53**, 3634 (1975).
14. S. J. GILL, N. F. NICHOLS, and I. WADSO. J. Chem. Thermodyn. **8**, 445 (1976).
15. N. NICHOLS and I. WADSO. J. Chem. Thermodyn. **7**, 329 (1975).
16. C. OSTIGUY, J. C. AHLUWALIA, G. PERRON, and J. E. DESNOYERS. Can. J. Chem. **55**, 3368 (1977).

Appendix 1

Apparent molar properties at 25°C, for aqueous, substituted benzene sulfonic acid sodium salts, $ArSO_3^-Na^+(aq)$

m (mol kg^{-1})	$\frac{c_p d}{c_{pw}\, d_w} - 1$	$^{\phi}C_p$ (JK^{-1}mol^{-1})	$(d-d_w)$ (g cm^{-3})	$^{\phi}V$ (cm^{3}mol^{-1})
Ar = benzene, Source 1 (acid)				
0.05407	−0.002173	254.8	0.004207	101.99
0.1087	−0.004331	256.7	0.008382	102.29
0.2197	−0.008539	259.0	0.016678	102.60
0.4510	−0.016934	262.1	0.033345	102.87
0.6890	−0.025016	263.4	0.049853	102.76
0.9462	−0.033095	268.3	0.066173	103.47
Ar = benzene, Source 2 (salt)				
0.09370	−0.003674	267.7	0.007034	104.44
0.2060	−0.007861	272.0	0.015203	104.85
0.3049	−0.011403	274.1	0.022243	104.97
0.4048	−0.014851	276.7	0.029124	105.24
0.5079	−0.018340	278.0	0.036121	105.33
0.6082	−0.021612	279.8	0.042695	105.55
0.7799	−0.027108	280.3	0.053902	105.46

Appendix 1 (*Concluded*)

m (mol kg^{-1})	$\frac{c_p d}{c_{pw}\, d_w} - 1$	ΦC_p (J K^{-1} mol^{-1})	$(d-d_w)$ (g cm^{-3})	ΦV (cm^3 mol^{-1})
Ar = 2,4-dimethylbenzene				
0.08182	−0.002887	402.9	0.006111	132.88
0.1359	−0.004745	403.9	0.010070	132.96
0.1806	−0.006287	403.6	0.013296	133.00
0.2169	−0.007354	406.9	0.015889	133.01
0.5802	−0.020927	391.1	0.040469	133.25
Ar = 2,5-dimethylbenzene				
0.08413	−0.002860	423.3	0.006000	136.26
0.1707	−0.005677	425.5	0.012003	136.43
0.2762	−0.009128	424.8	0.019115	136.59
0.5356	−0.017286	425.3	0.035607	137.06
0.7319	−0.023416	422.8	0.047503	137.01
Ar = ethylbenzene				
0.08551	−0.003310	379.9	0.006210	134.93
0.1547	−0.006081	394.6	0.011103	135.11
0.2179	−0.008579	394.2	0.015451	135.40
0.3233	−0.012892	390.0	0.022581	135.49
0.3783	−0.015193	387.8	0.026216	135.55
0.5176	−0.020898	384.4	0.035139	135.75
0.6269	−0.025614	380.2	0.041909	135.86
0.6809	−0.028076	377.6	0.045151	135.96
0.8390	−0.035753	368.4	0.054393	136.18
0.9991	−0.043471	361.2	0.063281	136.37
Ar = mesitylene				
0.1002	−0.003036	489.2	0.007286	148.64
0.2054	−0.006364	483.9	0.014732	148.56
0.3104	−0.010013	476.1	0.021935	148.54
0.4989	−0.017098	463.8	0.034272	148.68
0.6109	−0.021643	454.4	0.041567	148.27
0.7103	−0.025982	449.7	0.047208	148.98
Ar = *p*-toluene				
0.1264	−0.004840	341.9	0.009061	121.54
0.2059	−0.007874	341.3	0.014579	121.74
0.3109	−0.011784	341.3	0.021703	121.88
0.4065	−0.015340	340.5	0.028035	121.95
0.5066	−0.019036	340.1	0.034466	122.10
0.6062	−0.022715	339.1	0.040705	122.22
0.6062	−0.022637	339.7	0.040705	122.22
0.7028	−0.026254	337.5	0.046723	122.16
0.8670	−0.032224	336.2	0.056405	122.39

Selected-ion flow tube studies of reactions of the radical cation $(HC_3N)^{+\cdot}$ in the interstellar chemical synthesis of cyanoacetylene

A. Fox, A. B. Raksit, S. Dheandhanoo, and D. K. Bohme[1]

Department of Chemistry and Centre for Research in Experimental Space Science, York University, Downsview, Ont. Canada M3J 1P3

Received August 15, 1985

A. Fox, A. B. Raksit, S. Dheandhanoo, and D. K. Bohme. Can. J. Chem. **64**, 399 (1986).

The radical cation $(HC_3N)^{+\cdot}$ was produced in a Selected-Ion Flow Tube (SIFT) apparatus from cyanoacetylene by electron impact and reacted at room temperature in helium buffer gas with a selection of molecules including H_2, CO, HCN, CH_4, H_2O, O_2, HC_3N, C_2H_2, OCS, C_2H_4, and C_4H_2. The observed reactions exhibited a wide range of reactivity and a variety of pathways including charge transfer, hydrogen atom transfer, proton transfer, and association. Association reactions were observed with CO, O_2, HCN, and HC_3N. With the latter two molecules association was observed to proceed close to the collision limit, which is suggestive of covalent bond formation perhaps involving azine-like N—N bonds. For HC_3N an equally rapid association has been observed by Buckley *et al.* with ICR (Ion Cyclotron Resonance) measurements at low pressures and this is suggestive of radiative association. The hydrogen atom transfer reaction of ionized cyanoacetylene with H_2 is slow while similar reactions with CH_4 and H_2O are fast. The reaction with CO fails to transfer a proton. These results have implications for synthetic schemes for cyanoacetylene as proposed in recent models of the chemistry of interstellar gas clouds. Proton transfer was also observed to be curiously unfavourable with all other molecules having a proton affinity higher than $(C_3N)^{\cdot}$. Also, hydrogen-atom transfer was inefficient with the polar molecules HCN and HC_3N. These results suggest that interactions at close separations may lead to preferential alignment of the reacting ion and molecule which is not suited for proton transfer or hydrogen atom transfer.

A. Fox, A. B. Raksit, S. Dheandhanoo, et D. K. Bohme. Can. J. Chem. **64**, 399 (1986).

La réaction d'impact électronique sur le cyanoacétylène a permis de générer le radical cation $(HC_3N)^{+\cdot}$ dans un tube à écoulement, à ion sélectif; on l'a fait réagir, à la température ambiante et dans de l'helium agissant comme gaz tampon, avec diverses molécules comme le H_2, le CO, le HCN, le CH_4, le H_2O, le O_2, le HC_3N, le C_2H_2, le OCS, le C_2H_4, et le C_4H_2. Les réactions observées représentent un large éventail de réactivités et une grande diversité de voies réactionnelles, y compris les transferts de charge, d'atomes d'hydrogène et de protons ainsi que les réactions d'association. On a observé des réactions d'association avec le CO, le O_2, le HCN et le HC_3N. Dans les cas de ces deux dernières molécules, on a observé que les réactions d'association se produisent jusqu'à la limite des collisions et ceci suggère qu'il y a formation de liaisons covalentes impliquant peut-être des liaisons N—N du type azine. Dans le cas du HC_3N, Buckley *et al.* ont aussi observé une réaction d'association à l'aide de mesures ICR alors qu'ils opéraient à basses pressions; ces résultats suggèrent une association radiative. La réaction de transfert d'atomes d'hydrogène du cyanoacétylène avec le H_2 est très lente alors que des réactions semblables avec le CH_4 et le H_2O sont rapides. La réaction avec le CO ne produit pas de réactions de transfert de proton. Ces résultats ont des implications pour les schémas de synthèse du cyanocétylène qui ont été proposés dans des modèles récents de la chimie des nuages gazeux interstellaires. On a aussi observé que la réaction de transfert de proton n'est curieusement pas favorable avec aucune des autres molécules possédant une affinité protonique plus élevée que celle du $(C_2N)^{\cdot}$. De plus, le transfert d'un atome d'hydrogène est inefficace avec les molécules polaires HCN et HC_3N. Ces résultats suggèrent que les interactions, lorsque les séparations sont faibles, peuvent conduire à un alignement préférentiel de l'ion qui réagit et de la molecule, qui n'est pas approprié pour un transfert de proton ou d'un atome d'hydrogène.

[Traduit par le journal]

Introduction

The radical cation $(HC_3N)^{+\cdot}$ has been implicated as an intermediate in the chemical synthesis of cyanoacetylene in dense interstellar gas clouds rich in molecular hydrogen (1–3). Available models of the chemistry proceeding in such clouds presume a rapid hydrogenation as indicated by reaction [1].

[1] $(HC_3N)^{+\cdot} + H_2 \rightarrow H_2C_3N^+ + H^{\cdot}$

Cyanoacetylene can be formed if the product ion of the hydrogenation reaction recombines with electrons as in reaction [2]

[2] $H_2C_3N^+ + e \rightarrow HC_3N + H^{\cdot}$

or transfers a proton to a molecule X as in reaction [3].

[3] $H_2C_3N^{+\cdot} + X \rightarrow XH^+ + HC_3N$

Sources of the radical cation $(HC_3N)^{+\cdot}$ which have been adopted in the various chemical models for interstellar gas clouds include the reaction of $C_3H_2^{+\cdot}$ with atomic nitrogen (1–3), the protonation of $(C_3N)^{\cdot}$ by ions such as H_3^+ and HCO^+ (3), and the reaction of $C_2H_2^{+\cdot}$ with the $(CN)^{\cdot}$ radical (1). Also, laboratory evidence is available for the formation of $(HC_3N)^{+\cdot}$ by the reactions of C_2H_2 with CN^+ (4) and $(HCN)^{+\cdot}$ (5). Another loss process for $(HC_3N)^{+\cdot}$ that may compete with reaction [1] in dense interstellar clouds is the reaction with CO, which is the most abundant molecule in these environments next to H_2. This reaction has been presumed in one available model (6) to occur rapidly by proton transfer as indicated in reaction [4].

[4] $(HC_3N)^{+\cdot} + CO \rightarrow HCO^+ + {}^{\cdot}C_3N$

There appears to be no previous systematic laboratory study of the reactions of $(HC_3N)^{+\cdot}$. The study reported here was directed specifically towards an experimental elucidation of the kinetics and product distributions of the reactions with H_2 and CO that are important in the interstellar chemistry. However, it was also extended towards a more general investigation of the hydrogenation of $(HC_3N)^{+\cdot}$ in reactions of type [5] with sub-

[5] $(HC_3N)^{+\cdot} + XH \rightarrow H_2C_3N^+ + X^{\cdot}$

strates XH = H_2O, HCN, CH_4, C_2H_2, C_2H_4, and HC_3N. Of

[1]Author to whom correspondence may be addressed.

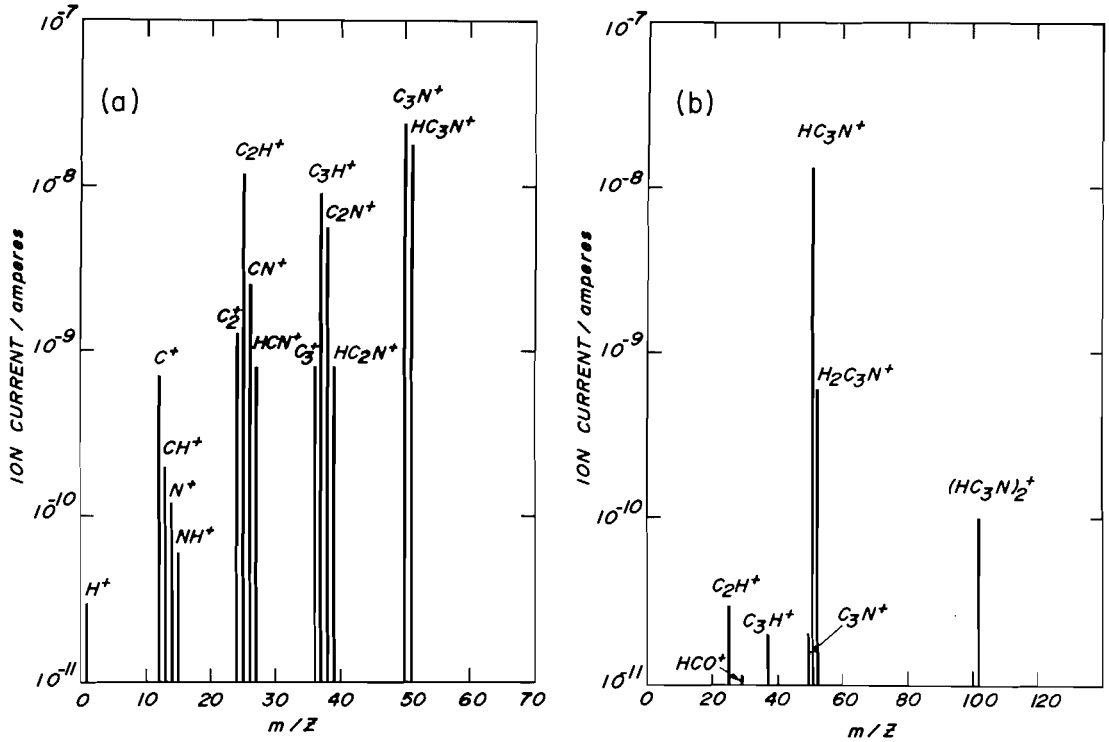

FIG 1. (a): SIFT spectrum for ions derived from cyanoacetylene (8% in helium) by electron impact at 28 eV. Ions are injected at 12 V; the buffer gas is helium at 0.315 Torr. (b): SIFT spectrum for HC_3N^+ derived from cyanoacetylene (10% in helium) by electron impact at 44.5 eV. The HC_3N^+ ions are injected at 12 V; the buffer gas is helium at 0.357 Torr. The background spectrum arises in part from ion–molecule reactions with water impurity and with cyanoacetylene leaking through the selection quadrupole.

additional interest was the competition of hydrogenation with charge transfer, which leads to the direct conversion of $(HC_3N)^{+\cdot}$ to cyanoacetylene as in reaction [6],

[6] $(HC_3N)^{+\cdot} + XH \rightarrow XH^{+\cdot} + HC_3N$

and the competition with proton transfer, as indicated by reaction [7],

[7] $(HC_3N)^{+\cdot} + XH \rightarrow XH_2^+ + (C_3N)^{\cdot}$

which drives one of the proposed sources of $(HC_3N)^{+\cdot}$ in its opposite direction to regenerate the $(C_3N)^{\cdot}$ radical.

Experimental

The measurements were performed with the Selected-Ion Flow Tube (SIFT) apparatus in the Ion Chemistry Laboratory (7,8). The $(HC_3N)^{+\cdot}$ was generated in an axial electron impact ionizer (Extranuclear Model 0413) from cyanoacetylene diluted with helium at electron energies from 25 to 45 eV. The ions that may be derived from cyanoacetylene using this source are shown in Fig. 1, which also displays the spectrum downstream when $(HC_3N)^{+\cdot}$ is selected upstream. The major impurity ion is $H_2C_3N^+$, which is thought to arise primarily from the reaction of $(HC_3N)^{+\cdot}$ with H_2O impurity in the buffer gas, while the $(HC_3N)_2^{+\cdot}$ ion is presumed to arise from a rapid addition reaction with cycanoacetylene leaking from the source through the selection quadrupole. The ions were injected into helium buffer gas at ca. 12 V. The total pressure was in the range from 0.30 to 0.36 Torr (1 Torr = 133.3 Pa) and the ambient temperature was 296 ± 2 K. The reagent gases and vapours as well as the helium buffer gas were generally of high purity, with a minimum purity of 99.5 mol%. Hydrogen cyanide was prepared according to the procedure described by Glemser (9). The cyanoacetylene was prepared from methyl propriolate (Aldrich) (10). Chemical ionization of the hydrogen cyanide and cyanoacetylene using H_3^+ indicated a purity of greater than 99% for both of these reagents.

Results

Table 1 summarizes the rate constants and product distributions obtained in this study and includes values for the collision rate constant, k_c, for the reactions investigated (11). It includes all the primary product ions that were observed to contribute more than 5% to the total product spectrum. The reactions are listed in order of decreasing ionization energy of the neutral substrate. Rate constants were derived in the usual manner (7) and product distributions were determined using the method of Adams and Smith (12).

H_2

Hydrogen was observed to react with $(HC_3N)^{+\cdot}$ only slowly. Two primary products were observed, as is indicated in Fig. 2. The ion at $m/z = 26$ was assigned to be the acetylene cation $C_2H_2^{+\cdot}$ and not the vinylidene cation or CN^+. The formation of the latter is endothermic. Also, the $C_2H_2^{+\cdot}$ was observed to react further with H_2 to produce $C_2H_4^{+\cdot}$ and some $C_2H_3^+$ in the manner reported previously for the reaction of $C_2H_2^{+\cdot}$ derived by electron impact from acetylene (13). The data also provided an upper limit of 1×10^{-13} cm^3 molecule^{-1} s^{-1} for the rate constants of the reactions of $C_2H_4^{+\cdot}$, $H_2C_3N^+$, and $(HC_3N)_2^{+\cdot}$ with H_2. The initial decay of the latter ion in Fig. 2 is due to the depletion of its source ion $(HC_3N)^{+\cdot}$.

CO

The measurement of the reaction of $(HC_3N)^{+\cdot}$ with CO was straightforward. The decay of $(HC_3N)^{+\cdot}$ provides an apparent second-order rate constant of 3.4×10^{-11} cm^3 molecule^{-1} s^{-1} at a total pressure of 0.31 Torr. Only the adduct ion $(HC_3N)^{+\cdot}\cdot CO$ was observed to be present in the product ion spectrum. Proton transfer was not observed. The adduct ion and the impurity ions

TABLE 1. Summary of rate constants (in units of 10^{-9} cm^3 molecule^{-1} s^{-1}) and product distributions measured for reactions of $HC_3N^{+\cdot}$ with the SIFT technique at 296 ± 2 K

Neutral reactant	Products	Branching[a] ratio	k_{exp}[b]	k_c[c]
H_2	$C_2H_2^{+\cdot}$ + HCN	0.5	0.0019	1.5
	$H_2C_3N^+$ + H$^\cdot$	0.5		
CO	$(HC_3N)^{+\cdot}\cdot$CO	1.0	0.034[d]	0.80
HCN	$(HC_3N)^{+\cdot}\cdot$HCN	1.0	0.89[e]	3.3
CH_4	$C_2H_3N^{+\cdot}$ + C_2H_2	0.5	0.59	1.1
	$C_3H_2N^+$ + $CH_3^\cdot$	0.3		
	$C_3H_4^{+\cdot}$ + HCN	0.1		
H_2O	$H_2C_3N^+$ + HO$^\cdot$	1.0	0.67	2.4
O_2	HCO^+ + $(C_2NO)^\cdot$	0.4	0.0025[e]	0.67
HC_3N	$(HC_3N)^{+\cdot}\cdot HC_3N$	1.0	1.2[e]	3.4
C_2H_2	$C_4H_2^{+\cdot}$ + HCN	0.8	0.64	1.0
	$C_2H_2^{+\cdot}$ + HC_3N	0.2		
OCS	$(OCS)^{+\cdot}$ + HC_3N	0.8	0.72	1.2
	$(HC_3NS)^{+\cdot}$ + CO	0.2		
C_2H_4	$C_2H_4^{+\cdot}$ + HC_3N	0.8	0.67	1.1
	$H_2C_3N^+$ + $C_2H_3^\cdot$	0.2		
C_4H_2	$C_4H_2^{+\cdot}$ + HC_3N	1.0	0.89	1.1

[a]Primary product ions which contribute more than 5%. The branching ratio has been rounded off to the nearest 5% and is estimated to be accurate to ±30%.
[b]The accuracy of the rate constants is estimated to be better than ±30%.
[c]Collision rate constants derived from the combined variational transition state theory – classical trajectory study of Su and Chesnavich (11).
[d]In helium buffer gas at a total pressure of 0.31 Torr and concentration of 1.0×10^{16} atoms cm^{-3}.
[e]In helium buffer gas at a total pressure of 0.34 Torr and concentration of 1.1×10^{16} cm^{-3}.

$(HC_3N)_2^{+\cdot}$ and $H_2C_3N^+$ were all observed not to react with CO, $k \leq 1 \times 10^{-12}$ cm^3 molecule^{-1} s^{-1}.

HCN, HC_3N

Hydrogen cyanide and cyanoacetylene were observed to react with $(HC_3N)^{+\cdot}$ in a similar fashion. With both molecules adduct formation was predominant and rapid at the few tenths of a Torr of helium pressure employed in these measurements. Proton transfer was observed to be almost absent although the data analysis allowed for as much as about 5% of the reaction with HCN and about 1% of the reaction with HC_3N to proceed in this fashion. The product ion spectra provided evidence for the successive addition of up to three molecules of HCN and two molecules of HC_3N to $(HC_3N)^{+\cdot}$ but, interestingly, the addition of the first molecule was by far the most rapid in each case, by more than about an order of magnitude. Figure 3 displays data that illustrate this point for HC_3N.

CH_4

A variety of products was observed for the rapid reaction of ionized cyanoacetylene with methane. However, the stoichiometry is such that the product assignments were not straightforward. Product ions were observed at m/z = 52 ($H_2C_3N^+$ or $C_4H_4^+$), 41 ($H_3C_2N^+$ or $C_3H_5^+$), 40 ($H_2C_2N^+$ or $C_3H_4^+$), 28 (H_2CN^+ or $C_2H_4^+$), and 66 ($H_4C_4N^+$). Experiments with CD_4 allowed the exclusion of the following products: $C_4H_4^+$, $H_2C_2N^+$, and $C_2H_4^+$. Also an upper limit of 5% could be assigned to the formation of $C_3H_5^+$. Formation of $H_2C_3N^+$ can be ascribed to hydrogen atom transfer. The $H_4C_4N^+$ will arise from condensation with hydrogen atom elimination and may be protonated methylcyanoacetylene. The $C_3H_4^+$ will result from condensation followed by elimination of HCN and may also give rise to H_2CN^+ if proton transfer proceeds before the products separate. The nature of the $C_3H_4^+$ ion is uncertain. Available heats of formation suggest that ionized allene, methylacetylene, and *cis*-cyclopropane are some of the possibilities. The nature of the major product ion $H_3C_2N^+$ that may be formed by condensation with elimination of acetylene is also uncertain. A number of isomers can be thought to be formed. The heat of formation of ionized methyl cyanide is too high. Formation of ionized methyl isocyanide is less endothermic but still energetically unfavourable by 10 kcal mol^{-1}. Other isomers are possible, e.g. ionized ethynylimidogen, but their heats of formation are not known.

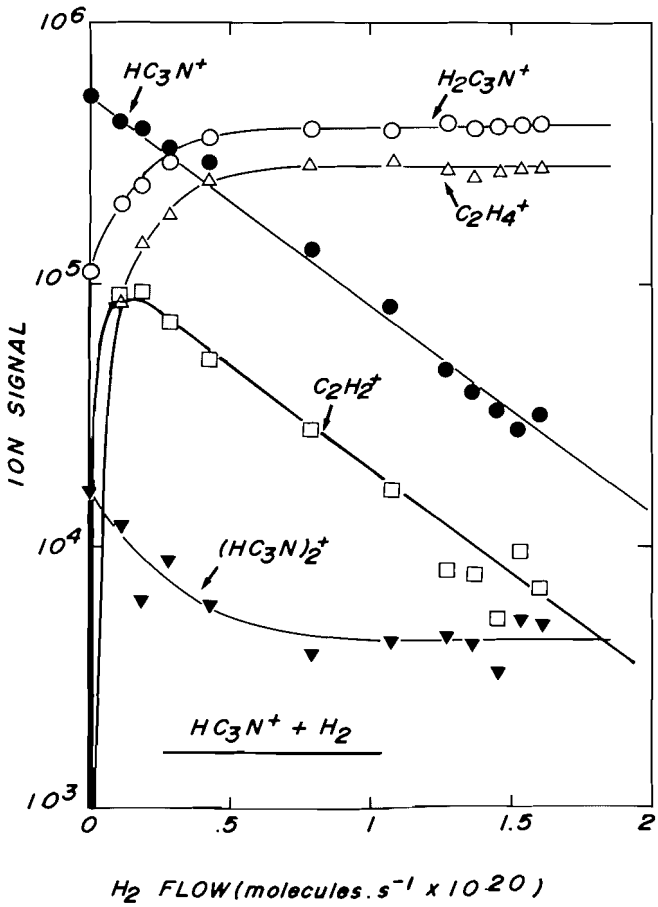

FIG. 2 The variations in ion signals recorded for the addition of hydrogen into the reaction region of the SIFT apparatus in which HC_3N^+ is initially established in helium buffer gas. P = 0.341 Torr, $\bar{v}$ = 7.0×10^3 cm s^{-1}, L = 46 cm, and T = 297 K. The HC_3N^+ is derived from cyanoacetylene at an electron energy of 44.5 eV and injected at 12 V.

H_2O

The predominant channel observed for the reaction with H_2O was hydrogen atom transfer. Formation of C_3O^+, which cannot be distinguished from $H_2C_3N^+$ with our mass spectrometer, was excluded on the basis of experiments with D_2O. Less than 5% of the reaction proceeded by proton transfer and there was no evidence for charge transfer, which is endothermic in any case. The impurity dimer ion $(HC_3N)_2^{+\cdot}$ did not react with H_2O. A secondary reaction was observed between the $H_2C_3N^+$ and H_2O to form the adduct.

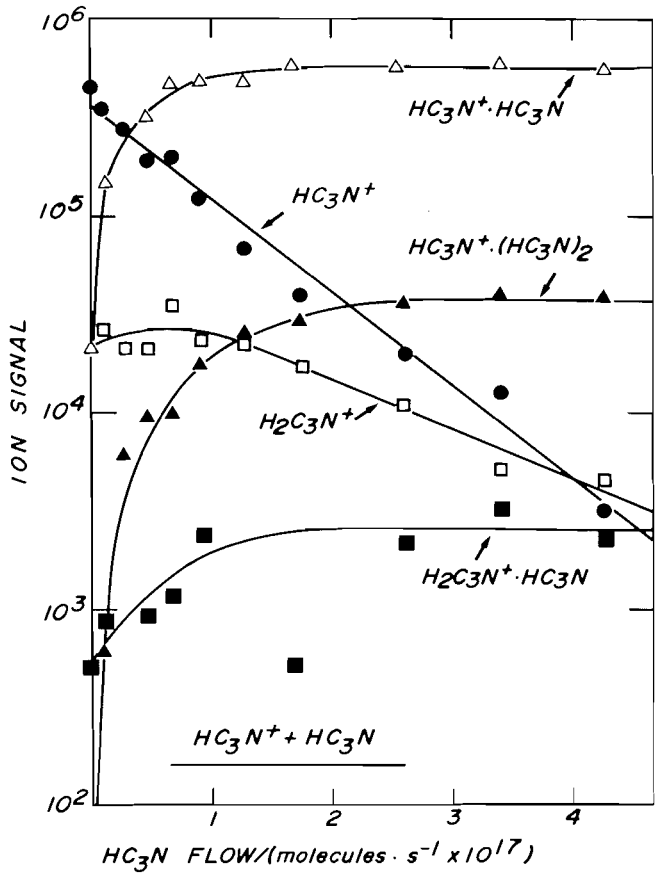

FIG. 3. The variations in ion signals recorded for the addition of cyanoacetylene into the reaction region of the SIFT apparatus in which HC_3N^+ is initially established in helium buffer gas. P = 0.319 Torr, $\bar{v}$ = 6.8 × 10^3 cm s^{-1}, L = 46 cm, and T = 298 K.

O_2

The reaction of $(HC_3N)^{+\cdot}$ with O_2 was the slowest reaction observed in this study with a measurable rate constant. HCO^+ and the adduct $(HC_3N)^{+\cdot} \cdot O_2$ were the only products observed and these were formed in approximately equal amounts.

C_2H_2

$C_2H_2^{+\cdot}$ and $C_4H_2^{+\cdot}$ appeared as the major product ions in this reaction. Formation of CN^+ and C_3N^+ is endothermic in this case. An abundance of secondary ion chemistry was observed since both of the primary product ions are reactive towards acetylene. We have established in separate experiments that $C_2H_2^{+\cdot}$ gives rise to $C_4H_2^{+\cdot}$, $C_4H_3^+$, and $C_4H_4^{+\cdot}$, which in turn add acetylene to give rise to the corresponding adduct ions. All of these conversions were observed to be initiated by the reaction of $(HC_3N)^{+\cdot}$ with acetylene. The $C_4H_3^+$ ion generated from $C_2H_2^{+\cdot}$, which also reacts further with acetylene, could not be distinguished with our mass spectrometer from $(HC_3N)^{+\cdot}$. Therefore it is conceivable that the decay of the ion at m/z = 51 provides only a lower limit to the rate constant of the primary reaction.

OCS

The predominant reaction observed with carbonyl sulphide was charge transfer, and the $(OCS)^{+\cdot}$ product ion reacted further to add one molecule of carbonyl sulphide. A minor channel was observed that corresponds to sulphur atom abstraction and so leads to the incorporation of sulphur into the cyanoacetylene ion. No reaction was observed with the $H_2C_3N^+$ ion that was also present initially. This is not surprising since proton transfer is endothermic in this case.

C_2H_4

$C_2H_4^{+\cdot}$ was the predominant product with ethylene and it rapidly reacted further to establish $C_3H_5^+$ and the adduct $(C_2H_4)_2^{+\cdot}$. The minor channel leading to the formation of $H_2C_3N^+$ corresponds to the transfer of a hydrogen atom.

C_4H_2

Charge transfer was the predominant reaction observed with diacetylene. The production of C_3N^+, which could not be distinguished with our mass spectrometer from $C_4H_2^{+\cdot}$, is endothermic. The $C_4H_2^{+\cdot}$ reacted further to form the adduct $C_4H_2^{+\cdot} \cdot C_4H_2$ as well as some $C_6H_2^{+\cdot}$. This latter reaction has been studied in separate experiments in more detail and will be reported elsewhere. It was also interesting to note that the $H_2C_3N^+$ reacted quite rapidly with diacetylene to add one molecule, while the addition of a second molecule was noted to be at least ten times slower. At 0.33 Torr of helium and a concentration of 1.1 × 10^{16} helium atoms cm^{-3} the apparent bimolecular rate constant for addition of the first molecule of diacetylene was (8.7 ± 2.6) × 10^{-10} cm^3 $molecule^{-1}$ s^{-1}. This is close to the collision limit and probably reflects the formation of a strong hydrogen bond in the adduct. Bonding of the second diacetylene molecule would then be much less favourable and lead to a much lower rate of adduct formation.

Discussion and conclusions

The efficiency of the hydrogenation of ionized cyanoacetylene by H atom transfer from H_2 according to reaction [1] has been established in the experiments reported here to be less than 0.05% at 296 K. The hydrogen atom transfer is more than 30 kcal mol^{-1} exothermic but its low efficiency suggests that it has a positive activation energy. Consequently it may not contribute significantly to the formation of $H_2C_3N^+$ at the much lower temperatures found in interstellar gas clouds. The reactions with CH_4 and H_2O provide more efficient routes for the hydrogenation of ionized cyanoacetylene and so may be more suited to the eventual synthesis of cyanoacetylene by reactions [2] and [3]. Of course other reactions operate in interstellar gas clouds to establish $H_2C_3N^+$ without $HC_3N^{+\cdot}$ as a precursor, such as, for example, the reaction of $C_3H_3^+$ with N atoms (2, 3) and the reaction of $C_2H_2^{+\cdot}$ with HCN (5).

Also, we have shown that proton transfer from ionized cyanoacetylene to carbon monoxide does not occur at room temperature and so is not a viable reaction in models of the chemistry of interstellar clouds. We have observed a slow addition reaction in a few tenths of a Torr of helium to form what may be the isocyanate ion, H—C≡C—C·=N⁺=C=O, but it is uncertain to what degree this happens in interstellar clouds in which radiative association would be the only means of stabilizing the adduct ion.

The reaction of ionized cyanoacetylene with carbonyl sulphide also has interesting implications for interstellar chemistry. The $(HC_3NS)^{+\cdot}$ ion formed in 20% of the reaction at room temperature is a potential source of ·S—C≡C—C≡N or :C=C=C=N—S·, which may be formed by the recombination of $(HC_3NS)^{+\cdot}$ with electrons.

The failure to observe significant amounts of proton transfer with any of the neutral reagents is curious. The proton affinities of the neutral molecules chosen as reagents span a range from 101 for H_2 to 184 kcal mol^{-1} for cyanoacetylene (14,15). The

proton affinity of $(C_3N)^{\bullet}$ can be calculated to be 140 kcal mol^{-1} from the known heats of formation of ionized cyanoacetylene, the proton, and the $(C_3N)^{\bullet}$ radical. The latter is based on the appearance potential of CN^- from dicyanoacetylene (16) and appears to be reliable. The proton affiinity of $(C_3N)^{\bullet}$ is therefore less than that for CO (142), OCS (151), C_2H_2 (153), C_2H_4 (163), H_2O (166), HCN (171), C_4H_2 (180), and HC_3N (184), where the proton affinity is given in parentheses in kcal mol^{-1}. Yet the proton transfer observed with any of these molecules was at most 5% of the total reaction pathway.

Charge transfer, H atom transfer, and adduct formation were the alternate channels that appeared to compete successfully with proton transfer. The recombination energy of $(HC_3N)^{+\bullet}$ is 11.60 eV, which exceeds the ionization energy of the molecules C_4H_2 (10.17), C_2H_4 (10.5), OCS (11.18), and C_2H_2 (11.41). Charge transfer is therefore exothermic and indeed was observed to be a predominant reaction channel for each of these four molecules. For the reaction with C_2H_2 the ultimate formation of the charge transfer product is minor but we speculate that $C_2H_2^{+\bullet}$ in part also reacts with HC_3N before the products separate to produce $C_4H_2^{+\bullet}$. We have shown in a separate study that this latter reaction proceeds readily when $C_2H_2^{+\bullet}$ is produced by electron impact from acetylene (17).

The hydrogen atom affinity of ionized cyanoacetylene is at least 10 kcal mol^{-1} higher than the homolytic X—H bond energy of any of the molecules of type XH chosen as reagents in this study. Yet hydrogen atom transfer was observed not to compete effectively with charge transfer when the latter was also exothermic, as for the reactions with ethylene, acetylene, and diacetylene. Also it did not compete significantly with adduct formation for the reactions with HCN and HC_3N. In fact, only for the reactions with H_2, CH_4, and H_2O was hydrogen atom transfer observed to compete effectively with other reaction channels.

We suggest that both the curious failure of proton transfer and the discriminating behaviour of hydrogen atom transfer may be accounted for by steric constraints that could operate at close separations because of the electrostatic interaction between the cyanoacetylene ion and the reacting molecule. Preferential attack at the nitrogen end of the lengthy $(H—C{\equiv}C—C{\equiv}N)^{+\bullet}$ ion would put the proton "out of reach" of the reacting molecule and so prevent proton transfer. Also, for hydrogen atom transfer, the hydrogen atom in the reacting molecule may become "out of reach" of the ion, depending on the length and preferred alignment of the reacting molecule. This is likely to be the case with HCN and HC_3N, for example. These strong dipoles are likely to approach the positive ion preferentially with their negative nitrogen end. Azine type N—N bonding would then be possible if the nitrogen end of the ion is the site of attack. The high rates of association observed for the reactions with HCN and HC_3N are consistent with this kind of chemical bond formation. The linkages may be the type shown in [8] and [9].

[8] $H—C{\equiv}C—C^{\bullet}{=}N—N{=}C^{+}—H$

[9] $H—C{\equiv}C—C^{\bullet}{=}N—N{=}C^{+}—C{\equiv}C—H$

Adduct formation was not observed with H_2, H_2O, and CH_4 because the hydrogen atom in these molecules is easily "within reach." Adduct formation was also not observed with C_2H_2, C_2H_4, and C_4H_2. In these cases charge transfer is preferred because of the relatively low ionization potentials of these molecules.

The association of cyanoacetylene molecules with ionized cyanoacetylene has also just recently been observed by Buckley *et al.* in an ICR (Ion Cyclotron Resonance) and a high pressure photoionization mass spectrometer (18). The apparent bimolecular rate constant that was reported for the addition of the first molecule in the ICR at a total pressure of 10^{-6} Torr is surprisingly large, $k = 7.4 \times 10^{-10}$ cm^3 $molecule^{-1}$ s^{-1}, and close to the value obtained at the much higher pressures of the SIFT experiments reported here. High rates of association under SIFT conditions are normally attributable to the formation of strongly bound adducts stabilized by collision with the buffer gas atoms. In this case, however, the almost equally high specific rate observed at the much lower pressures of the ICR suggests that this stabilization may proceed by the emission of a photon and so implies a truly bimolecular radiative association reaction. Buckley *et al.* (18) have also proposed several bonding possibilities for the association reaction other than the azine-like linkage discussed earlier. They have pointed out that C—C bonding could lead to an ion of type [10] while C—N bonding may result in an ion of type [11]. These alternatives are attractive in that addition of a second molecule of cyanoacetylene to these dimer ions can lead to some interesting cyclic structures (18).

[10] $^{+}CH{=}C(CN)—CH{=}C^{\bullet}—CN$

[11] $HC_2—C(=N)^{\bullet}—N{=}C^{+}—C_2H$

Acknowledgment

We thank the Natural Sciences and Engineering Research Council of Canada for financial support.

1. S. S. Prasad and W. T. Huntress. Astrophys. J. **239**, 151 (1980).
2. T. J. Millar and A. Freeman. Mon. Not. R. Astron. Soc. **207**, 425 (1984).
3. C. M. Leung, E. Herbst, and W. F. Huebner. Astrophys. J. Suppl. **56**, 231 (1984).
4. A. B. Raksit, H. I. Schiff, and D. K. Bohme. Int. J. Mass Spectrom. Ion Processes, **56**, 321 (1984).
5. H. I. Schiff, G. I. MacKay, G. D. Vlachos, and D. K. Bohme. *In* The Proceedings of the I.A.U. Symposium on Interstellar Molecules. *Edited by* B. H. Andrews. D. Reidel Publ. Co., Dordrecht. 1981. pp. 307–310.
6. E. Herbst. Astrophys. J. Suppl. **53**, 41 (1983).
7. G. I. MacKay, G. D. Vlachos, D. K. Bohme, and H. I. Schiff. Int. J. Mass Spectrom. Ion Phys. **36**, 259 (1980).
8. A. B. Raksit and D. K. Bohme. Int. J. Mass Spectrom. Ion Phys. **55**, 69 (1983).
9. O. Glemser. *In* The handbook of preparative inorganic chemistry. *Edited by* G. Brauer. Academic Press, New York. 1963. p. 658.
10. C. Moureu and J. C. Bongrand. Ann. Chim. (Rome), **14**, 47 (1920).
11. T. Su and W. J. Chesnavich. J. Chem.Phys. **76**, 5183 (1982).
12. N. G. Adams and D. Smith. J. Phys. B, **9**, 1439 (1976).
13. D. Smith and N. G. Adams. Chem. Phys. Lett. **47**, 383 (1977).
14. S. G. Lias, J. F. Liebman, and R. D. Levin. J. Phys. Chem. Ref. Data, **13**, 695 (1984).
15. A. B. Raksit and D. K. Bohme. Int. J. Mass Spectrom. Ion Processes, **57**, 211 (1984).
16. V. H. Dibeler, R. M. Reese, and J. L. Franklin. J. Am. Chem. Soc. **83**, 1813 (1961).
17. A. B. Raksit and D. K. Bohme. Can. J. Chem. **63**, 854 (1985).
18. T. J. Buckley, L. W. Sieck, R. Metz, and S. G. Lias. Int. J. Mass Spectrom. Ion Processes, **65**, 181 (1985).

Charge distributions and chemical effects. XL. Chemical bonds in benzenoid hydrocarbons

S. FLISZÁR, G. CARDINAL, AND N. A. BAYKARA
Département de Chimie, Université de Montréal, C.P. 6210, Succ. A, Montréal (Qué.), Canada H3C 3V1

Received June 26, 1985

S. FLISZÁR, G. CARDINAL, and N. A. BAYKARA. Charge distributions and chemical effects. XL. Chemical bonds in benzenoid hydrocarbons. Can. J. Chem. **64**, 404 (1986).

Benzenoid hydrocarbons were examined using a bond energy scheme featuring the role of atomic charges. The latter were conveniently deduced from appropriate correlations between theoretical results and ^{13}C nuclear magnetic resonance shifts. Atomization energies calculated in this manner agree with their experimental counterparts to within 0.36 kcal mol^{-1} (average deviation). It appears that benzenoid hydrocarbons can be efficiently described in terms of *local* charge density properties. In the absence of any distinctive specific feature characterizing benzenoids, this particular description of chemical bonds ultimately results in a unifying genealogy smoothly relating to one another the various possible types of CC and CH bonds which are formed by sp^2 and sp^3 carbons.

S. FLISZÁR, G. CARDINAL et N. A. BAYKARA. Charge distributions and chemical effects. XL. Chemical bonds in benzenoid hydrocarbons. Can. J. Chem. **64**, 404 (1986).

Utilisant un schéma d'énergie de liaison comportant le rôle des charges atomiques, on a étudié des hycrocarbures benzènoïdes. On peut facilement déduire les charges atomiques des corrélations appropriées entre les résultats théoriques et les déplacements chimiques du ^{13}C en rmn. Les énergies d'atomisation calculées de cette manière sont en accord, dans des limites de 0,36 kcal mol^{-1} (déviation moyenne). Il semble que les hydrocarbures benzènoïdes peuvent être décrits d'une manière efficace en fonction des propriétés de densité de charge *locale*. En l'absence de caractéristiques spécifiques distinctives des benzènoïdes, cette description particulière des liaisons chimiques resulte finalement en un généalogie reliant l'un à l'autre les divers types possibles de liaisons CC et CH formées par les carbones sp^2 et sp^3.

[Traduit par le journal]

Introduction

This study describes benzenoid hydrocarbons. It considers the role of electronic charges in chemical bonding and leads to reasonably accurate energy calculations using atomic charges deduced from ^{13}C nmr shifts. Moreover, it offers a vivid insight into the nature of chemical bonds.

The expression

$$[1] \quad \epsilon_{ij} = \epsilon^0_{ij} + a_{ij}\Delta q_i + a_{jk}\Delta q_j$$

indicates how their energies depend on the charges of the bond-forming atoms (1–3): ϵ^0_{ij} is for a reference bond with net charges q^0_i and q^0_j at atoms i and j, respectively, whereas ϵ_{ij} corresponds to modified charges, $q_i = q^0_i + \Delta q_i$ and $q_j = q^0_j + \Delta q_j$. The a_{ij} and a_{ji} parameters, "measuring" the changes in bond energy accompanying unit charge variations at atoms i and j, respectively, are discussed further below, as well as the ϵ^0_{ij}'s. Finally, the sum[1]

$$[2] \quad \Delta E^*_a \simeq \sum_{i<j} \epsilon_{ij}$$

is a valid approximation for the atomization energy of a molecule at its potential minimum. Indeed, the formula

$$[3] \quad \Delta E^*_a \simeq \Sigma\epsilon^0_{ij} + \Sigma_i\Sigma_j a_{ij}\Delta q_i$$

has proven accurate in over 130 comparisons between calculated and experimental energies (Fig. 1).

Equation [3] indicates the steps involved in these energy calculations. We begin with a description of the appropriate a_{ij} and ϵ^0_{ij} parameters, which will be conveniently tabulated. Next, we discuss the derivation of the required Δq_i charges, with the help of ^{13}C nmr shifts. Then it becomes a simple matter of assembling the pieces in order to deduce ΔE^*_a and,

[1]The omitted nonbonded contributions can safely be neglected in a first approximation (1–3).

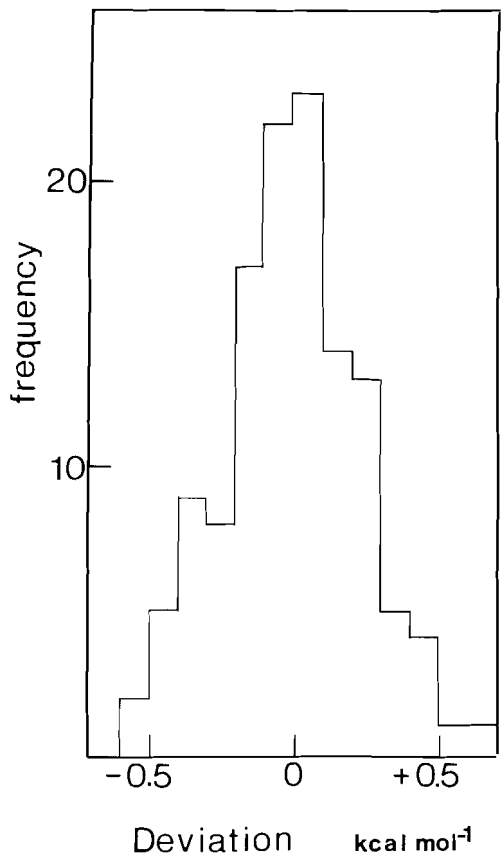

FIG. 1. Frequency of deviations between calculated and experimental atomization energies. This error distribution survey covers alkanes (1, 2) (including cycloalkanes constructed from chair and (or) boat cyclohexane rings), simple ethylenic (4) and polyunsaturated hydrocarbons (5), both conjugated and nonconjugated, as well as ethers, aldehydes, and ketones (6). The average deviation is ~0.23 kcal mol^{-1}.

TABLE 1. Most frequently used a_{ij} values[a], from eq. [4]

Bond	i—j	R_{ij} (Å)	a_{ij} (kcal mol^{-1} me^{-1})
1	C(Ar)—C(Ar)	1.40	$a_{CC}^{\sigma,\pi} = -0.358$
2	C(sp^3)—C(sp^3)	1.53	$a_{CC} = -0.488$
3	C(Ar)—H	1.08	$a_{CH}^{\sigma,\pi} = -0.083$
4	C(sp^3)—H	1.08	$a_{CH} = -0.247$
5	H—C	1.08	$a_{HC} = -0.632$
6	C(Ar)—C(sp^3)	1.53	$a_{CC}^{\sigma} = -0.450$
7	C(Ar)—H	1.08	$a_{CH}^{\sigma} = -0.210$
8	C=C (C_2H_4)	1.34	$a_{CC}^{\sigma,\pi} = -0.183$
9	C(sp^2)—C(sp^3)	1.53	$a_{CC}^{\sigma,\pi} = 0.275$
10	C(sp^2)—H	1.08	$a_{CH}^{\sigma,\pi} = 0.454$

[a]The values indicated $a_{ij}^{\sigma,\pi}$ are expressed for total ($\sigma + \pi$) electronic charges, eq. [5]; a_{ij}^{σ} refers to changes in σ electrons only. The results 2, 4, and 5 are from refs. 1 and 2; 8–10, describing ethylenic carbons, are from refs. 2 and 4.

therefrom, the corresponding enthalpies of formation, ΔH_f^0 (gas, 298.15 K).

Calculation of the a_{ij} *parameters*

The appropriate expression is (1, 2)

$$[4]\quad a_{ij} = \frac{3/7}{\nu_i K_i^{mol}}\left[\left(\frac{\partial E_i^{vs}}{\partial N_i}\right)^0 - \frac{1}{2}\left(\frac{\partial^2 E_i^{vs}}{\partial N_i^2}\right)^0 \Delta q_i\right] - \frac{3}{7} Z_j^{eff}\langle r_{ij}^{-1}\rangle^0$$

where Z^{eff} are effective nuclear charges (7–9) (e.g., 4 for C), ν_i = number of atoms attached to i, and $\langle r_{ij}^{-1}\rangle^0$ is the average inverse distance between the N_i electrons of atom i and the nucleus of atom j. K_i^{mol} is $\frac{1}{2}$ for H and 0.4287 for C (1, 2, 10). The factor $\frac{3}{7}$ translates nuclear-electronic into total (potential + kinetic) energy changes (1, 2, 10, 11). The derivatives of the appropriate valence state energy of atom i, E_i^{vs}, follow from SCF-Xα calculations (Appendix I). The second-order term being negligible for hydrogen and carbon, all the a_{ij}'s used in this work can be treated as constants. The most frequently occurring values are indicated in Table 1.

With sp^2 carbons, whose charges vary at both the σ and π levels, the $a_{ij}\Delta q_i$ term becomes $a_{ij}^{\sigma}\Delta q_i^{\sigma} + a_{ij}^{\pi}\Delta q_i^{\pi}$; a_{ij} is thus the weighted average of a_{ij}^{σ} and a_{ij}^{π} (2). Taking advantage of the relationship (12) $\Delta q_i^{\sigma} = m\Delta q_i^{\pi}$, this average is (4)

$$[5]\quad a_{ij} = (ma_{ij}^{\sigma} + a_{ij}^{\pi})/(1 + m)$$

For nonsubstituted aromatic carbons, it is found that $m \simeq -0.812$ (Appendix II); substitution (e.g. with a methyl group) changes m to ~ -0.90. For ethylenic carbons, $m = -0.955$ (4, 5). Equations [4] and [5] sum up the calculation of the a_{ij}'s.

Reference bond energies, ϵ_{ij}^0

The reference bonds ϵ_1–ϵ_5 (Table 2) were described earlier (1–3). Additional, frequently occurring reference energies are conveniently deduced with the help of the function[2] (1, 2, 13)

$$[6]\quad F = -\frac{3}{7}\sum_i\sum_j Z_i^{eff} q_j(\langle r_{ij}^{-1}\rangle - \langle r_{ij}^{-1}\rangle^0) - \frac{3}{7} \times \sum_i\sum_j Z_i^{eff} Z_j^{eff}[(R_{ij}^{-1}) - (R_{ij}^{-1})^0 - (\langle r_{ij}^{-1}\rangle - \langle r_{ij}^{-1}\rangle^0)]$$

which contains information regarding orbital shapes and internuclear distances, R_{ij}. This function is part of ΔE_a^* and nonzero if actual $\langle r_{ij}^{-1}\rangle$ and (or) R_{ij} parameters differ from those assumed in the definition of any ϵ_{ij}^0 included in $\Sigma\epsilon_{ij}^0$. (This situation arises, for example, if ethylene is constructed with ethane CH reference bonds.) In contrast, *when the* e_{ij}^0*'s are properly chosen, results derived from eq. [3] show that* $F \simeq 0$ *is a valid approximation*[3] (cf. Fig. 1), hence the merits of defining suitable ϵ_{ij}^0's. This is achieved by modifying ϵ_{ij}^0's deduced for $\langle r_{ij}^{-1}\rangle^0$ and $(R_{ij}^{-1})^0$ into values corresponding to $\langle r_{ij}^{-1}\rangle$ and (R_{ij}^{-1}), as requested by eq. [6].[4] Changes in reference charges, if desired, are made with the help of eq. [1]. Thus we deduce, for example, the ethylene and benzene CH bonds from that of ethane, or CC single bonds like those in biphenyl, *cis*-stilbene, etc., from that of ethane.

While a unified new genealogy of chemical bonds surfaces with eq. [6], the pivotal question rests here with our approximate way of applying it in a possibly rough, but certainly simple, scheme satisfying chemical intuition. The underlying hypotheses and detailed numerical examples illustrating the use of eq. [6] are given in Appendix III. These hypotheses are eventually going to be put on trial in extensive comparisons with experimental results. With the set of reference bond energies indicated in Table 2, F is ~0 again, and energy calculations can be made in a straightforward manner using eq. [3].

Charge calculations

Net charges of alkane carbon atoms are conveniently deduced from the remarkably accurate relationship (1, 2, 15)

$$[7]\quad \Delta q_C = -0.148\,\delta^{C_2H_6}\,\text{me}$$

where the ^{13}C nmr shift, $\delta^{C_2H_6}$ (ppm), and $\Delta q_C = q_C - q_C^0(C_2H_6)$ are expressed with reference to ethane. Similarly, for ethylenic sp^2 carbons we use (4)

$$[8]\quad \Delta q_C = 0.15\,\delta^{C_2H_4}\,\text{me}$$

where the nmr shifts, $\delta^{C_2H_4}$ and $\Delta q_C = q_C - q^0{}_C(C_2H_4)$ are expressed taking ethylene as reference. Finally, for aromatic carbons we use (Appendix II)

$$[9]\quad \Delta q_C = 1.20\,\delta^{C_6H_6}\,\text{me}$$

where both Δq_C and $\delta^{C_6H_6}$ are taken with reference to the benzene carbon atom. Note that eqs. [8] and [9] are for total ($\sigma + \pi$) net charges. These results serve two purposes, namely, the calculation of individual $a_{ij}\Delta q_i$ terms and that of the total net charge on all carbon atoms. The latter is obtained from a sum of

[2]The quantities appearing in eq. [6] are defined in terms of a suitable partitioning of the molecular electron density into atomic contributions, ρ_i, and of the equilibrium coordinates, r_i, of the nuclei, i.e.,

$$\int \frac{\rho_i(\boldsymbol{r})}{|\boldsymbol{r} - \boldsymbol{r}_i|}\,d\boldsymbol{r} = N_i\langle r_i^{-1}\rangle \text{ with } \int \rho_i(\boldsymbol{r})\,d\boldsymbol{r} = N_i$$

$$\int \frac{\rho_i(\boldsymbol{r})}{|\boldsymbol{r} - \boldsymbol{r}_i|}\,d\boldsymbol{r} = N_j\langle r_{ij}^{-1}\rangle \text{ with } \int \rho_j(\boldsymbol{r})\,d\boldsymbol{r} = N_j$$

The superscript zero indicates the corresponding expressions for the reference molecule.

[3]The first part is small because atomic net charges are small (e.g., <0.0351 e for sp^3 and ~0.007 e for ethylenic sp^2 carbons) and because small changes in electron populations are unlikely to modify their center of charge to any significant extent. The second part, in square brackets, is obviously zero for spherically symmetric electron clouds or small if the centers of electronic charge move along with the nuclei during small changes in internuclear distances.

[4]For example, eq. [6] predicts $F = -2.39$ kcal mol^{-1} for an ethylenic CH bond and -4.80 kcal mol^{-1} for a CC single bond formed by an ethylenic carbon (4, 5, 13, 14). Systematic inclusion of these results in the ϵ_{ij}^0's corresponding to these bonds takes care of F. Figure 1 includes ~50 olefins calculated in this manner.

TABLE 2. Frequently used reference bond energies[a]

Bond	i—j	Type	R_{ij} (Å)	Reference charge (me) i	Reference charge (me) j	ϵ_{ij}^0(kcal mol^{-1})
1	C—C	sp^3—sp^3	1.53	35.1	35.1	69.633
2	C=C	sp^2—sp^2	1.34	7.7	7.7	139.27
3	C—C	sp^2—sp^2	1.46	7.7	7.7	89.70
4	C:::C	Ar—Ar	1.40	14.8	14.8	114.21
5	C—H	sp^3—H	1.08	35.1	−11.7	106.806
6	C—C	Ar—Ar	1.40	14.8	14.8	91.56
7	C—C	Ar—sp^3	1.53	14.8	35.1	79.30
8	C—C	Ar—sp^2(nc)	1.49	14.8	7.7	86.89
9	C—C	Ar—sp^2(c)	1.48	14.8	7.7	90.40
10	C—C	sp^2—sp^3	1.53	7.7	35.1	77.70
11	C—H	Ar—H	1.08	14.8	−11.7	111.58
12	C—H	sp^2—H	1.08	7.7	−11.7	110.68

[a]Bond 8 is nonconjugated, 9 is conjugated, Ar = aromatic C atom, sp^2 indicates an ethylenic carbon. The following ϵ_{ij}^0's are taken from previous work: 1, 5 (1), 2, 10, 12 (4) and 3 (5). Bonds 1, 3, and 5 were used for deducing 6–12. The reference charge selected for benzene, 14.8 me, is discussed in Appendix II.

all Δq_i's to which are added 35.1 me for each sp^3 carbon, 14.8 me for each aromatic, and 7.7 me for each ethylenic sp^2 carbon of the molecule. This gives the sum Σq_C and $\Sigma q_H = -\Sigma q_C$. The reference for hydrogen being taken in all cases at −11.7 me, it follows that

[10] $\Sigma\Delta q_H = -\Sigma q_C + 11.8\, n_H$ me

where n_H is the number of hydrogen atoms. This concludes the derivation of the charges required in the forthcoming energy calculations.

The calculation of atomization energies, ΔE_a^*

We can now apply eq. [3]. The calculation of $\Sigma\epsilon_{ij}^0$ is straightforward, using Table 2. There is one point to be mentioned. The aromatic CC bond, ϵ_4, represents, so to speak, the average between a single and double bond as they are found in benzenoid structures: it is the CC bond of benzene. It is counted twice the number of double bonds one can write using classical Kekulé structures. The remaining CC bonds (e.g., 1 in naphthalene, 2 in anthracene, etc.) are treated as C(sp^2)—C(sp^2) single bonds—bond ϵ_6 in Table 2.

As regards the evaluation of $\Sigma_i\Sigma_j a_{ij}\Delta q_i$, first we calculate $\Sigma_j a_{ij}$ for each carbon atom, using Table 1. These sums are conveniently displayed in structure **I**. Next, we calculate the corresponding Δq_C's and form the product $\Delta q_i\Sigma_j a_{ij} = \Sigma_j a_{ij}\Delta q_i$ for each carbon, as in the example given in Table 3. The sum of these atomic terms over all carbon centers i yields the

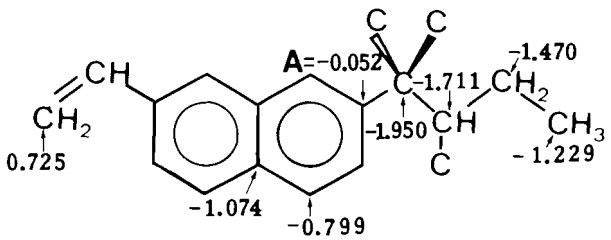

I

Sum of the a_{ij} terms for the various types of atoms, $\Sigma_j a_{ij}$, in kcal mol^{-1} me^{-1}.

TABLE 3. Calculation of $\Sigma_i\Sigma_j a_{ij}\Delta q_i$ (kcal mol^{-1}) for 2-methylnaphthalene, using the a_{ij}'s of Table 1 and eqs. [7] and [9][a]

Atom	δ	Δq	$\Sigma_j a_{ij}$	$\Sigma_j a_{ij}\Delta q_i$
1	−1.5	−1.80	−0.799	1.438
2	6.8		(−0.052)	−0.354
3	−0.45	−0.54	−0.799	0.431
4	−0.7	−0.84	−0.799	0.671
5	−0.7	−0.84	−0.799	0.671
6	−3.6	−4.32	−0.799	3.452
7	−2.7	−3.24	−0.799	2.589
8	−1.1	−1.32	−0.799	1.055
9	5.6	6.72	−1.074	−7.217
10	3.65	4.38	−1.074	−4.704
CH_3	16.35	−2.42	−1.229	2.974
$\Sigma\Delta q_H$		−61.88	−0.632	39.108

[a]The δ's are relative to benzene (1–10) and to ethane for the methyl carbon. From the Δq_c's (me), counting 14.8 me for each aromatic carbon and 35.1 me for the sp^3 reference, it is Σq_C = 178.88 and $\Sigma\Delta q_H = -178.88 - 10(-11.7)$ me. Note the contribution of C—2, $-0.052\,\delta = -0.354$ kcal mol^{-1}. The sum of all the $\Sigma_i\Sigma_j a_{ij}\Delta q_i$'s yields 40.11 kcal mol^{-1}, ready for use in eq. [3].

corresponding part of $\Sigma_i\Sigma_j a_{ij}\Delta q_i$. Finally, we calculate $\Sigma\Delta q_H$ and add $-0.632\ \Sigma\Delta q_H$ to the previous sum. This is now $\Sigma_i\Sigma_j a_{ij}\Delta q_i$, ready for use in eq. [3].

There is one case which is treated in a slightly different manner, with no loss in simplicity, that of an aromatic carbon attached to a non-aromatic carbon. Its contribution is $-0.052\ \delta^{C_6H_6}$ kcal mol^{-1}. This carbon is taken at 14.8 me in the computation of Σq_C. The reason for this approach stems from a situation of small differences between large numbers (explained in Appendix IV) arising in the evaluation of $\Sigma_j a_{ij}$.

In closing, let us mention a simple formula for nonsubstituted aromatic hydrocarbons, taking care of $\Sigma\Delta q_H$ by charge normalization and using the a_{ij}'s of Table 1, as well as eq. [9]. It is, indeed, readily deduced that

$$\Sigma_i\Sigma_j a_{ij}\Delta q_i = -0.33\,\Sigma N_{CC}\delta^{C_6H_6} + 0.46\,\Sigma\Delta^{C_6H_6} + 0.632\,(14.8\,n_C - 11.7\,n_H)$$

where N_{CC} = number of CC bonds formed by the carbon whose

TABLE 4. Energy calculations of selected planar benzenoid hydrocarbons, using ^{13}C nmr shifts (kcal mol^{-1})[a]

Molecule	$\Sigma N_{CC}\delta$	$\Sigma\delta$	$\Sigma_i\Sigma_j a_{ij}\Delta q_i$	$\Sigma\epsilon_{ij}^0$	ΔE_a^*
Benzene	0	0	11.76	1354.74	1366.50
Naphthalene	7.2	−1.6	31.27	2127.50	2158.77
Anthracene	50.1	17.6	48.57	2900.26	2948.83
Phenanthrene	−4.5	−8.0	54.81	2900.26	2955.07
Pyrene	−30.2	−17.1	77.81	3217.84	3295.65
Benz[*a*]anthracene	17.3	−0.7	73.60	3673.02	3746.62

[a]The average deviation between these calculated atomization energies and their experimental counterparts is 0.23 kcal mol^{-1} (see Table 5). The sources of the nmr shifts are indicated at the bottom of Table 5.

nmr shift is $\delta^{C_6H_6}$, n_C = number of C atoms, and n_H = number of H atoms in the molecule. Selected numerical examples are indicated in Table 4.

Now is the proper time to look at thermochemical results in order to assess the validity of our approach toward solving eq. [3].

Results

Most of the benzenoid hydrocarbons for which both the enthalpy of formation, ΔH_f^0 (gas, 298.15), and the carbon-13 nmr spectrum are experimentally known were examined in the present work. While experimental ΔH_f^0 results are typically reported with an error of 0.3–1.0 kcal mol^{-1}, independent measurements from different laboratories often differ from one another by much more than this. Pyrene, for example, is reported by Cox and Pilcher (16) with $\Delta H_f^0(g) = 49.94 \pm 0.64$, contrasting with the result cited by Kao and Allinger (17), 51.59 kcal mol^{-1}. Whenever reasonable, critically selected data given by Cox and Pilcher (16) were used. The structures of some of the compounds investigated here are shown in Fig. 2.

In order to offer valid comparisons with theoretical results, we must first deduce "experimental" atomization energies from enthalpies of formation, zero-point and heat-content energies, ZPE + $H_T - H_0$, and from the enthalpies of formation of the atoms, $\Delta H_f^0(A)$. The latter are taken from the literature (18), namely, $\Delta H_f^0(C) = 170.89$ and $\Delta H_f^0(H) = 52.09$ kcal mol^{-1} at 298.15 K. The appropriate equation is, for nonlinear molecules,

$$[11] \quad \Delta E_a^* = \sum_i n_i \left[\Delta H_f^0(A_i) - \frac{5}{2} RT \right] + \text{ZPE} + H_T - H_0 - \Delta H_f^0$$

Vibrational energy data are scarce, however, for the molecules considered in this study. Fortunately they can be constructed to a good approximation by means of additivity rules (2), e.g., ZPE + $H_T - H_0 \simeq 33.35 + 18.213\ (n-2) - 0.343\ n_{br}$ for a mono-olefin with n carbons and n_{br} = number of branchings, or ZPE + $H_T - H_0 \simeq 55.19 + 18.213\ (n-4) - 0.343\ n_{br}$ kcal mol^{-1} for diolefins (5). Similar equations are also found to apply in other homologous series of compounds, e.g., alkanes and cycloalkanes, ethers, and carbonyl compounds (2). Along these lines, we use the following formula for alkyl substitution, based on the experimental ZPE + $H_T - H_0$ value (66.22 kcal mol^{-1}) deduced for benzene in the harmonic oscillator approximation (2):

$$\text{ZPE} + H_T - H_0 = 66.22 + 18.21\, n - 0.343\, n_{br}$$

where n is the number of alkyl carbon atoms. Molecules like 9,10-dihydroanthracene or 1,2,3,4-tetrahydronaphthalene were treated in similar manner. In these situations, attention must be given to a lowering of ZPE + $H_T - H_0$ by 11.5 kcal mol^{-1} accompanying the loss of a pair of hydrogen atoms and by $\sim RT/2 = 0.296$ kcal mol^{-1} for each hindered rotation in cyclic compounds (2, 19). Moreover, the condensation of two fragments involves a correction of $4RT = 2.37$ kcal mol^{-1} because this term is included in the $H_T - H_0$ part of each molecule used as fragment and should not be counted twice in the final product. For example, the ZPE + $H_T - H_0$ value of 9,10-dihydroanthracene is obtained from dimethylbenzene ($66.22 + 2 \times 18.21$) and benzene, less 2×11.5, less $4RT$, and less $4RT/2$ kcal mol^{-1}. This type of estimate usually carries an uncertainty not exceeding 0.2 kcal mol^{-1}. Styrene, for example, can be constructed from benzene and ethylene to give ZPE + $H_T - H_0 = 66.22 + 33.35 - 11.5 - 4RT = 85.70$ kcal mol^{-1}.

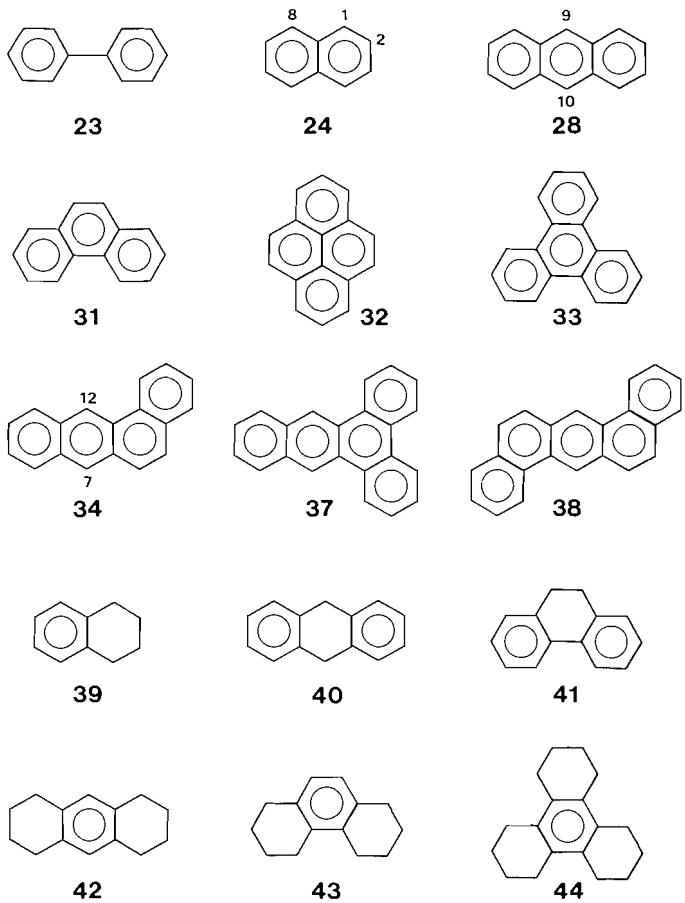

FIG. 2. A selection of molecules examined in this work. The numbering corresponds to that indicated in Table 5.

TABLE 5. Calculated and experimental energies of benzenoid hydrocarbons, kcal mol^{-1} [a]

Molecule	ΔH_f^0	ZPE + $H_T - H_0$	$\Sigma\epsilon_{ij}^0$	$\Sigma_i\Sigma_j a_{ij}\Delta q_i$	ΔE_a^* Calcd.	ΔE_a^* Exptl.
1 Benzene	19.81 ± 0.13	66.22	1354.74	11.76	1366.5	1366.5
2 Toluene	11.99 ± 0.10	84.43	1642.88	20.52	1663.4	1663.2
3 1,2-Dimethylbenzene	4.56 ± 0.26	102.64	1931.02	28.78	1959.8	1959.4
4 1,3-Dimethylbenzene	4.14 ± 0.18	102.64	1931.02	29.12	1960.1	1959.9
5 1,4-Dimethylbenzene	4.31 ± 0.24	102.64	1931.02	28.38	1959.3	1959.7
6 1,2,3-Trimethylbenzene	−2.26 ± 0.29	120.85	2219.15	37.26	2256.4	2255.1
7 1,2,4-Trimethylbenzene	−3.31 ± 0.26	120.85	2219.15	36.55	2255.7	2256.2
8 1,3,5-Trimethylbenzene	−3.81 ± 0.33	120.85	2219.15	37.47	2256.6	2256.6
9 1,2,3,4-Tetramethylbenzene	−10.02	139.06	2507.29	45.20	2552.5	2551.7
10 1,2,3,5-Tetramethylbenzene	−10.71	139.06	2507.29	44.80	2552.1	2552.4
11 1,2,4,5-Tetramethylbenzene	−10.82	139.06	2507.29	44.08	2551.4	2552.5
12 Pentamethylbenzene	−17.80	157.27	2795.43	52.46	2847.9	2848.3
13 Hexamethylbenzene	−25.26	175.48	3083.57	60.99	3144.6	3144.6
14 Ethylbenzene	7.15 ± 0.19	102.64	1926.12	30.55	1956.7	1956.9
15 *n*-Propylbenzene	1.89 ± 0.19	120.85	2209.37	40.97	2250.3	2250.9
16 Isopropylbenzene	0.96 ± 0.26	120.50	2209.37	42.14	2251.5	2251.5
17 *sec*-Butylbenzene	−4.15 ± 0.31	138.71	2492.61	52.37	2545.0	2545.5
18 *tert*-Butylbenzene	−5.40 ± 0.31	138.71	2492.61	54.84	2547.4	2546.7
19 1,2-Diphenylethane	32.4 ± 0.3	155.0	3141.78	61.18	3203.0	3202.9
20 Styrene	35.30 ± 0.25	85.80	1804.40	7.12	1811.5	1810.7
21 *cis*-Stilbene	60.31 ± 0.42	138.05	3020.73	36.05	3056.8	3056.8
22 *trans*-Stilbene	52.5	138.05	3027.75	36.20	3064.0	3064.6
23 Biphenyl	43.53 ± 0.60	116.91	2575.00	37.83	2612.8	2612.4
24 Naphthalene	36.25 ± 0.45	94.90	2126.30	31.27	2157.7	2157.6
25 1-Methylnaphthalene	27.93 ± 0.64	113.11	2414.44	40.88	2455.3	2454.8
26 2-Methylnaphthalene	27.75 ± 0.62	113.11	2414.44	40.11	2454.6	2454.9
27 1,8-Dimethylnaphthalene	See text	131.32	2698.97	46.01	2745.0	2745.0
28 Anthracene	55.2 ± 1.1	123.7	2897.86	48.57	2946.4	2946.3
29 9-Methylanthracene	(42.1)	141.8	3186.00	62.09	3248.1	
30 9,10-Dimethylanthracene	(31.6)	160.0	3474.14	73.34	3547.5	
31 Phenanthrene	49.5 ± 1.1	123.7	2897.86	54.81	2952.7	2952.0
32 Pyrene	53.94 ± 0.31	133.05	3217.84	77.81	3295.7	3295.7
33 Triphenylene	61.9 ± 1.1	152.3	3660.09	86.36	3746.5	3747.1
34 Benz[*a*]anthracene	65.97	152.3	3669.42	73.60	3743.0	3743.0
35 7-Methylbenz[*a*]anthracene	(56.2)	170.5	3957.56	84.06	4041.6	
36 7,12-Dimethylbenz[*a*]anthracene	66.4 ± 1.1	188.7	4245.70	90.31	4336.0	4320.2
37 Dibenz[*a*,*c*]anthracene	(77.2)	181.0	4440.98	98.36	4539.3	(4540.5)
38 Dibenz[*a*,*h*]anthracene	(79.6)	181.0	4440.98	95.90	4536.9	(4538.0)
39 1,2,3,4-Tetrahydronaphthalene	7.3 ± 1.3	126.1	2353.53	66.67	2420.2	2420.2
40 9,10-Dihydroanthracene	38.2 ± 1.1	142.3	3007.58	75.17	3082.8	3083.1
41 9,10-Dihydrophenanthrene	(37.8)	142.3	3007.82	75.68	3083.5	
42 (1–8)-Octahydroanthracene	(−4.3)	185.9	3352.31	120.58	3472.9	
43 (1–8)-Octahydrophenanthrene	(−4.9)	185.9	3352.31	121.17	3473.5	
44 (1–12)-Dodecahydrotriphenylene	(−16.4)	245.8	4351.10	175.10	4526.2	

[a]The experimental ΔH_f^0 results for **1–8**, **14–21**, **23**, **28**, **31**, **33**, **36**, and **40** are "selected values" reported in ref. 16. The results for **9–13** are given in ref. 24, that of **22** in ref. 25, and those of **24–26** in ref. 26. The value indicated for **32** is taken from ref. 27, **34** is reported in ref. 17, and **39** is taken from ref. 28. The ZPE + $H_T - H_0$ result given for **31** was deduced from a vibrational analysis described in ref. 29, in the harmonic oscillator approximation. The carbon-13 nmr spectra are from ref. 30 (**2–13**), ref. 31 (**14–19**), and from ref. 32 (**20**, **23**, **39–44**); **21** and **22** are from ref. 33; **24**, **31**, **32** from ref. 34; and **28** is from ref. 35; **25**, **26** are given in ref. 36; **27** is from ref. 37; and **29**, **30**, **34–38** are from ref. 38; **33** is described in ref. 39. In order to minimize possible solvent effects, whenever possible measurements made in benzene were selected.

From the vibrational spectrum of styrene (20), on the other hand, we find in the harmonic oscillator approximation that ZPE = 80.96 and $H_T - H_0 = 4.84$, for a total of 85.80 kcal mol^{-1}. Similarly, using ZPE + $H_T - H_0$ = 88.82 + 5.08 = 94.90 kcal mol^{-1} for naphthalene, deduced from its vibrational spectrum (21), we add to it the difference, 28.68 kcal mol^{-1}, between naphthalene and benzene, thus obtaining an estimate of 123.6 kcal mol^{-1} for anthracene. The same procedure is used for the higher homologues as well. Finally, using the fundamental frequencies of pyrene (22), we obtain (in the harmonic oscillator approximation) ZPE = 125.94, $H_T - H_0 = 7.11$, for a total of 133.05 kcal mol^{-1}.

While, of course, additional spectroscopic information would be welcome, we feel that the uncertainties affecting present estimates of ZPE + $H_T - H_0$ energies should not be blamed for possible discrepancies between calculated and observed ΔE_a^* (or ΔH_f^0) energies. With this in mind, we can now proceed with comparisons involving experimental enthal-

pies of formation (Table 5). In the absence of experimental results, predicted ΔH_f^0 values are indicated in parentheses. Two ΔE_a^* results listed in the column reporting "experimental values" are in parentheses: these are theoretical results offered for comparison, deduced from enthalpies of formation calculated by Dewar and de Llano (23).

Discussion

The average deviation between calculated and experimental energies is 0.36 kcal mol^{-1} for a collection of 35 benzenoid compounds. This result does not include 7,12-dimethylbenz-[*a*]anthracene: the discrepancy of ~16 kcal mol^{-1} between theory and experiment is in all likelihood due in part to an error in the latter. Although certainly real, steric interactions involving the methyl group in position 12 are probably not so severe as to cause a destabilization exceeding that found in 1,8-dimethylnaphthalene and 4,5-dimethylphenanthrene—molecules which are discussed further below.

At this stage it seems safe to conclude that the agreement between theory and experiment supports the general ideas underlying our energy analysis. On the other hand, the quality of this agreement should not be used to hide the limitations of our approach. These are best revealed by the following examples. *Trans*-stilbene was treated as a planar system and the C(sp^2)—Ph bonds were accordingly derived on the basis of a conjugated sp^2—sp^2 single bond (Appendix III, example 6). While the molecular structure of *trans*-stilbene appears to be approximately planar in the solid state (40), its gas phase structure is found to be nonplanar (41). However, the potential curve for energy vs. the dihedral angle is very shallow and the calculated energy barrier corresponding to the C_i conformation is only about 0.5 kcal mol^{-1} (17). Both these results and our calculation suggest that in *trans*-stilbene there is no great energy difference between conjugation and hyperconjugative stabilization of the sp^2—sp^2 single bond[5] but it is also clear that in this particular situation it could not be assumed *a priori* that our treatment would lead to a valid result, as it did. The case of *cis*-stilbene is clear-cut. Electron diffraction data (43) point to a C_2 symmetry in the gas phase and a structure that may be described as having a propeller-like conformation with phenyl groups rotated ca. 43° about the C—Ph bonds. The latter were thus treated as nonconjugated bonds: ϵ_s = 86.89 kcal mol^{-1} was deduced for R_{CC} = 1.49 Å, which is the experimental bond length (43). Similarly, the gas phase value (44) for the torsional angle about the central bond of biphenyl, 41.6°, and its bond length, R = 1.49 Å (17, 45), suggest that the central bond should be treated like a nonconjugated CC single bond, thus giving ϵ_{CC} = 88.68 kcal mol^{-1}. Finally, the same situation arises with triphenylene (**33**) which is significantly nonplanar (17, 46). The bonds joining the "external" rings to one another were thus calculated at ϵ_{CC} = 88.45 kcal mol^{-1} for R = 1.46 Å, following the approach used for biphenyl. It is clear that some advance knowledge is necessary in our calculations, namely, as regards planarity (or lack of it) of the benzenoid skeleton.

As an additional example, consider 4,5-dimethylphenanthrene. Using the ^{13}C nmr spectrum measured by Stothers *et al.* (47), we deduce ΔH_f^0 = 36.8 kcal mol^{-1} assuming planarity. Closely neighboring methyl groups which are separated by five bonds in the molecular skeleton, however, result in chiral nonplanar conformations (48). Modeling, where appropriate, the CC bonds on those described for biphenyl and *cis*-stilbene, we predict ΔH_f^0 = 47.8 for the nonplanar form, in acceptable accord with the reported value (16), 46.26 ± 1.46 kcal mol^{-1}, a result which is self-explanatory. Equally instructive examples are offered by dimethylnaphthalene isomers. With the substituents in the 1,8 position, our calculation yields ΔE_a^* = 2748.6 kcal mol^{-1} for the planar form, in error with respect to its experimental counterpart,[6] 2745.0 kcal mol^{-1}. The thermochemical stability is overestimated by ~3.6 kcal mol^{-1}, thus suggesting a possible loss of conjugation in this molecule which, as a matter of fact, is known to suffer considerable distortion from the normal naphthalene geometry (50). Indeed, a calculation following the lines described above for biphenyl and nonplanar 4,5-dimethylphenanthrene agrees with experiment. In contrast, 2,6-dimethylnaphthalene can safely be assumed to retain the planar geometry of naphthalene. The result deduced for this form, ΔE_a^* = 2751.3, agrees well with the experimental value,[6] 2751.0 kcal mol^{-1}. These examples illustrate possible applications of energy analyses based on ^{13}C spectra in problems regarding the origin of molecular stability, namely, as regards partial suppression of conjugation accompanying deformations of a benzenoid skeleton.

These examples are also there to remind us that our theory differs in its nature from variational calculations and thus lacks the flexibility of the latter, capable of predicting geometries as well as energies. Indeed, our approach applies only to molecules at equilibrium; in turn, it illustrates efficiently the role of local charges, namely, the way they affect chemical bonds. It is certainly gratifying to recognize how intimately bonds of different types are related to one another, e.g., the CH bonds of ethane, ethylene, and benzene or the CC single bonds of ethane, toluene, *cis*-stilbene, and biphenyl. Minor uncertainties plaguing numerical applications should not obscure the fundamental simplicity of the arguments describing bond energies in terms of local charges. The general concepts developed here, capable of describing chemical bonds in a unifying picture encompassing well-diversified situations, are more relevant, in our opinion, than the precision of the calculations supporting these views. At the present level, residual uncertainties resulting from occasional computational approximations are of the order of those affecting experimental results and are not of the sort that could threaten the essence of the basic ideas underlying our description of molecular energies.

While, of course, our approach does not have the potential of true density functional theory based on the Hohenberg–Kohn theorem (51), it offers at least a conceptually related, simple, and instructive solution when both local charges and nuclear positions are given for a ground-state molecule at equilibrium. At this relatively modest level, it becomes clear that the theory of chemistry and of the chemical bond are in essence a theory of electron density, a fact which can now be described in simple terms for a great variety of organic molecules.

Acknowledgements

The financial support given by the Natural Sciences and Engineering Research Council of Canada and the cooperation of the Centre de Calcul de l'Université de Montréal are gratefully acknowledged.

[5]Related analyses regarding the stabilization of sp^2—sp^2 single bonds are offered in ref. 42.

[6]These results were deduced from eq. [11] using thermochemical data at 350–370 K given in ref. 49.

1. S. FLISZÁR. J. Am. Chem. Soc. **102**, 6946 (1980).
2. S. FLISZÁR. Charge distributions and chemical effects. Springer Verlag, New York. 1983.
3. S. FLISZÁR. Int. J. Quantum Chem. **26**, 743 (1984).
4. M.-T. BÉRALDIN and S. FLISZÁR. Can. J. Chem. **61**, 197 (1983).
5. S. FLISZÁR and G. CARDINAL. Can. J. Chem. **62**, 2748 (1984).
6. S. FLISZÁR and M.-T. BÉRALDIN. Can. J. Chem. **60**, 792 (1982).
7. P. POLITZER and R. G. PARR. J. Chem. Phys. **61**, 4258 (1974); **64**, 4634 (1976).
8. S. FLISZÁR and H. HENRY. J. Chem. Phys. **67**, 2345 (1977); S. FLISZÁR and D. SALAHUB. J. Chem. Phys. **69**, 3321 (1978); R. J. BOYD. J. Chem. Phys. **66**, 356 (1977).
9. S. FLISZÁR. J. Chem. Phys. **79**, 3874 (1983).
10. S. FLISZÁR, M. FOUCRAULT, M.-T. BÉRALDIN, and J. BRIDET. Can. J. Chem. **59**, 1074 (1981).
11. P. POLITZER. J. Chem. Phys. **64**, 4239 (1976); S. FLISZÁR and M.-T. BÉRALDIN. J. Chem. Phys. **72**, 1013 (1980); T. ANNO. J. Chem. Phys. **72**, 782 (1980); P. POLITZER. J. Chem. Phys. **70**, 1067 (1979).
12. S. FLISZÁR, G. CARDINAL, and M.-T. BÉRALDIN. J. Am. Chem. Soc. **104**, 5287 (1982); W. J. HEHRE, R. W. TAFT, and R. D. TOPSOM. Progr. Phys. Org. Chem. **12**, 159 (1976).
13. S. FLISZÁR, G. DEL RE, and M. COMEAU. Can. J. Chem. **63**, 3551 (1985).
14. M.-T. BÉRALDIN. Ph.D. Thesis, Université de Montréal (1985).
15. S. FLISZÁR, A. GOURSOT, and H. DUGAS. J. Am. Chem. Soc. **96**, 4358 (1974).
16. J. D. COX and G. PILCHER. Thermochemistry of organic and organometallic compounds. Academic Press, London, New York. 1970.
17. J. KAO and N. L. ALLINGER. J. Am. Chem. Soc. **99**, 975 (1977).
18. D. R. STULL and G. C. SINKE. Adv. Chem. Ser. **18**, (1956).
19. S. FLISZÁR and J.-L. CANTARA. Can. J. Chem. **59**, 1381 (1981).
20. A. MARCHAND and J.-P. QUINTARD. Spectrochim. Acta Part A, **36**, 941 (1980).
21. S. S. MITRA and H. J. BERNSTEIN. Can. J. Chem. **37**, 553 (1959).
22. A. BREE, R. A. KYDD, T. N. MISRA, and V. V. B. VILKOS. Spectrochim. Acta. Part A, **27**, 2315 (1971).
23. M. J. S. DEWAR and C. DE LLANO. J. Am. Chem. Soc. **91**, 789 (1969).
24. S. H. HASTINGS and D. E. NICHOLSON. J. Phys. Chem. **61**, 730 (1957).
25. S. MARANTZ and G. T. ARMSTRONG. J. Chem. Eng. Data, **13**, 118, 455 (1968).
26. D. M. SPEROS and F. D. ROSSINI. J. Phys. Chem. **64**, 1723 (1960).
27. N. K. SMITH, R. C. STEWART JR., A. G. OSBORN, and D. W. SCOTT. J. Chem. Thermodyn. **12**, 919 (1980).
28. W. D. GOOD and S. H. LEE. J. Chem. Thermodyn. **8**, 643 (1976).
29. S. J. CYVIN, G. NEERLAND, J. BRUNVOLL, and N. B. CYVIN. Spectrosc. Lett. **14**, 37 (1981).
30. W. R. WOOLFENDEN and D. M. GRANT. J. Am. Chem. Soc. **88**, 1496 (1966).
31. Sadtler standard carbon-13 nmr spectra. Sadtler Research Laboratories, Inc., Philadelphia.
32. J. B. STOTHERS. Carbon-13 nmr spectroscopy. Academic Press, New York, NY. 1972.
33. T. W. PROULX and W. B. SMITH. J. Magn. Reson. **23**, 447 (1976).
34. T. D. ALGER, D. M. GRANT, and E. G. PAUL. J. Am. Chem. Soc. **88**, 5397 (1966).
35. R. J. PUGMIRE, D. M. GRANT, M. J. ROBINS, and R. K. ROBINS. J. Am. Chem. Soc. **91**, 6381 (1969).
36. D. DODDRELL and P. R. WELLS. J. Chem. Soc. Perkin Trans. 2, 1333 (1973).
37. A. J. JONES, T. D. ALGER, D. M. GRANT, and W. M. LITCHMANN. J. Am. Chem. Soc. **92**, 2386 (1970).
38. R. S. OZUBKO, G. W. BUCHANAN, and I. C. P. SMITH. Can. J. Chem. **52**, 2493 (1974).
39. A. J. JONES and D. M. GRANT. Chem. Commun. 1670 (1968).
40. C. J. FINDER, M. G. NEWTON, and N. L. ALLINGER. Acta Crystallogr. Sect. B, **30**, 411 (1974); A. KOEKSTRA, P. MEERTENS, and A. VOS. Acta Crystallogr. Sect. B, **31**, 2813 (1975).
41. M. TRAETTEBERG, E. B. FRANTSEN, F. C. MIJHOFF, and A. KOEKSTRA. J. Mol. Struct. **26**, 57 (1975).
42. H. KOLLMAR. J. Am. Chem. Soc. **101**, 4832 (1979); J. P. DAUDEY, G. TRINQUIER, J. C. BARTHELAT, and J. P. MALRIEU. Tetrahedron, **36**, 3399 (1980).
43. M. TRAETTEBERG and E. B. FRANTSEN. J. Mol. Struct. **26**, 69 (1975).
44. O. BASTIANSEN and M. TRAETTEBERG. Tetrahedron, **17**, 147 (1962).
45. A. ALMENNINGEN and O. BASTIANSEN. Skr. K. Nor. Vidensk. Selsk. **4**, 1 (1958).
46. P. R. PINNOCK, C. A. TAYLOR, and H. LIPSON. Acta Crystallogr. **9**, 173 (1956); F. R. AHMED and J. TROTTER. Acta Crystallogr. **16**, 503 (1963).
47. J. B. STOTHERS, C. T. TAN, and N. K. WILSON. Org. Magn. Reson. **9**, 408 (1977).
48. R. MUNDAY and I. O. SUTHERLAND. J. Chem. Soc. B, 80 (1968).
49. H. L. FINKE, J. F. MESSERLY, S. H. LEE, A. G. OSBORN, and D. R. DOUSLIN. J. Chem. Thermodyn. **9**, 937 (1977).
50. W. D. GOOD. J. Chem. Thermodyn. **5**, 715 (1973).
51. P. HOEHENBERG and W. KOHN. Phys. Rev. Sect. B, **136**B, 864 (1964).
52. B. I. DUNLAP, J. W. D. CONNOLLY, and J. R. SABIN. J. Chem. Phys., **71**, 4993 (1979); H. SAMBE and R. H. FELTON. J. Chem. Phys. **62**, 1122 (1975).
53. S. HUZINAGA. J. Chem. Phys. **42**, 1293 (1965).
54. T. H. DUNNING. J. Chem. Phys. **55**, 716 (1970).
55. F. HERMAN and S. SKILLMAN. Atomic structure calculations. Prentice–Hall, Englewood Cliffs, NJ. 1963.
56. A. H. STROUD. Approximate calculation of multiple integrals. Prentice–Hall, Englewood Cliffs, NJ. 1971.
57. J. C. SLATER. The self consistent field for molecules and solids. McGraw–Hill, New York, NY. 1974; K. H. JOHNSON. Adv. Quantum Chem. **7**, 143 (1973).
58. G. CARDINAL, N. A. BAYKARA, and S. FLISZÁR. To be published.
59. K. SCHWARZ. Phys. Rev. B, **5**, 2466 (1972).
60. W. J. HEHRE, R. F. STEWART, and J. A. POPLE. J. Chem. Phys. **51**, 2657 (1969).
61. R. S. MULLIKEN. J. Chem. Phys. **23**, 1833 (1955); **23**, 1841 (1955); **23**, 2338 (1955); **23**, 2343 (1955).
62. K. TAMAGAWA, T. IIJMA, and M. KIMURA. J. Mol. Struct. **30**, 243 (1976).
63. S. N. KETKAR and M. FINKI. J. Mol. Struct. **77**, 139 (1981).
64. A. ALMENNINGEN, O. BASTIANSEN, and F. DYVIK. Acta Crystallogr. **14**, 1056 (1961).
65. M. I. KAY, Y. OKAYA, and D. E. COX. Acta Crystallogr. Sect B, **27**, 26 (1971).
66. M. SAID, D. MAYNAU, J.-P. MALRIEU, and M.-A. GARCIA BACH. J. Am. Chem. Soc. **106**, 571 (1984).

Appendix I

The $\partial E/\partial N$ derivatives were obtained from LCAO-Xα calculations by means of the programs developed by Dunlap *et al.* (52). Huzinaga's (9*s*5*p*) basis (53) was used for ground-state carbon. Hydrogen was described by a (5*s*) basis obtained from Dunning's (3*s*) basis set (54). In the LCAO-Xα method it is necessary to fit the charge density and the exchange potentials to sets of auxiliary Hermite gaussian functions. The Xα exchange potentials were fitted to the auxiliary functions following the criterion given by Dunlap *et al.* (52), i.e.,

$$\int \rho(\widetilde{\rho^{1/3}})\,d\tau = \int (\widetilde{\rho^{1/3}})^4\,d\tau$$

TABLE A1. $(\partial E/\partial N)_\pi$ and $(\partial E/\partial N)_\sigma$ values (au) for use in eq. [4][a]

Molecule	Orbital	$(\partial E/\partial N)$, au		
		α_{HF}	$\alpha_{expt.}$	Selected
Benzene	π	−0.259	−0.264	−0.262
	σ	−0.372	−0.379	−0.375
Ethylene	π	−0.244	−0.248	−0.246
	σ	−0.373	−0.378	−0.375

[a]Additional results are reported in refs. 1 and 2.

where the tilde represents a fitted quantity. The sampling points for the exchange potentials were determined by taking each tenth point of the Herman–Skillman radial mesh (55) and an angular mesh consisting of the twelve vertices of a regular icosahedron (56). The auxiliary functions were selected as suggested by Dunlap *et al.* (52) for first-row diatomics: *s*-type functions were employed for the charge density fit, having orbital exponents twice those of the corresponding *s*-type gaussians used for the orbital basis. Five orbital exponents (5.0, 2.0, 0.6, 0.3, 0.1) were used for *p*-type functions. The exponents of every other *p* function used in the orbital basis were doubled to construct *d*-type Hermite gaussians for fitting the Coulomb potential. Bond-centered auxiliary *s* functions were also used, as suggested by Dunlap *et al.* (52). For the fit to the exchange potential, orbital exponents were taken at one-third of those of the corresponding charge density auxiliaries.

In LCAO-Xα calculations of heteronuclear systems one meets with the problem of choosing a single α value for the whole system because, contrasting with the Scattered Wave Method (57), the possibility of assigning different α values to different regions of space no longer exists. The general attitude has been to use the Kohn–Sham value of 2/3 or 0.7 in such situations. For a significant collection of organic molecules, on the other hand, we have found (58) that experimental atomization energies are well reproduced with an α value taken as an average of α_{ij}'s defined for the individual bonds, i.e.,

$$\alpha_{ij} = 1/2\,(\alpha_A + \alpha_B)$$

where (i, j) is a bond between centres A and B. The individual α_A's can be chosen following Schwarz (59), from a fit with Hartree–Fock values, or, else, from a fit with experimental energies of ground-state atoms (58). Selection of the latter α_A's yields atomization energies that are closer to their experimental counterparts (within a few kcal mol^{-1}) than the corresponding results deduced from the α_{HF} values given by Schwarz (59). The results are indicated in Table A1. The last column reports the $(\partial E/\partial N)$ values used in applications of eq. [4].

Appendix II

STO-3G charge analyses, following Pople's recipe (60) and Mulliken's scheme (61), are reported in Table A2, as well as the pertinent ^{13}C nmr shifts. Taking the σ–π separation, $\Delta q = \Delta q^\sigma + \Delta q^\pi$, into account as well as the relationships $\Delta q^\sigma = m\Delta q^\pi$, $\delta = c^\sigma \Delta q^\sigma + c^\pi \Delta q^\pi$ and $(d\delta/dq^\pi) = 157$ ppm/e (2, 12), we deduce $\delta = 0.835\,\Delta q + 178.66$ (ppm from TMS) and, hence, $\Delta q = 1.2\,\delta$ and $m = -0.812$. These results are admittedly crude. Extensive numerical analyses, however, such as those reported in Table 4, gave no reason for revision.

Mulliken's analysis involves a half-and-half partitioning of overlap populations. While charges of like C atoms (i.e., atoms forming the same type and number of bonds) are valid in comparisons involving them, lifting the constraint of halving overlap terms between dissimilar atoms becomes a must in realistic evaluations of absolute atomic charges (1, 2, 15). For benzene, we are presently unable to lift this constraint: hence the following approaches toward an estimate for the carbon net charge of benzene.

TABLE A2. Atomic charges (me) and ^{13}C nmr shifts (ppm from TMS) of selected benzenoid hydrocarbons[a]

Molecule	Atom	Net charge	δ
Benzene		−60.1	128.5
Naphthalene	C—1	−60.1	128.3
	C—2	−62.9	126.1
Anthracene	C—1	−57.9	130.3
	C—2	−62.6	125.7
	C—9	−56.0	132.8
Phenanthrene	C—1	−59.1	129.1
	C—2	−63.0	126.9
	C—3	−62.2	126.9
	C—4	−63.1	123.2
	C—9	−62.6	127.5

[a]Geometries were taken from electron diffraction studies of benzene (62), naphthalene (63), and anthracene (64) and from a neutron diffraction study of phenanthrene (65). The shift vs. charge correlation is generally acceptable. Atom C-4 of phenanthrene exhibits the largest deviation. The difference between calculated and experimental energies of phenanthrene is 0.76, using the shift value, and −0.34 kcal mol^{-1} using the charge result, while the reported experimental uncertainty is ±1.1 kcal mol^{-1}, a situation frustrating dedication to accuracy.

(*i*) The ^{13}C nmr shift of the methyl carbon in toluene, δ 21.3 ppm from TMS (32), gives $q_C = 32.77$ me, from eq. [7]. Using the correlation between methyl-C and methyl-H net charges (2), the latter are estimated at −12.38 me in toluene. The toluene CH_3 group is, in this approximation, 4.37 me negative. On the other hand, H replacing CH_3 (under otherwise identical conditions) is 9.05 me more negative than the latter (2). In this estimate, the benzene hydrogen should be negative by 13.4 me and, hence, $q_C(C_6H_6) \simeq 13.4$ me. This, of course, is a rough estimate. Now we look at an entirely different approach.

(*ii*) Applying eq. [2] to the benzene CH bond with ϵ^0_{11}, a_5, a_7, and $q^B_C = -q^B_H$ gives $\epsilon_{CH} = 107.29 + 0.422\,q^B_C$ kcal mol^{-1}, where the benzene carbon net charge, q^B_C, is now left as an unknown. Six of these CH bonds plus six CC bonds add up to give $\Delta E^*_a = 1366.5$ kcal mol^{-1}. Estimates of the CC bond energy based on SCF potentials at the nuclei (1–3) indicate that ϵ_{CC} is 1.62–1.65 times the CC bond energy of ethane, $\epsilon^0_1 = 69.633$ kcal mol^{-1}. With the ratio 1.62 there results $q^B_C = 18.1$ me; for 1.65 it is $q^B_C = 13.2$ me. Extensive numerical analyses involving all the experimental data included in Table 5 suggest that the ratio ~1.64 (giving ϵ_4) with $q^B_C = 14.8$ me represents a valid estimate. In this analysis, the uncertainty about q^B_C is unlikely to exceed 2 me. Finally, current work on graphite (to be published) shows that the uncertainty about $q^B_C = 14.8$ me is probably less than 1 me.

Appendix III

Approximate but valid estimates of eq. [6] can be obtained in a simple way. They are rooted in the following hypotheses (13). For CC and CH bonds involving sp^3 carbons, $\langle r^{-1}_{ij} \rangle$ is

adequately approximated by the inverse of the appropriate internuclear distance (1), a simplifying hypothesis that locates the centers of σ charges at their respective nuclear positions. Similarly, the charge centroids of aromatic carbons are taken at their nuclear positions. The situation differs with ethylenic sp^2 carbons because their overlapping $2p$ electrons forming a π bond shift their respective charge centroids inwards (4, 5, 13, 14). A simple recipe for single bonds formed by an ethylenic carbon j is as follows. (*i*) The centroid of the $(N_j - 1)$ σ electrons of ethylene (taken as reference) is located at its nuclear position. (*ii*) The "effective" distance of a bonded nucleus i (C or H) from the $2p$ electron of j is 0.02 Å larger than R_{ij}. (*iii*) Our estimate of the average inverse distance between the N_j electrons of the sp^2 carbon and nucleus i is thus

$$\langle r_{ij}^{-1}\rangle \simeq 0.529\,[(N_j - 1)R_{ij}^{-1} + (R_{ij} + 0.02)^{-1}]/N_j \text{ au}$$

ready for use in eq. [6]. This recipe, offered as a convenient replacement for equivalent but involved SCF analyses[7] of charge centroids (13), has proven accurate. Indeed, for a collection of ~50 olefins calculated in this approximation, the average deviation between theoretical and experimental atomization energies is ~0.25 kcal mol^{-1} (4, 5). Note that these considerations do not concern the benzenoid structures themselves, but only the ethylenic parts in molecules like styrene, stilbene, etc., reported here for the sake of completeness.

The numerical examples worked out below illustrate the use of eqs. [2] and [6] in the derivation of suitable reference bond energies, ϵ_{ij}^0. The conversion factors 1 bohr = 0.529 Å and 1 hartree = 627.51 kcal mol^{-1} were used. All a_{ij}'s are expressed in kcal mol^{-1} me^{-1} units and the energies in kcal mol^{-1}. The numbering of the a_{ij} and ϵ_{ij}^0 parameters is that indicated in Tables 1 and 2. The reference carbon net charges are (in 10^{-3} e units) 35.1 (C_2H_6), 7.7 (C_2H_4) and 14.8 (C_6H_6).

Example 1. Let us first apply the recipe given for $\langle r_{ij}^{-1}\rangle$ when j is an ethylenic C atom, with $N_i = 3.9923$ e. For a C_i—C_i single bond ($R = R^0 = 1.53$ Å) we find $\langle r_{ij}^{-1}\rangle = 0.34463$ au and $F = -4.80$ kcal mol^{-1}. For a CH bond ($R = R^0 = 1.08$ A) we find $\langle r_{ij}^{-1}\rangle = 0.48758$ au and $F = -2.39$ kcal mol^{-1}. These F values are incorporated in the new ϵ_{ij}^0's describing CC and CH bonds formed by ethylenic sp^2 carbons, as shown below.

Example 2. Starting with the ethane CC bond, ϵ_1^0, we construct the $C_j(sp^2)$—$C_i(sp^3)$ bond, ϵ_{10}, with $R_{CC} = 1.53$ Å, $q_j = 7.7$, and $q_i = 35.1$ me. The change from 35.1 to 7.7 me (using the average of $a_2 = -0.488$ and $\alpha_6 = -0.450$) modifies ϵ_1^0 to give $\epsilon_{CC} = 82.49$; adding $F = -4.80$, one obtains 77.7 for ϵ_{10}. Similarly, starting now with the ethane CH bond, ϵ_5, the change from 35.1 to 7.7 me at the C atom (using the average of $a_4 = -0.247$ and $a_7 = -0.210$ in eq. [2] leads to $\epsilon_{CH} = 113.07$; with $F = -2.39$, it follows that $\epsilon_{12} = 110.68$ for the $C(sp^2)$—H reference bond (13).

Example 3. For aromatic carbons, we keep the centers of charge as in the bond described above, $\epsilon_{CC} = 82.49$, hence $F = 0$. To obtain ϵ_7, we start with this result and modify the charge from 7.7 to 14.8 me, using $a_6 = -0.450$. Thus, $\epsilon_7 = 82.49 - 0.450\,(14.8–7.7) = 79.30$. Similarly, the 113.07 result quoted above leads to $\epsilon_{11} = 113.07 - 0.210\,(14.8–7.7) = 111.58$.

[7]Theoretical analyses, at the 4-31G level including polarization functions, account for over 80% of the results anticipated from empirical evaluations (13). Our recipe is, in principle, at the level of experimental accuracy.

Example 4. ϵ_7 was obtained from ϵ_1 by replacing one CH_3 of ethane by phenyl. The nonconjugated central bond of biphenyl is deduced from $2(\epsilon_7 - \epsilon_1) + \epsilon_1$ and $F = -0.29$, which reduces R from 1.53 to 1.49 Å with $q_C = 14.8$ me. The reference ϵ_8 (for a CC single bond, as in *cis*-stilbene) is deduced from ϵ_7 (R = 1.53 Å), which is reduced to 1.49 Å with $F = -5.40$. Using the average of a_2 and $a_{CC}^\sigma = -0.460$ (for 1.53 and 1.49 Å, respectively) for evaluating the change from 35.1 to 7.7 me at the sp^2 carbon, we find $\epsilon_8 = 79.30 - 5.40 + 12.99 = 86.89$.

Example 5. Here we begin with $\epsilon_3 = 89.70$ (a conjugated CC single bond formed by sp^2 carbons, as in 1,3-butadiene) (5) at its equilibrium distance, ~1.48 Å, and construct a C(Ar)—C(Ar) single bond modelled on benzene, with $R = 1.397$ Å. For $q_i = q_j = 7.7$ me, $F = 9.90$. Setting the charges at 14.8 me, using $a_{CC}^\sigma = -0.486$, reduces ϵ_{CC} by 6.90. The final result, 92.70, is in moderate agreement with its counterpart, 91.56, obtained from a numerical analysis of experimental data. Contrasting with the previous examples, this case illustrates a limitation of our simple evaluation of $\langle r_{ij}^{-1}\rangle$ for use in eq. [6].

Example 6. Taking now the above CC single bond, $\epsilon_6 = 91.56$, as input, we construct a CC single bond, $R = 1.445$ Å (66), like that found in styrene. The change from 1.397 to 1.445 Å translates into $F = -4.98$ with $q_i = q_j = 14.8$ me. Modification of the charge from 14.8 to 7.7 me at the ethylenic carbon, with $a_{CC}^\sigma = -0.472$, increases ϵ_{CC} by 3.35, thus giving $\epsilon = 89.93$. Similarly, for 1.48 Å (17) we find $\epsilon_9 = 90.40$ describing the C(Ar)—C(sp^2) reference bond, as in *trans*-stilbene.

Appendix IV

For an aromatic carbon linked to a non-aromatic carbon, $\Sigma_j a_{ij}$ is $2a_{CC}^{\sigma,\pi}(\text{Ar}) + a_{CC}^{\sigma,\pi}(\text{nAr})$, where $a_{CC}^{\sigma,\pi}(\text{Ar})$ is for the benzenic bond and $a_{CC}^{\sigma,\pi}(\text{nAr})$ for the bond formed with a non-aromatic carbon. The change in charge at the aromatic carbon is Δq_C (relative to benzene), contributing $\Delta q_C \Sigma_j a_{ij}$ to ΔE_a^*. On the other hand, this Δq_C is also part of Σq_C, hence, of $\Sigma \Delta q_H$, contributing $-\Delta q_C a_{HC}$. The total contribution of Δq_C is thus

$$[2a_{CC}^{\sigma,\pi}(\text{Ar}) + a_{CC}^{\sigma,\pi}(\text{nAr}) - a_{HC}]\Delta q_C$$

Of course, in this calculation, Δq_C must *not* be included in the evaluation of $\Sigma \Delta q_H$. Using eq. [5], as well as $\Delta q_C = (m + 1) \times \Delta q^\pi$ and $\delta = 157\ \Delta q^\pi$ (Appendix II), we find that the energy contributed by Δq_C is, in au,

$$m[2a_{CC}^{\sigma}(\text{Ar}) + a_{CC}^{\sigma}(\text{nAr}) - a_{HC}]\left(\frac{\delta}{157}\right) + [2a_{CC}^{\pi}(\text{Ar}) + a_{CC}^{\pi}(\text{nAr}) - a_{HC}]\left(\frac{\delta}{157}\right)$$

where δ is the ^{13}C shift relative to benzene. Inserting the appropriate a_{ij}'s (in au) gives the energy contributed by Δq_C, i.e., in kcal mol^{-1},

$$-(1.2562m + 1.1432)\left(\frac{627.51}{157}\right)\delta = -0.052\,\delta$$

for $m = -0.8997$. It is clear that the final result depends heavily on m, beyond the precision permitted by present SCF charge analyses. Inspection of molecules corresponding to this situation has consistently led to the −0.052 parameter. The corresponding m value, ~−0.90, seems intuitively reasonable when compared to −0.955 for ethylenic carbons (4) and to −0.812 for a benzenic carbon not engaged in a bond with a non-aromatic carbon.

The influence of ionic strength on the adsorption of azide ions on mercury electrodes

ARTUR J. MOTHEO, ERNESTO R. GONZALEZ,[1] AND LUIS A. AVACA
Instituto de Física e Química de São Carlos, Universidade de São Paulo, C.P. 369, São Carlos, SP, 13560 Brasil
Received April 1, 1985

ARTUR J. MOTHEO, ERNESTO R. GONZALEZ, and LUIS A. AVACA. Can. J. Chem. **64**, 413 (1986).

The adsorption of azide ions on mercury electrodes has been studied from constant ionic strength solutions of composition χ *M* NaN_3 + ($\mu - \chi$) *M* NaF with $\mu = 0.25$ and 0.5. Double layer parameters were obtained by taking into account the change in activity coefficients with solution composition. The results were analyzed together with those reported previously for $\mu = 0.95$, recalculated to take into account the change in activity coefficients. The influence of the ionic strength on the amount adsorbed, the properties of the inner layer, and the parameters of an adsorption isotherm for azide anions are discussed in terms of the electrostatic model of the double layer.

ARTUR J. MOTHEO, ERNESTO R. GONZALEZ et LUIS A. AVACA. Can. J. Chem. **64**, 413 (1986).

Opérant sur des solutions de force ionique constante et de composition χ *M* en NaN_3 + ($\mu - \chi$) *M* en NaF, avec $\mu = 0{,}25$ et 0,5, on a étudié l'adsorption des ions azotures sur des électrodes de mercure. On a obtenu les paramètres de double couche en tenant compte du changement des coefficients d'activité avec la composition des solutions. On a analysé ces résultats ainsi que ceux rapportés antérieurement pour $\mu = 0{,}95$ et recalculés pour tenir compte du changement dans les coefficients d'activité. On discute de l'influence de la force ionique sur la quantité de substance adsorbée, sur les propriétés de la couche interne et sur les paramètres de l'isotherme d'adsorption des ions azotures en fonction du modèle électrostatique de la double couche.
[Traduit par le journal]

Introduction

Because of its many advantages, most recent studies of adsorption of anions on mercury have been carried out in constant ionic strength solutions. A comparison with studies of the same anion in single salt solutions often showed differences in the amount adsorbed and, in some cases, in the double layer properties. Ions for which the adsorption is so strong that the adsorbed charge numerically exceeds the electrode charge, show higher specific adsorption in constant ionic strength solutions. Fawcett and McCarrick (1) showed this to be the case for iodide. More recently, the same situation was found in a study of thiocyanate adsorption at two different ionic strengths (2). A different behavior was found for ions that adsorb moderately. By comparing their results with a previous study by Payne (3), Fawcett and Sellan (4) concluded that for nitrate the adsorption increased with ionic strength at high concentrations of NO_3^- while the opposite situation was observed for low concentrations of NO_3^-.

In relation to the inner layer properties in constant ionic strength and single salt solutions, no differences were found for azide (5), and small ones for iodide (6), while widely differing behaviors were observed for chloride (7) and bromide (8). These results point to the necessity of detailed studies of the effect of the ionic strength on the double layer properties.

In a previous study on the adsorption of azide on mercury (5) at a constant ionic strength (μ) equal to 0.95, a comparison was made with the results in single salt solutions (9). This showed that the amount of N_3^- anions adsorbed depends on the ionic strength of the solution, but in both cases the same adsorption isotherm applies. Moreover, as mentioned above, the inner layer in single salt and mixed solutions seems to have the same characteristics. This is not a general case, so it is of interest to study the effect of the ionic strength on the adsorption of N_3^- in order to better understand the properties of the interface in the presence of this anion.

In the present work, the double layer properties of the system NaN_3 + NaF on mercury were studied at $\mu = 0.5$ and 0.25 and the results examined together with those obtained previously (5) for $\mu = 0.95$. In this work, the change of activity coefficients of the electrolytes with solution composition was taken into account so the double layer parameters for $\mu = 0.95$ were recalculated accordingly.

Experimental

Experimental details of the purification of reagents, electrochemical techniques for recording capacity–potential curves, and potentials of zero charge were given previously (5). Activity coefficients for NaN_3 were calculated as described below, from data obtained using the cell

[1] Na electrode/χ *M* NaCl + ($\mu - \chi$) *M* NaN_3/AgCl/Ag

The emf measurements were carried out with a Corning Electrometer 101, employing a Corning n° 476 210 electrode and an Ag/AgCl electrode prepared according to recommendations (10). All measurements were done at 25 ± 0.1°C.

Results and discussion

Capacity–potential curves

Figure 1 shows the capacity–potential curves for the system χ *M* NaN_3 + (0.25 − χ) *M* NaF. A similar set of curves was obtained for $\mu = 0.50$. The general features are the same as those observed previously (5) for $\mu = 0.95$ and resemble those of other halides and pseudo-halides (2, 7, 8). These systems differ from most oxyanions in the sense that no pronounced minimum is observed on the anodic side of the potential of zero charge (E_z). The base solution curve (μ *M* NaF) was integrated twice in the cathodic direction using the experimental value of E_z and taking for the surface tension at the potential of zero charge a reference value $\gamma_z^b = 0$ as integration constants. By back integration from $E = -1.65$ V of the remaining curves in each set, taking into account the influence of the variation of activity coefficients on the potential (see discussion in the next section), the values of $\Delta\gamma_z = \gamma_z^b - \gamma_z$ presented in Table 1 were obtained. A comparison of the values of $\Delta\gamma_z$ with those obtained for $\mu = 0.95$ (5) shows that this parameter has some dependence on the ionic strength only at high azide concentrations.

Change in activity coefficients with solution composition

As it was pointed out previously (1), in some constant ionic strength systems it becomes important to take into account the changes in activity coefficients with solution composition.

[1]Author to whom correspondence should be addressed.

Printed in Canada / Imprimé au Canada

TABLE 1. Coordinates of the point of zero charge for mercury electrodes in aqueous χ *M* NaN_3 + ($\mu - \chi$) *M* NaF at 25°C, for μ equal to 0.25 and 0.5 *M*

	$\mu = 0.25$			$\mu = 0.5$		
χ	E_z (*V* vs. SCE)*	C_z (μF cm^{-2})	$\Delta\gamma_z$ (mN m^{-1})	E_z (*V* vs. SCE)*	C_z (μF cm^{-2})	$\Delta\gamma_z$ (mN m^{-1})
0	−0.4339	23.65	0.0	−0.4340	24.95	0.0
0.001	−0.4393	25.03	0.0	−0.4392	26.00	0.0
0.0025	−0.4420	26.50	0.1	−0.4419	27.43	0.1
0.005	−0.4468	28.13	0.3	−0.4469	29.19	0.3
0.0075	−0.4518	29.69	0.4	−0.4517	30.28	0.4
0.01	−0.4560	30.42	0.5	−0.4560	30.80	0.5
0.015	−0.4625	30.74	0.7	−0.4625	32.35	0.7
0.025	−0.4720	33.07	1.0	−0.4719	33.70	1.1
0.05	−0.4871	35.26	1.6	−0.4870	35.65	1.8
0.1	−0.5048	36.85	2.4	−0.5057	37.05	2.7
0.25	−0.5262	38.24	3.9	−0.5308	38.30	4.5
0.5	—	—	—	−0.5489	38.97	6.0

*Voltage vs. standard calomel electrode.

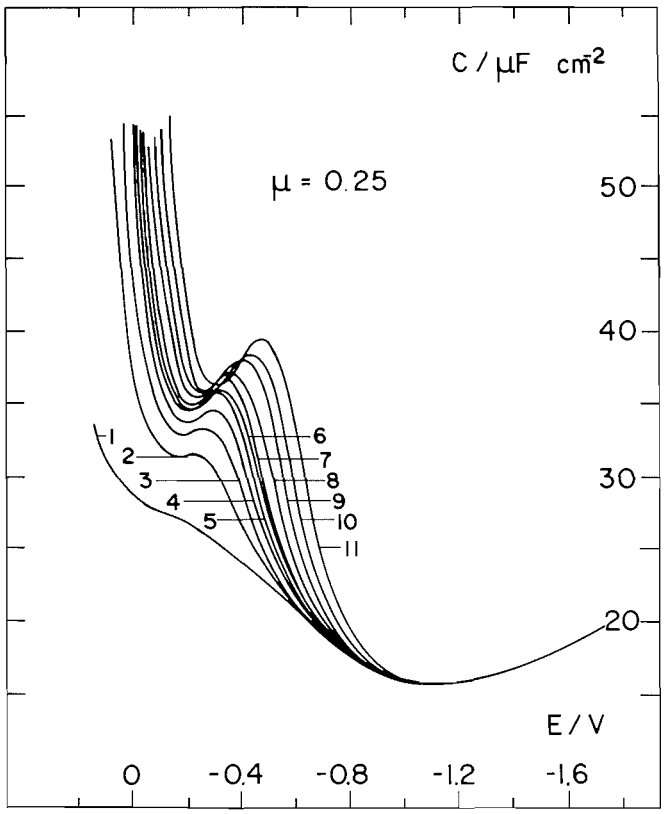

FIG. 1. Differential capacity of the double layer for a mercury electrode in aqueous χ *M* NaN_3 + (0.25 − χ) *M* NaF. χ = 0.0 (1), 0.001 (2), 0.0025 (3), 0.005 (4), 0.0075 (5), 0.01 (6), 0.015 (7), 0.025 (8), 0.05 (9), 0.1 (10), 0.25 (11).

As will be seen later, these affect the calculation of double layer parameters, in particular the specifically adsorbed charge determined by differentiation. Fawcett and McCarrick (1) took this into consideration for a system of two salts with a common cation, RA and RB, and at constant ionic strength, by introducing a parameter β defined as $\beta = d \ln \gamma_R/dx$, where γ_R is the activity coefficient of the cation and $x = C_{RA}/(C_{RA} + C_{RB})$. For such a system it is possible to write (11)

$$[2] \quad \frac{d \ln \gamma_{RA}}{dx} = \frac{1}{2}\left[\ln (\gamma^0_{RA})_\mu - \ln (\gamma^0_{RB})_\mu\right]$$

where γ_{RA} is the mean activity coefficient of the salt RA in the mixture, while the γ^0s are the corresponding values in single salt solutions at the same ionic strength of the mixture. This equation is derived from treatments based on a modified Debye–Hückel equation and does not take into account size effects (12).

For the system described, the activity coefficients of the anions γ_A and γ_B may be assumed to be independent of solution composition (12), so from eq. [2], the parameter β can be defined as

$$[3] \quad \beta = \frac{d \ln \gamma_R}{dx} = \ln (\gamma^0_{RA})_\mu - \ln (\gamma^0_{RB})_\mu$$

Thus, for NaN_3–NaF mixtures a β_1 will be introduced as:

$$[4] \quad \beta_1 = \ln \frac{(\gamma^0_{NaN_3})_\mu}{(\gamma^0_{NaF})_\mu}$$

Values of γ^0_{NaF} are available in the literature, but not those for $\gamma^0_{NaN_3}$. Attempts to measure these with a $Ag/AgN_3/N_3^-$ electrode were unsuccessful because of instability of the electrode. The alternative procedure of measuring β_1 directly using the cell

[5] Na electrode/χ *M* NaN_3 + ($\mu - \chi$) *M* NaF/F electrode

as described previously (1) also failed because the fluoride electrode was unstable in these solutions. The final procedure adopted here was to obtain the necessary values of $\gamma^0_{NaN_3}$ to be used in eq. [4] by the experimental determination of a β_2 defined as

$$[6] \quad \beta_2 = \ln \frac{(\gamma^0_{NaCl})_\mu}{(\gamma^0_{NaN_3})_\mu}$$

and corresponding to the mixtures NaCl–NaN_3 used in the cell described in the experimental section (eq. [1]). The Nernst equation for that cell is

$$[7] \quad \epsilon + \frac{RT}{F} \ln C_{Na} C_{Cl} = \epsilon_0 - \frac{RT}{F} \ln \gamma_{Na} \gamma_{Cl}$$

where ϵ_0 is the standard emf. Considering that at constant ionic strength γ_{Cl} is independent of composition (12), it follows that

$$[8] \quad \beta_2 = \frac{d \ln \gamma_{Na}}{dx} = -\frac{F}{RT}\frac{d}{dx}\left(\epsilon + \frac{RT}{F}\ln C_{Na}C_{Cl}\right)$$

The resulting values of β_2, together with the corresponding errors, were the following: -0.012 ± 0.003 for $\mu = 0.25$; -0.034 ± 0.006 for $\mu = 0.5$; and -0.0763 ± 0.0004 for $\mu = 0.95$. Introducing these values of β_2 and those of $(\gamma^0_{NaCl})_\mu$ from the literature (13) into eq. [6], the values of $\gamma^0_{NaN_3}$ were found to be 0.730, 0.705, and 0.709 for the ionic strengths 0.25, 0.5, and 0.95, respectively. It must be pointed out that owing to the form of eq. [6] the errors in β_2 represent at most a 1% uncertainty in the values of $\gamma^0_{NaN_3}$. Using those results in eq. [4] together with those of $(\gamma^0_{NaF})_\mu$ (13), the values of β_1 for the NaN_3–NaF mixtures were calculated as being 0.056, 0.109, and 0.208 for the ionic strengths 0.25, 0.5, and 0.95, respectively.

It is of interest to note that the values of $\gamma^0_{NaN_3}$ are very similar to those of γ^0_{NaSCN} (13). This justifies the approximation made by D'Alkaine *et al.* (9) in using values of γ^0_{NaSCN} in the work with NaN_3 in single salt solutions.

The adsorbed charge

Using the values presented in Table 1, capacity–potential curves were integrated twice to obtain the electrode charge density (q) and the surface tension (γ) as a function of potential, for each value of χ in each set. From these, Parsons' function $\xi_+ = qE_+ + \gamma$ was obtained. For this purpose, the experimental potential scale (E_R) was converted to a thermodynamic scale using the expression

$$[9] \quad dE_+ = dE_R - (\beta/f)\,dx$$

where $f = F/RT$. Values of the specifically adsorbed charge (q') due to N_3^- anions were then obtained at constant electrode charge from the expression

$$[10] \quad \frac{f}{1+\beta x}\left(\frac{\partial \xi_+}{\partial \ln \chi}\right)_q = q' + q^d_-\left(\frac{\beta x}{1+\beta x}\right)$$

where q^d_- is the anionic charge in the diffuse layer. In order to apply this equation, q^d_- was taken at first as being equal to $(RT\epsilon\mu/2\pi)^{1/2}$ and a value of q' calculated. By using diffuse layer theory, a new value of q^d_- was obtained. The procedure was then applied in an iterative way until the difference between two successive values of q' was less than 0.01 $\mu C\ cm^{-2}$. This calculation of q' was also applied to the experimental results obtained previously (5) for $\mu = 0.95$ because in that work the change of activity coefficients with solution composition was not taken into account. All the calculations described above were carried out with the use of computer programs.

If the influence of the change in activity coefficients is disregarded, values of q' are given by the simpler expression $q' = f(\partial \xi_+/\partial \ln \chi)_q$. A comparison with the more correct values obtained from eq. [10] shows that the correction is negligible for $\mu = 0.25$. For $\mu = 0.5$ and 0.95 differences are larger but they become significant only for the two highest values of χ.

For $\mu = 0.5$ and 0.25 the dependence of q' on q resembles that presented previously (5) for $\mu = 0.95$. The effect of the ionic strength on the adsorbed charge can be seen in Fig. 2 where the q' vs. q curves for three concentrations of N_3^- in the bulk are presented for each value of μ. For $\chi = 0.25$, it can be observed that q' increases with μ. This is because in this situation $|q'| > q$ and the potential at the outer Helmholtz plane

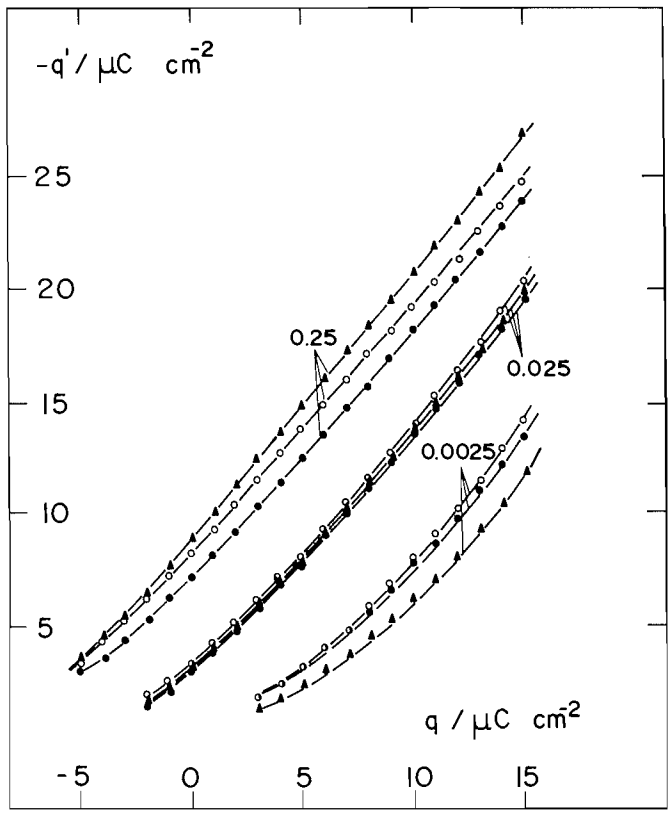

FIG. 2. Specifically adsorbed charge due to N_3^- anions on mercury for the ionic strengths 0.25 (●), 0.5 (○), and 0.95 (▲). Figures on the lines indicate the values of χ.

(oHp) ϕ_2 is negative. An increase of the ionic concentration in the diffuse layer makes ϕ_2 less negative, allowing larger values of q' to be attained. For $\chi = 0.0025$ the values for $\mu = 0.25$ and 0.5 are very close to each other and may be considered equal within experimental error. But those for $\mu = 0.95$ lie well below, indicating that for this value of χ the situation is reversed with respect to that for $\chi = 0.25$. Here, $|q'| < q$ and ϕ_2 is positive. An increase in the ionic concentration makes ϕ_2 less positive so q' decreases. An intermediate situation is observed for $\chi = 0.025$. This set of curves suggests that at some lower value of χ, for which ϕ_2 will approach a zero value, q' for a given concentration of NaN_3 will be independent of μ. The analysis done here in terms of electrostatic principles is quite straightforward; it has already been discussed in connection with the adsorption of SCN^- (2) and NO_3^- (4) but no results as illustrative as those in Fig. 2 were presented.

The inner layer properties

As usual, the properties of the inner layer will be analyzed in terms of plots of the potential drop across the inner layer (ϕ_{m-2}), obtained by subtracting the potential ϕ_2 of the oHp from the electrode potential, as a function of the adsorbed charge at constant q (Christie plots). Figure 3 shows the combined Christie plots for the three ionic strengths analyzed. The relevant region for the present system is that for $q > 0$, $|q'| > q$ and it is obvious that here the plots are independent of μ. This is in accordance with the fact that a previous comparison of the results for $\mu = 0.95$ (5) and single salt solutions (9) showed that the inner layer properties were the same in both systems. The slope of the plots seems to depend on μ when $q < 0$ and when $q > 0$ and $|q'| < q$. However, the reduced number of points and the larger errors

associated with low values of q' preclude the possibility of reaching definite conclusions. According to the classical model of the double layer, ϕ_{m-2} can be written

$$[11] \quad \phi_{m-2} = \frac{q}{K_{m2}} + \frac{q'}{K_{12}}$$

where K_{m2} is the integral capacity of the inner layer and K_{12} that between the inner Helmholtz plane (iHp) and the oHp. The slope of the Christie plots is then given by

$$[12] \quad \left(\frac{\partial\phi_{m-2}}{\partial q'}\right)_q = q\left(\frac{\partial 1/K_{m2}}{\partial q'}\right)_q + \frac{1}{K_{12}} + q'\left(\frac{\partial 1/K_{12}}{\partial q'}\right)_q$$

In the region where $q > 0$ and $|q'| > q$ the plots are linear and almost parallel, so that the two derivatives on the right-hand side of eq. [12] are zero and the slope is simply $1/K_{12}$. It must then be concluded that in this region K_{12} is independent of the ionic strength. This integral capacity can be written

$$[13] \quad K_{12} = \frac{\epsilon}{4\pi(x_2 - x_1)}$$

where ϵ is the permittivity of the inner layer, x_2 the distance from the metal to the oHp, and x_1 that between the metal and the iHp. Thus the conclusion above means that neither the ϵ profile nor the distances are affected by the ionic strength (unless they both vary in a compensating way, which is unlikely). This is not a general situation because in other cases, for example for the adsorption of SCN^- (2), the slope was found to be dependent on ionic strength. Figure 3 shows that in the region where $q \leq 0$ there is a definite tendency of the slope to increase with μ. This is a consequence of the weight of the points corresponding to the higher values of q'. Because the values of q' are small, it is unlikely that x_2 and (or) x_1 may be affected, so the smaller values of K_{12} for increasing μ are probably a consequence of a decreasing ϵ. This decrease in ϵ can be due to the fact that between the iHp and oHp more water is bound as the adsorbed charge and ionic concentration increase. Finally, in the region where $q > 0$ and $|q'| < q$ the effect of μ is not well defined, probably because q' is more inaccurate. Nevertheless, values of K_{12} are definitely larger. As already discussed (5), this is due to a replacement of Na^+ by F^- in the diffuse layer, which makes x_2 smaller.

The equivalent of eq. [13] for the integral capacity of the inner layer is $K_{m2} = \epsilon/4\pi x_2$. Then if a uniform value of the permittivity is assumed, the distance ratio $(x_2 - x_1)/x_2 = K_{m2}/K_{12}$ can be obtained. K_{12} and K_{m2} were calculated from the slope and the separation of the Christie plots, leading, in the region $q > 0$, to the average values $x_1/x_2 = 0.77$ for $|q'| > q$ and $x_1/x_2 = 0.86$ for $|q'| < q$. Because changes in x_1 are unlikely, these values show that the oHp is nearer the iHp when $|q'| < q$. Again this is due to the fact that the solvated F^- anion, which determines the diffuse layer charge in this region, has a smaller radius than the Na^+ cation (5).

The adsorption isotherm

According to the electrostatic model of the double layer and in the situation where discreteness-of-charge effects are estimated on the basis of the cutoff-disc model, the adsorption isotherm can be written (14, 15)

$$[14] \quad \ln(-q'/a_{N_3^-}) - \ln(q' - q_s') = \Phi + \frac{f}{K_{12}}q_s' + \frac{f}{K_{12}} \times \left(1 - g\frac{K_{m2}}{K_{m1}}\right)q' + f\phi_2$$

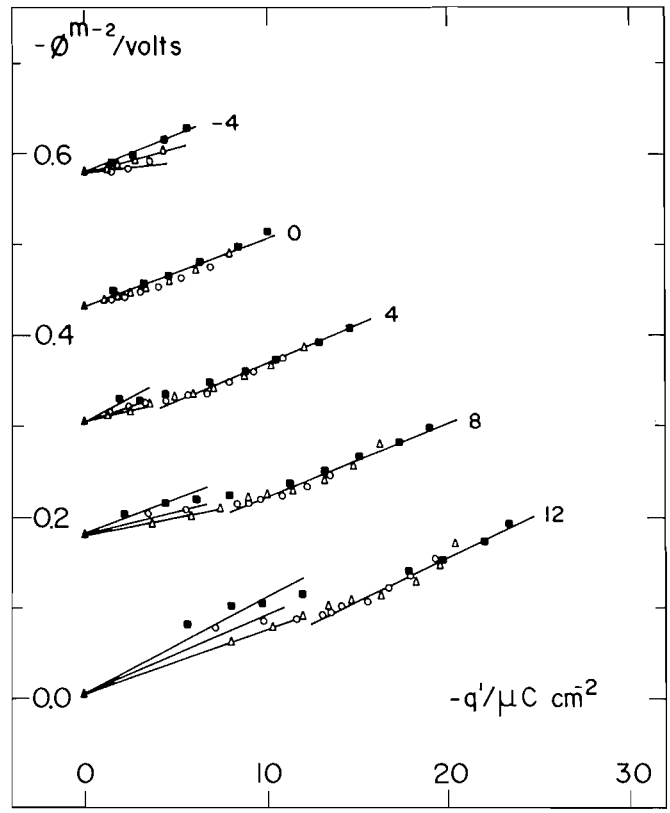

FIG. 3. Potential drop in the inner layer as a function of the specifically adsorbed charge due to N_3^- anions $\mu = 0.25$ (○), 0.5 (△), 0.95 (■). Figures on the lines indicate the electrode charge density in $\mu C\ cm^{-2}$. (▲) values correspond to the base solution.

where $a_{N_3^-}$ is the activity of N_3^- in the bulk, q_s' the maximum value of q', Φ a parameter related to the standard free energy of adsorption of an isolated particle, K_{m1} the integral capacity between the metal and the iHp, and g a dimensionless parameter related to the self-atmosphere potential of the adsorbed ion. As in previous cases (4, 16), the values of ϕ_2 are not large and can be approximated by the expression

$$[15] \quad f\phi_2 = \frac{q + q'}{A}$$

where $A = (RT\epsilon\mu/2\pi)^{1/2}$. Introducing eq. [15] into eq. [14] the result is

$$[16] \quad \ln(-q'/a_{N_3^-}) - \ln(q' - q_s') = \Phi + \left(\frac{f}{K_{12}} + \frac{1}{A}\right)q + \left(\frac{f}{K_{12}}\left(1 - g\frac{K_{m2}}{K_{m1}}\right) + \frac{1}{A}\right)q'$$

This isotherm was tested by plotting q' vs. $\ln(-q'/a_{N_3^-}) - \ln(q' - q_s')$ at constant q. Here it was assumed that the N_3^- anion adsorbs with the long axis perpendicular to the metal surface, giving for q_s' a value of 226 $\mu C\ cm^{-2}$. Figure 4 shows the results for $\mu = 0.25$. Plots with the same characteristics were obtained for $\mu = 0.5$ and 0.95. It is interesting to note that the isotherm plots present characteristics similar to those of the Christie plots. This statement is theoretically obvious but such a situation has not been apparent in experimental results presented for other systems. Figure 4 shows that straight lines are obtained for small values of q, but as q becomes larger it is apparent that there are two different slopes: one in the region $|q'| < q$ and

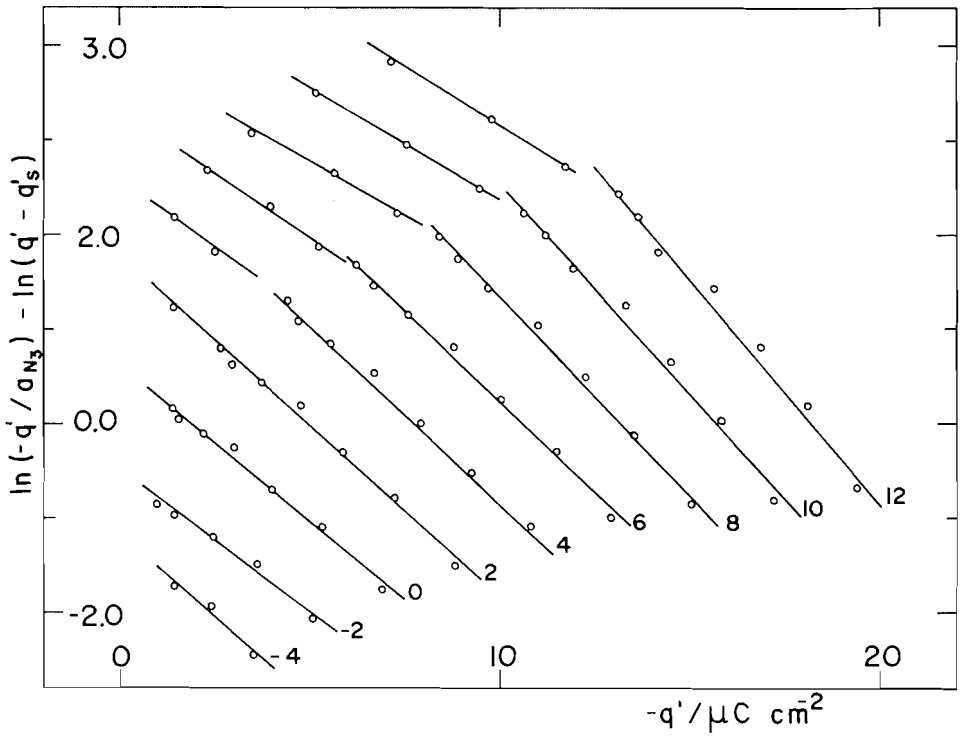

FIG. 4. Test of the adsorption isotherm (eq. [8]) for $\mu = 0.25$. Figures on the lines indicate the electrode charge density in $\mu C\ cm^{-2}$.

another one for $|q'| > q$. From the point of view of the isotherm parameters it is interesting to analyze the dependence of the parameter g on μ. This parameter was determined from slopes of plots like those in Fig. 4 using values of K_{m2} and K_{12} obtained from the corresponding Christie plots as described above. K_{m1} was evaluated from the relationship $K_{m2} = (1/K_{m1} + 1/K_{12})^{-1}$. In the region where $|q'| > q$, g depends somewhat on q but on average it was calcuated as being 1.14, 1.05, and 0.90 for the ionic strengths 0.25, 0.5, and 0.95, respectively. As discussed by Levine and Robinson (17, 18) g depends on the relative positions of the iHp and oHp and on the profile of variation of the permittivity of the inner layer with distance. As shown above, an increase in μ leads to an increase in q'. This increase is relatively small and unlikely to cause any alteration in the dimensions of the double layer. At the same time, an increase in μ means an increase in the ionic concentration in the diffuse layer. Thus there will be more bound water at the oHp and the permittivity in this region is likely to decrease. This may explain the fact that g decreases with increasing μ.

In the region where $|q'| < q$ the average values of g were 1.53, 1.30, and 1.13 for the ionic strengths 0.25, 0.5, and 0.95, respectively. Here g decreases with μ for the reasons just discussed. Also, it must be noted that the values of g are larger than those for the condition $|q'| > q$. The reason is again the fact that when F^- determines the diffuse layer charge the thickness of the inner layer is reduced. In other words, the oHp becomes nearer the iHp and consequently g increases (17, 18). The values of g obtained here are not very different from unity, falling well within the range discussed by Levine and Robinson (17, 18). This contrasts with the case of some oxianions where much higher values of g were observed (4, 16, 19). Finally, it must be noted that the values of g obtained here for azide anions are larger than those observed in single salt solutions (9), while according to the discussion above the opposite should be true. This was found to be due to the fact that the isotherm used in single salt solutions did not contain a term in q_s' which results in lower values of g. As an example, for $\mu = 0.25$, $q = 6\ \mu C\ cm^{-2}$, and in the region $|q'| > q$ the value obtained was $g = 1.14$. But if the therm in q_s' in the isotherm is disregarded it is found that $g = 0.75$. This value is indeed in good agreement with those obtained in single salt solutions (9).

This work presents a detailed evaluation of the effect of μ on the specific adsorbed charge for a system containing an active anion. The results were satisfactorily analyzed on the basis of the electrostatic model of the double layer. On the other hand, the double layer properties other than the amount adsorbed seem to be independent of μ. This observation cannot be generalized because there is some evidence that the situation may be different for other systems. The adsorption isotherm based on the electrostatic model is an adequate fit to the experimental results. In particular, the self-atmosphere parameter g and its dependence on μ are in accordance with this model but, again, this seems to be restricted to the present system.

Acknowledgements

Thanks are due to Dr. W. R. Fawcett of the University of Guelph, Canada, for helpful discussions. The authors acknowledge financial support from the Conselho Nacional de Desenvolvimento Científico e Tecnológico (CNPq) and the Fundação de Amparo à Pesquisa do Estado de São Paulo (FAPESP).

1. W. R. FAWCETT and T. A. MCCARRICK. J. Electrochem. Soc. **123**, 1325 (1976).
2. L. A. AVACA, E. R. GONZALEZ, and R. C. ROCHA-FILHO. Can. J. Chem. **61**, 388 (1983).
3. R. PAYNE. J. Phys. Chem. **69**, 4113 (1965).
4. W. R. FAWCETT and J. B. SELLAN. Can. J. Chem. **55**, 3871 (1977).
5. E. R. GONZALEZ. J. Electroanal. Chem. **90**, 431 (1978).
6. E. DUTKIEWICZ and R. PARSONS. J. Electroanal. Chem. **11**, 100 (1966).
7. R. PAYNE. J. Electroanal. Chem. **41**, 277 (1973).

8. G. J. HILLS and R. M. REEVES. J. Electroanal. Chem. **42**, 355 (1973).
9. C. V. D'ALKAINE, E. R. GONZALEZ, and R. PARSONS. J. Electroanal. Chem. **32**, 57 (1971).
10. D. J. G. IVES and G. J. JANZ. Reference electrodes. Academic Press Inc., New York. 1969.
11. D. R. ROSSEINSKY and R. J. HILL. J. Electroanal. Chem. **30**, App. 7 (1971).
12. E. A. GUGGENHEIM and J. C. TURGEON. Trans. Faraday Soc. **51**, 747 (1955).
13. R. A. ROBINSON and R. H. STOKES. Electrolyte solutions. Butterworths, London. 1955.
14. S. LEVINE. J. Colloid Interface Sci. **37**, 619 (1971).
15. W. R. FAWCETT. J. Electroanal. Chem. **84**, 3030 (1977).
16. E. R. GONZALEZ. Can. J. Chem. **60**, 1643 (1982).
17. S. LEVINE and K. ROBINSON. J. Electroanal. Chem. **41**, 159 (1973).
18. K. ROBINSON and S. LEVINE. J. Electroanal. Chem. **47**, 395 (1973).
19. E. R. GONZALEZ and S. SRINIVASAN. Electrochim. Acta, **27**, 1425 (1982).

Electrochemical gasification of lignite in phosphoric acid

KEITH E. JOHNSON AND LUC VERDET
Department of Chemistry, University of Regina, Regina, Sask., Canada S4S 0A2
Received March 11, 1985[1]

KEITH E. JOHNSON and LUC VERDET. Can. J. Chem. **64**, 419 (1986).

A combination of simple voltammetry, cyclic voltammetry, chronopotentiometry, glc, proximate and ultimate analyses, and petrography were applied to the investigation of lignite electrogasification in phosphoric acid. Conversion of ~40% lignite to CO_2 occurs, in part by thermal reaction. Electrooxidation of the lignite occurs in part through electrocatalysis due to incorporated Fe(II). Lesser amounts of CO are produced thermally.

KEITH E. JOHNSON et LUC VERDET. Can. J. Chem. **64**, 419 (1986).

On a utilisé une combinaison de voltamétries simple et cyclique, de chronopotentiométrie, de cpg, d'analyses approximative et ultime et de pétrographie pour étudier l'électrogazéification de la lignite dans l'acide phosphorique. Environ 40% de la lignite se transforme en CO_2 et cette réaction est en partie thermique. L'électro-oxydation de la lignite se produit en partie par le biais d'une électrocatalyse due à du Fe(II) qui est incorporé. Il se produit thermiquement des quantités moins importantes de CO.

[Traduit par le journal]

Introduction

The notion of using an electrochemical method to convert coal into a gaseous fuel was revived recently by Coughlin and Farooque (1) who electrolyzed slurries of various coals in dilute sulfuric acid and obtained hydrogen and lesser amounts of carbon dioxide and carbon monoxide. It was noted that the required potential for electrolysis was ~0.9 V, much less than that required for water electrolysis. In other words, coal electrogasification might also be viewed as an interesting water electrolysis with depolarization of the anode reaction. Further studies of the coal – sulfuric acid electrolysis reactions were undertaken by Baldwin *et al.* (2), Bockris and co-workers (3), Park and co-workers (4 – 6), and Marooka *et al.* (7) among others. It was observed (*a*) that iron(II) species were extracted into solution from the coal and were oxidized to iron(III), thus contributing to the current flow (2); (*b*) that some chemical as well as electrochemical conversion of the coal to CO_2 occurred (3); (*c*) that iron(II) and added cerium(III) catalysed the coal oxidation (4).

Since the earlier work (1) indicated that increased temperatures produced greater currents and the coals apparently passivated by electrolysis at low temperatures could be reactivated by heating, we studied a variety of electrolytes for the process (8). While a molten carbonate system has theoretical appeal and such media have been investigated in the fuel cell context, we chose another fuel cell system, 85% phosphoric acid, for a first detailed study since it showed better current levels than sulfuric acid. We would note in passing that the highest currents were obtained using methane sulfonic acid as the electrolyte; these currents were roughly 10 times those from comparable phosphoric acid slurries.

Experimental

The samples used were Bienfait, Saskatchewan lignite, Boundary Dam (lignite) char, and carbon graphite. Saskatchewan lignites approximately comprise 1/3 carbon, 1/3 the elements of water, and 1/3 clay minerals. 85% Phosphoric acid (Fisher) was used as electrolyte.

The electrolysis cells consisted of stoppered glass beakers containing the coal slurries stirred by a magnetic stirring bar with a gold or platinum sheet anode. The catholyte was pure solvent in a tube terminating in a frittered glass disc; the cathode was a platinum sheet. The reference electrode consisted of a silver wire dipping into an electrogenerated silver(I) solution in phosphoric acid in another tube similarly terminated by a glass frit/salt bridge. Provision for adding a thermometer, Pt or Au microelectrode, and gas bubbler to the cell existed. Exit gases, usually in a stream of nitrogen carrier, could be vented to a hood or collected in a gas bag for analysis by a Carle Model III-H chromatograph. The cells were immersed in a thermostat.

Current–voltage curves were measured with a simple ammeter and voltmeter circuit.

Cyclic voltammograms and chronopotentiograms were obtained using a PAR 170 Electrochemistry System with a HP7035B *X–Y* Recorder.

Proximate and ultimate analyses

The moisture content was determined by the ASTM:D 3173–73 procedure. This method has been criticized, especially when used with low rank coals (9). However, tests showed that with the lignite used in the present work the procedure gave good reproducibility, and that oxidation because of the use of air was negligible.

Volatile matter was determined using the ASTM:D 3172–73 procedure, with the modification for sparking fuels.

The ash content was determined using the ASTM:D 3174–73 procedure.

Carboxylic acid functions were determined by exchange of the samples with calcium acetate and titration of the liberated acetic acid with base.

Petrographic analyses were performed by W. McDougall, V. Nambudiri, and J. Potter of the Energy Research Unit of the University of Regina by standard procedures (10).

Results

Figure 1 demonstrates the enhanced current produced by adding carbon graphite, lignite, or char to 85% phosphoric acid at 125°C and Fig. 2 shows the effect of temperature on the current–voltage profile. Measurements of the current at 2 V at 20 temperatures yielded an activation energy of 28.9 kJ/mol (6.9 kcal/mol), slightly high for a diffusion-controlled process but comparable to the Ce(IV) in H_2SO_4 oxidation rate for coal (6). The decay of current at fixed potential was slow for lignite and not quite so slow for char. If the lignite was previously extracted with H_3PO_4, the recorded current was lower, whereas the extract produced a higher initial current but one falling off more rapidly.

Extraction of the coal with H_3PO_4 gave gases with a CO_2:CO ratio of 3.2 after 30-h electrolysis at (30°C) compared with ratios of 4.9 for unextracted coal and 2.3 for coal extracted with a benzene–alcohol mixture.

[1]Revision received October 7, 1985.

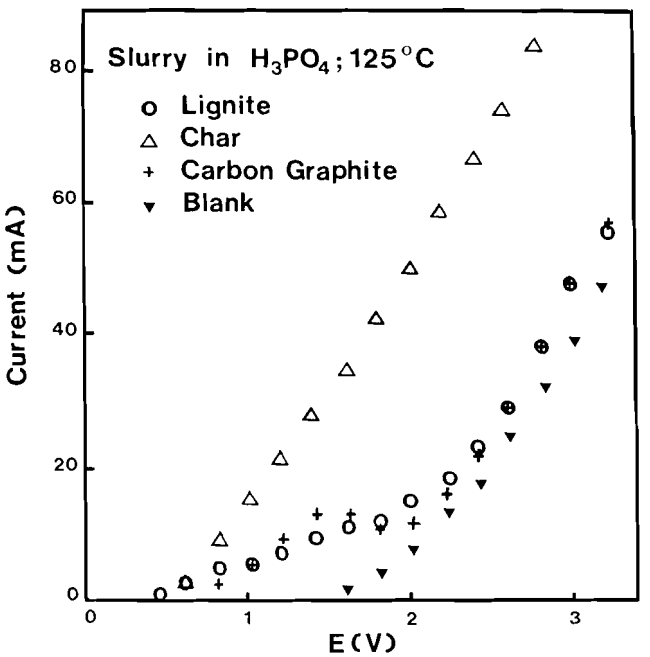

FIG. 1. Current–voltage profile for phosphoric acid at 125°C containing; o, lignite; Δ, char; and +, carbon graphite. Large platinum electrodes.

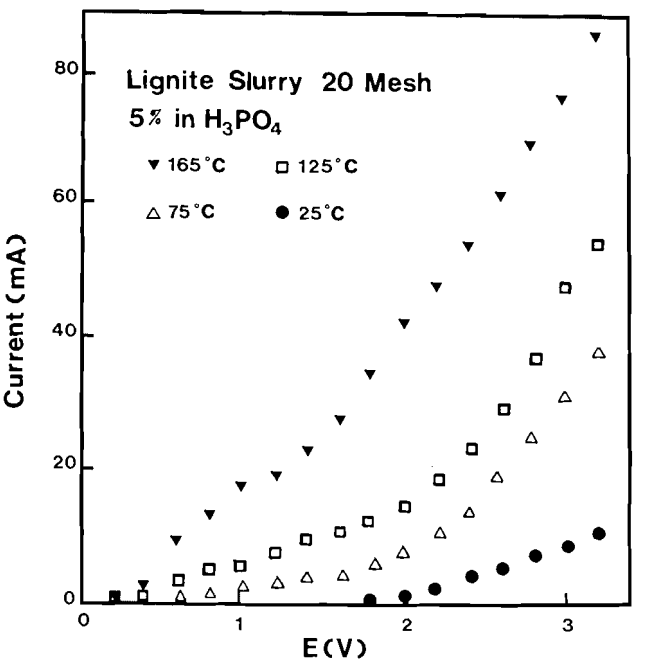

FIG. 2. The effect of temperature on the current–voltage profile of a 20-mesh lignite slurry in phosphoric acid. Large platinum electrodes.

Linear sweep voltammograms obtained with gold disc microelectrodes are shown for 30 and 150°C for H_3PO_4 alone and with added Fe(II) (Figs. 3 and 4) and for lignite in H_3PO_4 slurries (Figs. 5 and 6). The influence of formic acid on the voltammogram is noted in Fig. 5. The substitution of platinum for gold gave similar curves (Fig. 7) with lower current densities and no sharp anodic acid peak at ~0.8 V.

Chronopotentiograms obtained with currents of 75 and 130 μA merely highlighted the occurrence of electrode reactions at −0.4 and +0.8 V. Cyclic voltammograms showed the reversible Fe(III)/ Fe(II) peaks for Fe(II) solutions at ~−0.4 V, the

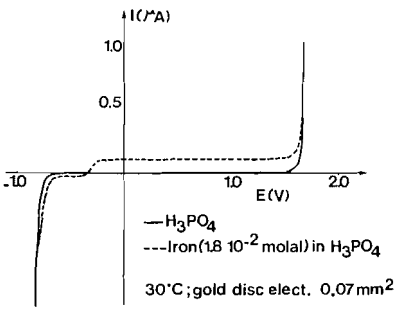

FIG. 3. Linear sweep voltammogram for (*a*) H_3PO_4 (*b*) Fe(II) in H_3PO_4 with gold microelectrode at 30°C.

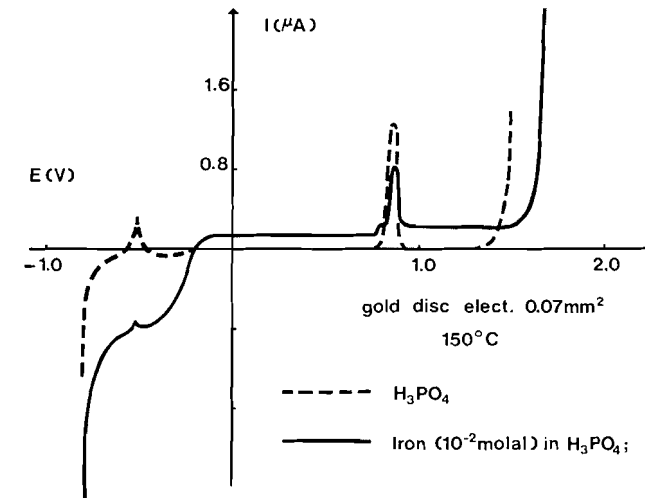

FIG. 4. Linear sweep voltammogram for (*a*) H_3PO_4 (*b*) Fe(II) in H_3PO_4 with gold microelectrode at 150°C.

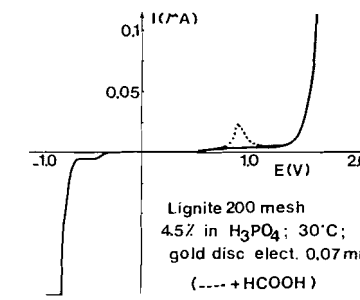

FIG. 5. Linear sweep voltammogram for lignite in H_3PO_4 with gold microelectrode at 30°C.

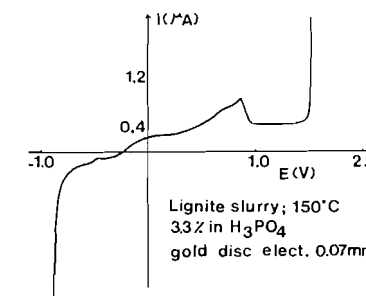

FIG. 6. Linear sweep voltammogram for lignite in H_3PO_4 with gold microelectrode at 150°C.

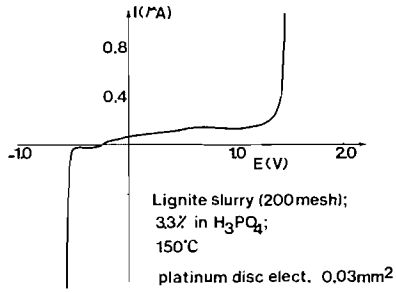

FIG. 7. Linear sweep voltammogram for lignite in H_3PO_4 at 150°C with platinum microelectrode.

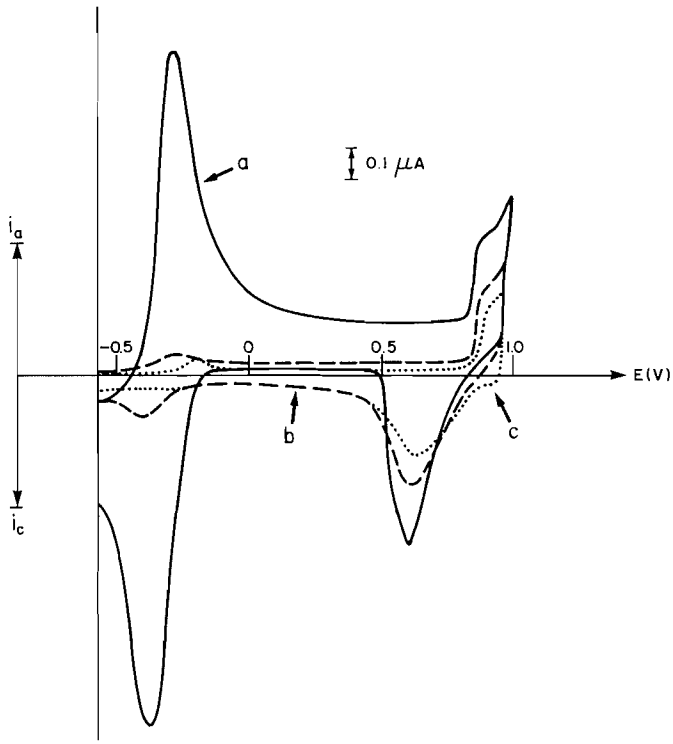

FIG. 8. Cyclic voltammograms in H_3PO_4 with 0.7-mm² gold microelectrode at 30°C: (*a*) 2×10^{-2} *m* Fe(II); (*b*) 3.3% lignite slurry; (*c*) base electrolyte.

same peaks for lignite slurries, gold oxide peaks in the 0.8 V region, and an additional anodic current rise around 0.5 V for slurries, the rise being more pronounced at 150°C. Figure 8 shows cyclic voltammograms for phosphoric acid, Fe(II) in phosphoric acid, and a slurry at 30°C, and Fig. 9 shows a similar set for 150°C. The cyclic voltammetry indicates the presence of iron ions, albeit trace amounts, in the H_3PO_4.

Several macroelectrolysis experiments were undertaken with platinum electrodes; the potential at constant current typically behaved as in Fig. 10, indicating several stages in electroactivity beyond the potential of Fe(II) oxidation. The evolved gases consisted of CO and CO_2 with traces of ethylene from thermal reaction of lignite and H_3PO_4 plus hydrogen when the slurry was electrolyzed. It was noted that the CO:CO_2 ratio was lowered once electrolysis commenced (Fig. 11).

Based on the overall electrode processes

$$H^+ + e^- \rightarrow \tfrac{1}{2}H_2 \text{ and } CO_2 + 4H^+ + 4e^- \rightarrow C + 2H_2O$$

the current efficiencies for H_2 and CO_2 production by constant

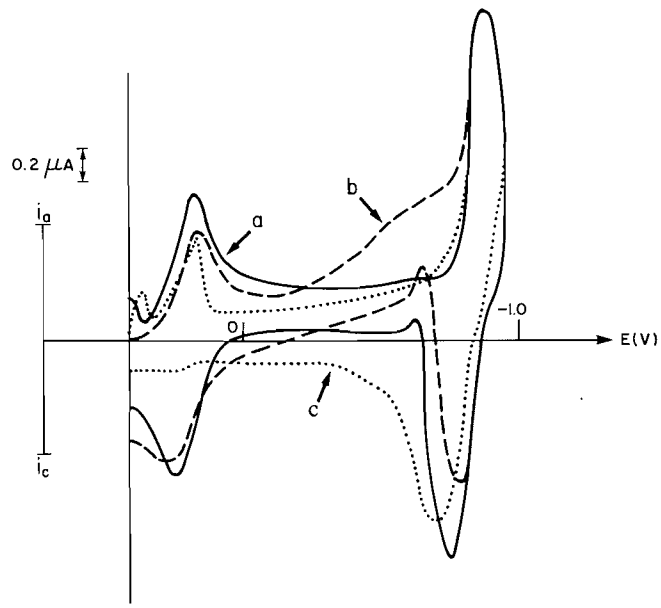

FIG. 9. Cyclic voltammograms in H_3PO_4 with 0.7-mm² gold microelectrode at 150°C: (*a*) 1×10^{-2} *m* Fe(II), (*b*) 5% lignite slurry; (*c*) base electrolyte.

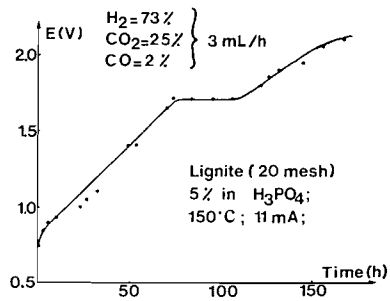

FIG. 10. Potential vs. time for Pt electrode in 5% slurry at 150°C.

TABLE 1. Determination of COOH functionalities by exchange with $Ca(OCOCH_3)_2$ and titration of liberated CH_3COOH

	A[a] (mequiv./g)	B[b] (mequiv./g)
Lignite	1.31	0.37
	1.32	0.36
Lignite after staying 15 days	1.06	1.35
in H_3PO_4 at 150°C	1.02	1.32
Lignite after electrolysis at 1.45V	1.06	1.21
for 11 days at 150°C	1.05	1.20
Char		0
		0
Char after electrolysis at 20 mA for		0.23
17 days at 150°C		0.22
Char after electrolysis at 1.50V for		0.34
16 days at 150°C		0.39

[a]A = with preliminary stay in HCl solution before exchange with Ca acetate.
[b]B = without HCl digestion time.

current electrolysis were 88 and 39%, respectively (a H_2:CO_2 ratio of 4.5 rather than 2).

Table 1 summarizes the —COOH function test results and Tables 2 and 3 the proximate ultimate analytical data. Electrolysis and heating of the lignite produced very little discernible

TABLE 2. Proximate and ultimate analysis of electrolyzed coal

	Moisture	Fixed	Volatiles[a]	Ash[a]	Heating value (S/g)	S	C[b]	H[b]	O[b,c]	N[b]
Lignite	3.51	47.76	39.21	9.52	24880.7	0.396	68.42	4.65	25.87	1.06
s.6d.;e.11.d. (1.45 V)	1.94	62.3	31.21	4.52	26679.1	0.794	71.22	3.95	23.8	1.03
s.12d.				(3.75)[d]			(70.29)[e]	(4.02)[e]	(24.66)[e]	(1.03)[e]
Char	1.52	73.34	9.22	15.92	26455.3	0.224	85.4	1.94	11.45	1.21
s.5d.;e.17.d. (20 mA; 10 mA)	1.07	74.49	8.22	16.22	26761.6	1.109	87.3	2.12	9.27	1.30
s.6d.;e.5d. (1.45 V)	1.09	72.40	8.46	18.05	26665.3	1.119	81.7	1.98	14.6	1.74
s.14d.;e.10.d. (1.0 V)	1.13	72.31	7.89	18.67	25721.6	1.829	82.8	1.88	14.3	1.03

[a]Air-dry basis.
[b]Dry, ash-free basis.
[c]Calculated by difference.
[d]Wet.
[e]Wet, ash-free basis.
Abbreviations: s. = stirred (155°C); d = days; e = electrolyzed (155°C).

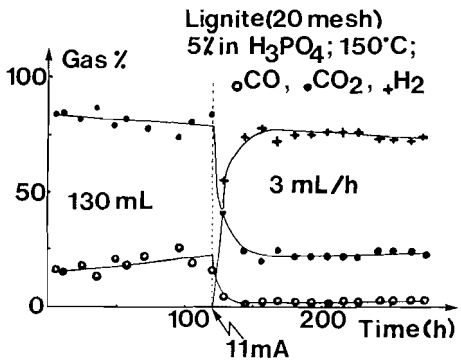

FIG. 11. Gas composition vs. time for lignite in H_3PO_4 at 150°C with electrolysis between platinum electrodes at 11 mA commencing after 125 h.

TABLE 3. Conclusions from ultimate and proximate analysis of electrolyzed lignite and char

1. Decrease in moisture content	Desorption, chemical dehydration, H_3PO_4 extraction
2. Decrease in volatiles (H:C)	CO_2 production, radical condensation and polymerization
3. Decrease in lignite ash	Inorganics dissolved by H_3PO_4
4. Increase in char ash	Char inorganics insoluble
5. Increase in calorific value	Decrease in moisture, H:C and ash
6. Increase in S content	S compounds involatile and insoluble

petrographic change; neither vesiculation nor any other evidence of devolatilization was noticed. The only recognizable difference between feedstock and residues was an increase in reflectance, R_0(av), from 0.39 to 0.43%. Detailed reflectograms of the chars showed a wide range of R_0(av) (0.40–4.79%) indicating nonuniform materials. This mitigated against any reliable measure of the effect of electrolysis but no vast changes were apparent.

Discussion

As in the case of sulfuric acid, lignite coal is chemically attacked by phosphoric acid with the production of gaseous CO and CO_2. This is due presumably to the dehydration of formyl and oxalyl groups. The rate of attack is slow but does increase with temperature. The formation of ethylene probably arises from the presence of some —OC_2H_5 groups on the coal. Electrolysis of coal slurries at 11 mA constant current produces a higher CO_2:CO ratio than does heating (12:1 vs. 4:1), suggesting Kolbe-type reactions of the —COOH groups on the coal (the —COOH groups were separately identified by infrared spectroscopy).

The linear voltammograms indicate the oxidation of Fe(II) to Fe(III) at −0.4 V, again as in sulfuric acid, but a further current flow occurs prior to the +0.8-V region. The current enhancement by formic acid addition suggests that isolated carbons in the coal macromolecules could be oxidized at this potential (+0.8 V). Comparison of Figs. 8 and 9 shows the distinct electroactivity of lignite at 150°C (+0.3→+0.8 V) as well as the iron redox peaks (−0.4 V) and the gold oxide peaks (+0.8 V oxidation, ~+0.7 V reduction).

The gold oxide formation peak is much more pronounced at 150°C and is decreased in the presence of added Fe^{2+} or lignite, presumably because the Fe^{2+}/Fe^{3+} exchange current is the higher one.

The current efficiency for H_2 production of only 88% could be due to slow leakage of Fe(III) into the catholyte or loss of gases from the apparatus, considering the length of the electrolysis time. The current efficiency for CO_2 production is surprisingly high at 39%. The rest of the charge presumably goes to humic acid and surface oxide production (cf. ref. 6 and references therein). The recent results of Dhooge and Park (6), in which 100% conversion to CO_2 by electro-oxidation of coal in H_2SO_4 was claimed, are not necessarily in conflict with our data. Their electrolyses were carried out at a *constant potential* of +1.0 V vs. NHE or ~+0.6 V vs. the Fe(III)/Fe(II) potential in 1 *M* H_3PO_4 (ref. 6, Table 1), which would correspond to ~+0.2 V vs. Ag^+/Ag in our system or close to the process following the Fe(II) oxidation. It is noteworthy that constant

current electrolysis produces substantially more (~10 times) CO_2 than CO. The experiments in which the CO_2 proportion in the gases is reduced by extraction confirm the availability of a soluble electroactive species (Fe(II)) and suggest that the CO is the product of a noncatalytic process. The coal moieties involved in the Fe(II)-catalysed reaction appear to dissolve in benzene–alcohol since the residue then produces even less CO_2.

In summary, the electrolysis of lignite slurries in phosphoric acid at 150°C gives rise to carbon dioxide and hydrogen with smaller amounts of carbon monoxide. While the carbon monoxide arises from a thermal reaction, the carbon dioxide has both thermal and electrochemical origins. Further, the electrooxidation of lignite is a mixed process of direct electrochemical oxidation and Fe(II) electrocatalysed oxidation. The ~40% conversion rate of lignite to CO_2 suggests that this electrogasification could be viable where low-cost or off-peak power is plentiful.

Acknowledgments

We are grateful to NSERC (Canada) and the Saskatchewan Research Council for financial support.

1. R. W. COUGHLIN and M. FAROOQUE. Nature, **279**, 301 (1979); **280**, 666 (1979); Fuel, **58**, 705 (1979); Ind. Eng. Chem. Process Des. Dev. **19**, 211 (1980); J. Appl. Electrochem. **10**, 729 (1980).
2. R. P. BALDWIN, K. F. JONES, T. T. JOSEPH, and J. L. WONG. Fuel, **60**, 739 (1981).
3. G. OKADA, V. GURUSWAMY, and J. O'M. BOCKRIS. J. Electrochem. Soc. **128**, 2097 (1981).
4. P. M. DHOOGE, D. E. STILWELL, and S.-M. PARK. J. Electrochem. Soc. **129**, 1719 (1982).
5. P. M. DHOOGE and S.-M. PARK. J. Electrochem. Soc. **130**, 1029 (1983); **130**, 1539 (1983).
6. S.-M. PARK. J. Electrochem Soc. **131**, 363C (1984).
7. S. MAROOKA, A. MURAKAMI, K. KUSAKOBE, Y. KATO, and K. KUSUNOKI. Fuel, **63**, 947 (1984).
8. F. W. YERHOFF and K. E. JOHNSON. *In* Energex '82. *Edited by* F. A. Curtis. Solar Energy Soc. Can., Regina. 1982. p. 1210.
9. C. K. KARR. Analytical methods for coal and coal products. Vol. 1. *Edited by* C. Karr. Academic Press, New York. 1978. Chap. 7.
10. E. STACH *et al.* (*Editors*). Stach's textbook of coal petrology. 3rd ed. Gebruder Borntraeger, Berlin. 1982.

Fluorination of uracil with acetylhypofluorite and fluorine in acetic acid: mechanistic investigation

MIRKO DIKSIC[1] AND SIMIN FARROKHZAD

Brain Imaging Centre, Montreal Neurological Institute and Hospital, and Department of Neurology and Neurosurgery, McGill University, Montreal, P.Q., Canada H3A 2B4

AND

LAWRENCE D. COLEBROOK

Department of Chemistry, Concordia University, 1455 de Maisonneuve Blvd. W., Montreal, P.Q., Canada H3G 1M8

Received October 15, 1984

MIRKO DIKSIC, SIMIN FARROKHZAD, and LAWRENCE D. COLEBROOK. Can. J. Chem. **64**, 424 (1986).

Fluorination of uracil with acetylhypofluorite and fluorine in acetic acid is described. The influence of the acetate ion on the products of the fluorination reaction was examined. Two stereoisomers (*cis* (**3**) and *trans* (**4**)) were found in the reaction mixture following fluorination in the absence of the acetate ion, but only one isomer (**4**) and 5-fluorouracil were found when the acetate ion was present during the fluorination reaction. ^2H nuclear magnetic resonance revealed that acetate from the solution containing acetate ion rather than from the residue from acetylhypofluorite binds to position 6 of uracil to form intermediates. The synthesis yields 5-fluorouracil isolated as pure compound in a chemical yield, relative to the fluorine introduced, of about 45%. The influence of inorganic cations on the yield of acetylhypofluorite was also evaluated.

MIRKO DIKSIC, SIMIN FARROKHZAD et LAWRENCE D. COLEBROOK. Can. J. Chem. **64**, 424 (1986).

On décrit la fluoration de l'uracil à l'aide de l'hypofluorite d'acétyle et de fluor dans l'acide acétique. On a étudié l'influence de l'ion acétate sur la nature des produits de la réaction de fluoration. Lors des réactions effectuées en l'absence d'ions acétates, on a démontré que les mélanges réactionnels contiennent deux stéréoisomères, soit les produits *cis* (**3**) et *trans* (**4**); toutefois, les mélanges obtenus après des réactions effectuées en présence d'ions acétates ne contiennent que du fluoro-5 uracil et de l'isomère **4**. La rmn du ^2H permet de démontrer que ce sont les ions acétates de la solution plutôt que ceux de l'hypofluorite d'acétyle qui se lient à la position 6 de l'uracil pour former des intermédiares. La synthèse conduit au fluoro-5 uracil qui a été isolé à l'état pur, avec un rendement, basé sur la quantité de fluor utilisé, qui est d'environ 45%. On a ausi évalué l'influence des cations inorganiques sur le rendement de l'hypofluorite d'acétyle.

[Traduit par le journal]

Introduction

^{18}F-labelled 5-fluorouracil (5-[^{18}F]FU) has been suggested as a tracer for in vivo investigation of the pharmacokinetics of uracil (1). Since its metabolic fragment continues to carry a positron-emitting radioisotope, the ^{18}F label, it can be used to investigate, in vivo, by means of positron emission tomography (PET), the metabolism of 5-[^{18}F]fluorouracil (2), possible incorporation of the [^{18}F]-labelled fluorouracil into RNA (3) in tumors, and, with this, the rate of RNA synthesis. The rate of RNA synthesis might, in turn, provide some indication of the activity of a tumor, which could be useful in assessing tumor therapy (4). Recently, the tissue distribution of 5-[^{18}F]fluorouracil was extensively evaluated in tumor-bearing animals (5, 6) and in humans with cancer (4). The results of these studies suggest that 5-fluorouracil indeed accumulates in different animal (5, 6) and human tumors (4).

Although attempts have been made to explain the reaction mechanism of the fluorination of uracil (7), it has never been completely understood. The intermediate, 5-fluoro-6-acetoxy-5, 6-dihydrouracil isomers **3** or **4** (Fig. 1), was isolated in 1979, but details of the reaction mechanism and stereochemical structure remained unexplained (7).

Uracil was first fluorinated with trifluoromethylhypofluorite (CF_3OF) (8). The synthesis of 5-[^{18}F]fluorouracil (**5**) (5-[^{18}F]FU) was first reported in 1973 (9) and the fluorination of uracil with [^{18}F]F_2 in acetic acid was reported in 1979 along with isolation of an intermediate. Recently we also reported a convenient high-yield synthesis of 5-[^{18}F]FU (10). In the present paper the isolation of intermediates produced in the fluorination of uracil, as well as their nmr spectra, is reported. Although positive stereochemistry of these intermediates could not be established by nmr spectra or chemical reactivity, we can now suggest a structure for these intermediates.

Results and discussion

Reactions of trifluoroacetylhypofluorite with stilbene (11), acetylhypofluorite with triacetylglucal (12–15), and trifluoromethylhypofluorite with uracil (16) have been reported. In all these cases, 100% regiospecificity was reported. Stereoselectivity in the syntheses of these fluoro compounds was also very good, but not always 100% (11, 20). This stereoselectivity is apparently influenced by the hardness of the base involved in the reaction (11). A mixture of *threo* and *erythro* forms was produced in the stilbene reaction with acetylhypofluorite in the presence of sodium acetate (11, 17). An addition of acetylhypofluorite across the double bond in triacetylglucal also resulted in two stereoisomers (18–20). Fluorination of uracil with molecular fluorine in acetic acid has also been reported, but the details of the reaction mechanism have never been established (7, 9, 22, 23).

Our results show that two major stereoisomeric adducts, *cis*- and *trans*-5-fluoro-6-acetoxy-5, 6-dihydrouracil, **3** and **4**, are produced by fluorination of uracil with molecular fluorine in acetic acid (reagent grade), or with acetylhypofluorite in acetic acid; however, 5-fluorouracil and one isomer, **4**, are found in the crude reaction mixture under both reaction conditions when an acetate ion is present during the fluorination reaction (Table 1). The ^1H nmr and ^{19}F nmr spectra were measured on the

[1]To whom correspondence should be addressed, at: Medical Cyclotron Unit, Montreal Neurological Institute, 3801 University St., Montreal, P.Q., Canada H3A 2B4.

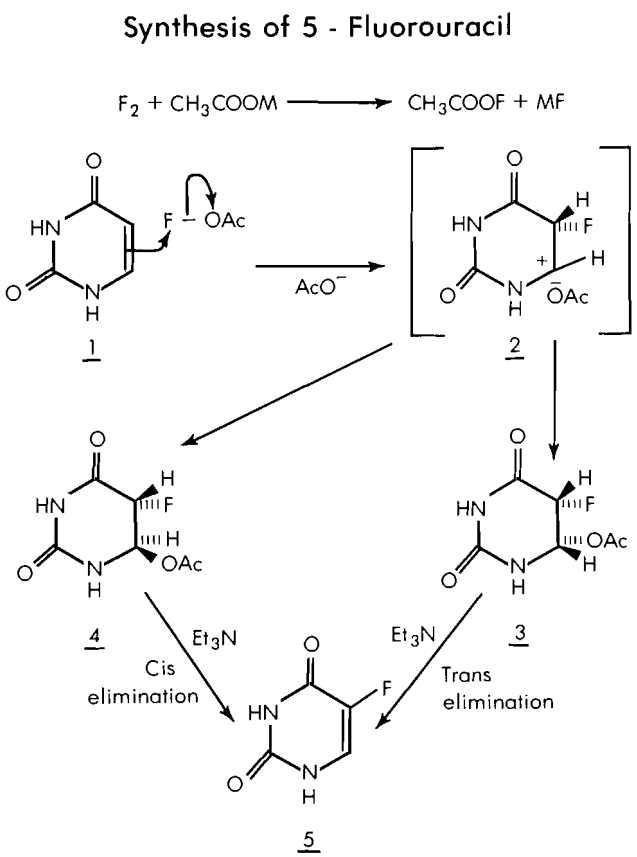

FIG. 1. Reaction scheme for the fluorination of uracil, **1**, with acethylhypofluorite.

relatively crude adducts prepared by fluorination of uracil (uracil present during bubbling) with F_2 in acetic acid (reagent grade). When acetate salt was not present during the reaction, the spectra revealed the presence of two geometric isomers (*trans* (**4**) and *cis* (**3**)) in a ratio of 1:2, but no 5-fluorouracil (Table 1). But when uracil was added (fluorination with CH_3COOF) after the end of bubbling, the ratio between *cis* (**3**) and *trans* (**4**) isomers was 4:1, and no 5-fluorouracil was found (Table 1). The presence of two geometric isomers indicates that the reaction does not have complete stereoselectivity. In contrast, in the presence of added acetate ion the spectra taken several hours after the end of bubbling showed the presence of a single isomer and 5-fluorouracil, suggesting that one of the isomers (Table 1) does not survive to the end of the reaction. We note that the reaction done in distilled acetic acid gave *trans* (**4**) and *cis* (**3**) isomers in a ratio of 2.5:1. This suggests that the removal of traces of impurities changes the mechanism of the reaction.

The ^1H and ^{19}F nmr spectra from positions 5 and 6 of the diastereomers were analyzed using iterative computer fitting, but positive identification of the stereochemistry at these positions could not be established on the basis of the coupling constants. Thus, $^3J_{H5-H6}$ is 3.9 and 4.3 Hz in **3** and **4**, respectively, while $^3J_{F5-H6}$ is 2.8 and 2.2 Hz in **3** and **4**, respectively. These values are too similar in magnitude to permit an unequivocal assignment of the configuration on the basis of the evidence of a coupling constant alone. Values of 4 and 2 Hz have also been reported for $^3J_{H5-H6}$ and $^3J_{F5-H6}$, respectively, for an isomer of 5-fluoro-6-acetyoxy-5,6-dihydrouracil prepared by fluorination of uracil in acetic anhydride – 5% acetic acid (23). Stereochemistry was not assigned (23).

TABLE 1. Ratios between *cis* (**3**) and *trans* (**4**) isomers formed under different fluorination conditions

Reaction medium	Ratio **3**:**4**	Acetate ion	Fluorinating reagent
AcOH (reagent)	Only **4***	Yes	F_2
AcOH (reagent)	2:1†	No	F_2
AcOH (distilled)	1:2.5†	No	F_2
AcOH (reagent)	4:1‡	No	CH_3COOF
AcOH (reagent)‡	8:1§	Yes	CH_3COOF

*Only one isomer (*trans* (**4**)) and 5-FUr found after evaporation of AcOH.
†Uracil present during bubbling.
‡Uracil added after the end of bubbling.
§Present in crude reaction mixture (before evaporation of AcOH), but after evaporation or about three hours after bubbling only *trans* (**4**) and 5-FUr were present.

Our results also suggest that the acetate ion is a strong enough base to facilitate acetic acid elimination in one of the isomers. This was confirmed in experiments where acetate ion was added to the crude reaction mixture containing the *cis*–*trans* mixture, ^{19}F nmr taken a few hours later showed that CH_3COOH was eliminated from the isomer assigned the *cis* configuration for that isomer (**3**), and the mixture contained only 5-fluorouracil and the *trans* isomer (**4**) in the same ratio in which the two isomers were present in the solution without acetate ion. The ease with which the *cis* isomer loses CH_3COOH supports our assignment, because the *cis* isomer (**3**) has H and CH_3COOH in the *trans* configuration favoured for the elimination of CH_3COOH.

Fluorination with fluorine

When fluorination with fluorine was carried out in the presence of an acetate ion, 60% of the fluorine was found in 5-fluorouracil (^{19}F nmr spectra), and the remainder (36–38%) in one stereoisomer (**4**), with a small admixture of 5,6-difluoro compound (2–4%). Fluorination of uracil with F_2 in CH_3COOH or CD_3COOD also yielded a minor product, which accounted for about 2–4% of the total F_2 approximately 1 h after introduction of F_2 was stopped. This compound was tentatively identified by its ^{19}F nmr spectrum as 5,6-difluoro-5,6-dihydrouracil. The $^{19}F\{^1H\}$ spectrum appeared as an AB quartet, $^3J_{F5-F6}=7.9$ Hz. When the fluorination reaction was carried out in CD_3COOD, the ^{19}F multiplet at δ −197.9 ppm showed loss of an H–F coupling (hydrogen on nitrogen-1). In consequence, this multiplet was assigned to F6, and the multiplet at −195.6 to F5. The geminal coupling constants, $^2J_{H5-F5}$ and $^2J_{H6-F6}$, were both 45.8 Hz.

Vine *et al.* (7), who investigated the fluorination of uracil with molecular fluorine in acetic acid with the addition of 25% (by volume) of acetic anhydride, reported the ^1H nmr spectrum of a single isomer with δ 2.13 (CH_3), 5.48 (J_{H5-F5} = 47 Hz, $J_{H5-H6}=4.5$ Hz, H5), and 6.27 ($J_{H5-H6}=45$ Hz, $J_{H6-F5}=2.22$ Hz, H6) ppm in acetic acid-d_4. They assigned the *cis* (H5—H6) configuration to this isomer on the basis of the magnitudes of the coupling constants. However, our experimental data on the two isomers show that the coupling constants are too similar to permit an unequivocal stereochemical assignment on the basis of coupling constants alone. In our work, the isomer produced in the fluorination of uracil in the presence of inorganic acetate has a ^1H nmr spectrum very similar to that reported by Vine *et al.* (7). The only difference is the value of J_{H-F} (geminal), for which 47 Hz was reported, compared with our value of 45.14 Hz. When we repeated the procedure of Vine *et al.* (7) we

TABLE 2. Yield of acetylhypofluorite as a function of acetate/fluorine ratio and cation

Cation X	CH_3COOX/F_2 (mmol/mmol)	Yield (%)	Number of determinations
Na^+	0.096	53 ± 3	2
	0.29	53 ± 4	2
	1.92	69 ± 3	3
	0.29	83 ± 4	3
	4	75 ± 3	3
	8	75 ± 3	2
	12	80 ± 2	3
	160	68 ± 3	3
K^+	0.9	71 ± 2	2
	1.9	78 ± 3	3
	2.9	90 ± 4	3
NH_4^+	0.096	55 ± 3	2
	0.29	60 ± 3	3
	1.9	70 ± 2	3
	2.9	90 ± 3	3
H^+	Glacial acetic acid	30 ± 3	3

obtained an isomer with J_{H-F} (geminal) = 45 Hz, which agrees well with the value obtained for the compound prepared by other procedures. On the basis of the nmr evidence, we conclude that the compound prepared by Vine *et al.* (7) is identical to the one we synthesized in the presence of an acetate ion. Our work indicates that the stereochemical assignments of Vine *et al.* (7), made on the basis of coupling constants, may not be correct. We consider that the opposite configuration is more likely.

The *trans* configuration of the intermediate 5-fluoro-6-acetoxy-5,6-dihydrouracil, **4**, obtained in the reaction of uracil and the fluorinating agent in the presence of inorganic acetate, was assigned on the basis of the observation that acetate from solution, rather than residue from CH_3COOF, adds in the 6 position and that this isomer is relatively more stable towards elimination of CH_3COOH. (See the experiments with deuterated acetate, analyzed by ^2H nmr, and discussion of possible reaction mechanisms.) The *trans* configuration of the intermediate is in accordance with other reactions involving ionic mechanisms, in which a halogen in the presence of a nucleophile is added to a double bond, yielding a compound with halogen and nucleophile in a *trans* configuration (24).

Indirect evidence for the stereochemistry of the *cis* isomer, **3**, is obtained from ^{19}F chemical shifts. This isomer has a chemical shift (δ −211.0 ppm) similar to *cis*-5-fluoro-6-methoxy-5,6-dihydrouracil (δ −208 ppm), for which the structure was positively assigned by X-ray crystallography (16). In this case, the fluorination reaction with CF_3OF proceeds with complete stereoselectivity (16), with only *syn* addition, and there is conclusive evidence that the nucleophile (methoxy) which adds to position 6 comes from the solvent rather than from the trifluoromethoxy residue of the CF_3OF (16). Values of $^3J_{H5-H6}(cis)$ = 4.0 and $^3J_{F5-H6}(trans)$ = 2.2 Hz were reported for *cis*-5-fluoro-6-methoxy-5, 6-dihydrouracil (16), comparable to the values noted above for the *cis*-acetoxy analogs (22). The ease with which stereoisomer **3** loses CH_3COOH also supports the assignment of the structure.

In the absence of added acetate ion, it is possible that fluorination (F_2 in CH_3COOH) of uracil proceeds through direct fluorination and *in situ* synthesis of acetylhypofluorite, which adds to the 5,6-double bond through a cation, **2**, (Fig. 1). The cation formed after the addition of fluorine (from F_2 or CH_3COOF) at C-5 will be more stable than fluorocarbon cations (16). This would allow the acetate ion to attack from either side and form two stereoisomers (equal probability would be expected only when the ion is planar and there is no hindrance of a nucleophilic attack).

The ratio between *trans* (**4**) and *cis* (**3**) isomers in the fluorination with F_2 in acetic acid differs from that observed in the fluorination with CH_3COOF (discussed later) (Table 1). This suggests that the reaction of molecular fluorine with uracil to form an intermediate occurs at a higher rate than that of fluorine with acetic acid to form acetylhypofluorite. The observation is not the same as that recently reported by Shiue *et al.* (21), who found no difference in the products in the fluorination of 2′,3′-di-O-acetyl-5′-deoxyuridine resulting from the two reactions.

Fluorination with acetylhypofluorite

The acetylhypofluorite yield is lower when it is synthesized in acetic acid without additional acetate ion (see Table 2 and ref. 13). As shown in Table 2, our results indicate that the yield of acetylhypofluorite is more a function of concentration than of the cation used. It is evident that the hypofluorite yield reaches a broad maximum when sodium acetate is used, while in other cases it increases with the concentration of acetate. A similar result was reported by Fowler *et al.* (13).

Fluorination of uracil with acetylhypofluorite (generated *in situ*) yielded intermediates **3** (*cis*) and **4** (*trans*) in different ratios (8:1) than fluorination with F_2, where it was 2:1 (Table 1). Fluorination done with acetylhypofluorite with acetate ion present during the reaction yielded mostly 5-fluorouracil (probably formed from *cis* isomer **3**) and a minor compound, *trans* isomer **4**. However, the fluorination of uracil with acetylhypofluorite when acetate ion was not present gave a ratio of 4:1 between the *cis* (**3**) and *trans* (**4**) isomers (Table 1).

That the incorporated acetate comes from the free acetate ion rather than from acetylhypofluorite was established by a labelling experiment (monitored by ^2H nmr) using deuterated acetate added to the reaction mixture after fluorine bubbling was stopped, but before uracil was added. No exchange between acetylhypofluorite and CD_3COO^- was observed. In this experiment, only one isomer was found, with deuterated acetate in position 6 of the intermediate. It was assigned the *anti*-configuration (*trans* (**4**)) as discussed above. The presence of deuterated, rather than regular, acetate in position 6, confirmed by ^2H nmr, supports the notion that the free acetate ion adds to position 6.

Fluorination of uracil with acetylhypofluorite also yields a small amount (2–4%) of the 5,5-difluoro adduct, 5,5-difluoro-6-acetoxy-5,6-dihydrouracil, identified by $^2J_{FF}$ = 284.2 Hz and the vicinal coupling constants $^3J_{FH}(cis)$ = 1.99 Hz and $^3J_{HF}(trans)$ = 6.73 Hz. The 6-methoxy analog of this compound has been reported by Robins *et al.* (16).

^{18}F-labelled 5-fluorouracil

The reaction scheme given in Fig. 1 for a non-radioactive synthesis was also applied when the ^{18}F-labelled compound was synthesized (10). ^{18}F-acetylhypofluorite was prepared first, and allowed to react *in situ* with uracil in the presence of acetate ion, yielding the intermediate, 5-[^{18}F]fluoro-6-acetoxy-5,6-dihydrouracil, **4**, which easily loses acetic acid, giving 5-[^{18}F]-fluorouracil (10).

Summary

On the basis of stability towards CH_3COOH, elimination of

one isomer, and the comparison of the ^{19}F chemical shifts with those of a related compound positively identified by X-ray crystallography (16), the stereochemistry of two intermediates formed in the fluorination reaction is suggested.

It was also observed that the ratio of *trans* (**4**) to *cis* (**3**) is greatly influenced by the purity of acetic acid, giving a ratio of 2.5:1 when the fluorination with F_2 was done in distilled acetic acid rather than in reagent grade, where it was 1:2. The fluorination in the presence of an acetate also yielded two isomers, but one (*cis* (**3**)) did not survive the work-up. Chemical and radiochemical yields were similar in both synthetic routes.

Experimental

General

Research grade chemicals obtained from regular suppliers were used in the syntheses. Thin-layer chromatography (tlc) was done on silica gel hard layer plates with a fluorescence indicator (254 nm). Two solvents were used for development of tlc plates: A, THF–hexane (65:35) and B, ethyl acetate – H_2O–HCOOH (13:1:1). ^{18}F compounds were investigated by visual identification under 254-nm uv light and by thin-layer radiochromatography, using a scanner with a windowless gas-flow proportional detector with a 1-mm opening. The final product was purified by simple filtration through a Sep-Pak column, using THF–hexane (40:6) as an elution solvent. In "cold" reactions, identification of reaction products was done by ^{19}F nmr, ^1H nmr, ^2H nmr, mass spectrometry, melting point, and tlc on silica gel. Reactions were followed by tlc.

The ^1H nmr spectra were obtained at 200 MHz on a Varian XL-200 spectrometer using DMSO-d_6 or acetic acid-d_4 solutions, with TMS as an internal reference. The ^{19}F nmr spectra were obtained at 75.39 MHz on a Bruker WP-80SY spectrometer, on a reaction mixture in acetic acid, acetic acid-d_4, or DMSO-d_6, using trichlorotrifluoroethane (^{19}F chemical shift, δ −82.20 ppm) as an external reference. Iterative analysis of nmr spectra was carried out using the PANIC program on a Bruker Aspect 2000 computer.

An authentic sample of 5-fluorouracil, used as a reference, was isolated from the drug, fluorouracil (Roche), by lowering the pH to about 6.5 (mp (uncorrected) 281°C (lit. (**25**) mp. 282–283°C).

In the first set of experiments, uracil (60–80 mg, 0.5–0.7 mmol) was fluorinated with acetylhypofluorite (prepared *in situ*) in acetic acid (10 mL) and acetic acid-d_4 (10 mL), with and without inorganic acetate.

In the second set of reactions, uracil (80 mg, 0.7 mmol) was suspended in glacial acetic acid, acetic acid-d_4, or in those acids (10 mL) in the presence of an acetate (deuterated or regular). Fluorine (0.1–0.6 mmol) in nitrogen was then introduced. The work-up was carried out as described later under B. In some experiments, the intermediates were analyzed directly in the acid solutions by ^1H nmr (deuterated acids) and ^{19}F nmr (regular and deuterated acids). When the intermediates were isolated, ^1H and ^{19}F nmr spectra were taken in DMSO-d_6 solution. In experiments done in acetic acid to which sodium deuteroacetate had been added, ^2H nmr spectra were taken on a crude reaction mixture.

A. *Reaction of acetylhypofluorite with uracil*

Acetylhypofluorite was prepared by reacting a 0.5–5% mixture of fluorine (0.1–0.6 mmol of F_2) in nitrogen with acetic acid in the presence of added acetate (generally 0.15 *M*) or with acetic acid without an acetate ion present, as described earlier (11–15). The presence of an OF group was established in the reaction mixture (from which all F_2 had been removed) by the appearance of a signal at 161.9 ppm in the ^{19}F nmr spectrum (acetic acid or acetic acid-d_4). At room temperature (about 22°C) the half-life of acetylhypofluorite is 20 min, as measured by ^{19}F nmr.

Acetylhypofluorite was allowed to react with uracil (80 mg, 0.7 mmol) by suspending it in a solution of hypofluorite in acetic acid, with (first set) and without (second set) added acetate ion. The reaction mixture from the first set was divided into two parts and a different work-up carried out on each. In the first part, acid was evaporated under reduced pressure (0.1 Torr; 1 Torr = 133.3 Pa) at a bath temperature of 60°C, the residue redissolved in DMSO-d_6 or acetic acid-d_4, and ^1H and ^{19}F nmr spectra taken. When the reaction was carried out in the presence of added acetate ion, *trans*-5-fluoro-6-acetoxy-5,6-dihydrouracil, **4**, was present, together with 5-fluorouracil. After evaporation of acetic acid, the residue proved to be over 80% final product, 5-fluorouracil, **5**, and only about 16–18% intermediate **4**. The second part was worked up by removing acid under reduced pressure and adding 0.7 mL of triethylamine to the residue. This was followed by a brief heating in a 60°C bath. The heating resulted in the complete elimination of CH_3COOH from the intermediate, giving pure 5-fluorouracil (**5**) in a quantitative yield.

In the second set (reaction done without addition of an acetate), the reaction mixture was divided and, on the first part, a similar work-up was done by evaporation under reduced pressure (0.1 Torr) in a 60°C bath. After evaporation, the residue consisted of about 88% of intermediate **3** and 12% of **4**, but no 5-fluorouracil in the first half. The second half of the reaction mixture was worked up with triethylamine as described above. Addition of 0.7 mL of triethylamine to the residue after evaporation, followed by brief heating in a 60°C bath, resulted in loss of CH_3COOH in both **3** and **4**, yielding 5-fluorouracil (**5**) or ^{18}F-labelled 5-fluorouracil. After evaporation of triethylamine, the residue was extracted with 1 mL of tetrahydrofuran–hexane (40:60) mixture, an the 5-fluorouracil or ^{18}F-labelled 5-FU was purified on a silica gel Sep-Pak column (10).

Purification of intermediate **3** was done only when working with non-radioactive materials. After fluorination in reagent grade acetic acid (no acetate added), isolation and purification were achieved using liquid chromatography (hplc) on silica gel with THF–hexane (35:75) as the solvent. It was not possible to determine the melting point because the intermediate was thermally unstable.

trans-*5-Fluoro-6-acetoxy-5,6-dihydrouracil (**4**)*

The ^1H nmr spectrum (acetic acid-d_4 δ : 2.07 (s, 3H, CH_3COO), 5.49 (d of d, 1H, $^2J_{H5-F5}$ = 45.1 Hz, $^3J_{H5-H6}$ = 4.27 Hz, H5), 6.31 (d, of d, 1H, $^3J_{H5-H6}$ = 4.38 Hz, $^3J_{H6-F5}$ = 2.26 Hz, H6); ^{19}F nmr spectrum (acetic acid-d_4) δ : −212.0 (d of d, 1F, $^2J_{F5-H5}$ = 45.24 Hz, $^3J_{F5-H6}$ = 2.19 Hz); (acetic acid/DMSO-d_6) δ : −212.0 (d of d, 1F, $^2J_{F5-H5}$ = 45.17 Hz, $^3J_{F5-H6}$ = 2.9 Hz). The ^{19}F nmr spectrum was best simulated by including a $^4J_{F5-H1}$ coupling of 2.2 Hz. The ^{19}F nmr spectra were analyzed by iterative computer fitting; TLC of the crude reaction mixture showed spots with R_f = 0.5 (5-FUr) and 0.81 in solvent A (*trans* (**4**) isomer). On heating, compound **4** was converted into 5-fluorouracil, mp 283°C, M^+ 130; tlc of the purified product showed R_f of 0.5 and 0.79, identical with an authentic sample of 5-fluorouracil, using, as developing solvent, solvent mixture A and solvent mixture B, respectively.

When the reaction was carried out in acetic acid in the presence of perdeuteroacetate, or in acetic acid-d_4 in the absence of acetate ion, the ^1H nmr spectrum of the reaction mixture showed no signal at 2.07 ppm, and it was unnecessary to use J_{F5-H1} in the simulation of the ^{19}F spectrum of the *trans* isomer.

Following fluorination with acetylhypofluorite in acetic acid (produced in acetic acid but no acetate), the solvent was evaporated and the resaidue dissolved in DMSO-d_6. The nmr analysis showed 10% of the residue to consist of 5-fluorouracil, the bulk of the remaining material being **3** and **4** in a 4:1 ratio. However, the ^{19}F nmr of the reaction mixture before evaporation had only two isomers present. A small amount (2–4%) of 5,5-difluoro-6-acetoxy-5,6-dihydrouracil, identified by its ^{19}F spectrum (acetic acid or acetic acid-d_4), was always present. On evaporation of the solvent, the 5,5-difluoro adduct was transformed into **3**.

5,5-Difluoro-6-acetoxy-5,6-dihydrouracil

The ^{19}F spectrum (acetic or acetic acid-d_4 δ: −114.3 ($^2J_{F5-F5'}$ = 284.20, $^3J_{F5-F6}$ (*cis*) = 1.99 Hz, F5), −132.0 ($^3J_{F5'-H6}$(*trans*) = 6.73 Hz, F5'). On broadband ^1H decoupling, the ^{19}F spectrum consisted of an AB quartet.

B. *Fluorination of uracil in acetic acid with molecular fluorine*

When uracil (0.7 mmol) suspended in acetic acid (10 mL) was

allowed to react with molecular fluorine (~0.5 mmol) in the absence of added inorganic acetate, a mixture of 1 part *trans*- (**4**) and 2 parts *cis*-5-fluoro-6-acetoxy-5,6-dihydrouracil (**3**) was obtained (the stereochemical assignments are given under Results and discussion). After evaporation of acetic acid and addition and subsequent evaporation of triethylamine, both isomers yielded 5-fluorouracil, with properties (mass spectrum, ^{1}H and ^{19}F nmr spectra, and melting point) identical to an authentic sample.

cis-5-Fluoro-6-acetoxy-5,6-dihydrouracil (3)

^{1}H nmr spectrum (acetic acid-d_4) δ : 2.10 (s, 3H, CH_3COO), 5.30 (d of d, 1H, $^2J_{F5-H5}$ = 46.69 Hz, $^3J_{H5-H6}$ = 3.96 Hz, H5), 5.34 (d of d, 1H, $^3J_{F5-H6}$ = 2.29 Hz, $^3J_{H5-H6}$ = 3.02 Hz, H6); ^{19}F nmr spectrum (acetic acid and acetic acid-d_4 δ : −211.0 (d of d, 1F, $^2J_{H5-F5}$ = 46.11 Hz, $^3J_{H6-F5}$ = 2.76 Hz). The ^{19}F spectra were analyzed by computer fitting. The ^{19}F spectrum of the acetic acid solution was best computer-simulated by allowing for a J_{F5-H1} coupling of 2.2 Hz. The *trans* isomer (**4**) had chemical shifts and coupling constants as described above.

5-Fluorouracil was identified by mp (281–283°C), ^{1}H and ^{19}F nmr spectra, and mass spectrometry (M^+ 130). The ^{1}H nmr spectrum in DMSO-d_6 was identical to that of an authentic sample of 5-fluorouracil.

In distilled acetic acid, 5-fluorouracil and the *trans* isomer **4** were found in the reaction crude when fluorination was done in the presence of an acetate ion, but a mixture of *trans* (**4**) and *cis* (**3**) isomers (in a ratio of 2:1) was formed when the reaction was carried out without addition of acetate ion. About 4% of 5,6-difluoro-5,6-dihydrouracil was identified in the reaction mixture by its ^{19}F nmr spectrum.

5,6-Difluoro-5,6-dihydrouracil

The ^{19}F nmr spectrum (acetic acid) δ : −195.6 (d of d, 1F, $^2J_{F5-H5}$ = 45.78 Hz, $^3J_{F5-F6}$ = 7.90 Hz, F5), −197.9 (d of d, 1F, $^2J_{F6-H6}$ = 45.78 Hz, $^3J_{F5-F6}$ = 7.90 Hz, F6).

Acknowledgments

This work was supported in part by a Medical Research Council of Canada Special Program Grant (SP-5), the Cone Memorial Fund, and a grant from the Killam Scholarship Fund of the Montreal Neurological Institute (to M. Diksic). The interest and encouragement of Drs. Y. L. Yamamoto and W. Feindel in this project are appreciated. We also express our thanks to Dr. Victoria Lees for editing and Ms. C. Elliot for typing this manuscript. A grant from the Faculty of Graduate Studies, McGill University, towards the purchase of a hplc unit is acknowledged. Funding towards the purchase of the nmr spectrometer (Concordia University) was provided by the Natural Sciences and Engineering Research Council of Canada. We wish to thank Dr. O. S. Tee for helpful discussions.

1. H. L. Davis, G. Ramirez and F. J. Ansfield. Cancer, **33**, 193 (1974).
2. A. D. Gani, P. B. Hitchcock, and D. W. Young. J. Chem. Soc. Chem. Commun. 898 (1983).
3. K. L.Mukherhee and C. Heidelberger. J. Biol. Chem. **235**, 433 (1960).
4. J. Shani, D. Young, T. Schlesinger, J. K. Siemsen, R. J. Chlebowski, J. R. Bateman, and W. Wolf. Int. J. Nucl. Med. Biol. **9**, 25 (1982).
5. J. Shani, W. Wolf, T. Schlesinger, A. L. Atkins, P. R. Bradley-Moore, V. Casella, J. S. Fowler, D. Greenberg, T. Ido, R. M. Lambrecht, R. MacGregor, C. Mantescu, R. Neirinckw, P. Som, A. P. Wolf, I. Wodinsky, and K. Meaney. Int. J. Nucl. Med. Biol. **5**, 19 (1978).
6. Y. Abe, H. Fukuda, K. Ishiwata, S. Yoshioka, K. Yamamda, S. Endo, K. Kubota, T. Sako, T. Matsuzawa, T. Takahashi, and T. Ido. Eur. J. Nucl. Med. **8**, 258 (1983).
7. E. L. Vine, D. Young, W. H. Vine, and W. Wolf. Int. J. Appl. Radiat. Isot. **30**, 401 (1979), and references therein.
8. D. H. R. Barton, R. H. Hesse, H. T. Toh, and M. M. Pechet. J. Org. Chem. **37**, 329 (1972).
9. J. S. Fowler, R. D. Finn, R. M. Lambrecht, and A. P. Wolf. J. Nucl. Med. **14**, 63, (1973).
10. M. Diksic, S. Farrokhzad, Y. L. Yamamoto, and W. Feindel. Int. J. Nucl. Med. Biol. **11**, 141 (1984).
11. S. Rozen and O. Lerman. J. Org. Chem. **45**, 672 (1980).
12. C.-Y. Shiue, P. A. Salvadori, A. P. Wolf, J. S. Fowler, and R. R. MacGregor. J. Nucl. Med. **23**, 899 (1982), and references therein.
13. J. S. Fowler, C.-Y. Shuie, A. P. Wolf, P. Salvadori, and R. R. MacGregor. Proc. 4th Int. Symp. Radiopharm. Chem., Jülich, W. Germany. August, 1982. p. 359.
14. M. Diksic and D. Jolly. Int. J. Appl. Radiat. Isot. **34**, 893 (1983).
15. R. E. Ehrenkaufer, J. F. Potocki, and D. M. Jewett. J. Nucl. Med. **25**, 333 (1984).
16. M. J. Robins, M. MacCoss, S. R. Naik, and G. Ramani. J. Am. Chem. Soc. **98**, 7381 (1976).
17. S. Rozen, O. Lerman, and M. Kol. J. Chem. Soc. Commun. 443 (1981).
18. D. M. Jewett, J. F. Potocki, and R. E. Ehrenkaufer. Synth. Commun. **14**, 45 (1984).
19. J. D. M. Herscheid, C. J. S. van Rijn, G. W. M. Visser, and A. Hoekstra. Proc. 5th Int. Symp. Radiopharm. Chem., Tokyo, Japan. 1984. p. 209 (abstract).
20. G. Bida, N. Satyamurthy, and J. Barrio. J. Nucl. Med. **25**, 1327 (1984).
21. C.-Y. Shiue, A. P. Wolf, and M. Friedkin. J. Label. Compd. Radiopharm. **21**, 865 (1984).
22. D. Cech and A. Holy. Collect. Czech. Chem. Commun. **41**, 3335 (1976).
23. A. Haas and D. Kortmann. Chem. Ber. **114**, 1176 (1981).
24. T. H. Lowry and K. S. Richardson. Mechanism and theory in organic chemistry. 2nd ed. Harper and Row, New York, 1981. p. 520.
25. R. Duschinsky, E. Plevin, and C. Heidelberger. J. Am. Chem. Soc. **79**, 4559 (1957).

Structural, magnetic, and spectroscopic studies of tetrakis(pyridine) complexes of iron(II) sulfonates

JOHN S. HAYNES, STEVEN J. RETTIG, JOHN R. SAMS, ROBERT C. THOMPSON,[1] AND JAMES TROTTER

Department of Chemistry, University of British Columbia, 2036 Main Mall, Vancouver, B.C., Canada V6T 1Y6

Received August 7, 1985

JOHN S. HAYNES, STEVEN J. RETTIG, JOHN R. SAMS, ROBERT C. THOMPSON and JAMES TROTTER. Can. J. Chem. **64**, 429 (1986).

The iron(II) complexes $Fe(NC_5H_5)_4(RSO_3)_2$ where R = CF_3, CH_3, and p-$CH_3C_6H_4$ have been prepared and their crystal structures determined by single crystal X-ray diffraction. Crystals of *trans*-bis(methanesulfonato-*O*)tetrakis(pyridine)iron(II) are monoclinic, a = 16.524(2), b = 9.1127(6), c = 18.684(2) Å, β = 109.903(6)°, Z = 4, space group *Pn*. The structure was solved by conventional heavy-atom methods and was refined by full-matrix least-squares procedures to R = 0.034 and R_w = 0.038 for 4243 reflections with $I \geq 3\sigma(I)$. Crystals of *trans*-bis(trifluoromethanesulfonato-*O*)tetrakis(pyridine)iron(II) are monoclinic, a = 10.456(1), b = 9.2981(8), c = 14.625(2) Å, β = 96.372(6)°, Z = 2, space group *Pn*. Structure solved and refined as above to R = 0.036, and R_w = 0.037 for 1483 reflections with $I \geq 3\sigma(I)$. Crystals of *trans*-bis(*p*-toluenesulfonato-*O*)tetrakis(pyridine)iron(II) are orthorhombic, a = 40.818(2), b = 9.8722(6), c = 17.3544(7) Å, Z = 8, space group *Fdd2*. The structure was solved by Patterson and Fourier syntheses and was refined by full-matrix least-squares procedures to R = 0.030 and R_w = 0.032 for 1851 reflections with $I \geq 3\sigma(I)$. All three structures show discrete octahedral molecules with monodentate *trans*-coordinated sulfonate groups. Two crystallographically independent molecules are observed in the R = CH_3 structure, the difference between them involving the orientation of the CH_3SO_3 groups with respect to the O—Fe—O vector. The FeN_4O_2 chromophore in each compound is a tetragonally compressed octahedron (approximate D_{4h} symmetry) with average Fe—N distances of 2.21, 2.23, and 2.24 Å and Fe—O distances of 2.11, 2.06, and 2.08 Å for the CF_3, CH_3, and p-$CH_3C_6H_4$ derivatives, respectively. The compounds were studied using vibrational, electronic, and Mössbauer spectroscopic methods, magnetic susceptibility measurements, and differential scanning calorimetry. Quadrupole splitting values from Mössbauer spectra indicate a $^5B_{2g}$ ground state for all three compounds and magnetic susceptibility data (310–4.2 K) have been analyzed assuming this ground state, using both a crystal field and a zero-field splitting model.

JOHN S. HAYNES, STEVEN J. RETTIG, JOHN R. SAMS, ROBERT C. THOMPSON et JAMES TROTTER. Can. J. Chem. **64**, 429 (1986).

On a préparé les complexes du fer(II) $Fe(NC_5H_5)_4(RSO_3)_2$ dans lesquels R = CF_3, CH_3 et p-$CH_3C_6H_4$ et on a déterminé leurs structures par diffraction des rayons-X sur des cristaux uniques. Les cristaux du bis(méthanesulfonato-*O*) tétrakis(pyridine)fer-(II) *trans* sont monocliniques avec a=16,524(2), b=9,1127(6), c=18,684(2) Å, β=109,903(6)°, Z=4 et groupe d'espace *Pn*. On a résolu la structure par les méthodes conventionnelles aux atomes lourds et on l'a affinée par la méthode des moindres carrés (matrice entière) jusqu'à des valeurs de R=0,034 et R_w=0,038 pour 4243 réflexions avec $I \geq 3\sigma(I)$. Les cristaux du bis(trifluorométhanesulfonato-*O*)tetrakis(pyridine)fer(II) *trans* sont monocliniques avec a=10,456(1), b=9,2981(8), c=14,625(2) Å, β=96,372(6)°, Z=2 et groupe d'espace *Pn*. On a résolu et affiinée la structure par les méthodes décrites plus haut jusqu'à des valeurs de R=0,036 et R_w=0,037 pour 1483 réflexions avec $I \geq 3\sigma(I)$. Les cristaux du bis(*p*-toluènesulfonato-*O*)tétrakis(pyridine) fer(II) *trans* sont orthorhombiques avec a=40,818(2), b=9,8722(6), c=17,3544(7) Å, Z=8 et groupe d'espace *Fdd2*. On a résolu la structure par des synthèses de Patterson et de Fourier et on l'a affinée par la méthode des moindres carrés (matrice entière) jusqu'à des valeurs de R=0,030 et R_w=0,032 pour 1851 réflexions avec $I \geq 3\sigma(I)$. Dans le trois structures, on retrouve des molécules octaédriques individuelles avec des groupements sulfonates monodentates coordonnées en *trans*. Dans la structure où R=CH_3, on observe deux molécules qui sont cristallographiquement indépendantes; la différence entre les deux implique l'orientation des groupements CH_3SO_3 par rapport au vecteur O—Fe—O. Dans chacun des composés, le chromophore FeN_4O_2 est un octaèdre qui est comprimé d'une façon tétragonale (symétrie approximative D_{4h}) et dans lequel les distances Fe—N moyennes sont 2,21, 2,23 et 2,24 Å alors que les distances Fe—O sont 2,11, 2,06 et 2,08 Å respectivement pour les dérivés CF_3, CH_3 et p-$CH_3C_6H_4$. On a étudié les composés en faisant appel aux spectroscopies vibrationnelles, électroniques et de Mössbauer, à des mesures de susceptibilité magnétique et à la calorimétrie de balayage différentiel. Les valeurs des dédoublements quadrupolaires obtenus à partir des spectres de Mössbauer indiquent que les trois composés existent dans un état fondamental $^5B_{2g}$; on a analysé les données de susceptibilité magnétique (de 310 à 4,2 K) à l'aide des modèles tant de champ cristallin que de dédoublement à champ zéro en faisant l'hypothèse que l'état fondamental est bien celui-là.

[Traduit par le journal]

Introduction

The study of the coordinating properties of sulfonate anions, RSO_3^-, is of interest for a number of reasons. In view of the fact that they are the anions of relatively strong acids, they might be expected to coordinate only very weakly to transition metal ions. Indeed, there are numerous examples where the trifluoromethanesulfonate (triflate) ion has been utilized as a noncoordinating counter-anion (1–5). Nevertheless, examples where $CF_3SO_3^-$ and other sulfonates coordinate as monodentate (6–10) as well as bidentate and tridentate (11–14) ligands are known.

We had earlier utilized spectroscopic and magnetic techniques to investigate the coordination of sulfonate anions in anhydrous salts (15, 16) as well as in pyridine complexes (17). The basic structure proposed for the latter group of compounds, involving octahedral stereochemistry with *trans*-coordinated sulfonate groups, is confirmed in the present work by single crystal X-ray diffraction studies on the iron(II) methane-, trifluoromethane-, and *p*-toluenesulfonate derivatives. The bonding parameters for these three complexes are examined here with a view to assessing the relative coordinating strengths of the anions and the effects of coordination on anion geometries. This assessment is aided by comparisons with published structural data on other sulfonates and on pyridine complexes

[1]Author to whom correspondence should be addressed.

with other anions (18–22). Finally, the structural information provided by the X-ray diffraction studies on these three closely related compounds permits a detailed examination of the effects of small variations in the nature of the ligand field on the spectroscopic and magnetic properties of octahedral iron(II) complexes.

Experimental

Materials

Anhydrous iron sulfonates, $Fe(RSO_3)_2$, where R is CH_3, CF_3, and p-$CH_3C_6H_4$, were prepared as described previously (16). These compounds, as well as the pyridine complexes, are both moisture and oxygen sensitive and were handled in a nitrogen atmosphere glove box. Pyridine was dried before use by refluxing over barium oxide, then distilling. Methanol was allowed to stand over molecular sieves (4A) before distillation and diethyl ether was dried by refluxing with sodiumbenzophenone followed by distillation. All solvents were degassed prior to use via several freeze–pump–thaw cycles.

Syntheses

The three pyridine complexes were prepared by analogous routes involving addition of an excess of pyridine to a methanol solution of the appropriate iron(II) sulfonate. Over a period of a few hours, crystals of the pyridine complex started to form and, after leaving overnight, the product was isolated by filtration and washed with small quantities of diethyl ether. All manipulations were performed in the glove box. Yields of 60–70% were obtained. As an example, detailed conditions for the preparation of $Fe(NC_5H_5)_4(CF_3SO_3)_2$ are given. To a methanol (5 mL) solution of $Fe(CF_3SO_3)_2$ (1.37 mmol) was added 4 mL of pyridine. Yellow-green crystals of the product which appeared overnight were isolated by filtration and washed with a small amount (~3 mL) of diethyl ether (yield 64%). *Anal.* calcd. for $FeC_{22}F_6H_{20}N_4O_6S_2$: C 39.41, H 3.01, N 8.36; found: C 39.41, H 3.10, N 8.28. *Anal.* calcd. for $Fe(NC_5H_5)_4(CH_3SO_3)_2$: C 46.98, H 4.67, N 9.96, O 17.07; found: C 46.70, H 4.67, N 9.72, O 17.01. *Anal.* calcd. for $Fe(NC_5H_5)_4(CH_3C_6H_4SO_3)_2$: C 57.13, H 4.80, N 7.84, O 13.43; found: C 56.87, H 4.82, N 7.64, O 13.20.

X-ray crystallographic analyses

trans-*Bis(methanesulfonato-*O*)tetrakis(pyridine)iron(II)*

A crystal bounded by the 11 faces (followed by their distances in mm from a common origin) ±(0 0 1), 0.20, ±(0 1 1), 0.27, ±(0 1 −1), 0.27, ±(0 2 1), 0.28 ±(1 0 −1), 0.30, (1 0 0), 0.31 mm was mounted in a general orientation. Unit-cell parameters were refined by least squares on 2 sin θ/λ values for 25 reflections (2θ = 35–42°) measured on a diffractometer with Mo-$K\alpha$ radiation ($\lambda(K\alpha_1)$ = 0.70930, ($\lambda(K\alpha_2)$ = 0.71359 Å). Crystal data at 22°C are:

$C_{22}H_{26}FeN_4O_6S_2$ fw = 562.44

Monoclinic, a = 16.524(2), b = 9.1127(6), c = 18.684(2) Å, β = 109.903(6)°, V = 2645.3(5) Å^3, Z = 4, ρ_c = 1.412 Mg m^{-3}, F(000) = 1168, μ(Mo-$K\alpha$) = 7.61 cm^{-1}. Absent reflections: $h0l$, $h+l$ odd, space group Pn (nonstandard setting of Pc, C_s^2, No. 7, equivalent positions: x, y, z; $1/2+x$, $-y$, $1/2+z$) from structure analysis.

Intensities were measured with graphite-monochromated Mo-$K\alpha$ radiation on an Enraf–Nonius CAD4-F diffractometer. An ω–2θ scan at 1.34–10.06° min^{-1} over a range of (0.85 + 0.35 tan θ) degrees in ω (extended by 25% on both sides for background measurement) was employed. Data were measured to 2θ = 55°. The intensities of three check reflections, measured every hour throughout the data collection, showed only small random fluctuations. After data reduction,[2] an absorption correction was applied using the Gaussian integration method (23, 24). Transmission factors ranged from 0.660 to 0.761 for 112 integration points. Of the 6042 independent reflections measured, 4243 (70.2%) had intensities greater than or equal to 3σ(I) above background, where $\sigma^2(I) = S + 2B + (0.04(S-B))^2$ with S = scan count and B = normalized background count.

The noncentrosymmetric space group Pn was indicated by the E-statistics. The structure was solved by conventional heavy atom methods. The coordinates of the Fe and S atoms from each of the two crystallographically independent molecules were determined from the Patterson function and those of the remaining non-hydrogen atoms from subsequent difference maps. Full-matrix least-squares refinement of the non-hydrogen atoms with anisotropic temperature factors resulted in R = 0.050. In subsequent stages of refinement the hydrogen atoms were included as fixed contributors in idealized positions (methyl groups based on observed positions, C(sp^2)—H = 0.97 Å, C(sp^3)—H = 0.98 Å), recalculated after each cycle of refinement. The scattering factors of ref. 25 were used for non-hydrogen atoms and those of ref. 26 for hydrogen atoms. Anomalous scattering factors from ref. 27 were used for the Fe and S atoms. The weighting scheme $w = 1/\sigma^2(F)$, where $\sigma^2(F)$ is derived from the previously defined $\sigma^2(I)$, gave uniform average values of $w(|F_o|-|F_c|)^2$ over ranges of both $|F_o|$ and sin θ/λ and was employed in the final stages of full-matrix refinement of 629 variables. Reflections with $I < 3\sigma(I)$ were not included in the refinement. Convergence was reached at R = 0.034 and R_w = 0.038 for 4243 reflections with $I \geq 3\sigma(I)$. For all 6042 reflections R = 0.078. The polarity of the structure (for the particular crystal used) was determined by parallel refinement, the resulting R and R_w factor ratios of 1.023 and 1.028, respectively, representing a probability of >99.5% that the correct polarity has been chosen. The function minimized was $\Sigma w(|F_o|-|F_c|)^2$, $R = \Sigma||F_o|-|F_c||/\Sigma|F_o|$ and $R_w = (\Sigma w(|F_o| - |F_c|)^2/\Sigma w|F_o|^2)^{1/2}$.

On the final cycle of refinement the mean and maximum parameter shifts corresponded to 0.02 and 0.16σ, respectively. The mean error in an observation of unit weight was 1.546. A final difference map showed maximum fluctuations of −0.85 to +0.36 e Å^{-3} near Fe atoms and was featureless elsewhere. The final positional and thermal parameters appear in Tables 1 and 5,[3] respectively. Measured and calculated structure factors have been placed in the Depository of Unpublished Data.[3]

trans-*Bis(trifluoromethanesulfonato-*O*-tetrakis(pyridine)iron(II)*

Experimental details are as above except where noted. The 8 bounding planes of the crystal used for data collection were: ±(−1 0 1), 0.09, ±(1 0 1), 0.31, ±(0 1 0), 0.06, ±(0 0 1), 0.33 mm. Reflections used in the refinement of the unit-cell constants had 2θ = 26–33°. Crystal data:

$C_{22}H_{20}F_6FeN_4O_6S_2$ fw = 670.38

Monoclinic, a = 10.456(1), b = 9.2981(8), c = 14.625(2) Å, β = 96.372(6)°, V = 1413.1(3) Å^3, Z = 2, ρ_c = 1.576 Mg m^{-3}, $F(000)$ = 680, μ(Mo-$K\alpha$) = 7.54 cm^{-1}. Absent reflections: $h0l$, $h+l$ odd, space group Pn from structure analysis.

An ω–2θ scan at 1.18–10.06° min^{-1} over a range of (0.65 + 0.35 tanθ)° in ω was employed. Of 2771 independent reflections measured (to 2θ = 52°), 1483 had intensities greater than 3σ(I) above background. An absorption correction was applied, transmission factors ranging from 0.895 to 0.909 for 88 sampling points.

The noncentrosymmetric space group Pn was suggested by both the E-statistics and by the Patterson function, from which the coordinates of the Fe and S atoms were determined. Refinement of the non-hydrogen atoms with anisotropic thermal parameters gave R = 0.047. Hydrogen atoms were included as fixed contributors in idealized positions in the final stages of refinement. Convergence was reached at

[2]The computer programs used include locally written programs for data processing and locally modified versions of the following: ORFLS, full-matrix least-squares, and ORFFE, function and errors, by W. R. Busing, K. O. Martin and H. A. Levy; FORDAP, Patterson and Fourier syntheses, by A. Zalkin; ORTEP II, illustrations, by C. K. Johnson; AGNOST, absorption corrections, by J. A. Ibers; TLS, thermal motion analysis, by V. Schomaker and K. N. Trueblood.

[3]The structure factor table, Table 5 (anisotropic thermal parameters), and other material mentioned in the text may be purchased from the Depository of Unpublished Data, CISTI, National Research Council of Canada, Ottawa, Ont., Canada, K1A 0S2.

$R = 0.036$ and $R_w = 0.037$ for 1483 reflections with $I \geq 3\sigma(I)$ (368 variables). For all 2771 reflections $R = 0.103$. The polarity was again determined by parallel refinement, the R and R_w ratios of 1.009 and 1.006 both corresponding to a >99.5% probability that the correct polarity has been chosen. The mean and maximum parameter shifts on the final cycle of refinement corresponded to 0.02 and 0.09σ, respectively, and the mean error in an observation of unit weight was 1.363. A final difference map showed maximum fluctuations of −0.56 to +0.47 e Å^{-3} near Fe and was featureless elsewhere.

trans-*Bis*(p-*toluenesulfonato*-O)*tetrakis(pyridine)iron(II)*

The six bounding planes of the crystal used for data collection were: ±(1 0 0), 0.15, (−1 2 −2), 0.19, (−1 −2 −2), 0.20, (−1 −1 1), 0.18, (−1 1 1), 0.21 mm. Reflections used for the refinement of the lattice constants had 2θ = 30–40°. Crystal data:

$C_{34}H_{34}FeN_4O_6S_2$ fw = 714.63

Orthorhombic, $a = 40.818(2)$, $b = 9.8722(6)$, $c = 17.3544(7)$ Å, $V = 6993.0(6)$ Å^3, $Z = 8$, $\rho_c = 1.358$ Mg m^{-3}, $F(000) = 2976$, μ(Mo-$K\alpha$) = 5.91 cm^{-1}. Absent reflections: hkl, $h+k$ odd and $k+l$ odd, $0kl$, $k+l \neq 4n$, and $h0l$, $h+l \neq 4n$, uniquely indicate the space group $Fdd2$ (C_{2v}^{19}, No. 43).

An ω–2θ scan at 0.84–10.06° min^{-1} over a range of (0.65 + 0.35 tan θ)° was employed. Of 2605 independent reflections measured (to 2θ = 60°), 1851 had $I \geq 3\sigma(I)$. Data were corrected for absorption, transmission factors ranging from 0.824 to 0.900 for 88 sampling points.

Space group symmetry requires the molecule to possess exact C_2 symmetry. The Fe and S coordinates were determined from the Patterson function and those of the remaining non-hydrogen atoms from a subsequent difference map. After refinement of the non-hydrogen atoms with anisotropic thermal parameters to $R = 0.043$, a difference map gave the positions of all hydrogen atoms, which were refined with isotropic thermal parameters in subsequent least-squares cycles. Convergence was reached at $R = 0.030$ and $R_w = 0.032$ for 1851 reflections with $I \geq 3\sigma(I)$ (280 variables). For all 2605 reflections $R = 0.073$. The polarity was determined by parallel refinement, the R and R_w ratios of 1.055 and 1.069 clearly indicating the correct choice ($p > 99.9\%$). The mean and maximum parameter shifts on the final cycle of refinement were 0.015 and 0.23σ and the mean error in an observation of unit weight was 1.346. Maximum fluctuations on the final difference map were −0.25 to +0.17 e Å^{-3}.

Analysis of thermal motion

The thermal motion in the three compounds (Figs. 1 and 2) has been analyzed in terms of the rigid-body modes of translation, libration, and screw motion (TLS model) (28). The rms errors in the U_{ij} (derived from the least-squares analyses) are 0.0031, 0.0053, and 0.0019 Å^2, respectively, for $Fe(NC_5H_5)_4(RSO_3)_2$, R = CH_3, CF_3, and p-$CH_3C_6H_4$. In each case, analyses of the entire molecule indicated significant independent motion of structural subunits, particularly the sulfonate groups. The subunits SO_3C, $O_2Fe(py)_4$, SCF_3, and tolyl were separately analyzed (rms $\Delta U_{ij} = 0.0012–0.0083$ Å^2). The appropriate distances have been corrected for libration (28, 29), using shape parameters q^2 of 0.08 for all atoms involved. Corrected bond lengths appear along with the uncorrected values in Table 2. Bond angles are given in Table 3. Calculated hydrogen atom parameters for $Fe(NC_5H_5)_4(CH_3SO_3)_2$ and $Fe(NC_5H_5)_4(CF_3SO_3)_2$, anisotropic thermal parameters, bond lengths and angles involving hydrogen for $Fe(NC_5H_5)_4(p\text{-}CH_3C_6H_4SO_3)_2$, and complete listings of torsion angles (Tables 4–8) are included as supplementary material.

Spectroscopy

Infrared spectra in the region 4000–250 cm^{-1} were recorded on samples mulled in Nujol held between KRS-5 plates (Harshaw Chemical Co.) using a Perkin Elmer 598 spectrophotometer. Electronic spectra (3.8–30 kK) were recorded on samples mulled in Nujol using a Cary 14 spectrophotometer. ^{57}Fe Mössbauer spectra were obtained as reported previously (30). Samples were contained in Nylon holders sealed with epoxy resin. The Doppler velocity scale was calibrated with a metallic iron foil absorber and isomer shifts are quoted relative to the centroid of the iron foil spectrum.

Magnetic susceptibilities

Variable temperature magnetic susceptibility measurements were made between 130 and 4.2 K using a vibrating sample magnetometer (31) and between 300 and 80 K using Gouy equipment (32). Magnetic susceptibilities were measured at room temperature at three different values of $H\,dH/dx$ with a Faraday magnetic balance (33). No field dependence was observed for any of the complexes. Molar magnetic susceptibilities were corrected for the diamagnetic susceptibilities of all atoms; corrections used were Fe^{2+} −13, NC_5H_5 −49, $CF_3SO_3^-$ −46, $CH_3SO_3^-$ −35, $CH_3C_6H_4SO_3^-$ −89 (units 10^{-6} cm^3 mol^{-1}).

Differential scanning calorimetry (DSC)

The DSC runs were performed using a Mettler DSC 20 cell programmed with a Mettler TC 10A processor. Powdered samples (~5 mg) contained in aluminum crucibles were heated (35–450°C at a rate of 4° min^{-1}) in an atmosphere of dry nitrogen (flow rate 50 mL min^{-1}). The temperature calibration was achieved using the known fusion temperatures of indium, lead, and zinc and the heat flow was calibrated using an accurately known quantity of indium.

Results and discussion

Crystal structure analyses

The molecular structures of the three $Fe(NC_5H_5)_4(RSO_3)_2$ molecules are given in Figs. 1 and 2 along with the atom numbering schemes; intermolecular bond distances and angles are given in Tables 2 and 3. With the exception of possible weak C—H···O hydrogen bonds (Table 9, deposited supplementary materials), each of the three structures consists of discrete molecules separated by normal van der Waals distances. Structure analyses show all three compounds to be octahedral with monodentate *trans*-coordinated sulfonate groups. Two conformations are observed in the R = CH_3 compound, the difference between them involving the orientation of the CH_3SO_3 groups with respect to the O—Fe—O vector. The two independent R = CH_3 molecules and the R = CF_3 molecule have approximate C_2 symmetry and for R = p-tolyl the molecules possess exact C_2 symmetry. In each case the twofold axis lies in the FeN_4 plane and bisects opposite N—Fe—N angles.

The FeN_4 groups are nonplanar in all three compounds. For R = CH_3 and CF_3 the maximum deviations from the mean plane are less than 0.021 Å, while for R = p-tolyl the maximum deviation is 0.284(4) Å. In the R = CF_3 structure the four pyridine N atoms are coplanar; the Fe is displaced 0.015(1) Å from the N_4 plane. The pyridine rings are generally planar to within experimental error. While the pyridine rings containing N(1), N(4), and N(6) in the R = CH_3 structure and N(2) in the R = p-tolyl structure are nonplanar, no atom deviates by more than 0.015(4) Å. The bond distances and angles in the pyridine rings are similar to those found for free gaseous pyridine by electron diffraction and microwave spectroscopy (34, 35). An interesting structural feature present in all three compounds is that the four pyridine molecules are arranged in a staggered propeller fashion and the rings *trans* to one another are nearly orthogonal. The *trans*-pyridine bonds are very close to linear, whereas the O—Fe—O bond angles deviate significantly from 180°. Nevertheless, the overall distortion of the FeN_4O_2 chromophore is not great and the environment around the iron atom in all three compounds may be described as approximately D_{4h}.

The average Fe—N distances for the CF_3, CH_3, and p-$CH_3C_6H_4$ derivatives are 2.21, 2.23, and 2.24 Å, respectively. These are comparable to the distances 2.23 Å reported for

TABLE 1. Final positional (fractional × 10^4, Fe and S × 10^5, H × 10^3) and isotropic thermal parameters ($U \times 10^3$ Å^2) with estimated standard deviations in parentheses[a]

Atom	x	y	z	U_{eq}/U_{iso}
		$Fe(NC_5H_5)_4(CH_3SO_3)_2$		
Fe(1)	40090	68958(6)	63300	37
Fe(2)	90418(6)	66988(6)	62924(5)	34
S(1)	49188(10)	91714(12)	78340(8)	43
S(2)	35615(10)	44572(15)	48373(9)	53
S(3)	86211(10)	94617(13)	49533(8)	49
S(4)	96112(9)	35613(13)	73588(8)	46
O(1)	4294(2)	8465(4)	7167(2)	56
O(2)	3596(3)	5326(4)	5495(2)	59
O(3)	8660(2)	8477(4)	5578(2)	48
O(4)	9304(2)	5035(4)	7085(2)	54
O(5)	5211(4)	8176(5)	8462(2)	85
O(6)	5602(3)	9844(4)	7654(3)	69
O(7)	3246(4)	5303(7)	4163(3)	114
O(8)	4361(3)	3759(6)	4933(4)	108
O(9)	8199(3)	8814(5)	4229(2)	75
O(10)	9486(3)	10013(5)	5041(3)	82
O(11)	10516(3)	3528(5)	7723(4)	98
O(12)	9261(4)	2481(4)	6798(3)	95
N(1)	3310(3)	5609(5)	6971(2)	45
N(2)	2842(3)	8207(4)	5735(2)	43
N(3)	4719(3)	8146(4)	5707(2)	44
N(4)	5179(3)	5584(4)	6892(2)	42
N(5)	7829(3)	5567(4)	5617(2)	41
N(6)	8394(3)	7831(4)	7014(2)	41
N(7)	10235(2)	7832(4)	6966(2)	39
N(8)	9714(3)	5687(4)	5575(2)	40
C(1)	4327(5)	10595(8)	8065(4)	84
C(2)	2814(6)	3064(9)	4803(6)	115
C(3)	8053(5)	10997(7)	5078(4)	76
C(4)	9162(8)	3212(10)	8066(6)	121
C(5)	3678(3)	5335(6)	7704(3)	50
C(6)	3329(4)	4370(6)	8094(3)	55
C(7)	2574(4)	3680(7)	7715(4)	64
C(8)	2174(4)	3992(7)	6959(4)	62
C(9)	2561(3)	4945(6)	6608(3)	51
C(10)	2413(3)	8901(6)	6123(3)	52
C(11)	1711(4)	9793(7)	5779(4)	63
C(12)	1440(3)	9947(7)	5012(4)	60
C(13)	1861(3)	9243(6)	4596(3)	54
C(14)	2564(3)	8396(6)	4978(3)	47
C(15)	4699(4)	9600(6)	5691(3)	55
C(16)	5092(4)	10451(6)	5288(4)	68
C(17)	5538(4)	9730(8)	4887(4)	76
C(18)	5577(4)	8237(8)	4910(4)	71
C(19)	5165(4)	7479(6)	5328(3)	56
C(20)	5138(4)	4123(5)	6946(3)	55
C(21)	5839(4)	3282(6)	7356(4)	67
C(22)	6595(4)	3957(7)	7713(4)	68
C(23)	6655(3)	5453(7)	7651(3)	61
C(24)	5937(3)	6221(5)	7235(3)	48
C(25)	7508(3)	5660(6)	4868(3)	48
C(26)	6751(4)	4996(7)	4429(3)	61
C(27)	6295(4)	4203(7)	4795(4)	63
C(28)	6614(4)	4084(7)	5560(4)	65
C(29)	7382(3)	4771(6)	5960(3)	54
C(30)	7667(4)	8587(6)	6689(3)	53
C(31)	7299(4)	9422(7)	7109(4)	76
C(32)	7695(6)	9505(8)	7873(5)	88
C(33)	8430(5)	8732(9)	8216(3)	77
C(34)	8747(4)	7873(6)	7756(3)	53
C(35)	10269(3)	9285(5)	7072(3)	44
C(36)	10989(4)	10003(6)	7534(4)	57
C(37)	11716(4)	9201(6)	7913(3)	58
C(38)	11702(3)	7717(6)	7804(3)	56
C(39)	10960(3)	7057(5)	7331(3)	48
C(40)	9624(4)	4273(5)	5386(3)	51
C(41)	9979(4)	3634(6)	4892(3)	57
C(42)	10457(4)	4469(7)	4581(3)	59
C(43)	10567(4)	5934(6)	4775(3)	58
C(44)	10187(3)	6502(5)	5270(3)	48
		$Fe(NC_5H_5)_4(CF_3SO_3)_2$		
Fe	46180	49617(16)	49420	37
S(1)	68694(23)	25378(29)	43403(18)	50
S(2)	28680(25)	74813(30)	60146(18)	50
F(1)	7322(7)	239(8)	3430(6)	106
F(2)	5526(7)	224(6)	4010(4)	87
F(3)	5718(7)	1490(8)	2821(4)	85
F(4)	1614(8)	9892(8)	5878(6)	107
F(5)	3071(7)	9703(7)	4959(5)	96
F(6)	1321(7)	8558(9)	4687(5)	104
O(1)	5659(6)	3246(7)	4450(5)	57
O(2)	7693(6)	3349(9)	3817(5)	78
O(3)	7431(8)	1896(8)	5164(5)	84
O(4)	3466(6)	6670(7)	5333(4)	49
O(5)	1798(7)	6761(9)	6331(5)	79
O(6)	3778(7)	8136(8)	6684(5)	72
N(1)	4607(7)	3841(9)	6284(5)	41
N(2)	4608(7)	6101(10)	3611(5)	46
N(3)	2873(7)	3798(9)	4405(5)	40
N(4)	6357(6)	6139(9)	5508(5)	43
C(1)	6318(9)	1058(11)	3614(7)	56
C(2)	2180(11)	8993(13)	5362(8)	72
C(3)	4487(9)	2407(11)	6314(7)	57
C(4)	4400(11)	1644(11)	7116(8)	69
C(5)	4387(11)	2401(18)	7927(7)	77
C(6)	4534(10)	3857(12)	7914(7)	65
C(7)	4624(10)	4525(9)	7084(7)	57
C(8)	3551(9)	6801(10)	3244(6)	57
C(9)	3495(9)	7604(12)	2457(7)	65
C(10)	4605(11)	7724(13)	2027(7)	62
C(11)	5675(10)	7023(12)	2376(7)	68
C(12)	5655(8)	6206(10)	3167(6)	51
C(13)	2805(8)	3078(10)	3607(6)	52
C(14)	1714(9)	2362(11)	3240(6)	60
C(15)	682(10)	2319(14)	3710(7)	63
C(16)	710(8)	3058(11)	4531(7)	56
C(17)	1832(8)	3778(9)	4861(6)	46
C(18)	6437(9)	7551(10)	5398(6)	58
C(19)	7541(11)	8315(11)	5662(7)	63
C(20)	8638(9)	7590(16)	6058(7)	61
C(21)	8552(8)	6156(12)	6167(7)	60
C(22)	7408(9)	5466(9)	5899(6)	54
		$Fe(NC_5H_5)_4(CH_3C_6H_4SO_3)_2$		
Fe	25000	25000	25000	31
S	18614(2)	3502(8)	21696(5)	43
O(1)	2140(<1)	1019(2)	2555(1)	44
O(2)	1628(1)	1335(3)	1905(2)	78
O(3)	1968(1)	−607(3)	1611(2)	71
N(1)	2253(1)	3772(3)	1619(2)	39
N(2)	2224(1)	3554(3)	3445(2)	39
C(1)	1669(1)	−573(3)	2916(2)	40
C(2)	1764(1)	−1870(4)	3082(2)	57
C(3)	1608(1)	−2583(4)	3651(3)	67
C(4)	1360(1)	−2029(4)	4083(2)	58
C(5)	1269(1)	−705(5)	3913(3)	65
C(6)	1419(1)	14(4)	3341(3)	55

TABLE 1. (*Concluded*)

Atom	*x*	*y*	*z*	U_{eq}/U_{iso}
C(7)	1188(2)	−2812(7)	4703(4)	88
C(8)	2241(1)	5125(3)	1714(2)	49
C(9)	2094(1)	5967(5)	1186(3)	63
C(10)	1952(1)	5438(5)	540(3)	72
C(11)	1969(1)	4054(6)	436(3)	69
C(12)	2118(1)	3266(4)	983(2)	50
C(13)	2373(1)	4113(4)	4051(2)	56
C(14)	2211(1)	4450(5)	4720(2)	68
C(15)	1884(1)	4246(5)	4773(2)	58
C(16)	1723(1)	3710(4)	4158(2)	50
C(17)	1899(1)	3371(3)	3504(2)	42
H(2)	189(1)	−221(5)	282(3)	64(14)
H(3)	166(2)	−357(8)	386(5)	137(23)
H(5)	110(2)	−35(8)	429(6)	164(31)
H(6)	136(1)	97(5)	325(3)	62(11)
H(7a)	115(1)	−380(7)	449(4)	111(20)
H(7b)	135(1)	−312(6)	491(4)	85(19)
H(7c)	98(3)	−254(9)	484(8)	187(39)
H(8)	233(1)	550(3)	211(3)	37(8)
H(9)	206(1)	685(6)	123(3)	75(14)
H(10)	188(2)	616(7)	11(5)	125(22)
H(11)	187(1)	371(5)	4(3)	74(14)
H(12)	214(1)	235(4)	95(2)	42(9)
H(13)	259(1)	421(3)	399(2)	44(9)
H(14)	233(1)	477(4)	511(3)	71(13)
H(15)	176(1)	446(6)	522(4)	99(18)
H(16)	148(1)	357(5)	417(3)	78(14)
H(17)	178(1)	296(3)	306(2)	35(8)

[a] U_{eq} = 1/3 trace (diagonalized *U*).

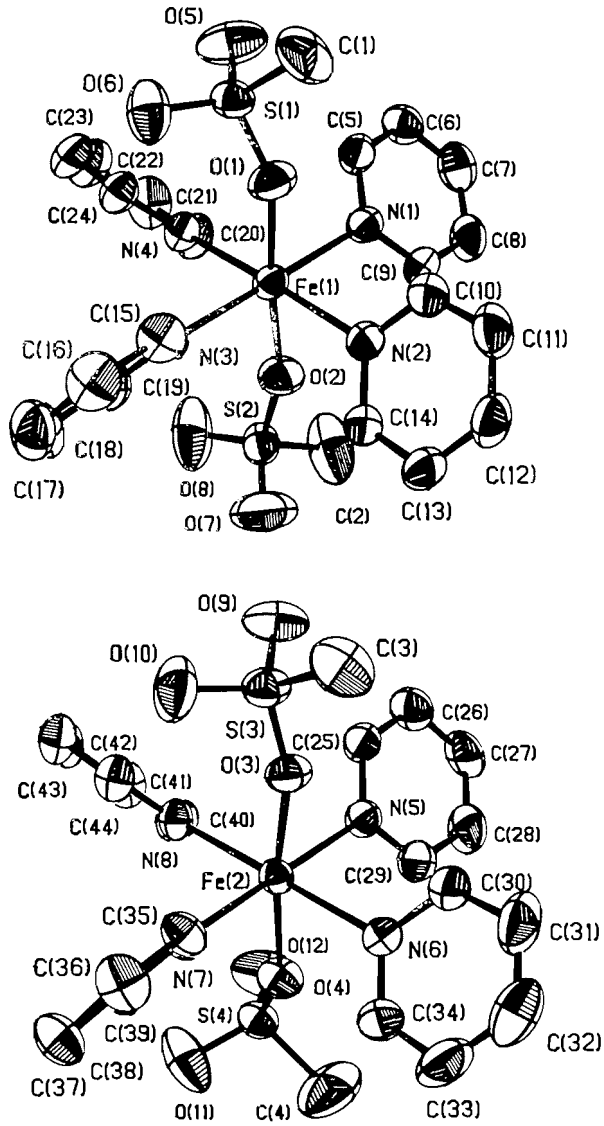

FIG. 1. Views of the two independent $Fe(NC_5H_5)_4(CH_3SO_3)_2$ molecules; 50% probability thermal ellipsoids are shown for the non-hydrogen atoms.

$Fe(py)_4Cl_2$ (18) and 2.26 Å for $Fe(py)_4(NCS)_2$ (19). The Fe—O distances range from 2.11 A in the trifluoromethanesulfonate complex to 2.06 Å in the methanesulfonate compound. Assuming that Fe—O bond distances in sulfonate complexes are good measures of the strength of the metal–anion coordination, it is interesting to note that in $[\eta^5\text{-}C_5(CH_3)_5](CO)_2FeOSO_2CF_3$ the Fe—O distance is only 2.007 Å (6). The presence of the strong π-acid ligands in this complex makes the iron centre strongly electrophilic and results in what is described in ref. 6 as a strong "electrostatic iron–triflate interaction."

Turning to a consideration of internal bonding parameters for individual anions, we note that the bond distances and angles observed here for $CF_3SO_3^-$ appear comparable to those seen in other unidentate coordinated trifluoromethanesulfonate groups (6–10). The anion assumes a staggered-ethane conformation about the S—C bond and, while the average C—F bond length is greater than those usually found in ionic $CF_3SO_3^-$ compounds (2–5), it is typical for the unidentate coordinated anion (6–10). The O—S—O angles are consistently greater than the C—S—O angles, a consequence of the fact that bond pair repulsions involving the multiply bonded S—O groups are greater than those involving the S—C group. The effect of coordination on the $CF_3SO_3^-$ group is most clearly seen in the S—O bond distances. The S—O bond involving the oxygen coordinated to iron is the longest such distance in this compound and the average bond length for the terminal S—O bonds (~1.44 Å) is close to the value found in ionic $CF_3SO_3^-$ compounds (2–5).

The methanesulfonate compound has the same staggered-ethane type structure for the anion with O—S—O angles greater and C—S—O angles smaller than the tetrahedral angle. The average S—C bond distance in this case (1.78 Å) is slightly shorter than in the $CF_3SO_3^-$ compound but longer than that seen in $Ca(CH_3SO_3)_2$ (ave. S—C = 1.75 A) (12). Again, the average S—O distance involving the iron-bound oxygens is longer (1.48 Å) than the average S—O distance involving terminal oxygens (1.45 Å). In the compounds $Ca(CH_3SO_3)_2$ (12) and $Cu(CO)(C_2H_5SO_3)$ (36) the sulfonate anion acts as a tridentate ligand and the range of S—O bond distances is much smaller, 1.429–1.456 Å and 1.445–1.462 Å, respectively. In these structures the effect of anion coordination only slightly affects the equality of S—O bond lengths. Two other methanesulfonates with known structures are relevant here, $Cu(CH_3SO_3)_2(H_2O)_4$ (10) and $Cd(CH_3SO_3)_2(H_2O)_2$ (14). In the copper complex the water molecules form the equatorial plane of a tetragonally distorted octahedron with two unidentate coordinated $CH_3SO_3^-$ groups in axial positions. Somewhat surprisingly, and in contrast to what is found here, the S—O bonds involving the terminal oxygens in the aquo complex are longer than those involving the oxygens bonded to the metal. This is likely a consequence of hydrogen bonding interactions

TABLE 2. Bond lengths (Å) with estimated standard deviations in parentheses

Bond	Length uncorr.	Length corr.	Bond	Length uncorr.	Length corr.
		$Fe(NC_5H_5)_4(CH_3SO_3)_2$			
Fe(1)—O(1)	2.052(3)	2.057	N(6)—C(30)	1.338(6)	1.339
Fe(1)—O(2)	2.054(3)	2.059	N(6)—C(34)	1.309(6)	1.310
Fe(1)—N(1)	2.254(4)	2.258	N(7)—C(35)	1.337(6)	1.339
Fe(1)—N(2)	2.219(4)	2.223	N(7)—C(39)	1.358(6)	1.360
Fe(1)—N(3)	2.227(4)	2.231	N(8)—C(40)	1.331(6)	1.332
Fe(1)—N(4)	2.211(4)	2.214	N(8)—C(44)	1.338(6)	1.339
Fe(2)—O(3)	2.057(3)	2.062	C(5)—C(6)	1.389(7)	1.390
Fe(2)—O(4)	2.059(3)	2.064	C(6)—C(7)	1.360(8)	1.362
Fe(2)—N(5)	2.224(3)	2.228	C(7)—C(8)	1.370(9)	1.372
Fe(2)—N(6)	2.239(4)	2.243	C(8)—C(9)	1.371(8)	1.373
Fe(2)—N(7)	2.201(4)	2.205	C(10)—C(11)	1.382(8)	1.383
Fe(2)—N(8)	2.213(4)	2.217	C(11)—C(12)	1.356(8)	1.358
S(1)—O(1)	1.469(4)	1.491	C(12)—C(13)	1.367(8)	1.368
S(1)—O(5)	1.431(4)	1.455	C(13)—C(14)	1.374(7)	1.374
S(1)—O(6)	1.422(4)	1.445	C(15)—C(16)	1.386(8)	1.387
S(1)—C(1)	1.764(6)	1.788	C(16)—C(17)	1.384(10)	1.386
S(2)—O(2)	1.446(4)	1.478	C(17)—C(18)	1.363(9)	1.364
S(2)—O(7)	1.416(5)	1.448	C(18)—C(19)	1.383(8)	1.384
S(2)—O(8)	1.421(5)	1.453	C(20)—C(21)	1.383(8)	1.383
S(2)—C(2)	1.758(7)	1.788	C(21)—C(22)	1.349(9)	1.350
S(3)—O(3)	1.456(3)	1.475	C(22)—C(23)	1.374(9)	1.376
S(3)—O(9)	1.422(4)	1.440	C(23)—C(24)	1.369(7)	1.370
S(3)—O(10)	1.470(4)	1.490	C(25)—C(26)	1.380(8)	1.382
S(3)—C(3)	1.745(6)	1.763	C(26)—C(27)	1.381(9)	1.383
S(4)—O(4)	1.466(3)	1.484	C(27)—C(28)	1.349(9)	1.352
S(4)—O(11)	1.417(5)	1.445	C(28)—C(29)	1.384(8)	1.386
S(4)—O(12)	1.411(4)	1.439	C(30)—C(31)	1.375(8)	1.375
S(4)—C(4)	1.750(9)	1.787	C(31)—C(32)	1.355(10)	1.357
N(1)—C(5)	1.319(6)	1.321	C(32)—C(33)	1.361(11)	1.362
N(1)—C(9)	1.336(6)	1.339	C(33)—C(34)	1.390(8)	1.390
N(2)—C(10)	1.332(7)	1.333	C(35)—C(36)	1.376(7)	1.376
N(2)—C(14)	1.341(6)	1.343	C(36)—C(37)	1.378(8)	1.379
N(3)—C(15)	1.326(6)	1.327	C(37)—C(38)	1.367(8)	1.369
N(3)—C(19)	1.330(7)	1.332	C(38)—C(39)	1.381(7)	1.381
N(4)—C(20)	1.339(6)	1.341	C(40)—C(41)	1.379(7)	1.380
N(4)—C(24)	1.330(6)	1.331	C(41)—C(42)	1.361(8)	1.362
N(5)—C(25)	1.319(6)	1.322	C(42)—C(43)	1.379(8)	1.380
N(5)—C(29)	1.344(6)	1.347	C(43)—C(44)	1.383(8)	1.384
		$Fe(NC_5H_5)_4(CF_3SO_3)_2$			
Fe—O(1)	2.102(6)	2.107	N(2)—C(8)	1.343(11)	1.345
Fe—O(4)	2.110(6)	2.115	N(2)—C(12)	1.337(11)	1.338
Fe—N(1)	2.223(8)	2.227	N(3)—C(13)	1.340(11)	1.342
Fe—N(2)	2.215(8)	2.219	N(3)—C(17)	1.338(10)	1.339
Fe—N(3)	2.190(7)	2.193	N(4)—C(18)	1.326(12)	1.328
Fe—N(4)	2.203(7)	2.206	N(4)—C(22)	1.337(11)	1.338
S(1)—O(1)	1.452(7)	1.471	C(3)—C(4)	1.383(13)	1.384
S(1)—O(2)	1.429(7)	1.449	C(4)—C(5)	1.38(2)	1.38
S(1)—O(3)	1.412(7)	1.427	C(5)—C(6)	1.36(2)	1.37
S(1)—C(1)	1.793(10)	1.813	C(6)—C(7)	1.375(13)	1.377
S(2)—O(4)	1.446(7)	1.461	C(8)—C(9)	1.368(13)	1.368
S(2)—O(5)	1.425(7)	1.441	C(9)—C(10)	1.383(13)	1.385
S(2)—O(6)	1.423(7)	1.439	C(10)—C(11)	1.346(14)	1.348
S(2)—C(2)	1.803(11)	1.822	C(11)—C(12)	1.385(13)	1.386
F(1)—C(1)	1.348(10)	1.372	C(13)—C(14)	1.377(12)	1.378
F(2)—C(1)	1.315(11)	1.339	C(14)—C(15)	1.343(14)	1.345
F(3)—C(1)	1.319(10)	1.343	C(15)—C(16)	1.381(14)	1.382
F(4)—C(2)	1.310(12)	1.330	C(16)—C(17)	1.391(11)	1.391
F(5)—C(2)	1.331(12)	1.354	C(18)—C(19)	1.374(13)	1.375
F(6)—C(2)	1.323(12)	1.348	C(19)—C(20)	1.400(14)	1.401
N(1)—C(3)	1.340(12)	1.342	C(20)—C(21)	1.35(2)	1.35
N(1)—C(7)	1.331(12)	1.332	C(21)—C(22)	1.376(12)	1.376

TABLE 2. (*Concluded*)

Bond	Length uncorr.	Length corr.	Bond	Length uncorr.	Length corr.
			$Fe(NC_5H_5)_4(CH_3C_6H_4SO_3)_2$		
Fe—O(1)	2.076(2)	2.080	C(2)—C(3)	1.371(6)	1.378
Fe—N(1)	2.221(3)	2.226	C(3)—C(4)	1.373(6)	1.387
Fe—N(2)	2.245(3)	2.248	C(4)—C(5)	1.391(6)	1.407
S—O(1)	1.474(2)	1.489	C(4)—C(7)	1.499(6)	1.504
S—O(2)	1.437(3)	1.452	C(5)—C(6)	1.364(6)	1.370
S—O(3)	1.421(3)	1.436	C(8)—C(9)	1.375(6)	1.377
S—C(1)	1.768(3)	1.777	C(9)—C(10)	1.365(7)	1.368
N(1)—C(8)	1.347(4)	1.349	C(10)—C(11)	1.380(8)	1.382
N(1)—C(12)	1.330(4)	1.333	C(11)—C(12)	1.372(6)	1.375
N(2)—C(13)	1.335(4)	1.335	C(13)—C(14)	1.376(6)	1.376
N(2)—C(17)	1.341(4)	1.343	C(14)—C(15)	1.355(6)	1.356
C(1)—C(2)	1.369(5)	1.384	C(15)—C(16)	1.360(6)	1.362
C(1)—C(6)	1.386(5)	1.401	C(16)—C(17)	1.384(5)	1.385

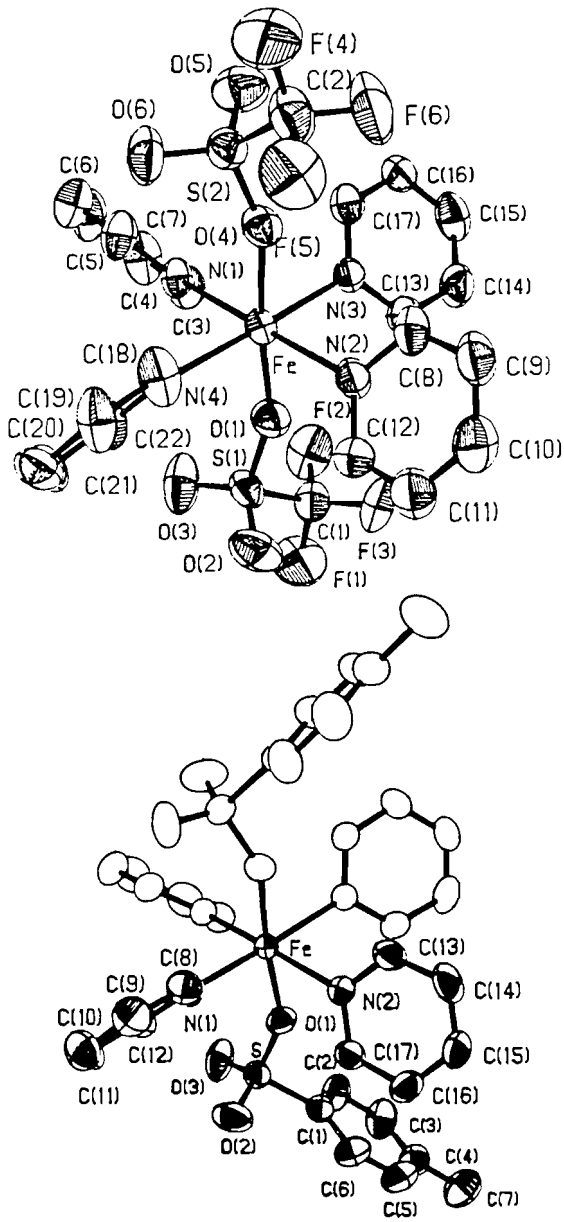

FIG. 2. Views of $Fe(NC_5H_5)_4(CF_3SO_3)_2$ (top) and $Fe(NC_5H_5)_4(p\text{-}CH_3C_6H_4SO_3)_2$ (bottom); 50% probability thermal ellipsoids are shown for the non-hydrogen atoms.

involving the terminal sulfonate oxygens that are present in the aquo complex but absent in the pyridine complexes studied here. The cadmium complex (14) contains metal atoms bridged by bidentate methanesulfonate groups to form an infinite chain structure. In this case the S—O terminal bond (1.436 Å) is shorter than the terminal S—O bonds in $Fe(py)_4(CH_3SO_3)_2$ (ave. 1.452 Å), as is expected due to the fact that in the cadmium complex the S—O π-bonding involves primarily only one terminal S—O bond while in the iron complex the π-bonding is shared between two such bonds.

In $Fe(py)_4(p\text{-}CH_3C_6H_4SO_3)_2$ the geometry around sulfur is, again, approximately tetrahedral with the largest distortion in the O(3)—S—O(2) angle (Fig. 2). The benzene ring is planar within experimental accuracy and the bond lengths and angles in the ring are as expected. Again, the terminal S—O distances are shorter (1.45 and 1.44 Å) than the S—O distance involving the oxygen coordinated to iron (1.49 Å). In organic *p*-toluenesulfonates (37–39), the S—O distances in the S—O—R groups are longer still (~1.57 Å). This is a clear illustration of the difference between bonding modes involving sulfonates and metals on the one hand and carbon on the other, the former being more ionic and one that does not distort the anion geometry as much. Consistent with this observation, we note that the S—O distances in the pyridine complex are closer to those observed in the parent acid hydrate (40), a compound that exists as an oxonium salt with all the S—O bonds approximately the same (ave. 1.454 Å).

Spectroscopy and magnetism

Partial infrared data with assignments are given in Table 10. Bands assigned to internal vibrations of the pyridine ligands are typical for complexes of this type and, in particular, the 8a, 6a, and 16b vibrations show the expected shift to higher frequencies on coordination (41–44). X-ray diffraction clearly showed that for all three complexes the CSO_3 moiety undergoes symmetry reduction from C_{3v} to approximate C_s on coordination. In C_{3v} symmetry six infrared active bands ($3E$ and $3A_1$) are expected for this group, while in C_s the E modes are split and nine bands are expected. In Table 10 infrared bands assigned to CSO_3 are listed according to the C_{3v} modes from which they are derived. Clearest evidence of symmetry reduction in all three complexes is the splitting by 80–90 cm^{-1} of the degenerate $\nu_4(E)$, SO_3 stretching mode in C_{3v} symmetry. Further evidence of symmetry reduction is seen in the SO_3 deformation regions of the spectra of the methyl and trifluoromethyl derivatives. In C_{3v} symmetry

TABLE 3. Bond angles (deg) with estimated standard deviations in parentheses

Bonds	Angle (deg)	Bonds	Angle (deg)
	$Fe(NC_5H_5)_4(CH_3SO_3)_2$		
O(1)—Fe(1)—O(2)	174.1(2)	Fe(1)—N(2)—C(10)	121.0(3)
O(1)—Fe(1)—N(1)	89.1(2)	Fe(1)—N(2)—C(14)	121.6(3)
O(1)—Fe(1)—N(2)	86.63(15)	C(10)—N(2)—C(14)	117.3(4)
O(1)—Fe(1)—N(3)	90.95(15)	Fe(1)—N(3)—C(15)	120.7(4)
O(1)—Fe(1)—N(4)	94.49(15)	Fe(1)—N(3)—C(19)	122.0(3)
O(2)—Fe(1)—N(1)	86.8(2)	C(15)—N(3)—C(19)	117.3(5)
O(2)—Fe(1)—N(2)	89.28(15)	Fe(1)—N(4)—C(20)	121.0(3)
O(2)—Fe(1)—N(3)	93.28(15)	Fe(1)—N(4)—C(24)	121.4(3)
O(2)—Fe(1)—N(4)	89.69(15)	C(20)—N(4)—C(24)	117.5(4)
N(1)—Fe(1)—N(2)	91.78(15)	Fe(2)—N(5)—C(25)	122.1(3)
N(1)—Fe(1)—N(3)	179.06(15)	Fe(2)—N(5)—C(29)	121.0(3)
N(1)—Fe(1)—N(4)	89.44(15)	C(25)—N(5)—C(29)	116.9(4)
N(2)—Fe(1)—N(3)	89.16(15)	Fe(2)—N(6)—C(30)	120.2(3)
N(2)—Fe(1)—N(4)	178.4(2)	Fe(2)—N(6)—C(34)	121.3(3)
N(3)—Fe(1)—N(4)	89.62(15)	C(30)—N(6)—C(34)	118.2(4)
O(3)—Fe(2)—O(4)	171.62(15)	Fe(2)—N(7)—C(35)	122.3(3)
O(3)—Fe(2)—N(5)	88.81(14)	Fe(2)—N(7)—C(39)	120.6(3)
O(3)—Fe(2)—N(6)	85.66(14)	C(35)—N(7)—C(39)	117.1(4)
O(3)—Fe(2)—N(7)	91.07(14)	Fe(2)—N(8)—C(40)	122.0(3)
O(3)—Fe(2)—N(8)	92.36(14)	Fe(2)—N(8)—C(44)	120.8(3)
O(4)—Fe(2)—N(5)	89.71(15)	C(40)—N(8)—C(44)	117.0(4)
O(4)—Fe(2)—N(6)	86.15(15)	N(1)—C(5)—C(6)	122.6(5)
O(4)—Fe(2)—N(7)	90.33(14)	C(5)—C(6)—C(7)	119.3(5)
O(4)—Fe(2)—N(8)	95.89(15)	C(6)—C(7)—C(8)	118.5(5)
N(5)—Fe(2)—N(6)	91.86(15)	C(7)—C(8)—C(9)	118.9(5)
N(5)—Fe(2)—N(7)	179.44(15)	N(1)—C(9)—C(8)	123.2(5)
N(5)—Fe(2)—N(8)	90.23(15)	N(2)—C(10)—C(11)	122.9(5)
N(6)—Fe(2)—N(7)	87.59(15)	C(10)—C(11)—C(12)	118.4(5)
N(6)—Fe(2)—N(8)	177.09(15)	C(11)—C(12)—C(13)	120.2(5)
N(7)—Fe(2)—N(8)	90.32(15)	C(12)—C(13)—C(14)	118.2(5)
O(1)—S(1)—O(5)	111.2(2)	N(2)—C(14)—C(13)	123.0(5)
O(1)—S(1)—O(6)	111.9(3)	N(3)—C(15)—C(16)	124.0(6)
O(1)—S(1)—C(1)	104.0(3)	C(15)—C(16)—C(17)	117.6(5)
O(5)—S(1)—O(6)	113.2(3)	C(16)—C(17)—C(18)	119.0(6)
O(5)—S(1)—C(1)	109.0(4)	C(17)—C(18)—C(19)	119.3(6)
O(6)—S(1)—C(1)	107.0(3)	N(3)—C(19)—C(18)	122.8(5)
O(2)—S(2)—O(7)	110.7(3)	N(4)—C(20)—C(21)	122.6(5)
O(2)—S(2)—O(8)	111.8(3)	C(20)—C(21)—C(22)	118.8(5)
O(2)—S(2)—C(2)	104.5(3)	C(21)—C(22)—C(23)	119.5(5)
O(7)—S(2)—O(8)	113.6(4)	C(22)—C(23)—C(24)	118.8(5)
O(7)—S(2)—C(2)	108.6(4)	N(4)—C(24)—C(23)	122.8(5)
O(8)—S(2)—C(2)	107.0(4)	N(5)—C(25)—C(26)	123.9(5)
O(3)—S(3)—C(9)	112.4(2)	C(25)—C(26)—C(27)	118.2(5)
O(3)—S(3)—C(10)	110.2(3)	C(26)—C(27)—C(28)	119.0(5)
O(3)—S(3)—C(3)	105.4(3)	C(27)—C(28)—C(29)	119.5(5)
O(9)—S(3)—O(10)	113.0(3)	N(5)—C(29)—C(28)	122.6(5)
O(9)—S(3)—C(3)	110.4(3)	N(6)—C(30)—C(31)	121.9(5)
O(10)—S(3)—C(3)	105.0(3)	C(30)—C(31)—C(32)	119.0(6)
O(4)—S(4)—O(11)	111.8(3)	C(31)—C(32)—C(33)	120.0(6)
O(4)—S(4)—O(12)	112.0(2)	C(32)—C(33)—C(34)	117.6(6)
O(4)—S(4)—C(4)	104.2(3)	N(6)—C(34)—C(33)	123.1(6)
O(11)—S(4)—O(12)	116.2(4)	N(7)—C(35)—C(36)	123.3(5)
O(11)—S(4)—C(4)	106.4(5)	C(35)—C(36)—C(37)	119.1(5)
O(12)—S(4)—C(4)	105.2(4)	C(36)—C(37)—C(38)	118.7(5)
Fe(1)—O(1)—S(1)	149.8(2)	C(37)—C(38)—C(39)	119.5(5)
Fe(1)—O(2)—S(2)	158.9(3)	N(7)—C(39)—C(38)	122.3(4)
Fe(2)—O(3)—S(3)	157.8(2)	N(8)—C(40)—C(41)	123.5(4)
Fe(2)—O(4)—S(4)	152.8(3)	C(40)—C(41)—C(42)	119.3(5)
Fe(1)—N(1)—C(5)	120.7(3)	C(41)—C(42)—C(43)	118.3(5)
Fe(1)—N(1)—C(9)	121.3(3)	C(42)—C(43)—C(44)	119.2(5)
C(5)—N(1)—C(9)	117.5(4)	N(8)—C(44)—C(43)	122.7(4)

TABLE 3. (*Concluded*)

Bonds	Angle (deg)	Bonds	Angle (deg)
	$Fe(NC_5H_5)_4(CF_3SO_3)_2$		
O(1)—Fe—O(4)	175.2(3)	C(13)—N(3)—C(17)	117.3(7)
O(1)—Fe—N(1)	90.0(3)	Fe—N(4)—C(18)	120.4(6)
O(1)—Fe—N(2)	90.8(3)	Fe—N(4)—C(22)	122.2(6)
O(1)—Fe—N(3)	86.8(3)	C(18)—N(4)—C(22)	117.1(7)
O(1)—Fe—N(4)	93.9(3)	S(1)—C(1)—F(1)	110.2(7)
O(4)—Fe—N(1)	93.1(3)	S(1)—C(1)—F(2)	111.6(7)
O(4)—Fe—N(2)	86.1(3)	S(1)—C(1)—F(3)	112.2(7)
O(4)—Fe—N(3)	89.5(3)	F(1)—C(1)—F(2)	107.3(9)
O(4)—Fe—N(4)	89.8(3)	F(1)—C(1)—F(3)	107.5(8)
N(1)—Fe—N(2)	179.2(4)	F(2)—C(1)—F(3)	107.8(8)
N(1)—Fe—N(3)	90.0(3)	S(2)—C(2)—F(4)	111.9(8)
N(1)—Fe—N(4)	89.2(3)	S(2)—C(2)—F(5)	111.3(7)
N(2)—Fe—N(3)	89.9(3)	S(2)—C(2)—F(6)	110.8(8)
N(2)—Fe—N(4)	90.9(3)	F(4)—C(2)—F(5)	108.8(10)
N(3)—Fe—N(4)	178.9(3)	F(4)—C(2)—F(6)	108.2(9)
O(1)—S(1)—O(2)	113.8(5)	F(5)—C(2)—F(6)	105.7(10)
O(1)—S(1)—O(3)	112.5(5)	N(1)—C(3)—C(4)	123.6(9)
O(1)—S(1)—C(1)	100.8(4)	C(3)—C(4)—C(5)	118.3(10)
O(2)—S(1)—O(3)	117.5(5)	C(4)—C(5)—C(6)	118.9(10)
O(2)—S(1)—C(1)	105.1(5)	C(5)—C(6)—C(7)	118.7(9)
O(3)—S(1)—C(1)	104.9(5)	N(1)—C(7)—C(6)	124.4(8)
O(4)—S(2)—O(5)	113.2(5)	N(2)—C(8)—C(9)	123.9(9)
O(4)—S(2)—O(6)	112.9(4)	C(8)—C(9)—C(10)	117.8(9)
O(4)—S(2)—C(2)	102.7(5)	C(9)—C(10)—C(11)	119.5(10)
O(5)—S(2)—O(6)	117.8(5)	C(10)—C(11)—C(12)	119.5(9)
O(5)—S(2)—C(2)	104.9(5)	N(2)—C(12)—C(11)	122.3(8)
O(6)—S(2)—C(2)	103.1(5)	N(3)—C(13)—C(14)	122.9(8)
Fe—O(1)—S(1)	150.8(4)	C(13)—C(14)—C(15)	119.5(9)
Fe—O(4)—S(2)	152.0(4)	C(14)—C(15)—C(16)	119.3(9)
Fe—N(1)—C(3)	120.3(6)	C(15)—C(16)—C(17)	118.5(8)
Fe—N(1)—C(7)	123.5(6)	N(3)—C(17)—C(16)	122.4(8)
C(3)—N(1)—C(7)	116.0(8)	N(4)—C(18)—C(19)	122.7(9)
Fe—N(2)—C(8)	120.4(6)	C(18)—C(19)—C(20)	119.4(10)
Fe—N(2)—C(12)	122.5(6)	C(19)—C(20)—C(21)	117.6(9)
C(8)—N(2)—C(12)	116.9(8)	C(20)—C(21)—C(22)	119.7(8)
Fe—N(3)—C(13)	121.4(6)	N(4)—C(22)—C(21)	123.4(8)
Fe—N(3)—C(17)	121.3(6)		
	$Fe(NC_5H_5)_4(CH_3C_6H_4SO_3)_2$		
O(1)—Fe—N(1)	96.22(9)	C(13)—N(2)—C(17)	116.4(3)
O(1)—Fe—N(2)	86.38(9)	S—C(1)—C(2)	120.6(3)
O(1)—Fe—O(1)′	174.69(14)	S—C(1)—C(6)	120.1(3)
O(1)—Fe—N(1)′	87.44(9)	C(2)—C(1)—C(6)	119.3(3)
O(1)—Fe—N(2)′	89.75(9)	C(1)—C(2)—C(3)	119.9(4)
N(1)—Fe—N(2)	90.73(9)	C(2)—C(3)—C(4)	122.2(4)
N(1)—Fe—N(1)′	92.99(14)	C(3)—C(4)—C(5)	117.0(4)
N(1)—Fe—N(2)′	173.10(10)	C(3)—C(4)—C(7)	122.2(5)
N(2)—Fe—N(2)′	86.18(14)	C(5)—C(4)—C(7)	120.8(5)
O(1)—S—O(2)	110.6(2)	C(4)—C(5)—C(6)	121.6(4)
O(1)—S—O(3)	111.8(2)	C(1)—C(6)—C(5)	120.0(4)
O(1)—S—C(1)	103.92(14)	N(1)—C(8)—C(9)	122.3(4)
O(2)—S—O(3)	115.8(2)	C(8)—C(9)—C(10)	120.1(4)
O(2)—S—C(1)	106.7(2)	C(9)—C(10)—C(11)	117.8(4)
O(3)—S—C(1)	107.0(2)	C(10)—C(11)—C(12)	119.5(4)
Fe—O(1)—S	147.1(2)	N(1)—C(12)—C(11)	123.0(4)
Fe—N(1)—C(8)	119.6(2)	N(2)—C(13)—C(14)	123.2(3)
Fe—N(1)—C(12)	123.1(2)	C(13)—C(14)—C(15)	119.6(4)
C(8)—N(1)—C(12)	117.3(3)	C(14)—C(15)—C(16)	118.7(3)
Fe—N(2)—C(13)	122.6(2)	C(15)—C(16)—C(17)	119.2(3)
Fe—N(2)—C(17)	119.3(2)	N(2)—C(17)—C(16)	122.9(3)

Here and elsewhere primed atoms have coordinates related to those in Table 1 by the symmetry operation: $1/2-x$, $1/2-y$, z.

TABLE 10. Infrared spectra, selected vibrations

Assignments	Infrared frequencies (cm^{-1})[a] $Fe(py)_4(CF_3SO_3)_2$	$Fe(py)_4(CH_3SO_3)_2$	$Fe(py)_4(CH_3C_6H_4SO_3)_2$
Anion[b]			
$\nu_4(E)$	1329 s	1252 s	1260 s
	1320 s	1162 s	1170 s
	1240 s		
$\nu_1(A_1)$	1035 s	1038 s	1030 s
$\nu_2(A_1)$	756 sh	779 sh	682 s
$\nu_3(A_1),\nu_5(E)$	636 s	556 s	557 m
	527 m	543 m	547 w
	518 m	523 m	
Pyridine[c]			
8a	1603 s	1601 m	1600 s
6a	632 sh	626 m	625 m
16b	428 m	427 m	425 m

[a]s = strong, m =medium, sh = shoulder.
[b]Assignments (CSO_3 part, C_{3v} symmetry) from ref. 16.
[c]Assigments from ref. 17.

TABLE 11. ^{57}Fe Mössbauer parameters[a]

Compound	T (K)	δ (mm s^{-1})	ΔE_Q (mm s^{-1})	Γ_1 (mm s^{-1})	Γ_2 (mm s^{-1})
$Fe(py)_4(CF_3SO_3)_2$	291	1.07	3.09	0.26	0.25
	78[b]	1.14	3.68	0.26	0.25
$Fe(py)_4(CH_3SO_3)_2$	291	1.07	3.53	0.28	0.26
	120	1.07	3.81	0.27	0.27
	78	1.07	3.83	0.27	0.26
	30	1.07	3.83	0.25	0.29
	8.38	1.08	3.83	0.30	0.31
$Fe(py)_4(p\text{-}CH_3C_6H_4SO_3)_2$	291	1.08	3.47	0.26	0.28
	78[b]	1.16	3.63	0.28	0.28

[a]Estimated precision of parameters is ±0.01 mm s^{-1}.
[b]Source is at 291 K and absorber at 78 K. In all other cases source and absorber are at the same temperature.

only two bands, assignable to $\nu_3(A_1)$ and $\nu_5(E)$, are expected. For these complexes, three absorptions are clearly assignable to SO_3 deformation modes. In the past, anion spectra very similar to those observed here have been used to infer unidentate sulfonate coordination (17). The present results validate the earlier conclusions and support the use of infrared criteria for determining the nature of sulfonate ion coordination in complexes.

Mössbauer data are given in Table 11 and a representative spectrum is shown in Fig. 3. At all temperatures employed, the Mössbauer spectra consisted of simple quadrupole-split doublets, as expected for distorted octahedral high-spin iron(II) complexes. The room temperature isomer shifts are virtually identical for the three complexes, and approximately 0.3 mm s^{-1} lower than those of the anhydrous iron(II) sulfonates, $Fe(RSO_3)_2$ (16, 45). The lower isomer shifts of the present complexes are attributabe to the covalent nature of the Fe—N (pyridine) bonding, which increases the *s* electron density at the iron nucleus. It is evident that in these complexes with FeN_4O_2 chromophores, differences in anion basicity are not large enough to have an appreciable effect on the isomer shift. This is in contrast to the results (41) for $Fe(py)_4X_2$ (X = Cl, Br, I), where the room temperature isomer shift decreases from 1.06 mm s^{-1} for the chloride to 0.99 mm s^{-1} for the iodide.

The quadrupole splittings, ΔE_Q, exceed 3 mm s^{-1} in all cases. We, as well as Long and co-workers (41, 46), have cautioned about the dangers of using the magnitude of ΔE_Q to deduce the orbital degeneracy of the iron(II) ground state, particularly when ΔE_Q is small. This is because the major contribution to the electric field gradient (efg) tensor results from an unequal distribution of the sixth iron $3d$ electron among the d_{xy} and d_{xz}, d_{yz} orbitals (in tetragonal symmetry). As the low-symmetry distortion and hence the splitting of the t_{2g} orbitals approach zero, so also will the quadrupole interaction, regardless of the orbital degeneracy of the ground state. On the other hand, since an orbitally degenerate ^5E_g state can produce a quadrupole splitting of at most about 2 mm s^{-1} (30), values substantially higher than this are diagnostic of an orbitally nondegenerate ground state. Thus the present results are consistent only with a $^5B_{2g}$ ground state, corresponding to the d_{xy} orbital lying lowest. This is precisely as required by the molecular structures discussed above, which show in each case an axially compressed octahedron of approximate D_{4h} symmetry. Thus V_{zz}, the principal component of the efg tensor, is positive in these complexes and presumably lies close to the pseudo-tetragonal molecular axis.

Solid state electronic spectra recorded at room temperature for the three complexes are typical for high-spin iron(II) in a

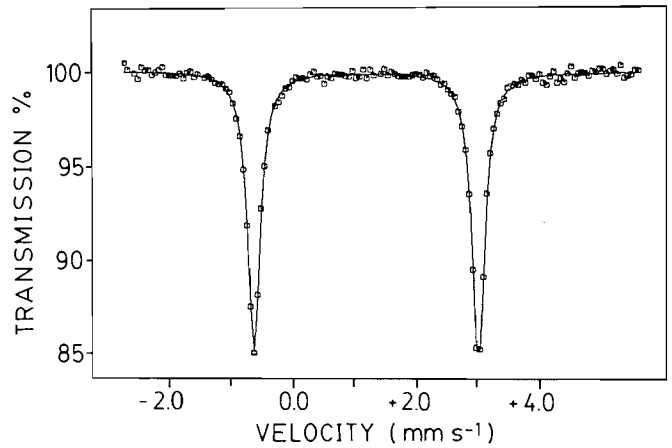

FIG. 3. Mössbauer spectrum of $Fe(NC_5H_5)_4(CH_3SO_3)_2$ at 78 K.

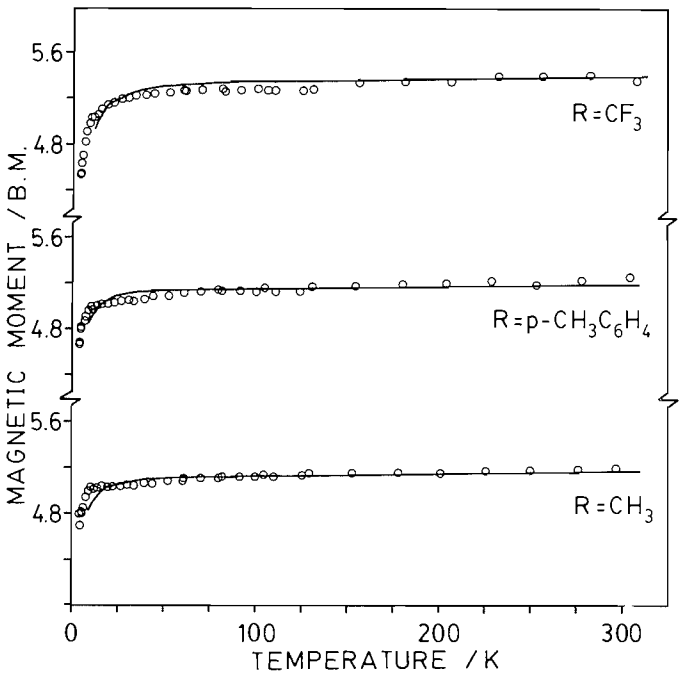

FIG. 4. Magnetic moment versus temperature plots for $Fe(NC_5H_5)_4(RSO_3)_2$. Solid lines are calculated (see text).

tetragonally distorted octahedral environment (47). Broad maxima are observed at 11.5, 11.4, and 11.0 kK for the R = CF_3, CH_3, and p-$CH_3C_6H_4$ derivatives, respectively. We tentatively assign these adsorptions to unresolved electronic transitions from the ground $^5B_{2g}$ state to the $^5A_{1g}$ and $^5B_{1g}$ levels derived from ^5E_g in cubic symmetry. The range of band energies observed is small, consistent with the relatively small differences in the FeN_4O_2 chromophores as shown by the X-ray structure determinations. We note, however, that on going from the CF_3 to the p-$CH_3C_6H_4$ derivative the energy decreases by about 500 cm^{-1}, a trend which parallels an increase in the average Fe—N distance from 2.21 to 2.24 Å. The triflate also exhibits a shoulder on its principal absorption band at about 9.2 kK. While this shoulder could result from some resolution of the $^5B_{2g} \rightarrow {}^5A_{1g}$, $^5B_{1g}$ transition, it is difficult to rationalize why the triflate should exhibit this feature and not the other two complexes, particularly in view of the fact that of the three pyridine complexes the triflate is the least tetragonally distorted. It is possible that the shoulder observed in the triflate arises from some other source, perhaps a weak spin-forbidden transition, and is a feature obscured in the spectra of the other two complexes by virtue of their relatively broader principal absorption bands.

Magnetic susceptibilities have been measured from 4.2 to 310 K for all three complexes and the data are given in Table 12 (deposited supplementary material). Magnetic moments as functions of temperature are displayed in Fig. 4. In both magnitude and temperature dependence the magnetic moments of these complexes are consistent with their formulation as pseudo-octahedral high-spin iron(II) compounds in which the orbital degeneracy of the $^5T_{2g}$ state is lifted by a low-symmetry crystal field. It is possible to analyze the temperature dependence of the magnetic moment as a function of distortion from O_h symmetry, spin-orbit coupling, and electron delocalization (48, 49). The distortion parameter Δ (or $3Ds$) is the separation of the $^5B_{2g}$ and ^5E_g states arising from the cubic field $^5T_{2g}$ ground term in the presence of a tetragonal ligand field. A positive value of Δ corresponds to the orbitally nondegenerate $^5B_{2g}$ state lying lowest. The spin-orbit coupling constant λ is expected to be reduced somewhat from its free-ion value of -100 cm^{-1} (50). The orbital reduction parameter k allows for electron delocalization in the t_{2g} orbital set. From powder magnetic susceptibility data it is difficult to determine the sign of Δ unambiguously. However, as discussed above, the Mössbauer data clearly show that the ground state in each of these complexes is an orbital singlet, as expected from the molecular geometries. Hence in analyzing the magnetic data only positive values of Δ have been considered.

The parameter values obtained by fitting the magnetic moment data (to ~10 K) are given in Table 13, and have been employed to construct the solid lines shown in Fig. 4. It will be seen that the fits are quite reasonable, especially at temperatures above about 20 K. In view of the approximate nature of this crystal field model (48, 49), the parameter values in Table 13 should be considered to be only semi-quantitative (i.e., ca. ±10%). With this in mind, it appears that the axial ligand fields are of about the same order of magnitude in all three cases. Values of λ are, as expected upon complex formation, substantially lower than the free ion value. For the methanesulfonate derivative, λ and k are reduced by corresponding amounts, although this correlation is not observed in the other two cases.

Disagreement at low temperatures between the observed moments and those calculated from the simple crystal field model (48, 49), is not unexpected. For example, the model ignores zero-field splitting of the spin quintet ground state of the iron(II) ion, which becomes particularly important at low temperatures. To show that zero-field splitting effects can account for the magnetic properties of these complexes, in particular in the low temperature region, we have analyzed the data in another way, utilizing the magnetic susceptibility equation for zero-field splitting of the $S = 2$ ground state multiplet (51). The axial zero-field splitting parameter D and the spectroscopic splitting parameter g were found for all three compounds by least-squares fitting of the molar susceptibilities as a function of temperature to the functions given in ref. 51. Information contained in the powder magnetic susceptibility data is insufficient to determine the sign of D and equally good fits are obtained using either positive or negative D values. For positive D, the best-fit parameters are given in Table 13 and the fitted magnetic susceptibility data for $Fe(py)_4(CH_3SO_3)_2$ are

TABLE 13. Parameters from fits of magnetic data

Compound	Crystal field parameters $\Delta(3Ds)$ (cm^{-1})	λ (cm^{-1})	k	Zero field splitting parameters D (cm^{-1})	g
$Fe(py)_4(CF_3SO_3)_2$	600	−80	1.00	6.1	2.15
$Fe(py)_4(CH_3SO_3)_2$	700	−70	0.70	3.4	2.08
$Fe(py)_4(p\text{-}CH_3C_6H_4SO_3)_2$	600	−60	0.80	3.9	2.09

TABLE 14. Differential scanning calorimetry data

Compound	Event 1 Temp. (°C)	Event 1 ΔH (kJ mol^{-1})	Event 1 % Mass loss[a] calcd.[b]	Event 1 % Mass loss[a] obs.	Event 2 Temp. (°C)	Event 2 ΔH (kJ mol^{-1})	Event 2 % Mass loss[a] calcd.[c]	Event 2 % Mass loss[a] obs.
$Fe(py)_4(CF_3SO_3)_2$	192	95	24	26	240	60	47	44
$Fe(py)_4(CH_3SO_3)_2$	141	91	28	28	*d*		56	55
$Fe(py)_4(p\text{-}CH_3C_6H_4SO_3)_2$	146	94	22	24	185	109	44	42

[a]Mass loss estimated by weighing sample in the aluminum crucible before and after the event.
[b]Calculated assuming loss of two moles of pyridine.
[c]Calculated assuming loss of four moles of pyridine.
[d]Several events are observed from 160 to 270° (see text). Observed weight loss after heating to 280°C.

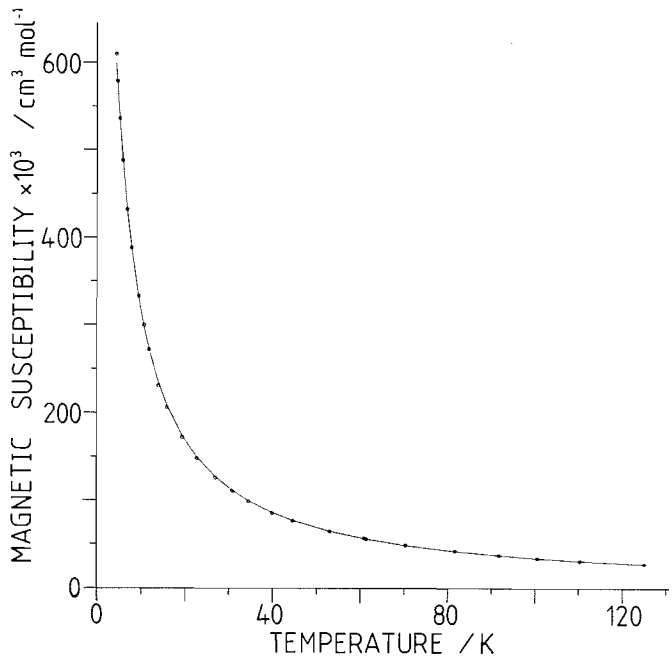

FIG. 5. Magnetic susceptibility versus temperature plot for $Fe(NC_5H_5)_4(CH_3SO_3)_2$. Solid line is calculated (see text).

displayed in Fig. 5. The agreement with experiment, particularly at low temperatures, is noticeably improved over that obtained with the crystal field model. The magnitude of the zero-field splitting is expected to be inversely proportional to the separation of the ^5E_g and $^5B_{2g}$ states (arising from the splitting of the $^5T_{2g}$ ground state) (52). Hence the relatively large D value obtained for the triflate derivative suggests a smaller $^5T_{2g}$ splitting, reflecting perhaps the lower degree of tetragonality for this complex as shown by the X-ray data.

Differential scanning calorimetry

In order to establish the range of thermal stabilities of these complexes and to evaluate the possibilities of obtaining complexes with lower pyridine-to-iron ratios through thermolysis, we studied the tetrakis(pyridine) complexes using differential scanning calorimetry. The results are summarized in Table 14. Thermograms of the triflate and *para*-toluenesulfonate derivatives show them to lose pyridine in two distinct steps. Approximate weight loss measurements indicate that the first step involves loss of two moles of pyridine per mole of complex to form bis(pyridine) derivatives. The remaining pyridine groups are lost in the second step at higher temperatures. The results for the methyl derivative are similar, in that two moles of pyridine are lost in a single first step. In this case, however, the higher temperature thermolysis is more complex, with the remaining two moles of pyridine dissociating in several endothermic steps. Similar results were obtained by Tominaga *et al.* (53) who observed that thermolysis of $Fe(py)_4Cl_2$ gave $Fe(py)_2Cl_2$, $Fe(py)Cl_2$, $Fe(py)_{2/3}Cl_2$, and, finally, $FeCl_2$ in distinct steps. In all three sulfonate complexes, infrared spectra and gravimetric analysis indicated that the residue remaining after removal of all pyridine was the corresponding anhydrous sulfonate compound.

Previous workers have used thermolysis as a preparative technique for obtaining bis(pyridine) complexes (41, 54). Our results suggest that it should be possible to obtain bis(pyridine)iron(II) sulfonates by heating bulk samples of the tetrakis(pyridine) complexes at appropriate temperatures. We have succeeded in obtaining $Fe(py)_2(CF_3SO_3)_2$ by this route and the preparation and characterization of such complexes is presently under study in this laboratory.

Acknowledgments

We thank the Natural Sciences and Engineering Research Council of Canada for financial support and the University of British Columbia Computing Centre for assistance. J. S. H.

thanks the U.B.C. Graduate Scholarship Committee for scholarship awards.

1. R. D. Howells and J. C. McCown. Chem. Rev. **77**, 69 (1977).
2. J. Cragel Jr., V. B. Pett, M. D. Glick, and R. E. DeSimone. Inorg. Chem. **17**, 2885 (1978).
3. G. B. Deacon, C. L. Raston, C. Tunaley, and A. H. White. Aust. J. Chem. **32**, 2195 (1979).
4. R. E. DeSimone and M. G. Glick. Inorg. Chem. **17**, 3574 (1978).
5. S.-M. Peng, J. A. Ibers, M. Millar, and R. H. Holm. J. Am. Chem. Soc. **98**, 8037 (1976).
6. M. B. Humphrey, W. M. Lamanna, M. Brookhart, and G. R. Husk. Inorg. Chem. **22**, 3355 (1983).
7. G. Nieuwpoort, G. C. Verschoor, and J. Reedijk. J. Chem. Soc. Dalton Trans. 531 (1983).
8. O. P. Anderson and A. B. Packard. Inorg. Chem. **18**, 1129 (1979).
9. S. Komiya, J. C. Huffman, and J. K. Kochi. Inorg. Chem. **16**, 2138 (1977).
10. F. Charbonnier, R. Faure, and H. Loiseleur. Acta Crystallogr. Sect. B, **33**, 1845 (1977).
11. P. L. Dedert, T. Sorrell, T. J. Marks, and J. A. Ibers. Inorg. Chem. **21**, 3506 (1982).
12. F. Charbonnier, R. Faure, and H. Loiseleur. Acta Crystallogr. Sect. B, **33**, 1478 (1977).
13. M. B. Dines and P. H. Bird. J. Chem. Soc. Chem. Commun. 12 (1973).
14. F. Charbonnier, R. Faure, and H. Loiseleur. Acta Crystallogr. Sect. B, **34**, 1504 (1978).
15. A. L. Arduini, M. Garnet, R. C. Thompson, and T. C. T. Wong. Can. J. Chem. **53**, 3812 (1975).
16. J. S. Haynes, J. R. Sams, and R. C. Thompson. Can. J. Chem. **59**, 669 (1981).
17. C. S. Alleyne and R. C. Thompson. Can. J. Chem. **52**, 18 (1974).
18. G. J. Long and P. J. Clarke. Inorg. Chem. **17**, 1394 (1978).
19. I. Søtofte and S. E. Rasmussen. Acta Chem. Scand. **21**, 2028 (1967).
20. P. J. Hamm, J. Bordner, and A. F. Schreiner. Inorg. Chim. Acta, **7**, 637 (1973).
21. A. S. Antsishkina and M. A. Porai-Koshitz. Sov. Phys. Crystallogr. (Engl. Transl.), **3**, 684 (1960).
22. M. A. Porai-Koshitz and G. N. Tischenko. Sov. Phys. Crystallogr. (Engl. Transl.), **4**, 216 (1960).
23. P. Coppens, L. Leiserowitz, and D. Rabinovich. Acta Crystallogr. **18**, 1035 (1965).
24. W. R. Busing and H. A. Levy. Acta Crystallogr. **22**, 457 (1967).
25. D. T. Cromer and J. B. Mann. Acta Crystallogr. Sect. A, **24**, 321 (1968).
26. R. F. Stewart, E. R. Davidson, and W. T. Simpson. J. Chem. Phys. **42**, 3175 (1965).
27. D. T. Cromer and D. Liberman. J. Chem. Phys. **53**, 1891 (1970).
28. V. Schomaker and K. N. Trueblood. Acta Crystallogr. Sect. B, **24**, 63 (1968).
29. D. W. J. Cruickshank. Acta Crystallogr. **9**, 747 (1956); **9**, 754 (1956); **14**, 896 (1961).
30. J. R. Sams and T. B. Tsin. Inorg. Chem. **14**, 1573 (1975).
31. J. S. Haynes, K. W. Oliver, S. J. Rettig, R. C. Thompson, and J. Trotter. Can. J. Chem. **60**, 2017 (1982).
32. H. C. Clark and R. J. O'Brien. Can. J. Chem. **39**, 1030 (1961).
33. F. G. Herring, B. Landa, R. C. Thompson, and C. F. Schwerdtfeger. J. Chem. Soc. A, 528 (1971).
34. A. Almenningen, O. Bastiansen, and L. Hansen. Acta Chem. Scand. **9**, 1306 (1955).
35. B. Bak, L. Hansen, and J. Rastrup-Andersen. J. Mol. Spectrosc. **2**, 1361 (1958).
36. G. Doyle, K. A. Eriksen, and P. Van Engen. Inorg. Chem. **22**, 2892 (1983).
37. V. J. James and J. F. McConnell. Tetrahedron, **27**, 5475 (1971).
38. P. L. Johnson, C. J. Cheer, J. P. Schaeffer, V. J. James, and F. H. Moore. Tetrahedron, **28**, 2893 (1972).
39. P. L. Johnson, J. P. Schaeffer, V. J. James, and J. F. McConnel. Tetrahedron, **28**, 2901 (1972).
40. S. K. Arora and M. Sundaralingam. Acta Crystallogr. Sect. B, **27**, 1293 (1971).
41. B. F. Little and G. J. Long. Inorg. Chem. **17**, 3401 (1978).
42. N. S. Gill, R. H. Nuttall, D. E. Scaife, and D. W. A. Sharp. J. Inorg. Nucl. Chem. **18**, 79 (1961).
43. C. H. Kline and J. Turkevich. J. Chem. Phys. **12**, 300 (1944).
44. L. Corsin, B. J. Fax, and R. C. Lord. J. Chem. Phys. **21**, 1170 (1953).
45. J. R. Sams, R. C. Thompson, and T. B. Tsin. Can. J. Chem. **55**, 115 (1977).
46. W. M. Reiff, G. J. Long, and B. F. Little. Inorg. Nucl. Chem. Lett. **12**, 405 (1976).
47. D. M. L. Goodgame, M. Goodgame, M. A. Hitchman, and M. J. Weeks. Inorg. Chem. **5**, 635 (1966).
48. B. N. Figgis, J. Lewis, F. E. Mabbs, and G. A. Webb. J. Chem. Soc. A, 442 (1967).
49. E. König, A. S. Chakravarty, and K. Madeja. Theor. Chim. Acta, **9**, 171 (1967).
50. T. M. Dunn. Trans. Faraday Soc. **57**, 1441 (1961).
51. C. L. Klein, C. J. O'Connor, R. J. Majeste, and L. M. Trefonas. J. Chem. Soc. Dalton Trans. 2419 (1982).
52. G. A. Eisman and W. M. Reiff. Inorg. Chim. Acta, **50**, 239 (1981).
53. T. Tominaga, T. Morimoto, M. Takeda, and N. Saito. Inorg. Nucl. Chem. Lett. **2**, 193 (1966).
54. G. J. Long, D. L. Whitney, and J. E. Kennedy. Inorg. Chem. **10**, 1406 (1971).

Metal ion – biomolecule interactions. X. Synthesis, spectroscopic and magnetic resonance investigations of methylmercury(II) complexes of the sulfur modified nucleosides 6-mercaptopurine riboside and 2-amino-6-mercaptopurine riboside

E. BUNCEL,[1] R. KUMAR, AND A. R. NORRIS

Department of Chemistry, Queen's University, Kingston, Ont., Canada K7L 3N6

Received May 21 1985

E. BUNCEL, R. KUMAR, and A. R. NORRIS. Can. J. Chem. **64**, 442 (1986).

A number of methylmercurated complexes of 6-mercaptopurine riboside and 2-amino-6-mercaptopurine riboside (6-MNucH_2) containing S-bound CH_3Hg(II) in neutral and cationic complexes (as in [CH_3Hg(6-MNucH)] and [CH_3Hg(6-MNucH_2)]NO_3), S- and N-bound CH_3Hg(II) (as in [$(CH_3Hg)_2$(6-MNucH)]NO_3), and S-, N-, C-bound CH_3Hg(II) (as in [$(CH_3Hg)_3$(6-MNuc)]NO_3) have been prepared in aqueous solution at appropriate pH and mole ratios of the constituents. The complexes were characterized by means of ^1H and ^{13}C nmr and ir spectroscopy and elemental analysis. Formation of C-bound methylmercurated species extends our previous results obtained with xanthosine, inosine, and imidazole derivatives, and substantiates our proposal that activation through electrophilic coordination at N(7) is a requirement for C(8)—H abstraction. $^2J(^1H–^{199}Hg)$ coupling constants, measured in $(CD_3)_2SO$ for a number of CH_3Hg(II) complexes of N-, S-, and C-donor heterocyclic ligands, including the 6-mercaptopurine riboside of the present study, correlate well with the $^1J(^{13}C–^{199}Hg)$ coupling constants, according to $^1J = 8.460^2J - 155.6$. The significance of this correlation in terms of the strength of the Hg–ligand bond is considered. The results could provide insight into the apparent selectivity of binding of CH_3Hg(II) by bio-ligands, as well as in the design of chemotherapeutic agents for the treatment of methylmercury poisoning.

E. BUNCEL, R. KUMAR et A. R. NORRIS. Can. J. Chem. **64**, 442 (1986).

Opérant en solution aqueuse et utilisant des pH et des rapports molaires appropriés, on a synthétisé un certain nombre de complexes du méthylmercure avec les ribosides de la mercapto-6 purine et de l'amino-2 mercapto-6 purine (M-6NucH_2) qui contiennent du CH_3Hg(II) lié soit au S dans des complexes neutres ou cationiques (comme dans le [CH_3Hg(M-6NucH)] et dans le [CH_3Hg(M-6NucH_2)]NO_3), soit au S ainsi qu'au N (comme dans le [$(CH_3Hg)_2$(M-6NucH)]NO_3) soit au S, au N et au C (comme dans le [$(CH_3Hg)_3$(M-6Nuc)]NO_3). On a caractérisé les complexes en faisant appel aux analyses élémentaires, à la spectroscopie ir et à la rmn du ^1H et du ^{13}C. La formation d'espèces contenant du méthylmercure lié au C étend nos résultats antérieurs obtenus à l'aide de dérivés de la xantosine, de l'inosine et de l'imidazole et donne plus de poids à notre proposition selon laquelle l'activation par le biais d'une coordination électrophile en N(7) est nécessaire à l'enlèvement du C(8)—H. Dans le cas des constantes de couplage $^2J(^1H–^{199}Hg)$, mesurées dans le $(CD_3)_2SO$ pour un certain nombre de complexes du CH_3Hg(II) avec des ligands hétérocycliques donneurs de N, S ou C et incluant ceux des ribosides de la mercapto-6 purine et de l'amino-2 mercapto-6 purine rapportés dans cette étude, on a pu établir une bonne corrélation avec les constantes de couplages $^1J(^{13}C–^{199}Hg)$ et elle est définie par l'équation $^1J = 8{,}460^2J - 155{,}6$. On considère la signification de cette corrélation en fonction de la force de la liaison Hg–ligand. Ces résultats pourraient fournir des explications relativement à la sélectivité apparente de la liaison du CH_3Hg(II) avec des bio-ligands ainsi que dans la préparation de modèles pour des agents chémothérapeutiques pour le traitement des empoisonnements par le méthylmercure.

[Traduit par le journal]

Introduction

In connection with our studies (1) of the interactions of methylmercury(II) and mercury(II) derivatives with nucleic acid constituents as free bases, nucleosides, and nucleotides, the thio derivatives of nucleosides appeared to be of particular interest. A number of such compounds can be found in limited quantities in nucleic acids. Transfer RNAs have been found to contain 2-mercaptouridine, 2-mercaptocytidine, 4-mercaptouridine, and other mercapto-containing compounds (2,3). Each polynucleotide may contain one or more of these species. In addition, 6-mercaptopurines are drugs of choice in the treatment of acute lymphocytic and chronic mylelocytic leukemias (4). We therefore deemed it of interest to determine the likely coordinating sites of 6-mercaptonucleosides (6-MNucH_2) towards heavy metal ions. The methylmercury(II) cation, which binds analogously to other heavy metal ions at a variety of ligand sites, serves as a good probe because, with few exceptions, it is essentially unifunctional and its equilibria involving nucleosides are quickly attained (5,6).

It is noteworthy that in some cases the metal complexes of 6-mercaptonucleosides have been found to be more active chemotherapeutic agents than the free ligands. The palladium(II) and bismuth(III) complexes of 6-mercaptopurine have recently been found to exhibit moderate anticarcinogenic activities (7). At present little is known about the structures of these complexes. A crystallographic study has proven the existence of chelate rings involving S(6) and N(7) in bis(6-mercapto-9-benzylpurinato)palladium(II) dimethylacetamide and in the isostructural platinum(II) compound (8). In two additional metal complexes with 6-mercaptopurine, the metal ions, viz. Hg(II) and Cd(II), have been found to bind preferentially to S(6) (9). The results of nmr studies of the reactions of $[Rh(PPh_3)_2CO]^+$ with 6-mercaptopurine riboside have been interpreted in terms of the formation of complexes containing S-bonded ligands (10).

In the present paper, we report on the isolation and characterization by ^1H and ^{13}C nmr, as well as by ir spectroscopy, of the products from the reactions of methylmercury(II) with 6-mercaptopurine riboside and 2-amino-6-mercaptopurine riboside.

Experimental

The ^1H nmr spectra of the complexes dissolved in $(CD_3)_2SO$ were recorded on a Bruker HX-60 instrument operating at 60 MHz in the Fourier transform mode. The ^{13}C nmr spectra were recorded on a

[1]Author to whom correspondence may be addressed.

TABLE 1. Analytical data for the isolated 6-mercaptonucleoside complexes

Compound	Microanalytical data[a] %C	%H	%N
2*a* [(CH_3Hg)(6-MPRH)]	26.59(26.46)	2.85(2.81)	11.09(11.23)
3*a* [(CH_3Hg)(6-MPRH$_2$)]NO_3	23.52(23.49)	2.84(2.67)	12.30(12.46)
4*a* [$(CH_3Hg)_2$(6-MPRH)]NO_3[b]	16.47(16.97)	2.13(2.94)	8.44(8.25)
2*b* [(CH_3Hg)(2-A-6-MPRH)]	25.72(25.69)	2.98(2.92)	13.34(13.62)
3*b* [(CH_3Hg)(2-A-6-MPRH$_2$)]NO_3	23.08(22.88)	2.72(2.77)	14.27(14.56)
4*b* [$(CH_3Hg)_2$(2-A-6-MPRH)]NO_3	18.41(18.20)	2.28(2.27)	10.44(10.61)

[a]Calculated values given in parentheses.
[b]Calculated values are for **4***a* formulated as [$(CH_3Hg)_2$(6-MPRH)]NO_3.4H_2O.

Bruker CXP-200 instrument operating at 50.307 MHz. Chemical shifts are referenced relative to internal tetramethylsilane (TMS). All spectra were recorded at room temperature (25 ± 2°C). The ir spectra were recorded as 1% (w/w) KBr discs on a Perkin–Elmer 598 spectrophotometer. Microanalyses were performed by Guelph Chemical Laboratories Ltd (Table 1).

6-Mercaptopurine riboside (Sigma), 2-amino-6-mercaptopurine riboside (Sigma), [$(CH_3Hg)_3O$]OH (Alfa), and CH_3HgCl (Alfa) were used as received. CH_3HgNO_3 was prepared from CH_3HgCl and $AgNO_3$ as described previously (11).

*Complexes of 6-mercaptopurine riboside (6-MPRH$_2$, **1**a)*

*[CH_3Hg (6-MPRH)] (**2**a)*

To a stirred solution of **1***a* (0.100 g, 0.352 mmol) in 20 mL of distilled water was added a suspension of [$(CH_3Hg)_3O$]OH (0.080 g, 0.353 mmol) in 5 mL water. The solution was stirred for 10 min and the white precipitate that formed was filtered, washed with ethanol and a small quantity of water, and finally dried *in vacuo* (0.165 g, 94%).

*[CH_3Hg(6-MPRH$_2$)]NO_3 (**3**a)*

A solution of CH_3HgNO_3 (0.098 g, 0.353 mmol) in 5 mL of water was added to a suspension of **1***a* (0.100 g, 0.352 mmol) in 20 mL water. The clear solution which resulted was evaporated slowly to dryness and the solid residue was stirred with ethanol, filtered, and dried *in vacuo* (0.178 g, 90%).

*[$(CH_3Hg)_2$(6-MPRH)]NO_3 (**4**a)*

To a solution of **2***a* (0.088 g, 0.176 mmol) in 10 mL of water was added a solution of CH_3HgNO_3 (0.049 g, 0.177 mmol) in 5 mL water, followed by 5 mL of ethanol. Crystallization was allowed to occur at 5°C and the product was filtered and dried *in vacuo* (0.098 g, 65%).

*[$(CH_3Hg)_3$(6-MPR)]NO_3 (**5**a)*

To a solution of **2***a* (0.102 g, 0.204 mmol) in 15 mL of water was added a solution of CH_3HgNO_3 (0.114 g, 0.205 mmol) in 5 mL water. The pH of the solution was adjusted to ca. 8 with 2 *M* NaOH and the solution heated at 70°C for 1 h. On standing, a yellowish oil separated and was stirred in ethanol to yield a yellow powder. This was collected by filtration and dried *in vacuo*. Some decomposition occurred in the course of recrystallizations from ethanol, as evidenced by the appearance of a small amount of black material that was filtered off before taking the ^1H nmr spectrum. Hence, elemental analysis on this product was not performed (0.165 g, 82%).

*Complexes of 2-amino-6-mercaptopurine riboside (2-A-6-MPRH$_2$, **1**b)*

*[(CH_3Hg)(2-A-6-MPRH)] (**2**b)*

To a stirred and heated solution of **1***b* (0.100 g, 0.334 mmol) in 15 mL of water was added a suspension of [$(CH_3Hg)_3O$]OH (0.076 g, 0.335 mmol) in 5 mL water. This resulted in the formation of a thick white precipitate. Following heating and stirring for an additional 20 min, the white precipitate was collected by filtration, washed with hot water, and dried *in vacuo* (0.168 g, 98%).

*[(CH_3Hg)(2-A-6-MPRH$_2$)]NO_3 (**3**b)*

To a suspension of **1***b* (0.100 g, 0.334 mmol) in 10 mL of water was added a solution of CH_3HgNO_3 (0.093 g, 0.335 mmol) in 10 mL water. The suspension dissolved to give a clear solution. After stirring for 2 h the solution was set aside to evaporate slowly. This procedure yielded a white solid which was stirred with ethanol for 20 min, filtered, and dried *in vacuo* (0.181 g, 94%).

*[$(CH_3Hg)_2$(2-A-6-MPRH)]NO_3 (**4**b)*

A solution of CH_3HgNO_3 (0.057 g, 0.205 mmol) in 5 mL of water was added to a hot stirred suspension of **2***b* (0.105 g, 0.204 mmol) in 25 mL water. On cooling to room temperature, the solution transformed to a gel. It was heated again with stirring for 30 min following which a clear solution resulted. The hot solution was filtered and left to evaporate slowly. The resulting white solid was stirred with ethanol, filtered and dried *in vacuo* (0.148 g, 91%).

*[$(CH_3Hg)_3$(2-A-6-MPR)]NO_3 (**5**b)*

A solution of CH_3HgNO_3 (0.120 g, 0.216 mmol) in 5 mL of water was added to a stirred suspension of **2***b* (0.111 g, 0.216 mmol) in 10 mL water. The pH of the resultant solution was increased to ca. 8 with 2 *M* NaOH, and the solution was heated at 70°C for 1 h, during which time some decomposition occurred as evidenced by the formation of a greyish-black precipitate. After filtration, the solution was allowed to stand, whereupon a yellowish-white solid precipitated. This was collected by filtration and found by ^1H nmr to consist mainly of **2***b*. The filtrate was set aside to evaporate slowly to dryness and the resulting residue was stirred with ethanol before filtration and drying *in vacuo*. An elemental analysis was not performed on this product since it was found, by using ^1H nmr techniques, to be contaminated with a small amount of **4***b* (0.093 g).

Results and discussion

Binding sites and complex formation

The S-modified nucleosides 6-mercaptopurine riboside (**1***a*) and 2-amino-6-mercaptopurine riboside (**1***b*) offer a number of potential binding sites towards CH_3Hg(II). In relation to the parent substrates studied previously, in which N(1), N(7), and C(8) were found to be possible binding sites in methylmercuration, the mercapto analogs contain the sulfur atom as a likely additional binding site (1*c*). Thus, depending on the reactant stoichiometry, the pH of the medium, and the relative affinities of the N, S, and C centers towards CH_3Hg(II), a number of possible products should be obtained in these interactions. Although coordination to the oxygen atoms of the ribose moiety could also be possible, no evidence for such a process has been found in this or previous work (1).

Studies of the $(CD_3)_2SO$ solutions of the complexes by ^1H and ^{13}C nmr have been found to be most informative in establishing the binding sites, while more limited information has been derived from ir absorption data. The complexes obtained from the interaction of **1***a* and **1***b* with CH_3Hg(II) are shown in Scheme 1. In all cases, the compounds **1***a* and **1***b* form

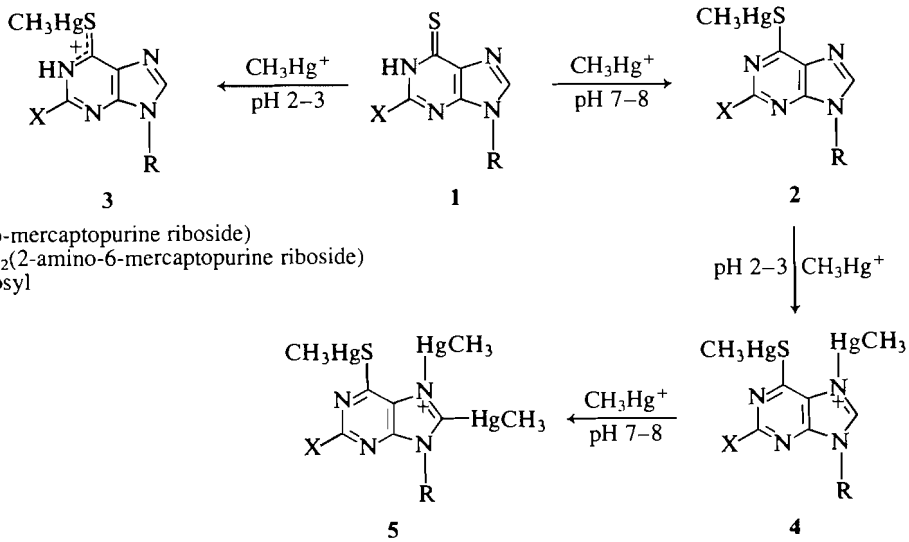

3 1 2

5 4

1*a*, etc. X = H(6-mercaptopurine riboside)
1*b*, etc. X = NH_2(2-amino-6-mercaptopurine riboside)
R = ribosyl

SCHEME 1

analogous complexes **2***a*/**2***b*, **3***a*/**3***b*, etc., which show very simple characteristics (*vide infra*).

In solution, 6-mercaptopurine riboside is generally considered to exist in the thione form —NH—C(S=S), **1**, although in one study evidence was given for the thiol form —N=C(—SH)—, **6**, as well (12). However, an X-ray crystal study of 6-mercaptopurine riboside reported, in addition to the thione form, a substantial contribution by the zwitterionic amidic form $—N^+H=C(—S^-)—$, **1′** (13).

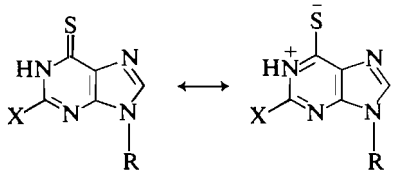

1 1′

Sites of metal ion binding in 6-mercaptonucleosides

(a) *S-methylmercuration (1:1 stoichiometry)*

Based on the above observations, we can view the deprotonation of **1** as giving rise to the delocalized anion **7** (14). This anion **7** has the potential to function as an ambidentate ligand with respect to both H^+ and metal ion coordination. According to HSAB theory, reaction of **7** with H^+ will occur at the "harder" site, that is, N rather than S, giving rise to **1**. On the other hand, reaction of **7** with CH_3Hg^+ can potentially lead to the formation of either **2** or **8** (Scheme 2). The tendency of heavy metal ions such as Hg(II) to favour the "soft" sulfur over the "hard" nitrogen donor atoms would point to the former as the most probable binding site for CH_3Hg^+. In accord with these considerations, reactions of thiolated nucleosides and thiolated polynucleotides with heavy metal ions have been shown to occur at sulfur rather than at nitrogen (17).

Thus the expected products in the reaction of **1***a* or **1***b* with CH_3Hg^+ at pH 7–8 will be **2***a* and **2***b*, respectively. The evidence we have obtained indicates that this is the case. The complex is found by microanalysis to correspond to [(CH_3Hg)-(6-MNucH)], where MNucH = purine riboside or 2-aminopurine riboside. Evidence in favour of the structure of **2** derives from the $^2J(^1H–^{199}Hg)$ value of ~185 Hz in $(CD_3)_2SO$, which is characteristic of S-bonded CH_3Hg(II) (15). Further evidence for the formation of **2** is the downfield shift of the C(8)—H

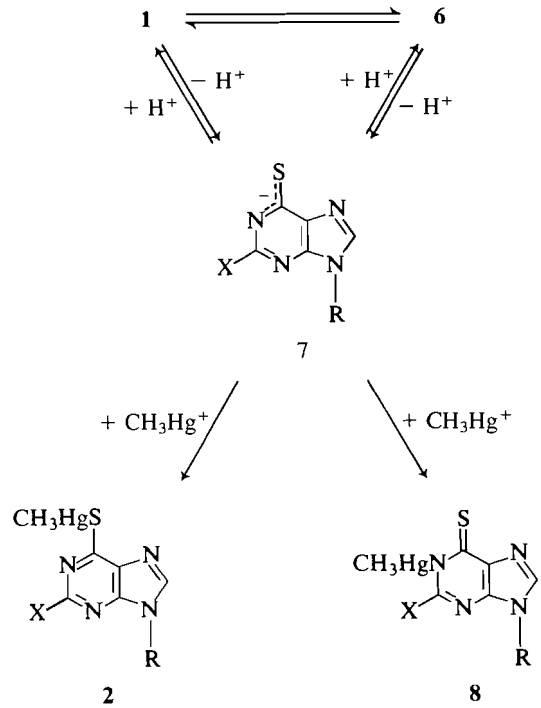

2 8

SCHEME 2

signal with respect to **1**. In the parent substrate, where N-bound CH_3Hg(II) has been documented in [CH_3Hg(NucH)], an upfield shift in the C(8)—H signal is observed with respect to the C(8)—H signal observed in the nucleoside itself (1*c*). Moreover, in the ^{13}C nmr spectrum, the C(6) resonance adjacent to the site of metal ion attack experiences a substantial upfield shift, together with a minor upfield shift in the C(5) resonance. The resonances due to C(2), C(4), and C(8) experience downfield shifts with respect to the corresponding resonances in **1**. A similar pronounced upfield shift in the C(6) resonance has been previously reported in 6-mercaptonucleosides on methylation (16). These results are in contrast to those obtained for the N-methylmercurated complexes [CH_3Hg(NucH)] (NucH = inosine or guanosine), where the C(2) and C(6) resonances adjacent to the site of coordination experience downfield shifts while the C(4), C(5), and C(8) resonances are relatively unaffected with respect to the parent (1*c*). Furthermore, the CH_3Hg(II) re-

TABLE 2. ^{1}H nuclear magnetic resonance spectral data for 6-mercaptonucleoside and its complexes

Compound	Chemical shifts[a,b] N(1)H	C(2)H	C(8)H	NH_2	H_1'	$CH_3Hg(II)$	Coupling constants, Hz $^2J(^1H-^{199}Hg)$
1*a* [6-MPRH$_2$]	13.85	8.23	8.55	—	5.90(d)	—	—
2*a* [(CH$_3$Hg)(6-MPRH)]	—	8.50	8.70	—	5.98(d)	0.83	185.54
3*a* [(CH$_3$Hg)(6-MPRH$_2$)]NO$_3$	[c]	8.80	8.90	—	6.01(d)	0.88	199.54
4*a* [(CH$_3$Hg)$_2$(6-MPRH)]NO$_3$	—	8.80	9.10	—	6.05(d)	0.91	218.92
5*a* [(CH$_3$Hg)$_3$(6-MPR)]NO$_3$	—	8.50	—	—	6.11(d)	0.75[d]	194.26[d]
						0.61[e]	146.72[e]
1*b* [2-A-6-MPRH$_2$]	11.97	—	8.15	6.82	5.70(d)	—	—
2*b* [(CH$_3$Hg)(2-A-6-MPRH)]	—	—	8.24	6.37	5.78(d)	0.80	184.86
3*b* [(CH$_3$Hg)(2-A-6-MPRH$_2$)]NO$_3$	[c]	—	8.62	6.91	5.79(d)	0.87	205.40
4*b* [(CH$_3$Hg)$_2$(2-A-6-MPRH)]NO$_3$	—	—	8.73	7.03	5.87(d)	0.89	215.38
5*b* [(CH$_3$Hg)$_3$(2-A-6-MPR)]NO$_3$	—	—	—	6.40	5.95(d)	0.76[d]	193.10[d]
						0.62[e]	156.70[e]

[a]Data for all **1***a* and **1***b* are taken from ref. 16.
[b]All resonances are singlets unless otherwise indicated: d = doublet.
[c]N(1)-H resonance is not observed due to exchange broadening caused by complexation at sulfur (27).
[d]N-, S-bound $CH_3Hg(II)$.
[e]C(8)-bound $CH_3Hg(II)$.

sonance at 9.0 ppm in **2**, when compared to the $CH_3Hg(II)$ resonance found at ca. 1.0 ppm in the N-methylmercurated species [CH_3Hg(NucH)], is good evidence in favour of structure **2** (1*c*). Further evidence in support of **2** is provided by our previous studies on the complex [CH_3Hg(MeImS)]. In this complex, methylmercuration at sulfur has been confirmed by X-ray crystal studies and the ^{13}C nmr spectrum exhibits a resonance associated with $CH_3Hg(II)$ at 8.7 ppm (1*d*).

When the reaction between **1** and CH_3HgNO_3 is carried out under acidic conditions (pH 2–3), a product **3** is obtained that corresponds to the formula [CH_3Hg(6-MNucH$_2$)]NO$_3$. The ^1H nmr spectrum of **3** (Table 2) exhibits a downfield shift in the C(8)—H resonance with respect to **1**, a feature characteristic of cationic complexes generated by addition of $CH_3Hg(II)$ at N(7). Also, the coupling constant, $^2J(^1H-^{199}Hg)$, of ca. 200 Hz is higher than the value of ca. 185 Hz found for the neutral complex with S-bonding in **2** (1*d*).

There are two possible structures for this cationic species, namely **3** and **9**. Evidence that coordination has not occurred at

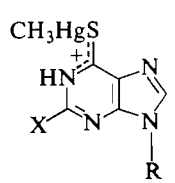

3

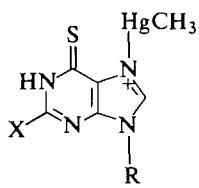

9

N(7) stems from the observation that N(7) coordination of $CH_3Hg(II)$ in inosine and guanosine leads to a $^2J(^1H-^{199}Hg)$ coupling constant of 229 Hz, significantly higher than that observed in the present case (1*c*). Also the $^2J(^1H-^{199}Hg)$ value in **3** is comparable to the $^2J(^1H-^{199}Hg)$ of 204.3 Hz for the complex [CH_3Hg(MeImSH)]NO$_3$, for which X-ray crystal studies have established sulfur to be the $CH_3Hg(II)$ binding site, with N protonated (1*d*, 1*f*). Further support for structure **3** is derived from the ^{13}C nmr spectrum. The resonances due to C(5) and C(6) experience upfield shifts while the C(2), C(4), and C(8) resonances experience downfield shifts with respect to **1** (Table 3). These observations are in contrast to the N(7)-methylmercurated complexes, e.g. [CH_3Hg(NucH$_2$)]NO$_3$, where upfield shifts in the C(2), C(4), C(5), C(6) resonances and a downfield shift in the C(8) resonance have been observed (1*c*). It is also pertinent that the N(7)-coordination of $CH_3Hg(II)$ in inosine and guanosine leads to a $CH_3Hg(II)$ carbon resonance of −0.7 ppm, which is significantly lower than the 8.0 ppm assignable to $CH_3Hg(II)$ coordinated at C(6)=S in **3** (1*c*). The ir spectrum shows the appearance of a characteristic band 1360 cm^{-1} due to free NO_3^- and is in accord with the proposed cationic nature of the complex (18).

(b) *N- and S-methylmercuration (2:1 stoichiometry)*

When the reaction of **2** with CH_3HgNO_3 is carried out at pH 3 under 2:1 stoichiometry of $CH_3Hg(II)$ / 6MNucH$_2$ one obtains a product that can be formulated as either **4**, **10**, or **11**.

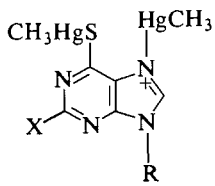

4

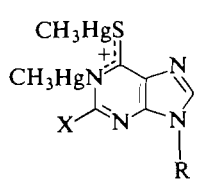

10

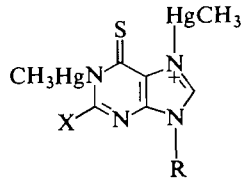

11

The ^1H nmr spectrum of the product of this reaction exhibits an appreciable downfield shift in the C(8)—H resonance relative to **1** (Table 2). The coupling constant, $^2J(^1H-^{199}Hg)$, of 215 Hz is intermediate between the values obtained previously for N(7)-bound $CH_3Hg(II)$ in [CH_3Hg(NucH)]NO$_3$ (229 Hz) and the value (185 Hz) for **2**, which indicates rapid exchange of $CH_3Hg(II)$ between the two environments (1*c*). In the ^{13}C nmr spectrum, a pronounced upfield shift in the C(6) resonance relative to **1** (Table 3) is characteristic of S-bound $CH_3Hg(II)$, which is in accord with either **4** or **10** (16). The latter possibility is less likely, as indicated from the trends in the chemical shifts of the other resonances in the ^{13}C nmr spectrum. The carbon resonances C(4), C(6), and C(8) adjacent to the site of methylmercuration are the most affected (Table 3). The C(2) resonance is also affected to an extent comparable to **2**, for which exclusive sulfur methylmercuration has been established. The C(8) resonance in **2** is almost unchanged with respect to **1**. If structure **10**

TABLE 3. ^{13}C chemical shifts and coupling constants for the $CH_3Hg(II)$–6-mercaptonucleoside complexes

Compound	Chemical shifts[a,b] Base carbons C(6)	C(2)	C(4)	C(8)	C(5)	Methylmercury(II) carbons CH_3Hg	Coupling constants Hz $^1J(^{13}C-^{199}Hg)$
1*a* [6-MPRH$_2$]	176.1	145.3	143.9	141.3	135.5	—	—
2*a* [(CH$_3$Hg)(6-MPRH)]	168.0	151.6	148.1	142.7	133.1	9.1	1452.5
3*a* [(CH$_3$Hg)(6-MPRH$_2$)]NO$_3$	167.2	149.9	147.9	143.9	133.0	8.1	1501.0
4*a* [(CH$_3$Hg)$_2$(6-MPRH)]NO$_3$	167.7	152.2	147.4	144.6	132.6	4.2	1694.3
5*a* [(CH$_3$Hg)$_3$(6-MPR)]NO$_3$	163.9	152.2	149.0	202.6	133.6	4.7[c] 7.2[d]	[e]
11*a* [(CH$_3$Hg)$_2$(6-MPRH$_2$)](NO$_3^-$)$_2$	167.4	151.6	147.5	145.7	132.8	4.2	1711.4
1*b* [2-A-6MPRH$_2$]	175.2	153.1	147.9	138.5	128.5	—	—
2*b* [(CH$_3$Hg)(2-A-6-MPRH)]	167.8	160.1	150.5	138.8	126.1	9.2	1440.0
3*b* [(CH$_3$Hg)(2-A-6-MPRH$_2$)]NO$_3$	163.7	155.3	151.6	143.3	126.2	7.7	1620.0
4*b* [(CH$_3$Hg)$_2$(2-A-6-MPRH)]NO$_3$	165.8	158.8	150.2	141.9	124.4	4.9	1670.2
5*b* [(CH$_3$Hg)$_3$(2-A-6-MPR)]NO$_3$	164.8	—	151.3	—	—	4.2[c] 6.9[d]	[e]
11*b* [(CH$_3$Hg)$_2$(2-A-6-MPRH$_2$)](NO$_3$)$_2$	164.4	156.9	151.0	143.0	125.5	4.4	1713.4

[a]In $(CD_3)_2SO$; chemical shifts measured from $(CH_3)_4Si$ internal standard at 50.307 MHz.
[b]Data for **1***a* and **1***b* are taken from ref. 16.
[c]N-, S-bound $CH_3Hg(II)$.
[d]C(8) bound $CH_3Hg(II)$.
[e]Not observed under experimental conditions.

were to be favoured, the C(8) resonance should be affected little or not at all, while larger changes in the C(2) resonance should have been observed, which is not the case. Also, on steric grounds, a more favourable situation for **4** as compared to **10** is anticipated. Since the —SHgCH$_3$ function on C(6) is expected to be electron withdrawing overall, one would expect the donor ability of N(1) towards CH_3Hg^+ (or H^+) to be decreased, thereby rendering N(7) as the most reactive centre. Thus the weight of evidence is in favor of structure **4**. The carbon resonance of $CH_3Hg(II)$ at ca. 4.5 ppm is significantly higher than the value (−0.13 ppm) obtained in N(1),N(7)-bound methylmercury(II) in the inosine and guanosine complexes [$(CH_3Hg)_2$-(NucH)]NO$_3$, (1*c*), which further supports S- and N-involvement in $CH_3Hg(II)$ binding. The appearance of a strong band at 1360 cm^{-1} due to NO_3^- in the ir spectrum supports the cationic nature of the complexes (18).

A different product of stoichiometry, 2 $CH_3Hg(II)$: 1 6MNucH$_2$, could result in principle if the reaction was carried out using **1** as the reactant rather than **2** as above. The complexes that could form under these conditions at pH 2–3 can be formulated as **12** and **13**. However, the isolated product corresponds

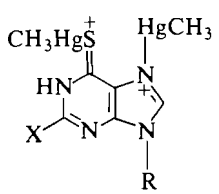

12

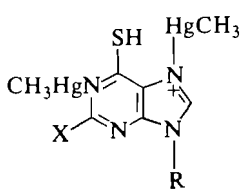

13

in fact to **4**, as shown by the analytical as well as the spectroscopic (^1H, ^{13}C nmr, and ir) data. This could be due to an increased acidity of N(1)—H on coordination of $CH_3Hg(II)$ at N(7) and S(6).

On the other hand, when **1** was titrated with two molar equivalents of CH_3HgNO_3 in $(CD_3)_2SO$, the ^1H nmr of the solution showed a downfield shift in the C(8)—H resonance, together with a higher value of the coupling constant $^2J(^1H-^{199}Hg)$ of 225 Hz. All ^{13}C nmr chemical shifts were very close to the values observed for **4** except for the $CH_3Hg(II)$ resonance, which occurred upfield by 0.5 ppm relative to **4** (Table 3). These results suggest that in $(CD_3)_2SO$ medium, the 2:1 complex has the structure given by **12**.

(c) *N-, and S-, and C-methylmercuration (3:1 stoichiometry)*

The complexes that could arise from a 3:1 interaction between $CH_3Hg(II)$ and the nucleosides under study are **14** and **5**.

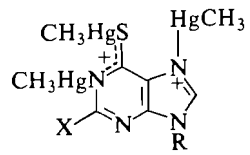

14

An attempt to obtain complex **14** via the reaction of **2** with CH_3HgNO_3 (2 moles) at pH 3 led only to the formation of **4**. Also, when **4** was treated with CH_3HgNO_3 (1 mole) at pH 3, no reaction occurred and only unreacted **4** could be recovered. Presumably, the lack of formation of **14** can be ascribed to adverse steric and electronic factors, as was also noted in the case of complex **10**.

However, when the reaction of **4** with CH_3HgNO_3 (1:1 mole ratio) was carried out at pH 7–8, the product obtained was found to have the structure given by **5**. The same product was obtained when **1** was reacted with CH_3HgNO_3 (3:1 mole ratio) at pH = 8. Interestingly, the reaction of **1***a* with CH_3HgNO_3 (3:1 mole ratio) yields **5** almost quantitatively, while with **1***b* an appreciable amount of **4** was found in addition to **5**.

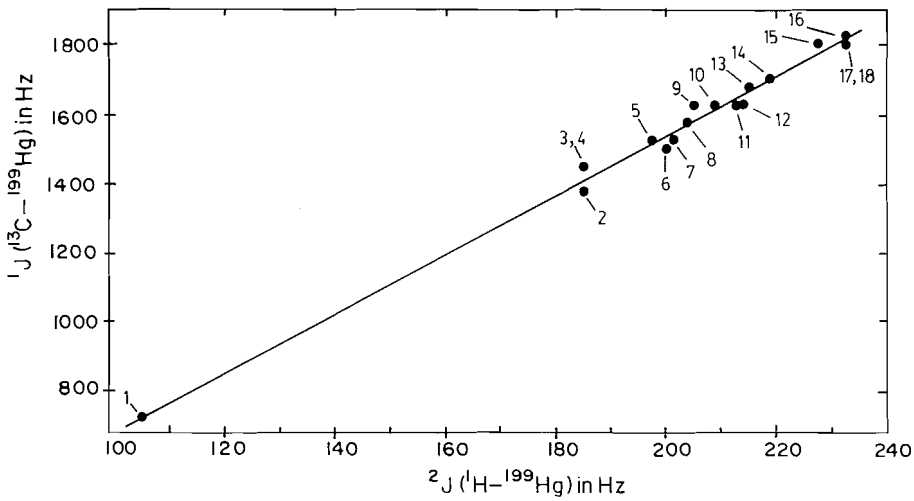

FIG. 1. The correlation between $^2J(^1H-^{199}Hg)$ and $^1J(^{13}C-^{199}Hg)$. Numbers 1 to 18 refer to compounds $(CH_3)_2Hg$; **1**; $[(CH_3Hg)(MeImS)]$, **2**; $[(CH_3Hg)(2\text{-A-6-MPRH})]$, **3**; $[(CH_3Hg)(6\text{-MPRH})]$, **4**; $[(CH_3Hg)_2(8\text{-ThioGuo})]$, **5**; $[(CH_3Hg)(6\text{-MPRH}_2)]NO_3$, **6**; $[(CH_3Hg)(uri)]$, **7**; $[(CH_3Hg)(MeImS)]NO_3$, **8**; $[(CH_3Hg)(2\text{-A-6-MPRH}_2)]NO_3$, **9**; $[(CH_3Hg)(Th)]$, **10**; $[(CH_3Hg)(8\text{-ThioGuoH}_2)]NO_3$, **11**; $[(CH_3Hg)_3(8\text{-ThioGuo})]NO_3$, **12**; $[(CH_3Hg)_2(2\text{-A-6-MPRH})]NO_3$, **13**; $[(CH_3Hg)_2(6\text{-MPRH})]NO_3$, **14**; $[(CH_3Hg)_2(Th)]NO_3$, **15**; $[(CH_3Hg)(Th)(NO_3)_2Hg]$, **16**; $[(CH_3Hg)(Th)]NO_3$, **17**; $[\{(CH_3Hg)(6\text{-MPRH})(NO_3)\}_2Hg]$, **18**; Data on coupling constants, $^2J(^1H-^{199}Hg)$ for complexes **1**, **2**, **5**, **7**, **8**, **10**, **11**, **12**, **15**, **16**, **17**, and **18** are taken from ref. 1.

The occurrence of carbon methylmercuration is in accord with our previous findings on the activation of C(8)—H in inosine and xanthosine, and C(2)—H in imidazole derivatives, as a result of coordination of $CH_3Hg(II)$ to N(7)/N(1) in these systems (1*a*,*c*,*e*). Proton abstraction gives an ylid (carbenoid) form that then reacts with $CH_3Hg(II)$ to give the observed product, as shown in eq. [1].

[1]

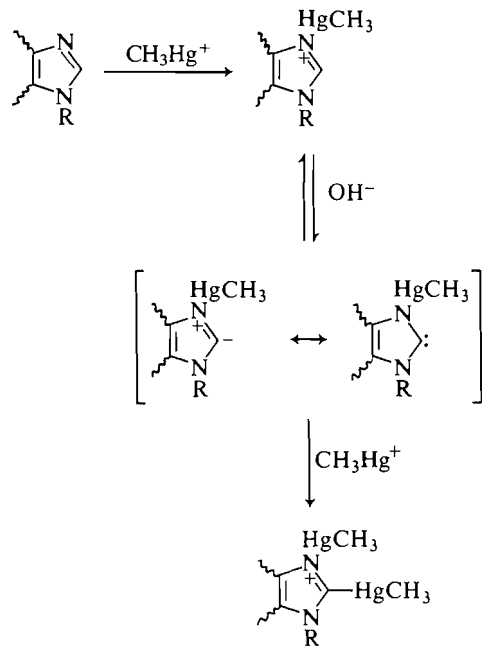

The most significant proof for the structure of **5** is the appearance of two ^1H nmr signals due to $CH_3Hg(II)$ in an integral ratio of ca. 2:1, one signal occurring at 0.74 ppm and assignable to an averaged, rapidly exchanging, S- and N-bound $CH_3Hg(II)$, and the other signal at 0.62 ppm assignable to C-bound $CH_3Hg(II)$. The latter signal is in the same region as previously found for C-bound $CH_3Hg(II)$ in the inosine, xanthosine, and N-methylimidazole complexes. As well, different coupling constants, $^2J(^1H-^{199}Hg)$, are observed for the $CH_3Hg(II)$ groups in the different environments, which is characteristic of simultaneous binding at two different sites. The ^{13}C nmr confirms the presence of $CH_3Hg(II)$ in two different environments, one resonance at 4.50 ppm for both S- and N-bound $CH_3Hg(II)$ and one at 7.00 ppm for carbon-bound $CH_3Hg(II)$. It is also noted that the C(8) resonance in **5** has experienced a downfield shift of 61 ppm, which is closely similar to the shift observed in the methylmercurated C(8) atoms of inosine and xanthosine (1*c*,*e*).

^{13}C chemical shifts and correlation of $^2J(^1H-^{199}Hg)$ and $^1J(^{13}C-^{199}Hg)$ couplings

The ^{13}C chemical shifts of $CH_3Hg(II)$ that have been observed in this work for S-bound $CH_3Hg(II)$ (8–9 ppm in **2** and **3**) are considerably larger than previously observed for N-bound $CH_3Hg(II)$ (−1.00 to 2.00 ppm in inosine and guanosine) (1*c*). In compounds **4** and **5**, containing both S- and N-bound $CH_3Hg(II)$, the ^{13}C signal of $CH_3Hg(II)$ (4.00 to 5.00 ppm) occurs at an intermediate value compared to the respective N-bound/S-bound 1:1 complexes, showing that there is rapid exchange of $CH_3Hg(II)$ on the nmr time scale. Thus ^{13}C chemical shifts of $CH_3Hg(II)$ provide a useful indicator of the nature of the donor ligand (19, 20).

The donor ligands that give rise to substantial ^{13}C chemical shifts also give rise to substantial $^1J(^{13}C-^{199}Hg)$ couplings (Table 3). As well, almost parallel changes are apparent in $^1J(^1H-^{199}Hg)$, methyl proton – mercury couplings (Fig. 1). The two quantities are correlated by eq. [2] (correlation coefficient = 0.9949).

$$[2] \quad {}^1J = 8.460\,{}^2J - 155.6$$

The origin of this relationship is presumably that a strongly bound ligand weakens the Hg—C bond *trans* to it and thus decreases the "s" character in the Hg—C bond. Since the Fermi contact term dominates the two-bond mercury–proton coupling, a decrease in "s" character in the Hg—C bond results in a smaller *J* value (21). In the present systems, $^1J(^{13}C-^{199}Hg)$ for **2***a* is lower by 175 Hz than in the neutral N-bound $CH_3Hg(II)$ complex $[(CH_3Hg)Th]$, and approximately 753 Hz higher than in

the carbon-bound $CH_3Hg(II)$ group in $(CH_3)_2Hg$. Also, $^1J(^{13}C-^{199}Hg)$ for **3***a* is lower by 301 Hz than in the cationic N-bound complex $[(CH_3Hg)(ThH)]NO_3$. However, in the 2:1 complex **4***a*, the ^1J value is lower by 100 Hz than in the 2:1 complex $[(CH_3Hg)_2Th]NO_3$.

Concluding remarks

We have found in the present study that 6-mercaptopurine riboside (**1***a*) and 2-amino-6-mercaptopurine riboside (**1***b*), under basic and acidic conditions, respectively, form 1:1 $CH_3Hg(II)$ / 6-$MNucH_2$ complexes **2***a*/**2***b* and **3***a*/**3***b*, involving binding of $CH_3Hg(II)$ via the sulfur atom. Under 2:1 stoichiometry of $CH_3Hg(II)$ / 6-$MNucH_2$, complexes **4***a*/**4***b* are obtained in which both sulfur and N(7) are involved in binding. The observation of C(8)-, N(7)-, and S(6)-binding under 3:1 stoichiometry of $CH_3Hg(II)$ / 6-$MNucH_2$, **5***a*/**5***b*, reinforces our previously proposed mechanism for the ready formation of the C-bonded adducts by means of initial activation by a coordinated electrophilic species at N(7) (1*a*,*c*,*e*). Thus 6-thionucleosides show different coordination behaviour with respect to the parent guanosine and inosine, with N(1) no longer being the primary donor atom (1*c*). This is in accord with the preference of Hg(II) for soft (class b) donor atoms such as sulfur (22). $^2J(^1H-^{199}Hg)$ coupling constants correlated well with $J(^{13}C-^{199}Hg)$ coupling constants and their magnitudes reflect the increase in the strength of the mercury–ligand bond in the order Hg—C > Hg—S > Hg—N (23).

Extrapolating to biological systems, the interaction of $CH_3Hg(II)$ with thiols to form S-bonded adducts is believed to be important in both the toxicology of $CH_3Hg(II)$ and the use of antidotes containing thiol groups (24). Although the formation constants for S-bonded $CH_3Hg(II)$ thionucleosides must be very large (25), these compounds are found to undergo extremely rapid nucleophilic ligand displacement reactions (e.g. glutathione model). Clearly these rapid ligand exchange reactions are the key to the bioavailability of $CH_3Hg(II)$. A similarly essential role exists in the treatment of mercury poisoning with chemotherapeutic agents, which complex $CH_3Hg(II)$ and Hg(II) in a more rapidly eliminated form (26). Carbon-bound $CH_3Hg(II)$ species such as those obtained in the present work provide another pathway for $CH_3Hg(II)$ and Hg(II) uptake since their formation is essentially irreversible. The toxicity of $CH_3Hg(II)$ in living beings may be due as much to this factor as to the extensive binding of $CH_3Hg(II)$ to S-centers. Finally, it is possible that 6-thionucleosides could be effective in competing with sulfur containing bio-ligands following intoxication by mercury and its organic derivatives (4).

Acknowledgments

This research was supported by the Natural Sciences and Engineering Research Council of Canada via the Strategic Grants Program in Environmental Toxicology.

1. (*a*) A. R. Norris, E. Buncel, and S. E. Taylor. J. Inorg. Biochem. **16**, 279 (1982); (*b*) S. E. Taylor, E. Buncel, and A. R. Norris. J. Inorg. Biochem. **15**, 131 (1981); (*c*) E. Buncel, A. R. Norris, S. E. Taylor, and W. J. Racz. Inorg. Chem. **20**, 98 (1981); (*d*) E. Buncel, A. R. Norris, S. E. Taylor, and W. J. Racz. Can. J. Chem. **60**, 3033 (1982); (*e*) E. Buncel, B. K. Hunter, R. Kumar, and A. R. Norris. J. Inorg. Biochem. **20**, 171 (1984); (*f*) A. R. Norris, S. E. Taylor, E. Buncel, F. Belanger-Gariepy, and A. L. Beauchamp. Can. J. Chem., **61**, 1536 (1983); (*g*) A. R. Norris, R. Kumar, and E. Buncel. J. Inorg. Biochem. **22**, 11 (1984).
2. L. Baczynskyj, K. Biemann, and R. H. Hall. Science, **159**, 1481 (1968).
3. J. Carbon, H. David, and M.H. Studier. Science, **161**, 1146 (1968).
4. S. K. Carter and L. M. Kershner. Pharm. Times, 56 (1975).
5. A. J. Canty and R. S. Tobias. Inorg. Chem. **18**, 413 (1979).
6. A. J. Canty and A. Marker. Inorg. Chem. **15**, 425 (1976).
7. (*a*) S. Kirschner, Y. Wei, D. Francis, and J. G. Bergmann. J. Med. Chem. **9**, 369 (1966); (*b*) S. M. Skinner and R. W. Lewis. Res. Commun. Chem. Pathol. Pharmacol. **16**, 183 (1977).
8. H. I. Heitner and S. J. Lippard. Inorg. Chem. 1974, **13**, 815.
9. (*a*) E. A. H. Griffith and E. L. Amma. J. Chem. Soc. Chem. Commun. 1013 (1979); (*b*) P. Lavertue, J. Hubert, and A. L. Beauchamp. Inorg. Chem. **15**, 322 (1976).
10. D. W. Abbott and C. Woods. Inorg. Chem. **22**, 1918 (1983).
11. L. W. Reeves, M. Suzuki, and J. A. Vanin. Inorg. Chem. **15**, 1035 (1976).
12. (*a*) M. Chenon, R. J. Pugmire, D. M. Grant, R. P. Panzica, and L. B. Townsend. J. Am. Chem. Soc. **97**, 4636 (1975); (*b*) S. F. Mason. Chem. Biol. Purines, Ciba Found. Symp. **2**, 161 (1963); (*c*) N. Hadjiliadis and T. Theophanides. Inorg. Chim. Acta, **15**, 167 (1975).
13. E. Shefter. J. Pharm. Sci. **57**, 1157 (1968).
14. D. Lichtenberg, F. Bergmann, and Z. Neiman. Isr. J. Chem. **10**, 805 (1972).
15. P. G. Simpson, T. E. Hopkins, and R. Haque. J. Phys. Chem. **77**, 2282 (1973).
16. M. Chenon, R. J. Pugmire, D. M. Grant, R. P. Panzica, and L. B. Townsend. J. Am. Chem. Soc. **97**, 4627 (1975).
17. (*a*) H. I. Heitner, S. J. Lippard, and H. R. Sunshine. J. Am. Chem. Soc. **94**, 8936 (1972); (*b*) H. R. Sunshine and S. J. Lippard. Nucleic Acids Res. **1**, 673 (1974).
18. C. C. Addison, N. Logan, S. C. Wallwork, and C. D. Gardner. Rev. **25**, 289 (1971).
19. (*a*) D. L. Rabenstein and M. T. Fairhurst. Inorg. Chem. **14**, 1413 (1975); (*b*) D. L. Rabenstein, R. Ozubko, S. Libich, C. A. Evans, M. Y. Fairhurst, and C. Suvanprakarn. J. Coord. Chem. **3**, 263 (1974); (*c*) A. P. Arnold and A. J. Canty. Can. J. Chem. **61**, 1428 (1983).
20. A. J. Brown. M.Sc. Thesis, University of Warwick, England (1975).
21. H. F. Henneike. J. Am. Chem. Soc. **94**, 5945 (1975).
22. (*a*) R. G. Pearson. J. Am. Chem. Soc. **85**, 3533 (1963); (*b*) J. Chem. Educ. **45**, 581 (1968).
23. A. J. Brown, O. W. Howarth, and P. Moore. J. Chem. Soc. Dalton Trans. 1589 (1976).
24. (*a*) W. L. Hughes. Ann. N.Y. Acad. Sci. **65**, 455 (1957); (*b*) J. T. McGregor and T. W. Clarkson. Adv. Exptl. Med. Biol. **48**, 463 (1974); (*c*) A. J. Canty. Am. Chem. Soc. Symp. Ser. **82**, 327 (1978).
25. D. L. Rabenstein and M. T. Fairhurst. J. Am. Chem. Soc. **97**, 2086 (1975).
26. J. Aaseth. Acta Pharmacol. Toxicol. **39**, 289 (1976).
27. K. W. Jennette, S. J. Lippard, and D. A. Ucko. Biochim. Acta, **402**, 403 (1975), and references therein.

Synthesis of *N,N'*-di(2-hydroxybenzyl)ethylenediamine-*N,N'*-diacetic acid (HBED) and derivatives

ARTHUR E. MARTELL,[1] RAMUNAS J. MOTEKAITIS, AND ERIC T. CLARKE
Department of Chemistry, Texas A&M University, College Station, TX 77843, U.S.A.

AND

J. J. HARRISON[1,2]
Gulf Research & Development Company, P.O. Drawer 2038, Pittsburgh, PA 15230, U.S.A.

Received April 10, 1985[3]

ARTHUR E. MARTELL, RAMUNAS J. MOTEKAITIS, ERIC T. CLARKE, and J. J. HARRISON. Can. J. Chem. **64**, 449 (1986).

Two synthetic approaches for the synthesis of *N,N'*-di(2-hydroxybenzyl)ethylenediamine-*N,N'*-diacetic acid (HBED) and derivatives are reported. The first involves conversion of *N,N'*-di(2-hydroxybenzyl)ethylenediamine to the diamide HBEDDA via reaction with formaldehyde and HCN followed by hydrolysis. Analysis of the species distribution curves of the Cu(II) chelates of *N,N'*-di(2-hydroxybenzyl)ethylenediamine-*N,N'*-diacetic acid (HBED) and its diamide, HBEDDA, and of the nature of the coordination in each complex species formed, suggest the selection of the reaction conditions most favorable for the Cu(II)-catalyzed hydrolysis of HBEDDA to HBED. The rate of conversion was found to be low, and the reasons for these findings are described. Iron(III) catalysis of the conversion of HBEDDA to HBED was found to be rapid and complete with a pseudo-first-order rate constant of 3.1×10^{-3} s^{-1} at 25.0°C. The results provide the final step of a new method for the synthesis of HBED. The second synthetic approach involves reaction of *N,N'*-ethylenediamine-diacetic acid (EDDA) with substituted phenols and formaldehyde. These approaches appear to be general for the synthesis of HBED and derivatives.

ARTHUR E. MARTELL, RAMUNAS J. MOTEKAITIS, ERIC T. CLARKE et J. J. HARRISON. Can. J. Chem. **64**, 449 (1986).

On rapporte deux méthodes de synthèse de l'acide *N,N'*-di(hydroxy-2-benzyl)-éthylènediamine-*N,N'*-diacétique (HBED) et de ses dérivés. La première implique le transformation de la *N,N'*-di(hydroxy-2-benzyl)éthylènediamine en diamide HBEDDA par le biais d'une réaction avec le formaldéhyde et le HCN qui est suivie d'une hydrolyse. Une analyse des courbes de distribution des espèces qui se forment lors de la chélation du Cu(II) avec l'acide HBED et son diamide HBEDDA ainsi que celle de la nature de la coordination dans chaque espèce complexe qui se forme permet de déterminer les conditions de réaction qui sont les plus favorables pour l'hydrolyse, catalysée par le Cu(II), du HBEDDA en HBED. On a trouvé que la vitesse de conversion est faible et on décrit les causes de ce résultat. On a trouvé que la transformation, catalysée par le Fe(III), du HBEDDA en HBED est rapide et que la constante de vitesse de pseudo premier ordre est égale à $3{,}1 \times 10^{-3}$ s^{-1}, à 25°C. Ces résultats fournissent l'étape finale d'une nouvelle méthode de synthèse de l'acide HBED. La deuxième voie de synthèse implique la réaction de l'acide *N,N'*-éthylènediaminediacétique (EDDA) avec des phénols substitués et du formaldéhyde.Ces méthodes semblent générales pour la synthèse de l'acide HBED et de ses dérivés.

[Traduit par le journal]

Introduction

The synthesis of *N,N'*-di(2-hydroxybenzyl)ethylenediamine-*N,N'*-diacetic acid (HBED, **1**) is of considerable interest because of its usefulness as a chelating agent for Fe(III) (1, 2) and for other trivalent ions (3–5). The free ligand and its esters have been found to be effective in the removal of iron from test animals (4, 6. 7) and are therefore of interest for the treatment of Cooley's anemia. The corresponding Ga(III) and In(III) chelates may also be useful as radiopharmaceuticals for tumor imaging purposes (4–7).

Unfortunately, the development of HBED as a ligand for these purposes has been held back by lack of a good synthetic method. The procedure described previously (1) suffers from the formation of a resinous polymeric by-product, which seems to be promoted by treatment with acid or base, and to sometimes form spontaneously during recrystallization of the material (decomposition seems to be a reverse Mannich reaction involving the splitting out of formaldehyde).

A new method of HBED synthesis, suitable for moderate to large scale production, has been developed by Strem Chemicals, Inc.,[4] but a description of the procedure employed is currently subject to proprietary restrictions.

We report two approaches for the synthesis of HBED and derivatives. The first approach involves conversion of *N,N'*-di(2-hydroxybenzyl)ethylenediamine to the diamide (HBEDDA) via reaction with formaldehyde and HCN followed by hydrolysis. Because of the difficulty of hydrolyzing HBEDDA, **2**, to HBED, **1**, it was decided to investigate the promotion of

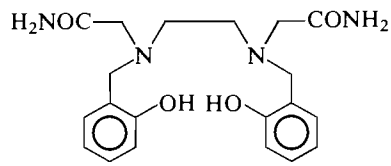

2

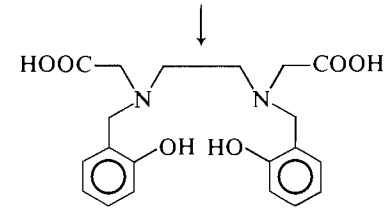

1

[1]Authors to whom correspondence may be addressed.

[2]Current address: Chevron Research Co., P.O. Box 1627. Richmond, CA 94802, U.S.A.

[3]Revision received October 22, 1985.

[4]M. Strem. Personal communication, 1984.

Printed in Canada / Imprimé au Canada

this reaction by Cu(II) and Fe(III) ions. To be successful, this must be done in such a manner as to utilize the formation of an HBED chelate of high stability as the driving force in reaction. This paper describes the selection of conditions most favourable for metal ion catalysis, and development of a procedure for the metal ion-catalyzed formation of HBED from its diamide.

A second approach for the synthesis of HBED derivatives, which involves reaction of *N,N'*ethylenediamine diacetic acid (EDDA) with substituted phenols and formaldehyde, is also reported.

Experimental

Materials

A pure sample of HBED was kindly donated by Mr. Mike Strem of Strem Chemicals, Inc., Newburyport, Massachusetts.

Potentiometry

Potentiometric measurements of hydrogen ion concentration were made in an apparatus of the type described previously (8). The potentiometric system was calibrated with dilute standard HCl and KOH solutions at 0.100 *M* ionic strength adjusted with KNO_3 so as to read p[H] directly, where p[H] = $-\log [H^+]$. The molar ligand to metal ion ratio was maintained at 1:1 for the determination of the formation constant of the Cu(II) chelates of HBEDDA and for the determination of the Fe(III) – potentiometric equilibrium curve.

Computations

Calculations of protonation constants of the ligand and its Cu(II) chelate, and of the formation constants of the chelate, were carried out with programs PKAS (9) and BEST (10), for the protonation constants and the Cu(II) chelate stability constants, respectively. The calculation of species distributions from equilibrium constants was carried out with program SPE, which employs the algorithm from BEST adapted to the Micromation computer system for graphic display on Houston Instruments DMP-29 HIPLOT X-Y plotter.

Kinetic measurements

The kinetics of conversion of the Cu(II) and Fe(III) chelates of HBEDDA to the corresponding HBED chelates was followed with a Perkin Elmer Model 553 fast scan uv/vis spectrophotometer. The absorptivities were such that $1.0 \times 1^{-4} M$ solutions (in 1.000-cm cells) provided sufficiently intense bands for quantitative measurements. The rates of conversion of the Cu(II) chelate were measured at p[H] 3.0 and 50.0°C, while those of the Fe(III) chelate were measured at p[H] values from 8 to 11 at 25.0°C.

Preparation of N,N'*-di(2-hydroxybenzyl)ethylenediamine*-N,N'*-di-acetonitrile, 4*

N,N'-di(2-hydroxybenzyl)ethylenediamine-*N,N'*-diacetonitrile, **4**, was synthesized, by a slight variation of published procedure (11), from the *N,N'*-di(2-hydroxybenzyl)ethylenediamine, **3** (12).

Preparation of HBEDdiamide.2HCl.2H$_2$O, 2

To a three-neck flask equipped with a magnetic stirrer cooling bath under argon were added 380 mL ethanol, 15.66 g HBEDacetonitrile (0.045 mol), and 34.8 g 30% H_2O_2 solution (0.307 mol). To this at 5°C was added 1.48 g (0.037 mol) sodium hydroxide dissolved in 16 mL water. This was stirred 3 h at 5–10°C, after which 31.1 g sodium bisulfite (0.30 mol) dissolved in 50 mL ice water was slowly added so that the temperature was held below 10°C. Then, after stirring at 10°C, the product was filtered to remove Na_2SO_4. The filtrate was mixed with 10 mL HCl and allowed to crystallize. A total of 4.75 g purified material was recovered, mp 200–205°C; 22% yield; ^{1}H nmr (CD_3OD/D_2O, NaOD)δ: 5.8–6.6 (m, 8H, ArH), 3.64 (s, 4H, H_2NOCCH_2N), 3.21 (s, 4H, $ArCH_2N$), 2.71 (s, 4H, NCH_2CH_2). *Anal.* calcd. for $C_{20}H_{26}N_4O_4.2HCl.H_2O$: C 50.32, H 6.33, N 11.75, Cl 14.85; found: C 50.29, H 6.20, N 11.56, Cl 15.22.

Fe(III)–HBED

The Fe(III)–HBED chelate was prepared in solution by mixing equivalent molar amounts of an Fe(III) salt and HBEDDA, adjusting the solution to neutral or alkaline pH, and stirring for 3–4 h at room temperature. The ammonia formed may be removed by refluxing briefly at pH 10.

Conversion of Fe(III)–HBED to HBED

To a 0.10 *M* solution of the Fe(III)–HBED reaction product obtained by Fe(III)-promoted hydrolysis of HBEDDA was added sufficient HCl solution to lower the p[H] to 5.0. To this solution an excess of 8-hydroxyquinoline in ethanol was added and the solution was warmed to about 50.0°C. The black precipitate of the Fe(III)–8-hydroxyquinoline chelate was filtered off, and the remaining deeply red-colored solution was repeatedly (5×) extracted at 50.0°C with chloroform containing 8-hydroxyquinoline. After three final extractions with pure chloroform, the remaining aqueous layer was shown spectrophotometrically to have been 96.6% converted to the metal-free ligand. The solution was acidified with HCl to p[H] 2 and the HBED was isolated by cooling the solution to 0°C. The first batch of nearly colorless crystals consisted of 55% of the theoretical amount. Additional material was obtained by reduction of the volume of the mother liquor and further crystallization at 0°.

Preparation of N,N'*-di(3,5-dimethyl-2-hydroxybenzyl)ethylenediamine*-N,N'*-diacetic acid 7a*

To a three-neck, 100-mL flask, equipped with a nitrogen source, thermometer, magnetic stirrer, heating mantle, SCM electrode and reference electrode, and dropping funnel was added 7 mL 30% NaOH solution and 15 mL methanol. To this was added 4.4 g (0.025 mol) ethylenediamine-*N,N*-diacetic acid and 12.2 g of 2,4-dimethylphenol (0.10 mol) dissolved in 12 mL methanol. The pH initially at 10.9 was adjusted by the addition of 10% HCl to pH 8.2. The reaction was heated to reflux and 8.1 g 37% formaldehyde solution (0.10 mol) in 24 mL methanol was added dropwise with stirring. The pH of the mixture was controlled at pH 8.0. This was heated at reflux for a total of 5 h, then the mixture was cooled to room temperature. The pH was adjusted with NaOH solution to 9.0 and a product precipitated. This was filtered and dried in a vacuum oven at 70°C overnight. A total of 8.08 g of product **7***a* as disodium salt was recovered, mp 181–183°C; 62% yield; ^{1}H nmr (CD_3OD) δ: 6.8 (br s, 2H, ArH), 6.5 (br s, 2H, ArH), 3.6 (s, 4H, HO_2CCH_2N), 3.1 (s, 4H, $ArCH_2N$), 2.6 (s, 4H, NCH_2CH_2), 2.20 (s, 6H, $ArCH_3$), 2.15 (s, 6H, $ArCH_3$). *Anal.* calcd. for $C_{24}H_{30}N_2O_6Na_2.2H_2O$: C 54.96, H 6.54, N 5.34, Na 8.77; found: C 54.54, H 6.26, N 5.35, Na 8.45.

Preparation of N,N'*-di(5-sodiumsulfonate-2-hydroxybenzyl)ethylenediamine*-N,N'*-diacetic acid, 7b*

To a three-neck flask equipped with nitrogen source, thermometer, magnetic stirrer, heating mantle, SCM electrode and reference electrode, and dropping funnel was added 4.4 g ethylenediamine diacetic acid (0.025 mol), 23.22 g *p*-phenolsulfonic acid sodium salt (0.10 mol), and 60 mL methanol. This was heated to reflux and 1.8 g NaOH in 3 mL water was added. The pH was 8.7. To this slurry at reflux was added 8.2 g 37% formaldehyde solution (0.10 mol). Midway through the formaldehyde addition, the mixture became a solution. This was refluxed for 5.5 h, then cooled to room temperature overnight. The white solids which precipitated were filtered and dried *in vacuo* to give 5.0 g product; ^{1}H nmr (D_2O) δ: 6.6–7.8 (m, 6H, ArH), 3.8 (br s, 4H, HO_2CCH_2N), 3.3 (br s, 4H, $ArCH_2N$), 2.9 (br s, 4H, NCH_2CH_2). Attempted purification of **7***b* by recrystallization was unsuccessful.

Results and discussion

N,N'-di(2-hydroxybenzyl)ethylenediamine-*N,N'*-diacetamide **2**, was synthesized according to Scheme 1. The known (11, 12) *N,N'*-di(2-hydroxybenzyl)ethylenediamine, **3**, was treated with HCN and formaldehyde to give *N,N'*-di(2-hydroxybenzyl)ethylenediamine-*N,N'*-diacetontrile, **4**, in 97% yield. The order of addition of reagents was important in this reaction. When the formaldehyde was added before the sodium cyanide, only 19% yield of **4** was obtained. Compound **4** could

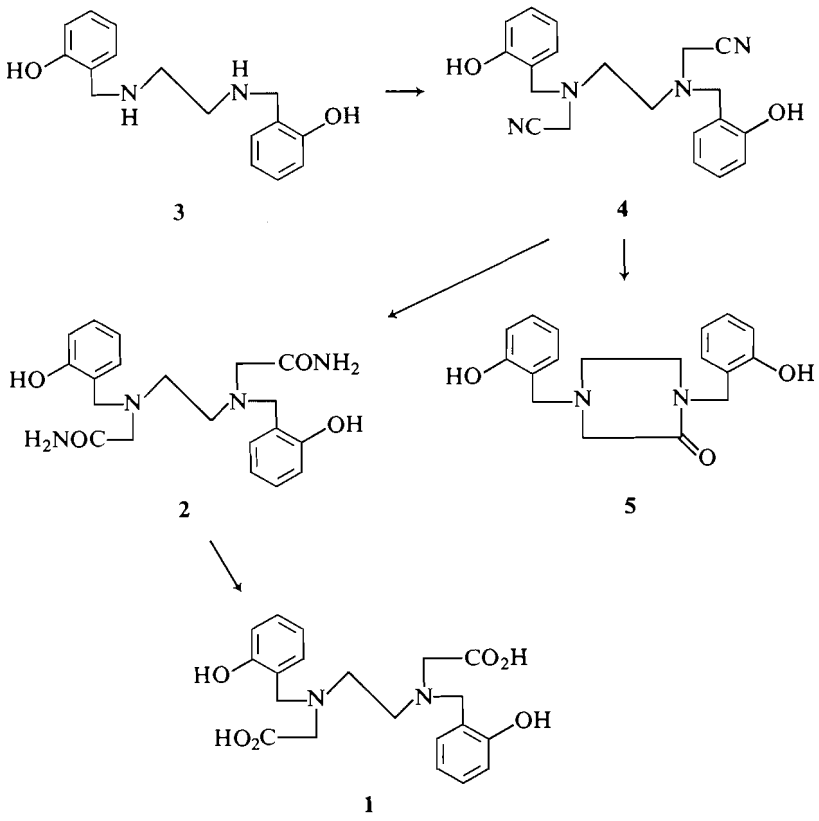

SCHEME 1

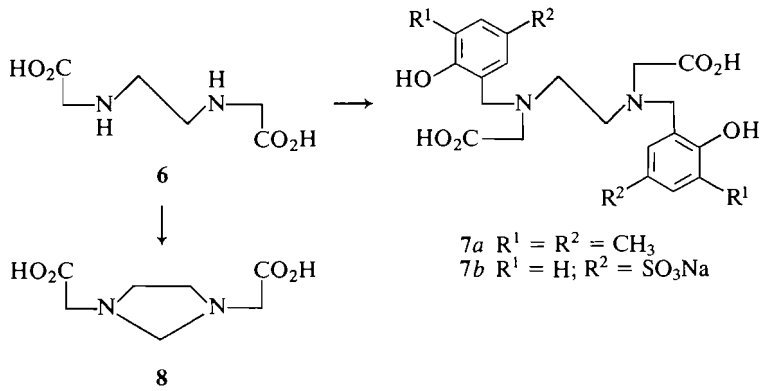

SCHEME 2

not be hydrolyzed to **1** by either acid or base catalysis (11). Instead, small amounts of *N*,*N*′-di(2-hydroxybenzyl)monoketopiperazine, **5**, were obtained. Compound **5** formed even after boiling **4** in water (11) at pH 7.

The diamide **2** was obtained by treating dinitrile **4** with excess H_2O_2 at 5–10°C using a catalytic amount of sodium hydroxide. The diamide could be precipitated as the di-HCl salt. Rather surprisingly, no evidence of an N-oxide was detected under these conditions where one might expect N-oxide to form.[5] This may be due to the unavailability of a reaction pathway for nitrogen atom substitution in these compounds **4** and **2**. Evidence supporting this was obtained by recovery after 8 h of unchanged **4** in the presence of excess H_2O_2 in methanol solution at room temperature. In contrast, when **4** was treated with H_2O_2 and a catalytic amount of sodium hyroxide at *room temperature* overnight, no amide could be recovered. Instead, a complex mixture that was not characterized was observed. Prolonged treatment of **4** with strong acid resulted in decomposition and loss of yield.

The diamide, **2**, could not be hydrolyzed in either acid or base solution or with sodium nitrite in acetic acid under a variety of conditions. Conversion to HBED, however, has been carried out by utilizing the catalytic effects of Cu(II) and Fe(III), as discussed below.

A second synthetic route suitable for the synthesis of derivatives of **1** substituted *para* to the phenolic hydroxyl group was accomplished by reacting ethylenediamine-*N*,*N*′-diacetic acid, **6**, with formaldehyde and a substituted phenol, as indicated in Scheme 2.

This reaction was examined using 2,4-dimethylphenol (14) under a variety of conditions and was found to be very sensitive

[5]See ref. 13 for conditions used in preparing nitrilotri(methylenephosphonic acid) N-oxide, for example.

TABLE 1. Effect of pH on synthesis of HBED derivatives[a]

Run	pH	Product yield (isolated) 7*a*	6
1	5	—	63%
2	7	Trace	53%
3[b]	8	62%	—
4[b]	9	27%	—
5[b]	11	21%	—
6[b]	13	Trace	—

[a]Reaction of 0.025 mmol EDDA, **6**, with 0.05 mmol 2,4-dimethylphenol and 0.05 mmol CH_2O solution in CH_3OH–H_2O at reflux for 5 h.
[b]Compound **8** was detected in the filtrate in large amounts.

to pH. At pH less than 7, only traces of desired product **7***a* were observed. Starting compound **6** was recovered unchanged and it appeared that only phenolformaldehyde reaction was occurring. Between pH 8 and 13, desired **7***a* could be isolated in moderate yield and all of **6** was consumed (Table 1). The best yield of desired product, **7***a*, 62% (see Experimental), could be obtained by reacting **6** and a twofold excess of 2,4-dimethylphenol at reflux temperature with a twofold excess of formaldehyde at pH 8.0. A by-product of this reaction, which became the predominant product under suitable conditions (deficiency of phenol or high pH), was identified by ^1H and ^{13}C nmr as **8** (Scheme 2). Compound **8** could be prepared in nearly quantitative yield in solution by reacting EDDA separately with 1 mol CH_2O and 1 mol base (Na_2CO_3 or NaOH).

The structural assignment of **8** follows by comparing its ^{13}C nmr spectrum (D_2O), δ: 176.0 (CO_2H), 75.9 (NCH_2N), 57.7 (NCH_2CH_2N), 51.6 (NCH_2CO_2H) with that of 1,3-dimethylimidazolidine (15) (CF_3CO_2H), δ: 74.48 (NCH_2N), 55.18 (NCH_2CH_2N), 42.70 (CH_3N), and from the ^1H nmr spectrum of **8** (D_2O), δ: 3.50 (2H, s, NCH_2N), 3.23 (4H, s, NCH_2CO_2H), 2.87 (4H, s, NCH_2CH_2N).

Presumably, by adding the formaldehyde last to a solution of **6** and 2,4-dimethylphenol at as low a pH as practical (pH 8), formation of **7***a* competes favorably with formation of **8**, which does not react further under these conditions to form **7***a*. The dimethyl derivative **7***a* prepared by this procedure precipitated as the disodium salt by adjusting the pH of the mixture at pH 9 and cooling.

A second HBED derivative **7***b* was also prepared by the reaction of **6** with formaldehyde and 4-phenolsulfonic acid sodium salt (14). Compound **7***b* was produced, as expected, and was characterized by nmr, but efforts to find a suitable crystalline derivative of **7***b* failed. As with compound **2**, the synthesis of **7***b* was sensitive to strong acid and at pH <4 yields starting compound phenol sulfonic acid and by-products. Compound **7***b* may hold promise as a very water-soluble iron chelating agent.

Hydrolysis of HBEDDA to HBED

Cu(II) complexes

The equilibrium data in the paper by L'Eplattenier *et al.* (1) were employed to determine the species formed from Cu(II) and HBED at a 1:1 molar ratio as a function of p[H]. The results for a 1.0×10^{-3} molar solution are presented in Fig. 1. It is seen that the three forms of the Cu(II) chelate, CuH_2L, $CuHL^-$, and CuL are related by chelate proton association constants (p*K*'s) of

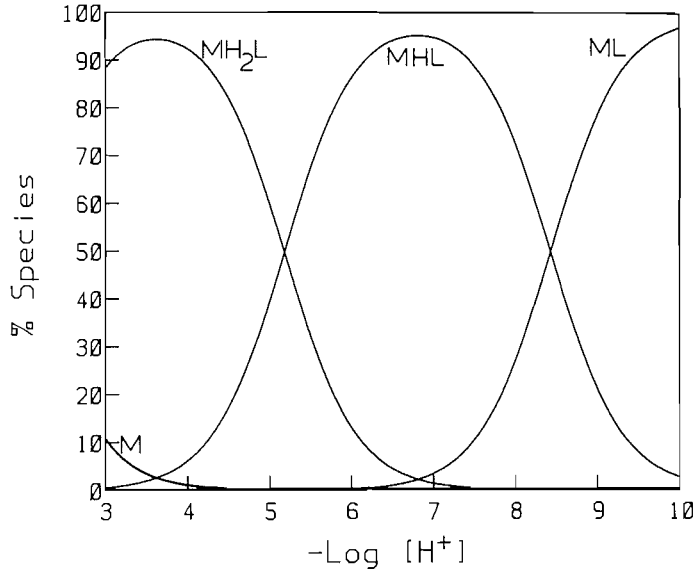

FIG 1. Species equilibrium distribution diagram for a 1:1 aqueous solution of Cu(II)–HBED as a function of −log [H] at 25.0°C; μ = 0.100 *M*; $T_L = T_M = 1 \times 10^{-3}$ *M*. Curve labelled M also represents the H_4L species.

8.63 and 5.18. Thus the low p[H] form, **9**, the intermediate p[H] species, **10**, and the high p[H] form, **11**, have been shown to have the conformations indicated below (1).

Because it was initially thought that the replacement of the carboxyl groups by amide groups would not have a major influence on the protonation constants of the Cu(II) chelates, it was reasoned that the corresponding amide groups of the Cu(II) chelates of HBED diamide would have conformations analogous to those of **9**, **10**, and **11**. Thus the low pH form would have the arrangement of coordinating donor groups indicated by **12**. At high pH values, by analogy with HBED itself, the diamide would be expected to involve phenolate coordination as indicated by **13**. In addition, an intermediate with a single coordinated phenolate group may also be formed in the mid-p[H] range.

Consideration of the factors involved in metal ion catalysis of amide hydrolysis (16) indicates that the most effective catalytic complex would be **12**, which should have its maximum concentration below pH 4. In **12**, coordination of the carbonyl oxygen should activate the carbonyl carbon toward nucleophilic attack by a base such as the water molecule or hydroxide ion. In **13**, the strong planar coordination by the Cu(II) ion is not directed toward the carbonyl oxygen. Because of the likelihood of weak axial coordination of the amide group, conformations such as that indicated by **14** should also be considered. It has been shown by Hopgood and Angelici (17) and others (18), however, that saturation of the coordination tendencies of Cu(II) by the planar donor groups leaves little additional coordination to be applied to the metal ion in the axial positions. In other words, the catalytic effect of Cu(II) directed toward the axial positions is relatively weak.

The amide nitrogen coordination, with proton dissociation of the type indicated by **15**, should be considered a definite possibility at intermediate and high pH. Such microspecies would be catalytically inactive, since coordinated amide groups are negatively charged and should have little or no tendency to react with nucleophiles. The inertness of such groups toward hydrolytic attack has previously been pointed out (19).

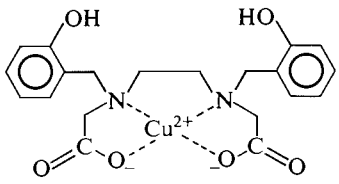

9 CuH_2L (below pH 5.18)

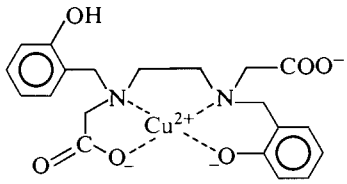

10 $CuHL^-$ (p[H] 5.18–8.63)

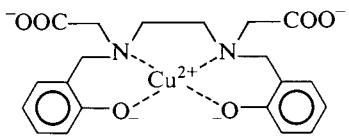

11 CuL^{2+} (above p[H] 8.63)

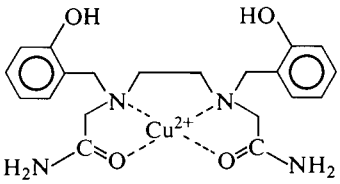

12 $CuH_2L'^{2+}$ (low p[H] form)

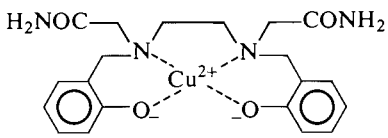

13 CuL′ (high p[H] form)

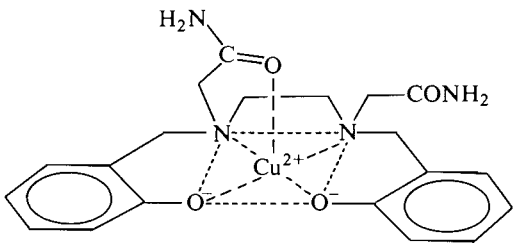

14 CuL′ (5-coordinate)

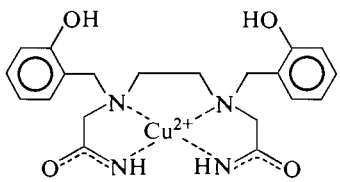

15 CuL′ (alternate high pH form)

It seems therefore, that the Cu(II) complexes below p[H] 5 would be the most catalytically active Cu(II) species in promoting amide hydrolysis, and p[H] 4.5 was therefore selected for carrying out the conversion of the HBED diamide to HBED. At this p[H], the hydrolysis of the aquo Cu(II) ion is minimal and may be neglected (19).

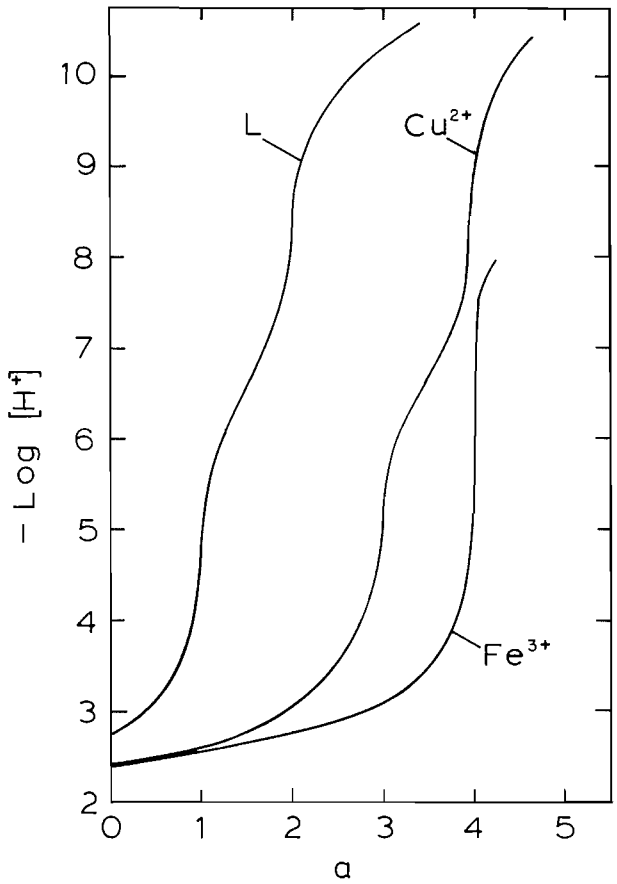

FIG 2. Potentiometric equilibrium curves for 2.000 millimolar solutions of HBEDDA (L), CuHBEDDA(Cu^{2+}) and FeHBEDDA(Fe^{3+}); μ = 0.100 *M* KCl; t = 25.0°C. The Fe^{3+} curve breaks after a = 4 (moles base/mole ligand) because of p[H] drift resulting from the initiation of Fe(III)-catalyzed hydrolysis of the amide groups of the ligand.

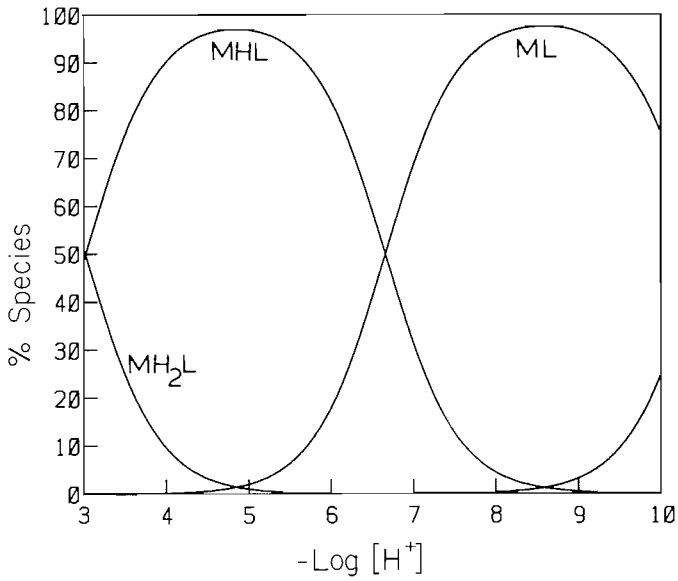

FIG 3. Species equilibrium distribution diagram for a 1:1 aqueous solution of Cu(II)–HBEDDA as a function of −log [H] at 25.0°C; μ = 0.100 *M*; $T_L = T_M = 1 \times 10^{-3}$ *M*.

TABLE 2. Protonation constants and chelate formation constants of HBED and HBEDdiamide (HBEDDA)[a]

Quotient	Log K HBED (H_4L)[b]	Log K HBEDDA (H_4L)[c]
$\frac{[HL]}{[H][L]}$	12.46	11.00
$\frac{[H_2L]}{[H][HL]}$	11.00	10.16
$\frac{[H_3L]}{[H][H_2L]}$	8.32	6.54
$\frac{[H_4L]}{[H][H_3L]}$	4.64	1.89
$\frac{[CuL]}{[Cu][L]}$	21.38	21.19
$\frac{[CuHL]}{[Cu][HL]}$	17.35	16.86
$\frac{[CuH_2L]}{[Cu][H_2L]}$	11.73	9.73
$\frac{[CuHL]}{[CuL][H]}$	8.63	6.67
$\frac{[CuH_2L]}{[CuHL][H]}$	5.18	3.03

[a] $\mu = 0.100\ M$ (KNO_3); $t = 25.00$°C.
[b] Reference 1.
[c] This work.

In order to quantify the reasoning described above, the protonation constants of HBED diamide and its Cu(II) complexes were measured potentiometrically by standard techniques, and the results are presented in the form of the potentiometric equilibrium curves illustrated by Fig. 2. From these data, the species distributions as a function of p[H] were calculated to give the distribution curves in Fig. 3. The protonation constants and metal chelate formation constants of HBEDDA, which were calculated from the data in Fig. 2, are given in Table 2, along with the corresponding value of HBED for comparison. It is apparent from the distribution curves in Figs. 1 and 3 that the partially deprotonated complex species $CuHL^+$ starts to form well below pH 3 and reaches its maximum value at pH 4.5, above which it is converted to the fully deprotonated complex, CuL, with a pK of 6.67. Thus even at low p[H] one of the phenolate donor groups is coordinated to Cu(II), and the catalytic effect of the metal on amide hydrolysis predicted above would be greatly diminished. At the low pH values at which Cu(II) coordinates the neutral ligand, H_2L, the catalytic activity of the metal ion would be expected to be quite low, because of the low concentrations of hydroxide ion under these conditions.

Cu(II) catalysis

This prediction has been verified by actually measuring the rate of conversion of HBEDDA to HBED at pH 3.0 and 50.0°C in the presence of an equivalent molar concentration of Cu(II). After 24 h only a small fraction of the diamide had been converted, with a pseudo-first-order rate constant of about $1.0 \times 10^{-7}\ s^{-1}$. This disappointing result is due to weak axial coordination in Cu(II) complexes, and to the formation of phenolate type Cu(II) complexes of HBEDDA at much lower p[H] than those of HBED. This striking difference in phenolate binding by these two ligands is now ascribed to the effective binding of Cu(II) by the EDDA moiety in HBED, which delays conversion to the phenolate type complexes to much higher p[H].

Fe(III) complexes

Because of the failure of Cu(II) as a catalyst for hydrolysis of the amide group of HBEDDA, it was decided to investigate catalysis by Fe(III). Although the completely deprotonated chelate, **16**, would be expected to form completely at low pH, it was felt that because of the additional charge on Fe(III), its strong octahedral coordination tendencies, and the high stability of the Fe(III)–HBED chelate, there would be considerable driving force favoring hydrolysis. This would be especially true at high pH, at which hydroxide ion concentration is high and the Fe(III) product chelate, **17**, would still be expected to be stable and soluble.

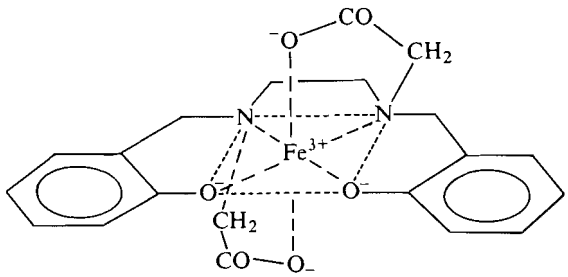

17 FeL^-

The potentiometric equilibrium curve of the Fe(III)–HBEDDA system at 25.0°C, 0.10 M ionic strength (Fig. 2), confirms that the phenolic protons are displaced initially at low p[H], leading to a strong acid titration curve. At and above p[H] 7.5 the system appeared to be unstable, presumably because of the onset of metal ion-catalyzed hydrolysis of the ligand.

Fe(III) catalysis

The reaction rate for conversion of Fe(III)–HBEDDA to Fe(III)–HBED was found to be so rapid in aqueous solution at p[H] 9.0 that the temperature was reduced to 25.0°C for convenience of measurement. The change of absorptivity with time, illustrated by Fig. 4, follows a pseudo-first-order rate law, and the value of k_{obs} was found to be $3.1 \times 10^{-3}\ s^{-1}$. The yield of Fe(III)–HBED was found to be essentially quantitative by comparison of the absorbance of the product of hydrolysis with that of an authentic sample of the HBED–Fe(III) chelate.

The absorbance curves for the Fe(III)-promoted conversion of HBEDDA to HBED at p[H] 9.0 are illustrated in Fig. 3. Although the reaction involving the hydrolysis of two coordinated amide groups (16) might be expected to occur in two steps, the isosbestic point in Fig. 4 clearly proves that the hydrolysis reactions are essentially concerted, and the Fe(III) chelate involving the coordination of one carboxylate group and one amide carbonyl oxygen is only an unstable intermediate present in negligible concentration.

The influence of p[H] on reaction rate was measured and the results are listed in Table 3. The expected increase in k_{obs} with increasing hydroxide ion concentration was observed, but was far below first-order dependence. The formation of hydroxo complexes at high pH could account for the low hydroxide ion dependence, because the formation of such complexes would reduce the concentration of the reactive intermediate **16**, as well as suppressing the catalytic activity of the iron(III) center by

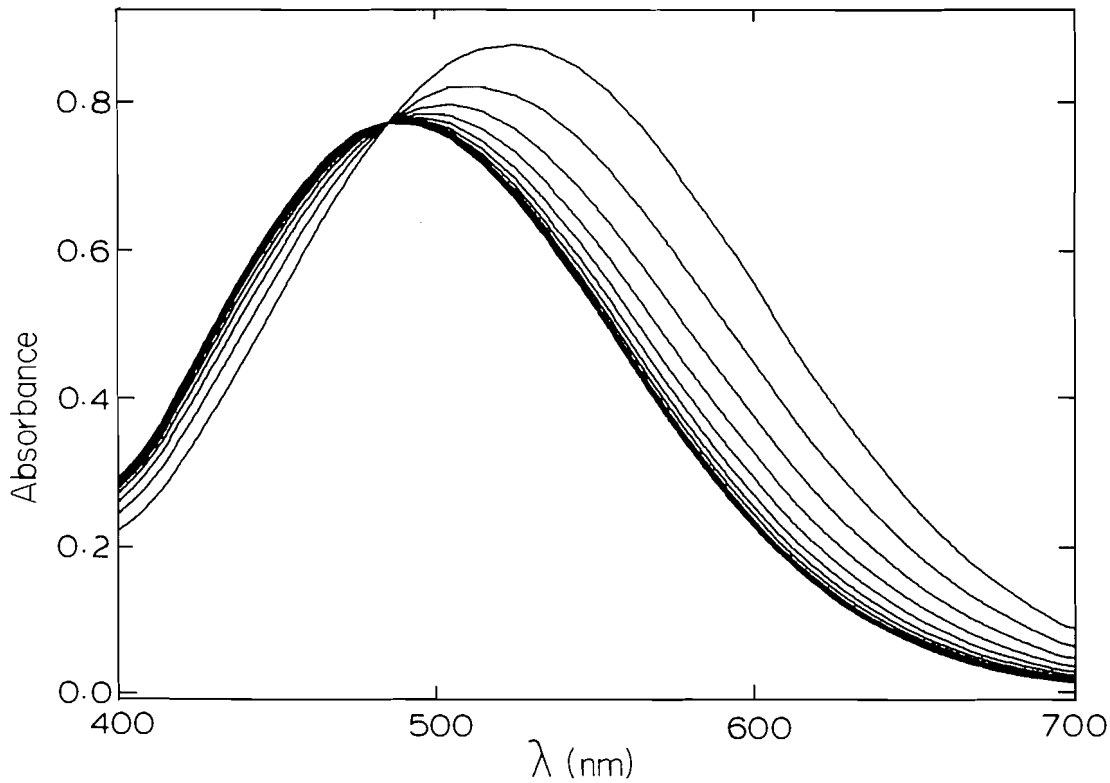

FIG 4. Spectral changes as a function of time (1-min intervals) for a solution of 2.30×10^{-4} *M* Fe HBEDDA at pH = 9.00 borax buffer; $\mu = 0.1000$ *M* at 25.0°C. The initial absorption band with a maximum at 517 nm for the Fe(III)–HBEDDA complex is rapidly converted to the 485-nm maximum band of the Fe(III)–HBED. the pseudo-first-order rate constant is computed as 3.1×10^{-3} s^{-1}.

TABLE 3. Pseudo-first-order rate constants for the conversion of Fe(III)–HBEDDA to Fe(III)–HBED (25.0°C, μ = 1.00 *M*)

p[H]	k_{obs}, $s^{-1} \times 10^3$	Buffer
8.0	2.7	Tris
9.0	3.1	Borate
10.0	6.7	Ammonia
11.0	9.3	Ammonia + NaOH

strong hydroxo coordination of the metal ion. Another factor that could account for low hydroxide dependence is the possibility of general base catalysis, whereby the catalytic effects of the buffer anions at the lower hydroxide ion concentrations would make significant contributions to the observed reaction rate.

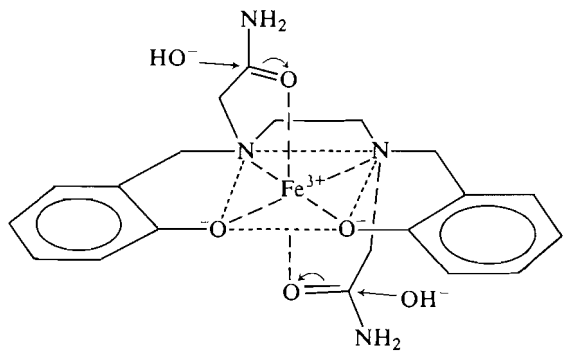

16

Fe(III)-promoted hydroxide-catalyzed hydrolysis of HBEDDA

Isolation of HBED

The conversion of the Fe(III) chelate of HBED to the free ligand involves special requirements. Because of its exceptionally high stability (20), treatment with strong excess mineral acid does not accomplish more than partial conversion. The sensitive methylene groups between the phenolic ring and the nitrogen atoms preclude the removal of Fe(III) by the use of excess alkali metal hydroxide, a method that works well for the related ligand, ethylenebis-*N*,*N*′-(*o*-hydroxyphenylglycine) (EHPG). The method that has been successful for the isolation of hydroxamate siderophores (21) from the corresponding iron(III) chelates resulted in only partial precipitation of the iron(III)–8-hydroxyquinoline chelate, apparently because the HBED–iron(III) chelate is much more stable than those of the hydroxamate siderophores. On the other hand, conversion to the oxine was sufficient to make it possible to remove nearly all of the remaining iron by successive extractions with chloroform. Conversion to the iron-free HBED was shown spectrophotometrically to be 96.6% complete.

Acknowledgments

This research was supported by a contract, AM-02208, from the National Institute of Arthritis, Diabetes and Digestive and Kidney Diseases.

We gratefully acknowledge the outstanding technical expertise of Mr. Ted Tabacchi. We would also like to thank Dr. D. C. Young for ^{13}C nmr spectra.

1. F. L'EPLATTENIER, I MURASE, and A. E. MARTELL J. Am. Chem. Soc. **89**, 837 (1967).
2. A. E. MARTELL. *In* Development of iron chelators for clinical use. *Edited by* A. E. Martell, D. G. Badman, and W. F. Anderson. Elsevier – North Holland, New York, 1981. pp. 67–104.

3. R. J. MOTEKAITIS and A. E. MARTELL. Inorg. Chem. **19**, 1646 (1980).
4. C. H. TALIAFERRO and A. E. MARTELL. Inorg. Chim. Acta, **85**, 9 (1984).
5. C. H. TALIAFERRO, R. J. MOTEKAITIS, and A. E. MARTELL. Inorg. Chem. **23**, 1129 (1984).
6. F. C. HUNT. Nucl. Med. **23**, 123 (1948).
7. F. C. HUNT and D. J. MADDALENA. J. Labelled Compd. Radiopharm. **19**, 1408 (1982).
8. R. J. MOTEKAITIS and A. E. MARTELL. Inorg. Chem. **23**, 18 (1984).
9. R. J. MOTEKAITIS and A. E. MARTELL. Can. J. Chem. **60**, 168 (1982).
10. R. J. MOTEKAITIS and A. E. MARTELL. Can. J. Chem. **60**, 2403 (1982).
11. I. MURASE. Mem. Fac. Sci. Kyushu Univ. Ser. C, **8**, 25 (1972).
12. A. FUNKE and J. P. FOURNEAU. Soc. Chim. Fr. **9**, 806 (1942).
13. R. P. CARTER, M. M. CRUTCHFIELD, and R. R. IRANI. Inorg. Chem. **6**, 943 (1967).
14. H. KROLL. U.S. Patent. No.2,967,196. 1955.
15. J. B. LAMBERT and M. W. MAJCHNZAK. J. Am. Chem. Soc. **102**, 3588 (1980).
16. A. E. MARTELL. Pure Appl. Chem. **17**, 129 (1968).
17. E. HOPGOOD and R. J. ANGELICI. J. Am. Chem. Soc. **90**, 2514 (1968).
18. A. E. MARTELL. *In* Proc. 3rd Symp. on Coordination Chemistry. Vol. 2. *Edited by* M. T. Beck. Akademiai Kiado, Budapest. 1970. p. 125.
19. A. E. MARTELL. Pure Appl. Chem. **17**, 1502 (1968).
20. R. M. SMITH and A. E. MARTELL. Critical stability constants. Vol. 1. Plenum, New York. 1974.
21. W. KELLER-SCHIEPLEIN, P. MARTENS, V. PRELOG, and A. WALSER. Helv. Chim. Acta, **48**, 710 (1965).

Isomerization of alkyl branched alkynoic acids[1]

SUZANNE R. ABRAMS

Plant Biotechnology Institute, National Research Council of Canada, Saskatoon, Sask. Canada S7N 0W9

Received May 3, 1985

SUZANNE R. ABRAMS. Can. J. Chem. **64**, 457 (1986).

Acetylenic acids are isomerized by alkali metal amides of 1,3-diaminopropane to 3,5-dienoic acids. An acid with a methyl branch at C-3 separating the carboxyl from the triple bond is rearranged to a mixture of the terminal alkynoic acid and two isomeric 3,5-dienoic acids. The corresponding 4-methyl compound affords the terminal alkynoic acid, one 3,5-dienoic acid, and two cyclized products, *cis*- and *trans*-3-methyl-5-(octylidene)-1-cyclopentanecarboxylic acids. Propargylic acids branched at C-5 and C-6 are rearranged to the appropriately substituted 3,5-dienoic acids in moderate yield.

SUZANNE R. ABRAMS. Can. J. Chem. **64**, 457 (1986).

Sous l'influence des sels alcalins des amidures du diamino-1,3 propane, les acides acétyléniques s'isomérisent en acides diène-3,5 oïques. Un acide portant un groupement méthyle en position C-3, qui sépare le groupement carboxyle de la triple liaison, se transpose en un mélange d'acide alcynoïque terminal et de deux acides diène-3,5 oïques isomères. Le composé équivalent comportant un méthyle en position 4 conduit à un acide alcynoïque terminal, un acide diène-3,5 oïque et deux produits de cyclisation, les acides méthyl-3 octylidène-5 cyclopentanecarboxylique-1 *cis* et *trans*. Les acides propargyliques portant des substituants dans les positions C-5 et C-6 se transposent, avec des rendements modérés, en acides diène-3,5 oïques substitués appropriés.

[Traduit par le journal]

Introduction

Exceedingly strong bases that effect multipositional isomerization of triple bonds along methylene chains (1) cause acetylenic acids to be rearranged to *E,E*- and *E,Z*-3,5-dienoic acids (2). Based upon this observation, an efficient synthesis of *E,Z*-3,5-tetradecadienoic acid, the pheromone of the black carpet beetle (*Attagenus megatomia*), has been developed. The key step is the isomerization of 7-tetradecynoic acid with the sodium salt of 1,3-diaminopropane in 1,3-diaminopropane to afford a 1:1 mixture of *E,E*- and *E,Z*-3,5-tetradecadienoic acids in 65% yield (2).

This novel rearrangement is interesting from the point of view of possible applications in natural product syntheses. Specific 3,5-dienoic acids substituted on the carbons of the double bonds, useful as diene components in Diels–Alder reactions, might be readily accessible by isomerization of appropriately substituted alkynoic acids. Diels–Alder reactions with the sodium salts of 3,5-dienoic acids are found to have greatly accelerated rates when performed in water. The dienes are prepared by deconjugation of the corresponding 2,4-dienoic compounds (3).

Previous studies have shown that rearrangements of unsubstituted acetylenic acids with other less basic reagents afford allenic, acetylenic, or 2,4-dienoic acids (4). Julia and Descoins (5) reported that isomerizations with the potassium salt of ethylene glycol of a variety of 3-methyl acids containing a triple bond proceeded much more slowly than the unsubstituted analogs. In only one case did they isolate rearrangement products, a mixture of stereoisomers of 2,4-dienoic acids.

The rearrangement of alkynoic acids with strong base is interesting from a mechanistic point of view. The carboxyl group obviously has a great effect on the course of the triple bond migration. How it influences the sequence of proton abstractions involved in the formation of the diene system is unknown.

To explore both the synthetic and mechanistic aspects of the rearrangement, some alkyl branched alkynoic acids have been prepared and the isomerization of these compounds with strong base studied.

[1]NRCC No. 25196.

Results and discussion

It had previously been established (2) that the carboxyl group of the acetylenic acid is converted to the dianion (**1**) in the isomerization reaction. It is postulated (Scheme 1) that the triple bond, when remote from the dianion, undergoes normal acetylene–allene interconversions along the methylene chain, and that the 4,5-allenic isomer **2** is a key intermediate. It is thought that the proton abstraction pattern is altered at this stage and that the doubly allylic protons on C-3 are more acidic than the vinyl protons on C-4 and C-6. Thus, proton abstraction from C-3 by the reagent, followed by protonation at C-5, breaks the allene–acetylene interconversions and affords a particularly stable intermediate **3**, which has an extensively delocalized conjugated π system. Protonation at C-2 on work-up gives the observed 3,5-dienoic acid product mixture **4**. If the postulated mechanism is correct, and **1**, which has a triple bond at C-5,C-6, is an obligatory intermediate, then neither C-5 nor C-6 may be substituted. However, one of the protons on C-3, and one on

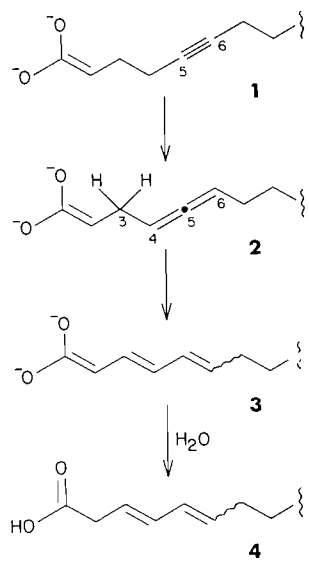

SCHEME 1

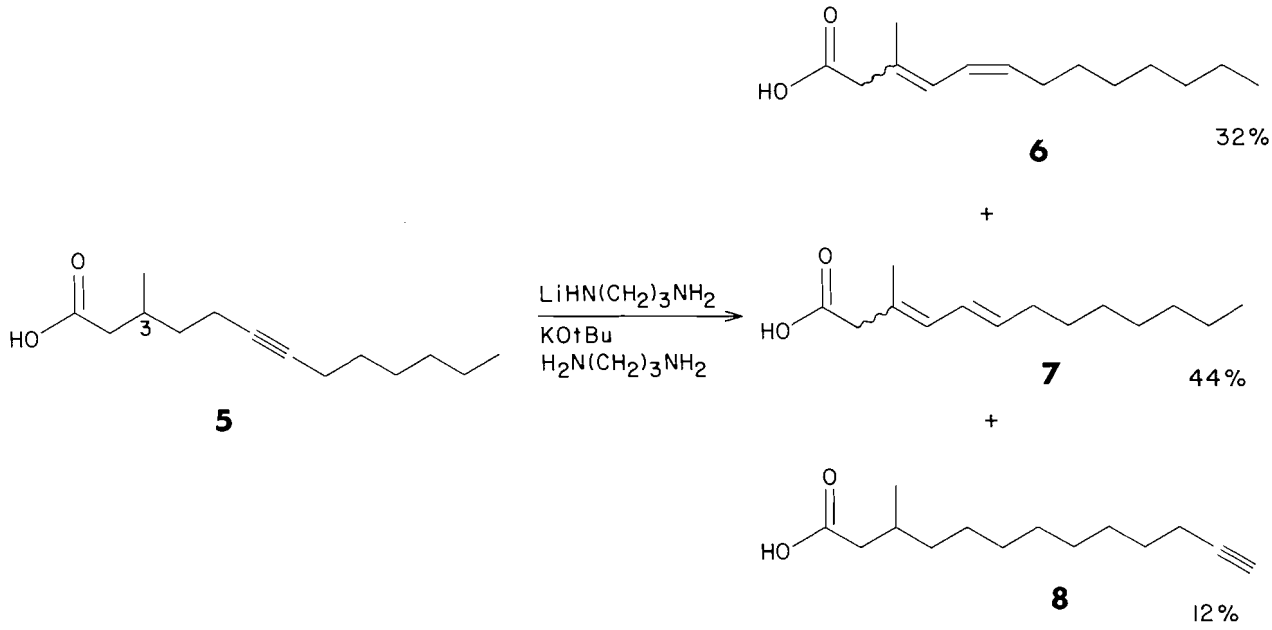

SCHEME 2

C-4, would not be required for the rearrangement to proceed. It ought to be possible to obtain dienoic acids with substitution at C-3 or C-4. To test this hypothesis, two alkynoic acids, one branched with a methyl group at C-3 and one at C-4, were synthesized by alkylation of the appropriately branched iodo-acid with octyne.

Rearrangement of 3-methyl-6-tridecynoic acid (**5**) with a mixed isomerization reagent (1) affords three products (Scheme 2), two dienoic acids **6** and **7**, and the terminal acetylenic acid **8**. In this case, and in all subsequent discussion, acids were methylated and structures of the isolated esters elucidated.

The formation of 3-methyl-12-tridecynoic acid (**8**) is evidence that the allene–acetylene interconversions are proceeding normally when the triple bond is remote from the carboxylate dianion.

The geometry of the C-5,C-6 double bonds of the diene systems of **6** (*Z*-) and **7** (*E*-) have been ascertained from the coupling constants for the protons on the double bond (**6**, $J_{5,6}$ = 8.4 Hz; **7**, $J_{5,6}$ = 15.2 Hz). The chemical shifts of the signal for the protons of the C-3 methyl group of **6** and **7** are nearly coincident (difference of 0.01 ppm), as are the chemical shifts of the methylene signals of C-2 (difference of 0.04 ppm). This suggests that the geometry about the C-3,C-4 bond is the same in both compounds. However, there is no direct evidence to allow an assignment of the geometry of the double bond. Indirect evidence supporting the assignment of the C-3,C-4 double bond as *trans* comes from two sources. First, in products of rearrangement reactions of the unsubstituted alkynoic acids and propargylic acids, in which the stereochemistry can be deduced from nmr using the coupling constants of H-3 and H-4, the *trans* geometry is found. As well, consideration of the geometry of intermediates postulated in the formation of the diene system supports the *trans* assignment (Scheme 3). The stereochemical assignment can be rationalized by considering abstraction of a proton from C-3 of **9** and the stability of the intermediate allylic allenic anion. Two conformations that **9** may adopt are **A**, in which a methyl group lies in the plane of the C-4,C-5 double bond, and **B**, in which the carboxylate dianion similarly is in the plane of the double bond. **A** would be expected to be of lower energy. If abstraction of a proton on C-3 is effected from **A**, then the allenic anion **C** should be formed preferentially (rather than **D** from **B**). The allenic anion **C** would be expected to be of much lower energy than the more hindered anion **D**. Protonation of **C** or **D** at C-5 could take place from either face of the allyl unit, affording **10** with both *Z* and *E* geometries at the C-5,C-6 double bond.

Attempts to synthesize isomeric 3-methyl-3,5-dienoic acids

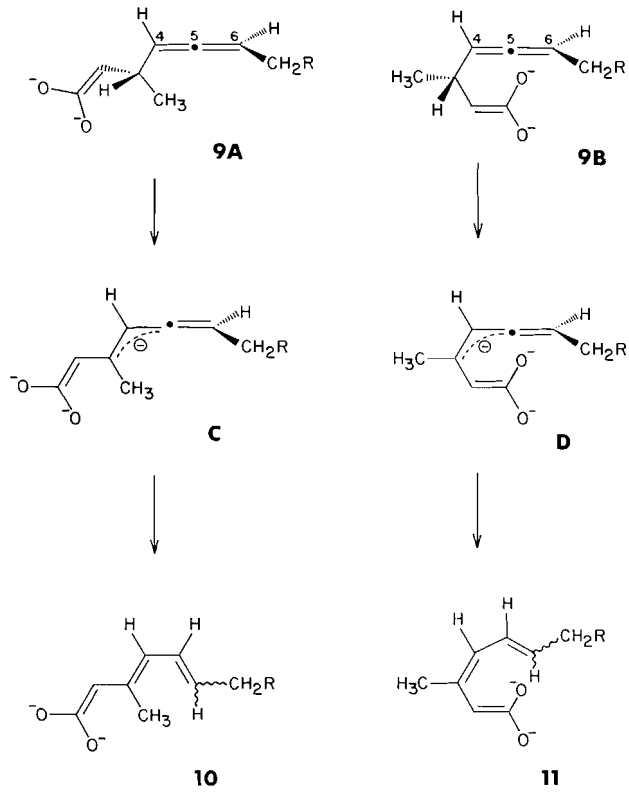

SCHEME 3

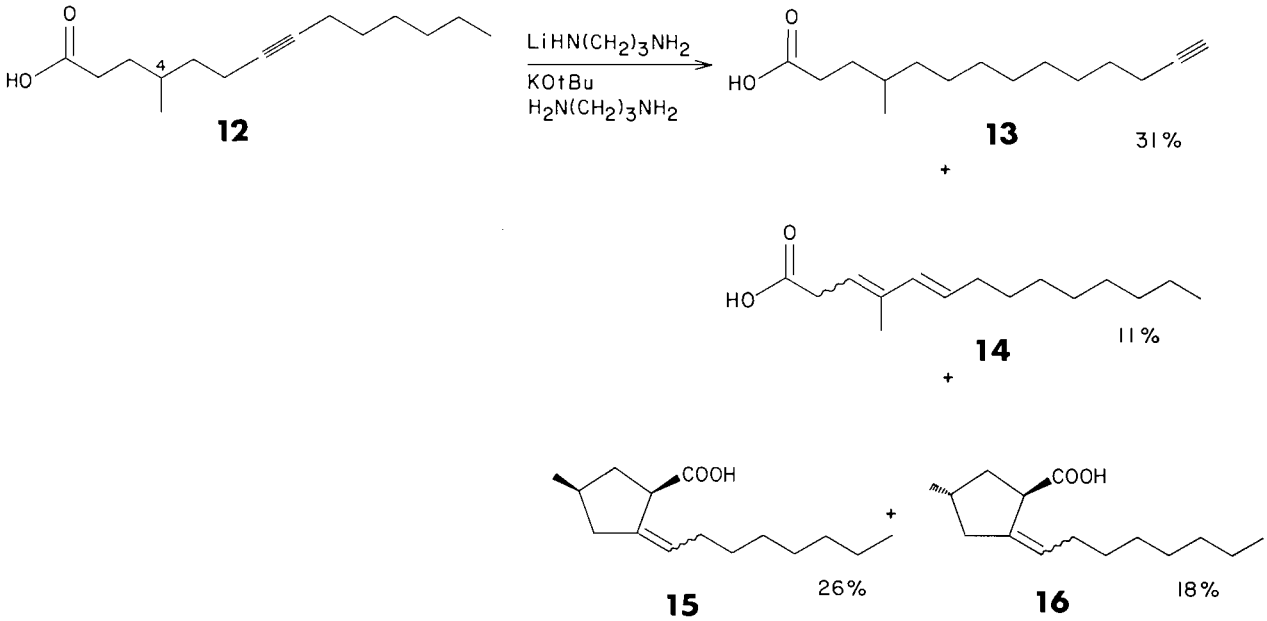

SCHEME 4

by equilibration of **6** and **7** with thiophenol (6) failed. Deconjugation of a mixture of ethyl (*E*,*E*)- and (*E*,*Z*)-3-methyl-2,4-decadienoate (7) with lithium diisopropylamide afforded only 3-methylene-4-decenoic acid. In this process a proton on the methyl group at C-3 was abstracted in preference to a proton on the chain at C-6.

From rearrangement of 4-methyl-7-tetradecynoic acid (**12**), under the same isomerization conditions, four products were isolated (Scheme 4). The most prominent component is 4-methyl-13-tetradecynoic acid (**13**). One 3,5-dienoic acid is observed. The stereochemistry of the C-3,C-4 double bond cannot be assigned. The C-5,C-6 double bond geometry is *trans* ($J_{5,6}$ = 15.5 Hz). The remaining two products, which account for 44% of the reaction mixture, are the result of the rearrangement taking a different course. It is proposed that the products are two cyclopentanecarboxylic acids **15** and **16**, differing only in the relative orientations of the methyl branch with respect to the carboxyl group. The assignment of relative stereochemistry is based on a chemical shift difference. The methyl signal for the isomer with the methyl and carboxyl groups on the same face of the ring is expected to be deshielded relative to the methyl signal for the isomer with the groups disposed *trans*. A difference of 0.09 ppm is observed. The geometry about the exocyclic double bond has not been established.

Others have observed analogous cyclizations of stabilized anions alkylating unactivated (8, 9) and activated triple bonds (10) to form five-membered cycles with exocylic double bonds. In the present case, the triple bond migrates from the C-7 to C-6 position before it is attacked by the stabilized dianion. This is an interesting example of a 5-*exo*-digonal taking precedence over a 6-*exo*-digonal ring closure. In theory both of these reactions should have the opportunity to take place. According to Baldwin's rules (11), both are favoured. In this example, only the five-membered ring is observed.

Acetylenic acids with the triple bond between the carboxyl and an alkyl branch were considered next. In the earlier study (2) it had been shown that the unbranched propargylic acid, 2-tetradecynoic acid, was also isomerized to 3,5-dienoic acids, and the homopropargylic acid was shown to be an intermediate. It is postulated that the rearrangement takes place as shown in Scheme 5. The dianion of the homopropargylic acid, **17**, is rearranged to the key intermediate **18**, at which point the allene–acetylene interconversions are terminated with the abstraction of a proton from C-6. The intermediate allenic anion is protonated at C-4, affording the dianion **4** with the extended delocalized π system. Substitution on either C-5 or C-6 should not hinder the rearrangement, but substitution at C-3 or C-4 should not be allowed if **17**, with its triple bond at C-3,C-4, is an obligatory intermediate. The formation of terminal acetylenic isomers is precluded by the positioning of the branch between the triple bond and the terminus of the chain, so the isomerization of propargylic acids should afford the 3,5-dienoic acids. A number of acetylenic acids branched at C-5 and C-6, and one at C-4 (Scheme 6), were prepared by alkylation of the tetrahydropyranyl ether of propargyl alcohol with the appropriate alkyl halide, followed by oxidation.

As for the unsubstituted case, isomerization of the 2-alkynoic

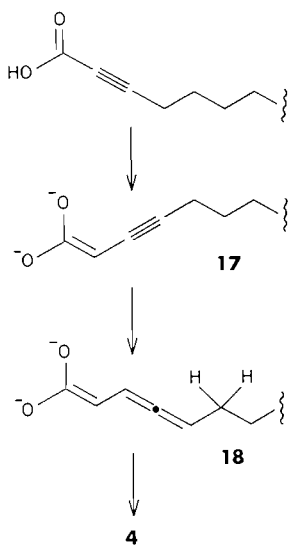

SCHEME 5

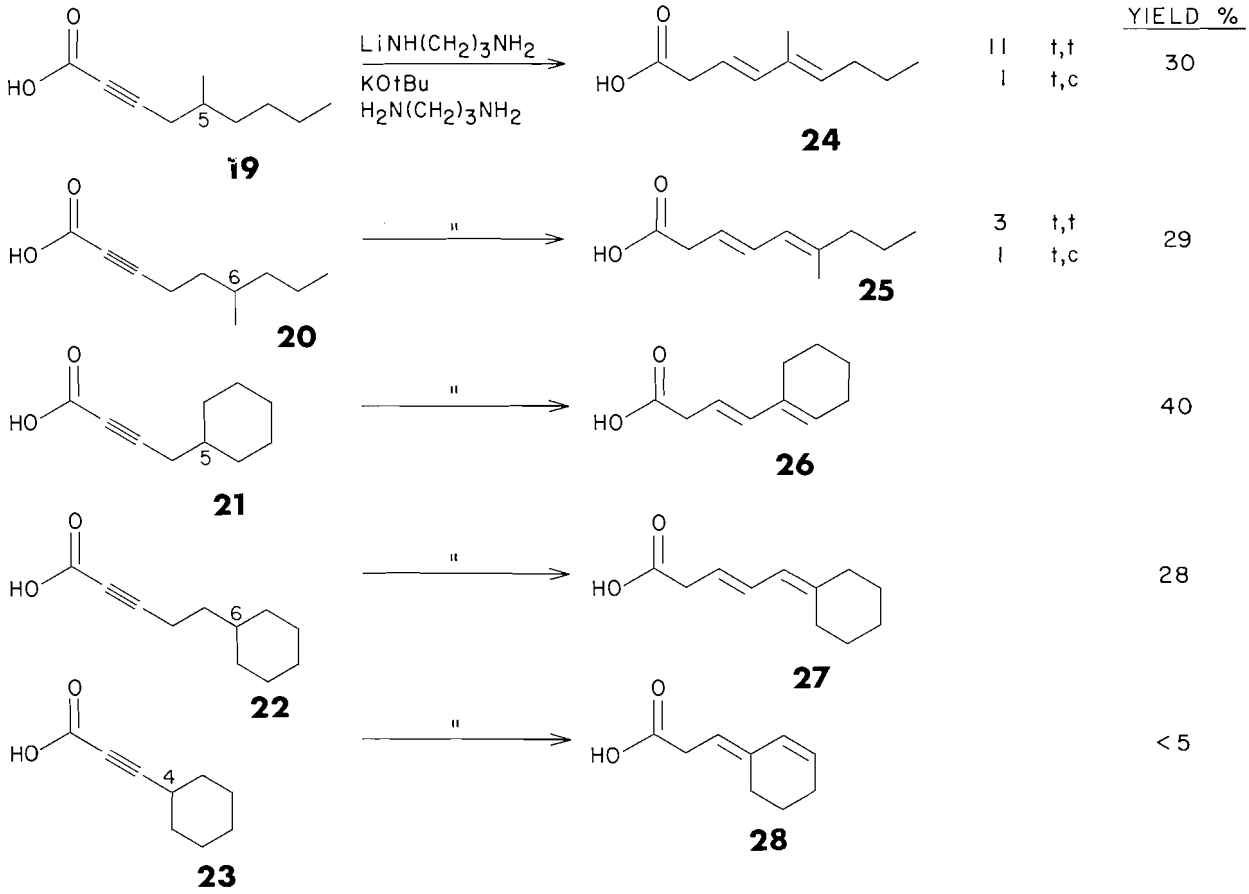

SCHEME 6

acids proceeded through the homopropargylic isomer. By carrying out the isomerization reaction at room temperature, 3-alkynoic acids could be isolated in good yield. One example is described in the experimental section.

It is interesting that, as predicted, 3-cyclohexylpropynoic acid (**23**) affords, on rearrangement, only traces of the 3,5-dienoic acids (**28**). The major products appeared to be dimeric and they were not investigated further.

Rearrangement of the substituted methyl- and cyclohexyl-alkynoic acids **19** to **22** using more vigorous reaction conditions (60°C) afforded the desired substituted 3,5-dienoic acids **24**–**27** in moderate yields. The C-3,C-4 double bond in each rearrangement product **24**–**27** is observed to be *trans*, from the coupling constants. Pairs of isomeric dienoic acids are formed in the case of the methyl branched series. The stereochemistry about the double bonds with the methyl group can be assigned by analysis of the chemical shifts of the protons adjacent to the double bond in question. Olefinic protons next to a *cis* double bond are shifted downfield relative to those adjacent to a *trans* double bond by 0.5 ppm, and methylene signals next to a *cis* double bond are similarly shifted by 0.2–0.3 ppm (2, 6, 12). In the 5-methyl case, the major product (78% of the mixture) is assigned the *trans,trans* configuration on analysis of the chemical shifts observed in comparison with those of the next most significant product (7% of the mixture). the signal for H-4 of the major component is observed at δ 6.12, while that of the minor component is found at δ 6.51. Similarly the methylene signal of C-7 is shifted downfield at 0.10 ppm in the case of the minor component. In the 6-methyl series, the (*E*,*E*)-compound is found to predominate by a ratio of 3:1. The signals in the olefinic region of the nmr spectrum are overlapped, but the methylene signals for C-7 are clearly separated, with the larger triplet at higher field (0.12 ppm).

There is no ambiguity in the geometry of the C-5,C-6 double bonds in the products **26** and **27**, and the C-3 and C-4 double bonds are found to be *trans*.

Conclusions

Alkyl branched acetylenic acids can be isomerized to substituted 3,5-dienoic acids. The position of the alkyl group, or the lack of one, on the chain affects the rate of the acetylene–allene interconversions and thus the distribution of products obtained. The 3-methyl branch (Scheme 2) does not appear to impede the formation of the 4,5-allenic dianon **2** relative to the unsubstituted case. From the synthetic point of view, 3-alkyl branched acetylenic acids offer good possibilities for construction of trisubstituted dienes. The 4-methyl branch does impede the rearrangement to 3,5-dienoic acids. The 4-alkyl branched isomers may, however, provide access to cyclopentanecarboxylic acid derivatives. Propargylic acids, which are readily accessible, should prove to be useful in the synthesis of 3,5-dienoic acids substituted at C-5 and C-6.

Experimental

All reactions requiring dry conditions were performed in vacuum flame-dried, or oven-dried (110°C for more than 2 h) glassware, under a positive pressure of argon. Solvents described as dry were obtained by distillation as follows: tetrahydrofuran (THF) from benzophenone ketyl; dichloromethane (CH_2Cl_2) and acetonitrile (CH_3CN) from CaH_2; hexamethylphosphorous triamide (HMPA) at reduced pressure

and subsequently stored over activated 4Å sieves; 1,3-diaminopropane from BaO, then stored over activated 4Å sieves.

Proton nmr spectra were recorded on a Varian EM 390 (90 MHz) or Bruker AM-360-WB (360 MHz) spectrometers, with $CDCl_3$ as solvent. Carbon spectra were recorded on the Bruker instrument in the Fourier transform mode at 90.6 MHz with proton noise decoupling, with $CDCl_3$ as solvent and lock. Infrared spectra were obtained with a Perkin Elmer 237B instrument. Gas chromatograms were obtained with a Varian 3700 instrument with FID, and 30-m SP 2100 capillary column. Retention times are given in minutes with the relative intensities in parentheses. Mass spectra were obtained on a Finnigan 4000E gc/ms instrument with an Incos 2300 data system and using an SP2100 column. Mass spectra are reported in mass to charge units (m/z) with the relative intensities given in parentheses as percentages of the base peak. Accurate mass measurements were provided by the Mass Spectrometry Laboratory, Psychiatric Research Unit, University of Saskatchewan, with an MS902S instrument with VG console update. Accurate masses were obtained at 1500 resolution and 3 s/decade using accurate-mass low-resolution software with PFTBA internal standard. Elemental analyses were performed by Spang Microanalytical Laboratory, Eagle Harbor, Michigan, U.S.A.

General isomerization procedure

Into a 25-mL pear-shaped flask fitted with magnetic stirring bar was charged lithium (42 mg, 7.0 mmol). 1,3-Diaminopropane (dry, 5.0 mL, **corrosive!**) was added by syringe and the mixture heated and stirred at 70°C until a white suspension of the lithium amide was formed. After cooling to room temperature, potassium *tert*-butoxide (500 mg, 5.0 mmol) was added, affording a lemon-yellow solution. A solution of the acetylenic acid (1.0 mmol) in a 1,3-diaminopropane (1.0 mL) was added by syringe, and the mixture stirred for 1.0 h, then poured into ice water. The mixture was acidified with HCl and extracted with $CHCl_3$ (3×). The combined organic phases were washed successively, once with 10% HCl, H_2O and NaCl solution, then dried over Na_2SO_4, filtered, and the solvent evaporated to afford a crude mixture of isomerized acids. Methyl esters were prepared either by reaction with methanolic HCl or with diazomethane, and then purified by chromatography.

The ratios of reagents in the different isomerization reactions were kept constant. The reaction temperature and time were varied with the particular substrate. Separations of the methylated products were effected either with silicic acid chromatography or hplc with reverse phase (Altex Ultrasphere ODS, 5 μm, 10 × 25 cm) or cation exchange (Whatman Partisil M9 10/50 SCX, Ag^+ form) columns.

3-Methyl-6-tridecynoic acid (5)

According to the method of Olah *et al.* (13), to a solution of 5-hydroxy-3-methylpentanoic acid (prepared by reduction of the half acid ester of 3-methylglutaric acid, followed by saponification, 3.7 g, 28 mmol) in CH_3CN (dry, 60 mL) was added first sodium iodide (18 g, 120 mmol), then chlorotrimethylsilane (15.3 mL, 120 mmol). The mixture was refluxed overnight, then cooled to room temperature, poured into ice water, and extracted with ether (3×). The combined ethereal extracts were washed first with H_2O (1×), then with 10% $Na_2S_2O_3$ solution (1×), and finally with $NaHCO_3$ (3×). The combined $NaHCO_3$ extracts were acidified with HCl and extracted with ether (3×). The combined ethereal extracts were washed with NaCl solution (1×), dried over Na_2SO_4, and the solvent evaporated to afford crude 5-iodo-3-methylpentanoic acid (4.8 g, 71%), which gave ^{1}H nmr δ: 3.2 (t, J = 7 Hz, CH_2I, 2H), 1.7–2.4 (m, 5H), and 1.0 (d, J = 6 Hz, CH_3, 3H). The crude acid was employed in the next step without further purification.

To a solution of 1-octyne (4.4 mL, 30.0 mmol) in THF (dry, 30 mL), at −70°C, was added first *n*-butyllithium (17.6 mL, 0.63 *M*, 28 mmol), then a solution of the lithium salt of 5-iodo-3-methylpentanoic acid (4.8 g, 20.0 mmol) in THF (100 mL) and HMPA (17 mL) (prepared by addition of *n*-butyllithium (11.3 mL, 0.63 M, 18 mmol) to the acid in THF–HMPA). The resultant mixture was stirred and allowed to warm to room temperature overnight, then poured into H_2O, acidified with HCl, and extracted with ether (3×). The combined ethereal extracts were washed with H_2O (1×), then with NaCl solution (1×), and dried over Na_2SO_4. Evaporation of the solvent afforded a brown oil (4.5 g) from which 3-methyl-6-tridecynoic acid (**5**) (860 mg, 20%) was isolated by chromatography of the methyl ester over a cation exchange column (Ag^+ form) eluting with methanol, followed by saponification. The acid **5** was distilled (bulb-to-bulb, over temp. 180°C, 0.1 Torr (1 Torr = 133.3 Pa)) and gave ν_{max} (film): 3500–2600, 1700 cm^{-1}; ^{1}H nmr (360 MHz) δ: 2.35 (dd, J = 14.5, 5.0 Hz, OOCCH, 1H), 2.0–2.2 (m, OOCCH, $H_2CC{\equiv}CCH_2$, 5H), 1.55 (m, $HCCH_3$, 1H), 1.20–1.48 (m, CH_2, 8H), 0.95 (d, J = 6.5 Hz, H_3CCH), and 0.85 (t, J = 7.1 Hz, H_2CCH_3); ^{13}C nmr; 179.1, 80.7, 79.3, 41.1, 35.8, 31.4, 29.4, 29.1, 28.6, 22.6, 19.2, 18.8, 16.5, and 14.0 ppm; gc/ms of methyl ester: 238 (0.05), 168 (13), 164 (10), 135 (8), 109 (12), 108 (20) and 95 (100). *Anal.* calcd. for $C_{14}H_{24}O_2$: C 74.95, H 10.78; found: C 74.95, H 10.71.

Rearrangement of 3-methyl-6-tridecynoic acid (5)

Isomerization of the acid **5** (224 mg, 1.0 mmol) as described above for 1.0 h at room temperature afforded a mixture of acids (176 mg, 75%), which was esterified with methanol HCl. Four major products, all isomeric, could be distinguished by glc (160°C, 16.3 (12), 17.7 (12), 18.1 (32), 20.8 (44)). Three of these were purified by hplc (reverse phase, eluting with 20% H_2O, 80% CH_3OH). Methyl 3-methyl-12-tridecynoate gave a single peak on glc (16.3 min); ir ν_{max} (film): 3300 and 1730 cm^{-1}; ^{1}H nmr (360 MHz) δ: 3.65 (s, OCH_3), 2.28 (dd, J = 14.6, 6.0 Hz, OOCCH, 1H), 2.16 (dt, J = 2.6, 7.0 Hz, $H_2CC{\equiv}C$, 2H), 2.09 (dd, J = 14.6, 8.1 Hz, OOCCH, 1H), 1.91 (t, J = 2.6 Hz, $C{\equiv}CH$, 1H), 1.2–1.6 (m, CH_2, CH, 15H), and 0.91 (d, J = 6.6 Hz, CH_3, 3H); gc/ms: 238 (missing), 207 (0.5), 195 (1.1), 164 (4.4), 101 (42), and 74 (100); accurate mass analysis of McLafferty rearrangement product calcd. for $C_{12}H_{20}$: 164.1565; found: 164.1453. Methyl 3-methyl-3,5-tridecadienoate (ester of **6**) gave a single peak on glc (18.1 min); ir ν_{max} (film): 1730 and 800 cm^{-1}; ^{1}H nmr (360 MHz) δ: 6.1–6.2 (m, H-4, H-5, 2H), 5.43 (dt, J = 7.2, 8.4 Hz, H-6, 1H), 3.67 (s, OCH_3, 3H), 3.06 (s, $OOCCH_2$, 2H), 2.13 (m, $C{=}CCH_2$, 2H), 1.80 (s, $H_3CC{=}C$, 3H), 1.2–1.4 (m, CH_2 10H), and 0.86 (t, J = 6.5 Hz, H_3C, 3H); irradiation of the signal δ 2.13 effects collapse of the signal δ 5.43 to a d, J = 8.4 Hz; gc/ms: 238 (51), 179 (8), 178 (7), 164 (32), 140 (40), 108 (45), 93 (100); accurate mass analysis for molecular ion calcd. for $C_{15}H_{26}O_2$: 238.1933; found: 238.1907. Methyl 3-methyl-3,5-tridecadienoate (ester of **7**) gave a single peak on glc (20.8 min); ir ν_{max} (film): 1730, 960, and 800 cm^{-1}; ^{1}H nmr (360 MHz) δ: 6.20 (dd, J = 10.3, 15.2 Hz, H-5, 1H), 5.87 (d, J = 10.3 Hz, H-4, 1H), 5.62 (dt, J = 15.2, 7.4 Hz, H-6, 1H), 3.66 (s, OCH_3, 3H), 3.02 (s, $OOCH_2$, 2H), 2.08 (dt, J = 7.6, 7.1 Hz, $C{=}CCH_2$, 2H), 1.79 (s, $H_3CC{=}C$, 3H), 1.2–1.6 (m, CH_2 10H), and 0.85 (t, J = 7.0 Hz, CH_3, 3H); gc/ms: 238 (61), 179 (11), 178 (8), 164 (31), 140 (40), 108 (42), and 93 (100); accurate mass analysis for molecular ion, calcd. for $C_{15}H_{26}O_2$: 238.1933; found: 238.1956.

4-Methyl-7-tetradecynoic acid (12)

According to the method of Whitesell *et al.* (14), to a stirred suspension of $NaHCO_3$ (8.4 g, 0.10 mmol) and *m*-chloroperbenzoic acid (85%, 9.6 g, approx. 0.05 mmol) in CH_2Cl_2 (dry, 50 mL) was added 4-methylcyclohexanone (5.6 g, 0.05 mmol). The temperature of the mixture was maintained between 18 and 30°C with an ice-water bath. After stirring for 5 h, H_2O was added and the CH_2Cl_2 layer was separated. The aqueous was extracted with CH_2Cl_2 (4×). The combined organic phases were washed with 10% Na_2CO_3 solution (2×), NaCl solution (1×), then were dried over Na_2SO_4, filtered, and the solvent evaporated to yield crude 4-methyl-7-oxacycloheptanone (15), 5.8 g, (90%), which gave ir ν_{max} (film): 1720 cm^{-1}; ^{1}H nmr (90 MHz) δ: 4.3 (m, OCH_2, 2H), 2.7 (m, $OCCH_2$ 2H), 1.3–2.2 (m, CH_2, CH, 5H), and 1.0 (d, J = 6 Hz, CH_3, 3H).

According to the method of Olah *et al.* (13), the lactone was converted to 6-iodo-4-methylhexanoic acid, 3.1 g (48%), which gave ir ν_{max} (film): 3400–2500, 1710 cm^{-1}; ^{1}H mnr (90 MHz) δ: 3.2 (m, CH_2I, 2H). 2.3 (t, J = 6 Hz, CH_2COO, 2H), 1.3–1.9 (m, CH_2CH, 5H), and 0.9 (t, J = 6 Hz, CH_3, 3H). The crude iodoacid was alkylated with the

lithium salt of octyne to afford 4-methyl-7-tetradecynoic acid (2.8 g). The acid **12** was converted to methyl ester with methanolic HCl and chromatographed over a cation exchange column (Ag^+ form), eluting with methanol, affording the methyl ester, 1.13 g (37%), which gave ms: 252 (0.6), 221 (3), 220 (2), 182 (21), 178 (12), 165 (11), 150 (24), 135 (17), 124 (26), 108 (55), 95 (92), and 81 (100). Saponification afforded the acid **12**, which was distilled (bulb-to-bulb, oven temp. 200°C, 0.1 Torr) and gave ^{1}H nmr (360 MHz) δ: 3.64 (s, OCH_3, 3H), 2.24–2.37 (m, $OOCCH_2$, 2H), 2.08–2.18 (m, $H_2CC{\equiv}C$, 4H), 1.2–1.7 (m, CH_2 CH, 13H), and 0.86 (m, CH_3, 6H); ^{13}C nmr: 180.5, 80.4, 79.8, 35.9, 31.8, 31.6, 31.4, 31.3, 29.1, 28.6, 22.6, 18.8, 16.5, and 14.0 ppm. *Anal.* calcd. for $C_{15}H_{26}O_2$: C 75.58, H 11.00; found: C 75.55, H 10.97.

Rearrangement of 4-methyl-7-tetradecynoic acid (12)

Isomerization of 4-methyl-7-tetradecynoic acid (230 g, 1.0 mmol) was carried out as described above for 1.0 h, at room temperature. The crude product (170 mg) was esterified with methanolic HCl, affording a mixture of methyl esters (200 mg) which gc/ms analysis indicated contained 4 major isomeric products that made up 86% of the mixture (170°C, 19.2 (18), 19.8 (26), 24.3 (31), and 27.5 (11)). Methyl 4-methyl-13-tetradecynoate was isolated by hplc (reverse phase, eluting with 10% H_2O, 90% CH_3OH) and gave a single peak on glc (24.1); ir ν_{max} (film): 3300 and 1730 cm^{-1}; ^{1}H nmr (360 MHz) δ: 3.65 (s, OCH_3, 3H), 2.25–2.35 (m, $OOCCH_2$, 2H), 2.16 (dt, J = 2.6, 7.0 Hz, $CH_2C{\equiv}C$, 2H),1.92 (t, J = 2.6 Hz, $C{\equiv}CH$, 1H), 1.2–1.7 (m, CH_2, 17H), and 0.85 (d, J = 6.3 Hz, 3H); ms: 252 (1–4), 237 (0.8), 109 (23), 95 (44), 87 (92), 81 (69), 74 (90), and 55 (100); accurate mass analysis for the molecular ion calcd. for $C_{18}H_{28}O_2$: 252.2088; found: 252.2058. Methyl *trans*-3-methyl-5-(1-octylidene)-1-cyclopentanecarboxylic acid was isolated by hplc (cation exchange column, eluting with 0.25% dimethoxyethane in hexane) and gave a single peak on glc (19.1); ir ν_{max} (film): 3320, 3310, and 1730 cm^{-1}; ^{1}H nmr (360 MHz) δ: 5.41 (m, HC=C, 1H), 3.65 (s, OCH_3, 3H), 3.37 (m, HCCOO, 1H), 2.49 (dd, J = 15, 7 Hz, H-4, 1H), 2.30 (m, H-3, 1H), 2.10 (m, H-2, 1H), 1.96 (q, J = 7 Hz, $H_2CC{=}C$, 2H), 1.80 (dd, J = 14, 7 Hz, H-4′, 1H), 1.43 (m, H-2′, 1H), 1.3–1.4 (m, CH_2 10H), 0.97 (d, J = 6.7 Hz, H_3CCH, 3H), and 0.86 (t, J = 7.0 Hz, H_3CCH_2, 3H); irradiation of the signal δ 2.30 causes the methyl doublet at δ 0.97 to collapse to a singlet, and the multiplets at δ 2.49 and 1.80 to collapse to doublets, J = 14 Hz; irradiation of the quartet at δ 1.96 causes collapse of vinyl signal at δ 5.41 to a singlet, and irradiation at δ 2.10 causes the signal at δ 3.31 to become a doublet, J = 8 Hz, and simplifies the multiplet at δ 1.43; ms: 252 (10), 237 (5), 193 (30), 192 (22), 164 (4), 150 (7), 139 (100), and 107 (84); accurate mass analysis for the molecular ion $C_{15}H_{26}O_2$ calcd.: 252.2088; found: 252.2081. The *cis* isomer **15** eluted after the *trans* compound and gave a single peak on glc (19.7); ir ν_{max} (film): 3320, 3300, 1720^{-1}; ^{1}H nmr (360 MHz) δ: 5.29 (m, HC=C, 1H), 3.68 (s, OCH_3, 3H), 3.31 (m, HCCOO, 1H), 2.49 (dd, J = 15.3, 6.3 Hz, H-4, 1H), 2.05 (m, H-2, 1H), 1.9–2.0 (m, $H_2CC{=}C$, H-3′, 3H), 1.79 (m, H-4′, 1H), 1.59 (q, J = 11 Hz, H-2′, 1H), 1.2–1.4 (m, CH_2, 10H), 1.06 (d, J = 6.2 Hz, H_3CCH, 3H), and 0.86 (t, J = 7.0 Hz, H_3CCH_2, 3H); irradiation of the signal δ 2.05 causes collapse of the signal at δ 3.31 to a doublet, J = 8 Hz, and simplifies the multiplet at δ 1.59; irradiation at δ 1.95 causes the multiplet at δ 2.49 to become a doublet, J = 6 Hz, and the methyl doublet at δ 1.06 and the vinyl proton δ 5.29 to become singlets; ms: 252 (12), 237 (5), 193 (38), 192 (33), 177 (11), 164 (13), 150 (21), 139 (96), and 107 (100); accurate mass analysis for the molecular ion $C_{15}H_{26}O_2$ calcd.: 252.2088; found: 252.2062. Methyl 4-methyl-3,5)tetradecadienoate was isolated using the same column, but with 1% dimethoxyethane in hexane, and gave a single peak on glc (27.5); ir ν_{max} (film): 1730, 960 cm^{-1}; ^{1}H nmr (360 MHz) δ: 6.30 (dd, J = 0.9, 15.5 Hz, H-5, 1H), 5.74 (dt, J = 7.2, 15.5 Hz, H-6, 1H), 5.38 (t further split, J = 0.6, 7.4 Hz, H-3, 1H), 3.67 (s, OCH_3, 3H), 3.18 (dd, J = 0.6, 7.4 Hz, $OOCCH_2$, 2H), 2.11 (dt, J = 6.9, 7.4 Hz, $H_2CC{=}C$, 2H), 1.82 (q, J = 1.1 Hz, $H_3CC{=}C$, 3H), 1.2–1.6 (m, CH_2, 12H), and 0.87 (t, J = 6.7 Hz, H_3CCH_2, 3H); ms: 252 (24), 221 (1.6), 178 (13), 165 (7), 154 (11), 140 (12), 135 (18), 105 (25), 95 (45), 94 (30), 93 (82), and 81 (100); accurate mass analysis for the molecular ion calcd.: 252.2088; found: 252.2091.

6-Methyl-2-nonynoic acid (20)

To a solution of the tetrahydropyranyl ether of propargyl alcohol (7.3 g, 47 mmol) in THF (dry, 50 mL) at 0°C was added a solution of *n*-butyllithium in hexane (33 mL, 52 mmol). After stirring for 0.5 h, a solution of 1-bromo-3-methylhexane (16) (8 g, 40 mmol) in HMPA (dry, 40 mL) was added dropwise. The stirred reaction was allowed to warm to room temperature over 3.5 h, then was poured into ice water, and was extracted with hexane (3×). The combined hexane extracts were dried over Na_2SO_4, filtered, and the solvent evaporated. The residue was taken up in CH_3OH (200 mL) and *p*-toluenesulfonic acid (approx. 100 mg) was added. The solution was refluxed overnight, then cooled, and the solvent evaporated. The residue was taken up in ether and washed with H_2O (1×), $NaHCO_3$ solution (1×), NaCl solution (1×), then dried over Na_2SO_4, filtered, and the solvent distilled. Chromatography over silicic acid afforded 6-methyl-2-nonyn-1-ol (2.65 g, 23% from 3-methyl-1-hexene), which gave ir ν_{max} (film): 3450, 2200, and 1010 cm^{-1}; ^{1}H nmr (90 MHz) δ: 4.2 (t, J = 2 Hz, OCH_2, 2H), 2.1–2.3 (m, $H_2CC{\equiv}C$, 2H), 1.0–1.7 (m, CH_2, CH, 7H), 0.8–1.0 (d and t superimposed, J = 7 Hz, $2CH_3$); ^{13}C nmr: 84.4, 78.4, 51.1, 38.9, 31.8, 20.0, 19.1, 16.5, and 14.3 ppm; ms of TMS ether: 226 (missing), 181 (20), 155 (8), 142 (8), 135 (9), 127 (17), 93 (19), 75 (100).

To a solution of the alcohol (2.25 g, 14.6 mmol) in acetone (60 mL) at 0°C was added dropwise a solution of CrO_3 (2.92 g, 29.2 mmol) in H_2O (11.2 mL) and H_2SO_4 (2.8 mL). After stirring for 0.5 h, isopropanol was added until the mixture was green, then the solvents were removed at reduced pressure. The residue was taken up in ether, then washed with H_2O (1×), and NaCl solution (1×), then dried over Na_2SO_4, filtered, the solvent evaporated, and the residue distilled (bulb-to-bulb, oven temp. 105°C, 0.075 Torr) to afford 6-methyl-2-nonynoic acid (**20**) (1.84 g, 75%). This compound gave ir ν_{max} (film): 3100 (br), 2220, and 1680 cm^{-1}; ^{1}H nmr (360 MHz) δ: 2.25–2.41 (m, $H_2CC{\equiv}C$, 2H), 1.04–1.66 (m, CH_2, CH, 7H), 0.87 (t, H_2CCH_3, J = 6.8 Hz, 3H), and 0.85 (d, $HCCH_3$, J = 6.6 Hz, 3H); ^{13}C nmr: 158.4, 92.9, 72.6, 38.8, 34.5, 31.9, 20.0, 19.1, 16.6, and 14.3 ppm; gc/ms of the methyl ester: 182 (missing), 151 (20), 139 (27), 125 (20), 121 (29), 111 (39), 107 (78), 93 (72), and 79 (100); accurate mass analysis for the TMS ester − CH_3 calcd.: 225.1310; found: 225.1297.

Rearrangement of 6-methyl-2-nonynoic acid (20) at room temperature

Using the standard conditions the acid **20** (500 mg, 3.0 mmol) was rearranged for 1.0 h at room temperature. The crude product was esterified with methanolic HCl, affording a mixture of esters (220 mg, 40%) that appeared by glc to contain four products (120°C, 17.0 (78), 17.7 (3), 19.8 (5) and 22.6 (14)). The major product, the methyl ester of 6-methyl-3-nonynoic acid, was obtained after chromatography (hplc, reverse phase eluting 30% H_2O–70% CH_3OH) and gave ir ν_{max} (film): 1740 cm^{-1}; ^{1}H nmr (360 MHz) δ: 3.72 (s, OCH_3, 3H), 3.25 (t, J = 2.5–Hz, $OOCCH_2$, 2H), 2.16 (ddt, J = 16.4, 5.6, and 2.5 Hz, $HCC{\equiv}C$, 1H), 2.03 (ddt, J = 16.4, 6.9, and 2.5 Hz, $HCC{\equiv}C$, 1H), 1.62 (m, $HCCH_3$, 1H), 1.1–1.4 (m, CH_2, 4H), 0.94 (d, J = 6.7 Hz, $HCCH_3$, 3H), and 0.87 (t, J = 7.1 Hz, H_2CCH_3, 3H); ms: 192 (missing), 167 (0.2), 122 (4), 112 (11), 108 (11), 84 (23), and 43 (100).

Rearrangement of 6-methyl-2-nonynoic acid (20) at 60°C

The acid **17** (500 mg, 3.0 mmol) was rearranged with the standard reagent at 60°C for 2.0 h. Methylation afforded a mixture of methyl 6-methyl-*E*,*E*- and methyl 6-methyl-*E*,*Z*-3,5-nonadienoates (280 mg), which gave 2 peaks on glc (120°C, 20.0 (26), and 22.9 (74)) but which could not be separated by any of the chromatographic techniques employed. In the 360-MHz nmr spectrum of the mixture, the olefinic, H_2CCOO, OCH_3, and methylene signals overlapped, but the allylic H δ 2.09 (t, J = 7.2 Hz) and 1.98 (t, J = 7.4 Hz) and the C-6 methyl signals δ 1.72 (s) and 1.69 (s) in the ratio of 1:3 could be distinguished. Superimposable gc/ms spectra were obtained for the isomeric products: (*1*) 182 (43), 123 (27), 108 (70), 93 (100), 81 (96), 67 (42), and 55 (27); and (*2*) 182 (42), 123 (26), 108 (67), 93 (98), 81 (97), 67 (41), and 55 (27). Accurate mass analyses of the molecular ions calcd. for $C_{11}H_{18}O_2$: 182.1306; found: 182.1289 (major product) and 182.1242 (minor product).

*5-Methyl-2-nonynoic acid (**19**)*

By a series of reactions analogous to that employed for the synthesis of 6-methyl-2-nonynoic acid, 5-methyl-2-nonynoic acid was prepared in about 12% overall yield starting from 2-methyl-1-hexene. The intermediate 5-methyl-2-nonyn-1-ol (distilled bulb-to-bulb, oven temp. 90°C, 0.05 Torr, 31% from 2-methyl-1-hexene) gave ir ν_{max} (film): 3350, 2200, and 1010 cm^{-1}; ^1H nmr (360 MHz) δ: 4.21 (t, J = 2.2 Hz, OCH_2, 2H), 2.16 (ddt, J = 16.6, 5.7, and 2.2 Hz, C≡CCH, 1H), 2.03 (ddt, J = 16.6, 7.0, and 2.2 Hz, C≡CCH, 1H), 1.58 (m, $HCCH_3$, 1H) 1.1–1.4 (m, CH_2, 6H), 0.92 (d, J = 6.6 Hz, $HCCH_3$, 3H), and 0.86 (6, J = 6.8 Hz, H_3CCH_2, 3H); ^{13}C nmr: 85.2, 79.3, 51.3, 35.8, 32.6, 29.3, 26.2, 22.9, 19.5, and 14.1 ppm; gc/ms of TMS ester: 226 (missing), 211 (10), 181 (24), 169 (7), 142 (6), 135 (8), 127 (12), 75 (100), and 73 (65). Jones oxidation gave the acid **16** (77%), which was distilled (bulb-to-bulb, oven temp. 120°C, 0.1 Torr) and gave ir ν_{max} (film): 3100, 2220, and 1670 cm^{-1}; ^1H nmr (360 MHz) δ: 2.31 (dd, J = 17.2, 5.7 Hz, C≡CCH, 1H), 2.21 (dd, J = 17.2, 7.0 Hz, C≡CCH, 1H), 1.72 (m, $HCCH_3$, 1H), 1.2–1.5 (m, CH_2 6H), 0.98 (d, J = 6.7 Hz, $HCCH_3$, 3H), and 0.87 (t, J = 6.8 Hz, H_2CCH_3, 3H); ^{13}C nmr: 158.4, 91.7, 73.7, 35.8, 32.1, 29.2, 26.1, 22.8, 19.5, and 14.0 ppm; gc/ms of TMS ester: 240 (missing), 225 (61), 181 (82), 156 (29), 96 (26), 75 (83), 73 (94), and 43 (100); accurate mass analysis for TMS ester − CH_3 calcd. for $C_{12}H_{21}O_2Si$: 225.1310; found 225.1392.

*Rearrangement of 5-methyl-2-nonynoic acid (**19**)*

The rearrangement of 5-methyl-2-nonynoic acid (336 mg, 2.0 mmol) was carried out under standard conditions for 2.0 h at 60°C, affording, after methylation and chromatography, a mixture of isomeric compounds (102 mg, 28%), the principal component (78%) of which was methyl 5-methyl-*E*,*E*-3,5-nonadienoate. This compound gave gc/ms: 182 (24), 108 (47), 93 (100), and 81 (49). The mixture gave an ir ν_{max} (film): 1740, 1640, 960, and 760 cm^{-1}; ^1H nmr (360 MHz) δ: 6.12 (dd, J = 15.6, 0.3 Hz, H-4, 1H), 5.59 (dt, J = 15.6, 7.2 Hz, H-3, 1H), 5.42 (t, J = 7.3 Hz, H-6, 1H), 3.66 (s, OCH_3, 3H), 3.10 (d, J = 7.2 Hz, H-2, 2H), 2.07 (dt, J = 7.3, 7.4 Hz, C=CCH_2, 2H), 1.72 (d, J = 0.3 Hz, H_3CC=CH, 3H), 1.32–1.42 (m, CH_2, 2H), and 0.88 (t, J = 7.4 Hz, H_3CCH_2, 3H), and other signals of low intensity at δ: 6.51 (d, J = 15 Hz, H-4), 3.67 (s, OCH_3), 2.17 (m, C=CCH_2), and 1.86 (H_3CC=C) due to the *E*,*Z*-isomer. An accurate mass analysis was obtained for the molecular ion of the major component calcd. for $C_{11}H_{18}O_2$: 182.1306; found: 182.1228.

*4-Cyclohexyl-2-butynoic acid (**21**)*

To a solution of 4-cyclohexyl-2-butyn-1-ol (17) (2.0 g, 13.2 mmol) in acetone at 0°C was added a solution of CrO_3 (3.3 g, 33 mmol) in H_2O (13 mL) and H_2SO_4 (4.4 mL). After stirring for 0.5 h, isopropanol was added until the mixture was green, then the solvents were evaporated and ether was added. The aqueous phase was washed with ether (3×), and the combined organic phases were washed with $NaHCO_3$ solution (2×). The combined $NaHCO_3$ phases were acidified with HCl, then extracted with ether (3×). The combined organic phases were then washed with NaCl solution (1×), dried over Na_2SO_4, filtered, the solvent evaporated, and the residue distilled (bulb-to-bulb, oven temp. 120–150°C, 0.075 Torr) affording 4-cyclohexyl-2-butynoic acid (**21**) (1.0 g, 50%). This compound gave ir ν_{max} ($CHCl_3$ solution): 3600, 3100, 2200, and 1680 cm^{-1}; ^1H nmr (90 MHz) δ: 2.26 (d, J = 6 Hz, H_2CC≡C, 2H), and 0.8–2.0 (m, 11H); gc/ms of TMS ester: 238 (0.8), 223 (72), 179 (100) and 156 (44); accurate mass analysis for the molecular ion of the TMS ester − CH_3 calcd. for $C_{12}H_{19}O_2Si$: 223.1164; found 223.1159.

*Rearrangement of 4-cyclohexyl-2-butynoic acid (**21**)*

Rearrangement of the acid **21** (664 mg, 4.0 mmol) for 2.0 h at 60°C under the standard conditions afforded, after methylation with CH_2N_2 and chromatography over silica gel, the dienoic methyl ester of **26** (280 mg, 40%), which gave ir ν_{max} (film): 1730 and 960 cm^{-1}; ^1H nmr (360 MHz) δ: 6.08 (d, J = 15.8 Hz, H-4, 1H), 5.58 (br t, J = 7.4 Hz, HC=CCH_2, 1H), 5.56 (dt, J = 15.8, 7.2 Hz, H-3, 1H), 3.66 (s, OCH_3, 3H), 3.08 (d, J = 7.2 Hz, $OOCCH_2$, 2H), 2.02–2.12 (m, H_2CC=C, 4H), and 1.5–1.7 (m, CH_2, 4H); gc/ms of methyl ester: 180 (30), 165 (0.5), 130 (8), 121 (33), 106 (39), 91 (57), and 79 (100); accurate mass analysis for the molecular ion of the methol ester calcd. for $C_{11}H_{16}O_2$: 180.1151; found: 180.1121.

*5-cyclohexyl-2-pentynoic acid (**22**)*

Employing an analogous set of conditions to that for the synthesis of 4-cyclohexyl-2-butynoic acid, 5-cyclohexyl-2-pentynoic acid was prepared starting with 1-bromo-2-cyclohexylethane. The acid **22** (distilled bulb-to-bulb, oven temp. 130–145°C, 0.05 Torr) gave ir ν_{max} (film): 3100, 2220, and 1680 cm^{-1}; ^1H nmr (90 MHz) δ: 2.3 (t, J = 7 Hz, H_2CC≡C, 2H), and 0.8–1.9 (m, CH_2, CH, 13H); ^{13}C nmr: 158.6, 92.9, 72.5, 36.6, 34.7, 32.6, 26.4, 26.0, and 16.1 ppm; gc/ms of TMS ester: 252 (missing), 237 (27), 193 (38), 162 (21), 133 (22), and 73 (100); accurate mass analysis for TMS ester − CH_3 calcd. for $C_{13}H_{21}O_2Si$; 237.1295; found: 237.1302.

*Rearrangement of 5-cyclohexyl-2-pentynoic acid (**22**)*

Rearrangement of the acid **19** for 2.0 h at 60°C with the standard reagent afforded, after methylation with CH_2N_2 and chromatography over silica gel, eluting with 20% ether – 80% hexane, the methyl ester of **27**, (110 mg, 28%). This compound gave ir ν_{max} (film): 1730, 960 and 760 cm^{-1}; ^1H nmr (360 MHz) δ: 6.30 (ddt, J = 15.0, 10.9, and 1.4 Hz, H-4, 1H), 5.71 (d, J = 10.9 Hz, H-5, 1H), 5.57 (dt, J = 7.2, 7.0 Hz, H-3, 1H), 3.62 (s, OCH_3, 3H), 3.06 (dd, J = 7.2 Hz, 1.0 Hz, H-2, 1H), 2.18–2.24 and 2.05–2.08 (m, C=CCH_2, 4H), and 1.46–1.52 (m, CH_2, 4H); gc/ms: 194 (62), 162 (7), 144 (11), 135 (40), 120 (99), 91 (87), 79 (90), and 67 (100); accurate mass analysis for the molecular ion of the methyl ester calcd. for $C_{12}H_{18}O_2$: 194.1307; found: 194.1305.

Acknowledgments

Professor J. E. Baldwin is thanked for a preprint of a manuscript on stereochemical generalizations and prediction for 1,3-prototropic shifts under basic conditions. Professor J. W. ApSimon gave up several hours of sunshine and presented this material, in my place, at the PAC Chem meeting in Honolulu, December 1984. I would like to acknowledge the expert technical assistance of Angela C. Shaw. L. Hogge, D. Olson, and T. Mazurek performed the gc–ms and nmr experiments.

1. S. R. Abrams. Can. J. Chem. **62**, 1333 (1984).
2. S. R. Abrams. Can. J. Chem. **60**, 1238 (1982).
3. P. A. Grieco, K. Yoshida, and P. Garnier. J. Org. Chem. **48**, 3137 (1983).
4. F. Theron, M. Verny, and R. Vessiere. *In* The chemistry of the carbon carbon triple bond. *Edited by* S. Patai, Wiley, Toronto. 1978. Chapt. 10.
5. M. Julia and C. Descoins. Bull. Soc. Chim. Fr. 2541 (1964).
6. R. A. Amos and J. A. Katzennelenbogen. J. Org. Chem. **43**, 555 (1978).
7. E. J. Corey and B. W. Erickson. J. Org. Chem. **39**, 821 (1974).
8. G. Eglinton and M. C. Whiting. J. Chem. Soc. 3052 (1953).
9. M. Miocque, M. Moskowitz, and S. Labidalle. Tetrahedron Lett. **32**, 2769 (1976).
10. M. A. Boeventura, J. Drouin, and J. M. Conia. Synthesis, 801 (1983).
11. J. E. Baldwin. J. Chem. Soc. Chem. Commun. 734 (1976).
12. L. M. Jackman and S. Sternhell. Applications of nuclear magnetic resonance inorganic chemistry. 2nd ed. Pergamon Press, New York. 1969. p. 225.
13. G. A. Olah, S. C. Narang, B. G. B. Gupta, and R. Malhotra. J. Org. Chem. **44**, 1247 (1979).
14. J. K. Whitesell, R. S. Matthews, and A. M. Hebling. J. Org. Chem. **43**, 785 (1978).
15. B. Phillips and P. S. Starcher. Chem. Abstr. **56**, 4624e (1962); German patent 1,086,686.
16. P. A. Levene and A. Rothen. J. Org. Chem. **1**, 76 (1936).
17. R. Gelin, R. Gelin, and M. Albrand. Bull. Soc. Chim. Fr. 4146 (1971).

The structure of $[Ir_2(CO)_2(\mu\text{-}H)(\mu\text{-}CO)(Ph_2PCH_2PPh_2)_2][BF_4]$ and comparisons with its rhodium analogue and other related doubly bridged A-frames

BRUCE R. SUTHERLAND AND MARTIN COWIE[1]

Department of Chemistry, University of Alberta, Edmonton, Alta., Canada T6G 2G2

Received August 7, 1985

BRUCE R. SUTHERLAND and MARTIN COWIE. Can. J. Chem. **64**, 464 (1986).

The structure of $[Ir_2(CO)_2(\mu\text{-}H)(\mu\text{-}CO)(DPM)_2][BF_4]$ (DPM=$Ph_2PCH_2PPh_2$) has been determined crystallographically. It crystallizes in the monoclinic space group $P2_1/n$ (a = 13.7740(6) Å, b = 15.277(2) Å, c = 23.581(2) Å, β = 97.015(5)°, V = 4924.9 Å^3, Z =4) and on the basis of 6628 unique observations and variation of 272 parameters, the structure converged to R = 0.031 and R_w = 0.043. This metal–metal bonded complex is similar to its rhodium analogue, having the two essentially identical Ir centres bridged by the carbonyl, hydride, and two diphosphine ligands. The major difference between this compound and the rhodium species (in the solid state) relates to the orientation of the phenyl groups of the diphosphine ligands; in the iridium complex four of these groups block the sites adjacent to the bridging hydride ligand, whereas these sites are relatively unobstructed in the rhodium analogue. This difference may result in different coordination sites for substrate molecules and therefore in different chemistry.

BRUCE R. SUTHERLAND et MARTIN COWIE. Can. J. Chem. **64**, 464 (1986).

Faisant appel à la cristallographie, on a déterminé la structure du complexe $[Ir_2(CO)_2(\mu\text{-}H)(\mu\text{-}CO)(DPM)_2][BF_4]$ (DPM=$Ph_2PCH_2PPh_2$). Il cristallise dans le groupe d'espace $P2_1/n$ (a = 13,7740(6) Å, b = 15,277(2) Å, c = 23,581(2) Å, β = 97,015(5)°, V = 4924,9 Å^3, Z = 4) et sur la base de 6628 observations uniques et de 272 paramètres, on a affiné la structure jusqu'à des valeurs respectives de R et R_w de 0,031 et 0,043. Ce complexe comportant une liaison métal–métal est semblable à son analogue contenant du rhodium et il possède deux centres Ir qui sont essentiellement identiques et qui sont liés par le carbonyle, l'hydrure et les deux ligands diphosphines. La principale différence entre ce composé et son analogue contenant du rhodium (à l'état solide) a trait à l'orientation des groupements phényles des ligands diphosphines; dans le complexe de l'iridium quatre de ces groupements bloquent les sites adjacents au ligand hydrure agissant comme pont alors que dans le complexe au rhodium ces sites ne sont pas bloqués. Il est possible que cette différence puisse provoquer des différences dans les sites de coordination pour les molécules de substrats et conduire ainsi à des chimies différentes.

[Traduit par le journal]

Introduction

We have recently shown (1) that catalysis of the water–gas shift (WGS) reaction, by complexes containing two metal centres, can be effectively modelled by using DPM-bridged (DPM = $Ph_2PCH_2PPh_2$), hydrido, and hydroxy complexes of iridium. In particular, the observation of $[Ir_2(CO)_2(\mu\text{-}H)(\mu\text{-}CO)(DPM)_2]^+$ in our WGS cycle prompted us to suggest that this cycle could serve as a model for the one in which the rhodium analogue, $[Rh_2(CO)_2(\mu\text{-}H)(\mu\text{-}CO)(DPM)_2]^+$, acted as catalyst or catalyst precursor (2). However, one notable difference in the chemistry of the above two hydrido-bridged complexes of Rh and Ir concerned their chemistry with acid; whereas the Rh species instantly evolved H_2 upon treatment with acid (2), the Ir complex yielded a stable dihydride from which H_2 could be evolved only under forcing conditions (1). Although this difference is in line with the well known greater stability of iridium-hydrides over those of rhodium (3), we were led to believe that an additional, equally important difference lay in the sites of protonation of the two complexes. We suggested (1) that protonation of the Rh complex occurred adjacent to the bridging hydride ligand such that reductive elimination of H_2 could be facile, whereas with the Ir complex initial protonation occurred opposite the bridging hydride ligand such that a ligand rearrangement would have to precede reductive elimination of H_2, thereby hampering the reductive elimination step.

In order to explain this postulated difference in protonation sites we undertook a structural determination of the above iridium hydride complex in order to compare it with the structure of the rhodium analogue (2). Furthermore, it was of interest to us to establish what differences might be present in the two compounds as an aid in determining how close an analogy could be drawn between complexes of rhodium and iridium. Such conclusions are important in studies in which rhodium-containing catalysts are modelled by their iridium analogues. Herein we report the results of this structure determination and a comparison between the two rhodium and iridium compounds.

[1]Author to whom correspondence should be addressed.

Experimental

The complex $[Ir_2(CO)_2(\mu\text{-}H)(\mu\text{-}CO)(DPM)_2][BF_4]$ was prepared by the protonation of $[Ir_2(CO)_3(DPM)_2]$ using $HBF_4\cdot OEt_2$, as has previously been reported (1). Dark orange crystals of the title complex of suitable X-ray diffraction quality were obtained from the slow diffusion of diethyl ether into a saturated CH_2Cl_2 solution of the complex. These crystals proved to be air stable so they were handled in air and the one chosen for the crystallographic study was mounted on a glass fibre using epoxy adhesive. Unit cell parameters were obtained from a least-squares refinement of the setting angles of 25 reflections, in the range of $20.0° < 2\theta < 25.0°$, which were accurately centred on an Enraf–Nonius CAD4 diffractomer using MoKα radiation. The systematic absences ($h0l$: $h+l$ = odd, $0k0$: k = odd) were consistent with the space group $P2_1/n$; this nonstandard setting of $P2_1/c$ was retained because of the convenient β angle.

Intensity data were collected on a CAD4 diffractometer in the bisecting mode employing the ω–2θ scan technique up to 2θ = 50.00° with graphite monochromated MoKα radiation. Backgrounds were scanned for 25% of the peak width on either end of the peak scan. The intensities of three standard reflections were measured at 1 h intervals of exposure to assess possible crystal decomposition or movement. No significant variation in these standards was noted, so no correction was applied to the data. A total of 8677 unique reflections were measured and processed in the usual way using a value of 0.04 for p (4); of these, 6628 were considered to be observed and were used in subsequent

TABLE 1. Summary of crystal data and details of intensity collection

Compound	$[Ir_2(CO)_2(\mu\text{-}H)(\mu\text{-}CO)(DPM)_2][BF_4]$
fw	1325.05
Formula	$Ir_2P_4F_4O_3C_{53}BH_{45}$
Cell parameters	
a, Å	13.7740(6)
b, Å	15.277(2)
c, Å	23.581(2)
β, deg	97.015(5)
V, Å^3	4924.9
d(calc), g cm^{-3}	1.786 (Z = 4)
Space group	$P2_1/n$
Temp, °C	22
Radiation	Graphite monochromated MoKα ($\bar{\lambda}$ = 0.71069 Å)
Receiving aperture, mm	2.00 × (1.00 tan θ) wide × 4.0 high 173 from crystal
Take-off angle, deg.	3.05
Scan speed, deg min^{-1}	Variable between 1.12 and 6.71
Scan width, deg	0.75 + (0.347 tan θ) in ω
2θ maximum, deg	50.00
No. of unique data collected	8677 (h, k, $\pm l$)
No. of unique observations ($F_0^2 \geq 3\sigma(F_0^2)$)	6628
Crystal faces	Of the form {1,0,1}, {0,0,1}, {1,0,$\bar{1}$}, {0,1,1}
Crystal dimensions, mm	0.11 × 0.33 × 0.22
Absorption coefficient, cm^{-1}	55.627
Range in transmission factors	0.2901–0.5664
Final no. of parameters varied	272
Error in observation of unit weight	1.101
R	0.031
R_w	0.043

calculations. Absorption corrections were applied to the data by using Gaussian integration (5).[2] See Table 1 for pertinent crystal data and details of intensity collection.

Structure solution and refinement

The structure was solved in the space group $P2_1/n$ using standard Patterson and Fourier techniques. All atoms, including hydrogens, were ultimately located. Atomic scattering factors were taken from Cromer and Waber's tabulations (6) for all atoms except hydrogen, for which the values of Stewart *et al.* (7) were used. Anomalous dispersion terms (8) for Ir and P were included in F_c. The carbon atoms of the phenyl rings were refined as rigid groups having D_{6h} symmetry, C—C distances of 1.39 Å and independent isotropic thermal parameters. All hydrogen atoms of the diphosphine ligands were located and included as fixed contributions but were not refined. Their idealized positions were calculated from the geometries about their attached carbon atoms using C—H distances of 0.95 Å. Each hydrogen atom was assigned an isotropic thermal parameter of 1 Å^2 greater than the B (or equivalent isotropic B of anisotropic atoms) of its attached carbon. The bridging hydride ligand was successfully located and was refined isotropically. All other non-hydrogen atoms were refined anisotropically.

The final model in the space group $P2_1/n$ with 272 parameters refined converged to R = 0.031 and R_w = 0.043.[3] On the final difference Fourier map, the 20 highest residuals (0.7–1.2 e/Å^3) were in the vicinities of the Ir and P atoms and the BF_4^- counterion; these compare with intensities of ca. 6.0 e/Å^3 on earlier Fourier maps for carbon atoms. Listings of coordinates and isotropic thermal parameters for nongroup and group atoms are given in Tables 2 and 3, respectively. Anisotropic thermal parameters, hydrogen parameters, and structure amplitudes have been deposited as supplementary information and are available on request (Tables 6, 7, and 8, respectively).[4]

TABLE 2. Positional and thermal parameters for the individual atoms

Atom	x[a]	y	z	B (Å^2)[b]
Ir(1)	0.11218(2)	0.24627(2)	−0.01014(1)	2.19
Ir(2)	0.26373(2)	0.36077(2)	0.02385(1)	2.24
P(1)	0.1400(1)	0.1659(1)	0.07390(7)	2.66
P(2)	0.3059(2)	0.2885(1)	0.10969(7)	2.61
P(3)	0.0875(1)	0.3028(1)	−0.10232(7)	2.31
P(4)	0.2522(1)	0.4266(1)	−0.06524(7)	2.37
F(1)	0.4155(7)	0.0432(7)	0.7232(4)	14.23
F(2)	0.5135(11)	0.1057(9)	0.6728(5)	21.39
F(3)	0.5620(8)	0.0037(7)	0.7254(5)	15.57
F(4)	0.5275(11)	0.1184(8)	0.7646(6)	21.85
O(1)	−0.0784(4)	0.1519(4)	−0.0346(2)	4.94
O(2)	0.3956(4)	0.5073(4)	0.0689(3)	5.53
O(3)	0.0577(4)	0.4197(4)	0.0424(2)	4.47
C(1)	−0.0050(5)	0.1873(5)	−0.0253(3)	3.27
C(2)	0.3447(5)	0.4507(5)	0.0512(3)	3.44
C(3)	0.1117(5)	0.3701(4)	0.0289(3)	2.98
C(4)	0.2036(5)	0.2286(5)	0.1132(3)	3.14
C(5)	0.1304(4)	0.4152(4)	−0.1052(1)	2.70
B(1)	0.5057(12)	0.0792(16)	0.7211(7)	8.73
H(1)	0.238(5)	0.264(5)	−0.012(3)	4.6(19)

[a]Estimated standard deviations in this and other tables are given in parentheses and correspond to the least significant digits.

[b]For all atoms except H(1), the values given are the equivalent isotropic thermal parameters.

Description of structure and discussion

The complex, $[Ir_2(CO)_2(\mu\text{-}H)(\mu\text{-}CO)(DPM)_2][BF_4]$, crystallizes from CH_2Cl_2 in two crystal modifications, a red form and an orange form (the orange form has ir spectral parameters very similar to those of the solution spectrum (1)). The structure of the orange form has been determined crystallographically and is reported here. The unit cell contains four anions and four cations, all of which are separated by normal van der Waals distances between the constituent atoms. A perspective view of the complex cation is shown in Fig. 1, and tabulations of distances and angles are given in Tables 4 and 5. The BF_4^- anion has the expected tetrahedral geometry, and as is common with such pseudo-spherical groups, displays some degree of disorder as indicated by the large thermal parameters. Nevertheless, the metrical parameters of this group are normal.

[2]All initial computing, including structure solution, absorption correction and least-squares refinement, was carried out on a PDP-11 PLUS computer using the Enraf–Nonius structure solution package. The final few refinements using the rigid-group approximation for the phenyl rings, and other structure completion operations were carried out on the University Amdahl computer using programs that are described in ref. 5.

[3]$R = \Sigma||F_o| - |F_c||/\Sigma|F_o|$; $R_w = [\Sigma w(|F_o| - |F_c|)^2/\Sigma wF_o^2]^{1/2}$.

[4]Complete set of data may be purchased from the Depository of Unpublished Data, CISTI, National Research Council of Canada, Ottawa, Ont., Canada K1A 0S2.

TABLE 3. Rigid group parameters

(*a*) Derived positions and thermal parameters

Atom	*x*	*y*	*z*	*B* (Å^2)	Atom	*x*	*y*	*z*	*B* (Å^2)
C(11)	0.2115(3)	0.0669(3)	0.0691(2)	2.7(1)	C(51)	0.1466(3)	0.2491(3)	−0.1576(2)	2.8(1)
C(12)	0.2213(4)	0.0336(3)	0.0152(2)	3.6(1)	C(52)	0.1233(3)	0.2759(3)	−0.2141(2)	3.8(1)
C(13)	0.2730(4)	−0.0437(3)	0.0099(2)	4.5(2)	C(53)	0.1705(4)	0.2385(3)	−0.2570(1)	4.3(2)
C(14)	0.3148(4)	−0.0877(3)	0.0585(2)	5.2(2)	C(54)	0.2412(3)	0.1742(3)	−0.2435(2)	5.0(2)
C(15)	0.3050(4)	−0.0543(3)	0.1125(2)	4.6(2)	C(55)	0.2645(3)	0.1473(3)	−0.1871(2)	4.5(2)
C(16)	0.2533(4)	0.0229(3)	0.1178(1)	4.2(2)	C(56)	0.2172(3)	0.1847(3)	0.1442(1)	3.4(1)
C(21)	0.0298(3)	0.1288(3)	0.1019(2)	3.3(1)	C(61)	−0.0408(3)	0.3067(3)	−0.1300(2)	2.8(1)
C(22)	−0.0320(4)	0.1907(2)	0.1219(2)	4.2(2)	C(62)	−0.1004(4)	0.3708(3)	−0.1106(2)	4.5(2)
C(23)	−0.1189(4)	0.1644(3)	0.1412(2)	5.3(2)	C(63)	−0.2009(4)	0.3690(3)	−0.1271(3)	5.6(2)
C(24)	−0.1441(3)	0.0762(4)	0.1407(3)	5.8(2)	C(64)	−0.2418(3)	0.3031(4)	−0.1632(3)	6.0(2)
C(25)	−0.0823(4)	0.0143(3)	0.1208(3)	5.4(2)	C(65)	−0.1822(4)	0.2389(3)	−0.1826(2)	5.3(2)
C(26)	0.0046(4)	0.0406(3)	0.1014(2)	4.2(2)	C(66)	−0.0817(4)	0.2407(3)	−0.1660(2)	4.2(2)
C(31)	0.3453(3)	0.3625(3)	0.1684(2)	3.1(1)	C(71)	0.2733(3)	0.5438(2)	−0.0624(2)	2.8(1)
C(32)	0.2752(2)	0.4163(3)	0.1882(2)	4.0(1)	C(72)	0.2071(3)	0.5970(3)	−0.0385(2)	4.9(2)
C(33)	0.3035(3)	0.4809(3)	0.2285(2)	4.9(2)	C(73)	0.2252(4)	0.6863(3)	−0.0319(3)	5.9(2)
C(34)	0.4019(4)	0.4915(3)	0.2490(2)	5.2(2)	C(74)	0.3096(5)	0.7224(2)	−0.0492(3)	6.0(2)
C(35)	0.4720(3)	0.4377(4)	0.2292(2)	4.7(2)	C(75)	0.3758(4)	0.6692(3)	−0.0732(3)	6.0(2)
C(36)	0.4437(3)	0.3731(3)	0.1889(2)	3.7(1)	C(76)	0.3576(3)	0.5799(3)	−0.0798(2)	4.5(2)
C(41)	0.4001(3)	0.2050(3)	0.1104(2)	3.2(1)	C(81)	0.3388(3)	0.3856(3)	−0.1105(2)	2.9(1)
C(42)	0.4292(4)	0.1772(3)	0.0589(2)	3.6(1)	C(82)	0.4171(4)	0.3345(4)	−0.0867(2)	4.3(2)
C(43)	0.4964(4)	0.1093(4)	0.0582(2)	5.2(2)	C(83)	0.4817(3)	0.2992(4)	−0.1216(2)	6.2(2)
C(44)	0.5344(4)	0.0690(3)	0.1090(2)	5.8(2)	C(84)	0.4682(4)	0.3150(4)	−0.1801(2)	6.1(2)
C(45)	0.5053(4)	0.0968(4)	0.1606(2)	5.1(2)	C(85)	0.3899(4)	0.3661(4)	−0.2039(2)	5.2(2)
C(46)	0.4382(4)	0.1647(3)	0.1613(2)	4.2(2)	C(86)	0.3253(3)	0.4014(3)	−0.1690(2)	4.0(1)

(*b*) Group parameters

	X_c*	Y_c	Z_c	phi†	theta	rho
Ring 1	0.2632(2)	−0.0104(2)	0.0638(1)	−1.93(2)	−1.765(3)	−0.90(2)
Ring 2	−0.0571(3)	0.1025(2)	0.1213(1)	−2.927(3)	2.914(3)	0.461(3)
Ring 3	0.3736(2)	0.4270(2)	0.2087(1)	−1.850(3)	3.031(3)	2.430(3)
Ring 4	0.4673(2)	0.1370(2)	0.1097(2)	−2.57(4)	−1.665(3)	−1.73(4)
Ring 5	0.1939(2)	0.2116(2)	−0.2006(1)	−2.397(4)	−2.476(2)	−1.634(4)
Ring 6	−0.1413(3)	0.3049(2)	−0.1466(2)	−3.013(3)	2.552(3)	−0.193(4)
Ring 7	0.2914(3)	0.6331(2)	−0.0558(1)	−1.697(3)	2.607(4)	3.037(4)
Ring 8	0.4035(3)	0.3503(2)	0.1453(2)	0.887(5)	2.307(3)	−1.470(5)

*X_c, Y_c, and Z_c are the fractional coordinates of the centroid of the rigid group.

†The rigid group orientation angles, phi, theta, and rho (radians), are the angles by which the rigid body is rotated with respect to a set of axes *X*, *Y*, and *Z*. The origin is the centre of the ring, *X* is parallel to *a**, *Z* is parallel to *c*, and *Y* is parallel to the line defined by the intersection of the plane containing *a** and *b** with the plane containing *b* and *c*.

As shown in Fig. 1, the cation has the typical geometry for a bis DPM-bridged complex (9), with both diphosphine ligands in an essentially *trans* arrangement on each metal. The remaining ligands lie in the plane which is essentially perpendicular to the metal phosphine vectors, and are arranged symmetrically such that each metal shares the bridging hydride and carbonyl ligands and also has a terminal CO group. If the Ir–Ir interaction is ignored, the metal geometries can be described as square pyramidal with the bridging carbonyl at the common apex of the two pyramids. The angles between the pseudo-*trans* ligands in the two pyramids average 169.29(6) and 155(2)° for the P—Ir—P and OC—Ir—H(1) angles, respectively. The major distortion from the square pyramidal geometry for each metal results because the bridging carbonyl group is offset towards the adjacent metal yielding an average H(1)—Ir—C(3) angle (86(2)°) which is much less than average C(3)—Ir—CO(terminal) angle (119.0(3)°).

The compound is clearly metal–metal bonded, with the Ir(1)—Ir(2) distance of 2.7661(4) Å corresponding to a normal Ir—Ir single bond; a range of distances between 2.779(1) and 2.893(2) Å seems to be typical in related Ir—Ir bonded species (10–13). Support for a metal–metal bonded formulation comes from the intraligand P–P separations (av. 2.999(2) Å), which indicate a compression along the Ir—Ir axis due to mutual attraction of the metals. The geometry of the bridging carbonyl ligand is typical for such a group accompanied by a metal–metal bond (14), therefore the Ir(1)—C(3)—Ir(2) angle, of 81.9(3)° is acute. Both terminal carbonyl groups are normal, with Ir—C distances much shorter than those on the bridging group. All parameters within the bridging DPM ligands are normal.

Refinement of the bridging hydride ligand proceeded well and the resulting Ir—H distances (av. 1.75(7) Å) are in good agreement with each other and are in the range normally observed for hydrides which bridge second and third row group VIII metals (15, 16). The angle at the bridging hydride is 105(4)°. These parameters agree rather well with those in the closely related Rh analogue (2) where Rh—H distances of 1.97(11) and 1.75(11) Å and a Rh—H—Rh angle of 94(5)° were observed.

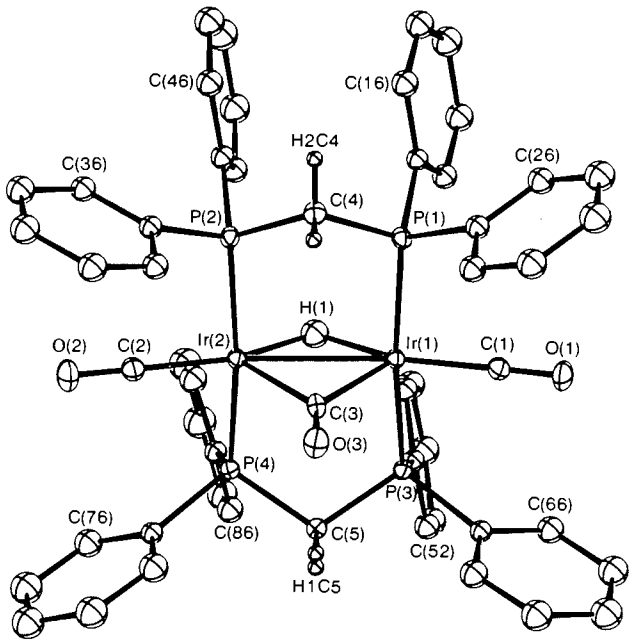

FIG. 1. A perspective drawing of the $[Ir_2(CO)_2(\mu\text{-}H)(\mu\text{-}CO)(DPM)_2]^+$ cation showing the numbering scheme. The numbering of the phenyl carbons starts at the one bound to phosphorus and proceeds sequentially around the rings. Thermal ellipsoids are shown at the 20% level except for the methylene hydrogen atoms, which are shown artificially small.

TABLE 4. Selected distances (Å) for $[Ir_2(CO)_2(\mu\text{-}H)(\mu\text{-}CO)(DPM)_2][BF_4]$

(*a*) Bonded distances

Bond	Distance	Bond	Distance
Ir(1)—Ir(2)	2.7661(4)	P(2)—C(4)	1.822(7)
Ir(1)—P(1)	2.323(2)	P(3)—C(5)	1.820(7)
Ir(1)—P(3)	2.325(2)	P(4)—C(5)	1.829(6)
Ir(2)—P(2)	2.316(2)	P(1)—C(11)	1.815(4)
Ir(2)—P(4)	2.317(2)	P(1)—C(21)	1.819(5)
Ir(1)—C(1)	1.845(7)	P(2)—C(31)	1.817(5)
Ir(2)—C(2)	1.837(7)	P(2)—C(41)	1.819(5)
Ir(1)—C(3)	2.104(7)	P(3)—C(51)	1.816(5)
Ir(2)—C(3)	2.116(7)	P(3)—C(61)	1.809(4)
Ir(1)—H(1)	1.76(7)	P(4)—C(71)	1.814(4)
Ir(2)—H(1)	1.73(7)	P(4)—C(81)	1.807(5)
C(1)—O(1)	1.144(8)	B(1)—F(1)	1.36(2)
C(2)—O(2)	1.157(8)	B(1)—F(2)	1.23(2)
C(3)—O(3)	1.135(8)	B(1)—F(3)	1.39(2)
P(1)—C(4)	1.828(7)	B(1)—F(4)	1.19(2)

(*b*) Nonbonded distances

Atoms	Distance	Atoms	Distance
P(1)–P(2)	2.996(2)	Ir(1)–H(56)	3.20
P(3)–P(4)	3.001(2)	Ir(2)–H(42)	3.06
Ir(1)–H(12)	3.02	Ir(2)–H(82)	3.01

The differences in the metal–hydrogen bond lengths between the two compounds are not significant and the more acute angle at the hydride ligand in the Rh complex results from the somewhat shorter Rh—Rh separation and the one slightly longer Rh—H distance.

The present compound is most clearly related to three other so-called (17) doubly bridged A-frame complexes: namely, $[Rh_2(CO)_2(\mu\text{-}H)(\mu\text{-}CO)(DPM)_2]^+$ (2), $[Rh_2(CO)_2(\mu\text{-}Cl)(\mu\text{-}CO)(DPM)_2]^+$ (18), and $[Ir_2(CO)_2(\mu\text{-}S)(\mu\text{-}CO)(DPM)_2]$ (13). All four compounds have pseudo-*trans* bridging DPM arrangements, one terminal CO on each metal, a bridging CO, a bridging formally anionic ligand, and a metal–metal bond. Superficially, the structures of all four complexes are essentially identical (apart from the obvious differences in the bridging anionic ligands). Although it is not surprising that Rh and Ir analogues are similar or that the two complexes containing bridging chloride and sulfide ligands are similar, it is surprising that the two bridging hydride complexes should so closely resemble the others since the hydride complexes have two fewer valence electrons. One might therefore expect differences in the metal–metal bond orders, although such is not observed. All four metal–metal separations correspond to normal single bonds (2.7661(4) (iridium hydride), 2.731(2) (rhodium hydride), 2.8415(7) (rhodium chloride), and 2.843(2) Å (iridium sulfide)). The longer distances in the chloride and sulfide complexes seem to result from the larger covalent radii of these bridging groups tending to force the metals apart. Consistent with these observations, extended Hückel calculations by Hoffman and Hoffmann (17) indicated that the molecular orbitals for $[Rh_2(CO)_2(\mu\text{-}H)(\mu\text{-}CO)(DPM)_2]^+$ and $[Rh_2(CO)_2(\mu\text{-}Cl)(\mu\text{-}CO)(DPM)_2]^+$ were rather similar so that in spite of the two valence-electron difference no metal–metal bond-order difference was predicted.

In addition to the obvious comparisons noted above, the present compound can also be compared with other binuclear group VIII diphosphine compounds in which the metal–metal bonds are simultaneously bridged by hydrido and carbonyl groups. Two such species are $[Rh_2Cl_3(\mu\text{-}H)(\mu\text{-}CO)(DPM)_2]$ (19) and $[Pt_2(\mu\text{-}H)(\mu\text{-}CO)(DPE)_2]$ (DPE = $Ph_2PCH_2CH_2PPh_2$) (20). Not unexpectedly, the parameters involving the $M_2(\mu\text{-}H)(\mu\text{-}CO)$ cores in these molecules are quite similar and are normal for metal–metal bonded species.

The structure determination of $[Ir_2(CO)_2(\mu\text{-}H)(\mu\text{-}CO)(DPM)_2]^+$ was undertaken to provide a basis for comparison between it and the analogous rhodium hydride. In particular, we sought to determine whether the structural information might suggest reasons for the apparent difference in protonation sites (1). The most obvious structural parameters which might explain these differences are the angles between the bridging hydrido and terminal carbonyl ligands and between the bridging and terminal carbonyl ligands; these would give a measure of the "openness" of the possible protonation sites. However, in our opinion, in the two hydride complexes these angles, averaging 153(4) and 113.5(9)°, respectively, for the Rh complex, and 155(2) and 119.0(3)° for Ir, do not differ enough to explain the different protonation sites, even though the Ir complex is somewhat more open adjacent to the bridging carbonyl ligand than the Rh analogue. There is one significant difference between the iridium hydride and the above three related A-frame complexes which may have a significant influence on the chemistry; this pertains to the orientations of the phenyl groups. In the three other complexes the diphosphine methylene groups are bent towards the bridging anionic ligands, thereby thrusting four phenyl groups (actually an *ortho* hydrogen from each) into the vacant sites between the bridging and terminal carbonyl ligands. This would effectively block these sites and would instead favour protonation at the sites adjacent to the bridging hydride ligand in $[Rh_2(CO)_2(\mu\text{-}H)(\mu\text{-}CO)(DPM)_2]^+$. The present iridium hydride differs significantly in this regard; its DPM methylene groups bend towards the

TABLE 5. Selected angles (deg) for $[Ir_2(CO)_2(\mu\text{-}H)(\mu\text{-}CO)(DPM)_2][BF_4]$

Bonds	Angle	Bonds	Angle	Bonds	Angle
H1)—Ir(1)—C(1)	155(2)	P(2)—Ir(2)—Ir(1)	92.97(4)	C(71)—P(4)—C(81)	104.5(2)
H(1)—Ir(1)—C(3)	86(2)	P(4)—Ir(2)—Ir(1)	92.65(4)	C(71)—P(4)—Ir(2)	113.7(2)
H(1)—Ir(1)—Ir(2)	37(2)	Ir(1)—H(1)—Ir(2)	105(4)	C(81)—P(4)—C(5)	107.1(2)
H(1)—Ir(1)—P(1)	93(2)	Ir(1)—C(1)—O(1)	178.9(7)	C(81)—P(4)—Ir(2)	114.1(1)
H(1)—Ir(1)—P(3)	87(2)	Ir(2)—C(2)—O(2)	179.4(6)	P(1)—C(4)—P(2)	110.3(3)
H(1)—Ir(2)—C(2)	154(2)	Ir(1)—C(3)—Ir(2)	81.9(3)	P(3)—C(5)—P(4)	110.7(3)
H(1)—Ir(2)—C(3)	87(2)	Ir(1)—C(3)—O(3)	139.5(5)	P(1)—C(11)—C(12)	118.4(2)
H(1)—Ir(2)—Ir(1)	38(2)	Ir(2)—C(3)—O(3)	138.4(5)	P(1)—C(11)—C(16)	121.6(2)
H(1)—Ir(2)—P(2)	92(3)	Ir(1)—P(1)—C(4)	112.9(2)	P(1)—C(21)—C(22)	118.9(2)
H(1)—Ir(2)—P(4)	86(2)	Ir(2)—P(2)—C(4)	112.6(2)	P(1)—C(21)—C(26)	121.1(2)
C(1)—Ir(1)—C(3)	118.4(3)	Ir(1)—P(3)—C(5)	112.0(2)	P(2)—C(31)—C(32)	117.9(2)
C(1)—Ir(1)—Ir(2)	167.6(2)	Ir(2)—P(4)—C(5)	112.5(2)	P(2)—C(31)—C(36)	121.7(2)
C(1)—Ir(1)—P(1)	87.5(2)	C(11)—P(1)—C(4)	105.8(3)	P(2)—C(41)—C(42)	119.1(2)
C(1)—Ir(1)—P(3)	88.6(2)	C(11)—P(1)—C(21)	104.3(2)	P(2)—C(41)—C(46)	120.8(2)
C(2)—Ir(2)—C(3)	119.5(3)	C(11)—P(1)—Ir(1)	115.0(1)	P(3)—C(51)—C(52)	118.8(2)
C(2)—Ir(2)—Ir(1)	168.3(2)	C(21)—P(1)—C(4)	103.2(3)	P(3)—C(51)—C(56)	121.2(2)
C(2)—Ir(2)—P(2)	88.5(2)	C(21)—P(1)—Ir(1)	114.6(1)	P(3)—C(61)—C(62)	119.6(2)
C(2)—Ir(2)—P(4)	88.0(2)	C(31)—P(2)—C(4)	104.5(3)	P(3)—C(61)—C(66)	120.1(2)
C(3)—Ir(1)—Ir(2)	49.2(2)	C(31)—P(2)—C(41)	106.4(2)	P(4)—C(71)—C(72)	118.8(2)
C(3)—Ir(1)—P(1)	96.4(2)	C(31)—P(2)—Ir(2)	112.9(1)	P(4)—C(71)—C(76)	121.1(2)
C(3)—Ir(1)—P(3)	93.8(2)	C(41)—P(2)—C(4)	102.8(3)	P(4)—C(81)—C(82)	119.5(2)
C(3)—Ir(2)—Ir(1)	48.8(2)	C(41)—P(2)—Ir(2)	116.5(1)	P(4)—C(81)—C(86)	120.5(2)
C(3)—Ir(2)—P(2)	97.3(2)	C(51)—P(3)—C(5)	102.9(3)	F(1)—B(1)—F(2)	111(1)
C(3)—Ir(2)—P(4)	93.6(2)	C(51)—P(3)—C(61)	105.0(2)	F(1)—B(1)—F(3)	100(2)
P(1)—Ir(1)—P(3)	169.70(6)	C(51)—P(3)—Ir(1)	118.5(1)	F(1)—B(1)—F(4)	108(2)
P(1)—Ir(1)—Ir(2)	92.69(4)	C(61)—P(3)—C(5)	105.3(2)	F(2)—B(1)—F(3)	103(2)
P(3)—Ir(1)—Ir(2)	93.15(4)	C(61)—P(3)—Ir(1)	112.0(2)	F(2)—B(1)—F(4)	126(2)
P(2)—Ir(2)—P(4)	168.87(6)	C(71)—P(4)—C(5)	104.2(2)	F(3)—B(1)—F(4)	106(1)

bridging CO ligand, and four phenyl groups (1,4,5, and 8) block the sites adjacent to the bridging hydride ligand. Two of the *ortho* hydrogen – iridium contacts are less than 3.02 Å and are much less than those contacts on the other side of the dimer where all are greater than 3.7 Å. Although the short Ir—H contacts are not particularly unusual (rhodium – *ortho* hydrogen contacts of ca. 2.8 Å are observed in Wilkinson's compound (21)) they are shorter than those in the rhodium analogue of our compound (2), where the shortest such contact is 3.18 Å, but more importantly they are on the *opposite* face of the dimer. If the observed solid state structures were maintained in solution, the reason for the apparently different protonation sites would seem to be clear; in the rhodium compound the *ortho* hydrogens of four phenyl groups block the sites *opposite* the bridging hydride ligand whereas in the iridium analogue the sites *adjacent* to the hydride ligand are blocked. However, the structures in solution will *not* be static and might be expected to fluctuate between the two extremes observed for the Rh and Ir compounds. Nevertheless, a difference in energy of only a few kilojoules per mole between the two extremes will have a very significant effect on the equilibrium concentration of these species. We therefore propose that the solid state structure observed for the iridium complex is the more thermodynamically favoured in solution (for which we can offer no explanation). This would tend to favour subsequent protonation at the site *opposite* the bridging hydride ligand. It may also be that with the Rh complex the thermodynamically favoured protonation product has the two hydride ligands mutually *cis* (before reductive elimination of H_2) whereas for Ir the favoured product has the two hydride ligands mutually *trans*. Again, it is worth reemphasizing that the ir spectrum of the crystals studied is very similar to that in solution, suggesting that there are no major differences between the solid state structure and the structure in solution.

The observed structural differences between the compounds, $[M_2(CO)_2(\mu\text{-}H)(\mu\text{-}CO)(DPM)_2]^+$ (M = Rh, Ir), have other potentially relevant consequences regarding modelling of rhodium-catalyzed reactions by the iridium analogues. Although this approach can yield useful information, caution must be taken not to extend analogies too far. We can see this in the two hydrides being discussed and in their potential reactions with substrate molecules such as olefins; with the rhodium compound, a substrate molecule reacting adjacent to the bridging hydride group is in a position for hydride migration (yielding an alkyl species) to occur, whereas with the iridium analogue it is conceivable that the substrate molecule might coordinate *trans* to the hydride ligand and consequently *not* be in a position for a facile hydride migration. Clearly the chemistry would then differ. We are currently pursuing these ideas.

Acknowledgments

We thank the University of Alberta and the Natural Sciences and Engineering Research Council of Canada (NSERC) for support of this work and NSERC for a graduate scholarship to B.R.S. and for partial funding of the diffractometer through a grant to M.C.

1. B. R. SUTHERLAND and M. COWIE. Organometallics, **4**, 1637 (1985).
2. C. P. KUBIAK, C. WOODCOCK, and R. EISENBERG. Inorg. Chem. **21**, 2119 (1982).
3. R. G. PEARSON. Chem. Rev. **85**, 41 (1985).
4. R. J. DOEDENS and J. A. IBERS. Inorg. Chem. **6**, 204 (1967).
5. M. COWIE and B. R. SUTHERLAND. Inorg. Chem. **23**, 2324 (1984).
6. D. T. CROMER and J. T. WABER. International tables for X-ray crystallography. Vol. IV. Kynoch Press, Birmingham, England. (1974). Table 2.2A.
7. R. F. STEWART, E. R. DAVIDSON, and W. T. SIMPSON. J. Chem. Phys. **42**, 3175 (1965).
8. D. T. CROMER and D. J. LIBERMAN. J. Chem. Phys. **53**, 1891 (1970).
9. R. J. PUDDEPHATT. Chem. Soc. Rev. 98 (1983).
10. B. R. SUTHERLAND and M. COWIE. Inorg. Chem. **23**, 2324 (1984).
11. B. R. SUTHERLAND and M. COWIE. Organometallics, **3**, 1869 (1984).
12. B. R. SUTHERLAND and M. COWIE. Submitted to Organometallics.
13. C. P. KUBIAK, C. WOODCOCK, and R. EISENBERG. Inorg. Chem. **19**, 2733 (1980).
14. R. COLTON and M. J. MCCORMICK. Cord. Chem. Rev. **31**, 1 (1980).
15. R. BAU, R. G. TELLER, S. W. KIRTLEY, and T. F. KOETZLE. Acc. Chem. Res. **12**, 176 (1979).
16. R. G. TELLER and R. BAU. Structure and bonding. Vol. 44. Springer-Verlag, Berlin. 1981. pp. 1–82.
17. D. M. HOFFMAN and R. HOFFMANN. Inorg. Chem. **20**, 3543 (1981).
18. M. COWIE. Inorg. Chem. **18**, 286 (1979).
19. B. R. SUTHERLAND and M. COWIE. Inorg. Chem. **23**, 1290 (1984).
20. G. MINGHETTI, A. L. BANDINI, G. BANDITELLI, F. BONATI, R. SZOSTAK, C. E. STROUSE, C. B. KNOBLER, and H. D. KAESZ. Inorg. Chem. **22**, 2332 (1983).
21. M. J. BENNETT and P. B. DONALDSON. Inorg. Chem. **16**, 655 (1977).

A bonded polyoxyethylene phase for gas and liquid chromatography[1]

PALITHA P. WICKRAMANAYAKE[2] AND WALTER A. AUE[3]
Department of Chemistry, Dalhousie University, Halifax, N.S., Canada B3H 4J3
Received July 14, 1983[4]

PALITHA P. WICKRAMANAYAKE and WALTER A. AUE. Can. J. Chem. **64**, 470 (1986).

Bonded phases were produced by reacting 2,4,7,9-tetramethyl-5-decyne-4,7-bis(polyethyleneoxide 30 mol) ether (Surfynol® 485) with silicic supports of high and low surface area. There is circumstantial evidence (a) that the nonextractable layer is held by multiple hydrogen bonding and (b) that the synthesis of these packings involves a reaction at the crosslinking site of the surfactant. The bonded phases, with layer thicknesses between 10 and 30 Å, were tested with three chromatographic techniques. In gas–solid chromatography, the phase proved well deactivated and yielded a reduced plate height of 2.5 (using a silica gel support). In gel permeation chromatography, polyethyleneglycols eluted within the mobile-phase volume. In liquid–solid (normal-phase adsorption) chromatography, the elution pattern differed significantly from that of unmodified silica gel. In each case, high-efficiency separations were obtained. The chromatographic experiments thus demonstrated the potential usefulness of the new phase for both gas and liquid chromatography. However, it was not tested in direct comparison with conventional phases nor was its utility established by subjecting it to routine analytical use.

PALITHA P. WICKRAMANAYAKE et WALTER A. AUE. Can. J. Chem. **64**, 470 (1986).

On a préparé des phases liées en faisant réagir du Surfynol® 485 avec des supports siliciques possédant des surfaces élevées ou basses. Des preuves circonstancielles permettent de croire (a) que la phase qui ne peut pas être extraite est liée par des liaisons hydrogènes multiples et (b) que la synthèse des ces garnissages implique une réaction au site de réticulation de l'agent de surface. On a vérifié l'utilité des phases liées, dont l'épaisseur varie entre 10 et 30 Å, en faisant appel à trois techniques chromatographiques. Dans la chromatographie gaz–solide, la phase s'avère bien désactivée et conduit à une hauteur réduit de plateau de 2,5 (en utilisant un support de gel de silice). Dans la chromatographie par perméation de gel, les polyéthylèneglycols sont élués avec le volume de la phase mobile. Dans la chromatographie liquide–solide (adsorption de phase normale), les caractéristiques de l'élution diffèrent beaucoup de celles observées avec une gel de silice qui n'a pas été modifié. Dans tous les cas, on a obtenu des séparations avec une grande efficacité. Les expériences chromatographiques ont donc démontrées l'usage potentiel de la nouvelle phase tant en chromatographie liquide que gazeuse. Toutefois, on ne l'a pas évalué par comparaison directe avec des phases conventionnelles et on n'a pas établi non plus son utilité en la soumettant à des utilisations analytiques de routine.

[Traduit par le journal]

Introduction

Ever since we described the "unexpected behavior of a common gas chromatographic phase" (1) in forming thin, nonextractable layers on typical gc supports, we wondered if polymers other than Carbowax-20M (CW-20M) could be used to achieve an equally surprising performance. A variety of materials were tried, from other polyethers to polyesters, silicones, and even hydrocarbons (2–5). Some rivaled, but none excelled, CW-20M.

The "bonded" layers made from this modified polyethyleneglycol (as well as from other common liquid phases) have rather interesting uses and properties (6–34). As far as one can tell from the commercial literature, similar separation media have been produced under different trade names by a variety of chromatographic supply houses and, more recently, by HNU, Dow (35). The high-temperature bonding technique has also been used with great success for the deactivation of, and the formation of insoluble layers in, glass capillaries (36–40).

It is primarily this aspect of deactivation that has made the bonded layers valuable for gas chromatography. In liquid chromatography, deactivation is usually a matter of choosing a suitable solvent mixture. Hence, it is not surprising that, as far as we can tell, these particular CW-20M-based phases have not found significant use in hplc.

Typical hplc phases are, of course, produced by reacting the silica surface with silane *monomers* (41–45). Still, several reports can be found in the literature of *polymers* being bonded to microparticulate supports. Of particular interest in the present context are early syntheses using short-chain polyethyleneglycols (46, 47) in analogy to the esterification of silica with alcohols (48), and the more recent development of cross-linked polyethyleneimine layers (49, and references quoted therein).

Our heat-treated, CW-20-M-based layer was assumed to derive its nonextractability (i.e., its bonded character) primarily from the polymer stretching out on the surface. Nonextractability was postulated to arise from multi-point sorption coupled with conformational changes in the chain, which made it orient to, and fit the silicic surface at minimum potential energy (27, 32). The multi-point contacts were presumed to involve hydrogen bonds between surface silanols and polyether oxygens.

Such hydrogen bonding is, of course, well-known and has been exploited to a variety of ends (50). To cite a chromatographic example, polyethyleneglycols and similar materials are frequently used to prevent denaturation and irreversible adsorption of proteins in size exclusion chromatography (51–53, and references therein). The distinguishing feature of the heat-treated Carbowax phase is, however, that a thin (≈15 Å on Chromosorb W) layer remains affixed to the surface even through week-long continuous extractions with protic solvents such as methanol.

More recent support for the postulated conformational

[1]Material taken in part from thesis of P.P.W. (Dalhousie University, 1980) and presented at the 64th Chemical Institute of Canada Conference, Halifax, N.S., June 1981.

[2]Present address: Division of Chemistry, National Research Council, Montreal Road, Ottawa, Ont., Canada K1A 0R6.

[3]To whom correspondence should be addressed.

[4]Revision received November 8, 1985.

changes induced by heat treatment (32) has come from interesting ir studies of Kaiser and Chase (54). The authors also claimed that the infrared spectra showed the terminal hydroxyls of the Carbowax entering ester bonds with the surface silanols.

Such a reaction is, of course, to be expected under aprotic conditions (48), provided the polymer did indeed contain terminal hydroxyls. If the heat-treated layers were extracted with, say, toluene, such terminal bonds should persist. If they were extracted with, say, methanol, the ester bonds should hydrolize (really, methanolize). As far as the bonded character of the layer is concerned, terminal ester linkages contribute, if at all, in a rather insignificant way; to wit, if nonextractability were primarily due to silicic ester bonds, the layer could not be stable to extended extraction by boiling methanol.

Whether in a synthetic, chromatographic, or analytical context, one can appreciate the potential magnitude of the two effects, terminal hydroxyl esterification versus hydrogen bonding of chain oxygens, by formally comparing the number of hydroxyls to the number of ether linkages in the polymer. Taking for demonstration a fictional, OH-terminated polyethyleneglycol of about 20 000 molecular weight, there are 227 —O— groups for a single —OH.

To characterize further the nature of the thin, bonded layers derived from CW-20M would clearly pose an interesting challenge. The present state of knowledge can perhaps be most aptly defined as reasonable conjecture. In a wider context, layers oriented within the range of surface forces are fascinating though complex objects of study. The interests involved range from basic investigations in physical chemistry (55, 56) and chromatography (57–65), over biological interfaces, adhesive joints, and the oceans' top layer, to dishwashing (66, 67). Some physicochemical aspects of thin layers, as seen by gas chromatography, have been reviewed (68). Not unexpectedly, the best performing of these systems exhibit a polarity lower than that of the polymer from which they originated. Furthermore, they are generally superior to conventional glc packings in resolving positional isomers; and their resistance to mass transfer in the stationary phase is very low.

Also of interest in this discussion is the excellent gas chromatography of alcohols on the CW-20M-based columns. A simple argument will show why. Alcohols often elute with poor peak shapes from conventional separation media, and this is commonly blamed on the interaction of their hydroxyl groups with the silanols of the silicic support. Now, one can exhaustively treat such a support with a small silanizing reagent. On the resulting thin, organic layer, atop mostly "capped" silanol groups, alcohols (of the same or larger size than the silanizing reagent) usually do migrate similarly with broad and (or) asymmetric concentration profiles. Compare this with the highly efficient alcohol chromatography on a Carbowax-modified surface, even though the latter kept its silanol groups intact (though partly hydrogen-bonded) under a comparably thin polyether layer. Clearly this situation is not adequately explained by the current conceptual framework.

The search for a new liquid phase to be used in the synthesis of improved bonded layers obviously raises the question of what constitutes improvement. In terms of one particular criterion, heat stability, this search has been successful. Verzele and coworkers developed a type of polyethyleneglycol free of polymerization catalyst and therefore of considerably higher stability (69). These low-bleed "Superox" phases have found extensive use as Carbowax substitutes. Similar to CW-20M, they can deactivate glass capillary columns (40). When used in our experiments like CW-20M on Chromosorb W, the material bonded well and the layer remaining after exhaustive extraction could be heated overnight at 300°C without loss of chromatographic performance.

With this exception, CW-20M has been by far the best of any polyethylene or polypropylene glycol tested. The only interesting fact to note from past attempts to find a superior material is that certain short polypropyleneglycol chains performed comparatively well with a wide-pore silica gel such as Davison grade 62. (The analogous reaction with CW-20M is troublesome since a high concentration of polymer is required and the support particles tend to stick together. There may also have been some difficulty for CW-20M molecules to migrate into some of the narrower pores, as discussed later.)

The unique structural characteristic of CW-20M among the polyethyleneglycols (including "linear CW-20M") is that it is "prepared by joining together two 7500 molecular weight alpha-*hydro*-omega-hydroxypoly(oxyethylene) molecules with a diepoxide" (70). That puts an aromatic "kink" in the structure and the obvious question arises whether this kink has anything to do with CW-20M's superior bonding ability.

The diepoxide employed for making CW-20M (as well as a series of other conventional cross-linking agents with two or more oxirane functional groups) did show some evidence of bonding when subjected to the same conditons as CW-20M in preliminary experiments. Without exception, however, the chromatographic performance was very poor. This suggested that the polyethyleneglycol chains were necessary for producing a chromatographically efficient layer. Furthermore, phases synthesized from CW-20M often had a phenol-like smell, a possible indication that (parts of) the cross-linking agent had indeed been liberated from its chains. Why this should lead to better bonding is not immediately clear. As far as the search for a competitor to CW-20M is concerned, however, it made empirical sense to look for a smaller molecule containing two polyethyleneglycol chains with a kink in the middle.

Fortunately, we became aware of an inexpensive commercial material that seemed to fit the bill. Figure 1 shows the structure of 2,4,7,9-tetramethyl-5-decyne-4,7-bis(polyethyleneoxide) 30 mol) ether. The material is known by its trademark as Surfȳnol® 485, a surfactant made by Air Products (71). Its acetylenic cross-linking agent, 2,4,7,9-tetramethyl-5-decyne-4,7-diol is also used as a surfactant, and is marketed as Surfȳnol® 104 (71). The performance of Surfȳnol 104 in bonding experiments was mediocre at best, not unlike that of its aromatic counterpart in CW-20M. Surfȳnol 485, on the other hand, did very well indeed.

Experimental

Chromosorb W, 45–60 mesh, and silica gel 62, 100–120 mesh, were exhaustively acid-washed. Lichrosorb and Lichrospher Si-100, 10 μm, were used as received.

The synthesis of the bonded phases was carried out in refluxing hexadecane under nitrogen as described earlier for CW-20M (4), followed by exhaustive extraction with methanol in a high-speed apparatus (72). Unless otherwise noted, Surfȳnol was added at 6 weight% load to Chromosorb and at 60% load to the other supports. Elemental analyses were carried out by Guelph Chemical Laboratories, Guelph, Ont.; surface area determinations were done by Micromeritics, Norcross, GA.

Gas chromatographic columns were 100 × 0.2 cm id, except as noted, and liquid chromatographic columns were 10 × 0.4 cm id. The latter were packed by the balanced-density method using tetrabromoethane and carbon tetrachloride.

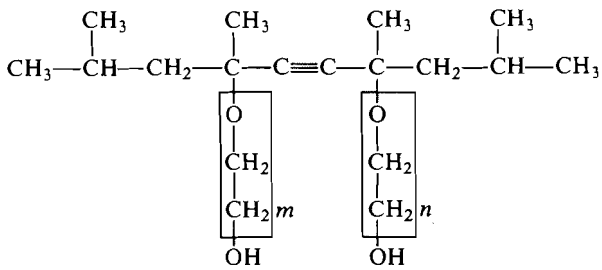

$(m + n) = 30 \rightarrow$ SURFYNOL® 485
$(m + n) = 0 \rightarrow$ SURFYNOL® 104

FIG. 1. Structure of two Air Products Surfynol® surfactants.

Ancillary experiment

The Si—OH group of both Chromosorb W and silica gel 62 were converted to Si—NH_2 by a modification of Peri's method (73). Typically, the support was treated in a quartz tube at 800°C for 2 h with a stream of chlorine and nitrogen. After cooling in nitrogen, a stream of ammonia was turned on and the temperature raised to 700°C where it remained for 1 h with ammonia, and a further hour with pure nitrogen flowing. The support was then allowed to cool in nitrogen. Treatment of this support with water liberated ammonia. Bonding of Surfynol and other compounds to the dry material was carried out as described above.

Results and discussion

The ancillary experiment with aminated silicic surfaces provided additional, though circumstantial, support for the multipoint sorption (as opposed to the terminal ester linkage) model of polyethyleneglycol (PEG) bonding: If there are no more silanol groups to be found on the surface, the ester bonding mechanism cannot be used to account for any extraction-resistant PEG layer.

On the other hand, hydrogen bonds between the ether oxygens and the surface amino groups would still be expected to exist, although being obviously weaker than those formed with surface hydroxyls. Therefore, one expects to find that bonding is possible, but that the resulting phase is chromatographically inferior. In part this should be due to the easier extraction of polymer by, or possible reaction of silamine groups with, methanol, and to the reduced stability of the phase against atmospheric moisture.

These expectations are borne out by the gas chromatographic test shown in Fig. 2. There is clear evidence of an organic layer, but alcohols elute with peak shapes noticeably worse than those of alkanes. In other words, the phase is not sufficiently deactivated.

In contrast, Surfynol 485 on regular, i.e., hydroxylated, Chromosorb W elutes alcohols with much better peak shape. Figure 3 shows this chromatography, which is equivalent to that obtained from CW-20M derived layers (and significantly better than those from a variety of conventional polyethyleneglycols and polyethyleneoxides of lower and higher molecular weight than CW-20M).

Elemental analysis shows 0.14% C, which translates to a layer thickness of ~26 Å on a (nominal) 1 m^2/g support. Carbowax phases on this type of support are generally considered to hold 0.1–0.2% polymer load (25). Elemental analysis is stretched to the limit here, but from the evidence available it seems that the Surfynol-derived layer is roughly comparable to (or perhaps a bit thicker than) the Carbowax-based film.

The heat stability of the Surfynol 485 phase is also comparable: an overnight exposure to 280°C did not destroy the chromatographic properties of this column. (However, for practical purposes, 250–260°C is likely to prove a more reasonable upper temperature limit. Also, as with CW-20M columns, the carrier gas should be essentially free of oxygen.)

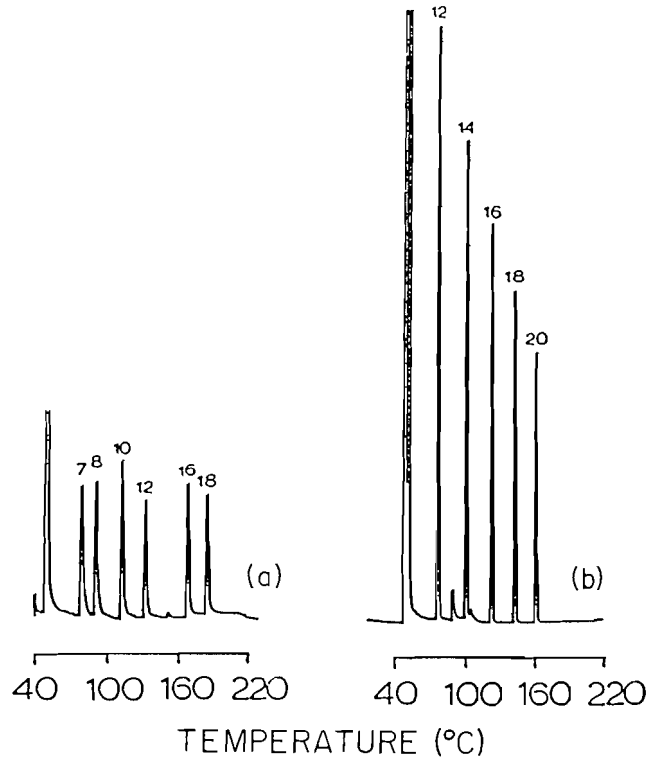

FIG. 2. Gas chromatography of (*a*) *n*-alkanols (carbon numbers 7, 8, 10, 12, 16, 18) and (*b*) alkanes (12, 14, 16, 18, 20) in an 8°C/min temperature program from 40 to 220°C on surface-aminated Chromosorb W, 45–60 mesh, modified with Surfynol 485.

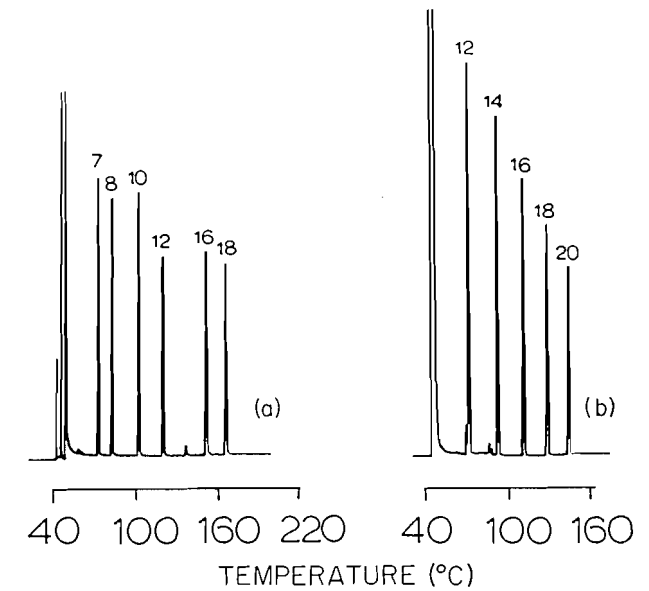

FIG. 3. Gas chromatography similar to that shown in Fig. 2 for (*a*) *n*-alcohols and (*b*) *n*-alkanes but on regular Chromosorb W modified with Surfynol 485.

Thus the gas chromatographic performance of Surfynol 485 and CW-20M does indeed turn out to be comparable on Chromosorb W. This lends credence to prior speculation that the presence of a cross-linking agent between two polyethylene-

glycol chains is conducive to obtaining a high-performance chromatographic phase by heat treatment. Aside from the reasons given earlier for believing in a rupture of link and chains, the following ancillary experiments support the viewpoint of a chemical change in the polymer during heat treatment.

Surfynol is typically bonded in boiling hexadecane (i.e., at 287°C). Similar runs with octadecane (316°C) or even eicosane (343°C) lead to a comparable product. Lower-boiling alkanes such as dodecane (216°C), however, do not. There the phase is yellow, bleeds heavily in the gas chromatograph, and changes with time in analyte retention. Only after conditioning at 250°C does it eventually settle down.

If Surfynol 485 is coated in heavy load, heat-treated in an inert atmosphere and then extracted (similar to the earlier procedure used on CW-20M, (1)), the gas chromatographic performance of the resulting material is poor and reminiscent of a thermosetting resin layer. For obvious reasons, no further experiments were conducted with that material.

In refluxing hexadecane, Surfynol 485 works as well as CW-20M on diatomaceous supports. But that would be of more academic than practical interest. However, Surfynol is decidedly superior to CW-20M on high-surface-area supports such as silica gels used for gas–solid or liquid chromatography.

For one, Surfynol can be used in the bonding reaction in almost any amount without fear of particle agglomeration. Subsequent extraction is easy and fast. This was demonstrated by adding Surfynol 485 to silica gel 62 at different weight ratios. The ratios were 0.3 (insufficient), 0.6, and 1.2. The latter 60 and 120% levels yielded essentially identical polymer loads.

The 60% material was subjected to prolonged extraction, monitored in this case for demonstration purposes. Right after the bonding reaction, and a few fast washes to remove the hexadecane, the phase's carbon content was about 16%. After about 10 h of continuous extraction with fast-flowing, hot methanol, it reached its final level of 15%, which it maintained for the duration of the experiment (40 h). Obviously, a long extraction is unnecessary for this material: a few washes will essentially do the job.

The carbon content corresponds to a layer of about 14 Å, which is significantly thicker than any achieved by using CW-20M. (This nominal layer thickness is less than the 26 Å mentioned above for the Chromosorb-based material. This is in agreement with the general trend of bonded layers to turn out thicker on low-surface-area supports (74). Assuming the elemental analyses to be reliable, 14 Å is, in fact, larger than would have been expected for analogous (74) extrapolation from 26 Å.)

Chromatographically that means a well-deactivated phase. And, indeed, as seen in Fig. 4, such solutes as 1-pentanol, hexanol, and heptanol separate with acceptable peak shapes, a behaviour rarely found with silica gel packings of (nominal) 300 m^2/g surface area.

This is still not a practical alcohol column, but it could serve very well for low-resolution work with highly volatile organics if one wants to avoid subambient programming. Figure 5 demonstrates this with a (composite) separation of *n*-alkanes from methane to tridecane starting at room temperature. A somewhat more applied example is shown in Fig. 6, the low-resolution chromatography of super unleaded gasoline.

Treatment with Surfynol 485 reduces the interaction of silica gel 62 even with alkanes: the bonded phase is somewhat less retentive; but it is more efficient, as shown in Fig. 7 by a comparison of Van Deemter plots. The solute nonane was run

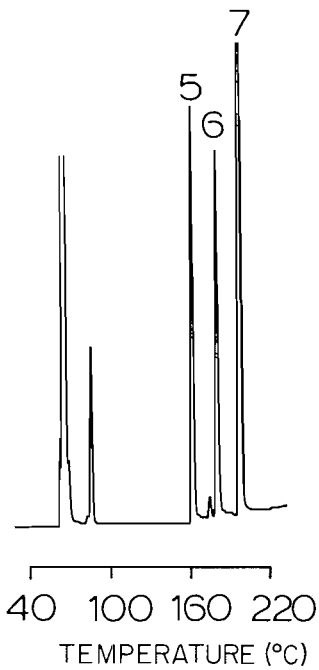

FIG. 4. Temperature-programmed gas chromatography of 1-pentanol, hexanol, and heptanol on modified silica gel 62.

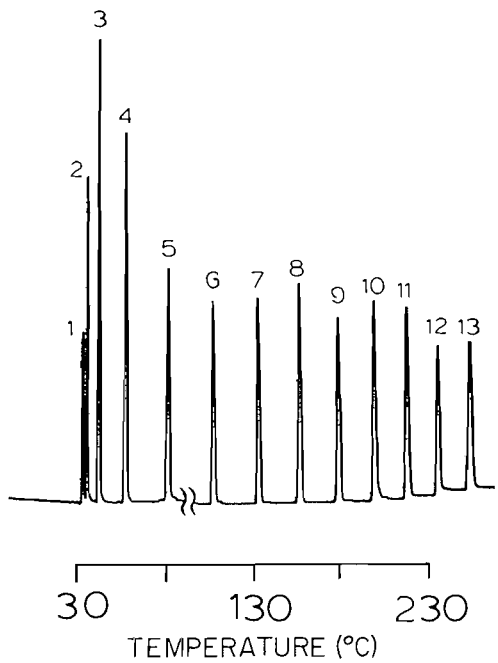

FIG. 5. Temperature-programmed gas chromatography of *n*-alkanes from methane to tridecane on modified silica gel 62, 100–120 mesh. Composite picture using a C-1–C-5 gas mixture and a C-6–C-13 solution. Column: 2 m × 2.1 mm id.

at 90°C on plain silica gel (upper curve) and at 80°C on the modified material (lower curve) in order to obtain roughly similar retention. The minimum plate height corresponds to about 2.5 particle diameters (i.e., a reduced plate height of 2.5), which is not all that far from the theoretically attainable limit.

The only disadvantage of the phase noted so far is its type of bleed. It made it unsuitable for high-sensitivity gc-ms analysis. Perhaps this bleed could be reduced by freeing the material of its polymerization catalysts, similar to the approach of Verzele *et*

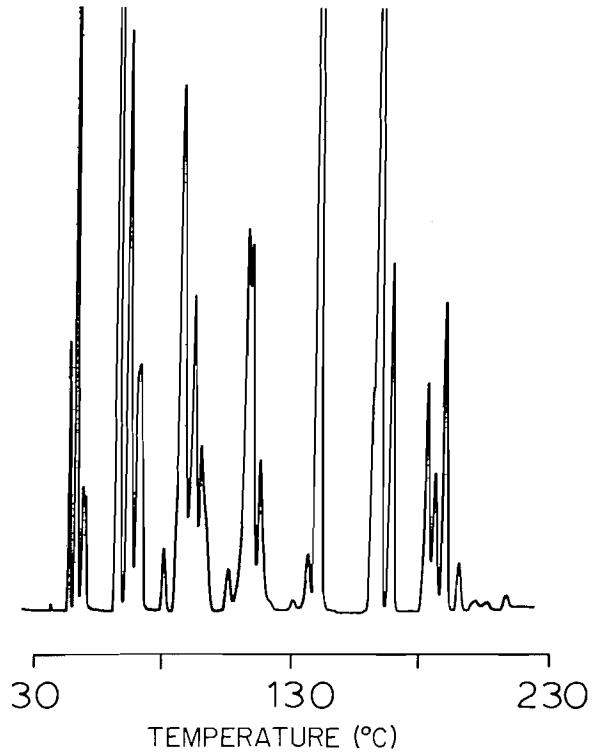

FIG. 6. Gas chromatography of super unleaded gasoline. Conditions as in Fig. 5.

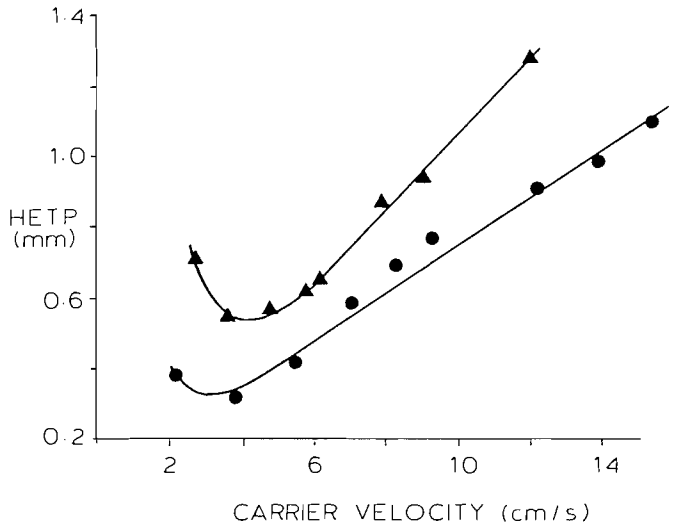

FIG. 7. Van Deemter plot for nonane at 90°C on plain (▲) and at 80°C on Surfynol 485 modified (●) silica gel 62, 100–120 mesh.

al. (69). The wetting ability of Surfynol 485 should make it an interesting candidate for the production of heat-immobilized layers of capillaries, similar to the earlier transfer of such technology from packed columns of CW-20M, SE-30, etc., but this possibility was not investigated.

Rather than investigating capillary gc, it was of greater interest at this stage to have a look at the performance of Surfynol-treated silica gel in liquid chromatography. It is obvious that the material would not serve well as a reversed phase (RP). It is easily wetted by water and, although RP-type behaviour can be observed under suitable conditions, the performance is poor. Besides, as Horvath has pointed out (75), it is possible to force even plain silica gel into RP behaviour.

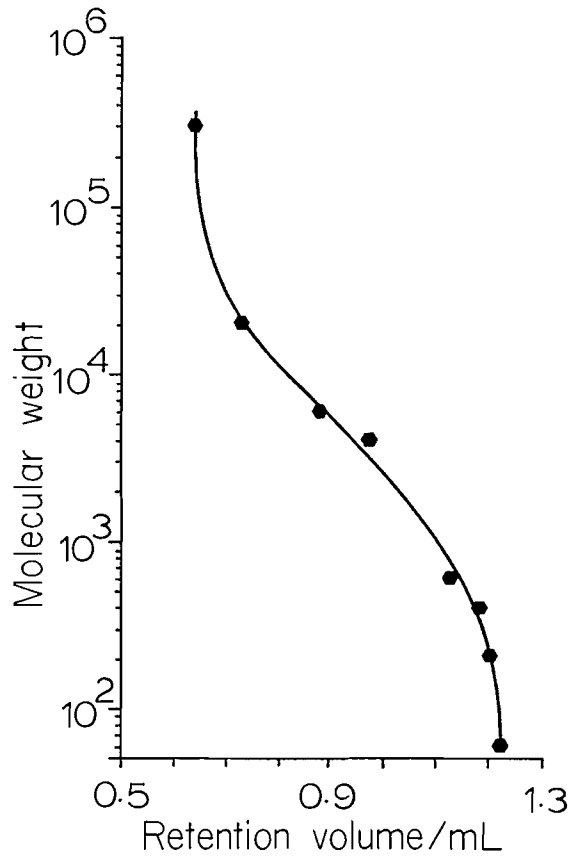

FIG. 8. Size exclusion chromatography of polyethyleneglycol molecular-weight standards, using methanol at 0.2 mL/min, a 0.4 × 10 cm column packed with 10 μm Lichrospher Si-100, and a refractive index detector. The Lichrospher particles were modified with Surfynol 485.

The more interesting aspect to pursue was the deactivated nature of the surface, even though, as mentioned before, deactivation in liquid chromatography is usually a question of choosing the right *mobile* phase.

A well-known problem in gel permeation chromatography is the undesirable sorption of hydrophilic molecules on silica-based surfaces (51–53). As a test, polyethyleneglycol molecular weight standards were chromatographed in methanol. The resulting calibration curve is shown in Fig. 8, corresponding to what one would expect from pure size-exclusion behaviour on a support of this porosity (76). It would have been interesting to follow this lead with more demanding analytes, enzymes for instance, to test for denaturation effects, etc. However, this was considered outside our primary area of interest.

Incidentally, Fig. 8 also provides an explanation, at least in part, why Surfynol 485 worked much better than CW-20M. This experiment used a Si-100 support and, for comparison, silica gel 62 has a mean pore diameter of 170 Å (77). It is obvious that the pores would have excluded intact CW-20M to a large extent while admitting the much smaller Surfynol 485. In this respect it may be worthwhile to mention that Surfynols of shorter polyethyleneglycol chains are available and these may be even better suited for treating narrow pores. (It bears repeating, however, that "regular" polyethyleneglycols of lower molecular weights, while showing evidence of bonding, gave inferior chromatographic performance.)

Another area of hplc where one would expect a modification of the surface to make a difference, is straightforward adsorp-

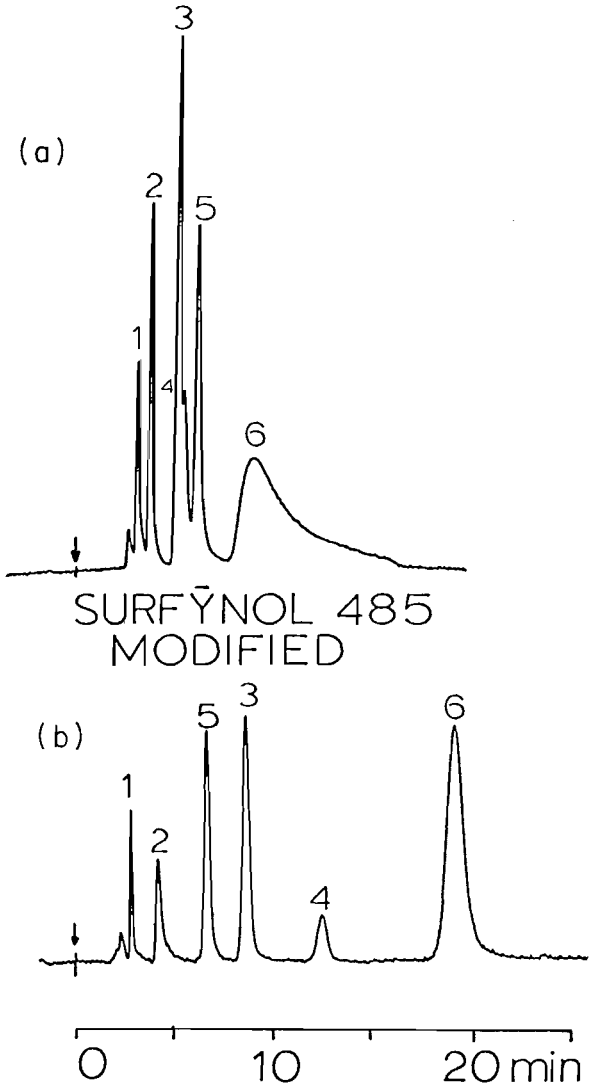

FIG. 9. Liquid–solid chromatography, using chloroform at 0.4 mL/min through a 0.4 × 10 cm column packed with 10 μm Lichrosorb Si-100 in (*a*) unmodified and (*b*) modified form. Peak designations are (1) *o*-chloroaniline, (2) *m*-chloroaniline, (3) phenol, (4), *p*-chlorophenol, (5) *p*-methoxyphenol, and (6) *p*-nitrophenol.

tion chromatography. That this is indeed so is shown in Fig. 9. Not only are the peak shapes different but the retention order itself shifts. It is not immediately obvious what effects did bring about these observed changes. One can think of a more homogeneous or a less acidic surface, one can envision different water retention by the particles, one can focus on the adsorbent properties of altered silanol groups on the surface or the additional ether oxygens in the layer, or one can speculate on the increased organic nature of the interface region. More experiments would have to be done to confirm or deny the applicability of such concepts to the case at hand and to capitalize on any that can be verified. Of more immediate importance, however, is to establish whether or not the new phase is sufficiently different from silica gel in selectivity across a wide range of solutes. Also important may be possible differences in response to water content of the mobile phase and in everyday ease of handling. In other words, the practical advantage of using such a phase in hplc still needs to be established.

Acknowledgments

This study was supported by the Natural Sciences and Engineering Research Council of Canada grant No. A-9604. We thank M. Verzele for a gift of Superox and M. Chinoy of Air Products for generous samples of Surfynol 104 and 485.

1. W. A. AUE, C. R. HASTINGS, and S. KAPILA. J. Chromatogr. **77**, 299 (1973).
2. C. R. HASTINGS, J. M. AUGL, S. KAPILA, and W. A. AUE. J. Chromatogr. **87**, 49 (1973).
3. W. A. AUE, C. R. HASTINGS, and S. KAPILA. Abstracts, IUPAC International Congress on Analytical Chemistry. Kyoto, Japan. April 1972. p. 83. Abstr. B1415.
4. M. M. DANIEWSKI and W. A. AUE. J. Chromatogr. **147**, 119 (1978).
5. T. R. EDGERTON and R. F. MOSEMAN. J. Chromatogr. Sci. **18**, 25 (1980).
6. F. W. KARASEK and H. H. HILL, JR. Research/Development. Dec. 1975. p. 30.
7. Z. SUPRYNOWICZ and J. Å. JÖNSSON. Chromatographia, **14**, 455 (1981).
8. A. A. AKHREM, G. V. AVVAKUMOV, and O. A. STREL'CHYONOK. J. Chromatogr. **176**, 207 (1979).
9. A. N. KOROL and T. I. DOVBUSH. J. Chromatogr. **238**, 291 (1982).
10. E. J. LORAH and D. D. HEMPHILL. J. Ass. Off. Anal. Chem. **57**, 570 (1974).
11. R. C. HALL and D. E. HARRIS. J. Chromatogr. **169**, 245 (1979).
12. W. L. WINTERLIN and R. F. MOSEMAN. J. Chromatogr. **153**, 409 (1978).
13. S. MORI. J. Chromatogr. **135**, 261 (1977).
14. K. LEKOVA, L. KARDJIEVA, A. ATANASOV, and V. NATAN. J. Chromatogr. **177**, 363 (1979).
15. H. L. CRIST and R. F. MOSEMAN. J. Chromatogr. **160**, 49 (1978).
16. R. F.MOSEMAN. J. Chromatogr. **166**, 397 (1978).
17. F. W. KARASEK, M. F. TCHIR, and W. D. BOWERS. J. Chromatogr. **151**, 321 (1978).
18. S. O. FARWELL and S. J. GLUCK. Anal. Chem. **52**, 1968 (1980).
19. C. R. FONTAN and H. H. HILL, JR. J. Chromatogr. **170**, 249 (1979).
20. A. N. KOROL, G. M. BELOKLEYTSEVA, and G. V. FILONENKO. J. Chromatogr. **194**, 145 (1980).
21. K. O. GERHARDT and W. A. AUE. J. Chromatogr. **82**, 382 (1973).
22. S. KAPILA, W. A. AUE, and J. M. AUGL. J. Chromatogr. **87**, 35 (1973).
23. C. R. HASTINGS, J. M. AUGL, S. KAPILA, and W. A. AUE. J. Chromatogr. **87**, 49 (1973).
24. C. R. HASTINGS and W. A. AUE. J. Chromatogr. **89**, 369 (1974).
25. W. A. AUE and D. R. YOUNKERS. J. Chromatogr. **88**, 7 (1974).
26. W. A. AUE, C. R. HASTINGS, and K. O. GERHARDT. J. Chromatogr. **99**, 45 (1974).
27. M. M. DANIEWSKI and W. A. AUE. J. Chromatogr. **147**, 395 (1978).
28. M. M. DANIEWSKI and W. A. AUE. J. Chromatogr. **150**, 506 (1978).
29. W. A. AUE and M. M. DANIEWSKI. J. Chromatogr. **151**, 11 (1978).
30. C. R. VOGT and W. A. AUE. J. Chromatogr. Sci. **16**, 268 (1978).
31. W. A. AUE, M. M. DANIEWSKI, and E. E. PICKETT. J. Chromatogr. **189**, 13 (1980).
32. W. A. AUE, C. R. HASTINGS, and S. KAPILA. Anal. Chem. **45**, 725 (1973).
33. W. A. AUE and P. P. WICKRAMANAYAKE. J. Chromatogr. **197**, 21 (1980).
34. P. P. WICKRAMANAYAKE and W. A. AUE. J. Chromatogr. **210**, 133 (1981).
35. T. J. NESTRICK, R. H. STEHL, J. N. DRISCOLL, L. F. JARAMILLO, and E. S. ATWOOD. Industrial Research and Development. Nov. 1980. p. 126.
36. D. A. CRONIN. J. Chromatogr. **97**, 263 (1974).
37. L. BLOMBERG. J. Chromatogr. **115**, 365 (1975).

38. E. SCHULTE. Chromatographia, **9**, 315 (1976).
39. K. GROB. J. Chromatogr. **168**, 563 (1979), and references cited therein.
40. R. F. ARRENDALE, R. F. SEVERSON, and O. T. CHORTYK. J. Chromatogr. **208**, 209 (1981).
41. R. E. MAJORS. J. Chromatogr. Sci. **18**, 488 (1980).
42. E. GRUSHKA (*Editor*). Bonded stationary phases in chromatography. Ann Arbor Science, Ann Arbor, MI. 1974.
43. E. GRUSHKA and E. J. KITKA, JR. Anal. Chem. **49**, 1004A (1977).
44. K. K. UNGER. Porous silica, Elsevier, Amsterdam. The Netherlands. 1979.
45. R. K. ISLER. The chemistry of silica. John Wiley, Toronto, Ont. 1979. pp. 677–710.
46. M. UIHLEIN and I. HALÁSZ J. Chromatogr. **80**, 1 (1973).
47. WATERS ASSOCIATES. Company literature, Waters Associates, Milford, MA. U.S.A.
48. R. K. ISLER. The chemistry of silica. John Wiley, Toronto, Ont. 1979. pp. 573, 689.
49. A. A.ALPERT and F. E. REGNIER. J. Chromatogr. **185**, 375 (1979).
50. R. K. ISLER. The chemistry of silica. John Wiley, Toronto, Ont. 1979.p. 395.
51. R. V. VIVILECCHIA, B. C. LIGHTBODY, N. Z. THIMOT, and H. M. QUINN. J. Chromatogr. Sci. **15**, 424 (1977).
52. H. D. CRONE, R. M. DAWSON, and E. M. SMITH. J. Chromatogr. **103**, 71 (1975).
53. S. D. ABBOT. American Laboratory. Aug. 1977. p. 14.
54. M. A. KAISER and D. B. CHASE. Anal. Chem. **52**, 1849 (1980).
55. J. C. HENNIKER. Rev. Mod. Phys. **21**, 322 (1949).
56. F. R. EIRICH. J. Colloid. Interface Sci. **58**, 423 (1977).
57. A. V. KISELEV. J. Chromatogr. **49**, 84 (1970).
58. J. SERPINET. J. Chromatogr. **68**, 9 (1972).
59. A. WAKSMUNDZKI and J. RAYSS. J. Chromatogr. **119**, 557 (1976).
60. R. R. STROMBERG, D. J. TUTAS. and E. PASSAGLIA. J. Phys. Chem. **69**, 3955 (1965).
61. J. C. GIDDINGS. Anal. Chem. **34**, 458 (1962).
62. F. BRUNER, P. CICCIOLI, G. CRESCENTINI, and M. T. PISTOLESI. Anal. Chem. **45**, 1851 (1973).
63. A. DI CORCIA and A. LIBERTI. Adv. Chromatogr. **14**, 305 (1976).
64. A. V. KISELEV, N. V. KOVALEVA, and YU. S. NIKITIN. J. Chromatogr. **58**, 19 (1971).
65. M. RYBA. Chromatographia, **9**, 105 (1976).
66. M. C. BOURNE and W. G. JENNINGS. Food Technol. (Chicago), **15**, 495 (1961).
67. R. M. ANDERSON, J. J. SATANEK, and J. C. HARRIS. J. Am. Oil Chem. Soc. **36**, 286 (1959).
68. J. R. CONDER and C. L. YOUNG. Physicochemical measurement by gas chromatography. John Wiley, Toronto, Ont. 1979. pp. 516–520.
69. M. VERZELE and P. SANDRA. J. Chromatogr. **158**, 111 (1978).
70. UNION CARBIDE CORPORATION. Carbowax polyethylene glycols. Interim Reprint F-4772F, 11/68-5M. 1968.
71. AIR PRODUCTS AND CHEMICALS, INC. Bulletins Surfȳnol® 104 and Surfȳnol® 400 series. Box 538, Allentown, PA. 18105, U.S.A.
72. W. A. AUE, P. P. WICKRAMANAYAKE, and J. MÜLLER. Anal. Chim. Acta, **125**, 175 (1981).
73. J. B. PERI. J. Phys. Chem. **70**, 2937 (1966).
74. P. P. WICKRAMANAYAKE and W. A. AUE. J. Chromatogr. **195**, 25 (1980).
75. C. HORVATH, W. MELANDER, and A. NAHUM. 13th International Symposium on Chromatography. Cannes, France. July 1980.
76. W. A. DARK and A. J. LIMPERT. J. Chromatogr. Sci. **11**, 114 (1973).
77. P. D. KLEIN. Anal. Chem. **34**, 733 (1962).

Crystal structure of tris(*o*-phenylenethiourea)selenium(II) bromide pentahydrate, $C_{21}H_{18}N_6S_3Br_2Se \cdot 5H_2O$

SP. CHIDAMBARAM AND G. ARAVAMUDAN

Department of Chemistry, Indian Institute of Technology, Madras - 600 036, India

AND

G. C. ROUT AND M. SESHASAYEE[1]

Department of Physics, Indian Institute of Technolgy, Madras - 600 036, India

Received January 31, 1985[2]

SP. CHIDAMBARAM, G. ARAVAMUDAN, G. C. ROUT, and M. SESHASAYEE. Can. J. Chem. **64**, 477 (1986).

The synthesis and crystal structure of the title complex are reported. Crystals are triclinic, space group $P\bar{1}$ with $a = 10.359(2)$, $b = 10.742(2)$, and $c = 13.604(2)$ Å, $\alpha = 87.25(1)$, $\beta = 88.89(1)$, $\gamma = 83.63(2)°$, and $Z = 2$. The structure was solved by the heavy atom method and refined by least squares to final R and R_w of 0.055 and 0.06 for 1707 unique reflections. The structure is comprised of planar $[Se_2(o\text{-phenylenethiourea})_6]^{4+}$ ions and bromide counterions with the water molecules providing extensive lattice stabilization through hydrogen bonding. The dinuclear complex arises by the fusion of two SeS_4 trapezoids with each Se bonded strongly to two terminal sulfur atoms Se—S(1) = 2.306(4), Se—S(3) = 2.286(5) Å and weakly to two other bridging sulfur atoms Se—S(2) = 2.840(5) and Se—S(2)′ = 2.852(5) Å.

SP. CHIDAMBARAM, G. ARAVAMUDAN, G. C. ROUT et M. SESHASAYEE. Can. J. Chem. **64**, 477 (1986).

On rapporte la synthèse et la structure cristalline du complexe mentionné dans le titre. Les cristaux sont tricliniques et cristallisent dans le groupe d'espace $P\bar{1}$ avec $a = 10,359(2)$, $b = 10,742(2)$, et $c = 13,604(2)$ Å, $\alpha = 87,25(1)$, $\beta = 88,89(1)$, $\gamma = 83,63(2)°$, et $Z = 2$. On a résolu la structure par la méthode des atomes lourds et on l'a affiinée par la méthode des moindres carrés jusqu'a des valeurs finales de R et R_w de 0,055 et 0,06 pour 1707 réflexions uniques. La structure comporte des ions plans de $[Se_2(o\text{-phénylènethiourée})_6]^{4+}$ et des contre-ions bromures avec des molécules d'eau qui fournissent une stabilisation importante de la maille par le biais de liaisons hydrogènes. Le complexe binucléaire provient de la fusion de deux SeS_4 sous forme de trapézoïdes dans lesquels chacun des Se est fortement lié aux deux atomes de soufre terminaux (Se—S(1) = 2,306(4) et Se—S(3) = 2,286(5) Å) et faiblement lié à deux autres atomes de soufre qui agissent comme ponts (Se—S(2) = 2,840(5) et Se—S(2)′ = 2,852(5) Å).

[Traduit par le journal]

Introduction

The interaction of selenium(IV) species with sulfur ligands has gained immense importance due to the formation of the Se(II)–sulfur ligated complexes which have been shown to be intermediates in the biochemical role of selenium (1, 2). Generally the interaction of selenium(IV) with sulfur containing ligands leads either to (*a*) reductive complexation, that is, reduction of selenium(IV) to selenium(II) and formation and stabilization of selenium(II) complexes with sulfur ligands (eg., thiosulphate (3), xanthates (4), dithiocarbamates (5), thiobenzoic acid (6), mercaptocarboxylic acids (7)) or to (*b*) reduction to elemental selenium (eg., hydrogen sulphide, thiourea). Very recently, with the use of concentrated hydrochloric acid medium, the highly unstable complex *cis*-dichlorobis(thiourea)-selenium(II) was isolated (8), and its structure determined. We have found (9) that, unlike thiourea, interaction of *o*-phenylenethiourea (ptu) with Se(IV) species leads to ready formation of Se(II) complexes, which are indefinitely stable at room temperature. In this paper we report the synthesis and structure of tris(*o*-phenylenethiourea)selenium(II) bromide pentahydrate. The structure consists of novel planar Se_2S_6 units (the first of its kind to be reported in Se(II) complexes with unidentate ligands) containing four moderately strong Se—S terminal bonds and four loose bridging Se—S bonds with each Se(II) displaying a trapezoidal sulfur coordination.

Experimental

Preparation of the complex

The reaction used for the preparation of the complex is

[1] 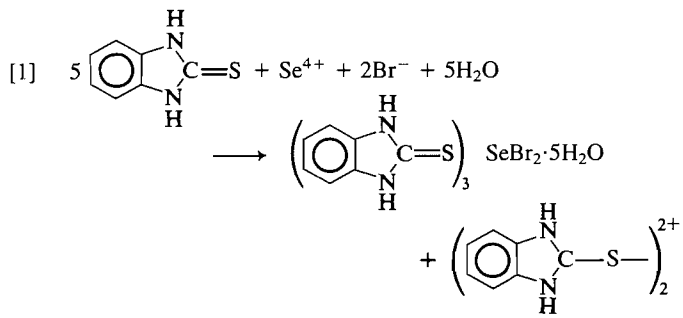

SeO_2 (BDH, 0.5 mmol (0.055 g)) dissolved in 3 mL of methanol and of *o*-phenylenethiourea (Aldrich Co. 99% pure, 3 mmol (0.45 g)) dissolved in 15 mL of methanol were mixed in the presence of 12.5 mL of 2 *N* hydrobromic acid. The yellow solution obtained, gave needle shaped, yellow-orange crystals of the title complex on evaporation at room temperature (30°C). *Anal.* calcd.: Se 10.14, Br 20.54, S 12.32, N 10.78. C 32.24, H 3.59; found: Se 10.09, Br 20.48, S 12.34, N 10.70, C 32.21, H 3.96. To prevent contamination with excess ligand or oxidized product, the crystals formed were washed with ether. The crystals were extremely stable when preserved in paraffin. In dry atmosphere, the crystals turned opaque and brittle due to loss of water of crystallization.

It is interesting to report that the disulfide oxidation product in reaction [1] was found to undergo disproportionation rapidly under acidic conditions to *o*-phenylenethiourea and a 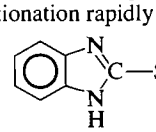 species, determination of whose composition and detailed characterization is in progress.

Crystal data (at 23°C)

$C_{21}H_{18}N_6S_3Br_2Se \cdot 5H_2O$ fw = 779.4

Triclinic, $a = 10.359(2)$, $b = 10.742(2)$, and $c = 13.604(2)$ Å, $\alpha =$

[1]To whom correspondence should be addressed.

[2]Revision received October 18, 1985.

87.25(1), β = 88.89(1), γ = 83.63(2)°, V = 1502.6 Å^3. Space group $P\bar{1}$, Z = 2, F(000) = 919.99, D_x = 1.72 Mg m^{-3}, μ(MoK$_\alpha$) = 4.11 mm^{-1}. Preliminary cell constants were obtained from Weissenberg photographs and a crystal of size 0.42 × 0.25 × 0.22 mm was mounted on a Enraf–Nonius CAD 4 diffractometer. Graphite monochromated MoK$_\alpha$(λ = 0.71069 Å) radiation was used. Lattice parameters were determined by least-squares refinement of θ values of 25 high angle reflections. The intensity data were collected by ω–2θ scan technique with scan interval Δω = (0.80 + 0.35 tan θ)°, extended by 25% on both sides for background measurements. Two check reflections ($42\bar{6}$ and $06\bar{1}$) recorded at the end of every hour of data collection time, showed no significant variation in intensity. A total of 5763 reflections were collected in the range of 2 < θ < 25° (h, 0–12; k, −12–12; l, −16–16). The 1707 reflections with $I > 3\sigma(I)$ formed a unique set. R_{int} equalled 0.01 after merging 123 reflections. No correction was made for absorption.

The SHELX-76 program (10) was used for all the computations done in solving the structure. Se and Br atoms were located from a Patterson map and the rest of the structure from Fourier maps. The function minimized in full matrix least-squares refinement was $\Sigma\omega(\Delta F)^2$. All but seven of the hydrogen atoms appeared in the final difference Fourier maps and were refined isotropically. Maximum peak height in the final difference Fourier map was 0.73 e Å^{-3}, maximum and average shift/esd in all non-hydrogen atom parameters were 1.615 and 0.022 in the final refinement cycle. Convergence was reached at R = 0.055 and R_w = 0.06 where w (the weighting scheme used) = $1/(\sigma^2(F_o) + 0.0599|F_o|^2)$.

Though the crystal used was of good quality as shown by the photographs and reflection profiles, only 30% of the possible reflections were observed, indicating that the diffractometer alignment should have been better, which would have yielded better quality data. This is also reflected in the large shift/esd in refinement, the data/parameter ratio being only 4.0.

Atomic scattering factors for non-hydrogen atoms, hydrogen atoms, and anomalous scattering factors are taken from refs. 11, 12, and 13, respectively.

The final positions are given in Table 1. Table 2 contains the bonding parameters in the structure. Fig. 1 was drawn using the ORTEP (14) program[3].

TABLE 1. The fractional atomic coordinates (×10^4) and equivalent thermal parameters (×10^3 Å^2) of nonhydrogen atoms

Atoms	X	Y	Z	U_{eq}
Se	314(1)	6884(2)	4733(1)	36(1)
Br(1)	3227(3)	373(3)	7944(2)	116(1)
Br(2)	−2208(2)	4556(2)	2614(2)	83(1)
S(1)	−1142(4)	8672(4)	4721(3)	48(2)
S(2)	1825(4)	4509(4)	4807(3)	44(1)
S(3)	2148(4)	7833(4)	4383(3)	45(1)
C(1)	−1336(17)	8785(13)	5999(12)	44(6)
N(1)	−2517(14)	8856(13)	6434(11)	51(6)
N(2)	−379(14)	8914(12)	6661(10)	42(5)
C(11)	−2288(18)	8990(15)	7439(14)	45(7)
C(12)	−1020(16)	9021(15)	7580(12)	47(6)
C(13)	−437(21)	9136(17)	8507(14)	62(8)
C(14)	−1337(23)	9202(19)	9280(15)	65(9)
C(15)	−2645(24)	9168(20)	9171(15)	72(9)
C(16)	−3244(22)	9082(17)	8250(16)	71(8)
C(2)	1976(17)	4425(16)	3548(12)	41(6)
N(3)	3110(12)	4456(13)	3046(10)	37(5)
N(4)	1018(12)	4244(12)	2918(9)	32(4)
C(21)	2905(18)	4336(15)	2051(14)	46(7)
C(22)	1579(16)	4253(14)	1962(13)	39(6)
C(23)	980(20)	4114(17)	1043(11)	55(7)
C(24)	1849(21)	4107(19)	228(13)	58(8)
C(25)	3156(22)	4277(18)	333(14)	63(8)
C(26)	3707(18)	4363(17)	1247(15)	56(7)
C(3)	2346(16)	7685(15)	3103(11)	42(6)
N(5)	3518(13)	7763(13)	2661(10)	50(6)
N(6)	1466(13)	7525(13)	2458(10)	44(5)
C(31)	3369(18)	7695(16)	1679(14)	44(7)
C(32)	2132(16)	7545(16)	1508(14)	46(6)
C(33)	1598(20)	7443(16)	575(14)	59(7)
C(34)	2460(22)	7492(19)	−207(15)	58(8)
C(35)	3744(26)	7682(18)	−46(16)	81(10)
C(36)	4267(19)	7769(17)	904(15)	93(8)
O(1)	−4969(15)	8784(21)	5646(12)	136(9)
O(2)	2309(16)	8322(14)	6648(12)	102(7)
O(3)	5293(15)	4494(30)	4079(13)	205(15)
O(4)	5777(14)	7665(18)	3714(12)	120(8)
O(5)	−1145(15)	7354(15)	2218(11)	100(7)

Results and discussion

Crystals of Se(ptu)$_3$Br$_2$·5H$_2$O are yellow-orange in colour, this being attributed to typical charge transfer bands. The compound is stable as such or when suspended in 2 N hydrobromic acid, but undergoes an immediate self-redox decomposition to Se and an oxidized product of the ligand when immersed in alkaline solution. The infrared spectrum of the complex does not have distinctive differences from that of the ligand which would enable positive conclusions regarding the coordination behaviour of the ptu ligand in the complex.

Figure 1 shows the ORTEP picture of the molecule. Only half of the centrosymmetrical [Se$_2$(ptu)$_6$]$^{4+}$ unit is featured in full. Additionally, the selenium and three sulfur atoms belonging to the other half are also shown for reasons of clarity. The structure is made up of an [Se$_2$(ptu)$_6$]$^{4+}$ cation, bromide counterions, and five water molecules of crystallization. In each cation, selenium, the soft acid site, is bonded to four phenylenethiourea ligands exclusively through sulfur atoms, the soft base site. The dinuclear complex arises by the fusion of two SeS$_4$ trapezoids with each selenium bonded strongly to two terminal sulfur atoms Se—S(1) = 2.306(4), Se—S(3) = 2.286(5) Å and weakly to two other bridging sulfur atoms Se—S(2) = 2.840, Se—S(2)′ = 2.852 Å. The SeS$_4$ group is planar to within 0.007 Å. The S—Se—S angles deviate substantially from 90°. The dihedral angle between the two SeS$_4$ trapezoids is nearly zero (0.03 (20)°). It is the first time in selenium(II) chemistry that a dimeric structure is reported with monodentate sulphur ligands. A [Te$_2$S$_6$]$^{4+}$ dimer with similar molecular geometry was reported (15) in the compound Te(tu)$_3$(HF$_2$)$_2$ (tu = thiourea).

It is interesting to comment on the coordination types of sulfur ligands reported till now around Se(II). The coordination number is observed to be two (bent) or four (square planar or trapezoidal). In two coordinated Se(II) complexes, the Se—S bond lengths are close to the sum of single covalent radii of selenium and sulfur (2.11 Å) as reported in refs. 3, 6, 7, 8, 16, and 17. This is because the ligands in these cases are mostly negatively charged and unidentate, and there are only two sulfur ligands bonded to selenium. In Se(S$_2$COCH$_3$)$_2$ (4) xanthate provides four sulfur atoms around the central metal atom selenium, two of these sulfurs (bridging ligands) are quite far from selenium so that their interaction with selenium is very weak, enabling the other thiolatosulfurs to bond strongly. Complexes such as Se(S$_2$CNC$_4$H$_8$O$_2$)$_2$ (5) and Se[N(Ph$_2$PS)$_2$]

[3]Anisotropic thermal parameters, bond lengths, and angles of the hydrogen atoms, mean plane calculations, and the structure factor tables may be purchased from the Depository of Unpublished Data, CISTI, National Research Council of Canada, Ottawa, Ont., Canada K1A 0S2.

TABLE 2. Bond lengths (Å) and bond angles (°), esd in parentheses

Atoms	Bond length	Atoms	Bond length
Se—S(1)	2.306(4)	C(21)—C(22)	1.394(25)
Se—S(2)	2.840(4)	C(22)—C(23)	1.428(24)
Se—S(3)	2.286(5)	C(23)—C(24)	1.414(26)
S(1)—C(1)	1.755(17)	C(24)—C(25)	1.397(32)
C(1)—N(1)	1.345(23)	C(25)—C(26)	1.390(29)
C(1)—N(2)	1.375(23)	C(26)—C(21)	1.362(24)
N(1)—C(11)	1.398(25)	C(3)—N(5)	1.354(21)
N(2)—C(12)	1.408(21)	C(3)—N(6)	1.308(21)
C(11)—C(12)	1.354(25)	N(3)—C(21)	1.389(24)
C(12)—C(13)	1.425(26)	N(4)—C(22)	1.414(21)
C(13)—C(14)	1.390(29)	N(5)—C(31)	1.354(24)
C(14)—C(15)	1.371(35)	N(6)—C(32)	1.454(23)
C(15)—C(16)	1.420(31)	C(31)—C(32)	1.335(26)
C(16)—C(11)	1.463(29)	C(32)—C(33)	1.408(27)
S(2)—C(2)	1.723(17)	C(33)—C(34)	1.378(30)
C(2)—N(3)	1.350(21)	C(34)—C(35)	1.391(36)
C(2)—N(4)	1.360(22)	C(35)—C(36)	1.422(31)
S(3)—C(3)	1.762(16)	C(36)—C(31)	1.398(27)

Atoms	Angle	Atoms	Angle
S(2)—Se—S(3)	89.9(2)	C(2)—N(3)—C(21)	110(1)
S(1)—Se—S(2)	172.6(2)	C(2)—N(4)—C(22)	107(1)
S(1)—Se—S(3)	97.6(2)	N(3)—C(21)—C(22)	106(1)
S(1)—Se—S(2′)	87.6(2)	N(4)—C(22)—C(21)	108(1)
S(2)—Se—S(2′)	85.0(3)	C(21)—C(22)—C(23)	123(1)
S(3)—Se—S(2′)	174.8(2)	C(22)—C(23)—C(24)	114(1)
Se—S(1)—C(1)	97.8(7)	C(23)—C(24)—C(25)	122(1)
S(1)—C(1)—N(1)	121(1)	C(24)—C(25)—C(26)	122(1)
S(1)—C(1)—N(2)	127(1)	C(25)—C(26)—C(21)	117(1)
C(1)—N(1)—C(11)	106(1)	Se—S(3)—C(3)	102.9(6)
C(1)—N(2)—C(12)	105(1)	S(3)—C(3)—N(5)	121(1)
N(1)—C(11)—C(12)	109(1)	S(3)—C(3)—N(6)	128(1)
N(2)—C(12)—C(11)	108(1)	N(5)—C(31)—C(32)	109(1)
C(11)—C(12)—C(13)	125(1)	N(6)—C(32)—C(31)	107(1)
C(12)—C(13)—C(14)	113(1)	C(31)—C(32)—C(33)	126(1)
C(13)—C(14)—C(15)	124(2)	C(32)—C(33)—C(34)	115(1)
C(14)—C(15)—C(16)	124(2)	C(33)—C(34)—C(35)	120(1)
C(15)—C(16)—C(11)	113(2)	C(34)—C(35)—C(36)	124(1)
Se—S(2)—C(2)	95(1)	C(35)—C(36)—C(31)	115(1)
S(2)—C(2)—N(3)	124(1)	Se—S(2)′—Se′	95.0(2)
S(2)—C(2)—N(4)	126(1)		

(18) though arising from bidentate ligands, are structurally very close to the present case, which have two weaker and two stronger bonds in its four coordination leading to a planar trapezoidal structure. $[Se(ptu)_4]Cl_2 \cdot 2HCl$ (9) is the only complex so far reported in Se(II) chemistry which shows a near square planar coordination. In the present case, in which the same sulfur compound features as the ligand, the smaller number of ligands per Se(II) alters the molecular geometry of SeS_4 coordination from square planar to trapezoidal and also provides a dimeric Se_2S_6 unit. In all the SeS_4 species the average Se—S bond length is 2.53 Å, showing that the Se—S interactions in these complexes are weaker than in two-coordinated complexes. This can be attributed to the larger number of sulfur atoms around selenium in the tetra-coordinated complexes.

The ptu ligands are planar to within 0.04 to 0.07 Å. The C—S distances in the ligands are 1.75(2), 1.72(2), and 1.76(2) Å showing partial double bond character. The C(1)—N(1) and C(1)—N(2); C(2)—N(3) and C(2)—N(4); C(3)—N(5) and C(3)—N(6) pairs show no significant variation in bond lengths, clearly indicating that the ptu ligand in the Se(II) complex occurs exclusively in thione form with the molecular parameters close to those observed in the structure of the free ptu ligand (19), $Se(ptu)_4 \cdot Cl_2 \cdot 2HCl$ (9), and in tellurium(II) complexes of the ligand (20). The ligand in all these cases is present in the thione form. The other bond parameters in the ligands are normal. The average N—H, C—H, and O—H bond lengths are 0.88(7), 0.91(2), and 0.83(1) Å, respectively.

There are two bromide ions per formula unit. The bromines, water oxygens, and nitrogen atoms of ptu ligand form an extensive hydrogen bonding network. Bromine atoms are well outside the coordination sphere of Se and form hydrogen bonds with six water molecules and one nitrogen atom, with Br...O and Br...N distances in the range of 3.08(2)–3.33(2) and 3.35(1) Å, respectively. The angles Br...H—O are in between 157 and 175° and the Br...H—N angle is 128°. Also oxygen

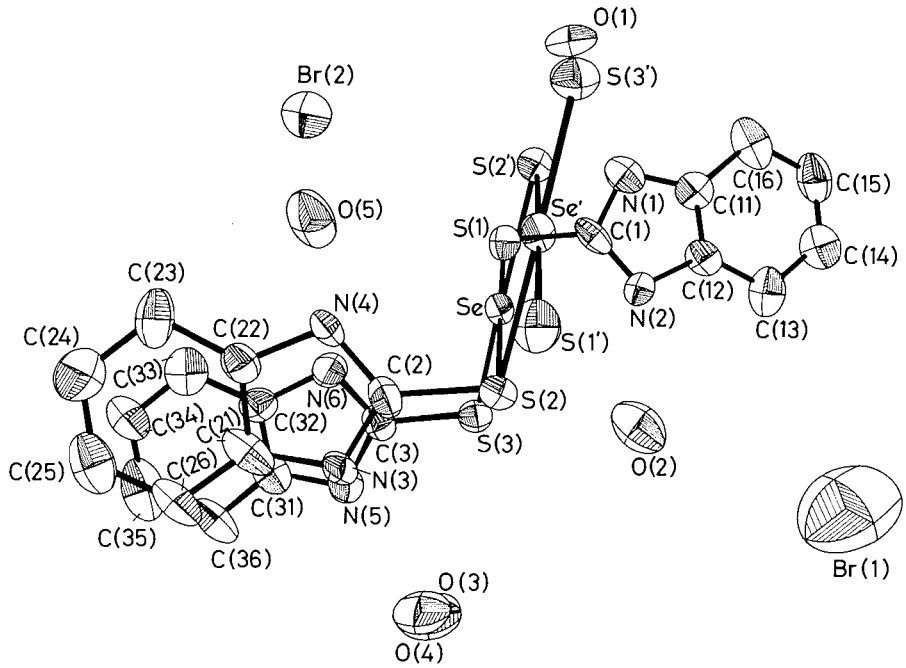

FIG. 1. Perspective view of the molecule showing atomic numbering, with 50% probability thermal ellipsoids.

atoms of water molecules form five hydrogen bonds with nitrogen atoms, as evidenced by the N...O distances of the order of 2.69(2) Å. N—H...O angles range between 163 and 176°. In addition, oxygen atoms among themselves form two hydrogen bonds with O...O distances 2.99(2) and 2.81(3) Å.

1. H. E. GANTHER. Biochemistry, **7**, 2898 (1968).
2. R. J. P. WILLIAMS. New trends in bio-inorganic chemistry. Academic Press, New York. (1978).
3. K. MAROY. Acta Chem. Scand. **26**, 45 (1972).
4. N. J. BRONDMO, S. ESPERAS, H. GRAVER, and S. HUSEBYE. Acta Chem. Scand. **27**, 713 (1973).
5. O. P. ANDERSON and S. HUSEBYE. Acta Chem. Scand. **24**, 3141 (1970).
6. G. ARAVAMUDAN, T. SUBRAHMANYAN, M. SESHASAYEE, and G. V. N. APPA RAO. Polyhedron, **2**, 1025 (1983).
7. G. V. N. APPA RAO, M. SESHASAYEE, G. ARAVAMUDAN, T. NAGESWARA RAO, and P. N. VENKATASUBRAMANIAN. Acta. Crystallogr. Sect B: Struct. Crystallogr. Cryst. Chem. **B38**, 2852 (1982).
8. S. V. BJORNEVAG and S. HAUGE. Acta Chem. Scand. Ser. A, **A37**, 235 (1983).
9. S. SOWRIRAJAN, G. ARAVAMUDAN, M. SESHASAYEE, and G. C. ROUT. Acta Crystallogr. Sect. C: Cryst. Struct. Commun. **C41**, 576 (1985).
10. G. M. SHELDRICK. SHELX program for crystal structure determination. University of Cambridge. England. 1976.
11. D. T. CROMER and J. B. MANN. Acta Crystallogr. Sect. A: Cryst. Phys. Diffr. Theor. Gen. Crystallogr. **A24**, 321 (1968).
12. R. F. STEWART, E. R. DAVIDSON, and W. T. SIMPSON. J. Chem. Phys. **42**, 3175 (1965).
13. D. T. CROMER and D. G. LIBERMAN. J. Chem. Phys. **53**, 1891 (1970).
14. C. K. JOHNSON. ORTEP report ORNL-3794. Oak Ridge National Laboratory. Tennessee. 1965.
15. O. FOSS and S. HAUGE. Acta Chem. Scand. **19**, 2395 (1965).
16. S. M. OHLBERG and P. A. VAUGHAN. J. Am. Chem. Soc. **76**, 2649 (1954).
17. S. FURBERG and P. OYUM. Acta Chem. Scand. **8**, 1701 (1954).
18. S. HUSEBYE and K. M. MOE. Acta Chem. Scand. Ser. A, **A37**, 219 (1983).
19. G. R. FORM, E. S. RAPER, and T. C. DOWNIE. Acta Crystallogr. Sect. B: Struct. Sci. **B32**, 345 (1976).
20. G. C. ROUT, M. SESHASAYEE, G. ARAVAMUDAN, and S. SOWRIRAJAN. J. Crystallogr. Spectrosc. Res. **15**, 375 (1985).

Some physical properties of long chain hydrocarbons

L. T. Chu, Carmen Sindilariu, Aaron Freilich, and Vojtech Fried

Department of Chemistry, The City University of New York, Brooklyn College, Brooklyn, NY 11210, U.S.A.

Received November 27, 1984[1]

L. T. Chu, Carmen Sindilariu, Aaron Freilich, and Vojtech Fried. Can. J. Chem. **64**, 481 (1986).

The densities, refractive indices, and viscosities of liquid *n*-nonadecane and *n*-nonadecyl benzene were investigated at temperatures not too far above their respective melting points. Except for the viscosities, no significant differences were observed in the behavior of the two hydrocarbons. The *n*-nonadecane + *n*-nonadecyl benzene system exhibits small positive excess volumes and small negative excess viscosities. The excess refractive index is zero in the entire concentration range.

L. T. Chu, Carmen Sindilariu, Aaron Freilich et Vojtech Fried. Can. J. Chem. **64**, 481 (1986).

Opérant à des températures juste au-dessus de leur point de fusion respectif, on a mesuré les densités, les indices de réfraction et les viscosités du *n*-nonadécane et du *n*-nonadécyl-benzène liquides. Excepté pour les viscosités, on n'a pas observé de différences significatives dans le comportement de ces deux hydrocarbures. Le système *n*-nonadécane + *n*-nonadécyl-benzène présente de faibles excès positifs des volumes et de faibles excès négatifs des viscosités. L'excès d'indice de réfraction est nul pour toute la gamme des concentrations.

[Traduit par le journal]

Introduction

Long chain aliphatic compounds have been the subject of many investigations. Ralston and coworkers (1, 2) measured the solubilities of long chain organic compounds in solvents of various polarities. They observed that in nonpolar and slightly polar solvents the solubility curves of substituted (with polar groups) aliphatic compounds and of the normal aliphatic compounds of corresponding chain length are qualitatively similar. If this is really so then the shape of the solubility curve depends mainly on the length of the alkyl chain. Seyer (3) observed that the solubility of diacetyl in normal aliphatic solvents, ranging from C_6 to C_{12}, obeys the ideal solubility law. Cáceres and coworkers (4–6) noticed that the excess volumes of *o*-, *m*-, and *p*-xylene solutions with normal aliphatic hydrocarbons vary from negative values for *n*-hexane to relatively large positive values for *n*-hexadecane. Heric and Coursey (7, 8) found that the excess volumes and the excess viscosities of solutions of *n*-hexadecane in 1-*n*-chloroalkanes of different chain length obey the congruence principle (9) very well.

Some normal long chain aliphatic hydrocarbons exhibit unusual behavior in the solid state. Aliphatic hydrocarbons containing from 18 to 36 carbons are polymorphous and undergo a solid–solid phase transition at temperatures slightly above their respective freezing points (10–15). In the higher temperature solid phase, designated as the "rotator phase", the molecules rotate about their long axes. In the lower temperature solid phase, designated as the "rigid phase," the rotation is severely restricted. The rotator phase formed from the melt at the freezing point is metastable and converts after a sufficient time, depending on the chain length, into the more stable low temperature solid rigid phase. Piper *et al.* (11) measured the transition temperatures for a large number of compounds.

To get some insight into the behavior of long chain hydrocarbons, we decided to investigate the physical properties of long chain hydrocarbons in the pure state and in mixtures. For convenience we studied the properties of melts rather than of solids. In this work we deal with the dependence of density (volume), refractive index, and viscosity of *n*-nonadecane (ND) and *n*-nonadecyl benzene (NDB) melts for the pure hydrocarbons and their mixtures.

[1]Revision received October 16, 1985.

Table 1. Some physical properties of *n*-nonadecane at various temperatures

Temp. (°C)	Density (g/cm^3)	Refractive index (n_D)	Viscosity (cp)
35	0.7752	1.4356	3.91
40	0.7719	1.4335	3.49
45	0.7686	1.4314	3.11
50	0.7653	1.4293	2.79
55	0.7620	1.4273	2.51
60	0.7587	1.4252	2.26
65	0.7554	1.4231	2.05
70	0.7521	1.4210	1.86

Experimental

The ND and NDB were Aldrich commercial chemicals of the highest purity (99%+). No impurities were detected in glc measurements of either hydrocarbon. The melting points, measured with an NBS certified mercury in glass thermometer, were in close agreement with the literature values, though we encountered some difficulties in reproducing the melting point of NDB. ND: mp 31.2°C (lit. (12, 16, 17) mp 31-32°C); NDB: mp 25.01°C (lit. (12) mp 24.94 ± 0.03°C).

The densities of the two hydrocarbons and their mixtures were measured pycnometrically with a 25-cm^3 volumetric flask, calibrated with deionized, twice-distilled water. Dissolved air was expelled from the water prior to the calibration. Air buoyancy corrections were employed in all the weighings. Because of the low volatility of both hydrocarbons, evaporation losses were negligibly small and were ignored in the density evaluation. The volumetric flask was placed in a thermostated water bath for 1 h. The temperature of the water bath was monitored with an NBS certified thermometer. The accuracy of the temperature reading was better than ±0.01°C at the lower temperatures and about ±0.02°C at the higher temperatures. The reproducibility of the density measurement was within $\pm 1 \times 10^{-4}$ g cm^{-3} for the pure melts and $\pm 1.5 \times 10^{-4}$ g cm^{-3} for the mixture. To check the accuracy of the method, we took density measurements with cyclohexane at 25°C. All of the measurements were within $\pm 1 \times 10^{-4}$ g cm^{-3} of the literature values (16, 17). The density measurements reported in Tables 1–3 represent averages of five measurements.

The viscosities were measured with an Ostwald-Ubbelohde viscosimeter made from pyrex glass in our glassblowing shop. The flow time in the given temperature interval varied between 400 and 1200 s. The small kinetic energy contributions to the viscosity of the samples were neglected. The viscosity, η, was calculated from the formula $\eta = \nu d =$

Printed in Canada / Imprimé au Canada

TABLE 2. Some physical properties of *n*-nonadecyl benzene at various temperatures

Temp. (°C)	Density (g/cm^3)	Refractive index (n_D)	Viscosity (cp)
35	0.8470	1.4742	9.56
40	0.8439	1.4722	8.33
45	0.8404	1.4702	7.27
50	0.8372	1.4681	6.39
55	0.8339	1.4661	5.62
60	0.8307	1.4641	4.98
65	0.8275	1.4621	4.42
70	0.8242	1.4600	3.94

TABLE 3. Some physical properties of *n*-nonadecane (1) + *n*-nonadecyl benzene (2) mixtures at 40°C

x_1	d_4^{40} ($g\ cm^{-3}$)	n_D	η (cp)
0.0000	0.8439	1.4722	8.33
0.1066	0.8372	1.4688	7.51
0.1924	0.8313	1.4655	7.01
0.4330	0.8145	1.4564	5.74
0.4887	0.8105	1.4543	5.47
0.6377	0.7996	1.4487	4.83
0.7465	0.7915	1.4445	4.38
0.8251	0.7856	1.4416	4.09
1.0000	0.7719	1.4335	3.49

Ctd where ν is the kinematic viscosity, d is the density, and t is the flow time. The viscosimeter constant, C, was determined from the flow time, density, and viscosity of highly purified glycerol ($d_4^{30} = 1.2552$ g cm^{-3}, $\eta = 5.87$ cp (16)). More than usual attention was paid in mounting the viscosimeter in the thermostated bath to ensure that the capillary was vertical. The thermostated bath was the same as that used for the density measurements. The reproducibility of the viscosity measurements was within $\pm 1 \times 10^{-2}$ cp at the lower temperatures and only $\pm 2 \times 10^{-2}$ cp at the higher temperatures. The values reported in Tables 1–3 are averages of at least five measurements.

The refractive indexes were measured with a Zeiss refractometer with a reproducibility of $\pm 1 \times 10^{-4}$ at the lower temperatures and $\pm 2 \times 10^{-4}$ at the higher temperatures. The values reported in Tables 1–3 are averages of five measurements.

Results and discussion

The experimental data are listed in Tables 1–3. The data for density and refractive index were fitted to

$$d = a + b(t/°C - 35°C)$$

$$n_D = a + b(t/°C - 35°C)$$

and for viscosity to

$$\ln \eta = \frac{a}{T} + b$$

The parameters of these expressions, obtained by a least-squares technique, are listed in Table 4.

According to the measured data, the molar volumes and refractive indices of the two hydrocarbons differ, but the rates of volume change and refractive index change with temperature are practically the same for the two hydrocarbons. Thus, with regard to volume and refractive index, the behavior of the two hydrocarbons is similar. If there is some rotational motion still present in the melt, it is not sufficient to cause deviations in the densities and refractive indices of the two hydrocarbons. This is not so when it comes to viscosity. At 35°C, the viscosity of NBD is about 2.4 times as large as that of ND. At 70°C, the viscosity of NDB is only 2.1 times as large as that of ND. Thus, the viscosity of NDB decreases more rapidly with temperature than that of ND. If this trend prevails, the viscosity vs. temperature curves of the two hydrocarbons will intersect. What is responsible for the different viscosity behavior of the two hydrocarbons? ND possesses dispersion forces only while NDB possesses dipole–dipole interaction forces in addition to the dispersion forces. It is our belief that it is the effect of temperature on the dipole–dipole forces (dispersion forces are practically temperature independent) and consequently on the rotational motion of the molecules that is responsible for the different viscosity–temperature behavior of the two hydrocarbons.

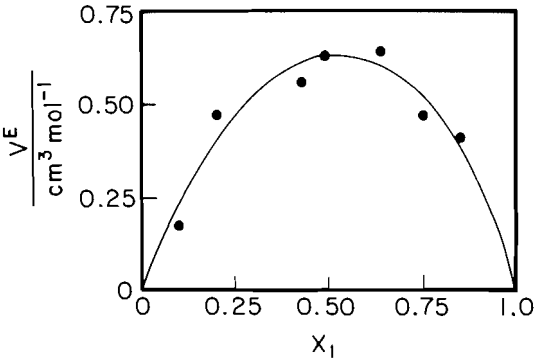

FIG. 1. The excess viscosity of the nonadecane + nonadecyl benzene system at 40°C.

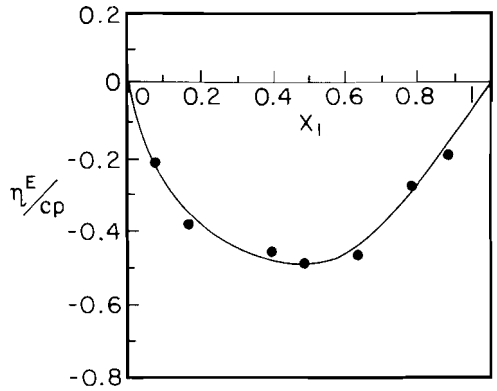

FIG. 2. The excess volume of the nonadecane + nonadecyl benzene system at 40°C.

The densities, refractive indices, and viscosities of the binary ND + NDB system, at 40°C, are given in Table 3. Analysis of the data reveals that the refractive index varies linearly with mole fraction: n_D^E is 0 in the entire concentration range. η^E and V^E are, however, different from zero (see Figs. 1 and 2). The V^E vs. mole fraction curve goes through a maximum and the η^E vs. mole fraction curve goes through a minimum. Because of the large molar masses of the two hydrocarbons, small errors in the densities and mole fractions affect substantially the V^E value ($V^E = (X_1M_1 + X_2M_2)/d - X_1M_1/d_1 - X_2M_2/d_2$). To a smaller extent this is also true for the η^E values.

TABLE 4. The parameters a and b obtained by the least-squares technique and the standard deviation, δ

	n-Nonadecane			*n*-Nonadecyl benzene		
	a	b	δ	a	b	δ
Density	0.7752	-6.60×10^{-4}	$\pm1.0\times10^{-4}$	0.8470	-6.50×10^{-4}	$\pm1.0\times10^{-4}$
Refractive index	1.4356	-4.16×10^{-4}	$\pm1.0\times10^{-4}$	1.4742	-4.05×10^{-4}	$\pm1.0\times10^{-4}$
Viscosity	2248.8	−5.9327	$\pm2.0\times10^{-3}$	2637.1	−6.3031	$\pm2.0\times10^{-3}$

Acknowledgments

The financial support of the Camille and Henry Dreyfus Foundation as well as of a City University of New York FRAP Grant (No. 6-63358) is deeply appreciated. Our special thanks goes to Mr. O. Safferling, our scientific glassblower, for his assistance.

1. A. W. RALSTON, and C. W. HOERR. J. Org. Chem. **9**, 319 (1944).
2. C. W. HOERR, H. J. HARWOOD, and A. W. RALSTON. J. Org. Chem. **9**, 267 (1944).
3. W. F. SEYER. J. Am. Chem. Soc. **60**, 827 (1938).
4. A. M. CÁCERES and D. J. NUÑEZ. J. Chem. Thermodyn. **13**, 1133 (1981).
5. A. M. CÁCERES and D. J. NUÑEZ. J. Chem. Eng. Data, **28**, 61 (1983).
6. A. M. CÁCERES and D. J. NUÑEZ. J. Chem. Eng. Data, **27**, 331 (1982).
7. E. L. HERIC and B.M. COURSEY. Can. J. Chem. **48**, 3911 (1970).
8. B. M. COURSEY and E. L. HERIC. Can. J. Chem. **49**, 2631 (1971).
9. J. N. BRONSTEAD and J. KOEFOED. Mat. Fys. Medd. K. Dan. Vidensk. Selsk. **22**, 1 (1946).
10. E. R. ANDREW. J. Chem. Phys. **18**, 607 (1950).
11. S. H. PIPER, A. C. CHIBNALL, S. J. HOPKINS, A. POLLARD, J. A. B. SMITH and E. F. WILLIAMS. Chem. Abstr. **26**, 2696 (1932).
12. E. F. MEYER and M. C. MEYER. J. Chem. Eng. Data, **28**, 148 (1983).
13. M. G. BROADHURST. J. Res. Natl. Bur. Stand. Sect. A, **66**, 241 (1962).
14. A. A. SCHAERER, C. J. BUSSO, A. E. SMITH and L. B. SKINNER. J. Am. Chem. Soc. **77**, 2017 (1955).
15. A. A. SCHAERER, G. G. BAYLE and W. M. MAZEE. Recl. Trav. Chim. Pays-Bas, **75**, 513 (1956).
16. J. TIMMERMANS. Physico-chemical constants of pure organic compounds. Elsevier, New York. 1950.
17. Handbook of chemistry and physics. 65th ed. Chemical Rubber Co., Cleveland, OH. 1984–1985.

Determination of solubility products of phosphate and vanadate apatites of lead and their solid solutions in 0.165 *M* sodium chloride solution

P. V. R. Rao, S. K. Gupta, and T. S. B. Narasaraju[1]

Department of Chemistry, North-Eastern Hill University, School of Physical Sciences, Shillong 793 003, India

Received November 19, 1984[2]

P. V. R. Rao, S. K. Gupta, and T. S. B. Narasaraju. Can. J. Chem. **64**, 484 (1986).

The solubility products of phosphate and vanadate apatites of lead and seven of their solid solutions, spread over the entire compositional range, were determined in 0.165 *M* sodium chloride solution at 37°C. These solubility products decreased with an increase in vanadium content. A theoretical interpretation was advanced based on changes in lattice and hydration energies resulting from isomorphous ionic substitutions. The aim of the studies was the understanding of the toxic effects of lead and vanadium on the human skeletal system.

P. V. R. Rao, S. K. Gupta et T. S. B. Narasaraju. Can. J. Chem. **64**, 484 (1986).

Opérant à 37°C et dans des solutions à 0,165 *M* de chlorure de sodium, on a déterminé les produits de solubilité du phosphate et du vanadate d'apatites de plomb et de sept de leurs solutions solides qui couvrent le spectre entier de compositions. Ces produits de solubilité diminuent avec une augmentation du contenu en vanadium. On propose une interprétation théorique qui est basée sur des changements dans le réseau et sur les énergies d'hydration qui résultent de substitutions ioniques isomorphes. Le but de ces études était de comprendre les effets toxiques du plomb et du vanadium sur le squelette humain.

[Traduit par le journal]

Introduction

Calcium phosphate apatite (CaPA), $Ca_{10}(PO_4)_6(OH)_2$, the principal inorganic constituent of human bones and teeth (1), undergoes several isomorphous cationic and anionic substitutions involving toxic ions. This constitutes the basis of the incorporation of toxic ions into the human skeletal system. It was established that the toxicity is controlled by the extent of incorporation of toxic ions during the principal bone processes calcification and resorption. Significant among such cationic substitutions has been the replacement of Ca^{2+} by Pb^{2+} forming lead phosphate apatite (PbPA), $Pb_{10}(PO_4)_6(OH)_2$, accounting for the incidence of plumbism, an occupational disease prevalent among workers of potteries and paints. While limited information on $Ca^{2+} \rightleftharpoons Pb^{2+}$ substitution in CaPA was available (2–4), substitution of PO_4^{3-} by VO_4^{3-} leading to the formation of lead vanadate apatite (PbVA), $Pb_{10}(VO_4)_6(OH)_2$, in the context of toxic effects of vanadium (5, 6) on human skeletal system, has not been studied. To investigate the combined effect of Pb^{2+} and VO_4^{3-} on calcification and resorption and to explore the possibility of their reversal, it was decided to study the solubility equilibria of PbPA, PbVA, and seven of their solid solutions spread over the entire compositional range, since these bone processes are controlled by the deposition and dissolution of CaPA at the interface of bone and body fluid. In addition, these studies were intended to clarify a few ambiguities associated with the available results on the solubilities of apatites.

Experimental

PbPA, PbVA, and a series of seven of their solid solutions were prepared through appropriate modifications of a wet method[3] and characterized to be of a high order of purity through X-ray, infrared, electromicroscopic, and thermal analyses, in addition to conventional chemical analyses.[3] The solubility product of each sample was determined at the biologically significant temperature of 37°C by analysis of its saturated solution, the pH of the dissolving medium being maintained constant using suitable buffer combinations. Each system was set up by adding 0.1 g of apatite to potassium hydrogen phthalate – hydrochloric acid buffer of required pH prepared in 100 mL of 0.165 *M* sodium chloride, the latter being needed to maintain the ionic strength of the medium effectively constant (7). Further, 0.165 *M* NaCl was considered as a standard reference solution (8), in which the activity coefficients of the dissolved ionic species could be taken as unity to avoid inaccuracies in their calculations, especially of polyvalent ions, and to enable products of ionic concentration in saturated solution of substances to be taken as their solubility products. Equilibration was carried out through shaking for about 12 h in air-tight polyethylene containers at a regulated speed using a mechanical shaker. The assembly was kept in a thermally insulated cabin maintained at 37 ± 0.5°C. The period of equilibration for attainment of saturation was found to be about 4 h based on a study of dissolution kinetics (9). To be doubly sure about the attainment of saturation, the equilibration period was extended to 12 h, at the end of which the pH of the system was measured. The colloidal component of the solute was separated from the solution by filtration through a 1G4 sintered glass crucible under suction at the temperature of equilibration, the suitability of the sintered glass crucibles for the purpose being verified by comparison with results obtained using colloidal filters (Millipore Filter Corporation, Bedford, U.S.A.) of pore size 10 mμm (10). From the saturated solutions thus obtained, lead was determined complexometrically (9) while phosphate and vanadate were estimated spectrophotometrically (11, 12), a separate aliquot being taken each time. Based on a series of such determinations the error limits were found to be ±1%.

Results and discussion

In Table 1 are included a few representative sets of results on the determination of the solubility products of PbPA, PbVA, and seven of their solid solutions. While the experimentally determined concentrations of lead, phosphorus, and vanadium are given in columns 2 to 4, the concentration of OH^- calculated from the final pH of each system is given in column 5, all the concentrations being taken as synonymous with activities as explained earlier. The gram atom ratios, Pb/P, Pb/V, and Pb/(P + V) calculated from the results of columns 2–4, are reported in column 8 of the table. It is evident that the ionic product K_{ip} of PbPA is equal to the product of the concentrations of the dissolved ions raised to appropriate powers, as given by $[Pb^{2+}]^{10}[PO_4^{3-}]^6[OH^-]^2$. While the concentrations of Pb^{2+} and

[1]Author to whom correspondence should be addressed.

[2]Revison received November 11, 1985.

[3]T. S. B. Narasaraju, S. K. Gupta, and P. V. R. Rao. Private communication.

TABLE 1. Solubility products of phosphate and vanadate apatites of lead and their solid solutions in 0.165 *M* sodium chloride

Sol'n. No. (1)†	Measured conc. (g atom/L) $[Pb] \times 10^4$ (2)	$[P_{Tot}] \times 10^4$ (3)	$[V_{Tot}] \times 10^5$ (4)	Calculated conc. (g ion/L) $[OH^-] \times 10^{11}$* (5)	$[PO_4^{3-}] \times 10^{19}$ (6)	$[VO_4^{3-}] \times 10^{22}$ (7)	Gram atom ratio $\frac{Pb}{P+V}$ (8)	pK_{ip} (9)	Average pK_{ip} (10)
Solute: lead phosphate apatite, $Pb_{10}(PO_4)_6(OH)_2$									
1.	8.200	5.069	—	0.2818	0.614	—	1.62	169.23	
2.	2.970	1.736	—	1.0233	4.758	—	1.72	167.20	
3.	2.480	1.340	—	1.2882	4.968	—	1.85	167.66	
4.	1.982	1.138	—	1.4791	7.116	—	1.74	167.57	167.91
Solute: solid solution no. 1, $Pb_{10}(PO_4)_{5.4}(VO_4)_{0.6}(OH)_2$									
5.	10.000	4.876	12.269	0.3548	1.061	1.143	1.64	168.53	
6.	2.970	1.615	0.393	0.9330	3.588	0.619	1.79	170.26	
7.	2.480	1.453	1.099	1.3200	7.024	4.648	1.59	168.64	
8.	1.790	1.162	0.314	1.4800	7.267	1.846	1.50	170.12	169.39
Solute: solid solution no. 2, $Pb_{10}(PO_4)_{4.5}(VO_4)_{1.5}(OH)_2$									
9.	2.970	1.615	0.982	0.6457	1.519	0.531	1.73	175.75	
10.	2.356	1.421	0.785	1.2590	6.217	2.923	1.57	172.31	
11.	1.988	1.162	0.259	1.5500	8.064	1.741	1.67	172.69	173.58
Solute: solid solution no. 3, $Pb_{10}(PO_4)_{3.69}(VO_4)_{2.31}(OH)_2$									
12.	2.970	1.485	2.110	0.6920	1.645	1.394	1.75	177.39	
13.	2.233	1.292	0.785	1.0700	3.936	1.844	1.63	176.57	
14.	1.988	1.074	2.042	1.5500	7.449	13.716	1.56	173.72	175.89
Solute: solid solution no. 4, $Pb_{10}(PO_4)_3(VO_4)_3(OH)_2$									
15.	2.970	1.615	3.485	0.8320	2.746	3.926	1.51	177.33	
16.	2.236	1.179	1.885	1.2000	4.644	6.137	1.64	176.98	
17.	2.087	1.074	2.788	1.7800	10.077	27.623	1.54	173.97	176.09
Solute: solid solution no. 5, $Pb_{10}(PO_4)_{2.6}(VO_4)_{3.4}(OH)_2$									
18.	9.500	3.713	19.631	0.3020	0.537	1.136	1.67	177.98	
19.	2.970	1.421	4.417	0.7250	1.756	3.343	1.59	179.33	
20.	2.144	0.969	1.220	1.2300	4.039	7.421	1.79	178.23	178.51
Solute: solid solution no. 6, $Pb_{10}(PO_4)_{1.9}(VO_4)_{4.1}(OH)_2$									
21.	2.970	1.292	4.859	0.6760	1.353	2.996	1.67	181.71	
22.	2.285	0.953	2.650	1.0700	2.902	6.224	1.87	180.52	
23.	1.998	0.827	7.852	1.1500	2.927	2.204	2.19	182.90	181.71
Solute: solid solution no. 7, $Pb_{10}(PO_4)_{1.2}(VO_4)_{4.8}(OH)_2$									
24.	1.980	0.517	6.478	0.6610	0.512	3.734	1.70	185.40	
25.	1.394	0.355	3.926	1.3489	1.324	11.914	1.86	183.50	184.45
Solute: lead vanadate apatite, $Pb_{10}(VO_4)_6(OH)_2$									
26.	0.800	—	4.711	1.4454	—	13.497	1.70	188.07	
27.	0.899	—	5.104	1.2882	—	20.237	1.76	186.40	187.24

*Calculated from the measured final pH of the equilibrated system.
†Column numbers referred to text.

OH^- were available directly from the measurements, that of PO_4^{3-} was calculated as shown below from the overall analytical concentration of PO_4^{3-} represented as $C_{(PO_4)}$.

$$[1] \quad C_{(PO_4)} = [H_3PO_4] + [H_2PO_4^-] + [HPO_4^{2-}] + [PO_4^{3-}]$$

$$[2] \quad [PO_4^{3-}] = \frac{C_{(PO_4)} \times K_1K_2K_3}{[H^+]^3 + K_1[H^+]^2 + K_1K_2[H^+] + K_1K_2K_3}$$

where K_1, K_2, K_3 are dissociation constants for H_3PO_4 (13, 14) given respectively by 7.51×10^{-3}, 6.33×10^{-8}, and 4.73×10^{-13}. A similar set of calculations (15) was done for the K_{ip} of PbVA, while a combination of the two gave K_{ip} values of the solid solutions. In all such calculations the dissociation of H_3VO_4 to $H_2VO_4^-$, HVO_4^{2-}, and VO_4^{3-} was considered. The possibility of existence of polyphosphates and polyvanadates in presence of cations such as Pb^{2+} is remote under conditions prevalent in the present systems. All these subdivided values, excepting those of PO_4^{3-} and VO_4^{3-} given in columns 6 and 7, are not reported for the sake of brevity. For the apatite phase, the calculated values of the pK_{ip} and their averages are given in columns 9 and 10 respectively of the table; the corresponding values of the other possible phases such as $Pb(HPO_4)$, $Pb(H_2PO_4)_2$, and $Pb_2(HPO_4)(OH)_2$ (16) and their vanadate counter parts are not reported, again for the sake of brevity.

Since the powers to which the ionic concentrations are to be raised to get K_{ip} values of apatites are high, the errors in their determinations play a significant role in deciding the fluctuations of the K_{ip} values calculated. While establishing the constancy of K_{ip} values of each one of the samples at 37 ± 0.5°C, care was taken to see that there was an unambiguous constancy after making allowance for the fluctuations caused by errors in the determination of ionic concentrations required. For this purpose sets of positive and negative error limits of determination of Pb^{2+}, PO_4^{3-}, VO_4^{3-}, and pH/OH^- obtained from pilot experiments with known quantities were chosen to calculate the upper and lower limits of K_{ip}/pK_{ip} values of each sample. A similar scrutiny was made before concluding the effect of ionic replacement on pK_{ip} values of PbPA, PbVA, and their solid solutions.

The results could unambiguously confirm that the samples exhibited a stoichiometric dissolution since the gram-atom ratios given in column 8 are in close proximity with the theoretical value of 1.67 and the pK_{ip} values of the apatite phase are constant for each system. The earlier results (16–18) (which were based on the supposition that the solubility of apatites is non-stoichiometric, being controlled either by the secondary phosphates or surface coatings of extraneous phases) are not substantiated by the present findings which confirm the thermodynamically expected stoichiometric dissolution (19–23). An important finding of the present investigations was that the solubilities of the samples exhibited a marked decrease with an increase in vanadium content, the average pK_{ip} values of PbPA and PbVA being 168 and 187, respectively, with the solid solutions having intermediary values. A theoretical interpretation of dependence of solubility of an ionic crystal on cationic and anionic replacement is possible through thermodynamic considerations (24).

For an ionic compound, the free-energy change accompanying dissolution, ΔG_{soln}, is related to K_{sp} as shown below at a given temperature T,

$$[3] \quad \Delta G_{soln} = -RT \ln K_{sp}$$

and can be calculated from experimental values of K_{sp}. Alternatively, it can be evaluated by considering dissolution of an ionic compound to be consisting of, (*i*) breaking down of its crystal architecture and (*ii*) the hydration of the constituent ions so set free resulting in the expression

$$[4] \quad \Delta G_{soln} = \Sigma \Delta G_{hi} - \Delta G_{lattice}$$

where $\Sigma\Delta G_{hi}$ is the sum of the free-energy changes of hydration of the constituting ions of the solute, while $\Delta G_{lattice}$ is the free-energy change of formation of the lattice. It is evident from this expression that a high solubility results when the hydration energy is high and lattice energy low, the converse being the case for low solubility. The terms on the right-hand side of the above equation can be calculated (24) by the following expression for an ionic crystal of general formula M_mN_n.

$$[5] \quad \Delta G_{soln} = \frac{-164Z_+{}^2m}{r_+ + 0.85} - \frac{164Z_-{}^2n}{r_- + 0.1} + \frac{332Az_-{}^2}{R_0}\left(1 - \frac{1}{n_B}\right) - 8.03\,(m+n)\ \text{kcal/mol}$$

where Z_+ and Z_-, r_+ and r_- given the charges and ionic radii, respectively of the concerned ions; A, the Madelung constant; n_B, the Born exponent; R_0, the crystallographic radius; and 0.85 and 0.1 are the correction terms in the respective ionic radii. If the cation remains the same, the dependence of ΔG_{soln} on r_- is given by the equation

$$[6] \quad \left(\frac{\partial \Delta G_{soln}}{\partial r_-}\right)_{r_+} = \left(\frac{164Z_-{}^2n}{(r_- + 0.1)^2}\right) - \left(\frac{332Az_-{}^2}{R_0{}^2}\left(1 - \frac{1}{n_B}\right)\right) \times \left(\frac{\partial R_0}{\partial r_-}\right)_{r_+}$$

while the corresponding expression in the case of anion remaining the same is given by

$$[7] \quad \left(\frac{\partial \Delta G_{soln}}{\partial r_+}\right)_{r_-} = \left(\frac{164Z_+{}^2m}{(r_+ + 0.85)^2}\right) - \left(\frac{332Az_-{}^2}{R_0{}^2}\left(1 - \frac{1}{n_B}\right)\right) \times \left(\frac{\partial R_0}{\partial r_+}\right)_{r_-}$$

in either case the term $(1 - 1/n_B)$ being assumed to be constant.

It could be shown that the above equations are adequate to explain qualitatively the dependence of solubility of ionic crystals on ionic replacement. The first and second terms on the right-hand side of eqs. [5] and [6] represent, respectively, changes in hydration and lattice energies consequent upon anionic replacement. It is evident that on increasing the value of r_- a constant r_+, both these terms diminish, although the diminution in the second is less than that in the first, contributing to a decrease in solubility. The lower solubilities of PbVA and the solid solutions over that of PbPA could thus be explained. These conclusions are found to be in agreement with the corresponding results on the halides of Cs. Further, it can be shown from eq. [5] that for systems involving comparable values of r_+ and r_- as is the case with Pb^{2+} and VO_4^{3-} a solubility decrease is expected relative to its counterpart for which the disparity is more.

1. A. S. Posner. *In* Phosphorus and its compounds. Vol. II. *Edited by* J. R. Van Wazer. Interscience Publishers, Inc., New York. 1961. p. 1429.
2. W. Boyd. A text-book of pathology. Lea Febiger, Philadelphia. 1962. pp. 428–429.
3. R. Klement. Z. Anorg. Allg. Chem. **237**, 161 (1938); Chem. Abstr. **32**, 6571 (1938).
4. G. I. Spielholtz and F. S. Kaplan. Talanta, **27**, 997 (1980).
5. S. Prakash. Advanced chemistry of rare elements. S. Chand & Co. (Pvt) Ltd., Delhi. 1975. p. 565.
6. M. Phull and P. C. Nigam. Indian J. Chem. Educ. **8**, 22 (1981).
7. J. N. Brönsted. Z. Phys. Chem. Stoechiom. Verwandtschaftse. **103**, 307 (1922).
8. V. K. La Mer. J. Phys. Chem. **66**, 973 (1962).
9. P. V. R. Rao. Studies on preparation and some physico-chemical aspects of solid solutions of phosphate and vanadate apatites of lead. Ph.D. Thesis. North-Eastern Hill University, Shillong, India.
10. N. S. Chickerur, R. P. Singh, and T. S. B. Narasaraju. Naturwissenschaften, **56**, 282 (1969).
11. T. S. B. Narasaraju and V. L. N. Rao. Z. Anal. Chem. **258**, 365 (1972).
12. G. Charlot. Colorimetric determination for elements. Elsevier Publishing Company, Amsterdam – London – New York. 1964, p. 427.
13. L. F. Nims. J. Am. Chem. Soc. **56**, 1110 (1934).
14. L. F. Nims. J. Am. Chem. Soc. **55**, 1946 (1933).
15. R. J. H. Clark and D. Brown. The chemistry of vanadium, niobium and tantalum. Pergamon Press, New York. 1975. p. 496.
16. H. M. Rootare, V. R. Dietz, and F. G. Carpenter. J. Colloid. Sci. **17**, 179 (1962).
17. R. M. Blitz, E. D. Pellegrino, S. T. Miller, and A. Moffit.

Clin. Orthop. Relat. Res. **71**, 219 (1970); Chem. Abstr. **76**, 58 090K (1972).
18. T. S. B. NARASARAJU and V. L. N. RAO. Z. Phys. Chem. (Leipzig), **255**, 655 (1974).
19. J. S. CLARK. Can. J. Chem. **33**, 1696 (1955).
20. E. C. MORENO, T. M. GREGORRY, and W. E. BROWN. J. Res. Natl. Bur. Stand. Sect. A, **72**, 773 (1968).
21. D. R. WIER, S. H. CHIEN, and C. A. BLACK. Soil Sci. **111**, 107 (1971).
22. T. S. B. NARASARAJU and U. S. RAI. Can. J. Chem. **57**, 2662 (1979).
23. T. S. B. NARASARAJU, K. K. RAO, and U. S. RAI. Can. J. Chem. **57**, 1919 (1979).
24. D. L. LEUSSING. *In* Treatise on analytical chemistry. Part 1. *Edited by* I. M. Kolthoff, P. J. Elving, and E. B. Sandell. The Interscience Encyclopaedia Inc., New York. 1959. p. 675.

A fast atom bombardment study of the lead isotope ratios in early nineteenth century Niagara Peninsula pottery glazes

JACK M. MILLER, TIMOTHY R. B. JONES, AND TINA KENNEY
Department of Chemistry, Brock University, St. Catharines, Ont., Canada L2S 3A1
DAVID W. RUPP
Department of Classics, Brock University, St. Catharines, Ont., Canada L2S 3A1
AND
BRIAN N. GREEN AND ROBERT S. BARDOLI
VG Analytical, Floats Road, Wythenshawe, Manchester, England M23 9LE

Received September 23, 1985

JACK M. MILLER, TIMOTHY R. B. JONES, TINA KENNEY, DAVID W. RUPP, BRIAN GREEN and ROBERT S. BARDOLI.Can. J. Chem. **64**, 488 (1986).

The application of fast atom bombardment (FAB) mass spectrometry to the determination of lead isotope ratios in nineteenth century pottery glazes from the Niagara Peninsula has been investigated with the aim of determining the source of the lead used in the glazes. Methods of sampling have been compared, including direct analysis of glass chips, analysis of powdered glaze scrapings, analysis of acid extracts of the former, and simple acid leaching of the surface of a piece of pottery. The latter method gave the best results. The FAB data, as obtained on an older mass spectrometer, can distinguish lead from igneous vs. sedimentary deposits, but is not adequate to determine specific mining locations. Although newer FAB instrumentation can narrow this range, the overlap of data from the Niagara Peninsula and England precludes a simple answer to the archeological question as to English vs. Canadian origin of the lead used in the Jordan pottery glazes. However, the data do suggest that the potter used a local source for the lead.

JACK M. MILLER, TIMOTHY R. B. JONES, TINA KENNEY, DAVID W. RUPP, BRIAN GREEN et ROBERT S. BARDOLI.Can. J. Chem. **64**, 488 (1986).

Faisant appel à la spectrométrie de masse par bombardement avec des atomes rapides et dans le but de déterminer la source du plomb utilisé pour fabriquer les émaux, on a déterminé les rapports des divers isotopes du plomb dans l'émail de poteries du dix-neuvième siècle provenant de la péninsule du Niagara. On a comparé les diverses méthodes d'échantillonnage, y compris l'analyse directe de morceaux de verre, l'analyse de poudres formées à partir de fragments d'émail, l'analyse d'extraits acides des premiers ou tout simplement en faisant un lavage acide de la surface des pièces de poterie. Cette dernière méthode donne les meilleurs résultats. Les données de la spectroscopie, telles qu'obtenues sur un spectromètre de masse plus vieux, permettent de distinguer du plomb provenant de sources ignées ou sédimentaires; toutefois, cette méthode n'est pas adéquate pour déterminer des sites spécifiques de mines. Même si les nouveaux appareils permettent de combler une partie de ces déficiences, le recouvrement des donnés provenant de la péninsule du Niagara et de l'Angleterre ne permet pas de donner une réponse simple aux questions archéologiques concernant l'origine anglaise ou canadienne du plomb utilisé dans les émaux de la poterie Jordan. Toutefois, les donnés suggèrent que le potier a fait appel à une source locale pour son plomb.

[Traduit par le journal]

Introduction

The application of the tools of modern analytical chemistry to archeological problems, when combined with the tools of classical archeology, forms the relatively new field of archeological chemistry. The ability to study trace element occurrences, isotope ratios, etc. can, especially when combined with the other archeological information available, permit dating of objects, or the determination of place of manufacture, place of origin of raw materials, or both. Such information can be particularly useful in determining trade patterns and social interactions. The chemical makeup of objects such as coins, tools, and pottery, the commonest artifacts, usually contain ratios of elements or isotopes that reflect their region of origin. A technique is especially valuable to the archeologist if it is nondestructive, and whether destructive or not, if it is sensitive enough to use with very small samples. Several reviews of this field have been published (1, 2).

Lead is a particularly important element archeologically and is often found in its metallic form or alloyed with various metals, and in glasses and glazes. All these forms have high "survival" factors, i.e., they are found as identifiable objects subject to characterization by classical methods. Stable lead isotope ratios differ with the source of the lead around the world as a result of differing radioactive precursors. Certainly, lead from igneous deposits is readily distinguished from lead derived from sedimentary deposits (3, 4).[1] Thus a comparison of the lead isotope ratios of lead of archeological origin should help to pinpoint the source of the lead used in the manufacture of the object. However, in practice this is only possible if the errors associated with the measurement are smaller than the variations in isotope ratio with the source of the lead. An igneous and sedimentary source of lead could readily be distinguished even with crude instrumentation but, as we shall show, to distinguish between Niagara Peninsula lead and some English leads is not a trivial problem.

The advent of fast atom bombardment (FAB) source for conventional organic mass spectrometers (5) now makes the measurement of isotope ratios from solid inorganic samples a widely available technique and, if the systematic errors can be minimized, a powerful and easily accessible tool for the archeological chemist. Dolnikowski *et al.* (6) have recently demonstrated the application of FAB mass spectrometry to the determination of metals in archeological artifacts, including the determination of lead isotope ratios. In their case it proved easy

[1]R. Farquar. Private communication. 1985.

to demonstrate that the American copy of the British pottery under examination clearly had a glaze of American origin. However, some North American and English lead isotope ratios overlap in their plots of $^{207}Pb/^{206}Pb$ vs. $^{204}Pb/^{206}Pb$. This is just the region where the data we discuss below appear on such a plot.

Our problem was with the origin of the lead for the glazes used in the Benjamin Lent pottery on the Niagara Escarpment near Jordan, Ont., a site active in the pioneer period between 1835–1836 and 1841–1842, and recently excavated by one of us (7). Several hypotheses exist. Firstly, native Niagara lead may have been used, there being surface deposits of galena (naturally occurring PbS) found in the face of the Niagara escarpment and in the surrounding area. Also, there appears to be some evidence of lead having been smelted in the nearby area in pioneer times. Secondly, a large number of broken bottles have been excavated at the site and it has been hypothesized that glass bottles, either from England or North America, might have been the source of material for the glaze. An alternative hypothesis suggests that the lead which lined the tea chests in which tea was imported via England might have served as the potter's source of lead for his glazes. Such lead is likely to have been reused scrap lead from a number of locations and might not match the expected isotope ratios for any specific area. The bottle hypotheses was eliminated at an early stage, the bottle glass having a much lower lead content than the glazes. In the work described below we explore the other two possibilities.

Experimental

(a) Instrumentation

Fast atom bombardment mass spectra were obtained on two instruments, an early AEI MS 30 at Brock University and a large double focussing mass spectrometer, the prototype VG ZAB SE, located at the VG factory in Wythenshawe. In both cases the atom beam was provided by an Ion Tech atom gun, with xenon as the bombarding gas; atom energies were on the order of 8 kV.

The MS-30 had a Kratos FAB source retrofit, including fast pumping, with samples being inserted via a stainless steel probe and lock which penetrates the end flange. Data were collected with a Kratos DS 55 data system (Nova 4X and fast preprocessor) and via a set of data acquisition programs written in house, based in part on programs written by Lapp[2]. This was necessary since our Kratos DS-55 data system could not average and process raw data. Experiments were also done with data acquisition on chart paper and via an integrating voltmeter while the instrument was operated in a static mode, with the magnet being set to the top of each peak of interest in turn. The best results were obtained using 30 s/mass decade narrow scans (170–230 Daltons) with data averaged using the time averaging capabilities of our raw data acquisition routines. Samples were run at a nominal resolving power of 1000, averaged in groups of 16, with typically eight sets of such data being acquired.

The ZAB was run at a resolving power of approximately 800, with narrow scans between m/z 230–200 at either 30 or 100 s/mass decade. There were 100 scans collected for each sample using the 11/250 data system. The ZAB data from the data system were consistent with trial runs obtained from the oscillographic recorder. Ten minutes of instrument time was all that was required per sample. Higher resolution could have been used to eliminate the lead hydride peaks rather than correcting for them as discussed below. However, at the lower sensitivity which comes with higher resolution, longer data acquisition time would have been required. Work is now underway to determine the optimum in the resolution–sensitivity tradeoff.

All data were corrected for background detected in the lead isotope region (0.1–0.2%), i.e., 4–8% of the ^{204}Pb peak, and for the presence of (typically) 0.5–1.0% PbH species, corrected on the basis of the 209/208 intensity ratio. The hydride peaks are time dependent, which complicates their correction.

Data were not corrected for mass discrimination of the detectors which we believe to be much smaller than the other systematic instrument errors. For both instruments the 5 mass unit range in question is a tiny fraction of the normal scanning range for which they are designed. The manufacturers have not recommended a mass discrimination correction, and previous work in our lab involving deuterium substitution suggests that neglecting this correction is valid for data with the accuracy we are obtaining.

(b) Sampling

Four methods of obtaining samples for insertion into the FAB source were attempted.

(i) Direct glaze chip method

In this, perhaps the simplest of the methods as far as sample preparation is concerned, a chip of glaze is lifted from a sherd using a flat hardened knife or spatula. The glaze chip is then attached directly to the probe tip with double-sided masking tape. This method presented two problems, first the difficulty of getting a flat chip of glaze from the sherd, and secondly the relatively poor signal-to-noise ratio in the MS-30 with the hardened fired glaze surface exposed to the atom beam. This method may be suitable for use with the ZAB which was observed to have between one and two orders of magnitude sensitivity advantage over the MS-30 for FAB work in this mass range. We did not however pursue this approach as ZAB time was limited.

(ii) Direct powder method

Glaze was scraped from the surface of a sherd using a carbide tipped scriber, and 1–2 mg of the solid powder obtained was placed directly on the tip of the FAB probe, again using double-sided tape. Some tests were done with the powdered glaze pressed into a pellet, but this did not seem critical. The MS-30 data thus obtained were adequate to distinguish sedimentary from igneous lead, but the reproducibility of the data precluded their use for serious studies. Using the ZAB with its greater sensitivity, good data were obtained, equivalent or better in quality than that reported by Dolnikowski *et al.* (7). In an attempt to get better sensitivity with the MS-30 we attempted two acid extraction procedures, discussed below, with some degree of success.

(iii) Powder-acid extraction method

The powdered glaze scraped from the sherds as described above was subjected to a 24 h hot aqua-regia extraction. Several milligrams of glaze were extracted, the undissolved glaze centrifuged off, and the lead–acid solution was allowed to evaporate to dryness. This material was then redissolved in a minimum amount of water and a drop of the concentrated solution was applied to the probe tip followed by evaporation of the water in an oven. Several applications could be made to thicken the layer on the probe tip. The extract from 4 mg of sample digested with 2 mL of acid was sufficient to do 15 separate determinations. The total ion current obtained in this way using the extracted lead salts was an order of magnitude higher than working with the unextracted powdered glazes.

(iv) Sherd-acid extraction method

Since the extraction procedure seemed to be such an advance, we then tried to determine if acid extraction of the glazed surface of a sherd would also provide a sufficient lead concentration for the analysis without the tedious scraping of the glaze, and perhaps without noticeably defacing the sherd. In this technique the glazed surface of the sherd was dipped for 2–3 min in a boiling aqua-regia solution. No visible sign of degradation of the glazed surface was observed. The resulting solution gave the best results of the four methods used for sample preparation with the MS-30. In addition to achieving the best mass spectrometric data from his technique, it was also the easiest in terms of sample preparation, though taking slightly longer than affixing the glaze directly to the probe tip with double-sided tape. With spare FAB probe tips one person could easily prepare ten samples in an hour.

Ultrapure acids should normally be used for lead isotope determinations (8, 9) because traces of lead occur in normal reagent grade acids. However, no lead could be detected by the MS-30 in a blank extraction

[2]R. Lapp. University of Nebraska. Private communication. 1984.

TABLE 1. MS 30 data for the direct powder method

Sherd no.	Colour	$^{208}Pb/^{206}Pb$	$^{207}Pb/^{206}Pb$
846	Green	2.094	0.8944
3043	Gold-purple	2.304	0.8123
1026	Red-green	1.908	0.7945
1835	Green red	2.104	0.8440
841	Yellow	2.147	0.8345
863	Green	2.232	0.8231
Average		2.132	0.8338

of lead-free glass, using high quality Baker Instra-analyzed reagent grade acids. Blank determinations on various grades of acids should be run with high sensitivity instruments before they are used in the extraction techniques described above.

Results and discussion

The sherds subjected to FAB-ms determination of their lead isotope ratios were obtained from the Jordan pottery site in Jordan, Ontario, in early nineteenth century pioneer pottery excavated by one of us (7).

In Table 1 we show the results of the isotope ratios measured using the direct powder method on the MS-30. The poor sensitivity made it difficult to measure the ^{204}Pb abundance with any accuracy. The data do, however, cluster in the region expected for English or Niagara Peninsula lead, and are distinct from data from most of the remainder of North America. The average value, however, falls outside the range of values expected. We did not have much confidence in these data although they were better than data obtained by directly examining a glaze chip. Detailed statistics were not collected on data points since it was obvious that improved methods would be needed. All the tabular ratio data are based on raw ion abundance that were first corrected for background and the presence of lead hydride species prior to calculation of the isotope ratios.

Dolnikowski *et al.* (6) in their FAB work used a plot of the $^{207}Pb/^{206}Pb$ ratio against that of $^{204}Pb/^{206}Pb$ as a visual indicator of the potential origins of lead samples. This plot has the disadvantage of using the ^{204}Pb abundance which is low and most subject to error. More commonly used is a plot of the 208/206 ratio vs. that of 207/206 (Fig. 1). The English data are taken from the literature (4),[1] while for the Niagara Peninsula and related areas in similar geological formations from northern New York State the data were kindly provided by Farquar.[1] It can be seen that the benchmark data for England and for the Niagara Peninsula overlap to a large extent so that we would expect to have difficulty in distinguishing between the two sources unless the standard deviations are very small. In the work of Dolnikowski *et al.* (6) it was suggested that there was a clear distinction between the lead isotope ratios from England and North America. However, their only points suggesting possible overlap come from the Niagara Peninsula. More detailed investigations[1] of the lead isotope ratios from the literature (3) point to further overlap of various lead sources from the original "Thirteen Colonies" with these of English lead, making life difficult for the archeologist.

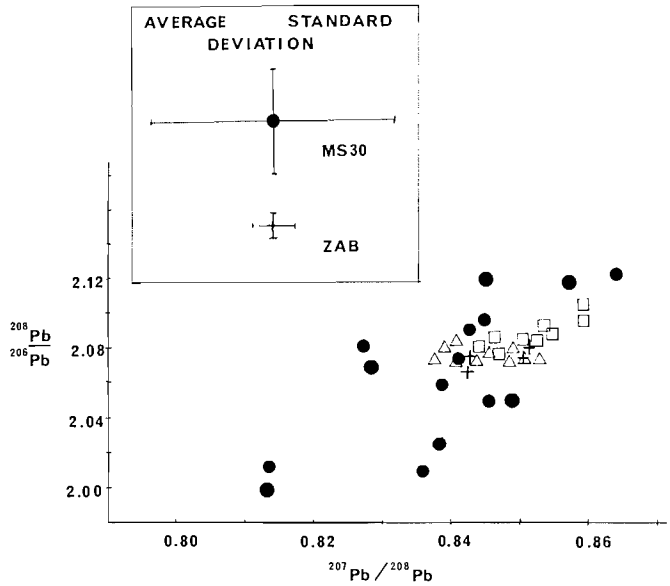

FIG. 1. Plot of $^{207}Pb/^{206}Pb$ vs. $^{208}Pb/^{206}Pb$ for (□) English (4)[1] and (△) Niagara Peninsula[1] lead, (and related escarpment samples from northern New York State), together with data from Jordan pottery sherds determined using (●) MS 30 and (+) ZAB SE mass spectrometers equipped with FAB sources. Standard deviations are shown for the two instruments.

It was clear that if the direct powder method was to be used successfully, higher sensitivity was needed. In Table 2 we show the data obtained on a VG ZAB SE prototype, a large high-mass, high-resolution, high-sensitivity reverse-geometry magnetic mass spectrometer. For the purposes of our experiments, only the stability of the instrument and its sensitivity were important to obtaining good results. The data obtained were of much higher quality, with standard deviations an order of magnitude smaller than for comparable runs on the MS 30. Figure 1 shows that the data from the ZAB fall directly on top of the Niagara Peninsula points. These also overlap with half of the values for English lead, so even with the greater precision, one cannot unequivocally state the origin of the lead in these glazes. However, the data appear to lie within the field of the Niagara Peninsula data points.

In an attempt to improve on the precision obtained with the MS 30 we experimented with the acid extraction techniques. Data are shown in Table 3 and plotted on Fig. 1. The standard

TABLE 2. ZAB SE data for the direct powder method

Sherd no.	Colour	$^{208}Pb/^{206}Pb$	$^{207}Pb/^{206}Pb$	$^{204}Pb/^{206}Pb$
846	Green	2.077±0.005	0.8513±0.002	0.0533±0.0004
3075	Wine	2.077±0.011	0.8505±0.0005	0.0569±0.0017
1166	Dk. brown	2.063±0.007	0.8420±0.006	0.0545±0.0009
1166*	Dk. brown	2.070±0.003	0.8425±0.003	0.0537±0.0009

*Scan speed was 100 s/mass decade.

TABLE 3. MS 30 data for the powder and sherd extraction methods

Sherd no.	Colour	$^{208}Pb/^{206}Pb$	$^{207}Pb/^{206}Pb$
1579	Green	2.021±0.007	0.8128±0.01
1497	Lt. brown	2.009±0.06	0.8353±0.01
1164	Red green	2.122±0.006	0.8639±0.03
1028	Orange red	1.945±0.007	0.8032±0.03
1028	Orange red	2.083±0.07	0.8268±0.04
1028	Orange red	2.058±0.02	0.8392±0.02
3161		2.021±0.04	0.8378±0.01
846	Green	2.097±0.05	0.8449±0.01
870	Gold brown	2.065±0.05	0.8407±0.01
870	Gold brown	2.028±0.04	0.8425±0.02
846*	Green	2.067±0.03	0.8504±0.01
846*	Green	2.084±0.02	0.8413±0.02
1500	Gold brown	2.001	0.8153
1170	Green slip	1.9745	0.8245
1164	Red green	1.9569	0.8871
1453	Red wine	2.1191	0.8573
846	Green	2.1214	0.8448
1170	Green	2.0510	0.8485
Average		2.046	0.8397

*Sherd extraction rather than the powder extraction method.

TABLE 4. Summary of data for sherd #846

Mass spec.	Sampling method	$^{208}Pb/^{206}Pb$	$^{207}Pb/^{206}Pb$
ZAB SE	Direct powder	2.077±0.005	0.8513±0.002
MS 30	Direct powder	2.094	0.8944
MS 30	Powder extn.	2.097±0.05	0.8449±0.013
MS 30	Sherd extn.	2.067±0.03	0.8504±0.014
MS 30	Sherd extn.	2.084±0.02	0.8413±0.015

deviations are reduced by a factor of two compared to the direct powder methods, but are still a factor of 5–10 worse than the ZAB powder data. This does suggest, however, that if the extraction techniques are used with the ZAB, data may be obtainable with sufficient precision to permit isolation of lead sources to particular mines. With the MS 30 data there is apparently some systematic error as the data seem shifted towards the lower left-hand side of the graph. However, the average value for all these lead extractions is very close to the Niagara Peninsula points, much closer to them than to the English data, again suggesting that the potter had a local source of lead.

One glaze sample from sherd #846, a green-glazed piece of pottery, was analyzed by both instruments, and the standard deviations calculated. These data are summarized in Table 4. Each MS 30 extraction method data point is within less than one standard deviation of the other MS 30 data points. The ZAB data fall close to the mean of the three MS 30 extraction samples.

Replicate determinations on separate samples of sherd #1166 were also done using the ZAB. Different scan speeds showed no significant differences (Table 2), although standard deviations were lower for the determination done using a 100 rather than 30 s/mass decade scan speed.

In conclusion, it would appear that if a modern mass spectrometer with a FAB source is used for lead isotope determinations for samples of archeological interest, it should be possible to develop the methodology to permit a rapid indication of probable origins of the lead in the artifact. Acid extraction techniques give the best results, and we predict that if these are used in conjunction with a modern high sensitivity instrument, high quality data can readily be obtained.

Acknowledgments

We wish to thank the Natural Sciences and Engineering Research Council of Canada for operating and capital grants, (JMM) and a summer studentship (TK) and the Shaver Foundation and a Joseph H. DeFrees Grant for assistance with acquisition of the FAB facilities at Brock. We also wish to thank Dr. R. Farquar, Geophysics Laboratory, University of Toronto, for helpful suggestions.

1. R. GOULD (*Editor*). Adv. Chem. Ser. No. 138 (1974).
2. R. GOULD (*Editor*). Adv. Chem. Ser. No. 171 (1978).
3. R. RUSSELL and R. FARQUAR. Lead isotopes in geology. Interscience, New York.
4. B. DOE. Lead isotopes. Springer-Verlag, New York. 1970.
5. J. M. MILLER. *In* Advances in inorganic chemistry and radiochemistry. Vol. 28, *Edited by* H. J. Emeléus and A. G. Sharpe. Academic Press, New York. 1984.
6. G. G. DOLNIKOWSKI, J. T. WATSON, and J. ALLISON. Anal. Chem. **56**, 197 (1984).
7. D. W. RUPP. Archaelogy, **33**, 44 (1980); Canadian Collector, **15**, 39 (1980).
8. E. C. KUEHNER, R. ALVAREZ, P. J. PAULSEN, and T. J. MURPHY. Anal. Chem. **44**, 2050 (1972).
9. I. C. BARNES, T. J. MURPHY, J. W. GROMLICH, and W. R. SHIELDS. Anal. Chem. **45**, 1881 (1973).

Complexes of hybrid ligands. Some Pd^{2+} and Pt^{2+} complexes of fluoro-alkoxy thioether ligands; the measurement of the *trans*-effect of phosphines on thioether inversion[1]

RENÉ T. BOERÉ AND CHRISTOPHER J. WILLIS

Department of Chemistry, The University of Western Ontario, London, Ont., Canada N6A 5B7

Received July 15, 1985

RENÉ T. BOERÉ and CHRISTOPHER J. WILLIS. Can. J. Chem. **64**, 492 (1986).

The hybrid ligands R—S—CH_2—$C(CF_3)_2$—O^- (R = CH_3 or C_6H_5) have been used in conjunction with the other donors to prepare complexes of Pt^{2+} and Pd^{2+}. Five-membered chelate rings are formed by coordination through the hard alkoxy and the soft thioether donor sites. Products are of two types: neutral $MCl\{RSCH_2C(CF_3)_2O\}(PR_3)$ or cationic $[M\{RSCH_2C(CF_3)_2O\}(PR_3)_2]^+$, and their geometry is assigned. Variable temperature nmr measurements are used to follow the inversion of the thioether function in the hybrid chelate ring, and values of $\Delta G\ddagger$ are calculated. From a comparison of the barrier to inversion in various complexes, the dynamic *trans* effect of various ligands is assessed including, for the first time using this criterion, the trialkylphosphines.

RENÉ T. BOERÉ et CHRISTOPHER J. WILLIS. Can. J. Chem. **64**, 492 (1986).

On a utilisé les ligands hybrides R—S—CH_2—$C(CF_3)_2$—O^- (R = CH_3 ou C_6H_5) en conjonction avec d'autres donneurs pour préparer des complexes du Pt^{2+} et du Pd^{2+}. Il se forme des chélates à cinq chaînons par coordination des sites donneurs dur de l'alcoolate et doux du thioéther. Les produits sont de deux types, soit neutres ($MCl\{RSCH_2C(CF_3)_2O\}(PR_3)$) ou cationiques ($[M\{RSCH_2C(CF_3)_2O\}(PR_3)_2]^+$) et on a attribué leur géométrie. On a utilisé des mesures de rmn à temperature variable pour examiner l'inversion de la fonction thioéther dans le cycle du chélate hybride et l'on a calculé les valeurs du $\Delta G\ddagger$. En se basant sur une comparaison de la barrière à l'inversion dans divers complexes, on a évalué l'effet dynamique *trans* de divers ligands dont les trialkylphosphines qui y ont été incluses pour la première fois en utilisant ce critère.

[Traduit par le journal]

Introduction

In the first part of this series (2), we described the synthesis of molecules of general formula $RSCH_2C(CF_3)_2OH$, containing both a fluorinated alcohol and a thioether function. In the mono-ionized form, these may act as bidentate, chelating, ligands toward transition metal ions. The combination of the hard —$C(CF_3)_2O^-$ donor with the soft thioether function enables them to form stable complexes with the softer transition metal ions, and we have described studies on the neutral bis-complexes $M[RSCH_2C(CF_3)_2O]_2$, which show *cis* geometry for M = Pt and both *cis* and *trans* for M = Pd.

In the present paper, we describe the extension of this study to the preparation of two additional types of complexes of these hybrid ligands, cationic complexes of type **1** with alkyl- and arylphosphine as coligand, and neutral type **2** complexes with phosphine and chloride as coligands.

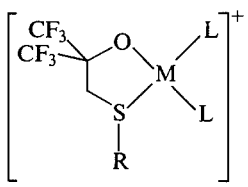

1

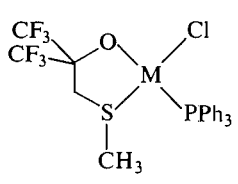

2

The cationic complexes are generally prepared with fluoroborate as counterion. Using phosphines as coligands, we have been able to make platinum(II) complexes with R = Me, L = PPh_3 (**3**), PPh_2Me (**4**), $PPhMe_2$ (**5**), or PMe_3 (**6**); R = Ph, L = PPh_3 (**7**), PPh_2Me (**8**), or $PPhMe_2$ (**9**). Palladium(II) phosphino complexes were more difficult to prepare, and were restricted to that with L = PPh_3, R = Me (**10**). Neutral type **2** complexes have been prepared for both Pt (**11**) and Pd (**12**).

In previous studies on related systems (2, 3) we have attempted to place the fluoroalkoxide function relative to other ligands in the dynamic *trans*-effect series by the measurement of the barrier to thioether inversion. Our object in synthesizing type **1** and **2** complexes was to extend this study and to include, for the first time, trialkylphosphines as coligands *trans* to the thioether group. The presence in these complexes of several nmr-active nuclei (^1H, ^{19}F, and ^{31}P), each of which may couple to ^{195}Pt, makes them particularly suitable for characterization by nmr.

Experimental section

General techniques and the preparation of the fluoroalcohol thioethers $CH_3SCH_2C(CF_3)_2OH$ and $C_6H_5SCH_2C(CF_3)_2OH$ have been described previously (2). As before, we will abbreviate the anionic forms of the ligands to Me—S—O^-, and Ph—S—O^-. Phosphine and thioether complexes of $PtCl_2$ and $PdCl_2$ were prepared by standard routes (3).

$[Pt(Me—S—O)(PPh_3)_2]BF_4$, 3

To *cis*-$PtCl_2(PPh_3)_2$ (1.0 g, 1.26 mmol) in CH_2Cl_2 (30 mL) was added $CH_3SCH_2C(CF_3)_2OH$ (0.29 g, 1.26 mmol) followed by the stoichiometric quantity of KOH in ethanol. (In this and following reactions, it was found convenient to measure out the required amount of KOH volumetrically using a standard solution, ~0.3 *M*, in ethanol). After stirring 3 h, the solution was centrifuged to remove KCl, then $AgBF_4$ (0.25 g, 1.26 mmol) was added, causing immediate precipitation of AgCl. The solution was centrifuged, stirred 16 h, filtered, and reduced in volume. Addition of pentane precipitated **3** as an off-white, air-stable solid (1.22 g, 94% yield) which was recrystallized from CH_2Cl_2–EtOH to give large colorless crystals, mp 294–296°C.

Complexes 4–9

Complexes **4**–**9** were prepared by the same general route, starting with the appropriate complex *cis*-$PtCl_2(PR_3)_2$ and the ligand alcohol $CH_3SCH_2C(CF_3)_2OH$ or $C_6H_5SCH_2C(CF_3)_2OH$. *$[Pt(Me—S—O)(PPh_2Me)_2]BF_4$*, **4**: colorless prisms from CH_2Cl_2–EtOH, mp 183–184°C. *$[Pt(Me—S—O)(PPhMe_2)_2]BF_4$*, **5**: Purification by dry-column chromatography on Florosil (CH_2Cl_2 eluant) yielded an oil which solidified to an amorphous cream solid when treated with ether, but could not be crystallized. *$[Pt(Me—S—O)(PMe_3)_2]BF_4$*, **6**: oil, giving light yellow powder, recrystallized from CH_2Cl_2–EtOH to give colorless crystals, mp 198–200°C. *$[Pt(Ph—S—O)(PPh_3)_2]BF_4$*, **7**:

[1]Taken in part from ref. 1. Presented in part at the XXIII International Conference of Coordination Chemistry. Boulder, CO. 1984.

TABLE 1. Analytical data for complexes

Compound	Formula	% Carbon		% Hydrogen		% Phosphorus		% Sulfur	
		calcd.	found	calcd.	found	calcd.	found	calcd.	found
3	$C_{41}H_{35}BF_{10}OP_2PtS$	47.64	46.54	3.41	3.49	5.99	6.07	3.10	3.23
4	$C_{31}H_{31}BF_{10}OP_2PtS$	40.94	40.98	3.43	3.42	6.78	7.36	3.53	3.77
6	$C_{11}H_{23}BF_{10}OP_2PtS$	19.98	19.99	3.51	3.56	9.37	8.54		
7	$C_{46}H_{37}BF_{10}OP_2PtS$	50.43	51.26	3.40	3.65	5.65	7.88	2.93	3.74
11	$C_{23}H_{20}ClF_6OPPtS$	38.37	38.37	2.90	2.59				
12	$C_{23}H_{20}ClF_6OPPdS$	43.76	43.58	3.19	3.34	4.91	5.42	5.08	6.22

pale yellow blocks from CH_2Cl_2 – 1-propanol, mp 225–230°C. *[Pt(Ph—S—O)(PPh$_2$Me)$_2$]BF$_4$*, **8**: oil, purified by dry-column chromatography (CH_2Cl_2 eluant), cream solid when treated with ether and vacuum-dried. *[Pt(Ph—S—O)(PPhMe$_2$)$_2$]BF$_4$*, **9**, similar to **8**.

[Pd(Me—S—O)(PPh$_3$)$_2$]BF$_4$, ***10***

To *trans*-$PdCl_2(PPh_3)_2$ (0.50 g, 0.72 mmol) suspended in benzene (40 mL) was added $CH_3SCH_2C(CF_3)_2OH$ (0.20 g, 0.72 mmol) followed by the stoichiometric amount of KOH in ethanol. As the base was added, the suspension passed through deep red to orange in color. KCl was removed, then $AgBF_4$ (0.14 g, 0.72 mmol) in EtOH was added and AgCl was immediately removed by centrifugation, giving a blood-red solution. Removal of solvent, followed by extraction with $CHCl_3$ and precipitation with ether gave a bright red powder, mp 200°C, which could not be recrystallized without decomposition; satisfactory analytical figures on the solid could not be obtained, but the compound was characterized by solution nmr data.

PtCl(Me—S—O)(PPh$_3$), ***11***

To *cis*-$PtCl_2(PPh_3)_2$ (0.50 g, 0.63 mmol) suspended in DMF (40 mL) was added $CH_3SCH_2C(CF_3)_2OH$ (0.14 g, 0.63 mmol) followed by KOH (0.63 mmol) in EtOH. After stirring 16 h, by which time the solids had dissolved, the solution was reduced in volume and the product precipitated in 44% yield by addition of hexane. Recrystallized from CH_2Cl_2–EtOH, beige flakes, mp 267–269°C.

PdCl(Me—S—O)(PPh$_3$), ***12***

To *trans*-$PdCl_2(PPh_3)_2$ (0.1 g, 1.43 mmol) suspended in benzene (150 mL) was added $CH_3SCH_2C(CF_3)_2OH$ (0.33 g, 1.43 mmol) and sulfur (0.046 g, 1.43 mmol) followed by KOH (1.43 mmol) in EtOH. The resulting deep-red solution was stirred 16 h, filtered, and solvent removed to give a yellow solid. After washing with ether, recrystallization from CH_2Cl_2–C_6H_{12} gave yellow platelets, mp 210°C.

Characterization

In all cases where a crystalline product was obtained, new complexes were characterized by elemental analysis. Data are given in Table 1; because of the variety of elements present, it was not possible to obtain reliable results for S and P analyses in every case.

Mass spectra of the cationic type **1** complexes gave peaks corresponding to the complete cation, $[M(PR_3)_2(Me—S—O)]^+$, only in the case of the Pt complexes with PR_3 = PPh_2Me and PMe_3. For all of the cationic Pt phosphine complexes, a strong peak appeared at a mass number corresponding to the loss of the substituent on sulfur, that is, the species $[Pt\{SCH_2C(CF_3)_2O\}(PR_3)_2]^+$, and for the species $[Pt(Pr_3)_2]^+$, where the complete fluoroalcohol thioether ligand has been lost. For the neutral type **2** complexes, the heaviest mass-number peak for both **11** and **12** corresponded to the loss of Cl^- from the molecule, together with typical fragmentation patterns corresponding to the loss of CF_3^-, etc. All species had infrared spectra consistent with their proposed structures. Nuclear magnetic resonance spectra, which provided the principal means for characterization, are discussed separately later in this paper.

Results and discussion

The synthesis of each of the complexes discussed in this work begins with the appropriate phosphine or thioether complex of the metal dichloride. Treatment with ligand and base (KOH) in the required molar ratio gives the type **2** chloro-complex, which may in some cases be isolated at that point. The addition of $AgBF_4$ then produces the cationic type **1** complex.

$$MCl_2(L)_2 + RSCH_2C(CF_3)_2OH + KOH \rightarrow MCl(L)\{RSCH_2C(CF_3)_2O\} + L + KCl$$

$$MCl(L)\{RSCH_2C(CF_3)_2O\} \xrightarrow{AgBF_4} [M(L)_2\{RSCH_2C(CF_3)_2O\}]BF_4 + AgCl$$

Careful choice of solvent and control of stoichiometry is needed in order to isolate these products, and yields at each stage were found to be very variable according to the nature of M, R, and L.

In the mass spectra of the cationic species, substantial peaks corresponding to the loss of the S-alkyl group in the ligand were observed in each case, and this suggested that it might be possible to prepare a neutral thiol complex by reductive dealkylation:

$$[M(L)_2\{RSCH_2C(CF_3)_2O\}]^+ + X^- \rightarrow M(L)_2\{SCH_2C(CF_3)_2O\} + RX$$

This is a well-recognized type of reaction carried out by nucleophilic attack on the thioether, although it has only been observed where the R—S group is attached to an aromatic ring (4, 5). Controlled dealkylation was not successful in our systems, however, since the stability of the complexes was not sufficient to prevent ligand displacement when treated with the strong nucleophiles needed (I^-, SCN^-).

Nuclear magnetic resonance studies

General features of the nmr spectra of the complexes are shown in Tables 2 and 3. Table 2 gives ^1H and ^{19}F data for the fluoroalcohol thioether ligand, while Table 3 gives ^1H and ^{31}P data for the phosphine ligands in the cationic complexes.

In a static situation, the pyramidal coordination of the thioether function induces inequivalence in the protons of the adjacent methylene group and in the geminal CF_3 groups attached to the ring. As we have previously demonstrated for the neutral bis-complexes of this ligand (2), this inequivalence may be removed by raising the temperature so that inversion of the chelate ring and inversion at sulfur becomes rapid (on the nmr time-scale), resulting in the chelate ring appearing dynamically planar. In each case, variable-temperature data are quoted under conditions designed to show, where possible, the limiting cases of such variations in the spectra.

(i) Neutral type 2 complexes

There are clearly two possible geometric isomers for these compounds; the *cis* form shown as **2** above, or the *trans* form in which positions of the Cl^- and PPh_3 ligands are reversed.

TABLE 2. ^1H and ^{19}F nmr data for alcohol-thioether ligands in complexes[a]

Compound	Solvent[b]	Temp. (°C)	CF_3 groups δ (ppm)	Δ_{AB} (Hz)	J_{AB} (Hz)	CH_2 group δ (ppm)	Δ_{AB} (Hz)	J_{AB} (Hz)	R—S δ (ppm)	^3J(Pt,H) (Hz)	^4J(P,H) (Hz)
3	M	−20	−76.21	(s, W = 4.2[c])		3.42	37.9	13.7	1.96	40.0	4.5
	A	32	[d]	(s, W = 18)		3.27	31	14	2.21	40	4.5
	M	40	−76.26	(s, W = 9.5)			(br singlet)		2.03	39.9	4.5
4	M	−20	−76.43	68.5	9.5	3.39	38.5	14	2.13	38	4.5
	M	30	−76.4	(br doublet)			(br doublet)		2.17	38	4.5
	C	50		(coalesced)		3.36	(br singlet)		2.21	39	4.3
4	C	90	−76.94	(s, W=7.5)		3.36	(s, J=20.5[c])		2.23	39	4.3
5	C	0	−74.4	155	9.5	3.40	49.3	14.5	2.74	37.5	4.0
	C	32	−74.4	~145 (br d)			(br d of d)		2.73	37.5	4.0
	C	90	−74.4	(s, W=33)		3.40	(s, J=17[c])		2.72	37.0	4.0
6	M	0	−76.95	184.4	9.6	3.36	45.6	15	2.79	36.8	3.8
	M	32		(br d of d)			(br d of d)		2.79	36.6	3.9
	C/D	23	[d]	178.5	9.4	3.48	26.8	~14	2.82	36.9	3.8
	C/D	105	[d]	(s, W=11)		3.45	(s, J=17.5[c])		2.81	36.5	3.8
7	C	−20	−76.6	42	~9.5	3.56	50.1	14			
	C	32		(br singlet)			(br doublet)		7.12–7.62[f]		
	C	60	−76.6	(s, W=3.8)		3.53	(s, J=22.5[c])				
8	C	−20	−76.4	54	~10	3.48	49.3	13			
	C	32		(br doublet)			(br doublet)		6.9–7.8[f]		
	C	80	−76.8	(s, W=9)		3.46	(s, J=18[c])				
9	C	−5	−76.9	112	~9	3.64	65.5	14.1			
	C	32		(br doublet)			(br doublet)		7.1–7.9[f]		
	C	88	−76.4	(s, W=8)		3.62	(s, $J \leq 20$[c])				
10	M	−40	−76.37	63	9.5	3.53	19.2	13.5	1.77	—	4.5
	M	−5					(br singlet)		1.82	—	5
	M	30	−76.24	(s, W=2.8)		3.50	(singlet)		1.85	—	6
11	C	32	−76.54	150	9.4	3.23	47.6	14.1	1.94	58.8	—
	M	32	−77.0	130	10	3.27	45.5	14.0	1.92	58.4	—
	A	32	−76.41	135	—	3.46	33.5	14.5	2.08	60.5	—
	D	32	[d]	140	~9.5	3.53	31.5	14.5	1.99	61.0	—
	D	180	[d]	(coalesced[g])		3.47	(s, J=31.0[c])		2.12	59.0	—
12 (*cis*)	M	32	−77.1	91	9.5	3.32	48.5	14	1.78	—	1.5
12 (*trans*)	C	−20	−76.5	(singlet)		3.16	49.0	14[h]	2.72	—	5
	C	32	−76.8	(singlet)			(br singlet)		2.69	—	5
	C	60	[d]			3.15	(singlet)		2.66	—	4.8

[a]Chemical shifts from TMS (^1H) or $CFCl_3$ (^{19}F).
[b]C = $CDCl_3$; M = CD_2Cl_2; D = d_6-DMSO; A = d_6-acetone.
[c]Half-height peak width, Hz.
[d]No $CFCl_3$ standard was added to solutions intended for high-temperature spectra.
[e]Value of ^3J(Pt,H), Hz.
[f]Multiplet, C_6H_5—S group.
[g]Very broad singlet at 150°C.

(Throughout, we use the term *cis* and *trans* with reference to the arrangement of the two soft ligands, phosphine and thioether, in the complexes.) It is immediately clear from the nmr spectra that the Pt complex **11** contains only one isomer, while the Pd analog **12**, is a mixture of two. In addition to the ^1H and ^{19}F data shown in Table 2, the Pt complex has a ^{31}P signal consisting of a singlet with ^{195}Pt satellites, δ = −1.87 ppm, ^1J(Pt,P) = 3455 Hz, while the Pd complex has two singlet ^{31}P signals, at 23.9 and 21.5 ppm.

Based on the known chemistry of the two metals, it would be expected that the antisymbiotic effect (6) would be stronger for the Pt complex, resulting in preferential formation of the isomer where the two soft ligands (PPh_3 and S—CH_3) are *cis* to each other. The nmr data are entirely consistent with this assignment. Firstly, there is no observed coupling from the CH_3—S group to phosphorus, whereas a value of 4–5 Hz for ^4J(P,H) is consistently observed for coupling to *one* phosphorus nucleus in the cationic type **1** complexes. It is well-established that *trans* coupling is considerably stronger than *cis*, so the absence of coupling is consistent with *cis* geometry in **11**. Secondly, ^3J(Pt,H) for the —SCH_3 group is 58–61 Hz, consistent with the presence of a *trans* chloride ligand, whereas in complex **3**, ^3J is only 40.8 Hz.

The CH_3 resonance in **11** is at 1.9–2.1 ppm, *more shielded* than the resonance in the free ligand (2.20 ppm), whereas the shift on coordination is in the opposite direction (to 2.8–2.9 ppm) in Pt(Me—S—O)$_2$ (2). This shielding is almost certainly due to the effect of the aromatic ring anisotropy of the phenyl groups in the *cis*-phosphine ligand in **11**, and similar effects occur for the cationic type **1** complexes. An upfield shift

on coordination has also been observed in a ruthenium complex, and attributed to nonbonding interactions between S—CH_3 and phenyl groups (5).

An analogous system in which chelated thioether and phosphine are coordinated to platinum has been reported (7).

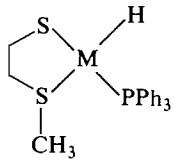

In this compound, the CH_3—S resonance is at 1.6 ppm, ^4J(P,H) = 1 Hz, and ^3J(Pt,H) = 14 Hz. The small coupling of the methyl protons to phosphorus, and the very greatly reduced coupling to platinum, are consistent with hydride *trans* to SCH_3, rather than the phosphine as the authors suggest.

The methylene signal of **11** consists of an AB pattern (67%) with $J_{AB} \approx 14$ Hz, a typical value for geminal protons, which is superimposed on a well-defined ABX pattern (33%) due to coupling with ^{195}Pt. The latter is symmetrical, with $J_{AX} = J_{BX} = 31.0$ Hz. On raising the temperature, the difference between inequivalent methylene protons decreases as thioether inversion becomes more rapid. Coupling to ^{195}Pt persists throughout, demonstrating a nondissociative mechanism of inversion. At 180°C, the highest temperature attainable in DMSO solution, the former have collapsed to a sharp singlet with satellites; ^3J(Pt,H) = 31.0 Hz. The peaks from the inequivalent CF_3 groups consist of a doublet of quartets at 32°C; the latter collapse into two broad singlets at ~110°C and to one very broad singlet around 150°C. The higher coalescence temperature is due to the greater difference in chemical shift of the ^{19}F signals.

With the palladium complex **12** it is possible to observe isomerization in solution. Freshly prepared samples show a preponderance of one isomer (*cis*) which corresponds to the solid-state form. After ~10 min in solution, this has equilibrated into the *cis–trans* mixture, whose composition is solvent and temperature dependent. At 32°C, the *cis* isomer amounts to 54% in CD_2Cl_2 but only 18% in $CDCl_3$, the latter dropping to 13% at 60°C.

Discrimination of these isomers is made on the same arguments as for **11**. The two CH_3—S signals are at 1.78 ppm with ^4J(P,H) = 1.5 Hz and at 2.72 ppm with ^4J = 5 Hz; the combination of greater shielding and smaller coupling clearly indicates that the former has CH_3—S *cis* to phosphine.

Signals from the methylene protons in **12** show AB patterns for both *cis* and *trans* isomers. The former is resolved at ambient temperature, but the latter only gives sharp signals on cooling to −20°C. Coupling to ^{31}P (^4J = ~2.5 Hz) then appears for one of the CH_2 protons of the *trans* isomer. On heating to 60°C, the methylene signal of the *trans* isomer collapses to a sharp singlet; it is not possible to observe this accurately for the *cis* isomer because its population drops as the temperature is raised, but it may be estimated that its coalescence temperature is at least 30°C higher than *trans*. This is in accord with the geometrical assignments, as the *trans* effect on thioether inversion of PPh_3 is expected to be significantly greater than that of Cl^- (8, 9).

The ^{31}P signals of *cis* and *trans* **12** were assigned from a comparison of their relative intensities in different solvents where populations had been established using ^{1}H and ^{19}F nmr spectra, from which the peak at 23.9 ppm is assigned to the *cis* isomer and that at 21.5 ppm to the *trans*. The latter is therefore slightly more shielded by the presence of the *trans* thioether, consistent with previous observation that a ligand of greater *trans* influence shifts a ^{31}P resonance to higher field (10).

The ^{19}F nmr spectra of complex **12** show an interesting difference between isomers. The *cis* form shows the usual doublet of quartets associated with inequivalent geminal CF_3 groups, but the *trans* form gives a singlet signal even at −20°C. As noted above, the methylene protons in this isomer give an AB doublet showing inequivalence because of the adjacent pyramidal thioether. The unusual nmr equivalence of the CF_3 groups is also seen in the cationic complex **3**.

(ii) Cationic type 1 phosphine complexes

In the presence of chloride, complexes of type **11** and **12** form by displacement of phosphine. Removal of Cl^- with Ag^+ leads to the isolation of the cationic complexes, in which the ligand *trans* to the thioether is also a phosphine. The ^{31}P data for these complexes are summarized in Table 3. The two phosphines are, of course, required to adopt *cis* geometry by the presence of the chelating coligand, and spectra are consistent with the presence of two inequivalent ^{31}P nuclei. We denote the phosphine *trans* as P_B. The coupling between them, $^2J(P_A,P_B)$ lies within the narrow range of 24.0–26.1 Hz. This is typical of *cis* phosphine complexes, for example, in the dihalide complexes $PtX_2(PMe_3)_2$, ^2J(P,P) is 18.9, 16.2, and 14.0 for X = Cl^-, Br^-, and I^-, respectively, compared to values of ~500 Hz in the *trans* isomers (11).

Two arguments may be used in the assignment of the ^{13}P signals to P_A and P_B. Firstly, in complexes of Me—S—O^-, coupling of 4–5 Hz is observed from CH_3 protons to *one* phosphorus nucleus. Selective decoupling experiments then show that, in all cases, this coupling is to the ^{31}P with the downfield resonance. There is ample precedent to show that the *trans* phosphine couples more strongly than the *cis* in square-planar complexes (12), so the downfield resonance may be assigned to P_A. Secondly, the cationic PPh_3 complex **3** may be compared with the neutral complex **11**, which we have shown to have the phosphine and thioether functions *cis*. The ^{31}P peak in **11** is at −1.87 ppm, whereas those in **3** are at 14.75 and 0.44 ppm, so the latter is more likely to correspond to P_B, *cis* to the thioether group.

The differences in the value of ^1J(Pt,P) between P_A and P_B for the various complexes are given in Table 3, and show a consistent trend. In the two series, using either Me—S—O^- or Ph—S—O^- as coligand, the value of Δ^1J(P) increases as phenyl groups in PR_3 are successively replaced by methyl. Although ^1J is decreasing for both P_A and P_B in these sequences, it drops more rapidly for P_B. Thus, in going from PPh_3 (**3**) to PPh_2Me (**4**), ^1J decreases by 125 Hz for P_B but only 54 Hz for P_A. The value of ^1J(Pt,P) for P_A *trans* to the thioether function of the hybrid ligand is consistently smaller by ~60 Hz. for each Me—S—O^- complex than for its Ph—S—O^- analog, showing the expected greater *trans* influence of the methylthioether. The value of ^1J for P_B only changes by ~10 Hz between each pair of complexes, consistent with our assignment that this phosphine is *trans* to alkoxide in each case.

For the palladium complex **10**, assignment of the two ^{31}P signals was carried out by comparison with neutral complex **12**. The downfield resonance (δ = 30.0 ppm) is associated with P_B, and that to higher field (δ = 25.6 ppm) with P_A. The difference between these (6.4 ppm) is greater than that found between *cis*

TABLE 3. ^1H and ^{31}P nmr data on phosphine

Compound	L	Solvent[b]	R_3P_A ligand[c] $\delta(P_A)$ (ppm)	$^1J(Pt,P_A)$ (Hz)	$\delta(CH_3)$ (ppm)	$^3J(Pt,H)$ (Hz)	$^2J(P_A,H)$ (Hz)
3	PPh_3	—	14.75	3410	—	—	—
4	PPh_2Me	M	6.77	3356	2.11	32	12
5	$PPhMe_2$	C	−8.71	3291	1.87, 1.72[f]	32	12
6	PMe_3	M	−14.78	3240	1.75	34.7	12.0
7	PPh_3	—	14.10	3466	—	—	—
8	PPh_2Me	C	3.91	3415	2.19	32.8	11.8
9	$PPhMe_2$	C	−8.31	3353	1.91	37, 30[f]	12

[a]At 32°C. ^{31}P chemicals shifts from $(MeO)_3PO$(ext), positive shifts to low field; all ^{31}P spectra proton decoupled.
[b]For ^1H spectra (M = CD_2Cl_2, C = $CDCl_3$); all ^{31}P spectra were run in CH_2Cl_2, 0.1 *M*.
[c]R_3P_A *trans* to sulfur, R_3P_B *trans* to oxygen.
[d]Chemical shift difference, $\delta(P_A) - \delta(P_B)$.
[e]Difference in coupling constants, $^1J(Pt, P_A) - (^1J(Pt,P_B)$.
[f]Complex at 32°C; chemical shifts refer to 0°C, see text.

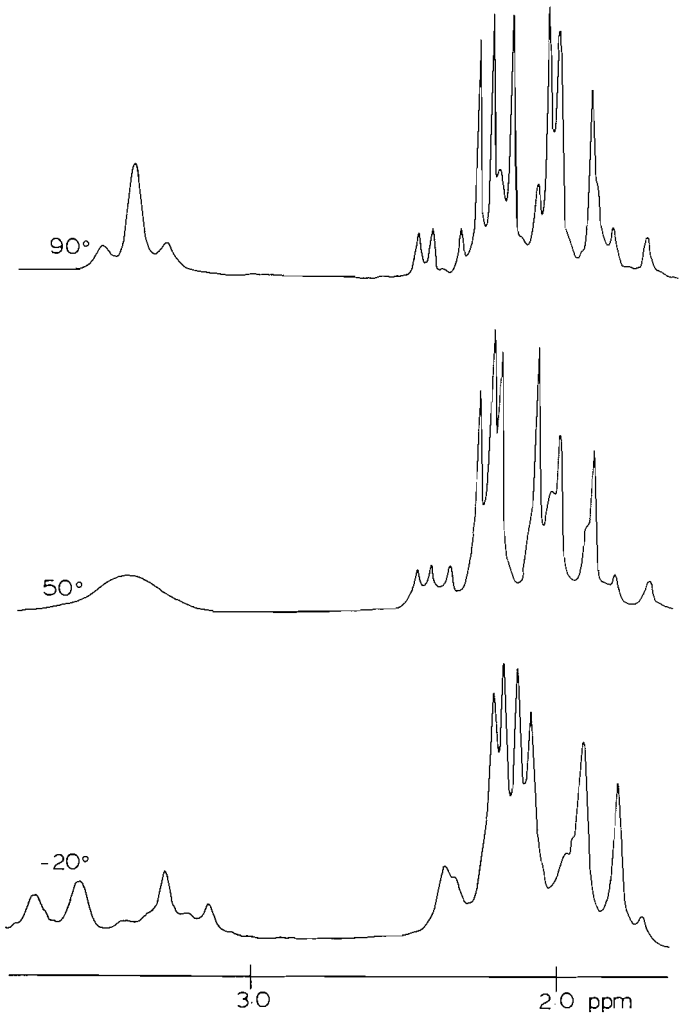

FIG. 1. The ^1H nmr spectrum of $[Pt(Me—S—O)(PPh_2Me)]^+$, **4**, showing coalescence of the CH_2 signal.

and *trans* forms of **12** (2.4 ppm), but less than the 14.3 ppm found in the Pt complex **3**. The value of $^2J(P_A,P_B)$ (23.7 Hz) is very similar to that in **3**. The relative positions of the ^{31}P resonances in the Pd complex are opposite to the assignments in the Pt series **3–9**, with P_B to low field of P_A, but such a reversal has been noted before in the *cis* and *trans* forms of the Pt and Pd complexes $MCl_2(PR_3)_2$ (13).

Variable temperature nmr studies were needed for a complete characterization of the ^1H and ^{19}F nmr spectra of the cationic complexes. Those of the Pt complexes with phosphines as coligand were generally similar, and the PPh_2Me complex **4**, shown in Fig. 1, will be discussed as an example.

At −20°C, the limiting[2] low temperature for this compound, the methyl region of the spectrum contains three doublets with doublet satellites, which are associated with CH_3S, CH_3P_A, and CH_3P_B. Each methyl group is coupled to both phosphorus and platinum, and ^4J for the CH_3S—P coupling is about half that of ^2J for CH_3—P coupling. The ^3J couplings for CH_3S—Pt and CH_3P_B—Pt are comparable, but that for CH_3P_A—Pt is smaller.

The ligand CH_2 resonance has a typical AB pattern (J_{AB} = 14 Hz, Δ_{AB} = 38.5 Hz) superimposed on a smaller ABX pattern due to coupling to ^{195}Pt. In contrast to the spectrum of the neutral complex **11**, this ABX pattern is unsymmetrical and buried under the major peaks, making analysis impossible. The ^{19}F spectrum[3] at −20°C consists of a doublet of quartets (J_{AB} = ~9.5 Hz, Δ_{AB} = 68.5 Hz), with slight second-order distortion, associated with the inequivalent geminal CF_3 groups.

The limiting high-temperature spectrum of complex **4** was run in $CDCl_3$ (sealed tube). All of the CH_3 resonances show some degree of temperature dependence in their chemical shifts, causing major changes in the appearance of the spectra (although the parameters are not greatly altered). The methylene signal is a fairly broad singlet, with ^3J coupling to ^{195}Pt of 20.5 Hz, less than ^3J for the CH_3S group (38 Hz). The ^{19}F signal has also collapsed to a singlet at 90°C; further sharpening would undoubtedly occur at higher temperatures, but no further information would be obtained.

In the spectrum of the $PPhMe_2$ complex **5**, most features are similar to those of **4** discussed above. However, there is a conspicuous difference in the low-temperature spectrum of the CH_3—P groups, which appear as *four* equal signals divided into two groups of two, all having essentially equal coupling to

[2]By limiting we imply that no significant change occurred in the spectrum when the temperature range was extended.

[3]No attempt was made to record the signal due to the BF_4^- counterion, which lies ~7000 Hz to high field of the CF_3 region.

ligands in cationic Pt complexes[a]

R_3P_B ligand[c]					P_A–P_B		
$\delta(P_B)$ (ppm)	$^1J(Pt,P_B)$ (Hz)	$\delta(CH_3)$ (ppm)	$^3J(Pt,H)$ (Hz)	$^2J(P_BH)$ (Hz)	$^2J(P_A,P_B)$ (Hz)	$\Delta\delta(P)$[d] (ppm)	$\Delta^1J(P)$[e] (ppm)
0.44	3374	—	—	—	24.0	14.31	36
−14.57	3249	1.88	37	11	25.2	21.34	107
−28.67	3170	1.78, 1.72[f]	34	11	25.2	19.96	121
−38.65	3090	1.84	35.0	11.1	26.1	23.87	150
−0.24	3384	—	—	—	24.2	14.34	82
−17.65	3255	1.80	36.4	11.0	25.1	21.56	160
−29.35	3181	1.51	34.0	11.0	25.3	21.04	172

^{31}P and ^{195}Pt. (The signals overlap, and selective decoupling was needed to resolve them.) They merge into the usual two peaks at high temperature. This low-temperature inequivalence can be explained by slow rotation (on the nmr time-scale) about the Pt–P bonds, associated with steric interaction, which could lead to conformational isomers having different environments for the methyl groups.

When the same phosphine is used as a coligand with the phenylthioether Ph—S—O^-, giving complex **9**, a similar effect is seen. In the low-temperature spectrum, two signals (each a doublet with ^{195}Pt satellites) are seen for CH_3—P_A, but only one signal for CH_3—P_B. This suggests that, in this complex, the steric restraints are such that there is restricted rotation about the Pt—P_A bond, but not the Pt—P_B bond. Alternatively, the preferred conformation may be such that the CH_3 groups attached to P_B are in similar environments.

For the PPh_3 complex **3**, the ^1H and ^{31}P nmr spectra are normal, but the ^{19}F signal is anomalous. It consists of a singlet, even at −20°C, indicating equivalent geminal CF_3 groups in the chelate ring. Under the same conditions, and up to 32°C, the adjacent methylene protons give the usual AB doublet because of the presence of the pyramidal thioether. A complete structural investigation of **3** (and, for comparative purposes, the PPh_2Me complex **4**) has been carried out to clarify this anomaly.[4]

The only cationic complex of palladium studied was $[Pd(PPh_3)_2(Me—S—O)]^+$, **10**. Its ^1H and ^{19}F spectra are similar to those of the Pt analog **3**, except that the coalescence temperature is considerably lowered; this difference is generally observed for thioether complexes of Pd and Pt (14). The CH_2 and CF_3 signals show the usual inequivalence at −40°C, but both have become equivalent at 32°C. The CH_3S signal is a doublet through coupling to the *trans* phosphine; $^4J(Pt,H)$ = 4.5 Hz, the same value as in **3**.

Thioether inversion studies

We have previously reported studies of inversion of coordinated thioethers in a number of systems where fluorinated alkoxide donors are also present, namely perfluoropinacol complexes $M(PFP)(SR_2)_2$, M = Pt or Pd (3), and neutral complexes of the hybrid ligands $M(R—S—O)_2$, M = Pt or Pd (2). In the present work, we have taken the same general approach; that is, we have obtained rate constants, and hence the inversion barrier $\Delta G^{\ddagger}$, from observations of band-widths at the coalescence point in variable-temperature nmr spectra. The treatment of data has been discussed in our previous papers and follows that given by Sandström (15).

In the complexes described in this paper, thioether inversion may be followed by observing the nmr signal of either the CH_2 protons or the CF_3 groups of the ligand, both of which will show inequivalence because of the presence of the pyramidal coordinated sulfur atom. In the former, this leads to AB type doublets at the lower limiting temperature, which coalesce to A_2 singlets. The spectral changes accompanying coalescence for complex **4** (Fig. 1) show the ^{195}Pt satellites in the limiting high-temperature spectrum, and the ABX pattern, at low intensity, visible under the dominant AB pattern at low temperatures. We have not attempted to account for Pt coupling in the inversion studies, and the contribution of the coupled nuclei to the linewidth at coalescence is assumed to be negligible.

A closed solution for the rate of exchange at the coalescence point for an AB spin system has been derived (15), and the rate constant, k, is given by

$$k = \pi \left[\frac{(w^*)^2 + 6J^2}{2} \right]^{1/2}$$

Here, w^* is the half-height linewidth at coalescence, and J is the coupling constant J_{AB}, which we have obtained from the low-temperature limiting spectra. The calculations are summarized, and the results presented in Table 4.

Inversion at sulfur exchanges ^{19}F signals from the CF_3 groups in A_3X_3 or A_3B_3 systems to yield eventually a singlet A_6 type spectrum. No closed analytical expression exists for this process, and previous Dnmr studies of CF_3 exchange have generally employed complete band-shape fitting. However, in cases where the value of Δ_{AB} is large, the effect on a doublet-of-quartets pattern of increasing the exchange rate is firstly to collapse the quartets internally into two broad singlets, then for this pattern to undergo further collapse into one broad singlet. We have, therefore, taken the simplified approach of applying the equation of Gutowsky and Holm (16) to the CF_3 spectra, taking the linewidth at half-height of this second coalescence point as Δ_{AB}. Calculations based on the ^{19}F spectra are summarized in Table 4; values of the activation energies

[4]R. T. Boeré, N. C. Payne, and C. J. Willis. Unpublished results.

TABLE 4. Calculations for the exchange of CH_2 and CF_3 signals

Compound	CH_2 signal data[a]				CF_3 signal data			
	w^*(Hz)	$k(s^{-1})$	T_c(K)	$\Delta G^{\ddagger}$(kJ/mol)	w^*(Hz)	$k(s^{-1})$	T_c(K)	$\Delta G^{\ddagger}$(kJ/mol)
3	34	106	315[b]	65±1				
4	28	98.4	317	66±1	55	122	328	67±1
5	48	133	329	67±1	165	367	338	67±1
6	22	90.5	321	67±1	133	296	343	68±1
7	35	109	311	64±1	23	51.1	303	64±1
8	32	100	323	67±1	40	89	318	66±1
9	42	120	318	65±1	85	189	327	66±1
10	17	82.6	268	56±1				
11	27.5	99.8	413	82±1	~130	~288	423	~85[c]
12 (*cis*)	~30	~101	343-8	71–72				
12 (*trans*)	31	103	301	62±1				

[a]J_{AB} values are given in Table 2.
[b]Estimated error on T_c values is ±5 K.
[c]Estimate; very broad line.

obtained in this way must be considered as approximations, especially as the value of Δ_{AB} decreases.

Mechanism of inversion of thioethers

The results of these studies further substantiate the application of the classical mechanism of inversion to coordinated thioethers, developed by Abel and coworkers (17). Key points of this approach, which we have developed in previous papers (2, 3), can now be applied to a further range of complexes.

(i) Metal dependence

Isostructural complexes of Pt and Pd can be compared in two cases in this series. For the neutral complexes **11** and **12**, $\Delta G^{\ddagger}$ is 10–11 kJ lower for Pd, while between the cationic pair with PPh_3 as coligand, **3** and **10**, the Pd complex is lower by ~8 kJ. We have previously noted a reduction of ~16 kJ in $\Delta G^{\ddagger}$ in the neutral bis-complexes M(R—S—O)$_2$ in going from Pt to Pd (2). The lower barriers in the case of Pd are consistent with its lower electronegativity (1.35 versus 1.44 (18)) and with the better π overlap between metal and sulfur, leading to stabilization of the transition state.

(ii) Substituent on sulfur

A comparison of the $\Delta G^{\ddagger}$ values for analogous complexes of Me—S—O$^-$ and Ph—S—O$^-$ shows little, if any, difference beyond experimental error. A reduction of the barrier has been observed when the backbone of a chelated thioether is replaced by an aromatic group, and this has been attributed to stabilization of the transition state by π conjugation with the ring (14, 19). However, in complexes with nonchelating aromatic substituents on sulfur, of the type M←S(R)Ph, a slight *increase* in $\Delta G^{\ddagger}$ compared to the Me—S analog (0.5–0.6 kJ mol^{-1}) has been noted (20), suggesting free rotation about the C—S bond and minimal conjugation effects. Such a change is below the experimental error in our data.

(iii) Trans *effect and the barrier to inversion*

The data available now, in conjunction with previous results (2), enable us to establish a *trans*-effect series for Pt and Pd thioether complexes that includes, for the first time, phosphines. Using the data in Table 4, where the thioether group is part of the hybrid ligand chelated to Pt in each case, the order of decreasing barrier height (that is, of *increasing trans* effect) as the *trans* ligand is varied is

	Compound		
	Pt(Me—S—O)$_2$	**11**	**3–6**
Trans-function	—C(CF$_3$)$_2$O$^-$	Cl	PR_3
Barrier, kJ/mol	89±1	82±1	65–67

Data from the Pd complexes show a parallel trend

	Compound			
	cis-Pd(Me—S—O)$_2$	*cis*-**12**	*trans*-Pd(Me—S—O)$_2$	**10**
Trans function	—C(CF$_3$)$_2$O$^-$	Cl$^-$	—S—CH$_3$	PR_3
Barrier, kJ/mol	73.5±1	71–72	68±1	56±1

Within the phosphine series, the differences are not significant, the barrier ranging from 67 ± 1 kJ with PMe_3 to 65 ± 1 kJ with PPh_3 as ligand. A recent study by Gosling and Tobe (21) of the kinetic *trans* effect on ligand substitution rates has given the order $SR_2 < OSR_2 < AsR_3 < PR_3 < P(OR)_3$. These workers also note that the effect of substitution of R groups in phosphines is small, and that the relative positions in the series of PMe_3 and PPh_3 depend on the nature of the reaction being studied. A study on various substituted thioethers led them to a similar conclusion (22).

Our results are, in general, complementary to those of Gosling and Tobe, and show that the use of thioether inversion barriers as a measure of the *trans* effect leads to the expected placing of the phosphines at the high end of the scale.

Acknowledgment

We are grateful to the Natural Sciences and Engineering Research Council of Canada for support of this work in the form of an operating grant to C.J.W. and a scholarship to R.T.B.

1. R. T. BOERÉ. Ph.D. Thesis, University of Western Ontario. London, Ont. 1984.
2. R. T. BOERÉ and C. J. WILLIS. Can. J. Chem. **63**, 3530 (1985).
3. R. T. BOERÉ and C. J. WILLIS. Inorg. Chem. **24**, 1059 (1985).
4. S. G. MURRAY and F. R. HARTLEY. Chem. Rev. **81**, 365 (1981).
5. D. M. ROUNDHILL, S. G. N. ROUNDHILL, W. B. BEAULIEU, and U. BAGCHI. Inorg. Chem. **19**, 3365 (1980).
6. R. G. PEARSON. Inorg. Chem. **12**, 712 (1973).
7. T. B. RAUCHFÜSS and D. M. ROUNDHILL. J. Am. Chem. Soc. **97**, 3386 (1975).
8. R. J. CROSS, G. J. SMITH, and R. WARDLE. Inorg. Nucl. Chem. Lett. **7**, 191 (1971).
9. R. J. CROSS, I. G. DALGLEISH, G. J. SMITH, and R. WARDLE. J. Chem. Soc. Dalton Trans. 992 (1972).
10. P. S. PREGOSIN and R. W. KUNZ. ^{31}P and ^{13}C NMR of transition-metal phosphine complexes. NMR basic principles and progress. Vol. 16. Springer-Verlag, Berlin. 1979.
11. R. J. GOODFELLOW and B. F. TAYLOR. J. Chem. Soc. Dalton Trans. 1676 (1974).
12. J. G. VERKADE. Coord. Chem. Rev. **9**, 1 (1972).
13. (*a*) S. O. GRIM, R. L. KEITER, and W. MCFARLANE. Inorg. Chem. **6**, 1133 (1967); (*b*) S. O. GRIM and R. L. KEITER. Inorg. Chem. Acta **4**, 56 (1970).
14. E. W. ABEL, S. K. BHARGAVA, K. KITE, K. C. ORRELL, V. SIK, and B. C. WILLIAMS. Polyhedron, **1**, 289 (1982).
15. J. SANDSTRÖM. Dynamic NMR spectroscopy. Academic Press, New York. 1982. p. 77.
16. H. S. GUTOWSKY and C. H. HOLM. J. Chem. Phys. **25**, 1228 (1956).
17. E. W. ABEL, K. G. ORRELL, and S. K. BHARGAVA. Prog. Inorg. Chem. **32**, 1 (1984), and references cited therein.
18. E. J. LITTLE and M. M. JONES. J. Chem. Educ. **37**, 231 (1960).
19. F. R. HARTLEY, S. G. MURRAY, W. LEVASON, H. E. SOUTTER, and C. A. MCAULIFFE. Inorg. Chim. Acta, **35**, 265 (1979).
20. E. W. ABEL, G. W. FARROW, K. G. ORRELL, and V. SIK. J. Chem. Soc. Dalton Trans. 42 (1977); 47 (1977).
21. R. GOSLING and M. L. TOBE. Inorg. Chem. **22**, 1235 (1983).
22. R. GOSLING and M. L. TOBE. Inorg. Chem. Acta **42**, 223 (1980).

Structural parameters for the chair or twist-boat conformations of 1,3-dioxa-5,6-benzocycloheptene and its 2-methyl and 2,2-dimethyl derivatives

ROBERT ST-AMOUR, MARC J. OLIVIER, MAURICE ST-JACQUES,[1] AND FRANÇOIS BRISSE[1]
Département de Chimie, Université de Montréal, C.P. 6128, Succ. A, Montréal (Qué.), Canada H3C 3J7
Received July 31, 1985

ROBERT ST-AMOUR, MARC J. OLIVIER, MAURICE ST-JACQUES, and FRANÇOIS BRISSE. Can. J. Chem. **64**, 500 (1986).

Low temperature X-ray studies of 1,3-dioxa-5,6-benzocycloheptene (**1**) and its 2-methyl (**2**) and 2,2-dimethyl derivatives (**3**) show that **1** and **2** exist in the crystal state exclusively in the chair (*C*) form while **3** exists exclusively in the twist-boat (*TB*) form. The final values of the agreement index, R_w, are 0.048, 0.059, and 0.046 for **1**, **2**, and **3**, respectively. Significant structural differences between the g^+g^+ arrangement of the acetal moiety with the *TB* form and the g^+g^- disposition in the *C* form are revealed. These differences can be interpreted as arising from a less efficient back-donation of an antiperiplanar lone pair on the oxygen atom in the g^+g^+ relative to the g^+g^- arrangement. Furthermore, the C—O bond lengths shed some light on the hybridization state of the lone pairs of electrons on oxygen. Finally the results are used to rationalize nmr observations in terms of molecular conformations in solution.

ROBERT ST-AMOUR, MARC J. OLIVIER, MAURICE ST-JACQUES et FRANÇOIS BRISSE. Can. J. Chem. **64**, 500 (1986).

L'étude par diffraction des rayons X à basse température du dioxa-1,3 benzo-5,6 cycloheptène (**1**) et de ses dérivés méthyl-2 (**2**) et diméthyl-2,2 (**3**) montre que **1** et **2** existent à l'état solide seulement sous la forme chaise (*C*) alors que **3** n'existe que sous la forme bateau-croisé (*TB*). Les valeurs finales du facteur d'accord R_w sont 0,048, 0,059 et 0,046 pour **1**, **2**, et **3** respectivement. Des différences structurales significatives entre l'arrangement g^+g^+ du groupe acétal dans la forme *TB* et la disposition g^+g^- dans la forme *C* sont mises en évidence. On interprète ces différences par une rétrodonation moins efficace du doublet antipériplanaire de l'oxygène dans l'arrangement g^+g^+ relativement à l'arrangement g^+g^-. De plus, les longueurs des liaisons C—O clarifient le type d'hybridation des doublets de l'oxygène. Finalement, ces résultats permettent de rationaliser les observations de rmn sur les conformations des molécules en solution.

Introduction

In recent years, we have studied the conformational properties of 1,3-dioxa-5,6-benzocycloheptene **1** and several derivatives in solution (1, 2) by means of ^1H and ^{13}C dnmr (dynamic nuclear magnetic resonance) methods. They reveal the existence of a mixture of the chair form **1***A* and the twist-boat form, **1***B*, in a ratio of 79:21 (in CHF_2Cl, at −130°C) (1).

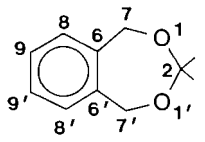

1

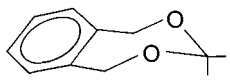

1A

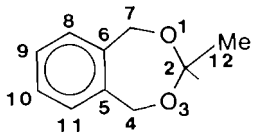

2

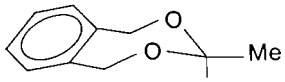

2A

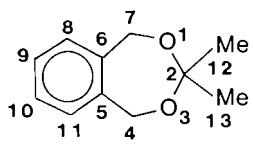

3

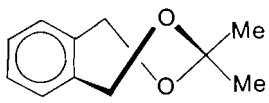

3B

Whereas the presence of a methyl group on the acetal carbon, C(2), slightly stabilizes the C_e form,[2] **2***A*, (96% at −115°C) (2), the addition of a second methyl on the same carbon destabilizes the *C* form completely in favor of the *TB* form, **3***B* (100%). This conformational behaviour was rationalized in terms of electronic and steric factors.

It is known that changes in electronic interactions can produce significant structural modifications in some organic compounds. For example, crystallographic studies (3) show that the bond distances in the C—O—C—O—C sequence in carbohydrates are dependent upon the orientation of the polar substituents on the anomeric carbon. The title compounds contain the same sequence of atoms, so that some structural differences between the chair and the twist-boat conformations might be expected.

To our knowledge, only the *TB* form of an analogue, 5,6-dichloro-2-*p*-nitrophenyl-1,3-dioxacyclohept-5-ene, **4**, has

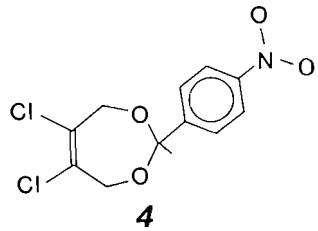

4

been characterized and no structural information regarding the chair form has been found. This lack of information suggests a crystallographic investigation of compounds **1**, **2**, and **3**, yielding a precise characterization of the shape of the two most important conformations of the seven-membered ring containing the acetal function. Such data also permit a more complete assessment of the dependence of the structural parameters on electronic factors.

Experimental

The three compounds were prepared by known procedures (1, 2). Crystals of **1** were obtained by a bulb-to-bulb sublimation in a Kugelrohr apparatus. Those of **2** were grown at room temperature by sublimation onto a cold finger while crystals of **3** were recrystallized in an ethanol–water mixture. All X-ray measurements have been made at low temperature using the locally modified Nonius liquid nitrogen low temperature attachment.

[1]Authors to whom correspondence may be addressed.

[2]The abbreviations *C* and *TB* are used for the chair and the twist-boat conformations, respectively. Furthermore, the chair form **2***A* with an equatorial methyl group is represented by C_e.

TABLE 1. Crystal data of interest

Parameter	Compound 1A	2A	3A
Molecular formula	$C_9H_{10}O_2$	$C_{10}H_{12}O_2$	$C_{11}H_{14}O_2$
Molecular weight	150.179	164.206	178.233
$F(000)$	320	352	768
Melting point (°C)	37–38	55–57	101–102
Unit cell	Orthorhombic	Monoclinic	Orthorhombic
a (Å)	8.450(6)	10.117(3)	6.354(6)
b	10.709(7)	7.975(4)	20.001(6)
c	8.412(4)	12.822(4)	15.068(3)
β (deg)	90	123.15(2)	90
V (Å^3)	761.2	866.1	1915.0
d_{calc} (g cm^{-3})	1.321	1.259	1.236
Z	4	4	8
Space group	*Pnma*	$P2_1/c$	*Pbca*
Radiation, Kᾱ (Å)	Mo, 0.71069	Cu, 1.54178	Cu, 1.54178
μ(Kα) (cm^{-1})	0.864	6.63	6.35
T (°C)	−70(2)	−50(2)	−50(2)
Crystal size (mm)	0.20 × 0.20 × 0.08	0.44 × 0.28 × 0.04	0.54 × 0.24 × 0.02

The accurate cell parameters and the intensity data were obtained on an Enraf–Nonius CAD4 diffractometer, using 25 reflections randomly found in the diffraction sphere. The space groups were chosen according to the symmetry of axial films and systematic absences in the measured intensities. Crystal data of interest are given in Table 1. The intensity data were collected by the ω/2θ scan technique using graphite monochromatized Kα radiation (either Cu or Mo). The intensities of three reference reflections were monitored every hour to assess the stability of the crystals. The orientation of the crystals was verified after every 100 measurements. Structure factors were obtained after scaling of the intensity data and Lorentz and polarization corrections were applied.[3] No attempt was made to correct for absorption because the absorption coefficients were small. Furthermore, the FLAT option of the Nonius diffractometer was used for both **2** and **3**. This option allows for the intensity measurement to be made in an orientation which minimizes the absorption effects. The details of the data collections are summarized in Table 2. The structures were solved using the MULTAN set of programs. All non-hydrogen atoms were revealed in each case in the first computed E-map. The weighted least-squares refinement of the atomic coordinates, minimizing $\Sigma w(|F_o| - |F_c|)^2$, was conducted with anisotropic temperature factors for C and O atoms and isotropically for H atoms. The weights were derived from the counting statistics of the intensities. The refinements were concluded when the largest (displacement/σ) ratio was less than 0.30. The details of the least-squares refinements are given in Table 2 for all three compounds.

The scattering curves for non-hydrogen atoms were taken from ref. 5 and those for H atoms for ref. 6. The atomic coordinates for the compounds under investigation are listed in Table 3. The tables of observed and calculated structure factors are part of the supplementary material.[4]

[3]The programs used here are modified versions of NRC-2, data reduction; NRC-10, bond distances and angles; and NRC-22, mean planes; FORDAP, Fourier and Patterson maps (A. Zalkin); MULTAN, multisolution program; NUCLS, least-squares refinement; and ORTEP, stereodrawings (7–10).

[4]Structure factor tables, anisotropic temperature factor tables, details of the least-squares planes calculations, and the list of REFCODES of 1,3-dioxane containing compounds taken from the Cambridge Data File have been deposited. Copies may be purchased from the Depository of Unpublished Data, CISTI, National Research Council of Canada, Ottawa, Ont., Canada K1A 0S2.

Results and discussion

The atomic numbering is indicated on the structures **1**, **2**, and **3**. The packing diagrams for the three molecules are shown in Fig. 1. The bond distances and bond angles of the three compounds are listed in Table 4 and are compared to the corresponding quantities in **4**. The torsion angles of interest are listed in Table 5.

The conformations of the molecules fall into two categories. Compounds **1** and **2** have the *C* conformation with the acetal in the g^+g^- arrangement while compounds **3** and **4** have the *TB* conformation and a g^+g^+ acetal arrangement.

Previous theoretical studies of a model compound (3*d*), dimethoxymethane, have shown that an acetal sequence in the g^+g^- arrangement without constraint has an ideal torsion angle of 60°. Our observations in compound **1** (Table 5) are −75.0(2)° and 75.0(2)° for O(1)—C(2)—O(3)—C(4) and O(3)—C(2)—O(1)—C(1), respectively. The same torsion angles in compound **2** have values of −75.1(2)° and 74.4(2)°. The equatorial methyl group in **2***A* hardly perturbs the conformation of the seven-membered ring. The torsion angles are significantly lower than the experimental value of 82.7° reported for the g^+g^- disposition of dimethoxymethane (15).

In the twist-boat **3***B* with a g^+g^+ disposition, the torsion angles of interest have values of 47.1(2)° and 49.1(2)°. In **4** the same torsion angles are 51.6(4)° and 45.9(4)°. These quantities are significantly different from the calculated 62.4° and experimental 63.3° values for the g^+g^+ arrangement of dimethoxymethane (11).

From a study of a large number of 1,3-dioxane derivatives in the chair form, the average of 67 bond angles O(1)—C(2)—O(3) in the acetal sequence is 111.7°, a value slightly larger than the ideal for sp^3 hybridization. In compound **1**, this angle has a value of 113.6(2)° while in compound **2** it is 112.8(2)°. In contrast, in the twist-boat **3***B* this bond angle is only 109.6(2)°, rather close to the 110.5(3)° in **4**. A similar difference in bond angles is calculated by van Alsenoy *et al.* (11) in dimethoxymethane, for which the O—C—O angles in the g^+g^- and the g^+g^+ conformations are evaluated to be 115.7 and 112.4°,

TABLE 2. Summary of data collection and refinement

Parameter	Compound		
	1*A*	**2***A*	**3***B*
Scan range (deg)	$(1.0 + 0.35 \tan\theta)$	$(1.0 + 0.14 \tan\theta)$	$(1.0 + 0.14 \tan\theta)$
Scan rate (deg min^{-1})	1.7 to 10.0	1.7 to 10.0	1.5 to 10.0
$2\theta_{max}$ (deg)	55.0	140.0	140.0
h, k, l ranges	$0 \leq h \leq 10$	$0 \leq h \leq 12$	$0 \leq h \leq 7$
	$0 \leq k \leq 13$	$0 \leq k \leq 9$	$0 \leq k \leq 24$
	$0 \leq l \leq 10$	$-15 \leq l \leq 15$	$0 \leq l \leq 18$
Max. fluctuation of standard reflections (%)	2.3	5.6	2.5
Number of reflections measured	1099	1644	2184
Number of reflections observed	670	1339	1170
If $I \geq k\,\sigma(I)$, $k =$	1.90	1.90	2.50
$R = \Sigma\lvert\Delta F\rvert/\Sigma\lvert F_o\rvert$	0.040	0.046	0.042
$R_w = [\Sigma w \Delta F^2/\Sigma F_o^2]^{1/2}$	0.048	0.059	0.046
$S = [\Sigma w \Delta F^2/(m - n)]^{1/2}$	1.74	2.33	1.39
$(\text{Displacement}/\sigma)_{max}$	0.01	0.05	0.29
$(\text{Displacement}/\sigma)_{average}$	0.00	0.01	0.05
Extreme fluctuations of residual electron density (e $Å^{-3}$)	−0.23, 0.19	−0.23, 0.27	−0.20, 0.19

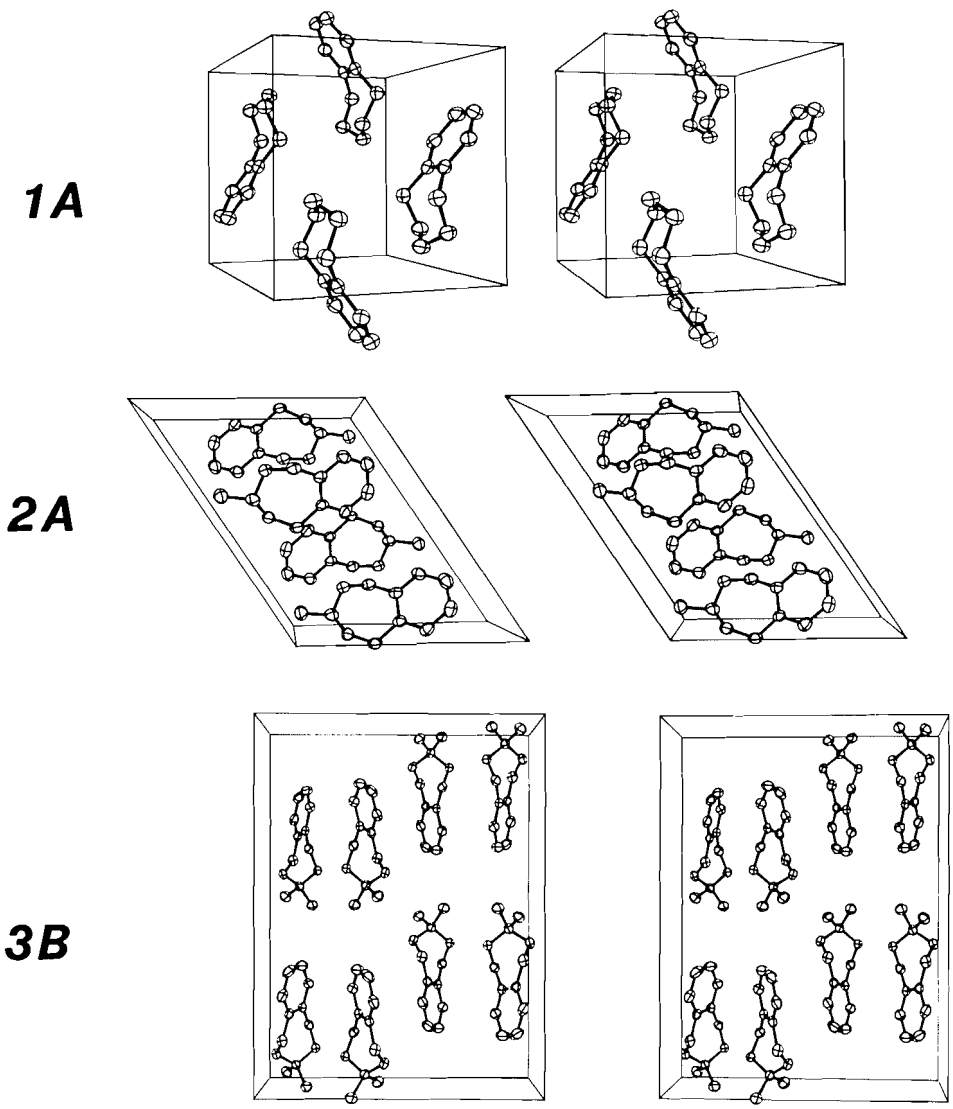

FIG. 1. Stereoviews of the molecules **1***A*, **2***A*, and **3***B* in their respective unit cells. For **1***A* and **2***A*, the *a* axis is horizontal while *c* is vertical. For **3***B*, *b* is horizontal and *c* is vertical.

TABLE 3. Fractional atomic coordinates for **1***A*, **2***A*, and **3***B*, ($\times 10^4$ for O and C atoms, $\times 10^3$ for H atoms), U_{eq} (Å^2, $\times 10^4$ for O and C), and U_{iso} (Å^2, $\times 10^3$ for H)

Atom	*x*	*y*	*z*	U_{eq}
1*A*				
O(1)	8203(1)	1399(1)	2110(1)	428
C(2)	7591(3)	2500	1429(3)	459
C(6)	8356(2)	1844(1)	4964(2)	312
C(7)	7558(2)	1124(2)	3656(2)	386
C(8)	9201(2)	1214(1)	6198(2)	384
C(9)	9853(2)	1857(2)	7415(2)	460
H(8)	908(2)	32(2)	619(2)	33
H(9)	1038(2)	138(2)	831(2)	51
H(21)	796(3)	250	35(4)	62
H(22)	643(3)	250	152(3)	39
H(71)	770(2)	22(2)	382(2)	36
H(72)	640(2)	130(1)	366(2)	33
2*A*				
O(1)	7503(1)	2558(2)	4774(1)	335
C(2)	7653(2)	1337(2)	4045(2)	347
O(3)	6271(1)	1162(1)	2849(1)	330
C(4)	5020(2)	274(2)	2824(2)	352
C(5)	4075(2)	1360(2)	3144(1)	305
C(6)	4805(2)	2186(2)	4299(1)	311
C(7)	6556(2)	2039(3)	5238(2)	375
C(8)	3886(2)	3137(2)	4576(2)	405
C(9)	2272(2)	3275(3)	3747(2)	477
C(10)	1548(2)	2466(3)	2605(2)	478
C(11)	2457(2)	1530(3)	2315(2)	396
C(12)	8950(2)	1893(3)	3884(2)	443
H(2)	798(2)	24(3)	452(2)	41
H(8)	437(2)	373(3)	536(2)	55
H(9)	164(3)	395(3)	393(2)	61
H(10)	38(3)	258(3)	201(2)	55
H(11)	190(2)	90(3)	149(2)	52
H(41)	431(2)	−15(2)	197(2)	29
H(42)	552(2)	−75(2)	341(2)	40
H(71)	688(2)	280(2)	597(2)	39
H(72)	686(2)	88(3)	555(2)	49
H(121)	995(3)	202(3)	468(2)	54
H(122)	912(3)	104(3)	339(2)	62
H(123)	869(3)	297(3)	345(2)	66
3*B*				
O(1)	3309(2)	1020(1)	1893(1)	289
C(2)	3839(3)	570(1)	1195(1)	300
O(3)	4918(2)	923(1)	511(1)	300
C(4)	6568(3)	1353(1)	816(1)	342
C(5)	5822(3)	2052(1)	1028(1)	307
C(6)	3863(3)	2175(1)	1420(1)	280
C(7)	2308(3)	1625(1)	1609(1)	312
C(8)	3309(4)	2831(1)	1621(1)	413
C(9)	4651(5)	3357(1)	1433(2)	546
C(10)	6572(4)	3237(1)	1045(2)	527
C(11)	7140(4)	2587(1)	842(1)	418
C(12)	1924(4)	271(1)	750(1)	401
C(13)	5188(4)	36(1)	1627(1)	418
H(8)	195(3)	291(1)	191(1)	50
H(9)	416(4)	381(1)	148(1)	54
H(10)	760(4)	361(1)	89(2)	67
H(11)	853(3)	249(1)	55(1)	48
H(41)	732(3)	114(1)	134(1)	47
H(42)	766(3)	135(1)	31(1)	47
H(71)	141(3)	175(1)	209(1)	47
H(72)	141(3)	155(1)	107(1)	36
H(121)	111(3)	62(1)	43(1)	46
H(122)	236(4)	−11(1)	37(1)	62
H(123)	88(3)	8(1)	121(1)	56
H(131)	431(4)	−23(1)	206(2)	80
H(132)	568(4)	−28(1)	118(1)	68
H(133)	642(3)	23(1)	191(1)	52

respectively. The larger angle values in g^+g^- may arise from *syn*-diaxial interaction between the two lone pairs on the oxygen. In our case, the *gem*-dimethyl effect (12) may also contribute to the 109° angle in **3***B*.

The structural parameters obtained for **1**, **2**, and **3** also allow us to assess the bond lengths to the anomeric carbon. A normal C—O bond length is 1.43–1.44 Å. For example, it is 1.425(5) Å in methanol and 1.435(5) Å in cyclopenteneoxide (16). These values are close to our results for the outer C—O bonds of the chair form **1***A*, 1.441(2) Å; **2***A*; 1.436(3) Å; and twist-boat **3***B*, 1.432(2) Å. On the other hand, the anomeric bond length of the acetal function is significantly shorter in the chair forms **1***A*, 1.409(2) Å; and **2***A*, 1.414(2), 1.408(2) Å; whereas in the twist-boat **3***B* the inner bond length is slightly longer, 1.425(2) Å. In the case of **4***B* one also notes that the anomeric C—O bonds are shorter than the outer C—O bonds.

The mean values of the inner and outer bond lengths in the acetal sequence reported for 67 1,3-dioxane rings in the Cambridge Data File are presented in Table 6. They are compared with their counterparts in dimethoxymethane and our own results.

It is of interest that, for the compounds studied here, it is also possible to rationalize the inner bond shortening in relationship to conformational changes in a manner similar to that used by Jeffrey (3*c*) for methylpyranosides.

According to many authors (3), the shortening of the inner C—O bond in a *gauche* conformation is due to the back-donation of one lone pair of an oxygen to the non-bonding orbital of the antiperiplanar C—O bond, as seen in **5**. The longer inner bond for the *TB* form **3***B*, which is in a g^+g^+ disposition compared to the *C* forms **1***A* and **2***A* possessing a g^+g^- conformation, may reflect a less efficient back-donation of the lone pair on the oxygen of the *TB* form because of a less favorable angular relationship.

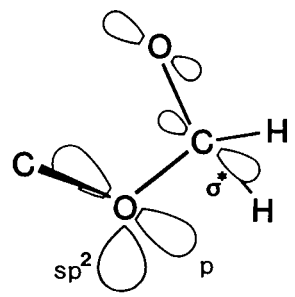

5

The difference in the extent of back-donation, and consequently of the inner C—O bond lengths, between the *C* and the *TB* forms can be readily explained if the oxygen is considered to be sp^2 hybridized instead of sp^3. Both hybridization states have been considered previously (3*b*, 13) without firm evidence for one or the other. Molecular models and the torsion angles in

TABLE 4. Comparison of bond distances and bond angles in various dioxabenzo cycloheptene molecular conformation

	Compound			
	1*A*	**2*A***	**3*B***	**4*B***
Distance				
O(1)—C(2)	1.409(2)	1.414(2)	1.425(2)	1.407(4)
O(3)—C(2)	*	1.408(2)	1.425(2)	1.413(4)
O(1)—C(7)	1.441(2)	1.438(3)	1.432(2)	1.428(4)
O(3)—C(4)	*	1.435(3)	1.432(2)	1.421(4)
C(6)—C(7)	1.503(2)	1.506(3)	1.506(3)	1.505(5)
C(5)—C(4)	*	1.504(3)	1.510(3)	1.497(4)
C(5)—C(6)	1.404(2)	1.406(2)	1.400(3)	1.324(4)
C(5)—C(11)	1.390(2)	1.387(3)	1.387(3)	—
C(6)—C(8)	*	1.388(3)	1.392(3)	—
C(11)—C(10)	1.386(2)	1.384(3)	1.383(3)	—
C(8)—C(9)	*	1.382(4)	1.384(3)	—
C(9)—C(10)	1.377(3)	1.387(3)	1.375(4)	—
C(2)—C(12)	—	1.502(4)	1.513(3)	—
C(2)—C(13)	—	—	1.516(3)	—
Angle				
O(1)—C(2)—O(3)	113.6(2)	112.8(2)	109.6(2)	110.5(3)
C(2)—O(1)—C(7)	112.6(1)	114.3(2)	114.7(1)	113.9(3)
C(2)—O(3)—C(4)	*	114.3(1)	114.7(1)	113.2(3)
O(1)—C(7)—C(6)	112.7(1)	113.9(2)	112.5(2)	111.8(3)
O(3)—C(4)—C(5)	*	113.2(2)	113.2(2)	111.2(3)
C(5)—C(6)—C(7)	120.9(1)	121.1(2)	122.3(2)	123.7(3)
C(4)—C(5)—C(6)	*	120.7(2)	122.1(2)	124.1(2)
C(7)—C(6)—C(8)	119.0(1)	119.8(2)	118.8(2)	115.1(3)
C(4)—C(5)—C(11)	*	120.5(2)	118.8(2)	113.3(3)
C(5)—C(6)—C(8)	119.0(1)	119.1(2)	118.9(2)	121.2(3)
C(6)—C(5)—C(11)	*	118.8(2)	119.1(2)	122.5(3)
C(6)—C(8)—C(9)	121.2(1)	121.5(2)	121.1(2)	—
C(5)—C(11)—C(10)	*	121.7(2)	121.5(2)	—
C(8)—C(9)—C(10)	119.8(2)	119.7(2)	120.1(2)	—
C(9)—C(10)—C(11)	*	119.3(2)	119.3(2)	—
O(1)—C(2)—C(12)	—	107.8(2)	112.8(2)	109.2(3)
O(3)—C(2)—C(12)	—	107.5(2)	105.2(2)	111.6(3)
O(1)—C(2)—C(13)	—	—	105.2(2)	—
O(3)—C(2)—C(13)	—	—	112.8(2)	—
C(12)—C(2)—C(13)	—	—	111.5(2)	—

*Value identical to that given just above due to crystallographic symmetry.

TABLE 5. Comparison of the torsion angles in the various dioxabenzocycloheptene molecular conformations

Bond	Compound			
	1*A*	**2*A***	**3*B***	**4*B***
O(1)—C(2)—O(3)—C(4)	−75.0(2)	−75.1(2)	47.1(2)	51.6(4)
O(3)—C(2)—O(1)—C(7)	75.0(2)*	74.4(2)	49.1(2)	45.9(4)
C(2)—O(1)—C(7)—C(6)	−81.7(2)	−80.5(2)	−90.5(2)	−86.7(4)
C(2)—O(3)—C(4)—C(5)	81.7(2)*	82.1(2)	−89.3(2)	−88.3(4)
O(1)—C(7)—C(6)—C(5)	59.4(2)	57.1(2)	37.2(3)	30.1(4)
O(3)—C(4)—C(5)—C(6)	−59.4(2)*	−59.2(1)	37.3(3)	28.3(4)
C(4)—C(5)—C(6)—C(7)	0.0(2)	1.3(2)	−3.7(3)	7.9(4)
C(11)—C(5)—C(6)—C(8)	0.0(2)	0.3(3)	−0.8(3)	5.5(2)
C(12)—C(2)—O(1)—C(7)	—	−167.1(2)	−67.7(2)	—
C(12)—C(2)—O(3)—C(4)	—	166.3(2)	168.5(2)	—
C(13)—C(2)—O(1)—C(7)	—	—	170.6(2)	169.0(5)
C(13)—C(2)—O(3)—C(4)	—	—	−69.7(2)	−70.0(4)

*Symmetry related.

TABLE 6. Relation between acetal conformation and relevant structural parameters in 1,3-dioxa compounds

Compound	Reference	Conformation	O—C—O—C torsion angles (degrees)		O—C—O angle (degrees)	Bond lengths (Å)	
						Inner C—O	Outer C—O
Dimethoxymethane	11	g^+g^-	82.7	−82.7	115.7	1.421‡	1.443
	15*	g^+g^+	63.3(9)	63.3(9)	114.3(7)	1.382(4)	1.432(4)
	11	g^+g^+	62.4	62.4	112.4	1.422	1.449
	3*d*	g^+g^+	60	60	113.9	1.423	1.444
	11	*gt*	57.4	179.4	109.5	1.409, 1.432	1.448, 1.442
	3*d*	*gt*	60	180	110.9	1.400, 1.425	1.443, 1.434
1,3-Dioxane	†	g^+g^-	60.5	−60.7	111.7	1.415	1.435
1*A*	This work	g^+g^-	75.0(2)	−75.0(2)	113.6(2)	1.409(2)	1.441(2)
2*A*	This work	g^+g^-	74.4(2)	−75.1(2)	112.8(2)	1.414(2), 1.408(2)	1.438(3), 1.435(3)
3*B*	This work	g^+g^+	49.1(2)	47.1(2)	110.5(3)	1.425(2), 1.425(2)	1.432(2), 1.432(2)
4*B*	4	g^+g^+	45.9(4)	51.6(4)	109.6(2)	1.407, 1.413	1.428, 1.421

*Gas phase electron diffraction.
†Averaged from the 67 rings in the Cambridge Data File.
‡When the molecule possesses a symmetry element, only one of the symmetry related distances is indicated.

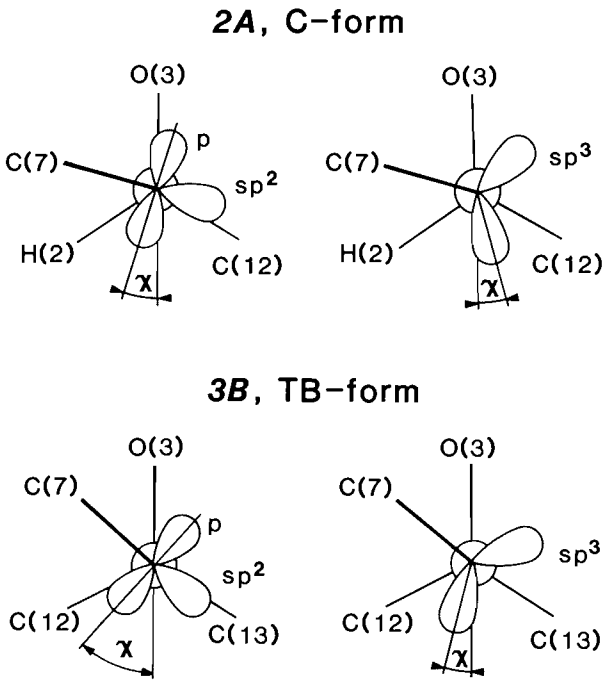

FIG. 2. Newman projections along O(1)→C(2) for **2***A* and **3***B*, where O(1) is either sp^2 or sp^3 hybridized. χ is the torsion angle between O(3) and the axis of the *p* or sp^3 orbital.

Table 5 for **2** (*C*) and **3** (*TB*) lead to the Newman projections along the O(1)—C(2) bond[5] shown in Fig. 2 for each of the possible hybridization states. When O(1) is sp^3, a similar torsion angle, χ, exists for **2***A* and **3***B* between a lone pair of O(1) and the σ* orbital of the C(2)—O(3) bond (χ ~ 15°). On the other hand, if O(1) is sp^2 hybridized, the torsion angle is more favorable for back-bonding in the *C* form **2***A* (χ ~ 15°) than the *TB* form **3***B* where χ is about 40°. The smaller χ value for *C* relative to *TB* in the latter case then explains the greater bond shortening observed for the *C* forms of **1** and **2**. This experimental observation in seven-membered rings constitutes the first evidence in favour of sp^2 hybridization for the acetal oxygen atoms.

[5]The same result will be observed in a projection along O(3)—C(2).

TABLE 7. Comparison of the dihedral angles (degrees) measuring the puckering in **1***A*, **2***A*, and 1,3-dioxane

	1*A*	**2***A*	1,3-Dioxane
[1]/[2]*	125.8	128.2	131.6
[2]/[3]	115.3	116.0	123.7

*Atoms included in the planes: [1] benzo group; [2] C(7), O(1), O(3), C(4); [3] O(1), O(3), C(2).

Although not included in the least-squares planes calculations (in each of the three compounds), atoms C(4) and C(7) are found to be coplanar with the benzo group, which forms plane [1]. Atoms C(7), O(1), O(3), and C(4) in the chairs **1** and **2** are also coplanar; they form plane [2]. Plane [3] is the acetal function made up of atoms O(1), O(3), and C(2). The puckering of the cycloheptene chair is measured by the angle between these planes. They are compared in Table 7 to those of 1,3-dioxane. It is clear that **1***A* and **2***A* have quite similar puckering. However, these two seven-membered rings are more puckered than 1,3-dioxane. The result of this puckering causes an increased interaction between an axial substituent on the anomeric carbon C(2) and the axial benzylic hydrogens H(41) and H(71) in **3**.

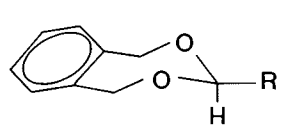

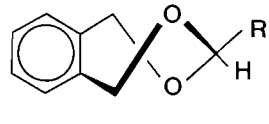

R = H	**1**	79%	21%
CH_3	**2**	96%	4%
C_6H_5	**6**	77%	23%

This also explains why only the *TB* form is observed for **3**.

Correlation between X-ray and nuclear magnetic resonance data

We now compare solid state information derived from the X-ray analyses with ^{13}C nmr information on the same compounds in solution (1, 2). As we will see next, the combination of these two techniques provides complementary information about the molecular geometry.

Whereas the two techniques reveal only the symmetrical *TB* form for **3** (dimethyl derivative) both in the crystalline state and

in solution at low temperature, slightly different results are obtained for the parent compound **1** and its monomethyl derivative **2**. The low temperature ^{13}C nmr spectra of **1** and **2** in solution show the presence of a major conformation (*C*) and a minor one (*TB*) in a ratio 79:21 for **1** (in CHF_2Cl at $-130°C$) and 96:4 for **2** (in CHF_2Cl at $-115°C$). The X-ray data identify only one conformation for each compound, the *C* form for **1** and the C_e form for **2**. Obviously, the absence of the *TB* form for **1** and **2** in the crystal state does not allow direct characterization of their *TB* geometries. Furthermore, the solution study of these compounds is complicated by the impossibility of slowing down, on the nmr time scale, the interconversion between the two identical *TB* forms, a fact which precludes observation of non-averaging *TB* signals by ^1H and ^{13}C nmr. In spite of this, the combined approach provides a better understanding of the features of the *TB* geometry of **2***B*.

In order to determine whether **2***B* is symmetrical or not, we use information from the two techniques. X-ray information (4) on the mono 4-nitrophenyl derivative, **4**, shows that it adopts a symmetrical *TB* ring **4***B*. But it is possible that the effect of the methyl group in **2** differs from that of the 4-nitrophenyl group in **4**. An answer to this question is provided by the analysis of the low temperature ^{13}C nmr results summarized under the structures below.

The reduced amount of the *TB* form for methyl substitution relative to phenyl substitution (**2** vs. **6**) was rationalized in terms of a larger non-bonding interaction for the methyl group. This stronger interaction could lead to a small deformation of the highly flexible *TB* form of **2**. Supporting evidence is provided by the value of the ^{13}C chemical shift γ-effect. As shown by Lambert and Vagenas (14) in carbocyclic rings, the γ-effect of a methyl substituent is linearly related to the dihedral angle θ between the methyl substituent and the γ-carbon. A similar linear relationship has already been proposed (2) to explain the γ-shift caused by a methyl group at C(2) on the benzylic carbons C(4) and C(7) in **2**. The average value of -2.83 ppm measured for **2***B* does not fit the linear relation, if we assume a symmetrical *TB* form with torsion angles taken as similar to the values of $-67.7°$ and $170.6°$ determined for **3***B* in the solid state (Table 5). But a slight twist, changing these angles by about 10° and leading to torsion angles of about $-80°$ and 180° for **2***B*, would increase the averaged γ-shift to about -3.1 ppm, a value that fits well with the linear relationship. The latter torsion angles, corresponding to an unsymmetrical geometry, then represent the extent of deformation brought about by steric interaction of the methyl group in the flexible *TB* conformation of **2**.

Acknowledgements

Financial support of this research by the Natural Sciences and Engineering Research Council of Canada and the Fonds FCAC of the Province de Québec is gratefully acknowledged.

1. A. Blanchette, F. Sauriol-Lord, and M. St-Jacques. J. Am. Chem. Soc. **100**, 4055 (1978).
2. R. St-Amour, M. T. Phan Viet, and M. St-Jacques. Can. J. Chem. **62**, 2830 (1984).
3. (*a*) B. Fuchs, L. Schleifer, and E. Tartakovsky. Nouv. J. Chim. **8**, 275 (1984); (*b*) A. J. Kirby. The anomeric effect and related stereoelectronic effects at oxygen. Springer Verlag, New York. 1983. pp. 52–61; (*c*) G. A. Jeffrey. *In* Anomeric effect; origin and consequences. *Edited by* Walter A. Szarek and Derek Horton. ACS Symposium Series. Vol. 87. Washington, DC. 1979. Chapt. 4; (*d*) G. A. Jeffrey, J. A. Pople, J. S. Binkley, and S. Vishveshwara. J. Am. Chem. Soc. **100**, 373 (1978).
4. V. N. Petrov, I. A. Litvinov, Yu. T. Struchkov, E. N. Klimovitskii, M. B. Tumirbaev, and B. A. Arbuzov. J. Gen. Chem. USSR, **53**, 112 (1983).
5. D. T. Cromer and J. B. Mann. Acta Crystallogr Sect. A, **24**, 321 (1968).
6. R. F. Stewart, E. R. Davidson, and W. T. Simpson. J. Chem. Phys. **42**, 3175 (1965).
7. F. R. Ahmed, S. R. Hall, M. E. Pippy, and C. P. Huber. J. Appl. Crystallogr. **6**, 309 (1973).
8. P. Main, S. E. Hull, L. Lessinger, G. Germain, J. Declercq, and M. M. Wolfson. MULTAN 78. A system of computer programs for the automatic solution of crystal structures from X-ray diffraction data. Universities of York, England, and Louvain, Belgium. 1978.
9. R. J. Doedens and J. A. Ibers. Inorg. Chem. **6**, 204 (1967).
10. C. K. Johnson. ORTEP, Report ORNL-3794. Oak Ridge National Laboratory, Tennessee. 1965.
11. C. van Alsenoy, L. Schäfer, J. N. Scarsdale, J. O. Williams, and H. J. Geise. J. Mol. Struct. **86**, 111 (1981).
12. F. Brisse, A. Battat, S. Pérez, H. Favre, and J.-C. Richer. Acta Crystallogr. Sect. B, **33**, 1503 (1977).
13. V. G. Rao. Can. J. Chem. **60**, 1067 (1982).
14. J. B. Lambert and A. R. Vagenas. Org. Magn. Reson. **17**, 265 (1981).
15. E. E. Astrup. Acta Chem. Scand. **27**, 3271 (1973).
16. L. E. Sutton. Tables of interatomic distances and configurations of molecules and ions. Supplement 1956–1959. The Chemical Society, London. 1965.

Structural studies of organoboron compounds XXIII:[1] preparation and crystal and molecular structures of 2,2-diphenyl-1,3-dioxa-4a-azonia-2-borata-1,2,3,4-tetrahydronaphthalene and 4,4-diphenyl-3-oxa-1-aza-4a-azonia-4-borata-1,2,3,4-tetrahydronaphthalene

W. KLIEGEL, H.-W. MOTZKUS, AND D. NANNINGA

Institut für Pharmazeutische Chemie, der Technischen Universität Braunschweig, 3300 Braunschweig, Beethovenstrasse 55, Bundesrepublik Deutschland

AND

STEVEN J. RETTIG AND JAMES TROTTER

Department of Chemistry, University of British Columbia, 2036 Main Mall, Vancouver, B.C., Canada V6T 1Y6

Received August 7, 1985

W. KLIEGEL, H.-W. MOTZKUS, D. NANNINGA, STEVEN J. RETTIG, and JAMES TROTTER. Can. J. Chem. **64**, 507 (1986).

Details of the synthesis, physical properties, and the crystal molecular structures of 2,2-diphenyl-1,3-dioxa-4a-azonia-2-borata-1,2,3,4-tetrahydronaphthalene, **5**, and 4,4-diphenyl-3-oxa-1-aza-4a-azonia-4-borata-1,2,3,4-tetrahydronaphthalene, **9**, are reported. Crystals of **5** are monoclinic, $a = 9.972(1)$, $b = 11.848(1)$, $c = 13.561(2)$ Å, $\beta = 106.231(5)°$, $Z = 4$, space group $P2_1/c$ and those of **9** are orthorhombic, $a = 20.676(1)$, $b = 15.4199(9)$, $c = 9.7533(4)$ Å, $Z = 8$, space group $Pbca$. Both structures were solved by direct methods and were refined by full-matrix least-squares procedures to R values of 0.036 and 0.045 for 1060 and 1700 reflections with $I \geq 3\sigma(I)$ respectively. Compound **5** has the expected cyclic *B,N*-betaine structure, resulting from *N*-aklylation of 2(1*H*)-pyridone with formaldehyde followed by reaction with $(Ph_2B)_2O$. The aza analog, however, does not have the analogous structure. The alkylation of 2-aminopyridine with formaldehyde in the presence of $(Ph_2B)_2O$ yields **9**, derived from alkylation of the amine rather than the pyridine ring nitrogen atom.

W. KLIEGEL, H.-W. MOTZKUS, D. NANNINGA, STEVEN J.RETTIG et JAMES TROTTER. Can. J. Chem. **64**, 507 (1986).

On rapporte les détails relatifs à la synthèse, aux propriétés physiques et aux structures cristallines et moléculaires du diphényl-2,2 dioxa-1,3 azonia-4a borata-2 tétrahydro-1,2,3,4 naphtalène (**5**) et du diphényl-4,4 oxa-3 aza-1 azonia-4a borata-4 tétrahydro-1,2,3,4 naphtalène (**9**). Les cristaux du composé **5** sont monocliniques, avec $a = 9{,}972(1)$, $b = 11{,}848(1)$, $c = 13{,}561(2)$ Å, $\beta = 106{,}231(5)°$, $Z = 4$ et groupe d'espace $P2_1/c$ alors que ceux du composé **9** sont orthorhombiques avec $a = 20{,}676(1)$, $b = 15{,}4199(9)$, $c = 9{,}7533(4)$ Å, $Z = 8$ et groupe d'espace $Pbca$. On a résolu les deux structures par des méthodes directes et on les a affinées par la méthode des moindres carrés (matrice entière) jusqu'à des valeurs R de 0,036 et 0,045 respectivement pour 1060 et 1700 réflexions avec $I \geq 3\sigma(I)$. Les composé **5** possède la structure attendue d'une *B,N*-bétaïne cyclique qui provient d'une *N*-alcoylation de la 1*H*-pyridone-2 avec le formaldéhyde suivie d'une réaction avec le $(Ph_2B)_2O$. Toutefois, l'analogue azoté ne possède pas une structure analogue. L'alcoylation de l'amino-2 pyridine par le formaldéhyde en présence de $(Ph_2B)_2O$ conduit au composé **9**, qui provient d'une alcoylation de l'amine plutôt que de l'atome d'azote du noyau pyridinique.

[Traduit par le journal]

Introduction

The tautomeric system 2(1*H*)-pyridone ↔ 2-hydroxypyridine **1** has been the subject of several experimental and theoretical studies (1–6). The alkylation of this bifunctional nucleophile still appears to be somewhat puzzling in spite of a number of detailed studies. For example, some thorough work is found in the literature (7–10) which demonstrates the possibility of both *N*- and *O*-alkylation to a variable extent depending on the alkylation reagent and the conditions of the reaction. The alkylation of 2(1*H*)-pyridones with formaldehyde has been shown to result in *N*-alkylation products (11,12). We have prepared 1-hydroxymethyl-2-pyridone **2** according to the literature (11) and allowed this compound to react with oxybis(diphenylborane) to yield the diphenylboron chelate **5**. The cyclic *B,N*-betaine **5** is a ring-enlarged analog (by formal methylene insertion) of the diphenylboron chelate **4** which has recently been synthesized (13) and characterized by X-ray structure analysis (14).

Since no unambiguous assignment of the structure of the chelate **5** could be made by chemical or spectroscopic means, an X-ray crystallographic study of **5** represented the best method for ruling out the alternate structure **6**, a possible result of hypothetical *O*-alkylation of **1** to **3**. A very similar analytical problem arose with the aza-analogous diphenylboron chelate which was obtained by the reaction of 2-aminopyridine (**7**), formaldehyde, and oxybis(diphenylborane) in a single step (without first forming the intermediate formaldehyde adduct). Since 2-aminopyridine also possesses two nucleophilic centers, both alternative structures, **8** and **9**, must be considered for the chelated alkylation product. Simple ir and nmr data were not sufficient for a definitive structural assignment, therefore an X-ray crystallographic analysis was undertaken.

Experimental

2,2-diphenyl-1,3-dioxa-4a-azonia-2-borata-1,2,3,4-tetrahydronaphthalene, 5

1-Hydroxymethyl-2-pyridone (0.50 g, 4 mmol), prepared according to the literature (11), and oxybis(diphenylborane) (0.70 g, 2 mmol) were dissolved in 20 mL ethanol. After reacting the solution under reflux conditions for 2–3 min and cooling down, colorless crystals were obtained. Intense cooling yielded 1.11 g (96%) of **5** mp 169–171°C (from benzene – petroleum ether); ir (KBr): 1650 cm^{-1} (C=N/C=O); ^1H nmr ($CDCl_3$–TMS) δ (ppm): 5.50 (s, N—CH_2—O), 6.30–6.73 (m, 14 H of Ph_2B and pyridone). *Anal.* calcd. for $C_{18}H_{16}BNO_2$: C 74.80, H 5.58, N 4.85; found: C 74.94, H 5.83, N 4.85. The substance gives a blue color reaction (15) with diphenylcarbazone in methanolic solution. Crystals suitable for X-ray

[1]For Part XXII, see ref. 30.

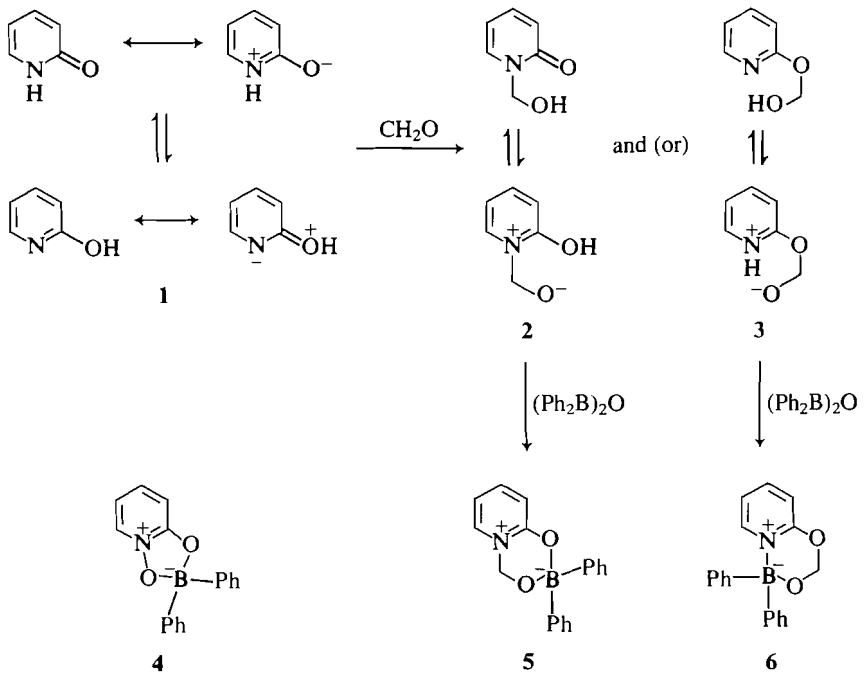

SCHEME A

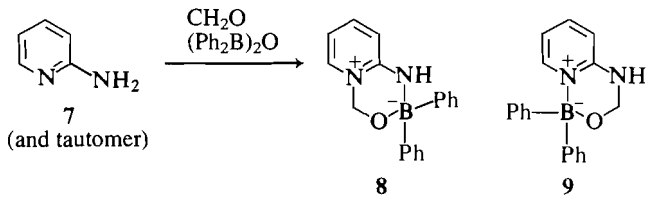

SCHEME B

analysis were obtained by recrystallization from benzene–cyclohexane.

4,4-Diphenyl-3-oxa-1-aza-4a-azonia-4-borata-1,2,3,4-tetrahydronaphthalene, 9

2-Aminopyridine (0.47 g, 5 mmol), formaldehyde (5 mmol, 40% aqueous solution), and oxybis(diphenylborane) (0.87 g, 2.5 mmol) were dissolved in 10 mL ethanol at room temperature. Intense cooling produced 1.08 g (75%) of colorless crystals, mp 164–168°C (from ethanol); ir (KBr): 3260 (N—H), 1640 cm^{-1} (C=N); ^1H nmr (d_6-DSMO – TMS) δ (ppm): 4.72 (s, N—CH_2—O), 6.52, 6.78, and 7.59 (3 m, 3 H of pyridine), 7.18 (s, 10 H of Ph_2B), 8.46 (m, N—H). *Anal.* calcd. for $C_{18}H_{17}BN_2O$: C 75.03, H 5.95, N 9.72; found: C 75.15, H 5.99, N 9.72. The substance gives a blue color reaction (15) with diphenylcarbazone in methanolic solution. Crystals suitable for X-ray analysis were obtained by recrystallization from ethanol.

X-ray crystallographic analyses

2,2-diphenyl-1,3-dioxa-4a-azonia-2-borata-1,2,3,4-tetrahydronaphthalene, 5

A crystal bounded by the 12 faces (followed by their distances in mm from a common origin): ±(1 −1 0), 0.12, ±(1 0 0), 0.08, ±(1 1 0), 0.14, ±(0 1 1), 0.19 ±(0 −1 1), 0.19, ±(1 0 2), 0.18 was mounted in a general orientation. Unit-cell parameters were refined by least-squares on the 2 sin θ/λ values for 25 reflections (2θ = 25–40°) measured on a diffractometer with Mo-Kα radiation (λ(Kα$_1$) = 0.70930, λ(Kα$_2$) = 0.71359 Å). Crystal data at 22°C are:

$C_{18}H_{16}BNO_2$ fw = 289.14

Monoclinic, a = 9.972(1), b = 11.848(1), c = 13.561(2) Å, β = 106.231(5)°, V = 1538.2(3) $Å^3$, Z = 4, ρ_c = 1.249 Mg m^{-3}, $F(000)$ = 608, μ(Mo-Kα) = 0.75 cm^{-1}. Absent reflections: $h0l$, l odd, and $0k0$, k odd, uniquely indicate the space group $P2_1/c$ (C_{2h}^5, No. 14).

Intensities were measured with graphite-monochromated Mo-Kα radiation on an Enraf-Nonius CAD4-F diffractometer. An ω–2θ scan at 1.06–10.06° min^{-1} over a range of (1.00 + 0.35 tan θ) degrees in ω (extended by 25% on both sides for background measurement) was employed. Data were measured to 2θ = 52°. The intensities of three check reflections, measured every 3600 s throughout the data collection, remained constant to within 4%. Of the 3018 independent reflections measured and processed,[2] 1060(35.1%) had intensities greater than or equal to 3σ(I) above background where $\sigma^2(I) = S + 2B + (0.04(S - B))^2$ with S = scan count and B = normalized background count. The majority of observed data had 2θ < 35°. Higher angle data were collected to maximize the number of observations. A 2σ cutoff would only increase the number of observed reflections by 32.

The structure was solved by direct methods. The positions of the non-hydrogen atoms being determined from an E-map. In the final stages of refinement the non-hydrogen atoms were refined with anisotropic thermal parameters and the hydrogen atoms were included as fixed contributors in idealized positions (C(sp^3)—H = 0.98, C(sp^2)—H = 0.97 Å), recalculated after each cycle of refinement. The scattering factors of ref. 16 were used for non-hydrogen atoms and those of ref. 17 for hydrogen atoms. The weighting scheme $w = 1/\sigma^2(F)$, where $\sigma^2(F)$ is derived from the previously defined $\sigma^2(I)$, gave uniform average values of $w(|F_o| - |F_c|)^2$ over ranges of both $|F_o|$ and sin θ/λ and was employed in the final stages of full-matrix refinement of variables. Reflections with $I < 3\sigma(I)$ were not included in the refinement. Convergence was reached at R = 0.036 and R_w = 0.040 for 1060 reflections with $I \geq 3\sigma(I)$. The function minimized was $\Sigma w(|F_o| - |F_c|)^2$, $R = \Sigma||F_o| - |F_c||/\Sigma|F_o|$ and $R_w = (\Sigma w(|F_o| - |F_c|)^2/\Sigma w|F_o|^2)^{1/2}$.

On the final cycle of refinement the mean and maximum parameter shifts corresponded to 0.007 and 0.04σ, respectively. The mean error in an observation of unit weight was 1.690. The final difference map was essentially featureless, residual densities ranging from −0.15 to

[2]The computer programs used include locally written programs for data processing and locally modified versions of the following: MULTAN 80, multisolution program by P. Main, S. J. Fiske, S. E. Hull, L. Lessinger, G. Germain, J. P. Declercq, and M. M. Woolfson; ORFLS, full-matrix least-squares, and ORFFE, function and errors, by W. R. Busing, K. O. Martin, and H. A. Levy; FORDAP, Patterson and Fourier syntheses, by A. Zalkin; ORTEP II, illustrations, by C. J. Johnson.

TABLE 1. Final positional (fractional) and isotropic thermal parameters ($U \times 10^3$ Å^2) with estimated standard deviations in parentheses

Atom	x	y	z	U_{eq}/U_{iso}
		5 ($\times 10^4$)		
O(1)	2079(2)	868(2)	1011(2)	48
O(2)	2990(2)	2614(2)	529(2)	49
N	3136(3)	895(2)	−294(2)	40
C(1)	2279(3)	414(3)	188(2)	37
C(2)	1606(3)	−584(3)	−199(2)	46
C(3)	1834(4)	−1076(3)	−1038(3)	56
C(4)	2732(4)	−579(3)	−1527(3)	63
C(5)	3359(4)	409(3)	−1157(3)	54
C(6)	3805(3)	2008(3)	66(3)	52
C(7)	1566(3)	2713(3)	1783(2)	43
C(8)	1205(3)	2416(3)	2672(2)	50
C(9)	206(4)	3011(3)	3004(3)	60
C(10)	−459(4)	3914(4)	2458(4)	70
C(11)	−149(4)	4226(3)	1573(3)	74
C(12)	849(4)	3626(3)	1243(3)	62
C(13)	4131(3)	1809(3)	2334(2)	41
C(14)	4377(4)	856(3)	2953(3)	55
C(15)	5574(5)	738(3)	3771(3)	72
C(16)	6573(4)	1577(4)	3984(3)	77
C(17)	6370(3)	2512(4)	3379(3)	66
C(18)	5185(3)	2628(3)	2574(2)	51
B	2729(4)	2046(3)	1421(3)	43
		9 ($\times 10^5$, H $\times 10^4$)		
O	22382(6)	51149(9)	41811(14)	53
N(1)	11847(7)	48549(10)	30563(17)	43
N(2)	20494(10)	54259(16)	18768(25)	71
C(1)	23412(12)	57239(18)	31384(30)	66
C(2)	14817(10)	50227(13)	18604(23)	52
C(3)	11832(14)	47659(19)	6109(27)	70
C(4)	5940(15)	43963(18)	6389(31)	73
C(5)	2784(12)	42576(16)	18686(28)	64
C(6)	5878(10)	44775(14)	30282(26)	51
C(7)	14753(9)	41344(12)	54097(20)	43
C(8)	18607(11)	34183(14)	50997(25)	57
C(9)	18153(15)	26473(16)	58283(32)	77
C(10)	13822(16)	25716(19)	68665(32)	80
C(11)	9899(15)	32555(20)	71967(28)	72
C(12)	10373(11)	40313(16)	64828(24)	56
C(13)	12538(10)	58828(13)	52214(21)	48
C(14)	7267(11)	63468(14)	47312(25)	59
C(15)	5215(16)	71148(17)	53404(33)	83
C(16)	8425(17)	74407(20)	64564(36)	92
C(17)	13536(17)	69885(22)	69858(42)	97
C(18)	15558(13)	62219(17)	63848(29)	75
B	15473(10)	50169(15)	45317(23)	44
H(N)	2250(12)	5413(17)	1128(25)	77(9)
H(1*a*)	2784(11)	5782(13)	2942(22)	62(6)
H(1*b*)	2152(11)	6315(17)	3424(21)	80(8)
H(3)	1425(12)	4886(16)	−195(28)	88(9)
H(4)	397(13)	4243(15)	−280(27)	92(9)
H(5)	−137(11)	4002(15)	2004(23)	74(7)
H(6)	418(8)	4382(11)	3881(20)	41(6)
H(8)	2157(10)	3480(13)	4288(22)	65(7)
H(9)	2127(14)	2199(20)	5571(28)	111(10)
H(10)	1333(12)	2052(17)	7447(29)	110(10)
H(11)	676(11)	3276(17)	7894(28)	90(9)
H(12)	762(10)	4542(16)	6740(19)	65(7)
H(14)	466(10)	6103(16)	3819(24)	84(7)
H(15)	150(12)	7470(20)	4950(25)	104(9)
H(16)	686(12)	7984(19)	6913(27)	107(9)
H(17)	1565(14)	7160(18)	7712(31)	105(11)
H(18)	1942(12)	5924(16)	6790(23)	82(8)

+0.14 e Å^{-3}. The final positional and thermal parameters appear in Tables 1 and 6 respectively.[3] Calculated hydrogen atom parameters appear in Table 5.[3] Measured and calculated structure factors have been placed in the Depository of Unpublished Data.[3]

4,4-diphenyl-3-oxa-1-aza-4a-azonia-4-borata-1,2,3,4-tetrahydronaphthalene, ***9***

Experimental details are as above except where noted. The 12 bounding planes of the crystal used for data collection were: {1 1 1}, 0.17, ±(0 1 0), 0.31, ±(1 0 0), 0.31 mm (from a common origin). Reflections employed in the refinement of the unit-cell parameters had 2θ = 30–41°. Crystal data:

$C_{18}H_{17}BN_2O$ fw = 288.16

Orthorhombic, a = 20.676(1), b = 15.4199(9), c = 9.7533(4) Å, V = 3110.1(3) Å^3, Z = 8, ρ_c = 1.231 Mg m^{-3}, $F(000)$ = 1216, μ(Mo-Kα) = 0.71 cm^{-1}. Absent reflections: 0kl, k odd, $h0l$, l odd, and $hk0$, h odd, uniquely indicate the space group $Pbca$ (D_{2h}^{15}, No. 61).

An ω–2θ scan at 1.01–10.06° min^{-1} over a range of (0.62 + 0.35 tan θ)° in ω was employed. Of 4517 independent reflections measured (to 2θ = 60°), 1700 had intensities greater than 3σ(I) above background. The intensities of the check reflections remained constant to within 3%.

The strucure was solved by direct methods, the non-hydrogen atoms being positioned from an E-map. After refinement of the non-hydrogen atoms with anisotropic thermal parameters to R = 0.082, the hydrogen atoms were positioned from a difference map and were subsequently refined with isotropic thermal parameters. Convergence was reached at R = 0.045 and R_w = 0.046 for 1700 reflections with $I \geq 3\sigma(I)$. The mean and maximum parameter shifts on the final cycle of refinement were 0.02 and 0.15σ and the mean error in an observation of unit weight was 1.813. The final difference map showed maximum fluctuations of −0.24 and +0.15 e Å^{-3}.

Analysis of thermal motion

The thermal motion in the two molecules (Fig. 1) has been analysed in terms of the rigid-body modes of translation, libration, and screw-motion (TLS model) (18). The rms errors in the U_{ij} (derived from the least-squares analyses) are 0.0021 and 0.0015 Å^2, respectively for **5** and **9**. Analyses of the entire molecules indicated independent motion of the phenyl groups. Subunits consisting of PhB groups and the ten atoms of the fused-ring systems were separately analysed for both structures (rms ΔU_{ij} = 0.0025–0.0034 Å^2 and 0.0024–0.0026 Å^2 for **5** and **9** respectively). The appropriate bond distances have been corrected for libration (18,19), using shape parameters q^2 of 0.08 for all atoms involved. Corrected bond lengths appear in Table 2 along with the uncorrected values; corrected bond angles do not differ by more than 1σ from the uncorrected values given in Table 3. Intra-annular torsion angles defining the conformations of chelate rings are listed in Table 4. Bond lengths and angles involving hydrogen and a complete listing of torsion angles (Tables 7–9) are included in the supplementary material.[3]

Results and discussion

Compound **5** has the expected structure derived from the ligand **2**, the *N*-alkylation product of 2(1*H*)-pyridone with formaldehyde. The molecule **5** is related to the cyclic *B*,*N*-betaine **4**, which may be regarded as a diphenylboron chelate of an "*O*-adduct" of pyridone while **5** may be thought of as the corresponding chelate of an "OCH_2-adduct" of pyridone. Surprisingly, the aza analog does not have the analogous structure **8** which would be less sterically hindered about the Ph_2B moiety than in the observed structure **9**, in which an

[3]The structure factor table, Table 6 (anisotropic thermal parameters) and other material mentioned in the text may be purchased from the Depository of Unpublished Data, CISTI, National Research Council of Canada, Ottawa, Ont., Canada K1A 0S2.

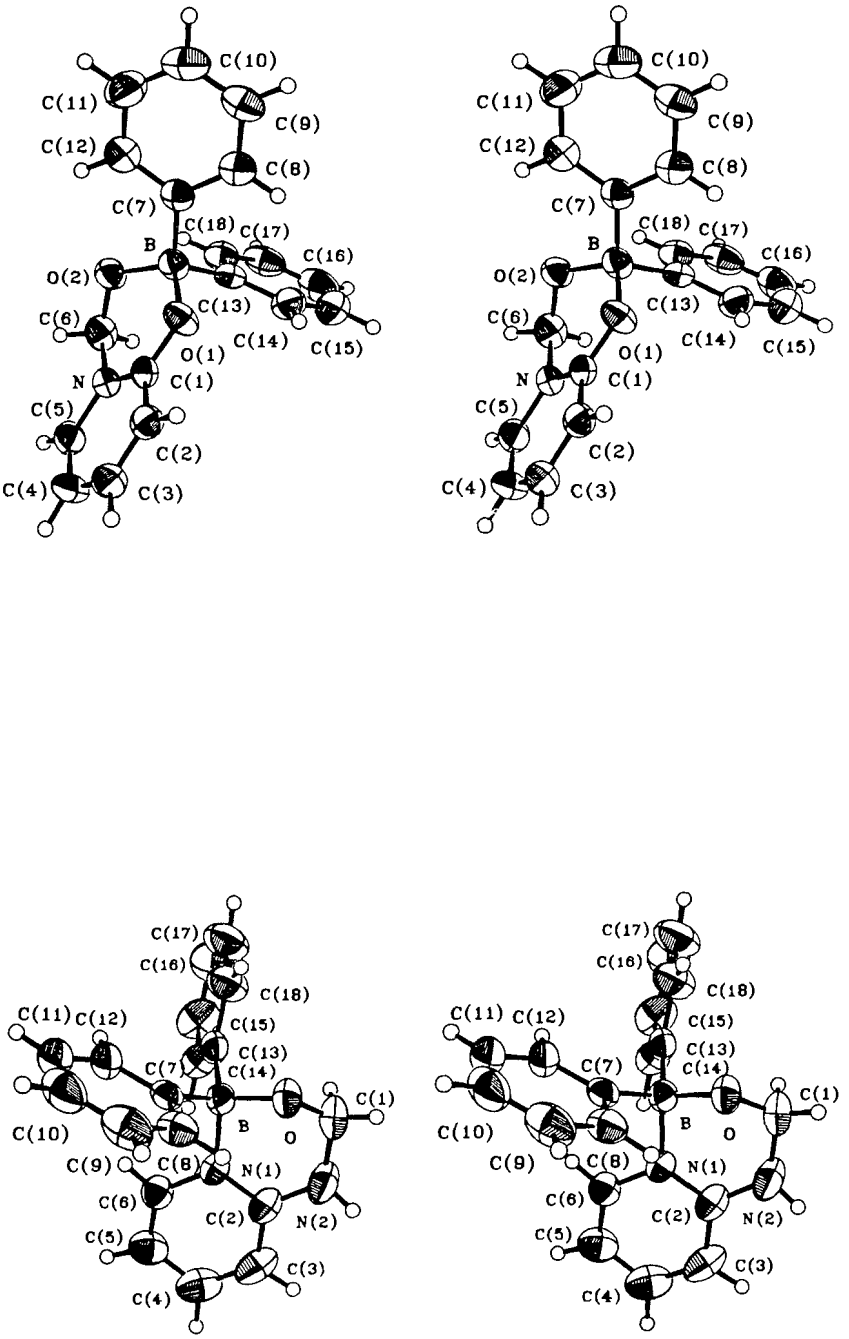

FIG. 1. Stereoscopic views of the 2,2-diphenyl-1,3-dioxa-4a-azonia-2-borata-1,2,3,4-tetrahydronaphthalene (top) and 4,4-diphenyl-3-oxa-1-aza-4a-azonia-4-borata-1,2,3,4-tetrahydronaphthalene (bottom) molecules; 50% probability thermal ellipsoids are shown for the non-hydrogen atoms. Hydrogen atoms have been assigned artificially small thermal parameters for the sake of clarity.

intramolecular N→B interaction involving the pyridine ring nitrogen occurs. The structure **9** is consistent, however, with that postulated by Gragg *et al.* (20) on the basis of mass spectral data of the addition products of (2-pyridylamino)diphenylborane and various carbonyl compounds. Similar addition products with the basic ring structure of **9** were also formulated by Dorokhov *et al.* (21) on the basis of spectroscopic data and by analogy with the chemical behavior of comparable amidine adducts (22).

The pyridone C—O distance[4] of 1.308(3) Å in **5**, similar to the corresponding value of 1.316(3) Å observed for a compound of the type **4** (14), is indicative of considerable single bond character. The intracyclic C(1)—N bond of the pyridine ring in **5** is short at 1.348(4) Å, indicating double bond character. The corresponding C—O and C—N distances in 2-pyridones (both

[4]Libration-corrected bond lengths are employed throughout the discussion and are compared with similarly derived parameters.

TABLE 2. Bond lengths (Å) with estimated standard deviations in parentheses

Bond	Uncorr.	Corr.	Bond	Uncorr.	Corr.
		5			
O(1)—C(1)	1.303(3)	1.308	C(7)—B	1.590(5)	1.596
O(1)—B	1.574(4)	1.578	C(8)—C(9)	1.394(4)	1.398
O(2)—C(6)	1.363(4)	1.369	C(9)—C(10)	1.363(5)	1.372
O(2)—B	1.470(4)	1.478	C(10)—C(11)	1.370(5)	1.379
N—C(1)	1.340(4)	1.348	C(11)—C(12)	1.396(5)	1.400
N—C(5)	1.377(4)	1.382	C(13)—C(14)	1.387(4)	1.397
N—C(6)	1.497(4)	1.502	C(13)—C(18)	1.401(4)	1.410
C(1)—C(2)	1.389(4)	1.394	C(13)—B	1.612(5)	1.618
C(2)—C(3)	1.352(4)	1.357	C(14)—C(15)	1.391(5)	1.397
C(3)—C(4)	1.385(5)	1.393	C(15)—C(16)	1.380(5)	1.388
C(4)—C(5)	1.355(5)	1.360	C(16)—C(17)	1.359(5)	1.369
C(7)—C(8)	1.396(4)	1.405	C(17)—C(18)	1.374(5)	1.380
C(7)—C(12)	1.387(4)	1.396			
		9			
O—C(1)	1.401(3)	1.411	C(7)—B	1.615(3)	1.621
O—B	1.477(3)	1.485	C(8)—C(9)	1.388(3)	1.394
N(1)—C(2)	1.343(3)	1.354	C(9)—C(10)	1.357(4)	1.365
N(1)—C(6)	1.365(2)	1.371	C(10)—C(11)	1.369(4)	1.380
N(1)—B	1.642(3)	1.648	C(11)—C(12)	1.388(4)	1.394
N(2)—C(1)	1.446(3)	1.451	C(13)—C(14)	1.389(3)	1.401
N(2)—C(2)	1.328(3)	1.335	C(13)—C(18)	1.397(3)	1.409
C(2)—C(3)	1.422(3)	1.428	C(13)—B	1.614(3)	1.619
C(3)—C(4)	1.345(4)	1.352	C(14)—C(15)	1.391(3)	1.397
C(4)—C(5)	1.382(4)	1.392	C(15)—C(16)	1.371(4)	1.382
C(5)—C(6)	1.343(3)	1.348	C(16)—C(17)	1.367(4)	1.380
C(7)—C(8)	1.395(3)	1.406	C(17)—C(18)	1.384(4)	1.390
C(7)—C(12)	1.393(3)	1.402			

experimental and calculated) have been summarized in ref. 14 and range 1.221–1.264 and 1.373–1.410 Å, respectively. The observed geometry of **5** is thus consistent with a greater contribution of structure **5***a* to the overall mesomeric structure **5***a* ↔ **5***b*.

The C(2)–N(2) bond in **9** between the 2-amino group and the pyridine ring is relatively short at 1.335(3) Å. The corresponding distances[5] in 2-aminopyridine (23) and 3-aminopyridine (24) (which does not have an amidine grouping) are 1.355(2) and 1.390(4) Å, respectively. The endocyclic C—N bond within the amidine grouping of **9**, 1.354(3) Å, does not differ significantly from the corresponding distance of 1.359(2) Å in 2-aminopyridine. The related N(1)—C(2) distance in 3-aminopyridine is slightly shorter at 1.345(4) Å. The structural data for **9** are consistent with a more important contribution of the canonical form **9***b* to the overall structure **9***a* ↔ **9***b*. It is noteworthy that the main contributing canonical forms **5***a* and **9***b* of the overall mesomeric structures of **5** and **9** both represent 1,4-betaines with the greatest spatial separation of the formal positive and negative charges on nitrogen and boron, respectively.

The pyridine ring in **5** exhibits a distinct and significant alternation of double and single bond character, the average difference between the short and long bonds being 0.035(6) Å. A similar, but more pronounced, situation is noted in the case of **9** where the short and long bonds differ by an average of 0.046(5) Å. This type of bond length alternation was not observed for closely related molecules of the type **4** (14).

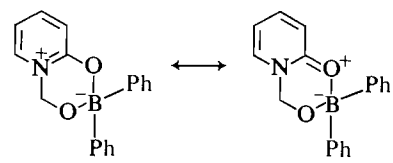

5*a* **5***b*

SCHEME C

The O—B distances in **5** are significantly different; the longer of the two (1.578(4) Å) involves the pyridone oxygen atom and is similar to the nearly equal O—B distances in compounds of the type **4** (1.557(3)–1.580(3) Å) and in other diphenylboron chelates with *N*-oxide[6] (25–27) or carbonyl (28, 29) oxygen coordinated to boron. The O(2)—C(6) distance of 1.369(4) Å in **5** is significantly shorter than the corresponding O—C(1) distance of 1.411(3) Å in **9**, indicating some double bond character in the former. Other bond lengths and angles in both structures (Tables 2 and 3) are normal.

[5]Corrected for libration from data in refs. 23 and 24 (rms ΔU_{ij} = 0.0012 and 0.0014 for the entire molecules).

[6]W. Kliegel, S. J. Rettig, and J. Trotter. 1.552(4) Å for 4,4-dimethyl-2,2-diphenyl-1,3-dioxa-4-azonia-2-boratacyclohexane. In preparation.

TABLE 3. Bond angles (deg) with estimated standard deviations in parentheses

Bonds	Angle(deg)	Bonds	Angle(deg)
	5		
C(1)—O(1)—B	121.5(2)	C(9)—C(10)—C(11)	119.5(4)
C(6)—O(2)—B	113.8(3)	C(10)—C(11)—C(12)	119.9(4)
C(1)—N—C(5)	120.9(3)	C(7)—C(12)—C(11)	122.4(3)
C(1)—N—C(6)	120.2(3)	C(14)—C(13)—C(18)	115.4(3)
C(5)—N—C(6)	118.8(3)	C(14)—C(13)—B	125.2(4)
O(1)—C(1)—N	120.9(3)	C(18)—C(13)—B	119.4(3)
O(1)—C(1)—C(2)	120.1(3)	C(13)—C(14)—C(15)	122.1(3)
N—C(1)—C(2)	118.9(3)	C(14)—C(15)—C(16)	120.2(3)
C(1)—C(2)—C(3)	120.5(3)	C(15)—C(16)—C(17)	118.9(3)
C(2)—C(3)—C(4)	120.2(3)	C(16)—C(17)—C(18)	120.7(4)
C(3)—C(4)—C(5)	118.8(3)	C(13)—C(18)—C(17)	122.6(3)
N—C(5)—C(4)	120.6(3)	O(1)—B—O(2)	105.4(2)
O(2)—C(6)—N	110.2(3)	O(1)—B—C(7)	106.6(2)
C(8)—C(7)—C(12)	115.7(3)	O(1)—B—C(13)	107.4(3)
C(8)—C(7)—B	121.9(3)	O(2)—B—C(7)	109.8(3)
C(12)—C(7)—B	122.5(3)	O(2)—B—C(13)	113.4(3)
C(7)—C(8)—C(9)	122.1(3)	C(7)—B—C(13)	113.6(3)
C(8)—C(9)—C(10)	120.3(4)		
	9		
C(1)—O—B	112.6(2)	C(9)—C(10)—C(11)	120.0(3)
C(2)—N(1)—C(6)	118.6(2)	C(10)—C(11)—C(12)	120.3(3)
C(2)—N(1)—B	121.5(2)	C(7)—C(12)—C(11)	121.4(3)
C(6)—N(1)—B	119.7(2)	C(14)—C(13)—C(18)	116.0(2)
C(1)—N(2)—C(2)	121.9(2)	C(14)—C(13)—B	125.3(2)
O—C(1)—N(2)	110.0(2)	C(18)—C(13)—B	118.7(2)
N(1)—C(2)—N(2)	118.9(2)	C(13)—C(14)—C(15)	122.1(2)
N(1)—C(2)—C(3)	119.5(2)	C(14)—C(15)—C(16)	120.2(3)
N(2)—C(2)—C(3)	121.6(2)	C(15)—C(16)—C(17)	119.2(3)
C(2)—C(3)—C(4)	119.6(3)	C(16)—C(17)—C(18)	120.6(3)
C(3)—C(4)—C(5)	120.7(3)	C(13)—C(18)—C(17)	121.9(3)
C(4)—C(5)—C(6)	117.8(2)	O—B—N(1)	104.73(15)
N(1)—C(6)—C(5)	123.7(2)	O—B—C(7)	107.3(2)
C(8)—C(7)—C(12)	116.3(2)	O—B—C(13)	112.1(2)
C(8)—C(7)—B	120.0(2)	N(1)—B—C(7)	107.13(15)
C(12)—C(7)—B	123.7(2)	N(1)—B—C(13)	108.7(2)
C(7)—C(8)—C(9)	121.9(3)	C(7)—B—C(13)	116.2(2)
C(8)—C(9)—C(10)	120.0(3)		

The chelate rings in **5** and **9** have slightly irregular O(2)- and O-envelope conformations (torsion angles in Table 4). The aromatic rings in **5** are all slightly but significantly nonplanar. (χ^2 = 10.1–21.5, maximum deviation from the mean plane 0.009(4) Å). In **9** the C(7)-phenyl ring is planar within experimental error while the C(13)-phenyl and pyridine rings are significantly nonplanar (χ^2 = 67.0 and 209.0, maximum deviations from the mean planes 0.015(3) and 0.019(2) Å). The pyridine ring in **9** is found to possess a flattened C(2),C(5)-boat conformation (see Table 4) with the B and N(2) atoms displaced from the mean plane by 0.170(2) and 0.078(2) Å in opposite directions, presumably a steric effect. The N(2) atom displays near planar geometry, being displaced 0.061(2) Å from the plane of its substituents, this plane being rotated 2.5(5)° with respect to the mean plane of the pyridine ring.

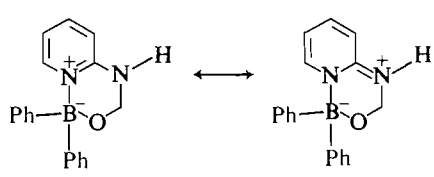

9a *9b*

SCHEME D

The crystal structure of **5** consists of discrete molecules separated by normal van der Waals distances and that of **9** consists of infinite chains of molecules linked by weak N(2)—H(N2)···O($1/2 - x, 1 - y, z - 1/2$) hydrogen bonds [H···O = 2.32(3), N···O = 3.127(3) Å, N—H···O = 161(2)°]. Both molecules show intramolecular interactions of possible significance [C(12)—H(12)···O(2) in **5**, C(8)—H(8)···O, and C(14)—H(14)···N(1) in **9** with H···(O/N) distances of 2.46, 2.53(2), and 2.54(2) Å; C···(O/N) distances of 2.844(4), 2.873(3), and 2.976(3) Å; and C—H···(O/N) angles of 103, 100(1), 102(1)° respectively], the C—H···N interaction in **9** involving the aromatic π-system of the pyridine ring.

TABLE 4. Intra-annular torsion angles (deg) standard deviations in parentheses

Atoms	Value(deg)
5	
B—O(1)—C(1)—N	5.3(4)
C(6)—N—C(1)—O(1)	−4.2(4)
C(1)—N—C(6)—O(2)	−27.6(4)
B—O(2)—C(6)—N	59.2(3)
C(6)—O(2)—B—O(1)	−55.6(3)
C(1)—O(1)—B—O(2)	22.5(4)
9	
B—O—C(1)—N(2)	−64.7(2)
C(2)—N(2)—C(1)—O	39.1(3)
C(1)—N(2)—C(2)—N(1)	−2.9(3)
B—N(1)—C(2)—N(2)	−8.3(3)
C(2)—N(1)—B—O	−15.0(2)
C(1)—O—B—N(1)	50.9(2)
C(6)—N(1)—C(2)—C(3)	−3.1(3)
N(1)—C(2)—C(3)—C(4)	3.2(3)
C(2)—C(3)—C(4)—C(5)	−0.5(4)
C(3)—C(4)—C(5)—C(6)	−2.1(4)
C(4)—C(5)—C(6)—N(1)	2.2(3)
C(2)—N(1)—C(6)—C(5)	0.4(3)

Acknowledgments

We thank the Natural Sciences and Engineering Research Council of Canada and the Fonds der Chemischen Industrie, Frankfurt am Main, for financial support and the University of British Columbia Computing Centre for assistance.

1. J. ELGUERO, C. MARZIN, A. R. KATRITZKY, and P. LINDA. The tautomerism of heterocycles. Adv. Heterocycl. Chem. Suppl. **1** (1976).
2. P. BEAK. Acc. Chem. Res. **10**, 186 (1977).
3. C. REICHARDT. Solvent effects in organic chemistry. Verlag Chemie, Weinheim. 1979. p. 66.
4. L. STEFANIAK. Tetrahedron, **32**, 1065 (1976).
5. H. B. SCHLEGEL, P. GUND, and E. M. FLUDER. J. Am. Chem. Soc. **104**, 5347 (1982).
6. C. KREBS, W. FÖRSTER, C. WEISS, and H. J. HOFMANN. J. Prakt. Chem. **324**, 369 (1982).
7. G. C. HOPKINS, J. P. JONAK, H. J. MINNEMEYER, and H. TIECKELMANN. J. Org. Chem. **32**, 4040 (1967).
8. H. J.-M. DOU, P. HASSANALY, and J. METZGER. J. Heterocycl. Chem. **14**, 321 (1977).
9. P. BEAK, J. LEE, and B. G. MCKINNIE. J. Org. Chem. **43**, 1367 (1978).
10. F. EFFENBERGER, W. BRODT, and J. ZINCZUK. Chem. Ber. **116**, 3011 (1983).
11. CILAG, LTD. Swiss patent 243101 (16/11/1946); Chem. Abstr. **43**, 7973 (1949).
12. SANDOZ, LTD. (W. Trueb and F. Reisser). Ger. Offen. 1934459 (15/1/1970); Chem. Abstr. **72**, 90 307 (1970).
13. W. KLIEGEL and D. NANNINGA. Pharmazie, **38**, 131 (1983).
14. W. KLIEGEL, D. NANNINGA, S. J. RETTIG, and J. TROTTER. Can. J. Chem. **61**, 2493 (1983).
15. R. NEU. Z. Anal. Chem. **176**, 334 (1960); B. FRIESE and F. UMLAND. Anal. Chim. Acta, **96**, 303 (1978).
16. D. T. CROMER and J. B. MANN. Acta Crystallogr. Sect. A: Cryst. Phys. Diffr. Theor. Gen. Crystallogr. **A24**, 321 (1968).
17. R. F. STEWART, E. R. DAVIDSON, and W. T. SIMPSON. J. Chem. Phys. **42**, 3175 (1965).
18. V. SCHOMAKER and K. N. TRUEBLOOD. Acta Crystallogr. Sect. B: Struct. Crystallogr. Cryst. Chem. **B24**, 63 (1968).
19. D. W. J. CRUICKSHANK. Acta Crystallogr. **9**, 747 (1956); **9**, 754 (1956); **14**, 896 (1961).
20. B. R. GRAGG, R. E. HANDSHOE, and K. NIEDENZU. J. Organomet. Chem. **116**, 135 (1976).
21. V. A. DOROKHOV. B. M. ZOLOTAREV, O. S. CHIZHOV, and B. M. MIKHAILOV. Izv. Akad. Nauk SSSR Ser.Chem. 1587 (1977); Bull. Acad. Sci. USSR Div. Chem. Sci. (Engl. Transl.), **26**, 1458 (1977).
22. V. A. DOROKHOV, V. I. SERENDENKO, and B. M. MIKHAILOV. Zh. Obshch. Khim. **45**, 1772 (1975); J. Gen. Chem. USSR (Engl. Transl.), **45**, 1737 (1975).
23. M. CHAO, E. SCHEMPP, and R. D. ROSENSTEIN. Acta Crystallogr. Sect. B: Struct. Crystallogr. Cryst. Chem. **B31**, 2922 (1975).
24. M. CHAO, E. SCHEMPP, and R. D. ROSENSTEIN. Acta Crystallogr. Sect. B: Struct. Crystallogr. Cryst. Chem. **B31**, 2924 (1975).
25. S. J. RETTIG, J. TROTTER, and W. KLIEGEL. Can. J. Chem. **52**, 2531 (1974).
26. S. J. RETTIG, J. TROTTER, W. KLIEGEL, and D. NANNINGA. Can. J. Chem. **56**, 1676 (1978).
27. W. KLIEGEL, H.-W. MOTZKUS, S. J. RETTIG, and J. TROTTER. Can. J. Chem. **62**, 838 (1984).
28. S. J. RETTIG and J. TROTTER. Can. J. Chem. **54**, 1168 (1976).
29. S. J. RETTIG and J. TROTTER. Can. J. Chem. **60**, 2957 (1982).
30. W. KLIEGEL, H.-W. MOTZKUS, S. J. RETTIG, and J. TROTTER. Can. J. Chem. **63**, 3516 (1985).

A new truxillate and some flavonoid esters from the leaf gum of *Traversia baccharoides* Hook. f.

PALANIAPPAN KULANTHAIVEL AND M. H. BENN[1]

Chemistry Department, The University, Calgary, Alta., Canada T2N 1N4

Received August 19, 1985

PALANIAPPAN KULANTHAIVEL and M. H. BENN. Can. J. Chem. **64**, 514 (1986).

Investigation of the leaf washings of *Traversia baccharoides* Hook. f. (Asteraceae: Senecionae) revealed the presence, besides typical cuticular lipids, of labd-13-ene-5,18-diol, 13-*epi-ent.*-manoyl oxide, *n*-butyl caffeate and its mono-*O*-isobutyrate derivatives, an α-truxillate photodimer of *n*-butyl caffeate (di-*n*-butyl traversate), (2*S*)-5,3′,4′-trihydroxy-7-methoxyflavanone, and various derivatives of quercetin including the 3-, 3′-, and 4′-mono-*O*-isobutyrates.

PALANIAPPAN KULANTHAIVEL et M. H. BENN. Can. J. Chem. **64**, 514 (1986).

Un examen des eaux de lavage des feuilles du *Traversia baccharoides* Hook. f. (Asteraceae: Senecionae) révèle qu'elles contiennent, en plus des lipides cuticulaires typiques, du labdène-13 diol-5,6, de l'oxyde du manoyle-13-*epi-ent.*, du caféate de *n*-butyle ainsi que son dérivé mono-*O*-isobutyrate, un photodimère α-truxillate du caféate de *n*-butyle (le traversate de di-*n*-butyle), la trihydroxy-(2*S*)-5,3′,4′ méthoxy-7 flavanone, et divers dérivés de la quercétine, dont les mono-*O*-isobutyrates en positions 3, 3′ ou 4′.

[Traduit par le journal]

Traversia baccharoides Hook. f. (Asteraceae: Senecionae) is a low shrub of montane to sub-alpine shrub habitat, indigenous to the South Island of New Zealand. Among the characteristic features of the plant is a distinct stickiness to the touch, a yellow stain with a delicately resinous aroma remaining upon the skin. We report here the results of an investigation of this leaf-gum.

Freshly collected sprigs of *T. baccharoides* were briefly rinsed in chloroform to yield a yellow solution, removal of solvent from which gave a thick orange-yellow gum with the odour of the plant. The major components of the gum were separated and characterized, as detailed in the Experimental, with the following results.

A set of straight-chain even-numbered fatty acids, principally C_{22}–C_{30}, was representative of commonly encountered plant cuticular lipids (1).

The resinous odour of the gum appeared to be largely due to two diterpenes, 13-*epi-ent.*-manoyl oxide (**1**) and labd-13-ene-5,18-diol (**2***a*). After we had identified the skeletons of these compounds by ^1H and ^{13}C nmr we anticipated that they would belong to the same stereochemical series. The $[\alpha]_D$ value of **2***a*, unlike that of **1**, is unreliable for assignation of absolute stereochemistry (2). However, the ord (optical rotatory dispersion) curve of our material followed that of an authentic specimen of **2***a*. We thus found the diterpenes to be antipodal.

A major component of the leaf-gum proved to be a $C_{13}H_{16}O_4$ compound that was quickly recognized as *n*-butyl caffeate (**3***a*) (cf. data in the Experimental, and Tables 1 and 4). *n*-Butyl esters are relatively rare among known natural products and this is the first report of the occurrence of **3***a* in nature. (*n*-Butanol was not employed at any stage in the extraction and processing of the plant material, neither was it, or **3***a*, present as a contaminant in the solvents or absorbents; i.e. we have considered and excluded the possibility that **3***a* was an artefact.)

Besides **3***a* we isolated a mixture of its mono-*O*-isobutyrates (**4***a*, **4***b*), which were only able to separate after *O*-methylation with diazomethane, although the structures of the major (**4***a*) and minor (**4***b*) isomers could be deduced from the ^{13}C nmr spectrum of the mixture. The identifications were confirmed by synthesis of authentic reference specimens of the methyl ethers (**5***c*, **5***d*) from *n*-butyl ferulate (**5***a*) and isoferulate (**5***b*).

[1]Author to whom correspondence may be addressed.

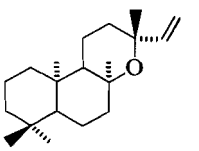

1

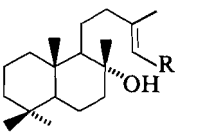

2*a* R = CH_2OH
2*b* R = CH_2OAc
2*c* R = CHO

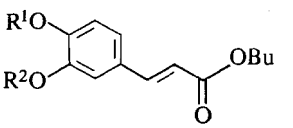

3*a* $R^1 = R^2 = H$
3*b* $R^1 = R^2$ = Ac
4*a* R^1 = H, R^2 = i-PrCO
4*b* R^1 = i-PrCO, R^2 = H
4*c* R^1 = Ac, R^2 = i-PrCO
4*d* R^1 = i-PrCO, R^2 = Ac
5*a* R^1 = H, R^2 = Me
5*b* R^1 = Me, R^2 = H
5*c* R^1 = i-PrCO, R^2 = Me
5*d* R^1 = Me, R^2 = i-PrCO

A further derivative of *n*-butyl caffeate was encountered in the form of a compound that we called di-*n*-butyl traversate (**6***a*). Our identification of this as an α-truxillate was based on the following evidence: (*i*) ms (mass spectra) measurements established the molecular composition as $C_{26}H_{32}O_8$, as required for a dimer of **3***a*; with (*ii*) the only fragment ions (**7***a*) corresponding to a truxillate rather than a truxinate (no ions seen for cleavage (b) in **7***b*) (3); (*iii*) in the 200-MHz ^1H nmr spectrum of **6***a* the cyclobutyl ring protons were observed as an AA′BB′ system (thus excluding isomers in which these nuclei form an A_2B_2 set) (3–5); and (*iv*) the chemical shift of the methyl function in dimethyl traversate (**6***c*), obtained by acid-catalysed methanolysis of **6***a*, corresponds to shielding by an adjacent *cis*-related aromatic ring (4).

It seemed reasonable to suspect that **6***a* was formed by the photochemical [2 + 2] dimerization of **3***a*, as the formation of other truxillates from cinnamates (3–6). Consistent with this idea, irradiation of **3***a* in aqueous suspension (6) with a medium-pressure Hanovia mercury vapour lamp produced **6***a*.

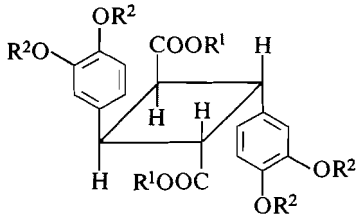

6*a* R^1 = Bu, R^2 = H
6*b* R^1 = Bu, R^2 = Ac
6*c* R^1 = Me, R^2 = H

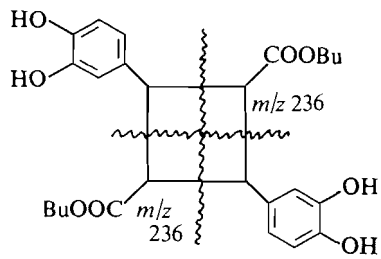

7a

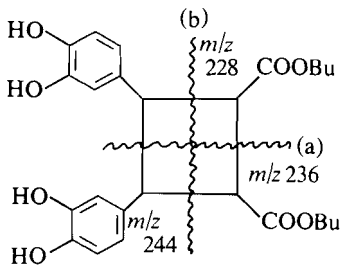

7b

The remaining seven compounds that we identified were flavonoids. Apart from the colourless (2*S*)-5,3′,4′-trihydroxy-7-methoxyflavanone (**8***a*), these were yellow and responsible for the colour of the leaf-gum. All these pigments proved to be derivatives of quercetin, three being the well-known methyl ethers rhamnazin (**9**), isorhamnetin (**10**), and rhamnetin (**11**), while the others were previously undescribed mono-*O*-isobutyrate ester derivates. Our identification of these latter substances as the 3-, 4′-, and 3′-esters (**12***a*, **13***a*, and **14***a*, respectively) can be summarized as follows. The ^{13}C nmr spectrum of **12***a* closely resembled that of quercetin (plus signals from the isobutyrate unit), except for the C-2 signal, which was shifted downfield by about 12 ppm, an observation consistent with acylation at C-3 (cf. the effect of glycosylation at this position) (7). Furthermore, the bathochromic shifts observed in the uv (ultraviolet) spectrum of **12***a* upon addition of $AlCl_3$, or $NaOAc–H_3BO_3$, were in accord with the ring-B diol system (8). The ms and ^1H nmr spectrum of the flavonoid and its tetra-*O*-acetate derivative were also in accord with structure **12***a*, and peresterification of **12***a* or quercetin with isobutyric anhydride yielded the same penta-*O*-isobutyrate (**12***c*).

Flavonoid acetate esters are well known as natural products (8) and a few other *O*-acyl derivatives have been described (9, 10) but, to our knowledge, **12***a* is the first example of an analogous isobutyrate.

Two more such compounds, **13***a* and **14***a*, were obtained as a mixture that we were unable to separate; they co-chromatographed in a variety of solvent systems, but both ^1H and ^{13}C nmr indicated their presence in ca. 1:3 ratio. We suspected that separation of these isomers (as also **4***a* from **4***b*) might be hampered by a facile O→O acyl migration moving the ester function between positions 3′ and 4′; however, after acetylating the mixture we were still unable to separate the isomers.

Phenolics have been demonstrated to contribute to plant defence both in the allelopathic inhibition of competitors (11), and as insect feeding-deterrents (12). *Traversia baccharoides* does not suffer from plant competition, and is markedly "under-utilized" by phytophageous insects (usually showing no sign of any such attack),[2] and it seems likely that *n*-butyl caffeate, the flavonoid esters, and possibly the truxillate contribute to the ecological defences of the plant.

Experimental

Instrumental and analytical methods were as described previously (14), supplemented by FT-IR using a Nicolet 5DX system. Analytical tlc was on 0.25-mm layers of Merck silica gel 60 F-254; and the radial centrifugal tlc was carried out on 2-mm-thick layers of Merck silica gel 60 PF 254 plus $CaSO_4 \cdot {}^1/_2H_2O$, using a Harrison Research Model 7924 Chromatotron.

Plant material, and the preparation of the leaf-gum extract

Traversia baccharoides (1.8 kg of fresh plant) was collected in early bloom in the N.W. Nelson region of New Zealand. A voucher specimen is deposited in the Herbarium of the University of Calgary. The twigs with flower heads and leaves were rinsed by swishing them for ca. 1–2 min in $CHCl_3$ (ca. 500 mL) contained in a beaker (1 L). When the wash liquid became bright yellow it was replaced by fresh solvent (a total of ca. 2.5 L of $CHCl_3$ were used). Evaporation of the combined washes at 40°C and under aspirator vacuum gave a yellow-orange gum (44.5 g).

Fractionation of the leaf-gum

The crude gum (44.5 g) was absorbed on silica gel (Woelm Pharma 70–230 mesh) by redissolving it in $CHCl_3$ (ca. 100 mL), stirring in the silica gel, and then removing the solvent under reduced pressure. This material was then loaded onto the top of a column (5 cm × 60 cm) of the

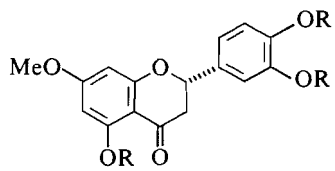

8*a* R = H
8*b* R = Ac

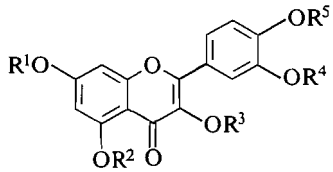

9 R^1 = R^4 = Me, R^2 = R^3 = R^5 = H
10 R^1 = R^2 = R^3 = R^5 = H, R^4 = Me
11 R^1 = Me, R^2 = R^3 = R^4 = R^5 = H
12*a* R^1 = R^2 = R^4 = R^5 = H, R^3 = i-PrCO
12*b* R^1 = R^2 = R^4 = R^5 = Ac, R^3 = i-PrCO
12*c* R^1 = R^2 = R^3 = R^4 = R^5 = i-PrCO
13*a* R^1 = R^2 = R^3 = R^4 = H, R^5 = i-PrCO
13*b* R^1 = R^2 = R^3 = R^4 = Ac, R^5 = i-PrCO
14*a* R^1 = R^2 = R^3 = R^5 = H, R^4 = i-PrCO
14*b* R^1 = R^2 = R^3 = R^5 = Ac, R^4 = i-PrCO

[2]J. S. Dugdale. Personal communication, 1985.

TABLE 1. ^{1}H nuclear magnetic resonance spectra of *n*-butyl caffeate (**3***a*) and derivatives[a]

	δ (ppm)									
H	**3***a*	**3***b*	**4***a*	**4***b*	**4***c*	**4***d*	**5***a*	**5***b*	**5***c*	**5***d*
2	6.23 d (16)	6.38	6.28	6.33	6.38	6.38	6.24	6.28	6.29	6.38
3	7.54 brd (16)	7.61	7.57	7.56	7.61	7.61	7.60	7.58	7.59	7.63
5	7.09 d (2)	7.35	7.26	7.19	7.34	7.35 m	7.02	7.13	7.23	7.09
8	6.85 d (8.5)	7.21	6.96	7.02	7.24	7.23	6.90	6.83	6.94	7.02
9	6.93 dd (2, 8.5)	7.40	7.28	7.02	7.40	7.40 m	7.06	7.02	7.35	7.11
1′	4.18 t (6.5)	4.20	4.19	4.20	4.20	4.20	5.20	4.19	4.19	4.21
2′	1.68 m	1.72	1.68	1.68	1.68	1.68	1.69	1.68	1.68	1.69
3′	1.47 m	1.48	1.44	1.44	1.42	1.42	1.43	1.43	1.45	1.46
4′	0.98 t (7)	0.96	0.96	0.96	0.96	0.96	0.96	0.96	0.96	0.97
CO–CH	—	—	2.88 hpt (7)	2.88	2.82	2.82	—	—	2.85	2.84
CH_3 CH_3	—	—	1.35 d (7)	1.34	1.32	1.31	—	—	1.33	1.32
OCH_3	—	—	—	—	—	—	3.90	3.84	3.84	3.83
Ac	—	2.30 s	—	—	2.27	2.28	—	—	—	—

[a]At 200 MHz, of solutions in $CDCl_3$. Coupling constants (*J*) in Hz, are shown in parentheses below δ values (rel. TMS=0) and multiplicities of the signals (s = singlet, d = doublet, t = triplet, hpt = heptet). Where not specified, multiplicities and *J*-values are as for the first entry for such groups.

same absorbent (500 g) packed in hexane. The column was eluted, and fractions collected as follows: F1–3, hexane (3 × 500 mL); 4–13, hexane – ethyl acetate (19:1 v/v) (2 × 500 mL, 13 × 250 mL); 14–21, hexane – ethyl acetate (9:1 v/v) (8 × 250 mL); 22–23, hexane – ethyl acetate (4:1 v/v) (12 × 250 mL); 34–44, hexane – ethyl acetate (3:2 v/v) (12 × 250 mL); 45–48, hexane – ethyl acetate (2:3 v/v) (4 × 250 mL); 49–52, hexane – ethyl acetate (1:4 v/v) (4 × 250 mL); 53–56, ethyl acetate (4 × 250 mL); 57–58, ethyl acetate – methanol (19:1 v/v) (2 × 50 mL); and ethyl acetate – methanol (9:1 v/v) (2 × 500 mL).

Purification of F4–5 (200 mg) by ptlc (benzene–hexane 1:1 v/v) afforded *ent*.-13-*epi*-manoyl oxide (**1**), mp 97–98°C (MeOH); $[\alpha]_D$ −28° ($CHCl_3$) (lit. (2) mp 100–101°C (15) mp 98–99.5°C). The ^{13}C nmr of **1** was identical with that reported in the literature for this compound (16) with the exception of the shift observed for the C-10 resonance, which we observed at δ 36.8 ppm. The literature value for this signal (δ 39.6) seems to represent a typographic error, i.e. should be 36.9 ppm.

Concentration of F24 resulted in the separation of a solid (17 mg), recognized from its ms as a mixture of long-chain fatty acids. After treatment of this material with ethereal diazomethane, gc–ms analysis revealed a series of straight-chain fatty acid methyl esters, predominant being the hexacosanoate, octacosanoate, and triacontanoate, accompanied by lesser amounts of tetracosanoate, docosanoate, and eicosanoate, and traes of tricosanoate, pentacosanoate, heptacosanoate, and nonacosanoate.

Evaporation of F27–33 gave a gum (1.5 g), which was near homogeneous by tlc (benzene – ethyl acetate 4:1 v/v). Further purification by rechromatography on silica gel with diethyl ether – hexane (3:7 v/v) as eluant gave a gum, homogeneous by tlc, which was, however, ca 2:1 mixture of **4***a* and **4***b*; ir (film): 3350 (br), 1760, 1710, 1640, and 1610 cm^{-1}; ms (positive ion CI-NH_3) *m/z*: 307 (6), 251 (55), and 71 (2). The ^{1}H and ^{13}C nmr data are given in Tables 1 and 4.

Acetylation of a portion (60 mg) of the mixture with acetic anhydride (0.5 mL) in pyridine (1 mL) at room temperature overnight gave a mixture of the acetate derivatives (**4***c*, **4***d*) that we were also unable to separate (see Table 1 for ^{1}H nmr data).

TABLE 2. ^{1}H nuclear magnetic resonance spectra of di-*n*-butyl traversate (**6***a*) and derivatives[a]

	δ (ppm)		
H	**6***a*	**6***b*	**6***c*
2	3.78	3.87 (10.5, 7)	3.81 (10.5, 7)
3	4.25 (10.5, 7)	4.42 (10.5, 7)	4.21 (10.5, 7)
5	6.80 d (2)	7.11	6.78
8	6.78 d (8)	7.15 m	6.78
9	6.63 dd (8, 2)	7.15 m	6.59 dd
1′	3.75 t (6.5)	3.82 dt (10.5, 6.5) 3.68 dt (10.5, 6.5)	3.36
2′	1.28 m	1.30	—
3′	1.14 m	1.14	—
4′	0.80 t (7)	0.81	—
Ac	—	2.29 s 2.27 s	—

[a]In $CDCl_3$–DMSO-d_6, at 200 MHz. Abbreviations and format as in footnote *a* to Table 1.

Methylation of another portion of the mixture of **4***a* and **4***b* with excess ethereal diazomethane for 4 h at room temperature, followed by removal of excess reagent and solvent, gave a mixture of the methyl ethers, which were separated by centrifugal radial centrifugal tlc (diethyl ether – hexane 3:7 v/v), first eluted being **5***c*, as a noncrystalline gum;

TABLE 3. ^{1}H nuclear magnetic resonance spectra[a] of the flavonoids **12***a*, **12***b*, **12***c*, **13***c*, **13***b*, and **14***b*

	δ (ppm)					
H	**12***a*[b]	**12***b*	**12***c*	**13***a*[b]	**14***a*[b]	**14***b*
6	6.28 d (2)	6.86	6.83	6.32	6.31	6.87
8	6.41 d (2)	7.32	7.31	6.44	6.43	7.33
2′	7.36 d (2)	7.65	7.65	7.86	7.85	7.66
5′	6.93 d (8.5)	7.34	7.32	7.09	7.08	7.34
6′	7.24 dd (8.5, 2)	7.70	7.71	7.68	7.99	7.71
CHCO	2.88 hpt (7)	2.87	2.99 2.81[d]	2.86	2.86	2.85
CH_3 CH_3	1.32 d (7)	1.29	1.37 1.32[c] 1.31 1.29	1.34	1.36	1.33
Ac	—	2.42	—	—	—	2.43
	—	2.34	—	—	—	2.33[c]
	—	2.32[c]	—	—	—	2.31

[a]At 200 MHz, in $CDCl_3$ unless otherwise specified. Abbreviations and format as in footnote[a] to Table 1.
[b]In $CDCl_3$–DMSO–d_6–D_2O.
[c]A six-proton signal.
[d]A four-proton signal.

TABLE 4. ^{13}C nuclear magnetic resonance[a] spectra of the cinnamates (**3***a*, **4***a*, **4***b*, **5***c*, and **5***d*) and di-*n*-butyl traversate (**6***a*)

	δ (ppm)					
C	**3***a*[b]	**4***a*	**4***b*	**5***c*	**5***d*	**6***a*[b]
1	161.7 s	167.6	167.6	167.1	166.9	174.0
2	155.5[c] d	116.7	122.9	116.7	118.4[c]	42.4
3	145.0[c] d	143.8	143.8	143.3	143.9	48.6[e]
4	126.9 s	127.6	133.2	127.5	133.2	131.9
5	114.4[c] d	122.1	116.6	121.8[c]	111.2	115.9[f]
6	144.9 s	138.9	147.7	140.2	151.5	145.6[g]
7	147.3 s	149.4	[d]	152.9	141.7	146.3[g]
8	115.0[c] d	117.8	120.9	112.2[c]	121.2	116.2[f]
9	121.8 d	127.2	118.4	124.4[c]	123.2	120.0
1′	64.2 t	64.5	64.7	64.3	64.6	65.6
2′	30.8 t	30.8	30.8	30.7	30.8	31.6
3′	19.2 t	19.2	19.2	19.1	19.2	20.1
4′	13.7 q	13.7	13.7	13.7	13.8	14.0
CO	—	175.6 s	175.6	174.9	175.0	—
CH	—	34.2 d	34.2	33.9	34.0	—
CH_3 CH_3	—	19.0 q	19.0	18.9	19.0	—
OCH_3	—	—	—	55.9 q	55.9	—

[a]At 50.4 MHz, in $CDCl_3$ unless otherwise specified. Signal multiplicities are as for the first entry.
[b]In CD_3OD.
[c]Assigned by selective proton decoupling experiments.
[d]Not observed.
[e]Partly under the solvent signal.
[f,g]Signals in the same vertical column may be interchanged.

TABLE 5. ^{13}C nuclear magnetic resonance spectra[a] of the flavonoids **8***a*, **12***a*, **13***a*, and **14***a*

	δ (ppm)			
C	**8***a* [b]	**12***a* [c]	**13***a*	**14***a*
2	79.2 d	158.6 s	145.6 s	145.6 s
3	43.0 t	131.6 s	135.3 s	136.6 s
4	196.2 s	117.1	178.4	178.4
5	163.9 s	163.1	161.9	161.9
6	94.8 d	100.2	99.0	99.0
7	167.8 s	166.2	164.9	164.7
8	94.0 d	95.1	94.3	94.3
9	163.0 s	158.4	157.6	157.4
10	103.0 s	105.0	103.9	103.9
1′	129.7 s	122.1	130.0	123.5
2′	113.9 s	116.4	116.9	123.3
3′	145.2 s	146.6	149.4	139.6
4′	145.6 s	150.2	137.4	151.3
5′	115.6 d	116.4	123.7	117.4
6′	118.1 d	122.3	120.0	127.0
CO	—	175.9 s	176.2	176.2
CH	—	35.1 d	34.3	34.3
CH_3 CH_3	—	19.3 q	19.0	19.0
OCH_3	55.6 q	—	—	—

[a]At 50.4 MHz in acetone-d_6 unless otherwise specified; format as in Table 4.
[b]In $CDCl_3$–DMSO-d_6.
[c]In CD_3OD.

ms: 320 (1), 250 (80), 194 (47), 177 (33), and 150 (20). Later fractions yielded **5***d*, also as a gum, with a ms nearly identical to that of **5***c*. The ^1H and ^{13}C nmr data for these derivatives are listed in Table 1 and 4, respectively. Their identity was confirmed by comparison of their ir spectra with those of authentic specimens (whose preparation is described later).

Trituration of F36–37 with hexane – ethyl acetate gave *n*-butyl caffeate (**3***a*) (2.53 g), mp 110°C (hexane – ethyl acetate) (lit. (17) mp 109–110°C). The ir spectrum (KBr) was superimposable upon that of synthetic **3***a*. The ^1H and ^{13}C data for this compound, as well as its diacetate derivative, are listed in Tables 1 and 4.

Fraction 38 (0.3 g) contained a mixture of **3***a* and **9**. The latter compound crystallized from F39 and was obtained as a yellow solid (0.18 g), mp 224–225°C (AcOH), identified as rhamnazin by direct comparison (ir, ^1H nmr, tlc and uv spectra) with an authentic specimen (lit. (18) mp 214–215°C).

Removal of solvent from F41 left a gum, which upon trituration with hexane – ethyl acetate gave (2*S*)-5,3′,4′-trihydroxy-7-methoxyflavanone (**8***a*) (refs. 19, 20), sternbin (ref. 21) (0.19 g), mp 222–223.5°C (lit. (19) mp 220°C). The cd (circular dichroism) (MeOH) revealed $[\theta]_{329}$ + 11 540°, $[\theta]_{312}$ 0°, and $[\theta]_{292}$ −32 980° (cf. ref. 22). The ^{13}C nmr data for **8***a*, not previously reported, are given in Table 5.

Concentration of F42–43 resulted in the crystallization of more **8***a* (0.64 g), then the separation of a mixture of **8***a*, **13***a*, and **14***a*, and finally a solid (0.43 g) that, although homogeneous by tlc in several solvent systems, was shown by ^1H and ^{13}C nmr to be a ca. 1:3 mixture of **13***a* and **14***a* (data in Tables 3 and 4). The ms of this material showed *m/z*: 372 (6.9), 302 (52), 153 (5), and 137 (5) as significant high-mass ions. The uv (MeOH) had λ_{max}: 372 (9 000), 304 sh (2 700), 272 (sh) (4 000), and 257 nm (6 600); upon addition of $AlCl_3$ (8), λ_{max}: 458 (13 300) (1 900), 271 (8 000), and 228 nm (6 100); with $AlCl_3$–HCl (8), λ_{max}: 428 (9 900), 360 (3 400), 304 (2 100), and 266 (7 400); with NaOAc, λ_{max}: 396 (5 900), 329 (5 100), and 275 nm (5 000); with NaOAc and H_3BO_3, λ_{max}: 386 (6 600), 296 (4 000), and 260 nm (5 900); and with NaOMe, λ_{max} 332 (10 000) and 246 nm (3 700), decomposition within minutes.

Acetylation (pyridine – acetic anhydride) gave a mixture of acetates (**13***b* and **14***b*) that co-chromatographed in several solvent systems. The ^1H nmr data for **14***b* are given in Table 3.

Evaporation of F45 and trituration of the residue with ethyl acetate gave a yellow solid (0.07 g) shown by tlc to be a mixture of two compounds. Separation of a portion (0.02 g) of this mixture by ptlc ($CHCl_3$–MeOH–EtOAc, 8:1:1 v/v) gave the less polar isorhamnetin (**10**) (7 mg), mp 296–300°C (MeOH) (lit. (13) mp 305–306°C). Comparison (uv, ir, ^1H nmr, and ms) with authentic isorhamnetin confirmed this identification. The more polar component (8 mg) formed a major part of F46 and was the sole constituent of F47, from which it was readily isolated (0.04 g). A yellow solid, the material had mp 292–294°C (MeOH), and it was identified as rhamnetin (**11**) by direct comparison (ir, ms, ^1H nmr, uv, and tlc) with an authentic reference sample (lit. (18) mp 290–295°C).

The mother liquors remaining after removal of **11** from F46 and 47 were combined and evaporated to yield a residual solid (3.1 g) that was rechromatographed on silica gel (160 g). Elution with chloroform–methanol (49:1 v/v) gave labd-13-ene-5,18-diol (**2***a*) (1.16 g), mp 127.5–128.5°C (hexane–benzene) (lit. (1) mp 130.5°C). Acetylation of **2***a* (acetic anhydride – pyridine) gave a monoacetate (**2***b*); ^1H nmr (200 MHz, $CDCl_3$) δ: 5.35 (qt, J = 1.2 and 7.5 Hz, H-14), 4.57 (brd, J = 7.5 Hz, H-15), 2.06 (Ac), 1.72 (brs, H-16), 1.13 (H-17), 0.87, 0.80, and 0.79 (H-18, -19, and -20). Oxidation of **2***a* (10 mg) with MnO_2 (50 mg) in chloroform (3 mL) overnight gave the unstable aldehyde (**2***c*); ^1H nmr (200 MHz, $CDCl_3$) δ: 9.99 (d, J = 8 Hz, H-15), 5.91 (brd, J = 8 Hz, H-14), 2.18 (d, J = 1 Hz, H-16), 1.16 (H-17), 0.88 (3H), and 0.79 (6H) (H-18, -19, and -20). Further elution of the column with chloroform–methanol (24:1 v/v) gave dibutyl traversate **6***a* (0.18 g) mp 182–183°C (EtOAc) ν_{max} (KBr): 3500, 3300, 2700, and 1610 cm^{-1}, $[\alpha]_D$ = 0 ($CHCl_3$); ms: 236 (44), 180 (85), and 163 (100). The ^1H and ^{13}C nmr data for **6***a* are given in Tables 2 and 4. Acetylation of **6***a* (25 mg) with acetic anhydride and pyridine gave the acetate derivative (**6***b*), mp 145–146.5°C (benzene); ν_{max} (KBr): 1771 and 1721 cm^{-1}; ms: 321 (8), 320 (7), 278 (48), 236 (90), 180 (39), and 163(33); the ^1H nmr data is in Table 2. Transesterification of **6***a* was achieved by boiling a solution of it (15 mg) in methanol saturated with HCl, under reflux for 4 h. Removal of solvent and recrystallization then gave dimethyl traversate (**6***c*), mp 268–271°C (MeOH); ν_{max} (KBr); 3390, 3322, 1709, and 1619 cm^{-1}; ms: 388 (4), 245 (11), 194 (65), 164 (51), and 136 (55); the ^1H nmr data are in Table 2.

From F50 a yellow solid (0.062 g) separated, and recrystallization gave pure quercetin 3-*O*-isobutyrate (**12***a*), mp 253–256°C ($CHCl_3$–MeOH); ν_{max} (KBr): 3417, 3293 (br), 1741, 1662, and 1613 cm^{-1}; uv (MeOH) λ_{max}: 347 (10 900, 262 (12 300), and 253 nm (12 600); after adding $AlCl_3$ (8), λ_{max}: 435 (17 400), 332 (3 700), 304 (4 900), and 275 nm (16 700); with $AlCl_3$–HCl (8), λ_{max}: 393 (10 900), 358 (10 900), 298 (7 200), and 268 (14 300); with NaOAc (8), λ_{max}: 366 (13 500), 260 sh (4 700), and 259 nm (17 000); with NaOMe (8), λ_{max}: 397 (15 600), 328 sh (6 500), and 269 (16 300); ms: 302 (14), 153 (5), 137 (17), and 109 (6); the ^1H and ^{13}C nmr data are in Tables 3 and 5. Acetylation of **12***a* with acetic anhydride and pyridine gave a tetra-*O*-acetate (**12***b*), mp 187–188°C (hexane–EtOAC); ν_{max}: 1775, 1648, and 1624 cm^{-1}; the ^1H nmr data are in Table 3.

*Photochemical synthesis of di-*n*-butyl traversate*

n-Butyl caffeate (**3***a*) (400 mg) was suspended in water (250 mL) and irradiated through a Pyrex filter with a 450-W Hanovia mercury vapour lamp, while a stream of nitrogen was bubbled through the solution. After 3 days tlc revealed the presence of the dimer **6***a*. Irradiation was continued for two more days and the mixture was then worked up to give a dark-brown gum, which was chromatographed on a column of silica gel (55 g). Elution with chloroform–methanol (49:1 v/v) gave first **3***a* and then (with 24:1 v/v eluant) crude dimer (110 mg), which was triturated with ethyl acetate to afford pure **6***a*, identical (ir, and ^1H nmr) with the natural product.

n-Butyl isoferulate 3-O-isobutyrate (5c)

Isoferulic acid (200 mg) was dissolved in *n*-butanol (25 mL) saturated with hydrogen chloride and the solution boiled under reflux for 4 h.

Removal of solvent and reagent under reduced pressure gave *n*-butyl ferulate (230 mg) as an oil; ν_{max} (film): 3400 (br), 1701, 1635, 1604, and 1592 cm^{-1}; ms: 250 (48), 194 (80), 177 (67), and 150 (37); the ^1H nmr data are given in Table 1. Acylation of this ester with isobutyric anhydride (2 mL) in pyridine (2 mL) overnight, at room temperature, followed by conventional work-up, gave **5***c* (245 mg).

n-*Butyl ferulate* 4-O-isobutrate (*5*d)

Ferulic acid (250 mg) was converted into **5***d* (250 mg) by the same procedure used to make **5***c* from isoferulic acid.

Quercetin penta-O-*isobutyrate (12*c)

Quercetin (0.2 g) was peracylated with isobutyric anhydride (3 mL) in pyridine (3 mL) at room temperature, overnight, and the reaction mixture worked up, in the usual way to give the penta-*O*-isobutyrate (**12***c*) (0.43 g), mp 169.5–171°C (acetone–hexane).

Acknowledgments

Financial support of this work was provided by way of a grant in aid of research to M. H. B. from the Natural Sciences and Engineering Research Council of Canada. We are grateful to Professor E. Wollenweber, Institute of Botany, Technische Hochschule Darmstadt, West Germany, and Professor P. R. Jefferies, Chemistry Department, University of Western Australia, for gifts of reference specimens of flavonoids, and labd-13-en-8,15-diol respectively. We also thank John Dugdale, Entomology Division, DSIR, Auckland, New Zealand, for his assessment of insect damage of *T. baccharoides*, and A. K. Walker and R. A. Galbreath, also of this address, for help in the collection of plant material.

1. P. E. KOLATTUKUDY. In The biochemistry of plants. Vol. 4. Lipids: structure and function. *Edited by* P. K. Stumpf. Academic Press, New York. 1980. p. 571.
2. P. R. JEFFRIES and T. G. PAYNE. Aust. J. Chem. **18**, 1441 (1965).
3. M. KUROYANAGI, Y. YAMAMOTO, S. FUKUSHIMA, A. UENO, T. NORO, and T. MIYASE. Chem. Pharm. Bull. Jpn. **30**, 1602 (1982).
4. G. MONTAUDO and S. CACAMESE. J. Org. Chem. **38**, 710 (1973).
5. R. B. FILHO, M. P. DE SOUZA, and M. E. O. MATTOS. Phytochemistry, **20**, 345 (1981).
6. D. G. FARNUM and A. J. MOSTASHARI. *In* Organic photochemical syntheses. Vol. 1. *Edited by* R. Srinivasan and T. D. Roberts. Wiley–Interscience, New York. 1971. p. 103.
7. K. R. MARKHAM, V. M. CHARI, and T. J. MABRY. *In* The flavanoids: advances in flavanoid research 1975–80. *Edited by* J. B. Harborne and T. J. Mabry. Chapman and Hall, London. 1982. p. 19.
8. K. R. MARKHAM. Techniques of flavonoid identification. Academic Press, New York. 1982.
9. E. WOLLENWEBER. Phytochemistry, **24**, 1493 (1985).
10. S. GHOSAL, K. BISWAS, and D. K. JAISWAL. Phytochemistry, **19**, 123 (1980).
11. E. E. RICE. *In* Allelopathy. 2nd ed. Academic Press, New York. 1983, and references therein.
12. R. T. PALO. J. Chem. Ecol. **10**, 499 (1984), and references therein.
13. L. JURD. J. Org. Chem. **27**, 1294 (1962).
14. H. RÜEGER and M. H. BENN. Can. J. Chem. **60**, 2918 (1982).
15. B. E. CROSS, R. H. B. GALT, and J. R. HAMJON. J. Chem. Soc. 2937 (1963).
16. F. WEHRLI and T. NISHIDA. Fortschr. Chem. Org. Naturst. **56**, 36 (1977).
17. R. A. ANDERSON and G. MOEGLING. Anal. Biochem. **27**, 397 (1969).
18. R. KUHN and I. LÖW. Ber. **77**, 211 (1944).
19. J. M. AMARO and A. M. MENDEZ. Rev. Latinoam. Quim. **14**, 86 (1982).
20. N. D. JOHNSON. Biochem. Syst. Ecol. **11**, 211 (1983).
21. A. GONZALEZ, B. M. FRAGA, V. P. GARCIA, and M. G. HERNANDEZ. Rev. Latinoam. Quim. **14**, 115 (1984).
22. W. GAFFIELD. Tetrahedron, **26**, 4093 (1970).

Transformation of β-diketones to β-chloro-α,β-unsaturated ketones induced by lithium hydride and phenyl dichlorophosphate

HSING-JANG LIU, GUY V. LAMOUREUX, AND MONTSE LLINAS-BRUNET
Department of Chemistry, University of Alberta, Edmonton, Alta., Canada T6G 2G2

Received August 19, 1985

HSING-JANG LIU, GUY V. LAMOUREUX, and MONTSE LLINAS-BRUNET. Can. J. Chem. **64**, 520 (1986).

The conversion of β-diketones to the corresponding β-chloro-α,β-unsaturated ketones is facilitated by using lithium hydride as a base and phenyl dichlorophosphate as an activating agent.

HSING-JANG LIU, GUY V. LAMOUREUX et MONTSE LLINAS-BRUNET. Can. J. Chem. **64**, 520 (1986).

La transformation des β-dicétones en β-chloro cétones α,β non saturées est facilitée par l'utilisation de l'hydrure de lithium comme base et du dichlorophosphate de phényle comme agent d'activation.

[Traduit par le journal]

During the course of our synthetic studies on cononafacic acid (1), it became necessary to convert diketone **1** to the corresponding β-chloro-α,β-unsaturated ketones **2** and (or) **3**. Several methods are known to effect this type of transformation using a variety of reagents, such as phosphorus trichloride (2), phosphorus oxychloride (2), acetyl chloride (3), thionyl chloride (4), phosgene (5), triphenylphosphine–carbon tetrachloride (6), oxalyl chloride (7), and triphenylphosphine dichloride (8), with or without the assistance of a base, usually a tertiary amine. Application of most of these methods to our system, however, met with little success. Invariably, the attempted reactions resulted in substantial loss of material without formation of the desired products in significant amount. As a consequence of these difficulties, alternative methods were investigated.

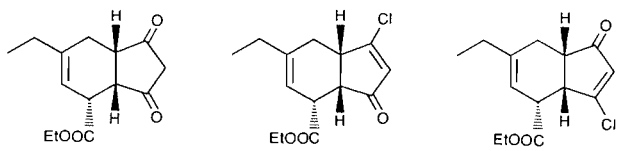

1 **2** **3**

Previously, phenyl dichlorophosphate was found in our laboratory to be an excellent activating agent for the condensation of carboxylic acids with alcohols (9) and thiols (10). Since 1,3-diones are normally completely enolized and possess characteristics similar to those of carboxylic acids, it is conceivable that phenyl dichlorophosphate can also serve as an activating agent to facilitate the desired transformation **1** → **2/3**. Contrary to this expectation, however, only a very small quantity of the desired products was formed when dione **1** was subjected to treatment with phenyl dichlorophosphate in tetrahydrofuran (THF) in the presence of triethylamine at room temperature. On the other hand, when the reaction was carried out subsequently, with lithium hydride substituting triethylamine and in the presence of hexamethylphosphoramide (HMPA), the results were rather promising and a substantial amount (~50% yield) of chloro enones **2** and **3** (3:2) was obtained for the first time. As the reaction is most likely to occur via the formation of a vinylogous mixed anhydride **4** followed by an overall replacement of the phosphate group with chloride (Scheme 1), a greater concentration of chloride ion is expected to facilitate the reaction, giving rise to an improved yield of the products. Indeed, when two equivalents of lithium chloride were added, the yield of **2** and **3** was increased considerably to 64% (1).

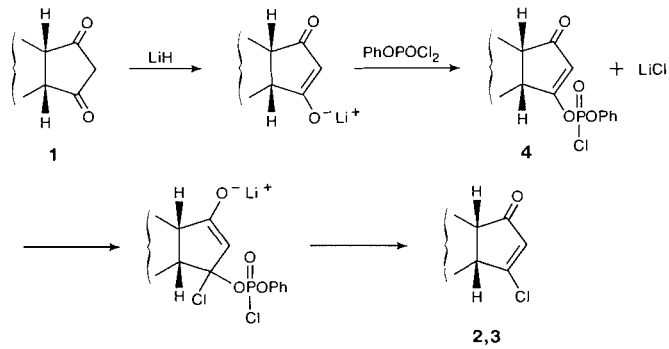

SCHEME 1

In search of a better activating agent, we have also examined phosphorus oxychloride and diphenyl chlorophosphate. Under comparable conditions, a 45% yield of **2** and **3**, again in 3:2 ratio, was obtained when the former reagent was applied, while an even lower yield of 25% resulted from the use of the latter reagent. Clearly, for the conversion of dione **1** to the corresponding chlorides **2** and **3**, phenyl dichlorophosphate is a more effective activating agent in the newly developed method, which in turn is superior to many existing methods attempted. The effectiveness of the new method could be attributed to the combination of a non-nucleophilic base and an adequately reactive and yet sufficiently stable activating agent.

The combination of LiH–$PhOPOCl_2$–LiCl proved to be generally useful for the transformation of β-diketones, cyclic ones in particular, to the corresponding β-chloro-α,β-unsaturated ketones. Table 1 summarizes the results obtained for a number of additional examples. During these studies, it was also recognized that the use of HMPA as a chelating agent was in fact unnecessary. The results were virtually unchanged in the absence of this reagent and a typical experiment could be simply carried out by sequential addition of lithium hydride (~1.3 equiv.), phenyl dichlorophosphate, and lithium chloride (~2 equiv. each[1]) to a solution of β-diketone in THF and allowing the reaction mixture to stir at room temperature for the required period of time.[2] The results obtained for cyclic β-diketones **5**–**8** (Entries 2–5) were uniformly good, with the

[1]With smaller quantities of the reagents, the reaction was considerably slower.

[2]The disappearance of the starting material and the intermediate mixed anhydride was monitored by thin-layer chromatographic analysis.

Table 1. Transformation of β-diones to β-chloro enones

Entry	Dione	Time (h)[a]	Product(s)	% Yield
1	**1**	16[b]	**2** + **3** (3 : 2)	64
2	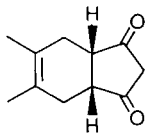 **5**	2	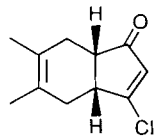 **12**	76
3	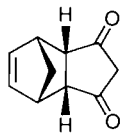 **6**	20	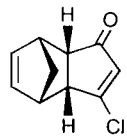 **13**	77
4	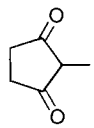 **7**	2	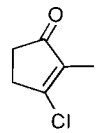 **14**	83
5	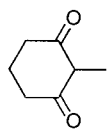 **8**	7	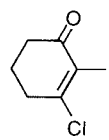 **15**	85
6	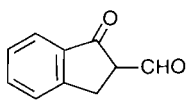 **9**	18	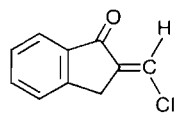 **16**	72
7	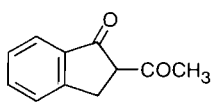 **10**	47	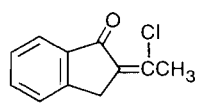 **17** (one isomer)	35
8	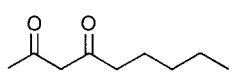 **11**	10	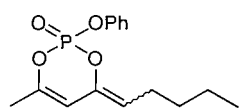 **18**	53

[a]Unless otherwise stated, all reactions were carried out in THF at room temperature using 1.3 equiv. of LiH and 2 equiv. each of $PhOPOCl_2$ and LiCl.

[b]HMPA (1.3 equiv.) was added.

corresponding chloro enones **12–15** produced, typically, in ~80% yield. For acyclic diketones, however, the results were less consistent because of the apparent structural dependency. For example, β-keto aldehyde **9**, which does not contain any α′-hydrogen atom, was found to undergo the reaction normally, with complete regio- and stereoselectivity, to give β-chloro enone **16** (Entry 6) as the only product. On the other hand, the result (35% yield of **17**[3]) obtained for the corresponding methyl diketone **10** (Entry 7) was rather disappointing due to the competing reaction leading to cyclic enol phosphate formation. The latter process was found to occur exclusively in the case of

[3]This compound was also obtained as a single stereoisomer. Its stereochemistry remains to be ascertained.

2,4-nonanedione (**11**) (Entry 8) to give enol phosphate **18** as the only isolatable product.

In conclusion, the procedure described above was shown to be effective for the conversion of β-diketones (with the exception of the acyclic ones, which are also readily enolizable towards the α′-carbon(s)) to β-chloro-α,β-unsaturated ketones of considerable synthetic utility.[4]

Experimental

General

Melting points were determined on a Kofler hot stage apparatus and are uncorrected. Elemental analyses were performed by the microanalytical laboratory of this department. Infrared (ir) spectra were recorded on a Nicolet 7-199 FT-IR spectrophotometer. Unless otherwise stated, ir samples were run as thin films. Proton nuclear magnetic resonance (^{1}Hmr) spectra were recorded on a Bruker WH-80, WH-200, or WH-400 spectrometer and, except where otherwise stated, were obtained on solutions in deuterochloroform with tetramethylsilane as internal reference. Carbon-13 nuclear magnetic resonance (^{13}Cmr) spectra were recorded on a Bruker WH-400 spectrometer and were obtained on solutions in deuterochloroform using tetramethylsilane as internal reference. Mass spectra (ms) were recorded using an A.E.I. model MS50 mass spectrometer.

*Transformation of β-diones **5**–**11** to β-chloro enones **12**–**17** and enol phosphate **18***

The reactions were carried out using the general procedure illustrated below with 2-methyl-1,3-cyclopentanedione (**7**). Times of reaction and yields of products are noted in Table 1. Products were purified by the following methods: **12**, **13**, **16**, and **17** by crystallization, **14** and **15** by distillation, and **18** by flash chromatography on silica gel (20% ether in petroleum ether).

At 0°C, to a solution of diketone **7** (508 mg, 4.5 mmol) in THF (20 mL) under an argon atmosphere, were sequentially added lithium hydride (45 mg, 5.6 mmol), phenyl dichlorophosphate (1.35 mL, 9 mmol), and lithium chloride (390 mg, 9.2 mmol). The reaction mixture was stirred at room temperature for 2 h. After cooling to 0°C, a solution of 10% aqueous sodium bicarbonate (20 mL) was added and the resulting solution extracted with dichloromethane (4 × 20 mL). The extracts were washed with water, dried over magnesium sulfate, filtered, and concentrated. Bulb-to-bulb distillation of the residue at 50°C (oven temperature)/1.5 Torr (1 Torr = 133.3 Pa) gave 492 mg (83% yield) of 3-chloro-2-methyl-2-cyclopentenone (**14**): ms M^+ 132.0153 and 130.0182 (calcd. for C_6H_7ClO: 132.0156 and 130.0186). The ir (1713 (C=O) and 1644 (C=C)cm^{-1}) and ^{1}Hmr (δ: 1.75 (t, 3H, J = 2 Hz, —CH_3), 2.58 (m, 2H, —CH_2CO—), and 2.83 (m, 2H, —CH_2CCl=)) spectra were found to be in agreement with those reported for **14** (8).

Compounds **12**, **13**, and **15**–**18** showed the following physical data:

*Chloro enone **12**:* mp 62–63°C (petroleum ether); ir: 1710 (C=O) and 1590 (C=C) cm^{-1}; ^{1}Hmr δ: 1.66 (br s, 6H, 2 × —CH_3), 2.30 (m, 4H, 2 × —CH_2—), 2.74 (ddd, 1H, J = J' = 6, J'' = 3.5 Hz, —CHCO—), 3.24 (dddd, 1H, J = 6, J' = 5, J'' = J''' = 1.5 Hz, —CHCCl=), and 6.21 (d, 1H, J = 1.5 Hz, —CH=); ms M^+: 196.0658 and 198.0630 (calcd. for $C_{11}H_{13}ClO$: 196.0655 and 198.0625). *Anal.* calcd. for $C_{11}H_{13}ClO$: C 67.18, H 6.66, Cl 18.02; found: C 67.11, H 6.58, Cl 17.87.

*Chloro enone **13**:* mp 67–68°C (petroleum ether); ir: 1699 (C=O) and 1580 (C=C) cm^{-1}; ^{1}Hmr δ: 1.62 (d, 1H, J = 8 Hz, —C*H*H—), 1.82 (ddd, 1H, J = 8, J' = J'' = 2 Hz, CH*H*—), 3.04 (dd, 1H, J = 5.5, J' = 4.5 Hz, —CHCO—), 3.16, 3.24 (both m, 1H each, 2 × =CCH—), 3.47 (ddd, 1H, J = 5.5, J' = 4.5, J'' = 1 Hz, —CHCCl=), 5.96 (d, 1H, J = 1 Hz, =CHCO—), 5.95 and 6.07 (both dd, 1H each, J = 5.5, J' = 3 Hz each, —CH=CH—); ms M^+: 180.0343 and 182.0317 (calcd. for $C_{10}H_9ClO$: 180.0341 and 182.0312). *Anal.* calcd. for $C_{10}H_9ClO$: C 66.49, H 5.02, Cl 19.63; found: C 66.53, H 5.06, Cl 19.61.

*Chloro enone **15*** obtained by bulb-to-bulb distillation of the crude product at 40°C (oven temperature)/0.5 Torr displayed ir (1679 (C=O) and 1627 (C=C) cm^{-1}) and ^{1}Hmr δ: 1.90 (t, 3H, J = 2 Hz, —CH_3), 2.02 (m, 2H, —CH_2—), 2.45 (t, 2H, J = 6 Hz, —CH_2CO—), and 2.73 (m, 2H, —CH_2CCl=) spectra in agreement with those reported (8). In the mass spectrum, molecular ions were observed at 144.0338 and 146.0312 (calcd. for C_7H_9ClO: 144.0342 and 146.0312).

*Chloro enone **16** (7):* mp 71–72°C (petroleum ether); ir: 1703 (C=O), 1636 (C=C), and 1610 (benzene) cm^{-1}; ^{1}Hmr δ: 3.76 (d, 2H, J = 2 Hz, —CH_2—), 7.38 (t, 1H, J = 2 Hz, =CHCl—), 7.40 (brdd, 1H, J = J' = 8 Hz, —CH=C*H*CH=), 7.48 (brd, 1H, J = 8 Hz, —C*H*=CCH$_2$—), 7.62 (ddd, 1H, J = J' = 8, J'' = 1.5 Hz, —CH=C*H*CH=), and 7.82 (br d, 1H, J = 8 Hz, CH=CCO—); ms M^+: 178.0180 and 180.0153 (calcd. for $C_{10}H_7ClO$: 178.0186 and 180.0156).

*Chloro enone **17**:* mp 102–103°C (petroleum ether): ir: 1696 (C=O), 1625 (C=C), 1605, and 1580 (benzene) cm^{-1}; ^{1}Hmr δ: 2.82 (t, 3H, J = 1 Hz, —CH_3), 3.80 (br s, 2H, —CH_2—), 7.39 (ddd, 1H, J = J' = 8, J'' = 1 Hz, —CH=C*H*CH=) 7.47 (ddd, 1H, J = 8, J' = J'' = 1 Hz, —C*H*=CCH$_2$—), 7.59 (ddd, 1H, J = J' = 8, J'' = 1 Hz, —CH=C*H*CH=), and 7.80 (dd, 1H, J = 8, J' = 1 Hz, —CH=CCO—); ^{13}Cmr; 190.9, 147.5, 146.6, 139.5, 134.4, 132.6, 127.5, 125.8, 124.2, 34.0, and 22.9; ms M^+: 192.0345 and 194.0317 (calcd. for $C_{11}H_9ClO$: 192.0342 and 194.0312). *Anal.* calcd. for $C_{11}H_9ClO$: C 68.58, H 4.71, Cl 18.40; found: C 68.45, H 4.68, Cl 18.24.

*Enol phosphate **18**:* ir: 1685, 1595 (C=C), 1305, and 950 (phosphate) cm^{-1}; ^{1}Hmr δ: 0.85 (t, 3H, J = 6 Hz, —$CH_2C\mathit{H}_3$), 1.28 (m, 4H, —$(C\mathit{H}_2)_2CH_3$), 1.93 (s, 3H, =CCH_3), 2.10 (m, 2H, =CH$C\mathit{H}_2$—), 4.79 (m, 1H, =C*H*CH_2—), 5.43 (br s, 1H, —C*H*=CCH_3), and 7.25 (m, 5H, —OC_6H_5); ms M^+: 294.1021 (calcd. for $C_{15}H_{19}PO_4$: 294.1021).

Acknowledgments

We are grateful to the Natural Sciences and Engineering Research Council of Canada for financial support of this work and for an Undergraduate Summer Studentship to G.V.L., and to the Alberta Heritage Foundation for Medical Research for a Studentship to M.L.

1. H. J. Liu and M. Llinas-Brunet. Can. J. Chem. **62**, 1747 (1984).
2. A. W. Crossley and H. R. Le Sueur. J. Chem. Soc. **83**, 110 (1903).
3. W. Hückel and K. Thiele. Chem. Ber. **94**, 96 (1961).
4. R. L. Frank and H. K. Hall, Jr. J. Am. Chem. Soc. **72**, 1645 (1950).
5. M. M. Shemyakin, Yu. A. Arbuzov, M. N. Kolosov, G. A. Shatenshtein, V. V. Onoprienko, and Yu. V. Konnova. J. Gen. Chem. U.S.S.R. **30**, 563 (1960).
6. L. Gruber, J. Tomoskozi, and L. Radics. Synthesis, 708 (1975).
7. R. D. Clark and C. H. Heathcock. J. Org. Chem. **41**, 636 (1976).
8. E. Piers, J. R. Grierson, C. K. Lau, and I. Nagakura. J. Chem. **60**, 210 (1982).
9. H. J. Liu, W. H. Chan, and S. P. Lee. Tetrahedron Lett. 4461 (1978).
10. H. J. Liu and S. I. Sabesan. Can. J. Chem. **58**, 2645 (1980).

[4]For a leading reference, see ref. 8.

Evaluation of the diffusion coefficient of the zincate ion using a rotating disk electrode

ELISABETE JORGE PESSINE,[1] SILVIA M. L. AGOSTINHO, AND HÉLIO C. CHAGAS
Department of Fundamental Chemistry, University of São Paulo, CP 20780, Brazil
Received December 11, 1984[2]

ELISABETE JORGE PESSINE, SILVIA M. L. AGOSTINHO, and HÉLIO C. CHAGAS. Can. J. Chem. **64**, 523 (1986).

Using a rotating Hg-film disc electrode, the diffusion coefficient of the zincate ion in a 1–4 *M* aqueous solution of NaOH was measured. Experiments covered a temperature range from 25 to 40°C. The experimental results are in agreement with the predictions of the Stokes–Einstein theory for diffusivity. The obtained Stokes radii decrease with increasing alkali concentration, but the ratio $D\eta/T$ is reasonably constant within the whole range of temperature investigated.

ELISABETE JORGE PESSINE, SILVIA M. L. AGOSTINHO et HÉLIO C. CHAGAS. Can. J. Chem. **64**, 523 (1986).

Utilisant une électrode à disque tournant de mercure sous forme de film et opérant à des températures allant de 25 à 40°C, on a mesuré le coefficient de diffusion de l'ion zincate dans des solutions aqueuses de NaOH de 1 à 4 *M*. Les résultats expérimentaux sont en accord avec les prévisions qui peuvent être faites à l'aide de la théorie de diffusivité de Stokes et Einstein. Les rayons de Stokes qui sont obtenus diminuent avec une augmentation de la concentration en base; toutefois, le rapport $D\eta/T$ est raisonnablement constant sur tout l'intervalle des températures étudiées.

[Traduit par le journal]

Introduction

The electrochemical behaviour of zinc in alkaline aqueous media has been the subject of a relatively large number of investigations (1–6) due to the importance of this system for both industrial electrodeposition processes and high density electrical batteries. With regard to the latter, corrosion is one of the principal factors that restricts the application of the zinc–zincate system as an efficient energy source over very long periods of time. In the range of 1—10 *M* alkali, the predominant corrosion product is the complex ion tetrahydroxyzincate (7–9).

Many authors have observed that transport of the zincate ion from the electrode surface to the bulk of the solution is the rate limiting step in the process of zinc dissolution. Any kinetic study of the zinc–zincate system thus requires a knowledge of the diffusion coefficient (D) of the zincate ion. However, since the available literature data for the diffusion coefficient of zincate ion is both very scarce and discordant (10), many authors have employed only an order of magnitude estimate of the diffusion coefficient in the analysis of their kinetic studies (4, 11–13). Several factors account for the existence of discrepancies in the available diffusion coefficient data: (*a*) most of the published results are based on the polarographic method (10) in alkaline media, conditions under which the zincate ion presents maxima of the second kind created by kinetic factors owing to the movement of solution past the drop surface, and these maxima overestimate the limiting current; (*b*) the zincate ion is reduced at a very negative potential, restricting the utilization of certain types of solid electrodes. In this case the hydrogen evolution occurs at potentials near those of zincate reduction (due to the low hydrogen overvoltage) making the evaluation of the cathodic limiting current of the reduced ion difficult.

In the present work we report a determination of the diffusion coefficient of the zincate ion in alkaline medium using an amalgamated gold rotating disk electrode. The rotating disk electrode provides one of the most accurate electrochemical methods for evaluation of diffusion coefficients (14, 15) due in part to the fact that the method is based on an exact mathematical solution for the diffusive–convective problem, and that the electrode has a uniformly accesible surface. As pointed out by Opekar and Beran (16), this method offers additional advantages in relation to conventional polarography and other such methods. From the dependence of the limiting current on the angular velocity of the disk, it is possible to separate currents from two different processes when only one is diffusion controlled; this is the case for simultaneous reduction of the zincate ion and hydrogen evolution, the former being controlled by diffusion while the latter is chemically controlled at the same potential (13, 17). The use of an amalgamated gold rotating disk electrode further facilitates the determination of the limiting current for zincate ion reduction due to the high hydrogen overvoltage of mercury.

Experimental

All solutions were prepared using analytical grade reagents and triply distilled water. The zincate solutions (1–10 m*M*) were prepared by adding appropriate aliquots of an aqueous zinc sulfate stock solution ($ZnSO_4 \cdot 7H_2O$ in water) to NaOH solution (1–4 *M*). The solutions were deoxygenated with purified nitrogen prior to all measurements. Prior to amalgamation, the gold disk electrode (ϕ = 0.465 cm) was mechanically polished with emery paper and with chromic oxide (1–5 μ) and rinsed with water and ethyl alcohol. Simply placing mercury on the electrode surface and removing the excess by rotating the disk at 10 000 rpm (18) failed to give reproducible results. This problem was overcome by leaving the electrode immersed in mercury for several days. Prior to each experiment a new layer of mercury was added and the excess removed as before.

All experiments were performed at 25, 30, 35, and 40°C. Viscosities of the sodium hydroxide solutions were determined at the same temperatures. The electronic equipment and cell has been described previously (19). A saturated calomel – potassium chloride electrode was used as reference electrode and a platinum foil as the counter electrode.

Results

Voltammograms were determined for solutions containing 1, 2, 4, 6, 8, and 10 m*M* zincate ion in aqueous NaOH (1, 2, 3, and 4 *M*) at several temperatures (25, 30, 35, and 40°C) and at different angular velocities of the disk electrode ($f^{1/2}$ = 2, 3, 4, 5, 6, 7 $Hz^{1/2}$).

Figure 1 shows a typical I–V curve for the reduction of the zincate ion (A) and the hydrogen evolution (B) on the rotating

[1]Comissão nacional de energia nuclear, Departamento de Metalurgia, Caixa Postal 11049. Pinheiros, São Paulo, Brazil.

[2]Revision received October 16, 1985.

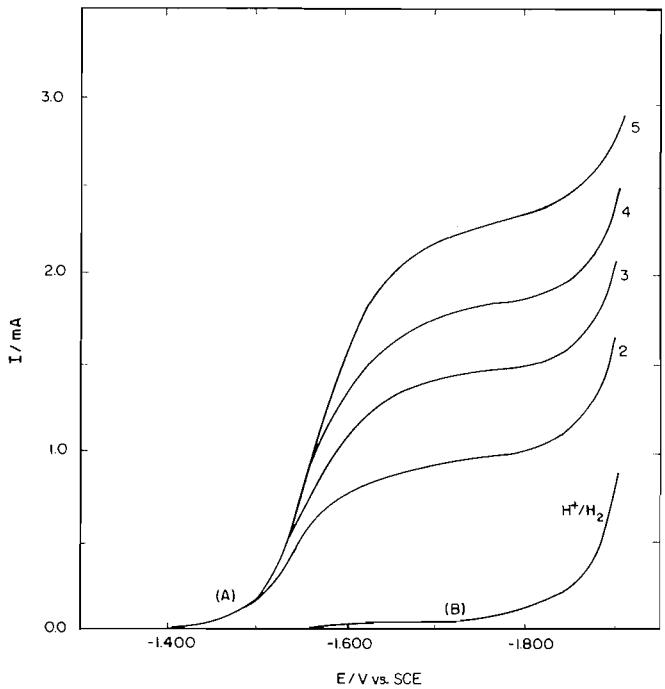

FIG. 1. Current–voltage relationships on Au-amalgamated disk electrode. (A) 2 m*M* $Zn(OH)_4^{2-}$ reduction. (B) Hydrogen evolution in free zincate ion solution. Both curves at 25°C, in 4 *M* aqueous NaOH with frequency of the rotating disk electrode varying from 2 to 5 $Hz^{1/2}$.

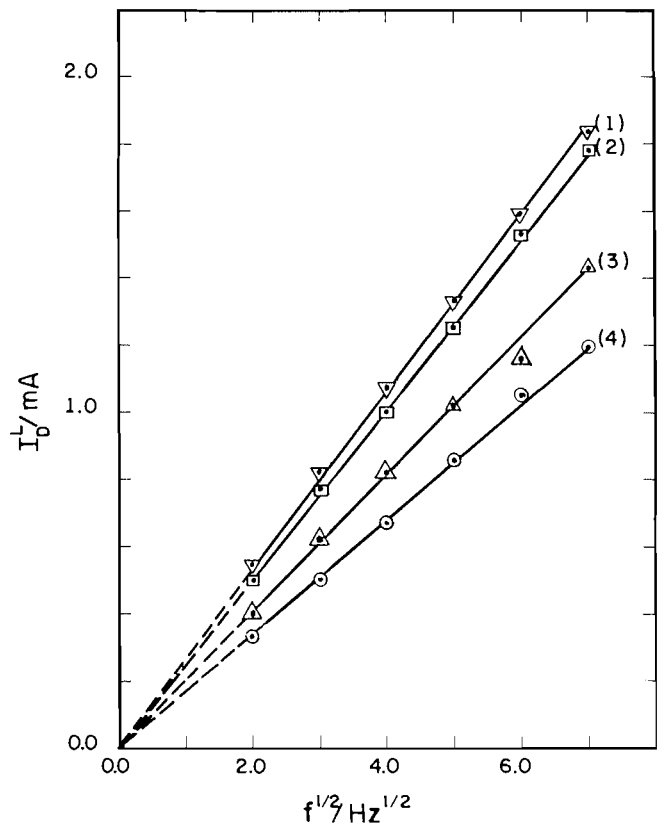

FIG. 2. Limiting diffusion current for $Zn(OH)_4^{2-}$: 8 m*M* deposition vs. $f^{1/2}$, varying NaOH concentrations. (1) 1 *M*, (2) 2 *M*, (3) 3 *M*, (4) 4 *M*. Area = 0.17 cm^2.

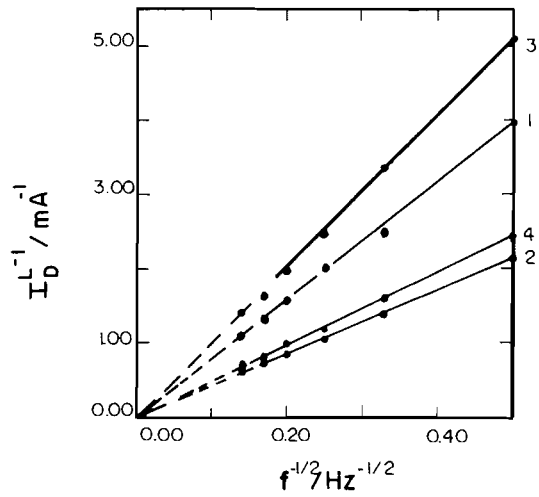

FIG. 3. Variation of $1/I_D^L$ with $f^{-1/2}$ at potential $E = -1.625$ vs. SCE and $T = 25$°C for: (1) 1 *M* NaOH, 4 m*M* $Zn(OH)_4^{2-}$; (2) 2 *M* NaOH, 8 m*M* $Zn(OH)_4^{2-}$; (3) 3 *M* NaOH,4 m*M* $Zn(OH)_4^{2-}$; and (4) 4 *M* NaOH, 10 m*M* $Zn(OH)_4^{2-}$.

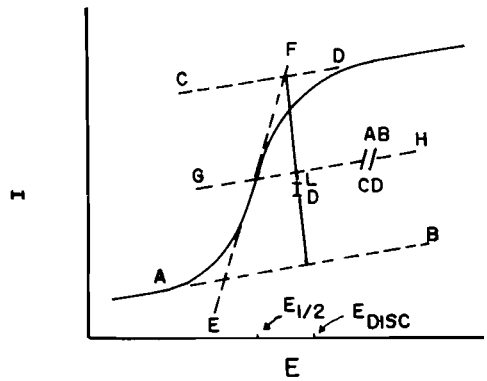

FIG. 4. Graphic evaluation of the limiting diffusion current without influence of H^+ ion discharge reaction and some residual current (22).

Hg-film disc electrode. Almost similar curves have been obtained in other situations studied here. This means that the wave of the zincate ion reduction begins at potentials less negative than the H^+ ion discharge waves. Thus, the influence of this last reaction on the measurements of the limiting diffusion current for the $Zn(OH)_4^{2-}$ reduction at the potential considered here is less pronounced.

Figure 2 demonstrates the linear dependence of the limiting diffusion current on the angular velocity at different concentrations of zincate ion in 1 *M* NaOH (25 ± 1°C). The same behaviour was observed for zincate solutions over the entire range of sodium hydroxide concentration and temperature studied. The diffusion coefficient of the zincate ion was calculated from these straight lines by linear regression using the Levich equation under diffusion control (20).

To compare the results obtained using both the Levich's diffusion and mixed controlled equations (20, 21), Fig. 3 has been constructed. Here are shown the variation of I^{-1} with $f^{-1/2}$ at $E = 1.625$ V vs. SCE (standard calomel electrode). This potential was taken after the determination of the limiting diffusion current of the $Zn(OH)_4^{2-}$ reduction using the scheme displayed in Fig. 4 (22). The calculated *D* values are listed in Tables 1 and 2.

TABLE 1. Average values of the zincate ion diffusion coefficient ($D \times 10^6$ cm^{2}s^{-1}) as a function of NaOH concentration and temperature*

NaOH concentration (M)	Temperature (°C)			
	25	30	35	40
1	4.90±0.20	5.40±0.30	7.10±0.10	6.70±0.10
2	4.60±0.20	4.70±0.20	4.90±0.20	6.30±0.10
3	3.80±0.10	4.00±0.10	4.80±0.20	6.40±0.10
4	3.10±0.10	3.40±0.10	4.10±0.20	5.50±0.20

*Each result of the table corresponds to an average of sixty measurements over a wide range of angular velocities of the disk electrode ($f^{1/2} = 2, 3, 4, 5, 6$ Hz$^{1/2}$) and zincate ion concentration (1, 2, 4, 6, 8, 10 mM); at least two independent voltamograms were constructed for each condition.

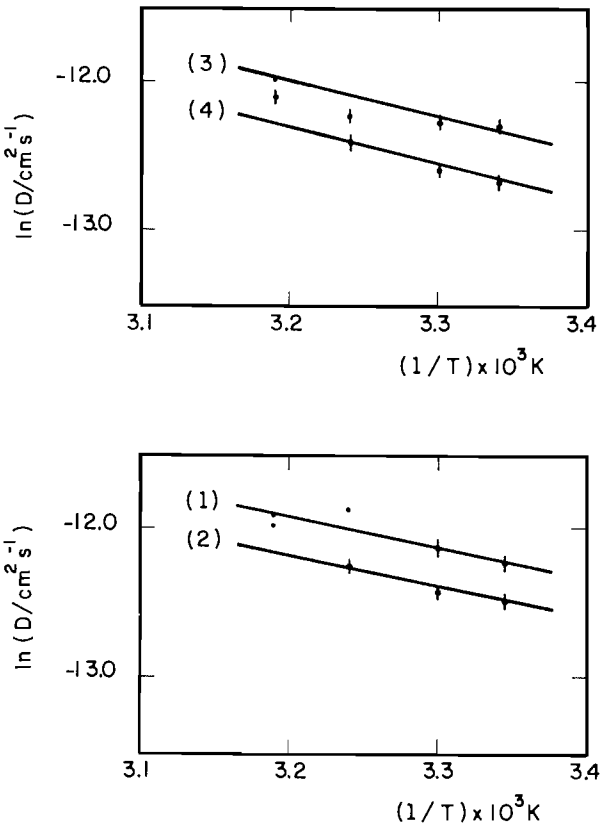

FIG. 5. Zincate ion diffusion coefficient vs. $1/T$ varying NaOH concentrations (1) 1 M, (2) 3 M, (3) 2 M, and (4) 4 M.

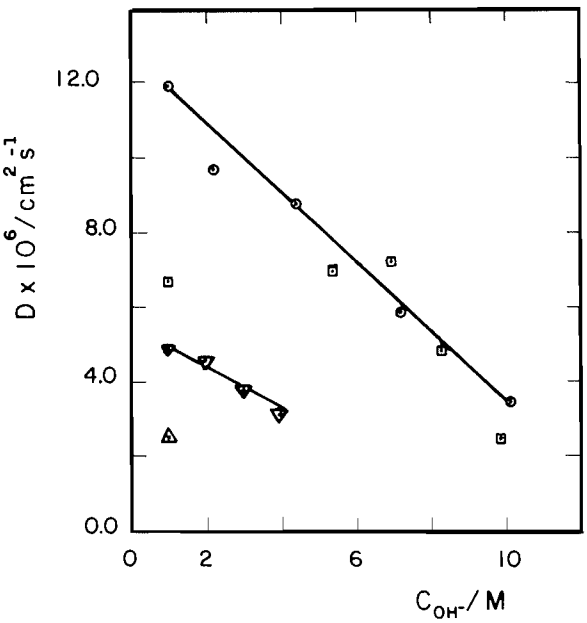

FIG. 6. Zincate ion diffusion coefficient at 25 C vs. OH^- concentrations. (⊙, ⊡) McBrien and Cairns (10); (△) Meites (24); and (▽) authors' data.

Figure 5 shows the temperature dependence of the diffusion coefficient at each sodium hydroxide concentration. From these data, we obtain the value of (10.00 ± 0.40) kcal/mol for the diffusion activation energy for zincate ion. The values of the solvodynamic radii (Table 3) were determined from the Stokes–Einstein equation (23).

Discussion and conclusion

Figure 6 compares the literature data for the zincate ion diffusion coefficient at 25°C in different alkaline media. The largest discrepancies in D values occur at alkali concentrations between 1 and 5 M. The polarographic values obtained by Dirkse (7) in KOH media are about five times larger than those of Meites (24) in NaOH media, a difference much too large to be ascribable to the change from potassium to sodium hydroxide. Indeed, McBreen's and Cairns' values (10) for the same alkali concentrations, are intermediate between these former values.

The value of 9×10^{-6} cm^2/s was used by Popova *et al.* (12) without reference to its origin and is listed in the Bard Encyclopedia (25). The results of Nanis (cf. 10) using the capillary method, indicate that the diffusion coefficient is independent of the zincate ion concentration over the range of 0.02–0.4 M. Finally, mention must be made of the values determined by Payne and Bard (26) using chronocoulometry (6.11×10^{-6} cm^2/s) and polarography (6.40×10^{-6} cm^2/s). These values were not included in Fig. 6 because it is not clear which alkali concentration was employed.

The results presented in this work (Tables 1 and 2), obtained through a great number of experiments and employing one of the most accurate electrochemical methods, show an accuracy of about 4% for the value of the diffusion coefficient of the zincate ion.

Quickenden and Jiang (27) have reported that the use of the diffusion control, instead of the mixed control, Levich equation in the evaluation of the diffusion coefficient introduces dispersion in the results obtained using the rotating disc method. The

TABLE 2. $Zn(OH)_4^{2-}$ diffusion coefficient ($D \times 10^6$ cm^2 s^{-1}) as a function of aqueous NaOH concentration and temperature using mixed control Levich equation

NaOH concentration (M)	Temperature (°C)			
	25	30	35	40
1	4.80±0.30	5.50±0.20	6.90±0.10	6.70±0.20
2	4.60±0.20	4.70±0.10	5.10±0.20	6.10±0.10
3	3.80±0.20	4.10±0.10	4.80±0.10	6.00±0.20
4	2.90±0.10	3.50±0.10	4.20±0.20	5.10±0.20

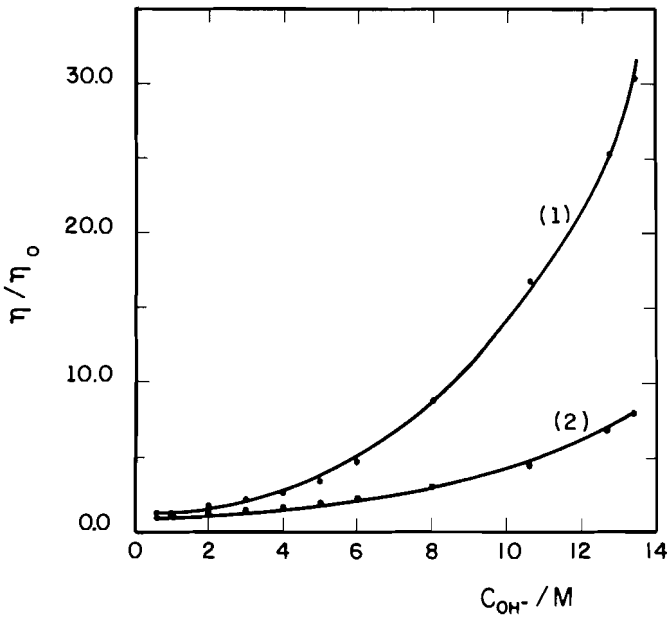

FIG. 7. Viscosity of (1) NaOH and (2) KOH vs. their concentrations.

TABLE 3. Solvodynamic radius of the zincate ion and the Stokes–Einstein coefficient

NaOH (M)	T(°C)	$(D\eta/T) \times 10^{10}$ (cm^{2}PK^{-1}s^{-1})	$r \times 10^8$ (cm)
1	25	1.97	3.71
	30	1.68	4.35
	35	1.94	3.75
	40	1.66	4.40
			$\bar{r} = 4.10 \pm 0.40$
2	25	1.98	3.69
	30	1.73	4.22
	35	1.56	4.68
	40	1.89	3.85
			$\bar{r} = 4.10 \pm 0.40$
3	25	2.04	3.58
	30	1.90	3.83
	35	2.02	3.62
	40	2.36	3.09
			$\bar{r} = 3.50 \pm 0.30$
4	25	2.14	3.41
	30	2.06	3.54
	35	2.16	3.38
	40	2.51	2.91
			$\bar{r} = 3.30 \pm 0.30$

zincate ion D values listed in Tables 1 and 2, evaluated with both Levich's equations varying over a narrow range, demonstrate that the nature of the surface reaction has more of an influence on the results than the way experimental data are treated.

The data in Table 3 indicate that the ratio $D\eta/T$ is temperature independent, within the experimental error, but increases with increasing sodium hydroxide concentration. The solvodynamic radius decreases about 20% in going from 1 to 4 M NaOH. Since both potentiometric and spectroscopic studies of the zincate ion system have shown that, in this hydroxide concentration range, the predominant species being tetrahydroxyzincate $Zn(OH)_4^{2-}$, the observed decrease in the solvodynamic radius can not be ascribed to a change in the complexation equilibria. We, therefore, attribute the decrease in the solvodynamic radius with increasing alkali concentration, to competition between solvation of $Zn(OH)_4^{2-}$, Na^+, and OH^-. This competition was especially important at sodium hydroxide concentrations above 2 M (Fig. 7). Indeed, at 4 M alkali there are only seven water molecules available for supporting electrolysis, or roughly the number of water molecules necessary to complete the first solvation shell of Na^+ and OH^-. In a study of the formate anion diffusion coefficient in different electrolytes (NaOH and KOH), Heitbaum and Gonzalez-Velasco (28) found that the solvodynamic radius of the formate anion is smaller in 5 M NaOH than in 5 M KOH. This can be explained in terms of the smaller ionic radius of the sodium ion (r = 0.95 Å) relative to the potassium ion (r = 1.33 Å) which results in a greater degree of solvation of the former. Consequently, in NaOH solution there will be less water available for hydration of the formate anion explaining the smaller solvodynamic radius as compared to the KOH medium.

The data (29) in Fig. 7 show that the viscosity is strongly dependent on the nature of the cation in the alkali concentration range above 2 M, being smaller for KOH solutions than for NaOH solutions. The source of this difference is probably the same as that outlined above. The data for the activation energy as a function of alkali concentration are not sufficiently precise to reveal a trend of the type expected on the basis of the significant change (20%) in the solvodynamic radius.

1. R. D. ARMSTRONG and M. F. BELL. J. Electroanal. Chem. **55**, 201 (1974).
2. R. D. ARMSTRONG and G. A. HERDMAN. J. Electroanal. Chem. **25**, 9 (1970).
3. R. D. ARMSTRONG and G. M. BULLMAN. J. Electroanal. Chem. **25**, 121 (1970).
4. J. O'M. BOCKRIS, Z. NAGY, and A. DAMJANOVIC. J. Electrochem. Soc. **119**, 285 (1972).
5. N. A. HAMPSON, G. A. HERDMAN and R. TAYLOR. J. Electroanal. Chem. **25**, 9 (1970).

6. J. P. G. FARR and N. A. HAMPSON. J. Electroanal. Chem. **18**, 407 (1969); **13**, 433 (1967).
7. T. P. DIRKSE. J. Electrochem. Soc. **101**, 328 (1954).
8. J. S. FORDYCE and R. L. BAUM. J. Chem. Phys. **43**, 843 (1965).
9. G. H. NEWMAN and G. E. BLOMGREEN. J. Chem. Phys. **43**, 2744 (1965).
10. J. MCBREEN and E. J. CAIRNS. Advances in electrochemistry and electrochemical engineering. Vol. II. *Edited by* H. Gerischer and C. W. Tobias. John Wiley and Sons, Inc., New York. 1978. p. 273.
11. B. KABANOV Electrochim, Acta, **6**, 253 (1962).
12. T. I. POPOVA, V. S. BAGOTSKII, and B.N. KABANOV. Russ. J. Phys. Chem. (Engl. Transl.), **36**, 766 (1962); **36**, 770 (1962).
13. Z. ZEMBURA. J. Electroanal. Chem. **46**, 243 (1973).
14. J. D. NEWSON and A. C. RIDDIFORD. J. Electrochem. Soc. **108**, 695 (1961).
15. S. BRUCKENSTEIN. J. Electrochem. Soc. **122**, 1215 (1975).
16. F. OPEKAR and P. BERAN. J. Electroanal. Chem. **69**, 1 (1976).
17. Y. PLESKOV. Zh. Fiz. Khim. **34**, 623 (1960).
18. B. MILLER and M. I. BELLAVANCE. J. Electrochem. Soc. **119**, 1510 (1972).
19. H. C. CHAGAS. Thesis. Universidade de São Paulo, Brazil. 1978.
20. V. G. LEVICH. Physicochemical hydrodynamics Prentice Hall, New Jersey. 1962.
21. A. J. BARD and L. R. FAULKNER. Electrochemical methods fundamentals and applications. John Wiley, New York. 1980.
22. L. MEITES. Polarographic techniques. John Wiley, New York. 1965.
23. J. O'M. BOCKRIS and A. K. N. REDDY. Modern electrochemistry. Vol. 2. Plenum Press, New York. 1970.
24. L. MEITES. *In* Handbook of analytical chemistry. *Edited by* L. Meites. McGraw–Hill, New York. 1963.
25. R. J. BRODD and V. E. LEGER. Encyclopedia of electrochemistry of the elements. Vol. V. *Edited by* A. J. Bard. New York. 1976. Chapt. V-1, p. 2.
26. D. W. A. PAYNE and A. J. BARD. J. Electrochem. Soc. **119**, 1665 (1972).
27. T. I. QUICKENDEN and X. JIANG. Electrochim. Acta, **29**, 693 (1984).
28. J. HEITBAUM and J. GONZALEZ-VELASCO. J. Electroanal. Chem. **63**, 23 (1975).
29. Handbook of chemistry and physics. 52nd ed. *Edited by* R. West. Chemical Rubber Company, Cleveland, OH. 1971–1972.

The He(I) and X-ray photoelectron spectra of *p*-*N*,*N*-dimethylaminobenzalmalonitrile

A. KATRIB AND B. D. EL-ISSA
Chemistry Department, Kuwait University, P.O. Box 1527, Kuwait City, Kuwait
AND
A. W. POTTS
Physics Department, King's College, London, U.K.
Received April 2, 1985[1]

A. KATRIB, B. D. EL-ISSA, and A. W. POTTS. Can. J. Chem. **64**, 528 (1986).

The assignment of the four outermost ionization energies obtained by uv-photoelectron spectroscopy (UPS) of *p*-*N*,*N*-dimethylaminobenzalmalonitrile is given. The X-ray photoelectron spectroscopy of the N 1*s* and C 1*s* core levels are also discussed. Two "shake-up" lines were observed at the high binding energy side of the N 1*s* spectral line. The energies of these spectral lines were found to correlate very well with the uv–visible spectrum. Also the energy difference of the two "shake-up" lines was found to be similar to the energy difference between the first and second ionization energies obtained by ups techniques. Only one "shake-up" line was observed in the case of C 1*s* photoionization. Theoretical studies by semiempirical methods including HAM/3, MINDO/3, and extended Hückel are also discussed.

A. KATRIB, B. D. EL-ISSA et A. W. POTTS. Can. J. Chem. **64**, 528 (1986).

On rapporte les attributions pour les quatre énergies d'ionisation les plus éloignées, obtenues par spectroscopie photoélectronique uv (spu), du *p*-*N*,*N*-diméthylaminobenzalmalonitrile. On discute aussi des spectroscopies photoélectroniques aux rayons X au niveau des noyaux N 1*s* et C 1*s*. On a observé deux raies "d'ébranlement" dans la partie de haute énergie de liaison de la raie spectrale du N 1*s*. On a trouvé qu'il existe une bonne corrélation entre les énergies de ces raies spectrales et les spectres uv–visible. On a aussi trouvé que la différence d'énergie entre les deux raies "d'ébranlement" est semblable à la différence d'énergie entre les première et seconde énergies d'ionisation qui ont été obtenues par les techniques de spu. On n'a observé qu'une seule des deux raies "d'ébranlement" dans le cas de la photoionisation du C 1*s*. On discute aussi d'études théoriques par des méthodes semi-empiriques incluant HAM/3, MINDO/3 et Hückel étendu.

[Traduit par le journal]

Introduction

In a study of some benzalmalonitrile derivatives, which are known to have the effect of sneeze and tear gases in addition to other physiological properties, some correlations in the uv, UP (uv-photoelectron) and XP (X-ray photoelectron) spectra have been found in the case of *p*-*N*,*N*-dimethylaminobenzalmalonitrile.

In order to assign the outermost molecular orbitals on the basis of ionization energies (IEs) obtained by UPS (uv-photoelectron spectroscopy) techniques, the photoelectron spectra of relevant molecules published previously have been used, as well as quantum mechanical calculations such as HAM/3, MINDO/3, and extended Hückel. In the case of aniline (1,2), the first IE was assigned to a ring π (b_1^{-1}) molecular orbital (MO). Also the second IE was assigned mainly to the nitrogen "lone pair" which has a similar binding energy to ammonia at 10.8 eV. The destabilization of the first orbital by 1.1 eV as compared to the $1e_g$ of benzene is explained in terms of conjugative and inductive effects. However, in the case of *p*-*N*,*N*-dimethylaniline (1), the first IE at 7.45 eV was assigned to a type of molecular orbital localized mainly on the nitrogen lone pair orbital, while the following two IEs are assigned to the benzene ring π orbitals. The molecule *p*-*N*,*N*-dimethylaminobenzalmalonitrile is expected to have similar behaviour concerning the outermost MOs especially since the nitrile group IEs are expected to be above 12 eV (3).

In the case of X-ray photoelectron spectroscopy (XPS), it has been found in certain types of compounds that the core level photoionization shows satellite structure which can be attributed to electronic transitions from the highest occupied (HOMO) to the lowest unoccupied molecular orbital (LUMO) {$\pi^* \leftarrow \pi$ transitions}; this is known as a "shake-up" process.

Shake-up lines are of relatively low intensity and are situated at the higher binding energy (lower kinetic energy) side of the main spectral line. Clark *et al.* (4–6) have used the shake-up lines to estimate the number of aromatic groups in polymers. A shake-up process was also observed in the case of —N=N— compounds (7) upon the removal of N 1*s* electrons. A correlation between the shake-up line and the uv–visible spectrum of the compound was also observed (7). It is expected that the shake-up process could provide valuable information concerning the nature of the outermost molecular orbital(s).

Theoretical methods

Three semiempirical theoretical methods were used to justify the assignment of the different IEs. Two of these methods, namely MINDO/3 (8, 9) and extended Hückel (EH) (10) employ the solution of the Schrödinger equation by using predefined overlap integrals between the different atomic orbitals. These methods are valuable in that they can be used to predict the order of the MOs and the composition of their respective eigenvectors. For practical purposes, the IEs can be taken as the negative of the orbital energies according to Koopmans' theorem (11), although this involves rather stringent approximations since the process of ionization is adiabatic and one would have to include relaxation effects. Nonetheless, if one were to assume that relaxation effects are approximately of the same order of magnitude for the outermost electrons, one can regard the difference in the orbital energies as a first approximation to the difference of ionization energies of the respective states. Invariably, the HAM/3 method (12–14) employs a suggestion first employed by Slater (15) in which the

[1]Revision received October 24, 1985.

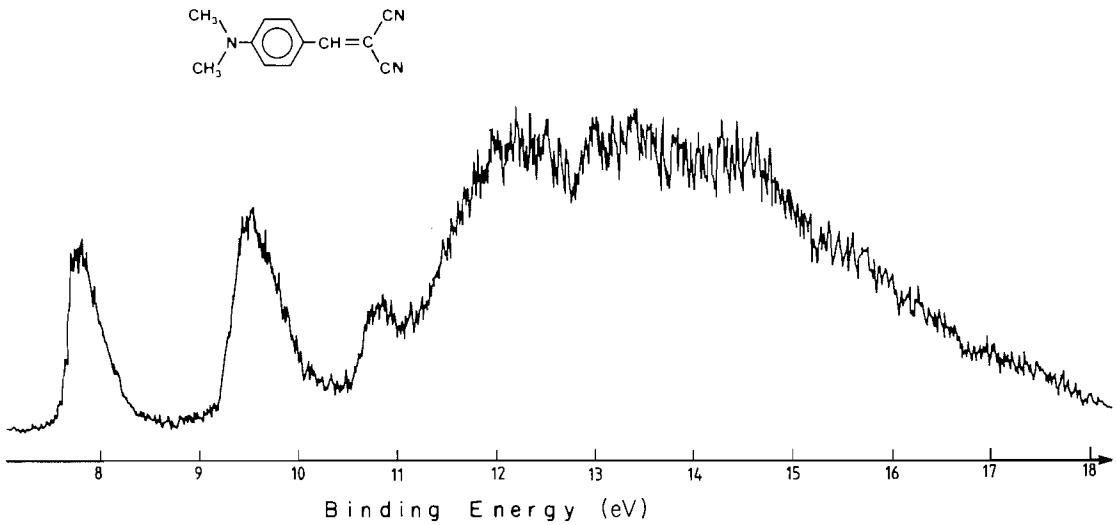

FIG. 1. The He(I) photoelectron spectrum of dimethylaminobenzalmalonitrile.

IE is calculated by removing half an electron from the respective orbitals. In HAM/3 the half electron is in effect equally removed from all the occupied MOs. The eigenvalues produced after such a condition is invoked, are then directly related to the ionization energies. Thus, unlike other semiempirical methods, but similar to the multiple scattering X-α method, HAM/3 makes a clear distinction between ionization and orbital energies. The difference between the two modes of energy is related to relaxation effects that accompany the process of ionization (16). Transition state excitation energies can be calculated by using configuration interaction of the molecule. Moreover, energies of core electrons can be calculated by taking the difference between the heat of formation of the molecule less the 1*s* electron from the heat of formation of the neutral molecule. In all three methods employed, the basis set used employed a minimal basis composed of one 1*s* Slater-type orbital (STO) of H, one 2*s*, and three 2*p* STOs for each of C and N. The bond lengths and bond angles used in the calculations are based on the equilibrium values of similar compounds (17).

Experimental

A McPherson ESCA-36 spectrometer with MgK_α source was used for measuring X-ray photoelectron spectra; a cryogenic pump in the sample chamber maintained a pressure of 10^{-8} Torr (1 Torr = 133.3 Pa). The sample was mounted on adhesive tape; its temperature was approximately ambient. The He(I) spectrum is obtained by using a Perkin Elmer P.S.16 spectrometer with a heated probe. To record the He(I) spectrum, the sample was heated to 125°C. The sample was prepared in the laboratory and its purity was tested spectroscopically.

Results and discussion

1.1 The He(I) spectrum

The uv photoelectron spectrum of *p-N,N*-dimethylaminobenzalmalonitrile shows the presence of three distinct peaks below 11 eV (Fig. 1). The first IE occurs at a vertical ionization potential of 7.8 eV and has no similar analogue in the photoelectron spectrum of benzal malonitrile.[2] However, in the case of *N,N*-dimethylaniline (1), the first IE occurs at 7.45 eV and is assigned to a π-type MO which is localized mainly on the nitrogen lone pair orbital, contrary to aniline, where the third IE at 10.8 eV is assigned to the nitrogen lone pair. The reason for this considerable change in the energy and position of the N lone pair orbital with respect to the two benzene π MOs can be explained in terms of resonance (conjugation) and inductive effects. In the case of aniline, the binding energy of the nitrogen lone pair moiety is expected to be close to that for ammonia at 10.8 eV, while the MO of the benzene ring occurs at 9.25 eV ($1e_g$). Therefore, the resonance interaction between the molecular orbitals would result in destabilization of the benzene ring π MOs and stabilization of the nitrogen lone pair orbital. On the other hand, the inductive effect of the nitrogen group will be of the opposite sign. In the case of *N,N*-dimethylaniline, the situation is reversed because the IE of the nitrogen lone pair is expected to be close to the dimethylamine at 8.93 eV, which is lower than was observed in the case of styrene (C=C π at 10.55 eV as compared to ethylene at 10.51 eV) (18).

The calculated orbital energies predicted by HAM/3, MINDO/3, and EH methods are given in Table 1. The type of each of the MOs is displayed next to the respective energies. The MINDO calculated value for the energy of the LUMO is positive and because this has no significant meaning, its value is not displayed. The measured and calculated IEs by HAM/3 taking into account relaxation effects are given in Table 2. Quantum mechanical calculations by using HAM/3, MINDO/3, and EH predict that the outermost molecular orbital (HOMO) is a π-type orbital localized mainly on the amino N (lone pair) orbital (Table 1). The IE predicted by HAM/3 by removing half an electron from the occupied orbitals at 7.5 eV is in good agreement with the experimental value at 7.8 eV (Table 2).

The second and third IEs predicted by HAM/3 at 8.78 and 9.36 eV (Table 2) are associated with π orbitals that are derived mainly from the conjugated C atoms of the benzene ring with some contribution of the nitrogen p_z orbital of the amino and nitrile groups. The EH and MINDO/3 calculations show that the second MO is a σ-type orbital involving interaction between the different atoms whereas the third MO is of a π-type character involving the benzene ring.

The HAM/3 method predicts a σ-type orbital close to the fourth π-derived orbital while the MINDO/3 and EH calculations predict that the fourth MO is a π type associated mainly

[2]A. Katrib. In preparation.

TABLE 1. Orbital energies for *p-N,N*-dimethylaminobenzalmalonitrile obtained by three different semiempirical methods

EH[a] (eV)	MINDO/3[a] (eV)	HAM/3[a] (eV)
−9.45(π*)	—	−5.65(π*)
−11.77(1π)	−7.62(1π)	−6.83(1π)
−12.17(1σ)	−8.76(1σ)	−7.44(2π)
−12.80(2π)	−9.33(2π)	−7.80(3π)
−12.93(3π)	−9.43(3π)	−8.74(1σ)

[a]The type of each of the orbitals is written next to the orbital energies.

TABLE 2. Correlation of the ionization energies obtained from photoelectron spectroscopy and theoretical values obtained from HAM/3 for *p-N,N*-dimethylaminobenzalmalonitrile

HAM/3 (eV)	Experimental (eV)	Assignment (eV)
7.50	7.8	π(:N)
8.78	9.6	π(ring)
9.36	9.8	π(ring)
10.67	10.9	π(C=C)

with the benzene C atoms. It is important to note that the presence of a σ-type orbital at binding energies below 12 eV is excluded in these types of molecules (1, 2). The fifth IE at 10.67 eV is predicted by HAM/3 to be a C=C π MO of the ethylenic moiety which is in good agreement with the measured IE at 10.9 eV.

1.2 X-ray photoelectron spectrum

The N 1*s* spectrum shows the presence of a main spectral line at 399.3 eV, with two relatively low intensity lines at 402.0 and 403.8 eV (Fig. 2*a*). From this spectrum, it can be deduced that the N 1*s* binding energies of the amino and nitrile nitrogens are identical. The first shake-up line at 402.0 eV (ΔE = 2.7 eV) is assigned to a shake-up process involving the π* ← 1π transition (HOMO to LUMO) in *p-N,N*-dimethylaminobenzalmalonitrile. This energy seems to correlate with the first uv–visible absorption line (Table 4) at 430 nm (2.88 eV). The second shake-up line (ΔE = 4.5 eV) is assigned to the π* ← 2π transition from the second occupied MO to the lowest unoccupied MO. This elecronic transition correlates with the uv absorption line at 267 nm (4.64 eV) of the neutral molecule. It is interesting to note that the energy difference between the two shake-up lines (ΔE = 1.8 eV) is the same as the difference between the first and the second measured IEs as well as the difference between the first and second absorption lines (ΔE = 1.7 eV) measured by uv–visible radiation (see Table 3). These results imply that both molecular orbitals suffer the same contraction (relaxation) as a result of photoionization from the outermost or from the N 1*s* electrons. The XPS of the C 1*s* energy region shows a broad line at 284.6 eV and a low intensity shoulder at the high binding energy side (Fig. 2*b*). This line is assigned to a shake-up process which might involve the π* ← 2π transition from the second occupied MO in the molecule. The first shake-up, however, is not visible. Although it was not possible to differentiate between the amino and nitrile N 1*s* electrons, it is

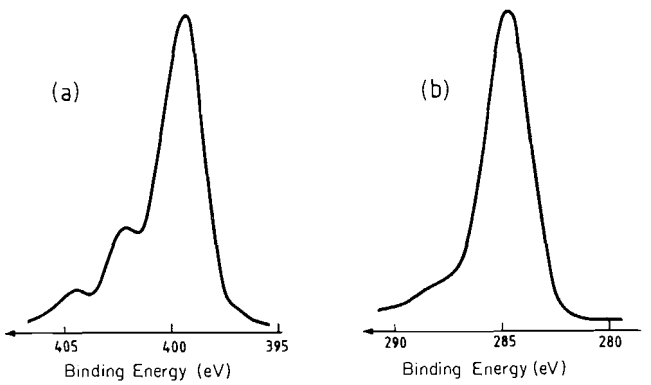

FIG. 2. The XPS of *p-N,N*-dimethylaminobenzalmalonitrile, (*a*) the N 1*s* energy region and (*b*) the C 1*s* energy region.

expected that the shake-up process should be associated with the photoionization of the amino N 1*s*, since the outermost molecular orbital is mainly localized on the amino group moiety. In Table 3, we display the difference in the IEs of the (1π) and (2π) MOs as obtained experimentally from the shake-up process and theoretically. The HAM/3 results are obtained from the difference of the IE of the (1π) and (2π) whereas this difference in the case of MINDO/3 and EH is derived from the difference in the energy of these orbitals. The HAM/3 difference of 1.22 eV seems to be underestimated relative to the experimental value which is reported as 1.8 eV. The MINDO/3 difference, however, is in agreement with the experimental value whereas the EH result is around 0.8 eV below the expected value. Table 4 displays the energies for the π* ← 1π and π* ← 2π transitions. The experimental transitions are obtained from the uv–visible spectrum whereas the theoretical results show the HAM/3 excitation energies with configuration interaction. The theoretical results are for singlet transitions which are obtained by adding to the energy difference of the orbitals involved in the transition the exchange integral that represents interaction between electrons having opposite spin, in comparison with triplet transitions that represent the same interaction between electrons having the same spin. The transition from 1π to the π* correlates very well with the experimental assignment whereas the second transition seems to be somewhat lower than the experimental value probably because the energy of the 2π MO is thought to be underestimated. The HAM/3 core level ESCA energies associated with the N 1*s* electrons were calculated by the method introduced earlier. The calculated energies for the three different types of N were found to be 402.77, 403.76, and 403.49 eV, the first being associated with the amino N while the other two are related to the nitrile nitrogen atoms. The experimental ESCA energy cannot differentiate between the N 1*s* electrons, a fact which may be due to the relative broadening of the N 1*s* spectral line (width at half maximum = 2.2 eV).

Conclusions

The He(I) photoelectron spectrum of *p-N,N*-dimethylaminobenzalmalonitrile shows that the outermost molecular orbital (HOMO) is a π-type MO predominantly of the amino nitrogen lone pair nature. Its stabilization by 0.3 eV as compared to the same MO in dimethyl aniline is attributed to the inductive effect of the nitrile groups in the molecule. The second and third π-type MOs are assigned to the benzene ring. The ethylenic group C=C π MO binding energy seems to be not affected as a result of conjugative and inductive effects with the benzene

TABLE 3. The difference between the energies of the 2π and 1π MOs as obtained theoretically and experimentally for *p-N,N*-dimethylaminobenzalmalonitrile.

Experimental (eV)			Theoretical (eV)		
He(I)	uv–visible	Shake-up	HAM/3[a]	MINDO/3[b]	EH[b]
1.8	1.7	1.8	1.22	1.70	1.03

[a]The HAM/3 results are obtained from the difference of the IEs of the respective states.
[b]The MINDO/3 and EH results are obtained from the difference in the orbital energy of these states.

TABLE 4. The shake-up process associated with transitions of electrons from the two upper-most HOMOs to the LUMO for *p-N,N*-dimethylamino-benzalmalonitrile

	Experimental uv–visible (eV)	HAM/3 singlet transitions (eV)
$\pi^* \leftarrow 1\pi$	2.9	2.95
$\pi^* \leftarrow 2\pi$	4.6	3.84

ring in a similar way to the situation in styrene. Quantum mechanical calculation on this molecule by using HAM/3, MINDO/3, and EH methods predicts that the outermost molecular orbital is mainly an amino nitrogen lone pair with a π-type character. The HAM/3 calculated IE of this MO is in good agreement with the experimental value. Similar results were obtained for the ethylenic —C=C— π MO. The presence of two shake-up lines of relatively low intensity associated with the photoionization of the N 1*s* electrons was assigned to $\pi^* \leftarrow \pi$ transitions of the HOMO (:N) and the second occupied orbital (π of the benzene ring) to the LUMO. The two shake-up line energies were found to correlate with the uv–visible absorption lines in the neutral molecule. It was also concluded that the highest two occupied MOs suffer the same contraction as a result of ionization by using He(I) or X-ray radiation of the valence or the N 1*s* electrons respectively. Such a conclusion was based on the energy difference between the two outermost orbitals, the two shake-up lines, and the two absorption lines observed by He(I), XP, and uv–visible spectra, respectively.

Acknowledgments

We thank the Research Council of the University of Kuwait for their support of this work. The authors would also like to express their gratitude to Dr. S. Hassan for providing the sample.

1. J. P. MAIER and D. W. TURNER. J. Chem. Soc. Faraday Trans. II, **69**, 521 (1973).
2. T. P. DEBIES and J. W. RABALAIS. J. Electron Spectrosc. Relat. Phenom. **1**, 355 (1972).
3. J. W. RABALAIS and R. J. COLTON. J. Electron Spectrosc. Relat. Phenom. **1**, 83 (1972).
4. D. T. CLARK, D. B. ADAMS, A. DILKS, J. PEELING, and H. R. THOMAS. J. Electron Spectrosc. Relat. Phenom. **8**, 51 (1976).
5. D. T. CLARK and A. DALKS. J. Polym. Sci. Chem. Ed. **14**, 533 (1976).
6. D. T. CLARK and A. DILKS. J. Polym. Sci. Chem. Ed. **15**, 15 (1977).
7. A. KATRIB and A. Y. KASSIM. Anal. Chem. **52**, 1546 (1980).
8. J. A. POPLE, D. L. BEVERIDGE, and P. D. DOBOSH. J. Chem. Phys. **47**, 2 (1967).
9. J. A. POPLE and G. A. SEGAL. J. Chem. Phys. **44**, 3289 (1966).
10. R. HOFFMANN. J. Chem. Phys. **40**, 2474 (1974).
11. T. A. KOOPMANS. Physica (Amsterdam), **1**, 104 (1933).
12. L. ÅSBRINK, C. FRIDH, and E. LINDHOLM. Chem. Phys. Lett. **52**, 63 (1977).
13. L. ÅSBRINK, C. FRIDH, and E. LINDHOLM. Chem. Phys. Lett. **52**, 69 (1977).
14. L. ÅSBRINK, C. FRIDH, and E. LINDHOLM. Chem. Phys. Lett. **52**, 72 (1977).
15. J. C. SLATER. Adv. Quantum Chem. **6**, 1 (1972).
16. E. LINDHOLM and L. ÅSBRINK. Lecture notes in chemistry: Molecular orbitals and their energies, studied by the semiempirical HAM method. *Edited by* G. Berthier, M. J. S. Dewar, H. Fischer, K. Filio, G. G. Hall, J. Hinze, H. H. Jafe, J. Jorther, W. Kutzelnigg, K. Rudenberg, and J. Tomasi. Springer-Verlag, Berlin. pp. 103–141. 1985.
17. CHEMICAL SOCIETY, LONDON. Tables of interatomic distances in molecules and ions. Chemical Society, London. 1958.
18. J. W. RABALAIS and R. J. COLTON. J. Electron Spectrosc. Relat. Phenom. **1**, 83 (1972).

An MNDO study of substituent effects in carbocations: the unimportance of inductive effects

AMIN MOHAMED AISSANI, JAMES CLAYTON BAUM, AND RICHARD FRANCIS LANGLER[1]
Department of Chemistry, Florida Institute of Technology, Melbourne, FL 32901-6988, U.S.A.

AND

JACK LEON GINSBURG
Department of Chemistry, St. Mary's University, Halifax, N.S., Canada B3H 3C3

Received March 26 1985[2]

AMIN MOHAMED AISSANI, JAMES CLAYTON BAUM, RICHARD FRANCIS LANGLER, and JACK LEON GINSBURG. Can. J. Chem. **64**, 532 (1986).

Stabilization effects for both saturated and unsaturated substituents were examined using MNDO calculations. (By "saturated substituents" we mean to imply that the substituent is attached to C^+ by sp^3 carbon, whether or not the substituent has a site of unsaturation at some point remote from the carbocationic center.) Relative gas phase stabilities of regioisomeric carbocations have been calculated. For simple groups, directly bound to $\overset{+}{C}$, π donation, σ donation, and polarization effects are found to be important. Saturated-substituent stabilization effects are examined by means of reaction enthalpies for isodesmic reactions between the appropriate neutral molecules and $\overset{+}{C}H_3$. Traditional analyses of substituent effects based solely on inductive effects for saturated groups have little or no significance. Inductive effects have no special importance in determining saturated substituent stabilization effects on carbocations.

AMIN MOHAMED AISSANI, JAMES CLAYTON BAUM, RICHARD FRANCIS LANGLER et JACK LEON GINSBURG. Can. J. Chem. **64**, 532 (1986).

On utilise des calculs MNDO sur des carbocations choisis pour déterminer les effets de stabilisation de substituants tant saturés que non saturés. (Par "substituant saturé", on entend un substituant qui est attache au C^+ par un carbone sp^3 même si le substituant porte un site d'insaturation en un autre point éloigné du centre carbocationique.) On a calculé les stabilités relatives de carbocations régioisomères. Pour des groupements simples qui sont directement liés au $\overset{+}{C}$, on a trouve que les effets de donation π ou σ ainsi que de polarisation sont importants. On a étudié les effets de stabilisation des substituants saturés à l'aide des enthalpies de réactions isodesmiques entre les molécules neutres appropriées et le $\overset{+}{C}H_3$. Les analyses traditionnelles des effets de substituants qui sont uniquement basées sur les effets inductifs des groupements saturés n'ont que peu ou pas de signification. Les effets inductifs n'ont pas d'importance spéciale dans la détermination des effets de stabilisation des substituants saturés des carbocations.

[Traduit par le journal]

Introduction

As part of our work in organosulfur chemistry, we have recently initiated a program of theoretical studies. Our initial study (1) has raised two questions: (*i*) how does sulfur compare to saturated carbon as a carbocation stabilizer? and (*ii*) how useful is the concept of inductive stabilization in anticipating substituent-stabilization effects in carbocations? Recent studies authored by Topsom *et al.* (2, 3) have further stimulated our interest in problems associated with inductive effects.

Inductive effects accompany a shift of electron density in a σ bond toward the more electronegative atom involved in the bond. Predictions may be improved by utilizing group electronegativities (4, 5). The shift of electron density in one σ bond is supposed to trigger a parallel but smaller shift in adjacent bonds with the result that each donor atom will lose electrons in greater proportion than it receives them (6). This view may be illustrated pictorially as shown below:

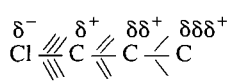

A second approximation (6) consideration involves the well-known hyperconjugative effect associated with simple aklyl groups.

Our previous study of thionium ions (1) led us to the conclusion that, "The relative degree of stabilization is independent of whether the substituent is a good σ donor or indeed whether it is a σ donor or σ acceptor." That study was focused on cations which had strong π donors attached to the carbocationic center. We felt that the relevance of inductive effects to relative carbocation stabilities might be more clearly revealed if the present study examined substituents which are poor π donors.

Our subsequent study of *S*-substituted radicals[3] led to the conclusion that the CF_3 group is a polarization destabilizer when attached to positively charged carbon and a polarization stabilizer when attached to radical carbon. Thus, a third question has arisen; are polarization effects useful in analyzing substituent effects in carbocations?

Our approach to the investigation of these questions has been to carry out MNDO calculations on a series of isomeric carbocations (structures **1** and **2**), the corresponding saturated molecules, the methyl cation, and methane. For the sake of completeness, we have also carried out calculations on the simpler cations $\overset{+}{C}H_2X$, (structures **3**).

Methods

All computations were done using the MNDO (modified neglect of differential overlap) semiempirical method (1*a*). A program written by

[1]Author to whom inquiries should be directed.

[2]Revision received October 29, 1985.

[3]J. C. Baum, J. L. Ginsburg, and R. F. Langler. Unpublished results.

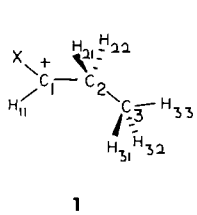

1

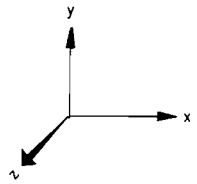

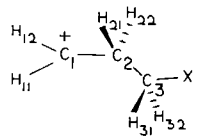

2

3

Walter Thiel and modified by the National Resource for Computation in Chemistry was used (1*b*). Dewar and Thiel (7*a*) compared MNDO calculated heats of formation with experimental heats of formation for various cationic species, including carbocations. The mean accuracy was comparable to that for neutral species.

The method used to calculate MNDO enthalpies of formation was discussed by Dewar and Thiel in their initial paper (7*b*). They used the relationship

$$\Delta H_f^{mol} = E_{tot}^{mol} - \sum_A E_{el}^A + \Sigma \Delta H_f^A$$

where ΔH_f^{mol} is the enthalpy of formation of the molecule in question, E_{tot}^{mol} is the total electronic energy of the molecule, E_{el}^A is the total electronic energy of atom A, and ΔH^A is the experimental enthalpy of formation of atom A at 298° K.

Since experimental molecular enthalpies of formation (298° K) are included in the criteria used to determine MNDO parameters, Dewar (7*a*) maintains that vibrational corrections are accounted for in the MNDO parameterization. Dewar (7*b*) established and supported this position for MINDO/3 computed enthalpies of formation.

Since its inception, the MNDO method has been used successfully for studies of carbocations and heterocarbocations (e.g., 7*c*–7*i*).

Results and discussion

Substitution at sp^2 *carbon*

The first portion of the discussion will deal with the effects of substituents directly attached to sp^2 carbon (C_1 in structure **1**). Table 1 presents calculated relative gas phase stabilities, $\Delta\Delta H_f$, for isomeric pairs of carbocation **1** and **2**. $\Delta\Delta H_f$ is a measure of the stabilizing ability of X relative to H when attached to C_1.

Table 2 presents data for bond orders arising from the interactions of the C_1p_z and C_2p_z orbitals. We note that the difference in these "π bond" orders for the isomeric carbocations presented in Table 2 and the corresponding differences in CS π bond orders reported in our previous study (1) (for cations with structures **4** and **5**) are virtually identical. The correlation

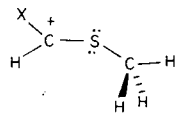

4

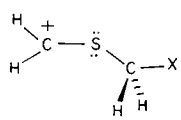

5

between these two results suggests that the hyperconjugative effect of the ethyl groups in structures **1** is qualitatively similar to the π bonding effect of sulfur in structures **4**. The principal impact of sulfur substitution as opposed to alkyl sustitution is that the stabilizing–destabilizing effect of those substituents which have the largest influence on $\Delta\Delta H_f$ is substantially diminished by the presence of the superior π bonder S. For example, X = OH in structures **1** and **2** affords a value for $\Delta\Delta H_f$ of −36.9 kcal/mol whereas X = OH in structures **4** and **5** gives rise to a $\Delta\Delta H_f$ of −20.0 kcal/mol. The stabilizing ability of

TABLE 1. Calculated relative stabilities of isomeric carbocations

Carbocation	X	ΔH_f(kcal/mol)	$\Delta\Delta H_f$(kcal/mol)
1*a*	CF_3	88.6	+10.8
2*a*		77.8	
1*b*	CN	250.0	−3.5
2*b*		253.5	
1*c*	$C(O)CH_3$	177.3	−4
2*c*		181.3	
1*d*	Cl	205.3	−5.7
2*d*		211.0	
1*e*	BH_2	205.6	−13.6
2*e*		219.2	
1*f*	CH_3	194.3	−13.9
2*f*		208.2	
1*g*	F	157.7	−16.6
2*g*		174.3	
1*h*	H	212.3	—
1*i*	C≡CH	243.0	−24.1
2*i*		267.1	
1*j*	$CH{=}CH_2$	201.0	−30.3
2*j*		231.3	
1*k*	OH	133.5	−36.9
2*k*		170.4	
1*l*	NH_2	166.5	−51.2
2*l*		217.7	

TABLE 2. Carbocation C_1 bond orders involving p_z orbitals

Carbocation	X	C_1—C_2	C_1—X
1*a*	CF_3	0.44	—
2*a*		0.39	—
1*b*	CN	0.35	0.36
2*b*		0.39	—
1*c*	$C(O)CH_3$	0.37	—
2*c*		0.39	—
1*d*	Cl	0.33	0.57
2*d*		0.40	—
1*e*	BH_2	0.33	—
2*e*		0.39	—
1*f*	CH_3	0.33	—
2*f*		0.39	—
1*g*	F	0.29	0.63
2*g*		0.40	—
1*h*	H	0.39	—
1*i*	C≡CH	0.28	0.55
2*i*		0.40	—
1*j*	$CH{=}CH_2$	0.26	0.64
2*j*		0.40	—
1*k*	OH	0.22	0.77
2*k*		0.41	—
1*l*	NH_2	0.20	0.85
2*l*		0.41	—

groups common to the present and previous studies is in the same order.

Another indicator of the tendency of ethyl groups to act as weak π donors can be adduced from a comparison of the data for structures **1** and **3** presented in Table 3. Ethyl groups tend to enhance total π donation into C^+ while diminishing the π bonding interaction of other substituents also attached to C^+ in the same way that sulfenyl sulfur does.

Table 4 details the results of our analysis of electron donation into C_1 for structures **1**. Consistent with the results of our previous study (1), the results in Table 4 indicate that the stronger

TABLE 3. Population numbers for C^+ and $\overset{+}{C}X$ π bond orders for structures **1** and **3**

Carbocation	X	Electron population in C_1p_z	CX π bond order
1*a*	CF_3	0.21	0.07
3*a*		0.01	0.08
1*b*	CN	0.26	0.36
3*b*		0.17	0.43
1*c*	$C(O)CH_3$	0.18	0.16
3*c*		0.05	0.20
1*d*	Cl	0.31	0.57
3*d*		0.26	0.64
1*e*	BH_2	0.23	0.31
3*e*		0.16	0.37
1*f*	CH_3	0.23	0.32
3*f*		0.15	0.38
1*g*	F	0.33	0.63
3*g*		0.27	0.68
1*i*	C≡CH	0.36	0.55
3*i*		0.33	0.61
1*j*	$CH{=}CH_2$	0.45	0.64
2*j*		0.44	0.70
1*k*	OH	0.44	0.77
3*k*		0.42	0.81
1*l*	NH_2	0.57	0.85
2*l*		0.55	0.89

π donors have a stabilizing effect which can be anticipated on the basis of their π donation into the "empty" C_1p_z orbital. The order so obtained is independent of σ-donation/withdrawal. The present study includes a larger selection of substituents which are poor π bonders than our previous study did. A brief examination of Table 4 shows that electron population in C_1p_z varies systematically with π donation from X when X is a strong π donor. For those groups which do not donate electron density from a π bond or lone pair, the electron population in C_1p_z is the only available indicator of π donation from X. There is no correlation between $\Delta\Delta H_f$ and electron population in the C_1p_z orbital for any of the poor π donors.

Table 5 presents more data for the poor π donors.[4] It is immediately obvious that $\Delta\Delta H_f$ values for the poor π bonders can *not* be correlated with (*i*) electron population in C_1p_z, (*ii*) transfer into C_1, or (*iii*) total electron transfer into C_1. In an attempt to rationalize the $\Delta\Delta H_f$ trends, we have examined the ionic bond orders for the cations of interest. Major polarization stabilization–destabilization in each case is associated with the bonds to C_1 so that the ionic bond orders listed in Table 5 are restricted to those involving C_1. There is some counterbalancing tendency for the poorer electron donors to enjoy polarization stabilization and for the better donors to suffer from polarization destabilization. The similarity of $\Delta\Delta H_f$ values for **1***b* and **1***c* suggests that a difference in ionic bond order of 0.0529 corresponds to a difference of ca. 0.12 e′ at C_1. From this relationship, it is possible to calculate effective electron donations into C_1 which account for π transfer, σ transfer, and polarization effects. Table 6 shows the results of our effective electron donation calculations. We conclude that polarization effects are comparable in importance to electron donation into the sp^2 carbon of carbocations substituted by poor π donors at sp^2 carbon.

Cyano-substituted carbonium ions have received a good deal of attention recently. In accord with both our present and past results (1), Gassman *et al.* (10–14) find that in comparison to H, the cyano group is a weak carbocation stabilizer when attached to C^+ but functions as a destabilizer at more remote centers in saturated substituents. Our calculations (on **1***c* and **2***c*) suggest a similar result for the acetyl group when that group is oriented perpendicular to the "empty" *p* orbital on C^+. Such an orientation avoids a direct interaction between the "empty" *p* orbital and the CO π bond. The possibility of α-keto stabilization of carbocations has been suggested previously (15) and is consistent with our own results on the carboethoxyl group (1).

Substitution at sp^3 *carbon*

Electron donations

In order to maximize the opportunity to focus on inductive effects, we have undertaken a series of calculations on systems which interpose an ethylene bridge between the carbocationic center and the groups examined in the first portion of this study. Substituent effects on carbocationic stability were evaluated by determining ΔH_r for the following isodesmic reaction

$$[1]\quad \underset{\mathbf{6}}{\overset{+}{C}H_3} + CH_3CH_2CH_2X \rightarrow \underset{\mathbf{2}}{\overset{+}{C}H_2CH_2CH_2X} + CH_4$$

The results of calculated gas phase heats of reaction, ΔH_r, are given in Table 7 along with the heats of formation for $\overset{+}{C}H_3$ and CH_4.

Typically, an analysis of carbocation stabilities, relying on inductive effects for saturated groups as outlined in the Introduction, proceeds in the following manner. Electron donation into sp^2 carbon is presumed to be the most important mechanism of carbocation stabilization. The substituent in question is expected to donate electron density in accord with its electronegativity. Group electronegativities are almost invariably ordered on the basis of the electronegativity of the most electronegative atom present in the substituent, e.g., CH_2F would be expected to be more electronegative than CH_2Cl because fluorine is more electronegative than chlorine. Since there are a variety of methods, currently available, for calculating group electronegativities, it is no longer necessary to use a single atomic electronegativity to estimate a group electronegativity.[5,6]

Table 8 presents a variety of group electronegativities for the groups included in our study along with MNDO electron donations from C_2H_2X into C_1 of structures **2**. While there is a tendency for the various approaches to substituent electronegativities to order the groups in the same way, our computational results cannot be anticipated from group electronegativities. For example, all approaches presented in Table 8 find that OH is more electronegative than Cl. As might be expected, both Huheey's original method (4, 5) and our modification of it (20) find that C_2H_4OH is more electronegative than C_2H_4Cl. How-

[4]Cl is excluded from consideration here because of the difficulty of comparing bonds involving only second shell orbitals with bonds involving both second and third shell orbitals.

[5]These methods have been developed in very different ways as an examination of refs. 4, 5, and 16 will show.

[6]Given the arbitrary nature of Mülliken population analyses, some caution is warranted in using substituent electronegativities derived from *ab initio* computations (16). An elaborate procedure has been developed to circumvent the problem of abstracting atomic electron densities from *ab initio* results (17*a*). The MNDO method avoids this ambiguity by using the density matrix system of population analysis which ignores the overlap integral (17*b*).

TABLE 4. Electron donation into $\overset{+}{C}_1$ in structures **1**

Carbocation	X	Electron population C_1p_z	Donation into $C_1p_z(\pi)$ and $C_1s,p_x,p_y(\sigma)$		
			X	C_2H_5	H
1*a*	CF_3	0.21	0.09(net)	0.33(net)	0.15σ
1*b*	CN	0.26	0.12π,−0.11σ	0.13π,0.13σ	0.13σ
1*c*	$C(O)CH_3$	0.18	0.18(net)	0.26(net)	0.13σ
1*d*	Cl	0.31	0.19π,−0.03σ	0.12π,0.14σ	0.14σ
1*e*	BH_2	0.23	0.27(net)	0.24(net)	0.12σ
1*f*	CH_3	0.23	0.22(net)	0.22(net)	0.11σ
1*g*	F	0.33	0.24π,−0.26σ	0.09π,0.16σ	0.15σ
1*h*	H	0.16	−,+0.10σ	0.16π,0.09σ	0.11σ
1*i*	C≡CH	0.36	0.27π,−0.05σ	0.08π,0.07σ	0.11σ
1*j*	$CH{=}CH_2$	0.45	0.37π,0.00σ	0.07π,0.05σ	0.09σ
1*k*	OH	0.44	0.39π,−0.18σ	0.05π,0.15σ	0.16σ
1*l*	NH_2	0.57	0.52π,−0.17σ	0.04π,0.15σ	0.13σ

TABLE 5. Electron donation and ionic bond orders for selected structures **1**

Carbocation	X	Electron donation into C_1			Ionic bond orders* for C_1			Sum of ionic bond orders for C_1 bonds (au)
		π	σ	Total	C_1—X	C_1—H_{11}	C_1—C_2	
1*a*	CF_3	0.21	0.37	0.58	−0.083	−0.030	+0.022	−0.091
1*b*	CN	0.26	0.15	0.42	+0.050	−0.038	+0.026	+0.038
1*c*	$C(O)CH_3$	0.18	0.39	0.58	−0.022	−0.025	+0.020	−0.027
1*e*	BH_2	0.23	0.41	0.64	−0.017	−0.021	+0.013	−0.029
1*f*	CH_3	0.23	0.32	0.56	+0.014	−0.023	+0.020	+0.011

*Ionic bond orders p^1 are defined as (8,9) $p^1_{AB} = -q_Aq_B/R_{AB}$ where q_A = atomic charge on A, q_B = atomic charge on B, and R_{AB} = AB bond length.

TABLE 6. Effective electron transfer for selected structures **1**

Carbocation	X	Total electron C_1	Total polarization effects for C_1 (au)	Equivalent electron donation*	Effective electron transfer	$\Delta\Delta H_f$ (kcal/mol)
1*a*	CF_3	0.58	−0.091	−0.20	0.37	+10
1*b*	CN	0.42	+0.038	+0.09	0.51	−3.5
1*c*	$C(O)CH_3$	0.58	−0.027	−0.06	0.51	−4.0
1*e*	BH_2	0.64	−0.029	−0.06	0.58	−13.6
1*f*	CH_3	0.56	+0.011	+0.02	0.59	−13.9

*These numbers correspond to the electron donation required to fully compensate for the removal of polarization effects. They were calculated using the following equation. 0.0529 au ≃ 0.12 e'.

ever, our MNDO calculations show that there is no significant difference in σ donation, π donation, or net electron donation from these two groups. We note that our modification (20) of Huheey's method for the calculation of group electronegativities tends to afford smaller differences in saturated substituent electronegativity values (4,5). As a result, our modification makes it somewhat easier to reach the unavoidable conclusion that *substituent electronegativities are not useful in attempting to assess either the electron donating ability of saturated substituents*[7] *or the relative impact of saturated substituents on the heats of reaction for carbocation formation.*

Table 9 displays results which permit an assessment of the more basic assumption that charge delocalization should correlate with substituent-stabilization effects. The differences in charge delocalization are very small. There is no systematic correlation of ΔH_r values with electron donation into C_1 or $C_1H_{11}H_{12}$. Furthermore, our introduction pictured a generalized scheme for the charge distributions accompanying inductive effects that is completely incompatible with our computational results. Typically, our calculations furnish partial charges of −0.10 on C_2 in structures **1** and −0.15 on C_2 in structures **2**. Systems which are denied strong π donation into C^+ invariably have a substantially *greater negative* charge built up on the carbon(s) adjacent to the carbocationic center. There is no correlation between the negative charge buildup on C_2 in structures **2** and the electronegativity of X or CH_2X. Some excess electron population on C_2 is accumulated in the C_2p_y orbitals.

A possible link between X and the buildup of electron population at C_2 in structure **2** is provided by the NH_2 group. Two configurations for the NH_2 group have been examined and

[7]By saturated substituents we mean to imply that the substituent is attached to $C^{\oplus}$ by sp^3 carbon, whether or not the substituent has a site of unsaturation at some point remote from the carbocationic center.

TABLE 7. Substituent effects on the energetics for the formulation of carbocation **2**

Species	X	ΔH_f (kcal/mol)	Substituent heat of stabilization* ΔH_r (kcal/mol)
2*a*	CF_3	77.8	−6.7
6*a*		−171.2	
2*b*	CN	253.5	−10.7
6*b*		8.5	
2*d*	Cl	211.0	−10.9
6*d*		−33.8	
2*g*	F	174.3	−11.3
6*g*		−70.1	
2*c*	$C(O)CH_3$	181.3	−15.3
6*c*		−59.1	
2*k*	OH	170.4	−17.6
6*k*		−67.7	
2*h*	H	212.3	−18.5
6*h*		−24.9	
2*e*	BH_2	219.2	−18.9
6*e*		−17.6	
2*f*	CH_3	208.2	−19.1
6*f*		−28.4	
2*i*	C≡CH	267.1	−19.3
6*i*		30.7	
2*j*	$CH{=}CH_2$	231.3	−20.0
6*j*		−4.4	
2*l*	NH_2	217.7	−21.3
6*l*		−16.7	
—	CH_3^+	243.8	
—	CH_4	−11.9	

*Isodesmic reaction defined in eq. [1].

are presented as Newman projections (**2***l*-1 and **2***l*-2) along with their calculated heats of formation.

Both orientation of the —NH_2 group and the near planarity at nitrogen in **2***l*-1 suggest that there is an interaction between the nitrogen lone pair orbital and the C_2p_y orbital. Buildup of electron population in the C_2p_y orbital supports the hyperconjugative donation of electron density from H_{11} and H_{12} into the C_1p_z orbital. The overall surplus of electron population on C_2 establishes significant polarization stabilization for the C_1C_2 bond.

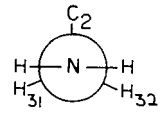

2*l*-1

ΔH_f = 217.7 kcal/mol

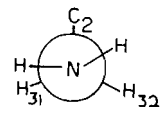

2*l*-2

ΔH_f = 223.2 kcal/mol

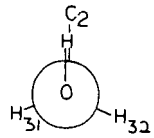

2*k*-1

We should also point out that a few groups (X) are oriented in structures **2**, in such a way as to indicate a preference for interaction with the C_2p_z orbital. A case in point is provided by the —OH group. A Newman projection of the energy minimized conformation of **2***k* is presented as **2***k*-1.

Differences in the net electron donations into C_1 or $C_1H_{11}H_{12}$ in the series of cations **2***a* → **2***l* are very small. Such differences never amount to more than a few hundredths of an electron. Allowance for polarization stabilization, using the relationship advanced in the discussion of sp^2 substituted systems, indicates that differences here are also equivalent to electron donations of the same magnitude. The consequent absence of any correlation between electron donations into C_1, even allowing for polarization effects, and ΔH_r values suggests that *conventional discussions of saturated-substituent*[7] *stabilization effects are simplified to the point of having little or no significance*.

There is some tendency for the cations **2**, which have poorer stabilizers (C_2H_4X groups), to suffer from greater polarization destabilization associated with the C_1H_{11} and C_1H_{12} bonds (due

TABLE 8. Substituent electronegativities and electron donation into C_1 for cations **2**

Cation	X	Huheey[a] (X)	Topsom[b] (X)	Inamoto[c] (X)	Wells[d] (X)	Huheey[e] (C_2H_4X)	Langler[f] (C_2H_4X)	σ donation from C_2H_4X	π donation from C_2H_4X	Net electron donation from C_2H_4X
2*a*	CF_3	3.46	0.17	2.47	3.35	2.69	2.37	0.08	0.15	0.23
2*b*	CN	3.84	0.31	2.61	3.3	2.63	2.40	0.08	0.16	0.24
2*d*	Cl	2.94	0.28	2.37	3.03	2.39	2.33	0.08	0.16	0.24
2*g*	F	3.88	0.52	3.10	3.95	2.46	2.40	0.07	0.16	0.24
2*c*	$C(O)CH_3$	2.69	0.14	2.39	—	2.48	2.31	0.08	0.16	0.25
2*k*	OH	3.51	0.43	2.79	3.7	2.52	2.38	0.09	0.17	0.26
2*h*	H	2.20	0.00	2.00	2.28	2.28	2.27	0.09	0.16	0.25
2*e*	BH_2	2.09	−0.04	—	—	2.21	2.27	0.10	0.16	0.26
2*f*	CH_3	2.27	0.17	2.14	2.3	2.27	2.28	0.08	0.17	0.26
2*i*	C≡CH	2.90	0.28	2.52	3.3	2.48	2.33	0.09	0.16	0.26
2*j*	$CH{=}CH_2$	2.41	0.17	2.34	3.0	2.34	2.29	0.09	0.16	0.26
2*l*	NH_2	2.61	0.33	2.47	3.35	2.39	2.31	0.09	0.17	0.27

[a]References 4,5.
[b]Reference 16.
[c]Reference 18.
[d]Reference 19.
[e]Calculated using method in refs. 4,5.
[f]Calculated using method in ref. 20.

TABLE 9. Residual positive charge on C_1 and $C_1H_{12}H_{11}$ in carbocations **2**

Carbocation	X	Partial charge on C_1	Partial charge on $C_1H_{11}H_{12}$
2*a*	CF_3	+0.52	+0.76
2*b*	CN	+0.52	+0.75
2*d*	Cl	+0.52	+0.75
2*g*	F	+0.52	+0.75
2*c*	$C(O)CH_3$	+0.51	+0.74
2*k*	OH	+0.51	+0.73
2*h*	H	+0.52	+0.74
2*e*	BH_2	+0.51	+0.73
2*f*	CH_3	+0.51	+0.74
2*i*	C≡CH	+0.51	+0.73
2*j*	$CH{=}CH_2$	+0.51	+0.73
2*l*	NH_2	+0.50	+0.72

to the buildup of adjacent like charges). Table 10 presents the pertinent data for cations **2** (listed in order of increasing substituent stabilization). This tendency offers some basis for the common practice of overlooking inductive stabilization from hydrogen attached to C^+.

In each cation **2**, the H_{21}–H_{22} separation is diminished by ca. 0.015 Å when compared with the H_{21}–H_{22} distance in the corresponding structure **6**. This result indicates the operation of hyperconjugative stabilization in structures **2** and underscores the need for a buildup of electron density in the C_2p_y orbital. The similarity of the magnitudes of contractions for the H_{21}–H_{22} distances in structures **2** is consistent with the observed similarities of the electron densities in the C_1p_z orbitals of structures **2** (see Table 8).

In addition to the contraction of the $H_{21}C_2H_{22}$ angles, the C_1C_2 bond lengths are consistently shorter in structures **2** than they are in the corresponding structures **1** (except for the **1***a*, **2***a* pair). A typical value for such a contraction is 0.03 Å. The magnitude of this contraction in C_1C_2 bond lengths is identical, for each substituent common to the present study[8] and our previous study of thionium ions (1), to the corresponding contraction of the CS_π bond of structures **5** when compared to structures **4**. For example, when X = OH, the $C(sp^2)S$ bond length in

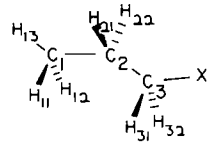

6

structure **5** is 0.06 Å shorter than the corresponding bond length in structure **4** and the C_1C_2 bond length is 0.06 Å shorter in structure **2** than the corresponding bond length in structure **1**. Along with our earlier discussion of C_1C_2 "π bond" orders in **1** and **2**, these bond length results make the analogy between a sulfur atom and a methylene group attractive.

As might be expected, the $C_1C_2C_3$ angle is wider in structures **2** where there is a relatively strong hyperconjugative effect, than it is in structures **1** where the hyperconjugative effect is considerably weaker. The same angle expansion can be observed by comparing the $C_1C_2C_3$ angles in structures **2** and **6**. The systematic contraction of the C_2C_3X bond angles in structures **2** (when compared with the corresponding angles in structures **6**) is a good deal more surprising. The sum of these skeletal angle differences for structures **2** and **6** correlates with C_1C_2 π bond order in structures **2**. Table 11 presents the bond angle information while Table 2 contains the C_1C_2 π bond orders for structures **2**. We note that those X groups which are the best π donors when attached to C_1, induce the greatest angle deformations when attached to C_3.

Conclusions

Good π donors attached to C^+ exhibit substituent-stabilization effects which correlate with electron donation into the "empty" *p* orbital on C^+.

Poor π donors attached to C^+ offer substituent-stabilization effects which can only be anticipated by a simultaneous accounting for π donation, σ donation, and polarization effects. These three factors are similar in importance for substituent-stabilization effects.

The usual view of inductive effects leads to expected charge distributions (for carbocations substituted at sp^2 carbon by saturated[7] substituents) which is intuitively unreasonable. This view requires the buildup of substantial *polarization destabilization* in order to achieve charge delocalization. The tra-

TABLE 10. C_1—H_{11}, C_1—H_{12} ionic bond orders

Carbocation	X	Ionic bond order C_1—H_{11} (au)	Ionic bond order C_1—H_{12} (au)	Total ionic bond order C_1—H_{11},C_1—H_{12} (au)
2*a*	CF_3	−0.300	−0.029	−0.059
2*b*	CN	−0.029	−0.028	−0.057
2*d*	Cl	−0.029	−0.028	−0.057
2*g*	F	−0.029	−0.029	−0.058
2*c*	$C(O)CH_3$	−0.029	−0.027	−0.056
2*k*	OH	−0.028	−0.026	−0.054
2*h*	H	−0.028	−0.026	−0.054
2*e*	BH_2	−0.028	−0.026	−0.054
2*f*	CH_3	−0.028	−0.026	−0.054
2*i*	C≡CH	−0.028	−0.026	−0.054
2*j*	$CH{=}CH_2$	−0.028	−0.025	−0.053
2*l*	NH_2	−0.026	−0.025	−0.051

[8]Groups common to both studies are: CH_3, OH, F, CN, CF_3, and Cl.

TABLE 11. Bond angle variations for structures **2** and **5**

Species	X	$C_1C_2C_3$ angle (°)	C_2C_3X angle (°)	Total angle difference (°)
2a	CF_3	116.8	116.1	3.2
6a		113.8	116.3	
2b	CN	117.4	111.9	4.3
6b		114.3	113.1	
2d	Cl	117.5	110.5	4.6
6d		113.9	111.5	
2g	F	117.3	110.6	5.0
6g		113.9	112.2	
2c	$C(O)CH_3$	117.1	113.2	2.7
6c		114.5	113.3	
2k	OH	117.0	107.4	5.4
6k		113.9	109.7	
2h	H	117.8	109.5	3.2
6h		115.4	110.3	
2e	BH_2	117.6	117.3	3.4
6e		114.9	118.0	
2f	CH_3	117.2	114.7	2.9
6f		114.7	115.1	
2i	C≡CH	117.2	112.0	4.1
6i		114.6	113.5	
2j	$CH{=}CH_2$	117.2°	113.6°	3.5
6j		114.2°	114.6°	
2l	NH_2	117.7°	107.8°	11.0
6l		114.2°	115.3°	

ditional view is entirely incompatible with our molecular orbital computations, which find that *sp^3 carbon attached to C^+ acquires substantial negative charge which results in significant polarization stabilization.*

There is no significant difference in electron donation into C^+ via inductive or hyperconjugative effects for the saturated substituents examined in this study. The heats of reaction reported here range over ca. 15 kcal/mol. Attempts to correlate differences in saturated substituent-stabilization effects in terms of electron donation appear to have no meaning whatsoever.

There is a useful analogy between the mode of stabilization of C^+ by sulfur and the mode of stabilization of C^+ by CH_2.

Acknowledgments

We wish to thank the staff of the computer center at the Florida Institute of Technology for technical assistance. The Florida Institute of Technology has provided both financial support and computing facilities which are gratefully acknowledged.

1. (*a*) J. L. GINSBURG and R. F. LANGLER. Can. J. Chem. **61**, 589 (1983), and references therein; (*b*) W. THIEL. Quantum Chemistry Program Exchange Bulletin, **11**, 379 (1979).
2. R. D. TOPSOM. Acc. Chem. Res. **16**, 292 (1983), and references therein.
3. S. MARRIOTT and R. D. TOPSOM. J. Am. Chem. Soc. **106**, 7 (1984).
4. J. E. HUHEEY. J. Phys. Chem. **69**, 3284 (1965).
5. J. E. HUHEEY. J. Phys. Chem. **70**, 2086 (1966).
6. C. K. INGOLD. Structure and mechanism in organic chemistry. 2nd ed. Cornell University Press, Ithaca, N.Y. 1969. pp. 70, 111.
7. (*a*) M. J. S. DEWAR and W. THIEL. J. Am. Chem. Soc. **99**, 4889 (1977); (*b*) R. BINGHAM, M. J. S. DEWAR, and D. H. LO. J. Am. Chem. Soc. **97**, 1285 (1975); (*c*) G. FRENKING, J. SCHMIDT, and H. SCHWARZ. Z. Naturforsch. B, **35**, 1031 (1980); (*d*) C. DECORET, J. ROYER, and J. J. DANNENBERG. J. Org. Chem. **46**, 4074 (1981); (*e*) D. J. BELLVILLE and N. L. BAULD. J. Am. Chem. Soc. **104**, 294 (1982); (*f*) D. J. BELLVILLE and N. L. BAULD. J. Am. Chem. Soc. **104**, 5700 (1982); (*g*) G. P. FORD and J. SCRIBNER. J. Comput. Chem. **4**, 594 (1983); (*h*) B. C. CHALLIS, J. N. ILEY, and H. S. RZEPA. J. Chem. Soc. Perkin Trans. **2**, 1037 (1983); (*i*) C. GLIDEWELL. J. Chem. Soc. Perkin Trans. **2**, 1175 (1984).
8. R. S. MULLIKEN. J. Chem. Phys. **23**, 1841 (1955).
9. M. H. WHANGBO, S. WOLFE, and F. BERNARDI. Can. J. Chem. **53**, 3040 (1975).
10. P. G. GASSMAN and K. SAITO. Tetrahedron Lett. **22**, 1311 (1981).
11. P. G. GASSMAN and J. J. TALLEY. J. Am. Chem. Soc. **102**, 1214 (1980).
12. P. G. GASSMAN, D. A. DIXON, and P. A. CHARLIER. J. Am. Chem. Soc. **102**, 3957 (1980).
13. P. G. GASSMAN and J. J. TALLEY. J. Am. Chem. Soc. **102**, 4138 (1980).
14. P. G. GASSMAN and T. L. GUGGENHEIM. J. Org. Chem. **47**, 3023 (1982).
15. X. CREARY. J. Am. Chem. Soc. **103**, 2463 (1981).
16. S. MARRIOTT, W. F. REYNOLDS, R. W. TAFT, and R. D. TOPSOM. J. Org. Chem. **49**, 959 (1984).
17. (*a*) D. L. GRIER and A. STREITWIESER, JR. J. Am. Chem. Soc. **104**, 3556 (1982); and (*b*) A. G. TURNER. Methods in molecular orbital theory. Prentice Hall. Englewood Cliffs, NJ. 1974.
18. (*a*) N. INAMOTO and S. MASUDA. Tetrahedron Lett. **18**, 3287 (1977); and (*b*) N. INAMOTO, S. MASUDA, K. TORI, and Y. YOSHIMURA. Tetrahedron Lett. **19**, 4547 (1978).
19. P. R. WELLS. Prog. Phys. Org. Chem. **6**, 111 (1968).
20. J. R. HANCOCK, W. R. HARDSTAFF, P. A. JOHNS, R. F. LANGLER, and W. S. MANTLE. Can. J. Chem. **61**, 1472 (1983).

Intrazeolite photochemistry. IV. Studies of carbonyl photochemistry on the hydrophobic zeolite Silicalite using time-resolved diffuse reflectance techniques[1]

F. WILKINSON AND C. J. WILLSHER

Department of Chemistry, University of Technology, Loughborough, Leicestershire, LE11 3TU, UK

AND

H. L. CASAL, LINDA J. JOHNSTON, AND J. C. SCAIANO

Division of Chemistry, National Research Council of Canada, Ottawa, Ont., Canada K1A 0R6

Received August 8, 1985

F. WILKINSON, C. J. WILLSHER, H. L. CASAL, LINDA J. JOHNSTON, and J. C. SCAIANO. Can. J. Chem. **64**, 539 (1986).

Transient absorption and luminescence from aromatic ketone triplets (xanthone, acetophenone, butyrophenone, valerophenone, *p*-methoxyacetophenone, β-phenyl-*p*-methoxypropiophenone and benzil) supported on the hydrophobic zeolite Silicalite have been obtained by time-resolved diffuse reflectance laser flash photolysis. These experiments were aimed at establishing the usefulness of this technique for studies of zeolite supported photoreactions. While the transient spectral properties can be used to examine the properties of the supporting media, the decays of the signals frequently follow complex kinetic behaviour. The decays for such heterogeneous systems cannot be easily fit to clean first or second order kinetics and are thought to be a mixture of several first order decays arising from triplets in different inclusion and adsorption sites. Evidence is presented for close-packing of the aromatic substrates and for triplet lifetime enhancement. Although the triplet spectrum of included benzil shows evidence for considerable axial freedom, the results for β-phenylpropiophenones indicate that other types of motion are restricted for included ketones. It is also found that the rate of the Norrish Type II reactions of valerophenone and butyrophenone supported on Silicalite are decreased with respect to the rates in solution.

F. WILKINSON, C. J. WILLSHER, H. L. CASAL, LINDA J. JOHNSTON et J. C. SCAIANO. Can. J. Chem. **64**, 539 (1986).

Faisant appel à la photolyse flash d'un laser à réflexion diffuse résolue, on a mesuré, l'absorption et la luminescence fugace d'états triplets de cétones aromatiques (xanthone, acétophénone, butyrophénone, valérophénone, *p*-méthoxyacétophénone, β-phényl *p*-méthoxypropiophénone et benzil) supportées sur le zéolite hydrophobe, Silicalite. On a réalisé ces expériences dans le but d'établir l'utilisé de cette technique pour des études de photoréactions supportées sur des zéolites. Alors que l'on peut utiliser les propriétés spectrales fugaces pour examiner les propriétés du support, les dégénérescences des signaux permettent souvent de suivre des comportements cinétiques complexes. Les dégénérescences de tels systèmes hétérogènes ne suivent pas exactement des cinétiques d'ordre un ou deux et on croit qu'elles sont des mélanges de plusieurs dégénérescences d'ordre un qui proviennent de triplets dans divers sites d'inclusion ou d'adsorption. On présente des données suggérant que les substrats aromatiques existent dans un arrangement compact et que les temps de vie des triplets sont augmentés. Même si le spectre triplet du benzil présente beaucoup de liberté axiale, les résultats obtenus avec les β-phénylpropiophénones indiquent que, pour ces cétones, d'autres types de mouvements sont restreints. On a aussi trouvé que les vitesses de réactions Norrish Type II de la valérophénone et de la butyrophénone supportées sur de la Silicalite sont plus faibles que les vitesses correspondantes en solution.

[Traduit par le journal]

Introduction

Organic photoreactions on zeolite supports have been the subject of attention during the last couple of years (1–4). Our own studies have concentrated on the hydrophobic zeolite Silicalite; this serves as a convenient substrate on which to probe both the effect of crystal lattices on organic photoreactions and the ways in which photochemical probes can be used to determine the nature of active sites in zeolites. Silicalite (5) is over 99% SiO_2, and its channel system consists of near-circular zigzag channels, cross-linked by elliptical straight channels. The diameter of the circular channels is 5.4 ± 0.2 Å and the free cross-section of the elliptical ones is 5.75 × 5.15 Å.

The recently developed technique of diffuse reflectance laser photolysis (6–9) has been successfully applied to the detection of excited states at interfaces and in various crystalline systems. We report here the results of an exploratory study of the photochemistry of various carbonyl compounds supported on Silicalite. Very recently Turro *et al.* have applied the same technique to study organic substrates on porous silicas (10).

Experimental section

Silicalite (from Union Carbide) had a particle size of ~1 μm and was calcined (500°C, 24 h) before use. All the ketones used were commercial materials and were purified by distillation or crystallization.

Samples were prepared using the techniques outlined in earlier reports in this series (1–3) and contained 1–3% ketone by weight. Based on a void volume of 0.19 mL/g for Silicalite (5) these inclusions would correspond to ≤20% occupancies. The samples (typically 0.5–1 g) were contained in a quartz spectrometer cell with an optical path of 3 mm, which in these experiments corresponds to the depth of the solid sample. The powder was shaken between laser shots to ensure that a fresh surface would be exposed each time.

Unless otherwise indicated, the samples had been purged with nitrogen. Earlier work (2) on similar samples has shown that a few minutes of purging with nitrogen are sufficient to remove oxygen.

The time-resolved diffuse reflectance measurements were carried out by exciting the samples with the frequency tripled (354 nm, 30–70 mJ) or frequency quadrupled (266 nm, ~10 mJ) pulses from a Nd-YAG laser. The monitoring source was a 200 W pulsed xenon lamp. The signals from the monochromator–photomultiplier system are captured by a Tektronix 7912-AD digitizer and processed using a PDP-11/03 computer. Special care was taken to minimize signals due to all specular reflections. Further details have been reported elsewhere (7).

All our kinetic analysis is based on the fraction of reflected light absorbed by the intermediate, i.e.,

$$\text{Signal} = \frac{J_0 - J}{J_0} = \frac{\Delta J}{J_0}$$

[1]Issued as NRCC No. 25018.

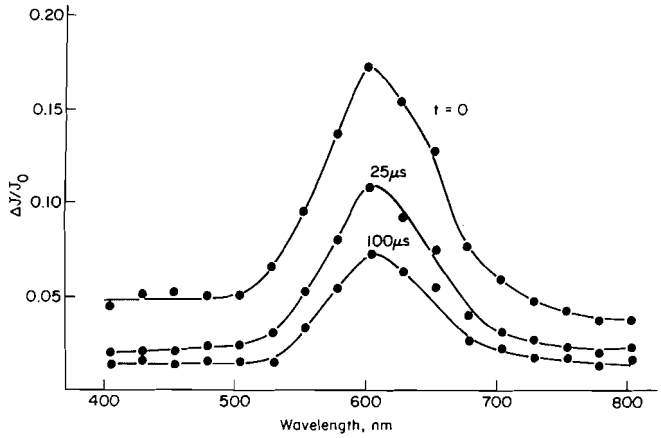

FIG. 1. Triplet diffuse reflectance spectrum of xanthone on Silicalite at 0, 25, and 100 μs after the laser pulse (354 nm excitation).

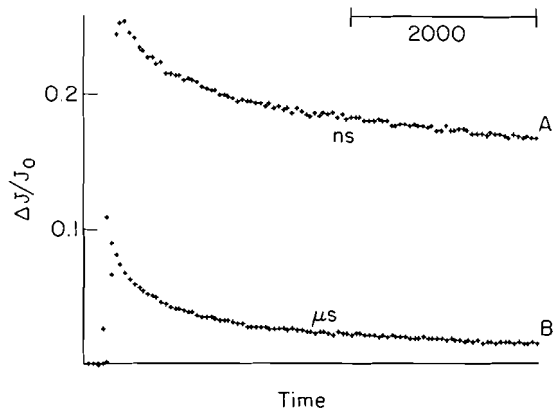

FIG. 2. Decay of triplet xanthone on Silicalite on time scales differing by a factor of 1000.

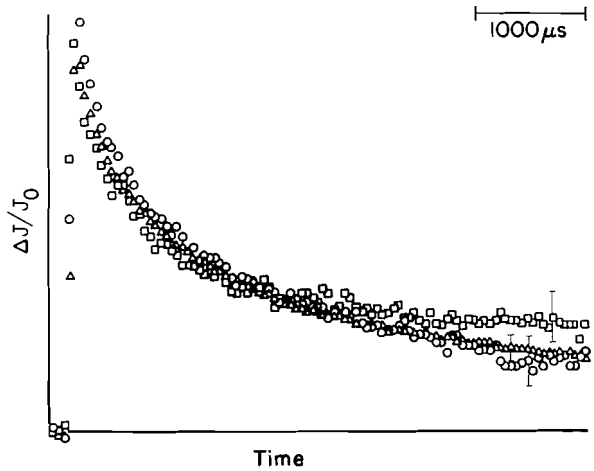

FIG. 3. Normalized decay traces for triplet xanthone on Silicalite as a function of laser dose: △, 100%; ○, 20%; □, 10%.

where J_0 and J refer to the photomultiplier signals before laser excitation and at time t after excitation, respectively. To a first aproximation this provides a suitable parameter for kinetic and spectroscopic analysis.

Results and discussion

In common with other zeolites, Silicalite offers more than one site for inclusion and (or) adsorption of organic compounds. Molecules with kinetic diameters comparable to that of benzene (~5.8 Å) are capable of being included in the channels of Silicalite. We have previously found that molecular geometry, size, and conformational flexibility play an important role in determining channel inclusion (2–3). Therefore, for the samples studied in this work there will be a combination of surface adsorption and channel inclusion. We use the term Silicalite-supported to describe these samples.

Xanthone

The molecular size and geometry of xanthone make it a borderline case for inclusion in the Silicalite channel framework. It seems likely that xanthone is located in a distribution of channel and surface sites.

The spectrum of the Silicalite-supported xanthone triplet, obtained using 354 nm excitation on a 4.88 μs per point time scale, is illustrated in Fig. 1 and shows its characteristic maximum at 605 nm, independent of how long after the laser pulse the signals were recorded. It is well known (11) that the position of λ_{max} for the xanthone triplet is a sensitive probe of the polarity of the environment, being ~610, 655, and 610 nm in 2-propanol, carbon tetrachloride, and sodium dodecyl sulfate (SDS) micelles, respectively (11). The value observed in Silicalite is in excellent agreement with the values of λ_{max} in polar media (2-propanol, SDS micelles) and suggests that xanthone is in a relatively polar environment in Silicalite. This result is rather surprising since other studies have shown that inclusion sites in Silicalite are nonpolar (12). However, we note that in the case of silica gel[2] the maximum is located at 580 nm, indicating that its surface sites may be substantially more polar in nature than those of Silicalite. This is a property that silica gel shares with other silicas (13).

The kinetics of triplet decay for xanthone on Silicalite are rather complex, extending over remarkably long periods of time. Figure 2 shows two traces obtained independently using the same sample with time scales differing by a factor of 1000. Note that the time per point in the longer time scale (trace B) is equivalent to 10 times the complete trace from the short time scale (trace A). The highest point in trace B corresponds to only a fraction of the initial signal in trace A since, on slower time scales, the fast information is not captured. The first point in trace B is actually an average or histogram of the earlier data. Not surprisingly, these data fail to fit either a first or second order decay. Bimolecular processes may play a role at very short time scales (*vide infra*), but at longer times these complex decays are probably best interpreted in terms of a distribution of first order decays arising from the multiple inclusion sites. While a more detailed understanding of the nature and number of decay modes would certainly be desirable, further elaboration is not warranted at the present time.

Luminescence lifetimes can be monitored using the same approach discussed above (but blocking the monitoring beam) and lead to traces in agreement with those recorded in the diffuse reflectance mode.

Attenuation of the laser dose, in either the diffuse reflectance or the luminescence mode, leads to signal reductions which are systematically less than the attenuation ratio itself. Figure 3 shows three normalized diffuse reflectance traces obtained with varying laser doses. The actual shape of the decay trace does not change significantly, suggesting that in the time scale monitored T–T annihilation does not play an important role. It should be

[2]Time-resolved diffuse reflectance studies of silica gel supported systems will be reported separately.

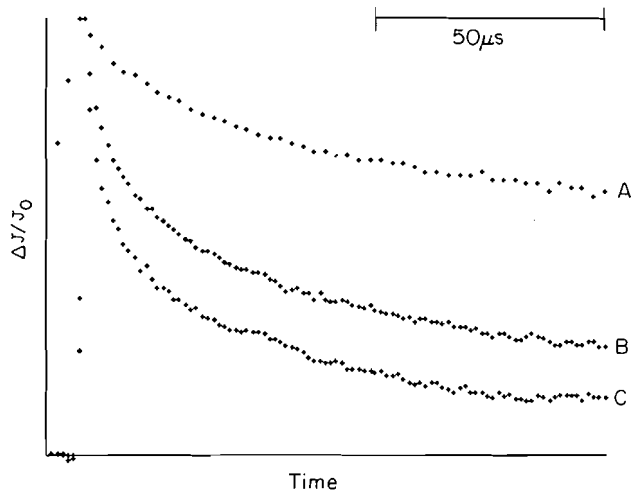

FIG. 4. Decay of triplet xanthone on Silicalite in the presence of nitrogen (A), air (B), and oxygen (C).

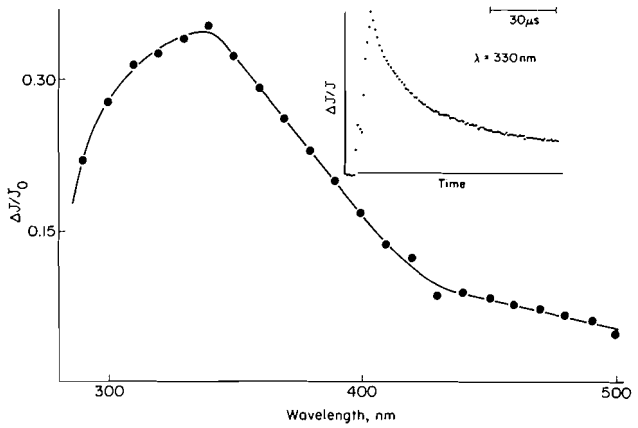

FIG. 5. Triplet diffuse reflectance spectrum of butyrophenone on Silicalite obtained by 266 nm excitation; the inset shows a decay trace at 330 nm.

noted that the small deviations in the latter parts of the decay traces are probably owing to the fact that the traces have been normalized, and the weaker signals obtained with the attenuated laser doses have large errors. The ratios of the initial signal intensities were 100:38:33 for laser doses of 100:20:10. Saturation effects of this type have also been observed for benzil triplets in crystals (8) and are to be expected based on current theory (14).

The effects of air and oxygen on the triplet decay were also examined. For a nitrogen purged sample the half-life of the decay was ~300 μs, whereas an air equilibrated sample had a half-life of 30 μs. The half-life was shorter still, ~5 μs, for an oxygen purged sample. Figure 4 illustrates this effect. We observe that while quenching does occur, the magnitude of the effect is substantially smaller than that which we have observed for oxygen quenching of xanthone on silica gel, where half-lives of 12 and 0.5 μs were measured for nitrogen and oxygen purged samples, respectively. This difference suggests that a large fraction of Silicalite-supported xanthone molecules are inside the channel structure and thus, not readily accessible to oxygen. To the extent that the exterior surface of Silicalite would resemble silica gel, the value of λ_{max} for T–T absorptions also supports extensive channel inclusion.

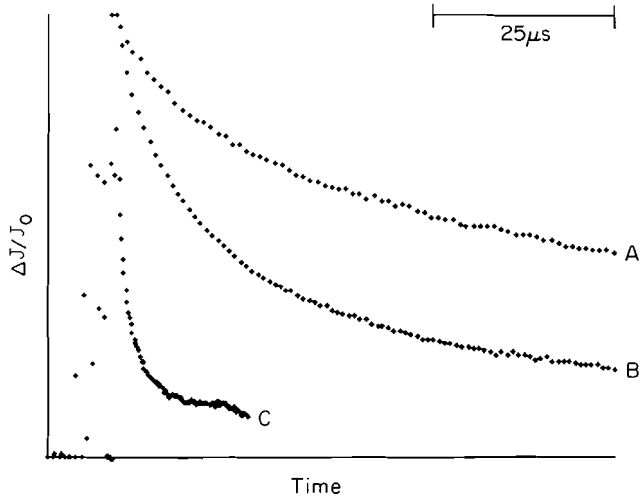

FIG. 6. Normalized decay traces for triplet acetophenone (A), butyrophenone (B), and valerophenone (C) on Silicalite (266 nm excitation).

Acetophenone, butyrophenone, and valerophenone

These ketones were selected because their kinetic diameters allow for easy channel inclusion. Furthermore, the Norrish Type II phototransformation of included valerophenone and butyrophenone could be compared with solution behaviour, thus, giving an idea of immobilization effects on this reaction.

Irradiation of Silicalite-supported butyrophenone samples yields the transient diffuse reflectance spectrum shown in Fig. 5. The spectrum is reasonable for a triplet benzoyl chromophore although somewhat broader than is normally observed in solution (15). Valerophenone and acetophenone in Silicalite give similar triplet spectra upon 266 nm excitation. The triplet decays for these three ketones all show complex kinetics. However, a comparison of the decays for each one on the same time scale (Fig. 6) showed that the lifetimes followed the order acetophenone > butyrophenone > valerophenone. For butyrophenone and valerophenone, which undergo the Norrish Type II reaction, the lifetimes are ~30 and ~2 μs, respectively; these represent a large increase in the triplet lifetime over those in solution (125 and ~5 ns) (16, 17).

Previous studies of valerophenone on Silicalite (2) have shown that the acetophenone produced in the Norrish Type II reaction plays a dominant role in determining the phosphorescence of the sample studied. This potential complication does not appear to be a problem here, since the two ketones which undergo the Type II reaction give transients which have different lifetimes and both of which are significantly shorter than that of the acetophenone triplet. Therefore, we conclude that the lifetime enhancement relative to the values in solution is real and attribute it to a decreased rate of the Norrish Type II reaction due to restrictions in molecular mobility. Similar results have recently been observed by Turro *et al.* for valerophenone and γ,γ-diphenylbutyrophenone adsorbed on porous silica (10). It is also interesting to note that the lifetimes for the two ketones still reflect the relative ease of abstraction of secondary vs. primary hydrogens. This suggests that the relative rates of decay are not determined by the rate at which the reactive conformation can be achieved. In other words, hydrogen abstraction remains the rate determining step for decay, with the favorable conformation for abstraction being less abundant in Silicalite than in solution.

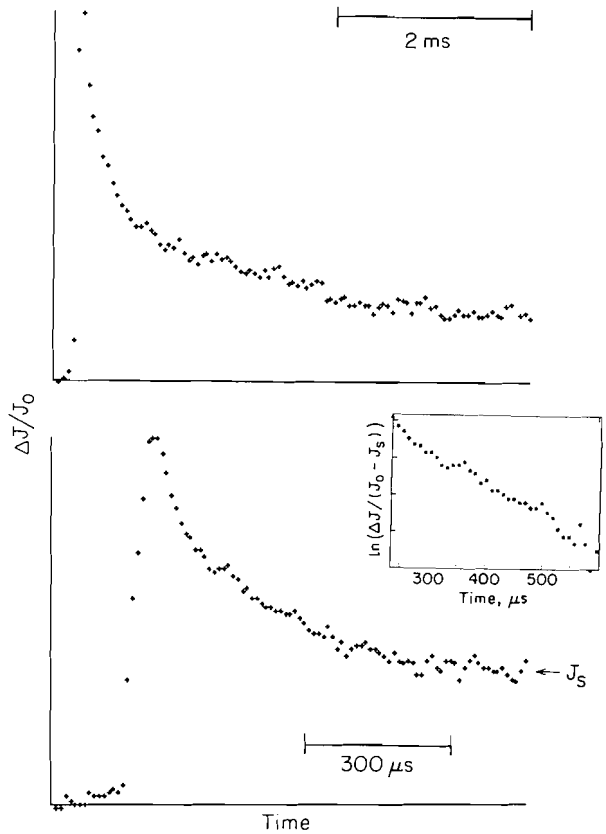

FIG. 7. Decay of triplet *p*-methoxyacetophenone on Silicalite (354 nm excitation), top. An expansion of the early part of this decay is shown at the bottom with an inset showing a first order analysis of the data (where $J_0 - J_s$ is the corrected baseline level).

p-*Methoxyacetophenone and* β-*phenyl*-p-*methoxypropiophenone*

The dimensions of these molecules are such that inclusion in Silicalite should be possible, although the methoxy substituent may restrict this process to some extent (3).

Figure 7 shows the decay of triplet *p*-methoxyacetophenone following 354 nm laser excitation. As in the case of xanthone the decay kinetics are complex and extend over a long period of time. However, in this case we observe a reasonably well defined "fast–slow" separation, as illustrated in Fig. 7 (top) for the time scale in which this differentiation is most evident. The fast part of the decay, shown in Fig. 7 (bottom) seems to approach first order kinetics (after an appropriate baseline shift) rather well (see insert in Fig. 7). The lifetime derived from this analysis was 230 μs; lifetimes of this magnitude had been determined previously using phosphorescence techniques for several aromatic ketones included in Silicalite (1, 2). The slow component's lifetime is too long to allow us to establish the dominance of first or second order decay modes (due to limitations of the digitizer); typical half-lives are of a few milliseconds. The luminescence from *p*-methoxyacetophenone also showed a fast and a slow component. The lifetime of the latter agreed well with the diffuse reflectance measurements; however, the fast component seems to incorporate luminescence from an additional (even shorter lived) species.

The diffuse reflectance spectrum of the triplet state of *p*-methoxyacetophenone is shown in Fig. 8. The intensity of the spectrum does, of course, change with time, but its spectral features do not. The value of λ_{max} = 410 nm is in excellent

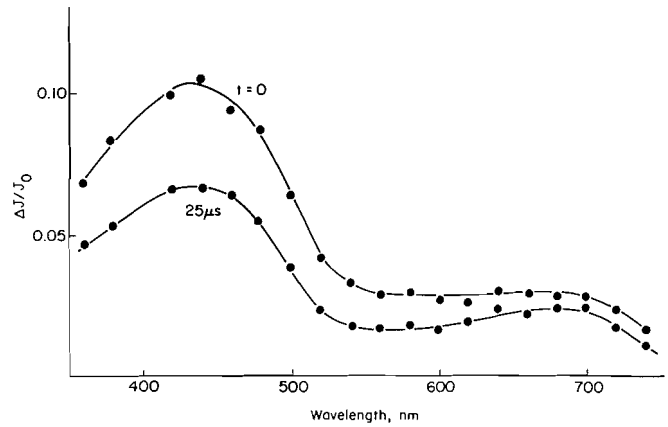

FIG. 8. Triplet spectrum of *p*-methoxyacetophenone on Silicalite (354 nm excitation).

agreement with that recorded in homogeneous solution for the same chromophore (18). The broad band in the 600 nm region is not present in the spectra of *p*-methoxybenzoyl monoketones in homogeneous solution; however, similar absorptions are observed in the case of poly(*p*-methoxyacrylophenone) (19), and to a lesser extent in its copolymers with other monomers (20). In the triplet spectra of polymers these broad bands around 600 nm have been suggested to reflect the close proximity of the chromophores (19, 20). Thus, correlation of this observation with the spectra of Silicalite-supported *p*-methoxyacetophenone suggests that the chromophores are also in close proximity on Silicalite.

β-Phenyl-*p*-methoxypropiophenone, like all β-arylpropiophenones, undergoes efficient deactivation in solution as a result of excited state interaction with the β-aryl moiety. Its triplet lifetime in isopentane at 300 K is 71 ns, compared with several microseconds for *p*-methoxyacetophenone (18).

Earlier work from our laboratory (3) has already shown that inclusion of ketones of this type in Silicalite essentially eliminates this decay mode as a result of restrictions of the molecular motions required to achieve an adequate conformation for quenching. Consistent with this, the behavior of β-phenyl-*p*-methoxypropiophenone triplet (354 nm excitation, monitoring diffuse reflectance transient absorption) was essentially the same as that of *p*-methoxyacetophenone; the only difference was some shortening of the fast decay.

Similar results were obtained upon 266 nm excitation of β-phenylpropiophenone. The triplet has a broad spectrum, λ_{max} ~320 nm, and decays within 500 μs with complex kinetics.

Benzil

Benzil (excited at 354 nm) gave a triplet spectrum (Fig. 9) with λ_{max} at 470 nm which is much closer to that of benzil triplet in solution (λ_{max} at 480 nm in cyclohexane or acetonitrile (21)) than to the spectrum for the crystalline material (λ_{max} at 520 nm (8)). The transient spectrum of the benzil–Silicalite sample showed an additional broad, weak band at long wavelengths, λ_{max} ~ 830 nm.

The emission spectrum has λ_{max} at 550 nm which is again shifted from those in glasses at 77 K and in the crystal which show λ_{max} at 510 (22) and 510 nm (8), respectively. These results confirm that we are not looking at microcrystalline benzil on the surface of the Silicalite but rather at adsorbed or included benzil molecules.

Benzil undergoes extensive conformational reorganization upon excitation into the triplet manifold; for example, the dipole

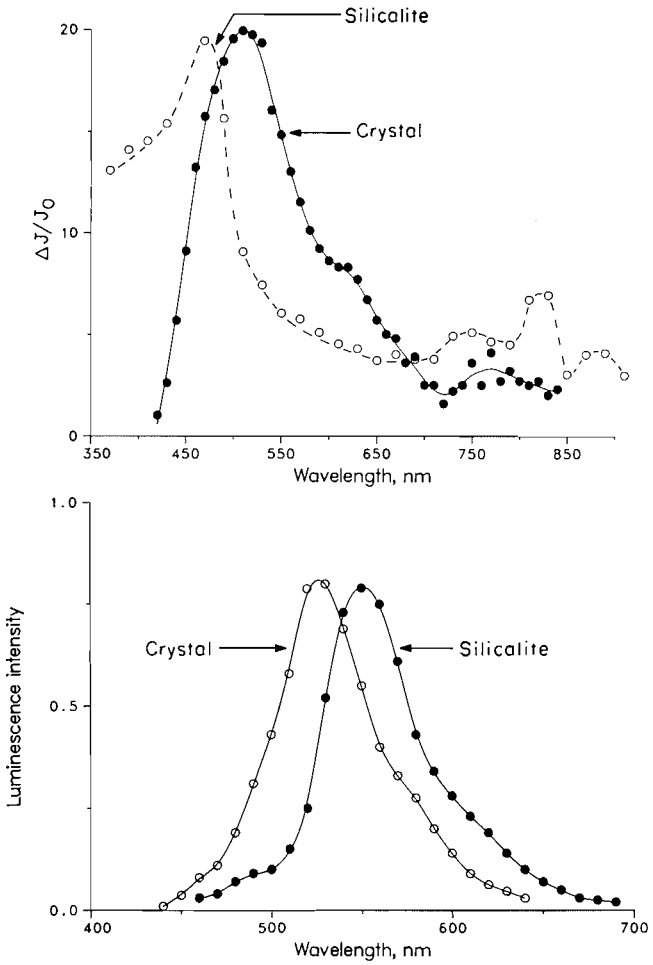

FIG. 9. Triplet diffuse reflectance (top) and emission (bottom) spectra of benzil crystals and benzil on Silicalite obtained by 354 nm excitation.

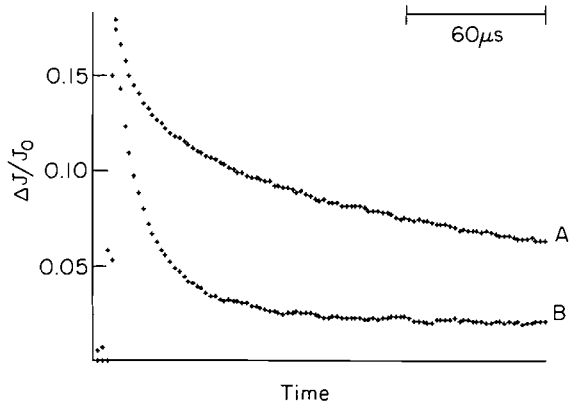

FIG. 10. Decay of triplet benzil on Silicalite in the presence of nitrogen (A) and air (B).

moment of the triplet is zero, as compared with 3.75 D for the ground state (23). The spectral characteristics mentioned above suggest that while the crystal structure of pure benzil severely limits this reorganization (8), the Silicalite framework allows it to occur rather freely. Since only axial motion is required this result is not entirely surprising; axial motions are not hindered on Silicalite (24).

Decay kinetics based on either the triplet absorption at 470 nm or emission at 550 nm gave similar results. The decays give reasonable fits to first order kinetics (except for a small amount of faster component at the beginning) and lead to lifetimes of ca. 360 μs. As with xanthone, the signal reductions upon laser attenuation do not match the laser attenuation ratio, following the order 100:36:31 for 100:20:10% of the laser dose. The presence of oxygen had a dramatic effect on the triplet lifetimes. Under air these lifetimes were reduced by a factor of approximately 20 from those measured under nitrogen. Thus, under air, over 80% of the decay took place with a lifetime of ca. 18 μs. Figure 10 shows a comparison of decay traces under air and under nitrogen. This dramatic oxygen effect on the triplet lifetime contrasts with the case of crystalline benzil where no effect was detected (8).

Conclusions

Time-resolved diffuse reflectance techniques can play an important role in developing an understanding of organic photoprocesses in zeolites. These studies can help us to understand the nature and properties of the active sites in these catalysts.

For aromatic ketones on Silicalite, complex triplet decay kinetics seem to be the rule, with decay processes extending over several orders of magnitude in time scale. Such complex kinetics would be expected for a heterogeneous system where ketone triplets in different channel or surface sites may decay with different rate constants. Similar behaviour has been observed in fluorescence decays of various aromatics adsorbed on solids (25).

Transient spectra can be quite useful in establishing some of the characteristics of the various adsorption sites on zeolites. Thus, the value of $\lambda_{max} = 605$ nm for triplet xanthone suggests a relatively polar environment, comparable with 2-propanol, but not as polar as in the case of silica gel where $\lambda_{max} = 580$ nm. The idea of closely packed guest molecules is supported by the spectral features of *p*-methoxyacetophenone triplet, and earlier evidence (2) for energy migration. The absorption and luminescence properties of benzil support the idea of considerable axial freedom for the included molecule. In the case of β-phenylpropiophenone, a similar degree of axial freedom cannot help the molecule undergo intramolecular quenching; in contrast, the folding motion required for deactivation is prevented by the Silicalite lattice. Butyrophenone and valerophenone show lifetime enhancements which reflect a decreased rate for the Norrish Type II reaction, owing to similar restrictions on molecular mobility.

Acknowledgments

The travel required to carry out the studies reported herein was generously supported by a NATO grant (372/84). This support is gratefully acknowledged. We are also grateful to Professor N. J. Turro for the communication of unpublished results.

1. H. L. CASAL and J. C. SCAIANO. Can. J. Chem. **62**, 628 (1984).
2. H. L. CASAL and J. C. SCAIANO. Can. J. Chem. **63**, 1308 (1985).
3. J. C. SCAIANO, H. L. CASAL, and J. C. NETTO-FERREIRA. ACS Symp. Ser. **278**, 211 (1985).
4. N. J. TURRO and P. WAN. Tetrahedron Lett. **25**, 3655 (1984).
5. E. M. FLANIGEN, J. M. BENNETT, R. W. GROSE, J. P. COHEN, R. L. PATTON, R. M. KIRCHENER, and J. V. SMITH. Nature (London), **271**, 512 (1978).
6. R. W. KESSLER and F. WILKINSON. J. Chem. Soc. Faraday Trans. 1, **77**, 309 (1981).
7. C. J. WILLSHER. J. Photochem. **28**, 229 (1985).

8. P. WILKINSON and C. J. WILLSHER. Appl. Spectrosc. **38**, 897 (1984).
9. F. WILKINSON and C. J. WILLSHER. Chem. Phys. Lett. **104**, 272 (1984).
10. N. J. TURRO, M. B. ZIMMT, I. R. GOULD, and W. MAHLER. J. Am. Chem. Soc. **107**, 5826 (1985); N. J. TURRO, I. R. GOULD, M. B. ZIMMT, and C. C. CHENG. Chem. Phys. Lett. **119**, 484 (1985).
11. A. GARNER and F. WILKINSON. J. Chem. Soc. Faraday Trans. 2, **72**, 1010 (1976); F. WILKINSON and A. GARNER. Photochem. Photobiol. **27**, 659 (1978); J. C. SCAIANO. J. Am. Chem. Soc. **102**, 7747 (1980).
12. N. B. MILESTONE and D. M. BIBBY. J. Chem. Technol. Biotechnol. **31**, 732 (1981); G. M. W. SHULTZ-SIBBEL, D. T. GJERDE, C. D. CHRISWELL, J. S. FRITZ, and W. E. COLEMAN. Talanta, **29**, 447 (1982).
13. P. A. LEERMAKERS, H. T. THOMAS, L. D. WEIS, and F. C. JAMES. J. Am. Chem. Soc. **88**, 5075 (1966).
14. W. HONNER, D. OELKRUG, C. J. WILLSHER, and F. WILKINSON. To be published.
15. H. LUTZ and L. LINDQVIST. Chem. Commun. 493 (1971).
16. P. J. WAGNER. Acc. Chem. Res. **4**, 168 (1971).
17. M. V. ENCINA, E. A. LISSI, E. LEMP, A. ZANOCCO, and J. C. SCAIANO. J. Am. Chem. Soc. **105**, 1856 (1983).
18. J. C. NETTO-FERREIRA, W. J. LEIGH, and J. C. SCAIANO. J. Am. Chem. Soc. **107**, 2617 (1985).
19. J. C. SELWYN and J. C. SCAIANO. Polymer, **21**, 1365 (1980).
20. J. C. SCAIANO and J. C. SELWYN. Macromolecules, **14**, 1723 (1981).
21. M. V. ENCINAS AND J. C. SCAIANO. J. Am. Chem. Soc. **101**, 7740 (1979).
22. S. C. BERA, R. MUKHERJEE, and M. CHOMDHURY. J. Chem. Phys. **51**, 754 (1969).
23. R. W. FESSENDEN, P. M. CARTON, H. SHIMAMORI, and J. C. SCAIANO. J. Phys. Chem. **86**, 3803 (1982).
24. J. B. NAGY, E. G. DEROUANE, H. A. RESING, and G. R. MILLER. J. Phys. Chem. **87**, 833 (1983).
25. P. DE MAYO. Pure Appl. Chem. **54**, 1623 (1982).

Synthèse de dérivés N-5 substitués des 5*H*-pyrido[4,3-*b*]benzo[*f*]indoles, isomères des 6*H*-pyrido[4,3-*b*]carbazoles (ellipticines)

CHI HUNG NGUYEN, ÉMILE BISAGNI[1] ET JEAN-MARC LHOSTE

Centre national de la recherche scientifique, Unité associée 40533, Laboratoire de synthèse organique, Institut Curie, Section de Biologie, Bâtiments 110–112, Centre Universitaire, 91405 Orsay Cédex, France

Reçu le 15 juillet 1985

CHI HUNG NGUYEN, ÉMILE BISAGNI et JEAN-MARC LHOSTE. Can. J. Chem. **64**, 545 (1986).

Les dérivés lithiés en 2 des alkyl-1 chloro-4 pyrrolo[3,2-*c*]pyridines réagissent avec les acétophénones en donnant les alcools tertiaires correspondants. Après déshydration, les diaryl-1,1 éthylènes formés sont réduits en diaryl-1,1 éthanes et la transformation de ces derniers en chloro-1 alkyl-5 5*H*-pyrido[4,3-*b*]benzo[*f*] indoles est réalisée soit directement par le dichlorométhylméthyléther en présence de chlorure stannique, soit indirectement par formylation suivie de cyclodeshydratation par l'acide polyphosphorique. La substitution de l'atome de chlore par les dialkylaminoalkylamines fournit enfin les dialkylaminoalkylamino-1 alkyl-5 5*H*-pyrido[4,3-*b*]benzo[*f*]indoles, isomères des dialkylaminoalkylamino-1 ellipticines N-6 substituées.

CHI HUNG NGUYEN, ÉMILE BISAGNI, and JEAN-MARC LHOSTE. Can. J. Chem. **64**, 545 (1986).

2-Lithio dérivatives of 1-alkyl-4-chloropyrrolo[3,2-*c*]pyridines react with acetophenones, giving the corresponding tertiary alcohols. After déhydration into 1,1-diarylethylenes and subsequent reduction to 1,1-diarylethanes, the synthesis of 1-chloro-5-alkyl-5*H*-pyrido[4,3-*b*]benzo[*f*]indoles was achieved either by direct cyclization with dichloromethylmethylether plus stannic chloride or by formylation and cyclodehydration with polyphosphoric acid. Finally, the substitution of the chlorine atom with dialkylaminoalkylamines leads to 1-amino substituted 5-alkyl-5*H*-pyrido[4,3-*b*]benzo[*f*]indoles, isomers of 1-dialkylamino-alkylamino 6-substituted ellipticines.

L'ellipticine **1***a*, dont les propriétés antitumorales sur la leucémie L1210 de la souris ont été reconnues vers la fin des années 60 (1) appartient à la famille des pyrido[4,3-*b*]carbazoles dont certains dérivés présentent des propriétés antitumorales plus importantes que l'alcaloïde **1***a*. C'est le cas,

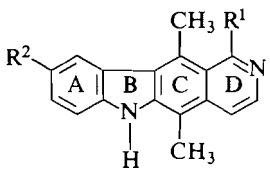

1*a* $R^1 = R^2 = H$
1*b* $R^1 = NH(CH_2)_3N(CH_2CH_3)_2$; $R^2 = OCH_3$

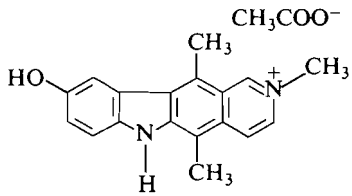

2

notamment, du composé **1***b* (2, 3) dont l'étude n'est pas achevée et du composé **2** qui est déjà utilisé chez l'homme (4, 5). Cette série hétérocyclique a donc largement retenu l'attention des chimistes et, depuis 15 ans, plus de 25 méthodes distinctes permettant d'y accéder en ont été décrites (6–9).

Par ailleurs, divers analogues structuraux du composé **1***a* ont également été préparés et, tandis que les dérivés oxygéné, soufré et hydrocarboné sur le sommet 6, respectivement **3** (10), **4** (11, 12) et **5** (13), sont dénués de toute activité, la série des aza-9 ellipticines ou pyrido[3′,4′:4,5]pyrrolo[2,3-*g*]isoquinoleines **6** (14, 15) a largement retenu l'attention des biologistes. Ainsi, le composé **7** s'est montré actif sur une grande variété de tumeurs expérimentales (16, 17) et il a même fait l'objet d'une étude clinique phase 1 dont les résultats semblent encourageants (18).

Cette série paraît donc intéressante et, puisque la présence de l'azote en 2 sur ce dernier système hétérocyclique se traduit en fait par une amélioration des propriétés antitumorales de ce type de substances, il nous a semblé utile de chercher à étudier les éventuelles propriétés biologiques des dérivés des 5*H*-pyrido-[4,3-*b*]benzo[*f*]indoles **8**.

En effet, en dehors de différentes quinones récemment synthéthisées par notre laboratoire (19), les dérivés de cet hétérocycle ne sont pas décrits et il s'agit de savoir si l'azote intracyclique en 2 peut en lui-même suffire au maintient de l'activité antitumorale, malgré le remplacement du système isoquinoléine des ellipticines par un noyau naphtalène. Cela devrait d'ailleurs permettre de préciser les caractéristiques

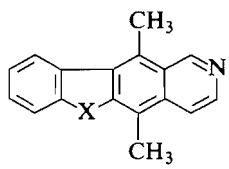

3 X = O
4 X = S
5 X = CH_2

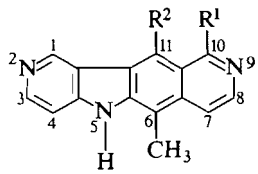

6 R^1 = H ou $NH(CH_2)_nN(R_3)_2$; $R^2 = CH_3$ ou H
7 $R^1 = NH(CH_2)_3N(CH_2CH_3)_2$; $R^2 = H$

structurales, et peut-être les propriétés chimiques, nécessaires à l'apparition d'une telle activité dans la famille des intercalants du type ellipticine.

Dans ce mémoire, nous décrivons les résultats de nos recherches concernant une première voie d'accès à certains dérivés des méthyl-6 5*H*-pyrido[4,3-*b*]benzo[*f*]indoles **8**.

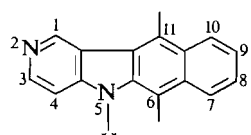

8

[1]Auteur à qui adresser la correspondance.

Chimie

Nous avons montré récemment que la lithiation de la méthyl-1 chloro-4 pyrrolo[3,2-*c*]pyridine **9***a* (20) par le *tert*-butyl lithium est régiospécifique de son sommet 2 (21).

De même qu'il réagissait avec l'acétaldéhyde pour donner 73,5% de la méthyl-1 (α-hydroxyéthyl)-2 chloro-4 pyrrolo-[3,2-*c*]pyridine (21), le dérivé lithié ainsi formé se condense avec l'acétophénone et la *p*-méthoxy-acétophénone pour engendrer, respectivement, 78% de la méthyl-1 (α-phényl α-hydroxy)-éthyl-2 chloro-4 pyrrolo[3,2-*c*]pyridine **10***a* et 71% de son analogue méthoxylé **10***b*. La deshydratation de ces deux composés, réalisée par l'anhydride acétique bouillant, conduit aux phényl-1 (et *p*-méthoxy phényl-1) (méthyl-1′ chloro-4′ pyrrolo-[3,2-*c*]pyridyl-2′)-1 éthylènes **11***a* et **11***b*. Cette réaction s'accompagne toutefois de l'hydrolyse partielle du chlore qui intervient probablement au cours du traitement du mélange réactionnel et, à côté de **11***a* (52,5%) et de **11***b* (44%), il se forme 23% de **12***a* et 26,5% de **12***b*. Ces derniers composés ont également été préparés à partir de la méthyl-1 méthoxy-4 pyrrolo[3,2-*c*]pyridine **13**. C'est ainsi que les alcools tertiaires **14***a* et **14***b* ont été préparés comme leurs analogues chlorés et que leur déshydratation en présence d'acide *p*-toluène sulfonique s'accompagne de leur déméthylation totale en **12***a* et **12***b*.

Par hydrogénation en présence de charbon palladié, ces derniers fournissent 90% des dérivés saturés correspondants **15***a* et **15***b*, normalement transformés par l'oxychlorure de phosphore bouillant en méthyl-1 (α-phényl)éthyl-2 (et α-(méthoxy-4′ phényl)éthyl-2 chloro-4 pyrrolo[3,2-*c*]pyridines **16***a* et **16***b*, également formés par hydrogénation de **11***a* et **11***b* en présence de rhodium sur alumine. Ce dernier catalyseur est toutefois le seul à avoir permis l'hydrogénation sélective de la double liaison. En effet, au cours des essais préliminaires réalisés à la température ambiante, le nickel de Raney commercial s'est avéré inefficace et le composé **11***a*, hydrogéné en présence de charbon palladié à 10%, a engendré, après absorption de la quantité théorique d'hydrogène, un mélange comprenant (en chromatographie en couche mince (ccm)) le composé de départ **11***a*, son dérivé d'hydrogénation **16***a* et un troisième produit correspondant très probablement au dérivé d'hydrogénolyse du chlore, que nous n'avons pas chercher à isoler.

Pour transformer les composés **16***a* et **16***b* en 5*H*-pyrido-[4,3-*b*]benzo[*f*]indoles **8**, deux voies distinctes ont été envisagées: d'une part, la formylation selon Vilsmeier–Haak, suivie de la cyclodéshydratation, et, d'autre part, la cyclisation directe. Bien que les rendements en aldéhydes **17***a* et **17***b* soient assez faibles, la formylation s'effectue dans les deux cas et la cyclodéshydratation en chloro-1 diméthyl-5,6 5*H*-pyrido-[4,3-*b*]benzo[*f*]indoles **18***a* et **18***b* est ensuite aisée. Au contraire, la cyclisation directe pour former **18** au départ de **16** au moyen du dichlorométhylméthyléther en présence de chlorure stannique est réalisable uniquement dans le cas de **16***a*. En effet, les essais réalisés dans les mêmes conditions experimentales au départ de **16***b* ont conduit à l'obtention d'un seul composé défini. Formé en très faible rendement, le spectre de rmn ^{1}H montre qu'il correspond à la formule **19**, indiquant ainsi que l'hétérocycle aza-5 indolique complexé par le chlorure stannique devient moins réactif que le cycle benzénique méthoxylé.

Disposant des dérivés chlorés **18***a* et **18***b*, il a été facile de les substituer par les dialkylaminoalkylamines pour former les dialkylaminoalkylamino-1 diméthyl-5,6 5*H*-pyrido[4,3-*b*]-benzo[*f*]indoles **20**–**23**. Cependant, pour compléter ce travail, nous avons cherché à accéder aux dérivés des 5*H*-pyrido-[4,3-*b*]benzo[*f*]indoles non substitués sur leur sommet 5. C'est pourquoi nous avons réalisé la même synthèse que précedemment au départ de la benzyl-1 chloro-4 pyrrolo[3,2-*c*]pyridine **9***c* (22, 23) lithiée et de la *p*-méthoxy-acétophénone.

En dehors de l'alcool tertiaire **10***c*, formé avec un rendement de 29% nettement inférieur à celui de **10***a* et **10***b* tous les autres intérmédiaires (**11***c*, **12***c*, **15***c*, **16***c*, **17***c* et **18***c*) ont été obtenus dans les mêmes conditions expérimentales et avec des rendements comparables à ceux de leurs analogues *N*-méthylés. De la même manière, la γ-diéthylaminopropylamine a bien transformé le composé **18***c* en dérivé aminé **24**. Malheureusement, les essais de débenzylation de ce dernier, tentés par hydrogénation catalytique sur charbon palladié dans diverses conditions expérimentales, ont conduit à un mélange comprenant principalement le composé de départ inchangé, à côté de traces d'un nouveau produit décelable en ccm mais que nous n'avons pas réuissi à isoler à l'état pur, même après plusieurs chromatographies sur alumine.

Conclusion

Nous avons montré que les 5*H*-pyrido[4,3-*b*]benzo[*f*]-indoles-5 substitués sont accessibles par une synthèse en 5–6 étapes au départ des chloro-4 pyrrolo[3,2-*c*]pyridines N-1 substituées. Celle-ci ne paraît toutefois pas applicable à la préparation des dérivés 5-NH correspondants, pourtant nécessaires pour pouvoir valablement comparer les propriétés biologiques des dérivés de cette série à celles des 6*H*-pyrido-[4,3-*b*]carbazoles (ellipticines) (24). Il sera donc utile d'en étudier une autre voie de synthèse car s'ils ne manifestent pas de propriétés antitumorales significatives sur la leucémie L1210,[2] les composés **20**–**23** N-5 méthylés sont néanmoins assez cytotoxiques in vitro pour justifier une étude plus complète de la série.

Partie expérimentale

Les points de fusion ont été pris au banc de Kofler. Les spectres de rmn ^{1}H ont été enregistrés sur un appareil Varian XL 100, dans les solvants indiqués, et les déplacements chimiques sont exprimés en ppm par rapport au Me_4Si.

Méthyl-1 (α-phényl α-hydroxy)éthyl-2 chloro-4 pyrrolo-[3,2-c]-pyridine ***10****a*

Le mélange formé par le composé **9***a* (21) (3,33 g, 20 mmol) en solution dans le THF anhydre (120 mL) est refroidi à −65°C et en maintenant l'ensemble sous agitation à la même température, le *tert*-butyl lithium (15,6 mL de la solution commerciale 1,6 *N*, soit 1,25 équivalent) est ajouté lentement. Après 10 min d'agitation à −65°C, l'acétophénone rectifiée (3,4 g, 30 mmol) dans le THF (10 mL) est ajoutée en 5 min. Le mélange est agité à −65°C pendant 45 min, puis 1 h à la température ambiante et versé dans 250 mL d'acide chlorhydrique 0,5 *N*. Après 1 nuit sous agitation, le mélange est extrait au chloroforme et l'évaporation du solvant fournit un résidu qui recristallise dans l'éthanol en donnant 3,92 g (68,4%) d'aiguilles incolores, *F* = 227–228°C; rmn ^{1}H ($(CD_3)_2SO$) δ: 1,95 (s, 3H, CH_3—C—OH), 3,46 (s, 3H, N—CH_3), 6,26 (s, 1H, OH), 6,77 (s, 1H, H-3), 7,34 (s, 5H, C_6H_5), 7,45 (d, 1H, H-7, J_{7-6} = 5,5 Hz), 8,03 (d, 1H, H-6). *Anal.* calc. pour $C_{16}H_{15}ClN_2O$: C 67,02; H 4,24; N 9,77; Cl 12,39; trouvé: C 66,93; H 5,45; N 9,92; Cl 12,19.

[2]Testés sur les cellules en culture dans les conditions habituelles (16, 17), les composés **20**–**23** inhibent la croissance de 50% des cellules aux concentrations de $0,5 \times 10^{-6}$ *M* (**20** et **21**) et 5×10^{-6} *M* (**22** et **23**). Ils sont toutefois toxiques pour la souris à 35 mg/kg et totalement inactifs sur la leucemie L 1210 à la dose de 12,5 mg/kg.

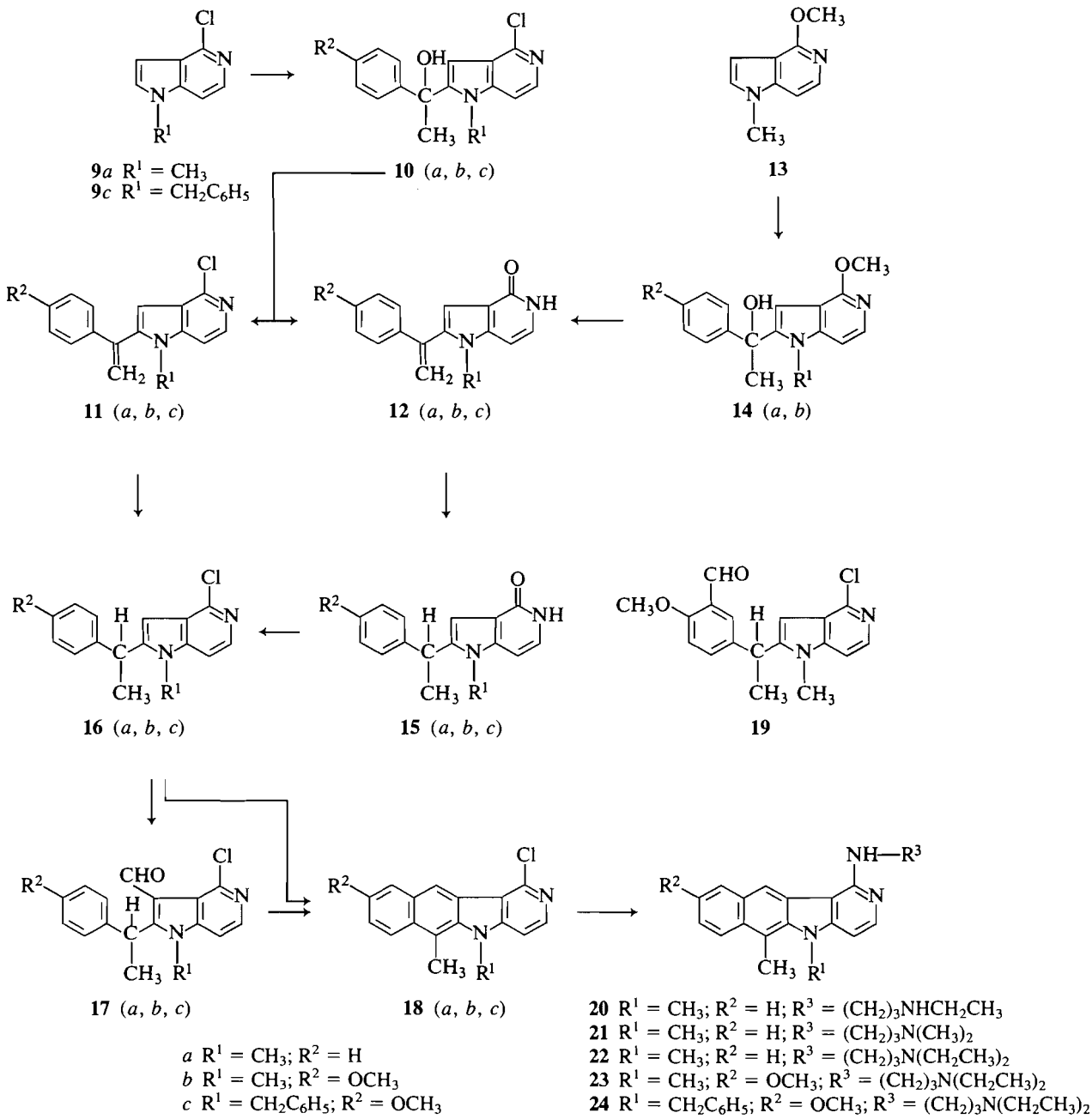

SCHÉMA 1

Méthyl-1 (α-méthoxy-4' phényl α-hydroxy)éthyl-2 chloro-4 pyrrolo-[3,2-c]pyridine ***10***b

Ce composé a été préparé comme le précédent à partir du dérivé chloré **9***a* (6,66 g, 40 mmol), lithié par 1,25 équivalent de *tert*-butyl lithium dans le THF (240 mL) et de la *p*-méthoxy-acetophénone (9 g, 60 mmol). Il recristallise dans l'éthanol en donnant 9 g (71%) d'aiguilles incolores, F = 210–212°C. *Anal.* calc. pour $C_{17}H_{17}ClN_2O_2$: C 64,46; H 5,41; N 8,84; Cl 11,19; trouvé: C 64,58; H 5,38; N 8,82; Cl 11,27.

Benzyl-1 (α-méthoxy-4' phenyl α-hydroxy)éthyl-2 chloro-4 pyrrolo-[3,2-c]pyridine ***10***c

La benzyl-1 chloro-4 pyrrolo[3,2-*c*]pyridine **9***c* (22, 23) 2,42 g, 10 mmol) en solution dans le diéthyléther sec (160 mL) est lithiée à −65°C par 11 mmol de *tert*-butyl lithium et traitée par la *p*-méthoxy acétophénone (1,8 g, 12 mmol) en solution dans l'éther (80 mL).[3] Après un traitement identique à celui mis en oeuvre dans les cas

[3]Dans le cas de la benzyl-1 chloro-4 pyrrolo[3,2-*c*]pyridine **9***c*, le rendement de la réaction est nettement abaissé si la lithiation est effectuée dans le THF. Ainsi, après réaction du lithien avec le DMF il se forme 58% de benzyl-1 formyl-2 chloro-4 pyrrolo[3,2-*c*]pyridine dans l'éther et seulement 29,6% dans le THF. Par ailleurs, en faisant réagir le lithien de **9***c* formé dans le THF avec l'acétaldéhyde, on isole environ 30% de benzyl-1 (α-hydroxyethyl)-2 chloro-4 pyrrolo[3,2-*c*]pyridine et 10% d'un mélange qui, après oxydation par le bioxyde de manganèse et chromatographie, fournit 2,5% de benzyl-1 chloro-4 acetyl-6 pyrrolo[3,2-*c*]pyridine, ce qui montre que la lithiation effectuée dans ces conditions n'est pas totalement spécifique du sommet 2 de **9***c*.

précédents, le mélange est extrait à l'éther et le résidu de l'évaporation du solvant est repris dans le minimum d'éthanol. Le solide insoluble est filtré pour donner 800 mg du composé **10***c* et l'évaporation des eaux mères fournit un résidu qui est chromatographié sur silice en éluant avec le dichlorométhane pur. La première fraction éluée correspond à la *p*-méthoxy-acétophénone, la seconde contient le composé chloré **9***c* inchangé et la troisième est constituée par une nouvelle quantité du composé attendu **10***c*. Les deux fractions de **10***c* réunies recristallisent dans l'éthanol pour donner des aiguilles incolores (1,15 g, 29%), F = 161–163°C. *Anal.* calc. pour $C_{23}H_{21}ClN_2O_2$: C 70,31; H 5,39; N 7,13; Cl 9,02; trouvé: C 70,34; H 5,62; N 7,17; Cl 8,85.

Méthyl-1 (α-phényl α-hydroxy)éthyl-2 méthoxy-4 pyrrolo-[3,2-c]-pyridine ***14***a

Le *tert*-butyl lithium (17 mL de la solution commerciale 1,6 *N*, soit 25 mmol) est ajouté à la solution de la méthyl-1 méthoxy-4 pyrrolo-[3,2-*c*]pyridine **13** (3,24 g, 20 mmol) dans le THF (100 mL) refroidie à −65°C. Après 5 min à cette température, le bain réfrigérant (acétone + Carboglace) est remplacé par un mélange glace + sel et le mélange réactionnel est agité pendant 15 min à −15°C.[4] La solution, devenue rose pâle, est de nouveau refroidie à −65°C et l'acétophénone (3,5 g, 30 mmol) en solution dans 10 mL de THF est ajoutée progressivement. Après 30 min d'agitation à −65°C et 1 h d'abandon à la température ambiante, le mélange est versé dans 250 mL d'acide chlorhydrique 0,5 *N*, agité pendant 15 min et extrait au dichlorométhane. Le résidu d'évaporation des phases organiques réunies est repris dans le minimum de toluène refroidi à −15°C et recristallisé dans le même solvant pour donner des cristaux incolores (4,5 g, 79,8%), F = 174–175°C. *Anal.* calc. pour $C_{17}H_{18}N_2O_2$: C 72,32; H 6,43; N 9,92; trouvé: C 72,34; H 6,43; N 9,90.

Méthyl-1 (α-méthoxy-4' phényl α-hydroxy)éthyl-2 méthoxy-4 pyrrolo-[3,2-c]pyridine ***14***b

Ce composé est obtenu suivant la même technique que le précédent à partir de **13** (6,5 g, 40 mmol), du *tert*-butyl lithium (50 mmol) et de la *p*-méthoxy-acétophénone (8 g, 60 mmol). Il recristallise dans le toluène pour donner des microcristaux incolores (7,6 g, 60,7%), F = 168–170°C; rmn ^{1}H ($(CD_3)_2SO$) δ: 1,88 (s, 3H, *CH*$_3$—C—OH), 3,43 (s, 3H, N—CH_3), 3,75 (s, 3H, C_6H_4—O*CH*$_3$), 4,02 (s, 3H, O*CH*$_{3-4}$), 6,01 (s, 1H, *OH*), 6,64 (s, 1H, H-3), 6,89 (d, 2H, H-3' + H-5'-Ar, $J_{3'-2'}$ = 9 Hz), 7,02 (d, 1H, H-7, J_{7-6} = 6 Hz), 7,24 (d, 2H, H-2' + H-6'-Ar), 7,78 (d, 1H, H-6). *Anal.* calc. pour $C_{18}H_{20}N_2O_3$: C 69,21; H 6,45; N 8,97; trouvé: C 69,43; H 6,49; N 8,70.

Phényl-1 (méthyl-1' chloro-4' pyrrolo[3,2-c]pyridyl-2')-1 éthylène ***11***a *et phényl-1 (méthyl-1' dihydro-4',5' oxo-4' (pyrrolo-[3,2-c]-pyridyl-2')-1 éthylène* ***12***a

Le composé **10***a* (7,5 g, 26 mmol) est chauffé à reflux pendant 18 h dans 105 mL d'anhydride acétique et le mélange est évaporé sous pression réduite. Le résidu est repris dans l'eau, alcalinisé par addition de soude *N* et extrait au chloroforme.

Après évaporation du solvant, le résidu est repris dans 20 mL du mélange dichlorométhane–éthanol 9:1. La partie insoluble est filtrée. Elle correspond au composé **12***a*.

Le filtrat est chromatographié sour colonne de silice en éluant avec le mélange dichlorométhane–éthanol 9:1.

(a) La première fraction éluée contient le composé **11***a* qui recristallise dans le cyclohexane en donnant des paillettes incolores (3,7 g, 52,6%), F = 130°C; rmn ^{1}H ($(CD_3)_2SO$) δ: 3,48 (s, 3H, N—CH_3), 5,68 (d, 1H, H-A CH_2═, J_{A-B} = 1 Hz), 6,07 (d, 1H, H-B CH_2═), 6,63 (d, 1H, H-3, J_{3-7} = 0,7 Hz), 7,41 (m, 5H, C_6H_5), 7,56 (q, 1H, H-7, J_{7-6} = 5,8 Hz), 8,08 (d, 1H, H-6). *Anal.* calc. pour $C_{16}H_{13}ClN_2$: C 71,51; H 4,84; N 10,43; Cl 13,22; trouvé: C 71,48; H 4,58; N 10,29; Cl 12.90.

(b) La seconde fraction éluée contient une nouvelle quantité du produit **12***a*. Après évaporation du solvant, celle-ci est jointe à la première partie filtrée précédemment et la recristallisation de l'ensemble dans le toluène fournit des microcristaux incolores (1,5 g, 22,9%), F = 235°C; rmn ^{1}H ($(CD_3)_2SO$) δ: 3,35 (s, 3H, N—CH_3), 5,53 (d, 1H, H-A CH_2═, J_{A-B} = 1,2 Hz), 5,85 (d, 1H, H-B CH_2═), 6,51 (d, 1H, H-7, J_{7-6} = 7,1 Hz), 6,55 (s, 1H, H-3), 7,11 (d, 1H, H-6), 7,38 (s, 5H, C_6H_5), 10,89 (s large, 1H, NH-5). *Anal.* calc. pour $C_{16}H_{14}N_2O$: C 76,78; H 5,64; N 11,19; trouvé: C 76,92; H 5,79; N 10,86.

Préparation du composé ***12***a *à partir de l'alcool tertiaire* ***14***a

Le composé **14***a* (3 g) est chauffé à reflux pendant 70 h dans 150 mL de toluène en présence de 4,4 g d'acide *p*-toluène sulfonique et le solvant est évaporé. Le résidu est repris dans l'eau, extrait au dichlorométhane dans lequel il est peu soluble, lavé avec une solution d'hydrogénocarbonate de sodium et le solvant est évaporé. Le résidu recristallise dans le toluène en donnant 2,2 g (82,7%) de microcristaux incolores, F = 235°C, identiques au produit **12***a* déjà obtenu précédemment.

p-*Méthoxyphényl-1 (méthyl-1' chloro-4' pyrrolo[3,2-c]pyridyl-2')-1 éthylène* ***11***b *et* p-*méthoxyphényl-1 (méthyl-1' dihydro-4',5' oxo-4' pyrrolo[3,2-c]pyridyl-2')-1 éthylène* ***12***b

Le composé **10***b* (5 g) est chauffé à reflux dans l'anhydride acétique (75 mL) pendant 18 h et le mélange résultant est traité suivant la technique déjà utilisée pour préparer **11***a* et **11***b*. Après chromatographie sur colonne de silice, les deux fractions éluées par le mélange dichlorométhane–éthanol 9:1 sont évaporées.

(a) La première fournit un résidu qui recristallise dans le cyclohexane en donnant 2,5 g (44%) du composé **11***b*, F = 157–158°C; rmn ^{1}H ($(CD_3)_2SO$) δ: 3,49 (s, 3H, NCH_3), 3,81 (s, 3H, OCH_3), 5,54 (d, 1H, H-A CH_2═, J_{A-B} = 1,1 Hz), 5,96 (d, 1H, H-B CH_2═), 6,61 (d, 1H, H-3, J_{3-7} = 0,8 Hz), 6,98 (d, 2H, H-3' + H-5' de C_6H_4, $J_{3'-2'}$ = 9 Hz), 7,29 (d, 2H, H-2' + H-6' de C_6H_4), 7,56 (q, 1H, H-7, J_{7-6} = 5,7 Hz), 8,08 (d, 1H, H-6). *Anal.* calc. pour $C_{17}H_{15}ClN_2O$: C 68,34; H 5,06; N 9,38; Cl 11,87; trouvé: C 68,18; H 4,97; N 9,34; Cl 12,14.

(b) La deuxième fraction contient le composé **12***b* qui recristallise dans l'éthanol en microcristaux incolores (1,4 g, 26,4%) qui se subliment et F = 260–270°C; rmn ^{1}H ($(CD_3)_2SO$) δ: 3,36 (s, 3H, N—CH_3), 3,81 (s, 3H, OCH_3), 5,40 (d, 1H, H-A CH_2═, J_{A-B} = 1,2 Hz), 5,76 (d, 1H, H-B CH_2═), 6,51 (d, 1H, H-7, J_{7-6} = 6,6 Hz), 6,52 (s, 1H, H-3), 6,97 (d, 2H, H-3' + H-5' de C_6H_4, $J_{3'-2'}$ = 8,8 Hz), 7,21 (d, 1H, H-6), 7,27 (d, 2H, H-2' + H-6' de C_6H_4), 10,83 (s large, 1H, NH). *Anal.* calc. pour $C_{17}H_{16}N_2O_2$: C 72,84; H 5,75; N 9,99; trouvé: C 72,57; H 5,58; N 10,08. N.B. Le même composé **12***b* a également été obtenu avec un rendement de 89% en chauffant au reflux pendant 24 h 1 g de l'alcool tertiaire **14***b* dans 70 mL de xylène, en présence de 2,66 g d'acide *p*-toluène sulfonique, et en traitant ensuite comme déjà indiqué pour transformer **14***a* en **12***a*.

Dérivés benzylés ***11***c *et* ***12***c

L'alcool **10***c* (6,8 g) est déshydraté en le chauffant dans l'anhydride acétique (150 mL) à reflux pendant 20 h. Le mélange résultant est traité comme déjà décrit pour préparer **11***a* et **12***a* et la chromatographie sur silice, en éluant avec le mélange dichlorométhane–éthanol 95:5, fournit les deux composés attendus: (a) 5,8 g (68,2%) de **11***c*, F = 144–146°C (cyclohexane); rmn ^{1}H ($(CD_3)_2SO$) δ: 5,16 (s, 2H, *CH*$_2$-Ar), 5,47 (s, 1H, CH-A, C*H*$_2$═), 5,86 (s, 1H, CH-B C*H*$_2$═), 6,69 (s, 1H, H-3), 6,84–7,30 (m, 9H, 5H-Ar + 4H-Ar', $J_{3'-2'}$ = 10 Hz), 7,5 (d, 1H, H-7, J_{7-6} = 6 Hz), 8,08 (d, 1H, H-6). *Anal.* calc. pour $C_{23}H_{19}ClN_2O$: C 73,69; H 5,11; N 7,47; Cl 9,46; trouvé: C 73,39; H 5,19; N 7,41; Cl 9,20. (b) 1,4 g (19,8%) de **12***c*, F = 216–217°C (toluène); rmn ^{1}H ($(CD_3)_2SO$) δ: 3,8 (s, 3H, OCH_3), 5,02 (s, 2H, CH_2-Ar), 5,32 (s, 1H, CH-A C*H*$_2$═), 5,66 (s, 1H, CH-B C*H*$_2$═), 6,44 (q, 1H, H-7, J_{7-6} = 7,3 Hz, J_{7-3} = 0,5 Hz), 6,59 (d, 1H, H-3), 6,85—7,27 (m, 10H, 5H-Ar + 4H-Ar' + H-6, $J_{2'-3'}$ = 9,3 Hz). *Anal.* calc. pour $C_{23}H_{20}N_2O_2$: C 77,50; H 5,66; N 7,86. trouvé: C 77,25; H 5,77; N 7,88.

[4]Comme nous l'avons déjà signalé (21), si la lithiation du composé **13** est réalisée sans "réchauffer" le mélange réactionnel à −15°C pendant 15 min, le rendement de la réaction est seulement de 8–10%.

Alkyl-1 (α-aryl)éthyl-2 dihydro-4,5 oxo-4 pyrrolo[3,2-c]pyridines ***15***a, ***15***b *et* ***15***c

Le composé **12** voulu (*a*, *b* ou *c*) (10 mmol) en solution dans l'acide acétique (100 mL) est hydrogéné en l'agitant sous atmosphère d'hydrogène à la température ambiante et à la pression normale en présence de 150 mg de charbon palladié à 10%, jusqu'à cessation de l'absorption d'hydrogène (30–45 min). Le catalyseur est filtré, lavé avec l'acide acétique et ce dernier est évaporé. Le résidu est repris trois fois dans 30 mL de toluène, réévaporé à chaque reprise sous pression réduite pour bien éliminer l'acide acétique restant et le solide obtenu est recristallisé dans le minimum de toluène pour donner des microcristaux incolores.

15*a*: Rendement 91%; F = 253–254°C; rmn ^{1}H ($(CD_3)_2SO$) δ: 1,60 (d, 3H, CH_3—CH, J_{CH_3-H} = 7,1 Hz), 3,36 (s, 3H, NCH_3), 4,32 (q, 1H, CH—CH_3), 6,44 (q, 1H, H-7, J_{7-6} = 7,1 Hz, J_{7-3} = 0,3 Hz), 6,53 (s, 1H, H-3), 7,01 (d, 1H, H-6), 7,14–7,46 (m, 5H, C_6H_5), 10,71 (s large, 1H, NH). *Anal.* calc. pour $C_{16}H_{16}N_2O$: C 76,16; H 6,39; N 11,10; trouvé: C 76,0; H 6,35; N 10,94.

15*b*: Rendement 85% F = 110–120°C, se resolidifie et F = 227°C; rmn ^{1}H ($(CD_3)_2SO$) δ: 1,57 (d, 3H, CH_3—CH, J = 7 Hz), 3,40 (s, 3H, N—CH_3), 3,75 (s, 3H, OCH_3), 4,26 (q, 1H, CH—CH_3), 6,45 (d, 1H, H-7, J_{7-6} = 8,2 Hz), 6,49 (s, 1H, H-3), 6,88 (d, 2H, H-3′ + H-5′ Ar, $J_{3'-2'}$ = 8,8 Hz), 7,01 (d, 1H, H-6), 7,12 (d, 2H, H-2′ + H-6′ Ar), 10,8 (s large, 1H, NH-5). *Anal.* calc. pour $C_{17}H_{18}N_2O_2 \cdot H_2O$: C 67,98; H 6,71; N 9,33; trouvé: C 68,38; H 6,84; N 9,15.

15*c*: Rendement 90% en produit brut, qui a été directement transformé en son dérivé chloré **16***c*.

Alkyl-1 (α-aryl)éthyl-2 chloro-4 pyrrolo[3,2-c]pyridines ***16***a, ***16***b *et* ***16***c

Technique A

Le composé **15** voulu (10 mmol) est chauffé dans l'oxychlorure de phosphore bouillant (70 mL) pendant 2 h 30 (**15***a*), 3 h (**15***b*) et 5 h (**15***c*) et l'excès d'oxychlorure est évaporé sous pression réduite. Le résidu est décomposé dans l'eau glacée, alcalinisé par l'ammoniaque et extrait au dichlorométhane. Après évaporation du solvant, le résidu est chromatographié sur colonne de silice, en éluant avec le mélange dichlorométhane–éthanol 9:1. L'évaporation de la fraction d'élution contenant le composé attendu fournit un solide qui recristallise dans l'hexane ou le cyclohexane en donnant des microcristaux incolores.

Technique B

Le rhodium sur alumine (125 mg à 5%) est placé dans un tricol muni d'un agitateur magnétique et après avoir fait passer un courant d'hydrogène pour éliminer l'air, 25 mL d'éthanol sont ajoutés par une première ampoule à additionner. Le composé **11** (*a*, *b* ou *c*, 50 mmol) en solution dans 100 mL d'éthanol et primitivement placé dans une seconde ampoule est ensuite ajouté et l'ensemble est agité à la température ambiante, en atmosphère d'hydrogène à la pression normale, jusqu'à absorption de la quantité théorique d'hydrogène (environ 48 h). Après filtration et évaporation du solvant, le solide résiduel est chromatographié sur silice comme déjà décrit avec la Technique A.

16*a*: Rendement A 78%; Rendement B 75%; F = 109–110°C; rmn ^{1}H ($(CD_3)_2SO$) δ: 1,67 (d, 3H, CH_3—CH, J_{CH_3-H} = 7 Hz), 3,54 (s, 3H, NCH_3), 4,48 (q, 1H, CH—CH_3), 6,60 (s, 1H, H-3), 7,24–7,34 (m, 5H, C_6H_5), 7,47 (d, 1H, H-7, J_{7-6} = 5,8 Hz), 8,0 (d, 1H, H-6). *Anal.* calc. pour $C_{16}H_{15}ClN_2$: C 70,98; H 5,54; N 10,35; Cl 13,12; trouvé: C 70,90; H 5,62; N 10,07; Cl 13,35.

16*b*: Rendement A 50%; Rendement B 85%; F = 114°C; rmn ^{1}H ($(CD_3)_2SO$) δ: 1,65 (d, 3H, CH—CH_3), 3,54 (s, 3H, N—CH_3), 3,74 (s, 3H, OCH_3), 4,53 (q, 1H, CH—CH_3), 6,56 (d, 1H, H-3), 6,9 (d, 2H, H-3′ + H-5′, $J_{3'-2'}$ = 9 Hz), 7,17 (d, 2H, H-2′ + H-6′), 7,46 (q, 1H, H-7, J_{7-6} = 5,8 Hz, J_{7-3} = 0,8 Hz), 8,0 (d, 1H, H-6). *Anal.* calc. pour $C_{17}H_{17}ClN_2O$: C 67,88; H 5,70; N 9,31; Cl 11,79; trouvé: C 67,82; H 5,73; N 9,35; Cl 11,49.

16*c*: Rendement A 64%; Rendement B 69%; F = 126–128°C; rmn ^{1}H ($CDCl_3$) δ: 1,65 (d, 3H, CH_3—CH, J_{CH_3-H} = 7,2 Hz), 3,78 (s, 3H, OCH_3), 4,0 (q, 1H, CH—CH_3), 5,05 (q, 2H, CH_2-Ar, J_{H-H} = 17,1 Hz), 6,72–7,29 (m, 11H, 5H-Ar + 4H-Ar′ + H-3 + H-7, $J_{2'-3'}$ = 9 Hz), 8,0 (d, 1H, H-6, J_{6-7} = 5,7 Hz). *Anal.* calc. pour $C_{23}H_{21}ClN_2O$: C 73,30; H 5,62; N 7,43; Cl 9,41; trouvé: C 73,45; H 5,63; N 7,75; Cl 9,58.

Méthyl-1 (α-phényl)éthyl-2 formyl-3 chloro-4 pyrrolo[3,2-c]pyridine ***17***a

À la solution du dérivé chloré **16***a* (500 mg, 1,8 mmol) dans le DMF (1,26 mL) on ajoute, sans refroidir, 1,48 mL d'oxychlorure de phosphore et le mélange résultant est chauffé au bain d'huile à 120°C pendant 2 h. Après avoir ajouté successivement 1,26 mL de DMF puis 1,48 mL d'oxychlorure, l'ensemble est de nouveau chauffé à 110–120°C pendant 2 h, décomposé à froid en le versant dans l'eau glacée (100 mL) et alcalinisé par une solution d'hydroxyde de sodium 3 *N*. Le précipité formé est extrait au dichlorométhane, lavé avec une solution d'hydroxyde de sodium *N*, puis à l'eau, et l'évaporation de la phase organique séchée fournit un solide qui est repris dans le minimum d'éthanol et recristallisé dans le même solvant en cristaux jaune-pâle (90 mg, 16,3%), F = 163–164°C; rmn ^{1}H ($(CD_3)_2SO$) δ: 1,8 (d, 3H, CH_3—CH, J_{CH_3-CH} = 7,4 Hz), 3,53 (s, 3H, NCH_3), 5,84 (q, 1H, CH—CH_3), 7,32 (m, 5H, C_6H_5), 7,67 (d, 1H, H-7, J_{7-6} = 5,8 Hz), 8,2 (d, 1H, H-6), 10,83 (s, 1H, CHO). *Anal.* calc. pour $C_{17}H_{15}ClN_2O$: C 68,34; H 5,02; N 9,38; Cl 11,89; trouvé: C 68,08; H 4,92; N 9,09; Cl 11,65.

Méthyl-1 (α-p-méthoxyphényl)éthyl-2 formyl-3 chloro-4 pyrrolo-[3,2-c]pyridine ***17***b

Le complexe formé à partir du diméthylformamide (9,2 mL, 0,12 mol) et de l'oxychlorure de phosphore (10,8 mL, 0,12 mol) est ajouté goutte à goutte à une solution du composé **16***b* (3 g, 10 mmol) dans du dichloro-1,2 éthane (10 mL) (rapport molaire 12:1). Le mélange résultant est chauffé au bain d'huile à 110°C pendant 24 h, versé dans l'eau, neutralisé par une solution d'hydrogénocarbonate de sodium et extrait au dichlorométhane. Le résidu de l'évaporation du solvant est repris dans le minimum d'éthanol pour donner 1,1 g d'un solide correspondant à l'aldéhyde attendu **17***b* pur. Les eaux mères sont évaporées et le nouveau résidu est chromatographié sur colonne d'alumine, en éluant avec le mélange éther de pétrole – acétate d'éthyle 4:1. La première fraction fournit 440 mg du composé **16***b* inchangé; la seconde contient une nouvelle quantité de **17***b* qui, réunie à la première, recristallise dans le méthanol en donnant au total 1,3 g, soit 38,6% d'aiguilles incolores, F = 184°C. Calculé par rapport au composé **16***b* réellement consommé, le rendement en **17***b* est de 46,4%; rmn ^{1}H ($(CD_3)_2SO$) δ: 1,76 (d, 3H, CH—CH_3, J = 7,3 Hz), 3,53 (s, 3H, N—CH_3), 3,76 (s, 3H, OCH_3), 5,77 (q, 1H, CH—CH_3), 6,92 (d, 2H, H-3′ + H—5′, $J_{3'-2'}$ = 8,9 Hz), 7,18 (d, 2H, H-2′ + H-6′), 7,66 (d, 1H, H-7, J_{7-6} = 5,7 Hz), 8,20 (d, 1H, H-6), 10,83 (s, 1H, CHO). *Anal.* calc. pour $C_{18}H_{17}ClN_2O_2$: C 65,75; H 5,21; N 8,52; Cl 10,78; trouvé: C 65,48; H 5,25; N 8,35; Cl 11.06.

Benzyl-1 (α-p-méthoxyphényl)éthyl-2 formyl-3 chloro-4 pyrrolo-[3,2-c]-pyridine ***17***c

La formylation de **16***c* est réalisée avec les mêmes proportions de réactifs et en suivant la même technique que dans le cas précédent. Après la chromatographie sur alumine, l'aldéhyde **17***c* recristallise dans le méthanol en microcristaux incolores, F = 182–184°C (rendement: 31,6%); rmn ^{1}H ($CDCl_3$) δ: 1,64 (d, 3H, CH_3—CH, J_{CH_3-H} = 7,5 Hz), 3,77 (s, 3H, OCH_3), 5,10 (s, 2H, CH_2-Ar), 6,02 (q, 1H, CH—CH_3), 6,75–7,27 (m, 1OH, 5H-Ar + 4H-Ar′ + H-7), 8,06 (d, 1H, H-6, J_{6-7} = 5,7 Hz), 11,08 (s, 1H, CHO). *Anal.* calc. pour $C_{24}H_{21}ClN_2O_2$: C 71,19; H 5,23; N 6,92; Cl 8,76; trouvé: C 70,99; H 5,35; N 7,09; Cl 8,63.

*Chloro-1 diméthyl-5,6 5*H*-pyrido [4,3-b]benzo[f]indole* ***18***a

Méthode A

L'aldéhyde **17***a* (100 mg) est chauffé à 120°C sous agitation, pendant 2 h, dans 5 g d'acide polyphosphorique et le mélange est versé dans l'eau froide, puis alcalinisé par l'ammoniaque. Le précipité formé est

recristallisé dans le minimum d'éthanol pour donner 72 mg (76%) du composé **18***a* partiellement hydraté, F = 202°C; rmn ^{1}H ($(CD_3)_2SO$) δ: 3,07 (s, 3H, CH_3-6), 4,14 (s, 3H, N—CH_3), 7,44–7,76 (m, 2H, H-8 + H-9), 7,60 (d, 1H, H-4, J_{4-3} = 5,9 Hz), 8,12–8,34 (m, 2H, H-7 + H-10), 8,35 (d, 1H, H-3), 8,84 (s, 1H, H-11). *Anal.* calc. pour $C_{17}H_{13}ClN_2 \cdot 1/2H_2O$: C 70,40; H 4,83; N 9,66; trouvé: C 70,63; H 4,59; N 10,04.

Méthode B

Le composé **16***a* (600 mg) est dissout dans le dichloroéthane (6 mL) et le chlorure stannique (1,02 mL, 4 équivalents) est ajouté à la température ambiante. À ce mélange, refroidi à 0°C, on ajoute le dichlorométhylméthyléther (0,35 mL, 1,7 équivalent). Après 1 h d'agitation à 0°C, l'ensemble est chauffé à reflux pendant 3 h, versé dans l'eau, alcanisé par l'ammoniaque et extrait au dichlorométhane. Le résidu de l'évaporation du solvant est chromatographié sur colonne d'alumine, en éluant avec le mélange éther de pétrole – acétate d'éthyle 4:1. La première fraction éluée contient le composé de départ inchangé (400 mg), la seconde fournit 110 mg (soit 53% par rapport au composé **16***a* consommé) du produit attendu **18***a*, F = 202°C, identique à celui préparé par la méthode A.

Chloro-1 méthoxy-9 diméthyl-5,6 5H-pyrido[4,3-b]benzo[f]indole ***18****b*

La solution de l'aldéhyde de **17***b* (200 mg) dans le mélange acide acétique (8 mL), plus anhydride acétique (5 mL) additionné de chlorure de zinc fondu sec (1,5 g), est chauffée à reflux pendant 2 h 30 et versée dans l'eau froide. Après avoir alcalinisé avec une solution d'hydroxyde de sodium *N* et extrait au dichlorométhane, le résidu de l'évaporation du solvant est chromatographié sur colonne d'alumine, en éluant avec le mélange éther de pétrole – acétate d'éthyle 1:1. L'évaporation de la principale fraction d'élution fournit un solide qui recristallise dans le toluène en donnant des microcristaux jaune-pâle (120 mg, 63,5%), F = 215–216°C, correspondant au composé **18***b* légèrement hydraté; rmn ^{1}H ($(CD_3)_2SO$) δ: 3,15 (s, 3H, CH_3-6), 4,01 (s, 3H, N—CH_3), 4,23 (s, 3H, OCH_3), 7,33 (q, 1H, H-8, J_{7-8} = 9,4 Hz, J_{8-10} = 2,8 Hz), 7,63 (d, 1H, H-10), 7,68 (d, 1H, H-4, J_{4-3} = 5,9 Hz), 8,24 (d, 1H, H-7), 8,38 (d, 1H, H-3), 8,88 (s, 1H, H-11). *Anal.* calc. pour $C_{18}H_{15}ClN_2O \cdot 0{,}25H_2O$: C 68,51; H 4,92; N 8,88; trouvé: C 68,54; H 4.97; N 8,61.

Méthyl-1 [α-(méthoxy-4′ formyl-3′ phényl)-1′ éthyl]-2 chloro-4 pyrrolo[3,2-c]pyridine ***19***

En cherchant transformer directement le composé **16***b* en dérivé tétracyclique **18***b* au moyen du dichlorométhylméthyléther en présence de chlorure stannique, dans les mêmes conditions expérimentales que celles utilisées précédemment pour former directement **18***a* à partir de **16***a*, 100 mg de **16***b* ont conduit, après chromatographie sur silice, à 8 mg d'un solide qui recristallise dans l'hexane en microcristaux jaunes, F = 186–188°C, dont le spectre de rmn ^{1}H présente les signaux suivants: ($(CD_3)_2SO$) δ: 1,66 (d, 3H, CH—CH_3), 3,56 (s, 3H, N—CH_3), 3,92 (s, 3H, OCH_3), 4,54 (q, 1H, CH—CH_3), 6,58 (s, 1H, H-3), 7,23 (d, 1H, H-5′, $J_{5'-6'}$ = 9 Hz), 7,56 (m, 3H, H-2′ + H-6′ + H-7), 7,99 (d, 1H, H-6, J_{6-7} = 5,8 Hz), 10,34 (s, 1H, CHO).

La faible quantité obtenue n'a pas permis de faire l'analyse centésimale de ce nouveau composé mais son spectre de rmn ^{1}H montre sans ambiguïté qu'il correspond à la structure **19** et son spectre de masse est en accord avec cette dernière. Ainsi, en desorption–ionisation (NH_3, 340 mA, 90 eV), il donne bien les pics moléculaires à 329 (M + 1, 100%) et à 331 (M + 1, pic isotopique Cl 37, 37%). De même, en impact électronique, (275°C, 0,25 Bar, 70 eV) les pics principaux sont à 328 ($M^{\cdot+}$, 100%) et à 313 (M − 15, —CH_3, 88,8%).

Chloro-1 benzyl-5 méthyl-6 méthoxy-9 5H-pyrido[4,3-b]benzo-[f]-indole ***18****c*

Le mélange constitué par l'acide acétique (20 mL), l'anhydride acétique (5 mL), l'acide *p*-toluène sulfonique anhydre (2,16 g) et l'aldéhyde **17***c* (270 mg) est chauffé sous agitation à 120°C pendant 4 h, versé dans l'eau (100 mL) alcalinisé à froid par l'ammoniaque et extrait au dichlorométhane. Le résidu de l'évaporation du solvant est chromatographié sur colonne d'alumine, en éluant avec le mélange éther de pétrole – acétate d'éthyle 3:2. Le composé **18***c*, qui se trouve dans la première fraction d'élution, recristallise dans l'hexane en microcristaux jaune pâle, F = 180–182°C; rmn ^{1}H ($(CD_3)_2SO$) δ: 2,87 (s, 3H, CH_3-6), 3,96 (s, 3H, OCH_3), 5,97 (s, 2H, CH_2), 7,05–7,12 (m, 2H de C_6H_5), 7,22–7,37 (m, 4H, H-8 +3H de C_6H_5), 7,62 (d, 1H, H-4, J_{4-3} = 5,9 Hz), 7,63 (s, 1H, H-10), 8,15 (d, 1H, H-7, J_{7-8} = 9,4 Hz), 8,35 (d, 1H, H-3), 8,94 (s, 1H, H-11). *Anal.* calc. pour $C_{24}H_{19}ClN_2O$: C 74,51; H 4,95; N 7,24; Cl 9,16; trouvé: C 74,69; H 5,13; N 7,20; Cl 8,92.

Dialkylaminoalkylamino-1 alkyl-5 méthyl-6 5H-pyrido[4,3-b]-benzo[f]indoles ***20–24***

Le chloro-1 méthyl-6 5*H*-pyrido[4,3-*b*]benzo[*f*]indole voulu (**18***a*, **18***b* ou **18***c*, 300 mg) est chauffé dans l'amine choisie (10 mL) au bain d'huile à 160°C pendant 20 h et l'excès d'amine est évaporé sous pression réduite. Le résidu obtenu est repris dans l'eau, alcalinisé par addition d'une solution d'hydroxyde de sodium *N* et extrait au dichlorométhane. Après évaporation du solvant, les composés **20**, **21**, **22** et **23** sont directement cristallisés, puis recristallisés dans le cyclohexane, et le composé **24** est recristallisé dans le même solvant, mais après chromatographie sur colonne d'alumine en éluant avec le mélange dichlorométhane–éthanol 97:3.

20: Rendement 78,4%; F = 134–136°C; rmn ^{1}H ($(CD_3)_2SO$) δ: 1,06 (t, 3H, CH_3—CH_2), 1,70–2,04 (m, 2H, CH_2-β), 2,6–2,81 (m, 4H, CH_2—CH_3 + CH_2-γ), 3,14 (s, 3H, CH_3-6), 3,62–3,82 (m, 2H, CH_2-α), 4,14 (s, 3H, N—CH_3), 6,88 (d, 1H, H-4, J_{3-4} = 6 Hz), 7,04 (s large, 1H, NH), 7,4–7,64 (m, 2H, H-8 + H-9), 8,10 (d, 1H, H-3), 8,16–8,33 (m, 2H, H-7 + H-10), 8,69 (s, 1H, H-11). *Anal.* calc. pour $C_{22}H_{26}N_4$: C 76,26; H 7,56; N 16,17; trouvé: C 76,12; H 7,49; N 15.97.

21: Rendement 74,3%; F = 183–185°C; rmn ^{1}H ($(CD_3)_2SO$) δ: 1,74–2,04 (m, 2H, CH_2-β), 2,31 (s, 6H, $N(CH_3)_2$, 3,15 (s, 3H, CH_3-6), 3,60–3,84 (m, 2H, CH_2-α), 4,14 (s, 3H, N-CH_3), 6,89 (d, 1H, H—4, J_{4-3} = 6 Hz), 6,98 (s large, 1H, NH), 7,42–7,64 (m, 2H, H-8 + H-9), 8,0–8,31 (m, 3H, H-3 + H-7 + H-10), 8,57 (s, 1H, H-11). Le signal du CH_2-γ est partiellement masqué par celui du DMSO: 1 pic à 2,43. *Anal.* calc. pour $C_{22}H_{26}N_4$: C 76,26, H 7,56; N 16,17; trouvé: C 76,11; H 7,51; N 15,95.

22: Rendement 47%; F = 138–140°C; rmn ^{1}H ($(CD_3)_2SO$) δ: 1,02 (t, 6H, CH_3—CH_2), 1,89 (m, 2H, CH_2-β), 2,52–2,70 (m, 6H, (CH_2—CH_3)$_2$ + CH_2-γ), 3,14 (s, 3H, CH_3-6), 3,72 (m, 2H, CH_2-α), 4,13 (s, 3H, N—CH_3), 6,8 (t, 1H, NH), 6,88 (d, 1H, H-4, J_{4-3} = 6 Hz), 7,52 (m, 2H, H-8 + H-9), 8,02–8,32 (m, 2H, H-7 + H-10), 8,11 (d, 1H, H-3), 8,60 (s, 1H, H-11). *Anal.* calc. pour $C_{24}H_{30}N_4$: C 76,96; H 8,07; N 14,96; trouvé: C 77,15; H 8,01; N 14,79.

23: Rendement 66%; F = 140–142°C; rmn ^{1}H ($(CD_3)_2SO$) δ: 1,03 (t, 2 × 3H, CH_3—CH_2), 1,89 (m, 2H, CH_2-β), 2,39–2,69 (m, 3 × 2H, CH_2—CH_3 + CH_2-γ), 3,12 (s, 3H, CH_3-6), 3,69–3,75 (m, 2H, CH_2-α), 3,95 (s, 3H, N—CH_3-5), 4,11 (s, 3H, OCH_3), 6,71 (t, 1H, NH-1), 6,86 (d, 1H, H-4, J_{4-3} = 6 Hz), 7,23 (q, 1H, H-8, J_{8-7} = 5,7 Hz, J_{8-10} = 2,4 Hz), 7,40 (d, 1H, H-10), 8,09 (d, 1H, H-3), 8,17 (d, 1H, H-7), 8,52 (s, 1H, H-11). *Anal.* calc. pour $C_{25}H_{32}N_4O$: C 74,22; H 7,97; N 13,85; trouvé: C 73,95; H 7,94; N 13,60.

24: Rendement 72,5%; F = 122–125°C; rmn ^{1}H ($(CD_3)_2SO$) δ: 1,06 (t, 2 × 3H, CH_3—CH_2), 1,90 (m, 2H, CH_2-β), 2,37–2,73 (m, 3 × 2H, CH_2—CH_3 + CH_2-γ), 2,85 (s, 3H, CH_3-6), 3,75 (q, 2H, CH_2-α), 3,92 (s, 3H, OCH_3), 5,85 (s, 2H, CH_2), 6,81 (d, 2H, H-4 + NH), 7,03–7,35 (m, 6H, H-8 + C_6H_5), 7,42 (d, 1H, H-10, J_{10-8} = 2,5 Hz), 8,06 (d, 1H, H-3, J_{3-4} = 6 Hz), 8,11 (d, 1H, H-7, J_{7-8} = 9,5 Hz), 8,60 (s, 1H, H-11). *Anal.* calc. pour $C_{31}H_{36}N_4O$: C 77,46; H 7,55; N 11,66; trouvé: C 77,60; H 7,67; N 11,25.

Remerciements

Les auteurs remercient l'Institut Curie et l'Institut national de

la santé et de la recherche médicale (contrat n° 842 001) qui ont partiellement financé ce travail.

1. L. K. DALTON, S. DEMERAC, B. C. ELMÈS, J. W. LODER, J. M. SWAN et T. TEITEI. Aust. J. Chem. **20**, 2715 (1967).
2. E. BISAGNI, C. DUCROCQ, J. M. LHOSTE, C. RIVALLE et A. CIVIER. J. Chem. Soc. Perkin Trans. **1**, 1706 (1979).
3. C. DUCROCQ, F. WENDLING, M. TOURBEZ-PERRIN, C. RIVALLE, P. TAMBOURIN, F. POCHON, E. BISAGNI et J. C. CHERMANN. J. Med. Chem. **23**, 1212 (1980).
4. J. B. LE PECQ, C. GOSSE, N. DATXUONG et C. PAOLETTI. C. R. Acad. Sci. D, **281**, 1365 (1975).
5. C. PAOLETTI, J. B. LE PECQ, N. DATXUONG, P. JURET, H. GARNIER, J. L. AMIEL et J. ROUESSE. Recent Results Cancer Res. **74**, 108 (1980).
6. M. SAINSBURY. Synthesis, 437 (1977).
7. B. BARONE et M. CHANON. Heterocycles, **16**, 1357 (1981).
8. M. J. E. HEWLINS, A. M. OLIVEIRA-CAMPOS et P. V. R. SHANNON. Synthesis, 289 (1984).
9. G. W. GRIBBLE et M. G. SAULNIER. Heterocycles, **23**, 177 (1985).
10. A. N. FUJIWARA, E. M. ACTON et L. GOODMAN. J. Heterocycl. Chem. **6**, 379 (1969).
11. A. N. FUJIWARA, E. M. ACTON et L. GOODMAN. J. Heterocycl. Chem. **5**, 853 (1968).
12. E. CAMPAIGNE et J. ASHBY. J. Heterocycl. Chem. **6**, 875 (1969).
13. V. M. DIXIT, J. M. KHANA et N. ANAUD. Ind. J. Chem. **16b**, 124 (1978).
14. C. RIVALLE, C. DUCROCQ et E. BISAGNI. J. Chem. Soc. Perkin Trans. **1**, 138 (1979).
15. C. DUCROCQ, E. BISAGNI, C. RIVALLE et J. M. LHOSTE. J. Chem. Soc. Perkin Trans. **1**, 142 (1979).
16. J. C. CHERMANN, J. GRUEST, L. MONTAGNIER, F. WENDLING, P. TAMBOURIN, M. PERIN, F. POCHON, C. DUCROCQ, C. RIVALLE et E. BISAGNI. C. R. Acad. Sci. D, **285**, 945 (1977).
17. R. LIDEREAU, J. C. CHERMANN, J. GRUEST, L. MONTAGNIER, C. DUCROCQ, C. RIVALLE et E. BISAGNI. Bull. Cancer, **67**, 1, (1980).
18. M. MARTY, C. JASMIN, P. POUILLART, C. GISSELBRECHT, G. GOUVELA et H. MAGDELAINAT. Proceedings A.S.C.O., 360 (1981).
19. C. ROBAUT, C. RIVALLE, M. RAUTUREAU, J. M. LHOSTE, E. BISAGNI et J. C. CHERMANN. Tetrahedron, **41**, 1945 (1985).
20. E. BISAGNI, J. D. BOURZAT et J. ANDRÉ-LOUISFERT. Tetrahedron, **26**, 2087 (1970).
21. E. BISAGNI, N. CHI HUNG et J. M. LHOSTE. Tetrahedron, **39**, 1777 (1983).
22. J. P. MARQUET, L. MONTAGNIER, J. GRUEST, J. D. BOURZAT, J. ANDRÉ-LOUISFERT et E. BISAGNI. Eur. J. Med. Chem.—Chim. Ther. **6**, 427 (1971).
23. C. DUCROCQ, E. BISAGNI, J. M. LHOSTE, J. MISPELTER et J. DEFAYE. Tetrahedron, **32**, 733 (1976).
24. C. RIVALLE, F. WENDLING, P. TAMBOURIN, J. M. LHOSTE, E. BISAGNI et J. C. CHERMANN. J. Med. Chem. **26**, 181 (1983).

An extension of the Beierbeck and Saunders parameters for the semiempirical calculation of the ^{13}C nuclear magnetic resonance chemical shifts: the *gauche*–γ(X) effect in epoxides

MARIA I. COLOMBO, DANIEL A. BUSTOS, MANUEL GONZALEZ-SIERRA, ALEJANDRO C. OLIVIERI, AND EDMUNDO A. RUVEDA

Instituto de Química Orgánica de Síntesis (CONICET–UNR), Facultad de Ciencias Bioquímicas y Farmacéuticas, CC 991, 2000 Rosario, Argentina

Received September 30, 1985

MARIA I. COLOMBO, DANIEL A. BUSTOS, MANUEL GONZALEZ-SIERRA, ALEJANDRO C. OLIVIERI, and EDMUNDO A. RUVEDA. Can. J. Chem. **64**, 552 (1986).

An additional substituent parameter, the gauche–γ(X), was derived and a correction for the HC parameter of Beierbeck and Saunders is proposed; this new parameter would allow the semiempirical calculation of ^{13}C nuclear magnetic resonance shifts of six-membered ring epoxides and, consequently, their stereochemistry.

MARIA I. COLOMBO, DANIEL A. BUSTOS, MANUEL GONZALEZ-SIERRA, ALEJANDRO C. OLIVIERI et EDMUNDO A. RUVEDA. Can. J. Chem. **64**, 552 (1986).

On a développé un paramètre de substituant additionnel, le paramètre *gauche*–γ(X), et on propose une correction au paramètre HC de Beierbeck et Saunders. Le nouveau paramètre permettrait de calculer semi-empiriquement les déplacements chimiques, en rmn du ^{13}C, des époxydes à six chaînons et, par voie de conséquence, leur stéréochimie.

[Traduit par le journal]

The epoxy group on six-membered rings is a common functionality in natural products. However, the unambiguous configurational assignment of the oxirane ring was difficult to establish until the advent of ^{13}C nmr spectroscopy. In fact, the pioneering work of Lukacs and co-workers (1) on steroidal epoxides showed that the influence of this functional group on the chemical shifts of neighbouring carbons was useful for solving the problem satisfactorily. It was shown that the introduction of an epoxide into a six-membered unsaturated ring causes the homoallylic-positioned carbon atom, bearing an axial proton *cis* to the oxygenated function, to undergo an upfield shift of 4–6 ppm. The same effect was observed on terpenoids having a rigid framework (2–4), on six-membered ring monoterpenes (5), and, also, in aliphatic chains with preferred conformations (6).

It was suggested that the main effect of introducing a *gauche* γ-substituent is the elimination of an HC interaction, associated with 1,3-diaxial HH interactions (7). However, if the observed chemical shift variation is larger than that caused simply by removal of the HC interaction, as in the case of cyclohexane epoxides, an additional γ(X) parameter may be required for semiempirical calculation of ^{13}C nmr shifts. This new *gauche*–γ(X) (γ_g(X)) parameter could be used as a complement to those previously reported (7) and, consequently, for the determination of the stereochemistry of six-membered ring epoxides.

Applying the semiempirical parameters derived by Beierbeck *et al.* (7), we have computed the shifts for the sequence: saturated hydrocarbon → olefin → epoxide, considering the epoxide as a *cis*-1,2-dihydroxylated compound (Scheme 1). A shielding effect of 5.8 ppm is predicted for the labelled carbon in going from A to the epoxide C, whereas an upfield shift of 2.7 ppm is expected for the Δδ (B → C). On the other hand, in going from B to the epoxide D, a deshielding effect of 1.9 ppm is computed.

We have found, as the result of the analysis of the experimental data listed in Table 1, that a γ_g(X) of ca.

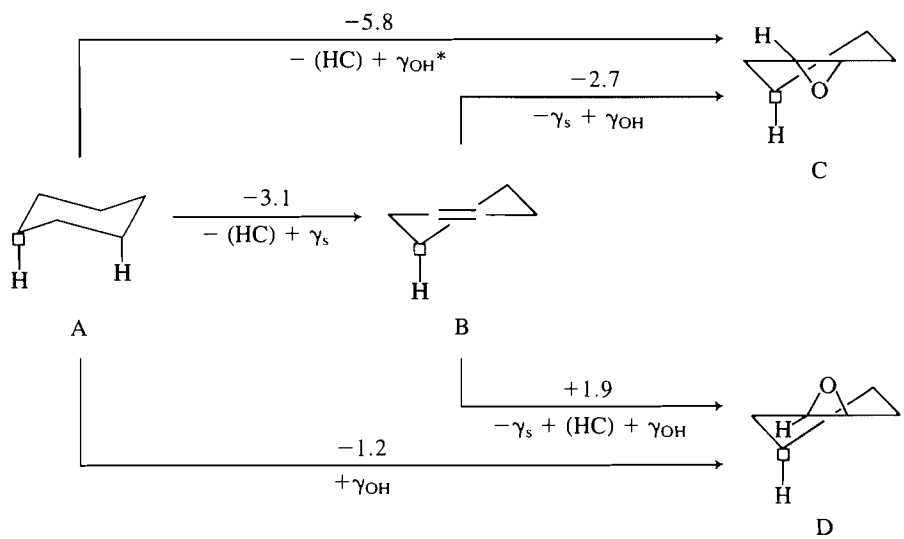

*The parameters (HC), γ_s, and γ_{OH} are defined in ref. 7

SCHEME 1

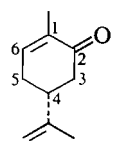

1*b* carvone
1*d* 1β,6β-epoxy

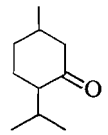

2*a* isomenthone
2*b* piperitone
2*c* 1α,2α-epoxy
2*d* 1β,2β-epoxy

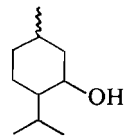

3*a* neomenthol
3*a′* neoisomenthol
3*c* 1α,2α-epoxy
3*d* 1β,2β-epoxy

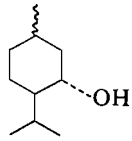

4*a* menthol
4*a′* isomenthol
4*c* 1α,2α-epoxy
4*d* 1β,2β-epoxy

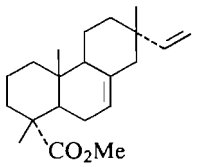

5*b* methyl isopimarate
5*c* 7α,8α-epoxy
5*d* 7β,8β-epoxy

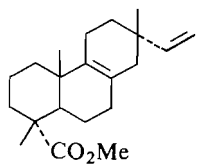

6*b* $\Delta^{8(9)}$ methyl isopimarate
6*c* 8α,9α-epoxy
6*d* 8β,9β-epoxy

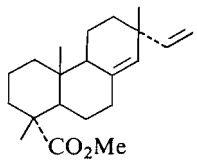

7*b* methyl sandaracopimarate
7*c* 8α,14α-epoxy
7*d* 8β,14β-epoxy

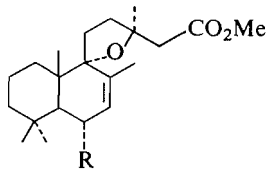

8*b* R = H methyl grindelate
8*c* R = H 7α,8α-epoxy
9*b* R = OH methyl 6α-hydroxigrindelate
9*c* R = OH 7α,8α-epoxy

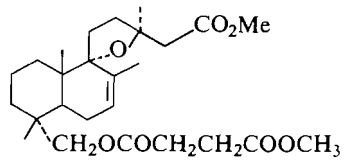

10*b* dimethyl 18-succinyloxygrindelate
10*c* 7β,8β-epoxy

−3.8 ppm, leading to the shifts shown in Scheme 2, is necessary to obtain good agreement with the observed values. This parameter does not apply at quaternary carbons. Furthermore, upon assigning a 3-ppm value for the HC interaction, which we suggest naming $(HC)_e$ for this type of compound, a $\Delta\delta(B \rightarrow D)$ value of practically zero, also in accord with the experimental data, is found (Scheme 2). Such a small value for this HC parameter could be attributable to the less effective 1,3-diaxial HH interaction in the half-chair conformation of the epoxide.

In Table 1 is shown a comparison between calculated and observed ^{13}C nmr values for the compounds studied, using the parameters given in Scheme 3.

The conclusions at which we have arrived seem to be quite

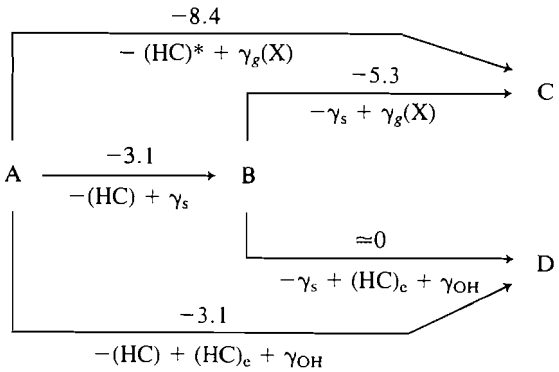

*The parameters (HC), γ_s, and γ_{OH} are defined in ref. 7

SCHEME 2

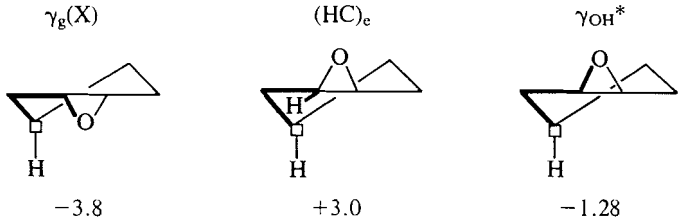

*This is the same parameter as that suggested in ref. 7

SCHEME 3. Parameters for the calculation of ^{13}C nmr of epoxides

TABLE 1. Calculated and observed chemical shifts for the compounds studied[a,b]

Carbon	Compound	Shift		Carbon	Compound	Shift	
		Calcd.	Obs.			Calcd.	Obs.
3	**1***b*	43.5	42.4	12	**6***c*	29.9	29.2
4	**1***b*	42.8	41.9	5	**6***d*	44.3	48.0
3	**1***d*	40.8	41.3	12	**6***d*	35.2	36.2
4	**1***d*	37.5	34.6	11	**7***b*	19.0	18.5
4	**2***a*	58.0	57.2	12	**7***b*	35.2	34.4
5	**2***a*	22.7	26.8	11	**7***c*	19.0	17.4
4	**2***b*	54.9	51.6	12	**7***c*	30.0	29.7
5	**2***b*	24.1	23.2	11	**7***d*	13.8	15.8
4	**2***c*	49.6	48.2	12	**7***d*	35.2	35.0
5	**2***c*	21.4	23.7	5	**8***b*	44.7	42.6
4	**2***d*	54.9	52.1	5	**8***c*	39.4	37.1
5	**2***d*	18.8	17.0	5	**9***b*	51.4	51.0
4	**3***a*	50.6	48.2	5	**9***c*	46.1	44.8
5	**3***a*	25.4	24.2	5	**10***b*	38.9	37.6
4	**3***a′*	50.6	47.4	5	**10***c*	38.9	37.7
5	**3***a′*	20.9	22.5	9	**11***a*	56.0	59.7
4	**3***c*	42.3	40.7	9	**11***b*	53.0	54.4
5	**3***c*	19.6	18.6	9	**11***c*	47.7	50.0
4	**3***d*	47.8	47.0	9	**11***d*	53.0	54.1
5	**3***d*	17.1	17.4	5	**12***a*	46.0	46.9
4	**4***a*	50.0	50.2	5	**12***b*	42.9	41.5
5	**4***a*	25.4	23.3	5	**12***c*	37.6	36.2
4	**4***a′*	50.0	49.7	5	**12***d*	42.9	41.2
5	**4***a′*	20.8	19.7	1	**13***a*	35.8	37.6
4	**4***c*	41.7	42.9	1	**13***b*	32.7	34.2
5	**4***c*	19.6	20.2	1	**13***c*	27.5	30.4
4	**4***d*	47.2	47.2	1	**13***d*	32.7	33.6
5	**4***d*	17.1	16.2	5	**14***b*	42.9	41.4
5	**5***a*	50.1	49.1	5	**14***c*	37.7	35.9
5	**5***b*	47.0	45.3	5	**14***d*	42.9	41.6
5	**5***c*	41.7	41.1	5	**15***b*	42.9	41.9
5	**5***d*	47.0	45.2	5	**15***c*	37.6	37.3
5	**6***a*	50.1	49.1	5	**15***d*	40.2	42.7
12	**6***a*	38.2	36.2	5	**16***b*	38.3	34.6
5	**6***b*	47.0	46.6	5	**16***c*	33.0	30.8
12	**6***b*	35.2	35.1	5	**16***d*	38.3	35.6
5	**6***c*	41.8	37.5				

[a]The chemical shifts for compounds **2***a*, **2***b*, **3***a*, **3***a′*, **4***a*, and **4***a′* were taken from ref. 10; for compounds **2***c*, **2***d*, **3***c*, **3***d*, **4***c*, and **4***d* from ref. 5; for compounds **5**, **6**, and **7** from ref. 2; for compounds **10***b* and **10***c* from ref. 11; for compound **11** from ref. 3, and those for compounds **12**, **13**, **14**, **15**, and **16** from ref. 1. The resonance values for compounds **1**, **8**, and **9** are data from this laboratory.

[b]Root-mean-squares deviation between calculated and observed resonances is 1.71 ppm.

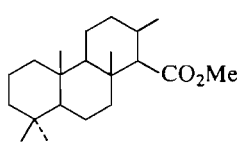

11*a* methyl isocopal-15-oate
11*b* methyl isocopal-12-en-15-oate
11*c* 12α,13α-epoxy
11*d* 12β,13β-epoxy

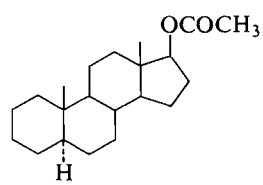

12*a* 17β-acetoxy-5α-androstane
12*b* 17β-acetoxy-5α-androst-2-ene
12*c* 2α,3α-epoxy
12*d* 2β,3β-epoxy
13*b* 17β-acetoxy-5α-androst-3-ene
13*c* 3α,4α-epoxy
13*d* 3β,4β-epoxy

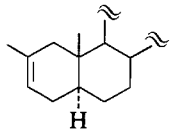

14*b* 2-methyl-17β-acetoxy-5α-androst-2-ene
14*c* 2α,3α-epoxy
14*d* 2β,3β-epoxy

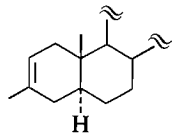

15*b* 3-methyl-17β-acetoxy-5α-androst-2-ene
15*c* 2α,3α-epoxy
15*d* 2β,3β-epoxy

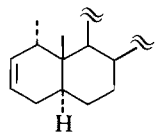

16*b* 1α-methyl-17β-acetoxy-5α-androst-2-ene
16*c* 2α,3α-epoxy
16*d* 2β,3β-epoxy

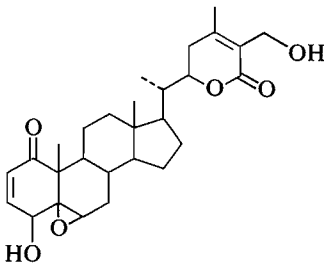

17

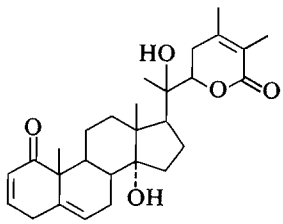

18

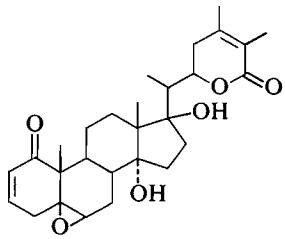

19

general; however, the effect of a 5β,6β-epoxide on the homoallylic carbon shift of the withanolides deserves some comment. As was previously reported by Gottlieb and Kirson (8), C-8 of withaferin A diacetate (**17**) does not suffer the expected shielding effect induced by the oxirane ring. Also, the same carbon of withanolide G (**18**) is practically unaffected compared to that of withanolide E (**19**). These apparently abnormal results could be explained by assuming that, in **17**, ring B adopts a distorted half-chair conformation leading to a reduced γ-*gauche* interaction. This assumption is supported by the reported X-ray analysis of withaferin A acetate *p*-bromobenzoate (9), which indeed shows such a distortion. Other cases that do not exhibit the expected effect on the homoallylic carbon shifts may be due to conformational distortion.

Acknowledgments

We thank CONICET (Consejo Nacional de Investigaciones Científicas y Técnicas) and UNR (Universidad Nacional de Rosario) for financial support and fellowships (D.A.B. and A.C.O.).

1. K. Tori, T. Komeno, M. Sangare, B. Septe, B. Delpech, A. Ahond, and G. Lukacs. Tetrahedron Lett. 1157 (1974).
2. B. Delmond, B. Papillaud, J. Valade, M. Petraud, and B. Barbe. Org. Magn. Reson. **12**, 209 (1979).
3. P. M. Imamura and E. A. Ruveda. J. Org. Chem. **45**, 510 (1980).
4. M. Gonzalez-Sierra, M. I. Colombo, M. E. Zudenigo, and E. A. Ruveda. Phytochemistry, **23**, 1685 (1984).
5. E. Gacs-Baitz, G. Kalaus, and P. Gyory. Org. Magn. Reson. **22**, 738 (1984).
6. M. Gonzalez-Sierra, D. A. Bustos, M. E. Zudenigo, and E. A. Ruveda. Tetrahedron. In press.
7. H. Beierbeck, J. K. Saunders, and J. W. ApSimon. Can. J. Chem. **55**, 2813 (1977).
8. H. E. Gottlieb and I. Kirson. Org. Magn. Reson. **16**, 20 (1981).
9. A. T. McPhail and G. A. Sim. J. Chem. Soc. (B), 962 (1968).
10. F. Bohlmann, R. Zeisberg, and E. Klein. Org. Magn. Reson. **7**, 426 (1975).
11. A. F. Rose. Phytochemistry, **19**, 2689 (1980).

Iminium ion-mediated cyclizations of 4-aryl-1,4-dihydropyridines. Alternate cyclization pathways

GEORGE D. HARTMAN,[1] WASYL HALCZENKO,[1] AND DAVID W. COCHRAN
Merck Sharp & Dohme Research Laboratories, West Point, PA 19486, U.S.A.

Received August 29, 1985

GEORGE D. HARTMAN, WASYL HALCZENKO, and DAVID W. COCHRAN. Can. J. Chem. **64**, 556 (1986).

Acid-catalyzed cyclization of dimethyl 2,6-dimethyl-4-[(2-ethenyl-5-methoxy)phenyl]-1,4-dihydropyridine-3,5-dicarboxylate affords novel products via competing intramolecular processes. The present mechanistic pathways differ from previous iminium ion-mediated cycloadditions, to afford conformationally constrained dihydropyridine analogs for study as calcium antagonists. These results illustrate the ability of the dihydropyridine nucleus to function as either a nucleophile or an electrophile, depending upon substituents in the aryl ring.

GEORGE D. HARTMAN, WASYL HALCZENKO et DAVID W. COCHRAN. Can. J. Chem. **64**, 556 (1986).

La cyclisation acido-catalysée du diméthyl-2,6 [(éthènyl-2 méthoxy-5)phényl]-4 dihydro-1,4 pyridinedicarboxylate-3,5 de diméthyle conduit à de nouveaux produits via des processus intramoléculaires qui sont en compétition. Les voies réactionnelles impliquées ici diffèrent de celles présumées antérieurement lors de cycloadditions impliquant des ions iminium et elles conduisent à des analogues de dihydropyridines ayant des contraintes conformationnelles et pouvant servir dans des études comme antagonistes du calcium. Ces résultats illustrent la facilité du noyau dihydropyridine à agir soit comme un nucléophile soit comme un électrophile suivant la nature des substituants attachés au noyau aromatique.

[Traduit par le journal]

Calcium antagonists encompass a heterogeneous group of compounds that inhibit calcium-dependent cellular processes (1). These agents are thought to decrease calcium influx through the slow calcium channel in the cell membrane, while having minimal effect on calcium extrusion or other ionic transport mechanisms (2). These attributes allow this class of compounds to inhibit calcium-mediated pathologic contractile events. Consequently, several calcium antagonists have gained clinical importance in the treatment of angina, hypertension, arrhythmias, and migraine (3). Among these, the 4-aryl-1,4-dihydropyridines, as characterized by nifedipine (**1**), have proven to be the most potent.

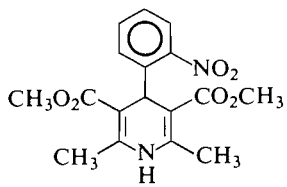

1

Development and further refinement of biologically active dihydropyridines have involved molecular classification according to drug receptor site and specific channel gating characteristics (4, 5). Pharmacologic progress in this area has hinged on the evolution of synthetic strategies that would provide molecules of appropriate topology. Inspired by suggestions that calcium entry blocker activity was correlated with the ring pucker in the dihydropyridine nucleus (6), a considerable amount of attention has lately been given to the preparation of conformationally constrained analogs (7, 8). As part of this effort we have described (9, 10) the synthesis of novel, rigid dihydropyridine derivatives arising from intramolecular biscyclization reactions between a 4-aryl substituent and the dihydropyridine/iminium species. Thus, treatment of dimethyl 2,6-dimethyl-4-(2-ethenyl)phenyl-1,4-dihydropyridine-3,5-dicarboxylate (**2**) with gaseous HCl gave cation **3**, which was

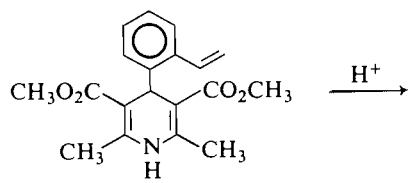

2

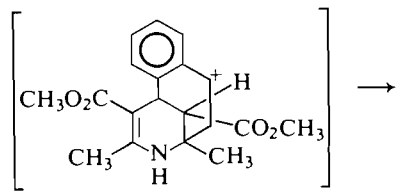

3

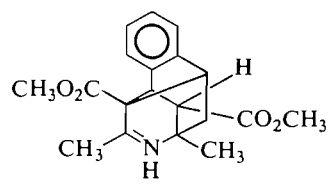

4

trapped internally by the aminocrotonate to provide **4**. In an effort to prepare more potent calcium entry blockers in this series, as well as with recognition that alternate reaction possibilities existed for intermediates such as **3**, we decided to explore the synthesis of aryl-substituted compounds. We now wish to report that acid-catalyzed cyclization of dimethyl 2,6-dimethyl-4-[(2-ethenyl-5-methoxy)phenyl]-1,4-dihydropyridine-3,5-dicarboxylate (**8**) affords products that are dramatically different from those observed for **2**, and which arise via competing intramolecular processes.

Results and discussion

The synthesis of dihydropyridine **8** is presented in Scheme 1. Treatment of the known 2-bromo-5-methoxybenzaldehyde acetal (**5**) (11) with *n*-BuLi followed by *N*-formylpiperidine gave

[1]Authors to whom correspondence may be addressed.

Printed in Canada / Imprimé au Canada

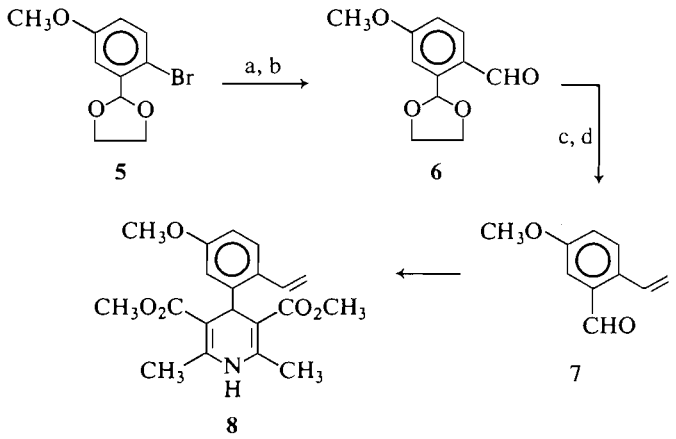

a: *n*-BuLi, THF, −70°C; b: *N*-formylpiperidine; c: $(C_6H_5)_3PCH_3Br$/*n*-BuLi, THF, 0°C to room temp. over 16 h; d: CH_3COCH_3,*p*-TSA, room temp. for 4 h; e: $CH_3COCH_2CO_2CH_3/H_2N(CH_3)C{=}CHCO_2CH_3$, CH_3OH, reflux for 72 h.

SCHEME 1

acetal aldehyde **6**. This compound was then methylidenated with the appropriate Wittig reagent and the aldehyde deprotected to give **7**, which was subjected to Hantzsch reaction with methyl acetoacetate and methyl 3-aminocrotonate to provide **8**.

When **8** in chloroform solution was treated with excess hydrogen chloride gas, starting material was consumed within 18 h and three new compounds were produced. The major products (Scheme 2) of reaction and basic work-up were dimethyl 1-methylidene-3,9-dimethyl-6-methoxy-2,4a-dihydro-9*H*-indeno[2,1-*c*]pyridine-4,9a-dicarboxylate (**14**) and its tautomer, **15**, which were obtained in 74% yield in a ratio of 1:1.25 as an inseparable mixture. The minor product of reaction was dimethyl 4,5-dihydro-10-methoxy-3,5-dimethyl-1,5-methano-1*H*-4-benzazonine-2,12α-dicarboxylate **11**, which was isolated in 12% yield. Surprisingly, none of the bis-cyclized adduct **12** was observed. The structure of **11** was proven by single-crystal X-ray analysis[2] and an ORTEP representation is presented in Fig. 1. The structures of **14** and **15** were assigned based upon 360-MHz ^{1}H nmr, elemental analysis, and mass spectral data. The assignment of the relative stereochemistry at the bridging carbon C-7 in **14** and **15** was made in the following manner. The mixture of **14** and **15** was reduced with sodium borohydride in acetic acid (12) to afford a single product whose 360-MHz ^{1}H nmr, elemental analysis, and mass spectral properties were correct for the gross structure of **16**. Nuclear Overhauser enhancement (nOe) experiments, wherein saturation of the C-6 methyl resonance at δ 0.62 gave an enhancement in the signals for N-H, N-6 and H-7, while saturation of the methyl resonance at C-7 produced an enhancement of the signals for H-4 and H-7, unequivocally indicated that the product had the relative stereochemistry shown in **16**.

The formation of cycloadducts **11**, **14**, and **15** from **8** suggests that reaction proceeds along two competing pathways. The major pathway (path a, Scheme 2) involves protonation of the styrenic double bond to give the methoxy-stabilized secondary benzylic cation **13**, which is attacked by C-3 of the dihydropyridine to provide **14** and **15**. Nucleophilic reactivity in this sense is directly analogous to that seen previously both in the

[2]Details of the structure will be published in full in the Journal of Medicinal Chemistry.

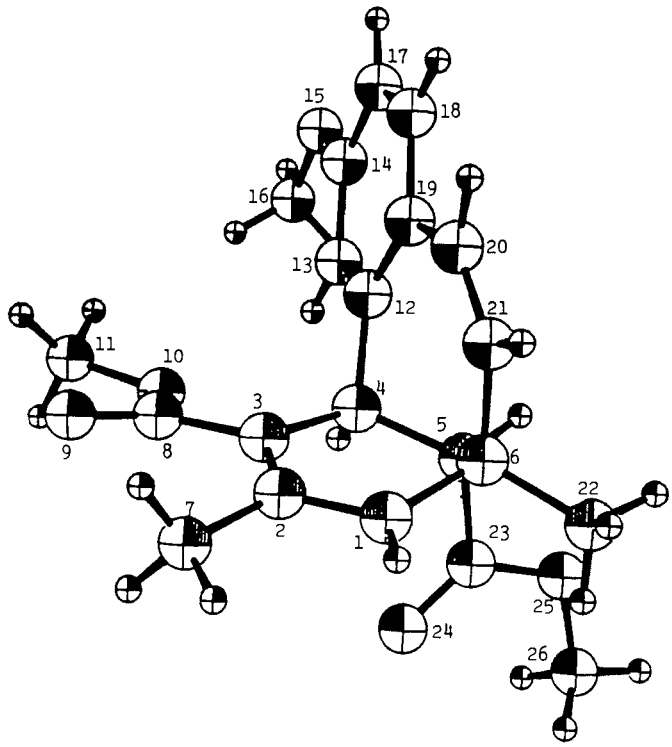

FIG. 1. ORTEP representation of **11**.

capture of cation **3** internally by the crotonate double bond (9), as well as in the acid-catalyzed opening of acetals (10). Similar reactivity has also been reported by Aritomi and Nishimura (13) in the internal capture of iminium salts by the dihydropyridine nucleus. It should also be noted that the formation of the indicated isomer at C-7 denotes, not unexpectedly, the capture of cation **15***b*. It is also apparent that the dramatic reversal in mechanism seen between **2** and **8** can be attributed to the rapid formation and trapping of the highly stabilized *p*-methoxybenzyl cation **13**.

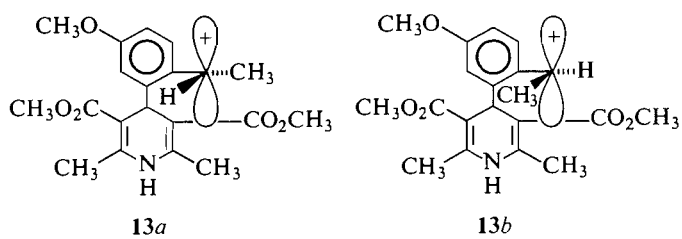

13*a* **13***b*

The minor pathway (path b) features formation of iminium ion **9** followed by attack of the styrenic double bond on C-2 to give cation **10**. Elimination of a proton, rather than internal capture as seen for **3**, then occurs to yield **11**.

The present results support and extend several concepts that have recently been advanced with regard to dihydropyridine reactivity (9, 10). As demonstrated in path a, where the dihydropyridine nucleus functions as a nucleophile, and in path b, where it acts as an electrophile, the net reactivity can encompass both polarities. Moreover, in contrast to styrene **2** and acetals (9) that display a single behavior, olefin **8** illustrates the ability to utilize its dihydropyridine nucleus as either nucleophile or electrophile competitively. We thus conclude that reactivity of 4-aryl-1,4-dihydropyridines in the present acid-catalyzed cyclization processes is a function both of aryl

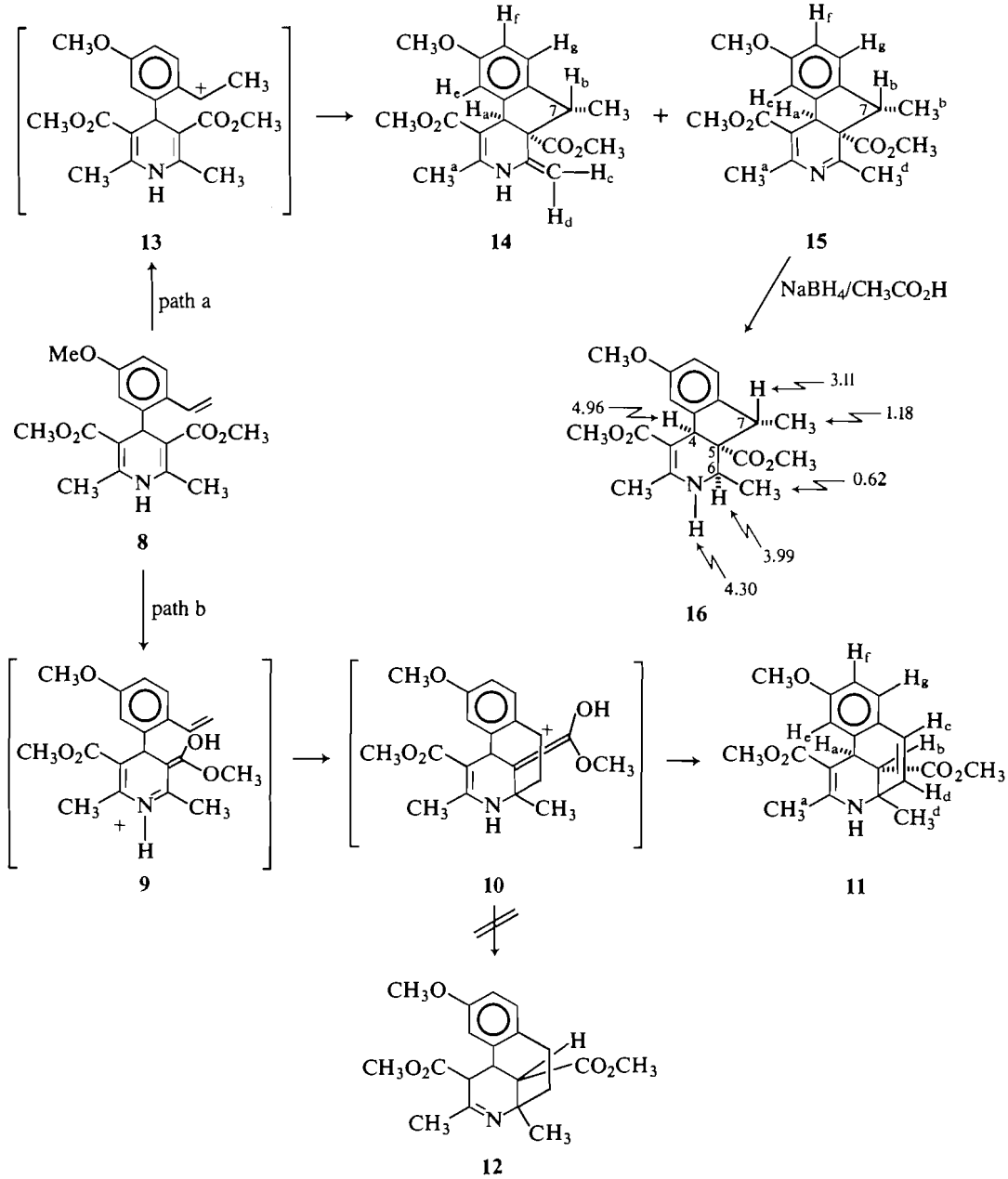

SCHEME 2

substituents that covalently interact with the nucleus, as well as those that only affect the stability of cyclization intermediates.

The compounds described in this paper represent novel, conformationally constrained dihydropyridine derivatives, which will be studied as calcium antagonists. Moreover, the pathways by which these cycloadducts arise represent a unique competitive reactivity previously unrecognized for 1,4-dihydropyridines. We feel that the application of these cyclization modes and preferences in analogous systems will be of synthetic utility.

Experimental

Melting points were taken on a Thomas–Hoover capillary apparatus and are uncorrected. The nmr spectra were recorded on an EM-390 or a Nicolet NT-360 spectrometer with Me_4Si as an internal standard. Mass spectra were obtained on a LKB-9000S mass spectrometer at 70 eV. *N*-formylpiperidine, methyl acetoacetate, and methyl 3-aminocrotonate were obtained from Aldrich and all were used without purification. *n*-Butyllithium (hexane) was purchased from Alfa.

2-[2-(1,3-Dioxalanyl)]-4-methoxybenzaldehyde (6)

To 38.87 g (0.15 mol) 2-bromo-5-methoxybenzaldehyde acetal (**5**) (11) in 500 mL tetrahydrofuran cooled to −75°C under nitrogen was added 0.15 mol *n*-butyllithium (in hexane) dropwise over 1.5 h. After stirring for 1 h at −70°C, a solution of 20.37 g (0.18 mol) *N*-formylpiperidine in 50 mL tetrahydrofuran was added dropwise while keeping the temperature < −70°C. The resulting yellow solution was allowed to come to room temperature with stirring overnight.

The reaction mixture was quenched with 75 mL of saturated ammonium chloride solution and extracted with 2 × 400 mL portions of ether. The combined organic extracts were washed successively with 4 × 100 mL portions of saturated ammonium chloride solution, then with brine, and dried. Solvent removal *in vacuo* gave an oil, which was fractionated through a 6-in. Vigreux column to give 22.8 g (73%) of **6** as an oil; ^1H nmr (90 MHz, $CDCl_3$): 3.55 (s, 3H, OCH_3), 3.80 (s, 4H, $-CH_2-CH_2-$), 6.15 (s, 1H, $HC(O)_2$), 6.72 (dd, 1H, aromatic, J = 2, 8 Hz), 6.95 (d, 1H, aromatic, J = 2 Hz), 7.65 (d, 1H, aromatic, J = 8 Hz), 10.05 (s, 1H, CHO).

2-Ethenyl-5-methoxybenzaldehyde (7)

To 95.0 g (0.226 mol) methyl triphenylphosphonium bromide suspended in 500 mL tetrahydrofuran and cooled to −75°C under nitrogen was added 0.252 mol *n*-butyllithium dropwise while keeping the temperature <−70°C. After addition was complete the temperature was allowed to gradually rise to 0°C over 3–4 h. Then, a solution of 21.5 g (0.103 mol) of **6** in 50 mL tetrahydrofuran was added dropwise while the temperature was kept <5°C. After addition was complete the reaction mixture was stirred in an ice bath overnight. The solvent was then removed *in vacuo* and the residue was taken up in 150 mL methylene chloride. This solution was passed through a pad of silica gel that was thoroughly rinsed with methylene chloride. The solvent was removed *in vacuo* to give a viscous oil that was purified by flash chromatography on silica gel, eluting with hexane – ethyl acetate, 85:15. The product acetal was isolated as a clear oil with R_f 0.5 in this solvent system. The yield was 14.9 g (70%).

Cleavage of the acetal was accomplished by treatment with *p*-toluenesulfonic acid monohydrate in acetone for 8 h at room temperature. The solvent was then removed *in vacuo* and the residue was taken up in either. This was washed with 2 × 50 mL portions of saturated sodium bicarbonate solution, then with brine, and dried. Solvent removal gave an oil, which was purified by flash chromatography on silica gel, eluting with hexane – ethyl acetate (9:1) to give pure **7**, R_f 0.5, as a slightly yellow oil, 8.02 g (48%); ^{1}H nmr (90 MHz, $CDCl_3$): 3.81 (s, 3H, OCH_3), 5.35 (dd, 1H, $=CH_2$), 5.54 (dd, 1H, $=CH_2$), 7.0–7.55 (m, 4H, aromatic + —CH=), 10.25 (s, 1H, CHO).

Dimethyl 2,6-dimethyl-4-[(2-ethenyl-5-methoxy)phenyl]-1,4-dihydropyridine-3,5-dicarboxylate (8)

To 8.0 g (0.049 mol) **7** dissolved in 50 mL methanol was added 5.68 g (0.049 mol) methyl 3-aminocrotonate and 5.72 g (0.049 mol) methyl acetoacetate and the resulting solution was heated at reflux for 3 days. The solvent was then removed *in vacuo* and the residue was triturated with ether. The pale yellow solid that separated was filtered off, washed with a small amount of cold ether, and air dried to give 6.55 g of **8**. The filtrate was purified by flash chromatography on silica gel, eluting with hexane–ether (1:2) to provide another 1.45 g of **8**, which had R_f 0.4 in this solvent system. The total yield of **8** was 8.0 g (46%), mp 141–143°C; ^{1}H nmr (360 MHz, $CDCl_3$): 2.32 (s, 6H, CH_3), 3.56 (s, 6H, CO_2CH_3), 3.74 (s, 3H, OCH_3), 5.19 (dd, 1H, $CH_2=$, J = 2, 12 Hz), 5.25 (s, 1H), 5.50 (dd, 1H, $CH_2=$, J = 2, 18 Hz), 5.60 (br, s, 1H, NH), 6.68 (dd, 1H, aromatic, J = 3, 9 Hz), 6.87 (d, 1H, aromatic, J = 3 Hz), 7.35–7.50 (m, 2H, aromatic), 7.45 (dd, 1H, —CH=, J = 12, 18 Hz); ms m/e: 357 (M^+). *Anal.* calcd. for $C_{20}H_{23}NO_5$: C 67.21, H 6.49, N 3.92; found: C 67.18, H 6.64, N 3.85.

Dimethyl 4,5-dihydro-10-methoxy-3,5-dimethyl-1,5-methano-1H-4-benzazonine-2,12α-dicarboxylate (11); dimethyl 1-methylidene-3,9-dimethyl-6-methoxy-2,4a-dihydro-9H-indeno[2,1-c]pyridine-4,9a-dicarboxylate (14); and dimethyl 1,3,9-trimethyl-6-methoxy-4a,9-dihydroindeno[2,1-c]pyridine-4,9a-dicarboxylate (15)

A stream of HCl gas was bubbled into a solution of 2.0 g (5.6 mmol) of **8** in 30 mL chloroform cooled to 0–5°C in an ice bath for 0.5 h. The reaction mixture was then stirred at room temperature overnight as the temperature gradually rose to ambient. The reaction mixture was diluted with 100 mL chloroform was 35 mL ice-cold water. This was neutralized with concentrated ammonium hydroxide solution and the phases were separated. The aqueous phase was extracted with 3 × 50 mL portions of chloroform and the combined organic extracts were washed with brine and dried. Solvent removal gave a yellow foam (2.1 g) which was a mixture of **11**, **14**, and **15**. This was purified by careful flash chromatography on silica gel (230–400 mesh), eluting with hexane–ether (1:2) to afford 1.48 g (74%) of a mixture of **14** and **15**, eluting first with an R_f 0.5, followed by 0.24 g (12% of **11**, R_f 0.4.

Compound **11**, mp 150–155°C; ^{1}H nmr (360 MHz, $CDCl_3$): 1.40 (s, 3H, CH_3^d), 2.23 (d, 3H, CH_3^a), 3.15 (s, 1H, H_b), 3.58 (s, 3H), 3.71 (s, 3H), 3.81 (s, 3H), 4.11 (br s, 1H, H_a), 4.21 (br, s, 1H, NH), 5.23 (d, 1H, H_d), 6.22 (d, 1H, H_c), 6.66 (d, 1H, H_f), 6.93 (d, 1H, H_g), 6.95 (d, 1H, H_e); ms m/e: 357 (M^+). *Anal.* calcd. for $C_{20}H_{23}NO_5$: C 67.21, H 6.49, N 3.92; found: C 66.90, H 6.64, N 3.92.

The tautomeric mixture **14/15** was determined, by integration of nmr peaks described below, to be a 1:1.25 ratio of these two compounds and had mp 170–172°C; ms m/e: 357 (M^+). *Anal.* calcd. for $C_{20}H_{23}NO_5$: C 67.21, H 6.49, N 3.92; found: C 67.50, H 6.65, N 3.99. **14** had ^{1}H nmr (360 MHz, $CDCl_3$): 1.21 (d, 3H, CH_3^b), 2.33 (s, 3H, CH_3^a), 4.45 (d, 1H, H_d), 4.69 (d, 1H H_c), 4.96 (s, 1H, H_a), 5.91 (br s, 1H, NH), 6.58 (br s, 1H, H_e), 6.68 (dd, 1H, H_f), 7.05, (d, 1H, H_c). **15** had ^{1}H nmr (360 MHz, $CDCl_3$): 1.18 (d, 3H, CH_3^b), 2.30 (s, 3H, CH_3^a), 2.42 (s, 3H, CH_3^d), 4.85 (s, 1H, H_a), 6.58 (br s, 1H, H_e), 6.72 (dd, 1H, H_f), 7.04 (d, 1H, H_g). In addition, the nmr spectrum of **14/15** contained absorptions that could not be specifically associated with either tautomer: 3.61 (q, 1H), 3.72 (s, 6H, CO_2CH_3), 3.79 (s, 3H, OCH_3), 3.74 (s, 3H, CO_2CH_3), 3.88 (s, 3H, CO_2CH_3).

Dimethyl 2,4a,9,9a-tetrahydro-6-methoxy-1,3,9-trimethyl-1H-indeno[2,1-c]pyridine-4-9a(α)-dicarboxylate (16)

To 5 mL glacial acetic acid was added 0.06 g (1.6 mmol) sodium borohydride at room temperature and, after the initial vigorous gas evolution, this suspension was stirred for 15 min. Then 0.10 g (0.28 mmol) of a mixture of **14/15** (1:1.25) was added in one portion and the resulting yellow solution was stirred at room temperature overnight.

The reaction mixture was then poured into 20 mL ice water, neutralized with saturated sodium bicarbonate solution, and filtered to give a tan solid. This was purified by flash chromatography on silica gel, eluting with hexane–ether (1:2) to give 0.32 g (31%) of **16**, R_f 0.4 in this solvent system, mp 134–140°C; ^{1}H nmr (360 MHz, $CDCl_3$): 0.62 (d, 3H, J = 7 Hz), 1.18 (d, 3H, J = 7 Hz), 2.25 (s, 3H, allylic CH_3), 3.11 (q, 1H, J = 7 Hz), 3.73 (s, 3H), 3.76 (s, 3H), 3.80 (s, 3H), 3.99 (m, 1H), 4.30 (br d, 1H, NH), 4.96 (s, 1H), 6.62–7.01 (3H, aromatic); ms m/e: 359 (M^+). *Anal.* calcd. for $C_{20}H_{25}NO_5$: C 66.83, H 7.01, N 3.90; found: C 66.93, H 7.30, N 3.67.

Acknowledgements

The authors wish to thank Mrs. Joan S. Murphy for the nmr spectra, Mr. John Moreau for elemental analyses, Dr. Harri Ramjit for mass spectral determinations, and Dr. James P. Springer for X-ray determinations. The authors also thank Dr. Steven M. Pitzenberger and Dr. Barry Trost for helpful discussions, and Mrs. M. Banker for preparation of the manuscript.

1. A. Fleckenstein. *In* Calcium antagonists and cardiovascular disease. *Edited by* L. H. Opie. Raven Press, New York. 1984. p. 9.
2. L. H. Opie. Pharmacol. Ther. **25**, 271 (1984).
3. R. A. Janis and D. T. Triggle. J. Med Chem. **26**, 776 (1983).
4. H. Glossmann, D. R. Ferry, A. Gall, and M. Rombusch. J. Cardiovasc. Pharmacol. **6**, S608 (1984).
5. M. Spedding. Trends Pharmacol. Sci. 114 (1985).
6. A. M. Triggle, E. Shefter, and D. Triggle. J. Med. Chem. **23**, 1442 (1980).
7. H. Meyer, L. Born, S. Kazda, and W. Dompert. Abstracts, Division of Medicinal Chemistry, 187th ACS National Meeting, St. Louis, Missouri. April 8–13, 1984.
8. D. A. Claremon, D. E. McClure, J. P. Springer, and J. J. Baldwin. Synthesis. In press.
9. G. D. Hartman, B. T. Phillips, and W. Halczenko. J. Org. Chem. **50**, 2423 (1985).
10. G. D. Hartman, W. Halczenko, and B. T. Phillips. J. Org. Chem. **50**, 2427 (1985).
11. T. Kametani, Y. Hirai, M. Kajiwara, T. Takahashi, and K. Fukumoto. Chem. Pharm. Bull. **23**, 2634 (1975).
12. R. O. Hutchins, W.-Y. Su, R. Sivakumar, F. Cistone, and Y. P. Stercho. J. Org. Chem. **48**, 3412 (1983).
13. J. Aritomi and H. Nishimura. Chem. Pharm. Bull. **29**, 1193 (1981).

Motional behavior of "asperlin" in solution. A ^{13}C spin-lattice relaxation study

PHOTIS DAIS[1] AND GEORGE FAINOS
Department of Chemistry, McGill University, Montreal, P.Q., Canada H3C 3G1
Received June 6, 1985

PHOTIS DAIS and GEORGE FAINOS. Can. J. Chem. **64**, 560 (1986).

^{13}C nuclear magnetic resonance spin-lattice relaxation times (T_1) have been used to probe the motional behavior of 5-acetoxy-5,6-dihydro-6-(1,2-epoxypropyl)-2-pyrone ("asperlin") in dimethyl sulfoxide solution. This molecule offers structural features suited to a study of internal motions, i.e., epoxypropyl and methyl internal motions superimposed on an anisotropic overall reorientation. The rigidity of the pyrone ring and its semiplanar conformation result in an overall ellipsoidal shape, and hence the rotational dynamics of asperlin are adequately approximated by the diffusion of a prolate ellipsoid with the major axis passing through the C(2)—H(2) bond. The description of the internal motion of the epoxypropyl ring is strongly model dependent. Furthermore, the relaxation data for the oxirane ring carbons do not uniquely define a dynamic model. Due to similarities in the activation energies of the overall and internal motions, based on temperature-dependent measurements, it has not been feasible to interpret the relaxation data by a single type of motion. Internal rotation of the epoxymethyl substituent is rationalized by applying the stochastic diffusion model of multiple internal rotations.

PHOTIS DAIS et GEORGE FAINOS. Can. J. Chem. **64**, 560 (1986).

On a utilisé les temps de relaxation spin-réseau (T_1) de la rmn du ^{13}C pour étudier le comportement des mouvements de l'acétoxy-5 dihydro-5,6 (époxy-1,2 propyl)-6 pyrone-2 ("asperlin") en solution dans le diméthylsulfoxyde. Cette molécule présente des caractéristiques de structure qui sont adaptées à une étude des mouvements internes; il s'agit des mouvements internes de l'époxypropyle et du méthyle qui se superposent à une orientation globale anisotrope. La rigidité du cycle pyrone et sa conformation semi-planaire lui font adopter une forme globale ellipsoïdale et l'on peut décrire adéquatement la dynamique de la rotation de l'asperlin en faisant l'approximation qu'elle ressemble à la diffusion d'une ellipsoïde allongée avec un axe majeur qui passerait par la liaison C(2)—H(2). La description du mouvement interne du cycle époxypropyle dépend beaucoup du modèle. De plus, les données de relaxation des carbones du cycle oxirane ne permettent pas de définir un modèle dyamique. À cause de similarités dans les énergies d'activation des mouvements globaux et internes, que l'on a obtenues à partir de mesures qui dépendaient de la température, on n'a pas pu interpréter les données de relaxation par un seul type de mouvement. On a rationalisé la rotation interne du substituant époxyméthyle en appliquant le modèle de diffusion stochastique des rotations internes multiples.
[Traduit par le journal]

Introduction

A large number of natural products contain α,β-unsaturated lactone structures. These include compounds of the coumarin series, macrolides, the steroid withaferin, and 2-pyrones of fungal origin. Among the latter group is 5-acetoxy-5,6-dihydro-6-(1,2-epoxypropyl)-2-pyrone) (**1**), produced by *Aspergillus nidulans* (1) and termed "asperlin," which possess antibiotic and antitumor activity. The structure of **1** has been studied (2–4) by ^1H and ^{13}C nmr spectroscopy, as well as by chemical synthesis. It was concluded that the pyrone ring of **1** assumes a semi-planar conformation, in which five of the six carbons are held coplanar, that the C(4)—H(4) bond approaches coplanarity with the olefinic bonds, and also that the 4,5-substituents of the ring have the L-*threo* configuration. In addition, the data confirmed that the oxirane ring is *trans*, and indicated that **1** is the 6*R*,7*S* diastereomer. Finally, it was shown that the H-5 and H-6 protons are *anti*, in the most probable conformation of the side chain about the C(5)—C(6) bond.

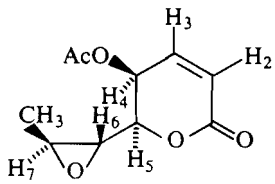

1

To obtain a fuller understanding of the properties of **1**, we have measured the ^{13}C spin-lattice relaxation times (T_1) of **1** in DMSO-d_6 solution over the temperature range 20–100°C, and calculated the diffusion coefficients of the overall and internal motions from the relaxation data. The data are consistent, approximately, with an overall axially symmetric diffusion, upon which internal rotations are superimposed. The interpretation of the relaxation data for the oxirane ring is found to be strongly dependent on the models adopted, whereas the methyl internal rotation is described by using the stochastic diffusion model for multiple internal rotations.

Experimental

^{13}C nuclear magnetic resonance relaxation experiments were conducted on a Varian XL-200 spectrometer operating at 50.3 MHz under conditions of full ^1H noise decoupling. The temperature was controlled to within ±0.1°C by means of a precalibrated copper–constantan thermocouple in the probe insert. The relaxation times were measured by the FIRFT technique (5) and analysed by a three-parameter non-linear procedure (6). The pulse duration for a 180° flip angle, checked at various temperatures, was 29.6 μs. Other details on relaxation experiments and ^{13}C nOe (nuclear Overhauser enhancement) measurements are given elsewhere (7). The rms error in the three-parameter fit was ±5% or better, whereas the reproducibility was ±5–10%, the upper limit pertaining at high temperatures. Samples of a 0.8 *M* solution of **1** in DMSO-d_6 were degassed by saturation with dry nitrogen gas for 1–2 min before use. All of the calculations were performed with algorithms written in APL.

Results and discussion

Carbon-13 T_1 values obtained from 20 to 100°C for the protonated carbons of **1** are summarized in Table 1. The nOe values for all protonated carbons,[2] at all temperatures, ap-

[1]Author to whom all correspondence should be addressed.

[2]For consistency with previous publications (2–4), **1** is numbered as a lactone. Accordingly, its carbonyl carbon is position 1 rather than, as in the pyrone system, position 2.

TABLE 1. ^{13}C spin-lattice relaxation times (in seconds) of "asperlin" in DMSO-d_6 solution

T (K)	C-2	C-3	C-4	C-5	C-6	C-7	CH_3	(C-3,C-4,C-5)/(C-6,C-7)
293	0.70	0.81	0.84	0.85	1.10	1.06	1.51	0.77
303	0.89	0.99	1.04	1.06	1.38	1.33	1.84	0.76
313	1.10	1.24	1.29	1.30	1.74	1.69	2.16	0.74
323	1.32	1.52	1.52	1.58	2.08	2.02	2.46	0.75
333	1.67	1.84	1.86	1.85	2.57	2.51	3.02	0.73
343	1.88	2.19	2.19	2.24	2.93	2.95	3.37	0.75
353	2.31	2.52	2.54	2.60	3.51	3.59	3.86	0.72
363	2.70	2.95	2.96	3.00	4.08	4.20	4.35	0.72
373	3.14	3.41	3.45	3.51	4.72	4.90	4.90	0.72

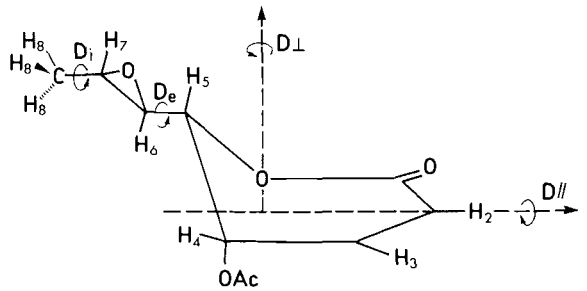

FIG. 1. Axes of rotation in "asperlin" and rotational diffusion coefficients.

proached the asymptotic value of 2.988 to within ±5%, indicating that these carbons relax predominantly via dipole–dipole interactions. The T_1 value of C-2 in the pyrone ring at all temperatures is smaller than the T_1's of the remaining ring carbons (Table 1). These differences, which are outside the experimental error, indicate that **1** reorients anisotropically about a preferential axis of rotation. Since C-3, C-4, and C-5 are characterized by similar T_1 values, their respective C—H vectors should form nearly equal angles with the preferential axis of rotation. Stereomodels indicate that this is the case, if the axis of rotation passes through, or forms small angles with, the C(2)—H(2) vector. The C(3)—H(3) vector forms an angle of 60° with this axis, whereas the C(4)—H(4) and C(5)—H(5) bonds form angles of 70.5° with the same axis. These qualitative relaxation characteristics reflect the molecular shape of **1**, which in turn determines the type of the overall molecular reorientation. The rotational dynamics of **1** can be adequately approximated by the diffusion of a prolate ellipsoid with a major axis passing through the C(2)—H(2) bond as in Fig. 1. The rotation about this axis is described by the rotational difusion coefficient, $D\|$, and the rotation of this axis is characterized by the rotational diffusion coefficient, $D\perp$.

Woessner has shown (8) that these two coefficients are related to the relaxation time by:

$$[1]\quad \frac{1}{T_1} = \frac{N\gamma_C^2\gamma_H^2\hbar^2}{r_{C-H}^6}(D\perp)^{-1}\left[\frac{A}{6} + \frac{B}{5+p} + \frac{C}{2+4p}\right], \qquad p = D\|/D\perp$$

where A, B, C are geometric functions (8) of the angle β formed by the pertinent C—H vector and the major axis of the ellipsoid. Because β = 0° for the C(2)—H(2) vector, its respective relaxation time is sufficient to determine $D\perp$ by means of the equation (8)

$$[2]\quad \frac{1}{T_1(\text{C-2})} = \frac{N\gamma_C^2\gamma_H^2\hbar}{r_{C-H}^6}(6D\perp)^{-1}$$

Using the relaxation data for C-4 (or C-5), a value of β = 70.5°, and of 1.09 Å for a C—H bond, the $D\perp$ and $D\|$ parameters displayed in Table 2 were calculated. By using the diffusion coefficients from Table 2 in eq. [1] with β = 60°, the angle formed by the C(3)—H(3) bond and the axis of rotation, the experimental T_1 values of C-3 are nicely reproduced (Table 3). This finding gives validity to the model used in the present treatment. Inspection of Table 2 reveals that over an 80°C temperature range the diffusion coefficients change by a factor of four, and that the pyrone ring rotates about the major axis ~1.5 times faster than about the perpendicular axis. The constancy of the $D\|/D\perp$ ratio is in accord with simple hydrodynamic theory (9), which requires that this ratio be determined by the molecular geometry. Plots of the diffusion coefficients $D\|$ and $D\perp$ on a semilogarithmic scale versus the reciprocal of the temperature (K^{-1}), in Fig. 2, give the following activation energies: 3.62 ± 0.46 kcal/mol for rotation about the major axis of the ellipsoid, and 4.07 ± 0.25 kcal/mol for rotation perpendicular to that axis.

The measured T_1 values of C-6 and C-7 are equal within the experimental error (Table 1), indicating that no puckering motion within the oxirane ring contributes to the relaxation of these carbons. The relaxation data may be interpreted in terms of motional anisotropy of a rigid molecule, since the major axis of the ellipsoid and the internal axis of rotation coincide, or, alternatively, by considering the superimposition of internal motion about the C(5)—C(6) bond upon the overall motion.

We first consider the effect of motional anisotropy, neglecting internal motion about the C(5)—C(6) bond. Anisotropic motion as described above will lead to differences in the T_1 values of the oxirane and pyrone ring carbons, if the angle formed by the C(6)—H(6) and (or) the C(7)—H(7) vectors and the axis of anisotropic motion is different from 109.5° or 120°, formed by the pertinent C—H vectors of C-4, C-5, and C-3, respectively. The HCH dihedral angle determined (10) for oxirane is 116.60°. A slightly larger value is probably expected for the disubstituted ring in **1**, due to increasing steric constraints caused by substitution.[3] However, such small angle differences, corresponding to a range ≤10°, must contribute very slightly to the T_1 calculated, assuming no internal motion. Therefore, the differences observed in the experimental T_1 values for the oxirane and pyrone carbons (Table 1), ranging

[3] A $HCC_{subst.}$ dihedral angle of 120° for the disubstituted oxirane ring was adopted in the following calculations.

TABLE 2. Rotational diffusion coefficients (in seconds^{-1}) for "asperlin" in DMSO-d_6 solution

T(K)	$D\perp \times 10^9$	$D\parallel \times 10^9$	$D\parallel/D\perp$	$D_e \times 10^9$	$D_e/D\parallel$	$D_i \times 10^{10}$
293	2.5	3.7	1.47	6.8	1.84	5.2
303	3.2	4.5	1.40	8.5	1.89	6.3
313	3.9	5.5	1.42	10.9	1.98	7.2
323	4.7	6.8	1.44	13.0	1.91	8.1
333	6.0	7.4	1.23	16.0	2.16	10.1
343	6.7	9.6	1.43	18.9	1.97	11.0
353	8.3	10.5	1.27	22.5	2.14	12.4
363	9.7	12.0	1.24	26.2	2.18	13.8
373	11.2	14.1	1.26	30.2	2.14	15.3

TABLE 3. Calculated and experimental T_1 values for C-3, C-6,7, and CH_3 of "asperlin"

T(K)	C-3 (exptl.)	C-3 (calcd)[a]	C-6,7 (exptl.)	C-6,7 (calcd.)[b,c]	C-6,7 (calcd.)[d,c]	C-6,7 (calcd.)[e,c]	CH_3-8 (exptl.)	CH_3-8 (calcd.)[f]
293	0.81	0.80	1.08	1.07 (26°)	1.08 (28°)	1.07 (26°)	1.51	1.50
303	0.99	1.02	1.36	1.35 (25°)	1.36 (29°)	1.33 (27°)	1.84	1.83
313	1.24	1.25	1.72	1.75 (26°)	1.72 (29°)	1.71 (28°)	2.16	2.15
323	1.52	1.52	2.05	2.06 (26°)	2.05 (29°)	2.03 (29°)	2.46	2.46
333	1.84	1.80	2.54	2.55 (25°)	2.54 (28°)	2.50 (28°)	3.02	3.03
343	2.19	2.15	2.94	2.92 (26°)	2.93 (29°)	2.95 (29°)	3.37	3.37
353	2.52	2.53	3.55	3.53 (26°)	3.54 (28°)	3.57 (30°)	3.86	3.87
363	2.95	2.93	4.14	4.10 (25°)	4.12 (28°)	4.13 (29°)	4.35	4.34
373	3.41	3.44	4.81	4.79 (26°)	4.82 (30°)	4.84 (32°)	4.90	4.89

[a]By employing Woessner's eqs. [1] and [2]; see text.
[b]By employing the two-states jump model with $\tau_A = \tau_B = 10^{-12}$ s.
[c]The values within parentheses are the angles θ that reproduce the experimental data.
[d]$\tau_A = 10^{-12}$ s, $\tau_B = 2 \times 10^{-12}$ s.
[e]$\tau_A = \tau_B = 10^{-11}$ s.
[f]By employing the model of multiple internal rotations as expressed by eqs. [9]–[11].

from 20 to 30%, are strong evidence against the possibility that overall anisotropic motion is responsible for the observed T_1 values of C-6 (or C-7).

A second approximate analysis is based on the assumption of an overall anisotropic reorientation, plus internal motion about the C(5)—C(6) bond. This analysis, however, is strongly model dependent. A model using unrestricted internal diffusion may be applied to this problem. Since the internal rotation axis is parallel to the major axis of the ellipsoid, the internal reorientation is independent of the reorientation of the remainder of the molecule about its symmetry axis (11). In this case, the relaxation of the oxirane ring can be described by eq. [1], in which $D\parallel$ is replaced by the internal rotational diffusion coefficient, D_e. The calculated diffusion coefficients for an angle $\beta = 120°$ are summarized in Table 2 and plotted vs. $(1/T)$ in Fig. 2. We find an activation energy of 4.06 ± 0.50 kcal/mol for the internal rotation of the epoxypropyl moiety. Moreover, inspection of Table 2 reveals that the epoxypropyl ring rotates about two times faster than the ellipsoid about its symmetry axis.

The temperature independence of the relaxation time ratio T_1(C-3,C-4,C-5)/T_1(C-6,C-7), observed in Table 1, can be explained by the constancy of the diffusion coefficient ratio $D_e/D\parallel$ throughout the temperature range of the measurements (Table 2). This result is a consequence of the similarity of activation energies for the internal and overall molecular diffusion processes. An analogous situation has been encountered in the study of the 3-chlorobiphenyl system (12). Activation energies for internal diffusion or jump models in a 25% solution of 3-chlorobiphenyl in DMSO-d_6 were found to be equal to that corresponding to the overall diffusion, within the experimental error.

A possible alternative to the approximate temperature independence of the relaxation time ratio could be that the internal motion is sufficiently rapid so that the relaxation rate falls within the geometric limit (13). In this case, the observed ratio becomes dependent on the diffusion coefficients of the overall motion only, with the rate reduced by the geometric factor $(3/2 \cos^2 \beta - 1/2)^2$ (13), i.e.,

$$[3] \quad \frac{T_1(\text{C-3,C-4,C-5})}{T_1(\text{C-6,C-7})} \rightarrow \frac{(3/2 \cos^2 120 - 1/2)^2}{\chi(p, \beta)}$$

where

$$[4] \quad \chi(p, \beta) = 1 + \frac{3(1-p)}{(5+p)} \sin^2 \beta + \frac{9(1-p)^2}{2(5+p)(1+2p)} \sin^4 \beta$$

Equation [4] is an alternative form (13*a*) of the expression in the brackets of eq. [1], with p and β defined previously. For $p = 1.5$ and $\beta = 109.5°$, expression [3] gives 0.0188. This geometric limit does not apply to the present data, since it predicts a relaxation time ratio that differs markedly from the observed value of ~0.75.

Next we consider restricted motion about the C(5)—C(6) bond. Some theoretical expressions (14–18) describe internal motion as a jump between several stable conformations.

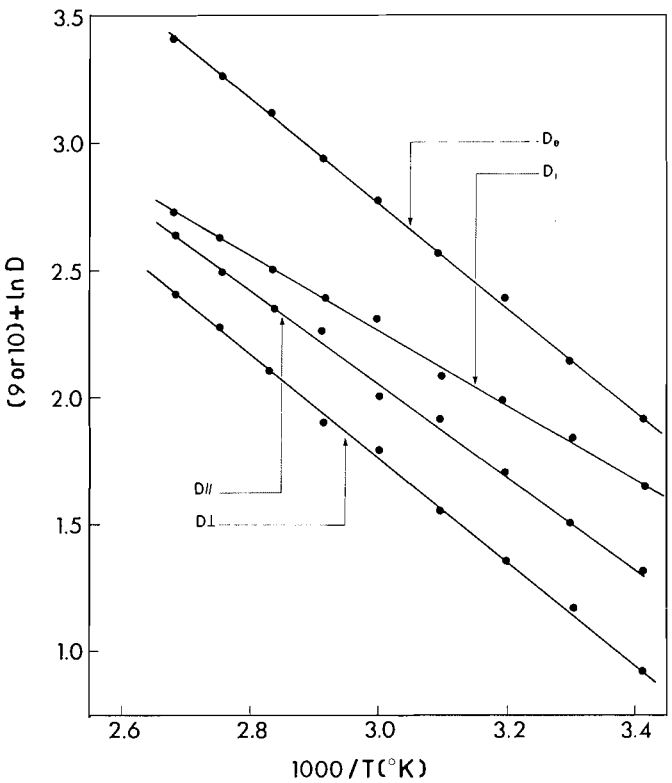

FIG. 2. Temperature dependence of the overall ($D\|$, $D\perp$), epoxypropyl (D_e), and methyl (D_i) rotational diffusion coefficients of "asperlin" in DMSO-d_6 solution.

According to these models, the rates of jumping or, equivalently, the lifetimes of the various conformations determine the relaxation rates. However, the fact that low amplitude diffusion is ineffective (15, 16) in causing relaxation suggests that a jump model involving relatively few conformations should be generally suitable for describing relaxation. Consequently, a model consisting of two alternate conformational states is taken to be an appropriate description of oscillation in the oxirane ring. The spectral density for such a model in the extreme narrowing region is given by (16, 17)

$$[5] \quad J(\omega) = \frac{(1 - C)}{6D\perp} + \frac{C}{6D\perp + 1/\tau_C}$$

where

$$[6] \quad \frac{1}{\tau_C} = \frac{1}{\tau_A} + \frac{1}{\tau_B}$$

and

$$[7] \quad C = \frac{3\tau_A\tau_B}{(\tau_A + \tau_B)^2}\{\sin^2\beta(1 - \cos 2\theta)\} \times \{2 - \sin^2\beta(1 - \cos 2\theta)\}$$

Expression [5] was derived by conceptualizing that the internal rotation axis is aligned with the symmetry axis of the ellipsoid. In eqs. [5]–[7], β is the angle formed by the C—H relaxation vector and the internal axis, τ_A and τ_B are the lifetimes of the two states, and θ is the half-range of the jump.

For very rapid internal jumping between the two states, this model would lead to a limiting relaxation time ratio of

$$[8] \quad \frac{T_1(\text{C-3,C-4,C-5})}{T_1(\text{C-6,C-7})} \rightarrow (1 - C)$$

Assuming $\tau_A = \tau_B$, the limiting value of the relaxation time ratio depends on the angle θ. Values of 0.72 and 0.70 were obtained for jumps between $\theta = \pm 20°$ and $\pm 90°$, respectively. These are in good agreement with the observed ratios in Table 1. In particular, an angle of $\theta = \pm 20°$ is commensurate with a very slight distortion of the *anti* orientation of the H-5 and H-6 protons deduced from the coupling data (4).

Although this model reproduces the experimental relaxation ratio, it does not give information about the actual rate of internal jumping nor a clear measure of the jumping amplitude. Of course, the internal motion does not have to be so fast that the observed relaxation ratio is described by a geometric factor only. The second term in eq. [5] could also contribute to the observed relaxation rate.

The problem of interpreting the relaxation data in terms of eqs. [5]–[7] is, clearly, unresolved. However, the temperature dependence of the relaxation data in Table 1 can be used to evaluate the validity of the approximations inherent in this model. T_1 values calculated for C-6,7 using different τ_A and τ_B lifetimes are summarized in Table 3 for comparison with experimental data. Good fits were obtained with $\tau_A = \tau_B = 10^{-12}$ s and $\tau_A = 10^{-12}$ s and $\tau_B = 2 \times 10^{-12}$ s, although these lifetimes gave small differences in the values of 2θ, i.e., 50–52° and 56–60° for the first and second case, respectively. It should be noted that plots of T_1 vs. θ corresponding to various values of $D\perp$ (Table 2) and $\tau_A = \tau_B$ are skewed, with the maximum T_1 value occurring at $\theta = 50°$. A maximal factor of 5 for τ_A/τ_B is possible in order to fit the data, although this value corresponds to a large range, $2\theta \simeq 120°$ for C-6,7. A factor of 6 is inconsistent with the data. Using $\tau_A = \tau_B = 10^{-11}$ s gives a range for $2\theta \simeq 60°$, which is similar to that when $\tau_A = 10^{-12}$ s and $\tau_B = 2 \times 10^{-12}$ s. Reducing τ_A and τ_B to 10^{-10} s renders even $\theta = 50°$ insufficient to fit the observed T_1 values of C-6,7. In summary, these calculations show that lifetimes in the range 10^{-11} to 10^{-12} s fit the data adequately, whereas longer lifetimes are inconsistent with the observed T_1 values.

The present findings demonstrate that the relaxation data for the protonated carbons of the oxirane ring of **1** do not uniquely define a dynamic model. The internal motion of the oxirane ring can be satisfactorily approximated either by free rotation about the C(5)—C(6) bond, or by a jumping process between two stable conformations. The problem of discriminating between these two models is due mainly to the fortuitous similarity in the activation energies of the internal and overall diffusional motions. However, inspection of molecular models indicates that geometrical constraints imposed on the rotation of the epoxypropyl moiety are not severe enough to justify restricted rotation about the C(5)—C(6) bond.

The relaxation of the carbon (CH_3-8) receives contributions from three types of molecular motion: (*1*) the internal rotation of the methyl group about its symmetry axis described by diffusion coefficient D_i; (*2*) the reorientation of the adjacent oxirane ring with diffusion coefficient D_e; and (*3*) the overall molecular motion characterized by diffusion coefficients $D\|$ and $D\perp$. Approximate separation of these relaxation contributions can be realized by applying the stochastic diffusion model of multiple internal rotations, developed initially by Wallach (19), and subsequently modified by Levine *et al.* (20, 21). In the present case, two motions about the C(5)—C(6) and C(7)—CH_3 bonds are considered to be free and independent of the overall molecular reorientation. Restricted rotation about the C(6)—C(7) bond ensures that the two internal motions are independent of one another. The spectral density used to

TABLE 4. Motional parameters and calculated relaxation times for **1**, including all C—H interactions[a]

T(K)	p	$D\perp \times 10^9$	$D\parallel \times 10^9$	T_1 (C-2)	T_1 (C-3)	T_1 (C-4)	T_1 (C-5)
293	1.48	2.6	3.8	0.69	0.78	0.81	0.82
323	1.46	4.8	7.0	1.30	1.48	1.55	1.55
353	1.28	8.5	10.9	2.28	2.51	2.57	2.58
373	1.26	11.4	14.4	3.14	3.34	3.43	3.45

[a]Using eq. [12].

calculate the required relaxation times is obtained by Fourier transformation of the appropriate autocorrelation function (19, 20):

$$[9] \quad J(\omega) = \sum_{\substack{m,a \\ b,c}} |d_{ma}(\beta_0)|^2 |d_{bc}(\beta_1)|^2 |d_{co}(\beta_2)|^2 \frac{\tau}{1 + \omega^2\tau^2}$$

where

$$[10] \quad \tau = (6D\perp + m^2(D\parallel - D\perp) + a^2D_e + c^2D_i)^{-1}$$

and $d_{ij}(\beta)$ are the second-rank Wigner rotation matrices (22). The angles β_0, β_1, β_2 correspond to angles between the first internal rotation axis and the major axis of the ellipsoid, the second and the third rotational axis, and the final rotation axis and the C—H relaxation vector, respectively. The subscripts, m, a, b, c are integers ranging from -2 to $+2$. It should be noted that the summation of the matrix elements $\sum_{a,b} |d_{ab}(\beta)|^2$ in eq. [9] is omitted, since it is equal to unity, as the second internal rotation about the C(6)—C(7) is frozen (19).

The relationship between spin-lattice relaxation times and spectral density is given by

$$[11] \quad \frac{1}{T_1} = \frac{N\gamma_C^2\gamma_H^2\hbar^2}{10r_{C-H}^6}\{J(\omega_H - \omega_C) + 3J(\omega_C) + 6J(\omega_H + \omega_C)\}$$

Using the spectral density eqs. [9]–[11], numerical results were obtained for values of $D\perp$, $D\parallel$, and D_e from Table 2. The parameter, D_i, fitting the experimental relaxation times, is depicted in the last column of Table 2 for each temperature, whereas Table 3 gives the T_1 values of the methyl carbons reproduced by the model of the multiple internal rotations. The agreement between the reproduced and experimental data is very good. The temperature dependence of the D_i diffusion coefficient, shown in Fig. 2, corresponds to an activation energy of 2.93 kcal/mol. This energy value implies that some resistance to free methyl internal rotation is likely to occur in **1**. This result is not unexpected due to the geminal disposition of the methyl group and H-7 in the oxirane ring of **1**.

The relaxation parameters of **1** shown in Table 1 are averages of at least two measurements. The effect of random noise and other sources of error (e.g., temperature fluctuations) contribute to the experimental uncertainty by 5–10%. The error introduced by nOe experiments was 5%. The overall effect of these sources of error results in a standard deviation of 7–11% for each individual T_1 measurements or a standard deviation of 5–8% for each mean value. This margin of experimental error appears to be quite substantial compared to the small anisotropy observed for **1**, which gives T_1 differences of the order of 10–16% (Table 1). Therefore, the legitimacy of the present quantitative analysis should be tested by considering those factors that may affect the anisotropy of the motion.

The first factor is related to the choice of the anisotropic axis of reorientation of the ellipsoid. A preferential axis of rotation that forms small angles with the C(2)—H(2) vector, it is not expected to modify the basic conclusions of this report. Larger deviations, however, may change the shape of the ellipsoid and consequently the interpretation of the relaxation data. Using Platzer's method (23), an anisotropic analysis for **1** was carried out by adjusting the anisotropic ratio, p, while varying the orientation of the anisotropic axis of rotation (i.e., the angles β relative to the various C—H vectors). The best agreement between the observed T_1 values of all the ring carbons and the bracketed quantity in eq. [1] was obtained when the axis formed angles of 10–20° with the C(2)—H(2) vector. For an angle of 20° between the C(2)—H(2) vector and the assumed symmetry axis of the ellipsoid for two sets of measurements, the motional parameters obtained by this approach were: $p = 1.37$, $D\perp = 2.4 \times 10^9\,s^{-1}$ at 293 K, and $p = 1.21$, $D\perp = 8.1 \times 10^9\,s^{-1}$ at 353 K. Consistent results were obtained for the remaining temperatures. Larger changes of the orientation of the anisotropic axis resulted in higher motional anisotropies than those reported in Table 2, but failed to reproduce the experimental data. Discrepancies of the order of 15, 25, and 40% were observed between the calculated and the experimental T_1 values for changes of the orientation of the anisotropic axis by 30, 40, and 50°, respectively.

The second factor we have investigated is the contribution of the intramolecular nonbonded C—H interactions to the relaxation of the ring carbons of **1**. T_1 values were calculated for each carbon, over a range of trial ratios p, with relaxation contributions summed over all protons in the molecule, i.e.,

$$[12] \quad \frac{1}{T_1^i} = \gamma_H^2\gamma_C^2\hbar^2\,(6D\perp)^{-1} \sum_j r_{ij}^{-6}\left(A_{ij} + \frac{6B_{ij}}{5+p} + \frac{6C_{ij}}{2+4p}\right)$$

where $A_{ij} = \frac{1}{4}(3\cos^2\beta_{ij} - 1)^2$, $B_{ij} = 3\sin^2\beta_{ij}\cos^2 B_{ij}$), $C_{ij} = \frac{3}{4}\sin^4\beta_{ij}$, and β_{ij} is the angle between the symmetry axis of the ellipsoid as in Fig. 1 and the vector joining the ith carbon with the jth proton. Internuclear separations, r_{ij}, were calculated using the ATCOOR computer program (24) assuming standard bond lengths and angles. Representative results at four temperatures are summarized in Table 4. Although no significant differences were found in the calculated diffusion coefficients from those obtained using bonded C—H interactions, it appears that contributions from nonbonded C—H interactions account for ~1.5% of the relaxation of the C-2 carbon and ~3% for each of the remaining ring carbons, which relax via two nonbonded protons at distances less than 2.5 Å. These contributions decrease the margin of the T_1 differences to 7–13%, which is comparable to the experimental uncertainty at high temperatures. This molecule, therefore, represents the borderline case, in which the overall motion may be described as isotropic at

high temperatures. The approximate assumption that **1** can be described by an overall isotropic motion plus internal rotation of the epoxypropyl ring leads to activation energies of 3.89 ± 0.16 kcal/mol and 4.28 ± 0.39 kcal/mol for the overall and internal motions, respectively. The latter value is considered as the upper limit for the internal rotation.

Acknowledgements

The authors acknowledge the valuable assistance of Prof. A. S. Perlin in the preparation of this manuscript, and wish to thank McGill University for financial support during the course of this investigation.

1. A. D. Argoudelis, J. H. Coates, and R. R. Herr. Antimicrob. Agents Chemother. 801 (1965); S. P. Owen and B. K. Bhuynan. Antimicrob. Agents Chemother. 804 (1965).
2. S. Lesage and A. S. Perlin. Can. J. Chem. **56**, 2889 (1978).
3. S. Lesage and A. S. Perlin. Can. J. Chem. **56**, 3117 (1978).
4. P. Dais and A. S. Perlin. Can. J. Chem. **63**, 1009 (1985).
5. G. C. Levy and I. R. Peat. J. Magn. Reson. **18**, 199 (1975).
6. M. Sass and D. Ziessow. J. Magn. Reson. **25**, 263 (1977).
7. P. Dais and A. S. Perlin. Can. J. Chem. **61**, 1542 (1983).
8. D. E. Woessner. J. Chem. Phys. **37**, 647 (1962).
9. C. M. Hu and R. Zwanzig. J. Chem. Phys. **60**, 4354 (1974).
10. C. Hirose. Bull. Chem. Soc. Jpn. **47**, 1311 (1974).
11. D. E. Woessner and B. S. Snowden, Jr. Adv. Mol. Relax. Processes, **3**, 181 (1972).
12. K. L. Oehme, G. Rudakoff, and R. Radeglia. Adv. Mol. Relax. Interact. Processes, **12**, 87 (1978).
13. (*a*) A. Allerhand, D. Doddrell, and R. Komoroski. J. Chem. Phys. **55**, 189 (1971); (*b*) G. C. Levy, J. D. Gargioli, and F. A. I. Anet. J. Am. Chem. Soc. **95**, 1527 (1973).
14. M. Baldo, K. J. Irgolic, and G. C. Papalardo. Mol. Phys. **38**, 1467 (1979).
15. D. Ghesquiere, B. Ban, and C. Chachaty. Macromolecules, **10**, 743 (1977).
16. R. E. London. J. Am. Chem. Soc. **100**, 2678 (1978).
17. R. London and M. A. Phillipi. J. Magn. Reson. **45**, 476 (1981).
18. B. Ban. J. Magn. Reson. **45**, 118 (1981).
19. D. Wallach. J. Chem. Phys. **47**, 5258 (1967).
20. Y. K. Levine, P. Partington, and G. C. K. Roberts. Mol. Phys. **25**, 497 (1973).
21. Y. K. Levine, N. J. M. Birdsall, A. G. Lee, J. C. Metcalfe, P. Partington, and G. C. Roberts. J. Chem. Phys. **60**, 2890 (1974).
22. D. M. Brink and G. R. Satchler. Angular momentum. Clarendon Press, Oxford. 1968.
23. N. Platzer. Org. Magn. Reson. **11**, 350 (1978).
24. J. E. Norlander. Quant. Chem. Progr. Exchange, QCPE No. 250.

Synthesis, characterization, and X-ray structures of Rh(I) monocarbonyl complexes containing unsymmetric tridentate pyrazolylgallate ligands

DAVID A. COOPER, STEVEN J. RETTIG, AND ALAN STORR[1]

Department of Chemistry, University of British Columbia, 2036 Main Mall, Vancouver, B.C., Canada V6T 1Y6

Received June 25, 1985

DAVID A. COOPER, STEVEN J. RETTIG, and ALAN STORR. Can. J. Chem. **64**, 566 (1986).

The reaction of the $[Rh(CO)_2Cl]_2$ dimer with the $Na^+[Me_2Ga(N_2C_3H_3)(OCH_2(C_5H_4N))]^-$ ligand has yielded the planar four-coordinate species $[Me_2Ga(N_2C_3H_3)(OCH_2(C_5H_4N))]Rh(CO)$, (LRh(CO)), displaying the tridentate gallate ligand in a meridional coordination mode. In addition, a second product, of similar geometry but with one of the Me groups on the Ga replaced by a Cl atom, viz, $[(Cl)MeGa(N_2C_3H_3)(OCH_2(C_5H_4N))]Rh(CO)$, has also been isolated and characterized. The former complex undergoes a facile oxidative addition reaction with MeI, the transient six-coordinate Rh(III) species produced being rapidly converted, in a methyl migration step, to the five-coordinate Rh(III) acetyl complex, LRh(COMe)I. Crystals of $[Me_2Ga(N_2C_3H_3)(OCH_2(C_5H_4N))]Rh(CO)$ are monoclinic, a = 13.139(2), b = 13.324(2), c = 17.352(2) Å, β = 103.251(7)°, Z = 8, space group $I2/a$, and those of $[(Cl)MeGa(N_2C_3H_3)(OCH_2(C_5H_4N))]Rh(CO)$ are triclinic, a = 8.846(2), b = 12.714(3), c = 7.631(2) Å, α = 93.82(1), β = 113.94(1), γ = 107.99(1)°, Z = 2, space group $P\bar{1}$. Both structures were solved by conventional heavy-atom methods and were refined by full-matrix least-squares procedures to final R values of 0.029 and 0.048 for 1890 and 1939 reflections with $I \geq 3\sigma(I)$, respectively. Both molecules display irregular square planar coordination geometry about Rh with Rh—O = 2.038(3) and 2.048(3), Rh—N(pyrazolyl) = 2.022(4) and 2.025(7), Rh—N(pyridyl) = 2.038(3) and 2.020(6), Rh—CO = 1.778(5) and 1.808(9) Å, respectively, for the two compounds. Molecules of $[Me_2Ga(N_2C_3H_3)(OCH_2(C_5H_4N))]Rh(CO)$ form weakly associated, centrosymmetric dimers via an intermolecular Rh···Rh interaction of 3.5445(7) Å.

DAVID A. COOPER, STEVEN J. RETTIG et ALAN STORR. Can. J. Chem. **64**, 566 (1986).

La réaction du dimère $[Rh(CO)_2Cl]_2$ avec le ligand $Na^+[Me_2Ga(N_2C_3H_3)(OCH_2(C_5H_4N))]^-$ conduit à la formation d'espèces tétracoordonnées planes $[Me_2Ga(N_2C_3H_3)(OCH_2(C_5H_4N))]Rh(CO)$, (LRh(CO)), dans lesquelles le ligand tridentate gallate est dans un mode de coordination méridional. De plus, on a isolé et caractérisé un deuxième produit, de géométrie semblable, dans lequel un des groupements méthyles du Ga a été remplacé par un atome de Cl. Le premier complexe subit une réaction d'addition oxydative facile sous l'influence du MeI; l'espèce hexacoordonnée du Rh(III) qui se produit d'une façon transitoire se transforme rapidement, par une migration de méthyle, en un complexe pentacoordonné du Rh(III) acétylé, le LRh(COMe)I. Les cristaux du $[Me_2Ga(N_2C_3H_3)(OCH_2(C_5H_4N))]Rh(CO)$ sont monocliniques avec a = 13,139(2), b = 13,324(2), c = 17,352(2) Å, β = 103,251(7)°, Z = 8 et groupe d'espace $I2/a$ alors que ceux du $[(Cl)MeGa(N_2C_3H_3)(OCH_2(C_5H_4N))]Rh(CO)$ sont tricliniques avec a = 8,846(2), b = 12,714(3), c = 7,631(2) Å, α = 93,82(1), β = 113,94(1), γ = 107,99(1)°, Z = 2 et groupe d'espace $P\bar{1}$. On a résolu les deux structures par les méthodes conventionnelles aux atomes lourds et on les affinées par la méthode des moindres carrés (matrice entière) jusqu'à des valeurs finales de R de 0,029 et 0.048 respectivement pour 1890 et 1939 réflexions avec $I \geq 3\sigma(I)$. Les deux molécules présentent des géométries de coordination autour du Rh qui sont du type plan carré irrégulier avec Rh—O = 2,038(3) et 2,048(3), Rh—N(pyrazolyle) = 2,022(4) et 2,025(7), Rh—N(pyridyle) = 2,038(3) et 2,020(6), Rh—(CO) = 1,778(5) et 1,808(9) Å respectivement pour les deux composés. Les molécules de $[Me_2Ga(N_2C_3H_3)(OCH_2(C_5H_4N))]Rh(CO)$ forment des dimères centrosymétriques, faiblement associés par le biais d'une interaction intermoléculaire Rh···Rh de 3,5445(7) Å

[Traduit par le journal]

Introduction

An earlier publication (1) reported the synthesis and complexation of the novel tridentate unsymmetric anionic organogallate ligand **1**. $[Me_2Ga(N_2C_3H_3)(OCH_2(C_5H_4N))]^-$. The ligand, containing both pyrazolyl and pyridyl donor groups, was shown to coordinate in a *facial* mode in a number of octahedral transition metal carbonyl compounds. The present account details the reaction of this ligand with the $[Rh(CO)_2Cl]_2$ dimer. The major product isolated, LRh(CO), has been shown by ir, ^1H nmr, mass spectrometry, and, definitively, by X-ray crystallographic analysis to display the L ligand in a *meridional* coordination mode. The complex undergoes a facile oxidative addition reaction with MeI, followed by a migratory insertion reaction to yield Rh(III) acetyl compound. A second product from the reaction of NaL with $[Rh(CO)_2Cl]_2$, namely, the chloro substituted species $[(Cl)MeGa(N_2C_3H_3)(OCH_2(C_5H_4N))]Rh(CO)$, has been fully characterized and its X-ray crystal structure determined.

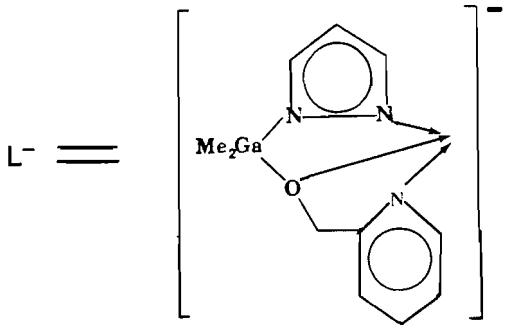

1

Experimental

Starting materials

Air-sensitive materials were handled in a glove-box under an atmosphere of oxygen-free dry nitrogen, in a nitrogen-blanketed apparatus, or on a high-vacuum line. Tetrahydrofuran (THF) was dried by refluxing over Na–benzophenone and was used immediately following distillation. Benzene, CH_2Cl_2, and hexane were dried by refluxing over potassium, calcium hydride, and calcium sulphate, respectively, followed by distillation. $[Rh(CO)_2Cl]_2$ (Strem Chemi-

[1]Author to whom correspondence may be addressed.

TABLE 1. Analytical and infrared data

Compound	Calcd. (%) C	H	N	Cl	Found (%) C	H	N	Cl	ν_{CO}(cm^{-1}) Nujol	CH_2Cl_2
LRh(CO)	35.49	3.70	10.35		35.09	3.75	10.35		1931	1962
L'Rh(CO)*	30.97	2.82	9.85	8.33	30.95	2.86	9.85	8.00	1942	1968
LRh(COMe)I	28.48	3.29	7.67		28.72	3.34	7.52		1694	1714

*L' = (Cl)MeGa($N_2C_3H_3$){$OCH_2(C_5H_4N)$}.

cals) and iodine (Aldrich) were used as supplied. MeI (Fisher) was distilled from P_2O_5 before use. The sodium salt, NaL, was prepared as a standard THF solution as described earlier (1).

Reaction of $[Rh(CO)_2Cl]_2$ with NaL

A two-molar equivalent of the NaL ligand solution was added dropwise to a stirred THF solution of $[Rh(CO)_2Cl]_2$ (0.276 g, 0.70 mmol) maintained at −78°C. The resulting reaction mixture was warmed slowly to room temperature and then refluxed for 18 h, during which time the original yellow solution turned dark reddish-brown. At this point the ir spectrum of the product mixture indicated complete disappearance of the starting rhodium carbonyl dimer and the presence of new carbonyl species giving ν_{CO} bands at 2018 and 1953 cm^{-1}. The solvent was then removed under vacuum and the resulting dark reddish-brown residue extracted with benzene. The benzene solvent was allowed to evaporate slowly from the filtered extracts to yield, first, orange cube-shaped crystals of LRh(CO) (~50% yield) and then, from more concentrated solutions, yellow platelet crystals of the chloro derivative [(Cl)MeGa($N_2C_3H_3$)($OCH_2(C_5H_4N)$)]Rh(CO) (~15%) yield). Analytical, ir, and ^{1}H nmr data for the two complexes are collected in Tables 1 and 2.

Reaction of LRh(CO) with MeI

A 1:1 molar ratio of LRh(CO) (0.056 g, 0.14 mmol) and MeI (0.020 g, 0.14 mmol) was stirred in CH_2Cl_2 at room temperature. The original solution gradually changed color from yellow to orange with the concomitant loss of the ν_{CO} band of LRh(CO) at 1962 cm^{-1} and the appearance of two new carbonyl bands at 1714 and 2042 cm^{-1} in the ir spectrum of the reaction mixture. After 2 h the solvent was allowed to evaporate slowly from the reaction mixture to yield small orange crystals of LRh(COMe)I in ~30% yield (see Tables 1 and 2).

Reaction of LRh(CO) with I_2

Iodine (0.030 g, 0.11 mmol) was stirred at room temperature with an equimolar amount of LRh(CO) (0.043 g, 0.11 mmol) in Ch_2Cl_2. The ν_{CO} band of the starting material (1962 cm^{-1}) gradually disappeared and was replaced by a new carbonyl band at higher frequency (2095 cm^{-1}) in the ir spectrum. A black solid was isolated from the solution at the end of the reaction but no analytically pure sample of the expected diiodide, $LRh(CO)I_2$, could be obtained.

X-ray crystallographic analyses

[Dimethyl(pyrazol-1-yl)(2-pyridylmethoxy)gallato-N^2,O,N^3]carbonylrhodium(I)

A crystal bounded by the 6 faces (followed by the distances in mm between parallel faces): {1 1 0}, 0.134, and {0 0 1}, 0.176, was mounted in a general orientation. Unit-cell parameters were refined by least squares on 2 sin θ/λ values for 25 reflections (2θ = 30–35°) measured on a diffractometer with Mo-Kα radiation (λ(Kα$_1$) = 0.70930, (λ(Kα$_2$) = 0.71359 Å). Crystal data at 22°C are:

$C_{12}H_{15}GaN_3O_2Rh$ fw 405.90

Monoclinic, a = 13.139(2), b = 13.324(2), c = 17.352(2) Å, β = 103.251(7)°, V = 2956.6(8) Å^3, ρ_m = 1.82 (flotation in $CHBr_3$–$CHCl_3$), Z = 8, ρ_c = 1.824 Mg m^{-3}. $F(000)$ = 1600, μ(Mo-$K\alpha$) = 29.2 cm^{-1}. Absent reflections: hkl, $h+k+l$ odd, and $h0l$, h (and l) odd, space group $I2/a$ (non-standard setting of $C2/c$, C_{2h}^6, No. 15 with equivalent positions: (0 0 0), (1/2, 1/2, 1/2)±(x, y, z; 1/2-x, y, -z)) from structure analysis.

Intensities were measured with graphite-monochromated Mo-Kα radiation on an Enraf–Nonius CAD4-F diffractometer. An ω–2θ scan at 0.84–6.71° min^{-1} over a range of (0.70 + 0.35 tan θ) degrees in ω (extended by 25% on both sides for background measurement) was employed. Data were measured to 2θ = 55°. The intensities of 3 check reflections, measured every 3600 s throughout the data collection, remained constant to within 3%. After data reduction,[2] an absorption correction was applied using the Gaussian integration method (2,3). Transmission factors ranged from 0.657 to 0.716 for 96 integration points. Of the 3388 independent reflections measured, 1890(55.8%) had intensities greater than or equal to 3σ(I) above background, where $\sigma^2(I) = S + 2B + (0.04(S-B))^2$ with S = scan count and B = normalized background count.

The centrosymmetric space group $I2/a$ was suggested by both the E-statistics and by the Patterson function, from which the coordinates of the Rh and Ga atoms were determined. The remaining non-hydrogen atoms were positioned from a subsequent difference map. In the final stages of refinement the non-hydrogen atoms were refined with anisotropic thermal parameters and hydrogen atoms were fixed in calculated positions (C(sp^2)—H = 0.97, C(sp^3)—H = 0.98 Å, U_H proportional to U_{eq} of the parent atom, methyl hydrogen positions based on observed positions). The scattering factors of ref. 4 were used for non-hydrogen atoms and those of ref. 5 for hydrogen atoms. Anomalous scattering factors from ref. 6 were used for the Rh and Ga atoms. The weighting scheme $w = 1/\sigma^2(F)$, where $\sigma^2(F)$ is derived from the previously defined $\sigma^2(I)$, gave uniform average values of $w(|F_o|-|F_c|)^2$ over ranges of both $|F_o|$ and sin θ/λ and was employed in the final stages of full-matrix refinement of 172 variables. Reflections with $I < 3\sigma(I)$ were not included in the refinement. Convergence was reached at R = 0.029 and R_w = 0.030 for 1890 reflections with $I \geq 3\sigma(I)$. For all 3388 reflections R = 0.093. The function minimized was $\Sigma w(|F_o|-|F_c|)^2$, $R = \Sigma||F_o|-|F_c||/\Sigma|F_o|$ and $R_w = (\Sigma w|F_o| \propto -|F_c|)^2/\Sigma w|F_o|^2)^{1/2}$.

On the final cycle of refinement the mean and maximum parameter shifts corresponded to 0.007 and 0.038σ, respectively. The mean error in an observation of unit weight was 1.143. The final difference map showed no unusual features, the largest peak (0.45 e Å^{-3}) being near the Rh atom. The final positional and thermal parameters appear in Tables 3 and 9[3] respectively. Bond lengths, bond angles, and intra-annular torsion angles appear in Table 4–6, respectively. Calculated hydrogen parameters (Table 8) and complete listings of torsion angles (Table 10) have been deposited.[3] Measured and calculated structure factors have been placed in the Depository of Unpublished Data.[3]

[2]The computer programs used include locally written programs for data processing and locally modified versions of the following: ORFLS, full-matrix least-squares, and ORFFE, function and errors, by W. R. Busing, K. O. Martin and H. A. Levy; FORDAP, Patterson and Fourier syntheses, by A. Zalkin; ORTEP II, illustrations, by C. K. Johnson.

[3]The structure factor table, Table 9 (anisotropic thermal parameters), and other material mentioned in the text may be purchased from the Depository of Unpublished Data, CISTI, National Research Council of Canada, Ottawa, Ont., Canada, K1A 0S2.

TABLE 2. ^{1}H nuclear magnetic resonance data for C_6D_6 solutions. ($\tau_{C_6D_5} \equiv 2.84$ ppm)

Compound	Ga—Me	—OCH_2—	—C(=O)—Me	Pyrazolyl and pyridyl protons†					
				H_δ	H_β	H_γ	H_ξ	H_η	H_θ	H_ι
LRh(CO)	10.00(s)	5.46(s)		2.32(d)	3.95(t)	2.69(d)	4.07(d)	4.15(t)	3.51(td)	1.90(dt)
L′Rh(CO)*	9.84(s)	$A=4.75, B=5.93$ ($J=16$ Hz)		2.50(d)	3.91(t)	2.68(d)	3.97(d)	4.00(t)	3.38(td)	2.08(dt)
LRh(COMe)I	9.92(s)	$A=4.78, B=5.24$ ($J=16$ Hz)	7.20(s)	1.12(d)	3.92(t)	2.76(d)	3.84(d)	4.00(t)	3.40(td)	0.44(dt)
	10.12(s)									

Abbreviations: s=singlet, d=doublet, t=triplet, td=triplet of doublets, dt=doublet of triplets.
*L′ = (Cl)MeGa($N_2C_3H_3$)($OCH_2(C_5H_4N)$).
†Consult Figs. 1, 4, and 5 for proton designations.

TABLE 3. Final positional (fractional × 10^4, Rh and Ga × 10^5) and isotropic thermal parameters ($U \times 10^3$ Å^2) with estimated standard deviations in parentheses*

Atom	x	y	z	U_{eq}
		[$Me_2Ga(N_2C_3H_3)(OCH_2(C_5H_4N))$]Rh(CO)		
Rh	32860(3)	35003(3)	22935(2)	38
Ga	23476(4)	51868(4)	34399(3)	47
O(1)	3174(3)	4019(3)	3376(2)	53
O(2)	3644(3)	2903(3)	749(2)	81
N(1)	1802(3)	5152(3)	2275(2)	50
N(2)	2164(3)	4491(3)	1789(2)	45
N(3)	4395(3)	2624(3)	2995(2)	42
C(1)	3481(4)	3111(4)	1358(3)	49
C(2)	3249(5)	6359(4)	3745(4)	71
C(3)	1212(4)	4869(4)	3976(3)	64
C(4)	3820(4)	3552(4)	4029(3)	49
C(5)	4537(3)	2800(3)	3778(3)	41
C(6)	5303(4)	2309(4)	4326(3)	59
C(7)	5939(4)	1620(5)	4078(3)	71
C(8)	5781(5)	1424(4)	3274(4)	71
C(9)	5009(4)	1937(4)	2763(3)	57
C(10)	1074(5)	5712(4)	1814(4)	67
C(11)	926(4)	5447(4)	1044(3)	69
C(12)	1629(4)	4680(4)	1049(3)	56
		[(Cl)$MeGa(N_2C_3H_3)(OCH_2(C_5H_4N))$]Rh(CO)		
Rh	53098(8)	41816(5)	27399(9)	40
Ga	15839(12)	20017(8)	−1266(14)	50
Cl	148(3)	1858(2)	1665(4)	72
O(1)	2846(7)	3559(5)	366(8)	53
O(2)	8810(9)	5085(6)	6200(10)	81
N(1)	3723(9)	1702(6)	1359(10)	49
N(2)	5266(9)	2575(6)	2566(10)	48
N(3)	4882(8)	5646(5)	2439(9)	42
C(1)	7464(12)	4766(7)	4864(13)	55
C(2)	86(12)	1193(9)	−2833(14)	72
C(3)	2072(11)	4382(8)	−215(13)	53
C(4)	3297(11)	5537(7)	937(12)	46
C(5)	2826(12)	6474(8)	542(13)	55
C(6)	3947(13)	7522(8)	1700(15)	64
C(7)	5563(13)	7648(8)	3241(15)	66
C(8)	5955(11)	6680(8)	3563(13)	53
C(9)	3993(14)	728(9)	1425(16)	76
C(10)	5755(15)	972(9)	2695(18)	86
C(11)	6493(11)	2113(8)	3340(14)	63

*U_{eq} = 1/3 trace (diagonalized U).

[(Chloro)methyl(pyrazol-1-yl)(2-pyridylmethoxy)gallato-N^2,O,N^3]-carbonylrhodium(I)

Experimental details are as above except where noted. The six bounding faces of the crystal are of the forms: {0 1 0}, 0.126, {−1 0 1}, 0.175, and {1 1 0}, 0.388 mm (between parallel pairs of faces). Reflections used for the determination of the lattice constants had 2θ = 30–38°. Crystal data are:

$C_{11}H_{12}ClGaN_3O_2Rh$ fw 426.31

Triclinic, a = 8.846(2), b = 12.714(3), c = 7.631(2) Å, α = 93.82(1), β = 113.94(1), γ = 107.99(1)°, V = 727.6(3) Å^3, ρ_m = 1.93, Z = 2, ρ_c = 1.946 Mg m^{-3}, $F(000)$ = 416, μ(Mo-Kα) = 31.5 cm^{-1}. Absent reflections: none, space group $P\bar{1}$ (C_i^1, No. 2, reduced cell, conventional orientation) from structure analysis.

An ω–2θ scan at 1.55-10.06° min^{-1} over a range of (0.95 + 0.35 tan θ)° in ω was employed. Of 3336 independent reflections measured,

TABLE 4. Bond lengths (Å) with estimated standard deviations in parentheses

Bond	Length(Å)	Bond	Length(Å)
	$[Me_2Ga(N_2C_3H_3)(OCH_2(C_5H_4N))]Rh(CO)$		
Rh—O(1)	2.038(3)	N(1)—C(10)	1.327(6)
Rh—N(2)	2.022(4)	N(2)—C(12)	1.339(6)
Rh—N(3)	2.038(3)	N(3)—C(5)	1.350(5)
Rh—C(1)	1.778(5)	N(3)—C(9)	1.341(6)
Ga—O(1)	1.915(3)	C(4)—C(5)	1.506(6)
Ga—N(1)	1.984(4)	C(5)—C(6)	1.380(7)
Ga—C(2)	1.958(6)	C(6)—C(7)	1.375(7)
Ga—C(3)	1.976(5)	C(7)—C(8)	1.387(8)
O(1)—C(4)	1.397(5)	C(8)—C(9)	1.368(8)
O(2)—C(1)	1.159(5)	C(10)—C(11)	1.354(8)
N(1)—N(2)	1.377(5)	C(11)—C(12)	1.376(7)
	$[(Cl)MeGa(N_2C_3H_3)(OCH_2(C_5H_4N))]Rh(CO)$		
Rh—O(1)	2.048(5)	N(1)—C(9)	1.332(11)
Rh—N(2)	2.025(7)	N(2)—C(11)	1.339(10)
Rh—N(3)	2.020(6)	N(3)—C(4)	1.362(9)
Rh—C(1)	1.808(9)	N(3)—C(8)	1.336(10)
Ga—Cl	2.194(3)	C(3)—C(4)	1.475(12)
Ga—O(1)	1.871(5)	C(4)—C(5)	1.391(11)
Ga—N(1)	1.942(6)	C(5)—C(6)	1.362(12)
Ga—C(2)	1.932(9)	C(6)—C(7)	1.386(13)
O(1)—C(3)	1.421(9)	C(7)—C(8)	1.389(12)
O(2)—C(1)	1.132(9)	C(9)—C(10)	1.378(14)
N(1)—N(2)	1.361(9)	C(10)—C(11)	1.353(13)

1939 had intensities greater than $3\sigma(I)$ above background. The variation in the standard reflections was less than 5%. Data were corrected for absorption, transmission factors ranging from 0.305 to 0.648 for 132 grid points.

The centrosymmetric space group was suggested by the Patterson function, from which the Rh, Ga, and Cl coordinates were determined. The remaining non-hydrogen atoms were positioned from a subsequent difference map and all non-hydrogen atoms were refined with anisotropic thermal parameters. Hydrogen atoms were fixed in calculated positions. Convergence was reached at $R = 0.048$ and $R_w = 0.055$ for 1939 reflection with $I \geq 3\sigma(I)$. For all 3336 reflections $R = 0.101$. Anomalous scattering corrections were also applied for Cl. On the final cycle of refinement the mean and maximum parameter shifts were 0.010 and 0.041 σ and the mean error in an observation of unit weight was 1.960. The final difference map showed maximum fluctuations of -2.8 and $+1.5$ e Å^{-3} near the Rh atom and was essentially featureless away from the heavier atoms.

Physical measurements

Infrared spectra were recorded on a Perkin–Elmer 598 spectrometer. The ^{1}H nmr spectra were obtained on Bruker WP80 and Bruker WH 400 MHz instruments using FT techniques. Mass spectra were recorded on a Kratos AES MS50 mass spectrometer at 120°C and 70 eV. Elemental analyses were performed by Mr. P. Borda of the U. B. C. microanalytical laboratory.

Results and discussion

The unsymmetric tridentate pyrazolylgallate ligand, **1**, has been incorporated in a *facial* coordination mode in numerous octahedral transition metal carbonyl complexes and in a tetrahedral "Ni(NO)" compound (1). The present study was initiated to demonstrate the capability of *meridional* coordination for this ligand system and this has been achieved in the formation of the four-coordinate square planar Rh(I) species, LRh(CO). Thus, the reaction of NaL with $[Rh(CO)_2Cl]_2$ in THF gave orange crystals of the target molecule in moderate yield. Infrared evidence indicates the formation of a transient dicarbonyl species, $LRh(CO)_2$, (ν_{CO} 2020, 2080 cm^{-1}) during the reaction but only the monocarbonyl complex (ν_{CO} 1962 cm^{-1}) could be isolated from solution. The incorporation of the related tridentate ligand systems $[Me_2Ga(N_2C_3H_3)(OCH_2CH_2NR_2)]^-$ (where R = H or Me) in similar square planar "Rh(I)CO" complexes has been reported recently (7). These complexes also formed via unstable dicarbonyl species, which again were not isolable from solution. The ν_{CO} stretching frequency of 1962 cm^{-1} for the present complex, LRh(CO), compares favorably with the values reported for the compounds $[Me_2Ga(N_2C_3H_3)(OCH_2CH_2NR_2)]Rh(CO)$ (ν_{CO} = 1955 cm^{-1} for R = H and 1957 cm^{-1} for R = Me). The slightly higher value in the present complex may well result from the π-acidity of the pyridyl ring in the L ligand.

The proton nmr of the LRh(CO) complex is shown in Fig. 1 and is clearly in agreement with a square planar complex in solution. Thus both the "$GaMe_2$" and —OCH_2— groupings give rise to singlets in the spectrum, as expected for the tridentate ligand in a *meridional* conformation about the Rh centre. The assignment of the other signals to the various pyrazolyl and pyridyl protons follows from previous studies (1, 7).

The mass spectrum of the LRh(CO) complex displayed a prominent signal due to the monomeric parent ion, P^+, with additional signals due to the $P-Me^+$, $P-CO^+$, and $P-Me-CO^+$ ions also being observed. The most intense signal in the spectrum was assigned to the $[OCH_2(C_5H_4N)]^+$ ion.

The molecular structure of LRh(CO) is shown in Fig. 2 and confirms the expected planarity about the Rh(I) centre with the fourth coordination site occupied by the terminal CO ligand (Rh—C—O = 176.2(5)°). Bond distances involving Rh are: Rh—O = 2.038(5), Rh—N(pyrazolyl) = 2.022(4), Rh—N(pyridyl) = 2.038(3), and Rh—CO = 1.778(5) Å. The coordination group (N_2OC) is significantly non-planar (χ^2 = 215), the atoms lying alternatively above and below the mean plane (O(1), 0.021(4); N(2), −0.027(4); C(1), 0.045(5); and N(3), −0.025(4) Å). The Rh atom is displaced from this mean plane by −0.0451(1) Å, a displacement greater than that of any of its substituents and, interestingly, in the direction of the symmetry-related Rh atom with which it interacts weakly (see below).

The pyrazolyl and pyridine rings are both planar within experimental error (χ^2 = 1.3 and 8.4, maximum deviations 0.005(6), and 0.009(6) Å, respectively). The chelate rings $RhOGaN_2$ and $RhONC_2$ are both significantly non-planar (χ^2 = 2095 and 99) but the deviations from planarity (max 0.069(4) and 0.042(6) Å) are relatively small (see torsion angles in Table 6). In fact, the entire non-hydrogen skeleton (excluding the Ga—Me carbon atoms) is planar to within ±0.325(1) Å.

Interestingly, the structure analysis also reveals the presence of weakly associated centrosymmetric dimer species in the solid state with a Rh···Rh interaction at 3.5445(7) Å (see Fig. 3). A weak metal–metal interaction is supported by the following facts: (a) the Rh—Rh distance is the shortest distance between non-hydrogen atoms of the two molecules forming the dimer; (b) the displacement of the Rh atom from its coordination plane is in the direction of the weak interaction (see above); and (c) the separation of 3.64 Å between the mean molecular planes (including all non-hydrogen atoms except C(2) and C(3)) is

TABLE 5. Bond angles (deg) with estimated standard deviations in parentheses

Bonds	Angle(deg)	Bonds	Angle(deg)
	[$Me_2Ga(N_2C_3H_3)(OCH_2(C_5H_4N))$]Rh(CO)		
O(1)—Rh—N(2)	88.73(14)	Rh—N(2)—N(1)	118.2(3)
O(1)—Rh—N(3)	80.61(14)	Rh—N(2)—C(12)	135.0(3)
O(1)—Rh—C(1)	175.1(2)	N(1)—N(2)—C(12)	106.8(4)
N(2)—Rh—N(3)	169.31(15)	Rh—N(3)—C(5)	114.6(3)
N(2)—Rh—C(1)	92.2(2)	Rh—N(3)—C(9)	127.5(3)
N(3)—Rh—C(1)	98.3(2)	C(5)—N(3)—C(9)	117.8(4)
O(1)—Ga—N(1)	89.95(14)	Rh—C(1)—O(2)	176.2(5)
O(1)—Ga—C(2)	110.3(2)	O(1)—C(4)—C(5)	111.5(4)
O(1)—Ga—C(3)	110.7(2)	N(3)—C(5)—C(4)	117.1(4)
N(1)—Ga—C(2)	110.4(2)	N(3)—C(5)—C(6)	121.4(4)
N(1)—Ga—C(3)	109.8(2)	C(4)—C(5)—C(6)	121.5(4)
C(2)—Ga—C(3)	121.3(2)	C(5)—C(6)—C(7)	120.1(5)
Rh—O(1)—Ga	119.4(2)	C(6)—C(7)—C(8)	118.6(5)
Rh—O(1)—C(4)	116.0(3)	C(7)—C(8)—C(9)	118.4(5)
Ga—O(1)—C(4)	124.2(3)	N(3)—C(9)—C(8)	123.7(5)
Ga—N(1)—N(2)	122.9(3)	N(1)—C(10)—C(11)	111.7(5)
Ga—N(1)—C(10)	130.0(4)	C(10)—C(11)—C(12)	104.1(5)
N(2)—N(1)—C(10)	107.0(4)	N(2)—C(12)—C(11)	110.5(5)
	[(Cl)MeGa($N_2C_3H_3$)($OCH_2(C_5H_4N)$)]Rh(CO)		
O(1)—Rh—N(2)	87.8(2)	Rh—N(2)—N(1)	119.2(5)
O(1)—Rh—N(3)	80.8(2)	Rh—N(2)—C(11)	134.5(6)
O(1)—Rh—C(1)	178.2(3)	N(1)—N(2)—C(11)	106.2(7)
N(2)—Rh—N(3)	168.7(2)	Rh—N(3)—C(4)	115.0(5)
N(2)—Rh—C(1)	93.7(3)	Rh—N(3)—C(8)	127.3(5)
N(3)—Rh—C(1)	97.6(3)	C(4)—N(3)—C(8)	117.8(7)
Cl—Ga—O(1)	104.5(2)	Rh—C(1)—O(2)	177.1(8)
Cl—Ga—N(1)	106.9(2)	O(1)—C(3)—C(4)	112.0(7)
Cl—Ga—C(2)	113.5(3)	N(3)—C(4)—C(3)	117.3(7)
O(1)—Ga—N(1)	92.9(3)	N(3)—C(4)—C(5)	121.4(8)
O(1)—Ga—C(2)	117.9(4)	C(3)—C(4)—C(5)	121.2(8)
N(1)—Ga—C(2)	118.5(4)	C(4)—C(5)—C(6)	119.8(8)
Rh—O(1)—Ga	115.7(3)	C(5)—C(6)—C(7)	119.6(8)
Rh—O(1)—C(3)	114.6(5)	C(6)—C(7)—C(8)	117.9(9)
Ga—O(1)—C(3)	125.3(5)	N(3)—C(8)—C(7)	123.5(8)
Ga—N(1)—N(2)	119.9(4)	N(1)—C(9)—C(10)	107.9(9)
Ga—N(1)—C(9)	130.5(6)	C(9)—C(10)—C(11)	105.9(9)
N(2)—N(1)—C(9)	109.6(7)	N(2)—C(11)—C(10)	110.4(8)

longer than the 3.4–3.5 Å normally associated with a π–π interaction that could occur between overlapping ligands. These dimeric units are well separated from adjacent dimers in the crystal lattice. Similar Rh···Rh interactions have been observed in other square planar Rh(I) carbonyl complexes (8–11), as indicated in Table 7. In the present LRh(CO) system the Rh···Rh interaction is limited to dimer species rather than molecular stacking on a more extended scale as observed in the other Rh(I) complexes in Table 7 for reasons analogous to those presented for similar dimers in the structure of tetraethylammonium [4,4′,5,5′-tetracyano-2,2′-biimidazolato-(2−)]dicarbonyliridium(I) (12) (Ir···Ir = 3.183(1) Å).

The reaction between LRh(CO) and MeI in CH_2Cl_2 is thought to proceed via a six-coordinate Rh(III) oxidative addition product to give the five-coordinate Rh(III) acetyl complex LRh(COMe)I:

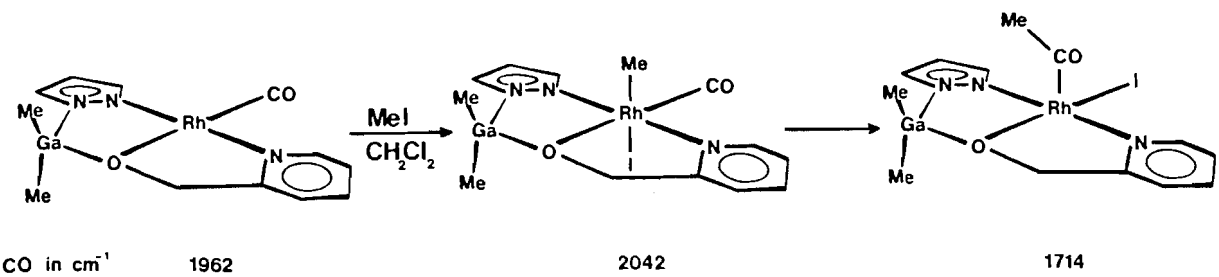

ν CO in cm^{-1} (CH_2Cl_2 soln.) 1962 2042 1714

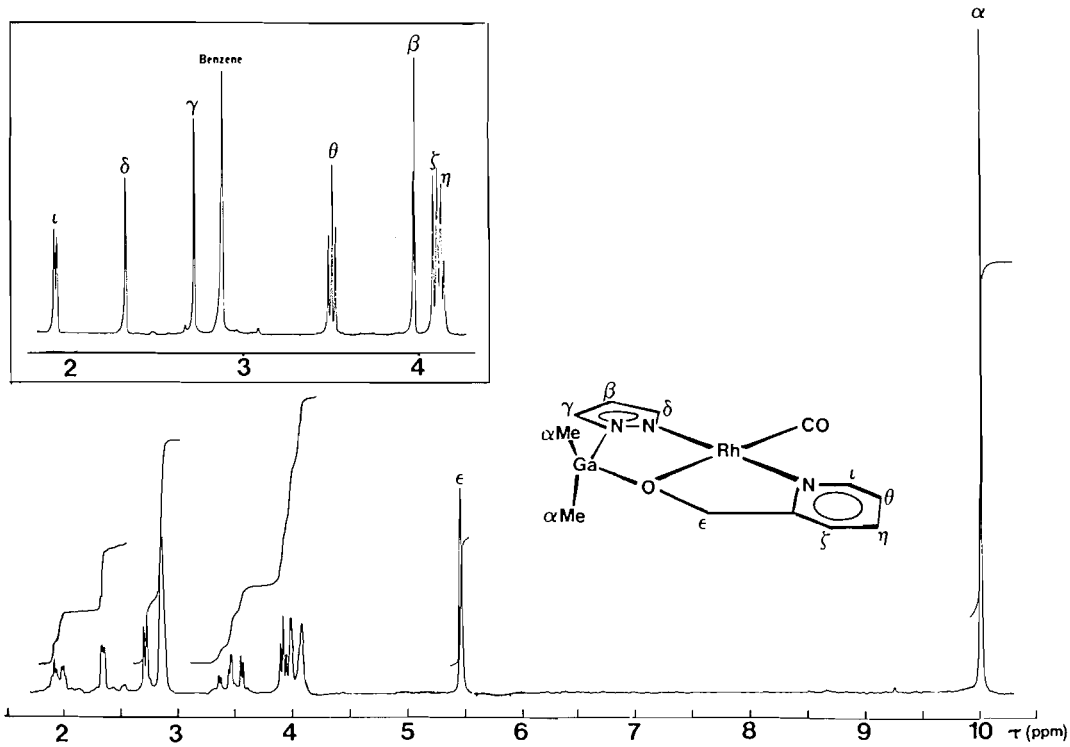

FIG. 1. Room temperature 80-MHz ^{1}H nmr spectrum of LRh(CO) in C_6D_6 (inset 400 MHz).

TABLE 6. Intra-annular torsion angles (deg) with standard deviations in parentheses

Atoms	Value(deg)
$[Me_2Ga(N_2C_3H_3)(OCH_2(C_5H_4N))]Rh(CO)$	
N(2)—Rh—O(1)—Ga	−8.7(2)
N(1)—Ga—O(1)—Rh	8.9(2)
O(1)—Ga—N(1)—N(2)	−6.0(3)
Ga—N(1)—N(2)—Rh	1.0(5)
O(1)—Rh—N(2)—N(1)	4.3(3)
N(3)—Rh—O(1)—C(4)	−2.1(3)
Rh—O(1)—C(4)—C(5)	4.6(5)
O(1)—C(4)—C(5)—N(3)	−5.8(6)
Rh—N(3)—C(5)—C(4)	4.3(5)
O(1)—Rh—N(3)—C(5)	−1.3(3)
$[(Cl)MeGa(N_2C_3H_3)(OCH_2(C_5H_4N))]Rh(CO)$	
N(2)—Rh—O(1)—Ga	19.8(4)
N(1)—Ga—O(1)—Rh	−20.7(4)
O(1)—Ga—N(1)—N(2)	13.7(7)
Ga—N(1)—N(2)—Rh	−1.3(9)
O(1)—Rh—N(2)—N(1)	−10.7(6)
N(3)—Rh—O(1)—C(3)	−2.8(5)
Rh—O(1)—C(3)—C(4)	4.8(9)
O(1)—C(3)—C(4)—N(3)	−4.8(11)
Rh—N(3)—C(4)—C(3)	2.5(9)
O(1)—Rh—N(3)—C(4)	0.2(5)

TABLE 7. Selected Rh···Rh interactions

Complex	Rh···Rh (Å)	Reference
LRh(CO)	3.5445	This work
(acac)Rh(CO)	3.253, 3.271	8
Rh(pzH)(CO) Cl	3.452	9
(8-hydroxyquinolinato)Rh(CO)	3.10	10
$(OC_2Rh(\mu\text{-pz})(\mu\text{-Cl})Rh(CO)$	3.511, 3.620	11

Thus the ν_{CO} band of the starting monocarbonyl species at 1962 cm^{-1} was replaced by two bands at 1714 and 2042 cm^{-1} in the metal carbonyl stretching region of the ir spectrum on addition of MeI, the 1714^{-1} band gaining in intensity with time. Attempts to isolate the species responsible for the 2042 cm^{-1} band were unsuccessful, only crystals of the Rh(III) acetyl complex LRh(COMe)I (ν_{CO} = 1714 cm^{-1}) being obtained from the product solution. It is postulated that the 2042 cm^{-1} band is due to the labile six-coordinate Rh(III) *trans*-addition product (this mode of addition being commonly found in oxidative addition reactions of alkyl halides on d^8 Rh(I) and Ir(I) complexes (ref. 13 and references therein)) and that this species readily undergoes a methyl migration to form a terminal acetyl group in the LRh(COMe)I complex. Interestingly, related rhodium complexes containing σ-bonded methyl groups have not been observed during the reaction of MeI with cyclopentadienyl rhodium carbonyls. For example, the reaction of MeI with $(\eta^5\text{-}C_5Me_5)Rh(CO)_2$ proceeds directly to the $(\eta^5\text{-}C_5Me_5)$-Rh(COMe)I complex at 50°C (14).

The ^{1}H nmr of the acetyl complex is shown in Fig. 4 and is consistent with the predicted formulation with a square pyramidal arrangement about the Rh atom. An X-ray structure determination has established this arrangement for the related compound $[Me_2Ga(N_2C_3H_3)(OCH_2CH_2NMe_2)]Rh(COMe)I$ (7). The position of the —CO*Me* signal is similar to those reported earlier for related rhodium acetyl species (7, 15), and no signal was observed in the region near 9 τ where one might expect Rh—*Me* signals (7, 15–17). In addition, the non-planarity of the complex renders inequivalent the two methyl groups on Ga and the —OCH_2— protons. Thus two singlets are observed for

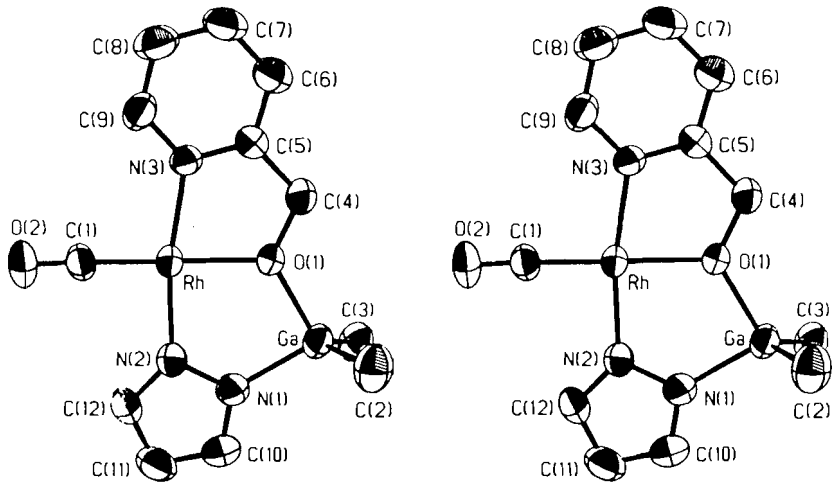

FIG. 2. Stereoscopic view of the [dimethyl(pyrazol-1-yl)(2-pyridylmethoxy)gallato-N^2,O,N^3]carbonylrhodium(I) molecule; 50% probability thermal ellipsoids are shown for the non-hydrogen atoms. Hydrogen atoms have been omitted for the sake of clarity.

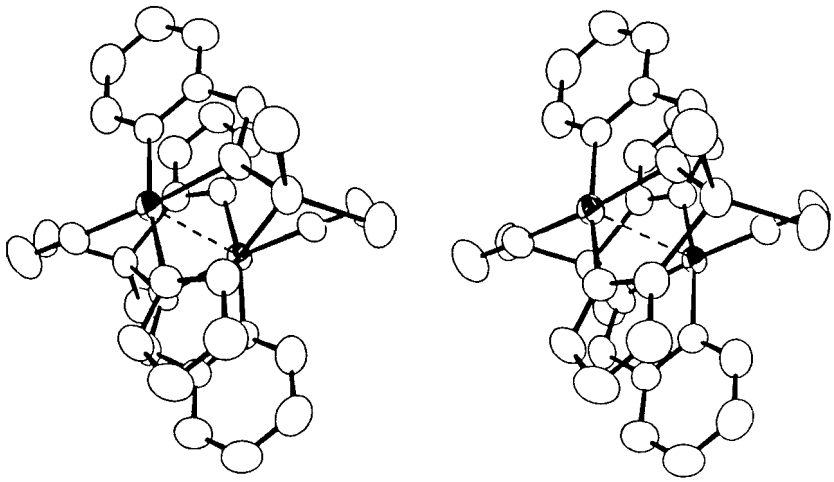

FIG. 3. Stereoscopic view of the [dimethyl(pyrazol-1-yl)(2-pyridylmethoxy)gallato-N^2,O,N^3]carbonylrhodium(I) dimer.

the "$GaMe_2$" moiety and an AB quartet for the methylene protons. A noteworthy feature of the spectrum is the significant downfield chemical shifts of the two signals due to the pyrazolyl and pyridyl protons that are adjacent to the iodine atom in the molecule, compared to their positions in the square planar LRh(CO) species, an effect possibly related to the deshielding influence of the electronegative halogen substituent.

The addition of iodine to a CH_2Cl_2 solution of LRh(CO) resulted in the immediate appearance of a new carbonyl band at 2095 cm^{-1} and the gradual disappearance of the ν_{CO} band attributable to the starting Rh(I) compound. This new band is probably due to the diiodide species $LRh(CO)(I)_2$, although analytically pure samples of this complex could not be obtained from the product solution. Difficulties in obtaining satisfactory elemental analyses for the complexes $[Me_2Ga(N_2C_3H_3)(OCH_2CH_2NR_2)]Rh(CO)(X)_2$ (X = I or Br, R = H or Me), with ν_{CO} ~2090 cm^{-1}, and for related pyrazolylborate dihalogen monocarbonyl species have been noted previously (7, 18, 19).

The second product isolated from the reaction of $[Rh(CO)_2Cl]_2$ with NaL, albeit in low yield, was in the form of yellow platelet crystals and analyzed as $[(Cl)MeGa(N_2C_3H_3)(OCH_2(C_5H_4N))]Rh(CO)$. The origin of the chlorine for methyl substitution on the gallium atom is puzzling since the only source of chlorine atoms is the $[Rh(CO)_2Cl]_2$ starting material, no chlorinated solvents being used in the reaction or work-up procedures. The ir spectrum of this chloro complex shows, in addition to a ν_{CO} band at 1968 cm^{-1} (CH_2Cl_2), a band at 360 cm^{-1} (C_6H_6), assigned to a ν_{GaCl} stretching vibration. This value is comparable to those found for other four-coordinate "GaCl" species (e.g. Me_3NGaH_2Cl, 345 cm^{-1} (C_6H_6) (20), Me_3NGaCl_3, 360 and 390 cm^{-1} (Nujol) (21), and Ph_3PGaCl_3, 352 and 391 cm^{-1} (CH_2Cl_2) (22)).

The predicted structure for the complex, with a square planar geometry about the Rh(I) center and a *meridional* coordination of the tridentate ligand, has been confirmed by X-ray structural analysis (see below) and is consistent with the ^1H nmr shown in Fig. 5. Thus, the —O*CH*$_2$— methylene protons are made inequivalent by the "(Cl)MeGa" moiety and give rise to an AB quartet in the spectrum. The remaining signals are readily assigned to the —Ga*Me*, pyrazolyl, and pyridyl protons, as indicated.

The mass spectrum of the $[(Cl)MeGa(N_2C_3H_3)(OCH_2(C_5H_4N))]Rh(CO)$ complex displayed a strong parent ion signal P^+, in addition to prominent signals due to the $P-CO^+$ and $P-Cl^+$ ions. The most intense signal in the spectrum corresponded to the $(Cl)Ga[OCH_2(C_5H_4N)]^+$ ion.

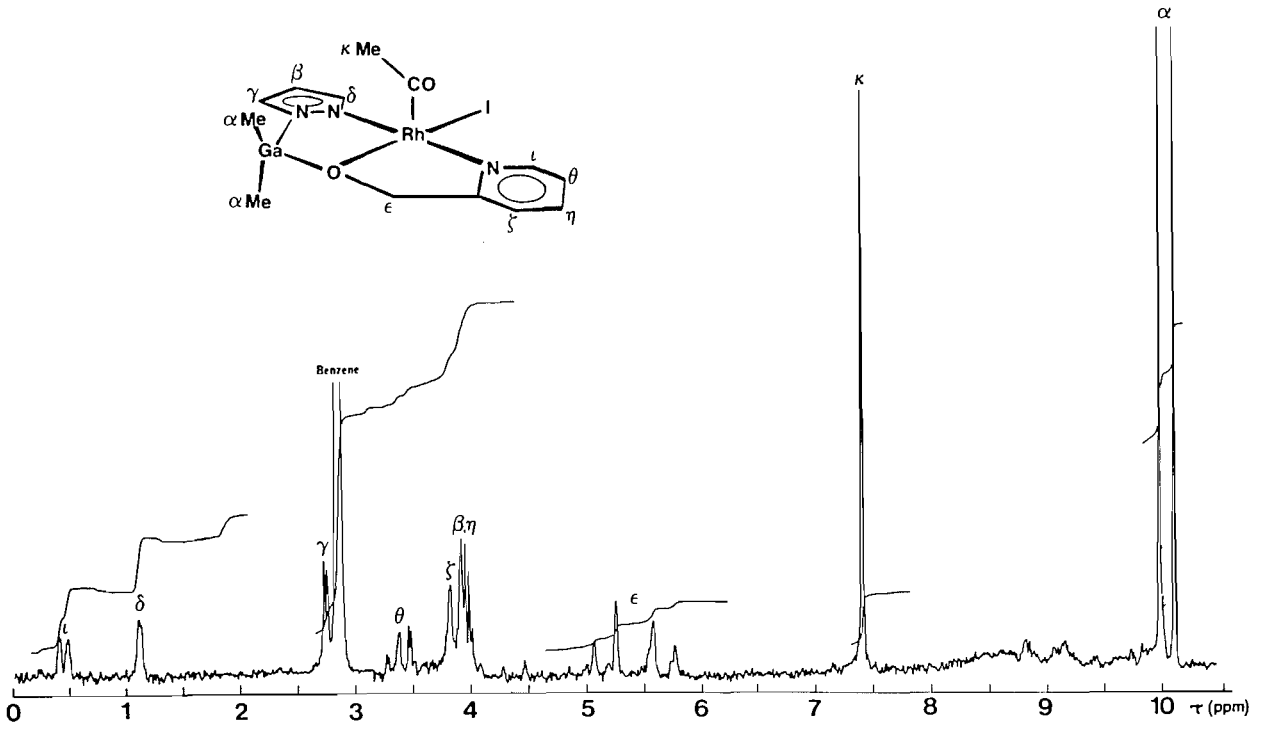

FIG. 4. Room temperature 80-MHz ^{1}H nmr spectrum of LRh(COMe)I in C_6D_6.

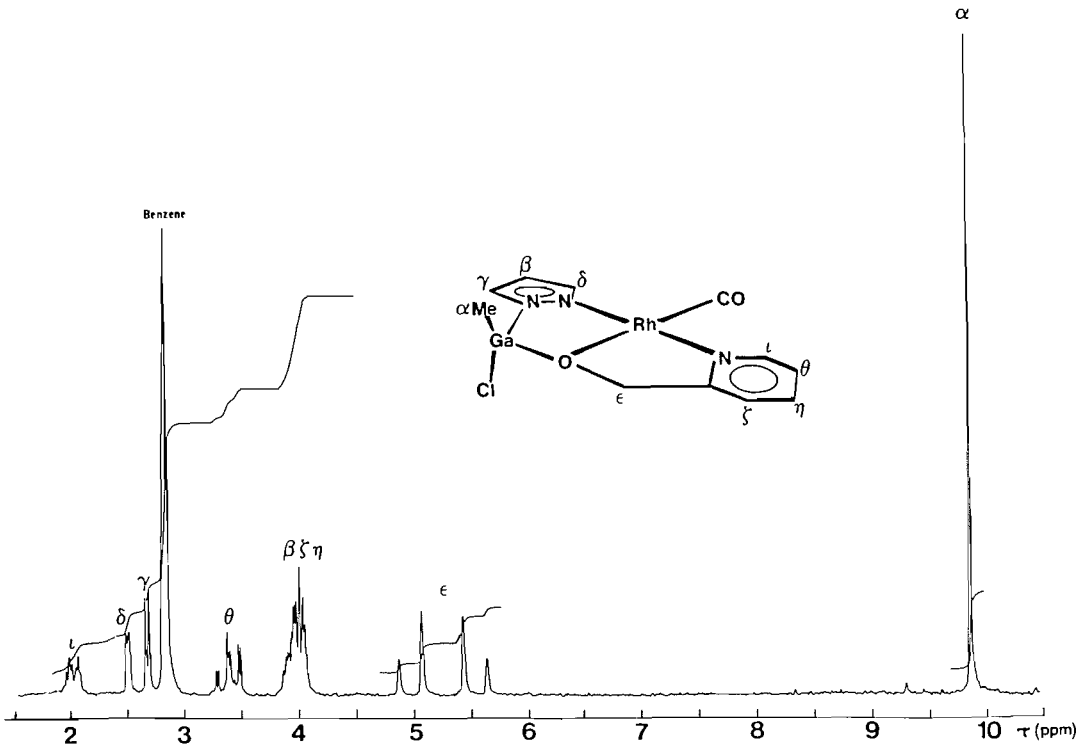

FIG. 5. Room temperature 80-MHz ^{1}H nmr spectrum of [(Cl)MeGa($N_2C_3H_3$)($OCH_2(C_5H_4N)$)]Rh(CO) in C_6D_6.

The molecular structure of the chloro complex, shown in Fig. 6, is very similar to that of the LRh(CO) compound described above. In [(Cl)MeGa($N_2C_3H_3$)($OCH_2(C_5H_4N)$)]Rh(CO) the coordination group (RhN_2OC) is planar within experimental error ($\chi^2 = 7.9$, maximum deviation 0.02(1) Å), in contrast to the situation observed for LRh(CO). The absence of the intermolecular Rh···Rh interaction in [(Cl)MeGa($N_2C_3H_3$)($OCH_2(C_5H_4N)$)]Rh(CO) (see below) is responsible for this difference. The Rh—C—O grouping is essentially linear with a bond angle of 177.1(8)° at carbon. Bond distances involving Rh are: Rh—O = 2.048(5), Rh—N(pyrazolyl) = 2.025(7), Rh—N(pyridyl) = 2.020(6), and Rh—CO = 1.808(9) Å. These values do not differ significantly from those in LRh(CO), but the Ga—O, Ga—N, and Ga—C bonds are all shorter than those in

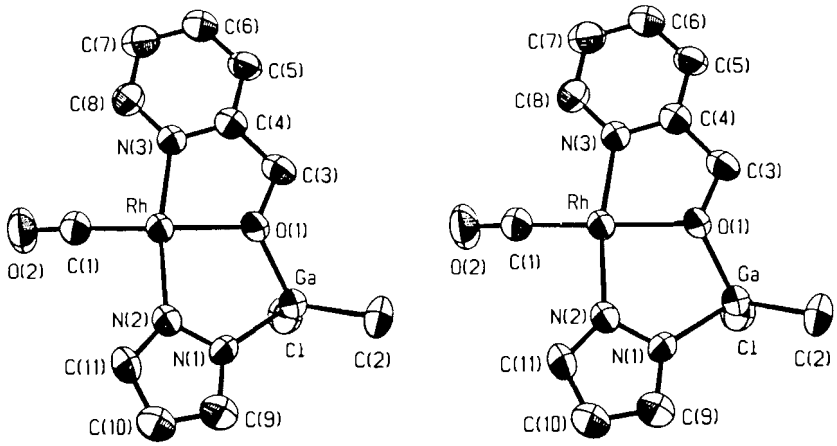

FIG. 6. Stereoscopic view of the [(chloro)methyl(pyrazol-1-yl)(2-pyridylmethoxy)gallato-N^2,O,N^3]carbonylrhodium(I) molecule; 50% probability thermal ellipsoids are shown for the non-hydrogen atoms. Hydrogen atoms have been omitted for the sake of clarity.

LRh(CO) (see Table 4) as a result of orbital contraction at Ga induced by the electronegative Cl substituent. The Ga—Cl distance of 2.194(3) Å is normal.

The pyrazolyl and pyridyl rings are planar within experimental error (χ^2 = 2.4 and 2.0, maximum deviations 0.009(10) and 0.010(10) Å) and the two chelate rings $RhOGaN_2$ and $RhONC_2$ are both significantly non-planar (χ^2 = 3550 and 26), the maximum deviation for the latter (0.042(10) Å) being the same as that found for LRh(CO). The $RhOGaN_2$ ring in [(Cl)MeGa-($N_2C_3H_3$)($OCH_2(C_5H_4N)$)]Rh(CO) deviates more from planarity than does the same ring in LRh(CO) (maximum deviation 0.163(6) Å compared to 0.069(4) Å). This is reflected in the larger magnitude of the intra-annular torsion angles (see Table 6) and represents an out-of-plane movement of the Ga atom that results in the Cl occupying a distinctively pseudoaxial position with respect to the five-membered ring. The entire non-hydrogen skeleton except chlorine is planar to within 0.57(1) Å, the Ga atom being displaced more than the pseudoequatorial methyl carbon atom C(2).

Unlike the dimethyl analog, [(Cl)MeGa($N_2C_3H_3$)(OCH_2-(C_5H_4N))]Rh(CO) does not form Rh···Rh linked dimer species in the solid state. The bulky chloro ligand in its pseudoaxial position effectively blocks any close approach of neighboring molecules from one side of each molecule, making stacking unlikely. The closest approach of Rh atoms from the "open" side of the molecule is 4.220(1) Å. This distance is long as a result of slipping, which may be due to a pair of weak intermolecular C—H···Cl interactions that link molecules into ribbons extending along the body diagonal of the unit cell (C(8)—H(8)···Cl($1-x,1-y,1-z$) and C(9)—H(9)···Cl($-x$, $-y,-z$), H···Cl = 2.84 and 2.84, C···Cl = 3.680(9) and 3.783(11) Å, C—H···Cl = 145 and 164°).

A more rational approach to ligands of the type [(Cl)MeGa-($N_2C_3H_3$)($OCH_2(C_5H_4N)$)]$^-$ is being developed, with the obvious possibility of producing novel tetradentate ligand systems.

Acknowledgemnts

We thank the Natural Sciences and Engineering Research Council of Canada for financial support, Professor James Trotter (Supervisor, University of British Columbia Crystallographic Service) for the use of laboratory facilities and computer programs, and the University of British Columbia Computing Centre for assistance.

1. S. J. RETTIG, A. STORR, J. TROTTER, and K. URICH. Can. J. Chem. **62**, 2783 (1984).
2. P. COPPENS, L. LEISEROWITZ, and D. RABINOVICH. Acta Crystallogr. **18**, 1035 (1965).
3. W. R. BUSING and H. A. LEVY. Acta Crystallogr. **22**, 457 (1967).
4. D. T. CROMER and J. B. MANN. Acta Crystallogr. Sect. A, **24**, 321 (1968).
5. R. F. STEWART, E. R. DAVIDSON, and W. T. SIMPSON. J. Chem. Phys. **42**, 3175 (1965).
6. D. T. CROMER and D. LIBERMAN. J. Chem. Phys. **53**, 1891 (1970).
7. B. M. LOUIE, S. J. RETTIG, A. STORR and J. TROTTER. Can. J. Chem. **63**, 3019 (1985).
8. F. HUQ and A. C. SKAPSKI. J. Cryst. Mol. Struct. **4**, 411 (1974).
9. M. J. DECKER, D. O. FJELDSTED, S. R. STOBART, and M. J. ZAWOROTKO. J. Chem. Soc. Chem. Commun. 1525 (1983).
10. L. G. KUZ'MINA, S. VERSHAVSKII, N. G. BOKII, Y. STRUCHKOV, and T. G. CHERKASOVA. J. Struct. Chem. (Engl. Transl.) **12**, 593 (1971).
11. B. M. LOUIE, S. J. RETTIG, A. STORR, and J. TROTTER. Can. J. Chem. **63**, 688 (1985).
12. P. G. RASMUSSEN, O. H. BAILEY, J. C. BAYON, and W. M. BUTLER. Inorg. Chem. **23**, 343 (1984).
13. P. UGUAGLIATI, A. PALAZZI, G. DEGANELLO, and U. BELLUCO. Inorg. Chem. **9**, 724 (1970).
14. J. W. KANG and P. M. MAITLIS. J. Organomet. Chem. **26**, 395 (1971).
15. M. C. BAIRD, J. T. MAGUE, J. A. OSBORN, and G. WILKINSON. J. Chem. Soc. Sect. A, 1347 (1967).
16. C.-H. CHENG, B. D. SPIVACK, and R. EISENBERG. J. Am. Chem. Soc. **99**, 3003 (1977).
17. C.-H. CHENG and R. EISENBERG. Inorg. Chem. **18**, 1418 (1979).
18. S. MAY, P. REINSALU, and J. POWELL. Inorg. Chem. **19**, 1582 (1980).
19. M. COCIVERA, T. J. DESMOND, G. FERGUSON, B. KAITNER, F. T. LALOR, and D. J. O'SULLIVAN. Organometallics, **1**, 1125 (1982).
20. N. N. GREENWOOD and A. STORR. J. Chem. Soc. 3426 (1965).
21. N. N. GREENWOOD, T. S. SRIVASTAVA, and B. P. STRAUGHAN. J. Chem. Soc. 699 (1966).
22. A. J. CARTY. Can. J. Chem. **45**, 3187 (1967).

The condensation of trimethylsilylium with water and the proton affinity of trimethylsilanol

JOHN A. STONE,[1] ANASTASIA C. M. WOJTYNIAK, AND WILLUM WYTENBURG
Chemistry Department, Queen's University, Kingston, Ont. Canada K7L 3N6
Received August 21, 1985

JOHN A. STONE, ANASTASIA C. M. WOJTYNIAK, and WILLUM WYTENBURG. Can. J. Chem. **64**, 575 (1986).

The proton affinity (PA) of trimethylsilanol has been determined by high pressure mass spectrometry from the enthalpy change for the reaction $Me_3Si^+ + H_2O \rightleftharpoons Me_3SiOH_2^+$. $\Delta H^0 = -30.1 \pm 1.9$ kcal mol^{-1} giving PA (Me_3SiOH) = 183.7 kcal mol^{-1}. This latter value is 10 kcal mol^{-1} less than that of the carbon analogue, *tert*-butanol.

JOHN A. STONE, ANASTASIA C. M. WOJTYNIAK et WILLUM WYTENBURG. Can. J. Chem. **64**, 575 (1986).

Faisant appel à la spectrométrie de masse à haute pression, on a mesuré le changement d'enthalpie pour la réaction $Me_3Si^+ + H_2O \rightleftharpoons Me_3SiOH_2^+$ et l'on en a tiré l'affinité protonique (AP) du triméthylsilanol. Le $\Delta H^0 = -30{,}1 \pm 1{,}9$ kcal mol^{-1} conduit à une AP (Me_3SiOH) = 183,7 kcal mol^{-1}. Cette valeur est 10 kcal mol^{-1} plus faible que celle de l'analogue carboné, le *tert*-butanol.

[Traduit par le journal]

Although the proton affinities of alcohols have been soundly established, those of their silicon analogues are virtually unknown. The one exception to this generalization is a bracketed proton affinity for trimethylsilanol (1). Non-alkyl substituted silanols are chemically unstable, readily forming siloxanes by an intermolecular elimination of water. Substitution of alkyl for H in the silyl group does lead to greater stability of a silanol but such silanols are still somewhat unstable and are not readily available.

A further problem encountered when attempts were made, by the usual mass spectrometric gas phase equilibrium methods, to determine the proton affinities of silicon compounds with silicon attached directly to a heteroatom was the propensity to transfer a silicon-containing group rather than the proton (2). We have indeed found that, in a pulsed electron beam high-pressure ion-source mass spectrometer (HPMS), advantages may be taken of the preference for silyl group transfer to obtain a ladder of Me_3Si^+ affinities for a variety of compounds in the same manner as for proton affinities (3). One of the compounds examined was water and it was found that the following equilibrium could be observed at the high temperatures (up to 600 K) available in our HPMS.

[1] $Me_3Si^+ + H_2O \rightleftharpoons \underset{\mathbf{1}}{Me_3SiOH_2^+}$

The carbon analogue of **1** is prepared by the reaction of the *tert*-butyl cation with water.

[2] $Me_3C^+ + H_2O \rightleftharpoons \underset{\mathbf{2}}{Me_3COH_2^+}$

The standard enthalpy change for reaction [2] was determined from a van't Hoff plot to be -11.2 kcal mol^{-1} (-46.9 kJ mol^{-1}), which, together with the enthalpies of formation of Me_3C^+ and H_2O, yielded an enthalpy of formation of **2** that was essentially the same as that derived using the measured proton affinity of *tert*-butanol (4). It was therefore concluded that **2** is protonated *tert*-butanol. By analogy we propose that **1** be identified as protonated trimethylsilanol.

Me_3Si^+ is readily formed in a high-pressure ion source using either tetramethylsilane alone (5, 6), or by proton transfer from the reagent ions in methane (CH_5^+, $C_2H_5^+$) to tetramethylsilane

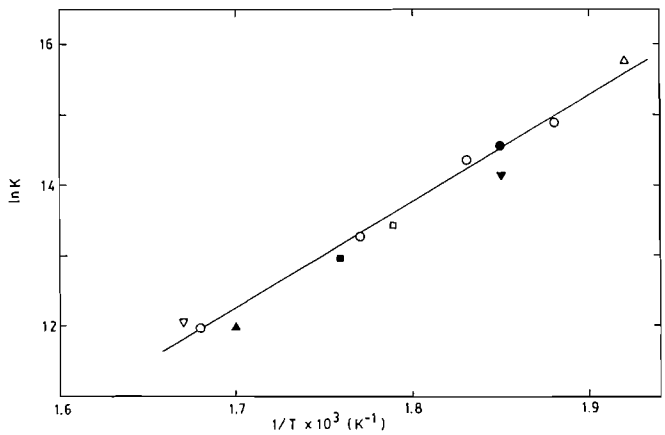

FIG 1. The van't Hoff plot for the reaction $Me_3Si^+ + H_2O \rightleftharpoons Me_3SiOH_2^+$. The ion source mixtures contained 99.5% CH_4, 0.5% Me_4Si, and 0.05 – 0.5% H_2O at total pressures between 400 and 600 Pa. Each different symbol represents a different sample. The standard state is 101 kPa and a least-squares analysis yields $\Delta H^0 = -30.1 \pm 1.9$ kcal mol^{-1} and $\Delta S^0 = -27.0 \pm 3.2$ cal K^{-1} mol^{-1} (the error limits represent one standard deviation).

(3, 7). The latter method yields only Me_3Si^+, while the former yields a more complicated spectrum due to the reactions of fragment ions with $SiMe_4$. In the presence of added water, equilibrium [1] is set up at 270–530 Pa and the equilibrium constant $i_{Me_3SiOH_2^+}/i_{Me_3Si^+}[H_2O]$ can be calculated, where i is a measured equilibrium ion current.

The standard enthalpy change obtained from the van't Hoff plot in Fig. 1 is -30.1 ± 1.9 kcal mol^{-1} while ΔS^0 is -27 ± 3.2 cal K^{-1} mol^{-1}. On the assumption that **1** is indeed protonated Me_3SiOH and taking $\Delta H_f^0(Me_3Si^+) = 150.5$ kcal mol^{-1}(8), $\Delta H_f^0(H_2O) = -57.8$ kcal mol^{-1}, and $\Delta H_f^0(Me_3SiOH) = -119.4$ kcal mol^{-1}(9), then the proton affinity of Me_3SiOH is 183.7 kcal mol^{-1}.

This value is far less than the range of 196 – 204 kcal mol^{-1} obtained by the bracketing technique with ion cyclotron resonance (icr) instrumentation (1).[2] The lower limit was

[1]Author to whom correspondence may be addressed.

[2]All values of proton affinities from the literature have been adjusted to be consistent with the value of 204 kcal mol^{-1} suggested for NH_3 in the compilation of ref. 10.

obtained using double resonance by observation of the reaction

[3] $Me_3SiOH_2^+ + Me_2C{=}CH_2 \rightleftharpoons Me_3SiOH + Me_2{}^+C{-}CH_3$

Irradiation of $Me_3SiOH_2^+$ led to a decrease in the product ion signal but there was no change in $Me_3SiOH_2^+$ when $Me_2C^+{-}CH_3$ was irradiated. We believe that this lower limit must be too high since the proton affinity of Me_3SiOH would then be higher than that of its carbon analogue Me_3COH, with a value of 193.7 kcal mol^{-1}(10). As discussed below, a compound with silicon bonded to the heteroatom being protonated appears to always have a proton affinity no greater than that of its carbon analogue. It is possible that the forward reaction, which could be perturbed, was a Me_3Si^+ transfer or the formation of a complex, although the latter is unlikely at the low pressures prevalent in icr studies. We do not have data on the Me_3Si^+ affinities of olefins.

The only equilibrium determination of the proton affinity of a compound in which silicon is bonded directly to the heteroatom that receives the proton involved (*t*-Bu)Me_2SiNMe_2 (2). This compound was found to have a proton affinity 5.2 kcal mol^{-1} less than its carbon analogue. Theoretical calculations carried out on silylamines lend credence to this difference. For example, the calculated proton affinities of MH_3NH_2, $(MH_3)_2NH$, and $(MH_3)_3N$ are higher for M = C than for M = Si by 8.9, 18.7, and 28.4 kcal mol^{-1}, respectively (11). The higher proton affinity of CH_3NH_2 relative to SiH_3NH_2 has been confirmed in another calculation, which yielded a difference of 6.9 kcal mol^{-1} (12). In addition, Me_2O is calculated also to have a proton affinity greater than that of its silicon analogue, $(SiH_3)_2O$, the difference being 11.8 kcal mol^{-1}(11). It is calculated that CH_3OH and SiH_3OH have identical proton affinities (12). The proton affinity of SiH_3OH has not been measured, but that of CH_3OH is 181.9 kcal mol^{-1} (10). While methyl substitution on silicon is calculated to stabilize silyl ions, it does so to a much smaller extent than does substitution on carbon in the analogous carbon compounds (13). If we accept equal proton affinities for SiH_3OH and CH_3OH, then substitution of Me for H on Si and C leads to a stabilization of the protonated species for silanol of only 2 kcal mol^{-1} compared with 12 kcal mol^{-1} for its carbon analogue.

It would be of value to confirm the validity of this proton affinity determination for Me_3SiOH by other equilibrium measurements, similar to that for reaction [1]. The next least strongly bound adduct containing the silicon oxygen bond is $Me_3SiOMeH^+$, obtained by the addition of MeOH to Me_3Si^+. Measurements of basicity differences by equilibrium measurements in our laboratory suggest that the binding energy for this complex is about 9 kcal mol^{-1} greater than that of the water complex. It is therefore too strongly bound for study at the temperatures available in our HPMS.

The very low enthalpy of dissociation of $Me_3COH_2^+$ to Me_3C^+ and H_2O (11.2 kcal mol^{-1}) reflects the great stability of Me_3C^+, solvation by a single H_2O molecule being unable to stabilize it further to any significant extent (4). Since an α-methyl group is far less effective in stabilizing a positive charge at silicon than at carbon (13), further substantial stabilization of Me_3Si^+ is therefore possible upon addition of H_2O to the positive Si centre, hence the much stronger bonding between Si and O in $Me_3SiOH_2^+$.

Experimental

The pulsed electron beam, high-pressure ion-source mass spectrometer and the method of determining gas phase equilibria have been described previously (14). Methane was Matheson Grade (99.99%) and tetamethylsilane, which was dried by standing over 13× molecular sieve, was from Merck Sharpe and Dohme, Canada Ltd.

Acknowledgments

The authors thank the Natural Sciences and Engineering Research Council of Canada for financial assistance.

1. C. G. Pitt, M. M. Bursey, and D. A. Chatfield. J. Chem. Soc. Perkin Trans. **2**, 434 (1976).
2. K. J. Shea, R. Gobeille, J. Bramblett, and E. Thompson. J. Am. Chem. Soc. **100**, 1611 (1978).
3. A. C. M. Wojtyniak. M.Sc. Thesis, Queen's University (1985).
4. K. Hiraoka and P. Kebarle. J. Am. Chem. Soc. **99**, 360 (1977).
5. T. J. Odiorne, D. J. Harvey, and P. Vouros. J.Phys. Chem. **76**, 3217 (1972).
6. L. Klevan and B. Munson. Int. J. Mass Spectrom. Ion Phys. **13**, 261 (1974).
7. D. Clemens and B. Munson. Org. Mass Spectrom. **20**, 368 (1985).
8. L. Szepes and T. Baer. J. Am. Chem. Soc. **106**, 273 (1984).
9. J. D. Cox and G.Pilcher. The thermochemistry of organic and organometallic compounds. Academic Press, London. 1970.
10. S. G. Lias, J. F. Liebman, and R. D. Levin. J. Phys. Chem. Ref. Data, **13**, 695 (1984).
11. C. Glidewell and C. Thomson. J. Comput. Chem. **3**, 495 (1982).
12. M. L. Hendewerk, R. Frey, and D. A. Dixon. J. Phys. Chem. **87**, 2026 (1983).
13. A. C. Hopkinson and M. H. Lien. J. Org. Chem. **46**, 998 (1981).
14. J. A. Stone and D. E. Splinter. Can. J. Chem. **59**, 1779 (1981).

Schmidt reaction of some constrained aromatic acids, and related topics

EDWARD H. RUEDIGER, SHAM S. GANDHI, AND MARTIN S. GIBSON[1]
Department of Chemistry, Brock University, St. Catharines, Ont., Canada L2S 3A1

AND

DAN FĂRCAŞIU[2] AND CORNELIA UNCUŢA
Institute of Atomic Physics, P.O. Box 35, Bucharest, Rumania

Received July 5, 1985

E. H. RUEDIGER, S. S. GANDHI, M. S. GIBSON, D. FĂRCAŞIU, and C. UNCUŢA. Can. J. Chem. **64**, 577 (1986).

Schmidt reaction of phthalic acid in 90–98% sulfuric acid gives anthranilic acid and anthranilazide (major products) by a process considered to involve 3,1-benzoxazin-2,4(1*H*)-dione as intermediate. Benzimidazol-2-one is produced in this reaction by a secondary process from anthranilazide; it is also produced by photolysis of anthranilazide. Under Schmidt reaction conditions, 1,2,3-benzotriazin-4(3*H*)-one gives *o*-azidobenzamide. Under similar conditions, the lactol of 4-formyl-5-phenanthroic acid gives 1-azapyren-2(1*H*)-one and phenanthrene-4,5-dicarboximide, while phenanthrene-4,5-dicarboxylic acid gives 1-azapyren-2(1*H*)-one. Diphenic acid yields phenanthridone and 2,2′-diaminobiphenyl in proportions dependent on the sulfuric acid concentration.

E. H. RUEDIGER, S. S. GANDHI, M. S. GIBSON, D. FĂRCAŞIU et C. UNCUŢA. Can. J. Chem. **64**, 577 (1986).

La réaction de Schmidt sur l'acide phtalique, dans l'acide sulfurique à 90–98%, conduit à l'acide anthranilique et à l'azoture de l'acide anthranilique (produits principaux) par un processus pour lequel on considère qu'il y a implication d'une 1*H*-benzoxazine-3,1 dione-2,4 comme intermédiaire. Au cours de cette réaction, l'azoture de l'acide anthranilique conduit à la formation de la benzimidazolone-2 par un processus secondaire; il s'en produit aussi par photolyse de l'azoture de l'acide anthranilique. Dans les conditions de la réaction de Schmidt, la 3*H*-benzotriazine-1,2,3 one-4 conduit au *o*-azidobenzamide. Dans des conditions semblables, le lactol de l'acide formyl-4 phénanthroïque-5 conduit à la 1*H*-aza-1 pyrènone-2 et au phénanthrènedicarboximide-4,5 alors que l'acide phénanthrènedicarboxylique-4,5 conduit à la 1*H*-aza-1 pyrènone-2. L'acide diphénique conduit à la phénanthridone et au diamino-2,2′ biphényle dans des proportions qui varient avec la concentration en acide sulfurique.

[Traduit par le journal]

The reactions of phthalic acid and of phthalic anhydride with sodium azide under acidic conditions have been variously reported as giving the following products: anthranilic acid and traces of *o*-phenylenediamine from phthalic acid in concentrated sulfuric acid (1); anthranilic acid, benzimidazol-2-one (**1**), and some 3,1-benzoxazin-2,4(1*H*)-dione (isatoic anhydride) (**2**) from phthalic anhydride in sulfuric acid (2); benzimidazol-2-one from phthalic anhydride in acetic acid (3); anthranilazide (**3**) and benzimidazol-2-one from phthalic acid and sodium azide in 90% sulfuric acid (1:6:15 molar ratio) (4). We now report details of our findings pertinent to these reactions together with details of experiments on several related topics.

In our experiments, phthalic acid in 1,2-dichloroethane (DCE) was treated with sodium azide in 90–98% sulfuric acid at 40–45°C. Under these conditions, the isolated products were anthranilic acid, anthranilazide, benzimidazol-2-one, and a small amount of *o*-phenylenediamine. The relative proportions of anthranilazide and benzimidazol-2-one were dependent both on reaction and isolation conditions, and separate experiments confirmed (5) that the former compound (by thermolysis) was the precursor of the later. In the cases previously noted (2, 3), benzimidazol-2-one presumably arose in the same way and we have since confirmed that anthranilazide is produced early in the reaction of phthalic anhydride with sodium azide in acetic acid (3).

This isolation of an acyl azide under Schmidt conditions is very unusual and the possibility that anthranilic acid, reported to be unreactive (1), might be the source of anthranilazide had to be considered. We found that anthranilic acid, when subjected to the same conditions, was consistently recoverable in 88–91% yields; anthranilazide was not detectable in the recovered samples. We conclude that anthranilic acid and its azide are formed from a common intermediate, most probably isatoic anhydride or its conjugate acid, by competing processes of hydrolysis and azidolysis in 90–98% sulfuric acid. Consistent with this view, we have observed that product compositions of anthranilic acid and anthranilazide from Schmidt reaction of isatoic anhydride and of phthalic acid are comparable under comparable conditions. Interestingly, the recently reported azidolysis of 2-amino-3,1-benzoxazin-4-one (**4**) follows a similar course, except that decarboxylation is blocked (6).

In a parallel experiment, we noted that 1,2,3-benzotriazin-4(3*H*)-one (**5**), unlike isatoic anhydride, did not function as an anthraniloylating agent under Schmidt conditions; instead, *o*-azidobenzamide was produced, an unusual example of formation of an azido compound from a triazinone under acidic conditions. We attribute this to acid-catalysed ring opening of the triazinone and reaction with hydrogen azide.[3]

Anthranilazide, now conveniently available by controlled Schmidt reaction of phthalic acid, was of interest in another connection, namely its photolysis. This might lead to a nitrene which could be trapped internally, by nitrene insertion into an

[1]Author to whom correspondence may be addressed.

[2]Present address: Corporate Research – Science Laboratories, Exxon Research and Engineering Company, Clinton Township, Annandale, NJ 08801, U.S.A.

[3]Terminal or 1,3-dipolar addition of hydrogen azide to protonated **5** ⇌ diazonium ion, followed by loss of nitrogen, would lead to *o*-azidobenzamide, as would direct displacement of the diazonium function as nitrogen.

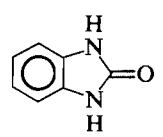

1

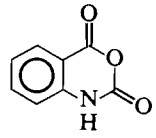

2

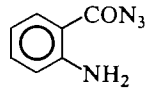

3

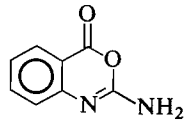

4

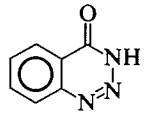

5

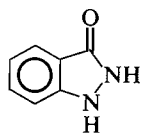

6

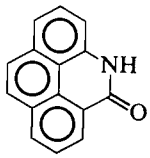

7

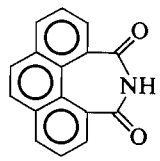

8

N—H bond, as indazol-3-one (**6**), or externally, using dimethyl sulfoxide, as *N*-(*o*-aminobenzoyl)-*S,S*-dimethylsulfoximine (7, 8); alternately, Curtius rearrangement could occur. Photolysis gave benzimidazol-2-one, showing that Curtius rearrangement was the dominant reaction.

Returning to our main concern, we gave consideration to the Schmidt reaction of 4-formyl-5-phenanthroic acid (lactol formulation (9)), previously reported by Medenwald (10) to give 1-azapyren-2(1*H*)-one (**7**). Formation of this product involves reaction at the latent aldehyde site, aryl migration (with electron pair), and deformylation. In this case, however, competitive hydrogen migration (with electron pair) is also possible. Reexamination of this Schmidt reaction confirmed the formation of **7**, but revealed that another major product was also produced. This was identified as phenanthrene-4,5-dicarboximide (**8**), the result (ultimately) of a competitive hydrogen migration.

Schmidt reaction of phenanthrene-4,5-dicarboxylic acid, prepared by oxidation of 4-formyl-5-phenanthroic acid (lactol), gave **7** as the major product. Unlike the case of phthalic acid, however, the Schmidt reactions of these phenanthrene derivatives were complex and it was not possible to characterize any minor products.

Finally, Schmidt reaction of biphenyl-2,2′-dicarboxylic acid (diphenic acid) has been reported to give mainly phenanthridone, with minor amounts of 2,2′-diaminobiphenyl (11), and we have confirmed this using 90% sulfuric acid. The formation of phenanthridone in this case parallels that of **7** from phenanthrene-4,5-dicarboxylic acid. However, the biphenyl system is less rigid than the phenanthrene system. Further examination of the diphenic acid case revealed that the product distribution was sensitive to the concentration of sulfuric acid employed; 2,2′-diaminobiphenyl was the major product, phenanthridone the minor, when 95–98% sulfuric acid was employed. Presumably both carboxyl groups in diphenic acid are significantly protonated in 95–98% sulfuric acid, repulsion then creating sufficient distancing between the charged groups for each to undergo Schmidt reaction independently. Product distributions in Schmidt reactions of other dicarboxylic acids are probably also susceptible to changes in sulfuric acid concentration in cases where molecular rotation or flexion are significant factors.

Experimental

Mass spectra were determined with an AEI MS-30 double beam spectrometer; *m/e* values are quoted for the lowest isotopic species. The ir spectra were recorded on Karl Zeiss Jena UR 10 and Perkin Elmer 237-B double beam spectrophotometers.

Thin-layer chromatography (tlc) was performed on silica gel 1B2-F plates (Baker); ligroin refers to the fraction bp 60–90′C.

Reference samples were prepared by previously published routes (4) or were purified commercial samples. After early experiments with phthalic acid in which products were separated by crystallization, product compositions were estimated by comparison with prepared mixtures of the possible products; the experiments described below were optimized for the isolation of anthranilazide and are representative of a number of runs.

Reaction of phthalic acid with sodium azide – sulfuric acid

During 40–50 min, NaN_3 (23 g, 0.35 mol) was added to a stirred mixture of phthalic acid (10 g, 0.06 mol), 1,2-dichloroethane (DCE) (50 mL), and 95–98% H_2SO_4(50 mL), the reaction temperature being maintained at 35–45°C. After being stirred at this temperature for a further 1.5 h, the mixture was chilled, diluted with water, and the pH was adjusted carefully (to avoid overheating) to 4–5 by addition of NaOH. The resulting mixture was extracted with ether (6 × 100 mL), and the extract was dried (Na_2SO_4) and evaporated carefully *in vacuo* (to avoid thermolysis of anthranilazide). This gave a brown solid (7.4 g), mp 68–70°C, shown by tlc (ligroin–ether) to contain anthranilic acid and anthranilazide (major products; ir and mass spectra), together with traces of other minor products; mass spectrum *m/e*: 137 (M^+, anthranilic acid) and 162 (M^+, anthranilazide).

Chromatography on Brockman alumina (activity class I) (ligroin–ether) gave, after careful evaporation of solvent, anthranilazide (3.5 g, 37%), mp 82°C (lit. (4) mp 83°C), identical (mixture mp, tlc, ir and mass spectra) with a reference sample. Later eluates (ether–acetone) gave trace amounts of *o*-phenylenediamine, identified by comparison (tlc; mass spectrum *m/e*; 108) with a reference sample. The column retained anthranilic acid.

A similar experiment using 90% H_2SO_4 gave 7.3 g of crude reaction products, mp 70–76°C, which yielded 3.4 g (35%) of anthranilazide after chromatography, followed by traces of *o*-phenylenediamine. Material insoluble in ether (prior to chromatography) was collected (730 mg, mp 250–255°C) and identified as impure benzimidazol-2-one (tlc; ir and mass spectra; mass spectrum, *m/e*; 134). From other experiments without temperature control or from those in which the crude products were allowed to remain for extended periods at room temperature prior to chromatography, benzimidazol-2-one, mp 305°C (lit. (4) mp 308°C) was isolated in larger quantities at the expense of anthranilazide.

Reaction of isatoic anhydride with sodium azide – sulfuric acid

Reaction of isatoic anhydride (4.9 g, 0.03 mol) with NaN_3 (7.6 g, 0.117 mol) in a mixture of 90% H_2SO_4 (27.1 mL), water (0.7 mL), and DCE (28 mL) was carried out as in the foregoing experiment (the amounts of NaN_3 and H_2O were adjusted to compensate for material used or produced in converting phthalic acid to isatoic anhydride in the former experiment). The crude product (4.2 g) possessed an ir spectrum virtually identical with that from the previous experiment; anthranilazide (1.35 g, 28%), recovered chromatographically, had mp 82°C.

Reaction of phthalic anhydride with sodium azide – acetic acid (ref. 3)

Phthalic anhydride (4.4 g, 0.03 mol) in glacial CH_3CO_2H (50 mL) was treated with NaN_3 (7.8 g, 0.12 mol) at 50°C as described previously, except that the reaction was quenched after 3 h. This gave a product consisting largely of phthalic anhydride, but clearly containing anthranilazide (ir spectrum). Chromatography, as above, gave 0.6 g (12%) of anthranilazide.

Reaction of 1,2,3-benzotriazin-4(3H)-one with sodium azide – sulfuric acid[4]

During 40 min, NaN_3 (6.8 g, 0.105 mol) was added to a stirred mixture of the triazinone (1.47 g, 0.01 mol), DCE (16.5 mL), and 90% H_2SO_4 (16.5 mL), the reaction temperature being kept at 40–50°C. After completion of the reaction as described above for phthalic acid, the pH was adjusted (NaOH) to 8–9 and the product (0.9 g) was isolated by extraction with ether. Crystallization from water gave *o*-azidobenzamide (0.8 g, 49%) as needles, mp 132–133°C (lit. 12) mp 135.5–136°C). *Anal.* calcd. for $C_7H_6N_4O$: C 51.85, H 3.70, N 34.57; found: C 52.33, H 3.73, N 34.66.

Photolysis of anthranilazide

A fused silica photolysis cell containing a solution of anthranilazide (0.2 g, 1.2 mmol) in acetone (5 mL) and cyclohexane (25 mL) was irradiated using a Hanovia Utility UV quartz lamp at 15-cm distance. The temperature of the reaction mixture remained below 30°C. The reaction was monitored by ir spectroscopy for the disappearance of starting material (azide band at ν_{max} 2135 cm^{-1}) and was complete within 60–90 min. Evaporation of the solvents gave a nearly quantitative yield of benzimidazol-2-one (0.11 g, 68% after purification), identical with a reference sample (tlc, ir and mass spectra).

A similar reaction in which dimethyl sulfoxide replaced cyclohexane gave, after purification, 0.09 g (56%) of benzimidazol-2-one. The mass spectrum of the crude product showed a minor peak at *m/e* 212, possibly due to traces of the sought sulfoximine, but this compound was not otherwise detectable.

Reaction of 4-formyl-5-phenanthroic acid (lactol) with sodium azide – sulfuric acid

A suspension of the lactol (13) (3.0 g, 12 mmol) in DCE (30 mL) and 95–98% H_2SO_4 (9 mL) was treated with NaN_3 (2.52 g, 39 mmol) in the manner described above for phthalic acid, but the reaction time was extended by 30 min. Ether extraction gave an ether-soluble yellow solid (780 mg) and an ether-insoluble brown solid (1.85 g). Thin-layer chromatography showed that the former fraction contained two major components, well resolved, together with several poorly resolved minor components; mass spectral evidence indicated that the predominant major component was probably **8**, the other **7**. Thin-layer chromatography of the ether-insoluble material revealed that it contained the same range of materials as the ether-soluble fraction, plus others (at least nine were discernible); there were two major components, **7** and, to a significantly lesser extent, **8** (mass spectrum).

Accordingly, a sample (500 mg) of the ether-soluble material was chromatographed on silica. Elution with benzene–ether (9:1) gave phenanthrene-4,5-dicarboximide **8** as a yellow solid (280 mg, pure by tlc), mp 237–238°C (from acetic acid) (lit. (10) mp 240°C) ir (KBr): 1672 and 1645 (C=O) cm^{-1}; mass spectrum, *m/e*; 247 (M^+, 100), 219 (54), 205 (29), 190 (11), and 176 (25).

Further elution with benzene–ether (3:1) gave 1-azapyren-2(1*H*)-one **7** as a yellow solid (45 mg, pure by tlc), mp 345°C after sublimation *in vacuo* (lit. (11) mp > 340°C); ir (KBr): 1664 (C=O) cm^{-1}; mass spectrum, *m/e*: 219 (M^+, 100), 190 (14), and 163 (6).

Further elution with ether, followed by acetone, gave a small amount of brown solid containing at least two compounds (tlc).

Medenwald's corresponding experiment (10) was repeated, but our procedure for work-up was followed. The ether-soluble and ether-insoluble fractions exhibited virtually the same tlc characteristics as those obtained in the foregoing experiment.

Reaction of phenanthrene-4,5-dicarboxylic acid with sodium azide – sulfuric acid

A suspension of the diacid (3.5 g, 13 mmol) in DCE (33 mL) and 95–98% H_2SO_4 (11 mL) was treated with NaN_3 (5.14 g, 78 mmol) in the manner described for the preceding lactol. An analogous procedure for isolation gave an ether-soluble material (0.94 g), mp 217–223°C, and an ether-insoluble residue (1.95 g), mp 267–272°C. Each solid was yellow-brown in colour, exhibited several spots on tlc, and contained the same major component, namely **7**. 1-Azapyren-2(1*H*)-one **7** was recovered from each fraction by sublimation *in vacuo*, 0.75 g from the former fraction and 1.17 g from the latter for a total recovery of 1.92 g (67%), mp 318–320°C. This sample was slightly impure (see preceding experiment), but its identity was satisfactorily established by ir and mass spectral correlations.

In the ether-soluble fraction there was evidence (tlc and mass spectrum) for the presence of **8** (mass spectrum, *m/e* 247), attributable to traces of lactol in the dicarboxylic acid, and other minor products.

Reaction of diphenic acid with sodium azide – sulfuric acid

Diphenic acid (5.0 g, 21 mmol) in DCE (23 mL) and 95–98% H_2SO_4 (17 mL) was treated with NaN_3 (8.0 g, 130 mmol) in the manner described above for phthalic acid, the reaction time being extended by 30 min. The extraction procedure gave a reddish-brown solid (2.8 g), together with some undissolved sediment. The reddish-brown solid was triturated with ether and the resulting ether-soluble material was chromatographed on alumina to yield 2,2′-diaminobiphenyl as beige crystals (1.65 g, 43%), mp 74–76°C (reference sample, mp 81°C); identity was confirmed by ir and mass spectral correlations.

The sediment from the original extraction was collected, washed, and dried to give a brown powder (0.3 g), mp 290–293°C. This was sublimed *in vacuo* to yield phenanthridone (0.24 g, 6%) as white needles, mp 293°C (reference sample, mp 293°C); identity was established by ir and mass spectral correlations. A further quantity of slightly impure phenanthridone (0.2 g), mp 287–290°C, was recovered as insoluble material from the intermediate ether trituration.

From a similar scale experiment conducted using 90% H_2SO_4, the quantities obtained of 2,2′-diaminobiphenyl and of phenanthridone were 0.18 g (5%) and 2.28 g (56%), respectively.

[4]With G. A. Pawelchak.

Acknowledgment

We thank the Natural Sciences and Engineering Research Council of Canada for partial financial support.

1. M. OESTERLIN. Angew. Chem. **45**, 536 (1932).
2. G. CARONNA. Gazz. Chim. Ital. **71**, 189 (1941).
3. S. MAFFEI and G. F. BETTINETTI. Ann. Chim. (Rome), **49**, 1809 (1959).
4. D. FĂRCAŞIU and M. ROMAN. Chem. Ind. 1225 (1967); 24 (1968), and references cited.
5. M. S. GIBSON and M. GREEN. Tetrahedron, **21**, 2191 (1965).
6. D. J. LE COUNT. J. Chem. Soc. Perkin Trans. **1**, 813 (1983).
7. N. FURUKAWA, M. FUKUMURA, T. NISHIO, and S. OAE. Bull. Chem. Soc. Jpn. **51**, 3599 (1978).
8. L. HORNER, G. BAUER, and J. DÖRGES. Chem. Ber. **98**, 2631 (1965), and references cited.
9. M. S. NEWMAN and H. S. WHITEHOUSE. J. Am. Chem. Soc. **71**, 3664 (1949); G. M. BADGER, J. E. CAMPBELL, J. W. COOK, R. A. RAPHAEL, and A. I. SCOTT. J. Chem. Soc. 2326 (1950).
10. H. MEDENWALD. Chem. Ber. **86**, 287 (1953), and references cited.
11. G. CARONNA. Gazz. Chim. Ital. **71**, 475 (1941).
12. E. BAMBERGER and E. DEMUTH. Ber. Dtsch. Chem. Ges. **35**, 1885 (1902).
13. R. E. DESSY and M. S. NEWMAN. Organic syntheses. Coll. Vol. IV. *Edited by* N. Rabjohn. Wiley, New York. 1963. p. 484.

Isolation of 5-methoxy-2,2-dimethyl-1-2*H*-benzopyran-6-propanoic acid methyl ester and characterization by two-dimensional nuclear magnetic resonance spectroscopy

HELEN JACOBS AND FRANK RAMDAYAL
Centre for Natural Products Chemistry, University of Guyana, Georgetown, Guyana
AND
WILLIAM F. REYNOLDS, JANUSZ POPLAWSKI,[1] AND STEWART MCLEAN
Department of Chemistry, University of Toronto, Toronto, Ont., Canada M5S 1A1

Received August 16, 1985

HELEN JACOBS, FRANK RAMDAYAL, WILLIAM F. REYNOLDS, JANUSZ POPLAWSKI and STEWART MCLEAN. Can. J. Chem. **64**, 580 (1986).

The structure of the title compound (**1**), isolated from *Hortia regia*, was established by nuclear magnetic resonance spectroscopy. The investigation demonstrates the value of indirect shift correlation experiments. The compound was further characterized by chemical and spectroscopic methods.

HELEN JACOBS, FRANK RAMDAYAL, WILLIAM F. REYNOLDS, JANUSZ POPLAWSKI et STEWART MCLEAN. Can. J. Chem. **64**, 580 (1986).

Faisant appel à la rmn, on a déterminé la structure du composé **1** qui est mentionné dans le titre. Cette étude a permis de démontrer la valeur des expériences de corrélations indirectes des déplacements. On a de plus caractérisé le composé en se basant sur des méthodes chimiques et spectroscopiques.

[Traduit par le journal]

As part of a collaborative investigation of the natural products of Guyana, samples of materials isolated in Guyana are sent to the Toronto laboratories for spectroscopic examination. It can be anticipated that many of these natural compounds will be of established structure and will simply require identification. Since we wished to test the potential of our nmr spectroscopic techniques to solve structural problems, the Toronto group has deliberately applied these techniques to some of the samples before any information regarding the type of compound expected, its formula, or any other spectroscopic data was made known to them.

The title compound was received as an oil, and ^1H, ^{13}C and DEPT-edited[2] (1) ^{13}C nmr spectra were used to arrive at a tentative assignment of its structure. The ^1H spectrum (Fig. 1) provided evidence for the presence of two equivalent C—Me groups (*gem*-dimethyl), two OMe groups, an apparent A_2B_2 spectrum in the aliphatic region, and two AX spectra, one (δ 5.66, 6.54) with J_{HH} = 9.9 Hz and the other (δ 6.50, 6.89) with J_{HH} = 8.4 Hz. The 9.9-Hz coupling suggested the presence of a *cis* disubstituted olefinic grouping and the 8.4-Hz coupling was attributed to *ortho*-related aromatic protons. Key features in the ^{13}C spectrum included a peak at δ 173.6 suggestive of an ester functionality, signals for two non-protonated aromatic carbons (δ 152.5, 154.3) with chemical shifts that indicated that they carried an OR substituent, and a relatively deshielded quaternary aliphatic carbon (δ 75.6). Complete data are summarized in Table 1.

Based on these data, **1** was deduced as the most probable

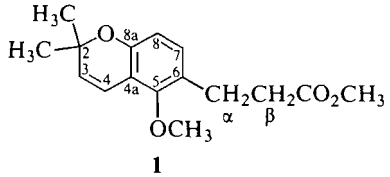

1

[1]On leave from the Institute of Chemistry, Białystok Branch of the University of Warsaw, Białystok, Poland.

[2]DEPT: dimensionless enhancement by polarization transfer.

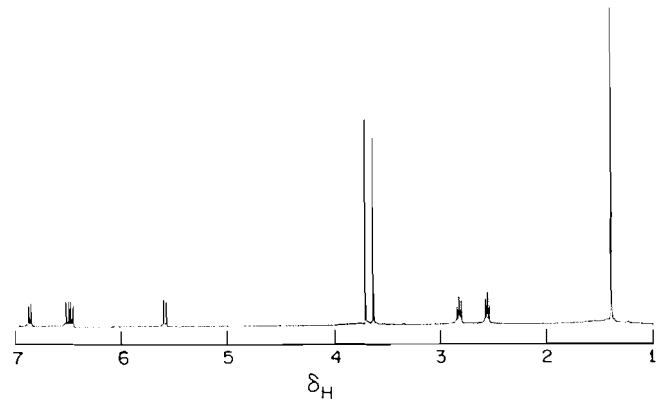

FIG. 1. 400-MHz ^1H spectrum for **1** in $CDCl_3$.

TABLE 1. Assigned ^1H and ^{13}C chemical shifts for **1** (in ppm relative to $(CH_3)_4Si$ in $CDCl_3$ solution)

Carbon	δ_C	δ_H	Coupling
C—2	75.51	—	
C—3	130.36	5.66	d, J = 9.9 Hz
C—4	117.21	6.54	d, J = 9.9 Hz
C—4a	114.79	—	
C—5	154.27	—	
C—6	125.05	—	
C—7	129.39	6.89	d, J = 8.4 Hz
C—8	112.26	6.50	d, J = 8.4 Hz
C—8a	152.54	—	
C—α	24.94	2.85	t, J = 7.5 Hz
C—β	34.91	2.57	t, J = 7.5 Hz
—CO_2—	173.57	—	
—CO_2CH_3	51.48	3.65	
—OCH_3	61.99	3.73	
$(CH_3)_2$	27.66	1.40	

Printed in Canada / Imprimé au Canada

structure. However, we were reluctant to rely so heavily on ^1H (ref. 2) and ^{13}C (ref. 3) chemical shift arguments for structural assignments, particularly since there were obvious discrepancies between earlier ^{13}C assignments for 2,2-dimethyl-1-2*H*-benzopyran (4) and some of its ring-substituted derivatives (5). Consequently, we believed that further verification was necessary, particularly with respect to the ring substitution pattern.

Examination of the literature revealed that structure **1** had previously been assigned (6) to one constituent of an inseparable mixture isolated from *Hortia badinii*. The assignment was made on the basis of the ^1H spectrum of the mixture, from which the peaks associated with other components were subtracted. This procedure provided a set of data very similar to ours, although some small differences (up to 0.08 ppm) in chemical shift are apparent. The reservations we held concerning the rigor of our structural assignment apply also to the earlier assignment.

Confirmation of the structure by two-dimensional nuclear magnetic resonance spectroscopy

Other substitution patterns of the benzenoid ring that had to be considered are represented by structures **2 – 6**. (We note that

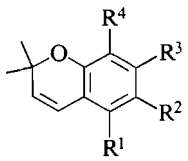

2 $R^1 = CH_2CH_2CO_2CH_3$, $R^2 = OCH_3$, $R^3 = R^4 = H$
3 $R^1 = R^2 = H$, $R^3 = CH_2CH_2CO_2CH_3$, $R^4 = OCH_3$
4 $R^1 = R^2 = H$, $R^3 = OCH_3$, $R^4 = CH_2CH_2CO_2CH_3$
5 $R^1 = CH_2CH_2CO_2CH_3$, $R^2 = R^3 = H$, $R^4 = OCH_3$
6 $R^1 = OCH_3$, $R^2 = R^3 = H$, $R^4 = CH_2CH_2CO_2CH_3$

some could, however, be considered improbable on the basis of chemical shifts observed.)

A standard direct ^1H–^{13}C shift-correlated experiment (7) was carried out first. This gives peaks for each directly bonded C—H pair at δ_H in F_1 and δ_C in F_2 (see Fig. 2), thus establishing direct ^1H–^{13}C connectivities. The experiment involves polarization transfer from ^1H to ^{13}C and requires a delay of $(2J_{CH})^{-1}$ to set up this polarization transfer. Consequently, it is possible to use the same experimental procedure to establish indirect ^1H–^{13}C connectivities by choosing delay times appropriate for geminal or vicinal ($^2J_{CH}$ or $^3J_{CH}$) couplings rather than one-bond ($^1J_{CH}$) couplings (8, 9). This experiment has already proved very useful for characterizing other natural products (10, 11). It does require some knowledge of $^2J_{CH}$ and $^3J_{CH}$ couplings, but extensive compilations of these are available (12, 13).

In the structures under consideration, values of $^3J_{CH} \sim 9$–10 Hz for *trans* couplings involving olefinic or aromatic protons and carbons are to be expected, while $^2J_{CH} \leq 2$ Hz. Both $^2J_{CH}$ and $^3J_{CH}$ are typically ca. 5 Hz for couplings involving aliphatic carbons. We chose the initial fixed delay prior to polarization transfer $\Delta_1 = 0.05$ s, with the second fixed delay $\Delta_2 = 0.033$ s, both optimized carbons (12). In fact, in addition to the cross peaks already noted for the *ipso* carbon, cross peaks are observed for the carbon peaks at δ 154.3 and δ 129.4 (not shown). This eliminates both **4** and **6** from consideration since both should show a cross peak with δ 152.5 (assigned to the carbon carrying the heterocyclic oxygen). Only structure **1** remains consistent in every respect with the spectroscopic data.

The structure of the compound is rigorously established on the basis of the data cited and the spectrum can be totally assigned with confidence (see Table 1). Although further confirmation appears unnecessary, we note that the experiment provides a number of additional cross peaks, all of which are in accord with the assignments already made. To cite just one example, a strong cross peak is observed between peaks assigned as C-6 and H-8 and confirms their *meta* relationship. All observed cross peaks are summarized in Table 2. In addition to the evidence cited above, the observation of a 0.6-Hz long-range coupling between H-4 and H-8 is also consistent with the proposed structure (14). The observation of this type of

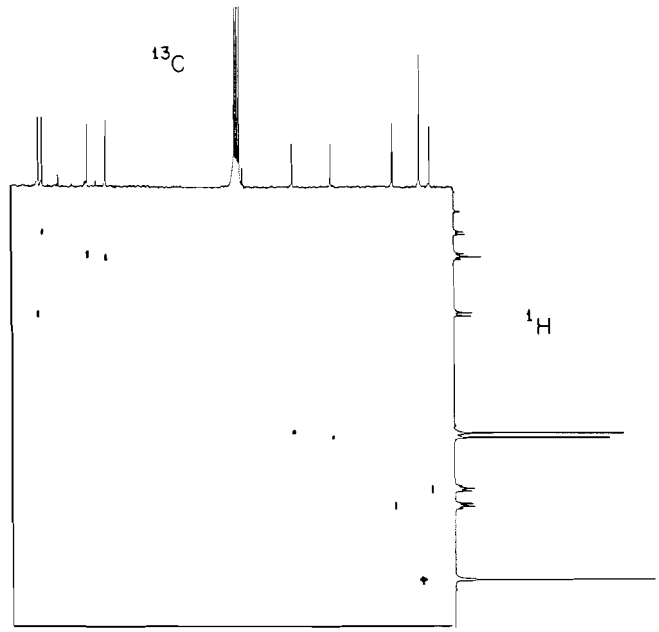

FIG. 2. Direct ^1H – ^{13}C shift correlated spectrum for **1**. ^{13}C frequencies are along the horizontal axis while ^1H frequencies are along the vertical.

TABLE 2. Hydrogen signals establishing indirect connectivities to each carbon from the indirect shift-correlated experiment

Carbon	Observed hydrogen connectivities
C—2	H—3,H—4,$(CH_3)_2$
C—3	$(CH_3)_2$
C—4	None observed
C—4a	H—3,H—8
C—5	H—7,H—α,OCH_3
C—6	H—8,H—α,H—β
C—7	H—8(w),[a]H—α
C—8	H—7(w)[a]
C—8a	H—7,H—4
C—α	H—β
C—β	H—α
—CO_2—	H—α,H—β,CO_2CH_3
—CO_2CH_3	None observed
—OCH_3	None observed
$(CH_3)_2$	$(CH_3)_2$[b]

[a]Low intensity peak. The adjacent oxygen functionality apparently increases the magnitude of $^2J_{CH}$ sufficiently (12) that a weak cross peak is observed corresponding to this coupling.

[b]A cross peak is observed corresponding to polarization transfer from the protons of one of the equivalent methyl groups to a ^{13}C atom in the second methyl group ($^3J_{CH}$).

coupling has been claimed to be diagnostic for the presence of the part structure **7** (14);

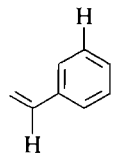

7

However, it should be noted that styrene derivatives also show ca. 0.5-Hz couplings between α and *ortho* protons (15). Thus the reliability of this diagnostic test for **7** is questionable.

The results presented here illustrate the great utility of the indirect shift-correlated experiment.[3] The main structural features of the compound were deduced from the ^1H and ^{13}C spectra, but it was not possible to use these data to distinguish between a number of isomeric possibilities differing in substitution patterns. The direct shift-correlation experiment was required to identify unequivocally aromatic C—H pairs, but provided little further structural information; it is at this point that the recognition of 2-bond and 3-bond connectivities becomes crucial and the power of the indirect shift-correlation experiment in distinguishing between isomeric possibilities becomes apparent. In the present case the data were compatible with only one of the isomeric possibilities, and allowed structure **1** to be assigned unequivocally. In fact, the combination of direct and indirect shift-correlated spectra has some distinct advantages over the alternative $^{13}C-^{13}C$ connectivity (INADEQUATE) experiment (16). The most obvious is sensitivity (10), since the INADEQUATE experiment appears to be an order of magnitude less sensitive. The second advantage is that, while the INADEQUATE experiment establishes only direct $^{13}C-^{13}C$ connectivities, the indirect shift-correlated experiment can often establish connectivities to several adjacent protons (and carbons) from a single ^{13}C cross section. Consequently, the same connectivity may be established and confirmed in more than one way. Thirdly, as illustrated in Fig. 3, the indirect experiment can establish connectivities even through heteroatoms, e.g. oxygen, something which is not possible with INADEQUATE. In previous applications this experiment has been used to assign the spectra of compounds of established structure (10, 11, 17–19), but the present results clearly demonstrate its potential in the field of structure elucidation of new compounds. It was to test this potential that the present investigation was carried out by the spectroscopic group before any other structural information concerning the compound in hand was available to them.

Although, as it happens, a compound of structure **1** has been described in the literature (6), it had not previously been obtained in a homogeneous form. Consequently, we have treated **1** as a new natural compound, and completed its characterization. These data, all of which are in accord with the assigned structure, are reported in the experimental section.

As a further confirmation of the assignments made, **1** was reduced to a dihydro derivative by catalytic hydrogenation. The ^1H spectrum of dihydro-**1** showed an AA′XX′ spectrum (δ 1.74, 2.73) in place of the AX spectrum (δ 5.66, 6.54) of **1**, while the other signals showed little change. In the ^{13}C spectrum, the δ 117.2 and δ 130.4 signals of **1** were replaced by methylene signals at δ 17.44 and δ 32.20 while the rest of the spectrum showed only small and predictable changes (see Experimental). These results clearly confirm the assignments made to the vinylic and aromatic C—H groupings in **1**.

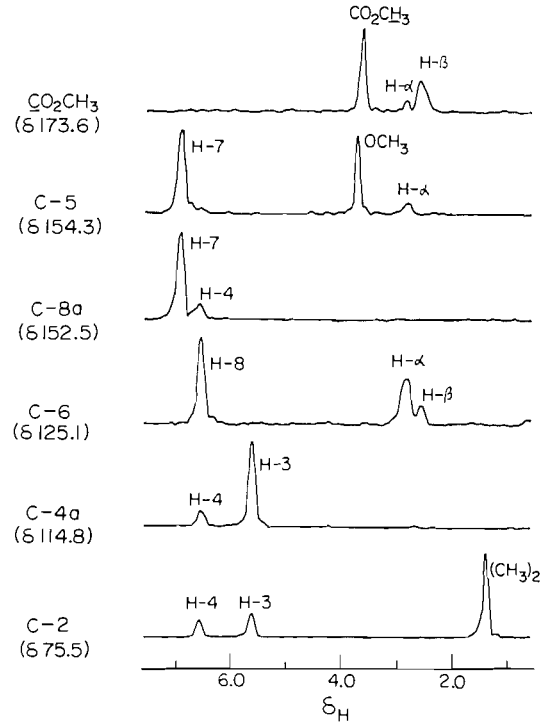

FIG. 3. ^1H cross sections through each non-protonated ^{13}C frequency from the indirect $^1H - ^{13}C$ shift-correlated spectrum for **1**.

Experimental

Infrared spectra were recorded on a Nicolet 5DX FTIR spectrometer with samples as liquid films. Ultraviolet spectra were recorded on a Carey 14 spectrometer with samples dissolved in 95% ethanol.

Standard ^1H and ^{13}C spectra were obtained on a Varian XL-400 spectrometer operating at 399.93 MHz for ^1H and 100.57 MHz for ^{13}C, using a sample containing 8 mg of **1** in 0.5 mL of $CDCl_3$ in a 5-mm tube. The ^1H spectral width was 4000 Hz and 32 768 data points were collected and zero-filled to 65 536 points. No weighting was applied during Fourier transformation. The ^{13}C spectrum contained the same number of data points for a 20 000-Hz spectral width and 1-Hz exponential line broadening was applied prior to Fourier transformation.

The 2D spectra were obtained on a Varian XL200 spectrometer operating at 50 MHz for ^{13}C and using 30 mg of **1** in 2 mL of $CDCl_3$. For the direct shift-correlated experiment, the ^{13}C spectral width was 6000 Hz while the ^1H spectral width was 1400 Hz. 1024 data points were collected for each spectrum with 64 transients/spectrum, and 256 time increments were used with zero filling to 1024. Five-hertz line broadening was used for both frequency axes. For the indirect shift-correlated experiment the ^{13}C spectral width was 8000 Hz with 2048 data points. The ^1H spectral width was 1400 Hz and 96 increments were used with 256 transients/spectrum. Weighting parameters were identical to those used in the previous experiment. Delay times are discussed in the text.

Standard Varian software was used to obtain the 2D spectra.

[3]We use the terms direct and indirect to describe the two shift-correlated experiments in the context of the connectivities established, i.e. between directly or indirectly bonded pairs of nuclei. A referee has argued that it would be better to refer to one-bond or long-range shift correlations. However, in nmr spectroscopy, long-range usually refers to couplings over four or more bonds. An alternative acceptable terminology would be ^1J-based or ^nJ-based shift correlation.

Isolation and characterization of **1**

Dried roots of *Hortia regia* Vand.[4] were ground and exhaustively extracted by percolation with cold methanol. The material obtained after the methanol had been removed under reduced pressure was chromatographed on neutral alumina (activity III). The fraction eluted with 20% ethyl acetate in hexanes was rechromatographed on silica gel, and the fraction eluted with 5% ethyl acetate in hexanes was substantially pure **1** as a colorless oil (0.5% from dried plant). Bulb-to-bulb distillation at 7 Pa and a bath temperature of 170°C provided the sample of **1** used for this study. ir: 1738 cm^{-1}; uv: λ_{max} 267 (ε 6 500), 278 (ε 5 500), 313 (ε 1 850); ms: (*m*/*z*(rel. intensity)): 276(16), 262(18), 261(100), 203(10), 187(16). *Exact Mass* calcd. for $C_{16}H_{20}O_4$: 276.3161; found: 276.1360. *Anal.* calcd. for $C_{16}H_{20}O_4$: C 69.54, H 7.30; found: C 69.53, H 7.28.

Compound **1** in ethyl acetate was hydrogenated over 10% palladium on carbon at ambient temperature and pressure, and was obtained as a colorless oil: ir: 1738 cm^{-1}; ^{1}Hmr (400 MHz; $CDCl_3$) (δ (multiplicity, *J*, number of protons)): 6.88 (d, 8.4 Hz, 1H), 6.50 (d, 8.4 Hz, 1H), 3.73 (s, 3H), 3.65 (s, 3H), 2.86 (m, 2H), 2.73 (m, 2H), 2.59 (m, 2H), 1.74 (m, 2H), 1.29 (s, 6H); ^{13}Cmr (100 MHz; $CDCl_3$) (δ (number of connected hydrogens from edited spectrum)): 17.44 (2), 24.90 (2), 26.68 (2 × 3), 32.20 (2), 34.98 (2), 51.44 (3), 60.20 (3), 73.61 (0), 112.95 (1), 114.84 (0), 123.75 (0), 127.71 (1), 153.57 (0), 156.45 (0), 173.66 (0).

Acknowledgments

The Centre at the University of Guyana is grateful for generous support from the Canadian International Development Agency. The research at the University of Toronto is supported by grants from the Natural Sciences and Engineering Research Council of Canada. We thank Professor D. B. MacLean for his help in obtaining mass spectra at McMaster University.

1. D. M. Doddrell, D. T. Pegg, and M. R. Bendall. J. Magn. Reson. **48**, 323 (1982).
2. L. M. Jackman and S. Sternhell. Nuclear magnetic resonance spectroscopy in organic chemistry. Pergamon Press, Oxford. 1969.
3. (*a*) J. B. Stothers. Carbon-13 NMR spectroscopy. Academic Press. New York. 1972; (*b*) E. Breitmaier and W. Voelter. ^{13}C NMR spectroscopy. Verlag Chemie, Weinheim. 1974; (*c*) F. W. Wehrli and T. Wirthlin. Interpretation of carbon-13 NMR spectra. Heyden, London. 1976.
4. A. M. Samat, G. J. Martin, and R. J. Anglielmetti. Org. Magn. Reson. **8**, 62 (1976).
5. P. C. Viera, M. A. deAlvarenga, O. R. Gottlieb, M. de Nazare, V. McDougall, and F. deA. M. Reis. Phytochemistry. **19**, 472 (1980).
6. D. deB. Corrêa, O. R. Gottlieb, and A. P. de Podua. Phytochemistry, **14**, 2059 (1975).
7. A. Pax and G. A. Morris. J. Magn. Reson. **42**, 501 (1981).
8. K. Hallenga and G. VanBinst. Bull Magn. Reson. **2**, 343 (1980).
9. A. Bax. *In* Topics in carbon-13 NMR spectroscopy. Vol. 4. *Edited by* G. C. Levy. Wiley, New York. 1984.
10. W. F. Reynolds, R. G. Enríquez, L. I. Escobar, and X. Lozoya. Can. J. Chem. **62**, 2421 (1984).
11. W. F. Reynolds, R. G. Enríquez, M. A. Chavez, A. L. Silva, and M. A. Martinez. Can. J. Chem. **63**, 849 (1985).
12. J. L. Marshall. Carbon–carbon and carbon–proton NMR couplings: applications to organic stereochemistry and conformational analysis. Verlag Chemie, Deerfield Beach. 1983.
13. P. E. Hansen. Prog. Nucl. Magn. Reson. Spectrosc. **14**, 175 (1981).
14. E. V. Lassak and J. T. Pinhey. J. Chem. Soc. (C), 2000 (1967).
15. M. Barfield, C. J. Macdonald, I. R. Peat, and W. F. Reynolds. J. Am. Chem. Soc. **93**, 4195 (1971).
16. (*a*) A. Bax, R. Freeman, and G. A. Morris. J. Am. Chem. Soc. **102**, 4849 (1980); (*b*) T. H. Mareci and R. Freeman. J. Magn. Reson. **48**, 158 (1982).
17. C. Wynants, K. Hallenga, C. vanBinst, A. Michel, and J. Zanen. J. Magn. Reson. **57**, 93 (1984).
18. H. Kessler, C. Griesinger, J. Zarbock, and H. R. Loosi. J. Magn. Reson. **57**, 331 (1984).
19. M. A. Debuc, J. Y. Lallemond, G. Dauphin, and G. Jeminet. J. Org. Chem. **49**, 1797 (1984).

[4]Voucher specimens are lodged in the University of Guyana Herbarium and in the Institute of Systemati Botany, Utrecht.

Synthesis of (±)-karahana ether and a (±)-labdadienoic acid by the electrophilic cyclization of epoxy allylsilanes

ROSEMARY J. ARMSTRONG AND LARRY WEILER[1]

Department of Chemistry, University of British Columbia, Vancouver, B.C., Canada V6T 1Y6

Received August 22, 1985

ROSEMARY J. ARMSTRONG and LARRY WEILER. Can. J. Chem. **64**, 584 (1986).

The epoxy allysilanes **7** and **16** were synthesized by stereoselective routes from β-keto esters and cyclized with Lewis acids in good yield. The monocyclic product from **7** was converted into (±)-karahana ether (**10**), and the bicyclic product from **20** was used in a synthesis of the 3-hydroxylabdadienoic acid **24***b*.

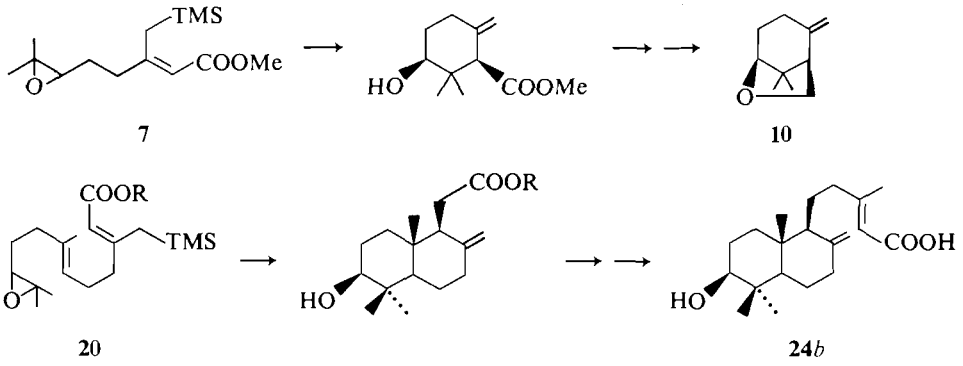

ROSEMARY J. ARMSTRONG et LARRY WEILER. Can. J. Chem. **64**, 584 (1986).

Utilisant des voies stéréosélectives appliquées à des β-céto esters, on a synthétisé les époxysilanes **7** et **16** et on les a cyclisés, avec de bons rendements, sous l'influence d'acides de Lewis. Le produit monocyclique obtenu à partir du produit **7** a été transformé en l'éther du (±)-karahana (**10**) alors que l'on a utilisé le produit bicyclique obtenu à partir du composé **20** pour effectuer la synthèse de l'acide hydroxy-3 labdadiènoïque (**24***b*).

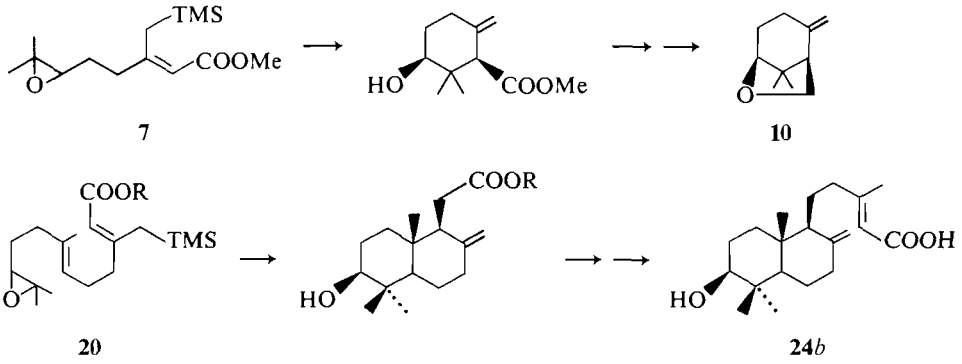

[Traduit par le journal]

Introduction

For the past fifty years, organic chemists have often sought biomimetic type routes in their syntheses of natural products (1). These routes, based on the presumed biosynthetic pathway, frequently were very efficient and led to the development of new synthetic reactions. The concept of biomimetic polyolefin cyclizations is based upon the Stork–Eschenmoser hypothesis, which was proposed in 1955 (2). These authors suggested that many cyclic terpenoid natural products arise via a cyclization of the appropriate polyolefin initiated by an electrophile. The conformation of the polyolefin and an *anti*-periplanar addition to the olefin determine the structure and stereochemistry of the final product. There have been a variety of successful natural products syntheses based on this concept (1, 3). In most cases, the cyclization has been initiated by the attack of a Lewis acid or a Bronsted acid on an alkene (3, 4), allylic alcohol (5), or an acetal (6). In the first case the product is not functionalized at the electrophilic terminus, and in the last two cases the functionality at this terminus is either an alkene or an ether—two groups that frequently require substantial manipulation to convert into the desired natural products.

In an effort to introduce other functional groups at the electrophilic terminus of the polyolefin, several research groups have studied the initiation of these cyclizations using other electrophiles, such as mercury(II) (7), brominating agents (8), and sulfinating or selinating reagents (9). This approach to functionalized products from polyolefin cyclizations has not been generally successful. In all but a few examples, the yield of polycarbocyclic products is very low, the exceptions being some recent mercury(II) cyclizations (7*a*, *b*). Following these cyclizations, it is necessary to convert the heteroatom into another functional group, such as an alcohol. In general this cannot be carried out stereoselectively.

[1]Author to whom correspondence may be addressed.

In 1962, Goldsmith showed that a terminal epoxide of a polyolefin could function as the electrophilic initiator in these cyclizations (3*g*, 10). In addition, Goldsmith recognized that, if the cyclization that leads to a six-membered ring proceeded via a transition state with ring A in a chair conformation, the resulting alcohol should be equatorial (eq. [1]). In 1966, Corey *et al.* (11)

[1] 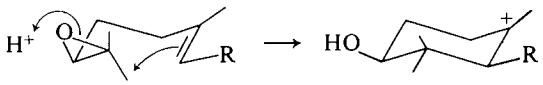

and van Tamelen *et al.* (12) showed that squalene 2,3-epoxide was enzymatically converted into a tetracyclic product that had an alcohol at C-3 with the α stereochemistry. Following these *in vivo* experiments, van Tamelen's group played a leading role in studying the *in vitro* cyclization of polyolefin epoxides (13). Without exception, these cyclizations had serious limitations as synthetic tools. Frequently, the regioselective synthesis of the terminal polyolefin epoxide was difficult to achieve in high yield. The cyclizations often proceeded in low yield and usually gave a large number of products that were difficult to separate. However, these studies proved that the transition state in these *in vitro* cyclizations did, in fact, proceed through a ring A chair conformation as shown in eq. [1].

Most of the early work on polyolefin cyclizations involved the use of unsubstituted alkenes as terminators. These alkenes had the disadvantage that, once cyclization was complete, the resulting carbonium ion could lose a proton from a number of positions or be trapped by nucleophiles, resulting in a variety of products being formed. Johnson and co-workers found that the styryl terminating group did lead to preferential formation of products resulting from an intermediate benzylic carbonium ion (3*b*). However, one was then faced with the problem of efficiently removing the aromatic ring to obtain useful products.

Subsequently it was found that allenes (3*b*), acetylenes (3*b*, 14), or vinyl halides (15) could function as efficient and useful terminators in these polyolefin cyclizations. Several groups have shown that the enol or enol phosphate of β-keto esters was also a very versatile terminating group in olefin cyclizations (16).

One of the major problems in polyolefin cyclizations, which was briefly alluded to above, is the lack of regioselectivity in quenching the carbonium ion intermediate produced in the cyclization. In 1976, Fleming *et al.* found that an allylsilane had a dramatic effect in controlling the regioselectivity in an olefiin cyclization (17). For example, Johnson and co-workers had found that the acetal **1**, on treatment with acid, gave a mixture of five products (including the three isomeric alkenes) as shown in eq. [2] (18). On the other hand, the acetal **2** cleanly cyclized to

[2] 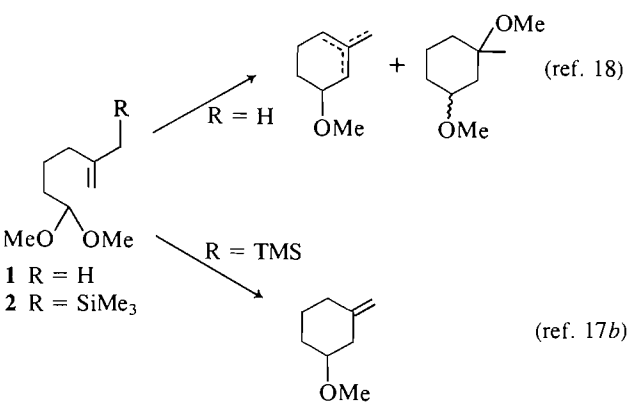

(ref. 18)

(ref. 17*b*)

3

the exocyclic alkene **3** (17). Presumably the regioselectivity in the latter reaction is controlled by the remarkable ability of silicon to stabilize a developing carbonium ion β to itself (19). In a subsequent paper Fleming and Pearce noted that the silicon also appeared to activate the terminal alkene in this cyclization (eq. [2]), compared to the unsubstituted case (17*b*).

Chow and Fleming extended these results to show that this type of cyclization could be controlled to regioselectively yield the exocyclic alkene **3** above, or either of the endocyclic alkenes as shown in eq. [3] (17*c*). Following the initial report on

[3] 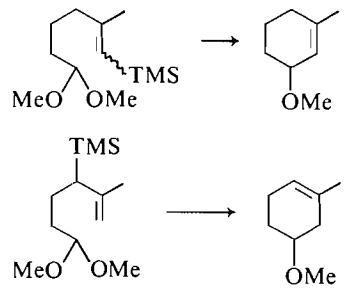

(ref. 17*c*)

the utility of allyl- and vinylsilanes in olefin cyclizations, this concept has been applied to the synthesis of five-membered rings (20), six-membered rings (21), seven-membered rings (22), and polycyclic systems (23). The results of Wang and Chan are particularly noteworthy (22). Electrophilic cyclizations to seven-membered rings are rare; however, the allylsilane shown in eq. [4] cyclized cleanly and efficiently to the cycloheptane derivative.

[4] 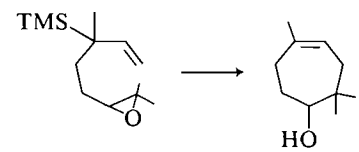

(ref. 22)

We recently introduced a stereoselective synthesis of carboxylated allylsilanes using the Grignard coupling to the enol phosphate of a β-keto ester (24) as shown in eq. [5] (25, 26). These allylsilanes could be cyclized with Lewis acids or mercuric salts to give mono- or bicyclic products in good yield, and we demonstrated the utility of this cyclization in the synthesis of trixagol (**4**) (26) and albicanyl acetate (**5**) (25). It was clear from these results that the conjugated alkene, although deactivated in electrophilic reactions by the ester moiety, was sufficiently activated by the silicon to allow these cyclizations to proceed efficiently. An additional bonus in these cyclizations was the remarkable ability of the silane group to control the regioselective generation of the exocyclic alkene.

We then turned our attention to the cyclization of epoxy allylsilanes with the expectation that the epoxide would be opened stereoselectively and that the resulting alcohol could be used to introduce other functional groups. As noted above, *in vitro* cyclizations of epoxy olefins usually proceed in low to moderate yields (13). We would like to report our results on the cyclization of epoxy allylsilanes and the utility of this cyclization in the synthesis of two representative natural products.[2]

The diene **6** (26) was regioselectively epoxidized in 84% yield to the epoxy allylsilane **7** using *m*-chloroperoxybenzoic acid (MCPBA). This reagent is known to preferentially attack electron-rich alkenes, thus the electron-withdrawing effect of the carbomethoxy group must be greater than the electron-

[2]A preliminary report of some of these results has appeared (ref. 27).

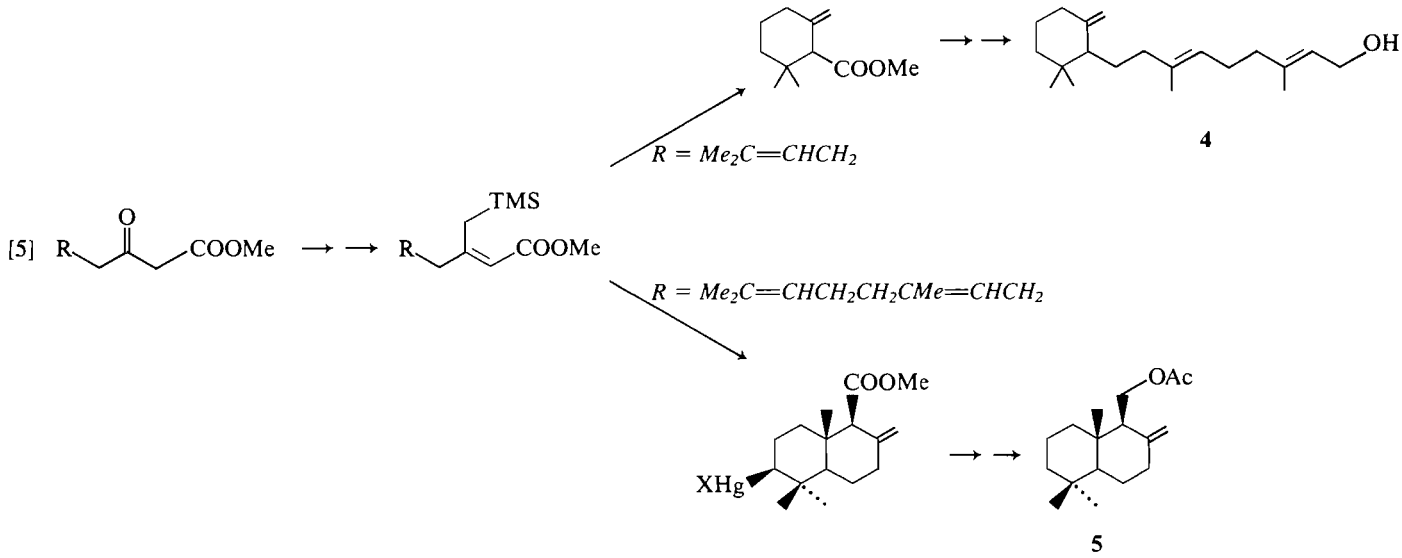

donating effect of the trimethylsilyl group. Cyclization of the epoxy allylsilane **7** proved to be extremely facile. Treatment of a solution of **7** in dry methylene chloride with either stannic chloride or boron trifluoride etherate effected conversion to the cyclic hydroxy ester **8** in good yield. Boron trifluoride was the Lewis acid of choice. Gas chromatographic analysis showed that the crude product contained approximately 80% of **8**, 10% of starting **7**, and 10% of two other unidentified products. This is at least a three-fold improvement in yield over the optimum cyclization of an olefinic epoxide reported to this time. It was clear that the trimethylsilyl group endowed the nucleophilic terminus with just the right electronic properties to efficiently participate in the cyclization.

Some loss of material was experienced on the column chromatographic purification of **8**. However, when the crude cyclization mixture was treated with lithium aluminum hydride, the diol **9** was isolated in 68% yield from **7**. The spectral and chromatographic properties of **8** and **9** indicated that each was a single diastereomer. The spectral data of the diol **9** were identical to those reported by Coates and Melvin (28) for a sample of **9** prepared by another unambiguous route.[3] The structure and *cis* stereochemistry of the diol **9** was further confirmed by its conversion to (±)-karahana ether (**10**) following the procedure of Coates and Melvin (28). Karahana ether is a volatile monoterpene, with a pleasant camphor-like odor, which has been isolated from Japanese hops (29). Two other syntheses of karahana ether have been reported recently (30).

This sequence of reactions proves that the ester and the alcohol groups in the cyclized product **8** must have the *cis* stereochemistry shown. This stereochemistry can result from a cyclization of the epoxy olefin via a chair-like transition state (2, 10).

The extension of the monocyclic epoxy allylsilane cyclization to the bicyclic case was achieved after some effort. The first problem to be solved involved the regioselective synthesis of the terminal epoxide **11**. Oxidation of the triene **12** (25, 31) with MCPBA gave a mixture of regioisomers (1:1) involving epoxidation of the 6,7 and 10,11 double bonds, and the two epoxides were difficult to separate on preparative scale. The enol phosphate **13** could be regioselectively epoxidized with MCPBA at low temperature (−50°C) to give the 6,7- and 10,11-epoxides in a ratio of 1:4. Unfortunately we were unable to separate these isomeric epoxides and the coupling of the mixture of enol phosphates with trimethylsilylmethyl magnesium chloride was inefficient.

The most successful approach to the synthesis of the 10,11-epoxy allylsilane utilized the terminal epoxidation method of van Tamelen and co-workers (13*a*, 32). This involved conversion of the triene **12** to the terminal bromohydrin with *N*-bromosuccinimide (NBS), and closure to the desired epoxy allylsilane **11** with potassium carbonate. The NBS reaction could be carried out either in DME–H_2O (3:1) or in THF–H_2O (5:1). The resulting bromohydrin was unstable, hence the crude reaction mixture was usually treated immediately with base. It

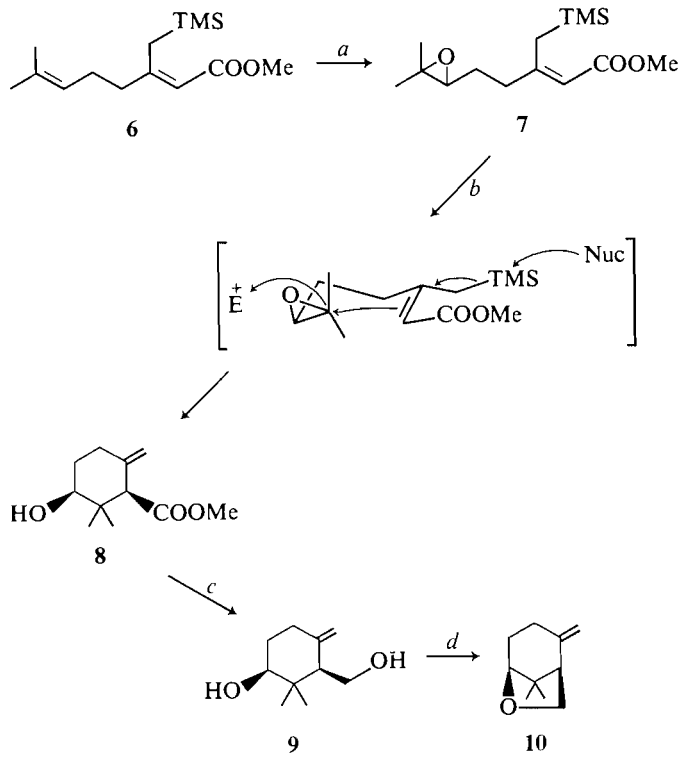

(a) MCPBA; (b) $BF_3{\cdot}Et_2O$; (c) LAH; (d) TsCl, py

SCHEME 1. Synthesis of (±)-kaharana ether (**10**).

[3]We are grateful to Professors Coates and Yamada for this data.

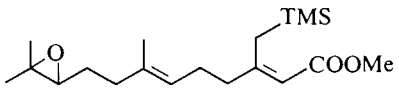

11

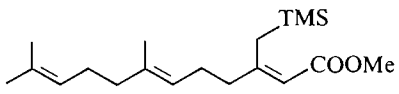

12

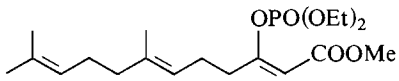

13

was necessary to carefully control the temperature of this cyclization and to monitor the progress of the reaction by tlc. The yield of terminal epoxide was generally from 45 to 55% after purification, and complete regioselectivity in epoxide formation was invariably obtained.

The epoxy allylsilane **11** was treated with a wide range of Lewis acids, and the ratio of products was determined by gas chromatography (gc) and ^{1}H nmr spectra (31). Boron trifluoride etherate in dry methylene chloride gave a good yield of the epimeric hydroxy esters **14**. Unfortunately the stereoselectivity in this reaction was poor, the two epimers, **14***a* and **14***b*, being formed in equal amounts. Cyclization at lower temperature (−50°C) gave improved stereoselectivity; however, a significant amount of a monocyclic product was obtained. Stannic chloride in dry methylene chloride gave the best yield and ratio of hydroxy esters **14***a* and **14***b*. On a small scale (<1 mmol), these esters were isolated in ca. 60% yield and the ratio of **14***a* to **14***b* was 1:2. Larger scale reactions (up to 5 mmol) gave ca. 55% yield of products, but the ratio of epimers fell to 2:3. On cooling the reaction, the stereoselectivity improved but again substantial amounts of monocyclic products were produced.

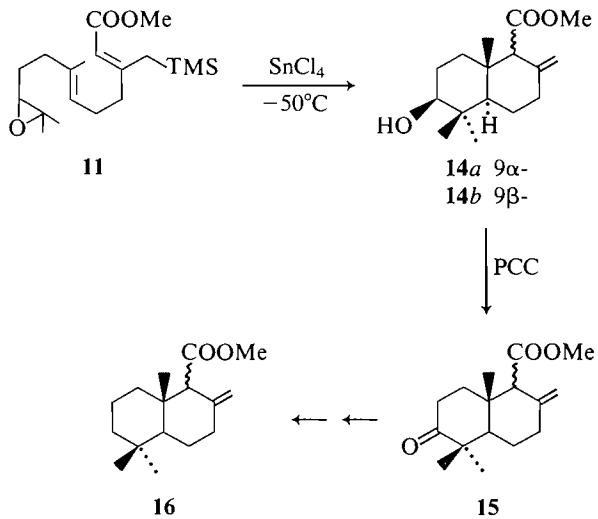

11 **14***a* 9α-
14*b* 9β-

16 **15**

The structures of the two cyclized products were confirmed by the following transformations. A mixture of cyclized esters, in a ratio of 2:3, was oxidized with pyridinium chlorochromate to give two ketones, **15**, also in a ratio of 2:3. This confirmed that the cyclized products were not epimeric at C-3. The ketone carbonyl of **15** was removed by formation of the tosylhydrazones and reduction with catecholborane (33) as shown above. Two products, **16**, were obtained in a ratio of 2:3 and they were shown to be the C-9 epimers by comparison with an authentic sample of these esters (25).

This clean cyclization of **11** can be contrasted with the cyclization of methyl 10,11-epoxyfarnesate (**17**), which on treatment with phosphoric acid or a Lewis acid gives a variety of products. The major bicyclic products in this latter example were the C-9 epimeric $\Delta^{7,8}$-alkenes which were isolated in 10–28% yield (eq. [6]) (13*a*). The ratio of the 9α/9β epimers varied with catalyst, but the 9α isomer was the major one. No exocyclic alkene **14** was found in the reaction mixture (13*a*).

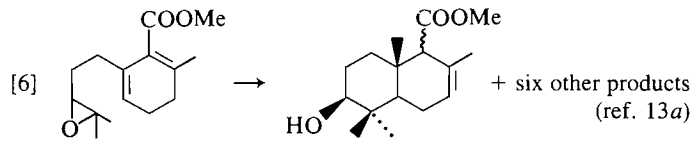

17

Although the above conversions of **11** and its derivatives give no indication of the stereochemistry of the hydroxyl group at C-3, they do confirm the structure of the remaining carbon skeleton. The stereochemistry of the alcohol was determined to be equatorial from the 400-MHz ^{1}H nmr spectrum of the esters, which showed the C-3 proton to be a double doublet with $J = 5$ and 11 Hz. This stereochemistry is also in accord with the Stork–Eschenmoser hypothesis of a ring A chair-like transition state for this cyclization.

If one assumes that the cyclization of the epoxy allylsilane **11** occurs via a chair–chair transition state to give ester **14***b*, and via a chair–boat transition state to give ester **14***a*, then the energies of these two transition states must be very similar, to give the observed product distributions. The cyclization is irreversible and the esters **14** do not equilibrate under the reaction conditions. The α-ester is the more stable product presumably because of the $A^{(1,3)}$ strain in **14***b*. Thus we conclude that the ratio of the two products is kinetically controlled and depends on the activation energy of the transition states leading to **14***a* and **14***b*. It is not immediately apparent what the controlling factors are in these transition states. However, it is expected that steric interactions of the ester with other groups might play an important role in the cyclization. To test this hypothesis, we synthesized esters with different sizes and studied their cyclization.

The *tert*-butyl ester of **11** decomposed under the cyclization conditions. The isopropyl, neopentyl, and di-*tert*-butylmethyl esters were synthesized as above from the corresponding acetoacetate esters, which were prepared from diketene as shown in Scheme 2 (34).

Cyclization of the isopropyl ester **20***a* gave an epimeric mixture of bicyclic products **21** in 51% yield and a ratio of 9α/9β of 1:3. This modest improvement in stereoselectivity over the methyl cyclization encouraged us to study the neopentyl ester **20***b* and the di-*tert*-butylmethyl ester **20***c*. No noticeable improvement in the product ratios was observed in the cyclization of the neopentyl ester **20***b*. There was a small increase in the ratio of α/β isomers in the cyclization of the di-*tert*-butylmethyl ester **20***c* using stannic chloride as catalyst. Changing the Lewis acid catalyst did not lead to any increase in the stereoselectivity in either of these cyclizations. An unexpected improvement in the product distribution was obtained with the di-*tert*-butylmethyl ester by the addition of a small amount of acetic acid to the stannic chloride catalyzed reaction. The maximum stereoselectivity was obtained when 0.1 equiv.

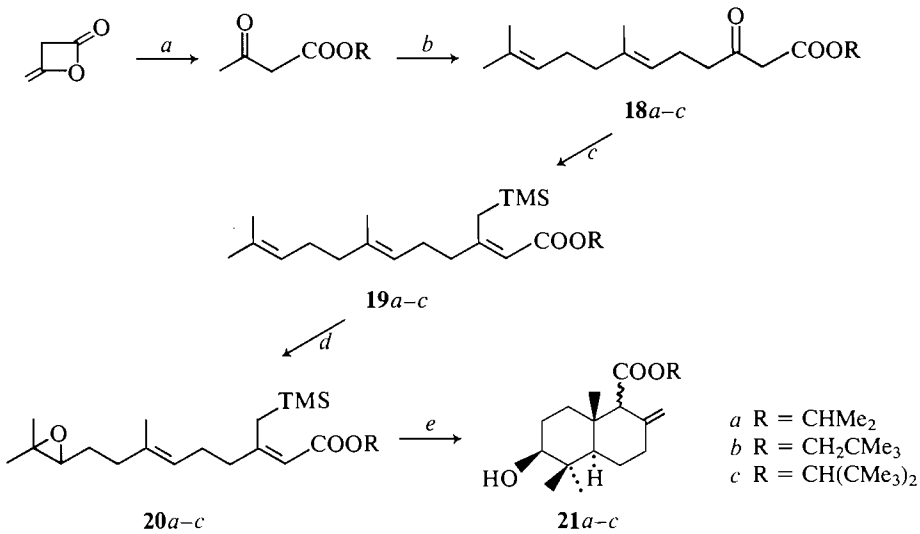

(a) ROH; (b) NaH, *n*-BuLi, $Me_2C{=}CHCH_2CH_2CMe{=}CHCH_2Br$;
(c) NaH, $ClPO(OEt)_2$ then Me_3SiCH_2MgCl, $Ni(acac)_2$;
(d) NBS, $THF–H_2O$ then K_2CO_3, MeOH; (e) $SnCl_4$, trace HOAc

SCHEME 2. Cyclization of diene epoxides.

of acetic acid was added, giving a ratio of α/β = 1:5 on small scale. The stereoselectivity fell to 1:3 for larger scale reactions. However, this still represented a 100% improvement over the methyl ester cyclizations. A summary of these results is contained in Table 1.

These results show that increasing the size of the ester group in the diene epoxide leads to an increase in the amount of β isomer obtained, and hence a larger difference in the activation energy of the chair–chair transition state relative to the chair–boat transition state. This difference can be rationalized by comparing the interaction of the ester group with the angular methyl group at C-10 and with the C-1 methylene of the incipient A ring. In the chair–chair transition state there is a *gauche* interaction between the ester COOR and both the C-10 methyl and the C-1 methylene (see **22**). In the chair–boat transition state **23** the ester is eclipsed with the C-1 methylene. This eclipsing interaction will increase as the size of the ester increases. Hence the chair–chair transition state leading to the 9β epimer is preferred for larger esters.

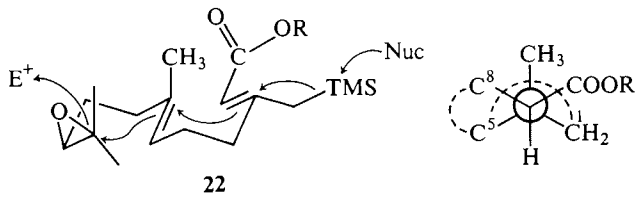

22

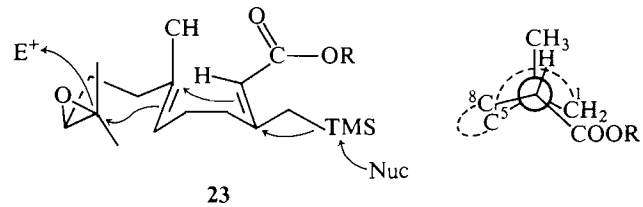

23

A large number of natural products possess the bicyclic carbon skeleton of **14** and **21**. However, those with a C-3 alcohol are less common. Two examples of these latter products are 3-acetoxylabda-8(20),13-dien-15-oic acid (**24***a*) and the corresponding alcohol **24***b*. The acetate **24***a* was isolated from the autumnal leaves of *Metasequoia glyptostroboides* (35), and its enantiomer was isolated from a Brazilian tree (popularly known as "Copaiba") as the alcohol **24***b* (36). The acid **25** is also a known natural product (37) and had been synthesized by Ohloff in 1958 (38). We outline below the first synthesis of the C-3 oxygenated labdadienes **24**.

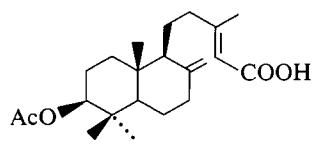

24*a*

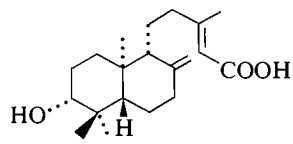

24*b*

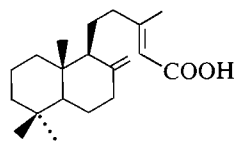

25

Our first approach to the synthesis of the labdadienes was patterned after our trixagol synthesis (26). The C-3 alcohol of **21***c* was protected as its *tert*-butyldimethylsilyl (TBDMS) ether. In the first instance the alcohol was reacted with TBDMS-Cl under standard conditions (39) for up to 10 days to achieve complete reaction. However, treating the alcohol with TBDMS triflate (40) produced complete conversion to the silyl ether within 15 min. In the next step we hoped to selectively reduce the less hindered 9α ester and thus achieve a facile separation of the 9α and 9β isomers. Careful reduction of the esters **26** enriched with the β isomer (α/β = 3:7) gave a 60% mixture to the two C-9 hydroxymethyl compounds and 40% recovered ester, which was greater than 90% β. This ester was reduced with DIBAL (diisobutylaluminum hydride) to give the 9β-hydroxymethyl compound **27**.

The alcohol **27** was converted into the mesylate in quantitative yield, and the mesylate was transformed to the sulfide with potassium thiophenoxide in 94% yield (26). We were unsuccessful in oxidizing this sulfide with MCPBA or potassium hydrogen persulfate (41). However, the sulfide was oxidized to

TABLE 1. Cyclization of epoxy allylsilanes **11** and **20**

Run	Ester	Conditions[a]	Yield (%)	Product (9α/9β)
1	**11**	1.2 equiv. $SnCl_4$,CH_2Cl_2,0°C	55	2:3
2	**20***a*, R = $CHMe_2$	1.2 equiv. $SnCl_4$,CH_2Cl_2,0°C	51	1:3
3	**20***b*, R = CH_2Me_2	1.2 equiv. $SnCl_4$,CH_2Cl_2,0°C	62	2:5
4	**20***c*, R − $CH(CMe_3)_2$	1.2 equiv. $SnCl_4$,CH_2Cl_2,0°C	60	1:3
5	**20***c*, R = $CH(CMe_3)_2$	1.2 equiv. $SnCl_2$ + 0.1 equiv. HOAc,CH_2Cl_2,0°C	55	1:5

[a]All reactions were run with 1 mmol of ester.

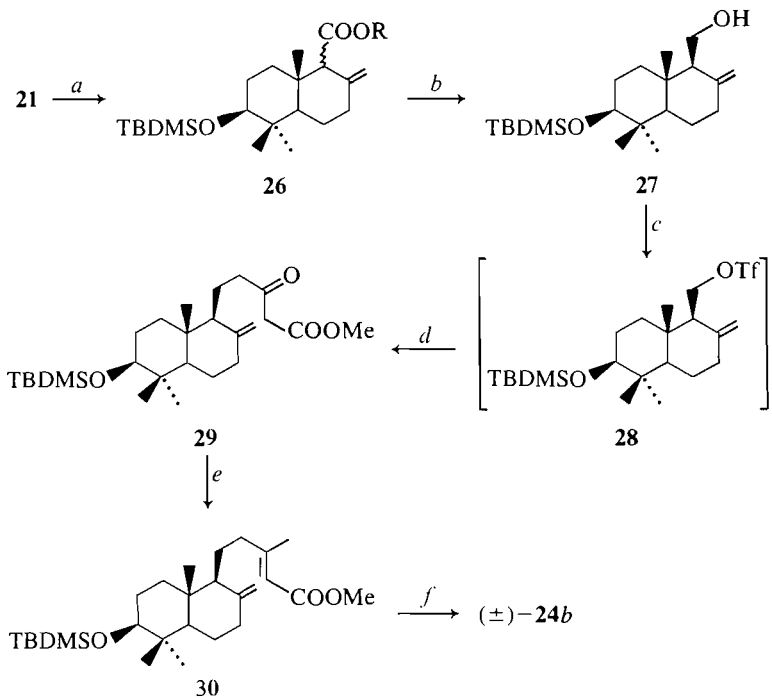

(a) TBDMS-Tf; (b) DIBAL, ϕMe–THF, 0°C then DIBAL, ϕMe;
(c) Tf_2O, CH_2Cl_2, −45°C; (d) $\bar{C}H_2COCHCOOMe$, THF,
−40°C; (e) NaH, $ClPO(OEt)_2$ then $LiMe_2Cu$; (f) HF, H_2O–MeCN then KOH, MeOH

SCHEME 3. Synthesis of 3-hydroxylabdadiene.

the sulfone in 85% yield with diphenyl diselenide and hydrogen peroxide (42). Although the anion from this sulfone could be alkylated with methyl iodide (<50%), we were totally unable to alkylate it with any other alkylating agent. Thus we were forced to explore another route to introduce the side chain at C-9.

Treatment of the alcohol **27** with *N*-methyl-*N*,*N*′-dicyclohexylcarbodiimidium iodide (43) resulted in a 65% yield of the corresponding iodide. Here we were thwarted in our attempt to introduce the side chain by alkylation of this iodide with the dianion of methyl acetoacetate (44). This is one of the very few examples we have found of the failure of this dianion to undergo alkylation. Alkylation with the methyl acetoacetate dianion was eventually achieved, albeit in low yield, with the triflate **28**. This triflate was prepared by adding the alcohol **27** to a cold (−40 to −50°C) mixture of pyridine and triflic anhydride in the minimum amount of methylene chloride. Because the triflate decomposed above 0°C, the reaction had to be worked up at low temperature (see experimental) and the crude triflate was added to a solution of the methyl acetoacetate dianion to give a 28% purified yield of the γ-alkylated β-keto ester **29**. This is the first example of the dianion alkylation of a β-keto ester with a triflate, and the use of triflates should extend the scope of the β-keto ester dianion reaction (44).

The synthesis of the hydroxy labdadienoic acid **24** from the β-keto ester **29** involved, first, formation of the *Z*-enol phosphate, followed by a cuprate coupling (24) to give the *E*-alkene **30** in 75% yield. Somewhat surprisingly, treatment of the silyl ether **30** with tetra-*n*-butylammonium fluoride did not effect cleavage of the *tert*-butyldimethylsilyl ether. Instead, hydrolysis of the methyl ester occurred. The silyl protecting group in **30** was hydrolyzed with 5% hydrofluoric acid in acetonitrile (45), and the methyl ester was hydrolyzed with aqueous methanolic KOH. The spectral data of the synthetic (±)-**24***b* were in good agreement with those of an authentic sample (36).[4]

Experimental[5]

Methyl (Z)-6,7-epoxy-7-methyl-3-[(trimethylsilyl)methyl]-2-octenoate (7)

To 7.63 g (0.030 mol) of diene **6** in dry CH_2Cl_2 at 0°C was slowly added a solution of 5.70 g (0.033 mol) of MCPBA in CH_2Cl_2. The

[4]We are grateful to Professor Mahajan for this data.

[5]For outline of procedures see ref. 26.

reaction mixture was stirred for 2 h at 0°C, then warmed to room temperature and diluted with ether. The organic layer was washed three times with saturated $NaHCO_3$, once with saturated NaCl, dried, and concentrated to give 8.1 g of crude **7**. Purification by flash chromatography (46) using petroleum ether–ethyl acetate (12:1) as eluant gave 6.83 g (84%) of epoxide **7** as a colourless oil. Preparative tlc of a small amount of this material using petroleum ether–ethyl acetate (7:1) gave **7** as a colourless liquid; bp (Kugelrohr distillation) 80°C/0.1 Torr (1 Torr = 133.3 Pa); ir ($CHCl_3$): 1700, 1615, 1250, 1160, and 850 cm^{-1}; ^1H nmr ($CDCl_3$) δ: 0.10 (s, 9H), 1.30 (s, 3H), 1.35 (s, 3H), 1.60–1.90 (m, 2H), 2.15–2.50 (m, 4H), 2.75 (bt, J = 6 Hz, 1H), 3.68 (s, 3H), and 5.58 (s, 1H); mass spectrum, m/z: 271(3), 270(M^+, 11), 255(8), 123(12), 121(20), 96(17), 95(42), 91(11), 89(41), 85(16), 82(31), 80(10), 75(20), 74(12), 73(100), 71(10), 69(10), 67(14), and 59(38). *Exact mass* calcd. for $C_{14}H_{26}O_3Si$: 270.1650; found (ms): 270.1650.

Methyl cis*-3-hydroxy-2,2-dimethyl-6-methylenecyclohexanecarboxylate (**8**)*

To a solution of 4.05 g (0.015 mol) of the trimethylsilyl epoxide **7** in 130 mL of CH_2Cl_2 at −56°C was slowly added a solution of 3.69 mL (0.030 mol) of $BF_3{\cdot}Et_2O$ in 20 mL of CH_2Cl_2. The reaction mixture was stirred for 4 h at −56°C, then quenched with saturated NaCl at −56°C. The organic layer was diluted with ether, washed four times with saturated NaCl, dried, and concentrated to give 3.41 g of crude product, which was used without further purification in the preparation of diol **9**. Purification of a small amount of this material by flash chromatography using petroleum ether–ethyl acetate (8:1) gave **8** as a colourless liquid; bp (Kugelrohr distillation) 95°C/0.1 Torr; ir ($CHCl_3$): 3420, 1710, 1650, 1155, and 1075 cm^{-1}; ^1H nmr ($CDCl_3$) δ: 0.93 (s, 3H), 1.04 (s, 3H), 1.70–2.80 (bm, 4H), 3.00 (s, 1H), 3.30–3.50 (m, 1H), 3.70 (s, 3H), 4.35 (bd, J = 10 Hz, 1H, exchangeable with D_2O), 4.85 (bs, 1H), and 4.95 (bs, 1H); mass spectrum, m/z: 198(M^+, 13), 180(20), 167(9), 139(12), 138(11), 123(14), 122(13), 121(100), 120(15), 109(10), 105(14), 97(14), 96(18), 95(80), 93(12), 83(16), 82(10), 81(13), 79(16), 69(13), 67(20), 59(14), and 55(25). *Anal.* calcd. for $C_{11}H_{18}O_3$: C 66.64, H 9.15; found: C 66.37, H 8.92.

cis*-3-Hydroxy-2,2-dimethyl-6-methylenecyclohexanemethanol (**9**)*

A slurry of 0.850 g (0.022 mol) of $LiAlH_4$ in dry ether was stirred at 0°C, and 3.41 g of the crude hydroxyl ester **8** in dry ether was slowly added to the slurry. The reaction mixture was heated at reflux for 2 h, then cooled to room temperature and quenched with 1 *M* HCl. The organic layer was washed once with 1 *M* HCl, twice with saturated NaCl, dried, and concentrated to give 1.95 g of crude **9**. Purification by flash chromatography using petroleum ether–ethyl acetate (1:1) as eluant gave 1.73 g (68% from trimethylsilyl epoxide **7**) of *cis*-diol **9** as a colourless oil. Preparative tlc of a small amount of this material using petroleum ether–ethyl acetate (1:1.5) gave **9** as a colourless liquid; bp (Kugelrohr distillation) 105°C/0.1 Torr; ir ($CHCl_3$): 3600, 3400, 1640, 1080, and 1010 cm^{-1}; ^1H nmr ($CDCl_3$) δ: 0.94 (s, 3H), 1.00 (s, 3H), 1.30–2.50 (m, 5H), 2.36 (bs, 2H, exchangeable with D_2O), 3.44 (dd, J = 4 Hz, 1H), 3.69 (A part of an ABX system, J_{AB} = 11 Hz, J_{AX} = 4 Hz, 1H), 3.91 (B part of an ABX system, J_{AB} = 11 Hz, J_{BX} = 7 Hz, 1H), 4.73 (bs, 1H), and 4.93 (bs, 1H); mass spectrum, m/z: 170(M^+, 0.5), 152(21), 138(8), 122(100), 121(55), 109(22), 108(20), 107(90), 96(26), 95(21), 93(30), 91(18), 81(37), 79(30), 71(21), 69(17), 67(31), 55(34), and 53(18). *Anal.* calcd. for $C_{10}H_{18}O_2$; C 70.55, H 10.66; found: C 70.40, H 10.70.

*8,8-Dimethyl-2-methylene-6-oxabicyclo[3.2.1]octane (karahana ether) (**10**)*

A solution of 0.850 g (5.0 mmol) of diol **9** in 7 mL of dry pyridine was stirred at 0°C, and 0.950 g (5.0 mmol) of *p*-toluenesulphonyl chloride was added to the solution. The reaction mixture was stirred for 5 h, while allowing it to warm to room temperature. The reaction mixture was diluted with ether, washed five times with 1 *M* HCl, once with saturated $NaHCO_3$, once with saturated NaCl, dried, and the solvent was removed to give 1.04 g of crude **10**. Purification by flash chromatography using petroleum ether–ether (9:1) as eluant gave 0.62 g (81%) of bicyclic ether **10** as a colourless liquid with a pleasant, camphor-like odour, whose spectral data (^1H nmr, ir, ms) are in good agreement with those of the literature (28–30).

General procedure A. Formation of epoxides from terminal bromohydrins (refs. 13a,32)

A solution of 1.0 equiv. of the olefin in THF–H_2O (5:1) (6 mL/mmol of olefin) was stirred at 10°C in the dark. To this solution was added NBS (1.1 equiv.) in small portions, and the reaction was stirred for 16 h while allowing it to warm to room temperature. The reaction was diluted with ether, washed three times with saturated NaCl, dried, and the solvent was removed. The crude bromohydrin was dissolved in anhydrous methanol and cooled to 0°C. Anhydrous potassium carbonate (K_2CO_3) (2.5 equiv.) was added to the reaction and the mixture was stirred for 15–30 min at 0°C, while monitoring the reaction by tlc. The reaction was diluted with ether, acidified with 1 *M* HCl, and the organic phase was washed once with 1 *M* HCl and three times with saturated NaCl. The aqueous washings were extracted three times with ether, the combined organic layers were dried, and the solvent was removed. Frequently the residue contained water, and was dissolved in ether, dried a second time, and the solvent was removed.

*Methyl (2Z,6E)-10,11-epoxy-7,11-dimethyl-3-[(trimethylsilyl)-methyl]-2,6-dodecadienoate (**11**)*

This compound was prepared according to the above general procedure A using 3.50 g (0.011 mol) of triene **12** and 2.13 g (0.012 mol) of NBS in 70 mL of a 5:1 solution of THF–H_2O. The crude bromohydrin obtained was moderately unstable, and was converted to epoxide **11** using 3.80 g (0.028 mol) of K_2CO_3 in anhydrous methanol. Work-up of the reaction mixture and purification of the crude product by flash chromatography using petroleum ether–ethyl acetate (15:1) as eluant gave 1.70 g (46%) of epoxide **11** as a colourless oil; bp (Kugelrohr distillation) 130°C/0.2 Torr; ir ($CHCl_3$): 1705, 1625, 1165, and 850 cm^{-1}; ^1H nmr ($CDCl_3$) δ: 0.04 (s, 9H), 1.25 (s, 3H), 1.29 (s, 3H), 1.61 (s, 3H), 1.45–1.76 (m, 2H), 1.95–2.26 (m, 6H), 2.39 (s, 2H), 2.69 (t, J = 6 Hz, 1H), 3.65 (s, 3H), 5.00–5.28 (m, 1H), and 5.55 (s, 1H); mass spectrum, m/z: 338(M^+, 3), 323(14), 253(13), 211(14), 186(18), 149(41), 107(36), 89(23), 85(21), 82(40), 81(22), 73(100), and 59(37). *Anal.* calcd. for $C_{19}H_{34}O_3Si$: C 67.41, H 10.12; found: C 67.33, H 10.22.

General procedure B. Cyclization of epoxy allylsilanes

A solution of the epoxy allylsilane (1.0 equiv.) in dry CH_2Cl_2 (30 mL/mmol of allylsilane) was cooled to 0°C and to this solution was added the desired amount of acetic acid while stirring under nitrogen. The Lewis acid was slowly added as a solution in CH_2Cl_2 and the reaction was either stirred for 1–4 h at 0°C, or was allowed to warm to room temperature. The mixture was quenched with aqueous KF, diluted with ether, and the organic layer was washed three times with aqueous KF, once with saturated NaCl, dried, and the solvent was removed.

Methyl trans*-decahydro-6β-hydroxy-5,5,8aβ-trimethyl-2-methylene-1ξ-naphthalenecarboxylate (**14**a, **14**b)*

These compounds were prepared according to general procedure B using 1.35 g (4.00 mmol) of compound **11** and 0.56 mL (4.8 mmol) of stannic chloride. The reaction was stirred for 3 h while allowing it to warm to room temperature. Work-up of the reaction mixture gave 1.14 g of crude product, which was purified by flash chromatography using petroleum ether–ethyl acetate (6:1) as eluant to yield 0.58 g (55%) of **14** (a/b = 1:1.5, as determined by ^1H nmr spectroscopy and gc (T = 180°C)). Preparative tlc of a small amount of this mixture using the same solvent system gave **14** as a viscous oil; bp (Kugelrohr distillation) 150°C/0.1 Torr; ir ($CHCl_3$): 3630, 3460, 1730, 1650, and 1160 cm^{-1}; ^1H nmr (400 MHz) ($CDCl_3$): δ: 0.77 (s, 1.2H), 0.80 (s, 1.8H), 0.92 (s, 1.2H), 1.00 (s, 1.8H), 1.04 (s, 1.2H), 1.06 (s, 1.8H), 1.25–1.76 (m, 7H), 1.95–2.16 (m, 1H), 2.28 (bd, J = 10 Hz, 1H, exchangeable with D_2O), 2.39–2.46 (m, 0.6H), 2.53–2.62 (m, 0.4H), 2.74 (s, 0.6H), 2.76 (s, 0.4H), 3.25 (dd, J = 11 Hz, 5 Hz, 1H), 3.62 (s, 1.2H), 3.64 (s, 1.8H), 4.66 (s, 0.6H), 4.73 (s, 0.4H), and 5.03 (s, 1H); mass spectrum, m/z: 266(M^+, 46), 248(27), 139(27), 135(100), 134(22), 121(28), 119(31), 114(28), 107(38), 105(24), 97(21), 95(29), 93(28), 91(24), 79(22), 69(26), 67(22), 55(34), 43(52), and

41(56). *Exact mass* calcd. for $C_{16}H_{26}O_3$: 266.1882; found (ms): 266.1881.

Methyl trans-*decahydro-5,5,8aβ-trimethyl-2-methylene-6-oxo-1ξ-naphthalenecarboxylate (**15**)*

A suspension of 0.310 g (1.5 mmol) of pyridinium chlorochromate, 0.040 g (0.48 mmol) of anhydrous sodium acetate, and 0.25 g (1% w/v of solvent) of 4 Å molecular sieves (dried and crushed) was stirred rapidly in 25 mL of CH_2Cl_2 at room temperature. To this solution was added 0.258 g (0.97 mmol) of alcohols **14** (a/b = 1:1.44) and the reaction was stirred for 2 h at room temperature. The reaction mixture was diluted with ether, stirred for 5 min, and the supernatant was passed through a 2.5 g Florisil column which had a layer of $MgSO_4$ on the top. The dark-brown residue was washed with ether, the ethereal extracts were passed through the column, eluted with ether, and the combined eluate was concentrated to give 0.250 g of **15** (a/b = 1:1.44, as determined by gc (T = 170°C)). Further purification by flash chromatography using petroleum ether–ethyl acetate (15:1) as eluant gave 0.228 g (89%) of **15** as an oil; bp (Kugelrohr distillation) 120°C/0.1 torr; ir ($CHCl_3$): 1735, 1705, 1650, and 1160 cm^{-1}; ^1H nmr ($CDCl_3$) δ: 1.05 (s, 1.2H), 1.08 (s, 1.8H), 1.12 (s, 1.8H), 1.15 (s, 2.4H), 1.30 (s, 1.8H), 1.45–1.95 (m, 5H), 2.15–2.96 (m, 5H), 3.64 (s, 1.2H), 3.69 (s, 1.8H), 4.72 (bs, 0.6H), 4.81 (bs, 0.4H), and 4.92 (bs, 1H); mass spectrum, m/z: 264(M^+, 86), 249(55), 246(35), 232(68), 217(33), 199(42), 161(49), 148(39), 147(54), 135(32), 133(100), 125(37), 123(49), 121(41), 120(41), 119(52), 114(36), 109(51), 107(73), 105(53), 95(65), 93(45), 91(67), 81(57), 79(55), 77(39), 69(61), 68(56), 59(35), 55(82), and 53(38). *Exact mass* calcd. for $C_{16}H_{24}O_3$: 264.1725; found (ms): 264.1727.

Methyl trans-*decahydro-5,5,8aβ-trimethyl-2-methylene-1ξ-naphthalenecarboxylate (**16**)*

To a solution of 0.053 g (0.20 mmol) of ketones **15** in 2 mL of dry ethanol was added 0.041 g (0.22 mmol) of *p*-toluenesulphonylhydrazine. The reaction mixture was heated at reflux for 4 h, cooled, and the solvent was removed to yield the *p*-toluenesulphonylhydrazones as a crystalline solid that was used without purification in the formation of compounds **16**; ir ($CHCl_3$): 1730, 1600, and 1160 cm^{-1}.

To a solution of these tosylhydrazones in chloroform (dried and distilled from $CaCl_2$) was added 0.026 g (0.22 mmol) of catecholborane at 0°C. The reaction was stirred for 1.5 h at 0°C; 0.082 g (0.60 mmol) of sodium acetate trihydrate was added, and the mixture was stirred at room temperature overnight. The reaction was diluted with ether, washed twice with saturated NaCl, dried, and the solvent was removed. Purification by flash chromatography using petroleum ether–ethyl acetate (10:1) gave 0.035 g (71%) of compounds **16** (a/b = 1.00:1.42, as determined by gc (T = 130°C)). The gc retention times were identical with those of an authentic sample of epimeric esters **16** (25).

General procedure C. Synthesis of alkyl acetoacetates from diketene (ref. 34)

A mixture of anhydrous sodium acetate (0.005 equiv.) and the alcohol (1.0 equiv.) was heated with stirring to 80–85°C, or to the boiling point of the alcohol. Diketene (1.05 equiv.) was added dropwise to the reaction mixture while maintaining the temperature below 115°C. The reaction was stirred for 2.5 h from the time of initial addition of diketene, and the product was distilled directly from the reaction mixture.

2-Propyl 3-oxobutanoate

This compound was prepared according to general procedure C using 8.2 mL (0.11 mol) of 2-propanol, 0.040 g (0.5 mmol) of anhydrous sodium acetate, and 8.8 mL (0.11 mol) of diketene. The product was distilled to give 13.3 g (86%) of β-keto ester as a colourless liquid; bp 90–100°C/45 Torr (lit. (47) bp 79–80°C/17 Torr); ir ($CHCl_3$): 1740, 1715, and 1105 cm^{-1}; ^1H nmr ($CDCl_3$) δ: 1.26 (d, J = 6 Hz, 6H), 2.26 (s, 3H), 3.42 (s, 2H), and 5.05 (septet, J = 6 Hz, 1H).

2,2-Dimethylpropyl 3-oxobutanoate

This compound was prepared according to general procedure C using 5.28 g (0.060 mol) of 2,2-dimethylpropyl alcohol, 0.025 g (0.30 mmol) of anhydrous sodium acetate, and 4.90 mL (0.063 mol) of diketene. The product was distilled to give 7.69 g (75%) of β-keto ester as a colourless liquid; bp 100–116°C/45 Torr (lit. (48) bp 60°C/3 Torr); ir ($CHCl_3$): 1740, 1705, and 1370 cm^{-1}; ^1H nmr ($CDCl_3$) δ: 0.93 (s, 9H), 2.25 (s, 3H), 3.46 (s, 2H), and 3.80 (s, 2H)

2,2,4,4-Tetramethyl-3-pentyl 3-oxobutanoate

This compound was prepared according to general procedure C using 13.2 g (0.092 mol) of 2,2,4,4-tetramethyl-3-pentanol (49), 0.038 g (0.5 mmol) of anhydrous sodium acetate, and 7.84 mL (0.10 mol) of diketene. The product was distilled to give 18.2 g (87%) of β-keto ester as a colourless liquid; bp 120°C/5 Torr; ir ($CHCl_3$): 1730, 1715, and 1380 cm^{-1}: ^1H nmr ($CDCl_3$) δ: 1.01 (s, 18H) 2.32 (s, 3H), 3.51 (s, 2H), and 4.65 (s, 1H); mass spectrum m/z: 228(M^+, 0.1), 171(11), 103(17), 87(42), 85(100), 69(17), 58(20), 57(85), 43(83), and 41(40). *Anal.* calcd. for $C_{13}H_{24}O_3$: C 68.39, H 10.59; found: C 68.57, H 10.80.

*2-Propyl (E)-7,11-dimethyl-3-oxo-6,10-dodecadienoate (**18**a)*

This compound was prepared from the dianion (44) using 3.08 g (0.077 mol) of sodium hydride (60% dispersion in oil), 10.1 g (0.070 mol) of 2-propyl 3-oxobutanoate, 29.6 mL (0.077 mol) of a 2.6 *M* solution of *n*-butyllithium in hexane, and 16.3 g (0.070 mol) of geranyl bromide. Work-up of the reaction mixture gave 20.9 g of crude product, which was used without further purification in the preparation of enol phosphate. Preparative tlc of a small amount of this compound using petroleum ether–ethyl acetate (8:1) gave **18***a* as a colourless liquid; bp (Kugelrohr distillation) 150°C/0.25 Torr; ir ($CHCl_3$): 1735, 1705, and 1100 cm^{-1}; ^1H nmr ($CDCl_3$) δ: 1.31 (d, J = 6 Hz, 6H), 1.63 (s, 6H), 1.73 (s, 3H), 1.9–2.25 (bs, 4H), 2.25–2.75 (m, 4H), 3.45 (s, 2H), 5.09 (septet, J = 6 Hz, 1H), and 5.0–5.3 (m, 2H); mass spectrum, m/z: 280(M^+, 5), 219(10), 169(17), 151(14), 136(33), 123(10), 109(81), 105(17), 93(15), 87(11), 81(26), 69(100), 68(14), 67(15), and 55(18). *Anal.* Calcd. for $C_{17}H_{28}O_3$: C 72.82, H 10.07; found: C 72.94, H 10.03.

*2,2-Dimethylpropyl (E)-7,11-dimethyl-3-oxo-6,10-dodecadienoate (**18**b)*

This compound was prepared from the dianion (44) using 1.63 g (0.041 mol) of sodium hydride (60% dispersion in oil), 6.35 g (0.037 mol) of 2,2-dimethylpropyl 3-oxobutanoate, 25.4 mL (0.041 mol) of a 1.6 *M* solution of *n*-butyllithium in hexane, and 9.04 g (0.039 mol) of geranyl bromide. Work-up of the reaction mixture gave 12.2 g of crude product, which was purified by distillation to yield 5.63 g (50%) of **18***b* as a yellow oil. Preparative tlc of a small amount of this compound using petroleum ether–ethyl acetate (5:1) gave **18***b* as a colourless liquid; bp 155°C/0.15 Torr; ir ($CHCl_3$): 1745 and 1720 cm^{-1}; ^1H nmr ($CDCl_3$) δ: 0.98 (s, 9H), 1.64 (s, 6H), 1.74 (s, 3H), 1.98–2.14 (m, 4H), 2.20–2.75 (m, 4H), 3.49 (s, 2H), 3.87 (s, 2H), and 4.95–5.25 (m, 2H); mass spectrum, m/z: 308(M^+, 12), 290(10), 247(12), 169(22), 136(36), 109(55), 93(20), 81(26), 71(68), 69(100), 57(24), 55(24), 43(87), and 41(74). *Anal.* calcd. for $C_{19}H_{32}O_3$: C 73.98, H 10.46; found C 74.05, H 10.40.

*2,2,4,4-Tetramethyl-3-pentyl (E)-7,11-dimethyl-3-oxo-6,10-dodecadienoate (**18**c)*

This compound was prepared via the dianion (44) using 3.30 g (0.083 mol) of sodium hydride (60% dispersion in oil), 17.1 g (0.075 mol) of 2,2,4,4-tetramethyl-3-pentyl 3-oxobutanoate, 53.2 mL (0.083 mol) of a 1.55 *M* solution of *n*-butyllithium in hexane, and 19.2 g (0.083 mol) of geranyl bromide. Work-up of the reaction mixture gave 30.5 g of crude product, which was used without further purification in the preparation of its enol phosphate. Preparative tlc of a small amount of this compound using petroleum ether–ethyl acetate (8:1) as eluant gave **18***c* as a colourless liquid; bp (Kugelrohr distillation) 120°C/0.1 Torr; ir ($CHCl_3$): 1735, 1710, and 1370 cm^{-1}; ^1H nmr ($CDCl_3$) δ: 1.00 (s, 18H), 1.61 (s, 6H), 1.69 (s, 3H), 1.90–2.12 (m, 4H), 2.20–2.75 (m, 4H), 3.49 (s, 2H), 4.65 (s, 1H), and 4.96–5.23 (bt, 2H); mass spectrum, m/z: 364(M^+, 0.1), 238(11), 195(10), 136(10), 109(27), 81(16), 71(26), 69(62), 57(100), and 41(48). *Anal.* calcd. for $C_{23}H_{40}O_3$: C 75.78, H 11.06; found: C 75.73, H 10.96.

General procedure D. Formation of (Z)-allylsilanes from (Z)-enol phosphates

The Grignard reagent was prepared from magnesium turnings (1.5–2.0 equiv.) and trimethylsilylmethyl chloride (1.5–2.2 equiv.) in ether at room temperature under nitrogen, and to this stirred solution was added 0.025–0.05 equiv. of anhydrous nickel(II) acetylacetonate. The resulting dark-brown mixture was stirred for 5 min at room temperature and a solution of enol phosphate (1.0 equiv.) in ether was slowly added (exothermic reaction). The reaction mixture was stirred at room temperature or at reflux for the desired time, and various amounts of catalyst were added during this time. The reaction was cooled to room temperature, quenched by the careful addition of 1 *M* HCl (until the mixture was acidic to litmus paper), and diluted with ether. The organic layer was washed once with 1 *M* HCl, twice with saturated NaCl, dried, and the solvent was removed.

*2-Propyl (2Z,6E)-7,11-dimethyl-3-[(trimethylsilyl)methyl]-2,6,10-dodecatrienoate (**19**a)*

The enol phosphate of **18***a* was prepared (24) using 3.08 g (0.077 mol) of sodium hydride (60% dispersion in oil), 20.9 g of crude β-keto ester **18***a*, and 11.1 mL (0.077 mol) of diethyl chlorophosphate. Work-up of the reaction mixture gave a quantitative yield of an orange oil, which was used without further purification in the preparation of silyl ester **19***a*. Preparative tlc of a small amount of this material using petroleum ether–ethyl acetate (2:1) gave pure enol phosphate as a viscous liquid; bp (Kugelrohr distillation) 190°C/0.2 Torr; ir ($CHCl_3$): 1720, 1670, 1270, 1105, and 1020 cm^{-1}; ^1H nmr ($CDCl_3$) δ: 1.28 (d, J = 6 Hz, 6H), 1.40 (dt, $J_{CH_2CH_3}$ = 7 Hz, $J_{POCH_2CH_3}$ = 1 Hz, 6H), 1.63 (s, 6H), 1.71 (s, 3H), 1.95–2.15 (m, 4H), 2.23–2.53 (m, 4H), 4.28 (dq, $J_{CH_2CH_3}$ = 7 Hz, J_{POCH_2} = 7 Hz, 4H), 4.87–5.25 (m, 3H), and 5.35 (s, 1H); mass spectrum, m/z: 416(M^+, 5), 357(12), 287(32), 220(48), 192(19), 165(19), 155(100), 133(19), 127(37), 105(20), 99(38), and 69(31). *Anal.* calcd. for $C_{21}H_{37}O_6P$: C 60.56, H 8.95; found: C 60.36, H 8.90.

The crude enol phosphate (31 g) was reacted according to the general procedure D using 3.40 g (0.14 mol) of magnesium turnings, 21.4 mL (0.154 mol) of trimethylsilylmethyl chloride, and 0.45–0.90 (1.8–3.5 mmol) of anhydrous nickel(II) acetylacetonate. A further portion of 0.45–0.90 g (1.8–3.5 mmol) of catalyst was added immediately after addition of the enol phosphate, and the reaction was stirred at room temperature for 1 h. Work-up of the reaction mixture gave 27 g of crude product, which was purified by flash chromatography using petroleum ether–ethyl acetate (30:1) as eluant to yield 17.0 g (70% from isopropyl acetoacetate) of **19***a* as a yellow oil. Preparative tlc of a small amount of this material using petroleum ether–ethyl acetate (20:1) gave **19***a* as a colourless oil; bp (Kugelrohr distillation)130°C/0.1 Torr; ir ($CHCl_3$): 1700, 1630, 1220, 1170, 1115, and 850 cm^{-1}; ^1H nmr ($CDCl_3$) δ: 0.08 (s, 9H), 1.27 (d, J = 6 Hz, 6H), 1.64 (s, 6H), 1.71 (s, 3H), 1.97–2.30 (m, 8H), 2.45 (s, 2H), .4.85–5.25 (m, 3H), and 5.54 (s, 1H); mass spectrum, m/z: 350(M^+, 5), 281(7), 239(15), 223(10), 156(7), 149(29), 81(14), 75(26), 73(100), 69(50), 43(17), and 41(49). *Anal.* calcd. for $C_{21}H_{38}O_2Si$: C 71.94, H 10.92; found: c 72.20, H 10.99.

*2,2-Dimethylpropyl (2Z,6E)-7,11-dimethyl-3-[(trimethylsilyl)-methyl]-2,6,10-dodecatrienoate (**19**b)*

The enol phosphate of **18***b* was prepared (24) using 0.80 g (0.020 mol) of sodium hydride (60% dispersion in oil), 5.63 g (0.018 mol) of β-keto ester **18***b*, and 2.76 mL (0.019 mol) of diethyl chlorophosphate. Work-up of the reaction mixture gave 5.44 g (67%) of an orange oil, which was used without further purification in the preparation of silyl ester **19***b*. Preparative tlc of a small amount of this material using petroleum ether–ethyl acetate (2:1) gave pure enol phosphate as a viscous oil; bp (Kugelrohr distillation) 180°C/0.1 Torr; ir ($CHCl_3$): 1720, 1670, and 1030 cm^{-1}; ^1H nmr ($CDCl_3$) δ: 0.96 (s, 9H), 1.37 (dt, $J_{CH_2CH_3}$ = 7 Hz, $J_{POCH_2CH_3}$ = 1 Hz, 6H), 1.67 (bs, 6H), 1.74 (bs, 3H), 1.90–2.17 (m, 4H), 2.26–2.64 (m, 4H), 3.82 (s, 2H), 4.27 (dq, $J_{CH_2CH_3}$ = 7 Hz, $J_{POCH_2CH_3}$ = 7 Hz, 4H), 5.0–5.26 (m, 2H), and 5.39 (s, 1H); mass spectrum, m/z: 444(M^+, 11), 308(17), 220(30), 155(100), 136(35), 127(39), 121(22), 109(49), 105(20), 99(45), 93(28), 85(27), 81(41), 71(60), 69(91), 67(24), 57(31), 55(34), 43(88), and 41(77). *Exact mass* calcd. for $C_{23}H_{41}O_6P$: 444.2651; found (ms): 444.2634.

This crude enol phosphate (3.44 g) was reacted according to general procedure D using 0.377 g (16 mmol) of magnesium turnings, 2.63 mL (17 mmol) of trimethylsilylmethyl chloride, and 0.050–0.10 g (0.19–0.33 mmol) of anhydrous nickel(II) acetylacetonate. A further portion of 0.050–0.10 g (0.19–0.33 mmol) of catalyst was added immediately after addition of the enol phosphate, and the reaction was stirred at room temperature for 1 h. Work-up of the reaction mixture gave 2.7 g of crude product, which was purified by flash chromatography using petroleum ether–ethyl acetate (40:1) as eluant to give 1.92 g (66% from β-keto ester **18***b*) of **19***b* as an orange oil. Preparative tlc of a small amount of this material using petroleum ether–ethyl acetate (30:1) gave **19***b* as a viscous liquid; bp (Kugelrohr distillation) 120°C/0.1 Torr; ir ($CHCl_3$): 1690, 1620, 1240, 1150, and 850 cm^{-1}; ^1H nmr ($CDCl_3$) δ: 0.10 (s, 9H), 0.98 (s, 9H), 1.64 (s, 6H), 1.73 (s, 3H), 1.92–2.30 (m, 8H), 2.47 (s, 2H), 3.80 (s, 2H), 4.98–5.25 (m, 2H), and 5.62 (s, 1H); mass specrum, m/z: 378(M^+, 22), 309(20), 239(35), 223(17), 149(38), 82(15), 81(19), 75(32), 73(100), 71(25), 69(51), 55(15), 43(45). and 41(27). *Anal.* calcd. for $C_{23}H_{42}O_2Si$: C 72.95, H 11.18; found: C 73.13, H 11.15.

*2,2,4,4-Tetramethyl-3-pentyl (2Z,6E)-7,11-dimethyl-3-[(trimethylsilyl)methyl]-2,6,10-dodecatrienoate (**19**c)*

The enol phosphate of **18***c* was prepared (24) using 3.80 g (0.083 mol) of sodium hydride (60% dispersion in oil), 30.5 g of crude β-keto ester **18***c*, and 11.5 mL (0.08 mol) of diethyl chlorophosphate. Work-up of the reaction mixture gave a quantitative yield of a yellow oil, which was used without further purification in the preparation of silyl ester **19***c*. Preparative tlc of a small amount of this material using petroleum ether–ethyl acetate (1:1) gave pure enol phosphate as a colourless oil; bp (Kugelrohr distillation) 140°C/0.1 Torr; ir ($CHCl_3$): 1715, 1670, and 1030 cm^{-1}; ^1H nmr ($CDCl_3$) δ: 1.01 (s, 18H), 1.36 (dt, $J_{CH_2CH_3}$ = 7 Hz, $J_{POCH_2CH_3}$ = 1 Hz, 6H), 1.62 (bs, 6H), 1.69 (bs, 3H), 1.90–2.16 (m, 4H), 2.25–2.55 (m, 4H), 4.26 (dq, $J_{CH_2CH_3}$ = 7 Hz, J_{POCH_2} = 7 Hz, 4H), 4.63 (s, 1H), 4.95–5.25 (bt, 2H), and 5.40 (s, 1H); mass spectrum, m/z: 500(M^+, 2), 357(22), 238(17), 220(38), 155(61), 136(16), 127(20), 109(30), 99(19), 81(22), 70(75), 69(25), 57(100), 55(18), 43(23), and 41(47). *Anal.* calcd. for $C_{27}H_{49}O_6P$: C 64.78, H 9.87; found: C 64.57, H 9.90.

This crude enol phosphate (20 g) was reacted according to general procedure D using 1.94 g (0.080 mol) of magnesium turnings, 12.2 mL (0.088 mol) of trimethylsilylmethyl chloride, and 0.25–0.50 g (1.0–2.0 mmol) of anhydrous nickel(II) acetylacetonate. The reaction mixture was stirred at room temperature for 2 h with no further addition of catalyst. Work-up of the reaction mixture, and purification by flash chromatography using petroleum ether–ethyl acetate (40:1) gave 12.20 g of **19***c* as a yellow liquid. Preparative tlc of a small amount of this material using the above solvent mixture gave **19***c* as a colourless oil; bp (Kugelrohr distillation) 120°C/0.1 Torr; ir ($CHCl_3$): 1690, 1620, 1155, and 850 cm^{-1}; ^1H nmr ($CDCl_3$) δ: 0.08 (s, 9H), 1.03 (s, 18H), 1.64 (s, 6H), 1.72 (s, 3H), 1.97–2.28 (m, 8H), 2.51 (s, 2H), 4.59 (s, 1H), 4.98–5.26 (m, 2H), and 5.62 (s, 1H); mass spectrum, m/z: 434(M^+, 0.1), 308(26), 293(18), 292(14), 291(40), 239(18), 109(20), 73(85), 71(16), 69(45), 57(100), and 41(3). *Anal.* calcd. for $C_{27}H_{50}O_2Si$: C 74.59, H 11.59; found: C 74.28, H 11.75.

*2-Propyl (2Z,6E)-10,11-epoxy-7,11-dimethyl-3-[(trimethylsilyl)methyl]-2,6-dodecadienoate (**20**a)*

This compound was prepared according to general procedure A using 10.3 g (0.029 mol) of triene **19***a* and 5.76 g (0.032 mol) of NBS in 175 mL of a 5:1 solution of THF–H_2O. Work-up of the reaction gave 13.3 g of crude bromohydrin, which was used without further purification and was converted to epoxide **20***a* using 10.1 g (0.074 mol) of K_2CO_3 in anhydrous methanol. Work-up of the reaction mixture and purification of the crude product by flash chromatography using petroleum ether–ethyl acetate (15:1) as eluant gave 6.0 g (56%) of epoxide **20***a*. Preparative tlc of a small amount of this material using petroleum ether–ethyl acetate (8:1) as eluant gave **20***a* as a colourless liquid; bp (Kugelrohr distillation) 160°C/0.15 Torr; ir ($CHCl_3$): 1700,

1625, 1255, 1210, 1170, 1110, and 850 cm^{-1}; ^1H nmr ($CDCl_3$) δ: 0.08 (s, 9H), 1.29 (d, J = 6 Hz, 6H), 1.30 (s, 3H), 1.34 (s, 3H), 1.65 (s, 3H), 1.55–1.80 (m, 2H), 2.00–2.30 (m, 6H), 2.44 (s, 2H), 2.73 (t, J = 6 Hz, 1H), 5.00 (septet, J = 6 Hz, 1H), 5.00–5.27 (m, 1H), and 5.51 (s, 1H); mass spectrum, m/z: 366(M^+, 5), 239(11), 149(16), 107(18), 81(18), 75(26), 73(100), 71(18), 59(17), 43(39), and 41(16). *Anal.* calcd. for $C_{21}H_{38}O_{39}Si$: C 68.00, H 10.45; found: C 68.92, H 10.39.

*2,2-Dimethylpropyl (2Z,6E)-10,11-epoxy-7,11-dimethyl-3-[(trimethylsilyl)methyl]-2,6-dodecadienoate (**20**b)*

This compound was prepared according to general procedure A using 1.13 g (3.0 mmol) of triene **19***b* and 0.590 g (3.3 mmol) of NBS in 20 mL of a 5:1 solution of THF–H_2O. Work-up of the reaction gave a quantitative yield of crude bromohydrin, which was used without further purification. The crude bromohydrin was converted into epoxide **20***b* using 1.04 g (7.5 mmol) of K_2CO_3 in anhydrous methanol. Work-up of the reaction mixture and purification of the crude product by flash chromatography using petroleum ether–ethyl acetate (20:1) as eluant gave 0.64 g (54%) of epoxide **20***b*. Preparative tlc of a small amount of this material using the same solvent system gave **20***b* as a colourless liquid; bp (Kugelrohr distillation) 130°C/0.1 Torr; ir ($CHCl_3$): 1700, 1625, 1260, 1220, 1160 and 860 cm^{-1}; ^1H nmr ($CDCl_3$) δ: 0.09 (s, 9H), 0.99 (s, 9H), 1.31 (s, 3H), 1.35 (s, 3H), 1.69 (bs, 3H), 1.59–1.81 (m, 2H), 2.04–2.31 (m, 6H), 2.47 (s, 2H), 2.74 (t, J = 6 Hz, 1H), 3.80 (s, 2H), 5.09–5.30 (m, 1H), and 5.59 (s, 1H); mass spectrum, m/z: 394 (M^+, 7), 379(10), 239(14), 149(20), 135(17), 121(16), 107(23), 85(17), 82(16), 81(24), 75(26), 73(100), 71(43), 69(17), 67(17), 55(17), 43(89), and 41(23). *Anal.* calcd. for $C_{23}H_{42}O_3Si$: C 70.00, H 10.73; found: C 69.83, H 10.80.

*2,2,4,4-Tetramethyl-3-pentyl (2Z,6E)-10,11-epoxy-7,11-dimethyl-3-[(trimethylsilyl)methyl]-2,6-dodecadienoate (**20**c)*

This compound was prepared via general procedure A using 13.5 g (0.031 mol) of triene **19***c* and 6.07 g (0.034 mol) of NBS in 180 mL of a 5:1 solution of THF–H_2O. Work-up of the reaction mixture gave a bromohydrin, which was used without purification. The crude bromohydrin was converted to epoxide **20***c* using 10.7 g (0.078 mol) of K_2CO_3 in anhydrous methanol. Work-up of the reaction mixture and purification by flash chromatography using petroleum ether–ethyl acetate (30:1) as eluant gave 7.9 g (57%) of epoxide **20***c*. Preparative tlc of a small amount of this material using the same solvent system gave **20***c* as a colourless liquid; bp (Kugelrohr distillation) 130°C/0.1 Torr; ir ($CHCl_3$): 1700, 1625, 1160, and 860 cm^{-1}; ^1H nmr ($CDCl_3$) δ: 0.07 (s, 9H), 1.03 (s, 18H), 1.28 (s, 3H), 1.32 (s, 3H), 1.67 (bs, 3H), 1.55–1.80 (m, 2H), 2.05–2.22 (m, 6H), 2.51 (s, 1H), 2.73 (t, J = 6 Hz, 1H), 4.58 (s, 1H), 5.15–5.30 (bt, 1H), and 5.59 (s, 1H); mass spectrum, m/z: 450(M^+, 1), 307(9), 239(10), 197(14), 135(12), 125(13), 109(14), 107(13), 75(16), 73(89), 71(27), 57(100), 43(30), and 41(19). *Anal.* calcd. for $C_{27}H_{50}O_3Si$: C 71.94, H 11.18; found: C 71.66, H 11.33.

2,2,4,4-Tetramethyl-3-pentyl trans*-decahydro-6β-hydroxyl-5,5-8aβ-trimethyl-2-methylene-1ξ-naphthalenecarboxylate (**21**c)*

These compounds were prepared via general procedure B using 0.62 g (1.4 mmol) of compound **20***c*, 7.8 μL (0.14 mmol) of acetic acid, and 0.18 mL (1.5 mmol) of stannic chloride. The reaction was stirred at 0°C for 2 h. Work-up of the reaction mixture and purification by flash chromatography using petroleum ether–ethyl acetate (8:1) as eluant gave 0.287 g (55%) of alcohols **21***c* in a ratio of 1:3, as determined by ^1H nmr spectroscopy and gc (T = 250°C). Preparative tlc of a small sample of this mixture using petroleum ether–ethyl acetate (6:1) gave **21***c* as white foam; bp (Kugelrohr distillation) 145°C/0.1 Torr; ir ($CHCl_3$): 3630, 3460, 1720, 1660, 1375, and 1165 cm^{-1}; ^1H nmr ($CDCl_3$) δ: 0.79 (s, 0.75H), 0.82 (s, 2.25H), 0.93 (s, 0.75H), 0.95 (s, 2.25H), 0.98 (s, 6.75H), 1.00 (s, 4.5H), 1.03 (s, 6.75H), 1.05 (s, 0.75H), 1.11 (s, 2.25H), 1.17–2.55 (m, 10H, 1H exchangeable with D_2O), 2.82 (bs, 1H), 3.07–3.44 (m, 1H), 4.54 (s, 0.25H), 4.59 (s, 0.75H), 4.75 (bs, 1H), and 4.86 (bs, 1H); mass spectrum, m/z: 378(M^+, 4), 252(38), 234(27), 233(22), 189(31), 135(21), 127(18), 119(8), 71(31), 57(100), and 41(21). *Anal.* calcd. for $C_{24}H_{42}O_3$: C 76.14, H 11.18; found: C 76.30, H 11.30.

2,2,4,4-Tetramethyl-3-pentyl trans*-decahydro-6β-[*tert*-butyldimethylsilyl)oxy]-5,5,8aβ-trimethyl-2-methylene-1ξ-naphthalenecarboxylate (**26**)*

These compounds were prepared (40) using 0.08 g (2.1 mmol) of alcohols **21***c*, 0.60 mL (5.1 mmol) of 2,6-dimethylpyridine, and 0.73 mL (3.2 mmol) of TBDMS triflate in 3 mL of CH_2Cl_2. Work-up of the reaction mixture gave 1.0 g (99%) of compounds **26**, which were used without further purification in the preparation of alcohols **27**. Purification of a small amount of this material by preparative tlc using petroleum ether–ethyl acetate (60:1) as eluant gave the pure 9β epimer of **26** as a colourless glass; bp (Kugelrohr distillation) 140°C/0.1 Torr; mp 116–118°C; ir ($CHCl_3$): 1720, 1660, 1160, 1100, and 835 cm^{-1}; ^1H nmr ($CDCl_3$) δ: 0.08 (s, 6H), 0.80 (s, 3H), 0.92 (s, 9H), 0.94 (s, 3H), 1.01 (s, 9H), 1.06 (s, 9H), 1.12 (s, 3H), 1.25–2.60 (m, 9H), 2.81 (bs, 1H), 3.27 (dd, J = 9 Hz, 6 Hz, 1H), 4.60 (s, 1H), 4.75 (bs, 1H), and 4.86 (bs, 1H); mass spectrum, m/z: 492 (M^+, 0.1), 309(6), 189(14), 91(17), 75(80), 73(41), 71(41), 69(21), 57(100), 55(44), 43(16), and 41(55). *Anal.* calcd. for $C_{30}H_{56}O_3Si$: C 73.11, H 11.45; found: C 73.07, H 11.40.

trans*-Decahydro-6β-[*tert*-butyldimethylsilyl)oxy]-5,5,8aβ-trimethyl-2-methylene-1ξ-naphthalenemethanol (**27**)*

To a solution of 0.984 g (2.0 mmol) of esters **26** in 50 mL of toluene was added 0.28 mL (3.5 mmol) of THF. The reaction was cooled to 0°C, 7.0 mL (7.0 mmol) of a 1 *M* solution of DIBAL in hexane was added, and the reaction was stirred at 0°C for 1 h. The reaction was quenched with 1 *M* HCl and diluted with ether. The organic phase was washed three times with 1 *M* HCl, once with saturated NaCl, dried, and the solvent was removed. Purification of the crude product by flash chromatography using petroleum ether–ethyl acetate (40:1) as eluant gave 0.400 g of esters **26** (9α/9β = 1:11, as determined by gc (T = 250°C)). The enriched β-ester **26** was dissolved in toluene and 3.52 mL (3.5 mmol) of a 1 *M* solution of DIBAL in hexane was added to the solution. The reaction was stirred at room temperature for 2 h, then diluted with ether, and quenched with 1*M* HCl. The organic layer was washed three times with 1 *M* HCl, once with saturated NaCl, dried, and the solvent was removed. Purification of the product by flash chromatography using petroleum ether–ethyl acetate (8:1) as eluant gave 0.271 g (95%) of alcohol **27**; bp (Kugelrohr distillation) 138°C/0.1 Torr; mp 65–67°C; ir ($CHCl_3$): 3620, 3450, 1650, 1100, and 840 cm^{-1}; ^1H nmr ($CDCl_3$) δ: 0.07 (s, 6H), 0.76 (s, 3H), 0.77 (s, 3H), 0.91 (s, 9H), 0.94 (s, 3H), 1.12–2.62 (m, 10H), 1.37 (bs, 1H, exchangeable with D_2O), 3.15–3.37 (m, 1H), 3.65–3.90 (m, 2H), 4.66 (bs, 1H), and 4.95 (bs, 1H); mass spectrum, m/z: 352(M^+, 1), 295(21), 147(13), 107(18), 105(24), 95(20), 81(15), 75(100), 73(34), and 69(15). *Anal.* calcd. for $C_{21}H_{40}O_2Si$: C 71.53, H 11.43; found: C 71.28, H 11.52.

Mesylate from alcohol 27

To a solution of 0.67 mL (4.8 mmol) of triethylamine in ether at 0°C was added a solution of alcohols **27** (9α/9β = 1:2, as determined by ^1H nmr spectroscopy) in ether at 0°C with stirring. After 5 min, 0.27 mL (3.5 mmol) of methanesulphonyl chloride was added to the reaction, and the mixture was stirred at 0°C for 2 h, then at room temperature for 2 h. The reaction was quenched with 1 *M* HCl, and the organic phase was washed three times with 1 *M* HCl, three times with saturated $NaHCO_3$, once with saturated NaCl, and dried. The solvent was removed to give 1.39 g (quantitative yield) of a mesylate, which was used without further purification in the preparation of sulfide. Preparative tlc of a small amount of this material using petroleum ether–ethyl acetate (6:1) gave pure mesylate (9α/9β = 1:2) as an oil which slowly crystallized; mp 72–77°C; ir ($CHCl_3$): 1360, 1175, 945, and 840 cm^{-1}; ^1H nmr ($CDCl_3$) δ: 0.06 (s, 6H), 0.78 (s, 3H), 0.86 (s, 1.2H), 0.91 (s, 10.8H), 0.94 (s, 1.8H), 0.99 (s, 1.2H), 1.15–2.58 (m, 10H), 3.00 (s, 1.2H), 3.02 (s, 1.8H), 3.05–3.35 (m, 1H), 4.20–4.50 (m, 2H), 4.61 (bs, 0.6H), 4.72 (bs, 0.4H), 4.85 (bs, 0.4H), and 4.92 (bs, 0.6H); mass

spectrum, *m/z*: 430(M^+, 3), 203(100), 153(32), 147(28), 135(22), 133(23), 119(24), 109(25), 107(39), 95(31), 93(23), 81(21), 75(61), and 73(35). *Exact mass* calcd. for $C_{22}H_{42}O_4SSi$: 430.2573; found (ms): 430.2572.

trans-*Decahydro-6β-[*tert*-butyldimethylsilyl)oxy-5,5,8aβ-trimethyl-2-methylene-1ξ-(phenylthiomethyl)naphthalene*

A slurry of 1.02 g (6.4 mmol) of KH (25% in oil) in dry ethanol was stirred at room temperature and 0.66 mL (6.4 mmol) of thiophenol was added to the slurry. After 10 min a solution of 1.39 g of the above mesylate (1α/1β = 1:1.5) in ethanol was added to the mixture, and the reaction was heated at reflux for 16 h. The ethanol was removed under reduced pressure and the residue was partitioned between ether and saturated NaCl. The two phases were acidified with 1 *M* HCl, and the organic phase was washed twice with saturated NaCl, dried, and concentrated. The crude product was purified by flash chromatography using petroleum ether as eluant to remove the mineral oil and diphenyl disulfide. The column was then eluted with petroleum ether–ethyl acetate (40:1) to give 1.33 g (94% from alcohols **27**) of sulfide as a pale yellow solid. Preparative tlc of a small amount of this material using the above solvent system gave pure sulfide (1α/1β = 1:1.5) as a colourless crystalline solid; bp (Kugelrohr distillation) 180°C/0.1 Torr; mp 73–89°C; ir ($CHCl_3$): 1100 and 840 cm^{-1}; ^1H nmr ($CDCl_3$) δ: 0.07 (s, 6H), 0.79 (s, 3H), 0.93 (bs, 15H), 1.15–2.50 (m, 10H), 2.81–3.30 (m, 3H), 4.70 (bs, 1H), 4.84 (bs, 0.4H), 4.99 (bs, 0.6H), and 7.15–7.48 (bs, 5H); mass spectrum, *m/z*: 445(13), 444(M^+, 27), 387(26), 203(28), 133(15), 123(27), 119(15), 117(15), 109(16), 107(17), 95(17), 93(15), 81(16), 75(100), 73(56), 69(18), 57(19), and 55(51). *Exact mass* calcd. for $C_{27}H_{44}OSSi$: 444.2882; found (ms): 444.2876.

trans-*Decahydro-6β-[*tert*-butyldimethylsilyl)oxy]-5,5,8aβ-trimethyl-2-methylene-1ξ-(phenylsulfonylmethyl)naphthalene*

To a solution of 0.504 g (1.6 mmol) of diphenyl diselenide in a 5:1 mixture of ether–CH_2Cl_2 at 0°C was added 0.92 mL (8.1 mmol) of a 30% (w/v) solution of hydrogen peroxide in water. To this oxidizing mixture was added 0.717 g (1.6 mmol) of the above sulfide (1α/1β = 1:1.5) and the reaction was refrigerated at 5°C for 16 h, during which time colourless crystals were observed to form. The reaction mixture was diluted with ether and ethyl acetate, and filtered to remove the insoluble crystals. The filtrate was washed three times with saturated NaCl, dried, and the solvent was removed to give 0.90 g of sulfone as an oil that was insoluble in petroleum ether. The crude product was dissolved in ethyl acetate and adsorbed into silica gel. Purification by flash chromatography using petroleum ether–ethyl acetate (6:1) as eluant gave 0.65 g (85%) of sulfone (1α/1β = 1:1.5). Preparative tlc of a small amount of this material using the same solvent system gave pure sulfone as a colourless glass; bp (Kugelrohr distillation) 195°C/0.1 Torr; ir ($CHCl_3$): 1660, 1315, 1150, 1105, and 840 cm^{-1}; ^1H nmr ($CDCl_3$) δ: 0.06 (s, 6H), 0.63 (s, 1.8H), 0.73 (s, 3H), 0.91 (s, 10.2H), 0.93 (s, 3H), 1.12–2.48 (m, 10H), 3.00–3.40 (m, 3H), 4.43 (bs, 1H), 4.60 (bs, 0.4H), 4.74 (bs, 0.6H), and 7.49–7.98 (m, 5H); mass spectrum, *m/z*: 476(M^+, 0.2), 420(29), 419(92), 217(61), 203(78), 201(34), 199(100), 147(23), 135(33), 109(20), 107(21), 95(24), 75(57), and 73(28). *Anal.* calcd. for $C_{27}H_{44}O_2SSi$: C 68.02, H 9.30; found: C 67.85, H 9.18.

A small portion of sulfone (1α/1β = 1:1.5), was crystallized from ether to give moderately pure β isomer; mp 156–159°C; ^1H nmr ($CDCl_3$) δ: 0.06 (s, 6H), 0.63 (s, 3H), 0.73 (s, 3H), 0.91 (s, 9H), 0.93 (s, 3H), 1.15–2.50 (m, 10H), 3.04–3.58 (m, 3H), 4.43 (bs, 1H), 4.74 (bs, 1H), 7.49–7.68 (m, 3H), and 7.80–7.98 (m, 5H).

*Methyl 5-[*trans-*decahydro-6'β-[(*tert*-butyldimethylsilyl)oxy]-5',5',8a'β-trimethyl-2'-methylene-1'β-naphthalenyl]-3-oxopentanoate (**29**)*

To a solution of 73 μL (0.91 mmol) of pyridine in 1 mL of CH_2Cl_2 at −40 to −50°C was added 139 μL (0.82 mmol) of freshly purified trifluoromethanesulphonic anhydride (triflic anhydride) with stirring. A white precipitate formed immediately and after 5 min a solution of 0.290 g (0.82 mmol) of alcohol **27** in 2 mL of CH_2Cl_2 was added to the mixture. The reaction was stirred at −40 to −50°C for 1 h, during which time the original precipitate disappeared and a new precipitate formed. The reaction was filtered through a glass sinter and the crystalline pyridinium triflate was washed with hexane that had been cooled to approximately −20°C. The filtrates were combined and the solvent was removed under high vacuum while maintaining the temperature below 0°C. The residue was dissolved in cold hexane (−20°C), and the insoluble matter was filtered through a glass sinter and washed with cold hexane. The filtrates were again combined and the solvent was removed under high vacuum while maintaining the temperature below 0°C. The resulting colourless to pink oil was dissolved in cold (−40°C) THF, and added to a preformed solution of the dianion of methyl acetoacetate in THF that was cooled to −40°C. (The dianion was prepared (44) from 0.056 g (1.4 mmol) of sodium hydride (60% dispersion in oil), 133 μL (1.2 mmol) of methyl acetoacetate, and 0.93 mL (1.4 mmol) of a 1.5 *M* solution of *n*-butyllithium in hexane.) The reaction mixture was allowed to warm to 0°C over a period of 1 h, then stirred at 0°C for a further 2 h. The mixture was quenched with 1 *M* HCl, ether, the organic phase was washed once with 1*M* HCl, once with saturated NaCl, and dried. The solvent was removed, while maintaining the temperature below 50°C, to yield an orange oil. Purification was performed, on the same day, by flash chromatography using petroleum ether as eluant to give 0.060 g (22%) of diene. The column was then eluted with petroleum ether–ethyl acetate (25:1) to remove any remaining nonpolar material. Elution with petroleum ether–ethyl acetate (10:1) gave the β-keto ester **29** (0.104 g, 28%) as a pale yellow oil. Preparative tlc of a small amount of this material using petroleum ether–ethyl acetate (6:1) gave **29** as a colourless oil; bp (Kugelrohr distillation) 170°C/0.1 Torr; ir ($CHCl_3$): 1750, 1720, 1255, 1100, and 840 cm^{-1}; ^1H nmr ($CDCl_3$) δ: 0.06 (s, 6H), 0.71 (s, 3H), 0.76 (s, 3H), 0.91 (s, 12H), 1.08–2.73 (m, 14H), 3.24 (bt, J = 7 Hz, 1H), 3.42 (s, 2H), 3.74 (s, 3H), 4.43 (bs, 1H), and 4.84 (bs, 1H); mass spectrum, *m/z*: 450 (M^+, 5), 394(32), 393(90), 149(19), 135(20), 121(17), 119(16), 107(17), 95(15), 81(15), 75(100), 73(50), 69(22), 55(20), 43(19), and 41(20). *Exact mass* calcd. for $C_{26}H_{46}O_4Si$: 450.3165; found (ms): 450.3168.

*Methyl (*E*)-3-methyl-5-[*trans-*decahydro-6'β-[*tert*-butyldimethylsilyl)oxy]-5',5',8a'β-trimethyl-2'-methylene-1'β-naphthalenyl]-2-pentenoate (**30**)*

The enol phosphate from **29** was prepared (24) using 11 mg (0.27 mmol) of sodium hydride (60% dispersion in oil), 80 mg (0.18 mmol) of β-keto ester **29**, and 31 μL (0.21 mmol) of diethyl chlorophosphate. Work-up of the reaction mixture gave a yellow oil, which was purified by flash chromatography using petroleum ether–ethyl acetate (2:1) as eluant to give 94 mg (90%) of enol phosphate as a viscous liquid; ir ($CHCl_3$): 1730, 1670, and 1035 cm^{-1}; ^1H nmr ($CDCl_3$) δ: 0.06 (s, 6H), 0.70 (s, 3H), 0.75 (s, 3H), 0.91 (s, 12H), 1.05–2.55 (m, 14H), 1.38 (dt, $J_{CH_2CH_3}$ = 7 Hz, $J_{POCH_2CH_3}$ = 1 Hz, 6H), 3.23 (bt, J = 7 Hz, 1H), 3.71 (s, 3H), 4.27 (dq, $J_{CH_2CH_3}$ = 7 Hz, $J_{POCH_2CH_3}$ = 8 Hz, 4H), 4.49 (bs, 1H), 4.85 (bs, 1H), and 5.35 (s, 1H); mass spectrum, *m/z*: 586(M^+, 0.6), 530(29), 529(86), 432(16), 375(17), 300(14), 253(19), 252(82), 230(13), 229(100), 220(24), 211(26), 201(18), 183(20), 155(57), 135(16), 127(18), 119(16), 99(23), 81(15), 75(56), and 73(41). *Exact mass* calcd. for $C_{30}H_{55}O_7PSi$: 586.3455; found (ms): 586.3435.

A suspension of 67 mg (0.33 mmol) of cuprous bromide–dimethyl sulphide complex ($CuBr{\cdot}Me_2S$) in 2 mL of ether was stirred at 0°C, and 0.39 mL (0.66 mmol) of a 1.7 *M* solution of methyllithium–lithium bromide complex in ether was slowly added to the suspension. The resulting light tan solution was cooled to −78°C and a solution of 64 mg (0.11 mmol) of the above enol phosphate in 1.5 mL of ether was added to the reaction. The reaction mixture was warmed to −50°C and stirred for 1 h while maintaining the temperature between −40 and −50°C. During this time the colour of the reaction mixture changed from bright yellow to a reddish-purple colour. The reaction was quenched at −40°C by the addition of a mixture of 50% aqueous ammonium chloride and concentrated ammonium hydroxide (ca. 5:1), and diluted with ether. The organic phase was washed three times with this ammoniacal solution to remove all copper salts, once with saturated NaCl, dried, and the solvent was removed. The crude product was purified by flash

chromatography using petroleum ether–ethyl acetate (40:1) as eluant to give 40 mg (82%) of **30** as a pale yellow oil. Preparative tlc of this material using the same solvent system gave **30** as a colourless liquid; bp (Kugelrohr distillation) 130°C/0.1 Torr; ir ($CHCl_3$): 1720, 1650, 1155, 1105, and 840 cm^{-1}; ^1H nmr ($CDCl_3$) δ: 0.08 (s, 6H), 0.72 (s, 3H), 0.77 (s, 3H), 0.92 (s, 12H), 1.06–2.55 (m, 14H), 2.18 (d, J = 1.5 Hz, 3H), 3.25 (bt, J = 7 Hz, 1H), 3.71 (s, 3H), 4.51 (bs, 1H), 4.88 (bs, 1H), and 5.65 (bs, 1H); mass spectrum, m/z: 448 (M^+, 2), 392(39), 391(100), 316(12), 285(11), 241(14), 171(12), 147(12), 135(23), 121(22), 119(16), 109(13), 107(17), 105(11), 95(29), 93(13), 81(13), 75(65), 73(34), and 69(12). *Anal.* calcd. for $C_{27}H_{48}O_3Si$: C 72.27, H 10.78; found: C 72.32, H 10.85.

*Methyl (*E*)-3-methyl-5-(*trans*-decahydro-5',5',8a'*β*-trimethyl-2'-methylene-6'*β*-hydroxy-1'*β*-naphthalenyl)-2-pentenoate*

The standard solution of 48% aqueous hydrofluoric acid and 10 volumes of acetonitrile was prepared (4.8% HF in CH_3CN), and 3 mL of this standard solution was added to 9.5 mg (0.02 mmol) of silyl ether **30**. This reaction was stirred at 0°C for 2 h while allowing it to warm to room temperature, then was diluted with ether. The organic phase was washed four times with water, dried, and the solvent was removed to give 7 mg (99%) of crude alcohol, which was used unpurified in the preparation of **24***b* (98% pure by gc (T = 250°C)). The spectral data (^1H nmr, ir, ms) are in good agreement with those found in the literature (35, 36); ir ($CHCl_3$): 3620, 3470, 1720, 1650, 1210, and 1155 cm^{-1}; ^1H nmr ($CDCl_3$) δ: 0.72 (s, 3H), 0.80 (s, 3H), 1.01 (s, 3H), 1.1–2.55 (m, 15H, 1H exchangeable with D_2O), 2.18 (d, J = 1.5 Hz, 3H), 3.15–3.40 (m, 1H), 3.70 (s, 3H), 4.53 (bs, 1H), 4.88 (bs, 1H), and 5.65 (bs, 1H); mass spectrum, m/z: 334(M^+, 6), 319(19), 316(16), 301(25), 260(19), 203(23), 175(21), 135(100), 134(25), 123(26), 121(38), 119(29), 114(55), 109(29), 107(53), 95(38), 93(35), 83(26), 82(26), 81(38), and 55(27). *Exact mass* calcd. for $C_{21}H_{34}O_3$: 334.2508; found (ms): 334.2512.

*(*E*)-3-Methyl-5-(*trans*-decahydro-5',5',8a'*β*-trimethyl-2'-methylene-6'*β*-hydroxy-1'*β*-naphthalenyl)-2-pentenoic acid (3-hydroxylabda-8(20),13-dien-15-oic acid) (**24**b)*

To a solution of 10 mg (0.03 mmol) of the above methyl ester in 3 mL of methanol was added 1 mL of a 10% (w/v) solution of aqueous KOH at 0°C. The reaction was stirred at room temperature for 30 h, then diluted with ether, washed three times with 1 *M* HCl, and once with saturated NaCl. The aqueous washings were extracted three times with ether, the combined organic layers were dried, and the solvent was removed. The crude product was purified by flash chromatography using petroleum ether–ethyl acetate (1:1.5) as eluant to give 8 mg (83%, 2 steps) of **24***b* as a crystalline solid whose spectral data (^1H nmr, ir, ms) are in good agreement with those found in the literature (35, 36); mp 173–174.5°C; ir ($CHCl_3$): 3000, 1700, and 1640 cm^{-1}; ^1H nmr ($CDCl_3$) δ: 0.72 (s, 3H), 0.81 (s, 3H), 1.03 (s, 3H), 1.0–2.6 (m, 16H, 2H exchangeable with D_2O), 2.19 (d, J = 1.5 Hz, 3H), 3.10–3.37 (m, 1H), 4.52 (bs, 1H), 4.89 (bs, 1H), and 5.68 (bs, 1H); mass spectrum, m/z: 320 (M^+, 7), 302(22), 152(25), 149(52), 136(27), 135(100), 134(26), 133(24), 123(31), 122(36), 121(48), 119(31), 109(40), 107(61), 105(28), 97(33), 96(31), 95(27), 93(48), and 91(39). *Exact mass* calcd. for $C_{20}H_{32}O_3$: 320.2351; found (ms): 320.2354.

Acknowledgments

We are grateful to Professors Coates, Yamada, and Mahajan for spectral data and comparison samples, and to the Natural Sciences and Engineering Research Council of Canada for financial support. One of us (R.J.A.) is grateful to the Canadian Commonwealth Scholarship and Fellowship Plan for the award of a graduate scholarship.

1. E. E. VAN TAMELEN. Acc. Chem. Res. **1**, 111 (1968).
2. (*a*) G. STORK and A. W. BURGSTAHLER. J. Am. Chem. Soc. **77**, 5068 (1955); (*b*) A. ESCHENMOSER, L. RUZICKA, O. JEGER, and D. ARIGONI. Helv. Chim. Acta, **38**, 1890 (1955).
3. (*a*) J. K. SUTHERLAND. Chem. Soc. Rev. **9**, 265 (1980); (*b*) W. S. JOHNSON. Bioorg. Chem. **5**, 51 (1976); (*c*) W. S. JOHNSON. Agnew. Chem. Int. Ed. Engl. **15**, 9 (1976); (*d*) E. E. VAN TAMELEN. Acc. Chem. Res. **8**, 152 (1975); (*e*) K. NAKANISHI, T. GOTO, S. ITO, S. NATORI, and S. NOZOE (*Editors*) Natural products chemistry. Vol. 1. Academic Press, Inc., New York, NY. 1974; (*f*) T. MONEY. Prog. Org. Chem. **8**, 29 (1973); (*g*) D. GOLDSMITH. Fortsch. Chem. Org. Naturst. **29**, 363 (1971); (*h*) W. S. JOHNSON. Acc. Chem. Res. **1**, 1 (1968).
4. M. A. TIUS and K. S. TAKAKI. J. Org. Chem. **47**, 3166 (1982).
5. W. S. JOHNSON, M. B. GRAVESTOCK, and B. E. MCCARRY. J. Am. Chem. Soc. **93**, 4332 (1971).
6. W. S. JOHNSON, K. WEIDHAUP, S. F. BRADY, and G. L. OLSON. J. Am. Chem. Soc. **90**, 5277 (1968).
7. (*a*) E. J. COREY, M. A. TIUS, and J. DAS. J. Am. Chem. Soc. **102**, 7612 (1980); (*b*) T. R. HOYE, A. J. CARUSO, and M. J. KURTH. J. Org. Chem. **46**, 3550 (1981); (*c*) M. NISHIZAWA, H. TAKENAKA, H. NISHIDE, and Y. HAYASHI. Tetrahedron Lett. **24**, 2581 (1983).
8. (*a*) E. E. VAN TAMELEN and E. J. HESSLER. J. Chem. Soc. Chem. Commun. 411 (1966); (*b*) T. KATO and I. ICHINOSE. J. Chem. Soc. Perkin Trans. 1, 1051 (1980); (*c*) T. KATO, K. ISHII, I. ICHINOSE, Y. NAKAI, and T. KUMAGAI. J. Chem. Soc. Chem. Commun. 1106 (1980).
9. (*a*) W. P. JACKSON, S. V. LEY, and A. J. WHITTLE. J. Chem. Soc. Chem. Commun. 1173 (1980); (*b*) M. ALDERDICE and L. WEILER. Can. J. Chem. **59**, 2239 (1981).
10. D. J. GOLDSMITH. J. Am. Chem. Soc. **84**, 3913 (1962).
11. E. J. COREY, W. E. RUSSEY, and P. R. ORTIZ DE MONTELLANO. J. Am. Chem. Soc. **88**, 4750 (1966).
12. E. E. VAN TAMELEN, J. D. WILLETT, R. B. CLAYTON, and K. E. LORD. J. Am. Chem. Soc. **88**, 4752 (1966).
13. (*a*) E. E. VAN TAMELEN, A. STORNI, E. J. HESSLER, and M. A. SCHWARTZ. Bioorg. Chem. **11**, 133 (1982); (*b*) E. E. VAN TAMELEN and R. M. COATES. Bioorg. Chem. **11**, 171 (1982); (*c*) E. E. VAN TAMELEN and R. G. NADEAU. Bioorg. Chem. **11**, 197 (1982); (*d*) E. E. VAN TAMELEN and S. A. MARSON. Bioorg. Chem. **11**, 219 (1982).
14. W. S. JOHNSON, C. E. WARD, S. G. BOOTS, M. B. GRAVESTOCK, R. L. MARKEZICH, B. E. MCCARRY, D. A. OKORIE, and R. J. PARRY. J. Am. Chem. Soc. **103**, 88 (1981).
15. P. T. LANSBURY. Acc. Chem. Res. **5**, 311 (1972).
16. (*a*) R. W. SKEEAN, G. L. TRAMMELL, and J. D. WHITE. Tetrahedron Lett. 525 (1976); (*b*) E. J. COREY, M. A. TIUS, and J. DAS. J. Am. Chem. Soc. **102**, 1742 (1980); (*c*) F. W. SUM and L. WEILER. Tetrahedron, **37**, Suppl. 1, 303 (1981); (*d*) E. E. VAN TAMELEN and J. R. HWU. J. Am. Chem. Soc. **105**, 2490 (1983); (*e*) W. P. JACKSON and S. V. LEY. J. Chem. Soc. Perkin Trans. 1, 1516 (1981); (*f*) J. D. WHITE, R. W. SKEEAN, and G. L. TRAMMELL. J. Org. Chem. **50**, 1939 (1985).
17. (*a*) I. FLEMING, A. PEARCE, and R. L. SNOWDEN. J. Chem. Soc. Chem. Commun. 182 (1976); (*b*) I. FLEMING and A. PEARCE. J. Chem. Soc. Perkin Trans. 1, 251 (1981); (*c*) H. F. CHOW and I. FLEMING. J. Chem. Soc. Perkin Trans. 1, 1815 (1984).
18. A. VAN DER GEN, K. WIEDHAUP, J. J. SWOBODA, H. C. DUNATHAN, and W. S. JOHNSON. J. Am. Chem. Soc. **95**, 2656 (1973).
19. I. FLEMING. *In* Comprehensive organic chemistry. Vol. 3. *Edited by* D. H. R. Barton and W. D. Ollis. Pergamon Press, Oxford. 1979. pp. 541–686.
20. (*a*) R. L. DANHEISER, D. J. CARINI, and A. BASAK. J. Am. Chem. Soc. **103**, 1604 (1981); (*b*) R. L. DANHEISER, D. J. CARINI, D. M. FINK, and A. BASAK. Tetrahedron, **39**, 935 (1983).
21. (*a*) T. K. SARKAR and N. H. ANDERSEN. Tetrahedron Lett. 3513 (1978); (*b*) M. OCHIAI, M. ARIMOTO, and E. FUJITA. J. Chem. Soc. Chem. Commun. 460 (1981); (*c*) A. ITOH, K. OSHIMA, and H. NOZAKI. Tetrahedron Lett. 1783 (1979); (*d*) I. KUWAJIMA, T. TANAKA, and K. ATSUMI. Chem. Lett. 779 (1979); (*e*) G. MAJETICH, R. DESMOND, and A. M. CASARES. Tetrahedron Lett. **24**, 1913 (1983).
22. D. WANG and T. H. CHAN. J. Chem. Soc. Chem. Commun. 1273 (1984).

23. (*a*) R. S. BRINKMEYER. Tetrahedron Lett. 207 (1979); (*b*) W. S. JOHNSON, T. M. YARNELL, R. F. MYERS, D. R. MORTON, and S. G. BOOTS. J. Org. Chem. **45**, 1254 (1980); (*c*) R. SCHMID, P. L. HUESMANN, and W. S. JOHNSON. J. Am. Chem. Soc. **102**, 5122 (1980); (*d*) L. R. HUGHES, R. SCHMID, and W. S. JOHNSON. Bioorg. Chem. **8**, 513 (1979).
24. F. W. SUM and L. WEILER. Can. J. Chem. **57**, 1431 (1979).
25. R. J. ARMSTRONG, F. L. HARRIS, and L. WEILER. Can. J. Chem. **60**, 673 (1982).
26. R. J. ARMSTRONG and L. WEILER. Can. J. Chem. **61**, 2530 (1983).
27. R. J. ARMSTRONG and L. WEILER. Can. J. Chem. **61**, 214 (1983).
28. R. M. COATES and L. S. MELVIN, JR. J. Org. Chem. **35**, 865 (1970).
29. Y. NAYA and M. KOTAKE. Tetrahedron Lett. 1645 (1968).
30. (*a*) Y. YAMADA, H. SANJOH, and K. IGUCHI. Tetrahedron Lett. 1323 (1979); (*b*) T. MUKAIYAMA, N. IWASAWA, T. TSUJI, and K. NARASAKA. Chem. Lett. 1175 (1979).
31. R. J. ARMSTRONG. Ph.D. Thesis, University of British Columbia, Vancouver, B.C., 1983.
32. (*a*) E. E. VAN TAMELEN and T. J. CURPHEY. Tetrahedron Lett. 121 (1962); (*b*) E. E. VAN TAMELEN, A. STORNI, E. J. HESSLER, and M. SCHWARTZ. J. Am. Chem. Soc. **85**, 3295 (1963); (*c*) E. E. VAN TAMELEN and K. B. SHARPLESS. Tetrahedron Lett. 2655 (1967).
33. G. W. KABALKA, J. D. BAKER, JR., and G. W. NEAL. J. Org. Chem. **42**, 512 (1977).
34. S. O. LAWESSON, S. GRONWALL, and R. SANDBERG. Org. Synth. Coll. Vol. V, *Edited by* H. E. Baumgarten. John Wiley and Sons, New York, NY. 1973 p. 155.
35. S. BRAUN and H. BREITENBACH. Tetrahedron, **33**, 145 (1977).
36. J. R. MAHAJAN and G. A. L. FERREIRA. An. Acad. Bras. Cienc. **43**, 611 (1971).
37. D. F. ZINKEL, J. K. TODA, and J. W. ROWE. Phytochemistry, **10**, 1161 (1971).
38. G. OHLOFF. Justus Liebigs Ann. Chem. **617**, 134 (1958).
39. E. J. COREY and A. VENKATESWARLU. J. Am. Chem. Soc. **94**, 6190 (1972).
40. E. J. COREY, H. CHO, C. RUCKER, and D. H. HUA. Tetrahedron Lett. **22**, 3455 (1981).
41. B. M. TROST and D. P. CURRAN. Tetrahedron Lett. **22**, 1287 (1981).
42. H. J. REICH, F. CHOW, and S. L. PEAKE. Synthesis, 299 (1978).
43. R. SCHEFFOLD and E. SALADIN. Agnew. Chem. Int. Ed. Engl. **11**, 229 (1972).
44. S. N. HUCKIN and L. WEILER. J. Am. Chem. Soc. **96**, 1082 (1974).
45. R. F. NEWTON, D. P. REYNOLDS, M. A. W. FINCH, D. R. KELLY, and S. M. ROBERTS. Tetrahedron Lett. **41**, 3981 (1979).
46. W. C. STILL, M. KAHN, and A. MITRA. J. Org. Chem. **43**, 2923 (1978).
47. F. KORTE and F. WUSTEN. Justus Liebigs Ann. Chem. **647**, 18 (1961).
48. R. TACKE, A. BENTLAGE, R. TOWART, H. MEYER, F. BOSSERT, W. VATER, and K. STOEPEL. Z. Naturforsch. Teil B, **35**, 494 (1980).
49. C. P. RADER. J. Am. Chem. Soc. **91**, 3248 (1969).

Des 6*H*-thiazines-1,3 aux céphèmes par cyclocondensation

J. P. PRADERE, J. C. ROZE ET H. QUINIOU[1]

Laboratoire de chimie organique 2, Unité associée au Centre national de la recherche scientifique 475, 2, rue de la Houssinière, 44072 Nantes CEDEX, France

R. DANION-BOUGOT ET D. DANION

Groupe de physico-chemie structurale, Unité associée au Centre national de la recherche scientifique 704, Université de Rennes 1, 35042 Rennes CEDEX, France

ET

L. TOUPET

Groupe de physique cristalline, Unité associée au Centre national de la recherche scientifique 804, Université de Rennes 1, 35042 Rennes, CEDEX, France

Reçu le 26 février 1985[2]

J. P. PRADERE, J. C. ROZE, H. QUINOIU, R. DANION-BOUGOT, D. DANION et L. TOUPET. Can. J. Chem. **64**, 597 (1986).

La synthèse de nouvelles thiazines est décrite. Leur détermination structurale et leurs paramètres spectroscopiques sont examinés. La cyclocondensation [2+2] de ces thiazines sur les cétènes est étudiée ainsi que la réversibilité de la réaction en fonction de la nature des substituants en positions 4 et (ou) 5 des 6*H*-thiazines-1,3.

J. P. PRADERE, J. C. ROZE, H. QUINIOU, R. DANION-BOUGOT, D. DANION, and L. TOUPET. Can. J. Chem. **64**, 597 (1986).

The synthesis of new thiazines is described. Their structural determination and their spectroscopic parameters are examined. The [2+2] cyclocondensation of these thiazines with ketenes is studied along with the reversibility of the reaction as a function of the nature of the substituents on position 4 and (or) 5 of 6*H*-1,3-thiazines.

[Traduit par le journal]

Introduction

Des travaux mentionnent l'utilisation des dihydrothiazines **4** (R^2 = groupement générateur de cycle β-lactamique) comme précurseurs de céphalosporines (1) ou de céphèmes **3** (2). La synthèse de ces composés bicycliques a été également effectuée par réaction de cycloaddition [2+2] à partir de 6*H*-thiazines-1,3 **2** non substituées en position 2 et comportant en position 4 un groupement fonctionnel électroattracteur (3).

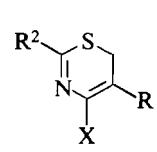

2

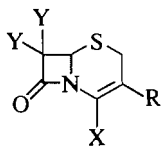

3

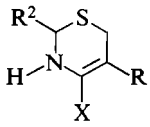

4

Les synthèses de composés β-lactamiques par action des cétènes sur la fonction imine de composés linéaires ou cycliques ont fait l'objet de nombreuses publications (4). Toutefois, peu de travaux concernent les 6*H*-thiazines-1,3 substituées en positions 2, 4 et 5. Dans certains cas, lorsque la position 2 des 6*H*-thiazines-1,3 **2** est substituée par un groupement aromatique, il n'a pas été possible d'obtenir le céphème correspondant (5).

Après avoir décrit l'accès à de nouvelles 6*H*-thiazines-1,3 polyfonctionnelles e leurs caractéristiques physico-chimiques (rayons X, rmn ^{13}C et ^{15}N), nous nous proposons de montrer l'influence de la température et de la nature des substituants en positions 4 et 5 sur la réactivité des phényl-2 6*H*-thiazines-1,3 vis-à-vis du diphénylcétène et du dichlorocétène.

1. Phényl-2 6*H*-thiazines-1,3 polysubstituées

1.1 Synthèse

Les 6*H*-thiazines-1,3 substituées **2** ont été obtenues selon une réaction de cyclocondensation [4+2].

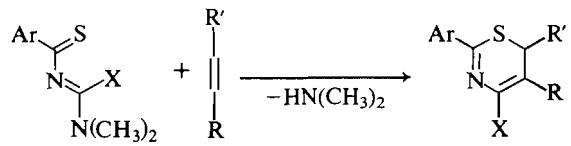

1*a* X = H
1*b* X = CH_3
1*c* X = $CO_2C_2H_5$
Ar = C_6H_5

R = CHO, $COCH_3$
R′ = H, CH_3

2

Le thia-1 aza-3 butadiène **1***a* opposé à l'acroléine dans le dichlorométhane, ou à la méthylvinylcétone sans solvant, conduit thermiquement aux 6*H*-thiazines-1,3 **2***a* et **2***b*. Lorsque la fonction imine de l'hétérodiène **1** est substituée par un groupement carboxylate (X = $CO_2C_2H_5$), l'accès aux thiazines correspondantes **2***e* et **2***f* nécessite une catalyse acide (7). On peut utiliser les acides de Lewis : chlorure d'aluminium, acétate de zinc ou les acides sulfoniques : Nafion-H (8), Amberlyst 15 dans le dichlorométhane. L'efficacité de l'Amberlyst 15 s'est avérée générale pour cette réaction de cyclocondensation [4+2]. Cette méthode permet l'introduction en positions 4 et (ou) 5 sur le cycle thiazinique de groupements électroattracteurs. Le caractère électroattracteur du substituant en position 5 peut être modifié par blocage de la fonction aldéhyde (R = CHO), selon les méthodes décrites dans la littérature (9,10) : l'action du thiophénol en présence d'acide de Lewis conduit aux thiazines **2***g*, **2***i*, **2***j* tandis que l'éthylèneglycol en présence d'acide paratoluène sulfonique (APTS) permet d'isoler le composé **2***h*.

L'hétérodiène **1***a* opposé à l'aldéhyde crotonique fournit la 6*H*-thiazine-1,3 **2***k* méthylée en position 6 (voir tableau 1).

1.2. Spectrométrie de rmn ^{13}C et ^{15}N

Nous avons effectué les mesures spectroscopiques par résonance magnétique nucléaire ^{13}C et ^{15}N afin d'établir une corrélation entre la réactivité de la fonction imine et la nature des substituants portés par la thiazine.

La comparaison des déplacements chimiques δ C2 en rmn ^{13}C des composés **2***a* et **2***g* d'une part, **2***c* et **2***i* d'autre part,

[1]Auteur à qui adresser la correspondance.
[2]Révision reçue le 24 octobre 1985.

TABLEAU 1. Phényl-2 6*H*-thiazines-1,3 **2**

Composés	R′	R	X	Rdt, %	^{13}C, ppm (TMS) C2	C4	C5	C6	$-\delta^{15}$N, ppm (CH_3NO_2)
2*a*(6)	H	CHO	H	75	169,0	154,8 $J(^{13}C–H) = 175$ Hz	117,1	20,2 $J(^{13}C–H) = 145$ Hz	89,5
2*b*(6)	H	COCH	H	96	168,5(13)	147.4 $J(^{13}C–H) = 177$ Hz	116,1	21,0 $J(^{13}C–H) = 146,5$ Hz	84,5
2*c*	H	CHO	CH_3	48	168,9	160,9	112,6	19,4 $J(^{13}C–H) = 146$ Hz	74,4
2*d*	H	$COCH_3$	CH_3	60	164,9	154,0	113,6	25,1 $J(^{13}C–H) = 145$ Hz	67,2
2*e*	H	CHO	CO_2Et	84	170,8	151,5	118,0	21,0 $J(^{13}C–H) = 147,5$ Hz	88,2
2*f*	H	$COCH_3$	CO_2Et	91	167,0	144,0	118,6	24,5 $J(^{13}C–H) = 145$ Hz	88,8
2*g*	H	$CH(SC_6H_5)_2$	H	70	161,1	136,8 $J(^{13}C–H) = 178,7$ Hz	114,9	23,6 $J(^{13}C–H) = 145$ Hz	85,4
2*h*	H	$CH(OCH_2)_2$	H	65	163,0	138,4 $J(^{13}C–H) = 177$ Hz	128,5	21,4 $J(^{13}C–H) = 145$ Hz	84,2
2*i*	H	$CH(SC_6H_5)_2$	CH_3	24	159,6	143,0	109,8	24,3 $J(^{13}C–H) = 143$ Hz	72,2
2*j*	H	$CH(SC_6H_5)_2$	CO_2Et	70	162,8	137,0	124,2	25,4 $J(^{13}C–H) = 145$ Hz	84,0
2*k*	CH_3	CHO	H	50	169,0	152,8 $J(^{13}C–H) = 177$ Hz	122,9	29,4 $J(^{13}C–H) = 145$ Hz	—

TABLEAU 2. Coordonnées atomiques et leurs écarts-type pour la 6*H*-thiazine-1,3 **2***b*

Atom	*x*	*y*	*z*	*B*(A2)[a]
S	0,96037(8)	0,1720(1)	0,9484(1)	5,77(2)
O	1,3112(2)	0,2269(3)	1,0913(3)	8,15(8)
N	0,9854(2)	0,4333(3)	1,8385(3)	3,78(6)
C1	1,0832(3)	0,2366(4)	1,0539(4)	4,94(9)
C2	1,1501(2)	0,3288(4)	0,9733(3)	4,03(8)
C3	1,2705(3)	0,3163(4)	1,0077(4)	5,36(9)
C4	1,3429(3)	0,4123(6)	0,9427(5)	8,1(1)
C5	1,0980(3)	0,4170(4)	0,8779(4)	4,22(8)
C6	0,9192(2)	0,3312(3)	0,8593(3)	3,52(7)
C7	0,8005(2)	0,3422(4)	0,8022(3)	3,75(7)
C8	0,7227(3)	0,2482(5)	0,8392(5)	6,2(1)
C9	0,6128(3)	0,2621(5)	0,7796(5)	7,5(1)
C10	0,5792(3)	0,3677(4)	0,6886(4)	6,6(1)
C11	0,6546(3)	0,4609(4)	0,6539(4)	6,1(1)
C12	0,7645(3)	0,4491(4)	0,7088(4)	4,74(9)
H1A	1,058(2)	0,289(3)	1,132(3)	4*
H1B	1,123(2)	0,155(3)	1,084(3)	4*
H4A	1,331(2)	0,409(3)	0,847(3)	4*
H4B	1,324(2)	0,511(3)	0,934(3)	4*
H4C	1,412(2)	0,384(3)	0,984(3)	4*
H5	1,140(2)	0,476(3)	0,834(3)	4*
H8	0,747(2)	0,174(3)	0,898(3)	4*
H9	0,569(2)	0,199(3)	0,808(3)	4*
H10	0,504(2)	0,374(3)	0,656(3)	4*
H11	0,631(2)	0,531(3)	0,590(3)	4*
H12	0,816(2)	0,512(3)	0,679(3)	4*

[a]Les atomes avec un astérique ont un coefficient d'agitation thermique isotrope fixe.

montre que l'introduction d'un groupement électroattracteur en position 5 provoque un déplacement vers les champs faibles d'environ 8 ppm pour ce carbone. Un groupement électroattracteur en position 4 a un effet très limité sur le déplacement chimique de C2. On peut toutefois remarquer que les effets des groupements électroattracteurs en positions 4 et 5 sont additifs (composés **2***a*, **2***e*, **2***g* et **2***j*) (voir tableau 1).

L'interprétation des déplacements chimiques $\delta^{15}N$, dans le cas des thiazines **2***c*, **2***d*, **2***i* est rendue difficile par l'existence de l'effet topologique β du groupement en position 4 qui pourrait entraîner une différence supérieure à 10 ppm entre la valeur observée et la valeur théorique (11).

Ainsi on observe pour ces composés, par rapport aux thiazines, **2***a*, **2***b*, **2***g*, un déplacement chimique vers les hautes fréquences du signal de l'atome d'azote comme il a été observé lorsque ce dernier est hybridé sp^3 (12).

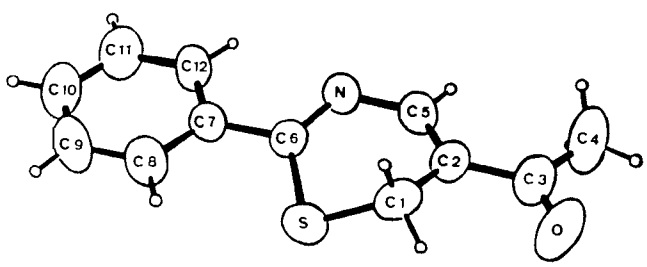

Vue en perspective du composé **2***b*[3]

[3]Les coordonnées de tous les atomes avec les β_{eq}, les longueurs et angles de liaisons avec écart-type ainsi que la liste des facteurs de structure sont disponibles. On peut les acheter en s'adressant au Dépôt de données non publiées ICIST, Conseil National de Recherche du Canada, Ottawa, (Ont.), Canada K1A 0S2.

TABLEAU 3. Paramètres angulaires et longueurs de liaison pour la 6*H*-thiazine-1,3 **2***b*

A : Angles dièdres entre plans moyens en degrés

Plan	Angle dièdre, degrés
C7—C8—C9—C10—C11—C12 / C6—N—C5—C2	3,7(6)
C6—N—C5—C2 / C3—C4—O	11,5(5)
C7—C8—C9—C10—C11—C12 / C3—C4—O	8,8(5)

B : Angles de torsion du cycle thiazinique en degrés

C6—S—C1—C2	−43,5
C1—S—C6—N	25,3
C6—N—C5—C2	−23,0
C5—N—C6—S	5,2
S—C1—C2—C5	37,6
C1—C2—C5—N	−1,9

C : Liaison	Longueur, Å
S—C1	1,792(4)
C1—C2	1,493(5)
C2—C5	1,330(5)
C5—N	1,384(4)
N—C6	1,287(4)
C6—S	1,754(3)
C3—O	1,219(5)

D : Liaison	Angle, degrés
C6—S—C1	98,9(2)
S—C1—C2	111,7(3)
C1—C2—C5	118.9(3)
C2—C5—N	127,8(3)
C5—N—C6	120,1(3)
N—C6—S	124,3(3)

1.3. Diffractométrie X

Les résultats de la détermination structurale de **2***b* font apparaître le cycle benzénique, le groupe acétyle et l'enchaînement hétéroatomique C2—C5—N—C6 dans des plans très voisins, ce qui laisserait supposer l'existence d'un système conjugué. En fait, les longueurs de liaisons observées par rayons X sont très proches des valeurs mesurées pour ces mêmes liaisons dans des systèmes isolés (14). Les paramètres cristallographiques de la 6*H*-thiazines-1,3 **2***b* sont rassemblés dans les tableaux 2 et 3.

2. Céphèmes

L'accès aux composés β-lactamiques **3** par action du diphénylcétène en solution toluénique (90°C) ou du dichlorocétène généré *in situ* dans le benzène sur les 6*H*-thiazines-1,3 substituées dépend de la nature des substituants en positions 4 et 5 de la thiazine **2** (voir tableau 4).

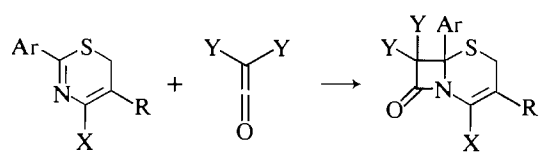

2 **3**

Ar = C_6H_5 Y = C_6H_5, Cl

2.1. Cyclocondensation et cycloreversion

L'accès direct aux composés β-lactamiques **3** a été possible,

TABLEAU 4. Céphèmes **3** : paramètres rmn ^1H et ^{13}C, ppm (TMS), et infrarouge, cm^{-1}

Composés	R	X	Y	Rdt %	δH_A	δH_B	$J_{H_A-H_B}$,Hz	J_{H_A-X},Hz	$\delta_{C=O}$ lactame	$\nu_{C=O}$ lactame
3*a*	CHO	H	C_6H_5	55	2,59	3,68	16,4	2	166,8	1780
3′*a*	$CH{=}CCl_2$	H	Cl	15	2,95	3,63	17,0	2,2	157,2	1800
3*b*	$COCH_3$	H	C_6H_5	95	2,59	3,85	17,4	2	167,3	1780
3′*b*	$COCH_3$	H	Cl	27	2,59	3,98	17,6	2,1	158,3	1815
3*c*	CHO	CH_3	C_6H_5	33	2,52	3,66	16,7	—	168,3	1785
3*d*	$COCH_3$	CH_3	C_6H_5	79	2,75	3,37	16,3	—	167,8	1775
3*g*	$CH(SC_6H_5)_2$	H	C_6H_5	82	2,79	3,54	16,5	2,1	165,8	1760
3′*g*	$CH(SC_6H_5)_2$	H	Cl	60	2,77	3,67	17,0	2,1	156,9	1805
3*i*	$CH(SC_6H_5)_2$	CH_3	C_6H_5	55	2,84	3,59	16,4	—	167	1770
3*j*	$CH(SC_6H_5)_2$	CO_2Et	C_6H_5	75	3,12	3,61	17,3	—	166,1	1780
3*l*	$CH(OCH_2)_2$	CO_2Et	C_6H_5	50	2,75	3,37	18,3	—	166,3	1760

lorsque les 6*H*-thiazines-1,3 ne sont pas simultanément substituées en positions 4 et 5 par un groupement carbonylé (composés **2***g* et **2***i*) ou lorsque ces thiazines possèdent un seul groupement carbonylé en position 4 (composé **2***j*) ou 5 (composés **2***a*, **2***b*, **2***c*, **2***d*).

Les réactions de cyclocondensation entre les 6*H*-thiazines-1,3 **2** et le diphénylcétène ont conduit aux céphèmes correspondants **3** avec de bons rendements (toluène, 90°C). Toutefois une élévation de température peut entraîner la thermolyse du céphème obtenu. Ainsi les céphèmes **3***a*, **3***b*, **3***c*, **3***d* conduisent respectivement par cycloreversion (toluène, 110°C) aux 6*H*-thiazines-1,3 précurseurs **2***a*, **2***b*, **2***c*, **2***d*.

Ces réactions de cycloreversion sont à rapprocher de celles mentionnées dans la littérature pour des cycles β-lactamiques (15).

L'analyse par spectrométrie de masse des céphèmes indique la formation de l'ion $(M - (C_6H_5)_2C{=}C{=}O)^{+\cdot}$ pic de base des spectres en bon accord avec les fragmentations observées pour des structures β-lactamiques (16).

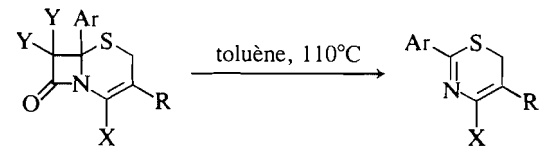

Y = Ar = C_6H_5
3*a*–**3***e* **2***a*–**2***e*

Dans les mêmes conditions nous n'avons pu accéder au céphème **3***e* par action du diphénylcétène sur **2***e*. La difficulté d'obtention de ce composé pourrait être liée à un écart relativement faible entre l'énergie nécessaire à la cyclocondensation et celle correspondant au seuil de reversibilité de la réaction. Nous avons pu vérifier que **3***e* obtenue par une synthèse indirecte se thermolysait effectivement.

En effet, l'action de l'éthylène glycol en présence d'APTS suivie de l'addition du diphénylcétène sur la 6*H*-thiazine-1,3 **2***e* fournit le céphème **3***l*. La libération de la fonction aldéhyde à partir de **3***l* permet d'accéder à **3***e*. La thermolyse de **3***e* (toluène, 110°C) redonne la 6*H*-thiazine-1,3 **2***e*.

La mise en évidence de la cycloreversion indique que les réactions entre thiazines et cétènes sont sous contrôle thermodynamique. Les corrélations entre structure et réactivité ne peuvent être envisagées qu'avec une extrême prudence malgré la similitude des déplacements chimiques observés pour le carbone C2 entre **2***a*, **2***b* d'une part et **2***e*, **2***f* d'autre part (voir tableau 1).

2.2. *Réactions particulières*

Ces réactions sont observées avec les 6*H*-thiazines-1,3 substituées en position 5 par un groupement aldéhyde.

L'action du dichlorocétène sur la 6*H*-thiazine-1,3 **2***a* conduit au céphème **3**″*a*. Dans ce cas, le dichlorocétène réagit aussi sur la fonction aldéhyde (17).

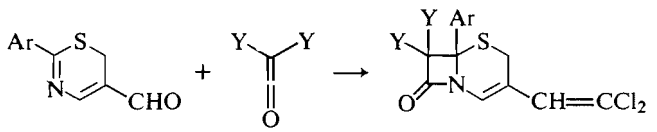

2*a* **3**″*a*
Ar = C_6H_5 Y = Cl

D'autre part, il est possible d'accéder au céphème **3***g* après protection de la fonction aldéhyde du céphème **3***a* sans altérer le cycle β-lactamique (action du thiophénol en présence d'acide de Lewis).

Les données spectroscopiques enregistrées (ir, rmn ^{13}C) pour les céphèmes **3** sont en bon accord avec celles de la littérature (16,18).

En résumé, les résultats expérimentaux ci-dessus permettent de penser que les cyclocondensations de cétènes et précurseurs sont d'autant plus aisées que l'encombrement stérique en position 4 et l'attraction électronique sur les carbones C4 et C5 des 6*H*-thiazines-1,3 sont plus faibles.

Partie expérimentale

L'Amberlyst 15 commercial (Janssen Chimica) est séché à l'étuve à 120°C.

Les chromatographies sur colonnes sont effectuées sur gel de silice Merck (Kieselgel 60, 70–230 mesh ASTM). Les points de fusion sont déterminés à l'aide d'un microscope Reichert à platine chauffante Kofler. Les spectres ir sont enregistrés à l'aide d'un spectrophotomètre UNICAM SP 1100. Les mesures sont faites sur les substances dispersées dans le bromure de potassium. Les fréquences sont exprimées en cm^{-1}.

Les spectres de rmn ^1H et ^{13}C sont enregistrés respectivement à l'aide des appareils Perkin–Elmer R-24-B (60 MHz) ou JEOL MH 100 (100 MHz) et Brucker WH 90 (20, 115 MHz). Les produits sont examinés en solution dans le $CDCl_3$, les déplacements chimiques (δ par rapport au TMS) sont exprimés en ppm et les constantes de couplage en hertz (Hz). Les spectres de rmn ^{15}N sont enregistrés à l'aide d'un appareil Brucker WM 250 (25, 355 MHz). Les déplacements chimiques sont exprimés en ppm par rapport à CH_3NO_2 utilisé comme référence interne.

Les spectres de masse sont enregistrés à l'aide d'appareils Varian MAT 311 et Varian MAT 112 à double focalisation (énergie d'ionisation 70 eV).

Les analyses sont effectuées par le service de microanalyse du CNRS.

Caractéristiques cristallographiques de **2**b

$C_{12}H_{11}NOS$ Monoclinique, $P2_1/c$, a = 12,258(3), b = 9,313(2), c = 9,785(2) Å, β = 98,90(2)°, V = 1103,6(4) Å^3, Z = 4, d_{calc} = 1,31 Mg m^{-3}, μ = 0,25 mm^{-1}. Le cristal utilisé (plaquette 0,4 × 0,2 × 0,05 mm obtenue d'une solution dans l'éthanol) a fourni 3360 réflexions uniques dont 1048 avec $\mathbf{I} > \sigma(I)$. Les mesures ont été effectuées avec un diffractomètre automatique CAD-4 Enraf–Nonius du Centre de Diffractométrie de l'Université de Rennes. (λ(MoKα) = 0,71069 Å, balayage $\omega/2\theta$ = 1, θ_{max} = 25° ; h : 0,17; k = 0,13; l = −13,13; R_{int} = 0,018).

Après corrections de Lorentz polarisation, dispersion anomale du soufre comprise (la source des facteurs de diffusion étant les tables internationales de cristallographie, volume IV, 1974), la structure a été résolue en utilisant les méthodes directes à l'aide du jeu de programmes SDP Enraf–Nonius sur un calculateur PDP 11/60 Digital. La carte de densité obtenue avec le meilleur set a révélé la totalité des atomes non hydrogène. Après affinements isotropes, puis anisotropes, une seule différence de Fourier a suffi pour déterminer la totalité des atomes d'hydrogène (entre 0,40 et 0,21 e Å^{-3}). Le meilleur affinement par moindres carrés par matrice complète de tous les paramètres (sauf les coefficients thermiques des atomes d'hydrogène fixés à 4 Å^2) a donné R = 0,049, R_w = 0,043 et S = 1,21, le schéma de pondération utilisé étant : $1/w = \sigma^2/F_o = \frac{1}{4} \mid (\sigma^2/I) + (0{,}04)^2 I \mid$ et la fonction minimisée : $\Sigma w(\Delta F)^2$. Le résidu de densité électronique est alors inférieur à 0,15 e Å^{-3}.

*Formyl-5 phényl-2 6*H*-thiazine-1,3* **2**a

À une solution de 25 mmol de **1***a* dans 50 cm^3 de dichlorométhane on ajoute 100 mmol d'acroléine en présence d'hydroquinone. On maintient l'agitation magnétique 2 h à température ambiante. Après évaporation des solvants, la 6*H*-thiazine-1,3 est chromatographiée (éluant : dichlorométhane). Par cristallisation dans un mélange éthanol – éther de pétrole, on obtient, 3,8 g de **2***a*.

*Acétyl-5 phényl-2 6*H*-thiazine-1,3* **2**b

Une solution de 25 mmol de **1***a* dans 125 mmol de méthylvinylcétone en présence d'hydroquinone est portée à reflux pendant 2 h. Après concentration, **2***b* cristallise dans un mélange éthanol – éther de pétrole. On obtient 5,2 g de thiazine.

On peut obtenir également **2***b* en ajoutant 5 mmol de chlorure d'aluminium et 25 mmol de méthylvinylcétone à une solution de 5 mmol de **1***a* dans 20 cm^3 de dichlorométhane à −20°C.

*Méthyl-4 phényl-2 6*H*-thiazines-1,3* **2**c *et* **2**d

À une solution de 1 mmol de **1***b* dans 20 cm^3 de dichlorométhane, à température ambiante, on ajoute, 0,3 g d'Amberlyst 15 et 10 mmol d'acroléine ou de méthylvinylcétone en présence d'hydroquinone sous agitation magnétique. L'évolution de la réaction est suivie par chromatographie sur couche mince. Après filtration, la solution est chromatographiée sur colonne (éluant : éther de pétrole – acétate d'éthyle 80:20). **2***c* : cristaux jaunes fondant à 88°C; m/z = 217. **2***d* : cristaux jaunes fondant à 75–77°C. *Anal.* calc. pour $C_{13}H_{13}NOS$: C67,50, H 5,67, S 13,86; tr. : C 67,93, H 5,63, S 13,94.

*Éthoxycarbonyl-4 phényl-2 6*H*-thiazines-1,3* **2**e *et* **2**f

À une solution de 3 mmol de **1***c* dans 20 cm^3 de dichlorométhane, dans la glace, on ajoute 3 mmol de chlorure d'aluminium pulvérisé, puis 24 mmol d'acroléine ou de méthylvinylcétone en présence d'hydroquinone. Le mélange est maintenu sous agitation magnétique et l'évolution de la réaction suivie par chromatographie sur couche mince. En fin de réaction on ajoute 60 cm^3 de dichlorométhane et 40 cm^3 d'eau. Après décantation, séchage et évaporation des solvants, la thiazine est purifiée par chromatographie sur colonne (éluant : éther de pétrole – acétate d'éthyle 80:20). La cristallisation est effectuée dans un mélange éthanol – éther de pétrole. **2***e* : cristaux jaunes fondant à 88–90°C. *Anal.* calc. pour $C_{14}H_{13}NO_3S$: C 61,07, H 4,76, S 11,64; tr. : C 60,87, H 4,63, S 11,63. **2***f* : cristaux jaunes fondant à 66–67°C. *Anal.* calc. pour $C_{15}H_{15}NO_3S$: C 62,26, H 5,23, S 11,08; tr. : C 62,00, H 5,22, S 10,96.

*Phényl-2 bis(phénylthio) méthyl-5 6*H*-thiazines-1,3* **2**g, **2**i, **2**j

À 3 mmol de **2***a*, **2***c*, ou **2***e* dans 20 cm^3 de dichlorométhane, on oppose 9 mmol de thiophénol en présence de 9 mmol d'éthérate de trifluorure de bore. L'agitation magnétique à température ambiante est poursuivie pendant 3 h. La solution est ensuite lavée par l'hydrogénocarbonate de sodium et extraite à l'éther diéthylique, puis chromatographiée sur colonne (éluant : dichlorométhane – éther de pétrole 50:50). Les composés obtenus sont recristallisés dans un mélange éthanol – éther de pétrole. **2***g* : cristaux jaunes fondant à 104–105°C. *Anal.* calc. pour $C_{23}H_{19}NS_3$: C 68,11, H 4,72, S 23,72; tr. : C 68,34, H 4,71, S 23,51. **2***i* : cristaux jaunes fondant à 79–81°C; m/z = 419. **2***j* : cristaux jaunes fondant à 82–83°C. *Anal.* calc, pour $C_{26}H_{23}NO_2S_3$: C 65,37, H 4,85, S 20,14; tr. : C 65,84, H 4,87, S 19,59.

*(Dioxolanne-1,3 yl-2)-5 phényl-2 6*H*-thiazine-1,3* **2**h

À 5 mmol de **2***a* dans 50 cm^3 de benzène anhydre, on oppose 15 mmol d'éthylène glycol en présence d'une trace d'acide paratoluène sulfonique. Le mélange réactionnel est porté à reflux pendant 16 h. L'eau formée est éliminée à l'aide d'un séparateur de Dean et Stark. La solution est lavée à l'hydrogénocarbonate de sodium, puis extraite à l'acétate d'éthyle. Après élimination du solvant et recristallisation dans un mélange acétate d'éthyle – éther de pétrole, **2***h* est obtenu sous forme de cristaux jaunes fondant à 89°C. *Anal.* calc. pour $C_{13}H_{13}NO_2S$: C 63,13, H 5,30, S 12,97; tr. : C 62,87, H 5,30, S 13,01.

*Formyl-5 méthyl-6 6*H*-thiazine-1,3* **2**k

À une solution de 10 mmol de **1***a* dans 15 cm^3 de toluène, on ajoute 5 cm^3 de crotonaldéhyde (5 équiv.) à 15% d'eau. On porte à reflux sous agitation magnétique. La disparition de **1***a* est suivie par chromatographie sur couche mince. Après concentration et chromatographie sur colonne (éluant : éther de pétrole – acétate d'éthyle 90:10), on isole une huile jaune, m/z = 217.

Triphényl-6,7,7 céphèmes **3**a, **3**b, **3**c, **3**d, **3**g, **3**i, **3**j

Le diphénylcétène est préparé selon la méthode décrite dans la littérature (19).

À une solution de 5 mmol de thiazines **2***a*, **2***b*, **2***c*, **2***d*, **2***g*, **2***i* ou **2***j* dans 20 cm^3 de toluène sec, sous atmosphère d'azote, sont ajoutées

7 mmol de diphényl cétène en solution dans 10 cm^3 de toluène sec. Le mélange réactionnel est porté à 100°C sous agitation magnétique. L'évolution est suivie par rmn. Les produits obtenus sont recristallisés dans l'éthanol. **3***a* : cristaux blancs fondant à 162–164°C. *Anal.* calc. pour $C_{25}H_{19}NO_2S$: C 75,54, H 4,82, S 8.07, tr. : C 75,64, H 4,89, S 8,15. **3***b* : cristaux blancs fondant à 148–150°C. *Anal.* calc. pour $C_{26}H_{21}NO_2S$: C 75,88, H 5,14, S 7,79; tr. : C 76,38, H 5,40, S 7,52. **3***c* : cristaux blancs fondant à 168°C. *Anal.* calc. pour $C_{26}H_{21}NO_2S$: C 75,88, H 5,14, S 7,79 ; tr. : C 75,58, H 5,44, S 7,37. **3***d* : cristaux blancs fondant à 163–165°C. *Anal.* calc. pour $C_{27}H_{23}NO_2S$: C 76,20, H 5,45, S 7,54 ; tr. : C 76,24, H 5,38, S 7,63. **3***g* : cristaux blancs fondant à 132–134°C. *Anal.* calc. pour $C_{37}H_{29}NOS_3$: C 74,09, H 4,87, S 16,04 ; tr. : 74,16, H 4,87, S 15,83. **3***i* : cristaux blancs fondant à 130–132°C. *Anal.* calc. pour $C_{38}H_{31}NOS_3$: C 74,35, H 5,09, S 15,67 ; tr. : C 74,57, H 5,22, S 15,31. **3***j* : cristaux blancs fondant à : 147–149°C. *Anal.* calc. pour $C_{40}H_{33}NO_3S_3$: C 71,50, H 4,95, S 14,32 ; tr. : C 71,80, H 4,97, S 14,02.

Dichloro-7,7 phényl-6 céphèmes **3**″a, **3**′b, **3**′g

Une solution de 5 mmol de thiazines **2***a*, **2***b* ou **2***g* et de 10 mmol du chlorure de l'acide dichloroacétique dans 50 cm^3 de benzène anhydre est portée à reflux sous atmosphère d'azote, avant addition goutte à goutte et sous agitation, d'une solution de 10 mmol de triéthylamine dans 25 cm^3 de benzène sec. L'avancement de la réaction est suivi par rmn. Le milieu réactionnel est ensuite lavé par HCl, 4 *N*, puis à l'eau, avant séchage et distillation du solvant.

3″*a* : Le reflux est maintenu 24 h et le meilleur résultat est obtenu en doublant les proportions de dichlorocétène (20 mmol pour 5 mmol de thiazine). Une chromatographie sur couche mince (gel de silice selon Stahl à 13% de plâtre; éluant ; éther de pétrole – éther diéthylique 2/3:1/3) permet l'obtention après recristallisation dans l'éther diéthylique de cristaux blancs fondant à 150°C, $m/z = 379$.

3′*b* : Après 5 h de reflux, les polymères formés sont éliminés par chromatographie sur colonne (éluant : éther diéthylique). La recristallisation dans un mélange chloroforme – éther diéthylique donne des cristaux blancs fondant à 137°C. *Anal.* calc. pour $C_{14}H_{11}Cl_2NO_2S$: C 51,23, H 3,38, Cl 21,61, N 4,27, S 9,77 ; tr. : C 51,29, H 3,33, Cl 21,40, N 4,31, S 9,94.

3′*g* : Après 4 h de reflux, par dilution à l'alcool de l'huile obtenue, le céphème donne des cristaux blancs fondant à 148°C. *Anal.* calc. pour $C_{25}H_{19}Cl_2NOS_3$: C 58,13, H 3,71, Cl 13,73, N 2,71, S 18,62 ; tr. : C 57,88, H 3,79, Cl 13,59, N 2,62, S 18,42.

(Dioxolanne-1,3 yl-2)-3 éthoxycarbonyl-4 triphényl-6,7,7 céphème **3**l

Après blocage de la fonction aldéhyde de la thiazine **2***e* selon le même mode opératoire que celui utilisé pour transformer **2***a* en **2***h*, on ajoute 5 mmol de diphénylcétène à 3 mmol du composé obtenu dans 10 cm^3 de toluène sec, sous atmosphère d'azote. Le mélange réactionnel est porté à 90°C pendant 6 h sous agitation magnétique. Après concentration et recristallisation dans l'éthanol, on isole un solide blanc fondant à 161–162°C. *Anal.* calc. pour $C_{30}H_{27}NO_5S$: C 70,15, H 5,30, S 6,24 ; tr. : C 70,28, H 5,34, S 6,20.

Déprotection de la fonction aldéhyde du céphème **3**l *: éthoxycarbonyl-4 formyl-3 triphényl-6,7,7 céphème* **3**e

À une mmol de **3***l* dans 50 cm^3 d'éthanol on ajoute 0,5 cm^3 d'acide sulfurique concentré. L'agitation magnétique à température ambiante est poursuivie jusqu'à disparition totale du produit de départ (contrôle par chromatographie sur couche mince). Après lavage à l'eau, puis extraction par le dichlorométhane, une chromatographie est effectuée sur colonne de gel de silice (éluant : éther de pétrole – acétate d'éthyle 85:15). La recristallisation dans l'éther de pétrole fournit des cristaux blancs fondant à 155–156°C; Rdt 50%; ir(KBr) : 1790 (C=O β-lactame), 1735 (C=O ester), 1670 (C=O aldéhyde) cm^{-1}; rmn ($CDCl_3$) δ : 2,62, (d, 1H, H_A), 3,86 (d, 1H, H_B), J_{AB} = 18,4 Hz, 9,95 (s, 1H, CHO); sm m/z : 469 $(M)^+$, 194 $((C_6H_5)_2C{=}C{=}O)$. *Anal.* calc. pour $C_{28}H_{23}NO_4S$: C 71,62, H 4,94, S 6,83; tr. : C 71,23, H 4,94, S 6,82.

Thermolyse de **3**a–**3**e

Une solution toluénique (10 cm^3) de 0,25 mmol de céphèmes **3***a*–**3***e* est portée à reflux. L'apparition d'une coloration jaune intense de la solution ainsi que le contrôle par chromatographie sur couche mince révèlent la présence des thiazines **2***a*–**2***e* correspondantes. Après séparation des produits réactionnels par chromatographie sur colonne de gel de silice, les 6*H*-thiazines-1,3 **2***a*–**2***e* sont identifiées par résonance magnétique nucléaire.

1. R. Heymes, J. Martel, et G. Nomine. Bull. Soc. Chim. Fr. 906, (1977).
2. J. C. Meslin, A. Reliquet, F. Reliquet et H. Quiniou. Synthesis, 453 (1980). J. C. Roze, J. P. Pradere, G. Duguay, A. Guevel, H. Quiniou et S. Poignant. Can. J. Chem. **61**, 1169 (1983). M. Lees, M. A. Riahi, M. Chehna, G. Duguay et H. Quiniou. J. Chem. Soc. Chem. Commun. 157 (1984).
3. N. G. Steingerg, R. W. Ratcliffe et B. G. Christensen. Tetrahedron Lett. 3567 (1974).
4. P. G. Sammes. Chem. Rev. **76**, 113 (1976); A. K. Mukerjee et A. K. Singh. Tetrahedron, **34**, 1731 (1978); G. A. Koppel. Small ring heterocycles. Part 2.*Édité par* A. Hassner. J. Wiley and Sons, New York. 1983. Chap. 2.
5. A. K. Mukerjee et R. C. Srivastava. Synthesis, 327 (1973).
6. J. C. Meslin et H. Quiniou. Bull. Soc. Chim. Fr. II, 347 (1979).
7. J. P. Pradere, J. C. Roze, G. Duguay, A. Guevel, C. Tea Gokou et H. Quiniou. Sulfur Lett. **1**, 115 (1983).
8. G. A. Olah, D. Meidar et A. P. Fung. Synthesis, 270 (1979).
9. F. A. J. Meskens. Synthesis, 501 (1981).
10. T. W. Greene. Protective groups in organic synthesis. Wiley–Interscience, New York. 1981.
11. G. J. Martin, M. L. Martin et J. P. Gouesnard. ^{15}N NMR spectroscopy. Springer Verlag, Berlin. 1981. p. 84.
12. J. P. Gouesnard et J. Dorie. Nouv. J. Chim. **6**, 143 (1982).
13. C. Rabiller, G. J. Martin, J. P. Pradere, J. C. Meslin et H. Quiniou. Org. Magn. Reson. **14**, 479 (1980).
14. J. B. Hendrickson, D. J. Cram et G. S. Hammons. Organic chemistry. McGraw–Hill, New York. 1970. p. 58.
15. H. Ulrich. Organic chemistry: cycloaddition reactions of heterocumulenes. Vol. 9. Academic Press, New York. 1967. p. 76.
16. R. B. Morin et M. Gorman (*Éditeurs*). Chemistry and biology of β-lactam antibiotics. Vol 2. Academic Press, New York. 1982. p. 52.
17. L. Muller et J. Hamer. 1–2 Cycloaddition reactions. Interscience, J. Wiley and Sons, New York. 1967. p. 143; W. T. Brady et A. D. Patel. Synthesis, 565 (1972).
18. J. W. Paschal, D. E. Dorman, P. R. Srinivasan et R. L. Lichter. J. Org. Chem. **43**, 2013 (1978).
19. H. O. House. Org. Synth. **52**, 36 (1972).

Bromation stéréosélective d'alcynes par le tribromure de tétrabutylammonium

JACQUES BERTHELOT[1]
Laboratoire de chimie organique structurale, Unité associée 455, Université Pierre et Marie Curie, 4, Place Jussieu, 75230 Paris CEDEX 05, France
ET
MICHEL FOURNIER
Laboratoire de physico-chimie inorganique, Équipe de recherche associée 608, Université Pierre et Marie Curie, 4, Place Jussieu, 75230 Paris CEDEX 05, France
Reçu le 22 mai 1985

JACQUES BERTHELOT et MICHEL FOURNIER. Can. J. Chem. **64**, 603 (1986).

L'action du tribromure de tétrabutylammonium ($TBABr_3$) sur différents alcynes (R—C≡C—R′, avec R et (ou) R′ = H, alcoyle, phényle, carboxyle, carbonyle) dans le chloroforme à 20°C conduit à la formation exclusive et stéréospécifique de l'isomère *E* de l'alcène 1-2 dibromé correspondant. Pour expliquer ce résultat nous proposons un mécanisme faisant intervenir comme intermédiaire un zwitterion bromé cyclique.

JACQUES BERTHELOT and MICHEL FOURNIER. Can. J. Chem. **64**, 603 (1986).

The reaction of tetrabutylammonium tribromide ($TBABr_3$) with alkynes (R—C≡C—R′, with R and (or) R′ = H, alkyl, phenyl, carboxyl, carbonyl) in chloroform at 20°C gives only the corresponding *E* 1,2-dibromo alkene in high yields. A mechanism involving a cyclic brominated zwitterion is suggested to account for the results, especially the stereospecificity of this *E*-addition.

De nombreux agents bromants, notamment les tribromures d'alkylammonium (triméthylphénylammonium (1), pyridinium, quinoleum (2)), ont été jadis utilisés pour éviter les inconvénients d'emploi du brome (très toxique et corrosif). En général, ils présentent l'inconvénient d'être peu stables, d'avoir un degré de brome actif diminuant rapidement au cours du temps ou d'être faiblement solubles.

Nous avons récemment décrit une méthode simple, pour additionner du brome sur les doubles liaisons éthyléniques (3) ou pour le substituer sélectivement en α d'acétals (3), qui utilise le tribromure de tétrabutylammonium ($TBABr_3$).[2] Ce réactif, solide orangé (F = 84°C), très stable, non toxique, à degré de brome constant, est facilement utilisable dans des conditions douces (20°C).

En outre, si l'addition électrophile du brome sur les oléfines a été très étudiée, les principaux détails étant bien connus (4), la réaction correspondante sur les alcynes l'est beaucoup moins et n'a suscité que peu d'attention (5).

L'halogénation des alcynes (chloration, iodation et surtout bromation) a été effectuée soit par l'halogène en solution (principalement dans l'acide acétique) (6*a, b*), soit à l'aide des halogénures métalliques (dérivés cuivriques essentiellement) en phase liquide et au reflux du solvant (7*a–e*). Dans tous les case, ces réactions conduisent à des mélanges d'alcènes 1–2 dibromés (*E* et *Z*), le plus souvent souillés de produits secondaires (alcènes monobromés, alcènes tribromés, composés d'addition du solvant) difficilement séparables. Dans les cas les plus favorables (absence de produits secondaires), il se forme toujours un mélange d'isomères *E* et *Z*, l'isomère *E* étant en général majoritaire (8). En outre, les rendements globaux en produits isolés purs sont souvent très moyens (45–65%) et l'halogène ou le sel cuivrique doivent être en large excès (de 5 à 20 fois la quantité d'alcyne). Dans la plupart des cas, il faut opérer au reflux du solvant. Par contre, nous signalons qu'en effectuant l'addition du brome, assistée d'ions bromures en

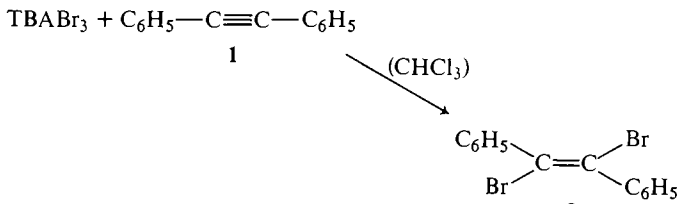

FIG. 1

milieu hydroacétique, sur l'ester éthylique de l'acide phénylpropionique, Berliner *et al.* n'obiennent que l'isomère *E* 1–2 dibromé (9, 10).

Pour ces raisons, il était tentant de comparer l'action de $TBABr_3$ sur les alcynes à celle des agents bromants habituellement utilisés en espérant un gain de rentabilité.

Résultats

Nous avons pris comme modèle d'étude la bromation du diphényl-1,2 acétylène (**1**) ou tolane (figure 1).

L'évolution de la réaction est suivie pour différents solvants, à diverses températures, en faisant varier les concentrations relatives des réactifs. Dans tous les cas, que ce soit à basse température avec des conditions stoechiométriques des réactifs ou en prolongeant la durée de réaction, à température plus élevée et avec une plus grande concentration en $TBABr_3$, seul l'isomère *E* est obtenu; nous n'avons jamais détecté (même en ccm (chromatographie sur couche mince)) la présence de l'isomère *Z* et aucun produit provenant de réactions secondaires ne vient perturber la réaction. Ces résultats sont résumés dans les tableaux 1 et 2.

Nous constatons que si la concentration relative de $TBABr_3$ augmente par rapport à celle du tolane, le rendement en alcène 1–2 dibromé diminue par suite de l'apparition d'une résinification, mais nous ne récupérons ni l'isomère *Z* de cet alcène, ni le produit de départ. Quels que soient la température et le rapport Br_3^-/alcyne, nous n'avons jamais obtenu le tétrabromo-1,1,2,2 diphényl-1,2 éthane. Comme nous l'avions déjà remarqué avec les alcènes (3) soumis à l'action bromante de $TBABr_3$, c'est le chloroforme, peu polaire, qui permet d'obtenir les

[1]Auteur à qui adresser toute correspondance.

[2]$TBABr_3$ est un produit pur et prêt à l'emploi, commercialisé par Janssen Chimica.

TABLEAU 1. Evolution de l'action de $TBABr_3$ sur le tolane dans différentes conditions*

Essai	$C_6H_5—C\equiv C—C_6H_5$	$TBABr_3$	Δ (°C)	Durée (h)	C_6H_5, Br, C=C, Br, C_6H_5 (%)	Tolane de départ (%)
a	1	1	−3	2	<3	95
b	1	1	−3	8	10	88
c	1	1	20	2	14	80
d	1	1	20	8	48	47
e	1	1	20	30	96	—
f	1	1	20	48	96	—
g	1	1	60	6	95	—
h	1	2	20	8	56	35
i	1	2	20	30	90	—
j	1	2	60	6	88	—
k	1	3	20	30	85	—
l	1	1	84	3	92	—
m	1	3	84	3	88	—

*Ces essais sont effectués sur 4 mmol de tolane, 4 mmol de $TBABr_3$ (1:1) dans 18 mL de $CHCl_3$. Les rendements indiqués sont ceux des produits isolés et purs après séparation par cp (éluant: éther de pétrole 95 – éther 5) s'il restait du produit initial. Les essais l et m ont été effectués en mélangeant $TBABr_3$ et le tolane solides et en portant à la fusion de $TBABr_3$ (84°C).

TABLEAU 2. Action de $TBABr_3$ sur le tolane dans différents solvants*

Solvant	Volume (mL)	**2** obtenu (%)	**1** restant (%)
$CHCl_3$	18	97	—
CCl_4	25	78	17
CH_3CN	20	80	15
THF	30	74	45
EtOH	45	25	70
MeOH	45	20	74

*Réactions toutes effectuées sur 4 mmol de tolane et 4 mmol de $TBABr_3$ à 20°C pendant 30 h. Les rendements sont indiqués en produits purs et isolés (cf. tableau 1). Les volumes de solvant utilisés sont fonction de la solubilité des réactifs.

meilleurs résultats; les alcools (plus polaires, mais solubilisant moins bien les réactifs) sont moins adaptés à ces réactions, ce qui avait déjà été remarqué par d'autres auteurs lors des différents essais d'halogénation (7*a*, 7*e*).

La différence de vitesse d'addition d'un même réactif conjointement sur un alcène et l'alcyne correspondant est bien connue (4, 10). Il en est de même lorsque nous faisons réagir $TBABr_3$ sur le *trans*-stilbène et le tolane dans la même solution chloroformique (à 20°) et en même concentration (tableau 3). En outre, si l'on soumet le dibromo-1,2 diphényl-1,2 éthylène *E* (**2**), lui-même, à l'action de $TBABr_3$ dans des conditions stoechiométriques et pendant dix jours à 20°C, seul (**2**) est récupéré quantitativement. Ces résultats obtenus avec le tolane comme modèle nous ont permis d'obtenir, dans les meilleures conditions et avec la même sélectivité, uniquement des alcènes 1–2 dibromés *E*, lorsque différents alcynes ont été soumis à l'action de $TBABr_3$ (tableau 4).

Dans tous ces essais, les rendements bruts sont pratiquement quantitatifs; les rendements en produits isolés sont plus faibles surtout dans le cas des liquides, s'ils sont purifiés par distillation, les alcènes 1–2 dibromés étant fragiles à la chaleur (polymérisation facile). Dans ce cas, la meilleure méthode de purification est la chromatographie préparative (cp) sur silice (cas de *d* notamment). La structure et la stéréochimie des produits **9–14** a été confirmée par comparaison avec des échantillons, connus, par leurs spectres de masse et de rmn ^1H (résonnance magnétique nucléaire) (cf. partie expérimentale). Il est à noter que, comme avec le tolane, nous n'avons jamais obtenu de composés tétrabromés.

Discussion

Dans les études antérieures (7*e*, 12) la bromation des alcynes, que ce soit par le brome ou par ses sels métalliques, semble toujours être de nature ionique. De même la bromation du tolane par $TBABr_3$ n'est par affectée par la présence de *méta*-dinitrobenzène ou d'oxygène (réputés capteurs de radicaux), et donne les mêmes résultats à la lumière ou à l'obscurité, sous gaz inerte (argon) ou à l'air. La réaction est toujours stéréospécifique, les rendements et les durées de réaction étant inchangés. Nous pensons donc que cette addition de $TBABr_3$ sur les alcynes est également de nature ionique. En utilisant le brome, ou $CuBr_2$, la formation du mélange en proportions variables des isomères *E* et *Z* pose des problèmes pour l'interprétation mécanistique du phénomène malgré des études approfondies (7*a*, 7*d*, 12). Il a déjà été montré que dans les tribromures d'ammonium, l'anion Br_3^- avait une structure linéaire (1), où les liaisons entre les atomes de brome étaient plus fragiles que celle de la structure moléculaire, et on a postulé qu'il pourrait réagir suivant:

$$Br_3^- \rightleftarrows Br^- + Br_2$$

Cette formation de brome moléculaire devrait donc conduire dans notre cas à la formation du mélange des isomères *E* et *Z* soit par addition analogue à celle du brome sur un alcyne soit par isomérisation ultérieure de l'alcène 1–2 dibromé *E* catalysée par le brome (7*e*). Or nous n'obtenons jamais d'isomère *Z*, même en laissant réagir d'une façon équimoléculaire du $TBABr_3$ et du diphényl-1,2 dibromo-1,2 éthylène pendant dix jours dans les conditions de la réaction. Par contre, si l'action du brome sur le méthylphénylacétylène conduit à un mélange d'isomères *E*, *Z*, seul l'isomère *E* est pratiquement (99%) obtenu quand il est soumis à l'addition du brome en présence de LiBr (16). De plus, comme nous l'avons déjà signalé, par addition de brome assistée d'ions bromures sur le phénylpropionate d'éthyle, seul l'isomère *E* est formé (9, 10). Ces résul-

TABLEAU 3. Différence d'action de $TBABr_3$ sur le tolane et le *trans*-stilbène*

Essai	C_6H_5(H)C=C(H)C_6H_5 (mmol)	C_6H_5—C≡C—C_6H_5 (mmol)	$TBABr_3$ (mmol)	Durée (h)	$(C_6H_5CHBr)_2$-*méso* (%)	Tolane récupéré (%)	C_6H_5(Br)C=C(Br)C_6H_5
a	4	4	4	1	98	100	—
b	4	4	4	30	98	100	Traces
c	4	4	8	1	97	100	5%
d	4	4	8	30	98	—	97%

*Les produits sont séparés par cp (éluant: éther de pétrole 97 – éther 3); pour l'essai a, cf. la réf. 3.

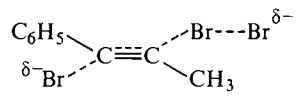

FIG. 2

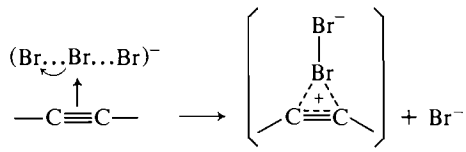

FIG. 3

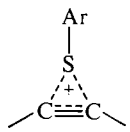

FIG. 4

tats avaient amené à postuler l'existence d'un ion Br_3^-, non dissocié, et son addition sur l'alcyne par un processus trimoléculaire de type Ad_E3, passant par un état de transition de nature comparable à celui de la fig. 2, après attaque du brome et de l'ion bromure sur les deux carbones de la triple liaison (10, 11). En ce qui concerne $TBABr_3$, nous pouvons rappeler que ce dernier, agissant sur un alcène *E*, tel que le *trans*-stilbène, conduit exclusivement à l'alcane 1–2 dibromé *méso* (3), donc à une addition en *anti* sur chaque carbone de la double liaison, compatible avec la formation intermédiaire, comme dans l'halogénation moléculaire (4), d'un ion bromonium cyclique.

De plus, nous opérons en solvant chloroformique alors que les essais d'addition du brome en présence d'ions bromures sont effectués dans l'acide acétique aqueux. C'est pourquoi, sans rejeter le mécanisme Ad_E3 cité précédemment, nous pouvons également supposer que l'action de $TBABr_3$ sur les alcynes se fait selon un mécanisme Ad_E2, impliquant le passage dans ce cas par un zwitterion cyclique bromé intermédiaire (fig. 3) suivi d'une addition *trans* d'ion Br^- (ou Br_3^-) sur ce zwitterion, conduisant à l'alcène 1–2 dibromé *E*. On peut noter que ce mécanisme avec un intermédiaire cyclique a déjà été établi dans le cas de l'addition d'halogénures de sulfényles sur le phényl-1 propyne (fig. 4), où aucune *cis* addition n'a été observée (17).

Conclusion

L'utilisation de $TBABr_3$, réactif non toxique, très facilement utilisable (stable et à degré de brome constant) dans des conditions expérimentales douces et dans les solvants usuels a donc permis de bromer, avec de bons rendements, des alcynes d'une façon très sélective (absence de produits secondaires) et très stéréospécifique puisque seul l'isomère 1–2 dibromé *E* est obtenu, ce qui est d'un intérêt synthétique évident. Bien que le mécanisme d'addition ne soit pas définitivement établi, nous apportons les indices sur sa nature très vraisemblablement ionique.

Partie expérimentale

Les points de fusion ont été déterminés au banc de Köfler, les spectres infrarouges (ir) ont été obtenus avec un spectromètre Pye–Unicam SP3-200, ceux de rmn ^1H (en solution dans $CDCl_3$, référence interne HMDS) avec un appareil Varian EM-360. Les spectres de masse (sm) ont été effectués sur un appareil AEI MS-30. Les chromatographie sur couche mince (ccm) et préparatives (cp) ont été réalisées sur gel de silice fluorescente "Merck PF 254." Les alcynes utilisés sont des produits commerciaux (Merck ou Alfa).

*Procédé général de bromation par $TBABr_3$ (cas du tolane **1**)*

À 4 mmol d'alcyne dans 18 mL de chloroforme on ajoute lentement, à température ambiante et sous agitation, 4 mmol de $TBABr_3$ (environ 20 min) ; la solution rouge intense vire lentement au rose puis au jaune. On laisse agiter pendant plusieurs heures en suivant l'évolution de la réaction par ccm (cf. tableau 1). La solution chloroformique est ensuite lavée deux fois par 20 mL d'une solution aqueuse contenant 5% de thiosulfate de sodium, puis trois fois par 20 mL d'eau, et enfin séchée sur sulfate de sodium. Le solvant est évaporé sous vide et le résidu est cristallisé (MeOH), puis recristallisé (MeOH). L'alcène 1–2 dibromé **2** est obtenu brut quantitativement, puis avec un rendement de l'ordre de 95% après purification (controlée par ccm) ; *F* net 214°C (litt. *F* (7*a*) 210°C). Quand le réaction est incomplète (cf. tableau 1) le tolane restant est séparé de **2** par cp. Comme nous l'avons déjà signalé (tableau 4), si les rendements bruts sont quantitatifs, avec les autres alcynes, ils sont plus faibles en produits purs quand ceux-ci sont liquides, après distillation (d'où l'emploi de la cp pour les obtenir, cas de **12** en particulier).

Principales caractéristiques spectrales des alcènes 1–2 dibromés E

La spectrographie de masse donne d'utiles indications, notamment par la présence déjà signalée (8) du pic moléculaire $M^{+\cdot}$ caractéristique d'un composé dibromé (formé de trois raies d'intensité relative 1, 2, 1). Ces alcènes dibromés présentent également tous les pics suivants : $(M - Br)^+$, formé de 2 raies d'égales intensités et $(M - 2Br)^+$ qui est souvent le pic de base (cas de **2**, **9**, **10**, **11** et **12** ; pour **11** il s'agit de $(M - (2Br + CO_2))^+$).

En ce qui concerne la rmn ^1H il a déjà été constaté, pour les alcènes dibromés vinyliques (8) ou contenant un groupement méthyle lié au carbone sp^2 (12), des déplacements différents pour les isomères *E* et *Z* en ce qui concerne cet hydrogène vinylique ou ce groupement méthyle. Avec les alcènes 1–2 dibromés de cette nature que nous obtenons, nous retrouvons bien uniquement ces pics caractéristiques d'isomères *E*: **9**: 6,7 ppm (s, 1H); **14**: 6,6 ppm (s, 1H); **10**: 2,6 ppm (s, 3H).

TABLEAU 4. Action de $TBABr_3$ sur différents alcynes*

Essai	Alcyne	Durée (h)	Produit	*F* ou Eb (°C/Torr) Ce travail	*F* ou Eb (°C/Torr) Litt. (réf.)	*R* (%)†	Spectre de masse $m/e = M^{+\cdot}$
a	$C_6H_5—C\equiv CH$ **3**	48	$C_6H_5(Br)C=C(Br)H$ **9**	130–134/12	132/15 (11)	86	264, 262, 260
b	$C_6H_5—C\equiv C—CH_3$ **4**	48	$C_6H_5(Br)C=C(Br)CH_3$ **10**	145/12	148/15 (12)	84	278, 276, 274
c	$C_6H_5—C\equiv C—CO_2H$ **5**	48	$C_6H_5(Br)C=C(Br)CO_2H$ **11**	136	136 (7*a*)	92	308, 306, 304
d	$C_6H_5—C\equiv C—CHO$ **6**	30	$C_6H_5(Br)C=C(Br)CHO$ **12**	44	44 (13)	86	292, 290, 288
e	$C_6H_5—C\equiv C—CH(OC_2H_5)_2$ **7**	36	$C_6H_5(Br)C=C(Br)CH(OC_2H_5)_2$ **13**	103	102 (14)	95	366, 364, 362
f	$(CH_3)_2—C(OH)—C\equiv CH$ **8**	25	$(CH_3)_2C(OH)(Br)C=C(Br)H$ **14**	90/15 $n_D^{20} = 1{,}5460$	77/7 (15) $n_D^{20} = 1{,}5469$	88	246, 244, 242

*Essais effectués sur 4 mmol d'alcyne et 4 mmol de $TBABr_3$ à 20°C dans 20 mL de $CHCl_3$ et suivis par ccm. Les produits obtenus ont été comparés à des échantillons connus (cas de a–f). Si l'essai d est effectué dans l'éthanol on n'obtient que **13**, mais avec un faible rendement (30% en produit brut).

†Les *R* (%) sont indiqués en produits isolés purs; pour d, **12** est obtenu par cp (éluant: éther de pétrole 75 – éther 25).

1. A. MARQUET, J. JACQUES et B. TCHOUBAR. Bull. Soc. Chim. Fr. 511 (1964).
2. K. W. ROSENMUND et W. KUHNHERM. Ber **56**, 1263 (1923); **56**, 2042 (1923).
3. M. FOURNIER, F. FOURNIER et J. BERTHELOT. Bull. Soc. Chim. Belg. **93**, 157 (1984).
4. P. B. DE LA MARE et R. BOLTON. Electrophilic addition to unsaturated systems. Elsevier, New York. 1966. chapt. 7.
5. R. C. FAHEY. Top. Stereochem. **3**, 279 (1968).
6. (*a*) G. H. SCHMID. *Dans* The chemistry of the carbon–carbon triple bond. Part I. *Édité par* S. Patai. John Wiley, New York. 1978. Chapt. 8; (*b*) P. B. DE LA MARE et R. BOLTON. Electrophilic addition to unsaturated systems. Elsevier, Amsterdam. 1982. chapt. 3.
7. (*a*) C. E. CASTRO, E. J. GAUGHAM et D. C. OWSLEY. J. Org. Chem. **30**, 587 (1965); (*b*) S. UEMURA, A. ONOE et M. OKANO. J. Chem. Soc. Commun. **23**, 925 (1975); (*c*) S. UEMURA, H. OKAZAKI, A. ONOE et M. OKANO. J. Chem. Soc., Perkin Trans. 1, 676 (1977); (*d*) S. UEMURA, H. OKAZAKI et M. OKANO. J. Chem. Soc. Perkin Trans. **1**, 1278 (1978); (*e*) S. UEMURA, H. OKAZAKI, M. OKANO, S. SAWADA et A. OKADA. Bull. Chem. Soc. Jpn. **51**, 1911 (1978).
8. J. KONIG et V. WOLF. Tetrahedron Lett. **19**, 1629 (1970).
9. S. DE YOUNG, S. EHRLICH et E. BERLINER. J. Am. Chem. Soc. **99**, 290 (1977).
10. S. EHRLICH et E. BERLINER. J. Am. Chem. Soc. **100**, 1525 (1978).
11. S. DE YOUNG et E. BERLINER. J. Org. Chem. **44**, 1088 (1979).
12. J. A. PINOCK et K. YATES. Can. J. Chem. **48**, 332 (1970).
13. BEILSTEIN. Handbuch der Organischem Chemie. E III, 7, 1385. Springer Verlag, Berlin. 1952.
14. K. AUWERS et M. SAYFRIED. Justus Liebigs Ann. Chem. **484**, 212 (1930).
15. I NAZAROV et L. BERGLESON. Zh. Obshch. Khim. **27**, 1540 (1957).
16. J. A. PINOCK et K. YATES. J. Am. Chem. Soc. **90**, 5643 (1968).
17. G. H. SCHMIDT et M. HEINOLA. J. Am. Chem. Soc. **90**, 3455 (1968).

Propriétés de solvation des solutions concentrées en acide phosphorique

C. Louis et J. Bessière

Laboratoire de chimie et d'electrochimie analytique, Faculté des sciences, Université de Nancy 1, B.P. 239, 54506 Vandoeuvre Les Nancy CEDEX, France

Reçu le 10 avril 1985

C. Louis et J. Bessière. Can. J. Chem. **64**, 608 (1986).

Les variations de solvatation d'espèces en solution dans les milieux H_2O–H_3PO_4 (1–14 *M*) sont caractérisées par des coefficients d'activité de transfert de solvatation *f*. Ils sont calculés à partir des valeurs de potentiels normaux de systèmes redox ou de mesures de solubilité. Leur analyse met en évidence une augmentation de la solvatation des anions et une desolvatation des cations lorsque la concentration d'acide croît. L'amplitude de la variation dépend du nombre de charges portées par l'espèce considérée, de la présence d'atomes d'oxygène dans sa structure, de son caractère basique. Les conséquences des variations de solvatation sur les réactions d'oxydo-réduction et de précipitation sont analysées.

C. Louis and J. Bessière. Can. J. Chem. **64**, 608 (1986).

Solvation properties of ions in H_2O–H_3PO_4 media (1–14 *M*) are characterized with their solvation transfer activity coefficients *f*. These are calculated from normal potential or solubility values, and indicate an increasing solvation for anions and decreasing solvation for cations in concentrated acid solutions. For each species, the range depends on its number of charges, on the existence of oxygen atoms in its structure, and on its basic properties. The consequences of variation of solvation on oxidation–reduction reactions and solubility properties are studied.

Les variations avec la teneur en acide de la réactivité de solutés dans les milieux eau – acide phosphorique ont été étudiées dans le cas de réactions d'oxydo-réduction et de précipitation (1, 2). Elles peuvent être interprétées d'un point de vue thermodynamique à partir des variations de solvatation des espèces mises en jeu. Celles-ci sont caractérisées par des coefficients d'activité de transfert de solvatation *f*.

Rappel théorique

Les coefficients d'activité d'anions et de cations sont calculés à partir des potentiels normaux de systèmes redox les mettant en jeu d'après les relations:

[1] système M^{n+}/M_s $\quad \log f_{M^{n+}} = n(E_0^{H_2O-H_3PO_4} - E_0^{H_2O})/0{,}059$

[2] système $M^{n+}/M^{(n-m)+}$ $\quad \log f_{M^{(n-m)+}} = m(E_0^{H_2O-H_3PO_4} - E_0^{H_2O})/0{,}059$

[3] système $MO_p^{n+}/MO_q^{[n+2(p-q)-m]+}$ $\quad \log f_{MO_p^{n+}}/f_{MO_q^{[n+2(p-q)-m]+}} = m(E_0^{H_2O-H_3PO_4} - E_0^{H_2O})/0{,}059 + 2(p-q)R_0(H) + (p-q)\log a_{H_2O}$

[4] système AX_n/A_s $\quad \log f_{X^-} = (E_0^{H_2O} - E_0^{H_2O-H_3PO_4})/0{,}059$

où $E_0^{H_2O-H_3PO_4}$ représente le potentiel normal du système redox dans le milieu phosphorique exprimé par rapport au système de comparaison ferricinium/ferrocène (Fc^+/Fc) et $E_0^{H_2O}$ son potentiel normal dans l'eau; R_0 (H) est la fonction d'acidité du milieu phosphorique (1) et a_{H_2O} son activité en eau.

Ils sont dans certains cas calculés à partir de valeurs de produits de solubilité d'après la relation:

[5] $\quad pK_s^{H_2O-H_3PO_4} - pK_s^{H_2O} = \log f_{M^+} = \log f_{X^-}$

où $pK_s^{H_2O-H_3PO_4}$ représente le produit de solubilité du composé MX dans le milieu phosphorique et $pK_s^{H_2O}$ son produit de solubilité dans l'eau. La détermination de la solubilité de phosphate, par exemple $XHPO_4$, permet également le calcul des coefficients d'activité selon des relations analogues à:

[6] $\quad \log f_{X^{2+}} = R_0(HPO_4^{2-}) - pK_s^{H_2O} - \log [X^{2+}]$

où $R_0(HPO_4^{2-})$ caractérise le pouvoir donneur de HPO_4^{2-} du milieu et $pK_s^{H_2O}$ est le produit de solubilité dans l'eau.

Résultats et discussion

L'étude de l'évolution des propriétés d'oxydo-réduction et de solubilité dans les milieux H_2O–H_3PO_4 (2) conduit aux valeurs de $\log f$ ou de $\log f_{ox}/f_{red}$ rassemblées dans le tableau 1 et représentées par les figures 1 et 2.

1. Variation de solvatation de cations

Les cations Ag^+, Hg_2^{2+}, Cu^{2+}, Pb^{2+}, Sn^{2+}, Zn^{2+}, Cd^{2+} sont caractérisés par des valeurs positives et croissantes des logarithmes des coefficients d'activité avec la concentration d'acide. Ils sont donc de moins en moins solvatés lorsque la concentration d'acide augmente. Pour une concentration donnée en acide, les valeurs de $\log f_{M^{n+}}$ dépendent de la charge de l'ion. Ainsi, les variations de $\log f_{Ag^+}$ sont moins importantes que celles observées pour l'ensemble des cations divalents: l'écart est de 3 unités lorsque l'on passe du milieu 2 *M* au milieu 11,5 *M* alors qu'il est de 7 unités au minimum pour un cation divalent. Elles sont du même ordre de grandeur que celles de $\log f_{Fe^{3+}}/f_{Fe^{2+}}$ et $\log f_{V^{3+}}/f_{V^{2+}}$ qui correspondent à des systèmes mettant en jeu une seule charge et n'impliquant l'oxygène. Les valeurs $\log f_{Cu^{2+}}$ et $\log f_{Sn^{2+}}$ sont négatives dans les milieux peu concentrés en acide phosphorique, de même que

[1]Revision reçu le 13 novembre 1985.

TABLEAU 1. Variation des coefficients d'activité d'espèces ioniques avec la concentration d'acide

	H_3PO_4 (*M*)				
	2,0	5,5	8,0	11,5	14,0
R_0(H)	−0,2	−1,9	−3,2	−6,1	−8,9
$\log f_{Ag^+}$	+0,7	+1,6	+2,6	+4,8	+6,4
$\log f_{Hg_2^{2+}}$	0,0	+2,2	+4,0	+7,3	+11,0
$\log f_{Pb^{2+}}$	+1,3	+3,4	+5,8	+8,7	+12,7
$\log f_{Cu^{2+}}$	−0,3	+2,0	+4,5	+8,3	+11,6
$\log f_{Sn^{2+}}$	−0,7	+2,7	+5,9	+10,7	+16,5
$\log f_{Cd^{2+}}$	+3,4	+6,9	+9,3	+13,1	+18,2
$\log f_{Zn^{2+}}$	+2,0	+5,5	+7,9	+11,8	+16,8
$\log f_{Fe^{3+}}/f_{Fe^{2+}}$	−4,3	−3,8	−3,1	−1,3	−0,2
$\log f_{V^{3+}}/f_{V^{2+}}$	−1,6			+0,9	
$\log f_{Fe(CN)_6^{3-}}/f_{Fe(CN)_6^{4-}}$	+6,4	+9,3	+11,9	+16,7	+21,9
$\log f_{UO_2^{2+}}/f_{U^{4+}}$	+4,0	+2,5	+1,3	−1,9	−10,8
$\log f_{VO_2^+}/f_{VO^{2+}}$	+1,3	+0,2	−0,9	−3,8	−7,0
$\log f_{VO^{2+}}/f_{V^{3+}}$	+1,9	+1,0	+0,5	−1,8	+3,8
$\log f_{H_3AsO_4}/f_{AsO^+}$	+2,0	−1,4	−3,9		
$\log f_{Cl^-}$	−1,0	−1,6	−2,1	−3,6	−4,9
$\log f_{Br^-}$	+0,7	−0,5	−1,5	−3,4	−4,8
$\log f_{I^-}$	−1,4	−1,9	−2,4	−3,5	−4,3
$\log f_{F^-}$	−3,4	−5,0	−6,1	−8,9	
$\log f_{SO_4^{2-}}$	−3,3	−6,0	−8,5	−11,5	−15,6
$\log f_{Fe(CN)_6^{4-}}$	−8,1	−12,7			
$\log f_{Fe(CN))_6^{3-}}$	−1,7	−3,3			
$\log f_{I_3^-}$	−3,3	−4,0	−5,5		

les valeurs $\log f_{Fe^{3+}}/f_{Fe^{2+}}$ dans tout le domaine de concentration de H_3PO_4. Les espèces Cu^{2+}, Sn^{2+}, Fe^{3+} sont donc plus solvatées dans les milieux phosphoriques correspondants que dans l'eau. Dans la mesure où les systèmes considérés dans le solvant de référence ne font pas intervenir les phénomènes de complexation, on devait s'attendre, pour les solutions diluées en acide, à des valeurs négatives de $\log f_{Fe^{3+}}$ et dans un moindre mesure de $\log f_{Cu^{2+}}$, la complexation en solution diluée étant assimilable à un accroissement de solvatation. Une augmentation de la concentration de H_3PO_4 entraîne pour ces espèces une décomplexation (ou une diminution de solvatation), ce qui accroît leur réactivité. Ainsi, le pouvoir oxydant de Fe(III) est, en milieu 14 *M*, voisin de celui qu'il a dans l'eau en milieu non complexant ($\log f_{Fe^{3+}}/f_{Fe^{2+}} = -0,2$). Les ions Cd^{2+} et Zn^{2+}, qui ne donnent pas de complexe en solution aqueuse diluée en acide, sont caractérisés par des valeurs $\log f_{Cd^{2+}}$ et $\log f_{Zn^{2+}}$ positives dans le milieu de concentration 2 *M* en H_3PO_4. Ces ions sont déjà moins solvatés dans ce milieu que dans l'eau en milieu non complexant. Le terme $\log f_{M^{n+}}$ intègre donc les phénomènes de complexation qui peuvent avoir lieu en solution diluée, les notions de complexation et de solvatation dans de tels milieux étant confondues. Parmi les cations divalent, Cu^{2+}, Pb^{2+}, Hg_2^{2+} se desolvatent moins vite que Zn^{2+} et Cd^{2+}. Or, en milieu phosphorique, les espèces Pb^{2+} et Hg_2^{2+} donnent des composés insolubles avec les anions de l'acide, ce qui traduit une forte affinité. D'autre part, dans l'eau la stabilité des phosphates de cuivre et de plomb est supérieure à celle des phosphates de zinc et de cadmium: $Pb_3(PO_4)_2$, $pK_s = 43,5$; $Cu_3(PO_4)_2$, $pK_s = 36,9$; $Zn_3(PO_4)_2$, $pK_s = 32,0$; $Cd_3(PO_4)_2$, $pK_s = 32,6$ (3). La désolvatation des ions semble donc d'autant plus aisée qu'ils donnent des complexes moins stables avec les espèces phosphate. Les valeurs de pK_s de $Ba_3(PO_4)_2$ et $Ca_3(PO_4)_2$ sont respectivement de 29,3 et 26 (4) et les coefficients d'activité qui peuvent être calculés pour les cations Ba^{2+} et Ca^{2+} caractérisent une désolvatation comparable à celle de Zn^{2+}.

Lorsque l'on compare les systèmes UO_2^{2+}/U^{4+}, VO_2^+/VO^{2+}, VO^{2+}/V^{3+}, H_3AsO_4/AsO^+, l'effet de l'acidité est le même pour les trois premiers: deux protons mis en jeu pour un électron. Il est moins prononcé pour le dernier: trois protons pour deux électrons et c'est dans tous les cas la forme réduite qui est la plus chargée. C'est donc la désolvatation de cette espèce qui est prédominante. En effet, la quantité $\log f_{ox}/f_{red}$ est décroissante et sa variation est d'autant plus importante que l'écart entre le nombre des charges portées par la forme oxydée et la forme réduite est grand: elle est de 14 unités pour $\log f_{UO_2^{2+}}/f_{U^{4+}}$ et de 8 et 5 unités pour $\log f_{VO_2^+}/f_{VO^{2+}}$ et $\log f_{VO^{2+}}/f_{V^{3+}}$ lorsque l'on passe du milieu 2 *M* au milieu 14 *M* en H_3PO_4. Contrairement à ce qui a été observé pour les systèmes Fe^{3+}/Fe^{2+} et V^{3+}/V^{2+}, $\log f_{ox}/f_{red}$ est positif dans les milieux dilués en acide pour les trois systèmes UO_2^{2+}/U^{4+}, VO_2^+/VO^{2+}, VO^{2+}/V^{3+} ainsi que pour H_3AsO_4/AsO^+. Ceci signifie que ce sont les formes réduites qui sont initialement les plus fortement associées aux anions du solvant. Dans les milieux plus concentrés en acide où $\log f_{ox}/f_{red}$ est négatif, les termes de solvatation d'une part, d'acidité et d'activité de l'eau d'autre part, jouent un rôle antagoniste dans la variation du potentiel normal apparent des systèmes, mais la solvatation ne compense que partiellement l'influence de l'acidité et de l'activité de l'eau.

Le nombre des charges portées par les formes oxydées et réduites ne joue pas seul. La présence d'oxygène dans l'un ou l'autre des cations mis en jeu dans le système redox intervient également. Les deux systèmes UO_2^{2+}/U^{4+} et VO^{2+}/V^{3+} présentent une certaine analogie: les formes oxydées comportent des atomes d'oxygène, les formes réduites n'en comportent pas. Seul, les distingue le nombre des charges portées par les formes réduites et on observe que la variation de $\log f_{UO_2^{2+}}/f_{U^{4+}}$ est deux fois plus importante que celle de $\log f_{VO^{2+}}/f_{V^{3+}}$; les varia-

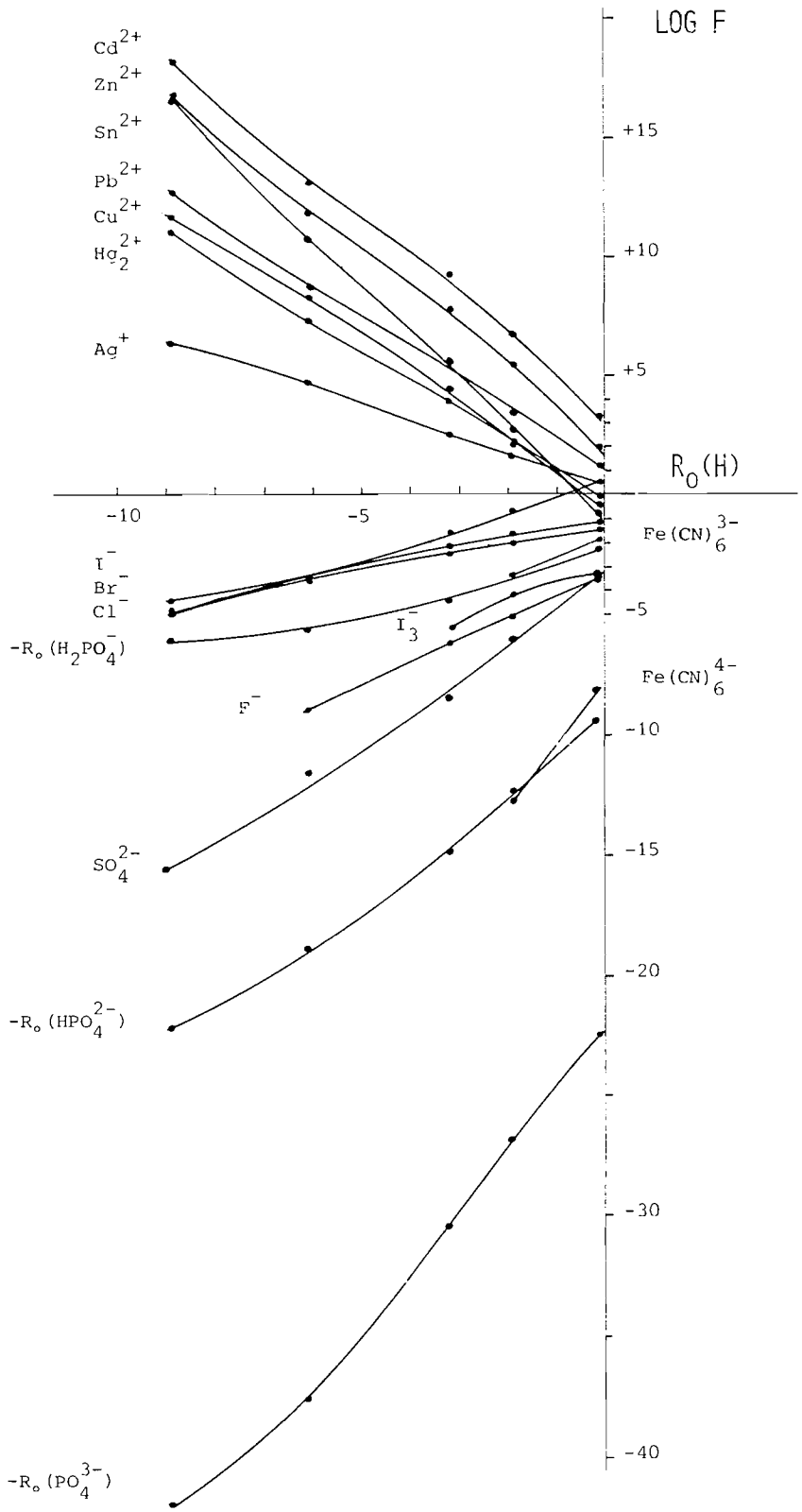

FIG. 1. Caractéristiques de solvatation des espèces en solution dans les milieux H_2O–H_3PO_4.

tions des potentiels normaux apparents de ces deux systèmes sont très voisines. La comparaison des systèmes VO_2^+/VO^{2+} et Fe^{3+}/Fe^{2+} ou V^{3+}/V^{2+}, pour lesquels le nombre de charges échangées est le même mais dont le premier seul met en jeu des espèces avec atome d'oxygène, montre que la variation de solvatation est deux fois plus grande dans le premier cas. L'effet de charge serait donc plus important pour les systèmes engageant deux espèces oxygénées.

2. Variation de solvatation des anions

La solvatation des anions croît avec la concentration de l'acide et sa variation est d'autant plus importante que les

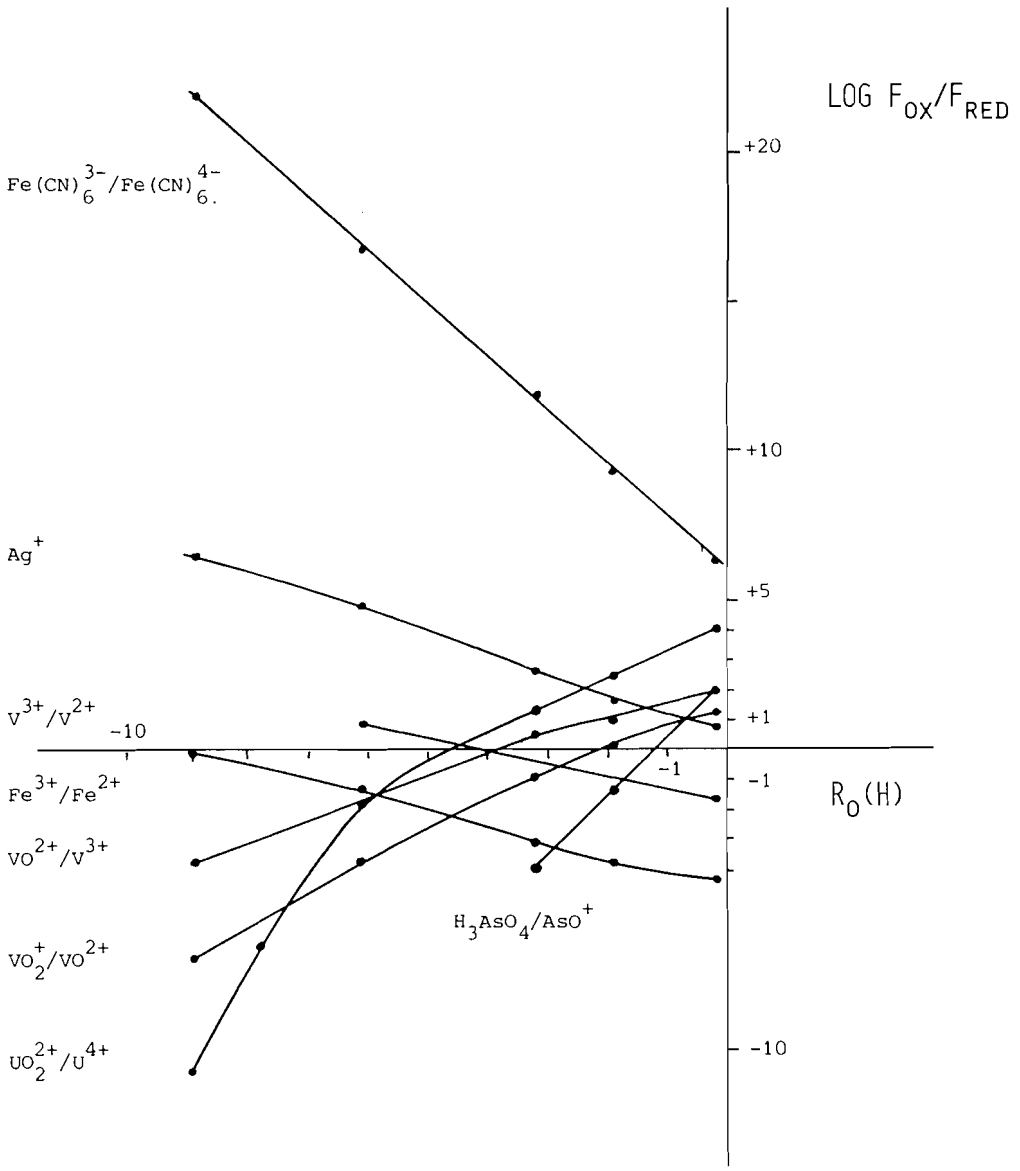

FIG. 2. Caractéristiques de solvatation dans les milieux H_2O–H_3PO_4 des espèces mises en jeu dans les systèmes de l'argent, du fer, de l'uranium, du vanadium, de l'arsenic et des hexacyanoferrate.

anions sont plus basiques. L'étude de la variation de la fonction H_0 par la détermination de la modification de la protonation de l'indicateur de Hammett: 4-chloro-2-nitroaniline (pK^{H_3O} = −0,9), lors de l'addition au milieu H_3PO_4 5,5 *M* de Cl^-, NO_3^-, SiF_6^{2-}, HSO_4^- à la concentration de 0,5 *M*, montre que ces anions sont dépourvus de propriétés basiques et que l'addition des acides conjugués se traduit par une augmentation du niveau d'acidité. Au contraire, les ions F^- et SO_4^{2-} basiques dans l'eau ($pK_{HF}^{H_2O}$ = 3,2, $pK_{HSO_4^-}^{H_2O}$ = 1,9) présentent des caractéristiques de basicité dans les milieux H_2O–H_3PO_4 et l'addition des acides conjugués ne modifie pas le niveau d'acidité de ces milieux.

Les anions Cl^-, Br^-, I^- ont un comportement voisin, l'effet de taille reste minime. Leur accroissement de solvatation est faible comparativement à celui de l'ion F^- dont les propriétés basiques expliquent que log *f* est trois fois plus élevé que celui des autres halogénures. Le coefficient d'activité des sulfates est supérieur au double de celui des chlorures dépourvus de basicité et à celui des fluorures. Ceci met en évidence l'intervention dans les caractéristiques de solvatation des anions de leur caractère basique et du nombre de charges qu'ils portent. De la même manière, les ions hexacyanoferrate(III), $Fe(CN)_6^{3-}$, dépourvus de propriétés basiques dans l'eau, ont des coefficients d'activité environ deux fois plus élevés que ceux des halogénures sans propriétés basiques dans l'eau. Au contraire, les hexacyanoferrate(II), $Fe(CN)_6^{4-}$, basiques dans l'eau $pK_{Fe(CN)_6H_2^{2-}}^{H_2O}$ = 3, $pK_{Fe(CN)_6H^{3-}}^{H_2O}$ = 4,2), ont des coefficients d'activité élevés et qui augmentent rapidement avec la concentration de l'acide.

La réactivité des anions du solvant est caractérisée par les fonctions $R_0(H_2PO_4^-)$, $R_0(HPO_4^{2-})$, $R_0(PO_4^{3-})$ (1). L'évolution des propriétés de solvatation d'une espèce en solution caractérisée par la variation de son coefficient d'activité se traduit par la modification de sa réactivité vis-à-vis des autres espèces présentes (ions du solvant ou solutés). Nous allons étudier les conséquences des phénomènes de solvatation dans le cas des réactions d'oxydo-réduction et de formation de composés insolubles.

3. Phénomènes de solvatation et réactions d'oxydo-réduction

Le diagramme potentiel – niveau d'acidité (2) est une traduction graphique des phénomènes de solvatation dans la mesure où la plupart des données concernant les coefficients d'activité ont été obtenues à partir de déterminations électrochimiques. Il rend compte de l'effet du niveau d'acidité, de l'activité de l'eau et de la solvatation relative des oxydants et des réducteurs conjugués sur la réactivité des espèces et permet de prévoir les réactions d'oxydo-réduction dans les milieux H_2O– H_3PO_4. Parmi les systèmes redox envisagés, trois groupes se dessinent: (*i*) les systèmes dont le potentiel varie fortement avec la teneur en acide. Ils engagent formellement deux protons pour un électron échangé (UO_2^{2+}/U^{4+}, VO_2^{+}/VO^{2+}, VO^{2+}/V^{3+}) et l'évolution est plus marquée pour les couples mettant en jeu une particule oxygénée. Les systèmes dont la forme réduite présente des propriétés basiques entrent également dans cette catégorie ($Fe(CN)_6^{3-}/Fe(CN)_6^{4-}$). (*ii*) Les systèmes dont le potentiel redox varie peu avec la teneur en acide: Fc^{+}/Fc et à un moindre degré I_3^{-}/I^{-}. (*iii*) Les systèmes intermédiaires: d'une manière générale, leur pouvoir oxydant évolue dans le même sens. Cependant, les couples pour lesquels la réactivité du proton intervient seule présentent une variation de leurs propriétés d'oxydo-réduction plus importante. Ainsi, le pouvoir réducteur de l'hydrogène et de l'hydroquinone évolue plus vite que celui des métaux seuls ou en présence d'anions. Lorsque les systèmes font intervenir le proton et des espèces ioniques ou moléculaires (H_2SO_3/H_2SO_2, H_3AsO_4/AsO^{+}) l'effet dû à l'acidité peut être limité par les termes $\log f_{ox}/f_{red}$ et le pouvoir réducteur de ces composés varie alors moins vite que celui des métaux. Les termes $\log f_{ox}/f_{red}$ peuvent se compenser en partie lorsque deux systèmes appartenant au même type et faisant intervenir le même nombre d'électrons sont en présence, alors qu'ils peuvent s'ajouter lorsque les deux systèmes appartiennent à des types différents comme Fe^{3+}/Fe^{2+} et UO_2^{2+}/U^{4+}.

4. Phénomènes de solvatation et réactions de précipitation

4.1 *Formation de composés insolubles n'engageant pas les phosphates*

La comparaison des valeurs $\log f_{M^{n+}}$ et $\log f_{X^{n-}}$ permet de prévoir l'évolution de la solubilité des sels MX avec la teneur en acide. Cependant, la solubilité réelle diffère de la quantité calculée si il se forme des espèces solubles MX ou $MX_m^{(n-m)-}$.

D'une manière générale, il y a compensation partielle des effets de changement de milieu sur l'anion et sur le cation. Les pK_s de quelques composés calculés d'après la relation [5] sont présentés dans le tableau 2. Lorsque l'anion est, comme Cl^{-}, dépourvu de propriétés basiques, l'effet de cation peut l'emporter sur l'effet d'anion. Ainsi, AgCl est plus stable en milieu H_3PO_4 14 *M* que dans l'eau. Il en est de même pour $PbCl_2$ et Hg_2Cl_2. Des résultats analogues seraient obtenus pour les bromures et les iodures puisque $\log f_{Br^-}$ et $\log f_{I^-}$ sont très peu différents de $\log f_{Cl^-}$. Dans le cas de $PbSO_4$, l'effet d'anion l'emporte sur l'effet de cation mais l'écart reste pratiquement constant dans tout le domaine de concentration; la solubilité de $PbSO_4$ varie donc peu avec la teneur en acide.

La présence d'acide peut modifier nettement la stabilité de sels engageant des cations dont la variation de solvatation se fait différemment. Ainsi, les hexacyanoferrates(II) de cuivre, de zinc et de cadmium, dont la stabilité est voisine dans l'eau, ont des caractéristiques de dissolution différentes en milieu H_3PO_4 2 et 5,5 *M*. Cu^{2+} et Pb^{2+} se desolvatent moins vite que Cd^{2+} et Zn^{2+}; l'effet d'anion est donc plus marqué dans le cas des sels de cuivre et de plomb que dans celui des sels de zinc et de cadmium. En milieu H_3PO_4 5,5 *M*, la stabilité du sel de cadmium est plus grande que dans l'eau bien que l'espèce $Fe(CN)_6^{4-}$ soit fortement solvatée en raison de sa basicité. Une inversion entre la stabilité dans l'eau et dans les milieux phosphoriques peut intervenir pour les sels engageant le même anion et les cations M^{n+} et N^{n+} lorsque la différence de leur pK_s dans l'eau est inférieure à $\log f_{M^{n+}}/f_{N^{n+}}$. Ainsi, l'iodate de cuivre ($pK_s^{H_2O} = 7,1$), qui est plus stable dans l'eau que l'iodate de zinc ($pK_s^{H_2O} = 5,4$) est moins stable que ce dernier en milieu acide.

TABLEAU 2. Effet de la concentration de H_3PO_4 sur la solubilité de quelques composés

		H_3PO_4 (*M*)				
pK_s	H_2O	2,0	5,5	8,0	11,5	14,0
AgCl	9,7	9,4	9,7	10,2	10,9	11,2
$PbCl_2$	4,8	4,1	5,0	6,5	6,5	7,7
Hg_2Cl_2	17,9	15,9	17,9	17,9	17,9	19,1
$PbSO_4$	7,7	5,7	5,1	5,0	4,9	4,8
$Pb_2[Fe(CN)_6]$	16,9	11,4	11,0			
$Cd_2[Fe(CN)_6]$	15,0	13,7	16,1			
$Cu_2[Fe(CN)_6]$	15,7	8,2	7,0			
$Zn_2[Fe(CN)_6]$	15,4	11,3	13,7			
$\log f_{Cd^{2+}}/f_{Cu^{2+}}$		3,7	4,9	4,8	4,8	
$\log f_{Zn^{2+}}/f_{Cu^{2+}}$		2,3	3,5	3,4	3,5	

Les réactions de précipitation engageant des anions peu basiques comme les halogénures ou les iodates sont favorisées dans les milieux concentrés en acide. Lorsque les anions sont basiques, l'effet de cation peut compenser dans certains cas l'accroissement de solvatation de l'anion. Mais de nombreuses espèces minérales qui précipitent dans l'eau sont solubles en milieu acide phosphorique. L'élimination d'une espèce par précipitation ou son dosage par formation d'un composé peu soluble seront donc plus difficiles.

4.2 *Précipitation des phosphates*

Phosphates de plomb

Lors de l'étude des systèmes mettant en jeu le plomb, nous avons déterminé la solubilité des phosphates de plomb $PbHPO_4$ dans les milieux de concentration inférieure à 8 *M* et du $Pb(H_2PO_4)_2$ dans les milieux plus concentrés. Puisque les fonctions basiques ont été évaluées indépendamment à partir des systèmes redox Hg_2HPO_4/Hg et $BiPO_4/Bi$, nous avons comparé (tableau 3) les valeurs expérimentales de solubilité du plomb à celles calculées à partir de relations analogues à [6] avec $pK_{s(PbHPO_4)}^{H_2O} = 9,9$ et $pK_{s(Pb_3(PO_4)_2)}^{H_2O} = 42,1$.

Il y a donc une concordance satisfaisante en ce qui concerne les limites des domaines de précipitation des différents phosphates. $Pb_3(PO_4)_2$ est soluble même pour de faibles concentrations de H_3PO_4. $PbHPO_4$ précipite jusqu'à une concentration d'acide de 8 *M*. Dans les milieux plus concentrés, c'est $Pb(H_2PO_4)$ qui est insoluble.

Phosphates d'argent

L'étude de la solubilité des phosphates d'argent dans les milieux H_2O–H_3PO_4 (5) montre que Ag_3PO_4 précipite pour des concentrations d'acide inférieures à 4 *M*, Ag_2HPO_4 pour des concentrations d'acide allant jusqu'à 9,5 *M* et que AgH_2PO_4 est insoluble dans les milieux plus concentrés. La solubilité de l'argent peut être calculée à partir du coefficient d'activité du

TABLEAU 3. Solubilité des phosphates de plomb dans les milieux H_2O–H_3PO_4

H_3PO_4 (M)	R_0 (HPO_4^{2-})	$\log f_{Pb^{2+}}$	$[Pb^{2+}]^a$	$[Pb^{2+}]^b$
2,0	9,4	1,3	1.6×10^{-2}	4×10^{-3}
5,5	12,2	3,4	8×10^{-2}	6×10^{-3}
8,0	14,8	5,8	0,1	7×10^{-3}
11,5	18,9	8,7	2	$Pb(H_2PO_4)_2$ insoluble $PbHPO_4$ soluble
H_3PO_4 (M)	R_0 (PO_4^{3-})	$\log f_{Pb^{2+}}$	$[Pb^{2+}]$	$[Pb^{2+}]$
2,0	22,4	1,3	0,4	$PbHPO_4$ insoluble
5,5	26,8	3,4	2,7	$Pb_3(PO_4)_2$ soluble

[a]Valeurs calculées.
[b]Valeurs expérimentales.

cation Ag^+ et de la fonction $R_0(PO_4^{3-})$ pour les faibles concentrations de H_3PO_4, où Ag_3PO_4 seul se forme, d'après la relation [6] où $pK_s^{H_2O} = 20,83$ (6). Les valeurs calculées et les résultats expérimentaux sont présentés dans le tableau 4.

Dans le domaine de concentration où la forme insoluble est Ag_3PO_4, les valeurs de solubilité expérimentales et calculées sont concordantes. La valeur élevée de 1,9 calculée en milieu 5,5 M est cohérente avec le fait qu'à cette concentration d'acide, il a été montré que la forme insoluble est Ag_2HPO_4.

Phosphates de baryum et de calcium

Les résultats des études de solubilité des phosphates de baryum (6–9) et de calcium (10, 11) dans les milieux phosphoriques nous ont permis de calculer les coefficients d'activité de Ba^{2+} et Ca^{2+} qui n'avaient pu être déterminés autrement. Les coefficients d'activité du cation Ba^{2+} sont calculés d'après la relation [6] où $pK_s^{H_2O} = 7,6$ (4) pour des concentrations d'acide de 3 M. Au delà de cette concentration c'est la forme $Ba(H_2PO_4)_2$ qui précipite; $\log f_{Ba^{2+}}$ est alors calculé d'après la relation

$$[7] \quad \log f_{Ba^{2+}} = 2\,R_0(H_2PO_4^-) - pK_s^{H_2O} - \log [Ba^{2+}]$$

Comme $pK_s^{H_2O}$ n'est pas connu, c'est la variation de $\log f_{Ba^{2+}}$ que nous avons calculée à partir de la limite de la zone de concentration d'acide où la forme insoluble est $BaHPO_4$ (3 M) jusqu'à une concentration d'acide de 13 M.

Pour les concentrations de H_3PO_4 inférieures à 3,8 M, $CaHPO_4$ est insoluble. La relation utilisée est analogue à [6] avec $pK_s^{H_2O} = 7,0$ (4). Pour des concentrations plus élevées d'acide, $Ca(H_2PO_4)_2 \cdot H_2O$ précipite. La relation:

$$[8] \quad \log f_{Ca^{2+}} = 2\,R_0(H_2PO_4^-) - pK_s^{H_2O} - \log [Ca^{2+}] - \log a_{H_2O}$$

conduit au calcul de la variation de $\log f_{Ca^{2+}}$.

Les valeurs de $\log f_{Ba^{2+}}$ et $\log f_{Ca^{2+}}$ sont rassemblées dans le tableau 5. Les cations Ba^{2+} et Ca^{2+} ont des caractéristiques de solvatation analogues à celles déterminées pour les autres cations divalents; ils sont voisins de Zn^{2+}, Sn^{2+}, Cd^{2+}, c'est-à-dire de ceux qui se désolvatent le plus. Ceci est en accord avec la stabilité dans l'eau plus faible de $Ba_3(PO_4)_2$ et de $Ca_3(PO_4)_2$ et avec le fait que le sulfate de baryum est stable même dans les milieux concentrés en acide: le renforcement de solvatation de l'anion est compensé par la désolvatation importante du cation.

TABLEAU 4. Solubilité des phosphates d'argent dans les milieux H_2O–H_3PO_4

H_3PO_4 (M)	R_0 (PO_4^{3-})	$\log f_{Ag^+}$	$[Ag^+]^a$	$[Ag^+]^b$	
1,0	20,8	0,2	0,6	0,2	
2,0	22,4	0,7	0,6		
3,0	23,4	0,9	0,9		
4,0	24,8	1,2	1,3	0,7	Ag_3PO_4 soluble
5,5	26,8	1,6	1,9		Ag_2HPO_4 insoluble

[a]Valeurs calculées.
[b]Valeurs expérimentales (5).

Phosphates d'uranium

L'étude de la solubilité des phosphates d'uranium(IV) en milieu phosphorique (12, 13) montre que, pour les concentrations d'acide inférieures à 9 M, la forme insoluble est $U(HPO_4)_2 \cdot 6H_2O$, et pour les concentrations plus élevées, c'est $U(HPO_4)_2H_3PO_4 \cdot H_2O$ qui précipite. En admettant que les solubilités des phosphates d'uranium(IV) ont été déterminées à l'équilibre et que les "gels" qui se forment peuvent être considérés comme des solides de structure définie et constante, les coefficients d'activité de l'espèce U^{4+} peuvent être calculés d'après la relation:

$$[9] \quad \log f_{U^{4+}} = -pK_s^{H_2O} + 2\,R_0(HPO_4^{2-}) - 6 \log a_{H_2O} - \log [U^{4+}]$$

avec $pK_s^{H_2O} = 27,5$ (12) en se limitant au domaine de concentration 2–8,8 M en H_3PO_4 où le solide est toujours $U(HPO_4)_2 \cdot 6H_2O$ et la solubilité de U^{4+} est inférieure à 0,5 M.

Des valeurs de $\log f_{UO_2^{2+}}$ peuvent en être déduites puisque $\log f_{UO_2^{2+}}/f_{U^{4+}}$ a été déterminé par une autre voie (tableau 1). Les résultats sont rassemblés dans le tableau 6. Pour les milieux de concentration d'acide inférieure à 4 M, la structure du phosphate d'uranium(VI) insoluble est $UO_2(HPO_4) \cdot 4H_2O$; dans les milieux plus concentrés, elle est $UO_2(H_2PO_4)_2 \cdot 3H_2O$ (14). La solubilité des phosphates d'uranium(VI) est beaucoup plus élevée que celle des phosphates d'uranium(IV): elle n'est inférieure à 0,5 ion g/L que pour des concentrations d'acide allant jusqu'à 2,5 M. Le domaine de concentration d'acide où il est possible de calculer à la fois $\log f_{UO_2^{2+}}$ et $\log f_{U^{4+}}$ à partir des solubilités des phosphates de U(VI) et U(IV) est donc très

TABLEAU 5. Coefficients d'activité des cations Ba^{2+} et Ca^{2+} en fonction de la concentration de H_3PO_4; valeurs calculées

H_3PO_4 (M)	1,2	1,8	2,9	5,6	6,5	9,2	10,5	11,5	12,0
$\log f_{Ba^{2+}}$	1,6	2,0	2,8	4,8	5,6	8,0	9,3	10,5	10,7
H_3PO_4 (M)	2,5	3,7	5,7	6,9	8,0	9,6	10,2	12,2	
$\log f_{Ca^{2+}}$	2,9	4,0	5,5	6,6	7,7	9,2	9,8	11,9	

TABLEAU 6. Coefficients d'activité des espèces UO_2^{2+} et U^{4+} calculés à partir de la solubilité de $U(HPO_4)_2 \cdot 6H_2O$

H_3PO_4 (M)	$[U^{4+}]^a$	R_0 (HPO_4^{2-})^b	$\log a_{H_2O}$	$\log f_{U^{4+}}$	$\log f_{UO_2^{2+}}/f_{U^{4+}}{}^c$	$\log f_{UO_2^{2+}}$
1,9	$6{,}2 \times 10^{-4}$	+9,3	−0,02	−5,6		
3,2	$3{,}9 \times 10^{-3}$	+10,2	−0,04	−4,4	+3,7	−0,8
4,2	$1{,}6 \times 10^{-2}$	+11,2	−0,06	−2,9	+3,2	+0,3
5,9	$4{,}3 \times 10^{-2}$	+12,5	−0,12	−0,2	+2,4	+2,2
7,1	0,19	+13,2	−0,17	+1,8	+1,7	+3,5
8,2	0,35	+15,0	−0,23	+4,3	+1,0	+5,3
8,8	0,52	+15,6	−0,27	+5,6	+0,6	+6,2

[a]D'après réf. 12.
[b]D'après réf. 1.
[c]D'après le tableau 1.

TABLEAU 7. Coefficients d'activité de l'espèce UO_2^{2+} calculés à partir de la solubilité de $UO_2(HPO_4) \cdot 4H_2O$

H_3PO_4 (M)	$[UO_2^{2+}]^a$	R_0 (HPO_4^{2-})^b	$\log a_{H_2O}$	$\log f_{UO_2^{2+}}$
0,9	0,1	+8,1	0	−1,6
1,3	0,2	+8,7	−0,01	−1,2
1,7	0,3	+9,1	−0,015	−1,0
2,4	0,6	+9,8	−0,025	−0,5

[a]D'après réf. 14.
[b]D'après réf. 1.

restreint. Nous donnons dans le tableau 7 les valeurs du coefficient d'activité de UO_2^{2+} calculées d'après la relation:

$$[10] \quad \log f_{UO_2^{2+}} = -pK_s^{H_2O} + R_0(HPO_4^{2-}) - 4 \log a_{H_2O} - \log [UO_2^{2+}]$$

avec $pK_s^{H_2O} = 10{,}7$.

Il semble donc que U^{4+} soit plus fortement solvaté dans les milieux phosphoriques dilués que dans l'eau, puis se désolvate très rapidement lorsque la concentration d'acide augmente, ce qui est conforme, en raison du nombre de charges portées par cette espèce, à l'analyse qui a été faite. UO_2^{2+} a, dans le même domaine de concentration d'acide, des caractéristiques de solvatation voisines de celles des cations divalents qui, comme Sn^{2+} ou Zn^{2+}, se désolvatent le plus lorsque la concentration d'acide augmente.

Conclusion

Les variations de solvatation des espèces ioniques en solution dans les milieux phosphoriques concentrés sont caractérisées par leurs coefficients d'activité de transfert de solvatation. Les cations sont moins solvatés lorsque la concentration d'acide augmente tandis que la solvatation des anions est renforcée. Pour une espèce donnée, l'amplitude de la variation de solvatation dépend du nombre de charges, de la présence d'oxygène dans sa structure, de son caractère basique. Les coefficients d'activité permettent d'interpréter ou de prévoir les réactions d'oxydo-réduction (diagramme potentiel – niveau d'acidité), l'évolution des propriétés de solubilité y compris celles des phosphates. Ils devraient également intervenir dans la prévision des réactions mises en jeu dans les processus de séparation comme l'extraction liquide–liquide et la flottation ionique.

1. C. LOUIS et J. BESSIÈRE. Can. J. Chem. **63**, 908 (1985).
2. C. LOUIS. Thèse de Doctorat d'Etat, Nancy, France. 1983.
3. G. CHARLOT. Les réactions chimiques en solution. L'analyse qualitative minérale. Masson et Cie., Paris. 1969. pp. 287–298.
4. G. CHARLOT. L'analyse qualitative et les réactions en solution. Masson et Cie., Paris. 1963. p. 210.
5. R. FLATT et G. BRUNIHOLZ. Helv. Chim. Acta, **34**, 692 (1951).
6. N. A. TANANAEV et R. A. LOVI. J. Appl. Chem. USSR, **15**, 214 (1942).
7. H. V. TARTAR et J. R. LORAH. J. Am. Chem. Soc. **51**, 1091 (1929).
8. H. GUERIN et A. ARTUR. Bull. Soc. Chim. Fr. 562 (1952).
9. A. ARTUR. Ann. Chim. **10**, 968 (1955).
10. K. L. ELMORE et T. D. FARR. Ind. Eng. Chem. **32**,. 580 (1940).
11. A. P. BELOPOL'SKII, M. T. SEREBRENNIKOVA et A. V. BILEVICH. J. Appl. Chem. USSR, **13**, 3 (1940).
12. J. M. SCHREYER. United States Atomic Energy Commission, ORNL 1747. 1 (1954).
13. J. M. SCHREYER. J. Am. Chem. Soc. **77**, 2972 (1955).
14. J. M. SCHREYER et C. F. BAES. J. Am. Chem. Soc. **76**, 354 (1954).

Dithiaphosphagermetannes-1,3,2,4 et dithiaphosphadigermolannes-1,4,5,2,3

J. BARRAU,[1] M. EL AMINE, G. RIMA ET J. SATGÉ[1]

Laboratoire de chimie des organominéraux, Unité associé N° 477 du Centre national de la recherche scientifique, Université Paul Sabatier, 118 route de Narbonne, 31062 Toulouse CEDEX, France

Reçu le 19 avril 1985[2]

J. BARRAU, M. EL AMINE, G. RIMA et J. SATGÉ. Can. J. Chem. **64**, 615 (1986).

Les hétérocycles germaniés et phosphorés anisyl-2 diméthyl-4,4 thio-2 dithiaphosphagermetanne-1,3,2,4, $Me_2GeSP(An)S$ (**1**), et anisyl-5 tétraméthyl-2,2,3,3 thio-5 dithiaphosphadigermolanne-1,4,5,2,3, $Me_2GeGe(Me_2)SP(An)S$ (**2**), sont obtenus par action de l'anisyltrithiophosphonate d'ammonium sur les dichlorures germaniés correspondants. Le composé **1** est instable à température ambiante et se décompose pour conduire à (Me_2GeS) et $(AnPS_2)_n$. Le composé **2** subit une fragmentation thermique à 200°C avec formation de $(Me_2GeS)_3$ et $(AnPS)_n$. Ces résultats sont expliqués par deux mécanismes de décomposition faisant intervenir les espèces doublement liées transitoires $(Me_2Ge{=}S)$ et $(AnPS_2)$ ou (AnPS) respectivement. Les réactions d'échange entre **2** et divers chlorures métallés (M_{IVB}) sont décrites. La réaction avec Me_2SiCl_2 conduit à la diméthylsilathione $[Me_2Si{=}S]$ via un dithiaphosphasiletanne intermédiaire.

J. BARRAU, M. EL AMINE, G. RIMA, and J. SATGÉ. Can. J. Chem. **64**, 615 (1986).

The synthesis of the new germylated and phosphorylated heterocycles 2-anisyl-4,4-dimethyl-2-thio-1,3,2,4-dithiaphosphagermetane, $Me_2GeSP(An)S$ (**1**), and 5-anisyl-2,2,3,3-tetramethyl-5-thio-1,4,5,2,3-dithiaphosphadigermolane, $Me_2GeGe(Me_2)SP(An)S$ (**2**), are described. The decomposition of **1** with formation of $(Me_2GeS)_3$ and $(AnPS_2)_n$ is observed at room temperature. At 200°C **2** undergoes thermal fragmentation leading to $(Me_2GeS)_3$ and $(AnPS)_n$. These results are explained by two mechanisms of decomposition involving formation of transient species $[Me_2Ge{=}S]$ and $[AnPS_2]$ or [AnPS], respectively. Exchange reactions between **2** and various metal (M_{IVB}) chlorides are described. With Me_2SiCl_2 the reaction leads to silathione $[Me_2Si{=}S]$, probably via transient dithiaphosphasiletane.

Introduction

Dans ce mémoire, nous présentons l'étude de nouveaux hétérocycles germaniés, l'anisyl-2 diméthyl-4,4 thio-2 dithiaphosphagermetanne-1,3,2,4, $Me_2GeSP(An)S$ (**1**), et l'anisyl-5 tétraméthyl-2,2,3,3 thio-5 dithiaphosphadigermolanne-1,4,5,2,3, $Me_2GeGe(Me_2)SP(An)S$ (**2**).

Ces hétérocycles sont les premiers représentants de thiophosphonates germaniés cycliques. Ils sont par décomposition intramoléculaire, comme diverses autres stuctures hétérocycliques germaniées (1–11), sources d'espèces à double liaison du germanium $[Me_2Ge{=}S]$ (12) et également du phosphore

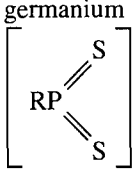

et [RP=S]. Ces éthers cycliques germaniés d'acides trithiophosphoniques peuvent également être utilisés comme agents de synthèse en chimie organogermaniée ou organophosphorée.

Résultats et discussion

Le dithiaphosphagermetanne **1** est obtenu à 20°C au sein de l'acétonitrile par action de l'anisyltrithiophosphonate d'ammonium (13) sur le dichlorodiméthylgermanium.

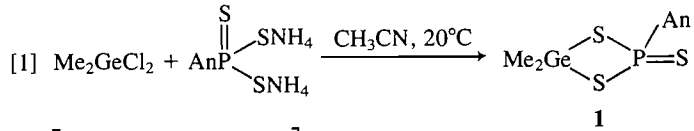

[1] $Me_2GeCl_2 + AnP(S)(SNH_4)_2 \xrightarrow{CH_3CN,\ 20°C} Me_2Ge(S)_2P(An)=S$ (**1**)

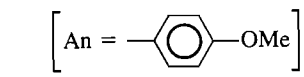

[An = —C₆H₄—OMe]

rmn ^1H δ_{Me} = 1,0 ppm (s) et 1,1 ppm (s)

^{31}P δ_P = 79,9 ppm (s)

Toute tentative de concentration sous vide ou distillation conduit à $(Me_2GeS)_3$ et $(AnPS_2)_n$ (14). La formation de ces entités peut être interprétée par un mécanisme de β-décomposition de l'hétérocycle **1** conduisant aux espèces monomères $[Me_2Ge{=}S]$

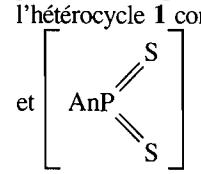

et

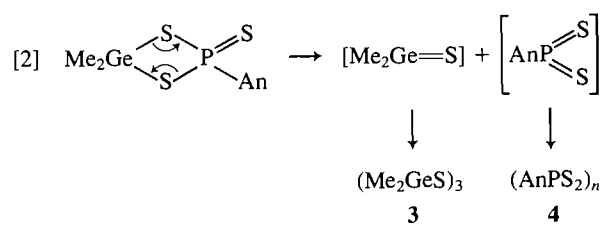

[2] $Me_2Ge(S)_2P(S)An \longrightarrow [Me_2Ge{=}S] + [AnP(S)_2]$

$(Me_2GeS)_3$ (**3**) $\quad (AnPS_2)_n$ (**4**)

L'addition de thiiranne au milieu réactionnel permet d'isoler le diméthylgermadithiolanne $Me_2GeSCH_2CH_2S$ (**5**) et le dithiaphospholanne-1,3,2, $AnP(S)SCH_2CH_2S$ (**6**). Ces hétérocycles représentent respectivement les adduits des deux espèces π liées

[1]Auteurs à qui adresser toute correspondance.

[2]Révision reçue le 8 novembre 1985.

$[Me_2Ge{=}S]$ et $\left[\text{AnP}(=S)(=S)\right]$ et du thiiranne.

[3] $Me_2GeCl_2 + AnP(=S)(SNH_4)_2 \xrightarrow[(2)\ -NH_4Cl]{(1)\ CH_3CN,\ 20°C} (3) + \text{thiiranne}$

Me_2Ge(dithiolane) + AnP(=S)(dithiolane)

5 **6**

Soulignons cependant que l'obtention du dithiaphospholanne-1,3,2 (**6**) n'est pas une preuve irréfutable de la condensation de l'intermédiaire monomère $\left[\text{AnP}(=S)(=S)\right]$ sur le thiiranne puisque ce même hétérocycle (**6**) peut être obtenu à partir du télomère $(AnPS_2)_n$.

[4] $(AnPS_2)_n$ + thiiranne $\xrightarrow{20°C}$ AnP(=S)(dithiolane) (Rdt ≥ 65%)

6

D'autre part, une insertion directe du thiiranne sur le dithiaphosphagermetanne **1** avec formation d'un hétérocycle à 7 chaînons instable (cf. réactivité de **2**) peut également expliquer la formation du dithiaphospholane **6** et du diméthylgermadithiolane **5** via $[Me_2Ge{=}S]$.

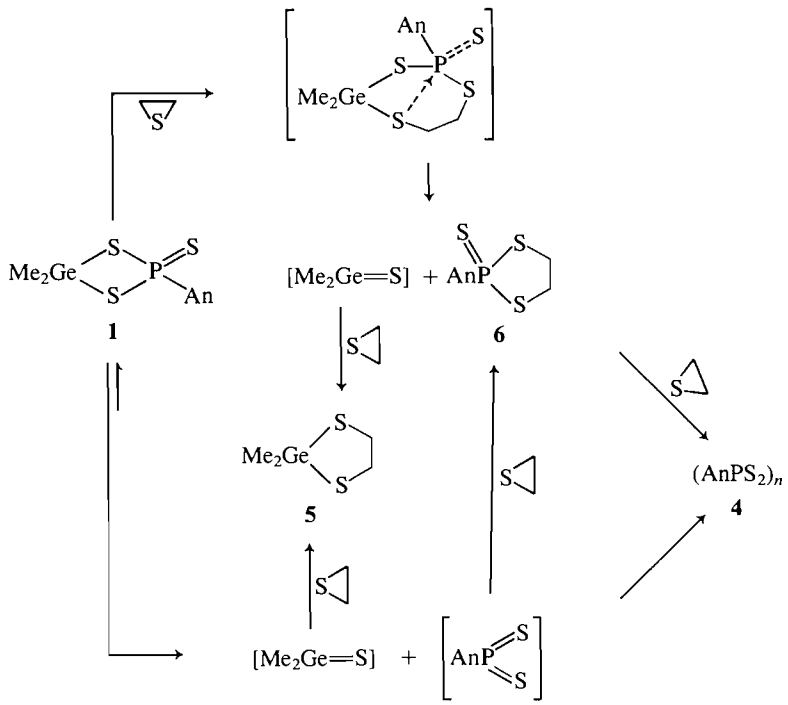

L'action directe de l'anisyltrithiophosphonate d'ammonium sur le tétraméthyl-1,1,2,2 dichloro-1,2 digermane (10) permet également d'accéder à l'anisyl-5 tétraméthyl-2,2,3,3 thio-5 dithiaphosphadigermolanne-1,4,5,2,3 (**2**) avec un rendement de l'ordre de 95%.

[5] $AnP(=S)(SNH_4)_2 + Me_2Ge(Cl)—Ge(Cl)Me_2 \xrightarrow[-2NH_4Cl]{CH_3CN,\ 20°C}$ Me_2Ge—$GeMe_2$(dithiolane)P(=S)An

2

Le dithiaphosphadigermolanne à phosphore tétracoordonné ainsi synthétisé a été caractérisé par analyse de rmn (^1H: δ_{Me} = 0,56 ppm (s) et 1,10 ppm (s); δ_{OMe} = 3,16 ppm (s); ^{31}P: δ_P = 86,0 ppm) et spectrométrie de masse.

La spectrographie de masse par désorption par champ permet d'observer uniquement le massif de l'ion moléculaire $M^{+\bullet}$ pour un courant de filament variant de 5 mA à 20 mA.

L'analyse du spectrogramme effectuée sous impact électronique (70 eV) révèle notamment la présence de quatre massifs correspondant à l'ion moléculaire $M^{+\bullet}$ et aux ions $[Me_2GeS]^{+\bullet}$, $[M - Me_2GeS]^{+\bullet}$ et $[AnPS]^{+\bullet}$. Faibles à 20°C, les intensités relatives de ces trois derniers pics augmentent très fortement lorsque la température de la source dépasse 100°C.

Une étude de filiation par identification des ions métastables permet de proposer le diagramme de fragmentation suivant:

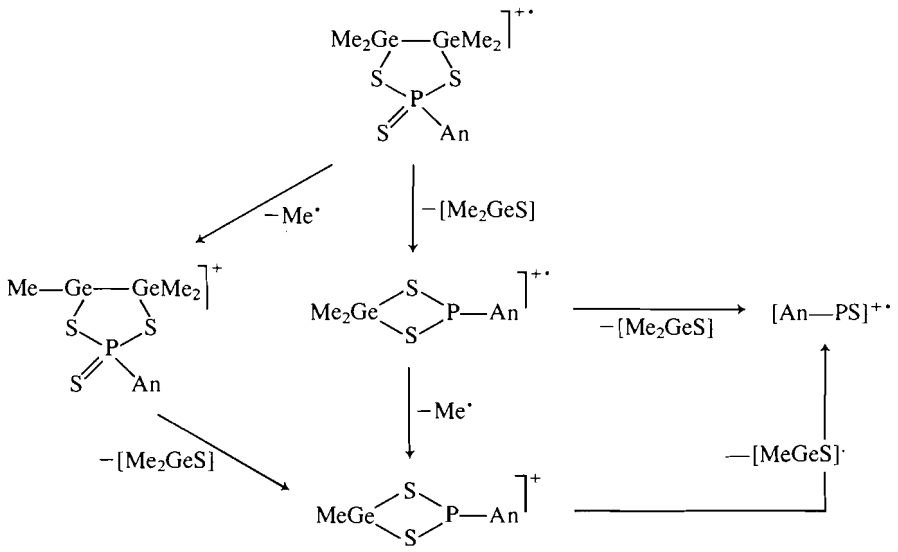

Le composé **2** est stable à température ordinaire mais instable à température plus élevée. Opérant à 270°C en tube scellé sa thermolyse et sa pyrolyse en phase vapeur conduisent à la formation exclusive de $(AnPS)_n$ (**7**) (15) et de $(Me_2GeS)_3$ (**3**) via les espèces monomères [AnP=S] et $[Me_2Ge{=}S]$.

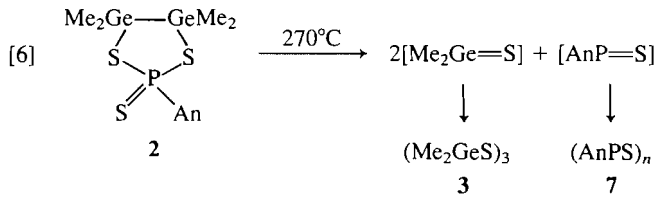

L'existence de corrélation entre les processus de fragmentation sous impact électronique et les comportements sous effet thermique de petits hétérocycles siliciés précurseurs d'espèces π liées du silicium (16) nous amène à proposer, pour rendre compte de cette thermolyse, un mécanisme de décomposition thermique de **2** en accord avec son comportement sous impact électronique. Ce mécanisme initié par attaque nucléophile d'un germanium par le soufre (P=S) conduit, à côté de $[Me_2Ge{=}S]$, à un dithiétanne intermédiaire (**8**) instable subissant lui-même une β-décomposition.

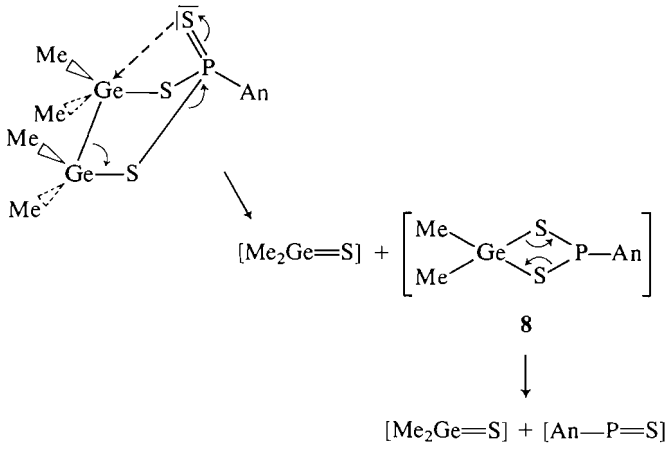

À l'appui de cette hypothèse, signalons que nous n'observons aucune décomposition de **2** à 270°C au sein de la triéthylamine. Celle-ci doit vraisemblablement former avec **2** un complexe instable non isolable, empêchant ainsi toute attaque nucléophile du soufre sur le germanium.

La réaction classique (4) de condensation de la diméthylgermathione monomère sur le thiiranne ne peut cependant pas être réalisée à partir de **2**. Le thiiranne réagit en effet à 20°C sur **2** avec formation de dithiaphospholanne, **6**, et d'hexaméthyl-2,2,3,3,5,5 trigerma-2,3,5 dithiolanne-1,4, **9** (10).

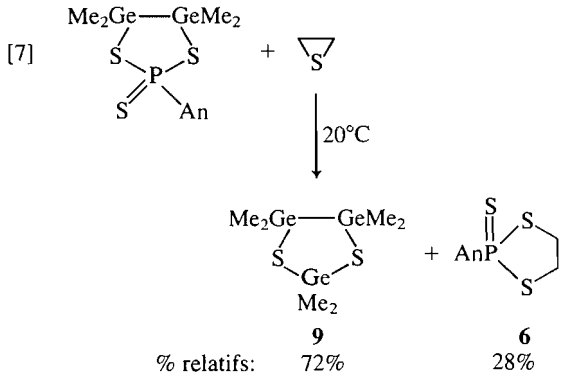

Ce bilan réactionnel peut s'interpréter par une insertion du thiiranne dans une liaison Ge—S de **2** suivie d'une décomposition (procédant par attaque nucléophile intramoléculaire d'un atome de S en α du germanium sur l'atome de phosphore) de l'hétérocycle ainsi obtenu. Le passage par un digermathiiranne intermédiaire qui se dimérise pour conduire à l'octaméthyltétragermadithiacyclohexane (**10**) instable (10) permet d'expliquer la formation de **9**.

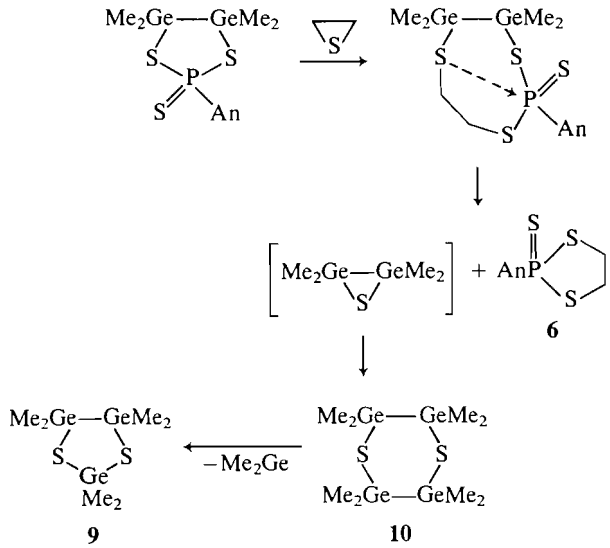

La diméthylgermathione peut cependant être caractérisée par addition sur la liaison germanium–soufre de $Me_2Ge(SMe)_2$ en réalisant la thermolyse de **2** en présence de ce dérivé. Le sulfure de bis(diméthylméthylthiogermanium) attendu (**11**) (4) est obtenu avec un rendement de 20%.

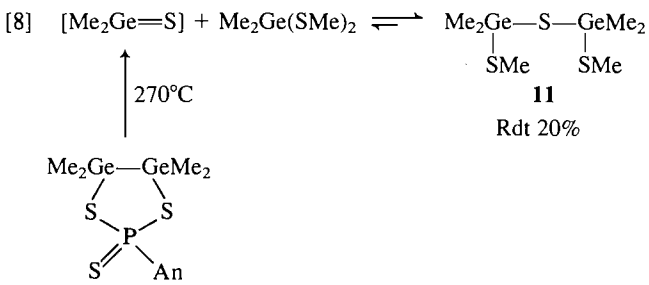

Bien que la spectroscopie photoélectronique ait déjà permis la mise en évidence de la diméthylgermathione $[Me_2Ge{=}S]$ (P. I exp:[3] n_S 8,6; π Ge—S 9,55; σ Ge—S 10,75; σ Ge—C 11,47 eV) lors de dépolymérisations thermiques de cyclogermathianes (17)

$$(R_2GeS)_3 \overset{\Delta}{\rightleftharpoons} [R_2Ge{=}S] + (R_2GeS)_2 \ (R = \text{alkyl})$$

nous ne pouvons pas utiliser cette technique pour suivre la décomposition de **2** puisque le phosphore porte un groupe anisyl —C_6H_4—OCH_3 dont les divers potentiels d'ionisation masquent ceux de $[Me_2Ge{=}S]$.

La sensibilité des liaisons Ge—S vis-à-vis des réactifs dipolaires a pu être mise à profit pour accéder à partir de **2** et divers chlorures métallés à d'autres espèces π liées $\left[\begin{smallmatrix}\diagdown\\ \diagup\end{smallmatrix} M_{IVB} = X\right]$

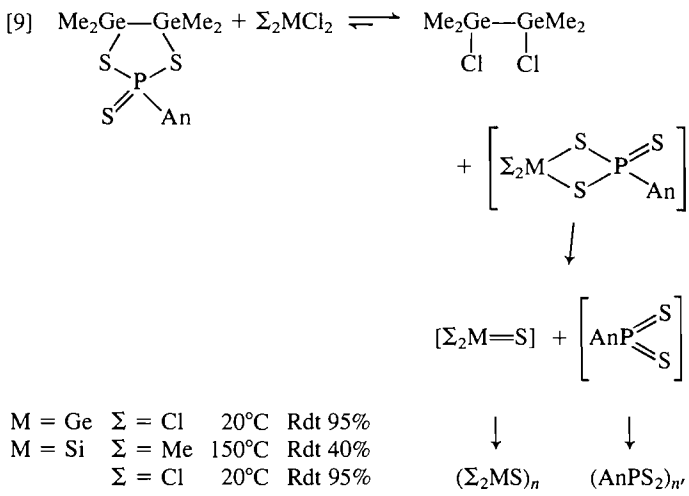

Avec M = Si et Σ = Me, la diméthylsilathione intermédiaire peut être caractérisée par condensation sur l'hexaméthyltrisiloxanne (16).

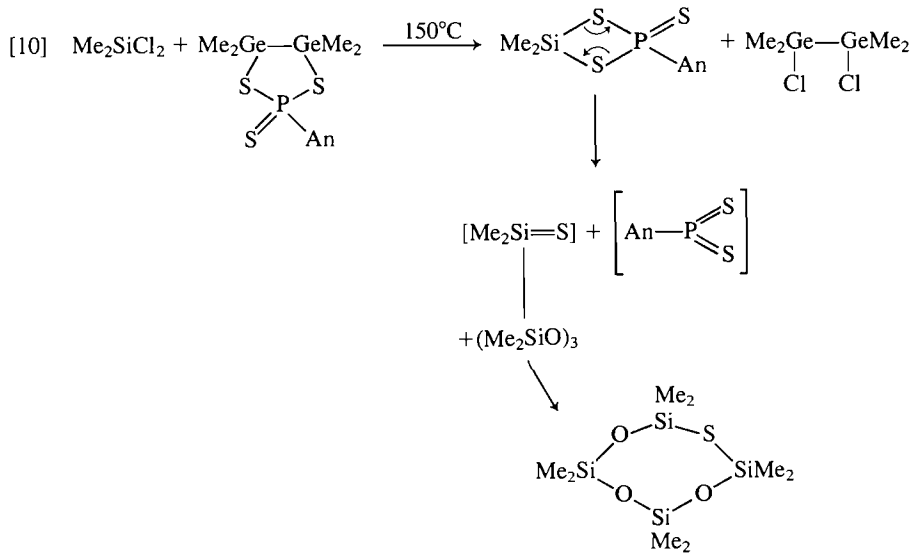

Avec le tétrachlorure de germanium (1/2 mole pour 1 mole de **2**) et le dichlorogermylène, les réactions d'échange ont lieu à 20°C et conduisent aux polymères $(GeS_2)_n$ et $(GeS)_n$ vraisemblablement via les intermédiaires disulfure de germanium monomère $[S{=}Ge{=}S]$ d'une part, et monosulfure de germanium ($:Ge{=}S$] d'autre part.

Partie expérimentale

Toutes les réactions ont été réalisées en atmosphère inerte d'argon. Les spectres de rmn ^1H ont été enregistrés sur spectromètre Varian EM 360A à 60 mégacycles; toutes les valeurs des déplacements chimiques sont données par rapport au TMS pris comme référence interne. Les spectres de rmn ^{31}P ont été réalisés sur spectromètre Bruker WP 90 à 36,4 mégacycles; les déplacements chimiques sont donnés par rapport à H_3PO_4 pris comme référence externe.

Les spectres de masse ont été effectués sur spectromètre de masse Ribermag R1010.

Anisyl-2 diméthyl-4,4 thio-2 dithiaphosphagermetanne-1,3,2,4, $Me_2GeSP(An)S$ (1)

Diméthyldichlorogermanium (1 g, 0,0057 mol) en solution dans 150 cm^3 de CH_3CN est traité par 1,55 g de $AnP(SNH_4)_2$ (13) (0,0057 mol). Après filtration, les analyses de rmn (^1H et ^{31}P) et de spectrométrie de masse du filtrat mettent en évidence la formation d'anisyl-2 diméthyl-4,4 thio-2 dithiaphosphagermetanne-1,3,2,4; rmn (CH_3CN) ^1H δ_{Me}:

[3] P.I exp = potentiel d'ionisation experimental.

1,0 ppm (s) et 1,1 ppm (s); ^{31}P δ_P: 79,0 ppm; spectre de masse, *m/e*: 338 $[Me_2GeSP(An)S]^{+\bullet}$.

Après concentration de ce filtrat sous 10 Torr (1 Torr = 133,3 Pa), les analyses cpv (chromatographie en phase vapeur), rmn et spectrométrie de masse dénotent la présence de $(Me_2GeS)_3$ (rmn (C_6H_6) ^1H δ_{Me}: 0,82 ppm) et de $(AnPS_2)_n$ ($n = 2$ essentiellement, rmn ($O—C_6H_4Cl_2$) ^{31}P δ_P: 14,5 ppm).

Anisyl-5 tétraméthyl-2,2,3,3 dithiaphosphadigermolanne-1,4,5,2,3, $Me_2GeGe(Me_2)SP(An)S$ (2)

Le mélange de 3,32 g de dichloro-1,2 tétraméthyldigermane (10) (0,0120 mol) et de 3,24 g de $AnP(SNH_4)_2$ (0,0120 mol) dans 500 cm^3 de CH_3CN est maintenu 24 h à température ambiante sous agitation. Après filtration, le filtrat est concentré sous 10 Torr. Les cristaux obtenus sont recristallisés dans le benzène. On obtient ainsi, 3,68 g d'anisyl-5 tétraméthyl-2,2,3,3 thio-5 dithiaphosphadigermolanne-1,4,5,2,3 (Rdt 70%); P_F = 150–151°C; rmn (C_6D_6) ^1H δ_{Me}: 0,56 ppm (s) et 1,10 ppm (s); δ_{OMe}: 3,16 ppm (s); $\delta_{C_6H_4}$: 8,50 ppm (dd, J_{PH} = 19 Hz) et 6,70 (dd, J_{PH} = 3 Hz); ^{31}P δ_P: 86,0 ppm. Spectre de masse *m/e*: 440 $[Me_2GeGe(Me_2)SP(An)S]^{+\bullet}$; 425 $[MeGeGe(Me_2)SP(An)S]^+$; 304 $[Me_2GeSP(An)S]^{+\bullet}$; 289 $[MeGeSP(An)S]^+$; 170 $[AnPS]^{+\bullet}$; 136 $[MeGeS]^{+\bullet}$; 121 $[MeGeS]^+$. *Anal.* calcd. pour $C_{11}H_{19}OS_3PGe_2$: C 30,05; H 4,32; S 21,85; tr.: C 30,10; H 4,35; S 21,78%.

Thermolyse de l'anisyl-5 tétraméthyl-2,2,3,3 thio-5 dithiaphosphadigermolanne-1,4,5,2,3

Un échantillon de $Me_2GeGe(Me_2)SP(An)S$ est maintenu en tube scellé à 200°C pendant 14 h. Les analyses de cpv, rmn et spectrométrie de masse dénotent la formation de $(Me_2GeS)_3$ (27%) et $(AnPS)_n$ ($n \geq 3$, *m/e* 510 $[AnPS]_3^{+\bullet}$) (15) à côté de 43% de dérivé de départ.

Pyrolyse de l'anisyl-5 tétraméthyl-2,2,3,3 thio-5 dithiaphosphadigermolanne-1,4,5,2,3

Une solution de 0,20 g de **2** dans 5 cm^3 de C_6H_6 anhydre est introduite goutte à goutte dans un pyrolyseur muni à sa sortie d'un piège refroidi à la neige carbonique et maintenu à 270°C sous courant faible d'argon (durée d'introduction 15 min). Après rétablissement de la température ordinaire le pyrolyseur est rincé avec quelques cm^3 de C_6H_6. Une analyse cpv du mélange permet de caractériser la formation de $(Me_2GeS)_3$ (76%) et l'absence totale de dérivé de départ.

Caractérisation de la diméthylgermathione

Le mélange de 0,39 g de diméthyldithiométhylgermanium (0,002 mol) et 1 g d'anisyl-5 tétraméthyl-2,2,3,3 thio-5 dithiaphosphadigermolanne-1,4,5,2,3 (0,0022 mol) est maintenu en tube scellé à 270°C pendant 4 h. Les analyses de cpv et de rmn ((C_6H_6) δ_{Me_2Ge}: 0,71 ppm (s); δ_{SMe}: 1,96 ppm (s)) permettent de mettre en évidence la formation de $[Me_2Ge(SMe)]_2S$ (20%) par comparaison avec un échantillon authentique synthétisé par ailleurs.

Synthèse du sulfure de bis(diméthylméthylthiogermanium)

Une quantité (0,69 g, 0,0017 mol) de $(Me_2GeS)_3$ est chauffé 14 h à 150°C en tube scellé en présence de 1 g de $Me_2Ge(SMe)_2$ (0,0051 mol). Les analyses de cpv, rmn et spectrométrie de masse permettent alors d'identifier $[Me_2Ge(SMe)]_2S$ (Rdt 26%) à côté de $(Me_2GeS)_3$ et $Me_2Ge(SMe)_2$ n'ayant pas réagi. $[Me_2Ge(SMe)]_2S$: rmn (C_6H_6) δ_{Me_2Ge}: 0,71 ppm (s); δ_{SMe}: 1,96 ppm (s). Spectre de masse, *m/e* 332 $[[Me_2Ge(SMe)_2]S]^{+\bullet}$.

Action du thiiranne sur l'anisyl-5, tétraméthyl-2,2,3,3 thio-5 dithiaphosphadigermolanne-1,4,5,2,3

Une quantité de thiiranne (0,28 g, 0,0046 mol) est ajouté goutte à goutte à 1 g d'anisyl-5 tétraméthyl-2,2,3,3 thio-5 dithiaphosphadigermolanne-1,4,5,2,3 (0,0022 mol) en solution dans 5 cm^3 de C_6H_6. Les analyses de cpv (comparaison avec un échantillon pur) et de rmn permettent de mettre en évidence la formation d'hexaméthyl-2,2,3,3,5,5 trigerma-2,3,5 dithiolanne-1,4 déjà décrit (10) (rmn (C_6D_6) $\delta_{Me_2GeGeMe_2}$: 0,56 ppm; δ_{SGeMe_2S}: 0,76 ppm) et de sulfure d'anisyl-2 dithiaphospholanne-1,3,2 (**6**) (synthétisé par ailleurs) (% relatifs 72 (28%)).

Anisyl-2 thio-2 dithiaphospholanne-1,3,2, $AnPSCH_2CH_2S$ (6)

À 5 g de dianisyl-2,4 dithio-2,4 dithiadiphospholanne-1,3,2,4 (0,0123 mol) en suspension dans 20 cm^3 de benzène anhydre, on ajoute 20 g de thiiranne (0,3333 mol). Le mélange est maintenu sous agitation pendant 4 h, puis concentré et distillé. On obtient ainsi 2 g d'anisyl-2 thio-2 dithiaphospholanne-1,3,2 (Rdt 31%); Eb = 112°C/0,1 Torr; rmn (C_6D_6) ^1H δ_{OMe}: 3,20 ppm (s); $\delta_{C_6H_4}$: 6,70 ppm (dd, J_{PH} = 3,5 Hz) et 8,18 ppm (dd, J_{PH} = 9,5 Hz); δ_{CH_2S}: 2,90 ppm (m); ^{31}P δ_P: 92 ppm. *Anal.* calc. pour $C_9H_{11}OS_2P$: C 41,22; H 4,19; S 36,64; tr.: C 41,35; H 4,21; S 36,72%.

Anisyl-5 tétraméthyl-2,2,3,3 thio-5 dithiaphosphadigermolanne-1,4,-5,2,3 et divers chlorures métallés

Le mélange de quantités stoechiométriques de dithiaphosphadigermolanne-1,4,5,2,3 et de chlorure métallé Σ_2MCl_2 est soit maintenu à 20°C, soit porté à 160°C pendant 4 h en tube scellé (cf. tableau de la réaction [9]).

Les analyses cpv et rmn révèlent alors la disparition quasi complète du dithiaphosphadigermolanne et la formation de dichloro-1,2 tétraméthyldigermane (10) et de $(AnPS_2)_n$ à côté des sulfures métallés correspondants $(\Sigma_2MS)_n$ ($(Me_2GeS)_3$ déjà décrit (18); $(Me_2SiS)_{2,3}$ déjà décrit (19), $(Me_2SiS)_2/Me_2SiS)_3 \simeq 1:2$; $(Cl_2GeS)_n$ caractérisé par analyse %tr. (calc.): Cl 40,12 (40,39); S 18,35 (18,23)).

Caractérisation de la diméthylsilathione

L'addition goutte à goute de 0,14 g de diméthyldichlorosilane (0,0011 mol) à un mélange anisyl-5 tétraméthyl-2,2,3,3 thio-5 dithiaphosphadigermolanne-1,4,5,2,3 (0,5 g = 0,0011 mol) et oxyde trimère $(Me_2SiO)_3$ (0,72 g = 0,0033 mol) donne un mélange réactionnel maintenu 1 h 30 à 150°C en tube scellé. Une analyse cpv du mélange permet de constater la formation de

$Me_2SiO(Me_2SiO)_2—SiMe_2S$ (25%)

déjà décrit (20).

1. M. Massol, D. Mesnard, J. Barrau et J. Satgé. C. R. Acad. Sci. Ser. C, **272**, 2081 (1971).
2. J. Barrau, M. Massol, D. Mesnard et J. Satgé. J. Organomet. Chem. **30**, C67 (1971).
3. J. Barrau, M. Bouchaut, H. Lavayssière, G. Dousse et J. Satgé. Helv. Chim. Acta, **62**, 152 (1979).
4. H. Lavayssière, G. Dousse, J. Barrau, J. Satgé et M. Bouchaut. J. Organomet. Chem. **161**, C59 (1978); H. Lavayssière. Thèse, Université Paul Sabatier, Toulouse, France. 1982.
5. J. Barrau, M. Bouchaut, H. Lavayssière, G. Dousse et J. Satgé. Synth. React. Inorg. Met.-Org. Chem., **10**, 515 (1980).
6. J. Barrau, H. Lavayssière, G. Dousse, C. Couret et J. Satgé. J. Organomet. Chem. **221**, 271 (1981).
7. J. Barrau, G. Rima et J. Satgé. J. Organomet. Chem. **252**, C73 (1983).
8. J. Barrau, G. Rima et J Satgé. Synth. React. Inorg. Met.-Org. Chem. **14**, 21 (1984).
9. J. Barrau, G. Rima, M. El Amine et J. Satgé. J. Chem. Research (S), 31 (1985).
10. J. Barrau, M. El Amine, G. Rima et J. Satgé. J. Organomet. Chem. **277**, 323 (1984).

11. J. BARRAU, N. BEN HAMIDA et J. SATGÉ. J. Organomet. Chem. **282**, 315 (1985).
12. J. SATGÉ. Adv. Organomet. Chem. **21**, 241 (1982).
13. E. FLUCK et H. BINDER. Z. Anorg. Allg. Chem. **377**, 298 (1977).
14. L. MAIER. Top. Phosphorus Chem. **10**, 129 (1978), et références citées.
15. G. A. ZANK et T. R. RANCHFUSS. Organometallics, **31**, 191 (1984).
16. L. E. GUSEL'NIKOV *et al.* J. Organomet. Chem. **214**, 145 (1981).
17. C. GUIMON, G. PFISTER-GUILLOUZO, H. LAVAYSSIÈRE, G. DOUSSE, J. BARRAU et J. SATGÉ. J. Organomet. Chem. **249**, C17 (1983).
18. E. G. ROCHOW. J. Am. Chem. Soc. **70**, 1801 (1948); H. SCHMIDBAUR et I. RUIDISCH. Inorg. Chem. **3**, 599 (1964).
19. Y. ETIENNE. C. R. Acad. Sci. Paris, **235**, 966 (1952); T. NOMURA, M. YOKOI et K. YAMASAKI. Proc. Jpn. Acad. **29**, 342 (1954).
20. H. S. D. SOYSA, I. N. JUNG et W. P. WEBER. J. Organomet. Chem. **171**, 177 (1979); H. S. D. SOYSA et W. P. WEBER. J. Organomet. Chem. **165**, C1 (1979).

Le lithio-2 naphtalène carbonitrile-1 et ses produits de substitutions

R. R. FRASER ET S. SAVARD[1]
Ottawa–Carleton Chemistry Institute, Université d'Ottawa, Ottawa, Ont., Canada K1N 9B4
Reçu le 23 juillet 1985

R. R. FRASER et S. SAVARD. Can. J. Chem. **64**, 621 (1986).

La lithiation du naphtalène carbonitrile-1 conduit à la formation du dérivé lithio-2 exclusivement. La réaction de cet intermédiaire avec dix différents électrophiles permet d'obtenir les dérivés substitués en position 2 avec des rendements de modérés à bons. Les alkyl-2 naphtalène carbonitriles-1 sont facilement lithiés et subséquemment alkylés pour donner un substituant alkyle modifié sur la position α. Les valeurs des pK_a pour les hydrogènes de la position 2 du naphtalène carbonitrile-1 et du méthyl-2 naphtalène carbonitrile-1 ont été déterminées et sont respectivement de 36,3 et 28,5.

R. R. FRASER and S. SAVARD. Can. J. Chem. **64**, 621 (1986).

Lithiation of 1-naphthonitrile provides the 2-lithio derivative exclusively. Reaction of this intermediate with ten different electrophiles produces 2-substituted derivatives in moderate to good yields. 2-Alkyl-1-naphthonitriles are readily lithiated and further alkylated to provide alkyl substituents modified at the α position. The pK_a values for the hydrogen at the 2-position of 1-cyanonaphthalene and 2-methyl-1-cyanonaphthalene have been determined to be 36.3 and 28.5, respectively.

L'*ortho*-lithiation directe de composés aromatiques est une méthode efficace pour la préparation d'intermédiaires aryllithiums utilisables ensuite dans les différentes synthèses. Plusieurs substituants sont bien connus pour diriger et stabiliser l'*ortho*-métalation, par exemple le $CH(OR)_2$, OCH_2OCH_3, $N(R)_2$ et $CH_2N(CH_3)_2$ (1). De même, certains électrophiles se sont avérés très efficaces comme agent activateur d'une telle lithiation dont le $CON\bar{R}$, le $CS\bar{N}R$, le $CONR_2$, l'oxazoline et le $OCONR_2$ (1). Dans ce dernier cas, trois méthodes ont été utilisées pour éviter la condensation du carbanion avec le produit de départ afin de permettre une concentration acceptable d'aryllithium avant l'addition d'un électrophile externe (2): (*i*) l'utilisation d'une basse température de réaction (−78°C ou moins); (*ii*) l'utilisation d'un électrophile stériquement (oxazoline (3)) ou électroniquement (carbamate, amide (1*c*)) déactivé qui réagit suffisamment lentement avec la base nucléophile (alkyllithium) ou avec l'anion formé, pour permettre l'attaque subséquente d'un agent électrophilique; (*iii*) l'addition *in situ* de l'électrophile pour piéger l'intermédiaire aryllithium immédiatement après sa formation par une base très stériquement encombrée, le tétraméthylpipéridine amidure de lithium (LTMP) (2, 4). Cette dernière méthode appliquée par Krizan et Martin permet d'obtenir des dérivés benzonitrile-2 et (dicyano-1,3 benzene)-2 dans d'excellents rendements, comme dans le cas des résultats obtenus précédemment avec un échange halogène–métal (5), contrairement à ceux obtenus par une lithiation directe (1*b*, 6).

Le groupement nitrile a été aussi utilisé comme agent activateur dans la métalation directe d'autres composés aromatiques, dont le thiophène (7, 8) et le sélénophène (8).

Nous voulons présenter ici la formation du lithio-2 naphtalène carbonitrile-1, **1** provenant d'une *ortho*-lithiation directe (LTMP, THF, −78°C). L'anion formé dans ces conditions est suffisamment stable pour réagir par la suite avec une grande variété d'électrophiles sans que de condensation nitrile–anion ne soit décelée. Cette réaction permet d'obtenir un naphtalène substitué-1,2 possédant le groupement nitrile-1 transformable par la suite de diverses façons.

La tableau 1 présente les divers électrophiles utilisés: les halogénures d'alkyles, les disulfures, l'iode ainsi que le chlorure de triméthylsilyle conduisent à de bons résultats. La constatation générale est, toutefis, que l'utilisation d'un équivalent de base ne permet pas un rendement supérieur à 85%.

L'utilisation de composés carbonylés comme agent électrophilique conduit à l'obtention de deux types de produits suivant la nature du produit de départ. Ces composés se forment probablement lors de l'isolement lorsque le mélange réactionnel est traité avec l'acide chlorhydrique dilué. Le benzaldéhyde avec le lithio-2 naphtalène carbonitrile-1, **2** donne la lactone cyclique **12**, identique à celle obtenue par Watanabe et Snieckus lors de la réaction du lithio-2 naphtalène carboxamide-1 *N*,*N*-diéthyle avec le benzaldéhyde (9). Lorsque la cycloheptanone est utilisée, la formation d'une lactame **11** (ir ($CHCl_3$): 1668 cm^{-1}; sm: 265 (M^+)) est constatée.

Le diéthylchlorocarbamate, le chlorure d'acétyle, le bromure de benzyle et la benzophénone ne permettent pas l'obention de résultats utilisables dans les conditions telles que décrites. Avec cette dernière, toutefois, la présence d'un composé de masse 335 correspondant au produit de substitution (alcool tertiaire, lactame ou imine) peut être détectée par gc–ms parmi les produits multiples de la réaction.

Le tableau 2 présente les pourcentages de deutération obtenus lors de la réaction du naphtalène carbonitrile-1, **1** avec le diisopropyl amidure de lithium (LDA) et le LTMP, suivi d'un piégeage avec D_2O. Avec le LTMP, 83% de deutération sur la position 2 est constaté alors qu'avec la LDA on n'en retrouve que 23%. Aucune deutération sur un autre site n'est observée. Ces résultats indiquent une acidité intermédiaire entre les deux bases qui correspond à un pK_a approximatif de 36,3 ± 0,6 (10). Cette mesure n'étaient valable que si la quantité de produit deutéré correspond à la valeur à l'équilibre de l'espèce lithiée en présence de base.[2] La métalation complète du nitrile aromatique est donc impossible avec le LTMP (pK_a = 37,3) (10*b*, *c*) si un équivalent de base est utilisé, expliquant le fait que le rendement maximum obtenu dans le tableau 1 soit de 85%. Le LDA n'est pas assez basique pour déprotonner de façon efficace le naphtalène carbonitrile-1, **1**. Il est intéressant de constater que le

[1]Présente adresse: CRIQ (Centre de Recherche Industrielle du Québec), 333, rue Franquet, C.P. 9038, Sainte-Foy (Qué.), Canada G1V 4C7.

[2]Une expérience démontrant que la quantité de produit lithié, mesurée par deutération après 15 et 45 min de réaction, est identique, permet de supposer une réaction à l'équilibre.

TABLEAU 1. Substitutions du naphtalène carbonitrile-1 par lithiation directe avec LTMP

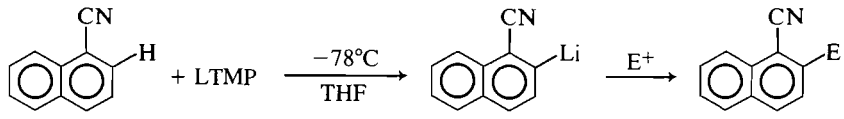

1 **2** **3–10**

Electrophile	Produit	Point de fusion (°C)[a]	Rendement[b]
$ClSi(CH_3)_3$	**3**, E = $Si(CH_3)_3$	70–71	85
CH_3I	**4**, E = CH_3	85–86 (Litt. (19) 87–88)	80[d]
CH_3CH_2I	**5**, E = CH_2CH_3	66–67 (Litt. (20) 66,5–67,5)	54[d,f]
$CH_3CH_2CH_2I$	**6**, E = $CH_2CH_2CH_3$	[c]	63[g,i]
CH_3SSCH_3	**7**, E = SCH_3	93,5–94,5	70[e]
PhSSPh	**8**, E = SPh	100–101	80[d]
I_2	**9**, E = I	97–99	72[d]
CH_2=$CHCH_2Br$	**10**, E = 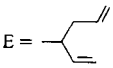	[c]	43[h,i]
Cycloheptanone	**11**, 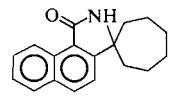	106,5–107,5	56[d,j]
Benzaldéhyde	**12**, 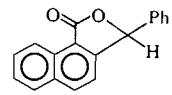	169–170 (Litt. (21*a*) 171–173) (Litt. (21*b*) 164–166)	20[e]

[a]Le composé isolé indique habituellement une pureté 98% par gc–ms.
[b]Matériel isolé après purification (recristallisation ou chromatographie). On utilise 10 équivalent de LTMP et 1.1 équivalent d'électrophile.
[c]Liquide incolore.
[d]Recristallisation dans l'hexane.
[e]Recristallisation dans l'éther.
[f]2 équivalents d'électrophile utilisés.
[g]4 équivalents d'électrophile utilisés.
[h]Rendement maximum avec l'équivalent de base et d'électrophile, 50%.
[i]Isolé par chromatographie.
[j]Une autre structure, l'iminolactone correspondante proposée par un examinateur, est aussi possible. L'évidence de l'infrarouge et de la rmn de ^{15}N n'est pas claire à cause du manque de modèles appropriés.

pK_a du produit **1** est environ de 2 unités (100 fois) plus acide que celui du benzonitrile (6).

Lors de l'addition des halogénures d'alkyles sur le lithionitrile **2**, un produit secondaire (de 3 à 8%) est détecté. Une analyse par gc–ms indique que pour l'iodure de méthyle, ce produit correspond au dérivé éthyl-2 naphtalène carbonitrile-1, **5**.[3] La séquence de formation de ce composé est présenté dans le schéma 1. Ainsi, après l'addition du groupement alkyle en position 2 (A, B) une faible quantité du produit formé réagit avec le lithio-2 nitrile **2** provenant de la métalation de **1** (C) pour donner le composé lithié en position benzylique qui réagit ensuite (D) avec l'halogénure d'alkyle. Un phénomène semblable a déjà été observé par Krizan et Martin (2) lors de l'addition *in situ* d'iodure de méthyle au lithio-2 dicyano-1,3 benzène, l'utilisation d'un équivalent de l'halogénure conduit à la formation presqu'exclusive du dérivé éthyl-2. Dans notre expérience, la quantité faible présente de ce dérivé **5** indique que l'attaque de l'électrophile (B) semble plus rapide que l'échange entre l'aryllithium et le dérivé alkyl-2 (C). Des résultats identiques sont obtenus avec l'utilisation de l'iodure d'éthyle (gc–ms, 5% d'un composé, 209 (M^+)) et de l'iodure de *n*-propyle (gc–ms, 3% d'un composé, 237 (M^+)). Avec l'utilisation du bromure d'allyle le seul produit d'alkylation isolé correspond au produit de diaddition **10**. Dans ce cas, l'acidité des protons allyliques est accrue par la présence du lien double.

Ces résultats suggèrent une acidité plus importante pour les protons benzyliques que pour le proton aromatique de la position 2. Dans l'article de revue de Ronald et Winkle (11), la réaction d'un alkyllithium sur différents toluènes *ortho*-substitués dont, par exemple, le 2-CH_2NMe_2, le 2-COOH (12) et le 2-CONHMe, conduit à une métalation exclusive de la position benzylique.

Le pK_a de cette position a donc été vérifié et le tableau 2 présente les pourcentages de deutération obtenus lors de la lithiation de **4**. Le produit est presque entièrement déprotonné par le *n*-propyltriméthylsilyl amidure de lithium (94% D, après addition de D_2O) alors qu'aucune réaction n'a lieu avec le bis-triméthylsilyl amidure de lithium (LHMDS) (13), indiquant

[3]Des fragmentation par spectroscopie de masse et rmn ^1H sont identiques au produit **5**.

TABLEAU 2. Lithiation et deutération du naphtalène carbonitrile-1 et de son dérivé méthyl-2

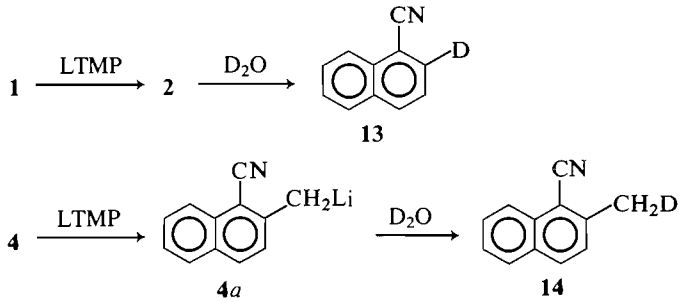

Lithio-nitrile	Base	% D^a	pK_a ^{b}
2	DIPA	23[d]	36,7 ± 0,6[e]
2	LTMP	83[c]	35,9 ± 0,6[e]
4*a*	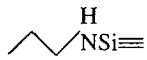	94[d]	28,5 ± 0,6
4*a*	HMDS	~0	>28,3

[a]Mesuré à partir des valeurs obtenues par rmn ^{1}H et sm.

[b]pK_a approximatif en tenant compte d'un équilibre atteinte entre la base et le nitrile et basé sur les valeurs suivantes d'acidité pour les bases, DIPA: 35,7; LTMP: 37,3; HMDS: 25,8; 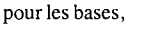 : 30,9 (10*c*).

[c]Valeur moyenne de 2 expériences avec des temps de lithiation de 15 et 45 min.

[d]Valeur moyenne de 2 expériences avec des temps de lithiation de 25 et 240 min.

[e]La valeur de 36,3 ± 0,6 dans le texte provient de la moyenne de ces deux valeurs.

un pK_a approximatif de 28,5 ± 0,6, les protons benzyliques étant environ 10^8 fois plus acides que celui de la position 2.

Cette grande acidité des protons benzyliques permet le prolongement ou la modification de la chaîne latérale de façon efficace (tableau 3). Ainsi la métalation, suivi de l'addition d'iodure de méthyle, sur le dérivé éthyl-2, **5** conduit à la formation du dérivé isopropyl-2, **15**.

L'influence du substituant nitrile-1 sur l'acidité du groupement méthyl-8 a été aussi étudiée. La lithiation du méthyl-8 naphtalène carbonitrile-1, suivie de l'addition de chlorure de triméthylsilyle conduit uniquement au dérivé triméthylsilyl-2, **17** (tableau 3). Si ce dérivé est traité à nouveau dans les mêmes conditions, aucun dérivé silylé sur les protons benzyliques de la position 8 n'est observé. L'utilisation d'une base plus forte (10*c*), le (cyclohexyl-1 néopentyl) *tertio*-butyl amidure de lithium conduit au même résultat. Ainsi l'acidité du méthyl-8 (pK_a 42) est beaucoup plus faible que celle retrouvée avec le méthyl-2.

Certains substituants en position 1 sur le naphtalène pouvant activer l'hydrogène de la position 8 (1*a*, 1*b*) (OCH_3 (14), NHR (15), $CH_2N(CH_3)_2$ (16), $SO_2NHC_4H_9$-*t* (17)), l'effet du nitrile a été analysé. En bloquant préalablement la position 2, la plus acide, par un groupement triméthylsilyle **3**, une tentative de lithiation avec le LTMP et ensuite le (cyclohexyl-1 néopentyl) *tertio*-butyl amidure de lithium, suivie d'une addition de chlorure de triméthylsilyle, n'a donné aucun résultat observable. Avec le *n*-butyllithium et le tétraméthylènediamine (TMEDA) dans le THF, suivi de l'addition de l'iodure de méthyle, le seul produit isolé correspond au produit d'addition de l'alkyllithium sur le nitrile et à la *N*-méthylation de l'imine formé.

Dans le cas du naphtalène carbonitrile-1, **1**, le groupement nitrile n'induit une forte influence qu'en position 2, l'acidité de la position 8 semblant très peu affectée par la présence de ce substituant.

La métalation directe du naphthalène carbonitrile-1, **1**, est une méthode efficace pour obtenir un dérivé substitué en position 2. L'aryllithium formé à partir d'une base non-nucléophile comme le LTMP est suffisamment stable à basse température (−78°C) pour effectuer ensuite l'addition d'un électrophile. De plus, les protons benzyliques obtenus lors de l'alkylation de la position 2 étant beaucoup plus acides que ceux sur le cycle aromatique, il est d'autant plus facile de modifier la chaîne latérale introduite antérieurement. Un autre avantage observé est que le groupement nitrile, activant très peu le proton

TABLEAU 3. Métalation et réacton des dérivés alkyl-2 et -8 du naphtalène carbonitrile-1

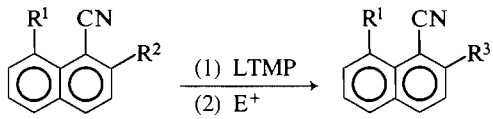

R^1	R^2	Électrophile	Produit (R^1, R^3)	Rendement[b] (%)	Point de fusion (°C)[a]
H	CH_3	CH_3I	**5**, R^1 = H, R^3 = CH_2CH_3	85[e]	66–67[d]
H	CH_2CH_3	CH_3I	**15**, R^1 = H, R^3 = $CH(CH_3)_2$	85[f]	[c]
H	CH_2CH_3	$ClSi(CH_3)_3$	**16**, R^1 = H, R^3 = $CH(Si(CH_3)_3)CH_3$	90[f]	[c]
CH_3	H	$ClSi(CH_3)_3$	**17**, R^1 = CH_3, R^3 = $Si(CH_3)_3$	88[e]	43–44

[a]Le composé isolé indique habituellement une pureté >98% par gc–ms.

[b]Matériel isolé après purification.

[c]Liquide incolore.

[d]Composé identique à celui obtenu précédemment (Tableau 1).

[e]Recristallisation dans l'hexane.

[f]Isolé par chromatographie.

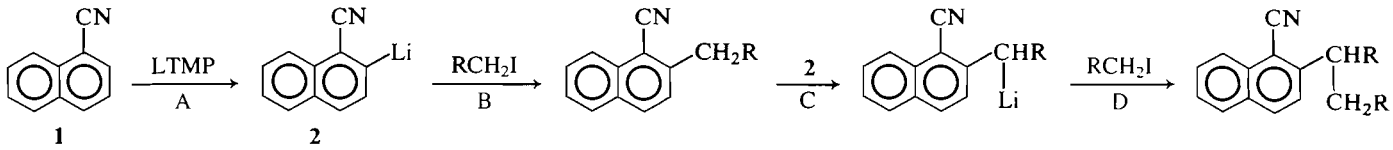

SCHÉMA 1

de la position 8, ou les protons benzyliques attachés à cette position, leur acidité demeure donc trop faible pour obtenir une déprotonation par les amines lithiés.

Partie expérimentale

Tous les nouveau composés ont été charactérisés par gc–ms ainsi que par rmn du ^1H (300 MHz) et du ^{13}C (20 MHz).

Les spectres du carbone 13 étaient enregistrés sur un spectromètre rmn Varian FT-80, opérant a une fréquence de 20 MHz. Les déplacements chimiques étaient obtenu dans des solutions de $CDCl_3$ utilisant comme référence interne la bande à 77,00 ppm du $CDCl_3$. L'attribution des résonances était faite à partir d'expériences de découplage hors-résonance et des effets de substituants connus (18). Les spectres des protons étaient enregistrés sur un spectromètre rmn Varian XL-300, opérant à une fréquence de 300 MHz. Les échantillons étaient en solution dans le $CDCl_3$ et la référence interne était la résonance à 7,24 ppm du chloroform. Les déplacements chimiques sont donnés en ppm, avec entre parenthèse la multiplicité et la constante de couplage en Hz (s = singulet, d = doublet, t = triplet, q = quadruplet, m = multiplet). Les spectres infrarouges étaient enregistrés sur un spectromètre ir Perkin Elmer 783 la valeur des absorptions est donnée en cm^{-1} et les échantillons étaient préparés en solution dans le chloroforme. Les spectres de masse étaient enregistrés sur un spectromètre VG 7070-E.

*Préparation du méthyl-2 naphtalènecarbonitrile-1, **4** (Procédure habituelle de lithiation et de substitution du naphtalène carbonitrile-1 et de ses dérivés alkyl-2)*

Une solution de 1,02 mL (0,006 mol) de TMP dans 25 mL de THF (anhydre) est refroidie à 0°C et agitée pendant 30 min sous atmosphère inerte (argon) après l'addition de 4,85 mL (0,006 mol) d'une solution de méthyl lithium dans l'éther diéthylique (1,25 *M*). On refroidit à −78°C et une solution du nitrile **1** (0,926 g, 0,006 mol dans 3 mL de THF) est additionnée lentement. La solution brune est agitée pendant 35 min avant l'ajout de l'iodure de méthyle (0,42 mL, 0,0066 mol). Après 2 h à −78°C, le mélange réactionnel est réchauffé à la température de la pièce et agité pendant 1 h. Pour isoler, 20 mL d'eau glacée sont ajoutés, la phase organique est lavée avec HCl 10% (2 × 50 mL), avec une solution de NaCl (saturé) (4 × 50 mL) et séchée sur $MgSO_4$ avant d'évaporer le solvant. Le solide obtenu est purifié par chromatographie sur gel de silice (hexane) et recristallisé dans l'hexane; 809 g (80%) d'un solide blanc (pf: 84–85°C) est ainsi recueilli, le méthyl-2 naphtalène carbonitrile-1, **4**.

Proprietés spectroscopiques

*Naphtalène carbonitrile-1, **1***: rmn ^1H: H2 = 7,92 (dd, 7,1, 1,2), H3 = 7,53 (dd, 7,1, 8,7), H4 = 8,09 (dd, 8,7, 1,2), H5 = 7,96 (d, 8,1), H6 = 7,62 (dd, 8,1, 7,0), H7 = 7,73 (dd, 8,5, 7,0), H8 = 8,25 (d, 8,5); rmn ^{13}C: C1 = 109,9, C2 = 132,1, C3 = 124,8, C4 = 132,4, C4a = 132,1, C5 = 128,6, C6 = 127,4, C7 = 128,4, C8 = 124,8, C8a = 132,7, CN = 117,6; sm: 153 (M^+, 100,0), 126 ($M^+ - 27$, 14,5).

*Triméthylsilyl-2 naphtalène carbonitrile-1, **3***: ir: 3018, 2960, 2222 (CN), 1588, 1255, 880, 855, 847; rmn ^1H: H3 = 7,66 (dd, 8,5), H4 = 8,01 (d, 8,5), H5 = 7,90 (d, 8,2), H6 = 7,61 (dd, 8,2, 7,0), H7 = 7,70 (dd, 8,2, 7,0), H8 = 8,33 (d, 8,2), Si≡ = 0,52 (s); rmn ^{13}C: C1 = 117,5, C2 = 147,0, C3 = 131,4, C4 = 133,1, C4a = 134,8, C5 = 130,1, C6 = 129,3, C7 = 130,1, C8 = 126,4, C8a = 134,9, Si≡ = −0,4, CN = 119,7; sm: 225 (M^+, 36,5), 211 ($M^+ - 14$, 35,6), 210 ($M^+ - 15$, 100,0), 183 ($M^+ - 42$, 20,0).

*Méthyl-2 naphtalène carbonitrile-1, **4***: ir: 3020, 2970, 2220 (CN), 1520, 1425, 1140, 1110, 930; rmn ^1H: H3 = 7,41 (d, 8,0), H4 = 7,96 (d, 8,0), H5 = 7,88 (d, 8,0), H6 = 7,56 (dd, 8,0, 7,0), H7 = 7,67 (dd, 7,0, 8,0), H8 = 8,21 (d, 8,0), CH_3 = 2,74 (s); rmn ^{13}C: C1 = 109,2, C2 = 142,9, C3 = 126,6, C4 = 132,6, C4a = 132,8, C5 = 128,4, C6 = 127,7, C7 = 128,5, C8 = 124,9, C8a = 131,2, CN = 117,1, CH_3 = 21,3; sm: 167 (M^+, 100,0), 166 ($M^+ - 1$, 38,9), 140 ($M^+ - 27$, 18,7), 139 ($M^+ - 28$, 16,1).

*Ethyl-2 naphtalène carbonitrile-1, **5***: ir: 3010, 2970, 2220 (CN), 1509, 825; rmn ^1H: H3 = 7,47, (d, 8,5), H4 = 8,02 (d, 8,5), H5 = 7,91 (d, 8,3), H6 = 7,58 (dd, 8,3, 7,0), H7 = 7,69 ((dd, 8,2, 7,0), H8 = 8,25 (d, 8,2), CH_2 = 3,09 (q, 7,0), CH_3 = 1,38 (t, 7,0); rmn ^{13}C: C1 = 108,4, C2 = 149,0, C3 = 126,3, C4 = 132,9, C4a = 133,2, C5 = 128,3, C6 = 126,6, C7 = 128,4, C8 = 124,9, C8a = 131,3, CN = 116,8, CH_2 = 28,6, CH_3 = 15,3; sm: 181 (M^+, 65,7), 180 ($M^+ - 1$, 7,5), 166 ($M^+ - 15$, 100,0), 140 ($M^+ - 41$, 12,8).

n-*Propyl-2 naphtalène carbonitrile-1, **6***: ir: 3015, 2960, 2220 (CN), 1508, 821; rmn ^1H: H3 = 7,40 (d, 8,5), H4 = 7,97 (d, 8,5), H5 = 7,86 (d, 8,5), H6 = 7,54 (dd, 8,5, 7,0), H7 = 7,66 (dd, 7,0, 8,3), H8 = 8,21 (d, 8,3), CH_2 = 3,01 (t, 7,0), CH_2 = 1,77 (sext, 7,0), CH_3 = 0,98 (t, 7,0); rmn ^{13}C: C1 = 108,9, C2 = 147,5, C3 = 126,6, C4 = 132,6, C4a = 132,8, C5 = 128,3, C6 = 126,9, C7 = 128,4, C8 = 125,0, C8a = 131,3, CN = 117,0, CH_2 = 37,2, CH = 24,3, CH_3 = 13,7; sm: 195 (M^+, 55,5), 194 ($M^+ - 1$, 9,4), 166 ($M^+ - 29$, 100,0), 140 ($M^+ - 55$, 16,0).

*Thiométhoxy-2 naphtalène carbonitrile-1, **7***: ir: 3010, 2927, 2218 (CN), 1585, 1502, 1434, 811; rmn ^1H: H3 = 7,41 (d, 8,8), H4 = 7,94 (d, 8,8), H5 = 7,81 (d, 8,5), H6 = 7,49 (dd, 8,5, 7,0), H7 = 7,62 (dd, 7,0, 8,2), H8 = 8,11 (d, 8,2), CH_3 = 2,62 (s); rmn ^{13}C: C1 = 107,2, C2 = 144,4, C3 = 124,1, C4 = 132,8, C4a = 133,1, C5 = 129,1, C6 = 126,5, C7 = 128,4, C8 = 123,0, C8a = 130,3, CN = 115,9, CH_3 = 15,9; sm: 199 (M^+, 100,0), 198 ($M^+ - 1$, 11,6), 167 ($M^+ - 32$, 12,6), 166 ($M^+ - 33$, 55,3), 140 ($M^+ - 59$, 56,6).

*Thiophénoxy-2 naphtalène carbonitrile-1, **8***: ir: 3020, 2220 (CN), 1583, 1501, 1134, 819; rmn ^1H: H3 = 7,14 (d, 9,0), H4 = 7,82 (d, 9,0), H5 = 7,81 (d, 8,0), H6 = 7,54 (dd, 7,0, 8,0), H7 = 7,67 (dd, 7,0, 8,5), H8 = 8,19 (d, 8,5), CH(*ortho*) = 7,52 (m), CH (*méta*, *para*) = 7,42 (m); rmn ^{13}C: C1 = 108,5, C2 = 143,2, C3 = 129,0, C4 = 132,8, C4a = 133,1, C5 = 128,4, C6 = 127,0, C7 = 128,9, C8 = 124,6, C8a = 131,6, CN = 115,8, C1′ = 130,8, C2′ = 133,6, C3′ = 129,7, C4′ = 125,9; sm: 261 (M^+, 100,0), 260 ($M^+ - 1$, 37,8), 259 ($M^+ - 2$, 13,0), 234 ($M^+ - 27$, 13,7).

*Iodo-2 naphtalène carbonitrile-1, **9***: ir: 3020, 2230 (CN), 1500, 1117, 818, 670; rmn ^1H: H3 = 7,83 (d, 9,0), H4 = 7,67 (d, 9,0), H5 = 7,80 (d, 8,5), H6 = 7,54 (dd, 7,0, 8,5), H7 = 7,61 (dd, 7,8, 8,5), H8 = 8,14 (d, 8,5); rmn ^{13}C: C1 = 110,2, C2 = 100,1, C3 = 133,4, C4 = 135,0, C4a = 131,6, C5 = 129,3, C6 = 127,8, C7 = 128,6, C8 = 125,2, C8a = 134,3, CN = 118,2; sm: 279 (M^+, 100,0), 152 ($M^+ - 127$, 49,0), 125 ($M^+ - 154$, 10,8).

*(Hexadiène-1,5 yl-3)-2-naphtalène carbonitrile-1, **10***: ir: 3082, 3065, 3015, 2220 (CN), 1640, 1625, 1596, 1508, 992, 922, 825; rmn ^1H: H3 = 7,43 (d, 8,0), H4 = 8,00 (d, 8,0), H5 = 7,86 (d, 8,5), H6 = 7,56 (dd, 7,0, 8,5), H7 = 7,66 (dd, 7,0, 8,0), H8 = 8,21 (d, 8,0), CH = 2,58 (m), CH = 2,66 (m), CH = 4,15 (m), CH_2 = 4,98 (m), CH_2 = 5,16 (m), CH = 5,71 (m), CH = 6,02 (m); sm: 233 (M^+, 10,1), 193 ($M^+ - 40$, 16,7), 192 ($M^+ - 41$, 100,0), 191 ($M^+ - 42$, 13,7), 190 ($M^+ - 43$, 16,2), 166 ($M^+ - 67$, 15,5), 165 ($M^+ - 68$, 29,5).

*Spiro [3H Benz[e] isoindole-1]-3, 1′-[cycloheptane], **11***: ir: 3290, 3010, 2930, 2860, 1668 (CO), 1519, 1158, 1080, 997, 980, 820; rmn ^1H: H3 = 7,43 (d, 8,2), H4 = 8,06 (d, 8,2), H5 = 7,93 (d, 8,0), H6 = 7,60 (dd, 7,0, 8,0), H7 = 7,76 (dd, 7,0, 8,1), H8 = 9,31 (d, 8,1), 12H = 1,60–2,06 (m); rmn ^{13}C: C1 = 122,0, C2 = 154,4, C3 = 124,4, C4 = 133,3, C4a = 133,2, C5 = 128,2, C6 = 126,4, C7 = 128,2, C8 = 117,8, C8a = 129,0, C—N = 90,4, CH_2 = 40,0, CH_2 = 29,2, CH_2 = 23,0, CO = 167,4; sm: 265 (M^+, 56,1), 209 ($M^+ - 56$, 19,8), 208

($M^+ - 57$, 71,2), 195 ($M^+ - 70$, 59,8), 180 ($M^+ - 85$, 35,7), 153 ($M^+ - 112$, 100,0), 152 ($M^+ - 113$, 18,7), 143 ($M^+ - 122$, 18,2), 126 ($M^+ - 139$, 27.6).

*Phenyl-3, naphto[1,2c]furane(3*H*) one-1,* ***12***: ir: 3060, 3020, 1752 (CO), 1580, 1520, 1108, 1040, 960, 820; rmn ^{1}H: H3 = 7,33 (d, 8,2), H4 = 8,07 (d, 8,2), H5 = 7,94 (d, 8,0), H6 = 7,63 (dd, 7,0, 8,0), H7 = 7,74 (dd, 7,0, 8,0), H8 = 9,04 (d, 8,0), CH(*ortho*) = 7,29 (m), CH (*méta, para*) = 7,37 (m), CH = 6,45 (s); rmn ^{13}C: C1 = 119,7, C2 = 151,2, C3 = 123,7, C4 = 135,7, C4a = 133,4, C5 = 129,2, C6 = 127,4 = 129,3, C7 = 129,3, C8 = 119,3, C8a = 129,0, CH = 82,1, CO = 170,8, C1′ = 136,0, C2′ = 127,2, C3′ = 129,0, C4′ = 128,4; sm: 260 (M^+, 39,7), 156 ($M^+ - 104$, 16,5), 155 ($M^+ - 105$, 100,0), 127 ($M^+ - 133$, 33,1), 126 ($M^+ - 134$, 12,6).

Deutéro-2 naphtalène carbonitrile-1, ***13***: rmn ^{1}H: H3 = 7,53 (d, 8,5), H4 = 8,09 (d, 8,5), H5 = 7,96 (d, 8,1), H6 = 7,62 (dd, 8,1, 7,0), H7 = 7,73 (dd, 8,5, 7,0), H8 = 8,25 (d, 8,5); sm: 154 (M^+, 100,0), 127 ($M^+ - 27$, 14,6).

Deutéro méthyl-2 naphtalène carbonitrile-1, ***14***: rmn ^{1}H: H3 = 7,41 (dd, 8,0), H4 = 7,96 (d, 8,0), H5 = 7,88 (d, 8,0), H6 = 7,56 (dd, 7,0, 8,0), H7 = 7,67 (dd, 7,0, 8,0), H8 = 8,21 (d, 8,0), CH_2D = 2,72 (t, 2,2); sm: 168 (M^+, 100,0), 167 ($M^+ - 1$, 36,0), 141 ($M^+ - 27$, 14,0), 140 ($M^+ - 28$, 15,9); t = triplet intensité 1:1:1.

Isopropyl-2 naphtalène carbonitrile-1, ***15***: ir: 3065, 3015, 2970, 2935, 2875, 2200 (CN), 1598, 825; rmn ^{1}H: H3 = 7,47 (dd, 8,5), H4 = 7,98 (d, 8,5), H5 = 7,83 (d, 8,0), H6 = 7,51 (dd, 7,0, 8,0), H7 = 7,62 (dd, 7,0, 8,5), H8 = 8,18 (d, 8,5), CH = 3,62 (sept, 7,0), CH_3 = 1,36 (d, 7,0); rmn ^{13}C: C1 = 107,9, C2 = 153,0, C3 = 125,1, C4 = 133,1, C4a = 132,7, C5 = 128,3, C6 = 126,6, C7 = 128,4, C8 = 123,0, C8a = 131,4, CN = 116,8, CH = 33,2, CH_3 = 23,2; sm: 195 ($M^+ - 38$,5), 180 ($M^+ - 15$, 100,0), 153 ($M^+ - 42$, 17,7), 152 ($M^+ - 43$, 12,4).

Triméthylsilyl-1 éthyl)-2-naphtalène carbonitrile-1, ***16***: ir: 3015, 2960, 2215 (CN), 1620, 1592, 1250, 840; rmn ^{1}H: H3 = 7,32 (d, 8,8), H4 = 7,94 (d, 8,8), H5 = 7,83 (d, 8,0), H6 = 7,50 (dd, 7,0, 8,0), H7 = 7,63 (dd, 7,0, 8,5), H8 = 8,16 (d, 8,5), CH = 3,02 (q, 7,0), CH_3 = 1,50 (d, 7,0), Si≡ = −0,02 (s); rmn ^{13}C: C1 = 107,0, C2 = 151,7, C3 = 124,9, C4 = 132,4, C4a = 132,9, C5 = 128,2, C6 = 126,0, C7 = 128,4, C8 = 124,3, C8a = 130,5, CN = 117,7, CH = 29,6, CH_3 = 14,8, Si≡ = −3,2; sm: 253 (M^+, 58,0), 258 ($M^+ - 1$, 17,5), 238 ($M^+ - 15$, 24,4), 73 ($M^+ - 180$, 100,0).

Méthyl-8 triméthylsilyl-2 naphtalène carbonitrile-1, ***17***: ir: 3020, 2980, 2960, 2215 (CN), 1462, 1420, 1253, 1140, 868, 840, 828; rmn ^{1}H: H3 = 7,68 (d, 8,1), H4 = 8,03 (d, 8,1), H5 = 7,77 (d, 7,5), H6, H7 = 7,46 (m), CH_3 = 3,16 (s), Si≡ = 0,53 (s); rmn ^{13}C: C1 = 114,3, C2 = 147,8, C3 = 131,2, C4 = 132,5, C4a = 132,5, C5 = 127,6, C6 = 126,9, C7 = 129,4, C8 = 128,3, C8a = 134,5, CN = 121,1, CH_3 = 23,4, Si≡ = −1.0; sm: 239 (M^+, 44,7), 225 ($M^+ - 14$, 21,9), 224 ($M^+ - 15$, 100,0), 197 ($M^+ - 42$, 5,7), 167 ($M^+ - 72$, 4,3).

(Lithio méthyl)-2 naphtalène carbonitrile-1, ***4***a: rmn ^{13}C: C1 = 143,0, C2 = 146,7, C3 = 115,2, C4 = 130,6, C4a = 129,8, C5 = 128,3, C6 = 127,8, C7 = 128,0, C8 = 118,3, C8a = 133,1, CH_2Li = 63,8, CN = 126,3.

1. (*a*) N. S. Narasimhan et R. S. Mali. Synthesis, 957 (1983); (*b*) H. W. Gschwend et H. R. Rodriguez. Org. React. **26**, 1 (1979); (*c*) P. Beak et V. Snieckus. Acc. Chem. Res. **15**, 306 (1984); (*d*) V. Snieckus et M. P. Sibi. J. Org. Chem. **48**, 1935 (1983).
2. T. D. Krizan et J. C. Martin. J. Org. Chem. **47**, 2681 (1982).
3. M. Reuman et A. I. Meyers. Tetrahedron, **41**, 837 (1985).
4. T. D. Krizan et J. C. Martin. J. Am. Chem. Soc. **105**, 6155 (1983).
5. W. E. Parham et L. D. Jones. J. Org. Chem. **41**, 1187 (1976).
6. R. R. Fraser, M. Bresse et T. S. Mansour. J. Am. Chem. Soc. **105**, 7790 (1983).
7. S. Gronowitz et B. Eriksson. Ark. Kemi, **21**, 335 (1983); Chem. Abstr. **59**, 13918 F(1963).
8. P. Dubus, B. Decroix, J. Morel et P. Pastour. Bull Soc. Chim. Fr. 628 (1976).
9. M. Watanabe et V. Snieckus. J. Am. Chem. Soc. **102**, 1457 (1980).
10. (*a*) R. R. Fraser, A. Baignée, M. Bresse et K. Hata. Tetrahedron Lett. 4195 (1982); (*b*) R. R. Fraser, M. Bresse et T. S. Mansour. Chem. Commun. 620 (1983); (*c*) R. R. Fraser et T. S. Mansour. J. Org. Chem. **49**, 3442 (1984); J. Org. Chem. **49**, 5284 (1984).
11. R. C. Ronald et M. R. Winkle. Tetrahedron, **39**, 2031 (1983).
12. P. L. Creger. J. Am. Chem. Soc. **92**, 1396 (1970).
13. R. R. Fraser, T. S. Mansour et S. Savard. J. Org. Chem. **50**, 3232 (1985).
14. N. S. Narasimhan et R. S. Mali. Synthesis, 796 (1975).
15. (*a*) C. Eaborn, P. Golborn et R. Taylor. J. Organomet. Chem. **10**, 171 (1967); (*b*) N. S. Narasimhan et A. C. Ranade. Ind. J. Chem. **7**, 538 (1969).
16. R. L. Gay et C. R. Hauser. J. Am. Chem. Soc. **89**, 2297 (1967).
17. J. G. Lombardino. J. Org. Chem. **36**, 1843 (1971).
18. (*a*) W. Kitching, M. Bullpitt, D. Gartshore, W. Adcock, T. C. Khor, D. Doddrell et I. D. Rae. J. Org. Chem. **42**, 2411 (1977); (*b*) P. E. Hansen. Org. Magn. Reson., **12**, 109 (1979).
19. R. C. Fuson, C. H. McKeever et L. C. Behr. J. Am. Chem. Soc. **63**, 2648 (1949); J. J. McCullough, W. K. MacKinnis, C. L. Lock et R. Faggiani. J. Am. Chem. Soc. **104**, 4644 (1982).
20. R. C. Fuson et D. H. Chadwick. J. Org. Chem. **13**, 484 (1948).
21. (*a*) J. M. Ruxer et G. Solladié. J. Chem. Res. (M), 4944 (1978); (*b*) V. Snieckus et M. Watanabe. J. Am. Chem. Soc. **102**, 1457 (1980).

Application des conditions de réaction par transfert de phase à la synthèse d'amino-éthers dérivés du *trans* phénoxy-2 cyclohexanol

P. DEPREUX ET A. MARCINCAL-LEFEBVRE

Laboratoire de chimie organique, Faculté de pharmacie de Lille, 3, rue du Professeur-Laguesse, 59045 Lille CEDEX, France

Reçu le 4 janvier 1985[1]

P. DEPREUX et A. MARCINCAL-LEFEBVRE. Can. J. Chem. **64**, 626 (1986).

On a préparé des amino-éthers du *trans* phénoxy-2 cyclohexanol en faisant appel à des méthodes impliquant des conditions anhydres (alcoolates de sodium dans le xylène) ou des conditions de catalyse par transfert de phase (CTP) (systèmes à deux phases liquide – liquide ou solide–liquide). On a optimisé divers facteurs. Dans le cas du système à deux phases liquide – liquide dans lequel on n'ajoute pas de catalyseur, la réaction se produit avec des rendements, qui sont comparables ou supérieurs à ceux obtenus avec adjonction de catalyseurs de transfert de phase, un ammonium quaternaire se formant *in situ*. En se basant sur le fait qu'il ne se produit pas d'extraction de OH^- dans la phase organique et que les rendements dépendent de la vitesse de l'agitation, on a pu démontrer que la déprotonation du ROH se produit à l'interface. En présence d'Aliquat, le rendement ne change pas avec la concentration organique du catalyseur. Les corrélations statistiques obtenues entre les variations de rendements et plusieurs paramètres étaient bonnes.

P. DEPREUX and A. MARCINCAL-LEFEBVRE. Can. J. Chem. **64**, 626 (1986).

Amino-ethers of *trans*-2-phenoxycyclohexanol were prepared by methods involving anhydrous conditions (sodium alkoxides in xylene) or phase transfer catalysis conditions (liquid–liquid or solid–liquid two-phase systems). Various factors were optimized. In the liquid–liquid two-phase system, when no catalyst was added, reaction proceeds with comparable or even better yields than with some PTC catalysts, a quaternary salt being formed *in situ*. It was shown that the deprotonation of ROH takes place at the interface, since there was no OH^- extraction in organic medium and the yield depends on the stirring speed. In the presence of Aliquat, the yield does not change with the organic concentration of the catalyst. Statistical correlations obtained between the variations in yield and several other parameters were good.

Dans le cadre de travaux sur les dérivés du *trans* phénoxy-2 cyclohexanol, nous avons étudié plus particulièrement la synthèse d'amino-éthers de type **1** (schéma 1), afin d'optimiser leurs conditions d'obtention par un procédé commode et peu coûteux, telle la catalyse par transfert de phase.

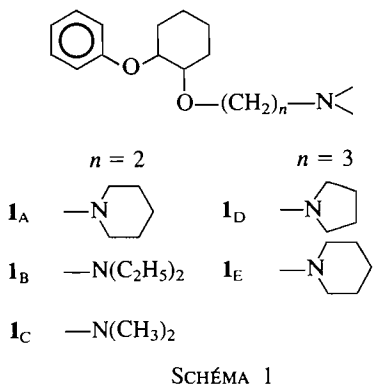

SCHÉMA 1

L'importance pharmacologique du chaînon—O—$(CH_2)_2$—N est reconnue; on le rencontre dans de nombreuses molécules à activités biologiques diverses. Ainsi le test de Winter appliqué au composé $\mathbf{1}_A$, en vue de déterminer son activité anti-inflammatoire potentielle, révèle une activité du même ordre de grandeur que celle de l'Indométhacine utilisée comme substance de référence.[2]

Nous avons réalisé la synthèse de type Williamson des éthers **1**, d'une part par réaction dans le xylène à reflux entre l'alcoolate de sodium du *trans* phénoxy-2 cyclohexanol et l'amine tertiaire halogénée aliphatique (schéma 2), et d'autre

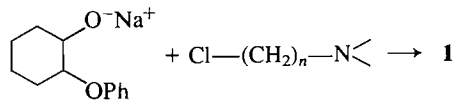

SCHÉMA 2

part par réaction de l'alcool lui-même dans des conditions de réaction par transfert de phase (schéma 3), catalysée par des ammoniums quaternaires (1) ou des éthers-couronnes (2), ou par addition d'amines tertiaires (3) ou de polyamines (4), susceptibles de former des ammoniums quaternaires (24), soit en présence de solution aqueuse de soude à 40% (système liquide – liquide (5)), soit en présence de soude en pastille (système solide – liquide (5)) et en employant différents solvants organiques.

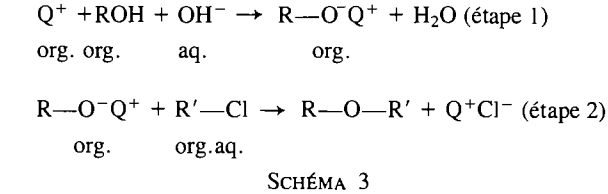

SCHÉMA 3

Les réactions de substitution nucléophile par transfert de phase ont été beaucoup étudiées (6–10) et il est particulièrement intéressant de pouvoir appliquer ce type de réactions par transfert de phase à la synthèse médicamenteuse qui se heurte souvent à la fragilité des molécules polyfonctionnelles préparées, dans les conditions de formation des alcoolates.

En ce qui concerne la réactivité et la stabilité des amines tertiaires halogénées, la présence de deux groupements fonctionnels dans ces composés laisse prévoir une réactivité complexe pour laquelle trois directions ont été mises en évidence (11) (schéma 4). Selon le milieu et sa constante diélectrique, la dimérisation en (b) se produit en proportions variables (11) et, lorsque $n = 2$, on a observé, dans l'eau, 70% de dimérisation

1. Révision reçue le 16 octobre 1985.

2. Réduction de l'œdème provoqué par la carraghénine dans le coussinet plantaire du rat (26): $\mathbf{1}_A$, 55.05% (3 h); Indométhacine, 79,36% (3 h).

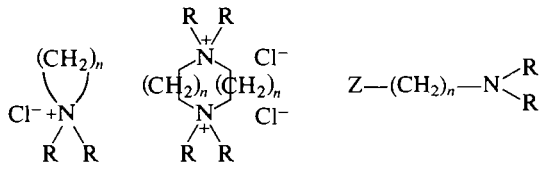

(a) (b) (c) S_N par $Z^{\bullet}$

SCHÉMA 4

(voie d'inactivation des amines tertiaires halogénées), alors que dans le benzène aucune réaction ne se produit.

Le dimère ainsi formé («diquat») possède deux groupements ammoniums et pourrait jouer le rôle de catalyseur par formation d'un alcoolate d'ammonium P^+ R—O^- dans des réactions de type transfert de phase. Cette hypothèse fut avancée par J. Jarousse (12) pour expliquer la réaction du cyclohexanol avec le chloro-2 *N,N*-diméthylaminoéthane en présence d'une solution aqueuse de soude à 50%. Néanmoins peu de précisions étaient données quant aux conditions opératoires et au rendement. De même, J. Dockx (13) a étudié la réaction d'alcools de type benzhydrol avec des dérivés halogénés en présence d'ammoniums quaternaires, mais n'a pas publié les résultats obtenus.

Les composés préparés ont été isolés sous forme d'oxalates recristallisés de l'acétate d'éthyle. Les rendements ont été calculés par rapport au *trans* phénoxy-2 cyclohexanol mis en réaction. Dans chaque essai, nous avons récupéré en fin de synthèse un pourcentage variable de cet alcool. Les corrélations entre différents paramètres et le rendement ont été établies.

Système biphasique liquide – liquide

Pour les réactions effectuées en *milieu biphasique liquide – liquide*, les conditions standards utilisées sont les suivantes: cinq équivalents de NaOH (solution aqueuse à 40%) par rapport au phénoxy-2 cyclohexanol (en solution benzénique) et un équivalent de chlorhydrate d'amine tertiaire halogénée. Le mélange est maintenu à reflux, sous agitation à 450 tours/min, pendant 4 h, en présence éventuellement de 0,1 équiv. de catalyseur. Les variations de conditions opératoires ont porté sur la quantité de soude, le solvant organique, le temps et la température de réaction ainsi que la nature du catalyseur.

(A) *Les résultats obtenus pour le composé* $\mathbf{1}_A$ sont rassemblés dans le tableau 1.

(a) Dans les conditions standards, en présence de *chlorure de benzyltriéthylammonium* (CBTEA) (réaction 1), d'Aliquat[3] ou de sulfate acide de tétrabutylammonium (TEBA) (réactions 4 et 6), les rendements sont respectivement de 14, 37 et 34%. Si l'on augmente la quantité de catalyseur et de soude (réaction 2), le rendement est comparable. Une température de réaction inférieure est défavorable (réactions 3 et 5).

(b) *Sans adjonction de catalyseur*, le rendement dans les conditions standards (réaction 7) est de 33%. Les variations des conditions (réactions 8–14) montrent l'influence favorable de l'augmentation de température (réaction 12, 43%, xylène à reflux) ou de l'augmentation de la quantité de soude, mais seulement si on opère à température ambiante (réaction 14).

(c) Une *amine tertiaire*, telle la triéthylamine, bien que pouvant avoir un rôle catalytique dans les réactions des dérivés halogénés par formation d'un ammonium quaternaire, provoque une chute du rendement de 27 (réaction 14) à 9% (réaction 17).

3. Aliquat: mélange de $(nC_8–C_{12})_3N^+CH_3Cl^-$.

Si l'on étudie la corrélation entre les variations de rendement observées et le rapport molaire NaOH – alcool, la température de réaction, le temps de réaction, la constante diélectrique de la phase organique et le nombre de carbone de l'ammonium (Q^+ ou P^+), on observe que 74% des variations de rendement peuvent être expliqués par la corrélation avec les paramètres cités précédemment. Si l'on compare, au moyen du test statistique F de Fischer – Snedecor, les variations de rendement expliquées par ces paramètres et celles dues au « hasard expérimental », il existe une différence significative entre ces deux types de variations au seuil de 3%. La *température de réaction* apparaît comme un facteur prépondérant dans les variations de rendement (coefficient de corrélation $r = 0{,}64$). De même, le *temps de réaction* n'est pas à négliger ($r = 0{,}46$); il est directement lié au facteur température ($r = 0{,}88$) et, si l'on ne tient pas compte du facteur temps dans les corrélations avec les variations de rendement, alors seulement 58% de celles-ci peuvent être expliquées et le seuil du test F est alors de 7%.

Herriot et Picker (14) ont étudié l'activité catalytique des ammoniums quaternaires et ont montré que deux facteurs intervenaient: d'une part, un grand nombre d'atomes de carbone (haute lipophilie) pour P^+ ou Q^+ et, d'autre part, une disposition symétrique autour de l'hétéroatome, ce deuxième facteur étant cependant moins important (24). Ainsi, le CBTEA (13 carbones) contient le nombre minimum d'atomes de carbone et son manque de symétrie est considéré comme peu favorable.

Sur la base de cette notion, nous avons, dans la corrélation, fait intervenir l'ammonium quaternaire par son *nombre d'atomes de carbone*. Ce facteur possède une corrélation positive ($r = 0{,}44$) avec les variations de rendement. Dans le cas du tétrabutylammonium (symétrique, 16 C), du trioctylméthylammonium (25 C) ou du dimère cyclique provenant du chloro-2 pipéridinoéthane (P^+ symétrique, 14 C), les cations sont volumineux; de ce fait, l'anion alcoolate semble moins associé, donc beaucoup plus réactif, comparativement aux cations hydrophiles et moins volumineux tels que le benzyltriéthylammonium et celui résultant de l'utilisation de triéthylamine, qui permet la formation de $(CH_2)_5N—CH_2—CH_2—N^+(C_2H_5)_3$.

Les baisses de rendement lors de l'addition de CBTEA ou de triéthylamine par rapport au rendement obtenu sans addition de catalyseur pourraient donc être expliquées par compétition entre paires d'ions et par une augmentation de l'hydrophilie dans le cas des ions triéthylammoniums, qui possèdent des propriétés tensio-actives défavorables (24).

Étant donné la lipophilie de l'alcool de départ (log *P* (calculé) = 3),[4] on peut penser que la formation de l'alcoolate s'effectue à l'interface de deux phases liquides, selon le mécanisme décrit pour les composés à CH acide qui sont eux-mêmes lipophiles (24, 25). Pour vérifier cette hypothèse, nous avons étudié les variations de rendement en fonction de la vitesse d'agitation et de la concentration en catalyseur, et montré[5] que, dans les conditions où nous opérons, l'Aliquat extrait les ions OH^- en phase organique ($3{,}6 \times 10^{-2}$ équiv. OH^- : 1 équiv. d'Aliquat dans le benzène), ce qui n'est pas le cas avec le pipéridinochloréthane, après 2 h d'agitation à 80°C uniquement en présence d'une solution de soude à 40% et de benzène; l'extraction de

4. log *P*: logarithme du coefficient de partage calculé par la méthode des constantes fragmentales de Rekker (voir réf. 15).

5. Titrage, par HCl 0,11 *N* en présence de fuchsine acide 1‰ et de 10 mL de H_2O, de 4 mL de la phase organique prélevés après 2 h d'agitation à 80°C d'une solution aqueuse de soude à 40% (5 mL) et de benzène (10 mL) en présence d'Aliquat (0.38 g).

TABLEAU 1. Réactions en présence de soude aqueuse à 40%. Variations de rendement en oxalate de $\mathbf{1}_A$ (agitation: 450 tours/min)

	Paramètres					
Catalyseur	Phase organique	Quantité de soude (équiv.)	Quantité de catalyseur (équiv.)	Temps de réaction (h)	Température de réaction (°C)	Rendement en $\mathbf{1}_A$ (%)
1. CBTEA	C_6H_6	5	0,1	4	80	14
2. CBTEA	C_6H_6	40	0,25	4	80	18
3. CBTEA	C_6H_6	40	0,25	24	20	0
4. Aliquat	C_6H_6	5	0,1	4	80	37
5. Aliquat	C_6H_6	5	0,1	4	70	28
6. TEBA	C_6H_6	5	0,1	4	80	34
7. Pas de catalyseur	C_6H_6	5		4	80	33
8. Pas de catalyseur	CH_2Cl_2	5		4	40	10
9. Pas de catalyseur	CH_2Cl_2	5		24	20	15
10. Pas de catalyseur	C_6H_6	5		4	70	27
11. Pas de catalyseur	C_6H_6	5		24	20	12
12. Pas de catalyseur	Xylène	5		4	110	43
13. Pas de catalyseur	C_6H_6	40		4	80	12
14. Pas de catalyseur	CH_2Cl_2	40		24	20	27
15. Benzo-15 crown-5	C_6H_6	40	0,05	24	20	0
16. Benzo-15 crown-5	C_6H_6	40	0,05	4	80	17
17. Et_3N	CH_2Cl_2	40	1	24	20	9

TABLEAU 2. Variations de rendement en oxalate de $\mathbf{1}_A$ en fonction de la vitesse d'agitation

Vitesse de rotation (tours/min)	200	300	450	500	950	1100
Rendement en $\mathbf{1}_A$ (oxalate) (%)	8	28	33	36	42	45

TABLEAU 3. Influence de la concentration en Aliquat sur le rendement en oxalate de $\mathbf{1}_A$

Nombre d'équivalents d'aliquat par rapport à l'alcool	Vitesse (tours/min)	Rendement en $\mathbf{1}_A$ (oxalate) (%)
0,05	700	44
0,1	700	46
0,1	450	37
0,15	700	46
0,20	700	43

l'anion OH^- est reconnue comme difficile et négligeable dans de nombreuses réactions (5, 16, 25).

En présence des seuls réactifs (soude, R—O—H et chloro-2 pipéridinoéthane dans le benzène), le catalyseur formé *in situ* (P^+) est moyennement hydrophile, relativement symétrique et volumineux; comme il n'extrait pas les ions OH^- en phase organique et que les rendements sont améliorés par augmentation de l'agitation (tableau 2) et donc de l'interface, on peut envisager un mécanisme interfacial pour l'arrachement de H^+ à ROH (étape 1) et que les étapes se produisant à l'interface limitent la vitesse de réaction[6] (schéma 2 où $P^+ = Q^+$). La paire d'ions $R—O^- P^+$ est formée d'un anion stabilisé par P^+ suffisamment volumineux pour ne pas lui être trop associé. La substitution (étape 2) peut se produire à la fois à l'interface, puisque le dérivé halogéné est soluble dans les deux phases, et simultanément dans la phase organique, puisque les rendements sont diminués en présence de catalyseurs plus hydrophiles, tels le CBTEA ou la triéthylamine. Par contre, l'addition aux réactifs d'un catalyseur plus lipophile, tel que l'aliquat, ou plus symétrique tel que le TEBA (réactions 4 et 6), augmente légèrement les rendements, par rapport à ceux obtenus dans les conditions standards (réaction 7) ; à la différence des catalyseurs précédents, y compris de P^+, ces catalyseurs extraient les ions OH^- en phase organique, ce que nous avons vérifié ; néanmoins la formation de RO^- reste prépondérante à l'interface, car les rendements ne sont pas augmentés par l'augmentation de la concentration en catalyseur, mais le sont par l'élévation de la vitesse d'agitation (tableau 3).

Cette légère augmentation des rendements peut signifier une amélioration de l'étape 2 par échange de cation: en faveur de $RO^- Q^+$ avec $:Q^+$: $(Bu)_4N^+$ ou $(octyl)_3N^+CH_3.Q^+$ étant plus lipophile, et donc plus efficace pour détacher RO^- de l'interface que P^+.

(B) Nous avons ensuite appliqué les différentes conditions de synthèse envisagées précédemment, en phase liquide – liquide, à l'obtention des amino-éthers $\mathbf{1}_{B,C,D}$ (schéma 1) ; et d'autre part, nous avons voulu comparer la réactivité d'un alcool moins lipophile, tel que le cyclohexanol (log P = 1,8) et l'avons fait réagir avec les chloro-2 pipéridino- (17) et diméthylamino-éthanes (18) (schéma 5) sans adjonction de catalyseur dans le benzène, 4 h à reflux en présence de 5 équiv. de soude (conditions standards). Les résultats obtenus lors de la *synthèse des éthers* $\mathbf{1}_{B,C,D}$ sont rassemblés dans la fig. 1.

Quelques soient les conditions opératoires, les dérivés $\mathbf{1}_{B,C,D}$ sont obtenus avec des rendements inférieurs à ceux du dérivé $\mathbf{1}_A$. Cette différence pourrait être expliquée par trois facteurs: la basicité de l'amine, l'encombrement stérique au niveau de son

6. Lors des réactions se produisant selon un mécanisme par extraction des ions OH^-, la vitesse de réaction augmente avec la lipophilie du catalyseur et sa concentration, mais est indépendante de la vitesse d'agitation au-dessus d'une certaine valeur (environ 300 tours/min (16)).

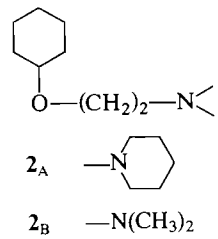

SCHÉMA 5

atome d'azote et la lipophilie ; ces facteurs interviennent essentiellement au niveau de l'activité du catalyseur et de sa formation *in situ* par dimérisation de l'amine chlorée. Il semble vraisemblable que les effets stériques interviennent de façon prépondérante, d'une part dans l'association du dimère avec l'anion alcoolate, et d'autre part dans la stabilité de ce dimère vis-à-vis des ions OH^- et, par exemple, de la température (19). Ainsi, le chloro-2 pipéridino-éthane donne de meilleurs rendements que le chloro-2 pyrrolidino-éthane, dont l'azote est moins encombré.

Si l'on compare les résultants obtenus dans le dichlorométhane (réactions 2′), on observe que les éthers **1** n'ont pu être obtenus qu'avec les chloro-2 pipéridino- et diéthylamino-éthanes qui sont plus lipophiles et plus encombrés que les dérivés pyrrolidiniques et diméthylaminés,[7] le meilleur rendement étant obtenu avec le dérivé le plus lipophile. Dans ces conditions opératoires le volume de soude est élevé et favorise la transformation irréversible en phase aqueuse des amines chlorées en dimère et particulièrement des plus hydrophiles, ce qui peut rendre compte du rendement quasi nul en $\mathbf{1}_C$ et $\mathbf{1}_D$ par consommation de ces dernières.

La *réactivité du cyclohexanol* n'est pas supérieure à celle du phénoxy-2 cyclohexanol. Avec le cyclohexanol, nous avons obtenu les dérivés $\mathbf{2}_A$ et $\mathbf{2}_B$ avec des rendements respectifs comparables à ceux obtenus pour $\mathbf{1}_A$ et $\mathbf{1}_C$, ce qui semble exclure pour le phénoxy-2 cyclohexanol l'intervention d'effets stériques (du groupement phénoxy en 2) ou de stabilisation de la paire d'ions Q^+ R—O^- par les doublets des deux atomes d'oxygène.

(C) Nous avons étudié pour l'obtention des dérivés de type **1** et **2** (25 essais) la *corrélation globale* entre les variations de rendement et les paramètres suivants: (*1*) rapport molaire NaOH–alcool ; (*2*) temps de réaction ; (*3*) température de réaction ; (*4*) constante diélectrique du solvant organique ; (*5*) nombre de carbone de Q^+ ; (*6*) log *P* de l'alcool ; (*7*) rapport molaire eau – amine chlorée ; (*8*) log *P* de l'amine chlorée. Les résultats amènent les commentaires suivants:

Dans les conditions d'étude (25 essais, 8 paramètres explicatifs), 65% des variations de rendement peuvent être expliqués par la corrélation. Il existe une différence significative au seuil de 1,22% entre les variations de rendement expliquées par le modèle et celles dues au hasard.

La lipophilie de l'alcool est peu corrélée ($r = -0,07$) mais ce résultat est peu indicatif, étant donné la faible gamme de lipophilie employée. Il existe naturellement une très bonne corrélation ($r = 0,97$) entre les paramètres 1 et 7 du fait de l'emploi dans tous les cas d'une solution aqueuse de soude à 40%. Une corrélation similaire ($r = -0,89$) existe entre temps et température de réaction.

Parmi les paramètres, nous pouvons noter une corrélation

7. log *P* des amines chlorées, calculé selon réf. 15: pipéridinique, 2,2; diéthylaminée, 2; pyrrolidinique, 1,6; diméthylaminée, 0,99.

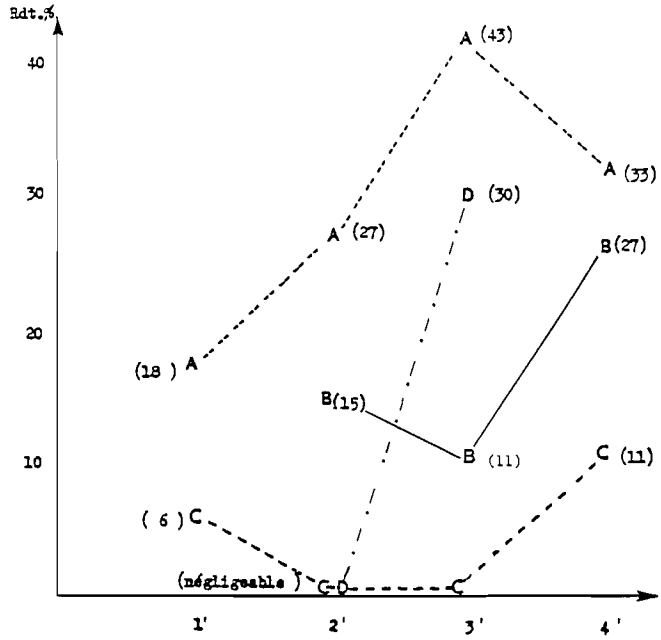

FIG. 1. Variations de rendement pour les amino-éthers **1**. 1′: CBTEA (0,25 équiv.) – C_6H_6 – 40 équiv. de NaOH, 4 h à 80°C; 2′: pas de catalyseur – CH_2Cl_2 – 40 équiv. de NaOH, 24 h à 20°C; 3′: pas de catalyseur – xylène – 5 équiv. de NaOH, 4 h à 110°C; 4′: pas de catalyseur – C_6H_6 – 5 équiv. de NaOH, 4 h à 80°C. A: pipéridino-amino-éther $\mathbf{1}_A$; B: diéthylamino-éther $\mathbf{1}_B$; C: diméthylamino-éther $\mathbf{1}_C$; D: pyrrolidinoamino-éther $\mathbf{1}_D$.

négative des variations de rendement avec le rapport molaire NaOH–alcool ($r = -0,44$), le temps de réaction ($r = -0,40$), la lipophile de l'alcool ($r = -0,07$), le rapport molaire eau – amine chlorée ($r = -0,41$) et la constante diélectrique ($r = -0,29$). Il existe une corrélation positive avec la température ($r = 0,38$), le nombre de carbone de Q^+ ($r = 0,57$) et le log *P* de l'amine chlorée ($r = 0,55$). Les paramètres 1–3, 5, 7, 8 apparaissent donc comme prépondérants dans les variations de rendement.

Étant donné les baisses de rendement observées dans le cas des composés $\mathbf{1}_B$ et $\mathbf{1}_C$, en présence de 5 équivalents de soude, sans adjonction de catalyseur, lors du passage du benzène à 80°C (réactions 4′ et 3′, fig. 1), baisse qui peut être expliquée par une décomposition à cette température (110°C) du dimère de l'amine chlorée, nous avons étudié la corrélation entre les variations de rendement et les paramètres 1–5 et 8 pour les essais effectués à une température inférieure à 110°C (21 essais). Dans ces conditions, 76% des variations de rendement sont expliquées et le test F indique une différence significative entre les variations expliquées par les facteurs envisagés et celles dues au hasard au seuil de 0,10%. La quantité de soude et d'eau ($r = -0,50$), le nombre de carbone de P^+ ou de Q^+ ($r = 0,60$) et le log *P* de l'amine chlorée ($r = 0,55$) sont les facteurs prépondérants. Si l'on fait intervenir la basicité de l'amine tertiaire, la corrélation n'est pas améliorée ($r^2 = 0,76$) et de plus ce paramètre intervient peu dans les variations de rendement ($r = 0,17$).

(D) Dans les conditions de réaction en milieu liquide–liquide, en présence de 40 équivalents de soude dans le benzène et de 0,05 équivalent d'un éther couronne, le "benzo-15-crown-5", les rendements en éther $\mathbf{1}_A$ sont semblables à ceux obtenus dans les mêmes conditions avec le CBTEA (18% après 4 h à 80°C) ; le complexe de l'éther couronne avec l'ion Na^+ étant

TABLEAU 4. Réactions dans un système solide–liquide. Variations de rendement en oxalate de $\mathbf{1}_A$ (agitation: 450 tpm)

	Paramètres						
Catalyseur	Phase organique	Quantité de soude (équiv.)	Na_2CO_3	Quantité de catalyseur (équiv.)	Temps de réaction (h)	Température de réaction (°C)	Rendement en $\mathbf{1}_A$ (%)
Pas de catalyseur	Benzène	3,5	+	0	4	70	12
Pas de catalyseur	Benzène	3,5	+	0	4	80	34
Benzo-15 crown-5	Benzène	3,5	+	0,1	4	70	18
Benzo-15 crown-5	Benzène	3,5	+	0,1	4	80	55
Benzo-15 crown-5	Xylène	3,5	+	0,1	4	110	36
Benzo-15 crown-5	Xylène	3,5	+	0,1	0,5	110	17
Kryptofix 5	Benzène	3,5	+	0,1	4	70	20
Benzo-15 crown-5	Benzène	3,5	○	0,1	4	70	20
Benzo-15 crown-5	Benzène	0	+	0,1	4	80	0
CBTEA	Benzène	3,5	+	0,1	4	80	21
TEBA	Benzène	3,5	+	0,1	4	70	17
Tétraméthyléthylène diamine	Benzène	3,5	+	0,1	4	80	28

comme la CBTEA, un catalyseur de transfert de phase trop hydrophiles (24).

Système biphasique solide–liquide

Afin d'étudier *l'influence de l'eau*, nous avons réalisé la synthèse du composé $\mathbf{1}_A$ dans un système biphasique solide–liquide en employant comme phase solide un mélange soude (3,5 équiv.) – Na_2CO_3 dans du benzène (70 ou 80°C). Dans ce type de catalyse, la déprotonation de l'alcool se produit à la surface du mélange solide. Les résultats obtenus avec un tel système sont réunis dans le tableau 4.

En absence de catalyseur, les résultats sont similaires à ceux obtenus en phase liquide–liquide. Comparativement à la réaction en phase liquide–liquide, la quantité d'eau étant faible (et provenant essentiellement de la déprotonation de l'alcool), la dimérisation serait plus lente, mais suffisante pour catalyser la réaction de l'anion alcoolate avec l'amine chlorée.

Les couronnes sont de bons catalyseurs dans les transferts de phase solide–liquide et l'utilisation du "benzo-15-crown-5" s'avère bénéfique. Dans le benzène, après 4 h à 80°C le rendement est de 55%. Avec un composé de type cryptand, le Kryptofix 5, les résultats sont similaires. Ces réactions sont classiquement réalisées en présence de NaOH + Na_2CO_3, mais la présence de carbonate, utilisé classiquement dans ce type de catalyse (20), n'est pas indispensable. A l'inverse, l'utilisation de Na_2CO_3 seul, décrite par certains auteurs (21), ne permet pas, dans le cas du composé $\mathbf{1}_A$, la condensation.

Dans ce procédé en phase solide–liquide, l'utilisation de CBTEA (0,1 équiv.), 4 h dans le benzène à 80°C, a donné un rendement de 21% (il était de 14% en phase liquide–liquide). De même le TEBA donne un rendement de 17% après 4 h à 70°C, équivalent à celui obtenu dans les mêmes conditions sans adjonction de catalyseur. Enfin en présence de tétraméthyléthylènediamine, le rendement est de 28%, après 4 h à 80°C dans le benzène.

Pour l'étude des *corrélations en phase solide–liquide*, nous avons utilisé comme paramètre dans le cas des essais à 70, 80, 110°C (12 essais), le temps et la température de réaction, le rapport molaire NaOH–alcool, le rapport molaire entre l'eau et l'amine chlorée, la constante diélectrique de la phase organique (2,3 pour le benzène et 2,11 pour le xylène) et pour différencier les ammoniums des éthers couronnes le nombre de carbone du contrion positif et le nombre de sites électroniques.

Nous pouvons constater que 95% des variations de rendement observés dans la catalyse solide–liquide peuvent être expliqués par la corrélation avec les paramètres envisagés. Dans des conditions de réaction identiques, c'est-à-dire 4 h à 70 ou 80°C dans le benzène en présence du mélange NaOH–Na_2CO_3 avec utilisation d'un éther couronne, d'une polyamine ou d'ammoniums quaternaires, nous avons envisagé la corrélation entre les rendements et la température de réaction, le nombre d'atomes de carbone du contrion positif et le nombre de sites électroniques, 76% des variations de rendement sont expliqués par ce paramètres. La température de réaction est un facteur prépondérant (r = 0,69).

Réactions en milieu anhydre

Lors de l'étude du procédé en milieu biphasique liquide–liquide, nous avons remarqué l'importance de la formation du dimère. Pour confirmer ce fait, nous avons effectué *la synthèse des éthers 1 en milieu anhydre*, en solution dans le xylène (D = 2) à reflux avec formation préalable du phénoxy-2 cyclohexanolate de sodium sous l'action du sodium fondu (1 équiv.). Après 3 h de réaction, les rendements de la condensation entre l'alcoolate de sodium et les amines chlorées sont les suivants: chloro-2 pipéridinoéthane, rendement 25%; chloro-2 diéthylaminoéthane, rendement 27%; chloro-2 pyrrolidinoéthane, rendement 20%. Dans ces conditions si l'on admet qu'il ne se forme pas de dimère, le contrion de l'anion est l'ion Na^+ et les trois amines donnent des rendements comparables. Nous avons étudié l'effet de l'addition de CBTEA ou de TEBA qui peuvent donner comme phase liquide–liquide la pair d'ions (b)

$$\underset{(a)}{RO^-Na^+} + R'_4N^+X^- \rightarrow \underset{(b)}{RO^-R'_4N^+} + Na^+X^-$$

dont la réactivité se rapprocherait de celle de l'anion dissocié et dans laquelle les interactions anion–cation seraient diminuées par rapport à (a) (22). Effectivement par ce procédé, les rendements sont améliorés: par exemple dans le cas du dérive $\mathbf{1}_A$, le rendement est de 40% en présence de CBTEA et de 46%

en présence de TEBA (0,1 équiv.); ayant dû ajouter de l'acétonitrile pour dissoudre le catalyseur, nous avons vérifié que l'amélioration de rendement résultait bien de l'utilisation d'un ammonium quaternaire et non de celle d'acétonitrile, solvant polaire qui peut également augmenter la vitesse de substitutions nucléophiles par solvation spécifique du cation (dans un mélange xylène–acétonitrile le rendement en $\mathbf{1}_A$ est de 19%). Nous avons confirmé l'effet favorable sur le rendement de l'addition de CBTEA avec le chloro-2 pyrrolidino-éthane (Rdt: 31%), le chloro-2 diméthylamino-éthane (27%) et avec la chloro-2 diéthylamino-éthane (30%). Si l'on utilise le chloro-3 pipéridinopropane en milieu anhydre, le rendement passe de 19% avec RO^-Na^+ seul comme nucléophile à 29% en présence de CBTEA.

Conclusion

La réaction entre le *trans* phénoxy-2 cyclohexanol et diverses amines tertiaires halogénées aliphatiques s'effectue avec des rendements moyens en général. Dans des conditions de transfert de phase en *milieu liquide–liquide*, les rendements dépendent principalement de la dimérisation d'une certaine quantité d'amine chlorée en ammonium quaternaire ; cette dimérisation, voie d'inactivation irréversible des amines chlorées, est fonction de la constante diélectrique du milieu et de la lipophilie de l'amine chlorée. Dans le cas du composé $\mathbf{1}_A$, l'amine chlorée est faiblement soluble dans l'eau ($\log P = 2{,}2$) ; de ce fait, si à 80°C on augmente le volume d'eau par utilisation de 8 fois plus de lessive de soude (40 équiv.) on favorise cette condensation irréversible en ammonium quaternaire, d'où la diminution de rendement par consommation d'amine chlorée. À température ambiante, la dimérisation est plus lente, de ce fait l'utilisation d'un volume d'eau plus important est favorable à la formation d'une quantité suffisante de catalyseur. Parallèlement à la lipophilie, l'encombrement de l'ammonium quaternaire (nombre de carbone de P^+ ou Q^+) apparaît déterminant dans le rendement.

Étant donné le lipophilie de l'alcool mis en réaction, les ammoniums jouent davantage le rôle de contrion vis-à-vis de l'anion alcoolate que de catalyseur de transfert de phase, la déprotonation se produisant vraisemblablement à l'interface.

L'étude en phase *solide–liquide* a confirmé l'intérêt des éthers couronnes dans ces conditions.

En milieu anhydre, dans le xylène, il n'y a vraisemblablement pas de dimérisation et l'utilisation de CBTEA ou de TEBA augmente le rendement en apportant un contrion moins associé à RO^-, l'amine chlorée réagissant sous la forme activée d'ion éthylène immonium (23).

Malgré des rendements moyens pour un cycle de réactions le procédé par transfert de phase s'avère donc intéressant dans la réaction d'éthérification de cyclohexanols par sa facilité de mise en œuvre et le recyclage possible de l'alcool n'ayant pas réagi.

Partie expérimentale

Lors du traitement du milieu réactionnel, les phases organiques, séchées sur sulfate de sodium anhydre, ont été évaporées sous pression réduite au moyen d'un évaporateur rotatif Büchi à la pression de la trompe à eau. Les résidus d'évaporation sont dissous dans de l'éther anhydre et transformés en oxalate par addition progressive d'une solution éthérée d'acide oxalique.

Les points de fusion non corrigés ont été déterminés par la méthode en tube capillaire.

Les spectres infrarouges (ir) ont été enregistrés avec un spectromètre Beckman IR20 à double faisceau ou un appareil Perkin Elmer 297. Les bases huileuses sont étalées en film entre deux pastilles de bromure de potassium. Les résultats sont donnés en cm^{-1}.

Les spectres de résonance magnétique nucléaire (^1H rmn) ont été réalisés à la fréquence de 60 MHz sur un appareil JEOL C.60HL. Les déplacements chimiques sont en ppm par rapport au tétraméthylsilane. Les signaux sont désignés par les abréviations suivantes: s (singulet), d (doublet), t (triplet), q (quadruplet), m (massif ou multiplet). Les constantes de couplage (J) sont données en Hz. La structure *trans* est vérifiée à cette fréquence par la largeur de signal à demi-hauteur.

Les différentes corrélations concernant les variations de rendement ont été déterminées par un programme informatique de régression multiple sans répétitions sur un ordinateur PDP 11.

Méthodes générales de synthèse

(A) *Procédé en milieu biphasique liquide–liquide*

À un mélange de 0,0156 mol de chlorhydrate d'amine tertiaire halogénée et 10 mL d'une solution aqueuse de soude à 40%, on ajoute ou non selon le cas 0,1 équiv. d'ammonium quaternaire, puis 0,0156 mol de *trans* phénoxy-2 cyclohexanol en solution dans 10 à 20 mL de benzène. On chauffe à reflux (80°C) 3 h sous agitation à une vitesse de rotation comprise entre 450 et 500 tours/min.

Après refroidissement, on sépare la phase organique, la lave à l'eau, puis l'évapore sous pression réduite après séchage. Le résidu d'évaporation est transformé en oxalate qui recristallise de l'acétate d'éthyle après filtration et concentration du filtrat.

(B) *Procédé en milieu biphasique solide–liquide*

Un mélange de *trans* phénoxy-2 cyclohexanol (0,026 mol) dans 20 mL de benzène, d'hydroxyde de sodium en pastilles (2,1 g), de carbonate de sodium (1,25 g) et de 10 mol% de catalyseur est agité vigoureusement vers 60°C pendant 30 min. À cette température, on ajoute ensuite goutte à goutte une solution de chloro-2 pipéridinoéthane (0.026 mol) dans 10 mL de benzène. L'agitation est alors poursuivie pendant 4 h à reflux (80°C). Après refroidissement on ajoute de l'eau et l'éther $\mathbf{1}_A$ est isolé, puis transformé en oxalate comme précédemment.

(C) *Procédé en milieu anhydre*

À une solution de phénoxy-2 cyclohexanolate de sodium (0,0156 mol) dans 20 mL de xylène anhydre, on ajoute à froid une solution de 10 mol% de CBTEA ou de TEBA dans 5 mL d'acétonitrile, puis 0,0156 mol d'amine tertiaire halogénée dans du xylène anhydre. On chauffe à reflux 3 h sous agitation. Après refroidissement on reprend par l'eau. Les amino-éthers sont extraits, puis isolés sous forme d'oxalate comme précédemment.

(Phénoxy-2 cyclohexyloxy)-2 pipéridinoéthane ($\mathbf{1}_A$). *F* (oxalate): 104–105°C; ir : 2960, 2880, 1600, 1490, 1240, 750, 690 cm^{-1}; rmn (CCl_4; base): 1,35 (m, 14H, CH_2); 2,3 (m, 6H, —CH_2—N<CH_2>); 3,3 (m, 1H, CH—O—CH_2); 3,5 (t, 2H, —O—CH_2—CH_2, J = 6 Hz); 4,03 (m, 1H, —CH—OC_6H_5, $W_{1/2}$ = 22,5 Hz); 7 (m, 5H, C_6H_5). *Anal.* (oxalate) calc. pour $C_{21}H_{31}NO_6$: C 64,09, H 7,94, N 3,56, O 24,39; tr.: C 63,66, H 7,92, N 3,62, O 24,79.

(Phenoxy-2 cyclohexyloxy)-2 diéthylaminoéthane ($\mathbf{1}_B$). *F* (oxalate): 105–107°C; ir: 2920, 2860, 2800, 1600, 1590, 1240, 750, 690 cm^{-1}; rmn (C_6D_6; base): 0,9 (t, 6H, CH_3, J = 7,5 Hz); 1,35 (m, 8H, CH_2); 2,4 (q, 4H, CH_2—CH_3, J = 7,5 Hz); 2,55 (t, 2H, CH_2—CH_2—N, J = 6 Hz); 3,5 (m, 3H, CH—O—CH_2); 4,1 (m, 1H, CH—OC_6H_5, $W_{1/2}$ = 20,5 Hz); 7 (m, 5H, C_6H_5). *Anal.* (oxalate) calc. pour $C_{20}H_{31}NO_6$: C 62,96, H 8,19, N 3,67, O 25,16; tr.: C 62,16, H 8,18, N 4,00, O 25,64.

(Phenoxy-2 cyclohexyloxy)-2 diméthylaminoéthane ($\mathbf{1}_C$). *F* (oxalate): 108–110°C; ir: 2920, 2840, 1600, 1590, 1490, 1240, 750, 690 cm^{-1}; rmn (CCl_4; base): 1,4 (m, 8H, CH_2); 2,1 (s, 6H, CH_3); 2,3 (t, 2H, CH_2—N, J = 6 Hz); 3,4 (m, 3H, CH—O—CH_2); 4 (m, 1H, CH—OC_6H_5, $W_{1/2}$ = 21 Hz); 7 (m, 5H, C_6H_5). *Anal.* (oxalate) calc. pour $C_{18}H_{27}NO_6$: C 61,17, H 7,70, N 3,96, O 27,16; tr.: C 60,18, H 7,66, N 4,28, O 27,61.

(Phénoxy-2 cyclohexyloxy)-2 pyrrolidinoéthane (1_D). F (oxalate): 92–93°C; ir : 2960, 2880, 2800, 1600, 1490, 1240, 750, 690 cm^{-1}; rmn (C_6D_6; base): 1,2 (m, 12H, CH_2); 2,4 (m, 4H, —N<CH_2 CH_2>); 2,6 (t, 2H, —CH_2—N, J = 6 Hz); 3,5 (m, 3H, CH—O—CH_2); 4 (m, 1H, CH—OC_6H_5, $W_{1/2}$ = 21 Hz); 7 (m, 5H, C_6H_5). *Anal.* (oxalate) calc. pour $C_{20}H_{29}NO_6$: C 63,30, H 7,70, N 3,69, O 25,30; tr.: C 62,87, H 7,76, N 3,86, O 25,49.

(Phénoxy-2 cyclohexyloxy)-2 pipéridinoéthane (1_E). F (oxalate): 119–120°C; ir : 2950, 2880, 2790, 1600, 1590, 1490, 1240, 750, 690 cm^{-1}; rmn (C_6D_6; base): 1,4 (m, 16H, CH_2); 2,2 (m, 6H, CH_2—N<CH_2 CH_2>); 3,45 (m, 3H, CH—O—CH_2); 4,15 (m, 1H, CH—OC_6H_5, $W_{1/2}$ = 21 Hz); 7 (m, 5H, C_6H_5). *Anal.* (oxalate) calc. pour $C_{22}H_{33}NO_6$: C 64,84, H 8,16, N 3,44, O 23,56; tr.: C 64,60, H 8,24, N 3,71, O 23,90.

Remerciements

Nous tenons à remercier Monsieur W. Werner (Institut für Pharmazeutische Chemie, Münster, République fédérale d'Allemagne) pour sa collaboration et ses encouragements pour ce travail.

1. P. Varughese. J. Chem. Educ. **54**, 666 (1977).
2. G. W. Gokel et H. D. Durst. Synthesis, 168 (1976).
3. W. P. Reeves et M. R. White. Synth. Commun. **6**, 193 (1976).
4. H. Normant, T. Cuvigny et P. Savignac. Synthesis, 805 (1975); M. C. Vanderzwan et F. W. Hartner. J. Org. Chem. **43**, 2655 (1978).
5. E. V. Dehmlow. Angew. Chem. Int. Ed. Engl. **16**, 493 (1977); Chimia, **34**, 12 (1980).
6. R. R. Galluci et R. C. Coing. J. Org. Chem. **48**, 342 (1983).
7. H. H. Freedman et R. A. Dubois. Tetrahedron Lett. **38**, 3251 (1975).
8. J. F. Biellmann, H. D'Orchymont et M. P. Goeldner. Tetrahedron Lett. **43**, 4209 (1979).
9. German Patent No. 2.842.217 (10 Apr. 1980).
10. N. V. Kuznetsov et I. I. Krasavtsev. Ukr. Khim. Zh. **45**, 158 (1979).
11. M. Miocque et J. P. Duclos. Chim. Ther. **4**, 363 (1969).
12. J. Jarrousse. C.R. Acad. Sci. **232**, 1424 (1951).
13. J. Dockx. Synthesis, 441 (1973).
14. A. W. Herriot et D. Picker. J. Am. Chem. Soc. **97**, 2345 (1975).
15. R. F. Rekker et H. M. Kort. Eur J. Med. Chem. **14**, 479 (1979).
16. M. Halpern, Y. Sasson et M. Rabinovitz. J. Org. Chem. **48**, 1022 (1983).
17. M. Protiva. Collect. Czech. Chem. Commun. **14**, 354 (1949).
18. F. G. Godfrey *et al.* J. Am. Chem. Soc. **74**, 1313 (1952).
19. L. Knorr. Ber. **37**, 3507 (1904).
20. K. Sjosberg. Aldrichimica Acta, **13**, 55 (1980).
21. M. Fedoryński, K. Wojciechowski, Z. Matacz et M. Mąkosza. J. Org. Chem. **43**, 4682 (1978).
22. F. Guibe et G. Bram. Bull. Soc. Chim. Fr. 933 (1975).
23. B. Tchoubar et M. Verrier. Bull. Soc. Chim. Fr. 2151 (1960).
24. F. Montanari, D. Landini et F. Rolla. Top. Curr. Chem. **101**, 147 (1982); F. Montanari. Cron. Chim. **71**, 3 (1982).
25. P. Caubere. Le transfert de phase et son utilisation en chimie organique. Masson, Paris. 1982.
26. P. Depreux et A. Marcincal-Lefebvre. Il Farmaco Ed. Sc. **40**, 565 (1985).

COMMUNICATION

The anesthetic potency of *n*-alcohols. A model spectroscopic study in inverted micelles

PIERRE MÉNASSA, THÉRÈSE LUSSIER, AND CAMILLE SANDORFY
Département de chimie, Université de Montréal, Montréal (Qué.), Canada H3C 3J7
Received December 12, 1985

PIERRE MÉNASSA, THÉRÈSE LUSSIER, and CAMILLE SANDORFY. Can. J. Chem. **64**, 633 (1986).

A relation has been found between the anesthetic potency of *n*-alcohols ($n = 1, 3, 6, 7, 9, 11, 14$, and 16) and their association constants with polar groups in inverted micelles. From this point of view, cholesterol and 7-dehydrocholesterol behave like short-chain *n*-alcohols while cholestanol behaves like a long-chain *n*-alcohol.

PIERRE MÉNASSA, THÉRÈSE LUSSIER et CAMILLE SANDORFY. Can. J. Chem. **64**, 633 (1986).

On a pu démontrer qu'il existe une relation entre le pouvoir anesthésique des *n*-alcools et leur constante d'association avec des groupements polaires dans des micelles inverses, qui a été determinée pour $n = 1, 3, 6, 7, 9, 11, 14$ et 16. De ce point de vue, le cholestérol et le dehydro-7 cholestérol se comportent comme des *n*-alcools à chaîne courte alors que le cholestanol s'apparente aux *n*-alcools à chaîne longue.

Alcohols are known to have anesthetic potency (1). Pringle *et al.* (2) have shown that this potency increases with the length of the hydrocarbon chain in *n*-alcohols. There is, however, a "cutoff" at C_{13}. While the latter still possesses a weak anesthetic potency, C_{14} has no anesthetic potency at all (3).

In an attempt to find a correlation between this behavior and the physico-chemical properties of alcohols, Wilson *et al.* (4) compared the hydrogen bond (H-bond) forming tendencies in the series of alcohols from C_1 to C_{18} by infrared spectroscopic means. They found that in neutral solvents, the free/H-bonded ratio for self-association is independent of the chain length. The same applies to ester carbonyl/*n*-alcohol association. Subsequently, Ménassa and Sandorfy (5) undertook similar studies in a membrane mimetic environment. Their system consisted of sodium di(2-ethylhexyl) sulfosuccinate (AOT) with traces of water in carbon tetrachloride to which an alcohol was added. The detergent AOT containing traces of water forms inverted micelles in carbon tetrachloride (6). The infrared spectra were recorded on a Nicolet model 5DXB Fourier-transform ir spectrometer with a resolution of $2\,cm^{-1}$. The method for computing association constants has been given previously (5, 7). The association constants of *n*-alcohols with AOT exhibit a pronounced dependence on chain length. The alcohol/AOT association constant decreases with increasing chain length as shown in Fig. 1. The spectra give evidence that association occurs between the alcohols and the SO_3^- group of AOT. The carbonyl bands were not observably affected with the dilute solutions that were used in those studies. However, with higher water content and alcohol concentrations, alcohol/carbonyl (AOT) association could also be detected.

More importantly, the H-bond association constants stopped decreasing at C_{10} (5) and remained constant at about $5\,L\,mol^{-1}$. Thus there appears to be a parallelism between the effect of the chain length on the H-bond equilibria of alcohols in these systems and their anesthetic potency. While AOT can only be a remote model for actual cell membranes, an analogy exists: the alcohol (anesthetic) must cross a hydrophobic region before reaching the polar groups. So the inverted micelles used in this work, which consist of a hydrophobic belt containing polar groups inside, mimic to some extent a lipid membrane surrounding a protein that contains an ion channel (8). It is perhaps

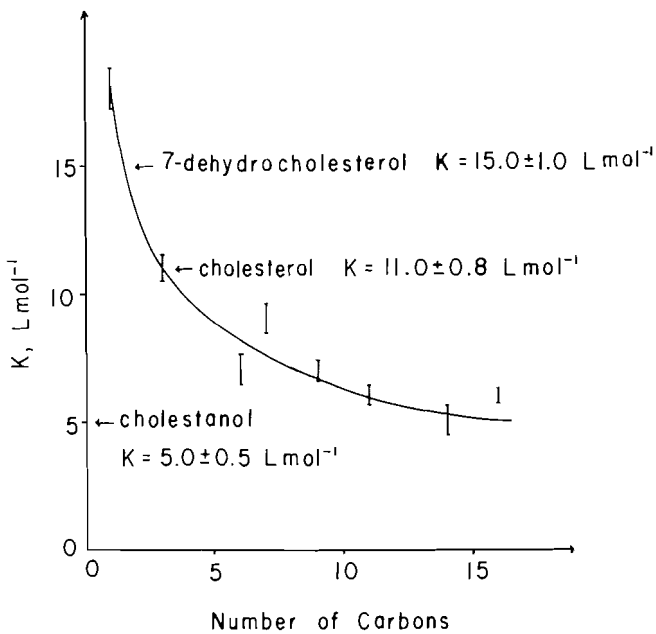

FIG. 1. The dependence of the AOT/alcohol association constants on the number of carbon atoms in *n*-alcohols (5). The association constants for the sterols depicted in Fig. 2 are also shown.

interesting in this respect that the breadth of the hydrophobic part of AOT (13 Å) is about the same as the length of C_{10}. In actual cell membranes, the breadth of the hydrophobic portion of the lipid is typically about 18 Å, about the same as the length of C_{14}.

A second observation made in our earlier work (5) concerns cholesterol. That cholesterol readily self associates by forming O—H...:O—H...:O—H... type H-bonds has been known for some time (9, 10). Now we have shown, by determination of H-bond association constants in the cholesterol/AOT/carbon tetrachloride system, that from this point of view cholesterol behaves like a short-chain alcohol (C_3), despite its bulky hydrocarbon moiety.

It then seemed interesting to us to ascertain whether this is a general property of sterols or if cholesterol represents a special

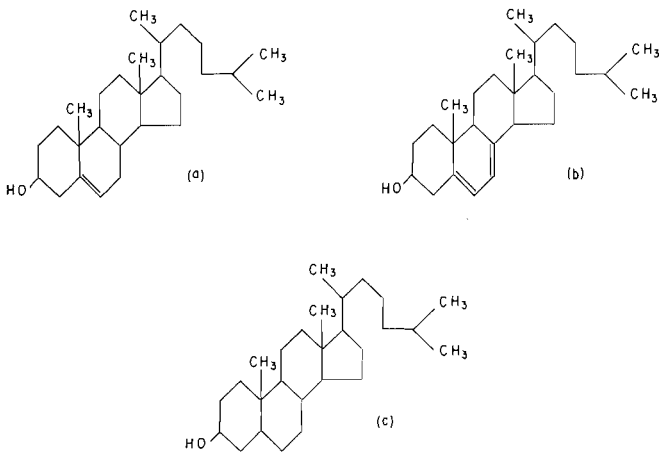

FIG. 2. The formulas of (a) cholesterol, (b) 7-dehydrocholesterol, and (c) cholestanol.

case. Cholestanol, a saturated sterol, and 7-dehydrocholesterol, which contains two conjugated double bonds, were studied (Fig. 2). The sterol/AOT association constants were found to be the following:

Cholesterol	$11.0 \pm 0.8\,L\,mol^{-1}$
Cholestanol	$5.0 \pm 0.5\,L\,mol^{-1}$
7-Dehydrocholesterol	$15.0 \pm 1.0\,L\,mol^{-1}$

Previously we found that cyclohexanol or *trans*-decahydro-2-naphthol have low alcohol/AOT association constants, like the long-chain *n*-alcohols (5). It appears then that the rings do not make it easier for the molecule to cross the hydrophobic belt of the AOT inverted micelles but that the double bonds, which make the molecules approach coplanarity, do.

Whether or not the above mentioned sterols possess an anesthetic potency is not known to us. However, certain steroids do possess anesthetic potency (11, 12) and the more potent ones contain the 3-OH group. All these observations seem to indicate that both hydrogen-bonding and hydrophobic interactions play a role in the anesthetic activity of alcohols. Their properties are likely to depend on a delicate balance between the two.

Acknowledgments

Financial help from the Natural Sciences and Engineering Research Council of Canada and le Ministère de l'Education du Québec are gratefully acknowledged. Our thanks are due to Dr. R. Buchet for helpful discussions.

1. J. POSTERNAK and E. ARNOLD. J. Physiol. **46**, 502 (1954).
2. M. J. PRINGLE, K. B. BROWN, and K. W. MILLER. Mol. Pharmacol. **19**, 49 (1981).
3. C. D. RICHARDS, C. A. KEIGHTLEY, T. R. HESKETH, and J. C. METCALFE. *In* Molecular mechanisms of anesthesia. Vol. 2. *Edited by* B. Raymond Fink. Raven Press, New York. 1980. p. 337.
4. L. WILSON, R. B. DE ALENCASTRO, and C. SANDORFY. Can. J. Chem. **63**, 40 (1985).
5. P. MÉNASSA and C. SANDORFY. Can. J. Chem. **63**, 3367 (1985).
6. M. UENO and H. KISHIMOTO. Bull. Chem. Soc. Jpn. **50**, 1637 (1977).
7. R. BUCHET, L. BEAUVAIS, and C. SANDORFY. J. Biomol. Struct. Dyn. **2**, 221 (1984).
8. R. BUCHET, C. SANDORFY, T. L. TRAPANE, and D. URRY. Biochim. Biophys. Acta. In press.
9. P. MERCIER, C. SANDORFY, and D. VOCELLE. J. Phys. Chem. **87**, 3670 (1983).
10. F. S. PARKER and K. R. BHASKAR. Biochemistry, **7**, 1286 (1968).
11. L. GYERMEK and L. F. SOYKA. Anesthesiology, **42**, 331 (1975).
12. T. J. O'LEARY, P. D. ROSS, and I. W. LEVIN. Biochemistry, **23**, 4636 (1984).

Estimation of heats of vaporization for non associating organic liquids from the boiling points at various pressures

J. PETER GUTHRIE

Department of Chemistry, University of Western Ontario, London, Ont., Canada N6A 5B7

Received May 30, 1985

J. PETER GUTHRIE. Can. J. Chem. **64**, 635 (1986).

At any pressure the heat of vaporization can be expressed as a quadratic function of the boiling point at that pressure. A seven parameter equation expressing the simultaneous dependence on boiling point and pressure can be fitted to the data; six pressures from 1 to 760 Torr (1 Torr = 133.3 Pa) were used. $\Delta H_{vap} = b_{11} + b_{12} \ln (p) + b_{13}p + (b_{21} + b_{22} \ln (p))t_{bp} + (b_{31} + b_{32} \ln (p))t_{bp}^2$. This relationship served as a guide for developing a relationship between vapour pressure at 25°C and the calorimetric heat of vaporization, and also a relationship between vapor pressure at 25°C and the boiling point at some other pressure. Parameters for both these relationships could be derived from the parameters obtained for ΔH_{vap} as a function of temperature and pressure. A third method was developed starting from an equation for vapor pressure and fitting to the heat of vaporization, the heat capacity of vaporization, and at least one t,p point. These methods allow the estimation of the vapor pressure at room temperature from very meager data. The problems of errors in estimated values are discussed.

J. PETER GUTHRIE. Can. J. Chem. **64**, 635 (1986).

À toutes les pressions, la chaleur de vaporisation peut être exprimée comme une fonction quadratique de son point d'ébullition à cette température. Toutes les données peuvent être accomodées par une équation à sept paramètres exprimant la dépendance simultanée sur le point d'ébullition et sur la pression; on a utilisé six pressions de 1 à 760 Torr. $\Delta H_{vap} = b_{11} + b_{12} \ln (p) + b_{13}p + (b_{21} + b_{22} \ln (p))t_{bp} + (b_{31} + b_{32} \ln (p))t_{bp}$. Cette relation a servi de guide pour développer une relation entre la pression de vapeur à 25°C et la chaleur de vaporisation calorimétrique ainsi que le point d'ébullition à d'autres pressions. On a pu obtenir les paramètres pour ces deux relations à partir des paramètres obtenus pour le ΔH_{vap} en fonction de la température et la pression. On a développé une troisième méthode à partir d'une équation pour la tension de vapeur et en y insérant la chaleur de vaporisation, la capacité calorifique de vaporisatin et au moins un point de t,p. Ces méthodes permettent d'évaluer la tension de vapeur à la température ambiante à partir de très peu de données. On discute des problèmes des erreurs dans les valeurs prédites.

[Traduit par la revue]

Introduction

In calculating the standard heat of formation of a gaseous compound, starting from a heat of formation determined by calorimetry on the liquid, it is necessary to have a value for the heat of vaporization at 25°C. Although there are standard methods for measuring heats of vaporization calorimetrically (1), the technique remains somewhat specialized and recourse is frequently had to estimation procedures (1). Of these, one of the simplest is that reported by Wadso (2), which needs only the normal boiling point.[1] The method is limited to non-hydrogen bonding liquids, with normal boiling points below 200°C. We have had occasion to determine heats of formation (3–8) which were used to calculate free energies of formation in aqueous solution. In the course of these calculations it was necessary to estimate the heat of vaporization. We have encountered difficulties when the normal boiling point could not be determined because of the thermal instability of the compound, or when the normal boiling point was higher than 200°C. Accordingly, we have sought for ways to extend the range of the Wadso equation, and took advantage of a report by Hildebrand and Scott (9) that ΔH_{vap} was a quadratic function of the normal boiling point. This approach could be applied at any vapour pressure. We have also had a need for estimates of the vapor pressures of organic liquids at 25°C, as part of the calculation of free energies of transfer from the gas to aqueous solution. In the present paper we wish to report the results of our attempts to generalize the Wadso equation. We have found empirical relations between the heat of vaporization at 25°C and the boiling point at various pressures, using a quadratic relation which allows a wider range of temperatures. The parameters of the quadratic can themselves be expressed as a function of pressure, allowing boiling points at any pressure to be used as the starting points for heat of vaporization estimates. Furthermore, the process can be inverted to allow the vapor pressure at any temperature to be estimated given only the heat of vaporization. We found that even better estimates of the vapor pressure can be obtained from any boiling point – pressure datum, using a relationship based on the empirical relationship found for ΔH_{vap}. Finally we have found that by fitting an equation, derived by Prausnitz *et al.* (10) from the theory of fluids, to ΔH_{vap}, ΔC_{vap}, and one p,t point we can obtain quite good vapor pressure estimates.

[1]Normal boiling point means boiling point at 1 atm = 101.325 kPa.

Results and discussion

The starting point for this work was the compilation of vapor pressure data by Stull *et al.* (11, 12), which gives boiling points at a series of pressures for a wide range of compounds. From this body of data, were selected those compounds which could not form hydrogen bonds, and for which there were calorimetric heats of vaporization available from the literature. For a number of ketones we used data from work by Ambrose *et al.* (13), and for the heavier hydrocarbons we replaced the values from ref. 12 by values from ref. 14 where these were significantly different; in both cases boiling points at the desired pressures were calculated from the empirical equations given by refs. 13 or 14. The set of data which we used is found in Table S1.[2] There are vapor pressure data for a number of large *n*-alkanes for which there are no heats of vaporization; since these compounds are solids with very low vapor pressures at room temperature, it is

[2]Copies of the supplementary material (Table S1, and larger versions of the graphs in Fig. 2) may be purchased from the Depository of Unpublished Data, CISTI, National Research Council of Canada, Ottawa, Ont., Canada K1A 0S2.

TABLE 1. Parameters for the quadratic dependence of ΔH_{vap} on t_{bp}

Pressure (Torr)	a_1 (kcal/mol)	a_2 (kcal/mol deg)	$10^4 a_3$ (kcal/moldeg^2)
	(a) Full data set		
1.	10.7(0.04)	0.0641(0.0015)	1.26(0.21)
10.	8.78(0.03)	0.0507(0.0008)	1.26(0.17)
40.	7.67(0.03)	0.0413(0.0011)	1.15(0.14)
100.	7.00(0.04)	0.0346(0.0014)	1.11(0.13)
400.	6.13(0.09)	0.0238(0.0020)	1.02(0.11)
760.	5.84(0.12)	0.0184(0.0023)	0.989(0.104)
	(b) Truncated data set		
1.	10.7(0.07)	0.0710(0.0058)	1.22(0.61)
10.	8.85(0.06)	0.0442(0.0038)	2.00(0.42)
40.	7.74(0.06)	0.0382(0.0026)	1.41(0.24)
100.	7.10(0.07)	0.0315(0.0023)	1.32(0.18)
400.	6.18(0.10)	0.0227(0.0022)	1.08(0.12)
760.	5.92(0.14)	0.0169(0.0026)	1.04(0.12)

unlikely that experimental values for the heats of vaporization of the supercooled liquids at 25°C will become available in the near future. For the *n*-alkanes the heat of vaporization is a very good linear function of number of carbon atoms for *n*-butane to *n*-heptadecane (15) or *n*-pentane to *n*-heptadecane (16) so that it seemed legitimate to include estimated values of the heat of vaporization for these compounds. This was done in order to have some data for high temperatures at the lowest vapor pressures. We used the equation $\Delta H_{vap} = 0.46 + 1.18 n_C$ (r = 0.99999), which is essentially identical to that reported by Mansson *et al.* (16). Similarly, values of ΔH_{vap} were estimated for 2-undecanone and 2-tridecanone by linear interpolation based on values for a series of 2-alkanones (17), for which we found $\Delta H_{vap} = (3.12 \pm 0.10) + (1.17 \pm 0.01 n_C)$ by least squares. The estimated values were given larger error limits to ensure that they were lightly weighted in the least squares calculations. For each pressure the data were fitted to the following quadratic expression in t_{bp} the boiling point (°C) at that pressure:

$$[1] \quad \Delta H_{vap} = a_1 + a_2 t_{bp} + a_3 t_{bp}^2$$

The fitting was done using a general least squares program which is based on the Marquardt algorithm[3] (18). The parameters evaluated in this way are found in Table 1. This table includes parameters fitting all the data in Table S1 and also a final restricted data set where all boiling points less than 0°C or greater than 300°C were excluded. This final set used only the range of practical interest and allowed a fit giving fewer serious deviations without needing additional parameters.

The parameters so determined are clearly all functions of pressure; Fig. 1 shows that they are all smooth functions of pressure, and in fact that a_2 and a_3 are linear in ln (p). For a_1 it is necessary to use a more elaborate function; in fact a constant term, a term linear in ln (p), and a term linear in p were required to account for the variation in a_1 with pressure.

$$[2] \quad a_i = b_{i1} + b_{i2} \ln (p) + b_{i3} p$$

Again, the best fit values of the parameters were determined by least squares, using eq. [2] with two or three parameters as needed. For eqs. [2] and [3] p is in atm (1 atm = 101.325 kPa).

[3]For polynomials it would actually be more efficient to use linear least squares, but the computational times are trivial and we have a convenient general program able to fit equations linear or nonlinear in the parameters.

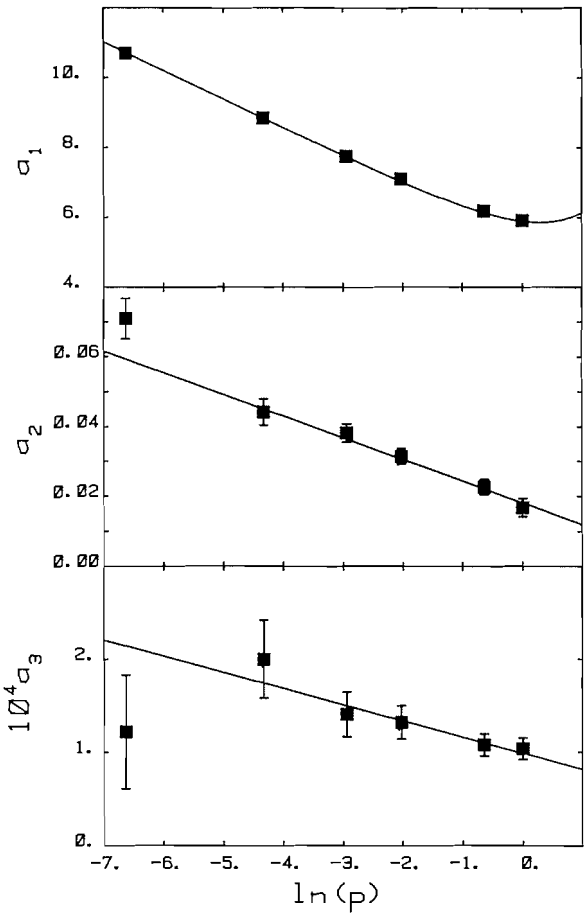

FIG. 1. Parameters for the quadratic relationship between heat of vaporization and boiling point, as a function of pressure. Parameter values from Table 1 for the full data set are plotted vs. ln (p) in atm, and the lines are drawn using the corresponding parameters from Table 2.

These parameters were used as initial estimates for the next stage of the calculations in which all the data in the full or the restricted set from Table S1 were fitted to the combined eq. [3], determining all the parameters at once to ensure that a set of parameters suited to fitting data at any pressure was obtained.

$$[3] \quad \Delta H_{vap} = b_{11} + b_{12} \ln (p) + b_{13} p + (b_{21} + b_{23} \ln (p)) t_{bp} + (b_{31} + b_{32} \ln (p)) t_{bp}^2$$

The parameters so determined are found in Table 2. The quality of the final fit is shown in Fig. 2.

With these parameters defined, it is clearly possible to calculate a version of eq. [1] for any pressure for which boiling point data at that pressure are available. It will, of course, be essential to exercise proper caution in evaluating the reliability of vapor pressure – temperature data from the literature, particularly when the data are simply physical properties of a compound and not measurements intended for high accuracy.

The fit to eq. [1] is actually very good at each pressure; for approximately 150 compounds, the weighted rms error is about 0.28 kcal/mol, and the worst deviations are only about 1.0 kcal/mol. The deviations may be summarized as: pressure (Torr), number of points, number of deviations greater than 1 kcal/mol, number of deviations greater than 2 kcal/mol; (full data set) 1, 142, 12, 4; 10, 150, 8, 0; 40, 154, 7, 1; 100, 154, 8, 0; 400, 154, 8, 0; 760, 154, 7, 0; (truncated data set) 1, 39, 5, 0; 10, 92, 10, 3; 40, 120, 3, 0; 100, 129, 3, 0; 400, 143, 4, 0; 760,

TABLE 2. Parameters for the dependence of the heat of vaporization parameters on the vapor pressure

Parameter	b_{i1}	b_{i2}	b_{i3}
	(a) Full data set		
a_1	5.14(0.04)	−0.841(0.010)	0.589(0.077)
a_2	0.0212(0.0010)	−0.00662(0.00023)	
a_3	$8.74(0.51)\times10^{-5}$	$-8.55(1.52)\times10^{-6}$	
	(a) Truncated data set		
a_1	5.28(0.07)	−0.822(0.017)	0.616(0.082)
a_2	0.0182(0.0014)	−0.00620(0.00060)	
a_3	$9.88(0.70)\times10^{-5}$	$-1.74(0.46)\times10^{-5}$	

140, 3, 0. The fit to eq. [3] is similarly good; the weighted rms deviation was 0.28 kcal/mol for either data set. For the full data set of 908 points there were only 50 deviations of more than 1.0 kcal/mol, and only 13 greater than 2.0 kcal/mol, while for the truncated data set of 526 points there were only 19 deviations of more than 1.0 kcal/mol, and none greater than 2.0 kcal/mol.

Although there was no improvement in the rms error using the restricted data set it seems better to use parameters based on this data set, because they give better description for high boiling compounds, even though there are severe deviations for boiling points less than 0°C. Leaving out points with boiling points less than 0°C has allowed a better description of the range of interest, at the price of a much poorer description of very low boiling compounds. The calculated curves begin to deviate seriously from the observed points at high temperatures (where the heats of vaporization are estimates and were accordingly given less weight in the fittng procedure). Clearly, the parameters reported allow a good calculation of ΔH_{vap} up to a boiling point of 300°C, but are not useful beyond this point. In a practical sense, however, it is rare to find compounds which are sufficiently thermally stable that meaningful boiling points above 300°C can be recorded, so the treatment reported here covers the normally accessible range of boiling points.

It is now possible to invert the procedure and develop an equation for estimating the vapor pressure given the heat of vaporization. For each parameter a_i in eq. [1] we substitute the appropriate form from eq. [2]; then by rearranging terms we get a transcendental equation, eq. [4], relating p and ΔH_{vap}

$$[4]\quad b_{13}p + [b_{12} + b_{22}\theta + b_{32}\theta^2]\,[\ln(p)] + [b_{11} + b_{21}\theta + b_{31}\theta^2 - \Delta H_{vap}] = 0$$

where θ is the temperature (°C) at which the vapor pressure (atm) is to be estimated. The term in p is insignificant at low pressures where the equation is of interest, so that in fact we have a linear equation in ln (p)

$$[5]\quad \ln(p) = [\Delta H_{vap} - b_{11} + b_{21}\theta + b_{31}\theta^2]/[b_{12} + b_{22}\theta + b_{32}\theta^2]$$

Substituting numerical values, and setting $\theta = 25$°C, we obtain eq. [6] giving the vapor pressure at room temperature, which is a quantity which we frequently need for free energy of transfer calculations.

$$[6]\quad \ln(p) = 5.66 - 0.988\Delta H_{vap}\ \text{(full data set)}$$
$$\ln(p) = 5.86 - 1.01\Delta H_{vap}\ \text{(truncated data set)}$$

The quality of the estimation was tested by using the data base in Table S1; for each compound the data were fitted to the simple Clausius Clapeyron equation, eq. [7], and the vapor pressure

$$[7]\quad \ln(p) = A + B/T$$

at 25°C was estimated. This value was compared to the value obtained by solving eq. [6] using the experimental heat of vaporization. The agreement is reasonable for pressures greater than 0.1 Torr, but becomes increasingly poor for lower pressures. Thus, eq. [6] is useful for interpolation. It should be borne in mind that the Clausius Clapeyron equation itself should not be used for long extrapolations because the heat of vaporization is not temperature independent, and consequently ln(p) is not a truly linear function of $1/T$. The curvature is slight, and a straight line is a remarkably good approximation (19). Nevertheless, any long extrapolation will be very sensitive to curvature or slight errors in the slope and will be unreliable.

Another approach is possible when there is no calorimetric heat of vaporization: since as we have shown ΔH_{vap} is a function of temperature and vapor pressure, $\Delta H_{vap} = f(t,p)$, it necessarily follows that $f(t_{bp},p_{obs}) = f(\theta,p)$ where t_{bp} is the boiling point (°C) at pressure p_{obs} (atm) and p is the vapor pressure at a reference temperature θ, normally 25°C. As before, since we are interested in the low pressure region, the term in eq. [3] linear in p can be neglected and we get

$$[8]\quad \ln(p) = \{b_{21}(t_{bp} - \theta) + b_{31}(t_{bp}^2 - \theta^2) + \ln(p_{obs})(b_{12} + b_{22}t_{bp} + b_{32}t_{bp}^2)\}/\{b_{12} + b_{22}\theta + b_{32}\theta^2\}$$

By collecting terms which are constant for a given value of θ taken as 25°C, we can simplify this to:

$$[9]\quad \ln(p) = c_1 + c_2\ln(p_{obs}) + (c_3 + c_4\ln(p_{obs}))t_{bp} + (c_5 + c_6\ln(p_{obs}))t_{bp}^2$$

The values of c_i were calculated from the values of b_{jk} given in Table 2; the values so calculated are given in Table 3.

This approach was tested using the data base from Table S1; the boiling point at 100 Torr was used as the reference point for calculating the vapor pressure at 25°C. Once again the agreement with the value obtained by a Clausius Clapeyron extrapolation was quite good for pressures greater than 0.1 Torr.

The most common situation where one needs to estimate a vapor pressure is one where the desired vapor pressure is quite low so that it is not practical to measure it without specialized apparatus. In order to estimate such vapor pressures one must take account of the nonlinear nature of the plot of ln (p) vs. $1/T$. Various methods have been suggested in the literature for the situation where good p–T data are available for a range of temperatures. King (20) and Ambrose (21) have proposed very similar equations involving four or five parameters which allow

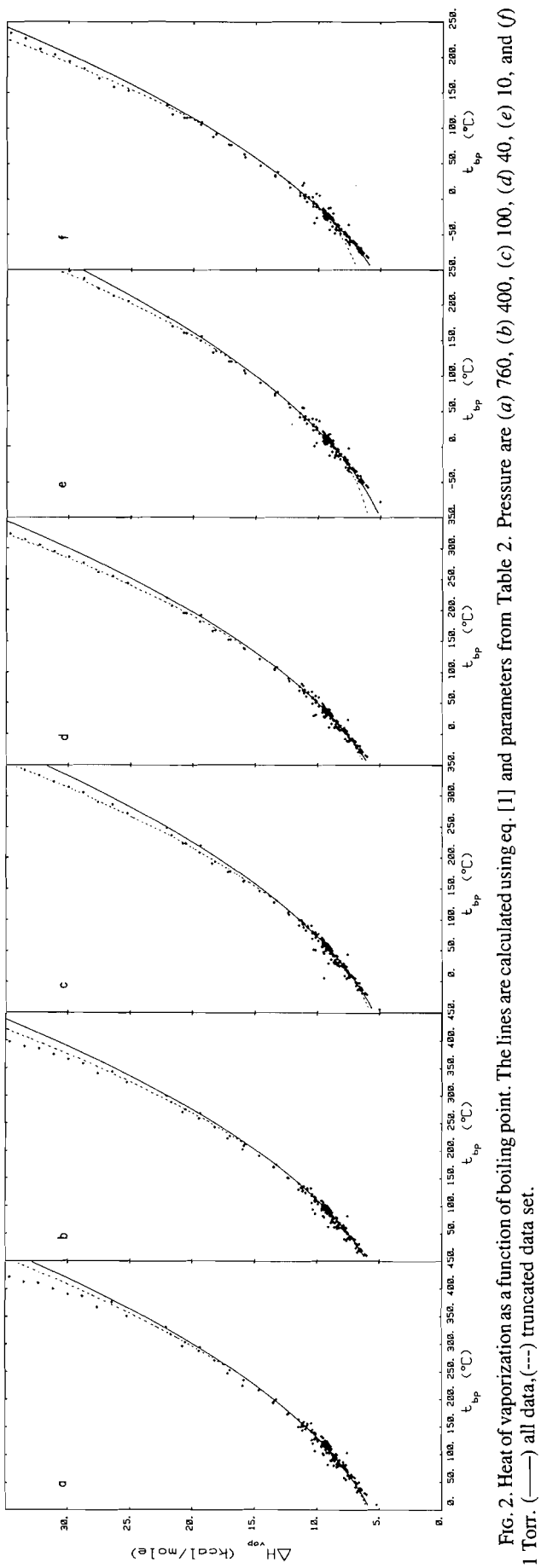

FIG. 2. Heat of vaporization as a function of boiling point. The lines are calculated using eq. [1] and parameters from Table 2. Pressure are (*a*) 760, (*b*) 400, (*c*) 100, (*d*) 40, (*e*) 10, and (*f*) 1 TORR. (——) all data, (---) truncated data set.

extrapolations down to very low pressures. Prausnitz (10) has proposed a five parameter equation which involves only two adjustable parameters from which the five parameters are calculated using relations based on the theory of fluids. For the situation where the data are not good enough for direct evaluation of the parameters, these (20, 21) and other (22, 23) authors have proposed making use of the approximate parallelism of $p-T$ curves by relations such as

$$[10] \quad \ln (p_A) = m \ln (p_B) + b$$

to estimate the pressure of substance A at a given temperature from the pressure of a reference substance B at the same temperature. Unfortunately this approach requires data over a significant range of temperatures and pressures in order to allow accurate determination of the slope and intercept required for extrapolation. If the range of data available is small then the extrapolation will be uncertain. This is precisely the situation in which we often find ourselves.

A solution to the dilemma is offered by the Prausnitz equation which requires only two adjustable parameters. Furthermore it differs from the equation favored by Ambrose and King in that the coefficients of the terms in T and T^2 are much smaller even though the overall curve is very similar. This suggests that the exact values of the parameters are not well determined by the data, but are subject to severe correlation. A similar conclusion is suggested by the fact that despite the empirical success of [10], which suggests that the coefficients for corresponding functions of T should be related by the slope parameter, m, we find that these coefficients frequently change sign as well as magnitude from one compound to another without impairing the fit. When the curvature is small the correction terms are not well defined and numerous sets of parameters may work equally well.

Our suggestion is that when the data are very sparse, one could obtain an estimate of the vapor pressure from the heat of vaporization, the heat capacity of vaporization, and a few $p-T$ points, even when these latter data would not themselves allow good extrapolation to lower temperatures. Since we have in this and previous papers (24, 25) reported methods for obtaining useful estimates of the heat and heat capacity of vaporization at 25°C, this seems an attractive way to make use of all of the limited information available. The procedure is to calculate Prausnitz' parameters, E_0/R and s, from the expressions for ΔH_{vap} and ΔC_{vap} derived from this equation. The equation is

$$[11] \quad \ln p = A + B/T + C \ln (T) + DT + ET^2 \; (p \text{ in atm}, T \text{ in K})$$

The first step was to express ΔH_{vap} and ΔC_{vap} in terms of the parameters as:

$$\Delta \mathrm{H}_{vap}/R = -B + CT + DT^2 + 2ET^3$$

$$\Delta \mathrm{C}_{vap}/R = C + 2DT + 6ET^2$$

where,

$$B = -E_0/R$$

$$C = 3/2 - s$$

$$D = (s - 1)/(E_0/R)$$

$$E = (s - 1)(s - 3)/2(E_0/R)^2$$

Then by an iterative solution E_0/R and s can be calculated. Although A could then be calculated (10), it seemed better to determine it empirically by fitting the equation to one or several

TABLE 3. Parameter values for eq. [9]

Parameter	Parameter value based on Full data set	Truncated data set
c_1	0.578	0.523
c_2	0.831	0.832
c_3	−0.0210	−0.184
c_4	0.00654	0.00628
c_5	-8.64×10^{-5}	-1.00×10^{-4}
c_6	8.45×10^{-6}	1.76×10^{-5}

p–T points to guarantee correctness at the lowest temperature for which the vapor pressure is known.

As a test of the procedure, we can use toluene, and from the following data:

$$\Delta H_{vap} = 9080 \text{ cal/mol } (1, 24)$$

$$\Delta C_{vap} = -12.5 \text{ cal/deg mol } (25, 26)$$

$$t = 1.5°\text{C at } p = 7.5 \text{ Torr } (21)$$

the parameters were determined to be: $A = 56.7632$, $B = -6594.12$, $C = -7.2539$, $D = 1.176\times10^{-3}$, $E = 5.130\times10^{-7}$, $E_0/R = 66594.12$, and $s = 8.7539$. The calculated pressure for 159 K was 0.00117 Pa; Ambrose (21) gives 0.001 Pa. This is a 17% error for a 115° extrapolation. Although this is not very good when compared to the performance of either the Ambrose or Prausnitz equations when they are fitted to good data, it is adequate for our purposes, which are to get vapor pressures accurate enough that the contribution from errors in vapor pressure is less than or comparable to the other errors in the thermochemical calculations, i.e., not more than a few tenths of a kcal/mol.

We may attempt to estimate the sensitivity to errors in ΔH_{vap} and ΔC_{vap} by using the Kirchhoff equation, eq. [12], in which ΔH_{vap} is taken as linear in temperature

$$[12] \quad \ln (p) = A + B/T + C \ln (T)$$

At temperature $\theta = 298$ K, $-\Delta H_\theta/R = -B + CT$, and $\Delta C_{vap} = \Delta C_\theta = -RC$; then $B = \Delta H_\theta/R - \Delta C_\theta/R$, and $C = -\Delta C_{vap}/R$. This leads to

$$\ln (p_\theta) = \ln (p_T) - \Delta H_\theta(1/\theta - 1/T)/R + \Delta C_\theta\theta(1/\theta - 1/T) + [\Delta C_\theta/R] \ln (T/\theta)$$

$$\sigma \ln p = [[-(1/R)(1/\theta - 1/T)]^2\sigma_{\Delta H}{}^2 + [(\theta/R)(1/\theta - 1/T) + (1/R) \ln (T/\theta)]^2\sigma_{\Delta C}{}^2]^{1/2}$$

The significance of the contributions can be seen by calculating the coefficients of $\sigma_{\Delta H}$ and $\sigma_{\Delta C}$ for various temperatures T, as shown in Table 4.

For errors of 1000 cal/mol in ΔH_θ and 1 cal/deg mol in ΔC_o and $T = 298$ K we expect an error of 1.27 in $\ln (p_\theta)$.

There are very few values of vapor pressures for high boiling liquids for use in testing these proposed extrapolation methods. Landolt-Bornstein (27) gives data for diethyl phthalate, for which $\ln (p_\theta) = -13.98$. The Clausius Clapeyron equation leads to $\ln (p_\theta) = -12.29$, with an error of 1.69, confirming that it is often a poor procedure for extrapolation . Equation [6] leads to $\ln (p_\theta) = -13.92$, in excellent agreement; eq. [9] leads to −14.77, in poorer agreement, and eq. [11] leads to −13.45 in useful agreement. Experimental values are available for hexadecane (20, 28, 29), $\ln (p_\theta) = -13.14$. The Clausius Clapeyron equation leads to $\ln (p_\theta) = -12.06$, again in poor agreement, eq. [6] leads to $\ln (p_\theta) = -14.00$, in poor agreement, eq. [9] leads to $\ln (p_\theta) = -13.76$, in only slightly better agreement; eq. [11], using the boiling point at 1 Torr to define A, leads to $\ln (p_\theta) = -13.22$, in excellent agreement.

TABLE 4. Sensitivity $\sigma \ln p$ to errors in ΔH and ΔC.

T (K)	Sensitivity to $\sigma_{\Delta H}$	$\sigma_{\Delta C}$
398	0.00042	0.27
498	0.00068	0.45
598	0.00085	0.60
698	0.00097	0.72

We found that $\ln (p_\theta)$ at 25°C is an excellent linear function of the number of carbon atoms for a series of n-alkanes from hexane to hexadecane (data from refs. 20, 28, 29), $\ln (p_\theta) = 5.206 - 1.1477n$ ($r = 0.99994$). Using this equation we could estimate values for the higher n-alkanes; these values were in reasonable agreement with those estimated using [6], [9], and [11], with errors of about 1 in $\ln (p_\theta)$ at $n = 29$.

The methods reported above extend and generalize the Wadso equation and make it possible to get useful thermochemical information from very meager physical data. We have encountered the need for such methods from our thermochemical investigations and hope that these methods will prove useful to other workers.

Acknowledgments

I thank the Natural Sciences and Engineering Research Council for financial support. I thank Kathleen F. Taylor for assistance with the development of some of the programs used in this work.

1. J. D. Cox and G. Pilcher. Thermochemistry of organic and organometallic compounds. Academic Press, London, U.K. 1970.
2. I. Wadso. Acta Chem. Scand. **20**, 544 (1966).
3. J. P. Guthrie. J. Am. Chem. Soc. **96**, 3608 (1974).
4. J. P. Guthrie. J. Am. Chem. Soc. **99**, 3991 (1977).
5. J. P. Guthrie. J. Am. Chem. Soc. **100**, 5892 (1978).
6. J. P. Guthrie. Can. J. Chem. **55**, 3562 (1977).
7. J. P. Guthrie and P. A. Cullimore. Can. J. Chem. **57**, 240 (1979).
8. J. P. Guthrie and P. A. Cullimore. Can. J. Chem. **58**, 1281 (1980).
9. J. H. Hildebrand and R. L. Scott. The solubility of nonelectrolytes. Reinhold, New York, 1950. p. 427.
10. D. S. Abrams, H. A. Massaldi, and J. M. Prausnitz. Ind. Eng. Chem. Fundam. **13**, 259 (1974); A. B. Macknick, J. Winnick, and J. M. Prausnitz. Ind. Eng. Chem. Fundam. **16**, 392 (1977).
11. D. R. Stull. Ind. Eng. Chem. **39**, 518 (1947).
12. Handbook of chemistry and physics. 48th ed. *Edited by* R. C. Weast. Chemical Rubber Co., Cleveland, 1967.
13. D. Ambrose, J. H. Ellender, E. B. Lees, C. H. S. Sprake, and R. Townshend. J. Chem. Thermodyn. **7**, 453 (1975).
14. R. C. Wilhoit and B. J. Zwolinski. Handbook of vapor pressures and heats of vaporization of hydrocarbons and related compounds. Thermodynamics Research Center. Texas A&M University, College Station, Texas, 1971.

15. E. MORAWETZ. J. Chem. Thermodyn. **4**, 139 (1972).
16. M. MANSSON, P. SELLERS, G. STRIDH, and S. SUNNER. J. Chem. Thermodyn. **9**, 91 (1977).
17. S. SUNNER, CH. SVENSSON, and A. S. ZELEPUGA. J. Chem. Thermodyn. **11**, 491 (1979).
18. P. A. BEVINGTON. Data reduction and error analysis for the physical sciences. McGraw–Hill, New York, 1969.
19. S. WALDENSTROM, K. STEGAVIK, and K. RAZI NAQVI. J. Chem. Ed. **59**, 30 (1982).
20. M. B. KING and H. AL-NAJJAR. Chem. Eng. Sci. **29**, 1003 (1974).
21. D. AMBROSE and R. H. DAVIES. J. Chem. Thermodyn. **12**, 871 (1980).
22. D. F. OTHMER and E.-S. YU. Ind. Eng. Chem. **60**, 22 (1968).
23. H. L. THOMAS and H. SMITH. J. Appl. Chem. **20**, 33 (1970).
24. J. P. GUTHRIE and K. F. TAYLOR. Can. J. Chem. **61**, 602 (1983).
25. J. P. GUTHRIE and K. F. TAYLOR. Can. J. Chem. **62**, 363 (1984).
26. R. SHAW. J. Chem. Eng. Data, **14**, 461 (1969).
27. LANDOLT-BORNSTEIN PHYSIKALISH-CHEMISCHE TABELLEN. Vol. 2. 6th ed. Springer, Berlin. 1960. part 2.
28. R. S. BRADLEY and A. D. SHELLARD. Proc. R. Soc. London **A198**, 239 (1949).
29. G. S. PARKS and G. E. MOORE. J. Chem. Phys. **17**, 1151 (1949).

Ion-molecule reactions with carbon chain molecules: reactions with diacetylene and the diacetylene cation

SEKSAN DHEANDHANOO, LEONARD FORTE, ARNOLD FOX, AND DIETHARD K. BOHME
Department of Chemistry and Centre for Research in Experimental Space Science, York University, Downsview, Ont., Canada M3J 1P3

Received September 6, 1985

SEKSAN DHEANDHANOO, LEONARD FORTE, ARNOLD FOX, and DIETHARD K. BOME. Can. J. Chem. **64**, 641 (1986).

Reactions of hydrocarbon and carbon/nitrogen ions with diacetylene and of the diacetylene radical cation with various molecules have been examined with a view to molecular growth by ion–molecule reaction. Measurements were performed with a Selected-Ion Flow Tube (SIFT) apparatus at 296 ± 2 K of the rate constants and product distributions for the reactions of C^+, CH_3^+, $C_2H_2^+$, C_3H^+, CN^+, C_2N^+, and $C_2N_2^+$ with C_4H_2 and of $C_4H_2^+$ with H_2, CO, C_2H_2, C_2N_2, and C_4H_2. Condensation and association reactions which build up the carbon content of the ion were observed to compete with charge transfer. For the reactions of CN^+ and $C_2N_2^+$ with C_4H_2 this growth involved the addition of cyanide to the carbon chain. The kinetics of protonation of diacetylene were also investigated. It was possible to bracket the proton affinity of diacetylene between the known proton affinities of HCN and CH_3OH with a value for $PA(C_4H_2)$ = 177 ± 5 kcal mol^{-1}, which results in a heat of formation for $C_4H_3^+$ of 305 ± 5 kcal mol^{-1}. Numerous secondary association reactions were observed to form adduct ions in helium buffer gas at total pressures of a few tenths of a Torr with rates near the collision rate. This was the case for $C_6H_4^+$ ($C_4H_2^+.C_2H_2$), $C_7H_5^+$ ($C_3H_3^+.C_4H_2$), $C_8H_4^+$ ($C_4H_2^+.C_4H_2$), $C_8H_5^+$ ($C_4H_3^+.C_4H_2$), $C_9H_3^+$ ($C_5H^+.C_4H_2$), $C_9H_4^+$ ($C_5H_2^+.C_4H_2$), $C_9H_5^+$ ($C_5H_3^+.C_4H_2$), $C_{10}H_4^+$ ($C_6H_2^+.C_4H_2$), $C_{10}H_5^+$ ($C_6H_3^+.C_4H_2$), $C_{11}H_7^+$ ($C_3H_3^+.(C_4H_2)_2$), $C_{12}H_6^+$ ($C_4H_2^+.(C_4H_2)_2$), $C_9H_3N^+$ ($HC_5N^+.C_4H_2$), and $C_{10}H_4N^+$ ($C_2N^+.(C_4H_2)_2$) where the reactants are indicated in parentheses. The observed high rates of association imply the formation of chemical bonds in the adduct ions but the structures of these ions were not resolved experimentally. In most instances there seems little basis for preferring acyclic over cyclic adduct ions.

SEKSAN DHEANDHANOO, LEONARD FORTE, ARNOLD FOX et DIETHARD K. BOME. Can. J. Chem. **64**, 641 (1986).

Dans le but d'évaluer la croissance des molécules par des réactions ion–molécule, on a étudié les réactions d'ions hydrocarbonés et d'ions carbone/azote avec le diacétylène ainsi que les réactions du radical cation du diacétylène avec diverses molécules. On a effectué les réactions à 296 ± 2 K et on les a étudiées à l'aide d'un appareil à tube à écoulement à ion choisi; on a mesuré les constantes de vitesse et les distributions de produits pour les réactions du C_4H_2 avec C^+, CH_3^+, $C_2H_2^+$, C_3H^+, CN^+, C_2N^+ et $C_2N_2^+$ et pour les réactions du $C_4H_2^+$ avec H_2, CO, C_2H_2, C_2N_2 et C_4H_2. On a observé que les réactions de condensation et d'association qui provoquent une croissance dans le contenu en carbone de l'ion sont en compétition avec le transfert de charge. Pour les réactions du CN^+ et du $C_2N_2^+$ avec le C_4H_2, cette croissance implique l'addition de cyanure sur la chaîne carbonée. On a aussi étudié la cinétique de la protonation du diacétylène. Il est possible de situer l'affinité protonique du diacétylène entre les affinités protoniques connues du HCN et du CH_3OH et ceci conduit à une valeur de $PA(C_4H_2)$ = 177 ± 5 kcal/mol et à une valeur de la chaleur de formation du $C_4H_3^+$ qui est égale à 305 ± 5 kcal/mol. On a observé que plusieurs réactions secondaires d'association forment des ions adduits dans un tampon d'hélium à des pressions totales de quelques dixièmes de Torr et avec des vitesses qui sont proches des vitesses de collision. Tel est le cas avec les ions suivants, où l'on a indiqué les réactifs entre parenthèses: $C_6H_4^+$ ($C_4H_2^+.C_2H_2$), $C_7H_5^+$ ($C_3H_3^+.C_4H_2$), $C_8H_4^+$ ($C_4H_2^+.C_4H_2$), $C_8H_5^+$ ($C_4H_3^+.C_4H_2$), $C_9H_3^+$ ($C_5H^+.C_4H_2$), $C_9H_4^+$ ($C_5H_2^+.C_4H_2$), $C_9H_5^+$ ($C_5H_3^+.C_4H_2$), $C_{10}H_4^+$ ($C_6H_2^+.C_4H_2$), $C_{10}H_5^+$ ($C_6H_3^+.C_4H_2$), $C_{11}H_7^+$ ($C_3H_3^+.(C_4H_2)_2$), $C_{12}H_6^+$ ($C_4H_2^+.(C_4H_2)_2$), $C_9H_3N^+$ ($HC_5N^+.C_4H_2$) et $C_{10}H_4N^+$ ($C_2N^+.(C_4H_2)_2$). Les taux élevés d'association observés impliquent qu'il y a formation de liaisons chimiques dans les ions adduits; toutefois, les structures de ces ions ne sont pas résolues expérimentalement. Dans la plupart des cas, il ne semble pas y avoir de préférence pour des ions adduits linéaires ou cycliques.

[Traduit par la revue]

Introduction

Extended "chain-like" molecules of bonded carbon atoms are formed naturally under a wide range of physical conditions. For example, cyanopolyynes with up to 11 carbon atoms have been identified at the low temperatures and low densities of the interstellar medium (1), while polyacetylenes with at least 12 carbon atoms have been found present at the high temperatures and the high densities of hydrocarbon flames (2). In the presence of ionization the formation and destruction of these chain molecules may involve ions (1, 2) and so it is of interest to establish the rates and products of ion–molecule reactions involving carbon chains. Here we report laboratory studies directed towards the identification and characterization of reactions of ions with diacetylene and reactions of the diacetylene radical cation with various molecules. Neutral and ionized diacetylene can be expected to be early intermediates in the growth of long carbon chain molecules from single carbon units.

Special emphasis is given in this investigation to reactions of diacetylene with the carbonaceous cations C^+, CH_3^+, $C_2H_2^+$, and C_3H^+, which are primal ions in the growth of molecules in the chemistry of interstellar gas clouds (3). Also, several reactions of carbon/nitrogen cations of the type $C_nN_m^+$ with diacetylene and of the diacetylene ion with C_2N_2 have been chosen for study because of their possible role in the chemistry of the ionosphere of Titan (4). Finally, a number of selected proton-transfer reactions have been investigated to estimate the proton affinity of diacetylene, which is useful in the elucidation of the neutralization of protonated diacetylene by proton transfer or electron–ion recombination.

Experimental

All measurements were taken with the Selected-Ion Flow Tube (SIFT) – flowing afterglow apparatus in the Ion Chemistry Laboratory at York University (5, 6). The reagent ions were derived from appropriate parent gases by electron impact at low pressures. An axial electron impact ionizer (Extranuclear, Model 041-3) was used as the ion source. Typical ion ejection energies were in the range 10–20 V. The initial spectrum for the experiments in which $C_4H_2^+$ was the selected ion is

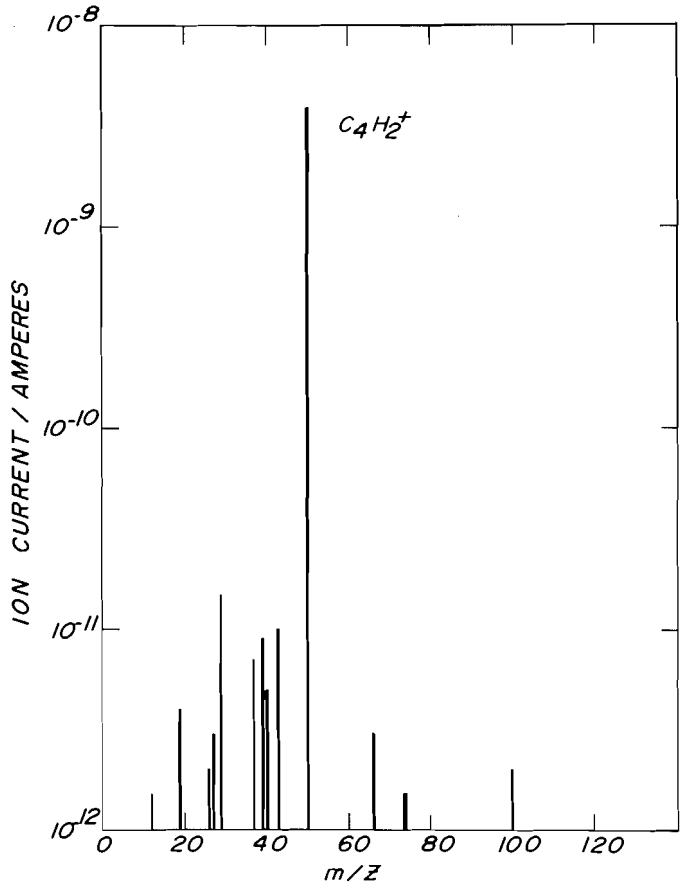

FIG. 1. SIFT spectrum for $C_4H_2^+$ derived from diacetylene (20% in helium) by electron impact at 53 eV. The $C_4H_2^+$ ions are injected at 16 V; the buffer gas is helium at 0.35 Torr. The background spectrum arises in part from collisional dissociation of $C_4H_2^+$ and in part from ion–molecule reactions with water vapour and other impurities in the helium, and with diacetylene leaking through the selection quadrupole.

shown in Fig. 1. Unless otherwise indicated, the individual reagent ions (and impurity ions) were generated in the manner described in a recent study of reactions with cyanoacetylene (7). The carrier gas was either helium or hydrogen. To remove traces of water vapour, the carrier gas was passed through zeolite traps (a 50:50 mixture of Union Carbide molecule sieves 4A and 13X) cooled to liquid nitrogen temperature. The diacetylene was prepared by the alkaline hydrolysis of 1,4-dichlorobut-2-yne (8) and was stored at Dry Ice temperature to avoid polymerization. Experiments with H_3^+ as the "chemical ionization" reagent indicated a purity of greater than 99%. All measurements were taken at an ambient temperature of 296 ± 2 K.

Results

Tables 1 and 2 present summaries of the reaction rate constants and product distributions obtained in this study for reactions of ions with diacetylene. Table 1 gives the results for reactions of carbonaceous ions and nitrogen-containing carbonaceous ions with cyanoacetylene, while Table 2 is restricted to results obtained for the proton-transfer reactions. Table 3 provides a summary for the reactions investigated with the diacetylene cation. Rate constants and product distributions were determined in the usual manner (5, 9). The tables include all of the primary product ions that were observed to contribute more than 5% to the total primary products. The branching ratios have been rounded off to the nearest 5% and are accurate to ±30%. The reaction rate constants are compared with collision rate constants derived with the Langevin theory (10)

TABLE 1. Summary of rate constants (in units of 10^{-9} cm^3 molecule^{-1} s^{-1}) and product distributions measured at 296 ± 2 K for ion–molecule reactions with diacetylene

Reactant ion	Products	Branching ratio	k_{exp}[a]	k_c[b]
C^+	$C_5H^+ + H$	0.50	2.9	1.84
	$C_4H_2^+ + C$	0.45		
	$C_3H^+ + C_2H$	0.05		
CH_3^+	$C_3H_3^+ + C_2H_2$	0.9	1.3	1.69
	$C_5H_3^+ + H_2$	0.1		
$C_2H_2^+$	$C_4H_2^+ + C_2H_2$	0.9	1.4	1.39
	$C_6H_3^+ + H$	0.1		
C_3H^+	$C_5H_2^+ + C_2H$	0.85	1.2	1.24
	$C_5H^+ + C_2H_2$	0.10		
	$C_4H_2^+ + C_3H$	0.05		
$C_3H_3^+$	$C_3H_3^+.C_4H_2$	1.0	~1	1.23
$C_4H_2^+$	$C_4H_2^+.C_4H_2$	0.9	1.3	1.15
	$C_6H_2^+ + C_2H_2$	0.1		
$C_4H_3^+$	$C_4H_3^+.C_4H_2$	0.9	~1	1.14
	$C_6H_3^+ + C_2H_2$	0.1		
C_5H^+	$C_5H^+.C_4H_2$	1.0	~1	1.09
$C_5H_2^+$	$C_5H_2^+.C_4H_2$	0.4	~1	1.09
	$C_7H_3^+ + C_2H$	0.6		
$C_5H_3^+$	$C_5H_3^+.C_4H_2$	1.0	~1	1.09
$C_6H_2^+$	$C_6H_2^+.C_4H_2$	1.0	~1	1.05
$C_6H_3^+$	$C_6H_3^+.C_4H_2$	1.0	~1	1.05
$C_3H_3^+.C_4H_2$	$C_3H_3^+.(C_4H_2)_2$	1.0	~1	1.01
$C_4H_2^+.C_4H_2$	$C_4H_2^+.(C_4H_2)_2$	1.0	~1	0.99
CN^+	$C_4H_2^+ + CN$	0.75	0.97	1.39
	$HC_5N^+ + H$	0.25		
C_2N^+	$C_5H^+ + HCN$	0.6	1.3	1.23
	$C_4H_2^+ + C_2N$	0.2		
	$C_2N^+.C_4N_2$	0.2		
$C_2N_2^+$	$C_4H_2^+ + C_2N_2$	0.9	1.2	1.14
	$HC_5N^+ + HCN$	0.1		
HC_5N^+	$HC_5N^+.C_4H_2$	1.0	~1	1.05
$C_2N^+.C_4H_2$	$C_2N^+.(C_4H_2)_2$	1.0	~1	1.02

[a]The accuracy of the rate constants is estimated to be better than ±30% unless the rate constant is indicated to be approximate. Only the apparent bimolecular rate constant is given. The measurements were taken at helium pressures in range from 0.27 to 0.37 Torr and helium densities in the range from 9.0×10^{15} to 1.2×10^{16} atoms cm^{-3}.

[b]Collision rate constants derived from the Langevin theory (10).

with an estimated polarizability for diacetylene of 6.0 Å^3 (11). Thermochemical data were taken from the usual sources (12, 13).

He^+/He_2^+

He^+ was derived from helium at 35 eV and injected into helium carrier gas at 0.32 Torr (1 Torr = 133.3 Pa). Approximately 30% conversion of He^+ to He_2^+ was observed downstream. Both ions reacted rapidly with diacetylene to yield a variety of product ions corresponding to charge transfer and dissociative charge transfer. No attempt was made to discern branching ratios for the reactions of the two helium ions. The rate constant for the reaction of He^+ was determined to be 2.7×10^{-9} cm^3 molecule^{-1} s^{-1}.

C^+

More than 95% of the C^+ was in the ^2P ground state (7). The C^+ was observed to react rapidly with diacetylene to produce three product ions, as can be seen from Fig. 2. The $C_4H_2^+$ arises from the charge transfer reaction, which is 25 kcal mol^{-1} exothermic. The other major product ion was C_5H^+, which is

TABLE 2. Summary of rate constants (in units of 10^{-9} cm^3 molecule^{-1} s^{-1}) measured at 296 ± 2 K for proton-transfer reactions with diacetylene

Reactant ion	Product	k_{exp}[a]	k_c[b]
H_3^+	$C_4H_3^+$	2.6	3.4
N_2H^+	$C_4H_3^+$	1.1	1.3
H_3O^+	$C_4H_3^+$	1.1	1.5
H_2CN^+	$C_4H_3^+$	1.4	1.3
$CH_3OH_2^+$	$CH_3OH_2^+.C_4H_2$	0.37[c]	1.3

[a]The accuracy of the rate constants is estimated to be better than ±30%.
[b]Collision rate constants derived from the Langevin theory (10).
[c]In hydrogen buffer gas at a total pressure of 0.36 Torr and concentration of 1.2×10^{16} molecules cm^{-3}.

TABLE 3. Summary of rate constants and product distributions measured at 296 ± 2 K for reactions with $C_4H_2^+$ derived from diacetylene

Neutral reactant	Products	Product distribution[a]	Rate constant[b]
H_2			≤5 (−13)
CO	$C_4H_2^+.CO$	0.5	1.9 (−11)
	$HC_5O^+ + H$	0.5	
C_2H_2	$C_4H_2^+.C_2H_2$	1.0	8.4 (−10)
C_4H_2	$C_4H_2^+.C_4H_2$	0.9	1.3 (−9)
	$C_6H_2^+ + C_2H_2$	0.1	
C_2N_2	$C_4H_2^+.C_2N_2$	0.98	4.3 (−11)
	$HC_5N^+ + HCN$	0.02	

[a]The branching ratio may be in error by as much as ±20%.
[b]Rate constants are expressed as a $(-b)$ to represent $a \times 10^{-b}$. The units are cm^3 molecule^{-1} s^{-1}. The accuracy is estimated to be better than ±30%. All rate constants are effective bimolecular rate constants for the disappearance of $C_4H_2^+$ in helium buffer gas at total pressures in the range from 0.26 to 0.36 Torr and helium concentrations from 8.4×10^{15} to 1.2×10^{16} atoms cm^{-3}.

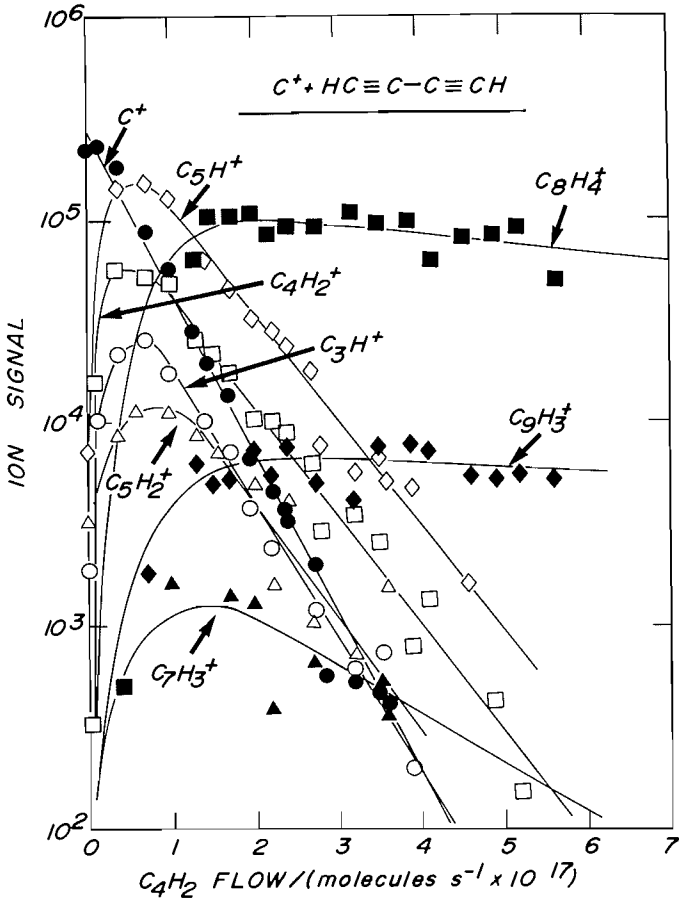

FIG. 2. The varieties in ion signals observed for the addition of diacetylene into the reaction region of the SIFT apparatus in which C^+ is initially established in helium buffer gas. $P = 0.275$ Torr, $\bar{v} = 5.6 \times 10^3$ cm s^{-1}, $L = 46$ cm, and $T = 295$ K. The C^+ is derived from cyanogen (10% in helium) at an electron energy of 60 eV.

probably the carbene cation HC≡C-C≡C-C:$^+$ that may be formed by C—H bond insertion with elimination of a hydrogen atom. Cyclic isomers of C_5H^+ are likely to be less stable. A minor channel of the reaction of C^+ with diacetylene leads to C_3H^+, which is probably the carbene cation HC≡C-C:$^+$ that may arise by C—C bond insertion with elimination of C_2H. The branching ratios observed for the production of C_3H^+ and C_5H^+ suggest that C—C bond insertion occurs 10 times less frequently than C—H bond insertion. C—H bond insertion can be expected to be more likely since it leads to a secondary carbocation intermediate in which the positive charge can be delocalized, while C—C bond insertion involves a primary carbocation intermediate in which the positive charge is localized.

Figure 2 also shows that secondary reactions were observed for all three primary product ions. The C_5H^+ was observed to rapidly add a molecule of diacetylene according to reaction [1].

[1] $C_5H^+ + C_4H_2 \rightarrow C_9H_3^+$

The structure of the $C_9H_3^+$ product ion is uncertain. However, if the C_5H^+ has carbene character, it can be expected to react with diacetylene by C—H bond insertion to form the acyclic cation $^+CH(C_4H)_2$. The high specific rate of association is consistent with such chemical bond formation in the adduct, as is the failure to observe rapid addition of a second molecule of diacetylene. The secondary reactions of $C_4H_2^+$ and C_3H^+ were similar to those observed in separate experiments, described later in the text, in which these ions were prepared directly in the electron impact source.

CH_3^+

Charge transfer is slightly (7 kcal mol^{-1}) endothermic in this case and was not observed. Figure 3 shows that the major product ion was $C_3H_3^+$ and that $C_5H_3^+$ was a minor product. The secondary reactions [2] to [4]

[2] $C_3H_3^+ + C_4H_2 \rightarrow C_7H_5^+$

[3] $C_7H_5^+ + C_4H_2 \rightarrow C_{11}H_7^+$

[4] $C_5H_3^+ + C_4H_2 \rightarrow C_9H_5^+$

were also observed to occur. They all involve the addition of diacetylene. The fast secondary reaction of $C_3H_3^+$ with diacetylene provides insight into the structure of this ion. Available thermochemical data indicate that the reaction of CH_3^+ with diacetylene may produce either the linear (propargyl) or the cyclic (cyclopropenium) isomer of $C_3H_3^+$. The ICR (ion cyclotron resonance) measurements of Smyth *et al.* (14) at low pressure have shown that only the linear isomer reacts with diacetylene. Our observation of the secondary reaction of $C_3H_3^+$ therefore implies that the reaction of CH_3^+ with diacetylene predominantly forms the linear isomer of $C_3H_3^+$. In the case of the formation of the minor $C_5H_3^+$ product ion, there is no basis for preferring an acyclic isomer (e.g.

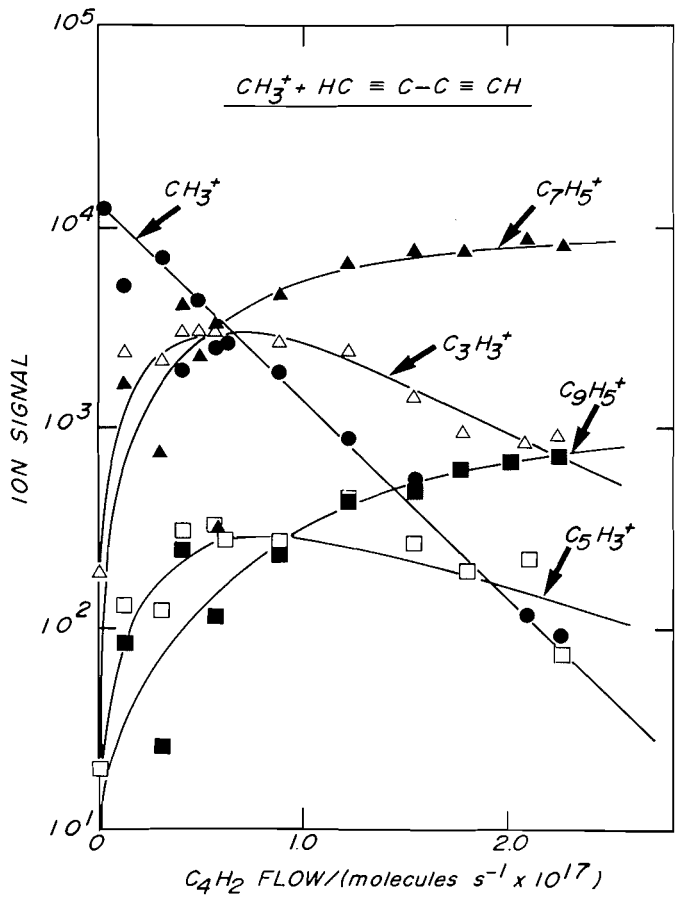

FIG. 3. The variations in ion signals observed for the addition of diacetylene into the reaction region of the SIFT apparatus in which CH_3^+ is initially established in helium buffer gas. $P = 0.335$ Torr, $\bar{v} = 5.3 \times 10^3$ cm s^{-1}, $L = 46$ cm, and $T = 293$ K. The CH_3^+ is derived from pure methane at an electron energy of 23 eV.

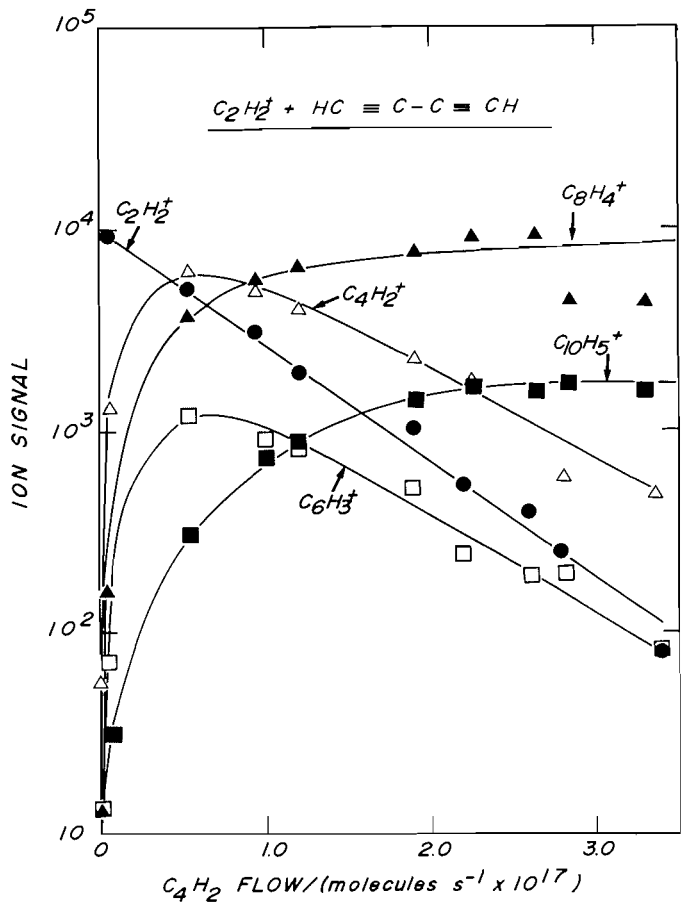

FIG. 4. The variations in ion signals observed for the addition of diacetylene into the reaction region of the SIFT apparatus in which $C_2H_2^+$ is initially established in helium buffer gas. $P = 0.372$ Torr, $\bar{v} = 6.7 \times 10^3$ cm s^{-1}, $L = 46$ cm, and $T = 295$ K. The $C_2H_2^+$ is derived from pure acetylene at an electron energy of 35 eV.

$^+CH_2$-C≡C-C≡CH) over a cyclic isomer (e.g. a C_2H substituted cyclopropenium ion), except perhaps by analogy with the preferred production of the linear propargyl isomer of $C_3H_3^+$.

The structures of the diacetylene adduct ions produced by reactions [2]–[4] are also not known. However, the high specific rates for their formation again imply formation of strong chemical bonds. A possible and interesting cyclic isomer of the $C_7H_5^+$ ion formed in reaction [2] is the phenyl carbene cation, $C_6H_5C:^+$. This carbene cation may add a second molecule of diacetylene, as in reaction [3], by C—H bond insertion to yield $^+CHC_4H(C_6H_5)$, a possible cyclic isomer of $C_{11}H_7^+$. Finally, the $C_9H_5^+$ ion formed in reaction [4] may also have a cyclic structure. One possibility is the formation of c-$C_5H_4(C_4H)^+$.

$C_2H_2^+$

Charge transfer was observed to be the main product channel for this reaction but there was a significant (10%) channel leading to carbon-chain lengthening with elimination of H in the formation of $C_6H_3^+$, which presumably is protonated triacetylene. This is evident in Fig. 4. Also, both product ions were seen to rapidly react further with diacetylene. The $C_6H_3^+$ responded to diacetylene with the addition reaction [5]. The

[5] $C_6H_3^+ + C_4H_2 \rightarrow C_{10}H_5^+$

resulting $C_{10}H_5^+$ is likely to be a proton-bound adduct of diacetylene and triacetylene but cyclic isomers again cannot be ruled out. The $C_4H_2^+$ responded to diacetylene in the manner indicated later in the text for the separate study of this reaction.

C_3H^+

The C_3H^+ carbene cation was observed to react with diacetylene primarily by condensation with elimination of C_2H or C_2H_2 leading to carbon-chain lengthening in the ion. Charge transfer appeared as only a minor channel. The predominant $C_5H_2^+$ product ion may result from C—H bond insertion with loss of C_2H and formation of HC≡C—CH=C=C$^{\bullet +}$ or from C—C bond insertion with loss of C_2H and formation of the radical cation $^\bullet C^+(C{\equiv}CH)_2$. The C_5H^+ formed by elimination of C_2H_2 is likely to be the carbene cation HC≡C—C≡C—C:$^+$. All three product ions were observed to react further. The C_5H^+ responded according to reaction [1] and the $C_4H_2^+$ reacted in the manner described later in the text. The $C_5H_2^+$ radical cation appeared to react further by addition and by condensation with elimination of C_2H in the following manner:

[6*a*] $C_5H_2^+ + C_4H_2 \rightarrow C_9H_4^+$

[6*b*] $\rightarrow C_7H_3^+ + C_2H$

In this case C—H insertion could lead to the acyclic radical cation HC≡C—CH=C=CH—C$^\bullet$=C$^+$—C≡CH, which may lose C_2H to form the carbon-chain cation HC≡C—CH=C=CH—C≡C$^+$.

$C_4H_2^+$

Ionized acetylene was reacted with carbon monoxide, acetylene, diacetylene, and cyanogen. No reaction was observed with hydrogen. Charge transfer and hydrogen atom transfer are endothermic with this molecule. Available heats of formation indicate that formation of the adduct ion $C_4H_4^+$ may be exothermic and that several isomers of $C_4H_4^+$ are possible, but it is not clear which one might be preferred. In any case, the very low upper limit to the rate constant for this reaction suggests that formation of the adduct involves a positive activation energy.

A slow reaction was observed with carbon monoxide. Approximately equal amounts were produced of the adduct ion $C_4H_2^+$.CO and the condensation product HC_5O^+, which involves elimination of H. No further reaction with CO was noticed with either product.

Acetylene was observed to add to $C_4H_2^+$ with a rate constant close to the collision limit but addition of a second molecule of acetylene was not rapid. It is not known whether the failure to add a second molecule of acetylene is indicative of the formation in the initial addition reaction of a cyclic product ion such as ionized benzyne, or an acylic product ion such as ionized 3-hexene-1,5-diyne, but both types of product are possible.

Addition was also the major channel with diacetylene, although in this case about 10% of the reaction led to the elimination of acetylene with formation of what may be ionized triacetylene. Again the measured rate constant for the loss of $C_4H_2^+$ is close to the collision limit. Results are shown in Fig. 5. The $C_6H_2^+$ is seen also to add a molecule of diacetylene but addition of a second molecule of diacetylene appears to be relatively unfavourable for both adduct ions in the product spectrum.

The primary product distribution observed for the reaction of $C_4H_2^+$ with C_4H_2 differs from that measured at lower pressures with an ICR (15), which indicates loss of C_2H_2 (83%), H_2 (17%), and H (1%) without any adduct formation. One cause of this difference may be the collisional stabilization of reactant and adduct ions, which proceeds at the moderate pressures of the SIFT experiments and which will be essentially absent in the ICR experiments. Observations that are consistent with such an interpretation have been made very recently in an ICR – high pressure mass spectrometer study (16). Loss from the adduct ion of both acetylene and hydrogen was noted in ICR experiments at $\sim 5 \times 10^{-6}$ Torr, but the loss of H_2 was observed to be entirely quenched in mass spectrometer experiments at pressures above ~0.01 Torr. Furthermore, the $C_6H_2^+$ produced by the reaction of $C_5H_2^+$ with C_4H_2 was seen to react further with C_4H_2, under ICR conditions, to produce $C_8H_2^+$ and $C_{10}H_2^+$ by elimination from the adduct ion of C_2H_2 and H_2, respectively. In contrast, all the adduct ions were observed to be stabilized in the high pressure mass spectrometer.

There is good agreement between the SIFT and ICR results on the rate constants for the loss of $C_4H_2^+$ and $C_6H_2^+$ in their reactions with C_4H_2. In the case of $C_4H_2^+$ the SIFT rate constant of $(1.3 \pm 0.4) \times 10^{-9}$ cm^3 molecule^{-1} s^{-1} is the same, within experimental error, as the ICR rate constants of 1.4×10^{-9} cm^3 molecule^{-1} s^{-1} (15) and $(1.39 \pm 0.5) \times 10^{-9}$ cm^3 molecule^{-1} s^{-1} (16). Also, for the reaction of $C_6H_2^+$ with C_4H_2, the ICR rate constant of $(1.06 \pm 0.4) \times 10^{-9}$ cm^3 molecule^{-1} s^{-1} is the same as the value of 1×10^{-9} cm^3 molecule^{-1} s^{-1} estimated from the SIFT results.

It is of interest to consider briefly the possible structures of the highly unsaturated hydrocarbon ions $C_8H_4^+$ and $C_{10}H_4^+$

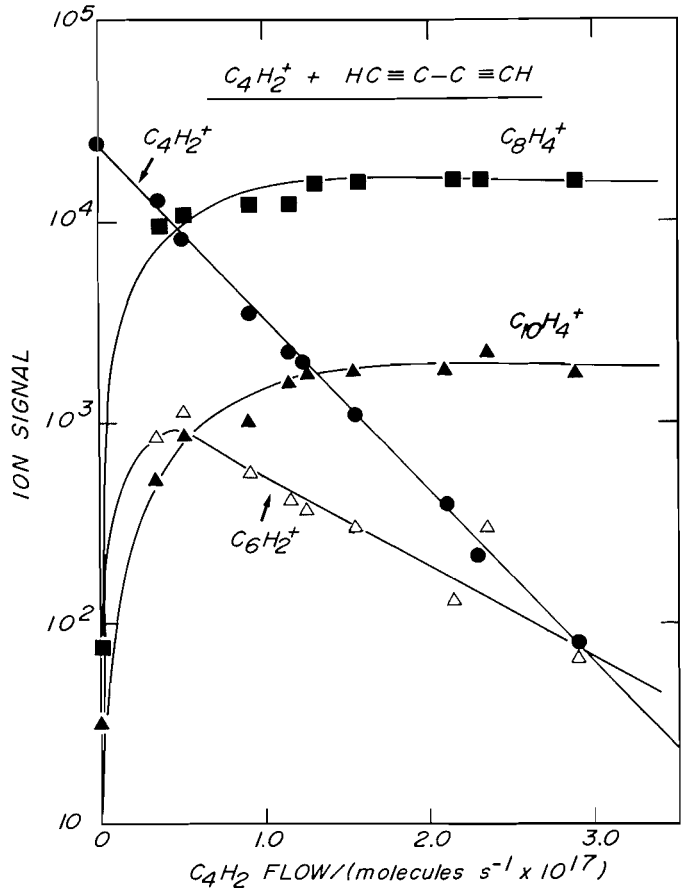

FIG. 5. The variations in ion signals observed for the addition of diacetylene into the reaction region of the SIFT apparatus in which the diacetylene radical cation is initially established in helium buffer gas. P = 0.259 Torr, $\bar{v} = 5.3 \times 10^3$ cm s^{-1}, L = 45 cm, and T = 297 K. The $C_2H_2^+$ is derived from diacetylene (10% in helium) at an electron energy of 35 eV.

produced in the addition reactions of $C_4H_2^+$ and $C_6H_2^+$ with C_4H_2. Carbon-chain isomers may be achieved by the addition of the C—H bond of one reagent across the triple bond of the other. The $C_8H_4^+$ isomer produced in this way would be HC≡C—C≡C—CH=CH—C≡CH$^+$, while HC≡C—C≡C—CH=CH—C≡C—C≡CH$^+$ would be a possible $C_{10}H_{4+}$ chain isomer. Formation of carbon-ring isomers can also be imagined. For example, $C_8H_4^+$ may have a cyclic structure with two alternating triple and double bonds while the analogous cyclic $C_{10}H_4^+$ structure would have an additional triple bond. Possible structures of $C_{2n}H_n^+$ and $C_{2n+2}H_n^+$ ions in general have been considered in more detail by Buckley *et al.* (16), who have observed sequential addition of diacetylene up to the formation of $C_{20}H_{10}^+$ and $C_{18}H_8^+$, respectively. Furthermore, these authors have identified reactivity patterns that suggest that the sequence initiated by $C_4H_2^+$ involves production of both cyclic and acyclic ions, with the latter being unreactive and increasingly preferred as the ion grows.

Adduct formation was also predominant in the SIFT experiments for the reaction of $C_4H_2^+$ with cyanogen, but there was also an indication of a minor channel (2%) leading to elimination of HCN and production of what is likely to be ionized cyano- or isocyanodiacetylene. Both product ions did not appear to rapidly react further with cyanogen. The specific rate for the addition of cyanogen to $C_4H_2^+$ is relatively low, so that the

adduct ion may not involve chemical bond formation in this case. The ion HC(CN)=C(CN)—C≡CH$^+$ would be one possible chemically bound adduct.

CN^+

The CN^+ ion was observed to react with diacetylene predominantly by charge transfer and by H atom elimination to form what is likely to be ionized cyanodiacetylene. The nature of these reaction channels and the measured branching ratios is very similar to those we have determined previously for the reaction of CN^+ with acetylene (17). Both product ions were observed to rapidly react further with diacetylene in the manner described earlier in the text in the case of $C_4H_2^+$, and by addition in the case of HC_5N^+ to form $HC_5N^+.C_4H_2$. The possible structures of the latter adduct are likely to be analogous to those discussed earlier for the $C_4H_2^+.C_4H_2$ adduct ion.

C_2N^+

The C_2N^+ was derived by electron impact at 60–80 eV from a 10% mixture of cyanogen in helium and exhibited only a single reactivity towards diacetylene (7). Product channels were observed corresponding to charge transfer, formation of C_5H^+, and adduct formation. Formation of C_5H^+ with elimination of HCN was the preferred channel. Since C_2N^+ may have carbene character, it seems likely that the formation of the adduct involves C—H bond insertion. Thus N≡C—CH$^+$—C≡C—C≡CH is a plausible intermediate, most of which eliminates HCN to form C_5H^+ and some of which is stabilized by collision to produce the $C_6H_2N^+$ product. Figure 6 shows that all three primary product ions add a molecule of diacetylene in rapid secondary reactions. The addition reactions with $C_4H_2^+$ and C_5H^+ have already been discussed, while the addition reaction with $C_6H_2N^+$ may proceed in analogy with the addition reaction of $C_5H_3^+$ noted earlier in the text.

$C_2N_2^+$

The $C_2N_2^+$ derived from cyanogen by electron impact was observed to react primarily by charge transfer. A minor channel was observed to lead to what is presumably ionized cyanodiacetylene. The observed secondary reactions of $C_4H_2^+$ and HC_5N^+ with diacetylene were as those described earlier in the text.

H_3^+, N_2H^+, H_3O^+, H_2CN^+, $CH_3OH_2^+$

Except for $CH_3OH_2^+$, these ions all reacted rapidly with diacetylene by proton transfer with rate constants close to the collision limit. The results are summarized in Table 2. The $CH_3OH_2^+$ was observed to react only by addition but with a high effective bimolecular rate constant. The high efficiency implies that the adduct is strongly bound, presumably by the proton. The secondary ion chemistry in helium buffer gas indicated a further rapid reaction of the $C_4H_3^+$ proton transfer product with diacetylene. The main channel of this secondary reaction was observed to correspond to addition to form $C_8H_5^+$ but a significant competing channel, about 10%, led to the formation of $C_6H_3^+$ as indicated in reaction [7].

[7*a*] $C_4H_3^+ + C_4H_2 \rightarrow C_8H_5^+$

[7*b*] $\rightarrow C_6H_3^+ + C_2H_2$

The $C_8H_5^+$ adduct may be the proton-bound diacetylene dimer but cyclic isomers are also possible, such as, for example, $C_6H_5C_2^+$. Complications arose in the secondary ion chemistry from the presence of hydrogen, which was added in the helium buffer gas experiments to generate the primary ions. Reactions with hydrogen became dominant in hydrogen buffer gas. They led to ions with $m/z = 103$ and 79 and the reactions are believed to be as indicated in [8] and [9].

[8] $C_8H_5^+ + H_2 \rightarrow C_8H_7^+$

[9] $C_8H_7^+ + H_2 \rightarrow C_6H_7^+ + C_2H_2$

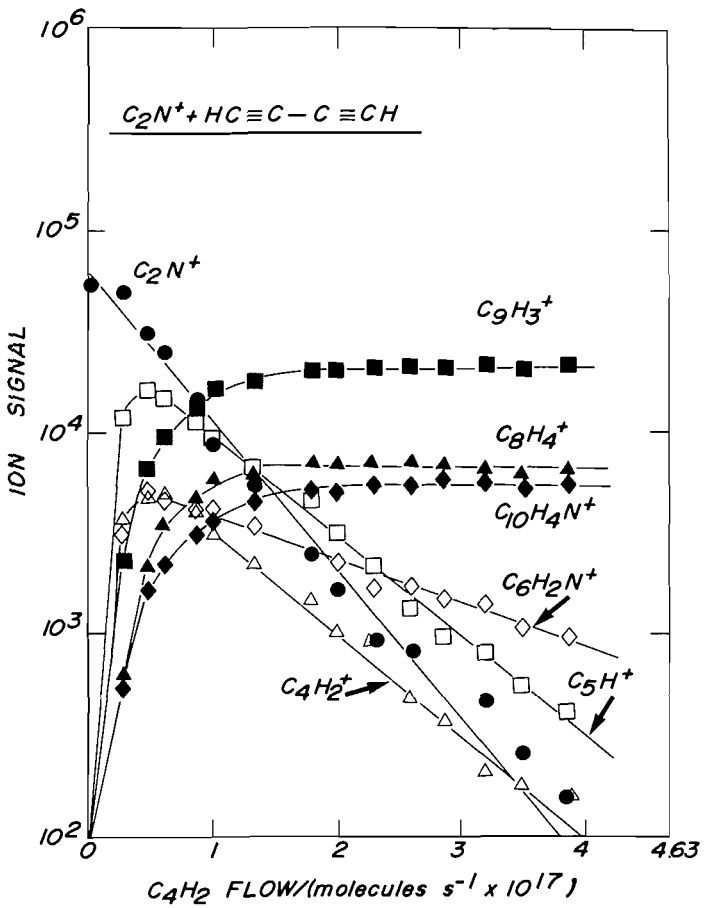

FIG. 6. The variations in ion signals observed for the addition of diacetylene into the reaction region of the SIFT apparatus in which C_2N^+ is initially established in helium buffer gas. $P = 0.296$ Torr, $\bar{v} = 5.8 \times 10^3$ cm s^{-1}, $L = 46$ cm, and $T = 296$ K. The C_2N^+ is derived from pure cyanogen at an electron energy of 80 eV.

Discussion

Diacetylene was found to be reactive towards all of the carbonaceous and carbon/nitrogen cations chosen for study. Aside from charge transfer, the predominant reaction channels observed correspond to condensation and association, both of which are suited for molecular growth by ion–molecule reactions. Condensation results when the adduct of the reacting ion and molecule dissociates into products before it is stabilized, while association refers to the process in which the adduct is stabilized by collision with a third molecule or by loss of radiation before separation into reactants or products.

Charge transfer was often an exothermic option because the ionization energy of diacetylene, 10.180 ± 0.003 eV, is relatively low in the range of the recombination energies of the selected reagent ions. Indeed, charge transfer was an observed product channel for all the primary ions with a recombination energy known to be larger than the ionization energy of diacetylene, including He^+ (24.6), CN^+ (14.5), $C_2N_2^+$ (13.374),

C_2N^+ (~13), $C_2H_2^+$ (11.41), C^+ (11.260), and C_3H^+ (10.35 ± 0.15) where the recombination energy is given in parentheses in eV (13, 6). The recombination energy of C_2N^+ is not well established. We can improve on the available approximate value by coupling the observation of charge transfer with diacetylene (ionization energy, IE = 10.180 eV) with the failure to observe charge transfer with cyanoacetylene (IE = 11.60 eV). These results imply a recombination energy of 10.9 ± 0.7 eV for the C_2N^+ generated in our experiments from cyanogen by electron impact. CH_3^+ was observed not to charge transfer. It is the only one of the selected ions with a recombination energy (9.842 eV) known to be smaller than ionization energy of diacetylene.

A number of the reaction channels observed to compete with charge transfer are of the condensation type leading to the lengthening of, or the addition of cyanide to the diacetylene carbon chain. Thus C_5H^+, $C_5H_2^+$, and $C_5H_3^+$ were produced from the reactions of C^+, C_3H^+, and CH_3^+ with diacetylene, respectively, and $C_6H_2^+$ and $C_6H_3^+$ were produced from $C_4H_2^+$ and $C_4H_3^+$, respectively. Both CN^+ and $C_2N_2^+$ were observed to produce HC_5N^+, which is presumably ionized cyano- or isocyanodiacetylene. In contrast, C_2N^+ reacted to produce C_5H^+ and thus to effect carbon-chain lengthening without cyanide addition. The most effective chain builders were C_3H^+, C_2N^+, and C^+.

The synthesis of molecules in an ionized environment by means of ion–molecule reactions requires the neutralization of the product ion as a final step. The neutralization may proceed in a number of different ways including electron–ion recombination (EIR), proton transfer (PT), or charge transfer (CT). Thus the carbonaceous neutrals C_5, C_5H, C_5H_2, and C_5H_3 may be derived from C_5H^+, $C_5H_2^+$, and $C_5H_3^+$ as, for example, in reactions [10] and [11]. However, these neutralization steps

[10] $C^+ \xrightarrow{C_4H_2} C_5H^+ \xrightarrow[EIR]{PT} :C{=}C{=}C{=}C{=}C:$

[11] $CH_3^+ \xrightarrow{C_4H_2} C_5H_3^+ \xrightarrow{CT} H_2C{=}C{=}C{=}C{=}\dot{C}H$

generally have not been studied in the laboratory and little is known about the relevant recombination energies or proton affinities. The $C_6H_2^+$ and $C_6H_3^+$ ions derived from the reactions of ionized and protonated diacetylene with diacetylene are likely to be ionized and protonated triacetylene, respectively, which may form neutral triacetylene by charge transfer and proton transfer, respectively. The reactions of CN^+ and $C_2N_2^+$ with diacetylene both produce some HC_5N^+ and so are potential sources of cyano- and isocyanodiacetylene, but other isomers are possible. It is interesting to note that under the SIFT conditions the HC_5N^+ was observed to react with diacetylene primarily to form the adduct, even though charge transfer is also exothermic if HC_5N^+ is ionized cyanodiacetylene.

Addition reactions were observed to be quite common, especially as secondary reactions, and several were observed to compete effectively with exothermic dissociation channels. Thus $C_3H_3^+$, C_5H^+, $C_5H_3^+$, $C_6H_2^+$, $C_6H_3^+$, and HC_5N^+ appeared to react with diacetylene to form stabilized adduct ions exclusively. In contrast, the addition of diacetylene to $C_4H_2^+$, $C_4H_3^+$, $C_5H_2^+$, and C_2N^+ was observed to occur in competition with dissociation channels. Also, the adduct ions $C_3H_3^+.C_4H_2$, $C_4H_2^+.C_4H_2$, and $C_2N^+.C_4H_2$ were observed to add a second molecule of diacetylene. The nature of the mechanism of stabilization of these adduct ions was not discerned and none of these reactions were studied systematically as a function of pressure. Also, no attempts were made to obtain structural information on the adduct ions, most of which may be cyclic or acyclic. In principle such information is available from comparative studies of ion reactivities. However, an elaborate experimental campaign would be required in practice to provide unequivocal results in this fashion.

In a few instances some insight into pressure dependence and stabilization mechanism is available from comparisons with results of photoionization mass spectrometer and ICR measurements performed at much lower pressures. The observation of dissociation products instead of adduct formation for the fast reaction of $C_4H_2^+$ with C_4H_2 in the ICR spectrometer (15, 16) implies collisional stabilization of the adduct at the moderate pressures of the SIFT apparatus. A similar situation appears to apply for the fast reaction of $C_6H_2^+$ with C_4H_2, which has been shown to lead to dissociation in ICR experiments (16) and to adduct formation in photoionization mass spectrometer experiments at ca. 0.01 Torr (16). Adduct formation is the reaction also observed in the SIFT experiments. The situation for the fast reaction of $C_3H_3^+$ with C_4H_2, which proceeds by adduct formation in the SIFT apparatus, is less clear. A similarly fast reaction has been observed with an ICR spectrometer for the linear isomer of $C_3H_3^+$, but products were not elucidated (14).

The diacetylene radical cation was observed to react primarily by addition to the molecules chosen for study, with the exception of hydrogen. The latter molecule failed to react with a measurable rate and this has implications for the lifetime of $C_4H_2^+$ in environments rich in H_2, such as dense interstellar clouds. With CO and C_2N_2, dissociative channels were observed, which lead to ions that, upon neutralization, allow for the growth of the carbon chain and the incorporation of a heteroatom. This is illustrated in the reaction sequences [12] and [13].

[12] $C_4H_2^+ \xrightarrow{CO} HC_5O^+ \xrightarrow[EIR]{PT} :C{=}C{=}C{=}C{=}C{=}O$

[13] $C_4H_2^+ \xrightarrow{C_2N_2} HC_5N^+ \xrightarrow[EIR]{PT} {}^{\cdot}C{\equiv}C{-}C{\equiv}C{-}C{\equiv}N$

The reaction of $C_4H_2^+$ with C_4H_2, only slightly dissociative at the moderate pressures of the SIFT apparatus, becomes completely dissociative at low pressures (15) without changing its overall reaction efficiency and allows for growth of molecules with up to eight carbon atoms. The reaction with C_2H_2 appears to have quite a different behaviour. Only adduct formation is observed, even at low pressures (18, 19). Also, there is some disparity of an unknown origin in the rate constants measured at moderate and low pressures. The SIFT rate constant is 2 to 3 times as large as those determined from measurements at low pressures. Recent ICR experiments have found the disappearance rate constant to be (3.3 × 0.8) × 10^{-10} cm^3 $molecule^{-1}$ s^{-1} and independent of pressure in the range from 2 × 10^{-6} to 3 × 10^{-5} Torr (18). Earlier trapped-ion measurements led to a rate constant of (2.3 ± 0.3) × 10^{-10} cm^3 $molecule^{-1}$ s^{-1} at ca. 10^{-4} Torr, which was also reported to be pressure independent (19). The pressure independence of the rate constant at low pressures has been rationalized both in terms of bimolecular radiative association (19) and in terms of saturated termolecular collisional association (18). The latter interpretation requires a lifetime for the $C_6H_4^+$ collision complex in the millisecond regime. The actual mechanism of stabilization remains unresolved.

There appears to be no previous information on the kinetics

of protonation of diacetylene. We have found that protonation occurs with considerable ease under our experimental conditions. The proton-transfer reactions that were observed all proceed essentially at the collision rate at room temperature. The occurrence of proton transfer with H_2CN^+ and the failure of proton transfer with $CH_3OH_2^+$ allow the proton affinity of diacetylene to be bracketed between the known proton affinities of HCN and CH_3OH. The proton affinities available for these two molecules (20) yield a proton affinity for diacetylene of 177 $\pm$ 5 kcal mol^{-1}. This value corresponds to a heat of formation for $C_4H_3^+$ of 305 $\pm$ 5 kcal mol^{-1}, which agrees well with the value of 307 kcal mol^{-1} that may be derived from the appearance potential for $C_4H_3^+$ from vinylacetylene (12). The bracketed value for the proton affinity agrees with the results of bracketing measurements performed recently with the techniques of ICR and high pressure mass spectrometry (20).

Acknowledgements

We thank the Natural Sciences and Engineering Research Council of Canada and the donors of the Petroleum Research Fund, administered by the American Chemical Society, for partial support of this research.

1. W. M. Irvine and A. Hjalmarson. *In* Cosmochemistry and the origin of life. *Edited by* C. Ponnamperuma. D. Reidel Publishing Co., Dordrecht. 1983. pp. 113–142.
2. H. F. Calcote. Combust. Flame, **42**, 215 (1981).
3. H. I. Schiff and D. K. Bohme. Astrophys. J. **208**, 237 (1976).
4. V. G. Kunde, A. C. Aikin, R. A. Hanel, D. E. Jennings, W. C. Maguire, and R. E. Samuelson. Nature, **292**, 686 (1981).
5. G. I. Mackay, G. D. Vlachos, D. K. Bohme, and H. I. Schiff. Int. J. Mass Spectrom. Ion Phys. **36**, 259 (1980).
6. A. B. Raksit and D. K. Bohme. Int. J. Mass Spectrom. Ion Phys. **55**, 69 (1983).
7. A. B. Raksit and D. K. Bohme. Can. J. Chem. **63**, 854 (1985).
8. L. Brandsma. Preparative acetylene chemistry. Elsevier Publishing Co., New York. 1971. pp. 122–124.
9. N. G. Adams and D. Smith. J. Phys. B, **9**, 1439 (1976).
10. G. Gioumousis and D. P. Stevenson. J. Chem. Phys. **29**, 294 (1958).
11. E. R. Lippincott and J. M. Stutman. J. Phys. Chem. **68**, 2926 (1964).
12. J. L. Franklin, J. G. Dillard, H. M. Rosenstock, J. T. Herron, K. Draxl, and F. H. Field. Natl. Stand. Ref. Data Ser. Natl. Bur. Stand. **26**, 41 (1969).
13. H. M. Rosenstock, K. Draxl, B. W. Steiner, and J. T. Herron. J. Phys. Chem. Ref. Data, Suppl. 1, **6** (1977).
14. K. C. Smith, S. G. Lias, and P. Ausloos. Combust. Sci. Technol. **28**, 147 (1982).
15. V. G. Anicich, G. A. Blake, J. K. Kim, M. J. McEwan, and W. T. Huntress. J. Phys. Chem. **88**, 4608 (1984).
16. T. J. Buckley, L. W. Sieck, R. Metz, S. G. Lias, and J. F. Liebman. Int. J. Mass Spectrom. Ion Processes, **65**, 181 (1985).
17. A. B. Raksit, H. I. Schiff, and D. K. Bohme. Int. J. Mass Spectrom. Ion Processes, **56**, 321 (1984).
18. F. W. Brill and J. R. Eyler. J. Phys. Chem. **85**, 1091 (1981).
19. P. G. Miasek and J. L. Beauchamp. Int. J. Mass Spectrom. Ion Phys. **15**, 49 (1974).
20. S. G. Lias and J. F. Liebman. J. Phys. Chem. Ref. Data, **13**, 695 (1984).

Cyanothiolacetate as a masked β-hydroxyproprionitrile carbanion in Michael reactions[1]

HSING-JANG LIU AND HLA WYNN
Department of Chemistry, University of Alberta, Edmonton, Alta., Canada T6G 2G2

Received August 21, 1985

HSING-JANG LIU and HLA WYNN. Can. J. Chem. **64**, 649 (1986).

A facile method for the introduction of a highly functionalized isopropyl unit, in the form of β-hydroxyproprionitrile or acrylonitrile, to the β carbon of an α,β-unsaturated ketone has been developed using *S-tert*-butyl cyanothiolacetate as a β-hydroxyproprionitrile equivalent in Michael reactions.

HSING-JANG LIU et HLA WYNN. Can. J. Chem. **64**, 649 (1986).

On a développé une méthode facile d'introduction d'une unité isopropyle hautement fonctionalisée, sous la forme d'un β-hydroxyproprionitrile ou d'acrylonitrile, au carbone β d'une cétone α,β-non saturée; la méthode est basée sur l'utilisation d'un cyanothiolacétate de *S-tert*-butyle comme carbanion équivalent à un β-hydroxypropionitrile dans des réactions de Michael.
[Traduit par la revue]

Introduction

One of the synthetically useful features of the thiolester group is its susceptibility to reduction with sodium borohydride to the alcohol level. This was first observed by Fujita and co-workers on the highly activated thiolesters derived from 2-mercaptothiazoline (3). Later it was found that ordinary thiolesters could also be reduced in the same way (4). It was further shown that the thiolester group could be selectively reduced in the presence of other commonly encountered acid derivatives such as amide, ester, and nitrile (4).

The ease of reduction of the thiolester group with sodium borohydride suggests a number of interesting possibilities for its use as a latent hydroxymethyl unit in synthesis, especially when such a unit, with or without protection, cannot be directly involved in a desired transformation. In a recent report (1), we described a convenient approach to β-hydroxypropionitrile and acrylonitrile derivatives involving alkylation or Knoevenagel-type reactions of cyanothiolacetate as the initiating step. As illustrated in Scheme 1, the synthetic approach is greatly

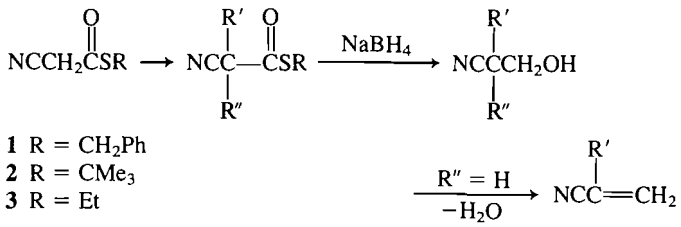

SCHEME 1

facilitated because of the ability of the thiolester group present in the starting material to serve both as an activating group for the carbon–carbon bond formation and as a convenient source of hydroxymethyl moiety. The overall transformation can be considered as the replacement of one to two α-protons of β-hydroxypropionitrile (or acrylonitrile) by electrophiles using cyanothiolacetate as a β-hydroxypropionitrile carbanion equivalent.

The use of cyanothiolacetate as a convenient source of a masked β-hydroxypropionitrile carbanion has a considerable potential in organic synthesis. One interesting application is in its use as a Michael donor to facilitate the introduction of a highly functionalized isopropyl unit to the β-carbon of an α,β-unsaturated ketone. This process, which is described herein, is expected to have broad utility in the synthesis of natural products, especially those of isoprene origin.

[1]Thiol esters in organic synthesis, Part XIII. For Parts XI and XII of this series, see refs. 1 and 2 respectively.

Results and discussion

A. *Michael reactions of cyanothiolacetates*

Three cyanothiolesters (benzyl (**1**), *tert*-butyl (**2**), and ethyl (**3**)) were examined. These compounds were readily prepared from the corresponding thiols and cyanoacetic acid according to the reported procedure (5). *S*-Benzyl cyanothiolacetate (**1**) was initially used but exploration on this compound was very brief due to its instability. On the other hand, cyanothiolester **2**, which was used extensively throughout this work, was shown to be stable and could be stored at room temperature for a prolonged period of time. In the large-scale preparation, this thiolester was purified first by distillation at 100°C/2 Torr (1 Torr = 133.3 Pa). The distillate was then chromatographed on silica gel as described (5). *S*-Ethyl cyanothiolacetate (**3**), bp 100°C/4 Torr, was purified in a similar manner.

1,4-Diazabicyclo[2.2.2]octane (DABCO), which was found to be a highly effective base to induce Michael reactions of β-keto thiolesters (6) and *S,S'*-diethyl dithiomalonate (7), was used initially for the present studies. The experimental results obtained for the addition of thiolester **2** to five α,β-unsaturated ketones are summarized in Table 1. These results showed that DABCO was only effective in a limited number of cases (Entries 1, 6, and 7). In most cases, however, the yields of adducts were rather disappointing (Entries 8–12) and occasionally bis-addition was observed (Entry 12).

In search of adequate conditions for the Michael reaction, we have examined a series of tertiary amine bases including 4-dimethylaminopyridine (DMAP), ethyldiisopropylamine (Hunig's base), *N,N*-dimethylaniline, pyridine, and imidazole. Apart from *S-tert*-butyl cyanothiolacetate (**2**), the corresponding ethyl derivative **3** was also used as a Michael donor. As shown by the experimental results compiled in Table 2, none of the amines applied was particularly effective. Consequently, alternative methods were sought. In the subsequent studies thiol ester **2** was used exclusively, since thiol ester **3** was shown, in spite of its smaller size, to be inferior as a Michael donor (cf. Table 1, Entry 1 and Table 2, Entry 2).

Generally, in Michael reactions in which the donor can also serve as a good leaving group, the rate-limiting step in which the new carbon–carbon bond is formed is reversible. The position of the equilibrium depends, to a large extent, on the stability of

TABLE 1. Michael reactions of thiolester **2** using DABCO as a base[a]

Entry	Enone (equiv.)	Equiv. of **2**	Equiv. of DABCO	Time (h)	Product(s)[b]	% Yield[c]
1.	 (1.0)	1.2	1.2	36	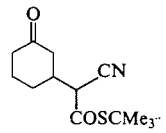 **4**	61
2.	(1.0)	1.2	1.2[d]	35	**4**	48
3.	(2.5)	1.0	1.0	36	**4**	54
4.	(1.5)	1.0	0.5	192	**4**	52
5.	(2.0)	1.0	0.3	168	**4**	58
6.	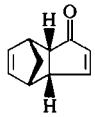 **5** (1.0)	1.5	1.2	25	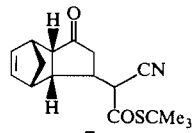 **7**	78
7.	(1.0)	1.5	1.2[e]	24	**7**	80
8.	 (2.5)	1.0	1.0	48	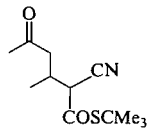 **8**	37
9.	(1.0)	1.2	1.2[e]	20	**8**	17
10.	 (1.0)	1.2	1.2	6	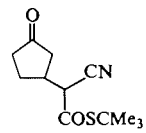 **9**	36
11.	(1.0)	1.0	1.0	23	**9**	46
12.	 **6** (1.0)	1.5	1.2	46	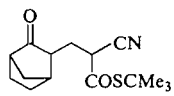 **10** + 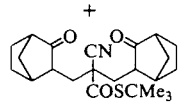 **11**	11 14

[a]Unless otherwise stated, these reactions were performed in DME at room temperature.
[b]All these products were obtained as diastereomeric mixtures.
[c]Yields were calculated on the basis of the yield-limiting reactant.
[d]This reaction was carried out in refluxing ether.
[e]These reactions were carried out in THF.

the intermediate enolate ion (8). In principle, the equilibrium could be shifted to the side of product formation by trapping the intermediate enolate ion with an adequate electrophile. As shown in Scheme 2, one such electrophile could be chlorotrimethylsilane, which is expected to react with the enolate ion rapidly to give a stable silyl enol ether that could then be converted to the desired ketone. Based on this principle, a general method for the Michael reaction was developed. Initially, the Michael reaction of thiolester **2** and 2-cyclohexen-1-one was examined in DME at room temperature in the presence of imidazole and chlorotrimethylsilane. The results were promising but not highly satisfactory. After a number of trials and modifications, it was found that the best results were obtained by the use of sodium hydride as a base, chlorotrimethylsilane as a trapping agent, and benzene as a solvent. By the use of this combination, a number of reactions were successfully explored. Results are compiled in Table 3.

In a typical experiment, thiolester **2** (1 equiv.) was treated with 1.2 equiv. of 2-cyclohexen-1-one, 0.9 equiv. of chlorotrimethylsilane, and 1.5 equiv. of sodium hydride in benzene at room temperature for 17 h. An 86% yield of adduct **4** was isolated after standard aqueous work-up and purification. In this case and two other cases (Entries 7 and 10) the normal work-up was found to be sufficient to generate the ketone carbonyl from the corresponding enol ether. In other cases (Entries 2–6, 8, and 9), however, the silyl enol ether moiety was shown to be rather

TABLE 2. Michael reactions using different tertiary amine bases[a]

Entry	Enone (equiv.)	Thiolester (equiv.)	Base (equiv.)	Time (h)	Product	% Yield
1.	 (1.0)	**3** (1.5)	DMAP (1.5)	19	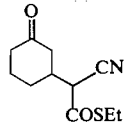 **12**	26
2.	(1.0)	**3** (1.2)	DABCO (1.2)	48	**12**	23
3.	(1.0)	**3** (1.2)	Hunig's base (1.2)	44	**12**	19
4.	(1.0)	**3** (1.5)	Imidazole (1.5)	52	**12**	16
5.	(1.0)	**3** (1.5)	*N*,*N*-Dimethylaniline (1.2)	52	*b*	—
6.	(1.0)	**3** (1.2)	Pyridine (1.2)	38	*b*	—
7.	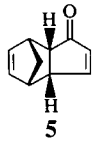 **5** (1.0)	**2** (1.5)	DMAP (1.2)	26	**7**	74
8.	(1.0)	**2** (1.5)	DABCO (1.2)	25	**7**	78
9.	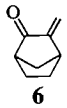 **6** (1.0)	**2** (1.5)	DMAP (1.2)	24	**10**	14
10.	(1.0)	**2** (1.5)	DABCO (1.2)	46	**10**	11

[a]All these reactions were performed in DME and at room temperature.
[b]No reaction.

stable and a brief treatment (10 min) of the crude product with potassium fluoride in methanol was necessary to secure the desired product.

During the studies, it was also noted that it was important to keep the amount of the trapping agent slightly less than that of the thiolester. In a number of experiments, when an excess of

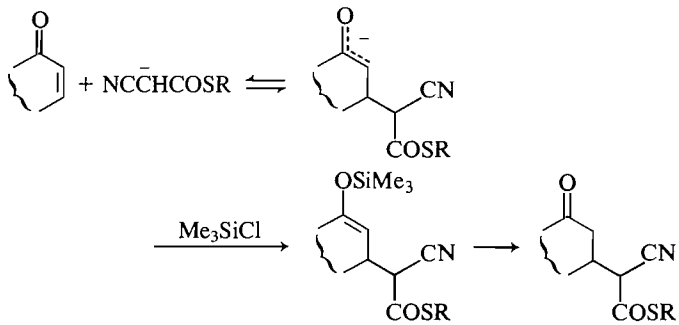

SCHEME 2

chlorotrimethylsilane was used, the desired product was not formed.[2]

Of the results shown in Table 3, three cases are particularly noteworthy. Whereas all the products possessing two or more chiral centers were obtained as mixtures of diastereomers, adducts **13** and **14** were produced, surprisingly, each as a single stereoisomer. Each compound displayed a single set of signals in the ^{1}Hmr spectrum as well as in the ^{13}Cmr spectrum. Another noteworthy case is the addition of thiolester **2** to methyl vinyl ketone (Entry 10), a highly reactive Michael acceptor. The best yield obtained for the adduct **15** was 48%, when the reaction was carried out in benzene at 10°C for 3 h. The low yield was partly due to the formation of a by-product, which was characterized as a diastereomeric mixture of compound **16**. This compound was apparently formed via bis-addition product **17**, involving an intramolecular aldol process. In order to suppress the formation of this bis-product, as well as to improve the yield of adduct **15**, the reaction was performed in toluene at low temperatures (−40°C and −60°C). Contrary to our expectation, the yields obtained for the desired product were lower and an increasing amount of compound **16** to the extent of 34% yield was obtained.

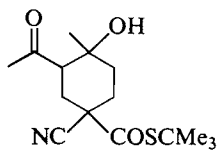

16

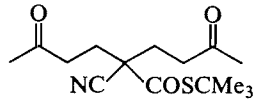

17

[2]To account for this observation, it is very likely that chlorotrimethylsilane reacts first with the thiolester and the resulting silyl enol ether is the effective trapping agent.

TABLE 3. Michael reactions of thiolester **2** using sodium hydride[a] in the presence[b] or absence of chlorotrimethylsilane

			With chlorotrimethylsilane					Without chlorotrimethylsilane			
Entry	Enone (equiv.)		Equiv. of **2**	Time (h)	Temp. (°C)	Product	% Yield	Time (h)	Temp. (°C)	Product	% Yield
1.		(1.2)	1.0	17	r.t.[c]	**4**	86	22	r.t.	**4**	90
2.	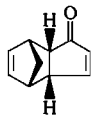 **5**	(1.0)	1.2	23	r.t.	**7**	84	25	r.t.	**7**	49
3.		(1.0)	1.2	8	7	**8**	62				
4.		(1.2)	1.0	27	−20[d]	**8**	68	24	−20[d]	**8**	58
5.		(1.0)	1.2	3	10	**9**	100	3.5	15	**9**	93
6.		(1.2)	1.0	2	10	**9**	64				
7.	 **6**	(1.0)	1.2	2	7	**10**	63	3	7	**10**	71
8.		(1.2)	1.0	16	r.t.	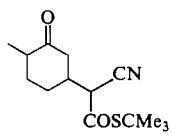 **13**	82	14	r.t.	**13**	49
9.	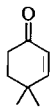	(1.2)	1.0	22	r.t.	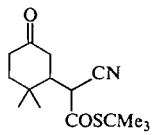 **14**	73	25	r.t.	**14**	46
10.		(1.0)	1.2	3	10	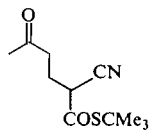 **15**	48				
11.		(1.0)	1.2	48	r.t.	*e*	—				
12.		(1.0)	1.2	22	r.t.	*e*	—				
13.		(1.2)	1.0	2	Reflux	*e*	—				

[a]The amount of sodium hydride used was 1.5 equiv. based on thiolester **2**.
[b]The amount of chlorotrimethylsilane used was 0.9 equiv. based on thiolester **2**.
[c]Room temperature.
[d]Toluene was used as a solvent.
[e]No reaction.

The reactions of thiolester **2** with β,β-disubstituted enones such as 3-methyl-2-cyclohexen-1-one (Entry 11) and α,β-disubstituted enones such as 3-methyl-3-penten-2-one and 2-methyl-2-cyclohexen-1-one (Entries 12 and 13) were also examined using the described conditions. In all of these cases, no detectable amount of adduct was produced. These two types of enones are known to be poor Michael acceptors, which do not usually undergo addition reaction with Michael donors of low nucleophilicity, such as malonic acid derivatives (9). Our case was no exception.

TABLE 4. Ketalization[a] and reduction[b] of Michael adducts

		Ketalization		Reduction			
Entry	Adduct	Time (h)	Product	Equiv. of $NaBH_4$	Time (h)	Product	Overall % yield
1.	**4**	7	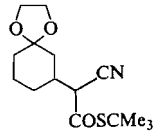 **18**	4	1	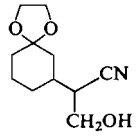 **19**	90
2.	**7**	21	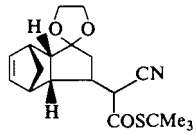 **20**	5	10	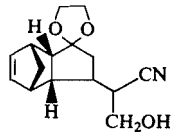 **21**	78
3.	**8**	22	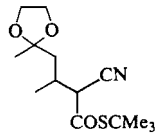 **22**	4	3	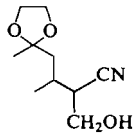 **23**	79
4.	**9**	24	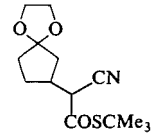 **24**	4	3.5	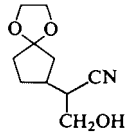 **25**	100
5.	**10**	12	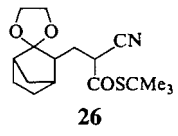 **26**	2	8	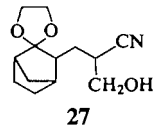 **27**	91

[a]These reactions were performed using ethylene glycol (10 equiv.) and *p*-toluenesulfonic acid (0.1 equiv.) in refluxing benzene.

[b]All the reactions were run at room temperature.

Table 3 also summarizes the results of several Michael reactions carried out under similar conditions in the absence of chlorotrimethylsilane. These experiments were performed in order to determine whether chlorotrimethylsilane indeed played a role in assisting the Michael reaction. An examination of the results reveals that, although in several cases (Entries 1, 4, 5, and 7) the yields of adducts were comparable, in other cases (Entries 2, 8 and 9) the adducts were obtained in substantially better yields when chlorotrimethylsilane was present.

Standard conditions for Michael reaction of analogous donors such as dialkyl malonate often involve the combination of a base, such as hydroxide and alkoxide, and a protic solvent, such as water and alcohol (10, 11). These conditions are apparently inadequate for the cyanothiolester under investigation, since the thiolester group is labile toward these strongly nucleophilic reagents. Experimentally, this was proven to be true. When the addition of cyanothiolester **2** to 4,4-dimethyl-2-cyclohexen-1-one was attempted in ethanol with potassium hydroxide at room temperature, adduct **14** was obtained in a poor yield of 19%.

B. *Conversion of Michael adducts to β-hydroxypropionitrile and acrylonitrile derivatives*

Since the ketone carbonyl is more reactive towards sodium borohydride than the thiolester carbonyl, its protection was necessary prior to the selective reduction of the latter functional group. In all the cases examined, the protection was readily achieved in the form of a ketal using standard ketalization conditions. Thus, treatment of adduct **4** with ethylene glycol in refluxing benzene in the presence of *p*-toluenesulfonic acid with continuous removal of water gave ketal **18** in virtually quantitative yield. Subsequent reduction of ketal **18** with sodium borohydride in ethanol at room temperature gave rise to the desired alcohol **19** in 90% yield over two steps (Table 4, Entry 1). Under similar conditions, four additional Michael adducts were ketalized and reduced to give the desired ketal alcohols in good overall yields. Particulars of these experiments are summarized in Table 4, Entries 2–5.

The conversion of ketal alcohols to the corresponding acrylonitriles was equally straightforward. Two methods were found to be readily applicable. Direct dehydration of ketal alcohol **19** with 1,3-dicyclohexylcarbodiimide (DCC) in refluxing ether in the presence of a trace amount of cuprous chloride (1, 12) proceeded smoothly to give a 79% yield of acrylonitrile derivative **28** (Table 5, Entry 1).

Ketal alcohol **21** was converted by two different methods into acrylonitrile derivative **29**. Direct dehydration with DCC gave a 60% yield of the latter compound (Entry 2). Indirectly, mesylation of **21** with methanesulfonyl chloride and triethylamine in dichloromethane at room temperature, followed by treatment of the resulting mesylate with 1,8-diazabicyclo[5.4.0]undec-7-ene (DBU) in refluxing benzene, gave the same compound in

TABLE 5. Dehydration of ketal alcohols

Entry	Ketal alcohol	Method[a]	Time (h)	Product	% Yield
1.	**19**	A	16	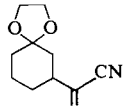 **28**	79
2.	**21**	A	48	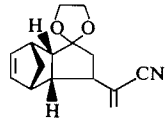 **29**	60
3.	**21**	B	*b*	**29**	58
4.	**23**	A	24	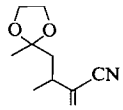 **30**	77
5.	**25**	A	31	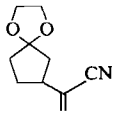 **31**	65
6.	**27**	A	21	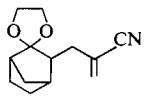 **32**	87

[a]Method A: A direct dehydration using DCC (1.5 equiv.) and a trace amount of copper(I) chloride in refluxing ether. Method B: A two-step procedure involving mesylation using methanesulfonyl chloride and triethylamine, followed by elimination with DBU in refluxing benzene.

[b]The time for mesylation was 24 h and the time required for elimination was 50 min.

comparable yield (Entry 3). Table 5 also summarizes the results obtained for the conversions of **23** → **30**, **25** → **31**, and **27** → **32** (Entries 4–6).

Having successfully completed the investigation on the conversion of Michael adducts to β-hydroxypropionitrile derivatives and, further, to acrylonitriles, the removal of the ketal protecting group was examined. Experimental results showed that the deprotection could be readily achieved without destruction of the rather labile acrylonitrile moiety. When exposed to *p*-toluenesulfonic acid in acetone at room temperature, both compounds **28** and **31** were found to undergo transketalization smoothly to give ketones **33** (81% yield) and **34** (97% yield) respectively.

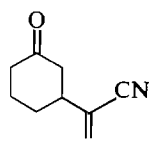
33

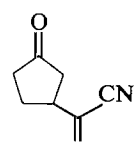
34

In conclusion, cyanothiolacetate **2** was shown to undergo Michael reaction with conjugated enones. The thiolester group of the products could be selectively reduced, after proper protection of the ketone carbonyl, with sodium borohydride to the alcohol level. Hence, a highly functionalized isopropyl unit in the form of β-hydroxypropionitrile could be easily introduced to the β-carbon of a conjugated enone, utilizing cyanothiolacetate as a masked β-hydroxypropionitrile carbanion equivalent. Furthermore, the β-hydroxypropionitrile group was readily dehydrated either directly with DCC or indirectly via a two-step sequence involving mesylation and elimination. Hence, cyanothiolacetate can also be conveniently used as a masked acrylonitrile unit in Michael reactions.

Experimental

General

Melting points were determined on a Kofler hot stage apparatus and are uncorrected. Elemental analyses were performed by the microanalytical laboratory of this department. Infrared (ir) spectra were recorded on a Perkin–Elmer model 457 or Nicolet 7-199 FT-IR spectrophotometer. Unless otherwise stated, ir samples were run as thin films. Proton nuclear magnetic resonance (^{1}Hmr) spectra were recorded on a Varian HA-100, HA-100/Digilab, Bruker WH-80, WH-200, or WH-400 spectrometer and, except where otherwise stated, were obtained on solutions in deuterochloroform with tetramethylsilane as internal reference. Carbon-13 nuclear magnetic resonance (^{13}Cmr) spectra were recorded on a Bruker HF-90/Nicolet 1085 system or a Bruker WH-200 or WH-400 spectrometer and were obtained on solutions in deuterochloroform using tetramethylsilane as internal reference. Mass spectra (ms) were recorded using A.E.I. model MS9, MS12, or MS50 mass spectrometers. Silica gel, 0.040–0.063 mm particle size, 230–400 mesh ASTM, was used as adsorbent for flash chromatography, and silica gel, 60–120 mesh, was used as adsorbent for column chromatography. Unless otherwise stated, anhydrous magnesium sulfate was used for drying organic solutions.

*Michael reactions of cyanothiolacetates **2** and **3** with α,β-unsaturated ketones*

The reactions were carried out using the general procedures illustrated below with 2-cyclohexen-1-one. Details of each reaction, such as temperature, time, yield, and relative quantities of reagents and reactants, are noted in Tables 1–3.

A. *Using tertiary amine as a base*

At 0°C, to a solution of *S-tert*-butyl cyanothiolacetate (**2**) (500 mg, 3.18 mmol) in DME (10 mL), were added DABCO (357 mg, 3.18 mmol) and 2-cyclohexen-1-one (0.26 mL, 2.65 mmol). After stirring at room temperature under an argon atmosphere for 36 h, the reaction mixture was poured into ice-cold 1 *N* aqueous hydrochloric acid (20 mL) and extracted with chloroform (4 × 20 mL). The extracts were washed with saturated aqueous sodium chloride, dried, filtered, and concentrated. Chromatography of the residue on silica gel, eluting with 10% ethyl acetate in petroleum ether, gave adduct **4** (410 mg; 61% yield) as a mixture of two diastereomers (ca. 1:1); ir ($CHCl_3$): 1677 (thiolester C=O), 1715 (ketone C=O), and 2240 (C≡N) cm^{-1}; ^{1}Hmr δ: 1.50 (s, 9H, —C(CH$_3$)$_3$), 3.45 (d, ~0.5H, J = 6 Hz, —CHCN of one isomer), and 3.60 (d, ~0.5H, J = 4 Hz, —CHCN of another isomer); ms M$^+$: 253.1137 (calcd. for $C_{13}H_{19}NO_2S$: 253.1136). *Anal.* calcd. for $C_{13}H_{19}NO_2S$: C 61.63, H 7.56, N 5.53, S 12.65; found: C 61.38, H 7.75, N 5.28, S 12.46.

B. *Using sodium hydride as a base in the presence of chlorotrimethylsilane*

Cyanothiolester **2** (348 mg, 2.21 mmol) was dissolved in benzene (8 mL) and stirred at ~5°C under an argon atmosphere. Chlorotrimethylsilane (0.22 mL, 1.73 mmol), 2-cyclohexen-1-one (0.25 mL, 2.56 mmol), and sodium hydride (50% dispersion in oil; 154 mg, 3.2 mmol) were sequentially added and the reaction mixture stirred for 17 h at room temperature. The reaction was worked up as in method A

and the crude product[3] purified by flash chromatography on silica gel (20% ethyl acetate – petroleum ether) to give adduct **4** (478 mg; 86% yield).

C. *Using sodium hydride as a base in the absence of chlorotrimethylsilane*

Cyanothiolester **2** (92 mg, 0.58 mmol) was dissolved in benzene (8 mL) and stirred at ~5°C under an argon atmosphere. Sodium hydride (50% dispersion in oil; 28 mg, 0.58 mmol) was introduced, followed by addition of 2-cyclohexen-1-one (0.07 mL, 0.7 mmol). After stirring for 22 h at room temperature, the mixture was worked up as in method A. Purification of the crude product by column chromatography on silica gel (20% ethyl acetate – petroleum ether) gave adduct **4** (132 mg; 90% yield).

The adducts **7–16** showed the following data:

Adduct **7**: mp 81–85°C (benzene – petroleum ether); ir ($CHCl_3$): 1675 (thiolester C=O), 1730 (ketone C=O), and 2240 (C≡N) cm^{-1}; ^{1}Hmr δ: 1.52 and 1.54 (both s, ~1:1, total 9H, —$C(Ch_3)_3$), 3.54, 3.64 (both d, ~1:1, 1H total, J = 10 Hz each, —CHCN), and 6.20 (br s, 2H, —CH=CH—); ms M^+: 303.1292 (calcd. for $C_{17}H_{21}NO_2S$: 303.1293). *Anal.* calcd. for $C_{17}H_{21}NO_2S$: C 67.30, H 6.98, N 4.62, S 10.57; found: C 67.48, H 7.15, N 4.48, S 10.31.

Adduct **8**: mp 42–43°C (benzene – petroleum ether); ir: 1685 (thiolester C=O), 1725 (ketone C=O), and 2260 (C≡N) cm^{-1}; ms M^+: 241.1138 (calcd. for $C_{12}H_{19}NO_2S$: 241.1136). *Anal.* calcd. for $C_{12}H_{19}NO_2S$: C 59.72, H 7.94, N 5.81, S 13.26; found: C 59.64, H 7.95, N 5.71, S 13.09. The ^{1}Hmr spectrum displayed two sets of signals in a ratio of 2:1, indicating the presence of two diastereomers. The following signals were attributed to the major isomer: δ 1.07 (d, 3H, J = 6 Hz, CH_3CH—), 1.54 (s, 9H, —$C(CH_3)_3$), 2.28 (s, 3H, CH_3CO—), and 3.90 (d, 1H, J = 4 Hz, —CHCN). The following signals were attributed to the minor isomer: δ 1.13 (d, 3H, J = 6 Hz, CH_3CH—), 1.49 (s, 9H, —$C(CH_3)_3$), 2.12 (s, 3H, CH_3CO—), and 3.52 (d, J = 6 Hz, —CHCN).

Adduct **9**: mp 57–60°C (crystallized on standing); ir ($CHCl_3$): 1679 (thiolester C=O), 1747 (ketone C=O), and 2250 (C≡N) cm^{-1}; ^{1}Hmr δ: 1.50 (s, 9H, —$C(CH_3)_3$), 3.60 (d, ~0.5H, J = 7 Hz, —CHCN of one isomer), and 3.67 (d, ~0.5H, J = 5 Hz, —CHCN of another isomer); ms M^+: 239.0980 (calcd. for $C_{12}H_{17}NO_2S$: 239.0980.

Adduct **10**: mp 65–69°C (crystallized on standing); ir: 1675 (thiolester C=O), 1740 (ketone C=O), and 2240 (C≡N) cm^{-1}; ^{1}Hmr δ: 1.50 (s, 9H, —$C(CH_3)_3$), 3.68 (dd, ~0.5H, J = 8, J' = 6 Hz, —CHCN of one isomer), and 4.00 (dd, ~0.5H, J = 9, J' = 5 Hz, —CHCN of another isomer); ms M^+: 279.1290 (calcd. for $C_{15}H_{21}NO_2S$: 279.1293. *Anal.* calcd. for $C_{15}H_{21}NO_2S$: C 64.48, H 7.58, N 5.02, S 11.45; found: C 64.55, H 7.63, N 4.93, S 11.23.

Adduct **11**: mp 58–60°C (crystallized on standing); ir: ($CHCl_3$): 1670 (thiolester C=O) and 1740 (2 × ketone C=O) cm^{-1}; ^{1}Hmr δ: 1.50 (s, 9H, —$C(CH_3)_3$) and 1.7–3.1 (complex, 22H); ms M^+: 401.2020 (calcd. for $C_{23}H_{31}NO_3S$: 401.2025.

Adduct **12**: ir: 1675 (thiolester C=O), 1710 (ketone C=O), and 2240 (C≡N) cm^{-1}; ^{1}Hmr δ: 1.34 (t, 3H, J = 8 Hz, CH_3CH_2), 3.02 (q, 2H, J = 6 Hz, CH_3CH_2—), 3.62 (d, ~0.5H, J = 5 Hz, —CHCN of one isomer), and 3.74 (d, ~0.5H, J = 4 Hz, —CHCN of another isomer); ms M^+: 225.0824 (calcd. for $C_{11}H_{15}NO_2S$: 225.0823.

Adduct **13**: ir ($CHCl_3$): 1680 (thiolester C=O), 1710 (ketone C=O), and 2260 (C≡N) cm^{-1}; ^{1}Hmr δ: 1.06 (d, 3H, J = 7 Hz, CH_3CH—), 1.54 (s, 9H, —$C(CH_3)_3$), and 3.44 (d, 1H, J = 5.5 Hz, —CHCN); ^{13}Cmr δ: 209.2, 190.4, 114.9, 51.5, 50.6, 45.6, 44.5, 40.4, 33.4, 29.5, 27.9, 14.1; ms M^+: 267.1290 (calcd. for $C_{14}H_{21}NO_2S$: 267.1293). *Anal.* calcd. for $C_{14}H_{21}NO_2S$: C 62.89, H 7.92, N 5.24, S 11.97; found: C 62.72, H 8.10, N 5.12, S 11.59.

Adduct **14**: mp 74–77°C (benzene in petroleum ether); ir 1680 (thiolester C=O), 1710 (ketone C=O), and 2250 (C≡N) cm^{-1}; ^{1}Hmr δ: 1.14, 1.22 (both s, 3H each, —$C(CH_3)_3$), and 3.74 (d, 1H, J = 2 Hz, —CHCN); ^{13}Cmr δ: 208.3, 191.2, 115.4, 50.6, 46.8, 46.6, 40.1 (2×), 37.7, 33.4, 29.5, 28.9, 19.9; ms M^+: 281.1444 (calcd. for $C_{15}H_{23}NO_2S$: 281.1449). *Anal.* calcd. for $C_{15}H_{23}NO_2S$: C 64.02, H 8.24, N 4.98, S 11.37; found: C 63.82, H 8.26, N 4.93, S 11.35.

Adduct **15**: ir 1685 (thiolester C=O), 1718 (ketone C=O), and 2250 (C≡N) cm^{-1}; ^{1}Hmr δ: 1.50 (s, 9H, —$C(CH_3)_3$), 2.14 (s, 3H, CH_3CO—), 2.63 (t, 2H, J = 7 Hz, —CH_2CO—), and 3.62 (dd, 1H, J = 8, J' = 6 Hz, —CHCN); ms M^+: 227.0975 (calcd. for $C_{11}H_{17}NO_2S$: 227.0980).

Adduct **16**: ir: 1680 (thiolester C=O), 1710 (ketone C=O), 2240 (C≡N), and 3500 (—OH) cm^{-1}; ms M^+ 297.1391 (calcd. for $C_{15}H_{23}NO_3S$: 297.1399). The ^{1}Hmr spectrum displayed two sets of signals in a ratio of 4:1. The following signals were attributed to the major diastereomer: δ 1.18 (s, 3H, —CH_3), 1.50 (s, 9H, —$C(CH_3)_3$), and 2.19 (s, 3H, —$COCH_3$). The following signals were attributed to the minor isomer: δ 1.25 (s, 3H, —CH_3), 1.52 (s, 9H, —$C(CH_3)_3$), and 2.16 (s, 3H, —$COCH_3$).

*Ketalization and selective reduction of Michael adducts **4** and **7–10***

The reactions were carried out using the general procedures illustrated below with adduct **4**. Reaction time and yield of individual reactions are noted in Table 4.

Ketone **4** (501 mg, 1.98 mmol) was dissolved in benzene (40 mL). Ethylene glycol (1.23 g, 19.8 mmol) and *p*-toluenesulfonic acid monohydrate (36 mg, 0.2 mmol) were added. The reaction flask was fitted with a Dean–Stark water separator charged with type 3A molecular sieves in the take-off arm. The reaction mixture was heated at reflux for 7 h under an argon atmosphere and then cooled to room temperature. Saturated aqueous sodium bicarbonate solution (10 mL) was added and the resulting solution extracted with dichloromethane (4 × 20 mL). The extracts were washed with saturated aqueous sodium chloride, dried, filtered, and concentrated to afford ketal **18** (596 mg); ir ($CHCl_3$): 1050–1100 (C—O), 1678 (C=O), and 2240 (C≡N) cm^{-1}; ^{1}Hmr δ: 1.50 (s, 9H, —$C(CH_3)_3$), 3.45, 3.49 (both d, 1H total, J = 7 Hz each, —CHCN), and 3.95 (br s, 4H, —OCH_2CH_2O—); ms M^+: 297.1409 (calcd. for $C_{15}H_{23}NO_3S$: 297.1399). *Anal.* calcd. for $C_{15}H_{23}NO_3S$: C 60.58, H 7.80, N 4.71, S 10.76; found: C 60.52, H 7.76, N 4.65, S 10.88.

Ketal **18** (248 mg, ~0.84 mmol) was dissolved in absolute ethanol (5 mL) and sodium borohydride (124 mg, 3.26 mmol) was added. The reaction mixture was stirred under an argon atmosphere at room temperature for 1 h. It was then poured into ice-cold saturated aqueous ammonium chloride solution (20 mL) and extracted with dichloromethane (4 × 20 mL). The extracts were washed with saturated aqueous sodium chloride solution, dried, filtered, and concentrated. The crude material was purified by column chromatography on silica gel (50% ethyl acetate – petroleum ether) to give a mixture of

[3]For compounds **7**, **8**, **9**, **13**, and **14**, the crude product was further treated with an equal amount (by weight) of potassium fluoride in water–methanol (1:2; 100 mL per each gram of the crude product) at room temperature for 10 min. This was followed by acidification with 1 *N* aqueous hydrochloric acid, extraction with chloroform, and work-up of the extracts in the usual manner.

diastereomeric alcohols **19** (163 mg; 90% yield from **4**); ir 2240 (C≡N) and 3400–3500 (—OH) cm^{-1}; ^{1}Hmr δ: 2.80 (m, 1H, —CHCN), 3.82, 3.86 (both d, 1H each, J = 6 Hz each; —CH_2OH), and 3.95 (m, 4H, —OCH_2CH_2O—); ms M^+: 211.1209 (calcd. for $C_{11}H_{17}NO_3$: 211.1208).

Compounds **20–27** displayed the following physical data:

Ketal **20**: ir: 1680 (C=O) and 2260 (C≡N) cm^{-1}; ^{1}Hmr δ: 1.49, 1.54 (both s, 9H total, —C(CH_3)$_3$), 3.60, 3.65 (both d, 1H total, J = 10 Hz each, —CHCN), 3.90 (br s, 4H, —OCH_2CH_2O—), and 6.20 (m, 2H, —CH=CH—); ms M^+: 347.1557 (calcd. for $C_{19}H_{25}NO_3S$: 347.1555).

Alcohol **21**: ir: 2260 (C≡N) and 3400–3500 (—OH) cm^{-1}; ^{1}Hmr δ: 3.80 (m, 2H, —CH_2OH), 3.90 (m, 4H, —OCH_2CH_2O—), and 6.20 (m, 2H, —CH=CH—); ms M^+: 261.1366 (calcd. for $C_{15}H_{19}NO_3$: 261.1365).

Ketal **22**: ir: 1680 (C=O) and 2250 (C≡N) cm^{-1}. *Anal.* calcd. for $C_{14}H_{23}NO_3S$: C 58.92, H 8.13, N 4.91, S 11.21; found: C 59.00, H 8.16, N 4.83, S 11.04. The following ^{1}Hmr data were attributed to the major isomer: δ 1.10 (d, 3H, J = 7 Hz, CH_3CH—), 1.36 (s, 3H, CH_3CO—), 1.52 (s, 9H, —C(CH_3)$_3$), 3.98 (s, 4H, —OCH_2CH_2O—), and 4.26 (d, 1H, J = 4 Hz, —CHCN). The following ^{1}Hmr data were attributed to the minor isomer: δ 1.22 (d, 3H, J = 7 Hz, CH_3CH—), 1.36 (s, 3H, CH_3CO—), 1.52 (s, 9H, —C(CH_3)$_3$), 3.60 (d, 1H, J = 4 Hz, —CHCN), and 3.90 (br s, 4H, —OCH_2CH_2O—).

Alcohol **23**: ir: 2260 (C≡N) and 3400–3500 (—OH) cm^{-1}; ms m/e: 184.0973 (M^+ −15; calcd. for $C_9H_{14}NO_3$: 184.0974). The following ^{1}Hmr signals were attributed to the major isomer: δ 1.10 (d, 3H, J = 6 Hz, CH_3CH—), 1.32 (s, 3H, CH_3CO—), 1.74 (d, 2H, J = 8 Hz, —CH_2CO—), 3.14 (td, 1H, J = 7, J' = 5 Hz, —CHCN), 3.80 (dd, 2H, J = 7, J' = 6 Hz, —CH_2OH), and 3.97 (s, 4H, —OCH_2CH_2O—). The following ^{1}Hmr data were attributed to the minor isomer: δ 1.20 (d, 3H, J = 8 Hz, CH_3CH—), 1.32 (s, 3H, CH_3CO—), 1.82 (d, 2H, J = 9 Hz, —CH_2CO—), 3.14 (td, 1H, J = 7, J' = 5 Hz, —CHCN), 3.80 (dd, 2H, J = 7, J' = 6 Hz, —CH_2OH), and 4.00 (s, 4H, —OCH_2CH_2O—).

Ketal **24**: ir: 1050–1100 (C—O), 1680 (C=O), and 2260 (C≡N) cm^{-1}; ^{1}Hmr δ: 1.50 (s, 9H, —C(CH_3)$_3$), 3.60 (d, ~0.5H, J = 7 Hz, —CHCN of one isomer), 3.67 (d, ~0.5H, J = 4 Hz, —CHCN of another isomer), and 3.95 (br s, 4H, —OCH_2CH_2O—); ms M^+: 283.1239 (calcd. for $C_{14}H_{21}NO_3S$: 283.1242).

Alcohol **25**: ir: 2260 (C≡N) and 3400–3500 (—OH) cm^{-1}; ^{1}Hmr δ: 2.75 (m, 2H, —CHCN and —OH), 3.80 (d, 2H, J = 6 Hz, —CH_2OH), and 3.90 (m, 4H, —OCH_2CH_2O—); ms M^+: 197.1043 (calcd. for $C_{10}H_{15}NO_3$: 197.1052).

Ketal **26**: ir: 1680 (C=O) and 2260 (C≡N) cm^{-1}; ^{1}Hmr δ: 1.50 (s, 9H, —C(CH_3)$_3$), 3.50 (m, 1H, —CHCN), and 3.90 (m, 4H, —OCH_2CH_2O—); ms M^+: 323.1558 (calcd. for $C_{17}H_{25}NO_3S$: 323.1555).

Alcohol **27**: ir: 2250 (C≡N) and 3400–3500 (—OH) cm^{-1}; ^{1}Hmr δ: 2.50 (br s, 1H, —OH), 2.70 (m, 1H, —CHCN), 3.76 (dd, 2H, J = 6, J' = 2 Hz, —CH_2OH), and 3.86 (m, 4H, —OCH_2CH_2O—); ms M^+: 237.1359 (calcd. for $C_{13}H_{19}NO_3$: 237.1365).

*Dehydration of alcohols **19**, **21**, **23**, **25**, and **27***

The dehydration reactions were carried out using the general procedures illustrated below with alcohol **21**. Time of reactions and yields of products are noted in Table 5.

A. *Direct dehydration*

Alcohol **21** (291 mg, 1.11 mmol) was dissolved in ether (5 mL). DCC (342 mg, 1.67 mmol) was introduced, followed by addition of a small amount of copper(I) chloride (15 mg). The mixture was heated at reflux for 48 h under an argon atmosphere, cooled to room temperature, and filtered. Concentration of the filtrate gave a residue which was dissolved in *n*-pentane, filtered, and concentrated. The crude product was purified by flash chromatography on silica gel (20% ethyl acetate – petroleum ether) to afford ketal olefin **29** (165 mg; 60% yield); ir: 1080 (C—O), 1630 (C=C), and 2220 (C≡N) cm^{-1}; ^{1}Hmr δ: 3.92 (m, 4H, —OCH_2CH_2O—), 5.76 (d, 1H, J = 2 Hz, =CHH), 5.86 (br s, 1H, =CHH), 6.10 (dd, 1H, J = 6, J' = 4 Hz, —CH=), and 6.34 (dd, 1H, J = 6, J' = 3 Hz, —CH=); ^{13}Cmr δ: 138.4, 132.3, 132.1, 128.8, 126.5, 115.4, 92.1, 64.5, 64.0, 55.1, 53.2, 50.8, 44.8, 44.7, 43.6; ms M^+: 243.1256 (calcd. for $C_{15}H_{17}NO_2$: 243.1259). *Anal.* calcd. for $C_{15}H_{17}NO_2$: C 74.04, H 7.05, N 5.76; found: C 74.06, H 7.20, N 5.59.

B. *Indirect dehydration*

Alcohol **21** (249 mg, 0.95 mmol) was dissolved in dichloromethane (10 mL). Methanesulfonyl chloride (0.22 mL, 2.85 mmol) and triethylamine (0.66 mL, 4.75 mmol) were added and the mixture stirred for 24 h at room temperature under an argon atmosphere. The resulting solution was evaporated to dryness *in vacuo* and the residue dissolved in benzene (5 mL). DBU (0.5 mL) was introduced and the solution refluxed for 50 min under an atmosphhere of argon. It was then cooled to room temperature, poured into 1 *N* aqueous hydrochloric acid (30 mL), and extracted with dichloromethane (4 × 20 mL). The extracts were washed sequentially with water, saturated aqueous sodium carbonate, and saturated aqueous sodium chloride, dried, filtered, and concentrated. Flash chromatography of the residue on silica gel (20% ethyl acetate – petroleum ether) afforded ketal olefin **29** (135 mg; 58% yield from alcohol **21**).

Ketal olefins **28** and **30–32** showed the following physical data:

Ketal olefin **28**: ir: 1080 (C—O) and 2220 (C≡N) cm^{-1}; ^{1}Hmr δ: 3.95 (s, 4H, —OCH_2CH_2O—), 5.70 (d, 1H, J = 2 Hz, =CHH), and 5.82 (br s, 1H, =CHH); ms M^+: 193.1102 (calcd. for $C_{11}H_{15}NO_2$: 193.1103).

Ketal olefin **30**: ir: 1050–1100 (C—O), 1630 (C=C), and 2220 (C≡N) cm^{-1}; ^{1}Hmr δ: 1.20 (d, 3H, J = 7 Hz, CH_3CH—), 1.36 (s, 3H, CH_3CO—), 3.96 (s, 4H, —OCH_2CH_2O—), 5.70, and 5.78 (both d, 1H each, J = 2 Hz each, =CH_2); ms m/e: 166.0868 (M^+ −15; calcd. for $C_9H_{12}NO_2$: 166.0868).

Ketal olefin **31**: ir: 1110 (C—O) and 2220 (C≡N) cm^{-1}; ^{1}Hmr δ: 3.94 (s, 4H, —OCH_2CH_2O—), 5.75 (d, 1H, J = 2 Hz, =CHH), 5.83 (br s, 1H, =CHH); ms m/e: 127.0759 (M^+ −52; calcd. for $C_7H_{11}O_2$: 127.0759).

Ketal olefin **32**: ir: 1120 (C—O), 1620 (C=O), and 2238 (C≡N) cm^{-1}; ^{1}Hmr δ: 3.80 (m, 4H, —OCH_2CH_2O—), 5.78, and 5.86 (both br s, 1H each, =CH_2); ms M^+: 219.1262 (calcd. for $C_{13}H_{17}NO_2$: C 71.19, H 7.82, N 6.39; found: C 71.06, H 7.93, N 6.23.

*Deketalization of ketal olefins **28** and **31***

A solution of ketal olefin **28** (62 mg, 0.32 mmol) and *p*-toluenesulfonic acid monohydrate (30 mg, 0.16 mmol) in acetone (5 mL) was stirred at room temperature under an argon atmosphere for 24 h. It was made basic with saturated aqueous sodium bicarbonate and extracted

with dichloromethane (4 × 10 mL). The extracts were washed with saturated aqueous sodium chloride, dried, filtered, and concentrated. The crude product was purified by flash chromatography on silica gel (20% ethyl acetate in petroleum ether) to afford ketone **33** (39 mg; 81% yield); ir: 1710 (C=O) and 2220 (C≡N) cm^{-1}; ^{1}Hmr δ: 5.80 (d, 1H, J = 2 Hz, =C*H*H) and 5.94 (br s, 1H, =CH*H*); ms M^+: 149.0839 (calcd. for $C_9H_{11}NO$: 149.0841).

Treatment of ketal olefin **31** (67 mg, 0.37 mmol) with *p*-toluenesulfonic acid monohydrate (70 mg, 0.37 mmol) and acetone (5 mL) under similar conditions for 36 h gave ketone **34** (49 mg; 97% yield); ir: 1620 (C=C), 1740 (C=O), and 2230 (C≡N) cm^{-1}; ^{1}Hmr δ: 3.10 (m, 1H, —CH—), 5.84, and 5.95 (both br s, 1H each, $=CH_2$); ms M^+: 135.0683 (calcd. for C_8H_9NO: 135.0684).

Acknowledgements

We are grateful to the Natural Sciences and Engineering Research Council of Canada and the University of Alberta for financial support.

1. H. J. Liu and H. Wynn. Tetrahedron Lett. **23**, 3151 (1982).
2. H. J. Liu and H. Wynn. Tetrahedron Lett. **26**, 4843 (1985).
3. Y. Nagao, K. Kawabata, and E. Fujita. Chem. Commun. 330 (1978).
4. H. J. Liu, R. R. Bukownik, and P. R. Pednekar. Synth. Commun. **11**, 599 (1981).
5. H. J. Liu and S. I. Sabesan. Can. J. Chem. **58**, 2645 (1980).
6. H. J. Liu, L. K. Ho, and H. K. Lai. Can. J. Chem. **59**, 1685 (1981).
7. H. J. Liu and I. V. Oppong. Can. J. Chem. **60**, 94 (1982).
8. H. O. House. Modern synthetic reactions. 2nd ed. W. A. Benjamin, Inc., Menlo Park, CA. 1972.
9. R. N. Ring, G. C. Tesoro, and D. R. Moore. J. Org. Chem. **32**, 1091 (1967).
10. N. C. Ross and R. Levine. J. Org. Chem. **29**, 2346 (1964).
11. A. Michael and J. Ross. J. Am. Chem. Soc. **52**, 4598 (1930).
12. C. Alexandre and F. Rouessac. Bull. Soc. Chim. Fr. 1837 (1971).

Thiol esters in organic synthesis. XIV.[1] The total synthesis of racemic α-costal

HSING-JANG LIU AND HLA WYNN
Department of Chemistry, University of Alberta, Edmonton, Alta., Canada T6G 2G2

Received July 29, 1985

HSING-JANG LIU and HLA WYNN. Can. J. Chem. **64**, 658 (1986).

The first total synthesis of α-costal (**1**) in racemic form has been achieved in an unequivocal manner whereby the structure previously assigned to the natural aldehyde is confirmed. A salient feature of the synthesis is the use of *S-tert*-butyl cyanothiolacetate to facilitate the introduction of the labile acrolein unit.

HSING-JANG LIU et HLA WYNN. Can. J. Chem. **64**, 658 (1986).

On a réalisé la première synthèse totale et non-ambigüe de l'α-costal (**1**) à l'état racémique et l'on a ainsi confirmé la structure qui a été antérieurement attribuée à cet aldéhyde naturel. La caractéristique principale de cette synthèse est l'utilisation du cyanothiolacétate de *S-tert*-butyle pour faciliter l'introduction de l'unité acroléine labile.

[Traduit par la revue]

Introduction

During the course of our studies on cyanothiolesters, we have established a methodology to facilitate the synthesis of β-hydroxypropionitrile and acrylonitrile derivatives through the use of cyanothiolacetate as a masked β-hydroxypropionitrile carbanion equivalent (Scheme 1) (1, 2). In essence, this method provides a convenient means for the incorporation of a highly functionalized isopropyl unit.[2] In order to test the applicability of this method in the area of natural product synthesis, α-costal (**1**) was chosen as a target molecule.

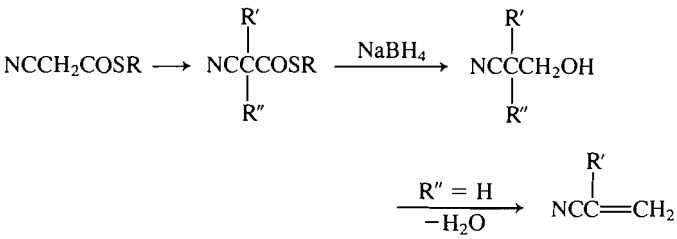

SCHEME 1

α-Costal (**1**) is one of the constituents of the leaf oil of *Thujopsis dolabrata* Sieb. et Zucc. It was first isolated in 1965 by Ito *et al.* (5), along with several other sesquiterpenes. This compound was found to be inseparable from its double-bond isomer, β-costal (**2**).[3] It was based solely on the information gathered on this mixture that the structure of α-costal was tentatively assigned (5).

In the approach to the synthesis of α-costal, the most suitable starting compound appeared to be ketone **3**, which was readily available from 2-methyl-1,3-cyclohexanedione (**4**) (6, 7). This compound already possesses some of the required features of the target molecule, such as a *trans*-decalin system, the angular and vinylic methyl groups, and a trisubstituted double bond. The transformation of ketone **3** to α-costal (**1**) requires the incorporation of an acrolein unit onto the carbon β to the ketone carbonyl. Involving the developed methods (1, 2) outlined in Scheme 1, this requirement could be achieved, in principle, by the three possible routes illustrated in Scheme 2.

Route A requires a 1,3-oxygen transposition of the ketone carbonyl. The resulting ketone is expected to undergo Knoevenagel-type condensation with cyanothiolacetate to facilitate the installation of the acrolein unit found in the target molecule. In route B, a leaving group will be introduced to the β carbon of the ketone carbonyl. This is to be followed by an alkylation reaction with cyanothiolacetate. In route C, the Michael addition of cyanothiolacetate is considered as a convenient means for the introduction of a highly functionalized isopropyl unit.

All of the outlined approaches were examined and, by the use of route A, the first total synthesis of α-costal (**1**) in racemic

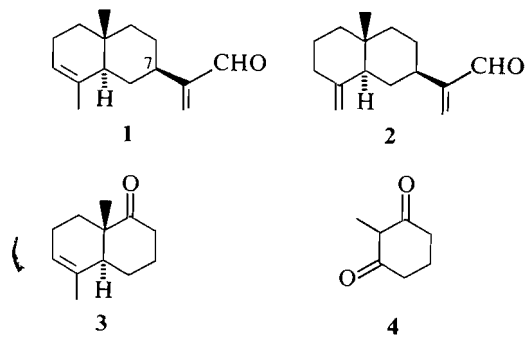

form has been achieved, confirming the structure and stereochemistry tentatively assigned to the natural aldehyde.[4]

Results and discussion

The starting 2-methyl-1,3-cyclohexanedione (**4**) was prepared in 90% yield by hydrogenation of the monosodium salt of 2-methylresorcinol at room temperature under 50 psi (1 psi = 6.89 kPa) pressure of hydrogen using 5% rhodium on alumina as a catalyst (9). This procedure compares favorably with the traditional one by Mekler (10), which requires substantially higher pressure using Raney nickel as a catalyst. Enedione **5** was prepared by modification of a reported procedure (11). Treatment of diketone **4** with ethyl vinyl ketone in 1,2-dimethoxyethane (DME) at room temperature in the presence of 1,4-diazabicyclo[2.2.2]octane (DABCO) (12) gave trione **6** in 90% yield. Intramolecular aldol condensation of **6** with benzoic acid and triethylamine in refluxing xylene (13) resulted in the formation of crystalline enedione **5**, mp 40–42°C (lit. (11) mp 39–40°C), in 89% yield. Ketalization of enedione **5** with an

[1]For part XIII of this series, see ref. 1.

[2]For other methods, see refs. 3 and 4 and references cited therein.

[3]In the original literature, α-costal was inadvertently named as β-costal and *vice versa*.

[4]Part of this work has been reported previously in a preliminary form (8).

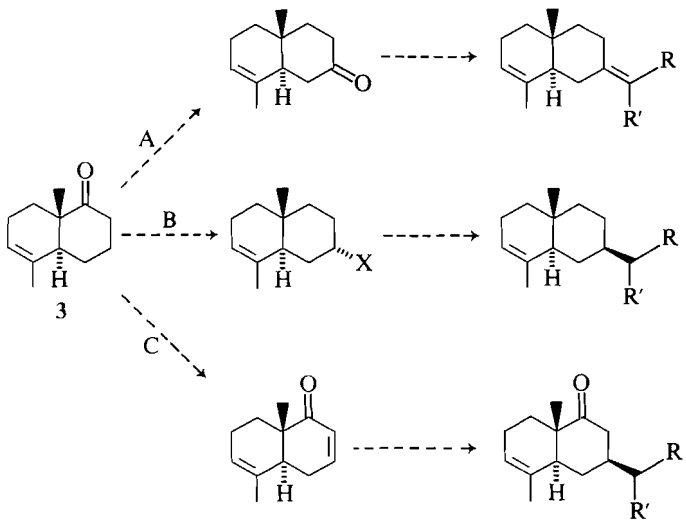

X = leaving group, R = CN, R′ = $COSC(CH_3)_3$

SCHEME 2

excess of ethylene glycol in the presence of a catalytic amount of either *d*-10-camphorsulfonic acid or *p*-toluenesulfonic acid in refluxing benzene gave ketal **7** (82–88% yield). In the case of camphorsulfonic acid, a small amount (~6% yield) of diketal **8** was also formed.

Ketal enone **7** was subjected to Birch reduction (14) in liquid ammonia at −78°C with an excess of lithium metal in the presence of *tert*-butyl alcohol. The resulting lithium enolate was trapped with diethyl phosphorochloridate in tetrahydrofuran (THF) at 0°C with (6) or without (7) the presence of *N,N,N′,N′*-tetramethylethylenediamine. The yield of the desired enol phosphate **9** ranged from 50 to 69%, comparable to that obtained by Ireland and Pfister (6). In addition to enol phosphate **9**, a variable amount (10–20%) of ketone **10**, apparently formed by the protonation of the intermediate enolate ion, was also obtained. In spite of the extreme care undertaken in carrying out the reaction, the formation of this ketone could not be suppressed.

Ketal enol phosphate **9** underwent reductive elimination of the phosphate group smoothly when treated with lithium in ethylamine in the presence of *tert*-butyl alcohol (6). Transketalization of the resulting ketal olefin **11** (84% yield) with acetone in the presence of *p*-toluenesulfonic acid gave rise to the known ketone **3** (6, 7) in quantitative yield. According to the synthetic plan shown in Scheme 2, three routes are conceivable to incorporate an acrolein unit onto the β-carbon of the ketone carbonyl. In order to activate the center to which the acrolein unit is to be attached, ketone **3** was converted to the α,β-unsaturated ketone **12** as follows.

Ketone **3** was treated sequentially with lithium diisopropylamide and phenylselenenyl chloride in THF at −78°C (15). After 3 h, the reaction was complete and selenide **13** was isolated in 88% yield as a single stereoisomer. The stereochemistry of the newly incorporated chiral center was deduced on the basis of the ^{1}Hmr spectrum, which showed a signal at δ 4.54 for the proton attached to this chiral center. The signal appeared as a doublet of doublets with coupling constants of 12 and 6 Hz, indicating that the proton was axial and thus the phenylselenenyl substituent equatorial. When selenide **13** was exposed to 30% hydrogen peroxide in THF at 0–15°C for 5 h, the α,β-unsaturated ketone **12** was isolated in 78% yield, resulting from concomitant oxidation of the phenylselenenyl group and elimination of the resulting selenoxide.

With enone **12** in hand, the three synthetic routes leading to α-costal (**1**) were individually explored as planned (Scheme 2). The first route to be examined was route A, in which a Knoevenagel-type condensation was conceived as a means for the introduction of a highly functionalized isopropyl unit required for the synthetic target.

Towards this end, enone **12** was converted to alcohol **14** by the use of Wharton's reaction (16). Epoxidation of enone **12** with 30% hydrogen peroxide in ethanol in the presence of sodium hydroxide afforded an 89% yield of epoxy ketone **15** as a single stereoisomer in crystalline form, mp 54–55°C. The stereochemistry of this compound could not be assigned unambiguously at this stage. However, the subsequent transformation requires its stereochemistry as shown, resulting from the epoxidation of enone **12** from the less hindered side. Initial attempts to induce the Wharton reaction on epoxy ketone **15** were carried out as follows, using standard conditions. Hydrazine hydrate (2 equiv.) and acetic acid (0.2 equiv.) were added sequentially to a methanolic solution of epoxide **15** and the resulting solution was stirred for 3 h at room temperature. The results were found to be rather unsatisfactory; the desired product **14** was isolated only in 38% yield, along with a substantial quantity of an unidentified material which appeared to be dimeric in nature (bishydrazone?), as suggested by its mass spectrum. When the reaction was carried out in neat hydrazine hydrate in the absence of glacial acetic acid at elevated temperature (17), a poor yield (18%) of the desired rearrangement product **14** was obtained. To avoid formation of the dimeric material, the reaction was performed with the following modifications. A dilute methanolic solution of epoxy ketone **15** was added slowly to a solution of hydrazine hydrate (5 equiv.) and glacial acetic acid (0.2 equiv.) in methanol. This experiment, involving the reverse addition and the use of a large excess of hydrazine hydrate, proved to be superior and the desired product **14** was obtained in a much improved yield of 74%. In the ^{1}Hmr spectrum, the C-7 proton appeared as a broad triplet at δ 4.22. Decoupling experiments showed that this proton was coupled with the axial proton on C-8 at δ 2.72 with a rather small coupling constant of 2.5 Hz. On the basis of this observed small coupling constant, the stereochemistry of compound **14** was deduced.

Oxidation of allylic alcohol **14** with pyridinium dichromate (18) gave an 89% yield of dienone **16**. The conversion of this compound to the corresponding saturated ketone **18** requires the selective reduction of the double bond conjugated with the ketone carbonyl. In the presence of Wilkinson's catalyst (tris(triphenylphosphine)rhodium chloride), hydrosilanes have been shown (19) to add to α,β-unsaturated ketones exclusively by 1,4-addition, to give silyl enol ethers which readily undergo hydrolysis to give saturated ketones. When enone **16** was subjected to hydrosilation with triethylsilane in the presence of Wilkinson's catalyst for 6 h at room temperature, silyl enol ether **17** was isolated in quantitative yield. On exposure to tetra-*n*-butylammonium fluoride in THF, this compound was converted to ketone **18** in 73% yield. An improved yield of 89% was obtained when the hydrosilation product was directly subjected to the fluoride treatment without purification.

Having successfully prepared the saturated ketone **18** from **3** via an overall 1,3-oxygen transposition, its condensation with *S-tert*-butyl cyanothiolacetate was investigated. Initially,

ketone **18** was treated with the latter reagent in THF in the presence of DABCO at room temperature. This set of conditions has been successfully used previously to effect the Knoevenagel-type condensation of *S-tert*-butyl cyanothiolacetate with various ketones (2). In the present case, however, the reaction was not highly effective. Although the reaction occurred readily at the outset, as indicated by thin-layer chromatographic (tlc) analysis, it could not be brought to completion even after 15 h at refluxing temperature, and only 21% yield of the desired product was formed. These results suggested that the reaction was probably reversible. In order to facilitate product formation, water, which was produced during the condensation, needed to be removed. Towards this end, magnesium sulfate was added to the reaction mixture. Surprisingly, this resulted in the rapid consumption of the thiolester reagent without substantial formation of the desired product, for reasons which have yet to be determined. In further attempts, sodium sulfate was used as a dehydrating agent. This experiment proved to be successful, giving an isomeric mixture of **19** along with compound **20** in ca. 4:1 ratio in a total of 73% yield.

To complete the synthesis of α-costal (**1**), it remained to modify the newly incorporated cyanothiolester unit to the required acrolein moiety, preferably with control of stereochemistry. Previously, it was shown (2) that the carbon–carbon double bond of α,β-unsaturated cyanothiolester systems present in the Knoevenagel-type condensation product could be selectively reduced with sodium borohydride under controlled conditions. In the presence of an excess of the reducing agent at higher temperature, further reduction of the thiolester to the alcohol level could also be simultaneously effected. The selective reduction of the carbon–carbon double bond of compound **19** was first examined in an attempt to determine the selectivity of the reduction. It was gratifying to find that when a mixture of **19** and **20** was subjected to sodium borohydride (1 mol equiv.) reduction at 0°C in ethanol, not only was the reduction of the former compound effected, but the carbon–carbon double bond of the latter compound was also smoothly reduced. Apparently, the conditions were sufficient to effect the isomerization of the double bond into conjugation with cyano and thiolester groups. The reduction product **21** obtained in 74% yield was found to be homogeneous by tlc. However, the ^{1}Hmr spectrum indicated the presence of all four diastereomers, showing four doublets in a ratio of 2:2:1:1 for the methine proton of the cyanothiolester group. Further reduction of cyanothiolacetate **21** with sodium borohydride in ethanol at room temperature gave an 88% yield of the corresponding alcohol **22** as a mixture of diastereomers. The same diastereomeric mixture could also be prepared directly from **19** and **20** using an excess of sodium borohydride (4 mol equiv.) in ethanol at −40°C[5] for 4 h and at room temperature for 12 h. The yield (91%) thus obtained was far superior to the two-step sequence.

Alcohol **22** was subjected to dehydration with dicyclohexylcarbodiimide in refluxing ether in the presence of a catalytic amount of copper(I) chloride (1, 2, 20) to give a mixture of cyano olefins **23** and **24** in 2:1 ratio and 94% total yield. These isomeric compounds were separated by Chromatotron. Both compounds showed in the ir spectrum, olefin absorption band at 1620 cm^{-1} and nitrile absorption band at 2210 cm^{-1}. The epimeric nature of these compounds was further confirmed by the mass spectra, each of which showed a molecular ion peak (215.1676 for the major and 215.1663 for the minor) in accordance with the molecular formula of $C_{15}H_{21}N$. The stereochemistry of these two compounds was assigned after careful examination of their respective ^{1}Hmr spectra. The major isomer showed a multiplet at δ 2.28 for the C-7 hydrogen atom. By decoupling experiments, this proton was found to be coupled to the vinylic protons of the acrylonitrile moiety at δ 5.74 (a doublet of doublets) and 5.82 (a broad singlet). Similarly, the C-7 proton of the minor isomer, which appeared at δ 2.72 as a multiplet, was also shown to couple with the terminal vinylic protons observed at δ 5.85 and 6.07, each as a doublet. It has been shown by sufficient examples that the axial and equatorial protons of cyclohexane derivatives (especially when rigid) are not equally shielded (21). The axial proton normally absorbs at a much higher field than the equatorial counterpart, with the relative chemical shift difference of ca. 0.2–0.8 ppm. The fact that the C-7 proton of the major isomer appeared at a much higher field (δ 2.28) than that of the minor isomer (δ 2.72) by 0.44 ppm indicated the axial orientation of this proton. Accordingly, the stereochemistry of **23** and **24** was deduced as shown.

The predominant formation of epimer **23** possessing the desired stereochemistry was apparently a result of preferential reduction of the conjugated carbon–carbon double bond of compound **19** with sodium borohydride, involving the addition of the hydride ion from the less hindered side of the molecule. In an attempt to improve the stereoselectivity, the mixture of compounds **19** and **20** was subjected to reduction with a bulky reducing agent. Unexpectedly, sequential reduction of the mixture of **19** and **20** with lithium tri-*tert*-butoxyaluminum hydride and then with sodium borohydride, followed by dehydration of the resulting alcohol, afforded mainly the undesired epimer **24** (~3 parts) and a smaller quantity of **23** (1 part).

Cyano olefins **23** and **24** were individually reduced with diisobutylaluminum hydride at −78°C in toluene for 3 h. From the former epimer an aldehyde was obtained in 59% yield. This compound was shown to be identical with natural α-costal (**1**) by comparison of its ^{1}Hmr spectrum with published values (5). Reduction of **24** gave a 60% yield of compound **25**, an epimer of α-costal (**1**). In agreement with the stereochemical assignments, the C-7 proton of this compound appeared, in the ^{1}Hmr spectrum, again at a much lower field (δ 3.04 in $CDCl_3$) than the corresponding one (δ 2.56) of α-costal (**1**).

After completing the first total synthesis of α-costal (**1**) in a stereoselective manner, the other two possible routes outlined in Scheme 2 were also examined in order to determine (*i*) the feasibility of these approaches leading to the natural product and (*ii*) the possible improvement of the total synthesis. For route B, alcohol **14**, which was produced as a single stereoisomer with a well-defined stereochemistry, provided an interesting opportunity to carry out the total synthesis with complete stereochemical control. It is conceivable that the replacement of the hydroxyl group with *S-tert*-butyl cyanothiolacetate with inversion of stereochemistry could lead eventually to the target molecule. The required replacement reaction could be directly effected using a Mitsunobu reaction (22). The best result was obtained when alcohol **14** and *S-tert*-butyl cyanothiolacetate (2 equiv.) were sequentially added to a THF solution of 1.5 equiv. each of diethyl azodicarboxylate and triphenylphosphine. After 3.5 h at −35°C, an inseparable mixture of the desired compound **26** and its isomer **27** (ca. 2:1) was isolated in

[5]When the reduction was carried out first at −78°C and then at room temperature, the same diastereomeric mixture was produced but in somewhat poorer yield.

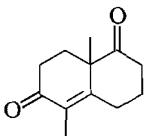

5

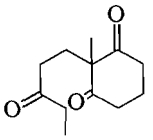

6

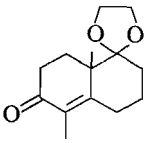

7

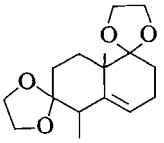

8

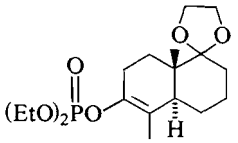

9

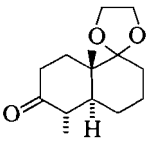

10

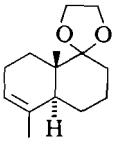

11

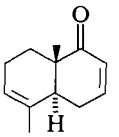

12

54% yield. Treatment of this mixture with sodium borohydride resulted in the exclusive reduction of compound **26** to give two epimeric alcohols **28** (1:1; 78% yield), with compound **27** recovered intact. The transformation of **28** to α-costal (**1**) requires the selective saturation of its disubstituted double bond. Unfortunately, this requirement could not be satisfactorily fulfilled in spite of numerous trials using different methods

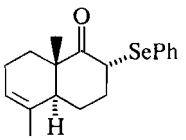

13

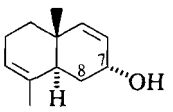

14

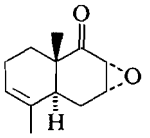

15

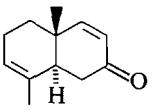

16

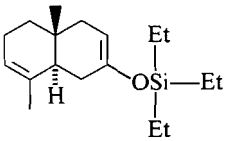

17

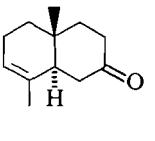

18

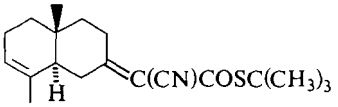

19

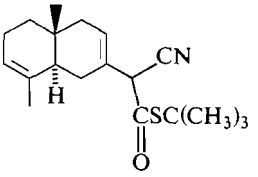

20

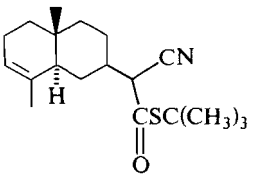

21

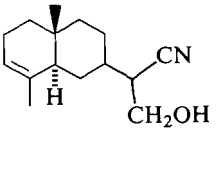

22

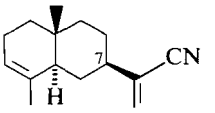

23

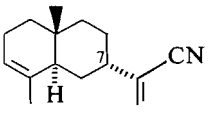

24

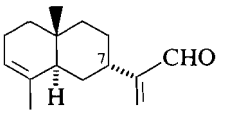

25

(catalytic hydrogenation, diimide reduction, and homogeneous hydrogenation with Wilkinson's catalyst) under various conditions.

The synthesis of α-costal (**1**) by route C requires the Michael addition of *S-tert*-butyl cyanothiolacetate to enone **12**. This was readily effected by treatment of the latter compound with the cyanothiolacetate and sodium hydride in the presence of chlorotrimethylsilane (1) in refluxing benzene for 16 h. A 76% yield of the desired adduct **29** was obtained. This material was shown to be a mixture of four diastereomers by the ^{1}Hmr spectrum, which displayed four doublets for the methine proton of the cyanothiolacetate group at δ 3.44, 3.53, 3.46, and 3.64,

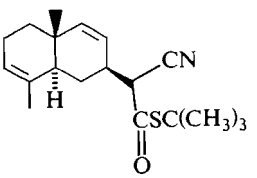

26

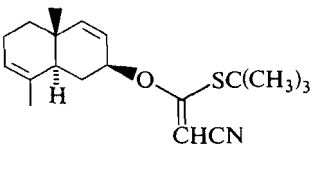

27

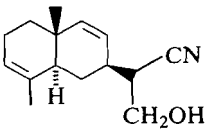

28

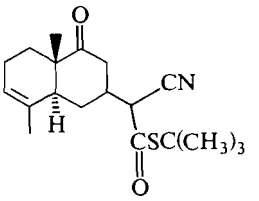

29

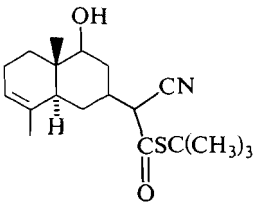

30

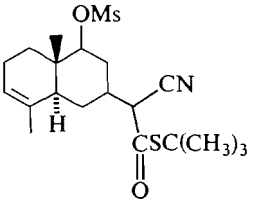

31

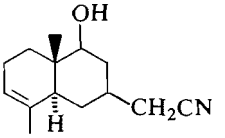

32

integrating to a 2:2:1:1 ratio. In order to remove its ketone carbonyl,[6] compound **29** was converted to the corresponding alcohol **30** by brief treatment with sodium borohydride at 0°C. Deoxygenation of **30** was examined but without any success; the reduction of the corresponding mesylate **31** with sodium iodide and zinc dust (23) in refluxing *N,N*-dimethylformamide (24) gave hydroxy nitrile **32** as the only isolatable product, while attempted preparation of halide and xanthate derivatives failed to yield any desired products. The poor stereoselectivity of the Michael addition (**12** → **29**) and the lack of simple solutions to effect the removal of the ketone carbonyl of the adduct made further exploration of route C to α-costal (**1**) unattractive.

Experimental

General

Melting points were determined on a Kofler hot stage apparatus and are uncorrected. Elemental analyses were performed by the microanalytical laboratory of this department. Infrared (ir) spectra were recorded on a Perkin–Elmer model 457 or Nicolet 7-199 FT-IR spectrophotometer. Unless otherwise stated, ir samples were run as thin films. Proton nuclear magnetic resonance (^{1}Hmr) spectra were recorded on a Varian HA-100/Digilab, Bruker WH-80, WH-200, or WH-400 spectrometer and, except where otherwise stated, were obtained on solutions in deuterochloroform with tetramethylsilane as internal reference. Carbon-13 nuclear magnetic resonance (^{13}Cmr) spectra were recorded on a Bruker HFX-90/Nicolet 1085 system or a Bruker WH-200 or WH-400 spectrometer and were obtained on solutions in deuterochloroform using tetramethylsilane as internal reference. Mass spectra (ms) were recorded using A.E.I. model MS9, MS12, or MS50 mass spectrometers. Unless otherwise stated, anhydrous magnesium sulfate was used for drying organic solutions.

Materials

DME and THF were freshly distilled over sodium metal. Benzene and ether were freshly distilled over lithium aluminum hydride. Dichloromethane was washed with an equal volume of 10% aqueous sodium carbonate and distilled over powdered calcium chloride. Gaseous ammonia was passed through potassium hydroxide pellets and distilled over sodium metal. *N,N,N′,N′*-Tetramethylethylenediamine was freshly distilled over sodium metal. Diethyl phosphorochloridate was distilled over powdered lead carbonate (25). Ethylamine, xylene, and diisopropylamine were freshly distilled over calcium hydride. Ethanol was distilled over magnesium turnings. *S-tert*-Butyl cyanothiolacetate was prepared according to the reported procedure (26).

2-Methyl-2-(3-oxopentyl)cyclohexane-1,3-dione (6)

2-Methylresorcinol (10 g, 0.08 mol) was dissolved in distilled water (70 mL). Sodium hydroxide (3.75 g, 0.09 mol) and 5% rhodium on alumina (1 g) were added and the hydrogenation bottle fitted in a Parr hydrogenation apparatus. The mixture was shaken under 50 psi pressure of hydrogen at room temperature for 9.5 h. The reaction mixture was then filtered through a sintered glass funnel and the filtrate acidified by dropwise addition of concentrated hydrochloric acid (~25 mL) to a pH of ~4. The resulting solution was extracted with ethyl acetate (4 × 200 mL). The extracts were dried, filtered, and concentrated to give dione **4** (9.1 g; ~90% yield), which was subjected to further reaction without purification.

Dione **4** (19 g, 0.15 mol) was dissolved in DME (300 mL). DABCO (19.38 g, 0.17 mol) was added. The solution was chilled to 0°C and stirred for 15 min under an argon atmosphere. Ethyl vinyl ketone (17.3 mL, 0.17 mol) was added dropwise and the reaction mixture stirred for 12 h at room temperature. The mixture was poured into ice-cold 1 *N* aqueous hydrochloric acid solution (~200 mL) and extracted with dichloromethane (4 × 300 mL). The extracts were washed with saturated aqueous sodium chloride, dried, filtered, and concentrated. The product **6** (28.37 g; ~90% yield) thus obtained was used directly for the next reaction. An analytical sample obtained by flash chromatography (20% ethyl acetate in petroleum ether) on silica gel showed the following spectral data: ir: 1715 (C=O) and 3500 (enol —OH) cm^{-1}; ^{1}Hmr δ: 1.02 (t, 3H, J = 7 Hz, CH_3CH_2—), 1.26 (s, 3H, CH_3—), and 1.8–2.9 (complex, 12H, 6 × —CH_2—); ms M$^+$: 210.1258 (calcd. for $C_{12}H_{18}O_3$: 210.1256).

5,8a-Dimethyl-3,4,8,8a-tetrahydro-1,6[2H, 7H]-naphthalenedione (5)

The crude trione **6** (3.95 g, ~19 mmol), obtained from the above experiment, and benzoic acid (2.47 g, 20 mmol) were dissolved in xylene (20 mL). Triethylamine (2.0 mL, 14 mmol) was added and the solution was heated at reflux with a Dean–Stark water separator. After 22 h, the solution was cooled and extracted with ether. The extracts were washed with water, 5% aqueous sodium bicarbonate, 2 *N* aqueous sulfuric acid, and water. Drying, filtration, and concentration gave the crude product, which was purified by flash chromatography on silica gel. Elution with 50% ether in petroleum ether gave enedione **5** (3.23 g; 89% yield based on crude **6**); mp 40–42°C (ether); ir 1610 (C=C), 1660 (conjugated C=O), and 1710 (saturated C=O) cm^{-1}; ^{1}Hmr δ: 1.38 (s, 3H, CH_3—) and 1.79 (s, 3H, CH_3C=); ^{13}Cmr δ: 212.1, 197.7, 158.2, 130.8, 50.7, 37.4, 33.3, 29.7, 29.5, 27.3, 23.4, and 21.6; ms M$^+$: 192.1149 (calcd. for $C_{12}H_{16}O_2$: 192.1150). *Anal.* calcd. for $C_{12}H_{16}O_2$: C 74.96, H 8.39; found: C 74.89, H 8.54.

5,5-Ethylenedioxy-1,4a-dimethyl-4,4a,5,6,7,8-hexahydro-2[3H]-naphthalenone (7)[7] and 1,1,6,6-diethylenedioxy-5,8a-dimethyl-1,2,3,5,6,7,8,8a-octahydronaphthalene (8)

A solution of *d*-10-camphorsulfonic acid (50 mg, 0.2 mmol) and ethylene glycol (2 mL, 38.61 mmol) in benzene (20 mL) was heated at reflux for 13 h with a Dean–Stark water separator. A portion of benzene (~10 mL) was distilled off and the solution cooled to room temperature. Enedione **5** (414 mg, 2.15 mmol) in benzene (10 mL) was added. The mixture was heated at reflux for 3 h under an argon atmosphere. After cooling to room temperature, the mixture was made basic with saturated aqueous sodium bicarbonate. The organic layer was separated and the aqueous solution extracted with ether (4 × 20 mL). The organic solutions were combined, dried, filtered, and concentrated. The crude product was purified by flash chromatography on silica gel (30% ethyl acetate in petroleum ether) to give ketal **7** (418 mg; 82% yield); ir: 1040–1200 (C—O), 1618 (C=C), and 1670 (C=O) cm^{-1}; ^{1}Hmr δ: 1.31 (s, 3H, CH_3—), 1.80 (s, 3H, CH_3C=), and 3.94 (br s, 4H, —OCH_2CH_2O—); ms M$^+$: 236.1410 (calcd. for $C_{14}H_{20}O_3$: 236.1412). *Anal.* calcd. for $C_{14}H_{20}O_3$: C 71.14, H 8.54; found: C 71.06, H 8.63.

Further elution with the same solvent system afforded diketal **8** (36 mg; 6% yield): ir: 1040–1180 (C—O) cm^{-1}; ^{1}Hmr δ: 1.04 (d, 3H, J = 7 Hz, CH_3CH—), 1.28 (s, 3H, CH_3—), 3.95 (m, 8H, 2 × —OCH_2CH_2O—), and 5.44 (br s, 1H, —CH=); ms M$^+$: 280.1671 (calcd. for $C_{16}H_{24}O_4$: 280.1675).

1,1-Ethylenedioxy-6-diethylphosphoryloxy-5,8aβ-dimethyl-1,2,3,4,4aα,7,8,8a-octahydronaphthalene (9)[8] and 5,5-ethylenedioxy-1α,4aβ-dimethyl-1,4,4a,5,6,7,8,8aα-octahydro-2[3H]-naphthalenone (10)

To a solution of lithium (169 mg, 0.02 g-atom) in ammonia (35 mL), was added dropwise a solution of ketal **7** (1.52 g, 6.35 mmol) in ether (25 mL) containing *tert*-butyl alcohol (0.5 mL, 5.31 mmol). The resulting solution was stirred under an argon atmosphere for 1.5 h at −78°C. Excess lithium was destroyed by dropwise addition of freshly distilled isoprene until the blue color discharged. The mixture was

[6]Standard methods for reducing a ketone to the hydrocarbon level are incompatible with other existing functionalities.

[7]Ketal **7** was obtained as the only product in 88% yield when the reaction was carried out using *p*-toluenesulfonic acid as a catalyst.

[8]The stereochemical designations used in this and all other chemical names in this section denote relative stereochemistry. All compounds used and obtained were racemic.

warmed to room temperature and concentrated under reduced pressure. The residue was cooled to 0°C and a solution of *N,N,N',N'*-tetramethylethylenediamine (13 mL) in ether (22 mL) was added slowly. After stirring for 5 min under an argon atmosphere, a solution of diethyl phosphorochloridate (3 mL, 20.76 mmol) in ether (10 mL) was slowly added. After stirring for 5 h, the mixture was poured into ice-cold water and extracted with ether (4 × 50 mL). The extracts were washed with water, dried, filtered, and concentrated. The crude product was chromatographed on silica gel. Elution with 40% petroleum ether in ether gave ketone **10** (151 mg; 10% yield); ir: 1050–1200 (C—O) and 1710 (C=O) cm^{-1}; ^{1}Hmr δ: 1.02 (d, 3H, J = 8 Hz, CH_3CH—), 1.25 (s, 3H, CH_3—), and 3.9–4.0 (m, 4H, —OCH_2CH_2O—); ms M^+: 238.1565 (calcd. for $C_{14}H_{22}O_3$: 238.1569).

Further elution with 30% petroleum ether in ether gave enol phosphate **9** (1.65 g, 69% yield); ir: 1690 (C=C) cm^{-1}; ^{1}Hmr δ: 0.98 (s, 3H, CH_3—), 1.38 (t, 6H, J = 7 Hz, 2 × CH_3CH_2O—), 1.63 (br s, 3H, CH_3C=), 3.95 (s, 4H, —OCH_2CH_2O—), 4.16 (qd, 4H, J = J' = 7 Hz, CH_3CH_2O—); ms M^+: 374.1851 (calcd. for $C_{18}H_{31}O_6P$: 374.1858).

*1,1-Ethylenedioxy-5,8aβ-dimethyl-1,2,3,4,4aα,7,8,8a-octahydronaphthalene (**11**)*

At 0°C, small pieces of lithium wire (2.0 g, 0.29 g-atom) were added to ethylamine (200 mL) under an argon atmosphere and the mixture was stirred for 1 h. A solution of ketal phosphate **9** (10.59 g, 28 mmol) and *tert*-butyl alcohol (4.5 mL, 48 mmol) in THF (194 mL) was added dropwise over 1 h. After stirring for 2 h at 0°C, ethylamine was removed under reduced pressure and water was added dropwise to discharge the blue color. The resulting mixture was extracted with ether (4 × 200 mL) and the extracts were washed with ice-cold water, dried, filtered, and concentrated. Flash chromatography of the residue on silica gel (30% ether in petroleum ether) afforded ketal olefin **11** (5.22 g; 84% yield); ir: 1080–1200 (C—O) cm^{-1}; ^{1}Hmr δ: 0.92 (s, 3H, CH_3—), 1.63 (br s, 3H, CH_3C=), 3.90 (s, 4H, —OCH_2CH_2O—), and 5.29 (m, 1H, —CH=); ^{13}Cmr δ: 134.9, 120.8, 113.0, 65.2, 65.1, 43.9, 41.4, 30.5, 26.9, 23.2, 23.0, 22.6, 21.5, and 14.1; ms M^+: 222.1617 (calcd. for $C_{14}H_{22}O_2$: 222.1620). *Anal.* calcd. for $C_{14}H_{22}O_2$: C 75.62, H 9.98; found: C 75.99, H 9.99.

*5,8aβ-Dimethyl-3,4,4aα,7,8,8a-hexahydro-1[2H]-naphthaleneone (**3**)*

Ketal olefin **11** (620 mg, 2.79 mmol) was dissolved in acetone (15 mL) and *p*-toluenesulfonic acid (530 mg, 2.79 mmol) was added. After stirring at room temperature under an argon atmosphere for 16 h, the reaction mixture was poured into ice-cold saturated aqueous sodium bircarbonate and extracted with dichloromethane (4 × 20 mL). The extracts were washed with saturated aqueous sodium chloride, dried, filtered, and concentrated. Flash chromatography of the residue on silica gel (10% ethyl acetate – petroleum ether) gave ketone **3** (500 mg; 100% yield); ir: 1710 (C=O) cm^{-1}; ^{1}Hmr δ: 1.06 (s, 3H, CH_3—), 1.66 (s, 3H, CH_3C=), and 5.35 (m, 1H, —CH=); ms M^+: 178.1360 (calcd. for $C_{12}H_{18}O$: 178.1358).

*5,8aβ-Dimethyl-2α-phenylselenenyl-3,4,4aα,7,8,8a-hexahydro-1[2H]-naphthalenone (**13**)*

Diisopropylamine (0.3 mL, 2.14 mmol) was dissolved in THF (9 mL) at −78°C under an argon atmosphere. Methyllithium (1.29 mL, 1.3 *M* solution in *n*-hexane) was added dropwise and the mixture stirred for 10 min. A solution of ketone **3** (250 mg, 1.4 mmol) in THF (0.5 mL) was added. After 10 min, a solution of phenylselenenyl chloride (320 mg, 1.67 mmol) in THF (0.5 mL) was added and the reaction mixture stirred for 3 h at −78°C. Ice-cold 1 *N* aqueous hydrochloric acid (10 mL) was added and the resulting solution extracted with ether (4 × 20 mL). The extracts were washed with saturated aqueous sodium chloride, dried, filtered, and concentrated. The residue was purified by flash chromatography on silica gel, eluting with 10% ethyl acetate in petroleum ether, to give selenide **13** (410 mg; 88% yield); ir: 1590 (aromatic) and 1710 (C=O) cm^{-1}; ^{1}Hmr δ: 1.15 (s, 3H, CH_3—), 1.65 (s, 3H, CH_3C=), 4.54 (dd, 1H, J = 12, J' = 6 Hz, —CHSe—), 5.34 (m, 1H, —CH=), and 7.45 (m, 5H, aromatic protons).

*5,8aβ-Dimethyl-4aα,7,8,8a-tetrahydro-1[4H]-naphthalenone (**12**)*

At 0°C, to a solution of selenide **13** (300 mg, 0.9 mmol) in THF (10 mL), were added 30% hydrogen peroxide (0.26 mL) and water (0.73 mL). The mixture was stirred for 5 h at 15°C, poured into saturated aqueous sodium bicarbonate (20 mL), and extracted with ether (4 × 20 mL). The extracts were washed with saturated aqueous sodium chloride, dried, filtered, and concentrated. Purification of the residue by flash chromatography (10% ethyl acetate – petroleum ether) afforded dienone **12** (130 mg; 78% yield); ir: 1690 (C=O) cm^{-1}; ^{1}Hmr δ: 1.02 (s, 3H, CH_3—), 1.68 (s, 3H, CH_3C=), 5.42 (m, 1H, —CH=C—), 5.94 (ddd, 1H, J = 11, J' = 3, J'' = 1.5 Hz, =CHCO—), 6.90 (ddd, 1H, J = 11, J' = 6, J'' = 2 Hz, —C*H*=CHCO—); ms M^+: 176.1198 (calcd. for $C_{12}H_{16}O$: 176.1201).

*2α,3α-Epoxy-5,8aβ-dimethyl-2,3,4aα,7,8,8a-hexahydro-1[4H]-naphthalenone (**15**)*

At 10°C, to a solution of dienone **12** (351 mg, 2 mmol) in ethanol (3 mL), were added with stirring a solution of sodium hydroxide (30 mg) in water (0.1 mL) and 30% hydrogen peroxide (0.34 mL, 3 mmol). After 1 h at room temperature, the mixture was diluted with water and extracted with dichloromethane (4 × 10 mL). The extracts were washed with saturated aqueous sodium chloride solution, dried, filtered, and concentrated. Purification of the crude product by flash chromatography on silica gel (5% ethyl acetate – petroleum ether) gave epoxide **15** (339 mg; 89% yield). Single recrystallization from petroleum ether gave pure white crystals (mp 54–55°C); ir: 1720 (C=O) cm^{-1}; ^{1}Hmr δ: 0.96 (s, 3H, CH_3—), 1.66 (s, 3H, CH_3C=), 3.20 (d, 1H, J = 4 Hz, —CHCO—), 3.56 (br s, 1H, —CH_2CHO—), and 5.40 (m, 1H, —CH=); ms M^+: 192.1153 (calcd. for $C_{12}H_{16}O_2$: 192.1150).

*7α-Hydroxy-1,4aβ-dimethyl-3,4,4a,7,8,8aα-hexahydronaphthalene (**14**)*

A solution of epoxide **15** (380 mg, 1.96 mmol) in methanol (5 mL) was added dropwise over a period of 1 h to a solution of hydrazine hydrate (0.48 mL, 9.77 mmol) and glacial acetic acid (0.02 mL, 0.38 mmol) under an argon atmosphere. The reaction mixture was stirred for 2.5 h at room temperature and then ice-cold water was added. The solution was extracted with dichloromethane (4 × 20 mL) and the extracts were washed with saturated aqueous sodium bicarbonate, dried, filtered, and concentrated. The residue was subjected to flash chromatography on silica gel. Elution with 20% ethyl acetate in petroleum ether gave allylic alcohol **14** (258 mg; 74% yield); ir: 1650 (C=C) and 3300–3400 (—OH) cm^{-1}; ^{1}Hmr δ: 0.86 (s, 3H, CH_3—), 1.68 (s, 3H, CH_3C=), 4.22 (br t, 1H, J = 4 Hz, —C*H*OH), 5.36 (m, 1H, —C*H*=CCH_3), 5.65 (ddd, 1H, J = 10, J' = 4, J'' = 1.5 Hz, —CH=C*H*CH—), and 5.78 (dd, J = 10 Hz, J' = 1 Hz, —C*H*=CHCH—); ms M^+: 178.1355 (calcd. for $C_{12}H_{18}O$: 178.1358).

*4aβ,8-Dimethyl-4a,5,6,8aα-tetrahydro-2[1H]-naphthalenone (**16**)*

Allylic alcohol **14** (64 mg, 0.36 mmol) was dissolved in dichloromethane (4 mL). Pyridinium dichromate (188 mg, 0.54 mmol) was added. The mixture was stirred at room temperature under an argon atmosphere for 4 h and filtered. The residue was washed thoroughly with dichloromethane. Concentration of the filtrate gave the crude product, which was subjected to flash chromatography on silica gel.

Elution with 10% ethyl acetate in petroleum ether gave dienone **16** (56 mg; 89% yield); ir: 1675 (C=O) cm^{-1}; ^{1}Hmr δ: 1.06 (s, 3H, CH_3—), 1.65 (br s, 3H, CH_3C=), 5.38 (m, 1H, —CH=C—), 5.86 (dd, 1H, J = 10, J' = 1.5 Hz, =CHCO—), and 6.83 (d, 1H, J = 10 Hz, —C*H*=CHCO—); ms M^+: 176.1198 (calcd. for $C_{12}H_{16}O$: 176.1201). *Anal.* calcd. for $C_{12}H_{16}O$: C 81.76, H 9.16; found: C 81.38, H 9.09.

7-Triethylsilyloxy-1,4aβ-dimethyl-3,4,4a,5,8,8aα-hexahydronaphthalene (17)

Dienone **16** (287 mg, 1.62 mmol) was dissolved in triethylsilane (10 mL). A catalytic amount (15 mg) of *tris*(triphenylphosphine)rhodium chloride was added. The mixture was stirred at room temperature under an argon atmosphere for 6 h and concentrated. The residue was then subjected to column chromatography, using 20% ethyl acetate in petroleum ether as an eluent, to give enol ether **17** (508 mg; 100% yield); ir: 1186–1208 (Si—OCH_2CH_3) and 1665 (C=C) cm^{-1}; ^{1}Hmr δ: 0.5–1 (complex, 15H, 3 × CH_3CH_2—), 1.00 (s, 3H, CH_3—), 1.63 (s, 3H, CH_3C=), 4.80 (br s, 1H, —CH=CO—), and 5.36 (br s, 1H, —CH=); ms M^+: 292.2224 (calcd. for $C_{18}H_{32}OSi$: 292.2222).

4aβ,8-Dimethyl-3,4,4a,5,6,8aα-hexahydro-2[1H]-naphthalenone (18)

Enol ether **17** (500 mg, 1.71 mmol) was dissolved in THF (10 mL) and tetra-*n*-butylammonium fluoride (1 *M* solution in THF; 1.7 mL, 1.71 mmol) was added at 0°C. The mixture was stirred for 1 h at room temperature under an argon atmosphere. Concentration of the solution gave a residue, which was purified by flash chromatography using 10% ethyl acetate in petroleum ether as an eluent to afford the saturated ketone **18** (226 mg; 73% yield); ir: 1710 (C=O) cm^{-1}; ^{1}Hmr δ: 1.00 (s, 3H, CH_3—), 1.58 (s, 3H, CH_3C=), and 5.40 (br s, 1H, —CH=); ms M^+: 178.1356 (calcd. for $C_{12}H_{18}O$: 178.1358). Under similar conditions, ketone **18** was obtained in 89% yield from enone **16** without purification of the intermediate enol ether **17**.

7[8H]-(tert-Butylthiocarbonylcyanomethylene)-1,4aβ-dimethyl-3,4,4a,5,6,8aα-hexahydronaphthalene (19) and 7-(tert-butylthiocarbonylcyanomethyl)-1,4aβ-dimethyl-3,4,4a,5,8,8aα-hexahydronaphthalene (20)

S-tert-Butyl cyanothiolacetate (458 mg, 2.92 mmol) and DABCO (330 mg, 2.95 mmol) were dissolved in THF (10 mL). Anhydrous sodium sulfate (622 mg, 4.38 mmol) was introduced, followed by the addition of a solution of ketone **18** (261 mg, 1.46 mmol) in THF (1 mL). The mixture was stirred at room temperature for 48 h, poured into ice-cold 1 *N* aqueous hydrochloric acid, and extracted with dichloromethane (4 × 20 mL). The extracts were washed with saturated aqueous sodium chloride, dried, filtered, and concentrated. Flash chromatography of the residue on silica gel (40% benzene in petroleum ether) afforded compound **19** (269 mg; 58% yield) as a mixture of two isomers (ca. 1:1); ir: 1670 (C=O), and 2240 (C≡N) cm^{-1}; ^{1}Hmr δ: 0.90, 0.94 (both s, total 3H, CH_3—), 1.52, 1.54 (both s, 9H total, —$C(CH_3)_3$), and 5.38 (br s, 1H, —CH=); ms M^+: 317.1814 (calcd. for $C_{19}H_{27}NOS$: 317.1813).

Further elution with the same solvent gave compound **20** (70 mg; 15% yield) as a mixture of two diastereomers (ca. 3:2); ir: 1670 (C=O) cm^{-1}; ^{1}Hmr δ: 0.78 (s, 3H, CH_3—), 1.50 (s, ~5.5H, —$C(CH_3)_3$, for major isomer), 1.52 (s, ~3.5H, —$C(CH_3)_3$, for minor isomer), 4.05 (br s, ~0.4H, —CHCN, for minor isomer), 4.75 (br s, ~0.6H, —CHCN, for major isomer), 5.38 (m, 1H, —C*H*=CCH_3), and 5.90 (m, 1H, —CH=); ms M^+: 317.1813 (calcd. for $C_{19}H_{27}NOS$: 317.1813).

7-(tert-Butylthiocarbonylcyanomethyl)-1,4aβ-dimethyl-3,4,4a,5,6,7,8,8aα-octahydronaphthalene (21)

A mixture of compounds **19** and **20** (113 mg, 0.35 mmol) was dissolved in absolute ethanol (7 mL) at 0°C. Sodium borohydride (3.3 mg, 0.09 mmol) was added and the mixture stirred for 2 h at 0°C under an argon atmosphere. Ice-cold saturated aqueous ammonium chloride was added and the resulting solution extracted with dichloromethane (3 × 10 mL). The extracts were washed with saturated aqueous sodium chloride, dried, filtered, and concentrated. Flash chromatography of the crude product on silica gel (50% benzene in petroleum ether) afforded saturated cyanothiolester **21** (83 mg; 74% yield) as a mixture of four diastereomers (2:2:1:1); ir: 1678 (C=O) and 2240 (C≡N) cm^{-1}; ^{1}Hmr δ: 0.80 (s, 3H, CH_3—), 1.52 (s, 9H, —$C(CH_3)_3$), 3.37, 3.39 (both d, ~0.33H each, J = 8 Hz each, —CHCN), 3.69, 3.70 (both d, 0.17H each, J = 12 Hz each, —CHCN), 5.33 (br s, ~0.33H, —CH=, for two minor isomers), and 5.34 (m, ~0.66H, —CH=, for two major isomers); ms M^+: 319.1971 (calcd. for $C_{19}H_{29}NOS$: 319.1970).

7-(1-Cyano-2-hydroxyethyl)-1,4aβ-dimethyl-3,4,4a,5,6,7,8,8aα-octahydronaphthalene (22)

A. *From reduction of compound 21*

Compound **21** (185 mg, 0.58 mmol) was dissolved in absolute ethanol (7 mL) at 0°C. Sodium borohydride (90 mg, 2.43 mmol) was added. The mixture was stirred at room temperature for 10 h under an argon atmosphere, poured into ice-cold saturated aqueous ammonium chloride solution, and extracted with dichloromethane (3 × 20 mL). The extracts were washed with aqueous sodium chloride solution, dried, filtered, and concentrated. The residue was chromatographed on silica gel (50% ethyl acetate in petroleum ether) to give alcohol **22** (119 mg; 88% yield) as a mixture of diastereomers; ir: 1060 (C—O), 2260 (C≡N), and 3400–3500 (—OH) cm^{-1}; ms M^+: 233.1778 (calcd. for $C_{15}H_{23}NO$: 233.1780). The ^{1}Hmr spectrum showed two sets of signals in ca. 2:1 ratio, with major signals at δ 0.80 (s, 3H, CH_3—), 1.60 (s, 3H, CH_3C=), 2.72 (dt, 1H, J = 7, J' = 6 Hz, —CHCN), 3.90 (m, 2H, —C*H*$_2$OH), and 5.36 (m, 1H, —CH=). The minor set of signals appeared at δ 0.87 (s, 3H, CH_3—), 1.66 (s, 3H, CH_3C=), 3.02 (m, 1H, —CHCN), 3.90 (m, 2H, —C*H*$_2$OH), and 5.36 (m, 1H, —CH=).

B. *From direct reduction of compounds 19 and 20*

The mixture of compounds **19** and **20** (124 mg, 0.39 mmol) was dissolved in ethanol (7 mL) and cooled to −40°C. Sodium borohydride (69 mg, 1.82 mmol) was added and the reaction mixture stirred for 4 h at −40°C under an argon atmosphere. Temperature was increased to room temperature and stirring continued for 24 h. Isolation and purification processes were performed in the same manner as mentioned above to give alcohol **22** (83 mg; 91% yield), identical in all respects with that obtained above.

7β-(1-Cyanoethenyl)-1,4aβ-dimethyl-3,4,4a,5,6,7,8,8aα-octahydronaphthalene (23) and 7α-(1-cyanoethenyl)-1,4aβ-dimethyl-3,4,4a,5,6,7,8,8aα-octahydronaphthalene (24)

The diastereomeric mixture of alcohols **22** (42 mg, 0.18 mmol) was dissolved in ether (5 mL). Dicyclohexylcarbodiimide (74 mg, 0.36 mmol) and a catalytic amount (2 mg) of copper(I) chloride were added. The mixture was heated at reflux under an argon atmosphere for 8.5 h, cooled to room temperature, diluted with ether, and filtered. Concentration of the filtrate, followed by purification of the crude product by flash chromatography on silica gel (40% petroleum ether in benzene), gave a mixture of two epimeric nitriles **23** and **24** (38 mg; 94% yield) in ca. 2:1 ratio, according to ^{1}Hmr integration. This mixture was subjected to separation by Chromatotron using 5% ether in petroleum ether as an eluent to give pure β-isomer **23** (11 mg) and pure α-isomer **24** (7 mg). The rest of the material was recovered as a mixture. The following spectral data were obtained for the β-isomer **23**: ir ($CHCl_3$): 1620 (C=C) and 2210 (C≡N) cm^{-1}; ^{1}Hmr δ: 0.82 (s, 3H, CH_3—), 1.62 (br s, 3H, CH_3C=), 2.28 (m, 1H, —C*H*C=CH_2), 5.36 (m, 1H, —CH=), 5.74 (dd, 1H, J = 2, J' = 1 Hz, =C*H*H), and

5.82 (br s, 1H, =CH*H*); ms M^+: 215.1676 (calcd. for $C_{15}H_{21}N$: 215.1674). The α-isomer **24** showed the following spectral data: ir ($CHCl_3$): 1620 (C=C) and 2210 (C≡N) cm^{-1}; ^{1}Hmr δ: 0.87 (s, 3H, CH_3—), 1.66 (br s, 3H, CH_3C=), 2.72 (m, 1H, —C*H*C=CH_2), 5.34 (m, 1H, —CH=), 5.85 (d, 1H, J = 2 Hz, =C*H*H), and 6.07 (d, 1H, J = 2 Hz, =CH*H*); ms M^+: 215.1663 (calcd. for $C_{15}H_{21}N$: 215.1674).

Nitriles **23** and **24** were also obtained in 1:2.8 ratio by reduction of compounds **19** and **20** with lithium tri-*tert*-butoxyaluminum hydride as follows. To a solution of the mixture of compounds **19** and **20** (99 mg, 0.31 mmol) in THF (5 mL) at 0°C, was added lithium tri-*tert*-butoxyaluminum hydride (119 mg, 0.47 mmol). The mixture was stirred under an argon atmosphere for 3.5 h at 0°C, acidified with ice-cold 1 *N* aqueous hydrochloric acid, and extracted with dichloromethane (3 × 10 mL). The extracts were washed with saturated aqueous sodium chloride, dried, filtered, and concentrated to give cyanothiolester **21**, which, without purification, was subjected to further reduction (**21** → **22**) with sodium borohydride and dehydration (**22** → **23** and **24**) with dicyclohexyl carbodiimide using described conditions (*vide supra*). Nitriles **23** and **24** (34 mg; 50% overall yield) thus formed were shown to be in a ratio of 1:2.8 by ^{1}Hmr analysis.

*(±)-α-Costal (**1**)*

Cyano olefin **23** (10 mg, 0.047 mmol) was dissolved in toluene (0.5 mL) and cooled to −78°C with stirring under an argon atmosphere. After 5 min, diisobutylaluminum hydride (25% by wt. in toluene; 0.05 mL, 0.07 mmol) was added. After stirring for 3 h at −78°C, the mixture poured into dilute aqueous oxalic acid and extracted with ether (2 × 2 mL). The extracts were dried, filtered, and concentrated. The resulting crude product was subjected to column chromatography on silica gel (40% petroleum ether in benzene) to give racemic α-costal (**1**) (6 mg; 59% yield); ir ($CHCl_3$): 1620 (C=C), 1694 (CHO), and 2700 (aldehyde C—H) cm^{-1}; ^{1}Hmr ($CDCl_3$) δ: 0.84 (s, 3H, CH_3—), 1.60 (s, 3H, CH_3C=), 2.56 (m, 1H, —CH—C=), 5.32 (m, 1H, —CH=), 5.90 (br s, 1H, =C*H*H), 6.30 (br s, 1H, =CH*H*), and 9.54 (s, 1H, —CHO); ^{1}Hmr (CCl_4) δ: 0.83 (s, 3H, —CH_3), 1.58 (s, 3H, CH_3C=), 2.53 (m, 1H, —CH—C=), 5.28 (m, 1H, =CH—), 5.90 (br s, 1H, =C*H*H), 6.21 (br s, 1H, =CH*H*), and 9.52 (s, 1H, —CHO); ^{13}Cmr δ: 194.6, 155.4, 134.7, 132.8, 121.2, 46.9, 40.2, 37.9, 37.2, 32.4, 29.7, 29.0, 27.0, 23.0, and 21.1; ms M^+: 218.1671 (calcd. for $C_{15}H_{22}O$: 218.1671).

*(±)-Epi-α-costal (**25**)*

Cyano olefin **24** (5 mg, 0.023 mmol) was dissolved in toluene (0.5 mL) and cooled to −78°C with stirring under an argon atmosphere. Diisobutylaluminum hydride (5% by wt. in toluene; 0.15 mL, 0.05 mmol) was added. The mixture was stirred for 3 h at −78°C, poured into dilute aqueous oxalic acid, and extracted with ether (2 × 2 mL). Drying, filtration, and concentration gave the crude product, which was subjected to column chromatography on silica gel. Elution with 40% petroleum ether in benzene gave racemic epi-α-costal **25** (3 mg; 60% yield); ir ($CHCl_3$): 1697 (CHO) and 2852 (aldehyde C—H) cm^{-1}; ^{1}Hmr δ: 0.85 (s, 3H, —CH_3), 1.54 (br s, 3H, CH_3C=), 3.04 (m, 1H, —CH—C=), 5.34 (m, 1H, —CH=), 6.11 (s, 1H, =C*H*H), 6.48 (d, 1H, J = 1.5 Hz, =CH*H*), and 9.48 (s, 1H, —CHO); ms M^+: 218.1672 (calcd. for $C_{15}H_{22}O$: 218.1671).

*7β-(tert-Butylthiocarbonylcyanomethyl)-1,4aβ-dimethyl-3,4,4a,7,8,8aα-hexahydronaphthalene (**26**) and 7β-(2-tert-butylthio-3-cyano-1-oxapropenyl)-1,4aβ-dimethyl-3,4,4a,7,8,8aα-hexahydronaphthalene (**27**)*

Triphenylphosphine (110 mg, 0.42 mmol) was dissolved in THF (3 mL) under an argon atmosphere at −15°C. Diethyl azodicarboxylate (0.07 mL, 0.42 mmol) was added and the solution cooled to −30°C with stirring. A solution of allylic alcohol **14** (50 mg, 0.28 mmol) in THF (0.5 mL) was introduced, followed by the addition of a solution of *S-tert*-butyl cyanothiolacetate (88 mg, 0.56 mmol) in THF (0.5 mL). After stirring for 3.5 h at −35°C, ice-cold water and then 1 *N* aqueous hydrochloric acid were added and the resulting solution was extracted with dichloromethane (4 × 15 mL). The extracts were washed with saturated aqueous sodium chloride, dried, filtered, and concentrated. The crude product was subjected to flash chromatography on silica gel (40% benzene in petroleum ether) to give a mixture of compounds **26** and **27** (50 mg; 54% yield) in ca. 2:1 ratio. The ^{1}Hmr spectrum of the mixture displayed two sets of signals in ca. 2:1 ratio. The major set of signals was attributed to compound **26** (a 1:1 diastereomeric mixture); δ: 0.95, 0.98 (both s, 1.5H each, —CH_3), 1.52 (s, 9H, —$C(CH_3)_3$), 1.66 (br s, 3H, CH_3C=), 3.50, 3.58 (both d, 0.5H each J = 6 Hz each, —CHCN), and 5.34 (m, 1H, —CH=). The minor signals were found to be identical with those observed for pure **27** (see the following experiment). The mixture also showed the following spectral data: ir: 1680 (C=O), 2210 (C≡N), and 2240 (C≡N) cm^{-1}; ms M^+: 317.1819 (calcd. for $C_{19}H_{27}NOS$: 317.1813).

*7β-(1-Cyano-2-hydroxyethyl)-1,4aβ-dimethyl-3,4,4a,7,8,8α-hexahydronaphthalene (**28**)*

The 2:1 mixture of compounds **26** and **27** (46 mg, 0.14 mmol) was dissolved in absolute ethanol (5 mL) and cooled to 0°C with stirring. Sodium borohydride (21 mg, 0.55 mmol) was added and stirring continued for 30 h at room temperature. The mixture was then poured into saturated aqueous ammonium chloride and extracted with dichloromethane (3 × 5 mL). The extracts were washed with saturated aqueous sodium chloride, dried, filtered, and concentrated. The residue was chromatographed on silica gel (20% ethyl acetate in petroleum ether) to give 15 mg of compound **27**; ir: 2210 (C≡N) cm^{-1}; ^{1}Hmr δ: 1.01 (s, 3H, CH_3—), 1.43 (s, 9H, —$C(CH_3)_3$), 1.66 (br s, 3H, CH_3C=), 5.00 (s, 1H, =CHCN), and 5.4–5.8 (complex, 4H, —CH= and —CH=CHCHO—); ms M^+: 317.1806 (calcd. for $C_{19}H_{27}NOS$: 317.1813).

Further elution with the same solvent system gave alcohol **28** (17 mg; ~78% yield based on **26**) as a mixture of two diastereomers (ca. 1:1); ir: 2260 (C≡N) and 3400–3500 (—OH) cm^{-1}; ^{1}Hmr δ: 0.93, 0.96 (both s, 1.5H each, CH_3—), 1.66 (br s, 3H, CH_3C=), 3.90 (br s, 2H, —CH_2O—), and 5.3–5.8 (complex, 3H, —CH= and —CH=CH—); ms M^+: 231.1617 (calcd. for $C_{15}H_{21}NO$: 231.1623).

*3-(tert-Butylthiocarbonylcyanomethyl)-5,8aβ-dimethyl-3,4,4aα,7,8,8a-hexahydro-1[2H]-naphthalenone (**29**)*

At 5°C, to a solution of *S-tert*-butyl cyanothiolacetate (160 mg, 1.01 mmol) in benzene (7 mL), were added chlorotrimethylsilane (0.11 mL, 0.92 mmol) and sodium hydride (50% dispersion in oil; 72 mg, 1.52 mmol). After stirring for 5 min under an argon atmosphere, a solution of dienone **12** (121 mg, 0.68 mmol) in benzene (0.5 mL) was introduced. The mixture was heated at reflux for 16 h. It was then cooled to room temperature, poured into 1 *N* aqueous hydrochloric acid, extracted with dichloromethane (3 × 10 mL), and the extracts concentrated. The residue was dissolved in methanol (20 mL) and treated with 5 mL of aqueous potassium fluoride solution (0.5 g/10 mL) for 10 min. The resulting solution was poured into 1 *N* aqueous hydrochloric acid (20 mL) and extracted with dichloromethane (4 × 20 mL). The extracts were dried, filtered, and concentrated. The crude product was purified by flash chromatography on silica gel (10% ethyl acetate – petroleum ether) to give 27 mg of starting dienone **12**. Further elution with the same solvent system gave 1,4 adduct **29** (136 mg; 76% yield based on consumed starting material) as a mixture of four diastereomers in ca. 2:2:1:1 ratio by ^{1}Hmr integration. The following ^{1}Hmr data were attributable to the two major isomers: δ 1.08, 1.12 (both s, 3H total, CH_3—), 1.52, 1.54 (both s, total 9H, —$C(CH_3)_3$), 1.68 (br s, 3H, CH_3C=), 3.44, 3.53 (both d, 1H total, J = 5 Hz each, —CHCN), and 5.42 (m, 1H, —CH=). The

following ^{1}Hmr data were attributable to the two minor isomers: δ 1.20, 1.28 (both s, total 3H, CH_3—), 1.56 (s, 9H, —$C(CH_3)_3$), 1.68 (br s, 3H, CH_3C=), 3.46, 3.64 (both d, 1H total, J = 5 Hz each, —CHCN), and 5.42 (m, 1H, —CH=). The following spectral data were also recorded on the mixture: ir ($CHCl_3$): 1679 (thiolester C=O), 1710 (ketone C=O), and 2220 (C≡N) cm^{-1}; ms M^+: 333.1765 (calcd. for $C_{19}H_{27}NO_2S$: 333.1762).

*3-(*tert*-Butylthiocarbonylcyanomethyl)-1-hydroxy-5,8aβ-dimethyl-1,2,3,4,4aα,7,8,8a-octahydronaphthalene (**30**)*

Ketone **29** (41 mg, 0.12 mmol) was dissolved in absolute ethanol (4 mL) and cooled to 0°C with stirring. Sodium borohydride (10 mg, 0.26 mmol) was added and the mixture stirred for 1.5 h at 0°C. Saturated aqueous ammonium chloride solution was added and the resulting solution extracted with dichloromethane (3 × 5 mL). Drying, filtration, and concentration gave the crude product, which was purified by flash chromatography on silica gel (40% ethyl acetate – petroleum ether) to give alcohol **30** (30 mg; 75% yield) as a mixture of diastereomers. The following spectral data were recorded on the mixture: ir: 1680 (C=O), 2250 (C≡N), and 3500–3600 (—OH) cm^{-1}; ^{1}Hmr δ: 0.84 (br s, 3H, CH_3—), 1.51 (br s, 9H, —$C(CH_3)_3$), 1.62 (br s, 3H, CH_3C=), 3.4–3.6 (m, 2H, —CHCN and —C*H*OH), and 5.40 (m, 1H, —CH=); ms M^+: 335.1919 (calcd. for $C_{19}H_{29}NO_2S$: 335.1919).

*3-Cyanomethyl-1-hydroxy-5,8aβ-dimethyl-1,2,3,4,4aα,7,8,8a-octahydronaphthalene (**32**)*

Alcohol **30** (74 mg, 0.22 mmol) was dissolved in chloroform (4 mL) and cooled to 0°C under an argon atmosphere. Methanesulfonyl chloride (0.05 mL, 0.66 mmol) and triethylamine (0.15 mL, 1.1 mmol) were added and the mixture stirred for 6 h at room temperature. The mixture was acidified with ice-cold 1 *N* aqueous hydrochloric acid and extracted with dichloromethane (4 × 8 mL). The extracts were washed with saturated aqueous sodium bicarbonate, dried, filtered, and concentrated. This crude mesylate **31** (134 mg) showed satisfactory ir and ^{1}Hmr spectra as follows: ir: 1185, 1360 (O=S=O), 1680 (C=O), and 2260 (C≡N) cm^{-1}; ^{1}Hmr δ: 0.81 (br s, 3H, CH_3—), 1.49 (s, 9H, —$C(CH_3)_3$), 1.58 (br s, 3H, CH_3C=), 3.00 (s, CH_3SO_3—), 3.4–3.6 (complex, 2H, —CHCN and —CHO—), and 5.33 (m, 1H, —CH=).

The crude mesylate was dissolved in *N*,*N*-dimethylformamide (7 mL). Sodium iodide (480 mg, 3.2 mmol) and zinc dust (420 mg, 6.4 mmol) were added. The mixture was heated at reflux for 7 h under an argon atmosphere. It was then cooled to room temperature and filtered and the residue washed thoroughly with dichloromethane. The filtrate was subsequently washed with water and the aqueous solution extracted with dichloromethane (4 × 5 mL). The extracts were washed with saturated aqueous sodium chloride, dried, filtered, and concentrated. The crude product was purified by flash chromatography (30% ethyl acetate in petroleum ether) to afford alcohol **32** (6 mg; 14% yield from **30**) as a mixture of diastereomers; ir: 2260 (C≡N) and 3400–3500 (OH) cm^{-1}; ^{1}Hmr δ: 0.80, 0.82 (both s, ~1.5 H each, CH_3—), 1.64 (br s, 3H, CH_3C=), 2.38 (d, 2H, J = 6 Hz, —CH_2CN), 3.39 (dd, 1H, J = 11, J' = 4 Hz, —C*H*OH), and 5.38 (m, 1H, —CH=); ms M^+: 219.1621 (calcd. for $C_{14}H_{21}NO$: 219.1623).

Acknowledgements

We are grateful to the Natural Sciences and Engineering Research Council of Canada and the University of Alberta for financial support.

1. H. J. Liu and H. Wynn. Can. J. Chem. **64**, 649 (1986).
2. H. J. Liu and H. Wynn. Tetrahedron. Lett. **23**, 3151 (1982).
3. R. K. Boeckman, Jr. and M. Ramaiah. J. Org. Chem. **42**, 1581 (1977).
4. L. C. Yu and P. Helquist. Tetrahedron Lett. 3423 (1978).
5. S. Ito, K. Endo, H. Honma, and K. Ota. Tetrahedron Lett. 3777 (1965).
6. R. E. Ireland and G. Pfister. Tetrahedron Lett. 2145 (1969).
7. L. C. Garver and E. E. Van Tamelen. J. Am. Chem. Soc. **104**, 867 (1982).
8. H. J. Liu and H. Wynn. Tetrahedron Lett. **26**, 4843 (1985).
9. J. C. Sircar and A. I. Meyers. J. Org. Chem. **30**, 3206 (1965).
10. A. B. Mekler. Org. Synth. Coll. Vol. 5, 743 (1973).
11. Y. Kitahara, A. Yoshikoshi, and S. Oida. Tetrahedron Lett. 1763 (1964).
12. H. J. Liu, L. K. Ho, and H. K. Lai. Can. J. Chem. **59**, 1685 (1981).
13. P. Wieland, H. Ueberwasser, G. Amuer, and K. Miescher. Helv. Chim. Acta, **36**, 376 (1953).
14. A. J. Birch and H. Smith. Q. Rev. (London), **12**, 17 (1958).
15. H. J. Reich, I. L. Reich, and J. M. Renge. J. Am. Chem. Soc. **95**, 5813 (1973).
16. P. S. Wharton and D. H. Bohlen. J. Org. Chem. **26**, 3615 (1961).
17. C. Djerassi, D. H. Williams, and B. Berkoz. J. Org. Chem. **27**, 2205 (1962).
18. E. J. Corey and G. Schmidt. Tetrahedron Lett. 399 (1979).
19. I. Ojima, M. Nihonyanagi, T. Kogure, M. Kumagai, S. Horinchi, K. Nakatsugawa, and Y. Nagai. J. Organomet. Chem. **94**, 449 (1975).
20. C. Alexandre and F. Rouessac. Bull. Soc. Chim. Fr. 1837 (1971).
21. L. M. Jackman and S. Sternhell. Applications of nuclear magnetic resonance spectroscopy in organic chemistry. 2nd ed. Pergamon Press, London. 1969.
22. O. Mitsunobu. Synthesis, 1 (1981).
23. Y. Fujimoto and T. Tatauno. Tetrahedron Lett. 3325 (1976).
24. H. J. Liu and T. K. Ngooi. Can. J. Chem. **62**, 2676 (1984).
25. T. D. Smith. J. Chem. Soc. 1122 (1962).
26. H. J. Liu and S. I. Sabesan. Can. J. Chem. **58**, 2645 (1980).

α-*N*,*N*-Dimethylaminoethylferrocene. A nuclear magnetic resonance study relating to stereoselective metalation

IAN R. BUTLER, WILLIAM R. CULLEN,[1] F. GEOFFREY HERRING, AND N. R. JAGANNATHAN

Chemistry Department, University of British Columbia, Vancouver, B.C., Canada V6T 1Y6

Received November 5, 1985

IAN R. BUTLER, WILLIAM R. CULLEN, F. GEOFFREY HERRING, and N. R. JAGANNATHAN. CAN. J. CHEM. **64**, 667 (1986).

A ^{1}H nmr study of Fe($C_5H_4CHMeNMe_2$-η)($C_5H_4PPh_2$-η), **2**, using the nOe difference experiment, shows a spatial correlation between the —NMe_2 group and the site of stereoselective lithiation.

IAN R. BUTLER, WILLIAM R. CULLEN, F. GEOFFREY HERRING et N. R. JAGANNATHAN. CAN. J. CHEM. **64**, 667 (1986).

Sur la base d'une étude à l'aide de la rmn du ^{1}H et faisant appel à une expérience de différence d'eOn effectuée sur le Fe($C_5H_4CHMeNMe_2$-η)($C_5H_4PPh_2$-η) (**2**), on peut démontrer l'existence d'une corrélation spatiale entre le groupement —NMe_2 et le site de la lithiation stéréosélective.

[Traduit par le journal]

One of the most frequently used starting materials for the synthesis of chiral ferrocene compounds is α-*N*,*N*-dimethylaminoethylferrocene, **1** (1). This compound is easily resolved into its enantiomers via its tartrate salts (2). The metalation of **1** with lithiumalkyls is stereoselective, the nitrogen atom directing the reaction as shown in eq. [1]. Thus

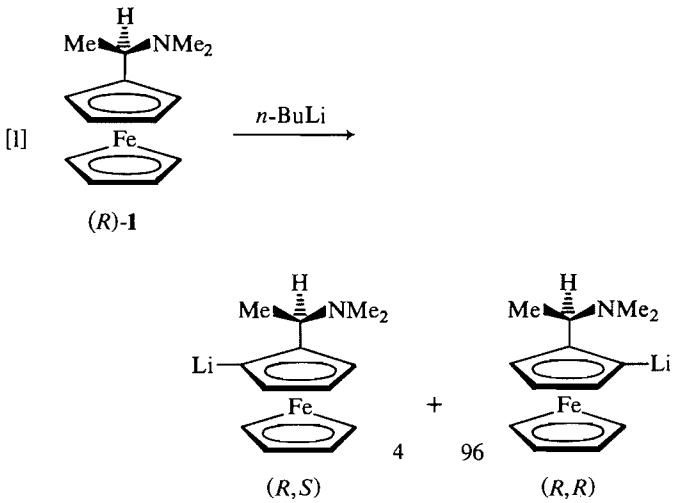

the use of chiral **1** allows the isolation of essentially optically pure products following substitution of the lithium with a variety of electrophiles. Ugi and co-workers have attributed this remarkable stereoselectivity to steric effects involving primarily the C-methyl group, which is presumed to prefer to stay above the plane of the upper ring (3).

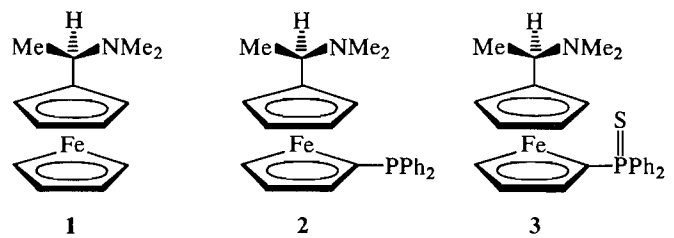

1 **2** **3**

X-ray crystallographic studies of products derived from the lithiation reaction indicate that there is no one preferred orientation for the $CHMeNMe_2$ group; there are examples showing that any one of the groups attached to the asymmetric carbon atom can be situated between the cyclopentadienyl rings (3–6).[2] In the absence of a structure for lithiated **1**, that of the dilithio derivative of **1** (7),

$$[Fe(\eta^5\text{-}C_5H_4Li)(\eta^5\text{-}C_5H_3(Li)(CHMeNMe_2)\text{-}1,2)]_4\text{-}[LiOEt]_2[TMED]_2$$

where TMED = tetramethylethylenediamine, should come closest to that of the transition state involved in the lithiation of **1**. Here one of the two different—NMe_2 groups in the molecule is situated well outside the interplane region, such that the methyl group—$CHMeNMe_2$ lies between the rings. This lithium atom, which is bonded to the —NMe_2 group and the deprotonated carbon atom, is also situated outside the interplane region. Nevertheless, this carbon atom is the one that would more likely be lithiated, according to eq. [1]. The other —NMe_2 is part of a —$CHMeNMe_2$ group of opposite chirality to the first. This amino function and its —$CHMeNMe_2$ group lie in the interplane region and the nitrogen is coordinated to a lithium atom that lies almost in the same plane as the cyclopentadienyl ring. However, this lithium atom is bonded to the carbon atom that would be less likely to be lithiated, according to eq. [1]. Thus, in the cluster of the dilithio derivatives the 4:96 ratio "expected" from eq. [1] is found to be 50:50. This observation has not been made previously (7) and probably accounts for the isolation of the unexpected (*S*,*S*) diastereomer of [Fe(η^5-C_5H_3($P(CMe_3)_2$-1,3][η^5-C_5H_3($CHMeNMe_2$)$P(CMe_3)_2$-1,2)] (6). This compound should have had the (*S*,*R*) configuration because the first step in its synthesis was the lithiation of (*S*)-**1** according to eq. [1].

Clearly the stereoselectivity observed in reactions involving **1** must be due to effects other than, or in addition to, those previously envisioned. This paper describes the probing of these effects using ^{1}H nmr spectroscopy.

The cyclopentadienyl proton resonances of **1** are overlapped even at 400 MHz and therefore a derivative is required in which the resonances are more dispersed and which retains the integrity of the $C_5H_4CHMeNMe_2$ group. The recently synthesized compound **2** has most of the required properties (8). The proton resonances overlap only slightly, as is seen in Figs. 1 and 2, the number of resonances being greater than might be expected at first sight because of the combination of the asymmetric center with the planar chirality of both rings. This makes all the protons inequivalent.

[1]Author to whom correspondence may be addressed.

[2]Also, I. R. Butler, W. R. Cullen, and S. J. Rettig, unpublished results.

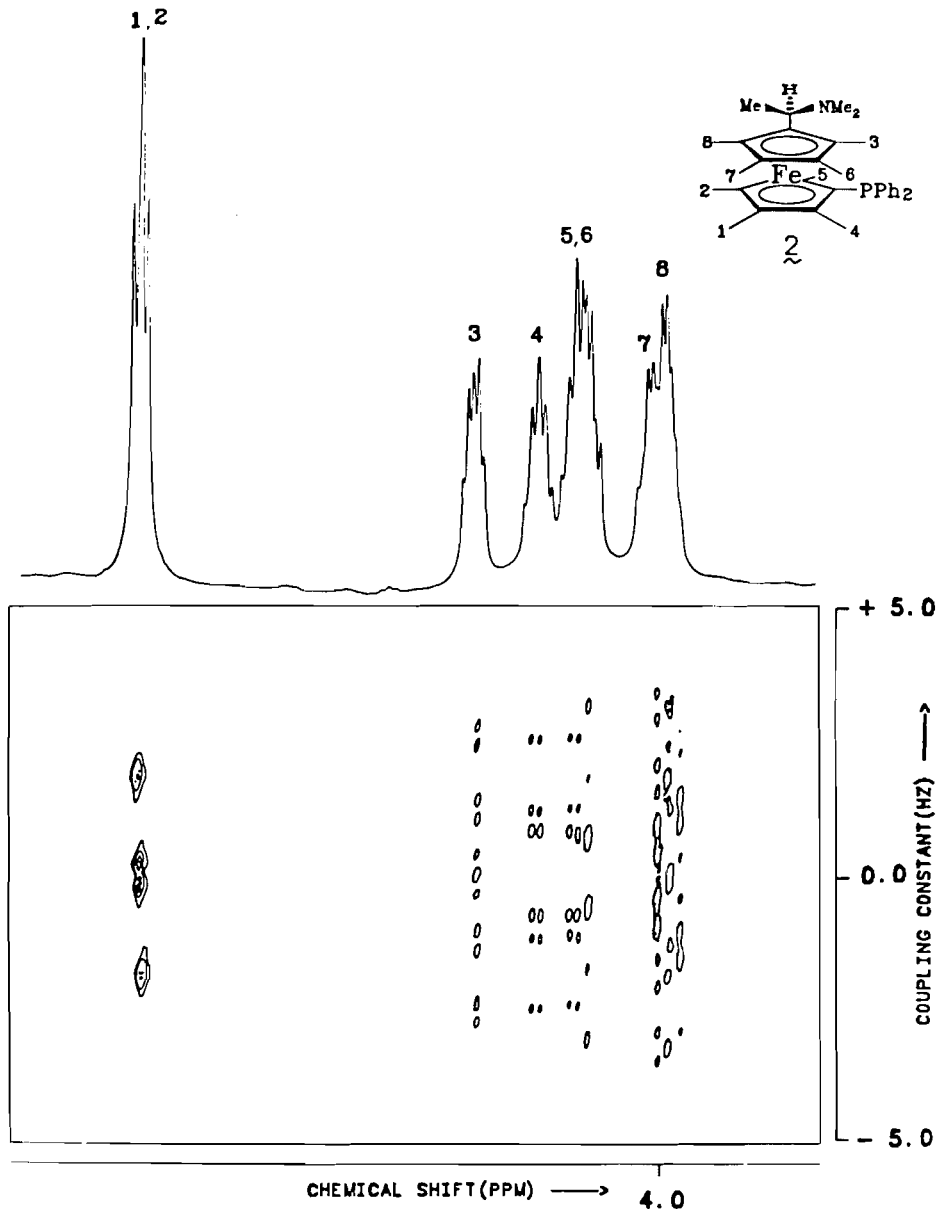

FIG. 1. 2D-*J* resolved contour plot of ferrocenyl proton region of **2**; 128 experiments in the t_1 axis with 1024 data points on the t_2 axis with a relaxation delay of 5 s and 32 scans for each t_1 experiment. Sinebell apodization was employed in both dimensions before Fourier transform.

Protons 1 and 2 have almost identical chemical shifts and give rise to the pseudo triplet. Protons 4 and 5 can be readily identified by their residual ^{31}P couplings observed in the 2D-*J* spectrum (Fig. 1). Each appears as a set of overlapping doublet of doublets of doublets in the one-dimensional spectrum. The ^{31}P couplings to 4 and 5 are ~3.5 Hz. Proton 3 is readily assigned from its splitting pattern (it shows the typical 1,2,2,2,1 pattern of a ferrocenyl proton adjacent to a single substituent) and homonuclear decoupling experiments. Similarly, resonances 6, 7, and 8 can be assigned, using the 2D-*J* spectrum to identify the resonance multiplicity and decoupling experiments to determine their relative positions.

To check the assignment, **2** was lithiated with *n*-butyllithium and the resulting product solution treated with D_2O. The ^1H nmr spectrum of the deuterated product indicates that site 3 has been deuterated almost exclusively.

Reaction of **2** with sulfur results in oxidation of the phosphorus, affording **3**. The enhanced electronegativity of the $PPh_2(S)$ side chain results in increased deshielding of the cyclopentadienyl resonances to which the phosphorus is attached. The nmr spectrum of **3** shows only 5 resonances because of overlap; however, these can be readily assigned as described for **2**. The two low-field resonances δ 4.45, 4.40 are due to the phosphorus-substituted cyclopentadienyl ring protons. The remaining three resonances δ 4.29, 4.11, 4.03 are assigned to protons in the 3, 6/7, and 8 positions, respectively. Oxidation of the phosphorus shifts all cyclopentadienyl resonances downfield. In both compounds **2** and **3** the resonances of protons 3 and 8 are separated by approximately 0.3 ppm, which is probably reflected in the stereoselectivity of the lithiation reaction.

Having assigned the resonances in **2**, a series of nOe (nuclear Overhauser effect) difference experiments were undertaken to garner further information about the preferred site of methalation. The first of these experiments was carried out by irradiating the NMe_2 singlet. As is seen in Fig. 2C, only two

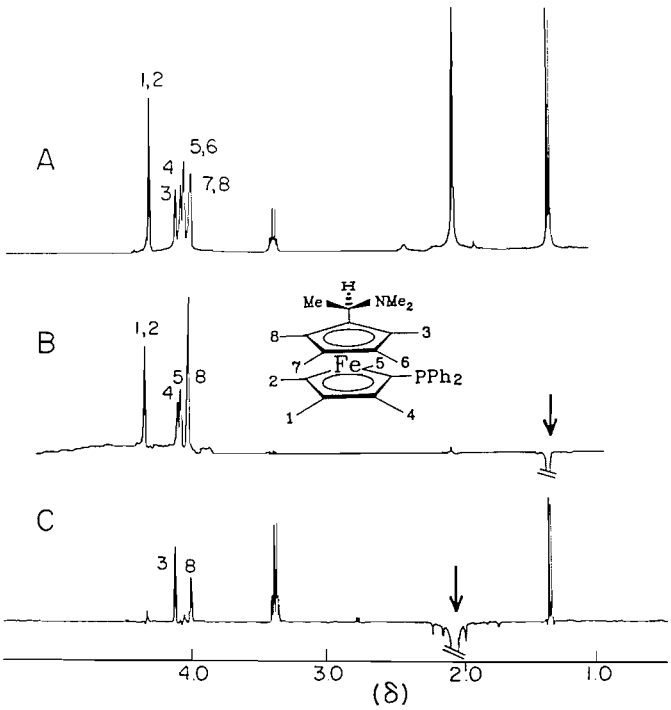

FIG. 2. 400-MHz ^{1}H spectra of **2** in $CDCl_3$ excluding phenyl region. A: normal spectrum, B: nOe difference spectrum with irradiation of CCH_3 (↓). C: nOe difference spectrum with irradiation at $N(CH_3)_2$ (↓).

proton sites are significantly enhanced, namely 3 and 8, with the greater effect on 3. If there is free rotation about the bond between the $CHMeNMe_2$ group and the ring, enhancement would be expected at 3 and 8 and, in addition, some effect on the bottom ring protons would be expected. Thus the $—NMe_2$ group seems to have a preference for a position above the rings and in proximity to the site of metalation at proton 3.

The second nOe difference spectrum shown in Fig. 2B was obtained by irradiation of the $C—CH_3$ resonance. In this case positive nOe enhancements are observed into proton sites 1, 2, 4, 5, and 8. By far the largest enhancement is observed at site 8, which is expected from the result of the first nOe experiment. However, since positive nOe effects are observed in all four proton sites on the lower cyclopentadienyl ring, the methyl group must lie preferentially between the rings as shown in **4**. Certainly this geometry is found in some known structures. A third nOe different experiment was conducted by irradiation of the *ortho* protons of the phenyl rings. Weak positive nOe enhancements were observed only into the ring proton sites 4

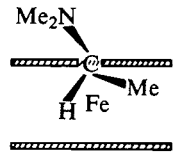

4

and 5, adjacent to the phosphorus. Thus there is little interaction of the PPh_2 group with the protons of any other rings and extrapolation of the results from **2** to **1** seems justified.

Indeed, nOe difference spectra of **1**, although more difficult to assign, do show these effects.

Thus it appears that in solution the NMe_2 group lies predominantly outside the rings, as indicated in **4**. Making the assumption that prior to metalation the incoming RLi coordinates to the amine function, it seems that the site of metalation is governed by the movement of the C-methyl group away from the area between the rings. This would result in stereoselectivity.

In this model the conformation of the transition state would look somewhat like that seen in **4** and in the appropriate part of the structure of the dilithio derivative described above. However, the result that the opposite diastereomer can be isolated suggests that the initial diastereoselectivity is a kinetic phenomenon associated with favored conformations such as **4** in solution. Apparently, there is little energy difference between the two possible diastereomers.

Acknowledgments

The authors would like to acknowledge the cooperation of the staff of the University of British Columbia for nuclear magnetic resonance service, as well as financial assistance from the Natural Sciences and Research Council of Canada.

1. (*a*) D. MARQUARDING, H. KLUSACEK, G. W. GOKEL, P. HOFFMANN, and I. K. UGI. J. Am. Chem. Soc. **92**, 5389 (1970); (*b*) C. R. HAUSER and J. K. LINDSAY. J. Org. Chem. **22**, 906 (1957).
2. G. W. GOKEL and I. K. UGI. J. Chem. Educ. **49**, 294 (1957).
3. L. F. BATTELLE, R. BAU, G. W. GOKEL, R. T. OYAKAWA, and I. K. UGI. J. Am. Chem. Soc. **95**, 482 (1973).
4. F. W. B. EINSTEIN and A. J. WILLIS. Acta Crystallogr. Sect. B, **36**, 39 (1980).
5. I. R. BUTLER, W. R. CULLEN, F. W. B. EINSTEIN, S. J. RETTIG, and A. J. WILLIS. Organometallics, **2**, 128 (1983).
6. T. D. APPLETON, W. R. CULLEN, S. V. EVANS, T. J. KIM, and J. TROTTER. J. Organometal. Chem. **279**, 5 (1985).
7. I. R. BUTLER, W. R. CULLEN, J. REGLINSKI, and S. J. RETTIG. J. Organometal. Chem. **249**, 183 (1983).
8. I. R. BUTLER and W. R. CULLEN. Can. J. Chem. **61**, 147 (1983).

The synthesis and structure of some 4-aryloxymethyl-2,2,6,6-tetramethyl-4-piperidinol and 4-aryloxymethyl-4-hydroxy-2,2,6,6-tetramethyl-1-piperidinyloxy derivatives

M. CYGLER[1] AND M. J. GRABOWSKI

Department of Crystallography, Institute of Chemistry, University of Łódź, 91-416 Łódź, Nowotki 18, Poland

AND

W. STRZYŻEWSKI, L. TURAŁA, AND R. SKOWROŃSKI

Institute of Chemistry, University of Łódź, 90-136 Łódź, Narutowicza 68, Poland

Received May 30 1985

M. CYGLER, J. GRABOWSKI, W. STRZYŻEWSKI, L. TURAŁA, and R. SKOWROŃSKI. Can. J. Chem. **64**, 670 (1986).

The synthesis of 5,5,7,7-tetramethyl-1-oxa-6-azaspiro[2.5]octane and modified synthesis of 5,5,7,7-tetramethyl-1-oxa-6-azaspiro[2.5]oct-6-yloxy are described. Reaction of these spiro-oxiranes with phenols gave corresponding 4-aryloxymethyl 4-piperidinols and their 1-piperidinyloxy derivatives. The same products have also been obtained by reaction with ethanol. The crystal structures of two derivatives: 4-phenoxymethyl-2,2,6,6-tetramethyl-4-piperidinol (**3***a*, 2880 reflections, $R = 0.054$) and 4-phenoxymethyl-4-hydroxy-2,2,6,6-tetramethyl-1-piperidinyloxy (**6***a*, 4395 reflections, $R = 0.084$) have been determined. Piperidine rings are in a chair conformation in both compounds with the phenoxymethyl substituent in an equatorial position. The

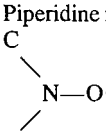

group is not planar, with the N—O bond inclined by 18.4° to the CNC plane. Although the space groups are different for these two compounds the molecules are packed in the crystal lattice in a topologically equivalent way.

M. CYGLER, J. GRABOWSKI, W. STRZYŻEWSKI, L. TURAŁA et R. SKOWROŃSKI. Can. J. Chem. **64**, 670 (1986).

On décrit la synthèse du tétraméthyl-5,5,7,7 oxa-1-aza-6 spiro[2.5]octane et une synthèse modifiée du tétraméthyl-5,5,7,7 oxa-1-aza-6 spiro[2.5]octyloxy-6. La réaction de ces spiro-oxiranes avec des phénols conduit aux aryloxyméthyl-4 pipéridinols-4 correspondants ainsi qu'à leurs dérivés pipéridinyloxy-1. On a aussi obtenu les mêmes produits par réaction avec de l'éthanol. On a déterminé les structures cristallines de deux dérivés: le phénoxyméthyl-4 tétraméthyl-2,2,6,6 pipéridinol-4 (**3***a*, 2880 réflexions et $R = 0{,}054$) et le phénoxyméthyl-4 hydroxy-4 tétraméthyl-2,2,6,6 pipéridinyloxy-1 (**6***a*, 4395 réflexions et $R = 0{,}084$). Dans chacun de ces composés, les cycles des pipéridines existent dans le conformation chaise et le substituant occupe la position équatoriale. Le groupement

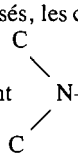

n'est pas polaire et la liaison N—O est inclinée de 18,4° par rapport au plan CNC. Même si les groupes d'espace de ces deux composés sont différents, les molécules sont entassées dans le réseau cristallin de façons qui sont topologiquement équivalentes.

[Traduit par la revue]

Introduction

Stable nitroxyl radicals incorporated in 2,2,6,6-tetramethylpiperidine have attracted the attention of chemists for over 10 years (1). These compounds have found many industrial applications. Together with their precursors, the free amines, they are recommended as light and heat stabilizers in the production of plastics (there are over 200 patents on that application of nitroxyl radicals cited in Chem. Abstr., e.g. ref. 2). Their utilization as spin labels in the investigation of biological systems (3) is one of the most important research applications. The synthesis of the title compounds was undertaken with a view to their potential further applications. We have chosen a method of synthesis based on spiro-oxirane chemistry to gain more insight into such reactions. The structural investigations described in this paper are a continuation of our interest in the conformation of substituted piperidine rings and the conformational differences between the nitroxy radicals and their parent amines.

[1]Author to whom correspondence may be addressed at the Department of Biochemistry, University of Alberta, Edmonton, Alta., Canada T6G 2H7.

Results and discussion

Synthesis

The steps in the synthesis of 4-aryloxymethyl-2,2,6,6-tetramethyl-4-piperidinol **3** and 4-aryloxymethyl-4-hydroxy-2,2,6,6-tetramethyl-1-piperidinyloxy **6** are shown in Scheme 1. 5,5,7,7-Tetramethyl-1-oxa-6-azaspiro[2.5]oct-6-yloxy **5** has previously been obtained by two methods: through the reaction of the ketone **4** with diazomethane (yield = 34%) (4) and by the method of Corey and Chaykovsky in the reaction of the ketone **4** with dimethylsulfonium methylide (yield = 71%) (5). We have applied a variant of the Corey reaction using dimethyloxosulfonium methylide (6), which is safer in use and more easily available. In addition to compound **5** we have obtained the epoxide **2**, which has not previously been described in the literature. The reaction yields were 54.0% and 51.8% for **5** and **2**, respectively. The structures of these intermediate compounds were confirmed by ir, ^{1}H nmr, and mass spectroscopy.

These epoxides (**2** and **5**) were then subjected to reaction with phenols under basic conditions. In each case only one product was obtained, which, as expected (7), turned out to be a tertiary alcohol. This was confirmed by the reaction of compounds **3**

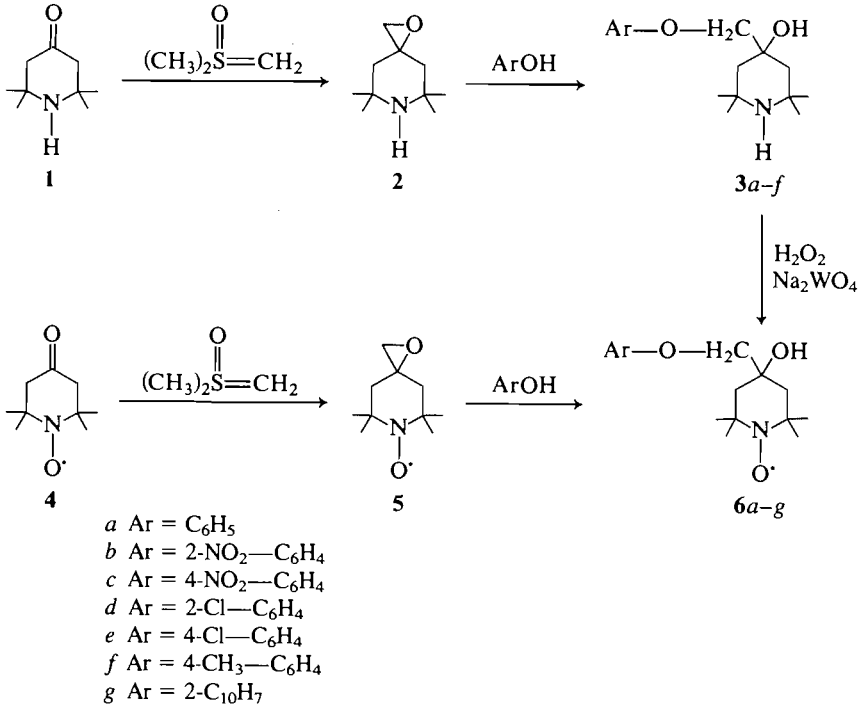

1 2 3*a–f* 4 5 6*a–g*

a Ar = C_6H_5
b Ar = 2-NO_2—C_6H_4
c Ar = 4-NO_2—C_6H_4
d Ar = 2-Cl—C_6H_4
e Ar = 4-Cl—C_6H_4
f Ar = 4-CH_3—C_6H_4
g Ar = 2-$C_{10}H_7$

SCHEME 1

with CrO_3 (this excludes primary and secondary alcohols). The oxidation of **3** with hydrogen peroxide in the presence of Na_2WO_4 and verseniane gave a product identical to **6**, which confirmed its deduced structure. X-ray analyses of **3***a* and **6***a* proved these assignments to be correct.

It is clear that the reaction of epoxides **2** and **5** with phenols proceeds typically, according to the S_N2 mechanism, with the expected reaction product (8). The approaching group attacks the least substituted carbon atom of the oxirane ring. The physical properties, results of analysis, and spectral data for the compounds obtained are presented in Tables 1 and 2.

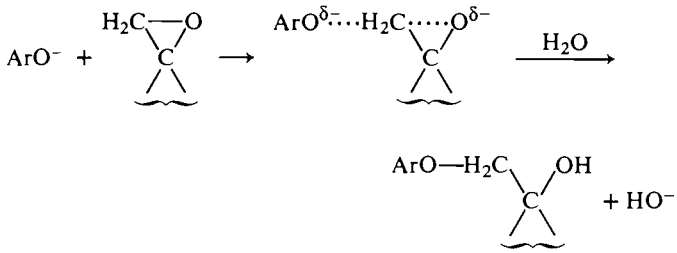

SCHEME 2

A different reaction mechanism was invoked for the reaction of aromatic amines with glycide esters (oxiranes substituted with polar groups), including the spiro-oxiranes (9). In this reaction only secondary alcohols were obtained, as is shown in Scheme 3:

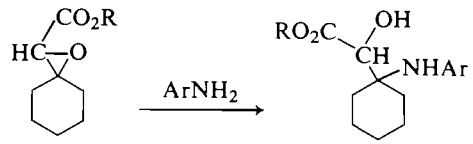

SCHEME 3

Reactions of alkyl derivatives of ethylene oxide with alcohols in acidic medium gave, on the other hand, a mixture of two isomers (7).

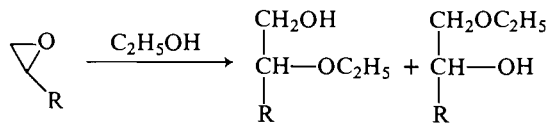

SCHEME 4

For these reactions an S_N1 mechanism has been proposed (8).

We have also followed the reaction of epoxides **2** and **5** with ethanol in a variety of conditions. In all cases (acidic or basic conditions), just as in the reactions with phenols, only one isomer of 4-ethoxymethyl-2,2,6,6-tetramethyl-4-piperidinol or 4-ethoxymethyl-4-hydroxy-2,2,6,6-tetramethyl-1-piperidinyloxy was obtained.

Crystal structure determination

Compounds **3***a* and **6***a* are representative of the two groups of end products and have been chosen for further crystallographic studies.

*Structure of 3*a

The final atomic coordinates are given in Table 3. A view of the molecule is shown in Fig. 1 and bond lengths, valence angles, and some torsion angles are given in Table 5. The piperidine ring exists in a chair conformation with an axial hydroxyl group. The phenyloxymethyl group is in a fully extended conformation with torsion angles around C(41)—O(42) and O(42)—C(7) bonds being 179.1(5)° and 179.7(5)°, respectively. The phenyl ring is nearly perpendicular to the mean plane of the piperidine ring. The hydroxyl group is not equally disposed toward the piperidine ring but is more inclined to one of the methylene groups (the exocyclic OCC angles differ by 5.2°). The distances between the axial substituents to the piperidine ring are listed in Table 5. The interactions of these substituents decrease the ring puckering significantly and lead to an increase of the valence angles at the ring methylene groups to 116.5(3)°. The average endocyclic torsion angle is 45.9°, as compared to 57° in an unsubstituted piperidine ring (10) and 53.5° in 2,2,6,6-

TABLE 1. Results, physical properties, and analysis of 4-aryloxymethyl-4-piperidinol derivatives

Compound	Melting point(°C)	Yield (%)	Mass spectra (15 eV) *m/e* (%)	Formula	Molecular mass	%N calcd.	%N found
3*a*	102.5–103.5	68.0	248 (100): 58 (45.2): 98 (19.4)	$C_{16}H_{25}NO_2$	263.19	5.31	5.25
3*b*	78–80	42.8	293 (100): 294 (30.3): 58 (19.8)	$C_{16}H_{22}N_2O_4$	308.17	9.06	8.83
3*c*	168.5–169.0	63.2	293 (100): 294 (17.8): 58 (16.2)	$C_{16}H_{24}N_2O_4$	306.17	9.06	8.89
3*d*	30	34.6	282 (100): 58 (50.9): 284 (35.8)	$C_{16}H_{24}ClNO_2$	297.68	4.69	4.46
3*e*	141–142	65.5	282 (100): 284 (33.8): 58 (19.6)	$C_{16}H_{24}ClNO_2$	297.68	4.69	4.53
3*f*	110–111	68.5	262 (100): 58 (38.1): 137 (22.7)	$C_{17}H_{27}NO_2$	277.20	5.41	5.39
6*a*	133–134	61.1	278 (100): 94 (55.4): 108 (37.2)	$C_{16}H_{24}NO_3$	278.17	5.03	4.98
6*b*	104–106	59.6	43 (100): 323 (69.6): 41 (62.8)	$C_{16}H_{23}N_2O_5$	323.16	8.67	8.49
6*c*	179–180	67.4	323 (100): 267 (44.7): 309 (37.0)	$C_{16}H_{23}N_2O_5$	323.16	8.67	8.51
6*d*	114–115	63.2	43 (100): 312 (78.2): 55 (56.3)	$C_{16}H_{23}ClNO_3$	312.67	4.47	4.37
6*e*	181.5–183	62.7	43 (100): 312 (95.3): 56 (60.4)	$C_{16}H_{23}ClNO_3$	312.67	4.47	4.45
6*f*	175–176	65.6	108 (100): 292 (84.2): 262 (39.7)	$C_{17}H_{25}NO_3$	291.19	5.13	5.07
6*g*	153–154	48.7	328 (100): 144 (44.3): 329 (37.4)	$C_{20}H_{26}NO_3$	328.18	4.27	3.98

tetramethylpiperidinium ion (TMP^+, ref. 11), where there are only two axial substituents. The flattening of the ring in **3***a* is nearly uniform, with the lowest puckering around C(4) where the mean CCCC torsion angle is 45.5(5)°. The degree of puckering of the ring at C(4) in 2,2,6,6-tetramethylpiperidine derivatives correlates well with the size of the axial substituent at this position. In TMP^+ (11) and *N*,*N*′-bis(2,2,6,6-tetramethyl-4-piperidyl)succinamide dihydrate (DTMP, ref. 12), where a H atom is axial to the ring at C(4), the CCCC torsion angle is similar to that in an unsubstituted piperidine ring (59.2(9)° in TMP^+, 55.8° and 57.9° in two independent molecules of DTMP). A related compound, 4-ethynyl-2,2,6,6-tetramethyl-4-piperidinol (TMPE, ref. 13) has an axial ethynyl group at C(4) and the CCCC torsion angle in this molecule is 49.7(8)°. Finally, in **3***a* with the axial hydroxyl group this torsion angle is even smaller. Hydrogen bonds also play a role in the ring distortion, as was shown in the case of DTMP (12) where two independent molecules with different geometry of H bonds display different degrees of puckering, which correlates with stretching or bending effects of the hydrogen bond interactions. The main effect is, however, observed at the end of the molecule around the N atom (hydrogen bond acceptor) with relatively small changes at the opposite side of the ring. The observed order of puckering around C(4) in **3***a* and TMPE can not be attributed to H bond interactions. The hydrogen bonds in TMPE are stronger (N...O = 2.790(9) Å *versus* 2.971(3) Å in **3***a*) and they are equatorial to the ring (stretching), while the effect of the hydrogen bond formed by the axial hydroxyl group of **3***a* must be less pronounced. Yet **3***a* displays smaller puckering at the C(4) part of the ring.

The size of an equatorial substituent has an opposite effect on the puckering of the ring, as was shown for *N*-methyl-2,2,6,6-tetramethyl-4-piperidinols (14). The magnitude of changes at the C(4) position is, however, smaller, with more pronounced changes occurring around the N atom. The degree of puckering of the ring is determined primarily by the bulkiness of the axial group. The size of an equatorial substituent plays a secondary role in defining the ring shape. This is exemplified by the structures of **3***a* and TMPE, where both axial and equatorial substituents are different and the degree of puckering at C(4) is determined by the size of the axial group.

The hydrogen atom at N(1) takes an axial position. As we have pointed out earlier (13), owing to a low energy difference between the axial and equatorial configuration, a hydrogen atom adopts a position which allows the free electron pair of the nitrogen atom to maximize the hydrogen bond interactions with a neighbouring molecule. Here a strong hydrogen bond is formed when the free electron pair is oriented equatorially with respect to the ring.

An increase of endocyclic angles at unsubstituted ring atoms (N(1), C(3), C(5)) observed here was also found in other derivatives with 2,4,6 axial substituents (13–15) and reveals the positions in the ring least resistant to deformation. The angles at the fully substituted C(2) and C(6) atoms are characteristic for an axial orientation of a substituent at N(1) (Table 4 in ref. 15).

Structure of **6***a*

The final atomic coordinates are given in Table 4. There are two independent molecules in the unit cell. Both have very similar conformations. The bond lengths, valence angles, and some torsion angles are given in Table 5. A view of one of the molecules (**I**) is shown in Fig. 2.

The overall conformation of **6***a* is similar to that of its free amine (compound **3***a*). The piperidine ring of the molecule assumes a chair conformation with an axially oriented hydroxyl group. The phenoxymethyl group exists in an extended conformation, with the phenyl ring nearly perpendicular to the mean plane of the piperidine ring (see Fig. 2). There are small but statistically significant differences in the torsion angles along the C(41)—O(42) and O(42)—C(7) bonds in both molecules. In molecule **II** these angles are −179.4(6) and 179.0(6)° respectively, while they are −174.6(6) and 175.2(6)°, respectively, in molecule **I**. A coupled change in both of these angles seems to be necessary to avoid clashes between hydrogens on the C(41) atom and on the phenyl ring. A rotation around the C(41)—O(42) bond alone would move the H(81) atom of the phenyl ring towards one of the hydrogens of the C(41) methylene group. A simultaneous rotation in the opposite direction along the O(42)—C(7) bond moves that hydrogen atom back towards its starting position. Such a concerted movement along these two bonds is obviously not changing significantly the energy of the molecule and shows that there is some rotational freedom along them.

The conformation of the piperidine ring is similar to that found in other six-membered nitroxyl derivatives (16,17). The ring is most flattened in the N part, with the CNCC torsion angles (36.4(4)° in mol **I** and 32.2(4)° in mol **II**) being in the range found in other compounds (16). As we have shown previously (16), the puckering of the C(4) part of the ring

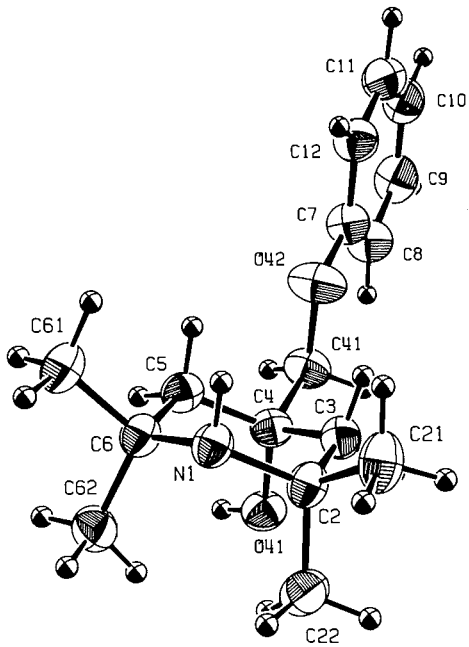

FIG. 1. A view of the molecule of 4-phenoxymethyl-2,2,6,6-tetramethyl-4-piperidinol, **3***a*.

depends on the degree of substitution of the C(4) atom. When an axial substituent to the ring is present at C(4) there is a significant decrease in the CCCC torsion angles. The average value of that torsion angle in both molecules of **6***a* is 53.0(1.0)° and agrees well with the value found for bisubstituted rings (53.7°). The flattening of that part of the ring is also reflected in an opening of the endocyclic angles at the methylene groups (C(3) and C(5) atoms). The distances between axial substituents are given in Table 5.

The average length of the N—O bond in both molecules is 1.280(4) Å. The 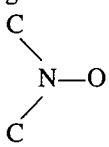 group is not planar. The N—O bond makes an angle of 18.6(2) and 18.3(2)° with the CNC plane in molecules **I** and **II**, respectively. The length of this bond, its inclination to the CNC plane, and the CNC angle are within the limits observed in other compounds (16). Similarly, as in **3***a*, the C(4)—C(41) bond is evenly disposed toward the piperidine ring while the C(4)—O(41) bond is somewhat inclined toward one side (the exocyclic OCC angles differ by 6°), probably as a result of hydrogen bond formation between H(O41) and O(1) from the neighbouring molecule (see Fig. 4).

The average C—C bond length in the phenyl ring is 1.376(14) Å. Some bonds in the ring are rather short but their calculated lengths are probably affected by a relatively large thermal motion of the phenyl ring.

Crystal packing

Diagrams representing packing of molecules are shown in Figs. 3 and 4. Molecules of both compounds form intermolecular hydrogen bonds. In **3***a* the H bond is formed between the hydroxyl group and the N atom of a neighbouring molecule. It is oriented equatorially to the ring. The geometry of that bond is: O—H = 0.89(3), O...N = 2.971(3), H...N = 2.11(3) Å, O—H...N = 163(2)°.

TABLE 2. Spectral data for 4-aryloxymethyl-4-piperidinol derivatives

Compound	^{1}H nmr[a] (ppm) 2,6—CH_3 eq.	2,6—CH_3 ax.	C—CH_2—C	C—CH_2—O	Other	Infrared spectra KBr (cm^{-1}) OH NH	C—O—C	C—O	Ar	N—O	Electron paramagnetic resonance spectra[b] H_0 (mT)[c]	a_N (mT)
3*a*	1.00(6H)s	1.40(6H)s	1.60(4H)d	3.60(2H)s	7.00(5H)m	3650–3100	1240	1150	1600			
3*b*	1.05(6H)s	1.35(6H)s	1.66(4H)d	3.72(2H)s	7.08(4H)m	3650–3050	1260	1160	1600			
3*c*	1.15(6H)s	1.47(6H)s	1.82(4H)d	3.82(2H)s	7.00(4H)m	3600–3100	1270	1120	1590			
3*d*	1.28(6H)s	1.60(6H)s	1.78(4H)d	3.97(2H)s	7.35(4H)m	3650–3050	1250	1150	1580			
3*e*	1.33(6H)s	1.62(6H)s	1.93(4H)d	3.90(2H)s	7.28(4H)m	3600–3100	1240	1170	1580			
3*f*	1.33(6H)s	1.63(6H)s	1.78(4H)d	3.87(2H)s	7.20(4H)m 2.52(3H)d	3650–3050	1240	1100	1620			
6*a*	1.38(6H)s	1.60(6H)s	1.96(4H)d	3.70(2H)s		3500–3200	1260	1030	1590	1345	328.6	1.49
6*b*	1.10(6H)s	1.34(6H)s	1.49(4H)d	3.65(2H)s		3550–3200	1250	1020	1620	1350	332.2	1.50
6*c*	1.14(6H)s	1.34(6H)s	1.68(4H)d	3.54(2H)s		3500–3200	1240	1040	1600	1360	328.3	1.51
6*d*	1.14(6H)s	1.36(6H)s	1.74(4H)d	3.56(2H)s		3500–3250	1250	1050	1590	1345	332.3	1.51
6*e*	1.12(6H)s	1.34(6H)s	1.63(4H)d	3.49(2H)s		3400–3200	1245	1030	1590	1345	328.3	1.48
6*f*	1.12(6H)s	1.32(6H)s	1.65(4H)d	3.46(2H)s		3400–3240	1240	1030	1600	1345	332.3	1.52

[a]The ^{1}H nmr spectra for compounds **6***a–f* were obtained by the reduction of radicals *in situ* to the hydroxylamine with excess of *N,N*-diphenylhydrazine.
[b]In toluene, 5×10^{-4} mol dcm^{-3}.
[c]Central signal of a triplet.

TABLE 3. Final atomic parameters and equivalent temperature factors ($\times 10^4$, $\times 10^3$ for H atoms) for 4-phenoxymethyl-2,2,6,6-tetramethyl-4-piperidinol **3***a*

Atom	*x*	*y*	*z*	U_{EQ}
N1	0.1941(1)	0.6993(2)	0.8761(1)	382
C2	0.0975(2)	0.6249(2)	0.8016(2)	399
C21	0.0645(2)	0.5549(3)	0.8982(2)	541
C22	0.0069(2)	0.7126(3)	0.7257(2)	523
C3	0.1208(2)	0.5243(2)	0.7176(2)	397
C4	0.1854(2)	0.5700(2)	0.6425(2)	394
O41	0.1158(1)	0.6398(2)	0.5362(1)	455
C41	0.2220(2)	0.4532(2)	0.5881(2)	468
O42	0.2922(1)	0.3782(2)	0.6881(1)	576
C5	0.2804(2)	0.6484(2)	0.7239(2)	418
C6	0.2603(1)	0.7505(2)	0.8098(2)	389
C61	0.3671(2)	0.7854(3)	0.9117(2)	488
C62	0.2120(2)	0.8722(2)	0.7379(2)	497
C7	0.3334(2)	0.2682(2)	0.6609(2)	457
C8	0.3118(2)	0.2215(2)	0.5401(2)	521
C9	0.3605(2)	0.1094(3)	0.5264(2)	589
C10	0.4280(2)	0.0433(3)	0.6273(3)	590
C11	0.4485(2)	0.0901(3)	0.7475(2)	544
C12	0.4017(2)	0.2011(2)	0.7641(2)	509

Atom	*x*	*y*	*z*	*U*
HN1	0.240(2)	0.646(2)	0.938(2)	49(3)
H211	0.007(2)	0.496(2)	0.851(2)	61(3)
H212	0.042(2)	0.621(2)	0.948(2)	52(3)
H213	0.125(2)	0.499(2)	0.957(2)	61(3)
H221	0.005(2)	0.788(2)	0.774(2)	60(3)
H222	0.017(2)	0.755(2)	0.652(2)	63(3)
H223	−0.061(2)	0.665(2)	0.700(2)	59(3)
H31	0.159(2)	0.453(2)	0.772(2)	46(3)
H32	0.051(2)	0.488(2)	0.658(2)	38(3)
HO41	0.152(2)	0.678(2)	0.496(2)	61(3)
H411	0.160(2)	0.400(2)	0.541(2)	64(3)
H412	0.256(2)	0.484(2)	0.534(2)	56(3)
H51	0.332(2)	0.585(2)	0.779(2)	47(3)
H52	0.315(2)	0.690(2)	0.674(2)	45(3)
H611	0.416(2)	0.814(2)	0.871(2)	58(3)
H612	0.357(2)	0.857(2)	0.966(2)	46(3)
H613	0.400(2)	0.709(2)	0.974(2)	78(3)
H621	0.192(2)	0.940(2)	0.793(2)	57(3)
H622	0.146(2)	0.859(2)	0.669(2)	64(3)
H623	0.265(2)	0.913(2)	0.708(2)	74(3)
H81	0.262(2)	0.265(2)	0.470(2)	82(3)
H91	0.349(2)	0.067(2)	0.444(2)	85(3)
H101	0.463(2)	−0.039(2)	0.619(2)	50(3)
H111	0.496(2)	0.041(2)	0.823(2)	61(3)
H121	0.415(2)	0.236(2)	0.847(2)	69(3)

In **6***a* the H bond is formed between the hydroxyl group of one molecule and the nitroxyl oxygen of the other independent molecule. The geometry is as follows: $O^{I}(1)\ldots O^{II}(4)$ = 2.776(3), $O^{II}-H^{II}(O4)$ = 0.85(2), $O^{I}(1)\ldots H^{II}(O4)$ = 1.94(2) Å, $O^{I}(1)\ldots H^{II}(O4)—O^{II}(4)$ = 168(2)°, $O^{II}(1)\ldots O^{I}(4)$ = 2.708(4), $O^{I}(4)—H^{I}(O4)$ = 0.93(2), $O^{II}(1)\ldots H^{I}(O4)$ = 1.78(2) Å, $O^{II}(1)\ldots H^{I}(O4)—O^{I}(4)$ = 174(2)°.

Chion and Lajzérowicz-Bonneteau (18) have analyzed the directionality of hydrogen bonds involving nitroxyl groups incorporated in five- and some six-membered rings. They found that in the majority of cases this bond is inclined by 10 to 30° (a_2) to the plane containing the N—O· group and parallel to the

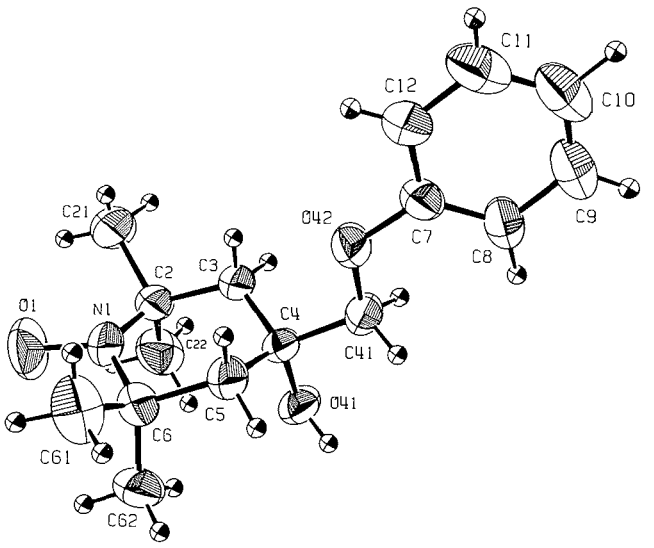

FIG. 2. A view of molecule **I** of 4-phenoxymethyl-4-hydroxy-2,2,6,6-tetramethyl-1-piperidinyloxy, **6***a*.

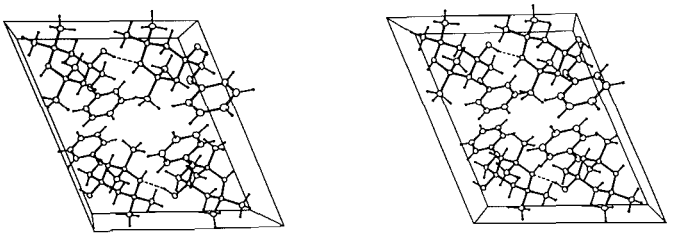

FIG. 3. A stereoscopic view of the unit cell of **3***a* with hydrogen bonds marked by dotted lines. The origin is in the lower left corner, the *Z*-axis is horizontal, the *X*-axis is vertical, and the *Y*-axis points toward the reader.

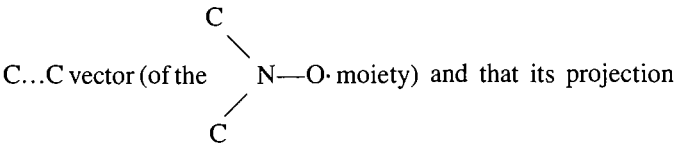

makes an angle of 20–50° (a_3) with the N—O vector. In all but one case the donor atom has also been found on the same side of this plane as the C...C atoms. In the present compound the corresponding angles are: a_2 = 10.3(3), a_3 = 32.5(3)° for the O atom involved in the hydrogen bond to the O(1) atom of molecule **I** and a_2 = 8.9(3), a_2 = 41.6(3)° for molecule **II**. The disposition of the donor group with respect to the above described plane containing the N—O group is, however, different in both molecules. In molecule **I** it is on the same side as the C...C atoms, while it is on the opposite side in molecule **II**.

Figures 3 and 4 show that the organization of the molecules of both compounds in the crystalline state is very similar although not identical. The same, topologically equivalent, system of H bonds is retained and nonbonded contacts of neighbouring molecules are similar. To accommodate the additional O(1) atom, by which the molecules of **6***a* differ from **3***a*, within the crystal structure of **3***a* and maintain favourable van der Waals interactions, the molecules have to move apart and slightly rotate. This results in changes in cell dimensions and lowering the crystal symmetry to triclinic. Such a similar packing arrangement can be rationalized on the basis that only a small

TABLE 4. Final atomic parameters and equivalent temperature factors ($\times 10^4$, $\times 10^3$ for H atoms) for 4-phenoxymethyl-4-hydroxy-2,2,6,6-tetramethyl-1-piperidinyloxy **6***a*

	Molecule **I**				Molecule **II**			
Atom	*X*	*Y*	*Z*	U/U_{eq}	*X*	*Y*	*Z*	U/U_{eq}
O1	0.4774(2)	0.3087(2)	0.2166(2)	1119	0.9504(2)	0.2237(2)	0.1653(2)	1399
N1	0.3930(2)	0.2433(2)	0.2041(2)	684	0.8772(2)	0.2947(2)	0.1688(2)	744
C2	0.3409(2)	0.1566(2)	0.0901(2)	648	0.8364(2)	0.2770(3)	0.2632(3)	799
C21	0.4377(3)	0.0950(3)	0.0742(4)	1055	0.9416(3)	0.2704(4)	0.3852(3)	1336
C22	0.2738(3)	0.2179(2)	−0.0248(2)	867	0.7638(3)	0.1618(3)	0.2199(4)	1213
C3	0.2662(2)	0.0658(2)	0.1072(3)	637	0.7701(2)	0.3811(2)	0.2783(3)	736
C4	0.1896(2)	0.1104(2)	0.1648(2)	531	0.6892(2)	0.4277(2)	0.1602(2)	536
O41	0.1019(1)	0.1695(1)	0.0736(2)	647	0.5957(1)	0.3472(1)	0.0801(2)	671
C41	0.1277(2)	0.0096(2)	0.1860(3)	627	0.6350(2)	0.5356(2)	0.1901(3)	611
O42	0.2112(1)	−0.0573(1)	0.2721(2)	678	0.7222(1)	0.6230(1)	0.2658(2)	718
C5	0.2594(2)	0.1876(2)	0.2860(2)	601	0.7538(2)	0.4550(2)	0.0877(2)	553
C6	0.3350(2)	0.2865(2)	0.2809(2)	620	0.8189(2)	0.3568(2)	0.0583(2)	575
C61	0.4252(3)	0.3275(3)	0.4122(3)	1007	0.9104(2)	0.4083(2)	0.0288(3)	831
C62	0.2661(3)	0.3895(2)	0.2250(3)	898	0.7412(3)	0.2700(2)	−0.0524(3)	809
C7	0.1733(2)	−0.1577(2)	0.2955(2)	617	0.6891(2)	0.7259(2)	0.3028(2)	655
C8	0.0595(2)	−0.1941(2)	0.2476(3)	722	0.5771(3)	0.7503(2)	0.2695(3)	815
C9	0.0332(3)	−0.3000(3)	0.2771(3)	905	0.5552(3)	0.8587(3)	0.3132(3)	1052
C10	0.1162(3)	−0.3657(3)	0.3502(3)	974	0.6404(4)	0.9379(3)	0.3878(3)	1134
C11	0.2285(3)	−0.3267(3)	0.3979(3)	944	0.7517(3)	0.9129(3)	0.4207(3)	1033
C12	0.2577(2)	−0.2231(2)	0.3711(3)	723	0.7765(3)	0.8072(3)	0.3775(3)	842
H21	0.396(1)	0.028(1)	−0.006(1)	106(2)	0.913(1)	0.264(1)	0.456(1)	112(2)
H22	0.487(1)	0.065(1)	0.155(1)	112(2)	0.995(1)	0.348(1)	0.419(1)	109(2)
H23	0.484(1)	0.144(1)	0.063(1)	105(2)	0.984(1)	0.210(1)	0.380(1)	108(2)
H24	0.247(1)	0.165(1)	−0.107(1)	100(2)	0.735(1)	0.155(1)	0.275(1)	111(2)
H25	0.316(1)	0.276(1)	−0.031(1)	99(2)	0.812(1)	0.097(1)	0.213(1)	97(2)
H26	0.198(1)	0.260(1)	−0.031(1)	95(2)	0.698(1)	0.169(1)	0.133(1)	109(2)
H31	0.315(1)	0.014(1)	0.163(1)	86(2)	0.826(1)	0.441(1)	0.341(1)	94(2)
H32	0.222(1)	0.015(1)	0.020(1)	84(2)	0.726(1)	0.358(1)	0.316(1)	85(2)
HO4	0.051(1)	0.193(1)	0.105(1)	98(2)	0.567(1)	0.343(1)	0.130(1)	82(2)
H41	0.073(1)	−0.044(1)	0.100(1)	91(2)	0.588(1)	0.514(1)	0.234(1)	72(2)
H42	0.077(1)	0.036(1)	0.226(1)	86(2)	0.584(1)	0.564(1)	0.116(1)	72(2)
H51	0.206(1)	0.223(1)	0.321(1)	78(2)	0.813(1)	0.525(1)	0.139(1)	88(2)
H52	0.307(1)	0.141(1)	0.349(1)	88(2)	0.708(1)	0.477(1)	0.008(1)	81(2)
H61	0.384(1)	0.351(1)	0.468(1)	111(2)	0.877(1)	0.455(1)	−0.039(1)	95(2)
H62	0.479(1)	0.385(1)	0.409(1)	107(2)	0.954(1)	0.353(1)	0.008(1)	96(2)
H63	0.472(1)	0.268(1)	0.443(1)	101(2)	0.969(1)	0.459(1)	0.107(1)	98(2)
H64	0.232(1)	0.420(1)	0.281(1)	103(2)	0.714(1)	0.307(1)	−0.130(1)	106(2)
H65	0.203(1)	0.373(1)	0.136(1)	101(2)	0.685(1)	0.241(1)	−0.034(1)	95(2)
H66	0.316(1)	0.450(1)	0.230(1)	94(2)	0.791(1)	0.216(1)	−0.068(1)	100(2)
H11	−0.009(1)	−0.151(1)	0.182(1)	98(2)	0.520(1)	0.692(1)	0.215(1)	96(2)
H12	−0.046(1)	−0.320(1)	0.247(1)	101(2)	0.472(1)	0.870(1)	0.287(1)	99(2)
H13	0.100(1)	−0.438(1)	0.376(1)	102(2)	0.629(1)	1.009(1)	0.422(1)	108(2)
H14	0.275(1)	−0.371(1)	0.441(1)	106(2)	0.823(1)	0.967(1)	0.480(1)	104(2)
H15	0.332(1)	−0.199(1)	0.399(1)	89(2)	0.857(1)	0.785(1)	0.397(1)	102(2)

TABLE 5. Bond distances, valence and torsion angles for **3***a* amd **6***a* (esd's in parentheses)

Bonds

Atoms	3a	6a		Atoms	3a	6a		Atoms	3a	6a	
		Molecule I	Molecule II			Molecule I	Molecule II			Molecule I	Molecule II
N(1)—O(1)	—	1.281(3)	1.279(4)	N(1)—C(2)	1.495(2)	1.490(3)	1.486(5)	N(1)—C(6)	1.483(2)	1.485(4)	1.482(3)
C(2)—C(3)	1.538(3)	1.528(4)	1.535(4)	C(2)—C(21)	1.531(3)	1.531(5)	1.513(4)	C(2)—C(22)	1.525(3)	1.531(4)	1.538(4)
C(3)—C(4)	1.524(3)	1.514(4)	1.510(3)	C(4)—C(5)	1.524(3)	1.512(3)	1.513(4)	C(4)—O(41)	1.436(2)	1.433(3)	1.431(2)
C(4)—C(41)	1.537(3)	1.531(4)	1.532(4)	C(5)—C(6)	1.546(3)	1.539(4)	1.531(4)	C(6)—C(61)	1.534(3)	1.513(4)	1.529(5)
C(6)—C(62)	1.525(3)	1.535(4)	1.523(3)	C(41)—O(42)	1.425(3)	1.435(3)	1.424(3)	O(42)—C(7)	1.366(3)	1.372(3)	1.372(3)
C(7)—C(8)	1.394(3)	1.382(4)	1.377(4)	C(7)—C(12)	1.392(3)	1.378(3)	1.378(4)	C(8)—C(9)	1.386(3)	1.402(5)	1.392(5)
C(9)—C(10)	1.368(4)	1.360(4)	1.348(5)	C(10)—C(11)	1.392(4)	1.372(5)	1.371(6)	C(11)—C(12)	1.372(3)	1.377(5)	1.379(5)

Angles

Atoms	3a	6a		Atoms	3a	6a	
		Molecule I	Molecule II			Molecule I	Molecule II
O(1)—N(1)—C(2)	—	117.2(3)	114.1(2)	O(1)—N(1)—C(6)	—	115.0(2)	116.6(3)
C(2)—N(1)—C(6)	118.2(1)	124.8(2)	126.4(2)	N(1)—C(2)—C(3)	111.6(2)	109.9(3)	109.2(3)
N(1)—C(2)—C(21)	105.7(2)	108.1(2)	106.8(3)	N(1)—C(2)—C(22)	111.6(2)	109.8(2)	107.9(3)
C(21)—C(2)—C(22)	107.8(2)	108.9(3)	110.3(3)	C(3)—C(2)—C(21)	108.4(2)	107.9(2)	109.4(3)
C(3)—C(2)—C(22)	111.5(2)	112.2(2)	113.1(3)	C(2)—C(3)—C(4)	116.2(2)	116.5(2)	116.9(2)
C(3)—C(4)—C(5)	111.2(2)	109.8(2)	109.0(2)	C(3)—C(4)—O(41)	107.2(2)	106.8(2)	112.9(2)
C(3)—C(4)—C(41)	109.1(2)	110.5(2)	111.0(2)	C(5)—C(4)—O(41)	112.9(2)	112.9(2)	107.7(2)
C(5)—C(4)—C(41)	110.2(2)	111.0(2)	110.7(2)	O(41)—C(4)—C(41)	105.7(2)	105.6(2)	105.6(2)
C(4)—C(5)—C(6)	116.7(2)	116.6(3)	116.5(2)	N(1)—C(6)—C(5)	111.5(2)	109.7(2)	109.9(2)
N(1)—C(6)—C(61)	106.4(2)	108.6(2)	107.9(2)	N(1)—C(6)—C(62)	110.8(2)	108.6(3)	108.7(2)
C(5)—C(6)—C(61)	107.8(2)	108.8(3)	109.0(2)	C(5)—C(6)—C(62)	111.9(2)	112.3(2)	112.5(2)
C(61)—C(6)—C(62)	108.1(2)	108.8(2)	108.7(3)	C(4)—C(41)—O(42)	109.4(2)	108.7(2)	109.5(2)
C(41)—O(42)—C(7)	119.3(2)	117.8(2)	117.5(2)	O(42)—C(7)—C(8)	124.7(2)	124.0(2)	124.1(2)
O(42)—C(7)—C(12)	115.5(2)	115.4(2)	115.5(3)	C(8)—C(7)—C(12)	119.7(2)	120.6(3)	120.4(3)
C(7)—C(8)—C(9)	118.5(2)	117.9(2)	118.2(3)	C(8)—C(9)—C(10)	122.0(2)	121.7(3)	121.7(4)
C(9)—C(10)—C(11)	119.0(2)	119.2(3)	119.8(4)	C(10)—C(11)—C(12)	120.3(2)	120.8(3)	120.1(3)
C(7)—C(12)—C(11)	120.4(2)	119.9(3)	119.8(3)				

TABLE 5. (*Concluded*)

Torsion angles

Atoms	3*a*	6*a* Molecule I	6*a* Molecule II	Atoms	3*a*	6*a* Molecule I	6*a* Molecule II
C(6)—N(1)—C(2)—C(3)	47.0(5)	−36.7(6)	−32.0(6)	C(2)—N(1)—C(6)—C(5)	−46.2(5)	36.2(6)	32.1(6)
N(1)—C(2)—C(3)—C(4)	−46.3(5)	43.3(6)	42.0(6)	C(4)—C(5)—C(6)—N(1)	45.1(5)	−42.6(6)	−41.7(6)
C(2)—C(3)—C(4)—C(5)	45.8(5)	−52.3(6)	−54.1(6)	C(3)—C(4)—C(5)—C(6)	−45.2(5)	51.9(6)	53.7(6)
C(21)—C(2)—C(3)—C(4)	−162.3(5)	160.7(6)	158.6(6)	C(22)—C(2)—C(3)—C(4)	79.3(5)	−79.2(6)	−78.1(6)
C(4)—C(5)—C(6)—C(61)	161.5(5)	−161.2(6)	−160.0(6)	C(4)—C(5)—C(6)—C(62)	−79.7(5)	78.3(6)	79.4(6)
C(2)—C(3)—C(4)—C(41)	167.5(5)	−175.3(6)	−176.4(6)	C(2)—C(3)—C(4)—O(41)	−78.3(5)	70.5(6)	65.3(6)
C(3)—C(4)—C(41)—O(42)	−64.8(5)	62.2(6)	59.8(6)	C(4)—C(41)—O(42)—C(7)	179.1(5)	−174.6(6)	−179.4(6)
O(41)—C(4)—C(41)—O(42)	179.8(5)	177.0(6)	−177.7(6)	C(41)—O(42)—C(7)—C(8)	−0.2(5)	−4.5(6)	−1.2(6)
C(41)—O(42)—C(7)—C(12)	179.7(5)	175.2(6)	179.0(6)				

Distances between axial substituents to the piperidine ring

Atoms	3*a*	6*a* Molecule I	6*a* Molecule II
C(22)...C(62)	3.219(4)	3.459(4)	3.533(5)
C(22)...O(41)	3.274(4)	3.046(4)	3.147(5)
C(62)...O(41)	3.156(4)	3.152(4)	3.076(5)

TABLE 6. Crystal data

Parameter	Compound 3a	Compound 6a
Formula	$C_{16}H_{25}NO_2$	$C_{16}H_{24}NO_3$
Molecular weight	263.2	278.2
Space group	$P2_1/c$	$P\bar{1}$
a	13.666(4) Å	13.080(3) Å
b	10.449(3) Å	11.648(3) Å
c	11.491(6) Å	12.034(4) Å
α	90°	96.33(3)°
β	111.98(3)°	116.33(3)°
γ	90°	90.25(3)°
V	1521.60(5) Å^3	1629.85(4) Å^3
Z	4	4
Molecule/asym. unit	1	2
$F(000)$	576	632
μ(CuKα)	5.15 cm^{-1}	5.88 cm^{-1}
D_x	1.149 g cm^{-3}	1.134 g cm^{-3}
ω–θ coupling n	1	4/3
Octants meas.	$hkl, -hkl$	$hkl, -hkl, h-kl, -h-kl$
No. of refl.	2880	6447
Refl with $I>3\sigma$	1953	2974
R	0.0537	0.0503 (0.0843)[a]
R_w	0.0601	0.0574 (0.0787)[a]
$S=\sqrt{(\Sigma w\Delta F^2/(m-n))}$	1.09	0.88
⟨shift/esd⟩	0.01	0.07
Wt. const. k[b]	0.00248	0.00398

[a]R-factors for 4395 reflections with $I > 0.5\sigma(I)$ are given in parentheses (see text).
[b]Weights: $w^{-1} = \sigma^2(F) + k|F|^2$ were used during refinement.

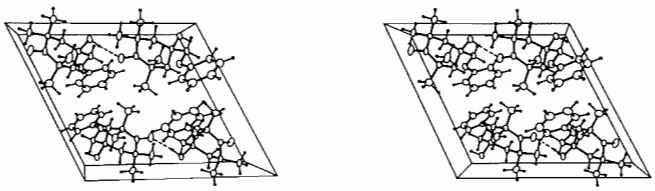

FIG. 4. A stereoscopic view of the unit cell of **6a** with hydrogen bonds marked by dotted lines. The origin is in the lower left corner, the X-axis is horizontal, the Z-axis is vertical, and the Y-axis points away from the reader.

part of the molecule has been modified, leaving its large hydrophobic surface unchanged. TMPE and 4-ethynyl-4-hydroxy-2,2,6,6-tetramethylpiperidine-1-oxyl (TMPEOx, ref. 19) form a pair of compounds that differ in a similar manner to **3a** and **6a**. With the smaller size of a substituent at C(4), however, an exchange of a hydrogen to an oxygen atom constitutes a much larger change of the molecular surface than in the above case. Consequently TMPE and TMPEOx display different modes of packing in the crystalline state.

Experimental

Melting points were determined with a Boetius apparatus and were not corrected. The ir spectra were recorded on a Perkin–Elmer PE-325 spectrometer with the KBr or liquid film technique. The ^{1}H nmr spectra were recorded on Tesla BS 487B (80 MHz) or Tesla 467 (60 MHz) spectrometers using TMS as an internal standard (δ = 0). Electron paramagnetic resonance (epr) spectra were measured on a JEOL JES-Me3X apparatus. Mass spectra were obtained on a LKB 2091 spectrometer at an ionization energy of 15 and 70 eV. Products from preparative scale reactions were isolated by column chromatography using Merck silica gel 60 (230–400 mesh) or Merck aluminium oxide 90 (70–230 mesh) packed in glass columns (1.5 cm in diameter, 40 cm length). The purity of separated compounds was controlled by thin-layer chromatography (tlc) using Merck silica gel 60 F 254 or aluminium oxide 60 F 254 analytical sheets.

2,2,6,6-Tetramethyl-4-piperidinone ***1***

This compound was obtained from acetone, NH_4Cl, and CaO as described earlier (20) and was converted to 2,2,6,6-tetramethyl-4-oxo-1-piperidinyloxy **4** (21).

5,5,7,7-tetramethyl-1-oxa-6-azaspiro[2.5]octane ***2***

Sodium hydride (3.1 g, 0.02 mol) and trimethyloxosulfonium iodide (5.28 g, 0.024 mol) were placed in a four-neck flask filled with dry nitrogen. DMSO (40 cm^3) was added dropwise, followed by 2,2,6,6-tetramethyl-4-piperidinone **1** (3.1 g, 0.02 mol) dissolved in 10 cm^3 DMSO. The contents of the flask were stirred at room temperature for 6 h under the N_2 atmosphere, then heated to 50°C, stirred for another 1.5 h, and slowly cooled to room temperature. Water (60 cm^3) was added to the mixture, followed by extraction with ether. The extract was washed 3 times with water and dried with anhydrous $MgSO_4$. After ether evaporation the sample was distilled under low pressure and fractions collected at 101–102°C/37 hPa. Yield 1.75 g (51.8%); ir (film) ν cm^{-1}: 1260 (C—O—C), 860 (oxirane), 3350 (NH); ^{1}H nmr (CCl_4), δ (ppm): 1.55 (s, 6H, 2,6-CH_3 eq.), 1.67 (s, 6H, 2,6-CH_3 ax.), 2.00 (s, 4H, —C—CH_2—C), 3.6 (s, 2H, —C—CH_2—O); ms (15 eV) m/e (%): 169$^+$ (2.6), 154 (100), 58 (53.3), 98 (39.5), 99 (15.3). *Anal.* calcd. for $C_{10}H_{19}NO$: C 70.96, H 11.31, N 8.28; found: C 71.29, H 11.37, N 8.21.

5,5,7,7-Tetramethyl-1-oxa-6-azaspiro[2.5]oct-6-yloxy ***5***

Synthesis was achieved as for compound **2**. The crude product was purified on a chromatography column filled with aluminium oxide (eluted with ethyl octane – hexane 1:4 mixture). A total of 1.98 g (yield 54.0%) of red crystals (mp 64–65°C) was obtained from 3.4 g (0.02 mol) of 2,2,6,6-tetramethyl-4-oxo-1-piperidinyloxy **4**; ir (KBr) ν

cm^{-1}: 1230 (C—O—C), 870 (oxirane), 1370 (N—O); ^1H nmr (CCl_4) (*in situ* reduction with the excess of *N,N*-diphenylhydrazine), δ (ppm): 1.14 (s, 6H, 2,6-CH_3 eq.), 1.19 (s, 6H, 2,6-CH_3 ax.), 1.59 (s, 4H, —C—CH_2—C), 2.51 (s, 2H, —C—CH_2—O); ms (15 eV) *m/e* (%): 184^+ (30.1), 56 (100), 98 (68.8), 83 (40.8), 70 (33.9), 81 (33.4).

4-Aryloxymethyl-2,2,6,6-tetramethyl-4-piperidinol **3** *or 4-aryloxymethyl-4-hydroxy-2,2,6,6-tetramethyl-1-piperidinyloxy* **6**

General procedure

The flask containing the mixture of phenol (0.03 mol), NaOH (0.44 g, 0.011 mol), and water (1.5 cm^3) was immersed in a boiling water bath. 5,5,7,7-Tetramethyl-1-oxa-6-azaspirol[2.5]octane **2** or 5,5,7,7-tetramethyl-1-oxa-6-azaspirol[2.5]oct-6-yloxy **5** (0.01 mol) was then added all at once. The heating was continued for 5 h. The reaction mixture was then transferred to 100 cm^3 of 4% NaOH solution having a temperature of 10–15°C. The product was extracted with ether. The ether extract was dried with anhydrous K_2CO_3 and the ether was distilled away under low pressure. The crude product was purified by crystallization. Compounds **3***a–d* were crystallized from *n*-hexane and **3***e–f* from a mixture of hexane – ethyl acetate, while compounds **6***a–g* were crystallized from water–methanol (1:1) mixtures. Physical properties, and spectral and analytical results are shown in Tables 1 and 2.

Oxidation of 4-aryloxymethyl-2,2,6,6-tetramethyl-4-piperidinols **3** *to 4-aryloxymethyl-4-hydroxy-2,2,6,6-tetramethyl-1-piperidinyloxys* **6** (shown below for the oxidation of **3***a* to **6***a*)

4-Phenoxymethyl-2,2,6,6-tetramethyl-4-piperidinol **3** (2.63 g, 0.01 mol) was dissolved in 15 cm^3 of methanol and mixed in a flask with Na_2WO_4 (0.4 g) and disodium versenate (0.4 g). Next, 10 cm^3 of water and 10 cm^3 fo H_2O_2 (30%) were added. The flask containing the solution was heated for 1 h in a water bath and then slowly cooled to room temperature. The crystalline product was filtered out. There was 2.7 g of 4-phenoxymethyl-4-hydroxy-2,2,6,6-tetramethyl-1-piperidinyloxy **6***a*, mp 133–134°C, yield 97.1%.

Compounds **3***b–f* were oxidized in a similar way to **6***b–f* with yields in the range of 90–98%.

Reaction of 5,5,7,7-tetramethyl-1-oxa-6-azaspiro[2.5]octane **2** *with ethanol*

Reaction condition 1

Sodium (0.23 g) was added to 5 cm^3 of absolute ethanol. After the reaction was completed compound **2** (1.69 g, 0.01 mol) was added (at boiling temperature). The temperature was maintained for 3 h. The alcohol was then distilled away under low pressure and 50 cm^3 of water was added, followed by extraction with ether. The extract was first dried with anhydrous $MgSO_4$ and then the ether was distilled away. The remaining material was recrystallized from *n*-hexane. 4-Ethoxymethyl-2,2,6,6-tetramethyl-4-piperidinol (1.2 g) was obtained (mp 70–71°C, yield 55.8%); ir (KBr) ν cm^{-1}: 3500–3100 (OH, NH), 1240 (C—O—C), 1115 (C—O); ^1H nmr (CCl_4), δ (ppm): 1.45 (d, 12H, 2,2,6,6-CH_3), 1.22 (3H, CH_3), 1.77 (s, 4H, —C—CH_2—C), 3.00 (q, 2H, —C—CH_2—O), 3.33 (m, 2H, —CH_2 ethoxy group); ms (15 eV) *m/e* (%): 200 (100), 58 (36.2), 182 (23.2), 98 (15.3).

Reaction condition 2

Ethanol (6.4 cm^3) was mixed in the flask with concentrated H_2SO_4 (0.55 cm^3) and compound **2** (1.69 g, 0.01 mol) was added at a temperature not exceeding 45°C. The mixture was left at room temperature for 24 h and a 20% NaOH solution was added. Ethanol was distilled away under low pressure, 50 cm^3 of water was added, and the product was extracted with ether. The extract was dried with anhydrous $MgSO_4$ and the ether distilled away. The remaining material (0.69 g, yield 32%) was recrystallized from *n*-hexane, giving a compound identical to the one obtained under reaction condition 1.

Reaction of 5,5,7,7-tetramethyl-1-oxa-6-azaspiro[2.5]oct-6-yloxy **5** *with ethanol*

The reaction was carried out using reaction condition 1 as in the synthesis of epoxide **2**. The crude product was crystallized from ethyl acetate – hexane (1:4) solution. Red crystals of 4-ethoxymethyl-4-hydroxy-2,2,6,6-tetramethyl-1-piperidinyloxy were obtained starting with compound **5** with the yield 69.8%; ir (KBr) ν cm^{-1}: 3400–3100 (OH), 1260 (C—O—C), 1130 (C—O), 1360 (N—O); ^1H nmr (CCl_2) δ (ppm): 1.03 (3H, CH_3), 1.14 (s, 6H, 2,6-CH_3 eq.), 1.32 (s, 6H, 2,6-CH_3 ax.), 1.58 (d, 4H, —C—CH_2—C), 3.10 (s, 2H, —C—CH_2—O), 3.42 (m, 2H, —CH_2 ethoxy group); ms (15 eV) *m/e* (%): 87 (100), 230^+ (87.5), 59 (63.6), 83 (58.0), 55 (34.5), 56 (32.1).

X-ray analysis

Suitable crystals of **3***a* were obtained from *n*-hexane and those of **6***a* from methanol–water (1:1) mixture. Diffraction data were collected on a CAD-4 diffractometer using monochromated CuKα radiation. The unit cell dimensions were obtained from a least-squares refinement of the angular settings for 25 reflections with θ in the range 18 –53° for **3***a* and 10 – 42° for **6***a*. The space group $P2_1/c$ for **3***a* was determined from systematic absences on Weissenberg photographs. Crystal data and pertinent details of refinement are given in Table 6.

An $\omega/n\theta$ scan technique was used for data collection with the scan width $\Delta\omega = (A + 0.2 \tan\theta)°$, extended by 25% on either side for background measurements (*A* equals 0.7 for **3***a* and 0.6 for **6***a*). One reflection was frequently monitored during the data collection and used for scaling purposes. The structures were solved with direct methods (SHELX 76, ref. 22). Compound **3***a* was refined using full-matrix least-squares while a block-diagonal least-squares method with one molecule per block was used for **6***a* (SHELX 76, ref. 22). Scattering amplitudes were taken from ref. 23. For **6***a* only 46% of measured reflections were above 3σ level. The percentage of "observed" reflections decreased rapidly with the θ angle. For $\theta > 57°$ only about 20% of the measured reflections were above the 3σ threshold. In the preliminary stages of refinement, reflections above the 3σ threshold were used. Since there are 553 parameters to refine, the reflections/parameter ratio was only 5.3. In the last few cycles of refinement, 4395 reflections with $I > 0.5\sigma(I)$ were used. Two reflections in the case of **3***a* and six for **6***a* were affected by extinction and were given zero weight in the refinement. Non-hydrogen atoms were refined with anisotropic temperature factors. The highest peaks in the difference map are 0.2 e/Å^3 and they appear near oxygen atoms. Final atomic coordinates for both compounds are given in Table 4.[2]

Acknowledgements

The authors acknowledge the help of the Microanalysis Laboratory, Center of Molecular and Macromolecular Chemistry, Polish Academy of Sciences, Łódź, in performing elemental analyses. We wish to thank Mr. S. Lecocq, Laboratoire de minéralogie–cristallographie associé au CNRS, Université Claude Bernard Lyon I, France, for collecting diffraction data.

1. E. G. Rozantsev. Free nitroxyl radicals. Plenum Press, New York, London. 1970.
2. N. Soma, T. Yoshioka, S. Morimura and T. Kurumada. German Patent No. 2,630,798 (1977); Chem. Abstr., **87**, 5815a (1977).
3. J. F. W. Keana. Chem. Rev. **78**, 37 (1978).
4. H. Schlude. Tetrahedron, **29**, 4007 (1973).
5. E. J. Rauckman, G. M. Rosen, and M. B. Abou-Donia. Org. Prep. Proced. Int. **84**, 159 (1976).
6. E. J. Corey and M. Chaykovsky. J. Am. Chem. Soc. **87**, 1353 (1976).
7. A. Rosovsky. *In* The chemistry of heterocyclic compounds. *Edited by* A. Weissberger. Heterocyclic compounds with three- and four-membered rings. Part one. Interscience Publishers, New York, London, Sydney. 1964. p. 1.

[2]Tables of anisotropic temperature factors and of observed and calculated structure factors have been deposited and may be purchased from the Depository of Unpublished Data, CISTI, National Research Council of Canada, Ottawa, Ont., Canada K1A 0S2.

8. R. E. PARKER and N. S. ISAACS. Chem. Rev. **59**, 737 (1959).
9. V. F. MARTYNOV. Zh. Obshch. Khim. **23**, 2006, (1953).
10. A. WAHLBERG. Acta Crystallogr. Sect. B, **36**, 2099 (1980); **B37**, 1240 (1981).
11. M. D. WALKINSHAW, A. H. COWLEY and S. K. MEHROTRA. Acta Crystallogr. Sect C, **40**, 129 (1983).
12. H. RUBEN, A. ZALKIN, and D. H. TEMPLETON. Acta Crystallogr. Sect. B, **31**, 334 (1974).
13. M. CYGLER, M. J. GRABOWSKI, J. SKOLIMOWSKI, and R. SKOWROŃSKI. Acta Crystallogr. Sect. B, **34**, 2327 (1978).
14. M. CYGLER, T. SKARŻYŃSKI, J. SKOLIMOWSKI, and A. THOZET. Acta Crystallogr. Sect. B, **36**, 2481 (1980).
15. M. CYGLER, T. MARKOWICZ, J. SKOLIMOWSKI, and R. SKOWROŃSKI. J. Mol. Struct. **68**, 161 (1980).
16. M. CYGLER. Can. J. Chem. **60**, 2392 (1982).
17. J. LAJZÉROWICZ-BONNETEAU. *In* Spin labelling. Theory and applications. *Edited by* L. J. Berliner. Academic Press, New York. 1976.
18. B. CHION and J. LAJZÉROWICZ-BONNETEAU. Acta Crystallogr. Sect. B, **36**, 998 (1980).
19. M. CYGLER. Acta Crystallogr. Sect. B, **35**, 195 (1979).
20. R. SKOWROŃSKI, W. STRZYŻEWSKI, and Z. CEBULSKA. Polish Patent No. 118992 (1982).
21. E. G. ROZANTSEV. Izv. Akad. Nauk SSSR, Ser. Khim. 2218 (1964).
22. G. M. SHELDRICK. SHELX 76. A program for crystal structure determination. University of Cambridge, England. 1976.
23. INTERNATIONAL TABLES FOR X-RAY CRYSTALLOGRAPHY. Vol. IV. Kynoch Press, Birmingham. 1974.

Excess thermodynamic properties of tetraalkyltin compounds with *Trans*-decalin and highly branched alkanes. Effect of steric hindrance

HONG PHUONG-NGUYEN AND GENEVIÈVE DELMAS

Chemistry department, Université du Québec à Montréal, P.O. Box 8888, Station A, Montréal, Que., Canada H3C 3P8

Received July 19, 1985

HONG PHUONG-NGUYEN and GENEVIÈVE DELMAS. Can. J. Chem. **64**, 681 (1986).

Molar excess thermodynamic quantities h^E, c_p^E, and v^E have been measured at 25°C over the whole composition range for mixtures of four globular $Sn(C_nH_{2n+1})_4$ (SnR_4) ($n = 1-4$) with *t*-decalin, and 2,2,4,4,6,8,8-heptamethylnonane (br-C_{16}) as well as h^E for the same SnR_4 compounds with 2,2,4-trimethylpentane (br-C_8). The excess viscosities are measured at −20, 25, and 40°C for the *t*-decalin + SnR_4 systems. By introducing g^E in the solution activation energy, the free energy of mixing can be related to and calculated from the excess viscosities. The steric hindrance contribution, corresponding to an increase of order or diminution of mobility in solution, known to occur either with compounds having highly substituted atoms or with flat-shaped molecules, was investigated. The free volume contribution to the different thermodynamic properties is calculated from the Prigogine–Patterson–Flory theory. The difference between the experimental and calculated excess data is associated with the steric hindrance contribution. Values of h^E, c_p^E, v^E, and s^E confirm the existence of a large steric hindrance contribution ($h^E < -200$ J mol^{-1} and $Ts^E < -400$ J mol^{-1} for two systems). Another contribution, found to occur for the two smaller globular SnR_4, may originate in the liberation of movement induced in solution by the second component.

HONG PHUONG-NGUYEN et GENEVIÈVE DELMAS. Can. J. Chem. **64**, 681 (1986).

Nous avons mesuré, à 25°C, sur tout le domaine de concentration les propriétés thermodynamiques d'excès suivantes: h^E, c_p^E et v^E pour des mélanges de *t*-décaline et de heptamethyl-2,2,4,4,6,8,8 nonane (ram-C_{16}) avec les quatre premiers composés de la serie SnR_4 ($R = C_nH_{2n+1}$, $n = 1-4$). Les h^E ont aussi été mesurées avec le triméthyl-2,2,4 pentane (ram-C_8). Des mesures de viscosités d'excès ont été faites à −20, 25 et 40°C sur les mélanges de *t*-décaline + SnR_4. En introduisant g^E dans l'énergie d'activation de la solution, on peut relier l'énergie libre de mélange (non-combinatoire) aux viscosités d'excès. La contribution d'empêchement stérique, qui se traduit par une diminution de mobilité ou une augmentation d'ordre en solution, était l'objet de ce travail. Elle se manifeste soit avec des molécules qui possèdent un atome très substitué soit avec d'autres qui ont une forme moléculaire assez plate. La théorie de Prigogine–Patterson–Flory est utilisée pour calculer les contributions de volume libre. La différence entre les valeurs expérimentales et calculées des viscosités d'excès est identifiée à la contribution à Ts^E venant de l'empêchement stérique. Les résultats de h^E, c_p^E, v^E et s^E confirment l'existence d'une contribution importante aux propriétés thermodynamiques venant de l'empêchement stérique ($h^E < -200$ J mol^{-1} et $Ts^E < -400$ J mol^{-1} pour deux systèmes). Pour les deux plus petits SnR_4, une autre contribution apparaît qui pourrait être reliée à la libération, par le deuxième composé, d'un mouvement dans ces molécules très symétriques.

Introduction

Previous work (1–3) on the tetraalkyltin compounds has shown that the long-chain molecules $Sn(C_nH_{2n+1})_4$ (or SnR_4) have orientational order which is destroyed in solution with globular molecules. The short-chain or globular SnR_4 seemed very interesting since the h^E (2, 3) and c_p^E (1) of their mixtures with long-chain compounds, either linear alkanes or SnR_4, show important irregularities instead of varying smoothly with the size or free volume of SnR_4.

Steric hindrance effect

Analysis of the h^E of the SnR_4 mixtures and of others leads to the definition of a new contribution to the thermodynamic properties of mixing arising from an increase of order or diminution of mobility of the molecules in solution in comparison to the pure liquids. This contribution, named steric hindrance contribution (2), condensation contribution (4), or coupling of torsional oscillations (5), occurs either when a molecule in the mixture has a crowded central atom, such as the highly branched alkanes, the SnR_4 compounds, and some disubstituted cyclohexanes (6*a*), or when it has a special flat shape such as cyclopentane or *trans*-decalin (6*b*). The steric hindrance character of many branched alkanes (with the carbon atom number $n \leq 8$) has been related (5) to the number of *trans* configurations of the molecule in the liquid state. The interaction of this type of molecule with the second component gives an exothermic contribution to h^E which makes the total h^E either negative or less endothermic than expected from comparison with similar systems. Since the steric hindrance contribution is less important at higher temperature, the c_p^E values associated with steric hindrance are positive. As can be expected from an increase of cohesion or from a contraction, steric hindrance gives a negative contribution to the excess volume v^E.

The aim of the present work was to study the steric hindrance effect in mixtures where the two components have either characteristic which is known to induce the steric hindrance effect. The compounds chosen were, on one hand, the four lower members of the SnR_4 series and, on the other hand, two highly branched alkanes namely, 2,2,4,4,6,8,8-heptamethylnonane (br-C_{16}) and 2,2,4-trimethylpentane (br-C_8) and the flat shaped molecule, *t*-decalin.

Values of the excess free energy are valuable to obtain the excess entropy and eventually the steric hindrance contribution to s^E. Since the g^E could not be measured by vapor pressure for the systems composed of nonvolatile compounds, they were calculated by an indirect method from excess viscosity data (7, 8).

For eight systems, namely the four lower members of the SnR_4 series, mixed with *t*-decalin and br-C_{16}, h^E, c_p^E, and v^E have been measured at 25°C as a function of concentration. For br-C_8, h^E values with the SnR_4 compounds with *t*-decalin have been obtained at −20, 25, and 40°C. The names of the tetraalkyltin compounds have been abbreviated in the following way: $SnMe_4$, $SnEt_4$, etc., for $Sn(methyl)_4$, $Sn(ethyl)_4$, etc.

Experimental

Materials

The SnR_4 compounds were purchased from the Organisch Chemisch

Instituut (Utrecht), *t*-decalin from Chemical Samples Co. (Columbus, OH), and the branched alkanes from the K and K Co. (White Plains, NY). The purity, as measured by gc was 99.8% for *t*-decalin and br-C_8 and 97.4% for br-C_{16}. The physicochemical constants of the SnR_4 compounds, measured together with those of other series (9) are given in ref. 1.

Apparatus

The density measurements were made with an Anton Paar densitometer, the characteristics of which have been described earlier (10).

The calorimeters are respectively a Picker flow apparatus for the c_p^E and a tilting Tian-Calvet calorimeter for the h^E. Details on the cells, accuracy, and calibration can be found in refs. 2 and 11 for h^E, and refs. 1 and 12 for c_p^E.

The viscosities are measured in an Ubbelohde viscosimeter installed in a constant-temperature water or water–methanol bath. The dynamic viscosities expressed in centipoises are obtained from the flow time, t, by the relation $\eta = (d_l - d_v)(Ct - B/t)$ where d_l and d_v are the liquid (pure or solution) and vapor densities, and C and B are calibration constants obtained as described in ref. 13.

Theory

Equation of state theory

The parameters required to characterize a liquid are V^*, the core volume or volume at 0 K, P^*, the pressure reduction parameter associated with the cohesive character of the liquid, and T^* the reduction temperature. Large, cohesive compounds have larger values of these parameters than volatile ones. The V^*, P^*, and T^* parameters and the reduced volume $\tilde{v}$ are calculated, with a model, from the density, the expansion coefficient α, and the thermal pressure coefficient γ of the pure liquid (14). The free volume contributions, h^E(fv), v^E(fv), g^E(fv), and c_p^E(fv) which depend on the difference in state of expansion of the liquids mixed can be calculated as described in the appendix of ref. 12*a* or in the original papers. They are negative for h^E, v^E, and c_p^E since the difference of expansion of the pure liquids leads to a kind of condensation of the more expanded component in the less expanded one, and since this difference of expansion becomes larger at higher temperature. In the present systems, the free volume contributions are of some size only in systems involving $SnMe_4$ and br-C_8 as seen in the corresponding columns in the tables. The term $X_{12}s_1^{-1}$ is the non equation-of-state part of h^E. It cannot be calculated *ab initio* but is obtained by subtracting from the experimental heats of mixing h^E(fv). s_1 and s_2 are the molecular surface-to-volume ratios of the molecules of liquids 1 and 2 obtained from molecular models.

Sign of X_{12}

In nonpolar systems, the h^E values are rarely negative because the free volume contribution is usually not large enough to overcome the positive h^E coming from the difference in force field between the two molecules and so the X_{12} values are also usually positive. The steric hindrance effect has been discovered both in systems with a negative h^E, more negative than the calculated h^E(fv), and in systems whose h^E value was less endothermic than could be expected by comparison with similar compounds. If the steric hindrance contribution is dominant, the X_{12} parameter will be found negative.

Separation of the different contributions to the thermodynamic functions

Excess heats and heat capacities. Measuring thermodynamic functions in a series helps to detect the different contributions and the variation of their relative importance from one system to another. The comparison of the sign of h^E and c_p^E is also a useful indication of the dominant contribution. The disordering and steric hindrance contributions are both diminishing when T increases. Accordingly, the corresponding contributions to c_p^E are negative and positive respectively (since the contributions to h^E are of contrary signs). Further, the presence of different contributions of comparable size can be inferred from the concentration dependence of the excess functions which can be either skewed or even can change sign over the composition range.

Excess volumes. The calculated v^E can be broken down into three terms (10) namely $v^E(h^E)$ which has the sign of h^E(exp.), v^E(fv) which is negative and $v^E(P^*)$ which can have either sign since it is proportional to $(\tilde{v}_1 - \tilde{v}_2)(P_1^* - P_2^*)$. This last term, which can give large contributions to v^E has been investigated in systems composed of liquids of different state of expansion and cohesive energy (11, 12, 15).[1]

Excess viscosity and free energy of mixing. Several definitions have been used for the excess viscosity but the more appropriate one for establishing the relation between the solution viscosity and g^E is

$$[1] \quad \Delta \ln \eta = \ln \eta - (x_1 \ln \eta_1 + x_2 \ln \eta_2)$$

where η_1, η_2, and η are the dynamic viscosities of the pure components and the solution respectively; the term in parentheses is considered as the logarithm of the viscosity of the ideal solution.

In order to be displaced and flow, a molecule has to overcome the attractive forces of its neighbours and find an empty site nearby. An expression which takes account of these requirements has been developed by Macedo and Litovitz (7) and has been applied by Bloomfield and Dewan (8).

$$[2] \quad \eta = A \exp(\Delta G^*/RT + (\tilde{v} - 1)^{-1})$$

where A is a parameter, ΔG^* the activation energy, and $\tilde{v}$ the reduced volume. A bridge can be made between the flow and thermodynamic properties of mixing if one assumes the simple relation between the pure liquids and solution activation energies ΔG_1^*, ΔG_2^*, ΔG^*, and the excess (noncombinatorial) free energy of mixing, g^E

$$[3] \quad \Delta G^* = x_1 \Delta G_1^* + x_2 \Delta G_2^* - g^E$$

If eq. [2] is applied to liquids 1 and 2 and to the solution and substituted in eq. [1] after using eq. [3] one finds

$$[4] \quad \Delta \ln \eta(\text{calcd.}) = -g^E/RT + (\tilde{v} - 1)^{-1} - (x_1(\tilde{v}_1 - 1)^{-1} + x_2(\tilde{v} - 1)^{-1})$$
$$= -h^E/RT + s^E/R + \ln \eta(v^E)$$
$$= \ln \eta(h^E) + \ln \eta(s^E) + \ln \eta(v^E)$$

where $\ln \eta(h^E) = -h^E/RT$

$$[5] \quad \ln \eta(s^E) = s^E/R$$
$$\ln \eta(v^E) = (\tilde{v} - 1)^{-1} - [x_1(\tilde{v}_1 - 1)^{-1} + x_2(\tilde{v}_2 - 1)^{-1}]$$

The physical meaning of eqs. [4] and [5] is as follows: a positive value of h^E which entails a loss of cohesive energy upon mixing the pure liquids will give a negative contribution to $\Delta \ln \eta$, corresponding to a solution less viscous than the ideal solution. The inverse will hold for a more cohesive solution displaying a negative h^E. The third term, $\ln \eta(v^E)$ will give a positive contribution to $\Delta \ln \eta$ or increase the viscosity of the solution if there is a contraction on mixing as is the case in systems with a difference in free volume between the components.

[1] S. N. Bhattacharyya and D. Patterson. Unpublished results.

TABLE 1. Excess enthalpies h^E, volumes v^E, and heat capacities c_p^E for the SnR_4 + *trans*-decalin systems at the
The A_i parameters are the coefficients of the Redlich–Kister equations. $h^E(fv)$, $X_{12}s_1^{-1}$, $v^E_{calcd.}$, and $(c_p^E)_v$ have been calculated at the same concentration

Component (1)	Component (2)	h^E (J mol^{-1})	x_1	A_0 (J mol^{-1})	A_1 (J mol^{-1})	A_2 (J mol^{-1})	h_v^E (J cm^{-3})	$h^E(fv)$ (J mol^{-1})	$X_{12}x_1^{-1}$ (J cm^{-3} Å^{-1})		σ^a
$SnMe_4$	+ *trans*-decalin	−71.7	0.30	−201.86	330.97	−80.70	−0.56	−29.3	−2.0		1.9 (7)
$SnEt_4$	+ *trans*-decalin	54.8	0.45	222.14	−61.17	−34.75	0.34	−6.3	1.9		1.8 (7)
$SnPr_4$	+ *trans*-decalin	−235.0	0.43	−904.82	366.69	−175.54	−1.41	−0.2	−6.4		2.8 (6)
$SnBut_4$	+ *trans*-decalin	−215.0	0.38	−799.34	372.13	−183.25	−1.14	−1.04	−5.3		3.4 (7)

	v^E (cm^3 mol^{-1})	x_1	B_0 (cm^3 mol^{-1})	B_1 (cm^3 mol^{-1})	B_2 (cm^3 mol^{-1})	$v^E_{calcd.}$ (cm^3 mol^{-1})	$v^E(h^E)$ (cm^3 mol^{-1})	$v^E(P^*)$ (cm^3 mol^{-1})	$v^E(fv)$ (cm^3 mol^{-1})	$v^E_{exp.} - v^E_{calcd.}$ (cm^3 mol^{-1})	σ^a
$SnMe_4$ + *trans*-decalin	−0.96	0.53	−3.86	−0.13	0.02	−0.824	−0.010	−0.505	−0.309	−0.14	0.04(5)
$SnEt_4$ + *trans*-decalin	−0.09	0.57	−0.35	−0.06	0.43	−0.074	−0.132	−0.065	−0.007	−0.01	0.01(5)
$SnPr_4$ + *trans*-decalin	−0.43	0.42	−1.68	0.41	0.07	−0.162	−0.149	−0.011	−0.002	−0.27	0.02(5)
$SnBut_4$ + *trans*-decalin	−0.38	0.38	−1.44	0.52	−0.11	−0.074	−0.132	−0.065	−0.007	−0.31	0.01(6)

	c_p^E (J mol^{-1} K^{-1})	x_1	C_0 (J mol^{-1} K^{-1})	C_1 (J mol^{-1} K^{-1})	C_2 (J mol^{-1} K^{-1})	$10^2(c_p^E)$ (J cm^{-3} K^{-1})	$c_p^E(fv)$ (J mol^{-1} K^{-1})	σ^a
$SnMe_4$ + *trans*-decalin	0.73	0.35	2.47	−2.26	0.05	0.59	−0.28	0.04(5)
$SnEt_4$ + *trans*-decalin	0.37	0.65	1.49	1.36	−2.45	0.25	<0 and >−0.07	0.06(5)
$SnPr_4$ + *trans*-decalin	0.26	0.56	9.98	1.10	−2.41	0.14	<0 and >−0.07	0.03(5)
$SnBut_4$ + *trans*-decalin	0.44	0.28	0.92	−1.64	2.16	0.26	<0 and >−0.07	0.04(5)

[a]Number of experimental points in parentheses.

TABLE 2. Excess enthalpies h^E, volumes v^E, and heat capacities $c_p{}^E$ for the SnR_4 + br-C_{16}[a] systems at the concentration x_1 of the maximum of the corresponding experimental curve. The A_i parameters are the coefficients of the Redlich–Kister equations. $h^E(fv)$, $X_{12}s_1{}^{-1}$, $v^E{}_{calcd.}$ and $(c_p^E)_v$ have been calculated at the same concentration

Component (1)	Component (2)	h^E (J mol^{-1})	x_1	A_0 (J mol^{-1})	A_1 (J mol^{-1})	A_2 (J mol^{-1})	h_v^E (J cm^{-3})	$h^E(fv)$ (J mol^{-1})	$X_{12}s_1{}^{-1}$ (J cm^{-3} Å^{-1})		σ^c
$SnMe_4$	br-C_{16}	67.5	0.65	198.28	287.82	134.13	0.44	−48.0	4.31		[b]
$SnEt_4$	br-C_{16}	93.1	0.46	372.76	24.48	12.76	0.46	−8.1	4.7		[b]
$SnPr_4$	br-C_{16}	−92.0	0.45	−362.54	85.37	−51.21	−0.40	−0.6	−2.0		3.30(5)
$SnBut_4$	br-C_{16}	−40.7	0.46	−161.18	−33.40	0.43	−0.16	−0.9	−0.4		[b]

	v^E (cm^3 mol^{-1})	x_1	B_0 (cm^3 mol^{-1})	B_1 (cm^3 mol^{-1})	B_2 (cm^3 mol^{-1})	$v^E{}_{calcd.}$ (cm^3 mol^{-1})	$v^E(h^E)$ (cm^3 mol^{-1})	$v^E(P^*)$ (cm^3 mol^{-1})	$v^E(fv)$ (cm^3 mol^{-1})	$v^E{}_{exp.} - v^E{}_{calcd.}$ (cm^3 mol^{-1})	σ^c
$SnMe_4$ + br-C_{16}	−0.20	0.50	—	0	0	−0.167	0.087	0.062	−0.316	−0.03	—(3)
$SnEt_4$ + br-C_{16}	0.21	0.50	0.80	0.03	—	0.197	0.078	0.187	−0.068	0.02	0.01(4)
$SnPr_4$ + br-C_{16}	−0.16	0.52	−0.64	0.02	0.60	0.014	−0.058	0.077	−0.005	−0.18	<0.01(5)
$SnBut_4$ + br-C_{16}	−0.27	0.64	−0.95	0.56	−0.59	0.081	−0.028	0.047	−0.006	−0.19	<0.01(5)

	c_p^E (J mol^{-1} K^{-1})	x_1	C_0 (J mol^{-1} K^{-1})	C_1 (J mol^{-1} K^{-1})	C_2 (J mol^{-1} K^{-1})	$10^2(c_p^E)$ (J K^{-1} cm^{-3})	$c_p^E(fv)$ (J mol^{-1} K^{-1})	σ^c
$SnMe_4$ + br-C_{16}	<0.1	—	—	—	—	<0.1	−0.44	—(4)
$SnEt_4$ + br-C_{16}	−0.76	0.50	−3.05	+0.40	—	−0.52	<0 and >−0.05	0.01(4)
$SnPr_4$ + br-C_{16}	0.52	0.78	1.77	2.09	2.57	0.26	<0 and >−0.05	0.01(5)
$SnBut_4$ + br-C_{16}	0.35	0.64	0.82	1.62	0.72	0.13	<0 and >−0.05	0.05(5)

[a] 2,2,4,4,6,8,8-Heptamethylnonane.
[b] Reference 8.
[c] Number of experimental points in parentheses.

TABLE 3. Excess enthalpies h^E for the SnR_4 + br-C_8 systems at the concentration x_1 of the maximum of the corresponding experimental curve. The A_i parameters are the coefficients of the Redlich–Kister equations. h^E(fv) and $X_{12}s_1^{-1}$ have been calculated at the same concentration

Component (1)	Component (2)	h^E (J mol^{-1})	x_1	A_0 (J mol^{-1})	A_1 (J mol^{-1})	A_2 (J mol^{-1})	$h^E{}_v$ (J cm^{-3})	h^E(fv) (J mol^{-1})	$X_{12}s_1^{-1}$ (J cm^{-3} Å^{-1})	σ^c
$SnMe_4$	+ 2,2,4-trimethylpentane	110.0	0.57	440.97	82.31	82.38	0.94	−1.4	4.3	3.5(6)
$SnEt_4$	+ 2,2,4-trimethylpentane	138.0	0.45	562.77	−112.86	−111.77	0.97	−8.9	4.7	1.5(6)
$SnPr_4$	+ 2,2,4-trimethylpentane	−64.0	0.40	−248.04	107.44	−5.67	−0.39	−27.3	−1.04	1.5(5)
$SnBut_4$	+ 2,2,4-trimethylpentane	−29.0	0.40	−101.80	97.40	11.20	−0.15	−45.8	0.43[a]	[b]

[a]The positive X_{12} is very likely due to the overestimation of h^E(fv).
[b]Reference 8.
[c]Number of experimental points in parentheses.

The second term, $\ln \eta(s^E)$ corresponds to the effect of the excess entropy of the system. Only the free volume part of s^E can be calculated by the theory used for the other free volume contributions. As with $\ln \eta(v^E)$, it is a function of the difference in reduced volumes of the components but the pressure parameter P^* and the core volume V^* come in the final expression

$$[6]\quad s^E/R = (3x_1P_1^*V_1^*/RT)(\ln(\tilde{v}_1^{1/3} - 1)/(\tilde{v}^{1/3} - 1)) + (3x_2P_2^*V_2^*/RT)(\ln(\tilde{v}_2^{1/3} - 1)/(\tilde{v}^{1/3} - 1))$$

The noncalculable excess entropy will be reflected in $\Delta \ln \eta$(exp) but not in $\Delta \ln \eta$(calcd.) so that the difference between the two will be a measure of Ts^E

$$[7]\quad Ts^E(\text{visc.}) = RT\delta = RT(\Delta \ln (\eta(\text{exp.}) - \Delta \ln \eta(\text{calcd.}))$$

Results and discussion

Tables 1 and 2 give the maximum of h^E, v^E, and c_p^E and the concentrations at which these functions are maximum for the mixtures with *t*-decalin and br-C_{16} respectively. Table 3 shows the h^E data with br-C_8 and Table 4 the excess viscosities of the SnR_4 compounds with *t*-decalin. Measurements have been done at 25°C but excess viscosities have been also measured at 40 and −20°C. The coefficients of the Redlich–Kister equations of the measured property y^E

$$[8]\quad y^E = x_1x_2 \sum_{i=0}^{i=2} Y_i(x_1 - x_2)^i$$

are also listed for most of the systems. The values $(h^E)_v$ and $(c_p^E)_v$ added in the tables are obtained by dividing the data at the maximum by the average core volume $x_1V_1^* + x_2V_2^*$. The equation of state contributions h^E(fv), c_p^E(fv), the different contributions to v^E, and the $X_{12}s_1^{-1}$ values have been tabulated also.

To compare the different systems, the maxima of h^E, c_p^E, and v^E have been plotted in Fig. 1 vs. V^* the core volume of the SnR_4 compounds for *t*-decalin (○), br-C_{16} (●), and br-C_8 (□).

In the following discussion, the steric hindrance contribution will be analysed in the series as it is reflected in turn from h^E, c_p^E, v^E, and $\Delta \ln \eta$.

Heats and excess heat capacities

Observation of Figs. 1*a* and 1*b* suggests that, as a simplifying assumption, the systems studied can be divided into two groups.

The first group consists of the six mixtures containing $SnPr_4$ and $SnBut_4$. The h^E values of these compounds with *t*-decalin, br-C_{16}, and br-C_8 are large and exothermic. This holds also for $X_{12}s_1^{-1}$ (see Tables 1–3) so that one can conclude that the steric hindrance contribution is dominant. The positive c_p^E values are also consistent with the above assumption.

The second group consists of the mixtures of $SnEt_4$ and $SnMe_4$ with *t*-decalin, br-C_{16}, and br-C_8 which, with the exception of the $SnMe_4$ + *t*-decalin system have a positive h^E. The h^E, larger for the $SnEt_4$ mixtures by 200–300 J mol^{-1} than for the next in the series, $SnPr_4$, are particularly striking and indicate that another contribution is active and dominant here. A difference in force-field between the two components of the mixture, a difference larger with $SnEt_4$ and $SnMe_4$ than with the other SnR_4 compounds, seems the obvious explanation for the endothermic heats. However, this effect cannot be the only one because it was not apparent in mixtures with other nonpolar molecules such as the linear alkanes or long-chain SnR_4 compounds. The positive h^E must be associated with a special contribution due to the shape of the present molecules, i.e., an effect of the disorder-type found with other systems (11) but not well understood presently.

Judged by the magnitude of h^E and $X_{12}s_1^{-1}$, the $SnMe_4$ + *t*-decalin system seems to be right at the temperature at which the two effects make comparable contributions to the thermodynamic functions. The concentration dependence of X_{12} shown in Fig. 2 (▽) supports this analysis. In decalin-rich solutions, the negative X_{12} suggests that steric hindrance is dominant while in $SnMe_4$-rich mixtures X_{12} is positive and has the same magnitude as in the $SnEt_4$ solutions. On the other hand, the moderate variation of X_{12} for the other systems reflects the rather symmetrical shape of their h^E (■, □, ○).

Figure 3 shows the concentration dependance of c_p^E in the *t*-decalin systems. The larger c_p^E for the $SnMe_4$ is indicative of a larger temperature dependence of h^E for this volatile liquid. The skewed or S-shaped curves of c_p^E for $SnBut_4$ and $SnPr_4$ seem in contradiction with the above description of a dominant contribution in h^E. However, the magnitude of the c_p^E is such that the predicted variation in h^E, even over a large temperature interval, is moderate. Results of excess viscosities at different temperatures (Fig. 4), confirm the small variation of the thermodynamic properties with temperature in the SnR_4 + *t*-decalin mixtures except for the $SnMe_4$ solutions. Consequently, the c_p^E data do not invalidate the above distinction between the two groups of systems.

Excess volumes

The values of v^E(exp.) − v^E (calcd.) listed in Tables 1 and 2 are large and negative indicating that the steric hindrance effect induces a contraction in the systems larger than that taken into account by the negative contribution coming from $v^E(h^E)$ or v^E(fv). In the present series, the values for the four more sterically hindered systems, $SnPr_4$ and $SnBut_4$ with *t*-decalin and br-C_{16} varies between −0.18 and −0.31 cm^3 mol^{-1}, the numbers for $SnMe_4$ being, as expected from the h^E value, intermediary (−0.14, −0.03) between those and the $SnEt_4$

TABLE 4. Excess viscosities $\Delta \ln \eta$ for the SnR_4 + *trans*-decalin systems at the concentration x_1 of the maximum. The A_i parameters are the coefficients of the Redlich–Kister equations. The different contributions to $\Delta \ln \eta$(calcd.) have been calculated for the SnR_4 *trans*-decalin systems at 25°C

Component	T (°C)	$\Delta \ln \eta$	x_1	A_0 (J mol^{-1})	A_1 (J mol^{-1})	A_2 (J mol^{-1})	σ^b	$\ln \eta(h^E)$	$\ln \eta(v^E)$	$\ln \eta(s^E)$	$\Delta \ln \eta$ (calcd.)	δ	$RT\delta$ (J mol^{-1})
$SnMe_4$ + *trans*-decalin	25	−0.007	0.55	−0.0293	−0.0155	−0.0043	0.0005(4)	0.029	0.055	−0.039	0.045	−0.052	−128.3
$SnEt_4$ + *trans*-decalin	25	−0.15	0.45	−0.6040	0.1305	−0.0913	0.0005(6)	−0.022	−0.027	−0.003	−0.052	−0.098	−241.7
$SnPr_4$ + *trans*-decalin	25	−0.12	0.44	−0.4656	0.1678	−0.1056	0.0030(6)	0.095	0.005	−0.020	0.080	−0.200	−493.3
$SnBut_4$ + *trans*-decalin	25	−0.05	0.35	−0.1705	0.1054	−0.0914	0.0007(6)	0.087	0.047	−0.019	0.115	−0.162	−399.6
$SnBut_4$ + br-C_{16}	25	−0.06	0.47	−0.245	0.039	0.013	0.0013[a]	0.008	0.008	−0.0008	−0.061	0.088	−217.0
$SnBut_4$ + br-C_{12}	25	+0.052	0.52	0.212	0.009	0.027	0.0016[a]	0.012	0.060	−0.0100	+0.052	−0.010	−24.7
$SnMe_4$ + *trans*-decalin	40	0.12	0.41	−0.4427	−0.3261	−0.1637	0.0070(4)						
$SnEt_4$ + *trans*-decalin	40	−0.14	0.45	−0.5299	0.1427	−0.049	0.0016(6)						
$SnPr_4$ + *trans*-decalin	40	−0.11	0.43	−0.4490	0.0799	−0.08785	0.0022(6)						
$SnBut_4$ + *trans*-decalin	40	−0.045	0.41	−0.1657	0.1201	−0.0428	0.0011(5)						
$SnMe_4$ + *trans*-decalin	−20	0.10	0.68	0.3531	0.2235	0.3203	0.0003(5)						
$SnEt_4$ + *trans*-decalin	−20	−0.23	0.45	−0.9080	0.1339	−0.2794	0.0006(5)						
$SnPr_4$ + *trans*-decalin	−20	−0.16	0.38	−0.6273	0.2493	−0.1461	0.0004(5)						
$SnBut_4$ + *trans*-decalin	−20	−0.04	0.30	−0.1127	0.1908	−0.0982	0.0014(5)						

[a]Reference 13*a*.
[b]Number of experimental points in parentheses.

values (−0.01, 0.02). It is worthwhile to compare the present $SnBut_4$ +br-C_{16} system with the $SnBut_4$ + *n*-C_{16} mixture. Due to the lack of the steric hindrance contribution, v^E(exp.) − v^E(calcd.) is small and positive (0.037) for the linear alkane while it is −0.19 cm^3 mol^{-1} with br-C_{16}.

Effect of P* *on* v^E

The two systems $SnMe_4$ (1) + *t*-decalin (2) and $SnMe_4$ (1) +br-C_{16} (2) are well suited to see the effect on v^E of the term $(\tilde{v}_1 - \tilde{v}_2)(P_1^* - P_2^*)$. The first factor $(\tilde{v}_1 - \tilde{v}_2)$ has the same value for the two systems. On the other hand, $(P_1^* - P_2^*)$ is negative and small for $SnMe_4$ +br-C_{16} and positive and larger for $SnMe_4$ + *t*-decalin (respectively 396 − 409 = −13 and 504 − 409 = 95 J cm^{-3}). Consequently, the v^E are predicted more negative for the first system than for the second and this is what is found experimentally namely −0.96 and −0.20 cm^{-3} mol^{-1} respectively.

Excess viscosities and excess entropies

In Table 4, the excess viscosity results are presented for the *t*-decalin mixtures, the experimental values on the left part and the calculated contributions, as defined in eq. [5], on the right. The coefficients of the Redlich–Kister equation are listed as well as the maxima of $\Delta \ln \eta$ and the concentration of the maxima. In the lower part of the table, experimental $\Delta \ln \eta$ values at 40 and −20°C are reported. In Fig. 4, the maxima of $\Delta \ln \eta$(exp.) are plotted against the temperature for the four systems. The trends of the temperature dependence are similar for the three higher SnR_4 compounds, a larger variation being reasonably found for $SnEt_4$. The rapid change of $\Delta \ln \eta$ for the $SnMe_4$ mixture between 25 and 40°C and between 25 and −20°C supports the analysis made from the h^E results of terms of opposite sign being in balance at 25°C. The positive value of $\Delta \ln \eta$ at 40°C can be accounted for by the increased difference between the free volume of *t*-decalin and $SnMe_4$ but the increase of $\Delta \ln \eta$ between 25 and −20°C is difficult to explain, considering the trend in the other systems. However, the positive (although small) values of $\Delta \ln \eta$ found at −20°C for the *t*-decalin +$SnBut_4$ system in $SnBut_4$-rich solutions ($x > 0.7$) shows that the trend for a positive $\Delta \ln \eta$ value at low temperature is not unique to the $SnMe_4$ system.

In Table 4, the difference δ between the experimental and calculated $\Delta \ln \eta$ values are reported as well as Ts^E(visc.) obtained from eq. [7] (7th and last column of the table).

In the present analysis, the question to be asked is whether the Ts^E values confirm the above analysis, namely the dominance of steric hindrance in the higher SnR_4 and the sharp change in the balance of the contributions for the two lower ones. From the negative values in Table 4, one sees that indeed the expected negative contribution for the steric hindrance effect is present and unexpectedly large (between −100 and −500 J mol^{-1}). It is interesting to note that although the difference in Ts^E between the propyl and ethyl derivatives is about as large as that between their h^E values, s^E is negative throughout the series. The positive Ts^E which could have been expected from the sign of h^E for the lighter SnR_4 compounds, does not occur because the contributions to Ts^E due to steric hindrance (as obtained from the excess viscosities) are about twice as large as the contributions to h^E due to steric hindrance. The negative values of v^E(exp.) − v^E(calcd.) are quite consistent with the Ts^E results.

In a previous study (13*a*) of long alkanes disordered by mixing with a globular molecule, the Ts^E(visc.) values in the series of the linear alkanes were found to correlate with

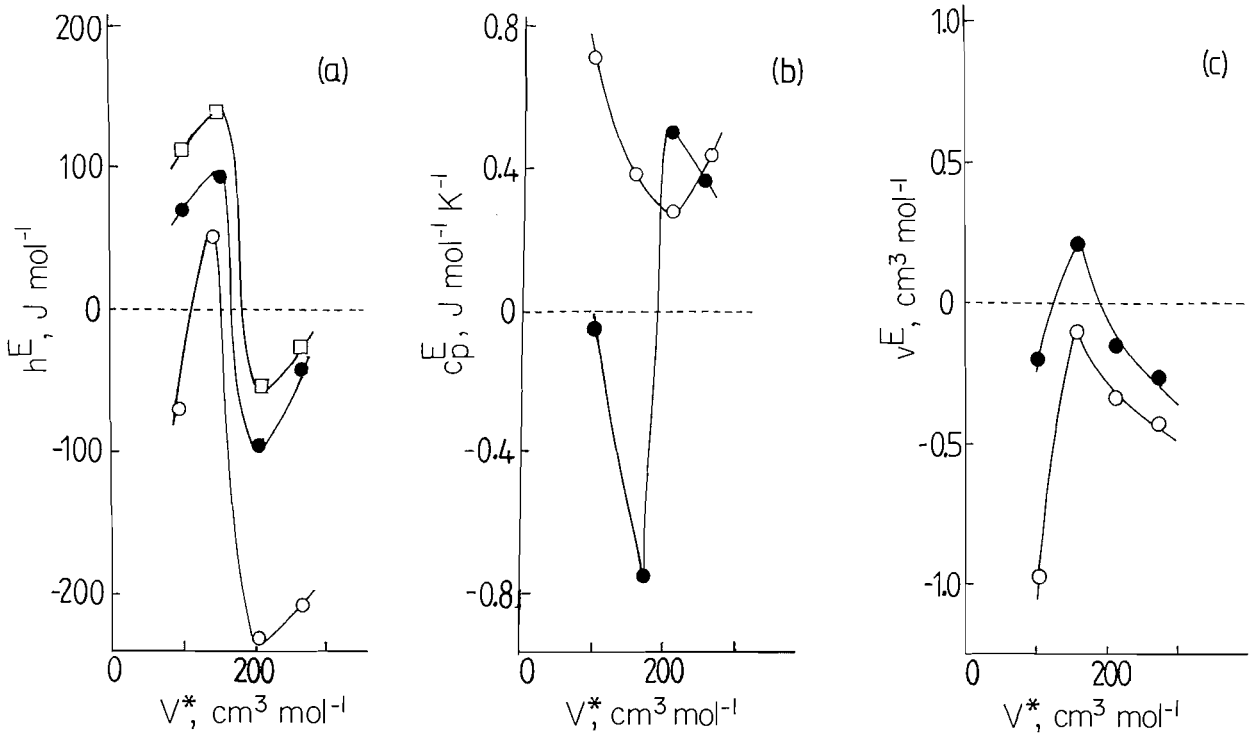

FIG. 1. Excess molar thermodynamic properties at 25°C, at the concentration of the maximum, plotted against the molar volume at 0 K, V^*, of the SnR_4 compound (methyl to butyl). The second component is *t*-decalin (○), br-C_{16}(●), or br-C_8 (□). Curves *a* for h^E, curves *b* for c_p^E, and curves *c* for v^E.

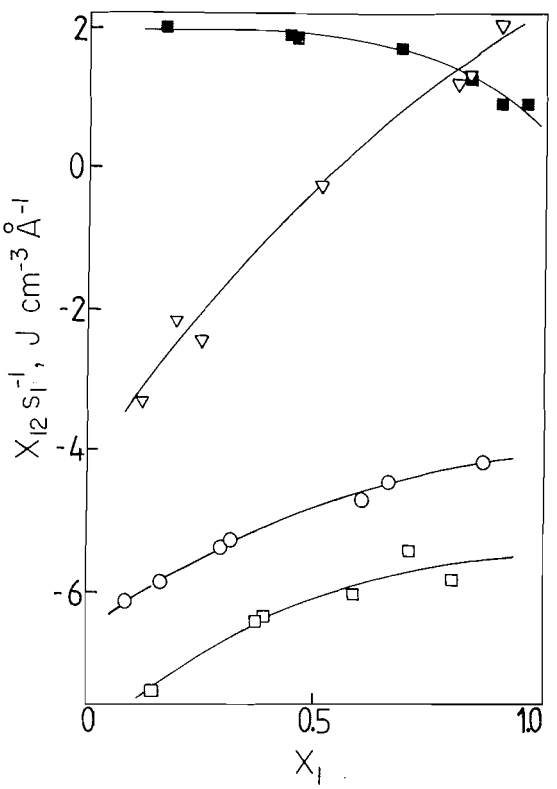

FIG. 2. The concentration dependence of the non-free-volume part of h^E, $X_{12}s_1^{-1}$, is shown for the mixtures of *t*-decalin with $SnMe_4$ (▽), $SnEt_4$ (■), $SnPr_4$ (□), and $SnBut_4$ (○).

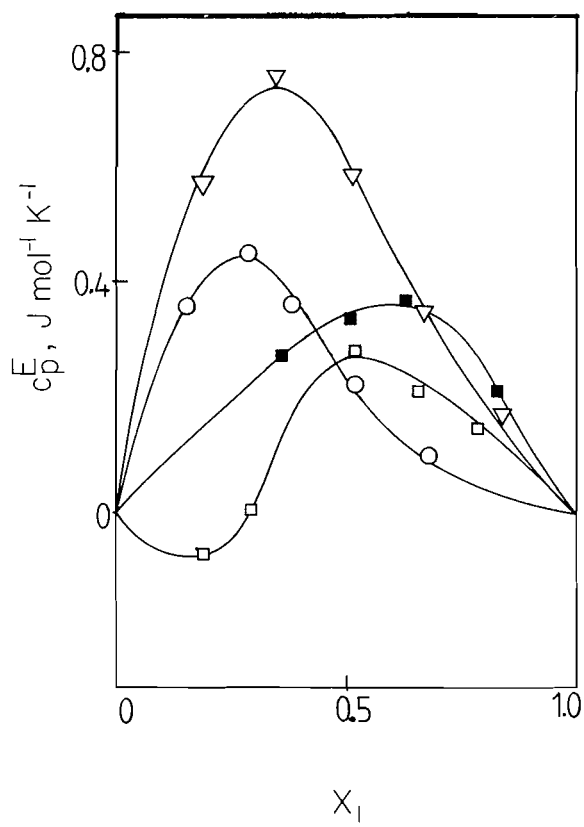

FIG. 3. The concentration dependance of c_p^E is given for the *t*-decalin + SnR_4 systems. Same symbols as in Fig. 2.

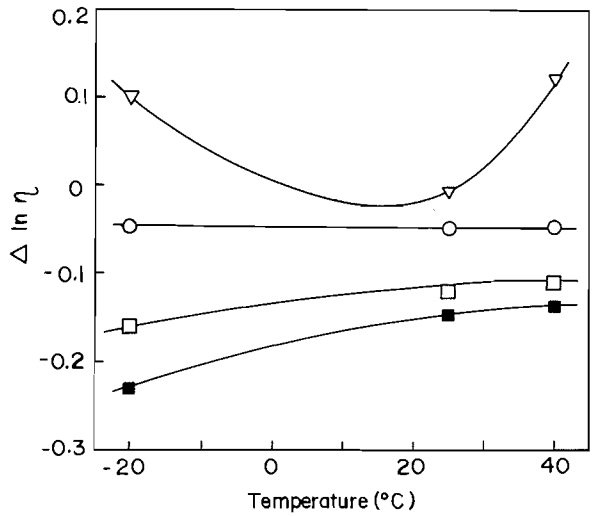

FIG. 4. The excess viscosities, $\Delta \ln \eta$, at the concentration of the maximum, are plotted for the *t*-decalin $+SnR_4$ systems versus the temperature. Same symbols as in Fig. 2.

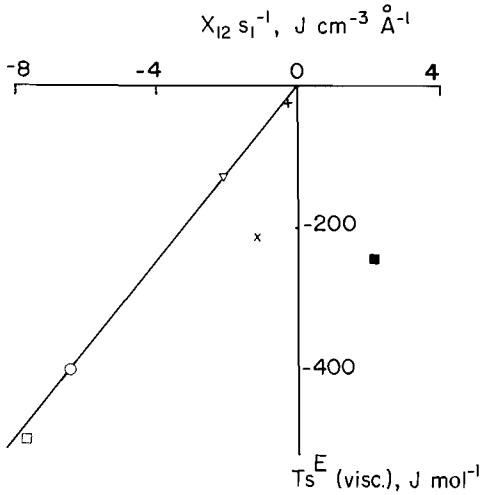

FIG. 5. The steric hindrance contributions to the excess viscosities, Ts^E(visc.) (Table 4, last column), are plotted for the *t*-decalin $+SnR_4$ systems at 25°C versus the corresponding contributions to h^E, $X_{12}s_1^{-1}$ (Tables 1 and 2). Same symbols as in Fig. 2. Data are given for two others mixtures (13*a*) showing the steric hindrance effect: $SnBut_4$ + br-C_{16} (×) and + br-C_{12} (+) (2,2,4,6,6-pentamethylheptane). The position of the $SnEt_4$ + *t*-decalin mixture on the graph (■) points to another effect.

h^E(disorder). Furthermore, in one system studied between 25 and 80°C, the decrease of Ts^E(visc.) was matching that of h^E(disorder) becoming zero at the temperature known for the disappearance of correlations of molecular orientations between the chains. The same type of correlation between the enthalpic and entropic contributions due to steric hindrance has been tested in Fig. 5 in which Ts^E(visc.) (at the maximum of $\Delta \ln \eta$) has been plotted against the X_{12} parameters (at the maximum of h^E). It is probably a coincidence that the point for $SnMe_4$ is in line with the others since X_{12} varies rapidly with concentration for this system. From previously obtained results (13*a*), data on $SnBut_4$ + br-C_{16} (×) and br-C_{12} (+) have been added in Fig. 5. They show that the steric hindrance effect exerted on the SnR_4 by *t*-decalin is stronger than that due to these branched alkanes. This had been found already by comparing the thermodynamic properties of *c*-C_5 and *t*-decalin (6*b*, 16) with that of *c*-C_5 and br-C_{16} (15). The other contribution is apparent in the $SnEt_4$ system whose positive X_{12} puts the point (■) quite distant from the correlating line.

In conclusion, the rapid change in h^E between $SnEt_4$ and $SnPr_4$ may be due to two effects: on one hand, to the diminution for the lower SnR_4 of the steric hindrance contribution as indicated by Fig. 4 and, on the other hand, to the existence for the $SnEt_4$ and $SnMe_4$ of the right conditions (free volume, molecular shape) for the liberation of movement in these compounds apparently quite cohesive (they have higher P^* than the longer homologues or than an alkane of the same molecular weight) in the liquid state.

Measurements of the ^{119}Sn relaxation times by nmr in the pure SnR_4 compounds and in their solutions in *t*-decalin are being made with the aim of obtaining a finer picture of the molecular changes associated with some of the unexpected values of the thermodynamic functions measured in the present work.

Acknowledgements

We would like to thank B. Riedl for some of the experimental results and the Natural Sciences and Engineering Research Council of Canada (NSERCC) for financial assistance.

1. B. RIEDL and G. DELMAS. Can. J. Chem. **62**, 1008 (1984).
2. (*a*) G. DELMAS and S. TURRELL. J. Chem. Soc. Faraday Trans. 1, **70**, 572 (1974); (*b*) G. DELMAS and NG. T. THANH. J. Phys. Chem. **81**, 1730 (1977); and (*c*) R. PHILIPPE, G. DELMAS, and H. PHUONG-NGUYEN. Can. J. Chem. **56**, 2856 (1978).
3. G. DELMAS and N. T. THANH. J. Chem. Soc. Faraday Trans. 2, **71**, 1172 (1975).
4. P. DE SAINT-ROMAIN, H. TRA VAN, and D. PATTERSON. J. Chem. Soc. Faraday Trans. 1, **75**, 1700 (1979).
5. C. L. DE LIGNY and W. E. HAMMERS. J. Solution Chem. **7**, 155 (1978).
6. (*a*) P. DE SAINT-ROMAIN and D. PATTERSON. J. Solution Chem. **11**, 119 (1982); and (*b*) P. DE SAINT-ROMAIN, H. TRA VAN, and D. PATTERSON. J. Chem. Soc. Faraday Trans. 1, **75**, 1708 (1979).
7. P. B. MACEDO and T. A. LITOVITZ. J. Chem. Phys. **31**, 1164 (1965).
8. V. A. BLOOMFIELD and R. K. DEWAN. J. Phys. Chem. **75**, 3113 (1971).
9. R. PHILIPPE, G. DELMAS, and M. COUCHON. Can. J. Chem. **56**, 370 (1978).
10. G. DELMAS, P. DE SAINT-ROMAIN, and P. PURVES. J. Chem. Soc. Faraday Trans. 1, **71**, 1181 (1975).
11. G. DELMAS and P. TANCRÈDE. Eur. Pol. J. **9**, 199 (1973).
12. (*a*) B. RIEDL and G. DELMAS. Can. J. Chem. **61**, 1876 (1983); and (*b*) H. PHUONG-NGUYEN, B. RIEDL, and G. DELMAS. Can. J. Chem. **61**, 1885 (1983).
13. (*a*) G. DELMAS, P. PURVES, and P. DE SAINT-ROMAIN. J. Phys. Chem. **79**, 1970 (1975); and (*b*) CL. JAMBON and G. DELMAS. Can. J. Chem. **55**, 1360 (1977).
14. P. J. FLORY. J. Am. Chem. Soc. **87**, 1833 (1965).
15. M. COSTAS and D. PATTERSON. J. Solution Chem. **11**, 807 (1982).
16. D. E. G. JONES, I. A. WEEKS, and G. C. BENSON. Can. J. Chem. **49**, 2481 (1971).

Sulphur anion chemistry in hydrocarbon flames with H_2S, OCS, and SO_2 additives

JOHN M. GOODINGS, DIETHARD K. BOHME, KAMAL ELGUINDI, AND ARNOLD FOX
York University, Department of Chemistry, 4700 Keele Street, Downsview, Ont., Canada M3J 1P3

Received July 8, 1985

JOHN M. GOODINGS, DIETHARD K. BOHME, KAMAL ELGUINDI, and ARNOLD FOX. Can. J. Chem. **64**, 689 (1986).

A premixed, fuel-rich, methane–oxygen flame at atmospheric pressure was doped separately with 0.2 mol% of H_2S, OCS, and SO_2 to probe the behaviour of fuel sulphur during combustion. These three additives represent compounds occurring early, intermediate, and late in the oxidation sequence of fuel sulphur. They are chemically ionized in the reaction zone of a hydrocarbon flame to give large signals of sulphurous negative ions. Those detected include S^-, SH^-, SO^- (uncertain), SO_2^- (S_2^-), SO_3^-, HSO_3^-, $CH_3O^- \cdot SO_2$, SO_4^- ($S_2O_2^-$, S_3^-), and HSO_4^-. Ion concentration profiles of these ions were measured along the conical flame axis by sampling the flame into a mass spectrometer. The shapes of the profiles are insensitive to the nature of the additive, but their relative magnitudes are indicative of the additive's position in the sulphur oxidation sequence. For each additive, the very large HSO_4^- signal has analytical implications as an indicator for total fuel sulphur. The sulphurous anion chemistry is discussed for each additive in terms of roughly twenty ion (electron)-molecule reactions of six basic types, whose rate constants were known previously, or were measured at room temperature using the York flowing afterglow apparatus.

JOHN M. GOODINGS, DIETHARD K. BOHME, KAMAL ELGUINDI et ARNOLD FOX. Can. J. Chem. **64**, 689 (1986).

Dans le but d'examiner le comportement de combustibles/soufre au cours de combustions, on a ajouté séparément 0,2 mol% de H_2S, de OCS et de SO_2 à des flammes prémélangées de méthane–oxygène, riches en combustibles et qui opéraient à la pression atmosphérique. Ces trois additifs représentent les composés qui se retrouvent respectivement dans les stades préliminaires, intermédiaires et finaux de la séquence d'oxydation de mélanges combustibles/soufre. Ils sont ionisés chimiquement dans la zone de la réaction de la flamme d'hydrocarbure pour donner des signaux importants des ions négatifs des entités sulfurées. Les entités détectées comportent: S^-, SH^-, SO^- (incertain), SO_2^- (S_2^-), SO_3^-, HSO_3^-, $CH_3O^- \cdot SO_2$, SO_4^- ($S_2O_2^-$, S_3^-) et HSO_4^-. On a mesuré les profils des concentrations ioniques de ces ions en fonction de l'axe conique de la flamme en faisant appel à un échantillonage de la flamme dans un spectromètre de masse. Les formes de ces profils ne varient pas avec la nature des additifs; toutefois, leurs amplitudes relatives sont reliées à la position de l'additif dans la séquence de l'oxydation du soufre. Pour chaque additif, le signal très important du HSO_4^- a des implications analytiques comme indicateur de la quantité totale du soufre/combustible. Pour chacun des additifs, on discute de la chimie des anions sulfureux en fonction d'environ vingt réactions ion (électron)/molécule de six types de base dont les constantes de vitesse étaient antérieurement connues ou qui ont été mesurées à la température ambiante en faisant appel à un appareil de phosphorescence continue de York.

[Traduit par la revue]

Introduction

The control of SO_x emissions from the combustion of fossil fuels has become important for reasons of public health and because of the impact on the environment by acid rain. Industry reports (1) indicate that the sulphur content of coal and heavy fuel oil can amount to 1–5% by weight; an average figure for gasoline is 0.03%. Increasing energy costs and problems of supply may necessitate the burning of high-sulphur fuels in the future, a trend which is at odds with an increasingly stringent body of environmental and health regulations.

Other combustion pollutants such as NO_x and soot are, to some extent, amenable to chemical modification during the combustion process. Undesirable products can be converted into less harmful forms by altering the combustion conditions or by means of additives (2). On the other hand, sulphur does not appear to offer the same possibilities for its chemical manipulation into harmless forms. The seemingly inevitable conversion of fuel sulphur into SO_2 has focussed effort in two other directions; namely, sulphur removal from the fuel before combustion, and stack-gas scrubbing of SO_2 from the burnt gas afterwards. However, continued study of the sulphur chemistry occurring in a flame may provide insight into more esoteric approaches to sulphur removal at source during the combustion process. It is also valid because of the analytical implications for the evaluation of sulphur-containing fuels.

An important insight was gained in a previous study (3) in which flame ionization was employed as a probe for sulphurous intermediates leading to SO_x formation in the reaction zone and burnt gas of a premixed, CH_4–O_2 flame doped with 0.2% of OCS. It was found that sulphur species readily form negative ions in the flame, and that these negative ions reveal features of the stepwise oxidation of OCS. These results encouraged us to extend the investigation further to include the addition of 0.2% of H_2S and of SO_2 for comparison with OCS. The three additives represent a progression in the sulphur oxidation chain with H_2S occurring early, OCS being intermediate and SO_2 being late as the final oxidation product.

For each additive, sulphurous negative ions are formed by chemical ionization (CI) processes of the neutral sulphur intermediates with the natural ions which are present in any hydrocarbon flame. The ion chemistry of the source and sink reactions is discussed, and comparisons are drawn amongst the three additives. The advantage of this method is that the sulphurous ions serve as a probe of the neutral sulphur chemistry in the flame reaction zone where it originates.

Experimental

All of the ion concentration measurements were performed on the same CH_4–O_2 flame of fuel-rich composition (equivalence ratio ϕ = 2.15) whose ion chemistry we have studied extensively in the past (4, 5). It was of the laminar premixed type with a conical luminous reaction zone (height $\simeq$ 5 mm, base diameter $\simeq$ 3 mm, thickness $\simeq$ 0.3 mm) to facilitate ionic sampling along the flame axis into a mass spectrometer. The flame has an adiabatic flame temperature of 2460 K and burnt gas velocity of approximately 1 m s^{-1}. It was stabilized at atmospheric pressure on a simple, tubular, quartz burner (2.3 mm id) surrounded by a flowing argon shield to minimize the entrainment of atmospheric air. Provision was made to add 0.2 mol% of H_2S or of SO_2 to the premixed gas in exactly the same way as was done previously for OCS (3). The additives could be introduced or removed without altering the flame. All gases were used straight from the cylinders

without further purification ($CH_4 > 99.0\%$, $O_2 > 99.6\%$, Ar > 99.9%, $H_2S > 97.5\%$, OCS > 97.5%, $SO_2 > 99.90\%$). The burner was mounted on a motor-driven carriage with accurate alignment of the flame axis with the sampling orifice of the mass spectrometer. The calibrated burner drive provided spatial resolution of ±0.02 mm along the flame axis (designated z) for measurements of ion concentration profiles.

The flame–ion mass spectrometer has been described previously in detail (4). The flame burned against a 60°, conical, chromium, sampling nozzle of orifice diameter *ca.* 0.1 mm mounted in a water-cooled flange of the type described by Hayhurst and Telford (6). The sampled ions pass through two stages of differential pumping into a quadrupole mass filter. The mass-analyzed ions are detected with a parallel-plate Faraday cage connected to a vibrating reed electrometer having a grid-leak resistance of 10^{11} ohms. The ion signal magnitudes in the figures are quoted in volts based on the detected ion current passing through 10^{11} ohms. Modifications to the quadrupole power supply have improved the resolution of the mass filter, particularly at high mass numbers. We have adopted the same normalization technique described in the paper with OCS additive (3). The profiles shown in the figures include a correction for mass discrimination in the filter against ions of high m/e measured at high resolving power. The dynamic range of sensitivity of the apparatus is five orders of magnitude. A method has been described (4) for locating a reproducible origin ($z = 0$) in the *flame* (not referred to the burner) corresponding to the downstream edge of the luminous reaction zone on the flame axis. In this way, a family of ion profiles at different mass numbers m/e can be accurately overlaid on the distance scale z.

The shapes of the profiles obtained for the three additives at the same mass number are very similar. However, some of the profiles presented in this work are somewhat different from those reported earlier (3) in that they are not as noticeably double-peaked. This is due to the use of a new chromium sampling nozzle having a larger orifice diameter such that the effect of boundary layer cooling, as discussed in the previous study (3), is less. In the present case, negative ion equilibria shift less in the exothermic direction, and electron attachment to form negative ions is reduced, particularly downstream where the temperature is high. That is, the free electron concentration is enhanced at the expense of the negative ion concentration, and distortion of the profiles due to sampling is reduced.

Results and discussion

Anion profiles

Figure 1 displays the dramatic enhancement observed in the total negative ion profiles with the separate additions of equimolar amounts of H_2S, OCS, and SO_2 into the premixed flame gas. In contrast, the total positive ion profiles showed no change in peak magnitude for these three cases. It is clear from Fig. 1 that SO_2 has the largest effect on the upstream concentration of negative ions and that H_2S and OCS also enhance negative ion formation and do so about equally. The bulk of the observed increases could be accounted for by the anions listed in Table 1. Individual profiles for the ions with m/e equal to 33, 64, 80, and 97 are shown in Figs. 2–5. While differences in the peak magnitudes of these profiles are again noticeable with the three different additives, the shapes of the individual profiles appear to be quite insensitive to the nature of the additive.

The ion assignments of the individual masses are given in Table 1. In making these assignments account has been taken of isotopic contributions as indicated previously (3). Increases in signal are apparent for all the ions in Table 1 with the following exceptions: $m/e = 32$ decreases for all three additives and $m/e = 33$ decreases for the addition of SO_2 only. The former ion is O_2^- in the undoped flame and reacts when the sulphur compounds are added. The $m/e = 33$ ion is HO_2^- in the undoped flame and it reacts when SO_2 is added to the premixed

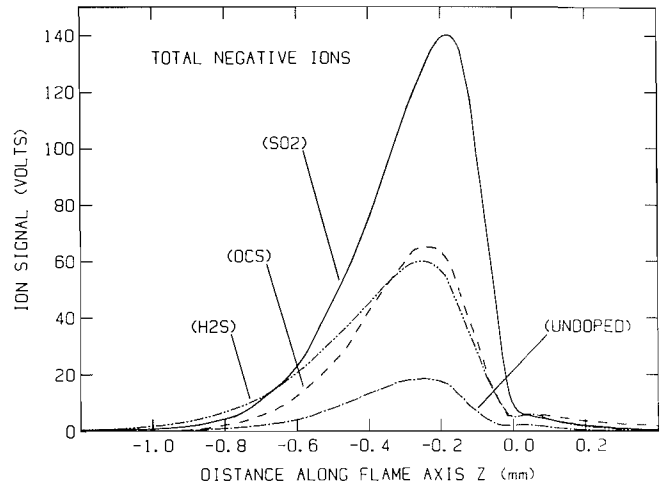

FIG. 1. Total negative ion profiles of the undoped flame and of the flame doped with 0.2 mol% of H_2S, OCS, and SO_2. The flame reaction zone is located upstream of $z = 0$.

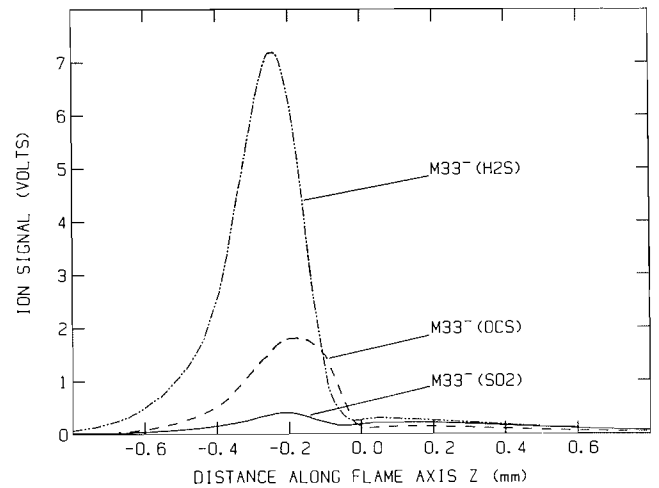

FIG. 2. Profiles of $m/e = 33$ representing SH^- and (or) HO_2^- when the flame is doped with 0.2 mol% of H_2S, OCS, and SO_2. The flame reaction zone is located upstream of $z = 0$.

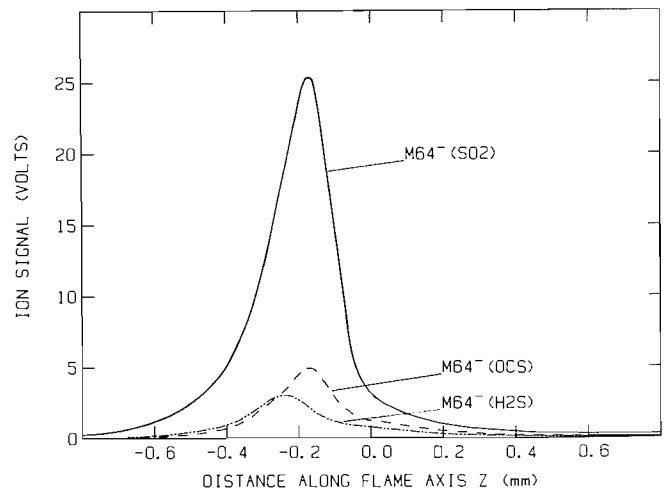

FIG. 3. Profiles at $m/e = 64$ representing SO_2^- (and possibly S_2^-) when the flame is doped with 0.2 mol% of H_2S, OCS, and SO_2. The flame reaction zone is located upstream of $z = 0$.

TABLE 1. Peak intensities of anion signals (in volts) in the reaction zone of the undoped flame, and with the flame doped with 0.2 mol% of H_2S, OCS, and SO_2

Parent ion	Mass number	No additive	H_2S	OCS	SO_2
Total positive		320	320	320	320
Total negative		18.5	60	65	140
S^-	$M32^-$	6.5 (O_2^-)	1.1	0.56	0.57
SH^-	$M33^-$	0.82 (HO_2^-)	7.2	1.8	0.40
SO_2^- (S_2^-)	$M64^-$	0.50	3.0	4.9	25.3
SO_3^-	$M80^-$	0.05	11.7	12.7	20.6
HSO_3^-	$M81^-$	0.01	2.3	3.0	3.1
$CH_3O^-SO_2$	$M95^-$	—	2.9	3.9	10.3
SO_4^- ($S_2O_2^-$, S_3^-)	$M96^-$	—	3.1	4.0	10.0
HSO_4^-	$M97^-$	—	29.5	38.0	88.3
Σ (sulphur anions)		—	60.8	68.9	158.6

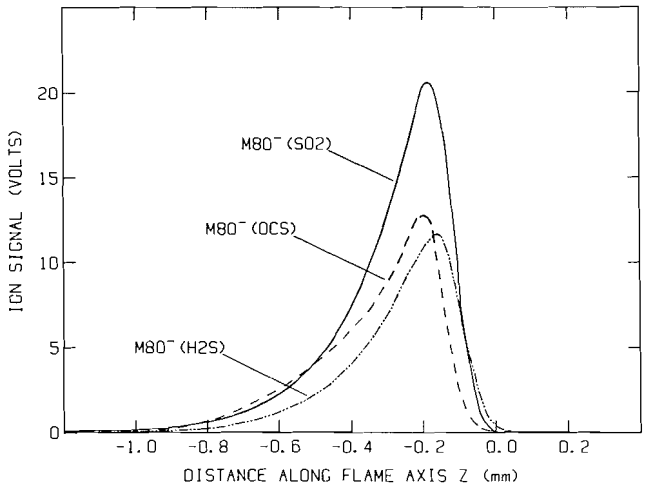

FIG. 4. Profiles at $m/e = 80$ representing SO_3^- when the flame is doped with 0.2 mol% of H_2S, OCS, and SO_2. The flame reaction zone is located upstream of $z = 0$.

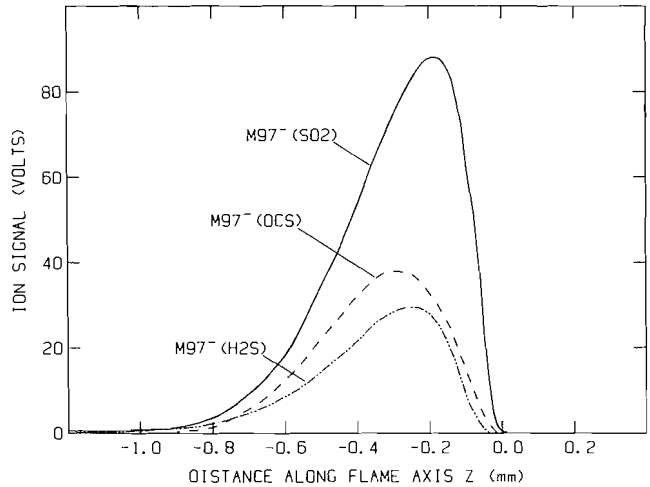

FIG. 5. Profiles at $m/e = 97$ showing the large signals of HSO_4^- obtained when the flame is doped with 0.2 mol% of H_2S, OCS, and SO_2. The flame reaction zone is located upstream of $z = 0$.

flame gas. The sulphur content of the residual peaks at $m/e = 32$ and $m/e = 33$ could not be determined with confidence due to the complications discussed previously (3). All the ions which were observed to increase contained at least one sulphur atom. Several of the sulphurous ions observed contained hydrogen and (or) oxygen and one at $m/e = 95$ must contain carbon.

Inspection of the ion peak intensities in Table 1 reveals that the appearance of sulphurous anions is dominated by HSO_4^- and, to a lesser extent, by SO_3^- in all three doped flames, approximately in proportion to the total negative ion peaks. Distinguishable features for the different additives are manifested with several of the relatively minor ions. The SO_2 flame is characterized by a considerably enhanced abundance of SO_2^- and a shortage of SH^-. The flame doped with H_2S clearly shows an enhanced SH^- peak. In general, the OCS peaks are intermediate between those of the other two additives.

Sulphurous anion chemistry

It is clear from the observed increases in the total negative ion profiles that the additives provide the flame with additional anions. These new anions may arise by attachment or dissociative attachment of electrons with the additive or with molecules derived from the additive by neutral chemistry. The ion assignments indicate that all of the new negative ions are sulphurous so that the sulphur in the additive becomes entrained in the ion directly in the initial formation by attachment or dissociative attachment, or indirectly through secondary ion–molecule reactions. The secondary ion chemistry will be complex but should be dominated by reactions of sulphurous anions with the dominant (non-sulphurous) neutrals in the flame. Secondary reactions with the additive itself or some of its neutral derivatives will have less impact but may still be noticeable.

Dissociative attachment in OCS should proceed in the manner indicated by reaction [1]

[1] $e^- + OCS \rightarrow S^- + CO$

since it is by far the least endothermic option of five possible channels (7). The endothermicity of reaction [1] is about 25 kcal mol^{-1}. The two channels given by reaction [2] appear likely with H_2S

[2*a*] $e^- + H_2S \rightarrow S^- + H_2$

[2*b*] $e^- + H_2S \rightarrow SH^- + H$

They are approximately 23 and 38 kcal mol^{-1} endothermic, respectively. Formation of H^- and SH is endothermic by more than 70 kcal mol^{-1} and is thus not expected to be significant. With SO_2, direct exothermic attachment to form SO_2^- is

expected (8) according to

[3] $e^- + SO_2 + M \rightarrow SO_2^- + M$

The channels leading to SO^-, S^-, O_2^-, or O^- in this case are all endothermic by more than 80 kcal mol^{-1}. We may therefore conclude that all the new primary ions formed from the three additives by electron attachment are sulphurous: S^- from OCS, S^- and SH^- from H_2S, and SO_2^- from SO_2.

Some of the secondary ion chemistry in OCS has been discussed previously in considerable detail (3). Briefly, with S^- as the primary ion we can expect the following secondary reactions to predominate

[4*a*] $S^- + O_2 \rightarrow SO_2 + e^-$

[4*b*] $S^- + O_2 \rightarrow SO^- + O$

[4*c*] $S^- + O_2 + M \rightarrow SO_2^- + M$

[5] $SO^- + O_2 + M \rightarrow SO_3^- + M$

[6] $SO_2^- + OH \rightleftharpoons SO_3^- + H$

[7] $SO_3^- + XH \rightleftharpoons HSO_3^- + X$

[8] $SO_2^- + O_2 + M \rightarrow SO_4^- + M$

[9] $SO_4^- + XH \rightleftharpoons HSO_4^- + X$

where M is a third body and XH is likely to be OH. Other reactions are possible if secondary sulphurous neutrals are present in sufficient concentration

[10] $S^- + SO_2 + M \rightarrow S_2O_2^- + M$

[11] $CH_3O^- + SO_2 + M \rightarrow CH_3O^- \cdot SO_2 + M$

Reaction [10] could account for the formation of some $S_2O_2^-$ at $m/e = 96$ although SO_4^- predominates from analysis of the ^{34}S isotope contribution at $m/e = 98$. Improved resolving power of the mass filter has led to the unequivocal identification of a sulphurous anion at $m/e = 95$, presumably formed by association of SO_2 with CH_3O^- via reaction [11]. It is noteworthy that the magnitude of this ion peak is approximately equal to that of SO_4^- at $m/e = 96$ for all three additives. This is the first sulphurous anion which must contain carbon that we have been able to detect. It is significant because it indicates the presence of appreciable SO_2 in the reaction zone of the OCS flame. It was also possible to detect the parent CH_3O^- ion at $m/e = 31$ in the undoped flame, which was not resolved previously because it occurs in the asymmetric foot of the very large O_2^- signal at $m/e = 32$. With OCS additive we can expect the following additional reactions to contribute

[12] $O_2^- + OCS \rightarrow SO_2^- + CO$

[13] $OH^- + OCS \rightarrow SH^- + CO_2$

[14] $S^- + OCS \rightarrow S_2^- + CO$

Isotope contributions of ^{34}S at $m/e = 66$ indicate that SO_2^- predominates over S_2^- at $m/e = 64$.

Reactions [10] and [12]–[14] have been examined separately at room temperature with the flowing afterglow technique in the Ion Chemistry Laboratory at York University. Reaction [10] has an effective second-order rate constant of 8.4×10^{-12} cm^3 $molecule^{-1}$ s^{-1} at 294 ± 2 K and a pressure of 1.5 Torr (1 Torr = 133.3 Pa).[1] This is a relatively high value for addition reactions of this type and suggests a stability for $S_2O_2^-$ brought about by covalent bonding. However, the ion has not often been observed in the gas phase although it has been identified previously in sulphur-doped crystals at low temperatures. Reactions [12]–[14] have all been found to occur rapidly with rate constants of (4.1 ± 1.2), (9.5 ± 2.9), and (9.1 ± 2.7) × 10^{-10} cm^{-3} $molecule^{-1}$ s^{-1}, respectively.[1] Also, no further reactions were observed for SO_2^-, SH^-, and S_2^- with OCS; i.e., $k \leq 10^{-12}$ cm^3 $molecule^{-1}$ s^{-1} in each case. Thus, reactions [1] and [4]–[14] together can account qualitatively for all the predominant sulphurous ions observed with the OCS additive; the importance of [10] and [14] is doubtful.

The enhanced abundance of SO_2^- in the flame seeded with SO_2 clearly is to be attributed to the direct attachment of electrons to SO_2. The lack of production of SH^- in this case is not unexpected. OH^- is known to add to SO_2 to produce HSO_3^- (9, 10) according to

[15] $OH^- + SO_2 + M \rightarrow HSO_3^- + M$

Production of SH^- from these reagents is about 20 kcal mol^{-1} endothermic and requires considerable bond redisposition. The ion signal at $m/e = 33$ actually decreases with SO_2 addition, presumably because of the charge transfer reaction

[16] $HO_2^- + SO_2 \rightarrow SO_2^- + HO_2$

The charge transfer is almost thermoneutral according to the known electron affinities of 1.16 eV for HO_2 (11) and 1.1 ± 0.1 eV for SO_2 (12).

The identifying features of the flame doped with H_2S can also be understood in terms of the ion chemistry with the additive. More SH^- can clearly be expected with H_2S than with OCS because of proton transfer reactions of the type

[17] $X^- + H_2S \rightarrow SH^- + XH$

which can be expected to occur between H_2S and a number of the anions present in the undoped flame. Also, some production of SH^- is expected from the dissociative attachment reaction [2*b*]. Starting with reaction [2*a*], the S_2^- and S_3^- ions might be expected to arise from the following two reactions with H_2S and (or) SH

[18] $S^- + H_2S\ (SH) \rightarrow S_2^- + H_2\ (H)$

[19] $S_2^- + H_2S\ (SH) \rightarrow S_3^- + H_2\ (H)$

Sulphur bond formation reactions of this type may be generalized by the reaction

[20] $S_n^- + XS \rightarrow S_{n+1}^- + X$

Their energies may be expressed with equation [21]

[21] $\Delta H^0 = D(X—S) - D(S_n—S) + EA(S_n) - EA(S_{n+1})$

where D and EA are the bond dissociation energy and electron affinity, respectively. $D(S_n—S)$ is approximately 70 kcal mol^{-1} for n = 2–7 and 103 kcal mol^{-1} for $n = 1$. $D(X—S)$ for H_2S is 72 kcal mol^{-1} and for SH is 85 kcal mol^{-1}. Values of 2.077, 1.663, and 2.0 eV are available for $EA(S)$, $EA(S_2)$, and $EA(S_3)$, respectively (11, 13). They indicate that reaction [18] is exothermic for both H_2S and SH; reaction [19] is exothermic for H_2S and slightly endothermic for SH. We have investigated the reactions of S^-, S_2^-, and S_3^- with H_2S separately with the flowing afterglow technique near room temperature. S_2^- and S_3^- were found not to react at 473 K while S^- reacted at 317 K primarily according to reaction [22], which may be either proton transfer or hydrogen atom transfer, with a rate constant of (5.2 ± 1.6) × 10^{-10} cm^3 $molecule^{-1}$ s^{-1};[1]

[22] $S^- + H_2S \rightarrow SH^- + SH$

[1] D. K. Bohme and co-workers. Unpublished results. York University, Downsview, Ont., Canada M3J 1P3.

Reaction channel [22] is only thermoneutral. The observation that it is preferred over the more exothermic reaction channel [18] near room temperature may reflect the kinetic barrier which is likely to be associated with the considerable bond redisposition required to bring about reaction channel [18]. Apparently the same chemistry is operative at flame temperatures; reaction channel [22] is the preferred route rather than the reaction sequence [18] + [19]. This behaviour is borne out by the ^{34}S isotope analysis which indicates the presence of SO_2^-, not S_2^-, at $m/e = 64$, 66 and SO_4^-, not S_3^-, at $m/e = 96$, 98.

Influence of the sulphurous neutral chemistry

It is possible that the discussion to this point underestimates the amounts of secondary sulphurous neutrals formed from the parent additives within the short time scale of the flame reaction zone. Certainly the observation of $CH_3O^- \cdot SO_2$ with all three additives gives pause for thought since neutral SO_2 must be involved in its formation. In this fuel-rich flame where H_2 is the major combustion product, relatively large concentrations of free H atoms will be present in the reaction zone and also upstream of it because of their very large diffusivities (4, 14). Thus, the following sequence of reactions may be near to being balanced

[23] $SO_2 + H \rightleftharpoons SO + OH$

[24] $SO + H \rightleftharpoons S + OH$

[25] $S + H_2 \rightleftharpoons SH + H$

[26] $SH + H_2 \rightleftharpoons H_2S + H$

Overall, the net reaction is

[27] $SO_2 + 2H_2 \rightleftharpoons H_2S + 2OH$

Since the OH concentration exceeds its equilibrium value in the reaction zone (4, 14), then the production of H_2S, and to a lesser extent SH, is suppressed with SO_2 additive. In contrast, the production of SO_2 with H_2S additive is enhanced. The entry and participation of OCS into the above scheme will occur via the reaction

[28] $OCS + H \rightleftharpoons SH + CO$

which has the same H-atom dependence as the reverse of reaction [26]. On the other hand, radical reactions of H and OH with sulphur species may be minimized if SO_2 catalyzes radical recombination according to

[29] $SO_2 + OH(H) + M \rightarrow HSO_3(HSO_2) + M$

[30] $HSO_3(HSO_2) + H \rightarrow SO_2 + H_2O(H_2)$

Other channels akin to reaction [30] might produce neutral SO_3

[31] $HSO_3 + H(OH) \rightarrow SO_3 + H_2(H_2O)$

or even sulphuric acid

[32] $HSO_3 + OH + M \rightarrow H_2SO_4 + M$

Thus, radical attack on the additives in the flame reaction zone may give rise to a variety of species (S, SH, SO, SO_2, HSO_2, SO_3, HSO_3, H_2SO_4) which can attach electrons to form sulphurous negative ions. The degree to which the neutral sulphur chemistry affects the observations of sulphurous anions is difficult to assess quantitatively, but its influence cannot be disregarded.

Conclusions

The present range of additives including H_2S, OCS, and SO_2 is representative of fuel sulphur compounds occurring early, intermediate, and late in the sulphur oxidation sequence. Thus, more general conclusions can be advanced than were possible with OCS in isolation (3).

(*1*) All three additives produce a dramatically increased concentration of sulphur anions in the flame reaction zone, and it is reasonable to assume that any fuel sulphur will do the same. This means that fuel sulphur gives rise to species (e.g., S, SH, SO_2, etc.) having higher stabilities than those of the C—H—O molecules normally present in a hydrocarbon flame.

(*2*) The ambient concentration of negative ions represents a balance between the rates of electron attachment and detachment. Three-body and dissociative attachment have a negative temperature dependence. Associative detachment by radicals and thermal detachment (near $z = 0$ in the profiles) have a positive temperature dependence. Thus, possible attempts to remove sulphur from combustion products as sulphurous anions will benefit from a lower temperature.

(*3*) The profile shape of a given sulphurous anion is remarkably insensitive to the nature of the additive. This will be the case if the rates of production and loss of the sulphurous anion are fast such that its profile essentially replicates that of the reagent C—H—O anion (or free electrons in the case of attachment).

(*4*) The profile magnitudes are not sufficiently distinct to predict the nature of the fuel sulphur from the anion signals. However, some useful qualitative trends are discernible at each end of the oxidation sequence; H_2S enhances SH^- at one end, while at the other end, SO_2 enhances SO_2^- and SH^- is absent.

(*5*) The anions are dominated by HSO_4^- which accounts for roughly half of the total ion signal present for each of the three additives. This has analytical implications for the detection of total sulphur. It does *not* necessarily imply the presence of sulphuric acid in the flame, however.

(*6*) The full range of sulphurous anions detected (in order of increasing m/e) includes S^-, SH^-, SO^- (uncertain), SO_2^- (S_2^-), SO_3^-, HSO_3^-, $CH_3O^- \cdot SO_2$, SO_4^- ($S_2O_2^- \cdot$, S_3^-), and HSO_4^-. Thus, S—H and S—O bonds may form, but evidently C—S and S—S bond formations are not favoured.

(*7*) The $CH_3O^- \cdot SO_2$ ion is revealing since its formation via reaction [11] requires the presence of SO_2 as a reagent. For the H_2S and OCS additives, appreciable secondary SO_2 must be present as a combustion product in the flame reaction zone. Evidently the oxidation of sulphurous neutrals (e.g., $H_2S \rightarrow SH \rightarrow SO \rightarrow SO_2$ or $OCS \rightarrow S \rightarrow SO \rightarrow SO_2$) proceeds very rapidly under flame conditions.

(*8*) The sulphurous anion chemistry is explicable in terms of roughly twenty ion (electron) – molecule reactions. The types of reactions are diverse and include attachment and dissociative attachment, association, atom transfer, proton transfer, and charge (electron) transfer.

(*9*) Sufficient time is available in the flame reaction zone for the occurrence of at least four consecutive ion–molecule reactions. This is evident from sequences such as $S^- \rightarrow SO_2^- \rightarrow SO_3^- \rightarrow HSO_3^-$ or $S^- \rightarrow SO_2^- \rightarrow SO_4^- \rightarrow HSO_4^-$ with the H_2S or OCS additives. The sequences might be longer except that we have not been successful in detecting sulphurous anions unambiguously having $m/e > 100$. Fast reaction rates are aided by the high (atmospheric) pressure of the flame (many of the reactions are termolecular) but not necessarily by the high flame temperature (many of the reactions have a negative or zero temperature dependence).

(*10*) These results bear out a general contention of flame-ion chemistry; namely, that the elevated flame temperature is

sufficient to overcome reaction endothermicities of at least 25 kcal mol^{-1}. Reactions [1] and [2*a*] are cases in point. This behaviour is in contrast to room-temperature studies, for example, using the flowing afterglow apparatus, in which endothermic reactions generally do not proceed at measurable rates.

Acknowledgements

Support of both the flame ionization work and the flowing afterglow studies by the Natural Sciences and Engineering Research Council of Canada is acknowledged. We wish to thank Dr. A. N. Hayhurst for his helpful comments with regard to the influence of the sulphurous neutral chemistry.

1. E. ROBINSON. Air quality monographs. Monograph #75-23, American Petroleum Institute, Washington, DC. 1976.
2. C. P. FENIMORE. Pollutant formation and destruction in flames. Frontiers of chemistry. *Edited by* K. J. Laidler. Plenary and keynote lectures presented at the 28th IUPAC Congress, Pergamon Press Ltd., Oxford, Great Britain. 1982. p. 41.
3. J. M. GOODINGS, K. ELGUINDI, and D. K. BOHME. Can. J. Chem. **61**, 1703 (1983).
4. J. M. GOODINGS, D. K. BOHME, and C.-W. NG. Combust. Flame, **36**, 27 (1979).
5. J. M. GOODINGS, D. K. BOHME, and C.-W. NG. Combust. Flame, **36**, 45 (1979).
6. A. N. HAYHURST and N. R. TELFORD. Combust. Flame, **28**, 67 (1977).
7. K. A. G. MACNEIL and J. C. J. THYNNE. J. Phys. Chem. **73**, 2960 (1969).
8. L. BOUBY, F. FIQUET-FAYARD, and C. BODERE. Int. J. Mass Spectrom. Ion Phys. **7**, 415 (1971).
9. F. C. FEHSENFELD and E. E. FERGUSON. J. Chem. Phys. **61**, 3181 (1974).
10. A. B. RAKSIT and D. K. BOHME. Can. J. Chem. **61**, 1683 (1983).
11. H. HOTOP and W. C. LINEBERGER. J. Phys. Chem. Ref. Data, **4**, 539 (1975).
12. R. J. CELOTTA, R. A. BENNETT, and J. L. HALL. J. Chem. Phys. **60**, 1740 (1974).
13. P. S. DRZAIC, J. MARKS, and J. I. BRAUMAN. Gas phase ion chemistry. Vol. 3, *Edited by* M. T. Bowers. Academic Press Inc., New York, NY. 1984. p. 167.
14. J. W. HASTIE. Combust. Flame, **21**, 187 (1973).

A photoconductivity study in γ-irradiated polyethylene at 77 K

TOYOAKI KIMURA,[1] YUTAKA UEDA, AND YOHICHI HIRAI[2]

Department of Synthetic Chemistry, Faculty of Engineering, Nagoya University, Chikusa-ku, Nagoya 464, Japan

Received July 17, 1985

TOYOAKI KIMURA, YUTAKA UEDA, and YOHICHI HIRAI. Can. J. Chem. **64**, 695 (1986).

A photoconductivity study was made on γ-irradiated low and high density polyethylene using 3-methylpentane, methylene chloride, and hexafluorobenzene as dopants. Electron spin resonance (esr) and optical absorption measurements were made together with photoconductivity. A study was also made for poly(4-methylpentene-1). The process of photocurrent generation is not ascribed totally to photodetrapping of trapped electrons in polyethylene; the process by photodetrapping of trapped electrons dominantly contributes to photocurrent generation in the ir region and may partly contribute in the visible region but not in the uv region. Another process for photocurrent generation other than photodetrapping of trapped electrons exists in the uv and perhaps partly in the visible region. We have tentatively ascribed this process to photodetachent of electrons from carbanions whch are formed by the reaction between radicals and electrons.

TOYOAKI KIMURA, YUTAKA UEDA et YOHICHI HIRAI. Can. J. Chem. **64**, 695 (1986).

On a effectué une étude de photoconductivité sur des polyéthylènes de basse et de haute densité, irradiés aux rayons γ et contenant les substances suivantes comme dopants: méthyl-3 pentane, chlorure de méthylène et hexafluorobenzène. En plus de la photoconductivité, on a aussi effectué des mesures de rpe et d'absorption. On a aussi étudié le poly(méthyl-4-pentène-1). On n'attribue pas tout le processus de la génération du photocurant au photodépiégeage des électrons piégés dans le polyéthylène; ce processus de photodépiégeage des électrons piégés contribue d'une façon dominante à la génération du photocourant dans le région de l'ir et peut aussi contribuer en partie dans la région du visible, mais pas dans la région de l'uv. En plus du photodépiégeage des électrons piégés, un autre processus de génération de photocourant existe dans l'uv et peut-être aussi dans le visible. Sur une base préliminaire, on a attribué ce processus au photodétachement des électrons des carbanions qui se forment par la réaction des radicaux et des électrons.

[Traduit par la revue]

Introduction

Trapped electrons generated by ionizing radiation have been widely investigated in organic solids especially in frozen organic glasses at the liquid nitrogen temperature (1). Concerning trapped electrons in nonpolar hydrocarbon glasses at 77 K, it is well known that the electron spin resonance (esr) spectra for those electrons show a singlet line with a line width of ~4 G(1), that absorption maxima of optical absorption spectra are ~1700 nm(1), and that photoconductivity maxima of photoconductivity spectra are ~1000 nm(2). It is also known that electrons are efficiently trapped in glassy matrices but not in crystalline matrices.

Hydrocarbon polymers such as polyethylene (PE), polypropylene (PP), or poly(4-methylpentene-1) (P4MP) have chemical unit structure similar to low molecular weight hydrocarbons such as 3-methylpentane (3MP) or 2-methylpentane (2MP). Thus it is interesting to compare the nature of electrons trapped in low molecular hydrocarbon glasses and the nature of those trapped in hydrocarbon polymers. Electron spin resonance spectra of trapped electrons in γ-irradiated polymers show singlet signals which are similar to those in low molecular hydrocarbon glasses although the line widths are slightly narrow: 3.4 G for PE and 2.6 G for P4MP (3). Concerning the optical absorption spectrum in a hydrocarbon polymer, Keyser and Williams have reported that the position of the absorption maximum (λ^{ab}_{max}) of trapped electrons in γ-irradiated P4MP at 77 K lies beyond 2000 nm (4). This result seems to be similar to that for low molecular weight hydrocarbon glasses, although the λ^{ab}_{max} in P4MP is longer than those in the glasses. On the other hand Partridge has shown a photoabsorption spectrum λ^{ab}_{max} which is ~280 nm in γ-irradiated low density polyethylene (LDPE) at 98 K and ascribed this to trapped electrons.

Polyethylene is widely used as electrical insulators. Thus, the nature of PE is widely studied in the field of electrical engineering by means of thermoluminescence (TL) (6–13), thermally stimulated current (TSC) (14–21), and photostimulated detrapping current (PSDC) (22,23). Trapped electrons, which are defined as electrons trapped physically in a matrix, are proposed to be the origin of TL (7–10), TSC (17,19), and PSDC (22,23). The reported PSDC spectra of trapped electrons in high density polyethylene (HDPE) X-irradiated at 90 K have shown only a small peak at ~1 eV and almost monotonous increase with considerable extent up to 5 eV (23).

The optical absorption and photoconductivity spectrum in γ- and X-irradiated PE in refs. 5 and 23, respectively, are dominant in the uv region and these have been ascribed to trapped electrons, as is described above. However, this is unacceptable from a viewpoint of trapped electrons in low molecular hydrocarbon glasses. It is conclusive that optical absorption and photoconductivity maxima lie in the ir region in low molecular hydrocarbon glasses. Freeman has demonstrated that even in highly polar media the upper limit of the absorption maximum of trapped electrons would be about 2.5 eV (24). Electron trapping in PE is an important and interesting phenomenon not only in the field of radiation chemistry but also in that of electrical engineering. Nevertheless, no further paper has been published since then.

Another point which we should note is the relationship between trapped electron yields in polymers and their crystallinities. It is reported that the higher the crystallinity of a polymer, the higher the trapped electron yield (4), which conflicts with the results from low molecular organic glasses as is described already.

In order to clarify these points described above we have measured optical, photoconductivity, and esr spectra for LDPE and HDPE γ-irradiated at 77 K. We have also studied the effect of doping using 3MP, methylene chloride, and hexafluoroben-

[1]To whom correspondence should be addressed.

[2]Present address is Tokai Kohgyo Co. Ltd., Ohbu, Aichi, Japan.

zene as dopants. In addition to LDPE and HDPE an investigation was also made for P4MP.

Experimental

Low density polyethylene and high density polyethylene were BE-R3000 (Ube Industries Ltd., the density was 0.919) and Sholex 6006M (Showa Denko K.K., the density was 0.958), respectively. LDPE and HDPB films made by hot press (1 mm thickness) were immersed in hot methylene chloride for a few days under argon atmosphere in a separable flask with three necks and a condenser. Following this, LDPE and HDPE were purified by hot hexane by the same procedure as above. On the other hand, another purification was made by dissolving PE pellets in hot xylene and then precipitating in methanol. However, no detectable difference in measured results can be observed between the samples purified by the former and latter method. Therefore, the former purification was mainly used through this work. Polyscience P4MP pellets were purified by the same procedure as that for PE. Purified PE and P4MP were dried *in vacuo*. Purified P4MP was pressed into a 1 mm thickness film by hot melt.

3-Methylpentane was Tokyo Kasei extra pure reagent and purified by molecular sieve 13X, which was evacuated at 300°C for 10 h. Nakarai Chemicals methylene chloride (spectro grade) and hexafluorobenzene (guaranteed reagent) were used as received.

Samples for photoconductivity measurements were made using films (1 × 9 × 50 mm) of LDPE, HDPE, and P4MP. Electrodes were made on the surfaces of both sides of a film by the following two methods. One is aluminum vapor deposition, where the front electrode was made to have a few slits through which incident photons were injected. The other is pressing brass meshes on both sides of a film by a flatiron. We have confirmed that the samples with aluminum deposited electrodes gave essentially the same results as those with mesh electrodes. However, since the adhesion between deposited aluminum and a film was poor which resulted in the poor reproducibility in the results and also the detachment of aluminum from the film when a dopant was used, the latter method was mainly used. Copper flat rings with a lead wire were contacted to the electrodes by a Teflon screw and nut which were set through a hole at the top of the film with electrodes. A sample in the photoconductivity cell, the main part of which was made of Supracil quartz, was evacuated on a vacuum line and sealed off immediately before the measurement. The scheme of the experiment was the same as that in ref. 25. A dc voltage of 500 V was applied for a sample of 1 mm thickness (5 kV/cm).

The samples for optical absorption measurement and for esr were a film (9 × 50 mm) and ~6–8 pieces of cut film (~1 × 50 mm), respectively. Samples in esr cells (Supracil quartz tube) and those in optical absorption cells (rectangular Supracil quartz) were evacuated on a vacuum line and sealed off. The esr measurements were made on a JEOL JES-3BX spectrometer with a ES-SCXA microwave unit. Optical absorption measurements were made on a Hitachi 323 spectrophotometer.

Doping for LDPE or HDPE was made by transferring a degassed dopant into the photoconductivity cell in which LDPE or HDPE was kept *in vacuo*. Then LDPE or HDPE was kept immersed in the dopant liquid overnight. After that the dopant was removed by vacuum distillation. The content of a dopant was measured by the difference in the weight before and after doping.

γ-Irradiation was made by γ-rays from a ^{60}Co source. The irradiation dose was 3.9×10^5 rad (1 rad = 10 mGy). γ-Irradiation and measurement were carried out at 77 K through this work.

Results and discussion

It is more difficult to purify polymers than low molecular hydrocarbons. In the latter case impurities such as olefines, aldehydes, ketones, etc. are satisfactorily removed from hydrocarbons by the use of a molecular sieve and purified hydrocarbons are separated from the molecular sieve by vacuum distillation. However, this technique cannot be used for polymers because the separation by vacuum distillation is practically inapplicable. Then, impurities may remain in polymers to some extent, which may lead to the difference in the results between low molecular hydrocarbons and PE as described before. There remains the following possibility: impurities in PE suppress the formation of trapped electrons and thus, the optical absorption spectrum ($\lambda_{max} \approx 280$ nm) in ref. 5 cannot be ascribed to trapped electrons. To check this possibility the effect of doping with a small amount of 3MP was investigated because it is expected that a small amount of 3MP does not compete with impurities for electrons. On the other hand, if trapped electrons do exist in γ-irradiated PE, doping of PE with electron scavengers such as methylene chloride or hexafluorobenzene will reveal the structure of trapped electrons in esr, optical absorption, and photoconductivity spectra. Thus, the effect of doping with electron scavengers was also investigated.

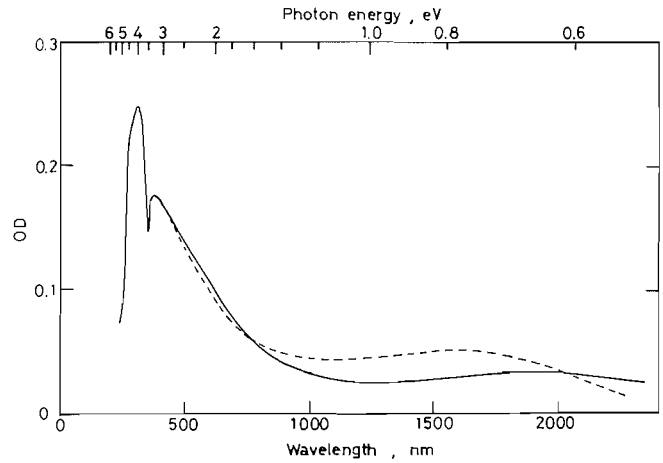

FIG. 1. Optical absorption spectra of photobleachable species in γ-irradiated nondoped LDPE (——) and LDPE doped with 3MP (---) system.

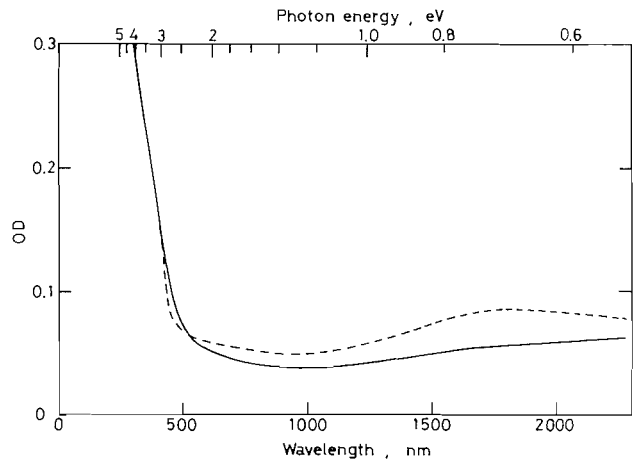

FIG. 2. Optical absorption spectra of photobleachable species in γ-irradiated nondoped HDPE (——) and HDPE doped with 3MP (---) system.

(1) Effect of 3MP doping on esr, optical absorption, and photoconductivity spectrum.

Some intermediate species produced in γ-irradiated LDPE and HDPE are photobleachable with visible light. We call these, "photobleachable species" through this work. Optical absorption spectra of photobleachable species in the γ-irradiated LDPE and HDPE sample were obtained by subtracting the

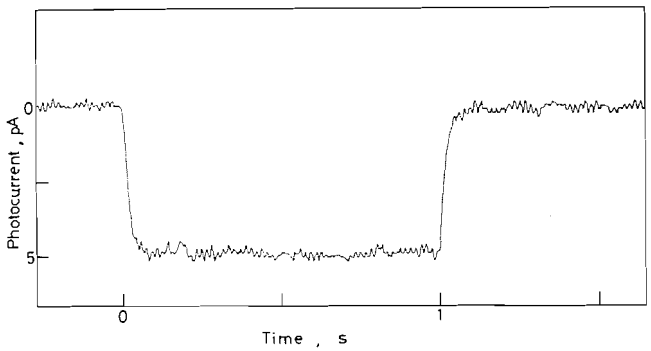

FIG. 3. Time profile of photocurrent in nondoped HDPE system. Wavelength of incident light was 1200 nm.

spectra of photobleached samples from those before the photobleach. Optical absorption spectra of photobleachable species in γ-irradiated nondoped LDPE and HDPE are shown as the solid line in Figs. 1 and 2, respectively. The optical absorption spectrum of bleachable species in LDPE in Fig. 1 is similar to that in ref. 5. In the case of HDPE, the spectrum was not measured at wavelengths shorter than ~300 nm because of the lack in transparency of HDPE films.

An example of photocurrent from γ-irradiated HDPE is shown in Fig. 3. The rise time of the amplifier was 100 or 300 ms through this work. In Fig. 3 it is shown that the photocurrent rises instantaneously when the shutter, through which the incident light comes, is opened and falls instantaneously to zero when the shutter is closed. Similar time profiles were obtained through this work. Photoconductivity spectra, meaning the photocurrent per incident photon versus the wavelength of incident light, for nondoped LDPE and HDPE system are plotted as circles in Figs. 4 and 5, respectively. The photoconductivity maxima at which the photocurrent per incident photon shows a maximum are ~280–300 nm for both nondoped LDPE and HDPE. This is similar to the result in ref. 26. It is interesting that for the nondoped LDPE system the photoconductivity spectrum is similar to the optical absorption spectrum (Figs. 1 and 4).

The amounts of 3MP dopant were 4 and 3 wt% for 3MP-LDPE and 3MP-HDPE systems, respectively. Doping of LDPE and HDPE with 3MP resulted in an increase in signal intensities of esr singlets. Since the amounts of samples for esr were not enough to neglect the quartz signal, we did not determine the increment of signal intensities as a result of 3MP doping. However, it can be obviously concluded from esr measurement that 3MP doping leads to an increase in esr singlet, which can be ascribed to trapped electrons. The nature of the singlets in 3MP-LDPE and 3MP-HDPE is different from those in nondoped LDPE and HDPE as will be described later.

The effect of 3MP doping on the optical absorption spectra of photobleachable species in LDPE and HDPE is clearly shown in Figs. 1 and 2, respectively. It is interesting to see that doping of LDPE and HDPE with 3MP causes the optical absorption spectra of photobleachable species to increase in the ir region and that the effect of 3MP doping is negligible in the visible and uv regions as is shown in Figs. 1 and 2.

Photoconductivity spectra for 3MP doped LDPE and HDPE are shown in Figs. 4 and 5, respectively together with those for nondoped LDPE and HDPE. The results from the photoconductivity spectra are similar to those from the optical absorption spectra in Figs. 1 and 2. In both cases of LDPE and HDPE in Figs. 4 and 5, doping with 3MP causes an enhancement in the spectrum in the ir region, but gives only a small and almost negligible effect in the visible and uv region, respectively.

From the results by esr it can be concluded that no impurity, which suppresses completely the formation of trapped electrons described above, exists in LDPE and HDPE systems and that 3MP doping causes the trapped electron yield to increase in LDPE and HDPE systems. Then both results by the optical absorption and photoconductivity measurements indicate that trapped electrons in 3MP doped systems are dominant in the ir region, which agrees well with the results on trapped electrons in low molecular hydrocarbon glasses.

The increase in the intensities in the optical and photoconductivity spectra as a result of 3MP doping in Figs. 1, 2, 4, and 5, indicates that new trapping sites for electrons are created by 3MP dopant molecules. The structure of the new trapping sites is not known at present. However, as is shown later, the nature of the new trapping sites is quite different from that in nondoped PE systems. It is generally expected that polymers swell when they absorb a low molecular substance. In the present case of LDPE and HDPE the increments in the volume after 3MP doping were 3.9 and 3.1% at room temperature, respectively. Although we did not measure the increase in the volume at 77 K, it can be said that the swelling of LDPE and HDPE is small at 77 K. If the swelling leads to a lower total density and if we ignore the role of doped 3MP molecules in new trapping sites, then the yield of trapped electrons in the swollen system would be lower than that in the nonswollen system. This is because the trapped electron yield is higher in HDPE than in LDPE (4). Therefore, doped 3MP molecules probably play an important role in the new trapping sites.

It is expected that 3MP molecules migrate into an amorphous region but not inside the crystalline region. The HDPE has less amorphous region than HDPE. Therefore the content of 3MP dopant in HDPE is actually less than that in LDPE. Nevertheless, the increment of trapped electrons as a result of 3MP doping in the HDPE system is even more than that in LDPE system as is seen in Figs. 1 and 2. This can be explained if we assume that electron traps are dominant in the interfacial region between the crystalline and amorphous part, which has been suggested by Kobayashi and Yahagi (17). Because of the existence of the esr singlet and optical absorption in the ir region and also from the reason which will be described later, we consider the existence of trapped electrons in γ-irradiated nondoped LDPE and HDPE. The role of doped 3MP molecules is not clear except that they contribute to form new trapping sites. New trapping sites are probably dominant in the interfacial region between the crystalline and amorphous parts as is described above. According to the cavity model for trapped electrons, potential wells with suitable depths and sizes are necessary (27). Therefore, some of doped 3MP molecules are arranged in PE to form suitable potential wells for new trapping sites.

In Fig. 6, power saturation curves, namely relative intensities of esr singlet signals versus square root of microwave power, for nondoped and 3MP doped HDPE system are shown. Since the power unit was not calibrated, only relative power values were available. The curves were adjusted to give the same intensity at the square root power of 2.236 au. It is seen from Fig. 6 that the signals for nondoped HDPE system saturate at a lower power than those for 3MP doped HDPE system. Namely, the new trapping sites which are formed as a result of 3MP doping show a different power saturation characteristic from that for trapping sites in nondoped PE system.

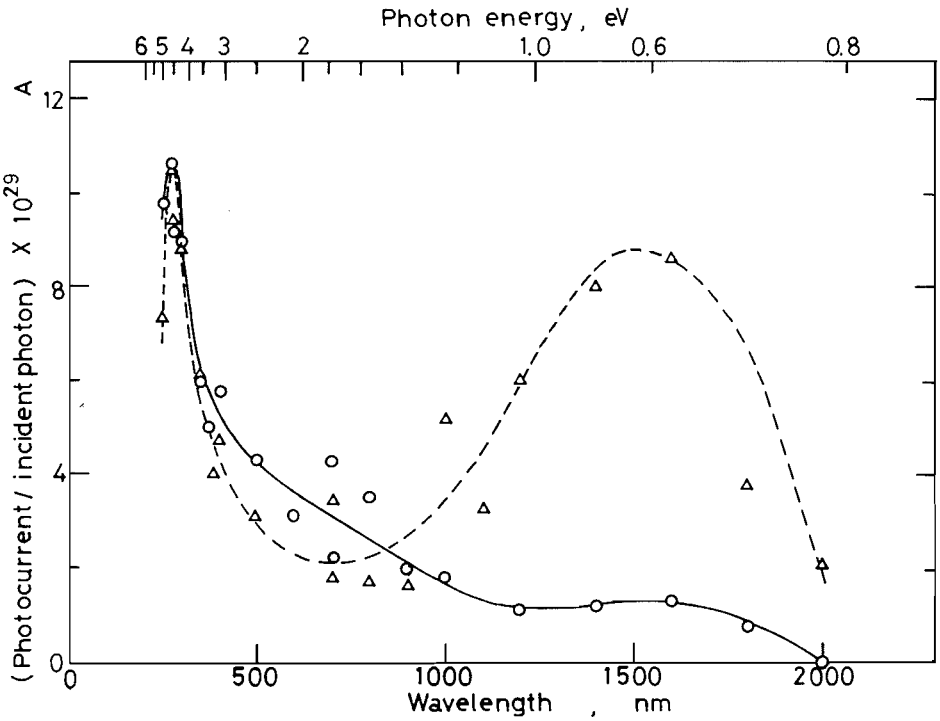

FIG. 4. Photoconductivity spectra for γ-irradiated nondoped LDPE (—○—) and LDPE doped with 3MP (--△--) system.

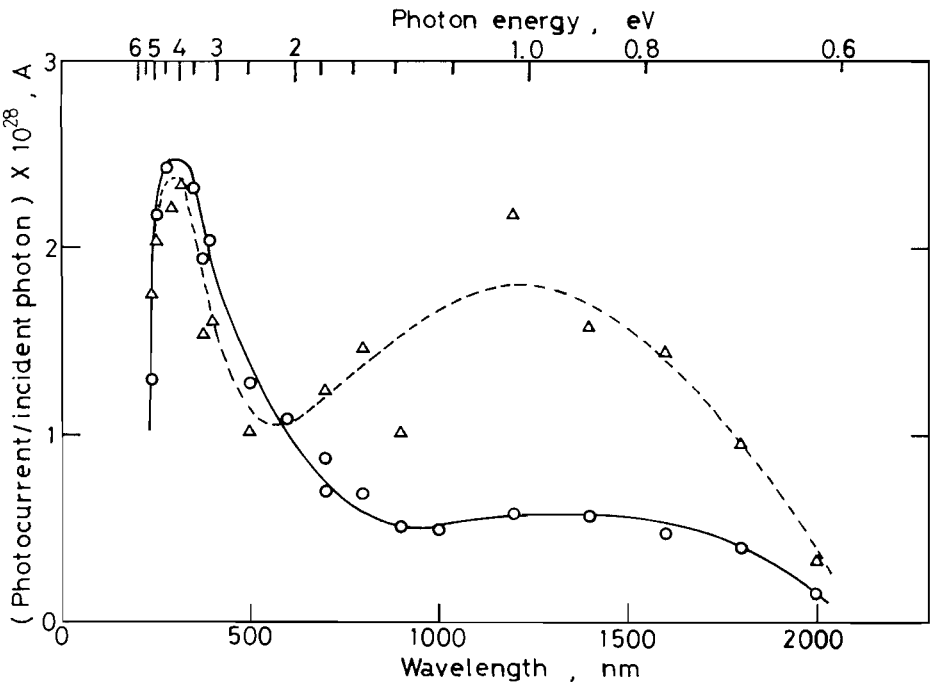

FIG. 5. Photoconductivity spectra for γ-irradiated nondoped HDPE (—○—) and HDPE doped with 3MP (--△--) system.

We do not intend to deny the existence of the cavity traps that include 3MP molecules in amorphous region. However, taking the fact that the increment of trapped electron yield as a result of 3MP doping in HDPE system is even more than that in 3MP doped LDPE system, it is better to say at present, that cavity traps that include 3MP are dominant in the interfacial region as is described above.

(2) Effect of doping with electron scavengers

It is well known that methylene chloride reacts with an electron to form Cl^- and the corresponding radical. It is also known that hexafluorobenzene reacts with an electron to form an anion (28). These dopants were used as electron scavengers. Contents of methylene chloride in LDPE and HDPE were 5 and 3 wt%, respectively and those of hexafluorobenzene in LDPE

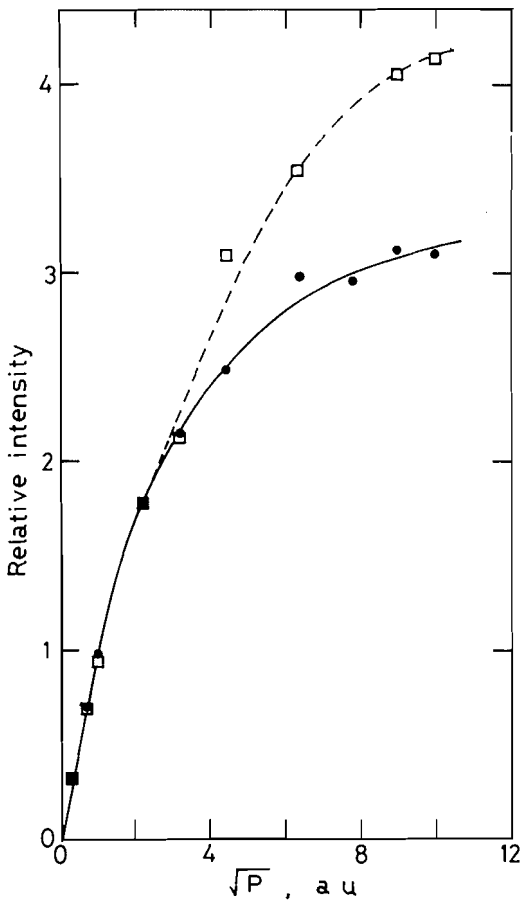

FIG. 6. Power saturation curves for singlet signals in esr spectra for nondoped HDPE (—●—) and HDPE doped with 3MP (--□--) system.

and HDPE were 4 and 2 wt%, respectively. Electron spin resonance measurements were made for LDPE and HDPE doped with methylene chloride and hexafluorobenzene γ-irradiated at 77 K. In each of these four systems (CH_2Cl_2-LDPE, C_6F_6-LDPE, CH_2Cl_2-HDPE, and C_6F_6-HDPE) it is hard to discern the singlet which is ascribed to trapped electrons. So, even if trapped electrons exist in these systems, the amount should be low.

Optical absorption measurements have also revealed that doping with methylene chloride or hexafluorobenzene reduces drastically the specrum in the ir region. This is shown in Fig. 7 for HDPE systems. In the case of C_6F_6 doping the spectrum in the visible region is higher than that in the nondoped HDPE because of the tail of $C_6F_6^-$ absorption. In the case of LDPE systems, similar results as those in Fig. 7 were obtained. However, the spectra in the ir region for the CH_2Cl_2 and C_6F_6 doped LDPE systems were almost negligible, indicating that electron scavenging by these scavengers in this system is more effective. In conclusion, dopants reduce drastically the spectrum in the ir region whereas the spectrum in the visible and uv regions is almost the same or increases because of the absorption of $C_6F_6^-$. Then it can be said that the optical absorption by trapped electrons in LDPE and HDPE is dominant in the ir region. This is also supported by the results from esr and agrees well with the results from low molecular hydrocarbon glasses.

Photoconductivity spectra for nondoped, CH_2Cl_2 doped, and C_6F_6 doped systems are shown in Figs. 8 and 9 in the case of

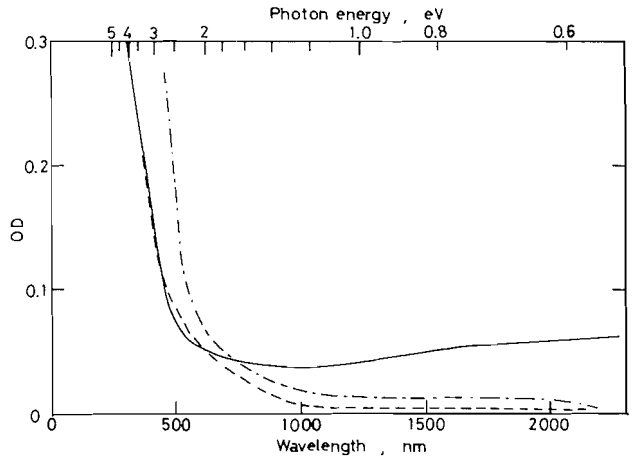

FIG. 7. Optical absorption spectra of photobleachable species in γ-irradiated nondoped HDPE (——), CH_2Cl_2 doped HDPE (– – –), and C_6F_6 doped HDPE (–·–·–) system.

LDPE and HDPE, respectively. It should be noted from Fig. 8 that doping with methylene chloride and hexafluorobenzene in LDPE systems suppresses considerably the photoconductivity spectra in the ir region but that the effect of doping is negligible in the uv region. In the case of HDPE, the photoconductivity spectra are suppressed by the doping as is seen in Fig. 9. In the uv region around the photoconductivity peak in Fig. 9, it can be said that the effect of the doping is small, although the curve for CH_2Cl_2-HDPE system and that for C_6F_6-HDPE system are somewhat higher and lower than that for the nondoped HDPE system, respectively. In both cases of LDPE and HDPE, the photoconductivity spectra in the visible region are suppressed by the doping with these electron scavengers. The reason for this may be as follows. Photoconductivity spectra of trapped electrons in LDPE and HDPE may have relatively high intensities compared with the photoconductivity maxima. This is observed in 3-methylheptane glass where the photoconductivity maximum lies at ~1000 nm but the intensity at 500 nm is 73% of the peak intensity at ~1000 nm (2). An alternative explanation for the suppression of photoconductivity spectra in the visible region by the doping may be that these dopants might suppress a precursor (other than trapped electrons) which gives the photocurrent. The photocurrent in γ-irradiated hydrocarbons is generally explained by the detrapping of electrons from their traps. However, we will suggest below a process of photocurrent generation which does not involve trapped electrons. This process is responsible for the photocurrent for the LDPE and HDPE systems doped with those electron scavengers in Figs. 8 and 9.

(3) Electron spin resonance, optical absorption, and photoconductivity spectrum for P4MP systems

No singlet which is ascribed to trapped electrons was observed in the esr spectrum for the γ-irradiated P4MP system. Optical absorption measurements for γ-irradiated P4MP showed that photobleachable species are produced also in this system. The optical absorption spectrum exists in the uv and the visible region, but only the absorption tail in the ir region up to 1400 nm. This indicates that trapped electrons are not produced in P4MP used in the present study. Nevertheless, we observed a photocurrent for the γ-irradiated P4MP system. In Fig. 10 the photoconductivity spectrum for the P4MP system is shown

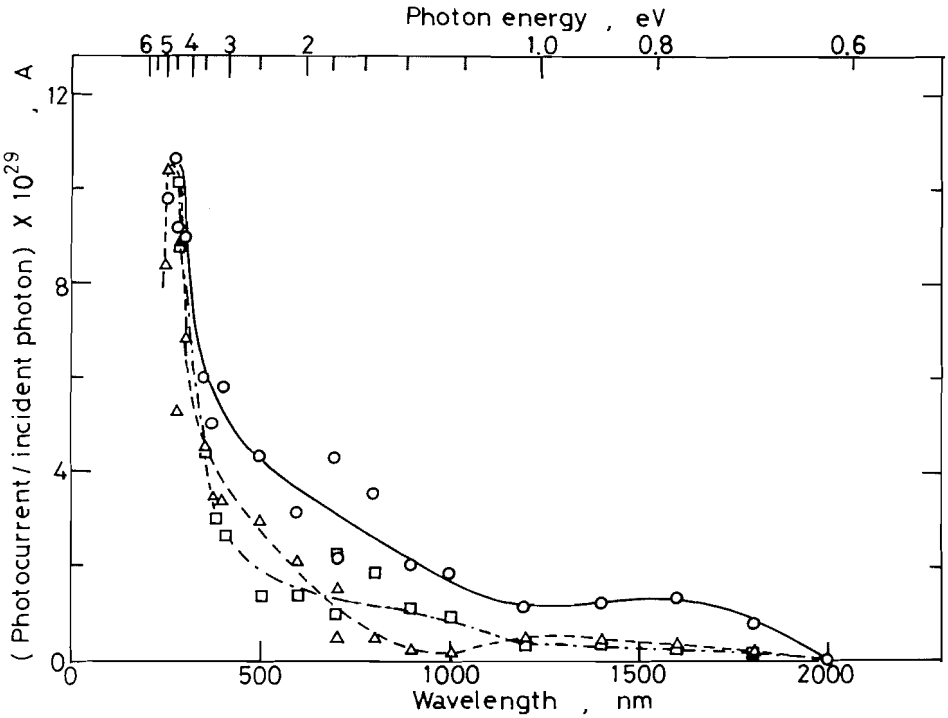

FIG. 8. Photoconductivity spectra for γ-irradiated nondoped LDPE (—○—), CH_2Cl_2 doped LDPE (--△--), and C_6F_6 doped LDPE (-·-□-·-) system.

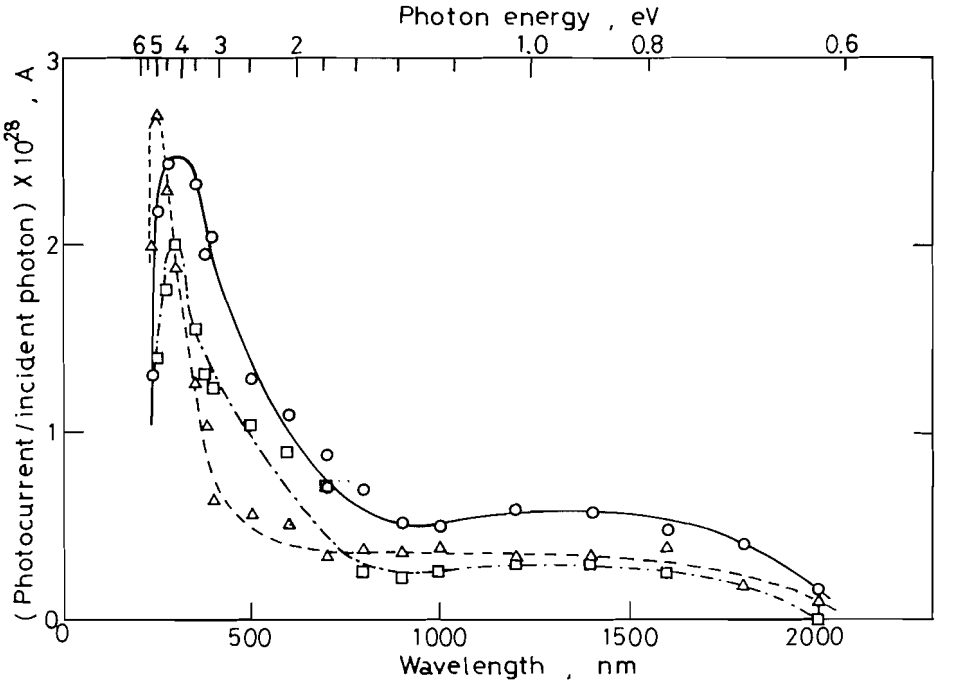

FIG. 9. Photoconductivity spectra for γ-irradiated nondoped HDPE (—○—), CH_2Cl_2 doped HDPE (--△--), and C_6F_6 doped HDPE (-·-□-·-) system.

together with the optical absorption spectrum of photobleachable species. It is interesting to note that the two curves in Fig. 10 fit well with each other except for the long wavelength side. It should be noted that the photoconductivity spectrum for the P4MP system in Fig. 10 is similar to those for the CH_2Cl_2 doped and C_6F_6 doped LDPE systems in Fig. 8 and, also, to those CH_2Cl_2 doped and C_6F_6 doped HDPE systems in Fig. 9. These five conductivity spectra described above indicate that photocurrent generation from the process of photodetrapping of trapped electrons is negligible because singlets in esr signals for these five systems are negligible. It is also interesting to note that the five photoconductivity spectra for the P4MP, CH_2Cl_2-LDPE, C_6F_6-LDPE, CH_2Cl_2-HDPE, and C_6F_6-HDPE systems have maxima at nearly the same position, 300 nm.

We did not observe photobleachable optical absorption in the ir region. This does not agree with the results in ref. 4. This

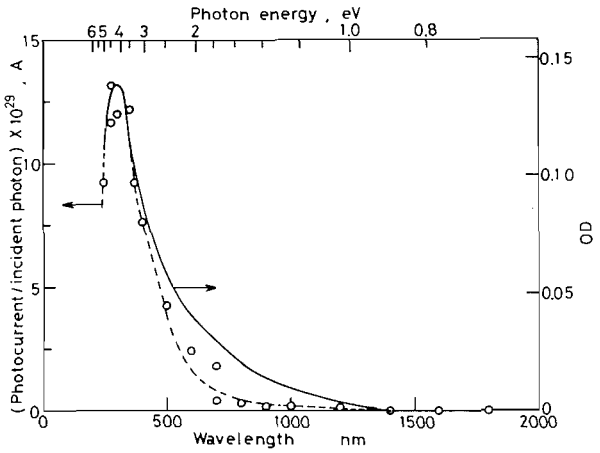

FIG. 10. Optical absorption spectrum of photobleachable species (——) and photoconductivity spectrum (––O––) for γ-irradiated P4MP system.

discrepancy may arise from the difference in P4MP itself. Unfortunately we could not obtain P4MP from the same company as that in ref. 4.

(4) Mechanism of photocurrent generation other than photodetrapping of trapped electrons

In TL studies heat detrapping of electrons from their traps and subsequent recombination are proposed as a mechanism of TL (7, 8, 10, 13). It has been found that similar glow peaks as those in TL are obtainable in TSC work. Then, photodetrapping of electrons from their traps has been proposed as a mechanism of photocurrent generation (17, 19). In the present study it is true that photocurrent by photodetrapping of trapped electrons is dominant in the ir region in the case of the LDPE and HDPE systems, as is described already. However, another mechanism other than photodetrapping of trapped electrons is necessary for photocurrent generation in the uv and perhaps in the visible region.

The mechanism of photocurrent generation other than photodetrapping of trapped electrons is not clear at present. One of the provable mechanisms is photodetachment of electrons from carbanions which are formed by the reaction between radicals and electrons:

$$RH \rightsquigarrow R^+ + e^-$$
$$R^+ + e^- \longrightarrow R\cdot + H$$
$$R\cdot + e^- \longrightarrow R^-$$
$$R^- \xrightarrow{h\nu} R\cdot + e^-$$

Willard *et al.* have shown that the absorption onset of 3-methylhexane carbanion is longer than 800 nm (29). It is not clear, however, whether electrons are photodetachable by the visible light. In the case of polyethylene it may be possible for electrons to be photodetached from carbanion by visible light because the electron affinities for $CH_3\cdot$, $C_2H_5\cdot$, n-$C_3H_7\cdot$, and iso-$C_3H_7\cdot$ are ~1.08–1.8, 1.4, 1.0, and ~1.0 eV, respectively (30). Optical absorption spectra of bleachable species in the uv region for the LDPE, HDPE, and P4MP systems, shown in Figs. 1, 2, and 10, respectively, could be ascribed to carbanions. The spectrum of 3MP carbanion in the uv region proposed by Willard *et al.* (31) is similar to ours but the absorption maximum is slightly shorter than ours.

Acknowledgment

Publication cost is supported by Tomonokai Research Laboratory of Physics and Chemistry.

1. L. KEVAN. *In* Advances in radiation chemistry. Vol. 4. *Edited by* M. Burton and J. L. Magee. Wiley-Interscience, New York. 1974. p. 181.
2. N. OKABE, T. KIMURA, and K. FUEKI. Can. J. Chem. **61**, 2799 (1983).
3. R. M. KEYSER, K. TSUJI, and F. WILLIAMS. *In* The Radiation chemistry of macromolecules. Vol. 1. *Edited by* M. Dole. Academic Press, New York. 1972. p. 145.
4. R. M. KEYSER and F. WILLIAMS. J. Phys. Chem. **75**, 1623 (1969).
5. R. H. PARTRIDGE. J. Chem. Phys. **52**, 1277 (1970).
6. A. CHARLESBY and R. H. PARTRIDGE. Proc. R. Soc. London A **271**, 170 (1963).
7. A. CHARLESBY and R. H. PARTRIDGE. Proc. R. Soc. London A **271**, 188 (1963).
8. I. BOUNSTEAD and A. CHARLESBY. Proc. R. Soc. London A **316**, 291 (1970).
9. I. BOUNSTEAD. Proc. R. Soc. London A **318**, 459 (1970).
10. K. ARAKI, M. ENDO, and K. YAHAGI. Jpn. J. Appl. Phys. **13**, 1787 (1974).
11. Y. SUZUOKI, K. YASUDA, T. MIZUNTANI, and M. IEDA. Jpn. J. Appl. Phys. **16**, 1339 (1977).
12. S. NAKAMURA, G. SAWA, and M. IEDA. J. Appl. Phys. **48**, 3626 (1977).
13. R. H. PARTRIDGE. Polymer, **23**, 1461 (1982).
14. G. SAWA, M, KAWADA, D. C. LEE, and M. IEDA. Jpn. J. Appl. Phys. **13**, 1547 (1974).
15. FISCHER and P. ROHL. J. Polym. Sci. Polym. Phys. Ed. **14**, 531 (1976).
16. S. NAKAMURA, G. SAWA, and M. IEDA. Jpn. J. Appl. Phys. **16**, 2165 (1977).
17. S. KOBAYASHI and K. YAHAGI. Jpn. J. Appl. Phys. **16**, 2053 (1977).
18. Y. SUZUOKI, T. MIZUNTANI, and M. IEDA. J. Phys. D, **10**, 1985 (1977).
19. S. KOBAYASHI and K. YAHAGI. Jpn. J. Appl. Phys. **18**, 261 (1979).
20. T. MIZUTANI, T. TSUKAHARA, and M. IEDA. J. Phys. D, **13**, 1673 (1980).
21. T. MIZUTANI, T. TSUKAHARA, and M. IEDA. Jpn. J. Appl. Phys. **19**, 2095 (1980).
22. Y. TAKAI, K. MORI, T. MIZUTANI, and M. IEDA. Jpn. J. Appl. Phys. **15**, 2341 (1976).
23. Y. SUZUOKI, T. MIZUTANI, Y. TAKAI, and M. IEDA. Jpn. J. Appl. Phys. **16**, 1929 (1976).
24. G. R. FREEMAN. J. Phys. Chem. **77**, 7 (1973).
25. T. KIMURA, K. HIRAO, N. OKABE, and K. FUEKI. Can. J. Chem. **62**, 64 (1984).
26. Y. TAKAI, T. INA, T. MIZUTANI, and M. IEDA. Jpn. J. Appl. Phys. **14**, 1251 (1975).
27. T. KIMURA. K. FUEKI, P. A. NARAYANA, and L. KEVAN. Can. J. Chem. **55**, 1940 (1977).
28. A. M. WANI, T. MUKERJEE, and J. P. MITTAL. Radiat. Eff. Lett. Sect. **43**, 13 (1979).
29. D. D. WILKEY, H. W. FENRICK, and J. E. WILLARD. J. Phys. Chem. **81**, 220 (1977).
30. V. I. VEDENEYEV, L. V. GURVICH, V. N. KONDRAT'YEV, V. A. MADVEDEV, and YE. L. FRANKEVICH. In Bond energies, ionization potentials and electron affiinities. Edward Arnold Ltd., London, U.K. 1966. p. 194.
31. D. BHATTACHARYA and J. E. WILLARD. J. Phys. Chem. **84**, 146 (1980).

Voltammetric studies of the electrochemical behaviour of salicylidene-2-aminopyridine at a hanging-mercury-drop-electrode

REFAT ABDEL-HAMID
Department of Chemistry, Faculty of Science, Sohag, Egypt

Received August 9, 1985

REFAT ABDEL-HAMID. Can. J. Chem. **64**, 702 (1986).

Electrochemical behaviour of salicylidene-2-aminopyridine has been investigated in 0.1 *M* tetraethylammonium perchlorate – dimethylformamide solutions by cyclic voltammetric and convolution potential sweep voltammetric methods. It was found that the depolarizer exhibits two well-defined diffusion-controlled irreversible one-electron waves. The cyclic voltammetric characteristics and the convolution, deconvolution, and logarithmic convolution analyses reveal that salicylidene-2-aminopyridine in such conditions follows a set of two one-electron transfer reactions each followed by an irreversible chemical reaction. The values of the first-order rate constant of the irreversible chemical reaction and $E_{1/2}$ were computed.

REFAT ABDEL-HAMID. Can. J. Chem. **64**, 702 (1986).

Faisant appel à des méthodes de voltamétrie cyclique et de voltamétrie à balayage de potentiel avec convolution et opérant dans des solutions à 0,1 *M* de perchlorate de tétraéthylammonium dans le diméthylformamide, on a étudié le comportement électrochimique de la base de Schiff formée par l'aldéhyde salicylique et l'amino-2 pyridine. On a trouvé que le dépolarisant présente deux vagues monoélectroniques, bien définies, irréversibles et contrôlées par la diffusion. Les caractéristiques de la voltamétrie cyclique, de la convolution, de la déconvolution et des analyses logarithmiques de la convolution suggèrent que, dans les conditions utilisées, la base de Schiff suit un mécanisme électronique–chimique–électronique–chimique. On a calculé les valeurs des constantes de vitesse du premier ordre de la réaction chimique irréversible ainsi que de $E_{1/2}$.

[Traduit par la revue]

Introduction

The electrochemical reduction mechanism of numerous aromatic imines or Schiff bases at a mercury electrode has been investigated in aprotic media (1–6). Relatively few studies, on the other hand, have concerned the electrochemical behaviour of heteroaromatic Schiff bases (7). In view of the considerable success achieved by others in clarifying the mechanism of reduction of aromatic hydrocarbons and carbonyl compounds through investigations in aprotic solvents, a study of the electrochemical reduction behaviour of heteroaromatic Schiff bases in *N,N*-dimethylformamide was undertaken.

This communication is concerned with electrochemical reduction of salicylidene-2-aminopyridine as investigated by cyclic voltammetry and convolution and deconvolution potential sweep voltammetry. The reduction mechanism at the hanging-mercury-drop-electrode (HMDE) is elucidated and discussed.

Experimental

Salicylidene-2-aminopyridine was synthesized by the condensation of salicylaldehyde with 2-aminopyridine in a 1:1 ratio in an ethanolic solution as reported earlier (8). The solid product obtained was recrystallized from ethanol. Tetraethylammonium perchlorate (Fluka) was recrystallized from methanol and dried in a vacuum oven at 60°C. *N,N*-Dimethylformamide (A.R. grade BDH) was purified by passing it through active neutral alumina as described elsewhere (9).

Fresh stock solution of tetraethylammonium perchlorate (TEAP) (0.1 mol dm^{-3}) in dimethylformamide (DMF) was prepared. Fresh stock solution of the Schiff base (10 m*M*) was prepared from a fresh electrolyte solution on the same day that measurements were carried out.

The experiments were performed using 0.1 *M* TEAP/DMF as supporting electrolyte. The measurements were done using a three electrode cell. It consists of a hanging mercury electrode with surface area of 1.05×10^{-2} cm^2 as working electrode, $Ag/AgNO_3$ (0.01 *M*) in 0.1 *M* TEAP/DMF as reference electrode and 1-cm^2 platinum sheet as auxiliary electrode.

Cyclic voltammetry was performed using an E.G. & G. PAR model 363 scanning potentiostat–galvanostat. The current response and potentials were stored on magnetic disk via a fast data-capture system based upon twin chanel 12-bit analogue-to-digital converter (50 μs conversion time) and a Gemini Galaxy 2 microcomputer. Data capture was written in Macro 80 assembler language which allowed a minimum acquisition time of 100 μs per point. In all experiments 500 data points were routinely captured, equally spaced in time, with a time interval appropriate to the time-scale of the particular experiment. Background data were also stored, and were subtracted from the experimental data set, minimizing effects such as double-layer charging currents.

Solutions were purged with nitrogen before each experiment and an atmosphere of nitrogen was maintained above the working solution. Internal resistance ohmic drop distortions were minimized by applying positive feedback compensation.

Convolution and deconvolution procedures were carried out according to the method described earlier (10). The convolution logarithmic analysis was carried out on the basis of the following general equations[1]

$$[1] \quad -\xi = \ln\left[\frac{(I_{lim} - I_1)}{I_2\left(\frac{D_A}{D_B}\right)^{1/2} + \frac{I_{lim} i \exp(1-\alpha)\xi)}{i_o}}\right]$$

and

$$[2] \quad -\alpha\xi = \ln\left[\frac{I_{lim} - I_1 - I_2(D_A/D_B)^{1/2}\exp(-\xi)}{I_{lim}\frac{i}{i_o}}\right]$$

where $\xi = (E - E^\theta)nF/RT$, α is the symmetry factor, I_1 and I_2 are the convolution currents given in eqs. [3] and [4], respectively, I_{lim} is the limit of I_1 and E approaches infinity and i_o is the exchange current for the electron-transfer process at $E = E^\theta$.

$$[3] \quad I_1'' = I_1(t) = \pi^{-1/2}\int_0^t \frac{i(u)}{(t-u)^{\frac{1}{2}}}du$$

$$[4] \quad I_2' = I_2(k',t) = \pi^{-1/2}\int_0^t \frac{i(u)\exp(-k_c'(t-u))}{(t-u)^{\frac{1}{2}}}du$$

[1]T. Boddington, I. D. Dobson, and N. Taylor. Unpublished results.

TABLE 1. First wave characteristics for salicylidene-2-aminopyridine in 0.1 *M* TEAP/DMF at 291 *K*

Sweep rate (mV s^{-1})	$-E_p$ (V)	i_p (μA)	$E_p - E_{p/2}$ (mV)	$i_p/\nu^{1/2}$ (μA $V^{-1/2}$)	$-E_p'$ [a] (V)	k_c [b] (s^{-1})	$-E_{1/2}$ [c] (V)
50	1.8610	0.53	70.2	2.37	1.8251	1.8	1.8252
100	1.8620	0.80	71.0	2.52	1.8262	3.8	1.8270
200	1.8645	1.17	69.5	2.62	1.8270	6.0	1.8290
500	1.8767	2.07	70.3	2.93	1.8278	9.0	1.8347

[a]Deconvoluted peak current potential.
[b]$k_c \pm 3\%$.
[c]$E_{1/2} \pm 0.5\%$.

Results and discussion

It has been found that salicylidene-2-aminopyridine was readily hydrolysed in aqueous and aqueous–organic solvent media into their parent constituents (8, 12). Thus, *N,N*-dimethylformamide is a convenient medium for this electrochemical investigation. Furthermore, studies in DMF give a more direct insight into the electrochemical properties of the azomethine group since, under the usual conditions, a preprotonation step can be excluded in this solvent.

Cyclic voltammograms of salicylidene-2-aminopyridine in anhydrous *N,N*-dimethylformamide containing 0.1 mol dm^{-3} tetraethylammonium perchlorate as supporting electrolyte show two well-defined irreversible waves. The reversal peaks of the two waves are almost nonexistent, indicating that the two waves correspond to two slow one-electron transfers or a fast one-electron transfer coupled with a rapid chemical reaction. The cathodic peak currents, i_p, of the two waves correlated with the square root of the sweep rate, $\nu^{1/2}$, with correlation coefficients of 0.9997 and 0.9987 for the first and second waves, respectively. They are also proportional to the concentration of the Schiff base in the range 0.49–1.19 × 10^{-3} *M* (r = 0.9967 and 0.9970, respectively). These are consistent with diffusion as the rate-limiting step (13). A number of electrochemical criteria are applied to establish the nature of the two waves.

The widths of the first cyclic voltammetric wave ($E_p - E_{p/2}$) at different sweep rates are observed to be insignificantly greater than the theoretical value expected for a reversible charge-transfer step (Table 1) (13). The peak potential, E_p, does shift in a negative direction with increasing scan rate. The plot of E_p against log ν yields a straight line with a slope less than 28.8 mV per decade (−6.9 ± 1 mV). Both observations are indicative of reversible electron transfer coupled with a follow-up chemical reaction (13, 14). This reaction could be regarded as a protonation of the Schiff base radical anion (2).

The variation of current function, $i_p/\nu^{1/2}$, with scan rate ν is an important diagnostic criterion for establishing the type of mechanism by cyclic voltammetry. For a reversible electronic process followed by an irreversible chemical process ($E_{rev}C_{irr}$) the current function should slightly increase with scan rate (15). The ratio slowly increases with scan rate (Table 1) revealing that the observed behaviour is consistent with a reversible electron-transfer process followed by a first-order irreversible chemical reaction.

Convolution of the cyclic voltammetric data of salicylidene-2-aminopyridine is carried out according to eqs. [3] and [4]. Figure 1 illustrates convoluted currents I_1 and I_2 cyclic voltammograms for the first wave of 1.19 × 10^{-3} *M* solution. It is clear that the convoluted current I_1 does not reach the same plateau value, regardless of the scan rate, and does not return

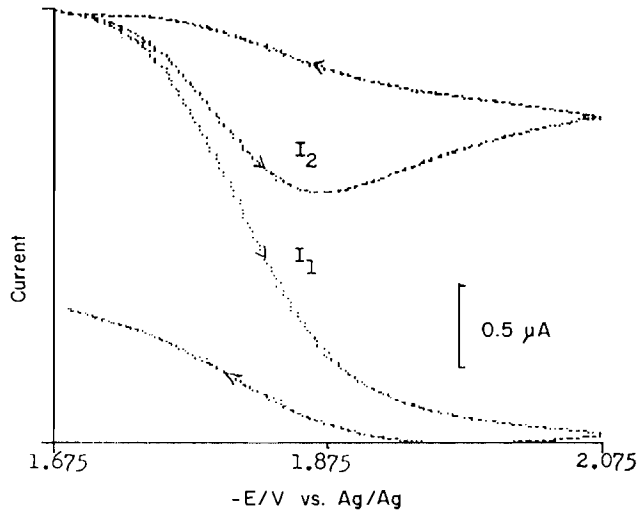

FIG. 1. Cyclic convoluted currents I_1 and I_2 voltammograms for the first wave of 1.19 × 10^{-3} *M* salicylidene-2-aminopyridine in 0.1 *M* TEAP/DMF solution at ν = 500 mV s^{-1}.

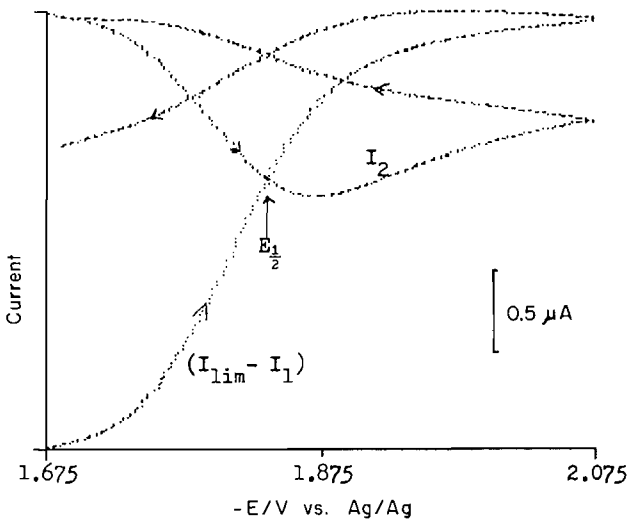

FIG. 2. Curves of ($I_{lim} - I_1$) for the correct treatment of k_c, I_2, and $E_{1/2}$ for the first wave of salicylidene-2-aminopyridine in 0.1 *M* TEAP/DMF solution at ν = 500 mV s^{-1}.

during the reverse half of the sweep to its initial (zero) value. This shows that the starting material is not conserved within the course of the cycle. This behaviour can be ascribed to irreversible electron-transfer or reversible electron-transfer coupled with a rapid chemical reaction.

Deconvolution cyclic voltammetric results reveal that the

TABLE 2. Second wave characteristics for salicylidene-2-aminopyridine in 0.1 *M* TEAP/DMF at 291 K

Sweep rate (mV s^{-1})	$-E_p$ (V)	i_p (μA)	$E_p - E_{p/2}$ (mV)	$i_p/\nu^{1/2}$ (μA $V^{-1/2}$)	$-E_p{}^a$ (V)	$k_c{}^b$ (s^{-1})
50	2.3950	1.16	68.6	5.18	2.3480	0.20
100	2.3994	1.40	69.1	4.43	2.3529	0.53
200	2.4165	1.67	70.0	3.73	2.3651	1.62
500	2.4215	2.16	63.7	3.05	2.3700	3.00

[a]Deconvoluted peak current potential.
[b]$k_c \pm 4\%$.

anodic to cathodic deconvoluted peak-current ratio, dI_{1pa}/dI_{1pc}, is almost less than unity (0.28) through the scan rate range used. This is consistent with the reversible electron-transfer process followed by an irreversible first-order chemical reaction ($E_{rev}C_{irr}$ mechanism), because the anion radical formed is removed from the vicinity of the electrode surface by reaction as well as by diffusion.

The first-order rate constant of the following chemical reaction, k'_c, the convoluted current I_2, and $E_{1/2}$ of the first wave are computed using the digital simulation and experimental data according to the method described earlier[1] (Table 1). The method relies on the equality of $(I_{lim} - I_1)$ and I_2 on both the forward and reverse halves of the sweep at $E = E_{1/2}$, where $E_{1/2} = E^\theta + (RT/nF) \ln (D_A/D_B)^{1/2}$. This is done by iterating different values of k'_c. If the k'_c value used to compute I_2 is large the crossing point of the $(I_{lim} - I_1)$ and $I_2 - E$ curves on the reverse sweep lies negative of the crossing on the forward sweep and I_2 rapidly changes sign after this point. For the low value of k'_c used, the crossing point on the return lies positive of the crossing on the forward scan and I_2 fails to return to zero at the end of the sweep. The correct treatment of data, the correct convoluted I_2 data, and the k'_c and $E_{1/2}$ values show zero displacement of the crossings which both lie at correct $E^{1/2}$. Also I_2 reaches zero at the end of the sweep. The crossing points of $(I_{lim} - I_1)$ and I_2 as a function of potential are demonstrated in Fig. 2 for the correct treatment of data as a representative example.

The convolution logarithmic analysis is tested for various reaction schemes (E_{rev}, EC, CE, E_{irr}, ECE, ...) according to eqs. [1] and [2]. In the sweep-rate range used, it is found that the data of the first wave fit satisfactorily the following equation

$$[5] \quad -\frac{(E - E^\theta)}{RT} nF = \ln[(I_{lim} - I_1)/I_2]$$

It gives rise to straight lines (correlation coefficients nearly one) with slopes close to 39.88 V^{-1} (at 18°C) expected for an $E_{rev}C_{irr}$ mechanism. This gives further support to the above conclusion that the first wave is ascribed to a reversible one-electron transfer followed by irreversible first-order chemical reaction.

The cyclic voltammetric results in the study of the second wave are recorded in Table 2. It can be seen that $(E_p - E_{p/2})$ is slightly greater than the value expected for a reversible process and E_p does shift towards more negative potentials, to the extent of −24.5 mV per log ν unit. Furthermore, the ratio $i_p/\nu^{1/2}$ decreases on increasing the scan rate. All the above evidence suggests that the irreversibility of the second wave is due to a moderately fast first-order reaction involving the product of the second electron-transfer.

Examination of the convoluted cyclic voltammetric data (I_1) for the second wave shows that I_1 during the reverse of the sweep, whatever the scan rate, does not coincide with I_1 on the forward scan and also it does not reach its initial (zero) value at the end of the sweep. Moreover, the anodic-to-cathodic deconvoluted peak-current ratio is always less than unity (0.37) through the scan rate range used. These facts indicate very good consistency of the data and provide a further verification of the $E_{rev}C_{irr}$ mechanism. The first-order rate constants of the follow-up reaction are computed as mentioned above and the values obtained are collected in Table 2.

Logarithmic analysis of the convoluted results is tested for various mechanisms and it is found that the data follow satisfactorily the $E_{rev}C_{irr}$ mechanism.

Taking into account the acid–base properties of the salicylidene-2-aminopyridine (HSAP) ($pK_a = 8.25$ in aqueous solutions (16)), the radical anions should be rapidly protonated by the starting compound through the "father–son" reaction (17) (reactions *ii* and *iv*).

Thus, the whole electrochemical reduction of HSAP in anhydrous *N*,*N*-dimethylformamide can be represented as follows:

$$[i] \quad HSAP + e \rightleftharpoons HSAP^{\cdot-}$$

$$[ii] \quad HSAP^{\cdot-} + HSAP \xrightarrow{k'_c} HSAPH^{\cdot} + SAP^- \quad \Big\} \text{1st wave}$$

$$[iii] \quad HSAPH^{\cdot} + e \rightleftharpoons HSAPH^-$$

$$[iv] \quad HSAPH^- + HSAP \xrightarrow{k'_c} HSAPH_2 + SAP^- \quad \Big\} \text{2nd wave}$$

Acknowledgement

This work has been performed at The University of Leeds, England. The author wishes to thank Dr. N. Taylor for the provision of facilities.

1. V. N. DMITRIEVA, N. A. ROZANEL'SKAYA, L. V. KONONENKO, B. I. STEPANOV, and V. D. BEZUGLYL. Zh. Obshch. Khim. **41**, 60 (1971).
2. C. P. ANDRIEUX and J. M. SAVEANT. J. Electroanal. Chem. Interfacial Electrochem. **33**, 453 (1971); and references therein.
3. M. USHARA and J-I. NAKAYA. Bull. Chem. Soc. Jpn. **43**, 3136 (1970).
4. V. D. BEZUGLYL, L. V. KONONENKO, A. F. KORUNORA, V. N. DMITRIEVA, and B. L. TIMAN. Kh. Obshch. Khim. **39**, 1680 (1969).
5. A. J. FRY and R. C. REED. J. Am. Chem. Soc. **91**, 6448 (1969).
6. J. M. W. SCOTT and W. H. JURA. Can. J. Chem. **45**, 2375 (1969).
7. F. MARTINEZ-ORTIZ, J. VERA, and P. MOLINA. J. Electroanal. Chem. Interfacial Electrochem. **154**, 193 (1983).
8. M. R. MAHMOUD, A. EL-NADY, R. ABDEL-HAMID, and A. A. EL-SAMAHY. Chem. Scr. **19**, 154 (1982).

9. O. HAMMERICH and V. D. PARKER. Electrochim. Acta, **18**, 537 (1973).
10. A. BLAGG, S. W. CARR, G. R. COOPER, I. D. DOBSON, J. B. GILL, D. C. GOODALL, B. L. SHAW, N. TAYLOR, and T. BODDINGTON. J. Chem. Soc. Dalton Trans. 1213 (1985).
11. J. C. IMBEAUX and J. M. SAVEANT. J. Electroanal. Chem. Interfacial Electrochem. **44**, 169 (1973).
12. A. C. DASH, B. DASH, and P. K. MAHAPATRA. J. Chem. Soc. Dalton Trans. 1503 (1983).
13. R. S. NICHOLSON and I. SHAIN. Anal. Chem. **36**, 706 (1964).
14. D. PLETCHER. Chem. Soc. Rev. **4**, 471 (1975).
15. A. J. BARD and L. R. FAULKNER. Electrochemical methods — fundamentals and applications. J. Wiley and Sons, New York. 1980.
16. M. T. EL-HATY. Ph.D. Thesis. Aswan, Egypt. 1978.
17. S. ROFFIA and C. GOTTARADI. J. Electroanal. Chem. Interfacial Electrochem. **142**, 263 (1982).

Mechanism of formation of serine β-lactones by Mitsunobu cyclization: synthesis and use of L-serine stereospecifically labelled with deuterium at C-3

SHAWN E. RAMER, RICHARD N. MOORE, AND JOHN C. VEDERAS[1]

Department of Chemistry, University of Alberta, Edmonton, Alta., Canada T6G 2G2

Received September 16, 1985

SHAWN E. RAMER, RICHARD N. MOORE, and JOHN C. VEDERAS. Can. J. Chem. **64**, 706 (1986).

The ring closure of *N*-benzyloxycarbonyl-L-serine (**1**) under Mitsunobu conditions (Ph_3P, dimethyl azodicarboxylate, −78°C) to give the corresponding β-lactone (**2**) is shown by deuterium and oxygen-18 labelling studies to proceed by hydroxy group activation, in contrast to analogous cyclizations of more hindered β-hydroxy acids, which usually occur by carboxy group activation. Samples of **1** stereospecifically labelled with deuterium at C-3 were prepared by hydrogenation of (*Z*)-2-acetamido-3-methoxyacrylic acid (**9**) with deuterium, followed by selective Acylase I deacetylation of the 2*S* isomer, removal of the protecting groups, and *N*-acylation of the resulting L-serine with benzyl chloroformate. Mitsunobu cyclizations of this 3*R* deuterated *N*-acyl serine, of the [hydroxy-^{18}O] analog **1***g*, and of the [carboxy-^{18}O] derivative **1***f* show that lactonization occurs with inversion of configuration at C-3, loss of the hydroxy oxygen, and retention of the carboxy oxygens. Similar labelling experiments demonstrate that aqueous sodium hydroxide opens the β-lactone ring by exclusive attack at the carbonyl to regenerate **1**, whereas acidic hydrolysis proceeds primarily by attack of water at the C-3 methylene group of **2**. This information allows interconversion of L-serines that are stereospecifically labelled at C-3 with hydrogen isotopes and affords access to other labelled β-substituted alanines.

SHAWN E. RAMER, RICHARD N. MOORE et JOHN C. VEDERAS. Can. J. Chem. **64**, 706 (1986).

Faisant appel à des études par marquage au deutérium et à l'oxygène-18, on a démontré que la cyclisation de la *N*-benzyloxycarbonyl L-sérine (**1**), dans des conditions de Mitsunobu (Ph_3P, azodicarboxylate de diméthyle, −78°C), qui conduit à la formation de la β-lactone corespondante se produit par le biais d'une activation du groupement hydroxyle; ceci est en opposition avec ce qui se produit lors de cyclisations analogues d'acides β-hydroxylés plus empêchés qui se produisent habituellement par le biais d'une activation du groupement carboxyle. On a préparé des échantillons de **1** marqués stéréospécifiquement par du deutérium en C-3 en procédant à une hydrogénation de l'acide acétamido-2 méthyoxy-3 acryliques-(*Z*) (**9**) avec du deutérium suivie d'une déacetylation sélective de l'isomère 2-(*S*) par l'Acylase I, de l'enlèvement des groupes protecteurs et finalement d'une *N*-acylation de la L-sérine qui en résulte par du chloroformate de benzyle. Les cyclisations, selon Mitsunobu, de cette *N*-acyl sérine deutérée en 3(*R*), de son analogue **1***g* portant un hydroxyle ^{18}O et du dérivé **1***f* portant un carboxyle ^{18}O démontrent que la lactonisation se produit avec une inversion de configuration en C-3, avec une perte d'oxygène de l'hydroxyle et avec rétention des oxygènes des groupements carboxyles. Des expériences semblables de marquage ont permis de démontrer que, sous l'influence de l'hydroxyde de sodium aqueux, le cycle de la β-lactone s'ouvre par une attaque qui se produit exclusivement au niveau du groupement carbonyle pour regénérer le composé **1** alors que l'hydrolyse acide se produit principalement par une attaque de l'eau au niveau de groupement méthylène en C-3 du composé **2**. Cette information permet une interconversion de L-sérine qui sont stéréospécifiquement marquées en C-3 avec des isotopes de l'hydrogène et permet un accès facile à d'autres alanines β-substituées qui seraient marquées.

[Traduit par la revue]

Introduction

The Mitsunobu reaction (1) of β-hydroxy carboxylic acids can produce alkenes and (or) β-lactones depending on substrate structure and solvent polarity (2–5). Although a number of earlier attempts to cyclize serine derivatives to β-lactones with various reagents proceeded in low to modest yields (≤1% to 45%) (6–11), we recently reported that reaction of optically pure *N*-acyl serines (e.g., **1**) under slightly modified Mitsunobu conditions (triphenylphosphine and dimethyl azodicarboxylate, −78°C) gives β-lactones (e.g., **2**), without racemization, in good yield (60–72%) (Scheme 1) (12). Previous investigations on the mechanism of the Mitsunobu reaction have shown that an initially-formed triphenylphosphine–azodicarboxylate adduct (13,14) can react with β-hydroxy acids to give either hydroxy group activation (HGA) or carboxy group activation (CGA) (2, 4). Although *intermolecular* Mitsunobu coupling of alcohols with carboxylic acids to form esters generally proceeds by the HGA pathway (1,13), this type of activation of β-hydroxy acids has been reported to result primarily in decarboxylative elimination to olefinic products (2–5). In the cases previously studied, β-lactone products arose principally by the CGA pathway (2,4). Since serine β-lactones are versatile intermediates for synthesis of important β-substituted alanines **3** (Scheme 1) (12), and the availability of the latter compouds stereospecifically labelled with hydrogen isotopes at C-3 would be useful for studies of enzyme mechanisms (15,16), we decided to examine the mode of formation of serine β-lactone **2** using *N*-benzyloxycarbonyl serine (**1**) labelled with oxygen-18 and deuterium at C-3. The site of nucleophilic attack on **1** by water and hydroxide to form **3** and **4** (Scheme 1, Nu = OH) was also investigated.

It is well established that ester or lactone formation by the HGA process in the Mitsunobu reaction proceeds with inversion of configuration at the carbon bearing the hydroxyl, whereas the CGA mechanism results in retention at that position (1, 2, 4). Therefore the position of activation during formation of serine β-lactones can be determined by cyclization of an *N*-protected serine that is stereospecifically labelled with deuterium at C-3. For example, a sample of protected L-serine **1** bearing deuterium in the H_B (pro *R*) position would cyclize to β-lactone **2***a* (^{2}H and nitrogen *cis*) or **2***b* (^{2}H and nitrogen *trans*) depending on whether the reaction follows the CGA or HGA pathway (Scheme 1). Similarly, nucleophilic opening at C-3 of **2***a* or **2***b* would result in inversion of configuration at that carbon to give

[1]Author to whom correspondence should be addressed.

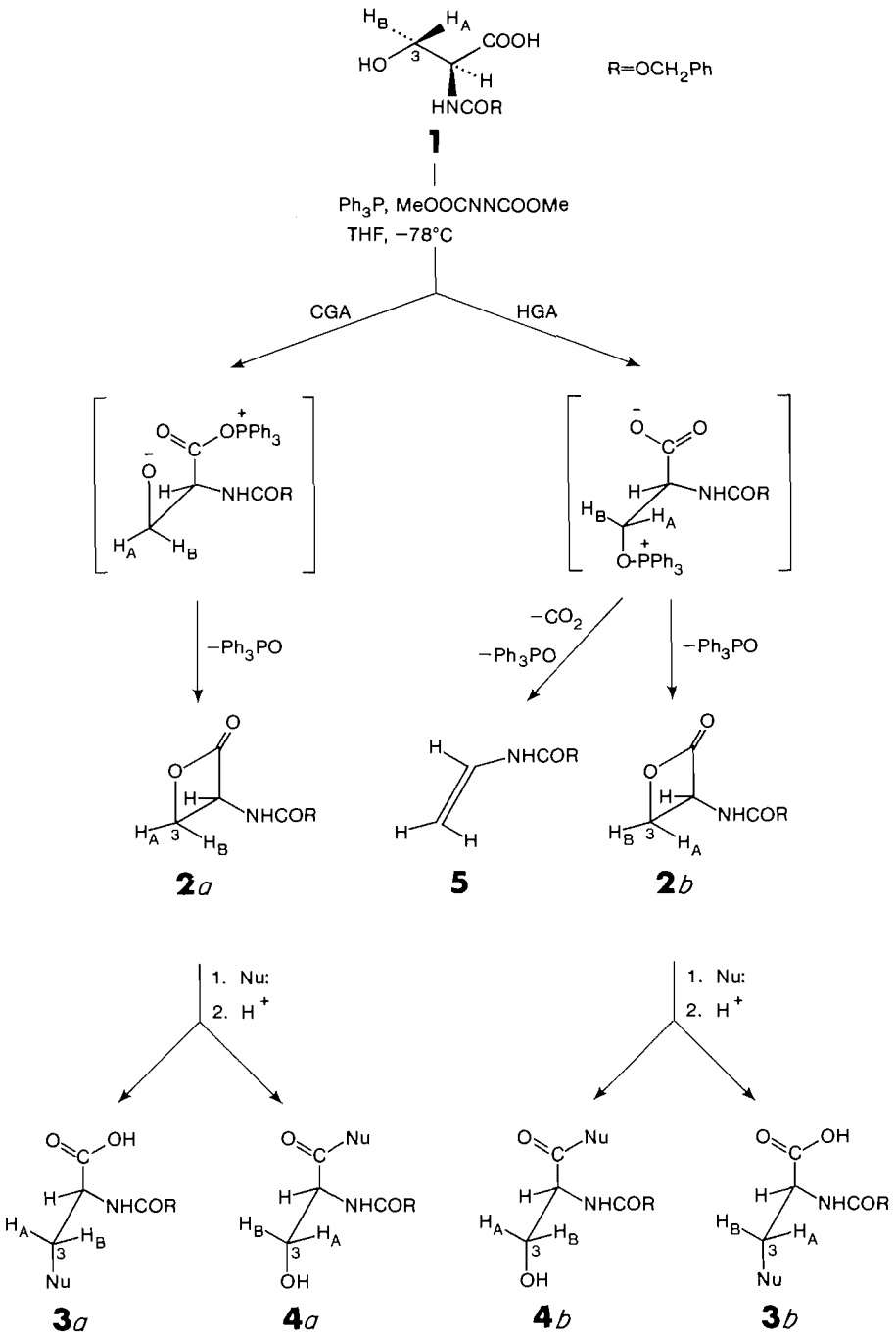

SCHEME 1

3*a* or 3*b*, respectively, whereas carbonyl attack would give 4*a* or 4*b*. If the nucleophile (Nu) is water or hydroxide, isotopic labelling is essential to distinguish between the two types of ring cleavage. Early studies on reaction of β-butyrolactone with [^{18}O]water (17) and on hydrolysis kinetics of β-propiolactone (18) report alkyl-oxygen cleavage at neutral pH and acyl-oxygen fission under strongly acidic or basic conditions.

A number of syntheses of serine labelled stereospecifically with deuterium or tritium at C-3 have been reported (19–26), but many either lack stereochemical purity or are able to produce only very small quantities of material after considerable effort. However, a recent synthesis published while our work was in progress utilizes an approach similar to the one described here (26).

Results

One of the required intermediates, *N*-benzyloxycarbonyl (2*S*, 3*R*)-[2,3-^{2}H$_2$]serine (**1***c*), was synthesized as shown in Scheme 2. Treatment of the known (27) protected chlorodehydroalanine **6** with sodium methoxide in methanol gives the acetal **7** in 96% yield. Elimination of methanol affords exclusively the *Z* isomer of the dehydroserine derivative **8**. The geometry of the double bond was confirmed by nmr spectral comparison to a large number of analogous compounds, including **16** and its *E*

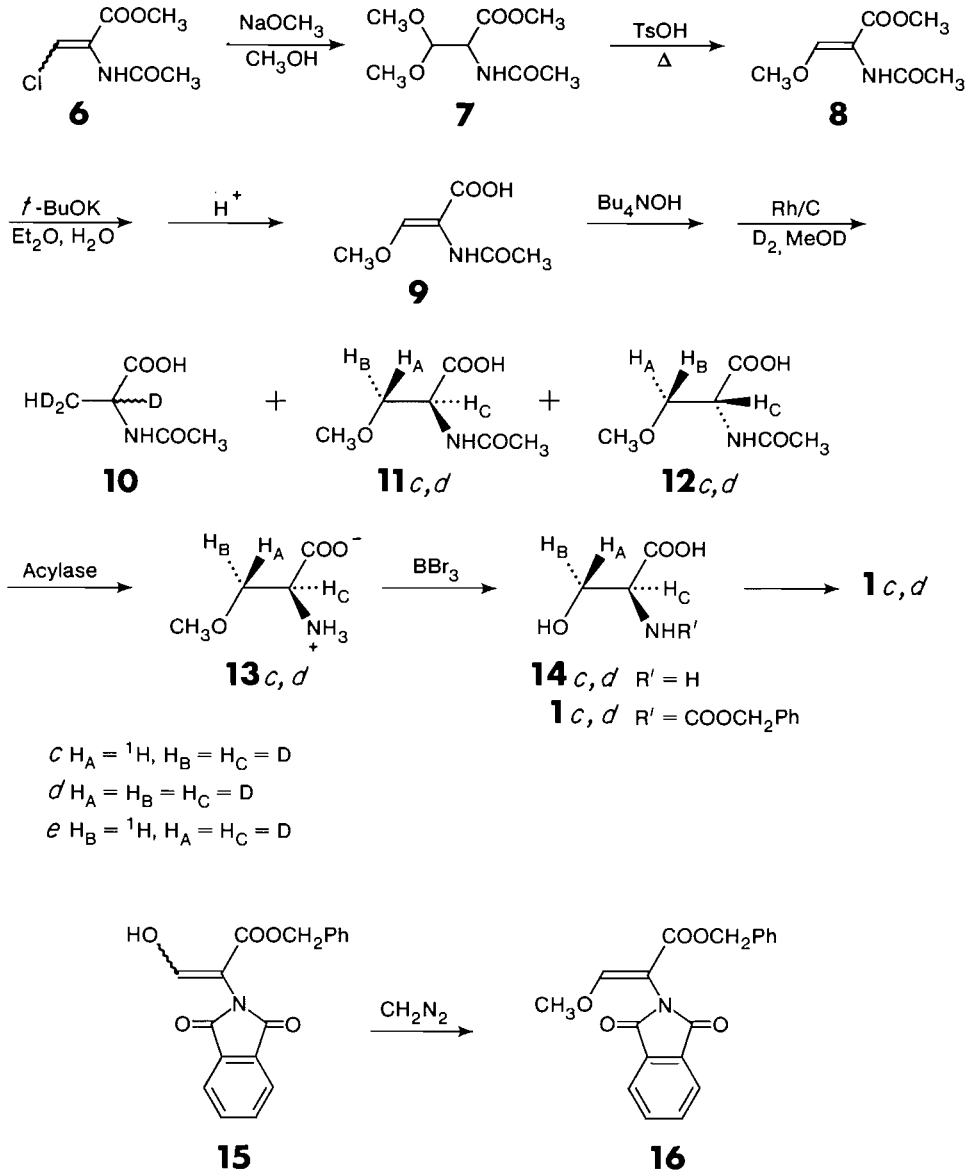

SCHEME 2

isomer, which were prepared by *O*-methylation of 3-oxoalanine derivatives (e.g., **15**) with diazomethane. The structure of the *Z* isomer **16** was determined by X-ray crystallographic analysis.[2] An ORTEP drawing is shown in Fig. 1.

Attempts to hydrogenate the ester **8** with deuterium gas using a variety of conditions gave a mixture of serine and alanine derivatives. Moreover, the ^1H nmr spectra of the resulting serine showed some hydrogen at C-2 and a significant scrambling of deuterium stereochemistry at the C-3 position. Therefore the methyl ester was hydrolysed to the acid **9** using conditions (28) that avoided Michael addition of hydroxide, and the correspoding tetrabutylammonium salt was prepared to decrease the amount of *N*-acetylalanine (**10**) formed during hydrogenation with deuterium. Under optimal conditions (5% Rh/C, methanol-d_1) the deuteration yields the desired 2*S*,3*R* and 2*R*,3*S* compounds **11***c* and **12***c*, respectively, as well as the corresponding trideuterio racemate, **11***d* and **12***d*, and the racemic over-reduction product, *N*-acetylalanine (**10**). However, nmr analysis clearly shows that no 2*R*,3*R* or 2*S*,3*S* serine derivatives are produced.

In general, the deuteration mixture was treated directly with Acylase I from hog kidney (29) to hydrolyse the *N*-acetyl group of the 2*S* amino acids, which are then easily separated from the *N*-acylated 2*R* isomers. The methyl ether of **13***c*,*d* is cleaved without epimerization using boron tribromide (30). Analysis of the product by ^1H and ^2H nmr spectroscopy showed that the dideuterated 2*S*,3*R*-[2,3-$^2H_2$] serine (**14***c*) and the trideuterated 2*S*-[2,3,3-$^2H_3$] serine (**14***d*) are formed in a 2:3 ratio by the hydrogenation procedure. The ^1H nmr spectrum (10% NaOD/D_2O) exhibits a single peak at 3.58 ppm for the H_S proton but has no signal at 3.72 ppm for the H_R proton of the unwanted isomer. The ^2H nmr (10% NaOH/H_2O, $CDCl_3$ internal standard) shows peaks at 3.72 ppm (1D), 3.59 ppm (0.6D), and

[2]Experimental details and tables of crystal data, positional and thermal parameters, anisotropic and isotropic thermal parameters, bond lengths, selected bond and torsional angles, weighted least-squares planes, and observed and calculated structure factors have been deposited and may be purchased from the Depository of Unpublished Data, CISTI, National Research Council of Canada, Ottawa, Ont., Canada K1A 0S2.

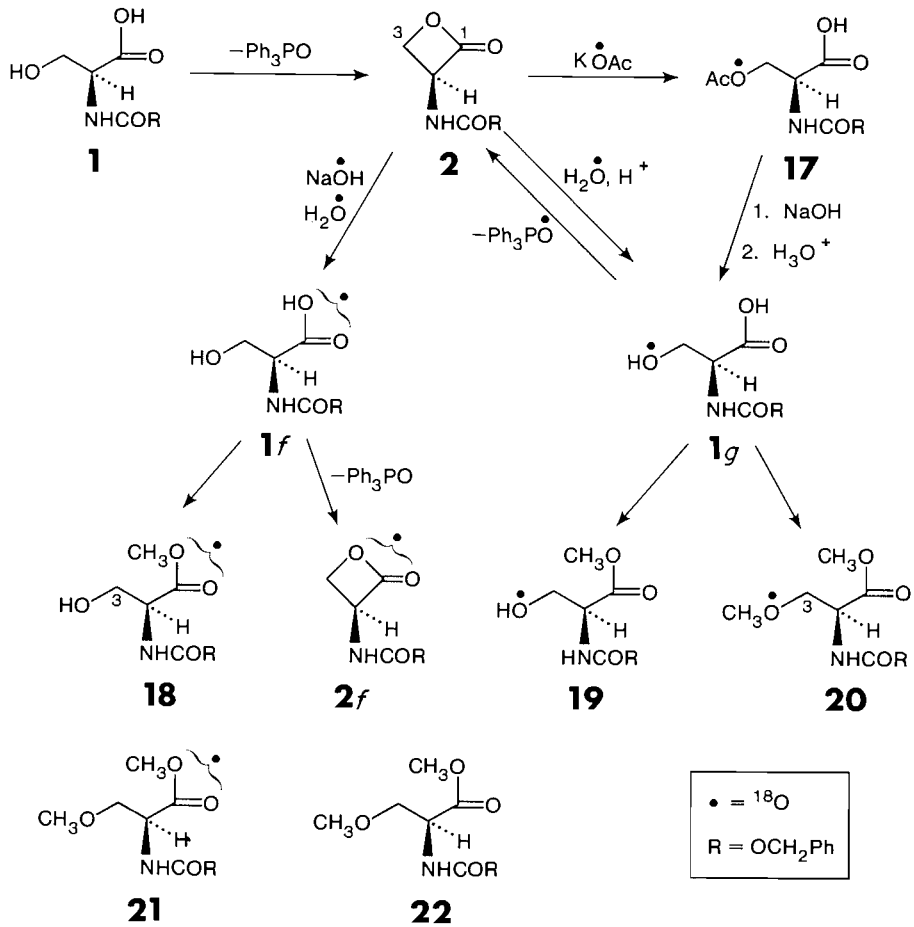

SCHEME 3

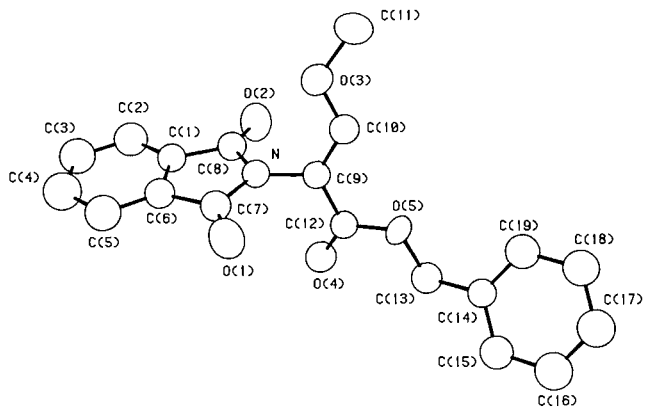

FIG. 1. An ORTEP drawing of (*Z*)-2-(*N*-phthalimido)-3-methoxypropenoic acid phenylmethyl ester **16**. The numbering of the atoms corresponds to that used in the Supplementary X-ray Material.

3.31 ppm (1D at C-2) for this mixture of trideuterated and stereospecifically dideuterated serines **14***d* and **14***c*. The spectra are in agreement with those reported previously for these labelled compounds (25). Treatment of **14***c*,*d* with benzyl chloroformate gave the required *N*-benzyloxycarbonyl serines **1***c*,*d* (31).

Cyclization of **1***c*,*d* afforded the corresponding mixture of trideuterated and dideuterated β-lactones **2**, which were isolated and subsequently opened with aqueous sodium hydroxide to regenerate the *N*-benzyloxycarbonyl-L-serines **1**. The benzyl group was removed by hydrogenolysis and the L-serine was analyzed by nmr spectroscopy as above. The results clearly showed that the process of Mitsunobu cyclization and basic ring opening proceeded with net *inversion* of configuration at C-3 to give **1***d*,*e*. This is consistent either with CGA cyclization and nucleophilic attack at C-3 to form **3***a* (Nu = OH) or with HGA cyclization and nucleophilic attack at the carbonyl to give **4***b* (Nu = OH) (Scheme 1).

The oxygen-18 labelling experiments depicted in Scheme 3 permit discrimination between these two possibilities. Treatment of unlabelled β-lactone **2** with sodium [^{18}O]hydroxide in [^{18}O]water (50% isotopic purity) and tetrahydrofuran (THF) rapidly cleaves the ring to generate the sodium salt of *N*-benzyloxycarbonyl-L-serine (**1***f*). This was acidified under nonaqueous conditions and trapped by diazomethane esterification as its methyl ester **18** to avoid possible exchange of oxygen at the carboxyl. Examination of the ^{13}C nmr spectra of **18** shows ^{18}O isotope shifts of the expected magnitude (32, 33) at the carbonyl carbon ($\Delta\delta$ = 0.015 and 0.038 ppm) and at the methyl carbon ($\Delta\delta$ = 0.026 ppm) but no detectable shift at the hydroxyl carbon, C-3. The complete lack of oxygen-18 at the hydroxyl was confirmed by comparison of the mass spectra of **18** and the isotopic isomer **19**. The latter compound was prepared by opening of the unlabelled β-lactone **2** with potassium [$^{18}O_2$]acetate (34) at C-3 (12) to form [$^{18}O_2$]acetyl-*N*-benzyloxycarbonyl-L-serine (**17**), followed by hydrolysis to hydroxy-labelled **1***g* and esterification (diazomethane) to give **19**. The high resolution electron impact mass spectra of **18** and **19** both display molecular ions and fission of a $COOCH_3$ fragment. With

compound **18** this results in complete loss of all ^{18}O label ($C_{10}H_{12}NO_3$ = 194.0810), but the hydroxy-labelled isomer **19** shows complete retention of ^{18}O ($C_{10}H_{12}NO_2{}^{18}O$ = 196.0684). The results demonstrate that hydroxide attacks the β-lactone **2** exclusively at the carbonyl carbon. Taken together with the deuterium labelling experiment above, it is clear that Mitsunobu cyclization of *N*-benzyloxycarbonyl serine (**1**) follows a hydroxy group activation (HGA) pathway to give β-lactone **2***b* with inversion at C-3; this is then cleaved by hydroxide at the carbonyl to produce **4***b* (Nu = OH) (Scheme 1).

To confirm these observations, the *N*-benzyloxycarbonyl serines **1***f* and **1***g* bearing oxygen-18 in the carboxyl and hydroxy group, respectively, were cyclized to β-lactones (Scheme 3). Mass spectral analysis of these prodcuts demonstrated that ring closure of **1***f* results in retention of all ^{18}O label to form **2***f*, whereas cyclization of **1***g* proceeds with complete loss of ^{18}O to give unlabelled lactone **2**.

Interestingly, reaction of unlabelled β-lactone **2** with [^{18}O]-water and HBF_4 at 20°C causes slow (ca. 11 days) ring opening to hydroxy-labelled *N*-benzyloxycarbonyl serine (**1***g*), which was isolated as its dimethyl derivative **20** by direct treatment with diazomethane. Since carboxylic acids exchange oxygen relatively rapidly under these conditions (35), ^{18}O label also appears in the carboxylate group. The location of label was determined by mass spectral comparison with reference samples of **20**, **21**, and **22**. These were obtained by diazomethane–HBF_4 methylation of the ^{18}O-hydroxy compound **1***g* (derived from acetate **17**), of the ^{18}O-carboxy analog **1***f*, and of unlabelled **1**, respectively. The high resolution electron impact mass spectra of **20**, **21**, and **22** display expected molecular ions as well as loss of a $COOCH_3$ fragment. This fission gives mass peaks $C_{11}H_{14}NO_3$ (208.0980) for compounds **21** and **22**, but produces peaks $C_{11}H_{14}NO_2{}^{18}O$ (210.1020) for the samples of **20** obtained after opening of β-lactone **2** either by [^{18}O]water/HBF_4 or by [^{18}O]acetate. Although the possibility of a certain amount of carbonyl attack on **2** by aqueous acid cannot be excluded under the experimental conditions, it is clear that at least a major portion of the nucleophilic opening occurs by attack at C-3.

Discussion

Our experiments show that Mitsunobu ring closure of *N*-benzyloxycarbonyl serine (**1**) proceeds by hydroxy group activation (HGA) with subsequent loss of the oxygen at C-3 and inversion of configuration at that site to give β-lactone **2***b* (Scheme 1). Opening of this lactone with aqueous hydroxide involves exclusive attack at the carbonyl to form **4***b* (Nu = OH). In contrast, under acidic conditions with water as the nucleophile, displacement at C-3 to give **3***b* (Nu = OH) is the major (if not exclusive) pathway of ring cleavage.

The vast majority of reported β-lactone formations by Mitsunobu coupling of β-hydroxy carboxylic acids occur by carboxyl group activation (CGA), (2,4). In a few cases where the α-carbon (C-2) has much greater steric bulk than the β-carbon (C-3), a minor amount (12–44%) of β-lactone formation by the HGA mechanism has been detected (4). Generally the HGA pathway with β-hydroxy acids has been described to give primarily decarboxylative elimination (2–5), presumably because of antiperiplanar alignment of the breaking bonds. However, these transformations were usually done at about 20°C, and we find that at such temperatures the primary product of Mitsunobu reaction of *N*-benzyloxycarbonyl serine (**1**) is the known (36) olefin **5**.[3] If the rate of addition of **1** to the triphenylphosphine–azodicarboxylate adduct is carefully controlled and the temperature is kept at −78°C, the olefin **5** becomes a minor product and 60% isolated yields of β-lactone **2** can be consistently achieved (12). Since thermal elimination of carbon dioxide from β-lactones once they are formed requires high temperatures (≥100°C) (5), it is the partitioning of the initial HGA adduct which accounts for formation of **5** and **2***b*. The precise factors that control this partitioning remain unknown. Possible explanations for the temperature effect may include the degree of ionization of the C-3 to oxygen bond, the participation of pentacoordinate phosphorus intermediates (13), and the conformational interconversion (2) of *syn* and *anti* coplanar alignments of the carboxy and activated hydroxy groups. Although increase of solvent polarity should promote charge separation and has been shown to affect the ratio of olefin to CGA β-lactone formation in other systems (2), preliminary indications are that a change from THF to acetonitrile has little effect on cyclization of *N*-acyl serines.[3] Apparently, steric interactions favor the HGA intermediate regardless of solvent polarity, and its partitioning to olefin **5** or β-lactone **2***b* is influenced primarily by temperature.

In the cleavage reactions, attack by hydroxide at the carbonyl to give **4***b* (Nu = OH) is in accord with earlier studies (17,18) and with behaviour of β-lactones with other "hard" nucleophiles like methoxide (12, 37). However, hydroxide, unlike methoxide (12), does not cause epimerization at the α-carbon (C-2). Most soft nucleophiles generally displace at C-3 to give **3***b* (12), in agreement with the observed mode of ring opening by [^{18}O]water under acidic conditions. Use of an acid with a non-nucleophilic counter ion (e.g., HBF_4) is essential to obtain attack by water; use of dilute aqueous HCl results in rapid formation of β-chloroalanine (Nu = Cl) (12, 38). Cleavage by nucleophiles other than water is probably a complicating factor in the early studies of acidic β-lactone hydrolysis (17, 18). However, the general observation of alkyl-oxygen fission at neutral to moderately low pH agrees with our results. The previously reported acyl-oxygen cleavage in very strong acid (8 *N* H_2SO_4) was not examined with serine β-lactones **2** because of product decomposition.

Knowledge of the stereochemical outcome of formation of serine β-lactones **2** and their cleavage mechanism permits synthesis of a large variety of β-substituted alanines **3** (12) that are stereospecifically labelled at C-3. Such compounds find continuing use in work on enzyme mechanisms (15, 16, 39, 40). In addition, Mitsunobu cyclization and hydroxide opening of *N*-acyl serines stereospecifically labelled with hydrogen isotopes at C-3 permits facile interconversion of the 3*R* and 3*S* isomers. These compounds are widely employed in biochemical studies, but generally each isomer has required an independent multistep synthesis.

Experimental

Melting points are uncorrected. Infrared (ir) spectra were recorded on a Nicolet 7199 FT system. Proton nuclear magnetic resonance spectra (^1H nmr) were measured using Bruker spectrometers, models WP80, WH200, and (or) WH400. Deuterium (^2H nmr) and carbon-13 (^{13}C nmr) nuclear magnetic resonance spectra were measured on the Bruker WH400. The internal standards were tetramethylsilane for organic solvents and sodium 3-trimethylsilyl-[2,2,3,3-D_4]-propionate for deuterium oxide. High resolution mass spectrometric (ms) measurements were obtained on a Kratos A.E.I. MS50 mass spectrometer using electron impact (EI) and chemical (NH_3) ionization (CI). Microanalyses were obtained using a Perkin Elmer 240 CHN analyser.

Cyclization of N*-benzyloxycarbonyl-*L*-serines* ***1***, ***1***c, ***1***g, *and* ***1***f *to* β*-lactones* ***2***, ***2***b, *and* ***2***f

Unlabelled β-lactone (**2**) was prepared on large scale in 60% yield

[3]Unpublished results, Lee D. Arnold and J. C. Vederas.

from *N*-benzyloxycarbonyl-L-serine (**1**) (Sigma) as previously described (12). In a typical smaller scale experiment, a solution of triphenylphosphine (157.9 mg, 0.601 mmol) in 2 mL of dry tetrahydrofuran was cooled to −78°C and dimethylazodicarboxylate (87.6 mg, 0.600 mmol) was added dropwise. After 10 min a white precipitate formed, to which was added over 10 min *N*-benzyloxycarbonyl-L-serine (**1**) (121.5 mg, 0.508 mmol) in 2 mL of dry tetrahydrofuran. This was stirred at −78°C for 25 min, then allowed to warm to room temperature and stirred for an additional 2.5 h. The solvent was removed and the residue was purified using flash silica chromatography (60:40 Skelly B–ethyl acetate). This gave 48.7 mg (43%) of the β-lactone **2** as a white solid; ir (film): 3363, 1845, 1685 cm^{-1}; ^1H nmr (CD_2Cl_2) δ: 4.48 (2H, d, CH_2-CH), 5.08 (1H, dd, C*H*), 5.15 (2H, s, CH_2-C_6H_5), 5.50 (1H, br s, N*H*), 7.37 (5H, s, aryl-*H*). *Exact Mass* calcd. for $C_{11}H_{11}NO_4$: 221.0688; found: 221.0685.

Similarly, when the ^2H labelled *N*-benzyloxycarbonyl-L-serine (**1***c*,*d*) (see below) was used, the labelled β-lactone **2***b* was formed and showed the expected chromatographic and spectral properties; ^1H nmr (CD_2Cl_2) δ: 4.44 (0.46H, s, C*H*D), 5.14 (1H, s, CH_2), 5.50 (1H, br s, N*H*), 7.38 (5H, s, aryl-*H*). *Exact Mass* calcd. for $C_{11}H_9{}^2H_2NO_4$: 223.0813; found: 223.0810.

From *N*-benzyloxycarbonyl-L-serine with ^{18}O in the carboxyl oxygen (**1***f*) (isotopic content: 71 ± 1% ^{18}O), the β-lactone **2***f* was formed with ^{18}O in the carbonyl and lactone oxygens. This had the expected chromatographic and spectral properties when compared to the unlabelled material (**2**). Isotopic content: 73 ± 1% ^{18}O by chemical ionization (NH_3) mass spectrometry.

From *N*-benzyloxycarbonyl-L-serine with ^{18}O in the hydroxyl oxygen (**1***g*) (isotopic purity: 76% ^{18}O, see below), β-lactone was formed, which showed identical properties to **2** and no indication of ^{18}O in the chemical ionization mass spectrum.

*2-Acetamido-3,3-dimethoxypropanoic acid methyl ester (**7**)*

A solution of sodium metal (1.85 g, 80 mmol) in 150 mL dry methanol was added to 2-acetamido-3-chloroacrylic acid methyl ester **6** (27) (14.3 g, 80 mmol) and the resulting solution was refluxed for 13 h. The methanol was removed *in vacuo* and saturated potassium bicarbonate solution was added. This was extracted with chloroform, and the extracts were dried over sodium sulfate and concentrated *in vacuo* to give 15.7 g (96%) of the dimethoxy compound **7** as an oil; ir (film): 3290, 1750, 1665 cm^{-1}; ^1H nmr ($CDCl_3$) δ: 2.05 (3H, s, $COCH_3$), 3.45 (6H, s, CH_3O-CH), 3.78 (3H, s, CO_2CH_3), 4.61 (1H, d, J = 3.5 Hz, $(CH_3O)_2$-C*H*), 4.88 (1H, dd, J = 3.5, 8.0 Hz, C*H*-NH) 6.33 (1H, br d, J = 8.0 Hz, N*H*); ms m/e: 174 ($M^+ - OCH_3$). *Anal.* calcd.: C 46.82, H 7.37, N 6.83; found: C 46.59, H 7.51, N 6.55.

*(Z)-2-Acetamido-3-methoxyacrylic acid methyl ester (**8**)*

To a solution of 2-acetamido-3,3-dimethoxypropanoic acid methyl ester (**7**) (20.1 g, 99 mmol) in 300 mL of dry toluene was added 500 mg of *p*-toluenesulfonic acid and 130 mg of hydroquinone, and the solution was refluxed for 3.5 h with azeotropic distillation of methanol/toluene. Additional dry toluene was added as necessary. The toluene was removed *in vacuo*, and the residue taken up in 225 mL of saturated sodium chloride solution and extracted with chloroform. The chloroform extracts were dried over sodium sulfate and concentrated *in vacuo* to yield a dark brown oil. This was repeatedly recrystallized from ethyl acetate to give 7.33 g (43%) of colourless vinyl methoxy compound **8**, mp 91–92°C (lit. (41) mp 93°C); ir (film): 3160, 3020, 1720 1660 cm^{-1}; ^1H nmr ($CDCl_3$) δ: 2.03 (3H, s, $COCH_3$), 3.68 (3H, s, CO_2CH_3), 3.83 (3H, s, vinyl-OCH_3), 7.23 (1H, s, vinyl *H*), 7.38 (1H, br s, N*H*). *Exact Mass* calcd. for $C_7H_{11}NO_4$: 173.0688; found: 173.0690. *Anal.* calcd.: C 48.55, H 6.40, N 8.09; found: C 48.57, H 6.34, N 7.90.

*(Z)-2-Acetamido-3-methoxyacrylic acid (**9**)*

To a suspension of potassium *tert*-butoxide (7.50 g, 66.8 mmol) in 150 mL anhydrous ether at 0°C was added 0.195 mL (10.8 mmol) of water. This was stirred for 5 min, methyl ester (**8**) (1.50 g, 8.66 mmol) was added, and stirring was continued at 20°C for 3 h. Ice was added and the separated aqueous phase was run down a 20 mm × 150 mm AG 50 acid-washed ion exchange column. The product was eluted with 100 mL of water and concentrated *in vacuo* to yield 1.32 g (96%) of the free acid **9** as a fluffy white powder; mp 172–174°C; ir (film): 3230, 3030, 1692, 1650 cm^{-1}; ^1H nmr (D_2O) δ: 2.05 (3H, s, $COCH_3$), 3.88 (3H, s, vinyl-OCH_3), 7.38 (1H, s, vinyl *H*). *Exact Mass* calcd. for $C_6H_9NO_4$: 159.0531; found: 159.0532. *Anal.* calcd.: C 45.28, H 5.70, N 8.80; found: C 45.14, H 5.60, N 8.54.

Deuterated L-*serine (**14**c,d)*

In a typical experiment the tetrabutylammonium salt of **9** was prepared by dissolving 0.51 g (3.2 mmol) in one eqivalent of tetrabutylammonium hydroxide and lyophilizing the resulting solution. This was lyophilized 3 times from D_2O if preparing deuterated serine. The oil was taken up in 40 mL of methanol (or CH_3OD) and added to 5% Rh(C) (0.20 g) prehydrogenated for at least 3 h in 100 mL of ethyl acetate. The resulting solution was stirred under 1 atm (101.3 kPa) of hydrogen (deuterium) for 3 h, filtered through Celite, and the solvent removed *in vacuo*. The free acid was obtained by stirring with acid-washed AG50 × 8 ion exchange resin, filtering, and lyophilizing to give a white solid (0.51 g, 96%). This is a mixture of *N*-acetyl-*O*-methylserine (**11** and **12**) and *N*-acetylalanine (**10**) in a 2:3 ratio. When the serine derivative was purified it was spectrally and chromatographically identical to authentic samples (42).

The 2*S* *N*-acetyl compounds (1.20 g of the above mixture) were selectively deacetylated by Acylase 1 using literature methods (29) and the resulting 2*S* amino acids were isolated by AG50 (H^+) ion exchange chromatography (372 mg, 42%). The (2*S*)-*O*-methylserine (**13**) obtained showed the expected spectral and chromatographic properties, compared to authentic *O*-methylserine (Sigma).

The above mixture (0.35 mg, 2.9 mmol) was treated with boron tribromide (12 mmol) in dichloromethane for 2.5 days at room temperature and the L-serine (**14**) (173 mg, 17% from **9**) was isolated from the L-alanine by careful ion exchange chromatography. This had identical spectral properties to authentic L-serine. The deuterated serine obtained in this manner was a 3:2 mixture of **14***d*/**14***c*, ir (film): 1755, cm^{-1}; ^1H nmr (10% NaOD/D_2O) δ: 3.58 (s, C*H*); ^2H nmr (10% NaOH/H_2O, $CDCl_3$ int. standard) δ: 3.31 (1D, s), 3.59 (0.6D, s), 3.72 (1D, s).

Deuterated N-*benzyloxycarbonyl*-L-*serine (**1**c,d)*

This material was prepared from the mixture of (2*S*, 3*R*)-[2,3-$^2H_2$]serine (**14***c*) and (2*S*)-[2,3,3-$^2H_3$]serine (**14***d*) by literature procedure (31); ir (film): 3340, 1715 cm^{-1}; ^1H nmr (D_2O) δ: 3.86 (0.4H, s, C*H*OH), 5.16 (2H, s, CH_2), 7.46 (5H, s, aryl-H). *Exact Mass* calcd. for $C_{11}H_{11}{}^2H_2NO_5$: 241.0919; found: 241.0919.

Hydrolysis of ^2H-labelled β-*lactone **2**b with sodium hydroxide: **2**b → **1**e*

To a cooled (0°C) solution of 0.5 mL tetrahydrofuran, 0.5 mL of water, and 0.194 mL of 0.587 *M* NaOH (0.114 mmol, 1.05 equiv.) was added dropwise a solution of the labelled β-lactone **2***b* (24.2 mg, 0.108 mmol) in 1 mL of tetrahydrofuran. This was stirred 10 min, the tetrahydrofuran removed *in vacuo*, and the water lyophilized. The residue was taken up in 1 mL of 1 *N* HCl and extracted with ethyl acetate. The solvent was removed to give 24.5 mg (95%) of the labelled *N*-benzyloxycarbonyl-serine **1***e* as a white solid; ir (film): 3340, 1715 cm^{-1}; ^1H nmr (D_2O) δ: 3.84 (0.4H, s, C*H*), 5.15 (2H, s, CH_2), 7.45 (5H, s, aryl-*H*). *Exact Mass* calcd. for $C_{11}H_{11}{}^2H_2NO_5$; 241.0919; found: 241.0921.

N-*Phthalimido-3-oxoalanine phenylmethyl ester (**15**)*

The literature preparation was adapted (43). A solution containing 30.0 g (0.101 mol) of *N*-(phthalimido)glycine phenylmethyl ester (44) in 250 mL of benzyl formate (dried over phosphorus pentoxide) was cooled to 5°C and 220 mL of a THF solution of potassium *tert*-butoxide (1 *M*) was added over 1 h. The mixture was kept at 5°C for 36 h and quenched at 0°C by the addition of 10 mL of glacial acetic acid (178 mmol) in 250 mL of dry benzene. After 30 min, the reaction mixture was added to 250 mL of 0.5 *M* aqueous hydrochloric acid and extracted with 4 L of benzene. The combined benzene extracts were concentrated *in vacuo* to yield 26.1 g of **15** (yield 80%); mp. 136.5–138°C; ir (film): 1790, 1720 cm^{-1}; ^1H nmr ($CDCl_3$) δ: 5.20 (s, 1H, N*H*), 5.38 (s, 2H, CH_2), 7.2–7.4 (m, 7H, Ar*H*), 7.85–7.95 (m, 2H, Ar*H*). *Exact Mass* calcd. for $C_{18}H_{13}NO_5$: 323.0794; found: 323.0794. *Anal.* calcd.: C 66.87, H 4.05, N 4.33; found: C 67.09, H 4.22, N 4.27.

Z-2-(N-Phthalimido)-3-methoxypropenoic acid phenylmethyl ester (16)

A solution containing 1.02 g (3.15 mmol) of *N*-phthalimido-3-oxoalanine phenylmethyl ester **15**, 0.5 mL of 1% aqueous HBF_4, and 300 mL of ether was cooled to 0°C. A solution of diazomethane in ether was added until a yellow colour persisted. The mixture was then warmed to 20°C, stirred for 15 h, filtered, and concentrated to a yellow solid. Column chromatography on silica gel (5 × 45 cm), using 32% ethyl acetate in chloroform followed by gradient elution to 100% ethyl acetate, gave 0.93 g of **16** (yield 87%); mp 116–117°C; ir (film): 1790, 1760, 1720, 1650 cm^{-1}; ^1H nmr ($CDCl_3$) δ: 3.89 (s, 3H, CH_3O), 5.21 (s, 2H, CH_2), 7.32 (m, 5H, Ar*H*), 7.71 (m, 3H, Ar*H*, vinyl-*H*), 7.87 (m, 2H, ArH). *Exact Mass* calcd. for $C_{19}H_{15}NO_5$: 337.0950; found: 337.0953. *Anal.* calcd.: C 67.65, H 4.48, N 4.15; found: C 67.58, H 4.50, N 4.11.

Potassium [$^{18}O_2$]acetate

This material was prepared by literature procedure (34) from unlabelled acetonitrile and [^{18}O]water. In order to determine the isotopic content, a portion was treated with α-bromo-*p*-phenylacetophenone using the method reported for preparation of *p*-bromophenacylformate (33). Mass spectrometric (CI) examination of the resulting purified *p*-phenylphenacylacetate (74% yield) gave an isotope ratio of 21.6% $^{18}O_1$ and 76.9% $^{18}O_2$; mp 105–106°C; ir (film): 1724, 1717, 1700, 1600 cm^{-1}; ^1H nmr ($CDCl_3$) δ: 2.23 (3H, s, CH_3), 5.34 (2H, s, CH_2), 7.35–8.08 (9H, m, aryl-*H*). *Exact Mass* calcd. for $C_{16}H_{14}O^{18}O_2$: 258.1029; found: 258.1031.

[^{18}O-Acetyl]-O-acetyl-N-benzyloxycarbonyl-L-serine (17)

The β-lactone **2** (59.6 mg, 0.27 mmol) was added to a solution of potassium [$^{18}O_2$]acetate (142 mg, 1.39 mmol) in dimethylformamide (6 mL) and water (0.5 mL). The mixture was stirred 1.5 h, water (6 mL) was added, and the solution was acidified to pH 2 with 1 *N* HCl. The solution was extracted with chloroform and the extracts were concentrated *in vacuo* to give 77 mg (99%) of pure ^{18}O-labelled *O*-acetyl-*N*-benzyloxycarbonyl-L-serine (**17**); ir (film): 3140, 1710, 1530 cm^{-1}; ^1H nmr ($CDCl_3$) δ: 1.93 (3H, s, $COCH_3$), 4.40 (3H, br, C*H* and CH_2OAc), 5.05 (2H, s, CH_2-C_6H_5), 5.95 (1H, br s, N*H*), 7.23 (5H, s, aryl-*H*). *Exact Mass* calcd. for $C_{13}H_{15}NO_4{}^{18}O_2$: 285.0984; found: 285.0987. Isotopic ratio: 21.4% ^{18}O, 77.1% $^{18}O_2$.

[Hydroxy-^{18}O]-N-benzyloxycarbonyl-L-serine (1g)

A solution of [^{18}O-acetyl]-*O*-acetyl-*N*-benzyloxycarbonyl-L-serine (**17**) (77 mg, 0.27 mmol), 2 mL THF, 2 mL water, and 0.59 *M* sodium hydroxide (1 mL) was stirred at 4°C for 2.5 h. This was acidified with 1 *N* HCl and extracted with ethyl acetate. The solvent was removed *in vacuo* to give 53 mg (82%) of pure ^{18}O-labelled *N*-benzyloxycarbonyl-L-serine (**1g**); ir (film): 3320, 1720 cm^{-1}; ^1H nmr (CD_3OD) δ: 3.85 (2H, d, J = 4.4 Hz, CH_2OH), 4.28 (1H, t, J = 4.2 Hz, C*H*), 5.09 (2H, s, CH_2-C_6H_5), 7.31 (5H, s, aryl-*H*). *Exact Mass* calcd. for $C_{11}H_{13}NO_4{}^{18}O$: 241.0836; found: 241.0830. Isotopic purity: 76.2% ^{18}O.

Hydrolysis of β-lactone 2 with sodium [^{18}O]hydroxide: 2 → 1f → 18

Sodium metal (10.9 mg, 0.473 mmol) was added cautiously to cold (0°C) [^{18}O]water (50% isotopic purity) under an argon stream. To this was added 0.5 ml of THF, followed by the dropwise addition of a solution of *N*-benzyloxycarbonyl-L-serine-β-lactone (**2**) (99.6 mg, 0.450 mmol) in 3 mL of THF. This was stirred for 0.5 h at 20°C, the THF was removed *in vacuo*, and the water was lyophilized to give the crude sodium salt of **1***f*. In preparative experiments the free acid of **1***f* was obtained by dissolving the sodium salt in water, acidifying with 1 *N* HCl, and extracting with ethyl acetate. The ethyl acetate extracts were dried (Na_2SO_4) and concentrated *in vacuo* to give the pure free acid **1***f* (89% yield) with the expected spectral and chromatographic properties. This had an isotopic ratio CI-ms of 71% ^{18}O (prepared from 90 at.% ^{18}O water). *Exact Mass* calcd. for $C_{11}H_{13}NO_4{}^{18}O$: 241.0836; found: 241.0833.

In studies of the mechanism of β-lactone opening, anhydrous ether (10 mL) and *p*-toluenesulfonic acid monohydrate (85.4 mg, 0.449 mmol) were added to the sodium salt of **1***f* and the mixture was treated with an ether solution of diazomethane until a slight yellow color persisted. This was stirred for 0.5 h, filtered, and the solvent was removed *in vacuo* to yield an oil (117.6 mg). This was purified on a silica gel column using Skelly B – ethyl acetate as the eluant to give 56.5 mg (50%) of the methyl ester **18** whose spectral and chromatographic properties were compared to unlabelled material and the corresponding [^{18}O-hydroxy] compound **19**. The ir and ^1H nmr were identical; for compound **18**, ^{13}C nmr ($CDCl_3$) δ; 52.69 (isotope shift 0.026 ppm upfield), 56.17, 63.18, 67.25, 128.16, 128.29, 128.60, 136.20, 156.39, 171.17 (isotope shifts 0.015 and 0.038 upfield). *Exact Mass* calcd. for $C_{12}H_{15}NO_4{}^{18}O$: 255.0992; found: 255.0995.

Acidic hydrolysis of β-lactone 2 with [^{18}O]water: 2 → 1g → 20

A solution of *N*-benzyloxycarbonyl-L-serine-β-lactone (**2**) (72.9 mg, 0.330 mmol) in 1.5 mL THF was added dropwise to a solution of [^{18}O]water (0.70 g, 50% isotopic purity), 0.5 mL THF, and HBF_4 (0.060 mL, 0.329 mmol). This was stirred at room temperature for 11 days, lyophilized, and the residue was taken up in ether. Excess diazomethane was added to the stirred ether solution and the solvent was removed *in vacuo*. The resultant oil **20** was compared spectrally (ir, ^1H nmr, ms) to the unlabelled analog **22** and the [carboxy-^{18}O] analog **21**; for compound **20**. *Exact Mass* calcd. for $C_{13}H_{17}NO_4{}^{18}O$: 269.1149; found: 269.1142.

Esterification of N-benzyloxycarbonyl-L-serine (1) and its [^{18}O-hydroxyl] analog: 1g → 19

A solution of diazomethane in ether was added to *N*-benzyloxycarbonyl-L-serine (**1**) (263 mg, 1.10 mmol) in ether (10 mL) until a yellow color persisted. This was stirred an additional 0.5 h and the solvent removed *in vacuo* to give the unlabelled methyl ester (279 mg, 99%); ir (film): 3350, 1708 cm^{-1}; ^1H nmr ($CDCl_3$) δ: 2.96 (1H, br, s, O*H*), 3.73 (3H, s, CH_3), 3.90 (2H, br, CH_2OH), 4.39 (1H, m, C*H*), 5.09 (2H, s, CH_2-C_6H_5), 5.88 (1H, br d, N*H*), 7.30 (5H, s, aryl-*H*). *Exact Mass* calcd. for $C_{12}H_{15}NO_5$: 253.0950; found: 253.0953.

Similarly, **19** was prepared from **1***g*; the product showed the expected spectral and chromatographic properties. *Exact Mass* calcd. for $C_{12}H_{15}NO_4{}^{18}O$: 255.0992; found: 255.0995.

N-benzyloxycarbonyl-O-methylserine methyl ester (22)

Unlabelled *N*-benzyloxycarbonyl-*O*-methylserine methyl ester was prepared by literature methods (45) from *O*-methylserine to give **22** as an oil; ir (film): 3345, 2947, 1723 cm^{-1}; ^1H nmr ($CDCl_3$) δ: 3.38 (3H, s, OCH_3), 3.78 (3H, s, CO_2CH_3), 3.7 (2H, br m, CH_2OCH_3), 4.5 (1H, m, C*H*), 5.15 (2H, s, CH_2-C_6H_5), 5.6 (1H, br d, N*H*), 7.33 (5H, s, aryl-*H*). *Exact Mass* calcd. for $C_{13}H_{17}NO_5$: 267.1106; found: 267.1104.

Acknowledgments

We are grateful to Lee D. Arnold and Jitendra Singh for helpful discussions and technical assistance, and to Dr. R. G. Ball for X-ray crystallographic analyses. We greatly appreciate financial support from the National Institutes of Health (GM29826), the Natural Sciences and Engineering Research Council of Canada, and the Alberta Heritage Foundation for Medical Research.

1. O. MITSUNOBU. Synthesis, 1 (1981).
2. W. ADAM, N. NARITA, and Y. NISHIZAWA. J. Am. Chem. Soc. **106**, 1843 (1984).
3. J. MULZER and O. LAMMER. Agnew Chem. Suppl. 887 (1983).
4. J. MULZER, G. BRÜNTRUP, and A. CHUCHOLOWSKI. Agnew. Chem. Int. Ed. Engl. **18**, 622 (1979).
5. J. MULZER, A. POINTNER, A. CHUCHOLOWSKI, and G. BRÜNTRUP. J. Chem. Soc. Chem. Commun. 52 (1979).
6. W. L. PARKER, M. L. RATHNUM, and W. LIU. J. Antibiot. **35**, 900 (1982).
7. A. SHANZER and J. LIBMAN. J. Chem. Soc. Chem. Commun. 846 (1983).

8. E. M. GORDON, M. A. ONDETTI, J. PLUSCEC, C. M. CIMARUSTI, D. P. BONNER, AND R. B. SYKES. J. Am. Chem. Soc. **104**, 6053 (1982).
9. V. JARM and D. FLES. J. Polymer Sci. **15**, 1061 (1977).
10. M. MIYOSHI, T. FUJII, N. YONEDA, and K. OKAMURA. Chem. Pharm. Bull. **17**, 1617 (1969).
11. J. C. SHEEHAN, K. HASSPACHER, and Y. L. YEH. J. Am. Chem. Soc. **81**, 6086 (1959).
12. L. D. ARNOLD, T. H. KALANTAR, and J. C. VEDERAS. J. Am. Chem. Soc. **107**, 7105 (1985).
13. E. GROCHOWSKI, B. D. HILTON, R. J. KUPPER, and C. MICHEJDA. J. Am. Chem. Soc. **104**, 6876 (1982).
14. M. VON ITZSTEIN and I. D. JENKINS. Aust. J. Chem. **36**, 557 (1983).
15. M. AKHTAR, V. C. EMERY, and J. A. ROBINSON. *In* New comprehensive biochemistry. Vol. 6. *Edited by* M. I. Page. Elsevier Biomedical Press, Amsterdam. 1984. pp. 303–372.
16. H. G. FLOSS and J. C. VEDERAS. *In* New comprehensive biochemistry. Vol. 3. *Edited by* Ch. Tamm. Elsevier Biomedical Press, Amsterdam. 1982. pp. 161–199.
17. A. R. OLSON and J. L. HYDE. J. Am. Chem. Soc. **63**, 2459 (1941).
18. F. A. LONG and M. PURCHASE. J. Am. Chem. Soc. **72**, 3267 (1950).
19. G. E. SYKE, R. POTTS, and H. G. FLOSS. J. Am. Chem. Soc. **96**, 1593 (1974).
20. C. FUGANTI, D. GHIRINGHELLI, D. GIANGRASSO, P. GRASSELLI, and A. S. AMISANO. Chim. Ind. (Milan), **56**, 424 (1974).
21. M. KAINOSHO and K. AJISAKA. J. Am. Chem. Soc. **97**, 5630 (1975).
22. H. G. FLOSS, E. SCHLEICHER, and R. POTTS. J. Biol. Chem. **251**, 5478 (1976).
23. Y. F. CHEUNG and C. WALSH. J. Am. Chem. Soc. **98**, 3397 (1976).
24. L. SLIEKER and S. J. BENKOVIC. J. Labelled Comp. Radiopharm. **19**, 647 (1982).
25. D. GANI and D. W. YOUNG. J. Chem. Soc. Perkin Trans. 1, 2393 (1983).
26. D. J. ABERHART and D. J. RUSSELL. J. Am. Chem. Soc. **106**, 4902 (1984).
27. A. J. KOLAR and R. K. OLSEN. J. Org. Chem. **45**, 3246 (1980).
28. P. G. GASSMAN and W. N. SCHENK. J. Org. Chem. **42**, 918 (1977).
29. M. JAEGER, S. ISKRIC, and M. WICKERHAUSER. Croat. Chem. Acta, **28**, 5 (1956).
30. M. V. BHATT and S. U. KULKHANI. Synthesis, 249 (1983).
31. J. A. MOORE, J. R. DICE, E. D. NICOLAIDES, R. D. WESTLAND, and E. L. WITTLE. J. Am. Chem. Soc. **75**, 2884 (1954).
32. J. C. VEDERAS. J. Am. Chem. Soc. **102**, 374 (1980).
33. J. M. RISLEY and R. L. VAN ETTEN. J. Am. Chem. Soc. **102**, 4609 (1980).
34. D. E. CANE, T. LIANG, and H. HASLER. J. Am. Chem. Soc. **104**, 7274 (1982).
35. D. SAMUEL and B. L. SILVER. Adv. Phys. Org. Chem. **3**, 123 (1965).
36. M. L. WOLFROM, G. H. MCFADDEN, and A. CHANEY. J. Org. Chem. **26**, 2597 (1961).
37. T. L. GRESHAM, J. E. JANSEN, and F. W. SHAVER. J. Am. Chem. Soc. **70**, 1001 (1948).
38. T. L. GRESHAM, J. E. JANSEN, and F. W. SHAVER. J. Am. Chem. Soc. **72**, 72 (1950).
39. J. L. VAN DER BAAN, J. W. F. K. BARNICK, and F. BICKELHAUPT. J. Chem. Soc. Perkin Trans. 1, 2809 (1984).
40. B. BADET, K. LEE, H. G. FLOSS, and C. WALSH. J. Chem. Soc. Chem. Commun. 838 (1984).
41. F. EFFENBERGER and T. BEISSWENGER. Chem. Ber. **117**, 1497 (1984).
42. J. P. GREENSTEIN and M. WINITZ. Chemistry of the amino acids. Vol. 3. John Wiley and Sons, New York. 1961. p. 2233.
43. G. JUST, B. Y. CHUNG, and K. GRÖZINGER. Can. J. Chem. **55**, 274 (1977).
44. D. A. HOOGWATER, D. N. REINHARDT, T. S. LIE, J. J. GUNNEWEG, and H. C. BEYERMAN. Recl. Trav. Chim. Pays-Bas, **92**, 819 (1973).
45. Z. BERNSTEIN and D. BEN-ISHAI. Tetrahedron, **33**, 881 (1984).

Nuclear magnetic resonance spectra of oriented bicyclic systems containing heteroatom(s): the spectrum of 2-thiocoumarin

S. ARUMUGAM AND C. L. KHETRAPAL[1]

Indian Institute of Science, Bangalore 560 012, India

Received September 27, 1985

S. ARUMUGAM and C. L. KHETRAPAL. Can. J. Chem. **64**, 714 (1986).

From the proton nmr studies of 2-thiocoumarin and coumarin, it is concluded that the relative interproton distances in the two oxygen heteroatom bicyclic systems are similar. The values for the phenyl ring protons do not deviate significantly from the regular hexagonal geometry, unlike bicyclic systems with nitrogens as the heteroatoms, such as diazanaphthalenes. Larger values of the indirect spin–spin couplings within the protons of the ring containing the oxygen heteroatom, compared to the values between the *ortho* protons in the phenyl rings in coumarin and 2-thiocoumarin, correspond to the olefinic nature of these protons. This is in contrast to results for the nitrogen heterocycles where both the rings are aromatic.

S. ARUMUGAM et C. L. KHETRAPAL. Can. J. Chem. **64**, 714 (1986).

Sur la base d'études rmn de la thio-2 coumarine et de la coumarine, on peut conclure que les distances relatives interprotons, dans ces deux systèmes hétérocycliques oxygénés, sont similaires. Les valeurs pour les protons des cycles aromatiques ne dévient pas beaucoup par rapport à la géométrie hexagonale régulière; cette observation est en opposition avec celle qui a été faite avec des systèmes hétérocycliques bicycliques contenant de l'azote, comme les diazanaphtalènes. Par rapport aux valeurs comparables pour les protons *ortho* des noyaux aromatiques de la coumarine et de la thio-2 coumarine, les valeurs observées pour les couplages indirects spin–spin entre le protons du cycle contenant l'oxygène comme hétéroatome sont plus élevées; ce résultat correspondrait à la nature oléfinique de ces protons et cette observation est en opposition avec les résultats obtenus avec les hétérocycles azotés dans lesquels les deux cycles sont aromatiques.

[Traduit par la revue]

Introduction

The proton nmr spectra of oriented bicyclic ring systems containing nitrogen, oxygen, and sulphur as heteroatom(s) have been investigated earlier (1–5). The systems examined are 1,3-, 2,3-, and 1,4-diazanaphthalenes (1–3), coumarin (4), and thialene (5). Except for the system with the oxygen heteroatom, in all the systems the arrangement of protons in the phenyl rings has been found to be distorted from the regular hexagonal geometry. In the oxygen compound (coumarin), no significant deviations from the regular hexagonal geometry have been observed for the relative arrangement of the phenyl protons. The bicyclic system 2-thiocoumarin, which is similar to coumarin, was studied and the results are reported in the present paper. It may be noted that the rings containing the heteroatoms attached to the phenyl ring are aromatic in all cases, except for coumarin and 2-thiocoumarin.

Experimental

A 5 mol% solution of 2-thiocoumarin was prepared in *N*-(*p*-ethoxybenzylidene-)*p'*-*n*-butylaniline (EBBA). The spectrum of the solution was recorded on a Bruker WH-270 FT nmr spectrometer equipped with a BNC-12 computer and 20 K data memory. At 303 K, 240 free induction decays were accumulated and Fourier transformed in order to obtain the frequency domain spectrum. A typical spectrum is shown in Fig. 1. An average line width of 10 Hz was obtained.

Spectral analysis

The iterative analysis of the spectrum was carried out as an ABCDEF system using the LAOCOONOR (6) programme on a DEC-1090 computer. All the 15 direct dipolar HH couplings between the interacting nuclei i and j (D_{ij}'s) were iterated upon, along with the 5 chemical shifts ($\nu_i - \nu_j$). The indirect spin–spin couplings used were taken from the analysis of the spectrum of coumarin in isotropic medium (4). A root-mean-square (rms) error of 0.8 Hz was obtained between the observed and the calculated line positions, with no line deviating by more than 2.0 Hz when 239 spectral lines were assigned for the analysis. The derived parameters are reproduced in Table 1.

[1]Author to whom correspondence should be addressed.

In another analysis, iterations on all the indirect spin–spin coupling constants were also carried out, in addition to those on the direct dipolar couplings and the chemical shifts. Within experimental error, values of the indirect couplings thus determined were similar to those for coumarin. A value for J_{12} of 9.56 Hz was thus obtained, compared to values for the *ortho* protons in the phenyl ring of 7.35 and 7.72 Hz.

Results and discussion

For the planar molecule of the type 2-thiocoumarin, 8 independent relative interproton distances and 3 order param-

TABLE 1. Spectral parameters* for 2-thiocoumarin oriented in the nematic phase of EBBA (values within parentheses are the "best-fit" calculated values)

Parameter	Value (Hz)	Parameter	Value (Hz)
D_{12}	−2284.7 (−2284.8)	D_{35}	126.0 (125.9)
D_{13}	−356.7 (−356.4)	D_{36}	69.3 (69.1)
D_{14}	−119.3 (−119.9)	D_{45}	564.4 (564.4)
D_{15}	−62.7 (−63.0)	D_{46}	−185.9 (−185.9)
D_{16}	−28.4 (−28.4)	D_{56}	−2383.4 (−2383.4)
D_{23}	−2187.6 (−2187.6)	$\nu_2 - \nu_1$	10.0†
D_{24}	−231.7 (−231.5)	$\nu_3 - \nu_1$	−7.6†
D_{25}	−23.8 (−23.5)	$\nu_4 - \nu_1$	−113.3†
D_{26}	64.9 (65.1)	$\nu_5 - \nu_1$	−104.5†
D_{34}	−788.8 (−788.8)	$\nu_6 - \nu_1$	−5.1†

*J values used: J_{12} = 9.56, J_{34} = 7.72, J_{35} = 1.47, J_{36} = 0.50, J_{45} = 7.35, J_{46} = 1.10, J_{56} = 7.72; all other J_{ij}'s = 0.00 Hz.
†At 270 MHz.

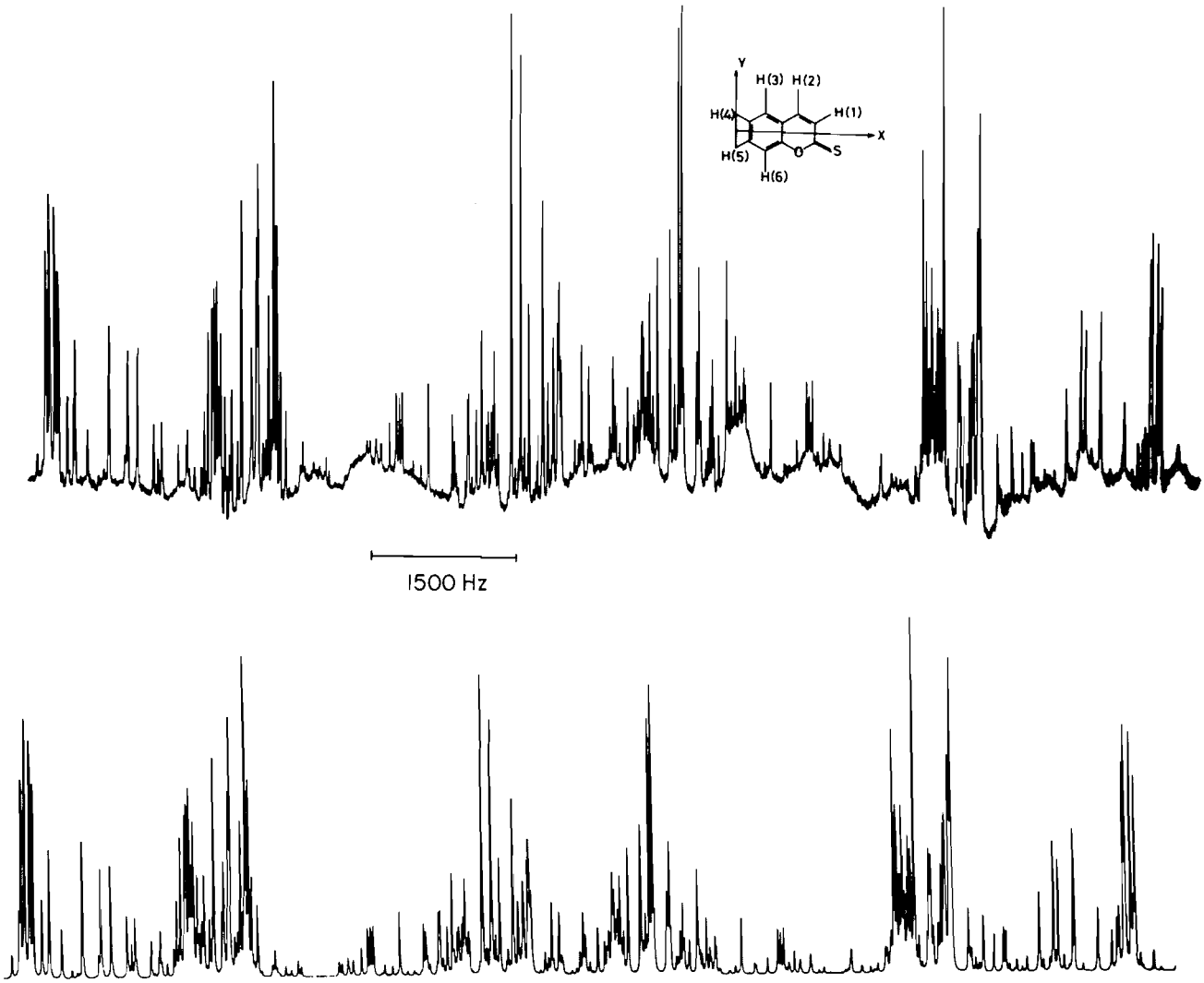

FIG. 1. Experimental (top trace) and calculated (bottom trace) proton nmr spectra of 2-thiocoumarin oriented in nematic phase of *N*-(*p*-ethoxybenzylidene)-*p'*-*n*-butylaniline. Solute concentration: 5 mol%; temperature: 303 K; spectrometer: WH-270; no. of free induction decays accumulated in the experimental spectrum: 240.

TABLE 2. Structural parameters in 2-thiocoumarin and coumarin. The values for the phenyl ring protons in diazanaphthalenes are also included for comparison. The numbering of protons corresponds to that given in Fig. 1, with protons 1 and 2 being those in the ring containing the heteroatoms

	Value				
Parameter	2-Thiocoumarin*	Coumarin (4)	Phthalazine (2)	Quinoxaline (1)	1,3-Diaza-naphthalene (3)
r_{12}/r_{45}	0.997 ± 0.001	0.994			
r_{14}/r_{45}	2.709 ± 0.003	2.707			
r_{15}/r_{45}	2.857 ± 0.003	2.857			
r_{25}/r_{45}	2.397 ± 0.002	2.396			
r_{34}/r_{45}	0.997 ± 0.001	0.998	1.008	1.01	1.003
r_{36}/r_{45}	2.003 ± 0.002	2.000	2.038	2.04	2.023
r_{46}/r_{45}	1.735 ± 0.002	1.733	1.748	1.75	1.738
r_{56}/r_{45}	1.004 ± 0.001	1.001	1.008	1.01	1.005

*The order parameters with respect to the right-handed Cartesian coodinate system with x, y axes being in the ring plane, such that the positive y-axis is the line joining proton 5 to 4, are: $S_{xx} = 0.2958 \pm 0.0009$, $S_{yy} = -0.0718 \pm 0.0001$, $S_{xy} = -0.1185 \pm 0.0005$. The value $r_{45} = 2.481$ Å was used for the calculation of the S-values.

eters (*S*-values) have to be obtained from 15 direct dipolar couplings. The least-squares-fit programme SHAPE (7) was used to determine the "best-fit" values of the relative interproton distances and the order parameters from the experimental dipolar couplings. A root-mean-square error of 0.2 Hz with a maximum deviation of 0.6 Hz between the observed and the "best-fit" computed dipolar couplings was obtained. The values of the calculated dipolar couplings are given in Table 1, within parentheses, and the derived geometrical and order parameters are reproduced in Table 2. The geometrical parameters for coumarin and some heteroaromatic bicyclic ring systems derived essentially from studies in aromatic liquid crystal solvents are included in Table 2 for comparison.

An agreement between the observed and the best-fit calculated dipolar couplings (Table 1) justifies the assumption of the planar structure of 2-thiocoumarin. A comparison of the geometrical data for coumarin and 2-thiocoumarin (Table 2) shows that the structures of the two are very similar and substitution of the sulphur atom for oxygen does not significantly alter the relative proton positions.

Furthermore, the relative interproton distances in the phenyl rings of coumarin and 2-thiocoumarin do not deviate significantly from the regular hexagonal geometry. On the other hand, there are significant distortions in the arrangement of the phenyl protons in the diazanaphthalenes (Table 2).

The larger value of J_{12} in coumarin and 2-thiocoumarin compared to the value for the *ortho* protons of the phenyl ring indicates that the 1 and 2 protons are olefinic in nature and the α-pyrone rings of coumarin and 2-thiocoumarin are both nonaromatic. On the other hand, in the diazanaphthalenes both the rings are aromatic.

Values of the order parameters with respect to the Cartesian coordinate system defined in Table 2 incidate that the principal axis of the order matrix is titled with respect to the selected Cartesian coordinate system by 16.4°.

Harmonic force fields for 2-thiocoumarin could not be located in the literature and hence vibrational corrections have not been applied. Furthermore, for a comparison of the structural data with other heteroaromatic systems where the vibrational corrections have not been applied, it is more reasonable to use the data without applying such corrections.

Conclusions

The structures of 2-thiocoumarin and coumarin are similar. No distortions in the phenyl ring protons are observed in these molecules. In contrast, the fused rings containing nitrogen heteroatoms produce significant distortions in the relative arrangements of the phenyl protons in diazanaphthalenes.

1. C. L. KHETRAPAL and A. C. KUNWAR. Mol. Cryst. Liq. Cryst. **15**, 363 (1972).
2. C. L. KHETRAPAL, A. SAUPE, and A. C. KUNWAR. Mol. Cryst. Liq. Cryst. **17**, 121 (1972).
3. S. ARUMUGAM, A. C. KUNWAR, and C. L. KHETRAPAL. Mol. Cryst. Liq. Cryst. **109**, 263 (1984).
4. E. CAPPELLI, A. DI NOLA, and A. L. SEGRE. Mol. Phys. **27**, 1385 (1974).
5. N. SURYAPRAKASH, C. L. KHETRAPAL, R. F. X. KLEIN, and V. HORAK. Magn. Reson. Chem. In press.
6. P. DIEHL, C. L. KHETRAPAL, and H. P. KELLERHALS. Mol. Phys. **15**, 333 (1968).
7. P. DIEHL, P. M. HENRICHS, and W. NIEDERBERGER. Mol. Phys. **20**, 139 (1971).

Heats of transport of some aqueous nonelectrolytes

A. K. MURKHERJEE
Department of Chemistry, Presidency College, Calcutta – 700 073, India
AND
S. K. SANYAL
Department of Agricultural Chemistry and Soil Science, Bidhan Chandra Krishi Viswavidyalaya, Kalyani – 741 235 Dt. Nadia, W.B., India

Received April 25, 1985

A. K. MUKHERJEE and S. K. SANYAL. Can. J. Chem. **64**, 717 (1986).

The thermal diffusion of aqueous solutions of glucose, sucrose, ethylacetate, and 1,4-dioxan (0.1 *m*) contained in the pores of a sintered glass disc (or porosity G4), which is subjected to a temperature gradient, has been studied. The resulting heat of transport data have been interpreted, in terms of local changes in entropy in the solvent brought forth by the presence of the solutes, and correlated to the hydrophobic hydration effects.

A. K. MUKHERJEE et S. K. SANYAL. Can. J. Chem. **64**, 717 (1986).

On a étudié la diffusion thermique de solutions aqueuses de glucose, de sucrose, d'acétate d'éthyle et de dioxanne-1,4 (0,1 *m*) contenues dans les pores d'un disque de verre fritté (de porosité G4) soumis à un gradient de température. On a interprété les données relatives au transport de chaleur qui en résulte en fonction de changements locaux d'entropie dans le solvant, qui sont causés par la présence de solutés et qui sont reliés à des effets d'hydration hydrophobe.

[Traduit par la revue]

Introduction

Experiments on thermal diffusion through coarsely porous diaphragm have been reported in the past (1–4), but little attention has been paid to the thermal diffusion of nonelectrolytes under these conditions. In the present communication, the thermodiffusive phenomenon of aqueous glucose, sucrose, ethylacetate, and 1,4-dioxan has been studied at a mean temperature of 25°C and a mean concentration ($\bar{m}$) of 0.1 *m* by using a diffusion call designed and fabricated for the present experiment.

Theoretical

A solution-filled pore in a highly porous nonisothermal diaphragm (e.g., a sintered G4 glass disc) may be considered to be equivalent to a microscopic Soret cell in which thermal diffusion proceeds at a moderately fast rate. Thus, the relations used for thermal diffusion in a binary system (5) (and for a solvent-fixed reference frame) can be adopted in the persent case, subject to a supposition (6, 7) that the chemical potential of the component *i* (μ_i) just within the diaphragm at each of its surfaces is the same as that in the adjacent layer of free solution outside the diaphragm. The latter holds true for the assumed equilibrium across each surface of the disc. The heat of transport of the solute ($\hat{Q}$) is thus given by eq. [1] (8)

$$[1] \quad \hat{Q} = RT^2\sigma\left(1 + \frac{\mathrm{d}\ln\gamma}{\mathrm{d}\ln m}\right)_T$$

where σ is the Soret coefficient, and is obtained as,

$$[2] \quad \sigma = -\left(\frac{\mathrm{d}\ln m}{\mathrm{d}T}\right)_{st} = -\frac{1}{\bar{m}}\left(\frac{\Delta m}{\Delta T}\right)_{st}$$

$\bar{m}$ the mean molal concentration, γ the mean activity coefficient on molality scale, and T the mean (absolute) temperature. Δm refers to the concentration difference between the two sides of the diaphragm at the steady state (denoted by subscript "st" in eq. [2], the solution in each half-cell of the glass being kept thoroughly mixed by means of magnetic stirrers (see below).

Experimental

(a) Thermodiffusive cell

The cell (Fig. 1) used is in two parts, containing glass tubes inverted onto each other. The one at the bottom has the G4 glass disc (of thickness 2 mm) fused onto its inner walls, and slips into the tube at the top through a ground glass joint, forming two compartments of nearly equal volumes (245.5 and 246.3 mL, respectively) above and below the diaphragm. A heating element of nichrome wire, covered by glass wool tape is wound around the top glass tube (Fig. 1) and forms a component of a thermoregulating system, also consisting of an electrical contact thermometer, inserted into the top compartment, and a relay unit. The contents of the lower compartment are cooled by passing cold thermostated water through glass cooling coils located inside the compartment. There are side filling tubes, one in each compartment just above and below the glass disc, which are connected through standard joints to graduated vertical glass capillary tubes. The lower compartment is provided with an additional inlet to facilitate the filling procedure. The temperature difference across the diaphragm is measured (to within ±0.02°C) by two pairs of face-to-face copper–constantan thermocouples, held fixed in the two compartments close to the diaphragm. Small magnetic stirrers are provided in two half-cells and are moved by means of a rotating magnet. The whole set-up is enclosed in a large air thermostat maintained at the mean temperature of the experiment.

(b) Materials and method

The nonelectrolytes used, i.e., glucose, sucrose, ethylacetate, and 1,4-dioxan were of high purity grade, and their solutions were prepared in double distilled (deaerated) water of conductivity less than 0.5 μmho cm^{-1}. The initial concentration of each solution studied was 0.1 *m*.

The cell was assembled and filled, from the bottom half-cell through the disc to the top half-cell, with solution, taking care to eliminate the entrapped air bubbles from the whole system. On applying a thermal gradient across the diaphragm, the temperatures were monitored by the thermocouples, and any solvent flow was ascertained by noting the rate of development of pressure difference between the glass capillary tubes emerging from the top and the bottom half-cells. Such solvent flow,

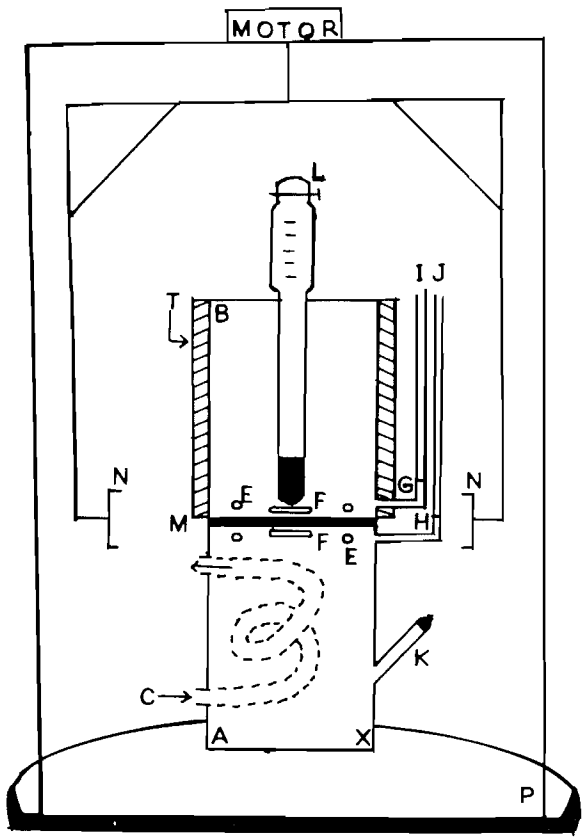

GLASS CELL

FIG. 1. Schematic diagram of the glass cell. Legend: A, lower compartment (246.3 mL); B, upper compartment (245.5 mL); C, glass cooling coil (diameter 1 cm, total length in the lower half-cell is 11.5 cm); E, thermocouple points; F, stirrer; G, H, outlets with standard joints; I, J, graduated tubes; K, inlet for solution; L, contact thermometer (the length of the immersed portion of the thermometer in the upper-half is 12.5 cm and the diameter of that portion is 1 cm); T, heating tape; N, rotating bar magnet; P, iron base; M, glass disc (2 mm thick). Total length of the cell, *AB* is 26.2 cm, diameter of the cell, *AX* is 5.0 cm.

however, turned out to be negligible after making proper correction for unequal thermal expansions in the two compartments.[1]

At the steady state, the aliquots were withdrawn from each compartment, and the concentration difference was determined by a Brice–Phoenix differential refractometer. The latter was previously calibrated with a number of standard pairs of solutions of each solute having known concentration differences.

A number of tests as follows have been applied to the present equipment to insure its satisfactory operation.

(*1*) Initial experiments were run with aqueous solutions of 0.1 *m* $CdSO_4$ and 0.417 *m* urea at 25.0°C to check the reliability of the results obtained with the present cell. The Soret coefficients (σ) thus obtained were within ± 1% of the corresponding values for 0.1 *m* $CdSO_4$ (9) and 0.417 *m* urea (10), determined by independent techniques.

(*2*) For a given solution at the mean temperature of 25°C, the apparatus has been operated at ΔTs from 4 to about 9°C and the same value of σ, within the limits of experimental error, were obtained. The temperatures were monitored throughout a run on a Leeds–Northrup potentiometer capable of recording electromotive force within ±0.5μV.

(*3*) In general, about 1 mL of solution was withdrawn from each compartment to determine the steady state concentrations and the separations obtained were found to be independent of these amounts provided that the volume removed were within 1–3 mL. Similar results were obtained for 0.1 *m* $CdSO_4$ and 0.417 *m* urea solutions of known Soret coefficients.

(*4*) The separation obtained was also found to be independent of the stirrer speed within the range of 140–160 rpm of the rotating magnet. A higher speed tended to lead to lower separations due presumably to some convective remixing which resulted from stirring into the diaphragm (1*b*).

(*5*) The relaxation time (τ) for the present solutions in the given cell was in the range of 800–1000 (taking the effective path length of diffusion to be equal to the thickness (0.2 cm) of the disc, i.e., by neglecting any probable internal structure of the porous disc, and assuming the diffusion coefficient of the given solutes to be of the order of 5×10^{-6} cm^2s^{-1}. Thus, for the composition of the solutions to reach within 1% of the final value at the steady state, a time of 5τ or about 70–90 min must be allowed. The given runs lasted for about 100 min. (Some runs were continued even longer up to 150 min without recording significantly different σ values.)

In addition, trial runs were performed for each solution to find out the time for attainment of the steady state concentrations in each half-cell, and the former turned out to be well within 100 min, in agreement with the requirement of relaxation times as above.

(*6*) The sintered diaphragm is known to be effective in preventing disturbance of the Soret equilibrium by convection (8), even though, for dilute electrolyte solutions (at concentrations less than 0.05 *m*) the results may be influenced by ionic adsorption or other surface effects (8). For the given nonelectrolyte solutions at 0.1 *m* concentrations, such surface effects are considered unimportant. Furthermore, essentially the same σ for a solution obtained for different ΔTs applied at a given mean temperature indicates that the convective remixing is not appreciable (the latter should have been more prominent at a higher ΔT leading to a larger separation). The absence of convective remixing was also ensured by virtue of obtaining a good agreement of σ values of 0.1 *m* $CdSO_4$ and 0.417 *m* urea with the corresponding literature data. It is also known that the amount of convection is inversely related to the sum of the two Rayleigh numbers, R_c and R_T (11) (for a given design of thermal diffusion cell). This sum ($R_c + R_T$), is of the same order of magnitude for 0.1 *m* glucose and 0.1 *m* $CdSO_4$ solutions. The latter is known to be relatively stable to convective remixing.

It may be noted here that the present design of the cell using a G4 sintered diaphragm for separating the hot and the cold compartments has some similarity to the design originally developed by Saxton *et al.* (1954) (1*b*) for the study of thermal diffusion in binary mixtures of organic liquids. Thus, the heating arrangement used for the top half-cell, the temperature measuring devices, and the sample withdrawing outlets, as well as the mode of analysis of the concentration differences have been similar in both cases. However, in the present case, one half-cell simply slips into the other through a ground glass joint with the sintered disc fused onto the walls of the former (Fig. 1), while in the design of Saxton *et al.*, the two half-cells were screwed together externally. Further, the cooling coil in the given case is located inside the lower half-cell unlike the external cooling arrangement used in the cell of Saxton *et al.* Instead of a single external magnet activating the magnetic stirrers in both compartments, as employed in the latter method, the present design uses a rotating framework with a pair of small bar magnets so fixed as to face each other across the diaphragm of the glass cell, and this ensures effective stirring of the solutions in the two compartments.

Results and discussion

The results are incorporated in Table 1. The errors in the determinations of σ and the heat of transport ($\hat{Q}$) are calculated as the standard deviations and shown in parenthesis below each value.

[1]By using the known volume of each half-cell, as well as thermal expansion coefficients of water and glass (the latter being about two order of magnitude less than the former), an allowance was made to account for the unequal thermal expansion of water while recording Δh values between the two glass capillary tubes at each mean temperature of study.

TABLE 1. Experimental parameters for the solutions studied

Solution (0.1 *m*)	T/A	B^a	$10^3\sigma_{mean}{}^b$ (deg^{-1})	$\hat{Q} = RT^2\sigma B$ ($J\,mol^{-1}$)
Glucose	298	1.0	1.69 (±0.03)	1248 (±22.1)
Sucrose	298	1.0	0.58 (±0.02)	428 (±14.8)
Ethylacetate	298	1.0	6.51 (±0.06)	4806 (±44.3)
1,4-Dioxan	298	1.0	6.12 (±0.02)	4518 (±14.8)

[a]The thermodynamic factor defined as $(1 + (d \ln \gamma)/(d \ln m))_T$.
[b]From eq. [2].

The value of the thermodynamic factor, $(1 + (d \ln \gamma)/(d \ln m))_T$, is assumed to be unity in the absence of relevant literature data on activity (or, osmotic) coefficients and is a reasonable approximation for such dilute solutions of nonelectrolytes. The steady state hydrostatic pressure differences (Δh), corrected for unequal thermal expansions, was found to be negligible in all the cases studied.

Positive $\hat{Q}$ corresponds to the promotion of "local" structure (8) of water, i.e., it finds an interpretation in terms of the local ordering (i.e., loss of entropy) of water adjacent to the solute molecules in dilute solutions. The much larger $\hat{Q}$ values of ethylacetate and dioxan than those of the sugars, evidently arise from a more hydrophobic character of the former, which further reinforces such ordering influences. Again, between the two sugars studied sucrose, having a greater number of structure breaking (free) hydroxyl groups than glucose, has a lower $\hat{Q}$. This also agrees with the above picture.

A somewhat higher $\hat{Q}$ for ethylacetate than that of dioxan may possibly be attributed to a ring structure of dioxan so that the (hydrophobic) surface area in contact with neighbouring water is reduced. This finds qualitative support from the reported larger "entropy loss" for the transfer of open chain amines and ethers from the gas phase (at 1 atm pressure) to dilute aqueous solution, as compared to their cyclic analogues (12).

1. (*a*) D. J. TREVOY and H. G. DIRCKAMER. J. Chem. Phys. **17**, 1120 (1949); (*b*) R. L. SAXTON, E. L. DOUGHERTY, JR. and H. G. DRICKAMER. J. Chem. Phys. **22**, 1166 (1954); (*c*) W. M. RUTHERFORD, E. L. DOUGHERTY, and H. G. DRICKAMER. J. Chem. Phys. **22**, 1289 (1954); and (*d*) W. M. RUTHERFORD and H. G. DRICKAMER. J. Chem. Phys. **22**, 1157 (1954).
2. K. F. ALEXANDER. Z. Phys. Chem. (Leipzig), **197**, 233 (1951).
3. F. BELLUCCI, M. BOBIK, E. DRIOLI, F. S. GAETA, D. G. MITA, and G. ORLANDO. Can. J. Chem. Eng. **56**, 698 (1978).
4. F. BELLUCCI, E. DRIOLI, F. G. SUMMA, F. S. GAETA, D. G. MITA, and N. PAGLIUCA. J. Chem. Soc. Faraday Trans. 2, **75**, 247 (1979).
5. J. N. AGAR. The structure of electrolyte solutions. *Edited by* W. J. Hamer. Wiley, New York. 1959. Chapt. 13. p. 200.
6. A. KATCHALSKY and P. F. CURRAN. Non-equilibrium thermodynamics in biophysics. Vol. 112. Harvard University, Cambridge, MA. 1965. p. 185.
7. J. G. KIRKWOOD. Ion transport across membranes. *Edited by* H. T. Clark. Academic Press, New York. NY. 1954. p. 119.
8. J. N. AGAR. Adv. Electrochem. Electrochem. Eng. **3**, 31 (1963).
9. L. G. LONGSWORTH. The structure of electrolyte solution. *Edited by* W. J. Hamer. Wiley, New York, NY. 1959. Chapt. 12. p. 183.
10. M. J. STORY and J. C. R. TURNER. Trans. Faraday Soc. **65**, 1810 (1969).
11. J. N. AGAR and J. C. R. TURNER. Proc. R. Soc. London A, **255**, 307 (1960).
12. S. CABANI, G. CONTI, and L. LEPORI. Trans. Faraday Soc. **67**, 1933 (1971); **67**, 1943 (1971).

Diastereoselectivity and asymmetric induction in the Diels–Alder reaction of *o*-quinodimethanes

JAMES L. CHARLTON

Department of Chemistry, University of Manitoba, Winnipeg, Man., Canada R3T 2N2

Received March 5, 1985[1]

JAMES L. CHARLTON. Can. J. Chem. **64**, 720 (1986).

The extent of asymmetric induction in the bimolecular Diels–Alder reactions of chiral *o*-quinodimethanes with dimethyl fumarate, methyl acrylate, and maleic anhydride has been studied. *o*-Quinodimethanes with chiral α-alkoxy groups were prepared from 1-alkoxy-1,3-dihydrobenzo[*c*]thiophene-2,2-dioxides **4***a–f* or 1-alkoxy-3-phenyl-1,3-dihydrobenzo[*c*]thiophene-2,2-dioxides **4***g–h* by thermolysis. These alkoxybenzosulfones were prepared from the corresponding hydroxybenzosulfones **8** and 1-phenylethanol, 2-phenyl-1-propanol, 4-phenyl-2-butanol, 1-phenyl-2-propanol, 3,3-dimethyl-2-butanol, or 1-cyclohexylethanol. The 1-phenylethoxy substituent yielded the largest asymmetric induction. The absolute configurations of the major cycloadducts of methyl acrylate with the *o*-quinodimethanes generated from 1-(*R*-1-phenylethoxy)- and 1-(*S*-1-phenylethoxy)-1,3-dihydrobenzo[*c*]thiophene-2,2-dioxides **4***i* and **4***j* have been determined to be 1*S*,2*S*-1-(*R*-1-phenylethoxy)- and 1*R*,2*R*-1-(*S*-1-phenylethoxy)-2-carbomethoxy-1,2,3,4-tetrahydronaphthalene **11***i* and **11***j*, respectively. The proposition that a chiral alkoxy substituent can block one face of the *o*-quinodimethane towards addition of a dienophile is discussed.

JAMES L. CHARLTON. Can. J. Chem. **64**, 720 (1986).

On a étudié le degré d'induction asymétrique qui se produit lors de réactions de Diels–Alder bimoléculaires d'*o*-quinodiméthanes chiraux avec le fumarate de diméthyle, l'acrylate de méthyle et l'anhydride maléique. On a préparé les *o*-quinodiméthanes portant les groupements α-alkoxy chiraux en procédant à la thermolyse d'alkoxy-1 dihydro-1,3 benzo[*c*]thiophène dioxydes-2,2 (**4***a–f*) ou d'alkoxy-1 phényl-3 dihydro-1,3 benzo[*c*]thiophène dioxydes-2,2 (**4***g–h*). On a préparé ces alkoxybenzosulfones à partir des hydroxybenzosulfones (**8**) et du phényl-1 éthanol, du phényl-2 propanol-1, du phényl-4 butanol-2, du phényl-1 propanol-2, du diméthyl-3,3 butanol-2 et du cyclohexyl-1 éthanol. Le substituant phényl-1 éthoxy a conduit aux inductions asymétriques les plus élevées. On a déterminé que les configurations absolues des principaux cycloadduits de l'acrylate de méthyle avec les *o*-quinodiméthanes générés à partir du (phényl-1*R* éthoxy)-1 et du (phényl-1*S* éthoxy)-1 dihydro-1,3 benzo[*c*]thiophène dioxydes-2,2 (**4***i* et **4***j*) sont respectivement les (phényl-1*R* éthoxy)-1*S*,2*S* et (phényl-1*S* éthoxy)-1*R*,2*R* carbométhoxy-2 tétrahydro-1,2,3,4 naphtalène (**11***i* et **11***j*). On discute de l'hypothèse selon laquelle un substituant alkoxy chiral peut bloquer une face d'un *o*-quinodiméthane lors de l'addition d'un dièNophile.

[Traduit par la revue]

Introduction

Due to their readiness to undergo Diels–Alder reactions, *o*-quinodimethanes (*o*-QDMs) have been used as intermediates in the synthesis of lignans, alkaloids, steroids, and anthracyclines (1–9). In contrast to the extensive work on asymmetric induction in Diels–Alder reactions of butadienes (10–12), relatively fewer studies have been made of asymmetric induction in Diels–Alder reactions of *o*-QDMs (5, 7, 9). Quinkert and Stark, Oppolzer *et al.*, and Kametani and Fukumoto exploited the stereoselectivity of the intramolecular Diels–Alder reaction of *o*-QDMs to prepare optically active steroids (9). Franck *et al.* have studied the reaction of an achiral *o*-QDM with a chiral dienophile to determine the relative roles of steric and secondary orbital interactions on the asymmetric induction (7). More recently Ito *et al.* (4) have reacted the oxazolidinium system **1** with fluoride ion to give the *o*-QDM **2** bearing a chiral auxiliary that partially controls the stereochemistry of the subsequent addition of dienophiles.[2]

In each of the cases cited above the asymmetric induction was attributed to the ability of the chiral auxiliary to block one face of the *o*-QDM, or to specifically direct the dienophile to one face of the *o*-QDM. In the case of the work of Ito *et al.* it was suggested that π-stacking of the substituent phenyl group blocked one face of the *o*-QDM, as shown by conformations **2A** and **2B**. This suggestion follows from a similar analysis of the addition of dienophiles to chiral butadienes made by Trost *et al.* (11) and Dauben and Bunce (12). By determining the absolute configuration of the cycloadduct **3**, it was concluded that reaction had occurred from conformation **2A**, despite the fact that nonbonded interactions would appear to favour conformation **2B**.

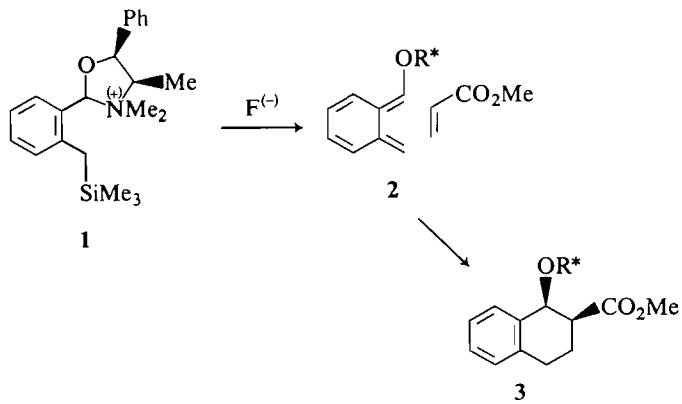

1 2 3

We have recently developed a simple synthesis of 1-alkoxy-

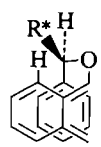

2A

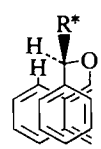

2B

[1]Revision received October 28, 1985.

[2]The absolute configuration of the molecules in the figure is inverted from Ito's work to facilitate comparison to later figures.

1,3-dihydrobenzo[*c*]thiophene-2,2-dioxides **4** (R^1=H, R^2=alkyl) and their 3-phenyl derivatives **4** (R^1=Ph), both of which can be thermalized to the α-alkoxy *o*-QDM **5** (13, 14).

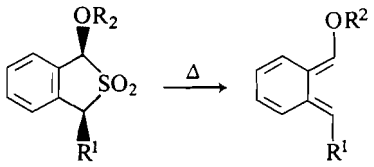

4 **5**

Using these precursors we have undertaken a study of the addition of dimethyl fumarate, methyl acrylate, and maleic anhydride to *o*-QDMs bearing a variety of chiral alkoxy groups, to determine the effect of structure of the chiral auxiliary on the extent of asymmetric induction (15). This study has also yielded information on the mechanism of the induction.

Results and discussion

The addition of α-alkoxy *o*-QDMs to fumarate has been shown previously to give exclusively the *cis*-1,2-*trans*-2,3 adduct (5, 13, 14). Similarly, addition to maleic anhydride has been shown to yield only the all-*cis endo* adducts (5, 16). Asymmetric induction results if a chiral and optically pure group R is able to favour formation of one of the diastereomers **6** or **7**. Separation of **6** and **7** followed by removal of the chiral auxiliary R would yield the optically pure adducts. Typically a large asymmetric induction is desirable as it enables selective synthesis of one of the desired stereoisomers **6** or **7**.

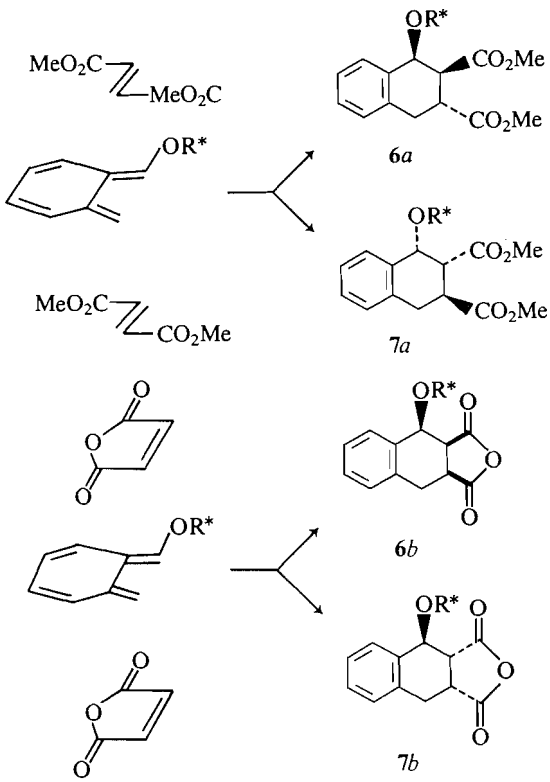

6a

7a

6b

7b

In order to test whether a particular auxiliary can induce asymmetry in the cycloadducts, it is not necessary to use an optically pure group R since the ratio of the diastereomeric cycloadducts can be determined by ^{1}H nmr of the racemic adducts. In this way we have tested several chiral auxiliaries for their ability to give diastereoselectivity in the addition reaction.

In two cases, **4***i* and **4***j*, we have used an optically pure auxiliary to prepare optically pure acrylate cycloadducts, which could be related to a compound of known configuration thereby establishing the absolute configuration of the major cycloadduct.

The chiral auxiliaries were specifically chosen to test the effect of varying the position of the phenyl group and the position of the chiral center, within the auxiliary, on its ability to control the addition sterically. Two auxiliaries having no phenyl group were chosen to investigate asymmetric induction by groups incapable of any π-stacking interactions.

Thus the alkoxysulfones **4***e–j* were synthesized using the approach described previously (13, 14) and illustrated below.

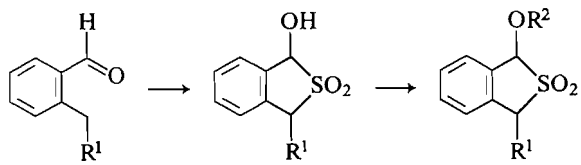

8*a* R^1 = H
8*b* R^1 = Ph

4

4*a* R^1 = H; R^2 = (+/−)-$CHCH_3Ph$
4*b* R^1 = H; R^2 = (+/−)-$CHCH_3CH_2Ph$
4*c* R^1 = H; R^2 = (+/−)-$CHCH_3CH_2CH_2Ph$
4*d* R^1 = H; R^2 = (+/−)-CH_2CHCH_3Ph
4*e* R^1 = H; R^2 = (+/−)-$CHCH_3$cyclohexyl
4*f* R^1 = H; R^2 = (+/−)-$CHCH_3$-tert-butyl
4*g* R^1 = Ph; R^2 = (+/−)-$CHCH_3$-tert-butyl
4*h* R^1 = Ph; R^2 = (+/−)-$CHCH_3Ph$
4*i* R^1 = H; R^2 = (*R*)-$CHCH_3Ph$
4*j* R^1 = H; R^2 = (*S*)-$CHCH_3Ph$

Sulfones **4***a–j* existed as a mixture of diastereomers and these mixtures could only be partially separated by chromatography on silica gel. The ratio of the diastereomers was determined in each case from the ratio of the methyl doublets in the nmr of the crude product and can be found in Table 1. In the case of **4***h* the two diastereomers were separated by chromatography on silica gel to give the individual diastereomers **4***h*-I and **4***h*-II. The yields of **4** (see Table 1) are based on the alcohol. The cycloadducts **9***a–h* were prepared by refluxing in toluene, benzene, or cyclohexane (see Experimental) (5 h) a mixture of **4** (100–200 mg) with four equivalents of dimethyl fumarate and 30 mg of anhydrous zinc oxide powder.

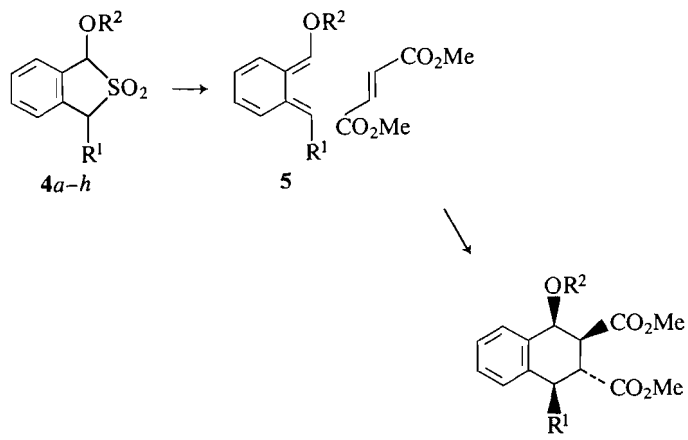

4*a–h* **5** **9***a–h* (+/−)

TABLE 1. Yields and diastereomer ratios

Sulfone	Sulfone yields[a]	Cycloadduct yields[b]	Elimination yields	Diastereomer ratios 4	Diastereomer ratios 9 or 10
4*a,i,j*	85	**9***a,i,j* 85(100)	81	4.3:1	2.8:1
		10*a* (100)			1.6:1
4*b*	83	**9***b* 77(87)	90	1.7:1	1.9:1
4*c*	93	**9***c* 79(91)	87	1.1:1	1:1
4*d*	84	**9***d* (63)	76	1.1:1	1:1
4*e*	65	**9***e* (56)	72	1:1	1:1
4*f*	78	**9***f* (83)	70	1.2:1	1.4:1
4*g*	90	**9***g* (92)	82	1.1:1	1.1:1
4*h*	68	**9***h* (91)	82	1.7:1	2.6:1
		10*h* (100)			1.8:1

[a]Yields are after chromatography.
[b]Includes 5–20% of the *trans*-1,2-adduct. Crude yields in brackets.

4*a* and **4***h* were likewise reacted with maleic anhydride in benzene to give **10***a* and **10***h*.

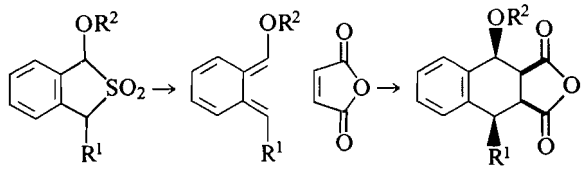

4*a*, **4***h* **5** **10***a*, **10***h* (+/−)

The zinc oxide markedly improves the yield of cycloadducts, presumably by preventing acid-catalysed hydrolysis of **5** due to adventitious water. The two optically active sulfones **4***i* and **4***j* were reacted with methyl acrylate by heating in toluene with an excess of methyl acrylate, in the presence of zinc oxide, at 150°C in a large sealed pressure flask. The adducts were isolated by filtering, evaporation, and recrystallization from hexane.

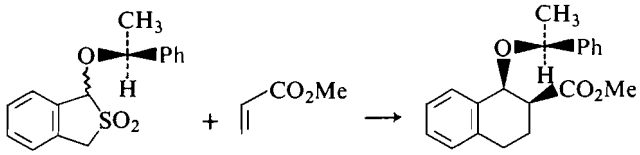

4*i* **11***i* (1′*R*, 1*S*,2*S*)

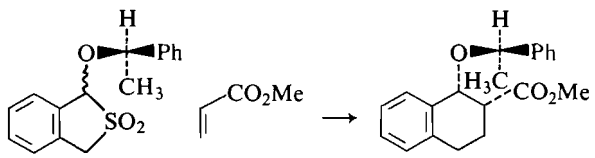

4*i* **11***j* (1′*S*, 1*R*, 2*R*)

Nuclear magnetic resonance spectra of the crude and recrystallized adducts **11***i* and **11***j* indicated that the crystalline material was the major 1,2-*cis* adduct, making up ca. 40% of the crude mixture (nmr). The enantiomeric relationship between **11***i* and **11***j* was confirmed by their opposite rotations (**11***i*, $[\alpha]_D^{20}$ −50.0°; **11***i*, $[\alpha]_D^{20}$ +48.0°; *c* 0.50, $CHCl_3$), and their mirror image cd (circular dichroism) spectra.

The structures of the cycloadducts **9***a–h* were confirmed by elimination (refluxing toluene, toluenesulfonic acid) to form the known dihydrophthalenes **12** and **13** (13).

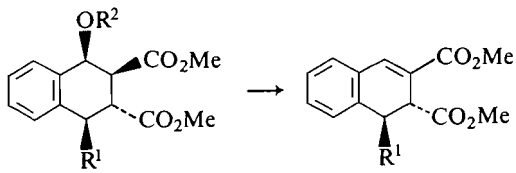

9 *a–f*(+/−) **12** (+/−) R^1 = H **13** (+/−) R^1 = Ph

The optically pure adduct **11***i* was reduced and hydrolysed to the acid **15**.

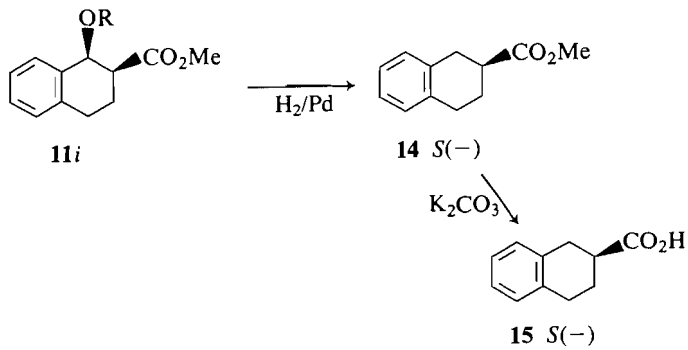

11*i* **14** *S*(−) **15** *S*(−)

The observed rotation of the acid **15** produced from **11***i* was −49.0°, which, when compared to the known configuration and rotation (*R*(+), $[\alpha]_D^{22}$ 55.5°) (17), establishes the configuration of **11***i* as 1′*R*,1*S*,2*S* and that of **11***j* as 1′*S*,2*R*,3*R* as shown.

The crude cycloaddition products **9***a–h* although primarily diastereomeric mixtures of the *cis*-1,2 adducts as determined by nmr (13), also contained 5–30% of the *trans*-1,2 adducts. Despite the complexity of the nmr spectra, it was possible to assign chemical shifts and coupling constants for some of the individual *cis*-1,2 diastereomers (see Experimental). In particular, the diastereomers of the phenyl substituted adduct **9***h* were both analyzable and the spectra confirmed the *cis*-1,2-*trans*-3,4 stereochemistry. This in turn confirmed the *cis* relationship of the phenyl and alkoxy groups in **4***h* since only the *cis*-sulfone could open via a pericyclic reaction to the *E,E o*-QDM **5** and give the observed adduct stereochemistry (13). The yields of the alkoxy sulfones, the cycloadducts, and the diastereomer ratios of each are given in Table 1. The greatest diastereoselectivity was found for the auxiliary 1-phenylethyl, both in the formation of the alkoxysulfones and in the formation of the cycloadducts.

Since the cycloadducts were prepared from the mixture of alkoxysulfone diastereomers, it is tempting to conclude that the diastereoselectivity in adduct formation is actually a chiral memory from the corresponding sulfone. This cannot be the case, however, since the chirality at the benzylic carbon of the sulfone is lost when it thermalizes to the *o*-QDM **5**. To confirm this, the diastereomeric sulfones **4***h*-I and **4***h*-II were each thermalized with fumarate and it was found that the two diastereomeric sulfones gave the identical mixture of cycloadducts.

Mechanism of asymmetric induction

The simplest mechanism that would explain the diastereoselectivity – asymmetric induction in the formation of cycloadducts from the chiral *o*-QDMs, **5**, is one in which the chiral group preferentially blocks one face of the *o*-QDM. In work on the Diels–Alder reactions of dienes, Trost has suggested that chiral auxiliaries containing a phenyl group might block one face of the diene (11). By the use of models we determined that π-stacking in the *o*-QDM should be sterically difficult for a 1-phenylethyl group although this group gave the largest diastereoselectivity. In addition, if one considers the two π-stacked conformations **2**A and **2**B (having an *R*-1-phenylethyl substituent), it can be seen that **2**B should be preferred due to fewer nonbonded interactions relative to **2**A. However, *endo* addition of acrylate to **2**B would have ultimately yielded the *R*(+) acid 15, which was the opposite to that observed. For these reasons we do not think that π-stacking is the mechanism by which the 1-phenylethyl auxiliary directs addition of dienophiles to *o*-QDMs. It should be noted that Ito *et al.* inexplicably came to the opposite conclusion in considering a similar example (4).

In alkyl phenyl esters it has been shown that the most stable conformation is one in which the alkyl group lies in the plane of the aromatic ring allowing *p*–π overlap (18). Rotational barriers of up to 6 kcal/mol have been observed. Based on this analogy we suggest that the preferred conformation of the α-(*R*-1-phenylethyl) *o*-QDM is given by **16**. The relative steric

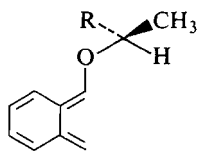

16 *a,b,c* R = Ph, cyclohexyl, *tert*-butyl

bulk of the phenyl and methyl groups serves to block the lower face of the *o*-QDM and cycloaddition of methyl acrylate to the upper face would give the 1′*R*,1*S*,2*S* cycloadduct, as was observed experimentally. This hypothesis is supported by the observation that the *o*-QDM **16***c*, which has a *tert*-butyl substituent in place of the phenyl of **16***a*, also induces asymmetry in the cycloadducts. The effect was smaller and may be because the phenyl group actually has a larger effective size due to specific and stronger solvation. The chiral auxilaries *c*, *d*, and *e* are less conformationally rigid and as such are not as effective in specifically blocking one face of the orthoquinodimethane.

Although we have not determined the absolute configuration of the fumarate and maleic anhydride adducts, we anticipate that this reaction will exhibit the same face selectivity as was observed with methyl acrylate.

Experimental

The nmr spectra were recorded on a Bruker AM-300 spectrometer using tetramethylsilane as an internal standard. The ir spectra were recorded on a Unicam 1000 spectrometer. Merck Kieselgel 60 was used for all column chromatography. Elemental analyses were performed by Guelph Chemical Laboratories Ltd., Guelph, Ontario, Canada. The structures of substituted sulfones **4***a–j* and the cycloadducts **9***a–h* and **11***i,j* are based on the conversion of the cycloadducts to known compounds (**9***a–h* to **12** or **13** and **11***i* to **14** and **15**). Elemental analyses are not included for these compounds.

1-Hydroxy-1,3-dihydrobenzo[c]thiophene-2,2-dioxide, **8**a

This compound was prepared from *o*-methylbenzaldehyde (9.4 g) using the method previously described (13, 14) to yield 6.4 g (34%). Traces of *o*-toluic acid were removed by trituration with a small volume of carbon tetrachloride at 30°C.

1-Hydroxy-4 phenyl-1,3-dihydrobenzo[c]thiophene-2,2-dioxide, **8**b

The sulfone was prepared as described previously (13, 14) from *o*-benzylbenzaldehyde (9.3 g) to yield 8.0 g (65%).

1-Alkoxy-1,3-dihydrobenzo[c]thiophene-2,2-dioxides and 1-alkoxy-3-phenyl-1,3-dihydrobenzo[c]thiophene-2,2-dioxide, **4**

The alkoxysulfones **4***a–j* were prepared by refluxing, for 5 h, a methylene chloride solution of 1.1–1.5 mmol of the corresponding hydroxy sulfone **8***a* or **8***b*, 5 mg of toluenesulfonic acid, and 1.0 mmol of the alcohols *rac*-1-phenylethanol, *rac*-2-phenylethanol, *rac*-3-phenylbutanol, *rac*-1-phenyl-2-propanol, *rac*-3,3-dimethyl-2-butanol, or *rac*-1-cyclohexylethanol. Compounds **4***i* and **4***j* were prepared from the pure enantiomers *R*-(+)-phenylethanol and *S*-(−)-phenylethanol. The alkoxy sulfones were isolated by washing the methylene chloride solution with 5% aqueous bicarbonate, drying, and evaporating, or more simply by filtering the mixture through a short silica gel column (5 cm × 1.5 cm) with methylene chloride, and evaporating. Crude yields were typically 90–100%. In most cases the mixture of diastereomeric sulfones was further purified by chromatography on silica gel using 20% ethyl acetate – hexane as eluant. In one case (**4***h*), the two constituent diastereomers were separated using the same solvent system. The following spectral data were obtained from the mixed diastereomers **4***a–h* and the separated diastereomers **4***h*-I and **4***h*-II.

4*a*: Major isomer I: ^{1}H nmr ($CDCl_3$) δ: 1.612 (d, J = 6.46, CH_3), 4.192 (d, J = 15.74, H-3A), 4.449 (d, J = 15.74, H-3B), 5.120 (s, H-1), 5.232 (q, J = 6.46, H-1′), 7.2–7.5 (m, aromatics).

4*a*: Minor isomer II: ^{1}H nmr ($CDCl_3$) δ: 1.691 (d, J = 6.44, CH_3), 4.187 (d, J = 15.6, H-3A), 4.371 (d, J = 15.6, H-3B), 5.176 (q, J = 6.44, H-1′), 5.531 (s, H-1), 7.2–7.5 (m, aromatics).

4*b*: Major isomer I: ^{1}H nmr ($CDCl_3$) δ: 1.461 (d, J = 6.22, CH_3), 2.905 (dd, J = 5.39, 13.75, H-1A′), 2.992 (dd, J = 7.76, 13.75, H-1B′), 4.145 (d, J = 15.59, H-3A), 4.312 (d, J = 15.59, H-3B), 4.4 (m, H-2′), 5.191 (s, H-1), 7.2–7.5 (m, aromatics).

4*b*: Minor isomer II: ^{1}H nmr ($CDCl_3$) δ: 1.289 (d, J = 6.08, CH_3), 2.771 (dd, J = 8.69, 13.23, H-1A′), 3.280 (dd, J = 4.67, 13.23, H-1B′), 4.221 (d, j = 15.60, H-3A), 4.394 (d, J = 15.60, H-3B), 4.4 (m, H-2′), 5.498 (s, H-1), 7.2–7.5 (m, aromatics).

4*c*: Mixture of two diastereomers: ^{1}H nmr ($CDCl_3$) δ: 1.398 (d, J = 6.08) and 1.458 (d, J = 6.25) H-1′, 1.90(m(and 2.06(m) H-3′, 2.7–2.9(m(H-4′, 4.151(m) and 4.25(m) H-2′, 5.492(s) and 5.470(s) H-1, 4.383 (d, J = 15.7), 4.383 (d, J = 15.6), and 4.373 (d, J = 15.7) H-3, 7.1–7.5 (m, aromatics).

4*d*: Mixture of two diastereomers: ^{1}H nmr ($CDCl_3$) δ: 1.323 (d, J = 6.85 and 1.366 (d, J = 6.98) H-3′, 3.164 (octet, J = 7.17) H-2′, 3.882 (dd, J = 7.45, 9.39) H-1A′, 3.918 (dd, J = 7.72, 9.50) and 4.33(m) H-1′, 4.171 (d, J = 15.8), 4.185 (d, J = 15.8), 4.329 (d, J = 15.8), and 4.334 (d, J = 15.8) H-3, 5.192(s) and 5.332(s) H-1, 7.026 (d, J = 5.35) H-4, 7.2–7.45 (m, aromatics).

4*e*: Mixture of two diastereomers: ^{1}H nmr ($CDCl_3$) δ: 1.15(m) and 1.75(m) cyclohexyl, 1.337(d, J = 6.17) and 1.354(d, J = 6.42) H-1′, 3.919(d of quart, J = 6.39, 5.42) and 3.988(quintet, J = 6.11) H-2′,

4.21(br d, J = 15.9) and 4.37(br d, J = 15.9) H-3, 5.506(s) H-1, 7.726(m) H-4, 7.743 (m, aromatics).

4*f*: Major isomer I: ^{1}H nmr ($CDCl_3$) δ: 0.984 (s, *tert*-butyl), 1.309 (d, J = 6.22, CH_3), 3.945 (q, J = 6.22, H-1′), 4.207 (d, J = 15.6, H-3A), 4.347 (d, J = 15.6, H-3B), 5.546 (s, H-1), 7.2–7.6 (aromatics).

4*f*: Minor isomer II: ^{1}H nmr ($CDCl_3$) δ: 1.024 (s, *tert*-butyl), 1.410 (d, J = 6.41, CH_3), 3.733 (q, J = 6.41, H-1′), 4.217 (d, J = 15.6, H-3A), 4.355 (d, J = 15.6, H-3B), 5.546 (s, H-1), 7.2–7.6 (aromatics).

4*g*: Isomer I: ^{1}H nmr ($CDCl_3$) δ: 0.926 (s, *tert*-butyl), 1.328 (d, J = 6.22, CH_3), 3.901 (q, J = 6.22, H-1′), 5.278 (s, H-1), 5.676 (s, H-3), 7.0–7.7 (aromatics).

4*h*-I: ^{1}H nmr ($CDCl_3$) δ: 1.733 (d, J = 6.44, H-2′), 5.213 (q, J = 6.44, H-1′), 5.270 (s, H-1), 5.708 (s, H-3), 7.07 (m, H-4), 7.2–7.6 (m, aromatics).

4*h*-II: ^{1}H nmr ($CDCl_3$) δ: 1.563 (d, J = 6.45, H-2′), 5.190 (q, J = 6.44, H-1′), 5.270 (s, H-1), 5.708 (s, H-3), 7.07 (m, H-4), 7.2–7.6 (m, aromatics).

trans-*1,2*-trans-*2,3-1-Alkoxy-2,3-dicarbomethoxy-1,2,3,4-tetrahydronaphthalene,* **9**a–f, *and* trans-*1,2*-trans-*2,3*-trans-*3,4-1-alkoxy-2,3-dicarbomethoxy-4-phenyl-1,2,3,4-tetrahydronaphthalene,* **9**g *and* **9**h

The cycloadducts were prepared by refluxing a solution (10 mL) of each of **4***a–g*, **4***h*-I, or **4***h*-II (100–200 mg), four equivalents of dimethyl fumarate, and 30 mg of anhydorus zinc oxide powder for 5 h. The following solvents were used: **4***a–f* toluene, **4***g* benzene, **4***h* cyclohexane. The solution was filtered through a 5 cm × 1.5 cm silica gel column with methylene chloride, evaporated to dryness, and then heated at 100°C at high vacuum to remove excess fumarate. The mixture of diastereomerers was then analysed by nmr. The structures of the cycloadducts were confirmed by elimination of the alcohol as described below.

9*a*: Major isomer I: ^{1}H nmr ($CDCl_3$) δ: 1.400 (d, 6.40, H-1′), 2.800 (dd, J = 10.85, 16.8, H-4a), 3.137 (dd, J = 3.19, 11.35, H-2), 3.259 (dd, J = 6.6, 17.0, H-4e), 3.622 (dt, J = 6.75, 11.15, H-3), 3.747 (s, OCH_3), 4.501 (q, J = 6.40, H-2′), 6.686 (d, J = 7.2, H-5), 6.95–7.40 (m, aromatics).

9*a*: Minor isomer II: ^{1}H nmr ($CDCl_3$) δ: 1.197 (d, 6.45, H-1′), 2.881 (dd, J = 9.45, 16.85, H-4a), 3.002 (dd, J = 2.285, 11.07, H-2), 3.392 (dd, J = 7.63, 16.8, H-4e), 3.74 (ddd, J = 7.6, 7.5, 11.1, H-3), 3.661 (s, OCH_3), 3.736 (s, OCH_3), 4.363 (q, J = 6.39, H-2′), 6.95–7.4 (m, aromatics).

9*b*: Mixture of two diastereomers: ^{1}H nmr ($CDCl_3$) δ: 0.845 (d, J = 6.11, CH_3), 1.106 (d, J = 6.04, CH_3), 2.4–3.8 (series of mult), 3.717 (s, OCH_3). 3.74 (s, OCH_3), 4.847 (d, J = 3.06, H-1), 4.931 (d, J = 2.98, H-1), 6.87 (m, H-5), 7.0–7.3 (m, aromatics).

9*c*: Mixture of (mainly) two diastereomers: ^{1}H nmr ($CDCl_3$) δ: 0.885 (d, J = 6.14, CH_3), 1.114 (d, J = 6.02, CH_3), 1.45–1.95 (m, H-3′), 2.1–3.65 (series of mult), 3.694 (s, OCH_3), 3.723 (s, OCH_3), 3.737 (s, OCH_3), 3.739 (s, OCH_3), 4.45 (d, J = 3.10, H-1), 4.876 (d, J = 2.98, H-1), 6.76 (d, H-5), 7.0–7.4 (m, aromatics).

9*d*: Mixture of two diastereomers: ^{1}H nmr ($CDCl_3$) δ: 1.136 (d, J = 7.01, CH_3), 1.193 (d, J = 6.88, CH_3), 2.75–3.8 (series of mult, H-2, H-3, H-4), 3.534 (s, OCH_3), 3.709 (s, OCH_3), 3.728 (s, OCH_3), 3.740 (s, OCH_3), 4.706 (d, J = 3.30, H-1), 4.724 (d, J = 3.28, H-1), 7.1–7.3 (m, aromatics).

9*e*: Mixture of two diastereomers: ^{1}H nmr ($CDCl_3$) δ: 0.694 (d, J = 6.33, CH_3), 1.053 (d, J = 6.19, CH_3), 1.1(br m, cyclohexyl), 1.6 (br m, cyclohexyl), 2.8–3.5 (series of mult, H-2–H-4), 3.743 (s, OCH_3), 3.738 (s, OCH_3), 3.728 (s, OCH_3), 4.111 (d, J = 3.11, H-1), 4.849 (d, J = 2.91, H-1), 7.1–7.3 (m, aromatics).

9*f*: Major isomer: ^{1}H nmr ($CDCl_3$) δ: 0.590 (s, *tert*-butyl), 1.031 (d, J = 6.18, CH_3), 2.8–3.4 (series of mult, 4H), 3.295 (q, J = 6.18, H-1′), 3.73 (s, OCH_3), 4.805 (d, J = 2.97, H-1).

9*f*: Minor isomer: ^{1}H nmr ($CDCl_3$) δ: 0.806 (s, *tert*-butyl), 0.490 (d, J = 6.3, CH_3), 2.8–3.4 (series of mult, 4H), 3.200 (d, J = 6.3, H-1′), 3.73 (s, OCH_3), 4.839 (d, J = 2.79, H-1).

9*g*: Major isomer: ^{1}H nmr ($CDCl_3$) δ: 0.723 (s, *tert*-butyl), 1.10 (d, J = 6.15, CH_3), 3.2–3.8 (series of mult, 5H), 3.455 (s, OCH_3), 3.707 (s, OCH_3), 4.088 (d, J = 11.3, H-4), 4.904 (d, J = 2.97, H-1), 6.81 (m, 1H), 7.1–7.4 (aromatics).

9*g*: Minor isomer: ^{1}H nmr ($CDCl_3$) δ: 0.855 (s, *tert*-butyl), 0.703 (d, J = 6.24, CH_3), 3.2–3.8 (series of mult, 5H), 3.505 (s, OCH_3), 3.707 (s, OCH_3), 4.088 (d, J = 11.3, H-4), 4.923 (d, J = 2.47, H-1), 6.81 (m, 1H), 7.1–7.4 (aromatics).

9*h*: Major isomer I: ^{1}H nmr ($CDCl_3$) δ: 1.447 (d, J = 6.38, CH_3), 3.300 (dd, J = 11.97, 2.77, H-2), 3.498 (s, OCH_3), 3.792 (s, OCH_3), 3.733 (br t, J = 11.44), 4.054 (d, J = 10.99, H-1), 4.645 (q, J = 6.35, H-1′), 5.022 (d, J = 2.72, H-1), 6.78 (m, H-5), 6.95–7.40 (m, aromatics).

9*h*: Minor isomer II: ^{1}H nmr ($CDCl_3$) δ: 1.310 (d, J = 6.44, CH_3), 3.179 (dd, 2.50, 12.12, H-2), 3.542 (s, OCH_3), 3.628 (s, OCH_3), 3.878 (dd, 10.58, 12.10, H-3), 4.119 (d, J = 10.59, H-4), 4.575 (q, J = 6.44, H-1′), 4.669 (d, J = 2.62, H-1), 6.78 (m, H-5), 6.95–7.40 (m, aromatics).

Maleic anhydride adducts **10**a *and* **10**h

The cycloadducts **10***a* and **10***h* were prepared by refluxing a benzene solution (10 mL) of **4***a* or **4***h*, (200–400 mg), four equivalents of maleic anhydride, and 30 mg of powdered zinc oxide for 20 h. The solution was filtered to remove zinc oxide, evaporated, and then heated to 100°C under high vacuum to remove maleic anhydride. The mixture of diastereomers was then analysed by nmr. Compound **10***a* recrystallized from benzene–hexane to give the major diastereomer as colourless crystals, mp 152–154°C; ir(CH_2Cl_2): 1790(s) and 1875(w) cm^{-1}; nmr ($CDCl_3$) δ: 1.192 (d, J = 6.47, C_3), 3.088 (dd, J = 8.9, 15.0, H-4), 3.232 (dd, J = 8.6, 15.0, H-4A), 3.317 (dd, J = 3.7, 10.5, H-4A), 3.463 (dt, J = 8.6, 10.5, H-3), 4.056 (q, J = 6.47, H-1′), 4.969 (d, J = 3.7, H-1), 6.9–7.4 (aromatics). Minor diastereomer, nmr ($CDCl_3$) δ: 1.403 (d, J = 6.39, 3.0–3.5 (m, 4H), 4.410 (q, J = 6.39, H-1′), 4.990 (d, J = 3.82, H-1), 6.9–7.4 (aromatics). *Anal.* calcd. for $C_{20}H_{18}O_4$: C 74.52, H 5.63; found: C 74.96, H 5.96.

Compound **10***h* recrystallized from benzene–hexane gave a mixture of diastereomers as colourless crystals; ir(CH_2Cl_2): 1790(s) and 1865(s) cm^{-1}; major isomer, nmr ($CDCl_3$) δ: 1.597 (d, J = 6.35, CH_3), 3.83 (m, H-2 and H-3), 4.243 (d, J = 5.5, H-4), 4.772 (d, J = 5.8, H-1), 4.915 (q, J = 6.35, H-1′), 6.9–7.5 (aromatics). Minor isomer, nmr ($CDCL_3$) δ: 1.366 (d, J = 6.41, CH_3), 3.83 (m, H-2), 3.364 (dd, J = 10.1, 4.9, H-3), 4.480 (q, J = 6.41, H-1′), 4.64 (d, J = 10.1, H-4), 4.656 (d, J = 4.9, H-1), 6.9–7.5 (aromatics). *Anal.* calcd. for $C_{26}H_{22}O_4$: C 78.37, H 5.57; found: C 78.49, H 5.82.

*(1S,2S)-1-(*R*-1-Phenylethoxy)-2-carbomethoxy-1,2,3,4-tetrahydronaphthalene,* **11**i

The alkoxysulfone **4**g (479 mg) was heated with methyl acrylate (1 mL), toluene (10 mL), and anhydrous powdered zinc oxide (30 mg) at 150°C under nitrogen in a sealed pressure flask (200 mL) for 2 hours with stirring. The solution was filtered through a 5 × 1.5 cm silica gel column with methylene chloride, evaporated, and recrystallized from hexane to give 96.1 mg (19%), mp 89–91°C, nmr of the crude reaction mixture indicted that the isolated adduct was the major adduct and made up ca. 40% of the crude reaction mixture.

11*i* ir(CH_2Cl_2): 1738 cm^{-1}; ^{1}H nmr ($CDCl_3$) δ: 1.419 (d, 6.44, CH_3), 2.064 (m, H-3e), 2.423 (m, H-3a), 2.724 (m, H-4a), 2.794 (m, H-2), 2.987 (m, H-4e), 3.820 (s, OCH_3), 4.590 (q, J = 6.40, H-1′), 4.857 (d, H-1), 6.71 (br d, J = 8.1, H-5), 6.9–7.45 (m, aromatics). The following coupling constants were determined by spectrum simulation and iterative fitting: $J_{1,2}$ = 3.26, $J_{2,3e}$ = 3.36, $J_{2,3a}$ = 12.01, $J_{3e,4e}$ = 2.991, $J_{3e,4a}$ = 6.68, $J_{3a,4e}$ = 6.30, $J_{3a,4a}$ = 11.12, $J_{3e,3a}$ = −13.66, $J_{4e,4a}$ = −17.32; $[\alpha]_D^{20}$ −50.0° (*c* 0.5, $CHCl_3$).

*(1*R*,2*R*)-(*S*-1-Phenylethoxy)-2-carbomethoxy-1,2,3,4-tetrahydronaphthalene,* **11**j

Compound **11***j* was prepared from 493 mg of **4***h* in a manner identical to that described for **11***i* to yield 125 mg of crystals (24%); ir and nmr spectra were identical to those of **11***i*; $[\alpha]_D^{20}$ +48.0° (*c* 0.5, $CHCl_3$).

Racemic ***11*** *(****11****i+****11****j)*

The racemic acrylate adduct was prepared from **4***a* in a manner identical to that described above for **11***i* and **11***j* and was recrystallized from hexane, mp 65–67°C; ir and nmr identical to **11***i*. *Anal.* calcd. for $C_{20}H_{22}O_3$: C 77.39, H 7.14; found: C 77.66, H 7.23.

2,3-Dicarbomethoxy-3,4-dihydronaphthalene, ***12****, and* trans*-1-phenyl-2,3-dicarbomethoxy-1,2-dihydronaphthalene,* ***13***

Elimination of the alcohol from the adducts **9***a–h* was accomplished by refluxing a toluene solution of each adduct (mixture of diastereomers) (50–150 mg) and toluene sulfonic acid (5 mg) in toluene (5–10 mL) for 5 h, filtering through a 5 cm × 1.5 cm silica gel column with methylene chloride and evaporating. The residue was chromatographed on silica gel (20% ethyl acetate – hexane) to give **12** (or **13**) in the yields given in Table 1. Compounds **12** and **13** were identified by comparison of their properties to those previously reported (13).

S*-(−)-2-Carboxyethyl-1,2,3,4-tetrahydronaphthalene,* ***14***

The adduct **11***i* (113 mg) was hydrogenated at 1 atm (1 atm = 101.3 kPa) and 20°C over 5% Pd/C (50 mg) in 10% acetic acid – methanol (10 mL). After 15 h the solution was filtered and evaporated to leave 75 mg of an oil, identified as the ester **14** by comparison to the literature (19); [α] −45° (*c* 1.34, $CHCl_3$).

S*-(−)-2-Carboxy-1,2,3,4-tetrahydronaphthalene,* ***15***

The ester **14** (75 mg) was refluxed with K_2CO_3 (200 mg) in 17% water–ethanol (20 mL) for 4 h. The solution was partially evaporated, diluted with water, acidified, and extracted with methylene chloride to yield 57.8 mg of **15** (83%); $[\alpha]_D^{20}$ −49.0° (*c* 0.5, $CHCl_3$), cf. $[\alpha]_D^{20}$ +55.5° (*c* 1.4, $CHCl_3$), for the *R*(+) isomer (17).

Acknowledgments

I would like to acknowledge the very capable technical assistance of Kirk Marat, who recorded and analysed the nmr spectra.

1. W. Oppolzer. Synthesis, 793 (1978).
2. R. L. Funk and K. P. C. Volhardt. Chem. Soc. Rev. **9**, 41 (1980).
3. W. Oppolzer. Heterocycles, **14**, 1614 (1980).
4. Y. Ito, Y. Amino, M. Nakatsuka, and T. Saegusa. J. Am. Chem. Soc. **105**, 1586 (1983).
5. P. G. Sammes. Tetrahedron, **32**, 405 (1976).
6. T. Kametani and K. Fukumoto. Acc. Chem. Res. **9**, 319 (1976).
7. R. W. Franck, T. V. John, and K. Olejniczak. J. Am. Chem. Soc. **104**, 1106 (1982).
8. A. G. Fallis. Can. J. Chem. **62**, 183 (1984).
9. G. Quinkert and H. Stark. Angew. Chem. Int. Ed. Engl. **22**, 667 (1983).
10. W. Oppolzer, C. Chapius, and G. Bernardinelli. Helv. Chim. Acta, **67**, 1397 (1984), and references therein.
11. B. M. Trost, D. O'Krongly, and J. L. Belletire. J. Am. Chem. Soc. **102**, 7595 (1980), and references cited.
12. W. G. Dauben and R. A. Bunce. Tetrahedron Lett. **23**, 4878 (1982).
13. T. Durst, E. C. Kozma, and J. L. Charlton. J. Org. Chem. **50**, 4829 (1985).
14. J. L. Charlton and T. Durst. Tetrahedron Lett. **25**, 2663 (1984).
15. J. L. Charlton. Tetrahedron Lett. **25**, 3413 (1985).
16. M. Pfau, S. Combrisson, J. E. Rowe, Jr., and N. D. Heindel. Tetrahedron, **34**, 3459 (1978); J. Mann and S. E. Piper. J. Chem. Soc. Chem. Commun. 430 (1982); J. Mann, S. E. Piper, and L. P. Yeung. J. Chem. Soc. Perkin Trans. 1. 2081 (1984); J. Mann, L. T. F. Wong, and A. R. Beard. Tetrahedron Lett. **26**, 1667 (1985).
17. A. Schoofs, J. P. Guette, and A. Horeau. Bull. Soc. Chim. Fr. 1215 (1976).
18. T. Schaefer, R. Laatikainen, T. A. Wildman, J. Peeling, G. Penner, J. Baleja, and K. Marat. Can. J. Chem. **62**, 1592 (1984).
19. Y. Ito, K. Yonezawa, and T. Saegusa. J. Org. Chem. **39**, 2769 (1974).

Alkylation of camphor imines of glycinates. Diastereoselectivity as a function of electronic factors in the alkylating agent[1]

JOHN M. MCINTOSH AND PRATIBHA MISHRA[2]
Department of Chemistry, University of Windsor, Windsor, Ont., Canada N9B 3P4

Received June 24, 1985

JOHN M. MCINTOSH and PRATIBHA MISHRA. Can. J. Chem. **64**, 726 (1986).

Alkylation of the (*R*)-camphor imine of *tert*-butyl glycinate with a variety of alkylating agents gave diastereoselectivities ranging from 0–100%. Simple alkyl halides larger than methyl give de's (diastereomeric excesses) of ca. 50% whereas those derived from allylic type systems afford de's of 75–100%. The results are best explained by invoking a transition state interaction between the π system of the alkylating agent and the imine which, for steric reasons, requires alkylation to occur from the pro-*R* face.

JOHN M. MCINTOSH et PRATIBHA MISHRA. Can. J. Chem. **64**, 726 (1986).

Les diastéréosélectivités des réactions d'alkylation de l'imine formée par la (*R*)-camphre et le glycinate de *tert*-butyle par divers agents alkylants varient de 0 à 100%. Les sélectivités des réactions affectuées avec des halogénures simples plus volumineux que le méthyle sont de l'ordre de 50% alors que celles effectuées avec des systèmes de types allyliques vont de 75 à 100%. La meilleure explication de ces résultats implique une interaction dans l'état de transition entre le système π de l'agent alkylant et l'imine qui, pour des raisons stériques, nécessite que l'alkylation se fasse par le face pro-*R*.

[Traduit par la revue]

Introduction

Some time ago, several reports on the alkylation of chiral imines of glycinates appeared. In particular, the use of menthone (1) and hydroxynopinone (**1**) (2) gave modest to fair stereoselectivities with the latter being the better *c*hiral *d*erivatizing *a*gent (CDA). The enhanced selectivity using **1** as CDA was attributed to the presence of the extra chelating center, which forced the enolate system into an arrangement in which the steric influence of the *syn*-methyl group could impede the attack of the electrophile from the top face of the molecule. While more recent developments (3) have displaced this methodology, the rationale given implied that camphor (**2***a*) might be more effective due to the closer proximity of the C-8 methyl group to the carbanionic center. In addition, the rigid

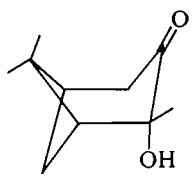

1

structure of **2** which would facilitate stereochemical reasoning, its ready availability in both enantiomeric forms, and the ease with which substituents can be introduced at many positions in stereospecific ways suggested that an investigation of its use as a CDA in glycinate alkylations would prove instructive.[3]

Because of the hindered nature of the carbonyl in **2***a*, its condensation with amines is known (5) to be a difficult reaction requiring vigorous reaction conditions. However, prior conversion into the thione **2***b* (6) markedly increases the facility of "carbonyl" additions (7). For derivatization with glycine esters, the use of **2***b* appears to be mandatory, as we have been unable to effect such condensations with **2***a* under a number of conditions.

Condensation of **2***b* with the hydrochlorides of methyl or ethyl glycinates in the presence of DABCO (1,4-diazabicyclo[2.2.2]octane) as a base required a large excess of amino ester and gave **3***a* or **3***b* severely contaminated with polyglycine. However, the corresponding *t*-Bu glycinate (free base) smoothly condensed with **2***b* to give **3***c* in high yield.

Two diastereomers of **3** are possible. However, both the 75-MHz ^{13}C nmr and the 300-MHz ^{1}H nmr were consistent only with the presence of one diastereomer. Models show that the *Z* isomer is severely destabilized by a steric interaction with the C-10 methyl group and, for this reason, **3***a*, *b*, *c* are assigned the *E* configuration as shown in Scheme 1 (5*b*).

Preliminary experiments on the alkylation of **3***a* gave the following results. Alkylation with MeI (**6***a*) or BzBr (**7**) gave

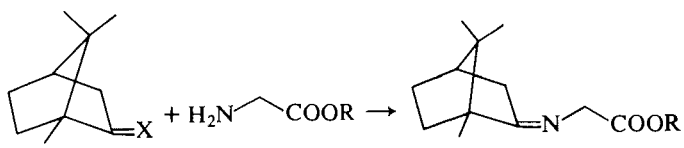

2*a* X = O
b X = S

3*a* R = Me
b R = Et
c R = *t*-Bu

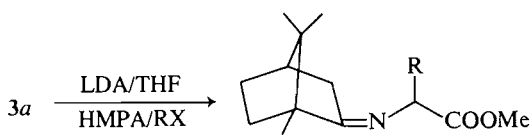

4*a* R = Me
b R = Bz

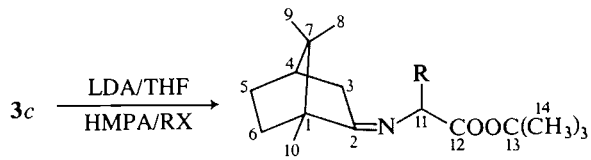

5 *a–m* (see Table 1).

SCHEME 1

[1]Presented in part at the annual conference of the Chemical Institute of Canada, Kingston, Ontario; June 1985.

[2]Holder NSERC predoctoral fellowship, 1981–present.

[3]Camphor has been used as a CDA in many other reactions. For some recent examples, see ref. 4.

TABLE 1. Products, yields, and stereochemical compositions of alkylation products **5**

Run	R	X (compound no.)	Temp. (°C)	Time (h)	Product	Yield (%)[a]	Ratio[b]	Diastereomeric excess
1	Me	I (**6***a*)	−78	1	**5***a*	82	1:1	0
2	Me	OTs (**6***b*)	−63	1.5	**5***a*	37(53)	1:1	0
3	$PhCH_2$	Br (**7**)	−78	1	**5***b*	89	>99:1	>98
4	MeO_2CCH_2	Br (**8**)	−78	1	**5***c*	78	73:27	46
5	EtO_2CCH_2	Br (**9**)	−78	1	**5***d*	86	66:34[c]	32
6	*t*-BuO_2CCH_2	Cl (**10**)	−78	0.5	**5***e*	32(84)	55:45	10
7	Bu	I (**11**)	−78	1	**5***f*	45(89)	75:25	50
8	i-Bu	Br (**12**)	−78–rt	1.5	**5***g*	48(95)	76:24	52
9	Allyl	Br (**13**)	−78	1	**5***h*	85	88:12	76
10	Methallyl	Cl (**14**)	−40	3	**5***i*	79	88:12	76
11	$PhSCH_2$	Cl (**15**)	−78–0	4	**5***j*	38	—	—
12	$PhSCH_2$	I (**15***a*)	−78	1	**5***j*	54(77)	82:18	64
13	4-Butenyl	Br (**16**)	−78–−20	4	**5***k*	68(94)	67:33[c]	34
14	2-Phenethyl	Br (**17**)	−78–−20	3	**5***m*	58(70)	67:33	34

[a]Isolated yields. Yields in parentheses are those based on unrecovered starting material.
[b]Based on the integration of the methine hydrogens at 300 MHz, unless otherwise noted.
[c]Based on the peak heights of the camphor methyl groups in the ^1H nmr spectrum.

diastereomeric mixtures of products **4***a* and **4***b* in ratios of 3:2 and 3:1, respectively. In hindsight, this former result was most useful, as the ^1H nmr of **4***b* showed a large difference ($\Delta\delta$ = 0.5) in the chemical shift of the C-8 methyl groups for the two diastereomers. Smaller differences were observed for the same signals in **4***a*. In addition, two doublets of doublets were evident for the methine proton in **4***b*. No dialkylated products were obtained. The presence of one equivalent of HMPA (hexamethylphosphoramide) in the reaction mixture was essential for good chemical yields. In its absence the yield of **4***b* fell to 40%, while the use of two equivalents gave a 2:1 mixture of diastereomers. When **4***b* was treated with LDA (lithium diisopropylamide) under the same conditions used for the alkylation of **3***c*, and the reaction was quenched with a 100-fold excess of either D_2O or CF_3COOD, ca. 50% of the recovered **4***b* was monodeuterated. (Previous workers (2*a*) have assumed that the absence of dialkylated material ensured that the product was a result of a kinetic process. Our deuteration result calls this into question.) As a result of steric factors, the imine bond in **5** is remarkably inert to many conditions. While this is advantageous in terms of the alkylation reactions, it causes some problems in the generation of the free amino ester. To date, the best method we have found for achieving this transformation is transamination using hydroxylamine (2*a*, *b*). Hydrolysis with citric acid (2*a*, *b*) was ineffective.

When the alkylation and deuteration experiments were repeated on imine **3***c* a high chemical yield of **5***a* was obtained, which consisted of a ca. 1:1 mixture of diastereomers. However, the **5***b* obtained was shown to be stereochemically homogeneous by hydrolysis to (*R*)-phenylalanine *tert*-butyl ester and by 300-MHz nmr. An AMX set of signals (J_{AM} = 13 Hz, J_{AX} = 10 Hz, J_{MX} = 4 Hz) was exhibited by the benzyl and methine protons. No sign of a second set of signals for the other possible diastereomer was evident. In addition, the methyl region was clean, whereas multiple signals were observed in all cases where two diastereomers were formed. Attempted deuteration of **5***a* and **5***b* failed completely. No deuterium incorporation could be detected by mass spectrometry. Thus it appears that the presence of the bulky ester group effectively ensures that the observed stereochemistry is a result of a kinetically controlled process. These results also clearly preclude attempts at further alkylation.

These results are most easily attributed to the differing steric requirements of the alkylating agent. The working model of the reacting system[4] involved an internally chelated enolate anion that is coplanar with the camphor moiety. Although models indicate that the C-8 methyl is somewhat removed from the path required for *exo*-attack (on the pro-*S* face), increasing the steric bulk of the alkylating agent might be expected to enhance the selectivity. To explore the stereoselectivity further, the alkylation of **3***c* with a range of alkylating agents that differ in reactivity (10) and steric requirements was examined. The results are shown in Table 1. The stereochemical composition of the product from each reaction was determined by integration of the nmr absorptions of the methine proton of the imine in the 300-MHz ^1H nmr spectrum (each diastereomer gave a doublet of doublets) and by comparison of the relative intensities of the two signals for C-8. It was also usually possible to estimate the diastereomeric ratio from the intensities of the camphor C-8 absorptions in the 60-MHz spectra. In the case of **5***b*, hydrolysis to the amino ester was performed and the optical purity determined by comparison of the specific rotation with the reported value. In all other cases, the absolute stereochemistry of the product present in the larger diastereomeric excess (de) was assumed to be *R*. Supporting this assumption is the fact that in all cases in which diastereomeric mixtures were obtained, the methine proton of the *R*,*R* isomer appeared at lower field than that of the *R*,*S* isomer. The same order was observed for the stereoisomeric mixtures of **4***a* and **4***b*.

While the tabulated chemical yields of products appear to correlate well with established concepts of reactivity, the stereochemical results do not. The more reactive halides

[4]It is well documented that *simple* lithio enolates are not monomeric (8) and also that coordinating solvents (HMPA, etc.) at least partially deaggregate the clusters (9). Thus, although the models proposed herein are undoubtedly a simplified version of the actual structure, they are useful in a *predictive* sense.

TABLE 2. ^{13}C nuclear magnetic resonance

Compound no.	R	C-1	C-2	C-3	C-4	C-5	C-6	C-7	C-8
3*c*	H	54.8	187.4	35.7	43.9	27.5	32.1	47.3	19.7
5*a*	Me	53.6	184.5	35.6	44.0	27.6	32.1	46.7	19.1
				[35.8]				[47.2]	
5*b*	Bz	53.8	184.8	35.8	43.5	27.1	31.7	47.0	19.3
5*c*	CH_2COOMe	54.1	186.6	36.1	44.0	27.5	32.2	47.4	19.8
				[36.0]			[32.0]		[19.4]
5*f*	Bu	54.0	184.1	36.2	44.0	27.6	32.7	47.3	19.6
		[54.1]		[35.9]		[27.6]	[32.6]	[46.9]	
5*g*	i-Bu	54.00	184.2	36.3	44.0	27.7	32.3	47.3	19.7
				[36.0]	[44.1]	[27.7]	[32.0]	[46.8]	[19.6]
5*h*	Allyl	54.0	184.8	36.3	44.0	27.5	32.5	47.3	19.6
							[31.8]		
5*i*	Methallyl	54.1	184.6	36.1	44.0	27.6	32.3	47.3	19.7
							[32.2]		[19.6]
5*j*	$PhSCH_2$	54.1	186.4	36.1	43.8	27.4	32.0	47.3	19.5
					[43.9]				[19.7]
5*k*	3-Butenyl	54.1	184.9	36.3	44.0	27.6	32.1	47.4	19.7
		[54.2]	[185.0]	[36.1]			[32.0]	[46.7]	
5*m*	$PhCH_2CH_2$	54.2	—	36.3	44.0	27.6	32.0	47.6	19.7
				[36.1]	[44.1]		[32.1]	[46.9]	

[a] At 75 MHz in $CDCl_3$.
[b] Values in brackets [ ] for the minor diastereomer.

(allylic, benzylic) should involve more reactant-like transition states and this should lead to lower stereoselectivities. A recent comprehensive review (11) is replete with such examples in which methyl iodide affords higher de's than benzyl bromide. Alkylation of glycine derivatized with **1** also shows this behaviour. Examination of Table 1 shows that our results with the camphor-derivatized glycinates are in complete conflict with this concept, that the reaction temperature has only a minor effect (compare runs 7 and 8, 9 and 10), and that the steric bulk of the alkylating agent does not correlate with the observed de's (compare runs 8 and 10).

The common feature of the alkylating agents which give de's of 75% or greater is the presence of a carbon π system immediately adjacent to the reacting center. Using the model previously mentioned, the *sterically* preferred transition state geometry for alkylation is undoubtedly that in which the R-group of RCH_2X is oriented away from the congested lithiated amine (A = H, B = R, Scheme 2). However, models

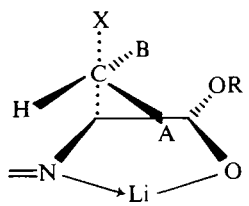

SCHEME 2

suggest that a much larger preference for attack on the pro-*R* face would result from a conformation in which the R group of the alkylating agent lies in an "eclipsed" arrangement with the lithiated imine (A = R, B = H, Scheme 2). The positive charge induced in the π system by the partial breaking of the carbon–halogen bond could favor A. This would account for the apparent abnormality of the α-haloesters, since such an interaction would be unfavorable. This thesis is also supported by comparison of the results obtained using **17** with **15** and **13** with **16**. In each case, when a favorable resonance interaction of the π system with a developing charge on the carbon undergoing substitution would cause an electron deficiency in the π system, increased diastereoselectivity is observed.

Catalytic hydrogenation of **5***i* gave **5***g*, the same product obtained using **12** as the alkylating agent but with a significant increase in selectivity. Catalytic reduction of **5***g* gave the propyl compound without loss of stereochemical integrity. Also it should be noted that the use of α-haloalkyl phenyl sulfides (e.g., **15**) as synthons for simple alkyl halides to achieve higher stereoselectivities may be generally useful in this system.

It is noteworthy that the imine (**18***a*) of fenchone and *t*-Bu

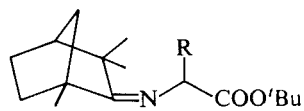

18*a* R = H
b R = Bz

glycinate can be prepared in an analogous manner, albeit with much more difficulty. In this case the stereochemistry of the imine is homogeneous and must be *syn* to the bridgehead methyl group (*E* stereochemistry). Alkylation of **18***a* with **7** affords the alkylated imine **18***b* as a 3:1 mixture of diastereomers. This is unexpected, as models indicate that little steric difference exists between the two diastereofaces of the lithiated imine.

The previously noted stability of the imine bond is illustrated by the observation that attempted deprotonation of **5***b* with BuLi led to the formation of two new products, which have been tentatively identified (mass spectroscopy) as **19** and **20**, the

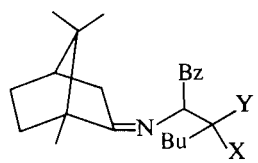

19 X = Y = O
20 X = OH, Y = Bu

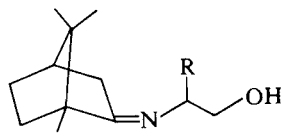

21*a* R = i-Bu
b R = Bz

data for alkylation products **5**[a,b]

C-9	C-10	C-11	C-12	C-13	C-14	R				
19.0	11.3	54.2	170.2	80.9	28.2					
18.7	11.4	60.3	173.2	80.9	28.2	19.7				
[18.9]		[60.2]				[19.7]				
18.8	11.5	66.7	171.2	80.8	28.0	138.9	129.8	128.0	126.1	38.7
19.1	11.4	61.8	172.1	81.3	28.0	37.4	170.1	51.5		
[19.0]	[11.3]	[61.5]	[172.2]			[37.6]				
19.1	11.6	65.3	171.9	80.5	28.1	32.4	28.3	22.6	14.1	
[19.0]	[11.5]	[65.0]				[32.0]	[28.4]	[22.5]		
19.1	11.6	63.6	172.1	80.6	28.1	23.4	41.9	21.9	24.8	
[19.0]	[11.5]	[63.1]				[23.6]	[41.8]	[21.6]		
18.9	11.5	64.9	171.2	80.8	28.1	37.4	135.0	117.0		
		[65.1]					[135.3]			
19.1	11.6	64.1	171.4	80.8	28.1	40.9	23.2	142.6	112.6	
		[64.3]							[112.4]	
19.0	11.4	64.7	170.1	81.4	28.0	36.4	125.8	128.8	128.9	136.6
		[64.8]				[36.5]				
19.1	11.6	64.3	171.6	80.7	28.1	30.2	32.4	138.4	115.1	
[19.0]	[11.5]	[64.0]	[171.5]			[30.3]			[115.0]	
19.1	11.5	64.1	—	80.8	28.2	32.5	34.3	141.8	128.7	128.5
[19.0]	[11.7]					[32.4]	[34.7]		128.4 125.9	

products of addition to the *t*-Bu ester. No addition to the imine bond was detectable. Further, LAH (lithium aluminum hydride) reduction of **5***g* did not occur until refluxing ether was employed. Under these conditions, **21***a* was obtained from **5***g* and **21***b* from **5***b* with little loss of stereochemical integrity observed (de = 48% and >98% respectively).

From the foregoing results, it seems clear that the use of camphor in place of menthone or **1** subtly alters the transitions states for alkylation. Further investigations into the use of modified camphor derivatives and other alkylating agents is required before more definitive conclusions regarding the transition state structure can be reached. Such work is currently in progress.

Experimental

Unless otherwise noted, infrared spectra were run as neat liquids on either a Perkin–Elmer Model 180 instrument or on a Nicolet 5-DX instrument in the FT mode. The five strongest peaks are reported. The nmr spectra were run on a Nicolet QE-300 instrument (^{1}H nmr at 300 MHz and ^{13}C nmr at 75 MHz) or at 60 MHz (^{1}H nmr) or 22.64 MHz (^{13}C nmr) in $CDCl_3$ solution, and are referenced to internal TMS. The data are presented in the format: (multiplicity, number of hydrogens, coupling constant) and are at 300 (proton) or 75 (carbon) MHz unless otherwise specified. Values in brackets ([ ]) are for the minor diastereomer. Optical rotations were measured on a Perkin–Elmer model 241 polarimeter in 95% ethanol solution with c = 10 unless noted to the contrary. Gas chromatographic analyses were performed using a 1.5 ft × 1/8 in. column packed with 5% OV-101 on Chromosorb W. Mass spectra were run on a Varian MAT CH-5 DF instrument in the field ionization (fi) mode. Solvents were removed at reduced pressure and the drying agent was anhydrous $MgSO_4$. Column chromatography utilized silica gel 60 (Merck) and 20% ether in petroleum ether as eluant unless otherwise specified. Satisfactory analyses (C, H, N) were obtained for all compounds (see Table 3). Microanalyses were performed by Canadian Microanalytical Services, Vancouver or Guelph Chemical Laboratories, Guelph, Ontario.

Imine **3**a

Camphorthione (**1***b*) (6) (13.7 g, 81 mmol), $[\alpha]_D^{25}$ −30.4°, 1.4-diazabicyclo[2.2.2]octane (DABCO) (10.1 g, 90 mmol), and methyl glycinate hydrochloride (40.2 g, 320 mmol) were dissolved in 500 mL of methanol and stirred at 45–50°C for 20 h. The solution was concentrated, diluted with ether, filtered, and the creamy solid washed with ether. The ether solution was concentrated and chromatographed to give 13.75 g (76%) of imine **3***a*, bp 93–95°C (0.8 Torr; 1 Torr = 133.3 Pa); ir: 2970, 1745, 1675, 1195, 1175 cm^{-1}; ^{1}H nmr (60 MHz): 4.03 (s, 2H), 3.67 (s, 3H), 2.60–0.90 (m, 7H), 0.98 (s, 3H), 0.92 (s, 3H), 0.77 (s, 3H); ^{13}C nmr (22.64 MHz): 187.1, 170.7, 54.1, 53.7, 51.6, 47.2, 43.8, 35.5, 31.9, 27.2, 19.3, 18.9, 11.1.

Imine **3**b

A mixture of ethyl glycinate hydrochloride (4 mmol), **1***b* (3 mmol), and DABCO (3 mmol) in 80 mL of xylene was stirred and heated at 145°C. Additional portions of ester and DABCO were added several times during the reaction. A tarry material (assumed to be polyglycine) formed during the reaction. The solution was cooled, decanted from the residue, concentrated, and chromatographed (3:2 hexane–ether) to give 0.38 g (54%) of imine **3***b*; ir: 2970, 1740, 1675, 1370, 1180 cm^{-1}; ^{1}H nmr (60 MHz): 4.14 (q, 2H, J = 7 Hz), 4.05 (s, 2H), 2.63–0.90 (m, 7H), 1.23 (t, 3H, J = 7 Hz), 0.98 (s, 3H), 0.92 (s, 3H), 0.78 (s, 3H); ^{13}C nmr (22.64 MHz): 187.2, 170.1, 60.5, 54.2, 53.8, 47.2, 43.9, 35.6, 31.9, 27.4, 19.4, 18.8, 14.0, 11.1.

Imine **3**c

tert-Butyl glycinate (12) (5.7 g, 44 mmol) and **1***b* (7 g, 42 mmol) were combined in 70 mL of toluene and refluxed for 24 h. The solution was cooled, concentrated, and the crude product chromatographed to give 9.7 g, (88%) of imine **3***c*; $[\alpha]_D^{26}$ −12.5°; ir: 2990, 1740, 1680, 1365, 1145 cm^{-1}; ^{1}H nmr: 3.97 (ABq, 2H, J = 16 Hz), 2.34–2.22 (m, 1H), 1.95–1.34 (m, 5H), 1.46 (s, 9H), 1.25–1.16 (m, 1H), 0.99 (s, 3H), 0.91 (s, 3H), 0.79 (s, 3H); ^{13}C nmr: (see Table 2).

Imine **18**a

tert-Butyl glycinate (1.3 g, 10 mmol) and fenchone thione (13) (1.7 g, 10 mmol) were combined in 70 mL of toluene and refluxed for 4 days. The solution was cooled, concentrated, and the crude product chromatographed to give 1.9 g (70%) of imine **18***a*; ^{1}H nmr: 4.26 (ABq, 2H, J = 18 Hz), 1.85–1.35 (m, 7H), 1.47 (s, 9H), 1.23 (s, 3H), 1.22 (s, 3H), 1.18 (s, 3H); ^{13}C nmr: 188.0, 170.2, 80.8, 53.6, 53.1, 50.1, 44.5, 42.3, 33.8, 28.2, 25.3, 24.6, 23.9, 17.6.

General alkylation procedure

LDA (8.3 mmol) was prepared at 0°C in 15 mL of dry THF and then

TABLE 3. Elemental analyses

Compound	Calculated (%)			Found (%)		
	C	H	N	C	H	N
3*a*	69.92	9.48	6.27	69.53	9.73	6.15
3*b*	70.85	9.77	5.90	67.79	9.39	5.81
3*c*	72.41	10.25	5.28	72.42	10.34	5.07
4*a*	70.85	9.77	5.90	70.34	9.94	5.64
4*b*	76.64	8.68	4.47	76.39	8.75	4.96
5*a*	73.07	10.46	5.01	72.94	9.89	5.49
5*b*	77.70	9.36	3.94	77.52	9.05	3.92
5*c*	67.62	9.26	4.15	67.74	9.26	4.15
5*d*	68.34	9.46	3.98	68.29	9.35	3.84
5*e*	69.62	9.83	3.69	69.15	9.49	3.57
5*f*	74.72	10.97	4.36	74.89	11.10	4.45
5*g*	74.72	10.97	4.36	74.11	11.10	4.28
5*h*	74.71	10.23	4.59	74.79	10.33	4.45
5*i*	75.19	10.41	4.38	74.45	10.58	4.13
5*j*	71.29	8.59	3.61	70.84	8.35	3.83
5*k*	75.19	10.41	4.38	75.02	10.68	4.45
5*m*	77.26	9.87	3.92	76.86	9.27	3.68
21*a*	76.44	11.63	5.57	76.73	11.62	5.52

cooled to −78°C. Imine **3***c* (2.0 g, 7.5 mmol) in 10 mL of THF was added. An orange solution resulted. HMPA (8.3 mmol) was added and the solution was stirred at −78°C for 10–15 min and then the alkylating agent (8 mmol) was added. The solution was stirred at −78° to −40°C (see Table 1) for 1–4 h, by which time the color of the solution usually became yellow. The reaction was quenched with 10 mL of water and allowed to warm to ambient temperature. Water (10 mL) was added, the layers were separated, and the aqueous phase was extracted with ether (2 × 50 mL). The organic layers were combined, washed with water (3 × 20 mL), dried, concentrated, and chromatographed to give the products listed in Table 1. No attempt was made to separate the diastereomers. When the de ratio of the products was greater than ca. 75%, the material frequently solidified. The ^{13}C nmr data for **5** are given in Table 2 and the ^1H nmr, infrared, and polarimetric data are given below.

5*a*: $[\alpha]_D^{26}$ −27.8°; ir: 2970, 1735, 1680, 1365, 1150 cm^{-1}; ^1H nmr: 3.90 (q, 1H, J = 7 Hz) [3.89 (q, 1H, J = 7 Hz)], 2.43–2.22 (m, 1H), 1.95–1.60 (m, 5H), 1.40 (s, 9H) [1.43 (s, 9H)], 1.34 (d, 3H, J = 7 Hz) [1.33 (d, 3H, J = 7 Hz)], 0.97 (s, 3H), 0.91 (s, 3H), 0.78 (s, 3H) [0.70 (s, 3H)].

5*b*: mp 69–72°C; $[\alpha]_D^{24}$ +86.5°; ir: 2980, 1730, 1680, 1370, 1145 cm^{-1}; ^1H nmr: 7.5–7.15 (m, 5H), 4.00 (dd, 1H, J = 4, 10 Hz), 3.25 (dd, 1H, J = 4, 13 Hz), 3.02 (dd, 1H, J = 10, 13 Hz), 2.25–2.15 (m, 2H), 1.73–1.41 (m, 3H), 1.42 (s, 9H), 1.10–0.90 (m, 2H), 0.96 (s, 3H), 0.84 (s, 3H), 0.72 (s, 3H).

5*c*: $[\alpha]_D^{26}$ +67.5°; ir: 2970, 1735, 1680, 1365, 1145 cm^{-1}; ^1H nmr: 4.34 (dd, 1H, J = 6, 8 Hz), 3.62 (s, 3H) [3.60 (s, 3H)], 2.99 (dd, 1H, J = 6, 16 Hz), 2.69 (dd, 1H, J = 8, 16 Hz), 2.59–2.38 (m, 1H), 2.07–1.58 (m, 4H), 1.39 (s, 9H) [1.40 (s, 9H)], 1.28–1.16 (m, 2H), 0.92 (s, 3H), 0.91 (s, 3H), 0.82 (s, 3H) [0.73 (s, 3H)].

5*d*: mp 52–58°C; ir: 2975, 1735, 1680, 1365, 1140 cm^{-1}; ^1H nmr (60 MHz): 4.47–4.20 (m, 1H), 4.08 (q, 2H, J = 7 Hz), 3.23–1.08 (m, 9H), 1.42 (s, 9H), 1.22 (t, 3H, J = 7 Hz), 0.93 (s, 6H), 0.82 (s, 3H) [0.73 (s, 3H)].

5*e*: ir: 2975, 1730, 1680, 1365, 1140 cm^{-1}; ^1H nmr (60 MHz): 4.47–4.13 (m, 1H), 2.60–1.00 (m, 9H), 1.42 (s, 18H), 0.95 (s, 3H), 0.92 (s, 3H), 0.83 (s, 3H) [0.75 (s, 3H)].

5*f*: $[\alpha]_D^{26}$ +59.2° (c = 6); ir: 2980, 1735, 1680, 1365, 1150 cm^{-1}; ^1H nmr: 3.78 (dd, 1H, J = 5, 9 Hz) [3.73 (dd, 1H, J = 5, 9 Hz)], 2.43–2.25 (m, 1H), 1.95–1.58 (m, 6H), 1.40 (s, 9H), 1.46–1.09 (m, 6H), 0.97 (s, 3H), 0.91 (s, 3H), 0.88 (t, 3H, J = 7 Hz), 0.79 (s, 3H) [0.73 (s, 3H)].

5*g*: $[\alpha]_D^{26}$ +52.4° (c = 8); ir: 2980, 1735, 1680, 1365, 1150 cm^{-1}; ^1H nmr: 3.89 (dd, 1H, J = 9, 5 Hz) [3.85 (dd, 1H, J = 10, 4 Hz)], 2.47–2.37 (m, 1H), 1.97–1.15 (m, 9H), 1.42 (s, 9H) [1.43 (s, 9H)], 0.99 (s, 3H) [0.98 (s, 3H)], 0.93 (s, 3H) [0.95 (s, 3H)], 0.81 (s, 3H) [0.75 (s, 3H)], 0.85 (d, 6H, J = 7 Hz) [0.93 (d, 6H, J = 7 Hz)].

5*h*: $[\alpha]_D^{24}$ +81.2°; ir: 2970, 1735, 1680, 1365, 1150 cm^{-1}; ^1H nmr: 5.80–5.65 (m, 1H), 5.11–4.92 (m, 2H), 3.85 (dd, 1H, J = 4, 8 Hz), 2.71–2.25 (m, 3H), 1.95–1.59 (m, 4H), 1.40 (s, 9H) [1.41 (s, 9H)], 1.46–1.13 (m, 2H), 0.97 (s, 3H), 0.91 (s, 3H), 0.79 (s, 3H) [0.73 (s, 3H)].

5*i*: $[\alpha]_D^{25}$ +75.6°; ir: 2970, 1735, 1680, 1365, 1145 cm^{-1}; ^1H nmr: 4.78–4.68 (m, 2H), 3.99 (dd, 1H, J = 6, 4 Hz), 2.69–2.37 (m, 3H), 2.00–1.58 (m, 7H), 1.45 (s, 9H) [1.46 (s, 9H)], 1.40–1.12 (m, 3H), 1.00 (s, 3H), 0.94 (s, 3H), 0.82 (s, 3H) [0.73 (s, 3H)].

5*j*: (from **15***a*) $[\alpha]_D^{22}$ +71.4°; ir: 2975, 1730, 1680, 1365, 1145 cm^{-1}; ^1H nmr: 7.42–7.14 (m, 5H), 4.04 (dd, 1H, J = 9, 5 Hz), 3.58 (dd, 1H, J = 5, 14 Hz), 3.28 (dd, 1H, J = 9, 14 Hz) [3.32 (dd, 1H, J = 9, 14 Hz)], 2.37–2.19 (m, 1H), 1.94–1.58 (m, 4H), 1.46 (s, 9H) [1.47 (s, 9H)], 1.43–1.09 (m, 2H), 0.98 (s, 3H), 0.94 (s, 3H), 0.79 (s, 3H).

5*k*: $[\alpha]_D^{26}$ +22.7°; ir: 2970, 1735, 1680, 1365, 1150 cm^{-1}; ^1H nmr: 5.87–5.69 (m, 1H), 5.05–4.89 (m, 2H), 3.79 (dd, 1H, J = 9, 14 Hz), 2.43–2.22 (m, 1H), 2.13–1.58 (m, 8H), 1.40 (s, 9H) [1.43 (s, 9H)], 1.46–1.09 (m, 2H), 0.97 (s, 3H), 0.91 (s, 3H), 0.79 (s, 3H) [0.74 (s, 3H)].

5*m*: $[\alpha]_D^{27}$ + 15°; ir: 2970, 1735, 1680, 1365, 1145 cm^{-1}; ^1H nmr: 7.42–7.20 (m, 5H), 3.80 (dd, 1H, J = 5, 9 Hz), 2.80–2.67 (m, 1H), 2.64–2.49 (m, 1H), 2.37–2.13 (m, 4H), 2.01–1.58 (m, 4H), 1.46 (s, 9H) [1.49 (s, 9H)], 1.31–1.16 (m, 1H), 1.02 (s, 3H), 0.97 (s, 3H) [0.99 (s, 3H)], 0.85 (s, 3H) [0.79 (s, 3H)].

tert-*Butyl phenylalaninate*

To a cold solution of NaOH (0.19 g, 4.6 mmol) in 50 mL of methanol was added hydroxylamine hydrochloride (0.32 g, 4.6 mmol) and acetic acid (0.28 g, 4.6 mmol). A solution of imine **5***b* in 20 mL of methanol was added and the mixture was stirred at ambient temperature for 20 h. The solution was concentrated, diluted with 10% hydrochloric acid, extracted with ether (3 × 50 mL), and the extracts were dried and concentrated to give 0.70 g (100%) of camphor oxime. The aqueous layer was basified and extracted with ether, the extracts dried and concentrated to give 0.416 g (45%) of *tert*-butyl phenylalaninate $[\alpha]_D^{24}$ − 22.4° (c = 10, EtOH) (lit. (14) $[\alpha]_D$ − 24.8° (neat).

When **5***a*, **5***b*, or **5***g* was treated with LDA in the same manner used for the alkylation, and the reaction was quenched at −78°C with a large excess of either CF_3COOD or D_2O, the isolated product showed no incorporation of deuterium (mass spectrum).

Alkylation of imine ***18****a*

In the same manner as described above, the alkylation of imine **18***a* was effected using 415 mg (1.6 mmol) of **18***a* and 0.3 g (1.7 mmol) of benzyl bromide. Chromatography afforded 0.49 g (84%) of imine **18***b*; ^1H nmr: 7.25 (m, 5H), 4.41 (dd, 1H, J = 4, 9 Hz) [4.43 (dd, 1H, J = 4, 9 Hz)], 3.27 (dd, 1H, J = 4, 13 Hz) [3.24 (dd, 1H, J = 4, 13 Hz)], 3.04 (dd, 1H, J = 9, 13 Hz) [3.03 (dd, 1H, J = 9, 13 Hz)], 1.67 (m, 2H), 1.55–1.20 (m, 5H), 1.48 (s, 9H) [1.51 (s, 9H)], 1.24 (s, 3H), 1.12 (s, 3H) [1.09 (s, 3H)], 0.58 (s, 3H) [0.61 (s, 3H)]; ^{13}C nmr: 171.4, 139.0 [138.9], 130.1 [130.0], 127.9 [128.0], 126.3 [126.4], 80.7 [80.7], 65.1 [65.0], 53.0, 50.3 [49.9], 46.3 [46.2], 44.5 [44.3], 42.3, 40.5 [40.3], 33.7, 33.4, 28.1, 25.3 [25.3], 24.6 [24.3], 17.9.

Hydride reduction of **5***b and* **5***f*

To a solution of **5***b* (750 mg, 2.1 mmol) in 15 mL of dry THF was added 80 mg (100% excess) of $LiAlH_4$. The suspension was stirred at reflux for 18 h, cooled and 25 mL of water was added cautiously. The aqueous layer was extracted with ether and the combined organic phases were dried and concentrated to give 582 mg (97%) of a gummy solid (**21***b*) that crystallized on standing. In the same way, but using ether as solvent, **5***f* was converted into **21***a*.

21*a*: mp 74–96°C; ir ($CHCl_3$): 3340, 2975, 1675, 1385, 1365, 1020 cm^{-1}; ^1H nmr: 3.61–3.52 (m, 2H), 3.49–3.38 (m, 1H), 2.52–

2.18 (m, 2H), 2.07–1.11 (m, 9H), 1.00 (s, 3H), 0.97 (s, 3H), 0.91 (d, 6H, J = 7 Hz) [0.89 (d, 6H, J = 7 Hz)], 0.79 (s, 3H) [0.80 (s, 3H)]; ^{13}C nmr: 183.6, 66.4, 60.5 [60.2], 53.9, 46.7 [46.5], 43.9, 41.3 [41.2], 36.0 [36.2], 32.9 [32.3], 27.4 [27.5], 24.8 [24.7], 23.3 [23.2], 22.5 [22.7], 19.5 [19.6], 18.9 [18.9], 11.6. The de ratio was the same as the starting ester, indicating no racemization had taken place during the reduction.

21*b*: ir ($CHCl_3$): 3450, 2970, 1675, 1450, 1090, 1015 cm^{-1}; ^{1}H nmr: 7.42–7.16 (m, 5H), 3.71 (dd, 1H, J = 11, 21 Hz), 3.69 (dd, 1H, J = 11, 18 Hz), 3.61–3.49 (m, 1H), 2.88 (dd, 1H, J = 4, 13 Hz), 2.72 (dd, 1H, J = 9, 13 Hz), 2.43–2.00 (m, 2H), 1.82–1.40 (m, 4H), 1.34–0.80 (m, 4H), 0.97 (s, 3H), 0.82 (s, 3H), 0.72 (s, 3H); ^{13}C nmr: 139.6, 129.9, 128.2, 126.1, 66.6, 64.3, 54.0, 46.6, 43.6, 38.7, 36.0, 32.2, 27.1, 19.6, 18.9, 11.7. The de ratio was 100%, which corresponds to complete retention of optical purity.

Catalytic reduction of **5**i

Hydrogenation of **5***i* over 10% Pd/C in ethanol solution led to the absorption of 1.0 equiv. of hydrogen. Filtration through Celite and evaporation afforded a quantitative yield of **5***g* (mp 52–58°C), whose ir and nmr spectra were identical in form to those obtained from the alkylation of **3***c*. The diastereomeric excess was determined to be 76% from the ^{1}H nmr, which corresponds to complete retention of optical purity, and the optical rotation was $[\alpha]_D^{25}$ +82.0°.

Acknowledgements

The financial assistance of the Natural Sciences and Engineering Research Council of Canada in the form of operating grants and a fellowship (to P.M.) made this work possible. The cooperation of the Chemistry Department of Wayne State University in running the high-field nmr spectra and Dr. R. D. Bach (W.S.U.) in donating time on the polarimeter is gratefully acknowledged.

1. T. OGURI, T. SHIOIRI, and S. YAMADA. Chem. Pharm. Bull. Jpn. **25**, 2287 (1977).
2. (*a*) S. YAMADA, T. OGURI, and T. SHIOIRI. J. Chem. Soc. Chem. Commun. 136 (1976); (*b*) T. OGURI, N. KAWAI, T. SHIOIRI, and S. YAMADA. Chem. Pharm. Bull. Jpn. **26**, 803 (1978); (*c*) J. A. BAJGROWICZ, B. COSSEC, C. PIGIERE, R. JAQUIER, and P. VIALLAFONT. Tetrahedron Lett. **24**, 3721 (1983).
3. U. SCHÖLLKOPF and U. GROTH. Angew. Chem. Int. Ed. Engl. **20**, 977 (1981); U. SCHÖLLKOPF, U. GROTH, and W. HARTWIG. Justus Liebigs Ann. Chem. 2407 (1981); U. SCHÖLLKOPF, W. HARTWIG, K-H. POSPISCHIL, and H. KEHNE. Synthesis, 966 (1981); 969 (1981).
4. (*a*) G. HELMCHEN, A. SELIM, D. DORSCH, and I. TAUFER. Tetrahedron Lett. **24**, 3213 (1983); (*b*) R. KELLY and A. ARVANTIS. Tetrahedron Lett. **25**, 39 (1984); (*c*) W. OPPOLZER, C. CHAPUIS, and G. BERNARDINELLI. Helv. Chim. Acta, **67**, 1397 (1984); (*d*) D. F. TABER and K. RAMAN. J. Am. Chem. Soc. **105**, 5935 (1983); (*e*) L. A. PAQUETTE and R. F. DOEHNER. J. Org. Chem. **45**, 5105 (1980); (*g*) C. R. NOE. Chem. Ber. **115**, 1576 (1982); **115**, 1591 (1982); **115**, 1607 (1982).
5. (*a*) I. SHAHAK and Y. SASSON. Synthesis, 535 (1973); (*b*) A. FORNI, I. MORETTI, and G. TORRE. Tetrahedron Lett. 2941 (1978).
6. B. S. PEDERSON, S. SCHEIBE, N. H. NILSSON, and S-O. LAWESSON. Bull. Soc. Chim. Belg. **87**, 223 (1978).
7. R. MAYER. Angew. Chem. Int. Ed. Engl. **3**, 277 (1964).
8. R. AMSTUTZ, W. B. SCHWEIZER, D. SEEBACH, and J. P. DUNITZ. Helv. Chim. Acta, **64**, 2617 (1981).
9. A. P. KRAPCHO and E. A. DUNDULIS. J. Org. Chem. **45**, 3236 (1980).
10. J. HINE. Physical organic chemistry. McGraw-Hill, New York. 1962. p. 176.
11. D. A. EVANS. *In* Asymmetric synthesis. Vol. 3B. *Edited by* J. D. Morrison. Academic Press, New York, NY. 1984.
12. A. T. MOORE and H. N. RYDON. Organic Syntheses Col. Vol. 5. p. 586.
13. D. H. R. BARTON, F. S. GUZIEC, and I. SHAHAK. J. Chem. Soc. Perkin Trans. 1, 1794 (1974).
14. G. W. ANDERSON and F. M. CALLAHAN. J. Am. Chem. Soc. **82**, 3359 (1960).

Synthesis and conformational analysis of 2-arylseleno-1,3-dithianes. Crystal and molecular structure of 2-(4-methoxyphenylseleno)- and 2-(4-trifluoromethylphenylseleno)-1,3-dithiane

B. Mario Pinto, Jesus Sandoval-Ramirez, R. Dev Sharma, Anthony C. Willis, and Frederick W. B. Einstein[1]

Department of Chemistry, Simon Fraser University, Burnaby, B.C., Canada V5A 1S6

Received July 12, 1985

B. Mario Pinto, Jesus Sandoval-Ramirez, R. Dev Sharma, Anthony C. Willis, and Frederick W. B. Einstein. Can. J. Chem. **64**, 732 (1986).

The synthesis of 2-(4-methoxyphenylseleno)-1,3-dithiane **3** and 2-(4-trifluoromethylphenylseleno)-1,3-dithiane **5** from 2-chloro-1,3-dithiane **1** and the corresponding sodium arylselenolates is described. Nuclear magnetic resonance spectroscopic investigation of the products indicates that the compounds exist predominantly in a conformation in which the arylseleno moiety adopts an axial orientation. X-ray crystallographic investigation indicates that the 1,3-dithiane ring exists in the chair conformation with the arylseleno moiety in the axial orientation. Compound **3** is orthorhombic, space group $P2_12_12_1$ with $a = 5.449(2)$ Å, $b = 9.217(2)$ Å, $c = 24.860(3)$ Å, $V = 1248.5$ Å^3, $Z = 4$. The structure was refined to $R = 0.038$ for 689 reflections with $I > 2.3\sigma(I)$. Compound **5** is monoclinic, space group $C2/c$, with $a = 28.628(7)$ Å, $b = 5.246(2)$ Å, $c = 21.342(5)$ Å, $\beta = 121.12(1)°$, $V = 2743.8$ Å^3, $Z = 8$. Its structure refined to $R = 0.064$ for 966 reflections with $I > 2.3\sigma(I)$.

B. Mario Pinto, Jesus Sandoval-Ramirez, R. Dev Sharma, Anthony C. Willis et Frederick W. B. Einstein. Can. J. Chem. **64**, 732 (1986).

On décrit la synthèse du (méthoxy-4 phénylséléno)-2 dithiane-1,3 (**3**) et du (trifluorométhyl-4 phénylséléno)-2 dithiane-1,3 (**5**) à partir du chloro-2 dithiane-1,3 (**1**) et des arylsélénolates de sodium correspondants. Une étude des produits par spectroscopie rmn indique que les composés existent principalement dans une conformation dans laquelle la portion arylséléno se trouve dans une orientation axiale. Des études par diffraction des rayons-X indiquent que le cycle dithiane-1,3 existe dans une conformation chaise et que les groupements arylséléno se trouvent dans une conformation axiale. Le composé **3** est orthorhombique, groupe d'espace $P2_12_12_1$, avec $a = 5{,}449(2)$, $b = 9{,}217(2)$ et $c = 24{,}860(3)$ Å, $V = 1248{,}5$ Å^3 et $Z = 4$. On a affiné la structure jusqu'à une valeur de $R = 0{,}038$ pour 689 réflexions avec $I > 2{,}3\sigma(I)$. Le composé **5** est monoclinique, groupe d'espace $C2/c$, avec $a = 28{,}628(7)$ Å, $b = 5{,}246(2)$ Å et $c = 21{,}342(5)$ Å, $\beta = 121{,}12(1)°$, $V = 2743{,}8$ Å^3 et $Z = 8$. On a affiné la structure jusqu'à une valeur de $R = 0{,}064$ pour 966 réflexions avec $I > 2{,}3\sigma(I)$.

[Traduit par la revue]

Introduction

As part of a program designed to investigate the nature and origin of conformational effects, we have been studying the interaction of X and Y atoms in X—C—Y fragments. Our approach is experimental in nature and focusses on the systematic evaluation of substituent effects on conformational equilibria. Although there have been many experimental (1) and theoretical (2) investigations of such X—C—Y anomeric interactions (3), these studies have generally dealt with interactions involving first- and second-row elements. For instance, the most recent reports by Juaristi *et al.* (4) and Mikolajczyk *et al.* (5) describe the nature of the interaction between the two second-row elements, sulfur and phosphorus. A noteworthy exception is the investigation by Drew and Kitching (6) of the interaction in S—C—Y fragments, in which Y is one of the Group IVa elements, Si, Ge, Sn, or Pb. Our principal interest was in the conformational behaviour of compounds containing the more electropositive elements in Group VIa, namely, the third- and fourth-row elements, selenium and tellurium. To the best of our knowledge, there have been only two reports of relevance to the work undertaken here: a brief mention of the conformational preference in 2-methylseleno-1,3-oxathiane (7), and a detailed study of the conformational analysis of 2-phenylseleno cyclohexanone (8). We now report the synthesis of two 2-arylseleno-1,3-dithianes, and their conformational properties in solution and in the solid state.

Experimental

Melting points were determined with a Fisher–Johns melting-point apparatus and are uncorrected. The ^{1}Hmr (400.13 MHz) and ^{13}Cmr (100.6 MHz) spectra were recorded on a Bruker WM400 spectrometer. Spectra were measured in chloroform-*d*. Chemical shifts are given in ppm downfield from TMS. Chemical shifts and coupling constants were obtained from first-order analyses of the nmr spectra. Assignments were confirmed by means of double irradiation experiments.

Analytical thin-layer chromatography (tlc) was performed on precoated glass plates with Merck silica gel 60F-254 as the adsorbent (layer thickness 0.25 mm). The developed plates were air-dried and exposed to uv light. Column chromatography was performed on silica gel (Kieselgel 60, 230–400 mesh) at a pressure of 300–500 kPa according to a published procedure (9).

Solvents were distilled before use and were dried, as necessary, by literature procedures. Solvents were evaporated under reduced pressure without heating. Reactions were performed under oxygen-free nitrogen in deoxygenated solvents. Transfers under nitrogen were effected by means of standard Schlenck tube techniques.

2-(4-Methoxyphenylseleno)-1,3-dithiane (3)

Sodium borohydride (0.155 g, 4.1 mmol) was added to a solution of 4,4′-dimethoxydiphenyl diselenide (10) (0.763 g, 2.05 mmol) in a mixture of ether (10 mL) and ethanol (10 mL) at ambient temperature. The orange solution became colourless. When evolution of gas had ceased (≈0.5 h), the solvent was removed under high vacuum to give a white solid. Anhydrous THF (15 mL) was added and the mixture was cooled to 0°C.

A solution of 1,3-dithiane (0.56 g, 4.16 mmol) in dry benzene (10 mL) at 0°C was treated with *N*-chlorosuccinimide (0.61 g, 4.58 mmol). The mixture was stirred at 0°C for 0.5 h, then at ambient temperature for 15 min. The solution of 2-chloro-1,3-dithiane (**1**) thus obtained was filtered under nitrogen directly into the solution of sodium 4-methoxyphenylselenolate, prepared as described above. The reaction mixture was stirred vigorously at 0°C for 0.5 h, then at ambient temperature for 0.5 h. Saturated ammonium chloride solution was added and the mixture was extracted with dichloromethane. The organic phase was washed successively with saturated sodium chloride

[1]Authors to whom correspondence may be addressed.

solution and water, was dried over anhydrous sodium sulfate, and the solvent removed under reduced pressure without heating. The crude product (1.26 g) contained only a trace of the starting diaryl diselenide, as indicated by tlc. Rapid chromatography (9) on silica gel using hexane – ethyl acetate (95:5) as eluant afforded the title compound **3** as a white solid (0.875 g, 70%). Recrystallization from ether yielded **3** as white prisms; mp 74°C. *Anal.* calcd. for $C_{11}H_{14}OS_2Se$: C 43.27, H 4.62; found: C 43.23, H 4.62.

2-(4-Trifluoromethylphenylseleno)-1,3-dithiane (5)

The title compound was prepared from 2-chloro-1,3-dithiane **1** and 4,4′-bistrifluoromethyldiphenyl diselenide (11), as described for the preparation of **3**. Compound **5** was obtained as white prisms from hexane; yield: 79%, mp 66°C. *Anal.* calcd. for $C_{11}H_{11}F_3S_2Se$: C 38.49, H 3.23; found: C 38.55, H 3.19.

r-*2-(4-Methoxyphenylseleno)*-trans-*4*-trans-*6-dimethyl-1,3-dithiane* **6** *and* r-*2-(4-methoxyphenylseleno*-cis-*4*-cis-*6-dimethyl-1,3-dithiane* **7**

Sodium 4-methoxyphenylselenolate (0.95 mmol) was treated with 2-chloro-*cis*-4,6-dimethyl-1,3-dithiane **9** (0.95 mmol) (prepared from *cis*-4,6-dimethyl-1,3-dithiane **8** (12) in analogous fashion to that described for the synthesis of **1**), as described for the preparation of **3**. The crude product (0.31 g) was chromatographed on silica gel using hexane – ethyl acetate (98:2) as eluant. Compound **6** was obtained as white prisms from hexane (0.178 g); mp 80°C. Compound **7** was obtained as a syrup (0.058 g); overall yield: 74%. *Anal.* calcd. for $C_{13}H_{18}OS_2Se$: C 46.84, H 5.44; found: C 47.01, H 5.60.

X-ray crystallographic analysis

Crystals of **3** and **5** were selected [0.22 × 0.05 × 0.16 mm for **3**; 0.18 × 0.26 × 0.24 mm for **5**][2] sealed in thin-walled glass capillaries and mounted on an Enraf–Nonius CAD4F diffractometer employing graphite-crystal monochromated MoKα radiation ($\lambda(\alpha_1) = 0.70930$ Å; $\lambda(\alpha_2) = 0.71359$ Å). Accurate cell dimensions and the orientation matrix were obtained by least-squares analysis of the setting angles of [25;23] reflections [20° < 2θ < 27°; 20° < 2θ < 32°], widely separated in reciprocal space, which were accurately centered on the detector.

Crystal data of 3

$C_{11}H_{14}OS_2Se$ fw = 305.32

Orthorhombic, $P2_12_12_1$, $a = 5.449(2)$, $b = 9.217(2)$, $c = 24.860(3)$ Å, $V = 1248.5$ Å^3, $Z = 4$, $D_c = 1.624$ g cm^3, μ(MoKα) = 32.69 cm^{-1}.

Crystal data of 5

$C_{11}H_{11}F_3S_2Se$ fw = 343.30

Monoclinic, $C2/c$, $a = 28.628(7)$, $b = 5.246(2)$, $c = 21.342(5)$ Å, $\beta = 121.12(1)°$, $V = 2743.8$ Å^3, $Z = 8$, $D_c = 1.662$ g cm^{-3}, μ(MoKα) = 30.10 cm^{-1}.

The intensities of unique data sets [*hkl*; *hkl* and *ħkl*] were collected for 2θ < 45° using ω–2θ scans with scan widths of ([0.71; 1.00] + 0.35 tan θ)° in ω and scan rates [3.29–0.66; 5.48–0.82]° min^{-1} in ω. Background counts were determined by extending the scans by 25% on each side. A total of [987;1798] reflections were measured of which [689;966] with $I > 2.3\sigma(I)$ were regarded as observed and used in structure solution and refinement. Two standards were measured at intervals of [90;60] min of X-ray exposure time. For **3** the standards varied from their mean < ∓2% and showed no systematic trends, so no scaling was applied, but in **5** the standards showed a systematic decrease in intensity of about 18% over the duration of the data collection, so a five-point smoothed curve was fitted to the standards and all reflection intensities were scaled by this curve. An analytic absorption correction (13) was applied to the data of **3** ($T = 0.64$–0.84) and an empirical absorption correction (14) based on Ψ-scans was applied to **5** (range 1.00–0.92).

Both structures were solved by conventional heavy-atom methods. Successive refinement and difference electron density maps led to the location of all non-H atoms, which were refined initially with individual isotropic temperature factors and then anisotropically. Non-methyl H atoms were positioned geometrically and assigned isotropic temperature factors derived from those of the C atoms to which they were attached; they were included in structure factor calculations but their parameters were not refined.

As its space group is polar, refinement of **3** was also performed with its atomic coordinates transformed by $(1 - x, 1 - y, 1 - z)$. The R value decreased from 0.058 to 0.049, establishing the latter as the correct hand of the molecule in this particular crystal, and so the transformed coordinates were used for all subsequent refinement. A difference map revealed two of the methyl H atoms and the other was calculated geometrically. These atoms were added to the model with fixed parameters. The least-squares refinement was continued until all shift/error ratios were <0.01. All features in a final difference map were of magnitude <0.41(3) e Å^{-3}. Final $R = 0.038$, $R_w = 0.034$ for 136 variables.

The structure of **5** was less well behaved. A difference map showed large peaks between the F atoms, suggesting that the CF_3 group was rotationally disordered about the C(8)—C(11) bond. A model was set up with three F atoms of occupancy g at the original positions and three of occupancy $(1 - g)$ between them; g was initially set at 0.55. In view of the instability of the refinement of these atoms, the "soft" constraints C(8)—F = 1.33(1) Å and F ... F = 2.17(1) Å within each group of three F atoms were applied within the least-squares refinement (15) and only one isotropic thermal parameter was assigned to all F atoms. Occupancy g refined to ca. 0.80, so F(1)—F(3) were next refined with individual isotropic temperature factors and, finally, individual anisotropic temperature factors. In addition, the H atom coordinates were recalculated and linked to ride on their respective C atoms. Refinement was continued until shift/error ratios were <0.4 for F atoms, <0.03 for non-F. A difference map showed no outstanding features (all peaks <0.51 e Å^{-3}). Final $R = 0.064$, $R_w = 0.058$ for 165 parameters.

Refinement of both structures was by full-matrix least squares minimizing the function $\sum w(|F_o| - |F_c|)^2$. The weights were initially unity but in the later cycles $w = [(\sigma(F_o))^2 + p(F_o)^2]^{-1}$ where $\sigma(F_o)$ was derived from the counting statistics and $p = 0.0003$ for **3** and 0.0004 for **5**. Neutral-atom scattering factors with anomalous dispersion corrections were used (16). Computer programs (17–19) were run on a VAX 11-750 computer.

Final atomic coordinates for non-H atoms are listed in Table 1 and selected bond lengths and angles in Table 2. Figures 1 and 2 show the molecular structure of **3** and **5**, respectively, with the atom labelling scheme. H atoms coordinates, anisotropic temperature factors, additional interatomic distances and angles, selected least-squares planes, torsion angles, and structure factor listings are deposited.[3]

Results and discussion

Synthesis

Initially, we envisaged the synthesis of the desired 2-arylseleno-1,3-dithianes by reaction of the anion of 1,3-dithiane (generated from 1,3-dithiane and butyl lithium, in THF) with the diselenides or their corresponding selenenyl halides. However, under these conditions the desired compounds were formed in low yield, large amounts of the diselenides being recovered after processing. This was in spite of the fact that initial discoloration of the solution of the selenium reagent was observed, indicating consumption of the reagent. This behaviour likely results from attack of the generated selenolate or halide ion at selenium in the 2-arylseleno-1,3-dithianes to regenerate the dithiane anion and the selenium reagent. We turned, therefore, to the reaction of the selenolate anions with 2-chloro-1,3-dithiane (**1**). Thus, reaction of 2-chloro-1,3-dithiane **1** (generated by *N*-chlorosuccinimide oxidation of 1,3-dithiane (20)) with sodium 4-methoxyphenyl selenolate **2** (obtained by sodium borohydride reduction of 4,4′-dimethoxy-

[2]Within this section, the values within square brackets are for **3** and **5**, respectively.

[3]A complete set of data may be purchased from the Depository of Unpublished Data, CISTI, National Research Council of Canada, Ottawa, Ont., Canada K1A 0S2.

TABLE 1. Fractional atomic coordinates and B_{eq}[a] of the non-hydrogen atoms

Atom	x	y	z	B_{eq}
2-(4-Methoxyphenylseleno)-1,3-dithiane, **3**				
Se	0.9374(2)	0.76011(14)	0.94252(4)	3.63
S(1)	0.7447(6)	0.4708(3)	0.98475(11)	3.62
S(2)	0.7310(7)	0.5119(4)	0.86481(12)	4.58
O(1)	0.713(2)	1.1560(9)	0.7553(3)	5.2
C(1)	0.711(2)	0.5977(10)	0.9299(4)	3.4
C(2)	1.040(2)	0.3989(11)	0.9692(4)	4.1
C(3)	1.066(3)	0.3246(12)	0.9153(5)	5.9
C(4)	1.031(3)	0.4299(14)	0.8693(4)	5.2
C(5)	0.855(2)	0.8850(11)	0.8837(4)	3.2
C(6)	0.653(2)	0.9669(14)	0.8850(4)	3.9
C(7)	0.596(2)	1.0671(12)	0.8426(4)	3.9
C(8)	0.748(2)	1.0696(12)	0.7986(4)	3.4
C(9)	0.948(2)	0.9793(14)	0.7964(4)	4.1
C(10)	1.001(2)	0.8855(12)	0.8380(5)	4.1
C(11)	0.500(3)	1.2492(18)	0.7538(4)	5.7
2-(4-Trifluoromethylphenylseleno)-1,3-dithiane, **5**				
Se	0.24087(6)	0.0511(3)	0.17337(7)	5.30
S(1)	0.3502(2)	−0.2089(8)	0.2628(2)	6.40
S(2)	0.2870(2)	−0.3238(7)	0.1007(2)	5.80
C(1)	0.2854(5)	−0.245(2)	0.1812(6)	5.1
C(2)	0.3792(5)	0.033(3)	0.2343(8)	7.4
C(3)	0.3819(6)	−0.032(3)	0.1678(9)	8.3
C(4)	0.3260(6)	−0.065(3)	0.0984(7)	7.2
C(5)	0.1723(5)	−0.041(3)	0.0888(7)	5.0
C(6)	0.1408(7)	−0.228(3)	0.0910(8)	8.9
C(7)	0.0897(7)	−0.279(4)	0.0293(11)	10.0
C(8)	0.0703(7)	−0.139(4)	−0.0314(10)	6.8
C(9)	0.1022(8)	0.039(4)	−0.0333(9)	10.2
C(10)	0.1537(7)	0.089(3)	0.0264(9)	8.4
C(11)[b]	0.0142(5)	−0.196(2)	−0.0965(7)	10.0
F(1)[b,c]	0.0102(8)	−0.443(3)	−0.1123(13)	16.8
F(2)[b,c]	−0.0237(5)	−0.130(6)	−0.0822(9)	17.4
F(3)[b,c]	0.0072(7)	−0.066(5)	−0.1544(8)	14.3
F(4)[b,d]	−0.0115(14)	−0.340(7)	−0.072(2)	9.6[e]
F(5)[b,d]	−0.0112(13)	0.028(3)	−0.118(2)	9.6[e]
F(6)[b,d]	0.0127(15)	−0.313(7)	−0.152(2)	9.6[e]

[a] $B_{eq} = 8\pi^2(U_1 + U_2 + U_3)/3$, where U_n (in Å^2) are the principal axes of the thermal ellipsoid.

[b] On account of the constrained refinement of C(11) and the F atoms, the esd's of these atoms are probably underestimated.

[c] Occupancy 0.68. The esd in the occupancy parameter is 0.03.

[d] Occupancy 0.32.

[e] Isotropic. One parameter was used for F(4), F(5), and F(6): B = 9.6(10).

TABLE 2. Selected interatomic distances and angles for 2-(4-methoxyphenylseleno)-1,3-dithiane, **3**, and 2-(4-trifluoromethylphenylseleno)-1,3-dithiane, **5**

Bond	Distance (Å) **3**	**5**
Se—C(1)	1.966(10)	1.963(12)
Se—C(5)	1.915(11)	1.920(12)
C(1)—S(1)	1.807(10)	1.781(12)
S(1)—C(2)	1.781(12)	1.786(14)
C(2)—C(3)	1.512(15)	1.500(16)
C(3)—C(4)	1.510(17)	1.528(17)
C(4)—S(2)	1.802(14)	1.774(14)
S(2)—C(1)	1.804(10)	1.790(11)
C(5)—C(6)	1.334(18)	1.348(17)
C(6)—C(7)	1.436(16)	1.399(18)
C(7)—C(8)	1.372(17)	1.338(20)
C(8)—C(9)	1.374(19)	1.318(20)
C(9)—C(10)	1.378(16)	1.388(19)
C(10)—C(5)	1.386(15)	1.337(17)
C(8)—O(1)	1.353(12)	—
O(1)—C(11)	1.442(18)	—
C(8)—C(11)	—	1.515(19)
Bonds	**Angle (°C) 3**	**5**
C(1)—Se—C(5)	100.8(4)	100.6(5)
Se—C(1)—S(1)	107.9(4)	107.5(6)
Se—C(1)—S(2)	116.0(5)	116.0(6)
S(1)—C(1)—S(2)	112.8(5)	115.7(6)
C(1)—S(1)—C(2)	99.8(5)	100.1(6)
S(1)—C(2)—C(3)	116.5(9)	115.0(10)
C(2)—C(3)—C(4)	111.6(9)	113.7(11)
C(3)—C(4)—S(2)	115.5(9)	114.8(10)
C(4)—S(2)—C(1)	100.6(5)	100.3(6)
Se—C(5)—C(6)	120.9(8)	121.8(12)
Se—C(5)—C(10)	119.6(9)	119.6(12)
C(6)—C(5)—C(10)	119.4(10)	118.5(13)
C(5)—C(6)—C(7)	121.7(10)	120.0(14)
C(6)—C(7)—C(8)	117.6(11)	121.0(17)
C(7)—C(8)—C(9)	120.2(10)	118.1(17)
C(8)—C(9)—C(10)	120.9(10)	122.0(16)
C(9)—C(10)—C(5)	119.9(10)	120.2(15)
C(8)—O(1)—C(11)	119.0(9)	—
C(7)—C(8)—O(1)	124.0(12)	—
C(9)—C(8)—O(1)	115.8(10)	—
C(7)—C(8)—C(11)	—	119.4(18)
C(9)—C(8)—C(11)	—	122.4(17)

diphenyl diselenide (10)) in a mixture of benzene and tetrahydrofuran at 0°C proceeded smoothly to give 2-(4-methoxyphenylseleno)-1,3-dithiane **3** in 70% yield (see Scheme 1). It was imperative that **3** be obtained in a pure state fairly rapidly to avoid significant decomposition. This was effected by means of rapid column chromatography on silica gel (9) followed by crystallization of the homogeneous product. Similar treatment of sodium 4-trifluoromethylphenyl selenolate **4** (obtained by sodium borohydride reduction of 4,4′-bistrifluoromethyldiphenyl diselenide (11)) with 2-chloro-1,3-dithiane **1** afforded, after processing as described above, 2-(4-trifluoromethylphenylseleno)-1,3-dithiane **5** in 79% yield (see Scheme 1).

Conformational analysis

The conformational equilibrium of interest is shown in Fig. 3. The conformational analysis of these systems was effected by means of nmr spectroscopy. Thus, the ^{1}Hmr spectra (400 MHz) of the conformationally-averaged systems in deuteriochloroform at ambient temperature were carefully analyzed. The H-2,

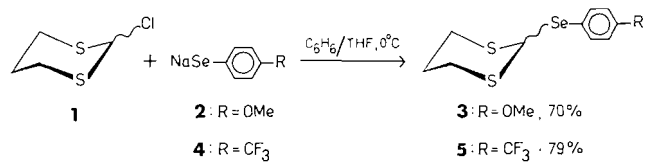

1 **2**: R = OMe **3**: R = OMe, 70%

4: R = CF_3 **5**: R = CF_3, 79%

SCHEME 1

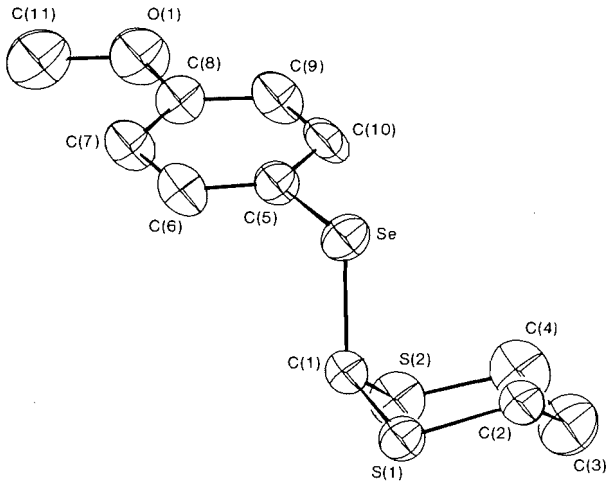

FIG. 1. SNOOPI diagram of 2-(4-methoxyphenylseleno)-1,3-dithiane, **3**. Thermal ellipsoids enclose 50% probabilities and hydrogen atoms have been deleted.

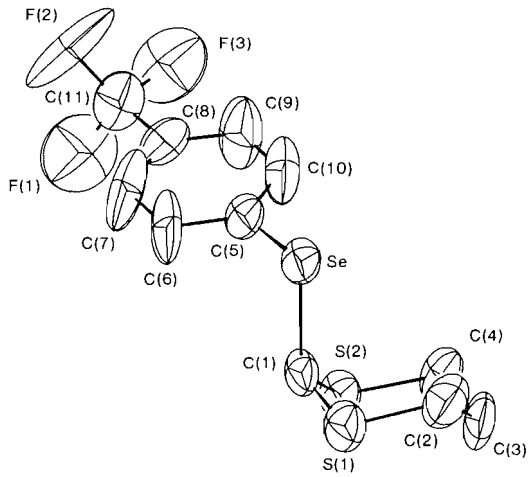

FIG. 2. SNOOPI diagram of 2-(4-trifluoromethylphenylseleno)-1,3-dithiane, **5**. Hydrogen atoms and the minor orientation of the disordered CF_3 group have been deleted. 50% probability ellipsoids are shown.

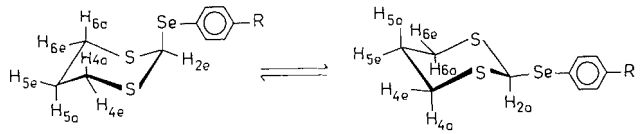

3: R = OMe

5: R = CF_3

FIG. 3. Conformational equilibrium in 2-arylseleno-1,3-dithianes.

H-4,6 axial, and H-4,6 equatorial signals appeared as distinct multiplets in the spectra of **3** and **5**, whereas partially overlapped multiplets were observed for the H-5 axial and H-5 equatorial signals (see, for example, Fig. 4); these were readily assigned on the basis of their vicinal coupling constants and the assignments were confirmed by means of spin-decoupling experiments. Analysis of the spectra yielded the chemical shifts and coupling constants listed in Table 3. The salient features of the spectra are (1) the chemical-shift differences observed for H-4,6 axial and equatorial proton signals, $\Delta\delta$(ax/eq) (0.54 ppm and 0.56 ppm in the spectra of **3** and **5**, respectively); (2) the appearance of the H-2 signals as broad singlets; and (3) the presence of significant long-range $^4J_{2,4e}$ and $^5J_{2,5e}$ couplings (see Table 3). The deshielding effect of an axial substituent at C-2 of 1,3-dithianes and 1,3,5-trithianes on H-4,6ax relative to H-4,6eq is well documented (4, 5, 21). Larger values of $\Delta\delta$(ax/eq) (H-4,6) have been noted for 2-diphenylphosphoryl-1,3-dithiane (1.2 ppm) (4)), 2-dimethoxyphosphoryl-1,3,5-trithiane (1.63 ppm (5)), and 2-phenylthio-1,3,5-trithiane (1.07 ppm (21)), which have been shown to exist predominantly in the conformation in which the 2-substituent adopts the axial orientation. Nonetheless, it would appear that the axial conformer is present to a significant extent in the equilibrium mixture of both **3** and **5**, since $\Delta\delta$(ax/eq) (H-4,6) in 2-*tert*-butyl-1,3-dithiane is reported to be only 0.09 ppm (4).

The appearance of the H-2 signals in the spectra of **3** and **5** as broad singlets ($W_{1/2}$ = 2.8 Hz) can be attributed principally to long-range four- and five-bond couplings to H-4e and H-5e, respectively. Thus, irradiation of the H-2 resonances resulted in loss of $^4J_{2,4e}$ (0.8 Hz in **3** and 1.0 Hz in **5**) and $^5J_{2,5e}$ (0.8 Hz in **3** and 1.0 Hz in **5**) in the signals corresponding to H-4e and H-5e, respectively. These results auger well for the predominantly axial orientation of the arylseleno moiety in the preferred conformations of **3** and **5**, since this orientation would permit significant long-range coupling between H-2e and H-4e and between H-2e and H-5e. The corresponding couplings to H-2a are known to be much smaller (6, 12, 22, 23).

The conformational preference was confirmed, for the *p*-methoxy derivative **3**, by synthesis of the corresponding anancomeric derivatives **6** and **7** (prepared from *cis*-4,6-dimethyl-1,3-dithiane **8** (12) in analogous fashion to that described for the synthesis of **3** and **5**) and by comparison of their spectroscopic properties with those of **3**. Thus, for example, the H-4a,6a resonance in the ^{1}Hmr spectrum of the axial isomer **6** resonates at lower field than that in the corresponding spectrum of the equatorial isomer **7**, in accord with the aforementioned deshielding effect of axial C-2 substituents. The chemical shift difference for H-4a,6a in **6** and **7** (0.53 ppm) compares

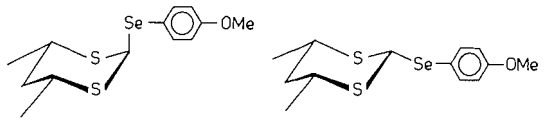

6 **7**

favourably with that observed for $\Delta\delta$(ax/eq) (H-4,6) in **3** and **5**. That H-2a resonates at higher field than H-2e ($\Delta\delta$ = 0.41 ppm) is also in accord with previous results (21) in 2-phenylthio thianes and 1,3,5-trithianes but not with the data on the unsubstituted compounds (12, 24). Interestingly, the H-2e resonance in the spectrum of **6** appears as a broad singlet ($W_{1/2}$ = 2.5 Hz), whereas H-2a in the spectrum of **7** appears as a sharp singlet ($W_{1/2}$ = 0.9 Hz) showing selenium satellites ($^1J_{^{77}Se,H\text{-}2a}$ = 12.3 Hz). Furthermore, the H-5e signal in the former spectrum displays long-range coupling to H-2e (confirmed by decoupling), whereas the corresponding signal in the latter spectrum shows little or no such coupling (see Fig. 5). The assignment of axial and equatorial orientations of the arylseleno substituent was further corroborated by the ^{13}Cmr data for **6** and **7** (see Table 4). Thus, C-4 and C-6 in the axial isomer **6** exhibit a shielding of 7.2 ppm relative to those in the equatorial isomer, owing to the γ-*gauche* effect (25).

It is clear, then, that the 2-arylseleno-1,3-dithianes **3** and **5** in solution exist predominantly in the conformation in which the arylseleno moiety adopts an axial orientation.

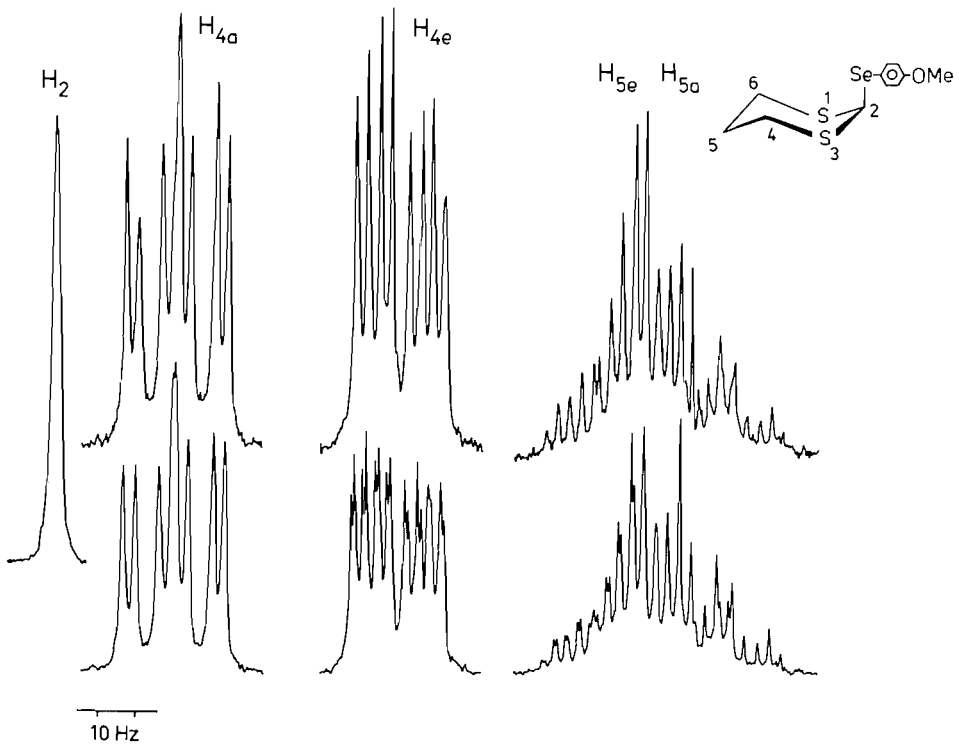

FIG. 4. Partial ^{1}Hmr spectrum of 2-(4-methoxyphenylseleno)-1,3-dithiane **3** recorded in deuteriochloroform at 400 MHz; top trace: with irradiation at ν(H-2).

TABLE 3. ^{1}H magnetic resonance spectroscopic data for 2-arylseleno-1,3-dithianes

Compound	Chemical shift (δ)[a] H-2	H-4a,6a	H-4e,6e	H-5a	H-5e	Ph	OCH_3	CH_3	Coupling constant (Hz)[b]
3	5.17 $W_{1/2}$ = 2.8 Hz	3.24	2.70	2.04	2.10	7.57 6.84	3.80	—	$^2J_{4a,4e} = -14.0$ $^2J_{5a,5e} = -14.0$ $^3J_{4a,5a} + {}^3J_{4a,5e} = 13.0$ $^3J_{4e,5e} + {}^3J_{4e,5a} = 9.0$ $^4J_{2,4e} \simeq 0.8$ $^5J_{2,5e} \simeq 0.8$
5	5.40 $W_{1/2}$ = 2.8 Hz	3.26	2.70	2.05	2.13	7.71 7.55	—	—	$^2J_{4a,4e} = -14.5$ $^2J_{5a,5e} = -14.0$ $^3J_{4a,5a} + {}^3J_{4a,5e} = 13.5$ $^3J_{4e,5e} + {}^3J_{4e,5a} = 9.0$ $^4J_{2,4e} \simeq 1.0$ $^5J_{2,5e} \simeq 1.0$
6	5.40 $W_{1/2}$ = 2.5 Hz	3.43	—	1.38	2.17	7.53 6.85	3.82	1.24	$^2J_{5a,5e} = -13.8$ $^3J_{4a,5a} + {}^3J_{4a,5e} = 13.7$ $^3J_{4a,CH_3} = 7.0$
7	4.99 $W_{1/2}$ = 0.9 Hz	2.90	—	1.22	2.06	7.67 6.86	3.82	1.20	$^2J_{5a,5e} = -14.0$ $^3J_{4a,5a} + {}^3J_{4a,5e} = 13.7$ $^3J_{4a,CH_3} = 7.2$ $^1J_{^{77}Se-H\text{-}2} = 12.3$

[a]Chemical shifts in ppm downfield from TMS in chloroform-*d*.
[b]Coupling constants represent measured spacings and are not calculated values.

X-ray crystallographic studies

In both structures, the 1,3-dithiane ring is in a chair conformation with the arylseleno moiety in the axial orientation. Atoms S(1), C(2), C(4), and S(2) form a plane at an angle of 58° to the plane C(1), S(1), S(2) and 55° to the plane C(2), C(3), C(4) in **3**; in **5** these values are both 56°. The aryl group is oriented to produce a staggered conformation of atoms about the Se—C(1) bond with S(1)—C(1)—Se—C(5) torsion angles of −176° for **3** and −175° for **5**. Steric effects derived from this orientation lead to the angles Se—C(1)—S(2) being greater than Se—C(1)—S(1) in both compounds (116.0(5)° cf. 107.9(4)° for **3**; 116.0(6)° cf. 107.5(6)° for **5**).

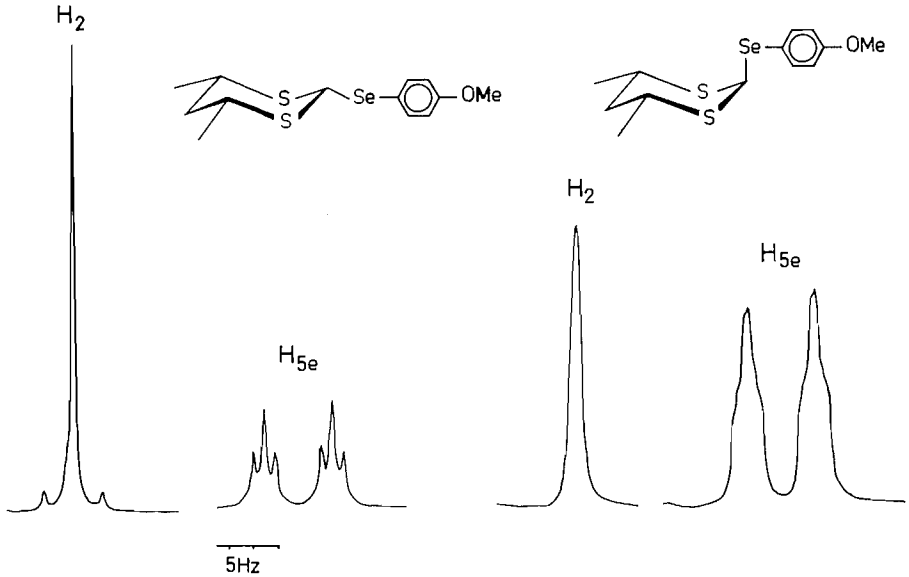

FIG. 5. Partial ^{1}Hmr spectra of *r*-2-(4-methoxyphenylseleno)-*trans*-4-*trans*-6-dimethyl-1,3-dithiane **6** and *r*-2-(4-methoxyphenylseleno)-*cis*-4-*cis*-6-dimethyl-1,3-dithiane **7** recorded in deuteriochloroform at 400 HMz.

TABLE 4. ^{13}C magnetic resonance chemical-shift data[a] for 2-arylseleno-1,3-dithianes

	Carbon						
Compound	C-2	C-4,6	C-5	Ph	OCH_3	CH_3	CF_3
3	42.0	27.7	25.0	160.1 137.6 121.0 114.4	55.1	—	—
	$^1J_{^{13}C-H-2}$ = 162 Hz $^1J_{^{13}C-^{77}Se}$ = 90 Hz						
5	41.9	27.5	25.0	135.7 134.6 125.7 122.6	—	—	130.0
	$^1J_{^{13}C-H-2}$ = 162 Hz $^1J_{^{13}C-^{77}Se}$ = 89 Hz						
6	44.7	35.3	43.9	160.1 137.6 122.9 114.5	55.1	20.9	—
	$^1J_{^{13}C-H-2}$ = 160 Hz $^1J_{^{13}C-^{77}Se}$ = 91 Hz						
7	43.0	42.5	42.3	160.5 137.9 117.6 114.6	55.2	21.1	—
	$^1J_{^{13}C-H-2}$ = 167 Hz						
8	44.7	39.3	33.4	—	—	21.8	—
1,3-Dithiane	31.6	29.5	26.2	—	—	—	—

[a]In ppm downfield from TMS in chloroform-*d*.

The axial disposition of the arylseleno group is consistent with expectations based on the anomeric effect (1–3). The expression of this effect would also be expected to influence structural features within the molecules. Within the framework of Perturbational Molecular Orbital (PMO) theory, increasing electronegativity of a substituent atom leads to a lowering of the energies of molecular orbitals associated with that atom (see for example ref. 26). Thus, the σ^*_{C-Se} orbital will be of lower energy in the *p*-trifluoromethyl derivative **5** than in the *p*-methoxy derivative **3** and it follows (27) that the n_S–σ^*_{C-Se} orbital interaction would be more important in the former compound. These arguments predict a smaller value for the angle C(1)—Se—C(5), a shorter Se—C(1) bond, and longer C(1)—S(1) and C(1)—S(2) bonds in **3** than in **5**. Unfortunately, these structure determinations are not sufficiently precise to confirm these predictions.

Conclusions

The axial conformational preference of the arylseleno moiety in the 2-arylseleno-1,3-dithianes **3** and **5** both in solution and in the solid state constitute support for the anomeric effect operating in S—C—Se fragments. The quantitation of this conformational effect in these and related compounds by means of low temperature nmr spectroscopy is in progress and the results will be reported elsewhere (for a preliminary account, see ref. 28).

Acknowledgements

We thank Ms. M. Vanderweyde for technical assistance, Mrs. M. Tracey for the recording of nmr spectra, and the Natural Sciences and Engineering Research Council of Canada for financial support.

1. J. T. EDWARD. Chem. Ind. (London), 1102 (1955); R. U. LEMIEUX and N. J. CHÜ. Abstr. Papers Am. Chem. Soc. Meeting, 133, 31N (1958); R. U. LEMIEUX. *In* Molecular rearrangements. *Edited by* P. de Mayo. Interscience, New York. 1964. p. 709; Pure Appl. Chem. **25**, 527 (1971); C. B. ANDERSON and D. T. SEPP. J. Org. Chem. **32**, 607 (1967); Tetrahedron, **24**, 1707 (1968); E. L. ELIEL and C. A. GIZA. J. Org. Chem. **33**, 3754 (1968); W. F. BAILEY and E. L. ELIEL. J. Am. Chem. Soc. **96**, 1798 (1974); H. PAULSEN, Z. GYORGYDEAK, and M. FRIEDMANN. Chem. Ber. **107**, 1590 (1974); H. PAULSEN. Die Starke, **27**, 397 (1975); C. ROMERS, C. ALTONA, H. R. BUYS, and E. HAVINGA. Top Stereochem. **4**, 39 (1969); E. A. C. LUCKEN. J. Chem. Soc. III, 2954 (1959); Z. ARDALAN, and E. A. C. LUCKEN. Helv. Chim. Acta, **56**, 1715 (1973); Z. DE WECKARDALAN, E. A. C. LUCKEN, and J. WEBER. J. Mol. Struct. **32**, 101 (1976); B. M. PINTO and S. WOLFE. Tetrahedron Lett. 3687 (1982); F. S. JORGENSEN and L. NORSKOV-LAURITSEN. Tetrahedron Lett. 5221 (1982); G. DESCOTES, M. LISSAC, J. DELMAU, and J. DUPLAN. C. R. Acad. Sci. Paris Ser. C, **267**, 1240 (1968); Y. BAHUREL, M. LISSAC-CAHU, G. DESCOTES, M. GELIN, J. DELMAU, and J. DUPLAN. Bull. Soc. Chim. Fr. 4006 (1970); P. DESLONGCHAMPS, D. D. ROWAN, N. POTHIER, T. SAUVÉ, and J. K. SAUNDERS. Can. J. Chem. **59**, 1105 (1981); P. DESLONGCHAMPS, D. D. ROWAN, N. POTHIER, and J. K. SAUNDERS. Can. J. Chem. **59**, 1122 (1981).
2. S. WOLFE, A. RAUK, L. M. TEL, and I. G. CSIZMADIA. J. Chem. Soc. B, 136 (1971); S. DAVID, O. EISENSTEIN, W. J. HEHRE, L. SALEM, and R. HOFFMAN. J. Am. Chem. Soc. **95**, 3806 (1973); S. WOLFE, M.-H. WHANGBO, and D. J. MITCHELL. Carbohydr. Res. **69**, 1 (1979); G. A. JEFFREY, J. A. POPLE, J. S. BINKLEY, and S. VISHVESHWARA. J. Am. Chem. Soc. **100**, 373 (1978); G. A. JEFFREY and J. H. YATES. J. Am. Chem. Soc. **101**, 820 (1979); L. SCHÄFER, C. VAN ALSENOY, J. O. WILLIAMS, J. N. SCARSDALE, and H. J. GEISE. J. Mol. Struct. Theochem. **76**, 349 (1981); C. VAN ALSENOY, L. SCHÄFER, J. N. SCARSDALE, J. O. WILLIAMS, and H. J. GEISE. J. Mol. Struct. Theochem. **86**, 111 (1981); F. S. JORGENSEN. J. Chem. Res. (S), 212 (1981); A. PROSS and L. RADOM. J. Comput. Chem. **1**, 295 (1980); P. v. R. SCHLEYER and A. J. KOS. Tetrahedron, **39**, 1141 (1983).
3. E. L. ELIEL. Acc. Chem. Res. **3**, 1 (1970); N. S. ZEFIROV and N. M. SHEKHTMAN. Russ. Chem. Rev. **40**, 315 (1979); W. A. SZAREK and D. HORTON (*Editors*). Anomeric effect origin and consequences. ACS Symp. Ser. No. 87, American Chemical Society, Washington, D.C. 1979; A. J. KIRBY. The Anomeric effect and related stereoelectronic effects at oxygen. Springer Verlag, Berlin. 1983.
4. E. JUARISTI, L. VALLE, C. MORA-UZETA, B. A. VALENZUELA, P. JOSEPH-NATHAN, and M. F. FREDRICH. J. Org. Chem. **47**, 5038 (1982); E. JUARISTI, B. A. VALENZUELA, L. VALLE, and A. T. MCPHAIL. J. Org. Chem. **49**, 3026 (1984).
5. M. MIKOLAJCZYK, P. BALCZEWSKI, K. WROBLEWSKI, J. KAROLAK-WOJCIECHOWSKA, A. MILLER, M. W. WIECZOREK, M. Y. ANTIPIN, and Y. T. STRUCHKOV. Tetrahedron, **40**, 4885 (1984).
6. G. M. DREW and W. KITCHING. J. Org. Chem. **46**, 558 (1981).
7. K. FUJI, M. UEDA, K. KAJIWARA, K. SUMI, E. FUJITA, and I. MIURA. Heterocycles, **16**, 178 (1981).
8. H. ÖZBAL and W. W. ZAJAC, JR. Tetrahedron Lett. 4821 (1979).
9. D. R. BUNDLE, T. IVERSEN, and S. JOSEPHSON. Int. Lab. 21 (1980).
10. H. J. REICH, M. L. COHEN, and P. D. CLARK. Org. Synth. **59**, 141 (1979); H. RHEINBOLDT. *In* Methoden der Organischen Chemie (Houben-Weyl). 4th ed. Vol. 9. *Edited by* E. Muller. Georg Thieme Verlag, Stuttgart, Germany. 1955. p. 1086.
11. H. J. REICH, J. M. RENGA, and I. L. REICH. J. Am. Chem. Soc. **97**, 5434 (1975).
12. E. L. ELIEL, A. A. HARTMANN, and A. G. ABATJOGLOU. J. Am. Chem. Soc. **96**, 1807 (1974).
13. J. DEMEULENAER and H. TOMPA. Acta Crystallogr. **19**, 1014 (1965).
14. A. C. T. NORTH, D. C. PHILLIPS, and F. S. MATHEWS. Acta Crystallogr. Sect. A, **24**, 351 (1968).
15. J. WASER. Acta Crystallogr. **16**, 1091 (1963).
16. INTERNATIONAL TABLES FOR X-RAY CRYSTALLOGRAPHY. Vol. IV. Kynoch Press, Birmingham, England. 1974.
17. A. C. LARSON and E. J. GABE. Computing in crystallography. Delft University Press, Delft, Holland. 1978; A. C. LARSON, F. L. LEE, Y. LEPAGE, and E. J. GABE. The N.R.C. VAX crystal structure system. Chemistry Division, N.R.C., Ottawa, Canada. 1984.
18. D. J. WATKINS and F. R. CARRUTHERS. CRYSTALS user guide. Chemical Crystallography Laboratory, University of Oxford. 1984.
19. E. K. DAVIES. CHEMGRAF user guide. Chemical Crystallography Laboratory, University of Oxford. 1983.
20. E. C. TAYLOR and J. L. LAMATTINA. Tetrahedron Lett. 2077 (1977); K. ARAI and M. OKI. Tetrahedron Lett. 2183 (1975); K. ARAI and M. OKI. Bull. Chem. Soc. Jpn. **49**, 553 (1976).
21. M. OKI, T. SUGAWARA, and H. IWAMURA. Bull. Chem. Soc. Jpn. **47**, 2457 (1971).
22. E. L. ELIEL and R. O. HUTCHINS. J. Am. Chem. Soc. **91**, 2703 (1969).
23. K. C. RAMEY and J. MESSICK. Tetrahedron Lett. 4423 (1965).
24. E. L. ELIEL, V. S. RAO, F. W. VIERHAPPER, and G. Z. JUARISTI. Tetrahedron Lett. 4339 (1975).
25. D. M. GRANT and B. V. CHENEY. J. Am. Chem. Soc. **89**, 5315 (1967).
26. A. PROSS, L. RADOM, and R. W. TAFT. J. Org. Chem. **45**, 818 (1980).
27. M.-H. WHANGBO and S. WOLFE. Isr. J. Chem. **20**, 36 (1980).
28. B. M. PINTO, J. SANDOVAL-RAMIREZ, and R. D. SHARMA. Tetrahedron Lett. 5235 (1985).

The crystal structure of an enol silyl ether

F. BRISSE

Department of Chemistry, Université de Montréal, P.O. Box 6218, Station A, Montréal, Qué., Canada H3C 3J7

AND

D. THORAVAL AND T. H. CHAN

Department of Chemistry, McGill University, 801 Sherbrooke St. West, Montréal, Qué., Canada H3A 2K6

Received December 5, 1985

F. BRISSE, D. THORAVAL, and T. H. CHAN. Can. J. Chem. **64**, 739 (1986).

The crystal structure of the enol silyl ether compound, $C_{28}H_{33}NO_3Si$, **1**, has been established by direct methods and refined to a final *R* value of 0.053 for 1825 observed reflections. The crystals belong to the monoclinic system, $a = 8.683(5)$, $b = 12.689(5)$, $c = 24.585(11)$ Å, $\beta = 105.33(4)°$, and the space group is $P2_1/c$. The C(sp^2)—C(sp^2) bond distance is normal but the Si(1)—O(1)—C(1) angle with a value of 132.5(4)° is larger than usual. This is attributed to an interaction between Si(1) and O(2) of the *N*-acetate group, d(Si ... O) = 3.320(4) Å. There is a distortion of the tetrahedral coordination around the silicon atom since the bond angles involving Si vary from 102.8(4) to 112.6(5)°. All three phenyl rings and the *N*-acetate group are planar. The two phenyls at C(3) are inclined by $\phi_1 = 66.5$, $\phi_2 = 58.7°$ with respect to the ethylenic group constituted of the two C(sp^2) atoms and their four substituents. The molecules are held in the crystal by van der Waals forces only.

F. BRISSE, D. THORAVAL et T. H. CHAN. Can. J. Chem. **64**, 739 (1986).

La structure cristalline de l'éther enolique silylé, $C_{28}H_{33}NO_3Si$, **1**, a été déterminée par des méthodes directes et affinée jusqu'à la valeur *R* finale de 0,053 pour 1825 réflexions observées. La maille monoclinique a pour dimension, $a = 8,683(5)$, $b = 12,689(5)$, $c = 24,585(11)$ Å, $\beta = 105,33(4)°$ et le groupe spatial est $P2_1/c$. La longueur de la liaison C(sp^2)—C(sp^2) est normale, par contre l'angle Si(1)—O(1)—C(1) avec une valeur de 132,5(4)° est plus ouvert que d'habitude. Ceci est attribué à une interaction entre Si(1) et O(2) du groupe *N*-acétate, d(Si ... O) = 3,320(4) Å. Les angles de valence autour de l'atome Si varient de 102,8(4) à 112,6(5)° reflétant ainsi la distortion de la coordination tétraédrique de cet atome. Les atomes de chacun des trois groupes phényles ainsi que du groupe *N*-acétate sont coplanaires. Les deux phényles fixés en C(3) sont inclinés de $\phi_1 = 66,5$ et $\phi_2 = 58,7°$ par rapport au plan éthylénique constitué des deux atomes C(sp^2) et de leurs quatre substituants. La cohésion moléculaire n'est assurée que par des forces de van der Waals.

Introduction

The chemistry of enol silyl ethers has undergone dramatic development since their first introduction into organic synthesis (1–4). Enol silyl ethers now rival enolate anions in importance. Reactions equivalent to aldol (5), Michael (6), Claisen (7), and Stobbe (8) can all be performed with enol silyl ethers. Compared to enolate anions, enol silyl ethers have several characteristic features which render them particularly useful. Whereas enolates are ionic compounds, enol silyl ethers are covalent molecules. For this reason, enol silyl ethers are in general less "reactive" than the corresponding enolates. In terms of experimental convenience, enolates are usually generated and used *in situ*, whereas enol silyl ethers can often be purified and stored for a finite period. Another important difference is that, whereas enolate anions are basic in character, enol silyl ethers are neutral molecules. Reactions of enol silyl ethers can be conducted under either neutral or acidic conditions, thus complementing the basic nature of enolate anion chemistry (8). Finally, it is possible to prepare *bis*- (10) or *tris*-enol silyl ethers[1] whereas generation of the corresponding enolate di- or trianions would be difficult. By using enol silyl ethers, one can extend the polyanion chemistry without many of the inherent difficulties.

In spite of the many reactions unravelled for enol silyl ethers and their growing popularity in organic synthesis, there is essentially no structural information regarding enol silyl ethers and few mechanistic studies on their reactions (11). As part of our overall interest in enol silyl ether chemistry, we have undertaken the first X-ray crystal structure study of an enol silyl ether. The compound under investigation is the *t*-butyldimethylsilyl ether (**1**) of the enol derived from a carbamate. Compound **1** was prepared according to the following reaction:

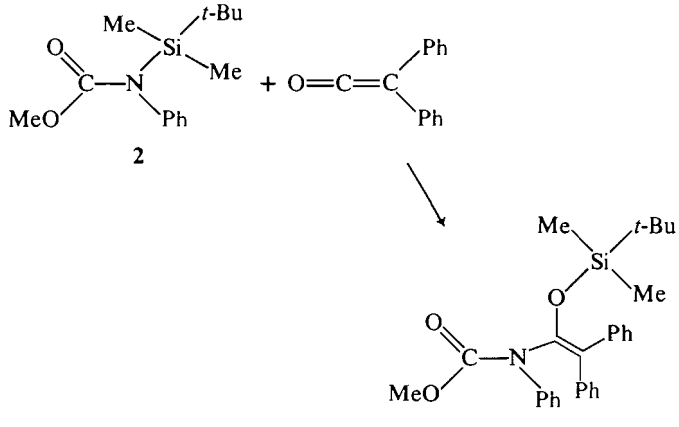

Methyl *N*-*t*-butyldimethylsilyl-*N*-phenylcarbamate (**2**) was first prepared from the silylation of the anion derived from methyl *N*-phenylcarbamate. Reaction of **2** with diphenylketene gave the enol silyl ether **1**. The reaction of *N*-silylamides with ketenes is the subject of a general study by us and will be reported separately.[2]

Experimental

Methyl N-*phenyl*-N-t-*butyldimethylsilylcarbamate (2)*

To a suspension of sodium hydride (50% in mineral oil, washed with dry hexane) in tetrahydrofuran at 0°C, methyl *N*-phenylcarbamate (10 mmol) was added. After hydrogen evolution had ceased, the

[1]T. H. Chan and D. Stossel. Private communication.

[2]T. H. Chan and D. Thoraval. Private communication.

TABLE 1. Crystal data and summary of data collection and structure refinement

Crystal

$C_{28}H_{33}NO_3Si$ mw = 459.666
Crystal system: monoclinic Space group: $P2_1/c$
a = 8.683(5), b = 12.689(5), c = 24.585(11) Å, β = 105.33(4)°,
V = 2612.5 Å^3, d_c = 1.168 g cm^{-3}, Z = 4, $F(000)$ = 984,
λ(MoKᾱ) = 0.71069 Å, μ(MoKα) = 1.12 cm^{-1}, T = 22°C
Crystal size: 0.12 × 0.20 × 0.36 mm

Data collection

ω–2θ scan, scan width Δω = (1.0 + 0.35 tan θ)°
Collection limits: 2θ ≤ 45°, $0 \leq h \leq 9$, $0 \leq k \leq 13$, $-26 \leq l \leq 26$
Fluctuations of the three standard reflections: 2.2, 2.3, 1.5%
Number of reflections measured = 3410
Number of reflections accepted = 1825
Acceptance threshold, $I \geq 1.96\,\sigma(I)$

Structure refinement

$R = \Sigma||F_o| - |F_c||/\Sigma|F_o| = 0.053$, $wR = [\Sigma w\Delta F^2/\Sigma wF_o^2]^{1/2} = 0.051$
$S = [\Sigma w\Delta F^2/(m-n)]^{1/2} = 0.73$
Average $\Delta/\sigma = 0.20$, maximum $\Delta/\sigma = 0.72$
Residual electron density −0.25, 0.17 e Å^{-3}

mixture was cooled to −78°C and treated with a THF solution of *t*-butyldimethylchlorosilane. The mixture was then warmed slowly to room temperature and stirred overnight. The solvent was then evaporated *in vacuo* and the residue treated with hexane. The mixture was filtered under N_2 and the filtrate was evaporated to dryness. The residual oil was purified by distillation to give **2** in 86% yield, bp 94–96°C (1.0 mm Hg (1 mm Hg = 133.3 Pa)); ir(neat)ν: 1700, 1590, 1485, 1435, 1310, 1250, 1085, 960, 930, 885 cm^{-1}; ^{1}H nmr ($CDCl_3$)δ: 0.05 (s, 6H), 1.01 (s, 9H), 3.6 (s, 3H), 6.9–7.3 (m, 5H); ^{29}Si nmr ($CDCl_3$)δ: 5.53 ppm.

Methyl N-*phenyl*-N-*(2,2-diphenyl-1-*t*-butyldimethylsiloxy)-vinyl-carbamate (**1**)*

To a stirred solution of **2** (200 mg) in ether (10 mL) at 0°C was added diphenylketene (1 equiv.) dropwise. The reaction can be followed by the disappearance of the orange colour of diphenylketene. At the end of the reaction (~20 h), the solvent was evaporated *in vacuo* and the residue was purified by flash chromatography (5% ether in hexane) to give **1** as a colorless oil in 85% yield. The pure **1** could be crystallized from hexane slowly to give crystals for X-ray analysis; ir(neat)ν: 1725, 1640, 1600, 1495, 1440, 1320, 1245, 1095, 835 cm^{-1}; ^{1}H nmr ($CDCl_3$)δ: 0.1 (s, 6H), 0.86 (s, 9H), 3.8 (s, 3H), 7.1–7.4 (m, 15H); ms *m/e*: 459 (M^+).

X-ray analysis of **1**

The unit-cell dimensions were obtained, from a single crystal mounted on a Nonius CAD4 diffractometer, by least-squares fit to the angular settings of 25 centered reflections in the range $13 \leq 2\theta \leq 28°$. The systematic absences of the type $0k0$, $k \neq 2n$ and $h0l$, $l \neq 2n$ uniquely determine the $P2_1/c$ space group. The crystal data of interest are presented in Table 1. Intensity data for both *hkl* and *hkl* octants were collected up to $2\theta_{max} = 45°$ using MoKᾱ radiation and a graphite monochromator. The data were corrected for Lorentz and polarization factors and reduced to structure factors in the usual manner.[3] The absorption coefficient for the MoKα radiation being small, no absorption correction was applied to the intensity data. The structure was solved by direct methods using the MULTAN set of programs. Most non-hydrogen atoms were revealed on the first E-map except for the *tert*-butyl group which was only found after a few refinement cycles followed by a difference Fourier synthesis. In the block-diagonal least-squares refinement, all non-hydrogen atoms were treated anisotropically. Then, another difference Fourier synthesis revealed all hydrogen atoms except those on the methyl groups. They appeared following a few more refinement cycles. The H atoms were refined with isotropic temperature factors. The function minimized was $\Sigma w||F_o| - |F_c||^2$. The scattering factors were taken from Cromer and Mann (16) for Si, O, N, and C and from Stewart *et al.* (17) for H atoms. The real and imaginary parts of the anomalous dispersion of Si were taken from Cromer and Liberman (18).

Results and discussion

The final atomic coordinates[4] for **1** ($C_{28}H_{33}NO_3Si$) are given in Table 2. A schematic of the atomic numbering adopted here is shown in Fig. 1. A stereopair showing the molecular conformation is shown in Fig. 2 while the bond distances, the bond angles, and the torsion angles are listed in Tables 3 and 4, respectively.

The enol silyl ether double bond

The C(1)—C(3) double bond, 1.346(8) Å long, is not significantly longer than that reported for unsubstituted ethylene. Values of 1.337(3), 1.339(2), and 1.333(2) Å were obtained by infrared spectroscopy (19), Raman spectroscopy (20), and electron diffraction in the gas phase (21), respectively. A more recent study (22) of the structure of C_2H_4 by X-ray diffraction at 85 K gives a C=C distance of 1.314(6) Å. The value measured here is, however, very close to that reported for a symmetrically substituted ethylene. In 1,1-bis(*p*-ethoxyphenyl)ethylene (23) the C=C bond is 1.342(3) Å long. The sum of the angles around C(1) and C(3) are 359.7 and 360.0° respectively, as expected for the sp^2 hybridization of these atoms. Both the C(21)—C(3)—C(31) and O(1)—C(1)—N(1) angles have values significantly lower than 120°. This is also observed in ethylene (19–22) where the H—C—H angle is found between 115.5(6) and 117.6(5)°.

[3]The programs used here are modified versions of NRC-2, data reduction, NRC-10, bond distances and angles, and NRC-22, mean planes (12), FORDAP, Fourier and Patterson maps (A. Zalkin), MULTAN, multisolution program (13), NUCLS, least-squares refinement (14), and ORTEP, stereodrawings (15).

[4]Tables of mean planes, anisotropic temperature factors, hydrogen atom coordinates, and lists of observed and calculated structure factors have been deposited and may be purchased from the Depository of Unpublished Data, CISTI, National Research Council of Canada, Ottawa, Ont., Canada K1A 0S2.

TABLE 2. Final atomic coordinates and their esd ($\times 10^4$) and U_{eq} ($Å^2$, $\times 10^4$)

Atom	X	Y	Z	U_{eq}
Si(1)	4307(2)	2231(1)	4349(1)	544
O(1)	5916(4)	1725(3)	4188(1)	548
O(2)	3206(4)	972(3)	3124(2)	629
O(3)	3755(4)	−764(3)	3206(2)	593
N(1)	5732(5)	408(4)	3507(2)	471
C(1)	6205(6)	1440(4)	3686(2)	479
C(2)	4124(6)	253(4)	3258(2)	483
C(3)	7042(6)	2058(4)	3426(2)	457
C(4)	2858(8)	1179(6)	4382(3)	801
C(5)	3429(8)	3265(6)	3841(3)	850
C(6)	5167(7)	2768(5)	5083(2)	626
C(7)	6397(9)	3612(7)	5087(3)	1072
C(8)	3780(9)	3243(7)	5291(3)	957
C(9)	5902(9)	1869(7)	5476(3)	1044
C(10)	2083(7)	−977(5)	3019(3)	702
C(11)	6897(6)	−393(5)	3611(2)	540
C(12)	7006(7)	−1126(5)	3217(3)	754
C(13)	8189(8)	−1847(6)	3317(4)	988
C(14)	9311(8)	−1891(6)	3823(4)	1053
C(15)	9222(8)	−1168(6)	4225(3)	968
C(16)	8032(7)	−440(5)	4129(3)	704
C(21)	7360(6)	1665(4)	2887(2)	487
C(22)	8952(7)	1558(5)	2864(2)	592
C(23)	9276(7)	1170(5)	2377(3)	708
C(24)	8061(8)	920(6)	1918(2)	755
C(25)	6512(7)	1050(6)	1932(2)	780
C(26)	6154(7)	1437(5)	2414(2)	619
C(31)	7718(6)	3077(4)	3649(2)	455
C(32)	8926(7)	3162(5)	4142(2)	642
C(33)	9558(7)	4130(6)	4330(3)	775
C(34)	9020(8)	5027(5)	4041(3)	766
C(35)	7818(8)	4959(5)	3553(3)	796
C(36)	7219(7)	3990(5)	3366(2)	658

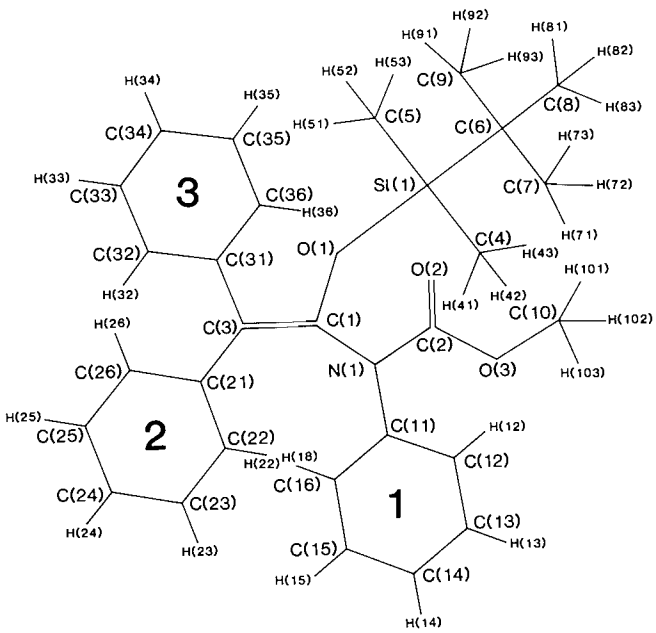

FIG. 1. Atomic numbering.

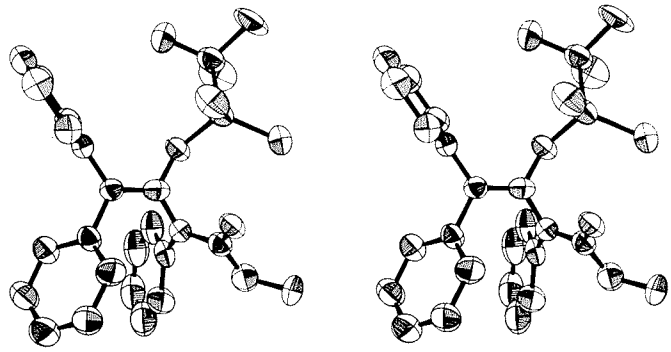

FIG. 2. Stereopair showing the molecular conformation of $C_{28}H_{33}NO_3Si$.

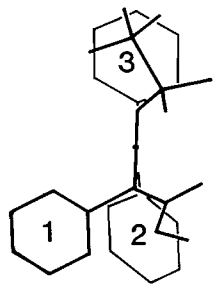

FIG. 3. Projection of the molecule along C(1)—C(3).

In the spectroscopic and electron diffraction studies, the C_2H_4 molecule was assumed to be planar and highly symmetrical. One finds here that there is a slight twist around the ethylenic bond. It is measured by the angle between the planes C(1), C(3), N(1), O(1) and C(1), C(3), C(21), C(31) and has a value of 4.2°. This distortion is also confirmed by a mean plane calculation. The atoms of the ethylenic bond and its four substituents are displaced by 5–20σ from their least-squares plane. This is not unusual for substituted ethylenes. It also suggests that the siloxy substituent does not confer unusual structural features on the double bond.

The phenyl groups

The atoms of each of the three phenyl groups are coplanar. However, the atoms C(3) and N(1) to which they are bonded significantly deviate from their corresponding phenyl planes. A view of the molecule, projected along the C(1)=C(3) bond (Fig. 3) reveals clearly the relative orientations of the three phenyl rings. The phenyl rings 1 and 2 are twisted around the C(11)—N(1) and the C(21)—C(3) bonds respectively in such a way that they are almost parallel to one another. At the same time, they are displayed laterally so that there is no overlap. The atoms constituting the phenyl rings 2 and 3, both attached at C(3), are in planes nearly perpendicular to one another. The relative orientation of the phenyl ring is described in a more quantitative manner using the conformational angles defined by Shields *et al.* (24). The dihedral angle between a phenyl plane and the group of atoms formed by C(1), C(3), C(21), C(31) is ϕ, while the dihedral angle between the two phenyls on C(3) is δ. Here ϕ_1 is 66.5° and ϕ_2 is 58.7° for the two phenyl groups at C(3) and δ_1 = 80.8°. These values compare well with ϕ_1 = 51.4, ϕ_2 = 54.5, and δ = 81.6° or ϕ_1 = 78.7, ϕ_2 = 45.4, and δ = 80.2° for the two molecules of 1,1-dichloro-2,2-bis(*p*-chlorophenyl)ethylene (24). These conformational angles take the values of $\phi_1 = \phi_2$ = 47.8 and δ = 82.9° for 1,1-dichloro-2,2-bis(*p*-methoxyphenyl)ethylene (23).

TABLE 3. Bond distances (Å) and angles (°) and their esd

Bond	Distance	Bond	Distance	Bond	Distance
C(1)—O(1)	1.372(6)	Si(1)—C(4)	1.851(8)	N(1)—C(11)	1.409(7)
C(1)—N(1)	1.407(7)	Si(1)—C(5)	1.833(7)	N(1)—C(2)	1.382(7)
C(1)—C(3)	1.342(8)	Si(1)—C(6)	1.888(6)	C(2)—O(2)	1.199(7)
C(3)—C(21)	1.510(7)	C(6)—C(7)	1.509(11)	C(2)—O(3)	1.328(7)
C(3)—C(31)	1.468(8)	C(6)—C(8)	1.548(10)	O(3)—C(10)	1.433(7)
O(1)—Si(1)	1.677(4)	C(6)—C(9)	1.521(10)		
C(11)—C(12)	1.363(9)	C(21)—C(22)	1.405(8)	C(31)—C(32)	1.380(8)
C(12)—C(13)	1.352(10)	C(22)—C(23)	1.392(9)	C(32)—C(33)	1.374(10)
C(13)—C(14)	1.363(12)	C(23)—C(24)	1.362(9)	C(33)—C(34)	1.357(10)
C(14)—C(15)	1.362(12)	C(24)—C(25)	1.364(10)	C(34)—C(35)	1.372(10)
C(15)—C(16)	1.362(10)	C(25)—C(26)	1.392(8)	C(35)—C(36)	1.367(9)
C(16)—C(11)	1.390(5)	C(26)—C(21)	1.375(8)	C(36)—C(31)	1.362(8)

Bonds	Angle	Bonds	Angle	Bonds	Angle
Si(1)—O(1)—C(1)	132.5(4)	O(1)—Si(1)—C(4)	110.5(3)	C(1)—N(1)—C(2)	116.6(4)
O(1)—C(1)—C(3)	121.6(5)	O(1)—Si(1)—C(5)	109.7(3)	C(1)—N(1)—C(11)	118.6(4)
O(1)—C(1)—N(1)	114.8(4)	O(1)—Si(1)—C(6)	102.7(3)	C(2)—N(1)—C(11)	124.8(5)
N(1)—C(1)—C(3)	123.2(5)	C(4)—Si(1)—C(5)	112.5(3)	N(1)—C(2)—O(2)	122.3(5)
C(1)—C(3)—C(21)	118.2(5)	C(4)—Si(1)—C(6)	108.7(3)	N(1)—C(2)—O(3)	111.8(5)
C(1)—C(3)—C(31)	123.6(5)	C(5)—Si(1)—C(6)	112.4(3)	O(2)—C(2)—O(3)	125.9(5)
C(21)—C(3)—C(31)	118.2(5)	Si(1)—C(6)—C(7)	111.3(5)	C(2)—O(3)—C(10)	115.5(4)
		Si(1)—C(6)—C(8)	108.1(5)	C(7)—C(6)—C(8)	109.3(6)
		Si(1)—C(6)—C(9)	109.2(5)	C(7)—C(6)—C(9)	110.4(6)
				C(8)—C(6)—C(9)	108.5(6)
N(1)—C(11)—C(12)	123.0(5)	C(3)—C(21)—C(22)	118.5(5)	C(3)—C(31)—C(32)	122.3(5)
N(1)—C(11)—C(16)	119.9(5)	C(3)—C(21)—C(26)	112.5(5)	C(3)—C(31)—C(36)	121.2(5)
C(12)—C(11)—C(16)	117.1(6)	C(22)—C(21)—C(26)	119.0(5)	C(32)—C(31)—C(36)	116.5(5)
C(11)—C(12)—C(13)	121.8(6)	C(21)—C(22)—C(23)	119.4(6)	C(31)—C(32)—C(33)	120.7(6)
C(12)—C(13)—C(14)	121.1(7)	C(22)—C(23)—C(24)	120.6(6)	C(32)—C(33)—C(34)	121.3(6)
C(13)—C(14)—C(15)	118.1(8)	C(23)—C(24)—C(25)	120.2(6)	C(33)—C(34)—C(35)	118.9(6)
C(14)—C(15)—C(16)	121.2(7)	C(24)—C(25)—C(26)	120.6(6)	C(34)—C(35)—C(36)	119.1(6)
C(15)—C(16)—C(11)	120.6(6)	C(25)—C(26)—C(21)	120.1(6)	C(35)—C(36)—C(31)	123.5(6)

TABLE 4. Torsion angles (°) of interest. The estimated errors are of the order of 0.8–1.0°

Angles	Value	Angles	Value
O(1)—C(1)—C(3)—C(21)	177.7	O(1)—Si(1)—C(6)—C(7)	61.2
O(1)—C(1)—C(3)—C(31)	0.1	O(1)—Si(1)—C(6)—C(8)	−178.7
N(1)—C(1)—C(3)—C(21)	5.7	O(1)—Si(1)—C(6)—C(9)	−61.0
N(1)—C(1)—C(3)—C(31)	−171.8	C(1)—N(1)—C(11)—C(12)	−135.7
C(1)—N(1)—C(2)—O(2)	10.6	C(1)—N(2)—C(11)—C(16)	42.4
C(1)—N(1)—C(2)—O(3)	−167.7	C(1)—C(3)—C(21)—C(22)	−121.0
N(1)—C(2)—O(3)—C(10)	172.2	C(1)—C(3)—C(21)—C(26)	60.8
C(3)—C(1)—O(1)—Si(1)	101.4	C(1)—C(3)—C(31)—C(32)	66.2
C(1)—O(1)—Si(1)—C(4)	81.6	C(1)—C(3)—C(31)—C(36)	−116.3
C(1)—O(1)—Si(1)—C(5)	−42.9		
C(1)—O(1)—Si(1)—C(6)	−162.6		

The *N*-acetate group of atoms (N(1), O(2), O(3), C(2), C(10)) is nearly coplanar. Its orientation and that of the phenyl group at N(1) are described by the dihedral angles ϕ_3 and ϕ_4 they make with the plane constituted of O(2), N(1), C(1), C(2), C(11). In this case one finds $\phi_3 = 11.4$, $\phi_4 = 43.4°$ while δ_2, the angle between the *N*-acetate and the phenyl plane is 54.0°.

The t*-butyl silyl group*

The bond distances and angles in this group of atoms compare well with their homologs in a penam (4-thia-1-azabicyclo[3.2.0]haptan-7-one) derivative,[5] **3**. In particular the bond angles show the same deformation of the tetrahedral coordination around Si. The smallest bond angle, O(1)—Si(1)—C(6) = 102.8(4)° and the largest, C(4)—Si(1)—C(5) = 112.6(5)° are found to be also the extreme values for the corresponding angles, 103.6(5)° and 112.6(6)°, respectively, in **3**. One has to note the particularly wide angle at O(1), C(1)—O(1)—Si(1) =

[5]A. Bedeschi, F. Bélanger-Gariépy, S. Hanessian, and F. Brisse. Acta Cryst. Submitted.

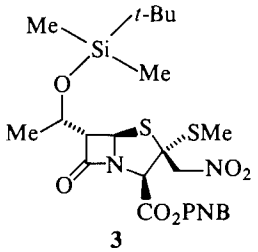

3

PNB = *para*-nitrobenzoate

132.4(4)°. The corresponding value in **3** is only 127.6(6)°. This is attributed to repulsions between O(2) and Si and its two methyl groups. The distances O(2) ... Si, O(2) ... C(4), and O(2) ... C(5) are among the shortest[6] in the molecule with values of 3.320(4), 3.197(8), and 3.381(8) Å, respectively. There are no short contacts between either C(4) or C(5) and any atom of the phenyl group 3.

Another interesting observation is the torsion angle for C(3)—C(1)—O(1)—Si(1) of 101.4(8)°. This places the O(1)—Si(1) bond in an orientation nearly parallel to the *p* orbitals of the C(1)—C(3) π bond suggesting the possibility of σ → π overlap.

ADDENDUM: Since the submission of our manuscript, a paper by Seebach *et al.* describing the structure of a number of lithium ester enolates (**4–6**) by X-ray diffraction has appeared (26).

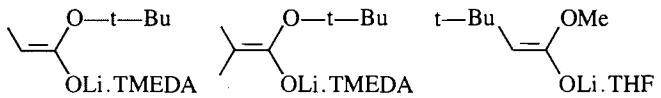

4 **5** **6**

Because of the complementary nature of the reactivities of enolates and enol silyl ethers, it is of interest to contrast the structures of these compounds. The first obvious difference is that in all lithium enolates, the crystalline compounds are either dimeric or tetrameric even with solvent of coordination. In the case of enol silyl ether **1**, the compound is monomeric. In spite of this difference, the C=C double bond length in **4–6** falls in between 1.350 and 1.341 Å, a value remarkably close to the double bond length in **1** (1.346 Å). The C—O bond length of the siloxy oxygen in **1** (1.372 Å) is in between the C—O bond length of the enol ether oxygen (1.379–1.419 Å) and of the enolate (1.304–1.314 Å). The siloxy C—O bond is, thus, more similar to the enol ether C—O bond. In their paper, Seebach *et al.* further argued that there is a correlation between bond length differences b − d and bond angle difference cd − bc (scheme 1)

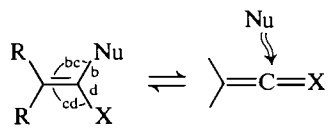

SCHEME 1

and this can be used to map the breakdown of the ester enolate into ketene and an alcoholate: Whether such an approach is valid and can be applied to map the breakdown of **1** to the precursor ketene and the silylated carbamate is of obvious mechanistic significance. Its answer will require X-ray structure determinations of several more enol silyl ethers of compounds analogous to **1**.

[6]When compared to the sum of van der Waals radii (25).

Acknowledgement

The financial support of this research by the Natural Sciences and Engineering Research Council (NSERC) is gratefully acknowledged. We are also thankful to Mr. M. J. Olivier for the X-ray data collection.

1. G. STORK and P. F. HUDRLIK. J. Am. Chem. Soc. **90**, 4462 (1968).
2. H. O. HOUSE, L. J. CZUBA, M. GALL, and H. D. OLMSTEAD. J. Org. Chem. **34**, 2324 (1969).
3. P. BROWNBRIDGE. Synthesis, 1 (1983); 85 (1983).
4. J. K. RASMUSSEN. Synthesis, 91 (1977).
5. T. MUKAIYAMA, K. BANNO, and K. NARASAKA. J. Am. Chem. Soc. **96**, 7503 (1974).
6. M. MIYASHITA. J. Am. Chem. Soc. **98**, 4679 (1976).
7. S. MURAI, Y. KUROKI, K. HASIGAWA, and S. TSUTSUMI. J. Chem. Soc. Chem. Commun. 946 (1972).
8. P. BROWNBRIDGE and T. H. CHAN. Tetrahedron Lett. **21**, 3427 (1980).
9. T. CHAN, I. PATERSON, and J. PINSONNAULT. Tetrahedron Lett. **18**, 4183 (1977).
10. T. H. CHAN and P. BROWNBRIDGE. J. Chem. Soc. Chem. Commun. 578 (1979).
11. T. H. CHAN and M. BROOK. Tetrahedron Lett. **26**, 2943 (1985).
12. F. R. AHMED, S. R. HALL, M. E. PIPPY, and C. P. HUBER. J. Appl. Crystallogr. **6**, 309 (1973). Accession Nos. 133–147.
13. P. MAIN, S. E. HULL, L. LESSINGER, G. GERMAIN, J. DECLERCQ, and M. M. WOOLFSON. Multan 78, a system of computer programs for the automatic solution of crystal structures from X-ray diffraction data. University of York, England, and Louvain, Belgium. 1978.
14. R. J. DOEDENS and J. A. IBERS. Inorg. Chem. **6**, 204 (1967).
15. C. K. JOHNSON. ORTEP, Report ORNL-3794, Oak Ridge National Laboratory, Oak Ridge, TN. 1965.
16. D. T. CROMER and J. B. MANN. Acta Crystallogr. Sect. A: Cryst. Phys. Diffr. Theor. Gen. Crystallogr. **A24**, 321 (1968).
17. R. F. STEWART, E. R. DAVIDSON, and W. T. SIMPSON. J. Chem. Phys. **42**, 3175 (1965).
18. D. T. CROMER and D. A. LIBERMAN. J. Chem. Phys. **53**, 1891 (1970).
19. H. C. ALLEN and E. K. PLYLER. J. Am. Chem. Soc. **80**, 2673 (1958).
20. J. M. DOWLING and B. P. STOICHEFF. Bull. Am. Phys. Soc. **3**, 313 (1958).
21. L. S. BARTELL and R. S. BONHAM. J. Chem. Phys. **31**, 400 (1959).
22. G. J. H. VAN NES and A. VOS. Acta Crystallogr. Sect. B: Struct. Crystallogr. Cryst. Chem. **B33**, 1653 (1977).
23. T. BANERJEE, S. CHAUDHURI, and P. T. MUTHAH. Acta Crystallogr. Sect. C: Cryst. Struct. Commun. **C41**, 269 (1985).
24. K. G. SHIELDS, C. H. L. KENNARD, and W. ROBINSON. J. Chem. Soc. Perkin Trans. **2**, 460 (1977).
25. W. W. PORTERFIELD. Inorganic chemistry. Addison-Wesley Publishing Company Inc., Reading, MA. 1984.
26. D. SEEBACH, R. AMSTUTZ, T. LAUBE, W. B. SCHWEIZER, and J. D. DUNITZ. J. Am. Chem. Soc. **107**, 5403 (1985).

Low temperature magnetic and Mössbauer studies on anhydrous iron(II) sulfonates

JOHN S. HAYNES, JOHN R. SAMS,[1] AND ROBERT C. THOMPSON[1]

Department of Chemistry, University of British Columbia, 2036 Main Mall, Vancouver, B.C., Canada V6T 1Y6

Received August 26, 1985

JOHN S. HAYNES, JOHN R. SAMS, and ROBERT C. THOMPSON. Can. J. Chem. **64**, 744 (1986).

Magnetic susceptibilities from 130 to 4.2 K are reported for a series of $Fe(RSO_3)_2$ compounds, where R is F, CF_3, CH_3, and p-$CH_3C_6H_4$. The β form of $Fe(CH_3SO_3)_2$ exhibits a maximum in susceptibility at approximately 22.5 K and a sharp drop in susceptibility below the maximum indicating a transition to a magnetically ordered state. None of the other compounds exhibit magnetic ordering although abnormally low magnetic moments down to 2.0 K are observed for α-$Fe(CH_3SO_3)_2$. Variable-temperature Mössbauer studies on $Fe(CF_3SO_3)_2$ and β- and α-$Fe(CH_3SO_3)_2$ are reported and the magnitude of axial field splitting is estimated for these compounds. The first two have trigonally elongated FeO_6 chromophores, whereas the third is trigonally compressed. The nature of the distortion in α-$Fe(CH_3SO_3)_2$ is confirmed by magnetic perturbation Mössbauer studies. Spectra in applied fields of 4.50 and 5.63 T show a doublet–triplet pattern, with the triplet at higher energy, indicating a negative V_{zz} and an orbital singlet ground state.

JOHN S. HAYNES, JOHN R. SAMS et ROBERT C. THOMPSON. Can. J. Chem. **64**, 744 (1986).

On a mesuré, de 130 à 4,2 K, les susceptibilités magnétiques d'une série de composés $Fe(RSO_3)_2$ dans lesquels R = F, CF_3, CH_3 et p-$CH_3C_6H_4$. Dans les cas de la forme β du $Fe(CH_3SO_3)_2$, on observe un maximum de susceptibilité à environ 22,5 K et une diminution marquée lorsqu'on diminue ensuite la température; ce résultat indique la présence d'une transition vers un état qui est magnétiquement ordonné. Aucun autre composé ne présente ce phénomène, même si des moments magnétiques anormalement faibles sont observés à 2,0 K avec l'α-$Fe(CH_3SO_3)_2$. On rapporte les résultats d'études de l'effet Mössbauer à diverses température sur le $Fe(CF_3SO_3)_2$ et sur les formes β et α du $Fe(CH_3SO_3)_2$ et l'on a évalué l'amplitude du dédoublement du champ axial dans ces composés. Les deux premiers possèdent des chromophores FeO_6 qui sont allongés trigonalement; par ailleurs, le troisième est trigonalement comprimé. La nature de la distorsion dans l'α-$Fe(CH_3SO_3)_2$ est confirmée par des études de perturbations magnétiques de Mössbauer. Les spectres obtenus lorsque des champs de 4,50 et 5,63 T sont appliqués mettent en évidence la présence d'un arrangement de doublet-triplet avec le triplet au niveau d'énergie le plus élevé. Ce résultat indique que le V_{zz} est négatif et qu'il existe une orbitale singulet dans l'état fondamental.

[Traduit par la revue]

Introduction

Previously we reported the preparation and study of a series of iron(II) sulfonate compounds, $Fe(RSO_3)_2$, where R is F, CF_3, CH_3, and p-$CH_3C_6H_4$ (1, 2). It was proposed that these compounds adopt a polymeric layered structure like that of $Ca(CH_3SO_3)_2$ (3), in which each RSO_3^- group acts as a tridentate bridging ligand to three different metal centres. This results in each metal being in an approximately octahedral environment of oxygen atoms, each oxygen atom being from a different sulfonate group (see Fig. 1, ref. 4). The methanesulfonate, unlike the others, was found in the earlier work to be obtainable in two isomeric forms (5) and the β form of this material was shown by Mössbauer spectroscopy to undergo a magnetic phase transition to an antiferromagnetically ordered state at approximately 23 K. None of the other sulfonates gave Mössbauer evidence for magnetic ordering, although magnetic susceptibility measurements from 80 to 300 K suggested the presence of weak antiferromagnetic exchange in α-$Fe(CH_3SO_3)_2$ (2). Our earlier studies on magnetic exchange effects in these materials were limited by the lack of suitable equipment for obtaining magnetic susceptibility data at cryogenic temperatures; this laboratory now has facilities which permit such studies down to 2.0 K and these are reported here.

Attempts to correlate magnetic properties with structure in these systems are hampered somewhat by the difficulty in obtaining precise structural information; unfortunately, the iron(II) sulfonates have not been obtainable in crystalline form suitable for single-crystal X-ray diffraction work. Nevertheless, considerable structural information was obtained previously for two of the sulfonates being considered here, namely $Fe(FSO_3)_2$ (6) and $Fe(p\text{-}CH_3C_6H_4SO_3)_2$ (4), from Mössbauer spectroscopy, particularly from the temperature dependence of the quadrupole splitting and from magnetic perturbation Mössbauer. Variable-temperature Mössbauer studies have now been completed on $Fe(CF_3SO_3)_2$ and on α- and β-$Fe(CH_3SO_3)_2$. In addition, magnetic perturbation Mössbauer spectra of α-$Fe(CH_3SO_3)_2$ are reported here and fits of the data to the phenomenological model of Varret (7) are discussed.

[1]Authors to whom correspondence may be addressed.

Experimental

The iron(II) sulfonates[2] were prepared as described previously (1, 2). Their purity was checked by microanalysis and by infrared and Mössbauer spectroscopy.

Magnetic susceptibility measurements (4.2–130 K) were made using a vibrating sample magnetometer as previously described (9). For α-$Fe(CH_3SO_3)_2$, additional data were collected to 2 K, temperatures below 4.2 K being achieved by reducing the vapor pressure of the helium in the sample zone of the magnetometer. The data reported here are in good agreement in the region of temperature overlap with the results reported earlier using the Gouy equipment (2, 6). The molar magnetic susceptibilities were corrected for the diamagnetism of all atoms: Fe^{2+} = 13, FSO_3^- = 40, $CF_3SO_3^-$ = 46, $CH_3SO_3^-$ = 35, and p-$CH_3C_6H_4SO_3^-$ = 89 (all 10^6 cm^3 mol^{-1}).

Samples for Mössbauer studies were contained in Nylon holders and sealed with epoxy resin to avoid hydrolysis and decomposition problems. The sample holder was attached to a copper ring before being mounted in the cryostat, to ensure good thermal contact.

[2]Recently, Sharma *et al.* (8) reported the preparation of $Fe(CH_3SO_3)_2$ by direct reaction of anhydrous iron(II) chloride with methanesulfonic acid, followed by washing with diethylether. Earlier (2) we had shown that this same reaction yields an acid solvate of composition $Fe(CH)_3SO_3)_2.CH_3SO_3H$ when the product is washed with CH_3SO_3H followed by drying in vacuum at 150°C. The data reported by the other workers (8) for their sample of $Fe(CH_3SO_3)_2$ do not correspond well with those reported by us for either the α or β forms.

TABLE 1. Magnetic data[a] for $Fe(RSO_3)_2$ compounds

T	χ_m	μ_{eff}	T	χ_m	μ_{eff}	T	χ_m	μ_{eff}
$Fe(p\text{-}CH_3C_6H_4SO_3)_2$			$\alpha\text{-}Fe(CH_3SO_3)_2$			$\beta\text{-}Fe(CH_3SO_3)_2$		
4.22	330	3.33	1.97	194	1.75	4.22	32.1	1.04
5.08	305	3.52	2.00	193	1.76	5.32	31.8	1.16
5.78	285	3.63	2.10	192	1.80	5.94	31.7	1.23
6.17	273	3.67	2.20	192	1.84	6.58	31.7	1.29
7.83	237	3.86	2.30	191	1.87	7.23	31.8	1.36
9.13	216	3.97	2.59	189	1.98	7.94	32.1	1.43
11.3	189	4.14	2.89	186	2.07	8.88	32.6	1.52
13.1	172	4.25	3.29	183	2.19	10.0	33.6	1.64
15.4	155	4.36	3.73	180	2.32	11.3	35.3	1.79
18.2	138	4.49	4.20	178	2.44	12.3	37.1	1.91
21.1	125	4.60	4.35	177	2.48	13.4	39.4	2.05
26.2	108	4.75	4.88	173	2.60	14.3	41.4	2.18
30.8	95.7	4.85	4.99	175	2.64	15.5	44.5	2.35
35.4	86.4	4.95	5.55	171	2.75	16.6	47.7	2.52
39.5	79.3	5.01	6.16	168	2.88	18.0	52.2	2.74
45.8	70.6	5.08	7.23	164	3.08	18.2	52.7	2.77
48.4	67.3	5.10	8.00	161	3.21	19.0	55.7	2.91
51.2	64.6	5.14	12.5	145	3.80	19.2	56.0	2.93
56.8	59.7	5.21	16.5	129	4.13	19.9	59.1	3.07
61.3	56.4	5.26	19.7	114	4.24	20.3	61.2	3.15
66.1	52.7	5.28	22.5	109	4.42	20.5	61.3	3.17
74.8	47.6	5.34	22.6	105	4.35	21.2	65.2	3.32
82.0	43.3	5.33	27.1	94.0	4.51	21.5	65.5	3.36
92.1	39.2	5.37	30.5	86.3	4.59	22.0	65.6	3.40
100.1	36.2	5.38	34.3	79.4	4.67	23.1	65.5	3.48
110.1	33.1	5.40	39.8	71.2	4.76	23.2	65.5	3.49
124.5	29.5	5.42	44.5	65.4	4.82	24.5	65.0	3.57
			52.8	57.0	4.91	25.1	64.8	3.61
			60.9	50.8	4.97	26.4	64.2	3.68
			61.6	50.3	4.98	26.9	63.8	3.70
			70.5	44.7	5.02	28.2	63.1	3.77
			82.2	39.0	5.06	28.8	62.7	3.80
			92.0	35.2	5.09	30.1	62.0	3.86
$Fe(FSO_3)_2$			100.3	32.4	5.10	30.7	61.5	3.88
			110.5	29.7	5.12	32.7	60.1	3.96
4.22	540	4.27	125.2	26.4	5.14	34.4	59.0	4.03
5.40	438	4.35				39.7	55.6	4.20
6.38	388	4.45				44.6	52.6	4.33
7.12	352	4.48				52.9	48.0	4.51
8.04	318	4.52	$Fe(CF_3SO_3)_2$			61.2	44.1	4.65
9.81	278	4.67				71.0	39.9	4.76
11.4	247	4.75	4.22	377	3.57	82.9	35.8	4.87
13.3	217	4.80	8.82	243	4.14	92.7	32.9	4.94
15.3	191	4.84	13.5	181	4.42	102.5	30.4	4.99
18.7	164	4.95	18.0	147	4.60	113.5	28.1	5.05
21.0	149	5.00	19.9	136	4.66	128.7	25.2	5.10
24.8	128	5.04	23.2	120	4.73			
28.8	113	5.10	27.4	106	4.82			
34.4	96.7	5.16	32.7	92.0	4.90			
41.5	82.5	5.23	42.8	74.6	5.05			
51.9	68.0	5.31	49.1	66.5	5.11			
60.8	59.3	5.37	55.9	60.1	5.19			
61.6	58.4	5.37	67.0	51.5	5.25			
70.2	52.0	5.40	78.7	44.5	5.29			
81.7	44.9	5.42	89.7	39.1	5.30			
91.2	40.4	5.43	94.1	38.0	5.35			
100.0	37.2	5.45	99.4	35.7	5.33			
110.4	33.8	5.46	111.1	32.1	5.34			
123.8	30.2	5.47	124.5	28.7	5.34			

[a]Temperatures (T) are in K; molar susceptibilities (χ_m) are in 10^3 cm^{-3} mol^{-1}; magnetic moments μ_{eff} are in BM.

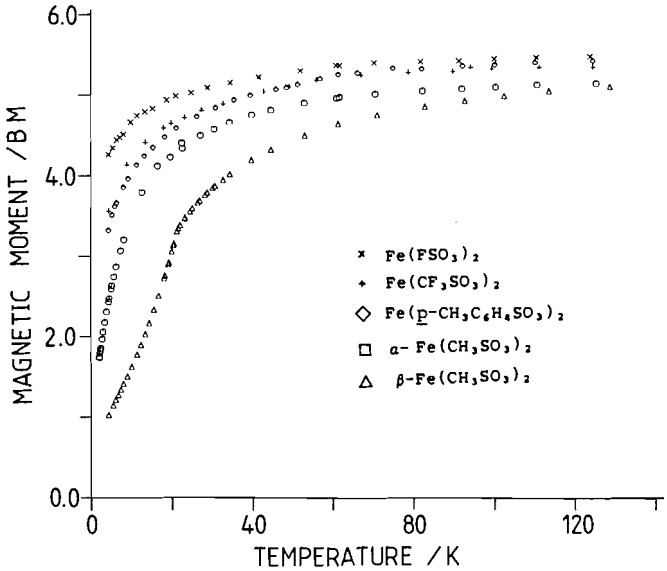

FIG. 1. Magnetic moment versus temperature for $Fe(RSO_3)_2$ compounds.

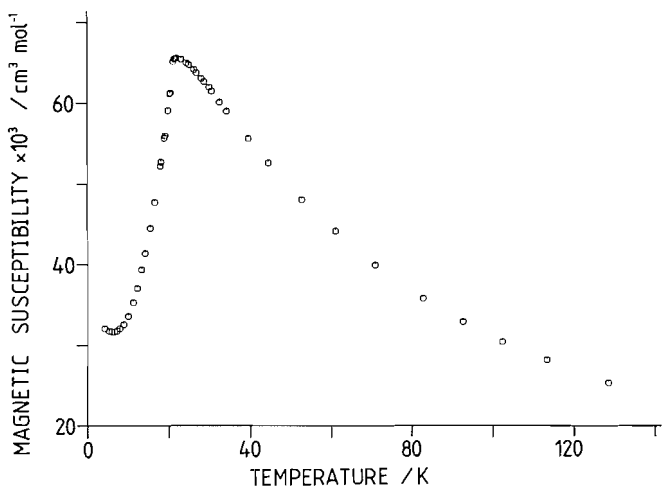

FIG. 2. Magnetic susceptibility versus temperature for β-$Fe(CH_3SO_3)_2$.

Zero-field Mössbauer spectra were recorded with the absorber in a Janis model DT-6 variable-temperature cryostat. Mössbauer spectra, at 4.3 K and below, and all applied field measurements were made with both source and absorber at the same temperature in a Janis model 11-MDT cryostat containing a Westinghouse superconducting solenoid. All spectra were recorded in transmission geometry and the Doppler velocity scale was calibrated with an enriched ^{57}Fe foil absorber; all isomer shifts are quoted relative to the centre of the iron foil spectrum. The Mössbauer spectrometers have been described previously (10, 11).

Results and discussion

Magnetic susceptibility data from 130 to 4.2 K for all $Fe(RSO_3)_2$ compounds (additional data to 1.97 K for α-$Fe(CH_3SO_3)_2$) are given in Table 1 and magnetic moments are plotted as a function of temperature in Fig. 1. For all compounds the moment is in excess of 5.0 BM (Bohr magneton) above 120 K and decreases with decreasing temperature, as expected for high-spin iron(II) in an octahedral ligand environment. With the exception of β-$Fe(CH_3SO_3)_2$, the moments decrease monotonically to a value in the range 2.4–4.3 BM at 4.2 K. The moment decreases more rapidly for β-$Fe(CH_3SO_3)_2$, reaching 1.04 BM at 4.2 K; moreover, the μ_{eff} versus T plot for this material shows an abrupt change in slope around 23 K. This phenomenon is more dramatically illustrated by the magnetic susceptibility versus temperature plot (Fig. 2), which shows a maximum in susceptibility at approximately 22.5 K, indicative of an antiferromagnetically coupled system, and a sharp drop in susceptibility at temperatures below the maximum, indicative of a phase transition to a magnetically ordered state. These findings coincide very well with the observations made earlier on variable-temperature Mössbauer studies, in which spectra were seen to change from a simple quadrupole doublet to a complex hyperfine pattern over a small temperature range around 23 K (5), a phenomenon ascribed then, and now confirmed, as due to magnetic ordering. The small increase in magnetic susceptibility below approximately 5.5 K may be due to a small amount of paramagnetic impurity, possibly a trace of the α form. This is quite plausible since the β form is prepared by conversion from α-$Fe(CH_3SO_3)_2$.

The magnetic exchange exhibited by β-$Fe(CH_3SO_3)_2$ is likely propagated by a superexchange mechanism involving the O—S—O bridging system. This is not the first example of exchange via such a system; in fact, the first definite observation of a susceptibility maximum corresponding to an antiferromagnetic transition was made on $FeSO_4$ (12, 13), where bridging sulfate anions form an extended three-dimensional lattice (14). Linear chain systems with either single or double O—S—O bridges arising from sulfate anions have also been found to have magnetic properties characteristic of low-dimensional magnetic exchange (15), and in some cases Mössbauer spectroscopy has revealed long-range magnetic ordering (16–18). For these linear chain systems, the magnetic properties have been analyzed using either the Ising or Heisenberg linear chain models. For two-dimensional layer systems, Lines (19) has proposed a quadratic layer Heisenberg antiferromagnetic model and this has been applied successfully in a number of cases (20–22). We find we can fit our experimental data for β-$Fe(CH_3SO_3)_2$ above the ordering temperature to the Lines model; however, we feel this is of questionable significance since the lattice which we propose for the sulfonate and that assumed in the Lines model are not compatible. The latter has each metal site interacting with four nearest-neighbour metal ions in a square or rectangular array, while the former has each iron interacting with six nearest neighbours.

The low-temperature magnetic moment data for the R = F, CF_3, and p-$CH_3C_6H_4$ compounds show a similar temperature dependence (Fig. 1) and the magnetic susceptibilities follow Curie–Weiss behaviour, no maximum being observed. The higher temperature (80–300 K) magnetic data for these compounds were previously fitted to a crystal field model (23) in which magnetic moments are determined by the values of λ, the spin-orbit coupling constant; ν, the axial field splitting parameter; and k, the orbital reduction parameter (2, 6). We have extended the theoretical curves, calculated employing the parameters determined by fits to the high temperature data, into the low temperature region and find generally that the agreement with experiment is poor. This is illustrated for $Fe(p\text{-}CH_3C_6H_4SO_3)_2$ in Fig. 3. In particular, at temperatures below approximately 50 K the observed magnetic moments are significantly less than the values predicted by the model. As noted earlier (2, 4, 6), several criticisms have been laid against this model and it appears that, for these compounds, either the model is not valid over the entire temperature region of 4.2–300 K or weak antiferromagnetic exchange interactions

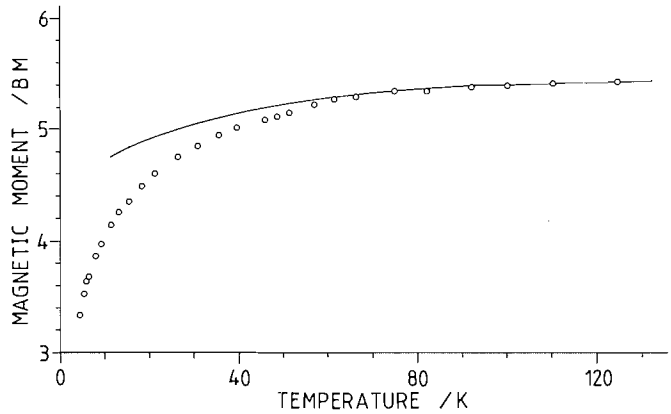

FIG. 3. Magnetic moment versus temperature for Fe(p-$CH_3C_6H_4SO_3$)$_2$. Line calculated from crystal field model with $\lambda = -90\ cm^{-1}$, $\nu = 3$, and $k = 0.75$.

TABLE 2. Mössbauer effect data[a] for iron(II) sulfonates

Temperature (K)	δ	ΔE_Q	Γ_1	Γ_2
	Fe(CF_3SO_3)$_2$			
6.5	1.46	2.01	0.49	0.52
17.7	1.46	1.98	0.52	0.54
38.8	1.45	1.95	0.55	0.55
64.4	1.45	1.91	0.51	0.49
78.8	1.39	1.82	0.28	0.31
80.0	1.45	1.84	0.47	0.44
104	1.46	1.88	0.50	0.50
115	1.43	1.81	0.33	0.33
131	1.42	1.78	0.55	0.54
183	1.40	1.68	0.41	0.39
233	1.37	1.59	0.46	0.44
272	1.35	1.51	0.45	0.41
293	1.32	1.44	0.28	0.26
	α-Fe(CH_3SO_3)$_2$			
4.2	1.35	3.31	0.52	0.54
10.5	1.21	3.39	0.40	0.40
35.2	1.44	3.34	0.55	0.51
60.0	1.42	3.35	0.56	0.54
84.7	1.45	3.37	0.41	0.37
110	1.44	3.36	0.41	0.38
140	1.42	3.30	0.47	0.44
170	1.41	3.29	0.39	0.36
200	1.40	3.24	0.40	0.38
235	1.37	3.19	0.40	0.37
264	1.36	3.12	0.44	0.41
293	1.34	2.95	0.41	0.39
	β-Fe(CH_3SO_3)$_2$			
25.3	1.37	1.54	0.41	0.39
30.0	1.49	1.55	0.39	0.37
80.0	1.48	1.41	0.45	0.44
109	1.46	1.38	0.35	0.34
139	1.46	1.33	0.35	0.33
169	1.43	1.28	0.34	0.33
209	1.43	1.20	0.33	0.33
239	1.41	1.14	0.34	0.32
260	1.40	1.10	0.33	0.32
293	1.31	0.94	0.28	0.33

[a]Units of δ, ΔE_Q, and Γ are all given in mm s^{-1}.

may be present. In general, however, it must be concluded that the low temperature magnetic susceptibility measurements show that any magnetic concentration present in these compounds must be very weak, a result consistent with the earlier Mössbauer studies on Fe(FSO_3)$_2$ (6) and Fe(p-$CH_3C_6H_4SO_3$)$_2$ (4), which show symmetric quadrupole doublets at 4.2 K with no evidence for magnetic hyperfine interactions. The spectrum of Fe(CF_3SO_3)$_2$ at 4.2 K is a quadrupole doublet that shows some assymmetry due to a slow spin-relaxation rate (see below).

In our earlier work on α-Fe(CH_3SO_3)$_2$ (5) the Mössbauer spectrum at 4.2 K was reported as a symmetric quadrupole doublet and the compound was described as acting as a fast-relaxing paramagnetic. Nevertheless, it was noted that the compound exhibits magnetic moment values significantly below those of other sulfonates (except for the β isomer) over the 80–300 K region, suggesting that this may be caused by weak antiferromagnetic coupling effects (2). In order to confirm this we were particularly interested in the low temperature magnetic behaviour and for this compound we extended the measurements below 4.2 K. As the data in Fig. 1 and Table 1 show, although the abnormally low moments continue to the lowest temperature studied, no maximum in magnetic susceptibility is observed even down to 1.97 K; hence there is no proof for magnetic exchange in this compound. It now seems more likely that the abnormally low moments observed for α-Fe(CH_3SO_3)$_2$ are a consequence of the fact that the compound has a well-isolated spin-orbit singlet ground state arising because, unlike the other sulfonates studied, it has a trigonally compressed FeO_6 chromophore (see below).

The present study has shown that the presence of significant magnetic exchange in a Fe(RSO_3)$_2$ compound is not simply related to electronic or steric effects associated with the substituent R. While magnetic ordering is seen in β-Fe(CH_3SO_3)$_2$, no ordering is seen in other systems whether R is more electronegative (F or CF_3) or the same or similar in electronegativity (α-CH_3 or p-$CH_3C_6H_4$). It seems likely that the different magnetic properties observed for these compounds arise more from differences in their detailed molecular geometries. The need for more structural information, particularly on the R = CF_3 compound and both forms of the R = CH_3 compound, prompted variable-temperature Mössbauer studies on these materials.

The Mössbauer spectra of Fe(CF_3SO_3)$_2$ and both α- and β-Fe(CH_3SO_3)$_2$ have been recorded at various temperatures from 4.2 to 300 K and the relevant parameters are given in Table 2. Agreement with values reported previously at 293 and 80 K (2) is good. As discussed in the earlier work, the isomer shift values, δ, are all relatively high, consistent with significant ionic character in the metal–ligand bonds. All three compounds exhibit a symmetric quadrupole doublet at room temperature and, for α-Fe(CH_3SO_3)$_2$, a symmetric doublet is retained down to 4.2 K. As described previously (4), β-Fe(CH_3SO_3)$_2$ shows the onset of complex hyperfine splitting below approximately 23 K. Fe(CF_3SO_3)$_2$ remains a symmetric quadrupole split doublet down to 8 K, below which it shows some assymmetry that may be caused by a slow spin-relaxation rate as observed in hexakis(pyridine-N-oxide) iron(II) perchlorate (24).

Values of the quadrupole splitting parameter, ΔE_Q, are plotted as a function of temperature in Fig. 4, where, for comparison, the data previously reported for Fe(FSO_3)$_2$ (6) and Fe(p-$CH_3C_6H_4SO_3$)$_2$ (4) are included. The magnitude and temperature dependence of ΔE_Q for Fe(CF_3SO_3)$_2$ follow very

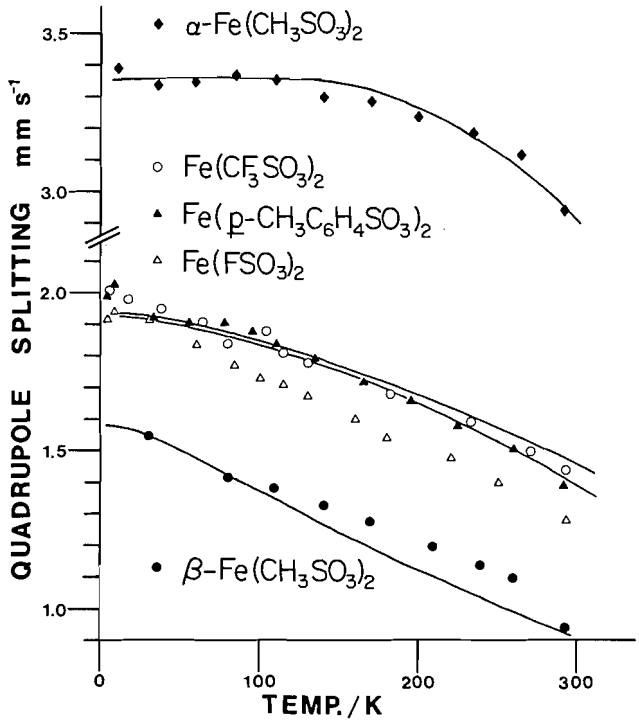

FIG. 4. Quadrupole splitting versus temperature for $Fe(RSO_3)_2$ compounds. Lines generated using parameters listed in Table 3.

TABLE 3. Crystal field splitting parameters derived from quadrupole splitting data

Compound	3Ds (cm^{-1})	λ (cm^{-1})	$D\sigma$ (cm^{-1})
$Fe(FSO_3)_2$[a]	−288	−90	−22
$Fe(CF_3SO_3)_2$	−320	−80	−20
α-$Fe(CH_3SO_3)_2$	+510	−100	−25
β-$Fe(CH_3SO_3)_2$	−160	−80	−16
$Fe(p\text{-}CH_3C_6H_4SO_3)_2$[a]	−280	−70	−28

[a]Data from ref. 4.

closely what was observed previously for $Fe(FSO_3)_2$ and $Fe(p\text{-}CH_3C_6H_4SO_3)_2$ and support the conclusion reached earlier (2) that the CF_3 compound, like the other two, has an FeO_6 chromophore that is distorted by a trigonal elongation along the C_3 axis. The ΔE_Q values observed for β-$Fe(CH_3SO_3)_2$ are significantly lower than those observed for the other compounds, suggesting that while this material in all probability also has a trigonally elongated FeO_6 chromophore, the magnitude of distortion from regular stereochemistry is significantly less. The very large ΔE_Q values observed for α-$Fe(CH_3SO_3)_2$ are consistent only with an orbital singlet ground state and, as earlier magnetic perturbation Mössbauer studies showed (5), this arises from a trigonal compression of the FeO_6 chromophore along the C_3 axis.

As described previously (4, 6), the quadrupole splitting data may be analyzed in terms of a crystal field model to provide estimates of the magnitude of axial distortions. The solid lines in Fig. 4 are calculated using the crystal field parameter values given in Table 3 where, for comparison, the values previously reported for the R = F and $p\text{-}CH_3C_6H_4$ compounds are also listed. The values of the spin-orbit coupling constant are, as expected, of the order of, or less than, the free ion value

TABLE 4. Parameters obtained from the Varret model for α-$Fe(CH_3SO_3)_2$[a]

H_{APP} (T)	Γ ($mm\ s^{-1}$)	ΔE_Q ($mm\ s^{-1}$)	η	HIX (T)	HIY (T)	HIZ (T)
4.50	0.40	−3.31	0.30	−1.00	−0.60	−2.00
5.63	0.40	−3.31	0.35	−1.00	−0.60	−2.50

[a]Temperature 4.2 K.

(−103 cm^{-1}) and the values of the fine-structure term, $D\sigma$, are of the same magnitude as those reported previously (4, 6). The magnitude of the axial field, as measured by 3Ds (magnitude of splitting of $^5T_{2g}$ state), is highest at 510 cm^{-1} for the one compound, α-$Fe(CH_3SO_3)_2$, that has a trigonally compressed FeO_6 chromophore. The values of 3Ds for the others are all approximately −300 cm^{-1} with the exception of that for β-$Fe(CH_3SO_3)_2$, which is only half that value. This represents the only clear correlation we have been able to find between the magnitude of magnetic exchange and structure in these iron(II) sulfonates. The compound which clearly exhibits magnetic ordering, β-$Fe(CH_3SO_3)_2$, is the one having the least distorted FeO_6 chromophore. Greater distortion, whether involving trigonal compression or elongation, seems to result in a damping of the magnetic exchange. Similar correlations between magnetic exchange effects and the geometry of the metal–ligand chromophore have been found for some copper(II) and manganese(II) phosphinate polymers (9, 25).

The presence of trigonally elongated FeO_6 chromophores and orbital doublet ground states in $Fe(FSO_3)_2$ and $Fe(p\text{-}CH_3C_6H_4SO_3)_2$ was confirmed earlier by magnetic perturbation Mössbauer studies (4, 6). In a preliminary report (5) we indicated that similar studies on α-$Fe(CH_3SO_3)_2$ confirm the presence of a unique (for iron(II) sulfonates) trigonally compressed FeO_6 chromophore and an orbital singlet ground state; however, few details were given. Moreover, at that time we reported that attempts to fit the applied field spectrum of α-$Fe(CH_3SO_3)_2$ assuming isotropic magnetic interaction were unsuccessful but that a treatment using a phenomenological model such as that suggested by Varret (7), which enables the anisotropy of the hyperfine field to be parameterized in the case of weak magnetization, should be more successful. We report here the details of our magnetic perturbation studies on α-$Fe(CH_3SO_3)_2$, including analysis using the Varret model.

Mössbauer spectra of α-$Fe(CH_3SO_3)_2$ have been recorded in longitudinal applied magnetic fields of up to 5.6 T at a temperature of 4.2 K. A field of 1.1 T serves only to broaden the spectral lines. However, in applied fields of 4.50 and 5.63 T a doublet–triplet pattern is produced (Fig. 5). The triplet is at higher energy relative to the doublet, indicating that V_{zz}, the principal component of the electric field gradient tensor, is negative (5, 10). This sign for V_{zz} is, as discussed previously (5), consistent with an orbital singlet ground state and a distortion from octahedral symmetry corresponding to a compression along the trigonal axis. Spectra computed employing the Varret model and the parameters given in Table 4 are shown as solid lines in Fig. 5. Reasonable fits of experimental and computed spectra may be obtained by assuming a zero value for the asymmetry parameter, η, and identical values of HIX and HIY, the internal magnetic fields in the X and Y directions. However, better agreement is obtained using the finite value of $\eta \approx 0.3$ and HIX ≠ HIY. This suggests a small rhombic

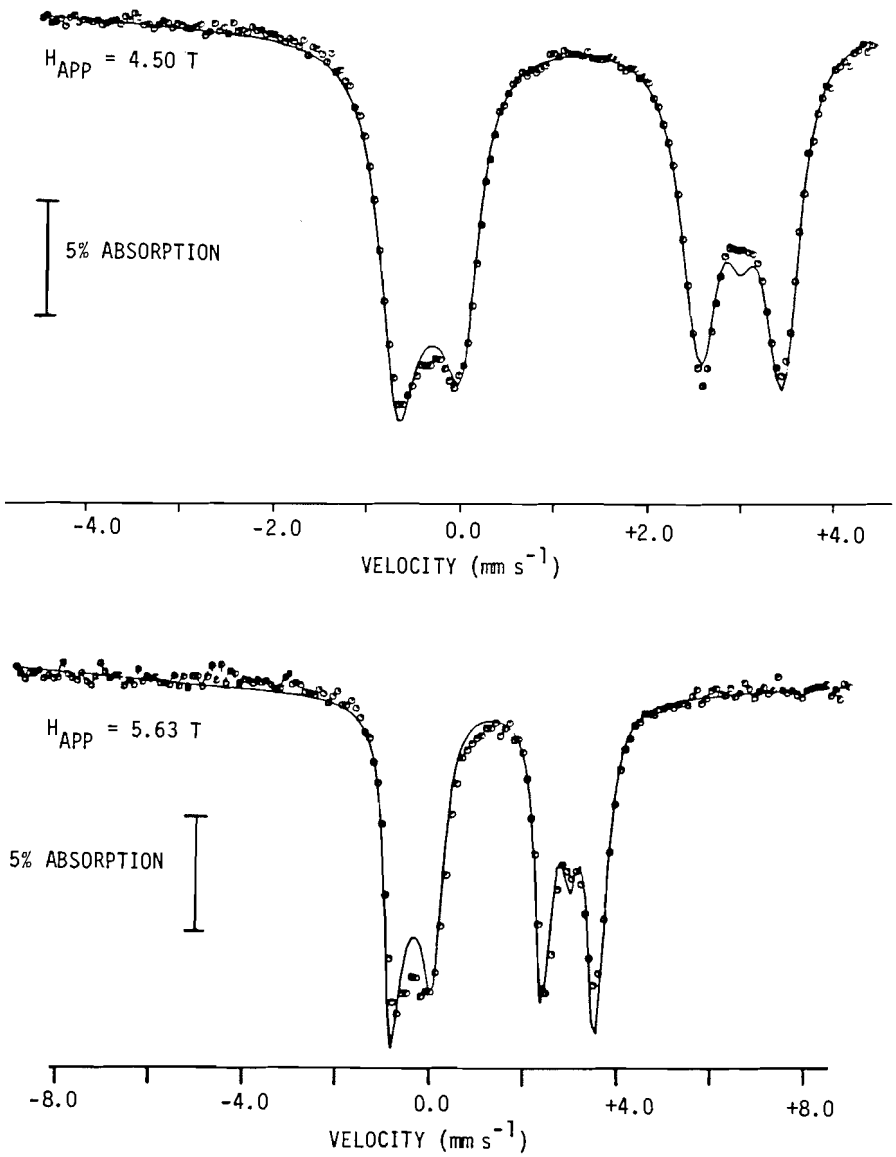

FIG. 5. Mössbauer spectra of α-$Fe(CH_3SO_3)_2$ at 4.2 K in applied magnetic fields of 4.50 and 5.63 T. Computed spectra generated by the parameters given in Table 4.

distortion in this compound, a fact which is consistent with infrared spectral data that show the anion to have C_s (rather than C_{3v}) symmetry (2).

Acknowledgements

Financial support from the Natural Sciences and Engineering Research Council of Canada is gratefully acknowledged. We thank Mrs. A. Sallos for financial assistance. J.S.H. thanks the U.B.C. Graduate Scholarship Committee for scholarship awards.

1. C. A. ALLEYNE, K. O'SULLIVAN MAILER, and R. C. THOMPSON. Can. J. Chem. **52**, 336 (1974).
2. J. S. HAYNES, J. R. SAMS, and R. C. THOMPSON. Can. J. Chem. **59**, 669 (1981).
3. F. CHARBONNIER, R. FAURE, and H. LOISELEUR. Acta Crystallogr. Sect. B, **33**, 1478 (1977).
4. J. S. HAYNES, A. R. HUME, J. R. SAMS, and R. C. THOMPSON. Chem. Phys. **78**, 127 (1983).
5. J. S. HAYNES, J. R. SAMS, and R. C. THOMPSON. Chem. Phys. Lett. **75**, 596 (1980).
6. J. R. SAMS, R. C. THOMPSON, and T. B. TSIN. Can. J. Chem. **55**, 115 (1977).
7. F. VARRET. J. Phys. Chem. Solids, **37**, 265 (1976).
8. S. K. SHARMA, R. K. MAHAJAN, B. KAPILA, and V. P. KAPILA. Polyhedron, **2**, 973 (1983).
9. J. S. HAYNES, K. W. OLIVER, S. J. RETTIG, R. C. THOMPSON, and J. TROTTER. Can. J. Chem. **62**, 891 (1984).
10. J. R. SAMS and T. B. TSIN. Inorg. Chem. **14**, 1573 (1975).
11. J. R. SAMS and J. C. SCOTT. J. Chem. Soc. Dalton Trans. 2265 (1974).
12. H. KAMERLINGH ONNES and A. PERRIER. Commun. Kamerlingh Onnes Lab. Univ. Leiden, **12**, 124a (1911).
13. H. KAMERLINGH ONNES and E. OOSTERHUIS. Commun. Kamerlingh Onnes Lab. Univ. Leiden, **12**, 129b (1912); **12**, 132e (1913).
14. B. C. FRAZER and P. J. BROWN. Phys. Rev. **125**, 1283 (1962).
15. H. T. WITTEVEN and J. REEDIJK. J. Solid State Chem. **10**, 151 (1974).

16. C. CHENG, H. WONG, and W. M. REIFF. Inorg. Chem. **16**, 819 (1977).
17. W. M. REIFF and B. W. DOCKUM. J. Solid State Chem. **31**, 407 (1980).
18. C. NICOLINI and W. M. REIFF. J. Solid State Chem. **44**, 141 (1982).
19. M. E. LINES. J. Phys. Chem. Solids, **31**, 101 (1970).
20. J. PARRIET, M. S. HADDAD, E. N. DUESLER, and D. N. HENDRICKSON. Inorg. Chem. **18**, 2679 (1979).
21. M. A. BABAR, L. F. LARKWORTHY, and S. S. TANDON. J. Chem. Soc. Dalton Trans. 1081 (1983).
22. M. J. STEAD and P. DAY. J. Chem. Soc. Dalton Trans. 1081 (1982).
23. B. N. FIGGIS, J. LEWIS, F. E. MABBS, and G. A. WEBB. J. Chem. Soc. (A), 442 (1967).
24. J. R. SAMS and T. B. TSIN. Chem. Phys. **15**, 209 (1976).
25. W. V. CICHA, J. S. HAYNES, K. W. OLIVER, S. J. RETTIG, R. C. THOMPSON, and J. TROTTER. Can. J. Chem. **63**, 1055 (1985).

Titanocene derivatives of purine and adenine. Synthesis and characterization of reaction products with $(\eta^5\text{-}C_5H_5)_2Ti(CO)_2$, $(\eta^5\text{-}C_5H_5)_2TiCl$, and $(\eta^5\text{-}C_5H_5)_2TiCl_2$[1]

DANIEL COZAK[2], ABDELHAKIM MARDHY, AND ANDRÉ MORNEAU

Department of Chemistry, Faculty of Science and Engineering, Université Laval, Québec, Que., Canada G1K 7P4

Received July 2, 1985

DANIEL COZAK, ABDELHAKIM MARDHY, and ANDRÉ MORNEAU. Can. J. Chem. **64**, 751 (1986).

The reaction of $CpTi(CO)_2$ (**1**), Cp_2TiCl (**2**), and Cp_2TiCl_2 (**3**) (Cp = η^5-C_5H_5) with purine (PuH) and adenine (AdH) in organic solvents is described. The compound **1** reacts with both molecules in an oxidative fashion giving $Cp_2Ti(C_5H_3N_4)(C_5H_4N_4)$ (**4**) and $(Cp_2Ti)_2(C_5H_3N_5)$ (**5**) with concomitant liberation of molecular carbon monoxide and hydrogen (4:1) following a first order rate law in metal complex. The compound **2** forms an adduct compound $Cp_2TiCl(C_5H_4N_4)$ (**6**) with PuH. Monosubstituted derivatives $Cp_2TiCl(C_5H_3N_4)$ (**7**) and $Cp_2TiCl(C_5H_4N_5)$ (**8**) are formed from the reaction of the deprotonated bases with **3**. In addition to the usual elemental analysis, the characteristic ir, ^1H nmr, epr, and ms results are given for the new compounds.

DANIEL COZAK, ABDELHAKIM MARDHY et ANDRÉ MORNEAU. Can. J. Chem. **64**, 751 (1986).

On décrit les réactions, en milieux organiques, des complexes $CpTi(CO)_2$ (**1**), Cp_2TiCl (**2**) et Cp_2TiCl_2 (**3**) (Cp = η^5-C_5H_5) avec la purine (PuH) et l'adénine (AdH). On a isolé et caractérisé les dérivés métallocéniques obtenus de ces réactions. Le composé **1** réagit avec ces ligands, par le biais d'une réaction oxydative, pour donner naissance aux produits $Cp_2Ti(C_5H_3N_4)(C_5H_4N_4)$ (**4**) et $(Cp_2Ti)_2(C_5H_3N_5)$ (**5**) avec un dégagement concomitant de monoxyde de carbone et d'hydrogène moléculaire (4:1) et en suivant une équation de vitesse du premier ordre par rapport au complexe métallique. La réaction de **2** avec la PuH donne le composé $Cp_2TiCl(C_5H_4N_4)$ (**6**). La réaction de **3** avec les bases déprotonées conduit aux produits monosubstitués $Cp_2TiCl(C_5H_3N_4)$ (**7**) et $Cp_2TiCl(C_5H_4N_5)$ (**8**). En plus des analyses élémentaires usuelles, on présente aussi les caractéristiques spectroscopiques ir, rmn ^1H, rpe et sm des nouveaux produits.

[Traduit par la revue]

Introduction

The titanocene dichloride complex, **3**, belongs to a group of metallocene compounds which have recently been found to be efficient antitumor agents (1–3). Biological tests and spectroscopic data indicate that the titanium complex has a similar biological and chemical action on tumor cells as the well known *Z*-dichlorodiaminoplatinum(II) class of antitumor complexes (4–6). However, **3** is an organometallic compound of the so called early groups of the transition metal series, by opposition to the platinum complex which belongs to the late groups. Hence, the physicochemical properties of these organometallic compounds are quite different. In the present case, this is particularly evident for the molecular and electronic structures of these complexes. Nevertheless, both are Lewis acids with 16 electrons in their metal valence shell (7).

In view of these facts we decided to examine the reactivity of **1**, **2**, and **3** with the free bases purine (PuH) and adenine (AdH), two molecular building blocks of DNA. The metallocene complexes chosen for study are tetragonal molecules with three oxidatively different titanium metals for which are known several cases of simple and oxidative substitution or addition reactions with nitrogen containing ligands or heterocyclic molecules related to the bases studied.

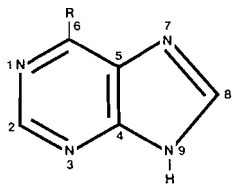

R=H (PuH), NH_2 (AdH)

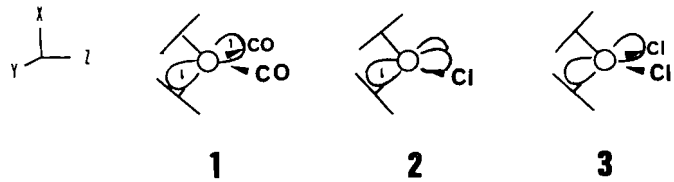

The molecular structures for the studied metallocenes are depicted above with the molecular orbital expected to contain the metal nonbonding electrons. These structures have been successfully interpreted from spectroscopic data by Petersen and Dahl (8) and by molecular calculations by Lauher and Hoffmann (9).

The low valent oxidation state of the titanium metal in **1** and the d^2 lone pair, which is exposed to the sides of the tilted rings, are largely responsible for the observed physicochemical properties of this complex. For example, the metal—carbonyl bond is unusually labile, as evidenced by the strong ir solvent dependent shifts observed for the CO stretching vibration and the facile CO substitution reaction known (10, 11). The carbonyl ligands are easily displaced by phosphine and phosphite derivatives (PR_3) to give the analogues $Cp_2Ti(PR_3)_2$ titanium(II) subsitution complex (12, 13). Carbonyl substitution by alkene, alkyne, ketone, aldehyde, acyl halide, carboxylic acid, and haloalkyl molecules has been amply studied and show that the nucleophilic attack by **1** follows an SN_2 mechanism (14–18). Noteworthy is a recent report by Stucky *et al.* for the reaction of **1** with thymine resulting in the metal oxidation to titanium(III) and liberation of molecular carbon monoxide and hydrogen (19). These authors also report the same type of oxidative substitution for titanium with several other analogous nitrogen containing aromatic heterocyclic molecules.

Monomeric **2** has only 15 electrons in its valence shell and will readily increase this number by addition of a lone pair of electrons from donating ligands such as amines or phosphines (20). In certain adduct complexes the neutral bidentate nitrogen containing ligand (L) is capable of displacing the chloride ion

[1]Taken in part from the M.Sc. thesis of A.M., Université Laval, 1984; presented in part at the XXIII International Conference on Coordination Chemistry, Boulder, CL, June 1984.

[2]To whom all correspondence should be addressed.

from the metal coordination sphere to form cationic $[Cp_2TiL]^+$ complexes. Oxidative addition to the metal or substitution involving the chloride ligands are the other two reaction paths commonly encountered for **2** (21). Closer to our interests, anionic uracil and different deprotonated imidazole, pyrimidine, benzimidazole, and pyrazole ring analogues are reported to give the substituted titanium(III) metallocenes when reacted with **2** (22, 23).

The reaction of **3** with the monoanions of chelating heterocyclic rings (XL), such as salicylaldimine and mercaptoquinazole, are reported to give mono or disubstitution compounds of the type $Cp_2Ti^{IV}Cl_x(XL)_{2-x}$, where ir spectroscopic data seem to indicate that an additional dative bond from the bidentate ligand is also involved in the metal bonding in these complexes (24, 25). Exchange of a chloride by an amino group occurs in liquid ammonia in the presence of excess amine (NH_2R) to give the $Cp_2TiCl(NHR)\cdot NH_2R$ metallocene and the corresponding hydrochloric ammonium salt (26). Deprotonation of naphthole by an alkyl amine has also been used to obtain the naphtholate complexes of mono and dichloride substituted **3** (27). Also, several substitution products can be obtained by metal exchange with the alkali salts of aromatic heterocyclic ligands (28, 29). In an earlier communication, we have reported the crystal structure of $Cp_2TiCl(Pu)$ synthesized from **3** and PuH in the presence of an amine base (30).

The complexes described hereafter all contain Cp_2Ti moiety and were obtained by reacting the ligand, or its deprotonated anion, with **1**, **2**, or **3** in aprotic organic solvents.

Experimental

Reactions and manipulation of the compounds were done under a blanket of purified nitrogen using Schlenk type vessels. Oxygen and water impurities from nitrogen were controlled by passing the gas first over supported copper catalyst (BASF-R3-11) heated at 200°C, purchased from Badische Anilin and Soda-Fabrik AG, W. Germany, and followed by 4A molecular sieve beds. The solvents used were refluxed for 1 h in a nitrogen atmosphere and over a drying agent before being distilled and stored. Sodium metal was used for drying aromatic solvents 1,2-dimethoxyethane (DME) and diglyme; sodium–benzophenone mixture for tetrahydrofuran (THF); 4A molecular sieve for pentane; and a magnesium – magnesium alkoxide mixture for drying methanol.

Melting and decomposition points were measured in nitrogen atmosphere sealed glass capillaries on a Thomas Hoover oil immersion type apparatus and are reported uncorrected. Mass spectra (ms) of the studied complexes were recorded on a Hewlett Packard 5995A mass spectrometer. The spectra were obtained by raising the temperature of the solid samples at a rate of 64°C/min to 200°C with 10^{-6} Torr (1 Torr = 133.3 Pa) pressure in the apparatus. Background subtracted spectra were regularly recorded for 15 min. Infrared (ir) spectra of air sensitive products were recorded on a Beckman IR-4250 spectrometer from KBr pellets of the samples prepared in a controlled atmosphere dry box (O_2 and H_2O < 5 ppm) equipped with a Teledyne Analytical Instrument oxygen analyzer model 317X. The spectra were calibrated (± 3 cm^{-1}) using the 2850.7, 1583.1, 1181.4, and 906.7 cm^{-1} bands of polystyrene film. A Varian EM 360A and a Bruker HX90 CW instrument were used to record the protonic nuclear magnetic resonance (nmr) spectra. Chemical shifts were measured relative to internal TMS or DSS in deuterated chloroform or dimethylsulfoxide (DMSO-d_6) and are reported in δ units from TMS. Electron paramagnetic resonance (epr) spectra were recorded on a JEOL JES-ME (9.3 GHz) spectrometer from polycrystalline solids or dilute (10^{-3} *M*) benzene solutions at ambient temperature. Diphenylpicrylhydrazyl (DPPH, g = 2.0036) was used as reference in epr spectra. Air sensitive samples were introduced in 3 mm od quartz tubing (5 mm od thin wall Pyrex glass tubing for nmr spectroscopy) mounted with a glass ground joint and stopper (5/20ST) to prevent their oxidation. Elemental C, H, and N analyses were performed in duplicate in our laboratory on a Hewlett Packard model 185 CHN analyzer using the appropriate anaerobic methods. X-ray intensity and cell parameter data for the structure determination were obtained with an Enraf-Nonius CAD4 diffractometer. Detailed structure data and methodology are described elsewhere (30).

Titanium trichloride, $TiCl_3$ 98%, was purchased from Ventron-Thiokol-Alfa; di(cyclopentadienyl)dichlorotitanium(IV), Cp_2TiCl_2 (**3**), and the thallium sulfate, $Tl_2(SO_4)$, from Aldrich Chemical Co.; purine, $C_5H_4N_4$, and adenine, $C_5H_5N_5$, from Sigma Chemicals Co. Di(cyclopentadienyl)monochlorotitanium(III), Cp_2TiCl (**2**), was prepared either by reduction of the dichloride **3** over aluminium metal (yield 85%) or by substitution from $TiCl_3$ and $Tl(C_5H_5)$ (yield 90%) as described in the literature (31, 32). Di(cyclopentadienyl)dicarbonyltitanium(II), $Cp_2Ti(CO)_2$ (**1**), was prepared by reduction of the dichloride complex **3** over aluminium in the presence of a CO atmosphere (33): yield 78%; ir (KBr) ν(CO): 1966 and 1871 cm^{-1}; ^{13}C nmr (C_6D_6) δ: 260.8 (s, CO) and 92.3 (s, Cp) ppm; ^{1}H nmr δ: 3.88(s) ppm; ms, m/z 234 (M^+, 5). We noticed while preparing this complex that special care must be taken to insure that the product is free of Cp_2TiCl and $Cp_2TiCl_2AlCl_2$ impurities. These partial reduction products are reaction intermediates resulting from the disproportion equilibrium between the unreacted starting complex **3** and the dicarbonyl product **1**, or the addition of $AlCl_3$ formed during the reduction reaction (34). The other reactants and the new titanocene derivatives described in this paper were prepared as described hereafter.

*Kinetic measurements. Reaction of **1** with PuH and AdH*

The experimental conditions described are those used for the kinetic curves given in the discussion (Fig. 1). Purine 0.302 g (2.52 mmol), or 0.590 g (4.37 mmol) AdH, was introduced in a nitrogen filled reaction cell thermostated at 85°C together with 10 mL diglyme. When the system reached thermal equilibrium the reaction was started by adding 10 mL of **1**, 80.0 m*M* (80.4 m*M* for the AdH experiment) in diglyme, from a dropping funnel. The reaction was followed by measuring the gas evolution with a mercury filled gas burette. Details of the experimental set-up and methodology are described elsewhere (35).

The gaseous reaction products were analyzed by gc on a Hewlett-Packard 7620A instrument equipped with a 13 m long column filled with molecular 13X sieves heated at 50°C and with a 21-620A mass spectrometer manufactured by Electro Dynamics Co. Kinetic experiments were carried out in a 1.3 L apparatus. Temperature of the reaction all-glass jacket-cell (300 mL) was regulated between 70 and 85°C (±0.05°C) using a Haake model F3-Q circulator bath.

Preparation of PuK

In a 100 mL flask, 1.93 g (16.1 mmol) purine was magnetically stirred together with 0.74 g (13.2 mmol) potassium hydroxide in 40 mL freshly distilled methanol for 1 h. The reaction mixture was then filtered to remove the excess purine and the filtrate was evaporated to dryness under reduced pressure on a rotary evaporator. The white solid was quantitatively recovered and used without any further purification; ir, see Table 1; ^{1}H nmr (DMSO-d_6) δ: 8.66 (s), 8.50 (s), 7.96 (s) ppm (lit. (H_2O) 9.2 (s, H6), 9.1 (s, H2), 8.9 (s, H8) ppm (36)).

Preparation of AdNa

In a 100 mL flask, 2.44 g (18.1 mmol) adenine was mixed together with 0.72 g (18.0 mmol) sodium hyroxide and 40 mL methanol. The reaction mixture was magnetically stirred for 1 h at room temperature and then filtered to remove the excess insoluble adenine. The methanol solvent was then vacuum evaporated on a rotary evaporator. Analytically pure adeninate was quantitatively recovered; ir, see Table 1; ^{1}H nmr (DMSO-d_6) δ: 7.90 (s), 7.66 (s), 6.30 (s) ppm (lit. 8.06 (s, H2), 7.96 (s, H8), and 6.85 (s, NH_2) ppm in 3 *N* aqueous NaOH; (DMSO-d_6) 7.83 (s, H2), 7.52 (s, H8) for AdK (37, 38)).

*Reaction of **1** with purine. Synthesis of $Cp_2Ti(C_5H_3N_4)(C_5H_4N_4)$ (**4**)*

In a 100 mL Schlenk flask, 1.69 g (7.22 mmol) dicarbonyl complex **1** was dissolved with 50 mL distilled THF. To this solution 1.74 g

(14.5 mmol) purine was added and the mixture heated on a paraffin bath at 55°C. The red solution turned violet within 15 min. Infrared spectroscopy showed that the reaction was over after 5 h (ν(C≡O): 1967 and 1889 cm^{-1} in THF). The cooled reaction mixture was then filtered over a fritted glass disk to remove a gray precipitate and the filtrate was evaporated to dryness under reduced pressure. The violet colored solid residue was then taken-up with a minimum quantity of THF and filtered. The filtrate was then reduced to half its volume and pentane was added to the solution till precipitation of the complex occurred. The compound was recovered by filtration and dried for 2 h at ambient temperature and 10^{-3} Torr. This yielded 1.83 g (61%) of a violet colored solid compound having the following analytical and spectroscopic properties. Mp 175°C; ir, see Table 1; epr (benzene) g = 1.981; ms, m/z (relative intensity >7%): 178 (7), 177 (9), 167 (11), 120 (10), 93 (16), 66 (29), 65 (12), 52 (12). *Anal.* calcd. for $C_{20}H_{17}N_8Ti$: C 57.56, H 4.11, N 26.85, Ti 11.48%; found: C 56.80, H 4.30, N 27.33, Ti 11.37%.

Reaction of ***1*** *with adenine. Synthesis of* $(Cp_2Ti)_2(C_5H_3N_5)$ ***(5)***

Following the same procedure given above for the purine reaction, 2.28 g (9.74 mmol) of **1** was reacted with 2.65 g (19.6 mmol) adenine in 50 mL THF at 55°C. The solution turned from red to blue in 15 min and the ir solution spectrum indicated that the reaction was over in 1 h. A greyish reaction precipitate was removed from the solution and the complex recrystallized from THF following the same work-up procedure given above for the reaction with PuH. After drying, a blue solid was recovered from the reaction in quantitative yield. The isolated compound has the following analytical and spectroscopic properties. Dec. point 230°C; ir, see Table 1; epr (benzene) g_1 = 1.981, g_2 = 1.975; ms, m/e (relative intensities >5%): 379 (15), 312 (7), 247 (5), 178 (100), 135 (7), 113 (30), 66 (19), 65 (25). *Anal.* calcd. for $C_{25}H_{23}N_5Ti_2$: C 61.37, H 4.74, N 14.31, Ti 19.57%; found: C 61.30, H 5.37, N 14.22, Ti 18.73%.

Reaction of ***2*** *with purine. Synthesis of* $Cp_2TiCl(C_5H_4N_4)$ ***(6)***

In a 100 mL Schlenk flask, 0.700 g (3.29 mmol) complex **2** was dissolved in 50 mL toluene. Then, 0.400 g (3.33 mmol) purine was added under a positive nitrogen pressure to the magnetically stirred solution. The purine slowly dissolved in a few minutes while the solution gradually changed color from green to violet and subsequently back to green. The reaction mixture was stirred for 48 h at ambient temperature. The product precipitated during this time and was recovered by filtration on a glass frit. After washing the solid with two 50 mL portions of cooled pentane, the compound was transferred to a Schlenk flask and thoroughly dried for 2 h at ambient temperature and 10^{-3} Torr. The analytically pure product was obtained by recrystallization from THF/pentane. This yielded 0.900 g (90%) of an air sensitive green complex. The compound gave the following analytical and spectroscopic data. Mp 120–130°C; ir, see Table 1; epr (solid) g_1 = 1.991, g_2 = 1.980, g_3 = 1.966; ms, m/e (relative intensities >8%): 213 (16), 178 (8), 148 (30), 120 (100), 93 (14), 83 (12), 66 (30), 65 (24). *Anal.* calcd. for $C_{15}H_{14}N_4ClTi$: C 54.00, H 4.23, N 16.79%; found: C 52.37, H 4.85, N 16.26%.

Similarly, the same reaction product was obtained using THF or DME instead of toluene as solvent. The total reaction time was 24 h. In these solvents **6** is soluble and was recovered by evaporating the solvent under reduced pressure after filtration to remove any unreacted solid purine.

Reaction of ***3*** *with purine and potassium purinate. Synthesis of* $Cp_2TiCl(C_5H_3N_4)$ ***(7)***

With PuH.

Complex **3**, 1.50 g (6.05 mmol) and purine 1.45 g (12.1 mmol) were placed together with 40 mL THF in a 100 mL Schlenk flask. To this solution, 1.68 mL (12 mmol) distilled triethylamine, $N(C_2H_5)_3$, was added and the mixture heated under positive nitrogen pressure. During the first few hours of reflux the solution darkened. The reaction was followed by nmr in deuterochloroform prepared from aliquots syringed regularly from the reaction mixture. After 18 h, no trace of the starting compound was found in the spectrum (^{1}H nmr ($CDCl_3$) δ: 6.60 (s) ppm for **3** and 6.70 (s) ppm for **7**) and the reaction mixture was then cooled to room temperature before being filtered to remove a white precipitate. The resulting filtrate was evaporated to dryness under reduced pressure and the red-brown residue taken up with a minimum amount of warm THF. The reaction product started to precipitate as the solution was left standing at ambient temperature. The resulting red crystals were recovered by filtration, washed with two 50 mL portions of cooled pentane and dried for 2 h at ambient temperature and 10^{-3} Torr. This yielded 1.65 g (82%) red crystalline product having the following analytical and spectroscopic data. Mp 155°C; ir, see Table 1; ^{1}H nmr (DMSO-d_6) δ: 9.00 (s, purine) and 9.23 (s, purine), 8.70 (s, purine), 6.73 (s, Cp); ms, m/e (relative intensities >5%) 332 (M^+, 5), 269 (19), 267 (46), 213 (19), 185 (33), 183 (43), 150 (31), 149 (17), 148 (81), 147 (12), 122 (18), 121 (15), 120 (100), 93 (18), 85 (17), 83 (29), 66 (36), 65 (34), 52 (16). *Anal.* calcd. for $C_{15}H_{13}N_4ClTi$: C 54.16, H 3.94, N 16.84%; found: C 54.68, H 3.53, N 16.93%.

With PuK.

A mixture of 1.20 g (4.84 mmol) **3** and 0.76 g (4.8 mmol) potassium purinate in 40 mL THF was refluxed for 18 h. The work-up procedure followed was identical to that given above for the reaction with PuH. This reaction yielded 1.09 g (68%) of product. The analytical and spectroscopic properties for this complex are identical with those given above for the PuH reaction.

Reaction of ***3*** *with sodium adeninate. Synthesis of* $Cp_2TiCl(C_5H_4N_5)$ ***(8)***

In a 100 mL Schlenk flask, 1.50 g (6.05 mmol) complex **3** and 2.84 g (18.1 mmol) sodium adeninate were reacted in 25 mL THF at ambient temperature and constant magnetic stirring. After 30 min, the original red color of the solution turned to pale orange. Progress of the reaction was followed by nmr. Aliquots were periodically taken from the reaction mixture and the THF replaced by deuterochloroform before checking for the presence of **3** (^{1}H nmr ($CDCl_3$) δ: 6.60 (s) ppm for **3** and 6.33 (s) for **8**). After 3.5 h, **3** had all reacted and the reaction mixture was filtered on a glass frit to remove a white precipitate. This solid product was washed, while on the frit, with 25 mL THF and the resulting filtrate was evaporated under reduced pressure. This gave 0.40 g (19%) of orange solid product which has the following analytical and spectroscopic properties. Dec. point 208°C; ir, see Table 1; ^{1}H nmr (DMSO-d_6) δ: 8.23 (s, adenine cycle), 8.20 (s, adenine cycle), 7.15 (s, NH_2), 6.46 (s, Cp); ms, m/z (relative intensities >5%): 381 (5), 380 (5), 379 (15), 377 (17), 376 (5), 374 (15), 312 (6), 215 (12), 214 (6), 213 (31), 211 (6), 185 (5), 183 (6), 180 (6), 179 (20), 178 (100), 177 (14), 176 (13), 152 (6), 150 (18), 148 (42), 129 (6), 122 (6), 113 (30), 83 (8), 66 (10), 65 (25). *Anal.* calcd. for $C_{15}H_{14}N_5ClTi$: C 51.82, H 4.02, N 20.14, Ti 13.78%; found: C 51.21, H 3.59, N 20.85, Ti 14.03%.

Results and discussion

The newly synthesized complexes **4**, **5**, and **6** are extremely air sensitive in solution and gave the expected epr spectra for titanium +3 complexes. Moreover, **7** and **8** gave normal diamagnetic proton nmr signals and did not show any signs of decomposition when exposed to air for short periods of time. Nevertheless, all compounds were prepared and kept under a purified nitrogen atmosphere as described in the experimental part.

The compounds isolated in this work were characterized by elemental analysis, ir, epr, ms, and ^{1}H nmr spectroscopy. The crystal structure of **7** has been determined by single crystal X-ray diffraction analysis and is reported in detail elsewhere (30).

Though both bases studied here are structurally quite similar, marked differences for their reactivity with the diferent titanocene complexes were observed. For instance, the oxidation product for the dicarbonyl complex **1** with PuH is monometallic (**4**) whereas, under similar conditions, the AdH derivative is

TABLE 1. Characteristic ir vibration frequencies recorded between 4000–250 cm^{-1} for the studied compounds[a,b]

Free ligand		Anion ligand			Complex				
PuH	AdH	PuK	AdNa	Assignments[c]	4	5	6	7	8
			3550 sh, w						
	3350 vw		3440 sh, m			3450 sh, m			
	3290 m		3350 m	$\nu(NH_2)$		3320 br, m			3300 br, m
3110 sh, s	3270 sh, w		3200 vw			3170 sh, m			
	3111 m		3152 s	$\nu(NH_2)$					3130 br, m
3100 m		3070 m		ν(C—H) Im cycle	3120 br, m	3100 br, m	3100 br, m	3115 sh, m	3100 s
3070 m		3040 m		ν(C—H) Py cycle	3080 m			3090 m	
3029 m		3010 m		ν(C—H) Py cycle	3035 w			3070 sh, s	
3010 sh, m									
2950 m	2960 w					2960 m	2960 w	2950 w	2960 w
								2920 sh, w	
2870 w							2860 w	2850 vw	
2790 br, m	2790 w			ν(N—H) Im cycle			2790 br, m	2800 vw	
2730 m				ν(N—H) Im cycle	2725 w		2680 w		2783 w
2687 m				ν(N—H) Im cycle			2560 w		2680 w
2618 w					2615 s				
						1740 w			
	1670 vs		1640 br, vs	$\delta(NH_2)$	1610 sh, s	1650 br, s	1620 sh, s		1665 vs
1618 vs	1602 vs	1595 vs	1617 vs	Py	1590 s	1600 s	1610 s	1608 m	1600 vs
1588 w									
1570 s		1543 s	1540 s	Py	1570 vs	1560 sh, s	1590 m	1595 vs	
1560 sh, s					1550 sh, s		1570 w		
1490 vw		1480 sh, m	1480 m	Im				1485 vw	
1460 s		1470 sh, m	1463 sh, m	Im, Py	1480 sh, m			1462 m	
	1450 w	1453 s	1455 s	Py	1470 s	1475 sh	1470 w	1448 sh, m	
				Cp	1440 m	1440 s	1440 w	1440s	1440 w
1427 s		1438 s		Im	1415 s	1413 m	1412 sh, s		
1402 vs	1420 m	1390 vs	1390 vs	Py	1400 vs	1395 m	1400 vs	1400 s	1415 m
		1383 sh, s						1390 s	
1350 vw	1365 m	1360 sh, m	1365 m	Py		1360 m		1365 sh, m	1365 m
			1328 w			1355 sh, w			
1330 s	1335 s	1332 m	1338 m	Im	1330 vs	1325 m	1328 s	1330 s	1330 m
	1310 vs		1318 s	$\nu(C—NH_2)$		1310 m			1305 vs
1310 vw		1298 s			1305 w		1305 w	1298 m	
							1270 sh, w	1290 m	
1273 vs	1252 m	1283 s	1255 m	δ(N—H) Im cycle, δ(C—H)	1270 sh, m	1262 s	1260 m	1270 s	1247 s
	1230 sh, w	1228 m	1235 sh, m	δ(C—H)	1230 m		1230 m	1230 m	
1213 s			1208 sh, m	δ(C—H)	1222 m		1220 sh, m	1220 sh, m	
1197 sh, m	1155 w	1192 vs	1195 s	δ(C—H)	1195 sh, m	1180 vw	1190 w	1185 m	
1140 vw	1125 m	1182 sh	1132 m	Im, Py	1137 w			1165 vs	1150 br, m
1096 m		1093 m		Im, Py	1105 m	1100 s	1105 s	1102 m	1121 w
						1070 sh, m		1070 sh, m	
							1058 w	1065 m	
								1032 sh, m	
	1022 m		1020 m	$\rho(NH_2)$	1020 m			1022 sh, m	1020 m
				Cp	1012 m	1020 vs	1015 s	1018 m	1010 m

TABLE 1. (*concluded*)

Free ligand		Anion ligand			Complex				
PuH	AdH	PuK	AdNa	Assignments[c]	**4**	**5**	**6**	**7**	**8**
965 s	940 s	960 vw	970 w	Im, Py	967 m	940 m		920 m	936 s
923 w		920 s	915 w	γ(C—H)	925 m		955 w	910 sh, m	
909 s	912 s	912 s	900 w	γ(C—H), Im, Py	910 s	915 w		905 m	910 w
860 br, m	870 br, m			γ(N—H) Im cycle			910 br, w		865 w
	848 m	880 w		Im, Py	840 sh, m	850 sh, m	845 w	860 m	840 w
				γ(N—H) Im cycle	820 s		815 vs	830 s	827 w
800 m	798 m	808 s	805 s	γ(C—H), Im, Py, Cp	808 s	800 br, m	798 vs	812 s	808 vs
790 w		795 m		γ(C—H)	800 s			800 vs	800 s
			730 w		792 sh, m	720 sh, m	725 s	720 s	750 w
	722 m	705 w	695 m	Im, Py					720 vs
	650 br, s	653 br, s		ω(NH_2)		660 m		665 w	
		648 sh, m	650 sh, m		640 m	640 sh, w	640 m	640 sh, w	632 br, s
600 s	628 m	625 w	615 w	Im, Py	600 s·		595 m	600 br, m	580 w
				ν(Ti—N)	570 sh, m	578 m	595 sh, m	570 sh, w	590 w
560 w	570 w		532 w	Im, Py	560 w		575 sh, m		
						550 sh, w	565 m		
	538 m		570 w	δ(C—NH_2)		525 sh, w			530 w
	465 w	465 m						462 w	
445 w				Im, Py	445 w			440 w	
				ν(Ti—Cp)	417 sh, w	395 m			
				ν(Ti—Cl)			395 m	395 m	390 m
	380 vw		385 w	ν(Ti—Cp)	385 m	385 w	382 w		
370 w	370 w	375 w	375 w		377 sh, w	375 w	372 w	350 w	
350 w		355 vw	355 vw		355 sh, w	355 w	352 w		
	332 s			Im, Py					320 w

[a]Main frequencies observed for **1**: 1968 vs, 1885 vs, 1260 m, 1070 m, 1018 s, 802 vs, 395 w, 355 vw cm^{-1}; **2**: 3088 w, 2960 w, 1445 m, 1439 m, 1271 m, 1065 w, 1023 sh, w, 895 m, 845 m, 813 vs, 799 vs, 782 sh, m, 390 m, 375 sh, w, 350 w cm^{-1}; **3**: 3100 s, 1435 s, 1025 sh, m, 1014 s, 860 m, 818 vs, 408 sh, w, 392 m, 349 w cm^{-1}.

[b]Legend: s = strong, m = medium, w = weak, v = very, sh = shoulder, br = broad; Py = pyrimidine ring modes, Im = imidazole ring modes.

[c]The assignments are those of the neutral and anion ligands taken from refs. 41–47 and the metallocene moiety from refs. 48 and 49.

bimetallic (**5**). Repeated attempts to react the neutral AdH ligand or its alkali (Li, Na, K) salts with the monochloride complex **2** resulted in the displacement of the cyclopentadienyl rings to give insoluble titanium containing products. This result is not completely unexpected since cyclopentadienyl has been reported to be displaced in **1** by strong bases such as *o*-phenantroline, and adducts of **2** are not isolable for bulky secondary or tertiary amines, or alkyls and aryl substituted phosphites (20, 32). Conversely, with PuH this reaction readily gives, in good yields, the adduct product **6** described hereafter. Finally, with **3** the chloride substitution product **8** was isolated only for the reaction with the adeninate salt AdNa, whereas PuH in the presence of NEt_3 or PuK gave in good yield the monosubstituted purine derivative **7**.

Carbon monoxide and hydrogen gas evolution was observed for the reaction of **1** with PuH and AdH. A 3.8–3.9:1 CO/H_2 molar ratio in the gas mixture over the reaction solution was determined by ms. This is very close to the expected 4:1 ratio for the overall oxidative addition reaction of **1** to these bases, as given in eqs. [1] and [2] below, corresponding to the formation of **4** and **5**. Moreover, reaction yields of 80–82% were found based on the evolved experimental–theoretical volume ratio and the unreacted base recovered after the reaction. Both reactions follow first order kinetics in the metal complex as evidenced by the linear $\ln(V_\infty - V_t)$ *vs.* time curves shown in Fig. 1. Using these plots, rate constants were calculated for a few ligand/complex ratios between 70 and 85°C to verify this first order dependence. The following results and observations were made.

The reaction rate constants measured at 85°C for PuH in xylene and diglyme solvents using a 3:1 ligand/complex molecular ratio are $0.97(\pm0.06) \times 10^{-4}\,s^{-1}$ and $2.0(\pm0.1) \times 10^{-4}\,s^{-1}$ (shaded circles in Fig. 1), respectively. The rate constants discussed here are for the reactions in diglyme at different temperatures. For the molecular ratios AdH/**1** = 1.5:2 and 11:2, the observed rate was the same, $0.49(\pm0.01) \times 10^{-4}\,s^{-1}$ (85°C, shaded squares in Fig. 1) and decreased to $0.325(\pm0.003) \times 10^{-4}$ when the reactant ratio was increased to 20:2. When the PuH/**1** ratio was increased from 3:1 to 40:1, an increased of the observed reaction rate constant from $1.39(\pm0.03) \times 10^{-4}$ to $2.9(\pm0.1) \times 10^{-4}\,s^{-1}$ resulted (80°C). In all cases, the activation enthalpies calculated from the Arrhenius plots give $\Delta H^* = 98$ and 108 (±8) kJ mol^{-1} ($\Delta S^* = -50$ and -34 J mol^{-1} K^{-1}), respectively for reactions [1] and [2]. More experimental results for different ligand concentrations are needed to verify the exact nature of these pseudo first-order laws. The decrease in reaction rates, above a given reactant ratio, observed for AdH/**1** indicates a more complicated rate law for this reaction. Moreover, the crude activation energy and entropy values (negative) calculated from the Arrhenius plots for these reactions agree well with the complex-ligand associative mechanism usually proposed as a limiting step in several oxidative SN_2 reactions of **1** and for other transition metal compounds in general (15, 16, 39, 40).

[1] $\underset{\mathbf{1}}{Cp_2Ti(CO)_2} + 2PuH \rightarrow \underset{\mathbf{4}}{CpTi(Pu)(PuH)} + 2CO + 0.5H_2$

[2] $2\underset{\mathbf{1}}{Cp_2Ti(CO)_2} + AdH \rightarrow \underset{\mathbf{5}}{(Cp_2Ti)_2(C_5H_3N_5)} + 4CO + H_2$

Formation of an insoluble amine salt, $[HNEt_3]^+$, during the reaction of **3** with PuH in the presence of NEt_3 was confirmed by ^1H nmr spectroscopy, $\delta(CD_2Cl_2)$: 3.08 (q, CH_2) and 1.36 (t, CH_3) ppm. Hence, our results point to the formation of the substitution product **7** given by eq. [3]. Attempts to prepare the disubstituted derivative by using an excess of ligand (PuH/complex ratio, 7:1) were to no avail. However, the ^1H nmr spectra of the crude reaction product with PuK showed the presence of a secondary titanocene product at $\delta(CDCl_3)$ 6.35 (s, Cp) ppm believe to be disubstituted. We were unable to properly isolate this product because of poor yields.

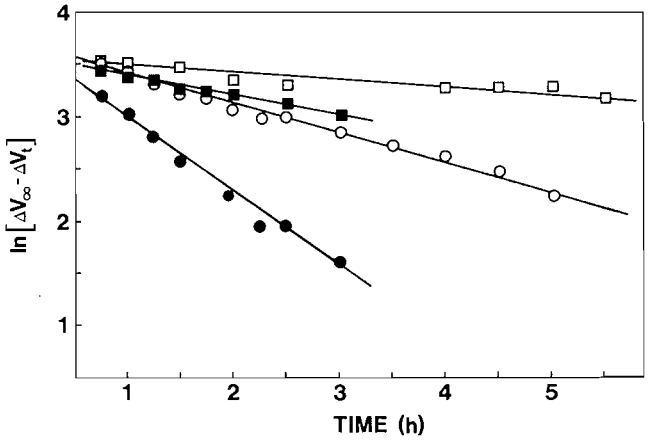

FIG. 1. Curves of $\ln[V_\infty - V_t]$ for the reaction of PuH (circles) and AdH (squares) with **1** in diglyme. The unshaded circles are for T = 75°C and shaded circles for 85°C using a PuH/**1** = 3:1 reactant ratio. The unshaded squares are for T = 75°C (AdH/**1** = 1.5:2) and the shaded squares for T = 85°C (AdH/**1** = 11:2). At 75°C, $k = 0.76(\pm0.01) \times 10^{-4}\,s^{-1}$ for PuH and $k = 0.172(\pm0.003) \times 10^{-4}\,s^{-1}$ for AdH. See text for details.

[3] $\underset{\mathbf{3}}{Cp_2TiCl_2} + PuH + NEt_3 \rightarrow \underset{\mathbf{7}}{Cp_2Ti(Pu)Cl} + [HNEt_3]Cl$

Infrared spectra

The observed infrared spectrum in the 4000–250 cm^{-1} range for the studied compounds are given in Table 1. The band assignment for the free ligands are those given in the literature (41–47). The frequencies for complexes **4–8** were tentatively correlated as much as possible with those of the ligands.

Hence, all the titanium complexes exhibit strong π-bonded cyclopentadienyl ligand around 1440, 1015, and 800 cm^{-1} expected for the titanocene unit (48, 49). The presence of the purine and adenine ligands in **4–8** is confirmed by the characteristic Py and Im ring skeleton vibrations which are given in the table. These skeleton modes can be divided into two groups. Those located around 1600, 1570, 1470, and 1400 cm^{-1} are due to the Py ring vibrations and those near 1460, 1415, and 1330 cm^{-1} to the Im ring. Also, the absorptions at 1440 cm^{-1} present for all the complexes is attributed to the Cp ring. However, several bands in the 800 cm^{-1} region renders difficult the unambiguous attribution of the characteristic frequencies in this region for the Cp or the purine ring modes.

A comparative look at the ir spectra of **4**, **6**, and **7** does not reveal major discrepancies for the observed frequencies. However, like PuH, the spectra of **4** and **6** have vibrations in the 2800–2400 cm^{-1} region superimposed to a broad base line deformation (not mentioned in Table 1) owing to the Im N—H stretching vibrations, whereas **7** has none. The only absorption seen at 2800 cm^{-1} for **7** is believed to be owing to a combination band. These observations are in agreement with spectroscopic and analytical results which indicate that **6** and **7** are, respective-

ly, titanium(III) addition and titanium(IV) substitution products with similar chemical compositions (i.e., $Cp_2TiCl(PuH_x)$, x = 1 and 0).

Another interesting feature is the presence of a medium intensity band at 395 cm^{-1} for **6** and **7** assigned to the Ti—Cl stretching. The weak band observed at 385 cm^{-1} for **4** must, in this case, be assigned to the other possibility, that is, the symmetric or asymmetric Ti–Cp metal–ring stretching of the metallocenic moiety (49). This vibration mode is also present in the spectrum of the nonchloride-containing complex **1** at 395 cm^{-1} (see footnote in Table 1). The bands near 570 cm^{-1} were assigned in each case to the Ti–N stretching frequencies. There was no evidence in the ir data whether N1, N3, N9, or N7 coordination to titanium is preferred in **4** or **6**, by way of comparison with **7**, or if the labile N7–H proton migrates to other nitrogen atoms in these complexes. This type of ligand rearrangement has been reported for several transition metal complexes of neutral or protonated purine, e.g., $[Cu(H_2O)_4(PuH)]SO_4$ (50), $ZnCl_3(PuH_2)$ (51), and $Cu_2Cl_6(PuH_3)$ (52). In general this type of structural nuance is difficult to detect by routine ir alone.

For the adenine derivatives **5** and **8**, the spectra are very similar to those of free AdNa and AdH, respectively. The vibrations for which these similitudes are most evident are in the 3400–2400 cm^{-1} and 1700–1600 cm^{-1} regions. More precisely, the AdNa and **5** spectra have both a very broad band near 1640 cm^{-1} attributed to the NH_2 deformation vibration which is slightly at higher frequencies and much sharper for AdH and **8**. Hence, in the latter spectra the NH_2 deformation band is well resolved from the sharp Py ring vibration near 1600 cm^{-1}, contrary to the former. Overlapping and very broad absorptions in the 3400–2800 cm^{-1} region have been assigned to the NH_2 stretching mode and a broad band in the 2800–2400 region to the Im N—H stretching, by Lautié and Novak (42). The two main absorption bands present at 3320 and 3100 cm^{-1} in the spectra of **5** can be assigned to a secondary rather than a primary amine if the low field band is assumed to be cause by a C—H stretching mode. Also, the 2800–2400 cm^{-1} region is void of the Im N—H stretching absorption for this complex. Furthermore, the important NH_2 wagging present at 650 cm^{-1} in the spectrum of AdH was not observed for **8** although a stretching mode is present as indicated by the absorptions at 3300 and 3130 cm^{-1}. The amino wagging mode should be manifest for the titanium derivative based on the spectra of the sodium metal salt, which contains a huge deformation of the base line ranging from 800 to 400 cm^{-1} owing to this mode (not mentioned in Table 1). Hence, based on its ir data, there is no evidence for the ring deprotonation in **8**, and the amino group should be involved in some type of bonding interaction. Data for **5** suggest that the amino group environment is significantly changed in this complex and clearly shows that the Im ring is deprotonated.

Several molecular and polymeric structures of purine base complexes with transition metals have been precisely determined by X-ray diffraction (53–55). In view of the great flexibility of the chelate–metal interactions in these solids, definitive structures based on ir data alone are difficult.

Electron paramagnetic resonance spectra

Solid and benzene solution spectra were recorded at room temperature for the paramagnetic **2**, **4**, **5**, and **6** compounds. The observed g values are typical of titanium +3 oxidation state.

The characteristic features of the solid state epr are as follows. The spectrum for polycrystalline **4**, see Fig. 2, has the general shape of an axially symmetric resonance with anisotropic tensors $g_{\|}$ = 1.994 and $g_{\perp}$ = 1.975. The powder spectrum of **6** is typical of a rhombic g tensor, giving rise to three g values: g_1 = 1.991, g_2 = 1.980, and g_3 = 1.966. The spectrum is also shown in Fig. 2. This type of spectrum has been observed for similar $Cp_2Ti^{III}XL$ addition complexes (56, 57). Contrasting with these special features, the powder spectrum for **5** gives an extremely broad single derivative shape resonance

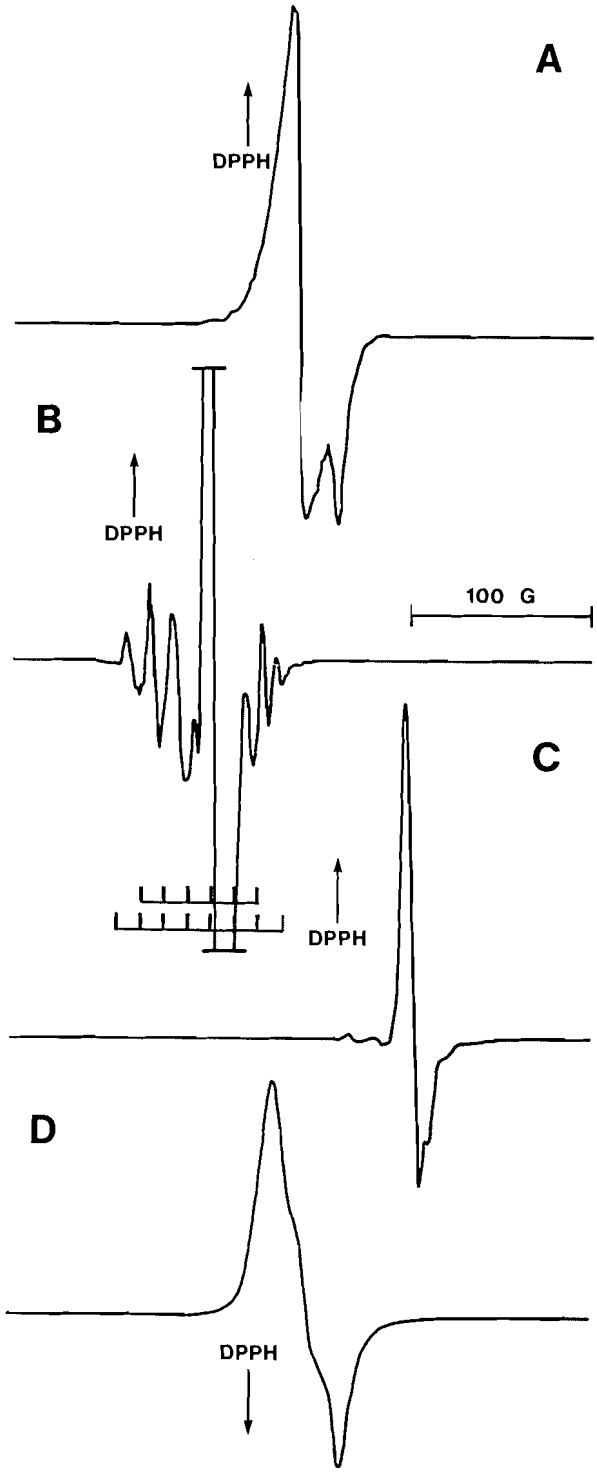

FIG. 2. Room temperature epr spectra of polycrystalline **4** (A) and in solution 10^{-3} M in benzene (B); of **5** in solution 10^{-3} M in benzene (C); and of polycrystalline **6** (D).

centered at $g = 2.001$ having approximately 82 G peak-to-peak, double the width observed in the spectra of the monochloride complex **2** which has a g value of 1.980.

Dilute solution spectra in benzene for the paramagnetic complexes show a narrow single resonance derivative signal. In addition to this, **5** has an unresolved resonance at high field of the main epr derivative resonance giving rise to two g values for this complex: $g_1 = 1.981$ and $g_2 = 1.975$. All the solution spectra showed hyperfine metal–spin coupling with ^{47}Ti ($I = 5/2$, natural abundance 7.5%) and ^{49}Ti ($I = 7/2$, natural abundance 5.5%) as shown in Fig. 2 for **4** ($g = 1.981$). The interline spacings measured are; for **2**, 15 G; for **5**, 10 G; for **4** and **6**, 13 G. The scale drawn for spectrum B of Fig. 2 depicts a sextet superimposed to an octet splitting centered around the more intense singlet resonance due to ^{46}Ti, ^{48}Ti, and ^{50}Ti (natural abundance 87.0%) metal atoms, $I = 0$ nuclei. The observed hyperfine resonance intensities coincide with those calculated from the natural isotopic abundance of titanium, 1:2.6:2.6:2.6:115:2.6:2.6:2.6:1 (58). Furthermore, the averaged interline splitting observed here is somewhat stronger than the 8–11 G range reported for bipyridine, imidazole, biimidazole, benzimidazole, and carboxylic acid complexes (59, 60).

Closer examination of the hyperfine structure in the solution spectra of **5** indicated the presence of a second less intense unresolved hyperfine splitting, with *ca.* 4 G interline spacing with the former. Similar splitting has been reported for dinuclear titanocene complexes of dicarboxylic acids (59, 61). Intramolecular magnetic exchange between neighboring titanium atoms [i.e., $J \gg A(\mathrm{Ti})$] has been shown to be the cause of this splitting. Hence, this feature is consistent with the dinuclear composition found by elemental microanalysis for **5**.

Mass spectra

The pertinent electron impact mass spectral data are given in the experimental part. The spectra of the studied compounds did not show any molecular ion fragments except **7** where a fragment at m/z 332 (5) corresponding to the molecular ion $[C_{15}H_{13}N_4ClTi]^+$ was present. For all the complexes, the $[C_{10}H_{10}Ti]^+$ and $[C_5H_5Ti]^+$ fragments typical for titanocene derivatives were more or less abundant at m/z 178 and 113 (percent relative intensity, 2–31%). For **6**, **7**, and **8** the mass peak at m/z 213 corresponding to the $[C_{10}H_{10}ClTi]^+$ ion can be explained by the loss of the neutral base ligand from the parent molecular ion. The base peak for the purine complexes were present at m/z 120 (100) due to the ionized pure ligand. The ms of the adenine complexes, on the other hand, gave a base peak corresponding to the titanocene unit at m/z 178 (100). Also, in the spectra of **8** several metal–adenine containing fragments were detected. The more intense fragments are at m/z 381 (5), 379 (15), 314 (4), and 312 (6), and coincide with the formulation of ions with two adenine rings $[(C_5H_5)(C_5H_xN_5)_2Ti]^+$ with $x = 4$ and 3, or one adenine ring $[(C_5H_5)_2(C_5H_yN_5)Ti]^+$ with $y = 6$ and 5 species, respectively. Primary elimination of neutral cyclopentadienyl fragments from the parent ion has been reported for several titanocene complexes with strong O, N, or S bonded chelating ligands (19, 23).

Structures

Crystallographic measurements for **7** show that the molecule contains a bent-cycle metallocene unit to which the deprotonated purine ligand is bonded through the N9 nitrogen (30). The ligands are tetragonally disposed around the metal with the purine ring pointing away as shown in the structure given below. This feature contrasts with the preferred N7 protonation

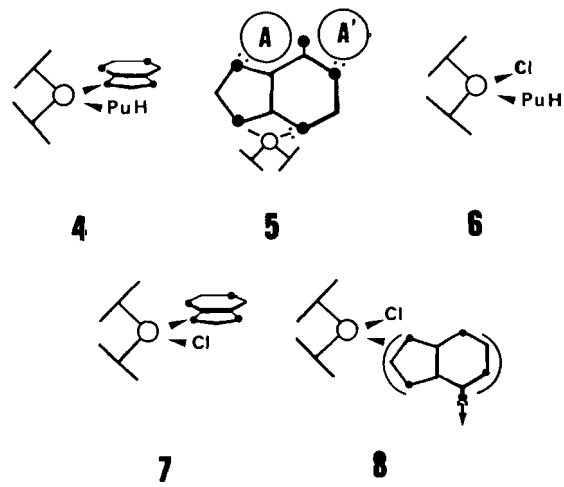

site of the free ligand and is probably due to the different Lewis acid properties of H^+ and the Cp_2Ti^+ cations. The titanium—ligand bond lengths and angles fall within previously reported values for titanium(IV) metallocenes.

The expected structures for complexes **4**–**6** and **8** are shown below. Analytical and spectroscopic results indicate the presence of π-cyclopentadienyl ligands in all four complexes. Moreover, titanium metallocenes generally adopt a tetragonally arranged *clino*-structure for its ligands. Also, the proposed structures are consistent with the 17 or 16 valence electron configuration usually encountered for titanium +3 and +4 oxidation state, respectively.

Kinetic, analytic, and spectroscopic results indicate that one of the two purine ligands in **4** is deprotonated and **5** must be a bimetallic complex with one doubly protonated adenine ligand. In **4** the deprotonated purine ligand is possibly coordinated through its N9 nitrogen as in **7**. Moreover, in these compounds and in **6** the titanium has a +3 oxidation state. Hence, structures **4** and **6** can reasonably be proposed and represent PuH addition compounds. The structure for **5** is more difficult to predict. If the assumption that the N9 and N6 nitrogens are the more probable deprotonation sites for adenine, then one $(\eta^5\text{-}C_5H_5)_2Ti$ unit can be expected to bond to the N9 nitrogen of the adenine ring, plus a dative bond from N3 is possible. The second titanium unit can then bond to the amino N6 nitrogen with an additional dative bond from either the N7 or the N1 atom of the ring. These two distinct structures are depicted in structure **5** by circles A and A′ respectively. For these two structures, it can be argued that formation of a five-member metallocycle (A) is expected to be favored over the smaller four-membered ring (A′). However, the greater basicity of N1 over N7 is an equally important property of the free adenine molecule in favor of the latter structure (A′).

Finally, for titanium compounds no information was available, as of yet, on the coordination properties of adenine. There are strong indications here, from ir and ms results for **8**, that the amino group is involved in inter- or intra-molecular chelation in the solid state, possibly with titanium. Seemingly, saturated penta-coordinated titanium(IV) complexes are rare but have been previously reported (24, 25).

Acknowledgments

Financial support from the "Fonds FCAC" Quebec government, Natural Sciences and Engineering Research Council of Canada, and the Moroccan Ministry of Education is gratefully acknowledged.

1. H. KÖPF and P. KÖPF-MAIER. Angew. Chem. Int. Ed. Engl. **18**, 477 (1979).
2. P. KÖPF-MAIER and H. KÖPF. Z. Naturforsch. B: Anorg. Chem. Org. Chem. **34B**, 805 (1979).
3. H. KÖPF and P. KÖPF-MAIER. Platinum, gold and other metal chimotherapeutic agents. Vol. 209. *Edited by* S. J. Lippard. ACS Symposium Series, Washington, D.C. 1983. p. 315.
4. P. KÖPF-MAIER, W. WAGNER, and H. KÖPF. Naturwissenschaften, **68**, 272 (1981).
5. P. KÖPF-MAIER and H. KÖPF. Naturwissenschaften, **67**, 415 (1980).
6. P. KÖPF-MAIER, B. HESSE, and H. KÖPF. J. Cancer Res. Clin. Oncol. **96**, 43 (1980).
7. C. M. LUKEHART. Fundamental transition metal organometallic chemistry. Brooks Cole Publ., Monterey, CA. 1985. p. 14.
8. J. L. PETERSEN and L. F. DAHL. J. Am. Chem. Soc. **96**, 2248 (1974).
9. J. W. LAUHER and R. HOFFMANN. J. Am. Chem. Soc. **98**, 1729 (1976).
10. J. G. MURRAY. J. Am. Chem. Soc. **83**, 1287 (1961).
11. G. FACHINETTI and C. FLORIANI. J. Chem. Soc. Chem. Commun. 66 (1974).
12. D. J. SIKORA, M. D. RAUSCH, R. D. ROGERS, and J. L. ATWOOD. J. Am. Chem. Soc. **103**, 982 (1981).
13. B. H. EDWARDS, R. D. ROGERS, D. J. SIKORA, J. L. ATWOOD, and M. D. RAUSCH. J. Am. Chem. Soc. **105**, 416 (1983).
14. B. DEMERSEMAN, M. PANKOWSKI, G. BOUQUET, and M. BIGORGNE. J. Organomet. Chem. **117**, 10 (1976).
15. C. FLORIANI and G. FACHINETTI. J. Chem. Soc. Chem. Commun. 790 (1972).
16. G. FACHINETTI and C. FLORIANI. J. Chem. Soc. Dalton Trans. 2297 (1977).
17. P. HONG, K. SONOGASHIRA, and N. HAGIHARA. Bull. Chem. Soc. Jpn. **39**, 1821 (1966).
18. G. FACHINETTI, C. BRIAN, C. FLORIANI, A. CHIESI-VILLA, and C. GUASTINI. Inorg. Chem. **17**, 2995 (1978); J. Chem. Soc. Dalton Trans. 792 (1979); J. Am. Chem. Soc. **100**, 1921 (1978).
19. D. R. CORBINS, L. C. FRANCESCONI, D. N. HENDRICKSON, and G. D. STUCKY. Inorg. Chem. **20**, 2084 (1981).
20. M. L. H. GREEN and C. R. LUCAS. J. Chem. Soc. Dalton Trans. 1000 (1972).
21. P. C. WAILES, R. S. P. COUTTS, and H. WEIGOLD. Organometallic chemistry of titanium, zirconium and hafnium. Academic Press, New York. 1974. p. 208.
22. B. F. FIESELMANN and G. D. STUCKY. Inorg. Chem. **17**, 2074 (1978).
23. D. R. CORBIN, L. C. FRANCESCONI, D. N. HENDRICKSON, and G. D. STUCKY. Inorg. Chem. **18**, 3069 (1979).
24. S. K. SENGUPTA and N. MUDDIN. Indian J. Chem. Sect A, **21A**, 426 (1982).
25. R. K. SHARMA, R. V. SINGH, and J. P. TANDON. J. Inorg. Nucl. Chem. **43**, 410 (1981); **42**, 1382 (1980).
26. A. ANAGNOSTOPOULOS and D. NICHOLLS. J. Inorg. Nucl. Chem. **27**, 339 (1965).
27. A. K. SHARMA and N. K. KAUSHIK. Synth. React. Inorg. Met. Org. Chem. **12**, 827 (1982).
28. K. ISSLEIB and G. BÄTZ. Z. Anorg. Allg. Chem. **369**, 83 (1969).
29. R. VANN BYNUM, W. E. HUNTER, R. D. ROGERS, and J. L. ATWOOD. Inorg. Chem. **19**, 2368 (1980).
30. A. L. BEAUCHAMP, D. COZAK, and A. MARDHY. Inorg. Chim. Acta, **92**, 191 (1984).
31. R. S. P. COUTTS, P. C. WAILES, and R. L. MARTIN. J. Organomet. Chem. **47**, 375 (1973).
32. L. E. MANZER. J. Organomet. Chem. **110**, 291 (1973); C. C. HUNT and J. R. DOYLE. Inorg. Nucl. Chem. Lett. **2**, 283 (1966).
33. B. DEMERSEMAN, G. BOUQUET, and M. BIGORGNE. J. Organomet. Chem. **101**, C24 (1975).
34. P. C. WAILES, R. S. P. COUTTS, and H. WEIGOLD. Organometallic chemistry of titanium, zirconium and hafnium. Academic Press, New York. 1974. p. 207.
35. F. CALDERAZZO and F. A. COTTON. Inorg. Chem. **1**, 30 (1962).
36. P. J. PUGMIRE and D. M. GRANT. J. Am. Chem. Soc. **93**, 1880 (1971).
37. C. D. JARDETZKY and O. JARDETZKY. J. Am. Chem. Soc. **82**, 222 (1960); W. M. BECK, J. C. CALABRESE, and N. D. KOTTMAIER. Inorg. Chem. **18**, 176 (1979).
38. H. BEHRENS and H. BRANDL. Z. Naturforsch. B: Anorg. Chem. Org. Chem. Biochem. Biophys. Biol. **22B**, 1216 (1967).
39. G. FACHINETTI and C. FLORIANI. J. Chem. Soc. Dalton Trans. 2433 (1974).
40. F. BOSOLO and R. G. PEARSON. Mechanisms of inorganic reactions. 2nd ed. John Wiley and Sons, New York. 1967. p. 571.
41. R. C. LORD and G. L. THOMAS, JR. Spectrochim. Acta Part A, **23A**, 2551 (1967).
42. A. LAUTIÉ and A. NOVAK. J. Chimie Phys. Phys. Chim. Biol. **71**, 415 (1974); **65**, 1359 (1968); **68**, 1492 (1971).
43. C. P. BEETZ, JR. and G. ASCARELLI. Spectrochim. Acta Part A, **36A**, 299 (1980).
44. R. SAVOIE, D. POIRIER, L. PRIZANT, and A. L. BEAUCHAMP. J. Raman Spectrosc. **11**, 481 (1981).
45. R. SAVOIE, J.-J. JUTIER, L. PRIZANT, and A. L. BEAUCHAMP. Spectrochim. Acta Part A, **38A**, 561 (1982).
46. J. C. CONNOLLY and H. LINSCHITZ. J. Heterocyclic Chem. **9**, 379 (1972).
47. J. R. LACHER, J. L. BITNER, D. J. EMERY, M. E. SEFFL, and J. D. PARK. J. Phys. Chem. **59**, 615 (1955).
48. H. P. FRITZ. Chem. Ber. **92**, 780 (1959).
49. H. P. FRITZ and R. SCHNEIDER. Chem. Ber. **93**, 1171 (1960).
50. W. S. SHELDRICK. Z. Naturforsch. B: Anorg. Chem. Org. Chem. **37B**, 653 (1982).
51. W. S. SHELDRICK. Acta Crystallogr. Sect B: Struct. Crystallogr. Cryst. Chem. **B37**, 945 (1981).
52. P. I. VESTUES and E. SLETTEN. Inorg. Chim. Acta, **52**, 269 (1981).
53. D. J. HODGSON. Prog. Inorg. Chem. **23**, 211 (1977); L. G. MARZILLI, Prog. Inorg. Chem. **23**, 255 (1977).
54. H. PEZZANO and F. PODO. Chem. Rev. **5**, 365 (1980).
55. U. WESER. Struct. Bonding (Berlin), **80**, 41 (1968).
56. L. C. FRANCESCONI, D. R. CORBIN, A. W. CLAUSS, D. N. HENDRICKSON, and G. D. STUCKY. Inorg. Chem. **20**, 2059 (1981).
57. B. F. FIESELMANN, D. N. HENDRICKSON, and G. D. STUCKY. Inorg. Chem. **17**, 1841 (1978).
58. B. A. GOODMAN and J. B. RAYNOR. Adv. Inorg. Chem. Radiochem. **13**, 135 (1970).
59. L. STECHER KRAMER, A. W. CLAUSS, L. C. FRANCESCONI, D. R. CORBIN, D. N. HENDRICKSON, and G. D. STUCKY. Inorg. Chem. **20**, 2070 (1981).
60. B. F. FIESELMANN, D. N. HENDRICKSON, and G. D. STUCKY. Inorg. Chem. **17**, 2078 (1978).
61. L. C. FRANCESCONI, D. R. CORBIN, A. W. CLAUSS, D. N. HENDRICKSON, and G. D. STUCKY. Inorg. Chem. **20**, 2078 (1981).

A study of lone-pair interactions of tetracyclic diamines by ultraviolet photoelectron spectroscopy

NICK HENRY WERSTIUK[1]
Department of Chemistry, McMaster University, Hamilton, Ont., Canada L8S 4M1

AND

DOUGLAS NEVE BUTLER AND SUSHIL DATTA
Department of Chemistry, York University, Downsview, Ont., Canada M3J 1P3

Received September 23, 1985

NICK HENRY WERSTIUK, DOUGLAS NEVE BUTLER, and SUSHIL DATTA. Can. J. Chem. **64**, 760 (1986).

The ultraviolet photoelectron spectra of 2,7-diazatetracyclo[3.3.3.0.^{4,9}0.^{8,11}]undecane (**1**) and its *N,N*-dimethyl- and methylene-bridged analogues **2** and **3** are documented. The spectrum of **2**, which exhibits a nitrogen lone-pair splitting of 0.95 ± 0.1 eV, is interpreted on the basis of an interaction of "inside" lone pairs of the 1,2-diamine. Apparently this is the first report of a study of such an interaction. The spectrum of **1** is consistent with our view that **1** is an intramolecularly hydrogen bonded species in which the lone pairs are "inside–outside".

NICK HENRY WERSTIUK, DOUGLAS NEVE BUTLER et SUSHIL DATTA. Can. J. Chem. **64**, 760 (1986).

On a mesuré les spectres photoélectroniques ultraviolets du diaza-2,7 tétracyclo[3.3.0.^{4,9}0.^{8,11}]undécane (**1**) et de ses analogues *N,N*-diméthylé (**2**) ou portant un pont méthylénique (**3**). Le spectre du composé **2** présente un couplage de la paire d'électrons libres de l'azote de 0,95 ± 0,1 eV que l'on interprète sur la base d'une interaction des paires d'électrons "internes" de la diamine-1,2. Le spectre du composé **1** est en accord avec notre hypothèse selon laquelle ce composé est une espèce qui possède des liaisons hydrogènes intramoléculaires dans lesquelles les paires libres sont du type "intérieur–extérieur".

[Traduit par la revue]

Introduction

Over the past fifteen years, studies of nitrogen, oxygen, and sulfur compounds by ultraviolet photoelectron spectroscopy have yielded a wealth of information on the factors that determine the magnitudes of through-space and through-bond interactions of lone pairs. Studies of diamines have been especially fruitful (1). In a significant paper in 1970, Heilbronner and Muszkat (2) confirmed early EH and MINDO/2 calculations that predicted significant interaction between the nitrogen lone pairs of 1,4-diazabicyclo[2.2.2]octane. They established that the lone-pair splitting was 2.13 eV, that n^+ was higher in energy than n^-, and thereby that interaction of the lone pairs occurred predominately through the ethano bridges. Subsequently, Nelsen and Buschek (3) studied 1,5-diazabicyclo[3.2.2]nonane, 1,5-diazabicyclo[3.2.1]octane (**7**), 1,5-diazabicyclo[3.3.1]nonane (**8**), and several piperazines and hexahydropyrimidines to evaluate through-space and through-bond interactions. They conclude that the magnitudes of the splittings of 1,1- and 1,2-diamines depend on the spatial orientation of the lone pairs, as shown in Fig. 1. More recently, Alder *et al.* (4), in a significant paper, described the effects of ring strain and three-electron σ-bonding on the ionization energies of bicyclic diamines.

In this paper we document and discuss the photoelectron spectra of 2,7-diazatetracyclo[3.3.3.0.^{4,9}0.^{8,11}]undecane (**1**) and its *N,N*-dimethyl- and methylene-bridged analogues **2** and **3**, the syntheses of which will be reported in a following publication. Diamine **2** provides an unique opportunity to investigate previously unknown (1) through-space interactions between the "inside" lone pairs of an alicyclic 1,2-diamine and **3** (essentially the "outside" analog of **2**). Diamine **1**, which is a stronger proton sponge[2] than 1,8-diaminonaphthalenes (1), provides an opportunity to study a rigid intramolecularly hydrogen-bonded 1,2-diamine.

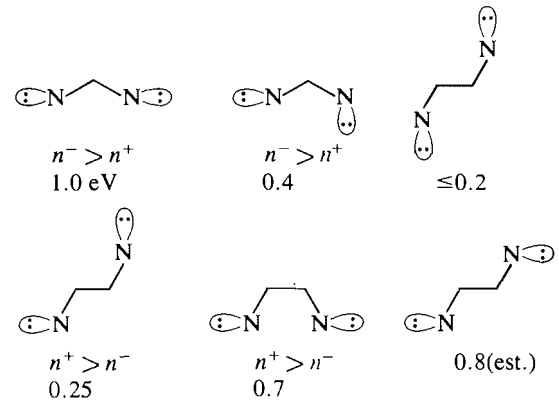

FIG. 1. Magnitudes of lone-pair splittings of 1,1- and 1,2-diamines as a function of spatial orientation.

Results

The photoelectron spectra of **1**, **2**, and **3** are given in Figs. 2(A), (B), and (C), respectively. The maxima of the lone pair IPs (ionization potentials) are taken as the vertical IPs, and splittings are listed in Table 1. Substantial splittings are observed for the diamines, and the lone-pair IPs of **2** are unusually low.

Aspects of the structures of diamines 1 and 2

Although the lone pairs of **3** are fixed, three limiting configurations are possible for **1** and **2**: **1**-i,i and **2**-i,i (i = in, o = out); **1**-i,o and **2**-i,o: **1**-o,o and **2**-o,o.

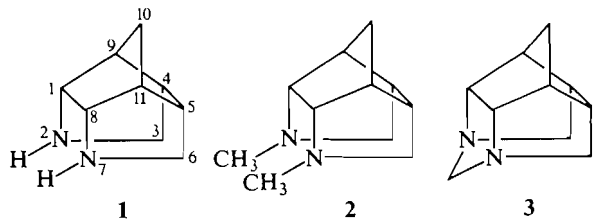

[1]Author to whom correspondence may be addressed.
[2]D. N. Butler, unpublished results.

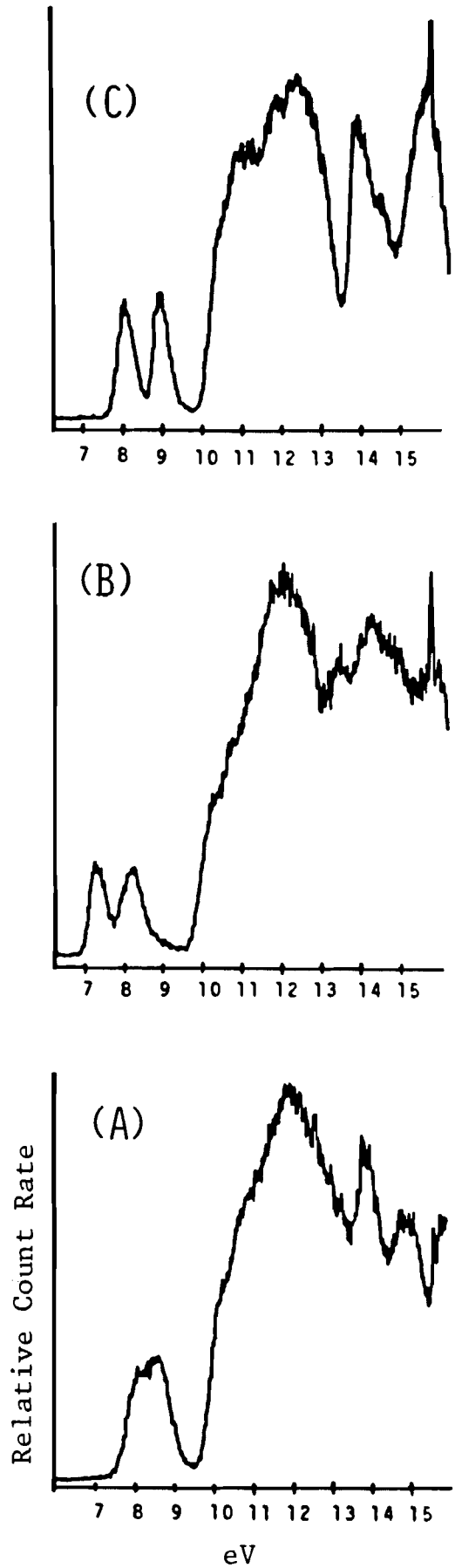

FIG. 2. (A) Photoelectron spectrum of diamine **1**; (B) photoelectron spectrum of diamine **2**; (C) photoelectron spectrum of diamine **3**.

TABLE 1. Ionization potentials and splittings of diamines

Diamine	IP^1_{max} (eV)	IP^2_{max} (eV)	ΔIP (eV)
1	8.20 ± 0.05 (n^-)	8.80 ± 0.05 (n^+)	0.6 ± 0.1[a]
2	7.29 ± 0.05 (n^-)	8.24 ± 0.05 (n^+)	0.95 ± 0.1
3	8.05 ± 0.05 (n^-)	9.00 ± 0.05 (n^+)	0.95 ± 0.1

[a]Estimated from the sum of two Gaussian peaks.

Although amine-to-amine hydrogen bonding is weak, it is expected that **1** is intramolecularly hydrogen bonded and the **1**-i,o is the most stable configuration. That partially alkylated 1,8-diaminonaphthalene **4** adopts a conformation with a N—H:N

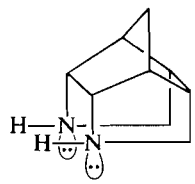

1-i,o

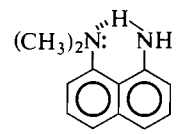

4

hydrogen bond (1), but 1,8-bis(dimethylamino)naphthalene is forced to adopt a structure with some lone-pair interaction, supports this expectation (6). While hydrogen bonding would provide a stabilization of approximately 10–15 kJ mol^{-1}, a further stabilization would result from a decrease of the lone-pair repulsion because the lone pairs would be directed away from each other. Our view that **1** is intramolecularly hydrogen bonded is further supported by the work of Vogel and Günther *et al.* (7). They established conclusively that *syn*-1,6:8,13-13-diimino[14]annulene (**5**) is intramolecularly hydrogen bonded and the $\Delta H\ddagger$ and $\Delta S\ddagger$ for inversion at nitrogen (**5***a* ⇄ **5***b*) are 26.1 kJ mol^{-1} and −76.5 J mol^{-1} K^{-1}, respectively. This was corroborated recently by a determination of the crystal and molecular structures of **5** (8).

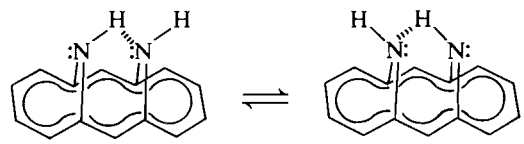

5*a* **5***b*

From models it is clear that **2**-o,o, with the nitrogens pyramidal, would be impossibly strained due to the steric interaction of the methyl groups. Similarly, in the case of **2**-i,o, if both nitrogens are sp^3-like, models show that there is severe crowding of the inside lone pair and the hydrogens of the methyl group. Furthermore, the stereoisomer in which the nitrogens are constrained to the triangular planar (sp^2 hybridized) would also be a high energy species due to angle strain and repulsion of the lone pairs that would be directed towards each other. Consequently, we expect that **2**-i,i with the nitrogens pyramidal is the most stable stereoisomer of the *N*,*N*-dimethyldiamine. In keeping with this expectation, the ^{13}Cmr of **2** exhibits only six

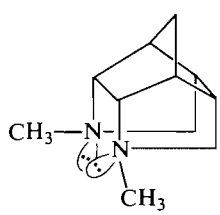

2-i,i

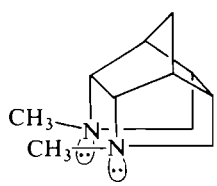

2-i,o

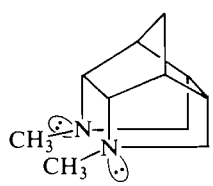

2-o,o

resonances: 67.9 ppm (C-1,C-8), 55.3 (C-3,C-6), 45.4 (CH_3), 42.9 (C-9,C-11), 41.3 (C-4,C-5), and 28.1 (C-10). Furthermore, the ^{13}Cmr spectrum obtained at −70°C showed no significant change relative to that obtained at ambient temperature. One aspect of the spectrum of **2** deserves comment. Unlike C-2- and C-3-*endo*-substituted bicyclo[2.2.1]heptanes that exhibit C-7 resonances at 35–40 ppm (5), C-10 of **2** appears at 28.1. In this connection, it is interesting to note that C-7 of quadricyclene appears at 32 ppm (5). Apparently the upfield shift is associated with bridging between C-2,C-6 and C-3,C-5. Although ^{13}Cmr results are consistent with our proposal that **2**-i,i is the stable isomer, **2**-i,o presumably would also exhibit six signals if inversion involving a "windshield-wiper" motion was rapid on the nmr time scale. Our expectation that **2**-i,i is the stable configuration of the *N,N*-dimethyl analogue of **1** is also supported by the work of Simonetta and co-workers (8). They established by X-ray diffraction that the *N,N*-dimethyl analogue of **5** has both *N*-methyl groups pointing outward.

Discussion and conclusions

The low values of the IPs for the lone pairs of **2** (7.29 and 8.24 eV; $\Delta IP = 0.95$ eV) are in keeping with our proposal that **2**-i,i is the most stable configuration of the *N,N*-dimethyldiamine. In fact, the onset of the low IP band is at 6.9 eV. By comparison, the IP of the "lone-pair" band in the PE spectrum of *N*-methylpyrrolidine is 8.41 eV (9). In the case of **2**-i,i, n^- should be higher in energy than n^+ and the IPs should be low because of the proximity of the lone pairs. The shift to lower binding energies in the case of **2** is similar to, but not as dramatic as, the shift observed for the "inside" lone pairs of 1,6-diazabicyclo[4.4.4]tetradecane (**6**) studied by Alder *et al.* (4). The authors (4) estimated the N...N distance in **6**-i,i (IPs 6.64 and

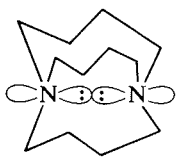

6-i,i

7.77 eV; $\Delta IP = 1.13$ eV), the most stable isomer of the diamine, to be 2.61 Å by a force field calculation.

In the case of **2**-i,i, models show that the N...N distance is slightly greater than the N...N distance of **6**-i,i but, more importantly, that the lone pair orbitals are not directed towards each other. Assuming that the N atoms are sp^3 hybridized, the angle between the lone pairs is approximately 70° (Fig. 3). These factors would account for the fact that the shift to lower binding energies is not as large as it is in the case of **6**-i,i and also that the splitting referred to is smaller as well.

In the case of **3**, the binding energies (8.05 and 9.00 eV) are essentially normal for a tertiary amine (*vide supra*). This fact provides additional support for our view that **2** has the i,i configuration. For **3** we propose that $n^- > n^+$, in keeping with Nelsen and Buschek's assignment for **7** (3). It is interesting to note that the splitting of 0.95 eV is somewhat larger than the splitting (0.75 eV) observed for **7** by Nelsen and Buschek. It may be that the back-lobes of the lone pair orbitals of **3** are slightly better aligned than they are in **7**. In the case of **8**, where the orbitals are exactly directed towards each other, the splitting is 1.03 eV.

For the parent diamine, if **1**-i,i is the most stable configuration, the ordering should be $n^- > n^+$ and the splitting, based on

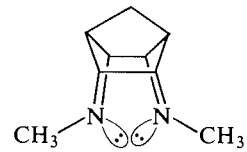

FIG. 3. Proposed structure of diamine **2**-i,i.

2-i,i, should be in the range of 0.95 eV. If, as expected, the diamine is intramolecularly hydrogen bonded, then n^- should be stabilized and n^+ destabilized or remain unaffected because the lone-pair interaction is decreased (Fig. 4). Since hydrogen bonding to nitrogen increases the lone-pair ionization energy, as established by Brown (10, 11), it is conceivable that hydrogen bonding to n^- also leads to a stabilization of n^-. Consequently,

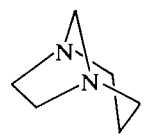

7

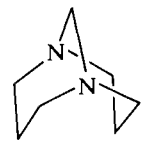

8

the splitting for **1**-i,o should be smaller than the splitting for **2**-i,i. In fact, this is observed experimentally—we estimate that the splitting for **1** is approximately 0.6 eV.

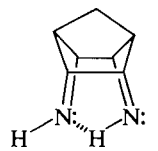

FIG. 4. Proposed structure of diamine **1**-i,o.

Experimental

The He(I) photoelectron spectra were obtained with a noncommercial instrument constructed from the design of Frost *et al.* (12) and based on a 10-cm diameter aluminum hemispherical electrostatic energy analyser. The photoelectrons are retarded and focussed onto a rectangular entrance slit (0.5 × 2 mm) by a suitable lens. He(I) photons were generated by an air-cooled DC discharge lamp operated at 1.3 kV. With this lamp the typical count rate on Ar $^2P_{3/2}$ is 100 000 Hz with a 40-meV fwhm. The spectra represent averages of 15–20 scans collected using an APPLE II+/ISAAC system that controls the spectrometer operations and data collection.

Diamines **1**, **2**, and **3**, whose syntheses will be reported in a following publication, exhibited ^{1}Hmr, ^{13}Cmr, and mass spectrometric spectral data consistent with the proposed structures, including, of course, the photoelectron spectra.

Acknowledgements

The authors thank the Natural Sciences and Engineering Research Council of Canada for financial support. Fruitful discussions with Professor S. Brown are gratefully acknowledged. N.H.W. wishes to thank Mr. F. Ramelan for invaluable assistance in constructing the photoelectron spectrometer at McMaster.

1. R. W. ALDER and R. B. SESSIONS. *In* The chemistry of amino, nitroso and nitro compounds. *Edited by* S. Patai. J. Wiley, New York. 1982. Chapt. 18.
2. E. HEIBRONNER and K. A. MUSZKAT. J. Am. Chem. Soc. **92**, 3818 (1970).
3. S. F. NELSEN and J. M. BUSCHEK. J. Am. Chem. Soc. **96**, 7930 (1974).

4. R. W. ALDER, R. J. ARROWSMITH, A. CASSON, R. B. SESSIONS, E. HEILBRONNER, B. KOVAC, H. HUBER, and M. TAAGEPERA. J. Am. Chem. Soc. **103**, 6137 (1981).
5. G. C. LEVY and G. L. NELSON. *In* Carbon-13 nuclear magnetic resonance for organic chemists. Wiley–Interscience, New York, 1972. pp. 46 and 48.
6. H. EINSPAHR, J.-B. ROBERT, R. F. MAISH, and J. D. ROBERTS. Acta Crystallogr. Sect. B, **29**, 1611 (1973).
7. E. VOGEL, F. KUEBART, J. A. MARCO, R. ANDREE, H. GÜNTHER, and R. AYDIN. J. Am. Chem. Soc. **105**, 6983 (1983).
8. R. DESTRO, T. PILATI, M. SIMONETTA, and E. VOGEL. J. Am. Chem. Soc. **107**, 3185 (1985).
9. D. H. AUE, H. M. WEBB, and M. T. BOWERS. J. Am. Chem. Soc. **98**, 311 (1976).
10. R. S. BROWN. Can. J. Chem. **54**, 642 (1976).
11. R. S. BROWN. Can. J. Chem. **54**, 1926 (1976).
12. D. C. FROST, S. F. LEE, C. A. MCDOWELL, and N. P. C. WESTWOOD. J. Electron Spectrosc. Relat. Phenom. **12**, 95 (1977).

Is the collision induced loss of ethene from the $(M - H^+)^-$ ion of butyrophenone a γ-hydrogen rearrangement?

MICHAEL B. STRINGER, DENNIS J. UNDERWOOD, AND JOHN H. BOWIE[1]
Department of Organic Chemistry, University of Adelaide, South Australia, 5001, Australia

AND

JOHN L. HOLMES,[1] ALEXANDER A. MOMMERS, AND JAN E. SZULEJKO
Department of Chemistry, University of Ottawa, Ottawa, Ont., Canada K1N 9B4

Received September 16, 1985

MICHAEL B. STRINGER, DENNIS J. UNDERWOOD, JOHN H. BOWIE, JOHN L. HOLMES, ALEXANDER A. MOMMERS, and JAN E. SZULEJKO. Can. J. Chem. **64**, 764 (1986).

The $(M - H^+)^-$ ion of butyrophenone undergoes the following reactions on collisional activation: losses of $CH_3^{\bullet}$, CH_4, $(C,H_5^{\bullet})$, C_2H_4, $C_3H_7^{\bullet}$, $(CO + CH_4)$, together with formation of $C_6H_5^-$ and $C_4H_5O^-$. Labelling studies (^{13}C and ^2H) show that the losses of $CH_3^{\bullet}$, $C_3H_7^{\bullet}$ and the formation of $C_6H_5^-$ and $C_4H_5O^-$ are specific and occur without hydrogen scrambling. All other reactions involve prior or accompanying hydrogen rearrangement. In particular, the loss of C_2H_4 is very complex: it involves loss of ethyl carbon atoms, but *all* hydrogen atoms are involved via specific rearrangement reactions. The phenyl–alkyl H rearrangements which are noted for this process occur *after* collisional activation of the $(M - H^+)^-$ ion.

MICHAEL B. STRINGER, DENNIS J. UNDERWOOD, JOHN H. BOWIE, JOHN L. HOLMES, ALEXANDER A. MOMMERS et JAN E. SZULEJKO. Can. J. Chem. **64**, 764 (1986).

Sous l'influence d'une activation par collision, l'ion $(M - H^+)^-$ de la butyrophénone subit les réactions suivantes: pertes de $CH_3^{\bullet}$, de CH_4, de $(C,H_5^{\bullet})$, de C_2H_4, $C_3H_7^{\bullet}$, de $(CO + CH_4)$ avec formation de $C_6H_5^-$ et de $C_4H_5O^-$. Des études de marquage (^{13}C et ^2H) ont démontré que les pertes de $CH_3^{\bullet}$ et de $C_3H_7^{\bullet}$ ainsi que les formations de $C_6H_5^-$ et de $C_4H_5O^-$ sont spécifiques et qu'elles se produisent sans redistribution des hydrogènes. Toutes les autres réactions impliquent des transpositions d'hydrogènes qui se produisent avant ou d'une façon concomitante avec les réactions. En particulier, la perte de C_2H_4 est très complexe: elle implique la perte des atomes de carbone de l'éthyle, mais *tous* les atomes d'hydrogène sont impliqués par le biais de réactions de transpositions spécifiques. Les transpositions des H des phényle–alkyle qui sont notées pour ce processus se produisent *après* l'activation par collision de l'ion $(M - H^+)^-$.

[Traduit par la revue]

Introduction

In the past decade there have been significant advances in the analytical applications of negative ion mass spectrometry, for example in the areas of electron capture, negative ion chemical ionization, secondary ion mass spectrometry, and fast atom bombardment (1). These "soft ionization" techniques often give molecular weight information, but in many cases fragment negative ions that in principle could yield structural information are absent in the spectra. Collision induced dissociations of negative ions can give structural information (1, 2); in addition, fundamental information concerning ion behaviour may be obtained by such studies (1, 3).

Hunt *et al.* have studied the collisional activation mass spectra of a variety of $(M - H^+)^-$ ions derived from ketones (4, 5). They have suggested (4) that the rearrangement peaks observed for dialkyl ketones may be explained by the γ-hydrogen rearrangements and olefin eliminations shown in Scheme 1. Deprotonation may occur at two positions in such systems and it is thus difficult to be certain which is the decomposing carbanion. In this paper we report the decompositions of the collisionally activated $(M - H^+)^-$ ion of butyrophenone. We chose this system for three reasons: (*i*) it should only deprotonate from one position to yield one initial carbanion; (*ii*) butyrophenone is relatively easy to label with ^2H and ^{13}C; and (*iii*) it is unable to undergo the type of γ-hydrogen rearrangement proposed by Hunt *et al.* (4) (see Scheme 1).

Results and discussion

All collisional activation (CA) mass spectra (6) were measured with a VG ZAB 2F mass spectrometer (7) operating at 70 eV in the negative chemical ionization mode. Water was used to produce HO^- reactant ions (8), and helium was used as the collision gas.

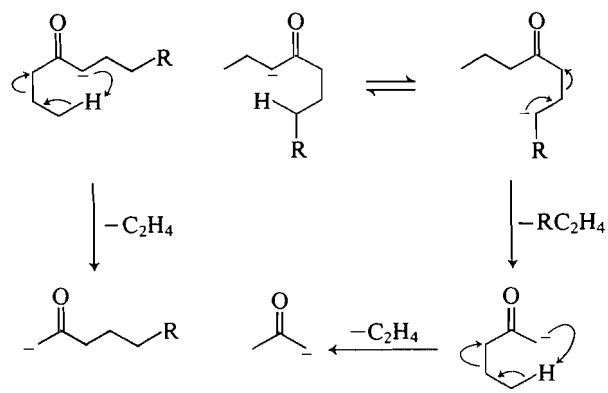

SCHEME 1

Details are provided in the experimental section.

The CA mass spectrum of the $(M - H^+)^-$ ion of butyrophenone is shown in Fig. 1. In order to determine the atoms involved in the fragmentations shown in Fig. 1, the corresponding spectra of the labelled compounds **2**–**9** were studied. Certain of the fragmentations are straightforward, others occur with or after extensive hydrogen scrambling. Let us deal first with some of the simpler fragmentations. The phenyl negative ion (m/z 77) is formed by simple cleavage, and this may be rationalized as shown in sequence [1]. The second *specific* reaction is that which produces $C_4H_5O^-$ (m/z 69). This ion is formed by loss of C_6H_6 (reaction [2]). The peak at m/z 69

[1]Authors to whom correspondence may be addressed.

Printed in Canada / Imprimé au Canada

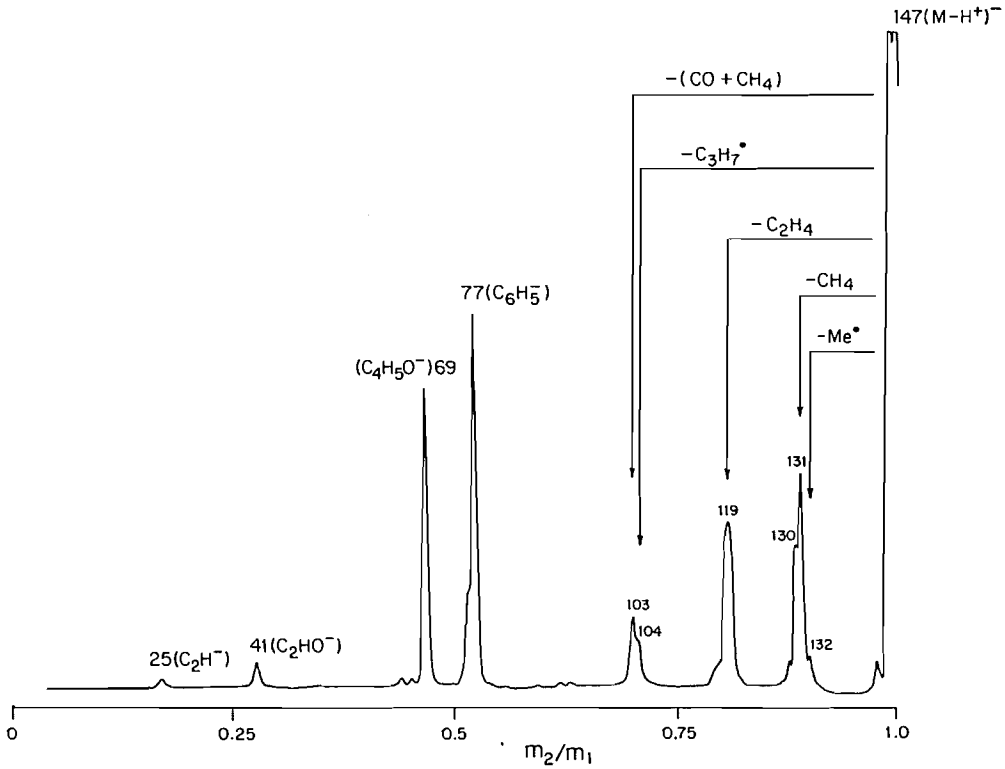

FIG. 1. The CA mass spectrum of the $(M-H^+)^-$ ion of butyrophenone. For full details see experimental section.

$PhCOCH_2CH_2CH_3$	**1**	$C_6D_5COCH_2CH_2CH_3$	**6**
$Ph^{13}COCH_2CH_2CH_3$	**2**	$PhCOCD_2CH_2CH_3$	**7**
$PhCOCH_2{}^{13}CH_2CH_3$	**3**	$PhCOCH_2CD_2CH_3$	**8**
$PhCOCH_2CH_2{}^{13}CH_3$	**4**	$PhCOCH_2CH_2CD_3$	**9**

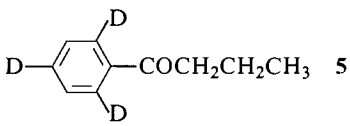

5

(Fig. 1) has a width at half height of 40 V, a value that corresponds to a small kinetic energy release, 0.050 V.

The losses of $CH_3^\bullet$, CH_4, and $C,H_5^\bullet$ (see Fig. 1) are complex and the appropriate relative peak abundances for ions derived from compounds **2**–**9** are listed in Table 1. From these figures

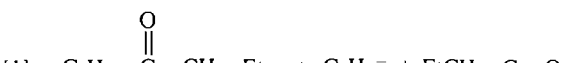

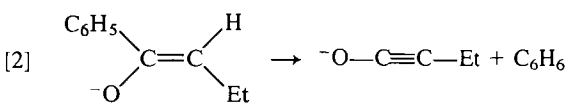

we may make the following observations. The loss of $CH_3^\bullet$ occurs exclusively from the terminal methyl group; neither carbon nor hydrogen scrambling precedes or accompanies this reaction (sequence [3]). Elimination of CH_4 involves the terminal methyl group together with a hydrogen atom from the phenyl ring. The CA mass spectrum of the $(M-H^+)^-$ ion of the ring d_3 derivative (**5**) shows that partial ring hydrogen scrambling precedes or accompanies the loss of the fourth hydrogen; further H/D mixing must be responsible for loss of 16 amu from **6**. This reaction is best rationalized by the first step of sequence [4]. The loss of the fifth hydrogen occurs primarily from the

TABLE 1. The losses of $CH_3^\bullet$, CH_4, and $C,H_5^\bullet$ (and labelled analogues)

	Loss					
Compound	−15	−16	−17	−18	−19	−20
1	8	54	33	6		
2	10	51	33	6		
3	13	48	31	8		
4		10	52	38	3	
5	6	39	33	18		
6	6	13	59	16	5	
7	10	49	25	15	2	
8	3	66	12	12	4	
9				11	51	38

position shown in the second stage of sequence [4]. The structures shown in sequence [4] are speculative: they are used solely to illustrate the two processes.

The peaks at m/z 103 and 104 in Fig. 1 are produced by the respective losses (CH_4+CO) and $C_3H_7^\bullet$. The relative peak abundances in this region are summarized in Table 2 for ions derived from compounds **1**–**9**. The loss of (CH_4+CO) follows precisely the first step of sequence [4], with additional loss of

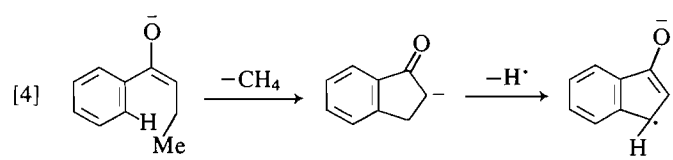

TABLE 2. The losses of (CH_4 + CO) and ($C_3H_7^{\bullet}$) and labelled analogues

	Compound								
Loss	**1**	**2**	**3**	**4**	**5**	**6**	**7**	**8**	**9**
−43	45	45			3	<1		<1	
−44	55	100	100	46	60	60	100	70	
−45		55		54	40	40		30	
−46					7	<2		1	40
−47									60

the original carbonyl group (of butyrophenone). The elimination of $C_3H_7^{\bullet}$ involves C_3H_6 from the side chain together with one phenyl hydrogen. The CA mass spectrum of the ring d_3 derivative (**5**) shows almost exclusive loss of $C_3H_6D^{\bullet}$; only a 3% peak corresponding to loss of $C_3H_7^{\bullet}$ is observed. We proposed an almost specific elimination of an *ortho*-hydrogen as shown in sequence [5].

[5] 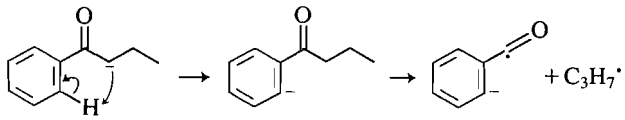

Our major interest in the CA mass spectrum shown in Fig. 1 concerns the loss of C_2H_4. Is this elimination a four-centre process [6], a six-centre reaction [7], or some more complex rearrangement?

[6] 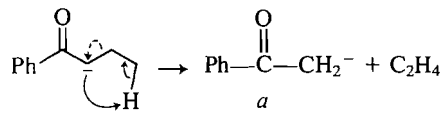

a

[7] 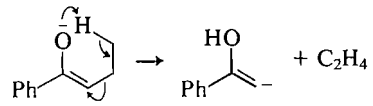

b

The first task was to determine whether the product ion of the reaction corresponds to *a* (sequence [6]) or *b* (sequence [7]). Thus we compared both the CA mass spectra and the charge inversion spectra (9) of *m/z* 119 and the $(M-H^+)^-$ ion of acetophenone (see Table 3). *Each pair of spectra are identical.* In particular, the charge inversion mass spectrum contains an ion corresponding to the process *m/z* 119 − CH_2, indicating the presence of a methylene group in the precursor negative ion. Thus we believe the product ion *m/z* 119 in Fig. 1 corresponds to the keto negative ion *a*. Whether it is formed directly (sequence [6]) or indirectly through *b* (sequence [7]) is not clear at this stage.

The collision-induced elimination of C_2H_4 from the butyrophenone $(M-H^+)^-$ ion produces a peak that shows no fine structure, is steep sided with a rounded top, and is unusually wide. The width of the peak of half height is 94 V (cf. the Gaussian type peak 40 V wide for reaction [2]), corresponding to a kinetic energy release of 0.44 eV. This is in keeping with a reaction having a reverse energy barrier.

The relative abundances of peaks arising from losses of ethene and deuteriated ethene from the $(M-H^+)^-$ (or $(M-D^+)^-$ where appropriate) negative ions from compounds **5**–**9** are summarized in Table 4. The corresponding spectra of the ^{13}C labelled compounds **3** and **4** show that the carbon atoms

TABLE 3. Collisional activation (CA) mass spectrum and charge exchange mass spectrum of ion $C_6H_5COCH_2^-$ from acetophenone

CA fragment anions (*m/z* (%) composition):
118(100) $C_8H_6O^{-\bullet}$, 101(2) $C_8H_5^-$, 89(2) $C_7H_5^-$, 77(40) $C_6H_5^-$, 64(2) $C_5H_4^{-\bullet}$, 41(40) C_2HO^-, and 25(1) C_2H^-

Charge exchange fragment cations (*m/z* (%) composition):
105(23) $C_7H_5O^+$, 103(28) $C_7H_3O^+$ or $C_8H_7^+$, 102(25) $C_7H_2O^+$ or $C_8H_6^+$, 91(49) $C_7H_7^+$, 89(28) $C_7H_5^+$, 77(100) $C_6H_5^+$, 75(12) $C_6H_3^+$, 65(26) $C_5H_5^+$, 63(18) $C_5H_3^+$, 51(31) $C_4H_3^+$, 50(31) $C_4H_2^{+\bullet}$, 41(7) $C_3H_5^+$ or C_2HO^+ and 39(13) $C_3H_3^+$

TABLE 4. Summary of ethene loss

Compound		Relative abundances
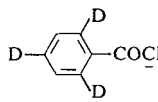	(**5**)	C_2H_4(80):C_2H_3D (20)
C_6D_5COCH Et	(**6**)	C_2H_4(65):C_2H_3D (35)
PhCOCD Et	(**7**)	C_2H_4(73):C_2H_3D (27)
$PhCOCHCD_2Me$	(**8**)	C_2H_4(3):C_2H_3D (26):$C_2H_2D_2$ (71)
$PhCOCHCH_2CD_3$	(**9**)	C_2H_3D(3):$C_2H_2D_2$ (59):C_2HD_3 (38)

eliminated are exclusively those of the terminal ethyl group. *No carbon scrambling accompanies the elimination of C_2H_4.* In marked contrast, *a number of specific hydrogen rearrangements precede or accompany the loss of C_2H_4.*

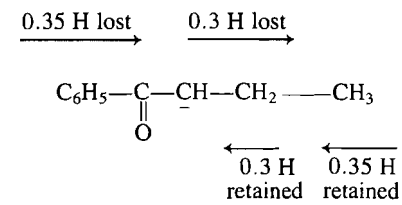

10

The data in Table 4 can be simplified as shown above in representation (**10**). Within experimental error, 0.65 of a hydrogen atom is transferred out of the ethyl substituent and is retained in the product ion while 0.65 of a hydrogen atom is transferred into the ethyl group and lost when ethene is eliminated. We propose the mechanisms in Scheme 2 in order to rationalize the experimental observations. The observation that the ion from **7** eliminates 27% of C_2H_3D (see Table 4) demands that there be a transfer of the remaining deuterium into the terminal ethyl substituent. We propose equilibrium *c* ⇄ *e* to account for this transfer. A comparison of the decomposition of the ions from **5** and **6** (Table 4) shows that ring hydrogens are involved in part *and that statistical ring hydrogen scrambling is co-occurring with aryl H transfer*. Either of the equilibria *c* ⇄ *g* or *d* ⇄ *h* together with *h* ⇄ *i* could account for the involvement of aryl hydrogen. Finally, a comparison of the losses of variously labelled ethenes from the $(M-H^+)^-$ ions from **8** and **9** shows that partial scrambling of the ethyl hydrogens also occurs. This could occur through either *e* or *f*: we prefer the equilibrium *f* ⇄ *i* because it involves the allylic species *i*. The mechanisms shown in Scheme 2 are speculative but they fit the experimental observations in a qualitative sense.

We believe that of the two possible decomposing intermediates, *e* and *f*, *e* is the more likely and that it decomposes

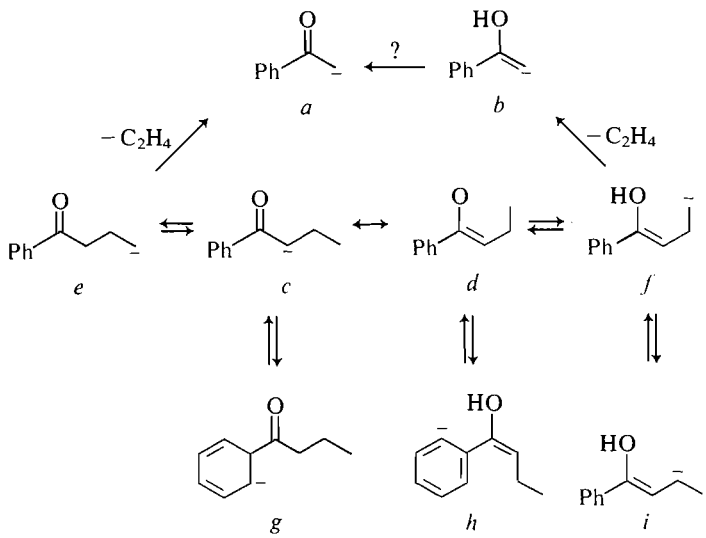

SCHEME 2

to *a* directly. It was explained above that the product ion corresponds to *a*; however, the possibility that some of *b* is formed from *f* and that *b* then tautomerizes to the more thermodynamically stable species *a* cannot be excluded.

There are few examples of hydrogen rearrangements in the *unimolecular* reactions of negative ions (1); e.g., aryl H scrambling is the exception (10) rather than the rule (1). The complex aryl–alkyl H rearrangements that occur in the CA mass spectrum of the butyrophenone $(M-H^+)^-$ ion have no prior analogy. Therefore it is of interest to determine whether these rearrangements occur in the negative ion *before or after* the collisional activation process. We cannot determine this for the aryl H scrambling, but the following experiment answers the question for aryl–alkyl H rearrangements. The charge inversion spectrum of the $(M-H^+)^-$ ion of 2,4,6-$^2H_3$-butyrophenone (**5**) shows two major peaks. These correspond to $C_6H_2D_3$—$C{\equiv}O^+$ (*m/z* 108) and $C_6H_2D_3^+$ (*m/z* 80). There is no evidence in the spectrum for the formation of ions $C_6H_3D_2$—$C{\equiv}O^+$ (*m/z* 107) or $C_6H_3D_2^+$ (*m/z* 79). Thus, even though the two experiments may not sample identical populations of ions, the results show that the aryl–alkyl H rearrangements observed for the CA mass spectrum are processes that occur *after* collisional activation of the $(M-H^+)^-$ ion.

Conclusions

The collision-induced fragmentations of the $(M-H^+)^-$ ion of butyrophenone provide interesting examples of differing decomposition time scales. Simple cleavages are fast (e.g., reactions [1] and [3]) and occur without any rearrangement of the side chain. Some rearrangement reactions are also fast: for example the loss of C_6H_6 (reaction [6]) occurs without hydrogen rearrangement in the side chain; elimination of $C_3H_7^\bullet$ (reaction [5]) is also fast since virtually no phenyl H scrambling is observed. All reactions involving loss of CH_4 co-occur with partial phenyl hydrogen scrambling. The loss of C_2H_4 is the slowest rearrangement; complete phenyl hydrogen randomization precedes or accompanies this reaction.

Experimental

Collisional activation mass spectra (7) and charge inversion spectra of negative ions (11) were recorded with a MM VG ZAB 2F spectrometer operating under the following conditions: negative ion chemical ionization mode, reactant ion HO^- formed from water (for full details see ref. 11), electron energy 70 eV, measured pressure of collision gas (He) in second field-free region collision cell 1.5 × 10^{-7} Torr (1 Torr = 133.3 Pa). The ion acceleration voltage was 8000 V.

The ^{13}C labelled 1-phenyl-1-butanones 2–4

1-(^{13}C)-1-phenyl-1-butanone (**2**), 3-(^{13}C)-1-phenyl-1-butanone (**3**), and 4-(^{13}C)-1-phenyl-1-butanone (**4**) were prepared in 60, 63, and 65% yield respectively by the following method. The labelled precursors 1-(^{13}C)-1-phenyl-1-ethanone (91.8% ^{13}C), 1-(^{13}C)-iodoethane (91.1% ^{13}C), and 2-(^{13}C)-iodoethane (90.6% ^{13}C) were commercial products.

Acetophenone was converted (in quantitative yield) to acetophenone dimethylhydrazone by a standard method (12). The hydrazone was allowed to react with lithium diisopropylamide (from butyllithium and diisopropylamine in tetrahydrofuran) by the method of Corey and Enders (13) to produce α-lithiated acetophenone dimethylhydrazone, which in turn was treated with iodoethane to produce 1-phenyl-1-butanone dimethylhydrazone (14). Treatment with copper^{II} acetate (14) gave 1-phenyl-1-butanone, which was purified by preparative hplc (Spectra Physics Chromatronix 3500 instrument using a Lichrosorb S 160 column of 10-μ particle size and dimensions 250 mm × 10 mm). Overall yield from acetophenone was in the range 60–65%.

The ^2H labelled 1-phenyl-1-butanones 5–9

1-(2,4,6-$^2H_3$-phenyl)-1-butanone (**5**) and 1-($^2H_5$-phenyl)-1-butanone (**6**) were prepared in 40 and 49% yield respectively by the following method. The labelled precursors used were 2,4,6-$^2H_3$-bromobenzene (from 2,4,6-$^2H_3$-aniline (15) ($^2H_3$ > 98%) by a standard method (16)), and $^2H_5$-bromobenzene ($^2H_5$ > 99%), which was a commercial product.

Bromobenzene was allowed to react with lithium (in diethyl ether) to form a solution of phenyllithium. Butyllithium was added to butanoic acid (in diethylether) to give the lithium salt as a suspension. The two lithium derivatives were allowed to react by the method of Levine *et al.* (17) to produce 1-phenyl-1-butanone, which was purified by thick-layer chromatography on silica gel, followed by distillation. The overall yield (from bromobenzene) was in the range 40–50%.

3-($^2H_2$)-1-phenyl-1-butanone (**8**) and 4-($^2H_3$)-1-phenyl-1-butanone (**9**) were prepared (both in 74% yield) by the general method described above for the ^{13}C labelled compounds **2–4**, expect that 1-phenyl-1-butanone dimethylhydrazone was hydrolysed using a mixture of diethyl ether and 2 *M* hydrochloric acid for 3½ h at 25°C. The 1-phenyl-1-butanone was purified by thick-layer chromatography on silica gel, followed by distillation. The labelled precursors, 1-($^2H_2$)-iodoethane (>99% $2H_2$) and 2-($^2H_3$)-iodoethane (>99% $^2H_2$) were commercial products.

2-($^2H_2$)-1-phenyl-1-butanone (**7**, $^2H_3$ > 98%) was prepared by exchanging 1-phenyl-1-butanone twice in refluxing 2 *M* sodium hydroxide for 16 h.

Acknowledgements

The synthetic part of this work was carried out with the aid of a grant from the Australian Research Grants Scheme. M.B.S. thanks the A.R.G.S. for the award of a postdoctoral fellowship. J.L.H. thanks the Natural Sciences and Engineering Research Council of Canada for continuing financial support. J.L.H. thanks the University of Adelaide (South Australia) for a Distinguished Visiting Scholar Award, and J.H.B. thanks the Natural Sciences and Engineering Research Council of Canada for an International Scientific Exchange Award during the tenures of which this work was completed.

1. J. H. BOWIE. Mass Spectrom. Rev. **3**, 161 (1984).
2. J. H. BOWIE, T. BLUMENTHAL, M. H. LAFFER, S. JANPOSRI, and G. E. GREAM. Aust. J. Chem. **37**, 1447 (1984); J. H. BOWIE, M. B. STRINGER, F. DUUS, S.-O. LAWESSON, F. C. V. LARSSON, and J. Ø. MADSEN. Aust. J. Chem. **37**, 1619 (1984).

3. F. W. McLAFFERTY (*Editor*). Tandem mass spectrometry. Wiley–Interscience, New York. 1983.
4. D. F. HUNT, J. SHABANOWITZ, and A. B. GIORDANI. Anal. Chem. **82**, 386 (1980); Environ. Health Perspect. **36**, 33 (1980).
5. D. F. HUNT, A. B. GIORDANI, J. SHABANOWITZ, and G. RHODES. J. Org. Chem. **47**, 738 (1982).
6. K. R. JENNINGS. Int. J. Mass Spectrom. Ion Phys. **1**, 227 (1968); F. W. McLAFFERTY and H. D. R. SHUDDEMAGE. J. Am. Chem. Soc. **91**, 1866 (1969); J. H. BOWIE. J. Am. Chem. Soc. **95**, 5795 (1973).
7. J. K. TERLOUW, P. C. BURGERS, and H. HOMMES. Org. Mass Spectrom. **14**, 307 (1979).
8. D. K. BOHME, A. B. RAKSHIT, and G. I. MACKAY. J. Am. Chem. Soc. **104**, 1099 (1982).
9. J. H. BOWIE and T. BLUMENTHAL. J. Am. Chem. Soc. **97**, 2959 (1975); I. HOWE, J. H. BOWIE, J. E. SZULEJKO, and J. H. BEYNON. Int. J. Mass Spectrom. Ion Phys. **34**, 99 (1980).
10. J. H. BOWIE and B. NUSSEY. J. Chem. Soc. Chem. Commun. 17 (1970); Org. Mass Spectrom. **3**, 933 (1970).
11. P. C. BURGERS, J. L. HOLMES, A. A. MOMMERS, and J. E. SZULEJKO. J. Am. Chem. Soc. **106**, 521 (1984).
12. G. R. NEWKOME and D. L. FISHEL. J. Org. Chem. **31**, 677 (1966).
13. E. J. COREY and D. ENDERS. Tetrahedron Lett. 3 (1976).
14. E. J. COREY and S. KNAPP. Tetrahedron Lett. 3667 (1976).
15. A. P. BEST and C. L. WILSON. J. Chem. Soc. 241 (1946).
16. A. I. VOGEL. A textbook of practical organic chemistry. 3rd ed. Longman, London. 1970. p. 602.
17. R. LEVINE, M. J. KARTEN, and W. M. KADANCE. J. Org. Chem. **40**, 1770 (1975).

A comparison of electron spin resonance α- and β-hyperfine coupling constants in *para*-substituted α-phenethyl radicals[1]

DONALD R. ARNOLD,[2] A. MARTIN DE P. NICHOLAS, AND KENT M. YOUNG
Department of Chemistry, Dalhousie University, Halifax, N.S., Canada, B3H 4J3

Received August 14, 1985

DONALD R. ARNOLD, A. MARTIN DE P. NICHOLAS, and KENT M. YOUNG. Can. J. Chem. **64**, 769 (1986).

The linear relationship between the electron spin resonance hyperfine coupling constants (hfc) of the α- and β-hydrogens of *para*-substituted α-phenethyl radicals provides experimental evidence that the magnitude of both the α- and β-hfc is determined largely by the extent of spin delocalization in these benzylic systems. The $\sigma_\alpha^\bullet$ scale, developed using substituted benzyl radicals, is shown to apply to phenethyl radicals as well.

DONALD R. ARNOLD, A. MARTIN DE P. NICHOLAS et KENT M. YOUNG. Can. J. Chem. **64**, 769 (1986).

La relation linéaire qui existe entre les constantes de couplages hyperfins (chf) de la rpe des hydrogènes α et β radicaux α-phénéthyles substitués en *para* fournit une preuve expérimentale du fait que, dans ces systèmes benzyliques, l'amplitude des couplages hyperfins α ainsi que β est principalement déterminée par le degré de délocalisation du spin. On démontre que l'échelle $\sigma_\alpha^\bullet$, qui a été développée pour les radicaux benzyles substitués, s'applique aussi aux radicaux phénéthyles.

[Traduit par la revue]

Introduction

Theory predicts that both the α- and β-hydrogen hyperfine coupling constants (hfc) in the electron spin resonance (esr) spectra of a radical are proportional to the spin density (2). This applies in spite of the fact that the mechanism of coupling is different for the two positions, the main cause of coupling being due to spin polarization for hydrogens in the α position and hyperconjugation in the case of β-hydrogens. Experimental proof of this conclusion is scarce because other factors, such as deviation from planarity at the radical center, differences in conformation of the hydrogens at the β-carbon relative to the half-filled orbital, and direct interaction (i.e. bridging) of groups in this β position with the radical center, can also influence the hfc. It is difficult to vary the spin density at the radical center and yet keep these other factors constant.

A series of *para*-substituted α-phenethyl radicals is ideally suited to test this theory. In this case the nature of the radical center should remain constant, all these radicals should be essentially planar, there should be free rotation of the adjacent methyl group that bears the β-hydrogens, and there can be no direct interaction of the substituent with the radical center other than that which is transmitted through the phenyl ring. Therefore, if spin density is the dominant factor influencing both α- and β-hfc, the two values should correlate throughout the series.

We have proposed that the magnitude of the α-hfc of substituted benzyl radicals is a measure of spin delocalization in benzylic radicals (3). We believe the substituent effect on spin density, expressed as $\sigma_\alpha^\bullet$ values (eq. [1]) will be generally

$$[1] \quad \sigma_\alpha^\bullet = 1 - [(\alpha - \mathrm{hfc_X})/(\alpha - \mathrm{hfc_H})]$$

useful in Hammett-type linear free energy relationships for radical reactions. If the α- and β-hfc of substituted α-phenethyl radicals correlate, indicating that both are affected primarily by spin density, and if they both correlate with the effect of substituents on the α-hfc of the benzylic radicals, the conclusion that $\sigma_\alpha^\bullet$ reflects the variation in spin density caused by the substituent will be confirmed.

[1]This is Part 6 of the series, "Substituent effects on benzyl radical hydrogen hyperfine coupling constants" (Part 5, see ref. 1).

[2]Author to whom correspondence should be addressed.

TABLE 1. Electron spin resonance hyperfine coupling constants for *para*-substituted α-phenethyl radicals[a,b]

	X	a_α	a_β	a_o	a_m	a_X
1.	$COCH_3$	15.03	16.65	4.70	1.65	0.30[c]
2.	COC_6H_5	15.08	16.69	4.70	1.65	
3.	CN	15.35	16.97[d]	4.88	1.65	0.80[e]
4.	$COOCH_3$	15.43	16.96	4.79	1.60	0.30[c]
5.	OCH_3	15.60[f]	17.25[g]	4.85[h]	1.50[h]	0.70[c,h]
				4.95[h]		
6.	C_2H_5	16.06[h]	17.51	4.72[h]	1.60[h]	2.95[h,i]
				5.12[h]		
7.	H	16.25	17.69[j]	4.95	1.65	5.90
8.	$OCOCH_3$	16.30	17.78	4.85	1.70	
				5.15		
9.	F	16.33	17.89	5.00	1.69	13.46[k]
				5.30		

[a]All values in G. Unless indicated otherwise uncertainty is ±0.03 G.
[b]Subscript indicates position; *o* = *ortho*, *m* = *meta*, and *X* = substituent.
[c]Hydrogens of methyl.
[d]A value of 16.90 G has been reported (5).
[e]Nitrogen of CN.
[f]Uncertainty of 0.10 G.
[g]A value of 17.25 G has been reported (5).
[h]Uncertainty of 0.06 G.
[i]α-Hydrogen of ethyl.
[j]A value of 17.70 G has been reported (5).
[k]^{19}F.

Results

The α-phenethyl radicals were generated photochemically in the microwave cavity of the esr spectrometer by hydrogen abstraction from the appropriately substituted ethylbenzene. The hydrogen was abstracted by *tert*-butoxy radicals formed from di-*tert*-butylperoxide. The procedure has been described previously (1, 3). Hyperfine coupling constants were measured directly from the spectra and then refined by iterative computer simulation (4). These results are summarized in Table 1.

The observed spectrum of the *para*-methoxyphenethyl radical was complicated by the competitive hydrogen abstraction from the methoxy methyl group. The experimental spectrum was simulated by a one-to-one mixture of the α-phenethyl

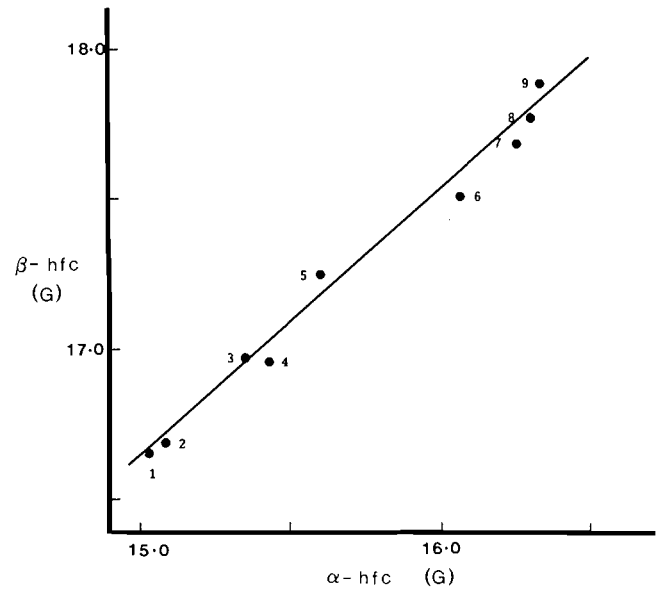

FIG. 1. A plot of the β-hfc versus the α-hfc of the α-phenethyl radicals. Points are numbered according to Table 1.

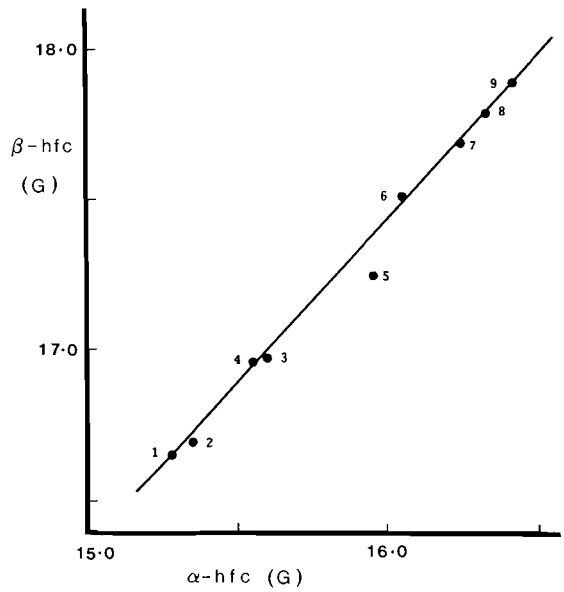

FIG. 2. A plot of the β-hfc of the α-phenethyl radicals versus the α-hfc of benzyl radicals. Points are numbered according to Table 1.

radical and aryloxymethyl radical with $a(CH_2)$ = 17.65 ± 0.1 G.

Discussion

The relationship between α- and β-hfc of *para*-substituted α-phenethyl radicals is illustrated in Fig. 1. A good (r = 0.993) linear correlation (β-hfc = (0.89 ± 0.09)α-hfc + (3.3 + 1.4)) is observed. This result indicates that both α-hfc and β-hfc are linearly related to the spin density at the benzylic position.

The relationship between the β-hfc of the α-phenethyl radicals and the α-hfc of the benzyl radicals is illustrated in Fig. 2. A good (r = 0.995) linear correlation (β-hfc(phen.) = (1.09 ± 0.09)α-hfc(benzyl) − (0.0 ± 1.5)) is observed. Of course, a similar correlation is observed between the α-hfc of these systems (Table 2). These results show that the $\sigma^{\bullet}_{\alpha}$ scale

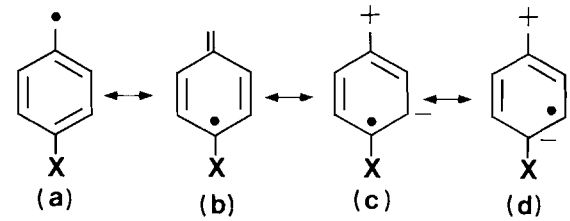

FIG. 3. Charge effects on spin delocalization in benzylic radicals.

should be directly applicable to reactions involving radicals of the α-phenethyl type.

A study comparing the effects of substituents on cumyl and benzyl radicals revealed charge effects acting on the β-hfc (3*c*). These effects were explained by proposing that dipolar valence bond structures, such as (c) and (d) in Fig. 3, contribute to provide additional spin delocalization in the cumyl radical series when the *para*-substituent is electron withdrawing. The correlation of β-hfc of the cumyl radicals and the α-hfc of the benzyl radicals was significantly improved by inclusion of the polar substituent parameter (σ_P) to account for the additional delocalization due to these charge-separated structures.

Notice that the correlation of α-hfc of the phenethyl radicals and the α-hfc of the benzyl radicals is not significantly improved by including the polar substituent parameter. Charge effects, if present, must be similar in these series. This, of course, is expected since the cumyl cation is significantly more stable than the benzyl cation, the α-phenethyl cation being intermediate in stability.

Conclusions

The correlation of α- and β-hfc in the α-phenethyl radical series indicates that both coupling mechanisms are proportional to spin density.

The differences that are observed between the α-hfc of substituted benzyl radicals and the β-hfc of the analogous cumyl radical are attributed to variation in the contribution of charge-separated valence bond structures, which influence spin density. The benzyl and α-phenethyl radicals are similar enough so that differences resulting from charge separation can be ignored.

Radical reactivity that depends upon variation in spin density should correlate directly with $\sigma^{\bullet}_{\alpha}$ so long as the radicals are as similar as benzyl and α-phenethyl. When the radicals are as different as benzyl and cumyl, polar factors that take into account the variation in spin delocalization due to the contribution of charge-separated valence bond structures must be included.

Experimental

General information

The esr spectra were recorded on a Varian Associates E-109 B electron paramagnetic resonance spectrometer, equipped with a liquid nitrogen variable temperature accessory, at 0.5 mW microwave power and 0.5–0.8 G modulation amplitude. All spectra were recorded with the aid of a Nicolet 1170 signal averager. Typically, 12, 100-G wide, scans were accumulated (0.5 min/scan). Coupling constants were measured directly from the oscilloscope and refined by computer simulation using an IBM-PC. Details of the procedure have been reported previously (1, 3).

The ^{1}H nmr spectra were recorded on a Varian CFT-20 spectrometer and are reported in parts per million downfield from TMS. Infrared spectra were recorded on either a Pye Unicam SP1000, or a Perkin–Elmer 283B or 1320 infrared spectrometer and are reported in wave numbers (relative to the 1601.8 cm^{-1} absorption of polystyrene). Mass

TABLE 2. A linear regression analysis of the relationship between the benzylic α- and β-hfc of benzylic radicals[a, b]

Regression equation[c]	r^d
β-hfc(phen) = (0.89±0.09)α-hfc(phen) + (3.3±1.4)	0.993
β-hfc(phen) = (0.87±0.13)α-hfc(phen) + (0.05±0.15)σ_p − (0.0±2.1)	0.992
β-hfc(phen) = (1.09±0.09)α-hfc(benzyl) − (0.0±1.5)	0.995
β-hfc(phen) = (1.14±0.12)α-hfc(benzyl) + (0.10±0.17)σ_p − (0.9±2.0)	0.995
β-hfc(phen) = (0.84±0.19)β-hfc(cumyl) + (4.1±3.1)	0.963
β-hfc(phen) = (1.08±0.21)β-hfc(cumyl) + (0.52±0.31)σ_p + (0.1±3.3)	0.986
α-hfc(phen) = (1.20±0.21)α-hfc(benzyl) − (3.4±3.3)	0.979
α-hfc(phen) = (1.27±0.31)α-hfc(benzyl) + (0.13±0.42)σ_p − (4.5±5.0)	0.978

[a]Hyperfine coupling constants for the phenethyl, benzyl, and cumyl radicals are taken from Table 1, and refs. 3*a* and 3*c*, respectively. The σ_p values are from ref. 6.
[b]Number of data points is nine. Phenethyl has been abbreviated as phen.
[c]Uncertainty indicated is the standard error at the 95% confidence interval.
[d]Correlation coefficient corrected for degrees of freedom.

spectra were obtained on a modified Du Pont CEC Model 21-104 mass spectrometer. Statistical calculations were done using the MINITAB statistical package, release 81.1, from Penn State University (University Park, Penn.).

The ethylbenzenes were purified by gas chromatography. A 5 ft. × 5/8 in. column packed with 5% SE-30 on Chromosorb-W (60/80) incorporating helium as the carrier gas was used.

Materials

Di-*tert*-butyl peroxide (DTBP) was obtained from Pfaltz and Bauer Inc. and was used without further purification. Ethylbenzene and *para*-diethylbenzene were obtained from Aldrich Chemical Co. and were purified by gas chromatography as described above. All solvents were distilled prior to use.

Synthesis

4-Ethylacetophenone

4-Ethylacetophenone (7) was prepared by the reaction of ethylbenzene and acetyl chloride in the presence of aluminum chloride, using carbon disulphide as the solvent (8). The reaction mixture was purified by vacuum distillation; 4-ethylacetophenone (bp 128–129°C/25 Torr; 1 Torr = 133.3 Pa) was obtained as a colourless oil in 54% yield; ir PE 1320 (neat): 1680, 1610, 1270, 835 cm^{-1}; ^1H nmr (80 MHz, $CDCl_3$) δ: 7.85 (d, 2H), 7.23 (d, 2H), 2.66 (q, 2H), 2.53 (s, 3H), 1.22 (t, 3H).

4-Ethylbenzophenone

4-Ethylbenzophenone (9) was prepared by a procedure similar to that used for the acetophenone except using benzoyl chloride. Vacuum distillation afforded 4-ethylbenzophenone as a colourless oil in 43% yield; ir PE 1320 (neat): 1660, 1610, 850, 705 cm^{-1}; ^1H nmr (80 MHz, $CDCl_3$) δ: 7.20–7.82 (m, 9H), 2.68 (q, 2HO), 1.23 (t, 3H).

Methyl 4-ethylbenzoate (ref. 10)

In a 250-mL 3-necked flask equipped with a magnetic stirrer, reflux condenser, and a constant pressure dropping funnel, was placed 12.2 g (91 mmol) of aluminum chloride. To the aluminum chloride was added 8.0 g (83 mmol) of ethylbenzene dissolved in 175 mL of carbon disulphide. The flask was cooled in an ice bath; to the cooled mixture was added a solution of 11.6 g (91 mmol) of oxalyl chloride in 25 mL of carbon disulphide. After the evolution of gases (**caution**: carbon monoxide) had ceased, the mixture was allowed to warm to room temperature. The mixture was then refluxed for 2.0 h and the cooled mixture was poured into 200 mL of methanol. The carbon disulphide was removed by distillation and the residue was poured into water and extracted with ether. The combined organic layers were washed with 5% sodium hydroxide, saturated salt solution, dried with magnesium sulphate, and evaporated. The yield of a pale yellow liquid was 8.2 g (60%). The product was distilled under vacuum to yield a colourless oil (bp 55–58°C/0.01 Torr); ir PE 1320 (neat): 1725, 1610, 1280, 1110 cm^{-1}; ^1H nmr (80 MHz, $CDCl_3$) δ: 7.94 (d, 2H), 7.20 (d, 2H), 3.85 (s, 3H), 2.65 (q, 2H), 1.21 (t, 3H).

4-Ethylphenyl acetate

4-Ethylphenyl acetate (8, 11) was prepared by the reaction between 4-ethylphenol and acetic anhydride in 3 *M* aqueous sodium hydroxide. The product was purified by vacuum distillation to give 2.7 g (82% yield) of a colourless oil (bp 82–85°C/1 Torr); ir PE 1320 (neat): 1770, 1515, 1375, 1220, 1025, 920, 855 cm^{-1}; ^1H nmr (80 MHz, $CDCl_3$) δ: 6.88–7.19 (m, 4H), 2.58 (q, 2H), 2.16 (s, 3H), 1.17 (t, 3H).

4-Cyanoethylbenzene

4-Cyanoethylbenzene (8, 12) was prepared by a Sandmeyer reaction using the diazonium salt formed from 4-ethylaniline and cuprous cyanide. The product was purified by chromatography over silica gel eluting with a hexane – methylene chloride gradient; the product was obtained in 62% yield as a colourless oil; ir SP 1000: 2240, 1610, 840 cm^{-1}.

4-Methoxyethylbenzene

4-Methoxyethylbenzene (13) was prepared by the reaction of 4-ethylphenol with dimethyl sulphate in 5% aqueous potassium hydroxide. The product was purified by vacuum distillation to give a 45% yield; ir PE 1320 (neat): 1615, 1590, 1515, 1250, 1180, 1040, 915, 830, 735 cm^{-1}; ^1H nmr (80 MHz, $CDCl_3$) δ: 7.10 (d, 2H), 6.79 (d, 2H), 3.74 (s, 3H), 2.57 (q, 2H), 1.19 (t, 3H).

4-Fluoroethylbenzene

4-Fluoroethylbenzene (8) was prepared by the thermal decomposition of the diazonium fluoroborate salt formed from 4-ethylaniline with fluoroboric acid. The product was purified by distillation to give a 35% yield of colourless oil, bp 140–144°C/760 Torr; ir PE 283B (neat): 1505, 1155, 830 cm^{-1}; ^1H nmr (80 MHz, $CDCl_3$) δ: 7.03 (m, 4H), 2.60 (q, 2H), 1.20 (t, 3H).

Acknowledgements

This work was supported by a grant from the Natural Sciences and Engineering Research Council of Canada. A.M.N. is grateful for the award of an Izaak Walton Killam Memorial Scholarship.

1. A. M. DE P. NICHOLAS and D. R. ARNOLD. Can. J. Chem. **64**, 270 (1986).
2. J. E. WERTZ and J. R. BOLTON. Electron spin resonance. McGraw–Hill, New York. 1972. Chapt. 6.
3. (*a*) J. M. DUST and D. R. ARNOLD. J. Am. Chem. Soc. **105**, 1211 (1983); **105**, 6531 (1983); (*b*) D. D. M. WAYNER and D. R. ARNOLD. Can. J. Chem. **62**, 1164 (1984); (*c*) D. R. ARNOLD, A. M. DE P. NICHOLAS, and M. S. SNOW. Can. J. Chem. **63**, 1150

(1985); (*d*) D. D. M. WAYNER and D. R. ARNOLD. Can. J. Chem. **63**, 2378 (1985).
4. U. M. OEHLER and E. G. JANZEN. Can. J. Chem. **60**, 1542 (1982).
5. H. G. VIEHE, Z. JANOUSEK, R. MERE'NYR, and L. STELLA. Acc. Chem. Res. **18**, 148 (1985).
6. O. EXNER. *In* Correlation analysis in chemistry. Recent advances. *Edited by* N. B. Chapman and J. Shorter. Plenum Press, New York. 1978. Chapt. 10.
7. A. KLAGES and G. TIDSROTH. Chem. Ber. **32**, 1558 (1899).
8. A. I. VOGEL. Practical organic chemistry. 4th ed. Longman Inc., New York. 1978. pp. 607, 703–706, 1102–1103.
9. C. SOLLSCHER. Chem. Ber. **15**, 1682 (1882).
10. F. VAN MEURS and H. VAN BEKKUM. J. Organomet. Chem. **133**, 321 (1977).
11. S. F. BIRCH, R. A. DEAN, F. A. FIDDLER, and R. A. LOWRY. J. Am. Chem. Soc. **71**, 1362 (1949).
12. G. ERRERA. Gazz. Chim. Ital. **14**, 485 (1885).
13. J. MOSCHNER. Chem. Ber. **34**, 1262 (1901).

A multinuclear nuclear magnetic resonance study of methylammonium nitrate

RODERICK E. WASYLISHEN
Department of Chemistry, Dalhousie University, Halifax, N.S., Canada B3H 4J3

Received June 19, 1985

RODERICK E. WASYLISHEN. Can. J. Chem. **64**, 773 (1986).

Deuterium nmr line shapes in the solid II phase of methylammonium nitrate (MAN) indicate that motion of the cation is restricted to internal rotations of the ND_3 group about the C—N axis. In the high temperature plastic phase, solid I, of MAN, ^2H, ^{14}N, and ^{17}O nmr results demonstrate that both the cation and anion undergo rapid overall rotations that result in complete averaging of all nuclear quadrupolar interactions. Spin-lattice relaxation results imply that rotations of the cation and anion are anisotropic and that the overall rotations are strongly coupled in both the solid I and liquid phases. At the melting point, overall rotations of the cation are only slightly faster in the liquid phase than in the solid I phase. In the solid I phase, in-plane rotations of the nitrate ion are about twice as rapid as end-over-end rotations of the C_3 axis. In the neat liquid, rotations of the NO_3^- ion are more isotropic, with overall rotations being slightly faster than rotations about the symmetry axis.

RODERICK E. WASYLISHEN. Can. J. Chem. **64**, 773 (1986).

Sur la base des formes des raies en rmn du ^2H de la phase solide II du nitrate de méthylammonium (NMA), on peut déduire que les mouvements du cation sont restreints aux rotations internes du groupement ND_3 autour de l'axe C—N. Dans la phase plastique qui existe à des températures plus élevées pour le solide I du NMA, les résultats de la rmn du ^2H, du ^{14}N et du ^{17}O démontrent que le cation ainsi que l'anion subissent des rotations globales rapides qui font que l'on n'observe qu'une moyenne de toutes les interactions quadrupolaires nucléaires. Les résultats de la relaxation spin-réseau impliquent que les rotations du cation ainsi que celles de l'anion sont anisotropes et que les rotations globales sont fortement couplées tant dans la phase solide I que dans le liquide. Au point de fusion, les rotations globales ne sont que légèrement plus rapides dans la phase liquide que dans la phase solide I. Dans la phase solide I, les rotations dans le plan de l'ion nitrate sont environ deux fois plus rapides que les rotations d'un bout à l'autre de l'axe C_3. Dans le liquide pur, les rotations de l'ion NO_3^- sont plus isotropes et les rotations globales sont légèrement plus rapides que les rotations autour de l'axe de symétrie.

[Traduit par la revue]

Introduction

Molecular motion involving the methylammonium ion has been the subject of numerous ^1H nmr studies (1–9). At atmospheric pressure many methylammonium salts are capable of existing in two or more solid phases depending upon temperature (1–10). For example, both methylammonium chloride (1) and methylammonium bromide (6, 7) exist in at least three different solid phases. Nuclear magnetic resonance studies indicate that although the CH_3 and NH_3 groups undergo rapid reorientation(s) about the C—N axis in many of these phases, the C—N axis itself does not reorientate (1–9).

Recent ^1H nmr studies of methylammonium nitrate, MAN, indicate an unusual phase transition at 352 K, approximately 32 degrees below the reported melting point (8). Although it was possible to conclude that the frequency of rotation of the cation exceeded 10^{10} Hz in this solid phase, no information on the rotations of the anion is available from the ^1H nmr study (8). Here we report the results of ^{14}N nmr relaxation measurements on both the methylammonium cation and the nitrate anion. These measurements permit us to calculate rotational correlation times for both the $CH_3NH_3^+$ and NO_3^- ions in the high temperature solid phase (solid I) and the liquid phase. Also, natural abundance ^{17}O nmr relaxation measurements yield information on the anisotropy of nitrate ion rotations. Finally, deuterium nmr results are reported for both the solid II phase ($T < 352$ K) and solid I phase (352 K $< T <$ 391 K) of $CH_3ND_3^+NO_3^-$.

Experimental

Methylammonium nitrate was prepared by neutralizing an aqueous solution of methylamine with nitric acid and subsequent drying under vacuum. Deuteration of the amino group was achieved by dissolving $CH_3NH_3NO_3$ in excess deuterium oxide. The resulting sample was dried on a vacuum rack at 343 K for several days before sealing in an nmr tube. All nmr measurements were performed on the deuterated sample, $CH_3ND_3NO_3$.

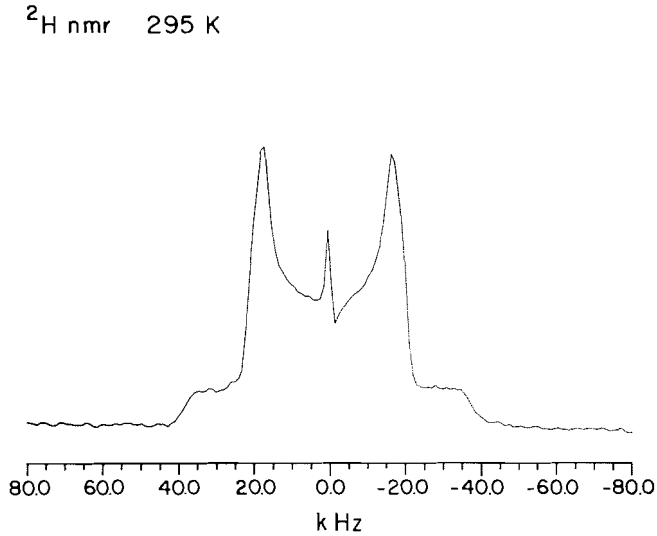

FIG. 1. The ^2H nmr powder pattern for $CH_3ND_3^+NO_3^-$ at 295 K (solid II) obtained at 30.72 MHz.

Spin-lattice relaxation measurements were performed on a Nicolet 360 NB (B_0 = 8.48 T) using the inversion recovery pulse sequence, which uses compensating pulses (11). The $\pi/2$ pulse widths were 40–55 μs. T_1 values were calculated from peak heights obtained at 12 or more different τ values using a nonlinear, three-parameter least-squares fitting procedure available on the Nicolet software (12).

Deuterium nmr spectra of MAN in the solid II phase were recorded on a Bruker MSL-200 (B_0 = 4.7 T).

Results and discussion

(b) *Solid II phase*

The deuterium nmr spectrum of $CH_3ND_3^+NO_3^-$ at 295 K is shown in Fig. 1. The observed quadrupolar splitting of 37 ± 2 kHz is approximately one-third the anticipated static value and

is indicative of rapid reorientation of the N—D bond about the CN axis, **I**.

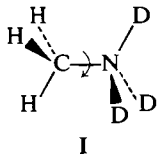

I

In general, the quadrupolar splittings between the spectral discontinuities of a ^2H nmr powder pattern are given by eq. [1] (13, 14),

$$[1]\quad \Delta\nu_1 = 3\chi(1-\eta)R/4$$
$$\Delta\nu_2 = 3\chi(1+\eta)R/4$$
$$\Delta\nu_3 = 3\chi R/2$$

where $\chi = e^2qQ/h$ is the ^2H quadrupolar coupling constant, 175 ± 10 kHz (15), η is the asymmetry parameter, less than 0.1 in the case of $CH_3ND_3^+$, and R is a reduction factor, $|(3\cos^2\beta - 1)/2|$, which results because of rapid rotation (or jumps) about some axis. β is defined as the angle between the largest principal component of the electric field gradient (the N—D bond) and the axis of rotation. For rotations of the ND_3 group about the C—N axis, **1**, $\beta = 109.5°$ and eq. [1] predicts $\Delta\nu_1 = \Delta\nu_2 = 43.7 \pm 2.5$ kHz. The smaller observed splitting may result from β values slightly larger than the tetrahedral angle and (or) averaging resulting from librations of the C—N axis.

We were unable to observe the nitrogen-14 nmr spectrum for the solid II phase of MAN. This was not unexpected since ^{14}N nmr studies indicate $\chi = 745$ kHz for the nitrate ion in sodium nitrate (16) and ^{14}N nqr studies show $\chi = 913 \pm 2$ kHz ($\eta = 0.109$) for the methylammonium cation in methylammonium chloride (17). A somewhat larger value for χ, 1106.7 ± 1.5 kHz, has been reported from a liquid crystal study of the methylammonium ion (18).

(b) *Solid I and liquid phases*

At temperatures above the solid II ↔ solid I phase transition, 352 K (8), the ^2H nmr powder pattern (Fig. 1) collapsed into a sharp single peak ($\nu_{1/2} < 40$ Hz); the ^{14}H nmr spectrum consisted of two chemically shifted peaks (Fig. 2). Also, above 352 K, a relatively sharp natural abundance ^{17}O nmr spectrum was observed for MAN. These results indicate that both the methylammonium cation and the nitrate anion are undergoing rapid overall rotations and (or) jumps that completely average all quadrupolar splittings (^2H, ^{14}H, and ^{17}O) to zero.

In order to gain further information about the time scale of these rotations, we have measured the temperature dependence of ^2H, ^{14}N, and ^{17}O spin-lattice relaxation time (Tables 1 and 2, Fig. 3). Our sample of MAN was solid at 388 K and melting occurred at 391 ± 2 K, approximately 7 K above the previously reported value (8); this is probably a deuterium isotope effect on the melting point. We summarize below the results obtained from each nmr active isotope investigated in this study.

(i) ^{14}N nuclear magnetic resonance

The ^{14}N resonances of the NO_3^- and $CH_3ND_3^+$ ions in the solid I phase of MAN are at 357.4 and −0.1 ppm, respectively, with respect to the ^{14}N resonance of the ammonium ion in a 5 *M* aqueous solution of $NH_4^+NO_3^-$. These nitrogen chemical shifts are in excellent agreement with those observed for the same ions in solution (19).

The temperature dependence of the experimental nitrogen

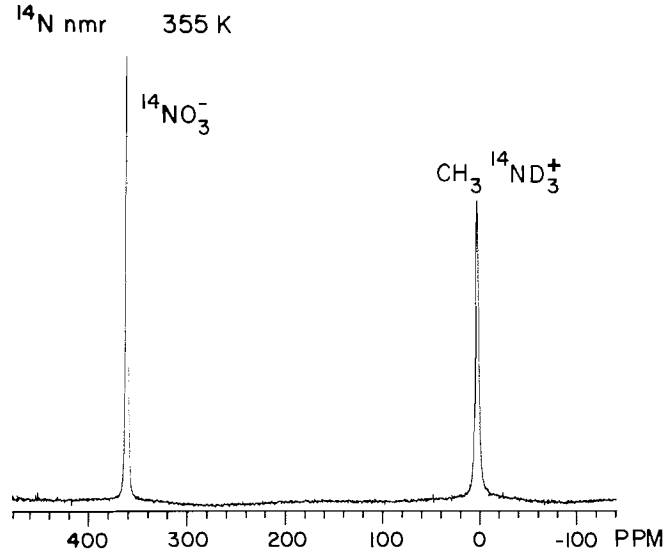

FIG. 2. ^{14}N nuclear magnetic resonance of $CH_3ND_3^+NO_3^-$ at 352 K (solid I) obtained at 26.08 MHz.

TABLE 1. Nitrogen-14 spin-lattice relaxation times[a] for $CH_3ND_3^+NO_3^-$

Temperature, K	$T_1(^{14}NO_3)$, ms	$T_1(^{14}ND_3)$, ms
393	31.6	11.9
361	33.4	12.4
367	35.1	12.6
373	37.1	13.2
381	39.7	14.1
387	42.7	15.0
393 (melt)	49.7	16.8

[a]Estimated experimental error less than ±7%.

TABLE 2. Oxygen-17 and deuterium spin-lattice relaxation times for $CH_3ND_3^+NO_3^-$

Temperature, K	$T_1(^{17}O)$,[a] ms	Temperature, K	$T_1(^2H)$,[b] s
355	2.28	355	1.17
361	2.39	359	1.31
368	2.52	363	1.33
369.5	2.56	371	1.38
378	2.92	373	1.41
383	3.08	381	1.56
385	3.14	385	1.70
383 (melt)	2.00	393 (melt)	1.42

[a]Estimated experimental error less than ±10%.
[b]Estimated experimental error less than ±7%; slope of Arrhenius plot is 11.9 ± 2 kJ mol^{-1}.

relaxation times for the nitrate and methylammonium ions in Fig. 3 can be described by

$$[2]\quad \ln T_1(NO_3^-) = 0.100 - 1.264\left(\frac{10^3}{T}\right)$$

and

$$[3]\quad \ln T_1(CH_3ND_3^+) = -1.716 - 0.969\left(\frac{10^3}{T}\right)$$

The slopes of these two linear equations correspond to activation energies of 10.5 ± 1.6 kJ mol^{-1} and 8.1 ± 1.2 kJ mol^{-1} for

TABLE 3. Representative rotational correlation times and diffusion constants for the solid I and liquid phases of MAN

	$CH_3{}^{14}ND_3{}^+$	$NO_3{}^-$		$NO_3{}^-$		
T, K	$\tau_\perp(^{14}N)$, ps	$\tau_\perp(^{14}N)$, ps	$\tau_{eff}(^{17}O)$, ps	$D_\perp$	$D_\parallel$	$D_\parallel/D_\perp$
355	4.71	3.88	2.93	4.3×10^{10}	8.0×10^{10}	1.9
385	3.80	2.94	2.13	5.7×10^{10}	11.2×10^{10}	2.0
393 (melt)	3.28	2.45	3.34	6.8×10^{10}	5.5×10^{10}	0.8

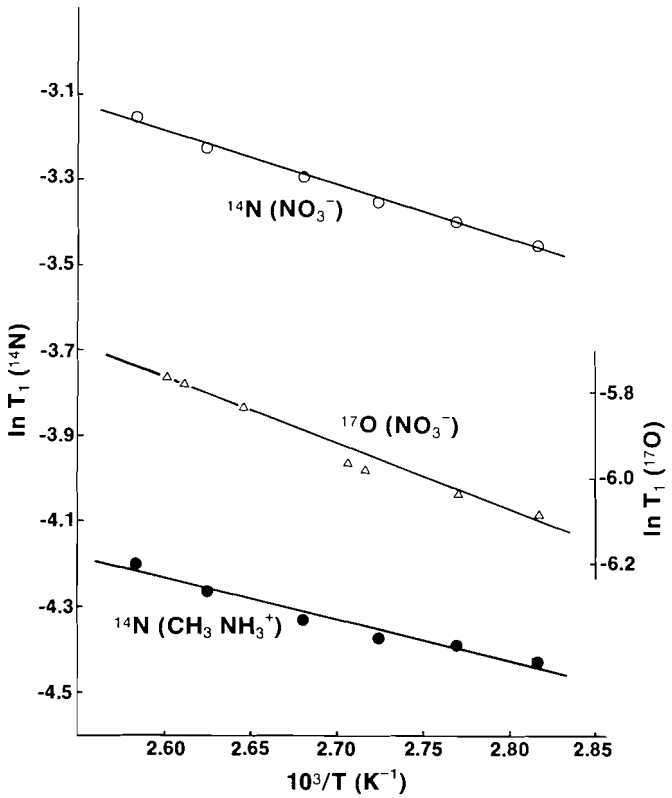

FIG. 3. Plots of ln $T_1(^{14}N)$ and ln $T_1(^{17}O)$ vs. $10^3/T$ for MAN (solid I).

the nitrate and methylammonium ions, respectively. The slopes are the same within the estimated experimental error (±15%). Nitrogen relaxation of both these ions is governed by the quadrupolar mechanism, eq. 4 (20), with $I = 1$.

$$[4]\quad \frac{1}{T_1} = \frac{3\pi^2}{10}\frac{2I+3}{I^2(2I-1)}\chi^2\tau_{eff}$$

Since the largest principal component of the electric field gradient for the nitrate ion is the C_3 symmetry axis, $\tau_{eff}(^{14}NO_3)$ is the correlation time describing rotations of the symmetry axis (i.e. end-over-end rotations). Similarly, the effective correlation time from ^{14}N measurements of the $CH_3ND_3{}^+$ resonance describes rotations of the C—N axis.

Substitution of experimental ^{14}N relaxation times at 355 K, $\chi(^{14}NO_3{}^-) = 745$ kHz (16) and $\chi(CH_3ND_3{}^+) = 1106.7$ kHz (18), into eq. [4] leads to overall rotational correlation times of 4.7 ps for the methylammonium ion and 3.9 ps for the nitrate ion. Calculated correlation times at 385 K and 393 K (liquid) are given in Table 3. Similar values of τ_{eff} for overall rotation of the nitrate and methylammonium ion suggest that the rotations of these ions are highly correlated or coupled. Because of the nonspherical shapes of these ions one might expect their rotational correlation times to be identical. Also, overall rotations of these two ions in the melt (liquid) are only slightly faster than those observed in the solid I phase. The consistently longer correlation times for the methylammonium ion (approximately 25%) compared to those of the nitrate ion may result from the substitution of inappropriate χ values into eq. [4]. (Note, any uncertainty in χ is squared in the calculation of τ_{eff}). Also, it is important to point out that there may be mechanisms for anion and cation rotations that permit different correlation times for the two ions.

The time scale for nitrate anion rotations in the solid I and liquid phases of MAN is slightly longer than what we have measured in dilute aqueous solutions of sodium nitrate (τ_{eff} = 1.1 ps) at 295 K (20*b*) but is significantly shorter than that observed in the solid I phase of ammonium nitrate at 413 K (τ_{eff} = 8.3 ps) (21).

(ii) ^{17}O nuclear magnetic resonance

At 373 K the ^{17}O nmr chemical shift of the nitrate ion of MAN is 419.2 ppm to high frequency of H_2O. The ^{17}O line width at half height was 120 ± 15 Hz at this temperature. Because of the low natural abundance of ^{17}O (0.037%), the error in the ^{17}O T_1 values is estimated to be ±10%. The best straight line describing the ^{17}O relaxation data is given by eq. [5], with a slope corresponding to 12.7 ± 2.5 kJ mol^{-1},

$$[5]\quad \ln T_1 = -1.79 - 1.53\left(\frac{10^3}{T}\right)$$

Oxygen-17 has a spin $I = 5/2$ and nuclear relaxation is governed by the quadrupolar mechanism, eq. [4]. For the nitrate ion, nqr studies (22) and *ab initio* molecular orbital calculations (20*b*, 22) indicate that the largest principal component of the ^{17}O electric field gradient (EFG) tensor lies along the N—O bond (x-axis), while the smallest component is along the C_3 symmetry axis (z-axis). The other principal component of the EFG tensor lies in the molecular plane of the ion, and is only slightly smaller than the x-component. Effective relaxation data will reflect rotations both parallel and perpendicular to the C_3 symmetry axis. Oxygen-17 τ_{eff} values calculated using χ = 12.57 MHz (22) and eq. [4] ($I = 5/2$) are summarized in Table 3. The shorter τ_{eff} values derived for the nitrate ion from the ^{17}O data compared to those derived from the ^{14}N data in the solid I phase imply that in-plane rotations are faster than overall rotations of the nitrate ion. In the liquid phase, in-plane rotations are slower than they are in the solid I phase.

By assuming that rotations of the nitrate ion can be described by a rotational diffusion model, one can relate $\tau_{eff}(^{17}O)$ for the

nitrate ion to the rotational diffusion constants $D_\perp$ and $D_\parallel$ (II),

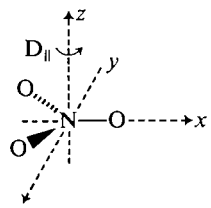

II

using eq. [6] (20).

[6] $\tau_{eff}(^{17}O) = \{[4 + (n_q - 1)^2]D_\perp + (n_q + 1)^2 D_\parallel\}/4D_r$

where

$$D_\perp = D_{xx} = D_{yy} = \frac{1}{6\tau_\perp(^{14}N)}$$

$$D_\parallel = D_{zz}$$

$$D_r = 3D_\perp(D_\perp + 2D_\parallel)$$

and $n_q = (q_{yy} - q_{zz})/q_{xx} = -0.747$ for the ^{17}O of the nitrate ion (20*b*, 22). The calculations indicate that the ratio, $D_\parallel/D_\perp \simeq 2$ in the solid I phase and approximately 0.8 in the neat liquid. Although it is important to recognize the possible limitations of a diffusion model, we feel that the qualitative results regarding the anisotropy of the nitrate ion rotations are significant; i.e., in-plane rotations or jumps of the nitrate ion are faster in the solid I phase than rotations of the C_3 symmetry axis. In the liquid phase rotations are more isotropic.

Similar calculations utilizing ^2H and ^{14}N relaxation data for the methylammonium ion yield, $D_\parallel/D_\perp$ ratios of 7.6 ± 2 and 4.3 ± 1, respectively, in the solid I and liquid phases. In this calculation we have assumed the CNH angle is tetrahedral. The qualitative result is that rotations of the $CH_3NH_3^+$ ion about the symmetry axis are faster than rotations of the symmetry axis. Again, rotations in the liquid phase are found to be more isotropic, as expected.

Conclusion

In this study we have demonstrated how one can combine ^2H, ^{14}N, and ^{17}O nmr relaxation data to characterize the temperature dependent rotations of the methylammonium cation and nitrate anion in $CH_3ND_3^+NO_3^-$ in both the solid and liquid state. In the solid I phase both ions are undergoing very rapid anisotropic rotations, which are strongly coupled. On melting, the rotations of each ion are more isotropic and the rate of overall rotations increases slightly. The high temperature orientationally disordered "plastic" phase is almost certainly cubic and similar to that of ammonium nitrate. Diffraction and calorimetry studies of this intriguing solid will lead to a better understanding of the structure and nature of the phase transition in methylammonium nitrate.[1]

[1] While this paper was in press the crystal structure of MAN appeared (23).

Acknowledgements

I wish to thank Dr. S. Peris and Mr. J. B. Macdonald for their assistance with some of the preliminary experimental work, Dr. A. M. de P. Nicholas, and Professors O. Knop and M. A. White for helpful discussions, and the Natural Sciences and Engineering Research Council of Canada for generous financial support in the form of equipment and operating grants. Also, I would like to thank one of the referees for carefully reading and commenting on this study.

1. J. Tsau and D. F. R. Gilson. Can. J. Chem. **48**, 717 (1970).
2. E. R. Andrew and P. C. Canepa. J. Magn. Reson. **7**, 429 (1972).
3. J. Tegenfeldt and L. Ödberg. J. Phys. Chem. Solids, **33**, 215 (1972).
4. J. Tegenfeldt, T. Keowsim, and C. Saterkvist. Acta Chem. Scand. **26**, 3524 (1972).
5. S. Albert and J. A. Ripmeester. J. Chem. Phys. **58**, 541 (1973).
6. H. Ishida, R. Ikeda, and D. Nakamura. Phys. Status Solidi A, **60**, K115 (1980).
7. H. Ishida, R. Ikeda, and D. Nakamura. J. Phys. Chem. **86**, 1003 (1982).
8. (*a*) H. Ishida, R. Ikeda, and D. Nakamura. Chem. Lett. 1943 (1982); (*b*) J. Chem. Soc. Faraday Trans. 2, 963 (1985).
9. H. Ishida, R. Ikeda, and D. Nakamura. Chem. Soc. Jpn. **5**, 3116 (1982).
10. N. G. Parsonage and L. A. K. Staveley. Disorder in crystals. Clarendon Press, Oxford. 1978. pp. 361–376.
11. R. Freeman, S. P. Kempsell, and M. H. Levitt. J. Magn. Reson. **38**, 453 (1983).
12. G. C. Levy and I. R. Peat. J. Magn. Reson. **18**, 500 (1975).
13. H. W. Spiess. NMR basic principles and progress. Vol. 15. Springer Verlag, Berlin. 1978. pp. 59–214.
14. (*a*) C. M. Gall, T. A. Cross, J. A. Diverdi, and S. J. Opella. Proc. Natl. Acad. Sci. USA, **79**, 101 (1982); (*b*) R. A. Kinsey, A. Kintanar, and E. Oldfield. J. Biol. Chem. **256**, 9028 (1981); (*c*) C. M. Gall, J. A. Diverdi, and S. J. Opella. J. Am. Chem. Soc. **103**, 5039 (1981).
15. M. J. Hunt and A. L. MacKay. J. Magn. Reson. **15**, 402 (1974).
16. M. Gourdji, L. Guibe, and A. Peneau. J. Phys. **35**, 497 (1974).
17. D. T. Edmonds, M. J. Hunt, and A. L. MacKay. J. Magn. Reson. **9**, 66 (1973).
18. P. Polatin, T. Barbara, and B. P. Dailey. J. Magn. Reson. **47**, 148 (1982).
19. G. C. Levy and R. L. Lichter. Nitrogen-15 nuclear magnetic resonance spectroscopy. John Wiley and Sons, New York. 1979.
20. (*a*) W. T. Huntress. Adv. Magn. Reson. **4**, 1 (1970); (*b*) A. M. de P. Nicholas and R. E. Wasylishen. J. Phys. Chem. **89**, 5446 (1985); (*c*) J. P. Kintzinger and J. M. Lehn. Mol. Phys. **27**, 491 (1974).
21. R. E. Wasylishen. Spectrochim. Acta Part A, **40**, 115 (1984).
22. C. P. Cheng and T. L. Brown. J. Am. Chem. Soc. **102**, 6418 (1980).
23. M. Mylrajan, T. K. K. Srinivasan, and G. Sreenivasamurthy. J. Crystallogr. Spectrosc. Res. **15**, 493 (1985).

Cation transport in gaseous nitrogen: density and temperature effects

TOSHINORI WADA, NORMAN GEE, AND GORDON R. FREEMAN
Chemistry Department, University of Alberta, Edmonton, Alta., Canada T6G 2G2

Received November 4, 1985

TOSHINORI WADA, NORMAN GEE, and GORDON R. FREEMAN. Can. J. Chem. **64**, 777 (1986).

The density-normalized mobility of $n\mu$ of cations in nitrogen gas at densities up to $n_c = 6.7 \times 10^{27}$ molecules/m^3 increases with temperature. At $n \leq 5.7 \times 10^{25}$ molecules/m^3 and $T > 250$ K, the dominating ion is N_4^+. At lower temperatures and higher densities, relatively loosely bound clusters $N_4^+(N_2)$, $N_4^+(N_2)_2$, ... form. Momentum transfer cross sections for $N_4^+-N_2$ are governed at low energies by the polarization potential, and at high energies by the hard body potential. The cross section for $N_2^+-N_2$ at high energies is larger than that for $N_4^+-N_2$.

TOSHINORI WADA, NORMAN GEE et GORDON R. FREEMAN. Can. J. Chem. **64**, 777 (1986).

La mobilité normalisée pour la densité, $n\mu$, de cations dans l'azote gazeux, à des densités allant jusqu'à $n_c = 6{,}7 \times 10^{27}$ molécules/m^3, augmente avec la température. Pour $n \leq 5{,}7 \times 10^{25}$ molécules/m^3 et $T > 250$ K, l'ion dominant est N_4^+. A des températures plus basses et à des densités plus élevées, il se forme des agrégats relativement faiblement liés de $N_4^+(N_2)$, $N_4^+(N_2)_2$, ... A basse énergie, les sections droites les transferts de moments, pour $N_4^+-N_2$, sont influencées par le potentiel de polarisation; par ailleurs, à des énergies plus élevées, elles sont gouvernées par les potentiels des corps durs. A des énergies élevées, la section droite pour $N_2^+-N_2$ est plus grande que celle pour $N_4^+-N_2$.

[Traduit par la revue]

Introduction

The mechanism of cation transport in simple molecular fluids undergoes a gradual transition from normal gas-phase-type to liquid-phase-type over a wide density range, $0.5 \lesssim n/n_c \lesssim 1.9$, where n_c is the number density of the vapor–liquid critical fluid (1). The transport mechanism does not change abruptly at the critical point. The mobility μ of ions in the low density gas is limited by binary collisions. In the normal liquid ($n/n_c \gtrsim 2.0$) it is limited by multibody, viscous interactions.

In the dense gas, at $n/n_c \gtrsim 0.5$, the density-normalized mobility $n\mu$ increases (1). This implies that the attractive ion–molecule scattering interactions interfere destructively when the ion interacts with several molecules at a time. The high density at which the increase of $n\mu$ takes place indicates that the scattering interaction has a relatively short range.

The present paper examines, in more detail, the temperature and density effects on cation transport in nitrogen gas.

Experimental

Ultra high purity nitrogen (99.9995%), obtained from Matheson, was further purified in a grease free vacuum line by: 1) passage through two cold traps at 113 K, 2) passage at 773 K through a 60-cm column of copper grains previously treated with hydrogen to remove oxide, 3) bubbling through a sodium–potassium alloy at 294 ± 1 K, and 4) contact as a gas with a series of potassium mirrors (2).

The conductance cell could contain ~6 MPa (3). The drift distance was 3.20 mm, measured with a small-hole caliper and micrometer. Prior to filling with sample, the cell was degassed by heating to 523 K while evacuating to 10^{-5} Pa.

The cations were generated with 100 ns pulses of 1.7 MeV X-rays (dose $\approx 9 \times 10^{-9}$ J/g). The mobility was measured by time of flight (4). Ion drift signals were averaged for eight pulses at each voltage to obtain the drift time. The mobility was independent of field strength, E/n, over the range 0.01–1 Td (Td = 10^{-21} V m^2/molecule). Each mobility reported herein is the average of about 15 values measured over the 100-fold range. The precision is ±2%.

The temperature was measured at the top, electrode level, and bottom of the cell with copper-constantan (Thermoelectric Canada Ltd. type t special) thermocouples connected to a Fluke 2100A digital thermometer. The temperature difference between the top and bottom of the cell was <1 K, except near T_c where it was 0.2 K (2). Constant temperature was maintained within ±0.2 K.

The amount of material put into the 15.0-cm^3 cell was measured by the gas pressure in the cell at 77 K for the smaller amounts, and by the volume of liquid transferred from a burette at 77 K to the cell at solid nitrogen temperature (63 K) for larger amounts.

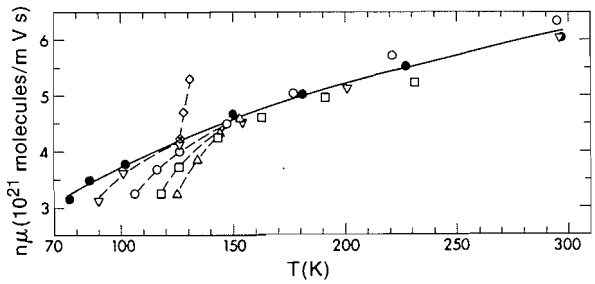

FIG. 1. Density-normalized mobility $n\mu$ of cations as a function of temperature at several densities. $n(10^{26}$ molecules/m^3): ●, 0.57; ▽, 2.30; ○, 7.8; □, 17.4; △, 32.0; ◇, 67.1 = n_c. The lines are guides for the eye.

The critical temperature, pressure, and density of nitrogen are T_c = 126.2 K, P_c = 3.3 MPa, and $n_c = 6.7 \times 10^{27}$ molecules/m^3 (5).

Results and discussion

A. Effect of temperature at different densities

The mobility increases with increasing temperature over the range 77–297 K (Fig. 1). To compare the results at different densities, the density-normalized mobility $n\mu$ is plotted against T. At $T > 150$ K the values of $n\mu$ are independent of n, within the experimental uncertainty of ±2%. At $T < 150$ K the $n\mu$ curves fan out, the value of $n\mu$ decreasing as n is increased from 0.57×10^{26} to 32×10^{26} molecules/m^3 (Fig. 1). However, at the density of the vapor–liquid critical fluid $n_c = 67 \times 10^{26}$ molecules/m^3, the values of $n\mu$ are higher, indicating a change of behavior.

The change of behavior is illustrated by plotting $n\mu$ against n at fixed T (Fig. 2). The value of $n\mu$ decreases gently with increasing n up to ~32×10^{26} molecules/m^3, then increases at higher densities. The increase of $n\mu$ with n signals destructive interference of the attractive ion–molecule scattering interactions as the ion interacts with several molecules at a time. This is the beginning of the transition region of densities, through which transport mechanism changes from gas-type to liquid-type (1).

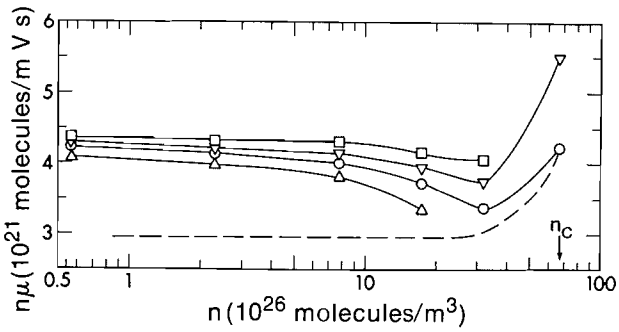

FIG. 2. Density-normalized mobility $n\mu$ of cations as a function of density at several temperatures. △, $0.95T_c$ = 119.9 K; ○, T_c = 126.2 K; ▽, $1.05T_c$ = 132.5 K; □, $1.10T_c$ = 138.8 K. ---, saturated vapor (1).

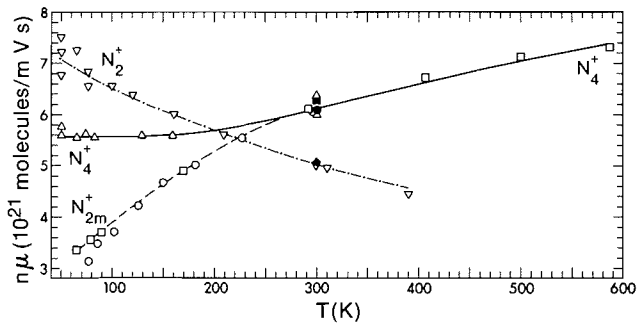

FIG. 3. Temperature dependence of the density-normalized mobility $n\mu$ in low density nitrogen gas. The gas density (10^{24} molecules/m^3) is the number following the point symbol. Unidentified N_{2m}^+: ○, 57, present work; □, ~0.3–0.8 (8). N_4^+: △, ≤0.5 (7); ■, 0.01–0.03 (6). N_3^+: ●, 0.001–0.03 (6). N_2^+: ▽, ≤0.5 (7); ◆, 0.001–0.03 (6). —— and –·–·–, calculated from eq. [6] using the corresponding (σ_m, ϵ) values from Fig. 4. --- is empirical. The different sets of N_4^+ and N_{2m}^+ data were normalized at 300 K to provide a more accurate shape of the temperature dependence: ○ and ■, 1.00 $n\mu$; □, $n\mu$/1.10; △, 1.07 $n\mu$. The stated uncertainties of $n\mu$ were ±4% in ref. 6 and ±10% in ref. 7.

The main question in the present work is why the curves in Fig. 1 fan out at T < 150 K and not at higher temperatures. The answer probably lies in the thermodynamics of the ion–molecule clustering reactions. At higher temperatures the ions are probably mainly N_4^+, and at low temperatures they are probably larger clusters.

The mobilities of mass-identified N_2^+, N_3^+, and N_4^+ have been measured at densities 10^2–10^3 times smaller than the lowest used in the present work (6, 7). The $n\mu$ of N_2^+ decreases with increasing temperature (Fig. 3); that of N_4^+ is independent of temperature between 50 and ~200 K, then increases gently at higher temperatures (Fig. 3). There is a crossover of $n\mu$ for N_2^+ and N_4^+ at 220 ± 20 K (7). The mobility of N_3^+ has only been measured at 300 K, where it is essentially the same as that of N_4^+ (6).

At 300 K the value of $n\mu$ of our mass-unidentified ions, designated N_{2m}^+, is essentially the same as that of N_4^+ (6, 7). At low temperatures $n\mu$ of N_{2m}^+ is smaller than that of N_4^+ (Fig. 3).

Early results of Tyndall and Pearce (8) in highly purified nitrogen, showed nearly the same temperature dependence as ours, even though we used a 100-fold larger density (Fig. 3). The $n\mu$ values calculated from the data of Tyndall and Pearce were approximately 10% greater than ours. Their value at 292 K is 10% higher than that of N_4^+ at 300 K at the same and lower densities; we attributed the difference to a 10% systematic error and divided their values by 1.10, to plot in Fig. 3.

The reaction

[1] $N_2^+ + 2N_2 \rightleftharpoons N_4^+ + N_2$

has $\Delta H^0_{2,4} = -95$ kJ/mol and $\Delta S^0_{2,4} = -84$ J/mol K, with standard state 1 atm (1 atm = 101 kPa) (9, 10). The equilibrium constant

[2] $K_{2,4} = \exp(-\Delta G^0_{2,4}/RT)$

therefore has the value 3×10^{12} atm^{-1} at 298 K, which is equivalent to 1×10^{-13} m^3/molecule. Thus equilibrium [1] is essentially completely on the side of N_4^+ when $n > 10^{14}$ molecules/m^3. Our system had $n \geq 57 \times 10^{24}$ molecules/m^3, so the concentration of N_2^+ was negligible.

The values of $n\mu$ indicate that at $T > 250$ K the main ions in our system were N_4^+ (Fig. 3). The lower values of $n\mu$ at $T <$ 250 K are attributed to the formation of larger clusters.

[3] $N_4^+ + 2N_2 \rightleftharpoons N_4^+(N_2) + N_2$

The results indicate that the equilibrium constant $K_{4,6}$ becomes > 1 at $T <$ 250 K, or $\Delta G^0_{4,5} \approx 0$ at 250 K. The value of $\Delta S^0_{4,6}$ is probably similar to that of $\Delta S^0_{2,4} = -84$ J/mol K. Hence, $\Delta H^0_{4,6} \approx -84 \times 250 = -21\,000$ J/mol = −21 kJ/mol.

The value $\Delta H^0_{2,4} = -95$ kJ/mol indicates that N_2^+–N_2 is held together by a one-electron bond, whereas $\Delta H^0_{4,6} = -21$ kJ/mol indicates that N_4^+–N_2 is a relatively loosely bound cluster.

The fanning out of $n\mu$ values with increasing density at $T <$ 150 K (Fig. 1) is attributed to an increase of the cluster size as in the following reactions:

[4] $N_4^+(N_2) + 2N_2 \rightleftharpoons N_4^+(N_2)_2 + N_2$

[5] $N_4^+(N_2)_2 + 2N_2 \rightleftharpoons N_4^+(N_2)_3 + N_2$

and so on. Assuming $\Delta S^0 \approx -80$ J/mol K and $\Delta G^0 = 0$ at ~140 K for each of reactions [4] and [5], one obtains $\Delta H^0 \approx -80 \times 140 = -11$ kJ/mol for each step.

The increase of reduced mass of the colliding pair is not enough to explain all the decrease of $n\mu$ in this region. The increasing hard core radius of the ion must also make a contribution.

B. Momentum transfer cross sections

The ions in Tyndall and Pearce's system (8) at $T > 250$ K would have been unclustered N_4^+ with a trace of N_3^+. The ratio of concentration $[N_3^+]/[N_4^+]$ would equal the ratio $[N^+]/[N_2^+]$ initially formed, which would be smaller in Tyndall's system than the 0.04 in a 70 V mass spectrum (11). The N_3^+ was therefore negligible in ref. 8 and in the present work.

To obtain a self-consistent view of the temperature coefficient of $n\mu(N_4^+)$ over the range $50 \leq T/K \leq 587$, the $n\mu$ values in refs. 7 and 8 were normalized at 290–300 K to those in ref. 6 and the present work. Thus, $n\mu$ values from ref. 8 were divided by 1.10, and those for N_4^+ from ref. 7 were multiplied by 1.07 (Fig. 3). The N_4^+–N_2 momentum transfer cross section as a function of collision energy ϵ was extracted from the ($n\mu$, T) values by numerically fitting them to eq. [6] (12).

$$[6] \quad n\mu = \frac{3}{8} e (k_B T)^{5/2} \left(\frac{2\pi}{M_r}\right)^{1/2} \Big/ \int_0^\infty \epsilon^2 \sigma_m \exp(-\epsilon/k_B T) d\epsilon$$

where e is the charge on the ion, k_B is Boltzmann's constant, and M_r is the reduced mass of the collision pair. The ions are in thermal equilibrium with the gas.

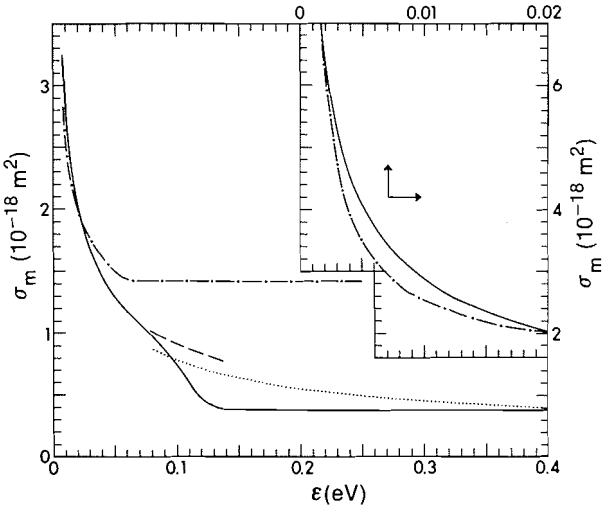

FIG. 4. Momentum transfer cross sections of N_2 for the cations N_4^+ (——) and N_2^+ (–·–·–), obtained by fitting the data in Fig. 3 to eq. [6]. – – –, σ_{pol} using α_m; ···, σ_{pol} using $\bar{\alpha}$ (see text).

The cross sections are shown in Fig. 4. At $\epsilon < 0.08$ eV the value of σ_m for N_4^+–N_2 collisions is equal to that expected from the polarization potential (13)

$$[7] \quad \sigma_{pol} = \left(\frac{2.21\pi e}{4\pi\epsilon_0 v}\right)\left(\frac{\alpha}{M_r}\right)^{1/2}$$

where ϵ_0 is the permittivity of vacuum and α is the polarizability of N_2. The value of α in eq. [7] is in SI units, C m^2/V (dipole moment (C m)/field strength (V m^{-1}); the non SI unit m^3 corresponds to $\alpha/4\pi\epsilon_0 = 8.99 \times 10^9\alpha$). If the values of the constants are inserted in eq. [7], and α is expressed in 10^{-40} C m^2/V and ϵ in eV, one obtains

$$[8] \quad \sigma_{pol}(m^2) = 1.76 \times 10^{-19}(\alpha/\epsilon)^{1/2}$$

At low energies the slowly moving molecule and ion interact for a sufficiently long time (>1 ps) during a collision that the nitrogen molecule tends to become oriented, such that its axis of maximum polarizability is directed towards the ion (1). Under these circumstances the maximum component $\alpha_m = 2.65 \times 10^{-40}$ C m^2/V (14) of the nitrogen polarizability matrix is used in eq. [8]. This gives the experimental values of σ_m for N_4^+–N_2 at $\epsilon < 0.08$ eV and the dashed line at $\epsilon > 0.08$ eV (Fig. 4).

At the higher energies the ion–molecule interaction time during a collision is too brief (≤1 ps) to allow the long polarization axis of the molecule to become oriented in the field of the ion. Under these circumstances the average value $\bar{\alpha} = 1.96 \times 10^{-40}$ C m^2/V (14) is used in eq. [8]. This gives the dotted line in Fig. 4.

The N_4^+–N_2 momentum transfer cross sections are therefore similar to those expected from the polarization interaction. The apparently low values in a broad region around $\epsilon \approx 0.15$ eV might be an artifact due to an imprecise normalization of the different sets of $n\mu$ values (ref. 7 values still too low). However, the constant σ_m at $\epsilon > 0.14$ eV is a hard body value similar to that for two nitrogen molecules, 4×10^{-19} m^2 (15).

Cross sections extracted from the $n\mu$ values of N_2^+ in Fig. 3 are also displayed in Fig. 4. The negative $d(n\mu)/dT$ indicates a relatively small dependence of σ_m on energy. The scattering potential for N_2^+–N_2 has a shorter range than that for N_4^+–N_2. The power p in the distance dependence of the interaction potential

$$[9] \quad V(r) \propto r^{-p}$$

is ~6–10 for N_2^+–N_2, and ~3–4 for N_4^+–N_2 at $\epsilon \approx 0.01$–0.13 eV (ref. 13, pp. 78–79).

The value of σ_m for N_2^+–N_2 at $\epsilon < 3$ meV in Fig. 4 has been arbitrarily drawn to join σ_{pol} at ~2 meV, although the $n\mu$ data at $T < 80$ K do not actually require such a large value of σ_m. At $\epsilon > 0.06$ eV, σ_m is constant with a value four times larger than the hard-body cross section for N_4^+–N_2 (Fig. 4) or the neutral N_2–N_2 (15). The larger cross section for N_2^+–N_2 can be attributed to resonant charge transfer (16).

Acknowledgements

We are grateful for financial assistance from the Natural Sciences and Engineering Research Council. We also thank the staff of the Radiation Research Center for maintaining the equipment.

1. N. GEE, S. S.-S. HUANG, T. WADA, and G. R. FREEMAN. J. Chem. Phys. **77**, 1411 (1982).
2. T. WADA and G. R. FREEMAN. Phys. Rev. A, **24**, 1066 (1981).
3. (*a*) T. WADA and G. R. FREEMAN. Phys. Rev. Lett. **42**, 715 (1978); (*b*) J.-P. DODELET and G. R. FREEMAN. Can. J. Chem. **55**, 2264 (1977).
4. N. GEE and G. R. FREEMAN. Can. J. Chem. **59**, 2988 (1981).
5. R. C. REID, J. M. PRAUSNITZ, and T. K. SHERWOOD. The properties of gases and liquids. McGraw–Hill, New York, 1977.
6. J. T. MOSELEY, S. M. SNUGGS, D. W. MARTIN, and E. W. MCDANIEL. Phys. Rev. **178**, 240 (1969).
7. H. BOHRINGER and F. ARNOLD. Int. J. Mass Spectrom. Ion Phys. **49**, 61 (1983).
8. A. M. TYNDALL and A. F. PEARCE. Proc. R. Soc. London. A, **149**, 426 (1935).
9. J. D. PAYZANT and P. KEBARLE. J. Chem. Phys. **53**, 4723 (1970).
10. R. PATRICK and D. M. GOLDEN. J. Chem. Phys. **82**, 75 (1985).
11. R. S. GOHLKE (*Editor*). Uncertified mass spectral data. Dow Chemical Co. and ASTM E-14, Midland, MI. 1963.
12. E. W. MCDANIEL and E. A. MASON. The mobility and diffusion of ions in gases. J. Wiley and Son, New York. 1973. pp. 139–140.
13. E. W. MCDANIEL. Collision phenomena in ionized gases. J. Wiley and Son, New York. 1964. Chapt. 3 and 9.
14. H. STUART. Landolt–Börnstein zahlenwerte und funktionen. *Edited by* A. Eucken and R. H. Hellwege. Springer-Verlag, Berlin. Germany. 1951. I Band, 3 Teil, Sec. 14207.
15. J. O. HIRSCHFELDER, C. F. CURTISS, and R. B. BIRD. Molecular theory of gases and liquids. Wiley, New York. 1954. p. 545.
16. E. W. MCDANIEL and E. A. MASON. The mobility and diffusion of ions in gases. J. Wiley and Son, New York. 1973. p. 42.

Electrostatic and nonelectrostatic, conventional and unitary thermodynamic quantities of reaction. I. Metal–ligand reactions in aqueous solvent

ROBERTO ARUGA

Department of Analytical Chemistry, University of Turin, via Giuria 5, 10125 Turin, Italy

Received July 25, 1985

ROBERTO ARUGA. Can. J. Chem. **64**, 780 (1986).

A calculation method of the electrostatic and nonelectrostatic parts of thermodynamic quantities of reaction, previously proposed and applied to complex-formation reactions of aminic and carboxylic ligands, is applied, in the present work, to association reactions of several other ligands. In particular, to check its reliability, this method is applied to ΔG^0, ΔH^0, and ΔS^0 data of literature for the formation of metal–anion pairs and for associations of metals with ligands containing pyridine nitrogen, ethereal oxygen, or thioethereal sulfur. Experimental data referring only to aqueous solutions are considered. The results obtained by this method are in agreement, in most cases, with those expected for the reactions examined. Therefore, it seems reliable and useful for a more significant interpretation of conventional thermodynamic parameters.

ROBERTO ARUGA. Can. J. Chem. **64**, 780 (1986).

Dans le présent travail, on applique à des réactions d'association de plusieurs autres ligands la méthode de calcul des composantes électrostatiques et non-électrostatiques de quantités thermodynamiques de réactions, qui avait été proposée et appliquée antérieurement à des réactions de formation de complexes de ligands amines et acides carboxyliques. Dans le but d'évaluer la fiabilité de cette méthode, on l'a appliquée en particulier à des données de ΔG^0, ΔH^0 et ΔS^0 relatives à la formation de paires de métal–anion et à des associations de métaux avec des ligands contenant l'azote d'une pyridine, l'oxygène d'un éther et le soufre d'un thioéther. On a considéré des données expérimentales se référant uniquement à des solutions aqueuses. Dans la plupart des cas, les résultats obtenus avec cette méthode sont en accord avec ceux que l'on pourrait espérer pour les réactions examinées. La méthode semble donc fiable et utile pour une interprétation significative des paramètres thermodynamiques conventionnels.

[Traduit par la revue]

Introduction

Two successive phases seem to have, in general, been characterized in the study of stabilities of metal–ligand complexes in solution. The former phase was characterized by the determination of stability constant data, the latter by the determination of Gibbs function together with its enthalpy and entropy contributions.

The determination of enthalpy and entropy data leads to a better comprehension of the causes which determine different complex stabilities in solution. Interpretation of entropy data is, in general, fairly simple, as this quantity is often determined by the so-called environmental factors, which consist of interactions of the solute with the surrounding solvent particles (1). The enthalpy value appears more complex, as it is affected by both environmental and internal factors, the latter being determined by the strength and nature of solute–solute and solute–solvent direct bonds. As a consequence of this fact, the need has been felt to divide the thermodynamic quantities, especially enthalpy, into two contributions which allow an evaluation of the relative importance of external and internal factors in the association process.

A method of calculation of electrostatic (or external) and nonelectrostatic (or internal) contributions of thermodynamic parameters was first proposed by Gurney (2) for the investigation of acid–base equilibria. Only later (3–6) the possibility was suggested to extend its application to metal–ligand reactions. Actual application of the Gurney method to experimental thermodynamic data for metal–ligand complexes is the subject of a limited number of papers (7–9). Moreover, the method was only used in the case of aminic and carboxylic ligands.

Taking into account these observations it was thought of interest, in the present study, to extend the experimental verification of Gurney's method to the case of ligands not yet investigated in previous works. This treatment, in particular, is applied here to several calorimetric data of literature for the formation, in aqueous solution, of the less stable ion pairs, and for ligands containing less investigated coordinating sites, such as pyridine nitrogen, ethereal oxygen, or thioethereal sulfur. Verifications of the above theory may also be useful in view of an extension of this treatment to association reactions in different solvents, which will be the subject of the next paper of this series (this issue, Can. J. Chem.).

Treatment of the experimental data

Referring to previous papers for fuller details (2, 9–12), it may be observed that the equilibrium constant for a general complex formation reaction

$$[1] \quad M + nL \rightleftarrows ML_n$$

can be expressed in terms of the mole fraction of the species (K^x) instead of the moles per liter. This is the same as assuming pure substance (i.e., unitary mole fraction) as the standard state for both the solute and the solvent. It can be demonstrated that K^x for equilibrium [1] is related to the conventional constant K in the following manner:

$$[2] \quad K = K^x M_s^{-n}$$

where M_s is the concentration of the solvent and n is the number of moles of the reagents minus the moles of the products. Therefore the conventional constant, as well as Gibbs function, consist of two parts: K^x, the unitary part, and M_s^{-n}, the cratic part.

The following observations can be made on the cratic term. (*a*) The existence of this term is due to different standard states for the solute and the solvent, as it disappears when K^x is used instead of K. (*b*) The cratic term is constant only for reactions of the same stoichiometric type and in the same solvent. On this basis several authors consider only the unitary part as a characteristic and specific quantity for every single reaction (2, 10). In general, the use of K^x is recommended when

Printed in Canada / Imprimé au Canada

TABLE 1. Electrostatic (el), nonelectrostatic (non), unitary (x), and cratic (c) contributions of the conventional thermodynamic parameters ΔX^0 ($X = G, H, S$)

ΔX^0	ΔX_{non}	ΔX_{el}
ΔG^0	$nRT \ln M_s + RCa$	$RCe^{T/\theta}$
ΔH^0	RCa	$RC(1 - T/\theta)e^{T/\theta}$
ΔS^0	$-nR \ln M_s$	$-e^{T/\theta}(RC/\theta)$
	ΔX^c	ΔX^x

quantities for reactions in different solvents or with different stoichiometry are compared, as different cratic parts are present in these cases. To eliminate any extraneous influence by the term M_s^{-n}, in the present study, it was also thought necessary to take the unitary term into consideration when the electrostatic and the covalent contribution of a certain thermodynamic quantity are compared with each other.

Unitary ΔG^0 may be divided into the electrostatic part (ΔG^x_{el}) and the nonelectrostatic part (ΔG^x_{non}) (2, 4, 8, 9). ΔG^x_{el} represents long-range electrostatic interactions, which are affected by the dielectric nature of the solvent and by the temperature. Therefore, it is determined by solute–solute electrostatic bonds and by long-range solute–solvent interactions. ΔG^x_{non} is determined by all short-range factors, independent of the dielectric constant and of the temperature. They consist mainly of solute–solute covalent bonds and of solute–solvent contact interactions (i.e., solvation interactions) (8). An evaluation of the above contributions can be made taking into account the following considerations. First of all, it may be shown that for an association reaction $\Delta G^x_{el} = \alpha/D$, where α is constant and D is the dielectric constant of the medium (2, 7, 9). The variation of D with temperature is expressed empirically by: $D = D_0 e^{-T/\theta}$, where D_0 is a constant and θ is a temperature characteristic of the solvent. From the values of D at various T, a value for θ of about 212 is obtained for water (13). From the above expressions, taking also into account that $\Delta G^x = \Delta G^x_{el} + \Delta G^x_{non}$, the following relation is obtained:

$$[3] \quad -\ln K^x = C(a + e^{T/\theta})/T$$

where $C = \alpha/RD_0$ and $a = \Delta G^x_{non} D_0/\alpha$. From eq. [3], using parameters C and a, the following expressions may be derived for the conventional thermodynamic quantities (9):

$$[4] \quad \Delta G^0 = nRT \ln M_s + RC(a + e^{T/\theta})$$

$$[5] \quad \Delta H^0 = RC[a + (1 - T/\theta)e^{T/\theta}]$$

$$[6] \quad \Delta S^0 = -nR \ln M_s - (RC/\theta)e^{T/\theta}$$

The electrostatic and nonelectrostatic contributions of conventional and unitary thermodynamic functions may be obtained from the preceding discussion. The corresponding expressions are summarized in Table 1. C and a are determined knowing the experimental values of ΔG^0 and ΔH^0 (or ΔG^0 and ΔS^0) and using eqs. [4] and [5] (or eqs. [5] and [6]).

It follows from the data in Table 1 that the cratic part of ΔH^0 is zero, i.e., $\Delta H^0 = \Delta H^x$. Therefore, comparisons between conventional quantities are valid, in the case of enthalpy, also for equilibria in different solvents. Moreover, it follows from Table 1 that $\Delta X_{el} = \Delta X^x_{el}$ and $\Delta H_{non} = \Delta G^x_{non}$.

Results and discussion

Thermodynamic quantities of the literature for associations in aqueous media at 25°C are collected in Table 2. According to the above statements, electrostatic and nonelectrostatic quantities are also listed in Table 2. Only the enthalpy values obtained by direct calorimetry are reported. Furthermore, values referred to the same ionic strength were compared when possible.

Evaluation of the reciprocal importance of electrostatic and nonelectrostatic factors for various types of equilibria (i.e., ΔG^x_{el} vs. ΔG^x_{non}, ΔH_{el} vs. ΔH_{non}) is an important point in the discussion of the present results. For metal–thiosulfate associations (14) negative values of ΔG^x_{el} are obtained, while values of ΔG^x_{non} are not distant from zero. This indicates prevailing electrostatic phenomena in the formation of the pairs, in accord with what is generally admitted for this kind of associations (1, 14). The only ΔG^x_{non} value considerably different from the others is that of cadmium ($\Delta G^x_{non} = -7.4$ kJ mol^{-1}). This value is in accord with a covalent character of the Cd—thiosulfate bond (14). It must be noted, in particular, that thiosulfate contains the —S^- group as bonding site and also that cadmium shows the greatest "soft" character among the metals listed in Table 2 for this anion.

The mean value of ΔG^x_{el} for the metal–thiosulfate associations (about -13 kJ mol^{-1}) is approximately determined by 5 kJ mol^{-1} of ΔH_{el} and by -18 kJ mol^{-1} of $-T\Delta S_{el}$. Taking into account that (*a*) ΔS_{el} is not affected by the association process (i.e., by the decrease from two to one solute particle) as the latter concerns the cratic part of ΔS^0 (see Table 1); (*b*) the endothermic values of ΔH_{el} show that they are not greatly affected by the formation of solute–solute bonds, the conclusion can be drawn that the above values of ΔH_{el} and $T\Delta S_{el}$ are mainly determined by external (i.e., solvent-destructuring) processes. It is also clear that the pair formation is a consequence of these processes, and that they favour the association through the entropy factors more than they oppose it through enthalpy. Similar considerations are also valid for the metal–sulfate associations (ref. 15, see Table 2). The only difference (which appears easily explainable) with respect to thiosulfate regards cadmium. In fact ΔG^x_{el} and ΔG^x_{non} of this metal with sulfate are similar to those of the other metals. Finally, a direct comparison of the thermodynamic quantities for sulfate and thiosulfate shows that the electrostatic parts of ΔH^0 and ΔS^0 for the former are more positive than for the latter, as though greater solvent-destructuring processes were present in the association of sulfate. This fact is in accord with a higher ionic strength ($I = 0.5$ mol L^{-1}) used for thiosulfate (and, consequently, with a more ordered structure of water in this case), while the results for sulfate refer to $I = 0$. It is also interesting to observe that differences in ionic strength do not remarkably affect the covalent part of the thermodynamic functions.

Comparisons of the electrostatic and nonelectrostatic part of Gibbs function may be interesting also for associations without charge neutralization. The results previously obtained in this laboratory for metal associations of 1-methylimidazole may be taken as an example (16). The second step of formation of certain mixed complexes where two electrically neutral particles take part in the association (17) is an even more typical example (see Table 2). Opposite results than for sulfate and thiosulfate are obtained in these cases. ΔG^x_{non} and ΔH_{non} are now clearly negative, while ΔG^x_{el} and ΔH_{el} are not distant from zero.

Previous experimental data for associations of pyridine-2-carboxylate with two groups of metals (the group from magnesium to barium and the nickel–zinc–copper group) are reported in Table 2 (18, 19). Different bonds may be formed by

TABLE 2. Molar thermodynamic quantities of literature for association equilibria: $M^{n+} + L^{p-} \rightleftarrows ML^{n-p}$, in aqueous solution at 25°C*

M	ΔG^0	ΔH^0	ΔS^0	ΔG_{non}	$\Delta G_{el} = \Delta G^x_{el}$	$\Delta H_{non} = \Delta G^x_{non}$	ΔH_{el}	$\Delta S^\dagger_{el}$
				L^{2-} = thiosulfate (14)				
Mg	−3.18	1.67	16.3	7.3	−10.5	−2.6	4.3	50
Ca	−3.97	2.68	22.2	7.8	−11.8	−2.1	4.8	56
Mn	−3.81	2.09	19.6	7.4	−11.2	−2.5	4.6	53
Co	−4.39	2.09	21.8	7.3	−11.7	−2.7	4.8	55
Ni	−4.44	1.84	20.9	7.1	−11.5	−2.9	4.7	54
Zn	−6.40	9.20	52.3	11.8	−18.2	1.8	7.4	86
Cd	−15.06	−0.17	49.8	2.5	−17.6	−7.4	7.1	83
				L^{2-} = sulfate (15)				
Mg	−13.18	5.31	61.5	6.9	−20.1	−3.0	8.2	95
Ca	−13.18	6.28	65.3	7.7	−20.9	−2.2	8.5	99
Ni	−13.10	6.36	65.7	7.9	−21.0	−2.0	8.5	99
Cu	−13.47	7.20	69.4	8.3	−21.8	−1.6	8.9	103
Zn	−13.22	5.69	63.6	7.3	−20.5	−2.6	8.4	97
Cd	−13.18	9.00	74.5	9.7	−22.8	−0.3	9.3	108
				L = 1-methylimidazole (16)				
Co	−13.68	−16.9	−10.9	−8.9	−4.8	−18.9	1.9	22
Ni	−17.40	−22.7	−18.0	−14.1	−3.3	−24.1	1.3	15
Cu	−24.52	−28.7	−14.0	−20.4	−4.1	−30.3	1.7	20
Zn	−15.40	−20.7	−17.8	−12.1	−3.3	−22.1	1.3	15
				M = CuL′‡; L = 2,2′-dipyridyl (17)				
(a)	−54.0	−49.8	13.8	−43.9	−10.0	−54.0	3.8	47
(b)	−52.7	−47.3	18.0	−41.8	−10.9	−51.9	4.2	51
(c)	−47.7	−49.4	−9.2	−42.7	−5.0	−52.3	2.1	24
(d)	−47.7	−49.8	−6.3	−41.8	−5.9	−51.9	2.5	27
(e)	−47.7	−48.5	−2.9	−41.0	−6.3	−51.0	2.5	30
(f)	−47.3	−54.0	−22.6	−44.8	−2.1	−54.8	0.8	11
(g)	−48.5	−48.9	−1.3	−41.8	−6.7	−51.5	2.9	32
(h)	−49.4	−43.9	18.4	−38.5	−10.9	−48.1	4.6	52
				L^- = pyridine-2-carboxylate (18, 19)				
Mg	−11.97	1.46	45.2	4.7	−16.6	−5.3	6.8	79
Ca	−9.71	−4.14	18.8	1.3	−11.0	−8.6	4.5	52
Sr	−9.12	−1.59	25.5	3.3	−12.5	−6.6	5.1	59
Ba	−8.83	−0.29	28.4	4.3	−13.1	−5.7	5.3	62
Ni	−37.40	−25.40	40.2	−21.8	−15.6	−31.8	6.3	74
Cu	−43.97	−26.94	56.9	−24.8	−19.1	−34.8	7.8	90
Zn	−29.04	−16.78	41.0	−13.3	−15.7	−23.2	6.4	74
				L^{2-} = pyridine-2,6-dicarboxylate (18, 19)				
Mg	−12.26	16.11	95.0	14.9	−27.2	5.0	11.0	128
Ca	−23.72	−12.26	38.5	−8.5	−15.2	−18.4	6.2	72
Sr	−20.92	−8.12	43.1	−4.7	−16.2	−14.7	6.6	77
Ba	−18.49	−8.08	35.1	−4.0	−14.5	−13.9	5.9	69
Ni	−37.57	−12.30	84.9	−12.5	−25.1	−22.5	10.2	118
Cu	−50.00	−15.82	115	−18.7	−31.3	−28.6	12.8	148
Zn	−34.23	−8.95	84.9	−9.2	−25.1	−19.1	10.2	118
				L^- = pyridine-2-acetate (21)				
Ni	−20.42	−15.4	16.7	−9.8	−10.6	−19.7	4.3	50
Cu	−31.00	−15.3	52.7	−12.8	−18.2	−22.7	7.4	86
Zn	−12.47	−3.9	28.4	0.6	−13.1	−9.3	5.3	62
	L = O—R—O—R—O—R—O—R—O—R (—R— = —CH_2—CH_2—) (22)							
Ag	−5.36	−13.5	−27.2	−4.1	−1.3	−14.0	0.5	6
Tl(I)	−7.03	−16.8	−32.6	−6.9	−0.2	−16.8	0.0	1
Pb	−10.54	−13.6	−10.5	−5.7	−4.8	−15.6	2.0	23
	L = S—R—O—R—O—R—O—R—O—R (—R— = —CH_2—CH_2—) (22)							
Ag	−28.53	−39.2	−35.1	−28.9	0.4	−38.9	−0.2	−2
Tl(I)	−4.56	−32.2	−92.9	−17.1	12.6	−27.1	−5.1	−59
Pb	−9.41	−21.5	−40.6	−10.9	1.5	−20.9	−0.6	−7

TABLE 2. (*concluded*)

M	ΔG^0	ΔH^0	ΔS^0	ΔG_{non}	$\Delta G_{el} = \Delta G^x_{el}$	$\Delta H_{non} = \Delta G^x_{non}$	ΔH_{el}	$\Delta S\dagger_{el}$
	L^{3-} = monohydrogen-2,2′-oxybis(ethyliminodiacetate); BATA (T = 20°C) (23)							
Mg	−46.7	14.7	209	4.7	−51.4	−5.1	19.7	243
Ca	−56.1	−28.7	94	−29.2	−26.9	−38.9	10.3	127
Mn	−77.2	−24.7	179	−32.2	−45.0	−42.0	17.2	212
Co	−85.6	−26.6	202	−35.9	−49.8	−45.6	19.1	235
Ni	−84.6	−19.8	221	−30.7	−53.8	−40.5	20.6	254
Cu	−101.5	−41.1	206	−50.8	−50.7	−60.6	19.5	240
Zn	−85.8	−25.1	207	−34.8	−51.0	−44.6	19.5	241
Cd	−90.9	−39.4	176	−46.6	−44.3	−56.4	17.0	209
Pb	−84.3	−55.0	100	−56.1	−28.2	−65.9	10.8	133
Hg(II)	−129.5	−85.8	149	−90.8	−38.7	−101	14.8	183
	L^{3-} = monohydrogen-2,2′-thiobis(ethyliminodiacetate); BSTA (T = 20°C) (23)							
Mg	−25.9	17.3	147	12.4	−38.2	2.6	14.6	180
Ca	−34.8	−10.5	83	−10.2	−24.7	−19.9	9.5	117
Mn	−56.5	−6.4	171	−13.3	−43.2	−23.0	16.6	204
Co	−78.5	−19.4	202	−28.7	−50.0	−38.5	19.1	235
Ni	−103	−32.2	242	−44.8	−58.3	−54.6	22.3	275
Cu	−93.0	−38.2	187	−46.3	−46.6	−56.1	17.9	220
Zn	−75.4	−15.5	204	−25.1	−50.3	−34.8	19.3	238
Cd	−80.7	−34.3	158	−40.1	−40.5	−49.9	15.6	192
Pb	−77.7	−54.4	80	−53.7	−24.0	−63.5	9.2	113
Hg(II)	−134	−95.4	132	−99.1	−35.0	−109	13.4	165

*Gibbs function and enthalpy are expressed in kJ mol^{-1}; entropy in J K^{-1} mol^{-1}. For the meaning of indexes and corresponding quantities see "Treatment of the experimental data" and Table 1.

†ΔS_{non} for the reactions listed in the table is constant: $\Delta S_{non} = -R \ln 55.35 = -33.4$ J K^{-1} mol^{-1}.

‡L′: (a) cyclopropane-1,1-dicarboxylate, (b) cyclobutane-1,1-dicarboxylate, (c) cyclopentane-1,1-dicarboxylate, (d) cyclohexane-1,1-dicarboxylate, (e) malonate, (f) succinate, (g) maleate, (h) phthalate.

this ligand: prevailingly, an electrostatic bond through the carboxylate group (8), and a covalent one through the pyridine nitrogen. The latter, in particular, is able to form π-bonds with the *d* electrons of the metal ion (20). The values of ΔH_{el} and ΔH_{non} seem in accord with these possibilities. In fact, similar ΔH_{el} values are obtained for all the above mentioned metals, in agreement with similar electrostatic phenomena (i.e., same charge-neutralization processes). On the other hand, very different values of ΔH_{non} are obtained: weakly exothermic values for group IIA metals (between −5 and −9 kJ mol^{-1}) and markedly exothermic values for Ni, Cu, Zn (between −23 and −35 kJ mol^{-1}). These results agree with a lower ability of the former metals to give covalent bonds. It must be noted, in particular, that they have no *d* electron. Similar observations can be made for the association of the above metals with pyridine-2,6-dicarboxylate (see Table 2).

Inversion of the stability order between magnesium and calcium with these two ligands is a fairly interesting point. In the case of pyridine-2-carboxylate the magnesium complex is more stable than that of calcium; for pyridine-2,6-dicarboxylate the order is reversed. This fact was previously justified considering the small dimensions of magnesium (1), which might have difficulty in forming stable bonds with the tridentate ligand. Such an explanation is related to short-range, steric factors, which should affect the nonelectrostatic part of enthalpy (8). The enthalpy data of Table 2 are in accord with this hypothesis. In fact, for both magnesium and calcium, the positive value of ΔH_{el} increases from the bidentate to the tridentate ligand, as a consequence of increasing charge-neutralization processes. ΔH_{non}, on the contrary, becomes more exothermic in the case of calcium, while it passes from −5.3 to +5.0 kJ mol^{-1} for magnesium. Therefore, ΔH_{non} seems to be the determining factor of the inversion of stabilities.

The presence of differently membered chelate rings is another example of a typical internal factor (8), which, in general, should affect the nonelectrostatic part of enthalpy. The above examined data for Ni, Cu, and Zn with pyridine-2-carboxylate (five-membered chelate ring), compared with the data of the same metals with pyridine-2-acetate (six-membered ring) (21) support this hypothesis. In fact (see Table 2), the higher stability of the pyridine-2-carboxylate complexes in comparison with those of pyridine-2-acetate is determined by ΔH_{non}, while ΔH_{el} values, for the three metal ions, show an opposite trend.

As regards the metal complexes of ethereal–oxygen or thioethereal–sulfur containing ligands (see Introduction), accurate calorimetric values are available in literature for "crown" ligands (22) and for polyaminopolycarboxylic ligands (23). Five oxygen atoms are present in the molecule of the first cyclic ether listed in Table 2, while one oxygen atom is replaced by one sulfur atom in the molecule of the second one. The following observations can be made on the thermodynamic quantities of reaction of these ligands with Ag, Tl(I), Pb. (*a*) The oxygen → sulfur replacement in the ligand molecule makes the covalent part of ΔG^x more negative. The decrease of ΔG^x_{non} is fairly limited for Pb and Tl(I), while it is greater for Ag. More precisely, the values of $\Delta\Delta G^x_{non}$ are −5.3 kJ mol^{-1} for Pb, −10.3 kJ mol^{-1} for Tl(I), and −24.9 kJ mol^{-1} for Ag. (*b*) The same sequence indicated at point (*a*) for $\Delta\Delta G^x_{non}$ is obtained when these metals are ordered following the increasing "soft" character: Pb < Tl(I) < Ag (24). (*c*) $\Delta\Delta G^x_{el}$ for the oxygen → sulfur replacement does not follow the above indicated sequence. The observations at points (*a*), (*b*), and (*c*) appear in accord

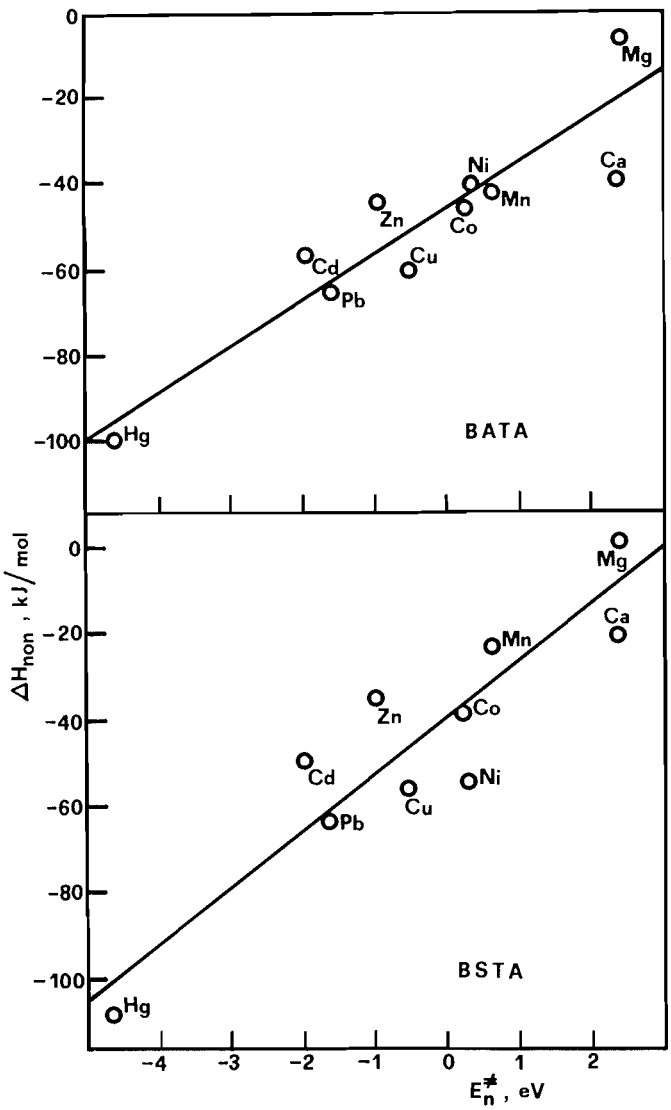

FIG. 1. Relationship between the nonelectrostatic contribution of enthalpy, ΔH_{non}, and the softness and hardness of metal ions, $E_n^{\neq}$ (24), for the complex formation reaction with BATA (above) and with BSTA (below) in aqueous solution.

with the nature and strength of the bonds which are probably formed between these metals and the sulfur atom. Similar considerations can be made also for ΔH_{el} and ΔH_{non}.

The ΔH_{el} and ΔH_{non} values for the bivalent metals listed in Table 2 with 2,2′-oxybis(ethyliminodiacetate) (BATA) and 2,2′-thiobis(ethyliminodiacetate) (BSTA) (23) suggest the following remarks. ΔH_{el} is almost constant; small endothermic deviations are only observed for smaller cations (Mg, Ni) and exothermic deviations for those with greater dimensions (Ca, Pb, Hg), in accord with different solvent-destructuring processes during the association. ΔH_{non}, on the other hand, becomes more negative with increasing softness of the metal ion, both in the case of BATA and of BSTA. An inversion is observed between ΔH_{non} for BATA (less negative) and for BSTA (more negative) in the case of Hg(II), which has the greatest soft character among the metal ions listed in Table 2. For a more significant examination of the ΔH_{non} dependence on softness of metal ions, the quantity $E_n^{\neq}$ should be considered. It was first introduced by Klopman (24) as a measure of hardness and softness of a metal ion in aqueous solution. A soft metal is characterized by a large negative value in $E_n^{\neq}$ and vice versa. Plots of ΔH_{non} vs. $E_n^{\neq}$ are reported in Fig. 1 for the association of BATA and BSTA with the bivalent metals of Table 2. Two straight lines are obtained by the least square method, with a slope of 10 and 13 for BATA and BSTA, respectively. A straight line with a slope of 10 (the same as for BATA) had been obtained previously for bivalent metals with EDTA (9). Taking into account that in metal complexes of BATA and BSTA both ethereal oxygen and thioethereal sulfur seem to form bonds with the cation (25), the conclusion can be drawn that the presence of an ethereal oxygen bound to the metal (as in the case of BATA) does not change (in comparison with EDTA) the trend of the ΔH_{non} values, while a considerable variation is caused by the sulfur atom of BSTA. If the electrostatic nature of an oxygen–metal bond and the covalent nature of a sulfur – soft metal bond are taken into account, the above conclusion is in agreement with the definition given for ΔH_{non}.

In conclusion, the present discussion shows that the calculation method of electrostatic and nonelectrostatic parts of thermodynamic quantities gives results which seem in satisfactory agreement with the nature and the course of the reactions examined. In particular, this method seems useful in clarifying phenomena which are implicit in conventional thermodynamic quantities but not immediately deducible from them.

1. G. H. NANCOLLAS. Interactions in electrolyte solutions. Elsevier, Amsterdam. 1966.
2. R. W. GURNEY. Ionic processes in solution. McGraw–Hill, New York. 1953.
3. J. LEWIS and R. G. WILKINS. *In* Modern coordination chemistry. *Edited by* F. J. C. Rossotti. Wiley, New York. 1960. Chapt. 1.
4. G. H. NANCOLLAS. Q. Rev. Chem. Soc. **14**, 402 (1960).
5. G. H. NANCOLLAS. Coord. Chem. Rev. **5**, 379 (1970).
6. A. E. MARTELL. *In* Coordination chemistry. Vol. I. *Edited by* G. Anderegg. Van Nostrand Reinhold, New York. 1971. Chapt. 8.
7. G. ANDEREGG. Helv. Chim. Acta, **51**, 1856 (1968).
8. G. DEGISCHER and G. H. NANCOLLAS. J. Chem. Soc. A, 1125 (1970).
9. S. MURAKAMI and T. YOSHINO. J. Inorg. Nucl. Chem. **43**, 2065 (1981).
10. A. W. ADAMSON. J. Am. Chem. Soc. **76**, 1578 (1954).
11. G. BEECH. Q. Rev. Chem. Soc. **23**, 410 (1969).
12. R. J. AGTERDENBOS. J. Chem. Educ. **45**, 230 (1968).
13. G. ÅKERLÖF. J. Am. Chem. Soc. **54**, 4125 (1932).
14. R. ARUGA. J. Inorg. Nucl. Chem. **36**, 3779 (1974).
15. J. W. LARSON. J. Phys. Chem. **74**, 3392 (1970).
16. R. ARUGA. Transition Met. Chem. **8**, 56 (1983).
17. G. ARENA, R. CALÌ, E. RIZZARELLI, S. SAMMARTANO, R. BARBUCCI, and M. J. M. CAMPBELL. J. Chem. Soc. Dalton. Trans. 581 (1977); 1090 (1978).
18. R. ARUGA. Bull. Soc. Chim. Fr. 79, (1983).
19. R. ARUGA. J. Inorg. Nucl. Chem. **41**, 845 (1979).
20. G. ANDEREGG. Helv. Chim. Acta, **43**, 414 (1960).
21. R. ARUGA. Atti Accad. Sci. Torino Cl. Sci. Fis. Mat. Nat. **114**, 365 (1980).
22. R. M. IZATT, R. E. TERRY, L. D. HANSEN, A. G. AVONDET, J. S. BRADSHAW, N. K. DALLEY, T. E. JENSEN, and J. J. CHRISTENSEN. Inorg. Chim. Acta, **30**, 1 (1978).
23. G. ANDEREGG. Helv. Chim. Acta, **47**, 1801 (1964).
24. G. KLOPMAN. J. Am. Chem. Soc. **90**, 233 (1968).
25. G. H. NANCOLLAS. Interactions in electrolyte solutions. Elsevier, Amsterdam. 1966. p. 158.

Electrostatic and nonelectrostatic, conventional and unitary thermodynamic quantities of reaction. II. Proton–ligand and metal–ligand reactions in mixed solvents

ROBERTO ARUGA
Department of Analytical Chemistry, University of Turin, via Giuria 5, 10125 Turin, Italy

Received July 25, 1985

ROBERTO ARUGA. Can. J. Chem. **64**, 785 (1986).

A calculation method of the electrostatic and the nonelectrostatic parts of thermodynamic quantities of reaction, previously proposed and applied to association reactions in aqueous medium, is applied, in the present work, to reactions in mixed solvents. The aim of the present treatment is to clarify the importance of the various factors (dependent and independent of the dielectric constant) through which the solvent affects complex stability. The method is applied to ΔG^0, ΔH^0, and ΔS^0 data of literature for proton–ligand and metal–ligand reactions in several water–methanol, water–ethanol, and water–dioxane mixtures. The conclusions of the present study seem to confirm a leading role of solvation equilibria in determining different stabilities of complex in different solvents, while a minor role is assigned to the dielectric properties of the solvent.

ROBERTO ARUGA. Can. J. Chem. **64**, 785 (1986).

Dans ce travail, on applique à des réactions dans des solvants mixtes, une méthode de calcul des portions électrostatiques et non-électrostatiques des quantités thermodynamiques de réactions, qui avait été proposée antérieurement et qui avait été appliquée à des réactions d'association dans des milieux aqueux. Le but du présent travail est de clarifier l'importance de divers facteurs (qui dépendent et qui sont indépendants de la constante diélectrique) par le biais desquels les effets de solvants affectent la stabilité des complexes. On applique la méthode aux données de ΔG^0, ΔH^0 et ΔS^0 trouvées dans la littérature pour des réactions proton–ligand et métal–ligand dans plusieurs mélanges de méthanol–eau, éthanol–eau et eau–dioxanne. Les conclusions de nos études semblent confirmer le rôle prépondérant de l'équilibre de solvatation dans la détermination des différents stabilitées des complexes dans divers solvants alors que les propriétés diélectriques du solvant ne joueraient qu'un rôle mineur.

[Traduit par la revue]

Introduction

The study of proton–ligand and metal–ligand equilibria, similarly to what took place in the study of aqueous media, passed through two successive phases also in the case of mixed and nonaqueous solvents (1). The former phase was, in general, characterized by the determination of stability data, while the latter saw the evaluation of the enthalpy and entropy contributions of ΔG^0.

Two principal facts take place passing from water to mixed or nonaqueous solvents. Firstly, a decrease is observed in the dielectric constant, at least for the most common organic solvents. Secondly, a general increase is observed in the stability of the reaction products, mainly in the case of associations between electrically charged particles (i.e., heteroelectric associations). From the above observations the conclusion was drawn that, for a metal–ligand or a proton–ligand system in different solvents (being equal the other experimental conditions), the dielectric constant of the medium has a determining influence on complex stability.

Afterwards, when sufficient amounts of enthalpy and entropy data were available for reactions in solvents other than water, this conclusion was remarkably modified. It was observed, for example, that the apparently simple and regular trend of ΔG^0 for various values of the dielectric constant was a consequence of more complex and not easily explainable variations in ΔH^0 and ΔS^0 (2). Other papers (3, 4) pointed out that not only the dielectric constant but solute–solvent direct interactions too, may have an important role in determining complex stability. In other words, the solvent may exert its influence in two ways, both through electrostatic (or environmental) factors and through short-range factors, the importance of which varies and is not always well understood.

To clarify this problem it may be of interest to extend, to equilibria in solvents other than water, the Gurney method of calculation of the electrostatic (or external) and nonelectrostatic (or internal) contributions of thermodynamic quantities of reaction. This method was previously used for reactions in aqueous medium (see ref. 1 and the relative bibliography).

Although enthalpy and entropy data of literature for complex-formation reactions in solvents other than water are not yet numerous (5), some accurate works are available at present on the subject. They treat proton–ligand as well as metal–ligand equilibria in aqueous–organic mixed solvents with variable water–cosolvent ratios (see Table 1).

Treatment of the experimental data

The concept of the electrostatic and nonelectrostatic parts of thermodynamic quantities of reaction, as well as the concept of the cratic and unitary contributions, were first introduced by Gurney (6). The electrostatic part represents long-range interactions, which are affected by the nature of the solvent and by the temperature. Therefore, it is determined by solute–solute electrostatic bonds and by long-range solute–solvent interactions (i.e., solvent-structuring and destructuring processes). The nonelectrostatic part is determined by all short-range factors, independent of the dielectric constant and temperature. They consist mainly of solute–solute covalent bonds and of solute–solvent contact interactions (i.e., solvation interactions) (7). Some notes about the use of this method in solvents other than water are reported below. Fuller details, together with general expressions for the calculation of the above partial quantities, are reported in the preceding paper of this series (1).

As concerns the present calculation method for equilibria in mixed solvents, the following observations must be taken into account. (*a*) For a correct comparison of thermodynamic parameters in different solvents the use of the unitary part of these quantities is recommended by some authors. The same applies when the electrostatic part of a quantity is compared with the corresponding nonelectrostatic part (1). Comparisons between conventional quantities are valid in the case of

Printed in Canada / Imprimé au Canada

TABLE 1. Molar thermodynamic quantities of literature for proton–ligand and metal–ligand equilibria in aqueous–organic mixed solvents at 25°C: $A^{n+} + L^{p-} \rightleftarrows AL^{n-p}$ (A^{n+} = proton or metal ion; L^{p-} = ligand)[a,b]

A	Organic cosolvent (wt%)	ΔG^0	ΔH^0	ΔS^0	ΔG^x	ΔS^x (= ΔS_{el})	ΔG_{non}	ΔG_{el} (= ΔG^x_{el})	ΔH_{non} (= ΔG^x_{non})	ΔH_{el}
					L = α-alaninate, react. site: —COO^-; org. cosolvent: dioxane (10)					
H	0	−13.39	−2.72	35.8	−23.35	69	1.2	−14.6	−8.8	5.9
	20	−15.10	−3.3	38	−24.64	71	−1.2	−13.8	−10.9	7.5
	35	−16.48	−3.8	42	−25.65	73	−3.0	−13.4	−12.1	8.4
	50	−18.54	−4.2	46	−27.28	77	−4.9	−13.6	−13.4	9.2
	65	−20.79	−5.0	54	−29.00	80	−6.7	−14.1	−14.6	9.6
					L = α-alaninate, react. site: —COO^-; org. cosolvent: methanol (10)					
H	0	−13.39	−2.72	35.6	−23.35	69	1.2	−14.6	−8.8	5.9
	20	−14.94	−4.2	38	−24.52	68	−1.2	−13.7	−10.9	6.7
	40	−16.61	−5.8	38	−25.82	67	−4.0	−12.6	−13.4	7.5
	60	−18.54	−6.2	42	−27.36	71	−6.0	−12.5	−14.6	8.4
	75	−20.79	−6.2	50	−29.29	77	−7.7	−13.1	−16.3	10.0
					L^- = α-alaninate, react. site: —NH_2; org. cosolvent: dioxane (10)					
H	0	−55.3	−47.3	26.8	−65.2	60	−42.5	−12.8	−52.3	5.0
	20	−55.8	−47.7	27	−65.3	59	−44.3	−11.5	−54.0	6.3
	35	−55.8	−47.3	28	−64.9	59	−44.9	−10.8	−54.0	6.7
	50	−56.5	−47.7	30	−65.2	59	−46.1	−10.4	−54.8	7.1
	65	−57.7	−46.4	38	−65.9	65	−46.2	−11.4	−54.4	7.9
					L^- = α-alaninate, react. site: —NH_2; org. cosolvent: methanol (10)					
H	0	−55.3	−47.3	26.8	−65.2	60	−42.5	−12.8	−52.3	5.0
	20	−55.0	−47.7	25	−64.6	57	−43.6	−11.4	−53.1	5.4
	40	−54.5	−47.3	24	−63.7	55	−44.1	−10.3	−53.1	5.9
	60	−54.1	−46.0	27	−62.9	56	−44.1	−10.0	−52.7	6.7
	75	−54.3	−44.8	32	−62.8	61	−44.1	−10.2	−52.7	7.9
					L^- = acetate; org. cosolvent: methanol (11)					
H	5	−27.45	0.42	93	−37.32	126	−0.7	−26.7	−10.6	11.0
	10	−27.95	−1.05	90	−37.70	123	−2.1	−25.9	−11.9	10.8
	20	−28.91	−1.46	92	−38.49	124	−3.9	−25.0	−13.5	12.0
	30	−30.00	−2.51	92	−39.41	124	−5.6	−24.4	−15.0	12.5
	40	−31.13	−1.67	99	−40.33	130	−6.7	−24.4	−15.9	14.3
	50	−32.47	−0.63	107	−41.51	137	−7.8	−24.7	−16.8	16.2
	60	−33.81	−0.42	112	−42.63	141	−8.7	−25.1	−17.6	17.1
	70	−35.77	0.84	123	−44.39	152	−10.0	−25.8	−18.6	19.4
	80	−38.07	1.26	132	−46.48	160	−11.0	−27.1	−19.4	20.7
					L^- = phenate; org. cosolvent: methanol (12)					
H	10	−57.55	−22.97	116	−67.24	149	−26.3	−31.2	−36.1	13.1
	30	−60.10	−22.55	126	−69.45	157	−29.0	−31.0	−38.4	15.9
	50	−62.53	−20.63	140	−71.50	171	−31.8	−30.7	−40.7	20.1
	70	−64.74	−19.46	152	−73.30	181	−34.0	−30.7	−42.6	23.1
	90	−69.27	−18.12	172	−77.40	199	−36.2	−33.0	−44.4	26.3
	100	−81.88	−35.56	156	−89.83	182	−48.7	−33.1	−56.7	21.1
					L^- = α-alaninate; org. cosolvent: dioxane (10)					
Cu	0	−46.0	−20.5	86	−56.0	119	−20.8	−25.2	−30.5	10.0
CuL	0	−38.3	−29.3	30	−48.3	64	−24.8	−13.5	−34.7	5.4
Cu	20	−48.2	−23.0	84	−57.7	116	−25.6	−22.6	−35.1	12.1
CuL	20	−39.2	−31.4	26	−48.8	58	−27.9	−11.3	−37.2	5.9
Cu	35	−49.8	−27.6	74	−59.0	105	−30.5	−19.3	−39.7	12.1
CuL	35	−40.7	−33.0	25	−49.8	56	−30.4	−10.3	−39.3	6.3
Cu	50	−52.9	−31.4	72	−61.6	101	−35.0	−17.9	−43.9	12.6
CuL	50	−42.5	−36.0	22	−51.2	56	−33.5	−9.0	−42.3	6.3
Cu	65	−55.0	−35.1	66	−63.2	94	−38.5	−16.5	−46.4	11.3
CuL	65	−43.8	−37.7	21	−52.0	48	−35.4	−8.4	−43.5	5.9
					L^- = α-alaninate; org. cosolvent: methanol (10)					
Cu	0	−46.0	−20.5	86	−56.0	119	−20.8	−25.2	−30.5	10.0
CuL	0	−38.3	−29.3	30	−48.3	64	−24.8	−13.5	−34.7	5.4
Cu	20	−47.8	−25.1	76	−57.4	108	−26.0	−21.8	−35.6	10.5
CuL	20	−39.6	−31.0	29	−49.2	61	−27.3	−12.3	−36.8	5.9
Cu	40	−50.0	−30.5	65	−59.2	96	−31.9	−18.1	−41.0	10.5

TABLE 1. (*concluded*)

A	Organic cosolvent (wt%)	ΔG^0	ΔH^0	ΔS^0	ΔG^x	ΔS^x (= ΔS_{el})	ΔG_{non}	ΔG_{el} (= ΔG^x_{el})	ΔH_{non} (= ΔG^x_{non})	ΔH_{el}
CuL	40	−41.0	−32.6	28	−50.2	59	−29.9	−11.1	−38.9	6.3
Cu	60	−52.3	−34.7	59	−61.1	89	−36.6	−15.7	−45.6	10.9
CuL	60	−42.6	−35.1	25	−51.4	54	−32.9	−9.6	−41.8	6.7
Cu	75	−54.0	−37.2	56	−62.5	85	−39.6	−14.4	−48.1	10.9
CuL	75	−43.7	−37.7	20	−52.2	49	−35.4	−8.3	−43.9	6.3
					L^- = α-alaninate; org. cosolvent: dioxane (10)					
Ni	0	−30.5	−16.7	46	−40.5	79	−13.6	−16.9	−23.4	6.7
NiL	0	−25.3	−19.2	20	−35.3	54	−13.9	−11.4	−23.8	4.6
Ni	20	−32.5	−17.6	50	−42.1	82	−16.6	−15.9	−25.9	8.4
NiL	20	−27.4	−20.9	22	−36.9	54	−16.9	−10.4	−26.4	5.4
Ni	35	−34.3	−17.6	56	−43.4	87	−18.4	−15.9	−27.6	10.0
NiL	35	−28.8	−20.9	26	−37.9	57	−18.3	−10.5	−27.6	6.7
Ni	50	−36.9	−20.5	54	−45.6	85	−22.1	−14.8	−31.0	10.5
NiL	50	−31.4	−23.4	27	−40.1	56	−21.5	−9.8	−30.1	6.7
Ni	65	−39.1	−21.8	58	−47.3	86	−24.1	−15.0	−32.2	10.5
NiL	65	−33.4	−25.1	28	−41.6	55	−23.7	−9.7	−31.8	6.7
					L^- = α-alaninate; org. cosolvent: methanol (10)					
Ni	0	−30.5	−16.7	46	−40.5	79	−13.6	−16.9	−23.4	6.7
NiL	0	−25.3	−19.2	20	−35.3	54	−13.9	−11.4	−23.8	4.6
Ni	20	−32.0	−17.1	50	−41.6	82	−15.5	−16.5	−25.1	7.9
NiL	20	−26.7	−19.2	25	−36.3	57	−15.2	−11.5	−24.7	5.4
Ni	40	−33.8	−17.1	56	−43.0	87	−17.4	−16.3	−26.8	9.6
NiL	40	−28.2	−20.1	27	−37.4	58	−17.3	−11.0	−26.4	6.3
Ni	60	−35.8	−18.4	58	−44.6	88	−20.2	−15.6	−28.9	10.5
NiL	60	−30.0	−20.1	33	−38.8	63	−18.9	−11.1	−27.6	7.5
Ni	75	−37.3	−17.6	66	−45.8	95	−21.2	−16.1	−29.7	12.1
NiL	75	−31.5	−20.5	37	−40.0	65	−20.4	−11.1	−28.9	8.4
					L^- = chloride ion; org. cosolvent: methanol (13)					
Cu	0	0.33	9.3	29	−9.62	63	13.8	−13.4	3.8	5.4
	4.0	0.04	12.1	42	−9.83	75	15.6	−15.6	5.7	6.4
	16.5	−0.33	13.4	46	−10.0	79	15.6	−16.0	6.0	7.4
	34.6	−3.01	11.7	50	−12.3	79	12.5	−15.6	3.2	8.4
	54.3	−5.86	14.8	71	−14.8	100	12.0	−17.8	3.0	11.8
	70.4	−8.16	11.1	64	−16.8	92	7.7	−15.9	−0.9	12.0
					L^- = chloride ion; org. cosolvent: ethanol (13)					
Cu	4.0	−0.04	12.0	42	−9.92	75	15.3	−15.4	5.5	6.5
	16.5	−0.92	13.8	50	−10.5	79	15.5	−16.4	5.9	7.9
	34.6	−3.56	11.1	50	−12.7	79	11.5	−15.1	2.4	8.7
	54.3	−5.77	13.6	65	−14.4	92	11.3	−17.1	2.7	10.9
	64.9	−10.21	9.4	67	−18.5	92	5.8	−16.0	−2.5	11.9

[a]For α-alaninate with Cu and Ni the second step of association is also considered. Therefore, A^{n+} indicates the 1:1 complex species too in these cases (see the table, first column).

[b]Gibbs function and enthalpy are expressed in kJ mol^{-1}; entropy in J K^{-1} mol^{-1}. For the meaning of indexes and corresponding quantities see ref. 1.

enthalpy, as its cratic part is zero ($\Delta H^0 = \Delta H^x$). (*b*) θ (see Table 1 of ref. 1) is a temperature characteristic of each solvent or solvent mixture. It is calculated by means of the empirical expression $D = D_0 e^{-T/\theta}$ (where D is the dielectric constant of the solvent and D_0 is a constant), knowing the values of D over a sufficiently wide range of temperatures. For the water–methanol, water–ethanol, and water–dioxane mixtures investigated in the present work the values of θ have been obtained from dielectric constant data published in previous papers (8, 9).

Results and discussion

The data of the literature for proton–ligand and metal–ligand equilibria in mixed solvents examined in the present work are listed in Table 1.

Besides the conventional thermodynamic parameters, the corresponding electrostatic, nonelectrostatic, and unitary parts have also been collected in the table. It must be pointed out that enthalpy values determined only by direct calorimetry were considered. Moreover, data for reactions in mixed solvents have been preferred to those in pure nonaqueous solvents and only the papers which report results for numerous water–cosolvent ratios have been considered. In fact the trend of thermodynamic quantities as a function of solvent composition is often complex, so that a sufficiently high number of mixtures is necessary for an accurate investigation.

The experimental data of Table 1 for proton, copper, and nickel associations with α-alaninate in water–dioxane and in water–methanol mixtures are those of the extensive work of Gergely and Kiss (10). The data in Table 1 suggest the following

observations on the protonation reaction of α-alaninate. In the first place, ΔG^x for the protonation of the amino group is about constant for increasing quantities of dioxane in the mixture, while it becomes a little less negative for increasing quantities of methanol. For the protonation of the carboxylate group, on the other hand, ΔG^x becomes much more favourable with increasing quantities of both the organic cosolvents. The different trends of Gibbs function for $—COO^-$ and $—NH_2$ were justified in the usual way (10), taking into account the decrease in the dielectric constant for increasing quantities of the organic cosolvent, and concluding that the protonation of $—NH_2$ should be less affected by this fact compared to the protonation of $—COO^-$, the former (at least partially) being isoelectric, the latter hetereoelectric. In reality, the values of ΔG^x_{el} for carboxylate indicate that factors depending on the dielectric constant have no determinant influence on the trend of ΔG^x of protonation. ΔG^x_{el} in fact shows an opposite trend with respect to ΔG^x over a wide range of solvent compositions, while the determinant sequence is that of ΔG^x_{non}.

In the second place, ΔG^x_{non} of protonation of the carboxylate group is very different than for the amino group (i.e., it is more favourable for $—NH_2$ than for $—COO^-$), while ΔG^x_{el} is about equal for these two groups. The conclusion should be drawn from these data that it is incorrect to consider protonation of $—NH_2$ as isoelectric, since in this case ΔG^x_{el} for $—NH_2$ should be of much smaller magnitude than for $—COO^-$. This conclusion is in complete agreement with a previous hypothesis (10) according to which an intramolecular hydrogen bond may develop in α-alaninate, via a water molecule between the carboxylate and amino groups. Because of the resulting electron shift, the protonation of the amino group should not be isoelectric.

As already mentioned above, an opposite trend of ΔG^x_{el} with respect to ΔG^x is observed for water-prevailing solvent compositions, while in the range of organic cosolvent prevalence (although data are less numerous in this case) ΔG^x_{el} shows the same trend as ΔG^x. More precisely, a minimum in stability is observed for ΔG^x_{el} at approximately 40–60 wt% of water. This fact is observed in several cases, as results from successive data of Table 1.

Other data of the table concern proton–acetate (11) and proton–phenate (12) associations, over a wide range of water–methanol mixtures. The results for these equilibria confirm the preceding observations for the protonation of the $—COO^-$ group of α-alanine. In this case, too, ΔG^x_{el} shows minimum stability at 40–60 wt% of water. It must also be noted that ΔH^0 and ΔS^0 for the protonation of phenate show maxima (i.e., minimal exothermicity for ΔH^0) at about 10% water. This does not appear from ΔG^0 because of the compensation of the enthalpy and entropy maxima. The present results show that the cause of such behavior of ΔH^0 and ΔS^0 is in the corresponding electrostatic part.

The data of copper and nickel with α-alaninate (Table 1) show the usual increase in complex stability with increasing amounts of organic cosolvent, both in the case of dioxane and of methanol. In this case too, calculation of the electrostatic and the nonelectrostatic contributions of ΔG^x indicates the latter as the determining factor of different stabilities in different solvents, for both the first and second step of association.

To investigate ion-pairing equilibria the data of a previous paper may be examined (13), concerning copper–chloride associations in several water–methanol and water–ethanol mixtures. ΔG^0 (and ΔG^x), as usual, becomes more negative with increasing concentrations of the organic cosolvent, for both methanol and ethanol mixtures (Table 1). Nevertheless, two new facts seem present in this case. Firstly, ΔG^x_{non} does not seem to be determinant on the ΔG^x sequence in different solvents, both in the case of methanol and of ethanol. Secondly, the magnitude of each ΔG^x value is determined by ΔG^x_{el}, while ΔG^x_{non} is in general not distant from zero and endothermic.

Within the limits of validity of the present theory, the following general conclusions can be drawn.

(*a*) The present results demonstrate that, in most cases, the trend of ΔG^x in different solvents is determined by nonelectrostatic, short-range factors (ΔG^x_{non}), while factors depending on the dielectric constant of the solvent (ΔG^x_{el}) show different trends, and do not appear to be determinant on stabilities. This conclusion is in accord with the results of recent works (3, 4).

(*b*) Taking the two main short-range factors into consideration (see "Treatment of the experimental data" and ref. 7), it may be observed that with a change of solvent, solute–solute covalent interactions are the same, while solute–solvent direct interactions (i.e., solvation interactions) are different. Consequently, the influence of the solvent on complex stability should be determined by the latter factor. This confirms the concept that a complex-formation equilibrium in a solvent, must be considered as a competition (with a consequent exchange reaction) between the ligand in a strict sense and the solvent–ligand (3, 4, 14).

(*c*) As concerns the role of the solvent in metal–ligand equilibria, outer-sphere associations should be considered as a particular case. It is interesting to consider again, in this connection, the data of copper with chloride, which appeared unusual with respect to the other data of Table 1. A prevailing outer-sphere character was suggested for these pairs (13). This fact should limit covalent solute–solute interactions and desolvation processes, i.e., internal processes taken as a whole. The small magnitude of ΔG^x_{non} may be justified in this way, as well as the fact that ΔG^x_{non} in this case is not determinant on the order of ΔG^x for different solvents.

(*d*) Taking into account that (*i*) the solvent seems to affect complex stability mainly through its own solvating ability (see point *b* above), (*ii*) the concept of donor number (DN, which is defined (14) as $-\Delta H^0$ of association in an inert medium between the solvent molecule and $SbCl_5$ reference acceptor) was shown to be useful as a measure of solvating abilities of donor solvents; the conclusion can be drawn that, among all the properties proposed previously to justify the solvent influence on complex stability (i.e., polarity, dielectric constant, donor number, autoprotolysis constant, hydrogen-bond forming ability), donor number is probably the most important. At the same time ΔG^x_{non} (which was demonstrated to be determinant on the ΔG^x sequence, see point *a* above) is equal to ΔH_{non}, being zero the corresponding entropy contribution (1). Therefore, it results from the present discussion that the influence of the solvent on complex stability is due to solute–solvent enthalpy factors. Taking into account the above definition of donor number, the equivalence of the two concepts becomes evident.

(*e*) Donor number does not always seem sufficient to justify experimental data of stability. Inadequacy of DN can be summarized in the following points. (*i*) Steric properties of solvents are not taken into account by DN, as it refers to the reaction of only one molecule of solvent with one molecule of $SbCl_5$ (14). In reality, when solute particles are surrounded by the solvent, bulk properties of the latter are important in determining the number and strength of solute–solvent bonds

and, consequently, the actual solvating properties of the solvent. (*ii*) For reasons similar to the preceding ones, DN does not consider the highly ordered structure of certain solvents. Water is a typical example of this fact. Taking into account that a DN of 18.0 is usually assigned to water and of 19.0 to organic solvents such as methanol and dioxane (15), the conclusion should be drawn that the latter have a slightly higher capacity than water for opposing metal–ligand complex formation. But for the most part the experimental data are in contrast with this conclusion (see, as an example, the ΔG^x values of Table 1). To eliminate this inconsistency, a DN value referring to the bulk donation properties of water is used by some authors (16), the magnitude of which is far greater than 18.0. (*iii*) Inert media in which the reaction enthalpy of the solvent with $SbCl_5$ may be measured correctly appear difficult to find. Dichloroethylene, which is the usual medium, shows unusual solvating properties which can affect experimental enthalpies. $SbCl_5$ too was shown, in some cases, to be a poor reference acid for the quantitative determination of donor strength (17). (*iv*) Since DN is a conventional ΔH^0, it may be affected, in addition to short-range factors, by external electrostatic factors too. The latter have no relationship with solvation bonds (7), so they could have an undue influence on DN.

The problem of evaluation of solvating properties could be treated in a more correct way by using the nonelectrostatic part of enthalpy instead of conventional ΔH^0. Let us for instance consider an association reaction $M + L \rightleftarrows ML$ in the solvent S_1 and in another solvent S_2 taken as reference. In accord with the present discussion and previous considerations (7), ΔH_{non} for this reaction may be considered as determined by two main factors: covalent interactions between M and L [ΔH(M–L)] and solvating bonds [ΔH(solv.)]. The former are equal in both solvents, while the latter are different. Consequently the difference of ΔH_{non} for this reaction in the two solvents may be indicated as follows:

$$[1] \quad (\Delta H_{non})_{S_1} - (\Delta H_{non})_{S_2} = [\Delta H(\text{solv.})]_{S_1} - [\Delta H(\text{solv.})]_{S_2}$$

The quantity at the left-hand side of eq. [1] has the same enthalpy nature as usual DN but, unlike DN, is not affected by external electrostatic factors. Moreover, as it refers to the real case of a solute surrounded by solvent molecules, it seems to eliminate the above mentioned disadvantages of usual DN. Therefore the concept of ΔH_{non}, at least in principle, could give an improved means, other than the usual DN, to measure solvating abilities of solvents.

(*f*) ΔH_{el} and ΔS_{el} of Table 1 are generally positive. This fact is usually due to the prevalence of solvent-destructuring processes over other processes, such as the formation of solute–solute bonds (which should give exothermic values of enthalpy). It may also be observed that ΔH_{el} and ΔS_{el}, few cases excepted, become more positive (i.e., solvent-destructuring processes increase) with increasing amounts of organic cosolvent. This fact may be justified, at least for heteroelectric associations, considering that the solvent, before the association reaction, is ordered by the electric field of ions. While the polar structure of water remains ordered after the association too, other solvents such as dioxane and alcohols become less ordered (4). Therefore, a greater increase of disorder is expected in the association as the quantity of the organic cosolvent increases.

1. R. ARUGA. Can. J. Chem. **64**, 0000 (1986).
2. R. M. IZATT, D. J. EATOUGH, and J. J. CHRISTENSEN. J. Phys. Chem. **72**, 2720 (1968).
3. K. K. MUI, W. A. E. MCBRYDE, and E. NIEBOER. Can. J. Chem. **52**, 1821 (1974).
4. W. A. E. MCBRYDE and H. K. J. POWELL. Can. J. Chem. **57**, 1785 (1979).
5. J. J. CHRISTENSEN, D. J. EATOUGH, and R. M. IZATT. Handbook of metal–ligand heats. 2nd ed. Marcel Dekker, New York. 1975.
6. R. W. GURNEY. Ionic processes in solution. McGraw–Hill, New York. 1953.
7. G. DEGISCHER and G. H. NANCOLLAS. J. Chem. Soc. A, 1125 (1970).
8. G. ÅKERLÖF. J. Am. Chem. Soc. **54**, 4125 (1932).
9. G. ÅKERLÖF and O. A. SHORT. J. Am. Chem. Soc. **58**, 1241 (1936).
10. A. GERGELY and T. KISS. J. Inorg. Nucl. Chem. **39**, 109 (1977).
11. L. AVEDIKIAN. Bull. Soc. Chim. Fr. 2832 (1971).
12. G. H. PARSONS and C. H. ROCHESTER. J. Chem. Soc. Faraday Trans. 1, **71**, 1069 (1975).
13. V. V. BLOKHIN, L. I. RAZMYSLOVA, M. I. SHALAEVSKAYA, YU. A. MAKASHEV, and V. E. MIRONOV. Zh. Fiz. Khim. **48**, 469 (1974).
14. V. GUTMAN. Coordination chemistry in non-aqueous solutions. Springer-Verlag, Wien, Austria. 1968.
15. U. MAYER. Coord. Chem. Rev. **21**, 159 (1976).
16. U. BIADER CEIPIDOR, V. CARUNCHIO, G. D'ASCENZO, and M. TOMASSETTI. Thermochim. Acta, **35**, 197 (1980).
17. Y. Y. LIM and R. S. DRAGO. Inorg. Chem. **11**, 202 (1972).

Measurement of some primary nuclear interferences in neutron activation analysis with a SLOWPOKE reactor

G. KENNEDY, J.-L. GALINIER, AND L. ZIKOVSKY
École Polytechnique, Montréal, Que., Canada H3C 3A7

Received April 15, 1985[1]

G. KENNEDY, J.-L. GALINIER, and L. ZIKOVSKY. Can. J. Chem. **64**, 790 (1986).

The interference factors were measured for 21 cases where the (n, p) and (n, α) reactions induced by fast neutrons produce the same radioisotopes as those used in the determination of F, Na, Mg, Al, S, Sc, Ti, V, Cr, Mn, Co, Ni, Cu, Ga, and As. The measured factors are compared with those calculated from data found in the literature.

G. KENNEDY, J.-L. GALINIER et L. ZIKOVSKY. Can. J. Chem. **64**, 790 (1986).

On a mesuré les facteurs d'interférence dans 21 cas pour lesquels les réactions (n, p) et (n, α) induites par des neutrons rapides produisent les mêmes radioisotopes que ceux utilisés lors de la détermination des éléments suivants: F, Na, Mg, Al, S, Sc, Ti, V, Cr, Mn, Co, Ni, Cu, Ga et As. On a comparé les facteurs mesurés avec ceux calculés sur la base des données que l'on peut retrouver dans la littérature.

[Traduit par la revue]

Introduction

In neutron activation analysis using reactors as a neutron source, it is usually assumed that each radioisotope detected is produced by the (n, γ) reaction on a stable isotope of the same element; however, in most irradiation sites, there is a significant component of fast neutrons which may produce the radioisotope of interest by (n, p) and (n, α) reactions on heavier elements. The analyst must be aware of which elements may be affected by these nuclear interferences and he may be able to correct them using an "interference factor" if the interfering element is also analysed.

In the case of the Canadian SLOWPOKE II reactor where the inner irradiation sites are located in the beryllium reflector, the fast neutron spectrum includes a component due to the (γ, n) reaction on beryllium as well as the fission neutrons. Using several (n, p) and (n, α) reactions of well-known cross section, this fast neutron flux has been determined (1) to be 0.21×10^{12} neutrons $cm^{-2} s^{-1}$ when the thermal neutron flux in these sites is 1.0×10^{12} neutrons $cm^{-2} s^{-1}$. With this significant fast neutron flux, it is estimated that the interferences from (n, p) and (n, α) reactions may be important for about 15 low- and medium-Z elements which are often analysed. The aim of this paper is to measure the "interference factors" for these elements with sufficient accuracy that they may be used to correct the interferences.

Several researchers have reported interference factors measured for interferences which occur with the analysis of sodium (2), aluminum (3, 4), sulfur (5), scandium (2), chromium (6), manganese (2, 5, 7), cobalt (2, 3, 7), and nickel (7). When the same factors were measured in several laboratories, the values measured varied by as much as several orders of magnitude, because of the widely varying ratios of fast to thermal neutron fluxes in the different reactors and irradiation sites used.

As a first approximation, the interference factors may be calculated using thermal neutron and fission neutron cross sections found in the literature as outlined by De Soete *et al.* (8). However, in a SLOWPOKE reactor the interference factors may be significantly different because of the influence of the beryllium reflector and other reactor components on the fast neutron spectrum. All the SLOWPOKE reactors currently in operation are of identical construction (including fuel, moderator, and reflector) and should, therefore, have identical neutron spectra. Any slight differences in the neutron spectra among these reactors would first be noticed as differences in the ratio of fast neutron flux to slow neutron flux. In the three reactors surveyed (1, 9)[2] this ratio has been measured as 0.21, 0.22, and 0.19, respectively, using various reactions for fast and thermal neutrons. These ratios appear to agree if one considers the uncertainties involved in their measurement. In addition, at the Montréal SLOWPOKE reactor this ratio was found to be constant, within the experimental error of 5%, over a period of seven years despite aging of the fuel and additions to the beryllium reflector. Thus, it is felt that a set of interference factors measured accurately with one SLOWPOKE II reactor will provide the data necessary for the accurate and reliable corrections of these interferences by analysts using any of the SLOWPOKE II reactors.

Experimental

In the analysis of an element with a given Z, the interference factor F for the (n, p) reaction is the weight, in micrograms, of element $(Z + 1)$ which produces the same activity of the radioisotope used for analysis as 1 μg of element Z via the (n, γ) reaction. For the (n, α) reaction, F is the weight of element $(Z + 2)$ which produces the same activity as 1 μg of element Z. Thus, the smaller the interference factor, the more severe is the interference.

The first step in determining the interference factors was to measure the activity produced by the (n, γ) reaction for each element under study. Known amounts of each element were sealed in 1.4 mL polyethylene vials and irradiated in an inner irradiation site and each was counted with a Ge(Li) detector in order to measure the area of the γ-ray peak per microgram of element. Elements $(Z + 1)$ or $(Z + 2)$ were irradiated in a similar manner to produce the same radioisotope by the (n, p) or (n, α) reaction. The peak area per microgram of interfering element was thus determined and the comparison with the peak area per microgram measured for element Z gives the interference factor.

The main difficulty in these measurements is that very small amounts of element Z in the standards of elements $(Z + 1)$ and $(Z + 2)$ produce a significant amount of the radioisotope under study since the (n, γ) cross sections are generally much larger than the (n, p) or (n, α) cross sections. In order to reduce this effect, only the purest compounds available were used for the standards of elements $(Z + 1)$ or $(Z + 2)$. In addition, all irradiations of elements $(Z + 1)$ or $(Z + 2)$ were performed with cadmium covers as well as in the normal manner. The presence of

[1]Revision received November 28, 1985.

[2]R. G. V. Hancock. Toronto SLOWPOKE Reactor. Private communication.

TABLE 1. The interference factors for some (n, p) and (n, α) reactions

X[a]	I[b]	Interfering reaction	Interference factor		Notes
			Measured	Calculated	
F	Na	$^{23}Na(n, \alpha)^{20}F$	89±9	80±18	
Na	Mg	$^{24}Mg(n, p)^{24}Na$	2330±120	2280±150	
Na	Al	$^{27}Al(n, \alpha)^{24}Na$	3770±400	4200±260	
Mg	Al	$^{27}Al(n, p)^{27}Mg$	5.8±0.3	5.7±0.6	
Mg	Si	$^{30}Si(n, \alpha)^{27}Mg$	4070±360	4980±640	
Al	Si	$^{28}Si(n, p)^{28}Al$	207±14	202±25	
Al	P	$^{31}P(n, \alpha)^{28}Al$	690±40	690±220	
S	Cl	$^{37}Cl(n, p)^{37}S$	3.0±0.2	1.6±0.8	c,d
S	Ar	$^{40}Ar(n, \alpha)^{37}S$	2.0±0.1	1.5±0.8	d
Sc	Ti	$^{46}Ti(n, p)^{46}Sc$	$138\times10^3\pm8\times10^3$	$134\times10^3\pm10\times10^3$	
Ti	V	$^{51}V(n, p)^{51}Ti$	84±10	58±7	c
Ti	Cr	$^{54}Cr(n, \alpha)^{51}Ti$	>12000	$66\times10^3\pm33\times10^3$	
V	Cr	$^{52}Cr(n, p)^{52}V$	$30\times10^3\pm2\times10^3$	$27\times10^3\pm2\times10^3$	c
Cr	Fe	$^{54}Fe(n, \alpha)^{51}Cr$	$47\times10^3\pm8\times10^3$	$102\times10^3\pm34\times10^3$	c
Mn	Fe	$^{56}Fe(n, p)^{56}Mn$	$68\times10^3\pm4\times10^3$	$70\times10^3\pm5\times10^3$	
Mn	Co	$^{59}Co(n, \alpha)^{56}Mn$	$\geq82\times10^3$	$463\times10^3\pm27\times10^3$	c
Co	Ni	$^{60}Ni(n, p)^{60}Co$	$321\times10^3\pm91\times10^3$	$328\times10^3\pm75\times10^3$	
Ni	Cu	$^{65}Cu(n, p)^{65}Ni$	550±60	643±321	
Cu	Zn	$^{66}Zn(n, p)^{66}Cu$	$13.1\times10^3\pm1.7\times10^3$	$20.2\times10^3\pm3.6\times10^3$	e
Ga	Ge	$^{72}Ge(n, p)^{72}Ga$	$\geq280\times10^3$	$2143\times10^3\pm580\times10^3$	
As	Se	$^{76}Se(n, p)^{76}As$	$252\times10^3\pm14\times10^3$	$714\times10^3\pm357\times10^3$	e

[a]X = element of interest.
[b]I = interfering element.
[c]Based on only one measured value of σ(n, p) or σ(n, α).
[d]Isotopic abundance is low and varies from compound to compound (13).
[e]Reactions (n, d) and (n, ^{3}H) may take place which would reduce the measured interference factor.

element Z in these standards was indicated by a higher peak area from the sample irradiated without cadmium cover.

Results and discussion

The measured interference factors are presented in Table 1. For $^{54}Cr(n, \alpha)^{51}Ti$, no ^{51}Ti activity was observed even with the irradiation under cadmium cover because of the more intense ^{51}Cr activity produced by the (n, γ) reaction on chromium. Thus, for this case, only a lower limit for the interference factor is given. For $^{59}Co(n, \alpha)^{56}Mn$ and $^{72}Ge(n, p)^{72}Ga$, the ^{56}Mn and ^{72}Ga activities were measurable only with the irradiation performed under cadmium cover. Thus, in these two cases, a part of the measured activity may be due to $^{55}Mn(n, \gamma)^{56}Mn$ and $^{71}Ga(n, \gamma)^{72}Ga$, respectively. For this reason, no experimental uncertainty is given with these interference factors, and the true interference factors may be higher than the values given in Table 1 for these two cases. For the other 18 cases, the uncertainty given includes the measurement error in the activities produced by both the (n, γ) and the (n, p) or (n, α) reactions.

Also shown in Table 1 are the interference factors calculated (8) using published cross sections. For the (n, p) interferences they were calculated with the formula

$$[1] \quad F = \frac{\theta_Z(\sigma_\gamma + 0.06R_\gamma)M_{Z+1}}{0.21\theta_{Z+1}\sigma_p M_Z}$$

where θ is the isotopic abundance, σ_γ the thermal-neutron (n, γ) cross section, R_γ the resonance integral including the $1/v$ contribution (8), M the atomic mass, and σ_p the (n, p) cross section for fission neutrons. For (n, α) interferences. σ_p is of course replaced by σ_α, the (n, α) cross section, and M_{Z+1} and θ_{Z+1} by M_{Z+2} and θ_{Z+2}. The term $0.06R_\gamma$ is included because the neutron flux has been measured to have a 6% component of epithermal neutrons. The factor 0.21 accounts for the previously mentioned 21% component of fast neutrons. The values of θ, M, σ_γ, and R_γ were taken from the Chart of the nuclides (10) and the recommended values of σ_p and σ_α from the Handbook on nuclear activation cross sections (11). For $^{40}Ar(n, \alpha)^{37}S$, $^{54}Cr(n, \alpha)^{51}Ti$, and $^{76}Se(n, p)^{76}As$ no measured cross sections were available. In these three cases, values extrapolated by Calamand (11) from cross-section systematics were used. The uncertainties listed with the calculated interference factors are those of the σ_p or σ_α cross sections since all the other factors in eq. [1] are known with much greater accuracy than these cross sections. All these data are shown in Table 2.

For 12 of the interferences listed in Table 1, the interference factors have been calculated (12) for the Halifax SLOWPOKE reactor whose construction is identical to the one used here. In general, their calculated values agree well with the values calculated in this work, which is to be expected since the two reactors have similar fast-to-thermal neutron-flux ratios (1, 9).

As can be seen from Table 1, there is generally very good agreement between the interference factors measured here and those calculated from measured cross sections found in the literature. This would lead us to believe that the component of the neutron spectrum due to the (γ, n) reaction on the beryllium of the reflector does not alter significantly the relative reaction rates for the (n, p) and (n, α) reactions on the elements studied in this work. But in the cases $^{37}Cl(n, p)^{37}S$, $^{51}V(n, p)^{51}Ti$, $^{54}Fe(n, \alpha)^{51}Cr$, $^{66}Zn(n, p)^{66}Cu$, and $^{76}Se(n, p)^{76}As$, the differences between the measured and calculated interference factors are significant. There are several possible reasons for these differences. In the first four cases it is possible that the (n, p) and (n, α) cross sections used in calculating the interference factors

TABLE 2. Nuclear data used in calculations of interferences factors

X	I	θ_Z (%)	M_Z	σ_γ (b)	R_γ (b)	$\theta_{Z+1,2}$ (%)	$M_{Z+1,2}$	$\sigma_{p,\alpha}$
F	Na	100	19.0	0.0095	0.020	100	23.0	0.77±0.17
Na	Mg	100	23.0	0.53	0.31	79	24.3	1.53±0.1
Na	Al	100	23.0	0.53	0.31	100	27.0	0.73±0.045
Mg	Al	11.0	24.3	0.038	0.025	100	27.0	4.0±0.45
Mg	Si	11.0	24.3	0.038	0.025	3.1	28.1	0.155±0.02
Al	Si	100	27.0	0.231	0.17	92.2	28.1	6.4±0.8
Al	P	100	27.0	0.231	0.17	100	30.9	1.9±0.6
S	Cl	0.015	32.0	0.15	0.64	24.2	35.5	0.38±0.19
S	Ar	0.015	32.0	0.15	0.64	99.6	39.9	0.11±0.06
Sc	Ti	100	45.0	26	8.6	8.0	47.9	12.5±0.9
Ti	V	5.3	47.9	0.179	0.12	99.8	50.9	0.87±0.11
Ti	Cr	5.3	47.9	0.179	0.12	2.36	52.0	0.033±0.016
V	Cr	99.8	50.9	4.91	2.7	83.8	52.0	1.09±0.08
Cr	Fe	4.35	52.0	15.9	7.6	5.8	55.9	0.6±0.2
Mn	Fe	100	54.9	13.3	14.2	91.7	55.9	1.07±0.08
Mn	Co	100	54.9	13.3	14.2	100	58.9	0.156±0.009
Co	Ni	100	58.9	37.0	75	26.1	58.7	2.3±0.4
Ni	Cu	0.9	58.9	1.49	1.0	30.9	63.5	0.34±0.17
Cu	Zn	30.9	63.5	2.17	2.2	27.8	65.4	0.62±0.11
Ga	Ge	40.0	69.7	4.70	31	27.5	72.6	0.022±0.006
As	Se	100	74.9	4.40	61	9	79.0	0.63±0.32

are erroneous since they are based on a single measurement which is not corroborated by other data. If the $^{67}Zn(n, d)^{66}Cu$ and $^{77}Se(n, d)^{76}As$ cross sections are high enough, this mode of production may be the reason why the measured interference factors are lower than those calculated from the (n, p) cross sections. Thus, in the five cases where a significant disagreement exists between the measured and the calculated interference factors, we prefer the present measurements because they are based on several individual determinations.

We recommend that the measured interference factors in Table 1 be used in the following manner. The sample is analysed for the element of interest and the interfering element, and the concentration of the interfering element is divided by the interference factor to yield the amount to be subtracted from the measured concentration of the element of interest. The accuracy of the corrected result thus depends on the accuracy of the determination of the interfering element and the uncertainty in the interference factor listed in Table 1. For $^{54}Cr(n, \alpha)^{51}Ti$, $^{59}Co(n, \alpha)^{56}Mn$, and $^{72}Ge(n, p)^{72}Ga$, for which only lower limits of the interference factors have been determined, the interferences will usually be negligible; their magnitude may be estimated from the calculated interference factors.

Conclusions

It is important to take into account interferences from (n, p) and (n, α) reactions in neutron activation analysis with reactors where the neutron flux has a significant fraction of fast neutrons. The interference factors measured in the present work make possible the accurate correction of these interferences. For any SLOWPOKE reactor, a verification of the ratio of fast-to-thermal neutron fluxes with one or two fast neutron reactions should be sufficient to permit the accurate correction of these 21 interferences with the factors measured here.

Acknowledgement

We would like to acknowledge the financial support of the Natural Sciences and Engineering Research Council of Canada which made this work possible.

1. L. ZIKOVSKY and J.-L. GALINIER. J. Radioanal. Chem. **67**, 1983 (1981).
2. R. W. DURHAM, M. P. NAVALKAR, and E. RICCI. Proceedings, Modern Trends in Activation Analysis, A & M College of Texas, College Station, TX. 1961. p. 67.
3. E. C. LIGHTOWLERS. Anal Chem. **34**, 1398 (1962).
4. V. K. YURTCHENKO. J. Radioanal. Chem. **41**, 137 (1977).
5. K. R. SHAH, R. H. FILBY, and W. A. HALLER. J. Radioanal. Chem. **6**, 185 (1970).
6. H. J. M. BOWEN. Analyst (London), **89**, 658 (1964).
7. G. PFREPPER, and H. KOCH. Mikrochim. Acta, **3**, 481 (1966).
8. D. DE SOETE, R. GIJBELS, and J. HOSTE. Neutron activation analysis. John Wiley and Sons Ltd., New York, NY. 1972. p. 478.
9. D. E. RYAN, D. C. STUART, and A. CHATTOPADHYAY. Anal. Chim. Acta, **100**, 87 (1978).
10. F. W. WALKER, G. J. KIRONAC, and F. M. ROURKE. Chart of the nuclides. General Electric Co. 1977.
11. A. CALAMAND. Handbook on nuclear activation cross sections. TRS-156, Int. Atomic En. Agency. 1974. p. 273.
12. Dalhousie University SLOWPOKE Reactor. Halifax. Annual Report 1979–1980.
13. H. G. THODE. Can. J. Res. Sect. B, **27**, 361 (1949).

E,E- and *E,Z*-α-phenyl-α′-acetoxyorthoquinodimethane: steric and electronic control of cycloaddition reactions

JAMES L. CHARLTON,[1] MIAN M. ALAUDDIN, AND GLENN H. PENNER
Department of Chemistry, University of Manitoba, Winnipeg, Man., Canada R3T 2N2

Received July 8, 1985

JAMES L. CHARLTON, MIAN M. ALAUDDIN, and GLENN H. PENNER. Can. J. Chem. **64**, 793 (1986).

E,E- and *E,Z*-α-phenyl-α′-acetoxyorthoquinodimethanes have been prepared from the corresponding *cis*- and *trans*-1-acetoxy-3-phenyl-1,3-dihydrobenzo[*c*]thiophene-2,2-dioxides. The regio- and diastereoselectivity of the addition reactions with dimethyl fumarate, dimethyl maleate, maleic anhydride, and methyl crotonate have been determined. *Ab initio* calculations have been carried out on orthoquinodimethane and its α-phenyl and α-oxy derivatives. A correlation has been made between the steric and electronic properties of the orthoquinodimethanes and the regio- and diastereoselectivity of their Diels–Alder reactions.

JAMES L. CHARLTON, MIAN M. ALAUDDIN et GLENN H. PENNER. Can. J. Chem. **64**, 793 (1986).

On a préparé les α-phényl α′-acétoxy *o*-quinodiméthanes-*E,E* et -*E,Z* à partir des acétoxy-1 phényl-3 dihydro-1,3 benzo[*c*]thiophènedioxydes-2,2-*cis* et -*trans*. On a déterminé les régio- et diastéréosélectivités de leurs réactions d'addition avec le fumarate de diméthyle, le maléate de diméthyle, l'anhydride maléique et le crotonate de méthyle. On a effectué des calculs *ab initio* sur l'*o*-quinodiméthane et sur ses dérivés α-phényle et α-oxy. On a établi une corrélation entre les propriétés stériques et électroniques des *o*-quinodiméthanes et les régio- et diastéréosélectivités de leurs réactions de Diels–Alder.

[Traduit par la revue]

Introduction

Recently there has been an interest in the use of orthoquinodimethanes as intermediates in lignan synthesis (1–5). This work has been stimulated by a growing interest in podophyllotoxin **1** and its derivatives, which show promise as cancer chemotherapeutic agents (6).[2]

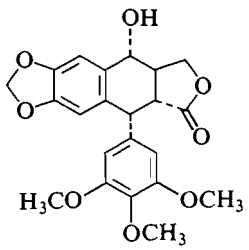

1

Our recent discovery of a simple route to α-oxy-α′-phenyl orthoquinodimethanes **2** (7, 8) has prompted us to investigate the reactions of these intermediates with dienophiles, to establish routes to the various diastereomers of the 1-aryl-4-oxy tetralin

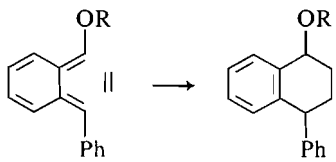

2

system. Previous work on the addition of oxy and phenyl substituted orthoquinodimethanes (*o*-QDMs) to alkenes (1, 2, 4, 7–9) indicated that the regio- and stereochemical course of the addition followed that expected for the Diels–Alder reaction of substituted dienes with alkenes. A *cis*-1,2 substituted pattern seemed to predominate, as shown by the following two examples (1, 9).

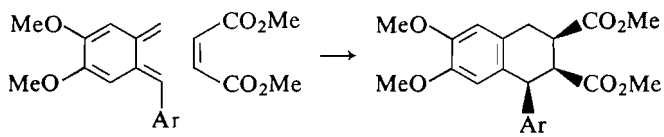

3 **4** 90%

Ar = 3,4-dimethoxyphenyl

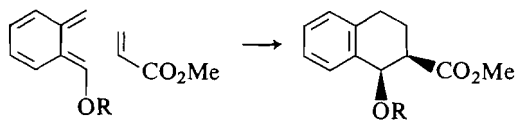

62%

R = —CHPh—CH(CH$_3$)—N(CH$_3$)$_2$

While the *cis*-1,2 substitution pattern is in accord with frontier molecular orbital predictions (10), there have been more recent claims of exceptions to the general pattern, which are in contrast to the previously observed directing effect of an aryl group as shown below (9, 11).

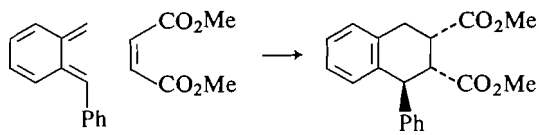

57%

To elucidate further the steric and electronic factors involved in these cycloadditions, we have carried out a study of the Diels–Alder reactions of both *E,E*- and *E,Z*-*o*-QDMs **6** and **16** (see Schemes 1 and 2) with the dienophiles dimethyl fumarate, dimethyl maleate, maleic anhydride, and methyl crotonate. Correlations have been drawn between the addition stereoselectivities and the steric and electronic properties of the *o*-QDMs.

Results

The acetoxyphenyl *o*-QDMs **6** and **16** were prepared by thermolysis of the *cis*- and *trans*-acetoxy sulfones **5** and **15** (5). We assume that **5** yields the *E,E*-*o*-QDM **6**, as it is much less

[1]Author to whom correspondence may be addressed.

[2]See also references cited in ref. 3.

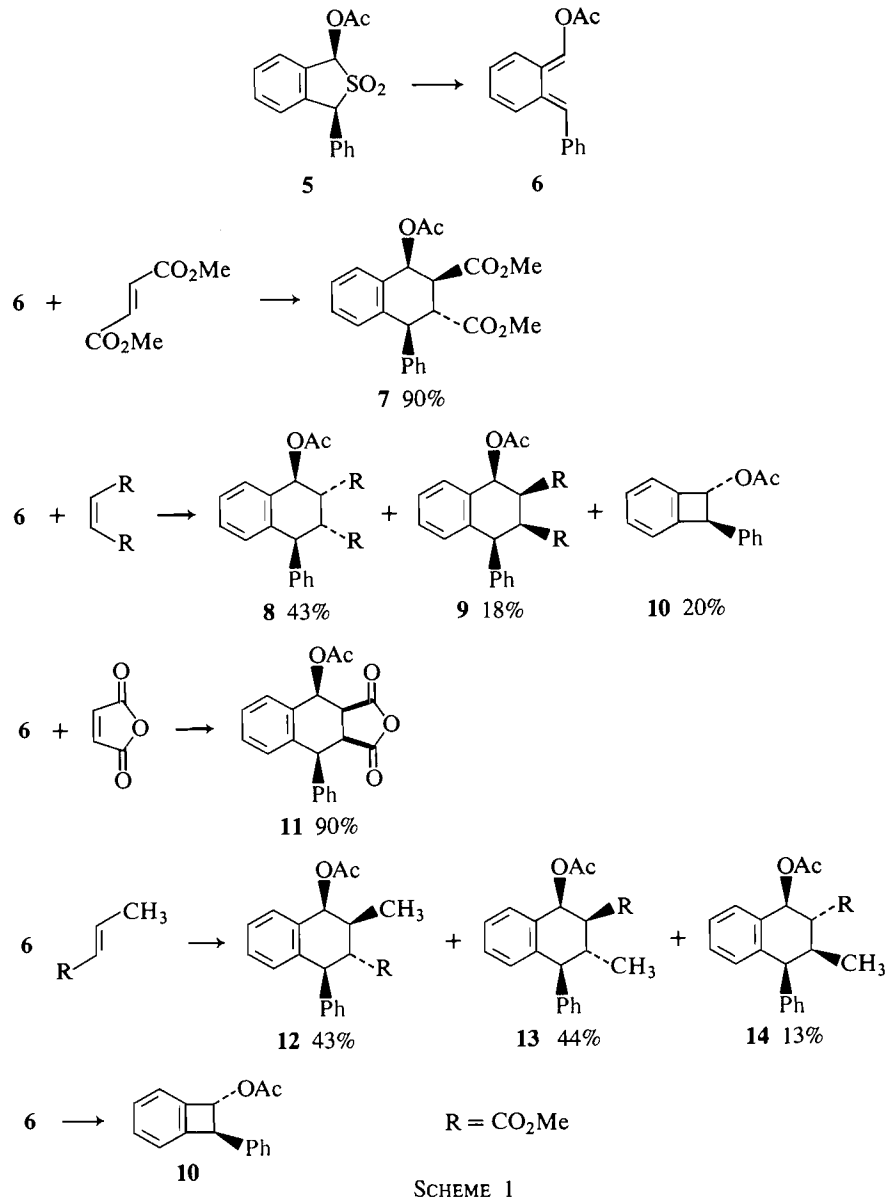

SCHEME 1

sterically hindered than the *Z,Z* configuration, which could have also formed by pericyclic extrusion of SO_2 from **5**. We also assume that **15** yields the *o*-QDM **16** with the *E*-acetoxy and *Z*-phenyl configuration, on the basis of arguments put forward by Sammes, who has noted a reluctance for oxy substituents to occupy the *Z*-position in *o*-QDMs (12).

TABLE 1. Reaction conditions for cycloadditions

Reactant	Diene[a]	Solvent	Temperature (°C)	Time (h)
5	DMF	T	140	5
5	DMM	T	180	5
5	MA	T	140	5
5	MC	T	140	10
5	—	T	140	15
16	DMF	T	180	5
16	DMM	T	180	18
16	MA	T	180	11
16	—	X	140	23

[a]Key: DMF = dimethylfumarate; DMM = dimethylmaleate; MA = maleic anhydride; MC = methyl crotonate; T = toluene; X = xylene.

The thermolysis conditions are given in Table 1. The product structures and yields are given in Schemes 1 and 2. The product structures were determined primarily on the basis of 300-MHz ^{1}H nmr spectra (see Table 2). The structures were further confirmed by elimination of acetic acid to form the 1-phenyl-2,3-dicarbomethoxy-1,2-dihydronaphthalenes.

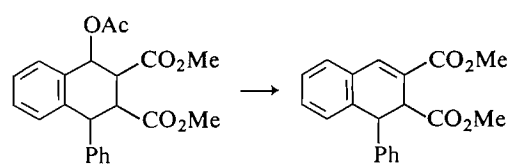

7, 8, 9, 17, or **18** → *trans* **20**, *cis* **21**

Thus adducts **7**, **8**, **17**, and **18** were converted to the known *trans*-alkene **20** and adduct **9** was converted to the *cis*-alkene **21**. The structure of the maleic anhydride adduct **11** was determined by treatment with methanol and diazomethane, which converted it to adduct **9**. The benzocyclobutenyl acetate **10**, which is formed as a minor product from **6** and dimethyl maleate, and as a major product in the absence of dienophile,

TABLE 2. Chemical shifts and coupling constants

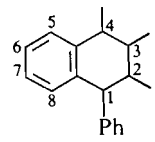

	7[a]	8[a]	9	11	12	13	14	17	18
H(1)	4.02	5.04	4.39	4.45	4.33	3.58	4.14	4.37	4.95
H(2)	3.82	3.76	3.68	3.98	3.10	2.71	2.55	3.48	3.43
H(3)	3.56	2.72	3.38	4.14	2.42	2.80	2.84	3.60	3.48
H(4)	6.69	6.93	6.63	6.14	6.13	6.38	6.47	6.80	6.49
OCH_3	3.22	3.13	3.43	—	3.72	3.54	3.72	3.45	3.62
OCH_3	3.78	3.21	3.77	—	—	—	—	3.65	3.67
OAc	1.60	1.67	2.04	2.27	2.12	2.10	2.19	2.18	2.10
CH_3	—	—	—	—	1.04	0.97	0.82	—	—
Arom	6.8–7.2[b]	6.8–7.2[c]	7.12–7.55	7.1–7.6	6.7–7.45	6.7–7.45	6.7–7.45	7.1–7.4	6.9–7.2
H(8)	6.71	—	7.13	—	—	—	—	—	—
$J_{1,2}$	11.26	7.24	5.32	5.59	11.20	10.28	6.6	10.69	10.69
$J_{2,3}$	12.26	4.49	4.1	9.99	—	12.16	2.8	10.76	10.76
$J_{3,4}$	3.16	4.99	4.26	7.45	3.00	2.72	9.39	8.85	8.85
$J_{x,CH}$	—	—	—	—	6.75	6.20	6.85		
Sol	C_6D_6	C_6D_6	$CDCl_3$	$CDCl_3$	$CDCl_3$	$CDCl_3$	$CDCl_3$	C_6D_6	$CDCl_3$

[a]For spectrum in $CDCl_3$, see ref. 8.
[b]Also 7.47 (d, 1H).
[c]Also 7.31 (d, 1H), 7.45 (d, 1H).

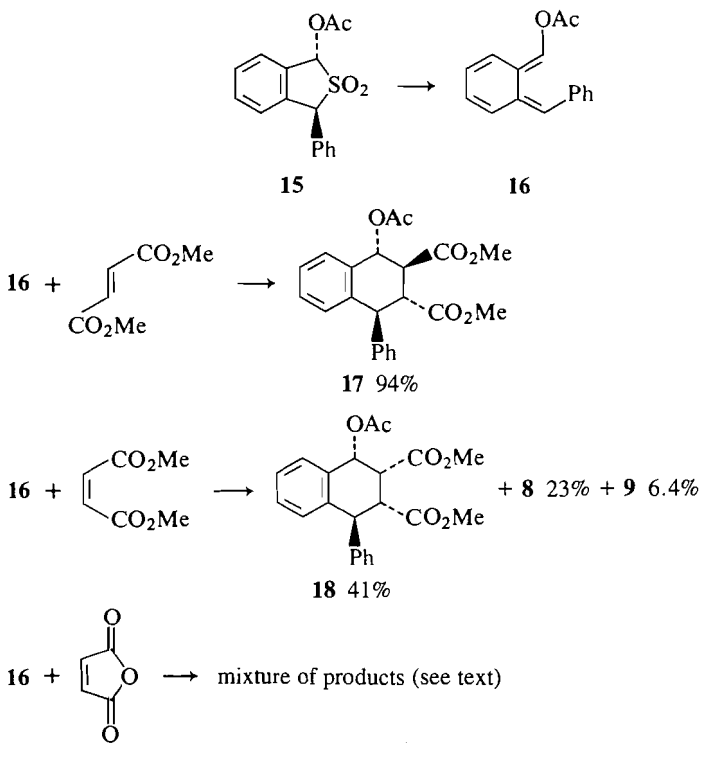

SCHEME 2

was identified by its ^1H nmr and ir spectra. It could also be converted to the adduct **7** by heating with dimethyl fumarate, which further confirmed its structure.

The adducts **12**, **13**, and **14** were not individually isolated. Their structures were deduced solely from ^1H nmr of the mixture using decoupling techniques to decipher the spectrum (see Table 2). Although the *E,Z-o*-QDM **16** plus maleic anhydride gave a mixture of products, the mixture could be converted to primarily the *trans*-alkene **20** by successive treatment with methanol (reflux) and diazomethane. This would indicate that the initial adduct of **16** and maleic anhydride was the *endo* adduct.

Discussion

The most notable feature of these cycloaddition reactions is the contrast between the stereoselectivity for addition of fumarate and maleate versus maleic anhydride. For fumarate and maleate the major products always have the phenyl and neighboring carbomethoxy group *trans*, irrespective of other factors. On the other hand, maleic anhydride added to both **6** and **16** to give predominantly the *cis*-1,2 stereochemistry via an *endo* transition state (assuming the acetoxy group is in the *E* configuration in both **6** and **16**).

It should be noted that the formation of **16** requires a higher temperature than does **6**. Thus **5** could be converted to **10** at 110°C whereas **15** was unaffected at this temperature. At 140°C, both were converted to anthracene in high yield. At the higher temperature, **10** is in equilibrium with **6** but must also be able to form the *Z,Z* isomer, which intramolecularly closes to eventually form anthracene. We were unable to find a temperature at which the *E,Z-o*-QDM **16** formed the *cis*-acetoxyphenylbenzocyclobutene as a stable product.

The difficulty that others have encountered in preparing a substituted benzocyclobutenol similar to **10** has not gone unnoticed (3). We are currently attempting to extend the scope of the reaction **5** → **10**.

The formation of **8** and **9** from the attempted reaction of **15** plus dimethyl maleate is probably due to the isomerization of **15** to **5**. Although zinc oxide, added to the reaction mixture as an acid scavenger, is relatively neutral, it may catalyse the conversion of **15** to **5** at high temperature. We have observed that this interconversion is readily catalysed by K_3PO_4 in *tert*-butanol or triethylamine in benzene.

Frontier orbital, secondary orbital, and dipole effects

Frontier orbital theory has often been used to predict regioselectivity of Diels–Alder reactions (10, 13–15). Generally, regioselectivity can be predicted on the basis of the most favourable overlap of the HOMO (highest occupied molecular orbital) of the diene with the LUMO (lowest unoccupied molecular orbital) of the dienophile (10). The predicted product has the larger HOMO coefficient of carbons 1 or 4 of the diene interacting with the larger LUMO coefficient of the dienophile. Thus, dienes with electron-releasing substituents add head-to-head with dienophiles bearing electron-withdrawing substituents.

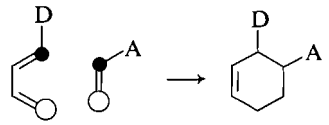

HOMO LUMO

Favourable secondary orbital overlap of the electron acceptor group of the dienophile with carbon 2 of the diene can lead to predominantly *endo* products (14–16).

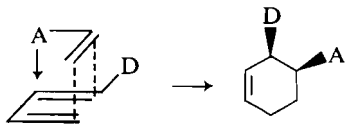

In cases where the primary orbital effects (carbons 1 and 4 of the diene) are approximately equal, the secondary orbital effect may also affect the regioselectivity (14). In the absence of any strong orbital effects, dipolar interactions may come into play to direct regioselectivity.

In Appendix A we describe *ab initio* calculations that have been used to find the optimum geometry, charge distribution, and molecular orbital coefficients for *o*-QDM, α-phenyl-, α-hydroxy-, and α-phenyl-α′-hydroxy-*o*-QDM. The calculations indicate that an *E*-α-phenyl substituent is rotated out of the plane of the *o*-QDM and has little effect on the orbital coefficients relative to the unsubstituted *o*-QDM. The fact that previously studied α-phenyl-*o*-QDMs add head-to-head with monoactivated dienophiles (1, 8, 11) may thus be related to dipolar effects rather than orbital effects since the phenyl group in *E*-α-phenyl-*o*-QDM does decrease the electron density on the carbon bearing the phenyl group (see Appendix A). It may also be due to the fact that α-phenyl-*o*-QDMs exist in the *Z* configuration, where orbital factors may be larger and direct the regiochemistry of addition. In the case of α-oxy-*o*-QDMs there are both a polar effect and secondary and primary orbital effects, which all favour head-to-head addition. The secondary orbital interaction should be large (large coefficient on C_2) and should favour a *cis*-1,2 adduct stereochemistry when fumarate is added. The α-oxy-*o*-QDMs do indeed give *endo* head-to-head addition (8, 9) as predicted. An analogous case dealing specifically with fumarate addition to 1-substituted dienes has been provided by Kakushima (15). However, for α-phenyl- and α-phenyl-α′-oxy-*o*-QDMs, only maleic anhydride gives the *endo* addition while fumarate and maleate always give the *trans*-phenyl carbomethoxy stereochemistry. In view of the out-of-plane rotation of the α-phenyl group in *E*-α-phenyl-*o*-QDM, it is likely that the preference for *exo* addition of dienophiles other than maleic anhydride is rooted in steric factors.

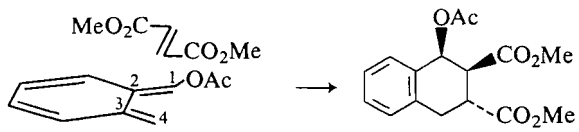

It should be noted that Mann and Piper have reported a case (see **3** → **4**) in which maleate undergoes *endo* addition to an α-aryl-*o*-QDM (2). This could be rationalized on the basis of increased secondary orbital effects, since the methoxy substituents on the *o*-QDM will raise the energy of the HOMO and increase orbital interaction with the dienophile LUMO.

Finally, we note that addition of crotonate to **6** gave a mixture of head-to-head and head-to-tail adducts indicating that, in this case at least, the directive effects of the phenyl and acetoxy group on the regiochemistry of addition are about equal.

Experimental

Proton magnetic resonance spectra were recorded on a Bruker AM-300 using tetramethylsilane as internal standard. Infrared (ir) spectra were recorded on a Unicam 1000 spectrometer. Mass spectra were recorded on a Finnegan 1015 mass spectrometer and only the major peaks are reported. Merck Kieselgel 60 was used for all chromatography. Elemental analyses were performed by Guelph Chemical Laboratories Ltd., Guelph, Ontario, Canada.

1-Acetoxy-3-phenyl-1,3-dihydrobenzo[c]thiophene-2,2-dioxide

The *cis* and *trans* acetates **5** and **15** were prepared as described previously (8). They were separated by a combination of crystallization and chromatography using 2% ethyl acetate in benzene as eluant.

Cycloaddition reactions

A procedure different from that previously used (8) was employed in this work. A toluene solution of the acetoxy phenyl sulfone **5** or **15** (100–200 mg), 30 mg of anhydrous, powdered zinc oxide, and four equivalents of the dienophile were sealed in a pressure flask (200 mL) and heated as described in Table 1. The solution was then filtered through a short column of silica gel with methylene chloride (through only filter paper for the maleic anhydride adducts), evaporated, and then heated at 100°C under high vacuum to remove excess dienophile.

The cycloadducts were then purified by recrystallization, sometimes after chromatography, as described below.

7: Recrystallized from hexane – ethyl acetate, mp 109–110°C; for spectra properties see ref. 8.

8: Chromatography, 20% ethyl acetate – hexane; recrystallized from hexane–CH_2Cl_2; for properties see ref. 8.

9: Chromatography, 20% ethyl acetate – hexane; recrystallized from hexane–CH_2Cl_2, mp 150–153°C; ir (CH_2Cl_2): 1747 cm^{-1}; mass spectrum *m/e* (rel. %): 382 (10), 339 (33), 322 (40), 307 (40), 262 (43), 221 (43), 203 (47), 188 (100). *Anal.* calcd. for $C_{22}H_{22}O_6$: C 69.10, H 5.80; found: C 68.92, H 6.09.

11: Recrystallized from hexane – ethyl acetate, mp 168–170°C; ir (CH_2Cl_2): 1750, 1760, 1795 cm^{-1}; mass spectrum *m/e* (rel. %): 336 (12), 293 (12), 276 (21), 248 (38), 204 (35), 195 (44), 178 (100). *Anal.* calcd. for $C_{20}H_{16}O_5$: C 71.42, H 4.79; found: C 71.55, H 5.09.

12, **13**, and **14**: Chromatography, 10% ethyl acetate – hexane. Separation of the three isomers was not possible by chromatography. The identity of the three isomers is based solely on the 300-MHz nmr spectrum of the mixture, which was analysed using decoupling and COZY techniques. The nmr data are given in Table 2.

17: Recrystallized from hexane–CH_2Cl_2, mp 135–137°C; ir (CH_2Cl_2): 1742 cm^{-1}; mass spectrum *m/e* (rel. %): 322 (7), 262 (36), 176 (44), 131 (65), 117 (76), 91 (100). *Anal.* calcd. for $C_{22}H_{22}O_6$: C 69.10, H 5.80; found: C 68.82, H 6.02.

18: Chromatography 10% ethyl acetate – hexane; recrystallized from hexane–CH_2Cl_2, mp 128–132°C; ir (CH_2Cl_2): 1745 cm^{-1}; mass spectrum *m/e* (rel. %): 382 (1), 351 (1), 339 (1.5), 322 (31), 294 (28), 231 (20), 204 (25), 43 (100). *Anal.* calcd. for $C_{22}H_{22}O_6$: C 69.10, H 5.80; found: C 68.98, H 6.00.

The cycloaddition product from **15** and maleic anhydride appeared to be a mixture by ^1H nmr. The crude reaction mixture was refluxed in methanol for 1 h, evaporated to dryness, and then treated with excess

diazomethane in ether. The ^{1}H nmr analysis showed the resulting product to be a mixture of **20** (major), **18** (minor), and **21** (minor).

trans-*1-Acetoxy-2-phenylbenzocyclobutene* ***10***

This compound was first isolated as a minor product from the reaction of the *cis*-sulfone **5** with dimethyl maleate by chromatography using 20% ethyl acetate – hexane (20%). Refluxing **5** (101.5 mg) in toluene with ZnO (33 mg) gave, after chromatography (20% ethyl acetate – hexane), 42 mg of **10** and 32.5 mg of **5** for a corrected yield of 76%. Recrystallized from hexane, mp 50–53°C; ir (CH_2Cl_2): 1740 cm^{-1}; ^{1}H nmr ($CDCl_3$): 2.15 (s, 3H), 4.67 (d, 1H, J_{12} = 1.63), 5.67 (d, 1H), 7.2–7.5 (m, aromatics); mass spectrum *m/e* (rel. %): 196 (27), 195 (47), 178 (100), 167 (67). *Anal.* calcd. for $C_{16}H_{14}O_2$: C 80.65, H 5.92; found: C 80.40, H 6.19. Refluxing **5** with ZnO in xylene (138°C) gave only anthracene.

Treatment of ***11*** *with methanol and diazomethane*

Compound **11** (10 mg) was refluxed for 1.5 h in methanol, evaporated, and then treated with diazomethane in ether; ^{1}H nmr showed the product of the reaction to be mainly **9**.

Elimination reactions to form ***20*** *and* ***21***

The cycloadducts **7**, **8**, **17**, and **18** could all be converted to **20** by refluxing (20 mg) in toluene (10 mL) with *p*-toluene sulfonic acid (5 mg) for 2 h. The product mixture was filtered through a short silica gel column with CH_2Cl_2 and evaporated to give a nearly quantitative yield of the alkene in each case. For properties see ref. 8. The all-*cis* tetralin, **9**, treated in the same way, gave the *cis*-alkene **21** as an oil; ir (CH_2Cl_2): 1720, 1735 cm^{-1}; ^{1}H nmr ($CDCl_3$): 3.34 (s, 3H), 3.79 (s, 3H), 4.02 (d, 1H, $J_{1,2}$ = 8.15), 4.61 (d, 1H), 7.01 (m, 1H), 7.18–7.38 (m, aromatics), 7.73 (s, 1H); mass spectrum *m/e* (rel. %): 322 (28), 290 (50), 262 (57), 204 (95), 203 (98), 202 (93), 178 (64), 105 (100). When **21** was dissolved in 0.1 *M* NaOMe and left at room temperature for 15 h, it was converted quantitatively to the alkene **20**.

1. J. Mann, S. E. Piper, and L. K. Yeung. J. Chem. Soc. Perkin Trans. 1, 2081 (1984).
2. J. Mann and S. E. Piper. J. Chem. Soc. Chem. Commun. 430 (1982).
3. M. E. Jung, P. Y-S. Lam, M. M. Mansuri, and L. M. Speltz. J. Org. Chem. **50**, 1087 (1985).
4. M. B. Glinski and T. Durst. Can. J. Chem. **61**, 573 (1983).
5. B. J. Arnold, S. M. Mellows, and P. G. Sammes. J. Chem. Soc. Perkin Trans. 1, 1266 (1973).
6. I. Jardine. *In* Anticancer agents based on natural product models. Medicinal Chemistry Monographs. Vol. 16. *Edited by* J. M. Cassady and J. D. Douras. Academic Press, New York. 1980. p. 319.
7. J. L. Charlton and T. Durst. Tetrahedron Lett. **25**, 2663 (1984).
8. T. Durst, E. C. Kozma, and J. L. Charlton. J. Org. Chem. **50**, 4829 (1985).
9. Y. Ito, Y. Amino, N. Nakatsuka, and T. Saegusa. J. Am. Chem. Soc. **105**, 1586 (1983).
10. I. Fleming. *In* Frontier orbitals and organic chemical reactions. Wiley, New York. 1976.
11. J. L. Charlton and T. Durst. Tetrahedron Lett. **25**, 5287 (1984).
12. P. G. Sammes. Tetrahedron, **32**, 405 (1976).
13. J. J. Dannenberg and R. W. Franck. J. Org. Chem. **50**, 2635 (1985), and references cited.
14. T. Cohen, R. J. Ruffner, D. W. Shull, W. M. Daniewski, R. M. Ottenbrite, and P. V. Alston. J. Org. Chem. **43**, 4052 (1978).
15. M. Kakushima. Can. J. Chem. **57**, 2564 (1979).
16. K. Alder, H. Vagt, and W. Voght. Liebigs Ann. Chem. **565**, 135 (1949); K. Alder and M. Schumacher. Liebigs Ann. Chem. **565**, 148 (1949).
17. M. R. Peterson and R. A. Poirier. MONSTERGAUSS, Department of Chemistry, University of Toronto, Toronto, Canada. 1981.

Appendix A

Ab initio molecular orbital calculations at the STO-3G level have been carried out on *o*-QDM **22**, α-hydroxy-*o*-QDM **23**, α-phenyl-*o*-QDM **24**, and α-hydroxy-α′-phenyl-*o*-QDM **25**. All bond lengths and bond angles were optimized with the constraint that the atoms of the *o*-QDM moiety remain planar. For the α-phenyl derivatives the benzene ring was held planar and the ring carbons were constrained to a hexagonal geometry.

TABLE 3. HOMO and LUMO molecular orbital coefficients and net atom charges

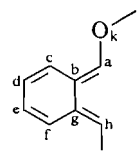

		Centre b	g	f	e	d	c	a	k	h
	H	+0.238	−0.238	+0.351	+0.322	−0.322	−0.352	+0.434	—	−0.434
22	L	−0.256	−0.256	−0.382	+0.347	+0.347	−0.382	+0.449	—	+0.497
	CD	+0.005	+0.005	−0.060	−0.066	−0.066	−0.060	−0.129	—	−0.129
	H	+0.327	−0.207	+0.316	+0.264	−0.337	−0.309	+0.408	−0.316	−0.442
23	L	−0.227	−0.261	−0.375	+0.352	+0.329	−0.381	+0.520	−0.204	+0.481
	CD	−0.031	+0.010	−0.063	−0.064	−0.073	−0.055	+0.061	−0.272	−0.144
	H	+0.232	−0.255	+0.345	+0.324	−0.311	−0.344	+0.435	—	−0.437
24	L	−0.253	−0.260	−0.377	+0.346	+0.340	−0.377	+0.491	—	+0.504
	CD	+0.005	−0.002	−0.062	−0.006	−0.066	−0.060	−0.132	—	−0.058
	H	+0.320	−0.222	+0.312	+0.267	−0.329	−0.304	+0.409	−0.314	−0.455
25	L	−0.224	−0.266	−0.370	+0.353	+0.322	−0.376	+0.514	−0.201	+0.488
	CD	−0.030	+0.005	−0.066	−0.064	−0.074	−0.056	+0.058	−0.273	−0.072

H, HOMO (highest occupied molecular orbital).
L, LUMO (lowest unoccupied molecular orbital).
CD, net charge density.

22

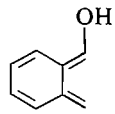

23

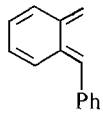

24

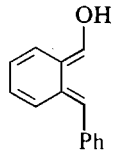

25

Calculations were performed on an Amdahl 470/V8 system using program MONSTERGAUSS (17).

Calculations on **25** were made for several different angles of the plane of the phenyl substituent relative to the plane of the *o*-QDM. The optimum angle appeared to be 60° with a small barrier (2.58 kJ/mol) at 90° and a prohibitive barrier at 0°. For comparison purposes, data given for **24** and **25** below are for calculations in which the phenyl group was held at 90°. Table 3 gives the HOMO and LUMO molecular orbital coefficients and the net atom charges for the four molecules studied.

Open chain nitrogen compounds. Part X.[1] Thermolysis of α-diazoacetanilides in methanol: a convenient synthesis of α-methoxyacetanilides from ethyl *N*-(arylazo)glycinate

KUMUDINI U. K. GAMAGE NICHOLAS AND KEITH VAUGHAN[2]
Department of Chemistry, Saint Mary's University, Halifax, N.S., Canada B3H 3C3
Received June 26, 1985

KUMUDINI U. K. GAMAGE NICHOLAS and KEITH VAUGHAN. Can. J. Chem. **64**, 799 (1986).

α-Diazoacetanilides (**4**), which are readily available from the open-chain triazenes (**2**), undergo thermolysis in methanol solution to afford the α-methoxyacetanilides (**5**), an apparently rare type of ether/amide derivative. The methanolic thermolysis is inhibited by the presence of a tertiary amine in the solvent, suggesting that a carbocation, rather than a carbene, intermediate is involved in the conversion of the diazo-amide to the methyl ether. This hypothesis is supported by the retardation of the reaction in the presence of an electron-withdrawing group in the *para* position of the anilide. The conversion **4** → **5** was also observed, on a small scale, under photolytic conditions. It is suggested that the α-diazoacetanilide represents a useful synthetic equivalent for the synthon $ArNHCOCH_2^+$.

KUMUDINI U. K. GAMAGE NICHOLAS et KEITH VAUGHAN. Can. J. Chem. **64**, 799 (1986).

Les triazènes (**2**) aliphatiques conduisent facilement aux α-diazoacétanilides (**4**) qui, en solution dans le méthanol, subissent une thermolyse conduisant aux α-méthoxyacétanilides (**5**), un type apparemment rare de derivé éther/amide. Les thermolyses en solution méthanolique sont inhibées par la présence d'amines tertiaires dans le solvant; ceci suggère que l'intermédiaire dans la conversion du diazo-amide en éther méthylique est un carbocation plutôt qu'un carbène. Cette hypothèse est en accord avec le fait que la réaction est retardée par la présence de groupes électro-atrtracteurs en position *para* de l'anilide. Opérant sur une faible échelle et dans des conditions photolytiques, on a pu aussi observé la conversion de **4** → **5**. On croit que l'α-diazoacétanilide représente un équivalent de synthèse utile pour le synthon $ArNHCOCH_2^+$.

[Traduit par la revue]

In a previous report (1), we described the base-catalysed cyclization of the ethyl *N*-(arylazo)glycinates (**2**), which affords the 5-hydroxytriazoles (**3**). The triazoles undergo rearrangement with Lewis acid catalysis to afford the α-diazoacetanilides (**4**). The triazenes (**2**) are readily obtained by diazotization of the arylamine (**1**) and diazonium coupling with ethyl glycinate. The diazoacetanilides (**4**) offer an interesting range of possible synthetic opportunities, since loss of nitrogen under thermal or photolytic conditions might afford the reactive intermediate carbene, Ar.NH.CO.C̈H. This paper describes a study of the thermolysis and photolysis of these diazo compounds (**4**) in methanol and other alcohols, which afford moderate yields of the ethers (**5** and **6**), formally the carbene O—H insertion product.

While a great number of studies have been carried out on the thermo- and photo-chemistry of diazo compounds, only a little of this work has been devoted to the study of α-diazoamides (>N—C(=O)—C(—)=N_2) and most of these studies involve photolysis. For example, photolysis of the α-diazoacetamides ($CH_3NH.CO.CN_2.CO_2Et$) in *tert*-butanol generates the appropriate carbene, which undergoes O—H insertion to give the corresponding ether $CH_3NH.CO.CH(Ot\text{-}Bu)CO_2Et$ (2). Similarly, photolysis of *N*,*N*-diethyl-α-diazoacetamide ($Et_2N.CO.CHN_2$) in methanol gives the O—H insertion product ($Et_2N.CO.CH_2OCH_3$), together with rearrangement and the

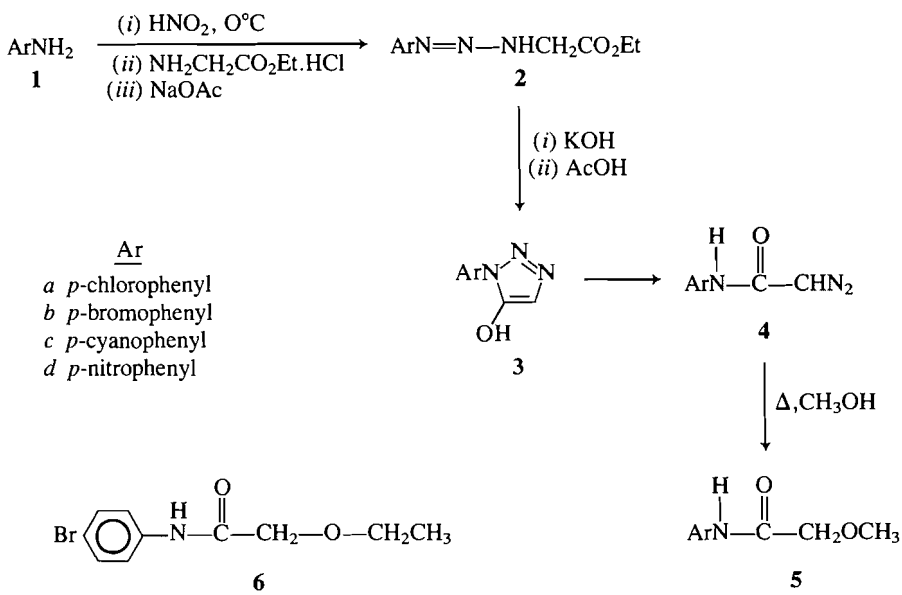

[1]For Part IX, see ref. 13.
[2]Author to whom correspondence may be addressed.

TABLE 1. Preparation and physical characteristics of the α-alkoxyacetanilides

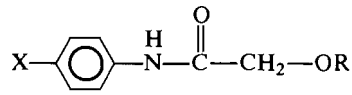

Compound no.	X	R	λ_{max}(nm)[a]	Reaction time (h)	Yield (%)	Melting point (°C)[b]	Crystals	Infrared (cm^{-1})	Nuclear magnetic resonance (δ) ($CDCl_3$)
5*a*	Cl	Me	273	7	47	76–76.5	White needles	3360 3250 1655 1575	3.5 (3H, s, O—CH_3) 4.0 (2H, s, CH_2) 7.28–7.55 (4H, AA'BB') 8.26 (1H, br s, NH)
5*b*	Br	Me	272	5½	50	82.5[c]	White needles	3400 3300 1670 1590	3.5 (3H, s, O—CH_3) 4.0 (2H, s, CH_2) 7.43–7.50 (4H, s, arom.) 8.26 (1H, s N*H*)
5*c*	CN	Me	288	46	46	83–85	Pale yellow plates	3250 3180 2230 1680 1595	3.5 (3H, s, —OCH_3) 4.0 (2H, s, CH_2) 7.62–7.73 (4H, AA'BB') 8.45 (br s, 1H, NH)
6	Br	Et	272	>48	79	65–67	Off-white plates	3400 3310 1710 (w) 1660 1590	1.2 (3H, t, *J* 7 Hz, CH_3)[d] 3.55 (2H, q, *J* 7 Hz, CH_2) 4.03 (2H, s, CH_2) 7.4–7.7 (4H, arom.) 9.85 (1H, br s, NH, exch D_2O)

[a]Absorption maximum in the uv spectrum of the starting diazo-amide.
[b]All ethers recrystallized from water.
[c]Literature (9) mp 85.3°C.
[d]Nuclear magnetic resonance in DMSO-d_6.

intramolecular C—H insertion products (3). Graziano, Scarpati, and co-workers (4) have extensively studied the photochemistry of diazoamide acetals (R—NHC(OMe)$_2$—C(=N$_2$)—), which have also been studied under thermolysis (5) and were found to be surprisingly stable up to 160°C.

The α-diazoacetanilides (**4***a*, *c*, and *d*) were prepared according to the published method (1). Diazotization of *p*-bromoaniline (**16**) and coupling of the diazonium salt with ethyl glycinate gave a high yield of the triazene (**2***b*), which has not been reported previously. Structural identification of **2***b* was based on comparison of spectroscopic features with other triazenes in the series. Cyclization of **2***b* in alcoholic KOH proceeded as expected to give the hydroxytriazole (**3***b*), which in turn underwent rearrangement over alumina in chloroform to give the α-diazoacetanilide (**4***b*).

Thermolysis of the diazoacetanilides was carried out in refluxing methanol. The progress of reaction was followed both by thin-layer chromatography, and by observing the disappearance of the uv absorption maximum of the reactant diazo compound. (The λ_{max} for each substrate is given in Table 1.) The time of reaction required for complete conversion of reactant to products, shown in Table 1, varied significantly with the substituent in the aryl group of **4**; electron-withdrawing groups retard the reaction significantly. Indeed the *p*-nitro-α-diazoacetanilide (**4***d*) was recovered unchanged after 120 h in refluxing methanol, whereas reaction of the *p*-bromo analogue (**4***b*) was complete after 5.5 h in refluxing methanol.

Structural identification of the methyl esters (**5** *a*, *b*, and *c*) obtained from these reactions is based on spectroscopic (Table 1) and elemental analyses. The ir spectra show absorption from NH and amide-carbonyl groups, and the ^{1}H nmr spectra exhibit characteristic O—Me resonance at 3.5 ppm, a methylene signal at 4.0 ppm, and NH resonance at ca. 8.2–8.4 ppm. The ^{13}C spectra (Table 2) were obtained for the *p*-bromo- and *p*-chloro-α-methyoxyacetanilides (**5***a* and **5***b*) to corroborate the structural assignment. The structures of **5***a* and **5***b* were also confirmed by elemental analysis. Refluxing **4***b* in ethanol afforded the analogous ethyl ether (**6**), which was identified by ir and nmr spectroscopy; the reaction of **4***b* in ethanol required longer time than in methanol, which is consistent with a polar mechanism and with the lower dielectric constant of ethanol (24.3) compared to methanol (32.6).

A simple, but attractive, mechanism for the conversion **4** → **5** is that shown in Scheme 1, path (b), in which loss of N_2 from the free diazo compound generates the carbene (**7**), followed by O—H insertion during reaction with the solvent. Such O—H insertion of diarylcarbene Ar_2C:, generated thermally in methanol from diaryldiazomethanes Ar_2CN_2, has been observed to give the ethers $Ar_2CH.OMe$; the mechanism proposed for this reaction involves the intermediate formation of an ylide, Ar—C$^-$—O$^+$(R)(H), rather than a carbenium ion intermediate (6). However, the alternative route for **4** → **5** shown in the scheme, path (a), should also be considered. Protonation of the amide carbonyl group by the protic solvent gives intermediate **8**, which would undergo prototropic shift to the diazonium ion (**9**) followed by loss of N_2 to give the carbenium ion (**10**). Nucleophilic attack by the solvent at the carbocation centre of **10**, and loss of H^+, affords the observed product (**5**).

In order to distinguish which of these mechanisms might be

TABLE 2. ^{13}C nuclear magnetic resonance chemical shifts of α-methoxyacetanilides

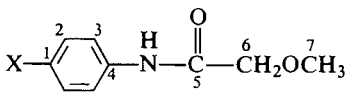

Compound no.	X	CH_3	CH_2	$C{=}O$	Arom.
5*a*	Cl	59.2	71.9	167.4	120.8 128.9 (129.5)[a] 135.6
5*b*	Br	59.2	71.9	167.4	117.0 121.1 131.9 136.1

[a]Partially obscured by δ 128.9 signal.

occurring, we investigated the effect of tertiary amines on the rate and course of the methanolysis of **4**. Accordingly, the *p*-bromo-α-diazoacetanilide (**4***b*) was refluxed in methanol containing 2% triethylamine. While the total time for the disappearance of the diazo compound was increased significantly, compared to the reaction in methanol alone, product analysis indicated the formation of a complex mixture not containing the expected ether (**5***b*). However, reaction of **4***b* in methanol containing 2% pyridine did afford the expected product (**5***b*) but the reaction time required for complete disappearance of the diazo compound was observed to be 2–3 times that in methanol alone. These observations support the suggestion that the methanolysis is acid catalysed and that path (a), Scheme 1, is the more likely route for the conversion **4** → **5**. Further support for the carbocation (**9**) pathway is the substituent effect described previously; electron-withdrawing substituents in Ar decrease the basicity of the amide group, thus shifting the equilibrium **4** ⇌ **8** away from the protonated form (**8**). (The effect of electron-withdrawing substituents on the rate of carbene generation by nitrogen loss from diazoalkanes is usually to accelerate the reaction (10).) Consequently, the lower concentration of **8** in the reaction mixture could be responsible for the lowering of the rate of reaction.

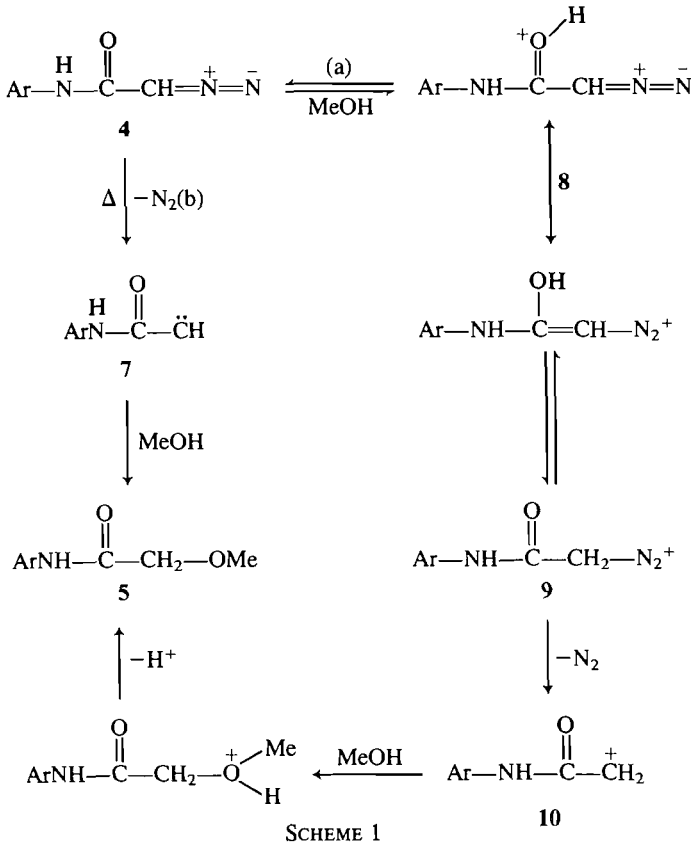

SCHEME 1

These arguments raise the question of the source and nature of the protic acid needed in part (a), Scheme 1. Normally the —OH group in an alcohol is not sufficiently acidic to react with a diazo-alkane (11); however, it has been observed that the reactivity of alcohols towards diphenylmethylene, generated by photolysis of diphenyldiazomethane, increases with increasing acidity of the hydroxy group (6*b*). Thus it is possible that the methanol functions as a weak acid, affording a low concentration of the highly reactive protonated species (**8**).

We also considered the possible intervention of a "Wolff" type rearrangement of the potential intermediate carbene (**7**). By analogy with the Wolff rearrangement of diazoacetyl esters (12), an expected product of the methanolysis of **4** would be the methyl α-anilinoacetate, $ArNH.CH_2CO_2Me$. However, spectroscopic analysis of the product mixtures from methanolysis of the diazo-amides (**4**) indicated the complete absence of any methyl esters.

It was also of interest to us to examine the behaviour of an α-diazoacetanilide when subjected to photolysis. Accordingly the *p*-bromo-α-diazoacetanilide (**4***b*) was photolyzed in methanol on a small scale using a low-power 254-nm uv lamp as the light source. The methyl ether (**5***b*) was observed to crystallize out of the solution during photolysis; the structures of this product was clearly evident from the nmr spectrum, which was identical with that of the thermolysis product from **4***b* in methanol. However, we have not pursued this reaction further to establish its preparative value.

A literature search of the substructure, —N(Ar)—CO.CH_2OR, revealed surprisingly few examples of this apparently simple type of molecule. Recent literature (7, 8) reports the investigation of the fungicidal and microbiocidal uses of *N*,*N*-disubstituted methoxyacetamides; the monosubstituted methoxyacetamides ($ArNHCO.CH_2OMe$) appear to have been ignored in this context. An earlier report (9) lists the *p*-bromo-α-methoxyacetanilide **5***b* as one of several anilides used in a study of their optical crystallography; the method of synthesis was acylation of the aniline by methoxyacetyl chloride, but no yield was reported. The method of synthesis reported here via the triazene **2** has an advantage over the aniline-acylation route for anilines with electron-withdrawing groups in the aryl moiety, which would have low reactivity as nucleophiles towards the acyl chloride. An electron-withdrawing group in Ar is a distinct advantage in the synthesis of the triazene **2**, which can only be obtained in good yield when Ar has an electron-withdrawing group attached. Accordingly, it appears that the synthesis of α-methyoxyacetanilides reported here is a new route to a seemingly rare group of simple amides.

In conclusion, it appears that α-diazoacetanilides of type **4** undergo thermal solvolysis in methanol by a carbenium ion, rather than by a carbene mechanism, and that the diazo compound $ArNH.CO.CHN_2$ is a convenient synthetic equivalent for the carbenium synthon ($Ar.NH.CO.CH_2^+$), which might be useful for other synthetic applications, presently being investigated in this laboratory.

Experimental

Melting points were measured with a Kofler hot-stage apparatus and are uncorrected. Infrared spectra were recorded in Nujol mulls with Perkin Elmer 1300 or 299 grating spectrometers, and uv spectra were obtained with a Unicam SP8-400 spectrophotometer. The nmr spectra were recorded with Varian EM360 (60 MHz) or Nicolet (360 MHz) spectrometers. Microanalyses were conducted by the Canadian Microanalytical Laboratory, Vancouver, B.C. Since the compounds were all prepared by the same sequence of reactions, and since the ^{1}Hmr and ^{13}Cmr spectra are so simple and consistent for the series, only representative compounds were analyzed.

Ethyl N-(p-*bromophenylazo)glycinate (***2***b)*

Diazotization of *p*-bromoaniline and coupling the diazonium salt with ethyl glycinate according to the published procedure (1) afforded the triazene (***2****b*), 90% yield, mp 69–70°C (hexanes); ir: 3395, 1734, 1580, and 840 cm^{-1}; nmr δ ($CDCl_3$): 1.35 (3H, t, Me), 4.25 (2H, q, CH_2), 4.36 (2H, s, CH_2), 7.16–7.5 (4H, AA′BB′, arom.), 8.4 (1H, br, s, NM).

*1-(*p*-Bromophenyl)-5-hydroxy-1,2,3-triazole (***3***b)*

The triazene (***2****b*) was treated with alcoholic potassium hydroxide according to the published method (1) and the resulting potassium triazolate dissolved in water and neutralized with acetic acid to give the triazole (***3****b*), 63% yield, mp 119–119.5°C (hexane); ir: 3150 and 1590 cm^{-1}; δ (DMSO-d_6); 7.06 (1H, s) and 7.75 (4H, s).

α-Diazoacetanilides ***4***

The α-diazoacetanilides (***4****a*, *c*, and *d*) were prepared as described previously (1) and had physical properties in agreement with those reported. *p*-Bromo-α-diazoacetanilide (***4****b*) was prepared from the triazole (***3****b*) by the same method. Yield of ***4****b* 70%, mp 130–135°C (yellow needles from benzene–nitromethane); λ_{max} (EtOH): 273 nm; ir: 2120, 1730, and 1630 cm^{-1}; nmr δ ($CDCl_3$): 5.5 (1H, s, C*H*N_2), 7.1 (4H, s, arom.), and 9.8 (1H, br s, NH; exchangeable with D_2O).

*α-Methoxyacetanilides (***5***). General procedure*

The α-diazoacetanilide (***4***) was dissolved in absolute methanol to a concentration 0.01 *M* (e.g. in the case of the *p*-bromo derivative ***4****b*, 60 mg of the diazoamide was dissolved in methanol (25 mL)). The methanolic solution was flushed with dry N_2 gas and then refluxed. Reaction was taken to completion by following the decrease of uv absorption of the diazo compound and by thin-layer chromatography; tlc of the final product mixtures showed only one major component. The methanolic solution was evaporated to dryness under vacuum and the residue recrystallized from an appropriate solvent (usually water) to afford the ether (***5***). Reaction times required for completion, product yields, and physical and spectroscopic characteristics are given in Tables 1 and 2.

p-*Bromo-α-methoxyacetanilide (***5***b)*

Anal. calcd. for $C_9H_{10}NO_2Br$: C 44.29, H 4.13, N 5.74, Br 32.74%; found: C 44.24, H 4.12, N 5.84, Br 32.48.

p-*Chloro-α-methoxyacetanilide (***5***a)*

Anal. calcd. for $C_9H_{10}NO_2Cl$: C 54.15, H 5.05, N 7.02, Cl 17.75%; found: C 53.94, H 5.05, N 7.09, Cl 17.61%.

1. K. M. Baines, K. Vaughan, D. L. Hooper, and L. F. Leveck. Can. J. Chem. **61**, 1549 (1983).
2. J. Wydila and E. R. Thornton. Tetrahedron Lett. **24**, 233 (1983).
3. R. R. Rando. J. Am. Chem. Soc. **92**, 6706 (1970).
4. M. L. Graziano, R. Scarpati, and D. Tafuri. Tetrahedron Lett. **13**, 2469 (1972).
5. M. L. Graziano, R. Scarpati, and E. Fattorusso. J. Heterocycl. Chem. **11**, 529 (1974).
6. (*a*) D. Bethell, D. Whittaker, and J. D. Callister. J. Chem. Soc. 2466 (1965); (*b*) W. Kirmse. Ann. Chem. **666**, 9 (1963); (*c*) P. D. Bartlett and T. G. Traylor. J. Am. Chem. Soc. **84**, 399 (1962).
7. W. Kunz, A. Hubele, and W. Eckhardt. Ciba-Geigy A.-G. Swiss Patent No. CH 642070 A, 20 Mar. 1984; Chem. Abstr. **101**, 110709z (1984).
8. J. Stoetter, W. Fuehrer, and W. Brandes. Bayer A.-G. Eur. Pat. Appl. EP 56161 A2, 21 Jul. 1982; Chem. Abstr. **97**, 215788b (1982).
9. W. M. D. Bryant and J. Mitchell, Jr. J. Am. Chem. Soc. **60**, 2748 (1938).
10. P. Kovacic, R. R. Flynn, J. F. Gormish, A. H. Kappelman, and J. R. Shelton. J. Org. Chem. **34**, 3313 (1969).
11. G. W. Corvell and A. Ledwith. Q. Rev. **24**, 165 (1970).
12. S. Patai (*Editor*). The chemistry of diazonium and diazo groups. Part 1. John Wiley and Sons, Ltd, New York. 1978. pp. 467–468, and references cited therein.
13. D. L. Hooper, H. W. Manning, R. J. LaFrance, and K. Vaughan. Can. J. Chem. **64**, 250 (1986).

Cyclic hydroboration of geraniol derivatives: a synthesis of the left-hand portion of X-14547A

RALPH ALLEN WHITNEY
Department of Chemistry, Queen's University, Kingston, Ont., Canada K7L 3N6
Received June 26, 1985

RALPH ALLEN WHITNEY. Can. J. Chem. **64**, 803 (1986).

The stereochemical consequences of the cyclic hydroboration–oxidation of geraniol derivatives have been examined; moderately high selectivity (85–88%) for the formation of one major diastereomer has been observed, presumably as a consequence of remote asymmetric induction in the cyclic hydroboration of these 1,5-dienes. An approach to the synthesis of the left-hand portion of the ionophore antibiotic X-14547A is described.

RALPH ALLEN WHITNEY. Can. J. Chem. **64**, 803 (1986).

On a évalué les conséquences stéréochimiques de l'hydroboration–oxydation cyclique de dérivés du géraniol. On a observé des séléctivités relativement élevées (85–88%) pour la formation du diastéréoisomère prépondérant; ce résultat est probablement la conséquence d'une induction asymétrique à distance qui se fait sentir lors de l'hydroboration cyclique de ces dienes-1,5. On décrit une approche à la synthèse de la portion de gauche de l'antibiotique ionophore X-14547A.

[Traduit par la revue]

One of the major objectives in the synthesis of complex natural products is to transform stereochemically simple compounds into topologically complex structures in the most efficient manner possible. In this regard, reactions that allow the formation and relative control of a number of asymmetric centres in one synthetic step are extremely important; intramolecular cycloaddition reactions have been particularly useful in achieving this objective, with the Diels–Alder reaction (for recent reviews, see ref. 1) having received notable attention. Other recent examples of specific reactions that generate multiple asymmetric centres are the permanganate oxidation of dienes (2), arene-olefin cycloadditions (3), and diene cyclic hydroboration–oxidation (4). In this last case, the hydroboration of 1,4- and 1,5-dienes was examined and moderate to high levels of stereochemical control were obtained in the formation of acyclic 1,4- and 1,5-diols containing two remote asymmetric centres.

X-14547A, **1**, is an ionophore antibiotic possessing interesting and unusual structural features (5); the left-hand portion of the molecule, **2**, contains a trisubstituted tetrahydropyran ring with *trans* substituents across the ring oxygen, while the right-hand portion, **3**, contains a *trans*-fused tetrahydroindan with an appended ketopyrrole unit, an unusual structural feature for this type of antibiotic. Several synthetic approaches to the left-hand (6) and right-hand (7) portions of X-14547A have been reported, as well as three total syntheses (8) of the compound. Interestingly, the intramolecular Diels–Alder route to the right-hand portion has allowed a high degree of relative stereochemical control in establishing four additional centres of asymmetry from one pre-existing asymmetric centre in the triene substrate. In considering the possibility of establishing four centres of relative asymmetry in one step from an achiral precursor through cyclic hydroboration, it was decided that the left-hand portion **2** of X-14547A was a suitable synthetic target upon which to test this notion.

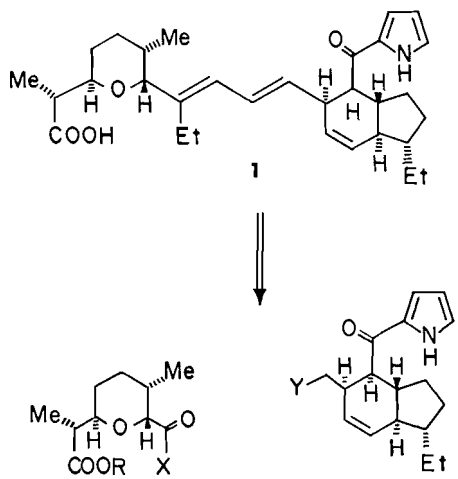

2*a*, R = H, X = Et
b, R = Me, X = OH
c, R = Me, X = OMe

Results and discussion

Geraniol tetrahydropyranyl ether **14***a* was the first diene examined; hydroboration was performed with borane–tetrahydrofuran complex at low temperature to suppress elimination in the β-alkoxyalkyborane intermediate (13). Subsequent oxidation followed by alcoholysis of the tetrahydropyranyl group provided 3,7-dimethyl-1,2,6-octanetriol (9) as a mixture of the diastereomers **5** and **6** in a 73% yield. Examination of the proton decoupled ^{13}C nmr spectrum indicated the presence of the two diastereomers in approximately an 85:15 ratio, by integration, but gave no indication as to the stereochemistry of the major isomer. Elucidation of the stereochemistry of the major diastereomer was accomplished using a precedented sequence (6*a*,*b*; 8*d*) in which the configuration at C-2 of **5** and **6** was inverted during the formation of the tetrahydropyran ring in **7***a* and **8***a*. The triol was selectively sulfonated at the primary hydroxyl group with *p*-toluenesulfonyl chloride to give a β-hydroxytosylate that, on treatment with base, afforded an epoxide. Intramolecular alcoholysis of the epoxide under acidic conditions proceeded to give a mixture of tetrahydropyranyl alcohols **7***a* and **8***a* with precedented inversion of configuration at C-2 (6*a*,*b*; 8*d*). Proton nmr data on the corresponding acetate indicated the presence of predominantly one stereoisomer, **7***b* or **8***b*, but did not unambiguously indicate which one of the two was the predominant isomer; mass spectral data showed fragment ions arising from α-cleavage of the C-2 and C-6 substituents as is characteristic of tetrahydropyrans (14). The ^{13}C nmr data on the alcohols were, however, very informative; **7***a* and **8***a* differ only in the axial versus equatorial disposition of the hydroxymethyl group at C-2 and the equatorial versus axial disposition of the methyl group at C-3. In general, axial sub-

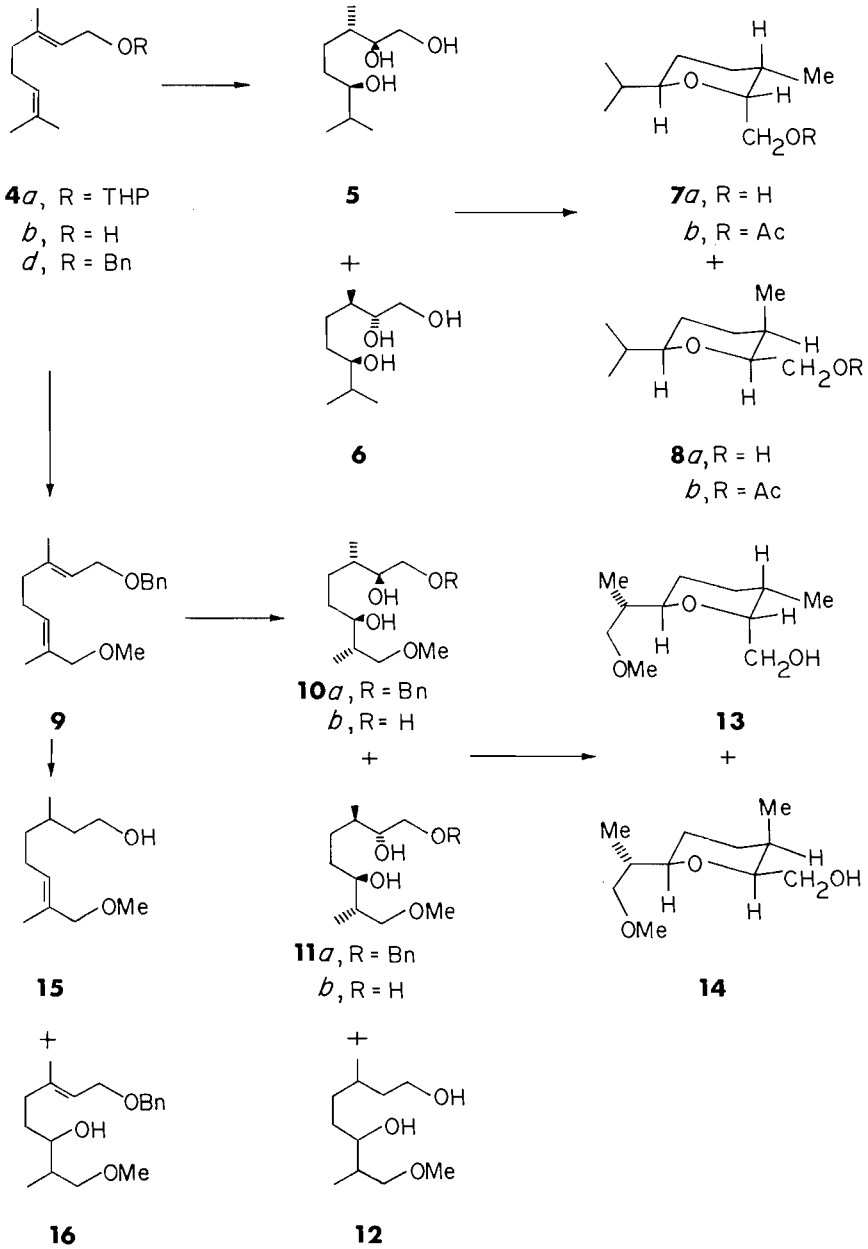

stituents in tetrahydropyranyl rings show a large upfield chemical shift compared to equatorial substituents (10); the nmr spectrum of the mixture of **7***a* and **8***a* showed the major isomer having chemical shifts of 64.7 and 12.1 ppm, respectively, for the C-2 hydroxymethyl and C-3 methyl groups, while the minor isomer had chemical shifts of 57.7 and 16.2 ppm, respectively. On this basis, **8***a* was the major diastereomer obtained and hence triol **6** was the major stereoisomer obtained from the cyclic hydroboration–oxidation of geraniol tetrahydropyranyl ether. Subsequent experiments showed that direct hydroboration of geraniol **4***b* with 2.5 molar equivalents of borane–tetrahydrofuran complex also gave triol **6** as the major diastereomer, obviating the need for an alcohol-protecting group during the hydroboration.

The use of thexylborane (13) as the reagent for hydroboration of **4***a* substantially altered the stereochemical outcome in that the mixture of triols obtained, on subsequent oxidation then alcoholysis of the tetrahydropyranyl group, showed a small predominance (60:40) of the diastereomer **5** over **6**, as evidenced by the proton decoupled ^{13}C nmr spectrum of the triol mixture. Conversion of this triol mixture to the mixture of tetrahydropyranylalcohols **7***a* and **8***a* showed the major isomer having chemical shifts of 57.7 and 16.2 ppm, respectively, for the C-2 hydroxymethyl and C-3 methyl groups, as expected for **7***a*.

Attention was next turned to diene **9**, prepared by selenium dioxide oxidation of *O*-benzylgeraniol (Sharpless catalytic procedure (11)) and subsequent methylation. The use of borane–tetrahydrofuran complex at low temperature as the cyclic hydroborating reagent led, on oxidation, to a mixture of nearly equal amounts of diols **10***a* and **11***a*, as determined by the proton decoupled ^{13}C nmr spectrum of the diol mixture. The use of thexylborane resulted in a substantial increase in diastereoselectivity (88:12 ratio of isomers) when the reaction was performed at $\leqq -10°C$; however, a competing β-elimination rehydroboration reaction led to the formation of a substantial amount of the diol **12** as well; we were unable to suppress the β-elimination without suppressing cyclic hydroboration. As a

consequence, the mixture of diastereomers **10***a* and **11***a* was obtained in only 31% yield upon chromatographic purification.

The mixture of diols was hydrogenolysed over palladium to give a mixture of triols **10***b* and **11***b*, which was converted to a mixture of the tetrahydropyranylalcohols **13** and **14** as described previously. The proton nmr spectrum did not readily identify the major diastereomer, while mass spectral data again showed typical fragment ions arising from α-cleavage of a tetrahydropyran. The ^{13}C nmr spectrum of the mixture of **13** and **14** showed the major diastereomer having a chemical shift of 57.4 ppm for the carbon of the hydroxymethyl group at C-2 and 16.3 ppm for the C-3 methyl group, clearly indicating (*vide supra*) **13** to be the major stereoisomer. The minor isomer **14** showed a hydroxymethyl group at 64.5 ppm and a C-3 methyl group at 12.1 ppm. That the stereochemistry of the major product was identical to that of the left-hand portion **2** of X-14547A was confirmed by oxidation of **13** to **2***b* with ruthenium tetroxide (Sharpless catalytic procedure (12)); treatment with ethereal diazomethane afforded the diester **2***c*. Both **2***b* and **3***c* have recently been reported (8*b*) as degradation products of X-14547A; comparison of the proton nmr spectra of our synthetic samples with spectra for samples obtained by degradation confirmed the structural assignment.

The difference in the stereoselectivities observed in the hydroboration–oxidation of dienes **4***a*/*b* and **9** can be rationalized as arising from opposite chemoselectivity in the initial site of hydroboration, followed subsequently by either an endocyclic or exocyclic intramolecular hydroboration step in which nonbonded interactions control the stereochemistry observed in the oxidation products. In the case of **4***a*/*b* it is well known that electrophilic reagents (e.g. ozone (15) and *N*-bromosuccinimide (16)) preferentially added to the C-6 double bond of geraniol; furthermore, recent studies by Nelson and Brown (17) have shown that an electronegative allylic heteroatom (chlorine) reduces the relative rate of reactivity of the alkene towards hydroboration. This strongly suggests that the first hydroboration of **4***a*/*b* is at the C-6 double bond, giving **17**, which undergoes an endocyclic hydroboration in a subsequent step that controls the stereochemical outcome. In the diene **9**, however, both double bonds are trisubstituted and have an allylic heteroatom substituent; again, the results of Nelson and Brown on allylic halogen substituent effects indicate that the relative rate of addition of boron to an alkene is slower when the site of boron addition is γ rather than β to the allylic heteroatom. This suggests that the initial site of hydroboration is reversed for diene **9**; that is, intermediate **18** is formed followed by an exocyclic ring-forming reaction. This latter case was verified experimentally by reacting diene **9** with 9-BBN (9-borobicyclo[3.3.1]nonane); the major hydroboration–oxidation product obtained was the alcohol **15** arising from hydroboration, β-elimination, then rehydroboration, prior to oxidation.

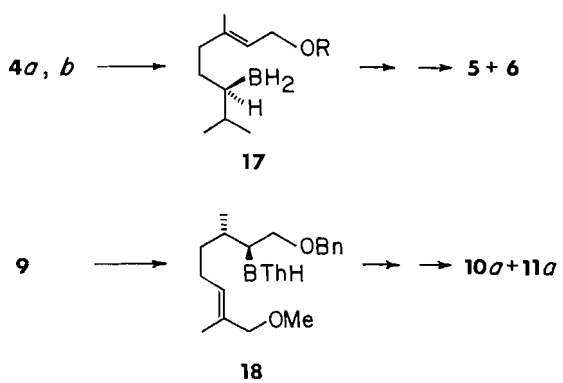

In summary, the cyclic hydroboration–oxidation of geraniol and certain of its derivatives has been shown to proceed to give moderately high levels of remote asymmetric induction in the formation of acyclic diols with the generation of up to four centres of relative asymmetry; the apparent importance of endocyclic versus exocyclic reaction pathways has been noted, as has the effect of electronegative allylic heteroatoms on relatives rates of alkene reactivity.

Experimental

General

Unless otherwise stated, sodium sulfate was used as the drying agent for organic solutions; organic solutions were concentrated by rotary evaporation at water aspirator pressure and temperatures below 40°C. All aqueous–organic partitioning was followed by a wash of the separated aqueous layer with an additional portion of the same organic solvent. Dry organic solvents were prepared by distillation from the following desiccants: magnesium (methanol), calcium hydride (pyridine, tetrahydrofuran). Column chromatography was performed with Merck silica gel 60 (70–230 mesh), while high performance liquid chromatography was performed on Merck Lobar columns. Melting points were determined on a Fisher–Johns or a Thomas Hoover melting point apparatus and are uncorrected. Infrared spectra were recorded on a Perkin–Elmer 528 instrument. Proton and carbon magnetic resonance spectra were recorded on Varian EM360, Bruker WH60, Bruker HX60, Bruker CXP200, or Bruker AM400 spectrometers; chemical shifts are recorded in δ values relative to tetramethylsilane, while coupling constants are generally reported to values of ±0.5 Hz. Mass spectra were recorded on an AEI MS12 at Trent University, Peterborough, Ontario, or on a V.G. 7070F at McMaster University, Hamilton, Ontario.

*(2RS,3RS,6RS)-3,7-Dimethyloctane-1,2,6-triol **6** and its diastereomer **5***

A solution of borane in tetrahydrofuran (1 *M*, 16 mL, 16 mmol) under a nitrogen atmosphere was cooled in a Dry Ice – isopropanol bath to −65°C, then geraniol tetrahydropyranyl ether (3 g, 12.6 mmol) was added neat by syringe. The resulting reaction mixture was allowed to warm to 0°C over 2 h, then aqueous sodium hydroxide (3 *M*, 16 mL), followed by 30% hydrogen peroxide (16 mL), was added. After stirring several hours the solution was extracted with methylene chloride (3 times) and the combined organic solutions were dried, filtered, then concentrated under reduced pressure. The residue obtained was dissolved in methanol (100 mL), a few crystals of *p*-toluenesulfonic acid were added, then the solution was stirred 24 h; addition of solid sodium carbonate, dilution with methylene chloride, filtration, and concentration under reduced pressure afforded an oil that was purified by kugelrohr distillation to give the triols **5** and **6** (bp 130°C/0.1 Torr; 1 Torr = 133.3 Pa) (lit. bp (9) 142°C/0.1 Torr) (1.73 g, 9.2 mmol, 73%); ^1H nmr ($CDCl_3/D_2O$): 3.8–3.3 (4H, m), 1.75–1.15 (6H, m), 0.91 (6H, d, J = 7 Hz); ^{13}C nmr ($CDCl_3$): 76.3, 76.1, 64.7, 35.3, 33.8, 30.3, 28.4, 18.8, 17.8, 15.5 (major isomer).

*(2SR,3RS,6RS)-2-Hydroxymethyl-3-methyl-6-methylethyltetrahydropyran **8**a and acetate **8**b, and their diastereomers **7**a and **7**b*

The mixture of triols (1.73 g, 9.2 mmol) was dissolved in methylene chloride (20 mL) and pyridine (8 mL) in a round-bottomed flask protected by a calcium chloride guard tube, then cooled in an ice–salt bath. *p*-Toluenesulfonyl chloride (2.0 g, 10.5 mmol) was added, and the reaction mixture was allowed to warm to room temperature and stirred overnight at room temperature. The reaction mixture was then partitioned between methylene chloride and dilute hydrochloric acid, with the organic layer being separated, dried, filtered, then concentrated under reduced pressure followed by high

vacuum to give the monotosylate: ^{1}H nmr ($CDCl_3$): 7.82 (2H, d, J = 9 Hz) 7.36 (2H, d, J = 9 Hz), 4.16 (1H, d of d, J = 10.5 and 3 Hz), 3.98 (1H, d of d, J = 10.5 and 7 Hz), 3.63 (1H, m), 3.32 (1H, m), 2.45 (3H, s), 1.9–1.2 (8H, m including OH), 0.88 (6H, d, J = 7 Hz), 0.84 (3H, d, J = 7 Hz); ^{13}C nmr ($CDCl_3$): 145.0, 133.3, 130.0, 128.0, 77.2, 73.5, 72.8, 35.6, 33.8, 30.9, 28.4, 21.6, 18.8, 17.4, 15.4 (major isomer).

The tosylate was dissolved in methanol, then freshly prepared sodium methoxide in methanol was added dropwise until the reaction mixture was basic. After stirring for an additional 15 min, the solution was concentrated under reduced pressure. The crude epoxide was dissolved in glacial acetic acid (8 mL), then stirred 2 days at room temperature. The reaction mixture was partitioned between ether and aqueous sodium carbonate, and the organic layer was separated, dried, filtered, then concentrated under reduced pressure. Purification by kugelrohr distillation (100°C/0.07 Torr) afforded a mixture of alcohols **7***a* and **8***a* (0.767 g, 4.5 mmol, 49%); ^{1}H nmr ($CDCl_3$): 3.75–3.4 (3H, m), 3.03 (1H, m), 1.99 (1H, br s), 1.81–1.31 (6H, m), 0.95 (3H, d, J = 7 Hz), 0.89 (6H, d, J = 7.5 Hz); ^{13}C nmr ($CDCl_3$): 83.4, 80.7, 64.7, 33.2, 31.3, 28.9, 22.9, 18.5, 18.3, 12.2 (major isomer); 76.7, 74.6, 57.7, 32.4, 31.7, 27.7, 27.7, 18.7, 18.5, 16.2 (minor isomer).

Treatment with acetyl chloride in pyridine gave the acetate **8***b* (bp 125°C/15 Torr); ^{1}H nmr ($CDCl_3$): 4.12 (1H, ABX, J = 12 and 8.7 Hz), 4.03 (1H, ABX, J = 12 and 4.5 Hz), 3.68 (1H, d of d of d, J = 8.7, 4.5, and 2 Hz, H-2), 3.06 (1H, m, H-6), 2.12 (3H, s), 1.9–1.3 (6H, m), 1.0 (6H, d, J = 7 Hz), 0.95 (3H, d, J = 7 Hz); ms *m/e*: 215 (M^+ +1) (23%), 214 (M^+) (12%), 213 (M^+ −1) (31%), 171 (73), 154 (91), 141 (52), 123 (67), 111 (72), 93 (60), 82 (98), 55 (100). Signals at 2.12 (s) and 4.58 (d of d) in the proton nmr spectrum were assigned to the acetate methyl group and one of the two diastereotopic hydrogens on the exocyclic methylene group, respectively, of the minor diastereomer **7***b*.

*(2*E*,6*E*)-1-Benzyloxy-8-methoxy-3,7-dimethylocta-2,6-diene* ***9***

Following the procedure of Umbreit and Sharpless (11), a solution of *tert*-butyl hydroperoxide (from 42 mL of 70% aqueous), salicylic acid (1.2 g, 8.7 mmol), and selenium dioxide (0.22 g, 2 mmol) in methylene chloride (54 mL) was prepared. To this solution was added slowly *O*-benzylgeraniol (18 g, 73.8 mmol), then the reaction mixture was stirred 2 days at room temperature after which time it was diluted with ether (200 mL), washed with aqueous sodium hydroxide (3 *M*, 30 mL, 3 times), dilute aqueous sodium bisulfite (twice), dried, filtered, then concentrated under reduced pressure. The crude product was dissolved in 95% ethanol (200 mL), then sodium borohydride (2 g) was added and the reaction mixture stirred overnight. After concentration under reduced pressure, the reaction mixture was partitioned between ether (350 mL) and water (100 mL). The ether layer was separated, dried, filtered, then concentrated under reduced pressure to give, after drying under high vacuum, an oil (16.3 g). The oil was dissolved in dry ether (100 mL) and then added to a stirred suspension of sodium hydride (7.5 g, 50% dispersion in oil, hexane washed, 156 mmol) in dry ether (150 mL). Methyl iodide (8 mL, 128 mmol) was added, then the reaction mixture was refluxed overnight under a calcium chloride guard tube. The organic solution was then washed with water, dried, filtered, and concentrated under reduced pressure. The crude product was purified by vacuum distillation to give the diether (bp 120–125°C/0.01 Torr, 8.3 g, 30.3 mmol, 41%); ir (neat): 2910, 2840, 1490, 1450, 1370, 1190, 1090 cm^{-1}; ^{1}H nmr ($CDCl_3$): 7.35 (5H, m), 5.45 (2H, m), 4.5 (2H, s), 4.05 (2H, d, J = 6 Hz), 3.8 (2H, s), 3.3 (3H, s), 2.4–1.4 (10H, m).

*(2*SR*,3*SR*,6*RS*,7*SR*)-1-Benzyloxy-8-methoxy-3,7-dimethyloctane-2,6-diol* ***10***a *and its diastereomer* ***11***a

The diether **9** (1.8 g, 6.57 mmol) was dissolved in dry tetrahydrofuran (10 mL) under a nitrogen atmosphere, then cooled in an ice–salt bath to −10 to −15°C. A solution of thexylborane (13) (1 *M*, 10 mL) was then added dropwise via a double-tipped cannula; the resulting reaction mixture was stirred for 2 h at −10°C. Aqueous NaOH (3 *M*, 20 mL) was added, followed by 50% aqueous hydrogen peroxide (10 mL); the resulting solution was stirred overnight, then partitioned between ether (100 mL) and water. The organic layer was separated, washed with aqueous sodium metabisulfite, dried, filtered, and concentrated under reduced pressure. Thin-layer chromatography (silica, ether) showed two major components, R_f 0.4 and 0.3. Chromatographic purification (Lobar, ether) gave a mixture of diols **10***a* and **11***a* (0.63 g, 31%) as the higher R_f component; ir ($CHCl_3$): 3600–3200, 2860, 1450, 1200, 1100 cm^{-1}; ^{1}H nmr ($CDCl_3$): 7.35 (5H, s), 4.58 (2H, s), 3.72–3.16 (9H, m including s at 3.36), 2.62 (1H, br s), 1.95–1.14 (7H, m), 0.90 (6H, d, J = 7 Hz); ^{13}C nmr ($CDCl_3$): 138.31, 128.41, 127.67, 77.22, 76.39, 74.31, 73.49, 72.82, 58.95, 38.35, 36.35, 32.35, 28.31, 15.62, 14.04 (major diastereomer).

The lower R_f component was the diol **12** (0.58 g, 44%) as an equal mixture of a pair of diastereomers, as evidenced by proton decoupled ^{13}C nmr; ir ($CHCl_3$): 3610, 3600–3100, 2920, 1450, 1090 cm^{-1}; ^{1}H nmr ($CDCl_3$): 3.75–2.85 (10H, m, including s at 3.34 and br —OH), 1.88–2.05 (8H, m) 0.98–0.82 (6H, m); ^{13}C nmr ($CDCl_3$): 77.5/77.45, 76.24/75.71, 60.63/60.58, 59.00, 39.99/39.64, 38.25/38.21, 32.54/32.07, 32.03/31.79, 29.78/29.17, 19.88/19.64, 13.93/13.85 (carbon chemical shifts have not been unambiguously assigned for each of the diastereomers).

*(2*SR*,3*SR*,6*RS*,7*SR*)-8-Methoxy-3,7-dimethyloctane-1,2,6-triol* ***10***b *and its diastereomer* ***11***b

The mixture of diols (0.490 g, 1.58 mmol) was dissolved in methanol (20 mL) containing glacial acetic acid (2 drops) and 5% palladium on charcoal (100 mg), then hydrogenolysed at atmospheric pressure until thin-layer chromatography (silica, ethyl acetate) showed no remaining starting material. The solution was then filtered through Celite, concentrated under reduced pressure, and dried under high vacuum to give the triol as a mixture of stereoisomers (0.338 g, 1.55 mmol, 98%); ir ($CHCl_3$): 3600–3100, 3000, 2930, 1450, 1190, 1090 cm^{-1}; ^{1}H nmr ($CDCl_3$): 3.82–3.30 (9H, m including s at 3.37), 3.3–1.9 (3H, br), 1.9–1.28 (6H, m), 0.9–0.8 (6H, pair of overlapping doublets); ms *m/e*: 201 (M^+ −H_3O) (7%), 187(17), 171(25), 139(48), 129(72), 103(95), 71(100). *Exact Mass* calcd. for $C_{11}H_{24}O_4$ − CH_5O: 187.1334; found: 187.1343.

*(2*RS*,3*SR*,6*RS*,1′*SR*)-6-(2-Methoxy-1-methylethyl)-2-hydroxymethyl-3-methyltetrahydropyran* ***13*** *and its diastereomer* ***14***

The mixture of triols (0.339 g, 1.55 mmol) was dissolved in dry pyridine (10 mL) under a nitrogen atmosphere, then cooled in an ice–salt bath to −10°C. *p*-Toluenesulfonyl chloride (0.325 g, 1.70 mmol) was added, then the reaction mixture was stirred 2 h at −10°C, followed by 2 h at room temperature. The solvent was then removed under high vacuum and the residue partitioned between methylene chloride (50 mL) and water (25 mL). The organic layer was separated, washed with dilute aqueous HCl, dried, filtered, and concentrated under reduced pressure to give the monotosylate; ir ($CHCl_3$): 3600–3300, 2960, 1450, 1350, 1160, 1085, 890 cm^{-1}; ^{1}H nmr ($CDCl_3$): 7.82 (2H, d, J = 6 Hz), 7.36 (2H, d, J = 6 Hz), 4.17–3.92 (2H, m, AB portion of ABX), 3.70–3.30 (7H, m including s at 3.36), 2.46 (3H, s), 2.4–2.00 (2H, br s), 1.86–1.20 (6H, m), 0.88 (3H, d, J = 7 Hz), 0.87 (2H, d, J = 7 Hz).

The tosylate was dissolved in dry methanol (25 mL), then freshly prepared sodium methoxide in methanol was added dropwise until thin-layer chromatography (silica, ether) showed complete consumption of the starting material. The reaction mixture was concentrated under reduced pressure, then partitioned between methylene chloride (50 mL) and water (25 mL). The organic layer was separated, dried, filtered, and concentrated under reduced pressure to give the epoxide, which was used without purification. The ^{1}H nmr spectrum showed multiplets centred at 2.73 and 2.48 δ in a 2:1 ratio, indicative of an epoxide structure.

The epoxide was dissolved in glacial acetic acid (4 mL), then stirred 3 days at room temperature, after which time the reaction mixture was partitioned between methylene chloride (50 mL) and aqueous NaOH (3 *M*, 25 mL). The organic layer was dried, filtered, then concentrated under reduced pressure to give the crude product. Purification by Lobar chromatography (ether–hexanes, 1:1; ether) gave a mixture of diastereomeric tetrahydropyrans with **13** as the major component and **14** as the minor component (0.13 g, 49%); ir ($CHCl_3$): 3650–3150, 2900, 1450, 1220, 1085, 1065, 1050, 900 cm^{-1}; ^{1}H nmr ($CDCl_3$): 4.0–3.84 (2H, m), 3.72 (1H, dd, J = 9 and 5 Hz), 3.51–3.26 (5H, m including s

at 3.34), 3.22 (1H, dd, J = 9, 3 Hz), 3.15 (1H, br OH), 2.06–1.18 (6H, m), 0.95 (3H, d, J = 7 Hz), 0.82 (3H, d, J = 7 Hz); doublets at 0.94 and 0.91 were attributed to the minor diastereomer; ^{13}C nmr ($CDCl_3$): 76.67, 75.24, 70.24, 58.93, 57.37, 38.13, 31.83, 28.54, 27.88, 16.27, 14.22 (major diastereomer); 80.88, 79.88, 75.16, 64.46, 58.78, 38.89, 31.32, 28.88, 22.92, 13.19, 12.09 (minor diastereomer); ms *m/e*: 203 (M^+ +1) (13%), 184 (11), 171(57), 139(53), 129(55), 111(53), 99(71), 93(60), 81(86), 69(97), 55(100). *Exact Mass* calcd. for $C_{11}H_{22}O_3 - CH_2OH$: 171.1385; found: 171.1385.

Methyl (2RS,5SR,6RS, αRS)-6-Carboxy-α,5-dimethyltetrahydropyran-2-acetate **2**b *and dimethyl ester* **2**c

Following the procedure of Sharpless and co-workers (12), to a solution of the alcohols **13** and **14** (30 mg, 0.15 mmol) in carbon tetrachloride (2 mL) and acetonitrile (2 mL) were added water (3 mL), ruthenium trichloride trihydrate (10 mg), and sodium periodate (360 mg, 1.68 mmol). The resulting reaction mixture was stirred 18 h at room temperature, then partitioned between methylene chloride (25 mL) and water (10 mL). The aqueous layer was separated, dried, filtered, and concentrated under reduced pressure to give the half-ester **2***b* (20 mg, 58%) on purification by Lobar chromatography (ether): ir ($CHCl_3$): 3700–3000, 2920, 1715 (br), 1450, 1430, 1310, 1200, 1170, 1080 cm^{-1}; ^{1}H nmr ($CDCl_3$): 8.25 (1H, br s, CO_2H), 4.35 (1H, d, J = 5 Hz, H-C6), 3.89 (1H, ddd, J = 11, 9 and 2.5 Hz, H-C2), 3.75 (3H, s, methyl ester), 2.65 (1H, d of q, J = 9 and 7 Hz, H-Cα), 2.18–0.9 (11H, m including doublets at 1.16 and 1.15 with J = 7 Hz); ^{13}C nmr ($CDCl_3$): 175.26, 172.16, 76.28, 75.07, 51.86, 43.95, 32.35, 27.02, 26.20, 16.09, 13.27; ms *m/e*: 231 (M^+ +1) (10%), 212 (21), 199(21), 185(45), 170(36), 153(54), 143(49), 125(72), 115(68), 97(75), 88(67), 69(78), 55(100). *Exact Mass* calcd. for $C_{11}H_{18}O_5 - CO_2H$: 185.1176; found: 185.1169.

Treatment of the half-ester **2***b* with ethereal diazomethane afforded the diester **2***c*; ir ($CHCl_3$): 2940, 1725, 1450, 1435, 1170, 1085 cm^{-1}; ^{1}H nmr ($CDCl_3$): 4.33 (1H, d, J = 5.6 Hz), 4.27 (1H, ddd, J = 2.9, 8.5, 10.8 Hz), 3.71 (3H, s), 3.68 (3H, s), 2.57 (1H, dq, J = 7.1, 8.2 Hz), 2.2–1.2 (5H, m), 1.11 (3H, d, J = 7 Hz), 0.92 (3H, d, J = 7 Hz).

Reaction of **9** *with 9-borabicyclo[3.3.1]nonane*

The diene **9** (0.36 g, 1.3 mmol) was dissolved in dry tetrahydrofuran (2 mL) under a dry nitrogen atmosphere in a round-bottomed flask. The flask was placed in a room-temperature bath, then 9-BBN (0.5 *M* in tetrahydrofuran, 5 mL) was added to the flask by syringe. After stirring the reaction mixture overnight, aqueous sodium hydroxide (3 *M*, 5 mL) was added, followed by hydrogen peroxide (30%, 5 mL). The resulting mixture was stirred several hours, then partitioned between methylene chloride and water. The organic layer was separated, dried, filtered, then concentrated under reduced pressure to give an oil that was chromatographed (Lobar; ether–hexanes, 1:1) to give recovered diene (0.19 g) and the alcohol **15** (0.054 g); ir ($CHCl_3$): 3610, 3600–3100, 2990, 2910, 1445, 1370, 1200, 1085 cm^{-1}; ^{1}H nmr ($CDCl_3$): 5.42 (1H, t, J = 7 Hz) 3.81 (2H, s), 3.68 (2H, m), 3.28 (3H, s), 2.55–1.13 (11H, m including s at 1.66), 0.92 (3H, d, J = 7 Hz); ^{13}C nmr ($CDCl_3$): 131.83, 128.63, 78.75, 60.88, 57.29, 39.84, 36.83, 29.24, 25.13, 19.52, 13.75. The alcohol **16** was detected by proton nmr as a minor and unquantifiable component in another fraction (5 mg).

Acknowledgements

Financial assistance of the Natural Sciences and Engineering Research Council is gratefully acknowledged, as is the technical assistance of Ms. S. Blake of the Queen's University Magnetic Resonance Laboratory, Nuclear Division. The author is indebted to Professor Steven V. Ley, Imperial College of Science and Technology, for providing copies of spectra for compounds **2***b* and **2***c* for the purpose of comparison.

1. A. G. Fallis. Can. J. Chem. **62**, 183 (1984); G. Breiger and J. N. Bennett. Chem. Rev. **80**, 63 (1980).
2. D. M. Walba and G. S. Stoudt. J. Org. Chem., **48**, 5406 (1983), and references therein.
3. P. A. Wender and G. B. Dreyer. Tetrahedron Lett. **24**, 4543 (1983), and references therein.
4. W. C. Still and K. P. Darst. J. Am. Chem. Soc. **102**, 7385 (1980).
5. J. W. Westley, R. H. Evans, Jr., C.-M. Liu, T. E. Hermann, and J. F. Blount. J. Am. Chem. Soc. **100**, 6784 (1978); C.-M. Liu, T. E. Hermann, M. Liu, N. J. Palleroni, B. L. T. Prosser, J. W. Westley, and P. J. Miller. J. Antibiot. **32**, 95 (1979); J. W. Westley, R. H. Evans, Jr., L. H. Sello, N. Troupe. C.-M. Liu, and J. F. Blount. J. Antibiott. **32**, 100 (1979).
6. (*a*) K. C. Nicolaou, D. H. Papahatjis, D. A. Claremon, and R. F. Dolle III. J. Am. Chem. Soc. **103**, 6967 (1981); (*b*) P.-T. Ho. Can. J. Chem. **60**, 90, (1980); (*c*) S. D. Burke, D. M. Armistead, and J. M. Fevig. Tetrahedron Lett. **26**, 1163 (1985).
7. M. P. Edwards, S. V. Ley, and S. G. Lister. Tetrahedron Lett. 361 (1981); K. C. Nicolaou and R. L. Magolda. J. Org. Chem. **46**, 1506 (1981); W. R. Roush and A. G. Myers. J. Org. Chem. **46**, 1509 (1981); G. Mansoor. M.Sc. Thesis, Queen's University. 1981.
8. (*a*) K. C. Nicolaou, D. A. Claremon, D. P. Papahatjis, and R. L. Magolda. J. Am. Chem. Soc. **103**, 6969 (1981); (*b*) M. P. Edwards, S. V. Ley, S. G. Lister, B. D. Palmer, and D. J. Williams. J. Org. Chem. **49**, 3503 (1984); (*c*) W. R. Roush, S. M. Peseckis, and A. E. Walts. J. Org. Chem. **49**, 3429 (1984); (*d*) K. C. Nicolaou, D. P. Papahatjis, D. A. Claremon, R. L. Magolda, and R. E. Dolle. J. Org. Chem. **50**, 1440 (1985).
9. J. Wolinsky and R. H. Bedoukian. J. Org. Chem. **41**, 278 (1976).
10. E. L. Eliel, K. D. Hargrave, K. M. Pietrusiewicz, and M. Manoharan. J. Am. Chem. Soc. **104**, 3635 (1982), and references therein.
11. M. A. Umbreit and K. G. Sharpless. J. Am. Chem. Soc. **99**, 5526 (1977).
12. P. H. J. Carlsen, T. Katsuki, V. S. Martin, and K. B. Sharpless. J. Org. Chem. **46**, 3936 (1981).
13. H. C. Brown. Organic syntheses via boranes. John Wiley and Sons, New York. 1975.
14. Q. N. Porter and J. Baldas. Mass spectrometry of heterocyclic compounds. Wiley–Interscience, New York. 1971.
15. G. Stork, M. Gregson, and P. A. Greico. Tetrahedron Lett. 1391 (1969).
16. M. Mori. Tetrahedron, **33**, 289 (1977).
17. D. J. Nelson and H. C. Brown. J. Am. Chem. Soc. **104**, 4907 (1982).

Complexes of 18-crown-6 macrocyclic ethers obtained from ethereal solvents. Complexes of potassium and sodium salts with host:guest ratios of 1:2 and 1:3

ANDRÉ RODRIGUE, JOHN W. BOVENKAMP,[1] BENOIT V. LACROIX, AND ROBERT A. B. BANNARD
Defence Research Establishment Ottawa, Ottawa, Ont., Canada K1A 0Z4

AND

GERALD W. BUCHANAN
Ottawa–Carleton Institute for Research and Graduate Studies in Chemistry, Carleton University, Ottawa, Ont., Canada K1S 5B6

Received August 9, 1985

ANDRÉ RODRIGUE, JOHN W. BOVENKAMP, BENOIT V. LACROIX, ROBERT A. B. BANNARD, and GERALD W. BUCHANAN. Can. J. Chem. **64**, 808 (1986).

This paper describes the synthesis, in ethereal solvents, of the complexes of 18-crown-6, the *cis–syn–cis* and the *cis–anti–cis* isomers of dicyclohexano-18-crown-6, and dibenzo-18-crown-6 with the potassium and sodium salts of phenoxide and thiocyanate (as well as some potassium oximate salts). In general, the macrocycles break down the aggregates of the potassium salts so that the complexes of the contact ion pairs are isolated. The complex of the *cis–anti–cis* isomer of dicyclohexano-18-crown-6, however, which has a low stability constant, complexes the dimer of potassium phenoxide to give a complex with a 1:2 host:guest ratio. This appears to be the first example of a 1:2 host:guest ratio of a potassium salt with an 18-crown-6 macrocycle. There is a greater tendency for the complexes of sodium salts to have host:guest ratios less than 1:1. Thus, 18-crown-6 gives complexes with sodium phenoxide and sodium thiocyanate which have 1:3 and 1:2 host:guest ratios, respectively. Host:guest ratios of 1:2 are also obtained for the two above-mentioned isomers of dicyclohexano-18-crown-6 and for dibenzo-18-crown-6 with sodium phenoxide. Sodium thiocyanate gives complexes with either 1:1 or 1:2 host:guest ratios depending on the macrocycle. With dibenzo-18-crown-6, sodium thiocyanate gives a 1:1 complex in which one molecule of the solvent used is incorporated into the complex. The infrared and ultraviolet spectra of the complexes are discussed.

ANDRÉ RODRIGUE, JOHN W. BOVENKAMP, BENOIT V. LACROIX, ROBERT A. B. BANNARD et GERALD W. BUCHANAN. Can. J. Chem. **64**, 808 (1986).

Dans cette communication, on décrit la synthèse, dans des solvants éthérés, des complexes de la 18-couronne-6, des isomères *cis–syn–cis* et *cis–anti–cis* de la dicyclohexano-18-couronne-6 et de la dibenzo-18-couronne-6 avec les phénolates et thiocyanates de potassium et de sodium (ainsi qu'avec quelques oximates de potassium). D'une façon générale, les macrocycles brisent les agrégats des sels de potassium et l'on peut donc isoler les complexes des paires d'ions de contact. Toutefois, la constante de stabilité du complexe de l'isomère *cis–anti–cis* de la dicyclohexano-18-couronne-6 est faible et il se complexe donc avec le dimère du phénolate de potassium pour donner un complexe dans le rapport 1:2. Il semble que ce soit le premier exemple d'un complexe dans le rapport 1:2 d'un sel de potassium avec un macrocycle 18-couronne-6. Dans le cas des complexes du sodium, il existe une grande tendance à avoir des complexes dans des rapports plus petits que 1:1. La 18-couronne-6 donne donc des complexes avec le phénolate de sodium et le thiocyanate de sodium dans des rapports respectifs de 1:3 et 1:2. On a aussi obtenu des rapports 1:2 lors de la formation de complexes entre le phénolate de sodium et les isomères mentionnés plus haute de la dicyclohexano-18-couronne-6 ainsi qu'avec la dibenzo-18-couronne-6. Dans le cas du thiocyanate de sodium, on obtient, suivant la nature des macrocycles, des complexes avec des rapports 1:1 ou 1:2. Avec la dibenzo-18-couronne-6, le thiocyanate de sodium donne un complexe 1:1 dans lequel une molécule du solvant utilisé est incorporée dans le complexe. On discute des spectres infrarouges et ultraviolets des complexes.

[Traduit par la revue]

Introduction

Since the pioneering paper by Pedersen (1) on the synthesis of cyclic polyethers and their complexes, there has been a great deal of interest in this area. Macrocyclic ether complexes have been shown to have 1:1 host:guest stoichiometry when the radius of the metal ion of the salt and the size of the cavity formed by the macrocycle are compatible (e.g. potassium salts with 18-crown-6 macrocycles (2)) but have 2:1 host:guest ratios when the metal ion radius is too large to fit into the cavity (e.g. (benzo-15-crown-5)$_2$·KNCS (3)). Alternatively, when the cavity of the cyclic polyether is large enough, two metal ions can be accommodated. Examples in this category are the 1:2 host:guest ratios exhibited by 18-crown-6·2LiNCS·2H$_2$O (4) and DB-24-crown-8·2KNCS (5).

Recently, we have carried out low temperature ^{13}C nmr stereochemical studies of the *cis–syn–cis* and *cis–anti–cis* isomers (isomers A and B, respectively) of dicyclohexano-18-crown-6 (6, 7). During our work with these compounds, it was found that on the addition of the commercial mixture of the two isomers to a 1,2-dimethoxyethane solution of potassium phenoxide, a solid precipitated. This solid had a narrow-range melting point and was shown by proton nmr to have a 1:2 host:guest ratio. Upon repeating the reaction with isomer B by itself, the same complex (**8** in Table 1) was obtained. It was apparent that an aggregate of potassium phenoxide, presumably a dimer, was being complexed by isomer B of DC-18-crown-6 instead of the contact ion pair that would have been expected.

The above result led to the present study in which the complexes of a series of sodium and potassium salts (mainly phenoxide and thiocyanate) were isolated from the ethereal solvents 1,2-dimethoxyethane (DME), tetrahydrofuran (THF), and diethyl ether. Whenever possible, a standard method was used, which involved reacting the macrocycle with an excess quantity of the sodium or potassium salt solubilized in anhydrous solvent (see experimental section). The complex that precipitated was then collected by filtration, washed with diethyl ether, and subjected to high vacuum. It was not possible to use this standard method with all of the complexes in Table 1

[1]Author to whom correspondence should be addressed.

TABLE 1. The complexes and their host:guest ratios

Number	Macrocycle[a]	Salt	Host:guest ratio
		Section A. Potassium complexes	
1	18-C-6	K^+OPh^-	1:1
2	18-C-6	$K^+(CH(COCH_3)_2)^-$	1:1
3	18-C-6	$K^+(CH_3COCCH_3)$ N—O	1:1
4	18-C-6	$K^+(PhCCH_3)$ N—O	1:1
5	18-C-6	K^+NCS^-	1:1
6	DC-18-C-6 (A)	K^+OPh^-	1:1
7	DC-18-C-6 (A)	K^+NCS^-	1:1
8	DC-18-C-6 (B)	K^+OPh^-	1:2
9	DC-18-C-6 (B)	$K^+(CH_3COCCH_3)$ N—O	1:1
10	DC-18-C-6 (B)	K^+NCS^-	1:1
11	DB-18-C-6	K^+OPh^-	1:1
12	DB-18-C-6	K^+NCS^-	1:1
13	Cryptand [2.2.2]	K^+OPh^-	1:1
		Section B. Sodium complexes	
14	18-C-6	Na^+OPh^-	1:3
15	18-C-6	Na^+NCS^-	1:2
16	DC-18-C-6 (A)	Na^+OPh^-	1:2
17	DC-18-C-6 (A)	Na^+NCS^-	1:1
18	DC-18-C-6 (B)	Na^+OPh^-	1:2
19	DC-18-C-6 (B)	Na^+NCS^-	1:2
20	DB-18-C-6	Na^+OPh^-	1:2
21[b]	DB-18-C-6	Na^+NCS^- (in dimethoxyethane)	1:1:1
22[b]	DB-18-C-6	Na^+NCS^- (in tetrahydrofuran)	1:1:1
23[b]	DB-18-C-6	Na^+NCS^- (in 1,3-dioxolane)	1:1:1

[a]DC-18-C-6 (A) designates the *cis–syn–cis* isomer and DC-18-C-6 (B) the *cis–anti–cis* isomer of this macrocycle.

[b]One molecule of solvent adheres very strongly to the complex of DB-18-C-6 and NaSCN. Thus, **20**, **21**, and **22** are 1:1:1 complexes containing one molecule of the solvents indicated (see text).

since in some cases the potassium salts were not soluble in the solvents used and in other cases the complex was too soluble to precipitate from the solvent in which it was formed. Dry solvents were used and the complexations were carried out in an argon atmosphere.

Results and discussion

In ethereal solvents like DME, THF, and Et_2O, many alkali metal salts form aggregates, $(R^-M^+)_n$. Jackman and Szeverenyi (8) have shown that lithioisobutyrophenone forms tetramers and dimers in this type of solvent. The authors (8) state that there did not appear to be any compelling reason to postulate free ions or monomeric ion pairs in the exchange process between the tetramer and the dimer in DME.

The degree of association of ion pairs depends on the solvent and on the size, charge density, and hardness of both the cation and the anion (9, 10). Reichle (11) has found that the degree of aggregation of 0.08 *M* potassium phenoxide in THF at 37°C is 3.2. Sodium and potassium alkoxides have been shown to form associated ion pairs even in more polar solvents than those used in this study (10, 12). Ion pairs of *t*-BuOLi were found to be more associated than those of *t*-BuOK (12). In Jackman and Lange's review (9), solvents are separated into four classes with respect to the occurrence of free ions, ion pairs, and aggregates of ion pairs. Weakly polar solvents like the ethereal solvents used in this study were called class B solvents. Evidence is presented that indicates that in this class of solvent "the 'tightness' of ion pairing (either as monomers or aggregates) will be greatest for Li^+, the smallest alkali metal cation, and will decrease monotonically with increasing ion radius of the cation" (9).

TABLE 2. Stability constants for sodium and potassium salt complexes in water and methanol (ref. 16)

	Sodium salts		Potassium salts	
Macrocycle	Log *K* (Water)	Log *K* (Methanol)	Log *K* (Water)	Log *K* (Methanol)
Cryptand [2.2.2]	3.90	7.98[a]	5.40	10.41[a]
18-Crown-6	0.8	4.36	2.03	6.05
DC-18-Crown-6				
Isomer A	1.21	4.08	2.02	6.01
Isomer B	0.69	3.68	1.63	5.38
DB-18-Crown-6	1.16	4.5	1.67	5.1

[a]All values are taken from ref. 16*a* except those for cryptand [2.2.2] in methanol, which are from ref. 16*b*.

It has been generally accepted that when 18-crown-6 macrocycles are added to solutions of sodium or potassium salts in ethereal solvents, the aggregates are broken up and 1:1 complexes with either the contact ion pair or the separated ion pair are formed (13, 14). In fact, Thomassen *et al.* (14) present kinetic evidence in support of this behaviour in the reaction of potassium phenoxide with butyl bromide in the presence of DC-18-crown-6. The study of Cornelis *et al.* (15) using sodium-23 nmr, however, has shown that the sodium salt of ethyl acetoacetate exists in THF as an equilibrium of monomeric and dimeric ion pairs, both of which interact with 18-crown-6 or 15-crown-5.

This work shows that, in some cases, complexes of 18-crown-6 macrocyclic ethers with potassium and sodium salts can be obtained from ethereal solvents with host:guest ratios smaller than 1:1. As shown in Table 2, the macrocyclic ethers used in this study had varying complexing abilities. "Hard" anions, such as phenoxide and oximates, as well as the "soft" thiocyanate anion were utilized. Sodium, as well as potassium, salts were used, since sodium salts would tend to form stronger aggregates (*vide supra*) and at the same time the stability constants of 18-crown-6 macrocycles are significantly smaller with sodium salts than with potassium salts (see Table 2).

Table 3 gives the melting points and elemental analyses of the isolated complexes while Table 4 gives the solvents used and the yields of the complexes obtained.

As the host:guest ratios for the potassium salts in Table 1 show, the 18-crown-6 macrocycles, with a single exception, give isolated complexes which have 1:1 host:guest ratios. As expected, cryptand [2.2.2], the strongest complexer in the table, also gives a 1:1 complex (**13**) with potassium phenoxide. The complex of DB-18-crown-6 with KNCS (**12**) gave the same 1:1 ratio when precipitated from DME as that obtained by Pedersen (3) from methanol. Also, the complex of 18-crown-6 with KNCS (**5**) gave the same 1:1 ratio as obtained by Dale and Kristiansen (17) and Seiler *et al.* (18) from methylene dichloride under non-anhydrous conditions. The B isomer of DC-

TABLE 3. Melting points and elemental analyses of the complexes

Complex number	Melting point (°C)	Calculated					Found				
		C	H	N	K	Na	C	H	N	K	Na
1	187.5–190	54.52	7.37				54.23	7.39			
2	147–148	50.72	7.76				50.40	8.09			
3	142–144	47.62	7.49	3.47			48.00	7.82	3.60		
4	140–142.5	54.89	7.37	3.20			54.45	7.77	3.36		
5[a]	190–192										
6	144–146	61.87	8.18		7.74		61.52	8.29		7.46	
7[b]	123–125	53.69	7.72	2.98	8.32		53.65	7.60	3.13	8.26	
8	188.5–191.5	60.35	7.28		12.28		60.30	6.77		12.53	
9	126–127.5	56.33	8.27	2.73	7.64		55.75	8.50	2.83	7.87	
10[b]	122–124	53.69	7.72	2.98	8.32		53.60	7.75	3.16	8.71	
11	202–204	63.38	5.93		7.93		63.15	5.94		8.06	
12[c]	243–245										
13[d]	109–112	56.67	8.12	5.51	7.69		54.77	8.67	5.18	7.81	
14	190.5–192.5	58.81	5.59			11.26	58.56	5.44			10.91
15[e]	137[+]	39.44	5.67	6.56		10.78	39.29	5.51	6.61		10.94
16	173–174.5	63.55	7.66			7.60	63.48	8.01			7.63
17	144.5–147	55.60	7.99	3.08		5.07	55.44	7.89	3.57		5.12
18	200.5–202.5	63.55	7.66			7.60	63.59	7.90			7.69
19[e]	178[+]	49.42	6.78	5.23		8.60	49.10	6.86	5.31		8.84
20	262–263.5	64.85	5.78			7.76	65.17	5.84			7.85
21	226.5–228	56.48	6.44	2.63		4.32	56.43	6.33	2.77		4.49
22	224.5–228	58.46	6.27	2.72		4.47	57.70	6.25	2.67		4.76
23	227–228	55.90	5.86	2.71		4.46	56.29	6.59	2.95		4.63

[a]Literature (17) mp 190°C.

[b]Pedersen (1) has reported the synthesis of the potassium thiocyanate complex of the mixture of A and B isomers of DC-18-crown-6 (mp (1) of the mixture was 72–122°C).

[c]Literature (3) mp 245–246°C.

[d]Complex **13** is especially sensitive to the atmosphere and to light (see the experimental section). Even so, it was possible to obtain a reasonable elemental analysis (except for the value for carbon, which was 1.9% low).

[e]At 137°C for **15** and 178°C for **19**, the solid turns into a mixture of liquid and solid. The solid in the mixture does not melt even up to 250°C. It is apparent that the 1:2 complex is decomposed at 137°C for **15** and 178°C for **19**, possibly to the 1:1 complex and NaNCS.

18-crown-6, however, gives a complex with a host:guest ratio of 1:2 (**8**). The crystal structure of this complex has been determined by X-ray diffraction techniques (19). Essentially, it is a dimer of potassium phenoxide that is being complexed. The potassium ions are related by symmetry and each is located approximately halfway between the crown ether and two phenoxide anions. Each individual crown molecule complexes one of the potassium ions of two dimers, one above the approximate plane of the macrocyclic ring and one below. Thus, it appears that the complexing ability of isomer B, DC-18-crown-6, a weak complexer (see Table 2), is not sufficient to break up the dimer to the contact ion pair stage.

Other examples of the potassium cation being out of the plane of the macrocycle ring have been reported. For example, in the 1:1 complex of 18-crown-6·potassium ethyl acetoacetate enolate, the K^+ is displaced by 0.9 Å out of the mean plane of the crown towards the strongly chelating anion of ethyl acetoacetate (20). With the NCS^- anion, the K^+ is situated exactly in the mean plane of the crown (18). The explanation must involve the competition between the crown and the anion for the K^+. If the anion is "hard", then it is closely associated with the K^+ and the crown cannot take the K^+ all the way into the "pocket" because of the repulsion between the crown oxygens and the negatively charged anion.

From Table 1, it is evident that the sodium salts have a much greater tendency to form complexes with multiple host:guest ratios than the potassium salts. A number of interesting comparisons can be made between the host:guest ratios obtained with sodium and potassium thiocyanates. Sodium thiocyanate gives a complex with 18-crown-6 which has a 1:2 host:guest ratio (**15**). This ratio can be compared with the 1:1 complex (18-crown-6·NaNCS·H_2O) formed by allowing a methylene dichloride solution of 18-crown-6 and NaNCS to evaporate in an open beaker to near dryness (17, 21, 22). The complex of NaNCS with DC-18-crown-6 (A) (**17**), however, has a 1:1 host:guest ratio, even though its complexing ability is not appreciably different from that of 18-crown-6 (see Table 2). It is thought that the cyclohexane rings, which are on the same side in DC-18-crown-6 (A), play a role in the explanation for this behaviour. That is, 18-crown-6 and also DC-18-crown-6 (B) would find it easier to complex two "out-of-pocket" cations than DC-18-crown-6 (A). In contrast to isomer A, DC-18-crown-6 (B) gives a NaNCS complex with a 1:2 host:guest ratio (**19**). The complex of DB-18-crown-6 with NaNCS has a 1:1 host:guest ratio (**21**, **22** and **23**) but it is interesting to note that the complex isolated is a 1:1:1 host:guest:solvent complex. Thus, solvent adheres very strongly to this complex and, even after 17 h in a drying pistol at 56°C under high vacuum, only a fraction of the solvent is removed from the 1:1:1 complexes that are formed in DME, THF, and 1,3-dioxolane. Complexes of DB-18-crown-6 with 1:1:1 ratios have been reported previously. For example, Hilgenfeld and Saenger (23) report the 1:1:1 complex of DB-18-crown-6 with potassium iodide and thiourea and Pedersen (24) reports 1:1:1 complexes of DB-18-crown-6 with sodium or potassium thiocyanate and thiourea. In the crystal structure of DB-18-crown-6 with potassium iodide and

TABLE 4. Solvents used and yields obtained for the complexes

Complex number	Solvent used[a]	Volume of solvent (mL)	Yield of complex (%)
1	DME	15	65
2	DME	20	51
3	DME	20	74
4	DME	20	73
5	THF	10	82
6	Et_2O	30	68
7	DME	10	55
8	DME	20	72
9	DME	30	63
10	DME	10	47
11	DME	15	74
12	DME	30	90
13	DME	14	51
14	THF + Et_2O	10 + 10	97
15	DME + Et_2O	10 + 5	64
16	THF + Et_2O	5 + 5	79
17	DME + Et_2O	10 + 5	83
18	DME	10	93
19	DME + Et_2O	10 + 5	81
20	THF	40	90
21	DME	30	89
22	THF	30	77
23	1,3-Dioxolane	30	97

[a]The solvent or solvent mixture in which the complex was formed. Et_2O, DME, and THF are used to designate diethyl ether, 1,2-dimethoxyethane, and tetrahydrofuran, respectively. See Experimental for isolation and purification procedures.

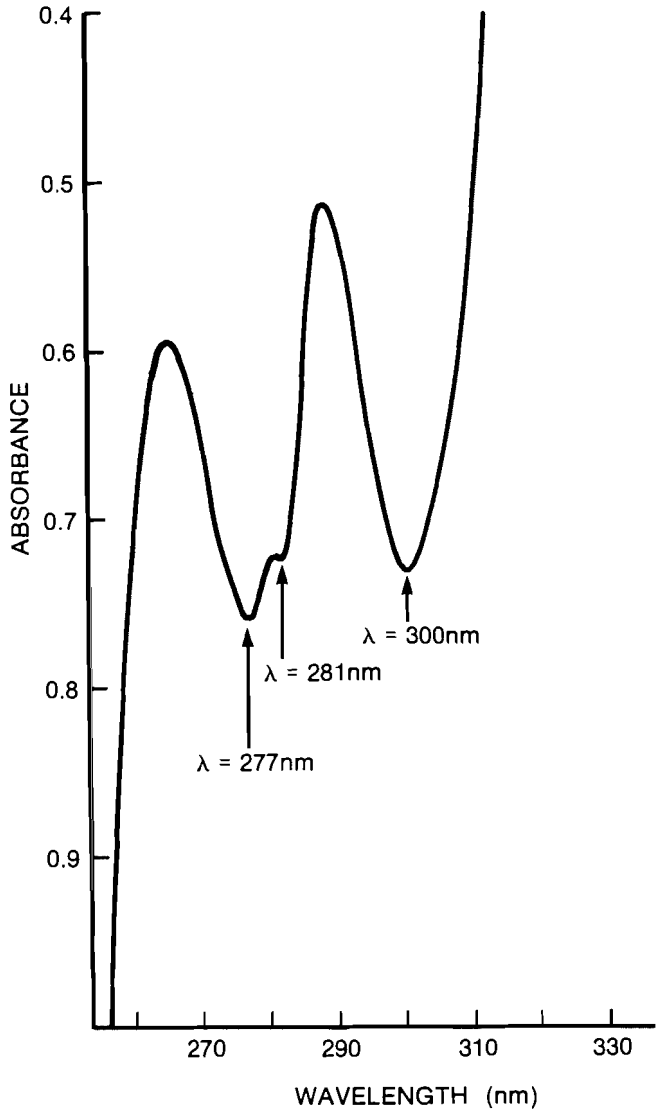

FIG. 1. The ultraviolet spectrum of DB-18-crown-6·2NaOPh in dimethoxyethane.

thiourea, the thiourea hydrogen bonds to the anion (23). This is not possible in **20**, **21**, and **22** and very likely the solvent molecule interacts with the Na^+. Solvent does not adhere as strongly to the 1:1 complex of DB-18-crown-6 with KNCS (12). This is in agreement with the work of Wong, Konizer, and Smid (25), who showed that THF is more strongly bonded to Na^+ than to K^+ in their system involving dimethyldibenzo-18-crown-6 and fluorenyl alkali salts.

Sodium phenoxide exhibits a greater propensity to form complexes with lower host:guest ratios than does KOPh (see Table 1). The reasons for this appear to be that Na^+ is not as strongly complexed by the crowns (see Table 2) and also that Na^+ is expected to form stronger associated ion pairs. Also, sodium phenoxide forms complexes with lower host:guest ratios than NaNCS. The proposed reason for this behaviour is that the "hard" phenoxide anion forms associated ion pairs more readily than the "soft" thiocyanate anion. Some support is obtained for this from the published crystal structure of 1:1 thiocyanate salt complexes. In the crystal structure of 18-crown-6·KNCS (18), the thiocyanate anions are disordered and interact only weakly with the K^+. Also, in 18-crown-6·NaNCS·H_2O, it is the water molecule that interacts with the Na^+ while the thiocyanate anion is hydrogen bonded to the water molecule (22).

18-Crown-6 forms a complex (**14**) with NaOPh that has a host:guest ratio of 1:3, the lowest ratio found in this study. It was readily precipitated using our standard method from a solution containing a 4:1 excess of salt to crown and has a melting point of 190.5–192.5°C. The reason why 18-crown-6 forms a complex with NaOPh with a 1:3 host:guest ratio, whereas the three substituted 18-crown-6 macrocycles give complexes with NaOPh with 1:2 ratios (**16**, **18**, and **20**), is not readily apparent. Attempts to grow suitable crystals of **14** for an X-ray diffraction structure determination have not yet been successful.

DC-18-crown-6 (A) forms a complex (**16**) with a 1:2 host:guest ratio with NaOPh as compared with the 1:1 ratio of its potassium analogue (**6**). The crystal structure of **16** has been determined (19) and differs considerably from that of DC-18-crown-6 (B)·2KOPh (**8**). The structure of **16** in the crystal form consists of a tetramer of NaOPh in which two macrocyclic ether molecules each complex two sodium ions. One sodium is coordinated to the six hexaether oxygens and to one of the phenoxide oxygens, while the other sodium is coordinated to only one of the crown oxygens and to three of the phenoxide oxygens. The crown adopts a highly irregular conformation. A full description of the structure of this interesting complex is given in ref. 19. The DC-18-crown-6 (B) complex with NaOPh (**18**) has the same host:guest ratio of 1:2 as its KOPh counterpart (**8**). However, DB-18-crown-6 gives a complex with NaOPh (**20**) with a host:guest ratio of 1:2, in contrast with its KOPh counterpart (**11**), which has a 1:1 ratio.

TABLE 5. λ_{max} from the ultraviolet spectra of the phenoxide anion in the complexes dissolved in dimethoxyethane

Macrocycle	Potassium phenoxide complexes			Sodium phenoxide complexes		
	Complex no.	Host:guest ratio	λ_{max} (nm)	Complex no.	Host:guest ratio	λ_{max} (nm)
18-C-6	**1**	1:1	317	**14**	1:3	299
DC-18-C-6 (A)	**6**	1:1	318	**16**	1:2	300
DC-18-C-6 (B)	**8**	1:2	311	**18**	1:2	300
DB-18-C-6	**11**	1:1	316	**20**	1:2	300
Cryptand [2.2.2]	**13**	1:1	322			
Potassium phenoxide		—	309			
Sodium phenoxide					—	300

TABLE 6. ν_{CN} and ν_{CS} infrared frequencies (cm^{-1}) for the free anion, the contact ion pair, and the dimer of sodium and potassium thiocyanate in solution (28, 29)

	Sodium thiocyanate[a]		Potassium thiocyanate[a]	
	ν_{CN}	ν_{CS}	ν_{CN}	ν_{CS}
Dimer	2042	769	2044	758
Contact ion pair	2056	760	2050	752
Free ion	2052	738	2052	738

[a]The solvent used was tetrahydrofuran except for the dimer of KNCS where dioxolane was used.

Ultraviolet spectra of the complexes

The ultraviolet spectrum of DB-18-crown-6·2NaOPh (**20**) in DME is shown in Fig. 1. Three peaks are present at λ_{max} 277, 281, and 300 nm. Only a single peak with a λ_{max} of 276 nm is present for DB-18-crown-6 in dimethoxyethane. The peak at λ_{max} 300 nm is that of the phenoxide anion. The appearance of a small peak like that at λ_{max} 281 nm has been shown by Pedersen (1) to be indicative of complex formation of DB-18-crown-6 with salts like KNCS, KI, and NaBr.

It is interesting to compare the λ_{max} values for the phenoxide anion for the applicable complexes. These are shown in Table 5 for DME solutions. The λ_{max} for potassium phenoxide itself, which is expected to exist as dimers and (or) higher aggregates of ion pairs, is 309 nm. The λ_{max} for phenoxide ion in the 1:1 complexes **1**, **6**, and **11** are shifted to 317, 318, and 316 nm, respectively. The phenoxide anion in these cases is expected to exist as a contact ion pair with the potassium ion. This ion pair is complexed by the crown ether. The λ_{max} for the phenoxide anion in the cryptand [2.2.2] complex (**13**) is shifted even further to 322 nm. In this case, the potassium ion is expected to be encased in the cryptand [2.2.2] molecule and contact between the cation and the phenoxide anion is expected to be greatly diminished (26). The λ_{max} value of the phenoxide ion in the complex formed by DC-18-crown-6 (B) with two KOPh salt molecules (**8**) is shifted to only 311 nm from the value of 309 nm for potassium phenoxide itself. Compound **8** in the crystalline state is essentially a complexed dimer of potassium phenoxide with the potassium ions above and below the plane formed by the ether rings (19) (*vide supra*). The small shift, compared to the larger ones for the 1:1 complexes in which contact ions pairs are expected, is evidence that this structure is maintained in solution.

In contrast, the λ_{max} values for the phenoxide anion in **14**, **16**, **18**, and **20**, which all have either 1:2 or 1:3 host:guest ratios, are essentially identical with that found for sodium phenoxide itself. This is a good indication that the Na^+ ions are not being complexed strongly and that the NaOPh salt molecules are associated more strongly with each other than with the macrocycles.

Ismail and El-Bayoumi (27) report that the λ_{max} of potassium *p*-methylphenoxide in THF increased from 317 to 326 nm when 18-crown-6 was added to the solution. This is similar to the magnitude of the shift difference found for potassium phenoxide and **1** (see Table 5). Thus, a 1:1 complex is probably formed in solution. On the other hand, for potassium *p*-methoxyphenoxide the λ_{max} of 334 nm did not change on the addition of 18-crown-6 (27). Also the λ_{max} of sodium *p*-methoxyphenoxide was found to be 323 nm by itself and 322 nm in the presence of 18-crown-6. These results would appear to indicate that 18-crown-6 complexes the dimer or higher aggregates of potassium and sodium *p*-methoxyphenoxide in THF. The sodium and potassium *p*-formyl phenoxide salts have λ_{max} shifts (27) in THF from 334 to 340 nm and from 347 to 357 nm, respectively, on the addition of 18-crown-6, indicative of 1:1 ion pair complexation.

Thus, single ion pairs are complexed more readily with substituted phenoxide in which the least charge is expected on the phenoxide oxygen (e.g. *p*-formyl) and associated ion pairs are complexed when the greatest amount of charge is expected on the phenoxide oxygen (e.g. *p*-methoxy). That is, the "harder" the anion, the stronger the associated ion pair aggregates and the more difficult it is for the crown to complex single ion pairs.

Infrared spectra of the complexes

Infrared spectra were obtained using the Nujol mull of the complexes. As noted by Pedersen (1) and others, for complexes that they studied, the infrared spectra of the complexes in Table 1 differ significantly from those of the macrocyclic ethers themselves, especially in the 700–1100 cm^{-1} region, which contains bands attributable to the wag, twist, and rock modes of vibration of the methylene groups of the macrocycle. Perhaps the most interesting aspect of the infrared spectra is the position and number of the ν_{CN} and ν_{CS} bands of the thiocyanate complexes.

Table 6 shows the position of these bands in the free anion, the contact ion pair, and the dimer, as determined by Chabanel and co-workers (28, 29) in tetrahydrofuran (dioxolane was used for $(KNCS)_2$). Table 7 shows the ν_{CN} and ν_{CS} frequencies

TABLE 7. ν_{CN} and ν_{CS} infrared frequencies (cm^{-1}) for the thiocyanate complexes[a]

Macrocycle	Sodium thiocyanate			Potassium thiocyanate		
	ν_{CN}	ν_{CS}	Host:guest ratio	ν_{CN}	ν_{CS}	Host:guest ratio
DC-18-C-6 (A)	2072	756	1:1 (**17**)	2057	749	1:1 (**7**)
DC-18-C-6 (B)	2050	767	1:2 (**19**)	2045	746	1:1 (**10**)
18-C-6	2067	756	1:2 (**15**)	2053	734	1:1 (**5**)
	2043	760				

[a]Obtained from the Nujol mull of the solid complexes.

obtained from the Nujol mulls of the solid complexes of Table 1. The thiocyanate complexes of DB-18-crown-6 are not included in Table 7 because the ν_{CS} peaks are masked by the peaks due to the aromatic carbon–hydrogen out-of-plane bending mode of vibration.

Although one must exercise caution in comparing the data in Table 6 for solutions of the thiocyanate salts with those in Table 7 for the Nujol mulls of the complexes, some speculation appears in order. The ν_{CS} frequency (734 cm^{-1}) found for the potassium thiocyanate complex of 18-crown-6 (**5**), is closest to that found for the free thiocyanate ion (738 cm^{-1}, see Table 6). The reason for this behaviour can be found in the published crystal structure of this compound (18), in which it was shown that the thiocyanate anion was disordered and interacted only weakly with the cation. The ν_{CS} frequencies of the 1:1 potassium thiocyanate complexes **7** and **10** (ν_{CS} = 749 and 746 cm^{-1}, respectively) are closest to that found for the contact ion pair of potassium thiocyanate in solution (752 cm^{-1}, see Table 6).

If it is assumed that the ν_{CS} and ν_{CN} frequencies of the 1:1 sodium thiocyanate complex of DC-18-crown-6 (A) (**17**) (see Table 7) are those for the contact ion pair (a not unreasonable assumption when these values are compared with those of Table 6), then some interesting comparisons can be made with **19** and **15**. For **19**, the ν_{CS} frequency increases by 11 cm^{-1} and the ν_{CN} frequency decreases by 22 cm^{-1} compared to the corresponding frequencies found for **17** (see Table 7). From Table 6, it can be seen that the ν_{CS} frequency of the dimer is higher by 9 cm^{-1} than that of the contact ion pair and the ν_{CN} frequency is lower by 14 cm^{-1}. Thus, it would be reasonable to expect that, in **19**, a dimer of sodium thiocyanate is being complexed. This would be a similar situation to that found in the crystal structure of **8**, in which the same macrocycle complexes a dimer of KOPh (19).

The ν_{CS} and ν_{CN} peaks for the 1:2 complex of 18-crown-6 with sodium thiocyanate (**15**) exist as doublets. Note that one set of ν_{CN} and ν_{CS} frequencies (2067 and 756 cm^{-1}, respectively) is close to that found for **17**, in which a contact ion pair was assumed, while the other set (ν_{CN} = 2043 and ν_{CS} = 760 cm^{-1}) has frequency values that are each 7 cm^{-1} less than those for **19** in which a dimer was postulated. Attempts are being made to prepare suitable crystals of **15** for an X-ray diffraction structure determination.

Experimental

Commercial anhydrous diethyl ether and toluene were dried over sodium wire. Reagent grade DME and THF were distilled from lithium aluminum hydride using a Stedman column and a variable take-off still head. Potassium and sodium thiocyanate were obtained commercially and were used after being subjected to high vacuum (<0.001 Torr; 1 Torr = 133.3 Pa) at 56°C for 18 h; mp 176–176.8 and >290°C, respectively (lit. (3) mp 173 and 287°C, respectively).

Isomers A and B of DC-18-crown-6 were separated from the commercial mixture by the method of Izatt *et al.* (30); mp 81.5–82.5°C (lit (30) mp 83–84°C) and 60.2–61.2°C (lit. (30) mp 61–62°C), respectively. DB-18-crown-6 was recrystallized from toluene; mp 161.5–163°C (lit. (3) mp 164°C and (31) mp 162.5–163.5°C). Commercial 18-crown-6 was precipitated as the acetonitrile complex (32) and the acetonitrile was removed under vacuum; mp 40.5–41.0°C (lit. (1) mp 39–40°C).

Preparation of the potassium salts of phenol, acetylacetone, E-acetophenone oxime (33), and 2,3-butanedione monoxime

These salts were obtained by reacting the starting material with powdered potassium in a nitrogen atmosphere. The safe handling procedures of Johnson and Schneider (34) were followed with potassium. Except in the case of the larger potassium salt preparations, where the initial filtration was carried out in the open air, the work-up of the reaction mixtures was conducted in a Dri-Lab (Vacuum Atmospheres) under an argon atmosphere. Purities of the potassium salts were checked by proton nmr and by potassium microanalyses. The procedure given below for potassium phenoxide is typical.

Potassium phenoxide

Potassium (9.21 g, 0.236 mol), freed of oxide crust, was added to a three-necked flask equipped with a reflux condenser, drying tube, stirring bar, and nitrogen gas inlet. Dry toluene (150 mL) was introduced and the potassium was powdered by heating the mixture to the boiling point while stirring vigorously. The mixture was allowed to cool and dry ether was added (150 mL). Phenol (25.00 g, 0.266 mol, sublimed under vacuum) dissolved in dry ether (150 mL) was added by dropping funnel. After being refluxed for 2 h, the mixture was filtered and the colourless solid was washed twice with dry ether. The salt was placed in a drying pistol under high vacuum (<0.001 Torr) at 56°C for 24 h. Yield, 28.2 g (91%); mp 285–289°C. *Anal.* calcd. for C_6H_5OK: K 29.57; found: K 29.17. Kornblum and Lurie (35) synthesized this salt by reacting phenol with potassium hydroxide in aqueous methanol.

Potassium acetylacetonate

A 9-day reflux period with powdered potassium was used; mp 210–215°C (dec.). *Anal.* calcd. for $C_5H_7O_2K$: K 28.33; found: K, 28.30. Carty *et al.* (36) report a potassium analysis for this salt which is 3.3% low.

Potassium 2,3-butanedione monoximate

The crude potassium salt obtained after a 1-week reflux period did not give a satisfactory potassium analysis. The solid was dissolved in warm ethanol, the solution was filtered while warm to remove undissolved material, and the salt was precipitated with dry ether; mp 224–226°C. *Anal.* calcd. for $C_4H_6NO_2K$: K 28.09; found: K 28.42.

E-*Potassium acetophenone oximate*

The crude potassium salt obtained after a 2-day reflux period was dispersed in a mixture of acetonitrile and dimethylsulfoxide (5:1 ratio). The mixture was heated to 70°C and filtered while hot. The solid that precipitated upon cooling had a mp of 267–270°C. *Anal.* calcd. for C_8H_8NOK: K 22.57; found: K 22.23.

Sodium phenoxide

Phenol and chunks of sodium metal in dry ether were refluxed under nitrogen for 3 days in a similar fashion to that described for the potassium

salt. The white salt was recrystallized from acetone. *Anal.* calcd. for C_6H_5ONa: Na 19.80; found: Na 19.74. Kornblum and Lurie (35) synthesized this salt using NaOH in methanol.

Synthesis of the macrocyclic ether complexes

It was possible to use a standard method for the synthesis of most of the complexes (see below). In this procedure, one equivalent of the macrocycle was added to a solution containing three equivalents of the salt. The complex was then allowed to precipitate from solution. The methods of synthesis of complexes for which the standard method was not used are given separately. Table 4 gives the solvent used, its volume, and the % yield (based on the macrocycle) for the complexes. All complexation reactions were carried out in a Dri-Lab (Vacuum Atmospheres) under an argon atmosphere. Table 3 gives the elemental analysis obtained for each complex.

*Standard synthetic method used for **1**, **5**, **8**, **10–12**, **16–23***

The sodium or potassium salt (5.1 mmol) was solubilized in anhydrous solvent. The crown was added (1.7 mmol) and the mixture was stirred for 1 h at room temperature. The precipitated complex was obtained by filtration, washed with diethyl ether, and subjected to high vacuum (<0.001 Torr) in a drying pistol (at 56°C) for approximately 17 h.

Solvents adhere very strongly to the complex between DB-18-crown-6 and NaNCS. One molecule of either dimethoxyethane, tetrahydrofuran, and 1,3-dioxolane is incorporated into the complex, when these are used as the complexing solvent (**21**, **22**, and **23**, respectively). Since only a fraction of this solvent was removed during the 17-h high vacuum treatment mentioned above, these complexes were only subjected to a 2-h period of high vacuum treatment. According to proton nmr and the elemental analyses, one molecule of solvent remained in the complexes in each case.

*Synthesis of **14** and **15***

The standard method was used except that 6.8 mmol of sodium phenoxide or sodium thiocyanate was used with 1.7 mmol of 18-crown-6.

*Synthesis of **7** and **10***

The complexes of isomers A and B of DC-18-crown-6 with potassium thiocyanate (**7** and **10**, respectively) were soluble in both dimethoxyethane and tetrahydrofuran and did not precipitate during the 1-h stirring period used in the standard method. Thus, the solvent was removed and methylene chloride (7 mL) was added. The insoluble solid was filtered off and washed with additional methylene chloride (3 mL). Diethyl ether (50 mL) was added to the combined methylene chloride filtrates to precipitate the complex.

*Synthesis of **6***

Isomer A of DC-18-crown-6 (1.7 mmol) was dissolved in diethyl ether (30 mL). Solid potassium phenoxide (1.7 mmol) was added. In about 4 min, only a trace of solid remained undissolved and this was filtered off. After several minutes, the complex began to precipitate from the filtrate and the mixture was filtered after being stirred for 30 min. After being washed with diethyl ether, the solid was subjected to high vacuum (<0.001 Torr) at 56°C for 17 h. The standard method could not be used to form this complex because the KOPh and the complex have similar solubilities in the solvents used. Both are very soluble in DME and the complex could not be precipitated without also precipitating the KOPh.

*Synthesis of **2** and **9***

The crown ether (1.7 mmol) and the potassium salt (5.1 mmol) were stirred in DME for 3 h. The excess potassium salt was filtered off. The solvent was removed from the filtrate and the residual complex was stirred for 30 min in diethyl ether. After being collected by filtration, the light-yellow salt was washed with diethyl ether and subjected to high vacuum (<0.001 Torr) at 56°C for 17 h.

*Synthesis of **3** and **4***

The potassium oximate (1.7 mmol) was dispersed in dimethoxyethane. Upon addition of the 18-crown-6 (1.8 mmol), the potassium salt dissolved and the complex soon precipitated. After the mixture was stirred for 1 h, the light-yellow solid was filtered off, washed with diethyl ether, and subjected to high vacuum (<0.001 Torr) at 56°C for 17 h.

*Synthesis of **13***

To potassium phenoxide (2.68 mmol) dissolved in DME (8 mL) was added cryptand [2.2.2] (2.66 mmol) in DME (6 mL). A clear light-yellow solution resulted. The beige precipitate that formed during the 18-h stirring period was collected by filtration and dried under high vacuum (<0.001 Torr) at 56°C for 9 h (0.687 g, 51%). Stirring the complex with fresh DME did not improve the elemental analysis (see Table 3), which was outside of the normally acceptable levels for carbon and hydrogen. In these experiments, flasks and sample bottles were covered with aluminum foil since cryptand [2.2.2] was stated to be light sensitive. Indeed, the complex (as a solid or in solution) turned purple when exposed to the atmosphere and to light.

Ultraviolet spectra of the phenoxide salt complexes

The complexes were dissolved in DME and a sample was inserted into the ultraviolet cells (0.1 cm) under an argon atmosphere. The ultraviolet spectra were obtained with a Varian Cary 2390 spectrophotometer. One of two methods was used to dissolve the complex in DME depending on its solubility. *Method A* (**6**, **13**, **14**, **16**, NaOPh, and KOPh): The complex (1 mmol) was weighed into a volumetric flask (50 mL) and anhydrous DME was added to the mark. A portion (5 mL) of this solution was diluted to 50 mL. The reference cell was filled with DME. *Method B* (**1**, **8**, **11**, **18**, **20**, and DB-18-crown-6): These materials were not soluble enough in DME to use Method A; however, about 0.05–0.1 mmol of each did dissolve in 50 mL of DME and this solubility was sufficient to give good ultraviolet spectra.

Intrared spectra of the thiocyanate salt complexes

A Perkin–Elmer infrared spectrophotometer (model 283) was used. Spectra were obtained on the Nujol mulls of the complexes using ZnSe optically flat windows (25 mm diameter × 2 mm thick).

Nuclear magnetic resonance studies of the complexes

^1H and ^{13}C studies of the complexes reported in this paper have been carried out. Some of this work has been published in refs. 6 and 7. Additional work will be reported in due course.

Acknowledgements

The Natural Sciences and Engineering Research Council of Canada (NSERCC) is thanked for a postdoctoral fellowship for A.R. and for financial assistance for G.W.B. We are grateful to George Morris of Agriculture Canada, Chemistry and Biology Research Institute, Analytical Chemistry Services, and Guelph Chemical Laboratories for carrying out the elemental analyses. We thank Dr. S. Fortier and M. Fraser of Queen's University for several stimulating discussions.

1. C. J. PEDERSEN. J. Am. Chem. Soc. **89**, 7017 (1967).
2. (*a*) R. M. IZATT and J. J. CHRISTENSEN (*Editors*). Synthetic multidentate macrocyclic compounds. Academic Press, New York. 1978; (*b*) G. A. MELSON (*Editor*). Coordination chemistry of macrocyclic compounds. Plenum Press, New York. 1979.
3. C. J. PEDERSEN. J. Am. Chem. Soc. **92**, 386 (1970).
4. P. GROTH. Acta Chem. Scand. Ser. A, **36**, 109 (1982).
5. N. S. POONIA. J. Am. Chem. Soc. **96**, 1012 (1974).
6. G. W. BUCHANAN, K. BOURQUE, J. W. BOVENKAMP, A. RODRIGUE, and R. A. B. BANNARD. Tetrahedron Lett. **25**, 3963 (1984).
7. G. W. BUCHANAN, K. BOURQUE, J. W. BOVENKAMP, and A. RODRIGUE. Can. J. Chem. **63**, 2747 (1985).
8. L. M. JACKMAN and N. M. SZEVERENYI. J. Am. Chem. Soc. **99**, 4954 (1977).
9. L. M. JACKMAN and B. C. LANGE. Tetrahedron, **33**, 2737 (1977).
10. O. A. REUTOV and A. L. KURTS. Russ. Chem. Rev. **46**, 1040 (1977).

11. W. T. REICHLE. J. Org. Chem. **37**, 4254 (1972).
12. V. A. BESSONOV, P. P. ALIKHANOV, E. N. GUR'YANOVA, A. P. SIMONOV, I. O. SHAPIRO, E. A. YAKOVLENA, and A. I. SHATENSHTEIN. Zh. Obshch. Khim. **37**, 109 (1967); Chem. Abstr. **66**, 115041U (1967).
13. A. L. KURTS, S. M. SAKEMBAERA, I. P. BELETSKAYA, and O. A. REUTOV. J. Org. Chem. USSR (Engl.), **10**, 1588 (1974).
14. L. M. THOMASSEN, T. ELLINGSEN, and J. UGELSTAD. Acta. Chem. Scand. **25**, 3024 (1971).
15. A. CORNELIS, P. LASZLO, and C. CAMBILLAU. J. Chem. Research (S), 462 (1978); J. Chem. Research (M), 5457 (1978).
16. (*a*) J. D. LAMB, R. M. IZATT, J. J. CHRISTENSEN, and D. L. EATOUGH. Coordination chemistry of macrocyclic compounds. *Edited by* G. A. Melson. Plenum Press, New York. 1979. Chapt. 3; (*b*) B. G. COX, H. SCHNEIDER, and J. STROKA. J. Am. Chem. Soc. **100**, 4746 (1978).
17. J. DALE and P. O. KRISTIANSEN. Acta. Chem. Scand. **26**, 1471 (1972).
18. P. SEILER, M. DOBLER, and J. D. DUNITZ. Acta Crystallogr. Sect. B, **30**, 2744 (1974).
19. M. E. FRASER, S. FORTIER, A. RODRIGUE, and J. W. BOVENKAMP. Can. J. Chem. **64**, 816 (1986).
20. C. RICHE and C. PASCARD-BILLY. J. Chem. Soc. Chem. Commun. 183 (1977).
21. J. D. DUNITZ, M. DOBLER, P. SEILER, and R. P. PHIZACKERLEY. Acta Crystallogr. Sect. B, **30**, 2733 (1974).
22. M. DOBLER, J. D. DUNITZ, and P. SEILER. Acta Crystallogr. Sect. B, **30**, 2741 (1974).
23. R. HILGENFELD and W. SAENGER. Angew. Chem. Int. Ed. Engl. **20**, 1045 (1981).
24. C. J. PEDERSEN. J. Org. Chem. **36**, 1690 (1971).
25. K. H. WONG, G. KONIZER, and J. SMID. J. Am. Chem. Soc. **92**, 666 (1970).
26. J. M. LEHN. Pure Appl. Chem. **52**, 2303 (1980).
27. K. Z. ISMAIL and M. A. EL-BAYOUMI. J. Solution Chem. **12**, 621 (1983).
28. M. CHABANEL and Z. WANG. J. Phys. Chem. **88**, 1441 (1984).
29. (*a*) D. PAOLI, M. LUCON and M. CHABANEL. Spectrochim. Acta, Part A, **34**, 1087 (1978); (*b*) Spectrochim. Acta, Part A, **35**, 593 (1979).
30. R. M. IZATT, B. L. HAYMORE, J. S. BRADSHAW, and J. J. CHRISTENSEN. Inorg. Chem. **14**, 3132 (1975).
31. C. J. PEDERSEN. Org. Synth. **52**, 66 (1972).
32. C. L. LIOTTA. U.S. Patent No. 3,997,562 (1976).
33. R. R. FRASER, R. CAPOOR, J. W. BOVENKAMP, B. V. LACROIX, and J. PAGOTTO. Can. J. Chem. **61**, 2616 (1983).
34. W. S. JOHNSON and W. P. SCHNEIDER. Org. Synth. Collect. Vol. **4**, 132 (1963).
35. N. KORNBLUM and A. P. LURIE. J. Am. Chem. Soc. **81**, 2705 (1959).
36. A. J. CARTY, D. G. TUCK, and E. BULLOCK. Can. J. Chem. **43**, 2559 (1965).

The crystal structures of the 1:2 host:guest complexes of dicyclohexano-18-crown-6 (isomers A and B) with sodium and potassium phenoxide

MARIE E. FRASER AND SUZANNE FORTIER[1]
Department of Chemistry, Queen's University, Kingston, Ont., Canada K7L 3N6
AND
ANDRÉ RODRIGUE AND JOHN W. BOVENKAMP
Defence Research Establishment Ottawa, Ottawa, Ont., Canada K1A 0Z4
Received August 15, 1985

MARIE E. FRASER, SUZANNE FORTIER, ANDRÉ RODRIGUE, and JOHN W. BOVENKAMP. Can. J. Chem. **64**, 816 (1986).

The crystal structures of the 1:2 host:guest complexes of dicyclohexano-18-crown-6 (isomer B) with potassium phenoxide and dicyclohexano-18-crown-6 (isomer A) with sodium phenoxide have been determined. The potassium phenoxide complex crystallizes in space group $P\bar{1}$ with a = 10.023(2), b = 11.238(2), c = 7.546(2) Å, α = 95.73(2), β = 103.04(2), γ = 92.03(2)°, and Z = 1. The sodium phenoxide complex crystallizes in space group $P2_1/n$ with a = 19.185(12), b = 13.266(5), c = 13.038(5) Å, β = 96.55(4)°, and Z = 4. Both structures were solved by direct methods and refined by full matrix least-squares calculations to a residual, R, of 0.035. The host conformation as well as the metal cation coordination differ considerably in the two structures. In the potassium phenoxide complex, the two cations are related by symmetry and have, consequently, the same chemical environment. Each potassium is located approximately halfway between the plane formed by the crown ether oxygens and the phenoxide anions and is coordinated to four of the crown oxygens and to two phenoxide oxygens. The oxygens of the crown are found to outline an elliptical cavity and to lie approximately in a plane. In the sodium phenoxide complex, the two sodiums have different crystallographic and chemical environments. One sodium is coordinated to the six hexaether oxygens, with distances ranging from 2.36 to 2.84 Å, and to one of the phenoxide oxygens. The other sodium is coordinated to only one of the crown oxygens and to three of the phenoxide oxygens. The hexaether adopts a highly irregular conformation.

MARIE E. FRASER, SUZANNE FORTIER, ANDRÉ RODRIGUE et JOHN W. BOVENKAMP. Can. J. Chem. **64**, 816 (1986).

On a déterminé les structures cristallines des complexes 1:2 de la dicyclohexano-18 couronne-6 (isomère B) avec le phénolate de potassium et de la dicyclohexano-18 couronne-6 (isomère A) avec le phénolate de sodium. Le complexe du phénolate de potassium cristallise dans le groupe d'espace $P\bar{1}$, avec a = 10,023(2), b = 11,238(2), c = 7,546(2) Å, α = 95,73(2), β = 103,04(2), γ = 92,03(2)° et Z = 1. Le complexe du phénolate de sodium cristallise dans le groupe d'espace $P2_1/n$, avec a = 19,185(12), b = 13,266(5), c = 13,038(5) Å, β = 96,55(4)° and Z = 4. On a résolu les deux structures par des méthodes directes et on les a affinées par la méthode des moindres carrés (matrice entière) jusqu'à des valeurs résiduelles de R de 0,035. La conformation de la molécule hôte ainsi que la coordination du cation métallique diffèrent considérablement dans les deux structures. Dans le complexe du phénolate de potassium, les deux cations sont reliés par de la symétrie et ont donc des environnements chimiques semblables. Chaque potassium est situé approximativement à mi-chemin entre le plan formé par les oxygènes de la couronne et celui des anions phénolates et chacun est coordonné à quatre oxygènes de la couronne et à deux oxygènes des phénolates. On a trouvé que les oxygènes de la couronne forment le contour d'une cavité ellipsoïdale et qu'ils se retrouvent approximativement dans un plan. Dans le complexe du phénolate de sodium, les deux cations de sodium se trouvent dans des environnements cristallographiques ainsi que chimiques qui sont différents. Un des cations de sodium est coordonné aux six oxygènes de l'éther, avec des distances variant de 2,36 à 2,84 Å, et à l'un des oxygènes des phénolates. L'autre sodium est coordonné à un seul des oxygènes de la couronne et à trois oxygènes des phénolates. La conformation de la couronne est hautement irrégulière.

[Traduit par la revue]

Introduction

Of the crown ethers, 18-crown-6 is probably the most extensively characterized. Nuclear magnetic resonance (nmr), infrared (ir), X-ray diffraction studies, as well as thermodynamics and molecular mechanics, have provided a basis for the understanding of the complexation of 18-crown-6 and its analogues, dicyclohexano-18-crown-6 and dibenzo-18-crown-6, with various guests (1–4).

Several factors contribute to the structural characteristics of host–guest complexes. It is well known that both ligand and salt (both cation and anion) parameters play a role in the structural features of the host–guest complex. This is seen in the results of the several crystallographic studies of alkali-metal complexes with 18-crown-6. The crystal structure analyses of the alkali thiocyanate complexes with 18-crown-6, for example, clearly show how the structures of the complexes are affected by the size of the cation relative to the size of the crown ether cavity (5–10). The "hole-size" criterion is not, however, the only one to be considered, as shown by the crystallographic study of the 18-crown-6 complex with potassium ethyl acetoacetate (11), where the counterion is seen to have a marked effect on the resultant structure: in spite of the fact that the size of the potassium ion is ideally suited to that of the 18-crown-6 cavity, a "hard" anion such as ethyl acetoacetate can pull the cation out of its ideal nesting position.

During a study of the *cis–syn–cis* and *cis–anti–cis* isomers (isomers A and B, respectively) of dicyclohexano-18-crown-6 (12), it was found that on the addition of the commercial mixture of the two isomers to a 1,2-dimethoxyethane solution of potassium phenoxide, a solid precipitated. The solid had a narrow-range melting point and was shown by proton nmr to have a 1:2 host:guest ratio. Upon repeating the reaction with isomer B by itself, the same complex was obtained. It was apparent that an aggregate of potassium phenoxide, presumably a dimer, was being complexed by isomer B of DC-18-crown-6 instead of the contact ion pair that would have been expected. The 1:2 host:guest ratio was surprising in view of the compatibility between the cation and the hexaether cavity size. In fact, this appears to be the first example of a 1:2 host:guest ratio complex of a potassium salt with an 18-crown-6 macrocycle. Also, a 1:2

[1]Author to whom all correspondence may be addressed.

TABLE 1. Crystal data[a]

Parameter	Crystal data	
Molecular formula	$K_2O_8C_{32}H_{46}$	$Na_2O_8C_{32}H_{46}$
Molecular weight	636.92	604.70
Space group; Z	$P\bar{1}$; 1	$P2_1/n$; 4
a, Å	10.023(2)	19.185(12)
b, Å	11.238(3)	13.266(5)
c, Å	7.546(2)	13.038(5)
α, deg	95.73(2)	90
β, deg	103.04(2)	96.55(4)
γ, deg	92.03(2)	90
V, Å^3	822.6	3297
Number of reflections used for the determination of unit cell parameters; 2θ range, deg	25; 16.3–20.9	25; 18.4–22.3
Density (calcd.), g cm^{-3}	1.286	1.218
Number of measured reflections	2885	3078
Number of observed reflections, $I > 3\sigma(I)$	2326	2472
2θ range scanned, deg	1–50	1–40
μ (MoKα), cm^{-1}	3.304	1.017
Crystal dimensions, mm	0.67 × 0.58 × 0.35	0.95 × 0.87 × 0.30
Isotropic secondary extinction correction, g	0.777 × 10^{-6}	0.323 × 10^{-6}
Final R; R_w	0.035; 0.061	0.035; 0.050
Largest shift/error in final least-squares cycle, Δ/σ	0.01	0.03
Maximum and minimum residual electron density in final difference Fourier map, e Å^{-3}	0.33; −0.16	0.21; −0.27
Standard deviation of an observation of unit weight, σ	1.830	1.608

[a]Estimated standard deviations are shown in parentheses.

host:guest complex of sodium phenoxide with DC-18-crown-6 (isomer A) was obtained from ethereal solvents (12). It was clear that, in both cases, the nature of the solvent used and the nature of the counterion played a role in the unusual host:guest ratios. This crystallographic study was undertaken to determine how the DC-18-crown-6 ligands were complexing the two salt molecules in these unusual complexes.

Experimental

The synthetic method used for the preparation of the two complexes has been described in a previous publication (12). Suitable crystals of DC-18-crown-6 (isomer A)·2NaOPh were obtained by dissolving the complex in dry tetrahydrofuran in a Dri-Lab (Vacuum Atmospheres) under an argon atmosphere and allowing the solvent to evaporate completely at room temperature. Crystals of DC-18-crown-6 (isomer B)·2KOPh were similarly obtained, except that the complex was initially dissolved in warm, dry 1,3-dioxolane. Pertinent data about the crystals used and the measurement of diffraction intensities are summarized in Table 1. The crystals used in the diffraction experiments were mounted inside a glass capillary in an oxygen-free atmosphere. The intensity data were collected on an Enraf–Nonius CAD-4 diffractometer using graphite monochromated MoKα ($\lambda = 0.71073$ Å) radiation. In each case, intensities were collected by the $\omega/2\theta$ scanning procedure and three reflections were measured after every 7200 s of exposure time to check on the stability of the crystals; in neither case was any evidence of crystal decay detected. The data were corrected for Lorentz and polarization effects; absorption corrections were not considered necessary. The structures were solved by direct methods using the program MULTAN 80 (13). For the K^+ complex, the positions of all the hydrogen atoms were found in the difference Fourier map. For the Na^+ complex, 44 out of 46 hydrogens were located in the maps; the remaining two were calculated. The structures were refined by full matrix least-squares using all reflections with $I > 3\sigma(I)$. Anisotropic temperature factors were used for the non-hydrogen atoms and isotropic temperature factors for the hydrogen atoms. All the hydrogen atoms were included in the calculations and refined except for the two calculated hydrogen atoms in the Na^+ complex, which were held fixed. The function minimized was $\Sigma w||F_o| - |F_c||^2$, where $w = 1/\sigma^2(|F_o|)$. A correction for isotropic secondary extinction effect was included in each refinement. The scattering factors were taken from Cromer and Waber (14). All the calculations were done on a PDP 11/23 computer using the Enraf–Nonius SDP program package (15).

Results and discussion

The 1:2 host:guest complex of DC-18-crown-6 (isomer B) with potasium phenoxide

ORTEP (16) drawings of the ligand and of the complex itself showing the atom numbering scheme are given in Figs. 1 and 2, respectively. The fractional coordinates and equivalent isotropic temperature factors of the non-hydrogen atoms are presented in Table 2. Oxygen–potassium bond lengths and angles appear in Table 4, average and range in the bond lengths and angles of the host and of the phenoxide are given in Table 5, and macrocyclic ring torsion angles appear in Table 6.[2]

Host geometry and conformation

In the present crystal structure, the *cis–anti–cis* isomer of DC-18-crown-6 has a crystallographic centre of symmetry. The cavity outlined by the oxygens of the hexaether is elliptical, a feature also observed in the uncomplexed ligand (17) although more pronounced there than in the present case. In 1:1 host:guest complexes of 18-crown-6 macrocycles in which the guest cation size is equal to or larger than the size of the host cavity, the cavity is generally found to be circular, with the oxygens outlining a nearly regular hexagon. This was also found to be the case in the 1:1:1 complex of DC-18-crown-6 (isomer B) with potassium phenoxide and phenol, in which the

[2]Complete tables of positional parameters, temperature factors, and observed and calculated structure factors may be purchased from the Depository of Unpublished Data, CISTI, National Research Council of Canada, Ottawa, Ont., Canada K1A 0S2.

TABLE 2. Final fractional coordinates and equivalent isotropic temperature factors for $K_2O_8C_{32}H_{46}$ with estimated standard deviations in parentheses

Atom	x	y	z	B_{eq} (Å^2)[a]
K	0.47340(5)	0.46887(4)	0.73784(6)	3.907
O(2)	0.2036(1)	0.4389(1)	0.5463(2)	4.02
O(5)	0.3548(1)	0.6439(1)	0.4822(2)	3.62
O(8)	0.6243(1)	0.7440(1)	0.4986(2)	3.81
O(14)	0.4868(2)	0.6525(2)	0.9791(3)	5.90
C(1)	0.1559(2)	0.3150(2)	0.5303(3)	3.99
C(3)	0.1685(2)	0.4956(2)	0.3856(3)	4.67
C(4)	0.2092(2)	0.6255(2)	0.4307(3)	4.41
C(6)	0.3926(2)	0.7695(2)	0.5131(3)	4.10
C(7)	0.5389(2)	0.7926(2)	0.6110(3)	4.21
C(9)	0.7675(2)	0.7664(2)	0.5802(3)	4.06
C(10)	0.8168(3)	0.8970(2)	0.5786(4)	5.14
C(11)	0.8016(3)	0.9310(2)	0.3860(4)	5.48
C(12)	0.8780(3)	0.8477(2)	0.2774(4)	5.57
C(13)	0.8308(2)	0.7178(2)	0.2771(2)	4.51
C(15)	0.3813(2)	0.7161(3)	0.9817(3)	4.50
C(16)	0.3966(3)	0.8424(2)	1.0135(3)	5.00
C(17)	0.2881(3)	0.9115(2)	1.0170(4)	5.99
C(18)	0.1591(4)	0.8625(3)	0.9896(4)	6.78
C(19)	0.1344(3)	0.7415(4)	0.9584(4)	7.32
C(20)	0.2471(4)	0.6674(3)	0.9546(4)	6.44

[a] $B_{eq} = \frac{4}{3}\Sigma_i\Sigma_j\beta_{ij}\,(a_i \cdot a_j)$.

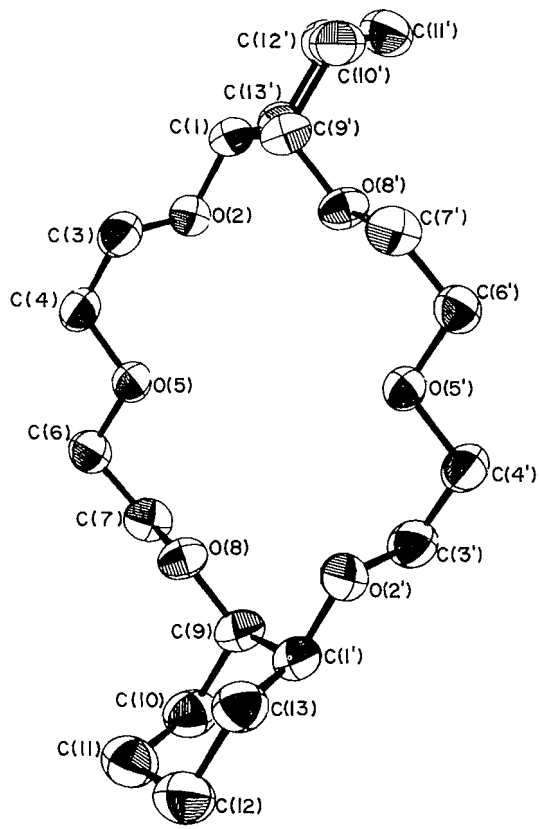

FIG. 1. ORTEP diagram and atom-numbering scheme for the isomer B of dicyclohexano-18-crown-6 in the potassium phenoxide complex.

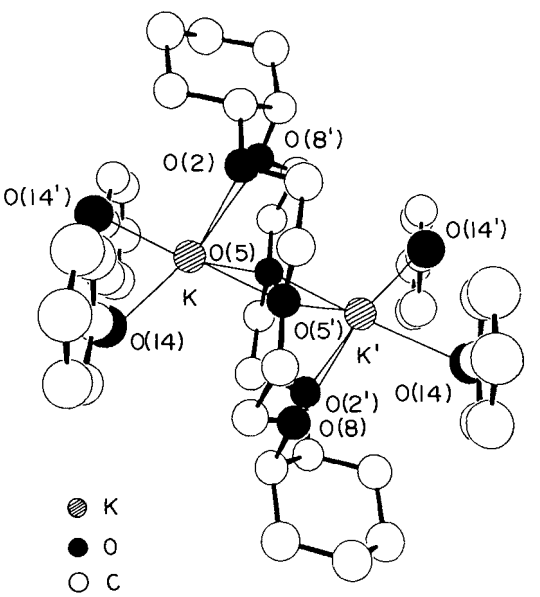

FIG. 2. ORTEP diagram and atom-numbering scheme for the potassium phenoxide complex.

potassium ion is found in the ideal nesting position,[3] and other 1:1 complexes of DC-18-crown-6 as well (18, 19). Thus the elliptical shape of the cavity is not a result of substituent effects but rather of host–guest interactions. In fact, it can be seen in Fig. 2 that with the donor atoms of the hexaether arranged in an elliptical shape, optimal $K^+ \ldots O$ distances can be achieved while keeping sufficient $K^+ \ldots K^+$ separation. Figure 3 shows the cavity geometry of the uncomplexed form (17), of the 1:1:1 complex containing potassium phenoxide and phenol,[2] and of the 1:2 host:guest complex of DC-18-crown-6 (isomer B) with potassium phenoxide. In the two cases where an elliptical shape is found, elongations are along the lines joining opposite oxygens, located on either side of the cyclohexyls. In contrast to the uncomplexed form, in the 1:2 complex the oxygens all point towards the centre of the cavity. They form an approximate plane and are found alternately ≈0.15 Å above and below their mean plane.

[3] M. E. Fraser, S. Fortier, A. Rodrigue, and J. W. Bovenkamp. Manuscript in preparation.

TABLE 3. Final fractional coordinates and equivalent isotropic temperature factors for $Na_2O_8C_{32}H_{46}$ with estimated standard deviations in parentheses

Atom	x	y	z	B_{eq} (Å^2)[a]
Na(1)	0.06478(5)	0.02195(7)	0.08230(7)	5.30
Na(2)	0.24079(5)	0.05192(7)	0.08807(7)	4.71
O(3)	0.20602(9)	0.0681(1)	−0.1291(1)	5.29
O(6)	0.13187(8)	0.1574(1)	0.0163(1)	4.54
O(9)	0.26243(8)	0.2265(1)	0.1041(1)	5.06
O(12)	0.36936(9)	0.0941(1)	0.1277(1)	5.61
O(15)	0.3132(1)	−0.0899(1)	0.1759(1)	5.99
O(18)	0.24718(9)	−0.1016(1)	−0.0167(1)	4.92
O(27)	0.15709(9)	0.0255(1)	0.2007(1)	5.51
O(34)	−0.03705(9)	0.1019(1)	0.0299(1)	6.01
C(1)	0.2165(2)	−0.1148(2)	−0.1209(2)	5.13
C(2)	0.2306(2)	−0.0192(2)	−0.1776(2)	5.42
C(4)	0.1326(1)	0.0845(2)	−0.1467(2)	5.43
C(5)	0.1171(1)	0.1770(2)	−0.0908(2)	5.76
C(7)	0.1391(1)	0.2450(2)	0.0806(2)	5.25
C(8)	0.2080(1)	0.2977(2)	0.0767(2)	5.73
C(10)	0.3315(1)	0.2616(2)	0.0910(2)	5.26
C(11)	0.3817(1)	0.1965(2)	0.1598(2)	6.17
C(13)	0.4066(2)	0.0204(3)	0.1926(3)	8.10
C(14)	0.3826(2)	−0.0806(2)	0.1587(3)	7.68
C(16)	0.2820(2)	−0.1830(2)	0.1407(3)	9.2
C(17)	0.2325(2)	−0.1749(2)	0.0546(2)	7.29
C(19)	0.3075(2)	−0.0032(2)	−0.1855(2)	6.60
C(20)	0.3401(2)	−0.0939(3)	−0.2333(3)	8.88
C(21)	0.3265(2)	−0.1888(3)	−0.1771(3)	8.95
C(22)	0.2488(2)	−0.2038(2)	−0.1710(2)	7.79
C(23)	0.3454(2)	0.2591(2)	−0.0199(2)	6.57
C(24)	0.4214(2)	0.2873(3)	−0.0312(3)	9.25
C(25)	0.4724(2)	0.2229(3)	0.0390(3)	10.0
C(26)	0.4567(2)	0.2298(3)	0.1494(3)	8.8
C(28)	0.1595(1)	0.0387(2)	0.2995(2)	4.28
C(29)	0.0986(1)	0.0481(2)	0.3499(2)	6.39
C(30)	0.1030(2)	0.0607(2)	0.4562(2)	8.30
C(31)	0.1663(2)	0.0650(2)	0.5148(2)	8.4
C(32)	0.2255(2)	0.0571(2)	0.4685(2)	6.78
C(33)	0.2227(2)	0.0448(2)	0.3638(2)	5.03
C(35)	−0.0443(1)	0.1964(2)	0.0512(2)	4.89
C(36)	−0.0415(1)	0.2318(2)	0.1526(2)	5.48
C(37)	−0.0495(2)	0.3326(2)	0.1747(2)	7.14
C(38)	−0.0594(2)	0.4023(2)	0.0994(2)	8.4
C(39)	−0.0621(2)	0.3714(3)	−0.0011(3)	8.21
C(40)	−0.0550(2)	0.2710(2)	−0.0253(2)	6.29

[a] $B_{eq} = \frac{4}{3}\Sigma_i\Sigma_j\beta_{ij}\,(\boldsymbol{a}_i\cdot\boldsymbol{a}_j)$.

In the regular hexaether conformation, all torsion angles about C—C bonds are synclinal and those about C—O bonds are antiplanar. As can be seen from Table 6, these values are found in the present structure with the exception of the torsion angle about the C—$O_{equatorial}$ bond. This distortion is responsible for the elliptical shape of the host cavity and thus allows for optimal host-guest interactions. In other cases, it was also found that the deformation strain was preferentially accommodated in torsion angles about the C—O bonds, without affecting the *gauche* arrangement of the OCH_2CH_2O units (20). In the hexaether, the C—C bond lengths show the characteristic shortening with an average value of 1.498 Å. As has been previously observed, the C—C distances in the cyclohexyl substituent, on the other hand, are in the normal range with an average value of 1.520 Å. The C—O bond lengths have an average value of 1.426 Å and the O—C—C and C—O—C angles, in the hexaether, have average values of 109.0° and 112.9°, respectively. The cyclohexyl ring is found in the chair conformation with an average absolute torsion angle value of 55.9°. All of these values conform with those obtained in previous studies (20).

Host–guest interactions

The potassium ions are related by a centre of symmetry and each is located approximately halfway between the crown ether and two phenoxide anions, as depicted in Fig. 2. The distance between the K^+ ion and the approximate plane defined by the crown oxygens is 1.678 Å, while a distance of 1.467 Å is found between the K^+ and the plane of the phenoxides. The $K^+ \ldots K^+$ distance is 3.87 Å. This value is very close to the $K^+ \ldots K^+$ distance of 3.8 Å found in the dibenzo-24-crown-8·2KNCS complex, where the cavity formed by the eight oxygens is larger and both potassium ions are approximately in the cavity (21). Addition of translational symmetry to Fig. 2 would show

TABLE 4. Oxygen – alkali metal bond lengths and angles for (a) $K_2O_8C_{32}H_{46}$ and (b) $Na_2O_8C_{32}H_{46}$ with estimated standard deviations in parentheses[a]

(a)

Bond	Length (Å)	Bonds	Angle (deg)
K—O(2)	2.754(1)	O(2)—K—O(5)	59.5(1)
K—O(5)	2.982(2)	O(2)—K—O(5′)	109.2(1)
K—O(5′)	2.891(2)	O(2)—K—O(8)	59.4(1)
K—O(8)	2.839(1)	O(2)—K—O(14)	106.1(1)
K—O(14)	2.591(1)	O(2)—K—O(14′)	110.5(1)
K—O(14′)	2.611(2)	O(5)—K—O(5′)	97.5(1)
		O(5)—K—O(8)	97.8(1)
		O(5)—K—O(14)	82.2(1)
		O(5)—K—O(14′)	159.6(1)
		O(5′)—K—O(8)	59.9(1)
		O(5′)—K—O(14)	138.6(1)
		O(5′)—K—O(14′)	102.8(1)
		O(8)—K—O(14)	161.5(1)
		O(8)—K—O(14′)	90.4(1)
		O(14)—K—O(14′)	84.2(1)

(b)

Bond	Length (Å)	Bonds	Angle (deg)
Na(1)—O(6)	2.425(2)	O(6)—Na(1)—O(27)	79.43(6)
Na(1)—O(27)	2.213(2)	O(6)—Na(1)—O(34)	91.19(6)
Na(1)—O(34)	2.259(2)	O(6)—Na(1)—O(34)	114.25(7)
Na(1)—O(34′)	2.224(2)	O(27)—Na(1)—O(34)	142.79(7)
Na(2)—O(3)	2.842(2)	O(27)—Na(1)—O(34′)	125.96(7)
Na(2)—O(6)	2.599(2)	O(34)—Na(1)—O(34′)	90.81(7)
Na(2)—O(9)	2.358(2)	O(3)—Na(2)—O(6)	60.85(5)
Na(2)—O(12)	2.525(2)	O(3)—Na(2)—O(9)	91.90(5)
Na(2)—O(15)	2.534(2)	O(9)—Na(2)—O(12)	66.79(6)
Na(2)—O(18)	2.463(2)	O(9)—Na(2)—O(15)	127.42(6)
Na(2)—O(27)	2.323(2)	O(3)—Na(2)—O(12)	107.46(6)
		O(3)—Na(2)—O(15)	124.10(6)
		O(3)—Na(2)—O(18)	62.04(5)
		O(3)—Na(2)—O(27)	122.72(6)
		O(6)—Na(2)—O(9)	68.24(5)
		O(6)—Na(2)—O(12)	132.91(6)
		O(6)—Na(2)—O(15)	159.96(6)
		O(6)—Na(2)—O(18)	109.54(5)
		O(6)—Na(2)—O(27)	73.93(5)
		O(9)—Na(2)—O(18)	147.36(6)
		O(9)—Na(2)—O(27)	102.67(6)
		O(12)—Na(2)—O(15)	66.42(6)
		O(12)—Na(2)—O(18)	100.82(6)
		O(12)—Na(2)—O(27)	129.33(6)
		O(15)—Na(2)—O(18)	64.97(5)
		O(15)—Na(2)—O(27)	89.15(6)
		O(18)—Na(2)—O(27)	107.90(6)

[a]The primed atoms are related to the unprimed atoms by the following symmetry operation: $-x, -y, -z$.

that each of the phenoxide oxygens is shared by two potassium ions and thus dimers of potassium phenoxide are formed. Each individual crown molecule complexes one of the potassium ions of two dimers, one above the approximate plane of the macrocyclic ring and one below. Each of the potassium ions is coordinated to four crown oxygens. The potassium–oxygen distance is somewhat closer for the oxygens attached to the cyclohexane rings (K^+ ... O(2) = 2.75 Å and K^+ ... O(8) = 2.84 Å) than for the oxygens in the middle of the macrocyclic ring (K^+ .... O(5) = 2.98 Å and K^+ ... O(5′) = 2.89 Å). The average of these K^+ ... O distances of 2.87 Å is only slightly larger than the value of 2.81 Å in the KNCS complex of 18-crown-6 (8), in which the K^+ is found in the ideal nesting position. Shorter distances are found between the K^+ ions and the oxygens of the two phenoxide goups, with an average value of 2.60 Å. This distance indicates that the potassium ions are strongly associated with the phenolate oxygens.

The 1:2 host:guest complex of DC-18-crown-6 (isomer A) with sodium phenoxide

ORTEP (16) drawings of the ligand and of the complete complex showing the atom numbering scheme are given in Figs. 4

TABLE 5. Average and range in the bond lengths (Å) and angles (deg) for the macrocyclic rings, cyclohexyl rings, and phenoxides of $K_2O_8C_{32}H_{46}$ and $Na_2O_8C_{32}H_{46}$ with estimated standard deviations in parentheses

$K_2O_8C_{32}H_{46}$			
Macrocyclic ring			
Average C—C	1.498	Average C—O	1.426
Range of C—C	1.487–1.519(3)	Range of C—O	1.407–1.440(2)
Average C—O—C	112.9	Average C—C—O	109.9
Range of C—O—C	109.7–115.8(1)	Range of C—C—O	108.9–112.4(1)
Cyclohexyl ring			
Average C—C	1.520	Average C—C—C	111.2
Range of C—C	1.513–1.534(3)	Range of C—C—C	109.0–112.6(2)
Phenoxide			
O(14)—C(15)	1.300(3)	O(14)—C(15)—C(16)	120.9(2)
		O(14)—C(15)—C(20)	123.9(2)
Average C—C	1.386	Average C—C—C	120.0
Range of C—C	1.350–1.431(4)	Range of C—C—C	115.1–122.3(3)
$Na_2O_8C_{32}H_{46}$			
Macrocyclic ring			
Average C—C	1.475	Average C—O	1.420
Range of C—C	1.389–1.511(5)	Range of C—O	1.381–1.433(4)
Average C—O—C	115.1	Average C—C—O	110.0
Range of C—O—C	113.8–117.1(3)	Range of C—C—O	106.2–114.9(3)
Cyclohexyl rings			
Average C—C	1.513	Average C—C—C	110.7
Range of C—C	1.496–1.529(6)	Range of C—C—C	106.2–122.6(4)
Phenoxides			
O(27)—C(28)	1.296(3)	O(34)—C(35)	1.295(3)
O(27)—C(28)—C(29)	122.6(2)	O(34)—C(35)—C(36)	122.2(3)
O(27)—C(28)—C(33)	122.4(2)	O(34)—C(35)—C(40)	122.8(3)
Average C—C	1.380	Average C—C—C	120.0
Range of C—C	1.346–1.410(5)	Range of C—C—C	115.1–122.6(4)

TABLE 6. Macrocyclic ring torsion angles

$K_2O_8C_{32}H_{46}$		$Na_2O_8C_{32}H_{46}$	
Bonds	Angle (deg)	Bonds	Angle (deg)
C(1)—O(2)—C(3)—C(4)	172.8(2)	C(1)—C(2)—O(3)—C(4)	−77.3(3)
O(2)—C(3)—C(4)—O(5)	67.4(2)	C(2)—O(3)—C(4)—C(5)	178.8(2)
C(3)—C(4)—O(5)—C(6)	176.1(2)	O(3)—C(4)—C(5)—O(6)	−66.4(2)
C(4)—O(5)—C(6)—C(7)	165.7(2)	C(4)—C(5)—O(6)—C(7)	162.9(2)
O(5)—C(6)—C(7)—O(8)	64.7(2)	C(5)—O(6)—C(7)—C(8)	−75.9(2)
C(6)—C(7)—O(8)—C(9)	177.8(2)	O(6)—C(7)—C(8)—O(9)	−56.0(2)
C(7)—O(8)—C(9)—C(1′)	166.2(2)	C(7)—C(8)—O(9)—C(10)	172.2(2)
O(8)—C(9)—C(1′)—O(2′)	−54.0(2)	C(8)—O(9)—C(10)—C(11)	158.5(2)
C(9)—C(1′)—O(2′)—C(3′)	−71.3(2)	O(9)—C(10)—C(11)—O(12)	58.4(2)
		C(10)—C(11)—O(12)—C(13)	−172.8(2)
		C(11)—O(12)—C(13)—C(14)	173.0(3)
		O(12)—C(13)—C(14)—O(15)	−65.7(4)
		C(13)—C(14)—O(15)—C(16)	176.6(3)
		C(14)—O(15)—C(16)—C(17)	−109.4(3)
		O(15)—C(16)—C(17)—O(18)	35.2(4)
		C(16)—C(17)—O(18)—C(1)	155.9(3)
		C(17)—O(18)—C(1)—C(2)	171.3(2)
		O(18)—C(1)—C(2)—O(3)	−55.0(3)

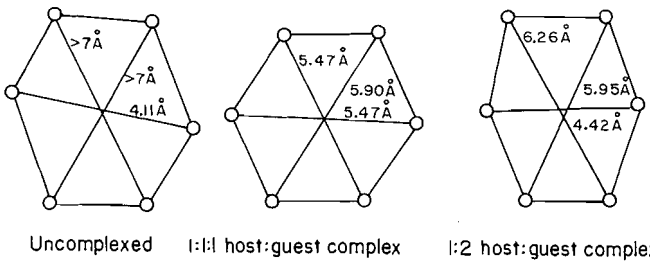

FIG. 3. Comparison of the cavity shape in uncomplexed and 1:1:1 and 1:2 host:guest complexes of dicyclohexano-18-crown-6 (isomer B).

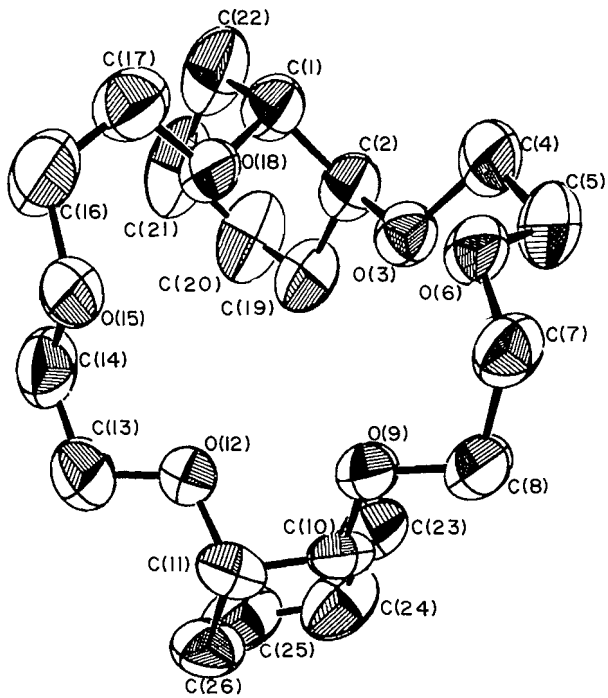

FIG. 4. ORTEP diagram and atom-numbering scheme for the isomer A of dicyclohexano-18-crown-6 in the sodium phenoxide complex.

and 5, respectively. The fractional coordinates and equivalent isotropic temperature factors of the non-hydrogen atoms are presented in Table 3. Oxygen–sodium bond lengths and angles appear in Table 4, average and range in the bond lengths and angles of the host and of the phenoxides are given in Table 5, and macrocyclic ring torsion angles appear in Table 6.[2]

Host geometry and conformation

As can be seen from Fig. 4 and Table 6, the host conformation is highly irregular. The irregular part of the hexaether consists of seven atoms, from C(17) to C(5). The remaining atoms are found in the regular crown conformation. As in the case of the NaNCS complex of 18-crown-6 (7), the irregular fragment of the hexaether is folded out of the mean plane of the ring to partially envelop the cation guest. Thus, while four of the oxygens are found to lie in an approximate plane, the remaining two, O(3) and O(18), are at distances of 1.903 and 2.655 Å from that plane. The distortion observed in the present structure is more pronounced than that observed in the NaNCS complex of 18-crown-6, where the irregular fragment consisted of five atoms and where five of the oxygen atoms were found to lie in an approximate plane (7).

The average C—C bond length in the hexaether is 1.475 Å, while a value of 1.513 Å is found in the cyclohexyls. In the hexaether, the average O—C—C and C—O—C angles are 110.0 and 115.1°, respectively, and the average C—O distance is 1.420 Å. The cyclohexyl rings are in the chair conformation with average absolute torsion angle values of 54.5 and 56.0°.

Host–guest interactions

Figure 5 shows four sodium ions complexed by two crown ethers so that the 1:2 DC-18-crown-6 (A) sodium phenoxide complex has essentially a tetramer of sodium phenoxides. The two sodium ions are in different chemical environments. Na(1) is coordinated to only one of the hexaether oxygens, O(6), at a distance of 2.425 Å and to three of the phenoxide oxygens at an average distance of 2.23 Å. Na(2) lies in the plane defined by the four oxygens of the regular crown fragment. It is coordinated to all six oxygens of the hexaether at distances ranging from 2.358 to 2.842 Å with an average value of 2.55 Å. In addition, Na(2) is coordinated to one phenoxide oxygen, O(27), located at a distance of 2.323 Å. It is worth noting that the distances between the Na^+ and the phenolate oxygens are all significantly shorter than those between the Na^+ and the crown oxygens. Thus, stronger interactions exist between the Na ions and the phenolate oxygens of the tetramer than between the Na ions and the crown oxygens. The Na(1)—Na(1), Na(2)—Na(2), and Na(1)—Na(2) distances are 3.147, 6.107, and 3.392 Å, respectively. By comparison, the $Na^+ \ldots Na^+$ distance in the complex of dibenzo-24-crown-8 with two sodium *o*-nitrophenolate salt molecules is 3.383 Å (22). With this larger macrocycle, the polyether ring folds around a pair of sodium ions. The two halves of the complex are related by a two-fold symmetry axis which passes through a pair of aliphatic C—C bonds on

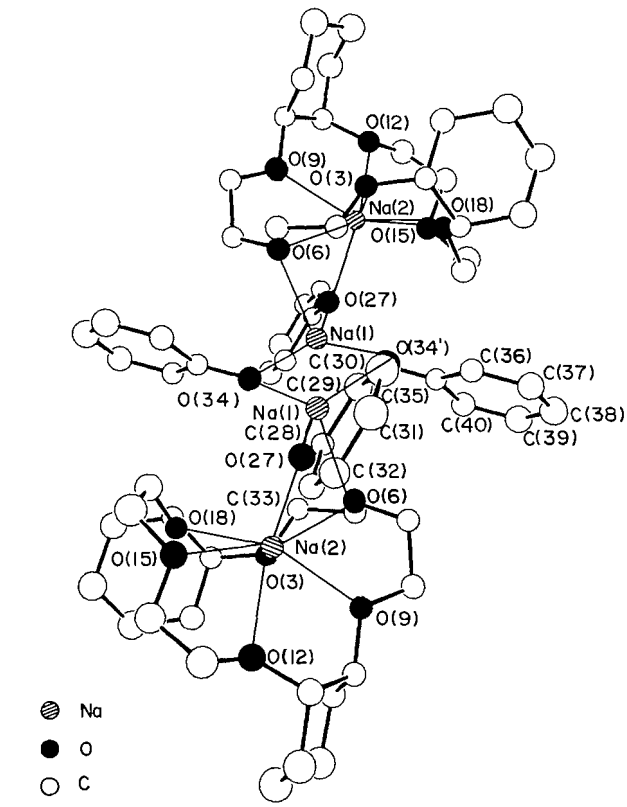

FIG. 5. ORTEP diagram and atom-numbering scheme for the sodium phenoxide complex.

opposite sides of the crown ring. The two phenolate oxygens, one on each side of the macrocyclic ring, bridge the pair of cations.

Conclusions

In this paper, the structures of two complexes of DC-18-crown-6 with unusual host:guest ratios were presented. Both complexes were obtained from relatively nonpolar ethereal solvents and in both cases, the "hard" phenoxide is the counterion. In the case of the K^+ complex, a dimer, and in the case of the Na^+ complex, a tetramer is being complexed instead of the contact ion pair that would have been expected for these 18-crown-6 macrocycles.

Further work on the structures of other unique complexes involving 18-crown-6 macrocycles is in progress and will be reported in due course.

Acknowledgements

Financial assistance in equipment grants and scholarships from the Natural Sciences and Engineering Research Council of Canada is gratefuly acknowledged.

1. F. VOGTLE and E. WEBER. *In* The chemistry of ethers, crown ethers, hydroxyl groups and their sulphur analogs. Supplement E1. *Edited by* S. Patai. Wiley, London. 1981. pp. 121–174.
2. M. HIRAOKA. Crown compounds. Elsevier, New York. 1982. pp. 1–276.
3. D. CRAM and K. N. TRUEBLOOD. *In* Host guest complex chemistry I. *Edited by* F. Vogtle. Springer Verlag, Berlin, Heidelberg, New York. 1981. pp. 43–106.
4. G. WIPFF, P. WEINER, and P. KOLLMAN. J. Am. Chem. Soc. **104**, 3249 (1982).
5. J. D. DUNITZ, M. DOBLER, P. SEILER, and R. P. PHIZACKERLEY. Acta Crystallogr. Sect. B, **30**, 2733 (1974).
6. J. D. DUNITZ and P. SEILER. Acta Crystallogr. Sect. B, **30**, 2739 (1974).
7. M. DOBLER, J. D. DUNITZ, and P. SEILER. Acta Crystallogr. Sect. B, **30**, 2741 (1974).
8. P. SEILER, M. DOBLER, and J. D. DUNITZ. Acta Crystallogr. Sect. B, **30**, 2744 (1974).
9. M. DOBLER and R. P. PHIZACKERLEY. Acta Crystallogr. Sect. B, **30**, 2746 (1974).
10. M. DOBLER and R. P. PHIZACKERLEY. Acta Crystallogr. Sect. B, **30**, 2748 (1974).
11. C. RICHE, C. PASCARD-BILLY, B. CAMBILLAU, and G. BRAM. J. Chem. Soc. Chem. Commun. 183 (1977).
12. A. RODRIGUE, J. W. BOVENKAMP, B. V. LACROIX, R. A. B. BANNARD, and G. W. BUCHANAN. Can. J. Chem. **64**, 808 (1986).
13. P. MAIN, S. J. FISKE, S. E. HULL, L. LESSINGER, G. GERMAIN, J.-P. DECLERCQ, and M. M. WOOLFSON. MULTAN 80. A system of computer programs for the automatic solution of crystal structures from X-ray diffraction data. Univs. of York, England, and Louvain, Belgium. 1980.
14. D. T. CROMER and J. T. WABER. International tables for X-ray crystallography. Vol. IV. Kynoch Press, Birmingham. 1974.
15. Enraf–Nonius. Structure determination package. *Revised by* B. A. Frenz. Enraf–Nonius, Delft. 1979.
16. C. K. JOHNSON. ORTEP. Report ORNL-3794, Oak Ridge National Laboratory, Tennessee. 1965.
17. N. K. DALLEY, J. S. SMITH, S. B. LARSON, J. J. CHRISTENSEN, and R. M. IZATT. J. Chem. Soc. Chem. Commun. 43 (1975).
18. D. L. HUGHES and M. R. TRUTER. J. Chem. Soc. Chem. Commun. 727 (1982).
19. N. K. DALLEY, D. E. SMITH, R. M. IZATT, and J. J. CHRISTENSEN. J. Chem. Soc. Chem. Commun. 90 (1972).
20. I. GOLDBERG. *In* The chemistry of ethers, crown ethers, hydroxyl groups and their sulphur analogs. Supplement E1. *Edited by* S. Patai. Wiley, London. 1980. pp. 175–214.
21. D. E. FENTON, M. MERCER, N. S. POONIA, and M. R. TRUTER. J. Chem. Soc. Chem. Commun. 66 (1972).
22. D. L. HUGHES. J. Chem. Soc. Dalton Trans. 2374 (1975).

Substitution régiosélective d'arènesulfonylhydrazones α,β-insaturées via la réaction de Shapiro

JEAN CLAUDE CAILLE, MICHEL FARNIER ET ROGER GUILARD[1]

Laboratoire de synthèse et d'électrosynthèse organométallique associé au Centre national de la recherche scientifique (UA 33), Faculté des sciences « Gabriel », 21100 Dijon, France

Reçu le 4 janvier 1985[2]

JEAN CLAUDE CAILLE, MICHEL FARNIER ET ROGER GUILARD. Can. J. Chem. **64**, 824 (1986).

Les arènesulfonylhydrazones de cyclopentanones α,β-insaturées de type isopropylidène et cyclopentylidène cyclopentanones, ont été soumises à l'action successive d'organolithiens à −78°C et de divers agents électrophiles. La réactivité des hydrazones dépend étroitement de la nature de l'électrophile dont le choix permet d'orienter régiosélectivement la substitution. La structure des produits est établie par analyse des spectres rmn ^1H et ^{13}C. Les hydrazones conservent leur configuration au cours de la réaction. Un mécanisme réactionnel faisant intervenir un intermédiaire a « six centres » est proposé. Par ailleurs, la réactivité de ces hydrazones est mise à profit pour élaborer une nouvelle stratégie de synthèse d'aldéhydes monoterpéniques.

JEAN CLAUDE CAILLE, MICHEL FARNIER, and ROGER GUILARD. Can. J. Chem. **64**, 824 (1986).

Arenesulfonylhydrazones of α,β-unsaturated cyclopentanones such as isopropylidene and cyclopentylidene cyclopentanones have been treated with alkyllithium reagents at −78°C followed by trapping with a variety of electrophiles. The reactivity of these hydrazones depends on the nature of electrophile that controls the regioselectivity of the reaction. The structure of all the products is established by ^1H and ^{13}C nmr. The reaction occurs with no inversion of configuration of the hydrazones. The formation of a "six centers" intermediate is discussed. Moreover, such a reactivity is used to prepare monoterpenic aldehydes.

Introduction

Opposés aux dérivés organolithiens, les tosylhydrazones présentent une réactivité singulière (1) mise à profit dans un grand nombre de synthèses (2). Les travaux de Lipton et Shapiro (3) démontrent de plus que l'action des alkyllithiens s'accompagne de la formation d'un *syn*-dianion réagissant très aisément avec de nombreux agents électrophiles pour conduire à une hydrazone substituée en α (voie A, fig. 1). Par ailleurs, la décomposition du dianion conduit à un lithien vinylique pouvant également réagir avec un électrophile (voie B, fig. 1). En outre la décomposition du dianion est plus aisée dans le cas d'hydrazones encombrées telles les trisylhydrazones (4), sans que la réactivité à l'égard des électrophiles soit altérée.

Cependant, peu de travaux ont été consacrés aux arènesulfonylhydrazones α,β-insaturées, depuis les études de Shapiro, Dauben et coll. (5). Dauben *et al.* ont toutefois montré le rôle déterminant de la stéréochimie de l'hydrazone et de la nature du solvant (6). Or nous avons rapporté dans une note préliminaire (7) qu'il était possible d'alkyler régiosélectivement la tosylhydrazone de la cyclopentylidène cyclopentanone. Dans ce travail nous nous sommes proposés de montrer l'influence de l'électrophile sur la régiospécificité de la réaction et d'étudier l'évolution de la stéréochimie des hydrazones. Dans ce but, nos travaux réalisés initialement au départ de la cyclopentylidène cyclopentanone ont été étendus à l'isopropylidène cyclopentanone, modèle plus proche de celui utilisé par Dauben *et al.* (6). De plus, nous avons tenté d'élaborer une voie d'accès à des aldéhydes monoterpéniques, applicable à la synthèse d'analogues naturels.

Résultats

Réactivité d'hydrazones α,β-insaturées vis-à-vis d'électrophiles

Les hydrazones **1** ont été soumises à l'action du butyllithium, puis de divers agents électrophiles, selon la voie A schématisée sur la figure 1. Les proportions des produits **2** et **3** obtenus (fig. 2) dépendent étroitement de la nature de l'électrophile, et l'ensemble de nos résultats est regroupé en tableau 1.

Au départ de l'hydrazone **1***b* de l'isopropylidène cyclopentanone, et après transformation en dianion correspondant, l'action de l'iodure de méthyle et du propionaldéhyde conduit uniquement et respectivement aux produits **2***c* et **2***d*, résultant de l'attaque de l'électrophile sur l'atome de carbone porteur du reste isopropényle. Dans le cas du sulfure de diméthyle, à côté de l'hydrazone **2***b* issue du même type d'attaque, il est possible d'isoler dans une faible proportion (5%) un mélange des isomères **3***d* correspondant à une attaque sur les sommets γ et γ′ du reste isopropylidène.

Dans la série des hydrazones de la cyclopentylidène cyclopentanone, l'action du sulfure de diméthyle est alors régiospécifique et ne conduit qu'à l'hydrazone **2***f*. Cette même régiospécificité est observée par action de l'iodure de méthoxy-2 éthyle : seules les hydrazones **2***e* et **2***g* sont isolées, ceci indépendamment de la nature du reste aryle, tosyl (—SO_2 *p*-tolyle) ou trisyl (—SO_2 triisopropyl-2,4,6 phényle), porté par l'hydrazone de départ. À l'opposé et, curieusement, lorsque l'on met en oeuvre le sulfure de diphényle, l'attaque ne porte jamais sur le carbone 2 de l'hydrazone de départ mais toujours sur les sommets γ et γ′ du reste alkylidène, quelle que soit la nature du reste alkylidène et celle du groupe aryle porté par l'hydrazone : dans tous les cas, seuls les mélanges d'hydrazones **3***a*, **3***c* et **3***f* sont obtenus. De plus, nous avons vérifié que l'introduction d'un groupe alkyle sur le sommet 5 de l'hydrazone **1** de départ ne modifie pas cette spécificité : à partir de l'hydrazone **1***c*, seul se forme le mélange **3***e*. Toutefois, la régiosélectivité n'est pas toujours aussi marquée puisque dans un cas, en utilisant le chloroformiate de méthyle, nous isolons conjointement les hydrazones **2***a* et **3***b* dans des proportions de 68 et 32%.

Ainsi la réactivité des hydrazones α,β-insaturées ne paraît dépendre ni de la nature du groupe alkylidène, ni de la nature du reste aryle porté par l'hydrazone. Par contre, le choix de l'agent électrophile est un facteur déterminant de la spécificité de la réaction.

Synthèse d'aldéhydes monoterpéniques

Selon le schéma réactionnel représenté en figure 1 (voie B), les hydrazones **1***b* et **1***c* sont traitées par le *sec*-butyllithium en excès dans le tétrahydrofuranne à −78°C. Le retour du milieu

[1]Auteur à qui adresser toute correspondance.

[2]Révision reçue le 8 novembre 1985.

Printed in Canada / Imprimé au Canada

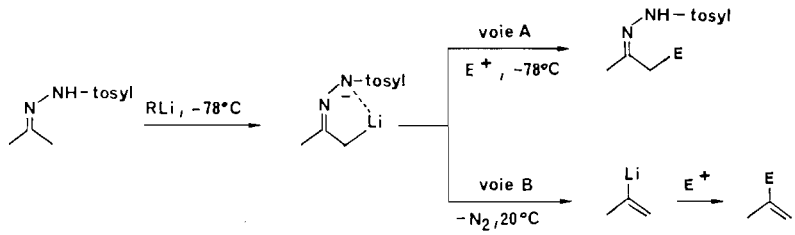

FIG. 1.

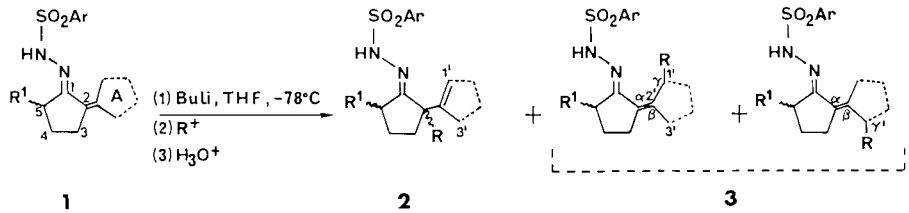

FIG. 2.

TABLEAU 1. Réactivité d'hydrazones **1** vis-à-vis d'agents électrophiles

Composé de départ	A	Ar	R^1	R	Hydrazones **2** (proportions relatives, %)	Hydrazones **3** (proportions relatives, %)	Rendement (%)
1*a*	Isopropylidène	*p*-Tolyle	H	SC_6H_5	—	**3***a* (100)	32
1*a*	Isopropylidène	*p*-Tolyle	H	CO_2Me	**2***a* (68)	**3***b* (32)	31
1*b*	Isopropylidène	Triisopropylphényle	H	SC_6H_5	—	**3***c* (100)	61
1*b*	Isopropylidène	Triisopropylphényle	H	SCH_3	**2***b* (95)	**3***d* (5)	58
1*b*	Isopropylidène	Triisopropylphényle	H	CH_3	**2***c* (100)	—	58
1*b*	Isopropylidène	Triisopropylphényle	H	$CH(OH)CH_2CH_3$	**2***d* (100)	—	48
1*c*	Isopropylidène	Triisopropylphényle	CH_3	SC_6H_5	—	**3***e* (100)	52
1*d*	Cyclopentylidène	*p*-Tolyle	H	$(CH_2)_2OCH_3$	**2***e* (100)	—	45
1*e*	Cyclopentylidène	Triisopropylphényle	H	SC_6H_5	—	**3***f* (100)	71
1*e*	Cyclopentylidène	Triisopropylphényle	H	SCH_3	**2***f* (100)	—	54
1*e*	Cyclopentylidène	Triisopropylphényle	H	$(CH_2)_2OCH_3$	**2***g* (100)	—	66

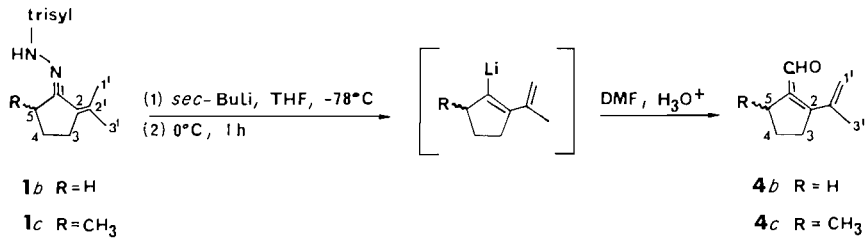

FIG. 3.

réactionnel à 0°C permet d'accéder aux lithiens vinyliques résultant de la déprotonation du sommet 1′ (fig. 3). La condensation du diméthylformamide (8) livre les aldéhydes correspondants **4***b* et **4***c* avec des rendements de l'ordre de 35%. Or, l'isomère **5** de l'aldéhyde **4***c* ainsi synthétisé est le précurseur du chrysomélidial (9).

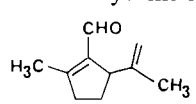

5

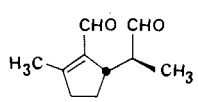

chrysomélidial

Nous avons tenté de proposer une voie d'accès plus simple à ce précurseur en utilisant les deux types de réactivité des arènesulfonylhydrazones. En effet, l'introduction d'un groupement *à priori* facilement éliminable devait permettre la formation de la double liaison dans la position recherchée. Nos résultats sont schématisés en figure 4.

Comme nous l'avons déjà décrit, l'hydrazone **1***b* traitée par le *sec*-butyllithium puis le sulfure de diméthyle conduit régiosélectivement au dérivé **2***b*. L'alkylation de ce dernier par l'iodure de méthyle fournit l'hydrazone **6** avec un rendement de 40%. Il est à noter que l'obtention de cette hydrazone a été également envisagée en traitant directement l'hydrazone **1***c* par le sulfure de diméthyle, mais cette voie ne permet d'isoler le composé **6** qu'avec un très faible rendement (de l'ordre de 10%). L'hydrazone **6**, traitée comme décrit précédemment pour

TABLEAU 2. Caractéristiques rmn ^1H d'hydrazones d'alkylidène-2 cyclopentanone-1, **1** et **3**

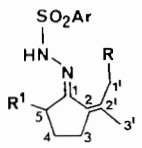
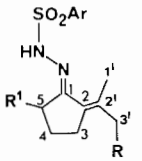

Composé	R	R^1	Déplacement chimique des protons (ppm) (CH_2)-3	(CH_2)-4	(CHR^1)-5	R	R^1	(CH_2R)-1′	(CH_2R)-3′	Constante de couplage (Hz)
1*a* (*E*)	H	H	2,39 (m)	1,74 (q)	2,30 (t, 2H)	—	—	2,05 (s, 3H)	1,77 (s, 3H)	7,40 (J_{34} et J_{54})
1*a* (*Z*)	H	H	2,06 (m)	1,65 (m)	1,94 (t, 2H)	—	—	1,42 (s, 3H)	1,28 (s, 3H)	7,40 (J_{54})
1*b*	H	H	2,43 (m)	1,73 (q)	2,31 (t, 2H)	—	—	1,87 (s, 3H)	1,73 (s, 3H)	7,40 (J_{34} et J_{54})
1*c*	H	CH_3	2,42 (m)	1,75–1,60 (m, 3H)		—	1,07 (d)	1,89 (s, 3H)	1,74 (s, 3H)	7,08 ($J_{5\text{-}CH_3}$)
3*a*	(SC_6H_5)-1′ (SC_6H_5)-3′	H	2,40 (m)	1,69 (q) 1,61 (q)	2,27 (t, 2H) 2,22 (t, 2H)	7,16 (M)	—	4,20 (s, 2H) 2,16 (s, 3H)	1,85 (s, 3H) 3,54 (s, 2H)	7,40 (J_{54})
3*b*	(CO_2CH_3)-1′ (CO_2CH_3)-3′	H	2,47 (m)	1,78 (m)	2,30 (t, 2H)	3,70 (s) 3,66 (s)	—	3,67 (s, 2H) 2,09 (s, 3H)	1,82 (s, 3H) 3,10 (s, 2H)	7,40 (J_{54})
3*c*	(SC_6H_5)-1′ (SC_6H_5)-3′	H	2,30 (m)	1,56 (m)	2,23 (t, 2H) 2,15 (t, 2H)	7,16 (M)	—	4,08 (s, 2H) 1,95 (s, 3H)	1,79 (s, 3H) 3,48 (s, 2H)	7,40 (J_{54})
3*d*	(SCH_3)-1′ (SCH_3)-3′	H	2,47 (m)	1,77 (m)	2,34 (t, 2H) 2,33 (t, 2H)	1,46 (s)	—	3,60 (s, 2H) 1,92 (s, 3H)	1,81 (s, 3H) 3,14 (s, 2H)	7,40 (J_{54})
3*e*	(SC_6H_5)-1′ (SC_6H_5)-3′	CH_3	2,31 (m)	1,64 (m)	2,15 (m, 1H)	7,16 (M)	1,00 (d) 0,90 (d)	4,30 (s, 2H) 1,92 (s, 3H)	1,78 (s, 3H) 3,47 (s, 2H)	7,32 ($J_{5\text{-}CH_3}$)

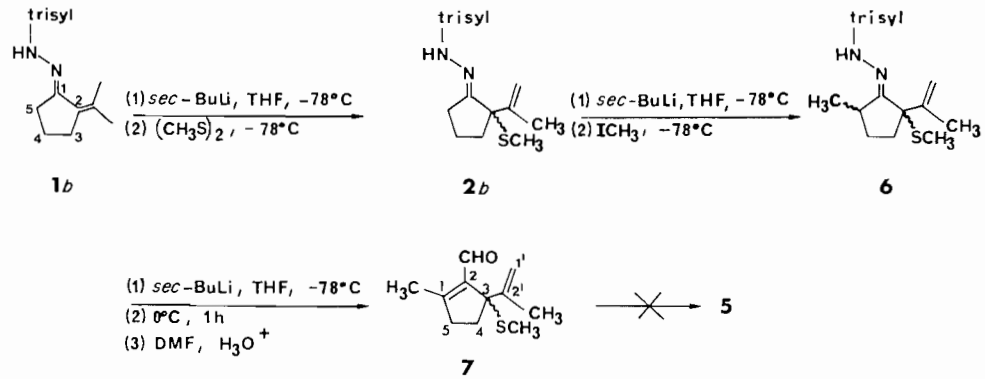

FIG. 4.

préparer les aldéhydes **4**, conduit à l'aldéhyde thiométhylé **7** (rendement : 38%).

Pour accéder à l'aldéhyde **5** recherché, la coupure du groupe thiométhyle a été tentée par action du lithium en présence d'éthylamine. En effet, cette méthode a déjà été utilisée avec succès (10) pour éliminer un groupe thiophényle en position allylique. Malheureusement, tous nos essais ont laissé inaltéré l'aldéhyde thiométhylé **7**. Par contre, dans le mémoire suivant, nous décrivons des exemples d'application de cette stratégie de synthèse permettant de proposer une nouvelle voie d'accès à des δ-lactones dont le squelette de base est celui des iridoïdes (11).

Établissement des structures

La structure de chacun des produits obtenus a pu être établie sur la base des données de l'analyse élémentaire et des résultats de rmn ^1H et ^{13}C. Nous avons regroupé dans le tableau 2 les caractéristiques de rmn protonique de la plupart des hydrazones d'alkylidène cyclopentanones **1** et **3**. Les caractéristiques rmn ^1H des autres hydrazones synthétisées et celles des aldéhydes **4***b*, **4***c* et **7** sont données dans la partie expérimentale où sont également reportées les caractéristiques rmn ^{13}C des hydrazones **2***c* et **3***d*. Dans le tableau 2 nous n'avons pas fait figurer les déplacements chimiques des protons du groupe aryle de la fonction hydrazone dont les caractéristiques sont en moyenne les suivantes : le reste tosyle donne un système AA′BB′ entre 7,2 et 7,9 ppm et un singulet vers 2,4 ppm; le reste trisyle, un singulet à 7,2 ppm pour les protons aromatiques, un doublet d'intensité 18 vers 1,3 ppm et deux heptuplets vers 2,9 et 4,2 ppm pour les protons des groupes isopropyle.

Comme il apparaît sur le tableau 2, les hydrazones **3** correspondent en fait à des mélanges des dérivés substitués respectivement en 1′ et 3′. Les deux isomères d'un mélange **3** n'ont pu être séparés, mais des caractéristiques rmn sont individualisables pour chacun de ces isomères : de façon générale, les protons du groupe méthyle en 1′ sont plus déblindés que ceux de groupe méthyle en 3′, ceci par analogie avec les résultats observés sur les hydrazones **1** de départ. Il en est de même pour les protons du reste (CH_2R). L'analyse des spectres de rmn ^1H montre également que les isomères des mélanges **3** se forment sensiblement dans les mêmes proportions. Une preuve supplémentaire de la présence d'un mélange pour les hydrazones **3** est apportée par l'examen du spectre rmn

^{13}C (écho de spin)[3] de **3***d*: des signaux distincts apparaissent pour les divers atomes de carbone des deux isomères. Nous avons de plus vérifié qu'après coupure de la fonction hydrazone (12) en cétone, ces dédoublements observés sur les spectres rmn ^{13}C persistent, ceci pour exclure l'existence éventuelle d'un mélange des deux configurations *syn* et *anti* d'hydrazones. D'autres arguments en faveur de la présence d'une seule configuration pour ces hydrazones sont discutés dans le paragraphe suivant.

Les spectres rmn ^1H de toutes les hydrazones **2** mettent en évidence des protons éthyléniques sous la forme de deux singulets entre 4,0 et 5,2 ppm pour un reste isopropényle, et d'un multiplet entre 5,1 et 5,7 ppm pour un reste cyclopentényle. De plus, la présence d'un carbone quaternaire en position 2 est confirmée dans un cas particulier par le relevé du spectre rmn ^{13}C (écho de spin) pour l'hydrazone **2***c*.

Enfin, il convient de souligner que l'hydrazone **6** correspond à un mélange de diastéréoisomères, ce qui se traduit sur le spectre rmn ^1H par la présence de deux doublets pour le groupe méthyle en position 5.

Stéréochimie des hydrazones

En opérant à température ambiante, il est classique (6) de n'obtenir que des hydrazones **1***a* (*E*) à partir des cétones correspondantes. Les caractéristiques rmn reportées au tableau 2 et dans la partie expérimentale pour les hydrazones **1**, correspondent toujours à la forme *E*, sauf dans le cas de l'hydrazone **1***a* où nous avons de plus préparé l'isomère *Z* aux fins de comparaison des données rmn ^1H. L'examen de ces données pour les hydrazones **1***a* (*E*) et **1***a* (*Z*) montre que les glissements chimiques des divers protons de la forme *E* sont toujours supérieurs à ceux de la forme *Z*. Les données rmn des autres hydrazones **1** synthétisées confirment la configuration *E* du produit obtenu sauf pour l'hydrazone **1***c*. Dans ce cas, nous obtenons en fait un mélange des configurations *E* et *Z* dans des proportions relatives de 80 et 20% : en effet, sur le spectre rmn ^1H, à côté des signaux relatifs aux groupes méthyle en 1′ et 3′ de la forme *E* respectivement à 1,89 et 1,74 ppm, apparaissent deux autres singulets à 1,61 et 1,54 ppm correspondant aux mêmes protons de la forme *Z*.

Nous avons voulu préciser si la configuration de l'hydrazone était conservée ou non au cours de la réaction conduisant aux hydrazones **2** et **3**. La stéréochimie des hydrazones d'alkénylcyclopentanones **2** est démontrée sur un cas particulier: par coupure de l'hydrazone **2***e*, on isole la cétone **8** à partir de laquelle l'hydrazone *E* est régénérée à température ambiante (2*g*) (fig. 5). Les caractéristiques physicochimiques et rmn ^1H du produit ainsi obtenu s'avèrent identiques à celles de l'hydrazone **2***e* mise en jeu qui doit donc être de configuration *E*.

La comparaison des glissements chimiques observés pour les protons des groupes méthyle en 1′ et 3′ des deux isomères **1***a* (*E*) et **1***a* (*Z*) et de ceux des mêmes groupes méthyle du mélange des hydrazones **3***a* issu de **1***a*(*E*) montre encore que la configuration de la fonction hydrazone est conservée lors de la transformation envisagée. L'examen des données rmn ^1H des autres hydrazones **3** permet de généraliser ce résultat. Un dernier argument confirme la stéréochimie *E* des hydrazones **2** et **3**: la protonation à −78°C du dianion issu de **1***b* de configuration *E* ne modifie pas la stéréochimie de cette hydrazone.

Le fait que la configuration *E* de l'hydrazone reste toujours inchangée lors de la préparation des composés **2** et **3** nous a conduit à proposer un mécanisme réactionnel précisant la nature du dianion intermédiaire.

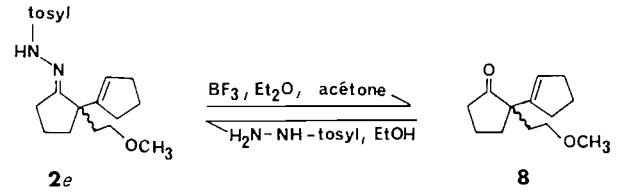

FIG. 5.

Mécanisme réactionnel

Lipton et Shapiro (3), puis Chamberlin et Bond (13), ont montré que l'alkylation d'hydrazones *E* en α procède par l'intermédiaire d'un *syn*-dianion (voie A, fig. 1). Le même mécanisme appliqué aux hydrazones α,β-insaturées **1** que nous avons étudiées, aurait dû conduire aux produits de substitution en position 5. Or, nous n'avons jamais pu isoler de tels composés, mais uniquement les hydrazones de type **2** et **3**. De plus, nous avons précisé dans le paragraphe précédent que la réaction s'effectue sans isomérisation de la fonction hydrazone *E*. Il n'est donc pas possible d'envisager un intermédiaire *syn*-dianion dans notre cas. L'hypothèse la plus plausible pour expliquer ces résultats paraît être l'intervention d'un intermédiaire à « six centres » qui se forme par déprotonation régiospécifique du sommet 1′. Le mécanisme réactionnel proposé est représenté en figure 6: l'intermédiaire à six centres (A) conduit au dianion allylique (B), précurseur des hydrazones **2** et **3**.

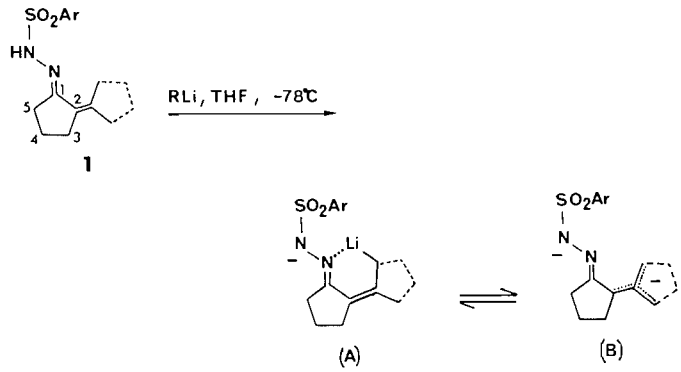

FIG. 6.

Il est à noter qu'un intermédiaire à six centres avait été évoqué par Bunnell et Fuchs (14) pour des hydrazones de β-céto ester. Une interprétation possible du changement de régiospécificité observé lors de l'emploi du sulfure de diphényle comme agent électrophile serait la suivante: à partir du dianion (B), il y aurait formation initiale d'une sulfimine conduisant ultérieurement aux hydrazones **3***a*, **3***c*, **3***e* et **3***f* selon

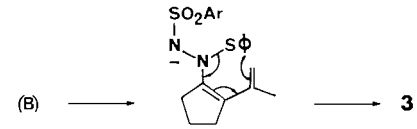

Conclusion

L'étude de la réactivité d'hydrazones α,β-insaturées vis-à-vis d'agents électrophiles montre que la déprotonation résultant de l'action de l'alkyllithien est régiospécifique et conduit à un

[3]Microprogramme d'écho de spin, « JMODXH.AU », Brüker.

intermédiaire à six centres. La configuration *E* des hydrazones est conservée au cours de la réaction. La formation d'un dianion allylique permet d'expliquer la formation concomitante ou non d'hydrazones d'alkényle et d'alkylidène cyclopentanones, la régiosélectivité de la réaction étant sous la dépendance essentielle de la nature de l'électrophile mis en jeu.

Cette réactivité particulière a été appliquée à la synthèse d'aldéhydes monoterpéniques et sera également mise en oeuvre dans l'article suivant pour proposer de nouvelles voies d'accès à des δ-lactones cyclopenténiques.

Partie expérimentale

Le déroulement des réactions est suivi par ccm (chromatographie sur couche mince) sur gel de silice (Kieselgel 60F254, Merck 5535). Les points de fusion mesurés sur banc Kofler ne sont pas corrigés. Les spectres infrarouges (ir) sont obtenus sur spectrophotomètre Perkin Elmer 580 B. Les spectres de résonance magnétique nucléaire (rmn) sont enregistrés à 400 MHz sur appareil Brüker WM 400. Les déplacements chimiques sont exprimés en ppm, le TMS étant pris comme référence interne (s, singulet; d, doublet; t, triplet; q, quintuplet; h, heptuplet; m, multiplet; M, massif). Les analyses sont effectuées par le Service central de microanalyses du Centre national de la recherche scientifique.

Le tétrahydrofuranne est distillé sur $LiAlH_4$, l'hexane et le tétraméthyléthylènediamine sur CaH_2. Les solutions d'alkyllithien sont commerciales. La lithiation des hydrazones est réalisée sous atmosphère d'argon.

Les produits de départ suivants sont préparés par les méthodes citées en référence : isopropylidène-2 cyclopentanone-1 (15); isopropylidène-2 méthyl-5 cyclopentanone-1 (16); tosylhydrazone de la cyclopentylidène-2 cyclopentanone-1, **1***d* (17).

Tosylhydrazones de l'isopropylidène-2 cyclopentanone-1 **1**a (E) *et* **1**a (Z)

(a) *Tosylhydrazone* **1**a (E)

On dissout au bain-marie 11,2 g (60 mmol) de tosylhydrazide dans 20 mL d'éthanol à reflux en présence d'une goutte d'acide chlorhydrique concentré, puis on ajoute, à température ambiante, l'isopropylidène-2 cyclopentanone-1 (7,5 g, 60 mmol). Après 12 h au réfrigérateur, puis filtration, on obtient 14 g (80%) d'un solide recristallisé dans l'éthanol; pf 216°C; R_f 0,27 (éther éthylique – hexane, 1 : 1); ν_{max}(KBr) : 3250 (NH), 1650 (C=C), 1600 aromatique, 1330 et 1150 (SO_2N) cm^{-1}. *Anal.* calc. pour $C_{15}H_{20}N_2O_2S$: C 61,63, H 6,90, N 9,58, O 10,95, S 10,95; trouvé : C 61,79, H 7,01, N 9,70, O 11,00, S 11,19.

(b) *Tosylhydrazone* **1**a (Z)

À une suspension de tosylhydrazide (5,0 g, 26,9 mmol) dans l'éthanol (50 mL), on ajoute l'isopropylidène-2 cyclopentanone-1 (3,33 g, 26,9 mmol) et 0,4 mL d'acide chlorhydrique concentré. Le mélange est porté à reflux pendant 3 h, puis évaporé sous pression réduite; l'huile brune obtenue est purifiée par chromatographie sur gel de silice (éluant : éther éthylique – hexane, 4 : 1). On recueille 4,7 g (60%) d'un solide recristallisé dans l'éthanol; pf 196°C; R_f 0,10 (éther éthylique – hexane, 1 : 1); ν_{max}(KBr) : 3200 (NH), 1640 (C=C), 1600 (aromatique), 1365 et 1160 (SO_2N) cm^{-1}. *Anal.* calc. pour $C_{15}H_{20}N_2O_2S$: C 61,63, H 6,90, O 10,95; trouvé : C 61,36, H 6,72, O 11,27.

Trisylhydrazones **1**b, **1**c *et* **1**e

Le même mode opératoire est utilisé pour préparer ces trois hydrazones : à une suspension de triisopropyl-2,4,6 benzènesulfonylhydrazide (29,8 g, 100 mmol) dans le méthanol (100 mL), on ajoute l'alkylidène cyclopentanone fraîchement distillée (100 mmol) et 1 mL d'acide chlorhydrique concentré. On agite vigoureusement jusqu'à formation d'un précipité abondant. Le mélange est ensuite déposé au réfrigérateur pendant la nuit. Le précipité obtenu est filtré, lavé au méthanol froid (3 × 50 mL), séché, puis recristallisé dans l'éthanol.

(a) *Trisylhydrazone de l'isopropylidène-2 cyclopentanone-1* **1**b

Rendement : 80%; pf 196°C; R_f 0,62 (éther éthylique – hexane, 1 : 1); ν_{max}(KBr) : 3250 (NH), 1655 (C=C), 1600 (aromatique), 1330 (SO_2N), 1160 et 1150 (SO_2N) cm^{-1}. *Anal.* calc. pour $C_{23}H_{36}N_2O_2S$: C 68,29, H 8,97, N 6,92; trouvé : C 68,21, H 8,98, N 6,81.

(b) *Trisylhydrazone de l'isopropylidène-2 méthyl-5 cyclopentanone-1* **1**c

Rendement : 40%; pf 158°C; R_f 0,69 (éther éthylique – hexane, 1 : 1); ν_{max}(KBr) : 3240 (NH), 1650 (C=C), 1600 (aromatique), 1330 (SO_2N), 1160 et 1150 (SO_2N) cm^{-1}. *Anal.* calc. pour $C_{24}H_{38}N_2O_2S$: C 68,87, H 9,15, N 6,69, S 7,64; trouvé : C 68,52, H 8,91, N 6,69, S 7,53.

(c) *Trisylhydrazone de la cyclopentylidène-2 cyclopentanone-1* **1**e

Rendement : 80%; pf 206°C; R_f 0,59 (éther éthylique – hexane, 1 : 1); ν_{max}(KBr) : 3240 (NH), 1665 (C=C), 1600 (aromatique), 1330 (SO_2N), 1160 et 1150 (SO_2N) cm^{-1}. *Anal.* calc. pour $C_{25}H_{38}N_2O_2S$: C 69,74, H 8,90, N 6,51, 0 7,43, S 7,43; trouvé : C 69,68, H 9,01, N 6,40, O 7,47, S 7,61.

Réactivité des tosylhydrazones **1**a (E) *et* **1**d *vis-à-vis d'agents électrophiles*

Le mode opératoire général est le suivant : à une solution de tosylhydrazone **1***a* ou **1***d* (6,84 mmol) dans le tétrahydrofuranne (30 mL) est ajoutée, à −78°C et goutte à goutte, une solution de *n*-butyllithium dans l'hexane (17,1 mmol). L'agitation est poursuivie pendant 20 min avant d'introduire goutte à goutte l'agent électrophile (10,26 mmol) en solution dans 5 mL de tétrahydrofuranne. À la fin de l'addition le milieu réactionnel est agité pendant 15 min à −78°C, puis 30 min à température ambiante. Après hydrolyse par NH_4Cl (50 mL), extraction par l'éther éthylique, lavage à l'eau et par une solution saturée en NaCl, puis évaporation du solvant, on obtient une huile éluée sur colonne de gel de silice par le mélange éther éthylique – hexane (1 : 1).

(a) *Action du sulfure de diphényle sur* **1**a (E)

Après recristallisation dans l'éthanol, on isole 0,87 g de tosylhydrazone de (phénylthio-1′(3′) isopropylidène)-2 cyclopentanone-1 **3***a*; pf 188–189°C; R_f 0,44 (éther éthylique – hexane, 1 : 1); ν_{max}(KBr) : 3200 (NH), 1650 (C=C), 1600 (aromatique), 1340 et 1170 (SO_2N) cm^{-1}. *Anal.* calc. pour $C_{21}H_{24}N_2O_2S_2$: C 62,98, H 6,04, 6,99, O 7,99, S 15,98; trouvé : C 63,27, H 5,89, N 6,85, O 8,53, S 15,69.

(b) *Action du chloroformiate de méthyle sur* **1**a (E)

Après recristallisation dans l'éthanol, on obtient successivement : 0,50 g de la tosylhydrazone de l'isopropényl-2 méthoxycarbonyl-2 cyclopentanone-1 **2***a*; pf 124°C; R_f 0,52 (éther éthylique – hexane, 3 : 2); ν_{max}(KBr) : 3200 (NH), 1725 (CO_2CH_3), 1640 (C=C), 1600 (aromatique), 1340 et 1170 (SO_2N) cm^{-1}; rmn ($CDCl_3$) δ : 7,82 et 7,29 (2d, 4H, —C_6H_4—), 4,93 et 4,64 (2s, 2H, —C=CH_2), 3,63 (s, 3H, —CO_2CH_3), 2,41 (s, 3H, —C_6H_4—CH_3), 2,31 (ddd, 1H, J_{3a3b} = 12,98, J_{3a4a} = 6,24 et J_{3a4b} = 9,83 Hz, H3a), 2,22 (dd, 2H, J_{4a5} = 6,11 et J_{4b5} = 8,81 Hz, (CH_2)-5), 2,04 (ddd, 1H, J_{3a3b} = 12,98, J_{3b4a} = 6,08, J_{3b4b} = 4,24 Hz, H3b), 1,80 (m, 1H, J_{4a5} = 6,11, J_{4a4b} = 12,15, J_{3a4a} = 6,24 et J_{3b4a} = 6,08 Hz, H4a), 1,73 (s, 3H, H_3C—C=C), 1,69 (m, 1H, J_{4b5} = 8,81, J_{4a4b} = 12,15, J_{3a4b} = 9,83 et J_{3b4b} = 4,24 Hz, H4b). *Anal.* calc. pour $C_{17}H_{22}N_2O_4S$: C 58,28, H 6,33, N 7,99, O 18,26, S 9,13; trouvé : C 58,13, H 6,24, N 8,24, O 18,11, S 9,02; et 0,24 g de la tosylhydrazone de (méthoxycarbonyl-1′(3′) isopropylidène)-2 cyclopentanone-1 **3***b*; pf (dec.) 90°C; R_f 0,36 (éther éthylique – hexane, 3 : 2); ν_{max}(KBr) : 3200 (NH), 1722 (CO_2CH_3), 1655 (C=C), 1600 (aromatique), 1340 et 1170 (SO_2N) cm^{-1}. *Anal.* calc. pour $C_{17}H_{22}N_2O_4S$: C 58,28, H 6,33, N 7,99, O 18,26, S 9,13; trouvé : C 58,46, H 6,28, N 7,96, O 17,92, S 9,05.

(c) *Action de l'iodo-1 méthoxy-2 éthane sur* **1**d

Après recristallisation dans le cyclohexane, on recueille 1,03 g de la tosylhydrazone de la cyclopentényl-2 (méthoxy-2 éthyl)-2 cyclopentanone-1 **2***e*; pf 127°C; R_f 0,23 (éther éthylique – hexane, 2 : 1); ν_{max}(KBr) : 3180 (NH), 1662 (C=C), 1600 (aromatique), 1360 et 1160 (SO_2N), 1120 (OCH_3) cm^{-1}; rmn ($CDCl_3$) δ : 7,86 et 7,25 (2d, 4H, —C_6H_4—), 5,10 (m, 1H, —C=CH—), 3,30 (m, 2H, —CH_2OCH_3), 3,23 (s, 3H, —OCH_3), 2,41 (s, 3H, —C_6H_4—CH_3), 2,00–1,60 (M, 14H, méthylènes cycliques et —$CH_2CH_2OCH_3$). *Anal.* calc. pour $C_{20}H_{28}N_2O_3S$: C 63,80, H 7,45, N 7,45, S 8,50; trouvé : C 64,17, H 7,52, N 7,38, S 8,33.

Réactivité des trisylhydrazones **1**b, **1**c *et* **1**e *vis-à-vis d'agents électrophiles*

Le mode opératoire général est le suivant: à une solution de trisylhydrazone (4,65 mmol) dans le tétrahydrofuranne (20 mL) à −78°C est ajoutée, goutte à goutte, une solution de *sec*-butyllithium dans le cyclohexane (11,62 mmol). Après agitation à −78°C pendant 1,5 h on ajoute lentement, et à cette même température, l'agent électrophile (7 mmol) en solution dans le tétrahydrofuranne (5 mL). On maintient le milieu réactionnel sous agitation pendant 7 h à −78°C. On réalise l'hydrolyse à l'aide d'une solution saturée de NH_4Cl, l'extraction par l'éther éthylique, puis on lave à l'eau et à l'aide d'une solution saturée de NaCl et l'on évapore les solvants organiques.

(a) *Action du sulfure de diphényle sur* **1**b

L'huile obtenue est éluée sur gel de silice, sous pression moyenne, par le mélange éther éthylique – hexane (1 : 2,5). Après recristallisation dans l'éthanol, on obtient 1,45 g de trisylhydrazone de (phénylthio-1′(3′) isopropylidène)-2 cyclopentanone-1 **3***c*; pf 120°C; R_f 0,55 (éther éthylique – hexane, 1 : 1); ν_{max}(KBr) : 3250 (NH), 1650 (C=C), 1600 et 1565 (aromatique), 1330 (SO_2N), 1165 et 1155 (SO_2N) cm^{-1}. *Anal.* calc. pour $C_{29}H_{40}N_2O_2S_2$: C 67,90, H 7,86, N 5,46, O 6,24, S 12,48; trouvé : C 67,89, H 7,86, N 5,34, O 6,17, S 12,39.

(b) *Action du sulfure de diméthyle sur* **1**b

Après chromatographie sur gel de silice (éluant : éther éthylique – hexane, 1 : 2,5), on recueille, après recristallisation dans l'éthanol, 1,15 g de trisylhydrazone de l'isopropényl-2 méthylthio-2 cyclopentanone-1 **2***b*; pf 140–141°C; R_f 0,63 (éther éthylique – hexane, 1 : 1); ν_{max}(KBr) : 3240 (NH), 1640 (C=C), 1600 et 1560 (aromatique), 1330 (SO_2N), 1165 et 1150 (SO_2N) cm^{-1}; rmn ($CDCl_3$) δ : 7,13 (s, 2H, aromatiques), 5,14 et 4,86 (2s, 2H, —C=CH_2), 4,19 (h, 2H, J = 6,80 Hz, *o*-*CH*(CH_3)$_2$), 2,88 (h, 1H, J = 6,80 Hz, *p*-*CH*(CH_3)$_2$), 2,47 et 2,33 (2m, 4H, (CH_2)-3 et (CH_2)-5), 1,77 (m, 2H, (CH_2)-4), 1,60 (s, 3H, H_3C—C=C), 1,37 (s, 3H, —SCH_3), 1,30 (d élargi, 18H, J = 6,80 Hz, —HC(*CH_3*)$_2$). *Anal.* calc. pour $C_{24}H_{38}N_2O_2S_2$: C 63,97, H 8,50, N 6,22, O 7,10, S 14,20; trouvé : C 63,90, H 8,69, N 6,09, O 7,27, S 14,20; et 0,062 g de trisylhydrazone de (méthylthio-1′(3′) isopropylidène)-2 cyclopentanone-1 **3***d*; pf 160°C; R_f 0,59 (éther éthylique – hexane, 1 : 1); ν_{max}(KBr) : 3250 (NH), 1650 (C=C), 1600 et 1565 (aromatique), 1335 (SO_2N), 1165 et 1150 (SO_2N) cm^{-1}; rmn ^{13}C ($CDCl_3$) δ : 160,3 et 160,2 (C-1), 153,9 et 153,8 puis 151,9 et 151,8 (2C, quaternaires aromatiques), 135,2 et 134,7 (C quaternaires aromatiques), 133,1 et 133,0 puis 131,9 et 131,8 (C-2 et C-2′), 41,2 et 35,6 (—*C*H_2SCH_3) ppm. *Anal.* calc. pour $C_{24}H_{38}N_2O_2S_2$: C 63,97, H 8,50, O 7,10, S 14,20; trouvé : C 63,90, H 8,69, O 7,27, S 14,20.

(c) *Action de l'iodure de méthyle sur* **1**b

L'huile obtenue traitée par le pentane abandonne 1,13 g de trisylhydrazone de l'isopropényl-2 méthyl-2 cyclopentanone-1 **2***c* recristallisée dans l'éthanol; pf 137°C; R_f 0,65 (éther éthylique – hexane, 1 : 1); ν_{max}(KBr) : 3240 (NH), 1635 (C=C), 1600 et 1560 (aromatique), 1330 (SO_2N), 1170 et 1155 (SO_2N) cm^{-1}; rmn ($CDCl_3$) δ : 7,12 (s, 2H, aromatiques), 4,55 et 4,31 (2s, 2H, —CH=CH_2), 4,19 (h, 2H, J = 6,80 Hz, *o*-*CH*(CH_3)$_2$), 2,88 (h, 1H, J = 6,80 Hz, *p*-*CH*(CH_3)$_2$), 2,20–1,60 (M, 6H, méthylènes cyclopentaniques), 1,45 (s, 3H, H_3C—C=C), 1,30 (d élargi, 18H, J = 6,80 Hz, —CH(*CH_3*)$_2$), 1,12 (s, 3H, C—CH_3); rmn ^{13}C ($CDCl_3$) δ : 162,9 (C-1), 153,9, 151,9 et 147,6 (3C, quaternaires aromatiques), 131,1 (C-2′), 124,3 (CH aromatique), 112,2 (C-1′), 52,8 (C-2 quaternaire), 38,2 (C-5), 34,9 (C-3′), 27,7 et 21,5 (C-3 et C-4) ppm. *Anal.* calc. pour $C_{24}H_{38}N_2O_2S$: C 68,87, H 9,15, N 6,69, O 7,64, S 7,64; trouvé : C 69,12, H 9,34, N 6,46, O 7,65, S 7,94.

(d) *Action du propionaldéhyde sur* **1**b

Après élution sur gel de silice, sous pression moyenne, par le mélange éther éthylique – hexane (1 : 1) et recristallisation dans l'éthanol, on isole 1,03 g de trisylhydrazone de 1′(hydroxy-1 propyl)-2 isopropényl-2 cyclopentanone-1 **2***d*; pf 150°C; R_f 0,33 (éther éthylique – hexane, 1 : 1); ν_{max}(KBr) : 3460 (OH), 3260 (NH), 1630 (C=C), 1600 et 1565 (aromatique), 1340 (SO_2N), 1170 et 1155 (SO_2N), 1110 (CHOH) cm^{-1}; rmn ($CDCl_3$) δ : 7,17 (s, 2H, aromatiques), 4,90 et 4,60 (2s, 2H, —C=CH_2), 4,15 (h, 2H, J = 6,80 Hz, *o*-*CH*(CH_3)$_2$), 3,73 (dd, 1H, J = 8,54 et 4,92 Hz, —*CH*OH—), 3,47 (d, 1H, J = 4,92 Hz, —CHO*H*—), 2,89 (h, 1H, J = 6,80 Hz, *p*-*CH*(CH_3)$_2$), 2,40 et 2,31 (2m, 4H, (CH_2)-3 et (CH_2)-5), 2,20–1,70 (M, 4H, (CH_2)-4 et (—CHOH*CH_2*CH_3)), 1,60 (s, 3H, H_3C—C=C), 1,30 (d élargi, 18H, J = 6,80 Hz, —CH(*CH_3*)$_2$), 0,83 (t, 3H, J = 7,32 Hz, —CH_2*CH_3*). *Anal.* calc. pour $C_{26}H_{42}N_2O_3S$: C 67,50, H 9,15, N 6,05, O 10,37, S 6,92; trouvé : C 67,59, H 9,22, N 6,00, O 10,51, S 7,20.

(e) *Action du sulfure de diphényle sur* **1**c

Après chromatographie sur gel de silice sous pression moyenne (éluant : éther éthylique – hexane, 1 : 5) et recristallisation dans l'éthanol, on recueille 1,27 g de trisylhydrazone de méthyl-5 (phénylthio-1′(3′) isopropylidène)-2 cyclopentanone-1 **3***e*; pf (dec.) 50°C; R_f 0,61 (éther éthylique – hexane, 1 : 1); ν_{max}(KBr) : 3200 (NH), 1650 (C=C), 1600 et 1570 (aromatique), 1330 (SO_2N), 1160 et 1150 (SO_2N) cm^{-1}. *Anal.* calc. pour $C_{30}H_{42}N_2O_2S_2$: C 68,42, H 8,04, S 12,15; trouvé : C 68,26, H 7,94, S 12,47.

(f) *Action du sulfure de diphényle sur* **1**e

Après élution sur gel de silice, sous pression moyenne, par le mélange éther éthylique – hexane (1 : 5) et recristallisation dans l'éthanol, on recueille 1,78 g de trisylhydrazone de (phénylthio-1′(3′) cyclopentylidène)-2 cyclopentanone-1 **3***f*; pf 140°C; R_f 0,55 (éther éthylique – hexane, 1 : 1); ν_{max}(KBr) : 3240 (NH), 1650 (C=C), 1600 et 1570 (aromatique), 1330 (SO_2N), 1165 et 1150 (SO_2N) cm^{-1}. *Anal.* calc. pour $C_{31}H_{42}N_2O_2S_2$: C 69,12, H 7,86, O 5,94, S 11,88; trouvé : C 69,01, H 7,94, O 5,75, S 12,11.

(g) *Action du sulfure de diméthyle sur* **1**e

L'huile obtenue abandonne dans le pentane 1,20 g de trisylhydrazone de la cyclopentényl-2 méthylthio-2 cyclopentanone-1 **2***f*, recristallisée dans l'éthanol; pf 163°C; R_f 0,65 (éther éthylique – hexane, 1 : 1); ν_{max}(KBr) : 3240 (NH), 1640 (C=C), 1600 et 1570 (aromatique), 1330 (SO_2N), 1170 et 1150 (SO_2N) cm^{-1}; rmn ($CDCl_3$) δ : 7,13 (s, 2H, aromatiques), 5,62 (m, 1H, —CH=C—), 4,20 (h, 2H, J = 6,80 Hz, *o*-*CH*(CH_3)$_2$), 2,88 (h, 1H, J = 6,80 Hz, *p*-*CH*(CH_3)$_2$), 2,40–1,50 (M, 12H, méthylènes cycliques), 1,37 (s, 3H, —SCH_3), 1,30 (d élargi, 18H, J = 6,80 Hz, —HC(*CH_3*)$_2$). *Anal.* calc. pour $C_{26}H_{40}N_2O_2S_2$: C 65,52, H 8,46, N 5,88, S 13,43; trouvé : C 65,44, H 8,52, N 5,87, S 13,07.

(h) *Action de l'iodo-1 méthoxy-2 éthane sur* **1**e

L'huile obtenue traitée par le pentane abandonne 1,50 g de trisylhydrazone de la cyclopentényl-2 (méthoxy-2 éthyl)-2 cyclopentanone-1 **2***g*, recristallisée dans l'éthanol; pf 144°C; R_f 0,48 (éther éthylique – hexane, 1 : 1); ν_{max}(KBr) : 3240 (NH), 1650 (C=C), 1600 et 1570 (aromatique), 1330 (SO_2N), 1165 et 1155 (SO_2N), 1114 (OCH_3) cm^{-1}; rmn ($CDCl_3$) δ : 7,13 (s, 2H, aromatiques), 5,11 (m, 1H, —C=CH—), 4,18 (h, 2H, J = 6,80 Hz, *o*-*CH*(CH_3)$_2$), 3,16 (m, 2H, —*CH_2*OCH_3), 3,14 (s, 3H, —OCH_3), 2,88 (h, 1H, J = 6,80 Hz, *p*-*CH*(CH_3)$_2$), 2,30–1,50 (M, 14H, méthylènes cycliques et —*$CH_2CH_2OCH_3$*), 1,30 (d élargi, 18H, J = 6,80 Hz, —CH(*CH_3*)$_2$). *Anal.* calc. pour $C_{28}H_{44}N_2O_3S$: C 68,82, H 9,07, N 5,73, O 9,82, S 6,55; trouvé : C 68,81, H 9,32, N 5,73, O 9,97, S 6,69.

Trisylhydrazone de l'isopropényl-2 méthyl-5 méthylthio-2 cyclopentanone-1 **6**

Selon le mode opératoire décrit pour préparer **2***c*, on obtient, à partir de 2,1 g (4,65 mmol) de **2***b* et 1,0 g d'iodure de méthyle, une huile éluée sur gel de silice, sous pression moyenne, par le mélange éther éthylique – hexane (1 : 5). Après recristallisation dans l'éthanol, on obtient 0,86 g (40%) d'un solide jaune pâle; pf 145°C; R_f 0,66 (éther éthylique – hexane, 1 : 1); ν_{max}(KBr) : 3172 (NH), 1635 (C=C), 1600 et 1560 (aromatique), 1380 (SO_2N), 1160 et 1154 (SO_2N) cm^{-1}; rmn ($CDCl_3$) δ : 7,13 (s, 2H, aromatiques), 5,07 et 4,83 (2s, —C=CH_2), 4,15 (h, 2H, J = 6,80 Hz, *o*-*CH*(CH_3)$_2$), 2,88 (h, 1H, J = 6,80 Hz, *p*-*CH*(CH_3)$_2$), 2,20–1,60 (M, 5H, protons cyclopentaniques), 1,66 (s, 3H, H_3C—C=C), 1,34 (s, 3H, —SCH_3), 1,30 (d élargi, 18H, J = 6,80 Hz, —CH(*CH_3*)$_2$, 1,29 et 1,14 (2d, $J_{5\text{-}CH_3}$ = 8,00 Hz, —CH*CH_3*). *Anal.* calc. pour $C_{25}H_{40}N_2O_2S_2$: C 64,63, H 8,68, N 6,03, O 6,88, S 13,77; trouvé : C 64,42, H 8,41, N 5,93, O 6,99, S 13,49.

Méthode générale de synthèse des aldéhydes **4**b, **4**c *et* **7**

À une solution de trisylhydrazone (10 mmol) dans le tétrahydrofuranne (20 mL) est ajoutée, à −78°C et goutte à goutte, une solution de *sec*-butyllithium dans le cyclohexane (35 mmol). À la fin de l'addition, le milieu réactionnel est agité pendant 1 h à −78°C, puis 1 h à 0°C. On ajoute alors le diméthylformamide (3,1 mL, 40 mmol) en solution dans le tétrahydrofuranne (5 mL). La solution obtenue est agitée à 0°C durant 1 h, hydrolysée par une solution saturée de NH_4Cl, puis extraite par l'éther éthylique. Les phases organiques sont lavées à l'eau et par une solution saturée en NaCl, puis évaporées. Après élution du résidu sur gel de silice (solvant : éther éthylique – hexane, 1 : 5), l'aldéhyde est isolé sous forme d'une huile jaune pâle.

(a) *Isopropényl-2 cyclopentènecarbaldéhyde-1* **4**b

À partir de **1***b*, on obtient 0,48 g (35%) de **4***b*; R_f 0,57 (éther éthylique – hexane, 1 : 4); ν_{max}(film) : 1661 (CHO), 1607 (C=C) cm^{-1}; rmn ($CDCl_3$) δ : 9,92 (s, 1H, —CHO), 5,20 et 5,08 (2s, 2H, —C=CH_2), 2,72 (tt, 2H, $J_{34\text{ ou }54}$ = 7,60 et J_{35} = 2,00 Hz, (CH_2)-3 ou -5), 2,63 (tt, 2H, $J_{54\text{ ou }34}$ = 7,60 et J_{35} = 2,00 Hz, (CH_2)-5 ou -3), 1,96 (s, 3H, CH_3—C=C), 1,90 (q, 2H, J_{43} et J_{45} = 7,60 Hz, (CH_2)-4). *Anal.* calc. pour $C_9H_{12}O$: C 79,37, H 8,88, O 11,75; trouvé : C 79,03, H 9,05, O 11,90.

(b) *Isopropényl-2 méthyl-5 cyclopentènecarbaldéhyde-1* **4**c

À partir de **1***c*, on obtient 0,55 g (37%) de l'aldéhyde **4***c*; R_f 0,60 (éther éthylique – hexane, 1 : 4); ν_{max}(film) : 1662 (CHO), 1605 (C=C) cm^{-1}; rmn ($CDCl_3$) δ : 9,88 (s, 1H, —CHO), 5,20 et 5,05 (2s, 2H, —C=CH_2), 3,14 (m, 1H, H-5), 2,75, 2,66, 2,09 et 1,51 (4m, 4H (CH_2)-3 et (CH_2)-4), 1,94 (s, 3H, H_3C—C=C), 1,13 (d, 3H, J = 6,89 Hz, —C—CH_3). *Anal.* calc. pour $C_{10}H_{14}O$: C 79,95, H 9,39, O 10,65; trouvé : C 80,20, H 9,01, O 11,12.

(c) *Isopropényl-3 méthyl-1 méthylthio-3 cyclopentènecarbaldéhyde-2* **7**

À partir de **6**, on obtient 0,74 g (38%) de l'aldéhyde **7**; R_f 0,33 (éther éthylique – hexane, 1 : 7); ν_{max}(film) : 1678 (CHO), 1615 (C=C) cm^{-1}; rmn ($CDCl_3$) δ : 9,76 (s, 1H, —CHO), 4,99 (m, 2H, —C=CH_2), 2,51–2,44 (M, 2H, (CH_2)-5), 2,23 (t, 3H, $J_{5\text{-}CH_3}$ = 1,10 Hz, H_3C—C=C—CHO), 2,20 (m, 2H, (CH_2)-4), 1,96 (s, 3H, —SCH_3), 1,83 (dd, $J_{1'a\text{-}CH_3}$ = 1,28 et $J_{1'b\text{-}CH_3}$ = 0,55 Hz, H_3C—C=C). *Anal.* calc. pour $C_{11}H_{16}OS$: C 67,32, H 8,22, O 8,15, S 16,31; trouvé : C 67,29, H 8,15, O 8,40, S 16,01.

Cyclopentényl-2 (méthoxy-2 éthyl)-2 cyclopentanone-1 **8**

À une solution d'hydrazone **2***e* (0,38 g, 1 mmol) dans le mélange acétone–eau (10 : 1, 11 mL) est ajouté l'éthérate de trifluorure de bore (0,63 mL, 5 mmol) (12). Le milieu réactionnel est agité pendant 48 à 72 h à température ambiante. Le solvant est évaporé puis le résidu repris par le pentane (3 × 20 mL). Les phases organiques sont réunies puis évaporées pour donner 0,13 g (61%) de cétone **8**; pé 135°C/3 Torr (1 Torr = 133,3 Pa); R_f 0,78 (éther éthylique – hexane, 1 : 1); ν_{max}(film) : 1735 (CO), 1638 (C=C), 1114 (OCH_3) cm^{-1}; rmn ($CDCl_3$) δ : 5,50 (m, 1H, —CH=C—), 3,33 (m, 2H, —CH_2OCH_3), 3,27 (s, 3H, —OCH_3), 2,30–1,83 (M, 14H, méthylènes cycliques et —$CH_2CH_2OCH_3$). *Anal.* calc. pour $C_{13}H_{20}O_2$: C 74,96, H 9,68, O 15,36; trouvé : C 74,89, H 9,76, O 15,37.

1. R. H. Shapiro. Org. React. **23**, 405 (1975).
2. (*a*) A. R. Chamberlin, J. E. Stemke et F. T. Bond. J. Org. Chem. **43**, 147 (1978); (*b*) R. M. Adlington et A. G. M. Barrett. J. Chem. Soc. Chem. Commun. 1071 (1978); (*c*) T. Nakai et T. Mimura. Tetrahedron Lett. 531 (1979); (*d*) R. M. Adlington et A. G. M. Barrett. J. Chem. Soc. Perkin Trans. **1**, 2848 (1981); (*e*) L. A. Paquette, W. E. Fristad, D. S. Dime et T. R. Bailey. J. Org. Chem. **45**, 3017 (1980); (*f*) F. T. Bond et R. A. DiPietro. J. Org. Chem. **46**, 1315 (1981); (*g*) R. Baudouy, J. Sartoretti et F. Choplin. Tetrahedron, **39**, 3293 (1983); (*h*) K. Kon et S. Isoe. Helv. Chim. Acta, **66**, 755 (1983); (*i*) J. C. Caille, F. Bellamy et R. Guilard. Tetrahedron Lett. 2345 (1984).
3. M. F. Lipton et R. H. Shapiro. J. Org. Chem. **43**, 1409 (1978).
4. N. J. Cusack, C. B. Reese, A. C. Risius et B. Roozpeikar. Tetrahedron, **32**, 2157 (1976).
5. W. G. Dauben, M. E. Lorber, N. D. Vietmeyer, R. H. Shapiro, J. H. Duncan et K. Tomer. J. Am. Chem. Soc. **90**, 4762 (1968).
6. W. G. Dauben, G. T. Rivers et W. T. Zimmerman. J. Am. Chem. Soc. **99**, 3414 (1977).
7. J. C. Caille et R. Guilard. Tetrahedron Lett. 2771 (1984).
8. P. C. Traas, H. Boelens et H. J. Takken. Tetrahedron Lett. 2287 (1976).
9. T. H. Jones, M. S. Blum et H. M. Fales. Tetrahedron Lett. 1701 (1980).
10. K. Kondo et M. Matsumoto. Tetrahedron Lett. 391 (1976).
11. A. F. Thomas. *Dans* The total synthesis of natural products. Vol. 2. *Éditeur* : J. ApSimon. Wiley – Interscience, New York. 1973. p. 62.
12. C. E. Sacks et P. L. Fuchs. Synthesis, 456 (1976).
13. A. R. Chamberlin et F. T. Bond. Synthesis, 44 (1979).
14. C. A. Bunnell et P. L. Fuchs. J. Am. Chem. Soc. **99**, 5184 (1977).
15. J. M. Conia et J. P. Sandré. Bull. Soc. Chim. Fr. 744 (1963).
16. R. Cornubert et C. Borrel. Bull. Soc. Chim. Fr. 301 (1930).
17. J. T. Sharp, R. H. Findlay et P. B. Thorogood. J. Chem. Soc. Perkin Trans. **1**, 102 (1975).

Sur une nouvelle méthode de synthèse de δ-lactones cyclopenténiques

JEAN CLAUDE CAILLE, MICHEL FARNIER ET ROGER GUILARD[1]
Laboratoire de synthèse et d'électrosynthèse organométallique (UA 33), Faculté des sciences « Gabriel », 21100 Dijon, France
ET
ANDRÉ AUBRY ET CLAUDE LECOMTE
Laboratoire de minéralogie et cristallographie (Équipe de recherche associée 162), Faculté des sciences, Centre de 2e cycle, B. P. N° 239, 54506 Vandoeuvre-les-Nancy, France
Reçu le 4 janvier 1985[2]

JEAN CLAUDE CAILLE, MICHEL FARNIER, ROGER GUILARD, ANDRÉ AUBRY et CLAUDE LECOMTE. Can. J. Chem. **64**, 831 (1986).

La synthèse de deux δ-lactones cyclopenténiques, l'hexahydro-1,3,4,4a,5,6 cyclopenta[*c*]pyrannone-1 et son analogue substitué en position 4a par un cyclopentényle, est décrite au départ de la cyclopentanone et de la cyclopentylidène-2 cyclopentanone. La réactivité singulière des tosylhydrazones permet la transformation de ces cyclopentanones en cyclopentènes fonctionnalisés en vue de leur cyclisation ultérieure en δ-lactone. Les conditions de cyclisation dépendent de la nature de la cyclopentanone. La structure des deux δ-lactones synthétisées est établie par analyse des spectres rmn ^1H, ^{13}C et de masse, et dans un cas, par analyse radiocristallographique.

JEAN CLAUDE CAILLE, MICHEL FARNIER, ROGER GUILARD, ANDRÉ AUBRY, and CLAUDE LECOMTE. Can. J. Chem. **64**, 831 (1986).

Synthesis of two cyclopentenic δ-lactones, 1,3,4,4a,5,6-hexahydrocyclopenta[*c*]pyran-1-one and its analogue possessing a cyclopentenyl group bonded to the carbon atom 4a is described, starting from the cyclopentanone or cyclopentylidene cyclopentanone. The remarkable reactivity of the tosylhydrazones allows transformation of these compounds into substituted cyclopentenes, which lead to δ-lactones by cyclization. The conditions of cyclization depend on the nature of the cyclopentanone. The structure of the two δ-lactones is established by ^1H and ^{13}C nmr data, mass spectrometry, and, in one case, by X-ray analysis.

Introduction

Dans le mémoire précédent (1), nous avons montré que la réaction de Shapiro (2) appliquée à des arènesulfonylhydrazones de cyclopentanones α,β-insaturées permet d'introduire régiospécifiquement un groupe alkyle sur l'atome de carbone substitué par un reste insaturé et situé en α de la fonction hydrazone. Le produit d'alkylation soumis à l'action d'un alkyllithien conduit à un dianion qui se décompose à température ambiante en un anion vinylique très réactif vis-à-vis d'électrophiles. En utilisant cette réactivité particulière et au départ d'hydrazones non cycliques, Adlington et Barrett (3) ont récemment mis au point une synthèse d'α-méthylène γ-butyrolactones. Nous nous sommes proposés d'utiliser des hydrazones de cyclopentanones pour accéder à des δ-lactones cyclopenténiques. En effet, ce motif δ-lactonique est fréquemment retrouvé dans un grand nombre de substances naturelles tels les monoterpènes bicycliques (4). Nous décrivons dans ce mémoire la synthèse de deux δ-lactones cyclopenténiques **1** et **2**, une partie de ce travail ayant déjà fait l'objet d'une note préliminaire (5).

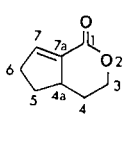

1

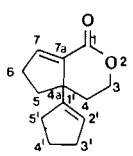

2

Résultats et discussion

Les premières étapes de la synthèse des δ-lactones cyclopenténiques **1** et **2**, communes à ces deux dérivés, sont schématisées en figure 1.

Les tosylhydrazones **3** et **4**, préparées selon des modalités classiques à partir des cyclopentanones correspondantes, sont alkylées après traitement par le *n*-butyllithium dans le mélange THF (tétrahydrofuranne) – hexane à −78°C, par l'iodo-1 méthoxy-2 éthane. Les dérivés alkylés **5** et **6** sont obtenus avec des rendements respectifs de 64 et 45%.

Les hydrazones **5** et **6** sont à nouveau traitées à −78°C par une solution de *n*-butyllithium dans le mélange TMEDA (tétraméthyléthylènediamine) – hexane. Les anions vinyliques générés après retour du milieu réactionnel à température ambiante sont soumis à un courant de CO_2; les acides obtenus après hydrolyse acide sont directement transformés en chlorures **7** et **8** correspondants par traitement au chlorure d'oxalyle (rendements de l'ordre de 50%).

Les divers essais de lactonisation des chlorures **7** et **8** sont respectivement représentés sur les figures 2 et 3. À partir du chlorure d'acide **7**, les esters méthylique **9***a*, éthylique **9***b* et tertiobutylique **9***c* sont préparés classiquement avec des rendements de l'ordre de 90%. Le trichlorure et le tribromure de bore ont déjà été utilisés avec succès (6, 7) pour lactoniser des esters porteurs d'un groupe méthoxy. Aussi, nous avons tout d'abord tenté une lactonisation directe de l'ester **9***a* en le traitant par le tribromure de bore, mais dans notre cas, la proportion de lactone **1** recherchée n'a jamais atteint 5%. Par ailleurs, une tentative de cyclisation de l'acide **10** obtenu par saponification de l'ester **9***b* s'est également soldée par un échec. Nous avons alors cherché à utiliser avec profit les réactifs préconisés par Olah *et al.* (8, 9) pour régénérer des fonctions acide et alcool à partir d'ester ou d'éther. Au départ de l'ester éthylique **9***b* et par action à température ambiante de l'iodure de dichlorométhylsilyle, l'alcool **11** uniquement est formé. Par contre, l'utilisation de l'ester tertiobutylique **9***c* permet d'obtenir la lactone **1** selon deux voies : en opérant au reflux de l'acétonitrile en présence d'iodure de dichlorométhylsilyle, la lactonisation s'effectue

1. Auteur à qui adresser toute correspondance.
2. Révision reçu le 8 novembre 1985.

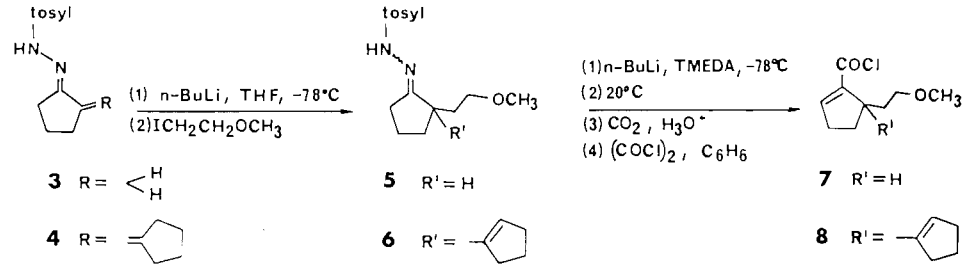

FIG. 1.

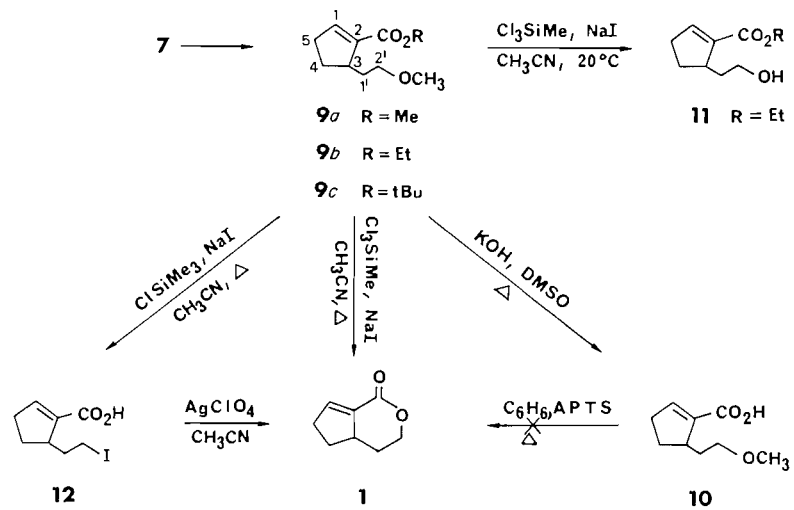

FIG. 2.

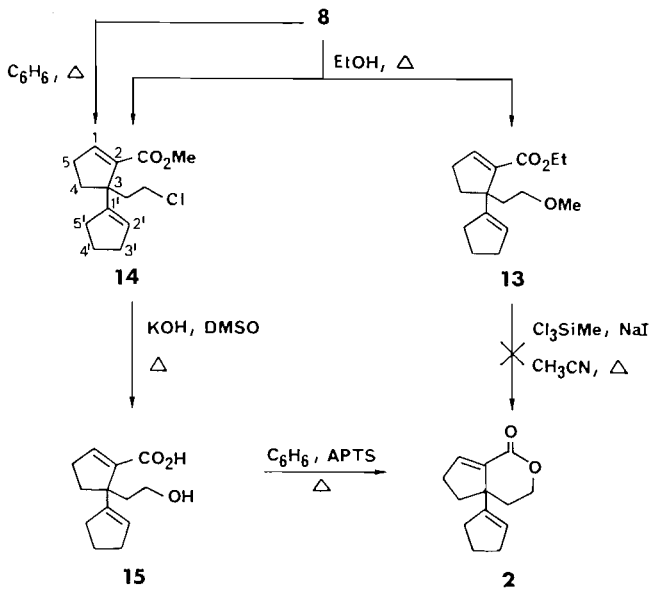

FIG. 3.

directement mais seulement avec un rendement de 44%; il est préférable d'employer l'iodure de triméthylsilyle, car celui-ci permet, via l'iodo-acide **12**, d'isoler la même lactone avec un rendement de 63%.

La même stratégie pouvait à priori être étendue à la synthèse de la lactone **2**. Lors de l'estérification du chlorure d'acide **8** par l'éthanol, outre l'ester **13** attendu, il y a formation de chloro-ester **14** dans une proportion d'environ 17% (fig. 3). Tous nos essais de lactonisation de l'ester **13** par l'iodure de dichloro-méthylsilyle se sont soldés par un échec. Pour accéder à la lactone **2** recherchée, nous avons utilisé le chloro-ester **14** qui peut par ailleurs être obtenu avec un rendement de 96% en chauffant le chlorure d'acide **8** au reflux du benzène. Le dérivé **14** traité par la potasse dans le DMSO (diméthyl-sulfoxyde) conduit à l'hydroxy-acide **15** avec un rendement de 80%. La cyclisation de ce dérivé est aisément réalisée par chauffage au reflux du benzène en présence d'acide *p*-toluènesulfonique et la lactone **2** est isolée avec un rendement de 80%.

Le chloro-ester **14** peut être également utilisé pour accéder au δ-lactame **17** correspondant (fig. 4), en le transformant en phtalimide **16** cyclisé en présence d'hydrate d'hydrazine.

Établissement des structures

La structure des divers produits synthétisés est établie par analyse des spectres de rmn (résonance magnétique nucléaire) protonique dont les données figurent dans la partie expérimentale. Dans le cas des lactones **1** et **2**, des informations structurales complémentaires sont apportées par la spectrométrie de masse et par la rmn ^{13}C et, pour l'une des deux lactones, **2**, une analyse radiocristallographique a été effectuée. Cette étude radiocristallographique montre la présence d'un cycle δ-lactonique accolé à un cyclopentène et porteur en 4a d'un reste cyclopenténylé, comme représenté en figure 5. L'angle formé par les plans moyens des cycles lactonique (C(4a)—C(7a)—C(1)—O(2)—C(3)—C(4)) et cyclopenténylé (C(4a)—C(5)—C(6)—C(7)—C(7a)) est égal à 17,9° et l'angle formé par le plan moyen du reste cyclopenténylé avec le plan moyen du bicycle lactonique est de 91,2°. Les valeurs des longueurs et angles de liaisons (tableau 1) confirment la

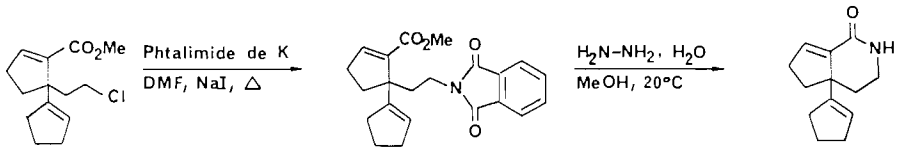

14 16 17

FIG. 4.

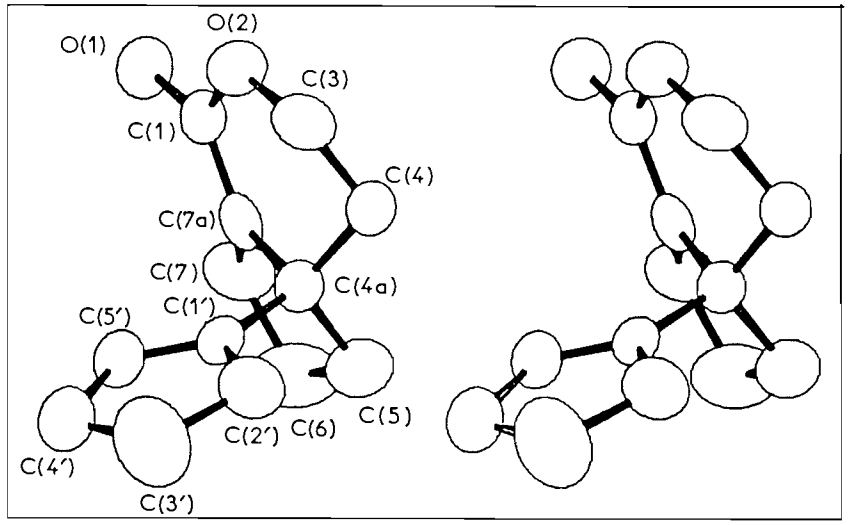

FIG. 5. Vue ORTEP de la structure cristalline de **2**.

TABLEAU 1. Longueurs (Å) et angles de liaisons (°)

Liaison	Longueur	Liaison	Longueur
C(1)—O(1)	1,208(5)	C(1)—O(2)	1,352(2)
O(2)—C(3)	1,459(5)	C(3)—C(4)	1,492(7)
C(4)—C(4a)	1,528(6)	C(4a)—C(5)	1,553(7)
C(5)—C(6)	1,532(9)	C(6)—C(7)	1,488(8)
C(7)—C(7a)	1,316(6)	C(1)—C(7a)	1,455(6)
C(4a)—C(7a)	1,516(5)	C(4a)—C(1')	1,518(4)
C(1')—C(2')	1,318(6)	C(2')—C(3')	1,496(6)
C(3')—C(4')	1,488(10)	C(4')—C(5')	1,500(8)
C(5')—C(1')	1,501(6)		

Liaisons	Angle	Liaisons	Angle
C(7a)—C(1)—O(1)	125,6(4)	O(1)—C(1)—O(2)	116,7(4)
C(7a)—C(1)—O(2)	117,6(3)	C(1)—O(2)—C(3)	121,9(3)
O(2)—C(3)—C(4)	114,2(4)	C(3)—C(4)—C(4a)	109,4(3)
C(4)—C(4a)—C(7a)	105,7(3)	C(7a)—C(4a)—C(5)	101,0(3)
C(4)—C(4a)—C(5)	115,4(4)	C(1')—C(4a)—C(4)	112,3(3)
C(1')—C(4a)—C(5)	110,6(3)	C(1')—C(4a)—C(7a)	111,2(3)
C(4a)—C(5)—C(6)	105,2(4)	C(5)—C(6)—C(7)	103,1(5)
C(6)—C(7)—C(7a)	112,1(4)	C(1)—C(7a)—C(4a)	121,8(3)
C(1)—C(7a)—C(7)	125,8(4)	C(4a)—C(7a)—C(7)	112,3(4)
C(4a)—C(1')—C(2')	127,0(3)	C(4a)—C(1')—C(5')	122,9(4)
C(2')—C(1')—C(5')	110,0(3)	C(1')—C(2')—C(3')	114,3(4)
C(2')—C(3')—C(4')	102,0(4)	C(3')—C(4')—C(5')	110,0(5)
C(1')—C(5')—C(4')	103,7(4)		

présence de deux liaisons doubles C(7)—C(7a) et C(1')—C(2'). Enfin l'examen des distances intermoléculaires montre que la cohésion du cristal est assurée par des forces de type van der Waals.

Les données spectrales sont en accord avec cet arrangement structural : le spectre rmn ^{13}C du composé **2** montre effectivement la présence d'un carbone quaternaire C(4a) à 51 ppm; en rmn protonique, pour cette lactone, seuls les protons éthyléniques et ceux du méthylène en position 3 peuvent être individualisés. Par contre, en rmn protonique à 400 MHz et à l'aide d'expériences de corrélation homonucléaire (COSY), l'attribution de tous les signaux des protons est possible pour la lactone **1** et ses précurseurs.

Enfin, la configuration des hydrazones **5** et **6** est différente : en effet, de façon classique (2*b*), l'hydrazone **5** est *Z*, alors que nous avons montré dans l'article précédent (1) que la configuration *E* de l'hydrazone **4** est conservée lors de sa transformation en **6**.

Conclusion

L'application de la réaction de Shapiro à des hydrazones de cyclopentanones constitue une voie d'accès aisée à des cyclopentènes fonctionnalisés. La lactonisation ultérieure des cyclopentènes dépend étroitement de la nature des fonctions portées par le cycle. Les réactifs silylés de Olah ont permis une lactonisation uniquement lorsque la δ-lactone cyclopenténique recherchée n'est pas substituée par un reste cyclopentényle. Dans ce cas, la lactonisation a été réalisée via la cyclisation classique d'un acide alcool.

Les deux nouvelles δ-lactones que nous avons synthétisées renferment le motif de base de divers produits naturels de la famille des monoterpènes bicycliques. La fonctionnalisation ultérieure des δ-lactones obtenues devrait permettre la préparation d'analogues structuraux d'iridoïdes.

Partie expérimentale

Le déroulement des réactions est suivi par ccm (chromatographie sur

couche mince) sur gel de silice (Kieselgel 60F254, Merck 5535). Les points de fusion mesurés sur banc Kofler ne sont pas corrigés. Les spectres infrarouges (ir) sont enregistrés sur spectrophotomètre Perkin Elmer 580 B. Les spectres de masse sont obtenus par impact électronique (30–70 eV) sur appareil Finnigan 3300. Les spectres rmn sont enregistrés à 100 MHz sur spectromètre JEOL FX 100 et à 400 MHz sur appareil Brüker WM 400. Les déplacements chimiques sont exprimés en parties par million et le tétraméthylsilane est pris comme référence interne (s, singulet; d, doublet; t, triplet; q, quadruplet; m, multiplet; M, massif). Les analyses sont effectuées par le Service central de microanalyses du Centre national de la recherche scientifique.

Le tétrahydrofuranne est distillé sur $LiAlH_4$, l'hexane et le tétraméthyléthylènediamine sur CaH_2. Les solutions d'alkyllithien sont commerciales. La lithiation des hydrazones est réalisée sous atmosphère d'argon.

Matières premières

Les produits de départ suivants sont préparés par les méthodes citées en référence : tosylhydrazone de la cyclopentanone, **3** (2); tosylhydrazone de la cyclopentylidène-2 cyclopentanone-1, **4** (10). La synthèse de la tosylhydrazone **6** est décrite dans le mémoire précédent (1).

Tosylhydrazone de la (méthoxy-2 éthyl)-2 cyclopentanone-1 **5**

À une solution de tosylhydrazone **3** (2,52 g, 10 mmol) dans le THF (60 mL) est ajoutée, goutte à goutte et à −78°C, une solution de *n*-butyllithium dans l'hexane (20 mmol). L'addition terminée, on ajoute, goutte à goutte et à −78°C, de l'iodo-1 méthoxy-2 éthane (2,05 g, 11 mmol) (11) dans le THF (10 mL). À la fin de l'addition l'agitation est maintenue 15 min, puis on laisse le milieu réactionnel revenir à température ambiante et maintient 30 min l'agitation. Après hydrolyse par une solution saturée de NH_4Cl (40 mL), on extrait par l'éther éthylique (3 × 20 mL). La phase organique lavée à l'eau (30 mL), puis séchée et évaporée, abandonne 2 g (64%) d'hydrazone **5** sous forme d'une solide blanc recristallisé dans l'éther isopropylique; pf 115°C; R_f 0,14 (éther éthylique – hexane, 2:1); ν_{max}(KBr) : 3140 (NH), 1645 (C=N), 1170 (SO_2N), 1120 (OCH_3) cm^{-1}; rmn 100 MHz ($CDCl_3$) δ : 7,85 et 7,30 (2d, 4H, —C_6H_4—), 3,39 (t, 2H, J = 6,59 Hz, —CH_2OCH_3), 3,28 (s, 3H, OCH_3), 2,42 (s, 3H, —$C_6H_4CH_3$), 2,20–1,20 (M, 9H, protons cyclopentaniques et —$CH_2CH_2OCH_3$). *Anal.* calc. pour $C_{15}H_{22}N_2O_3S$: C 58,06, H 7,09, N 9,03, S 10,32; trouvé : C 58,13, H 7,07, N 9,30, S 10,39.

Préparation des chlorures d'acide **7** *et* **8**

À une suspension de tosylhydrazone **5** ou **6** (30 mmol) dans le mélange TMEDA – hexane (1:1; 100 mL) est ajoutée à −78°C une solution de *n*-butyllithium dans l'hexane (105 mmol). La solution obtenue est agitée pendant 15 min à −78°C, puis 8 h à température ambiante. Après avoir à nouveau refroidi à −78°C, la solution est traitée par un rapide courant de CO_2. Après retour à température ambiante, la solution est hydrolysée par l'eau (300 mL) puis extraite par l'éther éthylique (3 × 50 mL). La phase aqueuse est acidifiée par l'acide chlorhydrique concentré jusqu'à pH 1 et extraite par l'éther éthylique (3 × 100 mL). Cette dernière phase éthérée lavée à l'eau (5 × 40 mL), puis séchée, fournit par évaporation l'acide correspondant.

À une solution de cet acide dans le benzène anhydre (100 mL) est ajouté goutte à goutte, sous courant d'azote et à température ambiante, le chlorure d'oxalyle (15 mL, 171 mmol). Après 3 h d'agitation à cette température, puis évaporation du solvant et de l'excès de réactif, on recueille le chlorure d'acide **7** ou **8** sous forme d'une huile (rendement ≃ 50%) utilisée sans autre purification pour les synthèses ultérieures.

Préparation des esters **9**a, **9**b *et* **9**c

(a) *(Méthoxy-2 éthyl)-3 cyclopentènecarboxylate-2 de méthyle* **9**a

Une solution de 2,65 g (14 mmol) du chlorure d'acide **7** dans 200 mL de méthanol est portée à reflux pendant 1 h. Le solvant est évaporé et le résidu est purifié par chromatographie sur gel de silice dans le solvant éther éthylique – hexane (1:4). On obtient 2,32 g (89%) d'une huile jaune; pé 125°C/3 Torr (1 Torr = 133,3 Pa); R_f 0,39 (éther éthylique – hexane, 1:4); ν_{max}(film) : 1715 (CO_2Me), 1625 (C=C), 1120 (OCH_3) cm^{-1}; rmn 400 MHz ($CDCl_3$) δ : 6,78 (m, 1H, H-1), 3,73 (s, 3H, —CO_2CH_3), 3,43 (dd, 2H, J = 6,40 et 7,38 Hz, —CH_2OCH_3), 3,32 (s, 3H, —OCH_3), 3,01 (M, 1H, H-3), 2,49 et 2,41 (2m, 2H, (CH_2)-5), 2,10 (m, 2H, H-4a et H-1′a), 1,75 (m, 1H, H-4b), 1,51 (m, 1H, H-1′b). *Anal.* calc. pour $C_{10}H_{16}O_3$: C 65,20, H 8,75, O 26,05; trouvé : C 64,87, H 8,82, O 26,40.

(b) *(Méthoxy-2 éthyl)-3 cyclopentènecarboxylate-2 d'éthyle* **9**b

Le mode opératoire est identique à celui décrit pour **9***a*, et on isole l'ester **9***b* avec un rendement de 94%; pé 130°C/3 Torr; R_f 0,42 (éther éthylique – hexane, 1:4); ν_{max}(film) : 1715 (CO_2Et), 1625 (C=C), 1120 (OCH_3) cm^{-1}; rmn 400 MHz ($CDCl_3$) δ : 6,77 (m, 1H, H-1), 4,19 (m, 2H, —$CO_2CH_2CH_3$), 3,43 (dd, 2H, J = 6,89 Hz et 7,38 Hz, —CH_2OCH_3), 3,32 (s, 3H, OCH_3), 3,00 (M, 1H, H-3), 2,48 et 2,40 (2m, 2H, (CH_2)-5), 2,10 (m, 2H, H-4a et H-1′a), 1,74 (m, 1H, H-4b), 1,51 (m, 1H, H-1′b), 1,30 (t, 3H, J = 7,39 Hz, —$CO_2CH_2CH_3$). *Anal.* calc. pour $C_{11}H_{18}O_3$: C 66,64, H 9,15, O 24,21; trouvé : C 66,37, H 8,86, O 24,41.

(c) *(Méthoxy-2 éthyl)-3 cyclopentènecarboxylate-2 de tertiobutyle* **9**c

Cet ester a été préparé selon la méthode décrite par M. Yamaguchi et coll. (12).

À une solution de 2,65 g de chlorure d'acide **7** dans le benzène anhydre (50 mL) sont ajoutés, sous courant d'azote, le cyanure d'argent (3,75 g, 30 mmol) et l'alcool tertiobutylique (15 mL). Le mélange est porté à reflux pendant 1 h, puis filtré. Après évaporation du filtrat et élution sur gel de silice dans le mélange éther éthylique – hexane (1:4), on recueille 2,91 g (92%) d'ester **9***c* sous forme d'une huile jaune; pé 140°C/3 Torr; R_f 0,45 (éther éthylique – hexane, 1:4); ν_{max}(film) : 1710 (CO_2tBu), 1625 (C=C), 1120 (OCH_3) cm^{-1}; rmn 400 MHz ($CDCl_3$) δ : 6,67 (m, 1H, H-1), 3,42 (dd, 2H, J = 6,90 et 7,38 Hz, —CH_2OCH_3), 3,33 (s, 3H, —OCH_3), 2,94 (M, 1H, H-3), 2,49 et 2,41 (2m, 2H, (CH_2)-5), 2,08 (m, 2H, H-4a et H-1′a), 1,71 (m, 1H, H-4b), 1,54 (m, 1H, H-1′b), 1,49 (s, 9H, —$C(CH_3)_3$). *Anal.* calc. pour $C_{13}H_{22}O_3$: C 68,99, H 9,80, O 21,21; trouvé : C 68,62, H 9,50, O 21,44.

(Hydroxy-2 éthyl)-3 cyclopentènecarboxylate-2 d'éthyle **11**

À une suspension d'iodure de sodium (5,25 g, 35 mmol) dans l'acétonitrile (60 mL) sont ajoutés, sous courant d'azote, le trichlorométhylsilane (5,23 g, 35 mmol) et l'ester **9***b* (6 g, 30 mmol). Le mélange est agité à température ambiante pendant 8 h, puis hydrolysé par l'eau (60 mL). Après extraction par l'éther éthylique (3 × 50 mL), la phase organique est lavée par une solution saturée de thiosulfate de sodium (30 mL) puis par l'eau (30 mL), séchée et évaporée. Après élution sur gel de silice par le mélange éther éthylique – hexane (4:1), on obtient 4 g (72%) d'ester alcool **11** sous forme d'une huile incolore; pé 143°C/1 Torr; R_f 0,23 (éther éthylique – hexane, 1:1); ν_{max}(film) : 3420 (OH), 1715 (CO_2Et), 1620 (C=C) cm^{-1}; rmn 400 MHz ($CDCl_3$) δ : 6,81 (m, 1H, H-1), 4,20 (q, 2H, J = 6,90 Hz, —$CO_2CH_2CH_3$), 3,64 (m, 2H, —CH_2OH), 3,08 (M, 1H, H-3), 2,50 (m, 2H, (CH_2)-5), 2,17 (m, 2H, H-4a et H-1′a), 1,84 (m, 1H, H-4b), 1,65 (m, 1H, H-1′b), 1,30 (t, 3H, J = 6,90 Hz, —$CO_2CH_2CH_3$). *Anal.* calc. pour $C_{10}H_{16}O_3$: C 65,21, H 8,70, O 26,08; trouvé : C 65,43, H 8,73, O 25,84.

Acide (iodo-2 éthyl)-3 cyclopentènecarboxylique-2 **12**

À une suspension d'iodure de sodium (1,35 g, 9 mmol) dans l'acétonitrile (15 mL) sont ajoutés, sous courant d'azote, l'ester **9***c* (0,60 g, 3 mmol) puis le triméthylchlorosilane (0.98 g, 9 mmol). Le mélange est porté à reflux pendant 16 h, puis hydrolysé par 15 mL d'eau. Après extraction par l'éther éthylique (3 × 10 mL), la phase organique est lavée par une solution saturée de thiosulfate de sodium (10 mL) puis par l'eau (10 mL), séchée et évaporée. On recueille 0,56 g (70%) de l'iodo-acide **12** recristallisé dans le cyclohexane; pf 104°C; R_f 0,30 (éther éthylique – hexane, 1:1); ν_{max}(KBr) : 3240 (OH), 1670 (CO_2H), 1625 (C=C); rmn 400 MHz ($CDCl_3$) δ : 6,97 (m, 1H, H-1), 3,25 (td, 1H, J = 4,75 et 9,63 Hz, H-2′a), 3,12 (td, 1H, J = 7,52 et 9,63 Hz, H-2′b), 3,00 (M, 1H, H-3), 2,51 (m, 2H, (CH_2)-5), 2,43 (m, 1H, H-4a), 2,17 (m, 1H, H-1′a), 1,80 (m, 1H, H-4b), 1,70 (m, 1H, H-1′b). *Anal.* calc. pour $C_8H_{11}O_2I$: C 36,00, H 4,13, I 47,74; trouvé : C 36,47, H 4,18, I 47,68.

Acide (méthoxy-2 éthyl)-3 cyclopentènecarboxylique-2 ***10***

À une solution d'ester **9***b* (1,21 g, 6,1 mmol) dans le DMSO (50 mL) est ajoutée une solution de potasse 2 *N* (20 mL). On chauffe pendant 4 h à 100°C. La solution est ensuite hydrolysée par l'eau (50 mL), puis extraite par l'éther éthylique (3 × 15 mL). La phase aqueuse est alors acidifiée par HCl concentré, puis à nouveau extraite par l'éther éthylique (3 × 20 mL). Cette dernière phase organique lavée jusqu'à neutralité, séchée, puis évaporée, abandonne 0,83 g (80%) de l'acide **10** sous forme d'un liquide incolore; ν_{max}(film) : 3240 (OH), 1685 (CO_2H), 1620 (C=C), 1114 (OCH_3) cm^{-1}; rmn 400 MHz ($CDCl_3$) δ : 6,92 (m, 1H, H-1), 3,44 (dd, 2H, J = 6,40 et 7,38 Hz, $-CH_2OCH_3$), 3,33 (s, 3H, —OCH_3), 3,02 (M, 1H, H-3), 2,50 (m, 2H, (CH_2)-5), 2,13 (m, 2H, H-4a et H-1′a), 1,75 (m, 1H, H-4b), 1,53 (m, 1H, H-1′b). *Anal.* calc. pour $C_9H_{14}O_3$: C 63,51, H 8,29, O 28,20; trouvé : C 63,39, H 8,40, O 28,28.

Hexahydro-1,3,4,4a,5,6 cyclopenta[c]pyrannone-1 ***1***

Cette lactone a été isolée soit à partir de l'ester **9***c*, soit à partir de l'acide **12**.

(a) *Synthèse à partir de l'ester* **9**c

À une suspension d'iodure de sodium (12,1 g, 81 mmol) dans l'acétonitrile (60 mL) sont ajoutés, sous courant d'azote, le trichlorométhylsilane (12,1 g, 81 mmol) et l'ester **9***c* (7 g, 31 mmol). Le mélange est porté à reflux pendant 24 h. On ajoute 50 mL d'eau puis on extrait par l'éther éthylique (3 × 50 mL). La phase organique est lavée par une solution saturée de thiosulfate de sodium (30 mL) puis par l'eau (30 mL), séchée et évaporée. L'huile obtenue est purifiée par chromatographie sous pression moyenne sur gel de silice avec le mélange éther éthylique – hexane (1 : 1). On isole ainsi 1,9 g (44%) de lactone **1**, sous forme d'une huile; pé 130°C/0,1 Torr; R_f 0,30 (éther éthylique – hexane, 1 : 1); ν_{max}(film) : 1721 (CO_2—), 1630 (C=C) cm^{-1}; rmn 400 MHz ($CDCl_3$) δ : 6,99 (m, 1H, H-7), 4,46 et 4,31 (2m, 2H, $J_{3\alpha4\beta}$ = 4,65, $J_{3\alpha4\alpha}$ = 2,05, $J_{3\beta4\alpha}$ = 2,76, $J_{3\beta4\beta}$ = 12,37 et $J_{3\alpha3\beta}$ = 11,47 Hz, (CH_2)-3), 2,98 (M, 1H, H-4a), 2,46 (m, 2H, (CH_2)-6), 2,37 (m, 1H, H-5α), 2,11 (m, 1H, H-4α), 1,66 (m, 2H, H-5β et H-4β); spectre de masse : $M^{+\bullet}$ 138 (69%), 108 (34), 94 (40), 80 (100). *Anal.* calc. pour $C_8H_{10}O_2$: C 69,56, H 7,25, O 23,19; trouvé : C 69,30, H 7,38, O 23,32.

(b) *Synthèse à partir de l'acide* **12**

À une solution de l'acide **12** (0,2 g, 0,75 mmol) dans l'acétonitrile (10 mL) on ajoute, sous courant d'azote, le perchlorate d'argent monohydraté (0,31 g, 1,5 mmol). On agite durant 48 h à température ambiante; le précipité obtenu est filtré et la phase organique est lavée à l'eau (3 × 20 mL) puis par une solution saturée en NaCl, séchée et évaporée. On recueille ainsi 93 mg (90%) de lactone **1**.

Préparation des esters ***13*** *et* ***14***

(a) *Action de l'éthanol sur le chlorure d'acide* **8**

Une solution de 3,58 g de chlorure d'acide **8** dans 200 mL d'éthanol est portée à reflux pendant 1 h. Après évaporation de l'éthanol, le résidu est élué sur gel de silice par le mélange éther éthylique – hexane (1 : 4) et on recueille dans l'ordre : 0,64 g (15%) de (chloro-2 éthyl)-3 (cyclopentényl-1′)-3 cyclopentènecarboxylate-2 de méthyle, **14**; pé 130°C/0,05 Torr; R_f 0,58 (éther éthylique – hexane, 1 : 4); ν_{max}(film) : 1718 (CO_2Me), 1620 (C=C), 655 (C—Cl) cm^{-1}; rmn 100 MHz ($CDCl_3$) δ : 6,87 (m, 1H, H-1), 5,37 (m, 1H, H-2′), 3,69 (s, 3H, —CO_2CH_3), 3,43 (m, 2H, —CH_2Cl), 2,65–1,60 (M, 12H, méthylènes cyclopenténiques et —CH_2CH_2Cl). *Anal.* calc. pour $C_{14}H_{19}O_2Cl$: C 66,14, H 7,48, O 12,59; trouvé : C 66,41, H 7,60, O 12,86; et 2,77 g (75%) de (cyclopentényl-1′)-3 (méthoxy-2 éthyl)-3 cyclopentènecarboxylate-2 d'éthyle, **13**; pé 135°C/0,05 Torr; R_f 0,37 (éther éthylique – hexane, 1 : 4); ν_{max}(film) : 1718 (CO_2Et), 1625 (C=C), 1114 (OCH_3) cm^{-1}; rmn 100 MHz ($CDCl_3$) δ : 6,84 (m, 1H, H-1), 5,35 (m, 1H, H-2′), 4,11 (q, 2H, J = 7,20 Hz, —$CO_2CH_2CH_3$), 3,34 (m, 2H, —CH_2OCH_3), 3,27 (s, 2H, —OCH_3), 2,43–1,60 (M, 12H, méthylènes cyclopenténiques et —$CH_2CH_2OCH_3$), 1,25 (t, 3H, J = 7,20 Hz, —$CO_2CH_2CH_3$). *Anal.* calc. pour $C_{16}H_{24}O_3$: C 72,69, H 9,15, O 18,16; trouvé : C 72,98, H 9,03, O 18,26.

(b) *Chauffage du chlorure d'acide* **8** *au reflux du benzène*

Une solution de 3,58 g de chlorure d'acide **8** dans le benzène (100 mL) est portée à reflux pendant 12 h. Après évaporation du solvant et purification sur gel de silice dans le mélange éther éthylique – hexane (1 : 4), on obtient 3,43 g (96%) du chloro-ester **14**.

Acide (cyclopentényl-1′)-3 (hydroxy-2 éthyl)-3 cyclopentènecarboxylique-2 ***15***

À une solution du composé **14** (0,3 g, 1,18 mmol) dans le DMSO (20 mL) est ajoutée une solution de potasse 2 *N* (5 mL). On porte à 100°C durant 4 h, puis on hydrolyse par l'eau (40 mL). La phase aqueuse est extraite par l'éther éthylique (3 × 10 mL), puis acidifiée par l'acide chlorhydrique concentré et extraite à nouveau par l'éther éthylique (3 × 20 mL). Cette dernière phase organique est lavée à l'eau (4 × 15 mL), séchée et évaporée. On recueille 0,21 g (80%) d'acide alcool **15**, recristallisé dans le benzène; pf 130°C; ν_{max}(KBr) : 3400 (OH), 1688 (CO_2H), 1618 (C=C) cm^{-1}; rmn 100 MHz ($CDCl_3$) δ : 7,00 (m, 1H, H-1), 5,40 (m, 1H, H-2′), 4,49 (M, 1H, —OH), 3,66 (m, 2H, —CH_2OH), 2,53–1,75 (M, 12H, méthylènes cyclopenténiques et —CH_2CH_2OH). *Anal.* calc. pour $C_{13}H_{18}O_3$: C 70,24, H 8,16, O 21,59; trouvé : C 69,89, H 8,29, O 21,82.

(Cyclopentényl-1′)-4a hexahydro-1,3,4,4a,5,6 cyclopenta[c]pyrannone-1 ***2***

On porte à reflux pendant 3 h dans un appareil Dean–Stark l'hydroxy-acide **15** (2,6 g, 11,7 mmol) dissous dans le benzène anhydre (100 mL) en présence d'acide *p*-toluènesulfonique (0,05 g). Le mélange réactionnel est versé sur de l'eau glacée et extrait par l'éther éthylique (3 × 50 mL). La phase organique est lavée à l'eau, séchée et évaporée. Le résidu élué sur gel de silice par le mélange éther éthylique – hexane (1 : 1) fournit, après recristallisation dans l'hexane, 1,90 g (80%) de lactone **2**; pf 74°C; R_f 0,41 (éther éthylique – hexane, 1 : 1); ν_{max}(KBr) : 1709 (CO_2—), 1630 (C=C) cm^{-1}; rmn 400 MHz ($CDCl_3$) δ : 7,00 (m, 1H, H-1), 5,38 (m, 1H, H-2′), 4,29 et 4,16 (2m, 2H, $J_{3\alpha4\beta}$ = 4,89, $J_{3\alpha4\alpha}$ = 1,60, $J_{3\beta4\alpha}$ = 2,84, $J_{3\beta4\beta}$ = 13,06 et $J_{3\alpha3\beta}$ = 11,36 Hz, (CH_2)-3), 2,41–1,62 (M, 12H, méthylènes cyclopenténiques et —CH_2CH_2O—); spectre de masse : $M^{+\bullet}$ 204 (100%), 176 (43), 148 (40). *Anal.* calc. pour $C_{13}H_{16}O_2$: C 76,47, H 7,84, O 15,69; trouvé : C 76,89, H 7,68, O 15,54.

(Cyclopentényl-1′)-3 (phtalimido-2 éthyl)-3 cyclopentènecarboxylate-2 de méthyle ***16***

À une solution du composé **14** (0,5 g, 1,97 mmol) dans le DMF (diméthylformamide) anhydre (10 mL) sont ajoutés, sous courant d'argon, le phtalimide de potassium (0,46 g, 2,5 mmol) et l'iodure de sodium (0,45 g, 3 mmol). On chauffe à 100°C durant 24 h. On hydrolyse par l'eau (30 mL) et extrait la phase aqueuse par l'éther éthylique (3 × 15 mL). La phase organique est lavée à l'eau, séchée et évaporée. Après élution sur gel de silice par le mélange éther éthylique – hexane (1 : 1), on obtient 0,3 g (42%) du phtalimide **16** recristallisé dans l'éthanol; pf 118°C; R_f 0,42 (éther éthylique – hexane, 1 : 1); ν_{max}(KBr) : 1771 (imide), 1711 (CO_2Me), 1614 (C=C), 1608 (aromatique); rmn 100 MHz ($CDCl_3$) δ : 7,82 et 7,69 (2m, 4H, aromatiques), 6,88 (m, 1H, H-1), 5,45 (m, 1H, H-2′), 3,65 (s, 3H, —CO_2CH_3), 3,64 (m, 2H, —CH_2N—), 2,58–1,63 (M, 12H, méthylènes cyclopenténiques et —CH_2CH_2N—). *Anal.* calc. pour $C_{22}H_{23}NO_4$: C 72,33, H 6,30, N 3,83, O 17,53; trouvé : C 72,25, H 6,39, N 3,75, O 17,77.

(Cyclopentényl-1′)-4a hexahydro-1,3,4,4a,5,6 2H*-cyclopenta[c]-pyridinone-1* ***17***

À une solution du composé **16** (1,5 g, 4,1 mmol) dans le méthanol (20 mL) est ajoutée une solution aqueuse d'hydrate d'hydrazine (13,7 mmol). On agite pendant 3 h à température ambiante, puis on ajoute une solution de 6,9 mL d'acide acétique dans 30 mL de méthanol. On agite pendant 5 min à 20°C et filtre le précipité formé. Après évaporation du filtrat, on ajoute 40 mL de CH_2Cl_2. La phase organique est lavée par une solution saturée de $NaHCO_3$ puis par l'eau, séchée et évaporée. L'huile obtenue est purifiée par chromatographie sous pression moyenne sur gel de silice à l'aide du mélange éther éthylique – hexane (1 : 1). On isole, après recristallisation dans le benzène, 0,2 g (24%) de lactame **17**; pf 200°C; R_f 0,17 (éther éthylique – hexane, 4 : 1); ν_{max}(KBr) : 3200 (NH), 1656 et 1639 (CONH—)

TABLEAU 2. Coordonnées fractionnaires des atomes de carbone et d'oxygène

Atome	x/a	y/b	z/c	B_{eq} (Å^2)
O(1)	0,9193(2)	0,3295(5)	0,5338(1)	5,16
O(2)	0,8543(2)	0,0307(5)	0,5330(1)	4,70
C(1′)	0,7868(2)	0,0168(6)	0,3662(2)	3,32
C(1)	0,8956(2)	0,1734(7)	0,5032(2)	3,70
C(2′)	0,7633(3)	0,2150(7)	0,3545(2)	4,3
C(3′)	0,6821(3)	0,2352(9)	0,3174(3)	5,6
C(3)	0,8190(3)	−0,1586(8)	0,5000(2)	4,9
C(4a)	0,8671(2)	−0,0566(6)	0,3994(2)	3,45
C(4′)	0,6586(3)	0,008(1)	0,3065(4)	8,5
C(4)	0,8610(3)	−0,2374(7)	0,4472(2)	4,5
C(5)	0,9231(3)	−0,0993(9)	0,3491(3)	5,5
C(5′)	0,7236(3)	−0,1351(8)	0,3370(3)	5,2
C(6)	0,9691(3)	0,109(1)	0,3454(3)	6,8
C(7a)	0,9105(2)	0,1221(6)	0,4384(2)	3,45
C(7)	0,9643(3)	0,2114(8)	0,4086(2)	5,0

cm^{-1}; rmn 400 MHz (acétone-d_6, D_2O) δ : 6,55 (m, 1H, H-1), 5,26 (m, 1H, H-2′), 3,24 (m, 1H, $J_{3\alpha3\beta}$ = 12,70, $J_{3\alpha4\alpha}$ = 5,30 et $J_{3\alpha4\beta}$ = 1,90 Hz, H-3α), 3,12 (m, 1H, $J_{3\alpha3\beta}$ = 12,70, $J_{3\beta4\alpha}$ = 12,70 et $J_{3\beta4\beta}$ = 3,69 Hz, H-3β), 2,33–1,64 (M, 12H, méthylènes cyclopenténiques et —CH_2CH_2NH—). *Anal.* calc. pour $C_{13}H_{17}NO$: C 76,81, H 8,43, N 6,89, O 7,87; trouvé : C 76,80, H 8,53, N 6,77, O 7,71.

Analyse radiocristallographique du composé **2**

$C_{13}H_{16}O_2$ M = 204

Monoclinique $I2/c$ ($h + k + l = 2n$; $h0l$, $l = 2n$); a = 17,144(7), b = 6,274(3), c = 20,977(7) Å; β = 98,66(3)°; V = 2231 Å^3; Z = 8; ρ_c = 1,21 g/cm^3; F (0, 0, 0) = 880; μ (MoKα) = 0,45 cm^{-1}.

Les cristaux du composé **2** ont été obtenus par recristallisation dans l'hexane. Après de multiples essais, un cristal de taille 0,2 × 0,4 × 0,1 mm a été utilisé pour enregistrer, sur un diffractomètre automatique CAD4 Enraf–Nonius, 2310 réflexions avec le rayonnement Kᾱ du molybdène monochromatisé au graphite ($1 < 2\theta < 60°$, largeur de balayage (0,90 + 0,35 tan θ)°). Seules 935 réflexions ont été conservées pour affiner la structure répondant au critère statistique $I > 3{,}3\sigma(I)$. Les intensités ont été corrigées des phénomènes de Lorentz et de polarisation, l'absorption a été négligée. L'ensemble des réflexions a été renormalisé par suite de la décomposition du cristal ($\Delta I_c/I_c$ = 0,25 à la fin de l'enregistrement) en ajustant une droite au sens des moindres carrés à l'intensité de deux réflexions de contrôle (312, 112). La structure a été résolue dans le groupe $I2/c$ (x, y, z; $\bar{x}, \bar{y}, \bar{z}$; $x, \bar{y}, 1/2 + z$; $\bar{x}, y, 1/2 - z$; $+1/2, 1/2, 1/2$) pour conserver un angle β proche de 90°. Les coordonnées fractionnaires des atomes de carbone et d'oxygène ont été déterminées à l'aide du programme MULTAN (13). Au cours de l'affinement (SHELX 76 (14)), chaque atome non-hydrogène a été affecté d'un coefficient d'agitation thermique anisotrope. L'ensemble des atomes d'hydrogène a été trouvé dans les sections de la différence de la densité électronique et affiné avec un facteur d'agitation thermique isotrope. L'affinement a convergé jusqu'aux indices suivants : $R(F)$ = 0,057; $R_w(F)$ = 0,051;[3] $R(F^2)$ = 0,058; S = 1,47;[3] N_p = 198; N_o = 935; $w = 1{,}7/[\sigma^2(F) + 0{,}0016\,F^2]$; max Δ/σ = 0,23 pour z de C(11); ρ résiduelle maximum = 0,2 ē/Å^3.

Les coordonnées fractionnaires des atomes autres que les atomes d'hydrogène sont rassemblées dans le tableau 2. La numérotation des atomes est visualisée en figure 5. Les coordonnées fractionnaires des atomes d'hydrogène, les facteurs d'agitation thermique et une liste des facteurs de structure ont été déposés sous forme de matériel supplémentaire.[4]

1. J. C. CAILLE, M. FARNIER et R. GUILARD. Can. J. Chem. **64**, 824 (1986).
2. (*a*) R. H. SHAPIRO. Org. React. **23**, 405 (1976); (*b*) M. F. LIPTON et R. H. SHAPIRO. J. Org. Chem. **43**, 1409 (1978).
3. R. M. ADLINGTON et A. G. M. BARRETT. J. Chem. Soc. Chem. Commun. 1071 (1978).
4. A. F. THOMAS. *Dans* The total synthesis of natural products. Vol. 2. *Éditeur* : J. ApSimon. Wiley – Interscience, New York. 1973. p. 62 et références citées.
5. J. C. CAILLE et R. GUILARD. Tetrahedron Lett. 2771 (1984).
6. K. MORI, T. TAKIGAWA et M. MATSUI. Tetrahedron Lett. 3953 (1976).
7. P. A. GRIECO, M. NISHIZAWA, T. OGURI, S. D. BURKE et N. MARINOVIC. J. Am. Chem. Soc. **99**, 5773 (1977).
8. G. A. OLAH, S. C. NARANG, B. G. BALARAM GUPTA et R. MALHOTRA. J. Org. Chem. **44**, 1247 (1979).
9. G. A. OLAH, A. HUSAIN, B. G. BALARAM GUPTA et S. C. NARANG. Angew. Chem. Int. Ed. Engl. **20**, 690 (1981); G. A. OLAH, A. HUSAIN, B. P. SINGH et A. K. MEHROTRA. J. Org. Chem. **48**, 3667 (1983).
10. J. T. SHARP, R. H. FINDLAY et P. B. THOROGOOD. J. Chem. Soc. Perkin Trans. 1, 102 (1975).
11. K. KUROSAWA, H. OBARA et H. UDA. Bull. Chem. Soc. Jpn. **39**, 530 (1966).
12. S. TAKIMOTO, J. INANAGA, T. KATSUKI et M. YAMAGUCHI. Bull. Chem. Soc. Jpn. **49**, 2335 (1976).
13. P. MAIN, M. M. WOOLFSON, L. LESSINGER, G. GERMAIN et J. P. DECLERCQ. MULTAN. A system of computer programs for the automatic solution of crystal structures from X-ray diffraction data. York University, Angleterre et Université de Louvain, Belgique. 1974.
14. G. M. SHELDRICK. Programs for crystal structure determination. Cambridge University, Angleterre. 1976.

3. $R_w(F) = \Sigma_H\, w^{1/2}|(F_o - F_c)|/\Sigma_H\, w^{1/2}F_o$; $S = [\Sigma\, w(F_o - F_c)^2 \div (m - n)]^{1/2}$.

4. On peut acheter ces données en s'adressant au Dépôt des données non publiées, ICIST, Conseil national de recherches du Canada, Ottawa (Ontario), Canada K1A 0S2.

The structures of huperzine A and B,[1] two new alkaloids exhibiting marked anticholinesterase activity

JIA-SEN LIU[2] AND YUAN-LONG ZHU
Shanghai Institute of Materia Medica, Academia Sinica, Shanghai, 200031, China
AND
CHAO-MEI YU, YOU-ZUO ZHOU, YAN-YI HAN, FENG-WU WU, AND BAO-FENG QI
Institute of Materia Medica, Zhejiang Academy of Medicine, Hangzhou, China
Received November 12, 1985

JIA-SEN LIU, YUAN-LONG ZHU, CHAO-MEI YU, YOU-ZUO ZHOU, YAN-YI HAN, FENG-WU WU, and BAO-FENG QI. Can. J. Chem. **64**, 837 (1986).

Huperzine A and B, two new Lycopodium alkaloids isolated from *Huperzia serrata* (Thunb.) Trev., are shown to possess structures **1** and **3**, respectively, on the basis of chemical and spectroscopic data.

JIA-SEN LIU, YUAN-LONG ZHU, CHAO-MEI YU, YOU-ZUO ZHOU, YAN-YI HAN, FENG-WU WU et BAO-FENG QI. Can. J. Chem. **64**, 837 (1986).

En se basant sur des données chimiques et spectroscopiques, on démontre que les deux nouveaux alkaloïdes du Lycopodium, les huperzines A et B, qui ont été isolés du *Huperzia serrata* (Thunb.) Trev., possèdent respectivement les structures **1** et **3**.
[Traduit par la revue]

Huperzine A (**1**) and B (**3**), two new Lycopodium alkaloids, were isolated from *Huperzia serrata* (Thunb.) Trev. = *Lycopodium serratum* Thunb., a Chinese folk medicine. They exhibit strong anticholinesterase activity in pharmacological studies (1) and markedly increase efficiency for learning and memory in animals.[3] Presently, the use of huperzine A in the treatment of myasthenia gravis (2), Alzheimer's dementia, and for the improvement of senile memory loss are under clinical investigation. In this paper we report chemical studies on the structures of huperzine A and B.

Huperzine A (**1**), $C_{15}H_{18}N_2O$ (M^+ 242.1426), mp 230°C, $[\alpha]_D^{24.5}$ −150.4° (*c* 0.498, MeOH), shows the characteristics of an α-pyridone in its uv spectrum (λ_{max} (EtOH) nm (log ε): 231 (4.01), 313 (3.89)), ir spectrum (3180, 1650, 1615, 1550 cm^{-1}), and ^1H nmr spectrum (see Table 1). Dehydrogenation of huperzine A over Pd/C at 300°C affords 6-methyl-2(1*H*)-pyridone, further attesting to the presence of an α-pyridone ring in the molecule. The presence of an endocyclic double bond and an exocyclic double bond as revealed in the ^1H and ^{13}C nmr spectra of huperzine A (Tables 1, 2), as well as the similarity of its mass spectrum with that of selagine (3), indicate that the structure of huperzine A (**1**) closely resembles that of the known alkaloid selagine (**2**) (4). The specific rotation (−99° in MeOH) of selagine (4) is much less than that of huperzine A. The olefinic proton of the endocyclic double bond in the ^1H nmr of 11,12-dihydroselagine appears as a singlet (4), while in the ^1H nmr of huperzine A (**1**) or in the ^1H nmr of 11,12-dihydrohuperzine A the olefinic proton appears as a doublet. This clearly accounts for the structural differences between **2** and **1** and

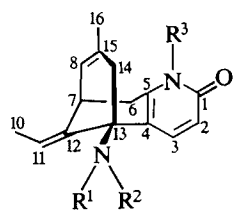

1 $R^1 = R^2 = R^3 = H$
1*a* R^1 = Me, $R^2 = R^3 = H$
1*b* $R^1 = R^2$ = Me, $R^3 = H$
1*c* $R^1 = R^2 = R^3$ = Me
1*d* R^1 = Ac, $= R^2 = R^3 = H$

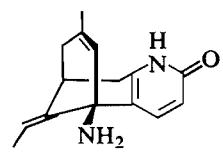

2

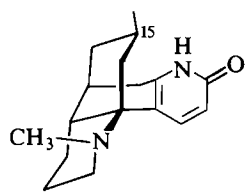

4

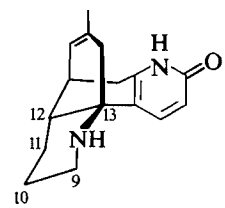

3

indicates the presence of a vicinal methine coupled to the olefinic proton in compound **1**. This partial structure can be accommodated in the molecule if the endocyclic double bond is located at C-8,C-15 with the olefinic proton at C-8. Corroborative evidence for the proposed structure is available from ^1H–{^1H} decoupling experiments and nOe (nuclear Overhauser effect) measurements. Irradiation at H-7 leads to simultaneous decoupling of H-8 and H-6, while irradiation at H-14 produces a 12.2% nOe enhancement at H-3.

Methylation of huperzine A with methyl iodide, formic acid/formaldehyde, and dimethyl sulfate provides *N*-monomethylhuperzine A (**1***a*), mp 235–236°C; *N,N*-dimethylhuperzine A (**1***b*), mp 243–245°C; and *N,N,N*-trimethylhuperzine A (**1***c*), viscous oil, respectively. Acetylation of **1** in Ac_2O/Py furnishes *N*-acetylhuperzine A (**1***d*), mp 276–277°C. Catalytic hydrogenation of **1** with Pt/EtOH gives 11,12-dihydrohuperzine A,

[1]Presented in part at the International Symposium on Organic Chemistry of Medicinal Natural Products (IUPAC), Shanghai, China, November 1985. After submission of the manuscript to the symposium, we found that an analogous alkaloid named isoselagine had been reported (9). From the published data, we conclude that huperzine A is not identical with isoselagine and that the latter may be the *Z* isomer of huperzine A.

[2]Author to whom correspondence should be addressed

[3]X-C. Tang. Personal communication.

TABLE 1. ^{1}H nuclear magnetic resonance data* of huperzine A (**1**) and B (**3**)

1 (100 MHz)		**3** (400 MHz)	
H-2	6.38, d, $J_{2,3} = 9$	H-2	6.43, d, $J_{2,3} = 9.3$
H-3	7.84, d, $J_{2,3} = 9$	H-3	7.68, d, $J_{2,3} = 9.3$
H-6	2.76, 2H, AB part of ABX, $J_{6\alpha,6\beta} = 16$, $J_{6\alpha,7} = 3$, $J_{6\beta,7} \cong 0$	H-6α	2.85, dd, $J_{6\alpha,6\beta} = 17.8$, $J_{6\alpha,7} = 5.4$
		H-6β	2.43, d, $J_{6\alpha,6\beta} = 17.8$, $J_{6\beta,7} \cong 0$
H-7	3.56, m	H-7	2.34, ddd, $J_{7,12} = 3.6$, $J_{7,8} = 4.7$, $J_{6\alpha,7} = 5.4$
H-8	5.38, d, $J_{7,8} = 5$	H-8	5.43, bd, $J_{7,8} = 4.7$
		H-9α	2.29, ddd, $J_{9\alpha,9\beta} = 13.5$, $J_{9\alpha,10\beta} = 12.5$, $J_{9\alpha,10\alpha} = 1.7$
		H-9β	2.74, ddd, $J_{9\alpha,9\beta} = 13.5$, $J_{9\alpha,10\beta} = 3.3$, $J_{9\beta,10\alpha} = 1.7$
H-10	1.62, 3H, d, $J_{10,11} = 7$	H-10α	1.54†
		H-10β	1.43, ddddd, $J_{10\beta,10\alpha} = J_{10\beta,11\alpha} = J_{10\beta,9\alpha} = 12.5$, $J_{10\beta,9\beta} = J_{10\beta,11\beta} = 3.3$
H-11	5.46, q, $J_{10,11} = 7$	H-11α	1.22, dddd, $J_{11\alpha,10\alpha} = 3.8$, $J_{11\alpha,12} = J_{11\alpha,11\beta} = J_{11\alpha,10\beta} = 12.5$
		H-11β	1.54†
		H-12	1.67, ddd, $J_{11\alpha,12} = 12.5$, $J_{11\beta,12} = J_{7,12} = 3.6$
H-14	2.12, 2H, s	H-14$_{endo}$	1.83, d, $J_{14,14} = 16.5$
		H-14$_{exo}$	2.02, d, $J_{14,14} = 16.5$
H-16	1.46, 3H, s	H-16	1.59, 3H, s
NH (in pyridone)	13.20, bs	NH (in pyridone)	13.20, bs

*In $CDCl_3$; chemical shifts, δ, in ppm relative to internal TMS; coupling constants, J, in Hz. The assignments are based on ^{1}H–{^{1}H} selective decoupling experiments.
†Overlapping signals.

TABLE 2. Carbon-13 chemical shifts* of huperzine A (**1**) and B (**3**)

Carbon	δ (multiplicity) **1** (22.63 MHz)	**3** (25.18 MHz)
1	165.52 (s)	165.39 (s)
2	116.97 (d)	117.90 (d)
3	140.25 (d)	140.37 (d)
4	122.95 (s)	117.90 (s)
5	142.59 (s)	143.27 (s)
6	35.24 (t)	29.45 (t)
7	32.95 (d)	34.59 (d)
8	124.36 (d)	126.12 (d)
9		48.03 (t)
10	12.31 (q)	25.34† (t)
11	111.23 (d)	28.13† (t)
12	143.30 (s)	40.70 (d)
13	54.35 (s)	53.22 (s)
14	49.25 (t)	41.67 (t)
15	134.09 (s)	132.23 (s)
16	22.57 (q)	22.68 (q)

*In $CDCl_3$, relative to internal TMS.
†May be interchanged.

mp 269–270°C, while use of Pt/AcOH gives tetrahydrohuperzine A, mp 264–265°C.

Examination of the ^{1}H nmr of huperzine A and its derivatives shows a remarkable upfield shift of the signals for H-3 and H-11 of 0.30 and 0.11 ppm in *N*-monomethylhuperzine A (**1***a*) and of 0.44 and 0.14 ppm in *N*-acetylhuperzine A (**1***d*). The remaining protons do not show any significant shift relative to the corresponding protons of huperzine A. This information reveals a close spatial relationship between H-3, H-11 and the *N*-methyl or the *N*-acetyl group, i.e., the exocyclic double bond of huperzine A has an *E* configuration. This assignment was confirmed by nOe experiments. Enhancements at H-7 of 11.7% upon irradiation of H-10 and 8.3% upon irradiation of H-6 were observed. Selagine (**2**) (5) has a *Z* configuration of the exocyclic double bond.

Huperzine B (**3**), $C_{16}H_{20}N_2O$ (M^+ 256.1558), mp 270–271°C, $[\alpha]_D^{25}$ −54.2° (*c* 0.203, MeOH), also possesses an α-pyridone and a C-8,C-15 endocyclic double bond. It is characterized by its uv spectrum (λ_{max} (MeOH) nm (log ε): 231 (3.95), 312 (3.85)), ir spectrum (3100, 1670, 1620, 1610, 1560 cm^{-1}), and ^{1}H and ^{13}C nmr spectra (see Tables 1, 2). The notable difference between **1** and **3** is the absence of signals corresponding to an exocyclic double bond in the ^{1}H and ^{13}C nmr spectra of **3**. Methylation of **3** with formic acid/formaldehyde provides *N*-methylhuperzine B, mp 272–273°C, a compound the spectral characteristics of which closely resemble those of the known alkaloid β-obscurine **4** (6). Dehydrogenation of huperzine B with Pd/C at 300°C furnishes 7-methylquinoline and 6-methyl-2(1*H*)-pyridone, providing further evidence that huperzine B possesses structure **3**.

An attempt to transform *N*-methylhuperzine B to β-obscurine by hydrogenation was unsuccessful. Hydrogenation of an acetic acid solution of *N*-methylhuperzine B in the presence of Pt gave a single product in nearly quantitative yield. The product was identified as 15-epi-β-obscurine, mp 281–283°C, characterized by the high-field chemical shift (δ 0.60) of the C-15 methyl in its ^{1}H nmr (7). This result suggests that, in *N*-methylhuperzine B, H-12 is β since in this configuration hydrogen addition to the C-8,C-15 double bond should proceed to produce 15-epi-β-obscurine. The stereochemistry at C-12 is verified by nOe experiments. Irradiation at H-12, H-10β, and H-11α causes a 7.9, 7.4, and 10.6% enhancement at H-14$_{exo}$, H-12, and H-6α, respectively, indicating the close spatial relationship between H-12, H-14$_{exo}$, and H-10β, and between H-11α and H-6α. The ^{1}H nmr line-broadening effect (8) in chloroform-*d* containing a trace of acid, which causes signals of H-12, H-14$_{exo}$, and H-10β to broaden and to shift downfield 0.21, 0.27, and 0.19 ppm respectively, also leads to the conclusion about the configuration of the three protons spatially close to the nitrogen lone-pair electrons, i.e., that H-12 is β configuration.

The assignment of absolute configuration for the bridgehead carbons C-13 and C-7 rests on the comparison of cd (circular dichroism) curves of 15-epi-β-obscurine derived from huperzine B **3** with that of β-obscurine **4**, a compound of known configuration (6). The cd curve of 15-epi-β-obscurine closely resembles that of β-obscurine except in the amplitude of the first Cotton effect at 310 nm. This phenomenon is also observed when the cd of huperzine B and 11,12-dihydrohuperzine A are compared, demonstrating that the configurations of the bridgehead carbons in β-obscurine, huperzine B, and huperzine A are similar. Thus, the 7*R*,13*R*,11*E* configuration may be assigned to huperzine A, and 7*S*,13*R*,12*R* to huperzine B.

Acknowledgements

The authors are deeply grateful to Professor William A. Ayer for providing an authentic sample of β-obscurine and for helpful discussion.

1. Y-E. Wang, D-X. Yue, and X-C. Tang. Acta Pharmacol. Sin. **7**, 109 (1986).
2. Y-C. Cheng, C-Z. Lu, Z-L. Ying, W-Y. Ni, C-L. Zhang, and G-W. Sang. New Drugs Clin. Rem. In press.
3. D. B. MacLean. Can. J. Chem. **41**, 2654 (1963).
4. Z. Valenta, H. Yoshimura, E. F. Rogers, M. Ternbah, and K. Wiesner. Tetrahedron Lett. 26 (1960).
5. M. Shamma, C. D. Jones, and J. A. Weiss. Tetrahedron, **25**, 4347 (1969).
6. W. A. Ayer, J. A. Berezowsky, and G. G. Iverach. Tetrahedron, **18**, 567 (1962).
7. F. A. L. Anet. Can. J. Chem. **39**, 2262 (1961).
8. R-S. Xu, Y-J. Lu, J-H. Chu, T. Iwashita, H. Naoki, Y. Naya, and K. Nakanishi. Tetrahedron, **38**, 2667 (1982).
9. C-H. Chen and S-S. Lee. J. Taiwan Pharm. Assoc. **36**, 1 (1984).

The reduction of (1-(4-cyanophenyl)-3-hydroxy-2-buten-1-one-*N*)pentaamminecobalt(III) by chromium(II)

ROBERT J. BALAHURA[1] AND A. JOHNSTON

Guelph–Waterloo Centre for Graduate Work in Chemistry, Department of Chemistry and Biochemistry, University of Guelph, Guelph, Ont., Canada N1G 2W1

Received June 3, 1985[2]

ROBERT J. BALAHURA and A. JOHNSTON. Can. J. Chem. **64**, 841 (1986).

The reduction of the title compound,

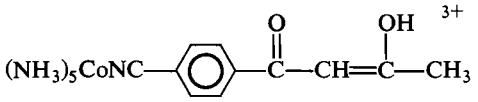

1

by chromium(II) is first order in Cr(II) and obeys the rate law $k_{obsd} = k_1K_a'/(K_a' + [H^+])$ at 25.0°C and $I = 1.0\,mol\,L^{-1}$ ($LiClO_4$) with $k_1 = (2.9 \pm 0.1) \times 10^4\,L\,mol^{-1}\,s^{-1}$ and $K_a' = 0.86 \pm 0.03\,mol\,L^{-1}$. In the rate law, k_1 refers to reduction of the 3+ ion above and the K_a' is the acid dissociation constant for the protonated form of **1**. The reduction occurs by a remote attack inner-sphere mechanism with complete transfer of the organic ligand to chromium.

ROBERT J. BALAHURA et A. JOHNSTON. Can. J. Chem. **64**, 841 (1986).

Le composé **1** mentionné dans le titre

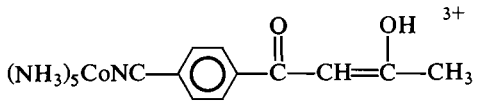

1

est réduit par le chrome(II); la réaction est du premier ordre en Cr(II) et, à 25,0°C, elle obéit à la loi de vitesse $k_{obs} = k_1K_a'/(K_a' + [H^+])$ alors que $I = 1,0\,mol\,L^{-1}$ ($LiClO_4$), $k_1 = (2,9 \pm 0,1) \times 10^4\,L\,mol^{-1}\,s^{-1}$ et $K_a' = 0,86 \pm 0,03\,mol\,L^{-1}$. Dans l'équation de vitesse, k_1 se rapporte à la réduction de l'ion 3+ mentionné plus haut alors que K_a' représente la constante de dissociation de la forme protonée du composé **1**. La réduction se produit par un mécanisme d'attaque à distance de la couche interne avec un transfert complet du ligand organique vers le chrome.

[Traduit par la revue]

Introduction

Electron transfer via "remote" substituents has been shown to occur in a wide variety of systems (1–5). For reduction of $(NH_3)_5CoNC—C_6H_4—R$ complexes by chromium(II), inner-sphere remote attack by the reductant takes place for R = CN (6), $C(O)CH_3$ (7), CHO (6), CO_2^- (8), and O^- (9). In all of these cases, the second-order rate constant determined is a composite of k_{et} (intramolecular electron transfer) and K_p (formation of precursor complex), which, in general, cannot be separated. However, for reduction of $(NH_3)_5CoNCacac^{2+}$, where NCacac = 3-cyano-2,4-pentanedionate, by chromium(II), saturation behaviour was observed with respect to the reductant concentration and individual values of k_{et} and K_p were obtained (10). This behaviour was attributed to three features of the remote β-diketonate group: (*1*) the large affinity of Cr^{2+} for hard oxygen donors, (*2*) the formation of a "stable" chelate with the reductant, and (*3*) a reduction of electrostatic repulsion by the presence of the delocalized negative charge.

In extending these studies, we attempted the synthesis of an analogous complex, $(NH_3)_5CoNC—C_6H_4—C(O)—acac^{2+}$. This preparation resulted in the isolation of **1**

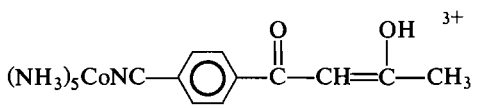

1

where a $COCH_3$ fragment has been lost. In this paper we wish to report on the preparation, characterization, and chromium(II) reduction of **1**.

Experimental

All reagent solutions were prepared in water that was deionized and distilled from alkaline permanganate in an all-glass apparatus. All metal salts, solvents, and organic starting materials were of reagent grade and used without further purification. Chromium(II) solutions were prepared as previously described (11). All kinetic measurements were performed on a Dionex model D-100 stopped-flow spectrophotometer interfaced with a digital storage unit. Reactions were carried out under pseudo-first-order conditions with the ratio Cr(II)/Co(III) > 15 at 314 and 360 nm. Observed rate constants were obtained directly from the exponential decay traces by curve matching with a calibrated decay generator.

The pK_a of $[(NH_3)_5CoNC—C_6H_4—C(O)CH=C(OH)—CH_3]^{3+}$ was determined by potentiometric titration with $0.01\,mol\,L^{-1}$ KOH (12).

Reaction mixtures from kinetic runs were subjected to ion exchange chromatography using SP-Sephadex cation exchange resin and Dowex 50W 50X8-200 cation exchange resin and eluted with gradually increasing concentrations of $NaClO_4/HClO_4$ solutions. Chromium concentrations were determined by oxidation to CrO_4^{-2} and measurement of the absorbance at 372 nm ($\varepsilon = 4815\,L\,mol^{-1}\,cm^{-1}$) (13).

Proton magnetic resonance spectra were obtained using Varian A60 or Bruker WP60FT spectrometers. Ultraviolet–visible spectra were recorded on a Beckman Acta CIII spectrophotometer, and infrared spectra were recorded using KBr pellets on a Beckman IR12 infrared spectrophotometer. Measurements of pH were made using a Radiometer model PHM26 pH meter.

[1]Author to whom correspondence may be addressed.

[2]Revision received December 13, 1985.

Syntheses

Preparation of 3-(4-cyanobenzoyl)-2,4-pentanedione

To a stirred solution of 5.0 g 4-cyanobenzoyl chloride in benzene was added 10.0 g thallium(I) 2,4-pentanedionate, and the reaction mixture was heated at 50°C for 30 min. The precipitate of thallous chloride was filtered off and the benzene solution reduced in volume under vacuum to yield a viscous oil. This oil was taken up in ethanol and a small amount of water added. Refrigeration of this solution yielded crystals of 3-(4-cyanobenzoyl)-2,4-pentanedione, which was washed with water and air-dried. The nitrile stretching frequency was observed at 2235 cm^{-1}; ^1H nmr spectrum (DMSO-d_6) δ: 8.20 (C_6H_4, 4H), 2.20 (CH_3, 6H), 17.2 (O—H, 1H). *Anal.* calcd. for $C_{13}H_{11}NO_3$: C 68.1, H 4.84, N 6.11; found: C 68.0, H 4.70, N 6.10.

*Preparation of (1-(4-cyanophenyl)-3-hydroxy-2-buten-1-one-*N*)-pentaamminecobalt(III) perchlorate, [$(NH_3)_5CoNC—C_6H_4—C(=O)—CH=C(OH)—CH_3](ClO_4)_3$*

To a solution of 5.0 g $[(NH_3)_5Co(CF_3SO_3)](CF_3SO_3)_2$ (14) in 25 mL sulfolane was added 2.2 g 3-(4-cyanobenzoyl)-2,4-pentanedione. The red solution was stirred for 1 day at 40°C, and the resultant orange solution was poured into 500 mL diethyl ether. The orange semisolid was washed with several portions of ether, dried, and dissolved in 500 mL water. The filtered aqueous solution was charged onto a CM-Sephadex column and eluted with 0.1–0.5 mol L^{-1} NaCl solution. The required complex moved down the column as a yellow band, with the characteristics of a 3+ ion. The band was physically removed and the complex removed from the resin by addition of 5 mol L^{-1} NaCl. Addition of sodium perchlorate resulted in precipitation of a light yellow powder, which was filtered, washed with water, ethanol, and finally ether, and then air-dried.

The electronic spectrum of the complex in water exhibited peak maxima at 466 (ε = 105 L mol^{-1} cm^{-1}), 320 (1.31 × 10^4), and 255 (2.2 × 10^4) nm. The nitrile stretching frequency was observed at 2295 cm^{-1}; ^1H nmr spectrum in DMSO-d_6 δ: 8.20 (C_6H_4, 4H), 2.23 (CH_3, 3H), 6.65 (CH, 1H), 4.20 (*cis*-NH_3, 12H), 3.80 (*trans*-NH_3, 3H). *Anal.* calcd. for $CoC_{11}N_6O_{14}H_{24}Cl_3$: C 21.0, H 3.84, N 13.3; found: C 21.4, H 4.40, N 13.4.

Results and discussion

Attempts to form the complex **2** by reaction of free ligand with $[(NH_3)_5Co(CF_3SO_3)](CF_3SO_3)_2$ in a noncoordinating solvent, sulfolane, resulted in isolation of a major species characteristic of a nitrile-bonded pentaamminecobalt(III) complex ($\nu(C\equiv N)$ = 2295 cm^{-1}) but which exhibited an nmr spectrum inconsistent with **2**. The ratio of phenyl protons to

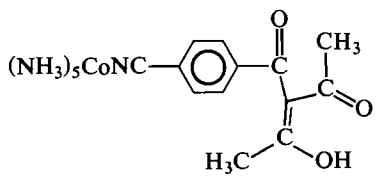

2

methyl protons in the nmr spectrum was 4:3 rather than 4:6 as expected. This fact, combined with elemental analysis and reactions of the free ligand (*vide supra*), indicated that the major product has structure **1**, which results from loss of a $COCH_3$ fragment. The mechanism of this transformation was believed to involve reaction of the free ligand with traces of trifluoromethanesulfonic acid in the $[(NH_3)_5Co(CF_3SO_3)](CF_3SO_3)_2$–sulfolane solution. The nmr spectra of the free ligand in DMSO-d_6 showed a decrease in the methyl peaks with time upon addition of a drop of trifluoroacetic acid.

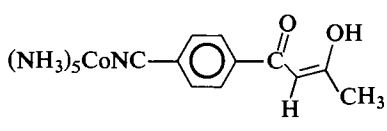

1

The pK_a for deprotonation of complex **1** was determined by potentiometric titration to be 6.92 ± 0.05. This value, as compared to that for the NCacac complex (10) (pK_a = 1.30) can be explained as being due to the change in position of the electronegative $(NH_3)_5CoNC$— group from the 3-position, which is directly adjacent to the β-diketone, to a more remote location in **1**, where the inductive effect is not nearly as great. Furthermore, small changes in the uv–vis spectrum of the complex **1** were observed in the acid range 0.10–1.0 mol L^{-1}, indicating a second equilibrium with pK_a value between 1 and 0. The changes were too small to allow a more accurate estimation of this equilibrium constant, which likely pertains to deprotonation of $[(NH_3)_5CoNC—C_6H_4—C(OH)=CH—C(OH)—CH_3]^{4+}$. Solutions of the complex in pure water were unstable and decomposition was evident after approximately 1 h.

Addition of Cr^{2+} to a solution of $[(NH_3)_5CoNC—C_6H_4—C(=O)—CH=C(OH)—CH_3]^{3+}$ resulted in a rapid decrease in absorbance at wavelengths corresponding to the maxima of the Co(III) complex. The stoichiometry of the reaction was determined to be 1:1 by reaction of the complex with excess Cr^{2+} followed by titrimetric determination of Cr^{2+} after the reaction.[3] Kinetic studies were limited to a rather narrow range of chromium(II) concentrations since runs at concentrations higher than 0.0122 mol L^{-1} resulted in rates too fast to be determined accurately by the stopped-flow method. Several runs were carried out at wavelengths corresponding to formation of product and in the ultraviolet region, and in all cases only one reaction was observed. At a constant acid concentration the rate of reduction was directly proportional to the chromium(II) concentration (Table 1). The variation of the observed rate constant with hydrogen ion concentration shows that the rate approaches a limiting value at low acid concentrations (Table 1). The data are consistent with a rate law of the general form [1] given below:

$$[1]\quad k_{obsd} = \frac{a}{b + [H^+]}$$

As predicted by eq. [1], a plot of k_{obsd}^{-1} vs. $[H^+]$ gives a straight line with intercept $(b/a) = (3.5 \pm 0.1) \times 10^{-5}$ *M* s and slope $(1/a) = (4.0 \pm 0.1) \times 10^{-5}$ s, yielding $a = (2.5 \pm 0.1) \times 10^4$ s^{-1} and $b = 0.86 \pm 0.03$ mol L^{-1}. A mechanism consistent with all the experimental results is given in Scheme 1. This mechanism leads to the rate law [2]:

$$[2]\quad k_{obsd} = \frac{k_1 K_a'}{[H^+] + K_a' + \dfrac{K_a K_a'}{[H^+]}}$$

If $K_aK_a'/[H^+] \ll ([H^+] + K_a')$, eq. [2] simplifies to eq. [3]:

$$[3]\quad k_{obsd} = \frac{k_1 K_a'}{[H^+] + K_a'}$$

which has the same form as eq. [1]. The analysis gives k_1 = (2.9

[3]Excess standard Fe^{3+} was added to the reaction mixtures and the excess Fe^{3+} determined by titration of liberated I_2 with standard sodium thiosulfate.

TABLE 1. Kinetic data for the reduction of (1-(4-cyanophenyl)-3-hydroxy-2-buten-1-one)-pentaamminecobalt(III) perchlorate by chromium(II)[a,b]

$[H^+]$, mol L^{-1}	$[Cr^{2+}] \times 10^3$, mol L^{-1}	$k \times 10^{-1}$,[c] s^{-1}	$k_{obsd} \times 10^{-4}$, L mol^{-1} s^{-1}	$k_{obsd}^{calcd} \times 10^{-4}$,[d] L mol^{-1} s^{-1}
0.0100	12.2	36	3.0	2.9
0.0297	12.2	35	2.9	2.8
0.0500	1.85	5.1	2.8	2.7
0.0500	8.90	24	2.7	2.7
0.0699	12.2	32	2.6	2.7
0.100	1.85	4.6	2.5	2.6
0.200	12.2	28	2.3	2.3
0.200	3.05	6.7	2.2	2.3
0.200	3.29	8.0	2.4	2.3
0.400	12.2	24	2.0	2.0
0.400	1.85	3.7	2.0	2.0
0.500	8.90	16	1.8	1.8
0.700	12.2	20	1.6	1.6
0.800	8.90	13	1.5	1.5
0.891	12.2	18	1.5	1.4
0.891	12.2	17	1.4	1.4

[a]Temperature = 25.0°C, I = 1.00 mol L^{-1} ($LiClO_4$).
[b][Co(III)] = 2.5×10^{-5} mol L^{-1}.
[c]Wavelength = 314 nm; rate constants are averages of at least six runs. Replicate runs agreed within 10% of each other. The fits of the individual runs were good to five half-times.
[d]Calculated on the basis of eq. [1] with $a = 2.5 \times 10^4$ s^{-1} and b = 0.86 mol L^{-1}.

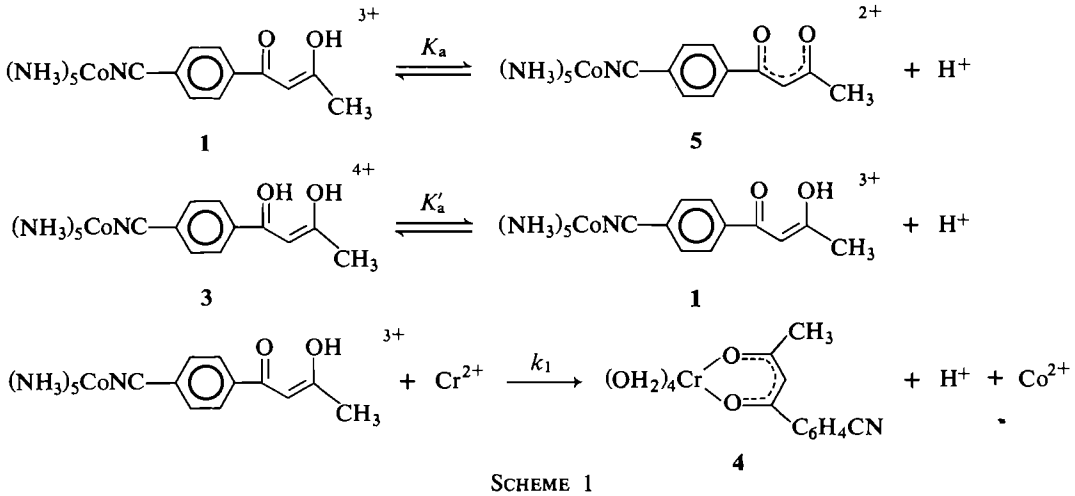

SCHEME 1

TABLE 2. Spectral parameters of β-diketone Cr(III) complexes[a]

Complex	λ_{max} (ε_{max}), nm (L mol^{-1} cm^{-1})	Reference
$(OH_2)_4Cr(acac)^{2+}$	533(27), 392(209)	15
$(OH_2)_4Cr(3\text{-formylacac})^{2+}$	557(30), 315(4640)	15
$(OH_2)_4Cr(3\text{-CNacac})^{2+}$	552(38), 357(242)	10
$(OH_2)_4Cr(2\text{-acetylbtdn})^{2+}$	547(35), 309(5100)	15
$(OH_2)_4Cr(1\text{-(4-cyanophenyl)btdn})^{2+}$	546(28), 356(12,000)	This work

[a]Aqueous solution, 25°C; btdn = butane-1,3-dionate.

$\pm$ 0.1) $\times 10^4$ L mol^{-1} s^{-1} and $K'_a = 0.86 \pm 0.03$ mol L^{-1}. The large value of K'_a is consistent with deprotonation of the 4+ species given in Scheme 1. The plot of k_{obsd}^{-1} vs. $[H^+]$ did not show any signs of downward curvature at low $[H^+]$, thus eliminating **3** as a reactant (16).

Cation exchange separation of reaction mixtures at various acidities (0.05–0.20 mol L^{-1} H^+) indicated only one chromium(III) complex as the major product. This species eluted as a 2+ complex and the electronic spectral parameters are consistent with the assignment of the product as the chelate **4** (Table 2 and Scheme 1). Quantitative experiments at a Co(III):Cr(II) ratio of 1:1 showed that this product accounted for ~90% of the Cr(II) initially added. Experiments at 1.0 mol L^{-1} H^+ gave increased amounts of $Cr(OH_2)_6^{3+}$ but repeated analyses were

TABLE 3. Kinetic data for reduction of pentaamminecobalt(III)L complexes by chromium(II)

L	$k^{25°C}$, L mol^{-1} s^{-1}	Mechanism	Reference
4-Acetylbenzonitrile	6×10^3	Inner sphere	7
4-Formylbenzonitrile	2.5×10^5	Inner sphere	6
4-Benzoylpyridine	4.7×10^4	Inner sphere	18
4-Acetoxybenzonitrile	0.021	Outer sphere	6
Benzonitrile	0.043	Outer sphere	9

inconsistent. It is likely that **4** hydrolyzes on the cation exchange column at the higher acidities.

Scheme 1 indicates that the reductant attacks the remote carbonyl oxygen adjacent to the benzene ring. Following electron transfer, rapid ring closure and deprotonation give the observed product **4**. The value of k_1, 2.9×10^4 L mol^{-1} s^{-1}, is similar to rate constants obtained for reduction by Cr^{2+} of other $(NH_3)_5Co^{3+}$ complexes with ligands containing remote carbonyl groups (Table 3). For these complexes, Cr^{2+} has been shown to attack at the remote carbonyl oxygen. The product analyses show that ligand transfer is essentially quantitative. In this sytem, the protonated form of the complex, **3**, would be expected to react via an outer-sphere pathway. This is a less facile process for nitrile complexes where rate constants in the range 0.02–0.06 L mol^{-1} s^{-1} are observed for outer-sphere processes (6, 8) (Table 3). The value of the acid dissociation constant of 0.86 mol L^{-1} obtained from the kinetic data is not unreasonable for protonation of a carbonyl oxygen. Similar values have been obtained for the acetato- and propionatopentaamminecobalt(III) complexes (0.35 and 0.24 mol L^{-1}, respectively) at high ionic strength (18). The proposed mechanism also provides a rationale for the fact that **5** does not react with Cr^{2+} even though the delocalized β-diketonate chelate has been shown to be an excellent lead-in group (10). In both **5** and **1** the carbonyl oxygen adjacent to the benzene group is available as a lead-in group for Cr^{2+}, but **1** is the predominant species in the acidity range studied. Even though **5** contains a chelate function it is unlikely that this is sufficient to make **5** much more reactive than **1**.

Acknowledgements

The authors wish to thank the Natural Sciences and Engineering Research Council of Canada for financial support of this work.

1. F. NORDMEYER and H. TAUBE. J. Am. Chem. Soc. **88**, 4295 (1966); **90**, 1162 (1968).
2. A. ZANELLA and H. TAUBE. J. Am. Chem. Soc. **94**, 6403 (1972); E. S. GOULD. J. Am. Chem. Soc. **96**, 2373 (1974).
3. W. C. KUPFERSCHMIDT and R. B. JORDAN. Inorg. Chem. **20**, 3469 (1981).
4. H. SPIECKER and K. WIEGHARDT. Inorg. Chem. **15**, 909 (1976).
5. A. H. MARTIN and E. S. GOULD. Inorg. Chem. **14**, 873 (1975); M. S. RAM, A. H. MARTIN, and E. S. GOULD. Inorg. Chem. **22**, 1103 (1983); M. HERY and K. WIEGHARDT. Inorg. Chem. **17**, 1130 (1978); B. H. BERRIE and J. E. EARLEY. Inorg. Chem. **23**, 774 (1984).
6. R. J. BALAHURA and W. L. PURCELL. J. Am. Chem. Soc. **98**, 4457 (1976).
7. R. J. BALAHURA and W. L. PURCELL. Inorg. Chem. **14**, 1469 (1975).
8. R. J. BALAHURA, W. C. KUPFERSCHMIDT, and W. L. PURCELL. Inorg. Chem. **22**, 1456 (1983).
9. R. J. BALAHURA, G. B. WRIGHT, and R. B. JORDAN. J. Am. Chem. Soc. **95**, 1137 (1973).
10. R. J. BALAHURA and A. J. JOHNSTON. Inorg. Chem. **22**, 3309 (1983).
11. R. J. BALAHURA and R. B. JORDAN. J. Am. Chem. Soc. **93**, 625 (1971).
12. A. ALBERT and E. P. SERJEANT. The determination of ionization constants. Chapman and Hall Ltd., London, England. 1971. p. 9.
13. G. W. HAUPT. J. Res. Natl. Bur. Stand. **48**, 414 (1952).
14. N. E. DIXON, W. G. JACKSON, M. J. LANCASTER, G. A. LAWRANCE, and A. M. SARGESON. Inorg. Chem. **20**, 470 (1981).
15. R. J. BALAHURA and N. A. LEWIS. Can. J. Chem. **53**, 1154 (1975).
16. A. ADIN and A. G. SYKES. J. Chem. Soc. (A), 351 (1968).
17. J. C. THOMAS, J. W. REED, and E. S. GOULD. Inorg. Chem. **14**, 1696 (1975).
18. C. CHEN and E. S. GOULD. J. Am. Chem. Soc. **95**, 5539 (1973).

Electron donor–acceptor complexes between naphthylamines and methyl viologen in aqueous sodium dodecyl sulphate solution

S. G. Bertolotti, J. J. Cosa, H. E. Gsponer,[1] M. Hamity, and C. M. Previtali
Universidad Nacional de Río Cuarto, Departamento de Química y Física, 5800 Río Cuarto, Argentina
Received August 26, 1985

S. G. Bertolotti, J. J. Cosa, H. E. Gsponer, M. Hamity, and C. M. Previtali. Can. J. Chem. **64**, 845 (1986).

The electron donor–acceptor (EDA) interaction between methyl viologen (MV^{2+}) and 1-naphthylamine (1NA), 2-naphthylamine (2NA), and *N*,*N*-dimethyl-1-naphthylamine (DMA) was studied in water and in aqueous sodium dodecyl sulphate (SDS). The experimental values of the association constants in water were 8.9, 9.8, and 2.8 M^{-1} for 1NA, 2NA, and DMA, respectively. In the presence of SDS the observed values were very much higher and strongly dependent upon the detergent concentration. The enhancement in the interaction is due to an increase in the local concentration of the partners in the micellar pseudophase. MV^{2+} itself was shown to strongly interact with the micelles. A new absorption is present at the red tail of the spectrum of MV^{2+} in the presence of SDS micelles. An association constant of 1700 M^{-1} was obtained from this absorption.

S. G. Bertolotti, J. J. Cosa, H. E. Gsponer, M. Hamity et C. M. Previtali. Can. J. Chem. **64**, 845 (1986).

Opérant dans l'eau et dans des solutions aqueuses de dodécylsulfate de sodium (DSS), on a étudié l'interaction de donneur–accepteur d'électrons (DAE) entre le viologène de méthyle (VM^{2+}) et la naphtylamine-1 (NA1), la naphtylamine-2 (NA2) et la *N*,*N* diméthyl naphtylamine-1 (DMA). Dans l'eau, les valeurs expérimentales pour les constantes d'association sont respectivement 8,9, 9,8 et 2,8 M^{-1} pour NA1, NA2 et DMA. En présence de DSS, les valeurs observées sont beaucoup plus élevées et elles dépendent beaucoup de la concentration du détergent. L'augmentation de l'interaction est due à une augmentation de la concentration locale des partenaires dans la pseudophase micellaire. On a démontré que le VM^{2+} lui-même interagit beaucoup avec les micelles. En présence de micelles de DSS, on a observé une nouvelle absorption à la fin de la région rouge du spectre du VM^{2+}. On a évalué à 1700 M^{-1} la constante d'association de cette absorption.

[Traduit par la revue]

Introduction

One of the key features responsible for the numerous current studies of micellar phenomena is the ability of charged micelles to solubilize and concentrate a wide variety of reagents, ranging from oppositely charged ions to hydrocarbons. Thus the formation of electron donor–acceptor (EDA) complexes between a hydrophobic donor solubilized within an anionic micelle and a cationic acceptor may proceed very efficiently (1, 2). It is known that methyl viologen cations (MV^{2+}) form EDA complexes with aromatic amines (3). In the present work we wish to report the effect of sodium dodecyl sulphate (SDS) concentration on the EDA equilibrium and charge transfer band between MV^{2+} and 1-naphthylamine (1NA), 2-naphthylamine (2NA), and *N*,*N*-dimethyl-1-naphthylamine (DMA).

Experimental

1NA and 2NA (Fluka, pure) were recrystallized at least three times from ethanol–water and subsequently vacuum sublimed. DMA (Fluka, pure) was purified by chromatography on an alumina column under nitrogen. Methyl viologen dichloride was obtained from a commercial solution and was recrystallized from methanol. Triply-distilled water was employed.

The uv–vis absorption measurements were recorded with a Cary 17 spectrophotometer.

The association of MV^{2+} with SDS was studied by means of the uv difference spectra between solutions containing MV^{2+} plus SDS versus MV^{2+}. In all cases the absorption measurements were corrected by the small absorption of SDS at the working wavelength. The concentration of MV^{2+} was held constant at 5×10^{-4} *M* and the SDS concentration was changed between 8×10^{-3} and 2×10^{-2} *M*.

Association of MV^{2+} and naphthylamines in SDS solutions was studied by absorption measurement on the charge transfer band. The reference cell always contained the same amount of MV^{2+} as that of the measuring cell in order to subtract the absorbance of the MV^{2+}–SDS complex. The concentration of MV^{2+} was changed between 2×10^{-4} and 2×10^{-3} *M*. In all cases the results were analyzed by a Benesi–Hildebrand (B–H) treatment or by a nonlinear regression analysis of the absorbance–concentration plots. Results in good agreement were obtained by both methods.

Results and discussion

Association of MV^{2+} with SDS micelles

The absorption spectra of $MVCl_2$ (10^{-4} *M*) in water, in the absence and in the presence of SDS 0.05 *M*, are shown in Fig. 1. The observed red shift of the absorption is typical of the EDA interaction of MV^{2+} with several anions (4, 5). The difference spectrum is shown in the inset in Fig. 1.

A B–H analysis of the difference band at 288 nm as a function of surfactant concentration yields a straight line. A value of 1700 M^{-1} is obtained for the apparent association constant (K_1) of MV^{2+} with SDS micelles, defined by eq. [1]

$$[1] \quad K_1 = \frac{[MV^{2+}]_m}{[MV^{2+}]_w[D]_m}$$

where $[MV^{2+}]_m$ and $[MV^{2+}]_w$ stand for the concentration of bound and free MV^{2+}, respectively, and $[D]_m$ is the micellized detergent concentration (D_{total} − cmc).

This result shows that MV^{2+} may be considered almost quantitatively bound to SDS under our working conditions. The same conclusion can be drawn from the earlier results of Schmehl and Whitten (6), who used an ionic exchange approach to study the binding of MV^{2+} to SDS micelles.

Interaction of naphthylamines with SDS micelles

When 1NA, 2NA, and DMA are dissolved in aqueous SDS a red shift is observed in the absorption spectra relative to water. The apparent association constants between the different naphthylamines and micelles can be obtained by employing an approach similar to that of Bunton *et al.* (7). The equilibrium constants (K_2) defined in the same way as eq. [1] were

[1]Author to whom correspondence may be addressed.

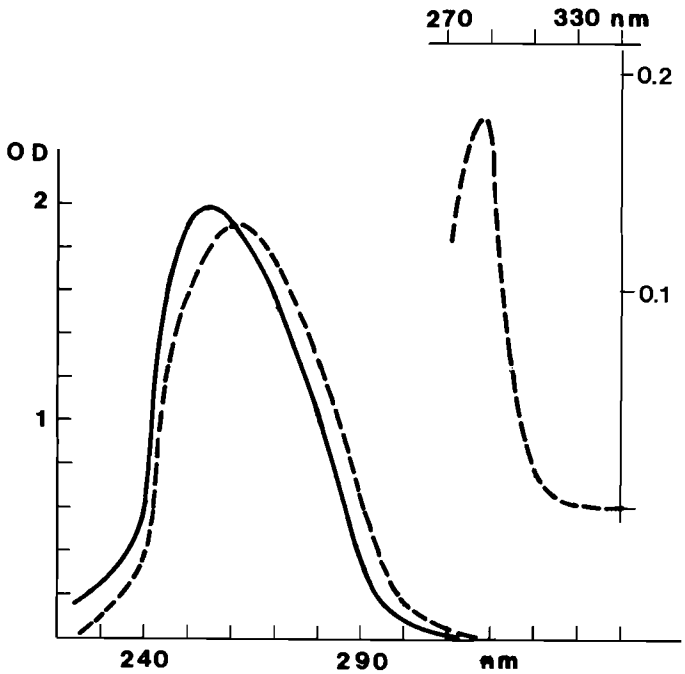

FIG. 1. Methyl viologen absorption spectrum. ——— 10^{-4} *M* aqueous solution. ---- 10^{-4} *M* in aqueous SDS 0.05 *M*. Inset: difference spectrum.

TABLE 1. Association constants of naphthylamines and methyl viologen with SDS micelles

	K (M^{-1})[a]
MV^{2+}	1700
1NA	250
2NA	275
DMA	320

[a]25°C. Estimated error ±5%.

determined using the equation:

$$[2] \quad (A - A_w)/[D]_m = K_2 A_m - K_2 A$$

where A is the observed absorbance, and A_w and A_m are the absorbances in the water and of the fully micellar-bound naphthylamine at a given wavelength. Equation [2] applies, provided that the concentration of bound amine is small compared with D_{total}. From a plot of $(A - A_w)/[D]_m$ vs. A, K_2 can be obtained. The values of the association constants are collected in Table 1.

Association of MV^{2+} with naphthylamines in the presence of SDS micelles

It is well known that MV^{2+} forms ground-state complexes of the EDA type with a variety of electron donors. These complexes are characterized by a broad charge transfer band, generally in the 400–500 nm region. These bands are red shifted and enhanced in intensity by the presence of anionic micelles (2). In Fig. 2 is shown the effect of SDS on the charge transfer band of the MV^{2+}–1NA system. Similar behaviour was found for the other naphthylamines.

From a B–H plot, the apparent equilibrium constant (K_{BH}) and the extinction coefficient for the EDA complex can be obtained. No deviation from linearity was observed in the plots

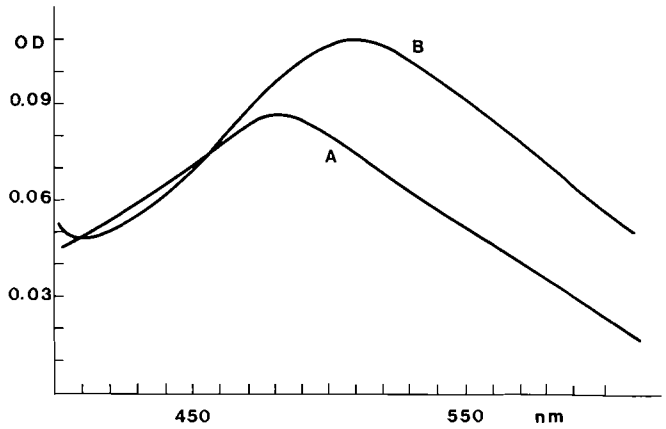

FIG. 2. Charge transfer absorption band of naphthylamine – methyl viologen complex. (A) 1NA 5×10^{-4} and MV^{2+} 0.1 *M* in aqueous solution. (B) 1NA 5×10^{-4} and MV^{2+} 0.1 *M* in SDS 0.1 *M*.

in the presence of micelles. The results are collected in Table 2. It can be seen that while the extinction coefficients are not much affected by the presence of the micelles, K_{BH} increases by two orders of magnitude with respect to pure water. From this it can be concluded that the enhancement is due to an increase in the local concentrations and not to a change in the electronic character of the transitions. Moreover, the red shift in the absorption maximum is indicative of the effect of a less polar medium on the charge transfer band (6). The absorption maximum in methanol for the system MV^{2+}–1NA was reported as 525 nm (3). This suggests that in our case the polarity of the region in which the transition takes place should be similar to that of methanol.

It is interesting to note that when cetyltrimethylammonium bromide (CTAB) was used as surfactant, the charge transfer band was suppressed.

Dependence of the association constant on surfactant concentration

According to the value of K_1, MV^{2+} can be considered almost quantitatively bound to SDS under our working conditions. Therefore the association of MV^{2+} and naphthylamines is taking place mainly in the micellar pseudophase and it is expected that changing the volume of the pseudophase would affect the equilibrium constants through a change in the local concentration of the reactants. The effect of detergent concentation on K_{BH} can be seen in Fig. 3 for the system MV^{2+}–1NA.

The behaviour of K_{BH} is similar to that observed for micelle catalyzed bimolecular reactions (7), where the observed rate constant generally goes through a maximum with increasing surfactant concentration. The sharp increase in K_{BH} with the SDS concentration before the critical micellar concentration may be due to several factors. The addition of MV^{2+} may induce change in the cmc and, in addition, it seems likely that some association is occurring in pre-micellar aggregates. The decrease in K_{BH} beyond the cmc can be fitted in all cases to a lienar plot of K_{BH}^{-1} versus micelle concentration, as shown in Fig. 4. From the association constants for the binding of reactants to micelle (Table 1), the fraction of reactants bound to the micelles can be calculated by eq. [3]

$$[3] \quad f = \frac{K[D]_m}{1 + K[D]_m}$$

where K is the observed binding constant.

TABLE 2. Parameters of EDA complexes for naphthylamines and methyl viologen in water and in 0.02 *M* SDS

System	Solvent	K_{BH} (M^{-1})[a]	λ_{max} (nm)	ε (M^{-1} cm^{-1})
1NA–MV^{2+}	H_2O	8.9	470	380
1NA–MV^{2+}	SDS (0.02 *M*)	530	510	361
2NA–MV^{2+}	H_2O	9.8	460	410
2NA–MV^{2+}	SDS (0.02 *M*)	750	505	397
DMA–MV^{2+}	H_2O	2.8	420	345
DMA–MV^{2+}	SDS (0.02 *M*)	570	450	194

[a]At 25°C. Estimated error ±5%.

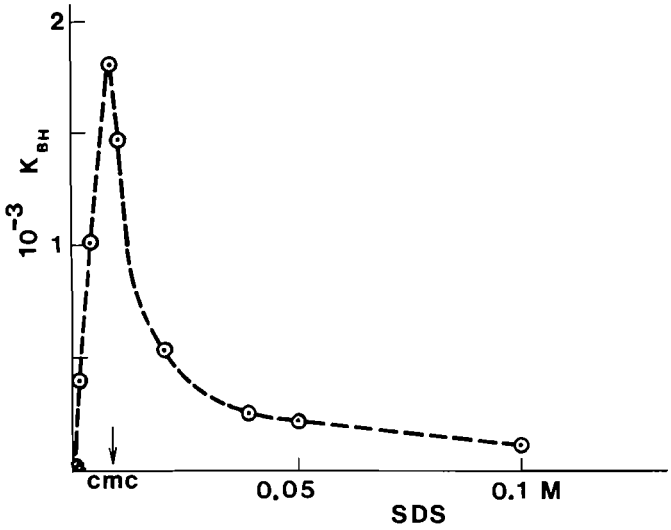

FIG. 3. Benesi–Hildebrand association constant (K_{BH}) of 1NA–MV^{2+} at different SDS concentrations.

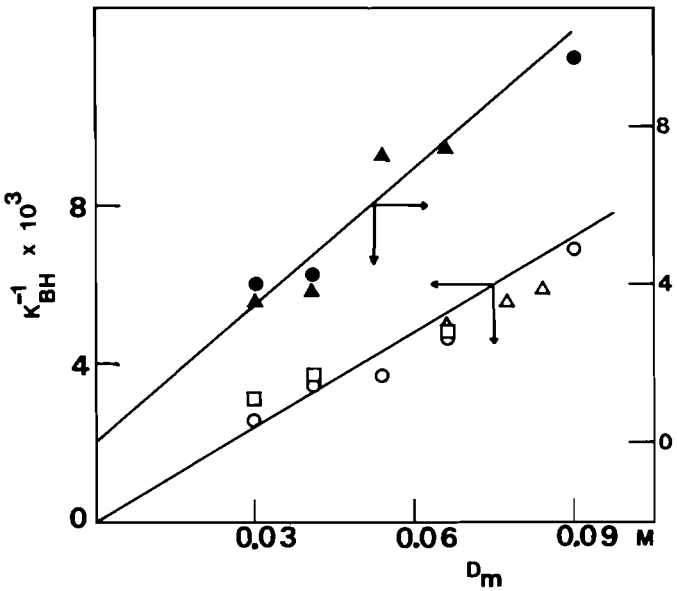

FIG. 4. Plots of the inverse of Benesi–Hildebrand constants versus micellized detergent. □, 2NA 1×10^{-4} *M*; ○, 2NA 5×10^{-4} *M*; △, 2NA 1×10^{-3} *M*; ▲, DMA 5×10^{-4} *M*; ●, 1NA 5×10^{-4} *M*.

For the detergent concentration range in Fig. 4, f is near unity for MV^{2+}, while for the naphthylamine, values between 0.75 and 0.97 are obtained. In these conditions the only equilibria to be considered are

$$[4] \quad A + M \overset{K_2}{\rightleftharpoons} (A)_m$$

$$[5] \quad (A)_m + (MV^{2+})_m \overset{K_3}{\rightleftharpoons} (AMV^{2+})_m$$

where A stands for any of the naphthylamines, M is the micelle, and $(AMV^{2+})_m$ is the EDA complex in the micellar pseudophase.

Equation [5] describes a reaction that occurs within the micelle and not an intermicellar reaction. From eq. [5], with the assumption that MV^{2+} is in excess over the amine,

$$[6] \quad \frac{[AMV^{2+}]_m}{f_A[A]_T - [AMV^{2+}]_m} = K_3 [MV^{2+}]_m$$

where $[A]_T$ is the total analytical concentration of the amine and f_A is the corresponding fraction incorporated with the micelles, eq. [3]. Rearranging, and assuming that Beer's law holds for the complex in the micellar phase, we obtain:

$$[7] \quad \frac{[A]_T}{OD} = \frac{1}{\varepsilon f_A} + \frac{1}{f_A \varepsilon K_3} \cdot \frac{1}{[MV^{2+}]_m}$$

where OD is the absorbance of the complex over 1 cm and ε the extinction coefficient. Now, the concentration of MV^{2+} in the micellar phase should be related to the analytical concentration

TABLE 3. Association constants in the micellar pseudophase

System	K_3 (M^{-1})
1NA–MV^{2+}	1.4
2NA–MV^{2+}	2.0
DMA–MV^{2+}	1.1

$[MV^{2+}]_0$ through:

$$[8] \quad [MV^{2+}]_m = \frac{[MV^{2+}]_0}{\bar{V}\,[D]_m}$$

where $\bar{V}$ is the molar volume of the micellized detergent. So, from the experimental B–H plots of $[A]_T/OD$ vs. $[MV^{2+}]_0$, the slope over intercept ratio gives

$$[9] \quad K_{BH}^{-1} = \frac{\bar{V}\,[D]_m}{K_3}$$

which predicts a linear relationship between K_{BH}^{-1} and $[D]_m$, as found in Fig. 4. From the slopes of these plots K_3 can be obtained, assuming a certain value for $\bar{V}$. Different opinions are sustained by several authors as to the correct value of $\bar{V}$. If it is assumed that the equilibrium takes place in the Stern region, a

value of $0.14\,L^{-1}$ (7) can be taken for $\bar{V}$. The equilibrium constants in the micellar phase calculated in this way are shown in Table 3. It can be seen that they are lower than in water but very similar to that found for MV^{2+} in methanol (3) when MV^{2+} is in excess of 1NA.

In summary, we have shown that the methyl viologen is strongly bound to SDS micelles. A charge transfer band appears in the difference spectrum, from which the association constant can be calculated. Naphthylamines are also incorporated with the micelles and the absorption of the EDA complex between the aromatic amines and MV^{2+} is enhanced by the presence of the surfactant. This can be explained as due to an increase in the local concentrations of the partners.

Acknowledgments

We wish to thank CONICOR (Provincia de Córdoba) and CONICET (República Argentina) for financial support.

1. H. Trimpe, G. Israel, H. G. O. Becker, I. R. Gould, and N. Turro. Chem. Phys. Lett. **99**, 275 (1983).
2. F. M. Martens and J. W. Verhoeven. J. Phys. Chem. **85**, 1174 (1981).
3. B. G. White. Trans. Faraday Soc. **65**, 2000 (1969); J. J. Cosa, H. E. Gsponer, and C. M. Previtali. J. Photochem. **19**, 271 (1982).
4. T. W. Ebbesen and G. Ferraudi. J. Phys. Chem. **87**, 3717 (1983).
5. M. Z. Hoffman, D. R. Prasad, G. Jones, and V. Malba. J. Am. Chem. Soc. **105**, 6360 (1983); J. P. Kuczynski, B. H. Milosavljevich, A. G. Lappin, and J. K. Thomas. Chem. Phys. Lett. **104**, 149 (1984).
6. R. H. Schmehl and D. G. Whitten. J. Am. Chem. Soc. **102**, 1938 (1980).
7. C. A. Bunton, G. Cerichelli, Y. Ihara, and L. Sepulveda. J. Am. Chem. Soc. **101**, 2429 (1979).

Preparation and X-ray crystal structures of the arsenic pentafluoride adducts of benzo-2,1,3-thiadiazole and benzo-1,2,3-thiadiazole

ALLEN APBLETT, TRISTRAM CHIVERS,[1] AND JOHN F. RICHARDSON
Department of Chemistry, University of Calgary, Calgary, Alberta, Canada T2N 1N4
Received October 23, 1985

ALLEN APBLETT, TRISTRAM CHIVERS, and JOHN F. RICHARDSON. Can. J. Chem. **64**, 849 (1986).

The reaction of arsenic pentafluoride with benzo-2,1,3-thiadiazole, **1**, or benzo-1,2,3-thiadiazole, **2**, in liquid SO_2 gave 1:1 adducts that were characterized spectroscopically (infrared and ^{13}C nmr) and by X-ray crystallography. Crystal data: for **1**·AsF_5, monoclinic, space group $P2_1/n$, $a = 6.932(1)$, $b = 9.113(1)$, $c = 15.136(2)$ Å, $\beta = 98.035(7)°$, $V = 946.8(2)$ Å^3, $Z = 4$; for **2**·AsF_5, monoclinic, space group $P2_1/a$, $a = 7.573(2)$, $b = 13.101(2)$, $c = 9.514(3)$ Å, $\beta = 90.95(2)°$, $V = 943.9(4)$ Å^3, $Z = 4$. The coordination of AsF_5 to one of the nitrogen atoms in **1** introduces asymmetry in the heterocyclic ring, with the longer bond lengths being associated with the coordinated nitrogen atom, d(S—N) = 1.633(5) and 1.577(6) Å, d(C—N) = 1.364(7) and 1.339(8) Å. The quinonoid character of the benzene ring is still apparent in the adduct. In **2**·AsF_5, the AsF_5 molecule is coordinated to the nitrogen atom that is bonded to carbon.

ALLEN APBLETT, TRISTRAM CHIVERS et JOHN F. RICHARDSON. Can. J. Chem. **64**, 849 (1986).

La réaction du pentafluorure d'arsenic avec le benzothiadiazole-1,2,3 (**1**) ou avec le benzothiadiazole-1,2,3 (**2**) dans le SO_2 liquide conduit à des adduits 1:1 que l'on a caractérisé par spectroscopie (infrarouge et rmn du ^{13}C) et par cristallographie des rayons-X. Les données cristallographiques sont les suivantes: le composé **1**·AsF_5 est monoclinique, groupe d'espace $P2_1/n$ avec $a = 6{,}932(1)$, $b = 9{,}113(1)$ et $c = 15{,}136(2)$ Å, $\beta = 98{,}035(7)°$, $V = 946{,}8(2)$ Å^3 et $Z = 4$ alors que le composé **2**·AsF_5 est monoclinique, groupe d'espace $P2_1/a$ avec $a = 7{,}573(2)$, $b = 13{,}101(2)$ et $c = 9{,}514(3)$ Å, $\beta = 90{,}95(2)°$, $V = 943{,}9(4)$ Å^3 et $Z = 4$. La coordination du AsF_5 à l'un des atomes d'azote du composé **1** introduit une asymétrie dans l'hétérocycle et les longueurs de liaison les plus longues sont associées avec l'atome d'azote coordonné, d(S—N) = 1,633(5) et 1,577(6) Å, d(C—N) = 1,364(7) et 1,339(8) Å. Le caractère quinonoïde du cycle benzénique est encore apparent dans l'adduit. Dans le composé **2**·AsF_5, la molécule de AsF_5 est coordonnée à l'atome d'azote qui est lié au carbone.

[Traduit par la revue]

Introduction

X-ray structural investigations of 2,1,3-benzothiadiazole **1** (1) and of numerous related 2,1,3-thiadiazoles (2) have indicated extensive π-delocalization in the heterocyclic ring and quinonoid character for the benzene ring, suggesting contributions from both resonance structures **1***a* and **1***b* to the overall structure of **1**. These conclusions are supported by ^1H nmr (3), microwave (4), and photoelectron spectra (5), and *ab initio* MO calculations (5) for **1**. The reactions of the parent 2,1,3-thiadiazole ring suggest that ionic forms such as **1***c* are also important contributors to the resonance hybrid (6).

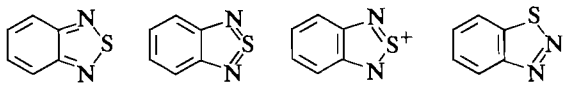

1*a* **1***b* **1***c* **2**

It has been demonstrated by nmr spectroscopy that **1** may coordinate to metals such as Pt(II) (7), Cr(O), Mo(O), and W(O) (8, 9), via one nitrogen, and *N,N'* dicoordinated binuclear adducts of Cr(O), Mo(O), and W(O) have been prepared very recently (10). Complexes of Hg(II), Ag(II), Cu(II), Cd(II) (11), (Co(II), Ni(II), and Fe(III) (12) have also been reported, but the mode of bonding of the ligand to the metal was not discussed. No X-ray structural data are available for any of these complexes.

In order to determine the effect of coordination on the structure of **1** we have prepared the AsF_5 adduct and determined its structure by X-ray crystallography. A similar investigation was also carried out for the AsF_5 adduct of benzo-1,2,3-thiadiazole, **2**, in order to establish the site of coordination of this unsymmetrical isomer of **1** with Lewis acids.

[1]Author to whom correspondence may be addressed.

Experimental

Reagents and general procedures

Benzo-2,1,3-thiadiazole (Eastman), benzo-1,2,3-thiadiazole (Fluka), and arsenic pentafluoride (Ozark–Mahoning) were obtained commercially and used without further purification. Liquid sulphur dioxide (Matheson) and $CFCl_3$ (Aldrich) were dried over P_2O_5 and transferred under vacuum into the reaction vessel, which consisted of two Pyrex bulbs separated by a medium porosity sintered glass frit and equipped with Kontes and J. Young Teflon-stemmed valves. Solid products were handled under a dry nitrogen atmosphere in a Vacuum Atmospheres dry box.

Instrumentation

Infrared spectra (4000–250 cm^{-1}) were recorded as Nujol mulls (CsI windows) on a Nicolet 5DX FT ir spectrometer. Mass spectra (EI/70 eV) were obtained on a Kratos MS80 RFA instrument. The nmr spectra were run on a Varian XL-200 spectrometer. Chemical shifts are reported in ppm downfield from Me_4Si.

Preparation of benzo-1,2,3-thiadiazole·AsF_5

Arsenic pentafluoride (1.01 g, 5.94 mmol) was condensed onto SO_2 (6.20 g) at −78°C in one bulb of the reaction vessel. The mixture was allowed to warm to room temperature and was then poured through the frit into the opposite bulb, which contained benzo-1,2,3-thiadiazole (0.80 g, 5.88 mmol) dissolved in SO_2 (4.10 g). Immediate reaction occurred to give a light tan solution and a white precipitate. After 18 h the solution was filtered through the frit into the empty bulb. The SO_2 was then slowly condensed into the opposite bulb by cooling it to 18°C in a thermostatted bath. This procedure produced colourless, rectangular crystals, which were used for the X-ray analysis after removal of solvent under vacuum. Infrared spectra indicated that the precipitate and the crystals were the same compound. The total yield of benzo-1,2,3-thiadiazole·AsF_5 was 1.79 g (5.85 mmol), mp 121°C (dec.). Infrared (major bands): 1533 (vs), 1482 (s), 1336 (s), 1280 (vs), 1247 (m), 1158 (s), 1135 (s), 949 (s), 906 (vs), 840 (s), 767 (vs), 754 (vs), 713 (vs), 661 (s), 647 (s), 592 (m), 541 (m), 533 (m), 422 (s), 388 (vs) cm^{-1}. The nmr data are given in Table 1.

TABLE 1. ^{13}C nuclear magnetic resonance data for benzo-2,1,3-thiadiazole, **1**, benzo-1,2,3-thiadiazole, **2**, and their AsF_5 adducts[a]

Compound	C-1	C-2	C-3	C-6	C-4	C-5
5,6-Me_2 derivative of **1**[b]	154.7	154.7	120.1	120.1	140.0	140.0
1[c,d]	150.6	150.6	119.8	119.8	136.9	136.9
1·AsF_5[e,f]	148.1	155.3	124.5	119.4	139.2	133.4
2[d,f]	138.8	156.2	121.7	117.3	127.2	124.9
2·AsF_5[e,g]	150.8		122.3		133.8	
	146.8		122.3		132.8	

[a]Chemical shifts in ppm downfield from Me_4Si. The numbering schemes for **1** and **2** and their AsF_5 adducts are indicated in Figs. 1 and 2, respectively.
[b]Data taken from ref. 19.
[c]The assignments of ^{13}C chemical shifts are based on those reported for 5,6-dimethyl-2,1,3-benzothiadiazole (19).
[d]In $CDCl_3$.
[e]In CD_3NO_2.
[f]The assignments for the inequivalent pairs of carbon atoms (C-1 and C-2, C-3 and C-6, C-4 and C-5) are made on the assumption that the carbon atom closest to AsF_5 in **1**·AsF_5 or to N(2) in **2** will have the higher downfield chemical shift in each pair.
[g]The accidental degeneracy for C-3 and C-6 and the closeness of the chemical shifts for C-1/C-2 and C-4/C-5 preclude an unambiguous assignment for these chemically inequivalent pairs of carbon atoms.

TABLE 2. Crystal data and experimental conditions

Parameter	**1**·AsF_5	**2**·AsF_5
Formula	$C_6H_4AsF_5N_2S$	$C_6H_4AsF_5N_2S$
Formula wt, amu	306.09	306.09
Space group	$P2_1/n$	$P2_1/a$
a, Å	6.932(1)	7.573(2)
b, Å	9.113(1)	13.101(2)
c, Å	15.136(2)	9.514(3)
β, deg	98.035(7)	90.95(2)
U, Å^3	946.8(2)	943.9(4)
Z	4	4
D_c, g cm^{-3}	2.15	2.15
μ, cm^{-1}	40.49	40.62
F(000)	592	592
Radiation	MoKα (λ = 0.7107 Å)	
Temp, °C	21	21
Scan range, deg	1.5 (0.80 + 0.347 tan θ)	1.5 (0.66 + 0.347 tan θ)
Scan speed, deg min^{-1}	3.4 to 0.7	3.4 to 0.6
max θ, deg	25	27.5
Data collected	$+h -k \pm l$	$+h +k \pm l$
No. unique data collected	1664	2154
No. observed data ($I > 3\sigma(I)$)	1263	1636
No. variables in final cycle	136	149
Extinction correction	—	$1.13(7) \times 10^{-4}$
GOF	1.17	0.97
R, R_w*	0.045, 0.041	0.048, 0.046
w	$[\sigma^2(F_o) + 0.00002(F_o^2)]^{-1}$	

*$R = \Sigma(||F_o| - |F_c||)/\Sigma|F_o|$; $R_w = [\Sigma w(|F_o| - |F_c|)^2/\Sigma w|F_o|^2]^{1/2}$.

Preparation of benzo-2,1,3-thiadiazole·AsF$_5$

The reaction of arsenic pentafluoride (1.00 g, 5.87 mmol) in SO_2 (5.02 g) with benzo-2,1,3-thiadiazole (0.78 g, 5.69 mmol) in SO_2 (7.23 g) was carried out using the procedure described above to give benzo-2,1,3-thiadiazole·AsF_5 (1.74 g, 5.68 mmol), mp 191°C. Yellow, cubic crystals suitable for X-ray analysis were obtained by slow removal of solvent from a solution of the adduct in SO_2 containing a trace of $CFCl_3$ into a bulb thermostatted at 17°C. Infrared (major bands): 1556 (s), 1350 (m), 1297 (m), 1271 (s), 1243 (m), 970 (s), 835 (m), 769 (s), 717 (vs), 707 (vs), 646 (s), 590 (m), 549 (m), 433 (m), 382 (vs) cm^{-1}. The nmr data are given in Table 1.

X-ray crystallography

The crystals used for data collection were fragments of approximate dimensions of 0.3 × 0.3 × 0.5 mm for **1**·AsF_5 and 0.3 × 0.5 × 0.5 for **2**·AsF_5, cut from larger samples. They were mounted in a glass capillary under an inert atmosphere. Intensity data were collected on an Enraf–Nonius CAD4F automated diffractometer using graphite monochromated MoKα radiation. Details concerning space group determination and data collection procedures were as described previously (13) while crystal data and experimental conditions are summarized in Table 2. The intensities of 3 standard reflections showed deviations of less than 3% in each case, indicative of crystal stability. Data were corrected for Lorentz, polarization, and absorption effects (empirical method using the program DIFABS (14)).

With each structure the coordinates of the As atom were determined by Patterson techniques and the remaining atoms located by difference Fourier techniques. Full-matrix least-squares cycles were based on F

TABLE 3. Positional parameters ($\times 10^4$) for the non-H atoms of $\mathbf{1}\cdot AsF_5$

Atom	x	y	z
As	70.0(10)	4804.3(6)	2857.8(5)
S	3681(2)	4726(2)	1837(1)
F(1)	2247(6)	4921(5)	3505(3)
F(2)	638(6)	3036(4)	2656(3)
F(3)	−1049(6)	4350(4)	3743(3)
F(4)	−391(7)	6591(4)	2992(3)
F(5)	−1985(5)	4634(4)	2136(3)
N(1)	4050(8)	5476(6)	937(4)
N(2)	1464(6)	5316(5)	1858(3)
C(1)	2462(9)	6235(6)	600(4)
C(2)	927(9)	6168(6)	1124(4)
C(3)	−807(9)	6941(7)	869(5)
C(4)	−901(11)	7733(7)	105(5)
C(5)	606(12)	7796(7)	−408(4)
C(6)	2285(11)	7085(8)	−181(4)

TABLE 4. Positional parameters ($\times 10^4$) for the non-H atoms of $\mathbf{2}\cdot AsF_5$

Atom	x	y	z
As	3261.4(8)	5687.3(4)	7545.3(6)
S	2036(2)	3108(1)	4888(2)
F(1)	1200(4)	5994(2)	6914(4)
F(2)	4105(5)	6068(2)	5976(4)
F(3)	3552(5)	6865(2)	8236(4)
F(4)	2378(5)	5219(3)	9043(4)
F(5)	5314(5)	5303(2)	8102(4)
N(1)	2266(6)	4277(3)	5449(5)
N(2)	2922(6)	4307(3)	6719(5)
C(1)	2842(7)	2567(4)	6391(5)
C(2)	3318(7)	3364(4)	7340(5)
C(3)	4029(8)	3156(4)	8674(6)
C(4)	4258(8)	2153(4)	9012(6)
C(5)	3799(8)	1350(4)	8102(7)
C(6)	3101(8)	1534(4)	6781(7)

minimizing the function $\Sigma w(|F_o| - |F_c|)^2$, where w is defined in Table 2. H atoms were located on a difference Fourier map and included in idealized positions but not refined for $\mathbf{1}\cdot AsF_5$, and were included in positions located with positional parameters refined for $\mathbf{2}\cdot AsF_5$. In each case thermal parameters were set to $1.1 \times B_{eq}$ of the C atom to which they are bonded, but not refined. In the final cycles of $\mathbf{1}\cdot AsF_5$, all non-H atoms were refined with anisotropic thermal parameters and the maximum shift/error was 0.05. An isotropic extinction parameter could not be refined. The highest peak in the final difference Fourier synthesis is 0.80 e Å^{-3} and is associated with the As atom. In the final cycles for $\mathbf{2}\cdot AsF_5$, all positional and non-H anisotropic thermal parameters were refined. The maximum shift/error was 0.14, the highest peak in the final difference Fourier synthesis is 0.94 e Å^{-3} and is associated with the As atom. All computations were done using the XRAY-76 system of programs (15) implemented on the Honeywell computer at the University of Calgary. Atomic scattering factors used for non-H atoms were those of Cromer and Mann (16) and were corrected for real and anomalous dispersion (17). Scattering factors for H atoms were from ref. 18. The final fractional atomic coordinates for $\mathbf{1}\cdot AsF_5$ and $\mathbf{2}\cdot AsF_5$ are given in Tables 3 and 4, respectively.[2]

Results and discussion

*Preparation and spectroscopic characterization of arsenic pentafluoride adducts of benzo-2,1,3-thiadiazole, **1**, and benzo-1,2,3-thiadiazole, **2***

The AsF_5 adducts of **1** and **2** were prepared in essentially quantitative yields as moisture-sensitive, colourless ($\mathbf{1}\cdot AsF_5$) or pale yellow ($\mathbf{2}\cdot AsF_5$) crystals by the reaction of the appropriate thiadiazole with the stoichiometric amount of AsF_5 in liquid sulphur dioxide. The adducts were characterized spectroscopically (mass, infrared, and ^{13}C nmr spectra) and by X-ray crystallography.

The base peak in the mass spectrum of $\mathbf{1}\cdot AsF_5$ at m/e 136 corresponds to the ion of the parent ligand, $\mathbf{1}^+$. The ion $\mathbf{2}^+$ (m/e 136, 70%) is also observed as a strong peak in the mass spectrum of $\mathbf{2}\cdot AsF_5$, but the base peak is at m/e 108 ($C_6H_4S^+$).

The ^{13}C nmr chemical shifts for the adducts $\mathbf{1}\cdot AsF_5$ and $\mathbf{2}\cdot AsF_5$ are compared with those of the parent ligands in Table 1. The symmetrically equivalent pairs of carbon atoms in **1** exhibit chemical shift differences of 5–7 ppm in $\mathbf{1}\cdot AsF_5$, indicating that coordination is via a nitrogen rather than the sulphur atom. In **2** all the carbon atoms are inequivalent and chemical shift differences are observed for those pairs of carbon atoms which are equivalent in the symmetrical isomer, **1**, the effect being most pronounced for the carbons bonded to the heteroatom. In the adduct $\mathbf{2}\cdot AsF_5$, however, these chemical shift differences are much smaller.

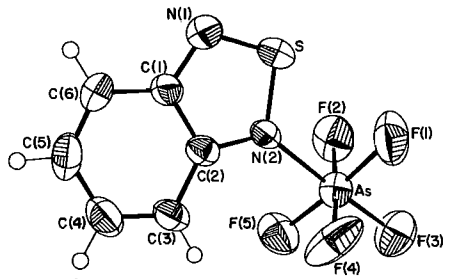

FIG. 1. An ORTEP drawing (50% probability ellipsoids) of $\mathbf{1}\cdot AsF_5$ showing the atomic numbering scheme. Hydrogen atoms are included as spheres of radius 0.1 Å.

Crystal and molecular structure of the AsF_5 adduct of benzo-2,1,3-thiadiazole

An ORTEP drawing of $\mathbf{1}\cdot AsF_5$ is depicted in Fig. 1. The bond lengths and bond angles are compared with those of the parent ligand **1** and $\mathbf{2}\cdot AsF_5$ in Table 5. The coordination site for the Lewis acid is, as expected, one of the nitrogen atoms. The X-ray structure of the parent ligand, **1**, was determined in 1951 (1), but the data are unreliable (the final R factor was 0.215). There is, however, a substantial bank of structural data for related thiadiazole ring systems (2), which can be used for comparison with the corresponding data for $\mathbf{1}\cdot AsF_5$. In summary the S—N and C—N bond lengths in 2,1,3-thiadiazoles are ca. 1.62 and 1.34 Å, respectively, and the angles at S and N are ca. 100 and 106°, respectively.

The coordination of AsF_5 to **1** does not distort the overall planarity of the heterocycle; the largest deviations are 0.02 Å for C(1) and S, which are on opposite sides of the molecular plane. As might be expected, however, adduct formation introduces asymmetry into the molecule so that bonds that were equivalent in **1** are no longer equal in the adduct. This effect is most

[2]Anisotropic thermal parameters, H atom parameters, and observed and calculated structure amplitudes may be purchased from the Depository of Unpublished Data, CISTI, National Research Council of Canada, Ottawa, Ont., Canada K1A 0S2.

TABLE 5. Bond lengths (Å) and angles (deg) for **1**,[a] **1**·AsF_5, and **2**·AsF_5

Bond	Distance		
	1	**1**·AsF_5	**2**·AsF_5
As—F(1)		1.684(4)	1.711(3)
As—F(2)		1.697(4)	1.708(3)
As—F(3)		1.690(5)	1.690(3)
As—F(4)		1.677(4)	1.699(4)
As—F(5)		1.677(4)	1.710(4)
As—N(2)		1.962(5)	1.986(4)
S—N(1)	1.60	1.577(6)	1.631(4)
S—N(2)	1.60	1.633(5)	
S—C(1)			1.700(5)
N(1)—N(2)			1.300(6)
N(1)—C(1)	1.34	1.339(8)	
C(1)—C(2)	1.41	1.414(9)	1.423(7)
C(2)—C(3)	1.46	1.400(8)	1.497(8)
C(2)—N(2)	1.34	1.364(7)	1.400(6)
C(3)—C(4)	1.29	1.357(10)	1.364(8)
C(4)—C(5)	1.46	1.387(12)	1.402(8)
C(5)—C(6)	1.29	1.334(10)	1.377(9)
C(6)—C(1)	1.46	1.404(9)	1.417(7)

Atoms	Angle		
	1	**1**·AsF_5	**2**·AsF_5
F(1)—As—F(2)		87.3(2)	88.7(2)
F(1)—As—F(3)		91.6(2)	92.0(2)
F(1)—As—F(4)		92.2(2)	90.6(2)
F(1)—As—F(5)		174.6(2)	175.8(2)
F(1)—As—N(2)		86.3(2)	87.9(2)
F(2)—As—F(3)		93.1(2)	91.5(2)
F(2)—As—F(4)		175.4(2)	175.4(2)
F(2)—As—F(5)		89.5(2)	90.3(2)
F(2)—As—N(2)		86.3(2)	88.2(2)
F(3)—As—F(4)		91.5)2)	93.1(2)
F(3)—As—F(5)		92.9(2)	92.1(2)
F(3)—As—N(2)		177.8(2)	179.6(2)
F(4)—As—F(5)		90.6(2)	90.1(2)
F(4)—As—N(2)		89.1(1)	87.3(2)
F(5)—As—N(2)		89.1(2)	88.0(2)
As—N(2)—C(2)		131.0(4)	127.7(3)
As—N(2)—S		120.2(2)	
As—N(2)—N(1)			116.1(3)
C(2)—N(2)—S	105	108.8(4)	
C(2)—N(2)—N(1)			116.2(4)
N(2)—S—N(1)	102	98.1(3)	
N(2)—N(1)—S			111.8(3)
S—N(1)—C(1)	105	109.2(5)	
N(1)—S—C(1)			94.6(2)
N(1)—C(1)—C(2)	114	114.0(5)	
N(1)—C(1)—C(6)		125.1(6)	
S—C(1)—C(2)			108.2(4)
S—C(1)—C(6)			131.6(4)
C(6)—C(1)—C(2)	119	120.8(6)	120.1(5)
C(1)—C(2)—C(3)	119	120.5(5)	121.6(5)
C(1)—C(2)—N(2)	114	109.9(5)	109.2(4)
N(2)—C(2)—C(3)		129.5(6)	129.2(5)
C(2)—C(3)—C(4)	120	116.1(6)	116.6(5)
C(3)—C(4)—C(5)	121	123.3(6)	123.2(6)
C(4)—C(5)—C(6)	121	122.3(6)	121.3(5)
C(5)—C(6)—C(1)	120	117.1(7)	117.1(5)

[a]Data taken from ref. 1.

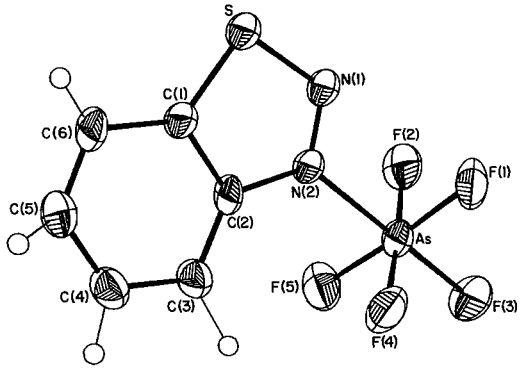

FIG. 2. An ORTEP drawing (50% probability ellipsoids) of **2**·AsF_5 showing the atomic numbering scheme. Hydrogen atoms are included as spheres of radius 0.1 Å.

pronounced for the S—N bonds, which now have lengths of 1.633(5) Å for the nitrogen bonded to AsF_5 and 1.577(6) Å for the uncoordinated nitrogen atom. The difference in the C—N bond lengths, 1.364(7) and 1.339(8), respectively, is on the borderline of the 3σ criterion of significance, but the longer bond also involves the coordinated nitrogen atom. The effect of coordination on the bond angles in the heterocyclic ring is small. The angle at sulphur is reduced to 98.1(3)°, whereas the average angle at nitrogen is increased to ca. 109° and there is no significant difference between the angles at the coordinated and uncoordinated nitrogen atoms. The most pronounced effect is for the carbon bonded to the coordinated nitrogen; the C(1)—C(2)—N(2) angle is reduced to 109.9(5)° from ca. 114° in **1** (1). In summary, the changes in the structural parameters of the heterocyclic ring in **1**, upon coordination, are small and indicate an increased contribution of the ionic resonance form **1***c* to the overall structure, consistent with removal of electron density from sulphur to nitrogen induced by the acceptor AsF_5 molecule.

Adduct formation also introduces some asymmetry in the C—C bond lengths of the aromatic ring. Nevertheless the quinonoid character is retained, albeit somewhat attenuated. Thus the average of the C(3)—C(4) and C(5)—C(6) distances is 1.345(10) Å, whereas the average of the other four C—C distances is 1.401(10) Å. The bond angles at C(3) and C(6) are 116.1(6) and 117.1(7)°, respectively, compared to 123.3(6) and 122.3(6)° for C(4) and C(5), respectively.

The As—N bond length of 1.958(5) Å is slightly longer and the mean As—F bond length of 1.685(5) Å is shorter than the corresponding distances in S_4N_4·AsF_5 (20) (d(As—N) = 1.910(5) and d(As—F) = 1.716(4) Å, cf. d(As—N) = 1.985(16) and d(As—F) = 1.695(10) Å in *N*-methyl-*S*,*S*-difluorosulphoximine·AsF_5 (21)).

Crystal and molecular structure of the AsF_5 adduct of benzo-1,2,3-thiadiazole

An ORTEP drawing of **2**·AsF_5 is shown in Fig. 2. Although the X-ray structure of **2** has not been determined, the following geometrical parameters were constructed on the basis of available structural data for related heterocycles and used for *ab initio* MO calculations (22): d(C—C) = 1.40, d(C—N) = 1.366, d(N—N) = 1.290, d(S—N) = 1.668, and d(C—S) = 1.724 Å. If these values can be taken as a reasonable guide to the structure of the parent ligand, it can be concluded that the effect of coordination on the bond lengths of the heterocyclic ring in **2**

is small. The C—N bond (1.400(6) Å) is slightly longer and the S—N bond (1.631(4) Å) is shorter in the adduct, whereas the N—N distance 1.300(6) Å is not changed significantly. The heterocyclic ligand in **2**·AsF_5 is planar within experimental error.

The trends in bond lengths and angles in the benzene ring of **2**·AsF_5 parallel closely those found for **1**·AsF_5, but the quinonoid character is less well developed (Table 5). The mean of the C(3)—C(4) and C(5)—C(6) distances is 1.370(9) Å compared to a mean value of 1.410(8) Å for the other four C—C bonds.

The As—N distance 1.986(4) Å is significantly longer than that in **1**·AsF_5, suggesting a slightly weaker interaction, but the mean As—F distance of 1.704(4) Å is longer.

Acknowledgements

We acknowledge the financial support of the Natural Sciences and Engineering Research Council of Canada in the form of a post-graduate scholarship (A.A.), an operating grant (T.C.), and an infrastructure grant (J.F.R.). We also thank Dr. K.A. Kerr for the use of the diffractometer.

1. V. Luzzati. Acta Crystallogr. **4**, 193 (1951).
2. A. Gieren, H. Beta, T. Hübner, V. Lamm, R. Neidlein, and D. Droste. Z. Naturforsch. Teil B, **39**, 485 (1984), and references cited therein.
3. N. M. D. Brown and P. Bladon. Spectrochim. Acta, Part A, **24**, 1869 (1968).
4. N. M. D. Brown, D. G. Lister, and J. K. Tyler. Spectrochim. Acta, Part A, **26**, 2133 (1970).
5. M. H. Palmer and S. M. F. Kennedy. J. Mol. Struct. **43**, 33 (1978).
6. W. G. Salmond. Q. Rev. **22**, 253 (1968).
7. J. Kuyper and K. Vrieze. J. Organomet. Chem. **86**, 127 (1975).
8. R. Meij, T. A. M. Kaandorp, D. J. Stufkens, and K. Vrieze. J. Organomet. Chem. **128**, 203 (1977).
9. W. Kaim. J. Organomet. Chem. **128**, 203 (1977).
10. W. Kaim and S. Kohlmann. Inorg. Chim. Acta, **101**, L21 (1985).
11. R. H. Hanson and C. E. Meloan. Inorg. Nucl. Chem. Lett. **7**, 461 (1971).
12. R. H. Hanson and C. E. Meloan. Inorg. Nucl. Chem. Lett. **7**, 467 (1971).
13. T. Chivers, R. T. Oakley, R. Pieters, and J. F. Richardson. Can. J. Chem. **63**, 1063 (1985).
14. N. Walker and D. Stuart. Acta Crystallogr. Sect. A, **39**, 158 (1983).
15. J. M. Stewart (*Editor*). Technical Report TR-446. Computer Science Centre, University of Maryland. 1976.
16. D. T. Cromer and J. B. Mann. Acta Crystallogr. Sect. A, **24**, 321 (1968).
17. International tables for X-ray crystallography. Kynoch Press, Birmingham, England. 1974.
18. R. F. Stewart, E. Davidson, and W. Simpson. J. Chem. Phys. **42**, 3175 (1965).
19. R. Meij, T. A. M. Kaandortp, D. J. Stufkens, and K. Vrieze. J. Organomet. Chem. **128**, 203 (1977).
20. R. J. Gillespie, J. P. Kent, and J. F. Sawyer. Acta Crystallogr. Sect. B, **36**, 655 (1980).
21. S. Bellard, A. V. Rivera, and G. M. Sheldrick. Acta Crystallogr. Sect. B, **34**, 1034 (1978).
22. M. H. Palmer and S. M. F. Kennedy. J. Mol. Struct. **43**, 221 (1978).

Ring cleavage of camphor derivatives: formation of chiral synthons for natural product synthesis

J. H. HUTCHINSON, T. MONEY,[1] AND S. E. PIPER
Department of Chemistry, The University of British Columbia, 2036 Main Mall, Vancouver, B.C., Canada V6T 1Y6
Received November 1, 1985

J. H. HUTCHINSON, T. MONEY, and S. E. PIPER. Can. J. Chem. **64**, 854 (1986).
Base-promoted ring cleavage of 9,10- and 8,10-dibromocamphor provides chiral intermediates for natural product synthesis.

J. H. HUTCHINSON, T. MONEY et S. E. PIPER. Can. J. Chem. **64**, 854 (1986).
Sous l'action de bases, il se produit une rupture de cycle des dibromo-9,10 (ou -8,10) camphres qui fournit des intermédiaires chiraux utiles dans la synthèse de produits naturels.

[Traduit par la revue]

The use of camphor as a chiral starting material in natural product synthesis (1) is dependent on the availability of methods for the regiospecific and stereoretentive functionalization of (+)-camphor (**1**) or (−)-camphor at the C(8) (2), C(9) (3), and C(10) (4) positions. Methods are also available for the synthesis of 8,10- and 9,10-disubstituted camphor derivatives (5). In addition, ring cleavage of the C(1)—C(2) (6) or C(2)—C(3) (7) bonds in camphor and its derivatives can be achieved, with variable efficiency, by a variety of methods.

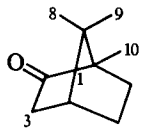

1

During our early investigations on the potential use of disubstituted camphor derivatives in steroid synthesis we attempted to synthesize 9,10-dicyanocamphor ethylene acetal (**3**) by treating (+)-9,10-dibromocamphor ethylene acetal (**2**) (Scheme 1) with sodium cyanide in dimethylsulphoxide (DMSO). The product of this reaction was a mixture of the required dinitrile (**3**) and, surprisingly, a monocyclic hydroxy-ethyl ester (**4**) whose structure was deduced from spectroscopic data (ir, nmr, and ms). It seemed reasonable to assume that the latter compound was produced by DMSO-promoted Grob-type cleavage (cf. Scheme 2) of the C(1)—C(2) bond in **2** and this was supported by the subsequent observation that treatment of **2** with DMSO alone resulted in a similar ring cleavage reaction to provide bromo-ester **5**. The extension of these investigations revealed that simple treatment of (+)-9,10-dibromocamphor (**6**) with KOH/THF/H_2O or NaOMe/MeOH for ~4 h at room temperature resulted in efficient ring cleavage and formation of bromo-acid **7** or the corresponding methyl ester (**8**) in 90–95% yield (8) (Scheme 3). Spectroscopic (nmr, ir) evidence indicated that the double bond in **7** and **8** was in the less stable (9), but synthetically useful, exocyclic position and this was confirmed by ozonolytic degradation to the corresponding cyclopentanone derivatives. Subsequent studies demonstrated that treatment of (+)-9,10-dibromocamphor (**6**) with KOH/DMSO–H_2O (5:1) for 12 h at 65°C provided hydroxy-acid **9** in ~90% yield (8*b*). The latter compound (**9**) can also be prepared by hydrolysis of the lactone **10** (8*a*) derived by cyclization of bromo-acid **7**, and tlc evidence indicated that lactone **10** is an intermediate in the "direct" conversion of 9,10-dibromo-camphor (**6**) to hydroxy-acid **9**.

As expected, (+)-8,10-dibromocamphor (**11**) (5) also undergoes ring cleavage when treated with NaOMe/MeOH to provide bromo-ester **12** (Scheme 4). However, in contrast, treatment with KOH/DMSO/H_2O provided a mixture (1:1) of lactone **13** and bicyclic acid **15**. The latter compound is presumably formed by initial formation of 10-bromo-3,8-cyclocamphor (**14**), followed by β-bromoketone cleavage in the usual way. Consistent with this explanation is our observation that (+)-8-bromocamphor (1, 2)[2] provides (+)-3,8-cyclo-camphor (1, 10) under the reaction conditions. Lactone **13** is obviously formed by spontaneous lactonization of the *cis* hydroxy-acid (Scheme 4) derived by ring cleavage of (+)-8,10-dibromocamphor (**11**) in the predicted fashion (cf. **6** → **7**).

The facile, efficient cleavage of the C(1)—C(2) bond in (+)-9,10-dibromocamphor (**6**) and (+)-8,10-dibromocamphor (**11**) are examples of a reaction that is characteristic of α,α-disubstituted β-bromoketones (11–22). Of particular relevance are reports in the early literature, by Forster (12) and Burgess (13), respectively, which claim that treatment of "β-bromocamphor" (**16**) (12) and "α,β-dibromocamphor" (**17**) (13) with refluxing KOH/EtOH for 5–8 h produces (+)-α-campholenic acid (**18**) (12) or the corresponding bromo-acid (**19**) (13). At that time (1900–1924) "β-bromocamphor" and "α,β-dibromocamphor" were assigned structures that, in modern nomenclature, would be named 6-bromocamphor (**16**) and 3,6-dibromocamphor (**17**), respectively, and their ring cleavage to (+)-α-campholenic acid (**18**) and its bromo derivative (**19**) were consistent with these structural assignments. However, the results of later investigations (24–26) indicated that "β-bromocamphor" (mp 78°C), derived from 1-hydroxy-camphene (**20**) (12), was identical to 10-bromocamphor (**21**), mp 78°C, prepared by thermolysis of 10-camphorsulfonyl bromide (**22**) (23) or camphor-10-mercurichloride (**23**) (26), and this structure assignment is now commonly accepted. It is interesting to realize, however, that a footnote in the paper by Burgess (13) refutes the suggestion by Lipp and Lausberg (25) that "α,β-dibromocamphor" has the 3,10-dibromocamphor structure (**24**), since this is inconsistent with its cleavage to bromo-α-campholenic acid (**19**). Despite these reservations it is now generally accepted that the early literature describes the conversion of 10-bromocamphor (**21**) and 3,10-dibromo-camphor (**24**) to (+)-α-campholenic acid (**18**) and its bromo derivative (**19**), respectively. These results, however, are inconsistent with our observations that ring cleavage of 9,10-dibromocamphor (**6**) provides unsaturated monocyclic compounds (**7**–**9**) in which the double bond is exclusively in the

[1]Author to whom correspondence may be addressed.

[2]We have been unable to repeat the yield quoted in ref. 2*a* and now find the overall yield of 8-bromocamphor to be 30–40%.

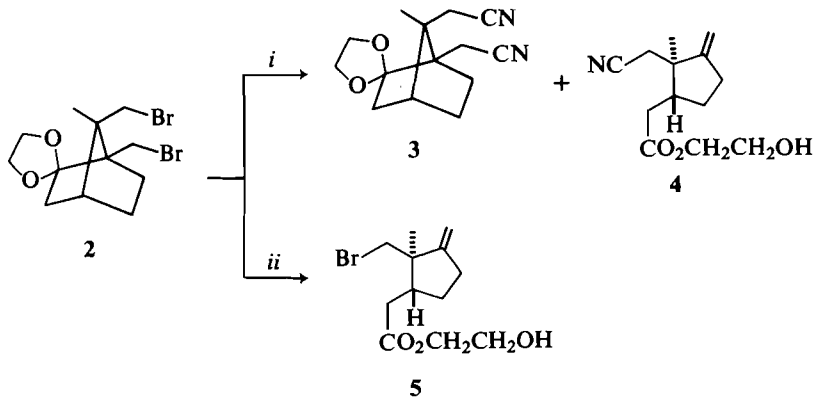

i, NaCN/DMSO/heat; *ii*, DMSO/heat

SCHEME 1

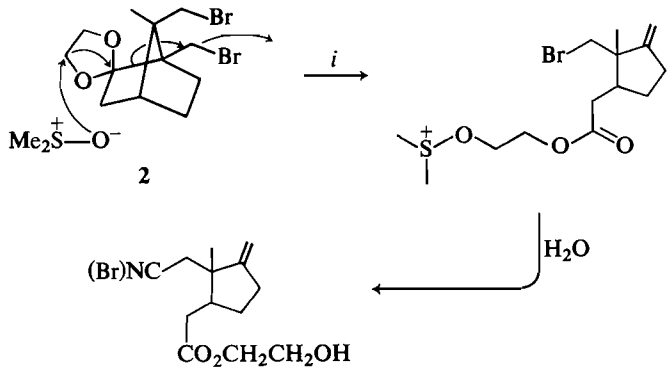

i, NaCN/DMSO/80°C or DMSO/80°C

SCHEME 2

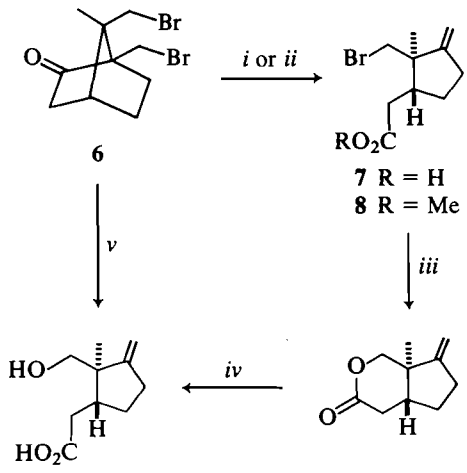

i, KOH/THF/H_2O; *ii*, NaOMe/MeOH; *iii*, KOH/DMSO–H_2O(99:1); *iv*, KOH/H_2O; *v*, KOH/DMSO–H_2O (7:1)/65°C/24 h

SCHEME 3

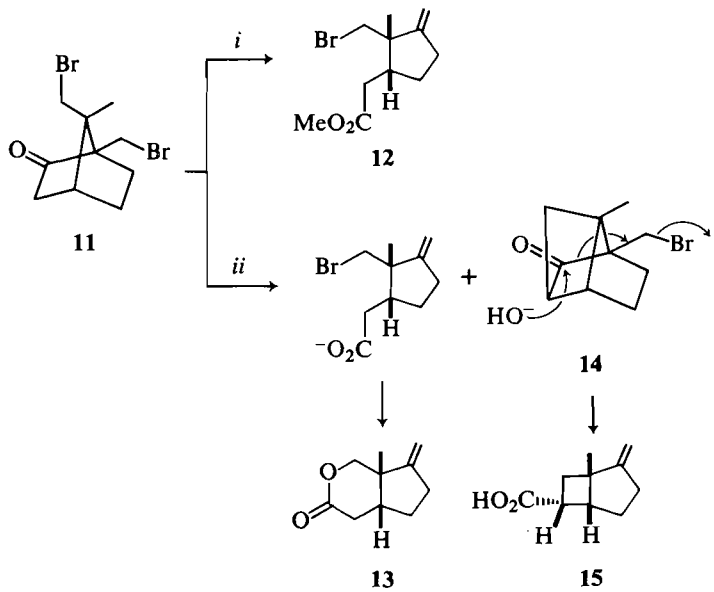

i, NaOMe/MeOH; *ii*, KOH/DMSO–H_2O (10:1)

SCHEME 4

exocyclic position.[3] As a result of these inconsistencies we treated 10-bromocamphor (**21**) under various conditions (cf. Scheme 2) used to cleave 9,10-dibromocamphor and found that the only major product formed was the exocyclic isomer (**25**) of (+)-α-campholenic acid (**18**). Since isomerization of these compounds does not seem to occur under basic conditions, the observed transformation of "β-bromocamphor" (i.e. 10-bromocamphor), to α-campholenic acid by the early workers is difficult to explain except in terms of their assumption (12, 13) that "α-bromocamphor" was 6-bromocamphor (**16**). As indicated above, however, this assumption is invalid.

As a footnote to the early literature it is interesting to note that treatment of authentic (−)-*endo*-6-bromocamphor (**30**)[4] with KOH/DMSO–H_2O (5:1) at 65°C for 36 h does indeed produce (+)-α-campholenic acid (**32**) as well as (+)-5,6-dehydrocamphor (**34**). In addition, more recent studies (27) indicate that treatment of (**30**) with KOBu^t/Bu^{t}OH followed by hydrolysis provides (−)-α-campholenic acid (**32**) as the major product in ~55% yield. Similarly, (−)-*endo*-6,9-dibromocamphor (**31**)

[3]10-Bromofenchone (**26**) also cleaves with base to provide an unsaturated monocyclic acid (**27**) with the double bond in the exocyclic position (14) (see Scheme 6).

[4](−)-*endo*-6-Bromocamphor (**30**) and (−)-*endo*-6,9-dibromocamphor (**31**) are readily prepared by acid-catalyzed arrangement of (+)-*endo*-3-bromocamphor (**28**) and (+)-*endo*-3,9-dibromocamphor (**29**), respectively. The mechanism of these fascinating rearrangements, in which the camphor configuration is inverted, will be described in a future report from our laboratory (cf. ref. 27).

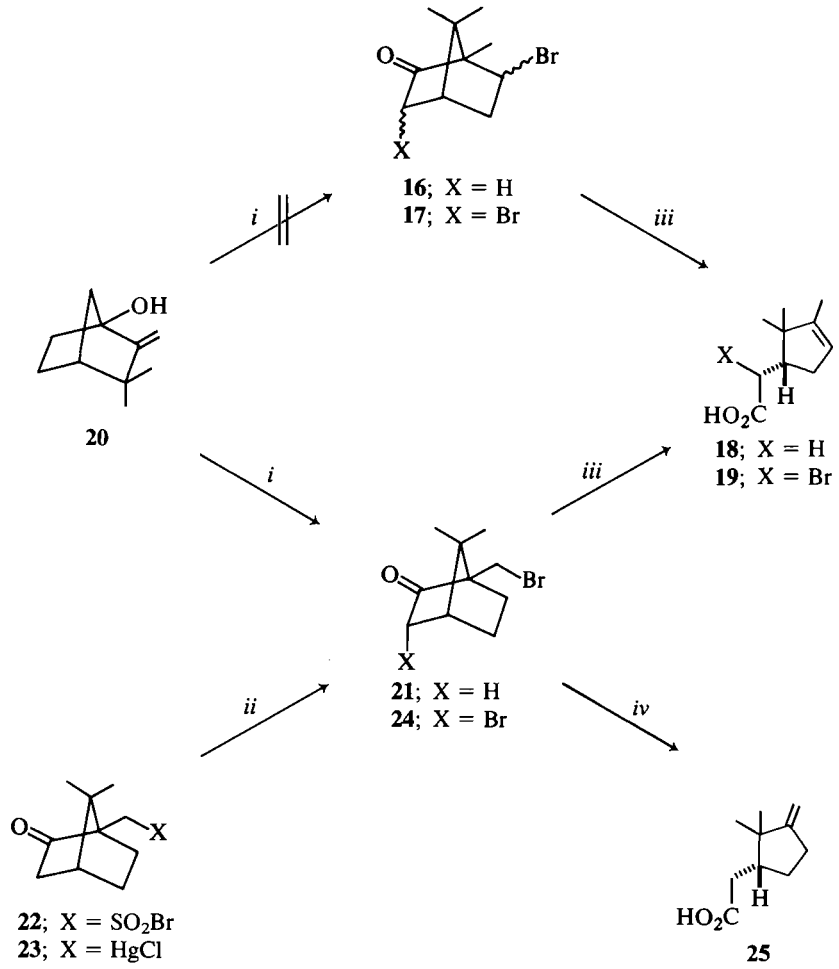

i, HBr; *ii*, *m*-xylene/heat *or* $Br_2/KBr/H_2O$; *iii*, KOH/EtOH/heat; *iv*, KOH/DMSO–H_2O (7:1)/65°C/1 h

SCHEME 5

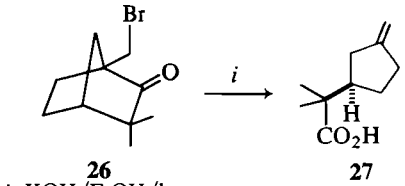

i, KOH/EtOH/heat

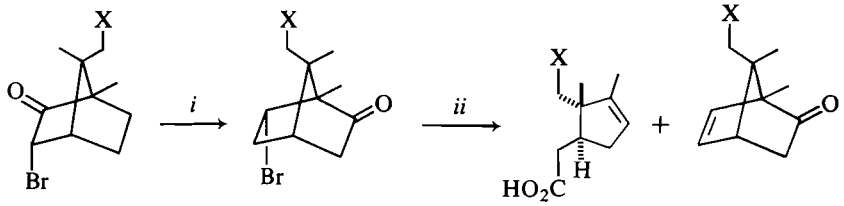

i, $ClSO_3H$/55°C/1 h; *ii*, KOH/DMSO–H_2O (7:1)/65°C/36 h *or* $KOBu^t/HOBu^t$

SCHEME 6

can be converted to hydroxy-α-campholenic acid (**33**) and (+)-5,6-dehydro-9-bromocamphor (**35**).

Aside from these mechanistic considerations, the ease and efficiency with which the bromo-acid **7**, hydroxy-acid **9**, and lactone **10** can be obtained from (+)-9,10-dibromocamphor (**6**) and bromo-ester **12**[5] from (+)-8,10-dibromocamphor (**11**) has prompted us to assess the potential of these compounds as chiral synthons in terpenoid and steroid synthesis and the results of our initial investigations have been described in recent reports (1, 8)[6] from this laboratory.

Experimental

Melting points (mp) were determined on a Kofler micro heating stage and are uncorrected. Infrared spectra were recorded on a Perkin–Elmer 137 spectrophotometer and optical rotations were made on a Perkin–Elmer 141 polarimeter. The ^{1}H nmr spectra were recorded on Bruker WH-400, Bruker WP-80, or Nicolet-Oxford H-270 instruments. Signal positions are given in delta (δ) with tetramethylsilane (TMS) as internal reference. The integrated areas and signal multiplicities are indicated in parentheses. Low resolution mass spectra were determined on a MAT CH-4 spectrometer and high resolution spectra were recorded on a Kratos MS-50 spectrometer. Gas–liquid chromatography was performed on a Hewlett–Packard model 5830A gas chromatograph with a 6 ft × ⅛ in. column (3% OV-17) or a Hewlett–Packard model 5880A gas chromatograph using 50 or 12 m × 0.2 mm columns (Carbowax 10M). Column chromatography was done using Merck silica gel 60 (230–400 mesh) and thin-layer chromatography (tlc) utilizing silica gel 1B2-F (Baker-flex) sheets. Microanalyses were performed by Mr. P. Borda, Microanalytical Laboratory, University of British Columbia.

(+)-9,10-Dibromocamphor (6) (5)[7]

To (+)-*endo*-3-bromocamphor (**28**) (Aldrich Chemical Co.) (100 g, 0.433 mmol) in an ice bath was added chlorosulphonic acid (80 mL) and bromine (35 mL, 0.683 mmol). The ice bath was then removed and the reaction stirred for 1 h before being added to ice/sodium bisulphite (solid). Extraction with ether (3 × 450 mL), followed by treatment of the ether layer with sodium bicarbonate, water (×3), and removal of the dried solvent provided (+)-3,9-dibromocamphor (**29**) as a white crystalline solid (133 g, 84% pure by glc; OV-17, 190°C). This material was used without further purification.

To the crude *endo*-3,9-dibromocamphor (133 g) at 0°C was added chlorosulphonic acid (160 mL) and bromine (40 mL, 0.78 mmol). The ice bath was removed, the flask covered with aluminum foil, and the reaction stirred for 6 days. Further portions of chlorosulphonic acid and bromine (20 mL and 15 mL and 15 mL, respectively) were added after the second and third days. The mixture was worked up as before to yield crude (+)-*endo*-3,9,10-tribromocamphor as a viscous dark orange oil (132 g). This was immediately dissolved in ether (250 mL) and glacial acetic acid (100 mL) and treated with zinc (35 g, 0.54 mmol) at 0°C (**care!**) over 20 min. The reaction was stirred vigorously for 45 min and then poured into water, extracted with ether (×3), and the excess acetic acid removed with sodium bicarbonate. Work-up in the usual way provided a viscous oil (72 g), which was a mixture of (+)-9,10-dibromocamphor (**6**) (55%) 9-bromocamphor (30%), and (−)-*anti*-7,9-dibromofenchone (8%) as determined by glc (OV-17, 190°C). (+)-9,10-Dibromocamphor (**6**) (30 g, 22% overall) was crystallized from the crude oil with methanol/petroleum ether.

In a separate experiment, the by-products were isolated and identified. Column chromatography (silica gel; petroleum ether/ether 24:1) provided (−)-*anti*-7,9-dibromofenchone as a white crystalline solid, mp 70.5–72°C; $[\alpha]_D$ −225.3° (*c* 1.13, MeOH); ν_{max} $(CHCl)_3$: 1740 cm^{-1}; δ ($CDCl_3$, 270 MHz): 1.11 (3H, s), 1.23 (3H, s), 1.44 (1H, m), 1.87 (2H, m), 2.30 (1H m), 2.53 (1H, d, J = 3.5 Hz), 3.36 (1H, d, J = 10.5 Hz), 3.48 (1H, d, J = 10.5 Hz), 4.19 (1H, br, s); *m/e* (relative intensity): 312/310/308 (M^+, 0.7/1.5/0.7), 231/229 (8/8), 203/201 (14/14), 121 (28), 107 (13), 93 (17), 81 (100), 79 (19). *Mol. Wt.* calcd. for $C_{10}H_{14}OBr_2$: 311.9371/309.9391/307.9411; found (high resolution mass spectrometry: 311.9362/309.9394/307.9367. *Anal.* calcd. for $C_{10}H_{14}OBr_2$: C 38.74, H 4.55, Br 51.55; found: C 38.81, H 4.50, Br 51.36. The structure and absolute configuration of this compound was confirmed by X-ray analysis.[8] Further elution provided 9-bromocamphor as a white crystalline solid.

(+)-9,10-Dibromocamphor ethylene ketal (2)

(+)-9,10-Dibromocamphor (**6**) (5.0 g, 16.1 mmol), ethylene glycol (15 mL), *para*-toluenesulphonic acid (100 mg), and dry benzene (60 mL) were refluxed in a Dean–Stark trap containing 4A molecular sieves for 1 week. The sieves were replaced every 24 h. The solution was poured into brine and extracted with ether (3 times). The combined organic layers were washed twice with water, dried ($MgSO_4$), and filtered through a silica gel pad. Removal of the solvent provided a crude oil (5.40 g). Column chromatography (silica gel, petroleum ether/ether 50:1) gave starting material (1.0 g) and (+)-9,10-dibromocamphor ethylene ketal (**2**) (3.66 g; 64% yield; 76% based on recovered starting material) as a white crystalline solid, mp 38–42°C; δ ($CDCl_3$, 400 MHz): 1.27 (3H, d, J = 1 Hz), 1.37 (1H, m), 1.50 (1H, d, J = 14 Hz), 1.80 (1H, m), 1.89 (1H, m), 2.02 (1H, m), 2.18 (2H, m), 3.43 (1H, d, J = 10 Hz), 3.51 (d) and 3.53 (d) (2H, AB quartet, J = 12 Hz), 3.69 (1H, dd, J = 10 Hz, 1 Hz), 3.72–3.99 (4H, m, ketal protons); *m/e* (relative intensity): 275/273 (M^+ − Br, 98/100), 193 (47), 149 (18), 131 (24), 121 (26), 107 (79), 105 (26). *Anal.* calcd. for $C_{12}H_{18}O_2Br_2$: C 40.71, H 5.12, Br 45.13; found: C 40.96, H 5.17, Br 45.00.

9,10-Dicyanocamphor ethylene ketal (3) and cyanoester (4)

(+)-9,10-Dibromocamphor ethylene ketal (**2**) (2.1 g, 5.9 mmol), sodium cyanide (0.87 g, 17.8 mmol), and potassium iodide (50 mg) were stirred in dry dimethylsulphoxide (25 mL) at 110°C under argon for 6 days. The mixture was poured into brine, extracted three times with ether, and the combined organic layers washed twice with brine, dried, and the solvent removed. The residue (1.1 g) was shown by glc (OV-17, 210°C) to be a mixture (4:3) of cyanoester (**4**) and 9,10-dicyanocamphor ethylene ketal (**3**). A portion of this material was subjected to column chromatography (silica gel; petroleum ether/ether 1:1) to provide a sample of 9,10-dicyanocamphor ethylene ketal (**3**), which was recrystallized from ether/petroleum ether to yield colourless needles, mp 73.5–74.5°C; ν_{max} ($CHCl_3$): 2250 cm^{-1}; δ ($CDCl_3$, 400 MHz): 1.33 (3H, s), 1.49 (1H, m), 1.45 (1H, d, J = 13.5 Hz; C(3) *endo* proton), 1.68 (1H, m), 1.81 (1H, m), 2.06 (1H, ddd, J = 13.5 Hz, 5 Hz and 3 Hz; C(3) *exo* proton), 2.18 (1H, dd, J = 4.5 Hz, 4.5 Hz; C(4) proton), 2.32 (1H, ddd, J = 13 Hz, 9 Hz, 4 Hz), 2.38 (d) and 2.46 (d) (2H, AB quartet, J = 18 Hz), 2.38 (d) and 2.54 (d) (2H, AB quartet, J = 18 Hz), 3.75–4.0 (4H, m, ketal protons); *m/e* (relative intensity): 246 (M^+, 0.9), 231 (1.1), 206 (100), 120 (56), 87 (96). *Mol. Wt.* calcd. for $C_{14}H_{18}O_2N_2$: 246.1368; found (high resolution mass spectrometry): 246.1376.

Further elution using pure ether provided the cyanoester (**4**) as a colourless oil; ν_{max} ($CHCl_3$): 2375, 1730, 1660 and 900 cm^{-1}; δ ($CDCl_3$, 400 MHz): 1.06 (3H, s), 1.42 (1H, m), 2.00 (2H, m, one proton exchangeable with D_2O), 2.29 (1H, dd, J = 16 Hz, 8 Hz), 2.35–2.50 (3H, m), 2.50 (2H, s, CH_2CN), 2.55 (1H, dd, J = 16 Hz, 4 Hz), 3.84 (2H, br s; sharpens to a multiplet on addition of D_2O; CH_2OH), 4.24 (2H, m; CH_2CH_2OH), 4.94 (1H, t, J = 2 Hz), 5.03 (1H, t, J = 2 Hz); *m/e* (relative intensity): 237 (M^+, 4.5), 176 (46),

[5]The enantiomers of **7**, **9**, **10**, **12**, and **13** are of course available from (−)-9,10-dibromocamphor and (−)-8,10-dibromocamphor, which can be prepared (5) from commercially available (−)-camphor or (−)-borneol.

[6]Some of these results were described at the C.I.C. Conference, Montreal, June 3–6, 1984, and at the International Symposium on the Chemistry of Natural Products, Edmonton, June 23–26, 1985.

[7]This is a modification of the method used by Dadson *et al.* (5*b*).

[8]S. J. Rettig and J. Trotter, U.B.C., unpublished results.

175 (25), 134 (96), 133 (29) 108 (100), 93 (46). *Mol. Wt.* calcd. for $C_{13}H_{19}O_3N$: 237.1365; found (high resolution mass spectrometry): 237.1366.

Bromohydroxy-ester (5)

(+)-9,10-Dibromocamphor ethylene ketal (**2**) (180 mg) was dissolved in dry dimethylsulphoxide (10 mL) and heated to 110°C for 4 h. The solution was cooled, acidified with 1 *N* hydrochloric acid, and extracted three times with ether. The ethereal layers were washed with water (3 times), dried, and evaporated to yield a colourless oil (94 mg). Purification by column chromatography (silica gel; petroleum ether/ether 2:1) gave starting material (34 mg) and the bromohydroxy-ester (**5**) (36.4 mg); ν_{max} (film): 3420 (br), 1740, 1660, 890 cm^{-1}; δ ($CDCl_3$, 400 MHz): 1.08 (3H, s), 1.35 (1H, m), 1.90 (1H, br s, exchangeable with D_2O), 1.97 (1H, m), 2.22 (1H, m), 2.30–2.47 (2H, m), 2.53–2.64 (2H, m), 3.37 (1H, d, J = 10 Hz), 3.46 (1H, d, J = 10 Hz), 3.85 (2H, m), 4.24 (2H, m), 4.85 (1H, t, J = 2.5 Hz), 5.00 (1H, t, J = 2.0 Hz); *m/e* (relative intensity): 292/290 (M^+, 0.1/0.1), 275/273 (1.4/1.3), 197 (45), 107 (100).

Methyl (1'R,2'R)-2-(2'-bromoethyl-2'-methyl-3'-methylenecyclopentyl)ethanoate (8); bromo-ester (8)

Sodium metal (0.41 g, 17.8 mmol) was added to dry methanol (50 mL) under argon at 0°C. When all the sodium had reacted, 9,10-dibromocamphor (**6**) (3.68 g, 11.9 mmol) was added, and after 6 h the reaction was terminated by acidifying with 1 *N* hydrochloric acid and then extracting three times with ether. The organic phase was washed with brine, dried ($MgSO_4$), and the solvent removed to yield the bromo-ester (**8**) (3.08 g, 99%), ν_{max} ($CHCl_3$): 1730, 1660, 900 cm^{-1}; δ ($CDCl_3$, 270 MHz): 1.05 (3H, s), 1.35 (1H, m), 1.93 (1H, m), 2.10 (1H, dd, J = 13.5 Hz, 11.5 Hz), 2.25–2.41 (2H, m), 2.46–2.59 (2H, m), 3.36 (d) and 3.45 (d) (2H, AB quartet, J = 12 Hz), 3.67 (3H, s; OCH_3), 4.84 (1H, t, J = 2.5 Hz), 4.98 (1H, t, J = 2 Hz); *m/e* (relative intensity): 262/260 (M^+, 0.1/0.1), 231/229 (1/1), 167 (57), 121 (15), 107 (100), 93 (22), 91 (24). *Mol. Wt.* calcd. for $C_{11}H_{17}O_2Br - OCH_3$: 231.0208/229.0228; found (high resolution mass spectrometry): 231.0211/229.0216.

(1'R,2'R)-2-(2'-Bromomethyl-2'-methyl-3'-methylenecyclopentyl) ethanoic acid (7); (−)-bromo-acid (7)

Method A

To a solution of (+)-9,10-dibromocamphor (**6**) (1.5 g, 4.8 mmol) in dimethylsulphoxide (51 mL) was added potassium hydroxide (1.35 g, 24 mmol) in water (10 mL). After 1 h, the yellow solution was poured into water and extracted once with ether. The ether layer was washed once with water and the combined aqueous layers were then carefully acidified with 6 *N* hydrochloric acid. This was extracted three times with ether and the combined ethereal layers washed with brine (twice), dried ($MgSO_4$), and evaporated to yield the bromo-acid (**7**) (1.17 g, 98%) as a white crystalline solid, one spot on tlc. Recrystallization of a small amount of this material from petroleum ether afforded pure bromo-acid (**7**), mp 62–64°C; $[\alpha]_D$ −45.8° (*c* 0.4, MeOH); ν_{max} ($CHCl_3$): 2950 (br), 1705, 1640, 890 cm^{-1}; δ ($CDCl_3$, 400 MHz): 1.08 (3H, s; angular methyl group), 1.39 (1H, m), 2.01 (1H, m), 2.18 (1H, dd, J = 16 Hz, 10 Hz), 2.32–2.48 (2H, m; allylic protons), 2.55 (1H, m; methine proton), 263 (1H, dd, J = 16 Hz, 4 Hz), 3.39 (d) and 3.47 (2H, AB quartet, J = 10 Hz), 4.86 (1H, t, J = 2 Hz), 5.00 (1H, t, J = 2 Hz); *m/e* (relative intensity): 248/246 (M^+, 0.4/0.4), 188/186 (4/4), 167 (7), 166 (17), 153 (100), 111 (32), 107 (98). *Anal.* calcd. for $C_{10}H_{15}O_2Br$: C 48.58, H 6.12, Br 32.35; found: C 48.47, H 6.16, Br 32.20.

Method B

(+)-9,10-Dibromocamphor (**6**), (1.0 g, 3.2 mmol), 0.5 *N* potassium hydroxide (80 mL, 40 mmol), and tetrahydrofuran (80 mL) were stirred at room temperature for 4.5 h. Work-up as described above gave the bromoacid (**7**) (0.75 g, 94%) as a white solid.

(1'R,2'R)-2-(2'-Hydroxymethyl-2'-methyl-3'-methylenecyclopentyl)ethanoic acid (9); (−)-hydroxy-acid (9)

Method A: From (+)-9,10-dibromocamphor (6)

A solution of (+)-9,10-dibromocamphor (**6**) (1.5 g, 4.8 mmol), potassium hydroxide (1.35 g, 24 mmol), dimethylsulphoxide (51 mL), and water (9 mL) was stirred at room temperature for 1.5 h, then at 65°C for 20 h. This was poured into ice-cold water and worked up as before to yield the hydroxy-acid (**9**) (0.807 g, 91%) as a white crystalline solid. A pure sample of **9** was obtained by recrystallization of a portion from ethyl acetate/petroleum ether, mp 118–119°C; $[\alpha]_D$ −21.4° (*c* 0.35, MeOH); ν_{max} ($CHCl_3$): 2850 (br), 1705, 890 cm^{-1}; δ ($CDCl_3$, 400 MHz): 0.88 (3H, s), 1.39 (1H, m), 1.99 (1H, m), 2.22 (1H, dd, J = 14 Hz, 9 Hz), 2.34 (1H, m), 2.40–2.56 (3H, m), 3.42 (d) and 3.53 (d) (2H, AB quartet, J = 11 Hz), 4.82 (1H, t, J = 2.5 Hz), 5.02 (1H, t, J = 2.0 Hz); *m/e* (relative intensity): 184 (M^+, 2), 166 (8), 154 (32), 153 (34), 107 (97), 95 (85), 94 (100), 93 (65), 79 (52). *Mol. Wt.* calcd. for $C_{10}H_{16}O_3$: 184.1100; found (high resolution mass spectrometry): 184.1096. *Anal.* calcd. for $C_{10}H_{16}O_3$: C 65.19, H 8.75; found: C 64.97, H 8.61.

Method B: From (1R,6R)-1-methyl-9-methylene-3-oxa-4-oxobicyclo[4.3.0]nonane (10); ((−)-lactone (10))

(−)-Lactone (**10**) (49 mg, 0.3 mmol) was dissolved in tetrahydrofuran (5 mL) and treated with 0.5 *N* potassium hydroxide solution (5 mL, 2.5 mmol) for 30 min. The solution was partitioned between ether and 1 *N* hydrochloric acid. After the usual work-up, the hydroxy-acid **9** was obtained as a white crystalline solid (54 mg, 100%).

(1R,6R)-1-Methyl-9-methylene-3-oxa-4-oxobicyclo[4.3.0]nonane (10); (−)-lactone (10)

A solution of the bromo-acid (**7**) (1.67 g, 6.8 mmol), potassium hydroxide in dimethylsulphoxide/water 9:1 (0.277 *M*, 24.55 mL, 6.8 mmol), silver(I) oxide (0.35 g, 1.5 mmol), and dimethylsulphoxide (111 mL) was stirred at room temperature for 1 h and then at 70°C for 1 h.

The solution was poured into brine, extracted with ether (×3), and the ether extracts washed with brine and dried. Removal of the solvent provided a yellow solid (1.23 g), which on trituration with cold petroleum ether gave the lactone (**10**) (1.04 g, 92%; 96% pure by glc; 3% OV-17, 160°C) as a crystalline solid. Subsequent recrystallization from petroleum ether provided pure lactone (**10**), mp 96.5–98.5°C; $[\alpha]_D$ −27.3° (*c* 0.42, CH_2Cl_2); ν_{max} ($CHCl_3$): 1740, 1650, 890 cm^{-1}; δ ($CDCl_3$, 400 MHz): 1.05 (3H, s; angular methyl group), 1.45 (1H, 9-line multiplet), 1.87 (1H, m), 2.01 (1H, 7-line multiplet; methine proton), 2.43 (1H, dd, J = 18 Hz, 13.5 Hz; H_A), 2.43 (1H, m), 2.62 (1H, m), 2.78 (1H, dd, J = 18 Hz, 5.5 Hz; H_B), 4.23 (d) and 4.37 (d) (2H, AB quartet, J = 10 Hz), 4.63 (1H, t, J = 2.5 Hz), 4.83 (1H, t, J = 2 Hz); *m/e* (relative intensity): 166 (M^+, 15), 107 (23), 95 (18), 94 (100), 93 (24), 79 (70). *Mol. Wt.* calcd. for $C_{10}H_{14}O_2$: 166.0994; found (high resolution mass spectrometry): 166.0994. *Anal.* calcd. for $C_{10}H_{14}O_2$: C 72.26, H 8.49, O 19.25; found: C 72.12, H 8.68, O 19.13.

Cleavage of (+)-10-bromocamphor (21); (+)-isocampholenic acid (25)

(+)-10-Bromocamphor (**21**) (28), (234 mg, 1.0 mmol) and potassium hydroxide (284 mg, 5.0 mmol) were stirred in dimethylsulphoxide (11 mL) and water (1.5 mL) at 65°C for 1 h. The solution was cooled, poured into brine, and extracted with ether. The aqueous phase was then acidified with 6 *N* hydrochloric acid and further extracted with ethyl acetate (×3). After two washings with brine, the organic extracts were dried ($MgSO_4$) and evaporated to yield a yellow oil (180 mg). Column chromatography (silica gel; petroleum ether/ether 1:1) gave isocampholenic acid (**25**) as a colourless oil (130.2 mg, 77%); $[\alpha]_D$ +1.6° (*c* 0.5, CH_2Cl_2); ν_{max} (film): 3000 (br), 1710, 1660, 885 cm^{-1}; δ ($CDCl_3$, 400 MHz): 0.85 (3H, s), 1.09 (3H, s), 1.38 (1H, m), 1.98 (2H, m), 2.15 (1H, dd, J = 15 Hz, 10 Hz), 2.36 (1H, m), 2.46 (1H, m), 2.46 (1H, dd, J = 15 Hz, 3.5 Hz), 4.78 (1H, t, J = 2.5 Hz), 4.80 (1H, t, J = 2 Hz); *m/e* (relative intensity): 168 (M^+, 2), 153 (26), 108 (100), 93 (97), 91 (37), 79 (33). *Mol. Wt.* calcd. for $C_{10}H_{16}O_2$: 168.1150; found (high resolution mass spectrometry): 168.1152. *Anal.* calcd. for $C_{10}H_{16}O_2$: C 71.39, H 9.59; found: C 71.13, H 9.59.

Cleavage of (−)-endo-6-bromocamphor (30)

(−)-*endo*-6-Bromocamphor (**30**) (27) (6.5 g, 0.028 mol), potassium

hydroxide (7.89 g, 0.14 mol), dimethylsulphoxide (280 mL), and water (40 mL) were stirred at 70°C for 96 h. The solution was diluted with water, extracted with ether (3 × 100 mL), and worked up in the usual way to yield a yellow oil (2.2 g). Flash chromatography on silica gel (petroleum ether/ether 9:1) afforded a volatile white solid, (+)-dehydrocamphor (**34**) (2.0 g, 47%); $[\alpha]_D$ +756° (*c* 0.50, CH_2Cl_2) (lit. (30), for enantiomer, $[\alpha]_D$ −735° (*c* 1.0, EtOH), lit. (31) $[\alpha]_D$ −731° (EtOH)); ν_{max} ($CHCl_3$): 1735 cm^{-1}; δ ($CDCl_3$, 400 MHz) (cf. ref. 32): 0.91 (3H, s), 1.01 (3H, s), 1.07 (3H, s), 1.93 (1H, d, *J* = 16.5 Hz; C(3) *endo* proton), 2.22 (1H, ddd, *J* = 16.5 Hz, 3.5 Hz, 1.0 Hz; C(3) *exo* proton), 2.68 (1H, br s; C(4) proton), 5.58 (1H, br d, *J* = 5.5 Hz; C(6) proton), 6.71 (1H, dd, *J* = 5.5 Hz, 3 Hz; C(5) proton); *m/e* (relative intensity): 150 (M^+, 12), 93 (58), 85 (59), 71 (92), 69 (100). *Mol. Wt.* calcd. for $C_{10}H_{14}O$: 150.1045; found (high resolution mass spectrometry): 150.1049. Further elution provided starting material (65 mg).

The aqueous phases were acidified with 1 *N* hydrochloric acid, then extracted with ether (3 × 300 mL), and the combined extracts washed with brine. Removal of the solvent gave (−)-α-campholenic acid (**32**) (1.88 g, 40%); $[\alpha]_D$ −8.2° (*c* 2.25, CH_2Cl_2) (lit. (33) $[\alpha]_D$ −9.0° (*c* 1.1, $CHCl_3$)); ν_{max} (film): 2950 (br), 1710 cm^{-1}; δ ($CDCl_3$, 400 MHz): 0.80 (3H, s), 1.02 (3H, s), 1.62 (3H, br s), 1.94 (1H, m), 2.20–2.35 (2H, m), 2.40–2.52 (2H, m), 5.24 (1H, br s); *m/e* (relative intensity): 168 (M^+, 28), 153 (64), 135 (28), 108 (100), 107 (82), 93 (80), 91 (42).

Cleavage of (−)-endo-6,9-dibromocamphor (31)

(−)-*endo*-6,9-Dibromocamphor (**31**) (34) (423 mg, 1.36 mmol), potassium hydroxide (382 mg, 6.8 mmol), dimethylsulphoxide (13 mL), and water (2 mL) were stirred at 60°C for 24 h. Work-up as before provided (before acidification of the aqueous phase) a crude oil (136 mg). Chromatography (silica gel; petroleum ether/ether 25:1) gave (+)-9-bromodehydrocamphor (**35**) (68.2 mg, 22%) as a white crystalline solid, mp 46.5–48.5°C (sealed tube); $[\alpha]_D$ +377.2° (*c* 0.5, CH_2Cl_2); ν_{max} ($CHCl_3$): 1740 cm^{-1}; δ ($CDCl_3$, 400 MHz): 1.05 (3H, s), 1.08 (3H, d, *J* = 1 Hz; C(9) methyl), 2.01 (1H, d, *J* = 17 Hz; C(3) *endo* proton), 2.22 (1H, ddd, *J* = 17 Hz, 3.5 Hz, 1 Hz; C(3) *exo* proton), 3.00 (1H, br s; C(4) proton), 3.22 (1H, d, *J* = 10 Hz), 4.02 (1H, dd, *J* = 10 Hz, 1 Hz), 5.68 (1H, br d, *J* = 6 Hz; C(6) proton), 6.49 (1H, dd, *J* = 6 Hz, 3 Hz; C(5) proton); *m/e* (relative intensity): 230/228 (M^+, 2/2), 188/186 (19/19), 107 (100), 91 (29), 79 (21). *Mol. Wt.* calcd. for $C_{10}H_{13}OBr$: 230.0129/228.0150; found (high resolution mass spectrometry): 230.0135/228.0149. *Anal.* calcd. for $C_{10}H_{13}OBr$: C 52.42, H 4.72, Br 34.87; found: C 52.40, H 5.60, Br 34.77.

Acidification of the aqueous phase and work-up as before provided a crude solid (139 mg), which after chromatography (silica gel; petroleum ether/ether/acetic acid 150:50:1) gave the hydroxy-acid (**33**) (59 mg) as a white crystalline solid, mp 102–103.5°C; $[\alpha]_D$ −19.52° (*c* 0.21, CH_2Cl_2); ν_{max} ($CHCl_3$): 3000 (br), 1705 cm^{-1}; δ ($CDCl_3$, 400 MHz): 0.82 (3H, s), 1.65 (3H, br s), 1.97 (1H, m), 2.34 (1H, dd, *J* = 16 Hz, 9 Hz), 2.64 (1H, dd, *J* = 16 Hz, 5.5 Hz), 2.64 (1H, m), 2.70 (1H, m), 3.42 (1H, d, *J* = 11 Hz), 3.54 (1H, d, *J* = 11 Hz), 5.41 (1H, br s); *m/e* (relative intensity): 184 (M^+, 0.01), 166 (17), 151 (32), 107 (59), 94 (100), 93 (80), 91 (63), 79 (95). *Mol. Wt.* calcd. for $C_{10}H_{16}O_3$: 184.1100; found (high resolution mass spectrometry): 184.1102. *Anal.* calcd. for $C_{10}H_{16}O_3$: C 65.19, H 8.75; found: C 65.01, H 8.70.

Cleavage of (+)-8,10-dibromocamphor (11) (ref. 5b)

(a) *With potassium hydroxide*

(+)-8,10-Dibromocamphor (**11**) (159 mg, 0.51 mmol), potassium hydroxide (144 mg, 2.56 mmol), dimethylsulphoxide (6 mL), and water (0.75 mL) were stirred for 1 h at room temperature. The mixture was poured into water, extracted with ether, and the aqueous layer subsequently acidified (1 *N* hydrochloric acid) and extracted with ethyl acetate (×3). After two washings with brine, the ethyl acetate extract was evaporated to provide a crude oil (118 mg). Flash chromatography on silica gel (petroleum ether/ether 1:1) gave bicyclic acid (**15**) (66.2 mg; 78%), as an oil that crystallized on standing, mp 45–48°C; $[\alpha]_D$ +167.9° (*c* 0.14, CH_2Cl_2); ν_{max} (film): 2950 (br), 1700, 1660, 890 cm^{-1}; δ ($CDCl_3$, 400 MHz): 1.33 (3H, s), 1.76 (2H, m), 1.99 (1H, ddd, *J* = 12 Hz, 9 Hz, 2 Hz), 1.32 (1H, dd, *J* = 12 Hz, 9 Hz), 2.37 (1H, m), 2.71 (1H, m; H_D), 2.77 (1H, m), 3.38 (1H, ddd, *J* = 9 Hz, 9 Hz, 9 Hz), 4.63 (1H, br s), and 4.75 (1H, br s); irradiation at δ 3.38 causes the signal at δ 1.99 to collapse to a doublet of doublets (*J* = 12 Hz, 2 Hz), δ 1.32 to collapse to a doublet (*J* = 12 Hz), and δ 2.71 is simplified. Irradiation at 1.76 causes the signal at δ 2.37 to collapse to a broad doublet (*J* = 16 Hz), δ 2.77 becomes a broad doublet (*J* = 16 Hz), and δ 2.71 becomes a broad doublet (*J* = 9 Hz); *m/e* (relative intensity): 166 (M^+, 1), 151 (6), 121 (15), 105 (21), 94 (76), 93 (31), 91 (37), 79 (100), 77 (37). *Mol. Wt.* calcd. for $C_{10}H_{14}O_2$: 166.0994; found (high resolution mass spectrometry): 166.0992. *Anal.* calcd. for $C_{10}H_{14}O_2$: C 72.26, H 8.49; found: C 71.99, H 8.52.

Further elution provided the lactone (**13**) (17.5 mg, 20%) as a crystalline solid; mp 55–56.5°C; $[\alpha]_D$ +29.6° (*c* 0.23, CH_2Cl_2); ν_{max} ($CHCl_3$): 1740, 1660, 890 cm^{-1}; δ ($CDCl_3$, 400 MHz): 1.20 (3H, s), 1.40 (1H, 6-line multiplet), 2.03 (1H, 6-line multiplet), 2.19 (1H, dddd, *J* = 7 Hz, 7 Hz, 7 Hz, 7 Hz), 2.33 (1H, dd, *J* = 15 Hz, 7.5 Hz), 2.43 (2H, m), 2.64 (1H, dd, *J* = 15 Hz, 7 Hz), 3.96 (1H, d, *J* = 11.5 Hz), 4.07 (1H, d, *J* = 11.5 Hz), 4.82 (1H, t, *J* = 2 Hz), 5.02 (1H, t, *J* = 2 Hz); *m/e* (relative intensity): 166 (M^+, 1), 136 (21), 107 (25), 94 (100), 79 (82). *Mol. Wt.* calcd. for $C_{10}H_{14}O_2$: 166.0994; found (high resolution mass spectrometry): 166.0993. *Anal.* calcd. for $C_{10}H_{14}O_2$: C 72.26, H 8.49; found: C 72.10, H 8.50.

(b) *With sodium methoxide*

Sodium metal (17 mg, 0.74 mmol) was added to dry methanol (2.5 mL) and, when all the metal had reacted, (+)-8,10-dibromocamphor (**11**) (105 mg, 0.34 mmol) was added in one portion. The reaction was stirred at room temperature under an argon atmosphere for 20 h and then acidified with a few drops of saturated ammonium chloride solution. Removal of methanol followed by extraction with ether yielded bromo-ester **12** as a colourless oil (88 mg, 98% yield); ν_{max} ($CHCl_3$): 1740, 1660, 890 cm^{-1}; δ ($CDCl_3$, 80 MHz): 1.23 (3H, s), 1.3–2.7 (7H, m), 3.32 (2H, s; CH_2Br), 3.70 (3H, s; OCH_3), 4.85 (1H, t, *J* = 2.5 Hz), 4.98 (1H, t, *J* = 2 Hz); *m/e* (relative intensity): 262/260 (M^+, 0.1/0.1), 231/229 (1/1), 167 (27), 107 (100).

Conversion of (+)-8-bromocamphor to (+)-3,8-cyclocamphor

(+)-8-Bromocamphor (447 mg, 1.94 mmol) and potassium hydroxide (542 mg, 9.68 mmol) were stirred in dimethylsulphoxide (22 mL) and water (3 mL) at room temperature. After 20 min, the dark orange solution was diluted with water and extracted with ether (×3). Removal of the solvent under reduced pressure afforded (+)-3,8-cyclocamphor (240 mg, 83%; 98% pure by capillary glc; OV-101, 120°C), which was crystallized (low temperature) from petroleum ether, mp 148–151°C (sealed tube), (lit. (29) mp 151–152.5°C); $[\alpha]_D$ +194.2° (*c* 0.652, $CHCl_3$) (lit. (29), for enantiomer, $[\alpha]_D$ −232° ($CHCl_3$)); ν_{max} ($CHCl_3$): 1745 cm^{-1}; δ ($CDCl_3$, 400 MHz): 1.05 (3H, s), 1.06 (3H, s), 1.39 (1H, ddd, *J* = 14 Hz, 8 Hz, 8 Hz), 1.60 (1H, m; C(5) *exo* proton), 1.64 (1H, d, *J* = 8 Hz; C(8) proton), 1.80 (1H, ddd, *J* = 13 Hz, 9 Hz, 2.5 Hz), 1.90 (1H, m), 1.97 (1H, dd, *J* = 8 Hz, 3 Hz), 2.49 (1H, dd, *J* = 5 Hz, 2.5 Hz; C(4) proton), 2.86 (1H, dd, *J* = 3 Hz, 2.5 Hz; C(3) *endo* proton). Decoupling of the proton at δ 1.97 causes the doublet at δ 1.64 to collapse to a singlet and the signal at 2.86 to a doublet (*J* = 2.5 Hz). Decoupling the signal at δ 2.49 causes the proton at δ 2.86 to appear as a doublet (*J* = 3 Hz) and the signal at δ 1.60 is simplified; *m/e* (relative intensity): 150 (M^+, 11), 122 (22), 107 (61), 95 (100), 91 (54), 79 (93). *Exact Mass* calcd. for $C_{10}H_{14}O$: 150.1045; found: 150.1041.

Acknowledgement

We are grateful to the Natural Sciences and Engineering Research Council of Canada for financial support.

1. T. MONEY. Nat. Prod. Rep. **2**, 253 (1985).
2. (*a*) C. R. ECK, R. W. MILLS, and T. MONEY. J. Chem. Soc. Perkin Trans. 1, 251 (1975); (*b*) P. CACHIA, N. DARBY, C. R.

ECK, and T. MONEY. J. Chem. Soc. Perkin Trans. 1, 359 (1976); (*c*) W. M. DADSON and T. MONEY. J. Chem. Soc. Chem. Commun. 112 (1982); (*d*) W. L. MEYER, C. E. CAPSHEW, J. H. JOHNSON, A. R. KLUSENER, A. P. LOBO, and R. N. MCCARTY. J. Org. Chem. **42**, 527 (1977).

3. (*a*) F. S. KIPPING and W. J. POPE. J. Chem. Soc. **63**, 548 (1893); (*b*) G. B. KAUFFMAN. J. Prakt. Chem. **33**, 295 (1966), and references cited; (*c*) W. L. MEYER, A. P. LOBO, and R. N. MCCARTY. J. Org. Chem. **32**, 1754 (1967); (*d*) H. NISHIMITZU, M. NISHIKAWA, and H. HAGIWARA. Proc. Jpn. Acad. **27**, 285 (1951); (*e*) E. J. COREY, S. W. CHOW, and R. A. SCHERRER. J. Am. Chem. Soc. **79**, 5773 (1957).
4. (*a*) A. REYCHLER. Bull. Soc. Chim. Paris, **19**, 120 (1898); (*b*) P. D. BARTLETT and L. H. KNOX. Org. Synth. **45**, 12 (1965), and references therein; (*c*) F. DALLACKER, K. ULRICHS, and M. LIPP. Liebigs. Ann. Chem. **667**, 50 (1963), and references cited.
5. (*a*) M. NISHIKAWA and H. HAGIWARA. J. Pharm. Soc. Jpn. **74**, 76, 81 (1954); (*b*) W. M. DADSON, M. LAM, T. MONEY, and S. E. PIPER. Can. J. Chem. **61**, 343 (1983).
6. (*a*) A. R. BATTERSBY, D. G. LAING, and R. RAMAGE. J. Chem. Soc. Perkin Trans 1, 2743 (1972), and references cited; (*b*) G. E. GREAM, D. WEGE, and M. MULAR. Aust. J. Chem. **27**, 567 (1974); (*c*) G. R. KROW. Tetrahedron, **37**, 2697 (1981), and references cited; (*d*) R. R. SAUERS. J. Am. Chem. Soc. **81**, 923 (1959), and references cited; (*e*) R. R. SAUERS and G. P. AHEARN. J. Am. Chem. Soc. **83**, 2759 (1961); (*f*) H. J. LIU and W. H. CHAN. Can. J. Chem. **57**, 708 (1979); **60**, 1081 (1982); (*g*) R. V. STEVENS, F. C. A. GAETA, and D. S. LAWRENCE. J. Am. Chem. Soc. **105**, 7713 (1983), and references cited; (*h*) J. D. CONNOLLY and K. H. OVERTON. J. Chem. Soc. 3366 (1961); (*i*) R. V. STEVENS and D. S. LAWRENCE. Tetrahedron, **41**, 93 (1985); (*j*) P. T. LANSBURY, D. J. MAZUR, and J. S. SPRINGER. J. Org. Chem. **50**, 1632 (1985).
7. (*a*) J. BREDT. Chem. Ber. **26**, 3047 (1893); (*b*) I. KITAGAWA, H. SHIBUYA, H. FUJIOKA, A. KAJIWARA, Y. YAMAMOTO, S. TSUJI, A. TAKAGI, and M. HORI. Chem. Pharm. Bull. **29**, 2540 (1981); (*c*) R. B. WOODWARD. Pure Appl. Chem. **17**, 519 (1968); **25**, 283 (1971); **33**, 145 (1973); (*d*) C. H. HASSEL. Org. React. **9**, 93 (1957); (*e*) D. MILJKOVIC, J. PETROVIC, M. STAGIC, and M. MILJKOVIC. J. Org. Chem. **38**, 3585 (1973); (*f*) F. S. KIPPING. J. Chem. Soc. **69**, 913 (1896); (*g*) F. S. KIPPING and W. J. POPE. J. Chem. Soc. **71**, 962 (1897); **71**, 989 (1897).
8. (*a*) J. H. HUTCHINSON, T. MONEY, and S. E. PIPER. J. Chem. Soc. Chem. Commun. 455 (1984); (*b*) J. H. HUTCHINSON and T. MONEY. Tetrahedron Lett. **26**, 1819 (1985); (*c*) J. H. HUTCHINSON and T. MONEY. Can. J. Chem. **63**, 3182 (1985); (*d*) J. H. HUTCHINSON, T. MONEY, and S. E. PIPER. J. Chem. Soc. Chem. Commun. 288 (1986); (*e*) J. H. HUTCHINSON and T. MONEY. Can. J. Chem. In press; (*f*) J. H. HUTCHINSON, T. MONEY, and S. E. PIPER. Can. J. Chem. In press.
9. (*a*) R. B. TURNER and R. H. GARNER. J. Am. Chem. Soc. **79**, 253 (1957); (*b*) R. FLECK. J. Org. Chem. **22**, 439 (1957).
10. E. J. COREY, M. OHNO, S. W. CHOW, and R. A. SCHERRER. J. Am. Chem. Soc. **81**, 6305 (1959).
11. K. B. BECKER and C. A. GROB. *In* The chemistry of double-bonded functional groups. Part 2, Suppl. *Edited by* A. S. Patai. Interscience, New York. 1977. pp. 653–723.
12. M. O. FORSTER. J. Chem. Soc. **81**, 264 (1902).
13. H. BURGESS. J. Chem. Soc. **125**, 2375 (1924).
14. D. S. TARBELL and F. C. LOVELESS. J. Am. Chem. Soc. **80**, 1963 (1958).
15. S. A. ACHMAD and G. W. K. CAVILL. Aust. J. Chem. **16**, 858 (1963); **18**, 1979 (1965).
16. (*a*) J. WOLINSKY and D. CHAN. J. Org. Chem. **30**, 41 (1965); (*b*) J. WOLINSKY and R. O. HUTCHINS. J. Org. Chem. **37**, 3294 (1972).
17. J. N. MARX and L. R. NORMAN. J. Org. Chem. **40**, 1602 (1975).
18. P. YATES, M. J. JORGENSEN, and P. SINGH. J. Am. Chem. Soc. **91**, 4793 (1969).
19. H. RUPE and K. SCHAFER. Helv. Chim. Acta, **11**, 463 (1928).
20. T. HUDLICKY and R. P. SHORT. J. Org. Chem. **47**, 1522 (1982).
21. J. L. BELLETIRE and D. R. WALLEY. Tetrahedron Lett. **24**, 1475 (1983).
22. E. WENKERT, P. BAKUZIS, R. J. BAUMGARTEN, C. L. LEICHT, and H. P. SCHENK. J. Am. Chem. Soc. **93**, 3028 (1971), and references cited.
23. H. E. ARMSTRONG and T. M. LOWRY. J. Chem. Soc. 1441 (1902); 1462 (1902).
24. E. WEDEKIND, D. SCHENK, and R. STUSSER. Chem. Ber. **56**, 633 (1923).
25. P. LIPP and F. LAUSBERG. Justus Liebigs Ann. Chem. **436**, 274 (1924).
26. J. D. LOUDON. J. Chem. Soc. 823 (1933).
27. J. H. HUTCHINSON. Ph.D. Thesis, University of British Columbia, Vancouver. 1985.
28. F. DALLACKER, K. ULRICHS, and M. LIPP. Justus Liebigs Ann. Chem. **667**, 550 (1963).
29. E. J. COREY, M. OHNO, S. W. CHOW, and R. A. SCHERRER. J. Am. Chem. Soc. **81**, 6305 (1959).
30. (*a*) D. E. BAYS, R. C. COOKSON, and S. MACKENZIE. J. Chem. Soc. (B), 215 (1967); (*b*) D. E. BAYS and R. C. COOKSON. J. Chem. Soc. (B), 226 (1967).
31. Y. ASAHINA, M. ISHIDATE, and T. TUKAMOTO. Chem. Ber. **69B**, 349 (1936); **69B**, 355 (1936).
32. P. J. MALKONEN and J. PAASIVIRTA. Suom. Kemistil. B, **43**, 457 (1970).
33. H. J. LIU and W. H. CHAN. Can. J. Chem. **60**, 1081 (1982).
34. M. NISHIKAWA. J. Pharm. Soc. Jpn. **72**, 634 (1952).

The dilemma of estimating forms of sulfur in low-sulfur low rank coals

SUJIT K. CHAKRABARTTY AND ANGELO IACCHELLI

Coal Research Department, Alberta Research Council, Devon Coal Research Centre, P.O. Bag #1310, Devon, Alta., Canada T0C 1E0

Received August 23, 1985

S. K. CHAKRABARTTY and A. IACCHELLI. Can. J. Chem. **64**, 861 (1986).

The analytical methods for estimating forms of sulfur in coals are reviewed on the basis of sulfur analyses of Western Canadian low sulfur subbituminous coals. The reasons for the variance in analyses are examined, and a novel method of analysis is recommended for evaluation

S. K. CHAKRABARTTY et A. IACCHELLI. Can. J. Chem. **64**, 861 (1986).

On présente une revue des méthodes analytiques permettant qu'évaluer diverses formes de soufre dans des charbons; cette revue est basée sur des analyses de soufre dans des charbons subbitumineux de l'ouest canadien contenant de faibles niveaux de soufre. On examine les raisons qui expliquent pourquoi les analyses conduisent à des résultats variables et on recommande une nouvelle méthode d'analyse pour l'évaluation.

[Traduit par la revue]

Introduction

The importance of coal as boiler fuel in power plants, particularly in North America, and the development of new coal resources have resulted in a renewed interest in coal analytical techniques. Having experienced the effect of acid rains, it is imperative that the forms of sulfur in coal should be determine precisely before it is combusted in a large utility boiler.

Sulfur in coal is recognized as existing in three forms: (*1*) inorganic sulfate (S_s), as ferrous sulfate and gypsum; (*2*) inorganic sulfides (S_p), generally as pyrites, although sulfides of zinc and lead may occur in some coals; and (*3*) as organic sulfur compounds (S_o) (1, 2). Elemental sulfur is occasionally detected and may be formed by weathering of exposed deposits (1). Most of the inorganic sulfur can be extracted by sequential treatment with hydrochloric and nitric acids. ASTM methods prescribe meticulous extraction of ground coal with dilute hydrochloric acid to remove soluble iron compounds including $FeSO_4$ and other sulfates. The HCl-washed coal is then treated with nitric acid, which dissolves pyrites (FeS_2), and iron is determined in the extracts (3). In the absence of standard methods for determining organic sulfur, S_o, the differences $S_o = S_T - (S_s + S_p)$ is denoted as sulfur present in the organic matrix as organo-sulfur compounds. The cumulative errors in determining S_T, S_s, and S_p are reflected in the values of S_o.

Simultaneous determination of iron and sulfur in various forms using suitable methods is more reliable than relying on either iron or sulfur analyses alone, but multifarious problems are encountered. Pyrites in coal occur as ultrafine particles frequently coated with, or encapsulated in, organic matter or minerals such as kaoline. Complete extraction of pyritic iron thus becomes difficult. Though it is claimed that nitric acid extractions isolate pyritic iron quantitatively, some of the non-pyritic iron may also be extracted along with pyrites and would be counted as pyritic iron. On the other hand, a loss of sulfur by oxidation during nitric acid extraction is a distinct possibility, and non-stoichiometry of iron-to-sulfur ratios poses a problem in assigning the analyses as pyrites, S_p. Young and Zawadzki (4) provided a convenient method for S_p determination, using the iron content of hydrochloric acid-washed coal as a measure of pyrite when extracted from 750°C ash, but a fair amount of sulfur is lost during ashing and could not be directly measured by this method. It has been suggested that a low temperature ashing method (5) could be used for simultaneous estimation of iron and sulfur, but the presence of alkali and alkaline-earth metals in coal minerals and in the organic matrix (as cations corresponding to carboxylate anions) would allow organic sulfur to be captured in low temperature ash and to interfere in the apparent pyrite stoichiometry.

The magnitude of errors is intensified when the total sulfur is low and a microanalytical technique is employed for analysis of forms of sulfur. For example, the sulfur content of Canadian Cretaceous coals used in power plant boilers is less than 1%. To meet emission standards and other regulations, a sound knowledge of the forms of sulfur and the associated chemistry should be at hand to provide a reliable guide to anticipated technological and environmental problems. The purpose of this paper is to review various modifications of the ASTM methods to analyse forms of sulfur in low-sulfur low rank coals. This review illustrated the dilemma of estimating the forms of sulfur in coal, and suggests the problem be resolved through the development of a procedure for the direct determination of organic sulfur or, alternatively, a method that permits the accurate determination of the iron-to-sulfur stoichiometry in the pyrite present in coal.

Analytical methods: experimental

Coal samples

Representative specimens of coals from eight deposits in central Alberta were used for this study. The specimens belong to three geological formations, and the ASTM ranking of samples was subbituminous A, B, and C (6).

Total sulfur determination

Total combustible sulfur in coal specimens was determined according to ASTM D4239 using the Leco SC-32 model sulfur determinator wherein 250-mg samples of −200 mesh air-dried coal are combusted in a stream of oxygen at 1350°C. The combustion products are freed from entrained particles and moisture by passage through a magnesium perchlorate trap, and an equilibrium mixture of SO_2 and SO_3 in the gas stream is determined by infrared absorption.

Total iron determination

Similar coal samples (2.0 g) were combusted to 750°C in a Fisher programmable furnace according to the ASTM D3174-82 procedure. Freshly ignited ash (200 mg) was placed in a 125 ml Teflon bottle containing 3 mL aqua regia and 5 mL hydrofluoric acid, and heated in a steam bath for 2 h. The excess HF was neutralized with 50 mL saturated boric acid solution. The volume of the solution was then made up to 100 mL with deionized water and the iron content was determined using an ICP spectrometer, ARL-34000 model, at wavelength 259.94 nm.

TABLE 1. Sulfur and iron content of the coal specimens (g/100 g dry coal)

Specimen	Geological "formations"	Total S	Total Fe	Atomic ratio S/Fe
Smoky Tower	Obed Marsh	0.451	0.443	1.77
Obed Marsh	Obed Marsh	0.367	0.255	2.50
Highvale	Scollard	0.131	0.350	0.65
Alix (Sisson's)	Scollard	0.345	0.479	1.25
Antelope Coulee	Scollard	0.665	1.470	0.79
Vesta	Horseshoe Canyon	0.940	0.685	2.39
Tofield	Horseshoe Canyon	1.108	0.916	2.11
Blackfoot	Horseshoe Canyon	0.580	0.654	1.54

Forms of sulfur

Different procedures used for this purpose are described below.

1. *Standard procedure*: ASTM D2492, Method 1

Sequential extractions of a 3-g coal sample, air-dried and pulverized to −200 mesh, were undertaken first with 50 mL 2.3 *N* HCl and then with 50 mL 1.7 *N* HNO_3 under reflux conditions. The extracts were diluted to 200 mL and analysed for iron and sulfur content using an ICP spectrometer, ARL-34000.

2. *Modified procedure*: Janke *et al.* (7), Young and Zawadzki (4), Method 2

Coal samples were first extracted with HCl according to ASTM D2492. The HCl-treated sample was then combusted in a furnace at 750°C. The resulting ash was then extracted with 2.3 *N* HCl under reflux conditions. The iron and sulfur content in the HCl extracts was measured separately using an ICP spectrometer, ARL-34000.

3. *Low temperature ashing (LTA) procedure*: Method 3

Coal samples were first extracted with HCl according to ASTM D2492. The HCl-treated coal was dried at 110°C for 1 h, transferred onto a 10 cm id Pyrex petri dish, and placed on a four-chamber oxygen plasma asher (manufactured by International Plasma Corporation) for low temperature combustion. When the inorganic matter was totally oxidized (25 h), the residual ash was sequentially extracted with HCl and HNO_3 according to ASTM D2492. The iron and sulfur content in the extracts was measured separately using an ICP spectrometer.

4. *Alternate LTA of coal*: Method 4

Oven-dried −200 mesh coal samples were oxidized in the oxygen plasma as in 3. No attempt was made at complete combustion of carbon, so that oxidation of pyrites could be avoided (8). Following sequential extraction with HCl and HNO_3 of the so-called LTA residue, determinations of the iron and sulfur content in the extracts were undertaken as in 3.

5. *Second alternate LTA of coal*: Method 5

The procedure for LTA described under 4 was modified to include more efficient ashing with combined oxygen–fluorine plasma (9). Fluorine plasma was generated *in situ* by using a Teflon petri dish instead of a Pyrex glass dish. All other steps for the estimation of the forms of sulfur were the same as in 4.

Results and discussion

The following results are described to demonstrate the dilemma coal analysts face when reporting the results of analysis according to some standard procedures. The results in Table 1, describing the coal samples, their geology, and analysis with respect to total iron and total sulfur content are precise and pose no problem. The error ranges within ±1.0% between replicate analyses. The atomic ratio, S/Fe, however, varies randomly according to sample origin.

In Table 2 these single-step analyses are compared with multiple-step iron analyses according to Methods 2 and 3, respectively. The results of multiple-step analyses are 4–25% lower than the single-step procedure. The error may be due to incomplete extractions, but both high and low temperature ashing procedures gave comparable results. Alternately, lower values may be assigned to handling losses during transfer, filtration, etc., or there may be forms of iron in the coal that are HCl/HNO_3 insoluble (after ashing), but soluble in HF.

Similar comparisons could not be made between single and multiple-step analyses of sulfur. Table 3 summarizes the results of total sulfur determination by "Leco" and by the multiple steps of Methods 1–5. The recovery of sulfur varies widely between different procedures. Between 15 and 57% sulfur is recovered by the standard ASTM D2492 (Method 1) procedure; this portion should be assigned as a combination of sulfate and pyritic sulfur. Using high temperature ashing, Method 2, recovery was extremely poor. Not only the organic sulfur was lost, but the pyrites probably decomposed to Fe_2O_3 and SO_2. Low temperature ashing (Method 4), on the other hand, gave more than 85% recovery in 7 out of 8 cases. The high recovery in the LTA procedure may have been due to the fixation of organic sulfur in the inorganic matrix without loss of pyritic sulfur. This possibility was suspected from the fact that the recovery of sulfur using Method 3 procedures, where low temperature ashing was done after HCl leaching of coals, was not as high as 85%. HCl leaching would remove alkali and alkaline-earth ions, which are responsible for fixing sulfur during low temperature ashing.

TABLE 2. Comparison of iron (g/100 g dry coal) analyses by different procedures

Coal sample	Single step, total Fe	Multiple steps, total Fe			
		High T (Method 2)	% Recovery	Low T (Method 3)	% Recovey
Smoky Tower	0.443	0.403	91.0	0.365	82.5
Obed Marsh	0.255	0.218	85.5	0.229	89.7
Highvale	0.350	0.335	95.7	0.310	88.6
Alix	0.479	0.430	89.9	0.426	89.0
coulee	1.470	1.123	76.4	1.110	75.5
Vesta	0.685	0.613	89.5	0.602	87.9
Totfield	0.916	0.825	90.0	0.859	93.7
Blackfoot	0.654	0.612	93.6	0.613	93.8

TABLE 3. Total sulfur (g/100 g dry coal) determined by various methods; single vs. multiple steps

Coal sample	Leco	Method 1	Method 2	Method 3	Method 4	Method 5
Smoky Tower	0.451	0.114	0.044	0.325	0.433	0.410
Obed Marsh	0.367	0.054	0.056	0.238	0.327	0.301
Highvale	0.131	0.075	0.038	0.172	0.233	0.290
Alix	0.345	0.128	0.044	0.236	0.362	0.385
Coulee	0.665	0.285	0.113	0.433	0.658	0.639
Vesta	0.940	0.165	0.020	0.231	0.918	0.780
Tofield	1.108	0.572	0.061	0.535	1.015	1.035
Blackfoot	0.580	0.159	0.032	0.242	0.542	0.499

TABLE 4. Iron (g/100 g dry coal) in various forms in coal

Coal sample	Fe_{total}	Fe_{HCl}	$Diff_a$ (Fe_p)	Fe* (Fe_s)	Fe_{ns}	
					$Diff_b$	% Fe_{total}
Smoky Tower	0.443	0.226	0.217	0.036	0.190	42.8
Obed Marsh	0.255	0.133	0.122	0.016	0.117	45.9
Highvale	0.350	0.266	0.084	0.035	0.231	66.0
Alix	0.479	0.315	0.164	0.044	0.271	56.6
Coulee	1.470	0.885	0.585	0.131	0.754	51.3
Vesta	0.685	0.467	0.218	0.022	0.445	65.0
Tofield	0.916	0.536	0.380	0.070	0.466	50.9
Blackfoot	0.654	0.532	0.122	0.031	0.501	76.6

$Diff_a = Fe_{total} - Fe_{HCl}$.
Fe* = Fe calculated from sulfate determination (Fe_s), assuming all sulfate occurs as $Fe_2(SO_4)_3$.
$Diff_b = Fe_{HCl} - Fe^*$.

TABLE 5. Sulfur (g/100 g dry coal) in various forms in coals

Coal sample	S_{total}	$S_{sulfate}$	S^*_{pyrite}	S_o		
				% dry coal	% daf coal	% S_{total}
Smoky Tower	0.451	0.031	0.249	0.171	(0.211)	37.9
Obed Marsh	0.367	0.014	0.140	0.213	(0.244)	58.0
Highvale	0.131	0.030	0.096	0.004	(0.004)	3.5
Alix	0.345	0.038	0.188	0.118	(0.154)	34.4
Coulee	0.665	0.113	0.672	?		?
Vesta	0.940	0.109	0.250	0.671	(0.793)	71.3
Tofield	1.108	0.060	0.436	0.611	(0.862)	55.2
Blackfoot	0.580	0.027	0.140	0.413	(0.476)	71.2

S* = calculated sulfur as pyrite from Fe_p in Table 4.
S_o = organic sulfur; parenthetical number is dry ash-free basis.

This discussion leads one to conclude that neither sulfur nor iron analysis according to the standard procedure can be applied in a straightforward way to estimate the distribution of sulfur in various forms. The data are difficult to interpret on the basis of a mass balance of sulfur and iron in single- and multiple-step analyses.

The ASTM procedures calculate pyritic sulfur from the nitric acid-extracted portion of iron analysis, the precision of which depends on completion of extraction without contamination from other iron minerals. An alternate procedure for calculating the distribution of sulfur in different forms may be carried out as shown in Tables 4 and 5. Here the pyritic iron is calculated from the differences between total iron and iron extracted with HCl. Iron in the HCl extract is assumed to be present as ferric sulfate and other soluble but non-sulfate iron compounds. Estimation of other sulfates, particularly gypsum, should be carried out to validate this interpretation of the iron distribution.

Between 43 and 76% of total iron in these coals is presumed to be present in a non-sulfide (or sulfate) form, according to the results in Table 4. If the iron distribution figures are correct, one

TABLE 6. S_o, organic sulfur (% S_{total}) estimated by different methods

Coal sample	ASTM D2492	Method 1*	Method 3*	Table 5
Smoky Tower	83.1	74.7	27.9	37.9
Obed Marsh	59.1	85.3	22.9	58.0
Highvale	49.6	42.7	(−31.2)	3.5
Alix	76.2	62.9	31.6	34.4
Coulee	57.6	57.1	34.9	?
Vesta	94.4	82.4	75.4	71.3
Tofield	67.0	48.4	51.7	55.2
Blackfoot	87.6	72.6	58.3	71.2

*Computed on the basis of sulfur analyses.

obtains the sulfur distribution results in Table 5. Here total and sulfate sulfur are analytical values and pyritic sulfur is calculated. These analyses suggest that the sulfur content of the organic matrix changes with the geology of the deposit; within the same formation a variation exists between deposits with respect to pyrite contents. This conclusion is based on the assumed distribution of the three types of sulfur compounds, and assumed association of sulfur with iron in coal (1, 3). Application of ASTM methods (3), however, gives contradictory results (Table 6) due to uncertainty regarding the validity of the assumptions and the estimation of pyrites.

The dilemma of correctly estimating organic sulfur depends on measuring pyritic sulfur accurately. Hyman and Rowe (10) have suggested a novel thermo-magneto-gravimetric analytical (TMGA) method that is based on the combined effects of temperature and a strong magnetic field on the apparent weight of a ferromagnetic material. TMGA results for 30 U.S. coals of various ranks were found highly reproducible with 0.09% standard deviation for pyrite measurement (11) and TMGA was recommended for routine application. The present discussion on the merit of standard procedures for estimating forms of sulfur in low-sulfur coals suggests that the TMGA approach may be more suitable for low-sulfur coals than these standard procedures.

1. W. H. ODE. *In* chemistry of coal utilization. *Edited by* H. Lowry. Suppl. Vol. John Wiley, New York. 1963. pp. 215–216.
2. H. J. GLUSKOTER, R. R. RUCH, W. G. MILLER, R. A. CAHIL, G. B. DREHER, and J. KUHN. Illinois State Geological Survey Circular 499. 1977.
3. Annual book of ASTM standards, gaseous fuels, coals and cokes. ASTM, Philadelphia, D3162-(1973), D2492-(1984).
4. R. K. YOUNG and E. A. ZAWADZKI. Fuel, **446**, p. 151–152 (1967).
5. R. N. MILLER, R. F. YARZAB, and P. H. GIVEN. Fuel, **58**, 4 (1979).
6. J. D. CAMPBELL and M. P. DU PLESSIS. Alberta Research Council Information Series #101. Alberta Plains coal regions: potential feedstock for coal conversion by liquefaction and pyrolysis. Edmonton, Alberta. 1983.
7. L. JANKE, R. DUREAU, J. GLASA, and W. J. MONTGOMERY. The determination of pyritic sulfur in coal by atomic absorption—a new approach. CANMET Report ERP/ERL 73-72(TR). Ottawa. 1978.
8. R. N. MILLER and P. H. GIVEN. A geochemical study of the inorganic constituents in some low rank coals. DOE Technical Report. Washington. Fe-2494-TR-1. 1978.
9. E. V. WILLIAMS. Low temperature oxygen–fluorine radio frequency ashing, etc. Analyst, **107**, p. 1006–1013 (1982).
10. M. HYMAN and M. W. ROWE. New approaches in coal chemistry. ACS Symposium Series, Amer. Chem. Soc. Washington, DC. 1982. p. 247.
11. D. M. AYLMER. A new method for the simultaneous determination of pyrite content and proximate analysis in coal and lignite. Ph.D. Thesis, Texas A&M University. 1983.

Relative complexing tendencies of O—O, O—N, and O—S donor (secondary) ligands in some lanthanide–EDTA mixed-ligand complexes

SUDHIR N. LIMAYE AND MAHESH C. SAXENA

Department of Chemistry, University of Sagar, Dr. Harisingh Gour Vishwavidyalaya, Sagar (M.P.) 470 003, India

Received May 28, 1985[1]

S. N. LIMAYE and M. C. SAXENA. Can. J. Chem. **64**, 865 (1986).

Metal–ligand association constants of 1:1 binary (ML) and 1:1:1 ternary (MAL) complexes of the type M + A ⇌ MA; MA + L ⇌ MAL (where M = La^{3+}, Ce^{3+}, Pr^{3+}, Nd^{3+}, or Sm^{3+}; A = primary ligand = EDTA; L = secondary ligand = O—O, O—N, O—S donor aliphatic or aromatic ligand) have been determined potentiometrically by the Irving–Rossotti titration technique at ionic strength 0.2 (mol dm^{-3} $NaClO_4$) and 25°C. Differences between log K_{ML} and log K_{MAL} are negative; this may be chiefly due to electrostatic repulsion between the primary binary complex and the incoming secondary ligand during the formation of the mixed-ligand complexes. The relative complexing tendencies of various secondary ligands have been found to follow the sequence O—O donor (aromatic) > O—N donor > O—O donor (aliphatic) ≥ O—S donor.

S. N. LIMAYE et M. C. SAXENA. Can. J. Chem. **64**, 865 (1986).

Utilisant la méthode de titration potentiométrique de Irving–Rossotti et opérant à 25°C et à une force ionique de 0,2 mol dm^{-3} $NaClO_4$, on a déterminé les constantes d'association métal–ligand des complexes binaires 1:1 (ML) et ternaires 1:1:1 (MAL) du type M + A ⇌ MA ou MA + L ⇌ MAL (où M = La^{3+}, Ce^{3+}, Pr^{3+}, Nd^{3+} ou Sm^{3+}; A = ligand primaire = EDTA; L = ligand secondaire = ligand donneur aliphatique ou aromatique O—O, O—N ou O—S). Les différences entre log K_{ML} et log K_{MAL} sont négatives; ce résultat est principalment dû à une répulsion électrostatique entre le complexe binaire primaire et le ligand secondaire qui approche au cours de la formation des complexes avec ligands mixtes. On a observé que les tendances relatives à la complexation de divers ligands secondaires sont dans l'ordre suivant: donneur O—O aromatique > donneur O—N > donneur O—O aliphatique ≥ donneur O—S.

[Traduit par la revue]

Introduction

The lanthanide metal ions are reported to display little tendency to form complexes with π-bonding ligands as their 4*f*-orbitals do not seem to be available for bonding (1–3). They exhibit class "a" (or hard acid) character as acceptor metal ions. Although earlier literature reveals that their coordination chemistry is limited mainly to complexes with oxygen, or oxygen–nitrogen donors (4, 5) some investigations have been carried out recently on their complexes with oxygen–sulphur (6, 7) and nitrogen donors (8, 9). Some β-diketone chelates have also been studied (10, 11).

The present work is intended to report the relative complexing tendencies of O—O, O—N, and O—S donor (secondary) ligands in the formation of 1:1:1 mixed-ligand complexes of the type LN–EDTA–L (charges omitted), where LN = La^{3+}, Ce^{3+}, Pr^{3+}, Nd^{3+}, or Sm^{3+}; EDTA = primary ligand; and L = O—O, O—N, or O—S donor secondary ligand. Aspects dealing with the effect of ring size of the secondary ligand on the stability of the mixed-ligand complex (12*a*), and occurrence of the intramolecular hydrophobic interaction (12*b*), have been communicated elsewhere.

Experimental

The lanthanides were supplied by Indian Rare Earths Ltd. (99.99% purity). Other chemicals were of standard purity (BDH Analar; E. Merck G. R.; Fluka). Solutions of La^{3+}, Ce^{3+}, and Sm^{3+} were prepared by dissolving the requisite quantities of the nitrate salts in double distilled water, and those of Pr^{3+} and Nd^{3+} by dissolving the oxides in the minimum quantity of perchloric acid and removing the excess by evaporation. The solutions were standardized by means of complexometric titrations (13). EDTA was used as the disodium dihydrate; the remaining two protons were neutralized before use. The secondary ligands were used as purchased.

Usual titration sets (14) were prepared for each system by using the final metal and ligand concentrations as 1×10^{-3} mol dm^{-3}. The ionic strength, *I*, was maintained constant at 0.2 (mol dm^{-3}, $NaClO_4$). These sets were equilibrated and titrated potentiometrically at 25°C with 0.2 mol dm^{-3} (carbonate free) NaOH using an Elico digital (model LI-120) pH meter. Reproducible pH readings were used for calculations. In the cases of salicyclic, phthalic, and anthranilic acids a partial aqueous medium (40% v/v ethanol–water) was used and the experimental pH-meter readings were corrected by using the Van-Uitert technique (15). The Irving–Rossotti approach (16) and its extension as applicable to ternary systems (17) were used for computing the proton–ligand and metal–ligand association constants.

Results

A representative set of pH titration curves for the system La(III) – EDTA – malic acid is shown in Fig. 1. The primary complex, MA (i.e., metal ion – EDTA chelate), is formed at a lower pH (below pH ~ 4.2) and remains stable over a fairly long range of pH (up to about 6.5–7.0). The secondary ligand, L, combines with MA in the pH region 4.0–5.0. The formation of the 1:1:1 ternary complex, MAL, in the present work may be represented as (charges omitted),

[1] M + A ⇌ MA

and

[2] MA + L ⇌ MAL

Similarly the formation of the binary complex may be written as,

[3] M + L ⇌ ML

and the association of protons with the secondary ligand as,

[4] H + L ⇌ HL; H + HL ⇌ H_2L; etc.

In eqs. [1]–[4] A represents deprotonated primary ligand and L deprotonated secondary ligand. The equilibrium constants corresponding to these equilibria are the metal–ligand association constants, K^{M}_{MA}, K^{MA}_{MAL}, K^{M}_{ML} (eqs. [1]–[3], respectively), and

[1]Revision received December 16, 1985.

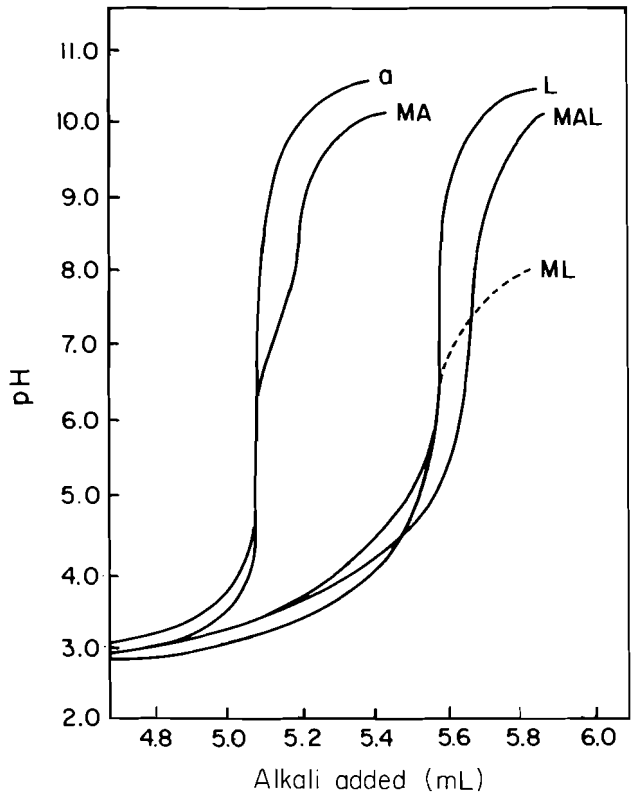

FIG. 1. Representative pH-titration plots for 1:1 binary (ML) and 1:1:1 ternary (MAL) La–EDTA–malic acid system.

proton–ligand association constants K^{H}_{HL}, $K^{HL}_{H_2L}$, etc. (or, K^{H}_{1}, K^{H}_{2}, etc.) (eq. [4]).

The quantity Δ log K used to quantify the stability of the ternary complex MAL (formed from MA) relative to that of the binary complex ML is defined as,

$$[5] \quad \Delta \log K = \log K^{MA}_{MAL} - \log K^{M}_{ML}$$

The formation functions of the protonated ligand, $\bar{n}_H$, and of the metal complex, $\bar{n}$, and the free-ligand exponent, pL, have been calculated from the titration curves in the usual manner (17).

The proton–ligand association constants have been calculated from the expression

$$[6] \quad \log K^{H}_{n} = B + \log \frac{\bar{n}_H}{1 - \bar{n}_H}$$

where B is the pH-meter reading. For a partially aqueous medium B was corrected (15) by means of the relationship

$$[7] \quad B = -\log [H] - [\log f + \log U_{H^0}]$$

where, f = activity coefficient of hydrogen ion in solution; U_{H^0} = correction at zero ionic strength.

In the case of amino acids it has been observed (see Fig. 2, for example) that the experimental curve MA diverges from curve A, indicating the formation of hydroxo species of the type $[MA(OH)_n]$; the secondary ligand L combines with MA in this higher pH region. The hydrolysis corrected values have been determined (18) in these cases and shown within square brackets in Table 3.

The values of log K^{M}_{ML}, log K^{MA}_{MAL}, and Δ log K have been reported in Tables 1–4. The quantities within parentheses are the standard deviations. The possibility of formation of species of the type MA_2 (including any disproportionation of MAL into MA_2 and ML_2) has been ignored in view of the hexadentate nature of EDTA. The use of sufficiently dilute solutions of metal ions and ligands (1×10^{-3} mol dm^{-3}) and smooth curves (not shown) between $\bar{n}$/[L] vs. [L] have been regarded as indicative of the absence of polynuclear species in the ternary systems.

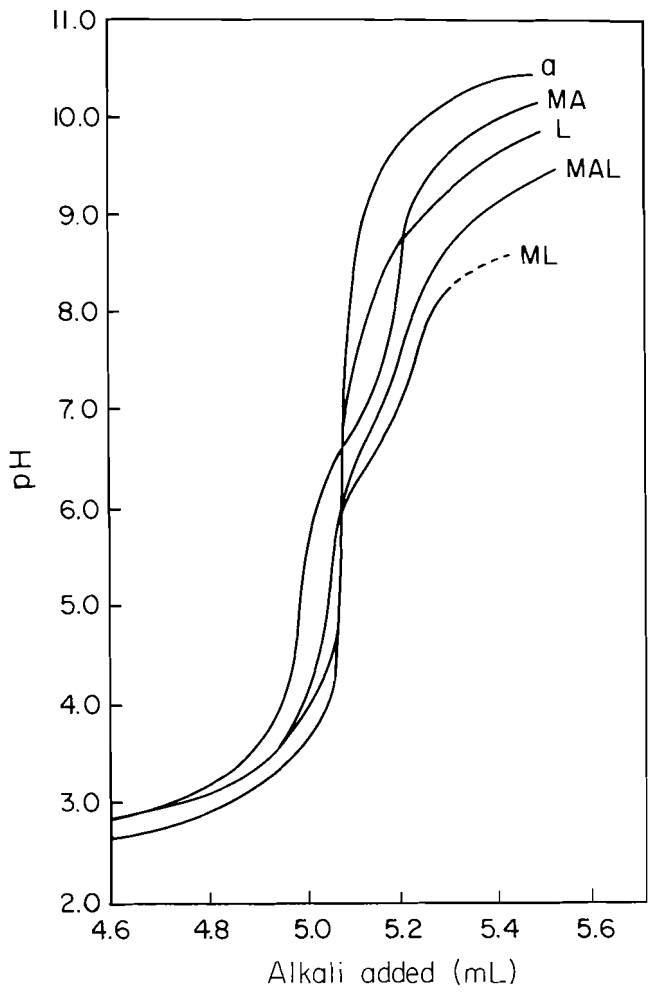

FIG. 2. Representative pH-titration plots for 1:1 binary (ML) and 1:1:1 ternary (MAL) La–EDTA–glycine system.

A representative figure (Fig. 3) has been incorporated to show the distribution of various species as a function of pH for the ternary system La(III)-EDTA-glycine. It may be seen that in this case the binary complex MA is formed (up to 90%) at pH 6.0 and the ternary complex MAL up to about 80% in the pH region 7.5 and above.

Discussion

A perusal of the data in Tables 1–4 reveals clearly that the association constants log K^{M}_{ML} and log K^{MA}_{MAL} follow the sequence $La^{3+} < Ce^{3+} < Pr^{3+} < Nd^{3+} < Sm^{3+}$ for all the O—O, O—N, and O—S donor ligands. This sequence is also of the order of increasing occupancy of the $4f$ orbitals of the lanthanides, and is accompanied by a regular decrease in ionic radii and hence a gradual increase in ionic potentials. Plots (not shown) of these metal–ligand association constants vs. r^{-1} (r = ionic radius of LN^{3+} ion), however, show some departure from linearity at Nd^{3+} and Sm^{3+} (electronic configuration: $4f^3$ and $4f^5$) which may well be due to a possible tetrad effect (19).

For related secondary ligands the association constants vary with ligand characteristics also. Thus, for the aliphatic hydroxy acids and the unsaturated carboxylic acids studied the trends are

TABLE 1. Association constants of 1:1 binary (log K^{M}_{ML}) and 1:1:1 ternary (log K^{MA}_{MAL}) lanthanide–EDTA complexes with O—O donor aliphatic ligands, and Δ log K values with I = 0.2 (mol dm^{-3}, $NaClO_4$) and a temperature of 25°C

Ligand	Property	La^{3+}	Ce^{3+}	Pr^{3+}	Nd^{3+}	Sm^{3+}
Malic acid	log K^{M}_{ML}	3.75 (±0.02)	4.10 (±0.01)	4.20 (±0.01)	4.45 (±0.01)	4.53 (±0.03)
CH(OH)COOH | CH_2COOH	log K^{MA}_{MAL}	3.38 (±0.04)	3.46 (±0.02)	3.53 (±0.01)	3.75 (±0.01)	4.11 (±0.01)
	−Δ log K	0.37	0.64	0.67	0.70	0.42
Lactic acid	log K^{M}_{ML}	3.68 (±0.02)	3.74 (±0.05)	3.98 (±0.03)	3.99 (±0.04)	4.12 (±0.03)
$CH_3CH(OH)$ | COOH	log K^{MA}_{MAL}	3.35 (±0.05)	3.43 (±0.02)	3.55 (±0.04)	3.68 (±0.02)	3.86 (±0.02)
	−Δ log K	0.33	0.31	0.43	0.31	0.26
Glycolic acid	log K^{M}_{ML}	3.60 (±0.02)	3.63 (±0.03)	3.71 (±0.03)	3.83 (±0.03)	3.92 (±0.06)
CH_2COOH | (OH)	log K^{MA}_{MAL}	3.28 (±0.06)	3.47 (±0.02)	3.58 (±0.03)	3.64 (±0.03)	3.72 (±0.02)
	−Δ log K	0.32	0.16	0.13	0.19	0.20
Gluconic acid	log K^{M}_{ML}	2.96 (±0.03)	3.16 (±0.03)	3.26 (±0.03)	3.40 (±0.02)	3.54 (±0.03)
CH_2OH | $(CHOH)_4$ | COOH	log K^{MA}_{MAL}	2.13 (±0.02)	2.46 (±0.01)	2.69 (±0.04)	2.80 (±0.03)	2.92 (±0.04)
	−Δ log K	0.83	0.70	0.57	0.60	0.62
Malonic acid	log K^{M}_{ML}	3.80 (±0.07)	4.11 (±0.08)	4.26 (±0.05)	4.50 (±0.09)	4.87 (±0.01)
COOH | CH_2 | COOH	log K^{MA}_{MAL}	2.96 (±0.02)	3.28 (±0.04)	3.43 (±0.04)	3.60 (±0.02)	3.70 (±0.01)
	−Δ log K	0.84	0.83	0.83	0.90	1.17
Succinic acid	log K^{M}_{ML}	3.73 (±0.02)	3.86 (±0.02)	4.11 (±0.08)	4.37 (±0.04)	4.49 (±0.05)
CH_2COOH | CH_2COOH	log K^{MA}_{MAL}	3.50 (±0.02)	3.61 (±0.02)	3.76 (±0.02)	3.87 (±0.03)	4.01 (±0.03)
	−Δ log K	0.23	0.25	0.35	0.50	0.48
Glutaric acid	log K^{M}_{ML}	3.70 (±0.04)	3.81 (±0.02)	4.02 (±0.01)	4.05 (±0.07)	4.26 (±0.03)
COOH | $(CH_2)_3$ | COOH	log K^{MA}_{MAL}	2.86 (±0.05)	3.08 (±0.03)	3.22 (±0.03)	3.37 (±0.01)	3.51 (±0.01)
	−Δ log K	0.84	0.73	0.80	0.68	0.75
Maleic acid	log K^{M}_{ML}	4.18 (±0.01)	4.35 (±0.06)	4.75 (±0.10)	5.05 (±0.05)	5.20 (±0.03)
HCCOOH ‖ HCCOOH	log K^{MA}_{MAL}	3.80 (±0.06)	4.26 (±0.03)	4.38 (±0.03)	4.53 (±0.03)	4.60 (±0.03)
	−Δ log K	0.38	0.09	0.37	0.52	0.60
Citraconic acid	log K^{M}_{ML}	4.61 (±0.06)	4.93 (±0.06)	5.03 (±0.04)	5.21 (±0.06)	5.34 (±0.03)
CH_3CCOOH ‖ HCCOOH	log K^{MA}_{MAL}	3.81 (±0.06)	3.99 (±0.02)	4.18 (±0.04)	4.30 (±0.05)	4.49 (±0.03)
	−Δ log K	0.80	0.94	0.85	0.91	0.85
Itaconic acid	log K^{M}_{ML}	3.81 (±0.02)	3.94 (±0.015)	4.09 (±0.01)	4.34 (±0.02)	4.47 (±0.02)
$H_2C{=}CCOOH$ | CH_2COOH	log K^{MA}_{MAL}	3.56 (±0.02)	3.74 (±0.04)	3.92 (±0.03)	4.10 (±0.01)	4.32 (±0.02)
	−Δ log K	0.25	0.20	0.17	0.24	0.15
Crotonic acid	log K^{M}_{ML}	3.32 (±0.03)	3.50 (±0.04)	3.67 (±0.03)	3.81 (±0.04)	3.96 (±0.04)
$HCCH_3$ ‖ HCCOOH	log K^{MA}_{MAL}	2.92 (±0.09)	3.07 (±0.03)	3.22 (±0.01)	3.46 (±0.03)	3.63 (±0.04)
	−Δ log K	0.40	0.43	0.45	0.35	0.33

TABLE 2. Association constants of 1:1 binary (log K^{M}_{ML}) and 1:1:1 ternary (log K^{MA}_{MAL}) lanthanide–EDTA complexes with O—O donor aromatic ligands and Δ log K values with I = 0.2 (mol dm^{-3}, $NaClO_4$) and a temperature of 25°C

Ligand	Property	La^{3+}	Ce^{3+}	Pr^{3+}	Nd^{3+}	Sm^{3+}
Salicylic acid* 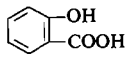	log K^{M}_{ML}	7.35 (±0.03)	7.55 (±0.01)	7.73 (±0.04)	7.83 (±0.01)	7.99 (±0.05)
	log K^{MA}_{MAL}	7.09 (±0.04)	7.35 (±0.01)	7.54 (±0.10)	7.63 (±0.09)	7.75 (±0.10)
	−Δ log K	0.26	0.20	0.19	0.20	0.24
Phthalic acid* 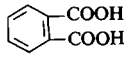	log K^{M}_{ML}	4.09 (±0.04)	4.37 (±0.05)	4.55 (±0.06)	4.72 (±0.05)	5.04 (±0.05)
	log K^{MA}_{MAL}	3.08 (±0.06)	3.48 (±0.04)	3.63 (±0.04)	3.96 (±0.05)	4.18 (±0.04)
	−Δ log K	1.01	0.89	0.92	0.76	0.86
Catechol 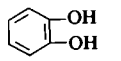	log K^{M}_{ML}	8.55 (±0.03)	8.65 (±0.04)	8.90 (±0.04)	9.10 (±0.07)	9.20 (±0.03)
	log K^{MA}_{MAL}	6.20 (±0.03)	6.50 (±0.02)	6.70 (±0.03)	7.00 (±0.05)	7.45 (±0.05)
	−Δ log K	2.35	2.15	2.20	2.10	1.75
Resorcinol 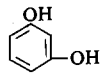	log K^{M}_{ML}	4.45 (±0.03)	4.55 (±0.02)	5.05 (±0.04)	5.35 (±0.04)	5.95 (±0.03)
	log K^{MA}_{MAL}	2.10 (±0.04)	2.20 (±0.04)	2.35 (±0.03)	2.50 (±0.02)	3.05 (±0.03)
	−Δ log K	2.35	2.35	2.70	2.85	2.90
Phloroglucinol 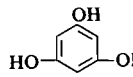	log K^{M}_{ML}	3.50 (±0.02)	3.75 (±0.04)	3.90 (±0.03)	4.10 (±0.07)	4.20 (±0.02)
	log K^{MA}_{MAL}	2.20 (±0.03)	2.40 (±0.03)	2.51 (±0.05)	2.65 (±0.02)	2.72 (±0.02)
	−Δ log K	1.30	1.35	1.39	1.45	1.48
Protocatechuic acid 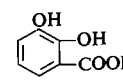	log K^{M}_{ML}	7.95 (±0.02)	8.15 (±0.07)	8.23 (±0.03)	8.45 (±0.04)	8.63 (±0.01)
	log K^{MA}_{MAL}	4.22 (±0.05)	4.44 (±0.025)	4.60 (±0.01)	4.88 (±0.02)	5.07 (±0.02)
	−Δ log K	3.73	3.71	3.63	3.57	3.56
β-Resorcyclic acid 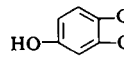	log K^{M}_{ML}	6.09 (±0.02)	6.21 (±0.03)	6.34 (±0.03)	6.48 (±0.04)	6.58 (±0.02)
	log K^{MA}_{MAL}	4.06 (±0.01)	4.13 (±0.03)	4.19 (±0.02)	4.33 (±0.03)	4.47 (±0.03)
	−Δ log K	2.03	2.08	2.15	2.15	2.11

*Indicates values in 40% (v/v) ethanol–water medium.

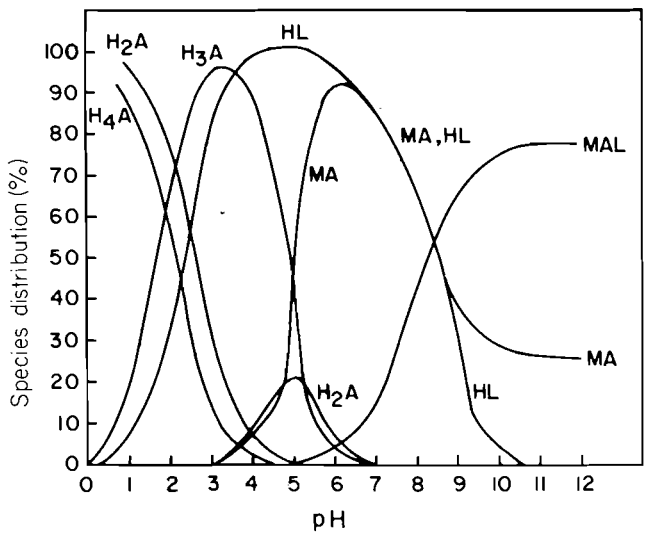

FIG. 3. Distribution of various species (%) as a function of pH in the La–EDTA–glycine ternary system.

malic acid > lactic acid > glycolic acid > gluconic acid (20) and citraconic acid > maleic acid > itaconic acid > crotonic acid, which are also the orders of ligand basicities. A similar sequence has been reported (21) for the ternary systems (LN-EDTA-L) where, LN = La^{3+}, Pr^{3+}, Nd^{3+}; L = malic acid, lactic acid, glycolic acid. For the saturated aliphatic dicarboxylic acids (12*a*) the order is malonic acid > succinic acid > glutaric acid, which may be due to a gradual increase in the size of the chelate ring formed by these ligands. In the case of O—N donors the sequence with respect to ligands has been found to be α-alanine < glycine < aspartic acid < leucine ≤ β-alanine < valine using the hydrolysis corrected values. For O—S donors thiomalic acid > thioglycolic acid is again the order of ligand basicities. A similar sequence has been observed for some 3*d* elements (22).

The Δ log K values are consistently negative for all the mixed-ligand complexes studied. This may be chiefly due to an electrostatic repulsion between the negatively charged primary complex and the incoming secondary ligand (also negatively charged) during the formation of mixed-ligand complexes.

TABLE 3. Association constants of 1:1 binary (log K^{M}_{ML}) and 1:1:1 ternary (log K^{MA}_{MAL}) lanthanide–EDTA complexes with O—O donor ligands, and Δ log K values with I = 0.2 (mol dm^{-3}, $NaClO_4$) and a temperature of 25°C

Ligand	Property	La^{3+}	Ce^{3+}	Pr^{3+}	Nd^{3+}	Sm^{3+}
Glycine	log K^{M}_{ML}	5.32 (±0.01)	5.38 (±0.02)	5.55 (±0.007)	5.68 (±0.02)	5.84 (±0.01)
CH_2NH_2COOH	log K^{MA}_{MAL}	4.09 (±0.01) [4.08]	4.32 (±0.01) [4.16]	4.63 (±0.02) [4.27]	4.89 (±0.03) [4.50]	4.97 (±0.02) [4.60]
	−Δ log K	1.23	1.06	0.92	0.79	0.87
α-Alanine	log K^{M}_{ML}	5.82 (±0.005)	6.03 (±0.01)	6.36 (±0.01)	6.52 (±0.02)	6.68 (±0.01)
CH_3CHNH_2COOH	log K^{MA}_{MAL}	4.28 (±0.03) [4.00]	4.40 (±0.01) [4.39]	4.99 (±0.04) [4.41]	5.17 (±0.02) [4.96]	5.37 (±0.01) [—]
	−Δ log K	1.54	1.63	1.37	1.35	1.31
β-Alanine	log K^{M}_{ML}	5.20 (±0.01)	5.90 (±0.05)	6.08 (±0.02)	6.24 (±0.02)	6.40 (±0.01)
$CH_2NH_2CH_2COOH$	log K^{MA}_{MAL}	4.33 (±0.10) [4.20]	4.37 (±0.10) [4.30]	4.49 (±0.10) [4.41]	4.72 (±0.10) [4.67]	4.99 (±0.10) [4.86]
	−Δ log K	0.87	1.53	1.59	1.52	1.41
Valine	log K^{M}_{ML}	5.94 (±0.04)	6.05 (±0.03)	6.28 (±0.04)	6.52 (±0.01)	6.68 (±0.02)
$(CH_3)_2CHCHNH_2COOH$	log K^{MA}_{MAL}	5.10 (±0.10) [—]	5.33 (±0.08) [—]	5.45 (±0.10) [—]	5.86 (±0.06) [—]	6.05 (±0.02) [—]
	−Δ log K	0.84	0.72	0.83	0.66	0.63
Leucine	log K^{M}_{ML}	5.61 (±0.03)	5.84 (±0.015)	5.99 (±0.02)	6.03 (±0.02)	6.18 (±0.03)
$(CH_3)_2CHCH_2CHNH_2COOH$	log K^{MA}_{MAL}	4.31 (±0.03) [4.21]	4.59 (±0.03) [4.35]	4.72 (±0.015) [4.40]	4.92 (±0.07) [4.82]	5.09 (±0.03) [5.00]
	−Δ log K	1.30	1.25	1.27	1.11	1.09
Aspartic acid	log K^{M}_{ML}	5.61 (±0.03)	5.77 (±0.015)	5.90 (±0.02)	6.04 (±0.02)	6.16 (±0.03)
$HOOCCH_2CHNH_2COOH$	log K^{MA}_{MAL}	4.55 (±0.02) [4.13]	4.71 (±0.03) [—]	4.91 (±0.02) [—]	4.98 (±0.02) [—]	5.37 (±0.02) [—]
	−Δ log K	1.06	1.06	0.99	1.06	0.79
Anthranilic acid*	log K^{M}_{ML}	2.05 (±0.10)	2.45 (±0.10)	2.90 (±0.10)	3.05 (±0.09)	3.36 (±0.05)
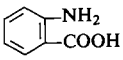	log K^{MA}_{MAL}	1.96 (±0.01)	2.25 (±0.10)	2.40 (±0.09)	2.95 (±0.09)	3.21 (±0.03)
	−Δ log K	0.09	0.20	0.50	0.10	0.15

*Indicates values in 40% (v/v) ethanol–water medium. Wherever necessary, the hydrolysis corrected values of log K^{MA}_{MAL} have been shown above in square brackets.

TABLE 4. Association constants of 1:1 binary (log K^{M}_{ML}) and 1:1:1 ternary (log K^{MA}_{MAL}) lanthanide–EDTA complexes with O—O donor ligands and Δ log K values with I = 0.2 (mol dm^{-3}, $NaClO_4$) and a temperature of 25°C

Ligand	Property	La^{3+}	Ce^{3+}	Pr^{3+}	Nd^{3+}	Sm^{3+}
Thiomalic acid	log K^{M}_{ML}	4.29 (±0.01)	4.41 (±0.01)	4.45 (±0.02)	4.56 (±0.02)	4.83 (±0.01)
CH(SH)COOH | CH_2COOH	log K^{MA}_{MAL}	4.04 (±0.01)	4.27 (±0.03)	4.34 (±0.02)	4.52 (±0.03)	4.56 (±0.04)
	−Δ log K	0.25	0.14	0.11	0.04	0.27
Thioglycolic acid	log K^{M}_{ML}	3.40 (±0.01)	3.52 (±0.03)	3.59 (±0.03)	3.67 (±0.10)	3.72 (±0.10)
$CH_2(SH)$ | COOH	log K^{MA}_{MAL}	3.32 (±0.03)	3.47 (±0.015)	3.53 (±0.02)	3.63 (±0.02)	3.68 (±0.03)
	−Δ log K	0.08	0.05	0.06	0.04	0.04

[8] $LN^{3+} + EDTA^{4-} \rightleftharpoons [LN\text{–}EDTA]^{-}$

$[LN\text{–}EDTA]^{-} + L^{n-} \rightleftharpoons [LN\text{–}EDTA\text{–}L]^{-(n+1)}$

The $-\Delta \log K$ values have been found to vary numerically from 0.04 to as much as 3.73; a general sequence in the $-\Delta \log K$ values has been observed to be

$$O\text{—}O_{(aromatic)} > O\text{—}N > O\text{—}O_{(aliphatic)} > O\text{—}S$$

for the different donor types, showing probably a discrimination of MA towards L. It is interesting to note that in the present case the highest $-\Delta \log K$ values have been obtained for catechol, resorcinol, and protocatechuic acid, which may be due to a greater electronic repulsion caused by a higher electron density associated with the π-electron cloud over the aromatic ring.

Sigel (23, 24) has observed a certain dependence of $-\Delta \log K$ on the proton–ligand association constants of the secondary ligands in complexes of the type M.Dipy.L. In the present work, a general parallel has also been noticed between the magnitudes of $-\Delta \log K$ and the proton–ligand association constants of the secondary ligands. A higher value of $\log K_n^H$ would imply that a relatively larger concentration of L^{n-} species exists in the ternary system, resulting in greater electronic repulsion during the formation of mixed-ligand complexes and a consequent enhancement in the magnitude of $-\Delta \log K$.

A significant conclusion that may be drawn from the experimental values of the association constants is that the $\log K_{MAL}^{MA}$ values lie in the sequence,

$$O\text{—}O_{(aromatic)} > O\text{—}N > O\text{—}O_{(aliphatic)} \geq O\text{—}S$$

with respect to the donor atoms of the secondary ligands. This trend is justified in view of the fact that the lanthanides are hard acids in terms of the "hard and soft" acid–base theory. The hard–hard interactions, being more facile, would result in more stable complexes with hard bases. It is also significant that the primary complex $(LN\text{–}EDTA)^{-}$ possesses enough hardness to show a preference towards O—O and O—N donors in the formation of the mixed-ligand complexes. The greater stability of the mixed-ligand complexes with O—O aromatic donors may result from the enhanced stabilizing capability of the aromatic ring due to resonance effects.

Acknowledgements

The authors are thankful to Prof. Y. G. Kher (retired) Head, Department of Chemistry, Doctor Harisingh Gour Vishwavidyalaya, Sagar for providing laboratory facilities. One of the authors (M.C.S.) is thankful to the M.P. Council of Science and Technology, Bhopal (India) for the award of a research grant.

1. W. B. Lewis, J. A. Jackson, T. F. Lamons, and H. Tube. J. Chem. Phys. **36**, 694 (1962).
2. J. J. Fritz, J. E. Field, and I. Grenthe. J. Phys. Chem. **65**, 2070 (1961).
3. T. Moeller and E. P. Hoewitz. J. Inorg. Nucl. Chem. **12**, 49 (1959).
4. S. P. Sinha. Complexes of rare-earths. Pergamon Press, New York. 1966.
5. J. C. Bailar. Comprehensive inorganic chemistry. Pergamon Press, New York. 1973.
6. R. S. Saxena and S. K. Bhatia. J. Inorg. Nucl. Chem. **37**, 309 (1975).
7. A. U. Malik and F. R. Rahmani. J. Inorg. Nucl. Chem. **37**, 1552 (1975).
8. J. H. Forsberg. Coord. Chem. Rev. **10**, 195 (1973).
9. S. P. Sinha. Anal. Chem. Acta, **52**, 193 (1970).
10. B. Liss Ivan and W. G. Boss. J. Inorg. Nucl. Chem. **39**, 449 (1977).
11. J. L. Sharma, B. S. Garg, and R. P. Singh. J. Inorg. Nucl. Chem. **42**, 452 (1980).
12. S. N. Limaye and M. C. Saxena. (*a*) J. Indian Chem. Soc. **61**, 448 (1984); (*b*) **62**, 352 (1985).
13. T. S. West. Complexometry with EDTA and related reagents. BDH Chemicals Ltd., Poole. 1969. p. 188.
14. S. N. Limaye and M. C. Saxena. J. Indian Chem. Soc. **59**, 698 (1982).
15. L. G. Van Uitert and C. G. Haas. J. Am. Chem. Soc. **75**, 451 (1953).
16. H. M. Irving and H. S. Rossotti. J. Chem. Soc. 3397 (1953); 2904 (1954).
17. M. V. Chidambaram and P. K. Bhattacharya. J. Inorg. Nucl. Chem. **32**, 3271 (1970).
18. C. R. Jejurkar and P. K. Bhattacharya. Indian J. Chem. **13**, 622 (1975).
19. R. J. P. Williams. Struct. Bonding (Berlin), **50**, 79 (1982); Chem. Abstr. **96**, 84118h (1982).
20. S. N. Limaye and M. C. Saxena. J. Indian Chem. Soc. **61**, 842 (1984).
21. H. S. Rana and J. P. Tandon. J. Inorg. Nucl. Chem. **39**, 1391 (1977).
22. M. V. Reddy and P. K. Bhattacharya. Indian J. Chem. **7**, 282 (1976); J. Prakt. Chem. **312**, 69 (1970).
23. R. Griesser, B. Prijs, and H. Sigel. J. Inorg. Nucl. Chem. Lett. **4**, 443 (1968).
24. H. Sigel. J. Inorg. Nucl. Chem. **37**, 507 (1975).

Kinetics and mechanism of dehydrochlorination of *N*-aryl-*C*-ethoxycarbonylformohydrazidoyl chlorides

AHMAD S. SHAWALI[1] AND HASSAN A. ALBAR

Department of Chemistry, Faculty of Science, King Abdulaziz University, P.O. Box 9028, Jeddah 21413, Saudi Arabia

Received September 27, 1985

AHMAD S. SHAWALI and HASSAN A. ALBAR. Can. J. Chem. **64**, 871 (1986).

The kinetics of triethylamine (TEA) catalyzed deydrochlorination of a series of *N*-aryl-*C*-ethoxycarbonylformohydrazidoyl chlorides **1***a–m* have been studied under pseudo-first-order conditions in 4:1 (v/v) dioxane–water solution at 30°C. For all compounds studied, the kinetics followed the rate law: $k_{obs} = k_2$ (TEA). The values of the overall second-order rate constants for the studied compounds were correlated by the equation: $\log k_2 = 0.533\,\sigma^- - 0.218$. The results are compatible with a mechanism involving a fast reversible deprotonation step leading to the anion of **1**, followed by rate-determining step involving the loss of the chloride ion from the anion. The reaction constants of these two steps were estimated to be 0.845 and − 0.312, respectively.

AHMAD S. SHAWALI et HASSAN A. ALBAR. Can. J. Chem. **64**, 871 (1986).

Opérant à 30°C et dans des solutions 4:1 (v/v) de dioxanne/eau, on a étudié les cinétiques du pseudo-premier ordre des réactions de déshydrochloruration catalysées par la triéthylamine (TEA) d'une série (**1***a–m*) de chlorures de *N*-aryl *C*-éthoxycarbonyl formohydrazidoyles. Dans tous les cas étudiés, l'équation de vitesse de la cinétique est la suivante: $k_{obs} = k_2$ (TEA). Pour tous les composés étudiés, on a établi une corrélation entre les constantes de vitesse globales du deuxième ordre qui est définie par l'équation suivante: $\log k_2 = 0{,}533\sigma^- - 0{,}218$. Les résultats sont compatibles avec un mécanisme impliquant une étape de déprotonation réversible rapide conduisant à l'anion de **1** qui serait suivie par une étape déterminante impliquant une perte de l'ion chlorure par l'anion. On a évalué les constantes de vitesses pour ces deux étapes à 0,845 et −0,312 respectivement.

[Traduit par la revue]

Introduction

The chemistry of *N*-aryl-*C*-ethoxycarbonylformohydrazidoyl chlorides **1** has been thoroughly investigated during the last decade (1–3). Due to their ease of preparation, such compounds have been extensively used in 1,3-dipolar cycloaddition reactions, where the intermediate nitrilimine **2**, formed *in situ* by the action of a base catalyst, reacts with a dipolarophile A=B, producing a cycloadduct **3**, eq. [1] (4,5).

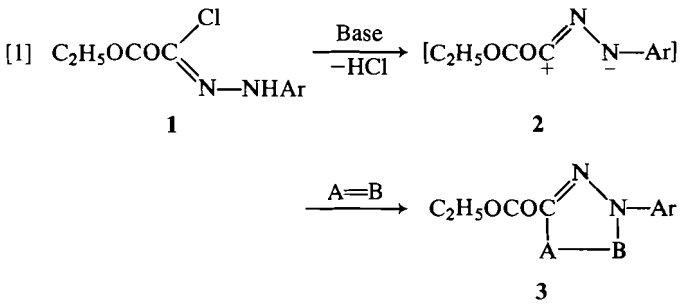

[1]

1 **2**

3

However, no attention has yet been given to the mechanism of formation of **2** from **1**. We wish to report here the results of our kinetic study of the triethylamine catalyzed dehydrochlorination of a series of substituted *N*-phenyl-*C*-ethoxycarbonylformohydrazidoyl chlorides **1***a–m* in 4:1 (v/v) dioxane–water mixture at 30°C in an attempt to shed some light on the mechanism of this elimination reaction.

Results and discussion

The sequence followed in the preparation of **1***a–m* is outlined in Scheme 1. Some of these hydrazidoyl chlorides were reported and others, namely **1***b* and **1***e–h*, are new. The structures of these chlorides were evidenced by their elemental and spectral analyses. For example, the infrared spectra of all compounds reveal the presence of characteristic bands near 3280–3220 (hydrazone NH), 1725–1695 (ester, CO), 1665–1600 (C=N), and 1080–1060 (ester C—O—C) cm^{-1}. In their ^{1}Hmr spectra, they exhibit a triplet signal at δ 1.3–1.4 (3H, J = 7 Hz, CH_3CH_2O), a quartet at δ 4.4–4.3 (2H, J = 7 Hz, CH_3CH_2O), and a singlet near 9.5–8.32 (1H, NH), in addition to the aromatic proton multiplet signal in the region 7.0–8.0 ppm.

On standing for 3 days at 25°C in 80% (v/v) dioxane–water mixture, these hydrazidoyl chlorides were recovered unchanged. However, addition of triethylamine (TEA) to the solution of **1** in this same solvent mixture liberated the chloride ion. Accordingly, the dehydrochlorination kinetics were followed at 30°C in 80% (v/v) dioxane–water mixture in the presence of a large excess, at least 10-fold, of TEA by determining the chloride ion concentration with an ion selective electrode (see Experimental). In all kinetic runs, the ionic strength in the reaction mixture was maintained at 0.10 by the addition of the appropriate volume of 5 *M* sodium nitrate solution in the same solvent system (80:20 dioxane–water, v/v).

The pseudo-first-order rate constant of the dehydrochlorination of **1** was estimated from the plot of log (C_∞ and C_t are the concentrations of chloride ion liberated at infinite time and at time t, respectively. The values of k_{obs} determined for the series of compounds studied are listed in Table 1. The value of k_{obs} was, in each case, a linear function of the triethylamine concentration as shown in Fig. 1, where k_{obs} is plotted vs. amine concentration. The fact that such plots have zero intercepts indicates that the water-assisted (i.e. the uncatalyzed) reaction is negligible.

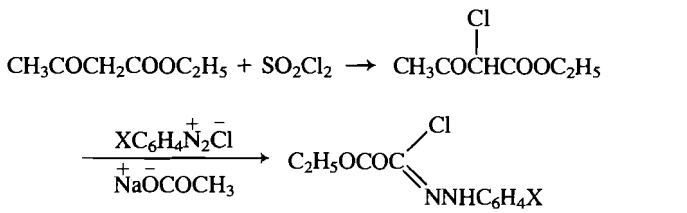

1

a, X = 4-CH_3 *b*, X = 3-CH_3 *c*, X = H *d*, X = 4-Cl
e, X = 3-Cl *f*, X = 4-$COOC_2H_5$ *g*, X = 3-NO_2 *h*, X = 4-$COCH_3$
i, X = 4-NO_2

SCHEME 1

[1]Author to whom correspondence may be addressed.

Printed in Canada / Imprimé au Canada

TABLE 1. Rate constants for dehydrochlorination of *N*-aryl-*C*-ethoxycarbonylformohydrazidoyl chlorides (0.002 *M*) ($C_2H_5OOCCCl{:}NNHC_6H_4X$) in 80% dioxane at 30°C and μ = 0.1; Et_3N = 0.02 *M*

X	log k_{obs}, $S.^{-1}$	log k_2[a]	σ_x^-
H	1.30	−0.191	0.00
p-CH_3	0.94	−0.327	−0.17
m-CH_3	1.15	−0.240	−0.07
p-Cl	1.53	−0.115	0.23
m-Cl	1.86	−0.032	0.37
m-NO_2	2.72	0.134	0.71
p-C_2H_5OOC	2.83	0.151	0.68
p-CH_3OC	3.50	0.243	0.84
p-NO_2	5.92	0.471	1.28

[a] $k_2 = k_{obs}/[(C_2H_5)_3N]$.

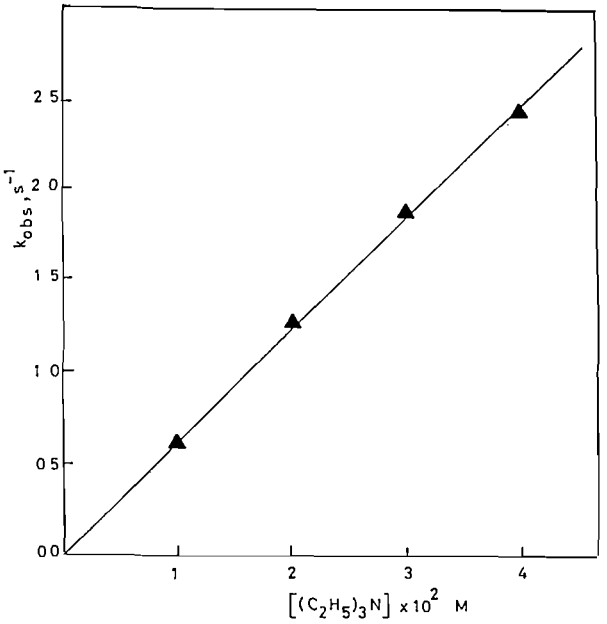

FIG. 1. Plot of the observed pseudo-first-order rate constants against triethylamine concentration for the dehydrochlorination of *N*-phenyl-*C*-ethoxycarbonylhydrazidoyl chloride in 4:1 dioxane–water at 30°C and μ = 0.1.

The plot of the log k_2 (where $k_2 = k_{obs} / [(C_2H_5)_3N]$) vs. the substituent constant σ_x^-, is linear (Fig. 2). The equation of the regression line is

$$[\log k_2 = 0.533\ \sigma_x^- - 0.218]$$

with correlation coefficient $t = 0.997$ and standard deviation $s = \pm 0.016$.

The most compatible mechanism that can account for the foregoing results is outlined in Scheme 2.

According to this sequence, it could be shown that,

$$\left[\log \frac{k_2}{k_2^0} = (\rho_1 - \rho_a)\sigma_x^- = \rho\ \sigma_x^-\right]$$

That is, the observed ρ value is the algebraic sum of the ρ values describing the separate stages.

For the reaction under study, it is expected that opposing effects will be operative in the 1,3-dipolar ion formation. That

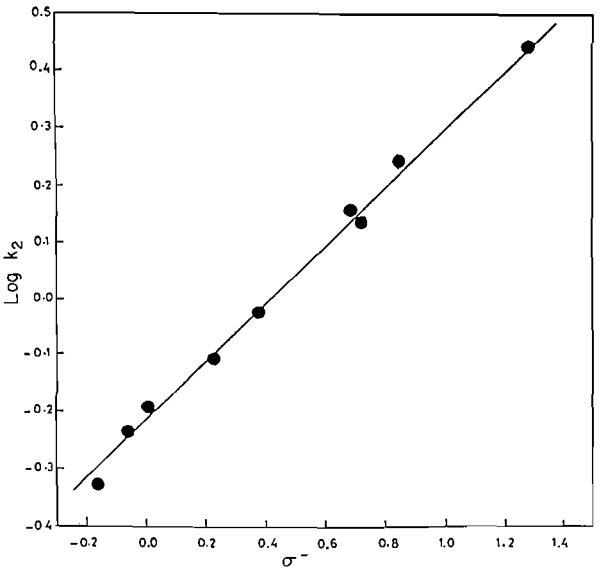

FIG. 2. Hammett plot of log k_2 versus σ^- constant for dehydrochlorination of the hydrazidoyl chlorides, $XC_6H_4NHN{:}C(Cl)COOC_2H_5$, in 4:1 dioxane–water at 30°C and μ = 0.1.

is, ρ_1 and ρ_a constants will have opposite signs, ρ_1 being negative whereas the value of ρ_a is positive. The positive sign of the ρ value obtained implies that $\rho_a < \rho_1$. To confirm this it was necessary to determine the acid dissociation constants K_a of the reaction series studied. However, the very high reactivity shown by these hydrazidoyl chlorides in basic solution made direct measurement of K_a difficult. Therefore, the rate of chloride ion loss from the hydrazidoyl chloride anion (k_2 in Scheme 2) could not be separated from the acidity constant K_a.

To overcome this difficulty, it was thought possible to estimate the value of ρ_a by determining the pK_a of the hydrazone series **4***a–h* in 80% (v/v) dioxane–water mixture at 30°C and ionic strength 0.1. The choice of **4** was based on the close similarity of the inductive effects of the CN and Cl groups. For example, the Taft σ constants of these two groups are σ^*_{CN} = 1.30 and σ^*_{Cl} = 1.05 (6). also, the values of σ_I of the CN and Cl groups were reported to be 0.60 and 0.47, respectively (6).

The compounds **4***a–h* required for such study were prepared by coupling ethyl cyanoacetate with diazotized arylamines in ethanol in the presence of sodium acetate. The structures of **4***a–n* were confirmed by their infrared and ^{1}Hmr spectra. Thus, the infrared spectra of all compounds reveal the presence of

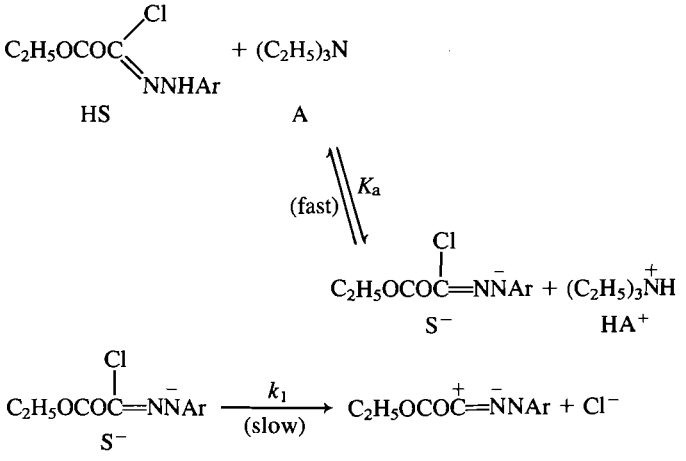

SCHEME 2

TABLE 2. Acid dissociation constants, pK_a, of ethyl cyanoglyoxalate arylhydrazones ($XC_6H_4NHN{=}C(CN)COOC_2H_5$) in 80% dioxane–water at 30°C and $\mu = 0.1$

X	acid λ_{max} nm	alkaline λ_{max} nm	pK_a	σ_x^-
m-CH_3	364	389	8.85	−0.07
H	362	388	8.75	0.00
p-Cl	352	392	8.52	0.23
m-Cl	354	396	8.47	0.37
m-Br	356	395	8.37	0.39
m-NO_2	340	387	8.09	0.71
p-CH_3CO	366	428	8.02	0.84
p-NO_2	376	472	7.63	1.28

characteristic bands near 3220 (hydrazone NH), 2220 (CN), 1710–1690 (ester CO), 1615 (C=N), and 1250 (ester C—O—C) cm^{-1}. In their ^{1}Hmr spectra, they exhibit a triplet signal at δ 1.3–1.4 (3H, $J = 7$ Hz, CH_3CH_2O), a quartet at δ 4.4 (2H, $J = 7$ Hz, CH_3CH_2O), and a singlet near 9.6 (1H, NH), in addition to the aromatic proton multiplet in the region 7.0–8.2 ppm.

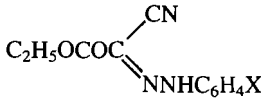

4

a, X = 3-CH_3 *d*, X = 3-Cl *g*, X = 4-CH_3CO
b, X = H *e*, X = 3-Br *h*, X = 4-NO_2
c, X = 4-Cl *f*, X = 3-NO_2

At pH < 8 each of the compounds **4***a–h* shows an intense π–π* absorption band near 360 nm. In alkaline medium, the corresponding anion shows π–π* band in the region 380–470 nm (Table 2). Spectra recorded at different pH values show an isobestic point near 380 nm. Typical spectra of an example of the series studied are reproduced in Fig. 3 and the values of λ_{max} of **4***a–h* in acid (pH < 3) and alkaline (pH > 11) media are summarized in Table 2. The absorbance of a freshly prepared solution measured at the wavelength of the absorption maximum of the anion plotted against pH shows a dependence in the shape of a dissociation curve of a monobasic acid. From the pH–absorbance data, the pK_a values of **4***a–h* were calculated. The results are summarized in Table 2.

A plot of pK_a vs. the substituent constant σ^- was linear (Fig. 4). The equation corresponding to this regression line is

$$[\log K_a = 0.845\ \sigma_x^- - 0.873]$$

with correction coefficient $r = 0.946$ and standard deviation $s = \pm 0.120$. As shown, the value of the slope (ρ_a) as expected is positive and has a value of 0.845. Since $\rho = \rho_i - \rho_a$ it follows that $\rho_i = -0.312$. This ρ_i value is negative, as expected for a reaction involving the generation of positive charge in the transition state.

These conclusions seem to be in agreement with literature data (7–9). Thus, for the thermolysis of 2,5-diaryltetrazoles **5**

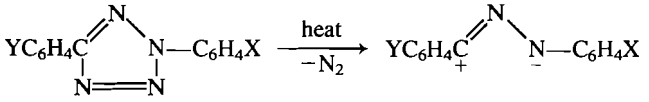

5 **6**

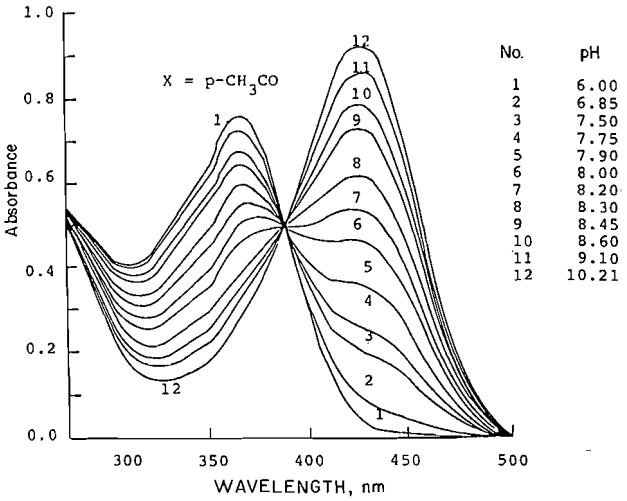

FIG. 3. Absorption spectra of ethyl α-cyanoglyoxalate arylhydrazones, $XC_6H_4NHN{:}C(CN)COOC_2H_5$, in 4:1 dioxane–water at 30°C and $\mu = 0.1$ at different pH values.

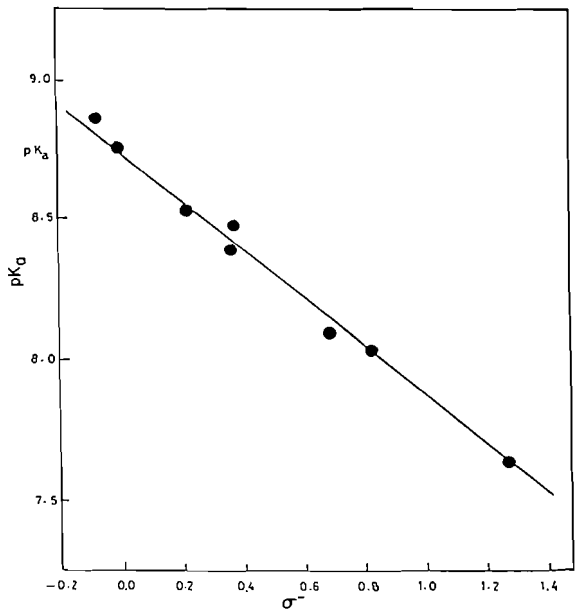

FIG. 4. Hammett plot of acid dissociation constant versus σ^- constant for ethyl α-cyanoglyoxalate aryl hydrazones, $XC_6H_4NHN{:}C(CN)COOC_2H_5$, in 4:1 dioxane–water at 30°C and $\mu = 0.1$.

the values of ρ_Y and ρ_X were found to be 1.16 and −0.23, respectively (7). Furthermore, a Hammett ρ value of −0.63 was reported for the formation of the azocarbonium ion **8** from the hydrazidoyl bromides **7** (8,9).

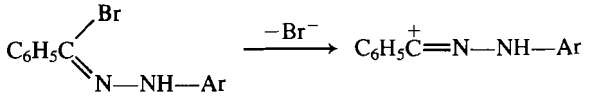

7 **8**

Ar = 2—Br, 4—XC_6H_3

The small value of ρ (−0.312) observed for series **1** undoubtedly results from the compensation of the trivalent anionic nitrogen centre for the positive charge buildup, such that the effect of substitution was reduced.

TABLE 3. *N*-Aryl-*C*-ethoxycarbonylformohydrazidoyl chlorides, $XC_6H_4NHN{=}C(Cl)COOC_2H_5$

X	Melting point °C (lit.) mp, °C	Yield, %	Molecular formula	*Anal.* calcd. (found), % C	H	N
4-CH_3	96–97 96–98(10)	80	$C_{11}H_{13}ClN_2O_2$			
3-CH_3	75	69	$C_{11}H_{13}ClN_2O_2$	54.88 (54.90)	5.55 (5.43)	11.64 (11.49)
H	80 77–79(10)	70	$C_{10}H_{11}ClN_2O_2$			
p-Cl	146 146(10)	83	$C_{10}H_{10}Cl_2N_2O_2$	45.98 (46.09)	3.86 (3.72)	10.72 (10.68)
m-Cl	95	70	$C_{10}H_{10}Cl_2N_2O_2$	45.98 (46.09)	3.86 (3.72)	10.72 (10.68)
p-$COOC_2H_5$	149	71	$C_{13}H_{15}ClN_2O_4$	52.27 (52.18)	5.06 (4.97)	9.38 (9.37)
m-NO_2	157	80	$C_{10}H_{10}ClN_3O_4$	44.21 (43.93)	3.71 (3.65)	15.47 (15.60)
p-$COCH_3$	157	75	$C_{12}H_{13}ClN_2O_3$	53.63 (53.44)	4.88 (4.83)	10.42 (10.39)
p-NO_2	192 191–193(10)	85	$C_{10}H_{10}ClN_3O_4$	44.21 (44.07)	3.71 (3.68)	15.47 (15.59)

Experimental

All melting points were measured on Bockmonoscop, Karlkolb Scientific Technical Supplies, West Germany, and are uncorrected. The infrared spectra were recorded in potassium bromide on a Zeiss infrared spectrophotometer model IMT16. The electronic absorption spectra were measured on a Pye–Unicam SP8000 spectrophotometer. The proton magnetic resonance spectra were obtained in deuterated chloroform with a Varian EM-390 90-MHz spectrometer. Microanalyses were performed on Perkin Elmer elemental analyzer model 240-B at the microanalytical laboratory of King Abdulaziz University. Ethyl 2-chloroacetoacetate was prepared by chlorination of ethyl acetoacetate with sulfuryl chloride in anhydrous ether as previously described (10).

Preparation of N-*aryl*-C-*ethoxycarbonylformohydrazidoyl chlorides* **1**a–i

A solution of ethyl 2-chloroacetoacetate (1.64 g, 0.01 mol) in ethanol (100 mL) was stirred for 15 min with 1.3 g sodium acetate trihydrate. The mixture was then chilled in an ice bath to 0.5°C. While the ester solution was cooling, the desired diazonium salt solution was prepared by diazotizing the appropriate arylamine (0.01 mol) in 6 *M* hydrochloric acid (6 mL) with cold 1 *M* sodium nitrite solution (10 mL) in the usual way. The diazonium salt solution was added to the cold ester solution over a period of 20 min while stirring and keeping the temperature below 5°C. The reaction mixture was then left in a refrigerator for 3 h. The precipitated solid was collected, washed with water, dried, and finally crystallized from ethanol. The compounds prepared, together with their physical constants, are listed in Table 3.

Preparation of ethyl cyanoglyoxalate arylhydrazones **4**a–h

These were prepared by coupling ethyl cyanoacetate with diazotized anilines following the same procedure described for **1***a–i*. The crude product, usually colored, was filtered, washed with water, and dried. Crystallization from acetic acid gave the corresponding ethyl cyanoglyoxalate arylhydrazone **4** in 70–85% yield. The compounds prepared are listed, together with their physical constants, in Table 4.

Kinetic studies

The kinetics of dehydrochlorination of the hydrazidoyl chlorides **1***a–i* were studied in dioxane–water (4:1, v/v) at 30°C(±0.1°C) and ionic strength μ = 0.1 ($NaNO_3$). The rates of dehydrochlorination were followed by recording the increase in the chloride ion concentration with time.

An Orion research microprocessor ion analyzer model 901 (Orion Research Incorporated, Mass., U.S.A.) with double junction reference electrode (90-02) and chloride ion electrode (94-17B) was used to record the chloride ion liberated during the dehydrochlorination of **1**.

Stock solutions of hydrazidoyl chlorides **1***a–i*, usually about 10^{-2} *M*, were prepared in 20% aqueous dioxane. A stock solution of triethylamine (1 *M*) was also prepared in the same solvent system. Appropriate concentrations of the amine and the hydrazidoyl chloride were prepared by dilution of the stock solutions and thermostated at 30°C in a constant temperature water bath.

Reactions were followed to 80% completion, with at least 15 readings taken. All kinetic runs were carried out in a double-wall cell, through which water at 30°C was circulated by means of a constant temperature MgW Louda circulating water pump.

In a typical kinetic run, the hydrazidoyl chloride solution (usually 2×10^{-3} *M*) was transferred to the cell. Then the appropriate volume of sodium nitrate stock solution (1.0 *M*) was added so that the ionic strength in the test solution was 0.1. The mixture was stirred with a magnetic stirrer. Then the chloride ion and the reference electrodes were introduced. The run was started by injecting the amine solution by means of a syringe and the stop watch was started at the moment of injection. the concentration of the chloride ion liberated was recorded at given intervals. In all kinetic runs, at least a tenfold excess of amine over the hydrazidoyl chloride was used in order to maintain pseudo-first-order kinetics. Duplicate or triplicate runs were performed for each concentration.

Good first-order plots of log ($C_\infty - C_t$) against time were obtained. The observed pseudo-first-order rate constants were calculated from the slopes of the straight lines obtained by the method of least squares (Table 1). The average deviation from the mean value of the rate constant in duplicate or triplicate experiments was ±5% or less.

Product analysis

A mixture of *N*-*p*-nitrophenyl-*C*-ethoxycarbonylformohydrazidoyl chloride **1***i* (0.71 g., 0.005 mol), triethylamine (0.71 mL, 0.005 mol), and sodium nitrate solution (5 *M*, 2 mL) in 100 mL 80% dioxane–water mixture was kept at the kinetic temperature 30°C until the chloride **1***i* disappeared, as evidenced by tlc (thin-layer chromatographic) analysis. The solvent in the mixture was distilled under reduced pressure and the residue was washed with water, dried, and subjected to preparative tlc separation using silica gel as adsorbent and the solvent system : toluene – ethyl acetate – acetic acid (12:4:0.5 by volume) as eluent.

TABLE 4. Ethyl cyanoglyoxalate arylhydrazones, $XC_6H_4NHN{=}C(CN)COOC_2H_5$

X	Melting point °C (lit.) mp, °C	Yield, %	Molecular formula	*Anal.* calcd. (found), % C	H	N
H	104 106(14)	75	$C_{11}H_{11}N_3O_2$	60.08 (59.87)	5.10 (4.97)	19.34 (18.97)
m-CH_3	92	80	$C_{12}H_{13}N_3O_2$	62.33 (62.21)	5.66 (5.51)	18.16 (17.87)
m-Cl	145–146	69	$C_{11}H_{10}ClN_3O_2$	52.49 (51.99)	4.00 (3.84)	16.69 (16.63)
p-Cl	151–152	78	$C_{11}H_{10}ClN_3O_2$	52.49 (52.19)	4.00 (3.92)	16.69 (16.49)
m-Br	155–156	68	$C_{11}H_{10}BrN_3O_2$	44.61 (44.38)	3.40 (3.39)	14.18 (14.07)
p-CH_3CO	159	75	$C_{13}H_{13}N_3O_3$	60.22 (60.04)	5.05 (4.83)	16.20 (16.07)
m-NO_2	135	85	$C_{11}H_{10}N_4O_4$	50.38 (49.98)	3.84 (3.76)	21.36 (20.98)
p-NO_2	193–194	83	$C_{11}H_{10}N_4O_4$	50.38 (50.58)	3.84 (3.74)	21.36 (21.17)

Two products were separated and identified as 1,4-bis-*p*-nitrophenyl-3,6-diethoxycarbonyl-1,4-dihydotetrazine **8** and ethyl oxalate mono-*p*-nitrophenylhydrazide **9**, by comparison with authentic samples prepared by literature methods (11).

The tetrazine derivative **8** was obtained in 35% yield, mp 237°C (AcOH) (Lit. (11) mp 236–237.5°C); ir (KBr) $\bar{\nu}$: 1746 (ester CO), 1580 (C=N), 1520, 1330 (NO_2), 1290 (C—N), 1175 (C—O—C) cm^{-1}; ^{1}Hmr ($CDCl_3$) δ: 1.2 (t, 6H, J = 7 Hz, $2CH_3$—CH_2), 4.3 (q, 4H, J = 7 Hz, $2CH_3$—CH_2O), 7.3 (d, 2H J = 9 Hz, 2 *p*-NO_2—ArH), 8.3 (d, 2H J = 9 Hz, 2 *p*-NO_2—ArH) ppm.

The hydrazide **9** was obtained in 60% yield, mp 170°C (ethanol); ir (KBr) $\bar{\nu}$: 3320 (NH), 1738 (ester CO), 1690 (anilide CO), 1505, 1320 (NO_2) cm^{-1} ^{1}Hmr ($CDCl_3$) δ: 1.43 (t, 3H, J = 7 Hz, CH_3—CH_2O), 4.52 (q, 2H, J = 7 Hz, CH_3—CH_2O), 7.06 (d, 2H, J = 9 Hz, *p*-NO_2—ArH), 8.26 (d, 2H, J = 9 Hz, *p*-NO_2—ArH), 8.7 (s, 1H, CONH), 10.90 (s, 1H, HNC_6H_4—NO_2-*p*) ppm. *Anal.* calcd. for $C_{10}H_{11}N_3O_5$: C 47.43, H 4.38, N 16.59; found: C 47.10, H 4.13, N 16.30%.

Determination of acid dissociation constants of **4**a–h

The acid dissociation constants of the compounds **4***a–h* were determined spectrophotometrically in 80% dioxane–water at 30 ± 0.1°C and an ionic strength of 0.1.

A Taccussel digital pH meter PHN 78 fitted with a glass electrode type C-285-725 and a reference electrode type TB/HS 286-506 was employed for the determination of pH. The instrument was accurate to ±0.01 pH unit. It was calibrated using two standard Beckman buffer solutions of pH 4.01 and 7.00. The pH meter readings (B) recorded in dioxane–water solutions were converted to hydrogen ion concentration [H^+] by means of the widely used relation of van Uitert and Hass (12), namely:

$$-\log [H^+] = B + \log U_H$$

where log U_H is the correction factor for the solvent composition and ionic strength used, for which B is read. For this purpose, readings were made on a series of solutions containing known amounts of hydrochloric acid and sodium chloride, such that the ionic strength was equal to 0.1 in 80% dioxane–water at 30.0 ± 0.1°C. The value of log U_H was found to be −0.55.

The experimental procedure in the determination of pK_a constants and their calculations from the absorbance–pH data were as described earlier (13). The pK_a values obtained were reproducible to within ±0.01 pK_a unit. The results are summarized in Table 2.

1. A. S. SHAWALI and C. PARKANYI. J. Heterocycl. Chem. **17**, 833 (1980), and references cited therein.
2. A. S. SHAWALI. Heterocycles, **20**, 2239 (1983).
3. R. HUISGEN. Angew. Chem. Int. Ed. Eng. **2**, 565 (1963).
4. R. S. TEWARI and P. PARIHAR. Tetrahedron, **39**, 129 (1983).
5. L. FODOR, M. S. ALGHARIB, G. SZABO, G. BERNATH, and P. SOHAR. Heterocycles, **22**, 537 (1984).
6. C. D. RITCHIE and W. F. SAGER. Progress in physical organic chemistry. Vol. 2. Interscience, New York. 1964.
7. S. Y. HONG and J.E. BALDWIN. Tetrahedron, **24**, 3767 (1965).
8. F. L. SCOTT, M. P. CASHMAN, and A. F. HEGARTY. J. Chem. Soc. Perkin Trans. **2**, 1607 (1971).
9. A. F. HEGARTY, M. P. CASHMAN, and F. L. SCOTT. J. Chem. Soc. Perkin Trans. **2**, 44 (1972).
10. R. HUISGEN and H. JACHIM. Ann. **591**, 220 (1955).
11. R. HUISGEN, E. AUDERHAAR, and G. WILLBILLICH. Chem. Ber. **98**, 1476 (1965).
12. L. G. VAN UITERT and C. G. HAAS. J. Am. Chem. Soc. **75**, 451 (1953).
13. A. S. SHAWALI and B. M. ALTAHOU. Can. J. Chem. **20**, 3260 (1976).
14. S. M. PARMERTER. *In* Organic reactions. *Edited by* R. Adams. John Wiley, New York. 1959. Chapt. p.1.

The crystal and molecular structure of *N*-(3,4,5-trimethoxycinnamoyl)-Δ^3-piperidine-2-one, an amide alkaloid (piperlongumine), $C_{17}H_{19}NO_5$

TAPATI BANERJEE AND SIDDHARTHA CHAUDHURI

Crystallography and Molecular Biology Division, Saha Institute of Nuclear Physics, Sector I, Block AF, Bidhannagar, Calcutta-700 064, India

Received March 15, 1985

TAPATI BANERJEE and SIDDHARTHA CHAUDHURI. Can. J. Chem. **64**, 876 (1986).

The crystals of $C_{17}H_{19}NO_5$ belong to the monoclinic space group $P2_1/n$ with $a = 15.793(3)$, $b = 4.089(4)$, $c = 24.649(5)$ Å, $\beta = 97.56(3)°$ $V = 1578(2)$ Å^3, and $Z = 4$. The structure was solved by MULTAN 78 and refined by full-matrix least-squares to a final R of 0.053 for 1863 observed reflections. X-ray crystallography has revealed that the molecule is the Δ^3 isomer and not the Δ^5 isomer suggested originally from nmr spectroscopy. The piperidyl nitrogen is sp^2 hybridized with its electron lone pair involved in conjugation with the carbonyl groups. The piperidone ring adopts a distorted boat conformation. An interesting feature of the structure is the formation of two C(ethylenic)—H...O(keto) intramolecular hydrogen bonds which stabilize the molecular conformation.

TAPATI BANERJEE et SIDDHARTHA CHAUDHURI. Can. J. Chem. **64**, 876 (1986).

Les cristaux du $C_{17}H_{19}NO_5$ appartiennent au groupe d'espace $P2_1/n$ avec $a = 15,793(3)$, $b = 4,089(4)$, et $c = 24,649(5)$ Å, $\beta = 97,56(3)°$, $V = 1578(2)$ Å^3, et $Z = 4$. On a résolu la structure par la méthode MULTAN 78 et on l'a affinée par la méthode des moindres carrés (matrice entière) jusqu'à une valeur finale de R de 0,053 pour 1863 réflexions observées. La cristallographie par diffraction des rayons X a permis de montrer qu'il s'agit de l'isomère Δ^3 et non pas de l'isomère Δ^5 qui avait été suggéré sur la base de la rmn. L'azote de la pipéridine est hybridée sp^2 et sa paire d'électrons libres est impliquée dans une conjugation avec les groupements carbonyles. Le cycle pipéridone adopte une conformation bateau déformé. Une caractéristique intéressante de la structure est la formation de deux liaisons hydrogènes intramoléculaires. C(éthylénique)—H...O(cétone) qui stabilisent la conformation moléculaire.

[Traduit par la revue]

Introduction

The amide alkaloid piperlongumine, **1**, isolated from the roots of the climbing plant *Piper Longum* L., is an effective drug in the treatment of asthma and chronic bronchitis (1). Earlier crystallographic (2–4) and spectroscopic (5) studies have shown that several alkaloids separated from *Piper* species, e.g., West African black or Ashanti pepper (3,4), contain the piperidine moiety; the amide alkaloids separated from the roots of *Piper Longum* L. are the exceptions (1). The present

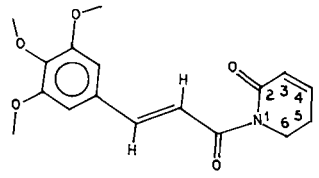

1

structural study has revealed certain interesting features of the piperlongumine molecule which are discussed here.

Experimental

Crystal data:

$C_{17}H_{19}NO_5$ fw=317.34

Monoclinic, $P2_1/n$, systematic absences: $h0l$, $h+l$ odd, $0k0$, k odd; $a = 15.793(3)$, $b = 4.089(4)$, $c = 24.649(5)$ Å, $\beta = 97.56(3)°$, $V = 1578(2)$ Å^3, $Z = 4$, $\rho_o = 1.35$ (by flotation in KI solution), $\rho_c = 1.33$ g cm^{-1}, $\lambda(CuK_\alpha) = 1.5418$ Å, $\mu(CuK_\alpha) = 8.3$ cm^{-1}.

The compound was recrystallized from ethanol. Initial symmetry information and unit cell dimensions were derived from oscillation and Weissenberg photographs. The intensity data were collected at 22°C on an Enraf-Nonius CAD4 diffractometer, using graphite monochromatized radiation, with a crystal of dimensions 0.40 × 0.18 × 0.10 mm. The data were collected in the needle option in which the intensities were recorded in the minimum absorption position of the crystal. Accurate cell parameters were obtained from the least-squares fit of the setting angles of 25 well-centred reflections with 2θ values ranging from 32.8 to 55.8°. The $\omega/2\theta$ technique was used for data collection up to a limit of $2\theta = 120°$. The peaks were scanned at the take-off angle of 4° with a scan width of $(0.60 + 0.15 \tan\theta)°$ and a variable scan time extending up to a maximum of 60 s. Three orientation control reflections and three intensity control reflections were monitored every 50 reflections and every hour of X-ray exposure, respectively, to ensure the stability of the crystal position and the crystal quality.

Out of 2350 unique reflections measured, 1863 were considered to

TABLE 1. Fractional coordinates, with esd in parentheses, and equivalent isotropic temperature factors for the non-hydrogen atoms

Atom	x	y	z	B_{eq} (Å^2)
N(1)	0.3629(1)	1.6656(6)	0.67699(9)	3.3
C(2)	0.4342(2)	1.7647(8)	0.6528(1)	3.6
C(3)	0.5083(2)	1.8690(10)	0.6901(1)	5.5
C(4)	0.5145(2)	1.8363(10)	0.7439(2)	6.6
C(5)	0.4417(2)	1.7094(9)	0.7696(1)	5.2
C(6)	0.3592(2)	1.7634(8)	0.7347(1)	4.0
O(7)	0.4345(1)	1.7661(6)	0.60350(8)	4.6
C(8)	0.2864(2)	1.5567(8)	0.6476(1)	3.2
O(9)	0.2203(1)	1.5872(7)	0.66767(7)	4.8
C(10)	0.2891(2)	1.3849(8)	0.5952(1)	3.2
C(11)	0.2192(2)	1.3320(8)	0.5618(1)	3.2
C(12)	0.2105(2)	1.1801(7)	0.5072(1)	3.2
C(13)	0.2796(2)	1.0231(7)	0.4883(1)	3.3
C(14)	0.2708(2)	0.9047(7)	0.4356(1)	3.1
C(15)	0.1941(2)	0.9350(7)	0.4015(1)	3.2
C(16)	0.1242(2)	1.0821(7)	0.4210(1)	3.0
C(17)	0.1337(2)	1.2021(7)	0.4739(1)	3.2
O(18)	0.3341(1)	0.7460(6)	0.41297(8)	4.5
C(19)	0.4130(2)	0.6966(9)	0.4472(1)	5.2
O(20)	0.1843(1)	0.8180(5)	0.34850(7)	4.0
C(21)	0.2235(3)	1.0160(10)	0.3115(1)	5.5
O(22)	0.0506(1)	1.0950(6)	0.38527(8)	4.1
C(23)	−0.0208(2)	1.2489(9)	0.4038(1)	4.5

TABLE 2. Bond distances (Å) and bond angles (°), with esd in parentheses

Bond	Distance	Bond	Distance
N(1)—C(2)	1.401(3)	C(12)—C(13)	1.397(4)
N(1)—C(6)	1.486(3)	C(13)—C(14)	1.376(3)
C(2)—C(3)	1.454(4)	C(14)—O(18)	1.370(3)
C(2)—O(7)	1.216(3)	O(18)—C(19)	1.425(3)
C(3)—C(4)	1.324(5)	C(14)—C(15)	1.387(4)
C(4)—C(5)	1.477(5)	C(15)—C(16)	1.396(4)
C(5)—C(6)	1.481(4)	C(15)—O(20)	1.381(3)
N(1)—C(8)	1.398(3)	O(20)—C(21)	1.420(4)
C(8)—O(9)	1.218(3)	C(16)—O(22)	1.365(4)
C(8)—C(10)	1.476(4)	O(22)—C(23)	1.418(4)
C(10)—C(11)	1.306(4)	C(16)—C(17)	1.383(3)
C(11)—C(12)	1.472(4)	C(17)—C(12)	1.376(4)

Bonds	Angle	Bonds	Angle
C(2)—N(1)—C(6)	117.6(2)	C(11)—C(12)—C(17)	119.2(2)
C(2)—N(1)—C(8)	124.0(2)	C(13)—C(12)—C(17)	119.8(3)
C(6)—N(1)—C(8)	116.3(2)	C(12)—C(13)—C(14)	119.3(3)
N(1)—C(2)—C(3)	116.1(2)	C(13)—C(14)—C(15)	120.9(3)
N(1)—C(2)—O(7)	124.3(3)	C(13)—C(14)—O(18)	124.2(2)
C(3)—C(2)—O(7)	121.5(3)	C(15)—C(14)—O(18)	114.9(2)
C(2)—C(3)—C(4)	123.5(3)	C(14)—C(15)—C(16)	119.8(3)
C(3)—C(4)—C(5)	120.3(3)	C(14)—C(15)—O(20)	121.6(2)
C(4)—C(5)—C(6)	111.9(3)	C(16)—C(15)—O(20)	118.6(2)
C(5)—C(6)—N(1)	111.9(2)	C(15)—C(16)—O(22)	116.1(2)
N(1)—C(8)—O(9)	119.0(3)	C(15)—C(16)—C(17)	118.9(3)
N(1)—C(8)—C(10)	118.9(2)	C(17)—C(16)—O(22)	124.9(2)
O(9)—C(8)—C(10)	121.9(3)	C(16)—C(17)—C(12)	121.3(3)
C(8)—C(10)—C(11)	120.8(3)	C(14)—O(18)—C(19)	117.0(2)
C(10)—C(11)—C(12)	128.5(3)	C(15)—O(20)—C(21)	113.9(2)
C(11)—C(12)—C(13)	120.9(3)	C(16)—O(22)—C(23)	117.1(2)

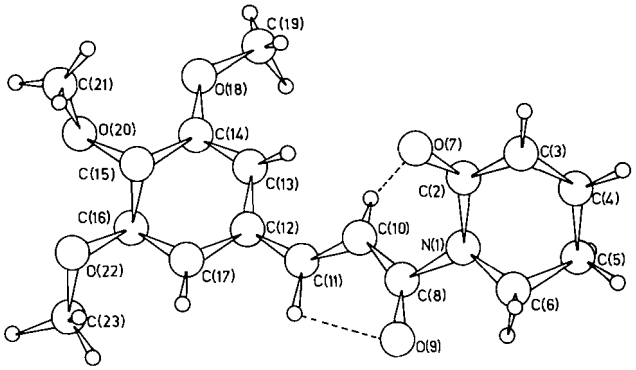

FIG. 1. A perspective view of the molecule down the *b* axis showing the C—H...O contacts.

be observed ($I \geq 3\,\sigma\,(I)$). The intensities were corrected for Lorentz and polarization factors but not for absorption. Corrections were also applied for the small variation (<2%) in the intensities of the control reflections.

The structure was determined by MULTAN (6) and refined by the full-matrix least-squares program ORFLS (7) to a final R of 0.053 (0.072 including unobserved reflections) and R_w of 0.066 ($w = 1/\sigma^2(|F_o|)$);[1] nine of the strongest reflections, namely $\bar{2}12$, $\bar{1}12$, 011, 012, $\bar{2}21$, $\bar{1}11$, $\bar{1}13$, 020, and 220, were removed from the least-squares refinement and marked as unobserved as their accuracy was doubtful because of the large differences between the intensity counts in the forward and reverse scans on the diffractometer. The hydrogen atoms, located from two successive difference electron density syntheses, were included in the refinement with isotropic thermal parameters. The maximum shift/error was less than 0.03 and peak heights ranging from −0.20 to 0.26 e Å^{-3} were found in a final difference synthesis computed at the end of the refinement.

The scattering factors for the non-hydrogen atoms were taken from Cromer and Waber (8) and those for the hydrogen atoms from Stewart, Davidson, and Simpson (9). The non-hydrogen scattering factors were corrected only for the real parts of the anomalous dispersion ($\Delta f'$ = 0.047, 0.029, and 0.017, for O, N, and C, respectively) from the International Tables for X-ray Crystallography (10). The geometrical parameters of the molecule were computed with the program PARST (11).

[1]Structure factor tables and the anisotropic thermal parameters may be purchased from the Depository of Unpublished Data, CISTI, National Research Council of Canada, Ottawa, Ont., Canada K1A 0S2.

Discussion

Figure 1 shows a perspective view of the piperlongumine molecule together with the atom labelling scheme. The coordinates for the non-hydrogen atoms together with their equivalent isotropic thermal parameters (12) are listed in Table 1. The interatomic bond distances and angles are given in Table 2, while Table 3 lists some selected torsion angles.

It is observed that the double bond in the piperidone ring is between C(3) and C(4); the compound is therefore the Δ^3 isomer rather than the Δ^5 isomer proposed from chemical and nmr spectroscopic studies (1). The N(1)—C(6) bond distance is in

TABLE 3. Some selected torsion angles (°) with esd in parentheses

Bonds	Angle
N(1)—C(2)—C(3)—C(4)	8.4(5)
C(2)—C(3)—C(4)—C(5)	−4.3(6)
C(3)—C(4)—C(5)—C(6)	−24.3(5)
C(4)—C(5)—C(6)—N(1)	47.1(4)
C(5)—C(6)—N(1)—C(2)	−45.3(3)
C(6)—N(1)—C(2)—C(3)	17.3(4)
O(7)—C(2)—N(1)—C(8)	0.7(3)
C(2)—N(1)—C(8)—C(10)	30.9(4)
C(2)—N(1)—C(8)—O(9)	−153.8(3)
C(6)—N(1)—C(8)—O(9)	9.4(4)
C(11)—C(10)—C(8)—O(9)	17.4(5)
C(13)—C(14)—O(18)—C(19)	1.4(4)
C(14)—C(15)—O(20)—C(21)	−75.8(3)
C(17)—C(16)—O(22)—C(23)	1.2(4)
C(11)—C(10)—C(8)—N(1)	−167.5(3)
C(8)—C(10)—C(11)—C(12)	176.8(3)
C(10)—C(11)—C(12)—C(13)	10.6(5)

good agreement with the values found in piperidine derivatives where C(6) is sp^3 hybridized (2–4,13–15).

As in other similarly substituted piperidine structures (2,3,13–16), the lone pair of electrons on the piperidyl nitrogen atom, N(1), is involved in conjugation with the carbonyl groups. This is indicated by the slight lengthening of the two C=O double bonds (1.216(3) and 1.218(3) Å) and the concomitant shortening of the two N—C(sp^2) single bonds (1.401(3) and 1.398(3) Å). Accordingly, the state of hybridization of the piperidyl nitrogen atom is sp^2 as shown by the sum (357.9(6)°) of the angles around it and the small deviation (−0.071(2) Å) of the atom from the plane of N(1), C(2), C(6), and C(8). The O(9)—C(8)—N(1)—C(6) torsion angle of 9.4(4)° is consistent with the partial double bond character of the N(1)—C(8) bond (17).

The bond distances and angles in the cinnamoyl moiety agree with those in other cinnamoyl derivatives (18,19). The progressive decrease in the C—C—C and C—C—N angles along the chain from the phenyl ring to the piperidone ring has also been observed in other cinnamoyl derivatives (2,3,16,18,19). This has been attributed to the steric repulsion between the hydrogen atoms of the chain (16).

The relative magnitudes of the C(phenyl)—O(methoxy) bond lengths C(14)—O(18), C(15)—O(20), and C(16)—O(22) (1.370(3), 1.381(3), and 1.365(4) Å) suggest considerable conjugation between the phenyl ring and the two methoxy groups substituted at C(14) and C(16). This conjugation appears to be favoured by the near coplanarity of these groups with the ring as indicated by the torsion angles C(13)—C(14)—O(18)—C(19) and C(17)—C(16)—O(22)—C(23) (Table 3). The extent of conjugation of the methoxy group at C(15) with the phenyl ring is comparatively smaller, possibly due to the accumulation of a considerable negative charge density at this carbon atom by the +R effects of the two adjacent methoxy groups. The noncoplanarity of the methoxy group at C(15) with the phenyl ring, indicated by the torsion angle C(16)—C(15)—O(20)—C(21), is obviously a result of the steric repulsion of the methoxy groups on either side of it.

The dissymmetry in the exocyclic angles at C(14) and C(16) may be attributed to the steric repulsive interaction between the

TABLE 4. Puckering parameters for different rings

Ring	q_2	q_3	Q	θ	φ
Piperidone (N(1), C(2), C(3), C(4), C(5), C(6))	0.36(2)	−0.20(1)	0.41(1)	119(3)	−8.4(7)
Phenyl (C(12), C(13), C(14), C(15), C(16), C(17))	0.024(1)	−0.005(3)	0.025(3)	102(7)	−171(7)
Hydrogen bonded six-membered ring (N(1), C(2), O(7) H(10), C(10), C(8))	0.54(1)	0.19(1)	0.57(2)	109.8(8)	−32(1)
Hydrogen bonded five-membered ring (C(8), O(9), H(11), C(11), C(10))	0.14(1)				−122(6)

TABLE 5. Geometries of C—H...O(keto) contacts

Structure	Contact	C—H (Å)	C—O (Å)	H...O (Å)	C—H...O(°)
Piperlongumine	C(10)—H(10)...O(7)	0.92(3)	2.761(4)	2.24(3)	115(2)
	C(11)—H(11)...O(9)	0.91(3)	2.808(3)	2.41(2)	106(2)
Piperx(2)	C(3)—H(3)...O(4)	0.87(1)	2.451(9)	1.72(1)	138.8(4)

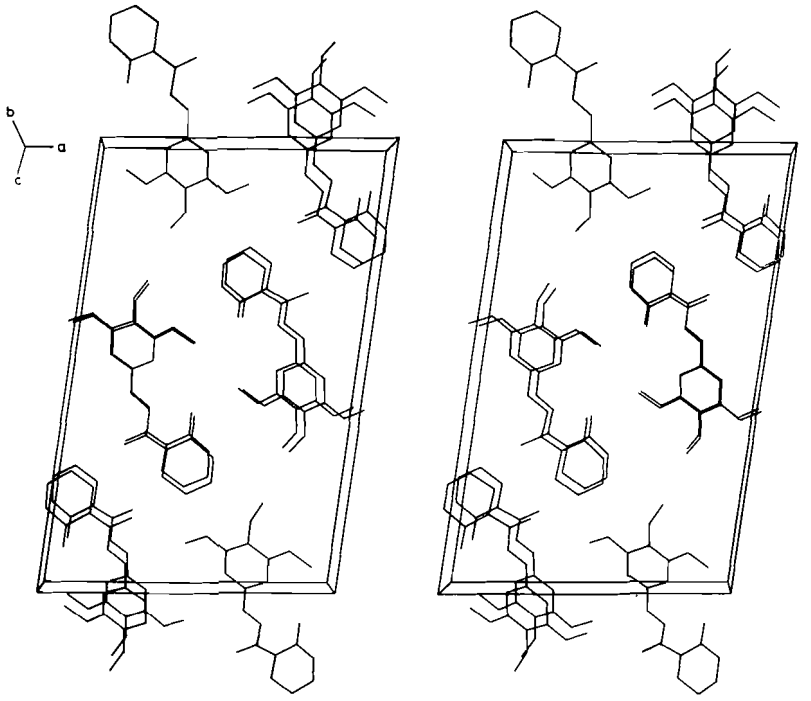

FIG. 2. A stereo view of the crystal structure.

corresponding methyl groups and the phenyl ring atoms.[2] A similar dissymmetry in th exocyclic angles has been observed in the structure of ethyl 3,4,5-dimethoxy-2-(3-methyl-2,2-pyridylsulphamoyl) phenyl propionate (20).

The torsion angles about the N(1)—C(8), C(8)—C(10), C(10)—C(11), and C(11)—C(12) bonds show that the molecule is nearly in the extended form. The acrylyl chain, O(9)—C(8)—C(10)—C(11)—C(12), makes dihedral angles of 18.7(2) and 24.3(1)° with the mean planes of the phenyl and piperidone rings, respectively.

The puckering parameters (21) for the different rings in the structure have been listed in Table 4. The piperidone ring is seen to have a distorted boat conformation. The piperidine ring, common in several amide alkaloids separated from *Piper* species (2–4) and in compounds containing piperidyl carbonyl groups (17), is found to be in the chair conformation.

The benzene ring is significantly nonplanar (11); the puckering parameters indicate a somewhat flattened distorted boat conformation for the ring (21).

The C—H groups that are near the electron withdrawing groups are capable of forming hydrogen bonds with a wide variety of acceptor atoms (22). The geometries of the intramolecular contacts C(10)—H(10)...O(7) and C(11)—H(11)...O(9), listed in Table 5, reveal that the ethylenic C—H groups in the present structure are indeed involved in such hydrogen bonds, leading to the formation of two hydrogen bonded rings. The six-membered ring, C(10)—H(10)—O(7)—C(2)—N(1)—C(8), is found to have a twist boat conformation while the five-membered ring, C(11)—H(11)—O(9)—C(8)—C(10), is in the twist form (Table 4) (21). In the course of the present study it has been found that a similar C—H...O bond, leading to the formation of a five-membered ring in the twist form, also exists in the structure of Piperx, *N*-piperidyl-5-(2-methoxy-4,5-methylenedioxyphenyl)-*trans*-2-*cis*-4-pentadienamide (2). Figure 2 shows a perspective view[3] of the crystal structure. The molecules are separated by unit cell translations along the *b* direction with translation related atoms superimposed. The unit vector along the *b* axis, 4.089(4) Å, is seen to be the sum of the van der Waals radii of the superimposing methyl groups.

[2]The C(13)—C(19), C(19)—H(13), C(17)—C(23), and C(23)—H(17) distances are 2.794(5), 2.51(3), 2.805(4), and 2.58(4) Å, respectively.

Acknowledgments

The authors thank Prof. (Mrs.) A. Chatterjee for a gift of the compound and their colleagues Dr. P. T. Muthiah and Mr. D. Chatterjee for useful discussions. They are also indebted to Prof. S. K. Mazumdar for his encouragement and keen interest in the work.

1. A. CHATTERJEE and C. P. DUTTA. Tetrahedron, **23**, 1769 (1967).
2. K. A. WOODE, F. L. PHILLIPS, I. ADDAE-MENSAH, J. C. J. BART, and S. CHAUDHURI. J. Nat. Prod. **47**, 1024 (1984).
3. F. H. HERBSTEIN, W.SCHWOTZER, I. ADDAE-MENSAH, F. G. TORTO, and K. A. WOODE. Acta Crystallogr. Sect. B: Struct. Crystallogr. Cryst. Chem. **B37**, 702 (1981).
4. J. BORDNER and P. MULLINS. Cryst. Struct. Commun. **3**, 693 (1974).
5. F. S. SPRING and J. STARK. J. Chem. Soc. 1170 (1950).
6. P. MAIN, S. E. HULL, L. LESSINGER, G. GERMAIN, J.-P. DECLERCQ, and M. M. WOOLFSON. MULTAN 78. A system of computer programs for the automatic solution of crystal structures from X-ray diffraction data. Universities of York, England and Louvain, Belgium, 1978.
7. W. R. BUSING, K. O. MARTIN, and H. A. LEVY. ORFLS. Report ORNL-TM-306. Oak Ridge National Laboratory. Oak Ridge, TN. 1962.
8. D. T. CROMER and J. T. WABER. Acta Crystallogr. **18**, 104 (1965).
9. R. F. STEWART, E. R. DAVIDSON, and W. T. SIMPSON. J. Chem. Phys. **42**, 3175 (1965).

[3]Coordinates for the stereo pair have been computed with the program STEREO. S. Chaudhuri, 1984. Unpublished.

10. INTERNATIONAL TABLES FOR X-RAY CRYSTALLOGRAPHY. Vol. IV. Kynoch Press. Birmingham. 1974.
11. M. NARDELLI. Comput. Chem. **7**, 95 (1983).
12. W. C. HAMILTON. Acta Crystallogr. **12**, 609 (1959).
13. E. ARTE, J. FENEAU-DUPONT, J.-P. DECLERCQ, G. GERMAIN, and M. VAN MEERSSCHE. Cryst. Struct. Commun. **6**, 493 (1977).
14. E. ARTE, J. FENEAU-DUPONT, J.-P. DECLERCQ, G. GERMAIN, and M. VAN MEERSSCHE. Cryst. Struct. Commun. **6**, 773 (1977).
15. D. TRANQUI, D. T. CROMER and A. BOUCHERLE. Acta Crystallogr. Sect. B: Struct. Crystallogr. Cryst. Chem. **B30**, 2237 (1974).
16. M. GRYNPAS and P. F. LINDLEY. Acta Crystallogr. Sect. B: Struct. Crystallogr. Cryst. Chem. **B31**, 2663 (1975).
17. G. GILLI and V. BERTOLASI. J. Am. Chem. Soc. **101**, 7704 (1979).
18. H. BRADACZEK, H. J. HEEHT, and P. REINHARDT. J. Cryst. Mol. Struct. **7**, 147 (1977).
19. M. COTRAIT and M. PESQUER. Acta Crystallogr. Sect. B: Struct. Crystallogr. Cryst. Chem. **B33**, 2826 (1977).
20. E. ELIOPOULOUS, B. SHELDRICK and S. HOMODRAKAS. Acta Crystallogr. Sect. C: Cryst. Struct. Commun. **C39**, 1693 (1983).
21. D. CREMER and J. A. POPLE. J. Am. Chem. Soc. **97**, 1354 (1975).
22. R. TAYLOR and O. KENNARD. J. Am. Chem. Soc. **104**, 5063 (1982).

Transferts d'électrons assistés par les métaux de transition : influence de la nature du cation métallique sur la réduction de composés carbonylés en milieu aprotique

FRANÇOISE FOURNIER
Laboratoire de chimie organique structurale, Centre national de la recherche scientifique, Unité associée 455, Université Pierre et Marie Curie, 4 Place Jussieu, 75230 Paris cédex 05, France
ET
MICHEL FOURNIER[1]
Laboratoire de physico-chimie inorganique, Centre national de la recherche scientifique, Unité associée 419, Université Pierre et Marie Curie, 4 Place Jussieu, 75230 Paris cédex 05, France
Reçu le 18 mars 1985[2]

F. FOURNIER et M. FOURNIER. Can. J. Chem. **64**, 881 (1986).

L'électropinacolisation de cétones est favorisée en présence de cations des métaux de transition. C'est un phénomène général qui se produit avec Cr^{2+}, Mn^{2+}, Fe^{2+}, Co^{2+}, Zn^{2+}, mais pas avec Ni^{2+}. La réduction conduit aux α-glycols, avec un bon résultat, sans résinification et à un potentiel moins négatif que celui de la cétone de départ. La répartition des composés isolés dépend du caractère acide, au sens de Lewis, et du pouvoir complexant du cation métallique. Ainsi, la plus grande spécificité, en dimère généralement, est observée avec Fe^{2+}, sauf pour la chalcone, où Zn^{2+} conduit à la meilleure stéréosélectivité. Aucun complexe préexistant, entre le dérivé carbonylé et l'ion métallique, n'a pu être mis en évidence.

F. FOURNIER and M. FOURNIER. Can. J. Chem. **64**, 881 (1986).

The pinacolisation of ketones is enhanced when a bivalent transition metal cation is present. This phenomenon is general and occurs with Cr^{2+}, Mn^{2+}, Fe^{2+}, Co^{2+}, Zn^{2+} but not with Ni^{2+}. The cathodic reduction leads to α-glycols with a good yield, without any resin production, and at a less negative potential than that of the ketone itself. The distribution of all isolated compounds is dependent on the Lewis character-acidity and complexing power of the metallic cation. Thus, for the dimerization, the greatest specificity is generally observed when Fe^{2+} is present. For the chalcone, the better stereoselectivity is obtained with Zn^{2+}. No evidence of initial carbonyl complex of the metal ion was shown.

Les réactions catalysées par transferts d'électrons et plus particulièrement celles assistées par les complexes de métaux de transition, font l'objet d'études intensives (1).

Le cas des composés carbonylés, spécialement celui des cétones aromatiques, suscite depuis ces dernières années quelques controverses (2). En effet, le problème essentiel qui se pose dans l'interprétation du mécanisme de la réduction électrochimique duplicative de la fonction carbonyle est celui de l'étape de couplage. Ainsi après formation initiale de l'anion radical $A^{\bar{\cdot}}$, éventuellement suivie de sa protonation, trois types de couplage peuvent être envisagés : (*1*) radical–radical ; (*2*) radical–substrat ; (*3*) ion–substrat. Ce qui peut être résumé par le Schéma suivant :

Étape initiale $A + \bar{e} \rightleftharpoons A^{\bar{\cdot}}$ et $A^{\bar{\cdot}} + H^+ \rightleftharpoons AH^{\cdot}$

Mécanisme 1 $2\,A^{\bar{\cdot}} \rightleftharpoons D^{2-}$, $A^{\bar{\cdot}} + AH^{\cdot} \rightleftharpoons DH^-$, $2\,AH^{\cdot} \rightleftharpoons DH_2$

D = dimère
DH^- = dimère anion protoné
DH_2 = dimère

Mécanisme 2 $A + A^{\bar{\cdot}} \rightleftharpoons D^{\bar{\cdot}}$, $A + AH^{\cdot} \rightleftharpoons DH^{\cdot}$

Puis éventuellement $D^{\bar{\cdot}} + \bar{e} \rightleftharpoons D^{2-}$, $DH^{\cdot} + \bar{e} \rightleftharpoons DH^-$

Mécanisme 3 $A^{\bar{\cdot}} + \bar{e} \rightleftharpoons A^{2-}$, $A^{2-} + H^+ \rightleftharpoons AH^-$

(fixation d'un 2ème $\bar{e}$) $A^{2-} + A \rightleftharpoons D^{2-}$, $AH^- + A \rightleftharpoons DH^-$
et éventuellement $A^{2-} + 2H^+ \rightleftharpoons AH_2$

ce qui se traduit sur le plan préparatif, par l'obtention de différents produits, monomères ou dimères.

Par exemple, avec les cétones aromatiques, on obtient uniquement des alcools (monoalcool ou diol). Par contre, avec les cétones α-β éthyléniques, les hydrodimères formés peuvent avoir des structures diverses, le radical anion créé existant sous plusieurs formes tautomères. Ainsi selon les liaison formées :

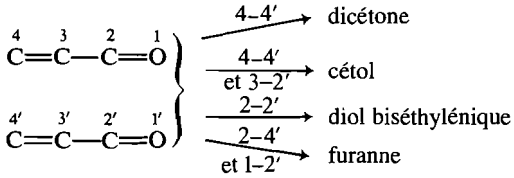

De plus, si le milieu est aprotique, DMF par exemple, l'électroréduction des cétones aromatiques conduit souvent à un fort pourcentage d'alcools par rapport à celui des glycols-α (3). Elle s'accompagne malheureusement d'une intense résinification. Le rapport monomère–dimère dépend de nombreux paramètres (4), et en particulier de la concentration d'éventuels donneurs de protons introduits en cours de réduction (2*b*, 2*c*). La résinification est souvent moins importante pour les cétones insaturées, les composés obtenus correspondant rarement à l'hydromérisation, mais à l'oligomérisation du réactif (dimérisation, trimérisation ...) (5, 6).

Des études polarographiques et voltampérométriques ont également montré que lors de l'électroréduction de quelques cétones aromatiques en présence de cations alcalins ou alcalino-terreux (2*e*, 7) (Na^+, Li^+, K^+, Ba^{2+}), il se forme des paires d'ions souvent instables qui disparaissent par dimérisation ou dismutation. Le schéma réactionnel couramment proposé est alors le suivant :

$$\left.\begin{array}{rl} 2\,R^{\bar{\cdot}} & \xrightarrow{k_1} \\ R^{\bar{\cdot}}....Me^+ + R^{\bar{\cdot}} & \xrightarrow{k_2} \\ 2R^{\bar{\cdot}}.....Me^+ & \xrightarrow{k_3} \end{array}\right\} \text{produits}$$

1. Auteur à qui adresser toute correspondance.
2. Révision reçu le 16 décembre 1985.

De notre côté, nous avions pu montrer qu'en présence d'un cation métallique de transition tel que Cr(III) ou Mn(II), la réduction électrochimique des cétones aromatiques (8, 9) ou α-β insaturées (5) conduisait préférentiellement aux hydrodimères avec inhibition totale des polymérisations, et ce, au potentiel même de réduction du métal(II) lorsque ce dernier a un potentiel de demi-vague plus positif que celui de la cétone.

Cet effet entraine un gain d'« énergie » pouvant atteindre 500 mV. L'interprétation de ce processus d'électroréduction assistée est complexe bien que certains auteurs pensent en avoir élucidé le mécanisme (10, 11). De plus, leurs études sont restées limitées au seul cas du chrome, alors que nous avons montré que le manganèse présente une action également bénéfique (9).

Il nous a paru indispensable d'établir la généralité du phénomène en variant la nature du cation métallique.

Notre choix, affecté par la solubilité dans le DMF du chlorure correspondant, a privilégié les éléments de la première série de transition (Cr, Mn, Fe, Co, Ni, Zn) pour étudier l'influence de la configuration électronique sur l'orientation du processus de réduction. Puisque nous avions suggéré antérieurement que le caractère acido-basique du cation métallique pouvait influer sur le mécanisme de l'hydrodimérisation (5), il nous a paru judicieux de pratiquer parallèlement l'étude électrochimique et les électrolyses préparatives en présence de Li^+, dont le caractère acide est bien connu dans ce milieu.

Pour éviter toute ambiguïté quant à la structure des composés formés et pour faciliter l'établissement des bilans réactionnels, notre étude s'est volontairement limitée à quelques cétones aromatiques, cycliquement ou linéairement encombrées, dont le potentiel de réduction diffère de, ou avoisine, celui du cation métallique, et à une cétone α-β éthylénique. Ces composés sont présentés dans la figure 1.

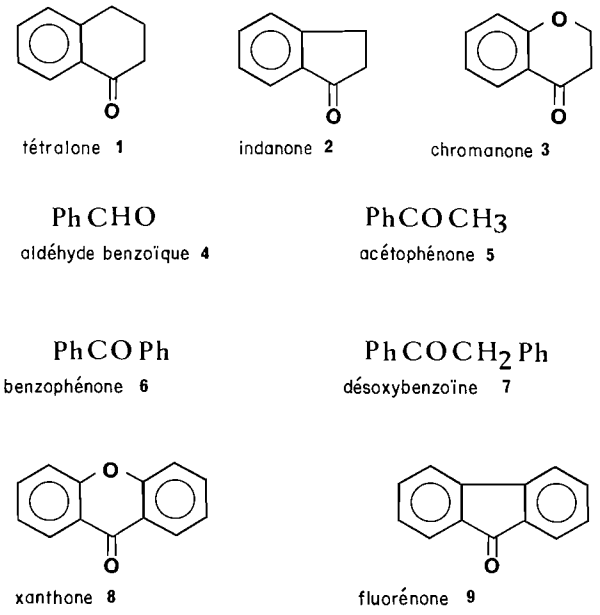

FIG. 1

A. *Analyse polarographique (tabl. 1) et voltammétrique (tabl. 2)*

I. Ions des métaux de transition

Les polarogrammes et voltammogrammes des espèces Cr(III) et Mn(II) dans le diméthylformamide (DMF) ont été précédemment décrits (8, 9). En ce qui concerne les autres cations, leur polarogramme, pour des solutions de concentration 10^{-3} *M* dans le DMF, présente, soit une seule vague de réduction biélectronique (cas de $FeCl_2 \cdot 4H_2O$ ou de $NiCl_2 \cdot 6H_2O$), soit deux vagues de réduction monoélectroniques de hauteurs sensiblement égales (cas de $CoCl_2 \cdot 6H_2O$).

L'analyse par voltamétrie cyclique de ces différents systèmes montre que les pics correspondants aux processus

$$\text{ou} \begin{cases} M^{II} + 2\bar{e} \longrightarrow M^0 \\ M^{II} + \bar{e} \longrightarrow M^I \\ M^I + \bar{e} \longrightarrow M^0 \end{cases}$$

sont de nature irréversible.

Sur électrode stationnaire, sans renouvellement de la goutte de mercure, les voltammogrammes se modifient à chaque cycle jusqu'à disparition complète du phénomène de réduction. Si l'on renouvelle la goutte après chaque balayage, et après agitation de la solution par barbottage d'argon, une variation linéaire du potentiel du premier pic de réduction E_{pc1} avec le logarithme de la vitesse de balayage (v) est observée. Ces résultats sont rassemblés dans le tableau 2.

La solution de $ZnCl_2$ anhydre ne présente pas de vague de réduction dans le domaine d'électroactivité accessible dans ces conditions.

Cette absence de réductibilité, surprenante au premier examen, méritait d'être confirmée. Des essais répétés en solvant anhydre nous ont permis d'établir ce résultat sans ambiguïté. Toutefois, l'addition de traces d'eau (1% en volume) ou l'utilisation de DMF insuffisamment déshydraté permet de révéler, vers −2 V, une vague de hauteur sensiblement égale à celle de Mn^{2+} lorsqu'on l'enregistre dans les mêmes conditions. Cette vague est très sensible à la présence d'eau et peut même se déplacer jusqu'à −1,8 V si le zinc est complètement hydraté.

Ce phénomène n'est pas affecté par la nature de l'anion du sel de fond puisque les résultats sont inchangés en présence de TBA ClO_4. Le cation Zn^{2+}, solvaté par le DMF, est donc non réductible dans ce domaine d'électroactivité (−0,4 V ; −3 V). Ce résultat fera l'objet d'une publication prochaine.[3]

II. *Cétones*

Elles présentent toutes une première vague de réduction polarographique qui correspond à l'échange d'un électron. En effet, leur hauteur est égale à moins de 10% près à celle de la vague de réduction du benzaldéhyde enregistrée dans les mêmes conditions et dont il est établi (12) qu'elle traduit un échange monoélectronique réversible.

Cette première vague est réversible, pour toute vitesse de balayage, dans le cas des cétones aromatiques (composés **1**–**9**). Par contre pour la chalcone **10**, si le balayage est inférieur à 0,5 V s^{-1}, la réduction devient irréversible.

Dans tous les cas, la seconde vague de réduction est, lorsqu'elle n'est pas masquée par la décharge de l'électrolyte support, irréversible et sensiblement monoélectronique.

III. *Mélanges cétone – cation métallique*

Dans un souci de simplicité évidente, nous n'avons considéré

3. Un des rapporteurs s'est étonné de la non réductibilité de Zn^{2+} dans ce milieu et suggère une intervention des anions halogénures introduits simultanément aux cations puisque les sels de départ sont des chlorures et le sel de fond un bromure. Il nous paraît, que la présence d'eau, même à l'état de traces, est le facteur essentiel, ce qui expliquerait nos divergences avec les résultats publiés antérieurement.

TABLEAU 1. Potentiels de demi-vague polarographique d'un mélange équimolaire 10^{-3} *M* de cation métallique et de cétone dans du DMF contenant TBABr 0,1 *M* (ECS)

	$-E^{1/2}$(V) cétone DMF – TBABr 0,1 *M*	Li^+	Cr^{2+}	Mn^{2+}	Fe^{2+}	Co^{2+}	Ni^{2+}	Zn^{2+}
$-E^{1/2}$(V) cation métallique		—	1,52	1,55	1,42	1,55 1,92	1,05	—
$-E^{1/2}$(V) cation métallique + cétone **1**	1,97	1,76	1,53	1,55	1,42	1,55 1,92	Δ[a]	1,92
2	2,01	1,84	1,53	1,57	1,42	1,55 1,95	Δ	1,95
3	1,90	1,75	1,53	1,565	1,42	1,55 1,86	Δ	1,85
4	1,80	1,65	1,53	1,56	1,42	1,55 1,75	Δ	1,77
5	1,98	1,80	1,52	1,56	1,42	1,55 1,95	Δ	1,92
6	1,72	1,45	1,45	1,57	1,42	1,55 1,67	Δ	1,66
7	1,89	1,77	1,48	1,56	1,42	1,55 1,87	Δ	1,86
8	1,63	1,54	1,44	1,505	1,42	1,54	Δ	1,58
9	1,24	1,17	1,15	1,15	1,15	1,16	Δ	1,19
10	1,39	1,19	1,26	1,33	1,21	1,34	Δ	1,34

[a]Δ: Additivité de tous les systèmes présents.

TABLEAU 2. Variation du premier pic de réduction en fonction de log *v*

		Li^+	Cr^{2+}	Mn^{2+}	Fe^{2+}	Co^{2+}	Ni^{2+}	Zn^{2+}
$\frac{\partial E_{pc1}{}^{c}}{\partial \log v}$ (mV s^{-1})		—	0	20	49,[a] 166	110,[a] 284	22	—
Tétralone	**1**	311	[b]	[b]	[b]	[b]	[b]	34,9,[a] 65
Benzophénone	**6**	498	[b]	0	[b]	[b]	[b]	0,[a] 35,8
Fluorénone	**9**	0	0	0	0	35	0	57
Chalcone	**10**	32	22	38	100,[a] 40	65,[a] 400	0	32

[a]Changement de pente pour v = 50 mV s^{-1}.
[b]Cas où il y a additivité des systèmes présents, le premier pic de réduction étant alors celui du cation métallique.
[c]Électrolyte support DMF – TBABr 0,1 *M*, v variant de 5 à 500 mV s^{-1} (ECS).

que l'influence du cation métallique sur la première vague de réduction du composé carbonylé.

(a) *Cations non réductibles : Li^+, Zn^{2+}*

Quelle que soit la cétone, leur action est un simple abaissement du potentiel de réduction dans un effet rappelant celui des protons. En voltamétrie cyclique, le pic correspondant devient alors irréversible pour toute vitesse de balayage.

Ceci rappelle l'effet bien connu des ions alcalins ou alcalino-terreux, habituellement interprété par la formation de paires d'ions entre le radical anion et le cation. Toutefois, cette interaction est souvent plus importante sur l'espèce A^{2-} que sur le radical anion $A^{\cdot-}$, ce qui se traduit, sur les polarogrammes, par un rapprochement des deux étapes monoélectroniques, pouvant même conduire à leur confusion. Ceci est particulièrement bien mis en évidence dans le cas des quinones (7*c*). Dans notre cas, seule la première vague est très notablement affectée et le zinc présente un effet moindre que celui du lithium.

(b) *Cation beaucoup plus réductible que la cétone : Ni^{2+}*

On observe alors (polarographie et voltammétrie cyclique) la simple additivité des systèmes en présence, sans intéraction.

(c) *Cations de potentiel de réduction voisin de celui du composé carbonylé : Cr^{2+}, Mn^{2+}, Fe^{2+}*

Dans le cas où le potentiel de réduction du cation métallique est plus négatif que celui de la première vague de réduction de la cétone (fluorénone **9**, chalcone **10**), la vague de réduction du système M(II)/M(0) disparaît et la première vague de réduction de la cétone se trouve avancée vers des potentiels plus positifs (de 50 à 100 mV selon les cas), rappelant ainsi l'action des cations non réductibles. Il en est de même avec le cation zinc aquo, $Zn{\cdot}(H_2O)_4{}^{2+}$ lorsque sa vague de réduction peut être observée.

Si le potentiel de réduction du cation métallique est moins négatif que celui de la cétone (cétones aromatiques **1**–**8**), la vaque de réduction de cette dernière disparaît complètement

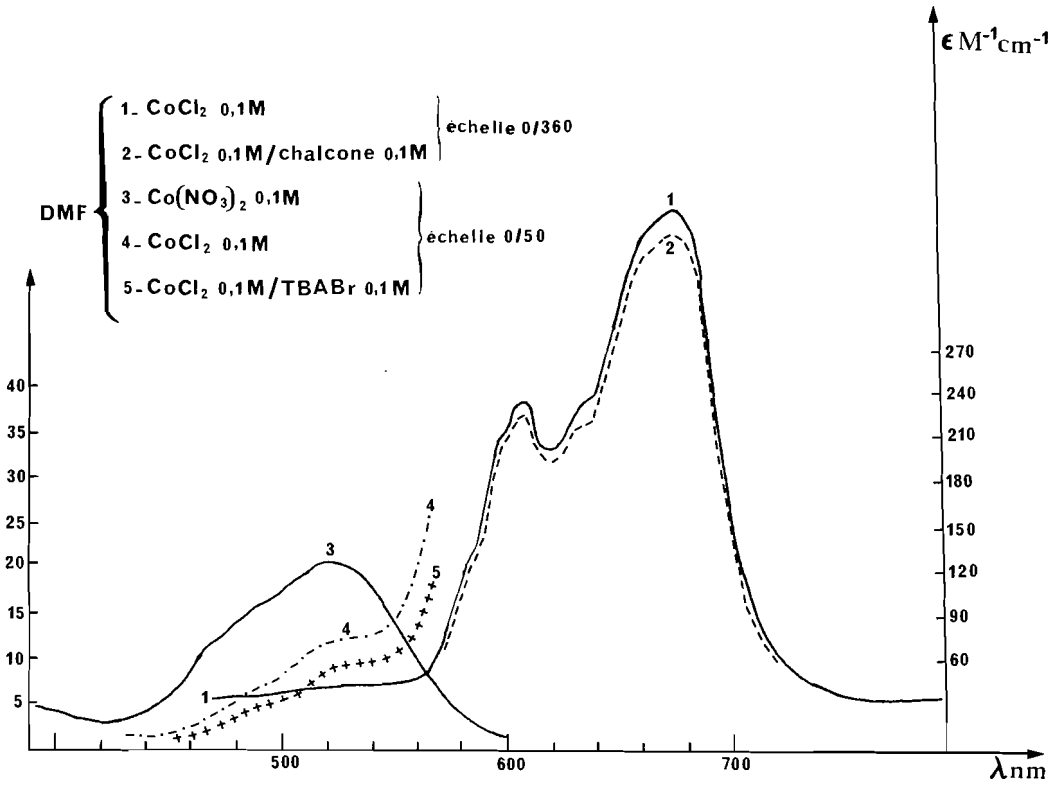

FIG. 2. Spectres d'absorption électronique des mélanges sel de cobalt – chalcone.

pour des quantités équimolaires de cétone et de sel métallique. La vague de réduction du métal M(II) → M(0) est très peu affectée et se déplace légèrement vers les potentiels positifs (de l'ordre de 10 mV).

La voltammétrie cyclique montre, pour toute vitesse de balayage supérieure à 5 mV s^{-1}, la simple additivité de systèmes en présence pour quasiment toutes les cétones aromatiques.

Par contre, pour la chalcone **10**, l'addition de quantités croissantes de cation métallique entraîne l'apparition d'un nouveau pic, irréversible, qui remplace progressivement le premier pic de réduction de la chalcone. Sa hauteur croit et le potentiel de pic E_{pc1} se déplace légèrement vers des potentiels moins négatifs. À l'équimolarité, ce nouveau pic, traduit une réaction monoélectronique. L'addition d'un excès de cation métallique n'affecte pas le potentiel de pic, mais augmente légèrement sa hauteur. Les pics de réduction propres au cation métallique ne réapparaissent jamais.

Le comportement des systèmes **6***d*, **7***c* et **8***b* est intermédiaire ; il dépend fortement de la vitesse de balayage, et nous verrons plus loin que dans ces cas le monoalcool est obtenu seul et quantitativement.

(d) *Cas du cobalt* Co^{2+}

Les vagues polarographiques sont mal définies en raison de la complexité du système $Co^{2+}/Co^{(0)}$. Toutefois, quelques effets marqués peuvent être observés. Pour les cétones dont la première vague de réduction est située entre les deux vagues de réduction $Co^{2+} \rightarrow Co^{+}$, $Co^{+} \rightarrow Co^{(0)}$ du cation métallique (cétone aromatiques **1**–**8**) la deuxième vague de réduction du cation métallique ($Co^{+} \rightarrow Co^{0}$) disparaît sans que la vague correspondant au système $Co^{2+} \rightarrow Co^{+}$ soit affectée. La vague de réduction de la cétone est alors légèrement déplacée vers des potentiels moins négatifs. Le phénomène est proche de celui observé dans le cas du chrome(III) et décrit antérieurement (5, 10, 11).

Pour les cétones dont la réduction se fait avant celle du système métallique (florénone **9** et chalcone **10**), les vagues du système Co^{2+}/Co disparaissent comme dans le cas précédent (III(c)) et la première vague de réduction de la cétone se déplace vers des potentiels moins négatifs.

En voltammétrie cyclique, le phénomène est analogue à celui décrit en III(c).

IV. *Discussion*

Dans tous les cas de cétones aromatiques, il apparaît que l'interaction composé carbonylé – espèce métallique est cinétiquement lente, puisqu'elle n'affecte les voltammogrammes que pour des vitesses de balayage inférieures à 5 mV s^{-1}, domaine où les processus de diffusion deviennent prépondérants. Aux vitesses supérieures, les systèmes cation métallique/métal – cétone/radical anion se comportent indépendamment, y compris en terme de réversibilité de la première étape du dérivé carbonylé. Les modifications observées aux faibles vitesses ne peuvent donc provenir que d'une réaction lente impliquant l'espèce métallique. Par contre, dans le cas d'insaturation (chalcone **10**) ou dans les cas **8***b*, **6***d* et **7***c*, l'interaction est soit très rapide, soit d'une autre nature ; puisque la disparition du pic de réduction du métal est observée même pour des vitesses supérieures à 5 mV s^{-1} et jusqu'à des vitesses égales à 500 mV s^{-1}, limite supérieure accessible avec notre appareillage. La variation du potentiel du premier pic de réduction du système cétone – cation métallique en fonction de log v^4 ($\delta E_{pc1}/\delta \log v$) est fortement dépendante du cation métallique présent comme le

4. Un des rapporteurs suggère de discuter plutôt de la dépendance de E_{pc} avec la concentration C_R du substrat, en considérant les valeurs des pentes $\delta E_{pc}/\delta \log C_R$. Cette remarque fondée nécessite toutefois de pouvoir explorer un domaine de concentration suffisamment étendu, ce qui nous était difficile compte tenu de la faible solubilité des halogénures utilisés.

montre le tableau 2, et ceci que cette première étape soit attribuée à la réduction du cation ou à la réduction du dérivé carbonylé.

Ceci suggère donc que l'échange électronique a lieu sur chaque espèce indépendamment, bien que suivi d'une interaction forte entre les espèces formées, interaction dont la cinétique peut être lente ou très rapide selon le cas.

B. *Étude spectrophotométrique*

Dans le but de mettre en évidence un éventuel complexe cétone – ion métallique préexistant dans la solution avant électrolyse et de déterminer l'influence des ions halogénures (chlorures et bromures) présents en concentration importante, nous avons choisi d'étudier l'influence du dérivé carbonylé sur le spectre d'absorption du cation métallique. Cette étude a été menée avec le cobalt, dont le spectre d'absorption électronique est caractéristique (fig. 2), dans les conditions de concentration des électrolyses préparatives.

Dans le DMF, pour l'ion cobalteux, si le contre ion n'est pas complexant (nitrate par exemple), le spectre est voisin de celui de l'ion hexa aquo (λ_{max} 520 nm, ϵ = 22,5). Par contre, à la même concentration, le chlorure cobalteux hexahydraté fournit un spectre caractéristique du complexe tétraédrique $CoCl_4^{2-}$ en présence de la quantité équivalente du complexe aquo. Si le sel est dissout en présence de TBABr 0,1 *M*, alors la proportion de cobalt cationique décroit au profit du mélange des complexes halogénés.

L'addition de benzophénone **6** à la solution dans le DMF du composé cationique aquo $Co{\cdot}(H_2O)_6^{2+}$ ne modifie pas le spectre du complexe cationique. Il en est de même dans le cas du complexe anionique. Aucune modification dans la répartition des deux espèces n'est perceptible. Ainsi, peut-on considérer qu'il n'y a pas d'interaction préexistante significative dans ce cas.

La même étude a été menée avec la chalcone **10**. Là encore, aucune interaction ne se manifeste sur le spectre de l'élément métallique. Il en est de même du spectre de la chalcone **10**, qui n'est pas influencé par la présence du cobalt. La même observation peut être faite pour une solution de chalcone dans LiCl 0,1 *M*.

C. *Électrolyses à potentiel contrôlé*

Les bilans réactionnels globaux, en produits effectivement isolés, pour chaque composé et chaque système métallique sont rassemblés dans le tableau 3. Les résultats des électrolyses préparatives confirment la différence de comportement des cétones aromatiques et d'un composé α-β insaturé, comme la chalcone, telle qu'elle est suggérée par la voltammétrie cyclique.

I. *Coulométries*

(a) *Chalcone **10***

Réalisées dans les conditions d'équimolarité cétone – cation métallique, au palier de la nouvelle vague de réduction de **10**, les coulométries confirment, pour tout métal, un échange monoélectronique (1–1,2 F/mol selon les cas).

(b) *Cétones aromatiques **1–9***

La proportion respective *R* de cation métallique et de cétone a été déterminée empiriquement par variation continue de telle sorte que ces conditions expérimentales permettent la conversion totale du composé carbonylé de départ.

Dans le cas où le cation métallique n'est pas réductible (Li^+, Zn^2), l'équimolarité (R = 1) des composants suffit pour transformer la totalité de la cétone par réduction au palier de sa première vague et après passage d'une quantité d'électricité Q variable selon le composé carbonylé et telle que

$$1{,}5\ \text{F} \leqslant Q \leqslant 2\ \text{F pour } Li^+$$

$$2\ \text{F} \leqslant Q \leqslant 3\ \text{F pour } Zn^{2+}$$

Lorsque le cation métallique est lui-même réductible (Cr^{3+}, Mn^{2+}, Fe^{2+}, Co^{2+}), mais de potentiel de réduction voisin de celui de la cétone, la réduction a été menée au potentiel du palier de la vague de réduction du cation métallique (système M^{II}/M^0) dans le cas des composés **1–8**. Dans le cas du composé **9**, c'est la première vague de réduction de la fluorénone qui est touchée et nous considérerons ce composé à part.

Pour un composé donné, les proportions respectives des constituants dépendent fortement du métal. Si l'équimolarité (R = 1) suffit pour Cr^{3+} et Mn^{2+}, il faut doubler la quantité du cation (R = 2) dans le cas où M = Fe ou Co. Ainsi, pour la tétralone **1** en présence de Fe^{2+}, l'électrolyse ne conduit après séparation qu'à un taux de conversion de 78% (60% de diol *d,l* et 18% de diol *méso*) si R = 1.

Ceci s'explique si l'on prend en compte les quantités respectives anion/cation dans ces deux cas précis (fig. 2) où l'étude spectrophotométrique indique une équipartition entre les complexes cationiques et anioniques, et si l'on admet que c'est l'espèce cationique qui intervient dans le phénomène d'électrocatalyse. Il en est vraisemblablement de même dans le cas du fer(II). Les quantités d'électricité sont telles que les taux de conversion de 100% ne sont obtenus que pour

$$Q = 4\ \text{F}\ (Cr^{3+});\ 3\ \text{F}\ (Mn^{2+})$$

$$3\ \text{F} \leqslant Q \leqslant 5\ \text{F}\ (Fe^{2+}, Co^{2+})$$

Si l'on considère (8) que le système $Cr^{3+} \rightarrow Cr^{2+}$ consomme 1 F sans intervenir dans le processus, ce qui est confirmé par l'utilisation de chrome(II), alors chrome et manganèse sont équivalents du simple point de vue de la coulométrie (3 F). Par contre, après prise en compte de l'excès d'espèce métallique, fer et cobalt induisent un échange tel que $1\ \text{F} \leqslant Q \leqslant 3\ \text{F}$ selon le cas; c'est-à-dire un comportement intermédiaire entre Li^+ et Cr^{2+} (Mn^{2+}). Si le cation métallique est beaucoup plus réductible que la cétone (Ni^{2+}), le taux de conversion T est toujours nul quel que soit R.

La fluorénone **9** se distingue des autres cétones aromatiques. Le taux de conversion est nul (T = 0) avec Li^+, Mn^{2+} et Ni^{2+} quel que soit R. Il est maximum (T = 100%) avec Cr^{3+}(R = 1, Q = 4 F); Co^{2+} (R = 2, Q = 1,7 F); (R = 2, Q = 1,2 F).

Dans ce cas encore, si le rapport fer/fluorénone est R = 1, le taux de conversion est T = 80% et après traitement le mélange comprend 80% de diol et 20% de fluorénone non transformée.

II. *Résultats et discussion*

L'influence de Ni^{2+} est nulle et les résultats des électrolyses préparatives confirment les prévisions qui pouvaient être faites de l'examen des polarogrammes et des voltammogrammes.

Par contre, comme le montre le tableau 3, la nature et la répartition des produits obtenus dépendent plus ou moins du cation présent selon la cétone étudiée.

(a) *Cétone α-β insaturée **10***

La structure des hydrodimères obtenus par électroréduction de la chalcone **10** a été résolue dans une publication antérieure (5). La prise en compte des facteurs orbitalaires et des données électrochimiques a permis de proposer, pour chaque hydrodimère, un mécanisme de formation. Dans ce mémoire (5), nous avions montré qu'en l'absence de cation métallique, la réduction électrochimique (DMF, TBABr 0,1 *M*) conduit, par une réaction d'oligomérisation radicalaire, à un trimère cétoni-

TABLEAU 3. Résultats des électrolyses préparatives

Cétones	Li^+ **a**	Cr^{3+} **b**	Mn^{2+} **c**	Fe^{2+} **d**	Co^{2+} **e**	Ni^{2+} **f**	Zn^{2+} **g**
1	Diol 88% { *dl* 84 / *méso* 4	Diol 85% { *dl* 68 / *méso* 17	Diol 84% { *dl* 65 / *méso* 19	Diol 84% { *dl* 64 / *méso* 20	Diol 84% { *dl* 64 / *méso* 20	Résinification	Diol 81% { *dl* 64 / *méso* 17
2	Diol 70% { *dl* 66 / *méso* 4	Diol 63% { *dl* 48 / *méso* 15	Diol 66% { *dl* 51 / *méso* 15	Diol 70% { *dl* 50 / *méso* 20	Diol 73% { *dl* 56 / *méso* 17	Résinification	Diol 68% { *dl* 54 / *méso* 14
3	Diol 64% { *dl* 60 / *méso* 4	Diol 78% { *dl* 62 / *méso* 16	Diol 74% { *dl* 63 / *méso* 11	Diol 93% { *dl* 88 / *méso* 5	Diol 83% { *dl* 80 / *méso* 3	Résinification	Diol 93% { *dl* 64 / *méso* 29
4	Diol 80% { *dl* 71 / *méso* 9	Diol 70% { *dl* 42 / *méso* 28	Diol 30%	Diol 100% { *dl* 61 / *méso* 39	Diol 78% { *dl* 53 / *méso* 25	Aldéhyde benzoïque	Diol 65% { *dl* 45 / *méso* 20
5	Diol 85% { *dl* 77 / *méso* 3	Diol 24% { *dl* 13 / *méso* 11 Alcool 10% Acétophénone 39%	Diol 49% { *dl* 33 / *méso* 13 Alcool 4% Acétophénone 49%	Diol 92% { *dl* 70 / *méso* 22	Diol 84% { *dl* 63 / *méso* 21	Acétophénone	Diol 64% { *dl* 43 / *méso* 21 Alcool 23%
6	Alcool 2% Diol 172°C 76%	Alcool 6% Diol 212°C 37% Diol 172°C 27%	Alcool 11% Diol 212°C 47% Diol 172°C 17%	Alcool 97%	Alcool 18% Diol 212°C 2% Diol 172°C 70%	Désoxybenzoïne	Alcool 25% Diol 172°C 44%
7	Benzhydrol 96%	Diol 74% Benzhydrol 18%	Benzhydrol 87%	Diol 85% Benzhydrol 4%	Diol 63% Benzhydrol 25%	Benzophénone	Benzhydrol 100%
8	Xanthone 26% Diol 56%	Xanthol 90% Diol 38%	Xanthone	Diol 97%	Xanthone 72% Diol 26% Diol 48%	Xanthone	Xanthol 100% Diol 21%
9	Fluorénone	Fluorénol 48%	Fluorénone	Diol 91%	Fluorénol 48%	Fluorénone	Fluorénol 60%
10	β-Cétols 92% (*cis* + *trans*)	Cétone saturée 4% Dicétone 20% β-Cétols 59% (*cis* + *trans*)	Cétone saturée 8% Furannes 20% β-Cétols 60% (*cis* + *trans*)	Cétone saturée 7% Dicétone 22% β-Cétols 58% (*cis* + *trans*)	Cétone saturée 11% Dicétone 27% β-Cétols 44% (*cis* + *trans*)	Chalcone 49% Dicétone 5% β-Cétols 18% (*cis* + *trans*), résines	β-Cétol *trans* 97%

que cyclique avec un rendement de 60%, à côté de résines non séparables. Nous avions montré également qu'en présence d'un cation métallique, tel que Cr^{3+}, le taux de conversion et le rendement chimique sont toujours de 100%, le produit majoritaire étant toujours un β-cétol.

Qu'en est-il, en présence d'ions métalliques de polarisabilité différente, mais qui, dans ce cas, se réduisent toujours après le composé carbonylé, et dont les voltammogrammes suggèrent une interaction cétone–cation forte et rapide qui pourrait être de type paire d'ions?

(*i*) *Cations non réductibles*

En présence de Li^+, le β-cétol est obtenu de façon sélective, avec un rendement très élevé, sous ses deux formes *cis* (46%) et *trans* (46%).

En présence de Zn^{2+} anhydre, le même cétol est obtenu avec un rendement de 97%, mais uniquement sous sa forme *trans*. Dans ces deux cas, un seul produit est formé et la variation du potentiel de pic de réduction de la cétone avec la vitesse de balayage est une droite de pente −32 mV. La pente théorique pour un mécanisme de couplage radical anion – substrat est de 30 mV (13). Ceci suggère que le mécanisme de formation du β-cétol débute par l'attaque d'un radical anion sur une molécule neutre. Un tel couplage a d'ailleurs été proposé par Savéant dans le cas de milieux aprotiques très secs (14). Le radical anion serait stabilisé par formation d'une paire d'ions avec le cation métallique, ce qui est conséquent avec la variation du ptoentiel de demi-vague du composé carbonylé vers les potentiels positifs. De telles interactions sont fondamentales dans les processus biochimiques où l'ion Zn^{2+} est particulièrement efficace dans l'hydrolyse des chaines peptidiques. De la même façon, l'influence de l'ion Mg^{2+} a déjà été signalée lors de la réduction de composés carbonylés (15).

(*ii*) *Cations réductibles : Cr^{2+}, Fe^{2+}, Co^{2+}, Mn^{2+}*

Les composés obtenus sont les mêmes pour tous ces cations : cétone, dicétone, β-cétols, mais leur répartition dépend sensiblement du cation métallique antagoniste. La différence de comportement est maximum avec Co^{2+}. Avec Mn^{2+}, on note la présence d'un composé nouveau hydroxy-4 furannique en place de la dicétone. Ce nouveau composé est présent sous forme d'au moins trois diastéréoisomères.

L'ensemble de ces observations peut se relier au caractère acide de Lewis de ces cations si l'on se réfère à l'échelle de dureté au sens de Jorgensen (16):

$$\sigma_A = \frac{E^0 + 4{,}5}{z}$$

σ_A représentant la douceur, E^0 le potentiel standard du couple M^{z+}/M^0, z la charge de l'ion, et l'on suppose que les cations sont solvatés d'une manière équivalente.

Dans ces conditions, les ions se classent comme ci-dessous :

Li^+	Mn^{2+}	Cr^{2+}	Zn^{2+}	Fe^{2+}	Co^{2+}	
1,48	1,65	1,79	1,87	2,03	2,11	douceur

Il apparaît bien que le caractère acide de Mn, Fe, Cr, est de même nature, l'ion Co^{2+} étant un peu moins dur d'où une moindre proportion de cétol si l'on admet que c'est bien une interaction de nature acide qui favorise ce composé (5).

Le mécanisme primaire est complexe puisque la nature des produits obtenus est variée et l'examen des pentes $\delta E_{pc}/\delta \log v$ est d'un faible secours puisque la compétition entre plusieurs mécanismes est probable. Le cas de Cr^{2+} est peut être le plus simple puisque le système métallique seul n'interfère pas (pente nulle pour l'ion isolé).

Dans ce cas, une pente de 22 mV est obtenue en présence de chalcone, ce qui peut être interprêté comme une dimérisation primaire du radical anion conduisant à la dicétone, ce processus imposant sa vitesse. Le caractère électrophile du substrat dépendant de la force de l'interaction avec le métal de transition, un acide dur orientera préférentiellement la duplication vers une réaction de type radical anion – substrat; un acide mou défavorisera cette interaction d'autant plus qu'il est mou et la réaction radical anion – radical anion ne s'en exprimera que mieux.

(b) *Cétones aromatiques **1–9***

La plupart des cations se réduisent avant le composé carbonylé et c'est sur cette vague que nous conduisons l'électrolyse. Dans les quelques cas où le cation métallique se réduit après le composé carbonylé (Li^+, Zn^{2+}), on conduit l'électrolyse au potentiel de réduction de la cétone, valeur déplacée vers les potentiels moins négatifs, vraisemblablement par un effet de type paires d'ions comme en la réf. 7. Les résultats des électrolytes préparatives sont plus complexes à analyser, quel que soit le cation métallique.

Toutefois, dans le DMF, en présence de cation métallique, nous dégageons quelques points importants :

Les résinifications sont totalement supprimées.

Les cétones aromatiques encombrées sont réduites au potentiel de réduction du cation métallique, ce qui représente souvent un gain supérieur à 400 mV (**1**, **2**, **3**, **5**, **7**) par rapport au potentiel de réduction de la cétone seule.

La répartition des produits obtenus, diols ou alcools, dépend beaucoup du métal. Les différences les plus marquées sont obtenues dans le cas des composés **5**, **6**, **7**, **8** et **9**.

De tous les cations Fe^{2+} est le plus sélectif puisque dans presque tous les cas le diol est obtenu comme produit unique, sous forme *méso* ou *dl*, avec un rendement supérieur à 85%.

Le rendement faradique (exprimé comme le rapport entre la coulométrie théorique de réduction de la cétone (1 F/mol) et la coulométrie réelle) est toujours inférieur à 1. Il est même quelque fois très faible (0,2) contrairement au cas de la chalcone **10** où le rendement faradique est toujours voisin de 1.

Dans tous les cas où le monoalcool est obtenu seul (cas **8***b* avec Cr^{2+}, **7***c* avec Mn^{2+}, **6***d* avec Fe^{2+}), on n'observe, en voltammétrie cyclique, que le pic de réduction du composé carbonylé et ceci quelles que soient les vitesses de balayage. Le pic du cation métallique n'apparaît jamais. Au contraire, dans le cas où le diol est formé, la voltammétrie cyclique montre une simple additivité des systèmes ; il est logique de supposer que le système métallique est le premier touché.

Les taux de conversion ne sont en général pas proportionnels à la quantité d'électricité échangée. Ainsi lorsque le diol est le seul produit formé, on attend un rendement de 0,33 F puisque 2 F sont consommés dans la réaction $M^{II} \rightarrow M^0$ en sus d'une éventuelle réduction du composé carbonylé. C'est en particulier le cas de Cr^{2+} et Mn^{2+}. Un test simple permet de confirme cette observation. Dans le cas de la tétralone **1**, si l'électrolyse en présence de Mn^{2+} est arrêtée après 2,2 F, seulement 63% de diol se sont formés et 20% de **1** n'ont pas été transformés ; 0,8 F sont donc nécessaire à la transformation des 20% restants. Le même test mené avec Cr^{2+}, conduit après passage de 1,5 F à un mélange de 60% de produit de départ **1** et 29% de diol. Il faut donc 1,5 F pour transformer les 60% restants.

La présence simultanée du cation métallique et du composé

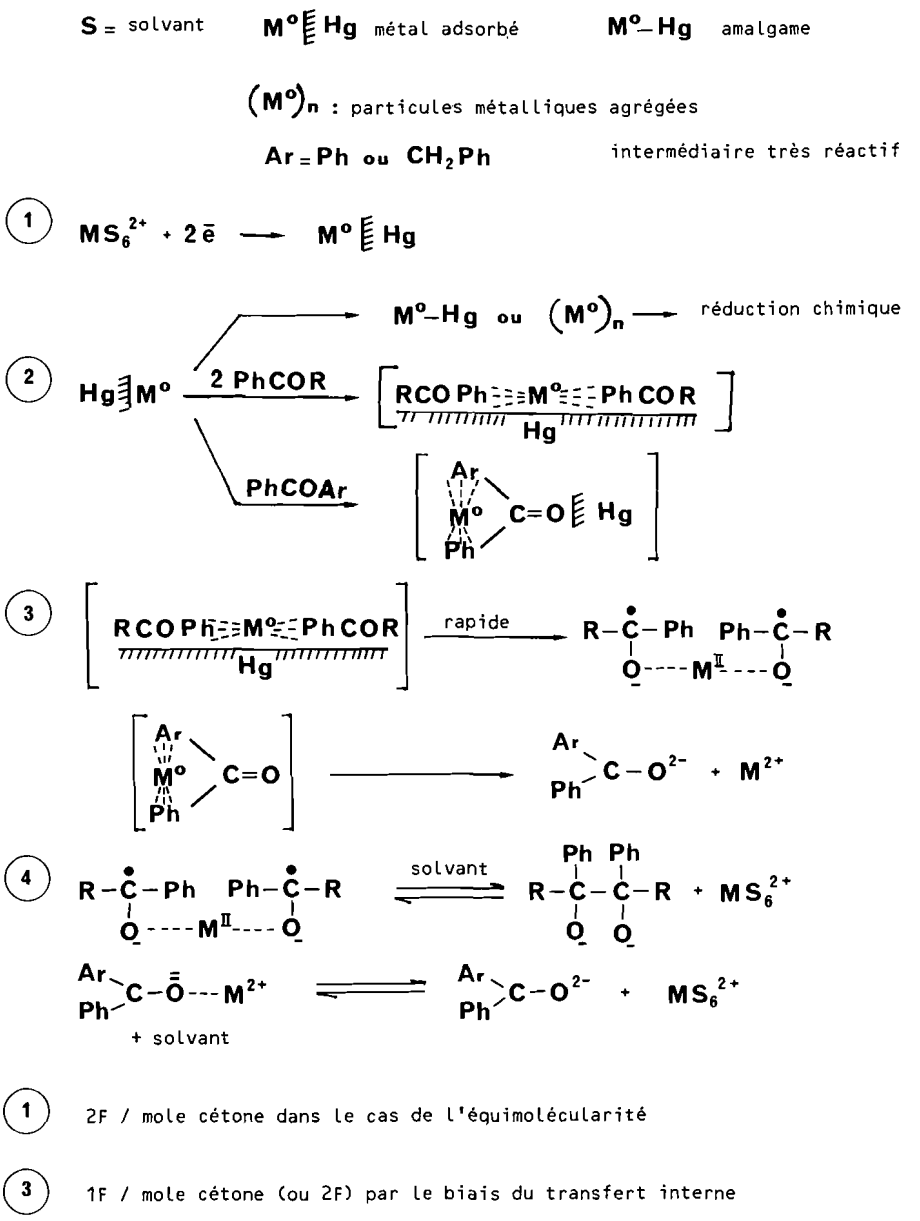

FIG. 3. Schéma réactionnel possible pour l'électroréduction catalysée de cétones aromatiques.

carbonylé est indispensable au processus d'électroréduction. Ainsi, un test de préélectrolyse du cation jusqu'à l'état métallique (2 F) suivi de l'introduction de la cétone **1** dans le compartiment cathodique en maintenant le potentiel du mercure au potentiel de réduction du métal ne conduit à aucune duplication (on récupère intégralement la cétone de départ si le cation est Mn^{2+} ; la résinification est totale avec Fe^{2+}).

Le rendement final dépend fortement de la quantité de cation présente. Ainsi si la préélectrolyse du cation n'est menée que jusqu'à 1,5 F (cas de $MnCl_2$) puis poursuivie normalement, après ajout de la cétone **1**, jusqu'à son terme (3 F), on récupère après séparation 50% de diol et 35% de résines. 25% de la quantité initiale de cation ont permis 50% de duplication.

D. *Interprétation*

L'ensemble de ces observations, bien que ne permettant pas d'élucider complètement et définitivement les mécanismes mis en jeu, suggère cependant quelques voies d'approche.

Dans les cas les plus simples (chalcone **10**, cations peu ou non réductibles), le composé carbonylé est le premier réduit et le radical anion formé interagit plus ou moins fortement avec le cation métallique dans une interaction de type paire d'ions $R^{\bar{\cdot}}$ ... M^+ ou $R^{\bar{\cdot}}$ ... M^{2+} ... $R^{\bar{\cdot}}$. Ceci est assez classique. Le radical ainsi stabilisé peut alors réagir sur une molécule neutre ou sur lui-même. Dans tous les cas, si le cation était réductible son potentiel de demi-vague devient plus négatif dans cette interaction et peut se trouver repoussé lors de la zone d'électroactivité.

L'interprétation des autres systèmes est plus délicate. La première étape de réduction doit être nécessairement le passage du cation à l'état métallique, le carbonyle n'étant pas touché ; une interaction de type paire d'ions entre le radical et l'ion métallique est impossible.

Comme l'étude spectrale, dans la zone des transferts électroniques du métal de transition, n'a mis en évidence aucune interaction préexistante importante, la présence nécessaire de la cétone en début d'électrolyse ne peut s'expliquer que par interaction entre des centres métalliques réduits à la surface du mercure et le système aromatique du composé carbonylé, avant que le métal ne puisse diffuser dans l'électrode (amalgame) ou

s'agréger en particules inertes (fig. 3). Cette participation du métal de la cathode (mercure) est suggérée par l'observation de la passivation d'une électrode à goutte de mercure déposée sur électrode d'or et polarisée au potentiel de réduction du cation métallique. Après un tel traitement l'électrode reste inactivé vis-à-vis du composé carbonylé même après lavage.

L'amalgame ou le métal divisé peut être réducteur et conduire à la formation de résines, comme dans une réduction classique.[5] La répartition des produits de réaction depend donc des cinétiques de toutes ces interactions. Le comportement de tous ces composés carbonylés peut, peut-être, s'expliquer par le passage progressif d'une interaction forte de type complexe à l'interaction faible de type « acide–base » selon la variation des facteurs orbitalaires, les deux types d'interaction pouvant se manifester conjointement. La force de l'interaction forte dépendrait essentiellement de l'aptitude de l'élément métallique à former des complexes intermédiaires de type π, donc du nombre d'électrons « *d* » du métal. Ainsi dans le cas du chrome (d^6) et lorsque le noyau benzénique (3 doublets π) n'est pas fortement conjugué avec le carbonyle (composés **1**, **2**, **3**, **4**, **5**), les composés type « sandwich » à 18 électrons sont sûrement favorisés. Dans le cas du manganèse, du fer et du cobalt, les complexes ainsi créés seraient à 19, 20 et 21 électrons, ce qui les rendrait particulièrement aptes au transfert électronique interne suivi de la dimérisation des radicaux anions formés et de la libération du métal dans son état d'oxydation 2+. Dans tous ces cas, ce modèle rend compte de la non réductibilité du ligand organique après interaction avec le métal.

Dans le cas où la conjugaison croit (**6**, **7**, **8**) à l'ensemble du système π, défavorisant le complexe « type sandwich » (20 ē pour Cr, puis 21, 22, 23 ē pour Mn, Fe, Co) au profit de l'interaction de type acidobasique au niveau du carbonyle, un échange biélectronique conduisant au monoalcool devient alors possible.

Toutefois trop de paramètres ne sont pas encore maîtrisés, rendant aléatoire une conclusion formelle. La répartition des produits obtenus dépend fortement du cation métallique pour un composé donné.[6] Retenons que, comme nous l'avions suspecté en considérant l'influence des ions Mn^{2+} (9), le phénomène de réduction duplicative observé en présence de Cr^{3+} n'est pas spécifique de ce cation métallique. Le phénomène est général pour toute la première série des éléments de transition et son mécanisme, malgré des indices nouveaux, reste encore à démontrer sans ambiguité.

Partie expérimenale

Les points de fusion ont été déterminés au banc de Köfler. Les spectres ir ont été obtenus avec un spectromètre Pye-Unicam SP 3-200, ceux de rmn ^{13}C avec un appareil Brüker WP 80 et ^1H avec un appareil Brüker SY 250. Les spectres uv ont été enregistrés sur Perkin–Elmer 555. Les spectres de masse ont été effectués sur un appareil AEI type MS 30. Les analyse élémentaires ont été effectuées au laboratoire de microanalyse de l'Université de Paris VI que nous tenons à remercier vivement. Les chromatographies sur couche mince ont été réalisées sur gel de silice fluorescente Merck PF-254 (plaque 20 × 20, e = 0,1 cm).

En électrochimie, tous les potentiels ont été mesurés par rapport à une électrode de référence au calomel – KCl saturé (ECS) munie d'une jonction remplie avec une solution de TBA Br 0,1 *M* dans le DMF (électrode Tacussel RDJ/C 10). Les polarogrammes ont été enregistrés sur une table traçante XY Iffelec IF 3802 couplée à un polarographe PAR 174 A. Les voltammogrammes ont été réalisés grâce à un potentiostat PAR 173 gouverné par un générateur de signaux PAR 175, sur goutte de mercure fournie par une électrode de Kémula à piston micrométrique (Tacussel).

Les électrolyses ont été réalisées en atmosphère d'argon, à température ambiante, avec un potentiostat PAR 173 muni d'un coulomètre PAR 179, sur une cathode de mercure de 26 cm^2 environ de surface et agitée avec un barreau aimanté. Les compartiments anodique et cathodique sont séparés par une pastille de verre fritté de porosité 4 et de 2,5 cm de diamètre. L'anode est un disque de platine de 2 cm de diamètre.

Le DMF utilisé est d'origine Merck; il est préalablement distillé sur P_2O_5. Il contient du bromure de tétrabutylammonium 0,1 *M* et un peu d'eau 2×10^{-2} *M* environ (dosage de Karl-Fischer). Ainsi pour les analyses voltammétriques avec des concentrations en $CrCl_3 \cdot 6H_2O$ ou $MnCl_2 \cdot 4H_2O$ de 10^{-3} *M*, la concentration d'eau est de l'ordre de $2–3 \times 10^{-2}$ *M*; pour les électrolyses où la concentration de sel métallique est en général de 7×10^{-2} *M* (5×10^{-3} moles dans 70 cm^3 de solvant), la concentration d'eau est de 0,45 *M* environ.

En fin de réaction (déterminée par analyse polarographique), le mélange obtenu est versé dans un grand volume d'eau (700 cm^3 au moins), extrait à l'éther et séché sur sulfate de sodium. Le solvant est chassé sous vide, le résidu séparé par chromatographie sur couche mince de silice.

Les produits résultants des électrolyses ont déjà été décrits (5, 17–20) et nous les avons identifiés par leurs caractéristiques physiques et spectroscopiques, par comparaison avec celles d'échantillons authentiques. Les particularités observés et les spectres de rmn des produits obtenus sont donnés dans les réfs. 5 et 21. Le pourcentage respectif des formes *méso* et *dl*, pour les diols de l'acétophénone **5** et du benzaldéhyde **4**, a été évalué par spectroscopie rmn (22, 23). Dans tous les autres cas, les deux isomères *méso* et *dl* ont pu être séparés.

Les halogénures métalliques hydratés sont des produits Prolabo, les composés anhydres étant fournis par Ventron. Dans le cas du chrome les mêmes résultats sont obtenus à partir de la solution de chlorure chromique électrolysée à l'état de chlorure chromeux ou à partir de chlorure chromeux anhydre.

Remerciements

Les auteurs remercient vivement les rapporteurs pour leurs pertinentes remarques et suggestions.

1. M. Chanon et M. L. Tobe. Angew. Chem. Int. Ed. Engl. **21**, 1 (1982).
2. (*a*) J. P. Seguin, J. P. Doucet et R. Uzan. C. R. Acad. Sci. Sér. C, **278**, 129 (1974); (*b*) M. A. Michel, G. Mousset et J. Simonet. J. Electroanal. Chem. **98**, 319 (1979); (*c*) C. P. Andrieux et J. M. Saveant. Bull. Soc. Chim. Fr. 3281 (1972); (*d*) E. Lamy, L. Nadjo et J. M. Saveant. Electroanal. Chem. **50**, 141 (1974); (*e*) W. R. Fawcett et A. Lasia. Can J. Chem. **59**, 3256 (1981); (*f*) P. H. Given, M. E. Peover et J. Sihoen. J. Chem. Soc. 2674 (1958); (*g*) A. Bewick et H. Cleghorn. J. Chem. Soc. Perkin Trans. 2, 1410 (1973).
3. M. M. Baizer. Organic electrochemistry. *Éditeur*: M. M. Baizer. Marcel Dekker, New York. 1973. Chap. 9.
4. K. Köster et H. Wendt. J. Electroanal. Chem. **138**, 209, (1982).
5. F. Fournier, J. Berthelot et J.-J. Basselier. Tetrahedron, **41**, 5667 (1985).
6. F. Fournier, D. Davoust et J.-J. Basselier. Tetrahedron, **41**, 5677 (1985).
7. (*a*) A. Lasia et M. K. Kalinowski. J. Electroanal. Chem. **36**, 511 (1972); (*b*) A. Lasia. J. Electroanal. Chem. **102**, 117 (1979); (*c*) T. Fujinaga, K. Izutsu et T. Nomura. J. Electroanal. Chem. **29**, 203 (1971).

5. Un des rapporteurs rappelle que la plupart des métaux étudiés sont peu solubles dans le mercure et qu'une adsorption du composé organique sur les cristallites métalliques est possible, modifiant le processus d'électroréduction. Ce phénomène est difficilement discernable d'une vraie complexation au sens organométallique comme nous le proposons.

6. Un des rapporteurs rappelle aussi l'influence des métaux de transition dans l'évolution de la réaction des réactifs organomagnésiens avec les fonctions carbonyles (24).

8. F. FOURNIER, J. BERTHELOT et Y. L. PASCAL. Tetrahedron, **40**, 339, (1984); C. R. Acad. Sci. Sér. 3, **294**, 849 (1982).
9. F. FOURNIER, J. BERTHELOT et Y. L. PASCAL. Can. J. Chem. **61**, 2121 (1983).
10. D. W. SOPHER et J. H. P. UTLEY. J. Chem. Soc. Chem. Commun. 1087 (1979); J. Chem. Soc. Perkin Trans. 2, 1361 (1984).
11. M. PERRIN, P. POUILLEN, G. MOUSSET et P. MARTINET. Tetrahedron, **36**, 221 (1980).
12. G. ANTHOINE, J. NASIELSKI et B. WILMET-DEVOS. Bull. Soc. Chim. Belg. **78**, 465 (1969).
13. E. LAMY, L. NADJO et J. M. SAVEANT. Electroanal. Chem. **42**, 189 (1973).
14. J. M. SAVEANT. Acta Chem. Scand. Sér. B, **37**, 365 (1983).
15. F. BASOLO et R. PEARSON. Mechanisms of inorganic reactions. John Wiley and Sons, Inc., New York 1967.
16. C. K. JORGENSEN. Top. Curr. Chem. **56**, 1, (1975).
17. G. MAJERUS, E. YAX et G. OURISSON. Bull. Soc. Chim. Fr. 4143 (1967).
18. D. SEEBACH, H. A. OEI et H. DAUM. Chem. Ber. **110**, 2316 (1977).
19. H. GOTH, P. CERUTTI et H. SCHMIDT. Helv. Chim. Acta, **48**, 1395 (1965).
20. Y. ALTMAN et D. GINSBURG. J. Chem. Soc. 1498 (1961).
21. Y. L. PASCAL, O. CONVERT, J. BERTHELOT et F. FOURNIER. Org. Magn. Reson. **22**, 580 (1984).
22. J. H. STOCKER, D. H. KERN et R. M. JENEVEIN. J. Org. Chem. **33**, 412 (1968).
23. H. J. STOCKER et R. M. JENEVEIN. J. Org. Chem. **33**, 2145 (1968).
24. J. K. KOCHI. Organometallic mechanisms and catalysis. Academic Press, New York. Chap. 14 p. 514.

Electrochemical behaviour of the Zn(II)–Zn(Hg) system in aqueous ethylene glycol solutions

R. M. RODRÍGUEZ, E. BRILLAS, AND J. A. GARRIDO
Departament de Química física, Universitat de Barcelona, Avda. Diagonal 647, 08028-Barcelona, Spain
AND
J. DOMÉNECH
Departament de Química física, Universitat Autónoma de Barcelona, Bellaterra (Barcelona), Spain
Received August 22, 1985

R. M. RODRÍGUEZ, E. BRILLAS, J. A. GARRIDO, and J. DOMÉNECH. Can. J. Chem. **64**, 891 (1986).

The electrochemical behaviour of the Zn(II)–Zn(Hg) system in aqueous ethylene glycol (EG) solutions containing 5.0×10^{-2} *M* $LiClO_4$ has been studied by polarography and cyclic voltammetry. The reversible half-wave potentials, the diffusion coefficients and the Walden products for Zn(II) have been polarographically determined. The standard free energies of transfer of 1 mol of Zn(II) ions from water to EG–water mixtures, ΔG_t^0, obtained from the reversible half-wave potentials vs. the ferrocene electrode scale, are always negative, indicating a greater stability of Zn(II) in EG–water mixtures than in pure water. The splitting of the ΔG_t^0 values into electrostatic and chemical contributions shows that the mixtures are more basic than water. The analysis of the variation of the Walden product with solvent composition indicates an enhancement of the solvent structure in the water-rich region. The diffusion coefficient for Zn in mercury, the transfer coefficients for Zn(II) electroreduction, and the apparent standard rate constants of the Zn(II)–Zn(Hg) system have been determined by cyclic voltammetry. The change in the kinetics with solvent composition is discussed in terms of existing models.

R. M. RODRÍGUEZ, E. BRILLAS, J. A. GARRIDO et J. DOMÉNECH. Can. J. Chem. **64**, 891 (1986).

Faisant appel à la polarographie et à la voltammétrie cyclique, on a étudié le comportement électrochimique du système Zn(II)–Zn(Hg) dans des solutions aqueuses d'éthylène glycol (EG) contenant $5{,}0 \times 10^{-2}$ *M* de $LiClO_4$. A l'aide de la polarographie, on a déterminé les potentiels réversibles de demi-vague, les coefficients de diffusion et les produits de Walden pour le Zn(II). On a déterminé que les énergies libres standards pour le transfert d'une mole d'ions Zn(II) de l'eau à des mélanges d'eau–EG, ΔG_t^0, qui ont été obtenues à partir des potentiels réversibles de demi-vague vs. l'échelle de l'électrode du ferrocène sont toujours négatives; ce résultat indique que le Zn(II) est plus stable dans des mélanges d'eau–EG que dans de l'eau pure. Le dédoublement des valeurs de ΔG_t^0 en contributions électrostatiques et chimiques permet d'établir que les mélanges sont plus basiques que l'eau. L'analyse de la variation du produit de Walden avec la composition du solvant indique qu'il se produit une augmentation de la structure du solvant dans la région riche en eau. Utilisant la voltammétrie cyclique, on a détermine le coefficient de diffusion du Zn dans le mercure, les coefficients de transferts pour l'électroréduction du Zn(II) et les constantes de vitesses apparentes standards du sytème Zn(II)–Zn(Hg). On discute du changement dans les cinétiques avec la composition du solvant en fonction de modèles existants.

[Traduit par la revue]

Introduction

The electrochemical behaviour of the Zn(II)–Zn(Hg) system has been studied in several organic solvent–water mixtures (1–5). The authors have shown that the kinetics of this system depend basically on the solvation energy which represents the main contribution to the activation energy, and on the adsorption of the organic solvent which modifies the structure of the double layer at the electrode surface. Two different changes in the rate constant with solvent composition have been found, depending on the organic solvent used. Thus, in mixtures of water with less basic organic solvents, the rate constants of the Zn(II)–Zn(Hg) system exhibit minima in the intermediate composition range (1–4). To explain this behaviour, Behr *et al.* (2) propose to determine the rate constant, k, in a given aqueous mixture by means of the expression

$$[1] \quad k = k_w P$$

where k_w is the rate constant in the pure aqueous solution and P a correction term which describes the surface concentration, c, of the reactant ion. This term can be regarded as the distribution coefficient of the reactant between the bulk (α) and surface (σ) phases and it has the following form:

$$[2] \quad P = c^\sigma / c^\alpha = \exp(-{}^\alpha\Delta^\sigma G_t / RT)$$

${}^\alpha\Delta^\sigma G_t$ being the change in the free energy of transfer of 1 mol of ions between both phases. These two phases differ in solvent composition due to adsorption of the organic solvent on the electrode.

On the other hand, in mixtures of water with more basic organic solvents, the rate constants of the Zn(II)–Zn(Hg) system change monotonically when the concentration of the organic component increases (4, 5). This behaviour has been explained using the model of Broda and Galus (6) who propose to calculate the value of k in a given aqueous mixture by the equation

$$[3] \quad k = k_w(1 - \theta_{sol}) + k_{sol}\theta_{sol}$$

where k_w and k_{sol} denote the rate constants in pure water and in pure organic solvent respectively, θ_{sol} is the surface coverage of the electrode by organic solvent molecules. This model considers that two parallel reactions take place due to reactant ions approaching the surface layer and reacting either with the surface organic solvent molecules or with the surface water molecules.

Ethylene glycol (EG) is a common solvent in electrochemistry. Some studies on the electroreduction of several cations with amalgam formation in this solvent and its aqueous mixtures have been reported in the literature dealing with the determination of the reversible half-wave potential and the diffusive properties of the species in solution (7–9). In this way, we have previously investigated (10) the polarographic reduction of Cd(II) in EG–water mixtures with $LiClO_4$ as supporting

electrolyte. Under these conditions, we have found that solvent structure is enhanced in the water-rich region, whereas the ion always has a greater stability in EG–water mixtures than in pure water, suggesting that the mixtures are more basic than pure water.

The purpose of this paper is to study the electrochemical behaviour of the Zn(II)–Zn(Hg) system in EG–water mixtures containing a concentration of 5.0×10^{-2} *M* of $LiClO_4$, to clarify the acid–base and structural properties of these mixtures, and to check the application of the existing models stated above to explain the changes in the kinetics under the influence of the organic solvent.

Experimental

Ethylene glycol (Fluka, A.R. grade) was dried over 3 Å molecular sieves; its water content determined by the Karl Fisher method was lower than 0.05%. Lithium perchlorate (Fluka, A.R. grade) was dried at 130°C under reduced pressure and kept dry afterwards. Zinc sulphate (Merck, A.R. grade) was used without further purification. All solutions were prepared by weight with water obtained using a Millipore Milli Q system.

The polarographic measurements were performed with an Amel model 471 multipolarograph. The cyclic voltammetric measurements were carried out with a P.A.R. model 175 universal programmer, connected to an Amel model 551 potentiostat. The cyclic voltammograms were done at scan rate *v*; values lower than 0.200 V s^{-1} were directly displayed on a Philips model 8043 X–Y recorder, whereas the measurements made at higher scan rates were previously recorded on a Nicolet model 3091 digital storage oscilloscope. The ohmic drop compensation of all voltammetric measurements was achieved with a positive feedback network of the same instruments.

All voltammetric experiments were conducted in a three-electrode cell under nitrogen presaturated with the solution to be investigated. The temperature was kept at 25.0°C. A satured calomel electrode (SCE), with aqueous solution of NaCl, was used as reference electrode and a Pt wire as counter electrode. The flow rate, *m*, of the dropping mercury electrode employed in polarography was 0.628 mg s^{-1} in 0.1 *M* KCl solution on open circuit at a mercury height of 50 cm. In cyclic voltammetry the working electrode was a hanging mercury drop electrode with an area, *A*, of 0.0222 cm^2.

Solutions of Zn(II) (5.0×10^{-4} *M*) in both water and EG–water mixtures of 0.10–0.70 EG mole fraction, containing a concentration of 5.0×10^{-2} *M* of $LiClO_4$ as background electrolyte, were studied. The polarograms of each solution were recorded using a mercury height of 50 cm and drop times, *t*, 0.5, 1.0, 2.0, and 3.0 s. Drop times were regulated with a Tacussel GCMS hammer. The cyclic voltammograms of each solution were recorded in a scan rate range between 0.020 and 20 V s^{-1}.

Results and discussion

Polarographic behaviour

The Zn(II) displayed a single, well defined, polarographic reduction wave in all solutions studied. The wave is always diffusion controlled since a good linear correlation between the logarithm of the limiting current, I_l, and the logarithm of *t*, with slopes close to 0.19, was obtained in all solutions. In each solution the half-wave potential, $E_{1/2}$, was found to be independent of the drop time. Moreover, as can be seen in Fig. 1, the plots of *E* (applied potential) vs. log $((I_l - I)/I)$ were always linear, with slopes of about 30 mV. These results indicate that, in all solutions, Zn(II) electroreduction is a two-electron reversible process (11).

Table 1 summarizes polarographic results obtained for Zn(II) under the experimental conditions tested. It can be observed that when the EG mole fraction increases, $E_{1/2}$ is shifted to more

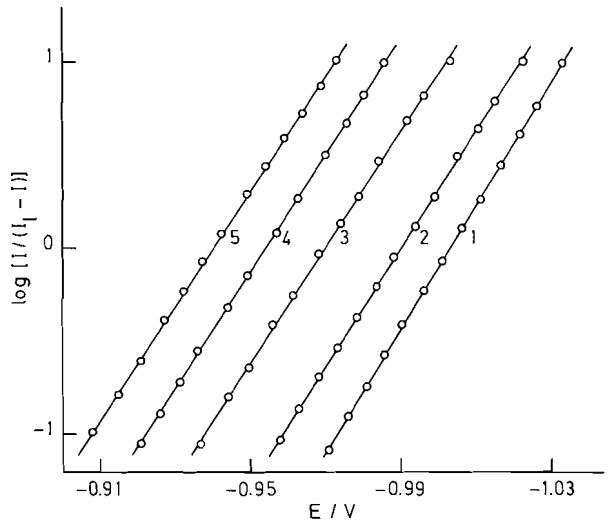

FIG. 1. Dependence of $\log (I/(I_l - I))$ on the applied potential for the polarographic reduction of Zn(II) in different aqueous EG solutions containing 5.0×10^{-2} *M* $LiClO_4$. EG mole fraction: (1) 0.00, (2) 0.10, (3) 0.30, (4) 0.50, (5) 0.70. Drop time 3.0 s and temperature 25.0°C.

positive values, whereas the value of the diffusion-current constant, I_d, gradually decreases. The diffusion coefficient of Zn(II), D_{ox}, also reported in Table 1, was calculated in each solution by substitution of the corresponding I_d value in the Ilkovič equation using a number of transferred electrons per reactant ion (*n* value) of 2.

To analyse the variation of $E_{1/2}$ with solvent composition, the liquid junction potential between the SCE (aqueous solution of NaCl) and each solution must be determined. In this way we have previously reported (10) that, in the EG–water media used, the liquid junction potentials can be estimated adopting the half-wave potentials of the ferrocene oxidation as internal reference. The half-wave potentials of Zn(II) expressed with respect to the half-wave potentials of ferrocene, $E_{1/2,Foc}$, are listed in Table 1. As can be seen, the $E_{1/2,Foc}$ values for Zn(II) become more negative as long as the EG mole fraction increases.

Taking into account these $E_{1/2,Foc}$ values, the standard free energies of transfer of one mole of Zn(II) ions from water to mixed solvents, ΔG_t^0, were calculated according to the following expression (2, 5, 6):

$$[4] \quad \Delta G_t^0 = 2F\,{}^{w}\Delta^{x}E^0$$

${}^{w}\Delta^{x}E^0$ being the difference between the standard potentials, E^0, of the Zn(II)–Zn(Hg) system in mixed solvent, x, and aqueous solution, w. Assuming that the diffusion coefficient of Zn in the amalgam formed by reduction of Zn(II) does not vary with solvent composition, as it has been confirmed from the cyclic voltammetric results which will be presented below, the differences ${}^{w}\Delta^{x}E^0$ were determined by means of the equation (12, 13):

$$[5] \quad {}^{w}\Delta^{x}E^0 = {}^{w}\Delta^{x}E_{1/2,Foc} + \frac{RT}{2F} \ln \frac{(\gamma_{ox})_w (D_{ox})_x^{1/2}}{(\gamma_{ox})_x (D_{ox})_w^{1/2}}$$

where γ_{ox} and D_{ox} are the activity coefficient and the diffusion coefficient, respectively, of Zn(II) in each solution. Then, to calculate ${}^{w}\Delta^{x}E^0$ a value of 0.570 was employed as activity coefficient $(\gamma_{ox})_w$ in the aqueous solution (14), whereas the

TABLE 1. Polarographic results for 5.0×10^{-4} *M* Zn(II) in water and EG–water mixtures containing 5.0×10^{-2} *M* $LiClO_4$, at 25°C

x_{EG}	$E_{1/2}$[a] (V)	$E_{1/2,Foc}$[b] (V)	I_d[c] ($\mu A\ mM^{-1}\ mg^{-2/3}\ s^{1/2}$)	$D_{ox} \times 10^7$ ($cm^2\ s^{-1}$)	γ_{ox}[e]	ΔG_t^{0f} (kJ mol^{-1})
0.00	−1.002	−1.143	3.26	72.3	0.570	0
0.10	−0.989	−1.149	2.33	36.8	0.514	−2.02
0.20	−0.979	−1.163	1.87	23.7	0.480	−5.44
0.30	−0.973	−1.179	1.49	15.1	0.442	−9.26
0.40	−0.960	−1.186	1.23	10.2	0.400	−11.38
0.50	−0.954	−1.201	1.07	7.7	0.365	−14.82
0.60	−0.946	−1.214	0.96	6.2	0.332	−17.83
0.70	−0.940	−1.224	0.88	5.2	0.302	−20.28

[a]Half-wave potential vs. SCE (aqueous solution of NaCl).
[b]Half-wave potential vs. ferrocene electrode scale.
[c]Diffusion-current constant calculated as $I_l/c\ m^{2/3}\ t^{1/6}$ where I_l = limiting current, c = Zn(II) concentration, m = flow rate, and t = drop time.
[d]Diffusion coefficient for Zn(II) calculated as $(I_d/607n)$ where n is the number of transferred electrons per reactant ion (see text).
[e]Activity coefficient for Zn(II) estimated from refs. 14–16 (see text).
[f]Standard free energy of transfer of 1 mol of Zn(II) ions from water to mixed solvent.

values used as activity coefficients $(\gamma_{ox})_x$ in mixed solvents (see Table 1) were estimated by means of the expression (15):

$$[6] \quad \log (\gamma_{ox})_x = (\epsilon_w/\epsilon_x)^{3/2} \log (\gamma_{ox})_w$$

where ϵ_w and ϵ_x denote the dielectric constants of water and the mixed solvent, respectively. These latter values were determined from the dielectric constants provided for several EG–water mixtures in ref. 16.

The ΔG_t^0 values obtained following the procedure stated above are given in the last column of Table 1. As can be seen, these values are more negative as long as the EG content in the solvent increases. This fact indicates that the transfer of Zn(II) from water to mixed solvents is thermodynamically favoured and also, that this process becomes more spontaneous when more EG is added to the mixed solvent. A similar behaviour has been previously reported for the transfer of Cd(II) from water to EG–water mixtures (10). This same effect has been described for the transfer of several ions, as Cd(II), Zn(II), and Pb(II), from water to dimethylsulfoxide–water mixtures (5), being ascribed to a higher solvating power of the dimethylsulfoxide, probably due to its greater basicity.

To gain a better understanding of this behaviour in EG–water mixtures, the ΔG_t^0 values for Zn(II) were split into two contributions: (*i*) an electrostatic one, $\Delta G_{t,el}^0$, which arises from the change in the dielectric constant of the solvent and (*ii*) a chemical one, $\Delta G_{t,ch}^0$, which depends on the solvation and other specific ion–solvent interactions. The electrostatic contribution to the standard free energy of transfer was estimated by means of the Born equation (17),

$$[7] \quad \Delta G_{t,el}^0 = \frac{N(ze)^2}{2r}\left(\frac{1}{\epsilon_x} - \frac{1}{\epsilon_w}\right)$$

where r is the crystallographic radius of Zn(II) (= 0.74 Å (18)). So, the chemical contribution to the standard free energy of transfer was determined by subtracting the $\Delta G_{t,el}^0$ found in each EG–water mixture from the corresponding ΔG_t^0. The dependence of the resulting $\Delta G_{t,ch}^0$ on EG mole fraction is shown in Fig. 2. It can be observed that the $\Delta G_{t,ch}^0$ values are more negative with increasing the EG content in the solvent. A similar behaviour has also been reported by Kundu *et al.* (19) for alkali

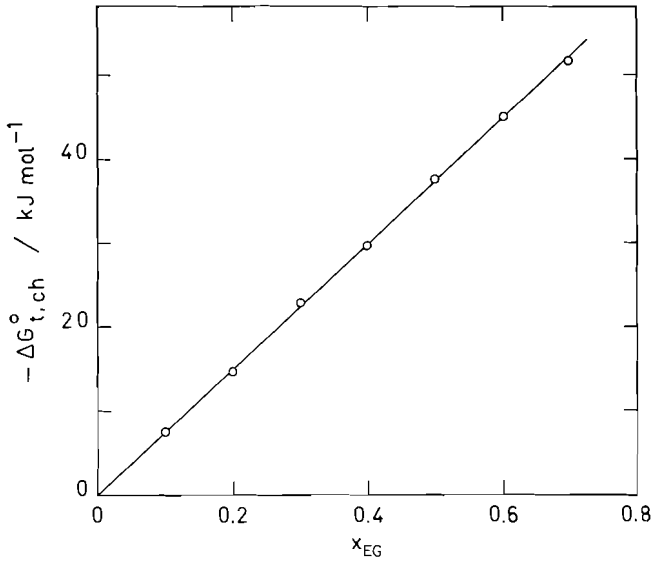

FIG. 2. Plot of the $\Delta G_{t,ch}^0$ for Zn(II) vs. EG mole fraction. Temperature 25.0°C.

cations in EG–water mixtures. According to these authors, the trend in the variation of $\Delta G_{t,ch}^0$ for Zn(II) with solvent composition could be explained considering the existence of specific acid–base interactions between the ion and solvent molecules. In this way these results indicate that the mixtures are more basic than water, increasing its basicity when EG is added to the solvent and hence, producing stronger ion–solvent interactions. In addition, the linear correlation found between $\Delta G_{t,ch}^0$ and x_{EG} (see Fig. 2) suggests a gradual increase in the Zn(II) solvation proportional to the EG mole fraction.

On the other hand, it should be noted that the gradual decrease in diffusion coefficient of Zn(II) when the EG content in the solvent increases (see Table 1) is mainly due to the progressive increase in viscosity, η, of the solution. The viscosities of the EG–water mixtures tested, containing 5.0×10^{-2} *M* $LiClO_4$, have been previously measured (10) and they are shown in Fig. 3*b*. Then, the change in the structure of the EG–water mixtures at different compositions can be analysed from the variation of

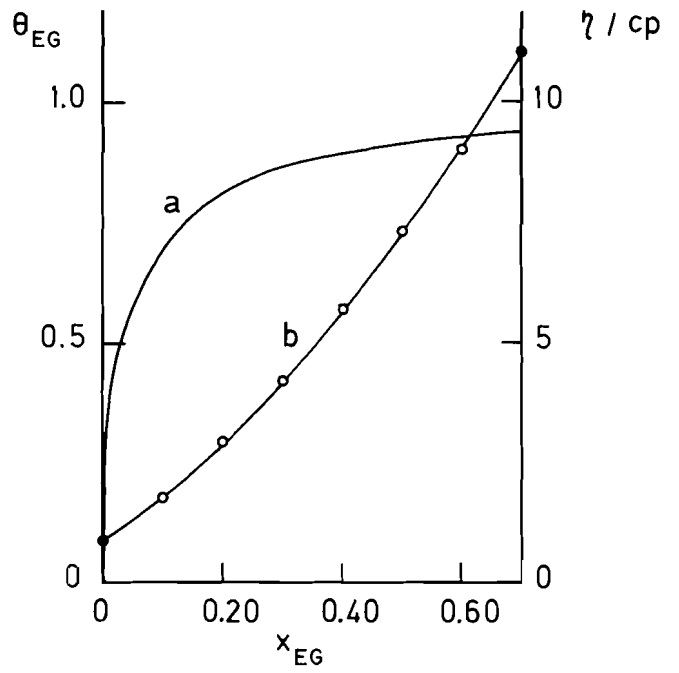

FIG. 3. (*a*) The surface coverage of the electrode by EG molecules in different EG–water mixtures at $E = -1.0$ V vs. SCE (aqueous solution of NaCl). Data estimated from refs. 25 and 26. (*b*) Viscosity of EG–water mixtures vs. EG mole fraction (10). Temperature 25.0°C.

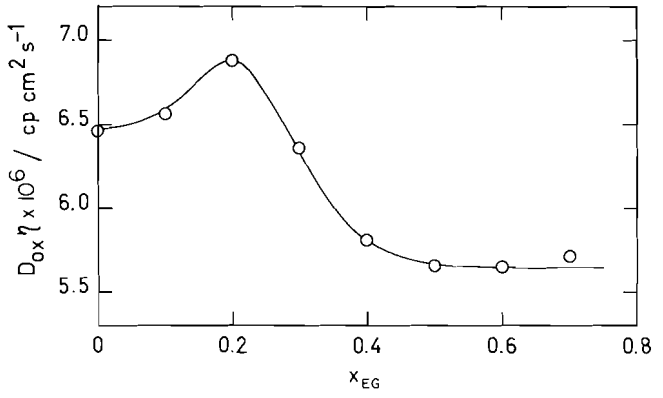

FIG. 4. Variation of the Walden product for Zn(II) with EG mole fraction. Temperature 25.0°C.

the Walden product, $D_{ox}\eta$, with solvent composition to avoid the effect of the bulk viscosity.

The dependence of $D_{ox}\eta$ for Zn(II) on EG mole fraction is shown in Fig. 4. As it can be seen, a maximum value of the Walden product is reached in the water-rich region, close to $x_{EG} = 0.2$. A similar behaviour for the Walden product of Cd(II) has also been previously described (10). This could be explained considering that in the water-rich region the solvent becomes more structured because small amounts of EG added to pure water promote the three-dimensional network building of the last solvent, as we have recently reported from viscosity measurements of several alkali cations.[1] Consequently, in the water-rich region, the Zn(II) ion, as well as the Cd(II) ion, become more structure breaking. This decreases local viscosity around the ion, leading to an increase in its mobility. At $x_{EG} > 0.2$, addition of EG to mixed solvent causes a decrease in solvent structure and hence, a loss in mobility of the Zn(II) ion, which partially causes the observed decrease in its Walden product. In addition, according to the Stokes–Einstein relation, the product $D_{ox}\eta$ is inversely proportional to the solvated radius of diffusive species. Thus, the gradual decrease in $D_{ox}\eta$ of Zn(II) at $x_{EG} > 0.2$ is also explained by an increase in the solvated radius of this ion due to the substitution of the more voluminous EG molecules by water ones. This fact is consistent with the progressive increase in the Zn(II) solvation, as stated above.

[1]J. Doménech, E. Brillas, J. A. Garrido, and R. M. Rodríguez. Private communication.

Cyclic voltammetric behaviour

The Zn(II)–Zn(Hg) system exhibits a redox couple under all the experimental conditions studied, which shows a different voltammetric behaviour depending on the EG content in the mixture and the scan rate. To determine the cyclic voltammetric parameters corresponding to this system in each tested solution, the cyclic voltammograms were carried out starting from −0.700 V and reversing the scan at −1.200 V.

Values of cathodic peak potential, E_p^c, cathodic half-peak potential, $E_{p/2}^c$, anodic peak potential, E_p^a, and cathodic peak current, I_p^c, obtained at a scan rate of 0.020 V s^{-1} are summarized in Table 2. It can be observed that E_p^c, $E_{p/2}^c$, and E_p^a are gradually shifted with increasing EG content in the mixture to less negative values. On the other hand, I_p^c progressively decreases as long as the EG mole fraction rises, in accordance with the gradual increase in viscosity of the reaction medium (see Fig. 3b). From the I_p^c values, the cathodic peak-current functions, ψ_p^c, were calculated employing an n value of 2 and the diffusion coefficients for Zn(II) previously determined by polarography (see Table 1). The ψ_p^c values thus obtained are also listed in Table 2. As can be seen, ψ_p^c is independent of the EG content in the mixture with a value of 0.46 ± 0.01, as is expected for a two-electron reversible reduction process (11, 20).

For a given solution and at scan rates lower than 0.150 V s^{-1}, the ratio of anodic to cathodic peak currents, I_p^a/I_p^c, is found to be higher than unity, its value dependent on the applied reversal potential, E_λ. This is due to the concentration effect of the Zn amalgam formed in the hanging mercury drop electrode because of the spherical diffusion and the limited volume of the electrode. Recently, Tokuda *et al.* (20) have studied theoretically, by cyclic voltammetry, this kind of process for a simple reversible system, such as

[8] $M^{n+} + ne^- \rightleftharpoons M(Hg)$

They established the following equations to calculate the diffusion coefficient, D_{red}, for metal M in mercury and the reversible half-wave potential, $E_{1/2}^r$, corresponding to the M^{n+} electroreduction:

$$[9] \quad D_{red} = [\{(I_p^a/I_p^c) - 1\}/4.130 D_{ox}^{0.172} r_0^{-1.273} \times (RT/nFv)^{0.637} \{(nF/RT)(E_p^c - E_\lambda)\}]^{0.719 - 0.469}$$

$$[10] \quad E_{1/2}^r = E_p^c + (RT/nF)[1.109 + 5.047 D_{ox}^{0.344} D_{red}^{0.168} \times r_0^{-1.024} (RT/nFv)^{0.512}]$$

r_0 being the electrode radius.

Because the Zn(II) electroreduction is reversible in all solutions at 0.020 V s^{-1}, as was pointed out above, it seems plausible to consider that the Zn(II)–Zn(Hg) system behaves as a simple reversible one at low v values and hence, D_{red} for Zn in mercury and $E_{1/2}^r$ for the Zn(II) electroreduction can be

TABLE 2. Cyclic voltammetric results of the Zn(II)–Zn(Hg) system in water and EG–water mixtures containing 5.0×10^{-2} *M* $LiClO_4$, at a scan rate of 0.020 V s^{-1} and at 25.0°C

x_{EG}	$E_p^{c\,a}$ (V)	$E_{p/2}^{c\,b}$ (V)	$E_p^{a\,c}$ (V)	$I_p^{c\,d}$ (μA)	$\psi_p^{c\,e}$	$D_{red} \times 10^{5\,f}$ ($cm^2\,s^{-1}$)	$E_{1/2}^{r\,g}$ (V)
0.00	−1.020	−0.990	−0.992	3.40	0.47	1.50	−1.002
0.10	−1.008	−0.977	−0.975	2.41	0.47	1.38	−0.991
0.20	−0.997	−0.967	−0.965	1.91	0.45	1.47	−0.980
0.30	−0.990	−0.960	−0.955	1.51	0.46	1.44	−0.974
0.40	−0.978	−0.949	−0.944	1.25	0.46	1.40	−0.962
0.50	−0.970	−0.941	−0.937	1.10	0.47	1.32	−0.954
0.60	−0.963	−0.932	−0.936	0.92	0.45	1.39	−0.947
0.70	−0.955	−0.922	−0.922	0.90	0.47	1.31	−0.939

[a]Cathodic peak potential vs. SCE (aqueous solution of NaCl).
[b]Cathodic half-peak potential vs. SCE (aqueous solution of NaCl).
[c]Anodic peak potential vs. SCE (aqueous solution of NaCl).
[d]Cathodic peak current.
[e]Cathodic peak-current function calculated as $I_p^c/nFAc(D_{ox}nFv/RT)^{1/2}$.
[f]Diffusion coefficient for Zn in mercury.
[g]Reversible half-wave potential for Zn(II) vs. SCE (aqueous solution of NaCl).

determined by means of eqs. [9] and [10], respectively. To corroborate all these suppositions, several cyclic voltammograms were recorded for each studied solution at 0.020 and 0.050 V s^{-1}, with different values of $(E_p^c - E_\lambda)$ between 0.080 and 0.200 V. The I_p^a/I_p^c ratio for each redox couple was determined following the method described in ref. 11. The mean value of D_{red} obtained for each solution by using eq. [9] is given in Table 2. It can be observed that the diffusion coefficient for Zn in mercury remains practically constant in all experimental conditions, taking a value of $(1.40 \pm 0.09) \times 10^{-5}$ $cm^2\,s^{-1}$ which agrees with those reported in the literature from other reaction media (5, 21). This indicates that the Zn(II)–Zn(Hg) system is always reversible at low scan rates. On the other hand, the $E_{1/2}^r$ values calculated from the eq. [10] are listed in the last column of Table 2. It should be noted that these values are in accordance with those determined by polarography (see Table 1), with a maximum deviation of ±2 mV. From an inspection of Table 2 it can be seen that there is a difference between $E_{1/2}^r$ and E_p^c of 17 ± 1 mV in all solutions, i.e., a value slightly higher than the 14 mV expected for a two-electron reversible process (11). Then, the fact that the values of $(E_p^a - E_p^c)$ and $(E_{p/2}^c - E_p^c)$ for the Zn(II)–Zn(Hg) system under reversible conditions (see Table 2) slightly differ from the 28 mV established for a two-electron reversible system (11), can be attributed to the amalgam formation process.

For each studied solution and at scan rates higher than 0.150 V s^{-1}, the I_p^a/I_p^c ratio remains close to unity, although it slightly decreases as the scan rate rises. With increasing v, there is always a progressive decrease in ψ_p^c, whereas, simultaneously, E_p^c is shifted to more negative values and E_p^a to less negative ones; hence, a gradual increase in $(E_p^a - E_p^c)$, as well as in $(E_{p/2}^c - E_p^c)$, is also observed. All these results are indicative of a quasi-reversible behaviour of the Zn(II)–Zn(Hg) system under these conditions. Experimental efforts were then concentrated on the determination of the kinetic parameters of this system in each solution.

The apparent standard rate constant, k_s, of a simple quasi-reversible system can be calculated by means of the expression (22)

$$[11] \quad k_s = D_{red}^{\alpha/2} D_{ox}^{(1-\alpha)/2} (\pi nFv/RT)^{1/2}\,\psi$$

where ψ is a function of $(E_p^a - E_p^c)n$ and of the transfer coefficient, α, for the reduction process. According to Matsuda and Ayabe (23), this transfer coefficient can be determined when the process is quasi-reversible from a given v_o value, because in such conditions, a linear correlation between E_p^c and $-\log v$, with a slope of $(0.0296/\alpha n)$ V at 25.0°C, is expected. Thus, eq. [11] can only be used to obtain k_s at scan rates lower than v_o.

TABLE 3. Kinetic parameters of the Zn(II)–Zn(Hg) system in water and EG–water mixtures containing 5.0×10^{-2} *M* $LiClO_4$, at 25.0°C

x_{EG}	$k_s \times 10^{3\,a}$ ($cm\,s^{-1}$)	α^b	$k_s^0 \times 10^{3\,c}$ ($cm\,s^{-1}$)
0.00	17.2	0.31	25.3
0.10	7.5	0.29	12.0
0.20	6.2	0.29	10.5
0.30	5.5	0.27	9.9
0.40	5.2	0.25	10.3
0.50	4.8	0.26	10.2
0.60	4.4	0.27	9.9
0.70	3.7	0.27	8.9

[a]Apparent standard rate constant of the Zn(II)–Zn(Hg) system.
[b]Transfer coefficient for Zn(II) electroreduction.
[c]Apparent standard rate constant of the Zn(II)–Zn(Hg) system at $\gamma_{ox} = 1$.

For the cathodic peak of the Zn(II)–Zn(Hg) system under quasi-reversible conditions, good linear correlations between E_p^c and $-\log v$ were always obtained at v values higher than 3 V s^{-1}. Assuming that the slope of these plots was $(0.0296/\alpha n)$ V per decade and $n = 2$, the transfer coefficient for the Zn(II) electroreduction is always found to be close to 0.3, as can be seen in Table 3. Similar α values have also been reported for this reduction process in other reaction media (5, 24).

In the scan rate range between 0.2 and 2 V s^{-1} the difference $(E_p^a - E_p^c)$ gradually increases with rising v from 0.045 to 0.110 V, approximately. Under these conditions, the ψ parameter for each redox couple was determined from the ψ vs. $(E_p^a - E_p^c)n$ plot established by Nicholson (22) and then, the corresponding k_s of the Zn(II)–Zn(Hg) system was calculated by using eq. [11]. For each solution, at least seven cyclic

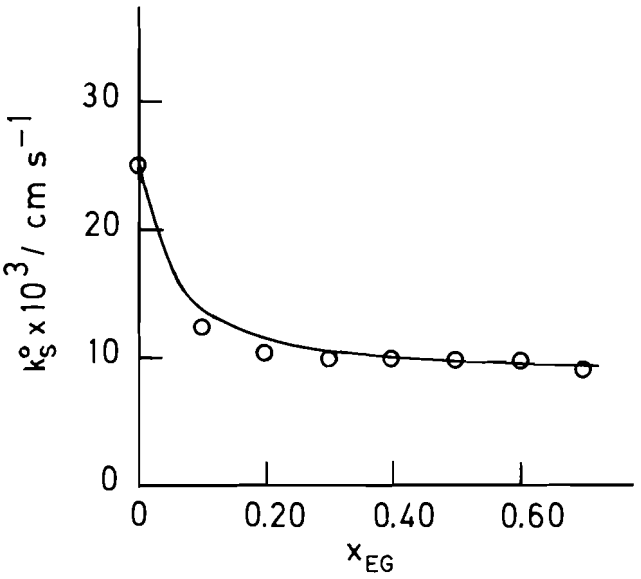

FIG. 5. Dependence of experimental values of k_s^0 for the Zn(II)–Zn(Hg) system on EG mole fraction. The solid line corresponds to the theoretical curve calculated from the model of Broda and Galus (6).

voltammograms with different scan rates were recorded to obtain a mean value of k_s. The resulting k_s values, with an accuracy of ±8%, are given in Table 3. A progressive decrease in k_s with increasing EG mole fraction can be observed.

A better insight into the variation of the apparent standard rate constant with the reaction medium can be gained taking into account that k_s depends on the activity coefficient, γ_{ox}, of Zn(II), according to the expression (23):

[12] $k_s = k_s^0 \gamma_{ox}^{1-\alpha}$

k_s^0 being the apparent standard rate constant at $\gamma_{ox} = 1$. The k_s^0 values were calculated using the γ_{ox} values reported in Table 1 and they are listed in the last column of Table 3. It was then tried to interpret the change in the kinetics of the Zn(II)–Zn(Hg) system with solvent composition in terms of existing models stated in the Introduction.

The monotonic decrease in k_s^0 as the EG mole fraction increases can only be explained by the model of Broda and Galus (6), which describes the change in kinetics by eq. [3]. This model seems plausible to use because the EG–water mixtures are more basic than water as was pointed out above.

To corroborate if eq. [3] can describe the change of k_s^0, the theoretical k_s^0 value for each solution was calculated. For this, the $k_{s,w}^0$ value was taken from Table 3, whereas the $k_{s,EG}^0$ value was obtained by extrapolation at $x_{EG} = 1$. On the other hand, the surface coverage of the electrode by EG molecules, θ_{EG}, at −1.000 V, i.e., at the potential of Zn(II) electroreduction, in the different EG–water mixtures studied was estimated from data reported in refs. 25 and 26. The variation of θ_{EG} with EG mole fraction is presented in Fig. 3*a*.

Figure 5 shows the dependence of the experimental k_s^0 values on EG mole fraction, as well as the corresponding theoretical curve (solid line) calculated by using eq. [3]. A very good agreement between the experimental and the calculated values is found, indicating that the model of Broda and Galus [6] explains the change of k_s^0 for the Zn(II)–Zn(Hg) system in EG–water mixtures.

Finally, according to the above-mentioned authors, a linear dependence of the activation energy on the surface coverage must be expected. This fact is difficult to interpret if the solvation energy (ΔG_t^0) is the main contribution to the activation energy, as it is usually considered, because ΔG_t^0 gradually increases with rising EG mole fraction (see Table 1), whereas most of the increase in activation enrgy should take place up to $x_{EG} = 0.4$, as can be deduced from Fig 3*a*. Then, the increase in activation energy could be ascribed to the activation energy needed for the reorganization of the solvation shell of the reactant ion entering the surface layer, as Jaenicke and Schweitzer (1) have suggested.

1. W. JAENICKE and P. H. SCHWEITZER. Z. Phys. Chem. N.F. **52**, 104 (1967).
2. B. BEHR, J. STROKA, and J. TARASZEWSKA. J. Electroanal. Chem. **58**, 71 (1975).
3. J. STROKA, K. MAKSYMIUK, and Z. GALUS. J. Electroanal. Chem. **167**, 211 (1984).
4. K. MAKSYMIUK, J. STROKA, and Z. GALUS. J. Electroanal. Chem. **181**, 51 (1984).
5. J. TARASZEWSKA and A. WALEGA. J. Electroanal. Chem. **171**, 243 (1984).
6. J. BRODA and Z. GALUS. J. Electroanal. Chem. **130**, 229 (1981).
7. C. H. R. GENTRY. Nature, **157**, 479 (1946).
8. D. B. BRUSS and T. DE VRIES. J. Am. Chem. Soc. **75**, 733 (1956).
9. T. RABOCKAI. Can. J. Chem. **57**, 1801 (1979).
10. E. BRILLAS, J. A. GARRIDO, R. M. RODRÍGUEZ and J. DOMÉNECH. Chem. Scr. **25**, 369 (1985).
11. Z. GALUS. Fundamentals of Electrochemical Analysis. Chapt. 7 and 17. Harwood, Chichester. 1976.
12. J. J. LINGANE. J. Am. Chem. Soc. **61**, 2099 (1939).
13. D. D. DEFORD and D. L. ANDERSEN. J. Am. Chem. Soc. **72**, 3918 (1950).
14. J. KIELLAND. J. Am. Chem. Soc. **59**, 1675 (1937).
15. A. AREVALO, A. VIVO, and E. TEJERA. An. Quím. **70**, 318 (1974).
16. F. ACCASCINA, S. PETRUCCI, and S. SCHIAVO. Sci. Tec. **3**, 242 (1959).
17. M. BORN. Z. Phys. **1**, 45 (1920).
18. R. PARSONS. Handbook of electrochemical constants. Butterworths Scientific Publications, London. 1959. p. 5.
19. K. K. KUNDU, A. K. RAKSHIT, and M. N. DAS. Electrochim. Acta, **17**, 1921 (1972).
20. K. TOKUDA, N. ENOMOTO, H. MATSUDA, and N. KOIZUMI. J. Electroanal. Chem. **159**, 23 (1983).
21. A. M. BOND, B. S. GRABARIC, R. D. JONES, and N. W. RUMBLE. J. Electroanal. Chem. **100**, 625 (1979).
22. R. S. NICHOLSON. Anal. Chem. **37**, 1351 (1965).
23. H. MATSUDA and Y. AYABE. Z. Elektrochem. **59**, 494 (1955).
24. S. KANG, K. MATSUDA, and R. TAMAMUSHI. Collect. Czech. Chem. Commun. **47**, 1433 (1982).
25. S. TRASATTI. J. Electroanal. Chem. **28**, 257 (1970).
26. B. V. APPARAO and M. V. RAMANAMURTI. J. Chem. Soc. Faraday Trans. 1, **75**, 2576 (1979).

Hydridoiridium(III) sulfoxide complexes and their reactivity toward dioxygen

BRIAN R. JAMES AND ROBERT H. MORRIS[1]

Department of Chemistry, University of British Columbia, Vancouver, B.C., Canada V6T 1Y6

AND

PAL KVINTOVICS[2]

Research Group for Petrochemistry of the Hungarian Academy of Sciences, University of Chemical Engineering, Veszprem, Hungary H-8200

Received August 19, 1985

BRIAN R. JAMES, ROBERT H. MORRIS, and PAL KVINTOVICS. Can. J. Chem. **64**, 897 (1986).

Synthetic routes to hydridoiridium(III) dimethylsulfoxide complexes via oxidative addition of HCl or H_2 to precursor *in situ* iridium(I) species are described. The complexes, *trans,mer*-$IrHCl_2(DMSO)_3$ (**1***a*) and *cis,mer*-$IrH_2Cl(DMSO)_3$ (**2**), have been characterized by ^1H nmr and ir, and contain only S-bonded sulphoxide, DMSO. Comparison is made with data for other isomers reported in the literature, and some discrepancies are discussed. The decomposition of **1***a* and **2** in chloroform leads to isomers of $IrCl_3(DMSO)_3$, while (**2**) with HCl generates *cis,cis*-$IrHCl_2(DMSO)_2(DMSO)$ with the O-bonded sulfoxide *trans* to hydride. The reaction of **1***a* in dichloromethane with dioxygen occurs with a 1:1 stoichiometry and generates two complexes tentatively formulated as $Ir(OH)Cl_2(DMSO)_2H_2O$ (**3**) and $IrCl_2(O_2)(DMSO)_2 \cdot DMSO$ (**4**); a hydroperoxide intermediate (Ir—OOH) initially formed from **1***a* is considered to react with further **1***a* in the rate-determining step. Oxidation of coordinated DMSO to the sulphone is not observed, implying that such a catalyzed O_2-oxidation reported earlier in aqueous 2-propanol proceeds via reaction of IrOOH with free DMSO, or else via free hydrogen peroxide.

BRIAN R. JAMES, ROBERT H. MORRIS, et PAL KVINTOVICS. Can. J. Chem. **64**, 897 (1986).

On décrit des voies de synthèses de complexes de l'hydroiridium(III) et du diméthylsulfoxyde qui impliquent l'addition de HCl ou de H_2 à des précurseurs d'iridium(I) préparés *in situ*. On a caractérisé les complexes, soit le $IrHCl_2(DMSO)_3$-*trans,mer* (**1***a*) et le $IrHCl_2(DMSO)_3$-*cis,mer* (**2**), en faisant appel à la rmn du ^1H et à la spectroscopie ir et ils ne contiennent que des sulfoxydes liés par le soufre, DMSO. On fait une comparaison avec les données publiées antérieurement pour d'autres complexes et on discute des divergences. La décomposition des composés **1***a* et **2** dans le chloroforme conduit à des isomères du $IrCl_3(DMSO)_3$ alors que la réaction du composé **2** avec du HCl conduit à la formation de $IrHCl_2(DMSO)_2(DMSO)$-*cis,cis* dans lequel le sulfoxyde est lié par l'oxygène en position *trans* par rapport à l'hydrure. Dans le dichlorométhane, le composé **1***a* réagit avec le dioxygène avec une stoïchiométrie 1:1 et conduit à deux complexes auxquels on a attribué, à titre d'essai, les formules $Ir(OH)Cl_2(DMSO)_2H_2O$ (**3**) et $IrCl_2(O_2)(DMSO)_2 \cdot DMSO$ (**4**); on a considère qu'un intermédiaire hydroperoxyde (Ir—OOH) qui se forme initialement à partir de **1***a* réagirait à nouveau avec le composé **1***a* dans l'étape déterminante. On n'a pas observé d'oxydation du DMSO coordonné en sulfone; ce résultat implique qu'une telle réaction catalysée d'oxydation par O_2, dont on a antérieurement suggéré l'existence pour des réactions dans le propanol-2 aqueux, se produirait soit par une réaction du IrOOH avec du DMSO libre soit via du peroxyde d'hydrogène libre.

[Traduit par la revue]

Introduction

We have become increasingly interested in transition-metal catalyzed oxygenations using O_2 in the presence of a co-reductant, for example (1–4),

$$[1] \quad O_2 + \text{substrate} + H^- \xrightarrow{H^+} \text{substrate(O)} + H_2O$$

In the particular case of a selective oxygenation of cyclooctene (X) to cyclooctanone using O_2–H_2 mixtures in the presence of an iridium catalyst (2), the suggested basic mechanism is outlined in eq. [2], a key feature being the formation of the iridium–hydroperoxide intermediate (Ir—OOH) by a net insertion of O_2 into the metal–hydride bond.

$$[2] \quad (X)IrH \xrightarrow{O_2} (X)Ir{-}OOH \longrightarrow Ir(OH) + XO$$

$$\uparrow \qquad\qquad +H_2, -H_2O \qquad\qquad \downarrow$$

Evidence was obtained for an Ir—OOH species and oxygen transfer to coordinated cyclooctene was considered to occur via a peroxometallocyclic intermediate. Other groups have reported on formation of Rh—OOH (5, 6) and Pt—OOH complexes (7) via reactivity of the platinum metal monohydride with O_2.

There is very intense interest generally in selective oxygenations utilizing O_2, (1, 3, 8–10). Those exemplified by eq. [1] resemble in stoichiometry those of cytochrome-P450, and here also, Fe(III)—OOH intermediates have been invoked but formed, in this case, via protonation of an Fe(III)peroxide (1, 2, 10, 11).

In addition, it is also known that "trace" O_2 can have marked effects on both stoichiometric and catalytic reactions of platinum metal complexes (12, 13). The catalytic reactions include hydrogenation of olefins and aromatics (13), and species formed from metal–hydrides with O_2 may play a role, although this was never suggested directly. Hydrogenolysis of O_2 to H_2O or H_2O_2 has been little studied using homogeneous catalysts (14, 15), but as the rate-determining step sometimes involves formation of a hydride from complex and H_2 (14), a subsequent step almost certainly involves metal–hydride plus O_2.

All of the above findings have encouraged us to pursue metal–hydride – O_2 chemistry. Previously, we had used the complex, *trans*-dichloro-*mer*-tris(dimethylsulfoxide)hydridoiridium(III), **1***a*, as a hydrogen transfer catalyst (16). This complex seemed a good candidate for a reactivity study

[1]Present address: Department of Chemistry and Scarborough Campus, University of Toronto, Toronto, Ont., Canada M5S 1A1.

[2]On leave at the University of British Columbia. 1981–1982.

toward O_2, particularly since Trocha-Grimshaw and Henbest (17) had used such a hydride (and one of Rh) in aqueous 2-propanol solutions for the air oxidation of DMSO to the sulphone, and we had discovered a similar rhodium-catalyzed oxygenation using O_2–H_2 mixture and had suggested a Rh—OOH intermediate (2, 18).

The communication describing the hydrogen transfer work (16) had noted differences with literature data (19) on various isomers of $IrHCl_2(DMSO)_3$.[3] A further interest in the hydrides themselves stems from their potential as catalysts (with chiral sulfoxides) for asymmetric hydrogenation of prochiral substrates. The present paper gives the details on the syntheses and full spectroscopic characterization of **1***a*, and other mono- and dihydrides of Ir(III), together with data on reactivity of **1***a* toward O_2.

Experimental

The iridium was obtained from Johnson, Matthey Ltd. as $IrCl_3 \cdot 3H_2O$ containing 51.76% of the metal, or as $IrCl_4$ from Platinum Chemicals; the cyclooctene precursor $[IrCl(C_8H_{14})_2]_2$ was prepared by a literature procedure (20). The sources of all the other materials used, the synthetic procedures, the procedure used for following gas (O_2) uptake at constant pressure, and the instrumentation for the spectroscopic methods and gc separations, can be traced largely through earlier papers (2, 21). The DMSO was dried with KOH and then vacuum distilled; CH_2Cl_2 was distilled from CaH_2. A Varian E-3 was used to record esr spectra, and the magnetic susceptibility was measured on a Faraday balance (22). Microanalyses were performed by Mr. P. Borda of this department.

Acid of cis-*tetrachlorobis(DMSO)iridate(III), [H(DMSO)$_2$][IrCl$_4$(DMSO)$_2$]*

To a red solution, formed by heating $IrCl_3 \cdot 3H_2O$ (0.3 g, 0.87 mmol) in aqueous HCl (1.1 mL, 2.4 *M*) at 80°C for 30 min, was added DMSO (0.52 mL, 7.5 mmol); heating was continued for 38 h in air in a closed, glass-stoppered Schlenk tube. When the tube was opened, the strong smell of Me_2S emanated from the orange solution; the solution was reduced to an oil by pumping, and the residue dissolved in 1 mL H_2O and extracted with CH_2Cl_2 (3 × 10 mL). Evaporation of the aqueous layer gave a syrup, to which addition of 2-propanol (5 mL) and DMSO (0.5 mL) yielded the acid as yellow needles (yield, 40%). Spectral data agree with those published (19). For example, nmr (D_2O): δ 3.52 (s, 12H, DM*S*O), 2.71 (s, 12H, free DMSO). The CH_2Cl_2 extracts yielded 20 mg of $IrCl_3(DMSO)_2(DMSO)$ (19).

Acid of trans-*tetrachlorobis(DMSO)iridate(III), [H(DMSO)$_2$][IrCl$_4$(DMSO)$_2$]*

After $IrCl_4$ (0.45 g, 1.3 mmol) had reacted with conc. HCl (0.3 mL, 4 mmol) in 5 mL 2-propanol for 4 h at 55°C, the resulting green-red solution was cooled to room temperature, and DMSO (2.5 mL, 35 mmol) added. The orange needles that crystallized overnight were filtered in air, washed with 2-propanol and ether, and dried *in vacuo* (yield, 52%, mp 152–154°C); ir (cm^{-1}): ν(SO) 1127(s), $\rho_r(CH_3)$ 1027(s), 980(s); ν(OHO) 1700–1100(m), 900–600(s), ν(Ir—Cl) 335(m), 326(s). nmr (D_2O): δ 3.50 (s, 12H, DM*S*O), 2.71 (s, 12H, free DMSO).

trans-*Dichloro*-mer-*tris(DMSO)hydridoiridium(III), IrHCl$_2$(DMSO)$_3$ (1a)*

(*a*) The precursor $[IrCl(C_8H_{14})_2]_2$ (0.1 g, 0.11 mmol) was dissolved in dry DMSO (0.4 mL, 5.6 mmol) and CH_2Cl_2 (3 mL) at 10°C under Ar to give a yellow solution. A few large crystals of DMA·HCl (27 mg, 0.22 mmol) were rapidly weighed and added,[4] and the resulting colourless solution reduced in volume to ~0.5 mL *in vacuo*; dry ether was added slowly until a turbidity appeared, the solution was then warmed until clear and left at 0°C to deposit white crystals. The product was filtered under Ar, washed with a little ether, and dried *in vacuo* (yield, 70%); the crystals, isolated as a mono-DMSO solvate (see nmr), were very hygroscopic (giving a yellow oil) and were also sometimes contaminated with a small amount of cyclooctene as evidenced by nmr (δ 5.5, 2.0, 1.4 ppm). Carbon content was typically high. For example, *Anal.* calcd. for $C_6H_{19}O_3S_3Cl_2Ir \cdot C_2H_6OS$: C 16.66, H 4.37; found: C 18.1, H 4.1. Infrared (cm^{-1}): ν(Ir—H) 2180(s), ν(SO) 1134(s), 1110(s), $\rho_r(CH_3)$+ν(SO) of solvate 1027(s), ν(Ir—Cl) 302(w); nmr ($CDCl_3$): δ 3.73 (s, 6H, DM*S*O), 3.57 (s, 12H, DM*S*O), 2.62 (s, 6H, free DMSO), −18.86 (s, 1H, IrH).

(*b*) The solvate-free complex may be obtained by adding DMA·HCl (68 mg, 0.56 mmol) to a degassed suspension of $[IrCl(C_8H_{14})_2]_2$ (0.25 g, 0.28 mmol) in 5 mL 2-propanol and 1.0 mL DMSO; the suspended compound turns from orange to white in 10 min at room temperature. The product was filtered, washed with ether, and recrystallized following dissolution in 1 mL DMSO and addition of 5 mL 2-propanol–ether, (1:2 v/v) (yield, 60%). The spectral data were essentially the same as above, but there were no free DMSO peaks; trace, free cyclooctene was always detected and resulted in high carbon content. *Anal.* calcd. for $C_6H_{19}O_3S_3Cl_2Ir$: C 14.46, H 3.81; found: C 15.5, H 4.2.

Several attempts starting with either the *cis* or *trans* acid complexes $[H(DMSO)_2][IrCl_4(DMSO)_2]$ (see above) failed to reproduce the published syntheses (19) of $IrHCl_2(DMSO)_3$, *trans*-Cl_2-*mer*$(DMSO)_3$, or *cis*-Cl_2-*mer*$(DMSO)_3$. A few milligrams of a yellow product could be realized, but this was a mixture of hydrides and other neutral complexes. Infrared (cm^{-1}): ν(Ir—H) 2180–2150(w), ν(SO) 1130–1100(s); nmr ($CDCl_3$): δ 3.51 (main DM*S*O peak), 3.73, 3.63, 3.57, 3.21 (minor DM*S*O peaks), 2.91 (minor DMS*O* peak), −18.85 (small amount of hydride **1***a*), −19.45 (main hydride).

Reaction of 1a *with* $CDCl_3$

On heating **1***a* at 40°C in $CDCl_3$ under Ar, the solution turned from colourless to yellow and contained $IrCl_3(DMSO)_2(DMSO)$ with equal intensity nmr peaks at δ 3.63, 3.52, 2.88 (19), and *mer*-$IrCl_3(DMSO)_3$ with peaks at δ 3.56 and 3.46 (ratio 1:2) (19), as well as $CHDCl_2$ (δ 5.2).

Reaction of 1a *with* O_2 *in* CH_2Cl_2

Complex **1***a* (0.1 g, 0.20 mmol) was dissolved in CH_2Cl_2 (10 mL) and the solution stirred under O_2. After about 1 h, a white solid was filtered off, washed with CH_2Cl_2 and dried *in vacuo* at room temperature (yield 35 mg; ~38% based on an "$Ir(OH)Cl_2(DMSO)_2H_2O$" formulation). Infrared (see text). Nmr (d_6-DMSO): δ 3.35, 3.2-(DM*S*O); see text. *Anal.* calcd. for $C_4H_{15}O_4S_2Cl_2Ir$: C 10.57, H 3.30, O 14.09, S 14.09, Cl 15.61; found: C 11.3, H 3.5, O 13.4, S 13.2, Cl 16.4.

Evaporation of the CH_2Cl_2 filtrate at room temperature yielded a yellow material. Addition of $CHCl_3$ (5 mL) dissolved all but a trace of material that was filtered off; addition of ether (~2 mL) to the filtrate led to slow deposition of a yellow compound (yield 60 mg; ~57% based on an "$IrCl_2(O_2)(DMSO)_3$" formulation). Infrared (see text), μ_{eff} = 1.28 BM; nmr ($CDCl_3$); δ 3.6–3.2(DM*S*O), 3.0–2.8(DMS*O*), 2.6(free DMSO); *Anal.* calcd. for $C_6H_{18}O_5S_3Cl_2Ir$: C 13.61, H 3.40, O 15.12, S 18.15, Cl 13.4; found: C 12.8, H 3.4, O 14.0, S 17.5, Cl 13.9.

[3]Abbreviations used: DMA = *N*,*N*′-dimethylacetamide; DMSO = dimethylsulfoxide (DM*S*O and DMS*O* imply S- and O-bonded, respectively); within structures, S = DM*S*O, and O = DMS*O*.

[4]We have found DMA·HCl a useful reagent for quantitative HCl additions; a crystal structure determination done here in 1976 (R. Ball, R. S. McMillan, B. R. James, and J. Trotter, unpublished) revealed protonation at the oxygen and essential planarity at the carbonyl carbon [—C(O$^-$)=$\overset{+}{\text{N}}$<]; the findings agree with those of a structural paper that has come to our attention recently (23).

*Chloro-*cis*-dihydrido-*mer*-tris(DMSO)iridium(III), $IrH_2Cl(DMSO)_3$ (2)*

The precursor $[IrCl(C_8H_{14})_2]_2$ (0.1 g, 0.11 mmol) was dissolved in dry DMSO (0.4 mL, 5.6 mmol) and CH_2Cl_2 (3 mL) under Ar. Upon introduction of 1 atm H_2 (1 atm = 101.3 kPa), the solution turned colourless; after 5 min, it was concentrated to ~0.5 mL under vacuum, when 1 mL of 2-propanol and sufficient ether were added to give a white, air-stable precipitate. The suspension was cooled for a few hours at −10°C, and then filtered. The product was washed with ether and dried *in vacuo* (yield 70%). Infrared (cm^{-1}): ν(Ir—H) 2177(s), 2087(s), ν(SO) 1128(s), 1120(sh), 1090(m), $\rho_r(CH_3)$ 1035(s), 978(w), ν(Ir—Cl) too weak; nmr ($CDCl_3$): δ 3.57 (s, 6H, DM*S*O), 3.53 (s, 6H, DM*S*O), 3.39 (s, 6H, DM*S*O), −16.3 (d, J = 6Hz, 1H, IrH), −19.5 (d, J = 6Hz, 1H, IrH); *Anal.* calcd. for $C_6H_{20}O_3S_3ClIr$: C 15.53, H 4.34; found: C 15.6, H 4.2.

Reaction of the dihydride with $CDCl_3$ and with DMA·HCl

On leaving the dihydride in $CDCl_3$ at room temperature for 20 h, small amounts of at least two decomposition products were observed: the only monohydride was **1***a* (δ 3.73, 3.57, −18.85); a peak at δ 3.45 may be due to *mer*-$IrCl_3(DMSO)_3$ (see above, **1***a* + $CDCl_3$) although the requisite second peak at δ 3.56 was hidden; $CHDCl_2$ was observed at δ 5.2.

A stoichiometric amount of DMA·HCl reacts rapidly with the dihydride in $CDCl_3$ to give the nmr spectrum shown in Fig. 1. The iridium product is considered to be $IrHCl_2(DMSO)_2(DMSO)$ with *cis*-chlorides, and DMS*O* *trans* to the hydride; nmr: δ 3.56 (s, 6H, DM*S*O), 3.51, (s, 6H, DM*S*O), 2.68 (s, 6H, DMS*O*), −20.60 (s, 1H, IrH); other *in situ* peaks are seen at: δ 2.63 (s, 1H, free DMSO), 3.01 (2, 6H, N—CH_3), 2.16 (s, 3H, C—CH_3). The equivalence of the N—CH_3 groups of DMA must result from proton exchange with unreacted DMA·HCl (the spectrum of DMA·HCl in $CDCl_3$ also shows a single peak for the *N*-methyl groups).

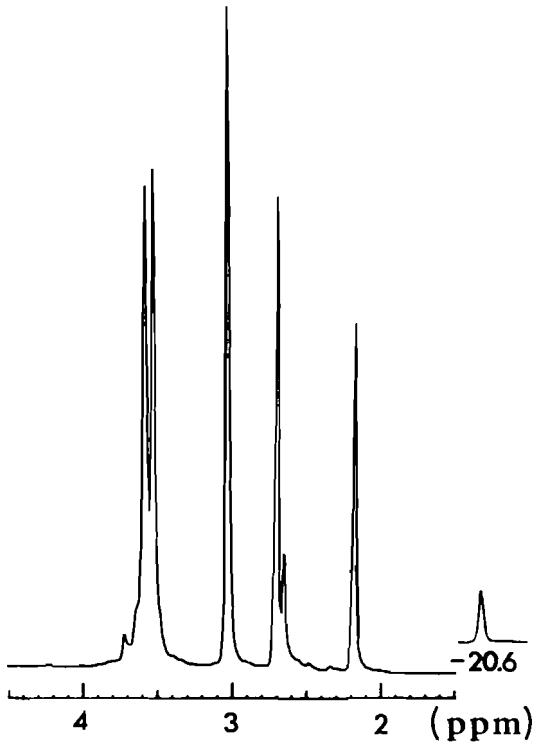

FIG. 1. ^1H nmr spectrum of a $CDCl_3$ solution containing *in situ* products from reaction of $IrH_2Cl(DMSO)_3$ (2) with HCl (added as DMA adduct) at room temperature and 100 MHz.

Results and discussion

Synthesis and characterization of the iridium(III) hydrides

It should be noted first that ^1H nmr and ir spectroscopy have been widely used to distinguish between O- and S-bonded sulfoxide ligands (21, 24), and we have extensively used such procedures in the present work.

The published routes (19) to $IrHCl_2(DMSO)_3$ isomers (**1**) via 2-propanol reduction of the acid complexes $[H(DMSO)_2][IrCl_4(DMSO)_2]$ were first investigated. The precursor *cis* and *trans* acids were readily synthesized from the available starting materials $IrCl_3·3H_2O$ or $IrCl_4$ by slightly modifying the methods of Haddad *et al.* (19). It is not clear whether these workers recognized the nature of the $[Me_2SO..H...OSMe_2]^+$ cation; the ir spectra show the typical broad ν_a(OHO) absorption (1700–600 cm^{-1}) of a symmetrically hydrogen-bonded system (25), with a region of decreased intensity at 1100–900 cm^{-1} and loss of ν(SO) of the cation, a phenomenon that we first encountered in the corresponding *trans*-$[H(DMSO)_2][RhCl_4(DMSO)_2]$ complex (26).

The spectroscopic data for the yellow *cis* and orange *trans* isomers of the Ir acids that we synthesized correspond closely to those given in the literature (19); the formulation of the yellow isomer as the *cis* acid seems reasonable based on its greater stability in polar solvents, and on the relative nmr shifts of the methyl protons (19). The Me_2S formed in our preparation of the *cis* acid may result from an acid-catalyzed decomposition of free or coordinated DMSO; formation and decomposition of hydridoiridium species is not a likely source of sulfide (as demonstrated for a corresponding Rh(III) system (18)), since no reducing agent was present. The only difference between our data and those in the literature (19) for the iridium acids is the melting point and colour of the *trans* isomer (mp 152–154°C, orange vs. 171.5–172°C, pink (19)), indicating different crystalline modifications. Our *trans* complex on warming at 65°C for 15 min in D_2O yielded the aquated species *trans*-$[IrCl_4(DMSO)(D_2O)]^-$, as evidenced by methyl peaks that grow in the ^1H nmr at δ 3.58. This reaction parallels that of the corresponding *trans* Rh acid (21), and supports the stereochemical assignment in view of the high kinetic *trans* effect of S-bonded sulfoxides (24, 27). Only minor amounts of the D_2O product from the *cis* acid were observed under corresponding conditions.

We were unable to generate significant amounts of $IrHCl_2(DMSO)_3$ isomers by the reported 2-propanol reduction of the *cis* or *trans* acids (19), and thus resorted to oxidative addition of HCl (added as the DMA adduct) to solutions containing Ir(I); see eq. [3] (written for a monomeric precursor).

[3] $IrCl(C_8H_{14})_2 + HCl \xrightarrow[-2C_8H_{14}]{DMSO}$ 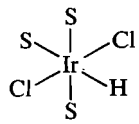

1*a*

$\xrightarrow[-CHDCl_2]{CDCl_3}$ 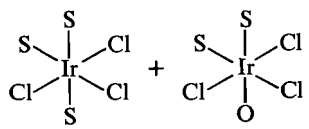

Excess DMSO is required to prevent formation of a mixed C_8H_{14}–DMSO complex that was obtained when a DMSO:Ir ratio of 3 was used; *in situ* ^1H nmr ($CDCl_3$) showed broad peaks of coordinated olefin (δ 4.7, 2.5, 1.5) along with a DMSO peak at δ 3.46. Use of excess HCl led to production of *trans*-

$[H(DMSO)_2][IrCl_4(DMSO)_2]$, presumably by protonation of a coordinated hydride with loss of H_2.

The stereochemistry shown in **1***a*, with *trans* chlorides and *mer*-DMSO ligands, is the only one consistent with the nmr data; other isomers should give three methyl peaks because the two methyl groups in some of the DMSO ligands become magnetically inequivalent. The isolated hydride (**1***a*, τ 28.86, 2180 cm^{-1}; ν(Ir—Cl) 302 cm^{-1}) was white, in contrast to two yellow isomers reported by Haddad *et al.* (19); one of these isomers was considered to be **1***a* by preliminary X-ray data[5], but the spectral data (τ 35.29, 2190 cm^{-1}; 334(s), 300(w) cm^{-1}) were quite different to those of our **1***a* complex. The methyl ^1H nmr resonances of the yellow **1***a* were said to be in the required 2:1 intensity ratio, but unfortunately the δ values were not reported. It is thus difficult to rationalize the differences; indeed, the brief mention of the X-ray work[5] does not specifically state that the DMSO ligands are all S-bonded. The yellow **1***a* had been made from *trans*-$[H(DMSO)_2][IrCl_4(DMSO)_2]$ (19); our efforts with this procedure (see Experimental) gave an *in situ* main hydride resonance at τ 29.45 and a minor one at τ 28.85, with no evidence for a hydride at τ 35.29.

To add to the confusion, the other yellow isomer reported by Haddad *et al.* (19), made by reduction of the *cis*-precursor acid, showed three equally intense methyl resonances in the ^1H nmr (again, δ values were not given), consistent with a *cis*-dichloro geometry; however, the spectral hydride data (τ 28.84, 2180 cm^{-1}) are identical to those for our white **1***a*, although the ν(Ir—Cl) region (335(s), 312(m), 282(m)) is different! Structure **1***b* was preferred over **1***c* for the *cis*-dichloro isomer, largely

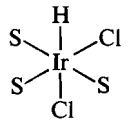

1*b*

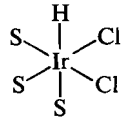

1*c*

because reaction with HCl gave *mer*-$IrCl_3(DMSO)_3$, this assuming that reactions of Ir(III) hydrides with HCl proceed without rearrangement of other ligands (but see below); this has been suggested based on data from corresponding tertiary phosphine systems (29).

Like both the yellow hydrides (19), our white hydride reacts with chalcone (PhCH=CHCOPh) to give the chelated alkyl $Ir[CH(Ph)CH_2C(Ph)O]Cl_2(DMSO)_2$, that has been fully characterized crystallographically (28) and spectroscopically (30). The methyl groups are all inequivalent in the nmr (δ 3.92, 3.50, 3.38, 2.04), and it is worth noting the previously unmentioned large upfield shift of an S-bonded DMSO (δ 2.04), that must result from a ring current of a proximal phenyl group (28). The white hydride decomposes in $CDCl_3$ and generates the products shown in eq. [3]; the nmr data noted for the products in this and previous work (19) allow for a fairly confident assignment of the stereochemistries shown. The expected (31) generation of the *mer*-$IrCl_3(DMSO)_3$ compound provides further indirect evidence for the **1***a* geometry for our white hydride.

A white, *cis*-dihydride $IrH_2Cl(DMSO)_3$, **2**, was prepared in good yield by the oxidative addition of H_2 to the cyclooctene dimer in DMSO (see eq. [1]). The nmr data are consistent only with the stereochemistry shown (see eq. [4] below); the mutually *trans* DMSO ligands contain magnetically inequivalent methyl groups. Haddad *et al.* (19) synthesized a further white isomer of **2** by treating their yellow **1***a* monohydride with aqueous 2-propanol. Their dihydride corresponds to structure **2** but with the DMSO *trans* to hydride being O-bonded; this is reflected in the nmr (δ 2.78 vs. δ 3.39 observed for **2**) and ir (ν_{IrH} 2250, 2170 cm^{-1} vs. 2177, 2087 for **2**), while the nmr data for the DMSO ligands and metal hydride (δ and *J* values) are essentially identical to those for our dihydride. The presence of the O-bonded DMSO in the dihydride of Haddad *et al.* is of interest, considering that full evidence for having all S-bonded DMSO in the precursor yellow **1***a* is not available for evaluation.

The major products of the decomposition of dihydride **2** in $CDCl_3$, eq. [4], are consistent with the assigned stereochemistries, cf. eq. [3], (31).

[4]

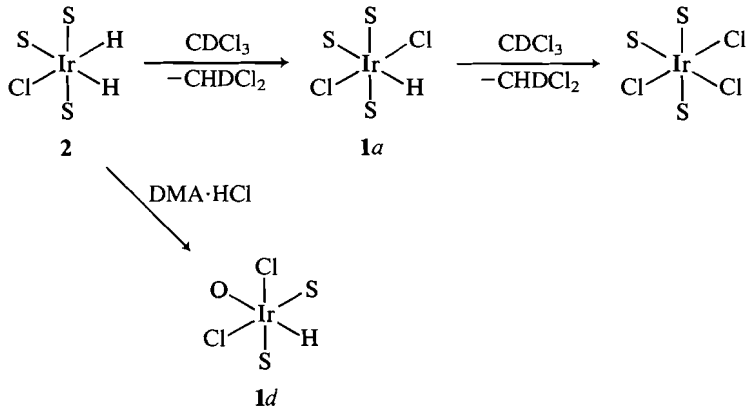

2 **1***a* **1***d*

The reaction of **2** with DMA·HCl results in the quantitative formation of a new monohydride **1***d* that contains O-bonded DMS*O*, eq. [4]; the observed stereochemistry is not consistent with that predicted by the iridium(III) hydride plus HCl "rule" referred to above.

[5]Unpublished work noted in ref. 28.

Reaction of $IrHCl_2(DMSO)_3$ (1a) with O_2

The reaction of **1***a* with O_2 was initially monitored in DMA or CH_2Cl_2 solution using the constant pressure gas uptake apparatus. The stoichiometry (and rates) were followed conveniently at 30°C under 1 atm total pressure (Fig. 2); the uptake curves reveal autocatalytic behaviour, and limited preliminary data in DMA for the maximum rates (Table 1) suggest a second-order

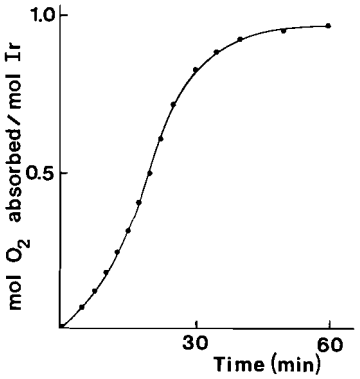

FIG. 2. Uptake of O_2 by DMA solution of $IrHCl_2(DMSO)_3$ (**1***a*) at 30°C, 1 atm O_2; [Ir] = 7.3×10^{-3} *M*.

TABLE 1. Maximum rates for reaction of $IrHCl_2(DMSO)_3$ (**1***a*) with 1 atm O_2 in DMA at 30°C (cf. Fig. 2)

[Ir]$\times 10^3$, *M*	Rate$\times 10^6$, *M* s^{-1}
3.34	1.1
~5.50	2.8
7.30	4.7

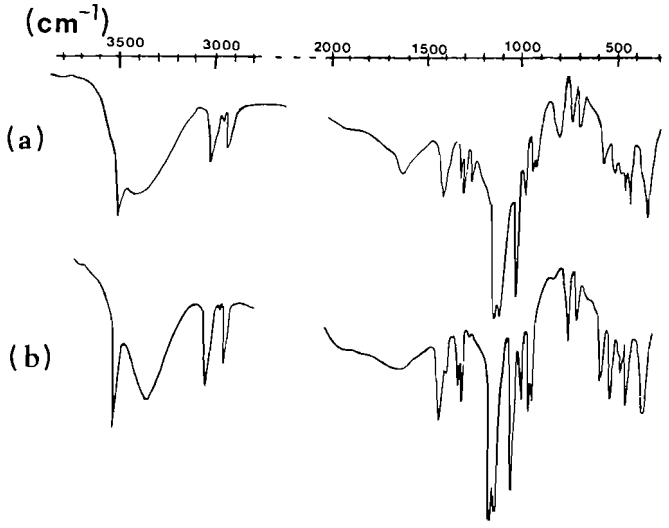

FIG. 3. Infrared spectrum (KBr) of complex **3**. (*a*) Sample dried *in vacuo*; (*b*) same sample, redissolved in DMSO and reprecipitated by addition of CH_2Cl_2.

dependence on metal. The net stoichiometry was invariably 0.95 ± 0.02 mol O_2/mol Ir, which seemed a good harbinger for possible formation of an IrOOH species (cf. eq. [2]). During the reaction in CH_2Cl_2 the initially colourless solution turned yellow and, towards completion of the O_2 uptake, a white precipitate appeared. Samples of the solution or filtrate taken after ~1 h, and analyzed by Karl–Fischer titration, showed the absence of water. Analysis for free DMSO by glc revealed ~0.8 mol/mol Ir; no sulphone ($DMSO_2$), readily identified by ir and mp, and an expected oxidation product (see Introduction), was ever detected.

The white solid is considered to be $Ir(OH)Cl_2(DMSO)_2H_2O$, **3**, (see Experimental). The ir (Fig. 3) reveals ν(OH) at 3500 cm^{-1} and coordinated or lattice water (3600–3100, ~1600 cm^{-1}); bands at 560, 510 cm^{-1}, not present in the hydride precursor, could be water librational modes (32). We had difficulty in obtaining completely satisfactory elemental analyses for **3** because of variable water content. Redissolving a

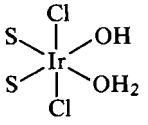

3

sample in DMSO and reprecipitating by adding CH_2Cl_2 gave changes in the ir (Fig. 3) that indicate loss of some water (changes in the 3600–3100, 1600 cm^{-1} regions; the loss of the 800 cm^{-1} band could result from loss of rocking–wagging modes of coordinated water (32)). The strong peak at 310 cm^{-1} is attributed to ν(Ir—Cl).

The metal–hydride bond of **1***a* (ν, 2180 cm^{-1}) has clearly undergone reaction, while the ν(SO) region of **3** is very similar to that of **1***a* and shows DM*S*O ligands. The ^{1}H nmr also reveals the S-bonded sulfoxides (δ 3.35, 3.22); the relative intensities, although comparable, were difficult to estimate because of a variable broad resonance around δ 3.3–2.8 that resulted from the variable water content. In total, the data are most consistent with the geometry shown; the broad ir absorption in the 1700–600 cm^{-1} region is again typical of ν_a(OHO) (see above), and an intra- or intermolecular H-bonded network within **3** is easy to visualize. A noted solubility of **3** in hot DMSO only is in accord with a polymeric type structure.

The other major iridium product formed in the reaction of **1***a* with O_2 was isolated from the yellow CH_2Cl_2 filtrate following removal of **3**. The elemental analysis is reasonable for the formulation $IrCl_2(O_2)(DMSO)_3$, **4**. Of major importance, treatment of **4** with aqueous HCl yielded 6.8 ± 0.1 mol% of H_2O_2 estimated by iodometric titration (7); The O_2, bound as peroxide (within a formally Ir(IV) complex), would generate a theoretical 6.43% of H_2O_2. Comparison of the ir of **4** with that of the residue following HCl treatment shows loss of a band at 795 cm^{-1} (Fig. 4), consistent with loss of coordinated, side-on, η^2 peroxide (33). A Faraday measurement at room temperature gave μ_{eff}=1.28 BM, which is low for a single unpaired electron, but is not unreasonable (34) for a low-spin, pseudo-octahedral d^5 Ir(IV) system (with O_2 occupying 2 sites as peroxide, and one DMSO being a solvate, see below). Furthermore, at room temperature, solid state esr measurement yielded a signal with a sharp component at g=2.11 and a broad component centred at g~4.5; low-spin d^5 complexes in (pseudo)octahedral fields typically give esr signals with $g_\perp > 2.00$ and $g_\parallel < 2.00$ that are detectable more readily at low temperatures (35). The low μ_{eff} value could result from a high spin–orbit coupling constant, which is characteristic of the heaviest ions, and (or) antiferromagnetic interactions. More detailed studies, including temperature dependence data, are needed in order to explain the magnetic properties of **4**. The ir (Fig. 4) reveals S-bonded DM*S*O (1130 cm^{-1}); the 1015 cm^{-1} band could be O-bonded DM*S*O and (or) methyl rocking modes. In CH_2Cl_2 the ir reveals an extra band at 1055 cm^{-1}, attributed to free DMSO, implying perhaps O-bonded DM*S*O or DMSO solvate in the solid state. The ^{1}H nmr spectrum (Experimental) gives paramagnetically broadened signals and is not very satisfactory, but is consistent with the ir data. A broad ir band at ~330 cm^{-1} is assigned to ν(Ir—Cl). Some broad absorption in the 3600–3300 cm^{-1} region (KBr) was considerably reduced in CH_2Cl_2

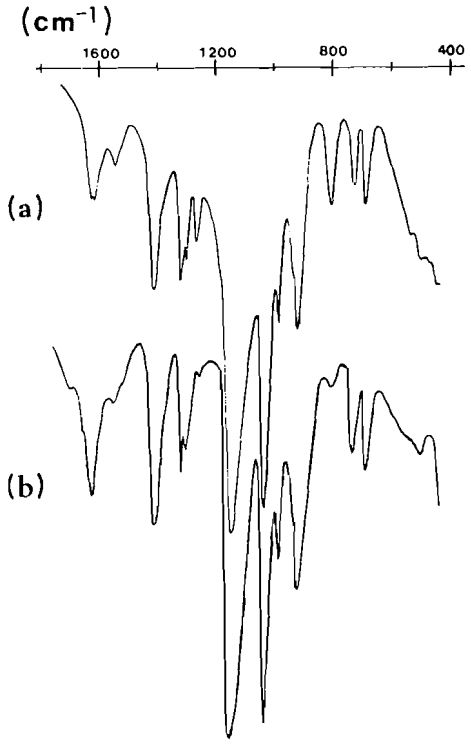

FIG. 4. Infrared spectrum (KBr) of complex **4** (*a*) before and (*b*) after treatment with HCl.

suggesting perhaps some H-bonding interactions in the solid state.

Thus, the favoured formulation of the yellow iridium oxidation product **4** is $IrCl_2(O_2)(DMSO)_2 \cdot DMSO$; its novelty, however, compels us to present this as a very tentative formulation. The possibility of a more realistic, diamagnetic Ir(III)–hydroperoxide formulation, $IrCl_2(OOH)(DMSO)_2 \cdot DMSO$ was considered, and such a species would similarly generate an equivalent of H_2O_2 (5), but the magnetic properties rule this out. An iridium(III) superoxide species would generate only 0.5 equivalents of peroxide, and would in any case be readily identified by esr (36).

Problems in distinguishing between peroxide and hydroperoxide have arisen before (5, 6, 37, 38), and key criteria of —OOH are certain ir bands: 3600–3500(w), ν(OO—H); 1260(w), δ(OO—H); 820(s), ν(O—OH). Sampling by ir the reacting CH_2Cl_2 solutions of $IrHCl_2(DMSO)_3$ under O_2 gave no firm evidence for such bands. It is worth noting that the ir changes in Fig. 3 ($a \rightarrow b$) reveal a loss of accompanying bands at 1260 and 800 cm^{-1}; we have attributed the loss of the 800 cm^{-1} band to removal of water, but presumably removal of some Ir—OOH species by the DMSO treatment could equally well explain the ir changes (including those in the 3500 cm^{-1} region).

It seems established that the final iridium products (**3** and **4**) are not hydroperoxides. Indeed, the overall reaction stoichiometry shown in eq. [5] is quite nicely established on consideration of all the data (no sulphone, no free H_2O, <1 free DMSO per Ir, ~38% of **3**, ~57% of **4**).

The autocatalytic nature of the O_2-uptake plot can be explained qualitatively by slow formation of an Ir(III)(OOH) intermediate that reacts subsequently with precursor **1***a*. The second-order dependence on Ir in the maximum rate region also accommodates such a suggestion, and resembles behaviour of

[5] $3\ IrHCl_2(DMSO)_3 + 3\ O_2 \longrightarrow Ir(OH)Cl_2(DMSO)_2H_2O + 2\ IrCl_2(O_2)(DMSO)_2 \cdot DMSO + DMSO$

1*a* **3** **4**

Co(II) systems that generate bridged-peroxo species via a corresponding $Co(II)O_2 + Co(II)$ pathway (39). In the present system, successive transfers of hydrogen from **1***a* to Ir(OOH) could formally result in **3** with concomitant generation of Ir(II), that subsequently binds O_2 to give the peroxide **4**. It is difficult not to invoke an Ir(OOH) intermediate for the reaction, and implies that the coordinated —OOH prefers to attack a metal–hydride rather than transfer an oxygen atom to coordinated DMSO. The observed catalyzed O_2-oxidation of DMSO to the sulphone via Ir(III) and Rh(III) hydrido(DMSO) complexes (17) thus almost certainly involves either oxygen transfer from M—OOH to free sulphoxide, or generation of free H_2O_2 (via protonation of M—OOH) that is known to effect the oxidation. The reported DMSO oxidation using the yellow **1***a* was effected using air in "hot" aqueous 2-propanol solutions containing excess DMSO.

An Ir—OOH moiety is considered to transfer an oxygen atom to a coordinated alkene via a peroxometallocyclic intermediate to give a ketone product (2); based on recent findings for some related Pt(II) systems (40), prior ionization of the moiety to Ir(III) and OOH^-, and external nucleophilic attack of the anion at the alkene would probably yield epoxide product. A coordinated alkene is more electrophilic than DMSO, and thus not surprisingly the nature of the substrate, and whether it is coordinated or not, will govern its susceptibility to, and mode of, oxidation via M—OOH species.

Concluding remarks

In summary, we have discovered efficient synthetic routes to hydridoiridium(III) species containing sulfoxide ligands via oxidative addition of a protonic acid to a labile, precursor iridium(I) complex in the presence of excess sulfoxide. Corresponding oxidative addition of H_2 yields dihydridoiridium(III) species. Some of the solution chemistry of the hydrides (decomposition in $CHCl_3$, and protonation) is briefly documented, while reactivity of an $IrHCl_2(DMSO)_3$ complex toward O_2 in solution has been studied in some detail. There is no oxidation of the coordinated sulfoxide, which has implications in catalysis utilizing metal–hydroperoxide species. The two iridium oxidation products are tentatively formulated as an aquo(hydroxy)iridium(III) species and a peroxoiridium(IV) species.

Acknowledgments

We thank Johnson, Matthey Ltd. for the loan of iridium, and the Natural Sciences and Engineering Research Council of Canada for financial support in terms of a research grant and a postgraduate scholarship (R. H. M.). Funding from a Guggenheim Fellowship (B. R. J.) supported a collaborative visit to Veszprem.

1. B. R. JAMES. *In* Fundamental research in homogeneous catalysis. Vol. 5. *Edited by* A. E. Shilov. Gordon and Breach, New York. 1986. In press.
2. M. T. ATLAY, M. PREECE, G. STRUKUL, and B. R. JAMES. Can. J. Chem. **61**, 1332 (1983).
3. H. MIMOUN. Angew Chem. Int. Ed. Engl. **21**, 734 (1982).
4. I. TABUSHI and A. YAZAKI. J. Am. Chem. Soc. **103**, 7371 (1981).

5. H. L. ROBERTS and W. R. SYMES. J. Chem. Soc. A, 1450 (1968).
6. L. E. JOHNSTON and J. A. PAGE. Can. J. Chem. **47**, 4241 (1969).
7. G. STRUKUL, R. ROS, and R. A. MICHELIN. Inorg. Chem. **21**, 495 (1982).
8. T. J. COLLINS. (*Editor*). Activation of dioxygen species and homogeneous catalytic oxidation. NATO workshop report. Galzignano. 1984.
9. M. A. ANDREWS and C. F. F. CHENG. J. Am. Chem. Soc. **104**, 4268 (1982).
10. A. R. MIKSZTAL and J. S. VALENTINE. Inorg. Chem. **23**, 3548 (1984).
11. A. M. KHENKIN and A. S. SHTEINMAN. J. Chem. Soc. Chem. Commun. 1219 (1984).
12. E. S. BOYER, D. S. MOORE, S. D. ROBINSON, B. R. JAMES, M. PREECE, and I. THORBURN. J. Chem. Soc. Dalton Trans. 617 (1985), and references therein.
13. B. R. JAMES. Homogeneous hydrogenation. Wiley, New York. 1973. p. 237.
14. B. C. HUI and B. R. JAMES. Can. J. Chem. **52**, 348 (1974).
15. R. C. MICHAELSON. U.S. Pat. 4,347,231, Chem. Abstr. **97**, 147066(1982): U.S. Pat. 4,347,232, Chem. Abstr. **97**, 165497(1982).
16. B. R. JAMES and R. H. MORRIS. J. Chem. Soc. Chem. Commun. 929 (1978).
17. J. TROCHA-GRIMSHAW and J. B. HENBEST. Chem. Commun. 1035 (1968).
18. B. R. JAMES, F. T. T. NG, and G. L. REMPEL. Can. J. Chem. **47**, 4521 (1969).
19. Y. M. Y. HADDAD, H. B. HENBEST, and J. TROCHA-GRIMSHAW. J. Chem. Soc. Perkin Trans. I, 592 (1974).
20. A. VAN DER ENT and A. L. ONDERDELINDEN. Inorg. Synth. **14**, 92 (1973).
21. B. R. JAMES and R. H. MORRIS. Can. J. Chem. **58**, 399 (1980).
22. F. G. HERRING, B. LANDA, R. C. THOMPSON, and C. F. SCHWERDTFEGER. J. Chem. Soc. A, 528 (1971).
23. E. BENEDETTI, B. DI BLASIO, and P. BLAINE. J. Chem. Soc. Perkin Trans. II, 500 (1980).
24. J. A. DAVIES. Adv. Inorg. Chem. Radiochem. **24**, 115 (1981).
25. D. HADZI and S. BRATOS. *In* The hydrogen bond. Vol. 2. *Edited by* P. Schuster, G. Zundal, and C. Sandorfy. North Holland, New York. 1976. p. 567.
26. B. R. JAMES, R. H. MORRIS, F. W. B. EINSTEIN, and A. WILLIS. J. Chem. Soc. Chem. Commun. 31 (1980).
27. Y. N. KUKUSHKIN. Inorg. Chim. Acta **9**, 117 (1974).
28. M. MCPARTLIN and R. MASON. J. Chem. Soc. A, 2206 (1970).
29. J. CHATT, R. S. COFFEY, and B. L. SHAW. J. Chem. Soc. 7391 (1965).
30. H. B. HENBEST and J. TROCHA-GRIMSHAW. J. Chem. Soc. Perkin Trans. I, 601 (1974).
31. R. A. SCHUNN. *In* Transition metal hydrides. *Edited by* E. L. Muetterties. Marcel Dekker, New York. 1971. p. 245.
32. D. M. ADAMS. Metal–ligand and related vibrations. Edward Arnold, London. 1967. p. 238.
33. J. P. COLLMAN and L. S. HEGEDUS. Principles and applications of organotransition metal chemistry. University Science, Mill Valley, CA. 1980. p. 154.
34. F. A. COTTON and G. WILKINSON. Advanced inorganic chemistry. 4th ed. John Wiley and Sons, New York. 1980. p. 948.
35. R. E. DESIMONE and R. S. DRAGO. J. Am. Chem. Soc. **92**, 2343 (1970); O. K. MEDHI and U. AGARWALA. Inorg. Chem. **19**, 1381 (1980).
36. B. R. JAMES, S. R. MIKKELSEN, T. W. LEUNG, G. M. WILLIAMS, and R. WONG. Inorg. Chim. Acta, **85**, 209 (1984).
37. W. P. GRIFFITH and T. D. WILKINS. J. Chem. Soc. A, 397 (1968).
38. R. D. GILLARD, B. H. HEATON, and D. H. VAUGHAN. J. Chem. Soc. A, 3126 (1970).
39. R. G. WILKINS. Adv. Chem. Ser. **100**, 111 (1971).
40. G. STRUKUL and R. A. MICHELIN. J. Chem. Soc. Chem. Commun. 1538 (1984).

The chemistry of the blue stain fungi. Part 1. Some metabolites of *Ceratocystis* species associated with mountain pine beetle infected lodgepole pine[1]

WILLIAM A. AYER, LOIS M. BROWNE, MEOW-CHEN FENG, HELENA ORSZANSKA, AND HOSSEIN SAEEDI-GHOMI
Department of Chemistry, The University of Aberta, Edmonton, Alta., Canada T6G 2G2
Received October 23, 1985

WILLIAM A. AYER, LOIS M. BROWNE, MEOW-CHEN FENG, HELENA ORSZANSKA, and HOSSEIN SAEEDI-GHOMI. Can. J. Chem. **64**, 904 (1986).

Metabolites formed in still culture by *Ceratocystis clavigera, C. ips*, and *C. huntii*, three of the four *Ceratocystis* species associated with the blue stain disease of pine, have been identified. In addition to the ubiquitous fungal metabolites ergosterol, ergosterol peroxide, and fatty acids we have isolated succinic acid, β-phenethyl alcohol (**1**), tryptophol (**2**), prolylleucyl anhydride (**3**), tyrosol (**4**), 3-phenylpropane-1,2-diol (**5**), 6,8-dihydroxy-3-methylisocoumarin (**8**), 6,8-dihydroxy-3-hydroxymethylisocoumarin (**9**), *p*-hydroxybenzaldehyde (**10**), phenylacetic acid (**11**), *p*-hydroxyphenylacetic acid (**12**), phenyllactic acid (**13**), *p*-hydroxyphenyllactic acid (**14**), and 2,3-dihydroxybenzoic acid (**15**). The complex formed by chelation of iron with 2,3-dihydroxybenzoic acid may be responsible, at least in part, for the blue staining of the sapwood of diseased pine.

WILLIAM A. AYER, LOIS M. BROWNE, MEOW-CHEN FENG, HELENA ORSZANSKA, et HOSSEIN SAEEDI-GHOMI. Can. J. Chem. **64**, 904 (1986).

On a identifié les métabolites qui se forment par culture à l'aide de *Ceratocystis clavigera, C. ips* et *C. huntii*, trois des quatre espèces de *Ceratocystis* associées avec la maladie des taches bleues des pins. En plus des métabolites de champignons que l'on retrouve partout, comme l'ergostérol, le peroxyde d'ergostérol et des acides gras, on a aussi isolé de l'acide succinique, de l'alcool β-phényléthylique (**1**), du tryptophol (**2**), de l'anhydride de prolylleucyle (**3**), du tyrosol (**4**), du phényl-3 propanediol-1,2 (**5**), de la dihydroxy-6,8 méthyl-3 isocoumarine (**8**), de la dihydroxy-6,8 hydroxyméthyl-3 isocoumarine (**9**), du *p*-hydroxybenzaldéhyde (**10**), de l'acide phénylacétique (**11**), de l'acide *p*-hydroxyphénylacétique (**12**), de l'acide phényllacétique (**13**), de l'acide *p*-hydroxyphényllacétique (**14**) et de l'acide dihydroxy-2,3 benzoïque (**15**). Le complexe qui se forme par chélation entre le fer et l'acide dihydroxy-2,3 benzoïque pourrait être responsable, au moins en partie, pour la couleur bleue qui se développe sur les pins malades.

[Traduit par la revue]

Fungi belonging to the genus *Ceratocystis* are important pathogens of forest trees, causing such problems as blue stain of conifers (1), oak wilt (2), and Dutch elm disease (3). In western Canada blue stain disease of conifers, so called because the sapwood of the diseased trees is stained a pronounced blue, currently causes death of about 40 million mature pines yearly (4). The disease is spread by the mountain pine beetle (*Dendroctonus ponderosae* Hopk.) (5), which lives symbiotically with a variety of microorganisms (6). The microflora associated with the mountain pine beetle has been the subject of several investigations (7*a–d*) and is reported to consist of yeasts and mycelial fungi including several species of blue stain fungi belonging to the genus *Ceratocystis*. Death of trees affected by blue stain disease results from the combined action of the bark beetle and its blue stain fungi. These organisms live in close mutualistic association. The bark beetle is the vector by which the disease spreads and the means by which the fungi gain access to the phloem and sapwood. The fungi kill the living host tissue, thus preventing resinosis (the production of copious amounts of resin and callus tissue), and this in turn facilitates beetle brood development (8). When the sapwood becomes girdled by blue stain fungi, the region above the infected area becomes water stressed; vital functions decline throughout the tree and it rapidly dies (8, 9*a–d*). The relationship, if any, of the characteristic blue stain in the sapwood to the etiology of the blue stain disease is a controversial question (10). Recently there have been several reports that, *concurrent with the development of blue stain* in the sapwood, the transpiration stream of bark beetle infected trees becomes restricted to the inner portions of sapwood and eventually transpiration fails completely (9, 11).

Currently we are engaged in a study of the metabolites produced by the various blue stain fungi thought to be involved in this disease in an attempt to determine the role that these metabolites may play in tree mortality and symptom expression. Since it has been inferred that water stress and the development of blue stain occur in the same time period (11), we have been especially interested in metabolites that may be responsible for the staining effect. Concurrently others have been reexamining the microflora associated with mountain pine beetle infested lodgepole pine (*Pinus contorta* Dougl. var *latifolia* Engelm.) at various stages of disease development.[2] Four species of blue stain fungi have consistently been isolated: *Ceratocystis clavigera* (Robins.-Jeff *et* Davison) Upadhyay, *Ceratocystis huntii* Robins.-Jeff., *Ceratocystis ips* (Rumb) Moreau, and *Ceratocystis minor* (Hedgc.) Hunt (12). As well, 15 other fungi (*Hormonema dematioides* Lagerb. and Melin, *Phialemonium dimorphosporum* Gams and Cooke, and *Rhinocladiella atrovirens* Nannf. have been positively identified) and ambrosial-like yeasts are frequently observed. In this paper we describe the metabolites produced on artificial medium by one strain of *C. clavigera*, two strains of *C. huntii*, and two strains of *C. ips*. *C. minor* was not included because its metabolites had been investigated previously.

Ceratocystis clavigera was grown in still culture for eight

[1]Presented at the 24th Annual Meeting of the Phytochemical Society of North America. Boston, MA, July 9–13, 1984.

[2]We thank Y. Hiratsuka and A. Tsuneda, Northern Forest Research Centre, Canadian Forestry Service, Edmonton, and L. Sigler, Curator, The University of Alberta Microfungus Collection, for their interest and active cooperation in this regard.

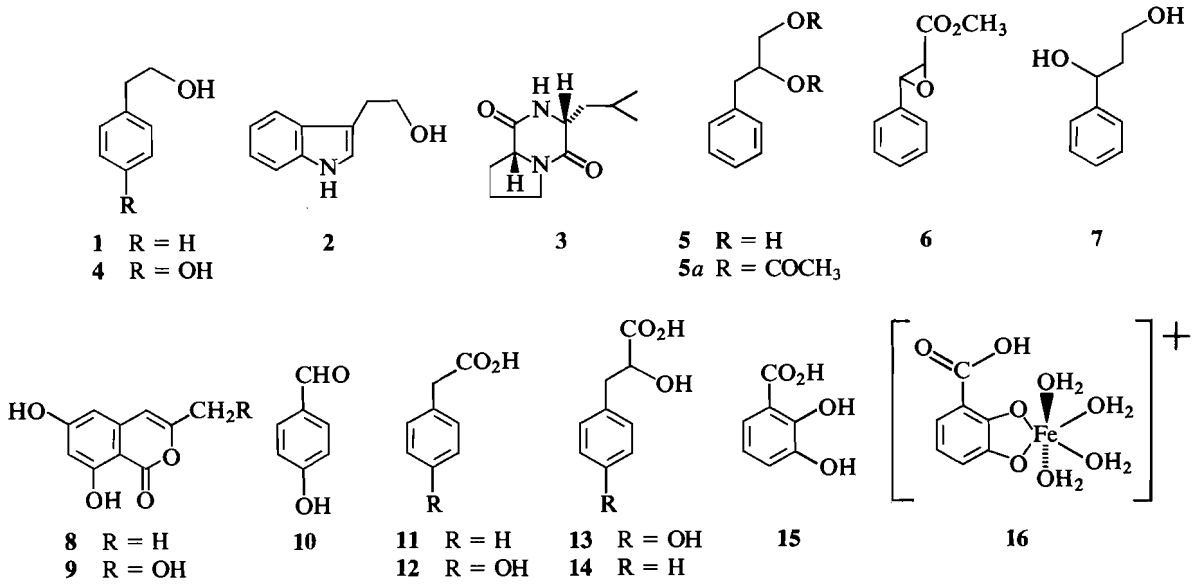

1 R = H
4 R = OH

2

3

5 R = H
5*a* R = $COCH_3$

6

7

8 R = H
9 R = OH

10

11 R = H
12 R = OH

13 R = OH
14 R = H

15

16

weeks. A production study using various media including potato dextrose broth (2.1%), yeast-malt broth (malt extract broth (Difco) 2.5%, glucose 1.3%, yeast extract 0.4%, peptone 0.07%), and V-8 broth (clarified V-8 juice 10% and glucose 1%) was undertaken for this and for each species of *Ceratocystis*. For each species the thin-layer chromatography (tlc) of the 3 broth extracts and 3 mycelial extracts showed the same metabolite production. The media chosen for routine metabolite production were based upon the best yield of extract obtained. In the case of *C. clavigera* a medium consisting of dextrose, malt extract, peptone, and yeast extract gave the best yield of metabolites. The mycelium was separated from the broth and the broth was concentrated at reduced pressure to approximately 5% of its original volume and extracted with ethyl acetate. The mycelium was extracted with methanol and the ethyl acetate soluble portion of the methanol extract was subjected to chromatographic separation. It was found that the mycelial extract contained squalene, linoleic acid, lignoceric acid, palmitic acid, linoleic acid triglyceride, ergosterol, and ergosterol peroxide. Each of these compounds was identified using mass spectrometry (ms), nuclear magnetic resonance (nmr), and infrared (ir) spectroscopy. Identity was confirmed by comparison with authentic samples.

The concentrated broth extract was shown by tlc to be a complex mixture of compounds and was separated by chromatography over silica gel. Squalene and linoleic acid triglyceride were identified as the least polar components of the mixture. The next metabolite isolated, with molecular formula $C_8H_{10}O$, was shown to be β-phenethyl alcohol (**1**), by its spectroscopic characteristics and by comparison with an authentic sample. The mixture also contained a crystalline nitrogen-containing compound with the molecular formula of $C_{10}H_{11}NO$. The melting point (mp) and spectral data for this compound suggested that it was tryptophol (**2**). Its primary hydroxyl function was readily acetylated at room temperature with acetic anhydride in pyridine. The identity of **2** was firmly established by comparison with an authentic sample prepared by $LiAlH_4$ reduction of the methyl ester of indole-3-acetic acid. Tryptophol has been reported as a metabolite of several fungi (13) including *C. fagacearum*, one of the blue stain fungi responsible for oak wilt (2). A second nitrogen-containing compound was present in the broth extract in small amounts. High resolution ms indicated the molecular formula $C_{11}H_{18}N_2O_2$. The base peak in the ms corresponds to the loss of a butene molecule. The ^{13}C nmr spectrum shows amide carbonyls at δ 170.0 and 166.2 as well as peaks at δ 59.0, 53.6, and 45.6, indicating three sp^3 carbons directly bonded to nitrogen atoms. The ^1H nmr spectrum has a singlet at δ 5.94 for the proton of a secondary amide function, an apparent triplet at δ 4.16 for a proton α to both a nitrogen and a carbonyl group, and a double doublet at δ 4.05 for another proton in a similar situation. The spectrum also indicates the presence of three consecutive methylene groups and an isobutyl group. The ir spectrum shows N—H stretching at 3260 cm^{-1} and amide carbonyl absorptions at 1670 and 1635 cm^{-1}. The mp, ir spectrum, and optical rotation are identical with those reported for prolylleucyl anhydride (**3**) (14*a*,*b*). Compound **3** which has been identified as a bitter testing component of sake (15*a*), has also been isolated from cultures of *Nocardia restricta* (15*b*) and reported as one of several phytotoxins produced by *Guignardia laricina*, the fungus responsible for larch shoot blight (15*c*). The major component of the broth extract has the molecular formula $C_8H_{10}O_2$. Inspection of its mp and spectral characteristics suggested that it is tyrosol (**4**). Its phenolic and primary hydroxyl functions were readily acetylated. Tyrosol was prepared from *p*-hydroxyphenylacetic acid by esterification with diazomethane followed by reduction with $LiAlH_4$. Comparison of the synthetic material with the natural product confirmed its identity. Tyrosol has been reported to possess phytotoxic activity against rice and germination inhibitory activity against lettuce seeds (16). The most polar metabolite isolated from the broth extract has the molecular formula $C_9H_{12}O_2$. Its ir spectrum shows a strong hydroxyl absorption at 3370 cm^{-1}. The ^1H nmr spectrum shows a complex multiplet for 5 aromatic protons centered at δ 7.27. It also displays a multiplet at δ 3.97 and a pair of double doublets at δ 3.72 and 3.54, suggesting the presence of a 1,2-diol group. Benzylic protons appear as doublets at δ 2.82 and 2.79. The spectral evidence suggests that the compound is 3-phenyl-1,2-propanediol (**5**). The diacetyl derivative **5***a* was prepared and shows spectral properties consistent with the assigned structure. Confirmation of the structure was obtained by synthesis. Cinnamic acid was esterified with diazomethane and the resulting methyl cinnamate was transformed to the epoxide **6** by treatment with *m*-chloroperbenzoic acid. Reduction of **6** with

$LiAlH_4$, provided 3-phenyl-1,2-propanediol (**5**) as well as a small amount of 3-phenyl-1,3-propanediol (**7**). To the best of our knowledge, 3-phenyl-1,2-propanediol has not previously been reported as a fungal metabolite.

The metabolites of two strains of *C. ips* were investigated. The differences observed between isolates are detailed in the Experimental. *C. ips* was grown in still culture in potato dextrose broth for eight weeks. The mycelium was separated from the broth and each was extracted as previously described. The mycelial extract was fractionated by chromatography over silica gel. It was found to contain a mixture of fatty acids and ergosterol peroxide. The fatty acid mixture was esterified with ethereal diazomethane and subjected to gas chromatography – mass spectral analyses. Eight peaks were observed in the gas chromatogram and the methyl esters of the following acids were identified: lauric palmitic, oleic, pentadecanoic, stearic, linoleic, linolenic, and heptadecanoic acids.

The broth was separated into neutral and acidic fractions and each fraction was subjected to chromatography over silica gel. The acidic fraction consisted mainly of one crystalline compound, which was identified a succinic acid. The neutral fraction was found to contain tyrosol (**4**) and about eight other compounds. The least polar components, **A** ($C_{10}H_8O_4$, mp 240–242°C) and **B** ($C_{10}H_8O_5$, mp 223–226°C) showed similar fragmentation patterns in their ms. The ir spectrum of each compound showed the presence of hydroxyl and α,β-unsaturated carbonyl functionality. The ^1H nmr spectra of **A** and **B** are very similar and reveal that a vinylic methyl group in the spectrum of **A** is replaced by a vinylic hydroxymethyl group in **B**. The molecular formulas, melting points, and spectral characteristics of **A** and **B** indicated that they are the isocoumarins **8** and **9**, respectively, metabolites that have previously been isolated from *C. minor*, the blue stain fungus associated with the southern pine beetle (17). The more polar fractions consisted of several simple aromatic compounds. One component was identified as *p*-hydroxybenzaldehyde (**10**) by comparison with an authentic sample. Two other components, **C** ($C_8H_8O_2$, mp 75–77°C) and **D** ($C_8H_8O_3$, mp 148°C) show similar fragmentation pätterns in their ms. The ir spectra of **C** and **D** show absorption bands characteristic fo a carboxylic acid. The ^1H nmr spectra indicated that **C** was phenylacetic acid (**11**) and **D** was *p*-hydroxyphenylacetic acid (**12**). These structural assignments were confirmed by comparison with authentic samples. Very small quantities (1 mg of each) of two very polar aromatic compounds, $C_{11}H_{12}O_5$ and $C_{12}H_{14}O_5$, and a phenolic acid, $C_{10}H_{10}O_5$, were isolated but were not identified.

We employed a rapid qualitative test to measure stem water conductivity in lodgepole pine seedlings. The stems of lodgepole pine seedlings were cut under water and the cuttings were placed in vials containing either test solution or control solvent. When metabolites produced by the blue stain fungi were isolated in sufficient quantity, their effect on stem water conductivity was measured. Several sets of replicate tests using three different concentrations of test solution were carried out for each of the following: *C. clavigera* broth and mycelial extracts, *C. ips* broth and mycelial extracts, *C. huntii* broth and mycelial extracts, ergosterol. ergosterol peroxide, tryptophol (**2**), tyrosol (**4**), *p*-hydroxybenzaldehyde (**10**), and 4-hydroxyphenyllactic acid (**13**). None of the metabolites tested (except **10**, which gave a weakly positive test) caused any pronounced effect in the bioassay, although the crude broth extracts and the crude mycelial extracts showed weak to moderate inhibition of water uptake. The differences between the individual metabolites and crude extracts in the bioassay may be due to synergistic effects of the metabolites or to difficulties in resolubilizing the crude extracts.

At this stage in the chemical investigations we sought further leads from biological studies as to where to focus our attention. Because of the complex nature of the disease it has not yet been possible to determine which, if any, of the *Ceratocystis* species is principally responsible for the death of the trees. Aware that the correlation between blue stain and failing transpiration may be faulty, we decided to study further the fungi which most rapidly caused the blue staining of pine chip medium and of pine bolts (18) inoculated with the individual fungi. It was found that *C. minor* caused staining most rapidly, followed by *C. huntii*. *C. clavigera* causes staining only slowly, and *C. ips* not at all. Since the metabolites of *C. minor* had been reported previously (17), we turned our attention to *C. huntii*.

Two stains of *C. huntii* were examined. *C. huntii* was grown in still culture in potato dextrose broth for eight weeks and extracted as before. The mycelial extract was fractionated by chromatography over silica gel. It was found to contain sterols, mainly ergosterol peroxide, fatty acids, and small amounts of tyrosol (**4**). Concentration of the broth extract yielded a white crystalline precipitate and a gummy residue. The crystalline precipitate, recrystallized from chloroform, was identified as succinic acid. The gummy residue was separated into neutral and acidic fractions by acid–base extraction and each fraction was subjected to chromatography over silica gel. The neutral fraction contained mainly one component, which was purified by crystallization from benzene, and identified as *p*-hydroxybenzaldehyde (**10**). The acidic fraction yielded further succinic acid and a residue, which was subjected to flash chromatography over silica gel. Only partial separation was achieved since succinic acid co-elutes with the small quantities of the other acids present in the extract. Other chromatographic techniques were investigated but simplification of the mixture by chromatography was not achieved. Further separation was accomplished by fractional crystallization from benzene – Skellysolve B to give three acids, **A**, **B**, and **C**. Compounds **A**, $C_9H_{10}O_4$, and **B**, $C_9H_{10}O_3$, are closely related compounds, as indicated by their ms. The ir spectra of both compounds show the presence of a carboxylic acid group. Their ^1H nmr spectra reveal that **A** is a *p*-substituted aromatic acid whereas **B** is its unsubstituted analog. On this basis and by comparison with authentic samples **A** was identified as (+)4-hydroxyphenyllactic acid (**13**) and **B** was identified as (+)-phenylactic acid (**14**). Both **13** and **14** are known oxidative enzyme inhibitors (19). Compound **C**, $C_7H_6O_3$, was identified (ms, ir, nmr) as 2,3-dihydroxybenzoic acid (**15**). Identity was confirmed by comparison with an authentic sample.

2,3-Dihydroxybenzoic acid (**15**) is a known iron-chelating agent (20) and it gives a bright blue color in the presence of ferric chloride. 2,3-Dihydroxybenzoic acid derivatives are common metabolites of microbes that have developed iron transport systems involving iron chelating agents, and which are called siderophores (21). We feel that the blue stain of the sapwood of infected lodgepole pine may be due, at least in part, to the siderophore **16** formed by chelation of iron with compound **15**. We are able to artificially induce blue staining on lodgepole pine by treating shavings of sapwood with a methanol solution of **15** and then adjusting the pH to near neutrality. Compound **15** also forms a greenish-brown complex with cobalt ions in weakly acid or basic medium; thus other metal complexes may be involved in the color formation.

In this paper we have described the metabolites produced by three of the four species of *Ceratocystis* responsible for blue staining of sapwood in blue stain diseased pine. 2,3-Dihydroxybenzoic acid (**15**) is probably the compound responsible for the staining effect of *C. huntii* since **15** readily forms a blue-colored siderophore in the presence of iron. None of the metabolites previously reported from *C. minor* (17) possesses the structural features for siderophore formation. Compounds **8** and **9**, which we also isolated from *C. ips*, do not show any apparent staining in the presence of iron. We, therefore, decided to reexamine the metabolites produced by *C. minor* and these results will form the topic of a separate communication. In the accompanying paper we report the results of a study undertaken to test the hypothesis that chelating metabolites produced by *Ceratocystis* species affect the essential metal balance, especialy that of iron, in diseased lodgepole pine.

Experimental

High resolution mass spectra were recorded on an A.E.I. MS-50 mass spectrometer coupled to a DS 50 computer. Unless diagnostically significant, only peaks greater than 20% of the base peak are reported. Infrared spectra were recorded on a Nicolet 7199 FT spectrometer. High field ^{1}H nmr spectra were recorded on a Bruker WH-200 or WH-400 spectrometers with an Aspect 2000 computer system. Optical rotations were obtained on a Perkin Elmer 141 polarimeter. Melting points were determined on a Fisher–Johns melting point apparatus and are uncorrected. E. Merck silica gel 60 (230–400 mesh) was used for flash column chromatography. Analytical thin-layer chromatography (tlc) was carried out on BDH precoated plates of silica gel 60 PF 254, with visualization by ultraviolet light or 5% phosphomolybdic acid in 5% sulfuric acid, followed by careful charring on a hot plate. All solvents were distilled prior to use. Skellysolve B refers to Skelly Oil Company light petroleum, bp 62–70°C.

Fungal strains

The blue stain fungi used in this study were obtained from Y. Hiratsuka, Northern Forest Research Center, Edmonton, and deposited with L. Sigler, Curator, The University of Alberta Microfungus Collection (UAMH).

C. clavigera: strain C837 (UAMH 4818) isolated by A. Tsuneda from *P. contorta* growing in southern Alberta in June 1983.

C. ips, formerly *C. montia*: strain C450 (UAMH 4910) isolated by R. C. Jeffrey from *P. contorta* growing in B.C. in August 1962 and strain C852 (UAMH 4838) isolated by A. Tsuneda from *P. contorta* growing in southern Alberta in June 1983.

C. huntii: strain C451 (UAMH 4997) isolated by R. C. Jeffrey from *P. contorta* growing in Alberta in August 1962, deposited at the Mycological Herbarium, Biosytematics Research Institute, Department of Agriculture, Ottawa, Canada (DAOM 90235) and C840 (UAMH 4825) isolated by A. Tsuneda from *P. contorta* growing in southern Alberta in June 1983.

Fungal strains were maintained at 4°C in slant tubes containing Difco potato dextrose agar. An aqueous suspension of mycelium was used to inoculate two potato dextrose agar plates. After 7–10 days at 17°C the culture was blended in a Waring blender with approximately 200 mL of sterile media and 20-mL aliquots were used to inoculate 10 × 1 L sterile media in 1-L Fernbach flasks. After inoculation the still cultures were kept at room temperature for 8 weeks. The culture broth was decanted from the mycelium, concentrated *in vacuo* to about 1 L, and continuously extracted with ethyl acetate for 24 h. The ethyl acetate extract was dried and concentrated to give crude broth extract. The mycelium was air-dried, pulverized, and subjected to Soxhlet extraction with ethyl acetate. The ethyl acetate extract was dried and concentrated to give crude mycelial extract.

Isolation of metabolites

The broth extract (1.8 g) was redissolved in ethyl acetate (150 mL) and extracted with saturated sodium bicarbonate (2 × 15 mL). The bicarbonate extract was washed with chloroform (2 × 10 mL), then cooled with ice and acidified to pH 3 with 6 *N* hydrochloric acid and extracted with chloroform (4 × 50 mL). The chloroform extract was dried (sodium sulfate) and evaporated to form a viscous oil (0.225 g). The ethyl acetate extract left after bicarbonate extraction was washed with water, brine, dried, and concentrated to give neutral material (0.480 g). The neutral material (0.470 g) was chromatographed using gradient elution (0–10% methanol in chloroform) to give, in order of increasing polarity, compounds **1**–**5**.

Phenethyl alcohol (1): Impure phenethyl alcohol obtained from the column was further purified by flash chromatography (eluent benzene – ethyl acetate 4:1) to give pure phenethyl alcohol (10 mg) as a colorless oil; ir(film): 3340, 1600, 1487, 1447, 1040 cm^{-1}; ^{1}H nmr ($CDCl_3$); identical with published spectrum (24); ms *m/z*: 122(M^+, 34), 92(62), 91(100).

Tryptophol (2): Flash chromatography of the impure tryptophol (eluant benzene – ethyl acetate 2:1) provided a crystalline sample of **2**, which was recrystallized from ether – Skellysolve B to give pure **2** (9 mg) as yellow needles, mp 57–58°C; ir(film): 3400, 3300, 1620, 1482, 1453, 1420, 1350, 1335 cm^{-1}; ^{1}H nmr ($CDCl_3$): identical with published spectrum (24); ms *m/z*: 161(M^+, 27), 131(11), 130(100)

Prolylleucyl anhydride (3): Crude anhydride **3** obtained from the original column was further purified by flash chromatography (eluent benzene – ethyl acetate, 1:1) to provide pure lactam **3** (5 mg) as white crystals, mp 147–150°C; $[\alpha]_D^{25}$ −102, (*c* 0.25, $CHCl_3$); ir (film): 3260, 1683, 1670, 1635, 1470, 1435, 1367, 1328, 1300 cm^{-1}; ^{1}H nmr ($CDCl_3$) δ: 5.94 (s, 1H), 4.16 (t, *J* = 8 Hz, 1H), 4.05 (dd, *J* = 4, 10 Hz, 1H), 3.60 (m, 2H), 2.38 (m, 1H), 2.10 (m, 3H), 1.96 (m, 1H), 1.78 (m, 1H), 1.56 (m, 1H), 1.04 (d, *J* = 7 Hz, CH_3), 0.99 (d, *J* = 7 Hz, CH_3); ^{13}C nmr ($CDCl_3$) δ: 170.0, 166.2, 59.1, 53.5, 45.6, 38.8, 28.2, 24.8, 23.3, 22.8, 21.8; ms *m/z*: 210 (M^+, 0.1), 154(100), 86(24), 70(64).

Tyrosol (4): Tyrosol (**4**), mp 91–92°C, was identified by the following spectral properties, ir(film): 3380, 3140, 1590, 1505, 1440, 1350, 1335, 1225, 1097, 1043, 1006 cm^{-1}; ^{1}H nmr($CDCl_3$) δ: 7.12 (d, *J* = 8 Hz, 2H), 6.80 (d, *J* = 8 Hz, 2H), 6.80 (br, s, 1H), 3.84 (t, *J* = 8 Hz, 2H), 2.81 (t, *J* = 6 Hz, 2H); ms *m/z*: 138(M^+, 24), 107(100).

3-Phenyl-1,2-propanediol (5): Impure **5** was subjected to flash chromatography (eluent benzene – ethyl acetate, 1:2) to provide pure 3-phenyl-1,2-propanediol (4.5 mg) as a colorless oil; $[\alpha]_D^{25}$ 0; ir (film): 3370, 1603, 1498, 1455, 1090, 1068 and 1032 cm^{-1}; ^{1}H nmr ($CDCl_3$) δ: 7.27 (5H), 3.97 (m, 1H), 3.72 (dd, *J* = 3.5, 11 Hz, 1H), 3.54 (dd, *J* = 7, 11 Hz, 1H), 2.82 (d, *J* = 1.5 Hz, 1H), 2.79 (d, *J* = 3 Hz, 1H), 2.05 (1H), 1.64 (1H); ms *m/z*: 152 (M^+, 4), 121, 103(19), 192(100), 91(44).

Acetylation of 5: Acetic anhydride (0.25 mL) was added to a solution of diol **5** (3.5 mg) in pyridine (0.5 mL). The reaction mixture was stirred at room temperature overnight. Toluene (5 mL) was added and the solvents were evaporated under reduced pressure. Flash chromatography of the residue (eluent ether – benzene 1:9) provided the diacetate **5***a* as a colorless oil (4 mg); ir (film): 1742, 1498, 1452, 1370, 1225, 1120, 1040 cm^{-1}; ^{1}H nmr ($CDCl_3$) δ: 7.27 (5H), 5.27 (m, 1H), 4.25 (dd, *J* = 3.5, 12 Hz, 1H), 4.02 (dd, *J* = 6, 12 Hz, 1H), 2.10 (s, 3H), 2.06 (s, 3H); ms *m/z*: 177 (M^+, 7), 176(58), 134(100), 133(67), 116(49), 105(24), 92(37), 91(52).

Preparation of diol 5: Cinnamic acid (0.6 g, 4.05 mmol) was dissolved in a 9:1 mixture of ether–ethanol (20 mL). Ethereal diazomethane was added until the yellow color of diazomethane persisted. The solvents were removed at reduced pressure to provide methyl cinnamate (0.65 g) as a colorless oil, which was dissolved in dichloromethane (50 mL). The solution was cooled in an ice bath and *m*-chloroperbenzoic acid (0.84 g) was added. The mixture was stirred at room temperature for 4 days. The reaction mixture was diluted with ether (200 mL) and the solution was successively washed with saturated sodium bicarbonate, water, brine, and then dried (sodium sulfate) and concentrated. The oily residue was purified by flash chromatography (eluent ether – Skellysolve B 1:4) to provide epoxide **6** (0.456 g) and unreacted methyl cinnamate (0.120 g). Epoxide **6** (0.180 g) was dissolved in dry ether and $LiAlH_4$ (0.100 g) was added.

After stirring at room temperature, excess $LiAlH_4$ was destroyed by addition of ethyl acetate. Water (20 mL) was added and the aqueous phase was adjusted to pH 4 by adding 6 *N* HCl. The mixture was diluted with ethyl acetate and the organic phase was separated, washed with water, brine, dried (sodium sulfate), and concentrated. The residue was purified by flash chromatography (eluant ethyl acetate – benzene, 3:1) to give 3-phenyl-1,2-propanediol **5** (0.135 g, 88%). The spectra data obtained for synthetic **5** were identical with that obtained for natural **5**.

Two strains of *C. ips* were investigated. The metabolites isolated were present in both strains (tlc) but quantities of metabolites varied between strains.

A portion of the mycelial extract (1.3 g) was chromatographed over silica gel (180 g). Gradient elution with ethyl acetate – methanol gave two major fractions. The less polar fraction (0.09 g) was purified by rechromatography over silica gel (3 g) and elution with ethyl acetate. It contained one component, which was identified as ergosterol peroxide, mp 163–165°C, by comparison with an authentic sample. A portion of the more polar fraction (0.16 g) was chromatographed over silica gel (20 g) by elution with Skellysolve B – acetone – acetic acid, 150:1:1. A white crystalline component **B** with a wide mp range (50–80°C) was obtained. The tlc of **B** showed a single spot in several solvent systems (R_f 0.7, toluene–acetone – acetic acid 75:25:1; 0.5, ethyl acetate – Skellysolve B – acetic acid 300:1:1; 6.2, chloroform–methanol 1:10). Recrystallization of **B** did not improve the mp range. The ir and ms of the crystalline component suggested that it was a mixture of fatty acids. Thus a portion of the component (0.008 g) was treated with ethereal diazomethane. After evaporation of the ether, the residue was analyzed by gas chromatography (column: 1/8 in × 6 ft., Apiezon on Chromasorb W; carrier gas: N_2, 40 mL/min; column temperature; 200°C; injection port: 250°C; detector: 250°C). Eight peaks were exhibited in the gas chromatogram. This mixture was subjected to gc–ms analysis and the following methyl esters were identified on the basis of their known mass spectral fragmentation patterns: methyl laurate, methyl palmitate, methyl oleate, methyl pentadecanoate, methyl stearate, methyl linoleate, methyl linolenate, and methyl heptadecanoate.

The broth extract (0.130 g) was redissolved in ethyl acetate and separated into acidic (0.149 g) and neutral (0.370 g) fractions by extraction with sodium bicarbonate solution as described before. The acidic fraction was treated with ethyl acetate – chloroform (1:1) and a crystalline compound, mp 187–188°C, identified as succinic acid by comparison with an authentic sample, was removed by filtration. The tlc of the mother liquors showed components present in the neutral extract, thus this fraction was not separated further. The neutral fraction was subjected to chromatography over silica gel. Tyrosol (**4**), identified by comparison with an authentic sample, and eight other components, listed in order of increasing polarity, were separated and identified.

6,8-Dihydroxy-3-methylisocoumarin (8): R_f 0.4 (chloroform – Skellysolve B – methanol, 25:25:1); mp 242–244°C (lit. (17) mp 240–242°C); ir (methanol cast): 3250, 1679, 1629, 1570, 1253 cm^{-1}; ^1H nmr (DMSO-d_6) δ: 2.20 (s, 3H), 6.29 (d, J = 2 Hz, 1H), 6.34 (d, J = 2 Hz, 1H), 6.48 (s, 1H), 10.90 (s, 1H); ms m/z: 192 (M^+, 100), 177(50), 163(10), 121(37).

p-*Hydroxybenzaldehyde (10)*: R_f 0.3 (chloroform – Skellysolve B – methanol, 25:25:1) was identified by comparison with an authentic sample.

6,8-Dihydroxy-3-hydroxymethylisocoumarin (9): R_f 0.5 (chloroform–methanol – acetic acid, 100:3:3); mp 223–226°C (lit. (17) mp 220–225°C); ir (methanol cast): 3200, 1682, 1636, 1500 cm^{-1}; ^1H nmr (acetone-d_6) δ: 6.6 (s, 1H) 6.5 (dd, 2H), 4.6 (s, 1H, D_2O exchange), 11.1 (s, 1H D_2O exchange); ms m/z: 208 (M^+, 99), 177(100), 121(62).

Phenylacetic acid (11): mp 75–77°C, was identified by comparison with an authentic sample.

p-*Hydroxyphenylacetic acid (12)*: mp 148°C, was identified by comparison with an authentic sample.

Compound $C_{11}H_{12}O_5$: R_f 0.5 (ethyl acetate – Skellysolve B – acetic acid, 100:100:1); mp 82–85°C.

Compound $C_{12}H_{14}O_5$: R_f 0.42 (ethyl acetate – Skellysolve B – acetic acid, 100:100:1); mp 112–117°C.

Compound $C_{10}H_{10}O_5$: R_f 0.23 (chloroform – methanol – acetic acid, 100:3:4), mp 138–141°C.

The major metabolites in *C. ips* (UAMH 4910) were compounds **4**, **6**, **7**, **8**, **11**, **12**, and the unidentified metabolites, whereas *C. ips* (UAMH 4838) contained **4**, **6**, **9**, and **10** as its major metabolites.

C. huntii

Two strains of *C. huntii* were examined.

The mycelial extract (0.2 g) was separated by silica gel chromatography utilizing gradient elution with chloroform–methanol. Elution with chloroform gave a crystalline compound (0.039 g, mp 178–179°C), which was identified as ergosterol peroxide by comparison with an authentic sample. Elution with chloroform–methanol (99:1) gave a component (0.045 g) whose spectral properties suggested it was a carboxylic acid. The component was esterified with diazomethane, then purified by chromatography over silica gel (eluent: benzene–ether (95:5)). The methyl ester (0.018 g) was identified as methyl linoleate by comparison with an authentic sample. Finally, elution with $CHCl_3$–methanol (96:4) gave a crystalline compound (2 mg) that was identified as tyrosol (**4**).

The broth extract, which contained large quantities of water soluble compounds, was redissolved in ethyl acetate (50 mL) and set aside in the refrigerator for 24 h. A solid precipitate (1.8 g) separated from the mother liquors. A portion of the white precipitate was recrystallized from chloroform–methanol to give white crystals (mp 188–192°C) identified as succinic acid by comparison with an authentic sample. The mother liquors from the crystallization were concentrated and the residue (6.68 g) was suspended in ethyl acetate (500 mL). The ethyl acetate extract was washed with saturated aqueous sodium bicarbonate (5 × 100 mL). The organic fraction was dried (anhydrous magnesium sulfate) and concentrated to yield neutral and phenolic compounds (0.336 g). The aqueous, alkaline extracts were acidified with 5% hydrochloric acid, then extracted with ethyl acetate (5 × 100 mL), dried (anhydrous magnesium sulfate), and concentrated to yield crude acids (1.20 g). The neutral extract (0.191 g), which was shown by tlc to be a complex mixture, was subjected to flash chromatography over silica gel. Elution with $CHCl_3$ – ethyl acetate – acetic acid (97:2:1) gave a fraction that contained mainly one compound. This material could not be further purified by chromatography but yielded *p*-hydroxybenzaldehyde **10** (0.052 g) after recrystallization, first from benzene – Skellysolve B, then from benzene. Attempts to isolate additional components from this extract were unsuccessful.

The crude acidic extract (1.20 g) was dissolved in $CHCl_3$ – ethyl acetate (1:1) and allowed to stand in the cold for 24 h. A crystalline precipitate (0.105 g) was removed by filtration and identified as succinic acid. The mother liquors were concentrated and subjected to flash chromatography over silica gel eluting with $CHCl_3$ – ethyl acetate – acetic acid (97:2:1). The chromatography resulted in a partial separation; the fractions from the chromatography contained 3 compounds in addition to succinic acid, which co-eluted with the others. No further chromatographic separation could be effected. Fractions 10–20 were combined (0.5 g). Crystallization from benzene – Skellysolve B gave a crystalline compound (**13**) (5 mg). Further crystallization of the mother liquors from benzene – Skellysolve B gave a second crystalline compound (**14**) (3 mg). A final crystallization from benzene – Skellysolve B yielded compound **15** (5 mg). The mother liquors from the crystallizations contained further quantities of the 3 compounds and succinic acid but these could not be further separated. Attempted purification by reverse phase chromatography was unsuccessful.

p-*Hydroxybenzaldehyde (10)*: mp 117–118°C (lit. (22) mp 116°C), was identified by its spectral properties and by comparison with an authentic sample; ir ($CHCl_3$ cast): 3180, 2880, 1678, 1612 cm^{-1}: ^1H nmr ($CDCl_3$) δ: 9.87 (s, C*H*O, 1H), 7.82 (d, J = 9 Hz, 2H), 6.98 (d, J = 9 Hz, 2H), 6.50 (s, O*H* 1H); ms m/z: 122(90), 121(100), 93(42), 65(41).

(+)-4-Hydroxyphenyllactic acid (13): mp 173°C (lit. (23) mp

168°C) gave a positive ferric chloride test and showed $[\alpha]_D$ +8.8° (*c* 0.5, methanol) (lit. (23) $[\alpha]$ +20° (*c* 2.5, ethanol); ir(KBr): 3470, 3240, 3190, 1740, 1610, 1600, 1510 cm^{-1}; ^1H nmr (CD_3OD) δ: 7.40 (d, J = 9 Hz, 2H), 7.02 (d, J = 9 Hz, 2H), 4.46 (dd, J = 4.5, 9 Hz, 1H), 3.14 (dd, J = 4.5, 14 Hz, 1H), 2.93 (dd, J = 9, 14 Hz, 1H); ms m/z: 182(11), 107(100).

*Phenyllactic acid (**14**)*: mp 116°C, $[\alpha]$ +19°C (*c* 0.3, methanol), was identified by its spectral properties and comparison with an authentic sample; ir ($CHCl_3$ cast): 3450, 2896, 2956, 1734, 1610, 1590 cm^{-1}; ^1H nmr ($CDCl_3$) δ: 5.74 (br, s, 2H), 4.78 (s, 1H), 3.38 (dd, J = 4, 8 Hz, 1H), 3.15 (dd, J = 8, 16 Hz, 1H); ms m/z: 166(6), 148(19), 91(100).

*2,3-Dihydroxybenzoic acid (**15**)*: mp 207–210°C, was identified by its spectral properties and by comparison with an authentic sample; ir (methanol cast): 3375, 3040, 2929, 1677, 1657, 1600 cm^{-1}; ^1H nmr (CD_3OD) δ: 7.46 (dd, J = 2, 8 Hz, 1H), 7.00 (dd, J = 2,8 Hz, 1H), 6.74 (t, J = 8 Hz, 1H); ms m/z: 137(9), 108(27), 80(23).

Water uptake bioassay

In this bioassay, the rate of water uptake depends upon the rate of transpiration and is meaningful when the rate of water uptake is relatively large. The seedling is washed free of soil, the root is removed by cutting under water, and the cutting is then immersed in the test solution. After a given time period (which varies according to seedling age), the test solution is replaced with acid fuschin dye for an equal time period. The degree of dye uptake in shoot cuttings that have been treated is measured (cm) and reflects the degree of inhibition of the tested compound on water conduction. Test solutions and control solvent were tested as described above and the measured water uptake is reported as a ratio, length of dye movement for test solution (cm)/length of shoot cutting (cm). In this assay three replicates per solution were tested on 1 and 2 year old lodgepole pine seedlings. The concentration of compound is expressed as fungal concentration, i.e., that isolated from 1 L of culture; 1/2 fungal concentration; and 10 times fungal concentration. In this assay the dye uptake for control solvent gave a ratio of 1. The ratio of dye uptake for metabolite treated seedlings (fungal concentration) divided by dye uptake for solvent treated seedlings: *C. clavigera* broth extract 1.0, mycelial extract 0.6; *C. ips* broth extract 0.5, mycelial extract 0.2; *C. huntii* broth extract 0.5, mycelial extract 0.5; ergosterol peroxide 0.98; succinic acid 1; tryptophol (**2**) 1; tyrosol (**4**) 1; *p*-hydroxybenzaldehyde (**10**) 0.7; 4-hydroxyphenyllactic acid 1; 2,3-dihydroxybenzoic acid (**15**) 1.

Acknowledgments

We wish to thank Dr. Y. Hiratsuka, Northern Forest Research Centre, Canadian Forestry Service, Edmonton for his interest and for cultures of *C. huntii*, *C. ips*, and *C. clavigera*, Anna Szenthe, Department of Chemistry, The University of Alberta, for growing the fungi, Dr. G. Lee, Department of Genetics, The University of Alberta, for helpful discussions, and the Alberta Forestry Service for plant materials. We gratefully acknowledge the financial support of the Natural Sciences and Engineering Research Council of Canada and the Alberta Forest Development Fund.

1. (*a*) L. Safranyik, D. M. Shrimpton, and H. S. Whitney. Forestry Technical Report 1. Canadian Forestry Service, October 1974; (*b*) *In* Management of lodgepole pine ecosystems. Symposium Proceedings. *Edited by* D. M. Baumgarten. 1975. p. 406.
2. (*a*) C. O. Rexode and H. D. Brown. USDA For. Serv. Forest and Insect Disease Leaflet, 1983; (*b*) J. N. Gibbs and D. W. French. USDA For. Serv. For. Exp. Station Res. Paper NC-185, 1980.
3. (*a*) R. J. Stipes and R. J. Campana. (*Editors*). Compendium of elm disease. Am. Phytopathol. Soc., St. Paul. 1981; (*b*) E. S. Kondro, Y. Hiratsuka, and W. B. G. Wagner (*Editors*). Proceedings: Dutch Elm Disease Symposium and Workshop, Winnipeg. 1981.
4. (*a*) B. H. Moody and H. F. Cereske. Northern Forest Research Centre, Canadian Forestry Service, Information Report NOR-X-261, 1984; (*b*) C. S. Wood, G. A. van Sickle, and T. L. Shore. Pacific Forest Research Centre, Canadian Forestry Service, Information Report BC-X-259, 1984.
5. J. H. Borden. *In* Bark beetles in North American conifers. *Edited by* J. B. Mitton and K. B. Sturgeon. University of Texas Press, Austin, TX. 1982. p. 74.
6. (*a*) C. Read. *In* Parasitism and symbiology, an introductory text. Ronald Press Co., New York. 1970; (*b*) W. Trager. *In* Symbiosis. Van Nostrand Reinhold, New York. 1970.
7. (*a*) R. C. Robinson. Can. J. Chem. **40**, 609 (1962); (*b*) R. C. Robinson-Jeffrey and A. H. Grinchenko. Can. J. Bot. **42**, 527 (1964); (*c*) R. C. Robinson-Jeffrey and R. W. Davidson. Can. J. Bot. **46**, 1523 (1964); (*d*) H. S. Whitney. Can. Entomol. **103**, 1495 (1971).
8. H. S. Whitney. *In* Bark beetles in North American conifers. *Edited by* J. B. Mitton and K. B. Sturgeon. University of Texas Press, Austin, TX. 1982. p. 183.
9. (*a*) R. W. Reid. For. Chron. **37**, 368 (1961); (*b*) D. E. Mathre. Contrib. Boyce Thompson Inst. **22**, 363 (1964); (*c*) H. G. Basham. Phytopathology, **60**, 750 (1970); (*d*) T. D. Paine. Can. J. Bot. **62**, 556 (1984).
10. (*a*) S. J. Barras and T. J. Perry. USDA For. Serv. Gen. Tech. Rept. SO-10 (1974); (*b*) H. S. Whitney and F. W. Cobb, Jr. Can. J. Bot. **50**, 1943 (1972).
11. R. G. Ballard, M. A. Walsh, and W. E. Cole. Can. J. Bot. **62**, 1724 (1984).
12. H. P. Upadhyay. *In* A monograph of *Ceratocystis* and *Ceratocystiopsis*. The University of Georgia Press, Athens, GA. 1981.
13. P. Fenn, R. D. Durbin, and J. E. Kuntz. Physiol. Plant. Pathol. **12**, 297 (1978).
14. (*a*) Y. S. Chen. Bull. Agric. Chem. Soc. Jpn. **24**, 372 (1960); (*b*) Y. Kodaira. Agric. Biol. Chem. **25**, 261 (1961).
15. (*a*) I. Belic, A. Cimerman, and H. Socic. Mikrobiologija, **9**, 251 (1972); (*b*) K. Takahashi, M. Tadenuma, K. Kitamoto, and S. Sato. Agric. Biol. Chem. **38**, 927 (1974); (*c*) H. Sato, T. Takashima, N. Otomo, and S. Sakamura. Nippon Nogei Kagaku Kaishi, **56**, 649 (1982).
16. A. Stoessl. *In* Toxins in plant disease. *Edited by* R. B. Durbin. Academic Press, New York. 1981. p. 116.
17. G. W. McGraw and R. W. Hemingway. Phytochemistry, **16**, 1315 (1977).
18. R. W. Hemingway, G. W. McGraw, and S. J. Barras. J. Agric. Food Chem. **25**, 717 (1977).
19. M. Schlamowitz, A. Shaw, and W. T. Jackson. J. Biol. Chem. **243**, 2821 (1968).
20. J. H. Graziano, R. W. Grady, and A. Cerami. J. Pharmacol. Exp. Ther. **190**, 570 (1974).
21. J. B. Neilands. Microbiol. Sci. **1**, 1 (1984).
22. P. G. Stecher (*editor*). The Merck Index. 8th ed. 1968. p. 548.
23. T. K. Narayan and G. R. Rao. Can. J. Microbiol. **22**, 384 (1976).
24. C. J. Pouchert. *In* The Aldrich library or NMR spectra. 2nd ed. 1983.

The chemistry of the blue stain fungi. Part 2. Some essential metal levels of diseased and healthy lodgepole pine

WILLIAM A. AYER, BYRON KRATOCHVIL, ERIC ALLEN, LOIS M. BROWNE, CLAUDE DUFRESNE, DANIEL FIGUEROA, AND ANNA SZENTHE

Department of Chemistry, The University of Alberta, Edmonton, Alta., Canada T6G 2G2

Received October 23, 1985

WILLIAM A. AYER, BYRON KRATOCHVIL, ERIC ALLEN, LOIS M. BROWNE, CLAUDE DUFRESNE, DANIEL FIGUEROA, and ANNA SZENTHE. Can. J. Chem. **64**, 910 (1986).

The concentrations of 13 trace elements were determined in the needles and wood of a closely grouped stand of lodgepole pine infected with blue stain disease. Over 100 samples each of needles and wood from both healthy and diseased trees were analyzed to assess possible correlation between metal levels and degree of infection. Statistical analysis showed no difference in the concentrations of essential trace elements in the wood at the 95% confidence level. Differences were observed at this confidence level in the needles, however, for calcium, iron, zinc, and chromium, calcium being lower and the other three elements higher in the diseased trees. Levels of aluminum, iron, manganese, and calcium in the needles increase 20–30% per year in both diseased and healthy trees.

WILLIAM A. AYER, BYRON KRATOCHVIL, ERIC ALLEN, LOIS M. BROWNE, CLAUDE DUFRESNE, DANIEL FIGUEROA, et ANNA SZENTHE. Can. J. Chem. **64**, 910 (1986).

On a déterminé les concentrations de 13 éléments présents à l'état de trace dans les aiguilles et dans le bois de pins bien regroupés infectés par le maladie des taches bleues. Dans le but d'essayer d'établir une corrélation possible entre les niveaux des métaux et le degré d'infection, on a effectué des analyses sur plus de 100 échantillons tant d'aiguilles que de bois provenant tant d'arbres malades que sains. À un niveau de confiance de 95%, on n'a pas pu noter de différence entre les concentrations des éléments essentiels à l'état de traces. Toutefois, à ce niveau de confiance, on a pu observé des différences dans les aiguilles pour le calcium, le fer, le zinc et le chrome; dans les arbres malades, le niveau de calcium est plus bas alors que les niveaux des trois autres éléments sont plus élevés que dans les arbres sains. Dans les aiguilles, tant des arbres sains que malades, les niveaux d'aluminium, de fer, de manganèse et de calcium augmentent 20–30% par année.

[Traduit par la revue]

Introduction

The disease of pine known as the blue stain disease currently causes the death of about 40 million trees each year in Western Canada (1). The disease is caused by a complex of fungi (2) that are spread by the mountain pine beetle (3). The fungi belong to the genus *Ceratocystis* and the name of the disease derives from the fact that the wood of the diseased trees is stained a pronounced blue color. As part of a collaborative research project with scientists at the Canadian Forestry Service, we have investigated the metabolites produced by these *Ceratocystis* species and this forms the topic of the accompanying paper. The blue coloration appears to be due to the iron chelate of 2,3-dihydroxybenzoic acid (4) and another siderophore isolated from *C. minor* (Hedgcock) Hunt, the structure of which forms the topic of a separate communication.

To test the hypothesis that the blue staining effect and subsequent blue stain disease symptoms (5) are related to metal ion levels, especially iron, we undertook a comparative study of micronutrient element levels of diseased and healthy lodgepole pine (*Pinus contorta* Loudon var *latifolia* Engelm) from one forest stand in southern Alberta. Our method of analyses allowed for the simultaneous determination of multiple element concentrations; thus the measurement of several physiologically important micronutrient metal concentrations, as well as those other elements accessible by the analytical method employed, was undertaken. Xylem sapwood and foliage samples were used in this analysis. Clement and Janin (6) have shown that metal concentrations vary significantly within different areas of the trunk in normal trees, with higher levels occurring in the central ring, then dropping rapidly across the heartwood to the sapwood. Within the sapwood, metal concentrations tend to remain constant. Since the staining of a diseased tree by the blue stain fungi occurs in the sapwood, our sampling of wood tissue was from this area. It is well documented that element concentrations on pine foliage vary with age and position along the crown (7*a*–*c*). For a single growing season nutrient levels are maximum during the summer months, stabilizing in the autumn. Yearly fluctuations arise from variations in moisture conditions and other environmental variables. Our sampling of pine tissue occurred during the summer and took into account tissue age and crown position. There have been few reported studies that compare trace element levels between healthy and diseased pine. On the other hand, several studies (8*a*–*d*) have tried to establish a relationship between environmental pollution and trace element levels observed in healthy and diseased trees. In most cases, however, fewer than three trees have been used for analysis. Because of the inherent tree-to-tree variability and the within-tree variability of element concentrations (7*b*), we chose to study a group of 20 trees, all located within a single stand a short distance from one another.

Experimental

Sample collection

Lodgepole pine (*P. contorta* Loudon var *latifolia* Engelm) located in an area of natural mountain pine beetle infestation near Blairmore, Alberta, were used for this study. The collection day was hot and sunny (25°C) with light winds blowing from the southeast. Samples from closely-grouped diseased (10 trees: tree number(base radius (cm)); 1(10), 2(10), 3(11), 4(11), 5(11), 6(10), 7(10), 8(8), 9(11), 10(9)) and healthy (10 trees: tree number(base radius (cm)); 11(8), 12(9), 13(9), 14(11), 15(11), 16(11), 17(10), 18(9.5), 19(6), 20(11)) trees were obtained.

Each tree was cut at its base. Four 5-cm cross-sections of wood were obtained: one section at the base of the trunk (for diseased trees the blue stain had often spread into the roots), two section about 3 m and 7 m

above the base (in diseased trees this is the area of bark beetle attack), and one section near the base of the crown (for diseased trees this section was just above the upper limit of the stained sapwood). The wood sections were labelled, placed in polyethylene bags, and taken to the laboratory, where three wedge-shaped sections of the sapwood, of about 5 g each, were collected at 120-degree intervals on the circumference of the sections. A total of 125 samples from healthy and 119 samples from diseased trees were obtained.

For each tree, needle samples were obtained from three positions in the crown (low, middle, and apex branches), and insofar as feasible from three ages of tissue (needles produced in 1984, 1983, and 1982 or older). A total of 89 samples from healthy and 53 samples from diseased trees were collected. The diseased trees did not have foliage from 1984, indicating that tree death occurred in the fall of 1983. The needle samples were placed in polyethylene bags, closed with twist ties, and labelled as to tree, position on the tree, and age of needles.

Sample preparation

The wood samples were placed on edge so that both faces of sapwood were exposed to the air for 7 days. Each sample was cut into small pieces (0.3 × 0.3 cm) using a stainless steel blade. The ends of each piece that had been in contact with the chain saw were removed and discarded. The wood pieces were ground to a coarse powder (20 mesh) in a tungsten carbide disk mill (Spex Shatterbox). The wood powder was dried at 85°C for 6 h, then allowed to cool to room temperature in a desiccator over anhydrous calcium sulfate. A sample (1.0 g) was accurately weighed, immediately placed in a dry Erlenmeyer flask (125 mL), and treated with concentrated HNO_3 (15 mL). The mixture was heated to boiling (glass boiling chips) and held at this temperature until it had concentrated to about 1/2 volume. Concentrated HNO_3 (10 mL) was added and the sample was digested and concentrated to a sample volume of 3.5–5 mL. The flask and contents were cooled to room temperature, 70% $HClO_4$ (5.5 mL) was added, and the mixture was heated in a stainless steel fume hood designed for perchloric acid use until dense, white fumes of $HClO_4$ evolved and the solution became colorless (maximum 10 min). The solution was cooled, diluted with doubly distilled water (10 mL), then transferred quantitatively to a volumetric flask (25 mL) and diluted to volume with water. A few clear particles, apparently mineral matter, could be seen in many of the flasks; therefore the solutions were filtered through low porosity, low ash filter paper (Whatman No. 42) into a polyethylene (50 mL) bottle.

The needle samples were dried in open plastic bags on the laboratory bench for 7 days. The dried needles were ground in a tungsten carbide disk mill to a coarse powder (20 mesh), then dried at 85°C for 2 h, and digested as described for the wood above. The digested needle samples contained an insoluble white precipitate of silica (1–3 mg), which was also removed by filtration.

To determine if the knives or grinding mill introduce metal contamination, two wood samples were frozen in liquid nitrogen, ground with a mortar and pestle, and the results compared with those obtained using stainless steel knives and the tungsten carbide disk mill. The only detectable differences observed were with Al, which was about 1 μg/g higher, and with Ni, which was about 0.1 μg/g higher when the knife and disk mill were used. It was concluded that the extent of contamination was sufficiently low that the knife–disk mill method could be used for all the samples.

Analysis

Samples were analyzed by inductively coupled plasma atomic emission spectroscopy (ICP-AE) on a direct reader instrument (Applied Research Laboratories, Model 16000). Plasma operating conditions and flow rates were as follows: frequency 27.12 MHz, forward power 1.25 kW, reflected power 0.05 kW, viewing zone 15 mm above load coil, coolant gas flow rate 10 L/min, auxilliary gas flow rate 0.65 L/min, nebulizer gas flow rate 0.5 L/min. All samples were introduced as aerosols using a standard concentric gas nebulizer. Measurements were made for all the elements listed below; several elements were at or below the detection limits; however, these are not included in the results section. Standard stock solutions (1 000 ppm) of metal salts were prepared by the method of Ward (9) employing the following salts: Al in 6 *M* HCl, $BaCl_2$ in H_2O, H_3BO_3 in H_2O, $CaCO_3$ in 0.5 *M* HNO_3, Cr in 4 *M* HCl, CuO in 4 *M* HNO_3, Fe in 4 *M* HCl, $MgCl_2.6H_2O$ in H_2O, Mn in 4 *M* HNO_3, $NiCl_2.6H_2O$ in H_2O, NaCl in H_2O, and Zn in 4 *M* HNO_3. The following standard solutions prepared from the above stocks were employed: standard 1, water; standard 2, Al, B, Cu, Fe, Mn, Mo, Ni, Zn, 3 ppm each; standard 3, Al, B, Cu, Fe, Mn, Mo, Ni, Zn, 30 ppm each; standard 4, Ba 1 ppm, Ca, Mg 10 ppm each; standard 5, Ba 10 ppm, Ca, Mg, 100 ppm each; standard 6, Na 3 ppm; standard 7, Na 30 ppm; standard 8, Cr 1 ppm; standard 9, Cr 10 ppm; standard 10, NBS pine needles standard reference material 1575, wet digested in the manner described above. Standard solutions of all the elements listed above were aspirated into the plasma at the beginning of data acquisition. These solutions were used to determine the concentration of the elements in the digested wood samples and the elements in the digested needle samples. Integration times were 10 s, and three replicate measurements were performed on each sample and standard solution.

Results and discussion

Results of the analyses are summarized in Table 1 for the needles and Table 2 for the wood. The values in general are similar to those reported by other workers on similar vegetation (7, 8). Because variations in the distribution of the elements also may provide useful information, the factors of needle age and needle and wood location were assessed using a MIDAS statistical package on the University of Alberta Amdahl 5860 computer. The conclusions can be summarized as follows.

No overall differences in the wood samples were observed between diseased and healthy trees by analysis of variance (ANOVA) at the 95% confidence level for any of the elements. Comparison of elements in the individual four wood sections of healthy vs. sick trees by the two sample t-test, however, showed calcium levels to be significantly higher in health sections A, B, and C (0.95 probability) but about the same in healthy and sick trees for section D. No significant trend was found for the other elements tested: B, Mg, Cu, Fe, Zn, Mn, and Ba. On the other hand, differences in the needles were found by ANOVA between diseased and healthy trees at the 95% confidence level for iron, zinc, magnesium, calcium, and chromium. The needles of diseased trees contained 12% less calcium, 15–20% greater levels of iron, zinc, and magnesium, and a four-fold increase in chromium. The magnitude of the differences does not indicate, however, that the blue stain fungi are causing a major perturbation in the levels of essential trace elements except perhaps for chromium.

The levels of aluminum, iron, manganese, and calcium in the needles increase at a rate of 20–30% a year as needle age increases. This trend is seen in both healthy and diseased trees. The accumulation of these trace elements in older foliage tissue has been observed by others (7*b*). The other eight elements studied did not show this trend.

The levels of aluminum and zinc in the needles increase from the base toward the crown of the tree (the overall increase amounting to about 50%), while the levels of calcium and possibly manganese decrease (calcium some 20–30% overall and manganese 15–20% for healthy, and variably for diseased, trees). The other elements showed no statistical change.

For the wood analyses, no trends in elemental composition with vertical location on the trunk were observed for any of the elements measured except magnesium, which shows an increase of 30–40% with height of the section from the ground in both healthy and diseased trees.

TABLE 1. Summary of trace element analyses for needles of diseased and healthy lodgepole pine from southern Alberta[a]

	Year of growth	No. of samples	Location on tree	Al	B	Cu	Fe	Zn	Ni	Mn	Ba	Mg	Ca	Na	Cr
Healthy trees	1984	9	Low	81±35	10±3	5.0±1.3	38±7	29±5	2.2±1.0	213±97	1.4±1.2	1010±113	1228±169	5±1	0.5±0.5
		9	Middle	104±50	12±8	4.6±0.6	41±11	32±6	2.3±2.0	208±111	0.9±0.9	986±136	1136±284	8±7	2±2
		8	High	131±56	14±5	5.3±1.1	46±13	44±10	3.9±4.9	178±78	1.4±1.4	1011±174	938±292	6±2	2±2
Healthy trees	1983	11	Low	117±57	10±2	3.4±1.5	61±16	25±6	1.2±0.6	278±128	2.0±1.4	1025±131	1876±402	9±5	5±6
		10	Middle	122±53	11±3	3.2±0.5	51±12	27±7	1.3±0.6	239±76	1.3±0.8	1031±122	1823±609	11±10	4±6
		10	High	179±65	17±10	4.7±2.5	76±49	42±7	2.1±2.1	231±111	1.1±0.8	1004±196	1530±445	15±15	5±7
Healthy trees	1982	10	Low	139±61	14±10	6±6	77±49	27±8	1.7±1.7	389±211	2.7±1.5	1076±201	2977±783	9±9	5±5
		11	Middle	158±80	16±14	3.5±1.4	63±12	28±7	1.1±0.3	355±165	2.0±0.8	1011±136	2487±713	14±14	4±4
		11	High	194±76	13±6	3.2±0.4	69±24	36±9	1.3±0.8	259±114	1.9±1.6	1037±240	1942±577	11±9	6±6
Overall	(1982–1983)	63		151±70	13±8	4±3	66±30	31±10	1.8±1.8	290±140	1.8±1.3	1030±160	2100±800	10±10	4±4
Diseased trees	1983	9	Low	125±46	12±3	3.7±1.1	64±11	28±5	1.3±0.5	220±91	1.8±0.4	1167±211	1603±403	24±13	15±2
		9	Middle	159±70	14±7	4.8±2.6	72±26	35±7	1.6±0.9	227±102	1.8±0.6	1146±143	1590±250	30±23	15±2
		8	High	178±59	25±22	5.4±2.1	77±18	48±9	2.0±1.2	195±58	1.3±0.6	1179±142	1316±183	32±32	15±2
Diseased trees	1982	9	Low	158±59	18±18	3.5±1.3	73±10	30±9	1.2±0.5	273±105	2.3±0.6	1234±249	2211±642	32±32	15±2
		9	Middle	196±62	16±6	3.2±1.6	83±19	36±16	1.8±1.8	319±164	2.4±0.7	1276±162	2515±537	23±17	16±1
		9	High	229±83	17±4	4.4±2.0	92±20	50±16	1.3±0.6	230±103	2.4±1.5	1300±243	1898±506	30±13	16±1
Overall		53		174±70	17±13	4±2	77±20	38±14	1.5±1.0	245±110	2.0±1.9	1220±200	1870±600	28±22	15±2
NBS SRM/1515	found[b]			512±110	12±1	3.0±0.1	146±10	69±4	3.0±0.4	598±40	8.0±0.6	1100±100	3900±300	26±1	2.0±1
	cert. val.[c]			545±30	—	3.0±0.3	200±10	—	(3.5)	675±15	—	—	4100±200	—	2.6±0.2
	lit. compiled val.[d]			491(2)	17(1)	—	—	—	2.2(1)	—	6.6(2)	—	4300(2)	40(2)	2.4(1)

[a]Values are averages and standard deviations in μg/g (ppm).
[b]Averages and standard deviation of two measurements on one sample solution.
[c]Provided by NBS. Uncertainties are 95% tolerance levels.
[d]Value compiled from analyses reported in literature (11). Number of independent reports in parentheses after values.

TABLE 2. Summary of trace element analyses for wood of diseased and healthy lodgepole pine from southern Alberta[a]

	No. of samples	Location on trees	Al	B	Cu	Fe	Zn	Ni	Mn	Ba	Mg	Ca	Na	Cr
Healthy trees	31	A	12±5	4±4	4±4	18±11	11±11	1.3±1.0	42±22	4±4	159±21	520±100	16±20	10±7
	30	B	11±3	2±2	4±4	20±13	7±5	1.5±1.1	38±16	4±4	174±23	520±64	13±12	10±7
	32	C	11±3	5±5	3±2	24±24	9±5	1.4±1.1	44±17	5±5	185±27	540±70	13±13	10±7
	32	D	11±3	8±8	6±6	17±10	7±3	1.3±0.9	48±16	2±1	205±41	530±61	17±17	10±7
Overall	125		11±3	5±5	5±5	20±16	9±9	1.5±1.0	43±18	4±4	181±34	530±74	15±15	10±7
Diseased trees	30	A	12±6	10±10	2.9±1.3	20±16	6±5	3±3	35±18	4±3	165±25	480±56	21±21	6±6
	30	B	12±3	6±6	3.2±1.4	19±11	9±19	1.9±1.9	37±16	3±2	176±28	490±58	14±14	5±5
	29	C	12±4	5±5	3.2±1.3	20±15	5±4	1.5±1.3	38±13	4±4	180±29	490±63	13±12	5±5
	30	D	16±16	6±6	3.3±2.1	22±22	7±7	1.5±0.7	40±16	3±2	231±48	520±76	18±18	6±6
Overrall	119		13±10	7±7	3.1±1.5	20±16	7±8	2±3	37±16	4±3	188±42	500±65	17±17	5±5

[a]Values are averages and standard deviations in μg/g (ppm).
[b]Section taken nearest ground denoted by A; section just under crown by D; sections B an

In addition to the above observations, an attempt was made to further reduce the effect of variability from highly localized parameters such as soil composition or drainage, by pairing diseased and healthy trees located near each other and performing statistical analysis on the pairs. Precision was not measurably improved, and so additional information could not be obtained by this approach. In fact, we found that trace element levels tended to differ significantly between adjoining healthy (or diseased) trees. It has been observed previously that tree-to-tree variability and within-tree variability of foliage are the main causes of deviation among foliar analyses for major and trace elements (8*b*,*c*). Statistically significant differences in trace element levels between healthy and diseased trees are thus difficult to detect, especially since reported trace element levels normally encompass a fairly wide range.

In conclusion, the magnitude of the natural variability of trace elemental composition of lodgepole pine is sufficiently great that within-tree differences in element levels that may be induced by fungal infection cannot be detected with a high degree of confidence. Previously we reported (4) that several species of blue stain fungi implicated in the blue stain disease of pine produce siderophores. Studies over the last several decades on the effects of chelating agents in plant nutrition have shown that the use of excess chelating agent can be toxic to plants (10*a*–*c*). Absorption of the chelator by the plant facilitates the movement of metals through the plant (11). Slight excesses of iron chelators produce increased iron uptake by plants as a result of an iron stress response (12). These studies are consistent with our findings: iron chelating agents are metabolites of blue stain fungi, and the foliage of blue stain diseased lodgepole pine shows increased levels of iron with respect to foliage of healthy lodgepole pine. It is interesting to note that other wilt diseases caused by microbes (13), e.g. *Fusarium*, produce wilt toxins that seem to chelate micronutritients and induce deficiencies and metal imbalances. Tree pathologists have observed that elms compartmentalize wood infected by the blue stain fungus that causes Dutch elm disease (14). In fact metal imbalances may serve as the "trigger" through which wilt diseases induce the tree to wall off and isolate (compartmentalize) wood infected by such fungi.

Acknowledgments

We wish to thank Mr. R. Miyigawa, Alberta Forestry Service, Edmonton, for help with plant material; Drs. I. Edwards and P. Addison, Northern Forest Research Center, Canadian Forestry Service, Edmonton, for helpful discussions; Mrs. L. Linarez for technical assistance in sample preparation; Mr. Y-B Shao for the ICP-AE analyses; Mrs. M. Duke for the analysis of the statistical data; and the Natural Sciences and Engineering Research Council of Canada for financial support.

1. (*a*) B. H. Moody and H. F. Cereske. Northern Forest Research Centre, Canadian Forestry Service, Information Report NOR-X-261, 1984; (*b*) C. S. Wood, G. A. van Sickle, and T. L. Shore. Pacific Forest Research Centre, Canadian Forestry Service, Information Report BC-X-259, 1984.
2. (*a*) R. C. Robinson. Can. J. Chem. **40**, 609 (1962); (*b*) R. C. Robinson-Jeffrey and A. H. Grinchenko. Can. J. Bot. **42**, 527 (1964); (*c*) R. C. Robinson-Jeffrey and R. W. Davidson. Can. J. Bot. **46**, 1523 (1964); (*d*) H. S. Whitney. Can. Entomol. **103**, 1495 (1971).
3. J. H. Borden. *In* Bark beetles in North American conifers. *Edited by* J. B. Mitton and K. B. Sturgeon. University of Texas Press, Austin, TX. 1982. p. 74.
4. W. A. Ayer, L. M. Browne, M. C. Feng, H. Orszanska, and H. Saeedi-Ghomi. Can. J. Chem. **64**, 904 (1986).
5. (*a*) R. G. Ballard, M. A. Walsh, and W. E. Cole. Can. J. Bot. **62**, 1724 (1984); (*b*) T. D. Paine. Can. J. Bot. **62**, 556 (1984).
6. A. Clement and G. Janin. Plant Soil **45**, 543 (1976).
7. (*a*) I. K. Morrison. Can. J. For. Res. **2**, 89 (1972); (*b*) M. Raupach. *In* Trace elements in soil–plant-animal systems. *Edited by* D. J. Nicholas and E. R. Egan. Academic Press, New York. 1975. p. 353; (*c*) A. L. Leaf. *In* Soil testing and plant analysis. *Edited by* L. M. Walsh and J. D. Beaton. Soil Science Society of America. Madison, WI. 1973. p. 427.
8. (*a*) R. E. Tout, W. B. Gilboy, and N. M. Spyron. J. Radioanal. **37**, 638 (1975); (*b*) J. Sheppard and W. Funk. Environ. Sci. Technol. **9**, 638 (1975); (*c*) J. Baker. Northern Forest Research Centre, Canadian Forestry Service, Information Report NOR-X-194, 1977; (*d*) C. F. Baes and S. B. McLaughlin. Science, **224**, 494 (1984); (*e*) G. P. Giuffre and R. Litman. J. Environ. Sci. Health, Part A, **14**, 65 (1977).
9. A. F. Ward. Technical Aid Note #4, Fisher Scientific Co., Waltham MA. 02154.
10. (*a*) E. Rogers. J. Am. Soc. Hortic. Sci. **100**, 531 (1975); (*b*) A. Wallace and R. T. Mueller. Hortic. Sci. **7**, 121 (1972); G. A. Wallace and A. Wallace. J. Plant Nutr. **6**, 461 (1983).
11. P. E. Powell, P. J. Szaniszlo, G. R. Cline, and C. P. Reid. J. Plant Nutr. **5**, 653 (1982).
12. A. Wallace. Soil Science **133**, 319 (1982).
13. A. Wallace. J. Plant. Nutr. **6**, 423 (1983).
14. A. L. Shigo. Sci. Am. 96 (1985).

Ab Initio SCF MO calculations on the reaction of hydroxyl radical with cytosine

BEVERLEY G. EATOCK, WILLIAM L. WALTZ, AND PAUL G. MEZEY

Department of Chemistry, University of Saskatchewan, Saskatoon, Sask., Canada S7N 0W0

Received September 5, 1985

BEVERLEY G. EATOCK, WILLIAM L. WALTZ, and PAUL G. MEZEY. Can. J. Chem. **64**, 914 (1986).

Ab initio calculations have been carried out on the relative stabilities of various possible products of the reaction between cytosine and the OH radical. These products are of importance in modelling radiation damage to living tissues. The preferred theoretical gas-phase addition site is the C6 ring atom according to these calculations. The analysis of a series of possible contributions to solvent effects strongly suggests the predominance of intermolecular H bonds in stabilizing the experimentally observed C5 adduct.

BEVERLEY G. EATOCK, WILLIAM L. WALTZ, et PAUL G. MEZEY. Can. J. Chem. **64**, 914 (1986).

On a effectué de calculs *ab initio* sur les stabilités relatives de divers produits possibles pour la réaction de la cytosine avec le radical OH. Ces produits sont importants dans l'élaboration d'un modèle pour les dommages dûs à la radiation dans les tissus vivants. D'après ces calculs théoriques, le site préféré pour l'addition en phase gazeuse est l'atome de carbone C6. L'analyse d'une série de contributions possibles aux effets de solvant suggère fortement la prédominance de liaisons hydrogènes intermoléculaires dans la stabilisation de l'adduit en C5 qui est observé expérimentalement.

[Traduit par la revue]

Introduction

Radiation damage to nitrogen heterocycles has attracted interest due to the relevance of such effects for biologically important systems. As an extension of studies on the reactions of OH radicals with N heterocyclic systems (pyridine, imidazole) (1, 2), we have investigated the attack of OH on the pyrimidine base cytosine. Experimental results on the reaction of OH with cytosine agree that ring addition occurs (3,4), but information on site preference for addition is obtained only by indirect methods (esr, pulse radiolysis) leaving results open to some controversy. *Ab initio* calculations, however, provide a direct aid to identification of favored product isomers, and have been shown to be useful in past studies, supplementing experimental results (1,2,5,6).

Radiation damage to cytosine is of interest because of its status as a component of DNA. Consideration of the N bases of DNA as subjects for *ab initio* studies favors the pyrimidines, both because of their greater susceptibility to OH attack (7) and the simpler problem that the electronic structure of the pyrimidines represents, as compared to the purine bases. Although more information exists regarding reactions of OH with thymine and uracil, the greater experimental controversy for site preference of OH addition to cytosine lent impetus to the choice of cytosine as a subject for these calculations. A recent paper (8) suggested that site selection of OH attack of cytosine is more discriminating than for the analogous reactions with thymine and uracil and that the major product, in opposition to expectations from the results of our previous studies on OH reactions with N heterocycles (1,2), was the species favored on account of electrophilic interactions rather than being the most electronically delocalized product. These factors contributed to the selection of cytosine as the subject for study. In particular, the following two types of processes are of interest:

[1] OH + 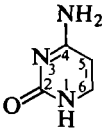 → H abstraction radicals + H_2O

[2] OH + 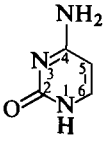 → OH adducts

Hydroxyl radicals are generally thought to add to the ring; however, some evidence also exists for the occurrence of H abstraction (3,4,9) either at the amino group or at N1 (10). Electron spin resonance spectra of the products arising from the reaction of OH with cytosine have yielded ambiguous results as line broadening occurs, obscuring finer splittings. However, all esr studies reported addition of OH at the C5—C6 bond (4,7,11–15). The conclusion by some authors that the C5 adduct is formed is not necessarily reliable as this is based on analogy with the reaction of OH with uracil (7,11,13–15). Both Joshi *et al.* (11) and Planinic (13) found evidence of the formation of two adducts. Planinic concluded that the preferred C5 adduct was kinetically favored by a ratio of 3:2 (13). Published pulse radiolysis work also supports the theory that two adducts are formed (9,16–18). Hissung and Von Sonntag used pulse radiolysis with both optical and conductimetric detection techniques to conclude that 55% of OH addition occurs at the C5 position (9). This preference for attack at the C5 site is supported by Hazra and Steenken who used pulse radiolysis and the oxidative–reductive characteristics of the nascent radicals (8). These authors however found a ratio of preference for the C5 adduct to the C6 adduct of 9:1.

In this paper, we present the results of *ab initio* calculations performed on the reaction of OH with cytosine. Both addition to the cytosine ring and H abstraction were considered as potential reactions. The products resulting from such reactions are depicted in Fig. 1; total energies and energy changes for the reactions [1] and [2] have been determined. Calculations were also performed on different tautometers as well as on various internally H-bonded forms of the adducts, and kinetic aspects of the reaction were investiated via the calculation of assumed reaction paths.

Computational methods

The total energies of reactants and possible products shown in Fig. 1 were calculated by *ab initio* SCF MO techniques using a version of the GAUSSIAN 76 program (19,20). Only the STO-3G minimal basis set was employed in the restricted Hartree–Fock (RHF) and unrestricted Hartree–Fock (UHF) calculations due to the prohibitively large number of functions required for extended basis set calculations. Due to the limitations on the basis set and the lack of the inclusion of correlation energy terms only large calculated energy differences can serve as basis for chemical conclusions. However, the

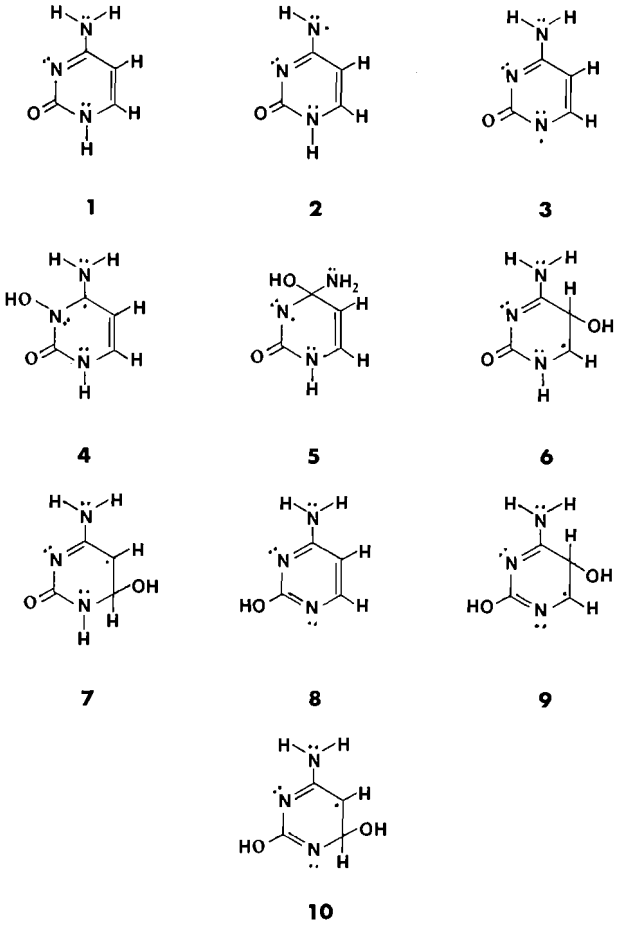

FIG. 1. Species studied and their designations.

high level of correlation between calculated 3G and 4-31G basis results of earlier model studies (2) on various imidazole + OH adducts suggests that an extension of the basis set would not overturn our conclusions. The geometry optimization for the most important species has been carried out to a uniform level of accuracy, higher than that routinely enforced in *ab initio* studies (*vide infra*).

Initial geometries for both cytosine and species **2–7** were obtained from X-ray diffraction data (21) with the local geometry of the OH addition site assumed to be tetrahedral (1,2,5,6). Initial geometries of species **9** and **10** were taken from modified optimized geometries of the analogous keto forms of the adducts. Geometry optimization was performed using the energy gradient method and continued until the average internal coordinate energy derivatives were less than or equal to 0.01 au. Optimization was not carried out as rigorously for species **3**, **4**, **9**, and **10** on the basis of the energetic unfavorability for formation of these species. Further refinement is not expected to change the relative energies of the products. The optimized geometries for all species calculated are reported in the appendix in Cartesian coordinate form. The energy of the OH radical was obtained from the study of OH with pyridines (1).

Quantitative aspects of the kinetics of the various reactions were obtained by calculating energy along assumed reaction paths. Points for each of the reaction path calculations were obtained by taking the mininum calculated energy of a choice of two different ring geometries: a geometry identical to that of the optimized adduct and a geometry intermediate between that of the optimized adduct and the starting reagent were used for the ring geometry with the C—OH bond length varied. There is some degree of arbitrariness in the choice of assumed reaction path. Note, however, that our purpose is to establish upper bounds for activation energies with the given basis set. Any optimization of the reaction path can lead only to an energy lowering, hence these assumed reaction paths provide upper bounds for the theoretical activation energies.

Results and discussion

Calculations were performed on potential products arising from the abstraction of H at N1 and at the amino group and from the addition of OH to the N3—C4 and C5—C6 double bonds.

Initially energies were calculated for the keto tautomeric forms of cytosine and the OH adducts. It is not within the scope of this paper to review the many articles published on the tautomerism of cytosine; here we refer only to some theoretical studies on the subject (22–29) including the first *ab initio* work (22), and a review by Kwiatkowski and Pullman (30) that gives an excellent perspective on this topic. The keto form of cytosine (species **1**) has been shown to be the form present in DNA and in solid crystals (30,31). Recent theoretical calculations (MINDO calculations and other calculations taking some components of solvation into account) (23–25, 29) concur with the results from the wide range of experimental techniques (30) supporting the general acceptance of the keto form as the predominant tautomer in aqueous solution despite the considerable controversy in earlier stages of research.

Tautomerism of the product of the OH reaction with cytosine (Cy) is an area where no direct experimental information exists. Hazra and Steenken (8) report that substitution at the N1 or N3 positions has little effect on site preference, thus implying a keto tautomeric form as shown in species **4–7** (Fig. 1).

Total and relative energies of the keto tautomers of potential products are presented in Table 1. Hydrogen abstraction at the N1 position and at the amino group and addition of OH at N3 are calculated to be unfavorable. The more extensively electron delocalized C6 adduct is calculated to be more stable relative to the C4 adduct and the experimentally found C5 adduct. In earlier theoretical studies (2,22,26–28), an arbitrary value of 40 kJ/mol was set as the limit of significant energy difference; thus, the small energy difference between the C4 and C5 adducts (5 kJ/mol) suggests similar stabilities, and no conclusive ordering in their relative stabilities can be made.

Hazra and Steenken's interpretation of their results (8) relies heavily on the assumption that the C4 and C6 adducts are oxidizing radicals while the C5 adduct has reducing properties. As a check on the veracity of these assumptions, *ab initio* calculations were performed on the optimized geometries of the adducts in question (species **5**, **6**, and **7**) with an electron added to each species. Energies (see Table 2) calculated for the addition of an electron to the adducts confirm that the C4 and C6 adducts are better oxidizing agents than the C5 adduct.

Because of the systematic disparity between the aqueous phase experimental results and the *ab initio* calculations involving heterocyclic compounds (2,22,23,29,30) it was decided to investigate the enol tautomers of the experimentally found C5 adduct and the theoretically preferred C6 adduct. This tautomeric form was chosen on the basis of the favorable relative energy of the enol tautomer of cytosine as suggested by various theoretical calculations (26–29). The results for these calculations, presented in Table 3, show that the enol tautomers are less stable than the corresponding keto forms for the adducts and that C6 is still the preferred addition site.

Energy was calculated for various geometry modifications to test the effect of internal H bonding. Figure 2 depicts the

TABLE 1. Calculated total energies for keto tautomeric forms and relative energies[a]

Species[b]	Molecule or radical	E(tot) (au)	ΔE(kJ/mol)
	OH	−74.3649	
	H_2O	−74.9659	
1	Cy (keto form)	−387.5451	
2	H abstracted from N1	−382.7847[c]	10920.5
3	H abstracted from NH_2	−386.8741	183.8
4	N3—OH—Cy	−461.8392[c]	185.9
5	C4—OH—Cy	−461.9561	−121.0
6	C5—OH—Cy	−461.9542	−116.0
7	C6—OH—Cy	−461.9862	−200.1

[a]Reaction energetics (ΔE) pertain to process for eq. [1] in text for species **2** and **3** and to process for eq. [2] in text for species **4–7**.
[b]See Fig. 1 for formula of species.
[c]The geometries for species **2** and **4** were not optimized to as high a degree as for other species (see text).

TABLE 2. Calculated total and relative energies for the addition of one electron to hydroxyl adducts

Species	Radical	E(tot) (au)	ΔE(kJ/mol)[a]
5	C4—OH—Cy	−461.7819	457.4
6	C5—OH—Cy	−461.7109	638.8
7	C6—OH—Cy	−461.8268	418.5

[a]Relative energy taken with respect to the energy for the appropriate adduct.

TABLE 3. Calculated total and relative energies for enol tautomeric forms[a]

Species[b]	Molecule or radical	E(tot) (au)	ΔE (kJ/mol)[a]
8	Cy (enol form)	−387.5444[b]	
9	C5—OH—Cy	−461.9097[c]	−1.1
10	C6—OH—Cy	−461.9420[c]	−88.9

[a]Reaction energetics are for eq. [2] in text using the energy of species **8** as the starting reactant.
[b]The energy for species **8** is taken from ref. 22.
[c]The geometries for species **9** and **10** were not optimized to as high a degree as for other species (see text).

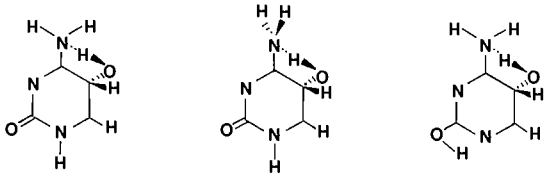

11 **12** **13**

FIG. 2. Modified geometries for the C5 adduct to test for internal hydrogen bonding.

modifications in geometry of the keto and enol forms of the C5 adduct used for the calculations. To increase the proximity between the hydroxyl protons and the lone electron pair of the N atom, both rotation of the amino group (species **12**) and displacement of the hydroxyl proton back into the plane of the ring (species **11** and **13**) were attempted in order to promote more internal H bonding with the N atoms. Results from these calculations show that these geometries destabilize the adducts

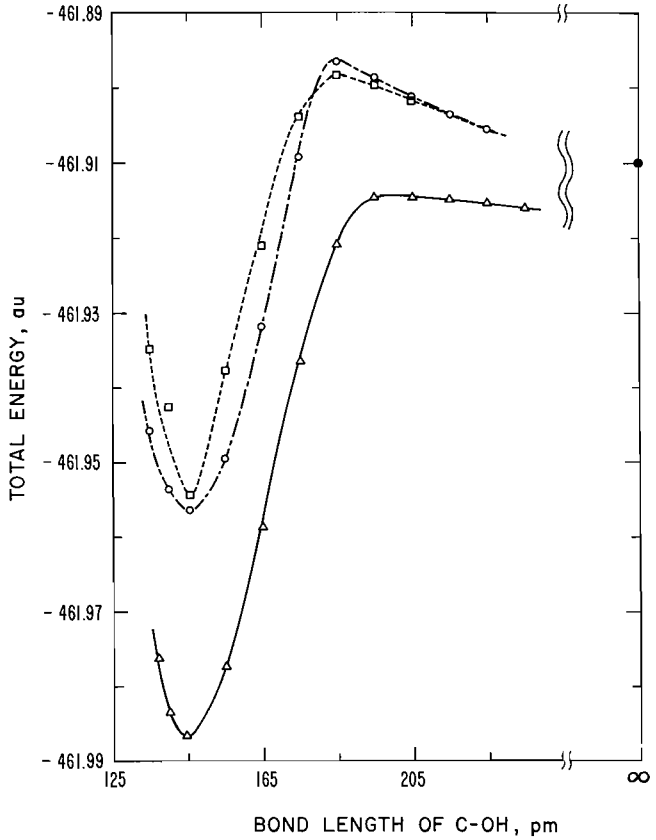

FIG. 3. Energy variation along approximate reaction paths calculated for addition of OH at the C4, C5, and C6 positions of cytosine. The reactions proceed from right to left. (——) C4—OH—Cy, (– – –) C5—OH—Cy, (———) C6—OH—Cy, (●) cytosine + OH at infinite separation.

TABLE 4. Calculated upper bonds for activation energies

Species[a]	Radical	E_a(kJ/mol)
5	C4—OH—Cy	35
6	C5—OH—Cy	31
7	C6—OH—Cy	0[b]

[a]See Fig. 1 for formula of species.
[b]See text.

TABLE 5. Calculated spins for radicals

Species[b]	Radical	S[a]
	OH	0.500
2	H abstracted from NH_2	1.030
4	N3—OH—Cy (keto form)	1.036
5	C4—OH—Cy (keto form)	0.810
6	C5—OH—Cy (keto form)	0.868
7	C6—OH—Cy (keto form)	0.844
9	C5—OH—Cy (enol form)	0.753
10	C6—OH—Cy (enol form)	0.816
Activated complexes of		
5	C4—OH—Cy (keto form)	0.945
6	C5—OH—Cy (keto form)	0.963
7	C6—OH—Cy (keto form)	0.996

[a]The expected S-value for doublet is 0.500.
[b]See Fig. 1 for formula of species.

TABLE 6. Energies corrected for electrostatic solute–water interaction

Species[b]	Molecule or radical	Dip. mom. D	Molec. polar. (Å^3)	Solute-H_2O interaction (kJ/mol)	Relative energy[a] (kJ/mol)	Corrected relative energy (kJ/mol)
2	H abs. NH_2	3.4	10.6	−13.1[b]	183.8	170.7
5	C4—OH—Cy	2.4	12.2	−7.0	−121.0	−128.0
6	C5—OH—Cy	3.8	11.6	−17.8	−116.0	−133.8
7	C6—OH—Cy	3.9	11.6	−18.4	−200.1	−218.5
9	C5—OH—Cy	3.6	11.5	−15.8	−1.1	−16.9
10	C6—OH—Cy	4.2	11.5	−21.4	−88.9	−110.3

[a]Energy is taken relative to eq. [1] for species **2** and eq. [2] for all other species. For species **9** and **10**, the enol form of cytosine (species **8**) was taken to be the starting reactant.

[b]Because species **2** is not an isomer of the other products, additional factors such as cavitation and van der Waal's forces are expected to contribute to a different extent to the solvation energy and hence should not be compared to the solvation energies of the other products.

(species **6** and **9**) by at least 50 kJ/mol, and hence the energy ordering of the OH adducts is unchanged.

To gain some insight into the kinetic aspects of the addition reactions, calculations were performed on assumed reaction paths for addition at the C4, C5, and C6 sites. Such assumed (not optimized) reaction paths, as shown in Fig. 3, are sufficient to give theoretical upper bounds for activation energies. As expected from the near diffusion-controlled rates of reaction (32), the upper bounds for the activation energies for OH addition, given in Table 4, are all small values. From these calculations, it can be seen that attack at the C6 position appears to lead to the kinetically as well as the thermodynamically favored product. No conclusions can be drawn regarding the relative kinetic preference for addition at the C4 vs. C5 positions due to the small difference in calculated approximate activation energies.

In Table 5, we have tabulated calculated spin eigenvalues for each of the radical species **2**–**10**. Comparing these values, S, to the expected value of 0.5 for doublets, it is evident that considerable spin contamination has occurred, as is common in UHF calculations. This likely results in lowered calculated energy values for the adducts while calculated energies for cytosine and OH are for the appropriate singlet and doublet states. Thus comparison of energies of the products to the energies of the starting reactants results in exaggerated low theoretical relative energies. The increase of calculated spins along the assumed reaction paths (shown in Table 5) suggests that the greatest degree of mixing of spin states occurs for the assumed reaction path of the C6 adduct, and thus this can possibly explain the apparent lack of an energy barrier for the addition of OH at C6.

An important aspect for consideration when comparing theoretical results of studies using isolated molecules with experimental results in solution is solvation. Hydrogen-bonding and electrostatic interactions between solute and solvent molecules are the main solvation features expected to modify the relative stabilities of the isomeric products (33, 34). Whereas in aqueous solution, H bonding is often the dominant effect, a direct, quantitative test of this effect with an *ab initio* model is prohibitively expensive. On the other hand, it is relatively simple to account for some electrostatic effects. In an attempt to explain the discrepancy between experimental results and calculated relative stabilities of tautomers of cytosine, Scanlan- and Hillier (23) corrected their calculated energies by including an estimate of electrostatic interaction. Despite the exclusion of consideration of H-bonding interactions, they were successful in showing the change in relative stabilities of tautomers in vapor phase as opposed to tautomers in solution.

Estimates of the water-adduct electrostatic interaction energy have been calculated using the reaction field continuum model (35) and are presented in Table 6. (Calculations are also presented for the product arising from H abstraction at the amino group, despite the nonisomeric nature of this product. Cavitation and van der Waals forces cannot be assumed to have the same effect as for the adduct products.) Molecular polarizabilities have been calculated using the method of Miller and Savchik (36) and the dipole moments have been obtained by *ab initio* STO-3G calculations. The dielectric constant of water was taken to be 78.54 and the radius of the spherical cavity assumed to be the same as for cytosine, 3.3 Å (23).

Although the small energy difference involved permits no definitive conclusions as to preference for attack between the C4 and C5 sites, the energies for electrostatic interaction with water show some reordering of relative stabilities of the adducts with the experimentally found C5 adduct now determined to be slightly more preferred than the C4 adduct. However, the small energy difference involved permits no conclusions as to preference of attack between C4 an C5.

Conclusions

Ab initio calculations have indicated that the preferred reaction of OH with cytosine is addition of OH to the C6 position, whereas the experimental results in aqueous solution indicate the preference for the formation of the C5 adduct. Interestingly, this experimental–theoretical discrepancy appears to be systematic for a number of N heterocyles (2,22,30). Various factors were considered as the basis for the disparity between experimental and theoretical results including tautomerism of the adducts, kinetic effects, mixing of higher order spin states in calculations of wave functions for doublet adducts, internal H bonding, and solvation aspects. Several plausible explanations have been excluded and using essentially a process of elimination, the results suggest that intermolecular hydrogen bonding is the major factor leading to the formation of the C5 adduct in solution as the predominant product.

Acknowledgments

We wish to express our appreciation to the Natural Sciences

and Engineering Research Council of Canada for financial assistance and for a postgraduate scholarship to B. G. E.

1. M. C. ANTHONY, W. L. WALTZ, and P. G. MEZEY. Can. J. Chem. **60**, 813 (1982).
2. B. G. EATOCK, W. L. WALTZ, and P. G. MEZEY. J. Comput. Chem. **6**, 68 (1985).
3. M. N. KHATTACK and J. H. GREEN.Int. J. Radiat. Biol. Relat. Stud. Phys. Chem. Med. **11**, 113, 137, 577 (1966).
4. M. G. ORMEROD and B. B. SINGH. Int. J. Radiat. Biol. Relat. Stud. Phys. Chem. Med. **10**, 533 (1966).
5. A. IMAMURA and K. HIRAO. Bull Chem. Soc. Jpn. **52**, 287 (1979).
6. E. WESTHOF and W. FLOSSMAN. J. Am. Chem. Soc. **97**, 6622 (1975).
7. C. NICOLAU and H. DERTINGER. Magn. Reson. Biol. Res. Rep. Int. Conf. 3rd. 215 (1969).
8. D. K. HAZRA and S. STEENKEN. J. Am. Chem. Soc. **105**, 4380 (1983).
9. A. HISSUNG and C. VON SONNTAG. Z. Naturforsch. B: Anorg. Chem. Org. Chem. **33B**, 321 (1978).
10. L. REN-ZHONG and L. NIAN-YUN. Radiat. Phys. Chem. **17**, 293 (1981).
11. A. JOSHI, S. RUSTGI, and P. REISZ. Int. J. Radiat. Biol. Relat. Stud. Phys. Chem. Med. **30**, 151 (1976).
12. H. TANAGUCHI. J. Phys. Chem. **94**, 3143 (1970).
13. J. PLANINIC. Int. J. Radiat. Biol. Relat. Stud. Phys. Chem. Med. **42**, 229 (1982).
14. H. DERTINGER and C. NICHOLAU. Biochim. Biophys. Acta, **199**, 316 (1970).
15. C. NICOLAU, M. MCMILLAN, and R. O. C. NORMAN. Biochim. Biophys. Acta, **174**, 413 (1969).
16. L. S. MYERS, M. L. HOLLIS, L. M. THEARD, F. C. PETERSON, and A. WARWICK. J. Am. Chem. Soc. **92**, 2875 (1970).
17. E. HAYON and M. SIMIC. J. Am. Chem. Soc. **95**, 1029 (1973).
18. L. S. MYERS, A. WARWICK, M. L. HOLLIS, J. D. ZIMBRICK, L. M. THEARD, and F. C. PETERSON. J. Am. Chem. Soc. **92**, 2871 (1970).
19. J. S. BINKLEY, R. A. WHITESIDE, P. C. HARIHARAN, R. SEEGER, J. A. POPLE, W. H. HEHRE, and M. D. NEWTON. GAUSSIAN 76. Quantum Chemistry Program Exchange, **11**, 368 (1978).
20. R. POIRIER and M. PETERSON. Modifications of GAUSSIAN 76 (MONSTERGAUSS). DEC Adaptation by R. E. Kari. Laurentian University, Sudbury, Ontario.
21. J. DONOHUE. Arch. Biochem. Biophys. **128**, 591 (1968).
22. J. D. GODDARD, P. G. MEZEY, and I. G. CSIZMADIA. Theor. Chim. Acta, **39**, 1 (1975).
23. M. J. SCANLAN and I. H. HILLIER. J. Am. Chem. Soc. **10**, 3737 (1984).
24. R. CZERMINSKI, B. LESYNG, and A. POHORILLE. Int. J. Quantum Chem. **16**, 605 (1979).
25. M. H. PALMER, J. R. WHEELER, J. S. KWIATKOWSKI, and B. LESYNG. J. Mol. Struct. **92**, 283 (1983).
26. P. G. MEZEY and J. J. LADIK. Theor. Chim. Acta, **52**, 129 (1979).
27. P. G. MEZEY, J. J. LADIK, and M. BARRY. Theor. Chim. Acta, **54**, 251 (1980).
28. E. C. HASS, P. G. MEZEY, J. J. LADIK, and M. BARRY. Theor. Chim. Acta, **60**, 283 (1980).
29. A. BUDA and A. SYGULA. J. Mol. Struct. **92**, 293 (1981).
30. J. S. KWIATKOWSKI and B. PULLMAN. Adv. Heterocycl. Chem. **18**, 199 (1975).
31. D. L. BARKER and R. E. MARSH. Acta. Crystallogr. **17**, 1581 (1964).
32. L. M. DORMAN and G. E. ADAMS. Natl. Stand. Ref. Data. Ser. (U.S. Natl. Bur. Stand.), **NSRDS - NBS 46** (1973).
33. P. BEAK and J. H. WHITE. J. Am. Chem. Soc. **104**, 7073 (1982).
34. P. BEAK. Acc. Chem. Res. **10**, 186 (1977).
35. R. REIN, V. RENUGOPAPKRISHNAN, S. NIR, and T. J. SWISSLER. Int. J. Quantum Chem. Quantum Biology Symp. **2**, 99 (1975).
36. K. J. MILLER and J. A. SAVCHIK. J. Am. Chem. Soc. **101**, 7206 (1979).

Appendix

The information given below is that for the optimized geometry for each species studied in terms of the cartesian coordinates with the units being in angstroms. The numbering of the atoms is that shown for cytosine (Cy) in eq. [1].

TABLE A1. Species **1**, Cy

Atom	*X*	*Y*	*Z*
N1	0.0000	0.0000	1.3102
C2	1.2509	0.0000	0.5891
N3	1.1653	0.0000	0.8518
C4	−0.0239	0.0000	−1.3957
C5	−1.2988	0.0000	−0.6537
C6	−1.2341	0.0000	0.6724
O	2.3099	0.0000	1.1982
N_{NH_2}	−0.0892	0.0000	−2.7854
H1	0.0440	0.0000	2.3289
H_{NH_2}	0.7682	0.0000	−3.3270
H'_{NH_2}	−0.9812	0.0000	−3.2676
H5	−2.2396	0.0000	−1.1784
H6	−2.1107	0.0000	1.3171

TABLE A2. Species **3**, H abstracted from NH_2

Atom	*X*	*Y*	*Z*
N1	0.0000	0.0000	1.3446
C2	1.2267	0.0000	0.5986
N3	1.2120	0.0000	−0.8228
C4	−0.0319	0.0000	−1.4157
C5	−1.2897	0.0000	−0.6842
C6	−1.2555	0.0000	0.6908
O	2.3511	0.0000	1.2351
N_{NH_2}	−0.0558	0.0000	−2.8023
H1	0.0622	0.0000	2.3597
H_{NH_2}	−0.0745	0.0000	−3.8099
H5	−2.2256	0.0000	−1.2232
H6	−2.1392	0.0000	1.3177

TABLE A3. Species **4**, N3—OH—Cy

Atom	*X*	*Y*	*Z*
N1	0.0000	0.0000	1.3950
C2	1.1865	0.0000	0.6850
N3	1.2476	0.0000	−0.7349
C4	0.1212	0.0000	−1.5402
C5	−1.1508	0.0000	−0.8672
C6	−1.3695	0.0000	0.4450
O	2.2145	0.0000	1.3854
N_{NH_2}	0.1960	0.0000	−2.9583
H1	0.0648	0.0032	2.4119
H_{NH_2}	1.0974	0.0000	−3.4222
H'_{NH_2}	−0.6616	0.0000	−3.4974
H5	−2.0564	−0.0033	−1.4557
H6	−2.3408	0.0071	0.9240
O	2.5951	0.0000	−1.3373
H	2.8372	0.0000	−0.3728

Table A4. Species **5**, C4—OH—Cy

Atom	*X*	*Y*	*Z*
N1	0.0000	0.0000	1.3537
C2	1.2369	0.0000	0.6396
N3	1.2828	0.0545	−0.7599
C4	−0.0564	0.2028	−1.4953
C5	−1.2715	−0.2433	−0.6673
C6	−1.1780	−0.3127	0.6851
O	2.3743	−0.0815	1.3194
N_{NH_2}	−0.0084	−0.4994	−2.7515
H1	0.0327	−0.0944	2.3677
H_{NH_2}	0.7279	−0.3127	−3.4180
H'_{NH_2}	−0.7267	−1.1670	−2.9935
H5	−2.1281	−0.6397	−1.1932
H6	−2.0035	−0.6466	−1.3023
O	−0.1604	1.6321	−1.7411
H	0.7303	1.9920	−1.5012

TABLE A5. Species **6**, C5—OH—Cy

Atom	*X*	*Y*	*Z*
N1	0.0000	0.0000	1.3478
C2	1.2233	0.0000	0.6142
N3	1.2079	−0.1226	−0.8044
C4	0.0113	−0.1450	−1.4117
C5	−1.3837	−0.0364	−0.7644
C6	−1.2519	0.1794	0.7366
O	2.3508	0.0408	1.2561
N_{NH_2}	0.0076	−0.3166	−2.8010
H1	0.0644	0.0435	2.3636
H_{NH_2}	0.8824	−0.4139	−3.3024
H'_{NH_2}	−0.8609	−0.4441	−3.3073
H5	−1.9043	0.8331	−1.1986
H6	−2.1066	0.3605	1.3747
O	−2.1040	−1.2388	−1.1213
H	−2.9527	−1.1645	−0.6144

TABLE A6. Species **7**, C6—OH—Cy

Atom	*X*	*Y*	*Z*
N1	0.0000	0.0000	1.3400
C2	1.2221	0.0000	0.5929
N3	1.2312	−0.2636	−0.7920
C4	−0.0472	−0.3807	−1.3728
C5	−1.2396	−0.0275	−0.7393
C6	−1.2236	0.5061	0.6901
O	2.3637	0.1624	1.2196
N_{NH_2}	−0.0242	−0.8178	−2.7116
H1	0.1070	0.2890	2.3143
H_{NH_2}	0.8544	−1.0685	−3.1469
H'_{NH_2}	−0.8785	−0.8878	−3.2487
H5	−2.1816	−0.0852	−1.2652
H6	−2.0973	0.1284	1.2484
O	−1.2041	1.9500	0.7526
H	−1.9854	2.2316	0.2116

TABLE A7. Species **9**, C5—OH—Cy (enol form)

Atom	*X*	*Y*	*Z*
N1	0.0000	0.0000	1.3179
C2	1.1393	0.0000	0.6571
N3	1.2679	−0.0373	−0.7577
C4	0.0797	−0.0407	−1.4132
C5	−1.3552	−0.0058	−0.8171
C6	−1.2911	0.1499	0.7271
O	2.2585	0.0057	1.4927
N_{NH_2}	0.1409	−0.1402	−2.8057
H2	1.8083	0.0021	2.4057
H_{NH_2}	1.0391	−0.1932	−3.2720
H'_{NH_2}	−0.7025	−0.2570	−3.3553
H5	−1.8756	0.8709	−1.2300
H6	−1.9766	0.8546	1.1979
O	−2.0070	−1.2095	−1.2771
H	−2.8825	−1.1958	−0.8126

TABLE A8. Species **10**, C6—OH—Cy (enol form)

Atom	*X*	*Y*	*Z*
N1	0.0000	0.0000	1.2810
C2	1.1331	0.0000	0.6571
N3	1.3312	−0.0502	−0.7399
C4	0.0562	−0.1101	−1.3957
C5	−1.2269	−0.0729	−0.7962
C6	−1.3529	0.1434	0.7385
O	2.1889	−0.0008	1.5878
N_{NH_2}	0.2021	−0.2332	−2.7920
H2	1.6738	−0.0663	2.4773
H_{NH_2}	1.1273	−0.2586	−3.2015
H'_{NH_2}	−0.6075	−0.2991	−3.3953
H5	−2.1154	−0.1360	−1.4107
H6	−2.0254	−0.5874	1.2143
O	−1.8703	1.4600	1.1469
H	−2.8266	1.4202	0.8841

Extraction of alkaline-earth metal *ortho*- and *para*-nitrophenoxides from aqueous media by crown ether and cryptand complexing agents

B. G. Cox[1]
Department of Chemistry, University of Stirling, Stirling, Scotland, FK9 4LA
E. Buncel[1] and H. S. Shin
Department of Chemistry, Queen's University, Kingston, Ont., Canada K7L 3N6
and
R. A. B. Bannard and J. G. Purdon
Chemical Detection Decontamination Section, Defence Research Establishment Ottawa, Shirley Bay, Ottawa, Ont., Canada K1A 0Z4

Received August 14, 1985

B. G. Cox, E. Buncel, H. S. Shin, R. A. B. Bannard, and J. G. Purdon. Can. J. Chem. **64**, 920 (1986).

A study has been performed on the extraction of alkaline-earth metal *ortho*- and *para*-nitrophenoxides, from aqueous medium into methylene chloride, in the presence of crown ether and cryptand complexing agents. The results are analyzed in terms of the various constituent complexation and extraction equilibria involved. Comparison is drawn with our previously reported study on extraction of potassium *p*-nitrophenoxide. The different anion stoichiometries in the two systems result in relatively more favorable extraction of M^+ systems at low anion concentrations. Furthermore, while extraction of MX (X = *o*- or *p*-nitrophenoxide) can be carried out in the presence of excess MOH, this is not possible in the case of MX_2 due to the limited solubility of $M(OH)_2$. The addition of excess MOH leads to more efficient extraction of M^+-phenoxides and prevents hydrolysis to free phenols. A noteworthy point in both MX and MX_2 systems is that at high concentrations of complexing agent a saturation effect occurs, which limits the overall extent of extraction achievable. Under these conditions the extraction is governed by the equilibrium constant, K_{dcs}, representing the partitioning of the complexed salt between the aqueous and organic phases, and is independent of the amount of ligand present.

B. G. Cox, E. Buncel, H. S. Shin, R. A. B. Bannard et J. G. Purdon. Can. J. Chem. **64**, 920 (1986).

On a réalisé une étude sur l'extraction des *ortho*- et *para*-nitrophénolates de métaux alcalino-terreux de milieux aqueux vers le chlorure de méthylène, en présence d'éthers couronnes et d'agents complexants cryptants. On analyse les résultats en fonctions des divers équlibres impliqués pour la complexation et l'extraction des constituants. On établit une comparaison avec l'étude que nous avons publiée antérieurement sur l'extraction du *p*-nitrophénolate de potassium. Les stoïchiométries anioniques différentes impliquées dans les deux systèmes font que les systèmes d'extraction de M^+ sont relativement plus favorables à des concentrations faibles d'anions. De plus, alors que l'extraction de MX (X = *o*- ou *p*-nitrophénolate) peut se faire en présence d'un excès de MOH, ceci n'est pas possible dans le cas de MX_2, à cause de la solubilité limitée du $M(OH)_2$. L'addition d'un excès de MOH conduit à une extraction plus efficace des phénolates de M^+ et élimine l'hydrolyse en phénols libres. On doit noter que, à des concentrations élevées d'agent complexant, tant de le système MX que MX_2, il se produit un effet de saturation qui limite les possibilités d'extraction. Dans ces conditions, l'extraction est gouvernée par la constante d'équilibre, K_{dcs}, qui représente la répartition du sel complexé entre les phases aqueuses et organiques, et elle est indépendante de la quantité de ligand qui est présente.

[Traduit par la revue]

Introduction

Efficient extraction of alkali-metal salts from aqueous media into organic solvents is often observed in the presence of macrocyclic complexing agents. This is especially true when the charge on the accompanying anion is highly delocalized as, for example, in the picrate anion (1–6).

Studies of extraction equilibria have considerable practical importance in relation to phase-transfer catalysis (7, 8) and analytical applications (9), and are also frequently used for comparative purposes in estimating the complexing capabilities of newly synthesized ligands (3, 10, 11). At a more fundamental level, a detailed analysis of the various equilibria involved in the overall extraction process is of some intrinsic interest, and is directly relevant to a better understanding of carrier-mediated ion transport in biological and synthetic membranes.

As part of a continuing investigation of the effect of macrocyclic complexing agents of cations on reaction rates and equilibria (12–14), we recently reported results of a comparative study on the extraction of potassium phenoxide, *p*-nitrophenoxide, and picrate from aqueous medium into methylene chloride in the presence of crown ether and cryptand complexing agents (5). In a parallel systematic study, the extraction of potassium phenoxide with macrocyclic ligands from aqueous medium into diverse organic solvents was investigated (6). In the present study we report the results of an investigation on the extraction of alkaline-earth *ortho*- and *para*-nitrophenoxides from aqueous medium into methylene chloride. The divalent cations could possibly serve in binding to two ligand sites in certain molecules of biological interest, which could be pertinent to studies concerning catalysis by metal cations and the effect of crown ethers and cryptands on such processes (14).

Experimental

Materials

The macrocyclic ligands (C) were purchased from BDH, Aldrich, Merck, or Parish Chemical Co., and used as received. Methylene chloride was dried and distilled. *o*-Nitrophenol and *p*-nitrophenol (Fisher, Reagent) were recrystallized from 2% v/v aqueous hydrochloric acid. The alkaline-earth salts of the *o*- and *p*-nitrophenols were prepared using the method of Poonia *et al.* (15, 16), from the alkaline-earth metal hydroxides (Mg^{2+}, BDH; Ca^{2+}, Anachemia;

[1]Authors to whom correspondence may be addressed.

Printed in Canada / Imprimé au Canada

TABLE 1. Initial concentrations of complexing agent (C) and alkaline earth nitrophenoxides (MX_2) in the extraction experiments

Salt (MX_2)	Complexing agent[a] (C)	$10^3[MX_2]$ *M*	$10^2[C]$ *M*	% Extraction
Magnesium	18-C-6	2.83	4.7	3.83
p-nitrophenoxide	B15-C-5	2.83	2.24	—
	(2,2,2)	2.83	4.15	8.55
	(2,2,1)	2.83	3.14	10.8
Magnesium	18-C-6	2.46	2.19	—
o-nitrophenoxide	(2,2,2)	2.46	2.78	8.64
	(2,2,1)	2.46	3.14	13.2
Calcium	18-C-6	3.86	4.7	6.28
p-nitrophenoxide	B15-C-5	3.86	3.24	—
	(2,2,2)	3.86	2.33	7.69
	(2,2,1)	3.70	3.14	5.71
Calcium	18-C-6	4.60	4.7	<1
o-nitrophenoxide	B15-C-5	4.60	3.24	—
	(2,2,2)	4.60	4.15	5.00
	(2,2,1)	4.60	3.14	2.32
Barium	18-C-6	5.10	4.70	2.91
p-nitrophenoxide	15-C-5	5.10	7.59	—
	B15-C-5	5.10	3.24	—
	DC24-C-8	5.10	3.46	2.89
	DB30-C-10	5.10	3.22	—
	(2,2,2)	5.10	3.34	4.29
	(2,2,1)	5.10	3.14	6.58
Barium	18-C-6	4.20	2.19	2.68
o-nitrophenoxide	15-C-5	4.20	5.64	—
	DC24-C-8	4.20	3.46	7.33
	(2,2,2)	4.20	2.67	5.36

[a]Complexing agents: 18-C-6, 18-crown-6 polyether; B15-C-5, benzo-15-crown-5 polyether; DB30-C-10, dibenzo-30-crown-10 polyether; DC24-C-8, dicyclohexano-24-crown-8 polyether; (2,2,1), cryptand [2,2,1]; (2,2,2), cryptand [2,2,2].

Ba^{2+}, Aldrich) and the *o*- and *p*-nitrophenols in the presence of ammonium hydroxide. As an example of the method, to a solution of *p*-nitrophenol (1.0 g, Fisher) in 95% ethanol (50 mL) was added concentrated ammonia (2 mL) followed by calcium hydroxide (0.27 g) in small portions. The reaction mixture was stirred for 3 h, filtered, and the filtrate was concentrated over a steam bath for 3 h to allow the ammonia to evaporate. The solution was further concentrated until crystallization started and was then allowed to cool. The yellow-orange needle-like crystals of calcium *p*-nitrophenoxide were filtered and dried *in vacuo* (0.10 g).

Extraction procedure

In the previous studies (5, 6) the potassium phenoxide salts were prepared *in situ* and used in the presence of excess hydroxide. The poor solubility of $M(OH)_2$ prevented this approach in the present series and this meant that, except where the basic cryptand ligands were involved, small amounts of the nitrophenoxides were extracted into the organic phase in the form of the free nitrophenol. All solutions (aqueous and organic), however, were analysed by uv, and any ArOH present was readily distinguished from ArO^- by virtue of its different absorption maxima. In other respects the extraction procedure was as previously described (5, 6). Control experiments showed that none of the nitrophenoxide salts were extracted in the absence of ligand. The initial concentrations of the complexing agent and the alkaline-earth nitrophenoxides used in the extraction experiments are listed in Table 1. The results are based on duplicate or triplicate determinations which usually agreed to ±2%.

Results

The equilibria involved in the extraction of the alkaline-earth nitrophenoxides MX_2 are represented in Scheme 1. The

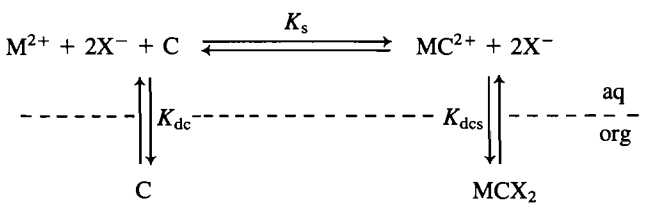

SCHEME 1

extraction of MX_2 in the absence of C is negligible under the present conditions and has not been included in Scheme 1. The three equilibrium constants involved, representing partitioning of the ligand (K_{dc}) and complexed salt (K_{dcs}), and complex formation in the aqueous phase (K_s), are defined in eqs. [1]–[3].

$$[1] \qquad K_{dc} = \frac{[C]_{org}}{[C]_{aq}}$$

$$[2] \qquad K_{dcs} = \frac{[MCX_2]_{org}}{[MC^{2+}]_{aq}[X^-]^2_{aq}}$$

$$[3] \qquad K_s = \frac{[MC^{2+}]_{aq}}{[M^{2+}]_{aq}[C]_{aq}}$$

The equilibrium constant for extraction (by C) of salt MX_2 is defined by eq. [4].

$$[4] \qquad K_e = \frac{[MCX_2]_{org}}{[M^{2+}]_{aq}[X^-]^2_{aq}[C]_{org}}$$

TABLE 2. Distribution constants (K_{dc}) between aqueous phase and methylene chloride for macrocylic ligands, and stability constants of alkaline-earth complexes (K_s) in water

	15-C-5	18-C-6	DC18-C-6	DB18-C-6	(2,2,2)	(2,2,1)
K_{dc}[a]	—	5.00	2×10^3	$>10^4$	5.00	5.00[b]
$K_{dc}(Ca^{2+})\ M^{-1}$	<1[c]	<3[c]			3.7×10^4[d]	8.9×10^6[d]
$K_s(Sr^{2+})\ M^{-1}$	89[c]	5.2×10^2[c]	1.74×10^3[c]		1.8×10^8[d]	2.2×10^7[d]
$K_s(Ba^{2+})\ M^{-1}$	51[c]	7.4×10^3[c]	3.7×10^3[c]		5.0×10^9[d]	2.0×10^6[d]

[a]Reference 5.
[b]Assumed the same as (2,2,2), see ref. 25.
[c]Reference 17.
[d]Reference 18.

TABLE 3. Equilibrium constants for extraction of alkaline-earth nitrophenoxides between water and methylene chloride[a]

Salt	Complexing agent	K'_e M^3	K_e M^3	K_{dcs} M^2
Magnesium	18-C-6	4.16×10^4	7.30×10^4	—
p-nitrophenoxide	(2,2,2)	1.23×10^5	ca. 1.9×10^5	—
	(2,2,1)	2.22×10^5	—	—
Magnesium	(2,2,2)	1.54×10^5	ca. 2.1×10^5	—
o-nitrophenoxide	(2,2,1)	2.38×10^5	—	—
Calcium	18-C-6	3.83×10^4	ca. 4.5×10^4	—
p-nitrophenoxide	(2,2,2)	1.00×10^5	1.73×10^7	2.14×10^3
	(2,2,1)	6.05×10^4	3.35×10^9	1.77×10^3
Calcium	18-C-6	$<4.01 \times 10^3$	—	—
o-nitrophenoxide	(2,2,2)	2.32×10^4	7.20×10^6	9.17×10^2
	(2,2,1)	1.32×10^4	7.39×10^8	4.04×10^2
Barium	18-C-6	1.03×10^4	7.25×10^5	4.89×10^2
p-nitrophenoxide	DC24-C-8	1.39×10^4	ca. 1.6×10^4	—
	(2,2,2)	2.56×10^4	7.45×10^{11}	7.51×10^2
	(2,2,1)	3.93×10^4	4.86×10^8	1.20×10^3
Barium	18-C-6	2.47×10^4	8.39×10^5	5.67×10^2
o-nitrophenoxide	DC24-C-8	4.93×10^4	ca. 5.5×10^4	—
	(2,2,2)	4.39×10^4	1.14×10^{12}	1.10×10^3

[a]Equilibrium constants referred to zero ionic strength, see Appendix.

Calculation of K_{dcs} (eq. [2]) and K_e (eq. [4]) requries knowledge of the stability constant for complexation in the aqueous phase (K_s), and the extent of partitioning of the free ligand between the aqueous and organic phases (K_{dc}). However, in cases where the free ligand is confined essentially to the organic phase and only weak complexes are formed between M^{2+} and C, we have $[M^{2+}]_{aq} \approx [M^{2+}]'_{aq}$, where $[M^{2+}]'_{aq} = [M^{2+}]_{aq} + [MC^{2+}]_{aq}$, and $[C]_{org} \approx [C]'$, where $[C]'$ is the total concentration of C exclusive of $[MCX_2]_{org}$. Then we may consider an approximate equilibrium constant K'_e given by eq. [5].

$$[5] \qquad K'_e = \frac{[MCX_2]_{org}}{[M^{2+}]'_{aq}[X^-]^2_{aq}[C]'}$$

Calculation of the fraction of M^{2+} (or X^-) extracted into the organic phase via eqs. [4] and [5] is considered in the discussion.

The data in Table 1 yield directly $[M^{2+}]'_{aq}$ and $[C]'$. Thus calculation of K'_e values is quite straightforward and does not require knowledge of either the partition coefficient of the ligand or the stability constant of MC^{2+}. The concentrations required for calculation of K_e (eq. [4]) and K_{dcs} (eq. [2]) may be obtained by appropriate manipulations of the terms contained in the definitions of $[M^{2+}]'_{aq}$, $[C]'$, K_{dc}, and K_s, as described in the Appendix. The ligand partition coefficients, K_{dc} (5, 6), and relevant complex stability constants, K_s (17, 18), used in the calculations are listed in Table 2. The equilibrium constants K'_e, K_e, and K_{dcs}, corrected to infinite dilution (see Appendix), are listed in Table 3.

Individual comments on calculation of the equilibrium constants for the various systems in Table 3 are as follows.

Calcium p-*nitrophenoxide*

An upper limit only is available for the stability constant of the 18-C-6 complex ($\log K_s \leqq 0.5$) (17). However, even assuming the maximum value, at the concentrations used (Table 1) the extent of formation of MC^{2+} is negligible.

Barium o- *and* p-*nitrophenoxide*

Values of K_{dc} and K_s are not available for DC-24-C-8, but K_s should be lower than that for 18-C-6 (17, 19) ($\log K_s = 3.9$) and K_{dc} should be similar to that of DC-18-C-6 ($\log K_{dc} = 3.3$). For any reasonable choice of K_s and K_{dc} it may be shown that the fraction of C and MC^{2+} in the aqueous phase is negligible, and hence $K_e = K'_e$.

Magnesium o- *and* p-*nitrophenoxide*

Stability constants are not available for Mg^{2+} complexes but size considerations suggest that they will be significantly lower than the corresponding values for Ca^{2+} complexes (17–19).

Thus for (2,2,2) and 18-C-6, complex formation in the aqueous phase has been neglected in calculating K_e. The stability constant of $Mg(2,2,1)^{2+}$ may, however, be large, and calculated K_e values are very sensitive to K_s $Mg(2,2,1)^{2+}$ for $K_s \geqq 10^2 M^{-1}$. Thus it is not possible to calculate K_e for extraction of Mg^{2+} salts by cryptand (2,2,1) with any certainty.

Discussion

In considering the extraction of M^{2+} salts, compared with the corresponding M^+ salts investigated previously (5, 6), two important differences may be noted. The first is that for a given cation size the solvation energy of M^{2+} is considerably larger than that of M^+. This leads to the practical result that in the present systems no extraction of M^{2+} salts was observed in the absence of added complexing ligand. This in turn simplifies the calculation somewhat and obviates the need of an iteration procedure in analyzing the data.

More importantly, there is also a difference in the stoichiometry of the extraction reaction. This means that the relative efficiencies of extraction of M^+ and M^{2+} systems will depend not only upon the differences in solvation energies of the cations and the extent to which these are modified or overcome by complexation with the ligands, but also on the total salt concentration range investigated. Thus extraction of MX_2 will be much more sensitive to the concentration and nature of the anion X^- than in the corresponding MX system. This is discussed quantitatively below, but it is clear that at low $[X^-]$ extraction of MX will be favoured relative to MX_2, and that the extraction of MX_2 becomes increasingly favoured with increasing $[X^-]$, as the latter has a second-order dependence on $[X^-]$. Thus any simple comparison of extraction percentages of M^{2+} and M^+ salts will be valid only for the concentrations at which the measurements were carried out.

A feature common to both M^+ and M^{2+} systems is that the extent of complex formation in the aqueous phase has a very strong influence on the overall extraction behaviour, especially for ligands with a significant tendency to partition into the aqueous phase. This is because in such cases a considerable proportion of M^{2+} (or M^+) may remain in the aqueous phase as MC^{2+} (or MC^+). Thus in the limit of high ligand concentrations, although eq. [4] (correctly) predicts that $[M^{2+}]_{aq}$ will approach zero, the extent of extraction of M^{2+} (as MCX_2) into the organic phase will not increase indefinitely, but rather will be governed by eq. [2], i.e., the extent to which the *complexed ion* partitions between the two layers. For purely practical purposes the percentage of extraction of a salt into the organic phase may be required, and it follows from the above that K_e values are often not of *direct* use in this respect. This is illustrated and amplified below in some detail for the extraction of M^{2+} salts as investigated in this work, but corresponding equations for M^+ may be written down by inspection.

The ratio of M^{2+} in the organic and aqueous phases, $[MCX_2]_{org}/[M^{2+}]'_{aq}$, and hence the percentage extraction is given by eq. [6].

$$[6] \qquad \frac{[MCX_2]_{org}}{[M^{2+}]'_{aq}} = \frac{K_e[X^-]^2_{aq}[C]_{org}}{1 + [C]_{org}K_s/K_{dc}}$$

Equation [6] follows directly from eq. [4] and the definition of $[M^{2+}]'_{aq}$ (= $[M^{2+}]_{aq}$ + $[MC^{2+}]_{aq}$, i.e. the total concentration of M^{2+} in the aqueous phase), together with eqs. [1] and [2]. There are two limiting cases corresponding to eq. [6].

(*i*) $[C]_{org}K_s/K_{dc} \ll 1$. This will occur at sufficiently low $[C]_{org}$, when the stability constant for complex formation is very small, or when the ligand partitions almost exclusively into the organic phase. Equation [6] then reduces to eq. [7].

$$[7] \qquad \frac{[MCX_2]_{org}}{[M^{2+}]'_{aq}} = K_e[X^-]^2_{aq}[C]_{org}$$

and the concentration ratio of M^{2+} in the two phases depends directly upon $[C]_{org}$.

(*ii*) $[C]_{org}K_s/K_{dc} \gg 1$. This corresponds to limiting high concentrations of $[C]_{org}$, very stable MC^{2+}, or strong partitioning of C into the aqueous phase. Under these conditions, quantitative conversion of M^{2+} in the aqueous layer to MC^{2+} occurs and the concentration ratio is given by eq. [8].

$$[8] \qquad \frac{[MCX_2]_{org}}{[M^{2+}]'_{aq}} = \frac{K_eK_{dc}[X^-]^2_{aq}}{K_s} = K_{dcs}[X^-]^2_{aq}$$

It is clear from the above that the relative efficiencies of two different ligands as extracting agents will depend upon the concentration range employed. This is illustrated by the results in Table 4, in which the extraction of $Ba(p\text{-}NO_2PhO)_2$ with a ligand of very strong complexing ability (2,2,2) is compared with one of moderate complexing ability (18-C-6). It may be seen that even at very low (excess) levels (10^{-4} *M*) of (2,2,2) the maximum extent of extraction is obtained. For 18-C-6, significantly higher levels are required to achieve maximum extraction, but the limiting value is only slightly lower than that for (2,2,2). This latter observation, which follows from the similar K_{dcs} values (Table 3), contrasts sharply with the behaviour of the corresponding K^+ salt (5, 6), results for which are also included in Table 4. In this case, although similar trends with ligand concentration are observed, the limiting extraction percentage is very much lower for 18-C-6 than for (2,2,2).

TABLE 4. Extraction of $Ba(p\text{-}NO_2PhO)_2$ (0.1 *M*) and $K(p\text{-}NO_2\text{-}PhO)$ (0.01 *M*) from water to methylene chloride by 18-C-6 and (2,2,2)

	% BaX_2 extracted		% KX extracted	
[Ligand]/M^a	(2,2,2)	18-C-6	(2,2,2)	18-C-6
10^{-4}	15.4	1.52	94.8	8.26×10^{-3}
10^{-3}	15.4	6.67	95.6	8.1×10^{-2}
10^{-2}	15.4	10.1	95.6	0.67
10^{-1}	15.4	10.6	95.7	2.40
1	15.4	10.7	95.7	3.32
∞	15.4	10.7	95.7	3.46

[a]Equilibrium excess ligand concentration.

The difference in behaviour of (2,2,2) and 18-C-6 with respect to extraction of the two cations K^+ and Ba^{2+} (which have similar ionic radii) may result from structural differences of the two ligands. For the essentially planar 18-C-6 ligand, cation coordination sites perpendicular to the ligand plane remain free, whereas the spherical cavity of the cryptand ligand totally encapsulates the ions. This would tend to make extraction of the 18-C-6 complexes more difficult, as in aqueous solution the remaining coordination sites would be occupied by water molecules, conferring extra stability on the complex. However, for the Ba^{2+} crown complex in methylene chloride the two associated anions can presumably satisfy both remaining coordination sites so that there is little difference between the extraction of Ba^{2+} as the (2,2,2) or 18-C-6 complexes. In the case of the K^+ crown complex there is only one anion available for coordination to K^+ in the organic phase.

It is of course difficult to compare the *absolute* extents of

extraction of M^+ and M^{2+} cations in any meaningful thermodynamic way, as the ratio of cation concentration in the organic and aqueous phases varies with $[X^-]$ in the former case and $[X^-]^2$ in the latter case. This means that for low salt concentrations extraction of KX will be favoured relative to BaX_2 and vice versa. It may readily be shown from the K_{dcs} values for the 18-C-6 extraction of barium *p*-nitrophenoxide (Table 3) and potassium *p*-nitrophenoxide ($3.60\,M^{-1}$) (5, 6) that at limiting high ligand concentrations the two salts are extracted to an equal extent when the salt concentrations are $3 \times 10^{-3}\,M$; the corresponding figure for extraction by (2,2,2) is $1.25\,M$.

Comparing the present overall results with those reported previously (5, 6), in practice the efficiency of extraction of *p*-nitrophenoxide achieved for the K^+ salt by the macrocyclic ligands was much higher than the values reported here. This is because it was possible to carry out the extractions in the presence of excess potassium hydroxide, which has the effect of driving the equilibrium position towards more favourable anion extraction percentages. This is not possible for M^{2+} systems because the limited solubility of $M(OH)_2$ necessitated the use of the prepared phenoxide salts. This represents a practical limitation in the extraction of phenoxides as their alkaline earth salts and also means that the hydrolysis of phenoxide to generate small quantities of (readily extractable) phenol could not be suppressed by the addition of excess hydroxide.

While the present results refer to the extraction of nitrophenoxide salts of the alkaline-earth cations, it is known from earlier work on K^+ salts (5, 6) that the extent of extraction is very sensitive to the nature of the accompanying anion. Thus for several crown ether and cryptand complexing ligands in a variety of solvents the order of extraction of K^+ salts was always phenoxide $\ll$ *p*-nitrophenoxide $\ll$ picrate, and in a number of cases extraction of picrate salts was observed even in the absence of added ligand. The extraction of salts of simple, highly solvated ions such as Cl^-, OH^-, etc. should be even more difficult than that of the phenoxide salts (20). These general trends relating to the nature of the anion should also be observed for M^{2+} salts, but are expected to be considerably amplified because of the involvement of two anions in the extraction process.

The results for extraction of Ca^{2+} and Ba^{2+} salts by cryptand ligands show that the *complexed* Ca^{2+} salts (K_{dcs} values) are extracted slightly more readily than the corresponding complexed Ba^{2+} salts. This is a good illustration of the extent to which the bicyclic cryptand ligands are able to shield the enclosed cations from the surrounding solvent. It has been shown, for example, that the extent of extraction of simple uncomplexed uni–univalent electrolytes such as alkali metal halides from water to organic solvents such as nitrobenzene and 1,2-dichloroethane decreases dramatically with decreasing cation (or anion) size (21, 22); e.g., for transfer between water and nitrobenzene, $K_{ds}(NaBr)/K_{ds}(KBr) = 2 \times 10^{-3}$. This is in line with the increased hydration energies of the small ions, and even larger differences would be expected for uncomplexed Ca^{2+} and Ba^{2+} salts, because of the much higher hydration energies involved ($\Delta G_{hyd}(Ca^{2+}) - \Delta G_{hyd}(Ba^{2+}) = 274\,kJ\,mol^{-1}$; cf. $\Delta G_{hyd}(Na^+) - \Delta G_{hyd}(K^+) = 73.5\,kJ\,mol^{-1}$) (ref. 23).

Acknowledgement

This research was supported by Supply and Services Canada, Department of National Defence (Contract No. 14SU-97714-2-1275).

1. C. J. Pederson. J. Am. Chem. Soc. **92**, 391 (1970).
2. H. K. Frensdorff. J. Am. Chem. Soc. **93**, 4684 (1971).
3. E. P. Kyba, R. C. Helgeson, K. Madan, G. W. Gokel, T. L. Tarnowski, S. S. Moore, and D. J. Cram. J. Am. Chem. Soc. **99**, 2564 (1977).
4. Y. Takeda. Bull. Chem. Soc. Jpn. **54**, 526 (1981).
5. E. Buncel, H. S. Shin, R. A. B. Bannard, and J. G. Purdon. Can. J. Chem. **62**, 926 (1984).
6. E. Buncel, H. S. Shin, R. A. B. Bannard, J. G. Purdon, and B. G. Cox. Talanta, **31**, 585 (1984).
7. C. M. Starks and C. Liotta. Phase transfer catalysis. Academic Press, New York. 1978.
8. D. Landini, A. Maia, and F. Montanari. J. Am. Chem. Soc. **106**, 2917 (1984).
9. I. M. Kolthoff. Anal. Chem. Rev. **51**, 1R (1979).
10. J. Jawaid and F. Ingman. Talanta, **25**, 91 (1978).
11. D. M. Dishong, C. J. Diamond, M. I. Cinoman, and G. W. Gokel. J. Am. Chem. Soc. **105**, 586 (1983).
12. E. Buncel and B. C. Menon. J. Am. Chem. Soc. **99**, 4457 (1977).
13. E. Buncel, B. C. Menon, and T. K. Venkatachalam. J. Org. Chem. **49**, 413 (1984).
14. E. Buncel, E. J. Dunn, R. A. B. Bannard, and J. G. Purdon. J. Chem. Soc. Chem. Commun. 162 (1984).
15. N. S. Poonia. J. Am. Chem. Soc. **96**, 1012 (1974).
16. N. S. Poonia, A. V. Bajaj, A. K. Arora, K. Joshi, and A. Banthia. Ind. J. Chem. **19**A, 37 (1980).
17. R. M. Izatt, R. E. Terry, B. L. Haymore, L. D. Hansen, N. K. Dalley, A. G. Avondet, and J. J. Christensen. J. Am. Chem. Soc. **98**, 7620 (1976).
18. B. G. Cox, Ng van Truong, and H. Schneider. J. Am. Chem. Soc. **106**, 1273 (1984).
19. G. W. Gokel, D. M. Goli, C. Minganti, and L. Echegoyen. J. Am. Chem. Soc. **105**, 6786 (1983).
20. J. D. Lamb, J. J. Christensen, S. R. Izatt, K. Bedke, M. S. Astin, and R. M. Izatt. J. Am. Chem. Soc. **102**, 3399 (1980).
21. M. H. Abraham and A. F. Danil de Namor. J. Chem. Soc. Faraday Trans. 1, **72**, 955 (1976).
22. A. F. Danil de Namor and T. Hill. J. Chem. Soc. Faraday Trans 1, **79**, 2713 (1983).
23. R. M. Noyes. J. Am. Chem. Soc. **84**, 513 (1962).
24. C. W. Davies. Ion association. Butterworths, London. 1962.
25. B. G. Cox, J. Garcia-Rosas, and H. Schneider. J. Am. Chem. Soc. **103**, 1384 (1981).

Appendix

The total concentrations of M^{2+} and C exclusive of $(MCX_2)_{org}$, $[M^{2+}]_t'$, and $[C]_t'$, respectively, are defined by eqs. [A1] and [A2],

$$[A1] \quad [M^{2+}]_t' = [M^{2+}]_{aq} + [MC^{2+}]_{aq} = [M^{2+}]_t - [MCX_2]_{org}$$

$$[A2] \quad [C]_t' = [C]_{org} + [C]_{aq} + [MC^{2+}]_{aq} = [C]_t - [MCX_2]_{org}$$

where $[M^{2+}]_t$ and $[C]_t$ are the total concentrations of M^{2+} and C in the system.

By combining eqs. [A1] and [A2] with eq. [1] (K_{dc}) and eq. [3] (K_s) it is possible to calculate all of the concentrations required to evaluate K_e (eq. [4]) and K_{dcs} (eq. [2]) as follows. Substituting eq. [1] into [A2] gives eq. [A3],

$$[A3] \quad [C]_{aq} = \frac{[C]_t' - [MC^{2+}]_{aq}}{1 + K_{dc}}$$

which, upon substitution into eq. [3], leads to eq. [A4]:

$$[A4] \quad [MC^{2+}]_{aq} = \frac{K_s[M^{2+}]_{aq}[C]_t'}{1 + K_{dc} + K_s[M^{2+}]_{aq}}$$

Substitution of eq. [A4] into eq. [A1] gives eq. [A5]:

$$[A5] \quad [M^{2+}]_{aq} = \frac{-b \pm (b^2 - 4c)^{1/2}}{2}$$

where

$$b = \frac{1 + K_{dc} + K_s([C]_t' - [M^{2+}]_t')}{K_s}$$

and

$$c = \frac{-(1 + K_{dc})[M^{2+}]_t'}{K_s}$$

This value of $[M^{2+}]_{aq}$ may then be substituted into eq. [A1] to give $[MC^{2+}]_{aq}$, which with eq. [A3] gives $[C]_{aq}$, and hence, from eq. [1], $[C]_{org}$.

Calculations carried out in this manner give equilibrium constants referred to the ionic strengths at which the measurements were carried out. K_e (and hence K_e') and K_{dcs} values may be corrected to infinite dilution via eqs. [A6] and [A7], in which γ is the activity coefficient.

$$[A6] \quad K_e = \frac{[MCX_2]_{org}}{[M^{2+}]_{aq}[X^-]^2[C]_{org}\,\gamma_{M^{2+}}\gamma_{X^-}^2}$$

$$[A7] \quad K_{dcs} = \frac{[MCX_2]_{org}}{[MC^{2+}]_{aq}[X^-]_{aq}^2\,\gamma_{M^{2+}}\gamma_{X^-}^2}$$

The required activity coefficients were calculated using the Davies equation (eq. [A8]) (ref. 24),

$$[A8] \quad \log \gamma_{\pm} = \frac{-AZ^2 I}{1 + I^{1/2}} + \frac{AI}{3}$$

in which $A = 0.5$ is the Debye–Hückel parameter and I is the ionic strength. The ionic strengths involved were quite low (0.007–0.015 M) but the overall activity coefficient correction, $\gamma_{M^{2+}}\gamma_{X^-}^2$, is not negligible, varying between 0.697 and 0.611. It is assumed also that $\gamma_{MC^{2+}} = \gamma_{MC^{2+}}$ (see eqs. [A6], [A7]).

Apparent molar heat capacities and volumes of aqueous solutions of several 1:1 electrolytes at elevated temperatures[1]

PREET P. S. SALUJA, JACQUES C. LEBLANC, AND HAROLD B. HUME[2]

Research Chemistry Branch, Atomic Energy of Canada Limited, Whiteshell Nuclear Research Establishment, Pinawa, Man., Canada R0E 1L0

Received November 20, 1985

PREET P. S. SALUJA, JACQUES C. LEBLANC, and HAROLD B. HUME. Can. J. Chem. **64**, 926 (1986).

The results of heat capacity (C_p) and density (d) measurements at 0.6 MPa and in the temperature range 298.15–373.15 K are presented for several 1:1 electrolytes in water. The flow microcalorimeter and densimeter used for these measurements were modificatons of the room-temperature designs. Data were obtained over concentrations ranging from 0.02 to 1.0 mol kg^{-1} (or to the solubility limit, whichever was lower). The heat capacity of a solution relative to that of water was measured with a precision of ± 0.1 mJ K^{-1} g^{-1} at all temperatures. The density of a solution relative to that of water was measured with a precision of ± 5 μg cm^{-3}. These C_p and d results were used to calculate the apparent molar heat capacities, ${}^{\phi}C_p$, and volumes, ${}^{\phi}V$, at 298.15, 323.15, 348.15, and 373.15 K, at a constant pressure of 0.6 MPa. These results are in good agreement with available literature data.

PREET P. S. SALUJA, JACQUES C. LEBLANC et HAROLD B. HUME. Can. J. Chem. **64**, 926 (1986).

Opérant à 0,6 MPa et à des températures allant de 298,15 à 373,15 K, on a mesuré les capacités calorifiques (C_p) et les densités (d) de plusieurs mélanges 1:1 d'électrolytes dans l'eau. Les densimètres et microcalorimètres à écoulement utilisés pour ces études étaient des appareils à température ambiante qui avaient été modifiés. On a obtenu des données à des concentrations allant de 0,02 à 1,0 mol kg^{-1} (ou, si elle était plus basse, jusqu'à la limite de solubilité). A toutes les températures, on a pu mesurer la capacité calorifique d'une solution relative à celle de l'eau avec une précision de $\pm 0,1$ mJ K^{-1} g^{-1}. On a mesuré la densité des solutions relative à celle de l'eau avec une précision de ± 5 μg cm^{-3}. On a utilisé ces résultats de C_p et de d pour calculer les capacités calorifiques, ${}^{\phi}C_p$, et les volumes, ${}^{\phi}V$, molaires apparents à des températures de 298,15, de 323,15, de 348,15 et de 373,15 K et à une pression constante de 0,6 MPa. Ces résultats sont en bon accord avec ceux disponibles dans la littérature.

[Traduit par la revue]

Introduction

Thermodynamic data for aqueous species at elevated temperatures are requried to understand, and model, various chemical processes in the vicinity of an underground nuclear fuel, waste disposal vault (1, 2), specifically the interactions of aqueous I^-, IO_3^-, Cs^+, and TcO_4^- with major constituents of groundwaters and mineral surfaces. Experimental heat capacities, C_p, are needed to determine partial molar heat capacities, $\bar{C}^0_{p,2}(T)$, and thereby standard Gibbs energies, $\bar{G}^0_2(T)$, for aqueous species as a function of temperature. Gibbs energies can then be used to calculate solubilities and chemical speciation in aqueous environments (2, 3).

The $\bar{G}^0_2(T)$ can be calculated at any temperature, T, using the following thermodynamic relation:

$$[1]\quad \bar{G}^0_2(T) = \bar{G}^0_2(T_R) - \bar{S}^0_2(T_R)(T - T_R) - T\int_{T_R}^{T} \frac{\bar{C}^0_{p,2}(T)}{T}\,dT + \int_{T_R}^{T} \bar{C}^0_{p,2}(T)\,dT$$

Standard Gibbs energy, $\bar{G}^0_2(T_R)$, and entropy, $\bar{S}^0_2(T_R)$, at room temperature (T_R) are usually available in the literature, in regularly updated compilations (4). To calculate Gibbs energies at elevated temperatures, we only need to determine $\bar{C}^0_{p,2}(T)$ as a function of temperature. The latter is identical to the apparent molar heat capacity, ${}^{\phi}C_p(T, m)$, extrapolated to infinite dilution ($m = 0$, m being the molality of solution in mol kg^{-1}) using a suitable ion-interaction approach for modelling ionic solutions (3, 5, 6). The ${}^{\phi}C_p(T, m)$ can be calculated directly from the heat capacity measurements, $C_p(T, m)$, over a wide range of concentrations and temperatures.

While $C_p(T, m)$, ${}^{\phi}C_p(T, m)$, and $\bar{C}^0_{p,2}(T)$ values for a few aqueous 1:1 species are available at room temperature (7–10), very few values (4, 11, 12) are available at higher temperatures. This is because both heat capacity and density measurements at elevated temperatures have been difficult. Consequently, the available data for aqueous species are often inconsistent. For example, the two $\bar{C}^0_{p,2}$ values for CsI in the literature agree only in the 300–323 K range. Data from adiabatic calorimetry (12) show a maximum, at about 353 K, in the $\bar{C}^0_{p,2}$ vs. temperature plot, whereas the data of Mitchell and Cobble (11) show no maximum in the 273–373 K range.

Recent advances in flow calorimeters (1, 5, 14, 15) and flow densimeters (1, 16, 17) allow determination of $C_p(T, m)$ and $d(T, m)$ data with improved precision, and make measurements in aqueous solutions at elevated temperatures easier. Thus, we have undertaken to measure heat capacities and densities of several 1:1 electrolytes, including fission product electrolytes (Cs, I). In this paper, we give measured heat capacities, calculated ${}^{\phi}C_p(T, m)$ values, measured densities, and calculated apparent molal volumes, ${}^{\phi}V(T, m)$, for nine 1:1 elctrolytes up to 373.15 K at a constant pressure of 0.6 MPa. In ref. 6, we apply Pitzer's ion-interaction model (1, 5) to our data to obtain $\bar{C}^0_{p,2}(T)$ and $\bar{V}^0_2(T)$ functions and to calculate thermodynamic properties of aqueous electrolytes at higher temperatures.

Experimental

(a) General approach

As discussed above, the $\bar{C}^0_{p,2}(T)$ and $\bar{V}^0_2(T)$ functions, two quantities of interest, are, respectively, identical to infinite-dilution ${}^{\phi}C^0_p(T)$ and ${}^{\phi}V^0(T)$ values, over a wide temperature range. Since ${}^{\phi}C_p(T, m)$ and ${}^{\phi}V(T, m)$ values can be experimentally determined only in finite concentration ranges, a theoretical ion-interaction approach (1, 5) is required to extrapolate these values to infinite dilution. To apply this model, a large number of $C_p(T, m)$ and $d(T, m)$ measurements are required, with a high degree of precision, for the parametric fit of the data to Pitzer's equations, to evaluate reliably the $\bar{C}^0_{p,2}(T)$ and $\bar{V}^0_2(T)$ functions and the temperature-dependent ion-

[1]Issued as AECL-8931.

[2]Co-op student at the University of Victoria, Victoria, B.C., Canada.

TABLE 1. Apparent molar heat capacities ($^{\phi}C_p$) of selected alkali halides and iodates in aqueous solutions as a function of temperature, at 0.6 MPa*

Molality (mol kg^{-1})	$^{\phi}C_p$ (J K^{-1} mol^{-1})
NaI, 323.15 K	
Water(0.0)	(75.28)
0.04911	−42.3
0.09791	−37.9
0.20115	−34.9
0.49648	−26.7
0.99059	−16.1
2.01000	+0.6
NaI, 348.15 K	
Water(0.0)	(75.50)
0.05266	−34.0
0.09847	−31.3
0.20365	−29.1
0.51703	−22.6
1.02118	−14.5
NaI, 373.15 K	
Water(0.0)	(75.92)
0.0485	−47.4
0.1051	−46.8
0.2136	−41.3
0.5267	−34.1
1.0030	−26.0
CsF, 298.15 K	
Water(0.0)	(75.26)
0.03185	−132
0.09585	−128.5
0.20930	−122.1
0.65802	−109.75
1.06028	−92.82
CsF, 323.15 K	
Water(0.0)	(75.28)
0.03185	−97.1
0.09585	−92.4
0.20930	−87.4
0.65802	−79.15
1.06028	−65.49
CsF, 348.15 K	
Water(0.0)	(75.50)
0.03185	−85.8
0.09585	−82.1
0.20930	−77.7
0.65802	−68.46
1.06028	−55.22
CsF, 373.15 K	
Water(0.0)	(75.92)
0.03185	−91.8
0.09585	−86.0
0.20930	−80.1
0.65802	−68.78
1.06028	−55.42
CsCl, 298.15 K	
Water(0.0)	(75.26)
0.04024	−142.3
0.10483	−137.3
0.20544	−131.1
0.42146	−123.5
0.59112	−116.2
0.79997	−110.1
1.02638	−104.24
CsCl, 323.15 K	
Water(0.0)	(75.28)
0.1114	−101.2
0.2120	−98.6
0.4068	−91.2
0.5942	−87.1
0.7885	−83.24
1.0189	−78.64
CsCl, 348.15 K	
Water(0.0)	(75.50)
0.1114	−93.7
0.2120	−86.8
0.4068	−80.3
0.5942	−76.0
0.7885	−72.16
1.0189	−68.55
CsCl, 373.15 K	
Water(0.0)	(75.92)
0.1114	−93.4
0.2120	−88.7
0.4068	−81.1
0.5942	−75.6
0.7885	−71.84
1.0189	−67.06
CsI, 298.15 K	
Water(0.0)	(75.26)
0.09843	−130.5
0.1964	−122.4
0.4153	−111.8
0.6115	−101.84
0.7969	−95.83
0.9907	−89.44
CsI, 323.15 K	
Water(0.0)	(75.28)
0.09843	−92.7
0.1830	−87.2
0.3914	−80.4
0.4153	−77.64
0.5684	−73.24
0.7969	−68.28
0.9907	−64.91
CsI, 348.15 K	
Water(0.0)	(75.50)
0.09434	−77.5
0.1830	−76.0
0.3914	−68.25
0.5684	−62.02
0.8242	−56.60
1.0090	−53.30
CsI, 373.15 K	
Water(0.0)	(75.92)
0.09843	−79.3
0.1964	−74.4
0.4153	−67.94
0.6115	−62.25
0.7969	−57.60
0.9907	−54.21
$NaIO_3$, 298.15 K	
Water(0.0)	(75.26)
0.05138	−22.58
0.10282	−8.80
0.15468	−0.10
0.25572	+16.17
0.36771	+31.18
0.45295	+42.53
$NaIO_3$, 323.15 K	
Water(0.0)	(75.28)
0.01019	+30.5
0.02044	+38.6
0.05092	+40.5
0.10283	+47.06
0.23165	+58.12
0.52556	+81.26
$NaIO_3$, 348.15 K	
Water(0.0)	(75.50)
0.01802	+49.7
0.04618	+58.0
0.05071	+58.6
0.09547	+63.1
0.20033	+71.2
0.20204	+71.7
0.35476	+82.14
0.41657	+85.18
$NaIO_3$, 373.15 K	
Water(0.0)	(75.92)
0.05138	+52.44
0.10282	+60.92
0.15468	+65.74
0.20390	+69.65
0.25572	+73.91
0.36771	+80.40
0.45295	+84.37
KIO_3, 298.15 K	
Water(0.0)	(75.26)
0.02018	−51.5
0.04271	−48.7
0.08321	−45.3
0.14193	−35.2
0.20525	−27.02
0.29825	−15.13
0.40571	−3.33
KIO_3, 323.15 K	
Water(0.0)	(75.28)
0.08321	+14.84
0.14193	+20.96
0.20525	+25.60
0.29825	+34.10
0.40571	+40.03
KIO_3, 348.15 K	
Water(0.0)	(75.50)
0.08321	+32.1
0.14193	+38.8
0.20525	+41.4
0.29825	+46.91
0.40571	+51.73
KIO_3, 373.15 K	
Water(0.0)	(75.92)
0.02018	+16.0
0.04271	+25.3
0.08321	+28.5
0.14193	+36.5
0.20525	+39.26
0.29825	+44.02
0.40571	+50.00
$CsIO_3$, 298.15 K	
Water(0.0)	(75.26)
0.00501	−113.4
0.00987	−106.3
0.02555	−90.7
0.04491	−82.0
0.05469	−80.6
0.06850	−77.9
$CsIO_3$, 323.15 K	
Water(0.0)	(75.28)
0.00987	−34.8
0.01994	−20.53
0.04376	−11.76
0.06556	−8.34
$CsIO_3$, 348.15 K	
Water(0.0)	(75.50)
0.00987	−5.66
0.01994	+8.42
0.04376	+17.44
0.06556	+18.73
$CsIO_3$, 373.15 K	
Water(0.0)	(75.92)
0.00517	−0.8
0.01165	+13.7
0.03329	+15.0
0.03976	+17.9
0.05116	+21.6
0.05924	+23.6

*Values in parentheses are heat capacities ($C^0_{p,1}$) for pure solvent (water) taken from compilations of Kell (18) and Raznjevic (19).

TABLE 3. (*concluded*)

Molality (mol kg^{-1})	ΦV (cm^3 mol^{-1})	Molality (mol kg^{-1})	ΦV (cm^3 mol^{-1})	Molality (mol kg^{-1})	ΦV (cm^3 mol^{-1})	Molality (mol kg^{-1})	ΦV (cm^3 mol^{-1})
$CsIO_3$, 322.04 K		0.04376	51.07	0.01994	52.92	0.03329	53.68
Water(0.0)	(18.22)	0.06556	51.39	0.04376	53.15	0.03976	53.98
0.00987	48.16	*$CsIO_3$, 347.03 K*		0.06556	53.44	0.05116	54.39
0.01994	50.31	Water(0.0)	(18.46)	*$CsIO_3$, 371.82 K*		0.05116	54.45
0.01994	50.46	0.00987	51.73	Water(0.0)	(18.77)	0.05924	54.63
0.04376	51.02	0.01994	52.87	0.01165	52.79		

*Values in parentheses are volumes (V_1^0) for pure water, calculated from equations of Fine and Millero (20).

TABLE 4. Apparent molar volumes ($^\Phi V$) of $KClO_4$ and HCl in aqueous solutions as a function of temperature, at 0.6 MPa*

Molality (mol kg^{-1})	ΦV (cm^3 mol^{-1})	Molality (mol kg^{-1})	ΦV (cm^3 mol^{-1})
$KClO_4$, 297.19 K		*$KClO_4$, 371.82 K*	
Water(0.0)	(18.06)	Water(0.0)	(18.77)
0.00897	52.92	0.00897	57.90
0.00897	53.03	0.04669	60.75
0.04669	53.36	0.04669	60.77
0.07681	53.47	0.07681	61.34
0.09582	53.64	0.07681	61.34
0.09582	53.67	0.11945	61.43
0.11945	53.73	0.11945	61.46
		HCl, 322.13 K	
$KClO_4$, 321.9 K		Water(0.0)	(18.22)
Water(0.0)	(18.22)	0.01007	17.57
0.00897	56.73	0.02532	17.84
0.04669	57.25	0.05088	18.18
0.04669	57.36	0.10133	18.36
0.09582	57.47	0.15204	18.65
0.09582	57.42	0.20630	18.66
0.11945	57.52	*HCl, 347.03 K*	
0.11945	57.48	Water(0.0)	(18.46)
		0.02085	16.81
$KClO_4$, 346.92 K		0.02565	16.93
Water(0.0)	(18.46)	0.05156	17.49
0.02956	59.10	0.10267	17.96
0.02956	59.14	*HCl, 371.97 K*	
0.04669	59.39	Water(0.0)	(18.78)
0.07681	59.75	0.01049	13.77
0.11945	59.90	0.02121	14.38
0.11945	59.89	0.05163	15.26

*Values in parentheses are volumes (V_1^0) for pure water, calculated from equations of Fine and Millero (20).

considering the uncertainties estimated in such measurements. This was expected, because the literature data were obtained recently with a room-temperature version of our flow microcalorimeter and flow densimeter system (1, 3).

For KIO_3, $CsIO_3$, and $KClO_4$, no room-temperature literature data are available for comparison. In the case of NaI and HCl, heat capacity and density measurements were not carried out at room temperature.

High-temperature values

Figure 2 shows a comparison of our data for CsCl, at 323.15

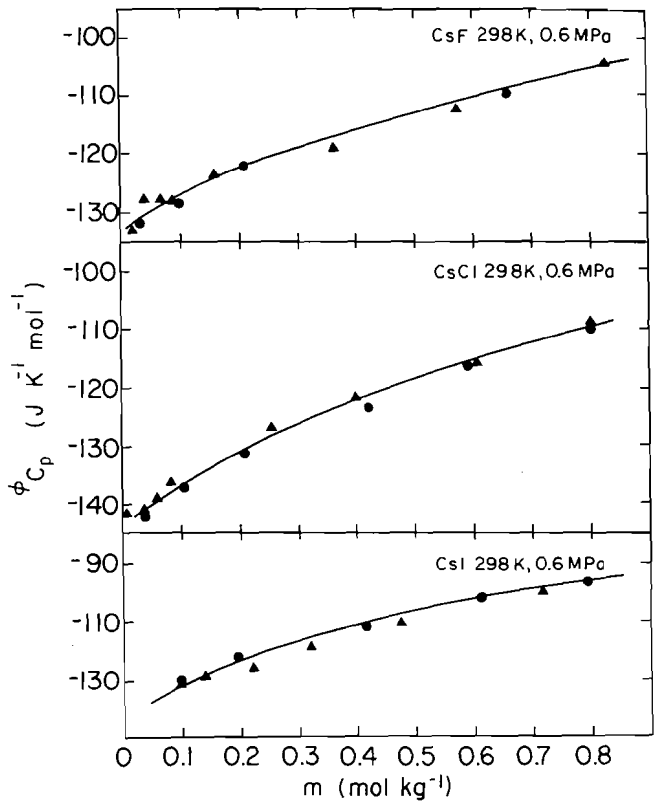

FIG. 1. Apparent molar heat capacities, $^\Phi C_p$, as a function of molality, m, for aqueous solutions of cesium halides; a comparison with 298.15 K data of Fortier *et al.* (7) and Desnoyers *et al.* (8). Present work, ●; data for refs. 7 and 8, ▲.

and 373.15 K, with existing data as a function of concentration (12). The literature data were obtained from adiabatic calorimetry measurements, and are based on only three, relatively high concentration (0.498, 1.084, and 1.606 mol kg^{-1}) of aqueous CsCl (12). The agreement is reasonable, but our $^\Phi C_p(T, m)$ values are about 5 J K^{-1} mol^{-1} less negative than the $^\Phi C_p(T, m)$ values of Rüterjans *et al.* (12). We believe the reason for the discrepancy at higher temperatures is that the adiabatic calorimetric measurements (12) require vaporization corrections, because both liquid and vapour phases of the sample coexist during the course of C_p measurement (12, 21). The large vaporization corrections at higher temperatures decrease the precision of the measured heat capacities and, consequently, of the $^\Phi C_p(T, m)$ values (12). The present flow calorimetric method does not require such vaporization corrections (1, 13).

Our $^\Phi C_p(T, m)$ values for CsI are about 13 J K^{-1} mol^{-1} less

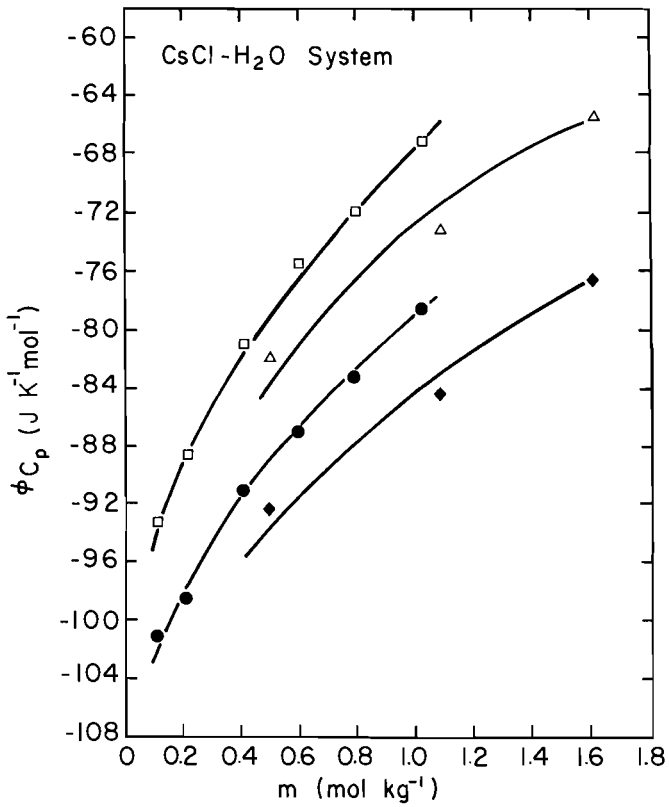

FIG. 2. Apparent molar heat capacities, ${}^{\phi}C_p$, as a function of molality, m, for aqueous CsCl solutions; a comparison with data of Rüterjans *et al.* (12) at 323.15 and 373.15 K. Data for 323.15 K: ◆, ref. 12; ●, present work. Data for 373.15 K: △, ref. 12; □, present work.

negative at 323.15 K and about 18 J K^{-1} mol^{-1} less negative at 373.15 K than the ${}^{\phi}C_p(T, m)$ values of Rüterjans *et al.* (12). We attribute the discrepancies between the two sets of data to uncertainties in the literature data associated with the vaporization corrections, as discussed above.

In the case of NaI, CsF, $NaIO_3$, KIO_3, $CsIO_3$, and $KClO_4$, no literature data at higher temperatures are available for comparison.

Conclusions

We have obtained the heat capacities (C_p and ${}^{\phi}C_p$), densities (d) and volumes (${}^{\phi}V$) of several 1:1 electrolytes in water, as a function of temperature and concentration. Our data are in good agreement with the sparse data available in the literature and determined by similar, or different, techniques. The present data are used in ref. 6 to determine reliable $\bar{C}^{o}_{p,2}(T)$ functions, which can then be used to calculate the thermodynamic properties of ions in water over an extended temperature range.

Acknowledgements

We are indebted to Professor Kenneth S. Pitzer for valuable discussions on this paper.

1. P. P. S. SALUJA. J. Nucl. Mater. **130**, 329 (1985).
2. D. F. TORGERSON, N. H. SAGERT, D. W. SHOESMITH, and P. TAYLOR (*Editors*). Underlying chemistry research for the nuclear fuel waste management program. Atomic Energy of Canada Limited Report, AECL-7786. 1984.
3. P. P. S. SALUJA and J. C. LEBLANC. Heat capacity data for selected cesium- and iodine-containing electrolytes in water at elevated temperatures. Atomic Energy of Canada Limited Report, AECL-8370. 1985.
4. D. D. WAGMAN, W. H. EVANS, V. B. PARKER, R. H. SCHUMM, I. HALOW, S. M. BAILEY, K. L. CHURNEY, and R. L. NUTTALL. NBS tables of chemical thermodynamic properties. Selected values for inorganic and C_1 and C_2 organic substances in SI units. U.S. National Bureau of Standards. J. Phys. Chem. Ref. Data Suppl. **11**, 1 (1982).
5. P. S. Z. ROGERS and K. S. PITZER. J. Phys. Chem. **85**, 2886 (1981).
6. P. P. S. SALUJA, K. S. PITZER, and R. C. PHUTELA. Can. J. Chem. In press.
7. J.-L. FORTIER, P.-A. LEDUC, and J. E. DESNOYERS. J. Solution Chem. **3**, 323 (1974).
8. J. E. DESNOYERS, C. DE VISSER, G. PERRON, and P. PICKER. J. Solution Chem. **5**, 605 (1976).
9. A. ROUX, G. M. MUSBALLY, G. PERRON, J. E. DESNOYERS, P. P. SINGH, E. M. WOOLLEY, and L. G. HEPLER. Can. J. Chem. **56**, 24 (1978).
10. J. J. SPITZER, I. V. OLOFSSON, P. P. SINGH, and L. G. HEPLER. Thermochim. Acta, **28**, 155 (1979).
11. R. E. MITCHELL and J. W. COBBLE. J. Am. Chem. Soc. **86**, 5401 (1964).
12. H. RÜTERJANS, F. SCHREINER, U. SAGE, and TH. ACKERMANN. J. Phys. Chem. **73**, 986 (1969).
13. P. PICKER, P.-A. LEDUC, P. R. PHILLIP, and J. E. DESNOYERS. J. Chem. Thermodyn. **3**, 631 (1971).
14. D. SMITH-MAGOWAN and R. H. WOOD. J. Chem. Thermodyn. **13**, 1047 (1981).
15. R. H. BUSEY, H. F. HOLMES, and R. E. MESMER. J. Chem. Thermodyn. **16**, 343 (1984).
16. P. PICKER, E. TREMBLAY, and C. JOLICOEUR. J. Solution Chem. **3**, 377 (1974).
17. H. J. ALBERT and R. H. WOOD. Rev. Sci. Instrum. **55**, 589 (1984).
18. G. S. KELL. Thermodynamics and transport properties of fluid water. *In* Water, a comprehensive treatise. Vol. 1. The physics and physical chemistry of water. *Edited by* F. Franks. Plenum Press, New York. 1973. Chapt. 10. pp. 363–412.
19. K. RAZNJEVIC. Handbook of thermodynamic tables and charts (English Translation). Hemisphere Publishing Corporation, Washington. 1976.
20. R. A. FINE and F. J. MILLERO. J. Chem. Phys. **59**, 5529 (1973).
21. A. J. B. CRUICKSHANK, TH. ACKERMANN, and P. A. GIGUE'RE. Heat capacity of liquids and solutions near room temperature. *In* Experimental thermodynamics. Vol. I. Calorimetry of non-reacting systems. *Edited by* J. P. McCullough and D. W. Scott. Plenum Press, New York. 1968. Chapt. 12. pp. 421–535.

The chemistry of some methoxychlor derivatives

WILLIAM H. BAARSCHERS[1] AND JAMES P. VUKMANICH
Department of Chemistry, Lakehead University, Oliver Road, Thunder Bay, Ont., Canada P7B 5E1
Received May 21, 1985[2]

WILLIAM H. BAARSCHERS and JAMES P. VUKMANICH. Can. J. Chem. **64**, 932 (1986).

The preparation of 1-chloro-2,2-bis(*p*-methoxyphenyl)ethylene (**3***a*) and of 1-chloro-2,2-bis(*p*-hydroxyphenyl)ethylene (**3***b*), required for a study of the microbial degradation of methoxychlor (**1***a*) was reinvestigated. The methoxy compound (**3***a*) was readily obtained by alkaline dehydrohalogenation of 1,1-dichloro-2,2-bis(*p*-methoxyphenyl)ethane (**2***a*), but similar treatment of 1,1-dichloro-2,2-bis(*p*-hydroxyphenyl)ethane (**2***b*) gave a chlorine-free compound, characterized as the diethyl acetal of 2,2-bis(*p*-hydroxyphenylacetaldehyde (**5***a*) on the basis of spectroscopic evidence and comparison with a model compound. Also, 2,2-bis(*p*-methoxyphenyl)acetic acid (**4***a*) and 2,2-bis(*p*-hydroxyphenyl)acetic acid (**4***b*) were prepared and the solubility and *p*-values (ethyl acetate/water) of these acids were determined.

WILLIAM H. BAARSCHERS et JAMES P. VUKMANICH. Can. J. Chem. **64**, 932 (1986).

On a réétudié la préparation du chloro-1 bis(*p*-méthoxyphényl)-2,2 éthylène (**3***a*) et du chloro-1 bis(*p*-hydroxyphényl)-2,2 éthylène (**3***b*) qui nous étaient nécessaires pour une étude de la dégradation microbienne du méthoxychlor (**1***a*). On obtient facilement le composé méthoxylé (**3***a*) par une déhydrohalogénation alcaline du dichloro-1,1 bis(*p*-méthoxyphényl)-2,2 éthane (**2***a*); toutefois, si l'on traite le dichloro-1,1 bis(*p*-hydroxyphényl)-2,2 éthane (**2***b*) de la même manière, on obtient un composé ne contenant pas de chlore. Sur la base de données spectroscopiques et par comparaison avec un composé modèle, on a établi qu'il s'agissait du diéthyl acétal du bis(*p*-hydroxyphényl)-2,2 acétaldéhyde (**5***a*). De plus, on à préparé l'acide bis(*p*-méthoxyphényl)-2,2 acétique (**4***a*) et l'acide bis(*p*-hydroxyphényl)-2,2 acétique (**4***b*) et l'on a déterminé leurs solubilités ainsi que leurs valeurs *p* (acétate d'éthyle/eau).

[Traduit par la revue]

Introduction

It was shown (1) that methoxychlor (**1***a*) and its hydroxy analogue (**1***b*) are reductively dechlorinated by *Klebsiella pneumoniae*. The resulting dichloro compounds (**2**) appeared to be further degraded, possibly (2) via the monochloro-olefins (**3**) to the substituted phenylacetic acids (**4**). Better evaluation of these preliminary results (1) required the preparation of the monochloro-olefins (**3**) and the acids (**4**) and measurement of the water solubility and extractability of the latter.

Most of the required compounds could be synthesized by methods published in earlier literature (3–5) and need no further discussion. However, attempts to prepare the dihydroxymonochloro-olefin (**3***b*) by alkaline dehydrohalogenation led to an unusual substitution product. The elucidation of structure **5***a* for this product on the basis of its spectroscopic properties and a comparison with the model compound **5***b* constitute a major part of this report.

Results and discussion

The dehydrohalogenation of substituted 2,2-diarylchloroethanes, including methoxychlor (**1***a*), has been studied by Cristol *et al.* (6). These authors found the rate of this E2 reaction to be primarily dependent on the acidity of the benzylic hydrogen, which in turn is determined by the electronic effects of the *p*-substituents on the aromatic rings and the degree of chlorine substitution on the α-carbon. Thus, the dehydrohalogenation of methoxychloro (**1***a*), hydrochlor (**1***b*), and the dimethoxydichloro compound (**2***a*) was found to proceed smoothly in ethanolic potassium hydroxide. In the case of hydroxychlor (**1***b*), the decrease in acidity of the benzylic hydrogen caused by the formation of the dianion (in alkaline medium) is sufficiently offset by the presence of the trichloromethyl group to allow elimination to proceed.

For the dihydroxydichloro compound (**2***b*) it appears that the decrease in chlorine substitution, as compared to hydroxychlor (**1***b*), has attenuated the acidity of the benzylic hydrogen to a point where alkaline dehydrohalogenation is no longer possible. Thus, treatment of the dichloro compound (**2***b*) with ethanolic potassium hydroxide gave a crystalline. chlorine-free product, $C_{18}H_{22}O_4$, in nearly quantitative yield. The elucidation of structure **5***a* (Scheme 1) for this new compound is relevant to the understanding of the chemistry of the 2,2-diarylchloroethanes.

The proton nuclear magnetic resonance (^{1}H nmr) spectrum of this unexpected reaction product contained multiple signals centered at δ = 9.04 and 3.20 ppm, characteristic of two equivalent ethoxy groups. A single 2-proton signal at δ = 4.21 ppm was initially assigned to the methylene group in a benzoin type structure (**7**), which could mechanistically be rationalized in terms of a modified Fritsch–Buttenburg–Wiechell rearrangement (7). However, a symmetrical 4-line pattern (8H), centered at δ = 6.94 ppm in this spectrum, indicated the equivalence of the two aromatic rings, which is inconsistent with structure **7**.

Treatment of the ethoxy compound with *p*-toluenesulfonic acid in dry acetone (8) gave a crude mixture in which the aldehyde (**6***a*) was the major component. Although attempts to purify this aldehyde failed due to slow and continuing decomposition during handling, the impure aldehyde (ν_{max} = 1719 cm^{-1}) gave a ^{1}H nmr spectrum in which the benzylic proton (H_a, **6**) gave a signal at δ = 4.69 ppm coupled (J = 1.5 Hz.) with the aldehydic proton (H_b) at δ = 9.75 ppm. The instability of the aldehyde (**6***a*) must be attributed to the *p*-hydroxy groups, since the commercially available diphenyl acetaldehyde (**6***b*) is a stable compound.

The anomalous chemical shift of the protons H_a and H_b of the acetal **5***a* must also be attributed to the presence of the *p*-hydroxy groups. Hexadeuteroacetone, routinely used in this study for solubility reasons, could form hydrogen bonds with these hydroxy groups, causing the benzylic proton H_a and the α-proton H_b to have the same chemical shift, so that only the single two-proton signal at δ = 4.21 is observed. Attempts to

[1]Author to whom correspondence may be addressed.
[2]Revision received Dec. 20, 1985.

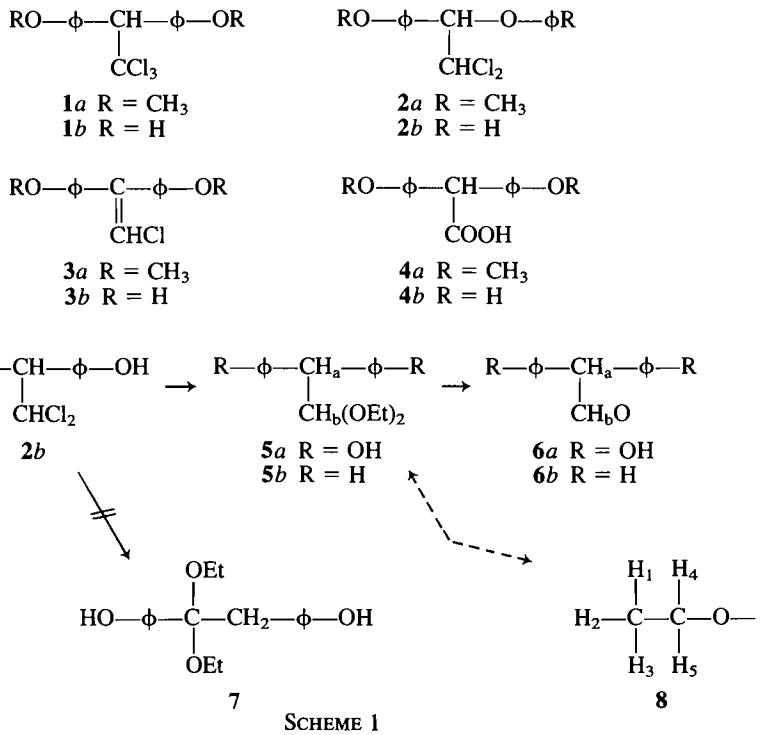

SCHEME 1

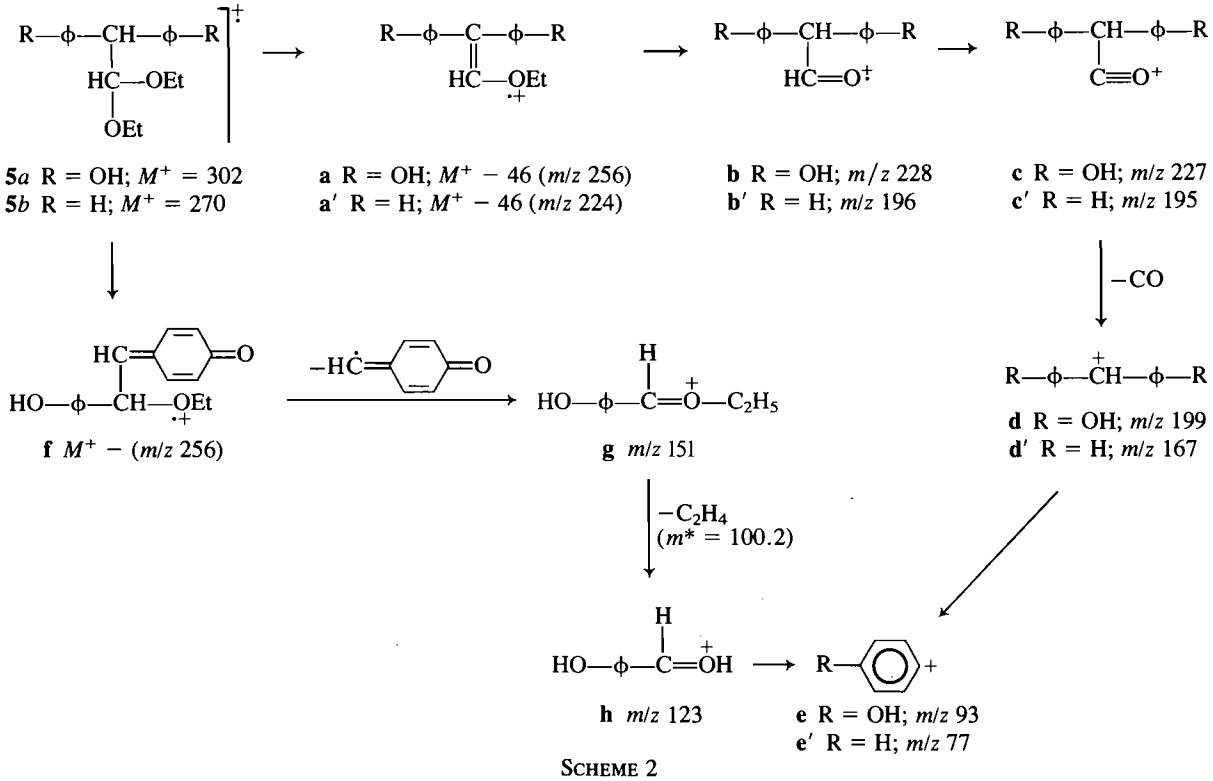

SCHEME 2

confirm this explanation by recording the ^{1}H nmr spectrum at 400 MHz were not successful.

Incidentally, the 400-MHz spectrum of the acetal (**5***a*) did provide the necessary resolution to show the considerable rigidity of this molecule in terms of the nonequivalence of the methylene protons of the ethoxy groups. A computer simulation of the observed 16-line signal was carried out using the ITRCAL program (9). Assignment of $\delta = 3.16$ and $\delta = 3.27$ ppm to protons H_4 and H_5 (**8**), respectively, and setting $J_{4,5} = 9.5$ Hz and $J_{1,4} = 7.27$ Hz gave a simulated spectrum identical to the observed pattern.

Final confirmation for the structure of the acetal (**5***a*) was obtained by comparison of its mass spectrum with that of the diethyl acetal (**5***b*) prepared from diphenyl acetaldehyde (**6***b*). The ions **a,a'** → **e'**, which result from fragmentations (see Scheme 2) that do not involve the *p*-hydroxy groups (of **5***a*), are

TABLE 1. Water solubility and *p*-values of the diarylacetic acids (**4**)

	Solubility (H_2O, ppm)	*p*-Value (EtOAc/H_2O)
Methoxy acid (**4***a*)	199	0.79
Hydroxy acid (**4***b*)	17 656	0.82

common to both spectra, and the ions **g**, **h**, and **e** are only found in the spectrum of **5***a*.

It may be noted that formation of acetals by direct substitution on a dichloromethyl group is not uncommon and, together with the analogous formation of aldehydes, is one of the standard routes for the preparation of these functional groups (10). However, such reactions usually involve substrates in which elimination is not a viable alternative. That this reaction has not been observed before with 2,2-diarylchloroethanes is probably because systematic studies of this group of compounds (5, 6, 11) have usually excluded compounds containing phenolic hydroxy groups.

For the preparation of the acids **4***a* and **4***b* by condensation of glyoxylic acid with anisole or phenol it was found that the use of glacial acetic acid with concentrated sulfuric acid substantially improved the yield of the methoxy acid (**4***a*) from 16% (12) to 80%, but this modification did not affect the yield of the hydroxy acid (**4***b*). The water solubilities of these acids were determined by gas chromatography and titration of carefully prepared, saturated solutions, and the *p*-values for the water/ethyl acetate system were determined according to Beroza *et al.* (13). The results of these measurements are presented in Table 1. It follows that, notwithstanding the relatively high water solubility of the hydroxy acid (**4***b*), the *p*-values of both acids are such that they may be expected to be recovered under conditions previously used for the extraction of *K. pneumoniae* cultures (1).

Experimental

General

Melting points are uncorrected. Infrared (ir) spectra were recorded on a Beckmann IR-12 spectrophotometer. Proton magnetic resonance (^{1}H nmr) spectra were recorded on a Bruker WP-80 and (or) a Bruker WP 400 spectrometer for hexadeuteroacetone solutions with tetramethylsilane as internal standard. Mass spectra (ms) were recorded on a Hitachi–Perkin–Elmer RMU-7 double focussing mass spectrometer. Combustion analyses were carried out with a Perkin Elmer Model 240 elemental analyser. A Perkin Elmer Model 3920 B gas chromatograph equipped with a flame ionization detector was used with silicone gum SE-30 (5%) on Gaschrom Q in a 1.8 × 6.4 mm column at 230–250°C. Nitrogen was the carrier gas at 25 mL/min.

1,1,1-Trichloro-2,2-bis(*p*-hydroxyphenyl)ethane ("Hydroxychlor", **1***b*), 1,1-dichloro-2,2-bis(*p*-methoxyphenyl)ethane (**2***a*), and 1,1-dichloro-2,2-bis(*p*-hydroxyphenyl)ethane (**2***b*) had been prepared earlier (1), according to Kapoor *et al.* (3). 1-Chloro-2,2-bis(*p*-methoxyphenyl)ethylene (**3***a*) was prepared according to Mendel *et al.* (4), and 1-chloro-2,2-bis-(*p*-hydroxyphenyl)ethylene (**3***b*) according to Davison *et al.* (5). All of these compounds had the required mp's, gave satisfactory elemental analysis results, and had spectral properties (^{1}H nmr and ms) in accordance with their structures.

*2,2-Bis(*p*-hydroxyphenyl)acetaldehyde diethyl acetal (**5**a)*

1,1-Dichloro-2,2-bis(*p*-hydroxyphenyl)ethane (**2***b*, 0.402 g) was added to a solution of potassium hydroxide (0.4 g) in ethanol (96%, 40 mL) and the mixture was refluxed for 1 h. The solvent was removed *in vacuo*, the residue dissolved in icewater (50 mL), and the resulting aqueous solution was acidified and extracted with ether (3 × 50 mL). The combined extract, after drying and removal of the solvent *in vacuo*, gave a crude product that, on recrystallization (chloroform–benzene – ethyl acetate), gave the pure acetal (**5***a*, 0.399 g, 93%); mp 190–192°C; ^{1}H nmr δ:0.94 (t, 6H, J = 7 Hz), 3.21 (m, 4H), 4.21 (s, 2H), 6.94 (q, 8H, arom.); ms: 302 (M^+, 1.5), 256 (30), 228 (11), 227 (14), 199 (40), 151 (100), 123 (80), 93 (22), 77 (18). *Anal.* calcd. for $C_{18}H_{22}O_4$: C 71.50, H 7.33; found: C 71.44, H 7.27.

*2,2-Bis(*p*-hydroxyphenyl)acetaldehyde (**6**a)*

To the diethylacetal (**5***a*, 0.902 g), in dry acetone (35 mL), was added *p*-toluenesulfonic acid (0.106 g) and the mixture was stirred at room temperature for 2 h. After removal of the solvent *in vacuo*, the residue was dissolved in water (80 mL) and sodium bicarbonate was added until pH = 7. Extraction with ether and removal of the solvent gave the crude aldehyde (**6***a*, 0.624 g). Thin-layer chromatography indicated the absence of starting material and the presence of minor impurities; ^{1}H nmr δ: 4.69 (d, 1H, J = 1.5 Hz), 6.90 (q, 8H, arom.), 9.75 (d, 1H, J = 1.5 Hz).

Attempts to purify the aldehyde (**6***a*), by recrystallization or by column or preparative thin-layer chromatography, led to increasingly impure products.

*2,2-Diphenylacetaldehyde diethyl acetal (**5**b)*

To a solution of diphenylacetaldehyde (**6***b*, 2.73 g) in ethanol (25 mL), was added concentrated sulfuric acid (0.5 mL), the mixture refluxed for 3 h, concentrated to small volume, and poured into icewater (50 mL) containing sodium carbonate (1 g). Extraction with ether gave a crude product (2.71 g) of which a small portion was purified by chromatography on silica gel. Elution with $CHCl_3$ gave the pure acetal (**5***b*) as a colourless oil; ^{1}H nmr δ: 0.99 (t, 6H, J = 7 Hz), 3.53 (m, 4H), 4.25 (d, 1H, J = 8 Hz), 5.20 (d, 1H, J = 8 Hz), 7.33 (m, 10H, arom.); ms: 270 (M^+, not observed), 224 (100), 196 (57), 195 (29), 167 (85), 77 (62).

*2,2-Bis(*p*-methoxyphenyl)acetic acid (**4**a) and 2,2-bis(*p*-hydroxyphenyl)acetic acid (**4**b)*

The acids were prepared by condensation of glyoxylic acid with anisole and phenol, respectively. The method of Hubacher (10) was modified by using glacial acetic acid as the solvent and concentrated sulfuric acid as the catalyst. The acid (**4***a*) was obtained in 80% yield and the yield of **4***b* was 42%. Both compounds were characterized by satisfactory combustion analysis results and had spectroscopic (^{1}H nmr, ms) properties in agreement with their structures.

Solubility measurements

(*i*) Methoxy acid **4***a* (25 mg) was added to water (50 mL) and the mixture stirred at room temperature for 48 h and filtered through a plug of glass wool. The first 20 mL of filtrate were discarded and, from the next 20 mL, triplicate 1-mL aliquots were transferred to 1-mL serum vials. After removal of the water with a stream of dry nitrogen, each sample was silylated (Tri-sil, 0.2 mL) and diluted with an internal standard solution (0.8 mL, DDT in benzene). Gas chromatographic analysis of these samples and of a series of similarly prepared standard solutions indicated the concentration of the acid **4***a* in water to be 199 ppm

(*ii*) Hydroxy acid **4***b* (2.0 g) was added to water (50 mL) and the mixture stirred and filtered as above. Triplicate 5.00-mL aliquots were titrated with sodium hydroxide solution to pH = 7.4. The average titer of 11.94 mL indicated the solubility of the acid to be 17 656 ppm.

p-Values

Stock solutions were prepared by dissolving the methoxy acid (45.51 mg) and the hydroxy acid (24.81 mg) in ethyl acetate (100 mL each). Aliquots (5.0 mL) of these stock solutions were transferred to 10-mL screw cap vials, containing distilled water (5.0 mL), previously equilibrated with ethyl acetate. The vials were shaken by hand, the layers allowed to separate, and 2-mL aliquots of the organic phase were withdrawn, placed in separate vials, and the solvent removed with a stream of dry nitrogen. Each dry residue was treated with Tri-sil reagent (Pierce, 0.2 mL) and made up to 1 mL with a DDT-containing internal standard solution. Gas chromatographic analysis of these

samples, as compared to a series of similarly prepared standard solutions, gave *p*-values (i.e., the ratio of the material in the organic phase to that originally present in the stock solution) as 0.79 for the methoxy acid (**4***a*) and 0.82 for the hydroxy acid (**4***b*).

Acknowledgments

The authors gratefully acknowledge financial support from the Natural Sciences and Engineering Research Council of Canada, and thank Dr. R. Lenkinski, Department of Chemistry, Guelph University, for recording the 400-MHz ^{1}H nmr spectra, and Dr. S. Maciaszek of this Department, for his help with the ITRCAL simulation.

1. W. H. Baarschers, A. I. Bharath, J. Elvish, and M. Davies. Can. J. Microbiol. **28**, 176 (1982).
2. G. Wedemeyer. Appl. Microbiol. **15**, 569 (1967).
3. I. P. Kapoor, R. L. Metcalf, R. F. Nystrom, and G. K. Sanga. J. Agric. Food Chem. **18**, 1145 (1970).
4. J. L. Mendel, A. K. Klein, J. T. Chen, and M. S. Walton. J. Assoc. Off. Anal. Chem. **50**, 897 (1967).
5. K. L. Davison, V. J. Feil, and C. H. Lamoreux. J. Agric. Food Chem. **30**, 130 (1982).
6. S. J. Cristol, N. L. Hause, A. J. Quant, H. W. Miller, K. R. Eilar, and J. S. Meek. J. Am. Chem. Soc. **74**, 3333 (1952).
7. J. G. Pritchard and A. A. Bothner-By. J. Phys. Chem. **64**, 1271 (1960).
8. R. D. Stipanovic and R. B. Turner. J. Org. Chem. **33**, 3261 (1968).
9. S. Castellano and A. A. Bothner-By. J. Chem. Phys. **41**, 3863 (1964).
10. C. A. Buehler and D. E. Pearson (*Editors*). Survey of organic synthesis. Vols. 1 and 2. John Wiley and Sons, New York. 1977. p. 468.
11. C. H. Lamoureux and V. J. Feil. J. Assoc. Off. Anal. Chem. **63**, 1007 (1980).
12. M. H. Hubacher. J. Org. Chem. **24**, 1949 (1959).
13. M. Beroza, M. N. Inscoe, and M. O. Bowman. Residue Rev. **30**, 1 (1969).

Dimeric rhodium(II) complexes containing bridging mandelate ligands

FLORIAN PRUCHNIK[1]
Institute of Chemistry, University of Wroclaw, 53-643 Wroclaw, Joliot - Curie 14, Poland
AND
BRIAN R. JAMES AND PÁL KVINTOVICS[2]
Department of Chemistry, University of British Columbia, Vancouver, B.C., Canada V6T 1Y6
Received November 8, 1985

FLORIAN PRUCHNIK, BRIAN R. JAMES, and PÁL KVINTOVICS. Can. J. Chem. **64**, 936 (1986).

The syntheses and characterization of some dimeric rhodium(II) complexes containing bridging mandelato ligands and a metal–metal bond are described. The compounds isolated are $Rh_2(O_2CR)_4(H_2O)_2$, previously described by Shchelokov and coworkers, and derivatives of the type $Rh_2(O_2CR)_2(N{-}N)_2X_2{\cdot}nH_2O$ (R = (*R*)—CH(OH)Ph, N—N = *o*-phenanthroline or 2,2′-dipyridyl, X = Cl, Br, I, and *n* is 4, 2, or 1). A mixture of species containing both bridged acetate and mandelate was isolated also. Infrared and electronic spectral data are reported. The chloride ligands of the dimers are displaced readily by alcohols, phosphines, phosphites, and amines; the metal centre also may be reduced by alcohols, $P(OEt)_3$, and $^nBu_2NH$. Preliminary studies point to the conditions necessary for the rhodium(II) mandelate and derivatives (phosphine or (N—N) substituted) to activate H_2 for catalytic hydrogenation of olefins and ketones, including prochiral substrates.

FLORIAN PRUCHNIK, BRIAN R. JAMES, et PÁL KVINTOVICS. Can. J. Chem. **64**, 936 (1986).

On décrit la synthèse et la caractérisation de quelques complexes dimères du rhodium(II) qui contiennent des ligands mandélato qui forment des ponts ainsi qu'une liaison métal–métal. Les composés isolés comportent le $Rh_2(O_2CR)_4(H_2O)_2$, qui a été décrit antérieurement par Shchelokov et ses collaborateurs, et des dérivés du type $Rh_2(O_2CR)_2(N{-}N)_2X_2{\cdot}nH_2O$ dans lesquels R = (*R*)—CH(OH)Ph, N—N = *o*-phénanthroline ou bipyridyle-2,2′, X = Cl, Br, ou I, et *n* = 4, 2, ou 1. On a aussi isolé des mélanges d'espèces contenant à la fois des ponts acétate et mandélate. On rapporte les données relatives aux spectres infrarouges et électroniques. Les ligands chlorures des dimères sont facilement déplacés par des alcools, des phosphines, des phosphites et des amines; le métal central peut aussi être réduit par les alcools, le $P(OEt)_3$, et $^nBu_2NH$. On a effectué des études préliminaires dans le but d'établir les conditions nécessaires pour que le mandélate de rhodium(II) et ses dérivés (substitués par des phosphines ou des N—N) puises activer le H_2 afin de réaliser une hydrogénation catalytique des oléfines et des cétones, y compris des substrates prochiraux.

[Traduit par la revue]

Introduction

Rhodium(II) carboxylato complexes such as $Rh_2(O_2CR)_4$ and bis-ligated adducts, $Rh_2(O_2CR)_2(N{-}N)_2X_2$ and $Rh_2(O_2CR)_2(L{-}L)_2$, where N—N = 2,2′-dipy, *o*-phen, X = halide, L—L = acac, dmgH, etc.,[3] have aroused considerable interest because of their interesting structures, catalytic properties, and anti-tumour activity (1,2). Our interests were based on the reported effectiveness of $Rh_2(O_2CR)_4$ (R = CH_3, C_3H_7) or $Rh_2(O_2CR)_2(dipy)_2Cl_2$ species for catalytic hydrogenation of olefins (3) and ketones (4), and cyclopropanation of substituted ethylenes (5,6). By using chiral carboxylates, we hope to develop catalytic systems for asymmetric hydrogenation of prochiral olefins and ketones, as well as for asymmetric cyclopropanation. Naturally occurring, inexpensive chiral ligands are especially attractive for use in asymmetric synthesis, and this paper describes the syntheses and characterization of some rhodium(II) complexes of the type $Rh_2(O_2CR)_2(N{-}N)_2X_2$ containing *R*- or *S*-mandelic acid. Reports on the synthesis and characterization of the *S*-mandelate complex $Rh_2(O_2CR)_4(H_2O)_2$, R = (*S*)—CH(OH)Ph, and a range of adducts formed with neutral ligands, have been published by Shchelokov *et al.* (7).

[1]On leave at the University of British Columbia, 1983.

[2]On leave from the University of Chemical Engineering, Veszprem, Hungary, 1981–1982.

[3]Ligand abbreviations used: 2,2′-dipy = 2,2′-dipyridyl, *o*-phen = 1,10-phenanthroline, Hacac = acetylacetone, $dmgH_2$ = dimethylglyoxime, py = pyridine, P(2-py)$_3$ = tris(2-pyridyl)phosphine.

Experimental

Rhodium(III) trichloride trihydrate (41.37% Rh) was supplied by Johnson, Matthey Ltd. The precursor rhodium complexes $Rh_2(O_2CCH_3)_4(MeOH)_2$ (8), $Na_4Rh_2(CO_3)_4{\cdot}2.5H_2O$ (9), and the 2-methylallyl complex $[RhCl_2(C_4H_7)]_2$ (10), were prepared by the literature methods. *R*- and *S*-Mandelic acid were used as supplied by Aldrich Chemical Co. Infrared spectra (KBr pellets) were measured on Perkin Elmer 283 and 598 instruments, uv–vis on Cary 15 and 17 instruments, and ^1H nmr on a Bruker WP-80 machine. Elemental analyses were carried out by Mr. P. Borda of the Chemistry Department at U.B.C. and at the Institute of Chemistry, University of Wroclaw. The procedures used to study the catalytic hydrogenation of the olefinic substrates have been described previously (11).

Diaquo-μ-tetrakis(R- *or* S-*mandelato)dirhodium(II), $Rh_2(O_2CR)_4(H_2O)_2$, **1**[4]*

The method used was similar to that given in the literature (7). The carbonate complex $Na_4Rh_2(CO_3)_4{\cdot}2.5H_2O$ (0.31 g, 5.3×10^{-4} mol) and (*R*)- or (*S*)-mandelic acid (0.685 g, 4.5×10^{-3} mol) in water (30 mL) were refluxed for 1 h. The blue colour of the carbonate faded and **1** precipitated as a green solid; the volume was reduced to 15 mL, and **1** was filtered off, washed with water, and recrystallized from CH_3OH–H_2O (1:1 v/v), yield 0.36 g (85%). *Anal.* calcd. for $C_{16}H_{16}O_7Rh$: C 45.41, H 3.81; found: C 45.9, H 4.1%. This method provides the simplest route to the tetrakis(mandelato) dimer; prior to the literature report of this synthesis (7), we had developed a procedure starting from $RhCl_3{\cdot}3H_2O$. Mandelic acid (0.46 g, 3×10^{-3} mol) was dissolved in EtOH (25 mL); freshly prepared ethoxide (3×10^{-3} mol Na/10 mL absolute EtOH) was then added under Ar, followed by $RhCl_3{\cdot}3H_2O$ (0.26 g, 1×10^{-3} mol), and the mixture refluxed for 1 h. Filtering

[4]R = (*R*) or (*S*)-CH(OH)Ph throughout this paper, unless stated otherwise.

yielded a green solution, which was concentrated to about 5 mL prior to addition of diethylether (10 mL) that precipitated out a green solid. This was dissolved in EtOH and loaded onto a silica-gel column; elution of the blue-green fraction with ethyl acetate gave $Rh_2(O_2CR)_4$, 0.20 g (50%). *Anal.* calcd. for $C_{16}H_{14}O_6Rh$: C 47.41, H 3.46; found: C 47.4, H 3.5. The ir data have been reported previously (7), but not the nmr data: ^{1}H nmr (DMSO-d_6), δ: PhC*H*(OH)— (4.88d, J_{HH} = 6 Hz, 1H); PhCH(O*H*)— (5.5d, J_{HH} = 6 Hz, 1H); C_6H_5 (7.1–7.3m, 5H); ^{13}C—{^{1}H} nmr(DMSO-d_6), δ: —*C*O_2 (193.3), *C*$_1$—CH(OH)CO_2 (140.8), Ph(C_2—C_6) (133–123), —*C*H(OH) (73.74).

Attempts to prepare pure mixed acetate–mandelate complexes were unsuccessful. Thus, for example, $Rh_2(O_2CCH_3)_4(MeOH)_2$ (5×10^{-4} mol) and (*S*)-mandelic acid (2×10^{-3} mol) were heated at 120°C for 4 h in 2-ethoxyethanol (7 mL); every hour ~1 mL of solvent was evaporated under vacuum to remove acetic acid. The remaining volume (~2 mL) was then filtered into diethylether (150 mL), and the mixture then refiltered. The filtrate was reduced in volume to 3–4 mL, when addition of toluene (5 mL) led to precipitation of a green solid. The precipitate was washed with toluene, dried, twice dissolved in dry diethylether and reprecipitated by adding hexane. A mixture of mixed-carboxylato ligand complexes containing both acetate and mandelate was obtained: ^{1}H nmr (CD_3COCD_3), δ: C*H*$_3CO_2$ 1.57 s, 1.62 s, 1.65 s, 1.70 s, 1.79 s; *H*$_2O$ + CH_3O*H* 2.89 s; C*H*$_3$OH 3.60 s; PhCH(O*H*)— 4.34 m; PhC*H*(OH)— 4.79 d, 4.87 m, 4.92 m; C_6H_5 7.1–7.3 m.

In $(CD_3)_2CO$ containing D_2O, the multiplets in the δ 4.79–4.92 region collapse to five singlets (loss of coupling to the mandelate–OH), the intensity ratios being the same as for the five acetate–CH_3 singlets. A mixture of $Rh_2[O_2CCH(OH)Ph]_n(O_2CMe)_{4-n}$ species, presumably with the possibility of *cis* and *trans* isomers for $n = 2$, is indicated, and an elemental analysis corresponded to $Rh_2[O_2CCH(OH)Ph]_{2.5}$-$(O_2CMe)_{1.5}\cdot 1.5H_2O\cdot 0.5CH_3OH$. *Anal.* calcd: C 39.46, H 3.80; found: C 39.5, H 4.0. Reaction of the rhodium acetate with mandelate in water gave mainly insoluble **1**; work up of the aqueous filtrate yielded water-soluble species with *n* being variable between 1 and 3.

Dichlorobis(phenanthroline)-μ-bis(S-mandelato)dirhodium(II)-tetrahydrate, $Rh_2(O_2CR)_2(phen)_2Cl_2\cdot 4H_2O$, 2

(*a*) Equimolar amounts (5×10^{-4} mol) of $[RhCl_2(C_4H_7)]_2$,phen, and (*S*)-mandelic acid, in 95% EtOH (15 ml) were refluxed for 5 h. A yellow-brown precipitate that formed was filtered off, and the red-brown filtrate left overnight under N_2 to yield red-brown crystals and a yellow powder that were separated by decantation. The red-brown compound was then recrystallized from 95% EtOH; yield 0.11 g (43%). *Anal.* calcd. for $C_{20}H_{19}O_5N_2ClRh$: C 47.50, H 3.79, O 15.82, N 5.54, Cl 7.01; found: C 47.2, H 3.8, O 15.6, N 5.6.

(*b*) A solution of $RhCl_3\cdot 3H_2O$ (10^{-3} mol), (*S*)-mandelic acid (5×10^{-3} mol) and NaOH (4×10^{-3} mol) in 95% EtOH (10 mL) were refluxed for 10 h. Some NaCl and Rh metal were filtered off to give a green solution thought to contain $[Rh_2(O_2CR)_4Cl_n]^{n-}$. Addition of 10^{-3} mol phen was followed by refluxing under N_2 for 4 h; a small quantity of a brownish-green precipitate was filtered off, and the filtrate left overnight to yield a red-brown precipitate that was recrystallized from 95% EtOH; yield 0.19 g (40%). *Anal.* found: C 47.8, H 4.0, N 5.4, Cl 7.1.

(*c*) A solution containing **1** (0.085 g, 10^{-4} mol), phen (0.040 g, 2×10^{-4} mol), and NaCl (0.013 g, 2.2×10^{-4} mol) in 75% EtOH (12 mL) was refluxed under N_2 for 2 h. The resulting dark green solution, on filtering hot in air to remove trace amounts of solid, became reddish-brown and yielded crystals of **2** on cooling; yield 70 mg (70%). *Anal.* found: C 47.5, H 3.5, N 5.7, Cl 7.4.

The bromo (3) and iodo (4) analogues of 2.

The bromo and iodo complexes were isolated in 70–80% yields as the tetra- and monohydrates, respectively, by the procedure described above in (*c*) but using NaBr or NaI. *Anal.* calcd. for $C_{20}H_{19}O_5N_2BrRh$: C 43.66, H 3.48, N 5.09, Br 14.52; found: C 43.3, H 3.2, N 4.8, Br 14.6. *Anal.* calcd. for $C_{40}H_{32}N_4I_2Rh_2$: C 42.13, H 2.83, N 4.91, I 22.26; found: C 41.7, H 2.5, N 4.6, I 22.5.

Dihalobis(dipyridine)-μ-bis(S-mandelato)dirhodium(II) dihydrate, $Rh_2(O_2CR)_2(dipy)_2X_2\cdot 2H_2O$; X = Cl (5), Br (6), I (7)

The procedure used was identical to that described in (*c*) but using dipy in place of phen, and the appropriate sodium halide; yields were 60%. *Anal.* calcd. for $C_{18}H_{17}O_4N_2ClRh$: C 46.62, H 3.70, N 6.04, Cl 7.65; found: C 46.4, H 3.4, N 6.2, Cl 7.9. *Anal.* calcd. for $C_{18}H_{17}O_4N_2BrRh$: C 42.55, H 3.37, N 5.51, Br 15.72; found: C 42.1, H 3.1, N 5.3, Br 15.4. *Anal.* calcd. for $C_{18}H_{17}O_4N_2IRh$: C 38.94, H 3.09, N 5.05, I 22.86; found: C 38.8, H 3.1, N 4.7, I 22.6.

Results and discussion

Although the metal–metal bonded μ-tetrakis(carboxylato)-dirhodium(II) species readily form adducts in which the axial sites are occupied by donor solvents or ligands (e.g., the mandelate species $Rh_2(O_2CR)_4$ readily and reversibly binds axial water ligands, and the nmr spectrum measured in DMSO-d_6 is certainly that of the bis(sulfoxide) adduct), the μ-carboxylates are thermally and substitutionally stable (1,2). The findings here confirm that substitution of the carboxylate ligands by other carboxylates, or chelating agents such as 2,2′-dipyridine or *o*-phenanthroline, is rather slow. Nevertheless, the best route that we found for the $Rh_2(O_2CR)_2(N—N)_2X_2$ complexes was via the precursor tetrakis-(mandelato) complex, rather than via $Rh_2Cl_4(C_4H_7)_2$ or $RhCl_3\cdot 3H_2O$ which gave more side products.

The extensive ir data in the literature for rhodium(II) carboxylates (1,2,12,13) allow for a fairly confident assignment of the bands listed in Table 1; ν_{asym}(RhO) almost certainly occurs at higher wavenumbers than ν_{sym}(RhO) (1). The relatively low ν(RhX) values indicate weakly held halide ligands as in the corresponding formate and acetate analogues (12,13), and ethanol solutions of the chloro and bromo complexes gave conductivities in the 140 ohm^{-1} cm^2 mol^{-1} range, while the iodo species gave about half this value; all the halide compounds show incomplete dissociation (see below). The tetrakis(mandelato) complex **1** has bands at 1380 and 1410 cm^{-1} in the $\nu_{sym}(CO_2)$ region, and a 1595 cm^{-1} band in the $\nu_{asym}(CO_2)$ region; the values are in the range given by Shchelokov *et al.* (7) for various tetrakis(mandelato) complexes, and are consistent with the familiar dimeric "lantern" structure with bridging carboxylates and a metal–metal bond. The free —OH group of the mandelate is seen at 3510 cm^{-1}. For complexes **2–7**, $\nu_{sym}(CO_2)$ and $\nu_{asym}(CO_2)$ are found in the ranges 1402–1410 and 1572–1577 cm^{-1}, respectively; the ir data, and electronic spectral data (see below), resemble very closely those of the formate and acetate $Rh_2(O_2CR)_2$-$(N—N)_2X_2$ analogues, and the type of structure, based on that determined for the formato-phenanthroline-chloro complex (12), is shown diagrammatically in Fig. 1.

The electronic spectra (Table 2) are typical of those of binuclear rhodium(II) complexes, and the lowest energy band (I) results from an allowed $\pi^*_{Rh—Rh} \rightarrow \sigma^*_{Rh—Rh}$ transition (1,7,12,14,15). The energy of this transition is higher for **2–7** than for **1**, and this we attribute to stabilization of the $\pi^*_{Rh—Rh}$ state by interaction with the π* orbitals of the unsaturated amine (12). The energy of band I has been shown previously to increase with increasing field strength of ligands coordinated along the Rh—Rh axis (1), and some limited data given in Tables 2 and 3 support further this claim. The aquo ligands of **1**, and the halide ligands of **2–7**, are readily displaced in ethanol solution and the data show an increase in energy within the series: L = ROH < RNH_2 ~ R_2NH ~ R_3N < PR_3 ~ $P(OR)_3$. A recent paper (16) has described formation of $Rh_2(O_2CCH_3)_2$-$(Ph_2P(C_6H_4))_2(CH_3CO_2H)_2$ from $Rh_2(O_2CCH_3)_4(MeOH)_2$ via

TABLE 1. Some infrared data of dimeric rhodium(II) mandelate complexes

Complex[a]	ν(RhO), cm^{-1}	ν(RhX), cm^{-1}
1	332s,364w,398m	—
2	330m, 390m	118s
3	336m, 395m	133s
4	335m, 397m	104s
5	330m, 375m, 390m	195s
6	303s, 347m	126s, 132s
7	327m, 388s	109s

[a] **1**, $Rh_2(O_2CR)_4(H_2O)_2$; **2**, (X = Cl), **3** (X = Br) within $Rh_2(O_2CR)_2$-$(phen)_2X_2 \cdot 4H_2O$; **4**, $Rh_2(O_2CR)_2(phen)_2I_2 \cdot H_2O$; **5** (X = Cl), **6** (X = Br), **7** (X = I) within $Rh_2(O_2CR)_2(dipy)_2X_2 \cdot 2H_2O$.

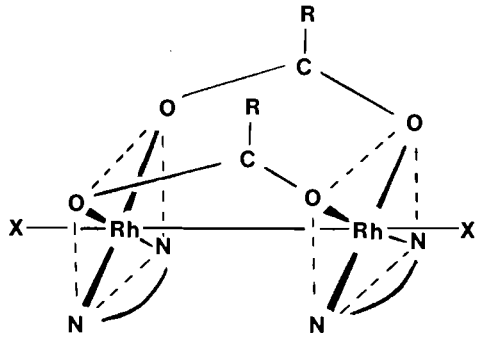

FIG. 1. Diagrammatic representation of the $Rh_2(O_2CR)_2(N{-}N)_2X_2$ complexes.

TABLE 2. Electronic absorption spectral data of the dimeric rhodium(II) mandelate complexes (**1**–**7**)

Complex[a]	Bands, μm^{-1} ($\epsilon \times 10^{-2}$, $M^{-1} cm^{-1}$)
1, EtOH	1.70(2.60)[b], 2.22(1.20)[c], 2.44sh(0.80), 3.00sh(1,70), 3.80sh(43), 3.89(51), 3.98(52), 4.31(103)
Mixture[d]	1.70(2.50)[b], 2.23(1.10)[c], 2.90sh(1.45), 3.80sh(47), 3.91sh(61), 3.98sh(66)
2, EtOH	1.80(3.70)[b], 2.30sh(32)[c], 2.63sh(54), 3.29sh(188), 3.55sh(275), 3.68sh(319), 3.86(396)
3, MeOH	1.80(2.00)[b], 2.31sh(25)[c], 2.62(42), 3.15(117)[e], 3.79sh(192), 3.89(265)
4, MeOH	1.81sh(4.20)[b], 2.22sh(50)[c], 2.55(92)[e], 2.80(97)[e], 3.31sh(102), 3.88(278)
5, EtOH	1.80(4.00)[b], 2.30(30)[c], 2.65(53), 3.23sh(230), 3.66(394)
6, MeOH	1.80(3.30)[b], 2.33sh(33)[c], 2.60sh(55), 3.03sh(166), 3.24(219)[e], 3.66(320)
7, MeOH	1.83sh(7.50)[b], 2.21sh(67)[c], 2.50(144)[e], 2.79(134)[e], 3.25sh(126), 3.58(230), 3.79sh(207), 3.86sh(198)

[a] See footnote *a* in Table 1.
[b] Band I.
[c] Band II.
[d] $Rh_2[O_2CCH(OH)Ph]_{2.5}(O_2CMe)_{1.5}$ product (see Experimental).
[e] Charge transfer, halide → Rh.

a refluxing procedure using PPh_3 in acetic acid, in which orthometallation has occurred at one phenyl ring on each phosphine; however, at the ambient conditions used in our work, simple ligand displacement to give $Rh_2(O_2CR)_4(EtOH)_{2-n}$ (phosphine)$_n$ from **1**, and $[Rh_2(O_2CR)_4(N{-}N)_2Cl_{2-n}(phosphine)_n]^{n+}$ from **2** and **5** (comparable to $Rh_2(O_2CCH_3)_2(dmg)_2(PPh_3)_2$ (17)), is considered to be occurring.

The electronic spectra of the bromo and iodo complexes (Table 2) show extra bands in 3.1–3.3 or 2.5–2.8 μm^{-1} regions, respectively, compared to the corresponding chloro complexes. The high extinction coefficients and relative positions of the peaks, based on differences between optical electronegativities of the metal and bromine and iodine (18), suggest they are halogen → Rh charge transfer bands; the halides probably remain partly coordinated in alcohol solutions. Assignment of the Cl → Rh bands, expected in the 3.6–4.0 μm^{-1} region, is difficult because of the presence of bands of the N—N ligands and phenyl groups.

The absorption occurring in the 2.2–2.35 μm^{-1} region (band II) (Tables 2, 3) arises from an allowed $\pi^*_{Rh-Rh} \rightarrow \sigma^*_{Rh-O}$ transition, with a weaker, forbidden $\delta_{Rh-Rh} \rightarrow \sigma^*_{Rh-Rh}$ component (1,7,14,15); without interference from charge transfer, the extinction coefficient of band II is less than that of band I. In the spectra of the phenanthroline and dipyridyl systems, band II is seen as a shoulder with much higher ϵ values because of charge transfer bands in the region (metal→ligand, or intraligand).

The $Rh_2(O_2CR)_2(N{-}N)_2X_2$ species on treatment with certain ligands in solution slowly undergo reduction. Thus, an ethanolic solution of **2** on treatment with a 100-fold excess of $P(OEt)_3$ under Ar at room temperature initially gives an electronic spectrum almost identical to that of the PPh_3 adduct (Table 3); on standing, the solution turns dark green ($t_{1/2} \sim 0.5$ h) with new, highly intense bands appearing at 1.49 and 1.66 μm^{-1} (670 and 602 nm), but on exposure to trace O_2, rapid reconversion to the Rh(II) species is observed. The intense, low energy bands are strongly indicative of Rh—Rh interactions within polynuclear $[Rh(I)]_n$ or $[Rh(I)Rh(II)]_n$ species (19); the bands result from metal to ligand charge transfer transitions ($d_{z^2} \rightarrow \pi^*$), the energies decreasing on increasing the number of interacting metal atoms. At refluxing temperatures, the ethanol solvent (or 2-propanol) can act as reductant, and air-sensitive green solutions again result. Green solutions formed by using $^nBu_2NH$ as reductant (Table 3) are somewhat more air-stable. Recent studies from one of our groups have revealed that reduction of Rh(III) to Rh(I) using alkyl amines occurs via a net dehydrogenation of the amine to give an enamine fragment (20); a similar redox process could be envisioned at two Rh(II) centres.

Preliminary studies show that complex **1** (or the unligated $Rh_2[O_2CCH(OH)Ph]_4$ species) in EtOH or dimethylacetamide solution will catalyze the H_2 hydrogenation of prochiral olefinic acids such as α-methylcinnamic or α-acetamidocinnamic under mild conditions (40°C, 1 atm H_2). A pretreatment of the complex with H_2 in the absence of substrate (30 min) is necessary for effective catalysis, during which time a color change from green to brown is observed: initial turnovers (mol H_2/mol Rh) for the catalysis at [Rh] = 2.5×10^{-3} M, [substrate] = 0.1 M, are about 1.0 min^{-1}, and final conversions are close to 100%. However, optical yields are close to zero, and the homogeneity of the systems is not established. Of interest, earlier work reporting on the ability of $Rh_2(O_2CCH_3)_4$ to catalyze the H_2 hydrogenation of terminal olefins in a range of solvents notes that the acetate dimer was unreactive toward H_2, although the hydride $HRh_2(O_2CCH_3)_3$ was postulated as a

TABLE 3. Electronic absorption spectral data for complexes **1**, **2**, and **5**, in the presence of added ligands (L)[a]

Complex + L	Bands, μm^{-1} ($\epsilon \times 10^{-2}$, M^{-1} cm^{-1})
1, PPh_3	2.12sh(22.0)[b], 2.65(252)[c], 3.17(111), 3.67sh(127), 3.77sh(153), 3.87sh(171), 3.97sh(190)
1 + P(2-py)$_3$	2.12sh(13.5)[b], 2.68(266)[c], 3.16(131), 3.79sh(210), 3.88(215), 3.97(203)
1 + py	1.84(2.60)[b], 2.19(1.20)[d], 3.22sh(31), 3.68sh(101), 3.80(119), 3.89(126), 4.00(132), 4.13(140), 4.31sh(128)
1 + ^{n}Bu$_2$NH	1.74(200)[b], 2.25(1.15)[d], 3.66sh(64), 3.79(69), 3.88(71)
2 + PPh_3	2.09sh(222)[b], 2.32(332)[c], 2.78(147), 3.68sh(392), 3.97sh(455)
2 + P(2-py)$_3$	2.13sh(281)[b], 2.35(360)[c], 2.96(138), 3.82(440)
2 + py	1.89sh(5.10)[b], 2.30sh(35)[d], 2.70sh(70), 3.31sh(240), 3.62sh(315), 3.89(525)
2 + ^{n}Bu$_2$NH[e]	1.31sh(10), 1.45sh(14), 1.67(29) 2.27sh(42), 2.63sh(69), 3.27sh(200), 3.86(770)
5 + PPh_3	2.08sh(248)[b], 2.31(348)[c], 2.78(121), 3.29(190), 3.85(384)
5 + P(2-py)$_3$	2.13sh(267)[b], 2.35(356)[c], 2.87(142), 3.12sh(150), 3.29(202), 3.89(550)
5 + py	1.89sh(6.10)[b], 2.27sh(34)[d], 2.66(65), 3.26sh(285), 3.68(385), 3.79sh(375), 3.86sh(340)
5 + ^{n}Bu$_2$NH	1.82sh(5.40)[b], 2.30sh(34)[d], 2.67(67), 3.25sh(243), 3.68(380)

[a]Dimeric complex + ligand (Rh_2:L = 1:2) in EtOH. **1** is considered to generate $Rh_2(O_2CR)_4(EtOH)_{2-n}L_n$ species; **2** and **5** are considered to generate $[Rh_2(O_2CR)_2(N{-}N)_2Cl_{2-n}L_n]^{n+}$ species.
[b]Band I.
[c]Charge transfer, phosphorus → Rh.
[d]Band II.
[e]Solution heated under Ar to give reduced, green species (see text).

catalytic intermediate (3). During the 30 min reaction of H_2 with **1**, ~0.65 mol gas/mol Rh_2 were taken up in solution, but reaction was still occurring slowly; no evidence for formation of a Rh hydride was obtained, and so presumably the H_2 reaction involves reduction to lower valent species. Addition of PPh_3 to solutions of **1** (PPh_3/Rh = 1) yields a catalyst system with *R*-mandelate effective for hydrogenation of E-α-methylcinnamic acid without the H_2 pretreatment; there is no darkening of colour, turnovers are now about 0.1 min^{-1}, and an enantiomeric excess of ~15% (*S*) was determined by rotation measurements on the $PhCH_2CH(CH_3)CO_2H$ product (21).

Complex **1** in the presence of phenanthroline or dipyridyl (N—N/Rh = 1) or complexes **2** and **5**, in basic alcoholic solutions, also catalyze the H_2 hydrogenation (at 30°C, 1 atm) of olefins. In the presence of excess of the chelating amines (5:1), **2** and **5** effect similar catalytic hydrogenation of ketones. Further studies are in progress on these systems, particularly with regard to use of prochiral substrates, and the relationship of the systems to other hydrogenations catalyzed by rhodium systems containing only the N—N ligands (22) or only carboxylate (3, 23), the latter sometimes utilizing hydrogen transfer from 2-propanol. Our preliminary findings on the catalytic hydrogenations suggest that π-acceptors (PPh_3, N—N) are necessary as ancillary ligands with the chiral carboxylates in order to effect any measurable asymmetric induction, and presumably this relates to stabilization of lower valent, most probably univalent, rhodium species. We have found recently that a trialkylphosphite is a required ancillary ligand for hydrogen transfer asymmetric hydrogenation of acetophenone using some iridium – chiral mandelate catalyst systems (24).

Acknowledgment

This work was supported in part by grants from the Natural Sciences and Engineering Research Council of Canada. We thank also Johnson, Matthey Ltd. for the loan of rhodium.

1. E. B. BOYAR and S. D. ROBINSON. Coord. Chem. Rev. **50**, 109 (1983).
2. T. R. FELTHOUSE. Progr. Inorg. Chem. **29**, 73 (1982).
3. B. C. Y. HUI, W. K. TEO, and G. L. REMPEL. Inorg. Chem. **12**, 757 (1973).
4. H. PASTERNAK, E. LANCMAN, and F. PRUCHNIK. J. Mol. Catal. **29**, 13 (1985).
5. D. HOLLAND and D. J. MILNER. J. Chem. Res. Miniprint, 3734 (1979).
6. H. B. KAGAN. *In* Comprehensive organometallic chemistry. Vol. 8. *Edited by* G. Wilkinson. Pergamon Press, Oxford. 1982. p. 463.
7. R. N. SHCHELOKOV, A. G. MAIOROVA, S. S. ABDULLAEV, O. N. EVSTAF'EVA, I. F. GOLOVANEVA, and G. N. EMEL'YANOVA. Russ. J. Inorg. Chem. (Engl. Transl.), **26**, 1774 (1981); I. F. GOLOVANEVA, S. S. ABDULLAEV, and R. N. SHCHELOKOV. Russ. J. Inorg. Chem. (Engl. Transl.), **27**, 1468 (1982).
8. G. L. REMPEL, P. LEGZDINS, H. SMITH, and G. WILKINSON. Inorg. Synth. **13**, 90 (1972).
9. C. R. WILSON and H. TAUBE. Inorg. Chem. **14**, 405 (1975).
10. F. PRUCHNIK. Inorg. Nucl. Chem. Lett. **9**, 1229 (1973).
11. B. R. JAMES and D. MAHAJAN. Isr. J. Chem. **15**, 214 (1977).
12. F. PRUCHNIK and M. ZUBER. Rocz. Chem. **51**, 1813 (1977); H. PASTERNAK and F. PRUCHNIK. Inorg. Nucl. Chem. Lett. **12**, 591 (1976).
13. F. PRUCHNIK, M. ZUBER, H. PASTERNAK, and K. WAJDA. Spectrochim. Acta, Part A, **34A**, 1111 (1978).
14. J. G. NORMAN, JR. and H. J. KOLARI. J. Am. Chem. Soc. **100**, 791 (1978); J. G. NORMAN, G. E. RENZONI, and D. A. CASE. J. Am. Chem. Soc. **101**, 5256 (1979).
15. D. S. MARTIN, JR., T. R. WEBB, G. R. ROBBINS, and P. E. FANWICK. Inorg. Chem. **18**, 475 (1979).
16. A. R. CHAKAVARTY, F. A. COTTON, D. A. TOCHER, and J. H. TOCHER. Organometallics, **4**, 8 (1985).
17. J. HALPERN, E. KIMURA, J. MOLIN-CASE, and C. S. WONG. J. Chem. Soc. Chem. Commun. 1207 (1971).
18. A. B. P. LEVER. Electronic spectroscopy. Elsevier, Amsterdam. 1968.
19. H. ISCI and W. R. MASON. Inorg. Chem. **14**, 913 (1975); K. R. MANN, J. G. GORDON, and H. B. GRAY. J. Am. Chem. Soc. **97**, 3553 (1975).
20. S. N. GAMAGE, R. H. MORRIS, S. J. RETTIG, and B. R. JAMES. J. Organomet. Chem. In press.
21. C. FISCHER and H. S. MOSHER. Tetrahedron Lett. 2487 (1977).
22. B. R. JAMES. *In* Comprehensive organometallic chemistry. Vol. 8. *Edited by* G. Wilkinson. Pergamon Press, Oxford. 1982. p. 285.
23. R. MARCEC. *In* Proceedings of the 4th International Symposium on homogeneous catalysis. Leningrad.1984. Book I. p. 133; S. SHINODA, T. KOJIMA, and Y. SAITO. J. Mol. Catal. **18**, 99 (1983).
24. B. HEIL, P. KVINTOVICS, L. TARSZABÓ, and B. R. JAMES. J. Mol. Catal. **33**, 71 (1985).

A simple, biogenetically modeled synthesis of 4-(methylthio)butyl thiocyanate: the reaction of thiocyanate anion with *S*-methyl-(1,*n*)-epithionium ions

M. H. Benn and Vinod K. Singh
Department of Chemistry, University of Calgary, Calgary, Alta., Canada T2N 1N4
Received October 21, 1985

M. H. Benn and Vinod K. Singh. Can. J. Chem. **64**, 940 (1986).

The reaction of *S*-methylthiolanium fluorosulphate with thiocyanate ion gives predominantly 4-(methylthio)butyl thiocyanate, a result which is in accord with a hypothesis for the biogenesis of this compound, and which has implications for the natural occurrence of analogous thiocyanates.

M. H. Benn et Vinod K. Singh. Can. J. Chem. **64**, 940 (1986).

La réaction du fluorosulfate du *S*-méthylthiolanium avec l'ion thiocyanate conduit principalement au thiocyanate de (méthylthio)-4 butyle; ce résultat est en accord avec une hypothèse relative à la biogénèse de ce composé et il a des implications relativement à l'existence à l'état naturel de thiocyanates analogues.

[Traduit par la revue]

Introduction

Glucosinolates are naturally occurring anions, characterized by the general structure **1**. They are commonly, but not exclusively, encountered within plants of families that constitute the Capparales and their decomposition is a matter of considerable current interest, because the products are known to be important factors in determining the palatability and toxicity of these plants to man and other animals (see ref. 1, and references therein).

Of the nearly 100 glucosinolates that have been isolated, or inferred to exist, all can be catabolized to isothiocyanates or nitriles. These products are known to arise from the aglucones that are released from **1** by myrosinase (thioglucoside glucohydrolase EC 3:2:3:1) (Scheme 1) (1). In contrast with this generality, only three, the allyl (2), benzyl (2, 3), and 4-(methylthio)butyl (4) compounds are known to be capable of yielding the corresponding thiocyanates, and they do so under conditions that indicate that these conversions involve other, plant-specific, enzymes.

To account for this striking restriction it has been postulated (5) that the thiocyanates are formed from aglucones by a fragmentation process in which departure of sulphate, instead of being concerted with the [1,2]-shift of the substituent R that yields the isothiocyanates, results in fragmentation to thiocyanate anion and a cation corresponding to R. Recombination of this ion pair would then be expected to preferentially form the thiocyanate as a consequence of the high nucleophilicity of the *S*-terminus of the ambident thiocyanate anion. Also plausible is the possibility that the fragmentation process is a consequence of a $Z \rightarrow E$ isomerization that destroys the geometry required for the concerted isothiocyanate-forming reaction (Scheme 2) (5). (The aglucone intermediates are shown in Schemes 1 and 2 in their free, protonated, forms. It may well be that they are bound, through bivalent sulphur, to a metal ion: this would inhibit tautomerism and interconversion of *E* and *Z* isomeric forms.)

Fragmentation should be favoured for substrates that yield relatively stable cations. The allyl and benzyl systems are textbook examples of such ions, and we visualized 4-(methylthio)butyl glucosinolate (**2**) ($n = 4$) as yielding the even more stable *S*-methylthiolanium cation. In this latter case there is then a requirement that attack by thiocyanate ion on the cation should favour ring opening over demethylation (path (b) of Scheme 3 rather than (a)), as well as preferential formation of thiocyanate. We reasoned that the first of these requirements would be met as a consequence of the release of torsional strain, as well as entropy, and statistical factors. Examination of the literature reveals excellent precedent for this in the report of Eliel *et al.* (6) that the reaction of azide and thiolate anions with **3***a* gave predominantly the products of ring opening, **4** and **5**, respectively, but we decided to submit the matter to direct test.

The reaction of thiolane (**6**, $n = 4$) with methyl fluorosulphate in dichloromethane gave the *S*-methylthiolanium salt (**3***b*). When this salt was treated with potassium thiocyanate in ethanol, or DMF, and the reaction monitored by gc, a single major product was observed (ca. 80%), together with two minor products (each ca. 10%). The latter two substances cochromatographed with authentic thiolane and methyl thiocyanate. The identity of the major product as 4-(methylthio)butyl thiocyanate (**7**) was first indicated by the results of a gc–ms analysis, and then confirmed by its isolation. The distilled material had physical properties (ir and ^{1}H nmr spectra) in excellent agreement with those reported for **7**, and the ^{13}C nmr spectrum was also in complete accord with this structure.

In order to assess the extent of isothiocyanate formation, we utilized the reaction of **3***b* with azide ion to make **4**, reduced this to the amine (**8**), and prepared from that an authentic specimen of **9**. We then established capillary gc conditions under which it was possible to obtain a base-line resolution of the isomeric thiocyanate–isothiocyanate pair. When the crude reaction products from **3***b* and potassium thiocyanate were reanalysed under these conditions, a trace (ca. 2–3%) of material chromatographically indistinguishable from the isothiocyanate (**9**) was detected. Similarly an analysis of the 200-MHz ^{1}H nmr spectrum of these crude reaction products, based on the relative integrals of the α-methylene groups of **7** and **9**, indicated the presence of the same amount of isothiocyanate.

Thus the biogenetically patterned synthesis of 4-(methylthio)butyl thiocyanate worked well, and provided a simple route to this compound, which previously had only been synthesized from 4-chloro-1-butanol, in several steps, in less than 10% yield (4).

It may also be noted that while good evidence has accumulated from the existence of a series of ω-(methylthio)alkylglucosinolates (**2**) ($n = 3$–8) (7), only the 4-(methylthio)butyl compound has been found to yield a thiocyanate. Were the higher homologues to fragment to form *S*-methyl-[1,*n*]-epithionium ions (**10***a*), our expectation would be that these would lack the torsional strain present in the thiolanium ion, and that the pre-

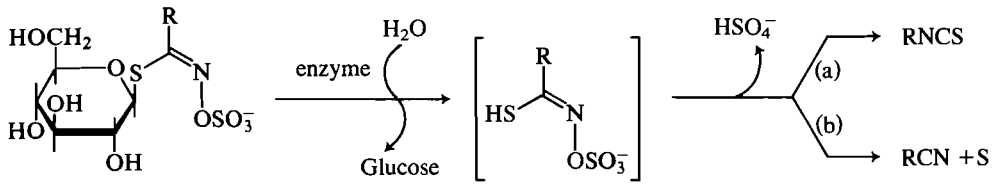

1

2 R = $CH_3S(CH_2)_n$

SCHEME 1. Catabolism of glucosinolates to isothiocyanates and nitriles

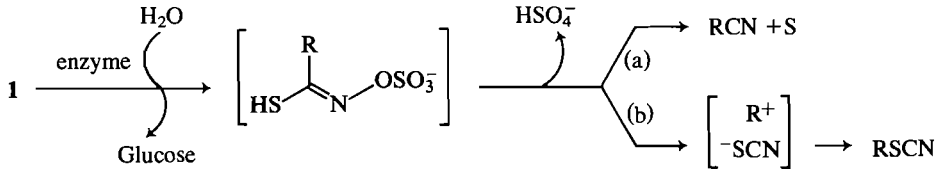

SCHEME 2. Hypothetical catabolism of glucosinolates to thiocyanates and nitriles

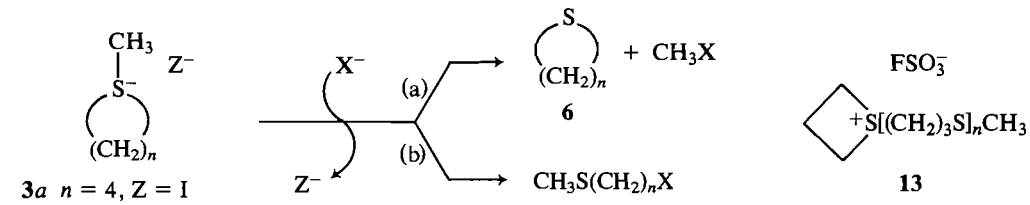

3*a* $n = 4$, Z = I
3*b* $n = 4$, Z = FSO_3
10*a* $n = 5$–8, Z = SCN
10*b* $n = 5$, Z = I
10*c* $n = 5$, Z = FCO_3
12*a* $n = 3$, Z = SCN
12*b* $n = 3$, Z = FSO_3

4 $n = 4$, X = N_3
5 $n = 4$, X = CH_3S
7 $n = 4$, X = SCN
8 $n = 4$, X = NH_2
9 $n = 4$, X = NCS
11*a* $n = 5$–8, X = SCN
14 $n = 3$, X = SCN

SCHEME 3. The reaction of *S*-methyl-1,*n*-epithionium ions with nucleophiles

ferred reaction with thiocyanate anion would be demethylation rather than ring opening; i.e., we predict that the glucosinolates **2** ($n = 5$–8) may be catabolized via cyclic *S*-methyl sulphonium salts to yield cyclic sulphides, but little, if any, of the thiocyanates **11***a*. On the other hand, **2** ($n = 3$) might give the highly strained and reactive sulphonium ion **12***a*, which we would expect to undergo ring-opening reaction with thiocyanate ion; i.e. **12***a* might give the lower homologue **14** of **7**.

In line with the first of these predictions, Eliel *et al.* have shown that azide ion attack on the *S*-methylthianium iodide (**10***b*) gives thiane and methyl azide (6). We found that thiocyanate ion behaved similarly: reaction of **10***c* with potassium thiocyanate gives thiane and only ca. 3% of **11***a*. At the other extreme, we could not control the methylation of thietane with methyl fluorosulphate on account of the very reactive nature of **12***b*: oligomerization of the theitane, to form **13**, competed with *S*-methylation. However, the reaction of potassium thiocyanate with the crude *S*-methylation products did give 3-(methylthio)propyl thiocyanate (**14**), albeit in low yield and accompanied by compounds arising from the oligomeric methylation products (see Experimental). Despite this, we think that rather than form **12***a*, 3-(methylthio)propyl glucosinolate is most likely to fragment to nitrile and elemental sulphur; i.e., since **12***a* is so highly energetic, **2** ($n = 3$) is most likely to avoid its formation and, instead, to behave as a glucosinolate incapable of yielding an efficiently charge-delocalized cation and follow path (a) of Scheme 2. Consistent with this idea are observations of the rates of solvolysis of ω-haloalkyl sulphides: little, if any, anchimeric assistance (via intramolecular cyclization to sulphonium ions) was seen when a 4-membered ring would result, in sharp contrast to the accelerated rates observed when 3-, 5-, or 6-membered rings would be formed (8, and references therein).

Thus the reactions of thiocyanate anion with *S*-methyl-(1,*n*)-epithionium ions are in accord with the fragmentation ion-pair recombination model for the biogenesis of 4-(methylthio)butyl thiocyanate, and suggest why homologues of this compound have not been observed in nature.

Experimental

Instrumental and analytical methods were as described before (9), augmented by gc and gc–ms. Packed-column gc analyses were performed with a Shimadzu 9A chromatograph (with fid) and C-R24X data processor using 3% OV-17 in 2 m × 4 mm glass columns, with a N_2 flow rate of 20 mL/min, and a temperature programme of 60 (1 min) – 250°C at 20°C/min. Capillary gc was done on a Carlo Erba instrument, using a 30 m × 0.32 mm, 0.25-μm, DB-1 column, a He flow rate of 1 mL/min, 60–200°C at 10°C/min. The gc–ms analyses were performed either with a HP 5992A instrument using similar conditions to those employed for the packed column gc work (but He as carrier gas), or a Kratos MS-80 spectrometer – data system interfaced with the Carlo Erba chromatograph.

Preparation of S*-methylthiolanium fluorosulphate (3*b*)*

Typically, to a stirred solution of thiolane (250 mg, 2.84 mmol) in dry CH_2Cl_2 (3 mL) was added a solution of methyl fluorosulphate (325 mg, 2.85 mmol) in CH_2Cl_2 (5 mL). A mildly exothermic reaction

ensued and the flask was cooled (water bath) so as to maintain an internal temperature of 20–25°C. The turbid reaction mixture was stirred for 1 h at room temperature and then evaporated to dryness under reduced pressure, finally under high vacuum. The residual free-flowing white solid (545 mg, 95%) was hygroscopic and was normally used directly. It could be recrystallized from EtOH–Et_2O (dry-box) to give the salt **3***b*, mp 188°C (sealed capillary); ^1H nmr (DMSO-d_6) δ: 2.30 (4H, m), 2.90 (3H, s), 3.46 (2H, m), 3.63 (2H, m); ^{13}C nmr (DMSO-d_6) δ: 24.9 q, 27.6 t, 44.3 t.

*Preparation of 4-(methylthio)butyl isothiocyanate (**9**)*

Treatment of the salt **3***b* with sodium azide, essentially as described by Eliel (6) but using dry DMF as solvent and conducting the reaction at 40°C for 20 h, gave **4** isolated as a colourless oil, bp 80–85°C/ca. 10 Torr (1 Torr = 133.3 Pa) (68%); ir (film): 2097; ^1H nmr ($CDCl_3$) δ: 1.7 (4H, m), 2.10 (3H, s), 2.53 (2H, m), 3.31 (2H, m); ^{13}C nmr ($CDCl_3$) δ: 15.3 q, 26.0 t, 27.8 t, 33.6 t, 51.0 t; ms: 117 ($M-N_2$, 6), 89 (16), 74 (20), 61 (78), 43 (100) (lit. (6) bp 86–87°C/15 Torr; ^1H nmr ($CDCl_3$) δ: 1.67 (4H, m), 2.08 (3H, s), 2.50 (2H, distorted t), 3.28 (2H, distorted t)).

The azide **4** was reduced with LAH according to a literature procedure (10) to give the amine **8**, which was obtained after distillation as a colourless oil, bp 80–82°C/12 Torr (54%) (lit. (11) bp 78–78.5°C/12 Torr); ir (film): 3480, 3287; ^1H nmr ($CDCl_3$) δ: 1.19 (2H, s, disappears after adding D_2O), 1.45–1.72 (4H, m), 2.1 (3H, s), 2.51 (2H, t, J = 7 Hz), 2.71 (2H, t, J = 7 Hz); ^{13}C nmr ($CDCl_3$) δ: 15.5 q, 26.5 t, 32.9 t, 34.1 t, 41.9 t; ms: 121 (6), 120 (20), 119 (100), 104 (37), 87 (18), 72 (24), 61 (33).

Following a general procedure (12), **8** (1.5 g, 12 mmol) was added to a mixture of CS_2 (2.0 g, 26.3 mmol) and H_2O (1 mL), followed by a solution of NaOH (800 mg, 40 mmol). This mixture was boiled under reflux for 10 min, then cooled to 25°C. Ethyl chloroformate (13 g, 119 mmol) was added and the mixture stirred for 15. h, after which more NaOH (800 mg) in H_2O (1 mL) was added and stirring continued for a further 1.5 h. The supernatant was decanted from a residue of salts that were washed with Et_2O (3 × 10 mL).

The combined supernatant and Et_2O extracts were then washed successively with 10% aqueous NaOH, H_2O, and brine. Removal of solvent from the dried (Na_2SO_4) Et_2O phase left a residual oil (2.46 g) that was shown by gc analysis to consist of two major components, one of which was recovered ethyl chloroformate. Column chromatography of the oil over silica gel (45 g) gave an oil (1.6 g) eluted with EtOAc–hexanes (5:95 v/v), a portion of which was further purified by distillation to give **9** as a light yellow oil, bp 90–92°/0.6 Torr (lit. (13) bp 136°C/12 Torr); ir (film): 2185, 2110 (br vs); ^1H nmr ($CDCl_3$) δ: 1.8 (4H, m), 2.11 (3H, s), 2.54 (2H, t, J = 7 Hz), 3.56 (2H, t, J = 7 Hz); ^{13}C nmr ($CDCl_3$) δ: 15.4, 25.9, 29.0, 33.3, 44.8, 130.3.

The reaction of potassium thiocyanate with sulphonium salts

(a) With S-methylthiolanium fluorosulphate

A solution of potassium thiocyanate (1.0 g, 10.3 mmol) in dry DMF (15 mL) was added to a stirred solution of **3***b* (prepared from 500 mg (5.7 mmol) thiolane) in dry DMF (10 mL), followed by a solution of KSCN (1.0 g, 10.3 mmol) in the same solvent (15 mL). The reaction mixture was stirred vigorously, and kept at 70°C (bath) for 7 h. It was then cooled to room temperature, diluted with H_2O (50 mL), and extracted with Et_2O (3 × 15 mL). The Et_2O extracts were combined, washed with H_2O (3 × 15 mL) and brine (15 mL), and then dried (Na_2SO_4). Packed column gc and gc–ms analyses revealed a single major product (ca. 80%) corresponding to **7**, together with small amounts (ca. 8% each) of thiolane and methyl thiocyanate. The oil remaining after careful removal of solvent from the Et_2O extract was distilled to yield **7** as a near colourless oil, bp 105–110°C/0.5 Torr (410 mg, 45%) ir (film): 2155; ^1H nmr ($CDCl_3$) δ: 1.75 (2H, m), 1.96 (2H, m), 2.1 (3H, s), 2.53 (2H, t, J = 7 Hz), 2.97 (2H, t, J = 7 Hz); ^{13}C nmr ($CDCl_3$) δ: 15.3 q, 27.0 t, 28.6 t, 33.1 t, 33.5 t, and 112.0 s; ms: 163 (2), 162 (2), 161 (100) (lit. (4) ir ($CHCl_3$): 2165; ^1H nmr (60 MHz, $CDCl_3$) δ: 1.5–2.0 (4H, m), 2.1 (3H, s), 2.3–2.7 (2H, m), 2.75–3.1 (2H, m)).

Capillary gc–ms revealed our distilled product to be ca. 98% pure, accompanied by ca. 2% of the isothiocyanate **9**. A similar conclusion was reached upon reexamining the ^1H nmr spectrum of the distilled **7**: traces of **9** were detectable as an absorption at δ 3.56, with an integrated intensity corresponding to the presence of 2–3% of this compound.

*(b) With S-methylthianium fluorosulphate (**10**c)*

Thiane (250 mg, 2.45 mmol) was converted to the sulphonium salt **10***c* by treatment with methyl fluorosulphate (285 mg, 2.50 mmol) in CH_2Cl_2. This salt was then dissolved in dry DMF (10 mL) containing KSCN (485 mg, 4.5 mmol) and the mixture heated at 80°C for 5 h. Work-up as described for the equivalent reaction of **3***b* yielded an Et_2O extract that was shown by gc–ms analyses to contain thiane and methyl thiocyanate as major components and only a small amount (ca. 4%) of a substance with the expected retention time and ms (176 (6), 119 (3), 117 (63), 101 (23), 61 (100)) of **11** (n = 5).

*(c) With S-methylthianium fluorosulphate (**12**b)*

To a stirred solution of methyl fluorosulphate (155 mg, 1.36 mmol) in CH_2Cl_2 (2 mL), at −5°C, was slowly added a solution of thietane (100 mg, 1.35 mmol) in CH_2Cl_2 (2 mL), the internal temperature of the reaction mixture being held at room temperature by external cooling. A gummy solid separated from the reaction mixture. After removal of solvent under reduced pressure and drying under high vacuum a sticky white solid was obtained. This material was dissolved in dry DMF (5 mL) containing KSCN (200 mg) and heated at 60°C for 1.5 h, with continuous stirring. After the usual work-up the solution of reaction products in Et_2O was analysed by gc–ms: a multitude of components were detected, among which the major were CH_3SCN (R_T 1.2 min, ca. 20%), **14** (R_T 7.5 min, ca. 25%) (149 (6), 148 (4), 147 (54), 120 (53), 61 (100)), and $CH_3S(CH_2)_4S(CH_2)_4SCN$ (R_T 12.5 min, ca. 18%) (221 (32), 206 (2), 121 (100), 73 (29), 61 (20)). Also present was $(CH_3SCH_2CH_2)_2$, (R_T 5.5 min, ca. 7%) (136 (100), 121 (18), 61 (43)).

Acknowledgement

Financial support of this work was provided via a grant-in-aid of research (to M.H.B.) from the Natural Sciences and Engineering Research Council of Canada.

1. (*a*) E. W. UNDERHILL. *In* Secondary plant products. Encyclopedia of Plant Physiology, New Series, Vol. 8. *Edited by* E. A. Bell and B. V. Charlwood. Springer Verlag, Berlin. 1980. p. 493; (*b*) G. R. FENWICK, R. K. HEANEY, and W. J. MULLIN. Crit. Rev. Food Sci. Nutr. **18**, 123 (1983).
2. R. GMELIN and A. I. VIRTANEN. Acta Chem. Scand. **13**, 1474 (1959).
3. M. SAARIVIRTA. Planta Med. **24**, 112 (1973).
4. M. SCHLÜTER and R. GMELIN. Phytochemistry, **11**, 3427 (1972).
5. (*a*) M. BENN. Pure Appl. Chem. **49**, 197 (1977); (*b*) X. HASAPIS and A. J. MACLEOD. Phytochemistry, **21**, 1009 (1982).
6. E. L. ELIEL, R. O. HUTCHINS, R. MEBANE, and R. L. WILLER. J. Org. Chem. **41**, 1052 (1976).
7. M. G. ETTLINGER and A. KJAER. *In* Recent advances in phytochemistry. Vol. 1. *Edited by* T. J. Mabry, R. E. Alston, and V. C. Runeckles. Appleton–Century–Crofts, New York. 1968. p. 60.
8. (*a*) B. CAPON and S. P. MCMANUS. *In* Neighbouring group participation. Plenum Press, New York. 1976. p. 195; (*b*) W. E. TRUCE, K. R. HOLLISTER, L. B. LINDY, and J. E. PARR. J. Org. Chem. **33**, 43 (1968).
9. H. RÜEGER and M. H. BENN. Can. J. Chem. **60**, 2918 (1982).
10. J. H. BOYER. J. Am. Chem. Soc. **73**, 5865 (1951).
11. A. KJAER and J. CONTI. Acta Chem. Scand. **8**, 295 (1954).
12. L. A. SPURLOCK and W. G. COX. J. Am. Chem. Soc. **91**, 2961 (1969).
13. A. KJAER and R. GMELIN. Acta Chem. Scand. **9**, 542 (1955).

Fastigiatine, a lycopodium alkaloid with a new ring system

ROBERT V. GERARD, DAVID B. MACLEAN,[1] ROMOLO FAGIANNI, AND COLIN J. LOCK[1]
Department of Chemistry, McMaster University, Hamilton, Ont., Canada L8S 4M1
Received September 6, 1985

ROBERT V. GERARD, DAVID B. MACLEAN, ROMOLO FAGIANNI, and COLIN J. LOCK. Can. J. Chem. **64**, 943 (1986).

Fastigiatine, $C_{19}H_{28}N_2O$, is a minor component of the alkaloids of *Lycopodium fastigiatum* R. Br. collected in New Zealand. Its structure and relative configuration have been resolved by an X-ray analysis of the free base. The pentacyclic ring system of fastigiatine has not been previously observed in the Lycopodium family of alkaloids or elsewhere. A proposal is presented for its derivation from the tetracyclic flabellidane ring system that is widely distributed among Lycopodium species. The mass spectrum and the ^{13}C and ^1H nmr spectra of fastigiatine are discussed.

ROBERT V. GERARD, DAVID B. MACLEAN, ROMOLO FAGIANNI, et COLIN J. LOCK. Can. J. Chem. **64**, 943 (1986).

La fastigiatine, $C_{19}H_{28}N_2O$, est un constituant mineur des alcaloïdes du *Lycopodium fastigiatine* R. Br. récolté en Nouvelle Zélande. On a résolu sa structure et sa configuration relative par l'analyse aux rayons-X de la base libre. On n'avait pas encore observé le système pentacyclique de la fastigiatine dans la famille des alcaloïdes du Lycopodium ou ailleurs. On propose une méthode de préparation de la fastigiatine à partir du système tétracyclique de la flabellidane que l'on retrouve souvent dans les espèces du Lycopodium. On discute du spectre de masse et des spectres rmn du ^{13}C et du ^1H de la fastigiatine.
[Traduit par la revue]

Introduction

The Lycopodium family of alkaloids comprises about 100 members of established structure distributed among some 20 different skeletal types (1). This surprisingly large number of alkaloids and ring systems has been derived from an estimated (2) 10% of the extant Lycopodium species. Recently, a number of species native to New Zealand have been investigated in this laboratory (3) and from one of them, *Lycopodium fastigiatum* R. Br., two new alkaloids, fastigiatine **1** ($C_{19}H_{28}N_2O$) and des-*N*-methylfastigiatine **2** ($C_{18}H_{26}N_2O$), have been isolated. We report here on the structure and on the nmr and mass spectra of **1**.

Fastigiatine and its lower homologue were initially detected in an extract of *L. fastigiatum* through examination by gas chromatography – mass spectrometry (gc–ms) (3). The alkaloids were then isolated from the extract by conventional liquid chromatographic procedures on alumina and silica columns. A detailed account of the isolation procedure is described elsewhere (3).

The initial examination of **1** by spectroscopic methods established its composition and the number and nature of its functional groups. An *N*-methyl, an *N*-acetyl group, a $CHCH_3$ group, and a trisubstituted double bond were evident from the nmr spectrum. The uv spectrum indicated that the double bond and the *N*-acetyl group were probably present in an enamide structure. However, the nmr spectrum and the mass spectrum of **1** did not lend themselves to simple interpretation and, because of the limited amount of compound available, an X-ray analysis was carried out. The structure derived from the X-ray study is shown in the accompanying formulas. The numbering system conforms with that commonly employed in this family of alkaloids (4).

The structure of fastigiatine is closely related to that of flabellidine **3** (1, 4) and one can envisage its formation from a derivative of *N*-methylflabellidine **4** through the iminium compound **5** by the route outlined in Scheme 1. It is noteworthy that lycopodane alkaloids functionalized at C-10 have recently been reported (5, 6), although flabellidanes similarly functionalized have not been found. The pentacyclic fastigiatine has a structural relationship to alkaloids of the tetracyclic flabellidane

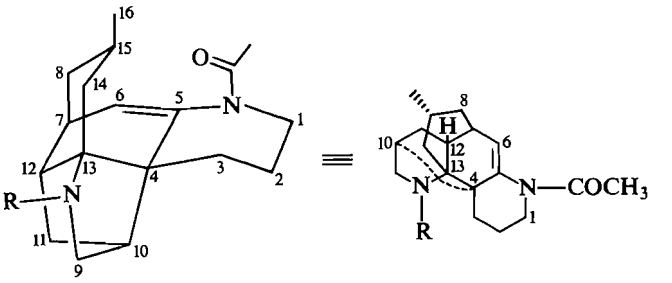

1 fastigiatine, R = CH_3 ≡ **2** des-*N*-methylfastigiatine, R = H

group that is analogous to that between the pentacyclic alopecurane group of alkaloid (1, 4, 7), e.g., dehydrolycopecurine **6** (1, 4, 8), and the lycopodane group, e.g., lycopodine **7** (1, 4). In each series the pentacyclic ring system may be formally derived from the corresponding tetracyclic ring system through formation of a bond between C-4 and C-10.

Since fastigiatine represents a new skeleton among the Lycopodium alkaloids, its mass spectrum was investigated in detail in the expectation that the information gained might be useful to others who may encounter this ring system in the future. Besides the molecular ion peak at m/z 300 and the peaks at m/z 176 and 124, there are prominent peaks at m/z 285 ($M-15$) and m/z 257 ($M-43$) in the mass spectrum of **1**. The composition of the ions corresponding to these peaks is recorded in Table 1. A B/E linked scan (9) carried out on the molecular ion at m/z 300 revealed that the ions, m/z 285, 257, and 124, are formed directly from the molecular ion, but the ion of m/z 176 was not observed in the B/E spectrum. However, its absence from the B/E spectrum does not preclude its formation from the molecular ion so long as the fragmentation leading to it occurs only in the ion source.

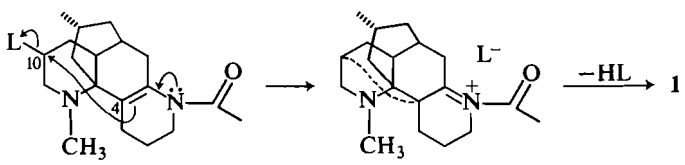

4 **5**

SCHEME 1

[1]Authors to whom correspondence may be addressed.

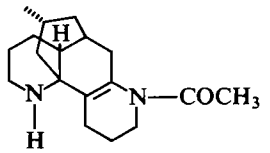

3

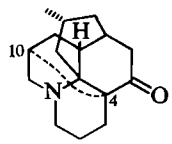

6

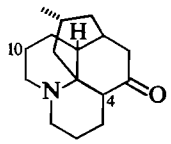

7

The ions at m/z 124 and 176 appear to arise from the fragmentation of fastigiatine into two parts, each of which can carry the charge. In the case of the spectrum of des-*N*-methylfastigiatine (3), the ion occurring at m/z 124 in **1** is shifted by 14 mass units (CH_2) to m/z 110. Thus these ions arise from the portion of the molecule bearing the N—H group in the case of des-*N*-methylfastigiatine and bearing the N—CH_3 group in the case of fastigiatine. It is apparent from the structures of **1** and **2** that the ions of m/z 124 and 176 cannot form in a simple manner. A fragmentation scheme for fastigiatine is proposed in Scheme 2, which accounts for the formation of the two ions, and in which the fragmentation is considered to be initiated in a retro Diels–Alder reaction resulting in fission of the bond between C-12 and C-7 and the bond between C-13 and C-4. Subsequent to the retro Diels–Alder process, the rupture of the bonds between C-9 and C-10 and between C-8 and C-15 is postulated and is predicted to be followed by the formation of bonds between C-9 and C-15 and between C-8 and C-10. At this stage there may be two ions, on one of which the charge is localized on N_α and on the other on N_β. The ion with the charge localized on N_α is postulated to fragment in the source leading to the ion of m/z 176, for which a metastable transition was not observed. The second ion with the charge localized on N_β is postulated to fragment more slowly, and for this fragmentation a metastable transition was observed. The charge is more delocalized on the ion of m/z 176, which may account for its more rapid formation. A reviewer[2] has suggested that the ion of m/z 176 may form by an entirely different and faster process from that of m/z 124. While this is an attractive proposal to account for the metastable transition in one case and its absence in the other, it is very difficult to envisage a simple and rapid process leading to m/z 176.

The loss of a methyl group can arise from various locations on the molecular ion. The loss of CH_3CO is a well-recognized loss from the N—$COCH_3$ group and the loss of C_3H_7 could arise in the same way as the loss of the corresponding fragment from the bridge atoms in a lycopodane system (10).

An analysis of the ^{13}C nmr spectrum of **1** has been carried out through application of two-dimensional (2D) heteronuclear and homonuclear nmr methods (11) (See Figs. 1 and 2, respectively). Many of the chemical shifts of the protons in the ^1H nmr spectrum were also revealed in this way. Through off-resonance and spin-sorted experiments, the 19 signals in the ^{13}C spectrum could be separated into four groups, carbon atoms devoid of hydrogen (four), methine carbon atoms (five), methylene carbon atoms (seven), and methyl groups (three). These data are recorded in Table 2.

The assignment of the ^{13}C signals (Fig. 1) to the nonprotonated carbon atoms was relatively simple. On the basis of their chemical shifts, peak 1 (170.0 δ) was assigned to the carbonyl carbon (C-17), and peak 2 (139.2 δ) to the vinylic quaternary carbon (C-5). The two tetrahedral quaternary signals, peaks 4 (65.4 δ) and 6 (55.0 δ), have been assigned to C-4 and C-13,

[2]We thank the reviewer for this comment and for others which led us to reconsider our original discussion on the fragmentation of **1**.

TABLE 1. Masses of selected ions of fastigiatine

Composition	Mass	
	Calculated	Observed
$C_{19}H_{28}N_2O$	300.2202	300.2198
$C_{18}H_{25}N_2O$	285.1967	285.1960
$C_{16}H_{21}N_2O$	257.1654	257.1625
$C_{17}H_{25}N_2$	257.2018	257.2017
$C_{11}H_{14}NO$	176.1075	176.1076
$C_8H_{14}N$	124.1126	124.1125

TABLE 2. Assignment of the signals in the ^{13}C spectrum of fastigiatine

Peak number	δ	Carbon type[a]	Carbon atom of fastigiatine
1	170.0	>C=O	17
2	139.2	=C<	5
3	123.1	=C<H	6
4	65.4	C	4 or 13
5	59.6	CH_2	9
6	55.0	C	13 or 4
7	45.5	CH	10
8	45.3	CH_2	1
9	40.2	CH	7
10	38.3	CH	12
11	37.4	CH_2	8
12	35.0	CH_3	19 (NCH_3)
13	34.6	CH_2	14
14	33.9	CH_2	11
15	25.5	CH	15
16	23.0	CH_2	3
17	22.3	CH_3	16 ($CHCH_3$)
18	21.5	CH_3	18 ($NCOCH_3$)
19	21.1	CH_2	2

[a]C, CH, CH_2, and CH_3 represent quaternary, tertiary, secondary, and primary aliphatic carbon atoms, respectively.

respectively, on the basis of their chemical shifts; however, these assignments are not secure and may be reversed.

Except in a few obvious cases the assignment of the ^{13}C signals of the protonated carbon atoms was not as straightforward, and resort to more refined techniques had to be taken. Accordingly, $^1H/^{13}C$ heteronuclear and $^1H/^1H$ homonuclear correlated spectra of fastigiatine were recorded and analysed as discussed below.

The doublet at 0.92 δ (3H, J = 6.5 Hz) in the proton spectrum of fastigiatine (Fig. 1 or 2) can be assigned to the protons on C-16 on the basis of its chemical shift, integrated area, and multiplicity. Accordingly, by making use of the 2D $^1H/^{13}C$ spectrum (Fig. 1), peak 17 (22.3 δ) can be assigned to C-16 of fastigiatine. The protons on C-16 are coupled to the proton on C-15 to form a multiplet near 1.9 δ as seen in the $^1H/^1H$ spectrum. With the chemical shift of the C-15 proton established, and referring now to the $^1H/^{13}C$ spectrum, peak 15 (22.2 δ) of the ^{13}C spectrum can be assigned to C-15 of fastigiatine. From the proton spectrum the singlet at 2.34 δ was

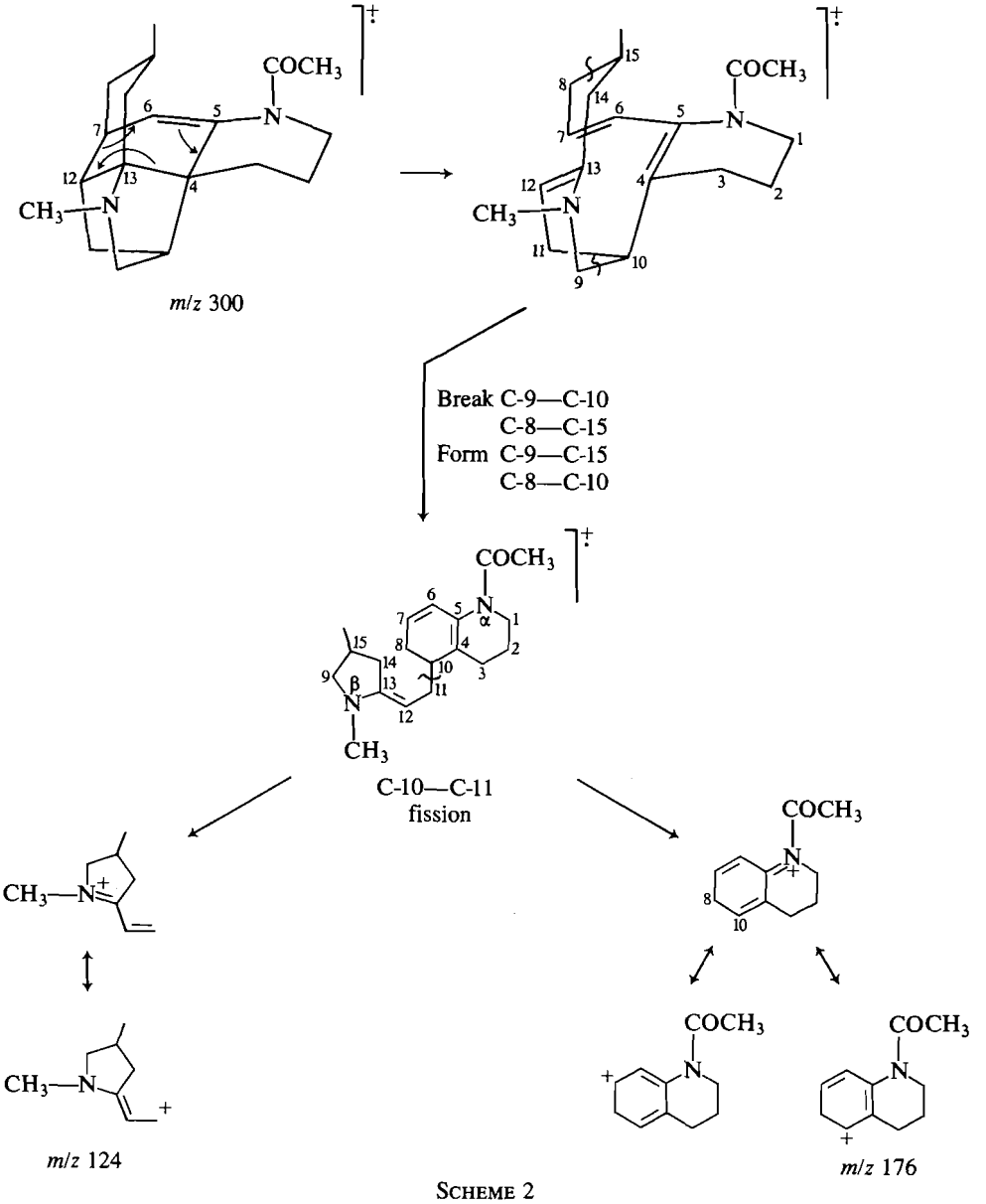

SCHEME 2

assigned to the NCH_3 group and the singlet at 2.15 δ to the $NCOCH_3$ group. The $^1H/^{13}C$ spectrum was then used to assign the NCH_3 group to peak 12 (35.0 δ) and the methyl of the $NCOCH_3$ group to peak 18 (21.5 δ).

Peak 3 (123.1 δ) in the ^{13}C spectrum may be assigned to the vinylic carbon C-6 on the basis of its chemical shift and multiplicity. The proton on C-6 is coupled to the proton on C-7 and shows a long range coupling, presumably to the proton on C-12 (*W* coupling), to form a doublet of doublets, 5.2 δ (dd, 1H, J = 1.1 and 5.5 Hz). From the $^1H/^1H$ spectrum (Fig. 2), couplings between the protons on C-6 and C-7 and between those on C-6 and C-12 are observed that enable a chemical shift to be assigned to the protons on each of these carbon atoms. By reference to the $^1H/^{13}C$ spectrum, peak 9 (40.2) in the ^{13}C spectrum may now be assigned to C-7, and peak 10 (38.3) to C-12.

The protons on C-1 and C-9 should resonate downfield since they are adjacent to a nitrogen atom, and therefore the multiplets centred near 3.7, 3.3, and 2.3 δ in the ^1H spectrum can be attributed to them. The protons on C-9 in fastigiatine should couple to each other and to the proton on C-10, a tertiary carbon atom. By examining the $^1H/^1H$ spectrum it may be observed that the multiplet at 3.3 δ couples to the multiplets at 2.3 δ and at 1.9 δ, the latter being assigned to C-10. With the determination of the chemical shifts of both C-9 protons and the proton at C-10, it was now possible, by examining the $^1H/^{13}C$ spectrum, to assign peak 5 (59.6 δ) to C-9, and peak 9 (45.5 δ) to C-10. The other set of protons adjacent to nitrogen at C-1 in fastigiatine should couple to the protons of C-2. By examining the $^1H/^1H$ spectrum, it can be observed that the multiplets at 3.7 and 3.3 δ couple to each other and to the multiplets at 1.5 and 1.7 δ. With the ^1H chemical shifts known it was possible, using Fig. 1, to assign peak 8 (45.3 δ) to C-1 and peak 19 (21.1 δ) to C-2. Turning now to C-3, it is evident that the protons on C-2 will couple to the protons on C-3 and, from an examination of the $^1H/^1H$ spectrum and the $^1H/^{13}C$ spectrum, peak 16 (23.0 δ) was assigned to C-3.

The proton at C-7 couples to the protons at C-8, as seen from the $^1H/^1H$ spectrum, and the chemical shift of each C-8 proton could then be determined. Thus, by examining the $^1H/^{13}C$

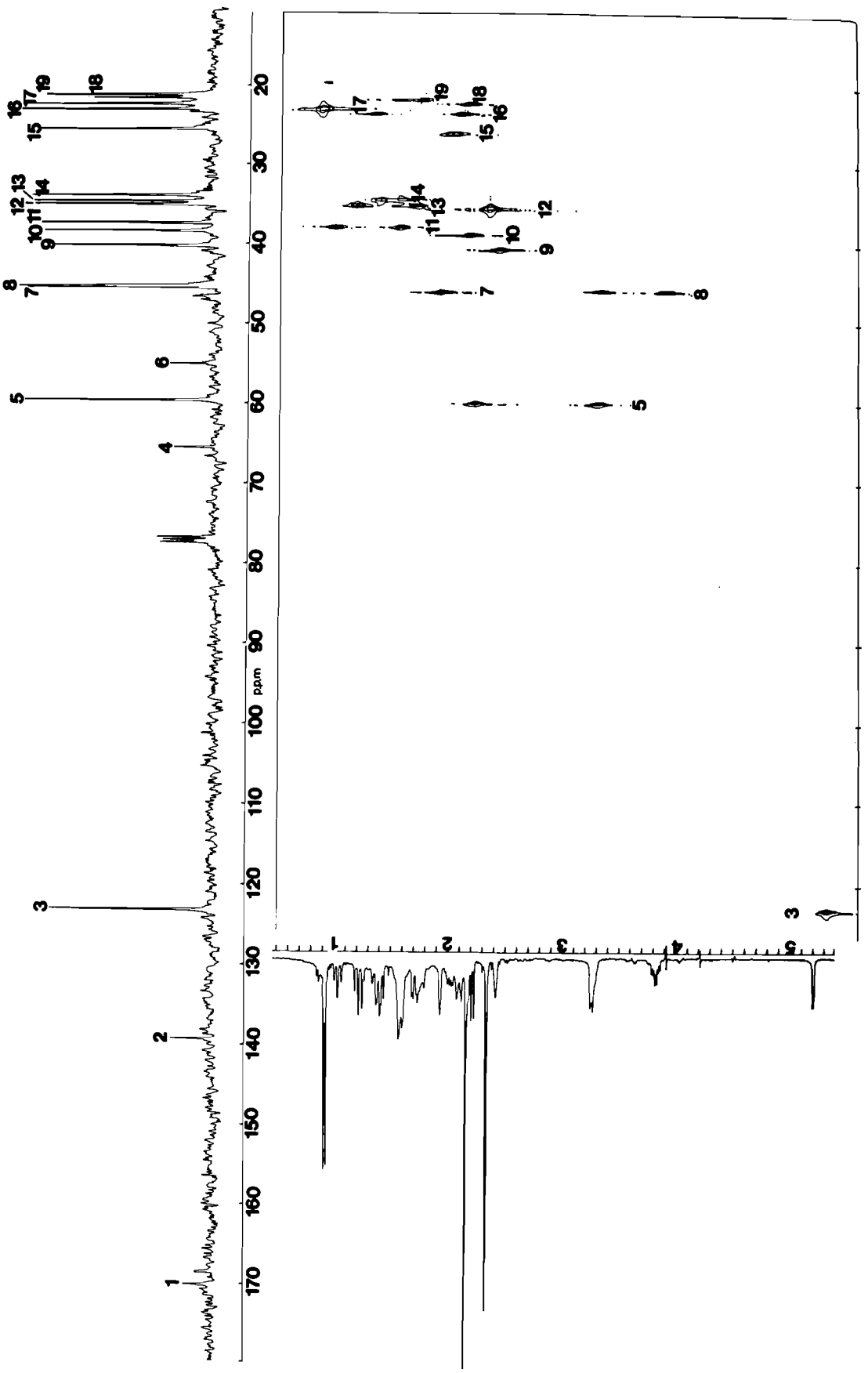

FIG 1. Heteronuclear (^1H,^{13}C) correlated spectrum of fastigiatine. N.B.: the ^{13}C spectrum is shown along the top of the figure and the ^1H spectrum at the side. The numbers assigned to the peaks are arbitrary but the assignment to specific carbon atoms may be found in Table 1.

TABLE 3. Selected interatomic distances and angles

Bond	Distance (Å)	Bond	Distance (Å)	Bond	Distance (Å)
N(1)—C(1)	1.47(1)	C(1)—C(2)	1.52(1)	C(2)—C(3)	1.53(1)
C(3)—C(4)	1.53(1)	C(4)—C(5)	1.52(1)	C(5)—N(1)	1.44(1)
C(5)—C(6)	1.31(1)	C(6)—C(7)	1.50(1)	C(7)—C(12)	1.54(1)
C(12)—C(13)	1.55(1)	C(13)—C(4)	1.58(1)	C(12)—C(11)	1.56(1)
C(11)—C(10)	1.54(1)	C(10)—C(4)	1.55(1)	C(7)—C(8)	1.57(1)
C(8)—C(15)	1.51(1)	C(15)—C(14)	1.55(1)	C(14)—C(13)	1.53(1)
C(13)—N(2)	1.49(1)	N(2)—C(9)	1.50(1)	C(9)—C(10)	1.49(1)
N(1)—C(17)	1.35(1)	C(17)—O	1.22(1)	C(17)—C(18)	1.49(1)
C(15—C(16)	1.52(1)	N(2)—C(19)	1.43(1)		

Bonds	Angle (deg)	Bonds	Angle (deg)	Bonds	Angle (deg)
C(5)—N(1)—C(1)	116.6(7)	C(5)—N(1)—C(17)	125.8(8)	C(17)—N(1)—C(1)	117.6(8)
N(1)—C(1)—C(2)	109.1(7)	C(1)—C(2)—C(3)	111.1(8)	C(2)—C(3)—C(4)	108.6(7)
C(3)—C(4)—C(5)	111.3(7)	C(3)—C(4)—C(13)	114.4(7)	C(3)—C(4)—C(10)	114.2(7)
C(5)—C(4)—C(10)	111.9(6)	C(5)—C(4)—C(13)	112.2(6)	C(10)—C(4)—C(13)	91.5(6)
C(4)—C(5)—N(1)	114.0(8)	C(4)—C(5)—C(6)	124.1(8)	N(1)—C(5)—C(6)	122.3(3)
C(5)—C(6)—C(7)	120.4(8)	C(6)—C(7)—C(8)	109.8(7)	C(6)—C(7)—C(12)	110.4(7)
C(8)—C(7)—C(12)	109.3(7)	C(7)—C(12)—C(13)	107.8(7)	C(7)—C(12)—C(11)	111.2(7)
C(11)—C(12)—C(13)	101.0(7)	C(12)—C(13)—C(4)	99.8(6)	C(12)—C(13)—C(14)	114.4(7)
C(12)—C(13)—N(2)	112.2(8)	C(4)—C(13)—N(2)	100.2(7)	C(4)—C(13)—C(14)	119.0(7)
N(2)—C(13)—C(14)	110.2(8)	C(7)—C(8)—C(15)	110.9(7)	C(8)—C(15)—C(14)	112.7(7)
C(8)—C(15)—C(16)	111.6(8)	C(14)—C(15)—C(16)	110.4(8)	C(15)—C(14)—C(13)	115.1(7)
C(12)—C(11)—C(10)	103.9(7)	C(11)—C(10)—C(4)	101.8(7)	C(11)—C(10)—C(9)	109.3(7)
C(9)—C(10)—C(4)	103.1(7)	C(13)—N(2)—C(9)	107.0(6)	C(13)—N(2)—C(19)	117.7(7)
C(9)—N(2)—C(19)	107.0(6)	N(2)—C(9)—C(10)	101.5(7)	N(1)—C(17)—C(18)	119.8(9)
N(1)—C(17)—O	120.0(1)	O—C(17)—C(18)	119.9(9)		

TABLE 4. Crystal and refinement data

Compound	$C_{19}H_{28}N_2O$
Formula weight	300.44
Crystal shape, size (mm)	plate, 0.17 × 0.30 × 0.37
Systematic absence	$h00$, $h = 2n+1$, $0k0$, $k = 2n+1$, $00l$, $l = 2n+1$
Space group	$P2_12_12_1$ (*19)
Unit cell parameters (Å)	a = 8.949(2), b = 22.302(5), c = 8.371(1) Å
V (Å^3)	1670.7(4)
Z	4
ρ_{calc}, ρ_{obs} (g cm^{-3})	1.19, 1.17(1)
Temperature (°C)	22
Linear absorb. coeff. (cm^{-1})	0.79
Reflections collected, max 2θ	$h,k,\pm l$,50°
Standard reflections (esd)	1 3 1, 0.018, 1 0 2, 0.012
No. of reflections collected	3257
No. of independent reflections	2516
R_{merg}	0.020
No. of reflections with $I > 0$, used	1163
Secondary extinction, x	0.00429
Final R_1,[a] R_2[a]	0.0664, 0.0744
Final shift/error max, ave.	0.082, 0.019
Final difference map, max, min (e Å^{-3})	0.34, −0.39
Weighting scheme	$W = (\sigma_F^2 + 0.000958\ F_o^2)^{-1}$
Error in an observation of unit weight	1.331

[a] $R_1 = \Sigma\|F_o|-|F_c\|/\Sigma|F_o|$; $R_2 = \{\Sigma\omega(|F_o|-|F_c|)^2/\Sigma\omega F_o^2\}^{\frac{1}{2}}$.

spectrum, peak 11 (37.4 δ) can be assigned to C-8. The assignment of the two remaining resonances was resolved in the following manner. The proton on C-10 is coupled to the two protons on C-11 and, by analysing the $^1H/^1H$ spectrum and the $^1H/^{13}C$ spectrum, C-11 can be assigned to peak 14 (33.9 δ). In like manner the protons on C-14 should couple to the proton on C-15, and by examining a slice of the $^1H/^1H$ spectrum along 1.9 δ the chemical shifts of the protons on C-14 were determined. In this way peak 13 (34.6 δ) in the ^{13}C spectrum was assigned to C-14. All assignments and ^{13}C chemical shifts are recorded in Table 2.

The molecular structure of fastigiatine is shown in Fig. 3.

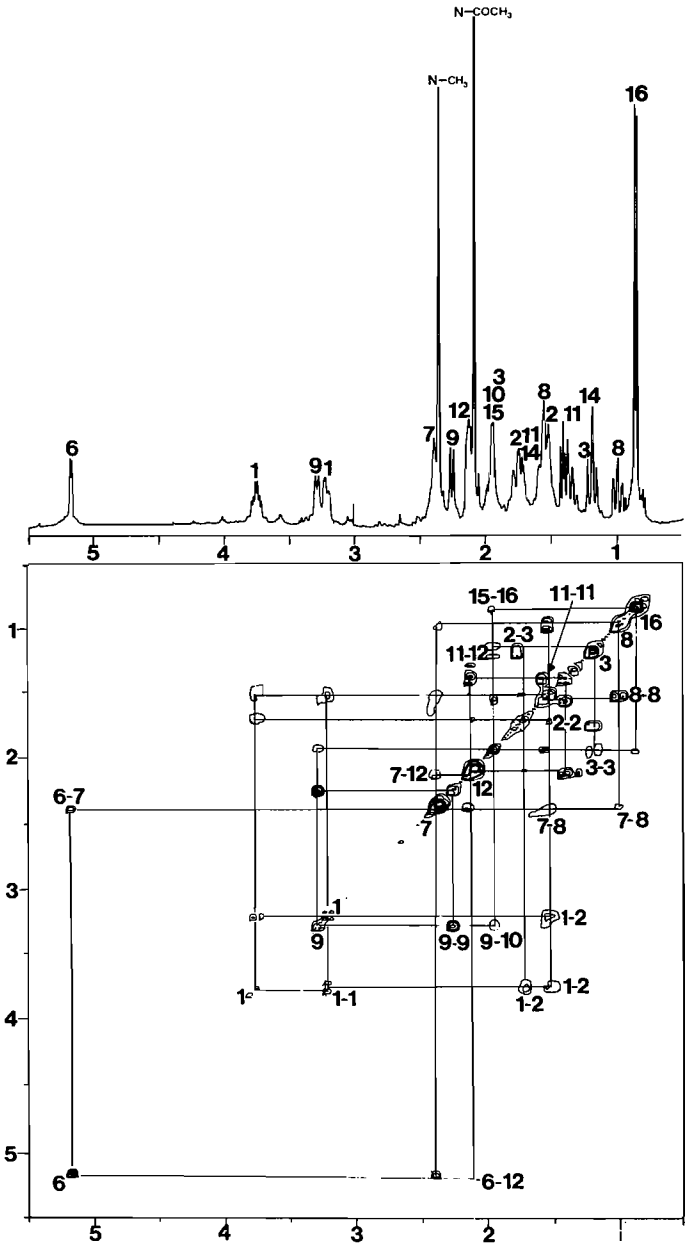

FIG. 2. Homonuclear (^1H,^1H) correlated spectrum of fastigiatine. N.B.: the numbers assigned to peaks in the ^1H spectrum refer to the position of the protons in the molecule.

Bond lengths and angles (Table 3) within the structure are normal when compared to similar structures. The *N*-acetyl features are like those in (−)-aspidospermine-*N*(b)-methiodide (12). Angles within the five-membered rings are considerably less than the tetrahedral angle and the averages are 99.6 and 100.5 for the respective rings C(10)C(4)C(13)C(12)C(11) and N(2)C(13)C(4)C(10)C(9). With the exception of C(10)—C(4)—C(13), 91.5(6)°, the range is similar to those observed in a keto lactam acid from lycoctonine (13) and the averages are only about 2° smaller. All rings are *cis*-joined, the two five-membered rings comprising an 2-aza-norbornane system. The six-membered rings have varying conformations, the N(1)C(1)C(2)C(3)C(4)C(5) ring being a twist boat, the C(4)C(5)C(6)C(7)C(12)C(13) ring being half-chair, and the third ring, C(7)C(8)C(15)C(14)C(13)C(12), a chair. Interactions between molecules in the cells are van der Waals and all intermolecular distances are equal to, or greater than, the van der Waals distances.

TABLE 5. Atomic positional parameters (× 10^4) and temperature factors (Å^2) (× 10^3)

Atom	*x*	*y*	*z*	U_{eq}[a]
C(1)	1316(10)	3492(4)	3369(9)	46
C(2)	1292(11)	4028(5)	2243(11)	60
C(3)	1595(10)	3834(4)	517(11)	51
C(4)	3204(9)	3601(3)	406(9)	29
C(5)	3775(10)	3398(4)	2028(9)	33
C(6)	5173(10)	3432(4)	2476(9)	36
C(7)	6338(9)	3674(4)	1359(10)	42
C(8)	6734(10)	4335(4)	1831(11)	51
C(9)	3048(11)	3436(4)	−2393(10)	53
C(10)	3446(10)	3118(4)	−893(9)	41
C(11)	5147(10)	3027(4)	−825(9)	43
C(12)	5765(9)	3661(4)	−374(9)	39
C(13)	4324(10)	4042(4)	−449(10)	41
C(14)	4495(10)	4678(4)	191(10)	44
C(15)	5359(11)	4731(4)	1784(9)	47
C(16)	5740(13)	5381(4)	2128(11)	69
C(17)	2708(11)	2573(4)	3668(11)	40
C(18)	3907(11)	2151(4)	3162(12)	59
C(19)	4563(12)	4267(5)	−3353(11)	67
N(1)	2649(8)	3128(3)	3034(8)	40
N(2)	3657(9)	4053(3)	−2073(8)	46
O	1765(8)	2411(3)	4621(8)	66

[a] $U_{eq} = \frac{1}{3}(U_{11} + U_{22} + U_{33})$.

Experimental

Apparatus, methods, and materials

The $^1H/^1H$ and $^1H/^{13}C$ 2D spectra were recorded on a Brüker WH400 spectrometer at the Southwestern Ontario NMR Centre, University of Guelph, Guelph, Ontario.

Electron impact (EI) mass spectra were recorded on a VG Micromass 7070F mass spectrometer at 70 eV. The high resolution spectra and the linked scan experiments were carried out on a Kratos MS50 instrument at the University of California, San Francisco, at the Bio-organic, Biomedical Mass Spectrometry Resource (A. L. Burlingame, Director) supported by NIH Division of Research Resources Grant RR01614.

Lycopodium fastigiatum R.Br. was obtained in 1967 through the Department of Scientific and Industrial Research, Botany Division, Christchurch, New Zealand, and carefully stored in a dry cupboard. It was collected at Mt. Robert, Nelson Lakes National Park, South Island, New Zealand. Fastigiatine, mp 143–46°C, was isolated as described elsewhere (3). The specimen used in this investigation was prepared by recrystallization from ether.

Measurement of the X-ray data

A platelike colourless crystal was mounted along the longest axis and used for X-ray studies. Precession photographs revealed the orthorhombic symmetry, and unit cell parameters were obtained from least-squares fit of χ, ϕ, and 2θ for 15 reflections in the range $18.3° < 2\theta < 23.8°$ recorded on a Syntex $P2_1$ diffractometer with use of graphite-monochromatized Mo$K\alpha$, radiation (λ = 0.70926 Å). Crystal data and other numbers related to data collected are given in Table 4. The density was measured by flotation in aqueous KBr. Intensities were also measured with the Syntex $P2_1$ diffractometer with use of a coupled θ(crystal) − 2θ(counter) scan. The methods of selection of scan rates and initial data treatment have been described (14, 15). Corrections were made for Lorentz polarization effects but not for absorption. This will give a maximum error in F_o of <1.0%.

The phases were determined by direct methods with use of 242 reflections with $|E| > 1.54$ and 12 sets of starting phases. Fourteen of

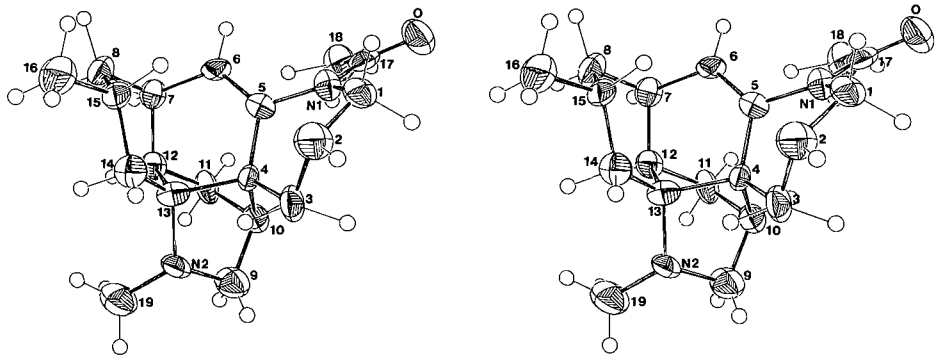

FIG. 3. The molecular structure of fastigiatine.

the non-hydrogen atoms were located on the *E* map and all atoms were located after refinement and subsequent difference syntheses. All non-hydrogen atoms were made anisotropic at this stage. In further refinement, which minimized $\Sigma\omega(|F_o| - |F_c|)^2$, hydrogen atoms were included but not refined. Corrections were made for secondary extinction (x(SHELX = 0.00429).[3] Scattering curves were taken from ref. 16. No attempt was made to determine the absolute configuration of the molecule. The configuration given here, to which all the data apply, is based on that commonly observed among the Lycopodium alkaloids (1). The atom parameters are listed in Table 5.[4]

Acknowledgments

We thank the Natural Sciences and Engineering Research Council of Canada for financial support of this work.

1. D. B. MACLEAN. *In* The alkaloids. Vol. 26. *Edited by* A. Brossi. Academic Press, New York. 1985. p. 241.
2. J. C. BRAEKMAN, L. NYEMBO, and J. J. SYMOENS. Phytochemistry, **19**, 803 (1980).
3. R. V. GERARD and D. B. MACLEAN. Phytochemistry. In press.
4. D. B. MACLEAN. *In* The Alkaloids. Vol. X. *Edited by* R. H. F. Manske. Academic Press, New York. 1968. p. 305; Vol. XIV, 1973, p. 347.

[3]All computations were carried out on CYBER 170/730 or 815 computers. Programs used for initial data treatment were from the X-ray 76 package (17). The structure was solved with SHELX (18). Planes were calculated using NRC-22 (19). Diagrams were prepared from ORTEP II (20).

[4]Tables of structure factors, anisotropic temperature factors, atomic positional parameters and bond lengths and angles involving hydrogen atoms have been deposited and may be purchased from the Depository of Unpublished Data, CISTI, National Research Council of Canada, Ottawa, Ont., Canada K1A 0S2.

5. Y. INUBUSHI and T. HARAYAMA. Yakugaku Zasshi, **102**, 434 (1982).
6. G. MORALES, L. A. LOYOLA, and M. CASTILLO. Phytochemistry, **18**, 1719 (1979); O. MUNOZ and M. CASTILLO. Heterocycles, **19**, 2287 (1982).
7. W. A. AYER, B. ALTENKIRK, N. MASAKI, and S. VALVERDE-LOPEZ. Can. J. Chem. **47**, 2449 (1969).
8. W. A. AYER and N. MASAKI. Can. J. Chem. **49**, 524, (1971).
9. U. P. SCHLUNEGGER. Advanced Mass Spectrometry Applications in Organic and Analytical Chemistry. Pergamon Press Ltd., New York. 1980.
10. D. B. MACLEAN. Can. J. Chem. **41**, 2654 (1963).
11. W. E. HULL. Two-dimensional NMR aspect 2000, 3000, Brüker Analytische Messtechnik. Karlsruhe, Germany. December, 1982.
12. J. F. D. MILLS and S. C. NYBURG. J. Chem. Soc. 1458 (1960).
13. M. CYGLER, M. PRZYBYLSKA, and O. E. EDWARDS. Acta. Crystallogr. Sect. B, **38**, 1500 (1982).
14. R. P. HUGHES, N. KRISHNAMACHARI, C. J. L. LOCK, J. POWELL, and G. TURNER. Inorg. Chem. **16**, 314 (1977).
15. B. LIPPERT, C. J. L. LOCK, B. ROSENBERG, and M. ZVAGULIS. Inorg. Chem. **16**, 1525 (1977).
16. D. T. CROMER and J. T. WABER. International tables for X-ray crystallography. Vol. IV. *Edited by* J. A. Ibers and W. C. Hamilton. Kynoch Press, Birmingham, England. 1974. Table 2.2A, p. 72ff.
17. J. M. STEWART. Technical report TR-446. University of Maryland, College Park, MD. 1976.
18. G. M. SHELDRICK. Cambridge University, Cambridge, England. 1976.
19. F. R. AHMED and M. E. PIPPY. National Research Council of Canada, Ottawa. 1978.
20. C. K. JOHNSON. Report ORNL-5138. Oak Ridge National Laboratory, Oak Ridge, TN. 1976.

Formation of a trimeric chloroguaiacol quinone in the preparation of tetrachloroguaiacol and crystal structure of its tetramethoxy derivative

NICK BURLINSON, STEVEN J. RETTIG, AND JAMES TROTTER

Department of Chemistry, University of British Columbia, 2036 Main Mall, University Campus, B.C., Canada, V6T 1Y6

AND

BRUCE MCKAGUE[1]

B.C. Research, 3650 Wesbrook Mall, Vancouver, B.C., Canada, V6S 2L2

Received December 23, 1985

NICK BURLINSON, STEVEN J. RETTIG, JAMES TROTTER, and BRUCE MCKAGUE. Can. J. Chem. **64**, 950 (1986).

A by-product formed in the preparation of tetrachloroguaiacol is shown to be a trimeric quinone. Derivatization of the quinone to a crystalline tetramethoxy derivative allowed X-ray determination of its crystal structure as 3,6-dichloro-4,5-dimethoxy-1,2-bis(2′-methoxy-3′,4′,5′,6′-tetrachlorophenoxy)benzene, **4**. Rarely observed long range J_{CH} coupling between ring carbons and methoxyl hydrogens as well as conformational isomerism were observed in ^1H and ^{13}C nmr studies of **4**. Crystals of **4** are triclinic, $a = 12.562$ (1), $b = 12.708(1)$, $c = 9.223(1)$ Å, $\alpha = 96.93(1)$, $\beta = 97.478(7)$, $\gamma = 101.285(8)°$, $Z = 2$, space group $P\bar{1}$. The structure was solved by direct methods and was refined by full-matrix least-squares procedures to $R = 0.056$ and $R_w = 0.056$ for 2946 reflections with $I \geq 1.5\sigma(I)$. The molecule contains a central six-membered dichloro-tetraoxo substituted aromatic ring, linked via oxygen bridges to two identical tetrachloro-dioxo substituted rings; intramolecular steric overcrowding causes significant deviations from a symmetrical conformation. Bond lengths, angles, and intermolecular distances are generally close to expected values.

NICK BURLINSON, STEVEN J. RETTIG, JAMES TROTTER, et BRUCE MCKAGUE. Can. J. Chem. **64**, 950 (1986).

Un sous produit obtenu lors de la préparation du tétrachloroguaïacol est en fait une quinone trimère. On a transormé cette quinone en un dérivé tétraméthoxylé dont l'analyse par cristallographie des rayons-X révèle que sa structure cristalline correspond à celle du dichloro-3,6 diméthoxy-4,5 bis(méthoxy,2′ tétrachloro-3′,4′,5′,6′ phénoxy)-1,2 benzène **4**. Des études par rmn du ^1H et du ^{13}C ont permis d'observer des constantes de couplage à longue distance. J_{CH}, assez rares entre les carbones du cycle et les hydrogènes des groupements méthoxyles, ainsi que de l'isomérie conformationnelle. Les cristaux appartiennent au groupe d'espace triclinique $P\bar{1}$ avec $a = 12{,}562(1)$, $b = 12{,}708(1)$, $c = 9{,}223(1)$ Å, $\alpha = 96{,}93(1)$, $\beta = 97{,}478(7)$, $\gamma = 101{,}285(8)°$, et $Z = 2$. On a résolu la structure par des méthodes directes et on l'a affinée par la méthode des moindres carrés (matrice complète) jusqu'à des valeurs de $R = 0{,}056$ et de $R_w = 0{,}056$ pour 2946 réflexions avec $I \geq 1{,}5\sigma(I)$. La molécule contient un cycle aromatique central à 6 chaînons portant un substituant dichloro-tétraoxo qui est lié par l'intermédiaire de deux ponts oxygène, à deux cycles identiques portant un substituant tétrachloro-dioxo. Un encombrement stérique intramoléculaire provoque des déviations importantes par rapport à une conformation symétrique. Les longueurs de liaison, les angles et les distances intermoléculaires sont généralement très près des valeurs attendues.

[Traduit par la revue]

Introduction

Tetrachloroguaiacol, **1**, a compound formed during the bleaching of pulp and paper (1, 2), is readily prepared by the chlorination of guaiacol, **2**, in acetic acid (3).

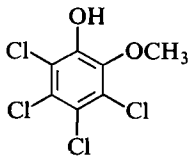

1

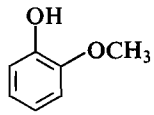

2

In the preparation of **1**, we frequently observed the formation of a bright orange, highly insoluble by-product, **3**, which could be separated from **1** during crystallization.

This paper reports the structural determination of the by-product, **3**, as a trimeric quinone as evidenced by the crystallographic structure determination of its tetramethoxy derivative, **4**. Additionally, the ^1H and ^{13}C nmr spectra of **4** are presented to suggest conformational isomerism in solutions of **4** due to steric crowding.

Experimental

Melting points were taken n a Kofler Micro Hot Stage and are uncorrected. Infrared (ir) spectra were recorded on a Unicam SP1100 spectrophotometer; ultraviolet (uv) spectra on a Beckman DB-GT spectrophotometer. A Kratos MS50 mass spectrometer was used to obtain mass spectra. Liquid chromatography (lc) was performed on a Hewlett Packard Model 1084B high performance liquid chromatograph equipped with a variable wavelength detector set at 254 nm. Reverse phase partition chromatography was done on a 4.6 mm × 20 cm RP-8 column, 5-μm particle size, using isocratic elution with acetonitrile–water, 90:10 and a flow of 1 mL/min.

^{13}C and ^1H magnetic resonance (nmr) spectra were obtained on a Varian XL-300 FT spectrometer operating at 75.429 MHz for carbon and 299.943 MHz for hydrogen. A 5-mm broadband probe was used. Solutions of 100 mg of each compound in 0.5 mL of *d*-chloroform, to which a small amount of tetramethylsilane (TMS) was added, were prepared. For the ^1H spectra, narrow spectral widths (200–500 Hz) and resolution enhancement processing of the FID were employed to obtain good peak resolution. Using aquisition times of 4 or 5 s and repetition rates of 5 s allowed digitization of 8–10 points/Hz.

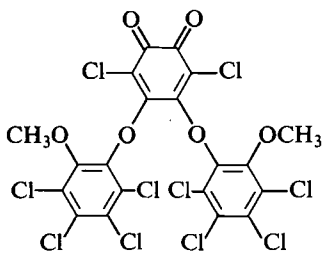

3

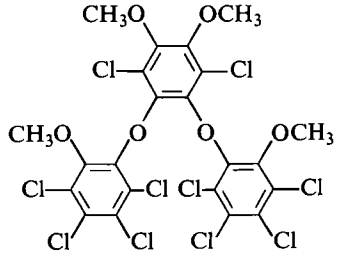

4

[1]Author to whom correspondence may be addressed.

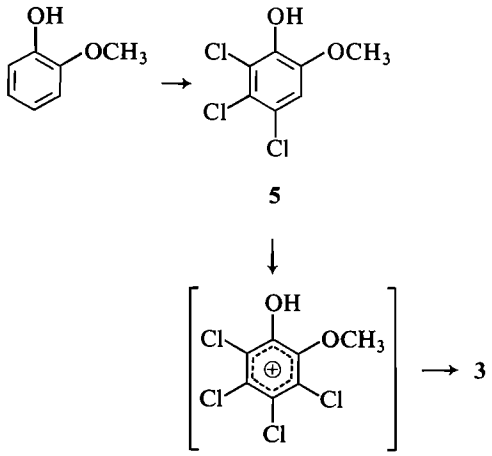

5

3

Isolation of the by-product

Tetrachloroguaiacol was prepared by the chlorination of guaiacol in acetic acid as described in the literature (3). The crude product was dissolved in hexane and the orange, insoluble by-product isolated by filtration. Two grams by-product was obtained from the chlorination of guaiacol on a 50-g scale. The orange compound, which was insoluble in common organic solvents, including dimethyl sulfoxide, had mp 250–255°C; ir (KBr): 1685, 1560 cm^{-1}; ms *m/e* (% relative intensity): 702 (25.6), 700 (42.8), 698 (51.4), 696 (38.2), 694 (13.6), 692 (5.8) M^+, 661 (42.9 M^+ −HCl), 247 (100). *Anal.* calcd. for $C_{20}H_6Cl_{10}O_6$: C 34.47, H 0.87; found: C 34.33, H 0.88.

Preparation of the tetramethoxy derivative

Sodium borohydride was added in small portions to a stirred suspension of the by-product (800 mg) in methanol (10 mL) until a clear solution formed (approximately 5 min). The product was poured into ice-water, acidified with sulphuric acid, and extracted thrice with ether. After washing the combined extracts with water, and drying with anhydrous magnesium sulfate, a few mL of the extract was evaporated with a stream of nitrogen to give a clear oil, ir (film): 3350 cm^{-1}, which rapidly turned orange in air. The remainder of the extract was methylated with diazomethane and evaporated to give a colourless white solid (700 mg). Extraction with hexane and concentration of the extract gave the product as a colourless solid (480 mg), mp 161.5–163°C. Three crystallizations from hexane gave the tetramethoxy derivative as colourless prisms (400 mg); mp 163–164°C; uv (ethanol), λ_{max}: 295 nm (ϵ 3900); ^1H nmr in $CDCl_3$, δ: 3.62 and 3.64 (singlets, total 3H), 3.93 (singlet, 3H); ^{13}C nmr in $CDCl_3$, δ: 61.46 and 61.74 (OCH_3), 119–128 (CCl), 140–150 (COR); ms *m/e* (% relative intensity): 730 (48.4), 728 (85.8), 726 (100), 724 (69.9), 722 (21.7)M^+. *Anal.* calcd. for $C_{22}H_{12}Cl_{10}O_6$: C 36.35, H 1.66; found: C 36.22, H 1.72.

X-ray crystallographic analysis of 3,6-dichloro-4,5-dimethoxy-1,2-bis(2'-methoxy-3',4',5',6'-tetrachlorophenoxy) benzene, 4

A crystal bounded by the 5 faces (followed by their distances in mm from a common origin): {1 $\bar{1}$ 0}, 0.104, (0 0 −1), 0.175, (1 1 0), 0.213, (−1 −1 1), 0.069 was mounted in a general orientation. Unit-cell parameters were refined by least squares on 2 sin θ/λ values for 25 reflections (2θ = 26–35°) measured on a diffractometer with Mo-$K\alpha$ radiation ($\lambda(K\alpha_1)$ = 0.70930, $\lambda(K\alpha_2)$ = 0.71359 Å). Crystal data at 22°C are:

$C_{22}H_{12}Cl_{10}O_6$ fw = 726.86

Triclinic, a = 12.562(1), b = 12.708(1), c = 9.223(1) Å, α = 96.93(1), β = 97.478(7), γ = 101.285(8)°, V = 1415.4(2) $Å^3$, Z = 2, = 1.705 Mg m^{-3}, $F(000)$ = 724, μ(Mo-$K\alpha$) = 10.28 cm^{-1}. Absent lections: none. Space group $P\bar{1}$ (C_i^1, No. 2, conventional reduced) from structure analysis.

ensities were measured with graphite-monochromated Mo-$K\alpha$ ion on an Enraf–Nonius CAD4-F diffractometer. An ω–2θ scan 5–10.06° min^{-1} over a range of (0.80 + 0.35 tan θ) degrees in ω (extended by 25% on both sides for background measurement) was employed. Data were measured to 2θ = 55°. The intensities of 3 check reflections, measured every 3600 s throughout the data collections, remained constant to within 4%. After data reduction,[2] an absorption correction was applied using the analytical method (4,5).

Transmission factors ranged from 0.697 to 0.822. Of the 6480 independent reflections measured, 2946 (45.5%) had intensities greater than or equal to 1.5σ(I) above background where $\sigma^2(I) = S + 2B + (0.04(S - B))^2$ with S = scan count and B = normalized background count.

The structure solution was initiated in the centrosymmetric space group $P\bar{1}$ on the basis of the E-statistics. The structure was solved by direct methods, the coordinates of 36 of the 38 non-hydrogen atoms being determined from an E-map. The remaining atoms, including hydrogen, were positioned from subsequent difference maps. In the final stages of refinement the non-hydrogen atoms were refined with anisotropic thermal parameters and the hydrogen atoms were included as fixed contributors in idealized positions (based on observed peaks, C—H = 0.98 Å, U_H = 1.25 U_C $Å^2$). The scattering factors of ref. 6 were used for non-hydrogen atoms and those of ref. 7 for hydrogen atoms. Anomalous scattering factors from ref. 8 were used for the Cl atoms. The weighting scheme $w = 1/\sigma^2(F)$, where $\sigma^2(F)$ is derived from the previously defined $\sigma^2(I)$, gave uniform average values of $w(|F_o|-|F_c|)^2$ over ranges of both $|F_o|$ and sin θ/λ and was employed in the final stages of full-matrix refinement of 343 variables. Reflections with $I < 1.5\sigma(I)$ were not included in the refinement. Convergence was reached at R = 0.056 and R_w = 0.056 for 2946 reflections with $I \geq 1.5\sigma(I)$. For all 6480 reflections R = 0.156. The function minimized was $\Sigma w(|F_o|-|F_c|)^2$, $R = \Sigma \||F_o|-|F_c|\|/\Sigma|F_o|$ and $R_w = (\Sigma w(|F_o|-|F_c|)^2/\Sigma w|F_o|^2)^{1/2}$.

On the final cycle of refinement the mean and maximum parameter shifts correspond to 0.002 and 0.03σ, respectively. The mean error in an observation of unit weight was 1.908. A final difference map showed maximum fluctuations of −1.51 to +0.55 e $Å^{-3}$ (near Cl(10) and C(14), respectively) and was essentially featureless elsewhere. The final positional and thermal parameters appear in Table 1. Bond lengths and angles appear in Tables 2 and 3, respectively. Calculated hydrogen coordinates and thermal parameters (Table 4), a complete listing of torsion angles (Table 5), and a listing of nonbonded distances (Table 6) are included as deposited material. Measured and calculated structure factors have been placed in the Depository of Unpublished Data.[3]

Results and discussion

The amorphous by-product, which normally comprised only a few percent of the product, had a melting point of 250–255°C and was insoluble in common organic solvents, including dimethyl sulfoxide. The material had infrared absorption at 1685 and 1560 cm^{-1} (KBr), suggesting the presence of a quinone group. No absorption was present in the hydroxyl region. Mass spectrometry indicated the compound was highly chlorinated and had a probable molecular weight of 692.

Addition of $NaBH_4$ to a methanol suspension of the by-product resulted in the immediate discharge of the orange colour and formation of a clear solution. The crude product had a large hydroxyl peak in the infrared spectrum (film) but no carbonyl absorption. Since it underwent air oxidation back to the starting

[2]The computer programs used include locally written programs for data processing and locally modified versions of the following: MULTAN 80, multisolution program by P. Main, S. J. Fiske, S. E. Hull, L. Lessinger, G. Germain, J. P. Declercq, and M. M. Woolfson; ORFLS, full-matrix least-squares, and ORFFE, function and errors, by W. R. Busing, K. O. Martin, and H. A. Levy; FORDAP, Patterson and Fourier syntheses, by A. Zalkin; ORTEP II, illustrations, by C. K. Johnson.

[3]The structure factor table, Table 7 (anisotropic thermal parameters) and other material mentioned in the text may be purchased from the Depository of Unpublished Data, CISTI, National Research Council of Canada, Ottawa, Ont,. Canada K1A 0S2.

TABLE 1. Final positional (fractional × 10^4, Cl × 10^5) and isotropic thermal parameters ($U \times 10^3$ Å^2) with estimated standard deviations in parentheses

Atom	x	y	z	U_{eq}
Cl(1)	16191(12)	48028(11)	38837(15)	63
Cl(2)	−8999(11)	83930(11)	25185(15)	64
Cl(3)	6180(16)	88309(15)	96070(17)	94
Cl(4)	29154(19)	103960(16)	105496(19)	121
Cl(5)	43612(17)	109664(19)	81463(27)	144
Cl(6)	34585(14)	100923(17)	48243(22)	110
Cl(7)	46470(14)	61284(15)	9226(18)	94
Cl(8)	65168(14)	60901(18)	34613(23)	113
Cl(9)	61886(13)	66877(20)	67574(21)	120
Cl(10)	40357(13)	73741(18)	74286(18)	102
O(1)	1280(3)	8769(3)	4282(4)	49
O(2)	2432(2)	7229(3)	4902(3)	53
O(3)	−457(3)	4475(3)	1895(4)	64
O(4)	−1663(2)	6060(3)	1427(4)	57
O(5)	−14(3)	8125(3)	6380(4)	60
O(6)	2710(3)	6759(4)	1878(5)	85
C(1)	831(4)	7680(4)	3760(5)	41
C(2)	1406(4)	6887(4)	4003(5)	43
C(3)	945(4)	5811(4)	3459(5)	45
C(4)	−73(4)	5533(4)	2544(5)	48
C(5)	−641(4)	6332(4)	2244(5)	41
C(6)	−191(4)	7393(4)	2869(5)	44
C(7)	1651(4)	9079(4)	5775(6)	43
C(8)	1007(4)	8806(4)	6815(6)	45
C(9)	1415(5)	9197(5)	8302(6)	59
C(10)	2442(6)	9877(5)	8714(6)	65
C(11)	3066(5)	10152(5)	7666(8)	72
C(12)	2677(4)	9752(4)	6181(7)	61
C(13)	3373(4)	6960(4)	4480(5)	43
C(14)	3528(4)	6744(4)	3044(6)	51
C(15)	4505(5)	6454(4)	2740(6)	59
C(16)	5321(4)	6419(5)	3874(7)	66
C(17)	5174(4)	6692(5)	5320(7)	62
C(18)	4202(4)	6957(4)	5632(5)	53
C(19)	−1420(6)	3903(5)	2297(7)	88
C(20)	−1706(5)	6006(5)	−135(6)	84
C(21)	−898(5)	8569(6)	6418(7)	90
C(22)	2758(5)	7623(6)	1452(6)	61

TABLE 2. Bond lengths (Å) with estimated standard deviations in parentheses

Bond	Length (Å)	Bond	Length (Å)
Cl(1)—C(3)	1.724(5)	O(6)—C(14)	1.392(6)
Cl(2)—C(6)	1.726(5)	O(6)—C(22)	1.202(6)
Cl(3)—C(9)	1.713(6)	C(1)—C(2)	1.372(6)
Cl(4)—C(10)	1.723(6)	C(1)—C(6)	1.388(6)
Cl(5)—C(11)	1.720(6)	C(2)—C(3)	1.380(6)
Cl(6)—C(12)	1.732(6)	C(3)—C(4)	1.394(6)
Cl(7)—C(15)	1.718(5)	C(4)—C(5)	1.383(6)
Cl(8)—C(16)	1.712(5)	C(5)—C(6)	1.379(6)
Cl(9)—C(17)	1.716(5)	C(7)—C(8)	1.366(6)
Cl(10)—C(18)	1.730(5)	C(7)—C(12)	1.379(6)
O(1)—C(1)	1.389(5)	C(8)—C(9)	1.394(7)
O(1)—C(7)	1.378(5)	C(9)—C(10)	1.384(8)
O(2)—C(2)	1.397(5)	C(10)—C(11)	1.357(8)
O(2)—C(13)	1.382(5)	C(11)—C(12)	1.390(8)
O(3)—C(4)	1.370(6)	C(13)—C(14)	1.367(6)
O(3)—C(19)	1.402(7)	C(13)—C(18)	1.389(6)
O(4)—C(5)	1.359(5)	C(14)—C(15)	1.401(7)
O(4)—C(20)	1.427(6)	C(15)—C(16)	1.378(7)
O(5)—C(8)	1.379(6)	C(16)—C(17)	1.382(7)
O(5)—C(21)	1.344(7)	C(17)—C(18)	1.385(7)

material rapidly, as evidenced by the formation of an orange colour on standing a few minutes, the methyl ether derivative was prepared by reaction with diazomethane in ether. After three recrystallizations from hexane, a colourless crystalline material with a melting point of 163–164°C was obtained in 50% overall yield.

Liquid chromatography indicated the methylated reduction product had a purity of 94%. The molecular weight from mass spectrometry was 722, consistent with the introduction of two methyl groups, and the intensities of the molecular ion isotope peaks were in agreement with a molecular formula of $C_{22}H_{12}O_6Cl_{10}$. The by-product was evidently a trimeric quinone **3**, which yielded the tetramethoxyderivative **4** on reduction and methylation.

The proton decoupled ^{13}C nmr spectrum of **4** revealed three groups of lines: one group has two resonances at δ 61.46 and 61.74, of integrated area 1:3, respectively, which are assigned to the four-methoxyl carbons; another group of resonances between δ 119 and 128 had 10 lines, consistent with 10 carbons each attached to chlorine; the third group of resonances had 6 lines in the region of δ 140–150, consistent with aromatic carbons attached to —OR groups. The 10 resonance lines in the C—Cl region would normally suggest an unsymmetrical structure for **4**; however, in light of the crystal structure, *vida infra*, the multiplicity of lines must be due to the presence of hindered rotations between rings as well as preferred methoxyl group orientations. The ring chlorines cause severe intramolecular steric crowding, and space filling models also suggest this.

A "coupled nOe" (nuclear Overhauser enhancement) ^{13}C nmr experiment resulted in collapse to quartets of the two resonances furthest downfield at δ 147.17 and δ 146.30 with 4.1 and 4.0 Hz coupling, respectively. This is indicative of long range $^3J_{CH}$ coupling between the ring carbons and the methoxyl hydrogens. This long range C—H coupling has been observed previously in anisole (9) but only as a broadening effect. To our knowledge these coupling values have not been reported. These $^3J_{CH} \cong$ 4 Hz are consistent with other $^3J_{CH}$ values, which in general are of the same order as $^3J_{HH}$ couplings of this geometry. Consequently, the resonance at δ 147.17 is assigned to three degenerate ring carbons containing a methoxyl group and the resonance at δ 146.30 to a fourth carbon with a methoxyl bonded. This assignment is also consistent with the above noted methyl carbon resonances, which gave two peaks but with integrated areas of 3:1.

The ^1H nmr spectrum of **4** has only three peaks (slightly broadened) all in the methoxy region at δ 3.62, 3.64, and 3.93. Scanning at a narrower sweep width to give 8 points/Hz digitization and using mathematical enhancement of the FID to improve resolution gave at least three resolved peaks of varying intensity for the broadened peak at δ 3.93 and two resolved peaks each for the lines at δ 3.64 and 3.62. This suggests the existence of more than one conformational isomer for each of the methoxyl groups in **4** and is in agreement with ^1H nmr work by T. Schaefer and R. Laatikainen (10) on 1,2-dimethoxybenzene, in which they suggest a predominance of a planar conformation in solution.

A similar multiplicity of chemical shifts for the ^1H resonance in tetrachloroveratrole (1,2-dimethoxytetrachlorobenzene) was also observed by us. The single peak at δ 3.91 upon enhanc

TABLE 3. Bond angles (deg) with estimated standard deviations in parentheses

Bonds	Angle (deg)	Bonds	Angle (deg)
C(1)—O(1)—C(7)	118.7(4)	Cl(3)—C(9)—C(8)	118.9(5)
C(2)—O(2)—C(13)	122.2(3)	Cl(3)—C(9)—C(10)	120.6(5)
C(4)—O(3)—C(19)	117.6(4)	C(8)—C(9)—C(10)	120.5(5)
C(5)—O(4)—C(20)	115.9(4)	Cl(4)—C(10)—C(9)	120.0(5)
C(8)—O(5)—C(21)	117.4(4)	Cl(4)—C(10)—C(11)	120.1(5)
C(14)—O(6)—C(22)	114.8(5)	C(9)—C(10)—C(11)	119.8(5)
O(1)—C(1)—C(2)	121.8(4)	Cl(5)—C(11)—C(10)	120.9(5)
O(1)—C(1)—C(6)	119.1(4)	Cl(5)—C(11)—C(12)	118.7(5)
C(2)—C(1)—C(6)	118.9(5)	C(10)—C(11)—C(12)	120.3(5)
O(2)—C(2)—C(1)	116.1(4)	Cl(6)—C(12)—C(7)	119.2(4)
O(2)—C(2)—C(3)	123.1(4)	Cl(6)—C(12)—C(11)	121.1(5)
C(1)—C(2)—C(3)	120.6(4)	C(7)—C(12)—C(11)	119.7(5)
Cl(1)—C(3)—C(2)	120.8(4)	O(2)—C(13)—C(14)	124.2(4)
Cl(1)—C(3)—C(4)	119.4(4)	O(2)—C(13)—C(18)	115.3(4)
C(2)—C(3)—C(4)	119.9(4)	C(14)—C(13)—C(18)	120.4(4)
O(3)—C(4)—C(3)	118.5(4)	O(6)—C(14)—C(13)	121.0(4)
O(3)—C(4)—C(5)	121.6(4)	O(6)—C(14)—C(15)	119.5(5)
C(3)—C(4)—C(5)	119.8(5)	C(13)—C(14)—C(15)	119.5(5)
O(4)—C(5)—C(4)	120.2(4)	Cl(7)—C(15)—C(14)	118.2(4)
O(4)—C(5)—C(6)	120.5(4)	Cl(7)—C(15)—C(16)	121.2(4)
C(4)—C(5)—C(6)	119.2(4)	C(14)—C(15)—C(16)	120.6(5)
Cl(2)—C(6)—C(1)	119.1(4)	Cl(8)—C(16)—C(15)	119.3(5)
Cl(2)—C(6)—C(5)	119.6(4)	Cl(8)—C(16)—C(17)	121.5(5)
C(1)—C(6)—C(5)	121.3(4)	C(15)—C(16)—C(17)	119.2(5)
O(1)—C(7)—C(8)	122.1(4)	Cl(9)—C(17)—C(16)	120.4(4)
O(1)—C(7)—C(12)	117.0(5)	Cl(9)—C(17)—C(18)	119.0(5)
C(8)—C(7)—C(12)	120.7(5)	C(16)—C(17)—C(18)	120.6(5)
O(5)—C(8)—C(7)	119.6(4)	Cl(10)—C(18)—C(13)	119.2(4)
O(5)—C(8)—C(9)	121.4(5)	Cl(10)—C(18)—C(17)	121.1(4)
C(7)—C(8)—C(9)	119.0(5)	C(13)—C(18)—C(17)	119.6(5)

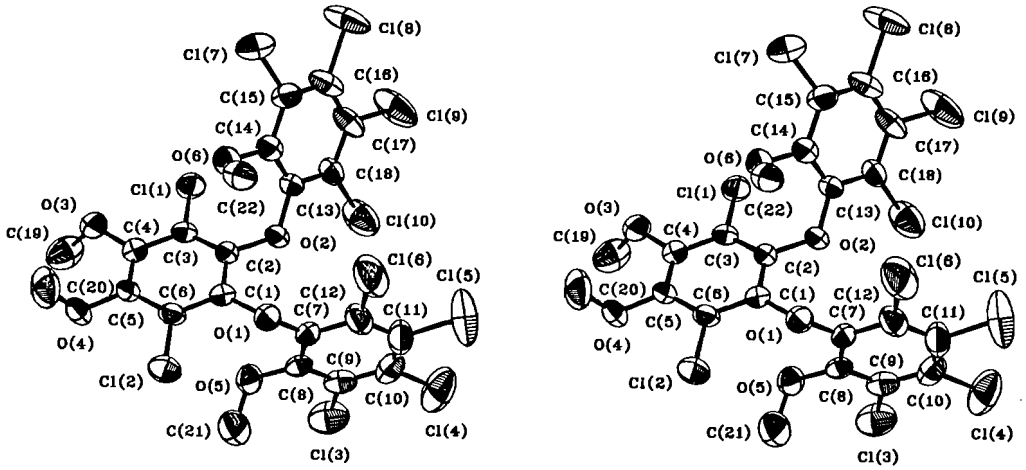

FIG. 1. Stereo view of **4**. 50% probability thermal ellipsoids are shown for the atoms.

resolution procedures split into two lines of area 2:1 with $\Delta\nu$ = 1.2 Hz, suggesting a *cis*:*trans* arrangement of methoxyl groups. The same long range $^3J_{CH}$ coupling referred to above was also observed for this model compound in a similar ^{13}C -"coupled NOe" experiment.

Formation of the trimer likely occurs during the final stage in the chlorination of guaiacol. The reaction progresses rapidly to tetrachloroguaiacol **5** under mild conditions, but introduction of the final chlorine is somewhat slower. Under forcing conditions, intermolecular reactions and oxidation may occur, possibly as shown, with the formation of condensation products such as the trimer **3**.

Discussion of crystal structure of ***4***

The molecule (Fig. 1) contains a central six-membered dichloro-tetraoxo substituted aromatic ring, linked via oxygen bridges to two identical tetrachloro-dioxo substituted rings. Although a structural formula has apparent C_{2v} symmetry, intramolecular steric interactions prevent the attainment of this symmetrical conformation. The observed molecular structure

has very rough C_2 symmetry, but with large deviations from exact symmetry; e.g. the outer-ring planes make angles of 91.5 and 68.3(5)° with the plane of the central ring (Fig. 1). Each six-membered ring is close to planar, with maximum displacements from the mean planes of 0.029(5) Å in the central ring, and 0.009(6) and 0.019(6) Å in the outer rings. The substituents are, however, more significantly displaced from the ring planes, presumably as a result of the steric overcrowding, by 0.005–0.137(2) Å for Cl and 0.005–0.092(4) Å for O atoms; the methoxy groups are oriented with the outer methyl carbon atoms displaced from the ring planes by 0.99–1.21(1) Å.

Some of the O—CH_3 bond distances seem anomalously short, particularly O(6)—C(22) at 1.202(6) Å, and to a lesser extent O(5)—C(21) at 1.344(7) Å. However, some of the thermal parameters of the atoms involved, particularly O(6), are quite large, although not physically unrealistic, and suggest possible librational or disorder errors in the positions of these outer atoms. Otherwise, the bond lengths in the molecule (Table 2) are generally close to expected values. Mean lengths (with standard deviations derived from rms deviations in parentheses) are C—Cl = 1.721(2), C—C = 1.382(3), C(sp^2)—O = 1.380(4), C(sp^3)—O = 1.415(13) Å. Bond angles (Table 3) are also close to normal values, relief of any steric strain apparently being accomplished by rotations and deviations from planarity, rather than bond angle distortions. Intermolecular distances are generally close to normal van der Waals separations; the shortest intermolecular Cl...Cl contacts of 3.481, 3.526, 3.604, 3.616(3) Å represent fairly strong interactions. Two C—H...Cl groupings (one intramoleclar, H...Cl = 2.89 Å, and one intermolecular, H...Cl = 2.80 Å) and one intramolecular C—H...O (H...O = 2.37 Å) may represent weak hydrogen-bond type interactions.

1. I. H. Rogers and L. H. Keith. Environ. Can. Fish. Marine Service Tech. Rep. No. 465 (1974).
2. K. P. Kringstad and K. Lindström. Environ. Sci. Technol. **18**, 236A (1984).
3. R. Fort, J. Sleziona, and L. Denivelle. Bull. Soc. Chim. Fr. 810 (1955).
4. P. Coppens, L. Leiserowitz, and D. Rabinovich. Acta Crystallogr. **18**, 1035 (1965).
5. J. De Meulenaer and H. Tompa. Acta Crystallogr. **19**, 1014 (1965).
6. D. T. Cromer and J. B. Mann. Acta Crystallogr. Sect A, **24**, 321 (1968).
7. R. F. Stewart, E. R. Davidson, and W. T. Simpson. J. Chem. Phys. **42**, 3175 (1965).
8. D. T. Cromer and D. Liberman. J. Chem. Phys. **53**, 1891 (1970).
9. L. Ernst, V. Wray, V. A. Chertkov, and N. M. Sergeyev. J. Magn. Reson. **25**, 123 (1977).
10. T. Schaefer and R. Laatikainen. Can. J. Chem. **61**, 224 (1983).

Kinetics of the interactions between dyes and micelles

VINCENT C. REINSBOROUGH[1] AND JOSEF F. HOLZWARTH
Fritz-Haber-Institut der Max-Planck-Gesellschaft, Faradayweg 4-6, D-1000 Berlin 33, West Germany

Received July 31, 1985[2]

VINCENT C. REINSBOROUGH and JOSEF F. HOLZWARTH. Can. J. Chem. **64**, 955 (1986).

The rates of association of three azo dyes, methyl red (MR), methyl orange (MO), and pyridine-2-azo-*p*-dimethylaniline (PADA), with sodium dodecylsulfate (SDS) and cetyltrimethylammonium bromide (CTAB) micelles in water were measured at 25°C over a wide pH range by the continuous flow method of integrating observation (CFMIO). The association was considered in 3 steps: bulk solution encounter, pH jump, and electrostatic and hydrophobic interactions. Either the first or third step is rate limiting depending on the charge of the dye. The rate constant of association of neutral PADA, MR, and MO with SDS micelles is approximately 2×10^6 dm^3 mol^{-1} s^{-1} while charging the dyes positively increases k to 10^9 dm^3 mol^{-1} s^{-1}. Increasing the hydrophobicity of dye or micelle increases k for the interaction with the neutral dye species. Changes in k with pH for the dye–CTAB association were less pronounced.

VINCENT C. REINSBOROUGH et JOSEF F. HOLZWARTH. Can. J. Chem. **64**, 955 (1986).

Opérant à 25°C, dans des solutions aqueuses à des pH très variés et faisant appel à une méthode d'écoulement continue d'intégration des observations, on a mesuré les vitesses d'association de trois colorants azo, le rouge de méthyle (RM), l'orange de méthyle (OM) et la pyridine-2-azo-*p*-diméthylaniline (PADA), avec des micelles de dodécylsulfate de sodium (DSS) ou du bromure de cétyltriméthylammonium (BCTA). On a considéré l'association en trois étapes : la rencontre globale des solutions, le changement rapide du pH et les interactions électrostatiques et hydrophobes. Suivant la charge du colorant, la première ou la troisième étape peuvent limiter la vitesse de la réaction. Les constantes d'association des entités neutres PADA, RM et OM avec les micelles de DSS sont de l'ordre de 2×10^6 dm^3 mol^{-1} s^{-1} alors que, si l'on charge les colorants positivement, la valeur de k augmente jusqu'à 10^9 dm^3 mol^{-1} s^{-1}. À cause de l'interaction avec les espèces colorantes neutres, une augmentation de l'hydrophobicité du colorant ou des micelles provoque une augmentation de k. Les variations de k avec le pH, pour l'association des colorants avec le BCTA, sont beaucoup moins prononcées.

[Traduit par la revue]

Introduction

Neutral molecules usually associate with ionic micelles in aqueous solution close to the diffusion-controlled limit, i.e., with a rate constant of 10^8–10^{10} dm^3 mol^{-1} s^{-1} (1–5). When the molecule and micelle are oppositely charged this should even more be the case, but when both have the same charge, it is not clear what effect the electrostatic repulsion has upon the solubilization process which, in this case, must proceed mainly through hydrophobic forces.

These three situations were examined in anionic micellar sodium dodecylsulfate (SDS) and cationic micellar cetyltrimethylammonium bromide (CTAB) solutions with azo dyes whose charges could be altered by altering the pH. The dye most extensively examined was methyl red (MR) which is positively charged, neutral (zwitterionic), or negatively charged depending upon the pH. Methyl orange (MO) came in for scrutiny also to confirm the trends noted with MR. The third dye, pyridine-2-azo-*p*-dimethylaniline (PADA), resembles the other two in structure but at ordinary pH values can only be neutral or positively charged. It was studied because it is widely used as an indicator reaction in its complexation with metal ions in micellar rate enhancement studies. It is usually assumed in these kinetics that the association step of PADA to the micelle is not rate limiting but it has never been measured.

Experimental

The continuous flow method of integrating observation (CFMIO) was used to obtain the rates of association of dye with micelle (6, 7). Solution A contained dye and surfactant at a concentration less than the critical micelle concentration (cmc) and solution B contained surfactant slightly higher than twice the cmc. As a result, the surfactant concentration after mixing was 25–50% higher than the cmc. No change in k_{obs} was noted within error when the final surfactant concentration did not greatly exceed twice the cmc, which took different values as the pH changed. Under these mixing conditions, both solutions contained surfactant monomer so that any dye–monomer interaction effects (8) in the mixing would be minimized. Micelle concentrations were calculated by subtracting the cmc from the final total surfactant concentration and dividing by the aggregation number. Values for the cmc and aggregation numbers as affected by ionic strength were taken from the literature (9, 10).

Pseudo-first-order conditions usually pertained with the micelles (10^{-5}–10^{-4} mol dm^{-3}) in at least 10-fold excess over the dye (10^{-6} mol dm^{-3}). For CFMIO to be effective, spectral differences on mixing must be at least 10–15%. This was not always possible when dye and micelle bore similar charges.

Three methods were used to calculate the rate constant of association of the dye with the micelles in the continuous flow method with integrating observation. If there are no interfering slower reactions, then the "constant speed" method is the most accurate. Most of the data could be collected by this technique. Solution absorbances of the reaction mixture at constant flow (E), the products (E_∞), and the two reactant solutions (averaged as E_0) are measured and combined in the ratio M defined as $(E - E_\infty)/(E_0 - E_\infty)$. The relationship between M and the rate constant takes different forms depending upon the order of the reaction (6). The error in k values determined by the constant speed method is usually 25–40%.

When more than one reaction occurs in the time it takes to register E_∞ (~0.1 s), then either one of two variants in approach can be used to eliminate E_∞ from the calculations. In the first, which could be called the "two speed" method, solution absorbances of the reaction mixture are obtained at two different mixing speeds (E_1, E_2) along with the absorbances of the reactants (E_0). The ratio M then takes the form $(E_1 - E_2)/(E_0 - E_2)$ where E_1 is associated with the faster flow rate (11). Then, for example, for a pseudo-first-order reaction

$$[1] \quad M = \frac{V_1[1 - \exp(-R/V_1)] - V_2[1 - \exp(-R/V_2)]}{R - V_2[1 - \exp(-R/V_2)]}$$

where $R = kc_0l$ in which k is the second order rate constant, c_0 is the

[1]On sabbatical leave from Mount Allison University, Sackville, N.B., Canada.

[2]Revision received January 14, 1986.

concentration of the reactant in excess, and l is the length of the observation tube. V_1 and V_2 are the two flow rates with $V_1 > V_2$.

The other variant in technique is the "three speed" method which eliminates E_0 and involves only the three solution absorbances (E_1, E_2, and E_3) of the reaction mixture at three different speeds (12). The ratio M is $(E_1 - E_3)/(E_2 - E_3)$ which for a pseudo-first-order reaction becomes

$$[2] \quad M = \frac{V_2[1 - \exp(-R/V_1)] - V_3[1 - \exp(-R/V_3)]}{V_2[1 - \exp(-R/V_2)] - V_3[1 - \exp(-R/V_3)]}$$

with V_1, V_2, and V_3 being the three flow rates and R having the same form as previously (12).

The difficulty with both these variants is that the absorbances E_1, E_2, and E_3 may not differ appreciably over the range of flow rates that are practical for the instrumentation. Errors in k thus usually lie in the 50–100% range. These two methods are often useful as a check only when one process is being viewed by the constant speed technique.

The surfactants and methyl red were obtained from Merck, methyl orange from Serva, PADA from ICN Pharmaceuticals, and 2-(5-bromo-2-pyridylazo)-5-diethylaminophenol (bromo-PADAP) from Janssen. Solutions were made from triply distilled water and used within an hour or two of preparation. The appropriate pH was obtained by adding NaOH or HCl solution to both reactant solutions.

Results

Methyl red interactions with SDS and CATB micelles

The spectra for MR in nonmicellized and micellized SDS solutions reveal sufficient spectral differences for kinetic exploitation by CFMIO as long as the pH is less than 8 (Fig. 1). The second order rate constant for the association of MR with SDS micelles obtained by CFMIO is shown in Fig. 2 for the pH range 1–8. The rate constant rises sharply from 2×10^6 dm^3 mol^{-1} s^{-1} at pH 8 to a value 2×10^9 dm^3 mol^{-1} s^{-1} or greater at pH 4. From pH 3 to 4, k is too large to be measured by CFMIO ($k \geq 2 \times 10^9$ dm^3 mol^{-1} s^{-1}). From pH 2.5 to 1, k drops rapidly being only 4×10^6 dm^3 mol^{-1} s^{-1} at pH 1.2.

With CTAB micelles, the applicable pH range for CFMIO is wider extending from pH 11 to 2.5 but the k values do not show the same dramatic changes as with SDS micelles (Fig. 2). Although it is tempting to draw a curve through the data points to yield a maximum in k around pH 5–6, it is not justified in view of the experimental error associated with each point (see error bars in Fig. 2). The best that can be said is that the rate of interaction of MR with CTAB micelles rises slowly but perceptibly over the pH range 2.5–11.

Salt additions were made at pH 4.5 and 8 in the MR–SDS system to see whether the changes in k were consistent with the different MR species postulated at each pH. At pH 4.5, the rate of interaction between dye and micelle was noticeably lowered, in regular fashion, with NaCl additions (Fig. 3) but at pH 8 a slight increase from $(2.0 \pm 0.5) \times 10^6$ to $(4.1 \pm 1.0) \times 10^6$ dm^3 mol^{-1} s^{-1} was detectable with the salt addition being 0.20 mol dm^{-3} NaCl. The uncertainties from the measurements justify saying only that k remains constant with salt additions at pH 8.

Methyl orange interactions with SDS micelles

Methyl orange differs from MR in structural detail only in having a *para*-SO_3^- group instead of an *ortho*-COO^- group as a substituent on one of the benzene rings (Figs. 4, 5). The spectra in micellar and nonmicellar SDS solutions are similar except that pH 4.2 catches the titration transition zone for MO (pH 3.5–4.5) and the acid region for MR (transition zone

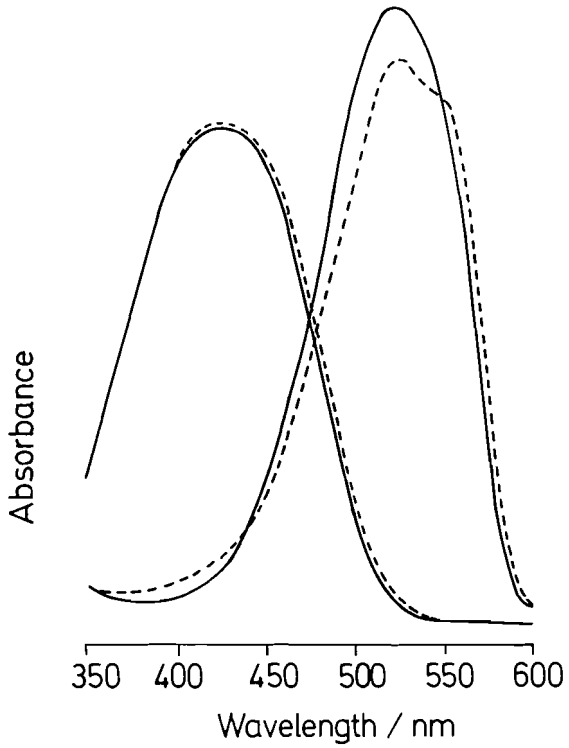

FIG. 1. Spectra for methyl red (MR) at pH 8.5 (left) and pH 4.2 (right) in micellar SDS (solid lines) and without any micelles (dotted lines) (MR 5×10^{-6} dm^3 mol^{-1} and SDS micelles 1×10^{-4} dm^3 mol^{-1}).

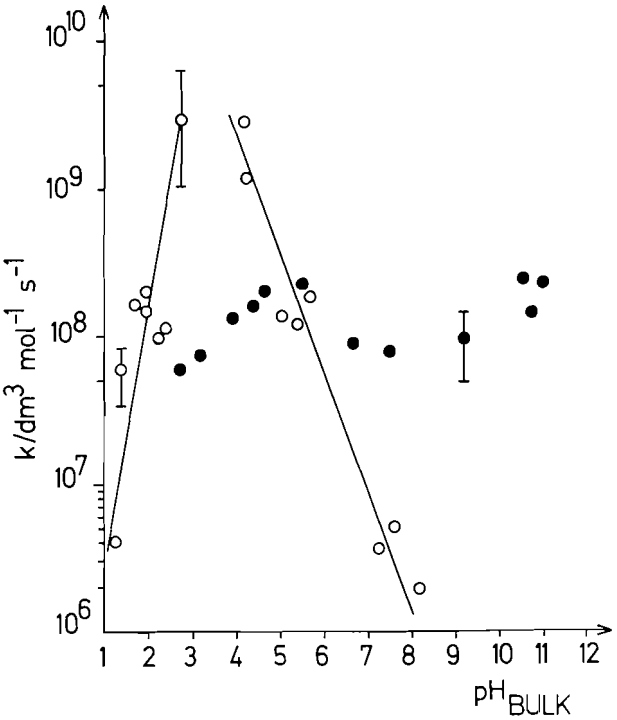

FIG. 2. Dependence on pH of the rate constant of association of methyl red with SDS micelles (○) and CTAB (●) with error bars drawn for representative points.

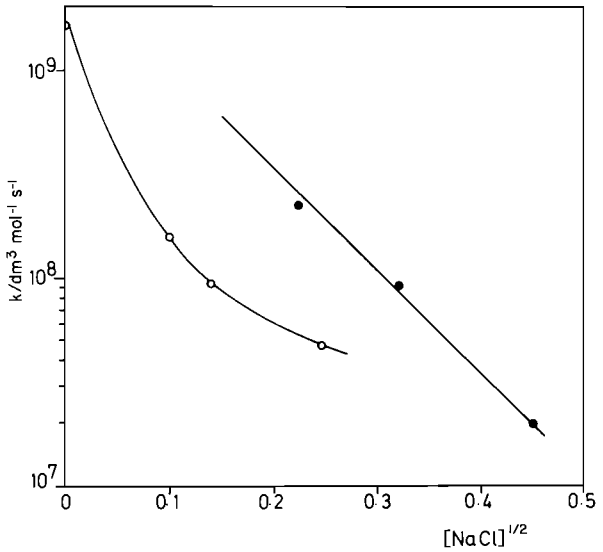

FIG. 3. Effect of NaCl concentration (in mol dm^{-3}) on the rate constant of association of SDS micelles with PADA at pH 5.0 (●) and with MR at pH 4.5 (○).

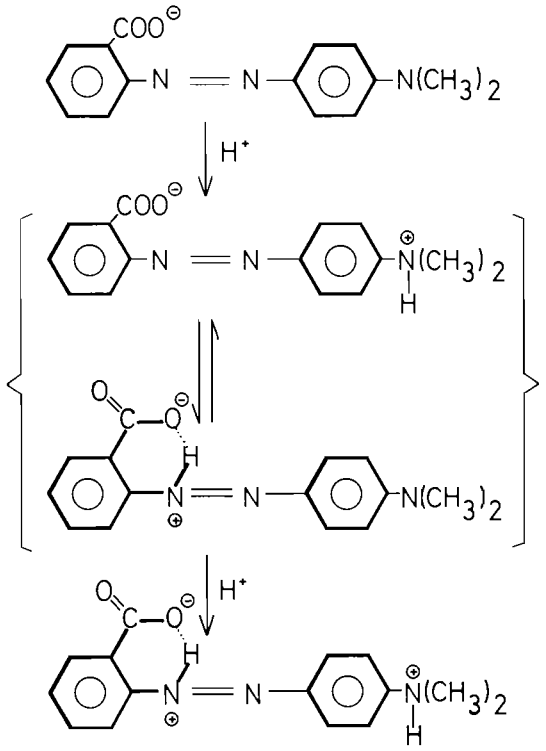

FIG. 4. Mechanism of protonation of methyl red (MR).

pH 5–6). For MO–SDS solutions above pH 6, there is no spectral difference from MO solutions without SDS (Fig. 6).

The k values for the MO–SDS system were measured by the less precise two speed CFMIO variant (see Experimental) because of an interfering secondary reaction. As with MR, the rate constant for the interaction between MO and SDS micelles rose from 2×10^6 to at least $5 \times 10^8\ dm^3\ mol^{-1}\ s^{-1}$ (Fig. 7) on decreasing pH in the acid region. Again, there was a short range at low pH (1.5–2.0 in pH) over which, the rate was too rapid to detect ($k \geq 5 \times 10^8\ dm^3\ mol^{-1}\ s^{-1}$). Below pH 1.5, k fell

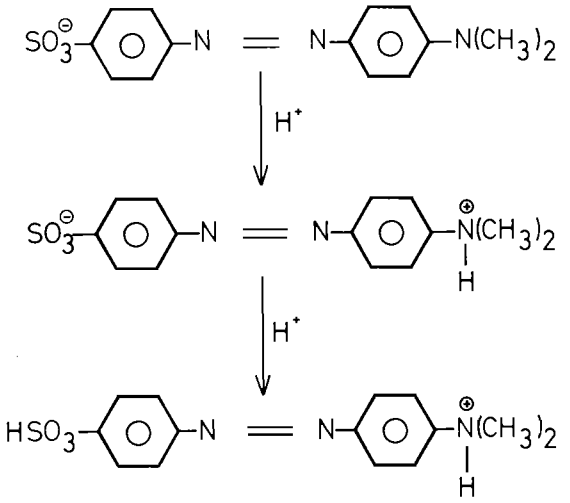

FIG. 5. Mechanism of protonation of methyl orange (MO).

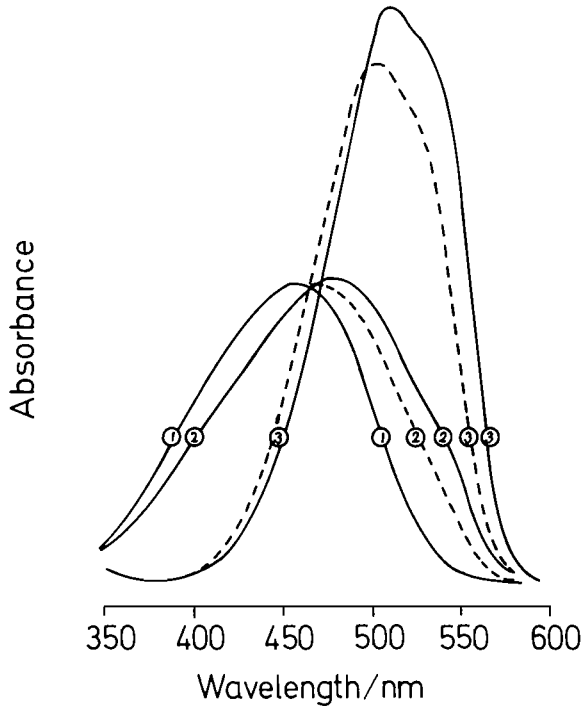

FIG. 6. Spectra for methyl orange in micellar (solid lines) and nonmicellar (dotted lines) SDS at pH 8.6 (1), pH 4.2 (2), and pH 1.0 (3). The two spectra at pH 8.6 are identical ($5 \times 10^{-3}\ dm^3\ mol^{-1}$ MO and $1 \times 10^{-4}\ dm^3\ mol^{-1}$ SDS micelles).

rapidly so that at pH 1.0 it was $2 \times 10^7\ dm^3\ mol^{-1}\ s^{-1}$ (Fig. 7). The identity of the interfering reaction was not pursued further since its effect could easily be eliminated by the two speed method.

Interactions of PADA with SDS and CTAB micelles

The pH dependence of the rate constant of interaction of PADA with micellar SDS solutions is shown in Fig. 8. Below pH 5.5, the reaction rate was too rapid to be observed without salt additions (Fig. 3) but dropped rapidly with increasing alkalinity to a constant value of $(2.0 \pm 0.5) \times 10^6\ dm^3\ mol^{-1}\ s^{-1}$ over the range pH 7–10.5. It should be noted that, unlike MO and MR associated with SDS micelles, with this diazo dye

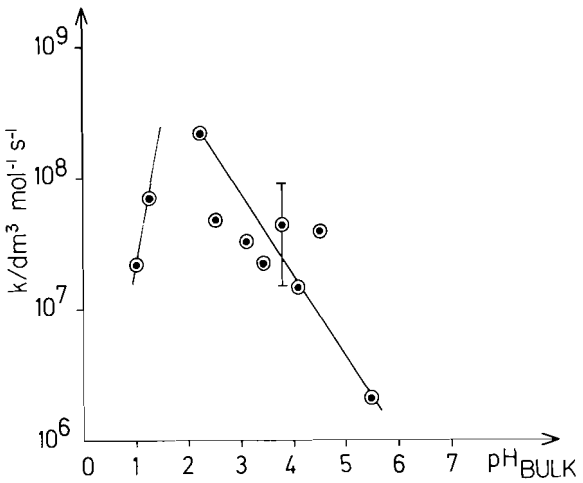

FIG. 7. Dependence on pH of rate constant of association of methyl orange (MO) with SDS micelles.

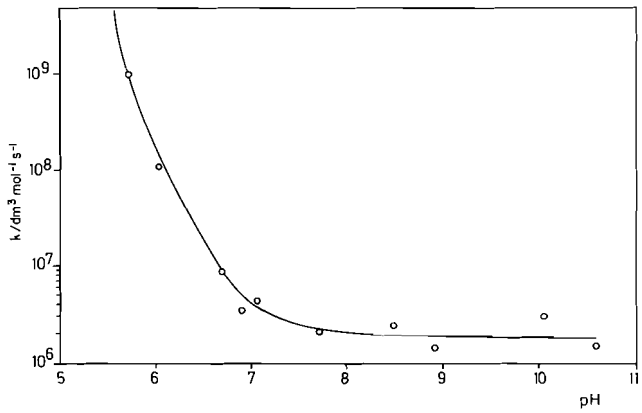

FIG. 8. Dependence on pH of rate constant of association of PADA with SDS micelles.

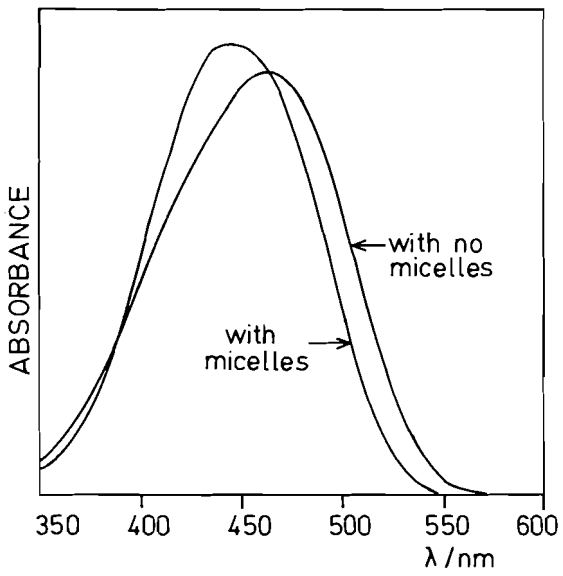

FIG. 9. Absorption spectra for PADA in water and in micellar CTAB solution at pH 9.

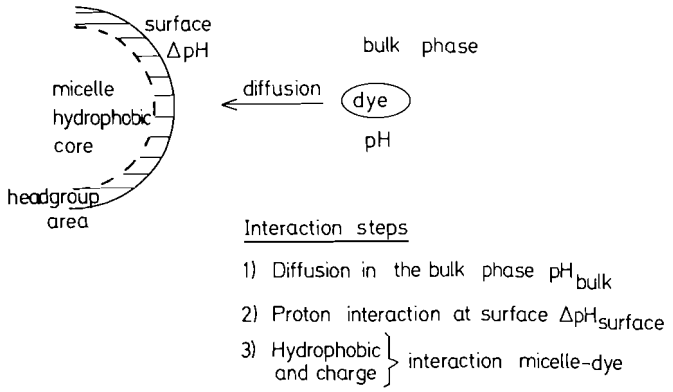

FIG. 10. Model of dye–micelle interactions.

sufficient spectral difference from the counterpart soapless solutions was maintained in the alkaline region (Fig. 9).

Discussion

The association of a dye molecule with a micelle may be divided into three stages corresponding to the three sites of interaction: the bulk solution, the micelle surface region, and the micelle interior (Fig. 10). In the first stage, the rate of interaction will be the bulk solution encounter rate which must be close to the diffusion-controlled limit of about 3×10^9 dm^3 mol^{-1} s^{-1} (13) especially when micelle and dye are oppositely charged. Dye protonation or deprotonation may occur in the second stage since the surface region pH will differ by approximately 2 pH units from the bulk solution value (14, 15). However, the rate of proton transfer in micellar media is also in the 10^9 dm^3 mol^{-1} s^{-1} range (16) so that this step should not ordinarily be rate-determining. The final stage of incorporation must be a complex interaction between electrostatic and hydrophobic forces as the dye settles into its binding site in the micelle core or surface or some intermediate position.

Methyl red and MO undergo protonation as depicted in Figs. 4 and 5. A more complete analysis would include quinoid forms (17, 18) but, for our purposes, a simplified scheme is sufficient. The *ortho* position of the COO^- group in MR as opposed to the *para* position of the SO_3^- substituent in MO affords stability to azo nitrogen protonation through the formation of a six-membered ring for MR. The pK_a values for MR in water are 4.9 and 2.4 while MO changes colour in the pH 3.1–4.1 range. The apparent pK_a for the dissociation of the neutral form of MR to the negative form is shifted to 6.7 in micellar SDS and to 3.55 in micellar decyltrimethylammonium bromide (15). Pyridine-2-azo-*p*-dimethylaniline is neutral in alkaline solution but positively charged in acid solution with its pK_a of 4.5 shifted to 6.7 in micellar SDS solutions (14).

Of the three dyes, only PADA gives rise to a spectral difference in alkaline SDS solutions. Only PADA is neutral above pH 7; MO and MR are negatively charged as are the SDS micelles. In acid solution, no spectral change results when positively charged PADA interacts with positively charged CTAB micelles. Apparently, when dye and micelle are similarly charged spectral differences are not found rendering CFMIO powerless to detect spectrophotometrically the kinetics of interaction between such species.

Thus, at pH 8 in the MR–SDS system (Fig. 2) where the observed rate of interaction is relatively slow at $2 \times$

10^6 dm^3 mol^{-1} s^{-1}, CFMIO senses only the association of the neutral MR species with negatively charged SDS micelles, even though negatively charged MR is the dominant species at this pH. Supporting evidence for this comes from salt additions to this system at pH 8. Even with 0.20 mol dm^{-3} NaCl, the rate constant remained unchanged. If the negative species were affecting the CFMIO-determined rate constants, they should have been dramatically affected by ionic strength changes of this order of magnitude.

As the pH is lowered from 8 to 4, negatively charged MR disappears, neutral MR waxes in concentration and then wanes as positively charged MR makes its appearance. The observed rate in this pH range is a blend of neutral MR and positively charged MR interactions with SDS micelles and rises sharply as a result. The increasing proportion of positively charged MR to neutral MR brings the rate close to the limit imposed by diffusion presumably due to the dominance of the electrostatic attractive forces as the hydrophobicity of the dye changes in character and strength with the charging of the dye. Salt additions at pH 4.5 depress k markedly (Fig. 3) as would be expected with Na^+ ions competing with positively charged MR for micelle surface sites. This same effect on k was noted in electron transfer reactions when salt was added (4).

In effect, this depression of k with salt addition explains why, at pH values lower than 4, the rate constant decreases markedly. The added H^+ ions act as added Na^+ ions in excluding positively charged MR from the micellar surface region. In fact, pH 2 and 10^{-2} mol Na^+/dm^3 are roughly equivalent in depressive power. The overall interpretation of the kinetic results for the MO–SDS system is similar.

For alkaline solutions in the PADA–SDS system where PADA is neutral, the rate constant of association is 2×10^6 dm^3 mol^{-1} s^{-1} for pH 7.5–10.5 (Fig. 8). Below pH 7, protonated PADA is formed and, as with MR, the sharp rise in k to the diffusion-controlled limit and the depressive effect upon k of salt additions reflect the strength of the electrostatic attractive forces.

Because cationic micelles shift the pK_a of dyes to lower pH, many of the protonation changes of these dyes are not available for study with CTAB micelles. Thus, in the MR–CTAB system, despite the wide pH range monitored, we see only the effect of the protonation of the negative species to the neutral form and it appears to have minimal effect on the rate constant of interaction. The hydrophobic force operative at intermediate pH values is relatively strong to yield a k value of 1×10^8 dm^3 mol^{-1} s^{-1}. At pH 11, k rises only to 2×10^8 dm^3 mol^{-1} s^{-1} with the electrostatic attractive contribution to the interaction but this contribution does not play the same dominant role as it did in the MR–SDS system.

This increase in the hydrophobic force of attraction with CTAB micelles is especially noticeable with PADA where the rate of interaction of neutral PADA with the micelles is so rapid as to be near or at the diffusion imposed limit. The longer carbon chain of CTAB as compared with SDS confers greater hydrophobicity to CTAB which is reflected also in its lower cmc. To test this further, the interaction rate constant was measured at pH 9 for neutral PADA associating with sodium tetradecylsulfate and sodium decylsulfate micelles. The k values thus determined were 2.4×10^8 and 1.6×10^5 dm^3 mol^{-1} s^{-1}, respectively, as compared with 2.0×10^6 dm^3 mol^{-1} s^{-1} for SDS. These data indicate that a two carbon increase in the chain length increases k by at least an order of magnitude in the C10–C14 range as the hydrophobic forces within the micelle are increased.

In summary, when the neutral dye species of MR, MO, and PADA interact with SDS and CTAB micelles the rate constants are 10^6 dm^3 mol^{-1} s^{-1} but when dye and micelle are oppositely charged k increases to 10^9 dm^3 mol^{-1} s^{-1}, the diffusion-controlled limit. Since even neutral molecules and micelles are thought to associate at this limit in solution (1–3), the slowness of the observed rate must be a consequence of the final stage of incorporation of the dye into the micelle when hydrophobic forces must chiefly be operative. The charging of the dye oppositely from the micelle must consequently affect the hydrophobicity of the dye and so the electrostatic forces now brought to bear upon the final interaction step are dominant. Increasing the hydrophobicity of the micelle by lengthening the carbon chain of the monomer serves to increase the rate of interaction. Increasing the hydrophobicity of the dye serves the same purpose. This was tested by investigating the association of the very hydrophobic dye, bromo-PADAP, in both SDS and CTAB and, even for neutral bromo-PADAP, k values were always too fast to be measured accurately by CFMIO despite sufficient spectral changes. With MR, MO, and PADA interacting with SDS and CTAB micelles, the hydrophobic forces responsible for the association are relatively weak causing the third stage of incorporation to be slow and rate-determining but this is not the case for bromo-PADAP associating with these same micelles.

Acknowledgements

We wish to thank Dr. B. H. Robinson for helpful discussions, the Fritz-Haber-Institut for financial support, and Mount Allison University for a sabbatical leave to V.C.R.

1. M. Almgren, F. Grieser, and J. K. Thomas. J. Am. Chem. Soc. **101**, 279 (1979).
2. J. E. Löfroth and M. Almgren. J. Phys. Chem. **86**, 1636 (1982).
3. J. C. Selwyn and J. C. Scaiano. Can. J. Chem. **59**, 663 (1981).
4. H. Bruhn and J. F. Holzwarth. Ber. Bunsenges. Phys. Chem. **82**, 1006 (1978).
5. S. Yiv and R. Zana. J. Colloid Interface Sci. **80**, 224 (1981).
6. J. F. Holzwarth. Techniques and applications of fast reactions in solution. *Edited by* W. J. Gettins and E. Wyn-Jones. D. Reidel Press, Dordrecht, Holland. 1979. p. 13.
7. V. Eck, M. Marcus, G. Stange, J. Westerhausen, and J. F. Holzwarth. Ber. Bunsenges. Phys. Chem. **85**, 869 (1981).
8. T. Ban, K. Kasatani, M. Kawasaki, and H. Sato. Photochem. Photobiol. **37**, 131 (1983).
9. M. Almgren and S. Swarup. Solution behavior of surfactants. *Edited by* K. Mittal and B. Lindman. Vol. 1. Plenum Press, New York. 1984. p. 613.
10. P. Mukerjee and K. J. Mysels. Nat. Stand. Ref. Data Ser. (U.S. Natl. Bur. Stand.), **NSRDS-NBS 36** (1971).
11. G. Stange. Diplomarbeit. Fritz-Haber-Institut. Berlin. 1982.
12. J. Westerhauser. Diplomarbeit. Fritz-Haber-Institut. Berlin. 1979.
13. M. Almgren, F. Grieser, and J. K. Thomas. J. Chem. Soc., Faraday Trans. 1, **75**, 1674 (1979).
14. A. D. James and B. H. Robinson. J. Chem. Soc., Faraday Trans. 1, **74**, 10 (1978).
15. M. Montal and C. Gitler. Bioenergetics, 4, 363 (1973).
16. H. Bruhn, S. Nigam, and J. F. Holzwarth. Faraday Discuss. Chem. Soc. **74**, 129 (1982).
17. T. R. Griffiths and P. J. Potts. Anal. Chim. Acta, **71**, 1 (1974).
18. J. C. Merlin, J. L. Lorriaux, A. Dupaix, and E. W. Thomas. J. Raman Spectrosc. **11**, 131 (1981).

Synthesis, structure, proton-nuclear magnetic resonance, and Fourier transform infrared spectroscopy of several transition and nontransition metal–adenosine-5-triphosphate complexes

H. A. TAJMIR-RIAHI, M. J. BERTRAND, AND T. THEOPHANIDES[1]

Department of Chemistry, Université de Montréal, Montréal, Que., Canada HC 3V1

Received September 20, 1985

H. A. TAJMIR-RIAHI, M. J. BERTRAND, and T. THEOPHANIDES. Can. J. Chem. **64**, 960 (1986).

Several complexes of adenosine-5-triphosphate disodium salt (Na_2H_2ATP) with the metal ions, Na^+, Mg^{2+}, Ca^{2+}, Mn^{2+}, Co^{2+}, Ni^{2+}, Cu^{2+}, and *cis*- and *trans*-$Pt(NH_3)_2Cl_2$ and K_2PtCl_4 at pH = 3.5 and 7.2 have been isolated, identified, and studied. Marked spectral similarities have been observed for the structurally known metal–phosphate bonded compounds, $[Cu(H_2ATP)(phen)]_2 \cdot 7H_2O$ and $[Zn(H_2ATP)(bipy)]_2 \cdot 4H_2O$ and all the metal–ATP complexes studied here, except the Pt–ATP complexes. The metal binding is through the α, β, and γ phosphate oxygen atoms when the N1-position of adenine is protonated. Spectral changes have also been observed for the Pt–ATP complexes in which there is a Pt–N7 and –N1 coordination. The sugar pucker in the $Na_2H_2ATP \cdot 3H_2O$ crystal dimers is C3′-*endo*–*anti* (in one) and C2′-*endo*–*anti* (in the other) with a characteristic infrared band at 818 cm^{-1}. In the corresponding Cu^{2+} and Zn^{2+} complexes the sugar has C3′-*endo*–*anti* conformation with the marker band at about 814 cm^{-1}. The C2′-*endo*–*anti* conformation is observed for all the metal–ATP complexes prepared here with a marker band at 825–822 cm^{-1}.

H. A. TAJMIR-RIAHI, M. J. BERTRAND et T. THEOPHANIDES. Can. J. Chem. **64**, 960 (1986).

Opérant à des pH de 3,5 et de 7,2, on a isolé, étudié et identifié plusieurs complexes du sel double de sodium du triphosphate-5 d'adénosine (Na_2H_2ATP) avec les ions métalliques Na^+, Mg^{2+}, Ca^{2+}, Mn^{2+}, Co^{2+}, Ni^{2+}, Cu^{2+} et avec les $Pt(NH_3)_2Cl_2$-*cis* et -*trans* ainsi que le K_2PtCl_4. On a remarqué des similarités spectrales marquées pour tous les composés structuraux connus comportant un phosphate lié à un métal, comme le $[Cu(H_2ATP)(phen)]_2 \cdot 7H_2O$, le $[Zn(H_2ATP)(bipy)]_2 \cdot 4H_2O$ et tous les complexes métal–ATP étudiés ici, excepté les complexes Pt–ATP. Lorsque la position N1 de l'adénine est protonée, la liaison du métal se fait par les atomes d'oxygène α, β et γ du phosphate. On a noté des changements spectraux dans les cas des complexes Pt–ATP dans lesquels il y a une cordination Pt–N7 et –N1. La conformation du sucre dans les cristaux dimères du $Na_2H_2ATP \cdot 3H_2O$ est C3′-*endo*–*anti* (dans l'un) et C2′-*endo*–*anti* (dans l'autre) et elle présente une bande infrarouge caractéristique à 818 cm^{-1}. Dans les complexes correspondants avec le Cu^{2+} et le Zn^{2+}, le sucre adopte une conformation C3′-*endo*–*anti* et il possède une bande caractéristique à 814 cm^{-1}. On observe une conformation C2′-*endo*–*anti* pour tous les complexes de métaux–ATP qui ont été préparés ici et ils sont tous caractérisés par une bande à 825–822 cm^{-1}.

[Traduit par la revue]

Introduction

Of all metal–mononucleotide complexes those involving ATP have been the subject of extensive investigations (1, 2). This is mainly due to the important role of ATP as a mediator in maintaining the energy balance in living cells by hydrolysis of its phosphoryl groups and by transfer to various acceptors. Since most of the reactions responsible for phosphoryl group transfer are catalyzed by metal ions the study of metal–ATP interactions is biologically significant. Although various spectroscopic techniques have been used (3–6) to characterize the nature of metal–ATP interactions, until recently the metal ion binding to the various potential coordination sites of the ATP molecule was the subject of speculation. A recent X-ray structural analysis of ternary complexes $[Cu(H_2ATP)(phen)]_2 \cdot 7H_2O$ (7) and $[Zn(H_2ATP)(bipy)]_2 \cdot 4H_2O$ (8) and several other complexes of Mg^{2+}, Ca^{2+}, Mn^{2+}, and Co^{2+} with ATP and dipyridylamine (9, 10) showed that the metal–ATP binding is through the α, β, and γ, phosphate oxygen atoms and that there is no interaction between the metal ion and the base adenine.

In the present work, several binary complexes of ATP with Na^{2+}, Mg^{2+}, Ca^{2+}, Mn^{2+}, Co^{2+}, Ni^{2+}, Cu^{2+}, Zn^{2+}, and Pt^{2+} have been isolated and studied by means of microanalysis, proton-nmr and Fourier transform infrared (FTir) spectroscopy. The spectroscopic results have been compared with those of the structurally known $[Cu(H_2ATP)(phen)]_2 \cdot 7H_2O$ and $[Zn(H_2ATP)(bipy)]_2 \cdot 4H_2O$ (8) complexes in order to detect the characteristic features of each structural type of complexes synthesized here and to establish a correlation between the spectral changes and the coordination sites involved. Furthermore, the marker bands of the sugar conformations C2′-*endo*–*anti* and C3′-*endo*–*anti* have been identified and tentative infrared assignments of the ATP absorption frequencies are reported. The molecular structure of the ATP anion (H_2ATP^{2-}) with the numbering of the atoms is shown below.

Experimental

Materials

Na_2H_2ATP was purchased from Raylo Chemicals Limited. K_2PtCl_4 was from Johnson Matthey Chemicals and was converted to *cis*- and *trans*-$Pt(NH_3)_2Cl_2$ as previously reported (11). These were purified according to a known procedure (12). D_2O (99.8%) was from Cambridge Isotope Laboratories. All the metal ion salts were reagent grade and were used as supplied.

Preparation of metal–ATP complexes

An aqueous solution of the metal ion salt (1 mmol) was added to a solution of Na_2H_2ATP (1 mmol) in H_2O (20 mL) and the pH was adjusted to 3.5 at room temperature. The solution was kept for 24 h and an ethanolic solution was added to precipitate the complex which was washed with ethanol several times and dried over $CaCl_2$. The analytical results agreed with the formula $M(H_2ATP) \cdot nH_2O$, where M = Mg^{2+}, Ca^{2+}, Mn^{2+}, Co^{2+}, Ni^{2+}, Cu^{2+}, and Zn^{2+} and n = 4–6. The platinum complexes were synthesized by addition of stoichiometric amounts of *cis*- or *trans*-$Pt(NH_3)_2Cl_2$ and K_2PtCl_4 to a solution of Na_2H_2ATP in H_2O (25 mL) in a similar fashion as stated for the other metal–ATP complexes. The complexes were isolated at pH = 3.5 and were analysed to give the composition of $[Pt(Na_2H_2ATP)_n]Cl_2 \cdot xH_2O$ and *cis*- and *trans*-$[Pt(NH_3)_2(Na_2H_2ATP)_2]Cl_2 \cdot 4H_2O$, where n = 1–4 and x = 2–6. The Mg^{2+}– and Pt^{2+}–ATP complexes were also prepared and isolated at pH = 7.2. The analytical data are given in Table 1.

[1]To whom correspondence should be addressed.

TABLE 1. Analytical data for ATP–metal complexes

Compounds	*Anal.* Calcd. (found), % C	H	N	M	pH
$[Cu(H_2ATP)(phen)]_2 \cdot 7H_2O$[a]	32.50 (32.65)	3.57 (3.18)	12.05 (11.65)	8.00 (7.85)	2.8
$[Zn(H_2ATP)(bipy)]_2 \cdot 4H_2O$[a]	31.50 (31.00)	3.41 (3.11)	12.86 (12.60)	8.53 (8.35)	4.0
$[Cu(H_2ATP)] \cdot 4H_2O$	18.69 (18.25)	3.42 (2.88)	10.90 (10.45)	10.12 (9.90)	3.5
$[Zn(H_2ATP)] \cdot 4H_2O$	18.70 (18.85)	3.42 (2.89)	10.90 (10.80)	9.98 (9.75)	3.5
$[Ni(H_2ATP)] \cdot 4H_2O$	18.90 (18.67)	3.46 (3.57)	11.02 (10.90)	9.14 (8.90)	3.5
$[Co(H_2ATP)] \cdot 4H_2O$	18.86 (18.40)	3.46 (3.31)	11.00 (10.50)	9.27 (9.10)	3.5
$[Mn(H_2ATP)] \cdot 4H_2O$	18.98 (18.45)	3.48 (3.30)	11.07 (11.71)	8.70 (8.65)	3.5
$[Mg(H_2ATP)] \cdot 5H_2O$	19.35 (19.18)	3.87 (3.65)	11.29 (10.85)	4.00 (3.85)	3.5
$[Mg_2(ATP)] \cdot 6H_2O$	18.20 (17.90)	3.64 (3.80)	10.61 (10.35)	7.42 (7.25)	7.2
$[Ca(H_2ATP)] \cdot 4H_2O$	19.45 (19.35)	3.57 (3.26)	11.13 (11.03)	6.48 (6.50)	3.5
$K[Pt(Na_2H_2ATP)Cl_3] \cdot 2H_2O$	12.95 (13.26)	1.95 (2.50)	7.55 (7.65)	21.02 (20.85)	3.05
$[Pt_2(Na_4ATP)_3Cl_4] \cdot 6H_2O$	14.85 (14.07)	1.98 (1.63)	8.65 (8.35)	16.08 (15.90)	7.2
$[Pt(Na_2H_2ATP)_2Cl_2] \cdot 6H_2O$	16.26 (15.61)	2.71 (2.63)	9.49 (9.01)	13.21 (13.05)	3.5
$[Pt(Na_2H_2ATP)_3Cl]Cl_2 \cdot 6H_2O$	17.76 (16.98)	2.66 (2.96)	10.36 (9.67)	9.62 (9.45)	3.5
$[Pt(Na_2H_2ATP)_4]Cl_2 \cdot 6H_2O$	18.62 (18.40)	2.64 (2.80)	10.86 (10.54)	7.56 (7.40)	3.5
cis-$[Pt(NH_3)_2(Na_2H_2ATP)_2]Cl_2 \cdot 4H_2O$	16.28	2.85	11.40	13.23	3.5
trans-$[Pt(NH_3)_2(Na_2H_2ATP)_2]Cl_2 \cdot 4H_2O$	16.28 (16.80)	2.85 (3.37)	11.40 (11.40)	13.23 (13.05)	3.5

[a]Structurally known.

Physical measurements

The solution pH values were measured on a Fisher Accumet Model 630 pH meter using 0.1 *N* NaOH or HCl solutions to control the pH. The ^{1}H-nmr spectra were recorded on a Varian EM 360–60 MHz. The solutions were in D_2O containing DSS as reference (δ = 0.00 ppm). The FTir spectra were recorded on a Digilab FTS-15C/D Fourier transform infrared interferometer equipped with a HgCdTe detector (Infrared Associates, New Brunswick, NJ), a KBr beam splitter, and a Globar source. The spectra were taken using KCl pellets and the resolution was 2–4 cm^{-1}. Previous procedures of data collecting and calculating the spectra were used (13). The compounds were analyzed for C, H, and N by Schwarzkopf Microanalytical Laboratory (U.S.A.) and the metal ions were determined complexometrically.

Results and discussion

Nuclear magnetic resonance spectra

The ^{1}H-nmr chemical shifts for Na_2H_2ATP and some of its metal adducts in D_2O solution are given in Table 2. Whereas the chemical shifts observed for H2 and H8 of ATP^{4-} are 8.03 and 8.43 ppm, those in Na_2H_2ATP are observed at 8.43 and 8.53 ppm, the downfield shifts of H2 and H8 protons are due to the protonation of the N1 position of the adenine ring, which is in agreement with the X-ray structural data for the Na_2H_2ATP compound (14). Complexation with the metal ions, Mg^{2+}, Ca^{2+}, and Zn^{2+} does not alter the chemical shifts of H2 and H8 considerably, while in Pt–ATP complexes drastic changes have been observed. It should be noted that the large downfield shifts of H8 in all the Pt–ATP complexes synthesized at pH = 3.5 and 7.2 are due to the direct Pt—N7 bonding (Table 2). The downfield shifts of H2 in all platinum–ATP compounds prepared at pH = 3.5 is attributed to the effect of Pt—N7

TABLE 2. The ^{1}H-nmr chemical shifts of 5′-ATP and its metal adducts in D_2O solution

Complexes	H8	H2	H1′
$Na_2H_2ATP \cdot 3H_2O$	8.53	8.43	6.13
Na_4ATP	8.45	8.03	6.15
$Mg(H_2ATP) \cdot 5H_2O$	8.50	8.35	6.12
$Mg_2(ATP) \cdot 6H_2O$	8.50	8.06	6.10
$Ca(H_2ATP) \cdot 4H_2O$	8.52	8.35	6.12
$Zn(H_2ATP) \cdot 4H_2$	8.58	8.40	6.20
$K[Pt(Na_2H_2ATP)Cl_3] \cdot 2H_2O$	8.70	8.55	6.25
$[Pt_2(Na_4(ATP)_3Cl_4] \cdot 6H_2O$	8.65	8.30	6.30
$[Pt(Na_2H_2ATP)_2Cl_2] \cdot 6H_2O$	8.75	8.60	6.20
$[Pt(Na_2H_2ATP)_3Cl]Cl \cdot 6H_2O$	8.80	8.55	6.25
$[Pt(Na_2H_2ATP)_4]Cl_2 \cdot 6H_2O$	8.85	8.60	6.35
cis-$[Pt(NH_3)_2(Na_2H_2ATP)_2]Cl_2 \cdot 4H_2O$	8.75	8.60	6.30
trans-$[Pt(NH_3)_2(Na_2H_2ATP)_2]Cl_2 \cdot 4H_2O$	8.75	8.65	6.30

TABLE 3. Selected FTir absorption bands for ATP anions and their metal

$Na_2H_2ATP \cdot 3H_2O$	Na_4ATP	$Mg(H_2ATP) \cdot 5H_2O$	$Ca(H_2ATP) \cdot 4H_2O$	$Mn(H_2ATP) \cdot 4H_2O$	$Co(H_2ATP) \cdot 4H_2O$
1705 s	1656 vs	1697 vs	1694 vs	1694 vs	1695 vs
1654 sh	1649 vs	1650 sh	1050 sh	1650 sh	1650 sh
1612 m	1611 s	1612 s	1612 s	1612 s	1612 s
1530 w	1580 m	1530 w	1535 vw	1530 vw	1530 vw
	1530 vw				
1500 m		1508 m	1508 m	1509 m	1510 m
1460 vw	1480 s	1477 w	1480 vw	1480 vw	1480 vw
1414 m	1410 s	1422 m	1421 m	1423 m	1424 m
1330 vs	1330 s	1333 sh	1322 w	1322 w	1320 w
1251 bs	1239 bs	1245 bs	1239 bs	1230 bs	1230 bs
1220 sh	1220 sh	—	—	—	—
1120 sh	1120 sh	1120 sh	1125 s	1122 s	1122 s
1105 bs	1106 bs	1108 sh	1110 sh	1099 s	1103 s
1051 s	1092 s	1093	1085 vs	1083 vs	1082 vs
1017 s	1010 sh	1001 m	1015 w	1013 w	—
1000 sh	—	—	1002 w	1002 m	999 m
965 s	—	959 w	945 sh	960 w	963 w
903 vs	905 bs	913 vs	913 vs	915 vs	912 vs
—	—	—	—	—	—
818 s	822 s	822 s	822 s	823 s	824 s
—	797 sh	782 vw	—	783 vw	783 vw
743 vw	740 vw	770 sh	740 sh	741 sh	742 sh
720 m	719 s	720 s	721 m	719 s	719 s
703 sh	—	681 w	690 sh	673 sh	670 w
671 s	644 m	637 m	637 w	638 w	638 m
630 sh	—	—	—	—	—
550 sh	550 sh	551 sh	550 sh	552 sh	551 sh
520 s	532 s	525 s	520 s	523 s	525 s

NOTE: s, strong; b, broad; w, weak; v, very; sh, shoulder; m, medium; ν, stretching; and δ, bending.

bonding. Moreover, platinum–N1 interaction has also been observed in the Pt–ATP complexes isolated at pH = 7.2, where deprotonation of the N1 position takes place. Upon a comparison of the proton-nmr spectra of Pt–ATP complexes with those of the corresponding Mg^{2+}, Ca^{2+}, and Zn–ATP compounds (Table 2), one can conclude that the binding of platinum to ATP occurs through the N7 site of the adenine ring in all the Pt–ATP adducts prepared in acidic media. The Pt–N1 coordination as well as the Pt—N7 bonding is inferred from the spectra of the platinum complexes isolated at pH = 7.2. There is no metal–base interaction in the Mg^{2+}, Ca^{2+}, and Zn^{2+}–ATP complexes (only metal–phosphate bonding is indicated from the spectra). It is worth mentioning that the sugar H1′ proton showed a considerable downfield shift in the spectra of all Pt–ATP complexes and this is most likely due to the direct metal–N7 coordination (Table 2). More conclusive evidence regarding the nature of the metal–ATP interaction is obtained from infrared spectroscopic studies discussed in the following section.

Fourier transform infrared species

Analyses of the crystal structure by X-ray showed that $Na_2H_2ATP \cdot 3H_2O$ exists as a dimer in which two of the Na^+ ions are bonded to the α, β, γ phosphate oxygens and the N7 nitrogen of the adenine ring. The other Na^+ ions are phosphate and water coordinated (14). In the crystal structures of $[Cu(H_2ATP)(phen)]_2 \cdot 7H_2O$ and $[Zn(H_2ATP)(bipy)]_2 \cdot 4H_2O$ complexes the metal ions are bonded only to the phosphate oxygen atoms with no metal–purine interaction (7, 8). The infrared spectra of these structurally known complexes have been recorded in the region of 4000–500 cm^{-1} and compared with the corresponding complexes of Mg^{2+}, Ca^{2+}, Mn^{2+}, Co^{2+}, Ni^{2+}, Cu^{2+}, Zn^{2+}, and Pt–ATP synthesized here. The results of the spectra analysis are described below in the two regions 3600–2700 cm^{-1} and 1800–500 cm^{-1}.

3600–2700 cm^{-1}

In this region, it is difficult to draw conclusions on the nature of metal–ligand bonding due to the presence of the strong hydrogen bonding network in the free Na_2H_2ATP and its metal adducts (7, 8, 14). The antisymmetric and symmetric stretching vibrations of NH_2, NH^+, H_2O sugar OH, CH_2, and CH groups are observed in this region and exhibit no major changes upon ATP–metal complexation.

1800–500 cm^{-1}

In this region of the spectra of the metal–ATP complexes, drastic changes occurred related to the base, phosphate and sugar vibrations and these are discussed below.

(a) Base vibrational frequencies. A strong and broad absorption band at 1705 cm^{-1} in the spectrum of Na_2H_2ATP, assigned to the protonated N1 position of the adenine base (3), showed shifting of about 10 cm^{-1} in the spectra of all the metal–ATP adducts synthesized at pH = 3.5 (Table 3). Upon deprotonation of the N1 position this absorption band disappeared and a new band was observed at 1656 cm^{-1} in the spectrum of the ATP^{4-} (Table 3 and Fig. 1). This absorption band is assigned to the NH_2 in-plane bending vibration (14). The small shifts of the

complexes in the region of 1800–500 cm^{-1} with possible assignments

$Ni(H_2ATP)\cdot 4H_2O$	$Cu(H_2ATP)\cdot 4H_2O$	$Zn(H_2ATP)\cdot 4H_2O$	$[Pt_2(Na_4ATP)_3Cl_4]^2\cdot 6H_2O$	Possible assignments
1697 vs	1695 vs	1694 vs	1565 vs	N1-protonated
1660 sh	1650 sh	1651 sh	1679 sh	δ NH_2
1612 s	1612 s	1612 s	1611 sh	Skeletal
1530 vw	1533 w	1530 vw	1584 sh	Pyrimidine
			1520 w	
1514 m	1509 m	1509 m	—	
1781 vw	1781 vw	1477 w	1728 w	ν N7—C— +
1428 m	1422 m	1423 m	1437 s	δ C8—H
1324 m	1325 w	1324 m	1350 m	ν Purine
			1325 w	
1233 bs	1223 bs	1233 bs	1239 bs	ν as PO_2
—	—	—	—	
1123 s	1112 bs	1122 vs	1108 vs	ν C—O (sugar)
1105 sh	1100 vs	1103 s	1100 sh	
1082 s	1085 vs	1085 s	1086 vs	ν as PO_2
—	—	—	—	
999 m	—	998 m	997 sh	
966 w	960 w	965 w	—	ν P—O—H
909 vs	918 vs	919 w	905 vs	ν O—P—O
—				
824 s	825 s	823 s	824 s	Sugar conformation
782 vw	782 vw	782 sh	787 sh	
755 sh	741 m	756 m	750 m	NH— out-of-plane
719 s	720 vw	720 m	722 m	Deformation
681 sh	680 vw	681 sh	680 sh	Ring vibration
638 w	638 w	636 m	638 m	Skeletal
—	—	—	591 sh	Deformation
552 sh	550 sh	555 sh	555 sh	δ H_2O
525 s	521 s	528 s	522 s	

bands at 1705–1695 cm^{-1} in the spectra of metal–ATP adducts are due to the rearrangement of the N1–H^+ hydrogen bonding system and are not due to the deprotonation or the participation of the N1 site in metal–ligand bonding. It should be noted that similar shifts of that absorption band were observed in the spectra of $[Cu(H_2ATP)(phen)]_2\cdot 7H_2O$ and $[Zn(Na_2H_2ATP)(bipy)]_2\cdot 4H_2O$ complexes where only metal–phosphate coordination has been reported (7, 8) (Fig. 1). It is worth mentioning that upon ionization of the N1–H^+ group and platination of the N1 position at a pH of 7.2, the absorption band at 1705 disappeared and a strong band at 1650 cm^{-1}, related to the NH_2 bending, was observed. This confirms the assignment of the band at 1705 cm^{-1} to the NH_2 bending upon protonation of the N1–H^+ group. The absorption band at 1612 cm^{-1} in the spectrum of the Na_2H_2ATP, attributed to the imidazol and pyrimidine ring skeletal vibrations, showed no changes in the spectra of the metal–ATP complexes (Table 3). A band with medium intensity appeared at about 1580 cm^{-1} in the spectra of deprotonated ATP^{4-}, $Mg_2(ATP)\cdot 6H_2O$, and $[Pt_2(Na_4ATP)_3Cl_4]\cdot 6H_2O$ complexes (Fig. 1 and Table 3) which is assigned to the pyrimidine ring vibration (14). This absorption is not present in the spectra of all the other metal–ATP complexes obtained in acidic media. A weak absorption band at 1500 cm^{-1}, in the free nucleotide spectrum, related to the pyrimidine ring vibration did not change upon ligand metalation. The two absorption bands with medium intensities at 1465 and 1414 cm^{-1} in the free ATP spectrum assigned to the purine N7—C8 stretching and C8—H bending vibrations (15), showed a small change in the spectra of all the metal–ATP compounds isolated from acidic solutions. Considerable shifting was observed in the spectra of platinum complexes (Table 3). Since the proton-nmr results indicated no direct N7–metal interaction, the small downfield shift of H8 (Table 2) and the infrared changes of the adenine ring vibrations are related to indirect metal–N7 interaction. This indirect interaction via H_2O molecules or the participation of the N7 atom in the base stacking interactions has been observed in the crystal structures of $[Cu(H_2ATP)(phen)]_2\cdot 7H_2O$, $[Zn(H_2ATP)(bipy)]_2\cdot 4H_2O$ (7, 8), and several other ternary Mg^{2+}– and Ca^{2+}–ATP complexes (9, 10). It should be noted that considerable changes ($\Delta\nu = 30\ cm^{-1}$) have been observed in the spectra of all the Pt–ATP compounds and they are, for the purine vibrational frequencies, caused by the direct Pt—N7 coordination. This is consistent with the major downfield shift of the H8 resonance in the platinum–ATP complexes described above (Table 2). Similar infrared spectral changes were observed for several platinum—N7 bonded mononucleotide complexes (15–19). A weak absorption band at 1330 cm^{-1} in the free nucleotide spectrum, assigned to the adenine ring vibration, exhibited considerable shifting and splitting in the spectra of Pt–ATP complexes (Table 3 and Fig. 1). The alteration observed for this absorption band is also related to the direct platinum—N7 bonding which is not observed in the spectra of the other metal–ATP complexes. Owing to the coupling of the vibrations, both in pyrimidine and imidazol rings, it is difficult to assign any individual absorption bands to the metal–N1 coordination and thus the Pt–N1 binding has been shown by the downfield shift of the H2 proton observed in aqueous solutions (Table 2).

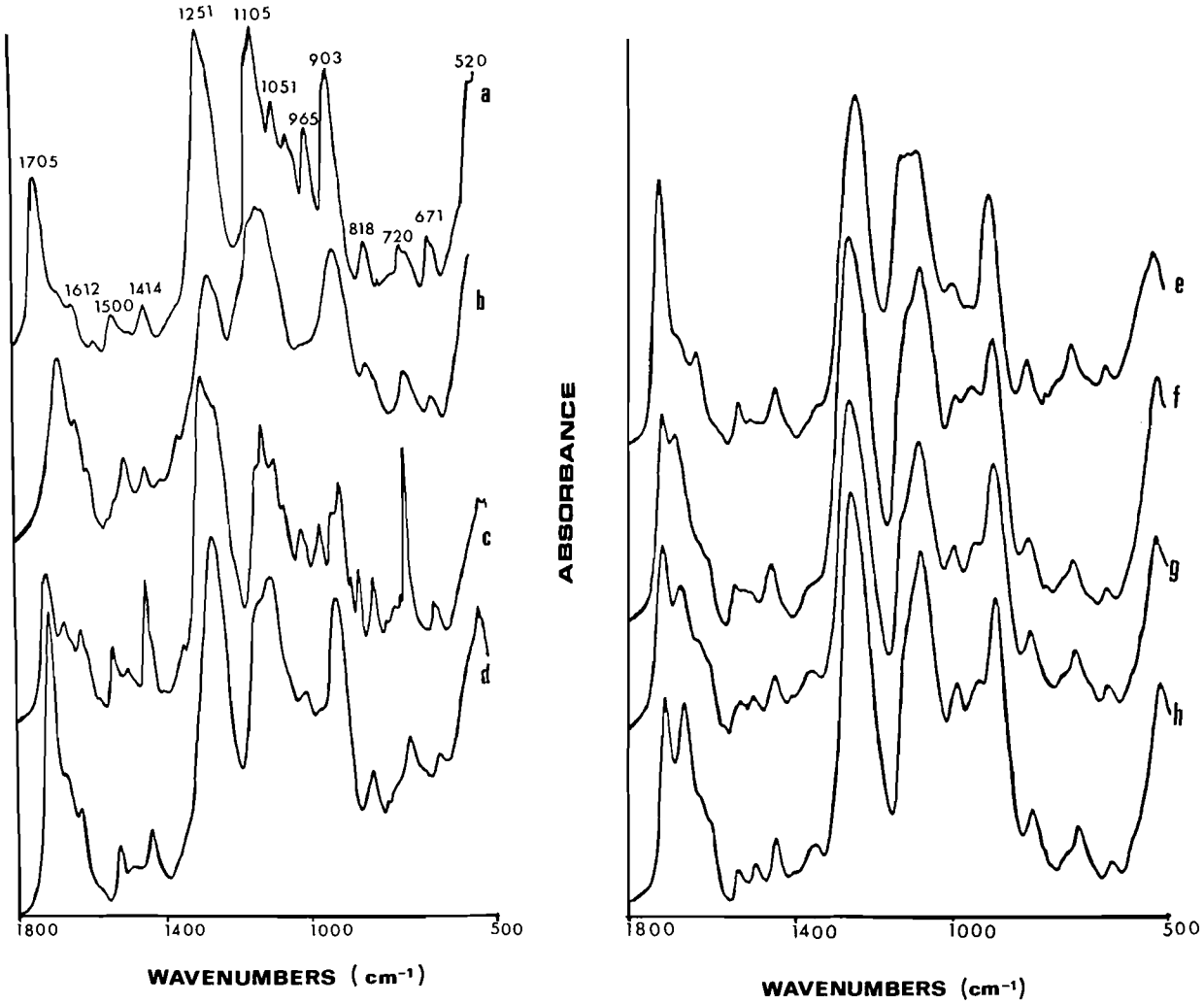

FIG. 1. The FTir spectra of $Na_2H_2ATP \cdot 3H_2O$ and metal–adducts in the region of 1800–500 cm^{-1} for (*a*) $Na_2H_2ATP \cdot 3H_2O$, (*b*) Na_4ATP, (*c*) $[Cu(H_2ATP)(phen)]_2 \cdot 7H_2O$, (*d*) $Mg(H_2ATP) \cdot 5H_2O$, (*e*) $Co(H_2ATP) \cdot 4H_2O$, (*f*) $Pt(Na_2H_2ATP)_2Cl_2 \cdot 6H_2O$, (*g*), *cis*-$[Pt(NH_3)_2(Na_2H_2ATP)_2]Cl_2 \cdot 4H_2O$, and (*h*) *trans*-$[Pt(NH_3)_2(Na_2H_2ATP)_2]Cl_2 \cdot 4H_2O$.

(b) Phosphate vibrational modes. The triphosphate chain in ATP is a potentially multidentate ligand, binding through the α, β, and γ phosphate oxygen atoms (7, 8). The phosphate group in H_2ATP^{2-} shows fundamental infrared vibrations in the region 1200–900 cm^{-1} which are assigned as follows: the two strong and broad absorption bands at 1252 and 1105 cm^{-1} are assigned to the PO_2^- antisymmetric and symmetric stretching vibrations, a strong band at 965 cm^{-1} is assigned to the P—O—H stretching, and the band at 903 cm^{-1} is assigned to the O—P—O stretching vibration (3). Upon dissociation of the H_2ATP^{2-} to ATP^{4-} at pH 7.2 the band at 965 cm^{-1} disappeared and two other strong absorption bands at 1120 and 1092 cm^{-1} were observed, which are assigned to the antisymmetric and symmetric stretching vibrations of the PO_3^{2-} (3) (Fig. 1). Upon phosphate coordination to the metals Cu^{2+} and Zn^{2+} in the ternary compounds $[Cu(H_2ATP)(phen))_2]_2 \cdot 7H_2O$ and $[Zn(H_2ATP)(bipy)]_2 \cdot 4H_2O$, the band at 1252 cm^{-1} shifted towards lower frequencies and the other phosphate band at 1105 cm^{-1} also showed shifting and splitting (Fig. 1). The band at 903 cm^{-1}, assigned to the O—P—O stretching, shifted towards higher frequencies. These spectral changes are due to the coordination of the α, β, and γ phosphate oxygen atoms to the metal cations which is in agreement with the X-ray structural

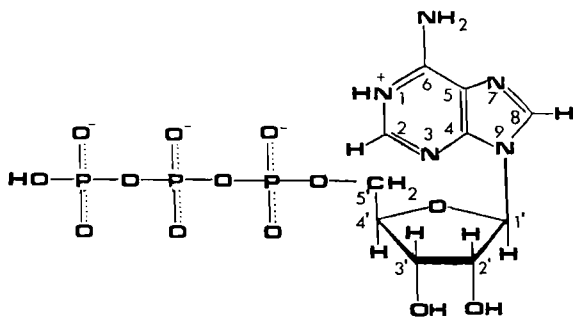

analysis (7, 8). Similar spectral changes were observed in the spectra of all the binary complexes synthesized here with the exception of the Pt–ATP compounds. This is indicative of a phosphate coordination mode in this series of metal–ATP complexes. The coordination of the α, β, and γ phosphate oxygen atoms in Mg^{2+} and Ca^{2+} in several other ternary metal–ATP complexes is known from X-ray crystallography (9, 10). In the spectra of the Pt–ATP complexes prepared here, the vibrations related to the phosphate group exhibited no major changes upon metal complexation (Fig. 1). This indicates that

TABLE 4. Sugar pucker in Na_2H_2ATP and in its metal adducts

Compounds	Sugar diagnostic band (cm^{-1})	Sugar conformation
$Na_2H_2ATP \cdot 3H_2O$ (dimer)	818	C3′-*endo–anti*
	818	C2′-*endo–anti*
$[Cu(H_2ATP)(phen)]_2 \cdot 7H_2O$	815	C3′-*endo–anti*
$[Zn(H_2ATP)(bipy)]_2 \cdot 4H_2O$	814	C3′-*endo–anti*
$Cu(H_2ATP) \cdot 4H_2O$	825	C2′-*endo–anti*
$Zn(H_2ATP) \cdot 4H_2O$	825	C2′-*endo–anti*
$Ni(H_2ATP) \cdot 4H_2O$	824	C2′-*endo–anti*
$Co(H_2ATP) \cdot 4H_2O$	824	C2′-*endo–anti*
$Mn(H_2ATP) \cdot 4H_2O$	823	C2′-*endo–anti*
$Ca(H_2ATP) \cdot 4H_2O$	822	C2′-*endo–anti*
$Mg(H_2ATP) \cdot 5H_2O$	822	C2′-*endo–anti*
$Mg_2(ATP) \cdot 6H_2O$	822	C2′-*endo–anti*
$K[Pt(Na_2H_2ATP)Cl_3] \cdot 2H_2O$	822	C2′-*endo–anti*
$[Pt(Na_2H_2ATP)_2Cl_2] \cdot 6H_2O$	822	C2′-*endo–anti*
$[Pt(Na_2H_2ATP)_3Cl]Cl \cdot 6H_2O$	822	C2′-*endo–anti*
$[Pt(Na_2H_2ATP)_4]Cl_2 \cdot 6H_2O$	823	C2′-*endo–anti*
cis-$[Pt(NH_3)_2(Na_2H_2ATP)_2]Cl_2 \cdot 4H_2O$	824	C2′-*endo–anti*
trans-$[Pt(NH_3)_2(Na_2H_2ATP)_2]Cl_2 \cdot 4H_2O$	823	C2′-*endo–anti*

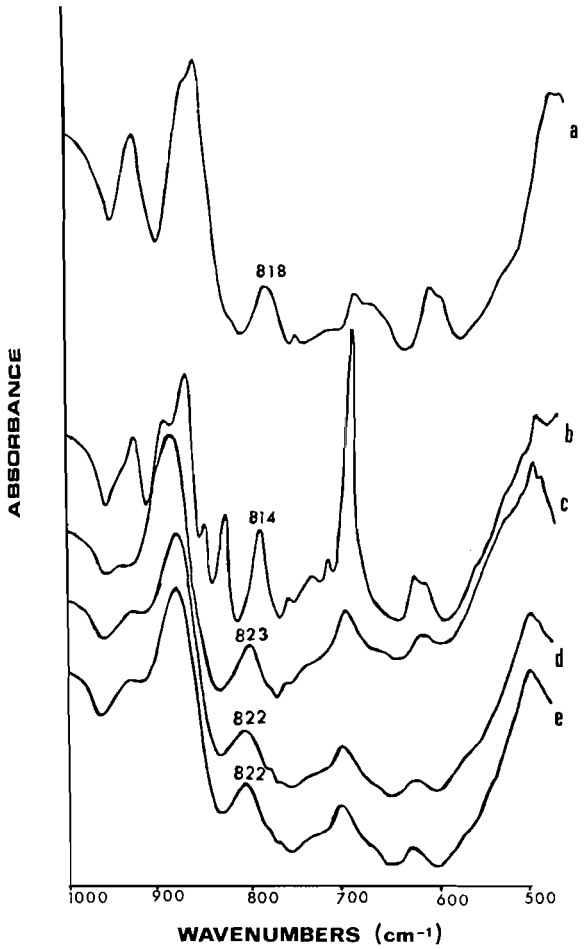

FIG. 2. The FTir spectra of $Na_2H_2ATP \cdot 3H_2O$ and metal–adducts in the region of 1000–500 cm^{-1} for (*a*) $Na_2H_2ATP \cdot 3H_2O$, (*b*) $[Cu(H_2ATP)(phen)]_2 \cdot 7H_2O$, (*c*) $Mg(H_2ATP) \cdot 5H_2O$, (*d*) *cis*-$[Pt(NH_3)_2(Na_2H_2ATP)_2]Cl_2 \cdot 4H_2O$, and (*e*) *trans*-$[Pt(NH_3)_2(Na_2H_2ATP)_2]Cl_2 \cdot 4H_2O$.

there is no direct Pt–phosphate interaction in the platinum–ATP complexes. However an indirect Pt–phosphate interaction via hydrogens of NH_3 or H_2O molecules can not be excluded.

(c) Characteristic sugar pucker bands. The OH stretching frequencies of the sugar are observed in the region 3500–3200 cm^{-1} and overlap with the base NH_2 and the water molecules bonded to the metal. The other absorption bands in the region 1400–600 cm^{-1} are masked by the strong and broad absorption bands of the phosphate group and the base (Fig. 1). A shoulder at 1120 cm^{-1} in the spectrum of Na_2H_2ATP is assigned to the sugar C—O stretching vibration which shows no changes upon nucleobase metalation (Table 3). However, a strong band at 818 cm^{-1} in the ligand spectra exhibited major changes upon sugar conformational transitions. The sugar pucker in $(Na_2H_2ATP \cdot 3H_2O)_2$ showed both C2′-*endo–anti* and C3′-*endo–anti* conformations (14) with a characteristic band at 818 cm^{-1}. This infrared band appeared at 814 cm^{-1} in the spectra of $[Cu(H_2ATP)(phen)]_2 \cdot 7H_2O$ and $[Zn(H_2ATP)(bipy)]_2 \cdot 4H_2O$ compounds which are known to contain only the C3′-*endo–anti* conformation (7, 8) (Fig. 3 and Table 4). In the spectra of the binary complexes of Mg^{2+}, Ca^{2+}, Zn^{2+}, Mn^{2+}, Co^{2+}, Ni^{2+}, Cu^{2+}, and Pt–ATP studied here, the sugar band appeared as a strong band at about 822 cm^{-1}, which corresponds to the C2′-*endo–anti* conformation (Fig. 2 and Table 4). A recent structural analysis of Mg^{2+} and Ca^{2+} complexes of ATP and dipyridineamine also exhibited the C2′-*endo–anti* sugar conformation in these metal complexes (10). It is interesting to note that in the ternary compounds of ATP with Cu^{2+} and Zn^{2+}, the sugar has C3′-*endo–anti* conformation (7, 8), whereas in the corresponding binary complexes the sugar showed the C2′-*endo–anti* conformation (Table 4). This could be due to the effect of the bulky ligands, 1,10-orthophenanthroline and 2,2′-bipyridyl on the sugar pucker.

Conclusions

Several new metal–ATP complexes have been prepared and comparison of the FTir spectra and X-ray structural information of the known compounds $[Cu(H_2ATP)(phen)]_2 \cdot 7H_2O$ and $[Zn(H_2ATP)(bipy)]_2 \cdot 4H_2O$ with that of the unknown binary M–ATP compounds (where M = M^{2+}, Ca^{2+}, Zn^{2+}, Mn^{2+}, Co^{2+}, Ni^{2+}, Cu^{2+}, and Pt^{2+}) leads to the following remarks: (1) All the binary metal–ATP complexes (except the Pt–ATP adducts) are bonded to the phosphate oxygen atoms with no direct metal–base interaction. (2) The Pt–ATP adducts synthesized in acidic media are N7-bonded, while the Pt–ATP complexes isolated here at pH = 7.2 are dimers $[Pt(Na_4ATP)_3Cl_4] \cdot 6H_2O$ having metal binding through the N1 and N7 atoms of the pyrimidine and imidazol rings. (3) The N1 atom of the pyrimidine ring is protoned in the acidic media and prevents metal–N1 coordination. (4) The phosphate spectral changes suggest that the metal coordination is via α, β, and γ phosphate oxygen atoms. (5) The sugar is not involved in metal complex formation and its conformation in $Na_2H_2ATP \cdot 3H_2O$ is both C2′-*endo–anti* and C3′-*endo–anti*. This changes to the C3′-*endo–anti* conformation in the ternary Cu^{2+}– and Zn^{2+}–ATP complexes. In all the other binary metal–ATP compounds studied here the sugar shows C2′-*endo–anti* conformation. The characteristic infrared band for C2′-*endo–anti* sugar pucker in ATP is at 822 cm^{-1} and the shift of this band to 814 cm^{-1} is a diagnostic of the transition to the C3′-*endo–anti* conformation.

Acknowledgements

The authors gratefully acknowledge the financial assistance

of the Natural Sciences and Engineering Research Council of Canada and the Fonds F.C.A.R. (Government of Quebec) in this work.

1. B. S. COOPERMAN. Metal ions in biological systems. Vol. 5. *Edited by* H. Sigel. Dekker, New York. 1976. pp. 79–125.
2. L. G. MARZILLI, T. J. KISTENMACHER, and G. L. EICHHORN. Nucleic acid–metal ion interactions. *Edited by* T. G. Spiro. Wiley, New York. 1980. pp. 179–250.
3. M. MATTHIES and G. ZUNDAL. J. Chem. Soc. Perkin Trans. 1, 1824 (1977); and J. Inorg. Biochem. **10**, 109 (1979).
4. A. LANIR and T. Y. YU. J. Biol. Chem. **254**, 5882 (1979).
5. S. J. KARLIK, G. A. ELGAVISH, and G. L. EICHHORN. J. Am. Chem. Soc. **105**, 602 (1983), and references cited therein.
6. (*a*) K. H. SCHELLER, F. HOFSTETTER, P. R. MITCHELL, P. PRIYS, and H. SIGEL. J. Am. Chem. Soc. **103**, 247 (1981); (*b*) H. SIGEL. Pure Appl. Chem. **55**, 137 (1983), and references cited therein.
7. W. S. SHELDRICK. Z. Naturforsch. B: Anorg. Chem. Org. Chem. **37B**, 863 (1982).
8. P. ORIOLI, R. CINI, D. DONATI, and S. MANGANI. J. Am. Chem. Soc. **103**, 4446 (1981).
9. R. CINI, M. SABAT, M. SUNDARALINGAM, M. C. BURLA, A. NUNZI, G. POLIDORI, and P. F. ZANAZZI. Inorg. Chim. Acta, **79**, 253 (1983); J. Biomol. Struct. Dyn. **1**, 663 (1983).
10. R. CINI, M. C. BURLA, A. NUNZI, C. P. POLIDORI, and P. F. ZANAZZI. J. Chem. Soc. Dalton Trans. 2467 (1984).
11. G. B. KAUFFMAN and D. O. COWAN. Inorg. Synth. 239 (1963).
12. G. RANUDASCHL, B. LIPPERT, and J. D. HOESCHELE. Inorg. Chim. Acta, **78**, L43 (1983).
13. H. A. TAJMIR-RIAHI and T. THEOPHANIDES. Can. J. Chem. **62**, 1429 (1984).
14. O. KENNARD, N. W. ISAACS, W. D. S. MOTHERWELL, T. C. COPPOLA, D. L. WAMPLER, A. C. LARSON, and D. G. WATSON. Proc. R. Soc. London A, **325**, 401 (1971).
15. H. A. TAJMIR-RIAHI and T. THEOPHANIDES. Inorg. Chim. Acta, **80**, 183 (1983).
16. H. A. TAJMIR-RIAHI and T. THEOPHANIDES. Inorg. Chim. Acta, **80**, 223 (1983).
17. H. A. TAJMIR-RIAHI and T. THEOPHANIDES. Can. J. Chem. **61**, 1813 (1983).
18. E. SCHERER, H. A. TAJMIR-RIAHI, and T. THEOPHANIDES. Inorg. Chim. Acta, **92**, 285 (1984).
19. H. A. TAJMIR-RIAHI and T. THEOPHANIDES. Can. J. Chem. **62**, 266 (1984).

The thermolysis and photolysis of malonic acid in the gas phase[1]

J.-R. CAO[2] AND R. A. BACK

Division of Chemistry, National Research Council of Canada, 100 Sussex Drive, Ottawa, Ont., Canada K1A 0R6

Received November 12, 1985

J.-R. CAO and R. A. BACK. Can. J. Chem. **64**, 967 (1986).

The thermolysis of malonic acid has been studied briefly in the gas phase at temperatures from 92 to 151°C at pressures around 0.1 Torr. Major products were CO_2 and acetic acid, while smaller amounts (< 5% of the CO_2) of CO, acetone, C_2H_6, and CH_4 were formed. Arrhenius parameters of E = 30.9 kcal/mol and log A (s^{-1}) = 13.27 were obtained, based on first-order rate constants for the formation of CO_2. It is suggested that the major products are formed by an internal hydrogen-atom transfer through a 4-centre transition state. The gas-phase photolysis was examined briefly using light of 228.8 nm, and gave products very similar to those of the thermolysis.

J.-R. CAO et R. A. BACK. Can. J. Chem. **64**, 967 (1986).

Opérant à des températures allant de 92 à 151°C et à des pressions d'environ 0,1 Torr, on a brièvement étudié la thermolyse de l'acide malonique en phase gazeuse. Les produits majoritaires sont le CO_2 et l'acide acétique qui se forment aux côtés de faibles quantités (< 5% par rapport aux quantités de CO_2) de CO, d'acétone, de C_2H_6 et de CH_4. En faisant l'hypothèse que les constantes de vitesse sont du premier ordre pour la formation du CO_2, on a déterminé les paramètres d'Arrhénius qui sont E = 30,9 kcal/mol et log A (s^{-1}) = 13,27. On suggère qu'un transfert interne d'hydrogène, par l'intermédiaire d'un état de transition à 4 centres, est responsable de la formation des produits majoritaires. On a examiné brièvement la photolyse en phase gazeuse, en utilisant une lumière de 228,8 nm; les produits obténus sont très semblables à ceux obtenus lors de la thermolyse.

[Traduit par la revue]

Introduction

Recent work in this laboratory has been concerned with the gas-phase photolysis and thermal decomposition of several carboxylic acids with adjacent carbonyl groups, including oxalic (1), pyruvic (2), and glyoxylic acids (3). Malonic acid, a β-dicarbonyl compound, is interesting for comparison. Its decomposition in the molten liquid and solid phase and in solution is well known, yielding CO_2 and acetic acid, but the gas-phase decomposition has not been reported. The present paper describes a brief study of the thermolysis and photolysis of malonic acid in the gas phase.

Experimental

Apparatus and methods were similar to those used before with other slightly volatile acids (1–3). The same reaction vessel, a quartz cylinder 10 cm long and 5 cm in diameter, was used for both pyrolysis and photolysis and was contained in an air thermostat. A Philips Cd spectral lamp was used for the photolysis. Malonic acid (obtained from Aldrich) is marginally volatile enough to work with as a vapor, as a useful vapor pressure is barely attained before thermal decomposition becomes prohibitive. After prolonged degassing at lower temperatures, solid malonic acid was sublimed at 92°C until the desired presure was reached in the reaction vessel, which was then isolated and the experiment begun. To minimize the amounts of products from the decomposition of the solid during vaporization, which took some time, small samples were used (5–10 mg) and renewed before each experiment. Substantial amounts of products were still present in the reaction cell at the beginning of an experiment, and corrections had to be made for these.

Products were analysed by fractionation at −196, −78, and 0°C, collected, and measured with a Toepler pump and gas buret, and by gas chromatography.

Results and discussion

The thermal decomposition

Major products were CO_2 and acetic acid, in roughly equal amounts, as found previously from liquid-phase decomposition (4). Minor products were CO (5%), acetone (3%), C_2H_6 (0.4%), and CH_4 (0.2%), with their yields relative to CO_2 at 92°C shown in parentheses. Formation of CO_2 followed approximate first-order kinetics over a range of conversions (up to 50%) and pressures between about 0.7 and 0.12 Torr (1 Torr = 133.3 Pa). First-order rate constants based on CO_2 formation are shown in Table 1, and in an Arrhenius plot in Fig. 1 together with the data of Clark (4) obtained in molten malonic acid. Each rate constant in Table 1 is based on 5 or 6 experiments at different reaction times, and is derived from the slope of a plot of CO_2 product (corrected for depletion of malonic acid, assuming first-order kinetics) against reaction time. From Fig. 1, Arrhenius parameters of E = 30.9 kcal/mol and log A (s^{-1}) = 13.27 were obtained, closer to those found for oxalic acid than to those for glyoxylic and pyruvic acids, which showed unusually low frequency factors (2). Realistic confidence limits of ±2 kcal/mol for E and ±0.2 for log A can be rather arbitrarily estimated. Although surface dependence was not tested, the Arrhenius parameters suggest that the present data probably correspond to a gas-phase reaction, which is also probably partly in its pressure-dependent region so that the high-pressure Arrhenius parameters may be somewhat higher than the measured values. The similarity of E and A to those for oxalic acid suggests a similar mechanism, i.e., a hydrogen-atom transfer through a 4-membered transition state:

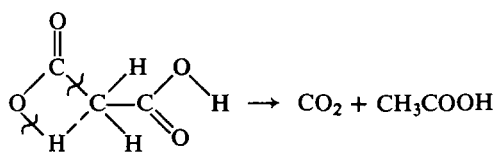

$\longrightarrow CO_2 + CH_3COOH$

TABLE 1. First-order rate constants for decomposition of malonic acid vapor

T (K)	k (s^{-1})
365.2	5.66×10^{-6}
372.2	1.32×10^{-5}
379.2	2.61×10^{-5}
389.2	7.63×10^{-5}
424.2	2.09×10^{-3}

[1]NRCC Publication number 25431.

[2]NRCC Research Associate, 1984–1985. Present address: Chemistry Department, Peking University, Peking, China.

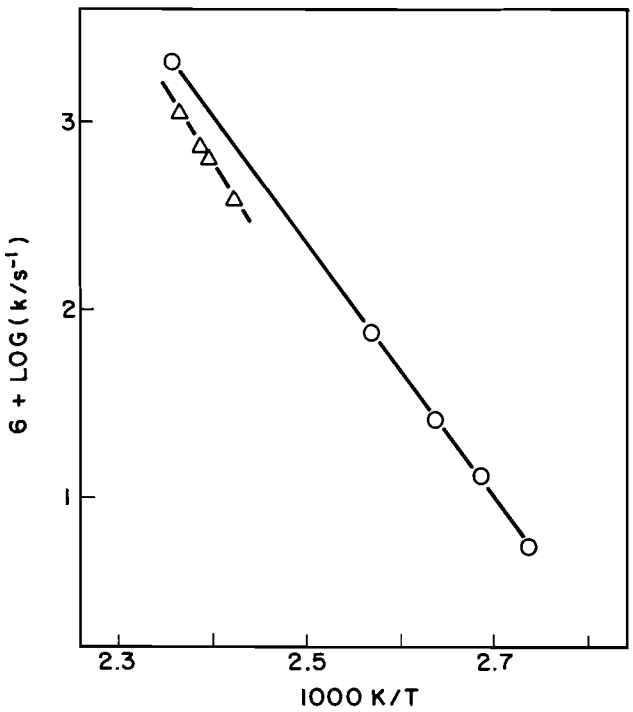

FIG. 1. Arrhenius plot for the thermal decomposition of malonic acid in the gas phase, based on first-order rate constants for the formation of CO_2. ○ = present data; △ = data for molten malonic acid (4).

The similarity of the rate constants for decomposition in the molten acid and in the gas phase indicates perhaps a similar mechanism in the former, although Clark suggested a biomolecular interaction (4) while Loudon *et al.* (5) preferred a unimolecular decomposition via a 6-centre transition state. The latter, yielding CO_2 and 1,1-ethylenediol (the enol form of acetic acid), is perhaps also a possibility for the gas-phase reaction, although it seems doubtful that the enol form would be energetically accessible in the gas phase in the absence of solvent stabilization.

The photolysis

Attempts to obtain an absorption spectrum of the vapor were unsuccessful, as no absorption significantly different from that of acetic acid was observed, and acetic acid was always present as a decomposition product. No structure was evident and no measurable absorption above about 250 nm. Under these circumstances, the radiation effective in the photolysis was almost entirely the 228.8-nm resonance line of the Cd lamp.

Major products at 92°C were again CO_2 and acetic acid in roughly equal yields, and minor products were also those found in the thermal reaction, with about the same product ratios. Sizeable corrections were made for the thermal decomposition in these experiments, but the rate of product formation was about 2.5 times larger with the light on than with the light off, and there is no doubt that a true gas-phase photolysis was taking place. It is interesting that the photolysis is so similar to the thermolysis despite the much higher energy of excitation (125 kcal/mol) available in the former. The mechanism of minor product formation in both systems is also curious. The nature of the products indicates formation of CH_3 and CH_3CO radicals, and while the energy in the photolysis is certainly high enough to generate such free radicals, their source in the thermal reaction at 92°C is not clear.

1. S. YAMAMOTO and R. A. BACK. J. Phys. Chem. **89**, 622 (1985).
2. S. YAMAMOTO and R. A. BACK. Can. J. Chem. **63**, 549 (1985).
3. R. A. BACK and S. YAMAMOTO. Can. J. Chem. **63**, 542 (1985).
4. L. W. CLARK. J. Phys. Chem. **67**, 138 (1963).
5. A. G. LOUDON, A. MACCOLL, and D. SMITH. J. Chem. Soc. Faraday Trans. 1, **69**, 894 (1973).

Oxidation of the mercurous ion by peroxidase

DONALD C. WIGFIELD AND SEASON TSE
The Ottawa–Carleton Institute for Research and Graduate Studies in Chemistry, Carleton University Campus, Ottawa, Ont., Canada K1S 5B6

Received July 2, 1985[1]

DONALD C. WIGFIELD and SEASON TSE. Can. J. Chem. **64**, 969 (1986).

The kinetics of oxidation of the mercurous ion by peroxidase have been measured by following the disappearance of mercurous ion using cold-vapour atomic absorption spectroscopy. Pseudo-first-order kinetics are observed with respect to mercurous ion, and the pseudo-first-order rate constants are linearly related to peroxidase concentration, showing first-order dependence on peroxidase. This behaviour is identical to oxidation of elemental mercury, and the second-order rate constant, $1.44 \times 10^4\ M^{-1}\ s^{-1}$ at 23°C, is also, within experimental error, the same as that for elemental mercury oxidation. The data are interpreted in terms of peroxidase-induced disproportionation of the mercurous dimer, followed by two-electron oxidation of zero-valent mercury.

DONALD C. WIGFIELD et SEASON TSE. Can. J. Chem. **64**, 969 (1986).

Faisant appel à la spectroscopie d'absorption atomique à vapeurs froides pour déterminer la disparition de l'ion mercureux, on a mesuré la cinétique de l'oxydation de l'ion mercureux par la peroxydase. Par rapport à l'ion mercureux, la réaction est d'un pseudo-premier ordre et on peut établir une corrélation linéaire entre les constantes de vitesse de pseudo-premier ordre et la concentration de peroxydase; ce résultat démontre que la réaction est aussi du premier ordre par rapport à la peroxydase. Ce comportement est identique à celui observé pour l'oxydation du mercure élémentaire et la constante de vitesse du deuxième ordre, $1{,}44 \times 10^4\ M^{-1}\ s^{-1}$ à 23°C, est aussi, à l'intérieur des limites expérimentales, la même que celle observée pour l'oxydation du mercure élémentaire. On interprète ces données en fonction d'une disproportionation du dimère mercureux qui est induite par la peroxydase et qui est suivie par une oxydation à deux électrons du mercure zéro-valent.

[Traduit par la revue]

Recently, in connection with the mechanism of toxicological action of elemental mercury, we have reported the kinetics of oxidation of elemental mercury by peroxidase, and proposed a mechanism for this transformation (1, 2). This, in combination with the powerful cold-vapour atomic absorption spectroscopy technique, which now allows analysis not only of total mercury (3) and zero-valent mercury (4), but also of the mercurous ion (5–7), leads to the possibility of studying the oxidation of the mercurous ion by peroxidase. We have completed this study and herein present the results.

Results

In our previous study on the oxidation of elemental mercury by peroxidase (1), in which pseudo-first-order behaviour with respect to elemental mercury was found, it was only possible to establish this first-order behaviour over a very limited concentration range. This resulted from the fact that the upper limit (solubility) and the lower limit (detection) differed only by one order of magnitude. A study of oxidation of a suitably soluble mercurous salt, such as nitrate, offered the possibility of a greater concentration range. In addition, it was of acute interest to investigate the oxidation of the mercurous ion, partly for its own sake, to compare its oxidation with that of elemental mercury, and partly because of the unknown role that the mercurous ion might play in the toxicological oxidation of elemental mercury.

Both elemental mercury and the mercurous ion give signals in cold-vapour atomic absorption analysis, whereas the mercuric ion does not, unless the analysis is carried out in the presence of a reducing agent (5). Thus the disappearance of the absorption signal represents a measure of formation of the mercuric ion, i.e. the oxidation of mercurous ion. We have previously investigated the size of the absorption signal from mercurous ion and found that, although the signal size can vary depending on experimental conditions, it does bear direct relationship to mercurous ion concentration under a particular set of reaction conditions and is therefore useful for following the reaction. Total mercury can also be determined (analysis in presence of a reducing agent) to ensure that one is indeed witnessing an interchange of mercury species, and not an absolute disappearance of mercury as a whole, e.g. by surface adsorption.

Figure 1 shows the disappearance of absorption signal when mercurous ion is in contact with horseradish peroxidase and its cofactor hydrogen peroxide, with various concentrations of the latter reagent. Two features are evident from this figure. The control points show that over the kinetic run more than 90% of the mercury is retained, showing that the potentially serious problem of mercury adsorption or evaporation at these trace levels is under control. Secondly, the change of hydrogen peroxide over several orders of magnitude makes no impact on the rate of mercurous ion oxidation. This was also observed in the oxidation of elemental mercury (1) and is consistent with the rapid and essentially irreversible formation of peroxidase Compound I (HRP-I) followed by slower oxidation of either form of mercury by HRP-I.

$$\text{HRP} + \text{H}_2\text{O}_2 \rightleftarrows \text{HRP-I} + \text{H}_2\text{O}$$

$$\text{HRP-I} + \text{mercury} \xrightarrow{\text{slow}} \text{oxidized mercury} + \text{HRP}$$

Under these circumstances, the rate of mercury oxidation is not dependent on hydrogen peroxide concentration.

In view of the finding that oxidation of elemental mercury by HRP-I obeyed normal chemical kinetics rather than Michaelis–Menten kinetics, over several half-lives of reaction(s),

$$\text{i.e. Rate} = k[\text{Hg}]^a[\text{HRP-I}]^b$$

where $a = b = 1$

we investigated the possibility that oxidation of the mercurous ion might show similar behaviour. Kinetic runs were therefore performed in which the rate of oxidation of the mercurous ion (disappearance of atomic absorption signal) was followed at

[1]Revision received January 27, 1986.

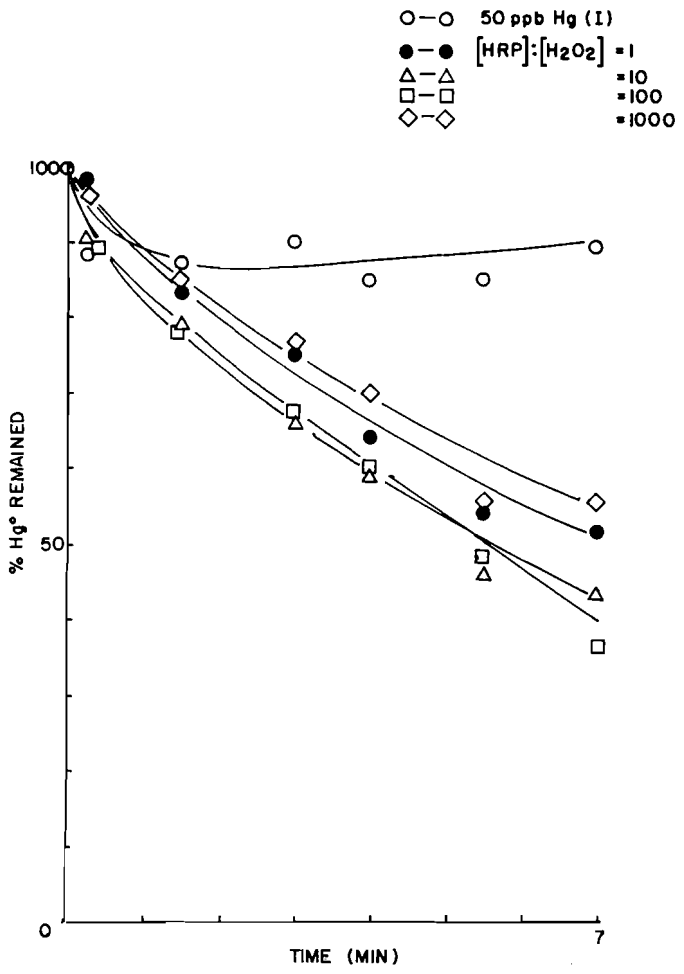

FIG. 1. Disappearance of mercurous ion in the presence of HRP and variable concentrations of H_2O_2.

various HRP-I concentrations. The logarithmic first-order test of these data is shown in Fig. 2, clearly establishing that, in common with oxidation of elemental mercury (1), oxidation of the mercurous ion is first order in mercury. In our previous paper (1) we have shown that the linearity of these plots, where the reaction is taken substantially to completion, requires that the enzyme is being constantly regenerated in the reaction, by re-oxidation to HRP-I with excess hydrogen peroxide; this in turn requires that, at least insofar as the enzyme is concerned, a two-electron oxidation is involved.[2]

Unlike the oxidation of elemental mercury, it is possible to study oxidation of the mercurous ion over a reasonable range of concentration. The pseudo-first-order rate constants summarized in Table 1 show that, consistent with the first-order process, these rate constant values are indeed independent of mercurous ion concentration. The rate constants are, however, heavily dependent on HRP-I concentration and a plot of these values as a function of each other is shown in Fig. 3, demonstrating that the reaction is first order with respect to HRP-I. The second-order rate constant that follows from these data is $1.44 \times 10^4\ M^{-1}\ s^{-1}$ at 23°C, and the overall rate equation is represented by:

$$\text{Rate} = k[Hg^{2+}{}_2][\text{HRP-I}]$$

[2]A one-electron process would cause formation of the species HRP-II, which cannot easily recycle either to HRP or HRP-I (1).

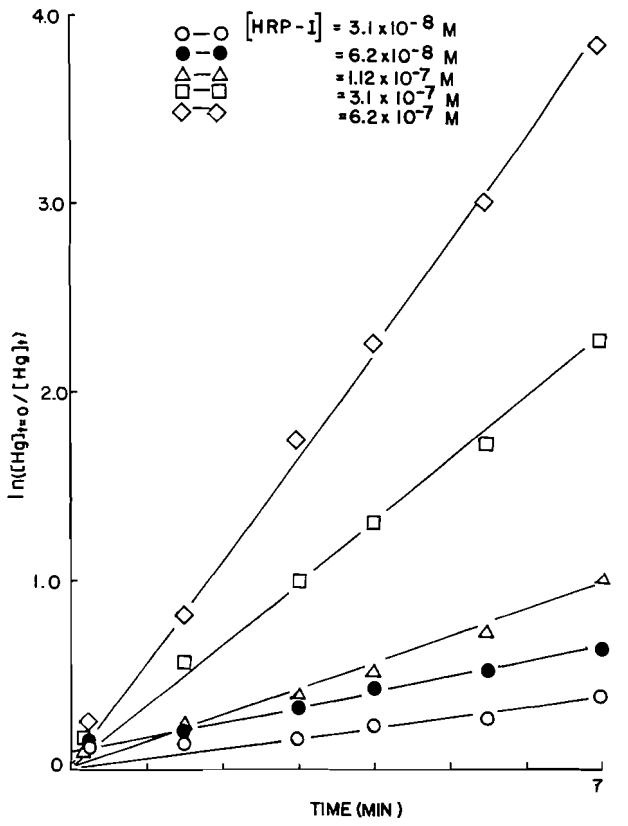

FIG. 2. First-order plot of the logarithm of remaining mercurous ion as a function of time ([Hg(I)] = 50 ppb initial).

TABLE 1. Pseudo-first-order rate constants for the oxidation of Hg(I) as a function of Hg(I) and HRP-I concentrations

[HRP-I] $\times 10^8$ (M)	[Hg(I)] (ppb)	$k^1 \times 10^3$ (min^{-1})	Correlation coefficient
3.10	50	0.6±0.2	0.927
6.20	50	1.0±0.2	0.980
12.4	50	2.0±0.2	0.996
12.4	100	2.1±0.2	0.993
12.4	250	2.0±0.1	0.995
12.4	500	2.0±0.1	0.993
31.0	50	4.6±0.6	0.998
62.0	50	9.1±0.2	0.998

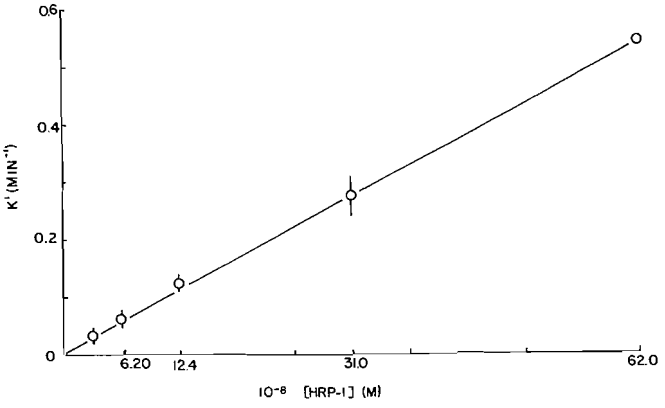

FIG. 3. Plot of pseudo-first-order rate constants of mercurous ion oxidation as a function of peroxidase Compound I concentration ([Hg(I)] = 50 ppb initial).

Discussion

The striking feature about the results presented above is the extraordinary similarity to oxidation of elemental mercury. Indeed they are indistinguishable. Both involve a second-order rate process, first order both in mercury (either Hg^0 or $Hg^{2+}{}_2$) and in enzyme. Both involve a two-electron oxidation process and, within experimental error, the rate constants are the same ($1.43 \times 10^4\, M^{-1}\, s^{-1}$ vs. $1.44 \times 10^4\, M^{-1}\, s^{-1}$). Conceptually the simplest mechanism that would accommodate the data would be one in which HRP-I somehow would accept an electron from each half of the mercurous dimer, giving two mercuric ions.

$$\text{HRP-I} + Hg^{2+}{}_2 \rightarrow \text{HRP} + 2Hg^{2+} + O^{2-}$$

This mechanism is, however, highly unsatisfactory on several grounds. The bulky mercurous dimer would have to approach the heme centre of the enzyme; it would have to do so in a fashion to enable both mercury atoms to give up an electron, and presumably only one of the mercuric ions produced would end up bound to the oxide ion of which HRP-I must divest itself in the process. Furthermore, to give an identical rate constant, this process would have to occur with precisely equal ease to the incomparably simpler oxidation of a mercury atom. This mechanism can probably be rejected.

The identity of rate constants suggests very strongly that disproportionation of the mercurous dimer is involved in the process, followed by two-electron oxidation of the mercury atom produced, i.e.

$$Hg^{2+}{}_2 \overset{K}{\rightleftarrows} Hg^0 + Hg^{2+}$$

$$Hg^0 + \text{HRP-I} \xrightarrow[\text{determining}]{\text{rate}} Hg^{2+} + \text{HRP}$$
$$k$$

In this way the rate-determining step in the reaction is the same two-electron oxidation involved in the oxidation of elemental mercury, which will clearly proceed at a rate independent of the source of Hg^0.

This simple process is, however, not consistent with the kinetic data because of the pre-equilibrium involved. In the absence of externally added Hg^{2+}, the concentrations of Hg^0 and Hg^{2+} are the same; thus

$$[Hg^0] = K^{1/2}[Hg^{2+}{}_2]^{1/2}$$

In this case, since the rate equation is:

$$\text{Rate} = k[Hg^0][\text{HRP-I}],$$

the reaction should have an initial half-order dependence on the concentration of mercurous ion.[3]

The disproportionation of the mercurous ion, however, is one that is dramatically dependent on experimental conditions. Although, in the absence of other ions, the equilibrium is far to the side favouring mercurous ion ($K = 5.5 \times 10^{-9}$) (8), it is an equilibrium that may be moved completely to the other side by ions that complex with the mercuric ion. Thus several potential salts of the mercurous species, such as cyanide and sulfide, simply do not exist (9). It is noteworthy that sulfide from cysteine is also a component of peroxidase (10). If the disproportionation mechanism is thus disturbed, the half-order dependence on mercurous ion disappears and is replaced by simple first-order kinetics, as is experimentally observed. The peroxidase thus apparently acts not only as the precursor of HRP-I, but also as the agent for the displacement of the disproportionation reaction, then to be followed by the two-electron oxidation of Hg^0. This process would not only have the kinetic properties experimentally observed, but would also demand a rate constant identical to that for elemental mercury oxidation. This overall mechanism is shown below.

$$Hg^{2+}{}_2 \xrightarrow{\text{peroxidase}} Hg^0 + Hg^{2+} - \text{peroxidase}$$

$$\text{HRP} + H_2O_2 \rightarrow \text{HRP-I} + H_2O$$

$$\text{HRP-I} + Hg^0 \xrightarrow[\text{determining}]{\text{rate}} \text{HRP} + Hg^{2+}$$

We have already commented on the detailed mechanism of the rate-controlling oxidation of Hg^0 (1).

From the data obtained it appears likely that the mechanism of oxidation of mercurous ion by the peroxidase system is best represented by the three steps outlined above.[4] It is noteworthy that complexation of Hg^{2+} by peroxidase evidently does not significantly affect the reaction rate, thus reinforcing the idea that only the heme portion of the peroxidase is important in the reaction and that this is basically a chemical reaction between two species (HRP-I and Hg^0). This is in contrast to the usual situation involving enzyme catalysis in which substrate binding and Michaelis–Menten kinetics are involved.

Experimental

Reagents and solutions

Horseradish peroxidase (E.C.1.11.1.7, Type X)

Horseradish peroxidase was obtained as a $(NH_4)_2SO_4$ suspension (Sigma Chemical Co., St. Louis, Mo., C-100). Solutions were freshly prepared by dissolving the desired amount of the enzyme in phosphate buffer (pH = 7.00, 0.05 *M*). The subsequent enzyme concentration was determined by the absorbance at 403 nm and the corresponding extinction coefficient ($\epsilon = 1.02 \times 10^4\, M^{-1}\, cm^{-1}$). The R.Z. value, an indicator of purity, was determined as the ratio of the absorbances at 403 and 280 nm.

Mercurous solutions

Stock mercurous solutions were prepared monthly by dissolving 1.0000 g of mercurous nitrate (Fisher Scientific, Toronto, Canada, M-168) in 1 L of 0.1% V/V nitric acid (Canlab, McGraw Ltd.). Serial dilutions from this solution were freshly made for each experiment. The concentrations were determined by cold vapour atomic absorption, under reducing conditions (5).

Hydrogen peroxide

Hydrogen peroxide solutions were prepared daily from 30% stock solution (Anachemiz Ltd., Montreal, Canada).

Water

All glassware used for solution preparation were cleaned by soaking in 35% nitric acid solution for at least a period of 48 h, and were thoroughly rinsed with distilled deionized water prior to use. All solutions were prepared using distilled deionized water (Millipore Corporation, Bedford, Mass.).

Mercury analysis

Mercury analysis by cold vapour atomic absorption, with separate determinations for elemental mercury and mercuric ion, has been fully described previously (4). Analysis of mercurous ion using the same apparatus is also fully documented (5).

Kinetic experiments

To 10 mL of mercury solution were added peroxidase and H_2O_2

[3]A referee has pointed out that after the initial period $Hg^0 \neq Hg^{2+}$ and thus the half order will gradually change.

[4]The analytical method cannot distinguish between Hg^0 and $\frac{1}{2}\, Hg^{2+}{}_2$; thus there is no inconsistency between the original use of mercurous ion and its ultimate analysis.

or previously prepared HRP-I. Mixing was done by means of the sampling syringe, for 15 s. The flask was stoppered with a glass stopper, and sampling done by momentary removal of the stopper.

Preparation of HRP-I

Compound I was prepared by mixing (Vortex) 0.9 mL of phosphate buffer and the desired amount of HRP, and various equivalents of H_2O_2, in a 1.5-mL disposable micro test tube. Its presence was confirmed by obtaining the spectra prior to addition to mercury solutions (1).

Acknowledgements

It is a pleasure to acknowledge the wise counsel of Professor Keith J. Laidler. We also acknowledge the financial support of the Natural Sciences and Engineering Research Council of Canada.

1. D. C. WIGFIELD and S. TSE. Can. J. Chem. **63**, 2940 (1985).
2. D. C. WIGFIELD and S. TSE. J. Appl. Toxicol. **6**, 73 (1986).
3. M. R. GREENWOOD, P. DHAHIR, T. W. CLARKSON, J.-P. FARANT, A. CHARTRAND, and A. KHAYAT. J. Anal. Toxicol. **1**, 265 (1977), and references therein.
4. D. C. WIGFIELD and S. L. PERKINS. J. Anal. Toxicol. **6**, 279 (1982).
5. D. C. WIGFIELD and S. L. PERKINS. Anal. Chim. Acta, **167**, 419 (1985).
6. D. C. WIGFIELD and S. L. PERKINS. Can. J. Chem. **63**, 275 (1985).
7. D. C. WIGFIELD and S. L. PERKINS. J. Appl. Toxicol. **5**, 339 (1985).
8. H. C. MOSER and A. F. VOIGT. J. Am. Chem. Soc. **79**, 1837 (1957).
9. N. V. SIDGWICK. The chemical elements and their compounds. Vol. 1. Oxford University Press. 1950. pp. 289–292.
10. K. G. WELINDER. Eur. J. Biochem. **96**, 483 (1979).

A rate and equilibrium study of the addition of acetone enolate ion to the 2-methyl-5-nitroisoquinolinium cation in aqueous solution

JOHN W. BUNTING AND JAMES W. TAM[1]
Department of Chemistry, University of Toronto, Toronto, Ont., Canada M5S 1A1

Received December 3, 1985

JOHN W. BUNTING and JAMES W. TAM. Can. J. Chem. **64**, 973 (1986).

Rate and equilibrium constants for the reaction between acetone and the 2-methyl-5-nitroisoquinolinium cation to give 1-acetonyl-1,2-dihydro-2-methyl-5-nitroisoquinoline (**2**) have been evaluated over the pH range 10.0–11.3 in aqueous solutions at 25°C. This reaction is shown to occur under much milder conditions (temperature, pH) and in much shorter reaction times than previously used for the synthesis of this adduct. Analogous data for the reaction of hexadeuteroacetone with this heterocyclic cation are also presented. The formation of **2** is shown to be first order in each of acetone, isoquinolinium cation, and hydroxide ion, and is not catalyzed by carbonate buffer species. These data are consistent with the rate-determining attack of the acetone enolate anion upon the isoquinolinium cation. The microscopic reverse of this reaction is the uncatalyzed decomposition of **2**, which is consistent with the observed pH independence of the first-order rate constant for this process. Quantitative comparisons of rates and equilibria for the addition of hydroxide ion and acetone enolate ion to this isoquinolinium cation and to substituted benzaldehydes are now available.

JOHN W. BUNTING et JAMES W. TAM. Can. J. Chem. **64**, 973 (1986).

Opérant en solutions aqueuses, à 25°C et dans un intervalle de pH allant de 10,0 à 11,3, on a évalué les constantes de vitesse et les constantes d'équilibre pour la réaction entre l'acétone et le cation méthyl-2 nitro-5 isoquinoléinium qui conduit à l'acétonyl-1 dihydro-1,2 méthyl-2 nitro-5 isoquinoléine (**2**). On a démontré que cette réaction s'effectue dans des conditions beaucoup plus douces (température, pH) et utilisant des temps de réaction beaucoup plus courts que ceux utilisés antérieurement dans la synthèse de cet adduit. On a également évalué les mêmes constantes pour la réaction de l'hexadeutéroacétone avec ce cation hétérocyclique. On a démontré que la réaction de formation du composé **2** est d'ordre un tant pour l'acétone que pour le cation isoquinoléinium et l'ion hydroxyde: toutefois, cette réaction n'est pas catalysée par des solutions tampon de carbonate. Ces données s'accordent avec un mécanisme impliquant une étape déterminante dans laquelle l'anion énolate de l'acétone attaque le cation isoquinoléinium. La réaction microscopiquement inverse est la décomposition non catalysée du composé **2**, ce qui s'accorde parfaitement avec les faits observés, à savoir que la constante de vitesse d'ordre un de cette réaction ne dépend pas du pH. Des comparaisons quantitatives de vitesses et des équilibres, dans le cas de l'addition de l'ion hydroxyde et ion énolate de l'acétone sur cet cation isoquinoléinium et sur des benzaldéhydes substitués, sont maintenant disponibles.

[Traduit par la revue]

Carbanion addition to heteroaromatic cations is a common route for the functionalization of heterocyclic rings (1–7).[2] These adducts can be reoxidized to the heteroaromatic system or, alternatively, can be employed as synthons for the further elaboration of the substitution pattern and (or) the extension of the ring system. Such adducts are particularly useful in isoquinoline chemistry, since the C-1 adducts derived from isoquinolinium cations are 1,2-dihydroisoquinolines that have enamine character. Such enamines have been shown to be useful intermediates for the introduction of sidechains by electrophilic attack at C-4 (3, 5, 10–13).

Despite the synthetic usefulness of such carbanion addition reactions, there do not appear to have been any quantitative studies of such processes. Quantitative information on the dependence of the rates and equilibria of such reactions upon the reactivity of the carbanion and the heterocyclic cation, and also upon other variables such as solution basicity, solvent, etc. would allow the straightforward prediction of the optimum conditions for the formation of such adducts. In an initial study in this area, we now report the rates and equilibria for the addition of the enolate ion of acetone to the 2-methyl-5-nitroisoquinolinium cation (eq. [1]), a reaction which has been found to be of synthetic use (5). In conjunction with literature information, this study also provides data that allow a quantitative comparison of nucleophilic addition to a heterocyclic cation and to the aldehyde carbonyl group.

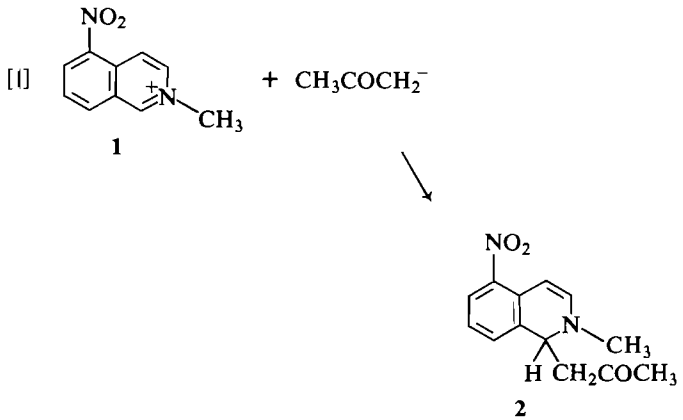

Experimental

2-Methyl-5-nitroisoquinolinium iodide was prepared by refluxing 5-nitroisoquinoline with methyl iodide in ethanol. After addition of a drop of concentrated HI, the salt precipitated upon cooling, and was recrystallized from a mixture of methanol and ethanol containing a few drops of concentrated HI. The presence of the acid is required to shift the equilibrium from the alkoxide adducts towards the cation. This salt was pure by Vollhard titration of the iodide ion and ^{1}Hmr spectral analysis.

[1]Recipient of a 1985 NSERC Summer Bursary for Undergraduate Research.

[2]To the best of our knowledge, there is no general review in this area. References given are to examples that come readily to mind, and are certainly not meant to be a complete survey of this area. The extensive studies (8, 9) based upon Reissert compound chemistry (cyanide adducts of heteroaromatic cations) also fall into this category. Analogous carbanion additions to electron-deficient neutral aromatic systems have recently been reviewed (23, 24).

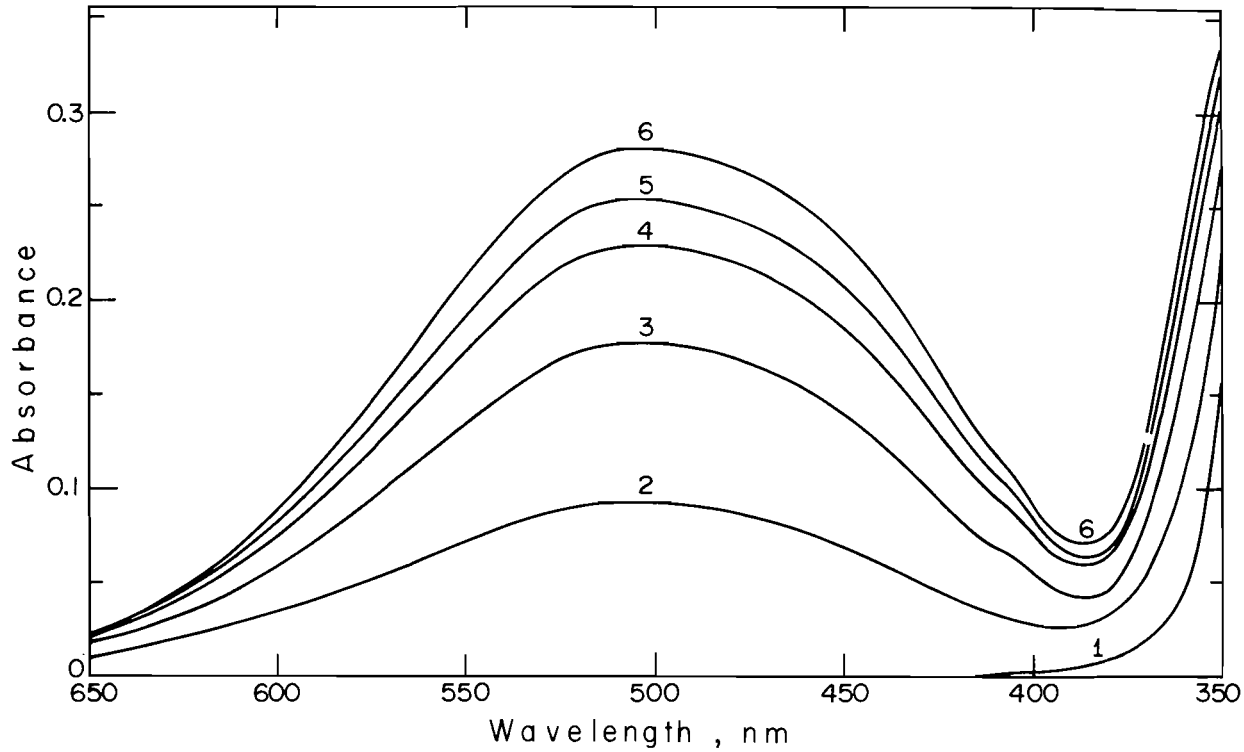

FIG. 1. Absorption spectra of solutions of the 2-methyl-5-nitroisoquinolinium cation (0.1 m*M*) equilibrated with various concentrations of acetone at pH 10.1 (25°C, ionic strength 0.1, 1-cm cell path length). Curve, [acetone]: 1, 0 *M*; 2, 0.226 *M*; 3, 0.452 *M*; 4, 0.678 *M*; 5, 0.904 *M*; 6, 1.356 *M*.

All kinetic studies employed spectral grade acetone or hexadeuteroacetone (99.9% D from MSD Isotopes, Montreal), and ACS Reagent grade KCl, KOH, HCl, and Na_2CO_3. Buffer solutions were prepared by the careful neutralization of a standard sodium carbonate solution with standard HCl solution to the appropriate pH, or by preparation of standard KOH solutions. All solutions for kinetic studies were adjusted to a final ionic strength of 0.1 by addition of the appropriate amount of KCl.

All kinetic data were obtained at 25°C by recording the time dependence of the increase in absorbance at 500 nm on a Unicam SP-1800 spectrophotometer equipped with an AR-125 linear recorder. Concentrations of the heterocyclic cation were in the range 0.05–0.2 m*M* (usually 0.1 m*M*), while acetone concentrations were in the range 7–500 m*M* depending upon the pH under study. The absorbance vs. time curves were digitized to give 15–20 data points covering approximately the first 90% of the reaction. These data points were fitted to the three-parameter first-order kinetic equation, $A = A_E + (A_0 - A_E)\exp(-k_{obs}t)$, where A is the absorbance at time t, A_0 and A_E are the initial and equilibrium absorbances respectively, and k_{obs} is the observed pseudo-first-order rate constant, by a computerized curve-fitting iteration procedure based upon the Marquardt algorithm. Replotting these data as $\ln(A_E - A)$ vs. t, gave plots that were strictly linear over at least the first 90% of the reaction, and slopes that were identical with the rate constants evaluated by the iterative fit.

The electronic absorption spectrum of the adduct **2** was observed to be unstable over extended periods of time, with the peak at 500 nm slowly disappearing in favour of a more intense absorption maximum in the vicinity of 435 nm. We have not investigated this very slow process (having a half-time of many hours), which did not interfere with the study of the much faster equilibration of the heterocyclic cation and its acetone adduct (half-time between 1 and 10 min under our experimental conditions).

A sample of the adduct for ^{1}Hmr spectral analysis was prepared by adjusting a solution containing 2-methyl-5-nitroisoquinolinium iodide (1 g) and acetone (1 mL) in water (10 mL) to pH 11.0 (pH meter) by the dropwise addition of 0.5 *M* NaOH. The dark red solution was extracted with several aliquots of chloroform and, after drying ($MgSO_4$), these extracts were evaporated to give a dark red oil, which was characterized by ^{1}Hmr spectroscopy.

Results

The electronic absorption spectrum of the 2-methyl-5-nitroisoquinolinium cation (**1**) after standing for 10 min at 25°C in aqueous solution at pH 10.1 in the presence of various concentrations of acetone is shown in Fig. 1. The appearance of a broad absorption maximum in the vicinity of 450–500 nm is characteristic of 1,2-dihydro-5-nitroisoquinoline derivatives (14, 15). Confirmation of the structure of the product of this reaction was obtained upon the isolation of a red oil from solutions containing higher concentrations of this cation. The ^{1}Hmr spectrum of this oil was identical to that previously reported by Somei *et al.* (5) for 1-acetonyl-1,2-dihydro-2-methyl-5-nitroisoquinoline (**2**).

The increase in absorbance at 500 nm proved to be cleanly kinetically first order in the 2-methyl-5-nitroisoquinolinium cation under all reaction conditions examined. However, the final absorbance at this wavelength displayed a pH dependence and also a dependence upon acetone concentration. This final absorbance increased with acetone concentration at constant pH (Fig. 1), and also increased with increasing pH at constant acetone concentration. These observations suggest a pH-dependent equilibrium between the 2-methyl-5-nitroisoquinolinium cation and the adduct **2**.

Since this isoquinolinium cation undergoes hydroxide ion addition to form the pseudobase **3** with pK_{R+} 11.7 (14), pseudobase formation competes with the formation of **2** in more basic aqueous solutions. Cation–pseudobase equilibration is essentially instantaneous (15), and is much faster than the reaction of the 2-methyl-5-nitroisoquinolinium cation with

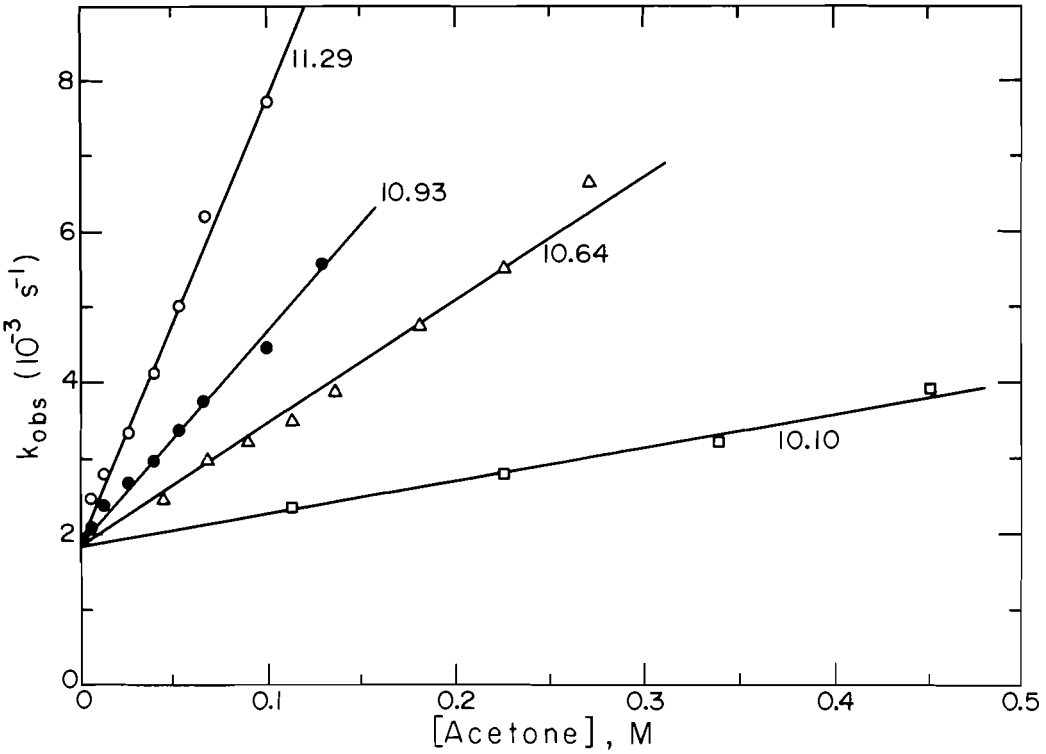

FIG. 2. Dependence of k_{obs} upon acetone concentration for the equilibration of **1** and **2** in solutions of various pH (as indicated on the figure).

acetone; however, spectral observations of the formation of **2** in more basic solutions are complicated by the similarity in the absorption spectra of **2** and **3**. We have therefore limited our quantitative study of the formation of **2** to the range pH 10.0–11.3. The lower limit to this range is determined by the low equilibrium concentrations of **2** that are present in solutions of lower pH, at acetone concentrations that are sufficiently small that they do not induce significant solvent effects (see below).

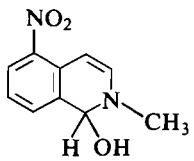

3

Pseudo-first-order rate constants (k_{obs}) for the equilibration of the 2-methyl-5-nitroisoquinolinium cation with the adduct **2** were evaluated as a function of acetone concentration and pH. At constant pH, k_{obs} is linear in acetone concentration up to 0.5 *M* (Fig. 2). At higher acetone concentrations, the observed rate constants show increasingly positive deviations from these linear relationships. We attribute this phenomenon to solvent effects upon the reaction rates at higher acetone concentrations. This interpretation is supported by our observation that such deviations can also be induced at lower acetone concentrations by the addition of acetonitrile to these predominantly aqueous reaction solutions. We have therefore restricted our studies to a maximum acetone concentration of 0.5 *M* (i.e. 3.5% v/v acetone in water) to avoid such solvent effects.

Values of k_{obs} proved to be independent of carbonate buffer concentration at constant acetone concentration, pH, and ionic strength (Table 1). Thus catalysis by buffer species is not involved in these reactions. This is confirmed by the data in Table 2 for studies at approximately constant pH (10.59 and 10.64) but quite different carbonate buffer concentrations.

TABLE 1. Pseudo-first-order rate constants for the equilibration of the 2-methyl-5-nitroisoquinolinium cation and acetone[a]

pH	[Carbonate] (*M*)	k_{obs} (s^{-1})
10.60	0.0390	$3.77(\pm0.05) \times 10^{-3}$
10.60	0.0312	$3.82(\pm0.04) \times 10^{-3}$
10.60	0.0234	$3.75(\pm0.05) \times 10^{-3}$
10.60	0.0156	$3.60(\pm0.04) \times 10^{-3}$
10.60	0.0078	$3.65(\pm0.03) \times 10^{-3}$
10.60	0.0039	$3.79(\pm0.05) \times 10^{-3}$
		Mean = $3.73(\pm0.08) \times 10^{-3}$

[a]All data at [acetone] = 0.136 *M*, ionic strength 0.1 (KCl + $NaHCO_3$ + Na_2CO_3). Carbonate concentrations in the table refer to total concentrations of carbonate and bicarbonate buffer species.

The dependence of k_{obs} upon acetone concentration is consistent with:

[2] $k_{obs} = k_f[\text{acetone}] + k_d$

Values of k_f and k_d were evaluated by least-squares analysis according to eq. [2] at each pH, and are collected in Table 2. While k_d appears to be pH independent within experimental error, k_f increases with pH in a way that is consistent with an approximate first-order dependence upon [$^-$OH]. The ratio k_f/k_d, which represents the apparent equilibrium constant (K_{app}) for the addition of acetone to the isoquinolinium cation at constant pH, is included in Table 2 and is also almost proportional to [$^-$OH]. It is shown below that these minor deviations from strict linearity in [$^-$OH] arise from the presence of small amounts of the pseudobase **3** in the most basic solutions.

Values of K_{app} could also be evaluated from the dependence

TABLE 2. Rate and equilibrium constants for the reaction of the 2-methyl-5-nitroisoquinolinium cation with acetone[a]

pH	$k_d(10^{-3}\ s^{-1})$	$k_f(10^{-2}\ M^{-1}\ s^{-1})$	$K_{app}(M^{-1})^b$	$K_{app}(M^{-1})^c$
10.10	1.8±0.1	0.46±0.05	2.6±0.4	2.3±0.2
10.59[d]	1.9±0.1	1.3±0.1	7±1	7.3±0.5
10.64	1.8±0.1	1.5±0.1	8±1	8.6±0.5
10.93	1.91±0.03	2.77±0.04	14.5±0.4	17±2
11.29	2.0±0.1	5.8±0.3	29±3	37±4
	Mean = 1.9±0.1			

[a]At 25°C, in ionic strength 0.1 carbonate buffer unless indicated otherwise.
[b]From $K_{app} = k_f/k_d$.
[c]From eq. [3].
[d]In carbonate buffer of ionic strength 0.05 + 0.05 *M* KCl.

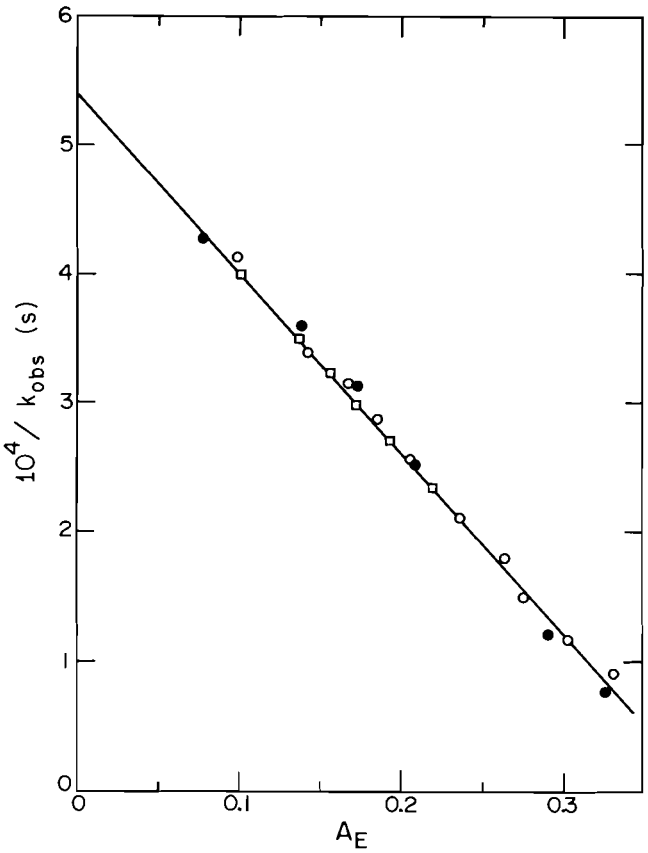

FIG. 3. Dependence of $1/k_{obs}$ on A_E according to eq. [5]. Data shown for pH 10.10 (●), pH 10.64 (○) (carbonate buffer $I = 0.1$), and pH 10.59 (□) (carbonate buffer $I = 0.05 + 0.05\ M$ KCl).

of the absorbance of equilibrated solutions upon acetone concentration. For an equilibrium of the form,

[3] $R^+ + CH \rightleftharpoons RC + H^+$

the apparent equilibrium constant at constant pH is given by $K_{app} = [RC]_E/[R^+]_E[CH]$ when [CH] (acetone) is in large excess over $[R^+]$ (isoquinolinium cation), as is the case in the current study. Since neither R^+ nor CH has significant absorbance at 500 nm, the observed absorbance at this wavelength is directly proportional to the concentration of the adduct (RC). If A_E is the equilibrium absorbance, then it follows that

[4] $A_E/[CH] = -K_{app}A_E + K_{app}\,\varepsilon_{RC}\,[R^+]_o$

where $[R^+]_o$ is the initial concentration of R^+. At pH 10.93 and 11.29, where there is a slight initial absorbance (A_o) at 500 nm because of the presence of small amounts of the hydroxide adduct of R^+, the left-hand side of eq. [4] must be modified to $(A_E - A_o)/[CH]$. Plots of this function were linear in A_E, and allowed the evaluation of K_{app} at each pH (Table 2), and the extinction coefficient of the adduct $\varepsilon_{RC} = 3900 \pm 200\ M^{-1}\,cm^{-1}$, which is pH independent.

Equations [2] and [4] may also be combined in the form:

[5] $1/k_{obs} = 1/k_d - A_E/(k_d\,\varepsilon_{RC}\,[R^+]_o)$

which predicts a linear dependence of $1/k_{obs}$ upon A_E (Fig. 3). The common line observed at the different pH and buffer concentrations in Fig. 3 further stresses the fact that k_d is independent of these variables. The data for pH 10.93 and 11.29 show small deviations from this line, but in a way that is consistent with the presence of minor amounts of hydroxide adduct in these more basic solutions.

TABLE 3. Rate and equilibrium constants for the reaction of the 2-methyl-5-nitroisoquinolinium cation with hexadeuteroacetone[a]

pH	$k_d(10^{-3}\ s^{-1})$	$k_f(10^{-3}\ M^{-1}\ s^{-1})$	$K_{app}(M^{-1})^b$
10.16	1.28±0.06	0.84±0.05	0.66
10.67	1.25±0.08	2.6±0.1	2.1
11.00	1.36±0.09	5.2±0.2	3.8
	Mean = 1.3±0.1		

[a]At 25°C, in ionic strength 0.1 carbonate buffer.
[b]From $K_{app} = k_f/k_d$.

The reaction of hexadeuteroacetone with the 2-methyl-5-nitroisoquinolinium cation was also investigated. This reaction was significantly slower than for acetone itself, but displayed the same dependence upon ketone concentration and pH as described above. Parameters for the hexadeuteroacetone addition reaction are summarized in Table 3.

For eq. [3], we define a pH-independent equilibrium constant $K = [H^+][RC]/[R^+][CH]$ that is related to the pH-dependent K_{app} of Tables 2 and 3 by:

[6] $K = K_{app}[H^+](1 + K_{R+}/[H^+])$

Using $pK_{R+} = 11.7$ for the 2-methyl-5-nitroisoquinolinium cation (14), eq. [6] may be used to convert each value for K_{app} in Tables 2 and 3 into values for K. Values for K calculated in this way are listed in Table 4, and are clearly pH independent within experimental error.

The pseudo-first-order rate constants k_{obs} are defined in terms of the equilibrium mixture of the isoquinolinium cation and its

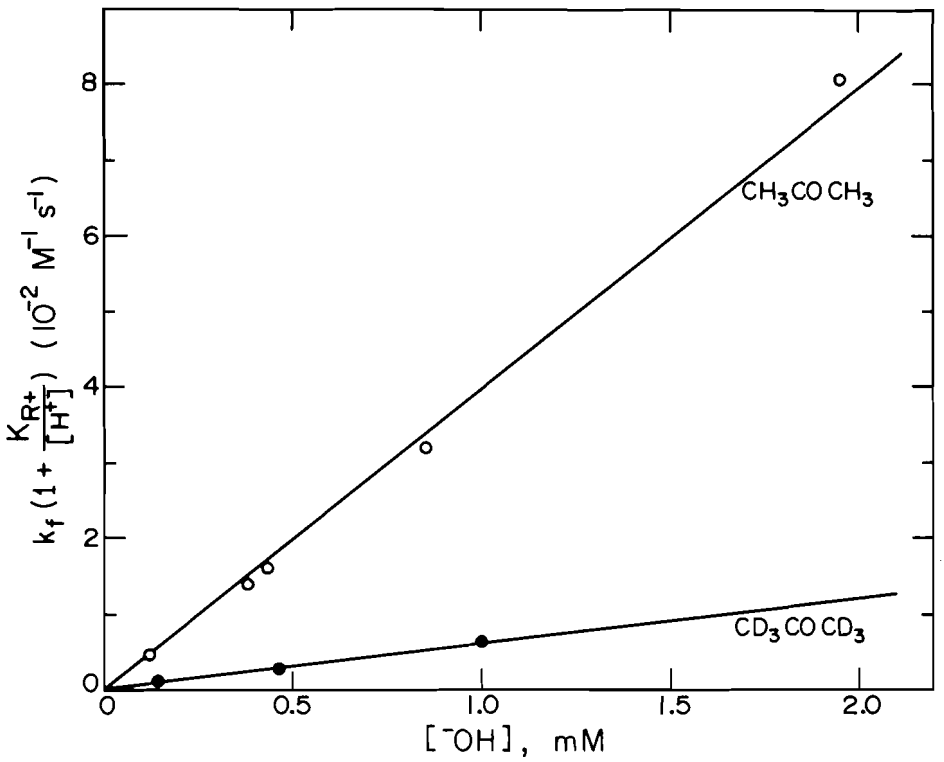

FIG. 4. Dependence of $k_f(1 + K_{R+}/[H^+])$ upon hydroxide ion concentration for acetone and hexadeuteroacetone addition to **1**.

TABLE 4. Values of K for the reaction of acetone and hexadeuteroacetone with the 2-methyl-5-nitroisoquinolinium cation[a]

Reagent	pH	$K \times 10^{10}$	K^H/K^D
CH_3COCH_3	10.10	2.0	
	10.59	2.0	
	10.64	2.1	
	10.93	2.1	
	11.29	2.4	
		Mean $K = 2.1(\pm 0.2) \times 10^{-10}$	
			4.5
CD_3COCD_3	10.16	0.47	
	10.67	0.49	
	11.00	0.46	
		Mean $K = 4.7(\pm 0.2) \times 10^{-11}$	

[a]Defined by eq. [6], at 25°C, ionic strength 0.1.

pseudobase at each pH. Whereas k_d is pH independent, k_f is pH dependent and should be corrected for the small amount of pseudobase present at each pH in the form $k_f(1 + K_{R+}/[H^+])$. This latter function is strictly proportional to $[^-OH]$ for both acetone and hexadeuteroacetone (Fig. 4). The slopes of these lines define pseudo-third-order rate constants (k_3) of 38 ± 2 $M^{-2}\,s^{-1}$ for acetone and 6.1 ± 0.1 $M^{-2}\,s^{-1}$ for hexadeuteroacetone. Thus $k_3^H/k_3^D = 6.2$.

Discussion

Somei *et al.* (5) report the preparation of 1-acetonyl-1,2-dihydro-2-methyl-5-nitroisoquinoline (**2**) by refluxing the 2-methyl-5-nitroisoquinolinium cation (**1**) with acetone in 0.2 *M* aqueous sodium hydroxide for 4 h. In the current work we have shown that the equilibrium of eq. [1] is established rapidly at room temperature in solutions that are much less basic than 0.2 *M* NaOH. For instance, at pH 11 in the presence of 0.5 *M* acetone, this equilibrium favours the adduct **2** over the cation **1** by a 10:1 ratio, with equilibrium being established with a half-time of less than 1 min at 25°C. The use of higher acetone concentrations would further displace the equilibrium in favour of the adduct, and so allow the use of even less basic solutions if desired. Thus the synthesis of **2** can be efficiently performed under much milder conditions than previously reported: lower temperatures, shorter reaction times, and less basic reaction medium.

The yield and rate of formation of the adduct are expected to decrease above pH 11.7 as the cation is preferentially converted into its pseudobase **3**. In 0.2 *M* NaOH (pH 13.3), the pseudobase predominates over this cation by a 40:1 ratio. Although in this pH region the concentration of the acetone enolate ion nucleophile is proportional to $[^-OH]$, the concentration of the isoquinolinium cation is inversely proportional to $[^-OH]$ and so there is no net increase in rate of adduct formation with increasing pH. In these more basic solutions the yield of adduct also suffers because its formation must compete with the disproportionation of the pseudobase to 2-methyl-5-nitro-1-isoquinolinone and 1,2-dihydro-2-methyl-5-nitroisoquinoline (16). Since this disproportionation is an irreversible process, whereas adduct formation from the cation is reversible, extended reaction periods (especially at high temperatures) will result in reduced yields of adduct and increased amounts of disproportionation products.

Similar considerations also apply to other carbanion additions to heteroaromatic cations, and suggest that in all such reactions yields will be optimized by the use of shorter reaction times in pH regions just below the pK_{R+} for pseudobase formation. Such low basicity reaction media also minimize side reactions in which the carbanion species may be involved (aldol condensations, etc.).

TABLE 5. Comparison of the addition of hydroxide ion and acetone enolate anion to 2-methyl-5-nitroisoquinolinium cation and to 4-nitrobenzaldehyde

	2-Methyl-5-nitroisoquinolinium cation			4-Nitrobenzaldehyde		
Parameter	H_2O[a]	MeCOMe[b]	MeCOMe/H_2O	H_2O[c]	MeCOMe[d]	MeCOMe/H_2O
pK_a	15.74	19.16		15.74	19.16	
$k_{Nu}(M^{-1}\,s^{-1})$	4.2×10^4	5.5×10^6	130	8.3×10^4	2.3×10^5	2.8
$k_{-Nu}(s^{-1})$	210	0.0019	9.0×10^{-6}	5200	0.0161[e]	3.1×10^{-6}
$K_{Nu}(M^{-1})$	200	2.9×10^9	1.5×10^7	16	1.4×10^7	8.8×10^5
K_{HNu}	3.6×10^{-14}	2.0×10^{-10}	5600	2.9×10^{-15}	1.0×10^{-12}	340

[a]Data from ref. 15.
[b]From current work.
[c]Data from McClelland and Coe (20).
[d]Data from Guthrie *et al.* (21).
[e]Using $pK_a = 14.0$ for alkoxide ion formation from the neutral aldol, as estimated from a linear free energy relationship for alcohol ionization (22).

Kinetics

Adduct formation from acetone and the 2-methyl-5-nitroisoquinolinium cation is found to be kinetically third order; i.e. first order in each of acetone, isoquinolinium cation, and hydroxide ion. Such a process is kinetically equivalent in this pH range to the reaction of the acetone enolate anion (C^-) with the isoquinolinium cation with second-order rate constant $k_2 = k_3K_w/K_a$, where K_w is the ionic product of water, and K_a is the acid dissociation constant of acetone in aqueous solution:

$$k_3[^-OH][CH][R^+] = (k_3K_w/K_a)[C^-][R^+] = k_2[C^-][R^+]$$

Thus $k_2 = 5.5 \times 10^6\ M^{-1}\ s^{-1}$ can be evaluated for the attack of the acetone enolate ion on the 2-methyl-5-nitroisoquinolinium cation in aqueous solution at 25°C, by making use of k_3 as evaluated above, $pK_w = 14.00$, and $pK_a = 19.16$ for acetone, as recently reported by Kresge and co-workers (17).

The first-order dependence upon isoquinolinium cation concentration indicates that enolate ion formation from acetone is not the rate-determining step for adduct formation in the kinetic scheme described in eq. [7], where k_1 and k_{-1} are respectively the pseudo-first-order rate constants for deprotonation of acetone and protonation of the enolate ion for the experimental conditions under consideration:

$$[7] \quad CH \underset{k_{-1}}{\overset{k_1}{\rightleftharpoons}} C^- \underset{k_{-2}}{\overset{k_2[R^+]}{\rightleftharpoons}} RC$$

This is confirmed by the fact that the rates of these reactions are not dependent upon the concentration of carbonate buffer species (Table 1).

We may therefore treat the enolate anion (C^-) as a steady-state intermediate according to the kinetic scheme of eq. [7]. We may readily evaluate k_1 and k_{-1} in eq. [7] for aqueous potassium hydroxide solutions using the reported second-order rate constant of $0.22\ M^{-1}\ s^{-1}$ for deprotonation of acetone by hydroxide ion and $pK_a = 19.16$ for this process at 25°C (17). Thus at pH 11, $k_1 = 2.2 \times 10^{-4}\ s^{-1}$ and $k_{-1} = 3.2 \times 10^4\ s^{-1}$. This value of k_{-1} is much larger than the maximum value of $k_2[R^+] = 5.5 \times 10^6 \times 1 \times 10^{-4} = 550\ s^{-1}$ for a reaction in which the initial concentration of isoquinolinium cation is 0.1 mM. This condition ($k_{-1} \gg k_2[R^+]$ holds over the entire pH region investigated in this work. Thus analysis of eq. [7], treating C^- as a steady-state intermediate, and with $[CH] \gg [R^+]$ and $k_{-1} \gg k_2[R^+]$, predicts the observed pseudo-first-order rate constant to be:

$$[8] \quad k_{obs} = k_2K_a[^-OH][CH]/K_w + k_{-2}$$

Equation [8] has the same form as the empirically deduced eq. [2], with k_f being proportional to $[^-OH]$ as is experimentally observed, and $k_d = k_{-2}$ being pH independent.

The values of k_2 and k_{-2} deduced in the current work may be combined with the extensive data available upon the rates of acetone – enolate ion equilibration (18, 19) to provide a complete description of the kinetics of eq. [7] for essentially any pH in any buffer solution at ionic strength 0.1 and 25°C.

The data in Tables 2 and 3 clearly indicate that there are significant kinetic and equilibrium isotope effects when the addition of the enolate ions of acetone and its hexadeutero derivative are compared. However, the interpretation of $K^H/K^D = 4.5$ and $k_3^H/k_3^D = 6.2$ is complicated by the fact that they contain contributions from the pK_a values of both acetone and hexadeuteroacetone. While the former value has been accurately measured as 19.16 (17), the latter value is not available, and strictly speaking is not simply definable for the reversible ionization of hexadeuteroacetone in H_2O. This latter point also applies to eq. [3], which for hexadeuteroacetone becomes:

$$[9] \quad R^+ + CD \rightleftharpoons RC + D^+$$

The reported K^D for eq. [9] can, strictly, only be considered as a pseudo-equilibrium constant in H_2O, since true equilibrium will only be achieved when essentially all deuterium in acetone molecules is exchanged for hydrogen, one atom at a time, via the equilibration of the adduct RC with R^+ and ketone.

The observed ratio $k_{-2}^H/k_{-2}^D = 1.5$ simply represents the relative first-order rate constants for the loss of the enolate ion and the pentadeutero-enolate ion of acetone from their respective adducts. This process should be influenced by only secondary isotope effects from replacement of two hydrogen atoms by two deuterium atoms on the methylene carbon atom of the adduct **2**. This secondary isotope effect will mainly reflect the change in hybridization of this carbon atom from sp^3 in the adduct to essentially sp^2 in the enolate anion. The observed isotope effect of 1.5 (for two deuterium atoms) is appropriate for a transition state in which enolate ion formation is well advanced. Such a product-like transition state is expected for an elementary reaction that generates the thermodynamically unstable enolate ion.

Comparison with related reactions

Analogous equilibria to eq. [1] can be written for essentially any nucleophilic addition to this heterocyclic cation. Such reactions can be summarized by eq. [10], [11], and [12].

[10] $HNu \overset{K_a}{\rightleftharpoons} H^+ + Nu^-$

[11] $R^+ + Nu^- \underset{k_{-Nu}}{\overset{k_{Nu}}{\rightleftharpoons}} RNu \qquad K_{Nu} = k_{Nu}/k_{-Nu}$

[12] $R^+ + HNu \overset{K_{HNu}}{\rightleftharpoons} RNu + H^+ \qquad K_{HNu} = K_{Nu}\,K_a$

To the best of our knowledge, the only analogous addition that has previously been quantitatively analyzed is the addition of hydroxide ion to give the pseudobase **3**. Rate and equilibrium constants for the addition of hydroxide ion and acetone enolate ion to the 2-methyl-5-nitroisoquinolinium cation are summarized in Table 5. This table also contains data from the literature for analogous addition reactions to the carbonyl group of 4-nitrobenzaldehyde, which was chosen since it is the most reactive substituted benzaldehyde for which quantitative data are available for both hydration (20) and acetone addition (mixed aldol condensation) (21). It can be readily seen that the relative rate and equilibrium constants for acetone and water addition to these two substrates are qualitatively similar. Quantitative agreement in such comparisons is unlikely since, in the case of the aldehyde, eqs. [11] and [12] represent addition to a neutral electrophile to give an anionic adduct rather than addition to a cationic electrophile to give a neutral adduct, as is the case for the heterocyclic cation. It should be noted that enolate addition to the carbonyl group is found to be the rate-determining step in the base-catalyzed addition of acetone to benzaldehydes (21). This is exactly analogous to the rate-determining addition of enolate ion to the isoquinolinium cation that is found in the current work.

Acknowledgement

We appreciate the support of this work by the Natural Sciences and Engineering Research Council of Canada.

1. N. J. Leonard, H. A. Dewalt, Jr., and G. W. Leubner. J. Am. Chem. Soc. **73**, 3325 (1951).
2. W. Kiel, F. Kroehnke, and G. Schneider. Justus Liebigs Ann. Chem. **766**, 45 (1972).
3. T.-K. Chen and C. K. Bradsher. Tetrahedron, **29**, 2951 (1973).
4. H. Takayama and T. Okamoto. Chem. Pharm. Bull. **26**, 2435 (1978).
5. M. Somei, F. Yamada, and C. Kaneko. Chemistry Lett. 123 (1979).
6. M. P. Sammes, C. W. F. Leung, and A. R. Katritzky. J. Chem. Soc. Perkin Trans. 1, 2835 (1981).
7. M. J. Wanner, G. J. Koomen, and U. K. Pandit. Tetrahedron, **38**, 2741 (1982).
8. F. D. Popp. Adv. Heterocycl. Chem. **9**, 1 (1968); **24**, 187 (1979).
9. J. V. Cooney. J. Heterocycl. Chem. **20**, 823 (1983).
10. M. Sainsbury, S. F. Dyke, D. W. Brown, and W. G. D. Lugton. Tetrahedron, **24**, 427 (1968).
11. S. F. Dyke, M. Sainsbury, D. W. Brown, M. N. Palfreyman, and E. P. Tiley. Tetrahedron, **24**, 6703 (1968).
12. M. Sainsbury, D. W. Brown, S. F. Dyke, R. D. J. Clipperton, and W. R. Tonkyn. Tetrahedron, **26**, 2239 (1970).
13. M. Somei, K. Hashiba, F. Yamada, T. Maekawa, T. Kimata, and C. Kaneko. Chem. Lett. 1245 (1978).
14. J. W. Bunting and W. G. Meathrel. Can. J. Chem. **52**, 972 (1974).
15. J. W. Bunting and D. J. Norris. J. Am. Chem. Soc. **99**, 1189 (1977).
16. J. W. Bunting, P. A. Lee-Young, and D. J. Norris. J. Org. Chem. **43**, 1132 (1978).
17. Y. Chiang, A. J. Kresge, Y. S. Tang, and J. Wirz. J. Am. Chem. Soc. **106**, 460 (1984).
18. M. L. Bender and A. Williams. J. Am. Chem. Soc. **88**, 2502 (1966).
19. J. R. Jones. The ionization of carbon acids. Academic Press, London. 1973. p. 135.
20. R. A. McClelland and M. Coe. J. Am. Chem. Soc. **105**, 2718 (1983).
21. J. P. Guthrie, J. Cossar, and K. F. Taylor. Can. J. Chem. **62**, 1958 (1984).
22. G. B. Barlin and D. D. Perrin. Q. Rev. Chem. Soc. **20**, 75 (1966).
23. F. Terrier. Chem. Rev. **82**, 77 (1982).
24. M. R. Crampton, E. Buncel, M. J. Strauss, and F. Terrier. Electron-deficient aromatic- and heteroaromatic-base interactions. Elsevier Scientific Publishing, Amsterdam. 1984.

A tellurium-125 and tin-119 Mössbauer and nuclear magnetic resonance study of the group IV organotellurides

C. H. W. JONES, R. D. SHARMA, AND S. P. TANEJA
Department of Chemistry, Simon Fraser University, Burnaby, B.C., Canada V5A 1S6

Received August 30, 1985

C. H. W. JONES, R. D. SHARMA, and S. P. TANEJA. Can. J. Chem. **64**, 980 (1986).

The ^{125}Te Mössbauer and nmr spectra of the compounds $(R_3X)_2Te$ (R = Me, X = C, Si, Ge, and Sn; R = Ph, X = Ge and Sn), R_3MTePh (R = Me, X = Si, Ge, and Sn; R = Ph, X = Ge, Sn, Pb), $R_2Sn(TePh)_2$ (R = Me and *t*-Bu), and the cyclic compounds $(Me_2SnTe)_3$, $(Me_2Sn)_3Te_2$, and $(t\text{-}Bu_2SnTe)_2$ have been measured. The trends in the Mössbauer and nmr data are discussed. The Mössbauer quadrupole splittings increase as the nmr chemical shifts become more positive, corresponding to a decrease in the shielding at the tellurium nucleus. The ^{119}Sn Mössbauer and nmr parameters of the compounds $(R_3Sn)_2E$ and R_3SnEPh (R = Me and Ph), $(Me_2SnE)_3$, $(Me_2Sn)_2E_2$, $(t\text{-}Bu_2SnE)_2$, and $Me_2Sn(EPh)_2$ (E = S, Se, and Te) are discussed. The ^{119}Sn Mössbauer quadrupole splittings are again observed to increase as the nmr chemical shifts become more positive. The ^{125}Te and ^{119}Sn nmr and Mössbauer data provide evidence that there is little transmission of bonding effects through the tin–tellurium bond as the chemical environment about the tin or tellurium is changed.

C. H. W. JONES, R. D. SHARMA et S. P. TANEJA. Can. J. Chem. **64**, 980 (1986).

On a mesuré les spectres de Mössbauer et de rmn du ^{125}Te des composés suivants: $(R_3X)_2Te$ dans lesquels R = Me et X = C, Si, Ge et Sn ou R = Ph et X = Ge et Sn; R_3MTePh dans lesquels R = Me et X = Se, Ge et Sn ou R = Ph et X = Ge, Sn et Pb; $R_2Sn(TePh)_2$ dans lesquels R = Me et *t*-Bu ainsi que les composés cycliques $(Me_2SnTe)_3$, $(Me_2Sn)_3Te_2$ et $(t\text{-}Bu_2SnTe)_2$. On discute des tendances qui se manifestent dans les données relatives aux spectres de rmn et de Mössbauer. Les couplages quadrupolaires de Mössbauer augmentent lorsque les déplacements chimiques de la rmn deviennent plus positifs; ceci correspond à une diminution du blindage au niveau du noyau du tellure. On discute des paramètres de la rmn et des spectres de Mössbauer des composés $(R_3Sn)_2E$ et R_3SnEPh dans lesquels R = Me et Ph ainsi que dans les composés $(Me_2SnE)_3$, $(Me_2Sn)_2E_2$, $(t\text{-}Bu_2SnE)_2$ et $Me_2Sn(EPh)_2$ dans lesquels E = S, Se et Te. Encore une fois dans ces cas, on observe que les couplages quadrupolaires dans les spectres de Mössbauer du ^{119}Sn augmentent lorsque les déplacements chimiques de la rmn deviennent plus positifs. Les donnés de la spectroscopie de Mössbauer et de la rmn du ^{125}Te et du ^{119}Sn mettent en évidence que les effets de liaison ne sont que faiblement ou peu transmis à travers la liaison étain-tellure lorsque change l'environnement chimique autour de l'étain ou du tellure.

[Traduit par la revue]

Introduction

As part of an on-going study of the ^{125}Te Mössbauer spectroscopy of organotellurium compounds (1–3) it was of interest to study the organotellurides of the group IV elements. In earlier studies the alkyl and aryl tellurides have been extensively investigated (1, 2) and the present experiments extend this work to include compounds of silicon, germanium, tin, and lead. In many of the compounds investigated the group IV organo ligand is of the form R_3X— where X = Si, Ge, Sn, and Pb. For this reason, it was of interest to synthesize and characterize di-*tert*-butyl telluride, $(Me_3C)_2Te$, for comparison with its group IV analogues and this work has been described in another paper (4). As another off-shoot of this work, the crystal structure of $(Ph_3Sn)_2Te$ was determined and this structure is compared with that of the sulphur and selenium compounds in ref. 5.

For some of the compounds under investigation, ^{125}Te nmr spectra have been reported in the literature (6, 10) and were initially used to aid in characterizing and identifying the compounds studied. However, the ^{125}Te nmr parameters are of some interest in their own right and a correlation has been observed between the ^{125}Te Mössbauer quadrupole splittings in the solid state and the solution nmr chemical shifts for the organotellurides.

The ^{119}Sn Mössbauer spectra of the organotin tellurides have been measured to complement the ^{125}Te data. The ^{119}Sn nmr spectra were recorded where these had not previously been measured. These experiments were extended to include the organotin selenides and sulphides so that comparisons could be made with regard to the trends observed in the Mössbauer and nmr parameters on variation of the chalcogen within the organotin chalcogenides. An empirical correlation was again observed between the ^{119}Sn Mössbauer quadrupole splitting in the solid state and the solution nmr chemical shifts.

Discussion

^{125}Te Mössbauer and nmr data

The Mössbauer quadrupole splittings, Δ, of both tellurium and tin are generally assumed to derive from an imbalance in the 5*p*-orbital populations, the 5*d* orbitals not being considered to contribute significantly. The Mössbauer isomer shifts, δ, reflect the relative *s*-electron densities at the nucleus and these in turn are dependent on the population of the 5*s* and 5*p* orbitals of the tellurium and tin atoms (11, 12).

In the series $(R_3X)_2Te$ (R = Me, X = C, Si, Ge, and Sn; R = Ph, X = C, Ge, Sn) the ^{125}Te quadrupole splittings range from 6.3 mm s^{-1} for $(Me_3Sn)_2Te$ to 10.5 mm s^{-1} for *t*-Bu_2Te, while the ^{125}Te isomer shifts are all very similar and are small and positive with respect to the reference standard (^{125}I in copper). A sample spectrum is shown in Fig. 1.

The large quadrupole splitting observed for *t*-Bu_2Te reflects the considerable imbalance in the 5*p*-orbital populations on tellurium resulting from the different hybrid characters and electron populations of the bonding and nonbonding orbitals. It would be expected that, as the electronegativity of the ligand bonded to tellurium decreases, the *p*-orbital imbalance, and hence the quadrupole splitting, should decrease and this is indeed so (Table 1). The similarity in the Δ values for $(Me_3Si)_2Te$, $(Me_3Ge)_2Te$, and $(Me_3Sn)_2Te$ reflects the similar group electronegativities of the trimethylsilyl, germyl, and stannyl ligands.

The quadrupole splittings of the compounds Ph_2Te (11.0 mm

TABLE 1. Tellurium-125 data

	^{125}Te Mössbauer*			^{125}Te nmr		
	δ ±0.08 (mm s^{-1})	Δ ±0.10 (mm s^{-1})	Γ av.	δ† (ppm)	J‡ (Hz)	Ref.§
Ph_2Te	+0.15	11.00	5.62	+688		C
t-Bu_2Te	+0.19	10.51	5.68	+993		C
				+979		7
t-Bu_2Te_2	+0.32	11.00	5.40	+487.2		C
				+477		6
$(Me_3Si)_2Te$	+0.29	6.40	5.38	−842		C
				−43		8
$Me_3SiTePh$	+0.23	9.52	6.24	+11.6		C
$(Me_3Ge)_2Te$	+0.23	6.67	5.54	−794.5		C
$(Ph_3Ge)_2Te$	+0.13	7.23	5.64	−832		C
$Me_3GeTePh$	+0.06	9.75	6.21	+40.2		C
$Ph_3GeTePh$	+0.13	9.30	5.93	−11.0		C
$(Me_3Sn)_2Te$	+0.05	6.27	5.40	−1225.9	2753	C
				−1214		9
$(Ph_3Sn)_2Te$	+0.28	6.60	5.45	−1310	3225	C
$Me_3SnTePh$	+0.32	9.46	6.56	−186.9	2614	C
$Ph_3SnTePh$	+0.24	9.05	5.68	−205.8	3245	C
$Me_2Sn(TePh)_2$	+0.33	9.22	5.52	−30.8		C
$(Me_2SnTe)_3$	+0.28	6.44	5.64	−860	3100	C
$(Me_2Sn)_3Te_2$	+0.13	6.23	5.70	−1082	(*a*)2630	C
					(*b*)3170	
$(t$-$Bu_2SnTe)_2$	+0.27	6.62	5.75	−1099		C
t-$Bu_2Sn(TePh)_2$	+0.29	9.59	6.08	−144.8	3158	C
$Ph_3PbTePh$	+0.34	9.57	5.58	−50.7	4058.7**	C

*δ ^{125}Te Mössbauer isomer shifts with respect to I/Cu, source and absorber at 4.2 K. Γ av. is the average linewidth.

†δ ^{125}Te nmr chemical shifts measured in $CDCl_3$ solution with respect to neat Me_2Te.

‡Except where noted these are $^1J(^{125}Te-^{119}Sn)$ values. For $Me_2Sn(TePh)_2$ and $(t$-$Bu_2SnTe)_2$ the signal-to-noise ratio at the tin side bands was poor. Values of $^1J(^{119}Sn-^{125}Te)$ were obtained from the ^{119}Sn spectra and are given in Table 3.

§C denotes this work and the measurements were made in $CDCl_3$ solution. Other referenced work is as shown.

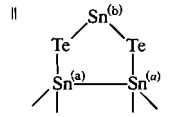

**Value is $^1J(^{125}Te-^{207}Pb)$.

s^{-1}), $Ph_3SnTePh$ (9.0 mm s^{-1}), and $(Ph_3Sn)_2Te$ (6.6 mm s^{-1}) show a similar trend with the changing electronegativity of the ligand, as do the compounds $Me_3GeTePh$ (9.75 mm s^{-1}) and $(Me_3Ge)_2Te$ (6.7 mm s^{-1}).

With regard to the ^{125}Te Mössbauer isomer shifts the large errors in δ, coupled with the small magnitude of the shifts, make it difficult to discern any systematic trends in δ as the ligand is changed.

The ^{125}Te Mössbauer quadrupole splitting for tellurium in a given moiety remains relatively constant within a given series of compounds. Thus, the Sn—^{125}Te—Ph group in $Me_3SnTePh$, $Me_2Sn(TePh)_2$, and t-$Bu_2Sn(TePh)_2$ has a very similar Δ value. Similarly, the Sn—^{125}Te—Sn groups in $(Ph_3Sn)_2Te$, $(Me_2Sn)_2Te$, and in the cyclic species $(Me_2SnTe)_3$, $(Me_2Sn)_3Te_2$, and $(t$-$Bu_2SnTe)_2$ also have similar values. For these latter compounds $(Me_2SnTe)_3$ is a six-membered ring (13), $(Me_2Sn)_3Te_2$ a five-membered ring containing the >Sn—Te—Sn—Te—Sn< macrocycle and $(t$-$Bu_2SnTe)_2$ is a four-membered ring. The crystal structures of the latter two have not been reported but those for $(t$-$Bu_2SnSe)_2$ and $(t$-$Bu_2SnS)_2$ have and show Sn—E—Sn bond angles of 82.5–87.6° (14).

The constancy of the ^{125}Te Mössbauer quadrupole splittings for the Sn—Te—Sn group in these different compounds indicates that this parameter is relatively insensitive to changes in the number or the nature of the organic groups bonded to the tin ligands or of inserting the tellurium into a six-, five-, or four-membered ring. This point will be returned to later.

The ^{125}Te nmr chemical shifts listed in Table 1 can be seen to span a very wide range from +993 to −1310 ppm with respect to Me_2Te. While the present data for t-Bu_2Te, t-Bu_2Te, and $(Me_3Sn)_2Te$ are in good agreement with the literature values, the value for $(Me_3Si)Te$ does not agree with that reported earlier by du Mont and Kroth (8). The present result was confirmed on samples of $(Me_3Si)_2Te$ prepared by two independent routes and characterized by ^{29}Si and proton nmr as well as by mass spectrometry.

The nmr chemical shifts appear to fall into three groups, those that are large and positive (Ph_2Te, t-Bu_2Te, t-Bu_2Te_2), those that are small and positive or negative (R_3XTePh where X = Si, Ge, Sn, R = Me; and X = Ge, Sn, R = Ph), and finally, those

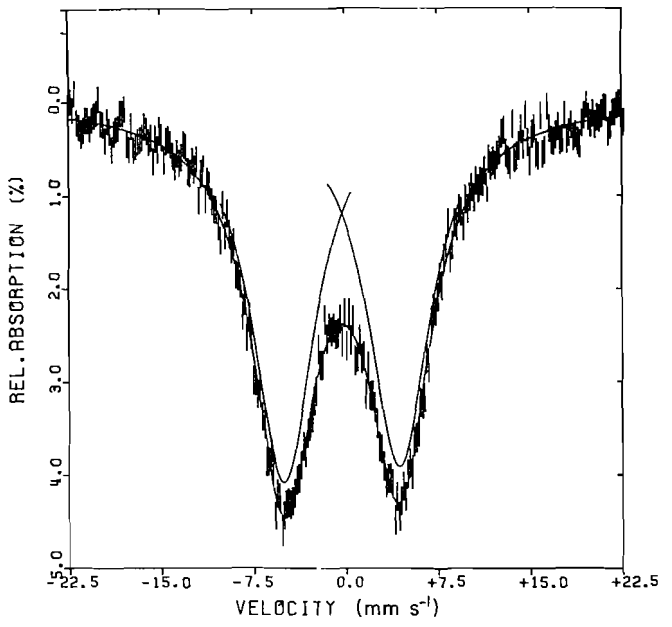

FIG. 1. The tellurium-125 Mössbauer spectrum of $Me_3SiTePh$.

TABLE 2. Relativistically corrected reduced coupling constants

	$^1K^{RC}$*			
	Pb—Te	Sn—Te	Sn—Se	$^1K^{RC}_{SnTe}/^1K^{RC}_{SnSe}$
$Ph_3PbTePh$	11.53			
$Ph_3SnTePh$		11.17		1.338
$Ph_3SnSePh$			8.35	
$(Ph_3Sn)_2Te$		11.111		1.274
$(Ph_3Sn)_2Te$			8.720	
$Me_3SnTePh$		8.998		1.306
$Me_3SnSePh$			6.85	
$Me_2Sn(TePh)_2$		10.833		1.243
$Me_2Sn(SePh)_2$			8.713	
$(Me_2SnTe)_3$		10.67		1.222
$(Me_2SnSe)_3$		8.73		
$(Me_2Sn)_3Te_2$		8.96(*a*)		1.269(*a*)
		10.87(*b*)		1.211(*b*)
$(Me_2Sn)_3Se_2$			7.06(*a*)	
			8.98(*b*)	
$(t\text{-}Bu_2SnTe)_2$		7.287		1.120
$(t\text{-}Bu_2SnSe)_2$			6.508	

*$^1K^{RC}$ values are in N A^{-2} m^{-3} when J is in Hz and are to be multiplied by 10^{21}.

that are large and negative ($(R_3X)_2Te$, where X = Si, Ge, Sn, R = Me; X = Ge, Sn, R = Ph). The nmr shifts in heavy atoms are generally taken to be dominated by the Ramsey paramagnetic shielding term (15–17) and the above trend then corresponds to the smallest shielding at tellurium when two carbon atoms are bonded to tellurium and the largest shielding when two Si, Ge, or Sn atoms are bonded to tellurium.

We note that this trend also follows the trend in the Mössbauer quadrupole splittings since Ph_2Te and t-Bu_2Te have Δ values of 11.0 and 10.5 mm s^{-1}, the R_3XTePh compounds Δ values of 9.05–9.75 mm s^{-1} and $(R_3X)_2Te$ splittings of 6.27–7.23 mm s^{-1}. Thus there appears to be a rough correlation between these two parameters for tellurium-125. The existence of such a correlation between nmr chemical shifts and nuclear quadrupole coupling constants has been commented on previously for terminal halogen ligands (17–22). The origin of this correlation in ^{125}Te organotellurides in particular will be discussed elsewhere.

The only previous correlation observed between tellurium Mössbauer and nmr data is that of Chadha and Miller (23) who reported a linear relationship between ^{13}C chemical shifts and ^{125}Te isomer shifts for diaryltellurides and diaryltellurium dihalides.

Other features of the ^{125}Te nmr data that should be commented on include the couplings to Sn and Pb. The tellurium–tin coupling constants obtained from ^{125}Te spectra are reported in Table 1 and the complementary data obtained from ^{119}Sn spectra are given in Table 2. Where coupling constants were obtained from both ^{125}Te and ^{119}Sn nmr spectra on the same compound the agreement was good, e.g., $Ph_3SnTePh$ $^1J(^{125}Te–^{119}Sn)$ = 3245 Hz, $^1J(^{119}Sn–^{125}Te)$ = 3242 Hz. In some cases the coupling constants were abstracted only from the tellurium spectra ($Me_3SnTePh$ and $(Me_3Sn)_2Te$) or from the tin spectra ($Me_2Sn(TePh)_2$ and $(t\text{-}Bu_2SnTe)_2$). Sample spectra are shown in Fig. 2.

The $^1J(^{125}Te–^{119}Sn)$ values are generally in the range of 3100–3250 Hz although smaller values are observed for $(Me_3Sn)_2Te$, 2753 Hz; for $Me_3SnTePh$, 2614 Hz; and for $(t\text{-}Bu_2SnTe)_2$, 2117 Hz. The coupling constants are more consistent in magnitude with those reported by Mathiasch (24) than with that of McFarlane (25). The tellurium–tin bond appears to have relatively constant s character, as monitored by the coupling constants, in $(Ph_3Sn)_2Te$, $Ph_3SnTePh$, $Me_2Sn(TePh)_2$, $(Me_2SnTe)_3$, $(Me_2Sn)_3Te_2$, and t-$Bu_2Sn(TePh)_2$. For $(t\text{-}Bu_2SnTe)_2$ the Te–Sn coupling constant is a minimum, and this may reflect the peculiar stereochemical requirements of the four-membered ring.

The $^1J(^{125}Te–^{207}Pb)$ value in $Ph_3PbTePh$ was found to be 4058.7 Hz (Table 1) and this appears to be the only compound in which the Pb–Te coupling has been observed. In order to facilitate a comparison of this coupling constant with that of $^1J(^{125}Te–^{119}Sn)$ in $Ph_3SnTePh$ it is necessary to correct for the different magnetogyric ratios for the two pairs of nuclei, Pb–Te and Sn–Te, and also for the relativistic effects which are extremely important in spin–spin coupling constants of heavy-metal elements. The application of these corrections has been described in detail by Burns *et al.* (26). Thus, the reduced coupling constant $^nK_{AB}$, corrected for the magnetogyric ratios γ_A and γ_B, is related to $^nJ_{AB}$ by:

$$^nK_{AB} = \frac{4\pi^2}{h\gamma_A\gamma_B}{}^aJ_{AB}$$

The relativistic correction factors taken from ref. 27 lead to the relativistically corrected coupling constants ($^nK^{RC}_{AB}$):

$$^nK^{RC}_{PbTe} = {}^nK_{PbTe}\left(\frac{1}{3.079}\right)\left(\frac{1}{1.459}\right)$$

$$^nK^{RC}_{SnTe} = {}^nK_{SnTe}\left(\frac{1}{1.426}\right)\left(\frac{1}{1.459}\right)$$

$$^nK^{RC}_{SnSe} = {}^nK_{SnSe}\left(\frac{1}{1.426}\right)\left(\frac{1}{1.155}\right)$$

The values for the relativistically corrected coupling constants are given in Table 2, together with a number of values for Sn—Te and Sn—Se which will be discussed later.

The point of note is that the relativistically corrected reduced coupling constants for $Ph_3SnTePh$ and $Ph_3PbTePh$ indicate very similar s-electron densities in the Pb—Te and Sn—Te bonds

in these compounds, although this, of course, was not immediately obvious from the $^1J_{AB}$ values. This again bears out the similarity in the bonding to tellurium reflected in the similar ^{125}Te nmr chemical shifts and the similar ^{125}Te Mössbauer parameters. In particular, the ^{125}Te Mössbauer isomer shifts which monitor the *s*-electron densities at the tellurium nucleus are very similar in both cases.

^{119}Sn Mössbauer and nmr data

There is already a substantial body of ^{119}Sn nmr data in the literature for the compounds investigated and these data, together with those measured in the present work, are given in Table 2. The ^{119}Sn Mössbauer data in Table 3 were primarily obtained in the present investigation.

The Mössbauer parameters of the compounds $(Ph_3Sn)_2E$, Ph_3SnEPh, and $(Me_3Sn)_2E$, where E = S, Se, or Te, show a simple trend with the changing electronegativity of the chalcogen. An increase in the electronegativity of E results in an increased removal of tin electron density along the Sn—E bond in those tetrahedral molecules (5), an increase in the *p*-orbital imbalance about the tin, and hence in Δ, and a small net decrease in *s*-electron density at the nucleus.

The ^{119}Sn nmr chemical shifts within each series become more positive with decreasing size and increasing electronegativity of the chalcogen, corresponding to a decreased shielding of the tin nucleus. As can be seen from Table 3 there again appears to be a rough correlation between the ^{119}Sn nmr and Mössbauer parameters, the nmr shift becoming more positive as the quadrupole splitting increases in magnitude. For example, in the series $(Me_3Sn)_2E$, E = S, Se, Te, the ^{119}Sn quadrupole splittings decrease from 1.68 to 1.49 (±0.03) mm s^{-1} while the nmr chemical shifts decrease from 94 to −63 ppm and a similar trend holds for the series $(Ph_3Sn)_2E$ and Ph_3SnEPh. However, in $(Me_3Sn)_2E$ or Me_3SnEPh the Mössbauer quadrupole splittings of the Me_3SnEPh compounds are significantly greater than would have been expected on the basis of their solution nmr chemical shifts. It would appear that the coordination about tin is not tetrahedral in Me_3SnEPh in the solid state and that this results in much larger quadropole splittings than those observed for Ph_3SnEPh.

In the five-membered rings $(Me_2Sn)_3E_2$ only one tin site is observed in the Mössbauer spectra while two are clearly resolved in the nmr spectra. This reflects the different inherent resolutions of the two techniques.

For the two- and six-membered ring cyclic compounds, the tin quadrupole splittings are comparable to those of the $Me_2Sn(EPh)_2$ analogues. The $^1J(^{125}Te–^{119}Sn)$ values are also comparable for the tellurium compounds ranging from 3095 ($(Me_2SnTe)_3$) to 3164 Hz (t-$Bu_2Sn(TePh)_2$). In the four-membered rings (t-$Bu_2SnE)_2$, the ^{119}Sn quadrupole splittings are greater than those observed in the five- and six-membered rings, while the $^1J(^{119}Sn–^{125}Te)$ coupling constant in (t-$Bu_2SnTe)_2$ is significantly smaller (2117 Hz) than that in $(Me_2SnTe)_3$ or $(Me_2Sn)_3Te_2$, as noted above. Similar trends are also observed in the corresponding selenides.

As noted above, it is also possible to compare coupling constants between different nuclei in similar or differing structural types if relativistically corrected reduced coupling constants are calculated. In Table 2 the $^1K^{RC}$ values for Sn–Te and Sn—Se bonds in pairs of isostructural selenium and tellurium compounds are given. It can be seen that there are only small differences in the Sn—Te and Sn—Se bond *s* characters in these different compounds and that these differences remain reasonably constant from one compound to another, although the Sn—Te *s* character is somewhat less in the four-, five-, and six-membered rings in comparison with $Ph_3SnTePh$.

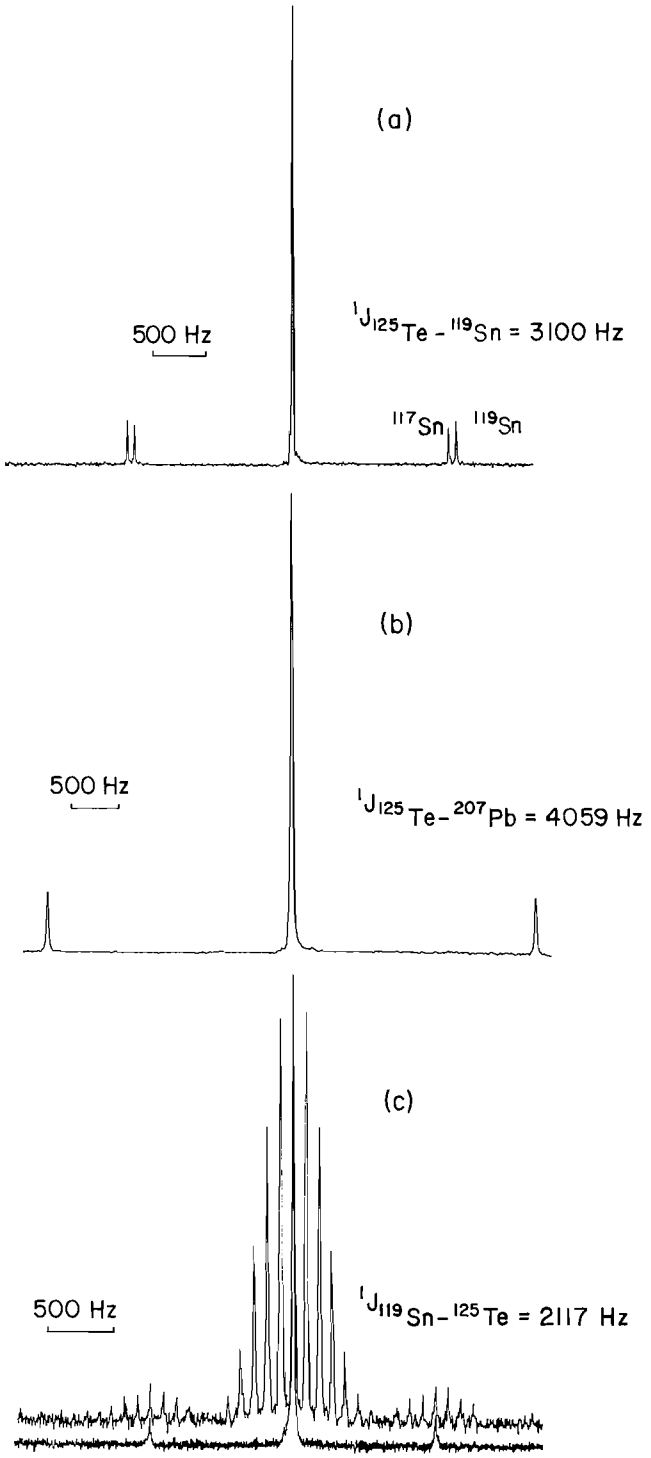

FIG. 2. Sample nmr spectra illustrating the couplings observed in the ^{125}Te spectra of (*a*) $(Me_2SnTe)_3$ and (*b*) $Ph_3PbTePh$, and in the ^{119}Sn spectrum of (*c*) (t-$Bu_2SnTe)_2$. In the latter the proton-coupled and -decoupled spectra are shown. The relative chemical shifts are not illustrated in this figure.

The $^1K^{RC}_{SnSe}$ value is always somewhat smaller than the $^1K^{RC}_{SnTe}$ value in a pair of isostructural compounds corresponding to somewhat less *s* character in the Sn—Se bonds than in the Sn—Te bonds. It is interesting that in all cases the ^{119}Sn Mössbauer isomer shift in the selenide is somewhat smaller than

TABLE 3. Tin-119 data

	^{119}Sn Mössbauer*			^{119}Sn nmr		
	δ ±0.03 (mm s^{-1})	Δ ±0.03 (mm s^{-1})	Γ av.	δ† (ppm)	J‡ (Hz)	Ref.§
$(Me_3Sn)_2S$	1.26	1.68	0.93	+93.9		C
				+86.5 (CH_2Cl_2)		10
				+84.9 (neat)		
$(Me_3Sn)_2Se$	1.29	1.59	1.02	+50.7		C
				+44.5 (neat)		10
$(Me_3Sn)_2Te$	1.32	1.49	1.07	−62.7	2753	C
				−66.8 (CH_2Cl_2)		10
				−62.8 ($CDCl_3$)		
					1385	25
$(Ph_3Sn)_2S$	(1.20)	(1.46)	0.94	−48.7 (neat)		10
$(Ph_3Sn)_2Se$	1.32	1.40	0.98	−75.5	$^1J(^{119}Sn-^{77}Se)$ = 1226	C
$(Ph_3Sn)_2Te$	1.33	1.23	1.01	−143.2	3228	C
Ph_3SnSPh	1.39	1.49	1.04	−65.2 (CH_2Cl_2)		10
				−62.1		
$Ph_3SnSePh$	1.37	1.43	1.02	−79.2	$^1J(^{119}Sn-^{77}Se)$ = 1174	C
$Ph_3SnTePh$	1.40	1.31	0.95	−125.0	3242	C
Me_3SnSPh	1.40	2.10	1.10	+91.3 (CH_2Cl_2)		10
				+90.5 (neat)		
$Me_3SnSePh$				+65.0	$^1J(^{119}Sn-^{77}Se)$ = 968	C
$Me_3SnTePh$	1.39	1.98	1.13	−29.6		C
$(Me_2SnS)_3$	1.34	1.88	0.95	+129 CH_2Cl_2		10
				+128 benzene		
				+131		19
$(Me_2SnSe)_3$	1.40	1.82	0.98	+42 benzene	$^1J(^{119}Sn-^{77}Se)$ = 1228	19
$(Me_2SnTe)_3$	1.46	1.64	1.14	−197.3	3095	
					3098	19
$(Me_2Sn)_3S_2$	1.65	1.95	1.19	+44 (*a*)		19
				+176 (*b*)		
$(Me_2Sn)_3Se_2$				+21 (*a*)	$^1J(^{119}Sn-^{77}Se)$	
				+82 (*b*)	= 992(*a*)	19
					= 1263(*b*)	

in the corresponding telluride indicating a smaller *s* electron at the tin nucleus in the selenide than in the telluride.

A comparison of the tellurium and tin data in the tellurides

Finally it is of interest to bring together some of the above points and to compare and contrast trends in the ^{119}Sn and ^{125}Te data within a related series of compounds.

	$(Me_3Sn)_2Te$ (1)	$(Ph_3Sn)_2Te$ (2)	$Me_3SnTePh$ (3)	$Ph_3SnTePh$ (4)
$^{119}\Delta$ (mm s^{-1})	1.49	1.23	1.98	1.31
$^{125}\Delta$ (mm s^{-1})	6.3	6.6	9.5	9.1
$^{119}\delta$ nmr (ppm)	−62.7	−143.2	−29.6	−125.0
$^{125}\delta$ nmr (ppm)	−1225.9	−1310.0	−186.9	−205.8
^1J(Te–Sn) (Hz)	2753	3225	2614	3245

For compounds **1** and **2** the ^{119}Sn Mössbauer quadrupole splittings show a small but significant difference, and the ^{119}Sn nmr chemical shifts an appreciable difference, when the Me_3Sn— group is replaced by the Ph_3Sn— group. On the other hand, the ^{125}Te quadrupole splittings and nmr chemical shifts show very little change at all. The change in the electronic environment about the tin is not transmitted through the tin–tellurium bond to any great extent.

Compounds **3** and **4** show similar trends although, as noted above, the environment about tin does not appear to be tetrahedral in the solid state.

In compounds **2** and **4** it can be seen that changing one Ph_3Sn— ligand on the tellurium for a phenyl ligand has a dramatic effect on the ^{125}Te quadrupole splitting and nmr chemical shift. However, it does not have a very significant effect on the ^{119}Sn parameters of the second Ph_3Sn— ligand, nor does it greatly affect the $^1J(^{119}Sn-^{125}Te)$ coupling constant. Thus, changes in the electronic environment about the tellurium are not reflected at the tin. It is also apparent that the $^1J(^{119}Sn-^{125}Te)$ coupling constants appear to be dominated by the coordination about the tin rather than about tellurium.

TABLE 3. (*concluded*)

	^{119}Sn Mössbauer*			^{119}Sn nmr		
	δ ±0.03 (mm s^{-1})	Δ ±0.03 (mm s^{-1})	Γ av.	δ† (ppm)	J‡ (Hz)	Ref.§
$(Me_2Sn)_3Te_2$	1.50	1.72	1.23	−38.4(*a*) −166.0(*b*)	2602(*a*)** 3156(*b*) $^1J(^{119}Sn-^{119}Sn)$ = 2784	C
				−38 (*a*) −164 (*b*)	2554 or 2643(*a*) 3159(*b*) $^1J(^{119}Sn-^{119}Sn)$ = 2554 or 2643	19
$(t\text{-}Bu_2SnS)_2$	1.69	2.09	0.95	+126.0		C
$(t\text{-}Bu_2SnSe)_2$	1.65	1.93	0.98	+54.6	$^1J(^{119}Sn-^{77}Se)$ = 915	C
$(t\text{-}Bu_2SnTe)_2$	1.83	1.87	1.15	−121.0	2117	C
$Me_2Sn(SPh)_2$	1.43	1.93	1.12	+123.5		C
				+125.6 (CH_2Cl_2) +122.5 (neat)		10
$Me_2Sn(SePh)_2$	1.38	1.80	1.01	+53.2	$^1J(^{119}Sn-^{77}Se)$ = 1225	C
				+54.1		10
$Me_2Sn(TePh)_2$	1.49	1.52	1.01	−154.4	3147	C
$t\text{-}Bu_2Sn(TePh)_2$				+16.4	3164	C

*δ Mössbauer isomer shift relative to $BaSnO_3$, source and absorber at 77 K, Γ av. is the average linewidth.

†δ nmr chemical shift relative to Me_4Sn.

‡Except where noted these are $^1J(^{119}Sn-^{125}Te)$ values. For $Me_3SnTePh$ and $(Me_3Sn)_2Te$ the signal-to-noise ratio at the tellurium side bands was poor and values for $^1J(^{125}Te-^{119}Sn)$ are quoted in Table 1. Similarly a value for $^1J(^{125}Te-^{77}Se)$ for $(Me_3Sn)_2Se$ was not obtained.

§C denotes this work and the measurements were made in $CDCl_3$ solution. Other referenced work is as shown.

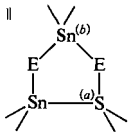

**$^1J(^{119}Sn-^{125}Te)$ and $^{119}Sn-^{119}Sn$ couplings were assigned noting that the $^1J(^{125}Te-^{119}Se)$ value obtained from the ^{125}Te spectrum was 2630 Hz.

For the cyclic compounds, on going from **5** to **7** it can be seen that

	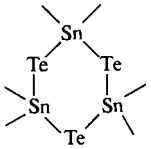 **5**	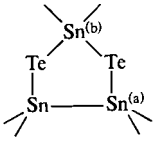 **6**	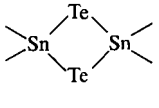 7
$^{119}\Delta$ (mm s^{-1})	1.64	1.72	1.87
$^{125}\Delta$ (mm s^{-1})	1.64	6.23	1.87
$^{119}\delta$ nmr (ppm)	−197.3	−38.4(a)	−121.0
$^{125}\delta$ nmr (ppm)	−860	−1082	−1099
^1J(Sn–Te) (Hz)	3100	2630(a) 3170(b)	2117

$^{119}\Delta$ becomes larger, the $^{119}\delta$ nmr chemical shifts become more positive, and the coupling constants markedly decrease.

However, neither the ^{125}Te quadrupole splittings nor the $^{125}\delta$ values show as significant a change. The constraints imposed within the four-membered ring in compound **7** appear to be greater for the four-coordinate tin than the two-coordinate tellurium.

Experimental

The syntheses were carried out under dry oxygen-free nitrogen and solvents were freshly distilled and flushed with nitrogen. The desired compounds were purified by either vacuum distillation or recrystallization. The preparations generally followed those reported in the literature.

Bis-*tert*-butyl telluride was prepared by reacting $TeCl_4$ with *t*-BuMgCl in THF and the ditelluride, $t\text{-}Bu_2Te_2$ was obtained by treating *t*-BuMgCl with tellurium metal in the presence of hexamethylphosphorustriamide (HMPTA) (4). The compounds $(Me_3X)_2E$, where X = Si, Ge, E = Te; and X = Sn, E = S, Se, and Te, were synthesized by the reaction of Li_2E with Me_3XCl in THF (28), while as an adaptation of this method, LiTePh in THF was reacted with Me_3SnCl, Me_2SnCl_2, and $t\text{-}Bu_2SnCl_2$ to give $Me_3SnTePh$, $Me_2Se(TePh)_2$, and $t\text{-}Bu_2Sn(TePh)_2$, respectively.

The compounds Ph_3XTePh (X = Ge, Sn, and Pb) were prepared by

TABLE 4. $^2J^{119}Sn-^1H$ coupling constants for methyltin chalcogenides

	$^2J^{119}Sn-^1H$ (Hz)	
$(Me_3Sn)_2S$	57.1	
$(Me_3Sn)_2Se$	56.1	
$(Me_3Sn)_2Te$	55.3	
Me_3SnSPh	56.0	
$Me_3SnSePh$	55.5	
$Me_3SnTePh$	55.3	
$Me_2Sn(SPh)_2$	59.8	
$Me_2Sn(SePh)_2$	57.0	
$Me_2Sn(TePh)_2$	55.0	
$(Me_2SnS)_3$	62.0	
$(Me_2SnSe)_3$	60.0	
$(Me_2SnTe)_3$	57.0	
$(Me_2Sn)_3S_2$*	63.1(*a*)	51.9(*b*)
$(Me_2Sn)_3Se_2$	60.5(*a*)	50.9(*b*)
$(Me_2Sn)_3Te_2$*	55.0(*a*)	48.0(*b*)

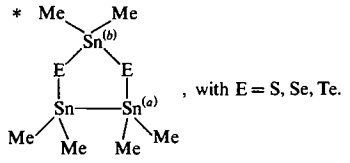

the addition of Ph_3XCl to NaTePh in an ethanol benzene solution (29). The selenide and telluride $(Ph_3Sn)_2Se$ and $(Ph_3Sn)_2Te$ were obtained by reacting NaHSe NaHTe with Ph_3SnCl in the presence of NaOH (5).

The reaction of Me_2SnCl_2 with Na_2S, NaHSe, and NaHTe produced $(Me_2SnS)_3$, $(Me_2SnSe)_3$, and $(Me_2SnTe)_3$ respectively, whereas ether solutions of Me_2SnH_2 containing small amounts of DMF reacted with S and Te to form $(Me_2Sn)_3S_2$ and $(Me_2Sn)_3Te_2$, respectively (30). The reaction of Li_2E, E = S, Se, or Te, with t-Bu_2SnCl_2 gave the dimers $(t\text{-}Bu_2SnE)_2$ (14).

Mössbauer spectra (256 channels) were recorded at 4.2 (tellurium) and 77 K (tin) using a standard constant acceleration drive and using the general methods previously described (1–3). For ^{125}Te a 5 mCi $^{125}Sb/Cu$ (1 Ci = 37 GBq) source was used and for ^{119}Sn, a 1 mCi $Ba^{119}mSnO_3$ source, these being provided by New England Nuclear. The spectra were computer fitted to independent Lorentzians and the ^{125}Te spectra gave linewidths (full width at half maximum, FWHM) of 5.2–6.5 mm s^{-1} and the ^{119}Sn spectra 0.9–1.1 mm s^{-1}. The ψ-squared values divided by the number of degrees of freedom lay in the range of 0.95–1.10.

The nmr spectra were measured on a Bruker WM 400 nmr spectrometer at 126.24 (^{125}Te) and 149.1 MHz (^{119}Sn) at ambient temperature, the general methods used having been previously described (4). The ^{125}Te chemical shifts are referenced with respect to neat Me_2Te and the ^{119}Sn chemical shifts to Me_4Sn. Positive chemical shifts are downfield from the reference standard. The linewidths (FWHM) were of the order of 5–10 (^{125}Te) and 1–2 Hz (^{119}Sn).

Acknowledgements

The authors wish to gratefully acknowledge a grant in support of this research from the Natural Sciences and Engineering Research Council of Canada. We also wish to thank one of the referees for pointing out the importance of correcting the nmr coupling constants to arrive at $^1K^{RC}$ values.

1. C. H. W. JONES, W. R. MCWHINNIE, and F. J. BERRY. Mössbauer effect methodology. *Edited by* J. J. Gruverman and C. W. Seidel. Plenum, New York. 1976. p. 227.
2. C. H. W. JONES, R. SCHULTZ, W. R. MCWHINNIE, and N. S. DANCE. Can. J. Chem. **54**, 3234 (1976).
3. N. S. DANCE and C. H. W. JONES. Can. J. Chem. **56**, 1746 (1978).
4. C. H. W. JONES and R. D. SHARMA. J. Organomet. Chem. **255**, 61 (1983).
5. F. W. B. EINSTEIN, C. H. W. JONES, T. JONES, and R. D. SHARMA. Can. J. Chem. In press.
6. D. H. O'BRIEN, N. DEREU, R. A. GRIGSBY, K. J. IRGOLIC, and F. F. KNAPP, JR. Organometallics, **1**, 513 (1982).
7. D. H. O'BRIEN, N. DEREU, C.-K. HUANG, K. J. IRGOLIC, and F. F. KNAPP, JR. Organometallics, **2**, 305 (1983).
8. W. W. DU MONT and H.-J. KROTH. Z. Naturforsch. B, Anorg. Chem. Org. Chem. **36B**, 332 (1981).
9. H. C. E. MCFARLANE and W. MCFARLANE. J. Chem. Soc. Dalton Trans. 2416 (1973).
10. P. J. SMITH and A. TUPCIAUSKAS. Annu. Rep. NMR Spectrosc. **8**, 291 (1978).
11. N. N. GREENWOOD and T. C. GIBB. *In* Mössbauer spectroscopy. Chapman and Hall Ltd., London. 1971. p. 379.
12. R. V. PARISH. Progr. Inorg. Chem. **15**, 101 (1972).
13. A. BLECHER and M. DRAGER. Angew Chem. Int. Ed. Engl. **18**, 677 (1979).
14. H. PUFF, R. GATTERMAYER, R. HUNDT, and R. ZIMMER. Angew. Chem. Int. Ed. Engl. **16**, 547 (1977).
15. C. A. RODGER, N. SHEPPARD, H. C. E. MCFARLANE, and W. MCFARLANE. *In* NMR and the periodic table. *Edited by* R. K. Harris and B. E. Mann. Academic Press, New York. 1978. p. 402.
16. C. J. JAMESON and H. S. GUTOWSKY. J. Chem. Phys. **40**, 1714 (1964).
17. M. KARPLUS and T. P. DAS. J. Chem. Phys. **34**, 1683 (1961).
18. Y. MASUDA. J. Phys. Soc. Jpn. **11**, 670 (1956).
19. E. L. MEUTERTIES and W. D. PHILLIPS. Adv. Inorg. Chem. Radiochem. **4**, 231 (1962).
20. K. J. JOHNSON, J. P. HUNT, and H. W. DODGEN. J. Chem. Phys. **51**, 4493 (1969).
21. Y. SAITO. Can. J. Chem. **43**, 2530 (1965).
22. B. LINDMAN and S. FORSEN. *In* NMR: basic principles and progress. *Edited by* P. Diehl, E. Fluck, and R. Kosfeld. Springer Verlag, New York, N.Y. 1976. p. 69.
23. R. K. CHADHA and J. M. MILLER. J. Chem. Soc. Dalton Trans. 117 (1982).
24. B. A. MATHIASCH and T. N. MITCHELL. J. Organomet. Chem. **184**, 175 (1980).
25. J. D. KENNEDY and W. MCFARLANE. J. Organomet. Chem. **94**, 7 (1975).
26. R. C. BURNS, L. A. DEVEREUX, P. GRANGER, and G. J. SCHROBILGEN. Inorg. Chem. **24**, 2615 (1985).
27. P. PYYKKÖ and L. WIESENFELD. Mol. Phys. **43**, 557 (1983).
28. M. R. DETTY and M. D. SEIDLER. J. Org. Chem. **47**, 1356 (1982).
29. H. J. GYSLING. Coord. Chem. Rev. **42**, 133 (1982).
30. B. MATHIASCH. Z. Anorg. Allg. Chem. **432**, 269 (1977).

A tellurium-125 Mössbauer study of bis(trifluoromethyl)- and bis(pentafluorophenyl)-tellurides and their dihalides

C. H. W. JONES[1] AND R. D. SHARMA

Department of Chemistry, Simon Fraser University, Burnaby, B.C., Canada V5A 1S6

AND

D. NAUMANN

Lehrbereich Anorganische Chemie der Universität, Dortmund, West Germany

Received August 30, 1985

C. H. W. JONES, R. D. SHARMA, and D. NAUMANN. Can. J. Chem. **64**, 987 (1986).

The ^{125}Te Mössbauer spectra for $(CF_3)_2Te$ and $(C_6F_5)_2Te$ have been recorded and exhibit significantly larger quadrupole splittings (14.02 and 13.40 mm s^{-1} respectively) than those of Me_2Te (10.5 mm s^{-1}) and Ph_2Te (11.0 mm s^{-1}). The dihalides $(CF_3)_2TeX_2$ and $(C6_6F_5)_2TeX_2$ (X = F, Cl,Br) have consistently smaller quadrupole splittings than the dihalides Me_2Tex_2 and Ph_2TeX_2. These observations are consistent with the greater electronegativity of the CF_3 and C_6F_5 ligands. The ^{125}Te nmr chemical shifts of $(C_6F_5)Te$ and its dihalides show a consistent trend to more positive values (increased deshielding) as the electronegativity of the ligands attached to tellurium increases ($(C_6F_5)Te$, 297.6 ppm; $(C_6F_5)_2TeF_2$, 1060 ppm). However, for $(CF_3)_2Te$ and its dihalides a more complex pattern is observed which may be explained by changes in the mean electronic excitation term in the Ramsey paramagnetic shielding term.

C. H. W. JONES, R. D. SHARMA et D. NAUMANN. Can. J. Chem. **64**, 987 (1986).

On a enregistré les spectres Mössbauer du ^{125}Te des composés $(CF_3)_2Te$ et $(C_6F_5)_2Te$. Ces spectres comportent des couplages quadrupolaires nettement plus élevés (respectivement de 14,01 et de 13,40 mm s^{-1}) que ceux observés pour le Me_2Te et le Ph_2Te (10,5 et 11,0 mm s^{-1} respectivement). Les couplages quadrupolaires des dihalogénures $(CF_3)_2TeX_2$ et $(C6_6F_5)_2TeX_2$ dans lesquels X = F, Cl ou Br) sont toujours plus faibles que ceux des dihalogénures Me_2TeX_2 et Ph_2TeX_2. Ces observations reflètent la plus grande électronégativité des ligands CF_3 et C_6F_5. Les déplacements chimiques, en rmn ^{125}Te, du $(C_6F_5)Te$ et de son dihalogénure rélèvent une tendance marquée vers des valeurs plus positives (augmentation du déblindage) lorsque l'électronégativité des ligands attachés au tellure augmente ($(C_6F_5)_2Te$ 297,6 ppm, $(C_6F_5)_2TeF_2$ 1060 ppm)). Cependant, dans la cas du $(CF_3)_2Te$ et de son dihalogénure, on observe un spectre plus complexe qui peut être expliqué par des changements dans le terme d'excitation électronique moyen du terme de blindage parmagnétique de Ramsey.

[Traduit par la revue]

Introduction

In earlier papers (1–4), we have reported the ^{125}Te Mössbauer parameters of a wide range of organotellurium compounds. Of particular interest for the present discussion were the dialkyl- and diaryl-tellurides, R_2Te, and their dihalide derivatives, R_2TeX_2.

It was found that, for the tellurides R_2Te, varying the alkyl ligand from Me to *tert*-Bu, for example, or the aryl ligand from phenyl to *p*-MeOPh or *p*-EtOPh, did not have any very significant effect on the ^{125}Te Mössbauer parameters, the quadrupole splittings, Δ, lying in the range 10.5–11.0 ±0.1 mm s^{-1}, and the isomer shifts, δ, in the range 0.10–0.30 ±0.08 mm s^{-1}. Similarly, incorporation of the tellerium into a heterocyclic ring, as in dibenzotellurophene, also had little effect on the observed Δ and δ values.

The dihalides R_2TeX_2 showed a systematic trend in the quadrupole splittings with a change in the halogen, the difluorides having the largest Δ values and the diiodides the smallest, while the isomer shifts showed very little dependence on the halogen. On changing the organic ligand R for different substituted phenyl groups, relatively little effect was observed on the quadrupole splittings for a given dihalide, except for the bis(2,2′-biphenyl)tellurides where there was some evidence for steric crowding about the tellurium.

In light of the above, it was of some interest to measure the Mössbauer parameters for dialkyl- and diaryl-tellurides, and their dihalides for compounds containing a significantly more electronegative organic ligand. We report here the ^{125}Te Mössbauer data for the bis(trifluoromethyl)- and bis(pentafluorophenyl-tellurides and their difluorides, dichlorides, and dibromides. The bis(trifluoromethyl) compounds have been synthesized previously (5,6). However, the syntheses of the dihalides of bis(pentafluorophenyl)telluride are reported here for the first time.

The ^{125}Te nmr chemical shifts of the $(CF_3)_2Te$ and $(CF_3)_2TeX_2$ (X F, Cl, or Br) have been reported by Gombler (7). We have measured the ^{125}Te nmr spectra of $(C_6F_5)_2Te$ and $(C_6F_5)_2TeX_2$ (X = F, Cl, or Br) and the data for the two series are compared.

Results and discussion

Mössbauer data

The ^{125}Te Mössbauer parameters are shown in Table 1 and a sample spectrum in Fig. 1. It is immediately apparent that $(CF_3)_2Te$ and $(C_6F_5)_2Te$ have significantly larger quadrupole splittings than those of Me_2Te (10.5 mm s^{-1}) and Ph_2Te (11.0 mm s^{-1}). The large quadrupole splittings arise from a considerable *p*-orbital imbalance on the tellurium, reflecting the difference between the Te—C bonds on the one hand and the two tellerium lone pairs on the other. The very electronegative CF_3 and C_6F_5 ligands result in a substantial increase in the *p*-orbital imbalance at tellerium in comparison with that in Me_2Te or Ph_2Te.

The Mössbauer isomer shifts for $(CF_3)_2Te$ and $(C_6F_5)_2Te$, with respect to the I/Cu as a reference standard, are similar to those of Me_2Te (0.06 mm s^{-1}) and Ph_2Te (0.12 mm s^{-1}). The range of isomer shifts for ^{125}Te is known to be relatively small and the similarity in the δ values is not unexpected. Moreover,

[1]Author to whom correspondence should be addressed.

TABLE 1. Tellurium-125 Mössbauer data

	$\delta^{*\dagger}$ (mm s^{-1})	$\Delta^{\dagger}$ (mm s^{-1})	$\Gamma^{\dagger}$ (mm s^{-1})
$(CF_3)_2Te$	−0.14	14.02	6.50
$(CF_3)_2TeF_2$	+0.59	7.36	6.21
$(CF_3)_2TeCl_2$	+0.58	6.89	5.64
$(CF_3)_2TeBr_2$	+0.64	5.60	6.30
$(C_6F_5)Te$	+0.14	13.40	5.94
$(C_6F_5)TeF_2$	+0.45	8.78	5.54
$(C_6F_5)TeCl_2$	+0.59	6.91	5.98
$(C_6F_5)_2TeBr_2$	+0.59	5.38	5.32

*Relative to I/Cu, source and absorbers at 4.2 K.
†Errors ±0.08 mm s^{-1}.

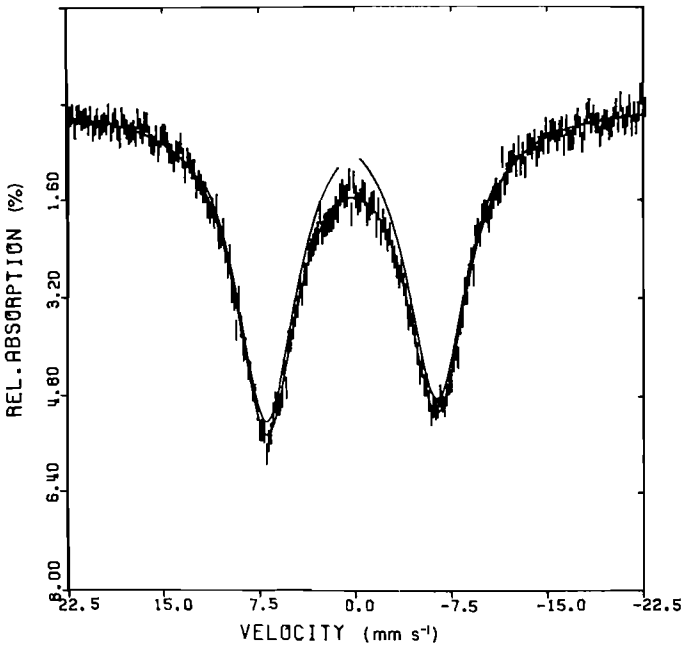

FIG. 1. Tellurium-125 Mössbauer spectrum of $(CF_3)_2Te$ at 4.2 K.

the Te—C bonds will have significant *s*–*p* hybrid character. The removal of *p*-electron density from tellurium in bonding will lead to an increase in the nuclear *s*-electron density, $|\psi_s(0)|^2$, through deshielding and hence to a more positive isomer shift, while the removal of *s*-electron density will decrease $|\psi_s(0)|^2$ and will make δ more negative. These off-setting factors appear to result in the similarity in the δ values observed.

The dihalides of $(CF_3)_2Te$ and $(C_6F_5)_2Te$ exhibit quadrupole splittings which are systematically smaller than those generally observed for dialkyl- and diaryl-tellurium dihalides. Thus, $(C_6F_5)_2TeF_2$ has a Δ value of only 8.8 mm s^{-1}, in comparison with 10.4 mm s^{-1} for Ph_2TeF_2; data for Me_2TeF_2 are not available. Similarly, $(C_6F_5)_2TeCl_2$ (6.9 mm s^{-1}) and $(CF_3)_2TeCl_2$ (6.9 mm s^{-1}) have significantly smaller splittings than those of Ph_2TeCl_2 (9.2 mm s^{-1}) and Me_2TeCl_2 (9.4 mm s^{-1}) while $(C_6F_5)_2TeBr_2$ (5.4 mm s^{-1}) and $(CF_3)_2TeBr_2$ (5.6 mm s^{-1}) have smaller splittings than Ph_2TeBr_2 (7.9 mm s^{-1}) and Me_2TeBr_2 (8.5 mm s^{-1}), respectively. Within each series of dihalides the quadrupole splittings follow a simple trend: F>Cl>Br.

The isomer shifts of the dihalides are all very similar and are more positive than those of the parent tellurides.

These trends in the Mössbauer parameters can be readily understood in terms of a simple valence–bond model for these compounds. The diphenyltellurium dihalides have crystal structures which show the tellurium to be in ψ-tbp environment, with the halogens occupying *trans*-axial positions and with the organic ligands and the presumed lone pair in the equatorial plane (8,9). The quadrupole splittings then reflect the *p*-orbital imbalance between the X—Te—X axial linkage and the Te—C bonds, and the lone pair in the equatorial plane. As the electronegativity of the organic ligand increases, this *p*-orbital imbalance might be expected to decrease, in agreement with the trend observed. Thus, $(C_6F_5)_2TeF_2$ has a significantly smaller quadrupole splitting than Ph_2TeF_2, consistent with a greater removal of electron density from the tellurium in the equatorial plane by the C_6F_5 ligand. A similar argument would apply to the chlorides and bromides. It is also of interest that consistent with this simple model, the difference in Δ between pairs of compounds in the CF_3 and Me series are all somewhat larger than those in the C_6F_5 and Ph series. Thus, the difference in Δ between $(CF_3)_2Te$ and Me_2Te is roughly reflected in the large difference in Δ between $(CF_3)_2TeBr_2$ and Me_2TeBr_2, while the smaller difference in Δ between $(C_6F_5)_2Te$ and Ph_2Te leads to a smaller difference in quadrupole splitting between $(C_6F_5)_2TeBr_2$ and Ph_2TeBr_2.

The isomer shifts for the dihalides reported in Table 1 are all more positive than those of the parent tellurides. This is consistent with the previous general observations on the R_2TeX_2 compounds. The bonding in the X—Te—X linkage appears to remove predominantly *p*-electron density from the tellurium, leading to a deshielding of the 5*s* electrons from the nucleus, an increase in $|\psi_s(0)|^2$, and a more positive isomer shift. The fact that isomer shifts are all similar again reflects the relative insensitivity of ^{125}Te isomer shifts to changes in the *s*- and *p*-orbital populations.

Nuclear magnetic resonance data

The ^{125}Te nmr chemical shifts are reported in Table 2 and the values for $(CF_3)_2Te$ and $(CF_3)_2TeX_2$ (X = Cl, Br) are in reasonable agreement with the literature values (7). To assist in an intercomparison of the data, we recorded the spectrum of $(CF_3)_2Te$ as a neat liquid and in solution in $CDCl_3$ and in CH_3CN. The ^{125}Te chemical shifts for $(C_6F_5)_2Te$ and $(C_6F_5)_2TeX_2$ (X = F, Cl, or Br) have not previously been measured.

The data for $(CF_3)_2Te$ and $(C_6F_5)_2Te$ and their dihalides are compared with those of Me_2Te and Ph_2Te and their dihalides in Fig. 2. It can be seen that $(CF_3)_2Te$ has a much more positive (downfield) shift than Me_2Te. The nmr chemical shifts for tellurium are generally assumed to be dominated by the paramagnetic shielding term. The increase in shift for $(CF_3)_2Te$, relative to Me_2Te, is consistent with a marked decrease in the shielding at the tellurium nucleus as a result of the greater electronegativity of the —CF_3 ligand. However, $(C_6F_5)_2Te$ has a less positive chemical shift than Ph_2Te, indicating that electronegativity is not the only factor involved.

It is of interest that in the dialkyltellurides and ditellurides, substitution of α-carbon protons by methyl groups leads to a more positive (downfield) shift, β-carbon proton substitution leads to a smaller negative (upfield) change in δ, and γ-substitution to a very small positive change in δ (4,10,11). An analogous situation is found in the phenyltellurides. As shown in Table 3, as the number of protons on the carbon atom bonded to tellurium decreases (*a*) δ becomes more positive; on *o*-substitution

TABLE 2. Tellurium-125 nmr chemical shifts

	δ* (ppm)	Solvent	Ref.
$(CF_3)_2Te$	1363.4	$CDCl_3$	
	1355.2	CH_3CN	
	1362.1	neat	
	1368	neat	7
$(CF_3)_2TeF_2$	1187	CH_3CN	7
$(CF_3)_2TeCl_2$	1118	CH_3CN	
	1114	CH_3CN	7
$(CF_3)_2TeBr_2$	1186	CH_3CN	
	1180	CH_3CN	7
$(C_6F_5)_2Te$	297.6	$CDCl_3$	
	278.9	CH_3CN	
$(C_6F_5)_2TeF_2$	1060.3	$CDCl_3$	
$(C_6F_5)_2TeCl_2$	656.5	$CDCl_3$	
$(C_6F_5)_2TeBr_2$	629.1	$CDCl_3$	

*Chemical shifts with respect to Me_2Te (neat) at ambient temperature. The shifts from ref. 7 are with respect to Me_2Te/C_6D_6.

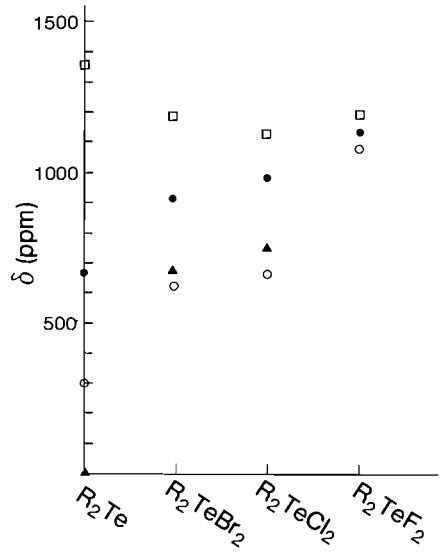

FIG. 2. A plot of ^{125}Te chemical shifts for (▲) R = Me (ref. 13); (●) R = Ph (ref. 16), the value for Ph_2TeF_2 is this work; (□) R = CF_3, this work; (○) R = C_6F_5, this work.

TABLE 3. Tellurium-125 nmr chemical shifts

	δ (ppm)	Δ(δ)*	Ref.
(*a*) MeTeMe	0		
PhTeMe	330	330	12
PhTePh	688	358	13—†
(*b*) PhTePh	688		
o-MeOPhTePh	579	−109	—†
o-MeOPhTePhOMe-*o*	445	−134	—†
(*c*) PhTeMe	330	+11	12
m-MeOPhTeMe	341		—†
(*d*) PhTePh	688	−20	
p-MeOPhTePh	668		14

*Δ(δ) is the difference in successive ^{125}Te nmr chemical shifts.
†D. H. O'Brien. Private communication.

(*b*) there is a smaller negative change in δ; on *m*-substitution (*c*) the effect on δ is small and positive; and finally, on *p*-substitution (*d*) a small, negative change in δ is observed.

On the basis of the above, $(CF_3)_2Te$ would be expected to have a much more positive δ than Me_2Te since there are no α protons in $(CF_3)_2Te$.

In $(C_6F_5)_2Te$, all the above effects will be superimposed. However, the full *o*-substitution for four fluorine ligands should have the dominant effect and a substantial negative change in δ, with respect to Ph_2Te, would be expected and is indeed observed.

The chemical shifts for the C_6F_5, Ph, and Me series appear to roughly parallel one another (Fig. 2), although data for Me_2TeF_2 is not available. The halides all exhibit more positive chemical shifts than the parent tellurides, consistent with less shielding at the tellurium nucleus in the presence of the electronegative halogens. The chemical shifts for these dihalides lie in the order F>Cl>Br.

The trend for the CF_3 series is more complex and, not only does $(CF_3)_2Te$ have a very large positive shift, but the values for the dihalides do not follow the trend referred to above. Rather, they exhibit a minimum value at $(CF_3)_2TeCl_2$. This may be rationalized in terms of the Ramsey paramagnetic shielding in the expression for nmr chemical shifts.

$$\sigma_p\alpha - \frac{1}{\Delta E}[\langle r^{-3}_p\rangle Pu + \langle r^{-3}_d\rangle Du]$$

where ΔE is the mean electronic excitation, *Pu* and *Du* are the "unbalance" in the valence *p* and *d* orbital populations, and $\langle r^{-3}_p\rangle$ and $\langle r^{-3}_d\rangle$ are the expectation values of the radii of the *p* and *d* valence orbitals.

Nuclear quadrupole coupling constants are also dependent on the valence *p* and *d* orbital populations and hence we might anticipate some correlation between the nmr chemical shifts and the Mössbauer quadrupole splittings for molecules of similar coordination. For $(C_6F_5)_2Te$ and $(CF_3)_2Te$ the quadrupole splittings are similar, suggesting similar valence orbital populations on the tellurium in these two molecules. However, the nmr chemical shifts are significantly different. This can be explained by a much smaller value for ΔE in $(CF_3)_2Te$ than in $(C_6F_5)_2Te$.

It is interesting that the difluorides all have very similar chemical shifts despite the differences in the shifts of the parent tellurides themselves (Fig. 2). In the difluorides, the shielding at the tellurium nucleus appears to be primarily determined by the fluorine ligands rather than the organic ligands.

Experimental

Bis(trifluoromethyl)telluride and the dihalides $(CF_3)_2TeX_2$ (X = F, Cl, or Br) were prepared and characterized as previously described (5,6).

Bis(pentafluorophenyl)telluride was prepared by heating an equimolar mixture of $(C_6F_5)_2Hg$ and tellurium in a sealed, evacuated tube at 225°C for 24 h (16). The corresponding dichlorides and dibromides were prepared by reaction of $(C_6F_5)_2Te$ with the elemental halogen in CCl_4. The difluoride was synthesized by reacting an excess of NaF with $(C_6F_5)_2TeCl_2$ in acetonitrile. In a second preparation, $(C_6F_5)_2Te$ was heated with a mixture of HNO_3 and 40% HF in a Teflon beaker for 12 h. The solution was then heated to dryness and $(C_6F_5)_2TeF_2$ was isolated by $CHCl_3$ extraction of the solid. Attempts to prepare the diiodide, either by halogenation of $(C_6F_5)_2Te$ or by reaction of KI with $(C_6F_5)_2TeCl_2$, were unsuccessful. Diphenyltellurium difluoride, whose ^{125}Te nmr chemical shift had not previously been reported, was prepared by the method of Sadekov (17).

The compounds were characterized by carbon analyis and by mass

spectrometry on a Hewlett–Packard 598B mass spectrometer: *Anal.* calcd. for $C_{12}F_{10}Te$: 31.16; found: C 31.17; m/e (^{130}Te) 464; *Anal.* calcd. for $C_{12}F_{12}Te$: 28.80; found: C 28.63; m/e 502; *Anal.* calcd. for $C_{12}F_{10}Cl_2Te$: 27.01, found: C 27.29; m/e 534; *Anal.* calcd. for $C_{12}F_{10}Br_2Te$: 23.15, found: C 23.19; m/e 543, corresponding to $(C_6F_5)_2TeBr^+$.

Mössbauer spectra were recorded using a Harwell Instruments constant acceleration drive, based on a Harwell 200 series wave-form generator and amplifier. A 2 mCi $^{125}Sb/Cu$ source (New England Nuclear) was used. The source and absorbers were immersed in liquid helium in a Harwell Instruments dewar. The 35.5 keV Mössbauer γ-ray was monitored through the 6 keV escape beak in a Xe/CO_2 proportional counter. The spectra were accumulated in a Nuclear Data 66 analyzer as 256-channel spectra and were subsequently computer-fitted to Lorentzians using the Nuclear Data 66 as a computer terminal for transmitting data to, and for computation on, the University IBM 4341 main-frame computer. The spectrometer was routinely calibrated using a $^{57}Co/Rh$ source and an iron foil absorber. The ^{125}Te isomer shifts were reported with respect to $^{125}I/Cu$ as a reference standard and this entailed adding 0.15 mm s^{-1} to the shifts measured against $^{125}Sb/Cu$ as the source.

The ^{125}Te nmr spectra were obtained on a Brüker WM 400 spectrometer at 126.24 MHz, operating at ambient temperature. The resonances were found by utilizing 166 kHz sweep widths, 10 μs (25°C) pulse widths, and a 0.01 s delay between acquisitions. Final spectra were obtained at the appropriate frequency, generally using a 5 kHz sweep width and 90° pulse widths with no delay. No broadband decoupling was employed. Data acquisition consisted of 16 000 data points, which were zero filled to 32 000 data points for the Fourier transform. The linewidths were 6–12 Hz. The ^{125}Te chemical shifts are reported with reference to neat Me_2Te.

Acknowledgment

The author (C.H.W.J.) wishes to acknowledge a grant in support of this research from the Natural Sciences and Engineering Research Council of Canada.

1. C. H. W. Jones, W. R. McWhinnie, and F. J. Berry. Mössbauer effect methodology. *Edited* by I. J. Gruverman and C. W. Seidel. Plenum, New York. 1976. p. 227.
2. F. J. Berry and C. H. W. Jones. Can. J. Chem. **54**, 3737 (1976).
3. N. S. Dance and C. H. W. Jones. Can. J. Chem. **56**, 1746 (1978).
4. C. H. W. Jones and R. D. Sharma. J. Organomet. Chem. **255**, 61 (1983).
5. (*a*) S. Herberg and D. Naumann. Z. Anorg. Allg. Chem. **494**, 159 (1982); (*b*) D. Nauman and S. Herberg. J. Fluorine Chem. **29**, 205 (1982).
6. S. Herberg and P. Naumann. Z. Anorg. Allg. Chem. **492**, 95 (1982).
7. W. Gombler. Z. Naturforsch. B: Anorg. Chem. Org. Chem. **36B**, 535 (1981).
8. G. Y. Chao and J. D. McCullough. Acta. Crystallogr. **15**, 887 (1962).
9. F. J. Berry and A. J. Edwards. J. Chem. Soc. Dalton Trans. 2306 (1980).
10. D. H. O'Brien, N. Dereu, C.-K. Huang, and K. J. Irgolic. Organometallics, **2**, 305 (1983).
11. D. H. O'Brien, N. Dereu, R. A. Grigsby, K. J. Irgolic, and F. F. Knapp. Organometallics, **1**, 513 (1982).
12. G. A. Kalabin, R. B. Valeev, and D. F. Kushnarev. Zh. Org. Khim. **17**, 947 (1981).
13. H. C. E. McFarlane and W. McFarlane. J. Chem. Soc. Dalton Trans. 2416 (1973).
14. R. K. Chadha and J. M. Miller. Can. J. Chem. **60**, 2256 (1982).
15. W. McFarlane, F. J. Berry, and B. C. Smith. J. Organomet. Chem. **113**, 139 (1976).
16. S. C. Cohen, M. L. N. Reddy, and A. G. Massey. J. Organomet. Chem. **11**, 563 (1968).
17. I. D. Sadekov, A. V. Bushov, V. L. Pavlova, V. S. Yur'eva, and V. I. Minkiv. Zh. Obshch. Khim. **47**, 1305 (1977).

The synthesis and seven-coordinate structure of $(CH_3)_2AsC(CF_3{=}C(CF_3)As(CH_3)_2W(CO)Br_2[P(OCH_3)_3]_2$

LYNN MIHICHUK,[1] MONICA PIZZEY, BEVERLY ROBERTSON, AND RICHARD BARTON

Faculty of Science, University of Regina, Regina, Sask. Canada S4S 0A2

Received December 8, 1985

LYNN MIHICHUK, MONICA PIZZEY, BEVERLY ROBERTSON, and RICHARD BARTON. Can. J. Chem. **64**, 991 (1986).

$(L{-}L)W(CO)_4$ (L–L = $(CH_3AsC(CF_3){=}C(CF_3)As(CH_3)_2$) is oxidized by Br_2 to yield the seven-coordinate complex $(L{-}L)W(CO)_3Br_2$, which reacts with monodentate phosphines or phosphites to form $(L{-}L)W(CO)Br_2P_2$ (P = phosphine or phosphite). Crystals of $(L{-}L)W(CO)Br_2[P(OCH_3)_3]_2$ are monoclinic, space group $P2_1/c$, a = 19.110(5), b = 9.208(3), c = 17.845(6) Å, β = 108.93(2)° at 21°C with Z = 4. The structure was solved from a Patterson map and refined by least squares to a conventional R value of 0.092 using 2330 independent reflections. The crystal structure indicated the tungsten atom to be seven-coordinate with the geometry most closely approximated by a capped trigonal prismatic environment, the capping group being a bromine atom (W—Br, 2.686(5) Å). The capped face consists of the remaining bromine atom (W—Br, 2.695(5) Å), a phosphorus atom (W—P, 2.465(9) Å), and the two arsenic atoms from the bidentate ligand (W—As, 2.619(3) and 2.526(4) Å). The W—As bond *trans* to a phosphite is significantly longer (by 0.093 Å) than the W—As bond *trans* to a bromine. The ^1H nmr data indicate that the complex is stereochemically rigid at 25°C and nonrigid at higher temperatures; however, the data at 25°C are not consistent with the configuration found in the crystal.

LYNN MIHICHUK, MONICA PIZZEY, BEVERLY ROBERTSON et RICHARD BARTON. Can. J. Chem. **64**, 991 (1986).

L'oxydation du $(L{-}L)W(CO)_4$ (L–L = $(CH_3AsC(CF_3){=}C(CF_3)As(CH_3)_2$) par le Br_2 donne le complexe heptacoordonné $(L{-}L)W(CO)_2Br_2$ qui réagit avec les phosphines ou les phosphites monodentates pour donner le $(L{-}L)W(CO)Br_2P_2$ (P = phosphine ou phosphite). Les cristaux de $(L{-}L)W(CO)Br_2[P(OCH_3)_3]_2$ appartiennent au groupe d'espace monoclinique $P2_1/c$ avec a = 19,110(5), b = 9,208(3), c = 17,845(6) Å, β = 108,93(2)° à 21°C et Z = 4. On a résolu la structure à partir d'une carte de Patterson et on l'a affinée par la méthode des moindres carrés jusqu'à une valeur de R = 0,092 pour 2330 réflexions indépendantes. La structure cristalline indique que l'atome de tungstène est heptacoordonné avec une géométrie approximative très voisine d'un environnement prismatique trigonal cappé par un atome de brome (W—Br, 2,686(5) Å. La face cappée comprend l'atome de brome résiduel (W—Br, 2,695(5) Å), un atome de phosphore (W—P, 2,465(9) Å) et les deux atomes d'arsenic du ligand bidentate (W—As, 2,619(3) et 2,526(4) Å). La liaison W—As qui est en position *trans* par rapport au phosphite est nettement plus longue (0,093 Å de plus) que la liaison W—As en position *trans* par rapport au brome. Les donnés de la rmn du ^1H indiquent que, à 25°C, le complexe est stéréochimiquement rigide, mais que ce n'est pas le cas à des températures plus élevées. Cependant, les données obtenues à 25°C ne concordent pas avec la configuration trouvée dans le cristal.

[Traduit par la revue]

Introduction

Studies of seven-coordinate complexes of metal carbonyls have shown that they can be described by either a capped octahedral geometry (1, 2) or a capped trigonal prismatic geometry (3, 4). The actual structures seldom match ideal polyhedral arrangements and, if the deviations are large, the choice of the most appropriate description may not be obvious. Various methods have been proposed to aid in the assignment of the best reference polyhedron (5–7).

This paper reports on the assignment of the polyhedron for the seven-coordinate complex $(L{-}L)W(CO)Br_2[P(OCH_3)_3]_2$ where L–L is the fluorocarbon-bridged ligand $(CH_3)_2AsC(CF_3{=}C(CF_3)As(CH_3)_2$. Variable temperature ^1H nmr studies have shown the complex to be stereochemically nonrigid, a common phenomenon observed in seven coordination (8). In an attempt to elucidate the mechanism of the motion of the ligands, which is generally poorly understood in seven coordination, we have undertaken to determine the solid-state geometry of the tungsten monocarbonyl complex.

Experimental

$C_{15}H_{30}As_2Br_2F_6O_7P_2W$ Mol. wt. = 991.88

Monoclinic, space group $P2_1/c$, a = 19.110(5), b = 9.208(3), c = 17.845(6) Å, β = 108.93(2)°, T = 21°C, V = 2970 Å^3, Z = 4, D_x = 2.22 g cm^{-3}, D_m = 2.20(5) g cm^{-3}, μ(MoKα) = 95.0 cm^{-1}, F(000) = 1880.

Initially, attempts were made to prepare the molybdenum analog of the compound reported here. Crystals were obtained but they proved to be extremely unstable in the X-ray beam. Their deterioration in the beam was not significantly attenuated by lowering their temperatures. Furthermore, a complex phase transformation occurs slightly below room temperature in the Mo compound.

The tungsten compound was prepared according to a method similar to that previously reported by Cullen and Mihichuk (9). The synthesis of the ligand *cis*-2,3-bis(dimethylarsino)-1,1,1,4,4,4-hexafluorobut-2-ene (L–L), and the $(L{-}L)W(CO)_4$ complex has been previously reported (10, 11).

Slow addition of bromine (0.070 g, 0.45 mmol) in dichloromethane to a rigorously degassed dichloromethane solution of an equimolar amount of $(L{-}L)W(CO)_4$ afforded orange-coloured crystals of $(L{-}L)W(CO)_3Br_2$ (0.25 g, 69%).

$(L{-}L)W(CO)_3Br_2$ (0.25 g, 0.31 mmol) and trimethyl phosphite (0.091 g, 0.73 mmol) were refluxed under argon in degassed benzene (25 mL) for 48 h, after which time the ir spectrum of the solution indicated complete reaction of the tricarbonyl complex. The benzene was removed under reduced pressure and recrystallization of the residue from a degassed dichloromethane–hexane mixture at −5°C afforded yellow plates of $(L{-}L)W(CO)Br_2[P(OCH_3)_3]_2$ (0.15 g, 48%). Their density was determined by flotation in a chloroform–bromoform mixture.

Preliminary investigation of the tungsten compound also showed evidence of crystal deterioration in the X-ray beam. The deterioration was not significantly influenced by lowering the temperature of the crystal, by coating it with collodion, or by isolating it in a capillary. It was decided that all diffraction data should be collected as quickly as was reasonably possible. A crystal in the form of a yellow plate of dimensions 0.2 × 0.2 × 0.3 mm was chosen for study. Laue symmetry and systematic absences (l = 2n + 1 for $h0\,l$, k = 2n + 1 for $0k0$) indicated the monoclinic space group $P2_1/c$.

[1]Author to whom correspondence may be addressed.

Intensity data were collected on a modified Picker FACS-1 diffractometer with graphite-monochromated Mo$K\alpha$ radiation ($\lambda = 0.71069$ Å), using the NRCC diffractometer control system (12). Diffraction intensities were measured first in the range $3° \leq 2\theta \leq 40°$ and then in the range $40° < 2\theta \leq 45°$, using a scan speed of 2 deg min^{-1} and a scan width of $(0.9 + 0.692 \tan \theta)°$. Data were collected in the octants with hkl and $\bar{h}kl$.

Three standard reflections were measured after every 47 reflections. Over the total period of the data collection their intensities decreased 15%, 25%, and 50%, respectively. It was decided that the data collected last was not reliable and only that collected between 3 and 40° was used in the structure determination. The standard deviations of the intensities ($\sigma(I)$) were calculated from the counting statistics of the individual reflections with a term added based on the extent to which the scatter in the intensities of the standard reflections exceeded that predicted from their own counting statistics. The inclusion of the third standard (12,0,0) with its high decay rate in this calculation led to unrealistically large standard deviations for strong reflections. The rate of fall-off of intensity did not appear to be anisotropic and the behaviour of the 12,0,0 reflection was anomalous. It was decided to exclude that reflection from all calculations. The intensities of the 2776 individual reflections in the range $3° \leq 2\theta \leq 40°$ were corrected for the fall-off in the intensities of two remaining standard reflections. The decrease in the intensity of each reflection, relative to its initial value, was calculated from a five-point interpolation of the curve of the sum of the intensities of the two remaining standards (0,6,0 and 0,0,12) and adjusted to the initial value of the sums of these standards. The maximum correction was 17%. Of these, 2330 showed $I > 2.0\sigma(I)$ and were treated as observed.

At the end of the data collection, attempts were made to measure the centered position of strong reflections with $2\theta > 30°$. However, the crystal had deteriorated to an extent that this was not possible. The remaining material was recrystallized but the crystals that were obtained were not the same as that for which data had been collected. New crystals were synthesized from the starting materials. They showed the same space group and approximate lattice constants as the original. Cell dimensions were calculated from all of the centered settings of 31 reflections using one of the new crystals with $30° \leq 2\theta \leq 40°$.

The intensity data from the original crystal was corrected for the effects of absorption using the Gaussian method and the XTAL system of programs (13). Scattering factors were those assigned by XTAL. Dispersion corrections taken from ref. 14 were applied.

The structure was solved by applying the Patterson method to the heavy atoms, with subsequent use of electron density and difference Fourier maps. It was refined by full-matrix least squares applied to the structure amplitudes using anisotropic temperature factors for tungsten, arsenic, bromine, and phosphorus atoms and isotropic temperature factors for the carbon, oxygen, and fluorine atoms. When anisotropic refinement was extended to other atoms, unrealistic values were obtained for the anisotropic temperature factors and the variation in similar bond lengths increased. The hydrogen atoms were not located. The final values of R and wR were 0.092 and 0.118, using σ^{-2} weights. The standard deviation of an observation of unit weight was 1.50, and the maximum value of Δ/σ was 2.4×10^{-4}. The only significant residual electron density consisted of several peaks in the neighbourhood of the W atom, with an electron density of approximately 2.5 e $Å^{-3}$. The atomic coordinates and isotropic or equivalent thermal parameters are given in Table 1. The important bond lengths and angles are given in Table 2.[2] The atomic labelling is given in Fig. 1 and a stereoscopic view of the molecule with thermal ellipsoids represented at 50% probability is shown in Fig. 2. Torsional angles in the five-membered ring of the chelate ligand and their estimated standard deviations are shown in Fig. 3.

[2]Tables of observed and calculated structure factor amplitudes, anisotropic temperature factors, and additional bond lengths and angles may be purchased from the Depository of Unpublished Data, CISTI, National Research Council of Canada, Ottawa, Ont., Canada K1A 0S2.

TABLE 1. Atomic and thermal parameters with estimated standard deviations

Atom	x[a]	y	z	U_{eq}/U_{iso}[b]
W	0.2165 (1)	0.4010 (2)	0.2128 (1)	3.95 (9)
Br(1)	0.2768 (2)	0.1541 (5)	0.1816 (2)	6.0 (2)
Br(2)	0.1676 (2)	0.2369 (5)	0.3106 (2)	6.0 (2)
As(1)	0.3511 (2)	0.4249 (5)	0.3127 (2)	4.8 (2)
As(2)	0.2922 (2)	0.4877 (5)	0.1289 (2)	5.0 (2)
P(1)	0.103 (1)	0.299 (1)	0.118 (1)	5.9 (6)
P(2)	0.200 (1)	0.570 (1)	0.306 (1)	6.1 (7)
F(1)	0.531 (1)	0.262 (3)	0.271 (1)	9.9 (8)
F(2)	0.547 (1)	0.484 (3)	0.306 (1)	9.8 (8)
F(3)	0.513 (1)	0.345 (3)	0.374 (2)	10.9 (9)
F(4)	0.421 (1)	0.513 (3)	0.062 (1)	8.5 (7)
F(5)	0.515 (1)	0.452 (3)	0.156 (1)	10.1 (8)
F(6)	0.438 (1)	0.297 (3)	0.088 (1)	11.1 (9)
O(1)	0.136 (1)	0.667 (3)	0.118 (1)	5.4 (6)
O(2)	0.067 (1)	0.144 (3)	0.125 (1)	7.2 (8)
O(3)	0.113 (1)	0.298 (3)	0.033 (1)	6.1 (7)
O(4)	0.033 (1)	0.392 (3)	0.109 (1)	5.8 (7)
O(5)	0.232 (1)	0.723 (3)	0.293 (1)	6.2 (7)
O(6)	0.120 (1)	0.613 (3)	0.317 (1)	7.3 (8)
O(7)	0.246 (1)	0.539 (3)	0.399 (1)	5.9 (7)
C(1)	0.167 (2)	0.562 (3)	0.158 (2)	3 (1)
C(2)	0.104 (2)	0.008 (5)	0.138 (2)	9 (1)
C(3)	0.055 (2)	0.233 (5)	−0.038 (2)	7 (1)
C(4)	−0.045 (2)	0.352 (4)	0.078 (2)	7 (1)
C(5)	0.237 (3)	0.852 (5)	0.354 (3)	9 (1)
C(6)	0.054 (2)	0.612 (5)	0.254 (3)	9 (1)
C(7)	0.216 (2)	0.511 (5)	0.463 (2)	7 (1)
C(8)	0.423 (2)	0.426 (4)	0.253 (2)	5 (1)
C(9)	0.400 (2)	0.435 (3)	0.177 (2)	3 (1)
C(10)	0.506 (2)	0.387 (5)	0.300 (3)	8 (1)
C(11)	0.444 (2)	0.433 (5)	0.121 (2)	7 (1)
C(12)	0.394 (2)	0.591 (4)	0.377 (2)	6 (1)
C(13)	0.373 (2)	0.281 (5)	0.393 (2)	7 (1)
C(14)	0.264 (2)	0.399 (4)	0.020 (2)	5 (1)
C(15)	0.302 (2)	0.703 (5)	0.115 (2)	8 (1)

[a]The numbers in parentheses refer to the estimated standard deviation in the last significant figure quoted.

[b]Thermal parameters are of the form $\exp[-2\pi^2(U_{11}h^2a^{*2} + U_{22}k^2b^{*2} + U_{33}l^2c^{*2} + 2U_{12}hka^*b^* + 2U_{13}hla^*c^* + 2U_{23}klb^*c)]$ and $U_{eq} = 1/3 \sum_{i=1}^{3}\sum_{j=1}^{3}[U_{ij}a_i^*a_j^*(\mathbf{a}_i.\mathbf{a}_j)]$.

Variable temperature ^1H nmr data were obtained using a Perkin–Elmer R12-B nmr spectrometer equipped with a variable-temperature probe. The variable-temperature controller was calibrated against standards and showed a maximum deviation of ±3 K in the temperature range investigated (233–373 K). Low temperature studies were done using $CDCl_3$ as solvent and high temperature studies using C_6H_6.

Discussion

The tungsten atom is seven-coordinate. Its coordination sphere includes the two arsenic atoms of the L–L ligand, two bromine atoms, two phosphorus atoms, and the carbon atom of the carbonyl group. The relevant seven-vertex polytopal polyhedra are the monocapped octahedron (C_{3v}), the quadrilaterally monocapped trigonal prism (C_{2v}) and the pentagonal prism (C_{5h}). Based on bond repulsion calculations, Kepert has shown that for identical ligands the capped trigonal prism is a transition state between two capped octahedral arrangements, reminiscent of the Berry rearrangement for five coordination (15). However, the barrier height in the seven-coordinate case is negligible, suggesting that facile rearrangement of the ligands is possible.

TABLE 2. Bond distances and angles with estimated standard deviations

(a) Bond	Distance (Å)
W—Br(1)	2.687 (5)
W—Br(2)	2.695 (5)
W—As(1)	2.619 (3)
W—As(2)	2.526 (4)
W—P(1)	2.465 (9)
W—P(2)	2.38 (1)
W—C(1)	1.86 (3)
As(1)—C(8)	2.00 (4)
As(1)—C(12)	1.93 (4)
As(1)—C(13)	1.89 (4)
As(2)—C(9)	2.01 (3)
As(2)—C(14)	2.01 (3)
As(2)—C(15)	2.01 (5)
O(1)—C(1)	1.24 (4)
C(8)—C(9)	1.28 (4)
C(8)—C(10)	1.56 (5)
C(9)—C(11)	1.50 (6)

(b) Bond	Angle (°)
Br(1)—W—Br(2)	85.5 (1)
Br(1)—W—As(1)	79.7 (1)
Br(1)—W—As(2)	77.2 (1)
Br(1)—W—P(1)	82.8 (3)
Br(1)—W—P(2)	149.7 (3)
Br(1)—W—C(1)	138 (1)
Br(2)—W—As(1)	94.4 (1)
Br(2)—W—As(2)	161.3 (1)
Br(2)—W—P(1)	79.5 (3)
Br(2)—W—P(2)	76.0 (3)
Br(2)—W—C(1)	124 (1)
As(1)—W—As(2)	75.7 (1)
As(1)—W—P(1)	161.8 (3)
As(1)—W—P(2)	78.2 (2)
As(1)—W—C(1)	120.7 (9)
As(2)—W—P(1)	105.0 (2)
As(2)—W—P(2)	116.3 (3)
As(2)—W—C(1)	74 (1)
P(1)—W—P(2)	116.2 (3)
P(1)—W—C(1)	76.1 (9)
P(2)—W—C(1)	71 (1)
W—As(1)—C(8)	109.5 (9)
W—As(1)—C(12)	127 (1)
W—As(1)—C(13)	112 (1)
C(8)—As(1)—C(12)	94 (2)
C(8)—As(1)—C(13)	112 (2)
C(12)—As(1)—C(13)	99 (2)
W—As(2)—C(9)	112 (1)
W—As(2)—C(14)	115 (1)
W—As(2)—C(15)	119 (1)
C(9)—As(2)—C(14)	103 (1)
C(9)—As(2)—C(15)	99 (1)
C(14)—As(2)—C(15)	107 (2)
As(1)—C(8)—C(9)	120 (3)
As(1)—C(8)—C(10)	117 (3)
C(9)—C(8)—C(10)	122 (4)
As(2)—C(9)—C(8)	115 (3)
As(2)—C(9)—C(11)	116 (2)
C(8)—C(9)—C(11)	128 (3)
W—C(1)—O(1)	176 (3)

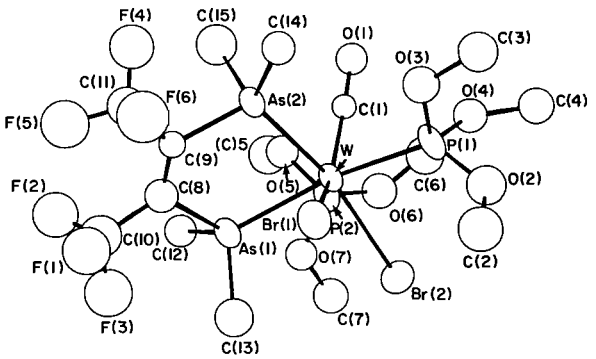

FIG. 1. Atomic labelling for $(CH_3)_2AsC(CF_3)=C(CF_3)As(CH_3)_2$-$W(CO)Br_2[P(OCH_3)_3]_2$

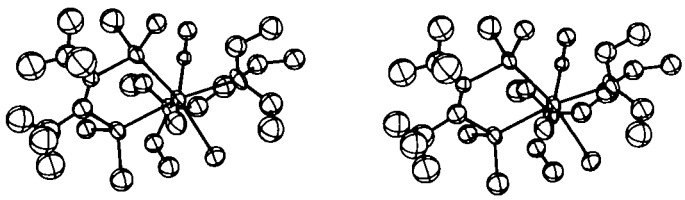

FIG. 2. Stereoscopic view of the molecule.

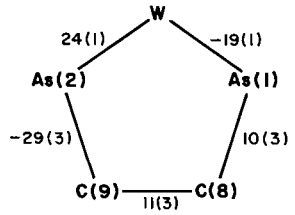

FIG. 3. Schematic diagram showing the torsional angles in the five-membered ring of the chelate ligand.

In order to describe the geometry of the observed polyhedron found here, we used the dihedral angles between the normals of adjacent faces of the polyhedron (δ angles) as suggested by Porai-Koshits and Aslanov (16). The δ angles for seven-coordinate polyhedra have been calculated by Muetterties and Guggenberger (5). It is convenient to focus attention on a subset of the δ angles for analysis of polyhedra. In this case the δ angles for three edges of the face, which is capped in the octahedral arrangement, are the relevant subset. In the capped octahedron their value is 24.2°. In the capped trigonal prism, two become zero as two quadrilateral faces are formed, and the third edge, which is also an edge at the base of the capped quadrilateral face of the trigonal prism, becomes 41.5° (5).

It has been suggested by Kouba and Wreford (17) that a preferable measure of polyhedral type is obtained if the polyhedron created by moving the vertices of the original polyhedron along their radii to the surface of a unit sphere is examined instead of the original polyhedron. One of us (18) has used this procedure for larger polyhedra and found that the use of the unit sphere provides superior discrimination among candidate ideal polyhedra.

The important δ parameters for $(L–L)W(CO)Br_2[P(OCH_3)_3]_2$, based on the unit sphere procedure, are 4°, 8°, and 30°, which are nearer those for the monocapped trigonal prism (0°, 0°, 41.5°) than the monocapped octahedron (24.2°, 24.2°, 24.2°). The capping atom is Br(1). The configuration is nevertheless on a plausible reaction path between a capped trigonal prism and a capped octahedron. If the polyhedron is described as an octa-

hedron, the capping atom is the carbon atom of the carbonyl group.

The structure of the closely related seven-coordinate compound (L–L)W(CO)$_3$I$_2$ has been reported by Mercer and Trotter (2). The configuration is similar but with δ angles (14°, 19°, 12°) that are closer to those of the capped octahedron. Based on an analysis of the edge lengths of the unit spheres, the small difference in configuration appears to be a direct consequence of the different spatial requirements of the two ligands that are carbonyl groups in the previously reported structure and phosphite groups in that reported here. The difference between the bonding radii of iodine and bromine seems less important in determining the small difference in configuration.

The bidentate ligand in both structures has a *bite* on the unit sphere ("normalized *bite*" in the terminology of Kepert (15)) of 1.23. According to the analysis by Kepert (15) of seven-coordinate polyhedra with one bidentate ligand and five unidentate ligands, all with equal metal–ligand bond lengths, such polyhedra may adopt, among others, a particular stereochemistry he labels as "D". In stereochemistry D in the capped trigonal prism, the bidentate ligand bridges an edge of the capped quadrilateral face that joins the trilateral faces of the prism. In the associated capped octahedron, the bidentate ligand joins the capped trilateral face to the trilateral face formed by the remaining three ligands. Keperts survey of seven-coordinate polyhedra suggests that for seven-coordinate polyhedra with a bidentate ligand having a normalized *bite* greater than 1.2, the D configuration is predominant.

The polyhedron in the compound reported here adopts stereochemistry D. Given the large variation in metal–ligand bond lengths in (L–L)W(CO)Br$_2$[P(OCH$_3$)$_3$]$_2$, we must conclude that the presence of the predicted stereochemistry D is either due to factors other than those considered by Kepert, or that the bond lengths are much less important than the normalized *bite* of the bidentate ligand in establishing stereochemistry.

The bidentate ligand forms a five-membered ring with the tungsten atom. The torsional angles for the ring are given in Fig. 3. The nature of the ring puckering was analyzed according to the method of Cremer and Pople (19). The relevant parameters are $q = 0.43$, $\phi = -13.2°$, indicating a highly puckered ring closer to the twist conformation than the envelope conformation. The W atom is above the plane of As(1), As(2), and C(9), and C(8) is below the plane. However, because of short bond lengths to C(8), the appearance of the ring in Fig. 1 is that of an envelope folded across the As–As line.

The parameters describing the ring in (L–L)W(CO)$_3$I$_2$ are essentially the same as in the present study. The fold about the As–As line is caused by the contact between the arsenic methyl groups and the carbonyl and the phosphite ligand containing P(2). The tetrahedral coordination of the arsenic atom is further distorted by these contacts. The reason that C(8) is also puckered out of the plane of the envelope is not clear. The fold may serve to optimize the *bite* of the ligand or it may be related by the packing requirements of the methyl and CF_3 groups.

Significant shortening of the W—As bonds from a predicted value of 2.73 Å (1) to the experimental values of 2.619(3) and 2.526(4) Å is thought to be due to some double-bond character in the W—As bonds caused by $d\pi$–$d\pi$ back donation from the tungsten atom. The two W—As bonds are also significantly different from each other, which can be explained by a consideration of their respective *trans* ligands. The Br(2) atom *trans* to As(2) is not as strong a $d\pi$ acceptor as P(1) *trans* to As(1), which should result in a greater back donation to As(2). This causes a shortening of the W—As(2) bond compared to the W—As(1) bond, the difference being 0.093 Å. Considerable back donation from W to the carbonyl group is evident from a comparison of the W—C(1) bond length of 1.86(3) Å to other carbonyl tungsten complexes. This in turn results in a longer C—O bond length (1, 2, 20). The two W—P bonds are significantly different from each other, which again can be explained on the basis of their respective *trans* ligands. Thus the W—P(2) bond, (P(2) *trans* to Br(1)) is shorter than the W—P(1) bond (P(1) *trans* to As(1)).

The geometry found in the solid state is not consistent with the structure in solution as deduced from ^{1}H nmr data. Two arsenic methyl resonances are observed at room temperature, which remained fairly sharp even at 233 K. However, as the temperature is increased the two resonances broaden, collapse, and coalesce into a single resonance line (coalescence temperature 343 K). The coalesced peak sharpened further in the range 343–373 K. The room temperature spectrum suggests a more symmetrical structure than observed in the solid state. The change in the ^{1}H nmr spectrum at higher temperature is indicative of stereochemical nonrigidity. The mechanism previously proposed for the related molybdenum complex (9), involving the migration of a capping CO group over faces of a more symmetrically capped octahedral polyhedron, is not consistent for the tungsten species in view of the geometry found in the solid state. A similar mechanism, as stated above, would explain the high temperature ^{1}H nmr results assuming the tungsten complex undergoes a rearrangement process to give a more symmetrical ligand arrangement, as stated for the Mo complex (9). Thus the ^{1}H nmr results suggest that there are two exchange processes occurring; a lower energy process which averages two sets of As—CH_3 groups (the spectrum recorded at 233 K is probably not the limiting spectrum) and a higher energy process which averages all four As—CH_3 groups.

If the reaction pathway between the octahedron capped by the carbonyl group and the trigonal prism capped by Br(1) is extended, another octahedron, capped by P(2), is obtained. None of these polyhedra show higher symmetry consistent with the room temperature nmr data, for which a pentagonal prism is required.

The δ angle for the edge P(1)–As(2) is smaller in both observed polyhedra than in the ideal polyhedron. This is consistent with a small distortion toward the geometry of the pentagonal bipyramid, unfortunately not a pentagonal bipyramid with higher symmetry required by the nmr results. A combination of concerted rearrangements of the ligands following pathways such as those discussed by King (21) would be required to generate a polyhedron (or time-averaged combination of polyhedra) with the required higher symmetry.

Acknowledgments

We are grateful to the Natural Sciences and Engineering Research Council of Canada for financial support of this work in the form of operating grants to R.B., L.M., and B.R. Technical assistance from K. Wolbaum, Yaoguang Luo, and Carolyn Giesinger, University of Regina, Regina, Saskatchewan, is gratefully acknowledged. The authors thank the University of Regina for provision of computational facilities.

1. F. A. Cotton, L. R. Falvello, and J. H. Meadows. Inorg. Chem. **24**, 514 (1985).
2. A. Mercer and J. Trotter. Can. J. Chem. **52**, 3331 (1974).
3. A. L. Beauchamp, F. Belanger-Gariepy, and S. Arali. Inorg. Chem. **24**, 1860 (1985).

4. M. G. B. DREW and J. D. WILKINS. J. Chem. Soc. Dalton Trans. 2664 (1973).
5. E. L. MUETTERTIES and L. J. GUGGENBERGER. J. Am. Chem. Soc. **96**, 1748 (1974).
6. M. G. B. DREW. Prog. Inorg. Chem. **23**, 67 (1977).
7. M. G. B. DREW and C. J. RIX. J. Organomet. Chem. **102**, 467 (1975).
8. F. A. VAN-CATLEDGE, S. D. ITTEL, and J. P. JESSON. Organometallics, **4**, 18 (1985), and references therein.
9. W. R. CULLEN and L. M. MIHICHUK. Can. J. Chem. **54**, 2548 (1976).
10. J. P. CROW, W. R. CULLEN, F. G. HERRING, J. R. SAMS, and R. L. TAPPING. Inorg. Chem. **10**, 1616 (1971).
11. W. R. CULLEN and L. M. MIHICHUK. Can. J. Chem. **53**, 3401 (1975).
12. A. C. LARSON and E. J. GABE. Computing in crystallography. *Edited by* H. Shenk, R. Olthof-Hazekamp, H. Van Koningsveld, and G. C. Bassi. Delft University Press. 1978. pp. 81–89.
13. J. M. STEWART, S. R. HALL, R. A. ALDEN, R. OLTHOF-HAZEKAMP, and R. M. DOHERTY. The XTAL system of crystallographic programs: users manual. Computer Science Centre, University of Maryland, College Park, MD. September, 1983.
14. International tables for X-ray crystallography. Vol. 4. Kynoch Press, New York. 1974. pp. 99, 149.
15. D. L. KEPERT. Inorganic chemistry concepts 6. Inorganic stereochemistry. Springer Verlag, New York. 1982.
16. M. A. PORAI-KOSHITS and L. A. ASLANOV. Zh. Strukt. Khim. **13**, 266 (1972).
17. J. H. KOUBA and S. S. WREFORD. Inorg. Chem. **15**, 1463 (1976).
18. B. E. ROBERTSON. Inorg. Chem. **16**, 2735 (1977).
19. D. CREMER and J. A. POPLE. J. Am.Chem. Soc. **97**, 1354 (1975).
20. M. G. B. DREW, A. W. JOHAMS, and A. P. WOLTERS. Chem. Commun. 819 (1971).
21. R. B. KING. Inorg. Chem. **24**, 1716 (1985).

Interactions between cations and sugars. II. Enthalpies, heat capacities, and volumes of aqueous solutions of Ca^{2+}–D-ribose and Ca^{2+}–D-arabinose at 25°C

JEAN-PIERRE MOREL[1], CLAUDE LHERMET, AND NICOLE MOREL-DESROSIERS
Laboratoire d'Étude des Interactions Solutés–Solvants, U.A. au C.N.R.S. n° 434, Université Clermont 2, 63170 Aubière, France

Received November 7, 1985

JEAN-PIERRE MOREL, CLAUDE LHERMET, and NICOLE MOREL-DESROSIERS. Can. J. Chem. **64**, 996 (1986).

The thermodynamic parameters characterizing the interaction between Ca^{2+} and the suitably positioned sequences of hydroxyls of some sugar isomers have been determined. This was done by comparing the properties of D-ribose which bears such sequences of hydroxyls with the properties of D-arabinose chosen as an inactive reference. The enthalpies of solution and of dilution, the apparent molal heat capacities, and the apparent molal volumes of the two pentoses have been first measured in water at 25°C. The measurement of these properties for the transfer of the sugars from water to $CaCl_2$ solutions (and, conversely, for the transfer of $CaCl_2$ from water to the sugar solutions) directly gives access to the Ca^{2+}–hydroxyls pair interaction parameters. The thermodynamic properties of this reaction of association may then be estimated: $\Delta H^\theta \cong -24$ kJ mol^{-1}; $\Delta S^\theta \cong -83$ J K^{-1} mol^{-1}; $\Delta V^\theta \cong 5$ cm^3 mol^{-1}; $\Delta C_p^\theta \cong 40$ J K^{-1} mol^{-1}. The analysis of these data shows that the weak association constant results from a large compensation between the favourable enthalpy and the unfavourable entropy of reaction.

JEAN-PIERRE MOREL, CLAUDE LHERMET et NICOLE MOREL-DESROSIERS. Can. J. Chem. **64**, 996 (1986).

Les paramètres thermodynamiques caractéristiques de l'interaction entre l'ion Ca^{2+} et les séquences d'hydroxyles en position favorable qui existent dans certains isomères des sucres sont déterminés. Pour ceci, on compare les propriétés du D-ribose qui comporte de telles séquences et celles du D-arabinose choisi comme référence non active. Les enthalpies de dissolution et de dilution, les capacités calorifiques molaires apparentes et les volumes molaires apparents sont d'abord déterminés dans l'eau à 25°C. La mesure des mêmes grandeurs relatives au transfert des sucres de l'eau pure aux solutions de $CaCl_2$ (et, inversement, de $CaCl_2$ de l'eau aux solutions de sucre) permet d'accéder aux paramètres correspondants relatifs à l'interaction par paire Ca^{2+}–hydroxyles. On peut alors évaluer les grandeurs thermodynamiques de cette réaction d'association: $\Delta H^\theta \cong -24$ kJ mol^{-1}, $\Delta S^\theta \cong -83$ J K^{-1} mol^{-1}, $\Delta V^\theta \cong 5$ cm^3 mol^{-1}, $\Delta C_p^\theta \cong 40$ J K^{-1} mol^{-1}. Celles-ci sont discutées; on observe en particulier que la constante d'association faible est due à une large compensation entre l'enthalpie favorable et l'entropie défavorable du processus.

Introduction

The study of the thermodynamics of hydration of sugars and sugar derivatives has raised, for a long time, a great deal of interest (1, 2). Amongst the most recent work based on precise thermodynamic determinations, some are concerned with the properties at infinite dilution (3–5), whereas others are interested in the excess properties which reflect the solute–solute interactions (6–8). The interactions between sugars and metal cations in aqueous solution are of great importance in biochemistry and have been closely looked at since Angyal's pioneering studies (9). The primary aim of Angyal's work was to compare the complexing ability of various cations with some sugars through the determination of the stability constants, a subject which was analysed in our previous paper (10).

The study of the interactions between D-arabinose or D-ribose and calcium ion by a very sensitive potentiometric method, which can be applied to solutions dilute in the metal ion, has led us to analyse the characteristics of the free energy of interaction. More precisely, the comparison of these two pentoses gives access to a pair interaction parameter g_{RCa} which is characteristic of the couple Ca^{2-} – axial–equatorial–axial sequence of oxygen atoms of the ribose isomers present at equilibrium. The presence in solution of many sugar anomers is one of the great difficulties of the thermodynamic, hence global, approach to the problem. Yet, it is essential to get this thermodynamic picture of the phenomena since it completes the interpretation which can be elaborated from, for instance, the nmr data. Indeed, the nmr methods (11, 12) allow one to "isolate" the interactions between the cation and the various isomers of the sugar but they can be used only on solutions with high salt concentrations, hence the following drawbacks: importance of the anion effects and of the activity coefficients. The thermodynamic methods we use are, on the contrary, based on extrapolation to infinite dilution and reflect the interaction between the sugar and the metal ion in this particular condition. The parameter g_{RCa}, which is characteristic of the free energy of interaction between calcium and ribose, can be directly related to the association constant β_1 (10) if one prefers to speak in terms of chemical equilibria to describe these weak interactions.

It is interesting now to determine other thermodynamic parameters which will help us to better characterize this interaction. Studies of this kind have already been performed on various solutes involving either nonelectrolyte–nonelectrolyte or electrolyte–nonelectrolyte pairs. Our previous work regarding the interactions between electrolytes and alcohols (13) in aqueous solutions will serve as a basis for the method and the formalism used in the present paper. We shall determine enthalpies of solution, volumes, and heat capacities which give access to the corresponding sugar–electrolyte (SE) pair interaction parameters h_{SE}, v_{SE}, c_{SE}.

Theoretical relations

It is well known that the excess thermodynamic functions can be expressed as virial expansions in concentration. These expansions, which are based on McMillan–Mayer theory, relate the nonideal component of any total thermodynamic function to a series of pair, triplet, and higher order interaction parameters. It is possible to evaluate these parameters through the determination of transfer functions. We shall only give here the relations which are necessary to the understanding of the present work; the details of the theoretical analysis have been given in a previous paper (13) and in the references cited therein. In these expressions, we shall designate the components of the ternary system water–nonelectrolyte–electrolyte

[1]To whom all correspondence should be addressed.

by the following letters: W for water, S for sugar (A: arabinose, R: ribose), and E for electrolyte.

The transfer function X of a nonelectrolyte S at molality m_S from pure water to a solution of electrolyte E at molality m_E is given by

$$[1] \quad \Delta_t X_S = 2\nu x_{SE} m_E + 3\nu^2 x_{SEE} m_E^2 + 3\nu x_{SSE} m_E m_S + \ldots$$

where ν is the number of ions into which E dissociates and x_{SE}, x_{SEE}, x_{SSE} are the pair and triplet interaction parameters. In the same way, the transfer function of the electrolyte at molality m_E from water to the solution of nonelectrolyte at molality m_S is given by

$$[2] \quad \Delta_t X_E = 2\nu x_{SE} m_S + 3\nu x_{SSE} m_S^2 + 3\nu^2 x_{SEE} m_S m_E + \ldots$$

For a standard function ($m_S \rightarrow 0$ in the first case and $m_E \rightarrow 0$ in the second one) the higher order terms in m_S or m_E on the right-hand side of eqs. [1] and [2] vanish. It immediately follows that

$$[3] \quad \left(\frac{\partial \Delta_t X_S^\theta}{\partial m_E}\right)_{m_E=0} = \left(\frac{\partial \Delta_t X_E^\theta}{\partial m_S}\right)_{m_S=0} = 2\nu x_{SE}$$

The pair interaction parameter is then readily measurable for any thermodynamic function from each of the studied transfers. Let us note that for an electrolyte with ν ions, x_{SE} characterizes all the pair interactions between the nonelectrolyte S and the various ions of E. Here, for instance, E$\equiv$$CaCl_2$ and it follows that

$$[4] \quad x_{SE} = \frac{x_{SCa^{2+}} + 2x_{SCl^-}}{3}$$

We have recently studied the case where $X \equiv G$ (10) and have shown that the measurement of the emf of a cell using electrodes which are reversible to Ca^{2+} and Cl^- gives access to the standard free energy of transfer $\Delta_t G_E^\theta$ and, accordingly, to g_{SE}. We shall examine here other functions, namely the enthalpy, the heat capacity, and the volume.

The measurement of the enthalpy of solution of the pure solid sugar $\Delta_{sol}H_S$ in water and in the electrolyte solution at sufficiently low final concentration ($m_S < 0.1$ mol kg^{-1}) gives directly access to the transfer function at infinite dilution. In fact, we observe that the enthalpies of solution do not, considering the uncertainty of the measurements, vary significantly with m_S; they may, thus, be assumed to be standard values. The standard enthalpy of transfer of the sugar from water to the electrolyte solution may be written

$$[5] \quad \Delta_t H_S^\theta(m_E) = \Delta_{sol}H_S(m_E) - \Delta_{sol}H_S = 2\nu h_{SE} m_E + 3\nu^2 h_{SEE} m_E^2 + \ldots$$

There is another method which gives access to the standard enthalpy and we shall use it for the transfer of the electrolyte E from water to the solution of sugar. This method is very useful when it is difficult to handle the pure solute (gas, hygroscopic product) (14). It involves the dilution of a concentrated aqueous solution of electrolyte E in water and in the sugar solutions. In the case studied here, the final concentrations in electrolyte are relatively low and, provided they are identical in water and in the sugar solution we may write

$$[6] \quad \Delta_t H_E^\theta(m_S) = \Delta_{dil}H_E(m_E, m_S) - \Delta_{dil}H_E(m_E) = 2\nu h_{SE} m_S + 3\nu h_{SSE} m_S^2 + \ldots$$

Through the measurement of the density of the solutions we get the apparent molal volume of the solute. Hence, the apparent molal volume of the sugar in water ϕ_{VS} is given by

$$[7] \quad \phi_{VS}(m_S) = M_S\rho^{-1} + 1000(\rho^{-1} - \rho_0^{-1})m_S^{-1}$$

where M_S is the molecular weight of the sugar and ρ and ρ_0 the densities (g cm^{-3}) of the solution of molality m_S and of pure water, respectively. One may also define the apparent molal volume of the sugar S in a solution of electrolyte of molality m_E by using the densities $\rho(m_S, m_E)$ and $\rho(m_E)$ (15). At low m_S concentrations, the transfer function $\phi_{VS}(m_S, m_E) - \phi_{VS}(m_S)$ may be assumed to be a standard value (infinite dilution) and we may write

$$[8] \quad \phi_{VS}(m_S, m_E) - \phi_{VS}(m_S) = 2\nu v_{SE} m_E + 3\nu^2 v_{SEE} m_E^2 + \ldots$$

Similarly, by considering the transfer of the electrolyte from water to the sugar solutions we get

$$[9] \quad \phi_{VE}(m_E, m_S) - \phi_{VE}(m_E) = 2\nu v_{SE} m_S + 3\nu v_{SSE} m_S^2 + \ldots$$

The apparent molal heat capacities at constant pressure are obtained by measuring the specific heats (J K^{-1} g^{-1}) of the solutions, c, and of the solvent, c_0, respectively,

$$[10] \quad \phi_{CS}(m_S) = M_S c + 1000(c - c_0)m_S^{-1}$$

The study of the ternary systems gives access, as outlined above, to the transfer function $\phi_{CS}(m_S, m_E) - \phi_{CS}(m_S)$ which is assumed to be the standard molal heat capacity of transfer if m_S is small enough. Equations similar to [8] and [9] may then be written

$$[11] \quad \phi_{CS}(m_S, m_E) - \phi_{CS}(m_S) = 2\nu c_{SE} m_E + 3\nu^2 c_{SEE} m_E^2 + \ldots$$

$$[12] \quad \phi_{CE}(m_E, m_S) - \phi_{CE}(m_E) = 2\nu c_{SE} m_S + 3\nu c_{SSE} m_S^2 + \ldots$$

Experimental

The two studied pentoses, D-arabinose and D-ribose, (Fluka puriss.) were dried under vacuum (no significant weight loss was observed), stored in a desiccator and used as such. The solutions of $CaCl_2$ (Merck pro analysis) were titrated by EDTA. All solutions were prepared by weight from triply distilled water degassed prior to use.

The enthalpies of solution and of dilution were measured with an LKB 8700 calorimeter by using the classical ampoule breaking technique. The densities were measured with a Sodev flow densimeter with a precision of about $\pm 5 \times 10^{-6}$ g cm^{-3} (16). The heat capacities were measured with a Picker flow microcalorimeter (Setaram) with, in the present case, an uncertainty on $\Delta c = c - c_0$ of the order of 0.5% (17).

All the measurements were carried out at 25.00 ± 0.01°C.

Results

Properties of the aqueous solutions of ribose and arabinose

The enthalpies of solution of both sugars have been measured in water, the final concentration varying from 0.01 to 0.1 mol kg^{-1}. The measurements were repeated six times and shown to be, considering the experimental uncertainty, concentration independent. The mean values may thus be assumed to be the standard values at infinite dilution. It follows that, for ribose,

$$\Delta_{sol}H_R^\theta = 13.60 \pm 0.06 \text{ kJ mol}^{-1}$$

and, for arabinose,

$$\Delta_{sol}H_A^\theta = 14.20 \pm 0.08 \text{ kJ mol}^{-1}$$

TABLE 1. Apparent molal heat capacities and apparent molal volumes of arabinose and ribose in water at 25°C

m (mol kg^{-1})	ϕ_C (J K^{-1} mol^{-1})	m (mol kg^{-1})	ϕ_V (cm^3 mol^{-1})
	Arabinose		
0.05001	282.3	0.01001	93.14
0.05009	282.7	0.02001	93.21
0.07493	282.5	0.04002	93.32
0.09999	283.9	0.06007	93.32
0.2503	283.6	0.07007	93.14
0.4976	285.0	0.08026	93.27
0.6525	285.4	0.09019	93.33
0.8022	286.2	0.10002	93.28
		0.5002	93.47
		0.5003	93.55
		0.9996	93.81
		1.0018	93.80
	Ribose		
0.02500	284.2	0.04004	94.87
0.05010	285.2	0.08006	95.10
0.07515	284.8	0.10006	95.22
0.1001	284.6	0.4968	95.36
0.2511	284.9	0.5022	95.38
0.5005	285.2	0.9965	95.57
0.6497	286.2	1.0035	95.52
0.8008	286.2		

The agreement with the values given in the literature (13.04 and 13.24 kJ mol^{-1}, respectively) (5) is not excellent.

We have reported in Table 1 the apparent molal volumes and heat capacities at various molalities. The variation with concentration is almost linear and the following relations may be proposed for ribose

$$\phi_{CR} = 284._5 + 2m_R \text{ J K}^{-1} \text{ mol}^{-1}$$
$$\phi_{VR} = 95.1 + 0.5m_R \text{ cm}^3 \text{ mol}^{-1}$$

and, for arabinose

$$\phi_{CA} = 282._5 + 4._5m_A \text{ J K}^{-1} \text{ mol}^{-1}$$
$$\phi_{VA} = 93.2 + 0.6m_A \text{ cm}^3 \text{ mol}^{-1}$$

The standard values at infinite dilution can be compared with those given in the literature: our ϕ_{VR}^θ is in good agreement with the value of 95.3 cm$^{3\ -1}$ given by Franks (18), but is slightly less than the value of 95.56 cm^3 mol^{-1} given by Jasra (5), the precision of the latter value being, however, overestimated. For ϕ_{VA}^θ, Jasra gives a value of 94.00 cm^3 mol^{-1} which is rather different from ours; as indicated above, we have also observed a large discrepancy between the enthalpy of solution of arabinose given by this author and our value. As regards the ϕ_{CR}^θ and ϕ_{CA}^θ values, we find two sets of data in the literature: on the one hand, 294 and 318 J K^{-1} mol^{-1} (5) and, on the other hand 271 and 278 J K^{-1} mol^{-1} (3) respectively. Jasra's data were determined from enthalpies of solution measured at 25 and 35°C and, obviously, their precision cannot be compared with that of heat capacities directly measured with the Picker flow microcalorimeter (17). The ϕ_C values given, at 30°C, by Kawaizumi (3) look more scattered as a function of m than ours but his values at infinite dilution, in particular that for arabinose, are in good agreement with those proposed here. Considering the precision of the methods used here and the low scattering of the results shown in Table 1, we believe that the ϕ_C and ϕ_V values we propose may be taken as reference values.

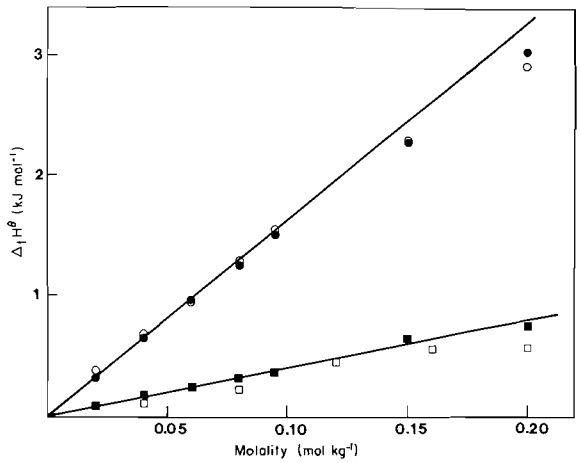

FIG. 1. Standard enthalpies of transfer of ribose (R) or arabinose (A) from water to aqueous solutions of $CaCl_2$ (E) and of transfer of $CaCl_2$ from water to aqueous solutions of ribose or arabinose. ●, $\Delta_t H_R^\theta$ versus m_E; ■, $\Delta_t H_A^\theta$ versus m_E; ○, $\Delta_t H_E^\theta$ versus m_R; □, $\Delta_t H_E^\theta$ versus m_A.

TABLE 2. Parameters characterizing the pair interaction between $CaCl_2$ and ribose or arabinose in water at 25°C

Parameters	Ribose	Arabinose
$2vg_{SE}$[a] (J mol^{-2} kg)	−2 200	−100
$2vh_{SE}$ (J mol^{-2} kg)	−16 500	−4000
$2vs_{SE}$ (J K^{-1} mol^{-2} kg)	−52	−10
$2vc_{SE}$ (J K^{-1} mol^{-2} kg)	350	80
$2vv_{SE}$ (cm^3 mol^{-2} kg)	5.0	2.5

[a]In ref. 10, the g_{SE} values are given in a molality scale which is relative to the aqueous sugar solution; here, the molality scale is relative to water. The difference between g_{RE} and g_{AE} is the same, i.e., −2100.

Transfer functions

Enthalpies

The dilution of a concentrated solution of $CaCl_2$ in water ($0.6948m$) is carried out into ribose and arabinose solutions of molality varying up to 0.2 mol kg^{-1}; the final $CaCl_2$ concentration is of the order of $0.0185m$. The enthalpies of dilution of transfer given by eq. [6] are reported in Fig. 1. Similarly, the dilution of concentrated solutions of ribose and arabinose ($0.6384m$) into $CaCl_2$ solutions of concentration varying up to $0.2m$ leads (by interchanging E for S in eq. [6]) to the transfer functions shown in Fig. 1. The extrapolation at $m = 0$ of the plots $\Delta_t H^\theta/m$ versus m gives (eqs. [5] and [6]) the parameters $2vh_{SE}$ shown in Table 2. The slope of the straight lines of Fig. 1 corresponds to $2vh_{RE}$ for ribose and $2vh_{AE}$ for arabinose; we see that relation [3] is verified.

Some transfer functions have been obtained by the solution method (relation [5]); these values are, although slightly less precise, in good agreement with those obtained by the dilution method.

Volumes

The apparent molal volumes of $CaCl_2$ have been measured at $0.1018m$ salt concentration in ribose and arabinose solutions of molality varying up to 0.8 mol kg^{-1}. Similarly, the apparent molal volumes of the sugars at $0.1000m$ have been measured in $CaCl_2$ solutions of molality varying up to 0.8 mol kg^{-1}. The transfer functions calculated from eqs. [8] and [9] are plotted in Fig. 2. Since the precision of the volumes of transfer is less than that of the enthalpies of transfer, it is necessary to work at higher

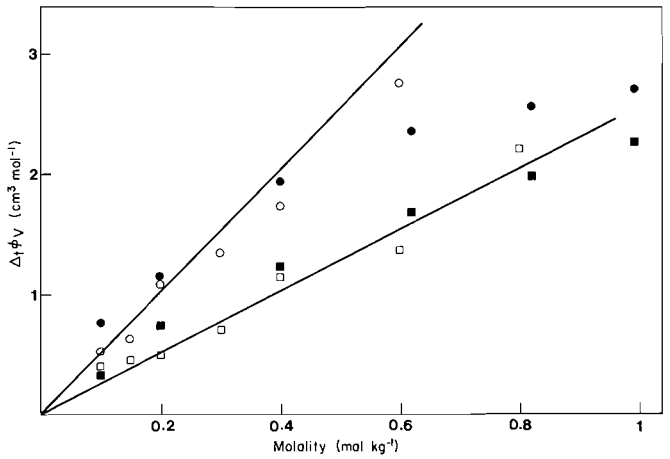

FIG. 2. Standard volumes of transfer of ribose (R) or arabinose (A) from water to aqueous solutions of $CaCl_2$ (E) and of transfer of $CaCl_2$ from water to aqueous solutions of ribose or arabinose. ●, $\Delta_t\phi_{VR}$ versus m_E; ■, $\Delta_t\phi_{VA}$ versus m_E; ○, $\Delta_t\phi_{VE}$ versus m_R; □, $\Delta_t\phi_{VE}$ versus m_A.

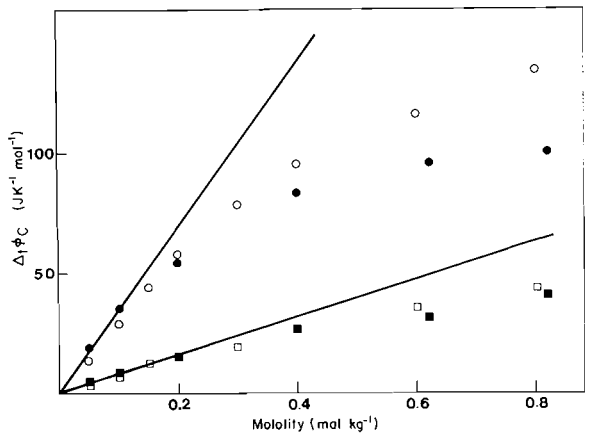

FIG. 3. Standard heat capacities of transfer of ribose (R) or arabinose (A) from water to aqueous solutions of $CaCl_2$ (E) and of transfer of $CaCl_2$ from water to aqueous solutions of ribose or arabinose. ●, $\Delta_t\phi_{CR}$ versus m_E; ■, $\Delta_t\phi_{CA}$ versus m_E; ○, $\Delta_t\phi_{CE}$ versus m_R; □, $\Delta_t\phi_{CE}$ versus m_A.

concentrations to be able to use a treatment similar to the one described above so as to get, after extrapolation at $m = 0$, the parameters $2\nu v_{SE}$ given in Table 2. These parameters of ribose and arabinose are represented by the straight lines of Fig. 2.

Heat capacities

The apparent molal heat capacities have been measured at the same concentrations as the volumes above. The transfer functions given by relations [11] and [12] are shown in Fig. 3. They give access to the pair parameters $2\nu c_{SE}$ which are reported in Table 2. Relation [3], again, is verified: the initial slopes are the same even if, in the case of ribose, both curves diverge rapidly. It thus looks as if the contribution of the triplet terms (relations [11] and [12]) is more important for ribose.

Discussion

In Table 2 are reported all the parameters which characterize the pair interactions between $CaCl_2$ and the two studied sugars, ribose and arabinose. These are mean values relative to both SCa^{2+} and SCl^- pairs, as shown by relation [4]. In our previous work (10), we have assumed that the difference observed between the interactions with each of the two isomeric pentoses was essentially due to some specific interaction between Ca^{2+} ion and the axial–equatorial–axial sequence of hydroxyls of ribose. This is analogous to say that the nonspecific interactions between Ca^{2+}, or Cl^-, and each of the two sugars are identical. We may then write (10)

[13] $2\nu g_{RE} - 2\nu g_{AE} = 2g_{RCa}$

as well as similar relations for the parameters corresponding to the other thermodynamic functions. It is then possible to evaluate by a simple subtraction all the parameters characteristic of the specific interaction between Ca^{2+} and ribose: $2g_{RCa} = -2100$ J mol^{-2} kg; $2h_{RCa} = -12\,500$ J mol^{-2} kg; $2s_{RCa} = -42$ J K^{-1} mol^{-2} kg; $2c_{RCa} = 270$ J K^{-1} mol^{-2} kg; $2v_{RCa} = 2.5$ cm^3 mol^{-2} kg. What do these parameters represent in a more familiar language? The chemical model which involves the following reaction of association (no R_2Ca^{2+} complex has been observed (10)) allows us to define the

[14] Ca^{2+} + 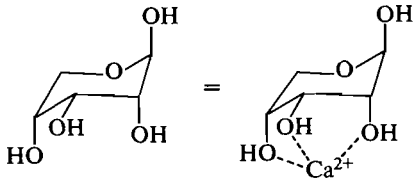 =

corresponding thermodynamic functions. We have shown in our previous work (10) that there is a coherence between the two languages by which we can express and estimate weak interactions. For instance, the association constant relative to reaction [14]

$$[15]\quad \beta = \frac{[RCa^{2+}]}{[Ca^{2+}][R]}$$

is directly related to the parameter g_{RCa} by the following good approximation

[16] $RT\beta = -2g_{RCa}$

It follows that $\beta = 0.85$. The pair interaction parameters x_{SE} defined by relations [1]–[3] correspond to the derivatives of the thermodynamic functions of transfer with respect to the concentration. It can readily be seen that the classical thermodynamic relations which exist between the various functions are also found between the x_{SE} parameters. Hence, we may write

$$\left(\frac{\partial g}{\partial T}\right)_P = -s; \quad \left(\frac{\partial (g/T)}{\partial T}\right)_P = -\frac{h}{T^2}; \quad \left(\frac{\partial g}{\partial P}\right)_T = v$$

and, also,

[17] $s = (h - g)/T$

with which we have calculated the s_{SE} parameters of Table 2. By integrating relation [17] we get the values of the g_{RCa} parameter at some characteristic temperatures and, as a result, the β values. We get, for instance,

[18] $\beta(0°C) = 1.44$; $\beta(25°C) = 0.85$; $\beta(37°C) = 0.63$

Each of the parameters characteristic of the pair interactions between Ca^{2+} and the suitably positioned hydroxyls is related in a simple way to each of the standard thermodynamic functions corresponding to the reaction of association (eq. [14]). Hence, the standard enthalpy of association can be calculated from the β constant by

$$[19]\quad \Delta H^\theta = RT^2\left(\frac{\partial \ln \beta}{\partial T}\right)_P$$

whence, from eq. [16],

[20] $2h_{RCa} = \beta\Delta H^{\theta}$

The meaning of this expression is obvious if we recall that the term $2h_{RCa}m_{Ca}$ corresponds to the enthalpy of transfer of ribose from water to an aqueous solution of Ca^{2+} of molality m_{Ca}; hence, if α which is the extent of association of the sugar is weak, as it is the case in the present conditions, we may write

$$[21]\quad \Delta_t H_R^{\theta}(m_{Ca}) = 2h_{RCa}m_{Ca} = \alpha\Delta H^{\theta} \cong \beta m_{Ca}\Delta H^{\theta}$$

Similarly, we may show that the relations corresponding to the entropy and the volume are given by

[22] $2s_{RCa} = \beta\Delta S^{\theta} - R\beta(\ln\beta - 1)$

[23] $2v_{RCa} = \beta\Delta V^{\theta}$

The interpretation of the heat capacity is, however, more complicated. We have shown (19) that the apparent molal heat capacity of transfer of a species which is involved in an association reaction (such as eq. [14]) contains a term equal to $(\partial\alpha/\partial T)\Delta H^{\theta}$ which corresponds to the equilibrium shift resulting from the temperature rise inherent in the heat capacity measurement. The apparent molal heat capacity of transfer is thus given by

$$[24]\quad \Delta_t\phi_{CR}(m_{Ca}) = 2c_{RCa}m_{Ca} = \alpha\Delta C_p^{\theta} + \left(\frac{\partial\alpha}{\partial T}\right)\Delta H^{\theta}$$

The case for which we have studied these problems into detail (19) is totally comparable to the present one except for the stability constants which were much higher. Relation [24] may thus be written

$$[25]\quad 2c_{RCa} = \beta\left(\Delta C_p^{\theta} + \frac{\Delta H^{\theta 2}}{RT^2}\right)$$

The equilibrium shift term is always positive; here, it is equal to 293 J K^{-1} and constitutes the major part of the $2c_{RCa}$ term. The ΔC_p^{θ} term is then obtained by subtraction. From eqs. [20], [22], [23], and [25] we get

$$\Delta H^{\theta} = -14.7 \text{ kJ mol}^{-1}$$

$$[26]\quad \Delta S^{\theta} = -51 \text{ J K}^{-1} \text{ mol}^{-1}$$

$$\Delta V^{\theta} = 3 \text{ cm}^3 \text{ mol}^{-1}$$

$$\Delta C_p^{\theta} = 24 \text{ J K}^{-1} \text{ mol}^{-1}$$

One must not forget that reaction [14] involves only the ribose isomers which bear a sequence of hydroxyls suitable for association: the β-pyranose 1C4 (~35%), the two α-pyranose conformers (~21%), and the α-furanose (~6%); percentages are given by Angyal at 31°C (9). The mean values given in eq. [26] characterize only the active isomers indicated above which represent about 60% of ribose. Hence, if we make the very crude approximation that all the isomers involved in an association process are characterized by identical thermodynamic functions of reaction, we may then propose the following values: $\Delta H^{\theta} \cong -24$ kJ mol^{-1}; $\Delta S^{\theta} \cong -83$ J K^{-1} mol^{-1}; $\Delta V^{\theta} \cong 5$ cm^3 mol^{-1}; $\Delta C_p^{\theta} \cong 40$ J K^{-1} mol^{-1}. But this is only, let us repeat it, a very crude estimation of the thermodynamic functions characterizing reaction [14]. As far as we know, these are the first values deduced from calorimetric measurements for the complex formation between a cation and a sugar. It is interesting to note that the ΔH^{θ} and ΔS^{θ} values proposed here are in good agreement with those determined by Lenkinski and Reuben (11) (−7 kcal mol^{-1} and −20 eu, respectively) for α-D-ribopyranose from nmr measurements at two temperatures. Even if our values are "mean" values, it is worthwhile underlining the fact that totally different methods lead to results in good agreement.

We thus notice that the enthalpic contribution to the cation–sugar association is favourable, and the weak value of the stability constant results from the very large unfavourable entropic term. Hence, as regards the energetic balance, the replacement of some water molecules in the hydration shell of Ca^{2+} by three hydroxyls of the ribose molecule results in a decrease of the enthalpy. Since the enthalpy of hydration of Ca^{2+} is large and the molecule of sugar has a hydrophilic character, the negative energetic balance for the association process indicates that the cation–sugar complex is itself strongly hydrated through the cation, which is probably largely accessible to the water molecules, and through the three lone pairs of the oxygen atoms of the hydroxyls involved in the complex formation with the cation. This complexation leads to a loss of degrees of freedom which gives a negative contribution to ΔS^{θ}, and to a partial dehydration of Ca^{2+} which gives a positive entropic contribution; the results given here show that the former is largely predominant. The three hydroxyls involved in the complex-formation process totally lose their rotational freedom: the lone pairs of the oxygen atoms cannot anymore be involved in the hydrogen bonds of the various hydration structures of the free sugar.

The positive value for the volume of reaction (~5 cm^3 mol^{-1}) may be logically explained through the classical "electrostriction" phenomena. The ion–solvent interaction gives a negative contribution to the partial molal volume of the cation and the replacement of part of the hydration shell of this cation by the sugar results in a positive ΔV^{θ} value.

The interpretation of the ΔC_p^{θ} of reaction is much more delicate, in particular because the values of the ionic heat capacities are unknown (19). We have shown that, as regards ΔS^{θ}, the negative contribution due to the loss by the sugar of internal and external degrees of freedom was predominant over the positive contribution due to the dehydration of the cation. Since the loss of internal degrees of freedom leads to a negative contribution to ΔC_p (19), it is obviously the balance of complicated hydration phenomena which is responsible for the positive ΔC_p^{θ} value observed here.

Conclusion

We have presented here the thermodynamic methods, in particular the calorimetric ones, which give access to the thermodynamic functions characterizing the reaction of weak association between an ion and a ligand through the determination of the pair interaction parameters.

The ΔH^{θ}, ΔS^{θ}, ΔV^{θ}, and ΔC_p^{θ} values have thus been estimated for the association between the complexing sequence of hydroxyls of the D-ribose molecule and the cation Ca^{2+} in aqueous solution. We have shown that the association constant is weak because of the large compensation between the favourable enthalpic term (~−25 kJ mol^{-1}) and the unfavourable entropic term (~−80 J K^{-1} mol^{-1}).

1. F. Franks and D. S. Reid. *In* Water a comprehensive treatise. Vol. 2. *Edited by* F. Franks. Plenum, New York. 1973. Chapt. 5. p. 323.

2. F. FRANKS. *In* Biochemical thermodynamics. *Edited by* M. N. Jones. Elsevier, New York. 1979. Chapt. 2. p. 15.
3. F. KAWAIZUMI, S. KUSHIDA, and Y. MIYAHARA. Bull. Chem. Soc. Jpn. **54**, 2282 (1981).
4. F. KAWAIZUMI, N. NISHIO, H. NOMURA, and Y. MIYAHARA. J. Chem. Thermodyn. **13**, 89 (1981).
5. R. V. JASRA and J. C. AHLUWALIA. J. Solution Chem. **11**, 325 (1982).
6. G. BARONE, P. CACACE, G. CASTRONUOVO, and V. ELIA. Carbohydr. Res. **91**, 101 (1981).
7. K. MIYAJIMA, M. SAWADA, and M. NAKAGAKI. Bull. Chem. Soc. Jpn. **56**, 1620 (1983).
8. G. BARONE, G. CASTRONUOVO, D. DOUCAS, V. ELIA, and C. A. MATTIA. J. Phys. Chem. **87**, 1931 (1983).
9. S. J. ANGYAL. Aust. J. Chem. **25**, 1957 (1972).
10. J.-P. MOREL and C. LHERMET. Can. J. Chem. **63**, 2639 (1985).
11. R. E. LENKINSKI and J. REUBEN. J. Am. Chem. Soc. **98**, 3089 (1976).
12. M. C. R. SYMONS, J. A. BENBOW, and H. PELMORE. J. Chem. Soc. Faraday Trans. 1, **78**, 3671 (1982).
13. G. PERRON, D. JOLY, J. E. DESNOYERS, L. AVEDIKIAN, and J.-P. MOREL. Can. J. Chem. **56**, 552 (1978).
14. Y. POINTUD, J.-P. MOREL, and J. JUILLARD. J. Phys. Chem. **80**, 2381 (1976).
15. C. DE VISSER, G. PERRON, and J. E. DESNOYERS. J. Am. Chem. Soc. **99**, 5894 (1977).
16. P. PICKER, E. TREMBLAY, and C. JOLICOEUR. J. Solution Chem. **3**, 377 (1974).
17. P. PICKER, P. A. LEDUC, P. R. PHILIP, and J. E. DESNOYERS. J. Chem. Thermodyn. **3**, 631 (1971).
18. F. FRANKS, J. R. RAVENHILL, and D. S. REID. J. Solution Chem. **1**, 3 (1972).
19. N. MOREL-DESROSIERS and J.-P. MOREL. J. Phys. Chem. **89**, 1541 (1985).

Synthesis of (±)-albicanyl acetate and (±)-isodrimenin by the electrophilic cyclization of olefinic allylsilanes

ROSEMARY J. ARMSTRONG, FRANCIS L. HARRIS,[1] AND LARRY WEILER[2]

Department of Chemistry, The University of British Columbia, Vancouver, B.C., Canada V6T 1Y6

Received November 11, 1985

ROSEMARY J. ARMSTRONG, FRANCIS L. HARRIS, and LARRY WEILER. Can. J. Chem. **64**, 1002 (1986).

The allylsilane **3** was synthesized and cyclized with Lewis acids or mercuric trifluoroacetate to give **5** or **6**, which were converted into albicanyl acetate (**7**) and isodrimenin (**12**).

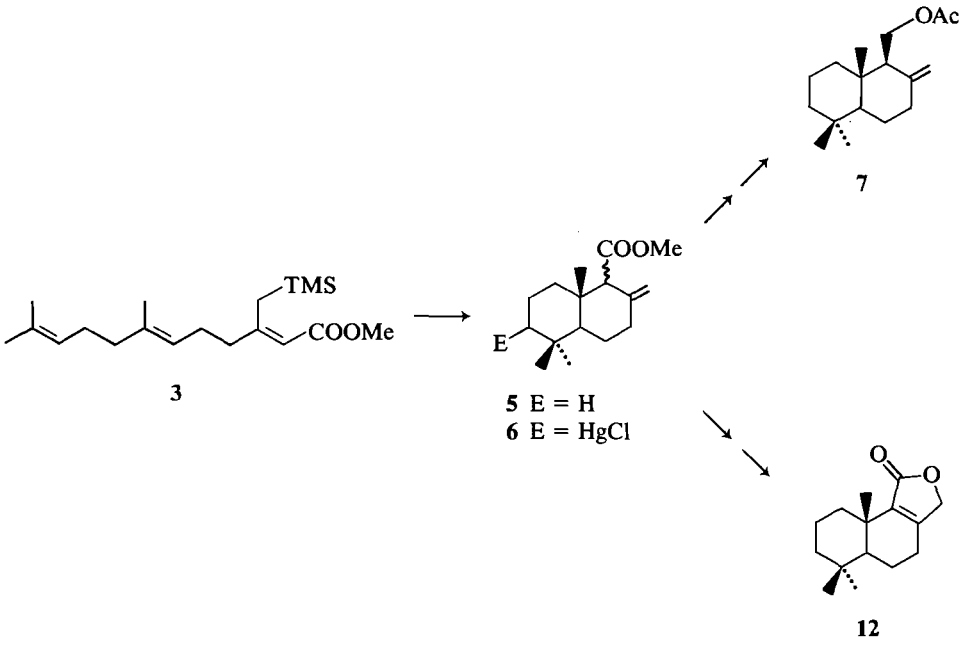

ROSEMARY J. ARMSTRONG, FRANCIS L. HARRIS, et LARRY WEILER. Can. J. Chem. **64**, 1002 (1986).

On a synthétisé l'allylsilane **3** et sa cyclisation, à l'aide d'acides de Lewis ou de trifluoroacétate mercurique, conduit aux composés **5** ou **6** que l'on a transformé en acétate d'abicanyle (**7**) ou en isodriménine (**12**).

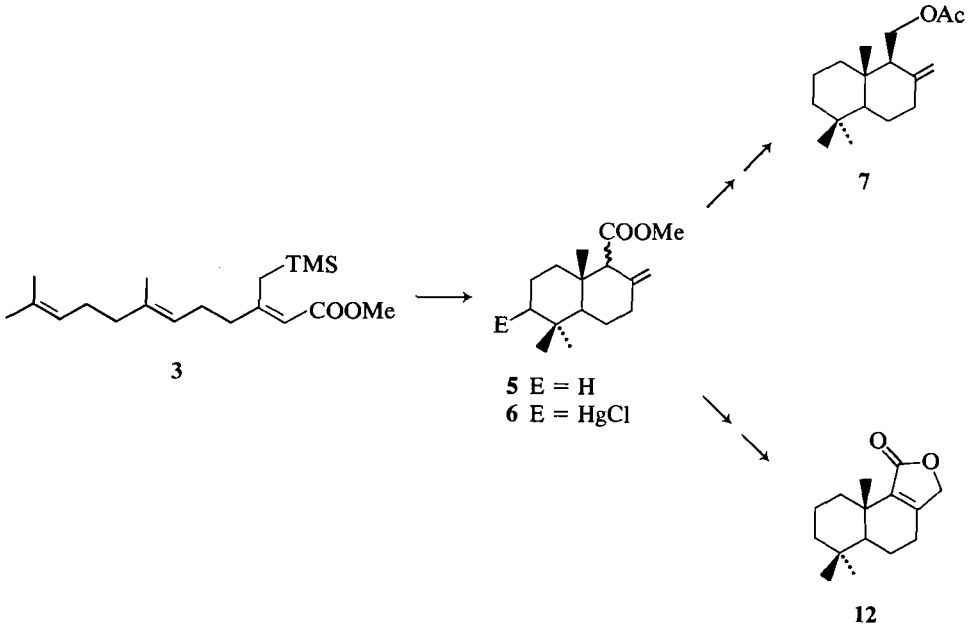

[Traduit par la revue]

[1]Permanent address: Department of Chemistry, California State University, Northridge, CA 91330, U.S.A.

[2]Author to whom correspondence may be addressed.

In 1976, Fleming *et al.* reported the first use of an allylsilane in an electrophilic cyclization (1). These results have been extended by Fleming and co-workers (2) and exploited by several other groups (3), including our own (4). In particular, we were able to show that the methyltrimethylsilyl group activated and controlled the regioselective alkene formation in the electrophilic cyclization of allylsilanes of α,β-unsaturated esters. This led to a method for the facile and efficient cyclization of epoxy alkenes (4*b*, 4*d*). Our initial efforts to cyclize olefinic allylsilanes involved a detailed study of the cyclization of the diene **1** to the exocyclic methylenecyclohexane shown below (4*c*). In this paper we report the details of the extension of this chemistry to the cyclization of trienes and the application of this cyclization in the synthesis of two drimane sesquiterpenes.[3]

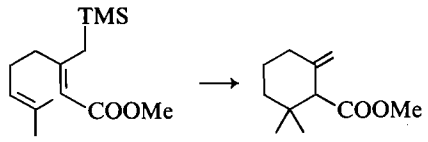

1

Synthesis of the (*E*,*Z*)-triene **3** is shown in eq. [1]. The β-keto ester **2** (5) was converted into the corresponding *Z*-enol phosphate (6) and coupled with trimethylsilymethylmagnesium chloride in the presence of nickel(II) bisacetylacetonate (7). The best yields of **3** were obtained by vigorous stirring of the reaction mixture, and by addition of fresh catalyst during the coupling reaction. The stereoselectivity in the formation of the conjugated alkene of **3** in this coupling reaction was greater than 95% as estimated from the ^{1}H nmr of the crude product.

[1]

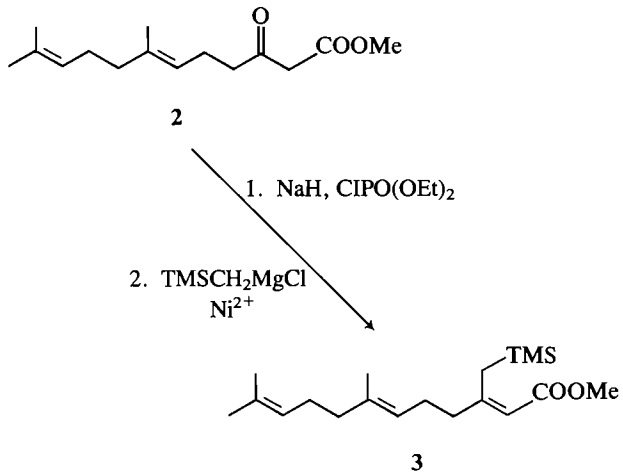

2 **3**

We carried out a study of the cyclization of triene **3** with a range of Lewis acids (4*c*) and determined the products by a combination of ^{1}H nmr spectroscopy and gas chromatography.[4] If titanium tetrachloride was used as the Lewis acid catalyst, the endocyclic compounds **4** were obtained in good yield. The ratio of the 1α:1β isomers was 1:1 and it was independent of the geometry of the terminal alkene in **3**.[5] It is interesting to note that the conjugated $\Delta^{1,2}$ alkene was not observed in any of our cyclization reactions. A number of Lewis acids, including boron trifluoride etherate, aluminum chloride, and stannic chloride, gave the exocyclic esters **5**. These reactions were quite solvent and temperature dependent. The optimum cyclization conditions for production of the exocyclic alkenes involved treating **3** with stannic chloride at −56°C in methylene chloride saturated with water. Under these conditions the esters **5** were obtained in 95% yield and the ratio of the 1α:1β isomers was 1:4. Under more vigorous conditions the exocyclic alkenes **5** isomerized to the more stable endocyclic compounds **4**. We were unable to separate the two epimers of **5** on preparative scale at this stage, nor were we able to epimerize either compound.

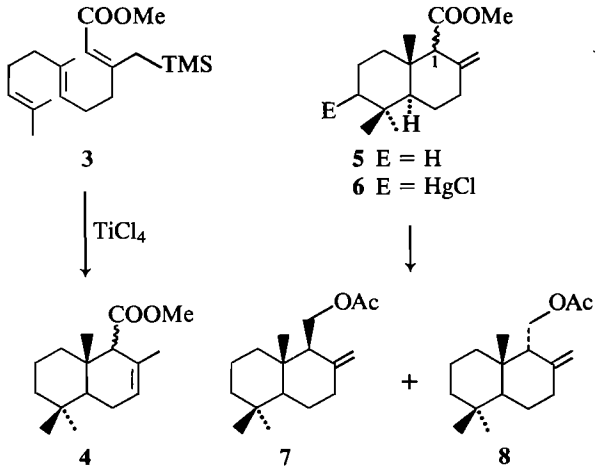

It was somewhat surprising to find that the cyclization of the allylsilane **3** gave an epimeric mixture of the products **5**. In accordance with the Stork–Eschenmoser hypothesis (9), cyclization of the triene **3** via the chair–chair conformation would be expected to yield the 1β isomer. The 1α epimer presumably arises via the chair–boat conformation. It seems that small steric interactions in the transition stage may play an important role in determining the product distribution (4*d*, 10).

Mercuric ion initiated cyclization (11) of the triene **3** was also investigated. Treatment of **3** with mercuric trifluoroacetate followed by a brine work-up gave the bicyclic products **6**, which were isolated, after chromatography, in 55–65% yield along with ca. 10% of a monocyclic product. We were unable to determine the number and structure of the stereoisomers of **6** present in the product. However, this problem was resolved in the subsequent reactions of **6**. The bicyclic product **6** was reduced with lithium aluminum hydride and acetylated to give the C-1 epimeric compounds **7** and **8** in good yield. The ratio of **7**:**8** was 3:1, which indicated that the energy difference between the chair–chair transition state and the chair–boat transition state for the Lewis acid cyclization and the mercuric trifluoroacetate cyclization must be very similar. Again, the crucial role of the trimethylsilyl group in controlling the high regioselectivity in the introduction of the exocyclic alkene cannot be underestimated (1–4). In a recent study of the mercuric cyclization of a range of trienes **9**, the $\Delta^{2,3}$-endocyclic compound was invariably the major product obtained (eq. [2]) (12).

[2]

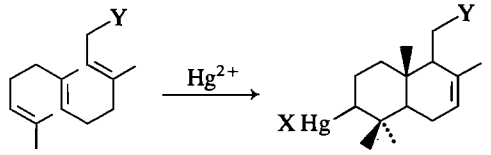

(ref. 12)

9

[3]A preliminary account of some of these results has been reported in ref. 4*a*.

[4]For details of this study see ref. 8.

[5]The *E* isomer of **3** was prepared from the *E*-enol phosphate of **2**; see ref. 15.

Recently the alcohol **10**, albicanol, and the corresponding acetate **7** have been isolated from a nudibranch (13). Albicanol (**10**) is also found in terrestrial sources (14). Albicanyl acetate (**7**) appears to have potent fish antifeedant activity and may well be of ecological importance in the marine environment. In the above sequence, we illustrated the conversion of the organomercurial compound **6** into albicanol (**10**) and its acetate **7**. This

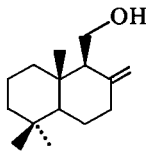

10

confirmed the expected *trans* ring fusion in the cyclized products from the triene **3**. In a similar fashion, the epimeric esters **5** were reduced to give albicanol (**10**) and *epi*-albicanol in high yield. These alcohols could be separated by column chromatography and albicanol (**10**) was obtained in 75% yield. Acetylation gave racemic albicanyl acetate (**7**) which had identical spectroscopic data to that of the natural product.[6] The racemic compound **7** from this synthesis was found to have antifeedant activity comparable to that of natural albicanol acetate, which is optically active.[7]

Warburganal (**11**) is another member of the drimane class of natural products that has attracted a great deal of interest recently. Much of this interest stems from the fact that warbuganal possesses potent insect antifeedant activity against the African army worms, *Spodoptera littoralis* and *S. exempta* (16). Difficulties are often encountered in the synthesis of the drimanic sesquiterpenes, including warbuganal, due to the variations in functionality at the C-1 and C-2 positions.[8] A similar problem has been encountered in some the syntheses of isodrimenin (**12**), which is an intermediate in one of the

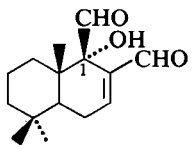

11

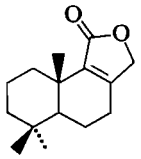

12

syntheses of warburganal (17). Several of the reported syntheses of isodrimenin have been characterized by a lack of regioselectivity in the introduction of the C-1 and C-2 substituents, by double bond isomerization to the $\Delta^{2,3}$ isomer, or by low yields (18).[9] A regioselective synthesis of isodrimenin (**12**) from the epimeric mixture of esters **5** is shown below. The exocyclic olefin in **5** was epoxidized using *m*-chloroperoxybenzoic acid (MCPBA) to give a mixture of all four isomers of **13** in 92% yield. The major isomer is thought to be the product obtained via α attack of MCPBA on the 1β isomer of **5**, since attack from the β direction would be hindered by the bridgehead methyl group. The epoxy esters **13** were then treated with 5 equivalents of lithium diisopropylamide in THF at −78°C, and allowed to stir at room temperature for 3 h. Isodrimenin (**12**) was isolated in 60% overall yield from **5**; the spectral data were in good agreement with that of an authentic sample.[10]

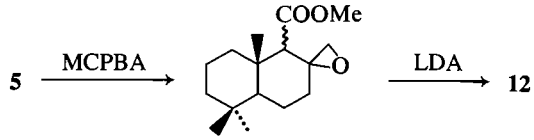

13

Experimental[11]

Methyl (2Z,6E)-7,11-dimethyl-3-[(trimethylsilyl)methyl]-2,6,10-dodecatrienoate (3)

The Grignard reagent was prepared from 1.05 g (0.080 mol) of magnesium turnings and 12.2 mL (0.088 mol) of trimethylsilylmethyl chloride in ether. To this solution was added 0.25–0.50 g (1.0–2.0 mmol) portions of anhydrous nickel(II) acetylacetonate 15.5 g (0.040 mol) of crude enol phosphate from **2** (6). The reaction mixture was heated at reflux for 4 h and further portions of 0.25–0.50 g (1.0–2.0 mmol) of catalyst were added after 0.5 and 1.5 h. Work-up of the reaction mixture gave 14.2 g of compound **3** as an orange oil. The crude product was purified by flash chromatography using petroleum ether – ethyl acetate (40:1) as eluant to yield 9.3 g (72%) of ester **3**. Preparative tlc of a small amount of this material using petroleum ether – ethyl acetate (20:1) gave **3** as a colourless liquid; bp (Kugelrohr distillation) 100°C/0.2 Torr (1 Torr = 133.3 Pa); ir ($CHCl_3$): 1700, 1620, 1435, 1245, 1160, and 855 cm^{-1}; ^1H nmr ($CDCl_3$) δ: 0.05 (s, 9H), 1.60 (s, 6H), 1.70 (s, 3H), 1.97–2.25 (m, 8H), 2.41 (s, 2H), 3.65 (s, 3H), 5.00–5.22 (m, 2H), and 5.55 (s, 1H); mass spectrum, *m/z*: 322(M^+, 15), 307(19), 253(18), 186(14), 150(12), 149(87), 121(19), 119(11), 117(36), 115(10), 95(12), 93(21), 89(25), 82(46) 81(25), 79(17), 75(10), 74(10), 73(100), 69(59), 59(19), 55(14), and 53(19). *Anal.* calcd. for $C_{19}H_{34}O_2Si$: C 70.75, H 10.62; found: C 70.90, H 10.60.

Methyl trans*-decahydro-5,5,8aβ-trimethyl-2-methylene-1ξ-naphthalenecarboxylate (5)*

To a solution of 1.60 g (5.0 mmol) of the ester **3** in 120 mL of CH_2Cl_2 saturated with water at −56°C was slowly added to a solution of 1.46 mL (12.5 mmol) of $SnCl_4$ in 20 mL of CH_2Cl_2 saturated with water. The reaction mixture was stirred for 3 h at −56°C, then quenched with aqueous KF solution, and diluted with ether. The organic phase was washed four times with aqueous KF, twice with saturated $NaHCO_3$, once with saturated NaCl, and dried. The solvent was removed to give 1.40 g of crude bicyclic esters **5**. Purification of **5** by flash chromatography using petroleum ether – ethyl acetate (40:1) gave 0.76 g (61%) of a mixture of α and β isomers of **5** as a colourless liquid (1α:1β = 17:83, as determined by gc (T = 160°C)); bp Kugelrohr distillation) 108°C/0.1 Torr; ir ($CHCl_3$): 1730, 1645, and 1165 cm^{-1}; ^1H nmr ($CDCl_3$) δ: 0.80 (s, 3H), 0.85 (s, 2.5H), 0.88 (s, 0.55H), 0.92 (s, 0.5H), 1.05 (s, 2.5H), 1.10–2.55 (m, 11H), 2.78 (bs, 1H), 3.65 (s, 3H), 4.63 (bs, 1H), and 4.81 (bs, 1H); mass spectrum, *m/z*: 250(M^+, 66), 235(25), 191(12), 175(24), 137(100), 136(17), 125(16), 124(23), 123(48), 121(24), 114(45), 109(30), 107(25), 105(19), 95(36), 93(20), 91(20), 82(22), 81(43), 79(22), 77(17), 69(49), 67(19), and 55(36). *Anal.* calcd. for $C_{16}H_{26}O_2$: C 76.75, H 10.47; found: C 76.58, H 10.41.

trans*-Decahydro-5,5,8aβ-trimethyl-2-methylene-1β-naphthalene-methanol (albicanol) (10)*

This compound was prepared using 0.190 g (5.0 mmol) of $LiAlH_4$ and 1.40 g of a mixture of esters **5** in ether. Work-up of the reaction

[6]We are grateful to Professor R. J. Andersen and J. Hellou for this data and for an authentic sample of albicanyl acetate.

[7]R. J. Anderson, S. W. Ayer, and M. E. LeBlanc. Unpublished observations, 1982.

[8]The numbering convention used in this paper is shown on structures **5** and **11**. This is not the usual convention for the drimane skeleton.

[9]For two recent syntheses of isodrimenin (**12**) that avoid these problems see ref. 19.

[10]We are grateful to Professor J. D. White for this data.

[11]For an outline of general procedures see ref. 4*c*.

mixture gave 1.11 g of compound **10** and the α isomer as a yellow oil (1α:1β = 17:83, as determined by gc (T = 170°C)). The crude product was purified by flash chromatography using petroleum ether – ether (2.5:1) as eluant. After six successive chromatographic separations of the mixture of isomers, 0.90 g of crude product gave 0.15 g (17%) of the α isomer and 0.67 g (75% from trimethylsilyl ester **3**) of alcohol **10**. The major alcohol **10** had spectral data identical to that of a sample of albicanol provided by Professor R. Andersen.

Methyl trans*-decahydro-6-chloromercurial-5,5,8aβ-trimethyl-2-methylene-1ξ-naphthalenecarboxylate (6)*

A sample of 0.363 g (1.13 mmol) of triene **3** was dissolved in 4 mL of dry nitromethane and cooled under N_2 to −20°C. A solution of 0.530 g (1.24 mmol) of mercuric trifluoroacetate in 1 mL of dry nitromethane was added dropwise to the above solution. The reaction mixture was stirred at −20°C for 1 h, then quenched with an aqueous solution of $NaHCO_3$ an NaCl. The mixture was extracted thoroughly with CH_2Cl_2. The combined organic extracts were washed, dried, and the solvent removed to yield 0.51 g of crude **6**. The crude product was purified by flash chromatography using petroleum ether – ether acetate (8:1) to give 0.33 g (60%) of **6** as a white solid that was characterized by its ^{1}H nmr spectrum and subsequent conversion to a mixture of **7** and **8**.

*Conversion of **6** to albicanol (**10**)*

Lithium aluminum hydride (33 mg, 0.87 mmol) was suspended in 3 mL of anhydrous ether. The above crude mercurial compound **6** (0.33 mg) was dissolved in 3 mL of anhydrous toluene and added to the hydride suspension. A second portion of 33 mg of $LiAlH_4$ was added and the mixture was refluxed for 3/4 h. Work-up of the reaction gave 0.14 g of crude product, which was purified by flash chromatography using petroleum ether – ether (3:1) to yield 95 mg of albicanol identical to that obtained above.

trans*-Decahydro-5,5,8aβ-trimethyl-2-methylene-1β-naphthalene-methyl acetate (albicanyl acetate) (7)*

A mixture of 0.16 mL (1.6 mmol) of acetic anhydride, 0.13 mL (1.6 mmol) of pyridine, and a catalytic amount of 4-dimethylaminopyridine was stirred in dry ether at room temperature. A solution of 0.33 g (1.5 mmol) of alcohol **10** in dry ether was added to the mixture, and the reaction was stirred for 2 h at room temperature. The reaction mixture was diluted with ether, washed three times with saturated $NaHCO_3$, three times with 1 *M* HCl, twice with saturated NaCl, dried, and concentrated to give 0.38 g (95%) of acetate **7**. Preparative tlc of this material using petroleum ether – ethyl acetate (10:1) gave **7** as a colourless liquid whose spectral data is in good agreement with that of an authentic sample of albicanyl acetate provided by Professor R. Andersen.

Methyl trans*-decahydro-5,5,8aβ-trimethyl-2-methylene-1ξ-naphthalenecarboxylate epoxide (13)*

To a solution of 0.678 g (2.7 mmol) of alkenes **5** in dry CH_2Cl_2 at 0°C was slowly added a solution of 0.56 g (3.4 mmol) of MCPBA in CH_2Cl_2. The reaction mixture was stirred for 2 h while allowing it to warm to room temperature, and was then diluted with ether. The organic layer was washed three times with saturated $NaHCO_3$, once with saturated NaCl, and dried. The solvent was removed to give 0.658 g of a mixture of crude epoxides, which was used without further purification in the preparation of isodrimenin. Preparative tlc of a small amount of this material using petroleum ether – ethyl acetate (20:1) gave a mixture of the four isomers of **13** as a colourless liquid; bp (Kugelrohr distillation) 100°C/0.1 Torr; ir ($CHCl_3$): 1730 and 1175 cm^{-1}; ^{1}H nmr ($CDCl_3$) δ: 0.90 (s, ≈2.4H), 0.95 (s, ≈2.4H), 1.00 (s, ≈0.6H), 1.05 (s, ≈0.6H), 1.10 (s, ≈0.6H), 1.15 (s, ≈2.4H), 1.00–2.10 (m, 11H), 2.43–2.72 (m, 2H), 3.30–3.50 (bs, 1H), 3.61 (s, ≈2.1H), 3.63 (s, ≈0.35H), 3.67 (s, ≈0.35H), and 3.68 (s, ≈0.2H); mass spectrum, m/z: 266(M^+, 4), 251(12), 248(39), 236(37), 235(31), 143(28), 141(100), 137(50), 130(76), 129(43), 128(33), 123(40), 121(26), 112(25), 109(51), 107(26), 95(56), 93(30), 91(28), 82(34), 81(61), 79(33), 69(74), 67(38), 59(26), and 55(76). *Exact Mass* calcd. for $C_{16}H_{26}O_3$: 266.1882; found (ms): 266.1881.

(4,5,aα,6,7,8,9,9aβ)-Octahydro-6,6,9a-trimethyl-naphtho[1,2-c]-furan-1(3H)-one (isodrimenin) (12)

To a solution of 0.70 mL (5.0 mmol) of diisopropylamine in dry THF at 0°C was added 2.94 mL (5.0 mmol) of a 1.70 *M* solution of *n*-butyllithium in hexane. The pale yellow solution was stirred for 15 min at 0°C, cooled to −78°C, and a solution of 0.266 g (1.0 mmol) of epoxy esters **13** was added. The reaction was allowed to warm to room temperature over a period of 1 h, stirred at room temperature for 3 h, then quenched with 1 *M* HCl and diluted with ether. The organic phase was washed once with 1 *M* HCl, twice with saturated NaCl, dried, and concentrated to give 0.266 g of crude product. Purification by flash chromatography using petroleum ether – ethyl acetate (5:1) as eluant gave 0.141 g (60% from esters **5**) of **12** as a white solid. Preparative tlc of a small amount of this material using petroleum ether – ethyl acetate (6:1) gave **12** as a crystalline solid whose spectral data (^{1}H nmr, ir, ms) are in good agreement with those of the literature (19); mp 88.5–90.0°C (lit. (19) mp 89–90°C).

Acknowledgments

We are grateful to Professors Andersen and White for spectral data and to the Natural Sciences and Engineering Research Council of Canada for financial support. One of us (R. J. A.) is grateful to the Canadian Commonwealth Scholarship and Fellowship Plan for the award of a graduate scholarship.

1. I. Fleming, A. Pearce, and R. L. Snowden. J. Chem. Soc. Chem. Commun. 182 (1976).
2. (*a*) I. Fleming and A. Pearce. J. Chem. Soc. Perkin Trans. 1, 251 (1981); (*b*) H. F. Chow and I. Fleming. J. Chem. Soc. Perkin Trans. 1, 1815 (1984).
3. (*a*) R. L. Danheiser, D. J. Carini, and A. Basak. J. Am. Chem. Soc. **103**, 1604 (1981); (*b*) R. L. Danheiser, D. J. Carini, D. M. Fink, and A. Basak. Tetrahedron, **39**, 935 (1983); (*c*) T. K. Sarkar and N. H. Andersen. Tetrahedron Lett. 3513 (1978); (*d*) M. Ochiai, M. Arimoto, and E. Fujita. J. Chem. Soc. Chem. Commun. 460 (1981); (*e*) A. Itoh, K. Oshima, and H. Nozaki. Tetrahedron Lett. 1783 (1979); (*f*) I. Kuwajima, T. Tanaka, and K. Atsumi. Chem. Lett. (1979); (*g*) G. Majetich, R. Desmond, and A. M. Casares. Tetrahedron Lett. **24**, 1913 (1983); (*h*) D. Wang and T. H. Chan. J. Chem. Soc. Chem. Commun. 1273 (1984); (*i*) R. S. Brinkmeyer. Tetrahedron Lett. 207 (1979); (*j*) R. Schmid, P. L. Huesmann, and W. S. Johnson. J. Am. Chem. Soc. **102**, 5122 (1980); (*k*) L. R. Hughes, R. Schmid, and W. S. Johnson. Bioorg. Chem. **8**, 513 (1979).
4. (*a*) R. J. Armstrong, F. L. Harris, and L. Weiler. Can. J. Chem. **60**, 673 (1982); (*b*) R. J. Armstrong and L. Weiler. Can. J. Chem. **61**, 214 (1983); (*c*) Can. J. Chem. **61**, 2530 (1983); (*d*) Can. J. Chem. **64**, 584 (1986).
5. S. N. Huckin and L. Weiler. J. Am. Chem. Soc. **96**, 1082 (1974).
6. F. W. Sum and L. Weiler. Tetrahedron, **37**, Suppl. 1, 303 (1981).
7. T. Hayashi, Y. Katsuro, and M. Kumada. Tetrahedron Lett. **21**, 3925 (1980).
8. R. J. Armstrong, Ph.D. Thesis, University of British Columbia, Vancouver, B.C., 1983.
9. (*a*) G. Stork and A. W. Burgstahler. J. Am. Chem. Soc. **77**, 5068 (1955); (*b*) A. Eschenmoser, L. Ruzicka, O. Jeger, and D. Arigoni. Helv. Chim. Acta, **38**, 1890 (1955).
10. E. E. van Tamelen, A. Storni, E. J. Hessler, and M. A. Schwartz. Bioorg. Chem. **11**, 133 (1982) and references therein.
11. (*a*) E. J. Corey, M. A. Tius, and J. Das. J. Am. Chem. Soc. **102**, 1742, (1980); (*b*) J. Am. Chem. Soc. **102**, 7612 (1980).
12. M. Nishizawa, H. Takenaka, H. Nishide, and Y. Hayashi. Tetrahedron Lett. **24**, 2581 (1983).
13. J. Hellou, R. J. Andersen, and J. E. Thompson. Tetrahedron, **38**, 1875 (1982).

14. Y. OHTA, N. H. ANDERSEN, and C. B. LIU. Tetrahedron, **33**, 617 (1977).
15. M. ALDERICE, C. SPINO, and L. WEILER. Tetrahedron Lett. **25**, 643 (1984).
16. (*a*) I. KUBO, Y. W. LEE, M. J. PETTEI, F. PILKIEWICZ, and K. NAKANISHI. J. Chem. Soc. Chem. Commun. 1013 (1976); (*b*) K. NAKANISHI and I. KUBO. Isr. J. Chem. **16**, 28 (1977); (*c*) W. C. MA and I. KUBO. Entomol. Exp. Appl. **22**, 107 (1977).
17. T. NAKATA, H. AKITA, T. NAITO, and T. OISHI. J. Am. Chem. Soc. **101**, 4400 (1979).
18. (*a*) E. WENKERT and D. P. STRIKE. J. Am. Chem. Soc. **86**, 2044 (1964); (*b*) Y. KITAHARA, T. KATO, T. SUZUKI, S. KANNO, and M. TANEMURA. J. Chem. Soc. Chem. Commun. 342 (1969); (*c*) H. AKITA and T. OISHI. Tetrahedron Lett. 3733 (1978); (*d*) H. AKITA, T. NAITO, and T. OISHI. Chem. Lett. 1365 (1979); (*e*) S. V. LEY and M. MAHON. Tetrahedron Lett. **22**, 4747 (1981).
19. (*a*) T. NAKANO and M. E. AGUERO. J. Chem. Soc. Perkin Trans. 1, 1163 (1982); (*b*) J. D. WHITE and L. P. BURTON. J. Org. Chem. **50**, 357 (1985).

Interdiffusion of acids and bases. HCl and NaOH in aqueous solution

DEREK G. LEAIST[1] AND BETTY WIENS
Department of Chemistry, University of Western Ontario, London, Ont., Canada N6A 5B7

Received November 12, 1985

DEREK G. LEAIST and BETTY WIENS. Can. J. Chem. **64**, 1007 (1986).

Stokes magnetically stirred diaphragm cells have been used to measure interdiffusion of hydrochloric acid and sodium hydroxide in aqueous solution at 25°C. Expressions are developed to estimate ternary diffusion coefficients for these mixtures. The analysis reveals sharp discontinuities between the diffusion properties of HCl-rich and NaOH-rich mixtures. Although the diffusion coefficients are sensitive to concentration, accurate analytic approximations for rates of interdiffusion can be obtained by averaging coefficients along the diffusion path. When HCl and NaOH interdiffuse, proton-coupled and hydroxide-coupled diffusion operating simultaneously on opposite sides of the diffusion boundary lead to rapid diffusion of inert Na^+ and Cl^- species.

DEREK G. LEAIST and BETTY WIENS. Can. J. Chem. **64**, 1007 (1986).

On a utilisé des cellules à diaphragme de Stokes agitées d'une façon magnétique pour mesurer l'interdiffusion de l'acide chlorhydrique et de l'hydroxyde de sodium dans des solutions aqueuses à 25°C. On a développé des expressions mathématiques pour évaluer les coefficients de diffusion ternaire pour ces mélanges. L'analyse révèle l'existence de discontinuités marquées entre les propriétés de diffusion de mélanges riches soit en HCl ou en NaOH. Même si les coefficients de diffusion sont sensibles à la concentration, on peut obtenir des approximations analytiques assez précises pour les vitesses d'interdiffusion si l'on fait des moyennes des coefficients le long du chemin de diffusion. Lorsqu'il se produit de l'interdiffusion du HCl et du NaOH, des diffusions liées soit au proton ou à l'hydroxyde qui opèrent simultanément de chaque côté de la frontière de diffusion provoquent la diffusion rapide d'espèces Na^+ et Cl^- inertes.

[Traduit par la revue]

1. Introduction

Interdiffusion of acids and bases occurs in many important absorption, extraction, and leaching operations. Transport in these and other reactive electrolyte mixtures is usually described by solving the Nernst–Planck equations (1, 2).

$$[1] \qquad \partial c_i/\partial t = D_i\nabla^2 c_i - (F/RT)z_iD_i\nabla(c_iE) + r_i$$

for the concentrations c_i of each diffusing species. Reaction rates per unit volume, r_i, are included for species produced or consumed by chemical reactions. The diffusion-induced electric field (E) couples transport of charged species. As a result of these complications, Nernst–Planck equations are difficult to solve. Solutions are usually obtained numerically by finite difference approximations (3, 4).

This research was undertaken to test a simpler treatment of acid–base diffusion, multicomponent Fick equations (5, 6)

$$[2] \qquad \partial C_i/\partial t = \sum_{k=1}^{N} \nabla(D_{ik}\nabla C_k)$$

which are phrased in terms of total concentrations C_i of neutral electrolyte components (such as HCl and NaOH) rather than concentrations c_i of charged species (such as H^+, Cl^-, Na^+, and OH^-). This approach offers several advantages:

(*a*) Fewer differential equations are required.

(*b*) Because total (reacted plus unreacted) components are conserved, reaction rate terms r_i can be dropped.

(*c*) Since the components are electrically neutral, it is not necessary to evaluate the electric field. (The effects of E are included implicitly in the values of the multicomponent diffusion coefficients.)

(*d*) If the diffusion coefficients are constant, or if suitable average coefficients can be defined, eq. [2] simplifies to

$$[3] \qquad \partial C_i/\partial t = \sum_{k=1}^{N} D_{ik}\nabla^2 C_k$$

for which analytic solutions exist.

To illustrate these ideas, we develop expressions to estimate multicomponent diffusion coefficients for aqueous hydrochloric acid + sodium hydroxide mixtures. Rates of diffusion for these mixtures predicted by multicomponent diffusion equations are then compared with rates measured by diaphragm cell experiments.

2. Experimental

Diffusion was measured by the Stokes diaphragm cell method (7). In these experiments solute diffuses between upper and lower magnetically stirred cell compartments through the pores of a sintered glass disc. The rate of diffusion is determined from changes in solute concentration after the cells are run for a timed interval.

Fine porosity pyrex diaphragms (3 cm diameter, 0.2 cm thick, mean pore diameter 5×10^{-4} cm) were used in this work. Cell compartment volumes (25–35 cm^3) of each cell were matched to within 0.5%. Each compartment was fitted with a greaseless teflon stopcock and a glass-coated iron stirrer which was rotated once per second by external magnets. Each cell was calibrated at frequent intervals by diffusing 0.5 *M* KCl into pure water at 25°C. Cell constants β (0.16–0.20 cm^{-2}) were computed from the relation

$$[4] \qquad \Delta c(t) = \Delta c(0)\exp(-\beta\bar{D}t)$$

where $\Delta c(t)$ is the measured difference in KCl concentration between upper and lower compartments at time t. The integral diffusion coefficient of aqueous KCl ($\bar{D}$) was evaluated by interpolation of the data reported by Stokes (8).

At the start of each experiment the lower compartment was filled with a binary solution of aqueous HCl or NaOH, whichever was denser. The upper compartment was filled with a binary solution of the other component. The cells were placed in a thermostat at 25 ± 0.01°C and stirred for about 2 h to establish steady state diffusion through the diaphragms. The cell compartments were rinsed, refilled with fresh solution, then returned to the thermostat for the duration of the run (0.2–5 days). Initial and final solute concentrations were determined

[1]To whom all correspondence should be addressed.

by potentiometric titration against silver nitrate and standardized HCl or NaOH.

Chemical reaction of HCl and NaOH produces heat. To maintain isothermal conditions during a run, dilute solutions with small heats of reaction were used. The rate of heat production in each diaphragm was never more than 1 mW (considerably less near the end of a run). We estimate the maximum increase in diaphragm temperature was only 0.001°C.

3. Theory

What is the minimum number of solute flows that must be specified to give a complete macroscopic description of diffusion in an isothermal electrolyte mixture containing s different solute species which undergo e chemical reactions? Because electrolytic reactions are rapid, e chemical equilibria exist locally. Electroneutrality provides one additional restriction. Therefore, only $N = s - e - 1$ solute concentrations are independent (9). We may choose N neutral solute components and describe diffusion of these components by multicomponent Fick equation [2].

Multicomponent diffusion equations, though simpler than Nernst–Planck equations, are of little practical use unless values of multicomponent diffusion coefficients D_{ik} are known. Fortunately, values of D_{ik} can be estimated by taking weighted averages of the diffusion coefficients D_i of the various solute species (9–12). This well-established procedure is illustrated in the Appendix for aqueous hydrochloric acid + sodium hydroxide mixtures.

Hydrochloric acid(1) + sodium hydroxide(2) + water (s = 4, e = 1, N = 2)

Four different solute species (H^+, Cl^-, Na^+, OH^-) are transported in aqueous HCl + NaOH mixtures. However, the conditions of chemical equilibrium ($H_2O \rightleftharpoons H^+ + OH^-$) and electroneutrality reduce the number of independent solute flows to only two. Therefore, a concise but complete description of interdiffusion of HCl and NaOH is given by ternary diffusion equations

$$[5a] \quad \partial C_1/\partial t = \nabla(D_{11}\nabla C_1) + \nabla(D_{12}\nabla C_2)$$

$$[5b] \quad \partial C_2/\partial t = \nabla(D_{21}\nabla C_1) + \nabla(D_{22}\nabla C_2)$$

where C_1 and C_2 denote total concentrations of HCl(1) and NaOH(2) components in moles per unit volume. Molar flux densities of the components are given by

$$[6a] \quad -J_1 = D_{11}\nabla C_1 + D_{12}\nabla C_2$$

$$[6b] \quad -J_2 = D_{21}\nabla C_1 + D_{22}\nabla C_2$$

Expressions developed in the Appendix together with the species diffusion coefficients listed in Table 1 were used to calculate ternary diffusion coefficients for aqueous HCl + NaOH mixtures at 25°C. The results are plotted against solute fraction of HCl (designated by X_1) in Fig. 1.

When HCl and NaOH interdiffuse, proton-coupled transport and hydroxide-coupled transport operate simultaneously on opposite sides of the diffusion boundary. This leads to remarkable diffusion properties, such as rapidly varying diffusion coefficients, large cross terms, and sharp discontinuities in diffusion properties. As expected for a strong electrolyte mixture (12), values of D_{ik} are sensitive to the ratio of solute concentrations, but not to total solute concentration.

The diffusivity of HCl in aqueous NaOH solutions (D_{11}) takes values from 2.0×10^{-9} to 6.3×10^{-9} m^2 s^{-1}. As the solute fraction of HCl approaches unity, D_{11} approaches the binary diffusivity of aqueous HCl, about 3.0×10^{-9} m^2 s^{-1}. In pure aqueous HCl, Cl^- and highly mobile H^+ diffuse at the same speed; the diffusion-induced electric field slows down H^+ and speeds up Cl^-, thereby preventing charge separation. If NaOH is added, it reacts with HCl to form NaCl. In the resulting ternary mixture, H^+ can diffuse more rapidly than Cl^-. Charge separation is avoided because the electric field established by the HCl gradient generates counterflow of Na^+. This mechanism increases the diffusivity of HCl and leads to large negative values for D_{21}, the cross coefficient that measures coupled flow of NaOH along the HCl gradient. Because the HCl gradient is unable to generate flow of NaOH in solutions free of NaOH, $D_{21} \rightarrow 0$ as $X_1 \rightarrow 1$.

TABLE 1. Species diffusion coefficients at 25°C[a]

Species	D_i (10^{-9} m^2 s^{-1})
H^+	9.31
Cl^-	2.03
Na^+	1.33
OH^-	5.30

[a]Estimated from published limiting ionic molar conductances (13) λ^0_i using the relation $D_i = RT\lambda^0_i F^2$. F is the Faraday, 96 487 C mol^{-1}.

There are sharp spikes in the diffusion coefficients near $X_1 = 0.5$. For example, D_{11} reaches a maximum value of 6.3×10^{-9} m^2 s^{-1} at solute fractions of HCl slightly above 0.5 where all but a trace of HCl is neutralized by NaOH. At these compositions, transport of HCl corresponds to tracer diffusion of H^+ in supporting NaCl solutions. Therefore, the HCl gradient ∇C_1 produces flow $-D_{H^+}\nabla C_1$ of H^+ with tracer diffusivity $D_{H^+} = 9.3 \times 10^{-9}$ m^2 s^{-1}. The HCl gradient also drives co-current flow $-D_{11}\nabla C_1$ of Cl^- and counter-current flow $-D_{21}\nabla C_1$ of Na^+. Electroneutrality requires that $D_{11} - D_{21} = D_{H^+}$ at $X_1 = 0.5^+$.

At solute fractions of HCl below 0.5, HCl reacts completely with excess NaOH. The disappearance of free H^+ leads to a sudden drop in the diffusivity of the HCl component. In this region the HCl gradient ∇C_1 produces an equal but opposite gradient $-\nabla C_1$ in free OH^-. At HCl solute fractions just below 0.5, trace amounts of OH^- diffuse in supporting NaCl solutions. In this case the Cl^- flux $-D_{11}\nabla C_1$ and Na^+ flux $-D_{21}\nabla C_1$ are balanced by the tracer OH^- flux $D_{OH^-}\nabla C_1$. Hence $D_{11} - D_{21} = D_{OH^-} = 5.3 \times 10^{-9}$ m^2 at $X_1 = 0.5^-$. In the limiting case of a trace of HCl in aqueous NaOH, D_{11} approaches the tracer diffusion coefficient of Cl^-, about 2.0×10^{-9} m^2 s^{-1}.

The diffusivity of NaOH in aqueous HCl solutions, D_{22}, ranges from 1.3×10^{-9} to 4.3×10^{-9} m^2 s^{-1}. At low solute fractions of HCl, values of D_{22} are close to the binary diffusivity of aqueous NaOH, about 2.0×10^{-9} m^{-2} s^{-1}. As more HCl is added, D_{22} increases. It reaches the value 2.8×10^{-9} m^2 s^{-1} just below $X_1 = 0.5$. At $X_1 = 0.5^-$, electroneutrality requires that $D_{22} - D_{12} = D_{OH^-}$.

In HCl-rich mixtures, proton-coupled transport of Na^+ leads to D_{22} values as large as 4.3×10^{-9} m^2 s^{-1}. A gradient in concentration of NaOH in an otherwise uniform solution of excess HCl establishes an equal but opposite gradient in free H^+. As H^+ diffuses rapidly towards the zone of higher NaOH concentration, counterflow of Na^+ is generated to prevent

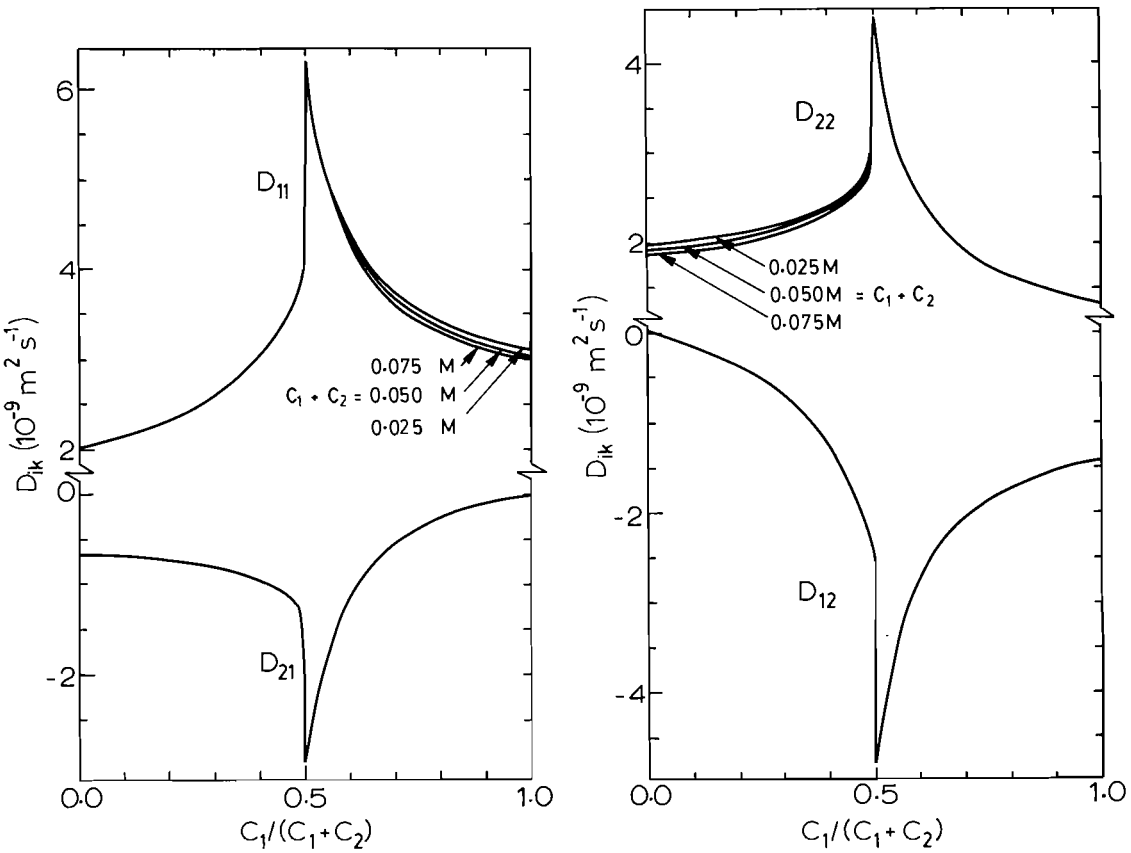

FIG. 1. Ternary diffusion coefficients at 25°C for aqueous HCl(1) + NaOH(2) plotted against HCl solute fraction $X_1 = C_1/(C_1 + C_2)$ for total solute concentrations $C_1 + C_2$ equal to 0.025, 0.050, and 0.075 M. Activity coefficient terms were included in the calculations.

charge separation. At $X_1 = 0.5^+$, $D_{22} - D_{12} = D_{H^+}$. In the limit $X_1 \rightarrow 1$, D_{22} equals the tracer diffusion coefficient of Na^+ in supporting HCl solutions, about $1.3 \times 10^{-9}\,m^2\,s^{-1}$.

4. Results and discussion

Figure 2 shows diaphragm cell results, for diffusion of 0.025, 0.050, and 0.075 M HCl into 0.075, 0.050, and 0.025 M NaOH, respectively. Component concentration differences across the cell diaphragms are plotted against βt.

The data shown in Fig. 2 can be used to calculate the apparent binary diffusion coefficients.

$$[7] \qquad D_{ai} = -\mathrm{d}\ln \Delta C_i/\mathrm{d}(\beta t)$$

for the HCl(1) and NaOH(2) components. When 0.075 M HCl diffuses into 0.025 M NaOH, for example, the initial slope of ΔC_1 versus βt corresponds to an apparent diffusivity of HCl equal to $8 \times 10^{-9}\ m^2\ s^{-1}$, an exceptionally large apparent diffusivity. In this case the HCl component diffuses rapidly because the main flow of HCl ($-D_{11}\nabla C_1$) is reinforced by a large co-current coupled flow of HCl ($-D_{12}\nabla C_2$) generated by the NaOH gradient. As further evidence for strongly coupled diffusion, note that the concentration difference for the HCl component can change sign. When this happens, the cell compartment that held no HCl at the start of the experiment now contains more HCl than the compartment which initially held all of the HCl. Thus HCl has diffused "up" its concentration gradient.

If the diffusion coefficients are constant, integration of the ternary diffusion equations gives simple analytic expressions (14)

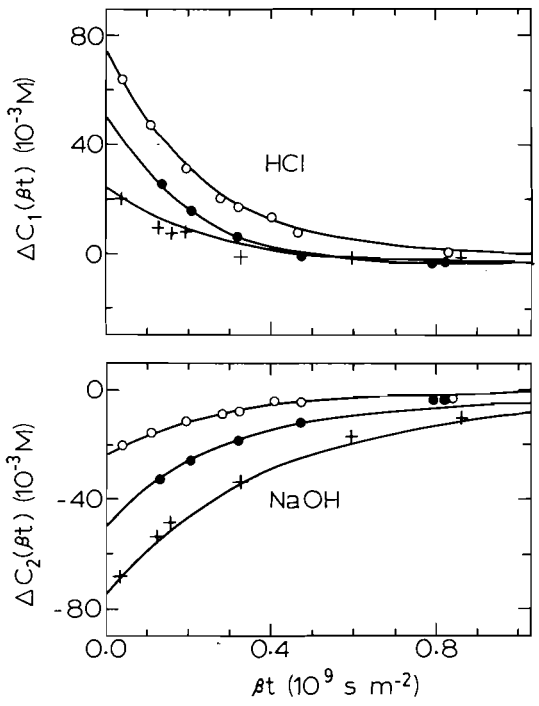

FIG. 2. Comparison of experimental and calculated concentration differences between upper and lower cell compartments for inter-diffusion of HCl(1) and NaOH(2) compartments: +, diffusion of 0.025 M HCl into 0.075 M NaOH; ●, 0.05 M HCl into 0.05 M NaOH; ○, 0.075 M HCl into 0.025 M NaOH. The plotted curves give concentration differences calculated from eqs. [8] using integral diffusion coefficients listed in Table 1.

TABLE 2. Integral diffusion coefficients for aqueous HCl(1) + NaOH(2)[a]

$\Delta C_1(0)$	$\Delta C_2(0)$	$\bar{X}_{1L}$	$\bar{X}_{1U}$	$\bar{D}_{11}$	$\bar{D}_{12}$	$\bar{D}_{21}$	$\bar{D}_{22}$
0.025	−0.075	0.50	0.10	2.59	−0.68	−0.83	2.19
0.050	−0.050	0.75	0.25	3.64	−1.93	−1.05	2.45
0.075	−0.025	0.10	0.50	3.75	−2.14	−0.63	2.00

[a] $\Delta C_i(0)$ and $\bar{D}_{ik}$ in units of M and 10^{-9} m^2 s^{-1}, respectively.

$$[8a] \quad \Delta C_1(t)/\Delta C_1(0) = A_1 \exp(-\beta D)^{(1)}t) + (1 - A_1)\exp(-\beta D^{(2)}t)$$

$$[8b] \quad \Delta C_2(t)/\Delta C_2(0) = (1 - A_2)\exp(-\beta D^{(1)}t) + A_2 \exp(-\beta D^{(2)}t)$$

for the concentration differences across the cell diaphragms. $D^{(1)}$ and $D^{(2)}$ denote eigenvalues of the diffusion coefficients matrix

$$[9a] \quad D^{(1)} = [D_{11} + D_{22} + (D_{11} - D_{22})(1 + 4D_{12}D_{21}/(D_{11} - D_{22})^2)^{1/2}]/2$$

$$[9b] \quad D^{(2)} = [D_{11} + D_{22} - (D_{11} - D_{22})(1 + 4D_{12}D_{21}/(D_{11} - D_{22})^2)^{1/2}]/2$$

Constants A_i are given by

$$[10a] \quad A_1 = [D_{11} - D^{(2)} + D_{12}\Delta C_2(0)/\Delta C_1(0)]/(D^{(1)} - D^{(2)})$$

$$[10b] \quad A_2 = [D_{22} - D^{(1)} + D_{21}\Delta C_1(0)/\Delta C_2(0)]/(D^{(2)} - D^{(1)})$$

Unhappily, diffusion coefficients for HCl + NaOH mixtures change by several hundred percent and pass through sharp discontinuities along the diffusion path. This rules out any hope of obtaining exact analytic descriptions of diffusion. However, it is helpful to define mean integral diffusion coefficients (15)

$$[11] \quad \bar{D}_{ik} = (\bar{X}_{1L} - \bar{X}_{1U})^{-1} \int_{\bar{X}_{1L}}^{\bar{X}_{1U}} D_{ik}\, dX_1$$

where $\bar{X}_{1L}$ and $\bar{X}_{1U}$ denote mean solute fractions in the lower (L) and upper (U) compartments, i.e., $\bar{X}_{1U} = [X_{1U}(t=0) + X_{1U}(t=\infty)]/2$. Values of $\bar{D}_{ik}$ calculated in this manner are listed in Table 2. Upon substitution of mean integral diffusion coefficients into eqs. [8], one obtains the calculated values for $\Delta C_1(t)$ and $\Delta C_2(t)$ given by the solid curves in Fig. 2. Experimental and calculated concentration differences are in close agreement. This comparison suggests that the calculated ternary diffusion coefficients correctly describe interdiffusion of HCl and NaOH. The calculated concentration differences corroborate negative experimental values for ΔC_1.

In conclusion, multicomponent diffusion equations provide accurate analytic descriptions of interdiffusion of acids and bases, a convenient alternative to finite difference approximations to the Nernst–Planck equations. The multicomponent analysis also provides direct information about the diffusivity of each electrolyte and the importance of coupled transport of other electrolytes in the mixture.

5. Acknowledgement

The authors gratefully acknowledge financial support by the Natural Sciences and Engineering Research Council of Canada.

1. W. NERNST. Z. Phys. Chem. Stoechiom. Verwandtschaftsl. **2**, 613 (1888); **4**, 129 (1889).
2. M. PLANCK. Ann. Phys. (Leipzig), **40**, 561 (1890).
3. A. EKMAN, S. LIUKKONEN, and K. KONTTURI. Electrochim. Acta, **23**, 243 (1978).
4. J. GARRIDO, S. MAFE, and J. PELLICER. J. Membr. Sci. **24**, 7 (1985).
5. H. J. V. TYRRELL and K. R. HARRIS. Diffusion in liquids. Butterworth, London. 1984. Chapt. 3.
6. D. D. FITTS. Nonequilibrium thermodynamics. McGraw–Hill, New York. 1962. Chapts. 7 and 8.
7. R. H. STOKES. J. Am. Chem. Soc. **72**, 763 (1950).
8. R. H. STOKES. J. Am. Chem. Soc. **73**, 3527 (1951).
9. D. G. LEAIST. J. Chem. Soc. Faraday Trans. 1, **78**, 3069 (1982).
10. D. G. LEAIST. J. Phys. Chem. **89**, 1486 (1985).
11. D. G. LEAIST. Aust. J. Chem. **38**, 249 (1985).
12. D. G. LEAIST and P. A. LYONS. J. Phys. Chem. **86**, 564 (1982).
13. R. A. ROBINSON and R. H. STOKES. Electrolyte solutions. 2nd ed. Academic Press, New York. 1959. App. 6.2.
14. E. L. CUSSLER and P. J. DUNLOP. J. Phys. Chem. **70**, 1880 (1966).
15. A. R. GORDON. Ann. N.Y. Acad. Sci. **46**, 285 (1945).
16. E. A. GUGGENHEIM and J. C. TURGEON. Trans. Faraday Soc. **51**, 747 (1955).

Appendix

The purpose of this appendix is to derive expressions for estimating ternary diffusion coefficients for aqueous HCl + NaOH mixtures. We will use the identity (5, 6)

$$[A1] \quad D_{ik} = \sum_{m=1}^{2} L_{im}\partial\mu_m/\partial C_k$$

where μ_m are the chemical potentials of the components. L_{im} are Onsager transport coefficients defined by flow equations for the components

$$[A2] \quad -J_i = \sum_{m=1}^{2} L_{im}\nabla\mu_m$$

According to the Nernst–Planck approximation, the flow of each species is proportional to the gradient in its electrochemical potential

$$[A3] \quad -j_i = l_{ii}\nabla\tilde{\mu}_i$$

where $l_{ii} = c_iD_i/RT$. R is the gas constant and T is the temperature. We number the solute species in aqueous HCl(1) + NaOH(2) as follows: $Cl^- = 1$, $Na^+ = 2$, $H^+ = 3$, and $OH^- = 4$.

The flux of the HCl component equals the flux of Cl^-. Also, the flux of the NaOH component equals the flux of Na^+.

$$[A4] \quad J_1(HCl) = j_1(Cl^-)$$

$$[A5] \quad J_2(NaOH) = j_2(Na^+)$$

The gradients in chemical potential of each component equals the sum of the gradients in electrochemical potential of the constituent species

$$[A6] \quad \nabla\mu_1(HCl) = \nabla\tilde{\mu}_1(Cl^-) + \nabla\tilde{\mu}_3(H^+)$$

$$[A7] \quad \nabla\mu_2(NaOH) = \nabla\tilde{\mu}_2(Na^+) + \nabla\tilde{\mu}_4(OH^-)$$

Electroneutrality and local chemical equilibrium of H^+ and OH^- provide the relations

$$[A8] \quad j_1(Cl^-) + j_4(OH^-) = j_2(Na^+) + j_3(H^+)$$

$$[A9] \quad \nabla\tilde{\mu}_3 + \nabla\tilde{\mu}_4 = 0$$

Substitution of eqs. [A3]–[A9] into eq. [A2] gives

[A10] $RTL_{11} = c_1D_1(c_2D_2 + c_3D_3 + c_4D_4)/A$

[A11] $RTL_{12} = RTL_{21} = c_1D_1c_2D_2/A$

[A12] $RTL_{22} = c_2D_2(c_1D_1 + c_3D_3 + c_4D_4)/A$

where A stands for

[A13] $A = c_1D_1 + c_2D_2 + c_3D_3 + c_4D_4$

The component chemical potentials are given by the expressions

[A14] $\mu_1(\mathrm{HCl}) = \mu_1^0(\mathrm{HCl}) + RT \ln [c_3(\mathrm{H^+})c_1(\mathrm{Cl^-})y_3y_1]$

[A15] $\mu_2(\mathrm{NaOH}) = \mu_2^0(\mathrm{NaOH}) + RT \ln [c_2(\mathrm{Na^+})c_4(\mathrm{OH^-})y_2y_4]$

in which y_i are ionic activity coefficients (molar concentration scale). Concentrations of H^+ and OH^- are related by

[A16] $K_w = c_3(\mathrm{H^+})c_4(\mathrm{OH^-})y_3y_4$

where K_w is the dissociation constant for water. We will assume that the activity coefficients are given by the Debye–Hückel equation (16)

[A17] $\ln y_i = -S_f z_i^2 I^{1/2}/(1 + I^{1/2})$

where I is the ionic strength and $S_f = 1.17$ for aqueous solutions at 25°C.

Excess HCl ($C_1 > C_2$)

For mixtures containing excess HCl: $c_1(\mathrm{Cl^-}) = C_1$, $c_2(\mathrm{Na^+}) = C_2$, $c_3(\mathrm{H^+}) = C_1 - C_2$ and $c_4(\mathrm{OH^-}) = K_w/(C_1 - C_2)y_3y_4 \cong 0$. Differentiation provides

[A18] $(RT)^{-1}\partial\mu_1/\partial C_1 = C_1^{-1} + (C_1 - C_2)^{-1} - S_f C_1^{1/2}/(1 + C_1^{1/2})^2$

[A19] $(RT)^{-1}\partial\mu_1/\partial C_2 = (RT)^{-1}\partial\mu_2/\partial C_1 = (C_2 - C_1)^{-1}$

[A20] $(RT)^{-1}\partial\mu_2/\partial C_2 = C_2^{-1} + (C_1 - C_2)^{-1}$

Finally, expressions for the ternary diffusion coefficients may be obtained by substituion of eqs. [A10]–[A12] and [A18]–[A20] into eq. [A1]. If activity coefficient terms are omitted, the expressions for D_{ik} simplify considerably,

[A21] $D_{11} = t_1D_3 + (1 - t_1)D_1$

[A22] $D_{12} = t_1(D_2 - D_3)$

[A23] $D_{21} = t_2(D_1 - D_3)$

[A24] $D_{22} = t_2D_3 + (1 - t_2)D_2$

Here t_i refers to the transference number of ion i defined by

[A25] $t_i = c_iz_i^2D_i \Big/ \sum_{k=1}^{4} c_kz_k^2D_k$

Excess NaOH ($C_2 > C_1$)

When excess NaOH is present, $c_1(\mathrm{Cl^-}) = C_1$, $c_2(\mathrm{Na^+}) = C_2$ as before, but $c_4(\mathrm{OH^-}) = C_2 - C_1$ and $c_3(\mathrm{H^+}) = K_w/(C_2 - C_1)y_3y_4 \cong 0$. Expressions for derivatives $\partial\mu_m/\partial C_k$ for these solutions can be obtained by interchanging subscripts 1 and 2 in eqs. [A18] and [A19].

If activity coefficient corrections are dropped, we obtain

[A26] $D_{11} = t_1D_4 + (1 - t_1)D_1$

[A27] $D_{12} = t_1(D_2 - D_4)$

[A28] $D_{21} = t_2(D_1 - D_4)$

[A29] $D_{22} = t_2D_4 + (1 - t_2)D_2$

Polarized overtone-combination bands in the near-infrared spectra of $K_2SnCl_4 \cdot H_2O$ and $KSnCl_3 \cdot H_2O$ at cryogenic temperatures

IAN M. WALKER
York University, Downsview, Ont., Canada M3J 1P3

AND

PAUL J. MCCARTHY
Canisius College, Buffalo, NY 14028, U.S.A.

Received November 4, 1985

IAN M. WALKER and PAUL J. MCCARTHY. Can. J. Chem. **64**, 1012 (1986).

The near-infrared (nir) spectra of $K_2SnCl_4 \cdot H_2O$ and $KSnCl_3 \cdot H_2O$ contain many highly polarized absorptions, due largely, if not completely, to combinations of vibrations of the water molecules in the crystals. The polarization of the absorptions can be related to the site symmetry of the water molecule. In $K_2SnCl_4 \cdot H_2O$ combination bands based on rocking, wagging, and twisting librations are seen, from which it is possible to definitively identify the rocking libration. The librations are much less in evidence in the spectra of $KSnCl_3 \cdot H_2O$. Sets of normal mode anharmonicity constants have been calculated from the energies of the absorptions.

IAN M. WALKER et PAUL J. MCCARTHY. Can. J. Chem. **64**, 1012 (1986).

Les spectres du $K_2SnCl_4 \cdot H_2O$ et du $KSnCl_3 \cdot H_2O$ dans le proche infrarouge (pir) contiennent plusieurs absorptions hautement polarisées qui sont dues principalement, si non uniquement, à des combinaisons de vibrations de molécules d'eau dans les cristaux. La polarisation des absorptions peut être reliée au site de symétrie de la molécule d'eau. Dans le $K_2SnCl_4 \cdot H_2O$, on peut observer des bandes de combinaison qui sont basées sur des librations de rotation, de balancement et de torsion; parmi celles-ci, on peut identifier d'une façon définitive la libration de rotation. Les librations sont beaucoup moins évidentes dans le spectre de $KSnCl_3 \cdot H_2O$. En se basant sur les énergies des absorptions, on a calculé des ensembles de constantes d'anharmonicité pour le mode normal.

[Traduit par la revue]

Introduction

The near-infrared (nir) spectra of water, alcohols, amides, etc., have proved most useful in the study of hydrogen bonding (1–3). In many cases, however, the vibrational overtone-combination features which appear in this region show severe broadening and overlap. This is a consequence of extensive coupling between the individual oscillators in concentrated media. This is especially true in ice, even at liquid nitrogen temperature (4).

In a recent article (5) we have shown that water overtone-combination bands in $M_2[FeCl_5H_2O]$ (M = Cs, K) are quite sharp at cryogenic temperatures. Since these nir features are considerably weaker than the fundamental bands, relatively thick (0.5 mm), oriented, single crystal samples may be used. The use of polarized light in this region has also revealed that these overtone-combination bands are excited only when the electric vector of the radiation is oriented along specific crystal directions. So far, our observations in this region have confirmed the notion that water molecules in salt hydrates are isolated from one another, and that they interact only modestly with neighboring halide ions via hydrogen bonding.

In this report we consider two further instances of this kind of salt hydrate, $K_2SnCl_4 \cdot H_2O$ and $KSnCl_3 \cdot H_2O$. The unusually high energies of the stretch fundamentals in these salts indicate that hydrogen bonding is considerably weaker than that encountered in $Cs_2[FeCl_5H_2O]$ (5). The spectrum of $K_2SnCl_4 \cdot H_2O$ in particular is remarkable for the number, sharpness, and distinct polarization of its bands. These features have enabled us to show that there is a definite relationship between the site symmetry of the water and the polarization of the spectrum, and to determine, possibly for the first time, values for the anharmonicities involving the librational modes.

Experimental

Crystal preparation

$K_2SnCl_4 \cdot H_2O$

Large needles of this substance appear when a solution containing 1 mol $SnCl_2$ and 2.5 mol KCl in 1 *M* HCl is evaporated under a stream of nitrogen. The crystals are for the most part cloudy in appearance, and examination under a microscope reveals an opaque band concentrated near the center of the crystal running along the needle axis. To obtain single-crystal spectra the needles must be mounted so that light passes through the clearer regions near the crystal edges.

$KSnCl_3 \cdot H_2O$

Clear transparent needles of this substance are obtained when a solution containing 1 mol $SnCl_2$ and 0.8 mol KCl in 1 *M* HCl is evaporated under nitrogen.

Both substances were dried *in vacuo*, and were characterized by ir spectroscopy using the highly distinctive water stretching vibrations reported in the literature (6, 7) as the criterion of purity.

Spectral data

Single crystals were mounted on the optical probe of a Displex cryogenic refrigerator and cooled to 10 K. Spectra were obtained on a Varian 2300 spectrophotometer. Polarized light, provided by Glan-Thompson prisms, was oriented along the extinction directions, which lie parallel and perpendicular to the needle axis in both cases.

Results and discussion

Structural data

The structure of $K_2SnCl_4 \cdot H_2O$ was solved originally in the space group *Pbnm* (D_{2h}^{16}, #62) with four formula units per unit cell (8). Subsequent authors (6) have transformed the data to the standard setting, *Pnma*, which we will use in our discussion. All atoms except hydrogen appear in the X-ray structure; this consists of trigonal pyramidal $SnCl_3^-$ units, K^+ ions, Cl^- ions, and water. The water is not attached to tin, but

rather, is weakly coordinated to potassium. There is a crystallographic plane of symmetry normal to the b axis, and the oxygen of water, two of the four chloride ions, and the tin atom all lie in this plane. The proton positions have been located by nmr studies (9, 10). One proton, H(1), is involved in a normal quasi-linear hydrogen bond to chloride ion, Cl(3), lying in the symmetry plane, while the other proton, H(2), forms a bifurcated hydrogen bond to two chloride ions, Cl(2), lying an equal distance above and below this symmetry plane. Thus the water molecule as a whole lies in the symmetry plane, the site symmetry being C_s. Deuteration studies on the ir fundamentals of $K_2SnCl_4 \cdot H_2O$ are entirely consistent with the presence of only one type of water in the unit cell (6). A list of all atomic coordinates has been reported (6).

The growth habit of $K_2SnCl_4 \cdot H_2O$ is such that needle growth takes place preferentially along the crystal b direction. Therefore a spectrum with electric vector E parallel to the needle axis ($E \| b$) excites vibrations which are normal to the plane of the water molecule (symmetry A''). These are the twisting (ρ_t) and the wagging (ρ_w) vibrations. The $E \perp b$ spectrum will contain the vibrations which take place in the plane of the water molecule (symmetry A'). These are the two OH stretches, the HOH bend, and the rocking (ρ_r) vibration. Thus in the reduction from C_{2v} (the symmetry of free water) to C_s, A_1 and B_1 become A', while A_2 and B_2 become A''.

The details of the structure of $KSnCl_3 \cdot H_2O$ have not been fully elucidated. The crystals are known to be orthorhombic, with diffraction symmetry *mmm* (7). Deuteration studies on the ir fundamental bands indicate that there is more than one water site in this lattice (7). These differences also appear in the ir stretch fundamentals of the fully protiated materials at low temperatures. From the general similarity of the nir spectra of the two compounds, however, we can conclude that the waters in $KSnCl_3 \cdot H_2O$ also lie in planes perpendicular to the needle axis.

Infrared fundamental spectra

The ir fundamentals for both crystals are listed in Table 1. In these compounds there is no distinction between the symmetric and antisymmetric stretches. We will, however, use these as convenient labels in the ensuing discussion. Three libration bands are found in the ir spectrum of $K_2SnCl_4 \cdot H_2O$; in environments of higher symmetry the ir spectrum of water can show only two such bands.

Overtone-combination spectra

It is well known that when water is engaged in hydrogen bonding the OH stretches are lowered and the HOH bend is raised in frequency (11). The stronger the hydrogen bonding the greater the effect. The frequencies of the fundamentals in $K_2SnCl_4 \cdot H_2O$ and $KSnCl_3 \cdot H_2O$ indicate that hydrogen bonding is weak in both, but weaker in the latter. Therefore, since almost all the combination bands contain at least one stretch, comparable bands in the spectra of the two compounds will in general be at higher energy in $KSnCl_3 \cdot H_2O$.

If one lists the normal vibrations of a crystal such as $K_2SnCl_4 \cdot H_2O$, then calculates the energy of all combinations which fall in the region 3800 – 12 000 cm^{-1}, then compares this long list with the observed spectrum, one reaches the conclusion that only a small fraction of the possible bands have appreciable intensity. The following general guidelines are useful for assigning bands in the water overtone-combination region:

(*a*) Binary combinations are in general considerably more intense than ternary combinations, while quaternary combinations are rarely seen unambiguously.

(*b*) The intensities of binary combinations usually fall off with increasing energy. This suggests that combination bands steal intensity from the fundamentals. The intensity-stealing mechanism appears to obey a $1/\Delta E$ law, where ΔE is the separation of the combination level from the stretch fundamentals around 3500 cm^{-1}.

(*c*) The fundamentals which combine to give observable bands must involve some significant motion of the water molecule. The commonest features are built on stretches, bends, and librations of water. We have been unable to find evidence that metal–oxygen or skeletal vibrations of metal chromophores contribute to the nir spectra of water in complexes. Translational motion of noncoordinated water could contribute to combination bands. There are, however, no instances where water translations have been unambiguously identified.

(*d*) Factor group splittings do not appear to be a major consideration in crystals where the water molecules are isolated from one another by several bonds. Therefore, for the compounds described here, our analysis will be based on site symmetries alone.

(*e*) The energy of a combination band will be close to, but usually somewhat less than, the sum of the energies of the fundamentals involved in it. This lowering is due to the varying degrees of anharmonicity in the combination bands.

(*f*) Finally, the normal electric dipole selection rules apply to the nir bands. The symmetry of a combination state is simply the direct product of the symmetries of the fundamentals of which it is composed.

TABLE 1. Fundamental bands in the infrared spectra of $K_2SnCl_4 \cdot H_2O$ and $KSnCl_3 \cdot H_2O$ at 113 K[a]

Mode	$K_2SnCl_4 \cdot H_2O$[b]	$KSnCl_3 \cdot H_2O$[c]
ν_1 (ν_s)	3436	3558, 3550
ν_2 (δ)	1622	1616, 1612, 1602
ν_3 (ν_a)	3543	3632
ν_4 (L_1)	530	427
ν_5 (L_2)	458	—
ν_6 (L_3)	427	—

[a]All data are in cm^{-1}. Symbol L refers to libration.
[b]Data from ref. 6.
[c]Data from ref. 7.

The spectra of the two compounds in the nir region are shown in Figs. 1 and 2. The great range of intensities should be noted. The weakest features near 10 000 cm^{-1} (not shown in the figures) can barely be seen above the background in clear, thick crystals. These features are about 0.002–0.003 times as intense as the strongest bands near 4000 cm^{-1}.

For $KSnCl_3 \cdot H_2O$ the polarizations are labeled 1 and 2, since the structure of the crystal is not known. The similarity of the spectra with those of $K_2SnCl_4 \cdot H_2O$ strongly suggest, however, that polarizations (pol.) 1 and 2 are perpendicular and parallel, respectively, to a unique axis. A general difference between the two compounds is this: the nir bands containing one or more librational quanta are stronger, sharper, and more numerous in the spectra of $K_2SnCl_4 \cdot H_2O$. This is related in part to the fact that this compound shows three librational bands in its ir fundamental spectrum while $KSnCl_3 \cdot H_2O$ shows only one (Table 1). Bands involving only stretches and bends have

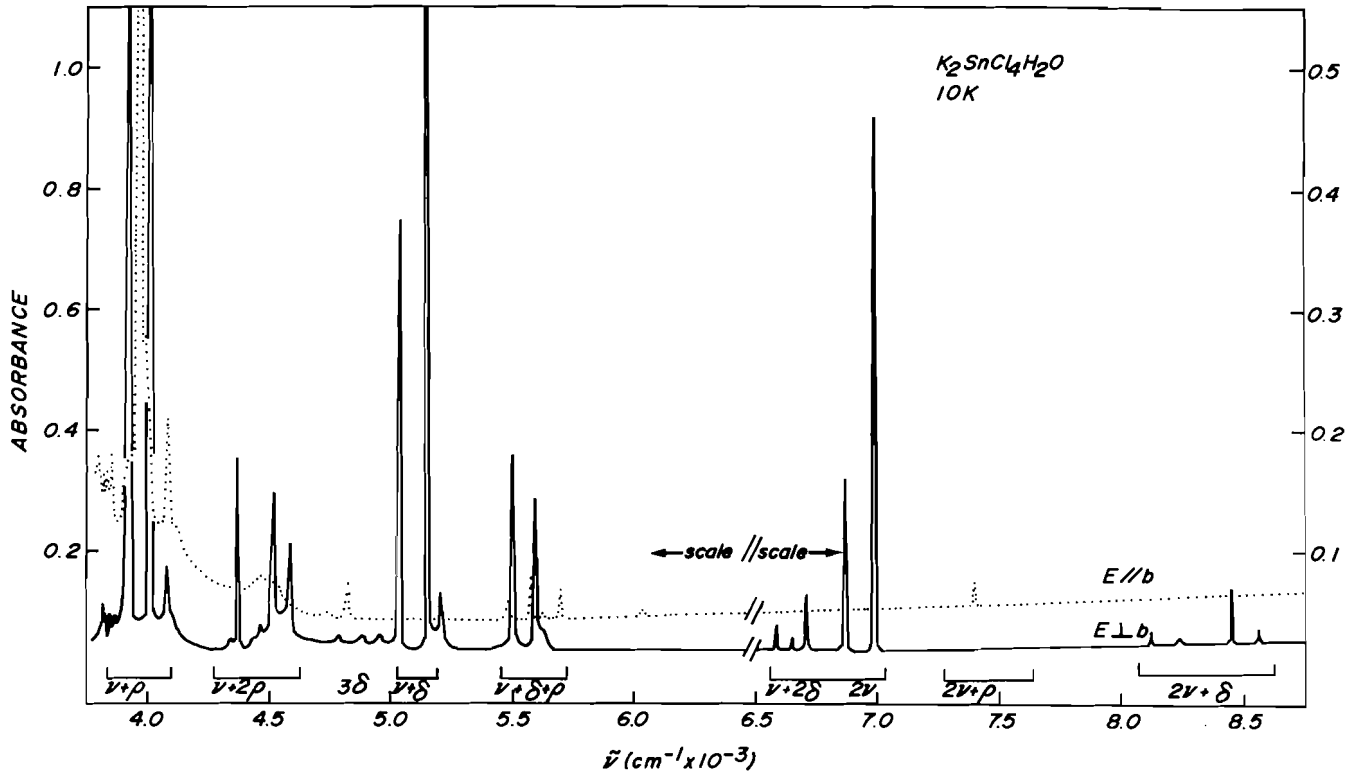

FIG. 1. Near-infrared spectra of single crystals of $K_2SnCl_4 \cdot H_2O$ at 10 K. The electric vector is oriented parallel (dotted line) and perpendicular (solid line) to the needle *b* axis. Rough assignments are shown beneath each band group. Band energies are listed in Table 2.

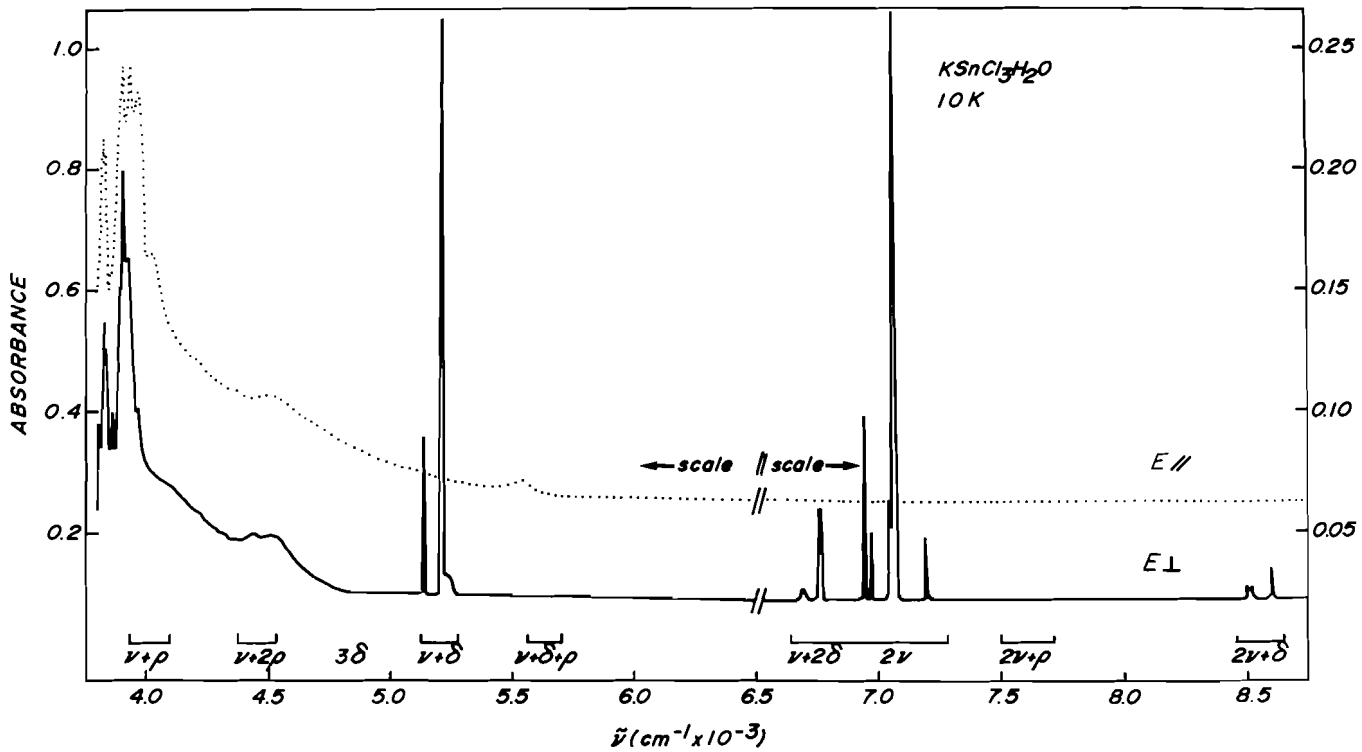

FIG. 2. Near-infrared spectra of single crystals of $KSnCl_3 \cdot H_2O$ at 10 K. The electric vector is oriented parallel (dotted line, pol. 2) and perpendicular (solid line, pol. 1) to the needle axis. Rough assignments are shown beneath each band group. Band energies are listed in Table 2.

similar intensity and sharpness in the two compounds. In Figs. 1 and 2 the general assignments for the various groups of bands are indicated. These are based on considerations of the symmetry, energy, and intensity of the bands. Table 2 lists the energies of all reproducible features of the spectra of both compounds (3800–9000 cm^{-1}) together with band assignments and calculated energies for most bands. The band positions are estimated to be accurate to $\pm 1\ cm^{-1}$. The method of energy calculation is discussed below.

To supplement the information contained in the figures and tables, we will make some comments on the various regions of the spectra.

Binary stretch–libration combinations (3800–4150 cm^{-1})

Since there are two OH stretches and three librations for $K_2SnCl_4 \cdot H_2O$, six possible binary states around 4000 cm^{-1} may arise. Two will have symmetry A' and should appear in the $E \perp b$ spectrum. The other four will be A'' and should appear in the $E \| b$ spectrum. Because of the high energy of the fundamental stretches in $K_2SnCl_4 \cdot H_2O$, almost all the expected features are actually seen in this region.

The $E \perp b$ spectrum shows two very strong bands at 3908 and 4010 cm^{-1}. Symmetry considerations indicate that these are the combinations of the two stretches with the rocking vibration. This analysis implies in turn that the middle of the three librations (458 cm^{-1}) must be the rocking vibration.

The $E \| b$ spectrum shows a very intense band whose peak (3959 cm^{-1}) could not be recorded even in a very thin crystal; it is flanked by two much weaker bands. The central band probably consists of two combinations which are expected to have almost the same energy, namely, $\nu_s + r_t$ and $\nu_a + \rho_w$. It is not clear why these combinations are so strong, while the other two ($\nu_s + \rho_w$ and $\nu_a + \rho_t$).

In this region the spectrum of $KSnCl_3 \cdot H_2O$ (pol. 1) shows two bands at 3823 and 3901 cm^{-1} (separation 78 cm^{-1}). These represent the combination of the OH stretches with a libration. The two OH stretches are separated by ca. 82 cm^{-1} in the ir spectrum, and the only libration observed there is at 427 cm^{-1} (7). The symmetry of this single libration is uncertain. The fact that nir bands appear around 3900 cm^{-1} in both polarizations with essentially the same energy may mean a near degeneracy of two librations of different symmetry. But, as in $K_2SnCl_4 \cdot H_2O$, the spectrum of pol. 2 in this region is somewhat more complex than that of the other polarization, an observation which suggests similar site symmetry for water in the two complexes. In addition to the two principal peaks (3826 and 3904 cm^{-1}), pol. 2 shows other features at higher energy which cannot, at present, be assigned.

Ternary stretch–libration combinations (4150–4700 cm^{-1})

At about 4500 cm^{-1} there is a series of bands in the spectra of $K_2SnCl_4 \cdot H_2O$. Combination of the two stretches with pairs of librations can give rise to 12 states. The $E \perp b$ spectrum is quite rich and seven absorptions of varying intensity and sharpness are seen, while the other spectrum is weaker and shows only three broad absorptions. The spectra agree with theory in that a larger number of bands (eight) is expected to occur in the A' ($E \perp b$) spectrum than in the A'' ($E \| b$) spectrum (four). Specific assignment of the bands in this region does not seem feasible at present.

The spectra of $KSnCl_3 \cdot H_2O$ in this region are poorer in detail, as is expected from the fact that only one libration is seen in the ir spectrum. Two principal bands in pol. 1 are separated by 80 cm^{-1}, the difference between the two fundamental stretches. The contrast of the sharpness of the bands in these spectra to those of $K_2SnCl_4 \cdot H_2O$ is worth noting.

(4700–5000 cm^{-1})

The polarized band at 4827 cm^{-1} in the $E \| b$ spectrum of $K_2SnCl_4 \cdot H_2O$ is totally absent at 292 K, and is barely visible above the background at 220 K. The crystal seems to go through a slight phase change at 202 K. This is seen as a sharp but noticeable rise in the baseline. On cooling the crystal from 160 to 10 K this band at 4827 cm^{-1} grows stronger with no change in baseline. It is not known what processes causes this absorption. No analogous band is found in $KSnCl_3 \cdot H_2O$.

The $E \perp b$ spectrum of $K_2SnCl_4 \cdot H_2O$ in this region contains three weak features, one of which (4782 cm^{-1}) is most likely the ternary $3\nu_2$ band. A similar very weak feature at 4716 cm^{-1} in pol. 1 of $KSnCl_3 \cdot H_2O$ is given the same assignment. The other features in both polarizations of $K_2SnCl_4 \cdot H_2O$ may be quaternary bands, several of which are calculated to appear in this region. They are of the type $\nu + 3\rho$.

Binary stretch–bend combinations (5000–5300 cm^{-1})

In this region both $K_2SnCl_4 \cdot H_2O$ and $KSnCl_3 \cdot H_2O$ show two intense, completely polarized bands, 5037, 5140 and 5137, 5213 cm^{-1}, respectively. These bands are readily assigned to the two stretch–bend combinations.

Since ν_1 of $KSnCl_3 \cdot H_2O$ is split into two components and ν_2 into three components, the band at 5137 cm^{-1} could have six components and the 5213 cm^{-1} band could have three components. This is, however, *not* seen. The sharp bands at 5137 and 5213 cm^{-1} are singlets with $\Delta\nu_{1/2} = 3.3$ and 4.4 cm^{-1}, respectively.

In $M_2[FeCl_5H_2O]$ (M = Cs, K) only one band is seen in this region (5), and it occurs in only one polarization. This transition was assigned in both cases to $\nu_a + \delta$, and in neither molecule was there any evidence for the corresponding $\nu_s + \delta$ transition. In $Cs_2[FeCl_5H_2O]$ the water lies on a C_{2v} site (5), while in $K_2[FeCl_5H_2O]$ there is evidence that a symmetry plane bisects the water molecule (12). Thus in these two crystals there is a symmetry distinction between the symmetric and antisymmetric stretching modes. The absence of the $\nu_s + \delta$ combination appears therefore to be a property of water in higher symmetry sites. In $K_2SnCl_4 \cdot H_2O$ the two stretches belong to the same symmetry species, and intensity transfer from one stretch–bend combination to the other can take place.

In $K_2SnCl_4 \cdot H_2O$ the weak band at 5209 cm^{-1} is assigned to the quaternary band $3\delta + \rho$ which appears to gain intensity from the nearby binary band $\nu_a + \delta$. The same assignment can be made for the double band at 5237, 5246 cm^{-1} in $KSnCl_3 \cdot H_2O$. The fit for the latter is poor because in the calculation x_{24} was set equal to zero. The splitting reflects the splitting in the fundamental bending vibration.

Stretch–bend–libration combinations (5300–6000 cm^{-1})

In $K_2SnCl_4 \cdot H_2O$ six such bands are expected some 500 cm^{-1} higher in energy than the stretched–bend combinations. They should show the same polarization as the binary stretch + libration modes. The A' spectrum of $K_2SnCl_4 \cdot H_2O$ contains two strong features which correspond to the two $\nu + \delta + L_2$ combinations. Each band is actually a closely spaced doublet, 5498 (sh) + 5504 cm^{-1}, and 5594 + 5606 cm^{-1} (sh). This may mean that at 10 K there are two slightly different sites for the

TABLE 2. Near-infrared spectra of $K_2SnCl_4 \cdot H_2O$ and $KSnCl_3 \cdot H_2O$ at 10 K

$K_2SnCl_4 \cdot H_2O$				$KSnCl_3 \cdot H_2O$			
		Obs.				Obs.[d]	
Mode[a]	Calcd.[b]	$\perp b(A')$	$\parallel b(A'')$	Mode[a]	Calcd.[b,c]	Pol. 1	Pol. 2.
(16)*	3859	3892(sh)	3859	(14)	3977	3823	3826
(15)	3908	3908	3908(sh)	(34)	4059	3901	3904
(14)(36)*	3959		3959				3924
(35)	4010	4010	4002(sh)			3944(sh)	3954
(34)*	4078	4076	4078				4030(sh)
(2255)	4104	4094					
(2256)*	4131		4118(sh)				
	4282	4340	4360			4161	4220
	to	4362					4364
	4613	4371(sh)		(144)	4404	4440	
	(12	4432		(344)	4486	4520	4516
	bands)	4455	4468				
		4513	4525				
		4579					
(222)	4782	4782		(222)	4716	4716	
(1666)*	4705						
			4748				
(3666)*	4791						
See text			4827				
(1456)	4854	4876					
(1445)	4954	4951					
(12)	5031	5037		(12)	5137	5137	
(32)	5139	5140		(32)	5213	5213	
(2225)	5219	5209				5237	
				(2224)	5143		
						5246	
(126)*	5476		5484	(124)	5564		5547
		5498(sh)		(324)	5640		
(125)	5496						
		5504					
(124)*	5572						
			5570				
(236)*	5577						
		5594					
(235)	5599						
		5606(sh)					
?			5619				
?		5635					
?			5674(sh)				
(234)*	5692		5693				
(2356)*							
	6037		6035				
(1245)*							
(122)	6598	6586		(122)	6686	6689	
						6760	
(322)	6707	6705		(322)	6756		
						6770	
						6941	
(11)	6648	6649		(11)	6956		
						6970	
						7045(sh)	
(13)	6869	6869		(13)	7052		
						7058	
(33)	6988	6988		(33)	7192	7191	
(336)*	7393						
			7398				
(134)*	7397						

TABLE 2. (*concluded*)

$K_2SnCl_4 \cdot H_2O$				$KSnCl_3 \cdot H_2O$			
		Obs.				Obs.[d]	
Mode[a]	Calcd.[b]	$\perp b(A')$	$\parallel b(A'')$	Mode[a]	Calcd.[b,c]	Pol. 1	Pol. 2.
(112)	8216	8125				8503	
				(112)	8520		
(2223)	8247	8244				8519	
(123)	8438	8454		(132)	8610	8611	
(233)	8558	8566		(332)	8744		

[a]Numbers in parentheses give the fundamentals used to calculate the energy. Fundamentals are listed in Table 1 and non-zero anharmonicities used in calculating the energies are shown in Table 3. Starred (*) combinations are those expected in the A'' spectrum.

[b]Symmetry of overtone containing a libration assumes L_2 (458 cm^{-1}) is ρ_r. A'' vibrations are ρ_w and ρ_t; rest are A'.

[c]Site symmetry of water assumed same as in $K_2SnCl_4 \cdot H_2O$; fundamentals used in calculations are $\nu_1 = 3550$, $\nu_2 = 1610$, $\nu_3 = 3632$, $\nu_4 = 427$ cm^{-1}.

[d]Pol. 1 and pol. 2 were recorded with the electric vector, E, perpendicular and parallel, respectively, to the needle axis.

water molecules. As noted above, a small phase change occurs at 202 K, and this could bring about such a situation. The A'' spectrum shows three principal peaks. Two of the four combinations expected here, $\nu_a + \delta + L_3$ and $\nu_s + \delta + L_1$ should have very nearly the same energy. This provides the basis for the assignments shown in Table 2. The nature of the other weak features seen in this region is unknown. No quaternary combinations are calculated to appear between 5400 and 5900 cm^{-1}.

In this region the pol. 2 spectrum of $KSnCl_3 \cdot H_2O$ shows one certain, broad band at 5547 cm^{-1} and possibly other bands at lower energy. The uncertainty arises from the fact that free water in the optical path of the spectrophotometer absorbs in this region and obscures weak absorptions that might occur here. The band(s) again represent $\nu + \delta + \rho$ combination(s).

Binary stretch and ternary strech–bend combinations (6000–7250 cm^{-1})

In both crystals these two sets of bands ($\nu + 2\delta$ and 2ν) are completely polarized, as expected. In $K_2SnCl_4 \cdot H_2O$ the two sets overlap, but in $KSnCl_3 \cdot H_2O$ they do not (see Table 2). For the $\nu + 2\delta$ set in each compound the separation is approximately the difference between the two fundamental stretches. In $KSnCl_3 \cdot H_2O$ the band at higher energy is a doublet of 9.5 cm^{-1} separation. Since the fundamental HOH bend is split into three components at 113 K (7), it is not surprising that some splitting of this overtone is observed. Perhaps more surprising is the fact that splitting of the lower-energy band is not observed, since the symmetrical stretch is also a doublet at 113 K.

For the 2ν combinations, $K_2SnCl_4 \cdot H_2O$ shows the expected three bands. They differ greatly in intensity, $2\nu_1$ being very weak, $2\nu_3$ strong, and $\nu_1 + \nu_3$ intermediate. But it is worth noting that the relative intensities of the three bands vary considerably as the face on which the light falls is changed. Such a change in crystal orientation can cause variation in the extent of mixing of the two stretches in the plane perpendicular to b and consequent variations in band intensity. The two $\nu + 2\delta$ bands show a similar variation in intensity upon change of crystal orientation, and in the various orientations $\nu_1 + 2\nu_2$ is weaker than $\nu_3 + 2\nu_2$.

The spectrum of $KSnCl_3 \cdot H_2O$ is considerably more complex in this region due to the splitting of the fundamentals. Reasonable assignments are listed in Table 2.

Other ternary combinations (7250–10 300 cm^{-1})

No clear example of the combination $2\nu + \rho$ is seen, with the possible exception of the weak 7398 cm^{-1} ($E \parallel b$) band in $K_2SnCl_4 \cdot H_2O$. Two possible assignments are shown in Table 2.

The set of bands at about 8500 cm^{-1} is in both compounds completely polarized, as expected for $2\nu + \delta$. The spectra of $K_2SnCl_4 \cdot H_2O$ contains four rather weak absorptions, three of them sharp and one quite diffuse. The three sharp bands, so alike in contour, are ascribed to the $2\nu + \delta$ absorptions. It seems most likely that the diffuse band is a quaternary combination, $\nu + 3\delta$. Fermi interaction of the various combinations may be the reason the fit between calculated and observed energies for the $2\nu_1 + \nu_2$ band is rather poor.

In $KSnCl_3 \cdot H_2O$ the lower energy band in this region is a doublet (16.0 cm^{-1} separation). This again seems to reflect the splitting of the fundamentals, ν_1 and ν_2. In the spectra we see no evidence of the $\nu_2 + 2\nu_3$ combination.

In the A' spectrum of $K_2SnCl_4 \cdot H_2O$ two very weak absorptions which may possibly be ascribed to 3ν are found at 9978 and 10 053 cm^{-1}. It is likely that an extremely weak absorption ca. 10 330 cm^{-1} in the analogous spectrum of $KSnCl_3 \cdot H_2O$ also represents this combination.

Calculation of band energies

For a molecule of more than three atoms without degenerate vibrations the combination and overtone bands will have energy (ref. 13, pp. 205–208)

$$[1] \quad G_0(v_1, v_2, \ldots) = \sum_i \omega^0{}_i v_i + \sum_i \sum_{k \geq i} x^0{}_{ik} v_i v_k$$

The energy is referred to the ground state and not to the minimum in the potential well. In this equation v_i is the vibrational quantum number of normal mode, i, $x^0{}_{ik}$ are the normal mode anharmonicity constants, and $\omega^0{}_i$ are the zero-order frequencies. The $\omega^0{}_i$ are related to the observed fundamentals, ν_i, as follows:

$$[2] \quad \omega^0{}_i = \omega_i + x_{ii} + \frac{1}{2}\sum_{k \neq i} x_{ik} + \ldots$$

$$[3] \quad \nu_i = \omega^0{}_i + x_{ii}$$

Here $x_{ik} = x_{ki}$ and, if higher powers are neglected, $x^0{}_{ik} = x_{ik}$.

Using the above equations and the observed absorptions we

TABLE 3. Anharmonicities[a,b]

	1	2	3	4	5	6
$K_2SnCl_4 \cdot H_2O$						
1	−112	−27	−110	−7	14	−4
2		−14	−26	18	−7	22
3			−49	5	9	−11
$KSnCl_3 \cdot H_2O$						
1	−72	−23	−130			
2		−19	−29			
3			−36			
Gaseous water[c]						
1	−42.6	−15.9	−165.8			
2		−16.8	−20.3			
3			−47.6			

[a]All data are in cm^{-1}. Anharmonicities not listed were assumed equal to zero in calculating band energies.
[b]Row and column numbers refer to the fundamentals in Table 1.
[c]Reference 14.

have calculated sets of normal mode anharmonicities (Table 3) which reproduce most of the bands nicely, as can be seen in Table 2.

The method used to calculate the anharmonicities for $K_2SnCl_4 \cdot H_2O$ is as follows: from the ir overtone, $2\nu_2$, x_{22} was calculated; from the $\nu + \delta$ bands x_{12} and x_{23}, from the 2ν bands x_{11}, x_{33}, and x_{13}, from the $\nu + \rho$ region x_{ik} ($i = 1, 3$; $k = 4, 5, 6$), and from the $\nu + \delta + \rho$ region x_{2k} ($k = 4, 5, 6$) were determined. The set of bands in the 4300–4600 cm^{-1} range, due to $\nu + 2\rho$, should in theory provide the basis for the calculation of the interlibrational anharmonicities. The specific identity of most of the bands is, however, uncertain, and we have not been able to determine values for these constants. Accordingly, in the calculations they have been equated to zero.

What precision can be attached to the anharmonicities listed in Table 3? Let us again consider $K_2SnCl_4 \cdot H_2O$. The calculations depend on the energies of the overtone and of the fundamentals of which it is composed. If each is accurate to ± 1 cm^{-1}, then there is a built-in uncertainty of ± 3 cm^{-1} for x_{ik} determined from a binary combination and ± 4 cm^{-1} for one from a ternary combination. Since the librations are broad in the fundamental spectrum, a larger uncertainty is expected in combinations involving them. Most ternary and quaternary combinations involve two or more different x_{ik} and so the uncertainties will be cumulative. A further source of uncertainty is the possibility of Fermi interaction between bands of the same symmetry and like energy. The observed value of the overtone might depend strongly on such interaction and, if used in calculating an anharmonicity constant, could lead to a completely misleading value. We have tried to avoid this, but have not had the mathematical apparatus to evaluate possible Fermi interactions. The consistency of the results and their comparison with gaseous water suggest that the x_{ik} involving only ν_i ($i = 1$, 2, 3) are quite acceptable. The other values listed are, we believe, also acceptable, but probably contain a greater uncertainty than the first set.

In the case of $KSnCl_3 \cdot H_2O$ the calculated anharmonicities are of lower precision than those for $K_2SnCl_4 \cdot H_2O$. The reasons for this are the multiplicity of two of the ir fundamentals with the consequent use of average energies in the calculation of the anharmonicities, and the lack of exact knowledge of the crystal structure. In addition, the appearance of only one libration instead of the expected three in the ir spectrum results in less rich overtone spectra. This, in turn, has made it impossible to calculate anharmonicities involving the libration.

While the anharmonicities of $KSnCl_3 \cdot H_2O$ are less precise than those of $K_2SnCl_4 \cdot H_2O$, the corresponding values for the two compounds show similar trends. These in turn are much like those of gaseous water. For comparison, values for the latter are also listed in Table 3 with, however, less precision than given in the original reference (14).

Certain specific points may be noted: (*1*) The anharmonicities involving only ν_i ($i = 1, 2, 3$) are all negative, as is also true for gaseous water. (*2*) About half of the anharmonicities involving librations are positive. While this is less usual, positive values have been found in many small molecules, as for example, gaseous CO_2, N_2O, and HCN (ref. 13, pp. 272–280). (*3*). In $K_2SnCl_4 \cdot H_2O$, in which there is no symmetry distinction between the two OH stretches, the anharmonicities x_{11} and x_{13} have nearly the same value. This is not true of $KSnCl_3 \cdot H_2O$ nor of gaseous water. (*4*) Certain anharmonicities show distinct trends in going from gaseous water to water in crystals: x_{11} is larger and x_{13} is smaller in crystals than in gas; x_{12} and x_{23} are slightly larger in crystals; x_{22} and x_{33} appear to be less affected. The variations in the stretch–stretch anharmonicity constants may be due to variations in the Fermi interaction on going from gas to crystal phase. Therefore we cannot rule out the possibility that there may actually be no difference between these gas and crystal anharmonicities once they have been corrected for this effect.

Finally, we should point out that the normal mode description of overtone bands is no longer considered to be accurate. Its use in the above analysis was dictated by convenience in the comparison of the small differences between our crystal data and the data for gas phase water (14). Current theory holds that analysis in terms of local excitation of individual O—H oscillators (local mode model) is a better description of reality (15). The implications of this for the overtone spectra of water in crystals will be explored in detail in later communications.

Conclusions

In both compounds of this study most bands are highly polarized, and the polarizations are consistent with the plane of the water molecules being perpendicular to the needle axis.

We have shown that for $K_2SnCl_4 \cdot H_2O$ it is possible to assign and characterize the librations of bound water. This could not be done on the basis of the fundamental ir spectrum (6).

An extensive list of normal mode anharmonicities has been calculated for both molecules. Those involving librations appear to be the first reported for such vibrations.

In future articles we will show how the nir spectrum can be used to study cooperative excitation in oriented chains of water molecules.

Acknowledgements

I.M.W. thanks the Natural Sciences and Engineering Research Council of Canada for its generous financial support. P.J.M. is grateful to Research Corporation for the funds to purchase the Displex cryogenic refrigerator.

1. H. YAMATERA, B. FITZPATRICK, and G. GORDON. J. Mol. Spectroscopy, **14**, 268 (1964); O. D. BONNER. Infrared Phys. **12**, 109 (1972).
2. J. G. BAYLY, V. B. KARTHA, and W. H. STEVENS. Infrared Phys. **3**, 211 (1963).

3. W. A. P. LUCK and W. DITTER. Z. Naturforsch. B: Anorg. Chem. Org. Chem. Biochem. Biophys. Biol. **24B**, 482 (1969).
4. D. KROH and A. RON. Chem. Phys. Lett. **36**, 527 (1975).
5. P. J. MCCARTHY and I. M. WALKER. Spectrochim. Acta Part A, **39A**, 827 (1983).
6. M. FALK, C. H. HUANG, and O. KNOP. Can. J. Chem. **52**, 2380 (1974).
7. M. FALK, C. H. HUANG, and O. KNOP. Can. J. Chem. **52**, 2928 (1974).
8. B. KAMENAR and D. GRDENIĆ. J. Inorg. Nucl. Chem. **24**, 1039 (1962).
9. A. A. SILVIDI and J. W. MCGRATH. Bull. Am. Phys. Soc. **4**, 471 (1959).
10. J. W. MCGRATH and A. A. SILVIDI. J. Chem. Phys. **34**, 322 (1961).
11. W. C. HAMILTON and J. A. IBERS. Hydrogen bonding in solids. W. A. Benjamin, New York. 1968. p. 85.
12. M. FALK, C. H. HUANG, and O. KNOP. Can. J. Chem. **53**, 51 (1975).
13. G. HERZBERG. Molecular spectra and molecular structure II. IR and raman spectra of polyatomic molecules. Van Nostrand, Princeton, NJ. 1945.
14. W. S. BENEDICT, N. GAILER, and E. K. PLYLER. J. Chem. Phys. **24**, 1139 (1956).
15. W. L. ELERT, P. R. STANNARD, and W. M. GELBART. J. Chem. Phys. **67**, 5395 (1977).

Isotope effects and activation parameters for the proton transfer reaction from 1-(4-nitrophenyl)-1-nitroethane to free anions and ion pairs of cesium *n*-propoxide in *n*-propanol solvent

ARNOLD JARCZEWSKI, GRZEGORZ SCHROEDER, AND PRZEMYSLAW PRUSZYNSKI
Department of Chemistry, Adam Mickiewicz University, Poznan, Poland

AND

KENNETH T. LEFFEK[1]
Department of Chemistry, Dalhousie University, Halifax, N.S., Canada B3H 4H6

Received June 20, 1985

This paper is dedicated to Professor Arthur N. Bourns

ARNOLD JARCZEWSKI, GRZEGORZ SCHROEDER, PRZEMYSLAW PRUSZYNSKI, and KENNETH T. LEFFEK. Can. J. Chem. **64**, 1021 (1986).

Rate constants for the proton and deuteron transfer from 1-(4-nitrophenyl)-1-nitroethane to cesium *n*-propoxide in *n*-propanol have been measured under pseudo-first-order conditions with an excess of base for four temperatures between 5 and 35°C. Using literature values of the fraction of cesium *n*-propoxide ion pairs that are dissociated into free ions, separate second-order rate constants for the proton and deuteron transfer to the ion pair and to the free ion have been calculated. The cesium *n*-propoxide ion pair is about 2.8 times more reactive than the free *n*-propoxide ion. The primary kinetic isotope effects for the two reactions are the same (k_H/k_D = 6.1–6.3 at 25°C) within experimental error. The enthalpy of activation is smaller for the ion-pair reaction and the entropy of activation more negative than for the free-ion reaction. For proton transfer, $\Delta H^{\pm}_{\text{ion pair}}$ = 8.3±0.2 kcal mol^{-1}, $\Delta H^{\pm}_{\text{ion}}$ = 9.6±1.0 kcal mol^{-1}, $\Delta S^{\pm}_{\text{ion pair}}$ = −12.3±0.6 cal mol^{-1} deg^{-1}, $\Delta S^{\pm}_{\text{ion}}$ = −10.1±3.4 cal mol^{-1} deg^{-1}. The greater reactivity of the ion pair relative to the free ion is interpreted in terms of the weaker solvation shell of the ion pair in the initial state.

ARNOLD JARCZEWSKI, GRZEGORZ SCHROEDER, PRZEMYSLAW PRUSZYNSKI et KENNETH T. LEFFEK. Can. J. Chem. **64**, 1021 (1986).

Opérant dans l'alcool propylique, dans des conditions de réactions de pseudo premier ordre, en présence d'un excès de base et à quatre températures allant de 5 à 35°C, on a mesuré les constantes de vitesse de réactions de transfert de protons et de deutérons du (nitro-4 phényl)-1 nitro-1 éthane vers le propylate de césium. Utilisant les données de la littérature relatives à la fraction des paires d'ions du propylate de césium qui sont dissociées en ions libres, on a calculé des constantes séparées de vitesse du deuxième ordre pour les transferts de protons et de deutérons vers les paires d'ions et vers les ions libres. La paire d'ions du propylate de césium est environ 2,8 fois plus réactive que l'ion propylate libre. À l'intérieur des erreurs expérimentales, les effets isotopiques cinétiques primaires sont les mêmes pour les deux réactions (k_H/k_D = 6,1–6,3 à 25°C). Par comparaison avec les valeurs correspondantes pour la réaction de l'ion libre, l'enthalpie d'activation de la réaction de la paire d'ions est plus petite alors que son entropie d'activation est plus négative. Pour la réaction de transfert de proton, $\Delta H^{\pm}_{\text{paire d'ions}}$ = 8,3 ± 0,2 kcal mol^{-1}, $\Delta H^{\pm}_{\text{ion}}$ = 9,6 ± 1,0 kcal mol^{-1}, $\Delta S^{\pm}_{\text{paire d'ions}}$ = −12,3 ± 0,6 cal mol^{-1} deg^{-1}, et $\Delta S^{\pm}_{\text{ion}}$ = −10,1 ± 3,4 cal mol^{-1} deg^{-1}. On interprète la plus grande réactivité de la paire d'ions par rapport à l'ion libre en fonction de la couche de solvatation plus faible de la paire d'ions dand l'état initial.

[Traduit par la revue]

Introduction

The different reactivity of free ion and ion-pair reagents in solution is well known (1, 2). Different relative reactivities for the two types of reagent have been observed under different circumstances, but it has frequently been assumed that ion-pair reactivity is negligibly small compared to that of the free ion. In 1956, Bevan and Monk (3) showed that the differences in second-order rate constants for the reaction of sodium, potassium, magnesium, calcium, and strontium thiosulfates with *n*-propyl bromide in mixed ethanol–water solvent could be eliminated completely if the rate constant was calculated with respect to the free thiosulfate ion. They assumed that ion pairs made no contribution to the reaction velocity and the rate constants for the free thiosulfate ion were found not only to be independent of the cation present, but also independent of the ion strengths of the solution (3). Cram *et al.* (4) investigated the rates of the racemization and exchange of 1-phenylmethoxyethane-1-*d* in dimethyl sulfoxide (DMSO) –potassium *tert*-butoxide. The order of the reaction with potassium *tert*-butoxide and other kinetic observations led them to conclude that potassium *tert*-butoxide in DMSO is largely in the form of ion pairs, but that only the dissociated *tert*-butoxide ion is chemically active, with the reactivity of the ion pairs vanishingly small in comparison. Leffek and Suszka (5) measured the second-order rate constants for the reaction of 4,4′-bis(dimethylamino)triphenylmethyl tetrafluoroborate carbonium ion with sodium methoxide in methanol and sodium ethoxide in ethanol. The results were used to evaluate the ion-pair dissociation constants for the two alkoxides, assuming that the ion-pair reactivity was negligibly small compared to that of the free ion. The dissociation constants based on this assumption were in good agreement with those determined from conductance measurements.

A spectrophotometric study of fluorenyl alkali metal salts by Hogen-Esch and Smid (6, 7) provided direct evidence for the existence of two types of ion pair. Chan and Smid (8), in a study of the deprotonation of triphenylmethane by polystyryl anions, showed that even though the bulk of the base is in the form of ion pairs, the free ions are responsible for the deprotonation.

[1]Author to whom correspondence may be addressed.

Printed in Canada / Imprimé au Canada

TABLE 1. Rate constants for the reaction of 1-(4-nitrophenyl)-1-nitroethane and its 1-d_1 analogue with cesium *n*-propoxide in *n*-propanol

(a) Normal substrate

	k_{obs} (s^{-1})					
Temp. (°C)	10^4[Base](M): 3.2	6.4	9.6	12.8	16.0	$10^{-3}k_f$($dm^3\,mol^{-1}s^{-1}$)
5	0.437	1.06	1.66	2.30	2.84	1.89±0.03
10	0.556	1.21	1.99	2.73	3.39	2.25±0.04
15	0.725	1.74	2.73	3.85	5.00	3.33±0.06
20	1.03	2.67	3.67	5.64	6.73	4.49±0.24
25	1.51	3.32	5.48	7.65	9.65	6.45±0.11
30	2.01	4.93	7.74	10.2	13.1	8.45±0.15
35	2.84	6.30	10.0	13.4	17.8	11.6 ±0.3

(b) Deuterated substrate

	k_{obs} (s^{-1})					
Temp. (°C)	10^{-4}[Base](M): 3.2	6.4	9.6	12.8	16.0	$10^{-3}k_f$($dm^3\,mol^{-1}s^{-1}$)
5	0.056	0.129	0.227	0.323	0.390	0.270±0.01
10	0.073	0.177	0.300	0.396	0.501	0.336±0.01
15	0.114	0.266	0.457	0.607	0.751	0.505±0.01
20	0.169	0.381	0.603	0.760	1.07	0.679±0.04
25	0.243	0.551	0.829	1.22	1.57	1.04 ±0.04
30	0.323	0.711	1.27	1.59	2.24	1.48 ±0.09
35	0.478	1.00	1.60	2.29	2.90	1.92 ±0.05

However, in some solvents the ion pairs did show a reactivity, leading to the suggestion that there were two forms of ion pairs, tight and loose, and that the latter were active reagents.

Proton transfer from 3,4-benzofluorene and 1,2-benzofluorene to various fluorenyl salts acting as bases showed (9) marked changes in second-order rate constant with concentration when the Li salt was used, but no such change when cesium or tetrabutylammonium salts were used. The latter reactions must be going via ion-pair reagents (1, 9) and it appears, therefore, that loose ion pairs in this system are much more reactive than tight ion pairs in the lithium salt reaction. Hogen-Esch and Smid (10) also found that aliphatic alcohols are relatively poor cation coordinators. Thus, in such a solvent a large ion pair would be expected to show considerable reactivity compared to the free ion.

These results suggest that it would be of interest to select a proton transfer reaction from a carbon acid to an alkoxide base, which might exist as free ions and also as loose ion pairs, and measure the rates of the two reactions to compare the primary isotope effects and activation parameters for the two transition states. Cesium *n*-propoxide was selected as the base since its large and poorly solvated cation should give its ion pair increased reactivity relative to ion pairs containing small cations such as lithium or sodium.

Results and discussion

In order to determine the individual rate constants and activation parameters for the proton transfer reaction between a carbon acid and alkoxide ions (k_i) and metal alkoxide ion pairs (k_{ip}) in the corresponding alcohol, independent and precise values of the ion association constants as a function of temperature are required. The necessary conductivity measurements for cesium *n*-propoxide in *n*-propyl alcohol were made by Barthel *et al.* (11, 12) at four temperatures between 5 and 35°C for a concentration range of $3.38 \times 10^{-4} - 32.12 \times 10^{-4}$ M propoxide, and the corresponding degrees of dissociation were calculated.

The reaction of 1-(4-nitrophenyl)-1-nitroethane with cesium *n*-propoxide in *n*-propyl alcohol solvent gives a single absorption peak, $\lambda_{max} = 410$ nm, identified (13, 14) as the carbanion ion-pair product of eq. [1].

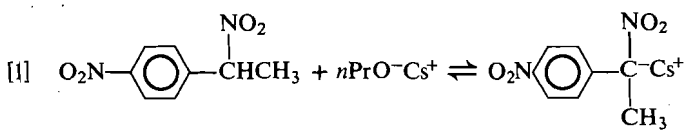

The absorptivity was found to be constant over a cesium *n*-propoxide range of $9.6 \times 10^{-4} - 2.8 \times 10^{-2}$ M, indicating that the equilibrium constant for the reaction is large.

The cesium *n*-propoxide exists in *n*-propanol as free ions and ion pairs in proportions that depend upon the concentration and temperature (11). For the overall reaction, with the base pesent in large excess, the pseudo-first-order rate constant, k_{obs}, is given by eq. [2], in which [B] is the stoichiometric concentration of cesium *n*-propoxide and k_f and k_b are the rate constants for the forward and backward reactions of eq. [1].

$$[2] \quad k_{obs} = k_f[B] + k_b$$

Provided that the interconversion of ions and ion pairs is fast compared to the reaction of both species with the carbon acid, k_f

TABLE 2. Rate constants for the proton and deuteron transfer reactions to cesium *p*-propoxide ion pairs and to free *n*-propoxide ions from 1-(4-nitrophenyl)-1-nitroethane in *n*-propanol

	Proton transfer		Deuteron transfer	
Temp. (°C)	$10^{-3}k_{ip}$ ($dm^3 mol^{-1} s^{-1}$)	$10^{-3}k_i$ ($dm^3 mol^{-1} s^{-1}$)	$10^{-3}k_{ip}$ ($dm^3 mol^{-1} s^{-1}$)	$10^{-3}k_i$ ($dm^3 mol^{-1} s^{-1}$)
5	3.43±0.44	1.21±0.13	0.57±0.06	0.13±0.02
15	5.76±0.29	1.81±0.11	0.86±0.11	0.30±0.04
25	10.2 ±0.4	3.59±0.17	1.60±0.10	0.58±0.05
35	16.2 ±0.7	7.06±0.40	2.67±0.14	0.15±0.08

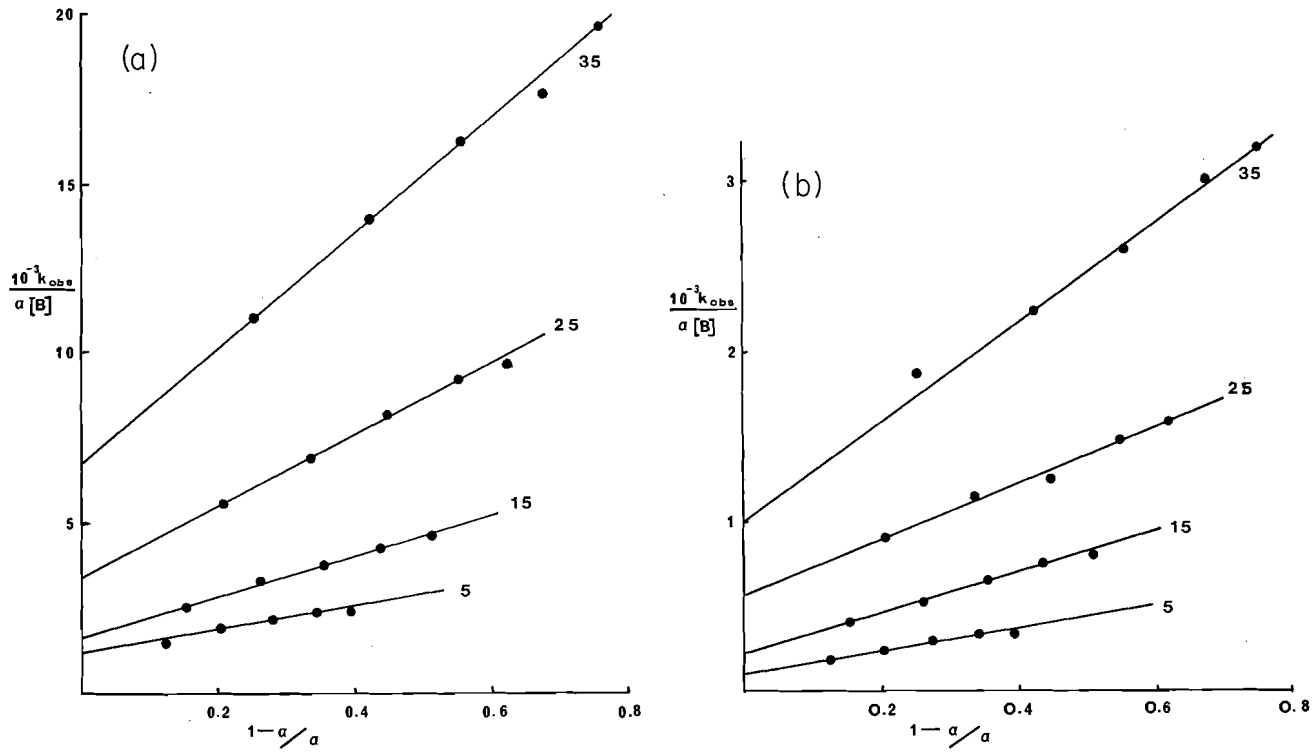

FIG. 1. Plots of 10^{-3} k_{obs}/α[base] vs. 1-α/α for (a) the proton and (b) the deuteron transfer from 1-(4-nitrophenyl)-1-nitroethane and its deuterated analogue to cesium *n*-propoxide in *n*-propanol.

is given by eq. [3]

[3] $k_f = \alpha\, k_i + (1\text{-}\alpha)\, k_{ip}$

in which α is the mole fraction of free ions, k_i is the first-order rate constant for the proton abstraction by free *n*-propoxide ions, and k_{ip} the first-order rate constant for proton abstraction in cesium *n*-propoxide ion pairs. Since k_b is essentially zero, k_{obs} is given by eq. [4], which may be rearranged to eq. [5].

[4] $k_{obs} = \alpha\, k_i[B] + (1 - \alpha)k_{ip}[B]$

[5] $k_{obs}/\alpha[B] = k_i + k_{ip}\,(1\text{-}\alpha/\alpha)$

Thus, from a plot of k_{obs}/α[B] vs. 1-α/α, k_{ip} is obtained as the slope and k_i as the intercept.

Table 1 shows the values of k_{obs} and the second-order rate constants k_f, calculated from the slopes of the plots of k_{obs} vs. base concentration, for the normal and 1-d_1 deuterated substrate at a series of temperatures between 5 and 35°C. Values of α at each of the cesium *n*-propoxide concentrations used in Table 1 were determined from plots of α vs. cesium *n*-propoxide concentration in *n*-propanol using the data of Barthel *et al.* (12), at the four temperatures shown in Table 2. Plots of k_{obs}/α[B] vs. 1-α/α are shown in Fig. 1 and k_i and k_{ip}, determined by a linear least-squares calculation, are recorded in Table 2, together with their standard deviations.

TABLE 3. The deuterium isotope effects for the reaction of cesium *n*-propoxide with 1-(4-nitrophenyl)-1-nitroethane in *n*-propanol

	k_H/k_D		
Temp. (°C)	Total concentration	Ion pairs	Free ions
5	7.0±0.3	6.0±1.0	9.2±1.6
10	6.7±0.2	—	—
15	6.6±0.2	6.7±0.9	6.1±0.9
20	6.6±0.5	—	—
25	6.2±0.2	6.3±0.5	6.1±0.6
30	5.8±0.3	—	—
35	6.0±0.2	6.1±0.4	6.1±0.5

TABLE 4. Activation parameters for the reaction of cesium *n*-propoxide with 1-(4-nitrophenyl)-1-nitroethane in *n*-propanol

	Total base concentration		Ion pairs		Free ions	
Parameter	H-transfer	D-transfer	H-transfer	D-transfer	H-transfer	D-transfer
$\Delta H^{\neq}$ (kcal mol^{-1})	10.1±0.4	11.0±0.4	8.3±0.2	8.3±0.6	9.6±1.0	11.6±0.2
$\Delta S^{\neq}$ (cal mol^{-1} deg^{-1})	−7.3±1.2	−7.7±1.4	−12.3±0.6	−15.9±2.0	−10.1±3.4	−6.8±0.7
$\Delta G^{\neq}$ (kcal mol^{-1})	12.3	13.3	12.0	13.0	12.6	13.6

The primary kinetic isotope effects, k_H/k_D, for k_f, k_i, and k_{ip} are given in Table 3 together with their standard deviations. Of the eight isotopic rate ratios reported in Table 3 for the ion-pair reaction and free-ion reaction, seven are identical within the limits of plus or minus one standard deviation. The remaining isotope effect of 9.2 ± 1.6 for the free-ion reaction at 5°C is just outside this limit but well within plus or minus two standard deviations. It is concluded, therefore, that there is no significant difference in isotope effect between the reaction going via the free ion and that going via the ion pair. The same conclusion is reached if the isotope effects on the activation parameters for the two reactions, shown in Table 4, are compared: $(\Delta H_D^{\neq} - \Delta H_H^{\neq})_{ip} = 0.0 \pm 0.8$ kcal mol^{-1}, $(\Delta H_D^{\neq} - \Delta H_H^{\neq})_i = 2.0 \pm 1.2$ kcal mol^{-1}, $(\Delta S_D^{\neq} - \Delta S_H^{\neq})_{ip} = -3.6 \pm 2.6$ cal mol^{-1} deg^{-1}, $(\Delta S_D^{\neq} - \Delta S_H^{\neq})_i = 3.3 \pm 4.1$ cal mol^{-1} deg^{-1}. These values show the differences between the two reactions that are just on the limit of plus or minus one standard deviation. Thus, values of isotope effects and activation parameters previously reported for proton transfers to alkoxide bases (15–17) based on k_f values are meaningful. The magnitude of the isotope effects, between 6 and 7, is consistent with the theory for the loss of one C—H or C—D stretching vibration. The constancy of the isotope effects for the two reactions indicates that the transition states for the proton transfers must be very similar.

The k_f, k_i, and k_{ip} values from Tables 1 and 2 yield the activation parameters by a linear least-squares fit to the transition state theory equation. These are shown in Table 4, with their standard deviations. These are typical values for reactions of carbon acids with alkoxide bases (15–17) and also similar to the values obtained for proton transfers from this substrate to nitrogen bases in aprotic solvents (13, 14, 18). The differences between the free ion and the ion-pair reactions are again very small.

From Table 2, it can be seen that the reactivity of the alkoxide ion pair is about 2.8 times greater than that of the free ion, although this rate difference is not large enough to give a detectable curvature of the plots of k_{obs} vs. base concentration. The ion-pair reaction has a lower free energy of activation than the ion reaction by about 0.6 kcal mol^{-1}, which arises from a lower enthalpy of activation offset by a more negative entropy of activation. Since a large part of the energy barrier to reaction for proton transfers to alkoxide bases is considered to arise from the energy required to break up the initial state solvation shell (15, 19), it is probable that the reactivity of the cesium *n*-propoxide ion pair arises from the nature of its solvation shell. The large size of the cesium ion gives it a weaker solvation shell than a smaller ion such as sodium and this results in the cesium *n*-propoxide ion pair being less strongly solvated than the *n*-propoxide ion. This effect is sufficient to give rise to the observed rate constant and activation parameter differences found for the two reactions.

However, it has been suggested by Cram and Gosser (20) that the cation within the ion pair may stabilize the transition state by interaction with the developing negative charge on the carbon atom. The larger negative entropies of activation for the ion-pair reactions, in our case, are consistent with the more highly structured transition state required by cesium interaction with the developing negative charge. Similar electrostatic effects have been observed by Kresge and co-workers for the hydrolysis of vinyl ethers and also for proton transfer reactions (21, 22). In the present reactions, however, the lack of dependence of the primary isotope effect on the nature of the reagent suggests that the initial state desolvation effect is the major contributor to the difference in the rate constants and activation parameters.

It may be concluded that in small cation alkoxide systems the free ions are generally more reactive than ion pairs because the latter are tightly bound by electrostatic forces. Only with large poorly solvated metal alkoxide ion pairs will the free-ion reaction be slower than the ion-pair reaction. However, since the two reactions show very similar activation parameters and primary isotope effects, no significant error is introduced by the interpretation of these parameters for the overall reaction, although it must be remembered that such parameters may be averages of two similar but separate reaction paths.

Experimental

1-(4-Nitrophenyl)-1-nitroethane and its α-deuterated analogue were prepared as described by Boyle (23) and earlier workers (24, 25). Commercial *n*-propanol was fractionally distilled over potassium metal. The fraction boiling at 97.0°C was collected. Commercial cesium metal (Aldrich) was used to prepare the cesium propoxide solutions under an atmosphere of argon.

The kinetic measurements were carried out under pseudo-first-order conditions using an acid concentration of 3.02×10^{-5} and base concentrations ranging from 3.2×10^{-4} to 16.0×10^{-4} *M*. The stock solutions were always freshly prepared and protected from moisture and carbon dioxide under an argon atmosphere. The reaction rates were measured with a stopped-flow spectrophotometer using the standard technique previously described (15).

1. M. SZWARC, A. STREITWIESER, and P. C. MOWERY. *In* Ions and ion pairs in organic chemistry. Vol. 2. *Edited by* M. Szwarc. Wiley, New York. 1974. Chapt. 2.
2. J. R. MURDOCH and A. STREITWIESER. Intra-Science Chemistry Reports, **7**, 45 (1973).
3. J. R. BEVAN and C. B. MONK. J. Chem. Soc. 1396 (1956).
4. D. J. CRAM, C. A. KINGSBURY, and B. RICKBORN. J. Am. Chem. Soc. **83**, 3688 (1961).
5. K. T. LEFFEK and A. SUSZKA. Can. J. Chem. **53**, 1537 (1975).
6. T. E. HOGEN-ESCH and J. SMID. J. Am. Chem. Soc. **87**, 669 (1965).
7. T. E. HOGEN-ESCH and J. SMID. J. Am. Chem. Soc. **88**, 307 (1966).
8. L. L. CHAN and J. SMID. J. Phys. Chem. **76**, 695 (1972).
9. T. E. HOGAN-ESCH and J. SMID. J. Am. Chem. Soc. **89**, 2764 (1967).

10. T. E. HOGAN-ESCH and J. SMID. J. Am. Chem. Soc. **94**, 9240 (1972).
11. J. BARTHEL, R. WACHTER, and M. KNERR. Electrochim. Acta. **16**, 723 (1971).
12. J. BARTHEL, J-C. JUSTICE, and R. WACHTER. Z. Phys. Chem. (Leipzig). **84**, 100 (1973).
13. K. T. LEFFEK and P. PRUSZYNSKI. Can. J. Chem. **60**, 1692 (1982).
14. A. JARCZEWSKI, P. PRUSZYNSKI, M. KAZI, and K. T. LEFFEK. Can. J. Chem. **62**, 954 (1984).
15. A. JARCZEWSKI and K. T. LEFFEK. Can. J. Chem. **50**, 24 (1972).
16. J-H. KIM and K. T. LEFFEK. Can. J. Chem. **51**, 2805 (1973).
17. J-H. KIM and K. T. LEFFEK. Can. J. Chem. **52**, 592 (1974).
18. K. T. LEFFEK and P. PRUSZYNSKI. Can. J. Chem. **59**, 3034 (1981).
19. E. F. CALDIN. J. Chem. Soc. 3345 (1959).
20. D. J. CRAM and L. GOSSER. J. Am. Chem. Soc. **85**, 3890 (1963).
21. W. K. CHWANG, R. ELIASON, and A. J. KRESGE. J. Am. Chem. Soc. **99**, 805 (1977).
22. D. B. DAHLBERG, M. A. KUZEMKO, Y. CHIANG, A. J. KRESGE, and M. F. POWELL. J. Am. Chem. Soc. **105**, 5387 (1983).
23. W. BOYLE, JR. Ph.D. dissertation, Northwestern University. 1971.
24. D. E. PEARSON and J. D. BRUTON. J. Org. Chem. **19**, 957 (1954).
25. W. D. EMMONS and A. S. PAGANO. J. Am. Chem. Soc. **77**, 4557 (1955).

Mechanisms of elimination reactions. 40. Attempted study of stereochemistry of elimination from 2-(*p*-nitrophenyl)ethyltrimethylammonium ion. Base-promoted *cis–trans* isomerization of *p*-nitrostyrene-β-*d*[1]

BRENT R. DOHNER AND WILLIAM H. SAUNDERS, JR.[2]

Department of Chemistry, University of Rochester, Rochester, NY 14620, U.S.A.

Received September 20, 1985

This paper is dedicated to Professor Arthur N. Bourns

BRENT R. DOHNER and WILLIAM H. SAUNDERS, JR. Can. J. Chem. **64**, 1026 (1986).

Stereospecifically deuterated $ArCHDCHDNMe_3^+I^-$ and $ArCHDCHDNMe_2O$ have been prepared, where Ar=C_6H_5 and *p*-$NO_2C_6H_4$. When Ar=C_6H_5, the elimination reaction of the quaternary salt with ethoxide in ethanol goes with >98% *anti* stereochemistry, and the Cope elimination of the amine oxide with >98% *syn* stereochemistry. When Ar=*p*-$NO_2C_6H_4$, however, both reactions lead to apparent 50:50 *anti*/*syn* product. Subjection of (*E*)-*p*-nitrostyrene-β-*d* to the conditions of both the ethoxide-promoted and Cope eliminations results in complete *cis–trans* equilibration. No loss of deuterium from *p*-nitrostyrene-α-*d* occurs under either set of conditions, excluding isomerization via an α-arylvinyl carbanion. The most likely mechanism for isomerization is reversible addition of ethoxide under E2 conditions and $ArCHDCHDNMe_2O$ under Cope conditions to the β-carbon of *p*-nitrostyrene. The *cis–trans* isomerization of the *p*-nitrostyrene is sufficiently rapid to preclude determination of the stereochemistry of base-promoted eliminations leading to it.

BRENT R. DOHNER et WILLIAM H. SAUNDERS, JR. Can. J. Chem. **64**, 1026 (1986).

On a préparé des $ArCHDCHDNMe_3^+I^-$ et des $ArCHDCHDNMe_2O$ spécifiquement deutérés, dans lesquels Ar=C_6H_5 et *p*-$NO_2C_6H_4$. Lorsque Ar=C_6H_5, la réaction d'élimination du sel quaternaire, sous l'influence de l'éthylate dans l'éthanol, se produit à >98% par une stéréochimie *anti* alors que l'élimination de Cope de l'oxyde d'amine se fait à >98% par une stéréochimie *syn*. Toutefois, lorsque Ar=*p*-$NO_2C_6H_4$, les deux réactions conduisent à un produit qui est apparemment 50:50 *anti*/*syn*. Lorsqu'on soumet le *p*-nitrostyrène-β-*d*-(*E*) à des réactions d'élimination tant de Cope que sous l'influence de l'éthylate, on obtient toujours un équilibre complet entre les isomères *cis–trans*. Ni l'une ni l'autre des conditions d'élimination ne provoque la perte de deutérium du *p*-nitrostyrène-α-*d*; ce résultat exclut la possibilité d'une élimination par le biais d'un carbanion α-arylvinyle. Le mécanisme le plus probable pour l'isomérisation est l'addition réversible d'éthylate, sous les conditions E2, et de $ArCHDCHDNMe_2O$, sous les conditions de Cope, au carbone β du *p*-nitrostyrène. L'isomérisation *cis–trans* du *p*-nitrostyrène est suffisamment rapide pour éliminer la possibilité de déterminer la stéréochimie des réactions d'élimination, effectuées sous l'influence de bases, qui lui donnent naissance.

[Traduit par la revue]

The mechanisms of base-promoted elimination from 2-arylethyl derivatives have been subjected to intensive scrutiny. Most of these reactions have been found to proceed via the E2 mechanism (2, 3). In the one reported stereochemical study in this series, 2-phenylethyl-1,2-d_2-trimethylammonium ion was found to give entirely (>95%) *anti* elimination when treated with ethoxide ion in ethanol or *tert*-butoxide ion in *tert*-butyl alcohol (4). Only when there is a second group, alkyl or aryl, in the 2-position is there appreciable *syn* elimination (1, 5).

Recently, evidence has been presented that 2-(*p*-nitrophenyl)ethyl quaternary ammonium salts eliminate by the E1cB mechanism (6, 7). The evidence included exchange of the β-hydrogens with solvent protons, an inverse solvent isotope effect on initial rates, and markedly curved plots of rate vs. buffer concentration. Even under conditions where there was no evidence for exchange, the lack of coupling between proton removal and leaving-group departure suggested an $(E1cB)_I$ mechanism.

In the light of these findings, the 2-arylethyl system seemed to offer an excellent opportunity to compare the stereochemical courses of E2 and E1cB reactions of closely similar substrates. What is to be expected in an E1cB reaction is by no means clear. A long-lived carbanion, free to rotate and invert prior to loss of the leaving group, should result in 50:50 *syn*/*anti* elimination. It is possible, however, that stereochemical randomization of the carbanion would be slowed by a hyperconjugative interaction of the lone pair with the bond between the α-carbon and the leaving group (8), by ion pairing (9), or simply by a very short lifetime. In such cases, considerable stereoselectivity, or even stereospecificity, could result.

In order to study the stereochemistry of elimination, we prepared 2-phenylethyl-1,1-d_2-trimethylammonium (**6**) and 2-(*p*-nitrophenyl)ethyl-1,2-d_2-trimethylammonium (**7**) iodides by stereospecific reactions. The synthetic sequence is shown in Scheme 1. The corresponding amine oxides, **8**, and **9***a*, were also prepared to provide checks on the stereochemical integrity of **6** and **7**. The commercial β-bromostyrene (**1**) was not stereochemically pure. It was shown by nmr to be 78.6% *E* and 21.4% *Z*. We thus needed to know whether this composition was preserved through the transformations leading to **6** and **7**. In order to do this, **5** was converted to **8**, which in turn was subjected to a Cope elimination, a reaction known to proceed via a stereospecifically *syn* pathway (10, 11). The products expected from *anti* and *syn* elimination are shown in Scheme 2.

By this procedure, **5** was shown to be 79.5% *RS,SR*. As a double check, **2** was deuteroborated as in Scheme 1, but then treated with NH_2OSO_3H (12). The resulting primary amine was converted to **5** by treatment with formaldehyde and formic acid (13). This sample of **5** was treated with hydrogen peroxide and the product subjected to Cope elimination, which showed it to be 79.0% *RR,SS*. It is clear that the synthesis of **5** is stereospecific, and there is no reason to believe that conversion of **5** to **6** or **8** affects its stereochemistry. Neither should the nitration to give **9**, but Cope elimination of **9***a* gave unexpected results, which will be discussed below.

[1]For previous paper in this series, see ref. 1.

[2]Author to whom correspondence may be addressed.

Printed in Canada / Imprimé au Canada

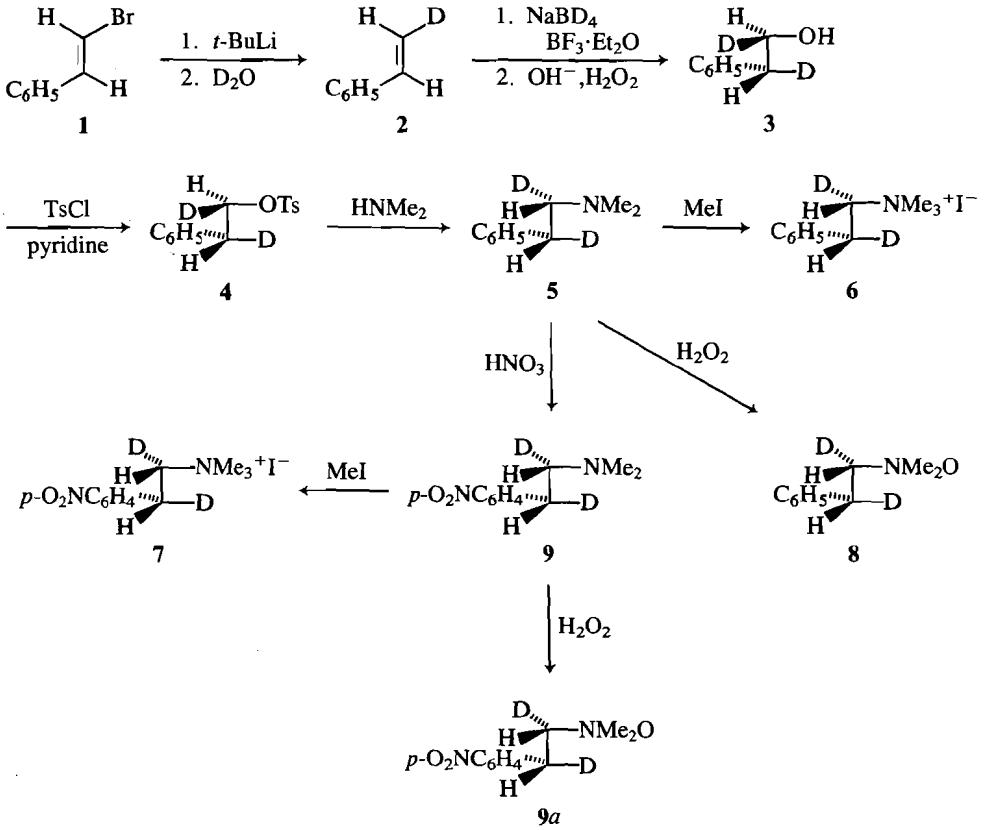

SCHEME 1. Synthesis of stereospecifically labeled 2-arylethyl-1,2-d_2-trimethylammonium salts and -dimethylamine oxides.

(*RS,SR*)-ArCHDCHDX

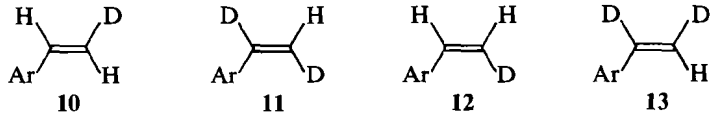

	10	**11**	**12**	**13**
Ar = C_6H_5:	5.80, d $J_{H,H}$ = 17.4 Hz	5.22, t $J_{H,D}$ = 1.4* Hz	5.23, d $J_{H,H}$ = 11.0 Hz	5.79, t $J_{H,D}$ = 2.8* Hz
Ar = *p*-$NO_2C_6H_4$:	5.94, d $J_{H,H}$ = 17.6 Hz	5.50, t $J_{H,D}$ = 1.5* Hz	5.50, d $J_{H,H}$ = 10.9 Hz	5.94, t $J_{H,D}$ = 2.5* Hz
	anti ⟶ **10** + **11**		*syn* ⟶ **12** + **13**	

*$J_{H,D}$ values are calculated from observed H,D splittings. Slightly different (and probably more accurate) values are obtained from the formula $J_{H,D} = J_{H,H}/6.5$ (2.7 Hz for *E* and 1.7 Hz for Z orientation of H and D)

SCHEME 2. Products expected in *anti* and *syn* elimination from ArCHDCHDX.

The two samples of **6**, which can be presumed to be 79.5% *RS,SR* and 79.0% *RR,SS*, respectively, permitted us to check the results of Bourns and Frosst (4). The high-field nmr spectrometers that we used permit more precise determination of the composition of the mixture of **10**–**13** than the 60-MHz nmr instrument available for the earlier work. On treatment with sodium ethoxide in ethanol at 80°C, the 79.5% *RS,SR* sample of **6** gave 78.7% **10** and **11**, while the 79.0% *RR,SS* sample gave 79.0% **12** and **13**. These results confirm that the elimination is entirely *anti* within experimental error. Any *syn* elimination must be less than 1–2% of the overall reaction.

Nitration of **5** with fuming nitric acid at −10°C (14) afforded a mixture that was 71% *para* and 29% *ortho*, from which the pure *para* isomer, **9**, was isolated by flash chromatography (15). **9** was converted to **7**, which was then treated with sodium ethoxide in ethanol at 60°C. Analysis of the mixture of deuterated *p*-nitrostyrenes gave 52.5% of **10** and **11** and 47.5% of **12** and **13**. Conversion of **9** to **9***a*, followed by Cope

elimination, gave 49.0% of **10** and **11** and 51% of **12** and **13**. This outcome indicates essentially complete loss of stereochemistry in *both* the base-promoted elimination of **7** and the Cope elimination of **9***a*. A random stereochemical outcome in the base-promoted elimination can be readily rationalized, but a nonstereospecific Cope elimination is, to the best of our knowledge, unprecedented. Consequently, we considered the possibility that stereochemistry was lost at some stage other than during the elimination reactions.

In principle, epimerization could occur during the nitration of **5** to **9**. The nmr spectra of **7** and **9** were too complex to give any information about proportions of stereoisomers, however, and the possibility of epimerization during nitration of **5** seemed farfetched in any case. A third possibility for loss of stereochemistry would be $E \rightleftharpoons Z$ isomerization of the deuterated nitrostyrenes under the conditions of the elimination reactions. This possibility was easiest to test experimentally, and was pursued first.

In order to obtain stereospecifically deuterium-labeled *p*-nitrostyrene, (*E*)-β-bromo-*p*-nitrostyrene was prepared by the method of Cristol and Norris (16), and converted to *p*-nitrophenylacetylene by treatment with sodium *tert*-butoxide in *tert*-butyl alcohol. Treatment of *p*-nitrophenylacetylene with 9-BBN (9-borabicyclo[3.3.1]nonane) (17) in tetrahydrofuran, followed by acetic-*O*-*d* acid, gave (*E*)-*p*-nitrostyrene-β-*d*. This *E* isomer showed a single nmr signal attributable to the β-proton at δ 6.01.

Treatment of the *E* isomer for 10 min with 0.1 *M* sodium ethoxide in ethanol led to a new vinyl proton nmr signal at δ 5.50, attributable to the *Z* isomer. The ratio of the signals at 6.01 and 5.50 was 47.7:52.2. Heating the *E* isomer at 80°C for 2.5 h in 80% Me_2SO – 20% H_2O containing 2-phenylethyldimethylamine oxide (Cope reaction conditions) led to a 50.0:50.0 mixture of the *E* and *Z* isomers. It is clear that complete equilibration between the *E* and *Z* isomers occurs under the conditions of both E2 and Cope eliminations.

Two possible mechanisms for the isomerization are outlined in Scheme 3. Here RO^- is EtO^- (base-promoted reaction) or $ArCH_2CH_2N^+Me_2O^-$ (Cope reaction). While path A seemed more likely than path B, we felt it necessary to distinguish between them, and chose an experiment which shed further light on path A as well. Reduction of *p*-nitroacetophenone by sodium borodeuteride, followed by tosylation and treatment of the resulting tosylate with sodium *tert*-butoxide in *tert*-butyl alcohol, afforded *p*-nitrostyrene-α-*d*. Neither under the E2 nor the Cope elimination conditions was there any observable loss of the α-deuterium, a fact which excludes path B. The method of synthesis also excludes path B for reaction with *tert*-butoxide in *tert*-butyl alcohol. Finally, the experiment excludes any significant *reversible* protonation of the carbanion **14**, resulting from addition of RO^- to *p*-nitrostyrene, for this, too, would lead to loss of α-deuterium. Irreversible protonation of **14** would give 2-(*p*-nitrophenyl)ethyl ethyl ether in the ethoxide-promoted isomerization, but no lines attributable to this compound appeared in the nmr spectrum of the isomerization product.

That nucleophilic addition to *p*-nitrostyrene occurs readily is not surprising, and there are literature precedents. Secondary amines give isolable adducts (18), and *N*-methyl-*C*-phenylnitrone (a model for the amine oxide) undergoes 1,3-dipolar addition, the nucleophilic oxygen going to the β-carbon of the *p*-nitrostyrene (19). Even more pertinent is the report of Alunni and Jencks that eliminations from 2-(*p*-nitrophenyl)ethyl quaternary ammonium salts are reversible (20), which means that tertiary amines as well can add to *p*-nitrostyrene.

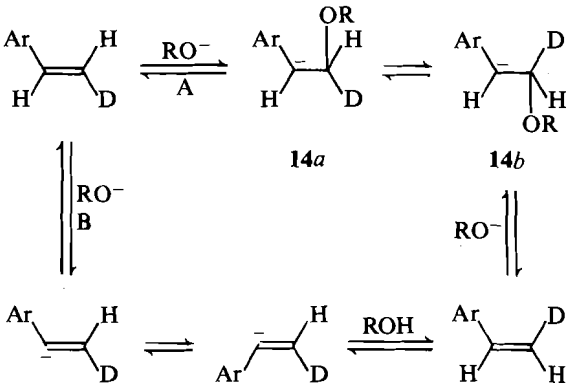

SCHEME 3. Possible mechanisms for stereoisomerization of (*E*)-*p*-nitrostyrene-β-*d*.

The data of Alunni and Jencks provide a means of estimating this rate of addition. The overall equilibrium (eq. [1]) is the sum of the two reactions of eqs. [2] and [3].

[1] $ArCH{=}CH_2 + HNMe_3^+ \leftrightharpoons ArCH_2CH_2NMe_3^+$

[2] $ArCH{=}CH_2 + NMe_3 \leftrightharpoons ArCHCH_2NMe_3^+$

[3] $ArCHCH_2NMe_3^+ + HNMe_3^+ \leftrightharpoons ArCH_2CH_2NMe_3^+ + NMe_3$

The equilibrium constant K_1 is not given by Alunni and Jencks, but there is a good linear correlation between log K_1 and $pK_a(R_3NH^+)$ for the other quaternary salts, which permits estimation of K_1 as 0.05. The equilibrium constant for eq. [3] is given by the ionization constant of Me_3NH^+ divided by the ionization constant of $ArCH_2CH_2NMe_3^+$. The former is quoted by Alunni and Jencks as $10^{-9.85}$, and the latter estimated by Keeffe and Jencks (7) as $10^{-15.5}$. With these numbers in hand, we can estimate K_2 to be $10^{-4.35}$. In turn, $K_2 = k_{addn}/k_{elim}$, and Keeffe and Jencks estimate k_{elim} to be 15 s^{-1}, which makes k_{addn} 7×10^{-4} M^{-1} s^{-1}. This compares with an *overall* rate of elimination reaction of 10^{-3} M^{-1} s^{-1} at 25°C in water.

Thus, even the back addition of trimethylamine to *p*-nitrostyrene is comparable in rate to the overall elimination, and the addition of the stronger hydroxide ion can be expected to be faster still. These conclusions apply to aqueous solution at 25°C, of course, rather than to our conditions of ethanolic solution at 60°C. It is probably safe, however, to assume that the difference in solvent and temperature does not drastically change the qualitative picture. Definitive evidence would require determination of the rates of both elimination and stereoisomerization. We did not consider this practicable, because both reactions are complete in less than ten minutes under our conditions. The available evidence strongly suggests that it will be difficult if not impossible to determine the stereochemistry of elimination from 2-(*p*-nitrophenyl)ethyltrimethylammonium ion without interference from stereoisomerization of the product.

Experimental

Solvents

Ether and tetrahydrofuran were refluxed over sodium, with benzophenone used as an indicator of dryness (21). They were then distilled. Dimethyl sulfoxide was stirred over calcium hydride for 2 days. It was distilled under reduced pressure and the first 10% discarded. Distilled water was refluxed over potassium permanganate for 2 h and distilled. Absolute ethanol was refluxed over magnesium turnings for 8 h and distilled. The first 10% of distillate was discarded.

General

All melting and boiling points are uncorrected. Most of the nmr spectra were recorded on a Bruker WH-400 or a Nicolet QE 300 nmr spectrometer. In a few cases a Varian EM-390 instrument was used. Chloroform-*d* and dimethyl-d_6 sulfoxide were used as nmr solvents.

(E)-Styrene-β-d was obtained from β-bromostyrene (Aldrich: 78.6% *E*, 21.4% *Z*) by the procedure used to prepare (*E*)-1-phenyl-1-(*p*-methoxyphenyl)ethylene-2-*d* (5). The product was extracted into ether and kept in solution to minimize possible polymerization or isomerization.

(RR,SS)-2-Phenylethanol-1,2-d_2

Deuteroborane was generated by the addition of boron trifluoride etherate (0.029 mol) to a solution of sodium borodeuteride (0.022 mol) in 200 mL of tetrahydrofuran at 0°C. (*E*)-Styrene-β-*d* was then converted to the desired product by the procedure used to prepare (*RR,SS*)-3-methyl-2-phenyl-1-butanol-1-*d* (5), except that ether was used to extract the product and the extract washed with aqueous ferrous sulfate before drying over magnesium sulfate.

(RR,SS)-2-Phenylethyl-1,2-d_2 *tosylate* was prepared by a standard procedure (22) and used without recrystallization.

(RS,SR)-2-Phenylethyl-1,2-d_2*-dimethylamine* was obtained from (*RR,SS*)-2-phenylethyl-1,2-d_2 tosylate and dimethylamine by the procedure used to prepare (*RS,SR*)-3-methyl-2-phenyl-1-(butyl-1-*d*)dimethylamine (5). It was shown to be 78% *RS,SR* isomer by analysis of its Cope elimination products (see below); ^{1}H nmr δ: 2.31 (s, 6H), 2.52 (d, 1H), 2.80 (d, 1H), 7.2–7.4 (m, 5H).

(RS,SR)-2-Phenylethyl-1,2-d_2*-trimethylammonium iodide*

Treatment of the above product with methyl iodide (5) gave material of mp 230–233°C; ^{1}H nmr δ: 3.02 (d, 1H), 3.12 (s, 9H), 3.50 (d, 1H), 7.35 (m, 5H).

(RR,SS)-2-Phenylethyl-1,2-d_2*-amine*

Deuteroboration of (*E*)-styrene-β-*d* was carried out as in the preparation of (*RS,SR*)-2-phenylethanol-2,3-d_2 (above), but instead of treating the borane with hydrogen peroxide, NH_2OSO_3H (1.1 equiv.) was added slowly and the reaction mixture heated to 95°C for 4 h. The reaction mixture was treated with concentrated hydrochloric acid, made basic, and the amine extracted with ether. The crude product was obtained in 14% yield.

(RR,SS)-2-Phenylethyl-1,2-d_2*-dimethylamine* was obtained by methylation of the above amine with formaldehyde and formic acid (13) and was shown to be 79% *RR,SS* by analysis of its Cope elimination products (see below).

(RR,SS)-2-Phenylethyl-1,2-d_2*-trimethylammonium iodide* was prepared by the same procedure as for the *RS,SR* isomer (above) and had mp 228–232°C.

(RS,SR)-2-(p-Nitrophenyl)ethyl-1,2-d_2*-dimethylamine* was prepared by adding (*RS,SR*)-2-phenylethyl-1,2-d_2-dimethylamine dropwise to fuming nitric acid at −10°C (14). The reaction mixture was allowed to warm to 0°C, made basic with sodium hydroxide, and the product extracted into ether. After removal of the ether, it was shown by nmr to be 71% *para* and 29% *ortho*. Separation was effected by flash chromatography (15). The solvent consisted of 120 mL of pentane, 30 mL of trimethylamine, and 100 mL of ether. A 230–240 mesh silica gel 60 column was used. The *ortho* isomer (R_f=0.36) preceded the *para* isomer (R_f=0.28), which was obtained in 56% yield; ^{1}H nmr δ: 2.31 (s, 6H), 2.51 (d, 1H), 2.80 (d, 2H), 7.80 (dd, 4H).

(RS,SR)-2-(p-Nitrophenyl)ethyl-1,2-d_2*-trimethylammonium iodide* was obtained by treatment of the above product with methyl iodide (5) and had mp 207–208°C; ^{1}H nmr δ: 3.13 (s, 9H), 3.31 (d, 1H), 3.58 (d, 1H), 7.95 (dd, 4H).

(E)-β-Bromo-p-nitrostyrene was prepared by the procedure of Cristol and Norris (16). It had mp 155–157°C (lit. (16) mp 156–157°C); ^{1}H nmr δ: 6.69 (s, 1H), 7.03 (s, 1H), 7.70 (dd, 4H).

p-Nitrophenylacetylene

(*E*)-β-bromo-*p*-nitrostyrene (0.044 mol) was dissolved in 250 mL of 0.1 *M* sodium *tert*-butoxide in *tert*-butyl alcohol and stirred at 30°C for 35 h. The reaction mixture was poured into water and the product extracted with ether. The ether extract was dried over magnesium sulfate and the ether removed to give 88% of the crude product; ^{1}H nmr δ: 3.30 (s, 1H), 7.85 (dd, 4H).

(E)-p-Nitrostyrene-β-d

p-Nitrophenylacetylene (0.0034 mol) in anhydrous tetrahydrofuran was added to a solution of 9-BBN (17) (0.0017 mol) in tetrahydrofuran at 0°C. The mixture was stirred for 1 h at 0°C and 2 h at room temperature. Acetic-*O*-*d* acid (0.034 mol) was added and the mixture stirred for 2 h. The mixture was poured into water and the product extracted with ether. It was stored in ether solution to minimize possible polymerization or isomerization. ^{1}H nmr δ: 6.01 (d, 1H), 6.65 (d, 1H), 7.81 (dd, 4H).

1-(p-Nitrophenyl)ethanol-1-d

To 0.0055 mol of *p*-nitroacetophenone in ethanol was added 0.0055 mol of sodium borodeuteride and the mixture stirred for 1 h at room temperature. The reaction mixture was poured into water and the product extracted with ether. The ether solution was dried over magnesium sulfate and evaporated to give 58% of crude product; ^{1}H nmr δ: 1.50 (s, 3H), 3.44 (s, 1H), 7.80 (dd, 4H).

1-(p-Nitrophenyl)ethyl-1-d *tosylate* was obtained from 1-(*p*-nitrophenyl)ethanol-1-*d* by a standard procedure (22). The crude product was used in the next step; ^{1}H nmr δ: 1.49 (d, 3H), 2.49 (s, 3H), 4.99 (q, 1H), 7.60 (dd, 4H), 7.80 (dd, 4H).

p-Nitrostyrene-α-d was obtained by heating 1-(*p*-nitrophenyl)ethyl-1-*d* tosylate (0.0032 mol) in excess 0.1 *M* sodium *tert*-butoxide in *tert*-butyl alcohol at 60°C for 12 h. The mixture was cooled, poured into water, and the product extracted with ether. It was kept in ether solution to minimize possible polymerization; ^{1}H nmr δ: 5.53 (t, 1H), 6.09 (t, 1H), 7.81 (dd, 4H).

Cope elimination reactions (23) of 2-arylethyldimethylamine oxides

The amine (0.00051 mol) was dissolved in 10 mL of methanol, cooled at 0°C, and 30% hydrogen peroxide (0.0015 mol) added dropwise. The mixture was warmed to room temperature, stirred for 24 h, and the excess peroxide decomposed by adding 5 mg of 10% platinum on carbon and stirring for 5 h. The mixture was filtered, the solvent removed under reduced pressure, and the residue dissolved in 80% dimethyl sulfoxide – 20% water and heated for 2.5 h (>5 half lives for 2-phenylethyldimethylamine oxide (24)). The solvent was removed and the mixture of mono- and di-deuterated styrenes analyzed by 300- or 400-MHz nmr (see Discussion).

Stereochemistry of base-promoted reactions of 2-arylethyl-1,2-d_2*-trimethylammonium iodides with sodium ethoxide in ethanol*

The substrate (ca. 20 mg) was dissolved in 5 mL of 0.1 *M* sodium ethoxide in ethanol at 80°C (unsubstituted) or 60°C (*p*-nitro substituted). The reaction was followed to completion by tlc (thin-layer chromatography). The reaction mixture was poured into water and the product was extracted with petroleum ether. The petroleum ether solution was dried over magnesium sulfate, filtered, 2 mL of dimethyl-d_6 sulfoxide added, and the petroleum ether removed on a rotary evaporator. The mixture of mono- and di-deutero styrenes was analyzed by 300- or 400-MHz nmr.

Acknowledgment

This work was supported by the U.S. National Science Foundation.

1. Brent R. Dohner and William H. Saunders, Jr. J. Am. Chem. Soc. **108**, 245 (1986).
2. W. H. Saunders, Jr. and A. F. Cockerill. Mechanisms of elimination reactions. Wiley–Interscience, New York. 1973. Chapt. II.
3. W. H. Saunders, Jr. Acc. Chem. Res. **8**, 19 (1976).
4. A. N. Bourns and A. C. Frosst. Can. J. Chem. **48**, 133 (1970).
5. Y.-T. Tao and W. H. Saunders, Jr. J. Am. Chem. Soc. **105**, 3183 (1983).
6. J. R. Gandler and W. P. Jencks. J. Am. Chem. Soc. **104**, 1937 (1982).
7. J. R. Keeffe and W. P. Jencks. J. Am. Chem. Soc. **105**, 265 (1983).

8. A. THIBBLIN. Chem. Scr. **15**, 121 (1980).
9. D. H. HUNTER and D. J. SHEARING. J. Am. Chem. Soc. **93**, 2348 (1971).
10. D. J. CRAM and J. E. MCCARTY. J. Am. Chem. Soc. **76**, 5740 (1954).
11. M. R. V. SAYHUN and D. J. CRAM. J. Am. Chem. Soc. **85**, 1263 (1963).
12. M. W. RATHKE, N. INOUE, K. R. VARMA, and H. C. BROWN. J. Am. Chem. Soc. **88**, 2870 (1966).
13. R. N. ICKE and B. B. WISEGARVER. Organic syntheses. Coll. Vol. III, Wiley, New York. 1955. p. 723.
14. F. R. GOSS, W. HANHART, and C. K. INGOLD. J. Chem. Soc. 250 (1927).
15. W. C. STILL, M. KAHN, and A. MITRA. J. Org. Chem. **43**, 2923 (1978).
16. S. J. CRISTOL and W. M. NORRIS. J. Am. Chem. Soc. **76**, 3005 (1954).
17. H. C. BROWN, C. G. SCOUTEN, and R. LIOTTA. J. Am. Chem. Soc. **101**, 96 (1979).
18. H. SHENHAV, Z. RAPPOPORT, and S. PATAI. J. Chem. Soc. B, 469 (1970).
19. R. HUISGEN, H. SEIDL, and I. BRÜNING. Chem. Ber. **102**, 1102 (1969).
20. S. ALUNNI and W. P. JENCKS. J. Am. Chem. Soc. **102**, 2052 (1980).
21. D. D. PERRIN, M. I. F. AMAREGA, and D. R. PERRIN. Purification of laboratory chemicals. 2nd ed; Pergamon Press, Oxford. 1980.
22. R. S. TIPSON. J. Org. Chem. **9**, 235 (1944).
23. A. C. COPE, R. A. PIKE, and C. F. SPENCER. J. Am. Chem. Soc. **75**, 3212 (1953).
24. W.-B. CHIAO and W. H. SAUNDERS, JR. J. Am. Chem. Soc. **100**, 2802 (1978).

Aza analogues of protoberberine and phthalideisoquinoline alkaloids[1]

JAHANGIR AND DAVID B. MACLEAN[2]
Department of Chemistry, McMaster University, Hamilton, Ont., Canada L8S 4M1

AND

HERBERT L. HOLLAND[2]
Department of Chemistry, Brock University, St. Catharines, Ont., Canada L2S 3A1

Received September 23, 1985

This paper is dedicated to Professor Arthur N. Bourns

JAHANGIR, DAVID B. MACLEAN, and HERBERT L. HOLLAND. Can. J. Chem. **64**, 1031 (1986).

Anions derived from furo[3,4-*c*]pyridin-3(1*H*)-one, by treatment with lithium diisopropylamide, react with substituted, 3,4-dihydroisoquinolines and 2-methyl-3,4-dihydroisoquinolinium salts yielding nitrogen analogues of the protoberberine and phthalideisoquinoline alkaloids, respectively.

JAHANGIR, DAVID B. MACLEAN et HERBERT L. HOLLAND. Can. J. Chem. **64**, 1031 (1986).

Les anions formés par la réaction de la furo[3,4-*c*]pyridine-(1*H*) one-3 avec le diisopropylamidure de lithium réagissent avec les dihydro-3,4 isoquinoléines substituées et avec les sels de méthyl-2 dihydro-3,4 isoquinolinium pour conduire respectivement aux analogues azotés des alcaloïdes de la protoberbérine et de la phtalideisoquinoléine.

[Traduit par la revue]

In several recent publications from this laboratory we have reported (1–5) the reactions of phthalide anions with imines and iminium salts. These reactions provided convenient routes to protoberberine (e.g., canadine **1**) and phthalideisoquinoline alkaloids (e.g., cordrastine **2**), respectively, and to related compounds in each series. The recent discovery of pyridine analogues of the protoberberines such as **3**, **4**, **5**, and **6** in *Alangium* species (6, 7) prompted us to investigate their synthesis by a route similar to that used for the synthesis of the protoberberine alkaloids from phthalide precursors (1, 2). To this end we prepared the anion derived from furo[3,5-*c*]pyridin-3(1*H*)-one (azaphthalide **7**) and studied its reaction with 3,4-dihydroisoquinolines **8** and also with the corresponding 2-methyl-3,4-dihydroisoquinolinium salts **9**. These reactions, which are reported below, provided, in the case of the reaction with imines, a straightforward route to the ring system of the *Alangium* alkaloids and, in the case of the reaction with iminium salts, a new class of compounds, which are pyridine analogues of the phthalideisoquinolines.

The imines **8***a*–**8***c* were prepared by cyclization of substituted *N*-formylphenylethylamines with $POCl_3$ as condensing agent. This procedure gave better yields than the usual method in which mixtures of acetonitrile and $POCl_3$ were employed. The imines **8***a*–**8***c* were converted to their methiodides **9***a*–**9***c* by standard procedures.

The furo[3,4-*c*]pyridin-3(1*H*)-one used in this study was prepared by reduction of cinchomeronic acid anhydride with sodium borohydride as outlined in Scheme 1. This major isomer was separated by crystallization from the minor regioisomer **10**. This preparation, an adaptation of a method developed by Kayser and Morand (8) for reduction of other acid anhydrides, proved superior to the previously reported reductions of cinchomeronic acid anhydride with LAH (lithium aluminum hydride) (9) and of the half ester of cinchomeronic acid with LAH (10).

Reaction of the lithium salt of the azaphthalide **7** with the 3,4-dihydroisoquinolines **8***a*, **8***b*, and **8***c* is outlined in Scheme 2. The initial products of the reaction were assigned structures **11** on the basis of spectroscopic examination of the compounds and of their *O*-acetates **12** and in analogy with the previously studied products of the reaction of lithium phthalide and 3,4-dihydroisoquinolines (1, 2). The relative configuration at C-13 and C-14 could not be established with certainty by examination

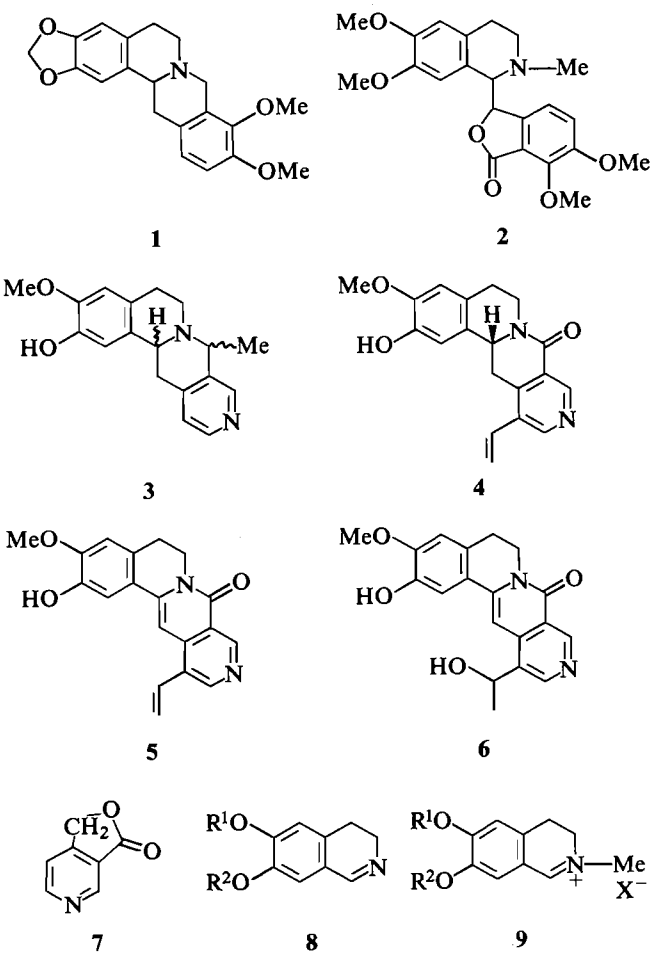

[1]A part of this work was presented at the 14th IUPAC International Symposium on the Chemistry of Natural Products, Poznan, Poland (see ref. 5).

[2]Authors to whom correspondence may be addressed.

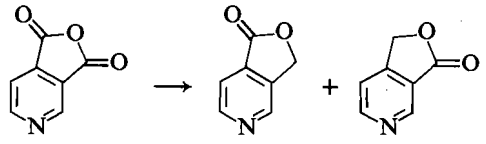

10 **7**

SCHEME 1

of the nmr spectra of compounds **11**, but their *O*-acetyl derivatives **12** showed that H-13 and H-14 were *trans* to one another, $J_{13,14}$ = 10.5 Hz (ref. 2, and references therein). The dehydration of **11***a*, **11***b*, and **11***c* was effected by treatment with $POCl_3$, yielding the isocarbostyril system found in compounds **13**. Again, these compounds showed the anticipated spectroscopic behaviour. Thus, the condensation of the azaphthalide with the imines provided a convenient route to the ring system found in the *Alangium* alkaloids.

Alternative routes to this ring system, which are not regiospecific, and which involve photochemical (11, 12) or thermal (12) cyclization of tricyclic enamides, have been described. Both methods have been applied successfully to the synthesis of the *Alangium* alkaloids, alamarine **6** and alangimarine **5** (13).

The mass spectral fragmentation of the compounds **11**(*a*–*c*) prepared in this study is analogous to that of the corresponding protoberberines examined in the previous study (2). The major fragmentation involves a retro-Diels–Alder opening of ring C of the azaberberine system. Ions corresponding to the isoquinoline moiety plus a hydrogen are observed in the three compounds at *m/z* 192, 176, and 268, respectively, and an ion derived from rings C and D is present in all three compounds at *m/z* 135.

We recently described the synthesis of phthalideisoquinoline alkaloids and related compounds by treatment of lithium phthalides with 2-methyl-3,4-dihydroisoquinolinium salts (3). Here we report that the lithium salt of furo[3,4-*c*]pyridin-3(*H*)-one behaves in an exactly analogous fashion to lithium phthalide in its reaction with isoquinolinium salts, as shown in Scheme 3, yielding mixtures of the racemic *threo* **14** and *erythro* **15** diastereomers. The yields reported for the two isomers refer to crystalline product isolated from the reaction system and should not be used as a measure of the *threo*:*erythro* ratio present in the crude reaction product, which is expected to be nearly 1:1.

The assignment of configuration to the *threo* and *erythro* isomers is based on a comparison of the properties of the isomeric compounds prepared in this study with those of phthalideisoquinoline alkaloids where the configurational assignments are secure (14, 15). In the *threo* compounds examined in this work, the proton at C-7′ is always deshielded relative to the corresponding proton in the *erythro* series. This situation is similar to that observed for the phthalideisoquinoline alkaloids themselves (16, 17), indicating that the isoquinoline–azaphthalide system in compounds **14** and **15** adopts the same preferred conformation as the corresponding rings in the alkaloids. In the *erythro* systems, the preferred conformation places the hydrogen at C-7′ in the shielding cone of the aromatic ring of the isoquinoline moiety, whereas in the preferred *threo* conformation this hydrogen is not in a position where it can be similarly affected. There is also consistency with respect to the coupling constants between the hydrogens at C-1 and C-1′. In each series the *threo* isomer has a smaller coupling constant than the *erythro* isomer. Moreover, the *erythro* and *threo* isomers also exhibit a similar chromatographic behaviour in each series. The *threo* isomer is less polar than the *erythro* on silica columns and shows a higher R_f value on tlc plates.

Experimental

Apparatus, materials, and methods

Unless otherwise stated, the ^1H nmr spectra were continuous wave, run at 90 MHz on a Varian EM 390 spectrometer. The samples were dissolved in $CDCl_3$ using tetramethylsilane (TMS) as the internal standard. Chemical shifts, quoted as δ values, were measured in relation to TMS. The symbols s, singlet, d, doublet, t, triplet, q, quartet, and m, multiplet are used in reporting spectra. The Fourier transform spectra were run on either a Bruker WP80 (80 MHz) or WM250 (250 MHz) spectrometer. The ^{13}C nmr spectra were run at 62.9 MHz on a Bruker WM250 FT spectrometer or at 20.115 MHz on a Bruker WP80 FT spectrometer, both at ambient temperature.

EI (electron impact) mass spectra were recorded on a V.G. Micromass 7070 F mass spectrometer at 70 eV and CI (chemical ionization) spectra on the same instrument using NH_3 at ca. 1 Torr (1 Torr = 133.3 Pa) as reagent gas. Infrared spectra were recorded on a Perkin–Elmer 283 spectrometer in $CHCl_3$ solution. Melting points were determined using a Gallenkamp apparatus and are uncorrected. The microanalyses were performed by the Guelph Chemical Laboratories Ltd., Guelph, Ontario.

Thin-layer chromatography (tlc) was performed using Polygram Sil G/UV_{254} or Polygram Aloxn/UV_{254} plates. Flash column chromatography (18) was employed using Kieselgel 60 (230–400 mesh).

All reactions involving lithiation steps were carried out in flame-dried apparatus under a blanket of argon, using septa and syringes for transfer of reagents. Diisopropylamine was refluxed over calcium hydride and distilled onto molecular sieves (4A). THF (tetrahydrofuran) was dried by distillation from Na/benzophenone under a nitrogen atmosphere just prior to use. The following compounds were obtained commercially or prepared according to literature procedures: cinchomeronic acid, cinchomeronic acid anhydride (19, 20); *N*-formyl-3,4-methylenedioxyphenylethyl amine (2); *N*-formyl-3,4-demethoxyphenylethyl amine (16); 6,7-methylenedioxy-2-methyl-3,4-dihydroisoquinolinium iodide (21); 6,7-dimethoxy-2-methyl-3,4-dihydroisoquinolinium iodide (22).

Preparation of 3,4-dihydroisoquinolines **8**a–**8**c

The appropriate formamides, *N*-formyl-3,4-dimethoxyphenylethyl amine, *N*-formyl-3,4-methylenedioxyphenylethyl amine, and *N*-formyl 3-methoxy-4-benzyloxyphenylethyl amine (25.0 g), were treated slowly and carefully at ice bath temperature with freshly distilled $POCl_3$ (60 mL) in a flask protected with a $CaCl_2$ tube. When the vigorous initial reaction subsided, the mixture was warmed to room temperature over a period of 10–20 min, then heated to 40°C for 5 min, and finally kept at room temperature for 2 h. The excess $POCl_3$ was destroyed by addition of the reaction mixture to crushed ice and the resulting solution made basic with concentrated aqueous NH_3. The mixture was extracted with $CHCl_3$, the $CHCl_3$ extract dried and evaporated, and the residue purified by bulb-to-bulb distillation. Compounds **8***a*–**8***c* were obtained in 80–90% yield; their spectroscopic properties were in accord with those reported in the literature: **8***a* (2), **8***b* (2), and **8***c* (23).

Reduction of cinchomeronic acid anhydride

A suspension of $NaBH_4$ (1.9 g, 0.05 mol) in freshly distilled THF (100 mL) and dry DMF (10 mL) was heated under reflux in a 2-necked, flame-dried, round-bottom flask under an argon atmosphere for 20 min. The reaction mixture was then cooled to 0°C in an ice bath and finely powdered cinchomeronic acid anhydride (7.48 g, 0.05 mol) was added in one portion. The mixture, which turned faintly pink, was stirred for 1 h at 0°C, the ice bath was removed, and stirring continued for a further 3 h. Excess $NaBH_4$ was destroyed by careful addition of a few drops of concentrated aqueous HCl at 0°C. The solvent was then evaporated, the residue taken up in 30 mL of 10 *M* HCl (aq) and the mixture heated under reflux for 1 h. The solution was then cooled and carefully neutralized to pH 8–9 with solid K_2CO_3. The neutral solution was extracted with $CHCl_3$, the extract washed with brine, and then dried over Na_2SO_4. The residue obtained on evaporation of the dried $CHCl_3$ extract was a mixture of azaphthalides 7 and **10** in a 4:1 ratio as estimated by ^1H nmr. The crude yields in a number of reactions ranged

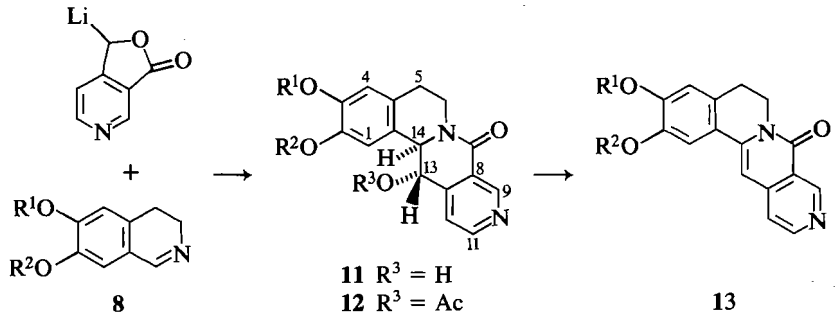

8 **11** R^3 = H; **12** R^3 = Ac **13**

Note: For compounds 8, 11, 12, and 13 in the (*a*) series, $R^1 = R^2 = CH_3$; in the (*b*) series $R^1 + R^2 = CH_2$, and in the (*c*) series $R^1 = CH_3$, $R^2 = C_6H_5CH_2$

SCHEME 2

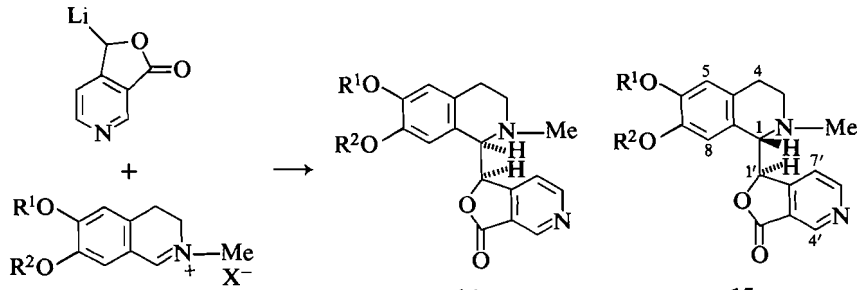

14 **15**

a $R^1 = R^2 = CH_3$
b $R^1 + R^2 = CH_2$

SCHEME 3

from 40–65%. The azaphthalides **7** and **10** were purified by fractional sublimation and by fractional crystallization from $CHCl_3$–Et_2O; azaphthalide (**7**), mp 142–143°C (lit. (10) mp 130–135°C; lit. (24) mp 145°C); azaphthalide (**10**), mp 116–118°C (lit. (23) mp 118°C). The spectroscopic properties of **7** and **10** were in agreement with literature values (10, 24).

Reaction of imine (8a) with the lithium salt of azaphthalide (7)

A solution of *n*-BuLi (2.44 mmol) in hexane 1.6 *M* was added dropwise with stirring to a solution of diisopropylamine (2.44 mmol) in THF at −20°C under an argon atmosphere. The LDA solution was stirred for an additional 5 min at the same temperature. After the addition was complete, the temperature of the reaction mixture was then lowered to −60°C and a solution of azaphthalide **7** (300 mg, 2.22 mmol) in THF (2 mL) was added dropwise to the LDA solution. The solution of the red anion so generated was stirred for a further 15 min at −60°C. Imine **8***a* (439 mg, 2.22 mmol) in 3 mL THF was then added dropwise and, when addition was complete, stirring of the solution was continued another 2 h. The temperature was raised to 20°C and the reaction mixture kept at this temperature for ca. 12 h. The mixture was worked up in the usual manner (1, 2) affording the condensation product **11***a* (590 mg, 81%), mp 230–235°C (dec.) ($CHCl_3$, acetone): R_f 0.22 (alumina, EtOAc); ir ($CHCl_3$), ν_{max}: 1645 cm^{-1}; ^1H nmr (90 MHz) δ: 2.8–3.0 (3H, m, C-5 H's and C-6 H_{ax}), 3.87 (3H, s, OCH_3), 3.90 (3H, s, OCH_3), 4.57–4.75 (2H, m, C-13 H and C-14 H), 4.85–5.05 (1H, m, C-6 H_{eq}), 6.75 (1H, s, C-4 H), 7.03 (1H, s, C-1 H), 7.70 (1H, d, J = 5.5 Hz, C-12 H), 8.74 (1H, d, J = 5.5 Hz, C-11 H), 9.13 (1H, s, C-9 H); ^{13}C nmr (62.9 MHz) δ: 30.3 (C-5), 39.3 (C-6); 56.3, 56.5, (2 × OCH_3); 61.4 (C-14), 71.3 (C-13); 112.4, 118.5, 123.3, 123.9, 129.2, 147.9, 149.1, 149.6, 149.7, 153.0 (aromatic carbon atoms);[3] 162.8 (C=O); ms (EI), *m*/*z* (%): 326 (26.5) $M^{+\cdot}$, 309 (4.5), 192 (100), 135 (10), 134 (6.5), 106 (18). *Anal.* calcd. for $C_{18}H_{18}N_2O_4$: C 66.26, H 5.52, N 8.59; found: C 66.11, H 5.59, N 8.58%. *Exact Mass* (hrms) calcd. for $C_{18}H_{18}N_2O_4$: 326.127; found: 326.127.

Reaction of imine (8b) with the lithium salt of azaphthalide (7)

This reaction was carried out in exactly the same manner as that described above. The condensation product **11***b* was separated as an oil but crystallized from ethyl acetate (420 mg, 61%), mp 230–231°C; R_f 0.46 (alumina, EtOAc); ir ($CHCl_3$), ν_{max}: 1640 cm^{-1}; ^1H nmr (90 MHz), δ: 2.80–3.13 (3H, m, C-5 H's and C-6 H_{ax}), 4.53–4.73 (2H, m, C-13 H and C-14 H), 4.83–5.03 (1H, m, C-6 H_{eq}), 5.97 (2H, s, OCH_2O), 6.73 (1H, s, C-4 H), 6.97 (1H, s, C-1 H), 7.67 (1H, d, J = 5.5 Hz, C-12 H), 8.77 (1H, d, J = 5.5 Hz, C-11 H), 9.20 (1H, s, C-9 H); ^{13}C nmr ($CDCl_3$ + DMSO-d_6) δ: 30.0 (C-5), 38.9 (C-6), 60.7 (C-14), 69.8 (C-13), 100.8 (OCH_2O); 108.1, 109.9, 119.0, 122.8, 125.4, 129.5, 145.4, 146.5, 148.6, 151.2, 152.4 (11 aromatic carbons); 162.0 (C=O); ms (EI), *m*/*z* (%): 310 (23) $M^{+\cdot}$, 176 (96.5), 135 (20.9), 106 (100). *Anal.* calcd. for $C_{17}H_{14}N_2O_4$: C 65.80, H 4.52, N 9.03; found: C 65.70, H 4.71, N 9.23%. *Exact Mass* for $C_{17}H_{14}N_2O_4$: 310.095; found: 310.094.

Reaction of imine (8c) with the lithium salt of azaphthalide (7)

The reaction was carried out in the manner described for the reaction between **8***a* and **7** except that 1.85 mmol of **8***c* was used and other quantities adjusted accordingly. The product (**11***c*) was recrystallized from $CHCl_3$–acetone (317 mg, 43%), mp 222–223°C; R_f 0.56 (alumina, EtOAc); ir ($CHCl_3$), ν_{max}: 1650 cm^{-1}; ^1H nmr (90 MHz), δ: 2.67–3.00 (3H, m, C-5 H's and C-6 H_{ax}), 3.97 (3H, s, OCH_3), 4.47–4.67 (2H, m, C-13 H and C-14 H), 4.87–5.03 (1H, m, C-6 H_{eq}), 6.70 (1H, s, C-4 H), 6.95 (1H, s, C-1 H), 7.30–7.53 (5H, m, C_6H_5), 7.60 (1H, d, J = 5.5 Hz, C-12 H), 8.75 (1H, d, J = 5.5 Hz, C-11 H), 9.20 (1H, s, C-9 H); ^{13}C nmr, δ: 29.8 (C-5), 39.0 (C-6), 55.9 (OMe), 60.6 (C-14), 70.2 (C-13 or OCH_2Ar), 71.0 (C-13 or OCH_2Ar); 111.7, 115.7, 119.0, 123.0, 124.4, 127.4, 127.5, 127.8, 128.4, 129.0, 137.0, 146.1, 148.8, 148.9, 151.1, 152.6 (aromatic carbons);[4] 162.5

[3]Ten signals were observed for 11 carbon atoms.

[4]16 signals observed for 17 aromatic carbon atoms.

(C=O); ms (EI), *m/z* (%): 402 (24.1) $M^{+\cdot}$, 268 (12.0), 177 (10.2), 135 (100), 134 (26.2), 106 (75), 91 (68.4). *Anal.* calcd. for $C_{24}H_{22}N_2O_4$: C 71.64, H 5.47, N 6.97; found: 71.98, H 5.76, N 7.14%.

O-*Acetyl derivative of* ***11***a

Compound **11***a* (50 mg) was dissolved in pyridine (0.5 mL) and treated with an excess of acetic anhydride (1.5 mL). The mixture was kept in a stoppered flask for ca. 12 h, the excess reagent removed under vacuum, and water (5 mL) added to the residue. The aqueous suspension was extracted with chloroform, and the chloroform extract washed with brine, dried over Na_2SO_4, and evaporated to dryness. The *O*-acetate (**12***a*) crystallized from methanol (47 mg, 83%), mp 249–250°C (dec.) (MeOH); R_f 0.36 (alumina, EtOAc); ir ($CHCl_3$), ν_{max}: 1645, 1745 cm^{-1}; ^1H nmr (250 MHz), δ: 2.23 (3H, s, $OCOCH_3$), 2.78–3.10 (3H, m, C-5 H's and C-6 H_{ax}), 3.88 (3H, s, OCH_3), 3.90 (3H, s, OCH_3), 4.92 (1H, d, *J* = 10.7 Hz, C-14 H), 4.90–5.00 (1H, m, C-6 H_{eq}), 6.05 (1H, d, *J* = 10.7 Hz, C-13 H), 6.72 (1H, s, C-4 H), 6.76 (1H, s, C-1 H), 7.15 (1H, d, *J* = 5.20 Hz, C-12 H), 8.76 (1H, d, *J* = 5.2 Hz, C-11 H), 9.27 (1H, s, C-9 H); ^{13}C nmr (62.9 MHz), δ: 21.0 (*CH*$_3$CO), 30.0 (C-5), 39.8 (C-6); 56.0, 56.4 (2 × OCH_3); 59.1 (C-14), 71.3 (C-13); 111.7, 111.8, 118.0, 120.8, 122.3, 125.5, 129.5, 146.2, 150.2, 153.0 (aromatic carbon atoms);[5] 160.57 (lactam C=O), 172.9 (CH_3*CO*); ms (EI), *m/z* (%): 368 (0.8) $M^{+\cdot}$, 325 (22.7), 308 (100), 293 (38.6), 135 (19.3), 134 (65.8). *Exact Mass* (hrms) calcd. for $C_{18}H_{17}N_2O_4$ ($M-C_2H_3O$): 325.119; found: 325.121; calcd. for $C_{18}H_{16}N_2O_3$ ($M-C_2H_4O_2$): 308.116; found: 308.121.

O-*Acetyl derivative of* ***11***b

This compound was prepared from 50 mg of **11***b* under the conditions used to prepare **12***a*. The product **12***b* crystallized from methanol (55 mg, 97%), mp 232–233°C (MeOH); R_f 0.63 (Al_2O_3, EtOAc); ir ($CHCl_3$), ν_{max}: 1650, 1750 cm^{-1}; ^1H nmr (250 MHz), δ: 2.23 (3H, s, *CH*$_3$CO), 2.76–3.05 (3H, m, C-5 H's and C-6 H_{ax}), 4.87 (1H, d, *J* = 10.7 Hz, C-14 H), 4.90–4.96 (1H, m, C-6 H_{eq}), 5.96 (2H, s, OCH_2O), 5.97 (1H, d, *J* = 10.7 Hz, C-13 H), 6.69 (1H, s, C-4 or C-1 H), 6.71 (1H, s, C-1 or C-4 H), 7.16 (1H, d, *J* = 5.2 Hz, C-12 H), 8.76 (1H, d, *J* = 5.2 Hz, C-11 H), 9.26 (1H, s, C-9 H); ms (EI), *m/z* (%): 352 (<1.0%) $M^{+\cdot}$, 2.09 (7.6), 292 (57.2), 277 (29.7), 176 (14.3), 135 (11.3), 134 (33). *Anal.* calcd. for $C_{19}H_{16}N_2O_5$: C 64.77, H 4.55, N 7.95; found: C 64.42, H 4.62, N 7.86. *Exact Mass* (hrms) calcd. for $C_{19}H_{13}N_2O_4$ ($M-C_2H_3O$): 309.088; found: 309.082.

O-*Acetyl derivative of* ***11***c

This compound was prepared from 25 mg of **11***c* under the conditions used to prepare **12***a*. The product **12***c* crystallized from chloroform–ether (23 mg, 83%), mp 182–185°C; R_f 0.80 (alumina, EtOAc), 0.52 (silica, EtOAc); ir ($CHCl_3$), ν_{max}: 1760, 1655 cm^{-1}; ^1H nmr (250 MHz), δ: 2.08 (3H, s, CH_3CO), 2.80–3.10 (3H, m, C-6 H's and C-5 H_{ax}), 3.88 (3H, s, —OCH_3), 4.80–5.00 (2H, m, C-14 H, C-5 H_{eq}), 5.08 (2H, s, CH_2Ar), 5.95 (1H, d, *J*=10.3 Hz, C-13 H), 6.72 (1H, s, C-1 or C-4 H), 6.80 (1H, s, C-1 or C-4 H), 7.09 (1H, d, *J* = 5.0 Hz, C-12 H), 7.30–7.50 (5H, m, C_6H_5), 8.72 (1H, d, *J* = 5.0 Hz, C-11 H), 9.24 (1H, s, C-9 H); ms (EI), *m/z* (%): 444 (3.1) $M^{+\cdot}$, 384 (44), 293 (20), 134 (20), 91 (100). *Exact Mass* (hrms) calcd. for $C_{24}H_{20}N_2O_3$ $(M-C_2H_4O_2)^{+\cdot}$: 384.147; found: 384.147.

Dehydration of alcohol ***11***a

To a solution of alcohol **11***a* (100 mg) in dry pyridine (5 mL) was added freshly distilled $POCl_3$ (1 mL) and the reaction mixture was left at ~20°C for 3 h. The excess of the reagent was evaporated *in vacuo* and the residue dissolved in water (10 mL), made basic with concentrated aqueous NH_3, and thoroughly extracted into chloroform. The combined chloroform extracts were washed with brine, dried over anhydrous Na_2SO_4, and evaporated *in vacuo*. The last traces of pyridine were removed by codistillation using benzene. The crude material on crystallization from MeOH gave product **13***a* (62 mg, 65.6%), mp 185–186°C (MeOH) (lit. (11) mp 169–172°C; R_f 0.37 (alumina, EtOAc); ir ($CHCl_3$), ν_{max}: 1650 cm^{-1}; ^1H nmr (250 MHz), δ: 2.97 (3H, t, *J* = 6.1 Hz, C-5 H's), 3.96 (3H, s, OCH_3), 4.00 (3H, s, OCH_3), 4.33 (2H, t, *J* = 6.1 Hz, C-6 H's), 6.77 (1H, s, C-1 or C-4 H), 7.27 (1H, s, C-13 H), 7.37 (1H, d, *J* = 5.5 Hz, C-12 H), 8.67 (1H, d, *J* = 5.5 Hz, C-11 H), 9.58 (1H, s, C-9 H); ^{13}C nmr, δ: 27.7 (C-5), 39.4 (C-6), 56.0, 56.3 (2 × OMe); 99.1, 108.5, 110.6, 118.9, 120.2, 129.5, 141.7, 142.9, 148.6, 150.4, 151.1, 151.2 (vinylic and aromatic carbons);[6] 161.6 (C=O); ms (EI), *m/z* (%): 308 (100) $M^{+\cdot}$, 307 (17), 294 (13.3), 293 (67.9), 291 (5.0), 277 (3.6), 265 (4.8). *Exact Mass* (hrms) calcd. for $C_{18}H_{16}N_2O_4$: 308.117, found: 308.116.

Dehydration of alcohol ***11***b

This reaction was carried out under the same conditions used for the preparation of **13***a*. The product **13***b* was obtained in 77% yield, mp 288–290° (dec.); R_f 0.58 (alumina, EtOAc); ir ($CHCl_3$), ν_{max}: 1650 cm^{-1}; ^1H nmr (250 MHz), δ: 2.94 (2H, t, *J* = 6.2 Hz, C-5 H's, 4.33 (2H, t, *J* = 6.2 Hz, C-6 H's), 6.05 (2H, s, OCH_2O), 6.75 (2H, s, C-1 and C-4 H's), 7.26 (1H, s, C-13 H), 7.34 (1H, d, *J* = 5.3 Hz, C-12 H), 8.67 (1H, d, *J* = 5.3 Hz, C-11 H), 9.58 (1H, s, C-9 H); ms (EI), *m/z* (%): 292 (97) $M^{+\cdot}$, 291 (34.3), 277 (100), 233 (26.3), 205 (23.6). *Exact Mass* (hrms) calcd. for $C_{17}H_{12}N_2O_3$: 292.085; found: 292.082.

Dehydration of alcohol ***11***c

This reaction was carried out in the same manner used for the dehydration of **11***a*. The product **13***c* was obtained in 95% yield, mp 180–182°C (EtOAc–hexane); R_f 0.68 (alumina, EtOac); ir ($CHCl_3$), ν_{max}: 1655 cm^{-1}; ^1H nmr (90 MHz), δ: 3.05 (2H, t, *J* = 6.2 Hz, C-5 H's), 4.05 (3H, s, OCH_3), 4.40 (2H, t, *J* = 6.2 Hz, C-6 H's), 5.34 (2H, s, OCH_2Ar), 6.73 (1H, s, C-1 H or C-4 H), 6.90 (1H, s, C-4 H or C-1 H), 7.30–7.67 (7H, m, C_6H_5, C-12 H and C-13 H), 8.87 (1H, d, *J* = 5.5 Hz, C-11 H), 9.58 (1H, s, C-9 H); ^{13}C nmr, δ: 29.9 (C-5), 41.5 (C-6), 58.1 (OMe), 74.0 (*OCH*$_2$Ar); 101.1, 113.1, 114.1, 120.7, 123.5, 129.6, 130.2, 130.7, 132.4, 138.9, 143.9, 149.8, 152.6, 153.6, 154.4 (vinylic and aromatic carbons);[7] 163.1 (C=O); ms (EI), *m/z* (%): 384 (74.3) $M^{+\cdot}$, 383 (8.8), 293 (29.0), 265 (7.2), 91 (100). *Exact Mass* (hrms) calcd. for $C_{24}H_{20}N_2O_3$: 384.147; found: 384.148.

*Reaction of iminium salt (****9***a*) *with the anion of azaphthalide (****7***)

n-BuLi (2.56 mmol) in hexane (1.6 *M*) was added to a stirred solution of disopropylamine (2.56 mmol) in dry THF (5 mL) at −78°C under an argon atmosphere. The temperature of the LDA solution was raised to 0°C for 10–15 min and then cooled again to −78°C before proceeding with the dropwise addition of a solution of the azaphthalide **7** (2.2 mmol in THF, 3 mL). Towards the end of the addition the initially formed red solution became turbid but became homogeneous again on raising the temperature to −40°C. The temperature was kept at −40°C during the remainder of the addition and for an additional 20 min. The solution was then transferred through a syringe tube into a flask fitted with a magnetic stirrer containing a suspension of 6,7-dimethoxy-2-methyl-3,4-dihydroisoquinolinium iodide (**9***a*) (740 mg, 2.2 mmol) in dry THF (3 mL). The mixture was stirred at −40°C for 3–4 h and then at ambient temperature overnight. The solvent was evaporated from the reaction mixture and the crude residue passed through a column of neutral alumina (activity I) using EtOAc as eluant. The residue obtained upon evaporation of the EtOAc was taken up in EtOH and from this solution the crystalline *threo* isomer **14***a* was obtained. The mother liquors were taken to dryness and the residue, dissolved in EtOAc, was separated into *threo* (**14***a*) and *erthryo* (**15***a*) components by flash chromatography.

Threo, **14***a* (213 mg, 25.6%); mp 198°C (from EtOH); R_f 0.48 (SiO_2, EtOAc); ir ($CHCl_3$), ν_{max}: 1762 cm^{-1}; ^1H nmr (250 MHz), δ: 2.4–3.2 (4H, m, C-3 H's, and C-4 H's), 2.71 (3H, s, —NCH_3); 3.71 (3H, s, OCH_3), 3.80 (3H, s, OCH_3), 4.19 (1H, d, *J* = 3.7 Hz, C-1 H), 5.75 (1H, d, *J* = 3.7 Hz, C-1′ H), 6.31 (1H, s, C-5 H), 6.66 (1H, s, C-8 H), 7.72 (1H, d, *J* = 5.1 Hz, C-7′ H), 8.63 (1H, d, *J* = 5.1 Hz,

[5] 10 signals observed for 11 aromatic carbon atoms.

[6] 12 signals observed for 13 carbon atoms.

[7] 15 signals observed for the 17 carbon atoms.

C-6′ H), 8.89 (1H, s, C-4′ H); ^{13}C nmr (62.9 MHz), δ: 29.5 (C-4), 45.1 (NCH_3), 50.8 (C-3); 55.8, 56.1 (2 × OCH_3); 65.5 (C-1), 81.4 (C-1′); 110.1, 111.2, 118.8, 152.4, 156.7, (5 × ArCH); 123.0, 123.5, 128.1, 147.3, 147.5, 148.0, (6 × ArC); 169.1 (C=O); ms (CI), *m/z* (%): 341 (16) $(M + 1)^+$, 207 (13.5), 206 (100), 136 (44). *Anal.* calcd. for $C_{19}H_{20}N_2O_4$: C 67.06, H 5.88, N 8.24%; found: C 66.92, H 5.62, N 8.32%. *Erythro*, **15***b* (65.8 mg, 9%); mp 108–110°C (from EtOH); R_f 0.22 (SiO_2, EtOAc); ir ($CHCl_3$), ν_{max}: 1768 cm^{-1}; ^{1}H nmr (250 MHz), δ: 2.17–2.9 (4H, m, C-3 H's, C-4 H's); 2.57 (3H, s, NCH_3), 3.80 (3H, s, OCH_3), 3.91 (3H, s, OCH_3), 4.16 (1H, d, J = 4.5 Hz, C-1 H), 5.66 (1H, d, J = 4.5 Hz, C-1′ H), 6.50 (1H, s, C-5 H), 6.64 (1H, s, C-8 H), 6.65 (1H, d, J = 5.1 Hz, C-7′ H), 8.66 (1H, d, J = 5.1 Hz, C-6′ H), 9.12 (1H, s, C-4′ H); ^{13}C nmr (62.9 MHz), δ: 27.0 (C-4), 45.6 (NCH_3); 50.0 (C-3), 56.3 (2 × OCH_3); 65.30 (C-1), 84.7 (C-1′); 111.1, 111.8, 118.5, 147.7, 152.6 (5 × ArCH); 123.5, 124.1, 129.5, 147.9, 148.9, 156.3 (6 × ArC); 168.5 (C=O); ms (CI), *m/z* (%): 341 (23) $(M+1)^+$, 206 (100). *Anal.* calcd. for $C_{19}H_{20}N_2O_4$: C 67.06, H 5.88, N 8.24; found: C 66.83, H 6.20, N 7.90%.

*Reaction of iminium salts (***9***b) with the anion of azaphthalide (***7***)*

This reaction was carried out in the same manner as that described in the previous section except that 6,7-methylenedioxy-2-methyl-3,4-dihydroisoquinolinium iodide (**9***b*) was used. The reaction mixture was worked up similarly and the mixture of isomeric products separated by flash chromatography using 1% MeOH in EtOAc as eluant.

Threo, **14***b* (212 mg, 30%), mp 151–153°C (dec.) (from EtOH, Et_2O); R_f 0.66 (SiO_2, EtOAc); ir ($CHCl_3$), ν_{max}; 1765 cm^{-1}; ^{1}H nmr (250 MHz), δ: 2.43–3.17 (4H, m, C-3 and C-4 H's), 2.62 (3H, s, —NCH_3), 4.14 (1H, d, J = 3.5 Hz, C-1 H), 5.70 (1H, d, J = 3.5 Hz, C-1′ H), 5.82 (2H, d, J = 4.9 Hz, OCH_2O), 6.34 (1H, s, C-5 H), 6.63 (1H, s, C-8 H), 7.69 (1H, d, J = 5.1 Hz, C-7′ H), 8.67 (1H, d, J = 5.1 Hz, C-6′ H), 8.96 (1H, s, C-4′ H); ^{13}C nmr (62.9 MHz), δ: 29.6 (C-4), 45.2 (NCH_3), 51.5 (C-3); 66.0 (C-1), 82.0 (C-1′), 101.1 (OCH_2O); 107.4, 108.5, 118.7, 147.6, 152.5 (5 × ArCH); 123.7, 124.3, 129.8, 146.3, 146.9, 156.6 (6 × ArC); 168.7 (C=O); ms (CI), *m/z* (%): 325 (5.0), $(M+1)^+$, 191 (28.2), 190 (100). *Anal.* calcd. for $C_{18}H_{16}N_2O_4$: C 66.66, H 4.94, N 8.64; found: C 66.32, H 5.31, N 8.28%. *Erythro*, **15***b* (180 mg, 25%); mp 144–146°C (dec.) (from EtOH, Et_2O); R_f 0.38 (SiO_2, EtOAc); ir ($CHCl_3$), ν_{max}: 1760 cm^{-1}; ^{1}H nmr (250 MHz), δ: 2.1–2.9 (4H, m, C-3 and C-4 H's), 2.54 (3H, s, —NCH_3), 4.11 (1H, d, J = 4.8 Hz, C-1 H), 5.57 (1H, d, J = 4.8 Hz, C-1′ H), 5.98 (2H, s, —OCH_2O), 6.62 (1H, s, C-5 or C-8 H), 6.65 (1H, d, J = 5.1 Hz, C-7′ H), 6.66 (1H, s, C-8 or C-5 H), 8.66 (1H, d, J = 5.1 Hz, C-6′ H), 9.13 (1H, s, C-4′ H); ^{13}C nmr (62.9 MHz), δ: 27.6 (C-4), 45.8 (NCH_3), 50.1 (C-3), 65.6 (C-1), 84.8 (C-1′), 101.3 (OCH_2O); 108.0, 108.8, 118.6, 147.8, 152.7 (5 × ArCH); 124.1, 124.7, 130.8, 146.6, 147.4, 156.1 (6 × ArC); 168.6 (C=O); ms (CI), *m/z* (%): 325 (34.5) $(M+1)^+$, 191 (38), 190 (100). *Anal.* calcd. for $C_{18}H_{16}N_2O_4$: C 66.66, H 4.94, N 8.64; found: C 66.26, H 5.15, N 8.33%.

Acknowledgements

We thank the Natural Sciences and Engineering Research Council of Canada for financial support of this work through grants to H.L.H. and D.B.M. We also thank B. Sayer for recording the 250-MHz spectra and F. Ramelan for the mass spectra.

1. R. Marsden and D. B. MacLean. Tetrahedron Lett. **24**, 2063 (1983).
2. R. Marsden and D. B. MacLean. Can. J. Chem. **62**, 1392 (1984).
3. R. Marsden and D. B. MacLean. Can. J. Chem. **62**, 306 (1984).
4. R. Marsden, D. B. MacLean, and L. Fodor. Can. J. Chem. **62**, 2682 (1984).
5. D. B. MacLean. *In* Natural products chemistry 1984. *Edited by* R. I. Zalewski and J. J. Skolik. Elsevier, Amsterdam. 1985. p. 113.
6. S. C. Pakrashi, R. R. Sinha, A. Bhattacharjya, R. Mukhopadhyay, and E. Ali. Heterocycles, **21**, 457 (1984).
7. S. C. Pakrashi, B. Acahri, E. Ali, P. P. G. Dastidar, and R. R. Sinha. Tetrahedron Lett. **21**, 2667 (1980); S. C. Pakrashi, R. Mukhopadhyay, R. R. Sinha, P. P. G. Dastidar, B. Achari, and E. Ali. Indian J. Chem. Sect B, **24**, 19 (1985).
8. M. M. Kayser and P. Morand. Can. J. Chem. **58**, 2484 (1980).
9. J. Kuthan, L. Musil, and V. Jehlicka. Collect. Czech. Chem. Commun. **42**, 283 (1977).
10. W. R. Ashcroft, M. G. Beal, and J. A. Joule. J. Chem. Soc. Perkin Trans. 1, 3012 (1981).
11. G. R. Lenz. J. Heterocycl. Chem. **16**, 433 (1979).
12. T. Naito and I. Ninomiya. Heterocycles, **14**, 959 (1980); T. Naito, O. Miyata, and I. Ninomiya. J. Chem. Soc. Chem. Commun. 517 (1979).
13. T. Naito, O. Miyata, I. Ninomiya, and S. C. Pakrashi. Heterocycles, **16**, 725 (1981).
14. M. Shamma. The isoquinoline alkaloids. Academic Press, New York. 1972. p. 360; M. Shamma and J. L. Moniot. Isoquinoline alkaloid research 1972–77. Plenum Press, New York. 1978. p. 307.
15. D. B. MacLean. *In* The alkaloids. Vol. XXIV. *Edited by* A. Brossi. Academic Press, New York. 1985. p. 253.
16. C. E. Slemon, L. C. Hellwig, J. P. Ruder, E. W. Hoskins, and D. B. MacLean. Can. J. Chem. **59**, 3005 (1981).
17. V. Elango, A. J. Freyer, G. Blasko, and M. Shamma. J. Nat. Prod. **45**, 517 (1982).
18. W. C. Still, M. Kahn, and A. Mitra. J. Org. Chem. **43**, 2923 (1978).
19. B. Fels. Ber. **37**, 2137 (1904).
20. A. Kirpal. Monatsh. Chem. **10**, 157 (1889).
21. T. Shono, H. Hamaguchi, M. Sasaki, S. Fujita, and K. Nagami. J. Org. Chem. **48**, 1621 (1983).
22. W. M. Whaley and M. Meadow. J. Chem. Soc. 1067 (1953).
23. T. Kametani and K. Ohkbo. Chem. Pharm. Bull. Jpn. **15**, 608 (1967).
24. G. Quequiner and A. Godard. C. R. Acad. Sci. **269**, 1646 (1969).

Properties of atoms and bonds in carbocations

R. F. W. BADER
Department of Chemistry, McMaster University, Hamilton, Ont., Canada L8S 4M1
Received October 15, 1985

This paper is dedicated to Professor Arthur N. Bourns

R. F. W. BADER. Can. J. Chem. **64**, 1036 (1986).

The quantum theory of atoms in molecules defines structures for and determines the properties of the atoms and bonds in the series of carbocations $[(CH_3)_nCH_{3-n}]^+$ with $n = 0$–3, and their parent hydrocarbons. In this theory, an atom in a molecule and its properties are defined by quantum mechanics. The quantum condition defining the atom is given in terms of a property derived from the charge density, as are the other concepts of the molecular structure hypothesis. In terms of the amount of electronic charge density accumulated between the carbon nuclei and its spatial distribution, a C—C bond of the carbocations exhibits an order greater than one. There is a transfer of charge from the hydrogens of methyl to the central carbon that destroys the axial symmetry of these C—C bonds and concentrates the charge in a plane perpendicular to the plane of substitution, in a manner consistent with the hyperconjugative mechanism of electron transfer. The positive charge of a carbocation is thus delocalized over all the atoms in the molecule, and the extent of this delocalization increases with increased methyl substitution. The electron population of each atom in a carbocation increases with this increase in the delocalization of positive charge and its energy is correspondingly decreased (the atom becomes more stable). These effects are most pronounced for the carbon atom bearing the methyl groups and they account for the observed increase in the relative stabilities of the carbocations with increasing methyl substitution. The electron populations and energies of the atoms in saturated hydrocarbons are also determined. The group additivity scheme for the energy in the homologous series of normal alkanes is predicted and explained in terms of the properties of the quantum atoms. It is the possibility of such transferability of the quantum atoms and their properties between systems that identifies them with the atoms of chemistry.

R. F. W. BADER. Can. J. Chem. **64**, 1036 (1986).

La théorie quantique des atomes dans les molécules définit les structures et détermine les properiétés des atomes et des liaisons dans une série de carbocations $[(CH_3)_nCH_{3-n}]^+$, dans lesquels $n = 0$–3, ainsi que dans leurs hydrocarbures de base. Dans cette théorie, la condition quantique qui définit l'atome ainsi que les autres concepts de l'hypothèse relative à la structure moléculaire sont définies en fonction d'une propriété dérivée de la densité de charge. En termes de la densité de la charge électronique qui est accumulée entre les noyaux de carbone et de leur distribution spatiale, une liaison C—C des carbocations présente un ordre qui est plus grand que un. Il se produit un transfert de charge des hydrogènes du méthyle vers le carbone central et ceci détruit la symétrie axiale de ces liaisons C—C et concentre la charge dans un plan perpendiculaire au plan de la substitution, d'une manière qui est en accord avec le mécanisme d'hyperconjugaison de transfert électronique. La charge positive d'un carbocation est donc délocalisée sur tous les atomes de la molécule et le degré de cette délocalisation augmente avec la substitution par des groupements méthyles. La population électronique de chaque atome d'un carbocation augmente avec cette augmentation dans la délocalisation de la charge positive et son énergie diminue d'une manière correspondante (l'atome devient plus stable). Ces effets se font sentir le plus sur l'atome de carbone qui porte les groupements méthyles et ils expliquent le fait que les stabilités relatives des carbocations augmentent avec une augmentation de la substitution par des groupements méthyles. On a aussi déterminé les populations électroniques et les énergies des atomes dans des hydrocarbures saturés. Le schéma d'additivité des groupements pour déterminer l'énergie dans des séries homologues d'alcanes normaux est prédit et expliqué en fonction des propriétés des atomes quantiques. C'est cette possibilité de tels transferts d'atomes quantiques et des leurs propriétés entre atomes qui les identifie avec les atomes de la chimie.

[Traduit par la revue]

Introduction

This paper relates the chemistry of carbocations and their parent hydrocarbons to the properties of their charge distributions. The molecules considered are the cations $[H_{3-n}C(Me)_n]^+$, $n = 0$–3, their parent hydrocarbons, and the additional hydrocarbons *n*-butane and *n*- and neo-pentane. The atoms, their properties, and the networks of bonds in these molecules are defined in terms of the quantum theory of atoms in molecules (1, 2). Trends in the properties of the atoms are determined within each set and compared between the sets. The primary static properties considered are the net charges and the energies of the atoms (3). The characters of the carbon–carbon bonds are summarized in terms of a bond order as determined by the value of the charge density ρ, at the bond saddle point, and a bond ellipticity as determined by the relative magnitudes of the two curvatures of ρ perpendicular to the bond path at the saddle point (4). The ellipticity of a bond measures its departure from radial symmetry and determines the plane in which charge density is preferentially accumulated. The atomic charges together with the orders and ellipticities of the bonds enable one to distinguish between the inductive and hyperconjugative electron release of charge to the carbon atom bearing the formal positive charge in the carbocations. The dominant factor determining the increasing stability of the carbocations with increasing methyl substitution is the corresponding increase in their ability to disperse the positive charge over the hydrogens of the methyl groups by both mechanisms of electron release.

The Laplacian of the charge density, the quantity $\nabla^2\rho$, determines the points within a molecule where electronic charge is locally concentrated and depleted (5, 6). The susceptibility of the carbocations to the addition of a nucleophile is related to the properties of their Laplacian distributions, and the relative inertness of the hydrocarbons to either nucleophilic or electrophilic attack is accounted for in the same manner.

Approximate single determinant state functions were obtained for all molecules using the 6-31G** basis set at 6-31G*

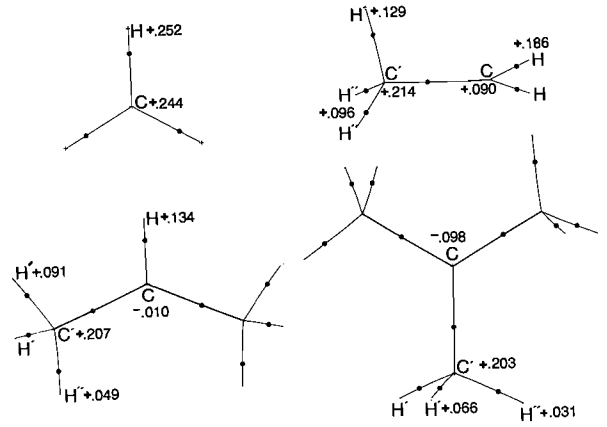

FIG. 1. Molecular graphs illustrating the structures of carbocations calculated from the charge distributions obtained in 6-31G**/6-31G* calculations. The dots indicate the positions of bond critical points. The existence of such a critical point in the charge distribution implies that the two neighbouring nuclei are linked by a line along which the charge density is a maximum with respect to any neighbouring line. In an equilibrium geometry, such a line is called a bond path. The bond paths between carbon nuclei are drawn in heavy line. A bond critical point lies in the interatomic surface denoting the common boundary shared by neighbouring atoms. Note that this surface is not equally placed between the carbon nuclei but is displaced from the midpoint in a direction away from the carbon bearing the methyl substituents. The numbers indicate the net charges on the atoms in atomic units.

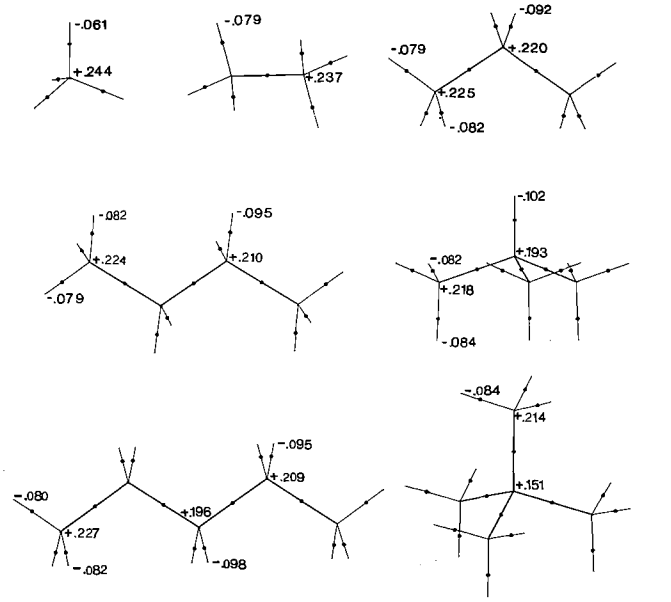

FIG. 2. Molecular graphs illustrating the structures of saturated hydrocarbons calculated from charge densities obtained in 6-31G**/6-31G* wave functions. See the caption for Fig. 1 for details.

optimized geometries, calculations denoted by 6-31G**/6-31G*.[1] The methyl cation is predicted to be of D_{3h} symmetry. The C_s structure reported for the ethyl cation (Fig. 1) is predicted to be most stable for all basis sets below 6-31G**. Using this larger basis a hydrogen bridged structure is found to be marginally more stable (7). The classical C_s structure is retained here for the purpose of comparing the abilities of hydrogen atoms and methyl groups to disperse the net positive charge of the cationic species. The C_{2v} structure for the 2-propyl cation is the most stable one for all basis sets that have been studied (7). The structure of the *tert*-butyl cation is found to be of C_{3h} symmetry. The structures of the saturated hydrocarbons are given in Fig. 2 from 6-31G* geometries determined by Wiberg and Wendoloski (8). In what follows, the carbon atom bearing the formal positive charge in a cation is denoted by C, as is the most substituted carbon in the neutral branched hydrocarbons. The carbon atom of a methyl group is denoted by C′. The properties of the atoms are calculated using the program PROAIM (9).

Atomic and bond properties

The principal differences between the distribution of charge in a hydrocarbon and in its corresponding carbocation are illustrated by comparing displays of their charge densities and associated gradient vector fields, as is done for the CH_4/CH_3^+ system in Fig. 3. The properties of a charge distribution are summarized by the properties of ρ at its critical points, points where the gradient vector field vanishes, i.e., where $\nabla\rho = 0$. For the molecules of interest here, which do not possess ring or cage structures, only two types of critical points are found, those where ρ is a local maximum (all three curvatures of ρ at the critical point are negative) and others, called bond critical points, where ρ possesses one positive and two negative curvatures (ρ at the critical point is a minimum along one direction and a maximum along the other two orthogonal directions). When the charge density is viewed in a plane containing one of the negative curvatures and the single positive curvature as in Fig. 3, a bond critical point has the appearance of a saddle.

The gradient vector of ρ points in the direction of maximum increase in ρ. One can follow the path of maximum increase in the charge density starting from some arbitrary point by following the path traced out by the gradient vector of ρ starting at that point. Every such gradient path originates and terminates at a critical point. The elements of molecular structure as embodied in the topology of the charge density are made evident in the flow of these gradient vectors, as shown in Fig. 3. The nuclear–electron attractive force dominates the interactions present in a molecule and, as a consequence, ρ exhibits a local maximum only at the position of a nucleus (Fig. 3). Because of this property, all of the paths traced out by the gradient vectors of ρ in the vicinity of a given nucleus terminate at that nucleus. The nucleus acts as an attractor in the gradient vector field and the region of space traversed by all the paths that terminate at a given attractor is called the basin of the attractor. Thus, as a result of the single dominant property that ρ exhibits a local maximum only at the position of a nucleus, all of space is partitioned into basins and associated with each basin is a single attractor or nucleus. An atom is defined as the union of an attractor and its basin, the basin being the region of space dominated by that nucleus.

Reference to Fig. 3 indicates that ρ exhibits a saddle point

[1]The total energies of all the molecules, quantities that are considered later, are given in Tables 2 and 3. The 6-31G* optimized geometries of the carbocations are as follows: CH_3^+, R(C—H) = 1.078 Å; $C_2H_5^+$, R(C—C) = 1.431 Å; R(C—H) = 1.079 Å, R(C—H′) = 1.117 Å, R(C—H″) = 1.081 Å, ∠(CCH) = 121.37°, ∠(CCH′) = 97.60°, ∠(CCH″) = 114.89°; $C_3H_7^+$, R(C—C) = 1.456 Å, R(C—H) = 1.080 Å, R(C—H′) = 1.093 Å, R(C—H″) = 1.079 Å, ∠(CCH) = 116.75°, ∠(CCH′) = 107.77°, ∠(CCH″) = 114.23°; $C_4H_9^+$, R(C—C) = 1.473 Å, R(C—H′) = 1.090 Å, R(C—H″) = 1.079 Å, ∠(CCH′) = 108.20°, ∠(CCH″) = 113.74°.

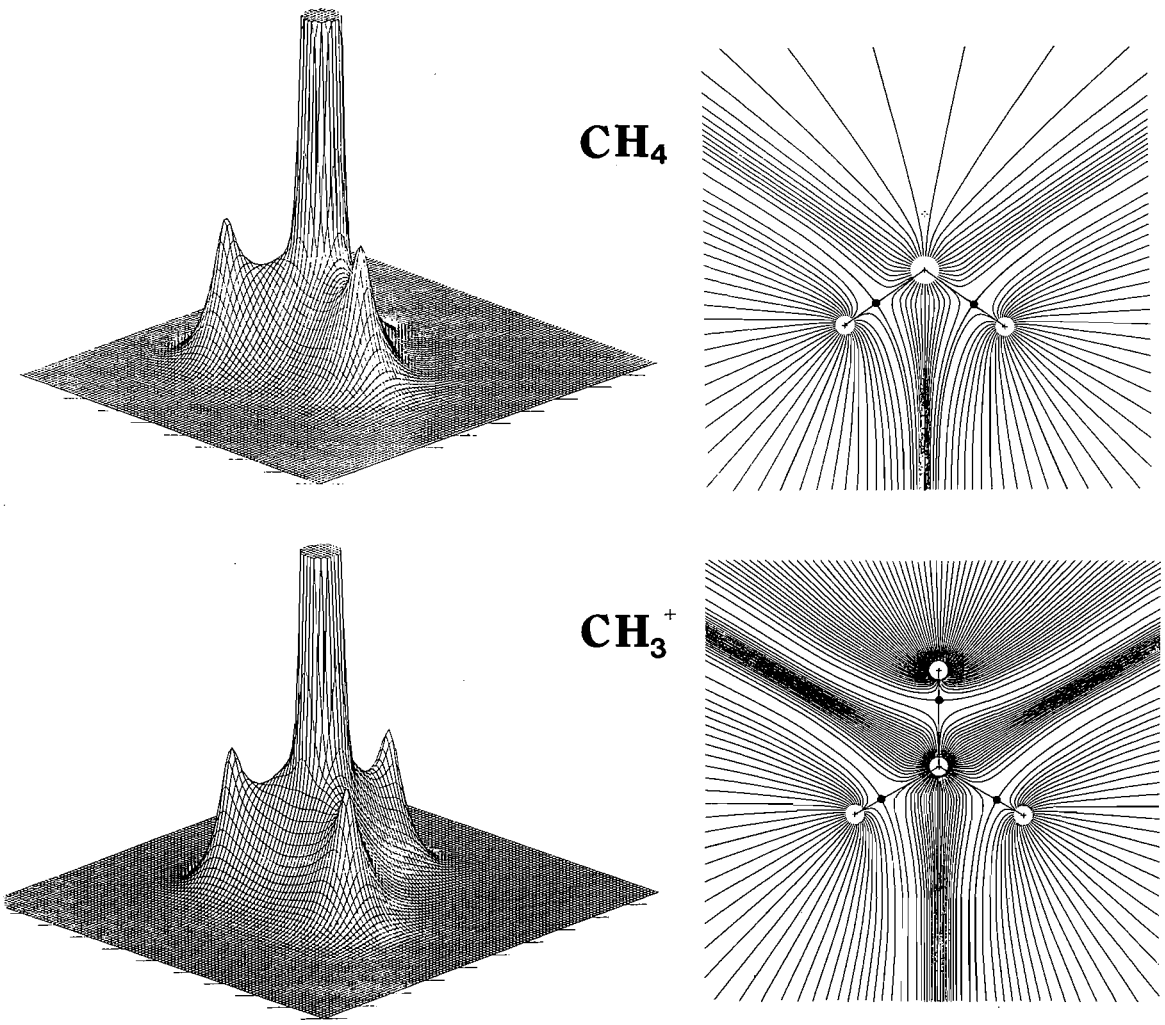

FIG. 3. Displays of the total electronic charge distributions of methane, in a plane containing the carbon nucleus and two protons, and of methyl cation, in a plane containing the carbon nucleus and three protons. Also shown are the gradient vector fields of the charge distributions for the same planes. These latter functions are displayed in terms of the trajectories traced out by the gradient vectors of the charge density. Most trajectories terminate at the local maxima in ρ located at the positions of the nuclei. The region of space traversed by all the trajectories that terminate at a given nucleus is called the basin of the atom. In these symmetry planes, two trajectories of ρ terminate at each of the bond critical points indicated by black dots. These pairs of paths indicate the intersection of the interatomic surface with the plane of the diagram. Two trajectories also originate at each of the bond critical points and terminate at the maxima on the neighbouring nuclei. The resulting lines define the bond paths.

between certain pairs of atoms. Such a critical point indicates that electronic charge is accumulated between the corresponding pairs of nuclei and for molecules in equilibrium geometries it is called a bond critical point. Two trajectories of $\nabla\rho$ originate at such a critical point and terminate at the neighbouring nuclei. They define a path along which the charge density is a maximum with respect to any neighbouring line, a bond path (see Fig. 3). While ρ is a minimum at a bond critical point in the direction of the bond path, it is a maximum with respect to all perpendicular directions and thus it serves as a terminus for gradient paths which form and define an interatomic surface (see Fig. 3). The network of bond paths defines a molecular graph and the structure of a molecule. The structures shown in Figs. 1 and 2 are representations of the molecular graphs as determined by the properties of the molecular charge distributions.

The value of ρ at the position of the proton is less in CH_3^+ than it is in CH_4, 2.79 compared to 2.90 e/Å^3. Its value at the carbon nucleus is greater in the cation than in the neutral molecule, 800.0 compared to 796.6 e/Å^3. The position of the bond critical point is shifted 0.09 Å closer to the proton and 0.08 Å away from the carbon nucleus in the cation, the difference in these two values representing the small difference in bond length between CH_4 and CH_3^+. These observations make quantitative what is qualitatively evident in Fig. 3: the removal of H^- from CH_4 to form the cation is accompanied by a general contraction of the charge density towards the carbon nucleus and by a transfer of charge from the hydrogen atoms to carbon. This result is typical of the systems studied here. As illustrated below, the positive charge of a carbocation is delocalized over all the hydrogens in the molecule and the extent of this delocalization increases with methyl substitution.

The average electron population of each atom Ω in a molecule is obtained by integrating $\rho(\boldsymbol{r})$ over the basin of the atom, eq. [1]

$$[1] \quad N(\Omega) = \int_{\Omega} \rho(\boldsymbol{r}) d\tau$$

The net charge on an atom, denoted by $q(\Omega)$, is obtained by subtracting this average number of electrons from the nuclear charge Z_Ω. The net charges obtained in this manner, with the use of charge densities obtained from the 6-31G**/6-31G* calculations, are indicated in Figs. 1 and 2.

The hydrogens in saturated hydrocarbons bear net negative charges (3). Since H is more electronegative than C in these molecules, the methyl group withdraws charge from the methylene group. In the normal paraffins, propane, butane, and pentane, the methyl groups have net charges of -0.018 ± 0.001 e, the charge being withdrawn from the methylenic groups. In propane this charge is withdrawn from a single CH_2 group, in butane, from two such groups, and the methylenic charges are +0.036 and +0.020 e, respectively. In pentane the charge is withdrawn only from the CH_2 groups linked to the methyl groups (they have the same net charge as they do in butane) and the central methylene group in this molecule has a zero net charge—the charge transfer is damped by a single methylene group. In the branched series $Me_nCH_{(4-n)}$ starting with methane, the magnitude of the negative charge on H increases with n from 0.06 e in methane to 0.10 e in isobutane. The charge on a methyl group is +0.06 e in methane and becomes more negative as n increases, equalling 0.00, −0.018, −0.029, and −0.038 in ethane, propane, isobutane, and neopentane, respectively. As a consequence of hydrogen being more electronegative than carbon, the relative electron-withdrawing ability of the functional groups in saturated hydrocarbons is H > CH_3 > CH_2 > CH > C. The positive charge on carbon C in the branched series decreases with increasing methyl substitution since Me withdraws fewer electrons than does H. The charge on this carbon atom exhibits the greatest dependence on structure.

The variation in atomic charges in the series of cations $[Me_nCH_{(3-n)}]^+$ is much greater than is found in the corresponding neutral series of molecules. In CH_3^+ the positive charge is almost equally delocalized over the C and H atoms. An increasing amount of electronic charge is transferred to C with increasing methyl substitution, and in the *tert*-butyl cation this atom bears a net negative charge. While the electron population of carbon atom C increases with increasing n, the net positive charges of the H atoms and methyl groups decrease with increasing n. That is, as more methyl groups are added, the total amount of electronic charge transferred to C is increased but, because of the increasing number of atoms able to donate charge, the net charges on these atoms are decreased. Thus the net charges on the methyl groups decrease through the series ethyl, 2-propyl, and *tert*-butyl. The values are respectively, +0.535, +0.438, and +0.366 e. Next to carbon atom C, the greatest variation in charge is found for the hydrogens, both the methyl hydrogens and those bonded directly to carbon atom C. In summary, increased methyl substitution at a carbon bearing a formal positive charge leads to an increase in the transfer of electronic charge to that atom and to an increase in the extent of delocalization of the positive charge over the methyl hydrogens.

The stabilities of the carbocations in the gas phase increase in the order of $CH_3^+ < CH_3CH_2^+ < (CH_3)_2CH^+ < (CH_3)_3C^+$. The energy changes underlying this ordering are discussed in a following section. Here we wish to note that the increase in stability parallels the increase in the dispersal of charge over the methyl hydrogens. A similar delocalization of charge over the methyl hydrogens has been found by Stutchbury and Cooper (10) to occur in protonated amines, thereby accounting for the observed order of increasing gas phase basicity, $NH_3 < CH_3NH_2 < (CH_3)_2NH < (CH_3)_3N$, and in alkoxide ions, thereby accounting for the observed order of increasing gas phase acidity, $H_2O < CH_3OH < CH_3CH_2OH < (CH_3)_2CHOH < (CH_3)_3COH$. In the alkoxide ions the methyl groups bear net negative charges (nearly all of which are located on the hydrogens) of −0.215, −0.191, and −0.184 e, respectively, in ethyl, isopropyl, and *tert*-butyl. In the protonated amines the methyl groups bear net positive charges of +0.569, +0.541, and +0.519 e, respectively, for the mono-, di-, and tri-metyl cations. Stutchbury and Cooper also observed that methyl substitution in the corresponding neutral molecules does not cause significant changes in the atomic populations, the variations in the net charges on the atoms in the saturated alcohols and amines being of the same order as the small variations reported here for the saturated hydrocarbons. The behaviour of the atomic charges in all three systems of molecules supports the following general conclusions: (a) In neutral, saturated molecules, replacement of hydrogen by methyl causes only small changes in atomic populations, the largest change being found for the atom at which the replacement occurs. (b) In corresponding anionic and cationic species, the replacement of hydrogen by a methyl group causes significant changes in the atomic popualtions, changes that correspond to a dispersal of the net charge over the methyl hydrogens. The variation in charge with the extent of methyl substitution is greatest for a system in which the site of substitution has an orbital vacancy. (c) The hydrogens of a methyl group may act effectively as either a sink or source of electronic charge (10).

Within the orbital model of electronic structure one differentiates between the inductive and hyperconjugative mechanisms of electron release from a methyl group to an unsaturated carbon or to a carbon with an orbital vacancy. If the hyperconjugative mechanism is operative, then the C—CH_3 bond should possess a bond order greater than one and exhibit some degree of π character. In addition, this mechanism can lead to differing extents of charge release from the methyl hydrogen atoms. The theory of atoms in molecules enables one to test for the presence of these anticipated consequences of hyperconjugation. Previous studies of hyperconjugation in these molecules employed the methods of a Mulliken population analysis (11).

The data in Table 1 characterize the properties of the C—C bonds in terms of the properties of ρ at the bond critical points. The value of ρ at a bond critical point, the quantity ρ_b, can be used to define a C—C bond order n (n = 1.0, 1.6, 2.0, 3.0, respectively, for ethane, benzene, ethylene, and acetylene) that provides a measure of the extent to which electronic charge is accumulated between the bonded nuclei (4). The C—C bonds in the saturated hydrocarbons are all of order 1.0. The values of ρ_b and of the bond ordr n increase slightly with methyl substitution and with chain length in the saturated hydrocarbons, notwithstanding small corresponding increases in the carbon–carbon bond lengths. In the carbocations, however, the C—CH_3 bond orders are all greater than unity, being largest in the ethyl cation. The observation of bond orders greater than unity for the C—CH_3 bonds in the cations correlates with the presence of partial double bond character.

In a bond with cylindrical symmetry the two negative curvatures of ρ at the bond critical point are of equal magnitude. However, if electronic charge is preferentially accumulated in a given plane (as it is for a bond with π character), then the rate of falloff in ρ, from its maximum value ρ_b at the bond critical point in the interatomic surface is less in this plane than in the one perpendicular to it and the magnitude of the corresponding

TABLE 1. Properties of C—C bonds (6-31G**/6-31G*)

A. In hydrocarbons

Molecule	Bond length R_e (Å)	$\rho(r_C)$ (e/Å^3)	Order n	Ellipticity ϵ	$\nabla^2\rho(r_c)$ (e/Å^5)	λ_3 (e/Å^5)
CH_3—CH_3	1.527	1.707	1.00	0.000	−16.04	7.15
CH_3—CH_2CH_3	1.528	1.718	1.01	0.008	−16.20	7.21
CH_3—$CH(CH_3)_2$	1.530	1.725	1.02	0.007	−16.28	7.24
CH_3—$CH_2CH_2CH_3$	1.528	1.719	1.01	0.007	−16.21	7.20
CH_3CH_2—CH_2CH_3	1.530	1.727	1.02	0.016	−16.29	7.28
CH_3—$CH_2(CH_2)_2CH_3$	1.527	1.722	1.01	0.006	−16.26	7.21
CH_3CH_2—$CH_2CH_2CH_3$	1.528	1.734	1.03	0.014	−16.42	7.27
CH_3—$C(CH_3)_3$	1.533	1.725	1.02	0.000	−16.25	7.25

B. In carbocations

Molecule	Bond length R_e (Å)	$\rho(r_C)$ (e/Å^3)	Order n	Ellipticity ϵ	$\nabla^2\rho(r_c)$ (e/Å^5)	λ_3 (e/Å^5)
CH_3—CH_2^+	1.431	2.028	1.37	0.091	−24.37	3.72
CH_3—$CH(CH_3)^+$	1.456	1.958	1.28	0.051	−22.50	4.86
CH_3—$C(CH_3)_2^+$	1.473	1.918	1.22	0.038	−21.21	5.69

curvature of ρ is smaller. If the two negative curvatures of ρ at a bond critical point are denoted by λ_1 and λ_2 with λ_2 being the curvature of smallest magnitude, the quantity $\epsilon = \lambda_1/\lambda_2 - 1$, the ellipticity of the bond, provides a measure of the extent to which charge is preferentially accumulated in a given plane (4). Thus, for example, the ellipticity of the C—C bond in ethane is zero, greater than zero for benzene, and greater still for ethylene (and equal to 0.45 in the 6-31G** basis). In the latter two molecules the curvature of smallest magnitude is directed perpendicular to the plane of the nuclei, as anticipated for bonds with π character. The C—C bonds in the saturated hydrocarbons are close to being axially symmetric and their ellipticities are in general close to zero. The ellipticities in the cations are significantly greater than zero and the trend in their values is the same as that found for the bond orders, being greatest in $C_2H_5^+$ and smallest in $C_4H_9^+$. In all three of these cations the major axis of the ellipticity is perpendicular to the plane containing the nuclei bonded to the C nucleus. That is, the charge density in the C—CH_3 bonds of the carbocations is preferentially delocalized in a direction parallel to the axis of the vacant $p\pi$ orbital on carbon atom C.

The final quantity listed in Table 1 is $\nabla^2\rho(r_c)$, the sum of the three curvatures of ρ at the bond critical point. The charge density is a maximum in an interatomic surface at the bond critical point. The two curvatures of ρ perpendicular to the bond path are, therefore, negative and charge is locally concentrated in the surface at this point. Since $\rho(r)$ is a minimum at r_c along the bond path, the third or parallel curvature of ρ at the bond critical point is positive. Charge is locally depleted at r_c with respect to neighbouring points along the bond path. Thus the formation of an interatomic surface and a chemical bond is a result of a competition between the perpendicular contractions of ρ, leading to a concentration or compression of electronic charge along the bond path, and the parallel expansion of ρ, leading to a depletion of charge in the interatomic surface and to its separate concentration in the basins of neighbouring nuclei. When $\nabla^2\rho < 0$, the perpendicular curvatures dominate the interaction and electronic charge is concentrated along the bond path. The result is a sharing of electronic charge between the nuclei as found in covalent or polar interactions. As one would anticipate, $\nabla^2\rho(r_C) < 0$ for all of the bonds in the hydrocarbon molecules. Its values for a C—C bond in the saturated molecules exhibits only small variations throughout the series, its magnitude being slightly larger in the branched systems and for the interior bonds linking methylene groups. To a first approximation, the C—C bonds in the saturated hydrocarbons exhibit autonomous behaviour. The small variations in the bond indices that are present indicate a slight increase in order and degree of binding as the extent of branching is increased or as the chain length is increased.

The values of $\nabla^2\rho$ for the C—CH_3 bonds in the cations become less negative through the series from ethyl to *tert*-butyl and are all greater in magnitude than the value for a C—C bond in the neutral molecules. Thus the greater the release of charge from methyl to carbon C, the greater is the bond order, the greater is the ellipticity and the more negative is the value of $\nabla^2\rho$. The value of $\nabla^2\rho(r_C)$ becomes more negative with an increase in bond order n as a consequence of two effects: (i) as n increases, charge is increasingly concentrated along the bond path, as reflected in an increase in magnitude of the perpendicular curvatures of ρ; (ii) the increase in the accumulation of charge in the internuclear region that accompanies an increase in n results in a decrease of λ_3, the (positive) curvature of ρ along the bond path. The C—CH_3 bonds of the carbocations all possess λ_3 values smaller than those for the neutral molecules, the smallest value being found for the ethyl cation for which the value of $\nabla^2\rho$ approaches that for a C—C double bond, −28.7 e/Å.

In terms of the amount of electronic charge accumulated between the carbon nuclei as measured by ρ_b, its mode of accumulation as measured by $\nabla^2\rho$, and its spatial distribution as measured by ε, the C—CH_3 bonds of the carbocations exhibit characteristics intermediate between those of a single and a double bond. It is clear that the transfer of charge from the hydrogens of methyl to carbon atom C occurs via a mechanism that destroys the axial symmetry of the C—CH_3 bond and concentrates the charge in a plane aligned with the direction of a $p\pi$ orbital on atom C. This alignment of the charge transfer is

reflected in the differing extents of charge removal from the hydrogen atoms of the methyl groups. There is no large differentiation between the charges on the methyl hydrogens in the saturated hydrocarbons. This is not the case in the carbocations. One notes that the net positive charge on a methyl carbon is not much changed from its value in the neutral precursor. The methyl hydrogens, however, bear net negative charges in the neutral molecules and net positive charges in the cations. Furthermore, the magnitude of this positive charge depends upon the orientation of H relative to the axis perpendicular to the plane of substitution at carbon C. In the ethyl cation the hydrogens of the methyl group are aligned such that the combination of orbitals depicted in **a** will be in-phase with the $p\pi$ orbital on carbon C. The loss of electronic charge is greater for the hydrogen labelled H′ (see Fig. 1) than it is for those labelled H″ and this is in line with the weighting of the coefficients of the atomic orbitals in **a**. This difference in extent of charge loss is reflected in the bond lengths as well, the values being 2.099 and 2.044 Å for the bonds to H′ and H″, respectively. In the 2-propyl and *tert*-butyl cations the methyl hydrogens are aligned such that the combination of orbitals depicted in **b** provides the overlap with the $p\pi$ orbital on carbon

a **b**

C. In both these molecules the hydrogens labelled H′ (Fig. 1) have approximately twice the net charge and slightly longer bond lengths than do the hydrogens labelled H″. If one accepts the simple orbital model of hyperconjugation, then the hydrogen atom populations of methyl may be used to determine what fraction of the charge loss from these atoms is caused by this mechanism. In the *tert*-butyl and 2-propyl cations the atoms H″ (see Fig. 1) cannot donate charge by the hyperconjugative mechanism and their net charges determine the inductive charge losses, which are 0.03 and 0.05 e, respectively. The 0.04 e lost in excess of this amount by the atoms H′ in these two molecules thus represents the charge released by the hyperconjugative mechanism. According to the model, the hyperconjugative release from H′ is twice that from H″ in the ethyl cation and, if the inductive loss is taken as 0.05 e, then the populations indeed yield hyperconjugative losses of 0.08 e from H′ and 0.04 e from H″.

Moments other than the monopole (the net charge) may be determined for an atom in a molecule. Of particular interest for the cations is the quadrupole moment of carbon atom C. The z^2 component of the traceless quadrupole moment tensor is (12)

$$[2] \quad Q_{zz}(\Omega) = -e\int_{\Omega} \rho(3z^2 - r^2)d\tau$$

with corresponding expressions for x^2 and y^2. For a spherical distribution all three components are zero. If the sphere is flattened at its poles to yield an oblate spheroid, then (taking the polar axis along z) $Q_{zz}(\Omega) > 0$ and $Q_{xx}(\Omega) = Q_{yy}(\Omega) = -\frac{1}{2}Q_{zz}(\Omega)$, reflecting the accumulation of negative charge in the xy-plane. The orbital model assigns a vacant $2p\pi$ orbital to atom C in CH_3^+ and one anticipates the charge distribution of this atom to exhibit the moments characteristic of an oblate spheroid. The magnitudes of these moments should be smaller for carbon C in *tert*-butyl cation, as some part of the charge transferred to this atom preferentially populates its $2p\pi$ orbital. These conjectures are borne out. Both methyl and *tert*-butyl cations possess a three-fold symmetry axis and the principal moments lie along the three cartesian axes. For CH_3^+ the value of $Q_{zz}(\Omega)$ is +1.22 au while for the *tert*-butyl cation its value is reduced to +0.43 au. The oblate nature of the C atom charge distribution is also reflected in the distribution of charge in the C—H bonds. These bonds exhibit significant ellipticities ranging from 0.054 in CH_3^+ to 0.050 in $C_3H_7^+$ and their major axes are in the same plane as that in which the sphere is flattened.

Reactivity

The susceptibility of a carbocation to nucleophilic addition can be predicted and understood in terms of the properties of the Laplacian of its charge distribution. The Laplacian of ρ is the sum of the three principal curvatures of ρ at each point in space:

$$[3] \quad \nabla^2\rho(\boldsymbol{r}) = \partial^2\rho/\partial x^2 + \partial^2\rho/\partial y^2 + \partial^2\rho/\partial z^2$$

When $\nabla^2\rho(\boldsymbol{r}) < 0$ the value of the charge density at $\boldsymbol{r}$ is greater than the value of $\rho(\boldsymbol{r})$ averaged over all the neighbouring points in space, and when $\nabla^2\rho(\boldsymbol{r}) > 0$, then $\rho(\boldsymbol{r})$ is less than this averaged value. These statements follow directly from the definition of the second derivative of a scaler function such as ρ (5, 6). The Laplacian distribution recovers the shell model of electronic structure by exhibiting a corresponding number of alternating pairs of shells of charge concentration and charge depletion. For an isolated atom with a complete outer shell, the valence shell of charge concentration (VSCC) possesses a sphere on whose surface charge is maximally concentrated. In general, this sphere of maximum charge concentration persists for an atom in chemical combination, but the charge is not uniformly concentrated over its surface. Instead, a number of local maxima are present on this surface and, in terms of their number, relative position, and size, they yield a faithful replica of the Lewis model of bonded and nonbonded electron pairs. A carbon atom in a saturated hydrocarbon possesses four bonded charge concentrations (see Fig. 4). Each of these maxima is linked to the other three by unique pairs of trajectories of the gradient of the Laplacian of ρ, which originate at intervening saddle points on the surface of charge concentration. These lines are the analogues of the bond paths defined by corresponding trajectories of the gradient of the charge density. This network of lines, called the atomic graph, partitions the surface of charge concentration into four segments and the basic structure is that of a tetrahedron with curved faces. In the centre of each face there is a local minimum in the surface of the VSCC. The uniform spherical surface of charge concentration of a free (sphericalized) carbon atom is transformed in methane, for example, into one with four tetrahedrally arranged concentrations of charge with charge depletions in the centre of each of the resulting faces. The surface of maximum charge concentration in the molecule is no longer perfectly spherical, the maxima and minima lying at slightly different distances from the nucleus, but all within the range of 0.54–0.55 Å.

It is well documented (6, 13, 14) that centres of charge concentration in the VSCC serve as sites of electrophilic attack, while the centres of charge depletion play the corresponding role in nucleophilic attack. The localized charge concentrations in the VSCC of carbon in a saturated hydrocarbon are, of course, all bonded concentrations and as such are relatively unreactive towards electrophiles. Because of the relatively small extent of charge transfer between atoms in saturated

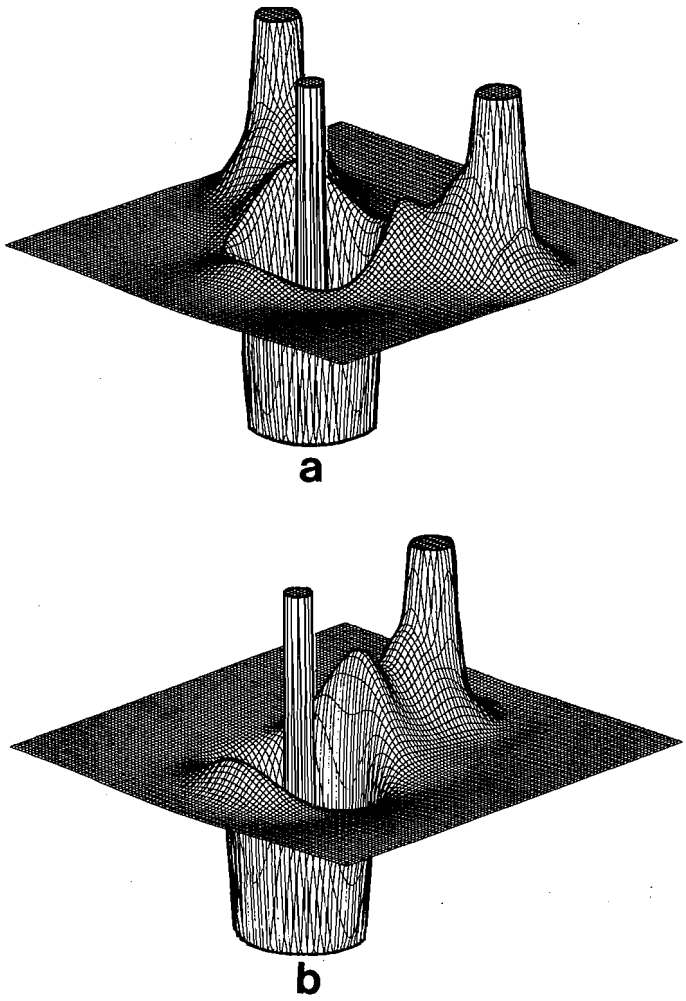

FIG. 4. Displays of the negative of the Laplacian of the charge distributions of (a) methane, in a plane containing the carbon and two hydrogen nuclei, and (b) of methyl cation in a plane containing the carbon nucleus and a single proton. A maximum (minimum) in $-\nabla^2\rho$ indicates a local concentration (depletion) of electronic charge. There is a local maximum at the position of each nucleus, which has been terminated at some arbitrary value. For carbon, this maximum and its neighbouring region of charge depletion denote the presence of an inner shell. Both drawings are to the same vertical scale. Note that the bonded maxima in the valence shell of carbon are larger in the cation than in the neutral molecule, a reflection of the contraction of charge towards the carbon nucleus in the former molecule. Most important is the absence of a "lip" separating the core region of the carbon in the cation from its valence region of charge removal. This puncturing of the valence shell of charge concentration (a shell which totally envelopes the carbon core in methane) is found in all of the cations and it gives approaching nucleophiles direct access to the region of charge removal in the carbon core.

hydrocarbons, the regions of charge depletion in the VSCC of a carbon atom are not pronounced and these atoms are also relatively unreactive towards nucleophilic attack. Substitution of a hydrogen in methane by fluorine greatly increases the extent of charge depletion in the VSCC of carbon in the face opposite the fluorine atom, thereby increasing the susceptibility of the carbon to nucleophilic attack (14).

The carbon atom in the methyl cation exemplifies the VSCC of a Lewis acid. The surface of maximum charge concentration of this atom is punctured on either side of the plane containing the nuclei, reducing the VSCC to an equatorial belt of charge concentration, the three bonded maxima being linked to form a ring by intervening saddle points. This behaviour is made evident in the relief map of the Laplacian (Fig. 4) by the absence of a "lip" at the corresponding positions of the core. Thus an incomplete valence shell of the Lewis model or a $p\pi$ orbital vacancy of the orbital model appears in the Laplacian distribution as two holes in the valence shell of charge concentration. These holes provide direct access to the region of charge depletion in the core of the atom, making it very susceptible to nucleophilic attack. The boron atom in trivalent systems exhibits similar behaviour, as does the carbon bearing the formal positive charge in the classical structure of the norbornyl cation (1). The two equivalent classical structures of this ion as determined by their charge distributions are separated by, and differ little in energy from, the symmetrical bridged or nonclassical structure. The Laplacian of this latter structure exhibits holes only on the *exo* side of the two carbons, which are alternately three-bonded in the two classical structures. On vibrational averaging, the most pronounced holes in the valence shells of these two atoms are those which, when combined with the charge concentration of a nucleophile, yield the mirror-image *exo*-norbornyl product, as is observed.

If purely electrostatic effects determined the reactivity of these systems, both the net charge and the quadrupole moment of carbon C would indicate that the reactivity should decrease through the series from methyl to *tert*-butyl. However, the very pronounced positive character of the Laplacian of the core as exposed by the holes in the VSCC of carbon atom C ensures the susceptibility of all these cations to nucleophilic attack, even though carbon C is essentially neutral in one, and bears a small negative charge in another, member of the series. Because of the ability of the methyl hydrogens to act as sinks as well as sources of electronic charge, the charge distribution of the carbon bearing the methyl groups is very polarizable, charge leaving the atom and migrating back to the methyl hydrogens with the approach of the negatively charged nucleophile.

Atomic energies

The topological atoms are quantum subsystems and, therefore, all of the theorems derivable from the Heisenberg equation of motion for any operator A apply to an atom in a molecule (2). In particular, the virial theorem applies (the operator A is set equal to $\boldsymbol{r}\cdot\boldsymbol{p}$) and one may define $E(\Omega)$, the energy of atom Ω in a molecule. These energies are additive and their summation over a molecule in an equilibrium geometry equals E, the total energy of the molecule,

$$[4] \quad E = \sum_{\Omega} E(\Omega)$$

It is important to realize that this partitioning of the total energy into atomic contributions includes a nontrivial partitioning of the nuclear–nuclear potential energy of repulsion.[2]

The viral theorem gives the following relationships between

[2]The partitioning of the nuclear–nuclear repulsive energy is obtained as a consequence of the potential energy being defined as the virial of the (Ehrenfest) forces exerted on the electrons. The virial of the forces that results from the electron–nuclear potential energy operator yields the electron–nuclear potential energy plus the virial of the Hellmann–Feynman forces exerted by the nuclei on the electrons. For an equilibrium geometry this latter contribution equals the nuclear–nuclear potential energy.

TABLE 2. Atomic energies in saturated hydrocarbons (6-31G**/6-31G*)

RH	E (au) and $\gamma = -V/T$	$E(CH_3)$ - A^a (kcal/mol)	$E(CH_2)$ - B^a (kcal/mol)	$\Delta E(C)^b$ of CH_3 (kcal/mol)	$\Delta E(C)^b$ of CH_2 (kcal/mol)	$E - \Sigma_\Omega E(\Omega)$ (kcal/mol)
CH_4	−40.20171 2.000499	+41.1	—	+14.4	—	+0.34
C_2H_6	−79.23824 2.000486	00.0	—	00.0	—	−1.11
C_3H_8	−118.27616 2.000450	−10.9	+21.7	−10.9	0.00	+0.56
C_4H_{10}	−157.31395 2.000354	−10.8	+10.8	−9.5	−10.0	−1.71
C_5H_{12}	−196.35159 2.000353	−9.9	+10.9	−9.1	−10.2	+0.97
$(CH_3)_3CH$	−157.31454 2.000389	−20.3	—	−19.4	—	−1.96
$(CH_3)_4C$	−196.35245 2.000298	−28.8	—	−26.5	—	+1.32

[a] $A = -39.61912$ au, the energy of CH_3 group in ethane; $B = -39.03775$ au, the energy increment in series $CH_3(CH_2)_nCH_3$.
[b] E(C) of CH_3 relative to E(C) in ethane = −37.63264 au and E(C) of CH_2, relative to E(C) of CH_2 in propane = −37.65449 au.

TABLE 3. Atomic energies in carbocations (6-31G**/6-31G*)

Cation R^+	E (au) and $\gamma = -V/T$	Atomic energies relative to C and H in CH_3^+ (kcal/mol)[a]						ΔE^{+b} (kcal/mol)		$E - \Sigma_\Omega E(\Omega)$ (kcal/mol)
		ΔE(C)	ΔE(H)	ΔE(C′)	ΔE(H′)	ΔE(H″)	$\Delta E(CH_3)$	Calcd.	Exp.[c]	
$[CH_3]^+$	−39.23629 2.000586	0.0	0.0	—	—	—	0.0	0.0	0.0	+0.63
$[CH_3CH_2]^+$	−78.32054 2.000592	−77.8	−21.1	−12.6	−14.9	−40.4	−108.4	−30	−41	−0.33
$[(CH_3)_2CH]^+$	−117.39328 2.000583	−123.7	−38.9	−16.4	−35.7	−56.4	−144.2	−52	−64	+0.43
$[(CH_3)_3C]^+$	−156.45830 2.000564	−154.6	—	−19.5	−44.8	−61.9	−171.7	−69	−81	+2.18

[a] Energies of atoms in CH_3^+ are: E(C) = −37.6824 au; E(H) = −0.5183 au.
[b] Energy change for reaction $CH_3^+ + RH \rightleftarrows CH_4 + R^+$.
[c] Experimental data for cations taken from ref. 18. The experimental values of ΔE^+ are calculated from $\Delta H_f^\circ(298)$ values.

the kinetic ($T(\Omega)$), potential ($V(\Omega)$) and total ($E(\Omega)$) energies of an atom in a molecule that is in an equilibrium geometry:

$$[5] \quad E(\Omega) = -T(\Omega), \quad 2T(\Omega) = -V(\Omega), \quad E(\Omega) = \tfrac{1}{2}V(\Omega)$$

where $E(\Omega) = T(\Omega) + V(\Omega)$. The kinetic energy of an atom in a molecule is easily obtained by integration of a corresponding density over the basin of the atom and the first of the relationships given in [5] is then used to obtain the total energy of the atom, $E(\Omega)$. The virial theorem is not exactly satisfied at the 6-31G** level of calculation and the ratio $-V/T$ for each molecule differs slightly from the correct value of two for an equilibrium geometry. This can be seen from the data in Tables 2 and 3, where this ratio is given under the heading γ. To correct for the small error in the virial, each atomic kinetic energy is multiplied by the factor $(\gamma - 1)$ to obtain a set of atomic energies that correctly sum to the total energy of the molecule. The nuber $(\gamma - 1)$ is in every case close to unity, the value it should equal at equilibrium. An atomic kinetic energy is obtained by numerical integration over the basin of an atom. As a test of the numerical methods, Tables 2 and 3 compare the sums of the atomic energies with the total energies (eq. [4]). The integration error is never greater than 2.0 kcal/mol. The relative precision of each integration may be determined[3] and, when the error in eq. [4] exceeds 0.5 kcal/mol, the results for the atom with the smallest precision are adjusted to yield the correct sum.

The most interesting property of the energies of the saturated hydrocarbons is that they obey an additivity relation wherein one assigns fixed energies to the CH_3, CH_2, CH, and C groups (15). The most important property of the topological atom is that its properties, including its energy, are determined by its spatial distribution of charge, that is, by its form in real space. Thus when two atoms or two functional groupings of atoms "look the same", i.e., when they have the same spatial distribution of charge, they have the same properties and they contribute identical amounts to the total energies of the systems in which they occur. This possibility of transferability in real space, together with the additivity of the atomic energies over a given

[3] As a consequence of the quantum condition of zero flux in the gradient vector of ρ through the surface of an atom, the integration of the Laplacian of the charge density over an atom must vanish (1, 2). The smallness of the value of this intergral may thus be used to judge the quality of an integration. Its value is a direct measure of the difference in the values of the two methods of calculating the average kinetic energy of an atom and normally it equals 0.1 kcal/mol or less.

molecule as expressed in eq. [4], are both necessary to account for additivity schemes in homologous series of molecules.

It is possible to fit the experimental heats of formation of the homologous series $CH_3(CH_2)_mCH_3$, starting with $m = 0$, with the expression $2A + mB$, where A is the contribution from the methyl group and B that from the methylene group. The generally accepted value for B at 25°C is -4.93 kcal/mol, while $A = -10.12$ kcal/mol. Wiberg has shown that the correlation energy correction, the zero point energies, and the change in H_f on going from 298 to 0 K are reasonably well represented by group equivalents (16*a*).[4] This is indeed the case, for the calculated 6-31G**/6-31G* energies (for the vibrationless molecules at 0 K) may also be fitted by the relationship $E = 2A + mB$, with $A = -39.61912$ au and $B = -39.03775$ au. Those constants reproduce the calculated energies with a maximum error of 0.13 kcal/mol, which is slightly smaller than the experimental errors in the measurements at 25°C. This means that the calculated state functions, energies, and charge distributions contain the necessary information to account for the additivity observed in this homologous series of molecules.

It is clear from the populations already considered that the methyl group in ethane is not identical to those found in the other members of the series and, similarly, the methylene group is different in the three molecules of the series considered here. The small differences found for these groups are to be expected, as their environments change by corresponding small amounts from molecule to molecule. In ethane, methyl is bonded to methyl, while in the other systems it is bonded to methylene, from which it withdraws charge. Table 2 lists the energies of the methyl groups relative to the constant A, the energy of a methyl group in ethane. To within the accuracy of the integrations, the population and energy of methyl are constant when it is bonded to methylene. That is, the methyl group is the same in all members of the homologous series past ethane. The methyl group in these molecules, relative to methyl in ethane, is more stable by an amount $\Delta E = -10.5 \pm 0.5$ kcal/mol and its electron population is greater by an amount $\Delta N = 0.018 \pm 0.001$ e. The charge and energy gained by the methyl groups are taken from the methylene groups. What is remarkable and what accounts for the additivity of energy in this series of molecules is that the energy gained by the methyl groups is equal to the energy lost by the methylene groups. Table 2 lists the energies of the methylene groups relative to the energy increment B and one finds that, in propane, the energy of the methylene group is $B - 2\Delta E$ and its charge is $+2\Delta N$. In butane, each methylene is bonded to a single methyl and their energies are given by $B - \Delta E$ and their charges by $+\Delta N$. The corresponding CH_2 groups in pentane, those bonded to a methyl group, have the same properties, implying that the central methylene in pentane, which is bonded only to methylene groups, should have an energy equal to B and a zero net charge. This is what is found, to within the uncertainties of the integrated values. Thus methylene groups bonded only to other methylenes, as found in pentane and all succeeding members of the series, possess zero net charges and contribute the standard increment B to the total energy. Also listed in Table 2 are the energies of the carbon atoms in the methyl and methylene groups relative to the corresponding energies in ethane and propane, respectively. These data show that essentially all of the increase in stability of CH_3 relative to its value in ethane, and of CH_2 relative to its value in propane, comes from the increase in the electron population of the carbon atom in these groups. The populations as well as the energies of the carbon of methyl are also remarkably constant after ethane, the net charge on a carbon of methyl in propane, butane, and pentane varying by only ± 0.002 e from the value 0.225 e.

Thus the additivity scheme for the energy in the hydrocarbons is not the result of the methyl and methylene groups having the same energies in every molecule in spite of small changes in their environments. Instead, their properties do change with changes in environment but the effect is damped by a single methylene group and, most important, the change in energy for a change in population, the quantity $\Delta E/\Delta N$, is the same for both the methylene and methyl groups. It is also necessary that the change in correlation energy for a change in population be the same for both groups to within the experimental uncertainty of ± 0.2 kcal/mol.

The branched molecules, isobutane and neopentane, are more stable than their normal isomers by 1.9 and 5.1 kcal/mol in terms of their ΔH_f values at 25°C and by 1.6 and 3.8 kcal/mol in their vibrationless states at 0 K (17). The 6-31G**/6-31G* calculated energies predict increased stabilities of only 0.4 and 0.5 kcal/mol, respectively, indicating that the change in correlation energy for a change in population for the CH and C groups is different from that for the CH_3 and CH_2 groups. As noted above, the relative electron-withdrawing abilities of the hydrocarbon groups are in the order $C < CH < CH_2 < CH_3$. Thus the charges on the methyl groups in the branched isomers are greater than those found in the normal alkanes, and they are correspondingly more stable. Relative to methyl in ethane, the ΔE and ΔN values for methyl in isobutane are 20.3 kcal/mol and 0.029 e and in neopentane they are 28.8 kcal/mol and 0.036 e, respectively, and the actual energies of the CH and C groups are less than the values assigned to them in the additivity scheme. Essentially all of the increase in stability of the methyl groups in the branched hydrocarbons resides in the carbon of the methyl group (see Table 2). Thus the ratio $\Delta E/\Delta N$ is greater for the branched isomers, where it equals 1.12 for isobutane and 1.27 au/e for neopentane, than it is for the normal alkanes for which it equals 0.88 au/e. The carbon exhibiting the greatest increase in stability is the one at which the branching occurs. In isobutane this atom is 26.6 kcal/mol more stable than the carbon atom in ethane, and in neopentane the corresponding increase in stability is 46.2 kcal/mol.

Table 3 lists the atomic and group energies for the carbocations, all relative to the values in CH_3^+. The final set of entries are the energy changes for the reaction of a carbocation R^+ with methane.

$$CH_3^+ + RH \rightarrow CH_4 + R^+ \qquad \Delta E^+$$

The experimental values for this energy change are also listed, calculated from heat of formation data at 298 K. The calculated values clearly reproduce the experimental increase in the stability of the cation with increased methyl substitution. The difference between the two sets of values is an almost constant 11 kcal/mol. As noted above, increasing methyl substitution leads to an increase in electron population of the carbon atom at which substitution occurs (carbon atom C in Fig. 1). There is also an increase in the extent of delocalization of the positive charge over the methyl hydrogens. This leads to an increase in the electron population of every atom with increased methyl substitution and to a corresponding increase in their stabilities, as indicated by the values of the relative energies listed in Table 3. The effect is most pronounced for carbon atom C because of

[4]For an extension of this work to other systems, see ref. 16*b*.

the transfer of charge to this atom, a transfer brought about by both inductive and hyperconjugative mechanisms of charge release. It is to be recalled that in the *tert*-butyl cation, the most stable of these cations, this carbon actually bears a net negative charge. While the branched neutral hydrocarbons also increase in stability with methyl substitution, the changes between members are less pronounced than between corresponding members of the cationic series and hence $\Delta E^{+} < 0$ and decreases through the series.

Acknowledgments

We thank Professor Wiberg for sending the optimized geometries and wavefunctions of the saturated hydrocarbons and for useful comments on the discussion of hyperconjugation. This paper is dedicated to Professor A. N. Bourns, the man who introduced me to organic chemistry, to scientific research, and to the art of teaching.

1. R. F. W. BADER. Acc. Chem. Res. **18**, 9 (1985).
2. R. F. W. BADER, T. T. NGUYEN-DANG, and Y. TAL. Rep. Prog. Phys. **44**, 893 (1981); R. F. W. BADER and T. T. NGUYEN-DANG. Adv. Quantum Chem. **14**, 63 (1981).
3. R. F. W. BADER, T.-H. TANG, Y. TAL, and F. W. BIEGLER-KONIG. J. Am. Chem. Soc. **104**, 940 (1982); **104**, 946 (1982). (1982).
4. R. F. W. BADER, T. S. SLEE, D. CREMER, and E. KRAKA. J. Am. Chem. Soc. **102**, 5061 (1983).
5. R. F. W. BADER and H. ESSEN. J. Chem. Phys. **80**, 1943 (1984).
6. R. F. W. BADER, P. J. MACDOUGALL, and C. D. H. LAU. J. Am. Chem. Soc. **106**, 1594 (1984).
7. L. RADOM, J. A. POPLE, V. BUSS, and P. v. R. SCHLEYER. J. Am. Chem. Soc. **94**, 311 (1972); K. RAGHAVACHARI, R. A. WHITESIDE, J. A. POPLE, and P. v. R. SCHLEYER. J. Am. Chem. Soc. **103**, 5649 (1981).
8. K. B. WIBERG and J. J. WENDOLOSKI. J. Am. Chem. Soc. **104**, 5679 (1982); K. B. WIBERG. J. Am. Chem. Soc. **105**, 1227 (1983).
9. F. W. BIEGLER-KONIG, R. F. W. BADER, and T.-H. TANG. J. Comput. Chem. **3**, 317 (1982).
10. N. C. J. STUTCHBURY and D. L. COOPER. J. Chem. Phys. **79**, 4967 (1983).
11. L. RADOM, J. A. POPLE, and P. v. R. SCHLEYER. J. Am. Chem. Soc. **94**, 5935 (1972); R. HOFFMANN. J. Chem. Phys. **40**, 2480 (1964); H. KOLLMAR and H. O. SMITH. Agnew. Chem. Int. Ed. Engl. **9**, 462 (1970); Theor. Chim. Acta, **20**, 65 (1971); J. E. WILLIAMS, V. BUSS, and L. C. ALLEN. J. Am. Chem. Soc. **93**, 6867 (1971).
12. J. O. HIRSCHFELDER, C. F. CURTISS, and R. B. BIRD. Molecular theory of gases and liquids. John Wiley and Sons, Inc., New York. 1964.
13. T.-H. TANG, R. F. W. BADER, and P. J. MACDOUGALL. Inorg. Chem. **24**, 2047 (1985).
14. R. F. W. BADER and P. J. MACDOUGALL. J. Am. Chem. Soc. **107**, 6788 (1985).
15. J. L. FRANKLIN. Ind. Eng. Chem. **41**, 1070 (1949); S. W. BENSON. Thermochemical kinetics. Wiley, New York. 1968; T. L. ALLEN. J. Chem. Phys. **31**, 1039 (1959); E. J. PROSEN, W. H. JOHNSON, and F. D. ROSSINI. J. Res. Natl. Bur. Stand. **37**, 51 (1946).
16. (*a*) K. B. WIBERG. J. Comput. Chem. **5**, 197 (1984); (*b*) M. R. IBRAHIM and P. VON SCHLEYER. J. Comput. Chem. **6**, 157 (1985).
17. S. FLISZAR. Charge distributions and chemical effects. Springer Verlag, Berlin. 1983.
18. H. M. ROSENSTOCK, K. DRAXL, B. W. STEINER, and J. T. H. HERRON. J. Phys. Chem. Ref. Data, **6**, Suppl. 1 (1977).

Gas-phase reactions of the hydroperoxide and peroxyformate anions

JOHN H. BOWIE,[1] CHARLES H. DEPUY,[2] SALLY A. SULLIVAN, AND VERONICA M. BIERBAUM
Department of Chemistry and Biochemistry, University of Colorado, Boulder, CO 80309, U.S.A.

Received October 23, 1985

JOHN H. BOWIE, CHARLES H. DEPUY, SALLY A. SULLIVAN, and VERONICA M. BIERBAUM. Can. J. Chem. **64**, 1046 (1986).

The flowing afterglow technique has been used to study the reactions of HO_2^- and HCO_3^- in the gas phase. The hydroperoxide ion reacts slowly with CO to form HO^-, and oxidizes CO_2, OCS, CS_2, NO, SO_2, CH_3NCO, and CH_3NCS in fast reactions to form CO_3^-, CO_2S^-, COS_2^-, NO_2^-, SO_3^-, $CH_3NCO_2^-$, and CH_3NCOS^-, respectively. Reactions of HO_2^- with certain amides and esters provide synthetic routes for a number of interesting peracyl anions. One of these, the peroxyformate ion, HCO_3^-, reacts with CO and NO in slow oxidation reactions to form the formate ion HCO_2^-. It also forms HCO_2^- upon reaction with acetone and pivalaldehyde, perhaps by Baeyer–Villiger oxidation.

JOHN H. BOWIE, CHARLES H. DEPUY, SALLY A. SULLIVAN et VERONICA M. BIERBAUM. Can. J. Chem. **64**, 1046 (1986).

Faisant appel à la technique de la phosphorescence dynamique, on a étudié les réactions des ions HO_2^- et HCO_3^- en phase gazeuse. L'ion hydroperoxyde réagit lentement avec le CO pour former du HO^- et il oxyde rapidement les substances suivantes: CO_2, OCS, CS_2, NO, SO_2, CH_3NCO et CH_3NCS pour former respectivement les ions suivants: CO_3^-, CO_2S^-, COS_2^-, NO_2^-, SO_3^-, $CH_3NCO_2^-$ et CH_3NCOS^-. Les réactions du HO_2^- avec certains amides ou esters s'avèrent des routes de synthèses intéressantes pour un certain nombre d'anions peracyles. Un d'eux, l'ion peroxyformate, HCO_3^-, oxyde lentement le CO et le NO pour donner l'ion formate HCO_2^-. Il forme aussi du HCO_2^- par réaction avec l'acétone et le pivalaldéhyde et cette réaction implique peut-être une oxydation de Baeyer–Villiger.

[Traduit par la revue]

Introduction

The gas phase ion chemistry of the hydroperoxy anion, HO_2^-, has been only sparsely investigated. The ion may be prepared in a flowing afterglow apparatus by sequential reactions involving hydride ion transfer to oxygen, for example from the cyclohexadienyl anion (1) or, better, from the anion derived by proton abstraction from 2,3-dimethyl-1-butene (eqs. [1] and [2]) (2).

[1] $NH_2^- +$ 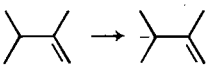 $\rightarrow$ 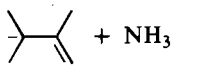 $+ NH_3$

[2] 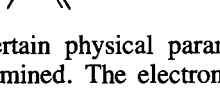 $+ O_2 \rightarrow HO_2^- +$ 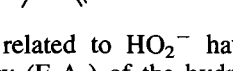

Certain physical parameters related to HO_2^- have been determined. The electron affinity (E.A.) of the hydroperoxy radical ($HO_2^- \rightarrow HO_2 + e^-$, ΔH = E.A.(HO_2)) is 1.078 ± 0.017 eV, and the gas-phase acidity of hydrogen peroxide ($H_2O_2 \rightarrow H^+ + HO_2^-$, $\Delta H = \Delta H^0_{acid}$ (H_2O_2)) is 376.4 ± 0.6 kcal mol^{-1} (2, 3). In a previous paper (1) we reported briefly that HO_2^- is a powerful oxidant, donating an oxygen atom to a number of substrates, and that it also can serve as a gas-phase base, reacting by proton abstraction with acidic organic molecules. In this paper we describe the chemistry of HO_2^- in its reactions as both oxidant and base in more detail, including its reaction rates with a variety of neutral substrates. In this context, HO_2^- reacts with certain amides to form peracyl anions. Dimethyl formamide, for example, reacts with HO_2^- to form the peroxyformate ion, HCO_3^-, and we describe some of the gas-phase reactions of this interesting ion.

Experimental

Experiments were performed at 300 K in a flowing afterglow (FA) system, which has been described previously (4). The system consists of a 100 cm × 7.6 cm id flow reactor affixed to a quadrupole mass spectrometer. A fast flow (80 m s^{-1}) and relatively high pressure (0.4 Torr; 1 Torr = 133.3 Pa) of helium buffer gas is maintained in the flow tube by a Roots blower. The HO_2^- ion was generated as follows. Amide ion was produced by electron impact on NH_3 (2×10^{-3} Torr) and 2,3-dimethyl-1-butene was added 10 cm downstream until no NH_2^- signal remained. Oxygen was then added at the same position until the signal corresponding to the anion of 2,3-dimethyl-1-butene disappeared. Care must be taken not to add too much oxygen as this causes the formation of O_4^-; subsequent reactions of this ion complicate the determination of branching ratios. The reaction sequence produces HO_2^- and O_2^- (normally in a 4:1 ratio), but the O_2^- has little or no effect on further reactions. The neutral reagent to be reacted with HCO_2^- was added through the movable inlet at least 10 cm downstream from the initial point of HCO_2^- generation.

In order to observe the reactions of the peroxyformate ion, HCO_3^-, dimethylformamide was introduced through a fixed inlet 10 cm downstream of HO_2^- formation. Since HCO_3^- reacts at a much slower rate than HO_2^- it is desirable that all HO_2^- ions be removed; therefore excess dimethylformamide is added. Nevertheless some experiments (see Table 2) show products formed by trace amounts of HO_2^-. The neutral reagent to be reacted with HCO_3^- was introduced through the movable inlet at a distance at least 10 cm downstream from the region of HCO_3^- generation.

Flow rates were determined by monitoring the pressure increase with time in a calibrated volume. Rate coefficients were measured by following reactant ion counts as a function of reaction distance. Measurements were made at several neutral flow rates, and reported values are averages of three measurements. The experimental precision of each rate constant is better than ±10%; the overall accuracy of the rate constants is estimated to be ±25%. Theoretical rates were calculated using the method of Su and Bowers (5). Branching ratios were measured as described previously (6).

All neutral reagents were obtained from commercial sources. Gases were of the following purities: He (99.997%), NH_3 (99.999%), O_2 (99.98%), N_2O (99.99%), NO (99.2%), CO (99.9%), CO_2 (99.5%), OCS (97.7%), and SO_2 (99.98%). Liquids were commercial reagent grade.

Results and discussion

Reactions of HO_2^-

The hydroperoxy anion reacts with many substrates by oxygen atom transfer and (or) proton abstraction. Those reactions for which we have determined rate constants are listed in Table 1. These data demonstrate that HO_2^- is a moderately

[1]On leave from the Department of Organic Chemistry, University of Adelaide, South Australia, 5001.

[2]Author to whom correspondence may be addressed.

TABLE 1. Reactions of HO_2^-. Products, branching ratios, rate constants, and efficiencies

Neutral reactant	Products	Branching ratios	k_{expt}[a]	k_{expt}/k_{ADO}[b]
CO	$HO^- + CO_2$	1.0	1.9×10^{-10}	0.22
CO_2	$CO_3^- + HO$	0.96	8.4×10^{-10}	0.91
	HCO_4^-	0.04		
OCS	$CO_2S^- + HO$	>0.95	[c]	
	$HS^- + CO_3$	<0.05		
CS_2	$COS_2^- + HO$	>0.95	[c]	
	$HS^- + CO_2S$	<0.05		
NO	$NO_2^- + HO$	1.0	5.0×10^{-10}	0.63
SO_2	$SO_3^- + HO$	0.78	2.1×10^{-9}	1.2
	$SO_2^- + HO_2$	0.20[d]		
	$HOOSO_2^-$	0.02		
CH_3NCO	$CH_3NCO_2^- + HO$	0.82	1.8×10^{-9}	0.72
	$CN^- + (CH_4O_3)$[e]	0.14		
	$NCO^- + CH_3O_2H$	0.02		
CH_3NCS	$CH_3NCOS^- + HO$	0.18	1.2×10^{-9}	
	$NCS^- + CH_3O_2H$	0.82		
CH_3COCH_3	$CH_3COCH_2^- + H_2O_2$	>0.98	2.2×10^{-9}	0.85
$(CH_3)_3CCHO$	$(CH_3)_3CCO_2^- + H_2O$	1.0	1.5×10^{-9}	0.60
$HCON(CH_3)_2$	$HCO_3^- + (CH_3)_2NH$	1.0	7.3×10^{-10}	0.23
$CH_3CO_2CH_3$	$^-CH_2CO_2CH_3 + H_2O_2$	0.52	1.9×10^{-9}	0.98
	$CH_3CO_3^- + CH_3OH$	0.48		

[a] In cm^3 $molecule^{-1}$ s^{-1}.
[b] Reaction efficiency. ADO rate constant calculated by the method of Su and Bowers (5).
[c] Since HS^- and HO_2^- are both m/z 33, the small buildup in HS^- makes the rate measurement inaccurate. The rate is less than that observed for the reaction: $HO_2^- + CO_2 \rightarrow CO_3^- + HO$.
[d] Some may come from O_2^-.
[e] Structure of the neutral product is not known.

strong base and a powerful oxidizing agent. Its basicity is demonstrated by the deprotonation of acetone (ΔH^0_{acid} = 368.8 kcal mol^{-1}) (7), which occurs at almost every collision, and of methyl acetate (ΔH^0_{acid} = 371.0 kcal mol^{-1}) (7), which occurs, on average, every second collision. These results are consistent with our previous determination of the acidity of H_2O_2 (*vide supra*).

The most interesting feature of the reactivity of HO_2^- is its power as an oxidizing agent. It readily oxidizes carbonyl compounds by donation of an oxygen atom, as exemplified by its reaction with CO_2, which we formulate as written in eq. [3].

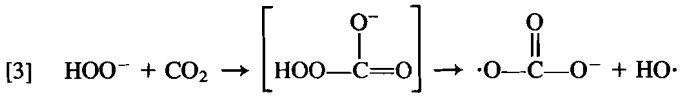

[3] $HOO^- + CO_2 \rightarrow [HOO{-}C(O^-){=}O] \rightarrow {\cdot}O{-}C(=O){-}O^- + HO{\cdot}$

This reaction occurs, within the experimental uncertainty, at every collision, and this rapid rate is consistent with other addition reactions to CO_2, which we reported in an earlier paper (8). A small amount of the adduct, $HOOCO_2^-$, is also formed. The exact amount formed is dependent upon the helium pressure since the reaction is termolecular. Provided that the adduct lives long enough ($\sim 10^{-7}$ s) to collide with one or more helium atoms, the reaction exothermicity can be removed and a stable adduct observed. An analogous reaction occurs with HO^- and CO_2 (8). A rapid reaction also occurs between HO_2^- and SO_2, OCS and CS_2.

With SO_2, SO_3^- is observed as the main product ion, with a smaller amount of the electron transfer product SO_2^- and a trace of adduct. Both OCS and CS_2 give mainly (>95%) the corresponding oxygen transfer products CO_2S^- and COS_2^-, respectively, but in both cases HS^- is produced in small amounts. Since HS^- and HO_2^- have the same mass, the determination of rate constants for these reactions is complicated; kinetic plots are curved because of buildup of a product ion of the same mass as that of the reactant whose intensity is being monitored. Qualitatively, however, both OCS and CS_2 react rapidly, but somewhat less so than do CO_2 or SO_2. The formation of HS^- must arise from proton transfer within the initial adduct, followed by fragmentation (eq. [4*b*]).

[4*a*] $HOO^- + OCS \xrightarrow{>0.95} CO_2S^- + HO$

[4*b*] $\xrightarrow{<0.05} HS^- + CO_3$

Since the electron affinity of the carbonate radical (2.69 eV) (9) is higher than that of HS· (2.32 eV) (9) and no CO_3^- is seen among the products, it is unlikely that CO_3 has the carbonate structure. We suggest instead that the following reaction occurs (eq. [5]).

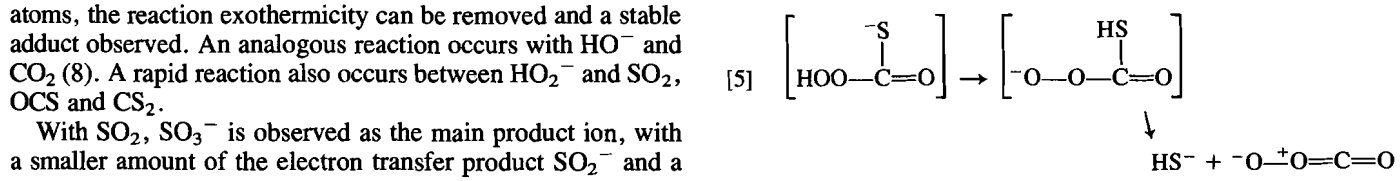

[5] $[HOO{-}C(S^-){=}O] \rightarrow [{}^-O{-}O{-}C(SH){=}O] \rightarrow HS^- + {}^-O{-}{}^+O{=}C{=}O$

The overall reaction would then be analogous to that which occurs between hydroxide ion and COS (eq. [6]) (8).

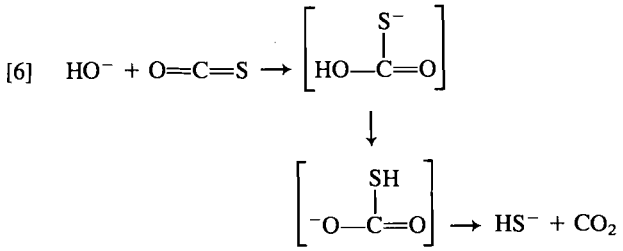

Reactions between HO_2^- and methylisocyanate and methylisothiocyanate offer an opportunity to compare substitution and oxidation reactions within the same molecule (eqs. [7] and [8]).

[7] $HO_2^- + CH_3NCO \rightarrow NCO^- + CH_3O_2H$
$\rightarrow CH_3NCO_2^- + HO$

[8] $HO_2^- + CH_3NCS \rightarrow NCS^- + CH_3O_2H$
$\rightarrow CH_3NCOS^- + HO$

For methylisocyanate only a trace (2%) of substitution, which generates NCO^-, is observed while with methylisothiocyanate NCS^- is the major product (82%). This is consistent with the fact that NCS^- is expected to be a better leaving group than NCO^- due to its lesser basicity (8). A more surprising product is cyanide ion (14%) from reaction of methylisocyanate with HO_2^-. A possible pathway for the formation of this ion is that shown in eq. [9].

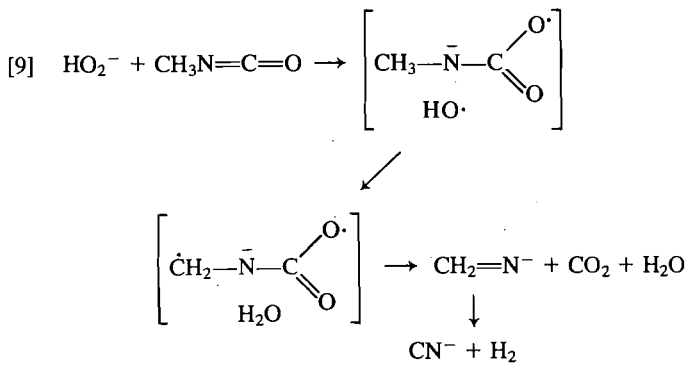

We have shown previously (10) that CN^- is formed readily when the formimine anion is produced in an exothermic reaction (eq. [10]).

The gas-phase hydroperoxy anion also oxidizes aldehydes to carboxylate ions, just as it does in solution. To avoid proton transfer reactions, which compete effectively, aldehydes without α-hydrogens must be used (eq. [11]).

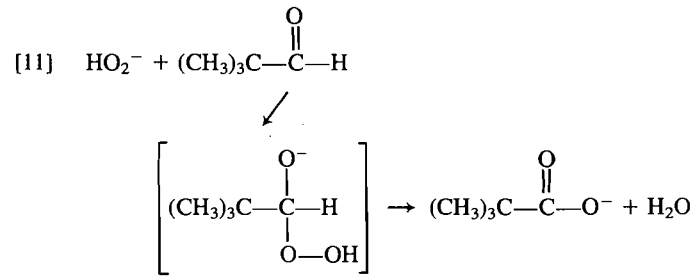

The mechanism by which water is eliminated from the adduct remains uncertain. The addition step should be only slightly exothermic, so that the adduct will not be energized sufficiently to promote even oxygen–oxygen bond cleavage. A seemingly related loss of water across a carbon–oxygen bond is observed upon addition of HO_2^- to ethylene oxide (eq. [12]).

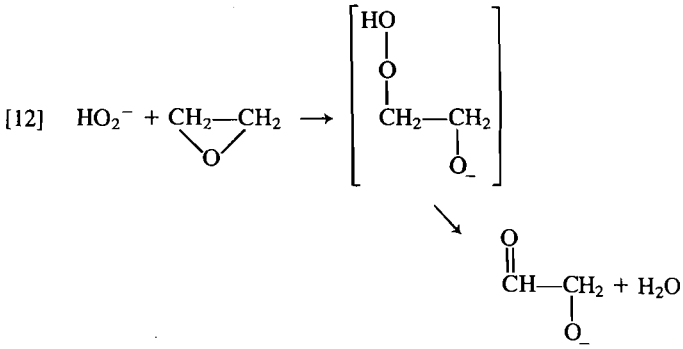

We reported previously (11) the reaction of HO_2^- with methyl formate, where proton abstraction resulting in the Riveros reaction ([13*a*]) gives rise to the major product ions, accompanied by smaller amounts of carbonyl addition ([13*b*]) and nucleophilic substitution products ([13*c*]).

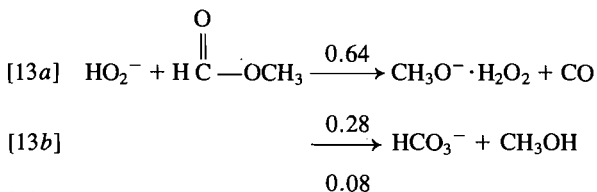

With methyl acetate as the substrate, a 50:50 mixture of products arising from proton abstraction and from carbonyl addition is observed. When dimethyl formamide is used, however, the peroxyformate ion is the exclusive ionic product (eq. [14]).

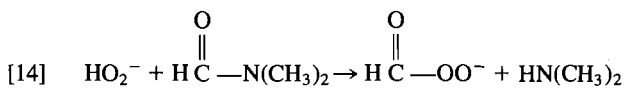

This reaction is somewhat slower than the others but still occurs at approximately one in four encounters. The chemistry of the peroxyformate ion will be considered briefly in a later section.

The reactions of HO_2^- with CO and NO are also appreciably slower than the encounter rates; the former produces hydroxide ion (eq. [15]), and the latter, NO_2^- (eq. [16]).

[15] $HOO^- + CO \rightarrow [HO—O—\bar{C}=O] \rightarrow HO^- + CO_2$

[16] $HOO^- + NO \rightarrow [HO—O—\dot{N}—O^-] \rightarrow NO_2^- + HO$

In either case the initial adduct is of higher energy than that, for example, from CO_2, and the difficulty in its formation probably presents a barrier along the reaction pathway and accounts for the slower rates. In the case of reaction with carbon monoxide, for example, the initial adduct is a formyl-type anion, a relatively high energy species. Subsequent decomposition gives HO^- and CO_2. Analogous decomposition of an adduct between HO_2^- and NO would be expected to form HO and NO_2^-, since NO_2 has a higher electron affinity (2.275 eV) (9) than does HO (1.83 eV) (9).

TABLE 2. Reactions of $H—\overset{O}{\overset{\|}{C}}—O_2^-$. Products, branching ratios, rate constants, and efficiencies

Neutral reactant	Products	Branching ratios	k_{expt}[a]	k_{expt}/k_{ADO}[b]
CO	$HCO_2^- + CO_2$	1.0	5.2×10^{-11}	0.07
CO_2	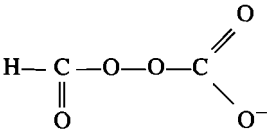	>0.95[c]	1.1×10^{-27} [d]	
	$HCO_2^- + CO_3$	0.02		
NO	$HCO_2^- + NO_2$	1.0[e]	7.0×10^{-11}	0.11
SO_2	$SO_2^- + HCO_3$	1.0	1.4×10^{-9}	1.1
CH_3COCH_3	$HCO_2^- + C_3H_6O_2$	1.0[f]	3.0×10^{-10}	0.13
$(CH_3)_3CCHO$	$HCO_2^- + C_5H_{10}O_2$	1.0[g]	8.4×10^{-10}	0.42

[a]In cm^3 $molecule^{-1}$ s^{-1}, unless otherwise noted.
[b]Reaction efficiency. ADO rate constant calculated by the method of Su and Bowers (5).
[c]This adduct is formed by a termolecular reaction; branching ratio is given for the pressure = 0.385 Torr.
[d]In cm^6 $molecule^{-2}$ s^{-1}.
[e]A small amount of NO_2^- is present (10% of HCO_2^- peak). The intensity of the signal increases markedly as the distance between the NO and DMF inlets is decreased. We believe NO_2^- is formed from residual HO_2^-.
[f]A small amount of $CH_3COCH_2^-$ is present (15% of HCO_2^- peak) but we believe this arises from residual HO_2^-.
[g]A small amount of $(CH_3)_3CCO_2^-$ is present (5% of HCO_2^- peak) but we believe this arises from residual HO_2^-. We cannot exclude the possibility that some $(CH_3)_3CCO_2^-$ is produced in the HCO_3^- reaction.

Reactions of HCO_3^-

Since the peroxyformate ion[3] can be formed readily from the reaction of HO_2^- with dimethylformamide, we have made a brief study of its chemistry and the results are summarized in Table 2. It is clear that the peroxyformate ion is significantly less reactive than the hydroperoxy anion. For example, it reacts with carbon monoxide at only a quarter of the rate at which HO_2^- reacts. This is consistent with HCO_3^- being a weaker base than is HO_2^-, as is shown by the fact that it does not deprotonate acetone, as HO_2^- does. To the extent, then, that a formyl-type anion is involved in the oxidation of CO, the peroxyformate ion should react more slowly (eq. [17]).

[17] 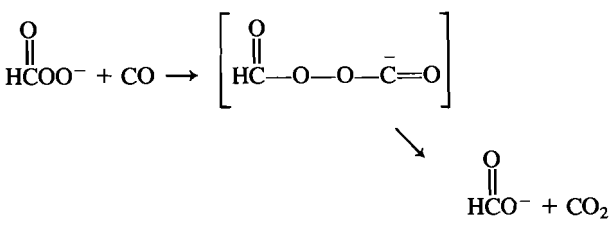

HCO_3^- also oxidizes NO more slowly than does HO_2^-. Since the formoxyl radical has a greater electron affinity (3.5–4 eV) than does NO_2, the formate ion is observed rather than NO_2^-.

Since HCO_3^- is not a strong enough base to abstract a proton from aldehydes and ketones, we were able to examine other, slower reactions of these neutrals. In particular we noted that acetone reacts rather slowly (eff. = 0.13) with HCO_3^- to produce HCO_2^-, and other carbonyl compounds react similarly. Obviously oxygen atom transfer has occurred to acetone, but the formate ion is such a weak base that it is the only ionic product. We suggest that when the peroxyformate ion reacts with aldehydes and ketones a gas-phase Baeyer–Villiger reaction occurs. For example, methyl acetate would be the neutral product from reaction with acetone as given in eq. [18].

[18] 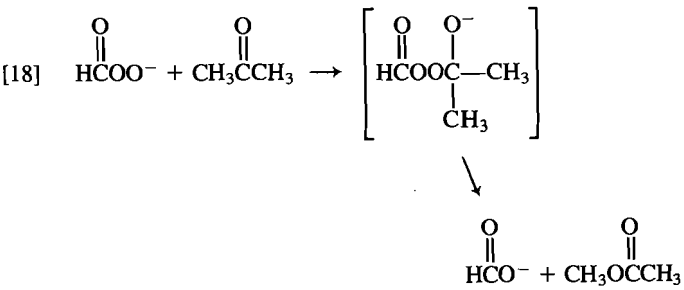

Pivalaldehyde reacts somewhat more rapidly (eff. = 0.42), also to form the formate ion.

Carbon dioxide reacts slowly with HCO_3^- in a termolecular reaction to form an adduct; only a small amount of the oxidation product is observed.

[3]There are two structures for an ion of molecular formula HCO_3^- that we must consider, namely the bicarbonate ion $HOCO_2^-$ and the peroxyformate ion HCO_3^-. We have prepared the bicarbonate ion by the termolecular process $HO^- + CO_2 + He \rightarrow HOCO_2^- + He$ (12). The bicarbonate ion undergoes ready exchange with (for example) D_2O or MeOD to form $DOCO_2^-$. The ion formed from HO_2^- and dimethylformamide does not exchange with either D_2O or MeOD; instead, it undergoes slow clustering reactions. Other reactions of the bicarbonate ion will be described in a subsequent publication.

Acknowledgement

We gratefully acknowledge support of this work by the U.S. Army Research Office under Contract #DAAG29-85-K-0046.

1. C. H. DEPUY, V. M. BIERBAUM, R. J. SCHMITT, and R. H. SHAPIRO. J. Am. Chem. Soc. **100**, 2920 (1978).
2. V. M. BIERBAUM, R. J. SCHMITT, C. H. DEPUY, R. D. MEAD,

P. A. SCHULZ, and W. C. LINEBERGER. J. Am. Chem. Soc. **103**, 6262 (1981).
3. J. M. OAKES, L. B. HARDING, and G. B. ELLISON. J. Chem. Phys. **83**, 5400 (1985).
4. C. H. DEPUY, and V. M. BIERBAUM. Acc. Chem. Res. **14**, 146 (1981).
5. T. SU, and M. T. BOWERS. Int. J. Mass Spectrom. Ion Phys. **12**, 347 (1973).
6. D. R. ANDERSON, V. M. BIERBAUM, and C. H. DEPUY. J. Am. Chem. Soc. **105**, 4244 (1983).
7. J. E. BARTMESS, and R. T. MCIVER, JR. *In* Gas phase ion chemistry. Vol. 2. *Edited by* M. T. Bowers. Academic Press, New York. 1979. Chapt. 11.
8. V. M. BIERBAUM, J. J. GRABOWSKI, and C. H. DEPUY. J. Phys. Chem. **88**, 1389 (1984).
9. B. K. JANOUSEK, and J. I. BRAUMAN. *In* Gas phase ion chemistry. Vol. 2. *Edited by* M. T. Bowers. Academic Press, New York. 1979. Chapt. 10.
10. S. R. KASS and C. H. DEPUY. J. Org. Chem. **50**, 2874 (1985).
11. C. H. DEPUY, E. W. DELLA, J. FILLEY, J. J. GRABOWSKI, and V. M. BIERBAUM. J. Am. Chem. Soc. **105**, 2481 (1983).
12. F. C. FEHSENFELD and E. E. FERGUSON. J. Chem. Phys. **61**, 3181 (1974).

Site of gas-phase ethyl ion attachment

ALEX. G. HARRISON
Department of Chemistry, University of Toronto, Toronto, Ont., Canada M5S 1A1
Received October 18, 1985

This paper is dedicated to Professor Arthur N. Bourns

ALEX G. HARRISON. Can. J. Chem. **64**, 1051 (1986).

The $[C_2D_5]^+$ species forms an adduct in the gas phase with ethyl acetate, ethylbenzene, and *p*-ethyltoluene, which subsequently unimolecularly eliminates C_2H_4 and C_2D_4 in approximately a 2:1 ratio. These results indicate that the adduct is not a weakly bound ion–molecule complex but a bonded species in which the C_2D_5 group has become equivalent to the C_2H_5 group present in the molecule; the preference for elimination of C_2H_4 is due to an isotope effect. From observations of the relative loss of C_2H_4 and C_2D_4 from $[C_2D_5]^+$ adducts with other molecules containing a C_2H_5 group, it is concluded that the $[C_2D_5]^+$ species attaches to the carboxyl group in ethyl benzoate, primarily to the ring in substituted phenetoles and in ethylphenols, primarily to the nitrogen in ethylpyridines, and primarily to the ring for *N*-ethyl- and *p*-ethyl-aniline.

ALEX G. HARRISON. Can. J. Chem. **64**, 1051 (1986).

En phase gazeuse, les espèces $[C_2D_5]^+$ forment des adduits avec l'acétate d'éthyle, l'éthylbenzène et le *p*-éthylbenzène qui, par le biais d'une réaction unimoléculaire, éliminent par la suite du C_2H_4 et du C_2D_4 dans un rapport de 2:1. Ces résultats indiquent que l'adduit n'est pas uniquement un complexe ion–molécule faiblement relié mais plutôt une espèce comportant une liaison et dans laquelle le groupement C_2D_5 est devenu équivalent au groupement C_2H_5 qui est présent dans la molécule; l'élimination préférentielle du C_2H_4 serait due à un effet isotopique. Sur la base des observations concernant les pertes relatives de C_2H_4 et de C_2D_4 à partir d'adduits du $[C_2D_5]^+$ avec d'autres molécules contenant un groupement C_2H_5, on en conclut que les espèces $[C_2D_5]^+$ s'attachent soit au groupement carboxyle du benzoate d'éthyle soit principalement au cycle aromatique des phénétoles substitués, des éthylphénols ou des anilines *N*- ou *p*-éthylées.

[Traduit par la revue]

There is considerable interest as to the site of protonation and alkylation of organic molecules in the gas phase; this interest is prompted not only by questions of intrinsic molecular properties such as proton affinities but also by the question of the effect of the site of attack on ionic fragmentation reactions under chemical ionization conditions. In considering the site of protonation/alkylation it is important to distinguish between conditions of thermodynamic control that apply when equilibrium proton affinities are measured and kinetic control that characterizes protonation and alkylation under chemical ionization conditions.

There now is a large body of equilibrium gas-phase proton affinity data (for a summary of data and methods of measurement, see ref. 1) including many bifunctional molecules. Although the thermodynamically favoured site of protonation has been elucidated from an investigation of substituent effects (2), for most bifunctional molecules, the site of protonation has been determined from correlations of gas-phase proton affinities with core binding energies. Thus, from correlations of the measured proton affinities of carboxylic acids and derivatives with O(1*s*) binding energies it has been established (3–5) that these compounds are protonated on the carbonyl oxygen. A similar study (6) has established that in the gas phase amides are protonated on the oxygen, which is in agreement with solution phase results (7). The correlation of proton affinity data of substituted pyridines with N(1*s*) binding energies (8) shows that protonation occurs on the nitrogen, while a similar correlation for substituted anilines (9) reveals a more complex behaviour where protonation on either the ring or a nitrogen depends on the substituent.

The position of proton or cation attack under the conditions of chemical ionization is much less clear. Much of the evidence has arisen from collision-induced dissociation (CID) studies (10) of the protonated and cationized products. Thus, Maquestiau *et al.* (11) found that the CID mass spectra of ethylated pyrrole and protonated *N*-ethylpyrrole showed substantial differences and they concluded that neither ethylation nor protonation occurred at the nitrogen. From similar studies of the ethylation of pyridine and the protonation of ethylpyridines they concluded that ethylation and protonation both occurred at the nitrogen. In the case of aniline they concluded from the similarity of the CID spectra of protonated 2-, 3-, and 4-ethylaniline with the CID spectrum of ethylated aniline that ring protonation and ethylation occurred. In contrast to these results, in a similar CID study Cooks and co-workers (12) concluded that aniline was both methylated and ethylated predominantly at the nitrogen, although in the ethylation reaction they concluded that 20% ring attack occurred. At the considerably higher pressures involved in radiolytic studies Attina and Cacace (13) observed ~20% nitrogen and ~80% ring ethylation of aniline. More recently, Burinsky and Campana (14) have studied the site of attachment of H^+, $[CH_3]^+$, and $[C_2H_5]^+$ to morpholine, thiomorpholine, and 1,4-thioxane by CID studies of the adducts. They concluded that the site of protonation followed the predicted trends in proton affinities of the heteroatoms (N > S > O) but that alkyl ion reactivities followed differences in electronegativity or electrophilicity (S > N > O).

Cooks and co-workers (12) observed that the ethyl ion adducts that they studied showed a strong tendency to eliminate ethylene in unimolecular (metastable) fragmentation reactions. They suggested that this arose because the adduct fragmenting in this way existed as a weakly bound ion–molecule complex such as a proton bound dimer of the substrate and ethylene, which would be expected to lose ethylene readily. To investigate this possibility we have reacted $[C_2D_5]^+$ with a number of substrates containing unlabelled ethyl groups. We have found that the adduct ion that fragments unimolecularly cannot be explained in terms of a weakly bound ion–molecule complex but rather that, in many cases, the labelled ethyl group added has become equivalent with the unlabelled ethyl group originally

present in the substrate molecule. As is indicated below, these studies also provide information on the site of attack when more than one site is possible.

In our initial studies we examined the unimolecular fragmentation of the $[C_2D_5]^+$ ethylbenzene and *p*-ethyltoluene adducts. In both cases we observed loss of both C_2H_4 and C_2D_4 in the ratio 2.3_9:1.0 (ethylbenzene) and 2.1_5:1.0 (*p*-ethyltoluene), favouring C_2H_4 loss. These results indicate that those adducts that are fragmenting unimolecularly cannot be described in terms of a weakly bound ion–molecule complex but rather that they are chemically bound species in which the C_2D_5 group has become equivalent with the C_2H_5 group originally present in the substrate molecule, i.e.

[1] $[C_2D_5]^+$ + 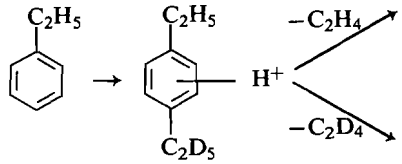 $-C_2H_4$, $-C_2D_4$

Fragmentation of protonated ethylbenzenes is known to involve elimination of ethylene (15). The preferred elimination of C_2H_4 compared to elimination of C_2D_4 undoubtedly arises from an isotope effect favouring H transfer over D transfer; isotope effects of this magnitude are observed frequently (16). The present experiment provides no information as to the exact position of attack, and attack at the *para* position as shown in reaction [1] is for illustrative purposes only.

Reaction of $[C_2D_5]^+$ with ethyl acetate leads to an adduct that subsequently loses C_2H_4 and C_2D_4 in the ratio 2.3_3:1.0. Again this indicates equivalence of the two ethyl groups, with elimination of C_2H_4 favoured by an isotope effect. We cannot distinguish between the two alternative sites of $[C_2D_5]^+$ attack exemplified by **1** and **2**, although the thermodynamically

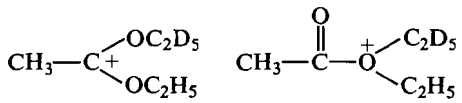

1 **2**

favoured product is **1** (3–5). The adduct formed between $[C_2D_5]^+$ and ethyl benzoate lost C_2H_4 and C_2D_4 unimolecularly in the ratio 2.1_5:1.0. This result indicates equivalence of the two ethyl groups and thus formation of an adduct similar to **1** or **2** rather than $[C_2D_5]^+$ addition to the aromatic ring.

Protonated and ethylated phenyl *n*-propyl ethers have been shown (17) to eliminate propylene, and a similar reaction would be expected for substituted phenetoles. Accordingly, we have studied the unimolecular fragmentation of the adduct of $[C_2D_5]^+$ with three substituted phenetoles, with the results summarized in Table 1. In all cases the observed ratio of C_2H_4 loss to C_2D_4 loss is greater than that expected for equivalence of the two ethyl groups, based on the results presented above. We interpret this result in terms of $[C_2D_5]^+$ addition at both the oxygen and the aromatic ring, viz.

[2] $[C_2D_5]^+$ + X– 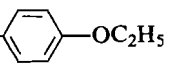 –OC_2H_5

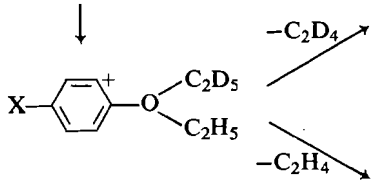

TABLE 1. Fragmentation of $[C_2D_5]^+$ adducts of substituted phenetoles

Phenetole	Fractional loss of C_2H_4	Fractional loss of C_2D_4	$-C_2H_4/-C_2H_4$
p-F	0.78_1	0.21_9	3.5_7
p-CH_3	0.85_4	0.14_6	5.8_5
p-Cl	0.92_1	0.07_9	11.6

[3] $C_2H_5^+$ + X– 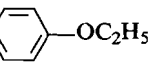 –OC_2H_5

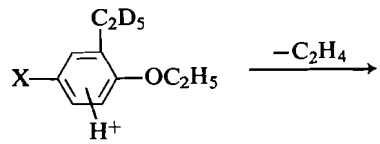

We can present no evidence concerning the exact position of attack on the ring; *ortho* attack is used for illustrative purposes only. If we assume that addition to oxygen (reaction [2]) will subsequently lead to C_2H_4 and C_2D_4 loss in the ratio 2.2:1.0 (see above) and that addition at the ring (reaction [3]) leads to loss of C_2H_4 only, we calculate that the percent of ring addition is 30% (*p*-F) 53% (*p*-CH_3), and 75% (*p*-Cl). The thermodynamically favoured site of protonation of the substituted phenetoles is not known, although it is known (2, 5) that the thermodynamically favoured site of protonation of anisole is the aromatic ring. It should be emphasized that the above results refer only to those ions that undergo fragmentation in the second field-free region of the mass spectrometer.

The $[C_2D_5]^+$ adducts with 2-ethylphenol and 3-ethylphenol showed unimolecular loss of C_2H_4 and C_2D_4 in the ratios 1.7_5(2-ethyl) and 2.0_1(3-ethyl). Again, the extensive loss of C_2H_4 is not consistent with a weakly bound ion–molecule complex between $[C_2D_5]^+$ and the phenol; such a complex would be expected to eliminate C_2D_4. Nor are the results consistent with addition of $[C_2D_5]^+$ to the hydroxyl group because, by analogy with the fragmentation of protonated phenetole (17), such a species also would eliminate C_2D_4. The results can be rationalized readily in terms of dominant addition to the ring, leading to equivalence of the labelled and unlabelled ethyl groups. Assuming that in such an intermediate C_2H_4 and C_2D_4 would be lost in the ratio 2.2:1.0, we estimate 79% ring ethylation of 2-ethylphenol and 92% ring ethylation of 3-ethylphenol. From CID studies, Cooks and co-workers (12) have concluded that phenol undergoes ring ethylation about 90% of the time. The ring is known (2) to be the thermodynamically favoured site of protonation.

Table 2 summarizes the results obtained for the $[C_2D_5]^+$ adducts with the isomeric ethylpyridines. The predominant loss of C_2D_4 in metastable ion fragmentation reactions clearly indicates that the added C_2D_5 has not become equivalent with the C_2H_5 group present in the molecule. While this might be taken as indicating that only a weakly bound ion–molecule complex is formed, we favour the alternative interpretation that the $[C_2D_5]^+$ species attacks the nitrogen, the thermodynamically favoured site of protonation (8). The fact that some loss of C_2H_4 is observed indicates a minor extent of ring ethylation. An unusual fragmentation is loss of CH_3 and CD_3 from the adduct ions. In other studies we have noted that protonated ethylpyri-

TABLE 2. Fragmentation of $[C_2D_5]^+$ adducts with ethylpyridines

Pyridine	Fractional loss of C_2H_4	C_2D_4	CH_3	CD_3
2-C_2H_5	0.05_3	0.72_4	0.14_2	0.07_5
3-C_2H_5	0.04_3	0.74_7	0.13_8	0.07_2
4-C_2H_5	0.01_5	0.69_2	0.23_4	0.05_9

TABLE 3. Fragmentation of $[C_2D_5]^+$ adducts of ethylanilines

Aniline	Fractional loss of C_2H_4	C_2D_4	C_2H_5	C_2D_5
N-Ethyl	0.04_3	0.54_0	0.05_4	0.36_3
p-Ethyl	0.44_8	0.34_8	0	0.20_4

dines lose CH_3 unimolecularly. The loss of CH_3 and CD_3 from the adducts also implies some ring ethylation. The conclusion that ethylation occurs predominantly at nitrogen is in agreement with the conclusion reached by Maquestiau *et al.* (11).

Table 3 summarizes the results obtained for the unimolecular fragmentation of the $[C_2D_5]^+$ adducts with *N*-ethylaniline and *p*-ethylaniline. For the adduct with *N*-ethylaniline, metastable ion fragmentation involves primarily loss of C_2D_4 and C_2D_5 with only minor loss of C_2H_4 and C_2H_5. Clearly the C_2D_5 group added has not become equivalent with the C_2H_5 attached to the nitrogen. While this might be explained in terms of formation of a weakly bound ion–molecule complex, we prefer the conclusion that ethylation has occurred predominantly on the ring. This conclusion is supported by the results for the adduct with *p*-ethylaniline where elimination of C_2H_4 exceeds elimination of C_2D_4, indicating a significant extent of ring ethylation. An unusual observation is that only C_2D_5 loss, and no C_2H_5 loss, is observed for the adduct with *p*-ethylaniline, while for the adduct with *N*-ethylaniline predominant loss of C_2D_5 is observed. These results suggest that C_2H_5 loss may be occurring from a weakly bound ion–molecule complex rather than from the σ-bonded adduct that leads to subsequent ethylation loss. The overall reaction is, of course, a charge transfer reaction and is not surprising, since the ionization energy of C_2H_5 (8.38 eV (18)) is greater than that of either of the ethylanilines (7.6 eV (18)). In any event, the present results are in agreement with the conclusions of Maquestiau *et al.* (11), that ethylation of anilines occurs primarily on the ring rather than at the nitrogen, even though, for the ethylanilines, the nitrogen is the thermodynamically favoured site of protonation (9).

In summary, ethylphenols and substituted phenetoles undergo ethyl ion addition primarily on the aromatic ring, the thermodynamically favoured site, while pyridines undergo ethyl ion addition primarily at the nitrogen, again the thermodynamically favoured site. By contrast, ethylanilines undergo attack primarily at the ring even though the nitrogen is the thermodynamically favoured site of attack. It is clear that the site of attack under conditions of kinetic control cannot always be predicted from the site of attack under thermodynamic control.

Experimental

The $[C_2D_5]^+$ adducts were prepared in the chemical ionization source of a VG Analytical ZAB-2FQ mass spectrometer by using CD_4 as reagent gas. Under chemical ionization conditions the CD_4 reagent gas gives a large yield of $[C_2D_5]^+$, which, in part, reacts by adduct formation with a variety of molecules. Source pressures were not measured directly but, from the extent of conversion of the methane primary ions to product ions, the pressure was estimated to be greater than 0.3 Torr (1 Torr = 133.3 Pa). The $M.C_2D_5^+$ adduct was mass selected by the magnetic sector of the reverse-geometry double-focussing mass spectrometer and underwent unimolecular fragmentation in the drift region between the magnetic and electric sector, with the ionic products of fragmentation being established from their kinetic energy by scanning the electric sector in the usual MIKES technique (19). Source temperatures were approximately 200°C with the electron energy 50 eV and the filament emission 500 μA. The ion accelerating voltage was 8 keV. Samples were admitted through a heated inlet system. All compounds were obtained commercially and they showed no detectable impurities in their mass spectra. The CD_4 was obtained from Merck, Sharp and Dohme, Montreal.

Acknowledgements

The purchase of the ZAB-2FQ mass spectrometer for the Ontario Regional Ion Chemistry Laboratory (ORICL) at the University of Toronto was made possible by a major installation grant from the Natural Sciences and Engineering Research Council of Canada. The operation of the laboratory is assisted by a grant from NSERC. The author is indebted to NSERC for the continued financial support of his research.

1. D. H. AUE and M. T. BOWERS. *In* Gas phase ion chemistry. Vol. 2. *Edited by* M. T. Bowers. Academic Press, New York. 1979. Chapt. 9.
2. Y. K. LAU and P. KEBARLE. J. Am. Chem. Soc. **98**, 7452 (1976).
3. T. X. CARROLL, S. R. SMITH, and T. D. THOMAS. J. Am. Chem. Soc. **97**, 659 (1975).
4. B. E. MILLS, R. L. MARTIN, and D. A. SHIRLEY. J. Am. Chem. Soc. **98**, 2380 (1976).
5. F. M. BENOIT and A. G. HARRISON. J. Am. Chem. Soc. **99**, 3980 (1977).
6. R. S. BROWN and A. TSE. J. Am. Chem. Soc. **102**, 5222 (1980).
7. (*a*) R. J. GILLESPIE and J. BIRCHALL. Can. J. Chem. **41**, 148 (1963); (*b*) P. STILBS, S. FORSEN, and J. S. HARTMAN. J. Chem. Soc. Perkin Trans. 2, 556 (1977).
8. R. S. BROWN and A. TSE. Can. J. Chem. **58**, 694 (1980).
9. Y. K. LAU, K. NISHIZAWA, A. TSE, R. S. BROWN, and P. KEBARLE. J. Am. Chem. Soc. **103**, 6291 (1981).
10. P. J. TODD and F. W. MCLAFFERTY. *In* Tandem mass spectrometry. Edited by F. W. McLafferty. John Wiley and Sons, New York. 1983. Chapt. 7.
11. A. MAQUESTIAU, Y. VAN HAVERBEKE, H. MISPREUVE, R. FLAMMING, J. A. HARRIS, I. HOWE, and J. H. BEYNON. Org. Mass Spectrom. **15**, 144 (1980).
12. K. V. WOOD, D. J. BURINSKY, D. CAMERON, and R. G. COOKS. J. Org. Chem. **48**, 5236 (1983).
13. M. ATTINA and F. CACACE. J. Am. Chem. Soc. **105**, 1122 (1983).
14. D. J. BURINSKY and J. E. CAMPANA. Org. Mass Spectrom. **19**, 539 (1984).
15. (*a*) A. G. HARRISON, P.-H. LIN, and H.-W. LEUNG. Adv. Mass Spectrom. **7**, 1394 (1978); (*b*) J. A. HERMAN and A. G. HARRISON. Org. Mass Spectrom. **16**, 423 (1981).
16. (*a*) P. J. DERRICK. Mass Spectrom. Rev. **2**, 285 (1983); (*b*) P. J. DERRICK and K. F. DONCHI. *In* Comprehensive chemical kinetics. Vol. 24. *Edited by* C. H. Bamford and C. F. H. Tipper. Elsevier, Amsterdam. 1983.
17. F. M. BENOIT and A. G. HARRISON. Org. Mass Spectrom. **11**, 599 (1976).
18. H. M. ROSENSTOCK, K. DRAXL, B. W. STEINER, and J. T. HERRON. J. Phys. Chem. Ref. Data, **6**, Suppl. 1 (1977).
19. R. G. COOKS, J. H. BEYNON, R. M. CAPRIOLI, and G. R. LESTER. Metastable ions. Elsevier, New York. 1973.

Oxidation of hydrocarbons. 17. Solvent and substituent effects on the oxidation of styrene derivatives by quaternary ammonium permanganates

DONALD G. LEE,[1] KEITH C. BROWN, AND HASAN KARAMAN
Department of Chemistry, University of Regina, Regina, Sask., Canada S4S 0A2
Received August 26, 1985
This paper is dedicated to Professor Arthur N. Bourns

DONALD G. LEE, KEITH C. BROWN, and HASAN KARAMAN. Can. J. Chem. **64**, 1054 (1986).

When alkenes are oxidized by quaternary ammonium or phosphonium permanganates in polar organic solvents, such as acetone, the structures of the cations have little or no effect on the rates of reaction. In less polar solvents, such as methylene chloride or toluene, the rates of reaction are, however, dependent on the identity of the quaternary ammonium or phosphonium ions. It thus appears as if the reacting species may exist as solvent-separated ion pairs in polar solvents and as intimate ion pairs in nonpolar solvents. The rates of reaction are also very sensitive to substituent effects, a nonlinear (concave upward) Hammett plot being obtained for the oxidation of substituted β-bromo and β-methoxystyrenes. The mechanism is best visualized as proceeding by way of a continuum of transition states that can vary from electron rich to electron poor depending on the capacity of the substrate structures to accommodate either negative or positive charges.

DONALD G. LEE, KEITH C. BROWN et HASAN KARAMAN. Can. J. Chem. **64**, 1054 (1986).

Lorsque des alcènes sont oxydés par des permanganates d'ammonium ou de phosphonium quaternaires, dans des solvants organiques polaires comme l'acétone, les structures des cations n'ont pas ou peu d'effet sur les vitesses des réactions. Dans des solvants moins polaires, comme le chlorure de méthylène ou le toluène, les vitesses dépendent toutefois de l'identité des ions quaternaires. Il semble donc que les entités qui réagissent peuvent exister sous la forme de paires d'ions solvatés dans les solvants polaires et de paires d'ions intimes dans les solvants non-polaires. Les vitesses de réaction sont aussi très sensibles aux effets de substituants: on obtient une courbe de Hammett qui n'est pas linéaire (concave vers le haut) lors de l'oxydation de β-bromo et de β-méthoxystyrènes substitués. La meilleure représentation du mécanisme de la réaction implique des états de transition continus qui varient suivant leur nature riche ou pauvre en électrons, qui dépend elle-même de la capacité des structures des substrats d'accommoder soit des charges positives ou négatives.

[Traduit par la revue]

Introduction

Recent studies have shown that a wide variety of organic functional groups may be oxidized by quaternary ammonium and phosphonium permanganates under mild, nonpolar conditions (1). For example, this reaction has been used for the oxidation of aliphatic hydrocarbons (2), arenes (2, 3), alcohols (4, 5), aldehydes (5, 6), ethers (7), sulfides (8), amines (9), and alkenes (10).

Because these reactions appear to have considerable synthetic potential and because they present an interesting example of electron transfer processes under nonaqueous conditions, we have undertaken a study of the oxidation of a number of styrene derivatives in three solvents, methylene chloride, toluene, and acetone. Our purpose was to investigate the reaction mechanism and to achieve a better understanding of the role that solvents play in these reactions.

Experimental

Reactants and solvents

The quaternary ammonium and phosphonium permanganates were prepared as previously described (11). The substituted methyl cinnamates were prepared by methylation of the corresponding cinnamic acids and purified by distillation or recrystallization (12). The physical properties of the esters corresponded well with those reported in the literature (Table 1). The substituted β-bromostyrenes were prepared, as described in the literature (12), by treating the corresponding cinnamic acids with bromine in hot chloroform, isolating the product (a substituted 2,3-dibromo-3-phenylpropanoic acid), and refluxing it in aqueous sodium bicarbonate. β-Bromostyrene was isolated by vacuum distillation and purified by prepartive glc using a 7-ft 15% Apiezon L on Chromosorb P column. The other substituted β-bromostyrenes, being volatile solids, were purified by vacuum sublimation. The physical properties of these compounds are summarized in Table 1. The substituted β-methoxystyrenes were prepared, as described in the literature (13), by treatment of the corresponding phenylacetylenes with potassium hydroxide in absolute methanol. The products were isolated from the reaction mixture by vacuum distillation and purified by radial chromatography, using a Harrison Research model 7924 chromatotron. The physical properties of these compounds are summarized in Table 1.

Proton magnetic spectra were recorded using a Perkin–Elmer 60-MHz R12B spectrophotometer.

The solvents (methylene chloride, toluene, and acetone) were purified by treatment with tetrabutylammonium permanganate for several hours, followed by fractional distillation from the solution.

Kinetics

Solutions of the substrate (0.8 M) and quaternary ammonium permanganate (4×10^{-4} M) were prepared in a particular solvent and thermostated for 15 min. Then an aliquot (3.0 mL) of the oxidant solution was transferred to a 10-mm cuvette in the thermostated cell compartment of a Hewlett–Packard 8450A spectrophotometer. A small portion of the reductant solution was injected from a syringe, and the absorbance was recorded at intervals. Plots of $\ln (A - A_\infty)$ against time were linear (10), thus indicating that the reaction is first order in permanganate. The pseudo-first-order rate constants, obtained from the slopes of these plots, were found to be directly proportional to the concentration of the reductant, thereby confirming that the reaction is also first order in reductant concentration (10).

Stoichiometry

The stoichiometry of the reaction was determined by adding small portions of a reductant solution to a standardized solution of permanganate and recording the spectrum of the product. A calculation of the number of moles of permanganate reduced, per mole of reductant added, indicated a 1:1 stoichiometry.

Products

The brown-yellow solution remaining after all of the permanganate had been reduced in methylene chloride by a typical alkene, 1-phenyl-1-

[1]Author to whom correspondence may be addresed.

TABLE 1. Properties of substituted styrenes

Substituted styrene	Melting or boiling point (°C) (lit. value)	Nuclear magnetic resonance (δ ppm)
Methyl (*E*)-cinnamate	mp = 34–36 (36.5(14))	3.73(s, 3H), 6.53(d, 1H, J = 2.8) 7.48(m, 5H), 7.73(d, 1H, J = 2.8)
Methyl (*E*)-*p*-methyl-cinnamate	mp = 56–57.4 (57–58(15))	2.34(s, 3H), 3.78(s, 3H), 6.50(3, 1H, J = 2.8), 7.40(m, 4H), 7.75(d, 1H, J = 2.8)
Methyl (*E*)-*m*-methyl-cinnamate	bp = 78–79/0.2 Torr	2.29(s, 3H), 3.73(s, 3H), 6.33(d, 1H, J = 2.7), 7.22(s, 4H), 7.64(d, 1H, J = 2.7)
Methyl (*E*)-*p*-methoxy-cinnamate	mp = 89–91.5 (94–95(15))	3.77(s, 3H), 3.86(s, 3H), 6.43(d, 1H, J = 2.8), 7.35(m, 4H), 7.73(d, 1H, J = 2.8)
Methyl (*E*)-*m*-methoxy-cinnamate	bp = 107–109/0.36 Torr (162/13 Torr(15))	3.71(s, 6H), 6.37(d, 1H, J = 2.8), 7.05(br, 4H), 7.63(d, 1H, J = 2.8)
Methyl (*E*)-*p*-chloro-cinnamate	mp = 74.5–76.5(76–76.5(16))	3.79(s, 3H), 6.59(d, 1H, J = 2.8), 7.57(m, 4H), 7.72(d, 1H, J = 2.8)
Methyl (*E*)-*m*-chloro-cinnamate	mp = 46–47.5	3.83(s, 3H), 6.60(d, 1H, J = 2.8), 7.59(m, 4H), 7.72(d, 1H, J = 2.8)
Methyl (*E*)-*p*-isopropyl-cinnamate	bp = 109–112/0.2 Torr	1.18(d, 6H), 2.85(m, 1H), 3.71(s, 3H), 6.37(d, 1H, J = 2.8), 7.32(m, 4H), 7.69(d, 1H, J = 2.8)
Methyl (*E*)-*m*-fluoro-cinnamate	bp = 91–92/0.7 Torr	3.78(s, 3H), 6.44(d, 1H, J = 2.8), 7.34(br, 4H), 7.67(d, 1H, J = 2.8)
(*E*)-β-Bromostyrene	bp = 80–83/5 Torr (108/20 Torr (14))	6.90(m, 2H), 7.28(s, 5H)
(*E*)-*p*-Methyl-β-bromo-styrene	mp = 46–46.5	2.34(s, 3H), 6.90(m, 2H), 7.18(s, 4H)
(*E*)-*p*-Methoxy-β-bromo-styrene	mp = 54.5–56 (55–55.5(17))	3.76(s, 3H), 6.90(m, 6H)
(*E*)-*p*-Chloro-β-bromo-styrene	mp = 47–49	6.94(m, 2H), 7.31(s, 4H)
(*Z*)-β-Methoxystyrene	bp = 70–72/3 Torr (44/0.3 Torr (15))	3.60(s, 3H), 5.15(d, 1H, J = 1.2), 5.99(d, 1H, J = 1.2), 7.19(br, 5H)
(*Z*)-*p*-chloro-β-methoxy-styrene	bp = 57–59/0.03 Torr	3.67(s, 3H), 5.07(d, 1H, J = 1.1), 6.03(d, 1H, J = 1.1), 7.33(m, 4H)
(*Z*)-*p*-Methoxy-β-methoxy-styrene	bp = 51–52/0.05 Torr	3.77(s, 3H), 3.75(s, 3H), 5.13(d, 1H, J = 1.1), 5.99(d, 1H, J = 1.1), 7.11(m, 4H)

pentene, was found by iodometric analysis (18) to contain manganese in the +4 oxidation state. Although no organic products could be detected in this solution when it was analyzed by glc, the corresponding diol, 1-phenyl-1,2-dihydroxypentane, could be isolated after treatment with base. On the other hand, when the yellow-brown methylene chloride solution was treated with aqueous acid, benzaldehyde was found to be a major product. similar results for other compounds have previously been reported (19).

The oxidation state of the manganese remained at +4 after treatment with aqueous base, but decreased to about +3 after treatment with aqueous acid. Thus, it appears that the organic product (diol) may be complexed to a manganese(IV) compound (MnO_2?) in organic solvents, and released only by hydrolysis. Under basic conditions no further redox reactions occur during hydrolysis, but under acidic conditions the diol is oxidatively cleaved with concurrent reduction of the manganese, as in eq. [1].

$$[1]\quad \text{Alkene} + MnO_4^- \xrightarrow{CH_2Cl_2} \text{Manganese(IV) complex}$$

$$\text{Manganese(IV) complex} \xrightarrow{OH^-/H_2O} \text{Diol} + MnO_2$$

$$\text{Manganese(IV) complex} \xrightarrow{H^+/H_2O} \text{cleavage products} + \text{Mn(III)}$$

Results and discussion

Although most salts exist as discrete ions in aqueous solutions, quaternary ammonium compounds when dissolved in organic solvents are more likely to form ion pairs (11). Brandstrom has shown that the probability of salts existing as ion pairs is inversely dependent on the distance between the centres of the two ions and the dielectric constants of the solvents (20). Using his method of calculation, we have previously shown that most quaternary ammonium permanganates would be expected to exist as ion pairs in all solvents except water (1). This can be demonstrated by examining the ^1H nmr spectrum of tetraethylammonium permanganate in three solvents, D_2O, acetone-d_6, and methylene chloride-d_2 (Fig. 1). In water a distinct triplet and quartet is apparent, while in acetone and methylene chloride the resolution is dramatically reduced, with the spectrum becoming two broad multiplets in the latter solvent. Assuming that the lack of resolution in the organic solvents is due to close association of the quaternary ammonium ion with the permanganate ion (11), it would appear that $Et_4N^+MnO_4^-$ exists as separate ions in water, as a loose ion pair in acetone, and as a tight ion pair in methylene chloride.

The data sumarized in Table 2 are also in agreement with this

TABLE 2. Second-order rate constants for the oxidation of methyl cinnamate by $Q^+MnO_4^-$ in three solvents[a]

Q^+	Acetone	Methylene chloride	Toluene[b]
Tetra-*n*-butylammonium	0.32±0.01	1.15±0.02	
Tetra-*n*-octylammonium	0.31±0.01	0.91±0.02	1.31±0.05
Methyltri-*n*-octylammonium	0.33±0.01	1.54±0.05	2.17±0.04
Methyltri-*n*-butylammonium		1.54±0.02	
Methyltriphenylphosphonium	0.34±0.02	1.35±0.02	
n-Butyltriphenylphosphonium	0.27±0.01	0.99±0.02	
Benzyltriphenylphosphonium	0.30±0.01	1.53±0.04	
18-Crown-6-K^+	0.27±0.01	1.64±0.01	

[a]Temperature = 22.0°C. $[Q^+MnO_4] = 4 \times 10^{-4}$ *M*. [Methyl cinnamate] = 8×10^{-3} *M*. Units are $M^{-1}\,s^{-1}$.
[b]Studies in toluene were limited by the insolubility of most quaternary ammonium and phosphonium salts in solvents of low polarity (11).

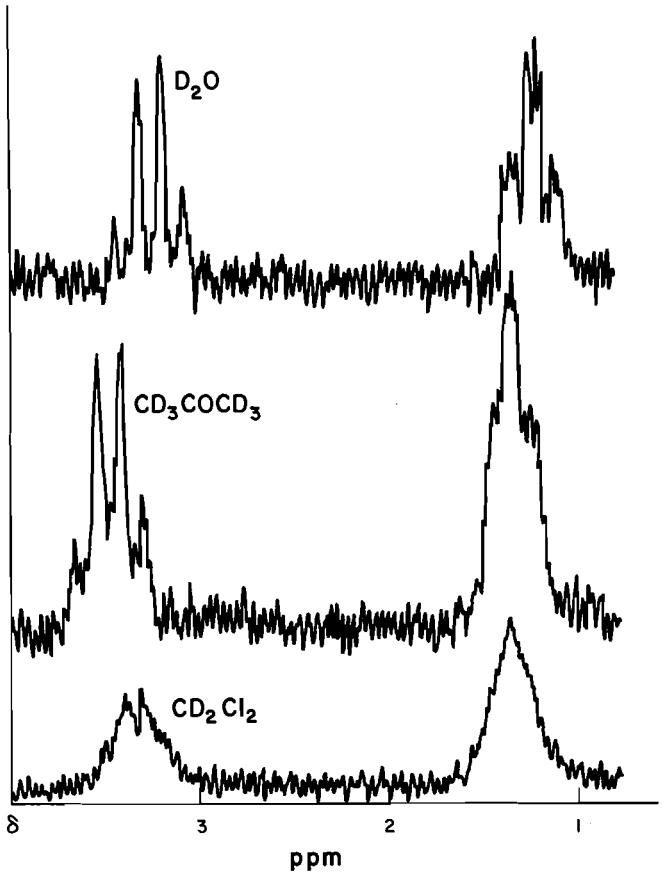

FIG. 1. Proton magnetic resonance spectra of tetraethylammonium permanganate in water-d_2, acetone-d_6, and methylene chloride-d_2.

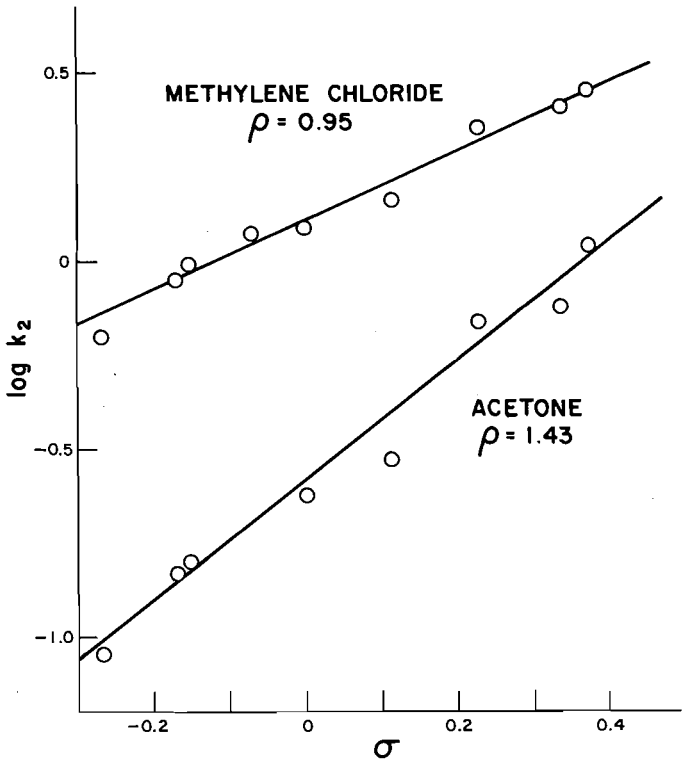

FIG. 2. Hammett plot for the oxidation of substituted methyl cinnamates by tetrabutylammonium permanganate in methylene chloride and acetone. $[QMnO_4] = 3.7 \times 10^{-4}$ *M*. [Methyl cinnamates] = 7.5×10^{-3} *M*. Temperature = 20.0 ± 0.1°C. For upper plot, slope = 0.95 ± 0.12, $r = 0.989$. For lower plot, slope = 1.43 ± 0.18, $r = 0.99$.

interpretation; the rate constants for the oxidation of methyl cinnamate in acetone are not dependent on the nature of the quaternary ammonium ion, whereas substantial variations in rates are found in the less polar solvents, methylene chloride and toluene. It thus appears as if the ion pairing in acetone is sufficiently loose to not affect the relative energies of the ground and transition states. However, in less polar solvents, where theory predicts tighter ion pairs (20), the ions must be intimately associated in either (or both) the ground state and the transition state. Furthermore, close contact within the ion pair seems to increase the rate of reaction. For example, the rate constants for oxidation of methyl cinnamate by methyltri-*n*-octylammonium permanganate are greater (in toluene and methylene chloride) than for tetra-*n*-octylammonium permanganate, presumably because the former allows for greater penetration of the anion into the structure of the cation (11, 21). Hence it appears as if quaternary ammonium permanganates may exist as solvent-separated ion pairs in acetone, but as intimate ion pairs in toluene and methylene chloride (22).

Additional evidence in support of this conclusion is obtained from a consideration of the effect of substituents on the rates of reaction. The Hammett ρ value for the oxidation of substituted methyl cinnamates by tetrabutylammonium permanganate is greater in acetone (ρ = 1.43) than it is in methylene chloride (ρ = 0.95). See Fig. 2. Since the ρ values are positive in both solvents, it is apparent that the transition state bears a greater

TABLE 3. Activation parameters for the oxidation of methyl cinnamate by methyltri-*n*-octylammonium permanganate[a]

Solvent	$\Delta H^{\ddagger}$ (kcal/mol)	$\Delta S^{\ddagger}$ (eu)	$\Delta G^{\ddagger}$ (kcal/mol)[b]
Acetone	8.06±0.50	−33.3±1.8	18.0±1.0
Methylene chloride	5.34±0.28	−39.2±1.0	17.0±0.6
Toluene	3.69±0.74	−44.1±0.3	16.8±0.8

[a]Temperature range from 0 to 30°C.
[b]At 25°C.

electron density than the ground state. However, the lower sensitivity of the reaction to substituent effects in methylene chloride suggests that, in this solvent, some of the increased negative charge is shared by the quaternary ammonium ions. In acetone, where the ion pair is much looser, the effect of substituents is greater because of a greater net charge developed in the transition state.

The thermodynamic parameters observed when different solvents are used could also be a consequence of ion pairing (Table 3). Since these reactions are clearly second order in all three solvents, the values of $\Delta H^{\ddagger}$ must reflect the differences in potential energies between the ground and transition states, while the relative magnitudes of $\Delta S^{\ddagger}$ must be associated with the different amounts of structure (or organization) in the ground and transition states. On this basis, the increase in organization on going from ground state to transition state is least in acetone ($\Delta S^{\ddagger} = -33.3 \pm 1.8$ eu) and greatest in toluene ($\Delta S^{\ddagger} = -44.1 \pm 0.3$ eu), with the value in methylene chloride being intermediate ($\Delta S^{\ddagger} = -39.2 \pm 1.0$ eu). Despite the fact that the reaction in toluene exhibits the least favorable entropy of activation, its rate of reaction is greatest because of the relatively low enthalpy of activation ($\Delta H^{\ddagger} = 3.69 \pm 0.74$ kcal/mol), the converse observation being true for the reaction in acetone ($\Delta H^{\ddagger} = 8.06 \pm 0.50$ kcal/mol). It therefore appears as if the formation of an intimate ion pair provides relatively greater organization and stability to the transition state than to the ground state during the oxidation of methyl cinnamate.

Current theory (23, 24) suggests that these reactions are initiated by formation of a π-complex between the alkene and manganese, as in eq. [2]. It is believed that this complex, **1**, can rapidly transform into a metallocyclooxetane, **2**, which then rearranges into a cyclic manganese(V) diester, **3**, long known to be an intermediate in these reactions (25). The latter is an example of a well-known group of reactions in which carbon migrates from metal to oxygen (23).

[2] 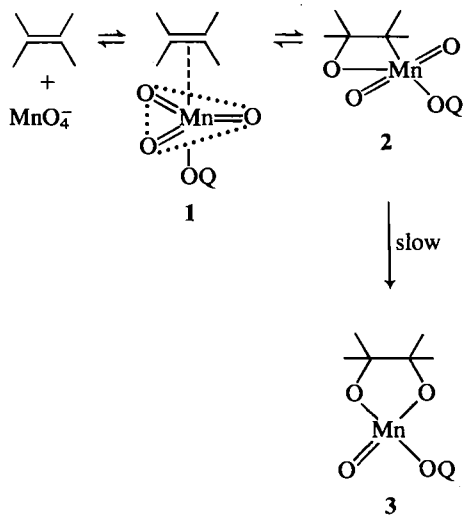

It is not possible to specify where, in this reaction sequence, the transition state is located. However, it may be noted that the formation of both **1** and **2** involves bond making, whereas conversion of **2** into **3** requires cleavage of the C—Mn bond. Hence it is not unreasonable, to assume, in the absence of other compelling evidence, that the last step in eq. [2] is likely to be rate limiting.

Since the effect of substituents indicates an electron-rich transition state when methyl cinnamate is oxidized, it seems reasonable to suggest that this rate-limiting step may involve heterolytic cleavage of the carbon–manganese bond to give an enolate-like transition state, as in eq. [3].

[3] 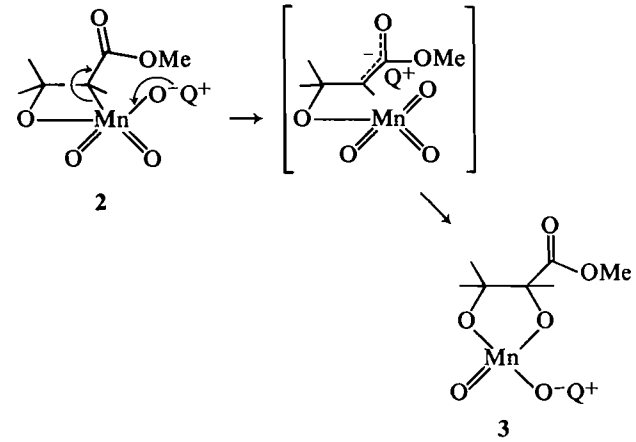

In this picture of the reaction, it is assumed that the proximity of the quaternary ammonium ion would increase the stability of the transition state in nonpolar solvents, but that this effect would be less in more polar solvents (such as acetone) where the cation could be surrounded by a sheath of solvent molecules.

Although the Hammett ρ value is observed to be positive for the oxidation of methyl cinnamates, previous work has shown that this observation is not universally true. For example, Toyoshima *et al.* (26) have reported that the oxidation of vinyl ethers by potassium permanganate in aqueous THF exhibited a negative ρ value (10), while Brownridge found that the ρ value for the oxidation of substituted cinnamic acids in aqueous acetic acid/$HClO_4$ solutions is essentially zero (27). Since some substituted alkenes (such as methyl cinnamates) that are capable of delocalizing negative charges exhibit positive ρ values, while other alkenes (such as vinyl ethers) that are able to stabilize positive charges exhibit negative ρ values, it is not surprising that for certain reactions, the sign of ρ actually changes when different substituents are present. The oxidation of substituted stilbenes, which has been studied by Henbest *et al.* (28), is one example of this phenomenon; the rate of reaction is accelerated by both electron-donating and electron-withdrawing substituents (10). The oxidation of substituted β-methoxy and β-bromostyrenes also gives Hammett plots with a distinctive

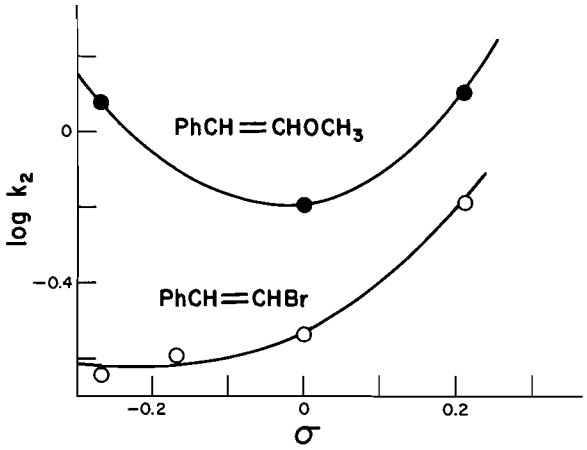

FIG. 3. Hammett plot for the oxidation of substituted β-bromostyrenes and β-methoxystyrenes by tetrabutylammonium permanganate in methylene chloride at 20.0°C.

upward curvature, as demonstrated in Fig. 3. Concave upward plots of this type are obtained only when the variation in substituents causes a change in mechanism (29). In other words, when substituents that are capable of stabilizing a positive charge are present, the reaction must be capable of selecting a pathway in which the transition state is electron deficient (eq. [3]), while the converse must be true when substituents that could stabilize a negative charge are present (eq. [4]).

[4] 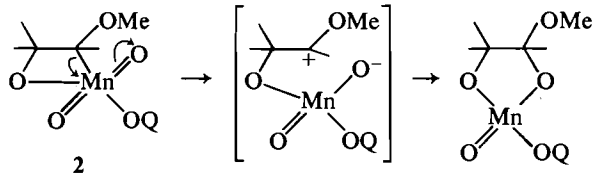

2 3

Since the mechanism chosen by the reaction can be altered from an electron-rich to an electron-deficient path merely by a change in substituents, it follows that the two transition states must be of similar energy and suggests that the reaction could best be visualized by use of a potential energy surface diagram (Fig. 4). According to transition state theory (30), the reaction would select the lowest energy pathway from **2** to **3**. When the substrate is capable of accommodating a negative charge, the reaction pathway would be shifted toward the lower right hand side of the surface, whereas the use of substrates capable of bearing positive charges would shift the reaction pathway toward the upper left hand corner of the diagram.

Although there is an overwhelming amount of evidence that **3** is an intermediate in these reactions, the yellow-brown product solution contains manganese in the +4 *not* the +5 oxidation state. Hence, it appears as if **3** may be a very reactive compound that rapidly undergoes a one-electron reduction, possibly by abstraction of a hydrogen atom from a molecule of solvent, as in [5].

[5] 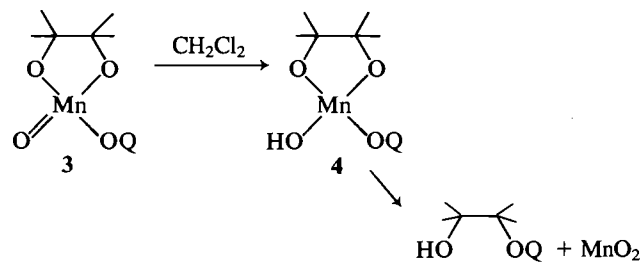

3 4 5

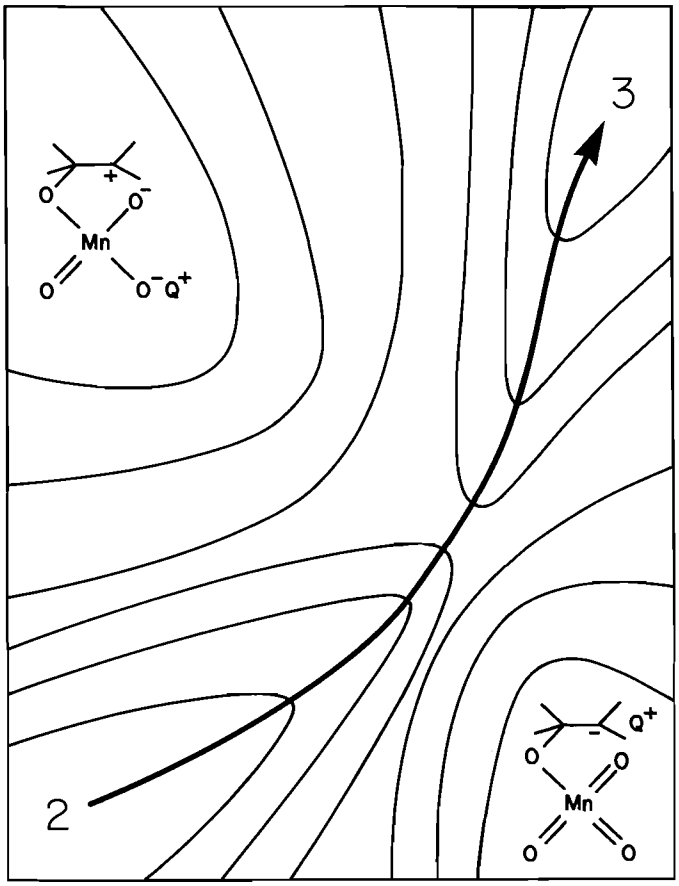

FIG. 4. Potential energy surface diagram for the rearrangement of structure **2** into structure **3**.

The product of this reaction would be a manganese(IV) cyclic diester, **4**, which could decompose to a diol anion, **5**, and manganese dioxide (31). Treatment of this product with aqueous base would release diol plus MnO_2, while addition of aqueous acid causes a further redox reaction in which the diol is oxidatively cleaved and manganese reduced to a lower oxidation state. The latter reaction is consistent with the higher reduction potential of manganese dioxide under acidic conditions (32).

Summary

1. A study of the effect of solvents on the rate of oxidation of methyl cinnamate by quaternary ammonium and phosphonium permanganates indicates that the cations are intimately associated with the transition state in nonpolar solvents, such as methylene chloride and toluene. In more polar solvents, such as acetone, the structure of the quaternary ammonium and phosphonium ions has no observable effect on the rate of reaction, presumably because they form solvent-separated ion pairs in both the ground state and the transition state.

2. A study of substituent effects on the rates of these reactions leads to the conclusion that they can proceed by way of continuum of transition states ranging from electron rich to electron poor. Although the mechanism is best visualized by use of a potential energy surface diagram (Fig. 4), the two extremes may be summarized as in Scheme 1.

3. The initial product of this reaction, **3**, is very reactive and rapidly undergoes a one-electron reduction to a manganese(IV) compound (or complex) that can be hydrolyzed under basic conditions to liberate a diol, or under acid conditions to produce cleavage products.

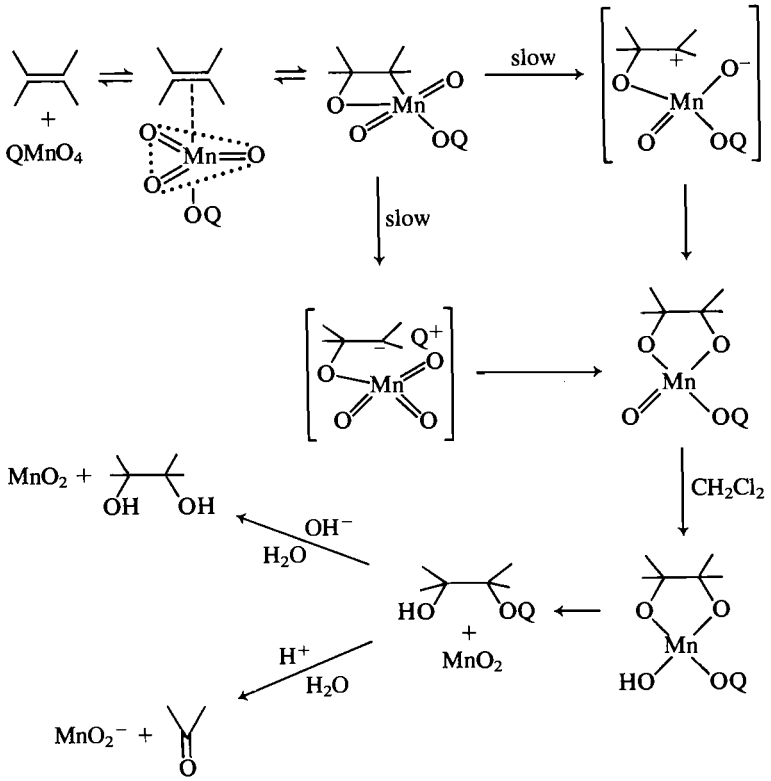

SCHEME 1. The reaction mechanism.

Acknowledgment

Financial assistance from the Natural Sciences and Engineering Research Council of Canada, and from Imperial Oil Limited, is gratefully acknowledged.

1. D. G. LEE. *In* Oxidation in organic chemistry. Part D. *Edited by* W. S. Trahanovsky. Academic Press, New York. 1982. Chapt. 2.
2. H. J. SCHMIDT and H. J. SCHAFTER. Angew. Chem. Int. Ed. Engl. **18**, 68 (1979).
3. R. SANGAIAH and G. S. KRISHNA RAO. Synthesis, 1018 (1980).
4. H. J. SCHMIDT and H. J. SCHAFER. Angew. Chem. Int. Ed. Engl. **20**, 104 (1981).
5. T. SALA and M. V. SARGENT. J. Chem. Soc. Chem. Commun. 253 (1978).
6. D. SCHOLZ. Monatsh. Chem. **110**, 1471 (1979).
7. H. J. SCHMIDT and H. J. SCHAFER. Angew. Chem. Int. Ed. Engl. **18**, 69 (1979).
8. D. G. LEE and N. S. SRINIVASAN. Sulfur Lett. **1**, 1 (1982).
9. H. J. SCHMIDT and H. J. SCHAFER. Angew. Chem. Int. Ed. Engl. **20**, 109 (1981).
10. D. G. LEE and K. C. BROWN. J. Am. Chem. Soc. **104**, 5076 (1982).
11. H. KARAMAN, R. J. BARTON, B. E. ROBERTSON, and D. G. LEE. J. Org. Chem. **49**, 4509 (1984).
12. B. S. FURNISS, A. J. HANNAFORD, V. ROGERS, P. W. G. SMITH, and A. R. TATCHELL. Vogel's textbook of practical organic chemistry. Longman, London. 1968.
13. K. AWERS. Chem. Ber. **44**, 3514 (1911).
14. R. C. WEAST (*Editor*). Handbook of chemistry and physics. Chemical Rubber Co., Boca Raton, FL. 1981–1982.
15. Dictionary of Organic Compounds. 5th ed. Chapman and Hall, London. 1982.
16. C. S. RONDESTVEDT and C. D. VER NOOY. J. Am. Chem. Soc. **77**, 4878 (1955).
17. E. R. TRUMBULL, R. T. FINN, K. M. IBNE-RASA, and C. K. SAUERS. J. Org. Chem. **27**, 2339 (1962).
18. D. G. LEE and J. F. PEREZ-BENITO. Can. J. Chem. **63**, 1275 (1985).
19. T. OGINO and K. MOCHIZUKI. Chem. Lett. 443 (1979).
20. A. BRANDSTROM. Adv. Phys. Org. Chem. **15**, 267 (1977).
21. S. R. C. HUGHES and D. H. PRICE. J. Chem. Soc. A, 1093 (1967); B. S. KRUMGAL'Z. Russ. J. Phys. Chem. **45**, 1448 (1971); J. E. GORDON and G. N. SUBBARAO. J. Am. Chem. Soc. **100**, 7445 (1978).
22. S. WINSTEIN, E. C. FRIEDRICH, and S. SMITH. J. Am. Chem. Soc. **86**, 305 (1964); F. A. CAREY and R. J. SUNDBERG. Advanced organic chemistry. Part A, 2nd ed. Plenum, New York. 1984. pp. 244–246; T. H. LOWRY and K. S. RICHARDSON. Mechanism and theory of organic chemistry. 2nd ed. Harper and Row, New York. 1981. pp. 320–323.
23. K. B. SHARPLESS, A. Y. TERANISHI, and J. E. BACKVALL. J. Am. Chem. Soc. **99**, 3120 (1977).
24. A. K. RAPPE and W. A. GODDARD. J. Am. Chem. Soc. **104**, 448, 3287 (1982).
25. R. STEWART. *In* Oxidation in organic chemistry. Part A. *Edited by* K. B. Wiberg. Academic Press, New York. 1965. p. 42.
26. K. TOYOSHIMA, T. OKUYAMA, and T. FUENO. J. Org. Chem. **45**, 1600 (1980).
27. J. R. BROWNRIDGE. M. Sc. Thesis, University of Regina, 1972; D. G. LEE and J. R. BROWNRIDGE. J. Am. Chem. Soc. **96**, 5517 (1974).
28. H. B. HENBEST, W. R. JACKSON, and B. C. G. ROBB. J. Chem. Soc. B, 803 (1966).
29. J. E. LEFFLER and E. GRUNWALD. Rates and equilibria of organic reactions. Wiley, New York. 1963. pp. 187–191; O. EXNER. *In* Advances in linear free energy relationships. *Edited by* N. B. Chapman and J. Shorter. Plenum, New York. 1972. pp. 12–17.
30. C. K. INGOLD. Structure and mechanism in organic chemistry. 2nd ed. G. Bell and Sons, London. 1969. pp. 45–48; K. J. LAIDLER. Chemical kinetics. 2nd ed. McGraw–Hill, Toronto. 1965. pp. 54–60.
31. J. F. PEREZ-BENITO and D. G. LEE. Can. J. Chem. **63**, 3545 (1985).
32. D. ARNDT. Manganese compounds as oxidizing agents in organic chemistry. Open Court, La Salle, Illinois. 1981. p. 27.

Solvolysis of 2-substituted-9-(*ortho*-substituted phenylmethyl)fluoren-9-yltrimethylammonium ions in various solvents. The effect of steric crowding on alkene formation

PETER JAMES SMITH[1] AND JYOTSNA PRADHAN[2]
Department of Chemistry, University of Saskatchewan, Saskatoon, Sask., Canada S7N 0W0
Received October 15, 1985
This paper is dedicated to Professor Arthur N. Bourns

PETER JAMES SMITH and JYOTSNA PRADHAN. Can. J. Chem. **64**, 1060 (1986).

The solvolytic reaction of several 9-(*ortho*-substituted phenylmethyl)fluoren-9-yltrimethylammonium salts has been investigated in several different solvents. Substitution and elimination products were found for the reactions in all the solvents studied, with the exceptions that reaction in both *tert*-butyl alcohol and chloroform led exclusively to the alkene product. The observed rate constants for alkene formation and the percent alkene were measured and it was found that the di-*ortho* compounds reacted at a faster rate but produced less alkene than the reaction of the corresponding mono-*ortho* salts. Hydrogen–deuterium isotope effects were also determined for the various reactions. The results are discussed in terms of the reaction proceeding by way of the E1 mechanism, where steric acceleration promotes the loss of the bulky ammonium leaving group to give the carbocation intermediate.

PETER JAMES SMITH et JYOTSNA PRADHAN. Can. J. Chem. **64**, 1060 (1986).

Opérant dans plusieurs solvants, on a étudié la réaction solvolytique de plusieurs sels triméthylammonium des ⟨phénylméthyles substitués en *ortho*)-9 fluorène-9 yles. À l'exception des réactions dans l'alcool *tert*-butylique ou dans le chloroforme, toutes les réactions étudiées dans les autres solvants ont conduit à la formation de produits de substitution ainsi que d'élimination. On a mesuré les constantes de vitesse pour la formation des alcènes ainsi que les pourcentages d'alcènes formés; on a trouvé que les composés doublement substitués en *ortho* réagissent plus rapidement mais qu'ils produisent moins d'alcènes que les réactions des sels correspondants qui ne portent qu'un substituant en *ortho*. On a déterminé les effets cinétiques hydrogène–deutérium pour diverses réactions. On discute des résultats en fonction d'une réaction qui se produirait par le biais d'un mécanisme E1 et dans lequel l'accélération stérique favoriserait le perte du nucléofuge ammonium encombrant au profit de la formation d'un carbocation intermédiaire.

[Traduit par la revue]

Introduction

Studies on the base-promoted 1,2 elimination reaction of quaternary ammonium salts have received considerable attention both from the experimental (1–6) and theoretical approaches (7, 8). Such substrates generally react with alkoxide bases by way of the one-step concerted E2 mechanism (9, 10) although reaction proceeding by the ylide mechanism (α', β) has been demonstrated by Cope and Mehta (11) for a substrate where approach of base to the β-hydrogen is unfavourable for steric reasons.

Generally, quaternary ammonium salts do not undergo elimination via a carbocation intermediate under solvolytic conditions and, hence, amines have been classified as "poor leaving groups" (poor nucleofuges (2, 12)). However, in a study on the degradation of ax-7-cholestanyltrimethylammonium iodide in boiling ethanol it was reported (13) that the reaction undoubtedly proceeded via an E1 process. Similarly, Hughes and Wilby (14) proposed that menthyltrimethyl- and neomenthyltrimethylammonium hydroxides, **1** and **2**, underwent reaction in water by the unimolecular E1 pathway. Since the neomenthyltrimethylammonium ion, where the $-\overset{+}{N}(CH_3)_3$ group is *cis* to the isopropyl substituent, showed a much larger propensity for reaction via the E1 mechanism than the menthyl substrate, the authors considered that carbocation formation is made favourable due to a relief in steric strain in the molecule.

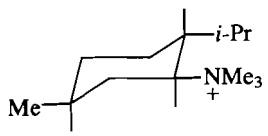

1

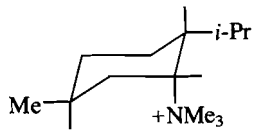

2

The effect of *para* substituents on the aryl ring on the nature of the E2 transition state was examined (2) for the reaction of 2-arylethyltrimethylammonium salts with ethoxide ion in ethanol, eq. [1]. It was found that when the *para* substituent was made more electron withdrawing the reaction rate *increased*. Also, measurements (2) and calculations (8) of both the primary hydrogen–deuterium and nitrogen (leaving group) isotope effects indicated that an increase in the electron-withdrawing power of the ring substituent leads to a corresponding transition state with *both decreased* C—H and C—$\overset{+}{N}$ bond weakening. This substituent effect on transition state geometry (a Hammond effect) was considered to be consistent with the theories of Thornton (15, 16), More O'Ferrall (17) and Jencks (18).

[1] 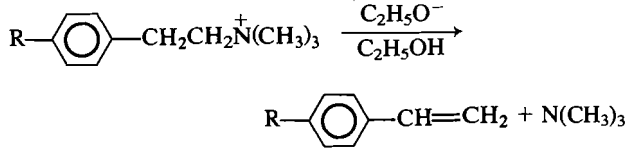

In an investigation (19) on the E2 reaction of 9-(4-substituted phenylmethyl)fluoren-9-yltrimethylammonium bromides, **3**, with ethoxide in ethanol, however, it was found that the

[1]Author to whom correspondence may be addressed.
[2]Present address: Department of Chemisty, University of Iowa, Iowa City, IA 52242, U.S.A.

variation of both the primary hydrogen–deuterium and nitrogen isotope effects with changes of the 4-substituent (R) on the phenyl ring were the *opposite* to those found in the earlier studies on the 2-arylethyl system. As well, the Hammett ρ value of +1.33 found for the reaction of **3** was very much less than the value of +3.77 found for the reaction of the 2-arylethyl salts with ethoxide (2), in spite of the fact that in both cases a benzylic hydrogen was being removed with ethoxide ion. It was concluded (19) that for reaction of **3** where the 4-substituent (R) is an electron withdrawer, which leads to an *increase* in the rate of reaction, the extent of both the β-carbon–hydrogen and the α-carbon–nitrogen bond rupture at the transition state is *more* advanced.[3] This apparent variance with the conclusions reached in the earlier studies (2) was discussed in the light of possible steric effects between the *ortho* hydrogens on the phenyl ring and the 1,8 hydrogens on the fluorene nucleus in the reactant and in the transition state.

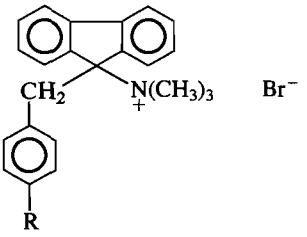

The effect of the nature of the leaving group has been extensively studied (20–30) for several elimination reactions in terms of mechanism as well as in transition-state structure. In all cases, nucleofugality was considered essentially as being entirely due to "electronic factors" (basicity, polarizability, etc). In order to test the proposal (19) that steric interactions might affect leaving group ability and, hence, are responsible for the unexpected results obtained from the study of the reaction of **3** in terms of transition-state geometry, several 9-(*ortho*-substituted phenylmethyl)fluoren-9-yltrimethylammonium salts have been prepared in order to investigate the possible effect of the *ortho* substituents on the phenyl ring in terms of mechanism and (or) transition-state structure. An examination of Dreiding models of the *para*-substituted salts, **3**, suggests that there is a possible steric interaction between the *ortho* hydrogens on the phenyl ring and the fluorenyl 1,8 hydrogens. Consequently, replacing the *ortho* hydrogens with bulkier groups should enhance the "steric effect".

In the present study,[4] the rate of reaction of a series of 2-substituted-9-(*ortho*-substituted phenylmethyl)fluoren-9-yltrimethylammonium salts, and their β-d_2 analogues, have been measured in a variety of protic solvents as well as in the aprotic solvent chloroform, and the product composition determined. Also, the effect of externally added trimethylamine and, as well, the effect of the addition of the strong base, sodium ethoxide, on both the rate of reaction and the product ratios have been examined for reaction of the *ortho*-substituted compounds in ethanol. Secondary β-hydrogen–deuterium isotope effects on carbocation formation have been measured and, as well, an estimate of the primary β-hydrogen–deuterium isotope effect for proton loss from the carbocation has been made by determining the product ratios. Activation parameters for the reaction of several 9-(*ortho*-substituted) salts in both absolute ethanol and 2-propanol were also determined.

Results

The compounds investigated in the present study are shown below:

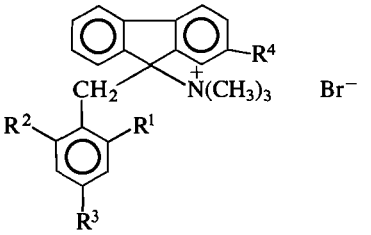

4, $R^1 = R^2 = CH_3$; $R^3 = R^4 = H$
5, $R^1 = R^2 = Cl$; $R^3 = R^4 = H$
6, $R^1 = CH_3$; $R^2 = R^3 = R^4 = H$
7, $R^1 = R^3 = CH_3$; $R^2 = R^4 = H$
8, $R^1 = R^2 = R^3 = CH_3$; $R^4 = H$
9, $R^1 = R^2 = CH_3$; $R^3 = H$; $R^4 = Br$

The observed rate constants for alkene formation, k_1, for reaction of the *ortho*-substituted salts, **4–9**, and their β-dideuterated analogues in absolute ethanol at 57.3°C are shown in Table 1. The secondary β-hydrogen–deuterium isotope effects, k_1^H/k_1^D, as well as the primary β-hydrogen–deuterium isotope effects,[5] k_E^H/k_E^D, determined from the product ratio data, are also given in this table. A comparison of the observed rate constant for alkene formation, k_1, for reaction of the bromine-substituted fluorenyl ring salt, **9**, with that for reaction of **4** at 68.4°C in absolute ethanol, $120 \pm 3.0 \times 10^{-5}$ (s^{-1}) and $109 \pm 0.5 \times 10^{-4}$ (s^{-1}), gives a Hammett ρ value of −2.5 for reaction of the 2,6-diMe substrate in ethanol.

The effect of externally added trimethylamine on the observed rate of alkene formation, k_1, and, as well, on the percent alkene product, was determined for the reaction of the 2-Me, **6**, and 2,4,6-triMe, **8**, salts in ethanol at approximately[6] 57°C, Table 2. The effect of the addition of a strong abstracting base, sodium ethoxide, on the observed rate constant for alkene formation, k_1, and on the percent alkene formed, was investigated for the reaction of the 2,4,6-triMe salt, **8**, in ethanol at the same temperature as used for the trimethylamine experiments, Table 2.

The effect of a change in solvent on the observed rate constant for alkene formation, k_1, the percent alkene, the secondary β-deuterium isotope effect, k_1^H/k_1^D, and the primary β-deuterium isotope effect, k_E^H/k_E^D, for the reaction of the 2-Me, 2,6-diMe, and 2,4,6-triMe salts, **6**, **4**, and **8**, respectively, were examined for reaction in a series of alcohol solvents as well as in two alcohol–water mixtures at 57.3°C, and the results are given in Table 3. The thermodynamic activation parameters were determined for the reaction of the 2-Me (**6**), 2,6-diMe (**4**), and 2,6-diCl (**5**) substrates in absolute ethanol and also for the reaction of the 2,6-diMe salt in 2-propanol. The observed rate constants for alkene formation, k_1, together with the per-

[3]This apparent "anti-Hammond" behavior on E2 transition state geometry can be accounted for by the More O'Ferrall theory (17) and will be discussed in a manuscript currently under preparation.

[4]A preliminary account of some of the studies has been published (31, 32).

[5]The method used for the determination of this effect will be given in the discussion section.

[6]The temperature was not exactly 57.3°C as used in the previous experiments and, hence, the rate constants differ slightly from those shown in Table 1.

TABLE 1. Hydrogen–deuterium isotope effects for reaction of a series of 9-(*ortho*-substituted phenylmethyl)fluoren-9-yltrimethylammonium bromides in absolute ethanol at 57.3°C

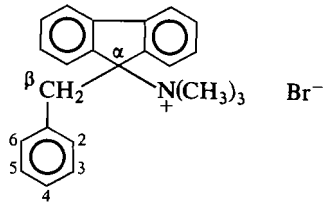

Substrate	$k_1 \times 10^5$ (s^{-1})	% alkene	k_1^H/k_1^D	$(k_E^H/k_E^D)^a$
2-Me (**6**)	2.35±0.09[b]	55±1.0[c]	1.22±0.05[d]	1.6±0.2[c]
6-d_2	1.92±0.04	43±1.0		
2,4-diMe (**7**)	2.85±0.03	57±1.0	1.16±0.01	2.0±0.2
7-d_2	2.46±0.02	40±1.0		
2,6-diCl (**5**)	9.59±0.20	29±1.0	1.45±0.04	2.5±0.6
5-d_2	6.60±0.12	14±2.0		
2,6-diMe (**4**)	295±4	28±1.0	1.62±0.03	3.1±1.0
4-d_2	182±2	11±2.0		
2,4,6-triMe (**8**)	297±16	30±1.0	1.39±0.10	4.9±2.0
8-d_2	214±10	8.0±2.0		

[a]Calculated from the product ratios: $k_E^H/k_E^D = \frac{(\%\text{alkene}/\%\text{ether})_H}{(\%\text{alkene}/\%\text{ether})_D}$, assuming $k_S^H = k_S^D$.

[b]Standard deviation.

[c]Estimated uncertainty.

[d]Ratios of observed rate constants for alkene formation: deviation = $\pm k^H/k^D[(r^H/k^H)^2 + (r^D/k^D)^2]^{1/2}$ where r is the standard deviation in k.

TABLE 2. First-order rate constants, k_1, and the percent alkene obtained for the reaction of the 2-Me, **6**, and 2,4,6-triMe, **8**, salts in the presence and absence of both externally added trimethylamine and sodium ethoxide in absolute ethanol at 57°C[a]

Substrate	[Substrate] $\times 10^4$ (M)	[Trimethylamine] (M)	[Sodium ethoxide] (M)	$k_1 \times 10^5$ (s^{-1})	% alkene
2-Me (**6**)	1.856	—	—	2.56±0.04[b]	55±1.0[c]
	1.856	3.5×10^{-3}	—	2.46±0.04	55±1.0
2,4,6-triMe (**8**)	1.570	—	—	330±14	31±1.0
	1.570	3.5×10^{-3}	—	345±8	31±1.0
	1.542	—	3.08×10^{-4}	312±8	31±1.0
	1.542	—	3.08×10^{-3}	340±9	31±1.0

[a]The temperature was slightly different for these experiments than that used to acquire the data shown in Table. 1.

[b]Standard deviation.

[c]Estimated uncertainty.

cent alkene values determined at three diferent temperatures for reaction of the three substrates, **4**, **5**, and **6**, are given in Table 4 alone with the values for E_A, $\Delta H^{\ddagger}$ (60°C), and $\Delta S^{\ddagger}$ (60°C).

The effect of an aprotic solvent, chloroform, on the observed rate constant for alkene formation, k_1, for reaction of the 2,6-diMe (**4**), 2,4,6-triMe (**8**), and 2-Me (**6**) salts and their β-dideuterated analogues was determined by both the uv (ultraviolet) spectroscopic method, used in all the preceding studies, and a nuclear magnetic resonance procedure (see the experimental section for details). The results are shown in Table 5 along with the secondary β-hydrogen–deuterium isotope effects, k_1^H/k_1^D. In all cases, the alkene was formed in 100 ± 5% yield. The rate constant for the bromine-substituted fluorene ring substituted salt, **9**, of 16.6 ± 0.2 × 10^{-5} (s^{-1}) can be compared with that of 128 ± 3 × 10^{-5} (s^{-1}) for reaction of **4** to give a ρ value for reaction of the 2,6-diMe salt in chloroform of −2.3 at 50°C.

Discussion

*Reaction of 2-substituted-9-(*ortho*-substituted phenylmethyl)-fluorene-9-yltrimethylammonium ions in absolute ethanol at 57.3°C*

In order to investigate the elimination reaction of the *ortho*-substituted quaternary ammonium salts **4–9** with ethoxide they were first dissolved in dry absolute ethanol and a uv spectrum was obtained for each solution. Surprisingly, it was found that the uv spectra of all the substrate solutions changed with time, indicating that reaction was taking place in the *absence* of base. It must be noted that the *para*-substituted analogues **3** (with hydrogens at the *ortho* positions) were completely stable in ethanol in the absence of ethoxide ion.

The products of the reaction of the *ortho*-substituted salts **4–9** in dry ethanol were found to be the corresponding alkene **10** as well as the ethyl ether, 9-ethoxy-9-(*ortho*-substituted phenylmethyl)fluorene, **11**, eq. [2]. The rate of reaction of the

TABLE 3. Hydrogen–deuterium isotope effects for reaction of the 2-Me, 2,6-diMe, and 2,4,6-triMe salts and their β-dideuterated analogues in various alcohol solvents at 57.3°C

Substrate	Solvent	$k_1 \times 10^5$ (s^{-1})	% alkene	k_1^H/k_1^D	$(k_E^H/k_E^D)^a$
2-Me (**6**)	MeOH	2.18±0.0[b]	43±1.0[c]	1.56±0.04[d]	1.3±0.1[c]
6-d_2	MeOH	1.40±0.02	37±1.0		
6	EtOH	2.35±0.09	55±1.0	1.22±0.05	1.6±0.2
6-d_2	EtOH	1.92±0.04	43±1.0		
6	95% EtOH	1.58±0.03	58±1.0	1.66±0.04	1.2±0.2
6-d_2	95% EtOH	0.95±0.01	53±1.0		
6	70% EtOH	0.93±0.02	54±1.0	—	—
6	*t*-BuOH	0.63±0.02	100±1.0	1.24±0.06	—
6-d_2	*t*-BuOH	0.51±0.02	100±1.0		
2,6-diMe (**4**)	EtOH	294±4	28±1.0	1.62±0.03	3.1±1.0
4-d_2	EtOH	182±2	11±2.0		
4	95% EtOH	212±3	30±1.0	1.32±0.02	3.1±1.0
4-d_2	95% EtOH	161±1	12±2.0		
4	2-PrOH	337±9	52±1.0	1.43±0.03	3.8±1.0
4-d_2	2-PrOH	236±3	22±1.0		
4	*t*-BuOH	195±11	100±1.0	1.57±0.09	—
4-d_2	*t*-BuOH	124±2	100±1.0		
2,4,6-triMe (**8**)	MeOH	245±6	21±1.0	1.10±0.06	5.1±2.0
8-d_2	MeOh	222±10	5±2.0		
8	EtOH	297±16	30±1.0	1.39±0.10	4.9±2.0
8-d_2	EtOH	214±10	8±2.0		

[a]Calculated from the product ratios assuming $k_S^H = k_S^D$.
[b]Standard deviation.

ortho-substituted salts in ethanol was determined by measuring the formation of the alkene product at 320 nm since the uv spectrum of the ether does not show any absorption at this wavelength. The percent alkene formed in the reaction was calculated from the absorbance reading at infinite time (see the experimental section for details).

[2]

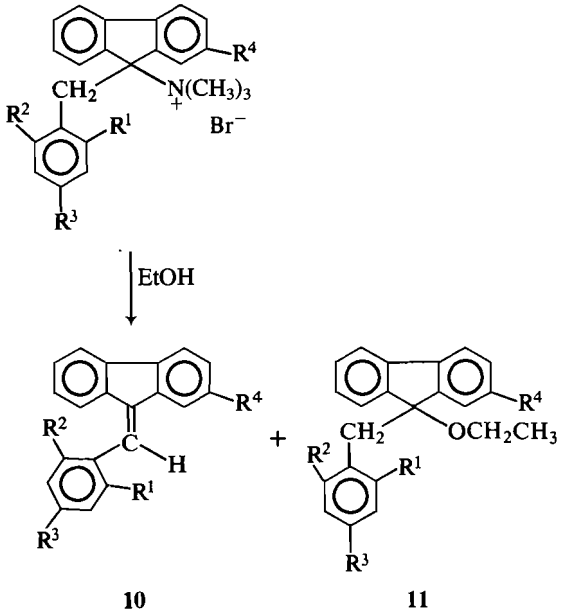

10 **11**

A consideration of the data in Table 1 indicates that the mono-*ortho*-substituted substrates react in ethanol to give a greater amount of alkene product, as compared with the reaction of the di-*ortho*-substituted salts; i.e., reaction of the undeuterated 2-Me and 2,4-diMe compounds give 55 and 57% alkene, respectively, while reaction of the 2,6-diMe salt gives approximately 28% alkene.

It can also be seen that the rate of reaction of the mono-*ortho*-substituted compounds is considerably slower than the rate of reaction of the di-*ortho*-substituted substrates. The observed rate constants for alkene formation, k_1, for reaction of the undeuterated 2-Me and 2,4-diMe salts in ethanol at 57.3°C are 2.35 and 2.85 × 10^{-5} (s^{-1}), respectively, while the corresponding rate constants for reaction of the 2,6-diCl, 2,6-diMe, and 2,4,6-triMe compounds are 9.59, 294, and 297 × 10^{-5} (s^{-1}), respectively. The compounds with only one *ortho* substituent react at a slower rate but give a greater yield of alkene product.

It is noteworthy that a 4-methyl substituent does not change significantly the observed rate constant for alkene formation, k_1, or the percent alkene, as compared to the reaction of compounds with only *ortho* substituents. The observed rate constants for alkene formation, k_1, together with the percent alkene for reaction of the undeuterated 2-Me and 2,4-diMe substrates are 2.35 × 10^{-5} (s^{-1}) (55%) and 2.85 × 10^{-5} (s^{-1}) (57%), respectively, while the corresponding values for reaction of the 2,6-diMe and 2,4,6-triMe compounds are 294 × 10^{-5} (s^{-1}) (28%) and 297 × 10^{-5} (s^{-1}) (30%), respectively.

The only mechanism that is consistent with the above results for reaction of the *ortho*-substituted salts in ethanol in the absence of a strong abstracting base is the E1 process involving carbocation formation. In principle, the formation of this carbocation can be a reversible process, eq. [3], and conse-

[3] *ortho*-Substituted salts $\underset{k_{-1}}{\overset{k_1}{\rightleftharpoons}}$ carbocation + trimethylamine

carbocation $\xrightarrow{k_2}$ products

TABLE 4. First-order rate constants k_1, E_A, $\Delta H^{\ddagger}$, $\Delta S^{\ddagger}$ values, and percent alkene formation for the reaction of the 2-Me, 2,6-diMe, and 2,6-diCl salts in absolute ethanol and 2-propanol at various temperatures

Substrate	Solvent	Temperature (°C)[a] (±0.01°C)	$k_1 \times 10^5$ (s^{-1})	% alkene	E_A (kcal mol^{-1})	$\Delta H^{\ddagger}$(60°C) (kcal mol^{-1})	$\Delta S^{\ddagger}$(60°C) (cal K^{-1} mol^{-1})
2-Me (**6**)	EtOH	47.2	0.458±0.025[b]	57±1[c]	36.9±0.5[b]	36.2±0.5[b]	29.9±1.6[b]
		57.3	2.35±0.09	55±1			
		67.3	13.1±0.3	53±1			
2,6-diCl (**5**)	EtOH	47.2	1.93±0.04	31±1	34.8±0.6	34.1±0.4	26.2±1.2
		57.3	9.59±0.20	29±1			
		69.1	63.7±0.8	27±1			
2,6-diMe (**4**)	EtOH	47.2	77.2±0.3	28±1	30.2±0.4	29.6±0.4	19.4±1.2
		57.3	294±4	28±1			
		67.3	1200±60	26±1			
	2-PrOH	48.3	93.4±2.7	52±1	28.4±1.8	27.7±1.8	13.7±5.5
		57.3	377±9	52±1			
		68.4	1230±40	52±1			

[a]The temperatures were determined using a platinum resistance thermometer.
[b]Standard deviation.
[c]Estimated uncertainty.

TABLE 5. Hydrogen–deuterium isotope effects for reaction of the 2-Me and 2,4,6-triMe salts and their β-dideuterated analogues in chloroform

Substrate	Temperature (°C)	$k_1 \times 10^5$ (s^{-1})	k_1^H/k_1^D
2,6-diMe (**4**)	50.6	128±3[a,b]	1.47±0.04[c]
4-d_2	50.6	87.2±1.3[a]	
4	50[d]	88.9±3.4[b,e]	1.88±0.12
4-d_2	50[d]	47.2±2.2[e]	
2,4,6-triMe (**8**)	50[d]	108±2[e]	1.55±0.03
8-d_2	50[d]	68.6±1.3[e]	
2-Me (**6**)	50[d]	0.760[e]	

[a]Determined using the uv method.
[b]Standard deviation.
[c]Deviation = $\pm k^H/k^D [(r^H/k^H)^2 + (r^D/k^D)^2]^{1/2}$ where r is the standard deviation in k.
[d]The approximate temperature in the probe of the nmr spectrometer.
[e]Determined using the nmr method.

quently the rate of alkene formation and the percent alkene were determined for reaction of both the 2-Me and 2,4,6-triMe substrates in absolute ethanol, both in the absence and presence of added trimethylamine, Table 2.

The results in Table 2 indicate that the rate of alkene formation, k_1, and the amount of alkene formed do not change for reaction of either the 2-Me or the 2,4,6-triMe compounds in ethanol when trimethylamine is added. Hence the formation of the carbocation in the system under study is irreversible, i.e. $k_2 >> k_1$ eq. [3].

The proton removal step to give the alkene product, k_E in eq. [4], was investigated for the reaction of the 2,4,6-triMe salt

[4] *ortho*-Substituted salts $\xrightarrow{k_1\ (\text{slow})}$ carbocation $\xrightarrow{k_E}$ alkene; carbocation $\xrightarrow{k_S}$ ether

when the strong base, sodium ethoxide, was added to the reaction solution, Table 2. It is seen that the observed rate constant for alkene formation, k_1, and the percent alkene were essentially unaffected when the concentration of the added ethoxide ion was either a factor of two or ten times as great as the substrate concentration. The loss of the proton from the carbocation must, therefore, not be rate determining, i.e. $k_1 \ll (k_E + k_S)$. Furthermore, the failure of the addition of ethoxide to change the alkene : ether ratio suggests that the solvent ethanol, and not ethoxide, is involved in the removal of the proton to give the alkene in the k_E step, as it is unlikely that ethoxide ion would affect the rate of alkene and ether formation in an identical fashion. The failure of ethoxide to affect the reaction can possibly be due to electrostatic control of the approach of $^-$OEt to a non-reacting site of the substrate, which leaves the β-proton and α-carbon open to attack by solvent.

The rate-determining formation of the 9-fluorenyl carbocation **12** is consistent with the observation of a Hammett ρ of −2.5, calculated from the k_1 values determined for the reaction of the 2,6-diMe salt **4** and the 2,6-diMe salt with a 2-bromo substituent on the 9-fluorenyl ring, **9**. Several groups of workers have prepared the 9-substituted 9-fluorenyl carbocations by reaction of the corresponding alcohol in acid media for spectroscopic (33, 34) and kinetic studies (35). As well, in spite of their "antiaromaticity", the 9-fluorenyl and the 9-methyl-9-fluorenyl carbocations have been proposed as intermediates in the solvolytic reaction of the 9-chloro (36) and 9-(3,5-dinitrobenzoate) (37) derivatives, respectively.

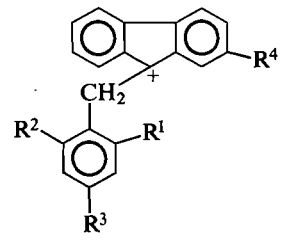

12

Reaction proceeding via the E1 mechanism where formation of the carbocation is rate determining, eq. [4], should give rise mainly to a secondary β-deuterium kinetic isotope effect (38) since rupture of the β-hydrogen bond occurs in a subsequent fast step. Applying the steady-state treatment to the reaction scheme

shown in eq. [4] leads to the expression for the rate of formation of the alkene product,

$$\frac{\mathrm{d[alkene]}}{\mathrm{d}t} = \left(\frac{k_1 k_E}{k_E + k_S}\right) A$$

where A represents the substrate concentration.

Setting E and S as the concentration of the alkene and ether products, respectively, it follows that the quaternary ammonium salt concentration, A, at a time T is given by

$$A_T = E_\infty - E_T + S_\infty - S_T$$

and since $k_E/k_S = E/S$ then

$$A_T = E_\infty - E_T + E_\infty\left(\frac{k_S}{k_E}\right) - E_T\left(\frac{k_S}{k_E}\right)$$

which becomes

$$A_T = (E_\infty - E_T)\left(\frac{k_E + k_S}{k_E}\right)$$

therefore

$$\frac{\mathrm{d}E}{\mathrm{d}T} = \frac{k_1 k_E}{(k_E + k_S)}\left(\frac{k_E + k_S}{k_E}\right)(E_\infty - E_T)$$

which reduces to

$$\frac{\mathrm{d}E}{E_\infty - E_T} = k_1 \mathrm{d}T$$

which integrates to $-\ln(E_\infty - E_T) = k_1 T + \text{constant}$. Since the alkene is the only absorbing species, then $\mathrm{OD}_\infty = \epsilon_E E l$ (OD is optical density), and the equation can be rewritten as

$$-\ln(\mathrm{OD}_\infty - \mathrm{OD}_E) = k_1 T + \text{constant}$$

Consequently the observed rate constant for alkene formation is, in fact, k_1 and the secondary β-deuterium isotope effect for carbocation formation is given by k_1^H/k_1^D.

The primary β-hydrogen–deuterium isotope effect for proton loss from the carbocation to give the alkene, k_E^H/k_E^D, can be determined from the product ratios. since

$$\frac{k_E^H}{k_S^H} = \frac{E^H}{S^H}$$

and

$$\frac{k_E^D}{k_S^D} = \frac{E^D}{S^D}$$

then

$$\frac{k_E^H}{k_E^D} = \frac{(\%E/\%S)_H}{(\%E/\%S)_D}$$

if the valid assumption is made that $k_S^H = k_S^D$.

It is seen that k_1^H/k_1^D varies between 1.16 ± 0.01 and 1.62 ± 0.03, while values for k_E^H/k_E^D vary between 1.6 ± 0.2 and 4.9 ± 2.0. In all cases the amount of alkene formed was decreased as a result of deuterium substitution at C_β; i.e. percent alkene was 55 ± 1.0 and 43 ± 1.0 for reaction of the 2-Me salt and its 2,2-d_2 analogue, respectively, while reaction of the 2,6-diMe compound and its 2,2-d_2 analogue led to values of percent alkene of 28 ± 1.0 and 11 ± 2.0, respectively. It is apparent, therefore, that a primary hydrogen–deuterium isotope effect is operative in the fast proton removal step. The values for the secondary β-deuterium isotope effects are consistent with literature values (38) for reactions proceeding by way of a slow rate-determining step involving carbocation formation, while the primary effects are reasonable in terms of the proposed mechanism where proton loss occurs in a fast step.

It appears from the data in Table 1 that the k_1^H/k_1^D values are significantly lower when the substrate has only one *ortho* substituent as compared to two, i.e. k_1^H/k_1^D = 1.22 ± 0.05 and 1.62 ± 0.03 found for reaction of the 2-Me and 2,6-diMe salts, respectively. As well, the magnitude of the primary β-hydrogen–deuterium isotope effect also is lower when the reactant has only one *ortho* substituent as compared to two, i.e. k_E^H/k_E^D = 1.6 ± 0.2 and 3.1 ± 1.0 found for reaction of the 2-Me and 2,6-diMe substrates, respectively. Although a comparison of the primary isotope effects, which are similar within experimental error, is difficult due to the error involved in the determination of the % alkene when elimination is a minor process, it may be concluded that the increase in the magnitude of the secondary β-deuterium effect is due to an increase in carbocation character at the transition state.

Secondary β-deuterium isotope effects of approximately 1.3 (for two hydrogens (deuteriums)) found in the present study are in accord with literature values found for other solvolytic reactions leading to carbocation formation (38–41). It is generally considered (38) that secondary β-deuterium isotope effects arise due to hyperconjugative assistance by the β-hydrogens to the formation of the carbocation. The magnitude of this isotope effect, in the absence of competing reactions, participation, ion-pairing, etc., depends on the ability of the β-CH(D) bond to overlap with the developing vacant orbital of an incipient carbocation at C_α. When they are orthogonal, a kinetic isotope effect of unity is expected (42, 43). Consequently, for the reaction under study where a normal secondary β-deuterium isotope effect is found, it appears that rotation is sufficiently free about the C_α—C_β bond to allow the required overlap.

As indicated earlier in the discussion section, the salts with only one *ortho* substituent react at a slower rate in ethanol but give a greater yield of elimination product, as compared to the reaction of the *ortho*-disubstituted compounds. As well, it was noted that a *para* substituent had a negligible effect on the solvolytic process, indicating the absence of a significant polar effect due to the alkyl groups. It appears, therefore, that the reaction of the ammonium salts in ethanol in the present investigation is promoted by "steric acceleration" due to the bulky trimethylammonium group (14, 44), leading to the favourable conversion of a tetrahedral carbon to a less crowded trigonal carbon. Dreiding stereomodels indicate considerable interaction between the *ortho* substituents and the 1,8 hydrogens on the fluorene ring as well as with the onium group. This supports the observation, Table 1, that the 2,6-diCl salt is less reactive than the 2,6-diMe compound but more reactive than the 2,4-diMe substrate since chlorine is "smaller" than methyl (Taft E_S steric substituent scale).

The accelerating effect of the relief of steric strain has been investigated by a series of workers for a variety of reactions (45–49). To our knowledge, however, the accelerating effect observed in the present study is only the second example (14) where a trialkylammonium salt (poor leaving group) undergoes solvolysis to give an alkene in an E1 process.

The observed variation of the alkene:ether ratio (% alkene) with the number of *ortho* substituents indicates that the alkene forming step (k_E) becomes less favourable relative to the competing ether forming step (k_S) for reaction of the di-*ortho*-

substituted compounds as compared to the reaction of the mono-*ortho*-substituted substrates. It is generally considered that, for reactions proceeding by way of a carbocation intermediate, the most important factor that determines the relative amount of elimination and substitution products is the stability of the alkene. The more stable the alkene the greater the amount of alkene product relative to the substitution product.

Extensive studies have been carried out on both the static and dynamic stereochemistry of "crowded" ethylenes (50–55) and it is now clear that bulky groups attached to the ethylenic carbons can lead to a twisting about the ethylene bond. Furthermore, it has been concluded (56, 57) that both 1,1-diphenylethylene and 9-diphenylmethylenefluorene **13**, which is related to the alkenes

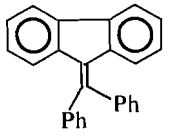

13

formed in the present study, have a phenyl group twisted out of the plane of the molecule due to steric interactions between the groups attached to the double bond. This is illustrated in **14** for the alkenes formed in the present study where the *ortho* methyl group "interacts" with the 1,8 hydrogens of the fluorene nucleus. The addition of a second *ortho* group to **14** (R^1 = CH_3) will lead to a further decrease in the planarity of the alkene, leading to decreased stability and hence a decrease in the percent alkene formed as observed.

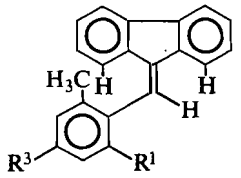

14

The proposal that the interaction between the *ortho* methyl groups with the 1,8 hydrogens on the fluorene nucleus leads to a decrease in the stability of the alkene receives support from uv spectroscopic data (see the experimental section). The λ_{max} values for the solutions of the *ortho*-substituted alkenes (obtained from compounds **4**–**9**) are the same within experimental error but are significantly lower[7] than those of the corresponding *para*-substituted alkenes where the *ortho* groups are hydrogens. The twisting of the aryl groups out of the plane of the double bond and the fluorenyl ring will lead to a decrease in the extent of conjugation and hence to higher energy electronic transitions. Such steric inhibition to effective conjugation has been observed in other systems (59, 60), where it was found that the conjugated 1,3 diene **15** did not have a uv maximum down to 200 nm whereas the structurally related conjugated diene **16** exhibited a more normal uv maximum at 232 nm.

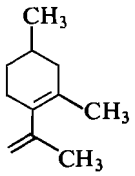

15

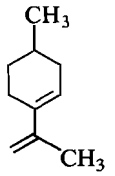

16

[7]P. J. Smith, D. S. K. Tsui, and G. S. Dyson. Unpublished results.

An alternative explanation for the changes in alkene:ether ratios effected by *ortho* substitution can be considered since it has been proposed that reaction to give the carbocation is induced by significant steric interactions in the substrate. The solvated carbocation can be neutralized by either proton loss from C_β with solvent acting as the base or by direct substitution of solvent to give the ether. Steric access of solvent to the carbocationic centre and the β-hydrogen could play a role in determining the relative amounts of the two products. This possibility will be discussed in the following section where the effect of solvent changes on both the rate of alkene formation and on product ratios is considered.

*Reaction of 9-(*ortho*-substituted phenylmethyl)fluoren-9-yltrimethylammonium ions in various solvents at 57.3°C*

A test for the carbocation mechanism proposed for the reaction of the *ortho*-substituted salts in ethanol, eq. [4], is determination of the effect of a change in the reaction medium on both reaction rate and product composition. Accordingly, the k_1 values for alkene formation as well as the percent alkene were determined for the reaction of three representative compounds, 2-Me, 2,6-diMe, and 2,4,6-triMe salts, in a variety of solvents, Table 3. The hydrogen–deuterium isotope effects, k_1^H/k_1^D and k_E^H/k_E^D, are also included.

It is seen that for reaction of all three substrates the amount of elimination product, % alkene, varies significantly when the alcohol solvent is changed; i.e. the percent alkene formed for reaction of the 2,6-diMe salt in ethanol, 2-propanol, and *tert*-butyl alcohol was 28, 52, and 100, respectively, while reaction of the 2-Me compound gave 43, 55, and 100% alkene for reaction in methanol, ethanol and *tert*-butyl alcohol, respectively. For reaction in all of the solvents studied, with the exception of the *tert*-butyl alcohol solvent where all the compounds gave exclusively the alkene product, the mono-*ortho* salt gave a greater percentage of alkene than the di-*ortho*-substituted compounds, in agreement with the results obtained for reactions in ethanol.

The increase in the amount of alkene formed when the solvent is varied from methanol to ethanol, 2-propanol, and *tert*-butyl alcohol can be attributed to an increase in the rate of proton abstraction as compared to the direct attack of solvent at the carbocationic centre. As the "size" of the alcohol molecule increases (primary < secondary < tertiary), the transition state for reaction proceeding to the ether products becomes more sterically crowded and, hence, of higher energy. This leads to a decrease in the amount of substitution relative to elimination.

Brown and Fletcher (61) were the first to suggest that steric effects are mainly responsible for the increase in olefin yields in reactions proceeding by way of a carbocation intermediate. They considered that since the trigonal carbocation is less strained than both the tetrahedral reactant and substitution product, an increase in the size of the groups attached to the reaction centre carbon would lower the rate of the substitution reaction relative to the elimination process.

With the *exception* of the results obtained for reaction in *tert*-butyl alcohol, the k_1 values for the reaction of the three compounds (**4**, **6**, and **8**) increased when the polarity of the alcohol solvent (as given by both *Y* and *Z* values) decreased. The k_1 values for reaction of the 2,6-diMe salt in 95% ethanol, ethanol, and 2-propanol were 212×10^{-5}, 294×10^{-5}, and 337×10^{-5} (s^{-1}), respectively. Similarly, the 2,4,6-triMe compound produced the alkene with rate constants of 245×10^{-5} and 297×10^{-5} (s^{-1}) for reaction in methanol and ethanol,

respectively. A study of the reaction of the 2-Me salt in 70% ethanol, 95% ethanol, methanol, and ethanol gave rate constants of 0.93×10^{-5}, 1.58×10^{-5}, 2.18×10^{-5}, and 2.35×10^{-5} (s^{-1}), respectively.

The observed trends in rate constants when the solvent is changed from methanol to the aqueous ethanol solutions, ethanol, and 2-propanol are predictable since the charged substrates, which will be solvated in the polar media, react via a transition state where there is charge dispersal. Consequently, reaction of a charged substrate proceeding via the rate-determining formation of a carbocation will proceed at a faster rate in a less polar solvent.

It was anticipated that the reaction of both the 2-Me and 2,6-diMe salts would proceed at the greatest rate in *t*-BuOH, the least polar solvent studied. However, the k_1 values were found to be the lowest in this solvent for reaction of both the 2-Me and 2,6-diMe compounds, Table 3. This unexpected effect of *tert*-butyl alcohol on the rate of reaction can perhaps be attributed to solvation effects. It has been suggested (8) that direct solvation of the positive nitrogen of the trimethylammonium group is unlikely, and that the interactions occur between solvent and the C—H dipoles induced by the positive nitogen. While *t*-BuOH and the other alcohol solvents can participate in this solvation, perhaps *t*-BuOH is less able to solvate the carbocationic intermediate for steric reasons.

In order to gain additional information concerning the reaction of the *ortho*-substituted salts, the thermodynamic activation parameters were determined for the reaction of the 2-Me, 2,6-diCl, and 2,6-diMe compounds in ethanol and also for the reaction of the 2,6-diMe substrate in 2-propanol. The appropriate rate constants and the percent alkene determined for reaction at three different temperatures along with values for E_A, $\Delta H^{\ddagger}$(60°C), and $\Delta S^{\ddagger}$(60°C) are given in Table 4. The Arrhenius plots all gave correlation coefficients better than 0.99.

The data in Table 4 indicate that the magnitude of $\Delta H^{\ddagger}$ decreases when a second *ortho* substituent is placed on the phenyl ring; $\Delta H^{\ddagger}$(60°C) = 36.2 and 29.6 kcal mol^{-1} for reaction of the 2-Me and 2,6-diMe substrates, respectively. As well, it is seen that the reaction of the 2,6-diMe salt (a charged substrate) has a lower enthalpy of activation when carried out in a solvent of decreased polarity; $\Delta H^{\ddagger}$(60°C) = 29.6 and 27.7 kcal mol^{-1} for reaction in absolute ethanol and 2-propanol, respectively. These results are consistent with the suggestion of steric acceleration promoting the ionization process via a charge-dispersed transition state.

The positive values for $\Delta S^{\ddagger}$ found for the reactions is consistent with reduced solvation at the transition state as compared with the initial state. A trend in $\Delta S^{\ddagger}$ is noted when the substrate is changed from 2-Me to 2,6-diCl to the 2,6-diMe compound for reaction in ethanol; $\Delta S^{\ddagger}$(60°C) = 29.9, 26.2, and 19.4 cal K^{-1} mol^{-1}, respectively. It may be concluded that reaction of the di-*ortho*-substituted compounds in ethanol are less entropically favoured due to decreased solvation of the ammonium ion for steric reasons. The change in the value $\Delta S^{\ddagger}$ when the solvent for the reaction of the 2,6-diMe compound is changed from ethanol to 2-propanol can be rationalized similarly, since 2-propanol will solvate the onium group to a lesser extent ($\Delta S^{\ddagger}$(60°C) = 13.7 and 19.4 cal K^{-1} mol^{-1} for the reaction of the 2,6-diMe salt in 2-propanol and ethanol, respectively).

The observed isotope effects, k_1^H/k_1^D, for reaction of the 2-Me, 2,6-diMe, and 2,4,6-triMe salts in the various solvents fall in the range between 1.1 and 1.7, Table 3. These values are consistent with the expected values for a secondary β-deuterium isotope effect associated with rate-determining carbocation formation. There does not appear to be a trend in the magnitude of these isotope effects for reaction of the three salts when the solvent is varied. The values for k_E^H/k_E^D lie in the range between 1.2 and 5.1. The error involved in the determination of these values does not allow a detailed discussion on the observed variations when the three substrates are reacted in the different solvents. It has been pointed out (62) that α- and β-deuterium effects in solvolytic reactions generally do not strongly depend on solvent changes.

As noted earlier, reaction of both the 2-Me and 2,6-diMe compounds in *tert*-butyl alcohol gave the alkene product in 100% yield. Consequently the values of k_1^H/k_1^D (the secondary β-deuterium isotope effect for slow rate-determining carbocation formation) of 1.24 and 1.57, for reaction of the 2-Me and 2,6-diMe compounds, appear to be significantly different. The difference between these two values indicates that the respective transition states for carbocation formation differ in the extent of positive charge developed at the 9-fluorenyl carbon and (or) that the extent to which the β-hydrogens can stabilize the developing charge by hyperconjugation is different (presumably for steric reasons).

*Reaction of 2-substituted-9-(*ortho*-substituted phenylmethyl)-fluoren-9-yltrimethylammonium ions in the aprotic solvent chloroform*

In order to further investigate the solvolytic reaction of the *ortho*-substituted compounds, it was decided to measure the rate of alkene formation for reaction of several substrates in the nonpolar aprotic solvent chlorform. It was reasoned that reaction in this nonpolar solvent would be favourable due to charge dispersal at the transition state for carbocation formation. Furthermore, reaction cannot proceed with solvent acting as either the base or nucleophile, and only the counterion, bromide, is capable of abstracting the β-hydrogen.

The rate of alkene formation, k_1, for reaction of the 2-Me, 2,6-diMe, and 2,4,6-triMe compounds was determined at 50°C in chloroform, Table 5, as well as the secondary β-deuterium isotope effects, k_1^H/k_1^D. In all cases the alkene was formed in 100 ± 5% yield. The present results are in contrast to earlier studies (63)[8] on the reaction of quaternary ammonium salts in chloroform, where substitution products were formed exclusively.

Reaction of the three salts in chloroform appears also, as in the other solvents, to proceed via the E1 mechanism. The observed ρ value of −2.3 and values of k_1^H/k_1^D = 1.47–1.88, which are unlikely to be primary effects, are consistent with reaction proceeding via a carbocation intermediate.

The variation in the k_1 values with changes in the *ortho* substituents follows the same trend for reactions of the salts in chloroform as in the other solvents. The observed rate constants for reaction of the di-*ortho*-substituted salts, 2,6-diMe and 2,4,6-triMe, at 50°C are 88.9×10^{-5} and 108×10^{-5} (s^{-1}), respectively, while the rate constant for reaction of the mono-*ortho*-substituted compound, 2-Me, is 0.76×10^{-5} (s^{-1}). Presumably, reaction in chloroform, as in the other solvents, is promoted by steric relief.

Reaction of the *ortho*-substituted salts in chloroform appears to be similar to that in the poorly solvating *tert*-butyl alcohol

[8]K. C. Westaway and H. Joly. Private communication.

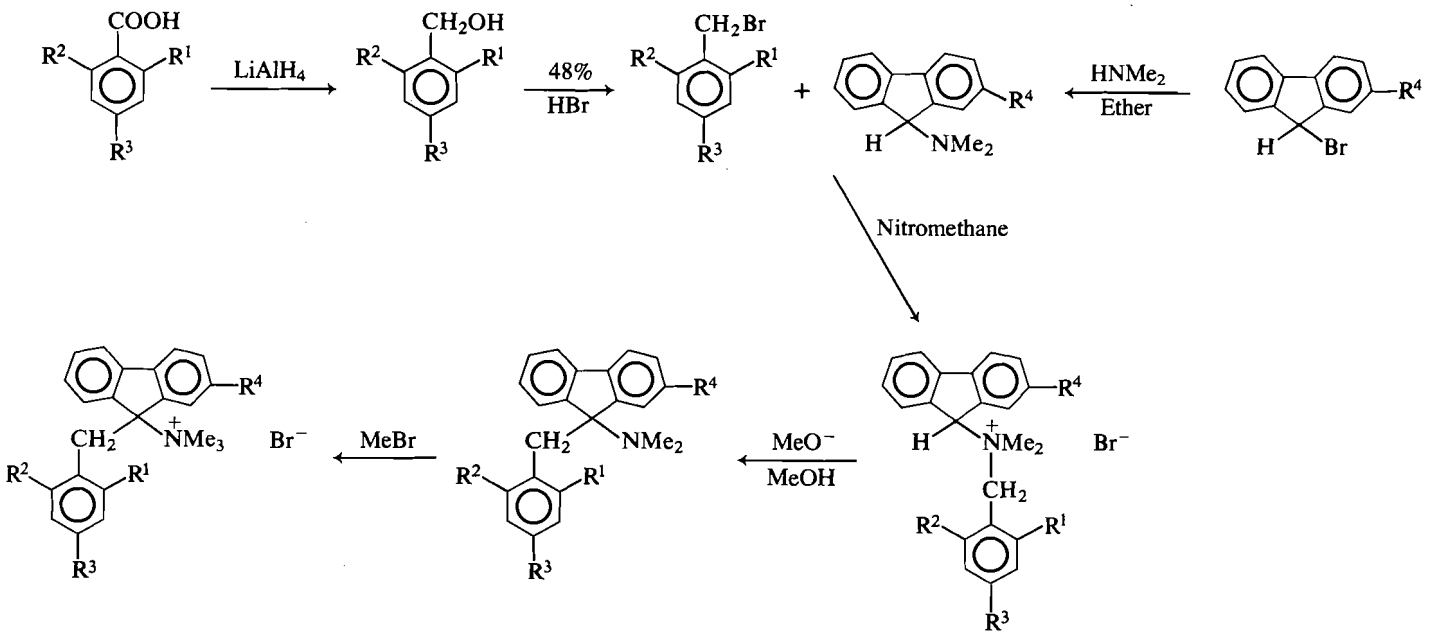

SCHEME 1. Synthetic route to 9-(*ortho*-substituted phenylmethyl)fluoren-9-yltrimethylammonium bromides.

solvent. This is reasonable since the onium group of the reactant and the developing carbocationic centre will be very poorly solvated in both solvents. Perhaps in chloroform the quaternary ammonium halides exist to a significant extent as ion pairs.

Experimental

Melting points are uncorrected. The ^1H nmr spectra were determined on a Varian T60 spectrometer. Mass spectra were obtained on an AEI M-12 mass spectrometer. Elemental analyses were carried out by the Guelph Chemical Laboratories, Guelph, Ontario, Canada. All reagents and solvents were reagent grade and were dried and purified by the usual procedures.

The synthetic pathways for most of the compounds in this study were similar and are outlined in Scheme 1. The deuterated substrates were all better than 95% deuterated since nmr and mass spectrometric analyses indicate complete deuteration.

Benzyl alcohols which were not commercially available and the α,α-dideuterated analogues of the benzyl alcohols were prepared by reduction of the corresponding benzoic acid or the methyl ester (65, 66).

2,6-Dimethylbenzyl alcohol

A solution of 2,6-dimethylbenzoic acid (80 g, 0.53 mol) in 500 mL of anhydrous diethyl ether was added to a slurry of $LiAlH_4$ (30 g, 0.79 mol) in 350 mL ether. After refluxing for 108 h the excess lithium aluminum hydride was destroyed using 30 mL water and 150 mL 10% sulphuric acid. The organic layer was separated and the aqueous layer washed three times with ether. The combined organic extracts were dried and evaporated to give 2,6-dimethylbenzyl alcohol, which was recrystallized from absolute ethanol; 77% yield, mp 80.5–81°C (lit. (67) mp 81–82°C).

2,6-Dimethylbenzyl bromide

2,6-Dimethylbenzyl alcohol (27.2 g, 0.2 mol) was refluxed with 48% HBr (105 g, 1.3 mol) for 5 h (58). After work-up, 35.9 g (0.18 mol) of 2,6-dimethylbenzyl bromide was obtained (90% yield). Since the nmr mass spectra showed no impurities and because of the extreme lachrymatory nature of the compound, it was used without further purification.

9-Fluorenyldimethylamine

Anhydrous dimethylamine gas was passed into an ice-cold solution of 49.4 g (0.2 mol) of 9-bromofluorene dissolved in 500 mL of anhydrous diethyl ether for 0.5 h. This mixture was stirred for a further 2 h and the resulting white precipitate was filtered off. The solvent was removed from the yellow filtrate using a rotary evaporator to give a solid, which on crystallization from *n*-hexane afforded pale yellow crystals (35.3 g, 0.17 mol) in 84% yield; mp 47.5–48°C; nmr and mass spectra confirmed the structure.

2,6-Dimethylphenylmethyl-9-fluorenyldimethylammonium bromide

A 10-mL solution of 18.5 g (0.093 mol) of 2,6-dimethylbenzyl bromide in nitromethane was added to a solution of 21 g (0.01 mol) of *N,N*-dimethylfluoren-9-ylamine in 20 mL of nitromethane. This mixture was stirred for 15 h and 200 mL of anhydrous diethyl ether was added to precipitate the salt. The white precipitate was filtered and dried and then recrystallized from ethanol–ether to give 29.3 g (0.072 mol) of pure compound in 78% yield, mp 169–170°C. The melting points of the various analogues of this compound are given in Table 6.

N,N-*Dimethyl-9-(2,6-dimethylphenylmethyl)fluoren-9-ylamine*

2,6-Dimethylphenylmethyl-9-fluorenyldimethylammonium bromide, 22.6 g (0.055 mol), was dissolved in 40 mL of methanol. Freshly cut metallic sodium, 4.6 g (0.2 mol), dissolved in 40 mL of methanol was added to the ammonium salt solution. This reaction mixture was stirred for 10 h at room temperature and then poured into 100 mL of water. This was extracted four times with 50-mL portions of chloroform. The combined organic extracts were dried over anhydrous $MgSO_4$ and rotary evaporated to give the crude amine, 17.2 g (0.053 mol) in 96% yield, mp 105–105.5°C. Repeated crystallization from 95% ethanol gave a pure white compound with satisfactory C, H, N analysis. The nmr and mass spectra confirmed the structure. The other *ortho*-substituted amines were similarly prepared by the Steven's rearrangement and the pertinent data is given in Table 7.

9,(2,6-Dimethylphenylmethyl)fluoren-9-yltrimethylammonium bromide

Pure *N,N*-dimethyl-9-(2,6-dimethylphenylmethyl)fluoren-9-ylamine, 2 g (0.0061 mol), was dissolved in 10 mL of sodium-dried benzene. This was refluxed with 20 mL of bromomethane at 0°C till turbidity was observed. The mixture was maintained at 5°C for a few days and the pure white solid was filtered off using a sintered glass funnel and washed three times with sodium-dried benzene (16% yield). Mass spectra and elemental analysis, Table 8, confirmed the structure.

2,6-Dimethylphenyldibenzofulvene

2,4-Dimethylbenzyltriphenylphosphonium bromide, 9.5 g (0.021 mol), prepared by Wittig's method (64), in 20 mL of dry benzene was

TABLE 6. The melting points of 2-substituted-9-fluorenyl-(*ortho*-substituted)-phenylmethyldimethylammonium bromides

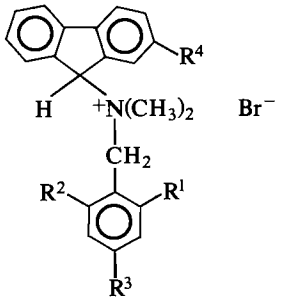

Compound		Melting point (°C)
$R^4 = H$	$R^1 = Me; R^2 = R^3 = H$	140–141
$R^4 = H$	$R^1 = R^3 = Me; R^2 = H$	120–121
$R^4 = H$	$R^1 = R^2 = Me; R^3 = H$	134–134.5
$R^4 = H$	$R^1 = R^2 = Cl; R^3 = H$	138–139
$R^4 = H$	$R^1 = R^2 = R^3 = Me$	116–119
$R^4 = Br$	$R^1 = R^2 = Me; R^3 = H$	220–222

stirred under nitrogen for 2 h with 3 g of sodium *tert*-butoxide. After the addition of 4 g (0.022 mol) of fluorenone in 50 mL of dry benzene the solution was stirred for another 2 h. The crude alkene obtained after work-up was separated on an alumina column (2 cm × 40 cm) using hexane as a solvent. The product was further purified by recrystallization from 95% ethanol, mp 165–165.5°C. The elemental analysis data for the above alkene and the related dibenzofulvenes are given in Table 9.

Kinetic measurements

The reactions were carried out in cuvettes with gas-tight covers inside a Bausch and Lomb Spectronic 710 instrument. The cuvette holder was linked to an external Haake FS circulator. The temperature of the water in the circulator was maintained at ±0.02°C. The temperature at which kinetic measurements were made was the actual temperature inside the cuvette, measured using a thermocouple attached to a digital thermometer. The fluctuations in the temperature in the cuvette were less than ±0.05°C.

Since the absorbance of the sample under study had to be directly measurable, the concentrations of the quaternary ammonium salt solution had to be appropriately adjusted. A stock solution of the compound under study was made using the dry ethanol (or the other solvents) at room temperature. These solutions were stored in the refrigerator and it was found that, except for the very reactive 2,6-diMe and the 2,4,6-triMe substrates, the storage did not affect the initial absorbance readings over a period of months.

Just before a kinetic run was initiated, the solution of the quaternary salt was brought to room temperature. A small amount was poured into a uv cell that had been rinsed with the solution. The tightly stoppered cuvette was fitted into the cuvette holder of the uv spectrometer and the timer started. A matched reference cell containing only the solvent was used to zero the absorbance before a reading was noted. In most cases the first reading was taken after at least 3 min so that the reaction mixture was in thermal equilibrium with the surroundings. The absorbance values were then taken at the appropriate time intervals. The reactions were generally followed up to 40–80% completion and at least three runs were made for each compound. Since it was not possible to measure more than one kinetic run at a time, the rates of reaction of the hydrogen and the deuterium substrates had to be measured consecutively within the least possible time.

The wavelength of the uv light used was fixed at 320 nm. It was determined that at this wavelength the product of the substitution reaction, the ether, did not have any significant absorption. Therefore, the change in the optical density that was monitored was due only to the increasing concentration of the alkene products.

The infinity readings were obtained by taking 5-mL aliquots of the initial salt solution in 10-mL volumetric flasks and filling to the mark. This was done in triplicate. These flasks were then lowered into an oil bath, which was maintained at the temperature of the reaction, and allowed to stand for at least 8–10 half-lives. These flasks were then withdrawn at different times and allowed to reach room temperature. If any solvent loss had occurred it was made up by addition of the pure solvent to the volumetric flask. A sample of this solution was used to measure the absorbance, which was the value at infinite time. This was repeated with the other two flasks. The infinity reading was taken as the average of the three readings. Using this average value of absorbance at infinite time, $\ln (A_\infty - A_t)$ was plotted versus time to obtain good linear first-order plots. At least three such plots for each compound were obtained. The experimentally obtained data were treated by least-squares analysis to determine the first-order rate constants using a HP 200A computer.

The *ortho*-substituted phenyldibenzofulvene solutions in the various solvents were used to determine values of the extinction coefficients at various wavelengths, Table 10. These extinction coefficients and the absorbance at infinite time were used to calculate the percent alkene formed in the reaction.

TABLE 7. The melting points and elemental analysis of the 9-(*ortho*-substituted phenylmethyl)fluoren-9-yldimethylamines

Compound		Melting point (°C)	Elemental analysis		
			C	H	N
$R^4 = H$	$R^1 = Me; R^2 = R^3 = H$	87–87.5	88.38 (88.14)	7.35 (7.40)	4.37[a] (4.47)[b]
$R^4 = H$	$R^1 = R^3 = Me; R^2 = H$	74.5–75	87.72 (88.03)	7.91 (7.70)	4.17 (4.28)
$R^4 = H$	$R^1 = R^2 = Me; R^3 = H$	105–105.5	87.96 (88.03)	7.58 (7.70)	4.11 (4.28)
$R^4 = H$	$R^1 = R^2 = Cl; R^3 = H$	135–135.5	71.62 (71.75)	5.14 (5.20)	3.72 (3.80)
$R^4 = H$	$R^1 = R^2 = R^3 = Me$	112–112.5	87.88 (87.93)	8.10 (7.97)	4.08 (4.10)
$R^4 = Br$	$R^1 = R^2 = Me; R^3 = H$	128.5–129	71.09 (70.94)	5.77 (5.95)	3.61 (3.45)

[a]Experimentally observed values.
[b]Theoretical values.

TABLE 8. Elemental analysis of the 9-(*ortho*-substituted phenylmethyl)-fluoren-9-yltrimethylammonium bromides

Compound number	C, H, N analysis		
	C	H	N
4	70.21	6.60	3.21[a]
	(71.09)	(6.68)	(3.32)[b]
4-d_2	69.94	6.60	3.38
	(70.75)	(7.12)	(3.30)
5	59.63	4.79	3.02
	(59.95)	(4.97)	(2.93)
5-d_2	59.54	5.23	3.11
	(59.38)	(5.20)	(3.01)
6	70.40	6.38	3.37
	(70.59)	(6.42)	(3.43)
6-d_2	69.12	6.71	3.37
	(70.24)	(6.88)	(3.41)
7	70.80	6.71	3.23
	(71.09)	(6.88)	(3.32)
7-d_2	70.30	7.00	3.35
	(70.75)	(7.12)	(3.30)
8	70.92	7.11	3.28
	(71.55)	(6.93)	(3.21)
8-d_2	68.69	7.00	3.66
	(71.23)	(7.36)	(3.20)
9	71.09	5.77	3.61
	(70.94)	(5.95)	(3.45)

[a]The top row numbers refer to the experimental value.
[b]These figures refer to theoretical values.

TABLE 9. The melting points and elemental analysis of the *ortho*-substituted phenyldibenzofulvenes

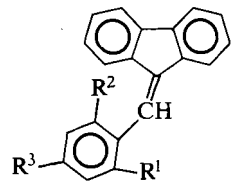

Substituent	Melting point (°C)	Elemental analysis
2-Me	110.5–111.5	C 93.84, H 5.94[a] (C 93.99, H 6.01)[b]
2,4-diMe	88–88.5	C 92.51, H 6.42 (C 93.62, H 6.38)
2,6-diMe	165–165.5	C 93.27, H 6.39 (C 93.62, H 6.38)
2,6-diCl	123–125.5	C 74.55, H 3.78 (C 74.32, H 3.74)
2,4,6-triMe	115.5–116	C 93.53, H 6.49 (C 93.20, H 6.80)

[a]Experimentally observed values.
[b]Theoretical values.

TABLE 10. The ultraviolet absorption data for the *ortho*-substituted phenyldibenzofulvenes in ethanol

Substituent	λ_{max} (nm)	Molar extinction coefficient at λ_{max} ($\times 10^{-4}$)	Molar extinction coefficient at 320 nm ($\times 10^{-4}$)
2-Me	311	1.36	1.20
2,6-diMe	310	1.16	0.753
2,4-diMe	311	1.37	1.36
2,4,6-triMe	309	1.52	1.08
2,6-diCl	310	1.39	0.868

Kinetic measurements by nuclear magnetic resonance method

The rates of reaction of the 2-Me, 2,6-diMe, and the 2,4,6-triMe substrates and the β-d_2 analogues of the 2,6-diMe and the 2,4,6-triMe compounds in chloroform at 50°C were determined by following the disappearance of appropriate hydrogen signals using a nmr spectrometer.

A dilute solution of the ammonium salt in $CDCl_3$ was prepared at room temperature and immediately placed in the probe of a Brüker WP-80 spectrometer maintained at 50°C. Several peaks in the spectrum (usually the peaks due to the hydrogen of the $—N^+(CH_3)_3$ and the ring methyl groups) were integrated at suitable times using chloroform as an internal standard. The slope of the plot of log (integral of the appropriate peak) against time was determined by least squares. The rate constants determined by monitoring the disappearance of several different hydrogen signals agreed to within 5% in all cases.

Acknowledgement

The authors gratefully acknowledge the financial support of this work by the Natural Sciences and Engineering Research Council of Canada.

1. W. H. SAUNDERS, JR. and A. F. COCKERILL. Mechanisms of elimination reactions. Wiley–Interscience, New York. 1973.
2. P. J. SMITH and A. N. BOURNS. Can. J. Chem. **52**, 749 (1974).
3. K. C. BROWN, F. J. ROMANO, and W. H. SAUNDERS, JR. J. Org. Chem. **46**, 4242 (1981).
4. P. J. SMITH and K. C. WESTAWAY. *In* The chemistry of amines, nitroso and nitro compounds. Supplement F. *Edited by* S. Patai. John Wiley and Sons Ltd., New York. 1982. p. 1261.
5. S. L. WU and P. J. SMITH. Can. J. Chem. **59**, 3016 (1981).
6. A. N. BOURNS and A. C. FROSST. Can. J. Chem. **48**, 133 (1970).
7. W. H. SAUNDERS, JR. Chem. Scr. **8**, 27 (1975).
8. D. E. LEWIS, L. B. SIMS, H. YAMATAKA, and J. MCKENNA. J. Am. Chem. Soc. **102**, 7411 (1980).
9. P. J. SMITH and A. N. BOURNS. Can. J. Chem. **48**, 125 (1970).
10. P. J. SMITH. *In* Isotopes in organic chemistry. Vol. 2. *Edited by* C. C. Lee and E. Buncel. Elsevier, Amsterdam. 1977. p. 39.
11. A. C COPE and A. S. MEHTA. J. Am. Chem. Soc. **85**, 1949 (1963).
12. A. F. COCKERILL and R. G. HARRISON. *In* The chemistry of double-bonded functional groups. *Edited by* S. Patai. Wiley, New York. 1977.
13. R. LEDGER, A. J. SMITH, and J. MCKENNA. Tetrahedron, **20**, 2413 (1964).
14. E. D. HUGHES and J. WILBY. J. Chem. Soc. 4094 (1960).
15. E. R. THORNTON. J. Am. Chem. Soc. **89**, 2915 (1967).
16. D. A. WINEY and E. R. THORNTON. J. Am. Chem. Soc. **97**, 3102 (1975).
17. R. A. MORE O'FERRALL. J. Chem. Soc. B, 274 (1970).
18. D. A. JENCKS and W. P. JENCKS. J. Am. Chem. Soc. **99**, 7948 (1977).
19. G. S. DYSON and P. J. SMITH. Can. J. Chem. **54**, 2339 (1976).
20. A. F. COCKERILL. Tetrahedron Lett. 4913 (1969).

21. P. SCHMID and A. N. BOURNS. Can. J. Chem. **53**, 3513 (1975).
22. C. J. M. STIRLING. Acc. Chem. Res. **12**, 198 (1979).
23. B. ISSARI and C. J. M. STIRLING. J. Chem. Soc. Perkin Trans. 2, 1043 (1984).
24. A. THIBBLIN. Chem. Scr. **15**, 121 (1980).
25. J. R. GANDLER and T. YOKOYAMA. J. Am. Chem. Soc. **106**, 130 (1984).
26. W. H. SAUNDERS, JR., D. G. BUSHMAN, and A. F. COCKERILL. J. Am. Chem. Soc. **90**, 1775 (1975).
27. S. ALUNNI and W. P. JENCKS. J. Am. Chem. Soc. **102**, 2052 (1980).
28. J. R. KEEFFE and W. P. JENCKS. J. Am. Chem. Soc. **103**, 2457 (1981).
29. J. R. GANDLER and W. P. JENCKS. J. Am. Chem. Soc. **104**, 1937 (1982).
30. J. R. KEEFFE and W. P. JENCKS. J. Am. Chem. Soc. **105**, 265 (1983).
31. J. PRADHAN and P. J. SMITH. Can. J. Chem. **59**, 911 (1981).
32. J. PRADHAN and P. J. SMITH. Tetrahedron Lett. **23**, 611 (1982).
33. E. A. CHANDROSS and C. F. SHELEY, JR. J. Am. Chem. Soc. **90**, 4345 (1968).
34. D. BETHEL, P. N. CLARE, and G. J. HARE. J. Chem. Soc. Perkin Trans. 2, 1889 (1983).
35. G. A. OLAH, G. K. S. PRAKASH, G. LIANG, P. W. WESTERMAN, K. KUNDE, J. CHANDRASEKHAR, and P. v. R. SCHLEYER. J. Am. Chem. Soc. **102**, 4485 (1980).
36. (*a*) A. LEDWITH and D. G. MORRIS. J. Chem. Soc. 508 (1964); (*b*) G. W. COWELL, A. LEDWITH, and D. G. MORRIS. J. Chem. Soc. B, 695 (1967); 697 (1967); (*c*) G. W. COWELL, T. D. GEORGE, A. LEDWITH, and D. G. MORRIS. J. Chem. Soc. B, 1169 (1966).
37. E. C. FRIEDRICH and D. B. TAGGART. J. Org. Chem. **43**, 805 (1978).
38. L. MELANDER and W. H. SAUNDERS, JR. Reaction rates of isotopic molecules. Wiley–Interscience, New York. 1980. Chapt. 6.
39. V. J. SHINER, JR. *In* Isotope effects in chemical reactions. *Edited by* C. J. Collins and N. S. Bowman. Van Nostrand–Reinhold, New York. 1970. Chapt. 2.
40. K. L. SERVIS and F. SHUE. J. Am. Chem. Soc. **102**, 7233 (1980).
41. J. S. LOMAS. J. Org. Chem. **46**, 412 (1981).
42. H. MASKILL. J. Chem. Soc. Perkin Trans. 2, 1889 (1976).
43. H. SIEHL and H. WALTER. J. Am. Chem. Soc. **106**, 5355 (1984).
44. F. LARKIN and R. A. MORE O'FERRALL. Aust. J. Chem. **36**, 1831 (1983).
45. H. C. BROWN and M. RAVINDRANATHAN. J. Am. Chem. Soc. **100**, 1865 (1978).
46. A. J. KIRBY and C. L. LOGAN. J. Chem. Soc. Perkin 2, 642 (1978).
47. K. LIU and M. KUO. Tetrahedron Lett. 355 (1985).
48. H. C. BROWN, S. IKEGAMI, and D. L. VANDER JAGT. J. Org. Chem. **50**, 1165 (1985).
49. K. B. WIBERG and R. R. SQUIRES. J. Am. Chem. Soc. **103**, 4473 (1981).
50. S. E. BIALI and Z. RAPPOPORT. J. Am. Chem. Soc. **106**, 477 (1984).
51. S. E. BIALI, G. DEPKE, Z. RAPPOPORT, and H. SCHWARZ. J. Am. Chem. Soc. **106**, 496 (1984).
52. L. ANDERSEN, U. BERG, and I. PETTERSSON. J. Org. Chem. **50**, 493 (1985).
53. M. BALLESTER, J. CASTAÑER, J. RIERA, G. DE LA FUENTE, and M. CAMPS. J. Org. Chem. **50**, 2287 (1985).
54. I. ARGRANAT and Y. TAPUHI. J. Am. Chem. Soc. **101**, 665 (1979).
55. M. KAFTORY, Y. APELOIG, and Z. RAPPOPORT. J. Chem. Soc. Perkin Trans. 2, 29 (1985).
56. J. E. DUBOIS and W. V. WRIGHT. Tetrahedron Lett. 3101 (1967).
57. M. RABINOVITZ, I. AGRANAT, and E. D. BERGMANN. J. Chem. Soc. B, 1281 (1967).
58. O. KAMM and C. S. MARVEL. Org. Synth. Coll. Vol. **1**, 25 (1941).
59. J. WAOLINSKY and D. CHAN. J. Am. Chem. Soc. **85**, 937 (1967).
60. D. A. LIGHTNER and B. V. CHRIST. Tetrahedron, **37**, 685 (1981).
61. H. C. BROWN and R. S. FLETCHER. J. Am. Chem. Soc. **72**, 1223 (1950).
62. V. J. SHINER, JR., D. A. NOLLEN, and K. HUMSKI. J. Org. Chem. **44**, 2108 (1979).
63. E. C. F. KO and K. T. LEFFEK. Can. J. Chem. **50**, 1297 (1972).
64. G. WITTIG and U. SCHOELLKOPF. Org. Synth. **40**, 66 (1960).
65. E. L. ELIEL, V. G. BADDING, and M. N. RERICK. J. Am. Chem. Soc. **84**, 2371 (1962).
66. O. H. WHEELER and J. L. MATEOS. Can. J. Chem. **36**, 1483 (1958).
67. N. LOFGREN and U. RANASSON. Acta. Chem. Scand. **17**, 1256 (1963).

Preparation of deuterium labelled styrenes and divinylbenzenes

NICK HENRY WERSTIUK AND GEORGE TIMMINS
Department of Chemistry, McMaster University, Hamilton, Ont., Canada L8S 4M1
Received October 18, 1985
This paper is dedicated to Professor Arthur N. Bourns

NICK HENRY WERSTIUK and GEORGE TIMMINS. Can. J. Chem. **64**, 1072 (1986).

Specifically deuteriated styrenes (1-*d*, 2,2′-d_2, and ring labelled), perdeuteriostyrene, and specifically deuteriated divinylbenzenes (1,1′-d_2, 2,2,2′,2′-d_4, and ring labelled) have been prepared by transforming suitably labelled phenylacetic (hydride or deuteride reduction and dehydration by solid KOH) and phenylenediacetic acids (esterification, hydride or deuteride reduction, and dehydration by solid KOH), respectively.

NICK HENRY WERSTIUK et GEORGE TIMMINS. Can. J. Chem. **64**, 1072 (1986).

On a préparé des styrènes deutérés d'une façon spécifique (*d*-1, d_2-2,2′ et marqué sur le cycle), du perdeutérostyrène et des divinylbenzènes deutérés d'une façon spécifique (d_2-1,1′,d_4-2,2,2′,2′ et marqué sur le cycle) en transformant respectivement d'acides phénylacétiques (réduction par l'hydrure ou le deutérure et déshydratation par le KOH solide) ou phénylènediacétiques (estérification, réduction par l'hydrure ou le deutérure et déshydratation par le KOH solide) marqués d'une façon appropriée.
[Traduit par la revue]

Introduction

The high temperature – dilute acid (HTDA) method has been used to prepare a wide range of deuteriated and tritiated organic compunds (1–8). In this paper we document its application to the preparation of deuteriated styrenes and divinylbenzenes (DVB's) that were required for solid-state ^{2}Hmr studies of cross-linked styrene polymers (9). Although initial studies established that styrene can be labelled directly at the 2-position under HTDA conditions (*vide infra*), it is not a viable route due to production of dimers and oligomers. Consequently, a general route to the specifically labelled styrenes was developed based on the H–D exchange of phenylacetic acid (PAA). To prepare specifically labelled divinylbenzenes (DVB's), phenylenediacetic acid (PDA) was used as a substrate.

Results and discussion

Attempted direct exchange of styrene and divinylbenzene

When styrene was reacted under HTDA conditions at 165°C, it was found that full equilibration of the C-2 hydrogens with the deuterium pool could be achieved. Unfortunately, although small amounts of styrene-2,2-d_2 (**1***b*) could be isolated by preparative gas chromatography (gc), it appeared that most of the styrene was lost as dimers and oligomers, making this route viable only for preparing **1***b* in relatively small amounts. Treatment of DVB under HTDA conditions resulted in rapid production of polymer, as expected, and this direction was pursued no further.

Preparation of deuteriated styrenes

Since direct deuteriation of styrene and DVB[1] was inefficient, PAA and PDA were selected as precursors. Labelled PAA **1***f* (1.90 excess D per molecule) was prepared from **1***e* by refluxing it twice in 1.3 *M* DCl/D_2O. Reduction of this product by LAH, followed by elimination of water by KOH, gave styrene-1-*d* (**1***a*) that contained 0.75 excess D atoms over natural abundance. The ^{2}Hmr spectrum of **1***a* showed signals at 6.6 and 2.7 ppm (<1%), the latter peak indicating that <0.5% of starting material was present. That **1***a* contined substantially less deuterium than expected (1.90/2), based on the deuterium content of the precursor PPA **1***f*, indicates that D–H exchange

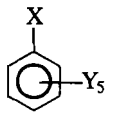

1

a X = CD=CH_2; Y = H
b X = CH=CD_2; Y = H
c X = CH=CH_2; Y = D
d X = CD=CD_2; Y = D
e X = CH_2CO_2H; Y = H
f X = CD_2CO_2H; Y = H
g X = CD_2CO_2H; Y = D
h X = CH_2COH_2; Y = D
i X = CD_2CH_2OH; Y = H
j X = CH_2CD_2OH; Y = H
k X = CH_2CH_2OH; Y = D
l X = CD_2CD_2OH; Y = D

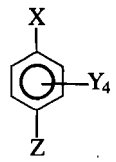

2

a X = Z = CD=CH_2; Y = H
b X = Z = CH=CD_2; Y = H
c X = Z = CH=CH_2; Y = D
d X = Z = CH_2CO_2H; Y = H
e X = Z = CD_2CO_2H; Y = H
f X = Z = CD_2CO_2H; Y = D
g X = Z = CH_2CO_2H; Y =D
h X = Z = CH_2CO_2Et; Y = H
i X = Z = CD_2CO_2Et; Y = H
j X = Z = CH_2CO_2Et; Y = D
k X = Z = CD_2CH_2OH; Y = H
l X = Z = CH_2CD_2OH; Y = H
m X = Z = CH_2CH_2OH, Y = D

competes with elimination. Nevertheless, back exchange can be minimized by using KOD and the O–D labelled alcohol.

When PAA was heated at 260°C in 0.26 *M* HCl/D_2O and recycled in 0.26 *M* DCl/D_2O, perlabelled acid **1***g* was obtained. Back exchange at the 2-position by KOH/H_2O (11) yielded ring-deuteriated acid **1***h*. LAH reduction, followed by elimination of water, gave **1***c* that contained 4.75 excess D atoms per molecule. The ^{2}Hmr spectrum of **1***c* exhibited a signal at 7.2 ppm and it was ascertained that <5% of starting alcohol was present.

Reduction of perlabelled PAA **1***g* by LAD, followed by elimination of water from **1***l*, yielded **1***d* (7.17 excess D atoms per molecule). It is evident from the ^{2}Hmr spectrum of **1***d* (Fig. 1) that a substantial amount (~25%) of D–H exchange occurred at the 1-position, as was observed in the preparation of **1***a*.

Reduction of PAA by LAD, followed by elimination of water, gave **1***b* (1.99 excess D atoms per molecule). The ^{2}Hmr spectrum of **1***b* exhibited signals at 5.1 and 5.6 ppm and no signals due to starting alcohol.

Preparation of deuteriated divinylbenzenes

Treatment of PDA **2**d with KOH/D_2O at 160°C yielded PDA-1,1,1′,1′-d_4 (**2***e*), and ^{1}Hmr analysis established that

[1]The commercially available material was a mixture of DVB, diethylbenzene, and the half-dehydrogenated compound.

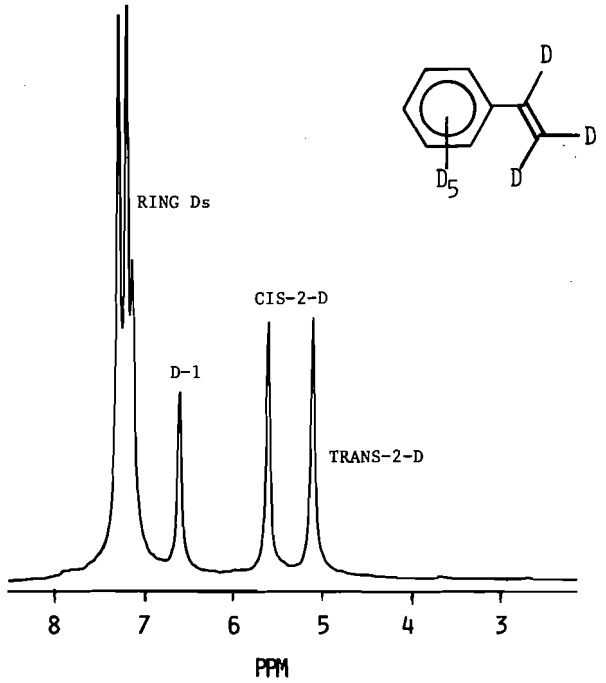

FIG. 1. The ^{2}Hmr (38.4 MHz) spectrum of styrene-d_8 in $CHCl_3$.

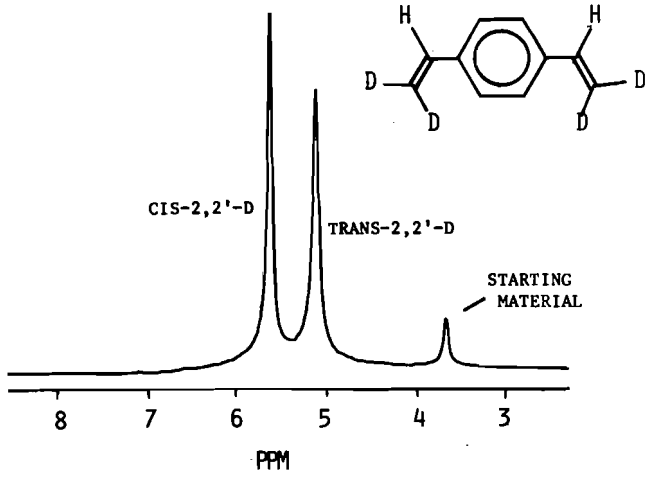

FIG. 2. The ^{2}Hmr (38.4 MHz) spectrum of divinylbenzene-2,2,2′, 2′-d_4 in $CHCl_3$.

exchange was >95% complete. Since direct reduction of the diacid proved to be unsatisfactory, the diethyl ester was prepared and reduced to **2***k* by LAH. KOH-promoted elimination of water from **2***k* gave DVB-1,1′-d_2 (**2***a*) (1.39 excess D per molecule). As observed in the preparation of styrene-1-*d*, **2***k* contained less deuterium (1.39 D) than expected (1.90 D) on the basis of the labelled PDA **2***e* (~3.8 D). As in the case of 2-phenylethanol, D–H exchange competes with elimination of water from **2***k*. The ^{2}Hmr spectrum of **2***a* exhibited signals at 6.6 and 2.8 ppm (6%), the latter establishing that the product contained 3% starting material.

At 260°C in 0.26 *M* DCl/D_2O **2***d* was perlabelled. Following back-exchange in aqueous KOH, the acid was converted, as described above, to DVB **2***c* (3.62 excess D atoms per molecule). The ^{2}Hmr spectrum of **2***c* showed, in addition to an intense signal at 7.4 ppm, weak signals at 7.2 (<5%) and 2.7 (<1%) due to starting material. A weak signal (<1%) at 6.7 indicated that a small amount of deuterium was located at the 1,1′-positions of **2***c*.

DVB-2,2,2′,2′-d_4 (**2***b*) (3.89 excess D atoms per molecule) was prepared by reducing diethyl ester **2***h* by LAD and eliminating water from **2***l* in the usual manner. The ^{2}Hmr spectrum (Fig. 2) of **2***b* indicates (signal at 3.7 ppm) that the product contains approximately 6% of **2***l*. The presence of 3–6% of starting material in the DVB's is due to the fact that it was necessary to carry out the elimination reactions at reduced pressure to minimize polymerization.

Conclusions

This study establishes that phenylacetic acid and phenylenediacetic acid are convenient starting materials for the preparation of specifically deuteriated styrenes and *p*-divinylbenzenes as well as the perlabelled compounds, even though the yields of the dehydration steps are modest as a consequence of the reactivity of the compounds. Although styrene-1,2,2′-d_3 was not prepared, its synthesis from PAA would be a simple matter. It should be possible to prepare a wide range of deuteriated substituted styrenes and the isomeric divinylbenzenes using the methodology documented in this paper. Furthermore, the corresponding tritiated compounds can be prepared using this approach as well.

In conclusion, we wish to comment on the facile elimination of water from the alcohols by solid KOH. Although base-promoted dehydration of alcohols is not discussed in general organic chemistry texts, it appears that it may be a very useful method for dehydrating fairly high-boiling alcohols that have an acidic hydrogen β to the hydroxyl group.

Experimental

Mass spectral deuterium analyses were carried out with a VG Micromass 7070F spectrometer at low ionizing voltage (12–15 eV) to minimize fragmentation. The nmr spectra were obtained on Varian EM-390 and Brüker WM-250 spectrometers; gc analyses were performed on a Tracor Model 560 gas chromatograph with a Varian Model 485 electronic integrator using a 6 ft × 4 mm id 3% OV-1 on 100–120 mesh Supelcoport column. For preparative gc a Varian A-700 gas chromatograph fitted with a 5 ft × 1/4 in. 15% SE-30 on 80–100 mesh Chromosorb W column was used. Ether for the hydride reductions was dried by distillation from LAH.

H–D exchange of styrene

Styrene (0.20 g), decalin (2 mL), and 0.26 *M* DCl/D_2O (5 mL) were sealed under vacuum in a medium-walled glass tube after degassing by three freeze–pump–thaw cycles. The tube was sealed in a Parr high pressure apparatus containing water to equalize pressure, and was heated at 165°C for 12 h. The organic solution was decanted from the frozen aqueous layer and styrene collected by preparative gc (5 ft × 1/4 in. 15% SE-30 on 80–100 mesh Chromosorb W). Mass spectral analysis indicated the incorporation of 1.94 excess D atoms per molecule (0.7% d_0, 4.3% d_1, 95.1% d_2); ^{1}Hmr ($CDCl_3$) showed that the C-2 Hs had been fully exchanged (δ:6.72 (m, H-1), 7.2–7.5 (m, aromatic Hs)). Gas chromatographic analysis indicated the presence of substantial amounts (~35%) of dimeric products; gc analysis of styrene was found to be inconsistent and unreliable, presumably due to reactivity of styrene on the column and injector block.

An attempt to distill styrene from a large-scale reaction (4.2 g styrene) resulted in the collection of no styrene. Using decalin as an internal standard, gc analysis indicated that only ~20% of the styrene was left in the product with dimeric material comprising ~10% more.

Phenylacetic acid-1,1-d_2 (**1***f*)

Phenylacetic acid (12.0 g) was refluxed for 142 h in 2.6 *M* HCl/D_2O (50 mL), the product was extracted with ether (50 mL, 3 × 20 mL), dried over anhydrous Na_2SO_4, and solvent removed on a roto-

evaporator to yield 11.8 g of **1***f* (97%, 1.57 excess D per molecule). This product (11.8 g) was then refluxed with 1.3 *M* DCl/D_2O (50 mL) for 72 h and extracted as above (yield 11.6 g, 98%; 1.90 excess D atoms per molecule).

Phenylethanol-2,2-d_2 (**1**i)

Phenylacetic acid-2,2′-d_2 (11.6 g) in dry ether (100 mL) was slowly added to a magnetically stirred slurry of LAH (3.0 g) in dry ether (100 mL) and refluxed for 2 h. More LAH (0.5 g) was added and reflux continued for 3 h. The reaction was quenched by careful addition of water (75 mL), then was acidified with concentrated HCl until most of the solid dissolved. The aqueous layer was saturated with NaCl and extracted with ether (4 × 40 mL) after removal of the organic layer. The extracts were washed with saturated aqueous $NaHCO_3$, dried over anhydrous Na_2SO_4, and filtered. The ether was removed by distillation through a 25-cm glass helices column and the last traces were removed under rotatory-pump vacuum to yield 9.9 g (95%) of **1***i*.

*Styrene-1-*d (**1**a)

Phenylethanol-2,2-d_2 (9.9 g) was heated with KOH pellets (4.3 g) (10) and styrene was rapidly distilled through a 15-cm Vigreux column into a Dry Ice – acetone cooled flask. Styrene-1-*d* was separated from water and dried over anhydrous Na_2SO_4 (yield 2.9 g, 35%). A considerable amount of polymer was produced. Mass spectral analysis indicated incorporation of 0.75 excess D atoms per molecule (27.5% d_0, 70.2% d_1, and 2.0% d_4 species) and ^{2}Hmr ($CHCl_3$) showed two resonances at 6.6 and 2.7 ppm (<1%). This analysis was confirmed by ^{1}Hmr ($CDCl_3$), δ:5.21 (m, *trans*-H-2), 5.72 (m, *cis*-H-2), 6.69 (q, H-1, po.3H), 7.1–7.5 (m, aromatic Hs).

Phenylacetic acid-d_7 (**1**g)

Phenylacetic acid (13.5 g) was heated at 260°C with 0.26 *M* HCl/D_2O (100 mL) for 72 h in a 600-mL Parr high pressure apparatus containing a glass liner. The product was extracted with ether (100 mL, 4 × 50 mL), the extracts were washed with saturated aqueous NaCl (25 mL), ether was removed on a roto-evaporator, and the remaining solvent was removed under vacuum to yield 11.2 g (83%) of **1***g*. The partially deuterated phenylacetic acid (10.9 g) was reacted with 0.26 *M* DCl/D_2O (100 mL) using the same procedure (yield 9.5 g, 87%). Mass spectral analysis showed the presence of 6.81 excess D atoms per molecule (0.5% d_4, 4.0% d_5, 20.2% d_6, 64.3% d_7, 11.0% d_8). The results indicate that not all of the carboxyl deuterons were exchanged during the work-up procedure.

Phenylacetic acid-d_5 (**1**h)

The deuteriated phenylacetic acid obtained above (9.2 g) was back-exchanged (11) by heating with H_2O (50 mL) and KOH (4.1 g) in a 600-mL Parr high pressure apparatus at 160°C for 24 h. The solution was acidified with concentrated HCl and extracted with ether (100 mL, 4 × 25 mL). The extracts were washed with saturated aqueous NaCl (25 mL), dried over anhydrous Na_2SO_4, decolorized with carbon, and the ether was stripped on a roto-evaporator and pumped off under vacuum to yield 9.0 g (98%) of **1***h*. Mass spectral analysis indicated that 4.9 excess D atoms per molecule remained (1.5% d_3, 16.6% D_4, 72.5% d_5, 7.9% d_6, 1.5% d_7); ^{1}Hmr ($CDCl_3$) confirmed that back exchange was essentially complete (δ:3.62 (2, H-2), 7.3–7.4 (residual aromatic Hs), 11.8 (s, —O—H).

Phenylethanol-d_5 (**1**k)

Phenylacetic acid-d_5 (8.9 g) in dry ether (150 mL) was added slowly to a magnetically stirred suspension of LAH (1.2 g) in dry ether (50 mL) and the mixture was refluxed for 5 h. The reaction was quenched by careful addition of water (75 mL), then acidified with concentrated HCl until the precipitates were disolved. After separation of the ether, the solution was further extracted with ether (5 × 20 mL), and the extracts were dried over anhydrous Na_2SO_4 and decolorized with carbon. The ether was stripped on a roto-evaporator and the remainder was removed under vacuum to yield 6.5 g (81%) of **1***k*; ^{1}Hmr ($CDCl_3$), δ:2.80 (t, H-1), 3.60 (s, —O—H), 3.80 (t, H-2), 7.3 (residual aromatic Hs).

Styurene-d_5 (**1**c)

Phenylethanol-d_5 (5.7 g) was heated with KOH (3.2 g, pellets) and styrene rapidly distilled through a 15-cm Vigreux column into a flask cooled in Dry Ice – acetone. The styrene was separated from water and dried over anhydrous Na_2SO_4 to yield 3.2 g (65%) of **1***c*. Mass spectral analysis indicated the presence of 4.75 excess D atoms per molecule (0.6% d_2, 4.0% d_3, 19.4% d_4, 72.1% d_5, 3.8% d_6, 0.1% d_7); ^{2}Hmr ($CHCl_3$) showed a resonance at 7.2 ppm; ^{1}Hmr ($CDCl_3$), δ:5.21 (d, *trans*-H-2), 5.72 (d, *cis*-H-2), 6.73 (q, H-1), 7.3 (residual aromatic Hs).

Phenylethanol-d_9 (**1**l)

To a slurry of LAD (3.0 g) in dry ether (100 mL) was slowly added perdeuteriated phenylacetic acid (10.2 g) in dry ether (100 mL). After refluxing for 2 h a further portion of LAD (0.5 g) was added and reflux continued for 6 h. After careful quenching of the reaction with wet ether (25 mL) and water (50 mL) and acidification with concentrated HCl, the aqueous layer was saturated with NaCl and extracted with ether (5 × 30 mL). The combined extracts were washed with saturated aqueous $NaHCO_3$ (30 mL), dried over anhydrous Na_2SO_4, decolorized with carbon, filtered, and solvent was removed by distillation through a 15-cm glass helices column. Traces of ether were removed under vacuum to yield 8.3 g (88.5%) of **1***l*.

Styrene-d_8 (**1**d)

Phenylethanol-d_9 from the previous reaction (8.2 g) was heated with KOH (3.7 g) and the styrene was distilled through a 15-cm Vigreux column into a Dry Ice cooled receiver as it was produced. After separation from water, the product was dried over anhydrous Na_2SO_4 and distilled through a 15-cm Vigreux column at reduced pressure (~10 Torr; 1 Torr = 133.3 Pa) to yield 5.4 g (77%) of **1***d*.

Mass spectral analysis indicated the incorporation of 7.17 excess D atoms per molecule (0.5% d_4, 6.0% d_5, 12.6% d_6, 37.0% d_7, 44.0% d_8); ^{2}Hmr ($CHCl_3$) (Fig. 1), δ:5.1 (*trans*-D-2), 5.6 (*cis*-D-2) 6.6 (D-1) 7.1–7.4 (aromatic Ds). Electronic integration established the following deuterium distribution; 1.88 D at C-2, 0.73 D at C-1, and 4.56 D in the aromatic ring.

Phenylethanol-2,3-d_2 (**1**j)

Phenylacetic acid (5.0 g) in dry ether (100 mL) was slowly added to a magnetically stirred slurry of LAD in dry ether (100 mL) and the mixture was refluxed for 4 h. The reaction mixture was carefully quenched with water, then acidified with concentrated HCl until precipitates were dissolved. The ether layer was separated, and the aqueous layer was saturated with NaCl and extracted with ether (4 × 15 mL). The combined extracts were dried over anhydrous Na_2SO_4, ether was stripped on a roto-evaporator, and the last traces were removed under vacuum to yield 4.2 g (95%) of **1***j*; ^{1}Hmr (CCl_4), δ:2.69 (s, H-1) 4.15 (s, —O—H), 7.0–7.3 (m, aromatic H5).

Styrene-2,2-d_2 (**1**b)

Phenylethanol-2,2-d_2 (3.6 g) was heated with KOH (2.0 g, pellets) and the styrene rapidly distilled through a 15-cm Vigreux column into a Dry Ice – acetone cooled receiver. The styrene was separated from water and dried over anhydrous Na_2SO_4 to yield 2.6 g (84%) of **1***b*. Mass spectral analysis indicated that 1.99 excess D atoms per molecule (2.5% d_1, 96.0% d_2, 1.5% d_3) were incorporated in the styrene; ^{2}Hmr, δ:5.1 (*trans*-D-2), 5.6 (*cis*-D-2).

Attempted H–D exchange of divinylbenzene

Divinylbenzene (0.20 g), decalin (2 mL), and 0.26 *M* DCl/D_2O (5 mL) in a medium-walled glass tube were degassed via three freeze–pump–thaw cycles and the tube was sealed under vacuum. Reaction was carried out at 160°C for 19 h in a Parr high pressure apparatus containing water to equalize pressure. A solid mass of polymer was formed and this deuteration approach was abandoned.

Phenylenediacetic acid-2,2,2′,2′-d_4 (**2**e)

The potassium salt of phenylenediacetic acid (9.6 g) was prepared by reaction with KOH (3.0 g) in water (20 mL). Water was removed with heating on a roto-evaporator and the salt was reacted with D_2O (50 mL)

and KOH (1.0 g) in a 600-ML Parr high pressure apparatus with a glass liner at 160°C for 28 h. The solution was acidified with concentrated HCl and the solid removed by filtration to yield 9.3 g (95%) of **1***e*; ^{1}Hmr (DMSO-d_6), δ:7.25 (s, aromatic Hs), 11.8 (s, —O—H), 3.53 (residual H-2).

Phenylenediacetic acid diethyl ester-2,2,2′,2′-d_4 *(2*i*)*

Phenylenediacetic acid **2***e* (8.9 g) was refluxed with absolute ethanol (38 mL), benzene (63 mL), and concentrated H_2SO_4(10 mL) with magnetic stirring in a Dean–Stark apparatus. After 12 h reaction, saturated aqueous NaCl (75 mL) was added and the mixture extracted with ether (50 mL, 3 × 20 mL). the combined extracts were washed with saturated aqueous $NaHCO_3$ (2 × 10 mL), dried over anhydrous Na_2SO_4, decolorized with carbon, and the ether was removed on a roto-evaporator, then with heating under vacuum. Removal of all the ethanol was difficult, to yield 9.6 g (84%) of **2***i*; ^{1}Hmr (CCl_4), δ:1.18 (t, CH_3), 4.07 (q, ethyl CH_2), 7.20 (s, aromatic Hs), 3.47 (residual 2,2′ Hs).

Benzenediethanol-2,2,2′,2′-d_4 *(2*k*)*

Phenylenediacetic acid diethyl ester (9.2 g) from the above reaction in dry ether (100 mL) was slowly added to a magnetically stirred suspension of LAH (1.9 g) in dry ether (50 mL). After a 6-h reflux, the reaction mixture was quenched by careful addition of water (50 mL) and acidified with concentrated HCl to dissolve the precipitate. Extraction with ether (9 × 50 mL) yielded 5.1 g (83%) of **2***k*; ^{1}Hmr (CDCl), δ:1.87 (s, —O—H), 2.82 (m, 1,1′ Hs), 3.97 (s, residual 2,2′ Hs), 7.20 (s, aromatic Hs).

Divinylbenzene-1,1′-d_2 *(2*a*)*

Benzenediethanol **2***k* (4.9 g) was heated rapidly with KOH pellets (2.5 g) and divinylbenzene (2.3 g, 62%) was quickly distilled through a 15-cm Vigreux column at ~60 Torr. Mass spectral analysis indicated the presence of 1.39 excess D atoms per molecule (11.6% d_0, 41.2% d_1, 45.0% d_2, 1.4% d_3, 0.9% d_4); ^{2}Hmr ($CHCl_3$), δ:6.6 (D-1), 2.8 (6%) (2,2,2′,2′-Ds) of **2***k*; ^{1}Hmr (CCl_4), δ:5.17 (m, *trans*-2,2′ Hs), 5.63 (m, *cis*-2,2′ Hs), 6.63 (residual 1,1′ Hs, 0.64H), 7.30 (s, aromatic Hs).

Phenylenediacetic acid-d_8 *(2*f*)*

Phenylenediacetic acid (10.0 g) was reacted with 0.26 *M* DCl/D_2O (100 mL) in a 600-mL Parr high pressure apparatus fitted with a glass liner at 260°C for 88 h. The solid was filtered off, washed with water (2 × 15 mL), and dried to yield 9.35 g (89.9%) of **2***f*. Mass spectral analysis disclosed the presence of 8.29 excess D atoms per molecule (0.9% d_5, 4.5% d_6, 16.2% d_7, 34.3% d_8, 31.2% d_9, 12.8% d_{10}); apparently not all of the carboxyl deuterons were washed out during isolation.

Phenylenediacetic acid-d_4 *(2*g*)*

Phenylenediacetic acid **2***f* (7.9 g) was reacted with KOH (5.0 g) in water (50 mL) to form the salt, and the water was removed on a roto-evaporator with heating and then with heating under vacuum. The salt was reacted in a glass-lined 600-mL Parr high pressure apparatus with KOH (1.0 g) and water (50 mL) at 160°C for 24 h. The reaction mixture was acidified, the precipitate filtered off, washed with water (4 × 15 mL), and dried by heating under vacuum to yield 7.4 g (96%) of **2***g*; ^{1}Hmr (DMSO-d_6), δ:3.56 (s, H-2,2′), 7.24 (s, residual aromatic Hs), 11.7 (s, —O—H).

Phenylenediacetic acid diethyl ester-d_4 *(2*j*)*

Phenylenediacetic acid **2***g* (7.2 g) was refluxed with magnetic stirring with absolute ethanol (35 mL), benzene (65 mL), and concentrated H_2SO_4 (12 mL) in a Dean–Stark apparatus for 18 h. To the reaction mixture was added ether (50 mL) and saturated aqueous NaCl and the organic solution separated. The aqueous layer was further extracted with ether (5 × 30 mL) and the combined extracts were washed with saturated aqueous $NaHCO_3$ (2 × 20 mL) and saturated aqueous NaCl (20 mL). After drying over anhydrous Na_2SO_4 and decolorizing with carbon, ether was stripped on a roto-evaporator, then with heating under vacuum, to yield 8.3 g (90%) of **2***j*. Mass spectral analysis demonstrated the presence of 3.75 excess D atoms per molecule (3.7% d_2, 23.5% d_3, 66.5% d_4, 5.9% d_5, 0.4% d_6); ^{1}Hmr ($CDCl_3$), δ:1.20 (t, CH_3), 3.60 (s, 2,2′ Hs) 4.18 (q, ethyl CH_2), 7.30 (s, residual aromatic Hs).

Benzenediethanol-d_4 *(2*m*)*

A solution of **2***j* (8.0 g) in dry ether (100 mL) was added slowly to a magnetically stirred suspension of LAH (1.3 g) in dry ether (50 mL) and the mixture refluxed overnight. The reaction was quenched by careful addition of water (50 mL) and then acidified by addition of concentrated HCl to dissolve the precipitate. The organic layer was separated, the aqueous phase extracted with ether (10 × 30 mL), and the combined extracts were washed with saturated aqueous NaCl (20 mL), dried over anhydrous Na_2SO_4, and decolorized with carbon. Ether was stripped on a roto-evaporator, then under vacuum, to yield 5.2 g (97%) of **2***m*; ^{1}Hmr ($CDCl_3$) δ:1.89 (s, O Hs), 2.81 (dt, 2,2′ Hs), 3.82 (t, 1,1′ Hs), 7.20 (s, residual aromatic Hs).

Divinylbenzene-d_4 *(2*c*)*

Benzenediethanol-d_4 **2***m* (5.0 g) was heated with KOH pellets (2.5 g) and the divinylbenzene (1.0 g, 26%) quickly distilled through a 15-cm Vigreux column at ~60 Torr. In this reaction the divinylbenzene polymerized very rapidly in the reaction flask. Mass spectral analysis indicated 3.62 excess D atoms per molecule (0.5%, d_0, 0.9% d_1, 5.7% d_2, 26.1% d_3, 63.0% d_4, 3.5% d_5, 0.3% d_6). The ^{2}Hmr spectrum showed, in addition to an intense peak at 7.4 ppm, weak signals at 7.2 (<5%) and 2.7 (<1%) due to starting material. A weak signal at 6.7 (<1%) indicated that a small amount of the deuterium was located at the 1,1′-positions of **2***c*. ^{1}Hmr (CCl_4), δ:5.11 (d, *trans*-2,2′ Hs), 5.59 (d, *cis*-2,2′ Hs), 6.66 (q, 1,1′ Hs), 7.30 (s, residual aromatic Hs, 0.35H).

Benezenediethanol-1,1,1′,1′-d_4 *(2*l*)*

The diester of PDA (11.0 g) in dry ether (150 mL) was slowly added to a magnetically stirred suspension of LAD (2.2 g) in dry ether (50 mL). After refluxing for 5 h, the reaction mixture was carefully quenched with water (50 mL) and acidified with concentrated HCl to dissolve the precipitate. After separation of the organic layer, the aqueous solution was extracted with ether (10 × 50 mL), and the combined extracts were washed with saturated aqueous NaCl (20 mL) and dried over anhydrous Na_2SO_4. Ether was stripped on a roto-evaporator, then the last traces were removed under vacuum to yield 7.5 g (88%) of **2***l*; ^{1}Hmr ($CDCl_3$), δ:1.58 (s, O Hs), 2.84 (s, 2,2′ Hs), 7.20 (s, aromatic Hs).

Divinylbenzene-2,2,2′,2′-d_4 *(2*b*)*

Benzenediethanol **2***l* (7.2 g) was heated with KOH pellets (2.6 g) and the divinylbenzene (2.5 g, 46%) was quickly distilled through a 15-cm Vigreux column at ~65 Torr. Mass spectral analysis showed that the product contained 3.89 excess D atoms per molecule (2.9% d_2, 6.6% d_3, 89.3% d_4, 1.1% d_5, 0.1% d_6 species). The ^{2}Hmr ($CHCl_3$) (Fig. 2) showed signals at 5.10 and 5.60 ppm corresponding to the 2,2′ deuterons and a signal at 3.7 pm that was due to starting material; ^{1}Hmr ($CDCl_3$), δ:6.67 (br s, 1,1′ Hs), 7.35 (s, aromatic Hs). Only a very small signal (<1%) was present for the 2,2 protons.

Acknowledgements

We thank the Natural Sciences and Engineering Research Council of Canada for fianancial assistance. We are indebted to Mr. B. Sayer for obtaining the ^{2}Hmr spectra.

1. N. H. Werstiuk and T. Kadai. Can. J. Chem. **51**, 1485 (1973).
2. N. H. Werstiuk and T. Kadai. Can. J. Chem. **52**, 2169 (1974).
3. N. H. Werstiuk and T. Kadai. U.S. Patent No. 3,989,705 (1976).
4. N. H. Werstiuk and T. Kadai. Canadian Patent No. 1048556 (1979).
5. N. H. Werstiuk and G. Timmins. Can. J. Chem. **59**, 1022 (1981).

6. N. H. WERSTIUK and G. TIMMINS. Can. J. Chem. **59**, 3218 (1981).
7. N. H. WERSTIUK and G. TIMMINS. Can. J. Chem. **63**, 530 (1985).
8. N. H. WERSTIUK. *In* Isotopes in physical and biomedical sciences. *Edited by* J. R. Jones and E. Buncel. Elsevier, New York. In press.
9. C. A. FYFE, E. C. KELUSKY, R. E. SOLEY, N. M. WIENCKE, N. H. WERSTIUK, and G. TIMMINS. Macromolecules. In press.
10. A. I. VOGEL. A textbook of practical organic chemistry. 3rd ed. Longmans, Green and Co. Ltd., London. 1956.
11. J. G. ATKINSON, J. J. CSAKVARY, G. T. HEBERT, and R. S. STUART. J. Am. Chem. Soc. **90**, 498 (1968).

Bridged polycyclic compounds. 88. Multiple intermediates in solvolysis of certain bridged bicyclic and tricyclic compounds[1]

STANLEY J. CRISTOL,[2] GEORGE C. SCHLOEMER, DIETER BRAUN, AND GWENDOLYN O. MAYO
Department of Chemistry, University of Colorado, Boulder, CO 80309, U.S.A.
Received August 26, 1985

This paper is dedicated to Professor Arthur N. Bourns

STANLEY J. CRISTOL, GEORGE C. SCHLOEMER, DIETER BRAUN, and GWENDOLYN O. MAYO. Can. J. Chem. **64**, 1077 (1986).

Acetolyses of 7-chloromethyl- and 7-bromomethyldibenzobicyclo[2.2.2]octatrienes, 8-chloro- and 8-bromo-7-methylenedibenzobicyclo[2.2.2]octa-2,5-dienes, 4-bromo-8-methylenedibenzobicyclo[3.2.1]octa-2,6-diene, and 2-chlorodibenzotricyclo-[3.2.2.$0^{2,4}$]nonadiene were carried out. The results observed were consistent with the involvement of two carbocations interconverting by a Wagner–Meerwein rearrangement, and with the absence of the 1-dibenzosemibullvalenylcarbinyl cation, which is the cyclopropylcarbinyl isomer of one of the cations produced. The preparations of the reactants and products are described.

STANLEY J. CRISTOL, GEORGE C. SCHLOEMER, DIETER BRAUN et GWENDOLYN O. MAYO. Can. J. Chem. **64**, 1077 (1986).

On a effectué les acétolyses des composés suivants: les chloromethyl-7 et bromomethyl-7 dibenzobicyclo[2.2.2]octatriènes, les chloro-8 et bromo-8 méthylène-7 dibenzobicyclo[2.2.2]octatriènes-2,5, le bromo-4 méthylène-8 dibenzobicyclo[3.2.1]octadiène-2,6 et le chloro-2 dibenzotricyclo[3.2.2.$0^{2,4}$]nonadiène. Les résultats observés sont en accord avec un mécanisme impliquant la présence de deux carbocations qui s'interconvertissent par une transposition de Wagner–Meerwein et l'absence du cation dibenzosemibullvalénylcarbinyle-1 qui est l'isomère cyclopropylcarbinyle de l'un des cations produits. On décrit les préparations des réactifs et des produits.

[Traduit par la revue]

Introduction

Some years ago (2), the solvolysis of **1**-Br (1-bromomethyldibenzosemibullvalene) and the solvolytic deamination of **1**-NH_2 were described and the nature of the intermediates involved in the formation of the solvolytic products was discussed. The purpose of this paper is to describe silver-ion assisted acetolyses of the corresponding allylic isomers (**2** and **3**, X = Cl, Br), the homoallylic bromide **4**-Br, and the cyclopropyl chloride **5**, all of which might be expected to share in the manifold of carbocations available to **1**. We were particularly interested in the nature of the products of these ground-state solvolyses, in order to compare them with those of ground-state solvolysis of **1** and those of photosolvolyses of similar or identical compounds.

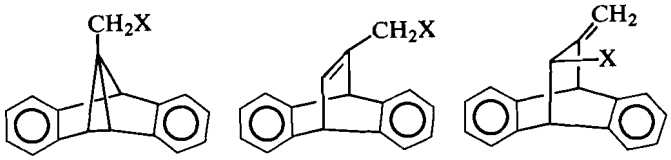

1 **2** **3**

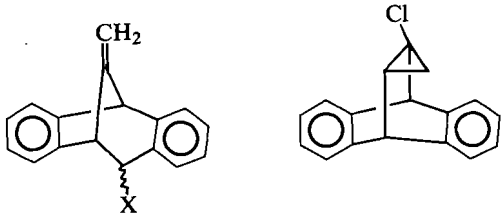

4 **5**

Silver-ion induced acetolysis (2) of **1**-Br gave, in addition to a small amount of 3,4-benzofluorene,[3] a mixture of the acetates **2**, **3**, and **4** (X = OAc). The ratios of the acetate products (rationalized to 100) are given in Table 1, as are corresponding results for **2**-Br, **3**-Br, and **4**-Br. The latter compounds gave no benzofluorene, consistent with the idea[3] that the progenitor of this hydrocarbon is a species not reached in the carbocation manifold from **2**-Br, **3**-Br, or **4**-Br. The ratios of products are, within experimental error, identical for the isomeric allylic compounds **2**-Br and **3**-Br. It was first assumed that the experiments conducted at 100°C for approximately an hour were kinetically controlled ones involving silver acetate. However, experiments on corresponding chlorides (see below) made clear that the experiments, which involved addition of silver acetate after the solution had been brought to temperature, allowed for substantial acetolysis and epimerization before solvolysis, and allowed for partial acid-catalyzed *exo–endo* transformation of the benzylic acetates **4** and for a partial conversion of **4**-OAc to the more stable **2**-OAc and **3**-OAc isomers.

When the acetate mixtures were allowed to stand in acetic acid containing 0.5 *M* perchloric acid for 90 h, conversion to **3**-OAc was substantially complete (95% could be isolated) (2).

It seems possible to conclude from these experiments that the carbocations **6** and **7** are involved, **6** leading to *exo* and *endo*-**4** acetates and **7** to **2**- and **3**-acetates. Reproducibility of conditions is not precise enough, in our opinion, to allow confidence in the assumption (2) that **6** and **7** are interconvertible at a rate substantially slower than capture, as this assumption would lead to substantially different mixtures from the benzylic and the allylic isomers, although the slightly greater amount of **4**-OAc

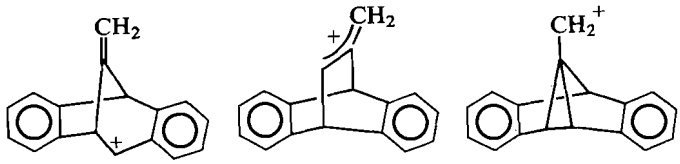

6 **7** **8**

[1]For previous paper in series, see ref. 1.
[2]Author to whom correspondence may be addressed.
[3]Plausible reaction paths for the formation of this hydrocarbon were discussed earlier (2), as were results on the deamination of **1**-NH_2.

TABLE 1. Silver-ion induced acetolysis of certain bromides

Substrate	Temperature, °C	Time, min	Order of AgOAc addition[a]	Composition of acetate product, % 2-OAc	3-OAc	4-OAc[c]
1-Br	100	65	Last	28	29	43
	90	45	Last	26	29	43
2-Br	100	45	Last	35	37	28
3-Br	100	45	Last	39	32	29
	97	840	Last	32	44	24
	23	300	Last	34	30	36
	100	1[d]	First	23	30	47
4-Br[b]	90	45	Last	21	23	56

[a]For those samples marked "last," the solutions of alkyl bromide were brought to temperature and silver acetate was then added; for that marked "first," the alkyl halide was added to a solution of silver acetate already at temperature.
[b]Composition of product computed from that of a reactant mixture of 72% **4**-Br, 10% **2**-Br, and 18% **3**-Br.
[c]The major portion of these product mixtures was *exo*; the fraction of *endo* epimer increased with increasing time and (or) severity.
[d]Time of heating after RBr added.

TABLE 2. Solvolyses of certain bicyclic and tricyclic chlorides in acetic acid at reflux

Substrate	Time	Order of AgOAc addition	RCl recovered	Composition of acetate product, % 2-OAc	3-OAc	4-OAc
2-Cl	2 h	None	32% **2**-Cl, 28% **3**-Cl	27	43	30
	35 min[a]	Last	0	26	43	31
	<1 min[a]	Last	19% **2**-Cl, 18% **3**-Cl	29	41	30
	1 min[b]	First	8% **3**-Cl	20	39	42
3-Cl	3 min[b]	First	62% **3**-Cl, trace **2**-Cl	21	35	44
	1 min[b]	First	36% **3**-Cl	22	34	44
5-Cl	23 h	Last	66% **5**-Cl	25	37	39
	72 h	Last	48% **5**-Cl	25	43	32
	9 d	Last	—	23	53	24

[a]Time of heating after AgOAc added.
[b]Time of heating after RCl added.

from **4**-Br suggests this. It is clear, however, from the absence of **1**-OAc and benzofluorene, that interconversion with **8** (homoallyl → cyclopropylcarbinyl isomerization) is not important in these experiments.

The chlorides **2**-Cl, **3**-Cl, and **5**-Cl were also subjected to acetolysis (Table 2). With **2**-Cl, in the absence of silver acetate (or when silver acetate was added after the solution had been brought to reflux and reaction was terminated by pouring into cold water as soon as possible after the addition), there was substantial conversion to the more stable allylic isomer **3**-Cl, along with solvolysis. On the other hand, solvolysis of **3**-Cl, which was significantly less reactive than **2**-Cl, was accompanied by, at most, trace rearrangement to **2**-Cl. Thus, like the acetates, **3**-Cl is thermodynamically more stable than its allylic isomer **2**-Cl.

In the experiments where the alkyl chlorides were added to a refluxing solution of silver acetate in acetic acid, and the reaction was terminated after a few minutes (presumably kinetic control) with **2**-Cl, **3**-Cl, and **3**-Br, the reaction mixture was somewhat richer in **4**-OAc (42–47%) and poorer in **2**-OAc than those prepared under more severe conditions. These results make it clear that **4**-OAc is converted to both **2**-OAc and **3**-OAc and, when previous work (2) on these acetates is considered, that, considerably less rapidly, **2**-OAc is converted to **3**-OAc. This same phenomenon can be noted in the silver-ion promoted acetolysis of **5**-Cl, which gives mixtures comparable to those from the other isomers at shorter times, and, at longer times, shows the tendency to give mixtures richer in **3**-OAc, consonant with its stability (2). The low reactivity of **5** is obviously a function of its being a chlorocyclopropane (3), and the products are consistent with those of other bridged systems (see, for example, ref. 4), and with the intervention of ions **6** and **7** as the reactive intermediates in the process.

Photochemical results are recorded in the accompanying paper (5), and discussions of the differences between the photoreactions and ground-state reactions are also given there.

Reagents and products

Compound **2**-Br was prepared, essentially as described by Shenoy (6), by treatment of **2**-OH (2, 6) with phosphorus

tribromide in pyridine. The other allylic isomer, **3**-Br, was prepared by a sequence in which allyl chloride was added to anthracene, elimination of hydrogen chloride gave the olefin **3**-H, and bromination with *N*-bromosuccinimide gave largely **3**-Br. The preparation of **4**-Br was carried out by heating **1**-Br (2) in xylene; a mixture containing 18% of **3**-Br, 10% of **2**-Br, and 72% of **4**-Br was produced. The lability of **4**-Br made purification difficult, hence this mixture was used in the reactions. The acetates **1**-OAc, **2**-OAc, **3**-OAc, and **4**-OAc have already been reported (2). **2**-Cl was prepared from **2**-OH using the method of Young *et al.* (7), for the conversion of primary allylic alcohols into the corresponding chlorides, without allylic rearrangement. We were unable to convert **2**-OH or **3**-OH into mixtures of allylic chlorides from which pure samples of **3**-Cl could be obtained (although it is now clear (see above) that thermolysis of these mixtures would have given **3**-Cl). We therefore prepared **3**-Cl by treatment of 7-chloro-8-chloromethyldibenzobicyclo[2.2.2]octa-2,5-diene (prepared from anthracene and 1,3-dichloropropene) with base, following the concept of Jarvis (8) regarding elimination in such systems. **5**-Cl was prepared by triplet-sensitized irradiation of **2**-Cl or **3**-Cl (5).

Experimental

The ^{1}H nmr spectra were determined with a Varian A-60A 60-MHz instrument (bromide work) and a Varian EM-390 (90-MHz) instrument (chloride work). Analyses were by Galbraith Laboratories, Inc., Knoxville, TN.

Preparation of 7-bromomethyldibenzobicyclo[2.2.2]octatriene (2-Br)

A mixture of 250 mg (1.07 mmol) of **2**-OH (2), 2.8 g (10.5 mmol) of PBr_3, 1 mL of pyridine, and 25 mL of reagent-grade benzene was heated and stirred for 20 min at 60°C, following the procedure of Shenoy (6). After being cooled, the mixture was extracted several times with water, aqueous $NaHCO_3$, and water. The benzene solution was dried ($MgSO_4$); evaporation of the solvent left an oil that crystallized from petroleum ether (bp 40–60°C) to give 282 mg (92%) of **2**-Br, mp 132–135°C (lit. (6) mp 142–144°C); ^{1}H nmr ($CDCl_3$), δ: 7.0 (dt, 1H, H-8, $J_{4,8}$ = 6.5 Hz, $J_{8,9}$ = 0.5 Hz), 5.28 (s, 1H, H-1), 5.22 (d, 1H, H-4, $J_{4,8}$ = 6.5 Hz), 4.40 (d, 2H, H-9, $J_{8,9}$ = 0.5 Hz).

Preparation of 7-methylene-8-bromodibenzobicyclo[2.2.2]octadiene (3-Br)

A solution of 7.73 g (35.4 mmol) of 7-methylenedibenzobicyclo-[2.2.2]octadiene (9), 7.9 g (35 mmol) of *N*-bromosuccinimide, and a catalytic amount of azobisisobutyronitrile in 90 mL of reagent-grade carbon tetrachloride was irradiated with a 100-W unfrosted tungsten lamp for 3½ h. The heat from the lamp caused the solution to reflux gently. The mixture was cooled and the insoluble succinimide was filtered. The filtrate was evaporated *in vacuo*. The resulting oil was chromatographed on Merck 71707 alumina and eluted rapidly with petroleum ether, bp 40–60°C. The major fraction was collected. Several recrystallizations from petroleum ether (bp 40–60°C) produced 6.2 g (60%) of **3**-Br, mp 121–122°C; ^{1}H nmr ($CDCl_3$), δ: 5.40 (d, 1H, H-9, $J_{8,9}$ = 1.5 Hz), 5.23 (d, 1H, H-9, $J_{8,9}$ = 2.0 Hz), 5.90 (m, 1H, H-8, $J_{4,8}$ = 3.0, $J_{8,9}$ = 2.0, 1.5 Hz), 4.72 (s, 1H, H-1), 4.54 (d, 1H, H-4, $J_{4,8}$ = 3.0 Hz).

Anal. calcd. for $C_{17}H_{13}Br$: C 68.70, H 4.41; found: C 68.75, H 4.57.

Thermal isomerization of 1-bromomethyldibenzotricyclo[3.3.0.0^{2,8}]octadiene (1-Br)

A solution of 70 mg (0.24 mmol) of **1**-Br in 50 mL of *m*-xylene was heated at reflux for 15 h. The *m*-xylene was removed *in vacuo* to give a yellow oily residue; ^{1}H nmr analysis showed 46% of *exo*-**4**-Br, 26% of *endo*-**4**-Br, 18% of **3**-Br, and 10% of **2**-Br. The mixture was analysed from the area of the following absorptions in the ^{1}H nmr spectrum: H-4, d, δ 5.90 of *endo*-**4**-Br; H-4, d, δ 5.65 of *exo*-**4**-Br; H-9, d, δ 4.40 of **2**-Br; H-1, s, δ 4.72 and H-4, d, δ 4.54 of **3**-Br. This mixture resisted attempts at separation and purification by either chromatography or crystallization due to the lability of the compounds. The yield of rearranged products was quantitative. The ^{1}H nmr spectra of *exo*- and *endo*-**4**-Br reported are those provided by analysis of the spectrum of the mixture: *exo*-**4**-Br: ^{1}H nmr ($CDCl_3$), δ: 5.65 (d, 1H, H-4, $J_{4,5}$ = 2.2 Hz), 5.07, 5.03 (2s, 2H, H-9), 4.40 (s, 1H, H-1); *endo*-**4**-Br: ^{1}H nmr ($CDCl_3$), δ: 5.90 (d, 1H, H-4, $J_{4,5}$ = 5.5 Hz), 4.98, 4.92 (2s, 2H, H-9), 4.40 (s, 1H, H-1), 4.05 (d, 1H, H-5, $J_{4,5}$ = 5.5 Hz).

Silver-assisted solvolysis of 7-bromomethyldibenzobicyclo[2.2.2]octatriene (2-Br)

To a solution of 500 mg (1.68 mmol) of **2**-Br in 15 mL of acetic acid at 100°C was added, with stirring, 300 mg (1.8 mmol) of solid silver acetate. The reaction mixture was stirred for 45 min, cooled, and filtered. Dilution of the filtrate with 150 mL of cold water produced a cloudy precipitate, which was extracted with several 50-mL portions of ether. The combined ether layers were washed with water and saturated sodium bicarbonate solution until neutral, then dried ($MgSO_4$). Evaporation of the solvent *in vacuo* produced 460 mg (98%) of an oil whose ^{1}H nmr spectrum[4] indicated it contained 35% of **2**-OAc, 37% of **3**-OAc, 22% of *endo*-**4**-OAc, and 6% of *exo*-**4**-OAc. This analysis was confirmed, as was that of all other solvolyses of the bromides, by reduction with $LiAlH_4$ to the corresponding alcohols and analysis of the ^{1}H nmr spectra of that mixture.

Silver-assisted solvolysis of 4-bromo-8-methylenedibenzobicyclo-[3.2.1]octadiene (4-Br)

To a solution of 70 mg (0.24 mmol) of the mixture of bromides from the thermolysis of **1**-Br described above, in 30 mL of acetic acid heated at 90°C, was added 100 mg (0.6 mmol) of silver acetate. The reaction was stirred at 90°C for 45 min, cooled, and filtered. The clear filtrate was diluted with 150 mL of water and extracted with several portions of ether. The combined ether layers were washed with water and saturated sodium bicarbonate solution until neutral, and dried ($MgSO_4$). Evaporation of the solvent gave 66 mg of an oil (100%) whose ^{1}H nmr spectrum[4] indicated a composition of 56% **4**-OAc, 23% of **3**-OAc, and 21% of **2**-OAc.

Silver-assisted solvolysis of 7-methylene-8-bromodibenzobicyclo [2.2.2]octadiene (3-Br)

A suspension of 1.24 g (4.18 mmol) of **3**-Br in 33 mL of acetic acid was heated to 100°C, after which silver acetate (0.70 g, 4.18 mmol) was added. The reaction mixture was heated at 100°C for 45 min, cooled, and filtered. Dilution of the filtrate with 150 mL of cold water resulted in a white precipitate, which was extracted with several 50-mL portions of ether. The combined ether portions were washed with water and saturated sodium bicarbonate solution. The ether was then dried ($MgSO_4$) and evaporated *in vacuo* to yield 1.65 g (97%) of an oil. The ^{1}H nmr spectrum of the mixture indicated the formation of 24% of *exo*-**4**-OAc, 5% of *endo*-**4**-OAc, 32% of **3**-OAc, and 39% of **2**-OAc.

Preparation of 8-chloro-7-methylenedibenzobicyclo[2.2.2]octadiene (3-Cl)

To a solution of 4.0 g (14 mmol) of 7-chloro-8-chloromethyldibenzobicyclo[2.2.2]octadiene (10) in 100 mL of dry dimethyl sulfoxide was added 2.3 g (21 mmol) of potassium *tert*-butoxide. The reaction mixture was stirred for 12 h at room temperature, and was then quenched by additon of 500 mL of water. The resulting suspension was extracted with several portions of ether. The combined ether layers were washed with 1 *M* hydrochloric acid and with water, then dried ($MgSO_4$). Evaporation of the solvent produced a yellow solid. Recrystallization from water–acetone yielded 2.5 g (71%) of crystalline **3**-Cl, mp 132 – 133°C; ^{1}H nmr ($CDCl_3$), δ: 5.35 (d, 1H, H-9, $J_{8,9}$ = 2.0 Hz), 5.17 (d, 1H, H-9, $J_{8,9}$ = 1.8 Hz), 4.71 (s, 1H, H-1), 4.70 (m, 1H, H-8, $J_{4,8}$ = 3.0, $J_{8,9}$ = 2.0, 1.8 Hz), 4.48 (d, 1H, H-4, $J_{4,8}$ = 3.0 Hz). *Anal.* calcd. for $C_{17}H_{13}Cl$: C 80.79, H 5.19; found: C 80.91, H 5.01.

[4]The properties of the acetate products and of the corresponding alcohols as well have already been reported (2).

Preparation of 7-chloromethyldibenzobicyclo[2.2.2]octatriene (2-Cl)

To a solution of 3.5 g (15 mmol) of 7-hydroxymethyldibenzobicyclo[2.2.2]octatriene **2**-OH (2) and 1.5 g (19 mmol) of pyridine in 200 mL of anhydrous ethyl ether was added (dropwise) a solution of 2.0 g (17 mmol) of thionyl chloride dissolved in 50 mL of anhydrous ether. After stirring overnight, the reaction mixture was poured into 350 mL of cold water. The ether layer was separated, and the water layer extracted twice with ether. The combined ether extracts were washed twice with sodium bicarbonate solution and twice with water. After the solution was dried ($MgSO_4$), removal of the solvent by distillation left a solid residue (3.8 g, 100%). Recrystallization from petroleum ether (bp 40–60°C) produced more than 90% of **2**-Cl, mp 147–148°C; ^{1}H nmr, δ: 7.41–6.91 (m, 8H, aromatic H), 6.80 (dt, 1H, H-8, $J_{4,8}$ = 6 Hz, $J_{8,9}$ = 1 Hz), 5.10 (s, 1H, H-1), 5.03 (d, 1H, H-4, $J_{4,8}$ = 6 Hz), 4.22 (d, 2H, H-9, $J_{8,9}$ = 1 Hz). *Anal.* calcd. for $C_{17}H_{13}Cl$: C 80.79, H 5.19; found: C 80.70, H 5.35.

Preparation of 2-chlorodibenzotricyclo[3.2.2.0^{2,4}]nonadiene (5)

A solution of 1.9 g (7.5 mmol) of **2**-Cl and 12 mL of acetophenone in 65 mL of acetonitrile in a Pyrex tube was deoxygenated by nitrogen bubbling for 20 min. It was then irradiated at 300 nm for 4 days with an Hanovia 500-W lamp (pyrex filter). The solvent was distilled off and the residual oil was chromatographed on 600 mL of a 60–200 mesh silica gel column. Elution with 10% benzene in petroleum ether (bp 40–60°C) gave **5**, contaminated with acetophenone. Steam distillation removed most of the acetophenone. The residue (1.2 g, 63%) contained 80% product and 20% acetophenone. Recrystallization from hexane gave pure **5**, mp 121–122°C; ^{1}H nmr ($CDCl_3$), δ: 7.40–7.00 (m, 8H, aromatic protons), 4.51 (s, 1H, H-1), 4.37 (d, 1H, H-5, $J_{4,5}$ = 5 Hz), 1.80 (dt, 1H, H-4, $J_{4,5}$ = 5 Hz, $J_{3anti,4}$ = 9 Hz, $J_{3syn,4}$ = 5 Hz), 1.17 (dd, 1H, H-3$_{anti}$, $J_{3anti,4}$ = 9 Hz, $J_{3anti,3syn}$ = 7 Hz), 0.55 (dd, 1H, H-3$_{syn}$, $J_{3anti,3syn}$ = 7, $J_{3syn,4}$ = 5 Hz). *Anal.* calcd. for $C_{17}H_{13}Cl$: C 80.79, H 5.19; found: C 80.59, H 5.13.

Thermal rearrangement of 2-Cl to 3-Cl

A solution of 66 mg (0.26 mmol) of **2**-Cl and 31 mg of anhydrous ferric chloride in 10 mL of carbon tetrachloride was heated at reflux for 2 h. After dilution with more carbon tetrachloride, the solution was washed with water, then chromatographed on a cold short silica-gel column to remove traces of ferric chloride. Elution with hexane gave a solution that, upon removal of the solvent by distillation, left a residue whose ^{1}H nmr spectrum was essentially that of **3**-Cl.

Acetolysis of 2-Cl in acetic acid

A solution of 18 mg (0.07 mmol) of **2**-Cl in 10 mL of acetic acid was heated at reflux for 2 h. After work-up similar to that described above for the bromides, ^{1}H nmr analysis indicated 32% of **2**-Cl remaining, 28% had been isomerized to **3**-Cl, while acetolysis was also seen (17% of **3**-OAc, 11% of **2**-OAc, and 12% of **4**-OAc).

Silver-assisted solvolyses of 2-Cl, 3-Cl, and 5-Cl

These experiments were generally conducted with about 0.01–0.04 *M* alkyl chloride in glacial acetic acid, and with 1.5–10 times the equivalent amount of silver acetate. Recoveries were close to quantitative. Conditions and results are tabulated in Table 2. When silver acetate is described as added "last," the alkyl chloride solution was heated to reflux before addition of silver acetate. In the "first" cases, a solution or suspension of silver acetate in acetic acid was brought to reflux before addition of solid alkyl chloride.

Acknowledgements

The authors are indebted to the National Science Foundation (Grants CHE-80-11933 and CHE-83-09927) for partial support of this work. G.C.S. is also indebted to the University of Colorado for fellowship support. Dieter Braun's stay in Boulder was sponsored by the student exchange program of the University of Colorado and the University of Regensburg, Federal Republic of Germany.

1. S. J. Cristol, M. W. Klein, M. H. Hendewerk, and R. D. Daussin. J. Org. Chem. **46**, 4992 (1981).
2. S. J. Cristol, G. C. Schloemer, D. R. James, and L. A. Paquette. J. Org. Chem. **37**, 3852 (1972).
3. (*a*) J. D. Roberts and V. C. Chambers. J. Am. Chem. Soc. **73**, 5034 (1951); (*b*) C. H. DePuy. Acc. Chem. Res. **1**, 33 (1968).
4. S. J. Cristol, R. M. Sequeira, and C. H. DePuy. J. Am. Chem. Soc. **87**, 4007 (1965).
5. S. J. Cristol, D. Braun, G. C. Schloemer, and B. Vanden Plas. Can. J. Chem. **64**, 1081 (1986).
6. P. K. Shenoy. Ph.D. dissertation, University of Arizona, Tucson, 1966.
7. W. G. Young, F. F. Caserio, and D. D. Brandon. J. Am. Chem. Soc. **82**, 6163 (1960).
8. B. B. Jarvis. J. Org. Chem. **33**, 4075 (1968).
9. S. J. Cristol and G. O. Mayo. J. Org. Chem. **34**, 2363 (1969).
10. S. J. Cristol and A. L. Noreen. J. Org. Chem. **41**, 4016 (1976).

Photochemical transformations. 42.[1] Photoreactions of certain bridged bicyclic and tricyclic chlorides and bromides containing aromatic chromophores

STANLEY J. CRISTOL,[2] DIETER BRAUN, GEORGE C. SCHLOEMER, AND BART J. VANDEN PLAS
Department of Chemistry, University of Colorado, Boulder, CO 80309, U.S.A.

Received August 26, 1985

This paper is dedicated to Professor Arthur N. Bourns

STANLEY J. CRISTOL, DIETER BRAUN, GEORGE C. SCHLOEMER, and BART J. VANDEN PLAS. Can. J. Chem. **64**, 1081 (1986).

Irradiations of a number of bicyclic and tricyclic bromides and chlorides containing aromatic rings have been carried out. With the allylic chlorides **2**-Cl and **3**-Cl, triplet-sensitized photoreactions in acetone (or in acetonitrile with acetophenone sensitizer) lead to allylic scrambling and allyl-to-cyclopropyl isomerization to **5**-Cl, while the corresponding bromides, under similar conditions, give allylic scrambling, photo-Wagner–Meerwein rearrangement, and photosolvolysis, but no allyl-to-cyclopropyl isomerization. The differences in reaction types are ascribed to the requirement for intramolecular electron transfer for the "ionic" reactions, which may be exothermic in the triplet states of the bromides, but not in those of the chlorides. In direct irradiations in acetic acid with 254-nm light, the singlet state of the chloride **2**-Cl is photoactive in the "ionic" sense, giving a mixture of acetates, benzofluorenes, and 1-methylfluoranthene. The latter hydrocarbon is the major product in the direct irradiation of **5**-Cl in acetic acid, along with a mixture of acetates. The photochemical results are contrasted with ground-state solvolyses of these compounds.

STANLEY J. CRISTOL, DIETER BRAUN, GEORGE C. SCHLOEMER et BART J. VANDEN PLAS. Can. J. Chem. **64**, 1081 (1986).

On a effectué des irradiations sur un certain nombre de bromures et de chlorures bicycliques et tricycliques contenant des noyaux aromatiques. Dans les cas des chlorures allyliques **2**-Cl et **3**-Cl, les photoréactions sensibilisées par un triplet et effectuées dans l'acétone (ou dans l'acétonitrile en utilisant l'acétophénone comme sensibilisateur) conduisent à des transpositions allyliques aléatoires et à une isomérisation de l'allyle en cyclopropyle au niveau du **5**-Cl. Par ailleurs, lorsqu'on soumet les bromures correspondants à des conditions semblables, il se produit des transpositions allyliques aléatoires, une photo-transposition de Wagner–Meerwein ainsi que de la photolyse; toutefois, il ne se produit pas d'isomérisation de l'allyle en cyclopropyle. On attribue les différences dans les types de réactions aux conditions requises pour que les réactions "ioniques" puissent procéder par un transfert électronique intramoléculaire qui peut être exothermique dans le cas des états triplets des bromures, mais pas dans le cas des chlorures. Lors d'irradiations directes par de la lumière à 254 nm dans de l'acide acétique, l'état singulet des chlorures **2**-Cl est photoréactif au sens "ionique" et il conduit à des mélange d'acétates, de benzfluorènes et de méthyl-1 fluoranthène. Lors des irradiations directes du **5**-Cl dans de l'acide acétique, ce dernier hydrocarbure est le produit principal aux côtés d'un mélange d'acétates. Les résultats photochimiques sont en opposition avec ceux observés lors des solvolyses de ces composés dans leur état fondamental.

[Traduit par la revue]

In connection with our continuing interest in photosolvolyses and photo-Wagner–Meerwein rearrangements (2), as well as in the photoreactions of allylic halides (3), we undertook a study of the photoreactions of certain chlorides and bromides of structures **1**–**5**, whose ground-state acetolyses have been reported in the accompanying paper (4), both upon direct irradiation and upon photosensitization.

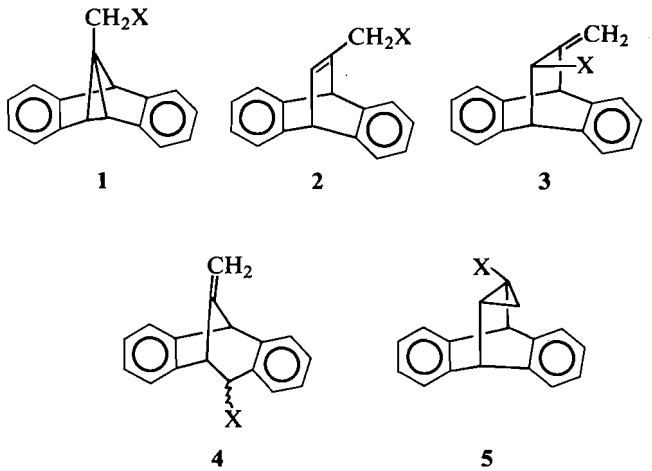

Triplet-sensitized reactions

Our initial interest in these compounds arose in connection with studies of allylic systems (3), and focussed on the allylic chlorides **2** and **3**, under triplet-sensitized conditions. When **2**-Cl was irradiated in acetone-d_6 in a Pyrex tube with a 450-W Hanovia lamp (Corex filter sleeve) or in an acetonitrile solution with acetophenone as sensitizer, it was rapidly converted to a roughly 1:6 mixture of **2**-Cl and **3**-Cl. Somewhat more slowly, this mixture was converted to **5**-Cl. A similar result occurred with **3**-Cl in acetonitrile, with either acetophenone or acetone as sensitizer. No evidence for photo-Wagner–Meerwein isomerization to **4**-Cl, for rearrangement to **1**-Cl, or for photosolvolysis was noted, although recovered chemical yields, when isomerization to **5**-Cl was carried out to completion, were only about 50%. Thus the results were comparable to those of other allylic chlorides (3), that is, allylic isomerization, with ultimate allyl-to-cyclopropyl rearrangement.

Irradiation of the corresponding allylic bromides gave rise to distinctly different results. While irradiation, in acetone, of allyl bromide itself gives cyclopropyl bromide (3*a*), no **5**-Br was produced when either **2**-Br or **3**-Br was irradiated through Pyrex in acetone-d_6. Instead, a steady-state ratio of **2**-Br to **3**-Br of 1.1:1.0 was set up, and the reaction mixture contained, in addition, significant amounts of the Wagner–Meerwein rearranged, less thermodynamically stable (4), bromide **4**-Br (largely the *endo* isomer) and the rearranged alcohol **4**-OH. The presence of **2**-OH and **3**-OH was not certain, as ^{1}H nmr data

[1]For preceding paper in series see ref. 1.
[2]Author to whom correspondence may be addressed.

were indistinct, but, when an experiment was conducted in a 1:3 mixture of acetone and methanol, evidence for **2**, **3**, and **4** methyl ethers was adduced. Whether the alcohol comes, in part at least, directly from the allylic bromides or via the benzylic bromides **4**-Br was not ascertained, but we did find that *exo*-**4**-Br was substantially more photoactive (solvolysis in acetone to **4**-OH) than its *endo* epimer. Wagner–Meerwein products were also formed in acetonitrile with acetophenone sensitizer, and **5**-Br was again absent.

These results are quite different from those (5) with the 1-halomethylnaphthalenes, which undergo, in addition to solvolysis under direct irradiation, sensitized photosolvolysis from triplet states when the halogen is either chlorine or bromine. The authors (5) believe that the triplet reactions occur via exciplex formation, while results on benzyl and substituted benzyl chlorides (6), which also undergo sensitized photosolvolysis, are well interpreted by the involvement of an upper triplet state.

While the disparity between the chloride and bromide results was at first puzzling, recent ideas (7) regarding photosolvolyses of β-arylethyl derivatives rationalize the results well. For some time (8) it has been proposed that there is a key requirement for these "ionic" reactions resulting in photo-Wagner–Meerwein rearrangements of β-arylethyl derivatives and (or) photosolvolysis. The requirement is that electron transfer of the photoexcited π^* electron to the σ^* orbital of the carbon–nucleofuge bond occurs to give a zwitterionic species. Thus, for example, **3** would give the zwitterionic biradical **6**. A variety of modes of fragmentation of **6** was proposed, all involving cleavage of the carbon—X bond. If that cleavage occurred prior to ring migration the biradical cation **7** (paired with X^-) would be produced, which could lead, by reverse electron transfer, to **8** or, by rearrangement followed by decay, to **9**. On the other hand, rearrangement concerted with cleavage would give a biradical cation excited-state precursor of **9**, which could decay to **9** and consequently to its equilibration (4) with **8**.

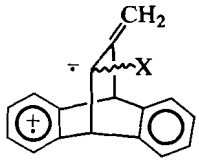

6

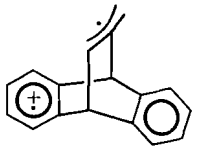

7

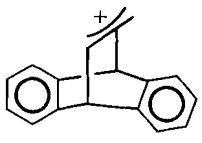

8

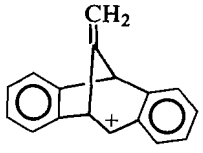

9

We have noted (7) that electron transfer from the π,π^* excited state to give a zwitterionic biradical may only be important when it is fast (and thus only when it is exothermic) and that the exothermicity may be judged from the Weller equation (9). A consequence of this requirement is that excited triplet states are less apt to be reactive than corresponding singlet states, as they are generally lower lying in energy (7*c*). In general, electron transfer from an excited benzene ring in its triplet state to a β carbon–chlorine bond is apt to be endothermic (7*c*). Thus, lacking the capability for ready electron transfer, the triplet of **3**-Cl (and that of its allylic isomer) undergoes the alternative allylic and allyl-to-cyclopropyl rearrangements.

Carbon–bromine bonds may be estimated to be at least 0.5 V more readily reducible than corresponding carbon–chlorine bonds (10). This energy difference is reflected in an equivalent lowering in energy requirement for electron transfer in **3**-Br vs. **3**-Cl (or to the allylic bromide system (11)) and thus, with the bromides, the "ionic" process is favored. In the dipolar aprotic solvent acetone, it is reasonable that tight ion pairs would be formed and that ion-pair return would be an important phenomenon. This, in fact, is the case, as allylic isomerization and rearrangement return to **4**-Br occur more rapidly than solvolysis. The latter undoubtedly involves capture of cation **9** by acetone (6), followed by hydrolysis of the resulting oxonium ion, enol ether, or hemiacetal by adventitious water or during work-up.

Direct irradiations

As the singlet energy of the aromatic ring is about 16 kcal/mol greater than its triplet energy (7*c*, 12) it might be anticipated (7, 9) that **2**-Cl and (or) **3**-Cl might be photoactive in the "ionic" sense upon direct irradiation. Accordingly, a solution of **2**-Cl in acetic acid was subjected to 254-nm irradiation. It disappeared rapidly, giving rise to a melange of hydrocarbon and acetate products including about 65% of a mixture of **3**-OAc, *exo*-**4**-OAc, and **10**-OAc, 15% of 3,4-benzofluorene (**11**), 10% of 1-methylfluoranthene (**12**), and small amounts of **1**-OAc and of

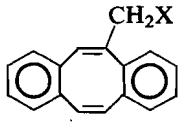

10

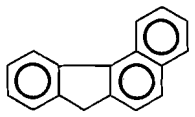

11

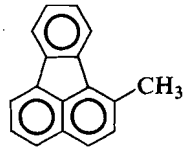

12

what is tentatively identified as 2,3-benzofluorene. (When the irradiation was interrupted before complete disappearance of alkyl chloride, **3**-Cl was also present.) In a separate experiment, it was shown that direct (254-nm) irradiation of **2**-OAc in acetic acid or in benzene led to a 4:1 mixture of **10**-OAc and **1**-OAc (so that **2**-OAc is undoubtedly the source of the **10**-OAc and the **1**-OAc), that **3**-OAc is photochemically inert, and that **4**-OAc is slightly active (with no identifiable products seen).

As discussed below, irradiation of **5**-Cl leads to **12**, so that the primary products of direct irradiation of **2**-Cl in acetic acid are undoubtedly **2**-OAc, **3**-OAc, **4**-OAc, **3**-Cl, **5**-Cl, and the benzofluorenes. Of these, one might speculate that **5**-Cl arises via intersystem crossing to the triplet of **2**-Cl and (or) **3**-Cl and that the others are the result of excited singlet reactions.

As the composition of the acetate mixture changed with irradiation time, an experiment was conducted in which the extent of acetate production from **2**-Cl was less than 15%. This led to a mixture of acetates containing approximately 50% of **4**-OAc, 28% of **3**-OAc, 13% of **2**-OAc, and 8% of **10**-OAc. The absorbance for **1**-OAc was too small to integrate. These ratios are not substantially different from those produced in the ground-state silver acetate induced acetolysis of **2**, **3**, and **4** chlorides (4). It therefore seems reasonable to assume that the acetates are formed by capture of the mixture of cations **8** and **9**, as in the ground-state system. It is generally true (1) that photosolvolysis products in systems such as these arise from thermally relaxed, that is, normal, cations, and this seems to be true here as well. As described above, it has been proposed (7, 8) that, following photoexcitation, β-arylethyl halides suffer electron transfer to give zwitterionic biradicals that may fragment to biradical cations and halide ion, and it is not unreasonable to

propose a similar initial course for **2**-Cl and **3**-Cl photoreactions. Where the branching to give benzofluorenes occurs is completely obscure.

It is of interest that benzofluorenes are not produced in observable amounts in the ground-state solvolysis of **2**, **3**, or **4** bromides or chlorides (4), but that **11** is produced (13) in small amounts by silver acetate promoted solvolysis of **1**-Br or by deamination of **1**-NH_2. No 2,3-benzofluorene was reported by these workers. As the process for the formation of **11** from **1**-Br is not clear, and as labelling experiments have not been done in either the ground-state work or the photoreactions, it seems wise to defer speculation at this time.

While **5**-Cl is stable under sensitization conditions (it, of course, is the product of triplet sensitization of **2**-Cl and **3**-Cl), irradiation with 254-nm light led to the formation of 1-methylfluoranthene (**12**) in about 50% yield, along with about 25% of a mixture of acetates. **12** was identified by its mass spectrum, its ^1H and ^{13}C nmr spectra, its ultraviolet spectrum, and its melting point (14). **12** is not observed in silver ion promoted acetolysis of **5**-Cl (4).

The acetate mixture produced in the irradiation of **5**-Cl was substantially identical with those produced by kinetic control in the ground-state reactions (4) or **2**-Cl, **3**-Cl, and **5**-Cl, comprising 43% of **4**-OAc, 36% of **3**-OAc, 11% of **2**-OAc, 8.5% of **10**-OAc, and 1.5% of **1**-OAc, if it is assumed that the latter two compounds are derived by photoreaction of **2**-OAc. It seems reasonable to assume that **4**-OAc, **3**-OAc, and **2**-OAc are derived by electron transfer from the π,π^* state to give the zwitterionic biradical **13**, or an isomeric species in which electron transfer has occurred from the other ring, which loses chloride ion to give the biradical cation **14**. Reverse electron transfer from **14** followed by, or concomitant with, ring opening would give the allylic cation **8** whose equilibration with **9** is discussed above.

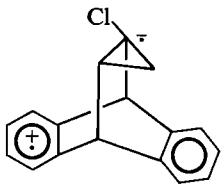

13

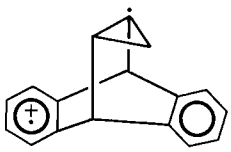

14

We are considering a number of possibilities for this remarkable rearrangement of **5**-Cl to **12**. It is known that irradiation of dibenzonorbornadienes (15), triptycenes (16), and dibenzohomobarrelenes, e.g., **5**-H (17), leads to products whose formation can be rationalized by an initial π,π bridging between two aromatic rings, followed by extrusion of a carbene from the frustrated di-π-methane biradical intermediate. It is possible to devise mechanisms for the reaction involving carbene intermediates. It is also possible to conceive of reaction paths involving an early electron-transfer process (1, 7, 8), consistent with the accompanying formation of acetolysis products. We are presently continuing work on this reaction and hope that experiments in progress or in prospect will allow us to choose among the various possibilities.

Experimental

General

The ^1H nmr spectra were determined with Varian A-60-A (60 MHz) (bromides), and EM-390 (90 MHz) and Brüker WM-250 (250 MHz) (chlorides) instruments. The preparation and properties of all compounds have been described (4). Solvents used were spectrograde quality. Irradiations in acetone with the Hanovia lamps were carried out in Pyrex tubes and the lamp had a Corex filter. Irradiations in acetic acid were carried out in a Srinivasan–Griffin Rayonet reactor with 254-nm lamps in quartz vessels.

Irradiation of 7-chloromethyl-2,3;5,6-dibenzobicyclo[2.2.2]octa-2,5,7-triene (2-Cl) in acetone

A solution of 100 mg (0.40 mmol) of **2**-Cl in 0.8 mL of acetone-d_6 in a Pyrex nmr tube was deoxygenated by bubbling nitrogen through the solution for 1 h while it was being cooled. Irradiation was conducted with a 450-W Hanovia lamp for 24 h, at which time the tube had become frosted with polymer. The ^1H nmr analysis showed a composition of approximately 65% of **5**-Cl, 30% of **3**-Cl, and 5% of **2**-Cl. The product ratios were obtained by integration of the following absorptions: H-8 (*exo*), 1H, dd, δ 1.30 (J = 7.0, 8.8 Hz) and H-8 (*endo*), 1H, dd, δ 0.55 (J = 7.0, 4.9 Hz) of **5**-Cl; H-9, 2H, d, δ 4.45 (J = 1.2 Hz) of **2**-Cl; H-9, 1H, d, δ 5.25 (J = 1.8 Hz) and H-9, 1H, d, δ 5.35 (J = 2 Hz) of **3**-Cl. Evaporation of the solvent under reduced pressure and chromatography of the residue on alumina (Merck 71707) gave **5**-Cl as the first fraction when eluted with petroleum ether – 10% benzene. The isolated yield of **5**-Cl was 41% (41 mg, 0.16 mmol), mp 116–117°C (lit. (4) mp 121–122°C). The reaction on a preparative scale in acetonitrile sensitized by acetophenone is described in the accompanying paper (4).

Irradiation of 8-chloro-7-methylene-2,3;5,6-dibenzobicyclo[2.2.2]-octa-2,5-diene (3-Cl) in acetone–acetonitrile

A solution of 100 mg (0.40 mmol) of **3**-Cl in 0.6 mL of acetonitrile-d_3 and 0.3 mL of acetone-d_6 in a Pyrex nmr tube was deoxygenated as above. The sample was then irradiated with a 450-W Hanovia lamp for 72 h, at which time ^1H nmr analysis indicated a composition of approximately 48% each of **5**-Cl and **3**-Cl and 4% of **2**-Cl.

Acetophenone-sensitized irradiation of 3-Cl

A solution of 150 mg (0.59 mmol) of **3**-Cl and 0.2 mL (205 mg, 1.67 mmol) of acetophenone dissolved in 0.7 mL of acetonitrile-d_3 in a Pyrex nmr tube was deoxygenated as above and was irradiated with a 450-W Hanovia lamp for three days, after which time the ^1H spectrum indicated a ratio of **5**-Cl to **3**-Cl of about 20:1. The contents were subjected to chromatography on silica gel and eluted with 10% benzene in petroleum ether (bp 40–60°C). The first fraction was collected. This contained 70 mg (47%) of **5**-Cl.

When biphenyl was attempted as sensitizer, no reaction ensued.

The ^1H nmr analysis of product mixtures of bromides

The areas of the following absorptions were used to calculate the ratios given in the following irradiation experiments (acetone-d_6): 4-*endo*-bromo-8-methylene-2,3;5,6-dibenzobicyclo[3.2.1]octadiene (*endo*-**4**-Br), H-4, 1H, d, δ 5.80, J = 5.5 Hz; 4-*exo*-bromo-8-methylene-2,3;5,6-dibenzobicyclo[3.2.1]octadiene (*exo*-**4**-Br), H-4, 1H, d, δ 5.52, J = 1.8 Hz; 8-bromo-7-methylene-2,3;5,6-dibenzobicyclo[2.2.2]octadiene (**3**-Br), H-9, 2H, d, δ 4.20, J = 1.2 Hz; 8-methylene-2,3;5,6-dibenzobicyclo[3.2.1]octadiene-4-ol (**4**-OH), H-4, 1H, d, δ 3.8–3.9, J = 2 Hz (*exo*-OH) and J = 5 Hz (*endo*-OH).

The experiments were conducted substantially as described above for the chlorides (through Pyrex). Compound **2**-Br gave a product mixture of approximately 17% of **4**-OH, 7% of **4**-Br, 40% of **2**-Br, and 37% of **3**-Br, and **3**-Br gave one of 14% of **4**-OH, 4% of **4**-Br, 43% of **2**-Br, and 38% of **3**-Br upon irradiation until the solutions turned brown. The ratio of solvolysis to isomerization was not affected by addition of small amounts of water. No peaks attributable to **5**-Br were noted.

Irradiation of 1-bromomethyl-3,4;6,7-dibenzotricyclo[3.3.0.$0^{2,8}$]-octa-3,6-diene (1-Br) in acetone

A solution of 80 mg (0.27 mmol) of **1**-Br in 0.6 mL of acetone-d_6 in a Pyrex nmr tube was deoxygenated as above for 1 h, and irradiated with a 250-W Hanovia lamp for 5 d; ^1H nmr analysis showed that no significant reaction had occurred.

Irradiation of 4-bromo-8-methylene-(2,3;6,7)dibenzobicyclo[3.2.1]-octa-2,6-diene (4-Br)

In a Pyrex nmr tube was placed a mixture of 80 mg (0.27 mmol) of 52% of *exo*-**4**-Br, 30% of *endo*-**4**-Br, 6% of **2**-Br, 9% of **3**-Br, and 3% of **1**-Br dissolved in 0.6 mL of acetone-d_6. The solution was degassed as above and the sample was irradiated with a 450-W Hanovia lamp. After 17 h of irradiation, ^{1}H nmr analysis showed a ratio of 31 of *endo*-**4**-Br/15 of *exo*-**4**-Br/12 of **3**-Br/13 of **2**-Br/10 of **1**-Br/20 of **4**-OH.

Direct irradiation of 2-Cl in acetic acid

In a typical experiment, a solution of 108 mg (0.43 mmol) of **2**-Cl in 30 mL of HOAc in a quartz tube, after 20 min of nitrogen bubbling, was irradiated in a Rayonet reactor at 254 nm for 20 h. The solution was poured into a mixture of water and ether. The water layer was extracted with ether and the combined ethereal solutions were neutralized with aqueous sodium bicarbonate, washed three times with water, and dried (Na_2SO_4). Evaporation of the solvent left 130 mg of a dark oil, which was separated into polar acetate fractions and nonpolar hydrocarbon fractions by thick-layer chromatography on silica gel. The hydrocarbon fractions moved with hexane and the acetates were extracted with ether. Analysis was by 250-MHz ^{1}H nmr spectroscopy, using peaks (4) at δ 5.51, 5.30, 5.00, 4.77, and 4.60 for **3**-OAc, at δ 5.95, 5.05, 4.93, 4.32, and 3.88 for *exo*-**4**-OAc, at δ 4.44 and 3.10 for **1**-OAc, at δ 4.87 for **10**-OAc, at δ 8.79, 8.42, and 4.02 for 3,4-benzofluorene (**11**) (18), at δ 8.21 and 4.09 for 2,3-benzofluorene (18), and at δ 2.90 for 1-methylfluoranthene (14*c*,*d*). The results averaged for several experiments are given in the discussion section.

In an experiment designed to measure initial products, a solution of 117 mg (0.46 mmol) of **2**-Cl in 65 mL of HOAc was irradiated for 30 min. Chromatographic separation gave 92 mg of less polar material containing largely **3**-Cl (major) and **2**-Cl (minor) and 16 mg of polar material; ^{1}H nmr analysis (250 MHz) with "cut-and-weigh" determination of the carbinyl proton(s) gave 51% of **4**-OAc, 28% of **3**-OAc, 13% of **2**-OAc, and 8% of **10**-OAc. **1**-OAc could not be measured accurately.

Direct irradiation of 7-acetoxymethyl-2,3;5,6-dibenzobicyclo[2.2.2]-octa-2,5,7-triene (2-OAc) in acetic acid

A solution of 10 mg of **2**-OAc in 1 mL of acetic acid-d_4 was deoxygenated and irradiated with 254-nm light for 17 h. The ^{1}H nmr analysis indicated that the mixture contained 80% of **10**-OAc and 20% of **1**-OAc. A larger scale reaction, carried out in benzene,[3] gave similar results: **10**-OAC, bp 90°C (1 Torr); ^{1}H nmr ($CDCl_3$), δ: 6.74 (s, 2H, H-7, H-8), 4.87 (d, 2H, CH_2, $J_{CH_2,4}$ = 1 Hz), 1.94 (acetate CH_3). *Anal.* calcd. for $C_{19}H_{16}O_2$: C 82.58, H 5.84; found: C 82.71, H 5.99.

Direct irradiation of 2-chloro-6,7;8,9-dibenzotricyclo[3.2.2.0^{2,4}]-nona-6,7-diene (5-Cl) in acetic acid

A solution of 168 mg (0.66 mmol) in 60 mL of HOAc in a quartz tube was deoxygenated (N_2 bubbling) for 25 min. After 3.4 h irradiation at 254 nm, the solvent was rotovapped off; ^{1}H nmr analysis of the residual oil indicated about 40% reaction using integration of H-1 and H-5 proton absorbances for **5**-Cl, that of the methyl group of 1-methylfluoranthene at δ 2.79, and the acetate methyl peaks (δ 1.9–2.3). Column chromatography and silica gel with methylene chloride – hexanes gave three fractions. The first fraction was **5**-Cl (72 mg, 43% of recovery).

The second fraction was 1-methylfluoranthene. It was identified by melting point, 67–72°C (lit. (14*a*,*b*) mp 72–73°C); its uv spectrum (λ_{max}: 275, 282, 285, 310, 325, 347, 362 nm); its mass spectrum (parent peak, 216); its ^{1}H nmr spectrum (14*c*,*d*), δ: 8.00–7.27 (m, 9H, aromatic H), 2.80 (s, 3H, CH_3). A ^{13}C nmr spectrum showed 16 carbon atoms in the range δ 140.0–119.8 (aromatic) and one at 20.1 (CH_3).

[3]This reaction was carried out by Dr. G. O. Mayo.

This fraction weighed 41 mg (50% yield based upon unrecovered **5**-Cl).

The third fraction was a mixture of five acetates and weighed 37 mg (26% yield based upon unrecovered **5**-Cl). The composition of this mixture was determined by ^{1}H nmr analysis (250-MHz nmr as described above for the irradiation of **2**-Cl, but using a cut-and-weigh procedure). It contained 43% of **4**-OAc, 36% of **3**-OAc, 11% of **2**-OAc, 8.5% of **10**-OAc, and 1.5% of **1**-OAc.

Acknowledgements

The authors are indebted to the National Science Foundation (Grant CHE-83-09927 and predecessor grants) for partial support of this work. D.B.'s stay in Boulder was sponsored by the student exchange program of the University of Colorado and the University of Regensburg, Federal Republic of Germany.

1. S. J. Cristol, R. J. Opitz, and E. O. Aeling. J. Org. Chem. **50**, 4834 (1985).
2. S. J. Cristol and T. H. Bindel. J. Org. Photochem. **6**, 372 (1983).
3. (*a*) S. J. Cristol and G. A. Lee. J. Am. Chem. Soc. **91**, 7554 (1969); (*b*) **95**, 7067 (1973); (*c*) S. J. Cristol and R. P. Micheli. J. Org. Chem. **40**, 667 (1975); (*d*) J. Am. Chem. Soc. **100**, 850 (1978).
4. S. J. Cristol, G. C. Schloemer, D. Braun and G. O. Mayo. Can. J. Chem. **64**, 1077 (1986).
5. G. H. Slocum and G. B. Schuster. J. Org. Chem. **49**, 2177 (1984).
6. S. J. Cristol and T. H. Bindel. J. Org. Chem. **45**, 951 (1980); S. J. Cristol and T. H. Bindel. J. Am. Chem. Soc. **103**, 7287 (1981).
7. (*a*) S. J. Cristol, D. G. Seapy and E. O. Aeling. J. Am. Chem. Soc. **105**, 7337 (1983); (*b*) S. J. Cristol and M. Z. Ali. Tetrahedron Lett. **24**, 5839 (1983); (*c*) S. J. Cristol, T. H. Bindel, D. Hoffman, and E. O. Aeling. J. Org. Chem. **49**, 2368 (1984); (*d*) S. J. Cristol and E. O. Aeling. J. Org. Chem. **50**, 2698 (1985).
8. S. J. Cristol and R. M. Strom. J. Am. Chem. Soc. **101**, 5707 (1979).
9. A. Weller. *In* 5th Nobel Symposium. Fast reactions and primary processes in chemical kinetics. *Edited by* S. Claesson. Interscience, New York. 1967. pp. 413–428.
10. (*a*) F. L. Lambert. J. Org. Chem. **31**, 4184 (1966); (*b*) F. L. Lambert and G. B. Ingall. Tetrahedron Lett. 3231 (1974); (*c*) F. G. Bordwell and A. H. Clemens. J. Org. Chem. **47**, 2510 (1982).
11. S. J. Cristol and G. A. Graf. J. Org. Chem. **47**, 5186 (1982).
12. S. L. Murov. Handbook of photochemistry. Marcel Dekker, New York. 1973. Sect. I.
13. S. J. Cristol, G. C. Schloemer, D. R. James, and L. A. Paquette. J. Org. Chem. **37**, 3852 (1972).
14. (*a*) N. Campbell and W. Hang. J. Chem. Soc. 1513 (1949); (*b*) S. H. Tucker. J. Chem. Soc. 2182 (1949); (*c*) E. Clar, A. Mullen, and Ü. Sanigok. Tetrahedron, **25**, 5539 (1959); (*d*) M. L. Lee, M. Novotny, and K. D. Bartle. Anal. Chem. **48**, 405 (1976).
15. J. Ipaktschi. Chem. Ber. **105**, 1989 (1972).
16. (*a*) H. Iwamura and K. Yoshimura. J. Am. Chem. Soc. **96**, 2652 (1974); (*b*) H. Iwamura. Chem. Lett. 5 (1974); (*c*) H. Iwamura and H. Tukeda. Tetrahedron Lett. 3451 (1978).
17. (*a*) H. Hemetsberger, W. Brauer, and D. Tartler. Chem. Ber. **110**, 1586 (1977); (*b*) H. Hemetsberger, W. Holstein, and F. Werres. Tetrahedron, **39**, 1151 (1983).
18. D. W. Jones, R. S. Mathews, and K. D. Bartle. Spectrochim. Acta, Part A, **28**, 2053 (1972).

Steric activation in prototropic reactions of pyrazine derivatives. I. Polar and conformational effects

T. W. S. LEE AND ROSS STEWART[1]
Department of Chemistry, University of British Columbia, Vancouver, B.C., Canada V6T 1Y6
Received September 13, 1985
This paper is dedicated to Professor Arthur N Bourns

T. W. S. LEE and ROSS STEWART. Can. J. Chem. **64**, 1085 (1986).

The rates of proton loss from methyl groups in a number of pyrazine derivatives have been measured in D_2O by monitoring the replacement of protium by deuterium at the acidic sites of the substrates; they include the reaction of four methylpyrazines with $NaOD/D_2O$ and nine alkylpyrazinium ions with D_2O/DCl. The reactive site, which is a methyl group conjugated to the aza or azonium group of the substrate, is in all cases activated by an adjacent alkyl group, with the greatest effect, a factor of about 30, occurring when a proton on nitrogen is replaced by a methyl group. The phenomenon is analysed in terms of polar effects, ring strain and inter-alkyl interactions (including gear effects), and hybridization changes at nitrogen.

T. W. S. LEE et ROSS STEWART. Can. J. Chem. **64**, 1085 (1986).

Opérant dans le D_2O et observant le taux de remplacement des protons par des deutérium au niveau des sites acides des substrats, on a mesuré les vitesses de perte de protons des groupements méthyles d'un certain nombre de dérivés de la pyrazine; les systèmes étudiés comportent les réactions de quatre méthylpyrazines avec le $NaOD/D_2O$ et de neuf ions alkylpyrazinium avec le D_2O/DCl. Dans tous les cas, le site réactif, qui est le groupement méthyle qui est conjugué avec le groupement azo ou azonium du substrat, doit sa réactivé à un groupement alkyle voisin et l'effet est maximal, par un facteur de 30, est obtenu lorsqu'on remplace un proton de l'azote par un groupement méthyle. On analyse le phénomène en fonction d'effets polaires, de tensions de cycles, d'interactions inter-alkyles et de changements d'hybridation au niveau de l'azote.

[Traduit par la revue]

Introduction

We have previously shown that alkyl groups adjacent to an acidic methyl group in a number of heterocyclic systems activate the methyl group with respect to proton loss. These systems include lumazines and 5-deazalumazines (1–3), 2-pyrimidones (4, 5), iminopyrimidines (4), and pyrimidonium salts (6).[2] We now report the results of a study of alkyl substituted pyrazines and their protonated or quaternized salts (eqs. [1] and [2]), where again activation by adjacent alkyl groups and

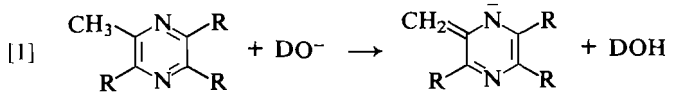

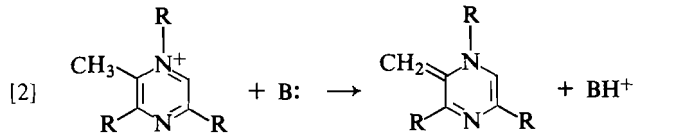

deactivation by more distant alkyl groups is observed. In the accompanying paper we have scrutinized the bases used to remove the proton from the reactive methyl group of one of the cationic substrates (eq. [2]). Using the Brønsted relationship we find that steric acceleration is present there also, but only with carboxylate bases; sterically hindered amines react more slowly than would be expected on the basis of their equilibrium base strengths.

Results and discussion

Pyrazines

The effect of methyl substitution on the reaction between pyrazines and hydroxide ion (eq. [1]) can be seen from the results in Table 1. The reaction of **1**, 2,3-dimethylpyrazine, with hydroxide ion is first order in substrate (highly linear first-order plots were obtained in all cases) and is also first order in hydroxide ion, as can be seen from the results in the table. Whereas the 2,3-dimethyl compound reacts faster than the 2-methyl compound, the 2,5- and 2,6-dimethyl compounds react more slowly. (Since all the methyl groups in the compounds in Table 1 are reactive, the comparisons are made on a per methyl basis.) The direction of this effect is consonant with those observed earlier. Though the magnitude is smaller than that observed in some of the earlier reactions, the deactivating effect of remote methyl is nonetheless quite substantial. A Hammett plot for compounds **2**, **3**, and **4**, using **2** as the parent and the σ values for *m*-methyl and *p*-methyl for **3** and **4**, gives a slope of +6.2. The magnitude of the latter shows that there is a strong electronic effect operating in this reaction and that it is in the conventional direction. That is, nonadjacent alkyl groups are substantially deactivating.

The electronic effect of an *ortho* group in aromatic systems is believed to be greater than that of the same group in the *meta* and *para* positions, though this may not always apply to alkyl groups (8–10).

Work with other heterocyclic systems had shown that a methyl group in a position "*meta*" to a reactive methyl centre is strongly deactivating, with effects that are generally considerably greater than that observed in this instance. It was suspected that the effects should be even greater for methyl at a "*para*" position and from the present results that appears to be so. (Such an arrangement could be achieved in only a few instances in the systems studied previously and then only when the "*para*" methyl was attached to nitrogen rather than to carbon. Since the geometrical changes that accompany those prototropic reactions are much greater at nitrogen than at carbon, *vide infra*, the significance of the observed effects was less clear than in the present case.) Similar effects of alkyl groups on the acidities of substituted benzenes have been observed previously (11, 12).

Pyrazinium ions

In order to compare the effect of hydrogen with alkyl at the cationic nitrogen centre, experiments were conducted in two

[1]Author to whom correspondence may be addressed.

[2]A case of steric acceleration involving enolization of a hindered aryl alkyl ketone has recently been reported (7).

TABLE 1. Rate data for reaction of alkylpyrazines with NaOD/D_2O at 30°C

	Compound	NaOD molarity	$10^7 k_{obs}$, s^{-1}	$10^7 k_2$, $M^{-1} s^{-1}$
1	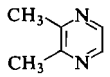	2.21	8.60	1.95
		1.77	7.00	1.98
		1.33	5.12	1.93
		0.88	3.32	1.89
		0.44	1.54	1.77
				1.90 ave.
2	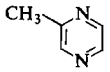	2.21	3.40	1.60
3	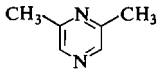	2.21	3.00	0.68
4	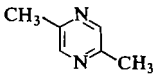	2.21	0.61	0.14

TABLE 2. Rate constants for exchange of hydrogens of the 2-methyl group of pyrazinium iodides in acid solution at 30°C

	Cation	k_{obs}, s^{-1}	
		D_2O/DCl (2.13 *M*)	D_2O, CF_3CO_2D (2.0 *M*)
5	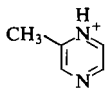	1.0×10^{-7a}	—
6	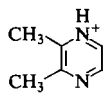	6.0×10^{-7}	1.8×10^{-6}
7	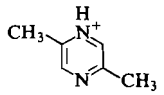	7.7×10^{-9}	—
8	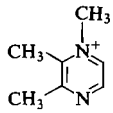	1.74×10^{-5}	4.6×10^{-5}
9	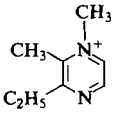	1.29×10^{-5}	—
10	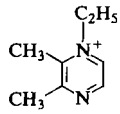	1.56×10^{-5}	2.4×10^{-5}
11	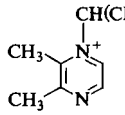	1.17×10^{-5}	1.5×10^{-5}
12	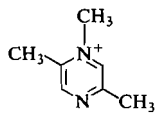	1.60×10^{-7}	—
13	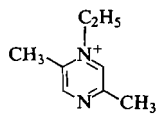	1.30×10^{-7}	—

[a]Estimated value after statistical correction, see text; actual $k_{obs} = 6.8 \times 10^{-8}$.

different acidic media, 2.13 *M* DCl in D_2O and 2.0 *M* CF_3CO_2D in D_2O, where the neutral bases **1**, **2**, and **4** are highly protonated (13). It can be seen from the results in Table 2 that similar trends are observed when the rate constants of the protonated and alkylated species are compared in the two media. The observed rates are slightly higher in the CF_3CO_2D/D_2O solution than in the DCl/D_2O solution, presumably because the trifluoroacetate ion makes a contribution to the proton abstraction process.

In the cases of **8**, **10**, and **11**, slow exchange was also observed at the C-3 methyl groups (~1/25th of the rate at the C-2 methyl) but we cannot be certain that this is not due to the presence of low concentrations of the protonated form of the quaternary salts. The pK_2 values of methylpyrazines, which would correspond to pK_1 of the quaternary salts, are in the region of −4.0 (13) but the higher prototropic reactivity expected for the dications might well compensate in part for their low concentrations and allow observation of exchange at the C-3 methyl groups.

In comparing the protonated and alkylated species one should note first that the difference in rate between the fast and slow isomers, those having a 1,2 and a 1,4 dimethyl arrangement, is much more striking in both of these cationic forms than in the neutral compounds **1** and **4**. The rate ratio for the latter reacting with hydroxide ion is 14 (Table 1), with the 1,2 compound being the more reactive. In the case of the protonated isomers **6** and **7** reacting with water the ratio is 78 and in the case of the pairs of alkylated isomers **8** and **12** and **10** and **13** the values are 109 and 120, again with the adjacent arrangement of methyl groups being the more reactive one.

The rate constant shown in Table 2 for methylpyrazinium ion, **5**, has been statistically corrected in an attempt to put it on the same basis as the other ions. In the other cases the exchanging methyl group is flanked at all times by cationic nitrogen, whereas **5** is in equilibrium with the other protonated form in which the methyl group and the cationic nitrogen are out of conjugation. Since **5** is expected to be present in larger amount than its isomer the correction factor should be less than two, leading to the estimated value given in the table.

Alkylation site

We recently examined the effect of neighbouring methyl on the prototropic reactivity of lumazines and deazalumazines and showed that the effect was greater when the neighbouring group was on nitrogen than when it was on carbon (1). The effect was as large as two orders of magnitude in one case, although for various reasons the precision of the measurements was less than in the present work.

In the present work the effect of replacing a proton on a neighbouring nitrogen atom with a methyl group can be seen by comparing the rate constants for **6** and **8**, the rate ratios being 29 in DCl/D_2O and 26 in D_2O/CF_3CO_2D. A similar result is seen when the values in DCl/D_2O of **7** and **12** are compared; here the rate ratio is 21.

How does the size of the alkyl group affect the degree of activation? It can be seen by comparing the rate constants for **8**, **10**, and **11** that going from methyl to ethyl to isopropyl causes the effect to subside. The rate ratio for hydrogen, methyl, ethyl, and isopropyl is 1:29:26:20 in the DCl/D_2O medium, with the drop-off being somewhat greater in D_2O/CF_3CO_2D. A similar effect is observed in the series **8** and **9** and in the series **7**, **12**, and **13**, where the ratio of rate constants for hydrogen, methyl, and ethyl is 1:21:17. As with the earlier system, the effect of alkyl at a neighbouring carbon is less, the rate ratio for **5** and **6** being 1:6.

It is clear that alkylation at nitrogen has a large effect on the adjacent reactive group; the size of the alkyl group is not critical, the effect being largest for methyl. (In 2-iminopyrimidinium ions, where the flanking alkyl groups are attached to carbon, the size of the alkyl group is again not critical, though in this case the isopropyl group has the largest effect (4).)

The large effect of *N*-alkylation is probably a result of relief of methyl–alkyl strain that accompanies conversion of the cation to the neutral intermediate **15** in eq. [3].

[3] 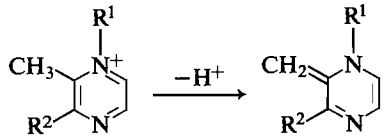

14 **15**

Each atom in the pyrazinium ring has sp^2 bonding and the ring can be assumed to be planar (14) or as close to planarity as the steric effect of the neighbouring substituents will allow; the intermediate **15**, however, has an sp^3 arrangement at nitrogen and it can adopt nonplanar conformations such as those shown in **16** and **17**. (See refs. 15*a* and *b* (p.75) for a description of the conformations of the analogous 1,3-cyclohexadiene and dihydropyrimidine systems.)

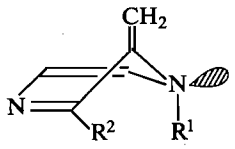

16

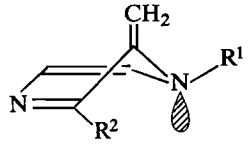

17

Molecular models of **15** show that the *N*-alkyl group R^1 can swing well away from the adjacent methylene group if it adopts the pseudoaxial conformation shown in **16**. As we have seen, the size of the alkyl group is not critical here though the effect is biggest in the present instance with methyl, the smallest alkyl group. Presumably the conventional steric effects that would be expected to be present in the transition state of any bimolecular reaction are present here and come into play with the larger groups.

When the neighbouring alkyl group is attached to carbon rather than to nitrogen the effect is smaller since here no hybridization change accompanies proton loss from the reactive site. Nonetheless, the bonds that join R^2 and methylene to the ring in the intermediate **16/17** make a significant dihedral angle, whereas in the starting materials the aromaticity of the ring ensures that these angles will be close to zero, at least in the absence of major strain. Accordingly, whatever strain accompanies the positioning of, say, two methyl groups at adjacent sites on an aromatic ring should be relieved to some extent by conversion to a nonaromatic system.

Can this explanation be applied to the heterocyclic systems studied previously, which all show activation by neighbouring methyl groups? Their structures are shown below, with the active site marked by an asterisk and the activating methyl groups marked by a dagger.

In the cases of **18–20** the alkylated nitrogen is formally sp^3 but in each case there is conjugation with a powerful electron sink, which will tend to make the ring planar. Indeed, in the case of **18** the geometry of the ring containing the exchanging groups

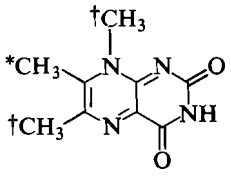

18

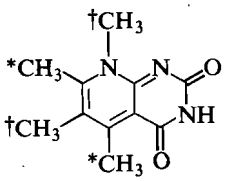

19

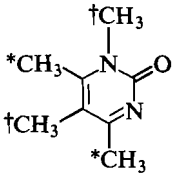

20

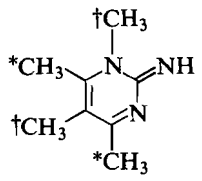

21

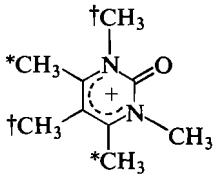

22

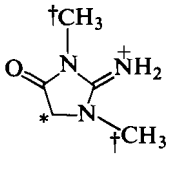

23

may closely resemble the quaternary pyrazine salts described herein. In the cases of **21** and **22** the rings will also tend toward a planar arrangement and will also form nonplanar intermediates when proton loss occurs. The creatinium salts, **23**, are an enigma. Here, methyl groups are slighly activating when present on endocyclic nitrogen and slightly deactivating when present on exocyclic nitrogen. The deprotonated intermediate in this case is mesoionic and it is difficult to assess the geometrical changes that accompany the loss of a proton from the activated methylene group in the ring.

Gear effects

It is known that *o*-xylene prefers the gear-clashed conformation **24** rather than the other gear-clashed form **25**, or the gear-meshed form **26** (16, 17).

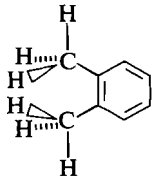

24

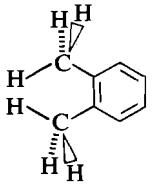

25

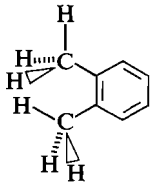

26

Roussel and co-workers (17, 18) have recently examined the interplay between alkyl groups attached to aromatic rings and have rationalized reactivity differences in a number of systems on the basis that adjacent methyl and similar alkyl groups prefer to avoid the interactions shown in **25** and **26**. Moreover, Schug and Viers (19) have calculated the energies of the rotational conformers of 2,3-lutidine and found that the gear-clashed rotamer **27** is more stable than the two gear-meshed rotamers **28** and **29** by 0.36 and 0.59 kcal mol^{-1}, respectively; it is more stable than the gear-clashed rotamer **30**, which has a frontal interaction of hydrogens, by 1.00 kcal mol^{-1}.

In an attempt to determine the extent of ring strain on rates of prototropic reactivity we have previously determined the geometry of a number of pyrimidonium salts, **22**, by means of X-ray crystallography. Although adjacent alkyl groups caused the ring to depart significantly from planarity in most cases, this did not always produce the higher reactivity that might have been expected. In addition to the matter of ring strain, bond deformations and inter-methyl conformational effects such as gearing may have significance. We showed that the inter-methyl distances were short in a number of the pyrimidonium ions but, as with ring strain, there was not a particularly good correspondence with high reactivity. The situation can be illustrated with

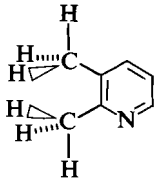

27

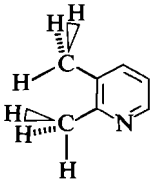

28

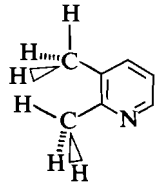

29

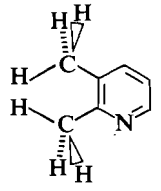

30

the three ions **31**–**33**, where the methyl group that undergoes proton loss is marked with an asterisk (Table 3).

The lower reactivity of **33** compared to **32** can be partly explained by the polar effect of the additional methyl group but it would be surprising if this alone were sufficiently large to overwhelm the effects of higher ring strain and lower inter-methyl distances.

In all three ions the adjacent methyl groups at positions 1 and 6 adopt the gear-clashed conformation shown in **24** and **27**. In **32** the methyl groups at positions 5 and 6 are close to being gear-meshed, as shown in **34**. In **33** the stable arrangement (at least in the crystal lattice) is that shown in **35**, where only gear-clashed arrangements are present (two favourable, one unfavourable).

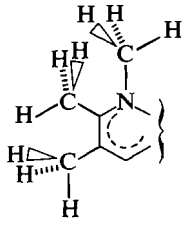

34

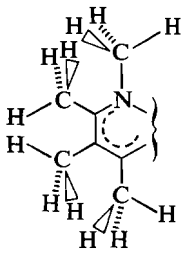

35

It is not certain what would be the favoured geometry of adjacent methyl and methylene groups in the intermediate species formed as a consequence of proton loss from the C-5 methyl group. However, it is clear that the unfavourable inter-hydrogen interaction between the central methyl groups in **35** (at C-5 and C-6) will be retained to a considerable extent in the intermediate since the methyl pair at C-4 and C-5 will presumably maintain their gear-clashed arrangement. The intermediate formed from **34**, on the other hand, will be free to adopt whatever conformation is most satisfactory, since there is now no buttressing methyl group present at C-4.

The energy difference calculated by Schug and Viers for the two gear-clashed rotamers of 2,3-lutidine is 1.0 kcal mol^{-1}. In the case of the isomeric pyrimidonium ions **31** and **32** the rate difference corresponds to an energy of some 1.8 kcal mol^{-1}, indicating that gear effects are large enough to be significant contributors to the rate effects we have observed.

In summary, the phenomenon of adjacent alkyl groups activating and remote methyl groups deactivating prototropic

TABLE 3. Prototropic reactivities and geometries of three pyrimidonium ions[a]

	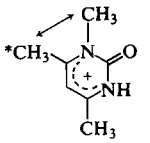 **31**	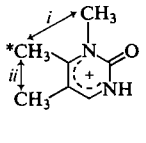 **32**	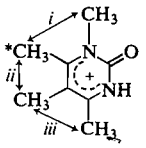 **33**
Relative reactivity[b]	1	20	2
Deviation of ring from planarity	1.6°	15.9°	17.4°
Intermethyl distances	2.30, 2.36 Å	(*i*) >2.40 Å (*ii*) 2.17 Å	(*i*) 2.23, 2.39 Å (*ii*) 1.99 Å (*iii*) >2.40 Å

[a]Data from ref. 6.
[b]For exchange of deuterium for protium at the C-5 methyl group (marked by an asterisk).

methyl sites in nitrogen heterocyclic systems has been rationalized on the basis of combinations of the following effects: (*a*) the polar effect of alkyl (deactivating), (*b*) ring strain in the starting materials (activating), (*c*) hybridization changes at nitrogen, which lead to less hindrance in the intermediate species than in the starting materials (activating), and (*d*) gear effects, which influence the energies of species containing alkyl groups (activating or deactivating).

Experimental

Compounds **1**–**4** are commercially available; the preparation of the iodide salts of **8**, **10**, **11**, and **13** has been described elsewhere (13).

The iodide salt of **12** was prepared by alkylation of 2,5-dimethylpyrazine with methyl iodide, essentially as previously described (13). Upon recrystallization from ethanol – ethyl acetate, yellow needles were obtained, mp 239–240°C. *Anal.* calcd. for $C_7H_{11}N_2I$: C 33.62, H, 4.43, N 11.20, I 50.75; found: C 33.51, H 4.56, N 11.15, I 50.60.

The iodide salt of **9** was prepared by alkylating 2-methyl-3-ethylpyrazine with methyl iodide. Analysis of the reaction mixture by nmr showed it to be a 3:1 mixture of **9** and the 2-ethyl isomer. Repeated recrystallization from ethanol – ethyl acetate gave **9**, as iodide, mp 186–188°C. *Anal.* calcd. for $C_8H_{13}N_2I$: C 36.24, H 5.34, N 10.56; found: C 36.51, H 5.20, N 10.60.

The rate measurements were made by following the exchange of deuterium for protium by nmr as previously described (4). In virtually all cases the reproducibility of the rate constants was ±5%.

Acknowledgement

We thank the Natural Sciences and Engineering Research Council of Canada for financial support.

1. R. STEWART and S. J. GUMBLEY. Can. J. Chem. **63**, 3290 (1985).
2. R. STEWART, S. J. GUMBLEY, and R. SRINIVASAN. J. Am. Chem. Soc. **102**, 6168 (1980).
3. R. STEWART, R. SRINIVASAN, and S. J. GUMBLEY. Can. J. Chem. **59**, 2755 (1981).
4. R. STEWART and T. W. S. LEE. J. Org. Chem. **47**, 2075 (1982).
5. R. SRINIVASAN, S. J. GUMBLEY, and R. STEWART. Tetrahedron, **35**, 1257 (1979).
6. T. W. S. LEE, S. J. RETTIG, R. STEWART, and J. TROTTER. Can. J. Chem. **62**, 1194 (1984).
7. A. G. PINCUS and G. GOPALAN. J. Am. Chem. Soc. **106**, 2630 (1984).
8. G. J. BIJLOO and R. F. REKKER. Quant. Struct.-Act. Relat. Pharmacol. Chem. Biol. **3**, 91 (1984).
9. M. CHARTON. Prog. Phys. Org. Chem. **13**, 119 (1981).
10. T. FUJITA and T. NISHIOKA. Prog. Phys. Org. Chem. **12**, 49 (1976).
11. J. E. HOFMANN, R. J. MULLER, and A. SCHRIESHEIM. J. Am. Chem. Soc. **85**, 3002 (1963).
12. A. STREITWIESER, JR., J. R. MURDOCH, G. HÄFELINGER, and C. J. CHANG. J. Am. Chem. Soc. **95**, 4248 (1973).
13. S. J. GUMBLEY, T. W. S. LEE, and R. STEWART. J. Heterocycl. Chem. **22**, 1143 (1985).
14. D. J. RABER and W. RODRIGUEZ. J. Am. Chem. Soc. **107**, 4146 (1985).
15. (*a*) B. SCHRADER and A. ANSMANN. Angew. Chem. Int. Ed. Engl. **14**, 364 (1975); (*b*) A. L. WEISS. Adv. Heterocycl. Chem. **38**, 1 (1985).
16. H. D. RUDOLPH, K. WALZER, and I. KRUTZIK. J. Mol. Spectrosc. **47**, 314 (1973).
17. U. BERG, T. LILJEFORS, C. ROUSSEL, and J. SANDSTRÖM. Acc. Chem. Res. **18**, 80 (1985).
18. C. ROUSSEL, A. T. BALABAN, U. BERG, M. CHANON, R. GALLO, G. KLATTE, J. A. MEMIAGHE, J. METZGER, D. ONICIU, and J. PIERROT-SANDERS. Tetrahedron, **39**, 4209 (1983).
19. J. C. SHUG and J. W. VIERS. Tetrahedron, **40**, 3971 (1984).

Steric activation in prototropic reactions of pyrazine derivatives. II. The Brønsted relation

K. NAGARAJAN, T. W. S. LEE, R. R. PERKINS, AND ROSS STEWART[1]
Department of Chemistry, University of British Columbia, Vancouver, B.C., Canada V6T 1Y6
Received September 13, 1985

This paper is dedicated to Professor Arthur N. Bourns

K. NAGARAJAN, T. W. S. LEE, R. R. PERKINS, and ROSS STEWART. Can. J. Chem. **64**, 1090 (1986).

The rate of deprotonation of the 2-methyl group in 1,2,3-trimethylpyrazinium ion by carboxylate, aniline, and pyridine bases has been measured in D_2O. Carboxylate ions containing bulky groups near the reaction centre, e.g. *ortho* benzoates, react faster than predicted by the Brønsted equation that correlates the reactions of unhindered carboxylates. Anilines and pyridines, on the other hand, show conventional steric effects. A tentative explanation for the activation engendered by groups adjacent to the carboxylate centre is based on the known effect that high concentrations of organic electrolytes have on the strengths of carboxylic acids but not of amines. Since *ortho* carboxylate ions have their relative basicities increased by an alkyl-rich environment, it is argued that the reactive methyl groups of the substrate might provide such an interaction in the transition state.

K. NAGARAJAN, T. W. S. LEE, R. R. PERKINS et ROSS STEWART. Can. J. Chem. **64**, 1090 (1986).

Opérant dans le D_2O, on a mesuré la vitesse de déprotonation du groupement méthyle de l'ion triméthyl-1,2,3 pyrazinium par les bases carboxylate, aniline et pyridine. Les vitesses de réaction des ions carboxylates qui comportent des groupements encombrants près du centre réactionnel, comme les *ortho* benzoates, sont plus rapide que celles prévues par l'équation de Brønsted qui établit une corrélation pour les réactions des carboxylates qui ne sont pas encombrés. Par ailleurs, on observe les effets stériques conventionnels avec les anilines et les pyridines. Comme explication préliminaire de l'activation engendrée par les groupements encombrants adjacents au centre réactionnel du carboxylate, on peut faire appel à l'effet connu des concentrations élevées d'électrolytes organiques sur les forces des acides carboxyliques qui n'influence pas les amines. Puisque les basicités relatives des ions *ortho* carboxylates sont augmentées par une environnement riche en groupements alkyles, on suggère que les groupements méthyles réactifs des substrats doivent fournir une telle interaction dans l'état de transition.
[Traduit par la revue]

Introduction

The role of steric effects in proton transfer reactions has been the subject of numerous publications from this laboratory (1–5). In particular, the accompanying paper deals with the increases in rate of proton removal from the activated methyl group of pyrazinium ions (eq. [1]) that are brought about by the presence of adjacent alkyl groups (1).

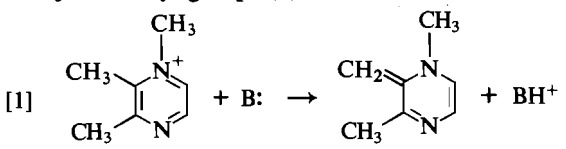

1

We turn our attention here to the matter of steric effects in the other component of the reaction, that is, the base. We report herein the results of a study of the reaction of carboxylate ions, anilines, and pyridines with 1,2,3-trimethylpyrazinium ion (**1**).

Results

Carboxylate ions

Reported in Table 1 are the rate constants for deprotonation of **1** by 35 different carboxylate bases. The latter can be subdivided into three categories: aliphatic, *meta*- and *para*-substituted benzoates, and *ortho*-substituted benzoates. The only one of these groups that gives a good Brønsted relation is that comprising the *meta*- and *para*-substituted benzoates, for which a coefficient of 0.447, (corr. coeff. 0.9913) is obtained. Considerable scatter is found in Brønsted plots of the other two groups, with the deviations being most apparent for those bases containing bulky substituents, e.g. diphenylacetate or 2,6-dimethoxybenzoate. The overall effect of bulk in the base can be seen in Fig. 1, where data for all the carboxylate ions appear. The straight line has been drawn for those carboxylates that have only monosubstitution at the α-carbon atom (included here are formate and acetate). The Brønsted coefficient for these points is 0.639, corr. coeff. 0.9987. All the other bases show positive deviations from this line, that is, they are more effective in abstracting a proton from **1** than would be expected on the basis of their equilibrium base strengths. It should be noted that over the years there have been isolated reports of other positive deviations from the Brønsted relation involving carboxylate ions, for example, in the anion catalyzed halogenation of certain ketones and esters (6) and the ionization of creatininium salts (7).[2]

Anilines and pyridines

Reported in Table 2 are the rate constants for the reaction of **1** with a series of anilines and a series of pyridines. The Brønsted plots for these two series are shown in Fig. 2. It can be seen that substitution at the 2-position gives rise to a conventional steric effect, that is, the bases are less effective kinetically than would be suggested by their equilibrium base strengths. Although the effect is small in the case of the anilines it is quite substantial in the case of the pyridines. There are many examples of this sort of behaviour in the literature (see, for examples, refs. 8–10). The Brønsted slope for the anilines is 0.707, corr. coeff. 0.9875, and for the pyridines is 0.566, corr. coeff. 0.9972, excluding in each case the 2-substituted compounds.

[1]Author to whom correspondence may be addressed.

[2]We have been informed by Dr. Brian Cox that analogous effects have recently been observed in his laboratory in the protonation of cryptands by *ortho*-substituted benzoic acids (B. G. Cox and N. van Truong, personal communication).

TABLE 1. Rate of isotopic exchange of the 2-methyl protons of **1** in aqueous (D_2O) carboxylate buffers, 30°C

	Buffer acid	10^6k_2, M^{-1} s^{-1}	pK_{DA}[a]
1	2,6-Dinitrobenzoic	1.94	1.57
2	2,6-Dichlorobenzoic	8.43	2.03
3	2-Nitrobenzoic	16.0	2.71
4	2-Iodobenzoic	101	3.36
5	2-Bromobenzoic	79.8	3.35
6	2-Chlorobenzoic	72.6	3.42
7	2-Fluorobenzoic	89.6	3.77
8	2,6-Dimethylbenzoic	225	3.75
9	2,4,6-Trimethylbenzoic	398	3.94
10	2,6-Dimethoxybenzoic	782	3.94
11	2-*tert*-Butylbenzoic	324	4.04
12	2-Isopropylbenzoic	229	4.13
13	2-Ethylbenzoic	278	4.29
14	2-Methylbenzoic	308	4.41
15	2-Methoxybenzoic	686	4.59
16	2-Ethoxybenzoic	723	4.66
17	2-Isopropoxybenzoic	813	4.74
18	3,5-Dinitrobenzoic	61.4	3.32
19	4-Nitrobenzoic	121	3.94
20	3-Nitrobenzoic	141	3.99
21	3-Chlorobenzoic	181	4.33
22	4-Chlorobenzoic	196	4.48
23	Benzoic	242	4.70
24	4-Methylbenzoic	341	4.87
25	Diphenylacetic	508	4.44
26	Isobutyric	659	5.36
27	Pivalic	1060	5.55
28	Chloroacetic	24.2	3.36
29	Bromoacetic	25.8	3.40
30	Iodoacetic	43.1	3.68
31	Methoxyacetic	67.3	4.07
32	Formic	94.7	4.25
33	Phenylacetic	216	4.81
34	Acetic	368	5.25
35	Propionic	507	5.37

[a]Values from refs. 16, 17, and ref. 12, Chapt. 2, corrected as described in ref. 7.

Discussion

It is clear from the results shown in Figs. 1 and 2 that steric hindrance in the base can have quite different effects on the rate of proton abstraction from **1**. Carboxylate ions that contain groups near the basic centre are more reactive than predicted by the Brønsted equation that correlates the reactivities of their unhindered analogues. A quite different situation is found in the case of anilines and pyridines, particularly the latter, where conventional steric effects appear to be operating.

In the accompanying paper we examined the effect of alkyl groups adjacent to the reactive site of the substrate; such groups invariably increase the rate of proton transfer, the effects being quite large when account is taken of the deactivating polar effect that more distant alkyl has on the acidic site.

Since amine bases are shown here to have conventional (deactivating) steric effects, we are not obliged to seek a universal explanation for what otherwise would have appeared to be a general (and surprising) phenomenon, viz. that groups adjacent to the reactive sites in both the acidic and basic components of the reaction accelerate the rate of proton transfer. Accordingly, we shall focus our attention on the carboxylate group in attempting to rationalize the present results.

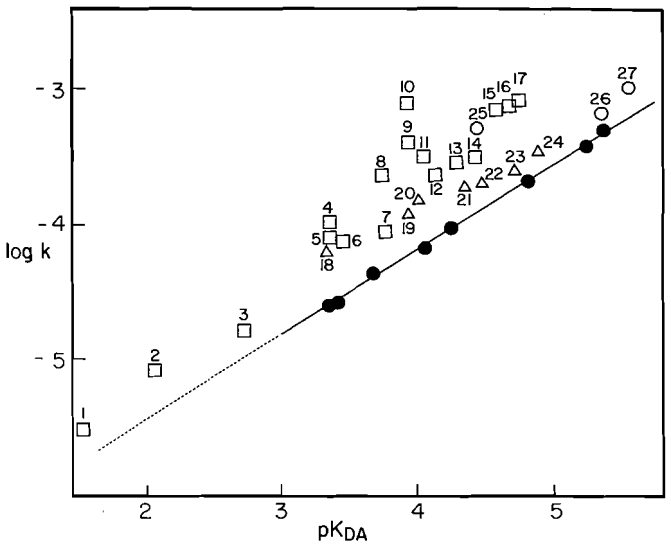

FIG. 1. Brønsted plot for the reaction of eq. [1] using carboxylate bases; numbers correspond to the carboxylic acids of Table 1; aliphatic acids (circles), *m*- and *p*-benzoic acids (triangles), *o*-benzoic acids (squares). The solid circles, which were used to determine the line, are the acids **28–35** in the table; Brønsted coefficient 0.639.

TABLE 2. Rate of isotopic exchange of the 2-methyl protons of **1** in aqueous (D_2O) amine buffers, 30°C

Buffer base	10^5k_2, M^{-1} s^{-1}	pK_{BD^+}[a]
Pyridines		
Unsubstituted	129	5.68
2-Methyl	154	6.36
2-Ethyl	133	6.32
2-Isopropyl	106	6.26
2-*tert*-Butyl	45.9	6.19
2,6-Dimethyl	145	7.17
3-Methyl	205	6.11
3-Fluoro	4.85	3.43
3-Bromo	4.11	3.30
3-Cyano	1.00	1.87
4-Methyl	311	6.47
Anilines		
Unsubstituted	191	5.08
2-Methyl	117	4.89
2-Ethyl	133	4.81
2-Isopropyl	116	4.86
2,4-Dimethyl	307	5.28
2,6-Dimethyl	57.7	4.40
3-Methyl	355	5.17
3,5-Dimethyl	457	5.35
3-Chloro	46.7	3.97
4-Methyl	493	5.51
4-Methoxy	866	5.77
4-Chloro	89.2	4.44

[a]Values from ref. 18 corrected to 30°C and D_2O according to ref. 7.

Although all the deviating points in Fig. 1 are on the positive side of the line, it must be pointed out that in most cases these do not correspond to absolute rate increases. For example, an *ortho* halo benzoate ion is less reactive than benzoate or, indeed, than the corresponding *meta* or *para* ions. The positive deviation

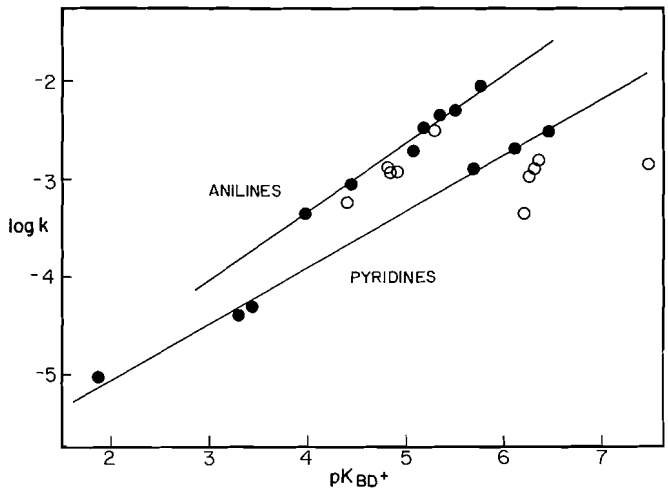

FIG. 2. Brønsted plots for the reaction of eq. [1] using aniline and pyridine bases (Table 2). The open circles represent compounds containing a substituent in the 2-position. The Brønsted coefficients are 0.707 (anilines) and 0.566 (pyridines).

arises to a great extent from the unusually low basicity of the *ortho* ions. Thus, as in all case of deviations from Brønsted relationships, it is necessary to examine the factors that affect both variables, that is, the reaction rate *and* the degree of the equilibrium ionization. The generally accepted explanation for *ortho* benzoates being weaker bases than their *para* counterparts is that there is hindrance to conjugation between the carboxyl group and the ring in the neutral acid, thus raising the energy of the latter and shifting the equilibrium toward the carboxylate ion. The moderately large Brønsted coefficient (0.639) and the fact that the proton transfer reaction is endergonic (uphill) suggests that the transition state should have a considerable amount of the character of the carboxylic acid (11, 12). It might be argued that the proton in the transition state is associated with both oxygen atoms, neither one of which would have significant carbonyl character, and in this case the deviation of the *ortho* compounds could be said to arise simply from anomalies in pK_{HA} rather than anomalies in rate. Since we have no grounds for believing that this situation obtains, and since it would not apply to the three aliphatic cases (**25**–**27**), we seek an explanation in other terms.

It was shown some time ago by Steigman and Sussman (13) that a high concentration of organic electrolyte, e.g. tetra-*n*-butylammonium bromide, has a profound effect on the pK of carboxylic acids. They become weaker acids and this change was found to be particularly marked in the case of *ortho*-substituted benzoic acids, which, in 7.75 molal $(n\text{-Bu})_4N^+Br^-$, become essentially equal in strength to their *para* isomers. Inorganic salts do not have this effect, and its was argued that the high concentration of alkyl units induces a high degree of structure in the water and that this has a greater effect on the *ortho* compounds than on their *meta* or *para* isomers. (There are indications that the effect is also present in aliphatic systems.)

Regardless of the precise origins of the pK changes, it is apparent that *ortho* carboxylate ions become relatively better proton acceptors (compared to their *meta* or *para* counterparts) in an environment that is alkyl rich. The transition state of the reactions under consideration here must have some of this character since the proton source is, in fact, an alkyl group and, indeed, adjacent alkyl groups in the substrate may also contribute to this sort of interaction when carboxylate bases are used. Accordingly, we tentatively ascribe the positive deviations from the Brønsted line for hindered carboxylates to an increase in effective basicity of the carboxylate group caused by the propinquity in the transition state of the carboxylate ion and the alkyl group(s) of the substrate. In the case of amine bases it is known that there is no increase in base strength in the presence of high concentrations of organic electrolyte and, indeed, in some cases, the base strength decreases. Conventional steric effects would thus be expected for amine bases, which is found to be the case.

Since polarizability effects can be important in acid–base reactions (see, for example, refs. 14 and 15) we consider briefly here the four *ortho* halo benzoates. If a high degree of polarizability in the nearby substituent helps stabilize the transition state, the deviations from the Brønsted (or Hammett) line should be in the order I > Br > Cl > F. This is, indeed, what is found, although it should be remembered that this is also the order of group size and, since *tert*-butyl has a larger deviation than the other *ortho* alkyl groups, the halogen order may simply reflect size rather than polarizability, although, of course, the two parameters are not unrelated. The use of thio substituents should clarify this point.

Experimental

The carboxylic acids, anilines, and pyridines were either obtained from commercial sources or were prepared by standard synthetic procedures.

The measurements of the rate of exchange for 1,2,3-trimethylpyrazinium iodide in D_2O were made using nmr spectroscopy, essentially as previously described (1, 4). For each compound two to four kinetic runs were performed at a given pH; in most cases the reproducibility of the derived second-order rate constants was ±10%.

Acknowledgements

We thank the Natural Sciences and Engineering Research Council of Canada for financial support.

1. T. W. S. LEE and R. STEWART. Can. J. Chem. **64**, 1085 (1986).
2. R. STEWART, S. J. GUMBLEY, and R. SRINIVASAN. J. Am. Chem. Soc. **102**, 6168 (1980).
3. R. STEWART and S. J. GUMBLEY. Can. J. Chem. **63**, 3290 (1985).
4. R. STEWART and T. W. S. LEE. J. Org. Chem. **47**, 2075 (1982).
5. R. STEWART, R. SRINIVASAN, and S. J. GUMBLEY. Can. J. Chem. **59**, 2755 (1981).
6. R. P. BELL, E. GELLES, and E. MÖLLER. Proc. R. Soc. A, **198**, 308 (1949).
7. R. SRINIVASAN and R. STEWART. J. Chem. Soc. Perkin Trans. 2, 674 (1976).
8. R. P. BELL. The proton in chemistry. 2nd ed. Cornell Univ. Press, Ithaca, NY. 1973. pp. 219–220.
9. J. A. FEATHER and V. GOLD. J. Chem. Soc. 1752 (1965).
10. J. HINE, J. G. HOUSTON, J. H. JENSEN, and J. MULDERS. J. Am. Chem. Soc. **87**, 5050 (1965).
11. A. J. KRESGE. *In* Proton-transfer reactions. *Edited by* E. F. Caldin and V. Gold. Chapman and Hall, London. 1975. Chapt. 7.
12. R. STEWART. The proton: applications to organic chemistry. Academic Press, Orlando, FL. 1985. p. 275.
13. J. STEIGMAN and D. SUSSMAN. J. Am. Chem. Soc. **89**, 6400 (1967); **89**, 6406 (1967).
14. R. W. TAFT. *In* Proton-transfer reactions. *Edited by* E. F. Caldin and V. Gold. Chapman and Hall, London. 1975. pp. 48 et seq.
15. F. G. BORDWELL, G. E. DRUCKER, and G. J. MCCOLLUM. J. Org. Chem. **47**, 2504 (1982).
16. G. KORTUM, W. VOGEL, and K. ANDRUSSOW. Dissociation constants of organic acids in aqueous solution. Butterworths, London. 1961.
17. E. P. SERJEANT and B. DEMPSEY. Ionization constants of organic acids in aqueous solution. Pergamon, Oxford. 1979.
18. D. D. PERRIN. Dissociation of organic bases in aqueous solutions. Butterworths, London. 1965; supplement, 1972.

Reactions of the 1-hydroxy-1,4-dimethylcyclohexadienyl cation,[1] an intermediate in the solvolysis of 1,4-dimethyl-4-nitrocyclohexa-2,5-dien-1-ol

ALFRED FISCHER, GEORGE N. HENDERSON, AND TREVOR A. SMYTH
Department of Chemistry, University of Victoria, Victoria, B.C., Canada V8W 2Y2
Received October 18, 1985
This paper is dedicated to Professor Arthur N. Bourns

ALFRED FISCHER, GEORGE N. HENDERSON, and TREVOR A. SMYTH. Can. J. Chem. **64**, 1093 (1986).

Solvolysis of 1,4-dimethyl-4-nitrocyclohexa-2,5-dien-1-ol in mixed aqueous organic solvents gives the diastereomers of 1,4-dimethylcyclohexa-2,5-diene-1,4-diol, 1,4-dimethylcyclohexa-3,5-diene-1,2-diol, 2-nitro-*p*-xylene, 2,4-dimethylphenol (all derived from the title cation, itself formed by ionization of the nitro group as nitrite), and 2,5-dimethylphenol. In aqueous methanol the diastereomers of 4-methoxy-1,4-dimethylcyclohexa-2,5-dienol are also obtained. Significant yields of 2,5-dimethylphenol are only obtained on the acid-catalysed further reaction of the dienediol (or the methoxydienol) and involve the intermediate formation of 1,4-dimethylcyclohexa-3,5-diene-1,2-diol. In the absence of added base the acid released in the solvolysis catalyses this reaction and leads to the aromatization of the dienes.

ALFRED FISCHER, GEORGE N. HENDERSON et TREVOR A. SMYTH. Can. J. Chem. **64**, 1093 (1986).

La solvolyse du diméthyl-1,4 nitro-4 cyclohexadiène-2,5 ol-1 dans des mélanges de solvants organiques aqueux conduit aux diastéréoisomères du diméthyl-1,4 cyclohexadiène-2,5 diol-1,4 et du diméthyl-1,4 cyclohexadiène-3,5 diol-1,2 ainsi qu'au nitro-2 *p*-xylène et au diméthyl-2,4 phénol (tous dérivés du cation mentionné dans le titre qui est lui-même formé par ionisation du groupement nitro sous forme de nitrite) et au diméthyl-2,5 phénol. Dans le méthanol aqueux, on obtient aussi les diastéréoisomères du méthoxy-4 diméthyl-1,4 cyclohexadiène-2,5 ol-1. On n'obtient des rendements importants de diméthyl-2,5 phénol que lors d'une réaction subséquente, catalysée par les acides, du dièndiol (ou du méthoxydiènol) et celle-ci implique la formation du diméthyl-1,4 cyclohexadiène-3,5 diol-1,2. Lorsqu'on n'ajoute pas de base, l'acide qui est formée lors de la solvolyse catalyse cette réaction qui conduit à l'aromatisation des dienes.

[Traduit par la revue]

Introduction

The adducts obtained on nitration of arenes in acetic anhydride, typically derivatives of 4-methyl-4-nitrocyclohexa-2,5-dienyl acetate, are labile and readily undergo rearomatization reactions in solution (1–6). A variety of rearomatization products have been obtained but the pathways to many of these appear to have one or other of two competitive initial steps, each of which involves the formation of a cyclohexadienyl cation (6, 7). For these routes rearomatization is initiated by unimolecular ionization of the nitro group as nitrite, forming a 1-acetoxy-4-methylcyclohexadienyl cation, or by acid-catalysed loss of the acetate function as acetic acid ($A_{Al}1$), forming a 4-methyl-4-nitrocyclohexadienyl cation. Formation of various substituted 4-methyl-4-nitrocyclohexadienyl cations and, more generally, substituted 4-alkyl-4-nitrocyclohexadienyl cations has been demonstrated by trapping experiments, e.g. both diastereomers of 4-ethyl-1-methyl-4-nitrocyclohexa-2,5-dienol were obtained when (*Z*)-4-ethyl-1-methyl-4-nitrocyclohexa-2,5-dienyl acetate was hydrolysed in acidified aqueous acetone (2). In the present paper we are concerned with the fate of the cyclohexadienyl cation obtained on solvolysis of the nitro group. We have investigated the solvolysis of 1,4-dimethyl-4-nitrocyclohexadienyl acetate (**1***a*), the corresponding dienol **1***b*, and the methyl ether **1***c*, and thus the formation and reactions of the 1-acetoxy-1,4-dimethylcyclohexadienyl cation (**2***a*) and its 1-hydroxy and 1-methoxy analogues **2***b* and **2***c*, respectively. Studies of the 1,4-dimethyl-4-nitrocyclohexa-2,5-dienyl acetate system have been reported by Moodie, Schofield, *et al.* (6), by Myhre and co-workers (7), and by Fischer and Ramsay (8). The 1-hydroxy-1,4-dimethylcyclohexadienyl cation and its 2-hydroxy isomer are simultaneously-formed intermediates in the acid-catalysed ring opening of 1,4-dimethylbenzene oxide (9, 10). In the present work the individual chemistries of the two cations can be distinguished since they are not formed simultaneously, and the 1-hydroxy cation can be studied in the absence of its isomer.

[1]In this paper enumeration of the cyclohexadienyl cations follows that of the parent cyclohexadienes.

Results and discussion

Configurations of 1,4-substituted cyclohexadienes

The configuration of (*E*)-1,4-dimethyl-4-nitrocyclohexa-2,5-dienol has been established by X-ray crystallography and those of the corresponding nitrodienyl acetates and methyl ethers by stereospecific interconversion reactions (11). Addition of methyllithium to 4-methyl-4-nitrocyclohexa-2,5-dienone gives preferentially the (*Z*)-dienol (12). Applying a similar argument, the major product isomer of the dienediol **3***bn* obtained on addition of methyllithium to 4-hydroxy-4-methylcyclohexa-2,5-dienone has been assigned the (*Z*) configuration (13). As would be expected, the (*E*)-dienediol has the higher melting point. The assignment is also supported by our shift reagent studies. There is only a small difference in the gradients of the shifts of the 4-CH_3 protons of the diastereomers produced on the addition of *tris*-(1,1,1,2,2,3,3-heptafluoro-7,7-[$^2H_6$]dimethyl-4,6[$^2H_3$]octanedionato)europium(III) (Eu([$^2H_9$]fod)$_3$). However, in accord with expectation, the (*E*) isomer, with the 4-CH_3 *cis* to the europium complexed at 1-OH, has the larger slope, 0.34 versus 0.31.

In the methylation reactions the stereochemistry at the asymmetric centres is not disturbed. Thus the configurations of the methoxydienols and the dimethoxydienes follow from the partial methylation of (*Z*)-**3***bn* to a mixture of (*Z*)-**3***bo* and (*Z*)-**3***co*, the methylation of (*Z*)-**3***bo* to (*Z*)-**3***co*, the partial methylation of (*E*)-**3***bn* to (*E*)-**3***bo*, and the methylation of (*E*)-**3***bo* to (*E*)-**3***co*.

Solvolysis reactions

Strongly ionizing solvents and low acidity are the conditions that favour the ionization of the nitro group over the competing

TABLE 1. Solvolysis of (*E*)-1,4-dimethyl-4-nitrocyclohexa-1,4-dien-1-ol ((*E*)-**1***b*) in 50% (v/v) methanol–water[a]

Expt. no.	*T* (°C)	*t* (h)	Base	[Base] [(*E*)-**1***b*]	**3***bo*	**3***bn*	**6***p*	**7***b*+**6***n*	Other
101	20	1	[b]	—	40	8	5	14	[c]
102	24	2	[d]	—	52	9	4	29[e]	*e,f*
103	25	3	Urea	2.2	43	19[g]	0	38[e]	*e,g*
104	40	4	—	—	9	0	0	62[e]	*e,h,i*
105	40	6	—	—	0	0	0	[j]	*j*
106	40	18	—	—	0	0	0	[j]	*j*
107	40	18	DPE[k]	1.1	28	20	0	52	
108	40	18	DPE	1.1	37	9	9	45	
109	40	1	DPE	1.1	26	29	4	42	
110	40	1	DPE	1.1	26	27	7	41	
111	40	1	DPE	2.2	22	14	7	58	
112	40	1	NBA[l]	0.5	49	12	12	27	
113	40	1	NBA	1.1	42	25	9	24	
114	40	1	NBA	2.2	36	14	11	39	
115	40	1	26LU[m]	1.6	59	13	12	17	
116	40	1	26LU	3.0	47	16	20	18	
117	40	1	KOAc	1.1	50	23	14	14	
118	40	1	KOAc	2.2	45	20	15	20	

[a]Procedures as described in the experimental section. Analysis by ^{1}H nmr in $CDCl_3$ in which (*E*)-**3***bn* is only partially soluble. Yields were reproducible to ±5 mol%.
[b]2,6-Lutidine (1.1 mol proportion) added immediately prior to work-up.
[c](*E*)-**1***b* (34%) unreacted.
[d]Diisopropylethylamine (1.1 mol proportion) added immediately prior to work-up.
[e]Anisoles present and included in the phenol fraction.
[f](*E*)-**1***b* (6%) unreacted.
[g]Dimethoxycyclohexadienes (**3***co*) present and included in the **3***bn* fraction.
[h]**3***co* (9%).
[i]Unidentified aromatic component (20%).
[j]Essentially complete rearomatization occurred. No attempt was made to identify the aromatic products, presumably dimethylphenols and dimethylanisoles.
[k]Diisopropyethylamine.
[l]*N*-Butylamine.
[m]2,6-Lutidine.

loss of the hydroxyl, acetate, or methoxyl group in the solvolysis of the nitrocyclohexadienols, their acetates, or methyl ethers (2, 5, 6). Accordingly, we studied initially the solvolysis of *E*-**1***b* in 50% aqueous methanol (Tables 1 and 2). Experiments 101–106, 201, 202, and 206 were carried out either in the absence of base or in the presence of the very weak base urea. For reaction times of up to ten solvolysis half-lives (i.e. up to 1 h at 40°C), dienes, including the methoxydienol **3***bo* and the diol **3***bn*, were obtained, as well as aromatic products, which were mainly phenols (expts. 102, 103, 201, 202, 206). However, after a longer reaction time (expt. 104) the diene components decreased and the aromatic components increased, and at very long reaction times only aromatic products were obtained as the initially formed dienes were aromatized (expts. 105 and 106). Except in the case of the shortest reaction time (expt. 101) the dienes obtained also included the dimethoxy compound **3***co* and the aromatic component also included dimethylanisoles, suggesting that these are secondary reaction products. In these reactions in the absence of base only minor amounts of 2-nitro-*p*-xylene (**6***p*) were formed and the amount did not increase with extended reaction times, which otherwise resulted in an increase in the total amount of aromatic product. Solvolysis in acidified aqueous methanol (pH 3.2) gave **3***co* (12%) and a complex mixture of aromatic products (88%) that included dimethylanisole(s).

When the solvolysis of (*E*)-**1***b* was carried out in the presence of base, formation of the dimethoxydienes and anisoles was suppressed and the methoxydienol **3***bo* and dienediol **3***bn* were either not subject to rearomatization or the rate of rearomatization was greatly reduced (compare expts. 104–106 with 107 and 108). The product distribution then was **3***bo* (44%), **3***bn* (22%), **6***p* (20%), 2,4-dimethylphenol (**7***b*, 11%), and 2,5-dimethylphenol (**6***n*, 2%) (expts. 209–211, 214, 215), both diastereomers of **3***bo* and **3***bn* being formed from the single diastereomer of the substrate. In the presence of potassium nitrite (in addition to potassium acetate) the yield of 2-nitro-*p*-xylene was greatly enhanced and that of the diene and phenol components correspondingly reduced (compare expts. 216 and 217). Solvolysis in methanol containing *N,N*-diisopropylethylamine gave **3***bo* (47%), **6***p* (36%), and **7***b* and **6***n* (17%). Solvolysis in the presence of base in aqueous acetone, aqueous tetrahydrofuran, and in ether–water mixtures gave both diastereomers of dienol **3***bn*, 2-nitro-*p*-xylene, and the 2,4- and 2,5-dimethylphenols (Table 3). Solvolysis in aqueous dioxan at pH 3.2 gave a complex mixture of aromatic products including nitrodimethylphenol(s).

Solvolysis of (*E*)-**1***c* in aqueous methanol containing *N,N*-diisopropylethylamine gave **3***co* (21%), **3***cn* (≡ **3***bo*, 34%), **6***p* (4%), and dimethylanisoles plus dimethylphenols (41%).

Solvolysis of (*E*)-**1***a* in aqueous methanol gave 2,5-dimethylphenyl acetate (**8***a*) as the sole product. In the presence of base, **8***a* was the very dominant (initial) product but partial solvolysis of **8***a* to **8***b* ensued. Solvolysis of 4-methyl-4-nitrocyclohexa-2,5-dien-1-ol in the presence of base gave *p*-cresol (90%) and unidentified diene (10%).

Reaction of (*E*)-**3***bn* with trifluoroacetic acid gave **7***b* (98%) and **6***n* (2%). In aqueous methanol at pH 3.2 **7***b* (68%) and **6***n* (32%) were obtained, although in a reaction carried out at a lower temperature, and which was therefore incomplete, some methoxydienes (12%) and dimethylanisoles (10%) were

TABLE 2. Solvolysis of (*E*)-1,4-dimethyl-4-nitrocyclohexa-1,4-dien-1-ol ((*E*)-**1***b*) in 50% methanol–water at 40°C[a]

Expt. no.	Base[b]	**3***bo*	**3***bn*	**6***p*	**7***b*	**6***n*	Other
201	—	22	2	0	33	7	[c]
202	Urea[d]	36	21[e]	0	25[f]	[g]	[h]
203	DPE	30	21	7	38	5	
204	26LU[k]	49	21	16	13	1	
205	KOAc	51	14	13	15	6	[j]
206	—	43	7	5	21	5	[k]
207	HPO_4[l]	0	0	20	50	[g]	[m]
208	DPE	39	14	11	32	5	
209	Tris[n]	43	23	23	12	1	
210	Tris	45	20	25	10	1	
211	$NaHCO_3$	47	25	18	11	1	
212	$NaHCO_3$	42	29	16	13	1	
213	C_5D_5N	36	28	13	12	[g]	[o]
214	C_5D_5N	43	28	17	9	4	
215	KOAc	42	17	16	17	6	[p]
216	KOAc	44	15	16	18	7	
217	KOAc[q]	16	18	56	11	[g]	

[a]Procedures as described in the experimental section. For experiments 201–205, substrate concentration = 0.075 mol dm^{-3}, reaction time = 1 h, precision ±5 mol%. For experiments 206–217, substrate concentration = 0.3 mol dm^{-3}, reaction time = 20 min, and precision ±3 mol%.

[b][Base] = 0.33 mol dm^{-3}.

[c]Dimethoxydienes **3***co* (16%), dimethylanisoles (10%), unidentified aromatic compound (11%).

[d][Urea] = 0.66 mol dm^{-3}.

[e]Includes dimethoxydiene **3***co*.

[f]**7***b* + **6***n*; hplc analysis was prevented by an interfering peak.

[g]**7***b*:**6***n* ratio not determined and the amount tabulated for **7***b* includes that of **6***n*.

[h]Dimethylanisoles (19%).

[i]2,6-Lutidine, removed after work-up by extensive pumping at reduced presure before ^1H nmr analysis.

[j]Dimethylanisoles (2%).

[k]Dimethoxydiene **3***co* (7%), dimethylanisoles (7%), unidentified aromatic compound (5%).

[l]Na_2HPO_4, only partially soluble.

[m]Diene **3***co* (15%), dimethylanisoles (16%). The presence of the anisoles prevented the determination of the ratio of **7***b*:**6***n* by nmr.

[n]Tris(hydroxymethyl)aminomethane.

[o]Diene (*E*)-**1***b* (11%); reaction incomplete because the use of a thick-walled reaction vessel reduced the period for which the reaction was at 40°C.

[p]Dimethylanisoles (3%).

[q]KNO_2 (3 mol dm^{-3}) also added.

TABLE 3. Solvolysis of (*E*)-1,4-dimethyl-4-nitrocyclohexa-1,4-dien-1-ol ((*E*)-**1***b*) in aqueous mixtures[a]

Expt. no.	Solvent[b]	*T* (°C)	*t* (h)	Base[c]	**3***bn*	**6***p*	**7***b* + **6***n*	Other
301	50% acetone	25	4.5	KOAc	23	24	39	[d]
302	33% acetone	40	1	DPE	38	11	43	[e]
303	9% acetone	40	0.5	DPE	39	8	37	[f]
304	9% acetone	20	2	KOAc	35	11	30	[g]
305	50% THF[h]	40	0.3	Tris[i]	14	7	7	[j]
306	33% THF	40	1	DPE	42	15	44	
307	50% ether	40	0.3	Tris	20	11	11	[k]
308	50% ether	40	2	Tris	22	15	13	[l]

[a]Analyses by ^1H nmr. The conjugated dienol **5***bn* was probably present in all of the reactions.

[b]Organic component and its percentage specified; the other component was water. The diethyl ether mixtures were heterogeneous.

[c]The mole ratio of base to (*E*)-**1***b* was 1.1 except for expts. 301 (2.2) and 304 (1.3).

[d](*E*)-**1***b* (14%).

[e]**5***bn* (8%).

[f]**5***bn* (6%), unidentified components with ^1H nmr peaks at 1.95 ppm (6%) and 2.25 ppm (4%).

[g]The 1.95-ppm (15%) and 2.25-ppm (9%) components.

[h]Tetrahydrofuran.

[i]Tris(hydroxymethyl)aminomethane.

[j](*E*)-**1***b* (72%).

[k](*E*)-**1***b* (59%).

[l](*E*)-**1***b* (51%).

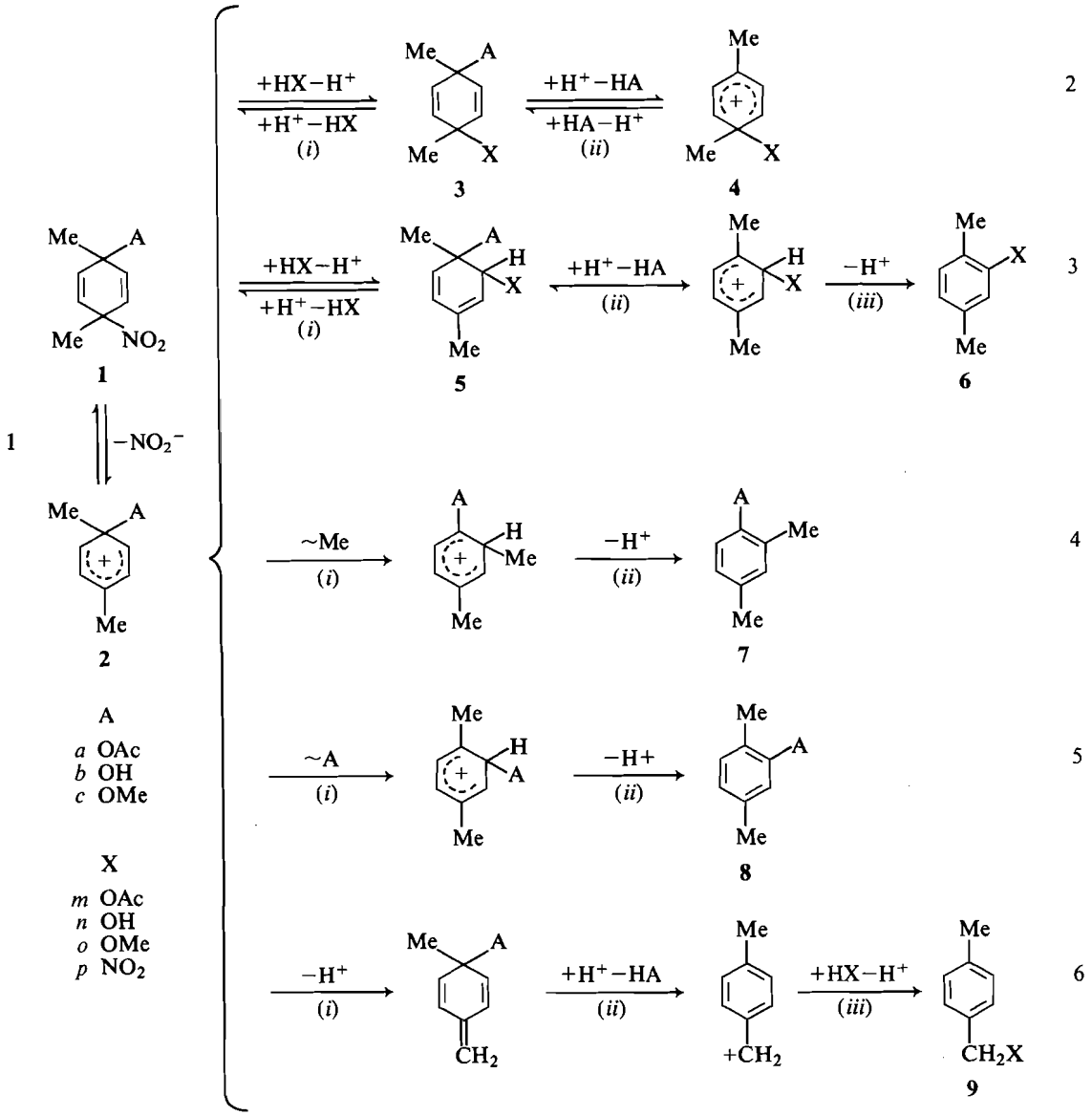

SCHEME 1

present in addition to the xylenols. In aqueous dioxan at pH 3.2 **7***b* and **6***n* were obtained in the 2:1 ratio. Reaction of (*Z*)-**3***co* with trifluoroacetic acid gave **7***c*.

We account for the solvolysis reaction products in terms of the formation and further reactions of a 1-A-1,4-dimethylcyclohexadienyl cation (**2**), as illustrated in Scheme 1, an elaboration of earlier schemes (2, 6, 7). Reactions 2(*i*) and 3(*i*) represent additions of a nucleophile to the electrophilic centre that is in a 1,4 or 1,2 relationship to the tetrahedral centre of the cation, respectively. As shown, these reactions may be followed by further reactions of the new cyclohexadienes. Reactions 4 and 5 in their initial steps (*i*) involve competing 1,2 migrations of the methyl and substituent A groups at the tetrahedral centre of the cation. Reaction 6 involves deprotonation of the cation to a triene followed by S_N1' substitution to form a benzylic derivative.

Unimolecular ionization of the nitro group in (*E*)-**1***b* leads to the hydroxycyclohexadienyl cation **2***b* (Scheme 1, reaction 1, A = OH). The methoxydienol **3***bo* and the dienediol **3***bn* are formed by solvent methanol or water, respectively, trapping **2***b* (reaction 2(*i*), A = OH and HX = HOMe or HOH). Reaction 2(*i*) is the dominant reaction of **2***b* since some 65% of the product consisted of **3***bn* and **3***bo*. The fact that both diastereomers of **3***bo* and **3***bn* are formed from a single diastereomer of **1***b* confirms the S_N1 substitution mechanism. 2-Nitro-*p*-xylene (**6***p*) was obtained in 19% yield. Addition of the nitrite ion, released in the ionization step, to the *ortho* position of **2***b* would give the nitrodiene **5***bp*, which, on elimination of water, would give the nitroarene. The addition–elimination would more likely follow the base-catalysed sequence depicted in Scheme 2 than the acid-catalysed sequence of reaction 3, Scheme 1. This is shown by the fact that only small amounts of **6***p* were formed in the reactions carried out in the absence of base, when the liberated nitrite would be present as the less nucleophilic nitrous acid. Our previous study of the methanolysis of 1-ethyl-4-methyl-4-nitrocyclohexadienol, which gave 4-ethyl-3-nitrotoluene in addition to 2-ethyl-4-methylphenol and the diastereomers of 1-ethyl-4-methoxy-4-methylcyclohexadien-1-ol, confirms that the nitro group is added at the position *meta* to its original position (2). The nitrite anion might also be expected to add to the *para* position of **2***b*. This reaction (2(*i*), X = NO_2) is just the reverse of the ionization reaction (reaction 1) and Myhre and

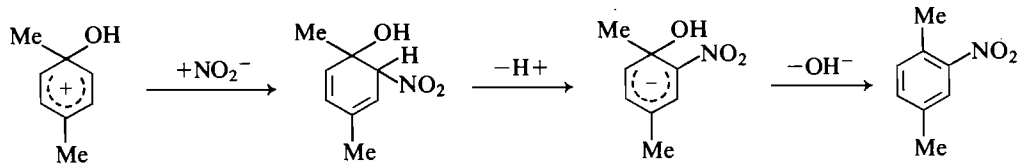

SCHEME 2

co-workers have argued that such return from the ion-pair is facile (7). The fact that in the presence of external nitrite the yield of 2-nitro-*p*-xylene from *E*-**1***b* increased to over 50% indicates that nitrite is a very effective competitor for cation **2***b* and establishes the intermolecular pathway of the formation of **6***p*. A 36% yield of **6***p* was obtained when the solvolysis reaction was carried out in methanol (containing diisopropylethylamine). This increased yield is presumably attributable to the effect of the lower dielectric constant solvent increasing the rate of the reaction between carbonium ion and nitrite anion, involving charge annihilation, relative to the rates of the other reactions of the carbonium ion, in which charge is preserved.

The 2,4-dimethylphenol (**7***b*), formed in 13% yield in the aqueous methanol solvolysis, arises via reaction 4. Since 2,5-dimethylphenol was formed in much lower yield (3%), it is evident that in cation **2***b* the methyl is much more prone to migrate (reaction 4(*i*)) than the hydroxyl (reaction 5(*i*)). This preference is even more marked than it appears since 2,5-dimethylphenol is also formed (and likely only formed) via reaction 3. The reaction of diol **3***bn* with trifluoroacetic acid, which gave 98% of 2,4-dimethylphenol, indicates that the relative migratory aptitude of methyl to hydroxyl in **2***b* is at least 50:1. The preference for methyl migration over migration of hydroxyl (or methoxyl) in cyclohexadienyl cations is well established in dienone–phenol rearrangement studies (14–16). Reaction of solvent at the position adjacent to the tetrahedral centre of **2***b* (reaction 3(*i*): S_N1') is slower than reaction at the *para* position (reaction 2(*i*): S_N1). On separation of the product of a large-scale reaction we obtained a small amount of the 1,2-diol (**5***bn*). It was difficult to establish the presence of **5***bn* and (or) **5***bo* in the solvolysis reaction mixtures because of the overlap of the methyl peaks with those of (*E*)-**1***b* (at 1.77 ppm) and of the products **3***bn* and **3***bo* (at 1.29 ppm). However, in a few reactions carried out in aqueous acetone and in aqueous tetrahydrofuran it was possible to establish from the absence of the quartet centred at 6.0 ppm that all of the reactant was consumed. The peak at 1.77 ppm could then be attributed to **5***bn*. In these reactions **5***bn* was present to the extent of 20% of the amount of **3***bn*, about 7% of the total reaction product. A further indication of the formation of **5***bn* was provided by the observation that in weakly acid solution (pH 3.2) the dienediol **3***bn* gave ca. 33% of **6***n*, presumably by the sequence **3***bn* → **2***b* → **5***bn* → → **6***n*. We conclude that the conjugated dienediol **5***bn* is a necessary intermediate between **2***b* and **6***n*. In dilute acid conditions the conversion of **5***bn* to **6***n* must be relatively efficient, since the extent of formation of **6***n* is half that of **7***b* although **5***bn* is only 20% of **3***bn*.

The formation of dienediol and (or) methoxydienol as intermediates in the solvolysis of the nitrocyclohexadienol has been inferred from kinetics studies (7). Our study of the products of solvolysis of 1-ethyl-4-methyl-4-nitrocyclohexa-2,5-dienol (2) and the present investigation provide the first reports of the positive identification of the dienediols and the methoxydienols as nitrocyclohexadienol solvolysis products and, in the case of the 1,2-diol, the first direct evidence of its formation in any reaction. The intermediate formation of **3***bn* in the second of two acid-catalysed mechanisms of ring opening of 1,4-dimethylbenzene oxide and its aromatization to **7***b* and **6***n* has been conclusively demonstrated by Bruice, Jerina, and co-workers (9). They proposed alternative pathways for the conversion of the diol to **7***b* and **6***n*, one being that depicted in Scheme 1 (**3***bn* → **2***b* → **5***bn* → → **6***n* and **3***bn* → **2***b* → → **7***b*), and the other, re-formation of the protonated oxide and its direct conversion to **7***b* and **6***n*. They preferred the second path. Our results, which demonstrate the intermediate formation of the 1,2-diol **5***bn* and the fact that **6***n* is not formed when **2***b* cannot be trapped by water (e.g. in trifluoroacetic acid), are in accord with the first. Our results also show that reversible formation of protonated oxide from cation **2***b* cannot occur since this would lead to a ratio **7***b*:**6***n* from the nitrodienol solvolysis reaction in the acid region (2:1), and from the reaction of the dienediol with acid, identical to that observed in reaction of the oxide with acid. However, the oxide reaction gives more **6***n* than **7***b* at pH 3.5 and **6***n* is even more favoured in stronger acid (9, 17).

No benzylic compounds were obtained in the solvolysis of (*E*)-**1***b* and thus the deprotonation of **2***b* (reaction 6(*i*)) must be slower than reactions 2(*i*), 3(*i*), or 4(*i*). Examples of reaction type 6 are known for nitrocyclohexadienyl cations, e.g. the nitrodimethylcyclohexadienyl cation formed by protonation of **1** at A and loss of HA (7, 8). However, there have been no reports of benzylic products being formed via cations such as **2***a*, **2***b*, or **2***c*.

The solvolysis reaction generates nitrous acid. In the absence of added base the solution becomes acidic and the initially formed dienes **3***bo* and **3***bn* can reform the cation **2***b* by acid-catalysed loss of methoxy or hydroxyl, respectively (reverse of reaction 2(*i*)), as discussed above. However, **3***bo* can also undergo acid-catalysed loss of hydroxyl (reaction 2) to generate the methoxycyclohexadienyl cation **4***o*. This, on reaction with methanol, would generate the dimethoxydiene **3***co*. Prolonged exposure to the acid conditions would lead to complete formation of aromatic products (phenols and anisoles) via reactions 3 and 4, and this was demonstrated by the results of solvolysis reactions carried out at pH 3.2 in which (*i*) little or no diene was obtained; (*ii*) in the case of the reaction in aqueous methanol, the small amount of diene obtained was largely **3***co*, reflecting the (acid-catalysed) exchange of the original hydroxyl group, and the aromatic compounds included anisoles, also indicative of this exchange; (*iii*) the phenols were nitrated under the acid conditions. We can thus understand why, in the aqueous methanol solvolyses of (*E*)-**1***b*, anisoles were significant components of the aromatic products and dimethoxydienes were formed only in the absence of added base and why these products were not obtained, even in the absence of added base, when the reaction time was very short.

Solvolysis of (*E*)-**1***c* in aqueous methanol follows analogous pathways to those described for (*E*)-**1***b* and does not require additional comment. Reaction of (*E*)-**1***c* with 50% trifluoroacetic acid in methanol gave **6***p*, **7***c*, and **6***o*. At such acidity this reaction presumably involves, at least in part, the nitrocyclohexa-

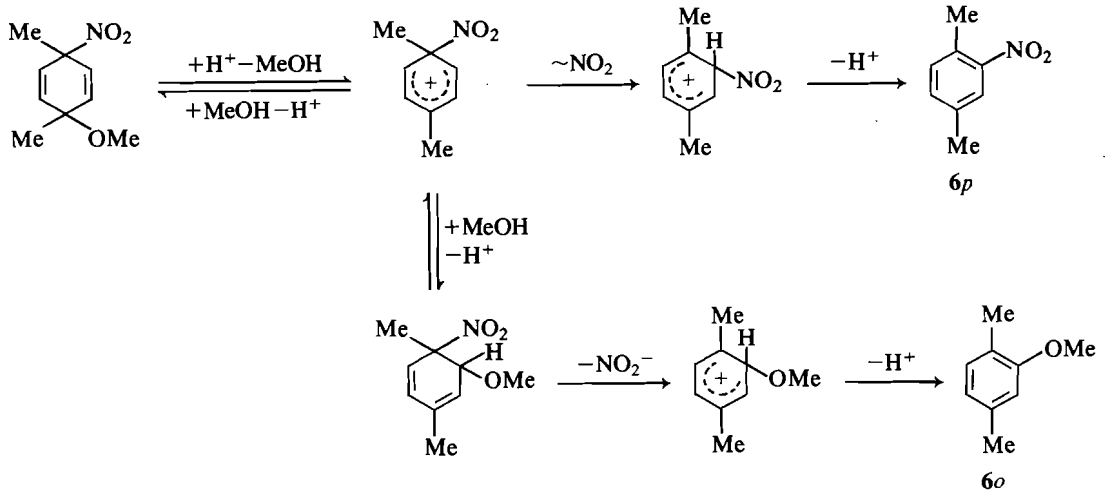

SCHEME 3

dienyl cation as shown in Scheme 3. However, the formation of **7***c* under these conditions must involve the methoxycyclohexadienyl cation **2***c*. Thus in this solvent mixture ionization of nitrite and the acid-catalysed loss of methanol are competitive. The reaction of (*Z*)-**3***co* with trifluoroacetic acid, which gave **7***c*, demonstrates the preferential migration of methyl rather than methoxyl in cation **2***c*.

Solvolysis of (*E*)-**1***a* differed from solvolysis of (*E*)-**1***b* and (*E*)-**1***c* in that essentially a single product (**8***a*) was obtained. The 1,2 shift of the acetate group in ion **2***a* should be facilitated by the formation of a bond to the carbonyl oxygen so that rearrangement (reaction 5) can occur via a cyclic transition state. We investigated the possibility that rearrangement of the acetate was concerted with the ionization of the nitro group by measuring the rates of solvolysis of (*E*)-**1***a* and (*E*)-**1***b*. Although (*E*)-**1***a* reacts faster than (*E*)-**1***b*, the rate ratio was only 2:1. The enhancement seems too small to require a concerted transition state, although it should be noted that formation of **2***a* should be slower than **2***b* since the acetoxy group is more electron withdrawing than the hydroxy group. Thus the true rate enhancement must be greater than is apparent. In any event, since cation **2***a* was not effectively trapped by nucleophiles, in contrast to **2***b* and **2***c*, the rearrangement of the acetate must occur very soon after **2***a* is formed if it is not synchronous with the ionization step.

Experimental

Infrared spectra were obtained on a Perkin–Elmer 283 spectrometer. The ^{1}H nmr spectra, at 90 MHz, were determined using a Perkin–Elmer R32 spectrometer. The ^{13}C nmr spectra, at 15.1 MHz, were obtained with a Nicolet TT-14 spectrometer. Mass spectra were determined on a Hitachi Perkin–Elmer RMU7 spectrometer. High pressure liquid chromatography (hplc) was carried out with a Waters system 500 (preparative) and on a Varian model 5000 (analytical) chromatograph. The gas–liquid chromatograph used was a Varian Aerograph model 2400.

2,4-Dimethylphenol, 2,4-dimethylanisole, 2,5-dimethylanisole, *N,N*-diisopropylethylamine, chlorotrimethylsilane, iodotrimethylsilane, bis(trimethylsilyl)acetamide, and 2,6-lutidine were from Aldrich. 2,5-Dimethylphenol, from Eastman, was recrystallized twice from *n*-heptane. Methyl iodide was from Mallinckrodt, trifluoroacetic acid was from Matheson, Coleman and Bell, and the Eu([^{2}H$_9$]fod)$_3$ shift reagent was from Merck, Sharp and Dohme. 2,5-Dimethylphenyl acetate was prepared by acetylation of the phenol with acetic anhydride (18).

1,4-Disubstituted cyclohexa-2,5-dienes

(*E*)-1,4-Dimethyl-4-nitrocyclohexa-2,5-dienyl acetate ((*E*)-**1***a*) was obtained by nitration of *p*-xylene (8, 11). Reaction of (*E*)-**1***a* with aluminum hydride gave (*E*)-1,4-dimethyl-4-nitrocyclohexa-2,5-dienol (*E*))-**1***b*) (11). Methylation of (*E*)-**1***b* gave (*E*)-**1***c* (11). Reduction of 4-methyl-4-nitrocyclohexa-2,5-dienone with sodium borohydride gave 4-methyl-4-nitrocyclohexa-2,5-dien-1-ol (12). Both diastereomers of 1,4-dimethylcyclohexa-2,5-diene-1,4-diol (**3***bn*) were obtained by addition of methyllithium to *p*-benzoquinone (13). Addition of methyllithium to 4-methoxy-4-methylcyclohexa-2,5-dienone (itself prepared from the chlorodienone by reaction with silver nitrate in methanol, cf. ref. 19) gave both isomers of 4-methoxy-1,4-dimethylcyclohexa-2,5-dienol (**3***bo*) in a 1:3 ratio. The isomers were separated by hplc. The minor isomer (*E*)-**3***bo* had mp 95–96°C (lit. (9) mp 94–95°C); ir (Nujol): 3415 (OH), 2820 (OCH_3), 1120, 1065 (C—O), 800 cm^{-1}; ^{1}H nmr ($CDCl_3$) δ: 1.30 (s, 3), 1.33 (s, 3), 1.80 (s, 1, O*H*), 3.02 (s, 3, OC*H*$_3$), 5.57 (d, 2, *J* = 10 Hz, 3-*H* and 5-*H*), 6.02 (d, 2, *J* = 10 Hz, 2-*H* and 6-*H*) ppm; ^{13}C nmr ($CDCl_3$) δ_C: 27.9 (1-*C*H$_3$ and 4-*C*H$_3$), 51.5 (O*C*H$_3$), 65.4 (*C*-1), 71.0 (*C*-4), 130.4 (*C*-3 and *C*-5), 136.4 (*C*-2 and *C*-6) ppm. The major isomer (*Z*)-**3***bo* was obtained as oil; ir (film): 3410 (OH), 2830 (OCH_3), 1135, 1085 (C—O), 780 cm^{-1}; ^{1}H nmr ($CDCl_3$) δ: 1.22 (s, 3), 1.28 (s, 3), 2.35 (s, 1, O*H*), 3.10 (s, 3, OC*H*$_3$), 5.59 (d, 2, *J* = 10 Hz, 3-*H* and 5-*H*), 5.95 (d, 2, *J* = 10 Hz, 2-*H* and 6-*H*) ppm; ^{13}C nmr δ_C: 28.0 and 29.0 (1-*C*H$_3$ and 4-*C*H$_3$), 51.9 (O*C*H$_3$), 65.4 (*C*-1), 71.0 (*C*-4), 130.3 (*C*-3 and *C*-5), 135.7 (*C*-2 and *C*-6) ppm.

(*E*)-3,6-Dimethoxy-3,6-dimethylcyclohexa-1,4-diene ((*E*)-**3***co*) was obtained by methylation of the methoxydienol (*E*)-**3***bo*. A mixture of freshly precipitated silver oxide (1.2 g), methyl iodide (4.5 cm^3), potassium hydroxide (0.03 g), and (*E*)-**3***bo* (0.30 g) was stirred at ambient temperature. The disappearance of the dienol (*E*)-**3***bo* was monitored by ^{1}H nmr and after 18 h, when none remained, the reaction mixture was filtered and the residue washed with ether (3 × 10 cm^3). The combined filtrate and washings were dried ($MgSO_4$) and the solvent evaporated at 30°C; ^{1}H nmr indicated that the solid residue (0.22 g) was essentially pure (*E*)-**3***co*. Crystals were obtained from pentane and a sample was sublimed at 40–60°C and had ir (KBr): 2820 (OCH_3), 1080 (C—O), 780 cm^{-1}; ^{1}H nmr ($CDCl_3$) δ: 1.29 (s, 6, 3-C*H*$_3$ and 6-C*H*$_3$), 3.03 (s, 6, 3-OC*H*$_3$ and 6-OC*H*$_3$), 5.75 (s, 4, 1-*H*, 2-*H*, 4-*H*, 5-*H*) ppm; ^{13}C nmr ($CDCl_3$, −10°C) δ_C: 27.6 (3-*C*H$_3$ and 6-*C*H$_3$), 51.6 (3-O*C*H$_3$ and 6-O*C*H$_3$), 71.0 (*C*-3 and *C*-6), 134.1 (*C*-1, *C*-2, *C*-4, *C*-5) ppm; ms (70 eV) *m/e* (relative intensity): 168 (0.5, *M*), 153.085 (100, M_r $^{12}C_9{}^1H_{13}{}^{16}O_2$: 153.092, *M* − CH_3), 137 (94), 122 (62), 121 (13), 105 (19), 91 (46), 79 (22), 78 (12), 77 (39), 65 (16), 53 (13), 51 (20), 43 (38). *Anal.* calcd. for $C_{10}H_{16}O_2$: C 71.39, H 9.59; found: C 71.20, H 9.61.

Similar methylation of the dienol (*Z*)-**3***bo* for 34 h gave (*Z*)-3,6-dimethoxy-3,6-dimethylcyclohexa-1,4-diene ((*Z*)-**3***co*) in essentially quantitative yield. The dimethoxydiene was also prepared by methyla-

tion of the dienediol (*Z*)-**3***bn* (0.8 g) by stirring with a mixture of methyl iodide (27 cm^3), potassium hydroxide (0.165 g), and silver oxide (14 g added in 1–3 g portions over the reaction period) for 8 days. After work-up, ^1H nmr showed that the residue consisted of (*Z*)-**3***co* (92%) and (*Z*)-**3***bo* (8%). Sublimation at 60–70°C gave colourless plates of (*Z*)-**3***co*, mp 56°C (with sublimation); ir (KBr): 2820 (OCH_3), 1090 (C—O), 800 cm^{-1}; ^1H nmr ($CDCl_3$) δ: 1.23 (s, 6, 3-CH_3 and 6-CH_3), 3.15 (s, 6, 3-OCH_3 and 6-OCH_3), 5.82 (s, 4, 1-*H*, 2-*H*, 4-*H*, 5-*H*) ppm; ^{13}C nmr ($CDCl_3$, −10°C) δ_C: 28.4 (3-*C*H_3 and 6-*C*H_3), 52.3 (3-O*C*H_3 and 6-O*C*H_3), 70.9 (*C*-3 and *C*-6), 134.0 (*C*-1, *C*-2, *C*-4 and *C*-5) ppm; ms (70 eV) *m/e* (relative intensity): 168 (0.3), 153.091 (100, M_r $^{12}C_9{}^1H_{13}{}^{16}O_2$: 153.092, $M - CH_3$), 138 (31), 137 (97), 123 (13), 122 (51), 121 (13), 107 (10), 106 (16), 105 (17), 91 (41), 79 (26), 78 (14), 77 (43), 65 (19), 53 (19), 52 (13), 51 (25), 43 (63), 41 (25). *Anal.* calcd. for $C_{10}H_{16}O_2$: C 71.39, H 9.59; found: C 70.93, H 9.47.

*Shift reagent studies on the diastereomers of 4-methoxy-1,4-dimethylcyclohexa-2,5-dienol (***3**bo*)*

A solution of Eu($[^2H_9]$fod)$_3$ (150 mg) in [^{2}H]chloroform (450 mm^3) was prepared and measured volumes were added, at 0°C, to solutions of the methoxydienols (*E*)-**3***bo* and (*Z*)-**3***bo* (30 mg) in [^{2}H]chloroform (300 mm^3) containing tetramethylsilane (20 mm^3). The ^1H nmr of each solution was measured at 0°C after addition of the shift reagent. Plots of the chemical shifts of the other protons against that of the 1-CH_3 protons gave relative shift gradients (gradient 1-CH_3 = 1.00) as follows: (*E*)-**3***bo*: 0.34 (4-CH_3), 0.35 (4-OCH_3), 0.45 (3-*H* and 5-*H*), 1.06 (2-*H* and 6-*H*); (*Z*)-**3***bo*: 0.31 (4-CH_3), 0.35 (4-OCH_3), 0.43 (3-*H* and 5-*H*), 1.02 (2-*H* and 6-*H*).

*Solvolysis of (*E*)-1,4-dimethyl-4-nitrocyclohexadienol ((*E*)-**1**b) in aqueous methanol*

Initial experiments (101–118) were carried out using (*E*)-**1***b* (100 mg, 0.6 mmol) in aqueous methanol (1:1 v/v, 8 cm^3), in both the presence and absence of a weak base, and at both ambient temperature and 40°C. These reactions were not stirred, as the nitrodienol appeared to dissolve completely. The products were worked up by first saturating the reaction mixture with sodium chloride, extracting with ether (3 × 20 cm^3), and washing the combined ether layers with saturated brine (3 × 10 cm^3). The ethereal solution was dried ($MgSO_4$) and the ether evaporated; ^1H nmr analysis ($CDCl_3$; 0°C) gave the results listed in Table 1.

Generally, integration of characteristic methyl peaks was the preferred means of determining the product ratios. The methyl peaks of 2-nitro-*p*-xylene were clearly separated from those of the dimethylphenols and the product dienes **3***bn* and **3***bo*. The C-CH_3 peaks of **3***bn* and **3***bo* overlapped but the total integral could be subdivided using the O-CH_3 peak to measure the amount of **3***bo*. In some cases, e.g. when *N*,*N*-diisopropylethylamine was used, the methyl region was partially obscured and the ratio of (**3***bn* + **3***bo*):**6***p*:(**7***b* + **6***n*) was determined from the integral of the vinyl and aromatic regions of the ^1H nmr spectrum. In subsequent experiments (below) the ratio of **7***b* to **6***n* was determined by analytical hplc. Careful examination of the aromatic phenol region of the ^1H nmr of mixtures of known phenol composition showed that it was possible to determine the ratio of **7***b*:**6***n* by ^1H nmr using solutions of known composition for standardization. The (*E*) isomer of the dienediol **3***bn* was not completely soluble in $CDCl_3$ and in later experiments [$^2H_6$]dimethylsulfoxide was the preferred solvent for ^1H nmr.

In the second set of experiments (201–205) a solution of (*E*)-**1***b* (1.0 g, 5.9 mmol) in aqueous methanol (1:1 v/v, 80 cm^3) was stirred at 40°C for 1 h. In most reactions a weak base was added. Each reaction mixture was worked up by cooling to 0°C, saturating the solution with sodium chloride, and extracting with cold ether (3 × 100 cm^3). The combined ethereal extracts were washed with brine (3 × 50 cm^3) and dried ($MgSO_4$). The ether was evaporated at 30°C and final traces of ether were removed under reduced pressure. Analysis was carried out by ^1H nmr using $(CD_3)_2CO$, $(CD_3)_2SO$, or $CDCl_3$ as solvent. The ratio of 2,4- to 2,5-dimethylphenol was determined by hplc. The peaks of the phenols overlapped and the amounts of each were determined by cutting and weighing the peaks, having first calibrated the system using solutions of known phenol ratios prepared from pure phenols. Results are listed in Table 2 (expts. 201–205).

In the third set of experiments (206–217) a solution of (*E*)-**1***b* (100 mg, 0.6 mmol) in aqueous methanol (1:1 v/v, 2 cm^3), also containing added reagent, was maintained at 40°C in an ultrasonic bath for 20 min. Ether (50 cm^3) was added and the solution dried, first over sodium sulfate and then over magnesium sulfate. The drying agents were washed with ether and the combined ether solution evaporated at 30°C. Analysis was carried out by ^1H nmr. The ratio of 2,4- to 2,5-dimethylphenol was determined by analytical hplc, or by nmr using the nmr of reaction mixtures in which the phenol ratio had previously been determined by analytical hplc as standards. Results are given in Table 2. Experiments 206–216 were carried out under the most carefully controlled conditions and using refined methods of product analysis. Of the reactions carried out in the presence of base, expts. 209–211, 214, and 215 were without complication and the results may be regarded as particularly reliable. Experiments 208, 212, and 216 are of less, but acceptable, reliability. Reaction 207 was complicated by the insolubility of the base disodium hydrogen phosphate and reaction 213 did not go to completion. The mean product distribution from the particularly reliable set of experiments is **3***bo* (44%), **3***bn* (22%), **6***p* (20%), **7***b* (11%), and **6***n* (2%) and from the particularly reliable plus reliable sets is **3***bo* (43%), **3***bn* (21%), **6***p* (18%), **7***b* (15%), and **6***n* (3%).[2]

A solvolysis reaction was also carried out under acid conditions. (*E*)-**1***b* (0.07 g, 0.4 mmol) was added to aqueous methanol (1:1 v/v, 10 cm^3) containing potassium chloride (7.5 mg, 1 mmol) after the pH of the solution had been adjusted to 3.2 by the addition of hydrochloric acid. The solution was stirred at ambient temperature for 22 h. The product, obtained after work-up as described above for expts. 101–118, contained (^1H nmr) dimethoxydienes (12%) and a mixture of aromatic compounds (88%) including dimethylanisoles, dimethylphenols, and, tentatively, dimethylnitrophenol(s).

In a larger-scale reaction (*E*)-**1***b* (3 g, 0.018 mol) was dissolved in aqueous methanol (1:1 v/v, 240 cm^3) and potassium acetate (1.9 g, 0.02 mol) was added. The solution was stirred at 40°C and then chilled. A sample (8 cm^3) was worked up to confirm completion of the solvolysis. The main reaction mixture was then saturated with salt, stirred for 5 min, and extracted with ether (3 × 200 cm^3). The combined ether layers were washed with brine (3 × 100 cm^3) and dried, first over sodium sulfate and then over magnesium sulfate. Evaporation of the ether at 30°C and removal of the final traces under reduced pressure gave an oil (2.4 g) that contained (by nmr) the methoxydienols **3***bo* (60%), dienediols **3***bn* (12%), dimethylphenols plus dimethylanisoles (16%), and 2-nitro-*p*-xylene (12%). Preparative hplc on silica and elution with ether gave four fractions, the first containing the aromatic compounds, the second was methoxydienol (*E*)-**3***bo*, the third its isomer (*Z*)-**3***bo* containing some (*E*)-**3***bo* (7%), and the fourth a mixture of (*Z*)-**3***bo* and the dienediols **3***bn*. Recrystallization of the second fraction from ether–pentane gave colourless crystals, mp 95–97°C (lit. (9) mp 94–95°C) with ^1H nmr identical to that of an authentic sample of (*E*)-**3***bo*. The ^1H nmr of the major component of the third fraction was identical to that of an authentic sample of (*Z*)-**3***bo*. Some crystals separated from the fourth fraction on standing. They were washed free of the oil with ether, dissolved in [$^2H_6$]acetone, and then had ^1H nmr identical to that of authentic (*E*)-**3***bn*.

*Solvolysis of (*E*)-**1**b in methanol*

A solution of (*E*)-**1***b* (70 mg, 0.41 mmol) and *N*,*N*-diisopropylethylamine (82 mm^3, 0.45 mmol) in CD_3OD (0.6 cm^3) was observed by nmr. Little or no reaction occurred over 1 h at 40°C. After 6 min at

[2]We have ignored the fact that the product distribution may be a function of the particular base used. The product distributions for reactions in which the same base was used are more closely similar than the product distributions for experiments involving different bases. However, such differences are small compared to those between reactions carried out with and without base. We have also ignored the likely presence of a small amount of **5***bn* and (or) **5***bo*.

60°C, formation of the two diastereomers of the methoxydienol **3***bo* was apparent. The reaction half-life at 60°C was 75 min and after 5.3 h the reaction mixture was worked up to give (^{1}H nmr) a mixture of **3***bo* (47%), dimethylphenols (17%), and 2-nitro-*p*-xylene (36%). A small amount of the dimethoxydiene **3***co* or dienediol **3***bn* was observed in the reaction mixture prior to work-up.

Solvolysis of (E)-**1**b *in aqueous tetrahydrofuran, aqueous ether, aqueous acetone, and aqueous dioxan*

The nitrodienol (100 mg, 0.59 mmol) was dissolved in the organic solvent, the requisite amount of water and the base were then added, and the solution stirred at the chosen temperature for the specified time. Work-up and ^{1}H nmr analysis gave the results summarized in Table 3.

Solvolysis was also carried out under acidic conditions in aqueous dioxan. The pH of the dioxan solution (1:1 v/v) containing potassium chloride was adjusted to 3.2 by the addition of hydrochloric acid. (*E*)-**1***b* was added and the mixture was stirred for 22 h at ambient temperature. After work-up, ^{1}H nmr indicated that aromatization was essentially complete and ^{1}H nmr and gc–ms indicated that the two major products were 2-nitro-*p*-xylene and dimethylnitrophenol.

In a larger-scale reaction a solution of (*E*)-**1***b* (10 g, 0.059 mol) in acetone (200 cm^3) and water (400 cm^3) containing *N*,*N*-diisopropylethylamine (11.7 cm^3, 0.065 mol) was stirred at 40°C for 1 h. The reaction mixture was saturated with salt, extracted with ether, and the combined ethereal extracts washed with brine, dried ($MgSO_4$), and the ether evaporated. The ^{1}H nmr analysis indicated that the mixture consisted of dienediol **3***bn* (35%), dimethylphenols (56%), and 2-nitro-*p*-xylene (10%). Addition of carbon tetrachloride gave colourless crystals of (*E*)-**3***bn* (0.7 g), which after recrystallization from acetone had mp 158–159°C; ir (KBr): 3370, 3330, 1125, and 1070 (OH), 1410 (C—CH_3), 780 (*cis* vinyl) cm^{-1}; ^{1}H nmr ($(CD_3)_2CO$, 0°C) δ: 1.18 (s, 6, 1-C*H*$_3$ and 4-C*H*$_3$), 3.02 (s, 2, 1-O*H* and 4-O*H*), 5.67 (s, 4, 2-*H*, 3-*H*, 5-*H*, and 6-*H*) ppm; ^{13}C nmr ($(CD_3)_2CO$) δ_C: 29.3 (1-*C*H$_3$ and 4-*C*H$_3$), 65.4 (*C*-1 and *C*-4), 133.9 (*C*-2, *C*-3, *C*-5, and *C*-6) ppm; ms (70 eV) *m/e* (relative intensity): 140 (1), 126 (17), 125.059 (100, M_r $^{12}C_7{}^1H_9{}^{16}O_2$: 125.060, $M - CH_3$), 124 (8), 122 (7), 111 (8), 110 (30), 108 (6), 107 (20), 106 (13), 105 (7), 97 (12), 91 (20), 79 (14), 77 (15). *Anal.* calcd. for $C_8H_{12}O_2$: C 68.55, H 8.63; found: C 68.62, H 8.61.

The carbon tetrachloride soluble extract contained 21% of dienes. After evaporation of the solvent a sample (5.5 g) of the residue was subjected to hplc on silica using ether eluant. The initial fraction (4.9 g) was a mixture of 2-nitro-*p*-xylene and dimethylphenols. The next fraction (0.19 g) was (*Z*)-**3***bn* containing a small amount of its (*E*) isomer and the final fraction (0.35 g) was a mixture containing **5***bn*. Purification by short-path distillation below 50°C at 50 Pa in a sublimator gave **5***bn* as an oil; ^{1}H nmr ($CDCl_3$, 270 MHz) δ: 1.29 (s, 3, 1-C*H*$_3$), 1.77 (t, 3, 4-C*H*$_3$), 2.81 (b, O*H*), 3.85 (bd, 1, 2-*H*), 5.61 (bd, 1, 3-*H*), 5.70 (dd, 1, J = 2, 10 Hz, 5-*H*), 5.75 (d, 1, J = 10 Hz, 6-*H*) ppm. In the 90-MHz spectrum, irradiation at 1.77 ppm collapsed the peaks at 3.85 and 5.61 to the doublets of an AB quartet (J = 4 Hz); irradiation at 3.85 collapsed the peak at 1.77 ppm to a doublet (J = 1.8 Hz) and sharpened the peak at 5.61 to an incompletely resolved quartet; irradiation at 5.61 collapsed the peak at 1.77 to an uneven doublet (J = 1.6 Hz) and sharpened the peak at 3.85 ppm to an incompletely resolved quartet.

Solvolysis of (E)-*3-methoxy-3,6-dimethyl-6-nitrocyclohexa-1,4-diene* ((E)-**1**c)

Solvolysis of (*E*)-**1***c* (100 mg, 0.55 mmol) was carried out for 5 h at 56°C in aqueous methanol (1:1 v/v, 8 cm^3) containing diisopropylethylamine (108 mm^3, 0.61 mmol). The substrate was not completely soluble. After work-up as described for expts. 101–118, the products obtained were (*E*)- and (*Z*)-**3***co* (21%), (*E*)- and (*Z*)-**3***cn* (34%), dimethylanisoles and dimethylphenols (41%), and 2-nitro-*p*-xylene (4%). The reaction was repeated at 40°C and at 25°C in the absence of added base. The reaction did not go to completion but a similar product distribution was obtained.

Reaction of (E)-**1**c *with methanol – trifluoroacetic acid*

Diene (*E*)-**1***c* (100 mg, 0.55 mmol) was dissolved in a mixture of methanol (250 mm^3) and trifluoroacetic acid (250 mm^3) at 0°C. After 16 h at 35°C aromatization was complete (^{1}H nmr). The solvent was evaporated and the residue was dissolved in ether (20 cm^3) and washed with aqueous sodium bicarbonate (3 × 10 cm^3) and water (10 cm^3). After drying ($MgSO_4$) the ether was evaporated to give an oil (55 mg) containing 2,4-dimethylanisole (16%), 2,5-dimethylanisole (34%), and 2-nitro-*p*-xylene (50%). Analysis by glc (10% FFAP) confirmed the presence of dimethylanisoles (single peak) and the 2-nitro-*p*-xylene. Similar results were obtained when the reaction was repeated at ambient temperature for 100 h.

Solvolysis of (E)-*1,4-dimethyl-4-nitrocyclohexa-2,5-dienyl acetate* ((E-**1**a)

Acetate (*E*)-**1***a* (100 mg, 0.47 mmol) was dissolved in aqueous methanol (1:1 v/v, 8 cm^3) and the mixture stirred at ambient temperature for 2 h. The reaction was worked up as described for expts. 101–118. 2,5-Dimethylphenyl acetate (47 mg) was the sole product (^{1}H nmr). The same result was obtained when the reaction was carried out for 1 h at 40°C. The reaction was also carried out in the presence of added base (diisopropylethylamine, potassium acetate) when partial solvolysis of the 2,5-dimethylphenyl acetate to 2,5-dimethylphenol occurred. A control experiment showed that 2,5-dimethylphenyl acetate was solvolysed to the phenol under these conditions. Any acetoxydienol formation could not have exceeded 3% of the product.

Solvolysis of 4-methyl-4-nitrocyclohexa-2,5-dien-1-ol

The nitrodienol (100 mg, 0.65 mmol) was weighed into a chilled flask and aqueous methanol (1:1 v/v, 2 cm^3), at −10°C, and sodium bicarbonate (57 mg, 0.68 mmol) were added. The mixture was heated in an ultrasonic bath at 40°C for 20 min. Ether (50 cm^3) was added, the solution dried over Na_2SO_4 and then over $MgSO_4$, and the solvent evaporated to give an oil (51 mg) consisting of *p*-cresol (90%) and unidentified dienes (δ: 1.57 and 5.95 ppm, 10%). Solvolysis was also carried out on a 0.16-mmol scale in D_2O–CD_3OD (1:1) containing C_5D_5N (0.18 mmol) and the reaction monitored by ^{1}H nmr. Again *p*-cresol (90%) and unidentified dienes (10%) were obtained. The half-life of **10** was 50 min at −10°C and 10 min at 0°C. When the solvolysis was carried out in acetone–water (1:2 v/v) containing sodium bicarbonate, *p*-cresol (90%) and unidentified diene (10%) were formed.

Rates of solvolysis of (E)-**1**a *and* (E)-**1**b

The diene (0.3 mmol) was dissolved in CD_3OD (1 cm^3) at 0°C, and cold D_2O (1 cm^3) and C_5D_5N (27 mm^3, 0.33 mmol) were added. A sample of the solution was quickly transferred to a nmr tube and the FT ^{1}H nmr spectrum observed (50 scans per spectrum) at the desired temperature. The time taken for the integral of the aliphatic methyl region to decrease to half of the original intensity was determined from a first-order plot. For (*E*)-**1***a*, $t_{1/2}$ = 2.5 min at 40°C and 75 min at 27°C. For (*E*)-**1***b*, $t_{1/2}$ = 5.5 min at 40°C and 210 min at 27°C.

Reaction of (E)-*1,4-dimethylcyclohexa-2,5-diene-1,4-diol* ((E)-**3**bn) *with trifluoroacetic acid*

The dienediol (*E*)-**3***bn* (40 mg) was dissolved in trifluoroacetic acid (0.5 cm^3) at 0°C in an nmr tube. After 15 min at 0°C and 10 min at 38°C, ^{1}H nmr indicated that aromatization was complete and that the product was largely 2,4-dimethylphenol. The same result was obtained when the experiment was repeated using (*E*)-**3***bn* (50 mg) in trifluoroacetic acid (1 cm^3) and allowing the solution to stand at ambient temperature for 1.5 h. The product phenol was isolated by neutralization of the trifluoroacetic acid with sodium bicarbonate solution and extraction with ether. The ^{1}H nmr of the isolated products from the two reactions confirmed that 2,4-dimethylphenol was the predominant product. Each reaction product was treated with bistrimethylsilylacetamide and the resulting mixtures of trimethylsilyloxydimethylbenzenes analysed by glc: the product from each reaction was determined to be trimethylsilyloxy-2,4-dimethylbenzene (98%) and trimethylsilyloxy-2,5-dimethylbenzene (2%).

Reaction of (E)-**3**bn *with dilute acid*

(*E*)-**3***bn* was solvolysed at 50°C for 5 h and at ambient temperature for 72 h, in aqueous methanol at pH 3.2, as described for (*E*)-**1***b*. After

work-up and ^{1}H nmr measurement, the ratio of dimethylphenols was determined by addition of bistrimethylsilylacetamide and analysis by glc: 2,4- (68%) and 2,5-dimethylphenol (32%) were the only products. In a second experiment, in which the mixture was heated for 21 h at 40°C, aromatization was not complete; ^{1}H nmr and glc–ms confirmed the presence of (*E*)-**3***co* (4%), (*Z*)-**3***co* (4%), (*E*)- and (*Z*)-**3***bo* (4%), **7***b* (55%), **6***n* (22.5%), and **6***o* plus **7***o* (10.5%). Solvolysis of (*E*)-**3***bn*, at ambient temperature for 26 h, was also carried out in aqueous dioxane at pH 3.2. Silylation and glc analysis gave the product distributions **7***b* (68.5%), **6***n* (31.5%) and **7***b* (64.4%), **6***n* (35.6%) in duplicate experiments.

Reaction of (Z)-3,6-dimethoxy-3,6-dimethylcyclohexa-1,4-diene ((Z)-3co) with trifluoroacetic acid

The ether (*Z*)-**3***co* (31 mg) was dissolved in trifluoroacetic acid (0.5 cm^3) and the reaction was monitored by ^{1}H nmr over 1 h, after which time rearomatization was complete. The nmr spectrum showed that 2,4-dimethylanisole was formed.

Acknowledgements

We thank Dr Orson Chan for the 270-MHz nmr spetrum and the Natural Sciences and Engineering Research Council of Canada for financial support.

1. D. J. Blackstock, A. Fischer, K. E. Richards, J. Vaughan, and G. J. Wright. Chem. Commun. 641 (1970).
2. A. Fischer and G. N. Henderson. Can. J. Chem. **59**, 2314 (1981).
3. R. C. Hahn and M. B. Groen. J. Am. Chem. Soc. **95**, 6128 (1973).
4. P. C. Myhre. J. Am. Chem. Soc. **94**, 7921 (1972).
5. T. Banwell, C. S. Morse, P. C. Myhre, and A. Vollmar. J. Am. Chem. Soc. **99**, 3042 (1977).
6. H. W. Gibbs, R. B. Moodie and K. Schofield. J. Chem. Soc. Perkin Trans. 2, 1145 (1978).
7. J. T. Geppert, M. W. Johnson, P. C. Myhre, and S. P. Woods. J. Am. Chem. Soc. **103**, 2057 (1981).
8. A. Fischer and J. N. Ramsay. Can. J. Chem. **53**, 3960 (1974).
9. G. J. Kasperek, T. C. Bruice, H. Yagi, N. Kaubisch, and D. M. Jerina. J. Am. Chem. Soc. **94**, 7876 (1972).
10. G. J. Kasperek, T. C. Bruice, H. Yagi, and D. M. Jerina. J. Chem. Soc. Chem. Commun. 784 (1972).
11. A. Fischer, G. N. Henderson, T. A. Smyth, F. W. B. Einstein, and R. E. Cobbledick. Can. J. Chem. **59**, 584 (1981).
12. C. E. Barnes, K. S. Feldman, M. W. Johnson, H. W. H. Lee, and P. C. Myhre. J. Org. Chem. **44**, 3925 (1979).
13. A. Fischer and G. N. Henderson. Tetrahedron Lett. 701 (1980).
14. E. Bamberger. Ber. **33**, 3600 (1901); Justus Liebigs Ann. Chem. **390**, 164 (1912).
15. V. P. Vitullo and E. A. Logue. J. Org. Chem. **37**, 3339 (1972).
16. J. N. Marx, J. C. Argyle, and L. R. Norman. J. Am. Chem. Soc. **96**, 2121 (1974).
17. E. A. Fehnel. J. Am. Chem. Soc. **94**, 3961 (1972).
18. A. I. Vogel. Practical organic chemistry. 4th ed. Longmans, London. 1978. p. 751.
19. A. Ronlan and V. D. Parker. J. Chem. Soc. (C), 3214 (1971).

Mechanism of azo coupling reactions. Part 34.[1] Reactivity of five-membered ring heteroaromatic diazonium ions

HEINZ DIENER AND HEINRICH ZOLLINGER
Technisch-Chemisches Laboratorium, Eidgenössische Technische Hochschule, CH-8092 Zurich, Switzerland
Received October 15, 1985

This paper is dedicated to Professor Arthur N. Bourns

HEINZ DIENER and HEINRICH ZOLLINGER. Can. J. Chem. **64**, 1102 (1986).

The azo coupling reactions of six five-membered ring heteroaromatic diazonium ions with 2-naphthol-3,6-disulfonic acid are investigated kinetically at various pH values. The dependence of the measured rate constants on the acidity of the aqueous reaction system is evaluated. It can be shown that the 2-naphtholate-3,6-disulfonate trianion reacts $4 \times 10^8 - 8 \times 10^8$ times faster than the 2-naphthol-3,6-disulfonate dianion. The rate constants of the six diazonium ions vary by more than four orders of magnitude. The logarithms of the rate constants of all comparable diazonium ions correlate linearly with ^{1}H nmr chemical shifts of the respective unsubstituted heteroaromatic parent compounds. An analogous correlation was found for azo couplings with substituted benzenediazonium ions. Diazotization of heteroaromatic amines does not go to completion, rather to an equilibrium. It is shown therefore that in acidic coupling systems the azo compound is only the kinetically controlled product. The thermodynamic products are 1-nitroso-2-naphthol-3,6-disulfonic acid and the heteroaromatic amine.

HEINZ DIENER et HEINRICH ZOLLINGER. Can. J. Chem. **64**, 1102 (1986).

Opérant à divers pH, on a étudié la cinétique de réactions de couplage azo entre six ions diazonium d'hétérocycles aromatiques à cinq chaînons et l'acide naphtol-2 disulfonique-3,6. On a évalué la dépendance des constantes de vitesses mesurées sur l'acidité du système aqueux de la réaction. On peut démontrer que le trianion naphtolate-2 disulfonate-3,6 réagit de 4×10^8 à 8×10^8 plus rapidement que le dianion naphtol-2 disulfonate-3,6. Les constantes de vitesse pour les six ions diazonium varient par plus de quatre ordres de grandeurs. Il existe une corrélation linéaire entre les constantes de vitesse de tous les ions diazonium comparables et les déplacements chimiques en rmn du ^{1}H des composés hétéroaromatiques de base qui ne sont pas substitués. On a pu établir une corrélation analogue pour les couplages azo avec des ions benzènediazonium substitués. La réaction de diazotation des amines hétéroaromatiques n'est pas complète; il s'agit plutôt d'un équilibre. On démontre alors que, dans les systèmes de couplages acides, les composés azo ne sont que les produits de contrôle cinétique. Les produits de contrôle thermodynamique sont l'acide nitroso-1 naphtol-2 disulfonique-3,6 et l'amine hétéroaromatique.

[Traduit par la revue]

Introduction

In contrast to the large number of investigations of the reactivity of carboaromatic diazonium ions in general and of the mechanism of their azo coupling reactions, very few comparable investigations have been made with heteroaromatic diazonium ions. Goerdeler and Haubrich (2) have made a semiquantitative comparison of the reactivity of 3-phenyl-1,2,4-thiadiazole-5-diazonium ion with 2-naphthol and the respective reaction with 2,4-dinitrobenzenediazonium ion. Sawaguchi *et al.* (3) have measured the rate of azo coupling of various heteroaromatic diazonium ions with 2-naphthol-3,6-disulfonic acid. There exists an extensive patent literature on azo dyes synthesized with heteroaromatic diazonium ions since Dickey and Towne realized in the early 1950s that industrially interesting disperse dyes can be obtained on this basis. Weaver and Shuttleworth (4) have reviewed that subject, but give no information on reactivities and yields.

Relations between the structure of heteroaromatic parent compounds and the reactivity of the respective diazonium ions have not been investigated in the past. The goal of this investigation is the measurement of the rates of azo coupling reactions of a series of five-membered ring heteroaromatic diazonium ions with the tri- and, if possible, the di-basic anion of 2-naphthol-3,6-disulfonic acid, and the correlation of the kinetic results with the chemical shift in ^{1}H nmr of the heteroaromatic compound that contains a hydrogen atom instead of the diazonio group. In addition, 1-nitroso-2-naphthol-3,6-disulfonic acid was identified as a by-product, as it is known that the yields of azo coupling reactions with heteroaromatic diazonium ions are in most cases significantly lower than those with carboaromatic diazonium ions.

The diazonium ions of the following amines were included in this investigation: thiazole-2-, -4-, and -5-diazonium ions (**1**, **2** and **3**), 1,2,4-thiadiazole-5-diazonium ion (**4**), 1,3,4-thiadiazole-2-diazonium ion (**5**), and 1,3,4-triazole-2-diazonium ion (**6**).

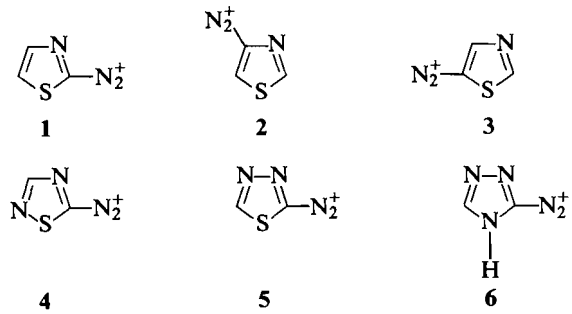

1 **2** **3**

4 **5** **6**

Experimental and kinetic results

The diazonium ions **1**–**6** were obtained by diazotization of the respective amines. For *2-aminothiazole* the synthesis of Traumann (5) was used.

4-Aminothiazole was synthesized from chloroacetonitrile and sodium thiocyanate, which form cyanomethylthiocyanate (NC—CH_2—S—CN). This compound was cyclized to 2-bromo-4-aminothiazole hydrobromide with HBr following a procedure described by Johnson and Nasutavicus (6). For the debromination of 2-bromo-4-aminothiazole the amino group has to be protected by acylation. Johnson and Nasutavicus used acetic anhydride for this purpose. We obtained

[1]Part 33: Kaminski *et al.* (1).

insufficient yields by using their procedure. Therefore we acylated with trifluoroacetanhydride: 28.6 g (0.11 mol) 2-bromo-4-aminothiazole hydrobromide was added in four batches to 75 g (0.36 mol) trifluoroacetanhydride. After 1 h at room temperature the solution was evaporated *in vacuo*. Yield: 34,75 g (81%) of the 1:1 addition product of 2-bromo-4-trifluoroacetamidothiazole with trifluoroacetic acid. Of this, 31.0 g were dissolved in 125 mL EtOH and purified on 80 g Amberlite IRC-50 (pretreated with 2 *M* NaOH and washed with 2 L water and afterwards with 200 mL ethanol). Afterwards, the EtOH solution was extracted with 150 mL hexane and treated at the boiling temperature with 0.5 g charcoal. After filtration and cooling, colorless needles precipitated, 16.78 g (76.6%) 2-bromo-4-trifluoroacetamidothiazole, mp 58°C; 16.78 g (61 mmol) of this product was debrominated with H_2 at normal pressure in a solution of 7.30 g (89 mmol) NaOAc in 500 mL absolute EtOH in the presence of 3 g Pd on coal (10%). After 6 h the filtrate was evaporated. The residue was extracted with warm CH_2Cl_2 and recrystallized from EtOH, 8.11 g (67.8%) 4-trifluoroacetamidothiazole, mp 139°C. *Anal.* calcd. for $C_5H_3N_2OSF_3$ (196.15): C 30.62, H 1.54, N 14.28%; found: C 30.57, H 1.65, N 14.31%. Then 392 mg (2 mmol) 4-trifluoroacetamidothiazole was dissolved in 3 mL water and 0.25 mL 50% NaOH. After 6 h at 35°C under Ar the solution was cooled in an ice bath and glacial acetic acid was added to pH 8. Water was evaporated under rotation at 40°C in an Ar atmosphere. The residue was distilled at 0.01 Torr/85°C (1 Torr = 133.3 Pa). We obtained a colorless oil that crystallized out at deep-freezer temperatures, 42 mg (21%). The melting point was not determined because the product rapidly became black. *Anal.* calcd. for $C_3H_4N_2S$ (100.14): C 35.98, H 4.03, N 27.97%; found: c 35.69, H 4.01, N 27.74%.

5-Aminothiazole was synthesized from aminoacetonitrile. Reaction with formic acid ethyl ester gave *N*-cyanomethylacetamide, as described by Sekiya and Osaki (7). As we were not successful in following the procedure of these authors for the next step, namely the addition of H_2S at the cyano group in order to form 2-formamido-thioacetamide, we used the method described by Sen *et al.* (8), in which gaseous H_2S was introduced into a pyridine solution of the substrate. As we did not obtain the desired product, rather again the substrate after evaporation at normal pressure, we evaporated the solvent *in vacuo* and did not purify the residue, but made the cyclocondensation to 5-aminothiazole directly with the help of $POCl_3$ as described by Masui and Tamura (9): 18.79 g raw 2-formamidothioacetamide gave 1.32 g 5-aminothiazole, which was chromatographed ($CHCl_3/CH_3OH$ 9:1, Kieselgel) and recrystallized from isopropanol under Ar, 0.537 g (3.5%) colorless crystals, mp 81°C (dec.). *Anal.* calcd. for $C_3H_4N_2S$ (100.14): C 35.98, H 4.03, N 27.97%; found: C 35.80, H 4.13, N 27.74%.

5-Amino-1,2,4- and *2-amino-1,3,4-thiadiazole* were synthesized by the methods of Goerdeler (10) and Stolle and Fehrenbach (11), respectively.

2-Amino-1,3,4-triazole: Fluka product, puriss; mp 154–155°C. *Anal.* calcd. for $C_2H_4N_4$ (84.08): C 28.57, H 4.80, N 66.63%; found: C 28.62, H 4.82, N 66.48%.

Methods of diazotization and azo coupling

After comparative studies of various methods, we used the following two procedures, which gave the best results with our amines **1–6**.

Method A: 1.0 mmol amine was dissolved in 5 mL 72% H_2SO_4 and diazotized by addition of 1.0 mmol powdered $NaNO_2$ at −10°C. After 1 h the solution was diluted to 50 mL with 72% H_2SO_4. For preparative azo coupling reactions 1 mmol of 2-naphthol-3,6-disulfonic acid (disodium salt, purified, containing 9% crystal water) was added. After 1 h the solution was carefully neutralized with Na_2CO_3. The precipitate consisted of a mixture of the azo compound, Na_2SO_4, and the products of decomposition, which were separated by preparative paper chromatography (*n*-butanol/ethanol/water 4:3:3). The colored zone on the paper was cut out and the azo compond extracted with water. Yields were low (1 to 5% pure azo compound). For kinetic measurements a 5-μL droplet of the diazo solution was put on the Teflon stopper of an uv cell that contained 3.0 mL buffer solution and 50 μL 0.211 *M* solution of 2-naphthol-3,6-disulfonic acid. The reaction was started by the shaking of the cell. Initial concentrations: 2-naphthol-3,6-disulfonic acid, 3.52×10^{-3} *M*; diazonium salt, 3.33×10^{-5} *M* (or lower).

TABLE 1. Azo couplings of thiazole-2-diazonium ion[a]

pH	$10^3 k_{ps}$ (s^{-1})	$10^{-8} k_1$ ($L\,mol^{-1}\,s^{-1}$)	k_2 ($L\,mol^{-1}\,s^{-1}$)
−1.72[b]	0.63±0.03	—	1.79×10^{-1}
0.51	1.15±0.03	1.15	
1.10	2.75±0.07	1.56	
1.55	7.18±0.11	1.44	
2.00	18.50±0.38	1.32	
Mean value (μ)		1.37±0.18[c]	

[a]Diazotization method A in 72% H_2SO_4; λ_{max} of azo compound: 486 nm.
[b]30% H_2SO_4 ($H_0 = -1.72$).
[c]95% confidence limits: $1.19 \times 10^8 < \mu < 1.55 \times 10^8$.

Method B: 1.0 mmol amine was dissolved in 1.0 mL 50% or 90% H_2SO_4 and diazotized at −10°C with 1.0 mL 1 *M* nitrosyl sulfuric acid (50% or 90% H_2SO_4). This solution was used directly for reactions on a preparative scale as described for method A. For kinetic measurements a 50-mL volumetric flask was filled with buffer and 100 μL of a 0.25 *M* solution of 2-naphthol-3,6-disulfonic acid and thermostatted. The diazo solution (5–20 μL) was dropped on the stopper. The volumetric flask was sealed with the stopper and the reaction was started by shaking. Afterwards a sample of the reacting solution was transferred into a quartz cell for spectrophotometric analysis. Initial concentrations: 2-naphthol-3,6-disulfonic acid, 5.00×10^{-4} *M*; diazo solution, $1.25–5.00 \times 10^{-5}$ *M*.

Method C: Due to the very low stability of 4-aminothiazole, the following procedure was used for diazotization: 0.196 g (1 mmol) 4-trifluoroacetamidothiazole was dissolved in 1.5 mL water by adding 0.125 mL 50% NaOH. The solution was stirred under Ar at room temperature for 24 h. After cooling to −10°C we added dropwise 2.5 mL (4.59) 96% H_2SO_4. This yielded a solution of 4-aminothiazole in 72% H_2SO_4. It was diazotized by adding 1.0 mL of 1 *M* nitrosylsulfuric acid (72% H_2SO_4) at −10°C.

Kinetic measurements were made in thermostatted 1.0-cm cells at 20.0 ± 0.1°C. Based on eq. [1], pseudo-first-order rate constants (k_{ps}) were obtained by linear regression from plots of $-\ln(A_\infty - A_t)$ against time (A_∞, A_t = optical density at the visible absorption maximum λ_{max} of the azo compound formed at times $t = \infty$, i.e. at least 10 half-life times, and t). All rate constants are mean values of the rate constants determined in three independent runs. Buffer solutions were made on the basis of the CRC Handbook (12).

$$[1] \quad -\ln(A_\infty - A_t) = k_{ps}t + C$$

Equation [1] has the advantage that k_{ps} can be determined without knowing the molar extinction coefficient of the azo compound at λ_{max}. The second-order rate constant is calculated as usual (13). Due to the high reactivity of the diazonium ions used and the relatively low pH values of the reacting solution (pH 1.72–5.97, see Results), the reaction rate consists of the sum of two independent reactions, namely that of the 2-naphtholate-3,6-disulfonate trianion RO^- (k_1) and that of the 2-naphthol-3,6-disulfonate dianion ROH (k_2). Equation [2] shows that by plotting log k_{ps} against pH, a straight line with a slope of 1.0 ± 0.1 is obtained if the reaction with RO^- is dominant. If $k_2[ROH] \gg k_1[RO^-]$ the overall rate is independent of pH.

$$[2] \quad \frac{d[Azo]}{dt} = k_{ps}[D] = k_1[RO^-][D] + k_2[ROH][D]$$

where D = diazonium ion. $[RO^-]$ and [ROH] were calculated as usual with the help of the acidity constant of the OH group of the coupling component: $pK_3 = 9.76$. This constant was calculated from data of Hashida *et al.* (14) for the ionic strength ($I = 0.08–0.10$) used in our experiments except for azo couplings of thiazole-2-diazonium (Table 1), which were run at $I = 0.20–0.25$. We determined $pK_3 = 9.40$ at this ionic strength. Results are given in Tables 1–6.

TABLE 2. Azo couplings of thiazole-4-diazonium ion[a]

pH	k_{ps} (s^{-1})	$10^{-6}k_1$ ($L\,mol^{-1}\,s^{-1}$)	k_2 ($L\,mol^{-1}\,s^{-1}$)
−0.31[b]	(7.94±0.37) × 10^{-6}	—	1.59×10^{-2}
1.01	(1.62±0.04) × 10^{-5}	9.29	
2.02	(7.46±0.18) × 10^{-5}	7.33	
3.03	(5.75±0.13) × 10^{-4}	6.18	
4.01	(6.52±0.19) × 10^{-3}	7.33	
4.53	(1.89±0.12) × 10^{-2}	6.42	
5.03	(6.97±0.31) × 10^{-2}	7.49	
μ		7.34±0.82[c]	

[a]Diazotization method C in 72% H_2SO_4; λ_{max} of azo compound: 485 nm.
[b]10% H_2SO_4.
[c]95% confidence limits: $6.62 \times 10^6 < \mu < 8.06 \times 10^6$.

TABLE 3. Azo couplings of thiazole-5-diazonium ion[a]

pH	k_{ps} (s^{-1})	$10^{-5}k_1$ ($L\,mol^{-1}\,s^{-1}$)
4.01	(4.49±0.13) × 10^{-4}	5.05
5.03	(3.72±0.13) × 10^{-3}	4.00
5.97	(2.95±0.08) × 10^{-2}	3.64
μ		4.23±0.73[b]

[a]Diazotization method B in 90% H_2SO_4; λ_{max} of azo compound: 473 nm.
[b]95% confidence limits: $3.40 \times 10^5 < \mu < 5.06 \times 10^5$.

TABLE 4. Azo couplings of 1,2,4-thiazole-5-diazonium ion[a]

% H_2SO_4	k_{ps} (s^{-1})	k_2[b] ($L\,mol^{-1}\,s^{-1}$)
30	(3.81±0.22) × 10^{-3}	7.62±0.44
50	(2.62±0.32) × 10^{-3}	5.25±0.65

[a]Diazotization method B in 90% H_2SO_4; λ_{max} of azo compound: 541 nm.
[b]$k_2 = k_{sp}/[ROH]$; $k_1[RO^-] \ll k_2[ROH]$. Štěrba and co-workers (19) and we (this paper) found ratios of reactivities of 2-naphtholate-3,6-disulfonate dianion $k_1/k_2 = 5.69 \times 10^8 - 7.94 \times 10^8$. Therefore we can calculate approximately k_1 for the azo coupling reaction of 1,2,4-thiadiazole-5-diazonium ion, based on k_2 in 30% H_2SO_4: $k_1 \cong 5.4 \times 10^9\ L\ mol^{-1}\ s^{-1}$.

TABLE 5. Azo couplings of 1,3,4-thiazole-2-diazonium ion[a]

% H_2SO_4	k_{ps}[b] (s^{-1})	k_2[c] ($L\,mol^{-1}\,s^{-1}$)
30	(1.87±0.13) × 10^{-3}	3.74±0.26
50	(5.33±0.85) × 10^{-4}	1.07±0.17

[a]Diazotization method B in 50% H_2SO_4; λ_{max} of azo compound: 544 nm.
[b]Calculated on the basis of initial rates.
[c]See footnote *b* of Table 4, $k_1 \cong 2.7 \times 10^9\ L\ mol^{-1}\ s^{-1}$.

In the azo coupling of the 1,3,4-thiadiazole-2-diazonium ion in 50% H_2SO_4 one observes that the absorption at $\lambda_{max} = 544$ nm goes through a maximum at approximately 1 h and decreases asymptotically thereafter (Fig. 1). Simultaneously, the optical density at 380 nm increases. This secondary band corresponds to the absortion maximum of 1-nitroso-2-naphthol-3,6-disulfonic acid. Pure 1-(1′,3′,4′-thiazolyl-2′-diazo)-2-naphthol-3,6-disulfonic acid in 50% H_2SO_4 solution shows the same

TABLE 6. Azo couplings of 1,3,4-thiazole-2-diazonium ion[a]

pH	k_{ps} (s^{-1})	$10^{-5}k_1$ ($L\,mol^{-1}\,s^{-1}$)
4.01	(1.66±0.10) × 10^{-4}	1.87
5.03	(1.89±0.15) × 10^{-3}	2.03
5.97	(1.13±0.11) × 10^{-2}	1.39
μ		1.76±0.33[b]

[a]Diazotization method B in 50% H_2SO_4; λ_{max} of azo compound: 495 nm.
[b]95% confidence limits: $1.39 \times 10^5 < \mu < 2.13 \times 10^5$.

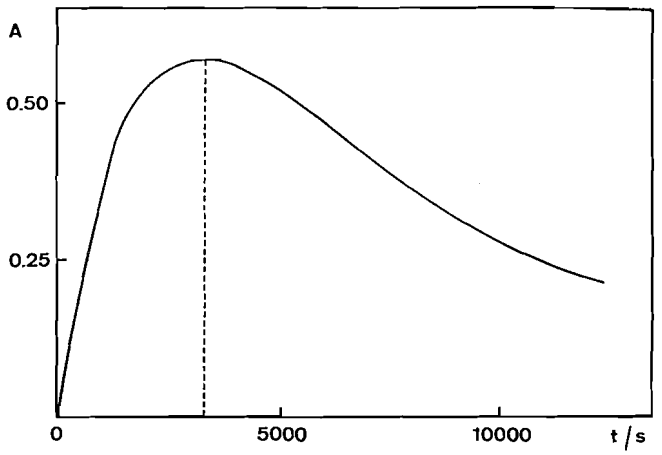

FIG. 1. Absorption of a mixture of the 1,3,4-thiadiazole-5-diazonium ion and 2-naphthol-3,6-disulfonic acid in 50% H_2SO_4 at 544 nm as a function of time.

decrease and increase, respectively, at the 544-nm and 380-nm bands, respectively. From such an experiment the rate of the retro-azo coupling reaction, i.e. the substitution of the heteroaryldiazo group by a proton, can be calculated: $k = (1.03 \pm 0.10) \times 10^{-4}\ s^{-1}$ (mean value of 3 measurements), 95% confidence limits; $0.92 \times 10^{-4} < \mu < 1.14 \times 10^{-4}\ s^{-1}$.

Discussion

The pseudo-first-order rate constants (k_{ps}) of the azo coupling reactions of the diazonium ions of six five-membered ring heteroaromatic amines with 2-naphthol-3,6-disulfonic acid show the typical dependence on the acidity of the aqueous solvent system that is known from respective investigations of carboaromatic diazonium ions with naphthols. The classical case is shown in Fig. 2 for the azo coupling of the thiazole-5-diazonium ion for the pH range 4–6: the measured values for log k_{ps} increase proportionally to pH, i.e. the rate is linearly dependent on the concentration of hydroxyl ions and therefore also linearly dependent on the concentration of the naphtholate ion (RO^-). It is the naphtholate ion that reacts with the diazonium ion (see ref. 13 and reviews (15, 16)).

Figure 3 demonstrates that the pH dependence of the azo coupling reaction of the thiazole-2-diazonium ion is in part different from that of the 5-isomer: the logarithm of the rate constant k_{ps} shows a linear dependence on pH with a slope of 1 only above pH 1. At lower pH values the curve gradually becomes horizontal. A similar figure results if our results with the 4-isomer are plotted. This is consistent with a dominant reaction of the naphthol relative to that of the naphtholate in the pH range below 0.5 ($k_2[ROH] > k_1[RO^-]$, because $[ROH] \gg [RO^-]$): in eq. [2] the first term can be neglected due to the ex-

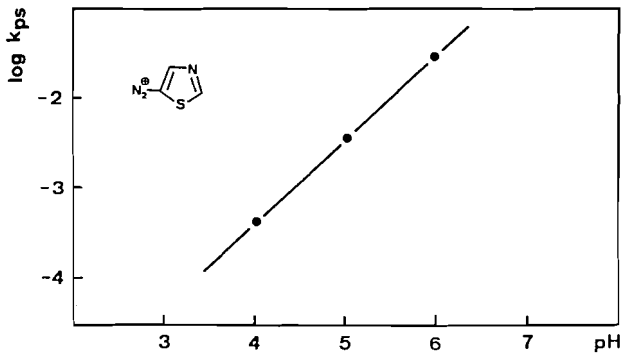

FIG. 2. Rate of azo coupling of the thiazole-5-diazonium ion with 2-naphthol-3,6-disulfonic acid as a function of acidity.

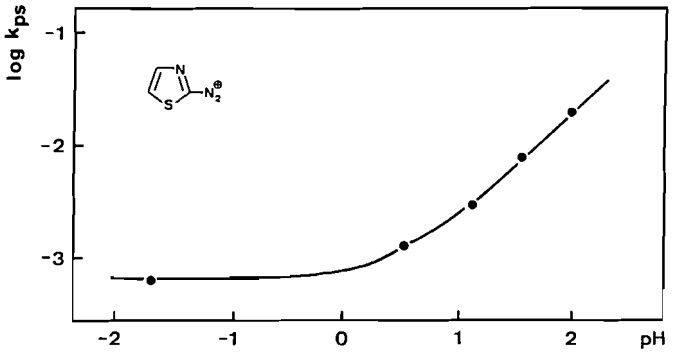

FIG. 3. Rate of azo coupling of a mixture of the thiazole-5-diazonium ion and 2-naphthol-3,6-disulfonic acid as a function of acidity.

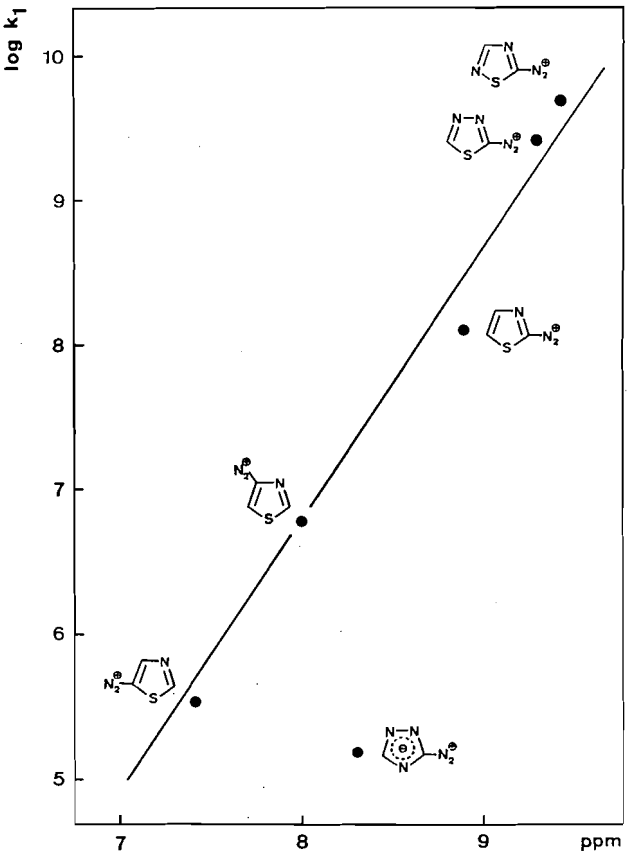

FIG. 4. Correlation between azo coupling rates of heteroaromatic diazonium ions with 2-naphtholate-3,6-disulfonate trianion and the chemical shifts of protons at the position of the diazonio group in ^{1}H nmr spectra of the respective heteroaromatic parent compound (nmr data from refs. 20 and 21).

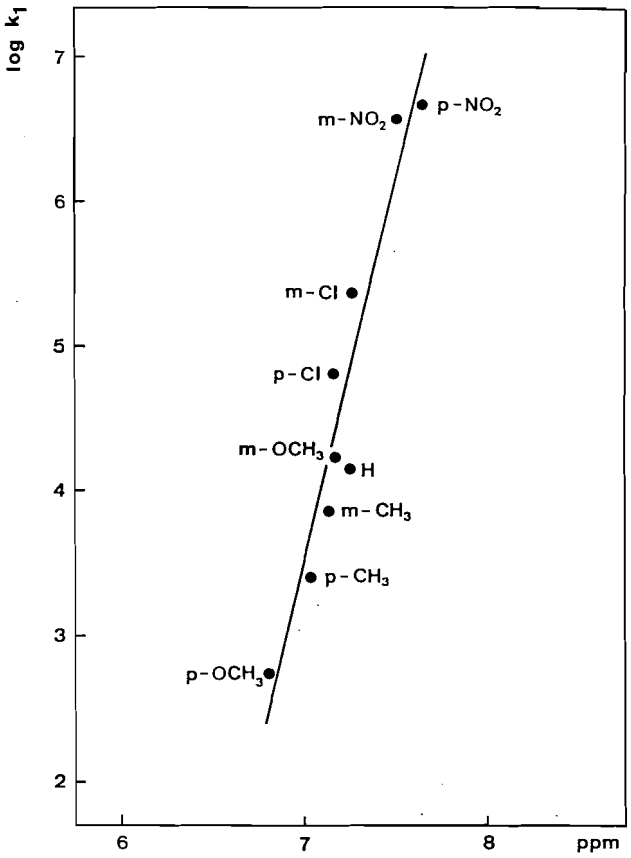

FIG. 5. Correlation between azo coupling rates of substituted benzenediazonium ions with the 2-naphtholate-3,6-disulfonate trianion (from ref. 15, p. 241) and the chemical shifts of protons at the position of the diazonio group in ^{1}H nmr spectra of the respective monosubstituted benzenes (nmr data from ref. 20).

tremely low numerical value of [RO^-]. For example, at pH 0, the equilibrium concentration of the naphtholate is $10^{9.76}$ times lower than that of the naphthol. An analogous pH dependence is expected for the thiazole-2-diazonium ion at lower pH values. Rates at pH < -2 are, however, too small to be measured accurately.

Semiquantitative work carried out in the fifties (17) suggests that undissociated naphthols and phenols do react with carboaromatic diazonium ions, but at rates that are several orders of magnitude lower than those of the respective naphtholates and phenolates. Quantitative evaluations of kinetic measurements carried out by Štěrba and co-workers (18, 19) in the seventies demonstrate that the naphtholates are 10^8–10^9 times more reactive than the naphthols.

The evaluation of the rate constants k_{ps} of the azo couplings of thiazole-2- and -4-diazonium ions with eq. [2] gives k_1 and k_2, i.e. the rate constants for reaction with the naphtholate and the naphthol, respectively (Tables 1 and 2). The ratios k_1/k_2 are 7.65×10^8 and 5.69×10^8. Very good agreement exists with the ratio k_1/k_2 of the reaction of the 3-nitrobenzenediazonium ion with 2-naphthol-3,6-disulfonic acid reported by Štěrba and co-workers (19): $k_1/k_2 = 7.94 \times 10^8$. This indicates strongly that, in this respect, azo coupling reactions of the heteroaromatic diazonium ion are mechanistically similar to those of carboaromatic analogs.

An interesting problem is the influence of the structure of the heteroaromatic ring on the reactivity of the respective diazonium ions. The results in Tables 1–6 show that the reactivities of the

six diazonium ions with the naphtholate ion (k_1) cover a range of more than 4 orders of magnitude ($1.76 \times 10^5 - 5.4 \times 10^9$ L mol^{-1} s^{-1}).

Is there a rationale behind the sequence of reactivities that we found? One may consider checking the results from MO calculations made with heteroaromatic compounds of the types used for this study. Literature data which we found could, however, not be compared because they were either not obtained with the same type of MO treatment or obtained with outdated methods. We preferred, therefore, a comparison with an experimental probe for the reactivity of heteroaromatic compounds, namely the ^{1}H nmr chemical shifts of the heteroaromatic compounds on which our six diazonium ions are based. In Fig. 4 we plotted the logarithms of our azo coupling rate constants k_1 against the chemical shift of that proton in the respective heteroaromatic parent compound which is substituted by the diazonio group in our diazonium ions. We found a surprisingly good linear relationship for all but one rate. This results should, in fact, not be astonishing: a change of the chemical shifts to lower field indicates lower nucleophilicity (i.e. higher electrophilicity) of a heteroaromatic compound, which is reflected in the higher electrophilicity of the diazonio group. More astonishing, in our opinion, is the fact that, to our knowledge, such a correlation between chemical shifts and a series of comparable electrophilic aromatic substitutions has not yet been reported in the literature.

It was therefore imperative to check if the same type of correlation also exists for azo coupling reactions of substituted benzenediazonium ions with 2-naphthol-3,6-disulfonic acid. This is indeed the case, as shown in Fig. 5.

The only heteroaromatic diazonium ion whose rate of azo coupling does not follow the linear relationship with the ^{1}H nmr data in Fig. 4 is the 1,3,4-triazole-2-diazonium ion. This apparent discrepancy is most likely based on the fact that the ion is easily deprotonated at the heterocyclic nitrogen atom in the 1-position. Under our azo coupling conditions (pH 4.01–5.97) the equilibrium is almost completely on the side of the zwitterion **7** in eq. [3]. The mesomeric structure **7***b* demonstrates

[3] 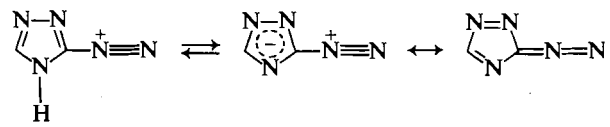

6 **7***a* **7***b*

that the reactivity of **7** is expected to be lower than that of **6** and the diazonium ions **1**–**5** used in this study. In Fig. 4 the chemical shift of 1,3,4-triazole is plotted (8.31 ppm). For the corresponding anion of 1,3,4-triazole a chemical shift of 8.10 ppm is reported (21). This value hardly improves the position of this diazo compound relative to the five others.

A comparison of Figs. 4 and 5 also offers an explanation for the deviation of the 1,3,4-triazole-2-diazonium zwitterion (**7**) in Fig. 4. The straight lines have different slopes. This is obviously due to the fact that the aromatic ring current is influenced by the type of aromatic systems involved, namely benzene (Fig. 5) and various heteroaromatic five-membered ring compounds (Fig. 4). It seems that the number and type of heteroatoms in these rings is of minor importance except for a (formally) anionic nitrogen as present in **7**.[2]

[2]A referee suggested that 1,3,4-triazole is the only compound in which the proton in question resides between two nitrogen atoms. This may be the cause for the deviation.

An additional factor for a decreased reactivity may be the addition (equilibrium [4]) of water to the diazo compound **7** to

[4] 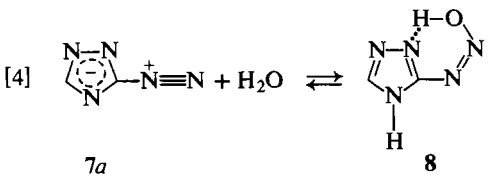

7*a* **8**

form the diazohydroxide **8**, which is probably not electrophilic at all. This possibility was, however, not investigated in more detail because of the low stability of solutions of this diazo compound.[3]

We explain the spectral change in kinetic runs of the azo coupling of the 1,3,4-thiadiazole-2-diazonium ion with time (Fig. 1) by the mechanism [5]. The diazonium ion **5** is present in

[5] 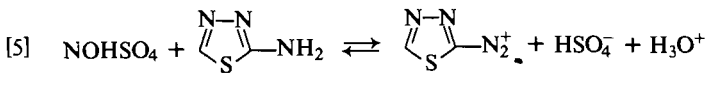

5

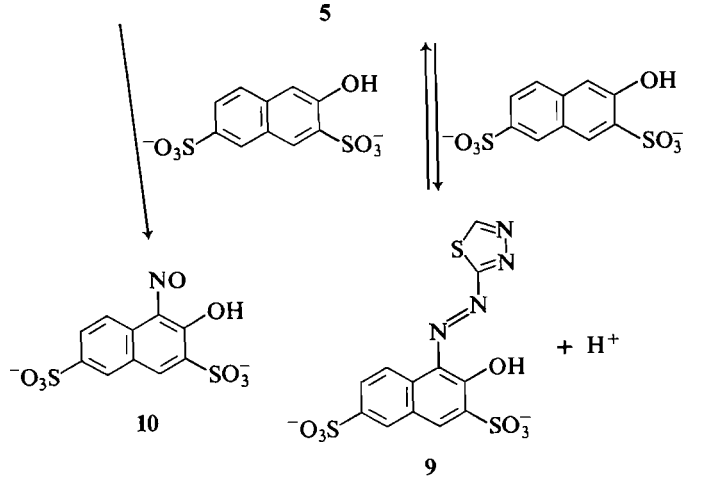

10 **9**

equilibrium with the nitrosating reagent[4] and forms the azo compound **9** as a kinetically controlled reaction product, whereas 1-nitroso-2-naphthol-3,6-disulfonic acid (**10**) is the thermodynamically controlled product. The back reaction of the azo coupling reaction **9** → **5** has been described in various cases involving carboaromatic diazonium ions.[5] Our results confirm that heteroaromatic diazonium ions also show the same behavior in this respect.

We will report on the mechanism of diazotization of heteroaromatic amines later (see ref. 22). In contrast to the diazotization of carboaromatic amines, which give quantitative yields of diazonium ions under the usual conditions, heteroaromatic amines are in equilibrium with the respective diazonium ions in the presence of nitrosating reagents. The formation of 1-nitroso-2-naphthol-3,6-disulfonic acid in reaction [5] is a consequence of that equilibrium.

1. R. KAMINSKI, U. LAUK, P. SKRABAL, and H. ZOLLINGER. Helv. Chim. Acta, **66**, 2002 (1983).
2. J. GOERDELER and H. HAUBRICH. Chem. Ber. **93**, 397 (1960).

[3]Note added Dec. 19, 1985: We only now became aware of the recent paper of Macháček *et al.* (23), who investigated the azo coupling mechanism of 5-methyl- and 5-phenyl-1,2,4-triazole-3-diazonium ions with phenols. In the context of diazo acid–base equilibria, they discuss structures analogous to **8** as potential intermediates.

[4]The formulation of the nitrosating reagent does not imply that it is not an ionic species.

[5]See summary, ref. 15, p. 241.

3. H. SAWAGUCHI, Y. HASHIDA, and K. MATSUI. Kogyo Kagaku Zasshi, **74**, 1859 (1971).
4. M. A. WEAVER and L. SHUTTLEWORTH. Dyes Pigm. **3**, 81 (1982).
5. V. TRAUMANN. Justus Liebigs Ann. Chem. **249**, 35 (1888).
6. F. JOHNSON and W. A. NASUTAVICUS. J. Org. Chem. **28**, 1877 (1963).
7. M. SEKIYA and Y. OSAKI. Chem. Pharm. Bull. **13**, 1319 (1965).
8. A. K. SEN and G. CHATTOPADHYAY. Ind. J. Chem. **178**, 222 (1979); A. K. SEN and A. K. MUKHOPADHYAY. Ind. J. Chem. **20B**, 275 (1981).
9. T. MASUI and T. TAMURA. Jap. Patents No. 7 103972 and 7 106049 (1971); Chem. Abstr. **74**, P 141756r (1971); **74**, P 141763r (1971).
10. J. GOERDELER. Chem. Ber. **87**, 57 (1954).
11. R. STOLLE and K. FEHRENBACH. J. Prakt. Chem. **122**, 289 (1929).
12. R. C. WEAST (*Editor*). Handbook of chemistry and physics. 59th ed. CRC Press, Boca Raton, Florida. 1979. p. D-186.
13. H. ZOLLINGER and C. WITTWER. Helv. Chim. Acta, **35**, 1209 (1952).
14. Y. HASHIDA, K. NAKAJIMA, S. SEKIGUCHI, and K. MATSUI. Kogyo Kagaku Zasshi, **72**, 1132 (1969).
15. H. ZOLLINGER. Azo and diazo chemistry. Interscience, New York. 1961.
16. I. SZELE and H. ZOLLINGER. Top. Curr. Chem. **112**, 1 (1983).
17. Z. J. ALLAN. Collect. Czech. Chem. Commun. **16**, 620 (1951); H. ZOLLINGER. Helv. Chim. Acta, **36**, 1070 (1953).
18. H. KROPACOVA, J. PANCHARTEK, V. ŠTĚRBA, and K. VALTER. Collect. Czech. Chem. Commun. **35**, 3287 (1970); J. KAVALEK, J. PANCHARTEK, V. ŠTĚRBA, and K. VALTER. Collect. Czech. Chem. Commun. **35**, 3470 (1970); V. ŠTĚRBA and K. VALTER. Collect. Czech. Chem. Commun. **37**, 270 (1972).
19. O. MACHACHOVA, V. ŠTĚRBA, and K. VALTER. Collect. Czech. Chem. Commun. **37**, 1851 (1972).
20. E. PRETSCH, T. CLERC, J. SEIBL, and W. SIMON. Tabellen zur Strukturaufklärung organischer Verbindungen. Springer, Berlin. 1976.
21. T. J. BATTERHAM. NMR spectra of simple heterocycles. John Wiley, New York. 1973.
22. H. DIENER. Ph.D. thesis, ETH Zurich, 1984.
23. V. MACHÁČEK, J. KOŘÍNEK, D. KREUZIGOVA, and V. ŠTĚRBA. Collect. Czech. Chem. Commun. **50**, 658 (1985).

The photo-Wallach rearrangement. Heavy-atom kinetic isotope effects and mechanism

HENRY J. SHINE, WITOLD SUBOTKOWSKI,[1] AND EWA GRUSZECKA[2]
Department of Chemistry, Texas Tech University, Lubbock, TX 79409-4260, U.S.A.
Received September 27, 1985
This paper is dedicated to Professor Arthur N. Bourns

HENRY J. SHINE, WITOLD SUBOTKOWSKI, and EWA GRUSZECKA. Can. J. Chem. **64**, 1108 (1986).

The photo-rearrangement of mixtures of azoxybenzene **4** and, successively, [^{15}N,^{15}N′]**4**, [^{18}O]**4**, and [2-^{14}C]**4** were carried out. Kinetic isotope effects (KIE) were calculated from measurements of isotopic ratios in both recovered **4** and the product, 2-hydroxyazobenzene (**6**). Analogous rearrangement of mixtures of 2,2′-azoxynaphthalene (**8**) with [^{15}N,^{15}N′]**8** and [1,1′-$^{13}C_2$]**8** were carried out and KIE were calculated from isotope ratios in the product. The results (particularly the lack of nitrogen KIE) collectively indicate that if an oxadiazole-like intermediate is involved in these rearrangements, an activation barrier exists in its formation rather than its decomposition.

HENRY J. SHINE, WITOLD SUBOTKOWSKI et EWA GRUSZECKA. Can. J. Chem. **64**, 1108 (1986).

On a réalisé des photo-transpositions sur des mélanges d'azoxybenzène (**4**) et successivement de composés **4** marqués au [^{15}N,^{15}N′], au [^{18}O] ou au [2-^{14}C]. On a calculé les effets isotopiques cinétiques (EIC) à partir de mesures des rapports isotopiques, tant dans le produit **4** qui était récupéré que dans le produit de la réaction, l'hydroxy-2 azobenzène (**6**). On a aussi réalisé des transpositions analogues sur des mélanges d'azoxynaphtalène-2,2′ (**8**) et de dérivés marqués au [^{15}N,^{15}N′] ou au [$^{13}C_2$-1,1′] et l'on a calculé les EIC en se basant sur les rapports isotopiques dans le produit. L'ensemble des résultats (et particulièrement le fait qu'il n'y a pas d'EIC de l'azote) indique que, si un intermédiaire ressemblant à un oxadiazole est impliqué dans ces transpositions, la barrière à l'activation existe plutôt dans sa formation que dans sa déomposition.

[Traduit par la revue]

Introduction

In recent years sporadic attempts have been made to detect intermediates in photochemical reactions in solution by measuring heavy-atom (other than hydrogen isotopes) kinetic isotope effects (KIE). The basis for this approach was expressed by Schutte and Havinga in 1967, who used the photo-Fries rearrangement to try to answer "the question that has been raised whether photochemical reactions after electron excitation pass through a transition state of appreciable energy of activation" (1). Schutte and Havinga used 4-methoxyphenyl-[^{14}C]acetate for measuring the carbon KIE in the photorearrangement of the ester into 2-acetyl-4-methoxyphenol, and found that within experimental error the rearrangement did not exhibit an isotope effect. They concluded, therefore, that rearrangement began in the electronically excited state (singlet) and proceeded very rapidly through vibrationally excited states in a process that required no thermal energy of activation.

The quest was later pursued by Kwart and co-workers (2), who sought evidence for a vibrationally excited ground state intermediate in the photochemical rearrangement of the ylide **1** into the diazepine **3**. In this case an inverse carbon KIE was found with the use of specifically labeled [^{13}C]**1**, and the result was attributed to the formation of the intermediate **2** in the pathway from excited **1** to product (**3**) (reaction [1]). To our knowledge this is the first time in which a heavy-atom KIE has been found in a photochemical rearrangement.

[1] 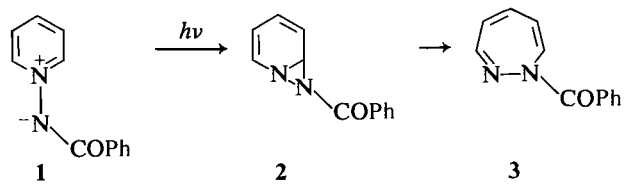

1 **2** **3**

We have been attracted to the idea of using heavy-atom KIE measurements in seeking evidence for activation barriers in photochemical rearrangements in solution. Such a barrier can exist in the electronically excited state (3). If we accept Ullman's view (4) and Kwart's conclusion, an activation barrier may also exist in a vibrationally excited ground state, reached by internal conversion from an electronically excited state. Internal conversion of this kind is known from photophysics studies to occur in the gas phase (3), but there is considerable doubt, because of rapid collisional deactivation, that a vibrationally excited ground state intermediate could exist long enough for detection in reactions in solution (5, 6).

Nevertheless, we have thought it worthwhile to continue the search for heavy-atom KIE in photochemical reactions, and have chosen the photo-Wallach rearrangement for study.

The photo-Wallach rearrangement is the intramolecular converison of an azoxyarene into a hydroxyazoarene (7). It is a singlet-state reaction (8), and does not involve radical pairs. Hence, in the use of ^{13}C labeling, it is not subject to the magnetic isotope effects associated with radical-pair reactions (9).

The photo-Wallach rearrangement is exemplified by the conversion of azoxybenzene (**4**) into 2-hydroxyazobenzene (**6**). The hydroxy group is known, from studies of substituent effects and nitrogen and carbon labeling, to migrate to the distant ring

[2] 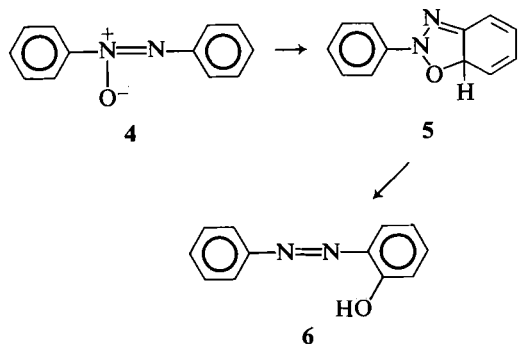

4 **5** **6**

[1]On leave from the Institute of Organic and Physical Chemistry, Technical University, Wrocław, Poland.

[2]Present address: Institute of Organic and Physical Chemistry, Technical University, Wrocław, Poland.

Printed in Canada / Imprimé au Canada

(7). It is now generally accepted that an intermediate is formed in the rearrangement, represented as **5** (eq. [2]) and attributed usually, but erroneously, to Badger and Buttery, in their finding and studies of the rearrangement's intramolecularity (10).[3]

Circumstantial evidence for the probable validity of **5** as an intermediate has been presented by Gegiou (13). That is, irradiation of 2,2′-azoxytoluene in solution at −70°C led to an absorption spectrum having a new band at approximately 436 nm. This was attributed to the dimethyl analog of **5** since it was thought to be the region in which an intermediate, similar to **5**, would absorb. This species was converted into the rearrangement product either by irradiation at 436 nm at −70°C or by warming the solution to room temperature without further irradiation. Although the corresponding band (i.e., for **5**) in the irradiation of **4** could not be detected, it was possible to irradiate **4** at temperatures in the range of −70 to −60°C and measure the rate of formation of **6** after irradiation was stopped. In this way an activation barrier for the formation of **6** of 12 kcal/mol was obtained and this was assigned to the decomposition of **5**. The several pieces of data when fitted together, then, showed that a ground-state intermediate is formed, consistent with the expectations for **5**, and that there is an activation barrier for its conversion into **6**. Noteworthy, also, is an additional report by the same authors that the formation of the ground-state intermediate appeared also to be temperature dependent; definitive supporting data for this report were not given, however (13).

The reports in the literature concerning rearrangement of **4** which we have briefly summarized suggested to us that we might be able to find heavy-atom KIE consistent with the formation and decay of an intermediate such as **5**. Our plan was to label **4** at its nitrogen, oxygen, and 2-carbon atoms and to measure the effects of labeling on the rate of rearrangement, seeking evidence thereby for bond-forming or bond-breaking steps in the conversion of **4** into **6**. Furthermore, because labeled precursors were available from earlier but unrelated work, we included the rearrangement of 2,2′-azoxynaphthalene (**8**) into 1-hydroxy-2,2′-azonaphthalene (**10**) in our plans, seeking evidence for the participation of the corresponding intermediate (**9**). The rearrangement of **8** into **10** had already been reported by Badger and Buttery (10).

[4]

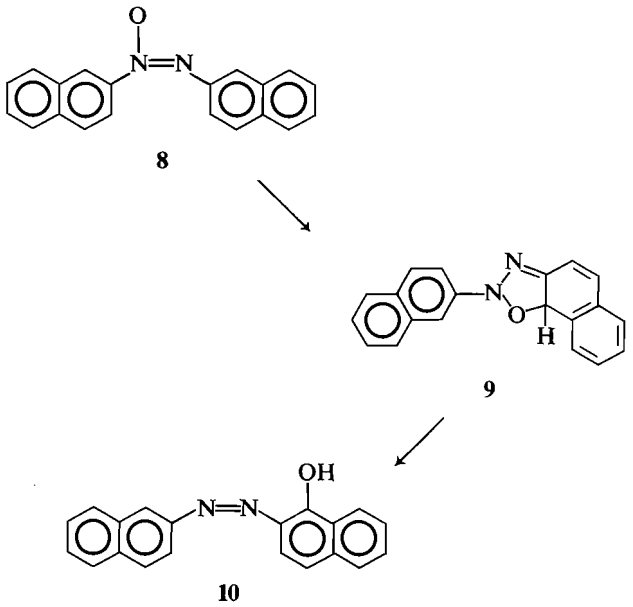

8 → **9** → **10**

Results and discussion

Preparation of labeled substrates

The labeled isomers of **4** which were prepared are designated as [^{15}N,^{15}N′]**4**, [^{18}O]**4**, and [2-^{14}C]**4**. Each of these was prepared by the reduction of the appropriately labeled nitrobenzene by heating with sodium hydroxide in methanol (14).

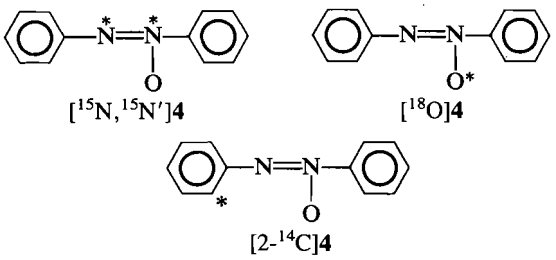

[^{15}N,^{15}N′]**4** [^{18}O]**4** [2-^{14}C]**4**

Labeled isomers of **4** have been prepared earlier in tracing the orientation and intramolecularity of the photorearrangement. The syntheses have been summarized by Dolenko and Buncel (15). These syntheses include singly labeled [^{15}N]**4** and [1-^{14}C]**4**. In our case we chose to use doubly labeled [^{15}N,^{15}N′]**4** and also [^{14}C]**4** which was a mixture of [2-^{14}C]**4** and [2′-^{14}C]**4**. The choice was made for convenience in preparation and also to avoid the raising of any question of ambiguity in our measurements from the possibility of isomerization of the azoxy group via an oxadiaziridine (16), prior to the photo-Wallach rearrangement. Such a possibility would appear to be ruled out by studies of orientation in the photo-Wallach rearrangement (10, 17), but isomerization of 4′- into 4-methoxyazoxybenzene has been reported, implicating the participation of an oxadiaziridine intermediate (17, 18), while the possible formation of diphenyloxadiaziridine as an initial side reaction in the photorearrangement of **4** has been proposed (19). Furthermore, Oae and co-workers found that a small amount of scrambling did, in fact, occur in the photo-rearrangement of [1-^{14}C]**4**. In that case the cause of the scrambling was attributed, however, to direct migrations to each *o*-position of **4** rather than to the initial involvement of a symmetrical oxadiaziridine ring (20).

[^{15}N,^{15}N′]**4** has been prepared earlier in our laboratory by the oxidation of [^{15}N,^{15}N′]azobenzene (21). In the present work it was more convenient to reduce [^{15}N]nitrobenzene containing 99 atom% of ^{15}N. In this way [^{15}N,^{15}N′]**4** was obtained containing

---

[3]It is curious that Badger and Buttery did not, in fact, claim that an intermediate with structure **5** was formed. Instead they concluded, from their studies with unsymmetrical azoxyarenes, that "an intramolecular mechanism is probably involved" and they represented this clearly as what we would now call a concerted process, as shown in reaction [3]

[3] **4** → 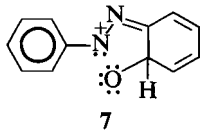 → **6**

7

Structure **7** is described by Badger and Buttery as "the quinonoid transition state," but whether they really meant transition state in its modern sense rather than (as is more likely) an intermediate is not now known. Lewis and Reiss (11), as has been reported by Buncel (12), proposed in 1966 that **5** is the intermediate in the rearrangement. Spence, Taylor, and Buchardt (7) although reproducing the scheme of Lewis and Reiss, represent **5** as an intermediate in what they describe as a *reformation* of the mechanism of Badger and Buttery. It may be, in this way, that the mechanism first set out by Lewis and Reiss is now attributed to Badger and Buttery, in whose work, however, no suggestion of an oxadiazole-like intermediate is made at all.

approximately 98% of doubly labeled **4**. This was diluted with ordinary **4** to give 10 mol% of [^{15}N,^{15}N′]**4** for rearrangement.

In the case of ^{14}C-labeling we began with [2-^{14}C]nitrobenzene which had been prepared earlier from 2-nitro-[1-^{14}C]aniline (22). This necessarily gave us a mixture of [2-^{14}C]**4** and [2′-^{14}C]**4**, which for convenience we designate here as solely [2-^{14}C]**4**. The final product had a radioactivity of approximately 16 mCi/mol.

In preparing [^{18}O]**4**, we found that the condensation of [^{18}O]phenylhydroxylamine with nitrosobenzene (23, 24), was inconvenient because of difficulties in preparing the labeled phenylhydroxylamine in reasonable yield and the loss of almost half of the initial ^{18}O content by this method. The method of choice, therefore, was by the reduction of [^{18}O]nitrobenzene (23) prepared by the nitration of benzene with [^{18}O]H_2O/NO_2BF_4 (25). After starting with [^{18}O]H_2O containing approximately 20 atom% of ^{18}O the **4** obtained had approximately 7 mol% of [^{18}O]**4**.

The compounds [^{15}N,^{15}N′]**8** and [1,1′-$^{13}C_2$]**8** were prepared from the corresponding 2,2′-azonaphthalene (26), by oxidation with *m*-chloroperbenzoic acid. Each labeled starting material contained approximately 10 mol% of the doubly labeled isomer.

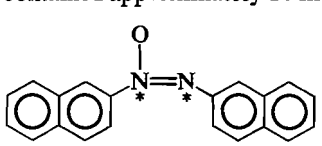

[^{15}N,^{15}N′]**8**

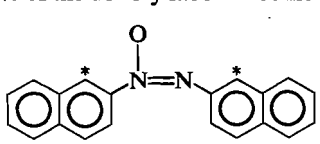

[1,1′-$^{13}C_2$]**8**

Rearrangements and KIE measurements

Rearrangements were carried out by broad-band irradiation with 350-nm lamps in a Rayonet reactor. Solutions of **4** in 95% ethanol and, because of solubility problems, of **8** in dimethoxyethane (DME), contained in a cyclindrical quartz flask were irradiated for pre-determined times so as to bring about either partial (5–20%) or complete conversion into product. Times for these conversions were obtained by monitoring the rearrangement of unenriched azoxy compound, at 410 nm for **4** and 505 nm for **8**. However, the extents of conversion used in calculating KIE were measured also by separation and isolation of unrearranged azoxy compound and product. The two measures of conversion (uv and isolation) were in good agreement in the work with **4**. We found that the planned complete conversion of **4** was never quite complete. Small amounts of **4** remained and were isolated. The data on conversions are given in Tables 1 and 2. The data in Table 1 concern calculations of KIE from isotopic abundances in isolated product (**6**). Table 2 concerns calculations of KIE from isotopic abundances in the starting material (substrate). In that table, therefore, only data for high conversions are given, which, in the calculations, are related to the isotopic abundances in the starting substrate.

The separations of unconverted substrate from product by column chromatography in the rearrangements of **8** were not as sharp as those in the rearrangements of **4**. Eluted fractions containing small amounts of both **8** and **10** were always obtained. Therefore, the amount of product isolated at low conversions was always 1–2% less than anticipated from absorption spectroscopy. Because of this, the extent of low conversion (i.e., F) used in calculating KIE is the spectroscopic conversion. We have used the spectroscopic measure also for 100% conversion of **8**. In this case, also, the amount of product after chromatography and crystallization was only about 75–80% of the expected yield. Lengthy irradiation of **10** itself caused the formation of a small amount of another, unidentified substance. Therefore, the low, isolated yield of **10** is attributable, not only to losses on separation and crystallization but also to a small amount of photochemical loss.

We measured isotopic abundances in the product (**6**) for rearrangements of [^{18}O]**4** and [^{15}N,^{15}N′]**4**, and in the substrate (**4**) for rearrangements of [2-^{14}C]**4** and [^{15}N,^{15}N′]**4**. In the rearrangements of **8** isotopic abundances only in the product **10** were measured.

Calculations of the oxygen and nitrogen KIE from isotopic abundances in the product (**6**) were made in two ways, A and B. It is important in calculating KIE from isotope ratios in products to know that complete conversion is indeed complete. If the isotope ratio is measured in a product at less than complete conversion but with the impression that conversion was complete ($F = 1.0$) the KIE calculated (eq. [5]) (27) will be smaller than the true KIE. This is to say, KIE both greater than or smaller than 1.000 will appear deceptively to be closer to 1.000. In that case eq. [6] is used for calculating KIE. In these equations R_0, R_p, and R'_p are the ratios of normalized abundances $(M + 2)/M$ in the product at molar conversions 1.0, F, and F', while k_2/k_1 is the KIE (k_H/k_L) for the reaction. The method of calculating KIE from low and almost 100% conversions with the use of eq. [6] and an iteration procedure has been described earlier (27). The columns A and B in Table 1 list KIE (k_1/k_2) calculated (A) on the assumption that complete conversion reached 100% and (B) with the use of real conversions based on isolations of unused **4**. The results of the two methods do not differ greatly, but are important particularly insofar as the ^{18}O KIE is concerned. The ^{18}O KIE is seen to be, within experimental error, an inverse one. On the other hand, there does not appear to be a nitrogen KIE. These data (Table 1) are averaged and listed in Table 3.

$$[5] \quad R_p/R_0 = [1 - (1 - F)^{k_2/k_1}]/F$$

$$[6] \quad R_p/R'_p = \frac{F'[1 - (1 - F)^{k_2/k_1}]}{F[1 - (1 - F')^{k_2/k_1}]}$$

In Table 2 are listed ^{14}C and ^{15}N KIE (k_1/k_2) obtained with recovered substrate in the rearrangement of **4**. It was necessary for these determinations to hydrogenolyze the substrate to aniline first, and to prepare the trifluoroacetyl derivative for ^{14}C and ^{15}N analyses. In the case of ^{14}C, both **4** and **6** are themselves unsuitable for scintillation counting because, being colored, each causes quenching. Hydrogenolysis of **4** goes quantitatively to aniline, and the colorless trifluoroacetyl derivative, also obtained quantitatively, can be purified by repeated sublimation. In the case of ^{15}N, the substrate itself is unsuitable for whole-molecule mass spectrometry. The abundance of the parent ion is low and the fragmentation pattern is unsuitable for use. Therefore, hydrogenolysis and trifluoroacetylation are again most useful. The mass spectrum of the trifluoroacetyl derivative is highly suitable for whole-molecule mass spectrometry. The results are summarized in Table 2 and averaged in Table 3. They show, again, that there is no nitrogen KIE and that there is a small ^{14}C KIE, averaging 1.0145.

Kinetic isotope effects (k_1/k_2) for the rearrangement of **8** are listed in Table 4. These were calculated on the assumption that 100% conversion was reached, as indicated spectroscopically. In the event that, like the rearrangement of **4**, the final conversion was a few percent short of 100% the results in Table 4 are minima. Our conclusion is that the rearrangement of **8**, like that of **4**, does not exhibit a nitrogen KIE. On the other hand there is a small, positive carbon KIE, averaging 1.07%.

TABLE 1. KIE based on analyses of product in the photorearrangement of azoxybenzene (**4**) in ethanol

Run	Isotope[a]	Time of irradiation	Conversion (%) Uv[b]	Conversion (%) Isol.[c]	KIE A[d]	KIE B[e]	σ
1	^{18}O	15 m	10.3	10.0	0.9915	0.9905	0.0014
		40 h		97.2			
2	^{18}O	20 m	12.0	12.3	0.9935	0.9919	0.0007
		20 h		93.5			
3	^{18}O	30 m	16.9	17.4	0.9929	0.9913	0.0016
		20 h		94.5			
4	^{18}O	40 m	20.6	20.2	0.9954	0.9948	0.0008
		20 h		97.2			
5	^{15}N	10 m	6.5	6.5	1.0019	1.0021	0.0031
		30 h		96.8			
6	^{15}N	10 m	8.1	8.1	1.0024	1.0025	0.0046
		20 h		96.0			
7	^{15}N	30 m	16.8	16.6	1.0010	1.0012	0.0015
		40 h		97.0			

[a]^{15}N means [^{15}N,$^{15}N'$]**4**.
[b]Based on change in absorption at 410 nm. Long irradiation (20–40 h) was assumed to have gone to 100% conversion. $[\mathbf{4}]_0$ was 1×10^{-3} *M* in each run.
[c]Based on recovered **4**.
[d]Assuming 100% conversion and calculated with eq. [5].
[e]Calculated with eq. [6], using % conversion based on recovered **4**.

TABLE 2. KIE based on analyses of substrate in the photorearrangement of azoxybenzene (**4**) in ethanol

Run	Isotope[a]	Time of irradiation (h)	Conversion (%) Uv[b]	Conversion (%) Isol.[c]	KIE[c]	σ
8	^{14}C	12	70	68.4	1.0090	0.0010
9	^{14}C	12	70	69.5	1.0116	0.0034
10	^{14}C	12	70	70.0	1.0229	0.0027
11	^{15}N	10	75.7	74.2	1.0018	0.0014
12	^{15}N	10.3	81.5	81.3	1.0019	0.0030
13	^{15}N	15	86.6	85.8	0.9937	0.0029

[a]^{15}N means [^{15}N,$^{15}N'$]**4**.
[b]Based on change in absorption at 410 nm. $[\mathbf{4}]_0$ was 2.0×10^{-3} *M* for ^{14}C and 1.5×10^{-3} *M* for ^{15}N runs.
[c]Based on recovered **4**.

TABLE 3. Summary of KIE in the photorearrangement of azoxybenzene (**4**)

Isotope	Basis	KIE[a]
^{18}O	Product	0.9921±0.0016
^{15}N	Product	1.0019±0.0006
^{15}N	Substrate	0.9991±0.0038
^{14}C	Substrate	1.0145±0.0060

[a]Average of data in Tables 1 and 2.

The meaning of the KIE

The absence of a nitrogen KIE in the rearrangements of both **4** and **8** indicates that if there is a step in the photo-Wallach rearrangement having a significant activation barrier, breaking of the N—O bond is not part of that step. The results are, then, not consistent with the barrier-less formation of an intermediate like **5** (and **9**) followed by its conversion over an activation barrier into product. The inverse oxygen KIE in the rearrangement of **4** and the positive, small carbon KIE in the formation of **6** and **10** suggest the surprising property of the rearrangement that it is in the formation of the intermediate that an activation barrier exists. The small size of the carbon KIE in the rearrangements of **4** and **8** is not inconsistent with the change in bonding which occurs at the aromatic position in a bond-forming reaction (27).

Bunce and co-workers (17) found that when an electron-donating group (CH_3) is placed in the ring which receives the migrating atom the quantum yield of rearrangement is greater than that when an electron-attracting group (CF_3) occupies the same position. For this reason it was proposed that the attack of the oxygen atom on the distant ring is an electrophilic rather than, as thought earlier, a nucleophilic reaction. This, in itself, suggests that the bonding of the oxygen atom with the ring is a ground-state reaction. Electrophilic attack was represented by Bunce and co-workers as in eq. [7]. This interesting proposal invites further analysis. Bunce noted that the photorearrangement involves an n,π^* singlet excitation, and proposed that excitation occurs from an *n* orbital on oxygen to an antibonding N—N oribital. If this is correct the oxygen atom has radical

TABLE 4. KIE[a] in the photo-rearrangement of 2,2′-azoxynaphthalene (**8**) in dimethoxyethane

Run	Isotope[b]	Conversion (%)[c]	KIE[d,g]	σ
14	^{15}N	4.0	0.9935[e]	
			1.0015[f]	0.0010
15	^{15}N	6.7	1.0060[e]	
			0.9999[f]	0.0006
16	^{15}N	6.7	1.0039[e]	0.0034
17	^{13}C	6.0	1.0090[e]	
			1.0071[f]	0.0005
18	^{13}C	6.0	1.0145[e]	
			1.0113[f]	0.0008
19	^{13}C	7.0	1.0115[e]	

[a]Based on analyses of product.
[b]^{15}N,$^{15}N'$ and 1,1′-$^{13}C_2$ labeling.
[c]Based on the amount of product isolated at low conversions.
[d]Calculated with eq. [5], using the low conversions shown in the table and assuming that 100% conversion (by uv) was indeed 100%.
[e]Measured at Texas Tech University.
[f]Measured at Rutgers University.
[g]Average for [^{15}N,$^{15}N'$] **8**, 1.0010; average for [1,1′-$^{13}C_2$] **8**, 1.0107.

character rather than positive-charge character in the excited state, and only after electronic reorganization can the intermediate **11**, with its electron-deficient oxygen atom, be formed.[4] Again, this likelihood suggests that the formation of **5** is a ground state rather than an electronically excited state reaction, the intermediate **11** being formed by demotion from the electronically excited state to a ground excited state. Our KIE results are in harmony with this description. An inverse (here, for oxygen) or a small positive (here, for carbon) KIE is consistent with the forming of a new bond in the transition state (29). The result is, by coincidence, similar to that found by Kwart and co-workers in the photo-rearrangement of **1** (reaction [1]) (2).

[7] 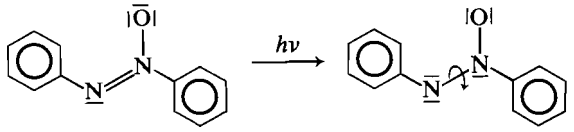

4 **11**

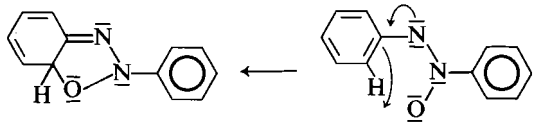

5 **12**

The photo-Wallach rearrangement then, appears to involve the formation, after excitation, of a ground-state intermediate in a step having an activation barrier. Collectively, the known information now indicates that this step is between ground-state intermediates.

Among Bunce's results on the effect of substituents on quantum yields it is seen that the greatest relative increases in quantum yield occur not when the methyl groups are in the acceptor ring but when the CF_3 groups are in the ring nearer to the N—O bond (17). For example, the quantum yields for rearrangement of 4′-CH_3-**4** and 4′-CF_3-**4** were, respectively, 0.37 and 1.70; the values for 3′,5′-$(CH_3)_2$-**4** and 3′,5′-$(CF_3)_2$-**4** were, respectively, 0.80 and 2.5. These results show that electron-attracting CF_3 groups in the nearby ring enhance rearrangement, and suggest that the n,π^* excitation may, in fact, be surprisingly from a nonbonding orbital on oxygen to a π^* orbital of the nearby ring. Thereafter electron reorganization to an intermediate such as **11** would follow.

If these representations are incorrect, we are left with the alternative possibility that bonding to form an intermediate such as **5** may occur in the electronically excited state between the electrophilic oxygen radical and the electron-rich distant ring. In other words, the closure is a radical reaction, albeit with electrophilic character in the transition state. The transition state, in that case, might have the character of **13**.

We might now ask about the fate of **5**. Our results indicate that the conversion of **5** into **6** does not have an activation barrier large enough to show up in the KIE measurements. We would anticipate that, in spite of changes which occur in bond orders (e.g., a single bond is broken and a double one is formed at nitrogen), we should have found significant positive KIE for nitrogen and oxygen if opening of the heterocyclic ring in **5** was the rate-determining process in the sequence of ground-state reactions. If then, **5** is to proceed on toward the final product (**6**) without isotopic fractionation, the reverting of **5** to **4** must no

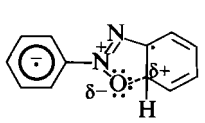

13

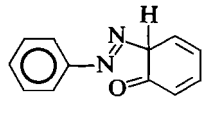

14

longer be possible. That is, return of **5** to **4** must be an unfavorable process as compared with going on completely to **6**, and the low quantum yield (13) for forming **6** from **4** is decided in one of the paths toward forming **5**. The way in which formation of **6** from **5** occurs is not known, but some possibilities are open to conjecture. One of them is, simply, ring opening accompanying deprotonation by basic solvents, in the present cases of ethanol or DME (reaction [8]), such as was proposed in the early work of Lewis and Reiss (11).

[8] 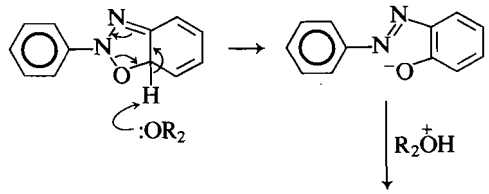

6

Another possibility arises as follows. Bunce has shown that diazonium ions are formed (and trapped by added 2-naphthol) during irradiations of **4** and other azoxyarenes in benzene solution. Diazonium ion formation was suppressed to very low amounts by the use of moderately basic solvents such as ethanol and diethyl ether (30). The origin of the diazonium ion was attributed by Bunce to an intermediate (**14**), obtained from **5** by

[4]An analogy can be drawn here with the electron distribution in an n,π^*-excited carbonyl group. This has been represented by Zimmerman (28) as having in one of its two resonance structures a positively charged, electrophilic oxygen atom in which two single electrons remain in separate orbitals. n,π^*-Excitation of the *N*-oxide group could be viewed similarly, that is as having positive charge character on the oxygen atom in the electronically excited state. But, we take structure **11** to represent a new, ground state, formed in Zimmerman's terminology, by electron demotion after excitation.

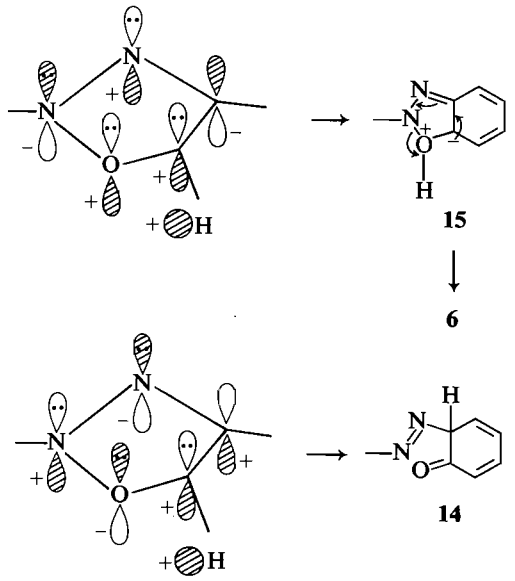

SCHEME 1

an intramolecular 1,2-hydrogen-atom shift, and undergoing either scission to give the diazonium ion or prototropy to form **6**. This proposal in itself could also account for the conversion of **5** into **6** in basic solvents. In connection with the intramolecularity of the H-migration, Bunce noted that *m*-cresol, obtained as the side product of irradiation of 2,2′-azoxytoluene in ethanol-*O*-*d*, contained no deuterium. We pose another possibility for intramolecular H-migration which may lead both to **6** and diazonium-ion formation, and this is a [1,5]-sigmatropic migration of hydrogen across the face of the heterocyclic ring, brought about by continuous broad-band irradiation. Suprafacial, solvent-dependent migration of the LUMO of the H atom across the HOMO of the excited eight-electron ring system could bring the H atom either to the *O*-terminus (**15**) or *C*-terminus (**14**), the former leading to **6** and the latter either to **6** by prototropy or diazonium ion by scission (Scheme 1). Perhaps these speculations may be related to the observations by Gegiou *et al.* that an intermediate was formed from 2,2′-azoxytoluene which, by continued irradiation (436 nm) at −70°C, went on to the rearrangement product (13).

Experimental

Preparation of labeled azoxybenzene (4)

Each labeled **4** was prepared from the reduction of the appropriately labeled nitrobenzene by heating with sodium hydroxide in methanol (14). Commercial (Merck, Sharpe and Dohme) [^{15}N]nitrobenzene, 99 atom% ^{15}N, was used for making [^{15}N,^{15}N′]**4**. [2-^{14}C]Nitrobenzene, previously prepared from 2-nitro-[1-^{14}C]aniline (22), was used for making [2-^{14}C]**4**. The product had an activity of approximately 16 mCi/mol. For making [^{18}O]**4** it was necessary first to prepare [^{18}O]nitrobenzene by the method of Høg (25) using $H_2{}^{18}O$ containing 20.3 atom% ^{18}O (Prochem BOC, Ltd.). The **4** finally obtained was found by mass spectrometry to contain approximately 7 mol% of [^{18}O]**4**. An example of the preparation of labeled **4** follows.

[^{15}N]Nitrobenzene (2.0 g, 16.3 mmol) was added during 50 min to a well-stirred solution of 3 g of sodium hydroxide in 8 mL of methanol at 75–80°C. The mixture was stirred at that temperature for 2.5 h and then diluted with crushed ice. After standing 12 h the yellow product was filtered, washed with water, and dried in air. The crude product was purified on a column of neutral alumina with benzene elution. Removal of the benzene left a liquid product (1.6 g, 8.0 mmol, 98%) which crystallized on standing overnight; mp 34.5°C. The solid was mixed with ordinary **4** and the mixture was crystallized from benzene, giving **4** containing 10 mol% of [^{15}N,^{15}N′]**4**.

Photo-rearrangements

Rearrangements were carried out in a Rayonet reactor with eight 350-nm U-tube lamps. Solutions to be irradiated were placed in a cylindrical quartz vessel and stirred gently during irradiation with a current of nitrogen. In order to specify particular extents of conversion, the disappearance of azoxy compound and the formation of product were first monitored spectroscopically with irradiations of unlabeled substrate. The formation of 2-hydroxyazobenzene (**6**) was monitored at 410 nm, while the formation of 1-hydroxy-2,2′-azonaphthalene (**10**) was monitored at 505 nm. Solvents for photo-rearrangement were 95% ethanol for **4** and 1,2-dimethoxyethane (DME) for **8**. Specific examples of rearrangement and workup follow.

Rearrangement of 4

(A) For product KIE measurement

A solution of 198 mg (1.0 mmol) of [^{18}O]**4** in 1.0 L of 95% ethanol was irradiated for 20 min. The solution was then divided into two parts. The larger part (750 mL) was evaporated at reduced pressure. The residue was dissolved in 20 mL of benzene and placed on a column of neutral alumina (Matheson, Coleman, Bell, AX0612-3, 80-200 mesh). Unrearranged **4** (130.2 mg 87.7%), mp 34.0–34.5°C, was eluted with benzene, while product, [^{18}O]**6**, was eluted with methanol. The crude product was dissolved in 80 mL of 10% aqueous sodium hydroxide, and the solution was acidified, after filtration, with hydrochloric acid. The product was then extracted with 3 × 50 mL of ether, giving 14.6 mg (9.6%) of [^{18}O]**6**. This was sublimed at low pressure to give [^{18}O]**6**, mp 81–82°C, for mass spectrometry.

The smaller part (250 mL) of the ethanol solution was irradiated again for 20 h to effect complete conversion of **4**. Workup as above then gave 3.2 mg (6.5%) of **4** and, for mass spectrometry, 41.4 mg (83.8%) of **6**. For the purpose of calculating KIE the extents of conversion of **4** were based on recovered **4**, namely 12% and 93.5% conversions.

Rearrangements of [^{15}N,^{15}N′]**4** designed for mass spectrometry of the product were carried out identically.

Results for all runs are listed in Table 1.

(B) For substrate KIE measurement

A solution of 297 mg (1.5 mmol) of [^{15}N,^{15}N′]**4** in 1 L of ethanol was irradiated for 12.2 h, the time calculated for 81% conversion. The solution was worked up as described above and gave 55.6 mg (18.7%) of recovered [^{15}N,^{15}N′]**4** and 226 mg (76.1%) of product. A portion (38.8 mg, 0.196 mmol) of recovered [^{15}N,^{15}N′]**4** was dissolved in 5 mL of absolute ethanol and was hydrogenolyzed over 5% Pd/charcoal at atmospheric pressure for 3 h. The ethanol solution was filtered and evaporated at 25°C, and the residue was dissolved in 15 mL of benzene. To this solution was added 2 mL of trifluoroacetic anhydride and the mixture was heated under reflux for 15 min. Evaporation gave crude product which was sublimed at low pressure to give 51.7 mg (0.27 mmol, 70%) of *N*-trifluoroacetyl[^{15}N]aniline, mp 87.5–88°C (lit. (31) mp 88.5–90°C). This was sublimed twice again for mass spectrometry.

A sample of unirradiated [^{15}N,^{15}N′]**4** was hydrogenolyzed and worked up in the same way to produce *N*-trifluoroacetyl[^{15}N]aniline for mass specrometry "at zero conversion".

Results are listed in Table 2.

(C) For scintillation counting and substrate KIE measurement

A solution of 400 mg (2.02 mmol) of [2-^{14}C]**4** in 1.0 L of ethanol was irradiated for 12 h, a time calculated for 70% conversion. Unrearranged substrate and product were separated on alumina as usual. The benzene eluate was evaporated at reduced pressure to give crystalline, unrearranged [2-^{14}C]**4**. This was again chromatographed on neutral alumina, crystallized, and hydrogenolyzed as described above, to give *N*-trifluoroacetyl-[2-^{14}C]aniline which was sublimed successively six times for scintillation counting. The final product had mp 87.6°C.

Preparation of labeled 2,2′-azoxynaphthalene (8)

Labeled **8** was prepared from [^{15}N,^{15}N′]- and [1,1′-$^{13}C_2$]-2,2′-azonaphthalene which had been synthesized earlier (26). Each of the

azonaphthalenes contained approximately 10 mol% of the doubly labeled isomer.

A solution of 1.06 g (3.76 mmol) of labeled 2,2′-azonaphthalene in 190 mL of benzene was kept at 27°C in a thermostated bath. To this solution was added a freshly prepared solution of 3.24 g (18.8 mmol) of *m*-chloroperbenzoic acid in 55 mL of benzene. The mixture was kept at 27°C for 17 h, during which time the reaction was monitored periodically by TLC. After oxidation was complete the solution was washed with dilute sodium bicarbonate solution and water, and then was dried and evaporated. The residue was chromatographed on a column of silica gel, eluting with cyclohexane, and the product was crsytallized from ethanol giving 1.01 g (3.38 mmol, 90%) of labeled **8**, mp 167–168°C (lit. (10) mp 166°C).

Rearrangement of 8 for product KIE measurements

A solution of 149 mg (0.50 mmol) of **8** containing approximately 10 mol% of labeled **8** in 1.0 L of DME was irradiated for 40 min, a time calculated to result in approximately 8% conversion. The solvent was removed in a rotary evaporator and the residue was separated by flash chromatography on silica gel (E. T. Baker) into recovered **8** and product **10**. The eluent was a mixture of cyclohexane, benzene, and piperidine (91:5:4 by volume). The recovered **8** was crystallized from ethanol giving 121 mg (81%). The crude **10** was dissolved in a small amount of chloroform and streaked on preparative-scale TLC plates (EM silica gel). Development with a mixture of cyclohexane, benzene, and piperidine (80:15:5) separated **10** from a small amount of another, unidentified, substance. After removal from the plate material, **10** was crystallized from ethanol giving 10.5 mg (7%) of labeled **10** for mass spectrometry.

For complete conversion of **8** a solution of 75.5 mg (0.25 mmol) of labeled **8** in 50 mL of DME was irradiated for 32 h. Workup as described gave 54 mg (72.5%) of **10** for mass spectrometry and 3 mg (4.0%) of recovered **8**.

These experiments were repeated three times for each of the [^{15}N,^{15}N′]**8** and [1,1′-$^{13}C_2$]**8**, with similar results. It is seen that the total recovery of material from the low-conversion irradiation was 88%. Losses occurred in the flash chromatography in which some fractions containing both **8** and **10** were discarded. The amount of **10** recovered (7%) was pleasingly close to that anticipated. The total recovery of material from 100% conversion (76.5%) was rather low, particularly **10** itself. Irradiation of **10** (14.9 mg in 100 mL of DME) for 10 h showed, by TLC, that a very small amount of a new compound having lower R_f was formed. Possibly, therefore, the lengthy irradiations needed for complete conversion of **8** may have also caused loss of some of the product **10**. The lengthy irradiations are taken as having achieved 100% conversion. Results are listed in Table 4.

KIE measurements

(A) Whole-molecule – ion mass ratios were measured with Hewlett–Packard mass spectrometers, Model 5985B (Rutgers University)[5] and 5995 (Texas Tech University). In the latter case multiple scanning was carried out in the selected-ion-monitoring (SIM) mode and the data were analyzed in blocks (27) with the aid of a program kindly supplied by Professor San Filippo. The number of scans made with the Model 5995 instrument was in the order of 5000 per run. The handling of samples was as described earlier (27).

Ions monitored, at 50 ms/ion dwell times, were M and $(M + 2)$ in the products (**6** and **10**) of rearrangement of [^{15}N,^{15}N′]**4**, [^{18}O]**4**, [^{15}N,^{15}N′]**8**, and [1,1′-$^{13}C_2$]**8**. Ions monitored when substrate was recovered and hydrogenolyzed in the rearrangement of [^{15}N,^{15}N′]**4** were the M and $(M + 1)$ of *N*-trifluoroacetylaniline.

(B) Scintillation counting was carried out with a Beckman Model LS 7000 liquid scintillation counter. The sample (approximately 5 mg) was dissolved in 10 mL of cocktail (Parkard, SCINT-0, No. 6103183) and counted ten times. Three separately weighed samples were counted for each conversion. Samples were weighed precisely (±0.001 mg) on a Cahn balance. Finally, the average of ten counts was expressed in counts per 1.000 mg and the results for the three samples were averaged for KIE calculations.

In making these calculations, it was assumed that equal amounts of [2-^{14}C]**4** and [2′-^{14}C]**4** were available for rearrangement. Therefore, in the labeled molecules, rearrangements to one labeled and three unlabeled *o*-position were possible, among which an intramolecular KIE existed and was assumed to have the same magnitude as the sought-after intermolecular KIE.

All KIE calculations were made as described earlier (27).

[5]We thank Dr. J. San Filippo, Jr. and Mrs. Marilyn Brownawell for these measurements, Table 4. Information on the way of making measurements has been given (27).

Acknowledgements

Acknowledgement is made to the Robert A. Welch Foundation, Grant No. D-028, the Donors of the Petroleum Research Fund administered by the American Chemical Society, Grant No. 15484-AC4, the National Science Foundation, Grants No. CHE-8026576 and CHE-8314947, and the Center for Energy Research, Texas Tech University, for support of this work. We thank Professor N. Bunce for stimulating discussion of this photo-rearrangement.

1. L. Schutte and E. Havinga. Tetrahedron, **23**, 2281 (1967).
2. H. Kwart, D. A. Benko, J. Streith, and J. L. Schuppiser. J. Am. Chem. Soc. **100**, 6502 (1978).
3. N. J. Turro. Modern molecular photochemistry. Benjamin-Cummings, Menlo Park, CA. 1968.
4. E. F. Ullman. Acc. Chem. Res. **1**, 353 (1968).
5. H. E. Zimmerman and J. W. Wilson. J. Am. Chem. Soc. **86**, 4036 (1964).
6. J. G. Calvert and J. N. Pitts. Photochemistry. Wiley, New York. 1966. pp. 312, 623, 624.
7. G. G. Spence, E. C. Taylor, and D. Buchardt. Chem. Rev. **70**, 231 (1970).
8. R. Tanikaga. Bull. Chem. Soc. Jpn. **41**, 1664 (1968).
9. (*a*) A. L. Buchachenko. Russ. Chem. Rev. (Engl. Transl.) **45**, 761 (1976); (*b*) R. A. Sagdeev, K. M. Salikhov, and Yu. N. Molin. Russ. Chem. Rev. (Engl. Transl.), **46**, 569 (1977); (*c*) I. R. Gould, N. J. Turro, and M. B. Zimmt. Adv. Phys. Org. Chem. **20**, 1 (1984).
10. G. M. Badger and R. G. Buttery. J. Chem. Soc. 2243 (1954).
11. G. E. Lewis and J. A. Reiss. Aust. J. Chem. **19**, 1887 (1966).
12. E. Buncel. *In* Mechanisms of molecular migrations. Vol. 1. *Edited by* B. S. Thyagarajan. Interscience, New York. 1971. pp. 61–119.
13. D. Gegiou, A. Tsoka, and E. Hadjoudis. J. Photochem. **21**, 149 (1983).
14. R. Ohme and A. Zubek. *In* Preparative organic chemistry. *Edited by* E. Hilgetag and A. Martini. Wiley, New York. 1968. p. 594.
15. A. J. Dolenko and E. Buncel. *In* The chemistry of the hydrazo, azo and azoxy groups. *Edited by* S. Patai. Wiley, New York. 1975. pp. 725–773.
16. F. D. Greene and S. S. Hecht. J. Org. Chem. **35**, 2482 (1970).
17. N. J. Bunce, J.-P. Schoch, and M. C. Zerner. J. Am. Chem. Soc. **99**, 7986 (1977).
18. N. J. Bunce. Can. J. Chem. **53**, 3477 (1975).
19. H. Mauser, G. Gauglitz, and F. Stier. Justus Liebigs Ann. Chem. **739**, 84 (1970).
20. S. Oae, T. Maeda, S. Kozuka, and M. Nakai. Bull. Chem. Soc. Jpn **44**, 2495 (1971).
21. H. J. Shine, H. Zmuda, H. Kwart, A. G. Horgan, and M. Brechbiel. J. Am. Chem. Soc. **104**, 5181 (1982).
22. H. J. Shine, J. Zygmunt, M. L. Brownawell, and J. San Filippo, Jr. J. Am. Chem. Soc. **106**, 3610 (1984).
23. S. Oae, T. Fukumoto, and M. Yamagami. Bull. Chem. Soc. Jpn. **36**, 728 (1963).
24. L. A. Neiman, V. I. Maimind, and M. M. Shemyakin. Tetrahedron Lett. 3157 (1965).
25. J. H. Høg. J. Labelled Compd. **7**, 179 (1971).

26. E. GRUSZECKA and H. J. SHINE. J. Labelled Compd. Radiopharm. **20**, 1257 (1983).
27. H. J. SHINE, E. GRUSZECKA, W. SUBOTKOWSKI, M. BROWNAWELL, and J. SAN FILIPPO, JR. J. Am. Chem. Soc. **107**, 3218 (1985).
28. H. E. ZIMMERMAN. Adv. Photochem. **1**, 183 (1963).
29. A. FRY. *In* Isotope effects in chemical reactions. *Edited by* C. J. Collins and N. S. Bowman. Van Nostrand Reinhold, New York. 1970. pp. 364–414.
30. N. J. BUNCE. Can. J. Chem. **55**, 383 (1977).
31. E. J. BOURNE, S. H. HENRY, C. E. M. TATLOW, and J. C. TATLOW. J. Chem. Soc. 4014 (1952).

Acid-catalyzed hydrolysis of 2-methylene-1,3-dithiolane. 2.[1] Remarkable effects of β substitution on reversibility of the carbon protonation

TADASHI OKUYAMA,[2] MASAYOSHI TOYODA, AND TAKAYUKI FUENO
Faculty of Engineering Science, Osaka University, Toyonaka, Osaka 560, Japan
Received October 25, 1985

This paper is dedicated to Professor Arthur N. Bourns

TADASHI OKUYAMA, MASAYOSHI TOYODA, and TAKAYUKI FUENO. Can. J. Chem. **64**, 1116 (1986).

Hydrolyses of 2-ethylidene- (**1***b*), 2-isopropylidene- (**1***c*), and 2-benzylidene-1,3-dithiolane (**1***d*) were kinetically investigated in aqueous solution. All the individual rate constants involved in this three-step reaction were evaluated. Initial carbon protonation is only partially reversible (k_2/k_{-1} = 1.33, 0.68, and 1.02 for **1***b*, **1***c*, and **1***d*, respectively) at higher pH, while the protonation becomes completely reversible below pH 2 where the third step is rate determining. Complete H–D isotope exchange at the β-carbon of **1***b* and **1***d* was observed in deuterium media before appreciable hydrolysis took place. It was demonstrated that reversion from the tetrahedral intermediate **3** to **1** occurs extensively during the reaction in the latter acidity range. Relative stabilities and reactivities of the olefinic substrates **1** are discussed.

TADASHI OKUYAMA, MASAYOSHI TOYODA et TAKAYUKI FUENO. Can. J. Chem. **64**, 1116 (1986).

Opérant en solutions aqueuses, on a examiné la cinétique des réactions d'hydrolyse des éthylidène-2 (**1***b*), isopropylidène-2 (**1***c*) et benzylidène-2 dithiolanes-1,3 (**1***d*). On a évalué toutes les constantes de vitesse individuelles de cette réaction en trois étapes. À des pH élevés, la réaction de protonation initiale du carbone n'est que partiellement réversible (k_2/k_{-1} = 1,33, 0,68 et 1,02 respectivement pour les composés **1***b*, **1***c* et **1***d*) alors que, à des pH inférieurs à 2, la protonation devient complètement réversible et que la troisième étape devient l'étape déterminante. Dans des milieux deutérés, on observe un échange complet des isotopes H/D au niveau du carbone β des composés **1***b* et **1***d* avant qu'une hydrolyse appréciable ne se produise. On a démontré que, au cours de la réaction, la transformation de l'intermédiaire tétraédrique **3** en **1** ne se produit que dans le dernier intervalle de pH. On discute des stabilités et des réactivités relatives des substrats oléfiniques **1**.

[Traduit par la revue]

Introduction

We recently accomplished complete kinetic analysis of a three-stage reaction process of the acid-catalyzed hydrolysis of 2-methylene-1,3-dithiolane, **1***a* (1). Main features of this reaction are: (*1*) Both steps 1 and 2 are partially rate determining above pH 2.5 (k_2/k_{-1} = 7.2) while step 3 becomes the slow step at higher acidities. (*2*) The equilibrium concentration of the tetrahedral intermediate (**3***a*) is greater than that of **1***a* (**3***a*/**1***a* = 27.5), and **3***a* builds up at the higher acidities.

In our continuing interest in this reaction, hydrolyses of the β-methyl and phenyl derivatives, 2-ethylidene- (**1***b*), 2-isopropylidene- (**1***c*), and 2-benzylidene-1,3-dithiolanes (**1***d*), have been examined in detail. The reactions follow essentially the same mechanism as that of the parent substrate **1***a* (eq. [1]). However, apparent kinetic behavior is much different from that of **1***a*. Buildup of the intermediate **3** was not observed because the equilibrium concentration of **1** (as compared with **3**) is greatly increased by the β substituent. A very rapid H–D isotope exchange at the β-carbon was found to precede the hydrolysis of **1***b* and **1***d* in deuterium media. The complete kinetic analysis enables us to make interesting comparisons of stabilities of olefinic substrates **1**, carbocations **2**, and tetrahedral intermediates **3**.

Results

Acid-catalyzed hydrolysis of β-substituted 2-methylene-1,3-dithiolane (**1***b*, **1***c*, and **1***d*) proceeds stepwise in the same way as that of other ketene dithioacetals (eq. [1]) (1–5). At high acidities was observed rapid formation of the absorption (λ_{max} 330 nm) of the carbocation intermediate **2**, which disappears slowly to give the thiolester product **4**. In less acidic solutions, however, the decay of **1** seems to occur with simultaneous formation of **4**. In the intermediate pH region 0–3, the decrease in the absorption of **1** was accompanied by a short induction period.

Reaction of the isolated salts of **2** was also examined independently. The spectral changes observed by the conventional uv spectroscopy were essentially the same as those observed by starting with **1** in the whole acidity range examined. Only the decay of **2** could be observed at higher acidities, while the reaction of **1** was observed at low acidities even when the reaction was started with **2**. That is, the initial rapid breakdown

[1] 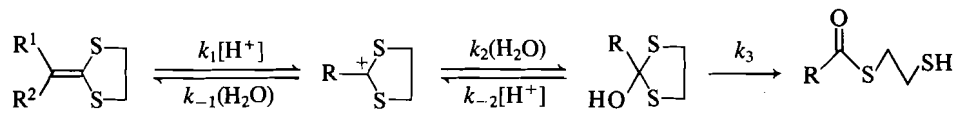

1 **2** **3** **4**

R = CHR^1R^2

a, $R^1 = R^2 = H$ *b*, $R^1 = H$, $R^2 = CH_3$
c, $R^1 = R^2 = CH_3$ *d*, $R^1 = H$, $R^2 = C_6H_5$

[1]For Part 1, see ref. 1.
[2]Author to whom correspondence may be addressed.

TABLE 1. Summary of the sigmoid correlations of the absorbances with the H_C and H_R acidity functions[a]

Substrate (conc. 10^4 M)	Absorbance	No. of data	pK_R[b]	Limiting absorbances at high and low acidities[b]	
1*b* (1.14)	A^0_{330}	8	−0.567(0.015)	0.887(0.011)	0.025(0.013)
1*b* (1.14)[b]	A^0_{235}	9	−0.609(0.020)	0.232(0.008)	0.736(0.008)
2*b* (1.12)	A^0_{330}	14	−0.609(0.010)	0.880(0.007)	0.005(0.008)
2*b* (1.12)	A^∞_{330}	11	−3.518(0.034)	0.898(0.006)	0.004(0.005)
1*c* (0.95)	A^0_{330}	7	−2.023(0.024)	0.688(0.011)	0.058(0.016)
1*c* (1.09)[c]	A^0_{230}	8	−1.957(0.013)	0.323(0.004)	0.841(0.008)
1*c* (0.95)	A^∞_{330}	7	−3.485(0.030)	0.662(0.013)	0.043(0.008)
1*d* (1.2)	A^0_{340}	7	−2.588(0.035)	0.855(0.021)	0.082(0.026)
1*d* (0.55)[d]	A^0_{304}	7	−2.665(0.033)	0.202(0.024)	1.101(0.025)
1*d* (1.2)	A^∞_{340}	7	−4.389(0.024)	0.814(0.010)	0.049(0.013)

[a]A^0 and A^∞ are correlated with the H_C and H_R acidity functions, respectively.
[b]Standard deviations are given in parentheses.
[c]Absorbance of **1***b* in H_2O was 0.846 at 235 nm.
[d]Absorbance of **1***c* in H_2O was 0.848 at 230 nm.
[e]Absorbance of **1***d* in H_2O was 1.034 at 304 nm.

of **2** largely results in the formation of **1** in less acidic solutions. This behavior of the carbocation is in contrast to that observed with the parent substrate **2***a* (1) and other dithio carbocations (3), which break down mainly to form **3** without any appreciable uv absorption, and slower formation of **4** follows.

The uv absorbance in acid solution was quantitatively examined on a conventional spectrophotometer. The "initial" absorbances A^0_{330} at 330 nm (λ_{max} of **2**)[3] as well as those at λ_{max} of **1** (**1***b*, 235; **1***c*, 230; **1***d*, 304 nm) were determined by rapidly introducing an aliquot of the stock solution of **1** into various acid solutions and extrapolating the absorbances to the time of mixing. The former absorbances increase and the latter decrease with increasing acidity. The decay of **2** was not complete in strong acid, leaving an equilibrium amount of **2**. The ultimate absorbances A^∞_{330} at 330 nm were also recorded. Results are given in Table S1 (supplementary material).[4] The initial absorbances are correlated with the H_C acidity function (6), which was obtained from protonation of the unsaturated carbon to give carbocations. The reason for the choice of the acidity function is given under Discussion. The correlations seem to be better than those with the H_R acidity function (7, 8). The initial absorbances at 330 nm and at λ_{max} of **1** respectively follow the sigmoid curves of the same midpoint (pK_R) as summarized in Table 1. The ultimate absorbances A^∞_{330} are correlated with H_R to give sigmoid curves with more negative pK_R (defined as pK_T in Table 5). Similar examinations were also carried out with the cation **2***b* and the results are the same as those obtained with **1***b* (Tables S1 and 1). The constant pK_T corresponds to the equilibrium between **2** and **4** (1, 9).

Pseudo-first-order rate constants k_0 were measured at 25°C by monitoring the decrease in the absorption of **1** in HCl solutions (<1 M) and that of **2** (330 nm) in $HClO_4$ solutions of higher acidities. The k_0 values determined at these two wavelengths coincide with each other as measured in some moderately strong acids. Rate constants obtained by starting with **2***b* were close to those obtained from the reaction of **1***b*. For some runs in the intermediate pH region where an induction period was observed, k_0 were determined from the later part of the first-order plots. Observed rate constants k_0 are summarized in Table S2[4] and plotted logarithmically against pH or the H_0 function (7) in Fig. 1. All the acidity–rate profiles are complicated with a maximum at pH 2–3 and a minimum around pH 1. That is, two acid-catalyzed regions were observed. In the case of **1***b* another maximum was observed at $H_0 \simeq -0.5$.

Reactions of **1** were also examined in deuterium solutions at both high and low DCl concentrations corresponding to the two different acid-catalyzed regions. The results are summarized in Table 2. Observed behavior is much different in the two acidity regions. First-order plots for **1***b* and **1***d* curved downward at the lower acidities while the plots were linear at the high acidities. In the former case, approximate initial and ultimate rate constants were determined from the slopes of the initial and later parts of the plots, respectively. Both of the rate constants are smaller than those obtained in the HCl solutions; the kinetic isotope effects are normal. By contrast, the rate constants obtained in DCl for the high acidity region are essentially identical with those found in HCl. The curvature of the first-order plots was not found with **1***c* but the kinetic isotope effects observed are similar to those found with **1***b* and **1***d*: normal at the low acidity and none at the high acidity.

Products from reactions of **1***b* and **1***d* in deuterium media were found to be deuterated extensively at the β position. Isotope exchange of **1***d* was kinetically examined in 80 vol% CH_3CN–D_2O at [DCl] = 0.1 and 0.002 M. Hydrolysis rates under these conditions were very small as measured spectrophotometrically (Table 3). Deuterium solvent isotope effects on the hydrolysis rate of **1***b* were negligibly small at 0.1 M but were normal at 0.002 M. The nmr analysis of the residues from the ether extract of the reaction mixture showed loss of the β-hydrogen of the substrates **1***b* and **1***d*. The intensity of the β-hydrogen relative to that of the phenyl group of **1***d* was calculated from the integration curves of the nmr spectra, and the rate constant k_{ex} for the isotope exchange was evaluated by the first-order plots as shown in Fig. 2. Values of k_{ex} are given in Table 3. The rate of the exchange is greater than that of the hydrolysis by factors of 10^3 and 60 at 0.1 and 0.002 M DCl, respectively.

Curved buffer dependences were observed in the hydrolyses of **1** in carboxylate buffers in the low acidity region as before

[3]The absorbances at 340 nm were measured for **2***d* rather than at 330 nm (λ_{max}) because absorption due to **1***d* is still large at 330 nm.

[4]Tables S1, S2, and S3 have been deposited as supplementary material and may be purchased from the Depository of Unpublished Data, CISTI, National Research Council of Canada, Ottawa, Ont., Canada K1A 0S2.

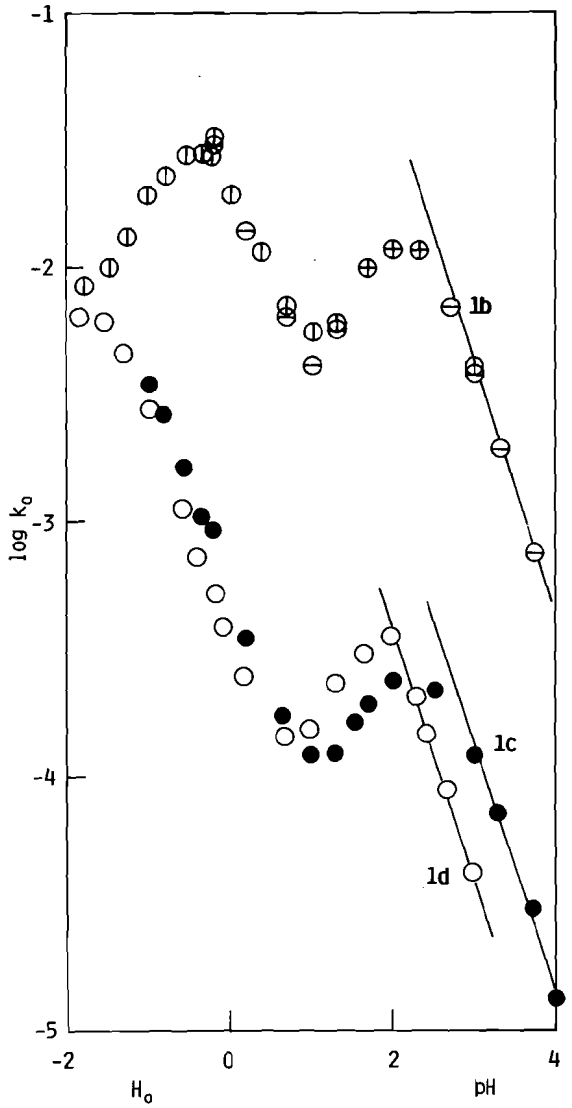

FIG. 1. Acidity–rate profiles for the hydrolysis of **1***b* (⊖), **2***b* (⊕), **1***c* (●), and **1***d* (○).

(1–5). The rate increase Δk ($= k_{obsd} - k_0$) induced by the buffer ($[B]_t$) follows the saturation curve according to eq. [2]. Parameters, K_{app} and Δk_{max}, were calculated by the least-

$$[2] \quad \Delta k = \Delta k_{max}[B]_t/(K_{app} + [B]_t)$$

squares treatments of $1/\Delta k$ vs. $1/[B]_t$, where k_0 ($k_{H^+}[H^+]$) was calculated from the results obtained in HCl solutions, and are given in Table 4.

Discussion

Low acidity region

The reaction concerned here involves three consecutive steps (eq. [1]) as was the case with the parent substrate **1***a* (1). In the high pH region (pH > 3 for **1***b* and **1***c* and pH > 2 for **1***d*) where the reaction is catalyzed by acid, the third step must be rapid and the first and second steps are both rate determining (eq. [3]). The rate constants k_0 observed in HCl solutions are given by eq. [4] (1).

$$[3] \quad 1 \underset{k_{-1}\ \ k'_{-1}[B]}{\overset{k_1[H^+]\ \ k'_1[BH^+]}{\rightleftharpoons}} 2 \xrightarrow{k_2} 3 \xrightarrow{\text{rapid}} 4$$

$$[4] \quad k_0 = k_{H^+}[H^+] = k_1k_2[H^+]/(k_{-1} + k_2)$$

Kinetic behavior is very similar to that of **1***a* in this pH region (1). Reactivity of **1***a* (k_{H^+}) is, however, greatly reduced by the β substitution as summarized in Table 5.

Curved buffer dependence observed in this pH region must arise from the fact that the buffer accelerates the first step but not the second step. The limiting rate constant k_{max} is described by eq. [5] (1).

$$[5] \quad k_{max} = k_1k_2[H^+]/k_{-1}$$

From the values of k_0 and k_{max}, the rate constant k_1 and the ratio k_2/k_{-1} ($= \Delta k_{max}/k_0$) can be evaluated (1). The results given in Table 4 show that the β substituent reduces this ratio. In other words, the substitution increases the reversibility of the carbon protonation in a kinetic sense.

The curvature of the pseudo-first-order plot for the reaction of **1***b* and **1***d* in deuterium media at higher pH must come from the isotope exchange occurring during the reaction (eq. [6]). The

[6] 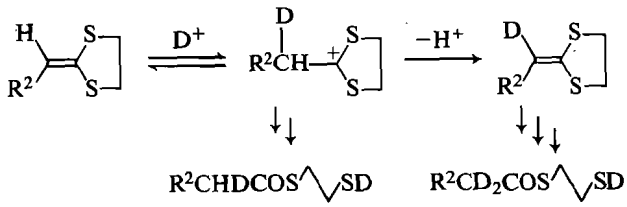

deuterated substrate is more reactive owing to the secondary kinetic isotope effects and for some other reasons (2). The disubstituted substrate **1***c*, which has no hydrogen capable of exchange, showed linear first-order behavior. Normal kinetic isotope effects observed are consistent with the carbon protonation involved in the rate-determining steps. The isotope effects k_{H_2O}/k_{D_2O} decrease in the order **1***b* > **1***c* > **1***d*, in agreement with the diminishing contribution from the first step to the rate (i.e., decreasing k_2/k_{-1}).

High acidity region

As the pH is lowered, the rate of the reverse of the second step ($k_{-2}[H^+]$) increases and the third step becomes rate determining. This occurs because the third step (k_3) is catalyzed by both acid and base and the acid-catalyzed reversion (k_{-2}) is faster than the acid-catalyzed decay of **3**. This situation will be seen below in Fig. 4 and is the same as that for the parent substrate **1***a*. However, the apparent kinetic behavior observed with the derivatives is much different from that found with **1***a*. In the latter case, the rate of decay of **1***a* increases with acidity beyond the pH at which $k_{-2}[H^+]$ exceeds k_3, but appearance of the product **4***a* becomes slower with increasing acidity. The intermediate **3***a* accumulates. By contrast, in the cases of the β-substituted derivatives, the rate of decay of **1** decreases and the decay seems to occur with simultaneous formation of **4**. The rate increases again with acidity beyond the minimum near pH 1. These differences found between **1***a* and its derivatives in this acidity region can be explained by the same mechanism but different equilibrium behavior involving the first and second steps. At equilibrium, **3***a* is favored over **1***a* (1), while the β-substituted derivatives of **1***a* are much favored over the corresponding **3**. Another decrease in the rate of reaction of **1***b* in strong acid will also be rationalized by this mechanism.

Equilibrium involving cation 2

The equilibrium involving the first and second steps was examined by the conventional uv method in the higher acidity range where the third step is slow enough. The "initial"

TABLE 2. Solvent isotope effects on the rates of hydrolysis of **1**[a]

[HCl], *M*	$10^4 k_{obsd}$, s^{-1}[b]	[DCl], *M*	$10^4 k_{obsd}$, s^{-1}[b]	k_{H_2O}/k_{D_2O}
		1b		
5.00×10^{-4}	20.2	5.02×10^{-4}	5.7(6.92)[c]	3.5(2.9)
1.00×10^{-3}	38.5	1.004×10^{-3}	9.5(13.1)[c]	4.0(2.9)
0.200	64.5	0.201	54.0	1.21
0.500	140	0.502	111	1.27
1.000	308	1.004	179	1.73
		1c		
5.00×10^{-4}	0.722	5.02×10^{-4}	0.463	1.57
1.00×10^{-3}	1.22	1.004×10^{-3}	0.637	1.92
0.500	3.78	0.502	3.95	0.96
1.000	10.08	1.004	9.75	1.04
		1d		
2.00×10^{-3}	0.894	2.01×10^{-3}	0.35(0.508)[c]	2.6(1.77)
5.00×10^{-3}	2.26	5.02×10^{-3}	0.8(1.39)[c]	2.8(1.63)
1.00×10^{-2}	3.51	1.004×10^{-2}	0.8(1.57)[c]	4.4(2.24)
0.500	2.23	0.502	2.06	1.09
1.000	5.52	1.004	5.51	1.01

[a]Measured at 25°C and the ionic strength of 0.50 *M*.

[b]Obtained as averages of 2–4 measurements, and estimated errors are less than ±5% except for those for the initial slopes.

[c]Pseudo-first-order plots were curved, and approximate rate constants obtained both from the initial slopes and from the ultimate slopes are given, with the latter in parentheses.

TABLE 3. Rate constants for the hydrolysis and isotope exchange of **1b** and **1d** in 80 vol% aqueous acetonitrile[a] at 25°C

Substrate	Acid conc., *M*	k_0, s^{-1} H_2O	k_0, s^{-1} D_2O	k_{ex}, s^{-1}
1b	0.1	1.02×10^{-4}	1.00×10^{-4}	
1b	2×10^{-3}	3.3×10^{-6}	1.6×10^{-6}	
1d	0.1	1.07×10^{-6}		1.1×10^{-3}
1d	2×10^{-3}	0.7×10^{-7}		0.4×10^{-5}

[a]No salt was added.

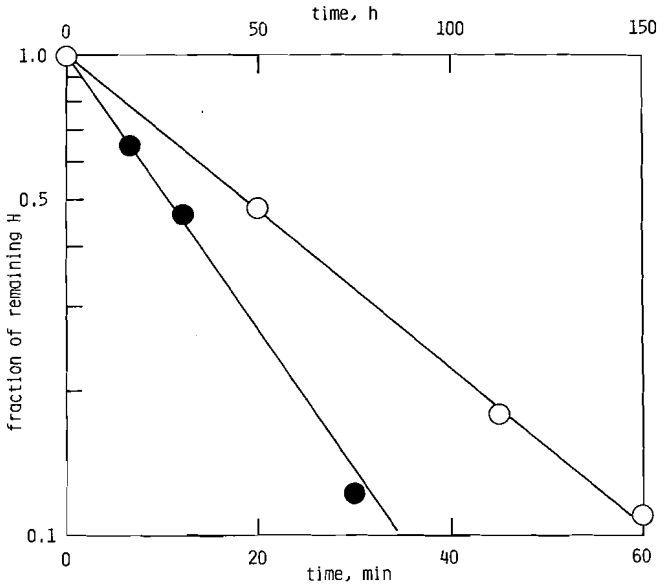

FIG. 2. Loss of the β-hydrogen of **1d** in 80 vol% CH_3CN–D_2O at 25°C. [DCl] = 0.002 *M* (○) against the upper abscissa and 0.10 *M* (●) against the lower abscissa.

absorbances due to **2** and **1** changed sigmoidally with acidity. Choice of the acidity functions is a problem here. If the equilibrium reflected mainly the second step, as was found with **1a** (1), the H_R acidity function defined by dehydration of alcohols (7) would be appropriate. On the other hand, if the first step is a main contributor, the H_C acidity function, which was defined by protonation of the unsaturated carbon bases (6), may be more suited for the correlation. The latter was found to be the case for all the β-substituted derivatives as analyzed below. Thus, the initial absorbances were correlated with H_C to give pK_R as listed in Table 1. The pK_R values obtained from the different wavelengths agree well and appropriate values are given in Table 5.

The equilibrium constant K_R is a composite of the two constants K_1 and K_2 for the first and second steps (eq. [7]).

$$[7] \quad K_R = 1/K_1 + K_2$$

Relative concentrations [**1**]/[**3**] in equilibrium would be found at the lower acidity limit where the contribution from **2** becomes negligibly small. Since **3** may absorb little light at wavelengths longer than 230 nm, the limiting absorbance at the absorption maximum of **1** at lower acidity must result from the absorption of **1**. The limiting absorbances for **1b**, **1c**, and **1d** are 86.9 (±1.0), 99.2 (±1.0), and 106.5 (±2.5)% of the absorbance of **1** for the same concentration in unbuffered water (no reactions), respectively.[5] Since the reactions of **1** are rapid enough and the equilibrium should be attained within a second in the acidity range examined, as evaluated from the rate constants obtained,

[5]Quenching of the isolated salt of **2d** in weakly acidic solutions revealed that (*1*) the initial absorbances at 304 nm in 1.2–2.4 *M* $HClO_4$ correspond to 100% formation of **1d**, and (*2*) the absorbance in HCl solutions decreases with decreasing concentration of acid below 1 *M*, limiting absorbance showing about 65% formation of **1d**. The limiting value should reflect the partitioning ratio k_{-1}/k_2 but the value was somewhat too high as compared with that calculated from the rate constants. Insufficient mixing may in part be responsible for this discrepancy.

TABLE 4. Buffer effects in the reaction of **1** at 25°C

Buffer	pH^a	K_{app}, M^b	$10^4 k_{max}$, s^{-1} [b]	k_2/k_{-1} [c]
		1*b*		
Chloroacetate	2.72	0.28(0.02)	93.4(4.4)	1.25
Methoxyacetate	3.06	0.084(0.006)	46.0(1.4)	1.34
Methoxyacetate	3.45	0.150(0.003)	17.7(0.2)	1.27
Formate	3.59	0.074(0.015)	14.6(0.9)	1.44
				Average 1.33
		1*c*		
Methoxyacetate	3.46	0.027(0.002)	0.339(0.005)	0.661
Formate	3.61	0.030(0.003)	0.250(0.006)	0.689
				Average 0.675
		1*d*		
Chloroacetate	2.99	0.028(0.002)	0.474(0.004)	1.03
Methoxyacetate	3.46	0.029(0.010)	0.157(0.008)	1.01
				Average 1.02

[a]Constant within ±0.01.
[b]Standard deviations are given in parentheses.
[c]$k_2/k_{-2} = \Delta k_{max}/k_H[H^+]$.

TABLE 5. Kinetic parameters for the reaction of **1** at 25°C

Parameter	**1***a* [a]	**1***b*	**1***c*	**1***d*	Origin of the values
$k_{H^+}/M^{-1}\,s^{-1}$	130	3.93	0.148	0.0451	k_{obsd} at high pH
k_2/k_{-1}	7.24	1.33	0.68	1.02	Buffer dependence
pK_R	0.25	−0.60	−1.99	−2.63	Initial absorbance
pK_T [b]	−4.6	−3.52	−3.48	−4.39	Ultimate absorbance
$k_1/M^{-1}\,s^{-1}$	148	6.90	0.367	0.0893	Footnotes *c*, *d*, *e*
k_{-1}/s^{-1}	2.9	24	36	38	K_1 or k_2/k_{-1}
k_2/s^{-1}	21	32	24	39	k_2/k_{-1} or K_2
$k_{-2}/M^{-1}\,s^{-1}$	39[c]	62[d]	120[e]	20[e]	Eq. [4] and k_2/k_{-1}
k_3/s^{-1} k_a	0.28	0.18	0.22	0.05	Eqs. [9] and [10]
$10^{-11}k_b$	1.4	1.8	2.2	2.0	
K_1/M^{-1}	51	0.29	1.03×10^{-2}	2.36×10^{-3}	K_R or k_1/k_{-1}
K_2/M	0.54	0.52	0.20	2.0	k_2/k_{-2} or K_R
$1/K_1K_2$ [f]	0.036	6.63	490	212	
ΔG_1/kcal mol^{-1} [g]	2.0	−1.1	−3.7	−3.2	

[a]Taken from ref. 1.
[b]For the equilibrium between **2** and **4**.
[c]Determined from the biphasic kinetics.
[d]Calculated from k_2 and K_2.
[e]See text for the estimation.
[f]Ratio of the equilibrium concentrations, [**1**]/[**3**].
[g]Free energy change on going from **3** to **1**.

the limiting absorbances no doubt correspond to the equilibrium concentrations of **1**. The results indicate that **1** is much more stable than **3**. The first step mainly contributes to the observed equilibrium. This must be responsible for the more negative pK_R values obtained as compared with that of **1***a*, which comes mainly from the second step (1).

We have to mention here that the conventional uv analyses of the initial absorbances successfully gave the equilibrium values in the present cases although the same analysis of the parent substrate **1***a* was unsuccessful, probably owing to some mixing problems (1). The present equilibrium reflects the first step and the very rapid equilibration may adjust the initial failure by insufficient mixing, if any, before any measurable decay of **3** takes place. By contrast, the second step is mostly responsible for the equilibrium **1***a* ⇌ **2***a* ⇌ **3***a* and the ensuing reaction of **3***a* may occur appreciably before initial mixing errors are corrected. This would have resulted in the poor reproducibility of the experiments with **1***a*.

The relative concentrations [**1**]/[**3**] in equilibrium should be equal to $1/K_1K_2$. In the case of **1***b*, $K_1 = 0.29$ and $K_2 = 0.52$ can be calculated from the observed values, $1/K_1K_2 = 86.9/13.1 = 6.63$ and $K_R = 3.98$. Since we also know values of k_1 and k_2/k_{-1}, all rate constants for the first two steps can be evaluated as listed in Table 5. For **1***c* and **1***d*, however, $K_R \simeq 1/K_1$ and we cannot evaluate reasonably the values of K_2. We now know k_{-2} values for **2***a*, **2***b*, and unsubstituted 1,3-dithiolanylium ion and the 2-*tert*-butyl derivative (9), and they correlated well with the σ* substituent constants (10) as shown in Fig. 3 (ρ* = −2.0). From this correlation, k_{-2} for **2***c* and **2***d* are estimated to be 100 and 15 $M^{-1}\,s^{-1}$, respectively. However, this correlation could be fortuitous, because it may not be well rationalized that the effects of alkyl substitution in the carbocation-

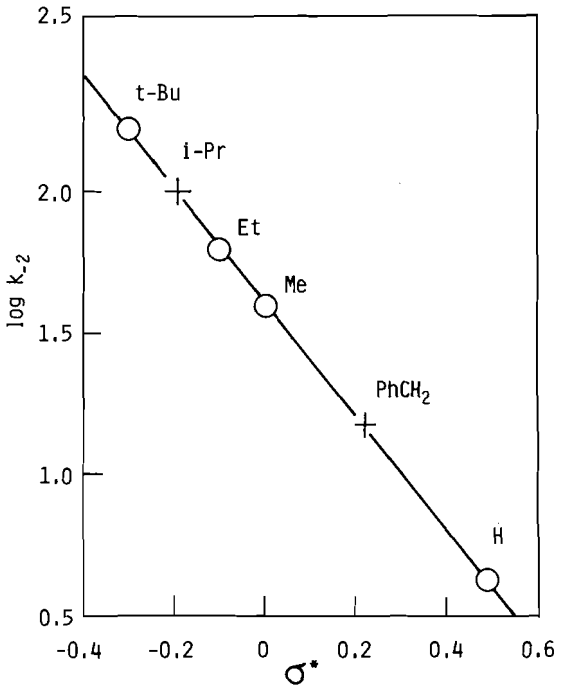

FIG. 3. Correlation of log k_{-2} with σ* of the 2-alkyl substituents of 2-hydroxy-1,3-dithiolane. Crosses indicate the estimated values.

forming reaction conform to the σ* constants, which refer mainly to the inductive effects. This reaction must be accelerated by the steric strain, which is relieved on going from the tetrahedral intermediate **3** to the planar cation **2**. The observed rate may be a compromise of the steric and electronic effects, and the σ* constants happen to be a good measure of the reactivity. Rate constants for another related reaction (eq. [8]) were determined before (4).

$$[8]\quad RC(SCH_3)_3 + H^+ \xrightarrow{k_{H^+}} RC^+(SCH_3)_2 + CH_3SH$$

The rate constants k_{H^+} (in $M^{-1}\,s^{-1}$) obtained at 30°C are: R = CH_3, 6.0×10^{-3}; C_2H_5, 1.8×10^{-2}; $(CH_3)_2CH$, 0.14; $C_6H_5CH_2$, 2.1×10^{-3}. With these limited number of data, the linear free-energy relationship between k_{H^+} and k_{-2} gives 140 and 25 $M^{-1}\,s^{-1}$ for k_{-2} of **2***c* and **2***d*, respectively. From these estimations, k_{-2} values for **2***c* and **2***d* of 120 and 20 $M^{-1}\,s^{-1}$ are used for the evaluation of other rate and equilibrium constants, as summarized in Table 5.

Decay of tetrahedral intermediate

Having K_1 and K_2 values at hand, we can calculate the fraction of tetrahedral intermediate **3** and the rate constant k_3 for its decay by eq. [9].

$$[9]\quad k_3 = (K_R + h_C)k_0/K_2$$

The k_3 values calculated in this way are logarithmically plotted against pH or the H_S acidity function[6] in Fig. 4. The profiles show that the k_3 process is catalyzed by both acid and base (eq. [10]).

$$[10]\quad k_3 = k_aH_S + k_b[OH^-]$$

Probable values of k_a and k_b are given in Table 5.

[6]The H_S acidity function is defined by $H_S = 1.3H_0 + 0.3$ (log $[H^+]$) for sulfur protonation (1, 9).

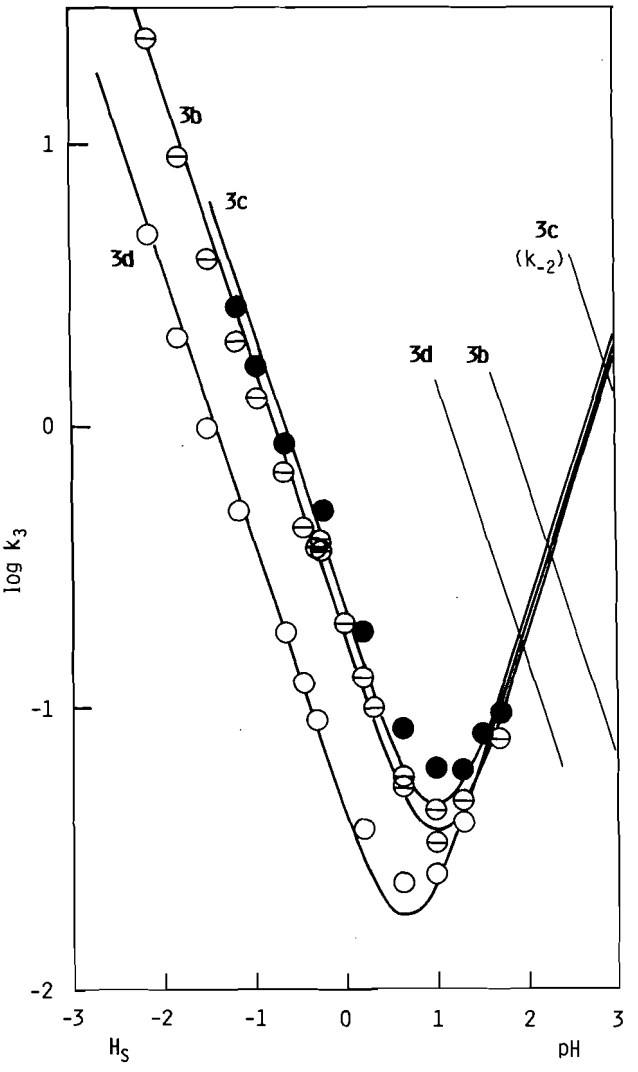

FIG. 4. Acidity – log k_3 correlations for the decay of the tetrahedral intermediates **3***b* (⊖), **3***c* (●), and **3***d* (○). Solid curves are calculated with the rate constants given in Table 5. Straight lines indicate rates of the reversion from **3** to **2** ($k_{-2}[H^+]$).

The acid-catalyzed reaction conforms to the H_S acidity function defined for sulfur protonation. This may be rationalized by a mechanism presented in eq. [11]. The rate-determining step would be opening of the ring. Kinetic solvent isotope effects were found to be very small at 0.1–1.0 *M* HCl (DCl), where the reactions involved are the pre-equilibrium formation of **3** and the acid-catalyzed decay of **3**. The observed isotope effects are not inconsistent with this mechanism (1).

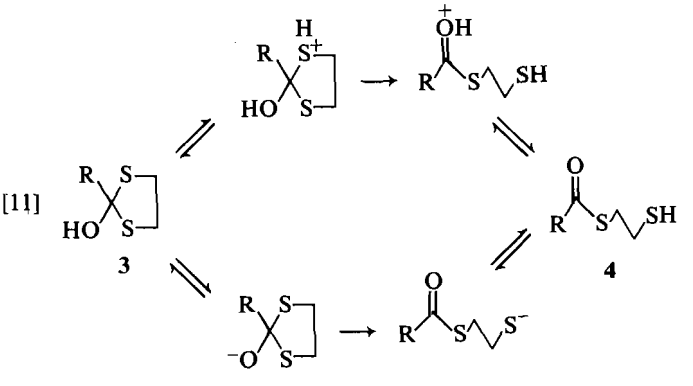

The values of k_b obtained here may be those when the deprotonation of **3** is a rapid equilibrium, although the proton transfer step was found to be involved in the rate-determining step of the base-catalyzed decay of **3** at higher pH when R = *tert*-butyl (9). We could not examine the present reaction at higher pH. The rate constants k_a and k_b are not much influenced by the substituent. This is understandable because the reaction center is remote from the substituent.

Isotope exchange

The nmr spectra of the extracted mixtures from the reaction of **1***b* and **1***d* in acidic acetonitrile–D_2O solutions showed that extensive loss of the β-hydrogen occurred before the hydrolysis proceeded. The loss is due to the isotope exchange with solvent deuterium. The doublet for the methyl group of **1***b* changed to a poorly separated triplet (coupled with the deuterium) as the quartet for the β-hydrogen disappeared. Quantitative evaluation of the rate constant k_{ex} for the isotope exchange of **1***d* in 80 vol% CH_3CN–D_2O showed that the exchange is much faster than the hydrolysis (10^3- and 60-fold at 0.1 and 0.002 *M* of DCl, respectively), as seen from the data of Table 3. This is consistent with the mechanism involving the pre-equilibrium steps and the conclusion that the pre-equilibrium is more complete at higher acidities. With the acyclic analogue $PhCH{=}C(SMe)_2$, the exchange was only 3-fold as rapid as the hydrolysis under similar conditions, although the kinetic reversibility of the protonation in terms of k_2/k_{-1} (0.36) was greater in mostly aqueous solutions (2). The isotope exchange of **1***d* occurs largely through reversion from the tetrahedral intermediate **3**, while that of the acyclic analogue takes place from the carbocation intermediate (eqs. [12] and [13]).

[12] 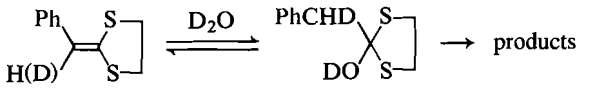

[13] 

Stability and reactivity

The equilibrium constants K_1 for protonation of the double bond refer to carbon basicity. Similar determinations of which we are aware are those with 1,1-diarylethylenes (6, 11) and enamines of propiophenone (12). The most basic is the enamine ($\log K_1 \simeq 10$) (12). The dithioolefins ($\log K_1 = 1.7$ to -2.9 for **1***a*–**1***d*) are more basic than diarylethylenes ($\log K_1 = -4.4$ for $(p\text{-}CH_3OC_6H_4)_2C{=}CH_2$ and -9.4 for $(C_6H_5)_2C{=}CH_2$) (6).

The equilibrium constants K_2 for hydration of the 2-alkyl-1,3-dithiolanylium ions **2** are only slightly influenced by the change in alkyl structure. The stability of **2** (relative to **3**) increases in the order R = $C_6H_5CH_2 < CH_3 \simeq C_2H_5 < (CH_3)_2CH < (CH_3)_3C$ (9). This order is opposite to the electron-donating ability of the alkyl group to the cationic center as deduced from, e.g., the σ_p^+ substituent constants. The steric strain in the tetrahedral form **3** is larger than that in the planar form **2** and this may contribute to the apparent stability of **2**. If we examine the rate constants k_2 and k_{-2}, the alkyl structure greatly influences k_{-2} but k_2 only slightly. The transition state for the second step may be closer to the state of the cationic intermediate **2**. A similar trend is also seen for the first step by comparing the magnitudes of k_1 and k_{-1}; the transition state for this step may also be close to the state of **2**.

Stability of the olefinic substrate **1** relative to the tetrahedral intermediate **3** is given by $1/K_1K_2$ as listed in Table 5. These values can be transformed to free energy differences ΔG_1 between **1** and **3** (Table 5). The unsubstituted **1***a* is less stable than **3***a* by 2 kcal/mol but the β-substituted derivatives **1** are a few kcal/mol more stable than the corresponding **3**. The β substitution would not affect appreciably the total energy of saturated compounds **3** but stabilizes the olefinic linkage of **1**. That is, the methyl, dimethyl, and phenyl groups stabilized the double bond by 3.1, 5.7, and 5.0 kcal/mol, respectively. These amounts of stabilization (in free energy) are close to those found in alkene stabilization (in enthalpy terms) (13, 14).

Effects of monomethyl and phenyl substitutions on the reactivity of **1***a* in protonation (k_1) are similar to those observed with the acyclic analogue $CH_2{=}C(SCH_3)_2$ (2–4), vinyl ethers (15–18), and vinyl sulfides (19). A second methyl group of **1***c* reduces the reactivity of **1***b* by nearly the same factor as the first (**1***a*/**1***b*), as shown below.

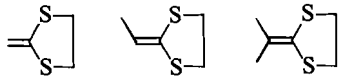

1 : 1/21 : 1/400

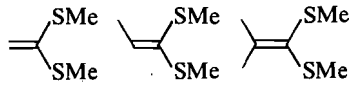

1 : 1/23 : $1/(8.8 \times 10^5)$

By contrast, a large reduction in the reactivity of the acyclic derivative was previously observed by dimethyl substitution (4). This was ascribed to a steric factor (4), but we suspected that a change in rate-determining step had been overlooked. Reexamination revealed, however, that the rates of hydrolysis of dimethylketene dimethyldithioacetal in 1 *M* and 0.1 *M* HCl nearly coincide with the extrapolation of those obtained in strong acid, and deuterium kinetic solvent isotope effects are normal ($k_{H_2O}/k_{D_2O} = 2.7$–3.0). That is, the largely reduced reactivity of the dimethyl derivative in protonation is real, and some steric factor that cannot operate in the dithiolane system should be the cause for this reduction in the acyclic system.

Summary

The carbon protonation of the β-substituted 2-methylene-1,3-dithiolanes was found to be completely reversible at higher acidities but only partially reversible at lower acidities during the hydrolysis. This is rationalized by the change in the rate-determining step and the stability of the olefinic substrates.

Experimental

Materials

2-Ethylidene- (**1***b*), 2-isopropylidene- (**1***c*), and 2-benzylidene-1,3-dithiolane (**1***d*) were obtained by deprotonation of the corresponding dithiolanylium perchlorates **2**, which were prepared from the reaction of the acyl chlorides with 1,2-ethanedithiol in the presence of perchloric acid as described elsewhere (20).

Equilibrium measurements

Initial (A^0) and equilibrium absorbances (A^∞) of the substrates in acid were measured on a Shimadzu UV-200 spectrophotometer at 25.0 ± 0.1°C. A sample of 30 μL of a stock solution of the substrate in dry acetonitrile was introduced from a microsyringe into 3.0 mL of acid solution, which was thermally equilibrated in a quartz cuvette, and time-dependent absorbance change was recorded. The absorbance was extrapolated to the time of mixing by a pseudo-first-order plot to obtain A^0, and A^∞ was read after 6 half-lives. The absorbances were plotted

against the H_C or H_R acidity function (6, 8) and pK_R was calculated by linear least-squares treatment according to the literature (21).

Kinetic measurements

Kinetic measurements were made in the same way as before (1). Reactions were carried out in aqueous solutions containing 0.5–1.0 vol% of CH_3CN at 25.0 ± 0.1°C and the ionic strength of the solutions of low acidity was maintained at 0.50 *M* by adding KCl. Reactions were followed spectrophotometrically on a Shimadu UV-200 or UV-140 spectrophotometer. The values of pH were determined with a Hitachi–Horiba F-7 pH meter.

Product analysis

In a 0.1 *M* HCl solution in 80 vol% CH_3CN–H_2O (20–30 mL) was dissolved 50 mg of the substrate **1** and the solution was kept at 25°C for about 5 half-lives. The products were taken up in ether after quenching with 10% $NaHCO_3$, washed with saturated NaCl, and dried over $MgSO_4$. The ether was removed under reduced pressure and the residues were subjected to nmr analysis by a JNM-C-60HL spectrometer. The spectra were consistent with the thiolester structure **4**; nmr (CCl_4) δ: **4***b*, 1.17 (t, 3H), 1.47 (t, 1H), 2.2–3.2 (m, 6H including q at 2.54 ppm); **4***d*, 1.42 (t, 1H), 2.3–3.4 (m, 4H), 3.70 (s, 2H), 7.2 (br s, 5H).

Isotope exchange

Reactions were carried out in 80 vol% CH_3CN–D_2O containing DCl. The DCl solutions were prepared by bringing 20 parts by volume of an appropriate DCl solution in D_2O (Merck, 99.75%) to 100 parts with dry acetonitrile in a volumetric flask. In a typical reaction, about 150 mg of **1***b* or **1***d* was dissolved in 100 mL of the DCl solution equilibrated thermally at 25°C. The mixture was shaken and left standing at 25°C. After appropriate reaction time, a 25-mL aliquot of the mixture was taken by a syringe, quenched with 10% $NaHCO_3$, extracted with ether, washed with saturated NaCl, and dried over $MgSO_4$. The ether was removed under vacuum and the residues dissolved in CCl_4 were subjected to nmr analysis. During the reaction of **1***b* in 0.1 *M* DCl, the quartet due to the β-hydrogen (5.4 ppm) was mostly (ca. 80%) lost in 10 min and the doublet due to the methyl group (1.7 ppm) changed to a broad singlet (or a poorly separated triplet). A similar change was also observed at 0.002 *M* of DCl. In the case of **1***d*, the intensity of the singlet at 6.5 ppm (β-hydrogen) was quantitatively evaluated in reference to that of the phenyl group. The rate of isotope exchange was calculated from the first-order plots of the intensity (Fig. 3). Kinetic analysis of the hydrolysis in this medium as well as in the corresponding HCl solution was also undertaken by uv spectrophotometry in the same way as above.

Acknowledgments

We thank W. Fujiwara for preliminary experiments and H. Okuda for measurements of nmr spectra.

1. T. Okuyama. J. Am. Chem. Soc. **106**, 7134 (1984).
2. T. Okuyama and T. Fueno. J. Am. Chem. Soc. **102**, 6590 (1980); **105**, 4390 (1983).
3. T. Okuyama, S. Kawao, and T. Fueno. J. Am. Chem. Soc. **105**, 3320 (1983).
4. T. Okuyama, S. Kawao, and T. Fueno. J. Org. Chem. **49**, 85 (1984).
5. T. Okuyama, S. Kawao, W. Fujiwara, and T. Fueno. J. Org. Chem. **49**, 89 (1984).
6. M. T. Reagan. J. Am. Chem. Soc. **91**, 5506 (1969).
7. C. H. Rochester. Acidity functions. Academic Press, New York. 1970.
8. A. J. Kresge, H. J. Chen, G. L. Capen, and M. F. Powell. Can. J. Chem. **61**, 249 (1983).
9. T. Okuyama and T. Fueno. J. Am. Chem. Soc. **107**, 4224 (1985).
10. R. W. Taft. *In* Steric effects in organic chemistry. *Edited by* M. S. Newman. Wiley, New York. 1956. Chapt. 13.
11. N. C. Deno, P. T. Groves, and G. Saines. J. Am. Chem. Soc. **81**, 5790 (1959).
12. P. Y. Sollenberger and R. B. Martin. J. Am. Chem. Soc. **92**, 4261 (1973).
13. S. W. Benson, F. R. Cruickshank, D. M. Golden, G. R. Haugen, H. E. O'Neal, A. S. Rodgers, R. Shaw, and R. Walsh. Chem. Rev. **69**, 279 (1969).
14. J. Hine. Structural effects on equilibria in organic chemistry. Wiley, New York. 1975. pp. 265–276.
15. T. Okuyama, T. Fueno, H. Nakatsuji, and J. Furukawa. J. Am. Chem. Soc. **89**, 5826 (1967).
16. P. Salomaa and P. Nissi. Acta Chem. Scand. **21**, 1386 (1967).
17. T. Okuyama, T. Fueno, and J. Furukawa. Bull. Chem. Soc. Jpn. **43**, 3256 (1970).
18. Y. Chiang, A. J. Kresge, and C. I. Young. Can. J. Chem. **56**, 461 (1978).
19. T. Okuyama, M. Nakada, and T. Fueno. Tetrahedron, **32**, 2249 (1976).
20. T. Okuyama and T. Fueno. Bull. Chem. Soc. Jpn. **59**, 453 (1986).
21. W. M. Clark. Oxidation–reduction potentials of organic systems. Williams and Wilkins, Baltimore, Md. 1960. pp. 149–155.

^{15}N Nuclear polarisation in the rearrangement of 2,6-dichloro-*N*-nitroaniline and 2,6-dibromo-*N*-nitroaniline

ADEL M. A. ABU-NAMOUS AND JOHN H. RIDD[1]
Chemistry Department, University College, 20 Gordon Street, London WC1H OAJ, England

AND

JOHN P. B. SANDALL
Chemistry Department, Royal Holloway and Bedford New College, Egham Hill, Egham, Surrey TW20 OEX, England

Received October 17, 1985

This paper is dedicated to Professor Arthur N. Bourns

ADEL M. A. ABU-NAMOUS, JOHN H. RIDD, and JOHN P. B. SANDALL. Can. J. Chem. **64**, 1124 (1986).

The acid-catalysed rearrangements of 2,6-dichloro-*N*-nitroaniline and 2,6-dibromo-*N*-nitroaniline to give the corresponding 4-nitro derivatives have been followed by ^{1}H and ^{15}N nmr spectroscopy in deuteriochloroform at 30°C. When $^{15}NO_2$-labelled nitramines are used, the ^{15}N nmr signals for both the substrate and product show enhanced absorption during reaction. When one labelled nitramine and one unlabelled nitramine are rearranged together, isotopic exchange occurs and ^{15}N nmr signals are seen for both substrates and both products. For the initially unlabelled nitramine and its product, these signals are in emission. The change in the enhancement of the signals during reaction shows that the nuclear polarization arises from the rearrangement, not from a preliminary equilibrium.

ADEL M. A. ABU-NAMOUS, JOHN H. RIDD et JOHN P. B. SANDALL. Can. J. Chem. **64**, 1124 (1986).

Opérant à 30°C, dans des solutions de deutérochloroforme et faisant appel à la rmn du ^{1}H et du ^{15}N, on a pu suivre l'évolution des transpositions acido-catalysées des dichloro-2,6 et dibromo-2,6 *N*-nitroanilines en dérivés nitro-4 correspondants. Lorsqu'on utilise des nitramines marquées avec des $^{15}NO_2$ et que l'on suit l'évolution de la réaction par rmn du ^{15}N, on observe une augmentation de l'absorption tant pour le substrat que pour le produit. Quand on effectue une transposition entre une nitramine marquée et une autre qui ne l'est pas, il se produit des échanges isotopiques et les signaux de la rmn du ^{15}N sont observés tant dans les substrats que dans les produits. Pour la nitramine qui n'était initialement pas marquée, ces signaux correspondent à des émissions. Les changements qui se manifestent par une augmentation des signaux au cours de la réaction indiquent que la polarisation nucléaire provient de la transposition et non pas d'un équilibre préliminaire.

[Traduit par la revue]

Introduction

Although a number of mechanisms have been put forward for the nitramine rearrangement (1), that most generally accepted, at least for nitramines from the more basic amines, is the radical pair interpretation first put forward by W. N. White *et al.* (2). On this interpretation the protonated nitramine undergoes homolysis to form the cation radical of the amine and nitrogen dioxide. One weakness of this mechanism is the lack of direct evidence for the intermediate radicals (3) and a related problem is the ill-defined borderline between the radical mechanism and the heterolytic processes expected for the rearrangement of nitramines containing strongly electron-withdrawing groups (1).

In our preliminary communication on this work (4), we showed that the rearrangement of $^{15}NO_2$-labelled 2,6-dibromo-*N*-nitroaniline gave strongly enhanced ^{15}N nmr signals during reaction for both the substrate and the 4-nitro product. This evidence for nuclear polarization shows that a radical pair is involved in some way in the reaction. However, since strong nuclear polarization was present in both the substrate and the product, it was recognised that this work did not provide unambiguous evidence for the radical pair interpretation of the rearrangement. The nuclear polarization could have been generated by a preliminary equilibrium involving the nitramine and then carried over into the product by a non-radical process. This complication has been rendered less likely by the recent work of Shine *et al.* (5), for these authors have used heavy element isotope effects to show that the rearrangement is not a concerted process. The present work was carried out to provide more direct evidence for the involvement of radical pairs in the rearrangement reaction.

2,6-Dibromo-*N*-nitroaniline and 2,6-dichloro-*N*-nitroaniline were chosen as the substrates partly because of the ease with which these compounds can be prepared from nitric acid (the source of the isotopic label) and partly because of the relative cleanliness of the corresponding rearrangements. The early work of Orton and Pearson (6) has, however, shown that the rearrangement of the bromo compound is accompanied by the formation of some 2,4-dibromo-6-nitroaniline.

Results

For this work, it was necessary to obtain conditions in which a relatively high concentration of the nitramine would rearrange smoothly in solution with a half-life of ca. 10 min. The conditions chosen involved reaction in deuteriochloroform at 30°C with trifluoroacetic acid as the catalyst. The reaction was studied first by ^{1}H nmr spectroscopy with nitromesitylene present as an inert standard.

The spectrum of 2,6-dibromo-*N*-nitroaniline in deuteriochloroform is as expected (δ: 7.19(t, 4-H, J = 8.14), 7.65(d, 3, 5-H), 9.62(s, N-H)). As reaction proceeds, the signal for the product appears at δ 8.34. The progress of the reaction was followed from the height of this peak and from the larger of the two peaks for the reactant at δ 7.65, both measured relative to the height of the peak for nitromesitylene (δ 6.92). A similar procedure was used for following the rearrangement of 2,6-dichloro-*N*-nitroaniline. In this compound, the aromatic protons give rise to a multiplet (δ: 7.44(m, 3, 4, 5-H), 9.44(s,

[1]Author to whom correspondence may be addressed.

Printed in Canada / Imprimé au Canada

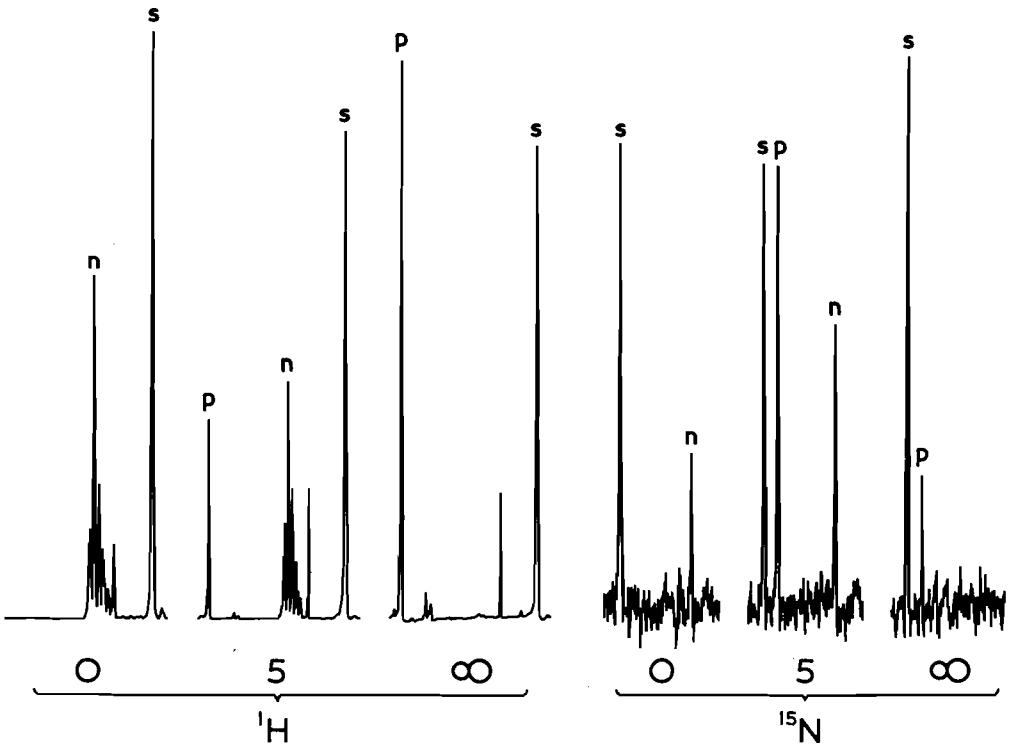

FIG. 1. The ^{1}H and ^{15}N nmr spectra for the rearrangement of 2,6-dichloro-*N*-nitroaniline at t/min = 0, 5, and infinity. Conditions: ^{1}H spectra from run 2, Table 1; ^{15}N spectra from the run with R = Cl in Table 2. Lettering: n, nitramine; s, standard; p, 4-nitro product. The main unlabelled signal in the last ^{1}H nmr spectrum comes from the protons in the solvent.

TABLE 1. First-order rate coefficients (k_N, k_P)[a] for the acid-catalysed rearrangement of the nitramines 2,6-$R_2C_6H_3NHNO_2$ (R = Br, Cl) in deuteriochloroform at 30°C. [Nitramine] = 0.05 mol kg^{-1}; [CF_3CO_2D] = 0.79 mol kg^{-1}; [CF_3CO_2H] = 0.85 mol kg^{-1}

R	10^4k_N (s^{-1})	10^4k_P (s^{-1})
Cl	8.9[b]	10.3[b]
Cl	9.1[c]	14.2[c]
Cl	6.1[b,d]	7.4[b,d]
Cl	7.0[c,d]	8.1[c,d]
Br	5.1[c]	6.4[c]
Br	3.6[b,d]	4.4[b,d]
Br	3.4[c,d]	5.2[c,d]

[a]Calculated from the ^{1}H nmr peaks for the nitramine (N) or the product (P).
[b]Using CF_3CO_2D.
[c]Using CF_3CO_2H.
[d]From a kinetic run involving the simultaneous rearrangement of both nitramines.

N-H), and the product signal is at δ 8.15. The dichloro compound gave reasonable first-order kinetics when followed from either the disappearance of the starting material or the appearance of the products: the conditions of the reactions and the rate coefficients obtained are shown in Table 1. The spectra for the rearrangement of the dichloro compound in the first series of Fig. 1 show the separation of the peaks and the cleanliness of the overall reaction. Some very small additional peaks can be seen in the final spectrum coming from the by-products formed. The results with the dibromo compound were less reproducible (see Discussion).

The runs with the $^{15}NO_2$-nitramines were carried out in a similar way and were followed by ^{15}N nmr spectroscopy using ^{15}N-nitrobenzene as an internal standard. For the dibromo compounds, the nitramine signal was 24.7 ppm to high field of the standard and the product signal was 5.1 ppm to high field of the standard. For the dichloro compounds, the corresponding values are 24.2 and 4.7. These slight differences in the positions of absorption of the dibromo and dichloro compounds made possible the observation of crossover experiments.

The changes in the heights of these nmr signals for the separate rearrangement of the two nitramines are shown in Table 2. It is immediately obvious that the intensity of the signals depends more on the nuclear polarization present than on the concentrations of the species concerned. Thus, the intensity of the peak for the nitramines rises over the first five minutes of reaction and remains above the initial intensity over almost all of the period studied (several half-lives). The intensity of the peak for the product also rises rapidly over the first five minutes and then decreases more slowly. The form of these spectra is illustrated for the dichloro compound in the second series of Fig. 1.

Studies have also been carried out on the simultaneous rearrangement of the two nitramines in the same solution, but with only one of the nitramines labelled with ^{15}N. The dichloro and dibromo nitramines used here are very suitable for this kind of experiment since they rearrange at similar rates (Table 1). If no isotopic exchange occurs then, when the reaction mixture is studied by ^{15}N nmr spectroscopy, only the rearrangement of the labelled nitramine should be seen. However, in these experiments, peaks were seen for both nitramines and both products. The peaks could be clearly distinguished since those for the initially unlabelled nitramine and the corresponding product were in emission. The heights of the peaks relative to the

TABLE 2. Relative peak heights[a] for the nitramines (n, n′) and the products (p, p′) in the ^{15}N nmr spectra during the rearrangement of the nitramines 2,6-$R_2C_6H_3NH^{15}NO_2$ (R = Br, Cl) (0.05 mol kg^{-1}) in $CDCl_3$ in the presence of CF_3CO_2D (0.9 mol kg^{-1}). Temperature = 30°C. The solutions also contained $Ph^{15}NO_2$ (0.05 mol kg^{-1})

	R = Br		R = Cl	
Time (min)	n′	p′	n	p
0	1	0	1	0
2	2.1	2.7	1.4	1.5
5	3.7	5.4	2.3	2.8
8	2.4	3.9	1.9	2.8
11	2.2	3.3	1.9	2.9
14	1.9	2.9	1.7	2.8
17	1.6	2.7	1.2	2.4
20	1.3	2.6	1.3	2.4
23	1.4	2.3	1.0	1.8
26	0.95	2.3	1.1	2.0

[a]Obtained by dividing the peak heights by the peak height of the standard and adjusting the scale to bring the value for the substrate at the start of the reaction to unity.

TABLE 3. Relative ^{15}N nmr peak heights[a] for nitramines (n, n′) and products (p, p′) during the concurrent rearrangement of 2,6-dibromo-*N*-nitroaniline and 2,6-dichloro-*N*-nitroaniline with only one of the substrates initially labelled with ^{15}N in the nitro group. The concentrations and conditions are as set out in Table 2. Negative values indicate an emission signal

	Bromo compound		Chloro compound	
Time (min)	n′	p′	n	p
(^{15}N-Label in bromo compound)				
0	1	0	0	0
2.5	2.9	4.8	−0.5	−2.5
6.5	4.6	8.2	−1.2	−5.3
10.5	4.2	7.5	−0.4	−4.1
14.5	3.8	6.1	−0.3	−3.4
18.5	3.5	5.5	−0.9	−3.1
22.5	2.7	4.4	−0.5	−2.7
26.5	3.1	4.4	−0.2	−1.5
30.0	1.2	4.0	−0.2	−1.4
34.5	1.5	2.9	−0.1	−1.4
38.5	1.7	2.8		−1.2
(^{15}N-Label in chloro compound)				
0	0	0	1	0
2.5	−0.5	−2.3	2.7	4.7
6.5	−1.9	−3.8	4.7	7.8
10.5	−1.2	−3.3	4.2	6.7
14.5	−0.8	−2.9	3.5	6.1
18.5	−1.1	−2.5	3.1	5.5
22.5	−0.5	−2.1	2.7	5.3
26.5	−0.7	−1.7	2.3	4.4
30.5	−0.5	−1.7	2.4	3.9
34.5	−0.3	−1.5	2.1	3.6
38.5	−0.3	−1.0	1.3	3.1

[a]See footnote *a*, Table 2.

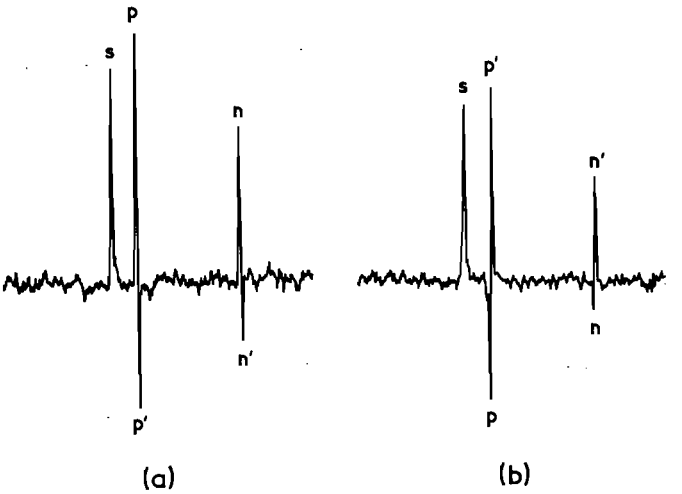

FIG. 2. The ^{15}N nmr spectra (t = 6.5 min) during the simultaneous rearrangement of 2,6-dichloro-*N*-nitroaniline and 2,6-dibromo-*N*-nitroaniline under the conditions defined in Table 3: (a) with the label in the dichloro compound; (b) with the label in the dibromo compound. The lettering follows that in Fig. 1 with the dashed symbols (n′, p′) indicating the nitramine and product from the dibromo series.

standard are listed in Table 3 and the form of the spectra is shown in Figure 2.

Discussion

The rearrangement will be discussed in terms of the radical pair mechanism originally proposed by White *et al.* (2) and shown in Scheme 1. The reverse reaction of the radical pair (**1**) to reform the nitramine has been added to the original mechanism to explain the polarization of the substrate observed in the present work.

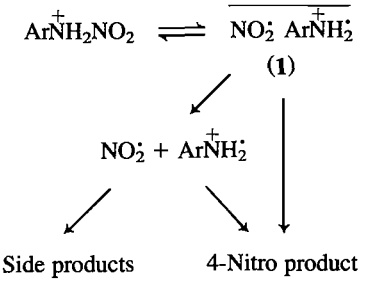

SCHEME 1

The present results provide support for this mechanism in several ways. First, the presence of nuclear polarization in the product of rearrangement is clear evidence for the involvement of radical pairs at some stage on the reaction path. If the radical pair is considered to be formed from the cation radical of the amine and nitrogen dioxide (as implied by the scheme), then Kaptein's rules (7) permit the phase of the polarization to be calculated from the sign of the difference between the g-values of the amine cation radicals ($g > 2.00249$) (8) and nitrogen dioxide ($g = 2.0000$) (9).[2] The application of Kaptein's rules also requires the sign of the hyperfine coupling constant (a_N) for the nitrogen atom in nitrogen dioxide; this should be negative because of the negative magnetogyric ratio of the ^{15}N nucleus (10). The negative magnetogyric ratio also has the consequence

[2]Several values exist for this quantity; the reasons for selecting g = 2.0000 are given in ref. 10.

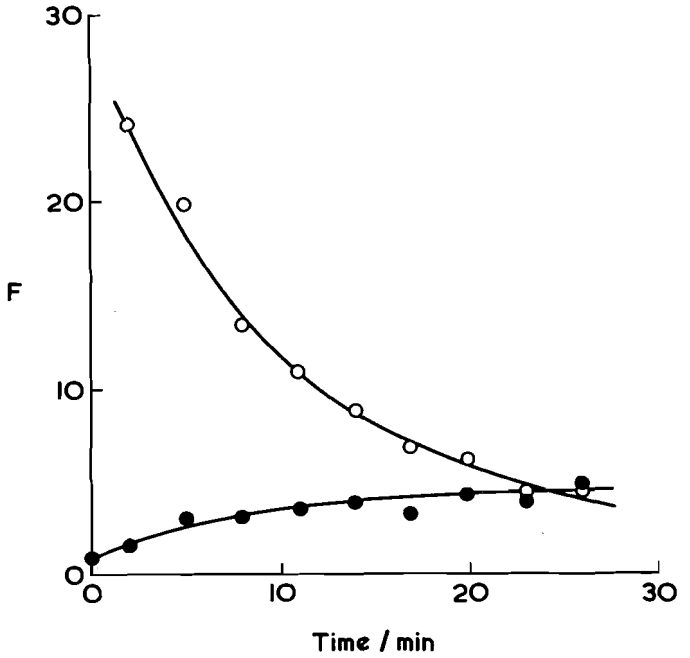

FIG. 3. The variation in the enhancement of the ^{15}N nmr signals during the rearrangement of 2,6-dichloro-*N*-nitroaniline: dots, nitramine; open circles, 4-nitro product.

that an additional negative sign should be added to the normal equation expressing Kaptein's rule for net polarization (11). The rule then takes the form of eq. [1], where the sign of Γ is positive for absorption and negative for emission. The sign of μ is positive when the radical pair is formed by the diffusion together of the radicals and negative when the radicals are formed from a singlet precursor (e.g., by homolysis of the protonated nitramine). The sign of ε is positive for cage products and negative for products formed from radicals that have escaped from the cage.

$$[1] \quad \Gamma = -\mu\varepsilon a_N(g_{NO_2} - g_{ArH+\cdot})$$

When the signs appropriate for the present reaction are inserted in this equation, it is clear that the recombination of the radical pair within the cage either to reform the nitramine or to form the rearranged product should lead to enhanced absorption, as observed (Fig. 1). Most of the radicals that separate should eventually diffuse together to form the same products but some of the polarization of the free nitrogen dioxide radicals should be lost through nuclear relaxation; the overall polarization should therefore be that for the recombination reaction within the cage.

This picture of the reaction also accords with the polarization observed when one labelled nitramine and one unlabelled nitramine are rearranged together, for the signals for the initially unlabelled nitramine and the corresponding rearranged product appear in emission (Fig. 2 and Table 3). These signals derive from species that have undergone isotopic exchange and it is reasonable, therefore, that they should reflect the polarization of the nitrogen dioxide molecules that have escaped from the original cage. This is of opposite phase to that of the cage products because the CIDNP (chemically induced dynamic nuclear polarization) effects derive from a degree of partitioning of the nitrogen dioxide molecules according to the ^{15}N nuclear spin.

The enhanced absorption signals observed in the rearrangement of a labelled substrate and the emission signals seen during the crossover experiments could also be explained by a reaction scheme in which the protonated nitramine dissociates reversibly to form the radical pair (1) but undergoes the nitramine rearrangement by a separate non-radical process. To eliminate this possibility, it is necessary to consider the relative polarization of the nitramine and the rearranged product. From the magnitude of the ^{15}N signals in Table 2 and the concentrations of the nitramine and rearranged product calculated from the rate coefficients in Table 1, it is possible to calculate the changes in the enhancement factor (F) of the ^{15}N signals during reaction (see experimental section). Such enhancement factors are plotted for the rearrangement of the 2,6-dichloronitramine in Fig. 3; the results for the rearrangement of the 2,6-dibromonitramine are very similar. The results show that, at the start of reaction, the enhancement factor for the product is much greater than that for the reactant; the greater part of the polarization of the product must therefore be generated in the rearrangement stage.

There are several possible complications in the above argument that require consideration. One is the possibility that the ^1H nmr measurements are distorted by nuclear polarization and so do not provide a true measure of the extent of reaction. When Kaptein's rules (7) are applied to the ^1H nmr spectra, the predicted result at the 3,5-position is emission, since calculations[3] suggest that the sign of the hyperfine coupling constant is positive at this position in the cation radical of dichloroaniline. A contribution from such nuclear polarization would therefore give an apparent increase in the rate of disappearance of the nitramine and a decrease in the rate of appearance of the rearranged product. The rate coefficients calculated from the heights of the peaks for the substrate and product are not identical (Table 1), but the discrepancy is in the opposite direction to that expected. However, in a number of runs, a curious variation exceeding the expected experimental error was observed in the height of the peaks for the dibromonitramine at the start of reaction; the above argument concerning the enhancement factors is therefore based on the results for dichloro compound (Fig. 3).

The discrepancy in the values of k_N and k_P (Table 1) could arise from the side reactions present. A concurrent first-order process would not interfere with the calculation of k_P but the presence of any subsequent reaction would decrease the height of the signal for the product at the end of reaction and thus cause the extent of reaction at earlier times to be overestimated. In this connection, it is interesting that some deamination does appear to occur in the reaction (see experimental section). Fortunately, the difference between the enhancement factors for the nitramine and product (Fig. 3) is far too great for the conclusions to be affected by such small uncertainties in the rate coefficients.

The relative enhancement factors for the nitramine and the rearranged product are also affected by the relaxation times of the ^{15}N nucleus in these compounds. The relaxation time of this nucleus in the N-$^{15}NO_2$ position of the dichloronitramine has therefore been measured (152 s). The result is slightly less than that found for an aromatic C-$^{15}NO_2$ group (170 s in nitrobenzene (12), 182 s for the 2-nitro group of 2,4-dinitrophenol (13)). This difference is insufficient to require any change in the above argument concerning the generation of the polarization in the rearrangement stage.

[3] J. Courtneidge, personal communication of results of MNDO calculation.

Because of this similarity in the relaxation times, the greater polarization found for the product in the exchange experiments (Fig. 2) implies that the radical pairs (**1**), at least when formed by diffusion, react mainly at the 4-position rather than at the nitrogen atom. What happens when the radical pair is formed by the homolysis of the protonated nitramine is less clear because the extent of nuclear polarization depends on the lifetime of the radical pair. If the initial orientation of the radical pair favours rapid recombination at the nitrogen atom, the contribution of this to the nuclear polarization could be slight because of the short lifetime involved. For a more complete discussion of this, it would be necessary to distinguish between different types of radical pairs, including solvent-separated pairs (14).

The extent of isotopic exchange during the concurrent rearrangements (Table 3) can be estimated from the relative heights of the ^{15}N peaks for the two rearranged products at the end of reaction. The results are not very accurate because, in the absence of nuclear polarization, the signal-to-noise ratio is low. However, the extent of exchange is clearly very considerable, for the peak height of the product formed by exchange is 70% of that formed from the initially labelled substrate when the initial label is in the dichloronitramine. The corresponding figure is 60% when the initial label is in the dibromo compound. These results accord with the extensive exchange observed by White and Golden (15) in the concurrent rearrangement of *N*-nitro-*N*-methylaniline and 4-fluoro-*N*-nitro(^{15}N)-*N*-methylaniline. Thus, the complete set of results are in full agreement with the mechanism proposed by White (2) (with the addition of some return of the radical pairs to the nitramine). The generation of nuclear polarization in the rearrangement stage provides unequivocal evidence for the involvement of radical pairs in the rearrangement.

Experimental

Materials

The nitramines were prepared by a modification of the method used by Orton and Smith (16) for the preparation of 2,6-dibromo-*N*-nitroaniline. The modifications were to facilitate the preparation of the labelled compounds. Nitric acid (2.8 mL, 40%) was added to a solution of the amine (0.014 mol) in glacial acetic acid (31 mL) followed, after cooling to 12°C, by the addition of acetic anhydride (2.1 mL). The reaction mixture was maintained below 20°C for 9 min and then poured into ice-water (51 g). After extraction with $CHCl_3$ (100 mL) and washing with water (3 × 100 mL), the chloroform solution was extracted with sodium carbonate (2 × 50 mL, 4%) and the extract was cautiously neutralized with hydrochloric acid. The precipitated nitramines were washed with water and dried under vacuum. 2,6-Dibromo-*N*-nitroaniline was formed in a yield of 71% and had mp 107°C (lit. (16) mp 108°C). *Anal.* for $C_6H_4N_2O_2Br_2$: C 24.4, H 1.4, N 9.5; found: C 24.2, H 1.4, N 9.5. 2,6-Dichloro-*N*-nitroaniline was formed in a yield of 80% and had mp 94–95°C (lit. (17) mp 102–103°C(dec.)). *Anal.* for $C_6H_4N_2O_2Cl_2$: C 34.8, H 2.0, N 13.5; found: C 34.5, H 1.9, N 13.7. The ^{15}N-labelled nitramines were prepared in the same way using nitric acid (95–99% ^{15}N, 40%) from B.O.C. Prochem. The trifluoroacetic acid was prepared by the addition of D_2O or H_2O to trifluoroacetic anhydride and standardized by titration with sodium hydroxide. The $CDCl_3$ used in the kinetic studies was from Aldrich (Gold Label).

Products

The ^1H nmr spectrum of the products of rearrangement of 2,6-dichloro-*N*-nitroaniline includes a number of small peaks with a total height of ca. 10% of the peak for the 4-nitro product (Fig. 1). The rearrangement of this nitramine (0.2828 g) followed by separation of the products by hplc gives 2,6-dichloro-4-nitroaniline (0.2135 g) together with other fractions (0.0336 g). The yield of the main product is therefore 86% of the isolated material or 75.5% overall. The other products have not been investigated in detail but an analysis by glc–ms indicated a complex mixture including some *meta*-dichlorobenzene and 3,5-dichloronitrobenzene. The results with the 2,6-dibromonitramine were very similar. Separation by hplc showed that the 4-nitro product was 89% of the isolated material.

Kinetics

The kinetic studies followed by ^1H and ^{15}N nmr spectroscopy were carried out on a Varian XL-200 FT spectrometer; the measurement of the relaxation time was made on a Jeol FX 90Q FT spectrometer using the fast inversion recovery method (18).

The nitramine or mixture of nitramines (usually 0.15 mmol) and an equivalent amount of the standard (nitromesitylene or ^{15}N-nitrobenzene) were dissolved in $CDCl_3$ (usually 1 or 2 mL) and brought to the required temperature (usually 30°C). The nmr spectrum was measured and the reaction was started by the addition of CF_3CO_2D or CF_3CO_2H (usually 0.1 mL); nmr spectra were then taken every 2 or 3 min for ca. 2 half-lives using 50 pulses, delay time 2 or 3 s. More acid was then added (0.1 mL) and the final spectrum was taken after ca. 10 half-lives.

For the runs followed by ^1H nmr spectroscopy, the rate coefficients obtained from the concentration of the nitramine were calculated from a plot of $\ln(h_n/h_s)$ against time, where h_n and h_s are the heights of the peaks for the aromatic protons in the nitramine and in nitromesitylene respectively (for the dibromo compound, the larger of the two peaks for the 3,5-protons was used). As expected, the height of the peak for nitromesitylene was almost constant throughout the run.

The rate coefficients for the runs followed from the concentration of the rearranged product were calculated from a plot of $\ln((h_p/h_s)_{t=\infty} - (h_p/h_s)_t)$ against time, where h_p is the height of the peak for the 3,5-protons in the product. Ten points were usually taken over about 2 half-lives but, in some runs, the first one or two points were neglected since these seemed subject to greater error. Regression coefficients were 0.99 ± 0.01.

The enhancement factors (F) for the nitramine plotted in Fig. 3 were calculated from eq. [2] and those for the product were calculated from eq. [3].

$$[2] \quad F = \frac{(h_n/h_s)_t a}{(h_n/h_s)_{t=0}(a - x)}$$

$$[2] \quad F = \frac{(h_p/h_s)_t a}{(h_p/h_s)_{t=\infty} x}$$

In these equations, the heights (h_n, h_p, h_s) refer to the peaks in the ^{15}N nmr spectra for the nitramine, product, and standard. The initial concentration of the nitramine is a and the concentration of the product (x) is calculated from the mean rate coefficient ($k = 9.6 \times 10^{-4}\ s^{-1}$) for the appropriate kinetic run.

Acknowledgement

One of us (A.M.A.A.-N.) thanks H. H. Sabah Al-Salem Al-Sabah for financial support.

1. R. B. Moodie. *In* Aromatic nitration. *Edited by* K. Schofield. Cambridge University Press, Cambridge. 1980. Chapt. 15.
2. W. N. White and J. R. Klink. J. Org. Chem. **42**, 166 (1977); W. N. White, H. S. White, and A. Fentiman. J. Org. Chem. **41**, 3166 (1976), and earlier papers in this series; W. N. White. *In* Mechanisms of molecular migrations. Vol. 3. *Edited by* B. S. Thyagarajan. Wiley–Interscience, New York. 1971. p. 109.
3. D. L. H. Williams. *In* Comprehensive chemical kinetics. Vol. 13. *Edited by* C. H. Bamford and C. F. H. Tipper. Elsevier, Amsterdam. 1972. Chapt. 3.
4. J. H. Ridd and J. P. B. Sandall. J. Chem. Soc. Chem. Commun. 261 (1982).
5. H. J. Shine, J. Zygmunt, M. L. Brownawell, and J. S. Filippo. J. Am. Chem. Soc. **106**, 3610 (1984).
6. K. J. P. Orton and C. Pearson. J. Chem. Soc. **93**, 725 (1908).

7. R. KAPTEIN. J. Chem. Soc. Chem. Commun. 732 (1971).
8. M. S. BLOIS, H. W. BROWN, and J. E. MALING. Neuvieme Colloque Ampere, Geneva: Librairie Payot, 242 (1960); cf. Landolt–Bornstein. Numerical data and functional relationships in science and technology. Vol. 9. *Edited by* K.-H. Hellwege. Springer Verlag, Berlin. 1980. Part d2, p. 28 et seq.
9. J. R. MORTON, K. F. PRESTON, and S. J. STRACH. J. Phys. Chem. **83**, 533 (1979).
10. A. H. CLEMENS, J. H. RIDD, and J. P. B. SANDALL. J. Chem. Soc. Perkin Trans. **2**, 1659 (1984).
11. N. A. PORTER, G. R. DUBAY, and J. G. GREEN. J. Am. Chem. Soc. **100**, 920 (1978).
12. D. SCHWEITZER and H. W. SPIESS. J. Magn. Reson. **16**, 243 (1974).
13. A. H. CLEMENS, J. H. RIDD, and J. P. B. SANDALL. J. Chem. Soc. Perkin Trans. **2**, 1667 (1984).
14. A. R. LEPLEY and G. L. CLOSS. Chemically induced magnetic polarisation. Wiley, New York. 1973. Chapt. 3.
15. W. N. WHITE and J. T. GOLDEN. J. Org. Chem. **35**, 2759 (1970).
16. K. J. P. ORTON and A. E. SMITH. J. Chem. Soc. **87**, 389 (1905).
17. B. CROSS and D. H. DAWE. U.S. Patent No. 4130645 (1978).
18. J. KOWALEWSKI, G. C. LEVY, L. F. JOHNSON, and L. PALMER. J. Magn. Reson. **26**, 533 (1977).

Organic reactions in liquid crystalline solvents. 4. Nanosecond laser flash photolysis studies of intramolecular motions of rod-like solutes in liquid crystals

WILLIAM J. LEIGH[1]

Department of Chemistry, McMaster University, Hamilton, Ont., Canada L8S 4M1

Received August 16, 1985

This paper is dedicated to Professor Arthur N. Bourns

WILLIAM J. LEIGH. Can. J. Chem. **64**, 1130 (1986).

The rates of triplet decay of a series of β-aryl-(4-alkoxypropiophenone)s in the smectic, nematic, and isotropic phases of 4′-butyl- and 4′-ethylbicyclohexyl-4-carbonitrile (BCCN and ECCN, respectively) have been measured over the 30–95°C temperature range by nanosecond laser flash photolysis. The rates of triplet decay for these probe molecules in fluid solution are governed by the rates of Cα—Cβ bond rotation, which allows intramolecular quenching of the carbonyl triplet state by the β-aryl ring. The ketones are substituted with alkyl groups of varying length, shape, and flexibility in the *para* positions of the β-phenyl (H, n-hexyl, cyclohexyl) and benzoyl (meth-, n-pent-, and n-octoxy) rings. With the exception of β-phenyl-(4-methoxypropiophenone), for each ketone the Arrhenius parameters for triplet decay in the smectic phase of BCCN are similar to those in the nematic phase of the same solvent, and in all cases, the Arrhenius plots exhibit perfect continuity at the S—N transition temperature. A solvation model is tentatively advanced to explain these results. In the nematic phase of BCCN, the Arrhenius activation energy and entropy are significantly more positive than those in isotropic ECCN for all the ketones studied, but variations in the energetics of triplet decay in the nematic phase as a function of solute structure are parallelled in the isotropic solvent. Thus, the inhibiting effect of the nematic solvent on the bond rotations leading to intramolecular triplet quenching in these probes is attributed to the predominant influence of microviscosity (viscous drag) effects; the presence of solvent orientational order appears to have little or no effect on the intramolecular mobility of these ketones. The results and conclusions of earlier studies of unimolecular reactions in nematic solvents are discussed in light of these results.

WILLIAM J. LEIGH. Can. J. Chem. **64**, 1130 (1986).

Faisant appel à la photolyse flash au laser dans le domaine des nanosecondes et opérant à des températures allant de 30 à 95°C, on a mesuré les taux de dégénérescence des triplets d'une série de β-aryl alkoxy-4 propiophénones dans des phases smectiques, nématiques et isotropes des butyl-4′ et éthyl-4′ bicyclohexylcarbonitriles-4 (BCCN et ECCN). Les taux de dégénérescence de ces molécules sondes dans des solutions fluides sont gouvernées par les vitesses de la rotation autour de la liaison Cα—Cβ qui permet un piégeage intramoléculaire de l'état triplet du carbonyle par le cycle β-arylique. Les positions *para* des groupements phényle (H, n-hexyle, cyclohexyle) ou benzoyle (méthoxy, n-pentoxy ou n-octoxy) des cétones sont substitués par les groupements alkyles indiqués qui ont diverses longueurs, formes et flexibilités. A l'exception de la β-phényl méthoxy-4 propiophénone, les paramètres d'Arrhénius de chacune des cétones, pour la dégénérescence de l'état triplet dans la phase smectique du BCCN, sont les mêmes que ceux mesurés dans la phase nématique du même solvant; de plus, dans tous les cas, les courbes d'Arrhénius présentent toutes une continuité parfaite à la température de transition S—N. Sur une base préliminaire, on suggère un modèle de solvatation pour expliquer ces résultats. Pour toutes les cétones étudiées dans la phase nématique du BCCN, les énergies et les entropies d'activation d'Arrhénius sont toutes beaucoup plus positives que celles mesurées dans la phase isotrope du ECCN; toutefois, les variations dans les facteurs énergétiques de la dégénérescence de l'état triplet dans la phase nématique, en fonction de la structure soluté, sont parrallèlles à celles observées dans le solvant isotrope. Ainsi, l'effet inhibiteur du solvant nématique sur les rotations des liaisons, qui conduit à un piégeage intramoléculaire du triplet dans ces sondes, est attribué à l'effet prédominant des effets de microviscosité (attraction visqueuse); l'influence de l'ordre orientationnel du solvant semble n'avoir que peu ou pas d'effet sur la mobilité intramoléculaire de ces cétones. A la lumière de ces résultats, on discute des résultats et des conclusions d'études antérieures sur des réactions unimoléculaires dans des solvants nématiques.

[Traduit par la revue]

Introduction

The effects of liquid crystalline order on the dynamics of uni- and bimolecular reactions of dissolved solutes is an area of increasing interest. Several investigations have examined the possible effects of these media on cyclization reactions, both thermally (2) and photochemically (3) induced. The premise behind these investigations is that the conformational mobility of a reactive molecule dissolved in an orientationally ordered solvent might be restricted in favour of those conformations which "fit" the best into the surrounding solvent framework. Nematic and smectic liquid crystals are formed by compounds whose molecular shape is rod-like,[2] and the dominant feature of the ordering in these materials is that the long molecular axes of the constituent molecules are oriented parallel to one another, on the average. Thus, cyclization of a similarly oriented, rod-like solute molecule is expected to be inhibited in a liquid crystal, to the extent that extended or rod-like conformations are favoured over those which are more globular (or less rod-like) in shape, and that formation of the globular conformer and subsequent transition state for cyclization involves some local disruption of liquid crystalline order.

With a couple of exceptions (*2e*, *3e*, *f*), the investigations reported to date have established only small or negligible effects of liquid crystalline solvents on the energetics of cyclization reactions. Several factors may be contributing to these results. The first (and most obvious) relates to the degree and rigidity of the orientational ordering in the various types of liquid crystals employed in these studies. Most have examined the effects of nematic or cholesteric liquid crystals on solute cyclization (*2a–d*, *3a–d*). These are the most fluid types of liquid crystalline phase, and their relatively low degree of orientational

[1]Natural Sciences and Engineering Research Council (Canada) University Research Fellow, 1983–1986.

[2]For comprehensive descriptions of the nature and properties of liquid crystals and leading references, see ref. 4.

ordering and rigidity is apparently insufficient to significantly inhibit the conformational mobility of solutes. On the other hand, the smectic types are more crystalline in character (4), with the result that substantial effects on cyclization energetics can be observed in these types of mesophase (2*e*, *f*, 3*e*, *f*).

The second factor which presumably contributes to the ability of liquid crystals to affect solute cyclization is the structure of the solute itself (5). Bulky, globular solutes have a more disruptive effect on macroscopic liquid crystalline order (as measured by mesophase transition temperatures) than do rod-like solutes (2*e*, 3*d*, 5, 6), an effect which is presumably the result of microscopic (in the vicinity of the solute) disruption of solvent order (3*e*, 5). This local isotropization of the solute's environment effectively truncates the potential effects of the ordered solvent on the solute's conformational (3*e*) or configurational (5) mobility. Recent results from our laboratory suggest that for smectic phases, the molecular length of the solute in relation to the smectic layer thickness may be an important factor in determining the extent to which solvent order inhibits the conformational mobility of the solute (7). In general, it appears that liquid crystalline effects on solute intramolecular motions are greatest for solutes whose sizes and shapes are similar to that of the solvent molecules (3*c*–*f*, 7).

While it is clear that solute mobility can be affected to some extent in nematic and cholesteric liquid crystals, it is difficult to ascertain the nature of the effect. Considering the rather high bulk viscosities of these mesophases (8), the magnitude of the effect which is generally observed (<3 kcal/mol in E_a; <5 eu in $\Delta S^{\ddagger}$) might just as reasonably be attributed to microviscosity (viscous drag) effects as to the presence of solvent order. In principle, a distinction between the two effects should be possible by comparing the conformational mobilities of a series of probes of varying molecular lengths in isotropic and liquid crystalline solvents. For a suitable series of probes, microviscosity effects should be revealed by parallel behaviour of the probes in the two solvents, while solvent order effects should be revealed by varying changes in probe dynamics in the two solvents depending on the structures of the probes.

A number of techniques have been used to investigate solute molecular mobility in liquid crystals, including nmr (9), esr (10), fluorescence decay (3*c*–*e*, 11), and nanosecond laser flash photolysis (3*f*, 7) methods. In particular, the latter two techniques are the most useful for investigating *intramolecular* solute motions, since such motions can be monitored directly by examining the dynamics of intramolecular excited state quenching processes, such as intramolecular excimer or exciplex formation (3*c*–*e*) or triplet quenching (7). These experiments involve measuring the competition between normal, unimolecular decay of the initially excited end of a probe molecule and its quenching by a moiety at the other end. As long as the quenching step occurs irreversibly, and at a rate which exceeds both those of collapse of the quenching geometry prior to quenching and the competing unimolecular decay process, then the observed rate of excited state decay reflects the rate(s) of the conformational changes which are required in order for quenching to occur.

The time scale over which a particular probe system is useful depends primarily on the excited state lifetime of the isolated chromophore in the absence of quencher. For fluorescence decay methods, this limits the usable time range to 1–250 ns. While this appears to be adequate for nematic and cholesteric phases, difficulties arise in smectic solvents, where bond rotations occur on a time scale which is apparently of the same order of magnitude (or perhaps longer) than the isolated lumophoric lifetime (3*e*). Nanosecond laser flash photolysis techniques allow the investigation of intrinsically longer-lived species, such as aromatic ketone triplet states, which affords more flexibility for monitoring the much slower rates of intramolecular quenching which may obtain in smectic phases.

Recently, we reported preliminary results of a nanosecond laser flash photolysis study of the effects of nematic and smectic solvent order on the triplet lifetime of β-phenyl-(4-methoxypropiophenone) (**1***a*) (7). β-Phenyl ketones such as **1***a* owe their photoinertness (12, 13) and unusually short triplet lifetimes (13, 14) to intramolecular quenching of the carbonyl triplet state via exciplex interactions between the β-phenyl ring and the carbonyl group (reaction [1]) (13–15).

[1] 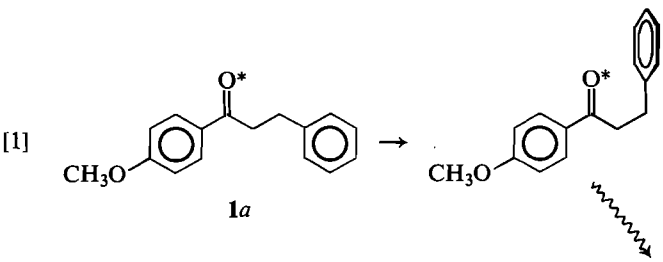

1*a*

Attainment of the quenching geometry, which requires rotation about the Cα—Cβ bond (13–17), is severely inhibited in the smectic phase of *trans*,*trans*-4′-butylbicyclohexyl-4-carbonitrile (BCCN); the activation energy and entropy for triplet decay of **1***a* are 12 kcal/mol higher and 35 eu more positive, respectively, relative to their values in a model isotropic solvent (*trans*,*trans*-4′-ethylbicyclohexyl-4-carbonitrile, ECCN). In the nematic phase of BCCN, E_a and $\Delta S^{\ddagger}$ were found to be 1.5 kcal/mol and 4 eu more positive, respectively, than their values in isotropic ECCN.

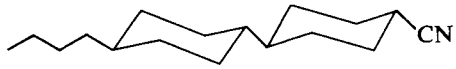

BCCN

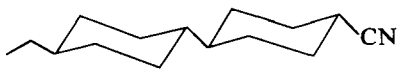

ECCN

The similarity between the molecular shapes of **1***a* (in its *trans*-conformation) and BCCN-type analogues, and the ease with which solute structural features can be altered via appropriate substitution, make this system a seemingly ideal probe with which to examine how the conformational mobility of solutes in liquid crystals depends on solute length and substituent shape and flexibility. To this end, we have synthesized a series of β-aryl-(4-alkoxypropiophenone)s (**1**–**3**) and measured their triplet lifetimes as a function of temperature in the smectic, nematic, and isotropic phases of BCCN and ECCN by nanosecond laser flash photolysis. The results of this study are reported below.

Results

The substituted β-phenylpropiophenones (**1**–**3**) were prepared by condensation of 4-hydroxy- or 4-methoxyacetophenone with the appropriate *para*-substituted benzaldehyde (18), hydrogenation of the resulting α,β-unsaturated ketones over Raney nickel, and alkylation of the β-aryl-(4-hydroxypropio-

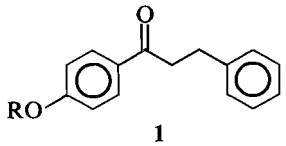

1

a, R = CH_3
b, R = $CH_2(CH_2)_3CH_3$
c, R = $CH_2(CH_2)_6CH_3$

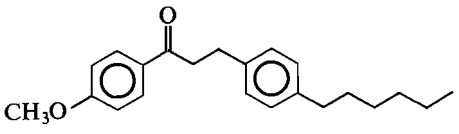

2

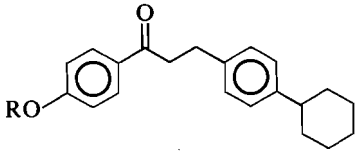

3

a, R = CH_3
b, R = $CH_2(CH_2)_3CH_3$
c, R = $CH_2(CH_2)_6CH_3$

phenone) with the appropriate alkyl bromide or dialkyl sulfate. The ultraviolet absorption and phosphorescence emission spectra of each of these compounds are similar to those of the parent compound **1***a*.

Transition temperatures for BCCN, ECCN, and mixtures ca. 0.04 molal (1 mol%) in each of the ketones studied were measured by thermal microscopy and are listed in Table 1.

The ultraviolet absorption spectra of **1***a* in methylcyclohexane, acetonitrile, and isotropic BCCN are shown in Fig. 1. The spectra of this compound as non-oriented solutions in the nematic and smectic phases of BCCN (prepared by simple cooling of the isotropic melt) were indistinguishable from that in the isotropic phase.

Laser flash photolysis experiments were carried out using the pulses (337.1 nm, <10 mJ, ~8 ns) from a nitrogen laser for excitation, and monitoring transient absorptions using a system with nanosecond time response (19). Samples for these experiments were ~1.0 mol% solutions of the ketones in BCCN and ECCN, and were contained in Pyrex cells of 0.7 mm pathlength. Optical densities of the isotropic solutions were in the range of 0.15–0.20 at the excitation wavelength. Liquid crystalline samples were prepared by normal cooling from the isotropic melts. Smectic samples prepared in this way were typically somewhat opaque and caused considerable scattering of the monitoring light, which necessitated more extensive signal averaging (compared to nematic and isotropic samples) in order to obtain reproducible decay traces. Annealing these samples at 40°C for 2–7 days results in homeotropically aligned samples, which are much more suitable for transient absorption measurements within a limited temperature range (40 ± 6°C). Above and below this temperature range, the glassy samples develop imperfections and turn opaque. Triplet lifetimes from annealed samples were identical to those obtained from unannealed ones, within experimental error. The former yield pseudoisotropic nematic phases upon warming; the characteristic turbid appearance of the nematic phase could be obtained by simple agitation of the sample cell.

Transient absorption spectra, recorded for **1***b* and **3***a* in the nematic phase of BCCN (~60°C), are shown in Fig. 2. These

TABLE 1. Transition temperatures for pure BCCN and ECCN and mixtures doped with 1 mol% **1–3** and MAP[a]

	BCCN		ECCN	
Ketone	Sm–N	N–I	Sm–N	N–I
None	53.5–54	80	46–46.5	48.5
1*a*	52.5–53	78.5–79	45–45.5	47.5–48
1*b*	51.5–52	77–77.5	45–45.5	46.5–47
1*c*	51–52	77–77.5	45–45.5	46.5
2	51.5–52.5	77–77.5	44.5–45.5	47–47.5
3*a*	52–52.5	78–78.5	44.5–45.5	47.5
3*b*	50.5–52	77–77.5	45–45.5	47–47.5
3*c*	51–52	77–77.5	45.5–46	47–47.5
MAP	51.5–52.5	78–78.5	45–45.5	47.5

[a]Measured by thermal microscopy. Temperatures are in °C and are corrected.

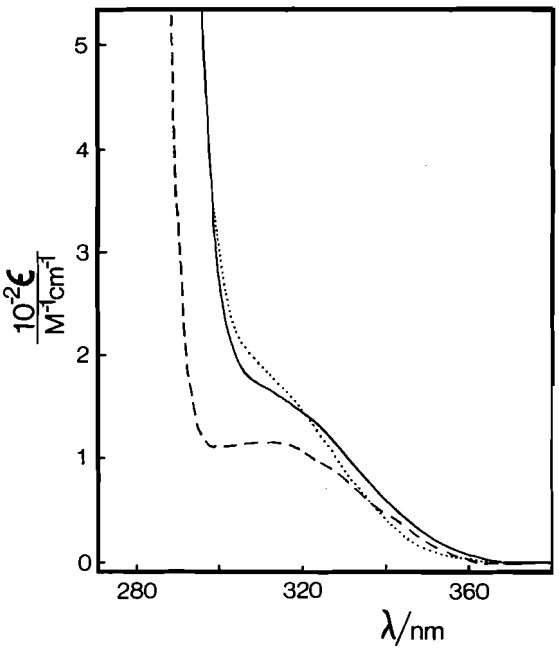

FIG. 1. Ultraviolet absorption spectra of **1***a* in methylcyclohexane (---), acetonitrile (···), and the isotropic phase of BCCN (—).

spectra, as well as those of the other ketones studied (**1***a*, *c*, **2**, and **3***b*, *c*) agree well with that previously reported for the triplet state of **1***a* (17*a*, 20).

The triplet states of **1–3**, monitored at 390 nm, decayed with clean first-order kinetics in every case. Representative decay traces, recorded for **1***b* and **3***a* in nematic BCCN (60°C), are included as inserts in Fig. 2. Generally, the transient absorptions decayed completely to baseline, although residual absorption did occur occasionally in the smectic phases. These absorptions were irreproducible and resulted in slightly larger errors in the calculated decay rates.

For each ketone, the triplet decay was monitored at several temperatures between 30 and 95°C in both BCCN and ECCN. Arrhenius plots of $-\log \tau_T$ versus $1/T$ in the two solvents are shown in Figs. 3 and 4 for **1***c* and **3***a*, respectively. With the exception of **1***a* in BCCN (7), and possibly **3***c* in the same solvent, the data appear to fit to a single line in each case. Arrhenius parameters for triplet decay in the nematic and smectic phases of BCCN and the isotropic phase of ECCN,

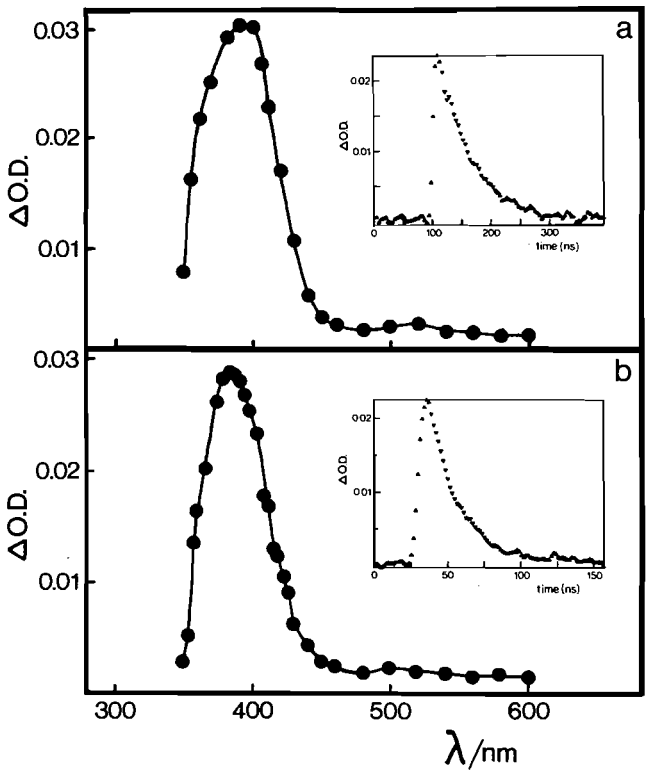

FIG. 2. Triplet–triplet absorption spectra of (*a*) **1***b* and (*b*) **3***a* in nematic BCCN, recorded at 58°C. Inserts: Representative decay traces, monitored at 390 nm for (*a*) **1***b* at 57°C and (*b*) **3***a* at 61°C.

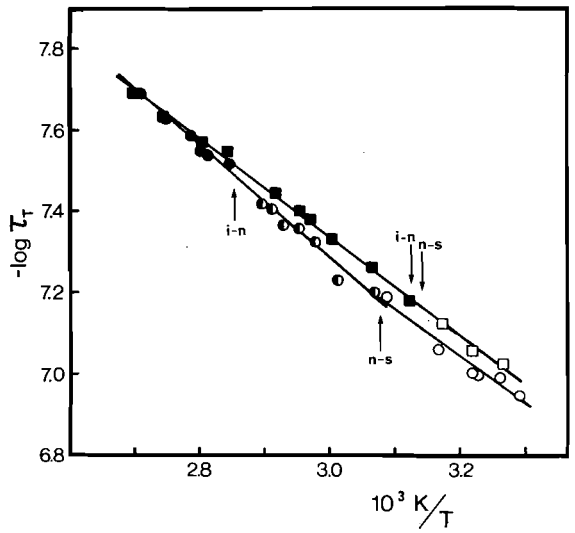

FIG. 3. Arrhenius plot ($-\log \tau_T$ vs. $1/T$) for triplet decay of **1***c*, monitored at 390 nm, in the nematic and smectic phases of BCCN (●) and the isotropic and smectic phases of ECCN (■). Open symbols denote smectic phase, half-symbols denote nematic phase, and closed symbols denote isotropic phase results. Transition temperatures for the mixtures are indicated.

obtained from least squares analysis of the data for each ketone, are summarized in Table 2. Entropies of activation, $\Delta S^{\ddagger}$, were obtained from standard Eyring plots of the same data. The errors listed in Table 2 for E_a, log A, and $\Delta S^{\ddagger}$ are listed as $\pm 2\sigma$ (i.e. 95% confidence limits), as obtained from the least squares analyses. Table 2 also includes triplet lifetimes for each ketone

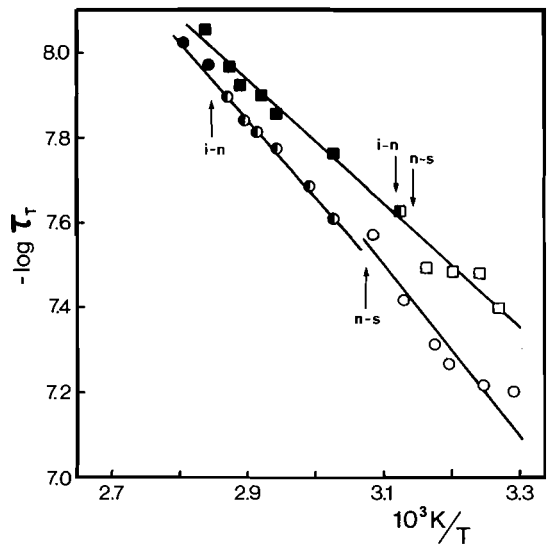

FIG. 4. Arrhenius plot ($-\log \tau_T$ vs. $1/T$) for triplet decay of **3***a*, monitored at 390 nm, in the nematic and smectic phases of BCCN (●) and the isotropic and smectic phases of ECCN (■). Open symbols denote smectic phase, half-symbols denote nematic phase, and closed symbols denote isotropic phase results. Transition temperatures for the mixtures are indicated.

in nematic and smectic BCCN and isotropic ECCN at 30 and 50°C, calculated from the corresponding Arrhenius parameters.

Owing to the limited temperature range over which we are able to obtain data in the isotropic phase of BCCN, we have employed ECCN as the model isotropic solvent with which to compare the behaviour of **1**–**3** in nematic and smectic BCCN. While ECCN is isotropic only above 48°C, the isotropic phase Arrhenius parameters reported in Table 2 were obtained from analysis of the ECCN data *over the full temperature range studied* (30–90°C). This treatment is justified on the basis that separate analysis of the smectic and isotropic phase data for this solvent yields identical Arrhenius parameters for each of the ketones studied. Similarly, the limited number of data points obtained in isotropic BCCN are indistinguishable from the nematic phase data in each case, and thus the two sets were combined and analysed as one to obtain the nematic phase Arrhenius parameters. For BCCN, separate calculations were performed for nematic and smectic phase data, even though in most cases (**1***b*, *c*, **2**, and **3***a*, *b*) triplet behaviour appears to be phase independent. This apparent phase independence *may* be the result of the somewhat greater scatter in the smectic phase data, caused by the usual semi-opaque nature of these samples.

Triplet lifetimes were also measured for 4-methoxyacetophenone (MAP) in the smectic, nematic, and isotropic phases of BCCN and ECCN by laser flash photolysis, and the results are plotted in Fig. 5. The factor of ca. 10 shorter lifetime of MAP in the isotropic and nematic phases of these solvents compared to those in smectic BCCN is presumably the result of more efficient impurity quenching in the former phases, reflecting their considerably lower viscosities relative to those of smectic BCCN (8).

Discussion

The triplet lifetime of β-phenylpropiophenone in fluid solution at room temperature is exceedingly short (ca. 1 ns (14)), and it is now reasonably well established that this is the result of efficient intramolecular deactivation via exciplex interactions

TABLE 2. Activation parameters and extrapolated triplet lifetimes for the triplet decay[a] of **1–3** in the nematic[b] and smectic phases of BCCN and the isotropic phase of ECCN[c]

Ketone	Phase	$\tau_T^{60°}$ (ns)	$\tau_T^{30°}$ (ns)	E_a (kcal/mol)	log A (s^{-1})	$\Delta S^{\ddagger}$ (eu)[d]
1*a*	Isot	34	74	5.2±0.3	10.9±0.2	−10.9±0.8
	Nem	41	113	6.7±0.3	11.8±0.2	−6.7±0.8
	Sm	28	346	16.7±1.3	18.5±1.1	24±4
1*b*	Isot	46	100	5.3±0.3	10.8±0.2	−11.8±1.3
	Nem	53	138	6.4±0.6	11.5±0.3	−8.1±1.8
	Sm	54	120	5.3±1.4	10.8±1.0	−11.4±4.6
1*c*	Isot	47	106	5.5±0.2	10.9±0.1	−10.7±0.5
	Nem	52	133	6.2±0.3	11.4±0.2	−8.7±1.1
	Sm	54	118	5.2±1.3	10.7±0.9	−11.8±4.1
2	Isot	14	34	5.8±0.5	11.7±0.4	−7.3±1.6
	Nem	19	58	7.4±0.9	12.6±0.6	−4.1±1.5
	Sm	19	54	7.1±2.5	12.4±1.8	−4±8
3*a*	Isot	16	44	6.6±0.4	12.1±0.3	−5.1±1.2
	Nem	22	77	8.3±0.7	13.1±0.4	−0.3±1.5
	Sm	19	85	9.9±3.1	14.2±2.1	5±10
3*b*	Isot	23	61	6.6±0.4	12.0±0.4	−5.9±1.3
	Nem	30	108	8.6±0.6	13.2±0.4	−1.1±1.0
	Sm	27	106	9.1±1.7	13.5±1.1	1±5
3*c*	Isot	22	58	6.4±0.6	11.8±0.5	−7.0±2.0
	Nem	31	104	8.0±0.6	12.7±0.4	−2.5±1.9
	Sm	28	123	9.8±0.9	14.0±0.8	3.4±2.8

[a]Measured by laser flash photolysis. Errors are quoted as $\pm 2\sigma$.
[b]Analyses performed using the data for both isotropic and nematic phases of this solvent.
[c]Analyses performed using the combined data for all phases of this solvent.
[d]Calculated from standard Eyring plots.

between the carbonyl group and the β-phenyl ring (14–16) (see reaction [1]). The activation energy for triplet decay of this molecule in fluid solution (2.3 kcal/mol (14)) is approximately that for rotation about the Cα—Cβ bond (14, 21); that these bond rotations are necessary for intramolecular quenching to occur is demonstrated by the fact that when the molecule is incorporated in zeolites (of such dimensions that the solute can reside in the channels only when it assumes the *trans*-conformation), the triplet lifetime is extended to ca. 2 ms at room temperature and phosphorescence is observed (16).

Ketones such as **1–3** have lowest π,π* triplet states (17*a*, 20), and the somewhat longer triplet lifetime and higher activation energy for triplet decay of **1***a* relative to that observed for β-phenylpropiophenone in fluid solution has lead to the conclusion that like the Norrish Type I and Type II reactions (22), β-phenyl quenching *requires* the proximity of the n,π* state (17*a*). This introduces an extra energy requirement for the process in addition to that of the bond rotations involved in assuming the correct quenching geometry, viz., thermal population of the n,π* triplet state. Accordingly, the activation energy for triplet decay of **1***a* in fluid solution (4.4 kcal/mol in toluene) and that of β-phenylpropiophenone in the same solvent (2.3 kcal/mol) corresponds roughly to the energy difference between the π,π* and n,π* triplet states of **1***a* (17*a*).

The triplet lifetime of 4-methoxyacetophenone (MAP) in BCCN and ECCN is 50–80 times greater than that of **1***a* under the same conditions of temperature and solvent phase, as comparison of the lifetime data in Table 2 and Fig. 5 shows. Furthermore, the fact that samples of **1***a* have been subjected to prolonged irradiation in these solvents with no apparent change in the appearance of the triplet decay profile or lifetime attests to the expected (14, 17*b*) photoinertness of these compounds.

These results indicate that the observed triplet decay rates for **1–3** in liquid crystalline as well as isotropic solution are dominated by unimolecular decay processes, and that bimolecular quenching by adventitious impurities or hydrogen abstraction from the solvent is unimportant. As well, these results demonstrate that the observed Arrhenius parameters for triplet decay of **1–3** in the various phases of BCCN and ECCN reflect the energetics of those molecular motions which must occur in order for the correct geometry for β-phenyl quenching to be attained. These motions are, presumably, Cα—Cβ bond rotation (interconverting *trans*- and *gauche*-conformers) and Cβ—C_{phenyl} bond rotation (which brings the β-phenyl group into a position such that its π-system overlaps with the carbonyl n-orbital).

Solvent properties

The dominant feature of the molecular ordering in liquid crystals is that the long molecular axes of the constituent molecules are oriented parallel to one another, on the average.[2,3] In nematic phases, this is the only type of ordering present, and hence these are the most fluid type of liquid crystalline phase. While molecular tumbling is on the whole anisotropic in these phases, the constituent molecules undergo nearly free rotation about their long molecular axes (24). In smectic phases, the constituent molecules are further arranged in layers in which the orientational vector is at some angle, or perpendicular, to the plane of the layer. Several types of smectic phases are known, and these are characterized according to the

[3]For the sake of brevity, we confine our discussion to smectic, nematic, and cholesteric phases of rod-like mesogens. The molecular ordering in discotic liquid crystals is quite different. For a review of this type of liquid crystal, see ref. 23.

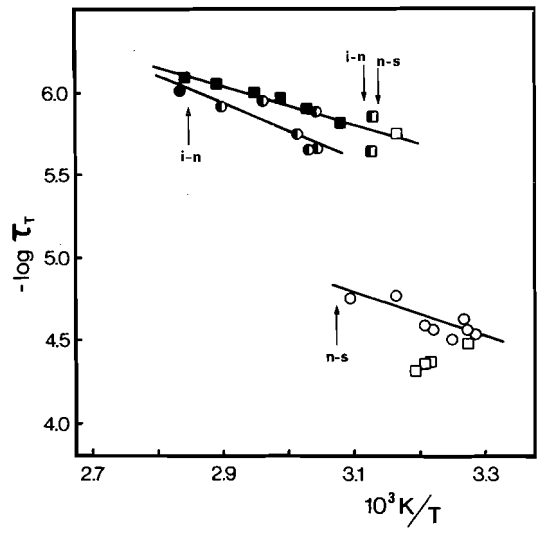

FIG. 5. Arrhenius plot ($-\log \tau_T$ vs. $1/T$) for triplet decay of MAP, monitored at 390 nm, in the nematic and smectic phases of BCCN (●) and the isotropic and smectic phases of ECCN (■). Open symbols denote smectic phase, half-symbols denote nematic phase, and closed symbols denote isotropic phase results. Transition temperatures for the mixtures are indicated.

nature of the molecular packing within the layers (25). In smectic A phases for example, the packing within the layers is nematic-like; thus, this type of smectic phase might be expected to resemble a nematic phase with respect to its effects on the motions and unimolecular reactivity of dissolved solutes. The smectic B phase is more crystalline in nature; within the layers, the constituent molecules are hexagonally close-packed (25).

BCCN forms a single smectic phase between 29–54°C and a nematic phase between 54–79°C, while ECCN is smectic between 28–44°C, nematic between 44–48°C, and is an isotropic liquid at temperatures above 48°C (26). The smectic phases of these two compounds have not yet been conclusively assigned with respect to mesomorphic type. X-ray diffraction studies have been carried out with the homologous *trans,trans*-4′-propylbicyclohexyl-4-carbonitrile (PCCN), a polymorphic smectic (26), from which it has been established that the high temperature smectic modification of this compound is Sm B (27). Thermal microscopy (28, 29) and DSC investigations with mixtures of BCCN/PCCN and BCCN/ECCN indicate that BCCN forms a smectic phase of similar but higher order than the SmB phase of PCCN, and that the smectic phase of ECCN is of even higher order than that of BCCN (28).

Incorporation of a solute in a liquid crystal results in some degree of disruption of solvent order in the vicinity of the solute (2*e*, 3*d*, 5, 6), the extent of which depends on the structure of the solute in relation to that of the mesogen (6), and is reflected in the transition temperatures of the liquid crystalline mixture (6, 30). Rigid, rod-like solutes tend to be oriented in a liquid crystal with their long axes parallel to those of the solvent (31). Flexible molecules cause more disruption of local order, and may be oriented to a lesser extent than rigid solutes (9*g*). Nevertheless, while such solutes retain a high degree of conformational mobility in liquid crystals, the conformational distribution is altered relative to that in isotropic solvents in favour of those conformers which are most compatible with solvent ordering (9*g*).

The transition temperatures listed in Table 1 for the ketone-doped samples of BCCN and ECCN indicate that incorporation of 1 mol% of each of the ketones studied has pronounced effects on both the Sm → N and N → I transition temperatures of the two mesogens. n-Alkyl substituents at either end of **1***a* (compare **1***a* with **1***b*, *c* and **2**) apparently result in somewhat greater disruption of local solvent order than a cyclohexyl substituent (cf. **1***a* and **3***a*) does. This is to be expected (6) considering the conformational motions available to the flexible alkyl chains compared to the relatively rigid cyclohexyl group, and the fact that the size and shape of the β-(4-cyclohexylphenyl) group in **3***a–c* is very similar to that of the solvent molecules.

The ultraviolet absorption spectra of **1***a* shown in Fig. 1 reveal that chromophore solvation in BCCN and ECCN is more like that in acetonitrile than in methylcyclohexane. Presumably, the fact that the position of the π,π* absorption is shifted to longer wavelengths in acetonitrile from its position in methylcyclohexane while the n,π* band is unaffected suggests that solvation in the nitrile solvents is such that there are strong interactions between the CN-group of the solvent and the benzoyl π-system.

The behaviour of 1–3 in nematic BCCN

Variation in the length and flexibility of the alkoxy substituent (**1***a–c*) has no effect on the Arrhenius parameters for triplet decay in either the nematic phase of BCCN or in isotropic ECCN, although the activation energy for decay in the nematic solvent (E_a^{nem}) is consistently higher than that in the isotropic solvent (E_a^{isot}). The same trend is observed in the nematic and isotropic phase data for the homologous series **3***a–c*. This indicates that increasing the length of the alkoxy group with flexible substituents has no effect on the ability (albeit slight) of the nematic solvent to impede the bond rotations leading to β-phenyl quenching. Averaging the differences between E_a^{nem} and E_a^{isot} and between $\Delta S^{\ddagger}$ values in the nematic and isotropic solvents over all the ketones studied yields $\Delta E_a = 1.4 \pm 0.5$ kcal/mol and $\Delta(\Delta S^{\ddagger}) = 3.9 \pm 1$ eu.

On the other hand, increasing the size of the β-aryl group within the series of 4-methoxy ketones **1***a*, **2**, and **3***a* results in continuous increases in both E_a^{nem} and E_a^{isot}, and similar trends are observed in $\Delta S^{\ddagger}$ (to more positive values). Along with the trends in the Arrhenius parameters observed for **1***a–c* and **3***a–c*, this suggests that solvation of the probes in these two solvents is such that solvent–solute interactions are strongest at the benzoyl end. This conclusion is supported by comparison of the uv absorption spectra of **1***a* in BCCN, acetonitrile, and methylcyclohexane. Thus, the benzoyl end of the ketone is apparently "anchored", and the β-aryl group constitutes the more mobile portion of the molecule. As the size of the mobile portion increases, the activation energy and entropy for intramolecular quenching tend to more positive values. This appears to be the case in both isotropic and nematic phases.

An explanation for the substituent effect on the energetics of β-phenyl quenching observed for **1***a*, **2**, and **3***a* which is based on a substituent effect on the quenching step (i.e. that which occurs after the correct geometry has been attained) can be discounted. Substitution on the β-phenyl ring by electron-donating substituents might be expected to increase the rate of intramolecular quenching of the electron-deficient n,π* triplet state. While the somewhat shorter triplet lifetimes of **2** and **3** compared to that of **1** in the isotropic solvent appear to be consistent with this, examination of the trends in E_a and $\Delta S^{\ddagger}$ show that this cannot be the origin of the observed substituent effect on τ_T. It is known that an increase in the activation energy

for an endothermic quenching process is accompanied by a *decrease* in the entropy of activation (a higher enthalpic requirement for quenching demands a tighter activated complex) (32). The trend to more positive $\Delta S^{\ddagger}$ values as E_a^{isot} increases which is observed for **1***a*, **2**, and **3***a* is clearly consistent with Cα—Cβ and Cβ—C_{phenyl} bond rotations being rate determining, since both will tend to more positive values as the viscous drag of the solvent on intramolecular motion increases. This provides further support for the explanation of the lack of a clear trend in the τ_T values for a series of β-arylpropiophenones with lowest n,π* triplet states (17*a*), from which it was concluded that bond rotations, and not the actual quenching process, form the rate determining step for β-phenyl quenching.

The effect of an ordered environment such as that found in liquid crystals on the intramolecular and diffusive mobility of solutes can be the result of microviscosity (viscous drag) effects or orientational ordering effects, or some combination of the two. Ultimately, the effects of high microviscosity and solvent orientational order on the Arrhenius parameters for solute motions are the same; E_a will increase and $\Delta S^{\ddagger}$ will become more positive as molecular motions become more difficult and require greater displacement of the surrounding solvent matrix, whether it is ordered or not. Solvent microviscosity will heighten the barrier to conformational interconversions only as a result of effects on the transition state energy; it should have little or no effect on the relative energies of the ground state conformers. On the other hand, solvent orientational order will affect the energies of both the ground state conformers (9*g*) and the transition state for their interconversion (2*e*, 3*c*–*e*, 5, 6). In the present case, the presence of solvent order should stabilize the rod-like *trans*-conformer and destabilize the transition state for formation of the quenching (*gauche*-like) geometry.

It is important to note that the Arrhenius parameters for triplet decay of **1**–**3** obtained by the present method represent average values over all conformations present in solution. If microviscosity alone is responsible for the observed effects on the triplet decay of **1**–**3** in nematic BCCN, then parallel changes in activation parameters in the nematic and isotropic solvents with changes in solute structure should be observed. On the other hand, if solvent order plays the dominant role, then the difference between the activation parameters for triplet decay in nematic and isotropic phases should vary depending on solute structure, if the difference in conformational distribution between nematic and isotropic phases varies with solute structure. Clearly, the results obtained for **1**–**3** in nematic BCCN and isotropic ECCN indicate that microviscosity effects are almost entirely responsible for the slightly higher E_a and more positive $\Delta S^{\ddagger}$ for solute bond rotations in the nematic phase. Either solute conformational energies are not altered enough in the nematic relative to isotropic phase to significantly contribute to the increase in activation parameters, or the changes do not vary appreciably throughout the series **1**–**3**.

The behaviour of ***1***–***3*** *in smectic BCCN*

The ability of the smectic phase of BCCN to inhibit β-phenyl quenching is strongly dependent on the structure of the probe (7). Inhibition is strong for probes which are shorter than (i.e. **1***a*) (7) or of a similar length to BCCN (28). For probes such as **1***b* and **1***c*, which are longer than BCCN, triplet decay is phase-independent (or almost so); this demands that the nature of the solvation of such probes in this smectic phase is much different than that experienced by **1***a*. The results imply that the environment experienced by **1***b* and **1***c* in smectic BCCN is essentially isotropic (or perhaps nematic; *vide infra*) with respect to its effects on the conformational mobility of the solute, although *bulk* smectic order is preserved in the samples.

Other workers have observed analogous variations in solute behaviour in smectic solvents as a function of solute structure. The product distribution from the Norrish Type II reaction of phenylalkyl ketones in smectic n-butyl stearate varies quite dramatically with reactant length; the effect of smectic solvent order in this case is greatest when the reactive solute is similar in length to the mesogen, and falls off as the solute increases or decreases from this optimal length (3*f*). Electron spin resonance investigations of nitroxide spin probes in smectic phases have led to the suggestion that, depending on solute/solvent structural relationships, solutes can reside in either the relatively rigid, core portion of the layers or the more fluid, hydrocarbon interlayer region (10*c*, *f*), or be partitioned between the two (10*b*). Solute mobility is very different in these two regions. For small solutes, mobility can apparently be greater in Sm B phases than in the lower order Sm A types (10*b*). This has been attributed to the solute residing in cavities in the hydrocarbon interlayer region, which become better-defined and afford less restriction to solute motion as the region increases in its overall rigidity.

BCCN is not a typical smectogen, in that the relatively short n-butyl end-chain does not allow for as much fluidity in the interlayer region as is usually the case in smectic phases (4). The Sm B phase of PCCN is regarded as being more crystalline in character than typical Sm B phases (27). This is the result of intercalation of the short n-propyl end-chains of one layer with nitrile groups in the next. For smectic BCCN, it thus seems unlikely that a solute which is unable to be incorporated unobtrusively *within* a smectic layer might reside instead in the interlayer region; there is simply just not enough room.

The perfect continuity in the Arrhenius plots for triplet decay of **1**–**3** at the S–N transition temperature may offer a clue as to the nature of the solvation of these probes in the smectic phases of both BCCN and ECCN, and allow a tentative explanation for the behaviour of **1**–**3** in these solvents. Normally, properties affected by diffusive mobility or viscosity are substantially altered at the S–N transition (4, 8*b*). The drastic change in the triplet lifetime of MAP at this transition (Fig. 5) is a perfect example of this behaviour; since the lifetime in this case is determined by impurity (e.g., oxygen) quenching, the large difference in the viscosities of the nematic and smectic phases (8) results in substantial differences in triplet lifetime in the two phases. The similar lifetimes above and below the bulk S–N transition temperature observed for **1**–**3** indicate that the microviscosity of the probes' *local* environment does not change detectably at the phase transition.

For all the probes studied except **1***a*, the results suggest that in the smectic phases of BCCN and ECCN, the local probe environment retains the order that was present in the nematic phase. Thus, the solvation shell for **1***b*–**3***c* in these smectic phases might be viewed as a small, isotropized nematic "pool" surrounded by the bulk smectic phase. In each case, the effective microviscosity in the solvation shell depends on probe structural features. Probes with long, flexible substituents create more disorder and a less compact solvation shell, with microviscosity similar to that in the bulk nematic phase. Elongated probes with inflexible, solvent-like substituents (**3**) experience a slightly greater microviscosity since the overall shape change in proceeding to the quenching geometry is more pronounced.

In the smectic phase of ECCN, these solvation pools may be intrinsically larger or better-defined than in BCCN, because the more crystalline-like interlayer packing renders the bulk smectic phase less miscible with the disordered regions surrounding the solute molecules. We note that the disordered microenvironment in a probe molecule's vicinity can only involve a few solvent molecules (certainly less than about ten) in order to maintain bulk smectic order at the high probe concentrations employed. The above description is essentially that of a mixed phase system, consisting of a ketone-rich nematic phase in coexistence with the smectic phase of the pure solvent.

In the case of **1***a* in BCCN, there is clearly a microscopic change in solvent phase which accompanies the bulk N → S phase transition, but the difference in local microviscosity just below the transition is apparently negligible. This is surprising, considering the very much higher degree of order and rigidity present in the smectic phase of pure BCCN relative to the nematic (27, 28). Further experiments are clearly necessary in order to conclusively define the nature of the solvation of **1** in this phase.[4]

Summary and conclusions

The Arrhenius parameters for triplet decay of a series of β-aryl-(4-alkoxypropiophenone)s reflect those of the simple conformational motions which allow intramolecular quenching of the carbonyl triplet state, and are significantly affected in the smectic and nematic phases of BCCN relative to their values in the isotropic phase of ECCN. The probes vary in the size and flexibility of substituents, and in their completely extended conformations, vary over a factor of two in length. Smectic solvent order results in large increases in E_a and $\Delta S^{\ddagger}$ for small, relatively compact probes, small increases for probes bearing a large inflexible substituent, and has no effect on the Arrhenius parameters for triplet decay of probes with flexible, long-chain alkyl substituents. The perfect continuity in the Arrhenius plots at the S–N transition temperature of BCCN suggests that for probes longer than the smectic layer thickness, their microenvironment in the smectic phase is similar to that in the nematic phase.

In the nematic phase, E_a and $\Delta S^{\ddagger}$ are consistently ca. 1.5 kcal/mol and 4 eu higher, respectively, than the corresponding values in the isotropic solvent. Variation of the alkoxy substituent has no effect on the Arrhenius parameters, while variation of the β-aryl substituent results in systematic increases with substituent size and rigidity. Parallel effects are observed in the isotropic phase, which leads to the conclusion that higher microviscosity, and not an orientational ordering effect, is responsible for the slight inhibition to solute conformational motion in the nematic phase relative to that in isotropic solvents.

From the present results, and previous studies of unimolecular reactions in nematic and cholesteric phases (2, 3), several conclusions can be derived with respect to the ability of these types of liquid crystals to inhibit intramolecular motion. It appears that the most one can expect in the way of an effect on the activation energy for such a process is about 3 kcal/mol, and it is likely that this is almost solely the result of microviscosity effects. Furthermore, an effect can only be expected when substantial changes in the *overall* shape of the molecule occur on the way to the transition state for reaction. The result that nematic solvents have no effect on the energetics of the Claisen rearrangement of cinnamyl phenyl ether (2*c*), for example, can be readily explained in this context; examination of molecular models shows that the bond rotations which interconvert the fully extended conformation of this molecule and that in the transition state for cyclization do not in fact alter the overall rod-like shape of the molecule appreciably. This same explanation can rationalize the small effects of cholesteric and compensated nematic solvents on the Norrish Type II reaction of α-diketones (3*a*).

Further investigation of the balance between solute/solvent structural features and the ability of smectic phases to inhibit the intramolecular mobility of solutes is in progress and will be reported in the near future.

Experimental

Melting points and transition temperatures were measured on a Reichert micro-hot stage microscope with polarizing lenses and are corrected. ^{1}H nmr spectra were recorded in deuterochloroform solution on a Varian EM390 nmr spectrometer, and are reported in parts per million downfield from TMS. Infrared spectra were recorded on a Perkin-Elmer Model 283 infrared spectrometer, and are reported in wavenumbers, calibrated against the 1601.8 cm^{-1} polystyrene absorption. Mass spectra were recorded on a VG Micromass 70-70F mass spectrometer, and exact masses have been calculated using an atomic mass of 12.00000 for carbon. Ultraviolet absorption spectra were recorded on a Hewlett Packard HP-8451 spectrometer.

Laser flash photolysis experiments employed the computerized facility which has been described in detail elsewhere (19), and the pulses (337.1 nm, ~8 ns, <10 mJ) of a nitrogen laser for excitation. Sample temperatures were recorded using a calibrated platinum thermometer, and are considered accurate to ±0.5°C. Samples of **1–3** as ~1.0 mol% solutions in BCCN and ECCN were contained in 0.7 mm × 7 mm rectangular Pyrex (Vitro Dynamics) sample cells. They were prepared by adding an aliquot of a standard solution of the ketone in dichloromethane to a cell by microlitre syringe, evaporating off the solvent with a stream of nitrogen, and then weighing the required amount of the mesogen into the cell. The samples were then either sealed with rubber septa and deoxygenated by bubbling dry nitrogen through the isotropic melts or subjected to three freeze–pump–thaw degassing cycles followed by sealing on a high vacuum line (10^{-3} Torr). Decay of laser-generated transients was monitored by uv absorption. The optical densities of the isotropic solutions were in the range 0.15–0.20 at 337 nm. While the isotropic solutions were optically clear at the transient monitoring wavelength (390–395 nm), and the nematic solutions almost so, the smectic samples generally had optical densities in the range 0.6–1.3 as a result of light scattering. For the smectic samples, decay traces represent the average of 40–60 shots, each corrected for background scattering from the excitation pulse. Annealing the smectic samples at 40°C for 2–7 days results in homeotropically aligned (i.e. glassy) samples, which have considerably better light transmission characteristics. The triplet lifetimes obtained using these samples do not differ significantly from the lifetimes obtained from the samples used immediately after cooling from the isotropic melts.

Methylcyclohexane (BDH Omnisolv), acetonitrile (Caledon HPLC), and dichloromethane (Caledon HPLC) were used as received. 4′-Butylbicyclohexyl-4-carbonitrile (BCCN; EM Licristal ZLI1538) and 4′-ethylbicyclohexyl-4-carbonitrile (ECCN; EM Licristal ZLI1537) were used as received from E. Merck, Co. 4-Methoxyacetophenone (Aldrich) used for laser flash photolysis experiments was recrystallized twice from methanol.

4-(n-Hexyl)benzaldehyde (bp 118–119°C, 3 mm Hg) and 4-cyclo-

[4]NOTE ADDED IN PROOF: The 4-ethoxy and 4-propoxy derivatives of **1** also show phase dependent behaviour in BCCN. However, the break in the Arrhenius plot does not occur at the bulk N → S transition temperature; rather it moves to progressively lower temperatures with increasing alkoxy chain length. The behaviour of the 4-^{n}butoxy derivative is phase independent (27).

hexylbenzaldehyde were prepared by formylation of 1-phenylhexane and cyclohexylbenzene (Aldrich), respectively, with hexamethylenetetramine in trifluoroacetic acid (33). The 4-cyclohexylbenzaldehyde that was obtained as a yellow oil after column chromatography of the crude reaction mixture on silica gel exhibited ^{1}H nmr, infrared, and mass spectra that were consistent with its structure. It was used without further purification or characterization.

The β-phenyl ketones **1***a* and **3***a* were prepared by condensing 4-methoxyacetophenone with benzaldehyde and 4-cyclohexylbenzaldehyde, respectively (18*a*), and hydrogenation of the resulting chalcone derivative over Raney nickel in ethyl acetate. Ketones **1***b*, *c*, **2**, and **3***b*, *c* were prepared by condensing 4-hydroxyacetophenone with the appropriate 4-alkylbenzaldehyde (18*b*), hydrogenation of the resulting chalcone over Raney nickel in 10% sodium hydroxide, and finally alkylation of the β-aryl-4′-hydroxypropiophenone with 1-bromopentane, 1-bromooctane, or dimethyl sulfate and potassium carbonate in refluxing acetone (34). 3-(4-Methoxyphenyl)-1-phenylpropen-3-one (**5***a*) had mp 105–106°C (lit. 101–103°C (1), 3-(4-hydroxyphenyl)-1-phenylpropen-3-one (**4***a*) had mp 171–172°C (lit. 177.5°C (18*b*), 1-(4-methoxyphenyl)-3-phenylpropan-1-one (**1***a*) had mp 96–97°C (lit. 96–97°C (18*b*)), and 1-(4-hydroxyphenyl)-3-phenylpropan-1-one (**6***a*) had mp 104–105°C (lit. 104°C (18*b*)). Spectral data for the other ketones which were synthesized as precursors to **1–3** are as follows:

*3-(4-Hydroxyphenyl)-1-(4-^{n}hexylphenyl)propen-3-one (**4**b)* (from 4-hydroxyacetophenone and 4-^{n}hexylbenzaldehyde) was recrystallized once from aqueous ethanol to afford light yellow needles, mp 108–112°C. ^{1}H nmr: δ 0.88(t, 3H), 1.32(m, 6H), 1.61(m, 2H), 2.65(t, 2H), 6.89(br s, 1H), 7.00(d, 2H), 7.34(d, 2H), 7.53(d, 1H), 7.59(d, 2H), 7.87(d, 1H), 8.04(d, 2H). Ir (CCl_4): 3608(w), 3415(m, br), 2960(w), 2925(m), 2855(w), 1667(m), 1653(m), 1598(s, sh), 1530(s, br), 1329(m), 1209(m), 1161(m), 980(m), 705(s, br). Mass: calcd. for $C_{21}H_{24}O_2$, 308.1776; found, 308.1754.

*1-(4-Cyclohexylphenyl)-3-(4-hydroxyphenyl)propen-3-one (**4**c)* (from 4-hydroxyacetophenone and 4-cyclohexylbenzaldehyde) was recrystallized once from 95% ethanol to afford light yellow plates, mp 190–192°C. ^{1}H nmr: δ 1.40(m, 5H), 1.83(m, 5H), 2.46(m, 1H), 6.41(br s, 1H), 6.95(d, 2H), 7.27(d, 2H), 7.48(d, 1H), 7.58(d, 2H), 7.84(d, 1H), 8.03(d, 2H). Ir (KBr): 3100(br, s), 2918(m), 2840(m), 1646(m), 1595(s), 1552(s, sh), 1405(m), 1328(s), 1296(m), 1218(s), 1161(s), 1022(m), 980(m), 810(m), 579(w), 538(w). Mass: calcd. for $C_{21}H_{22}O_2$, 306.1620; found, 306.1630.

*1-(4-Cyclohexylphenyl)-3-(4-methoxyphenyl)propen-3-one (**5**c)* (from 4-methoxyacetophenone and 4-cyclohexylbenzaldehyde) was chromatographed on silica gel (hexane/dichloromethane mixtures), and recrystallized once from 95% ethanol to afford light yellow plates, mp 95–96°C. ^{1}H nmr: δ 1.40(m, 5H), 1.83(m, 5H), 2.52(m, 1H), 3.89(s, 3H), 6.98(d, 2H), 7.37(d, 2H), 7.50(d, 1H), 7.59(d, 2H), 7.83(d, 1H), 8.07(d, 2H). Ir (CCl_4): 3006(w), 2927(s), 2847(m), 1666(s), 1604(s, br), 1418(w), 1329(m), 1252(m), 1167(s), 1022(m). Mass: calcd. for $C_{22}H_{24}O_2$, 320.1776; found, 320.1792.

*3-(4-^{n}hexylphenyl)-1-(4-hydroxyphenyl)propan-1-one (**6**b)* (from **4***b*) was recrystallized from aqueous ethanol to yield a colourless solid, mp 94–95°C. ^{1}H nmr: δ 0.87(t, 3H), 1.30(m, 6H), 1.56(m, 2H), 2.57(t, 2H), 3.13(m, 4H), 6.33(br s, 1H), 6.90(d, 2H), 7.15(s, 4H), 7.94(d, 2H). Ir (CCl_4): 3603(m), 3366(m, br), 3016(w), 2949(m), 2928(s), 2850(m), 1687(s), 1663(s), 1602(s, br), 1435(m), 1362(m), 1286(m), 1266(m), 1166(s). Mass: calcd. for $C_{21}H_{26}O_2$, 310.1933; found, 310.1930.

*3-(4-Cyclohexylphenyl)-1-(4-hydroxyphenyl)propan-1-one (**6**c)* (from **4***c*) was recrystallized from aqueous ethanol to yield a colourless solid, mp 147–150°C. ^{1}H nmr: δ 1.37(m, 5H), 1.81(m, 5H), 2.42(m, 1H), 3.11(m, 4H), 6.31(s, 1H), 6.90(d, 2H), 7.16(s, 4H), 7.95(d, 2H). Ir (CCl_4): 3608(m), 3372(m, br), 3010(w), 2928(s), 2850(m), 1688(s), 1667(m, sh), 1602(s, br), 1458(m), 1262(m), 1166(s). Mass: calcd. for $C_{21}H_{24}O_2$, 308.1776; found, 308.1759.

Substituted β-phenylpropiophenones 1–3

*1-(4-Pentoxyphenyl)-3-phenylpropan-1-one (**1**b)* (from **6***a* and 1-bromopentane) was recrystallized twice from methanol to yield colourless plates, mp 63–64°C. ^{1}H nmr: δ 0.91(t, 3H), 1.42(m, 4H), 1.80(m, 2H), 3.15(m, 4H), 4.02(t, 2H), 6.94(d, 2H), 7.31(s, 5H), 7.99(d, 2H). Ir (CCl_4): 3024(w), 2948(m), 2928(m), 2867(w), 1683(s), 1595(s, sh), 1532(s, br), 1303(m), 1338(m, br), 1306(w, sh), 1168(s), 978(m, br), 709(s, br). Mass: calcd. for $C_{20}H_{24}O_2$, 296.1776; found, 296.1759.

*1-(4-Octoxyphenyl)-3-phenylpropan-1-one (**1**c)* (from **6***a* and 1-bromooctane) was recrystallized twice from methanol to yield colourless plates, mp 48–49°C. ^{1}H nmr: δ 0.87(t, 3H), 1.31(m, 10H), 1.78(m, 2H), 3.13(m, 4H), 4.00(t, 2H), 6.90(d, 2H), 7.28(s, 5H), 7.94(d, 2H). The ir spectrum was similar to that of **1***b* except for minor differences in the C—H stretching region. Mass: calcd. for $C_{23}H_{30}O_2$, 338.2246; found, 338.2289.

*3-(4-^{n}hexylphenyl)-1-(4-methoxyphenyl)propan-1-one (**2**)* (from **6***b* and dimethylsulfate) was recrystallized twice from ethanol to yield colourless plates, mp 56–57°C. ^{1}H nmr: δ 0.87(t, 3H), 1.31(m, 6H), 1.53(m, 2H), 2.58(t, 2H), 3.12(m, 4H), 3.85(s, 3H), 6.92(d, 2H), 7.15(s, 4H), 7.97(d, 2H). Ir (CCl_4): 3003(w), 2948(m), 2920(s), 2846(m), 1685(s), 1594(s, sh), 1535(s, br), 1462(w), 1416(w), 1357(w), 1302(m), 1244(s), 1165(s), 1030(m), 966(w), 706(s, br). Mass: calcd. for $C_{22}H_{28}O_2$, 324.2090; found, 324.2067.

*3-(4-Cyclohexylphenyl)-1-(4-methoxyphenyl)propan-1-one (**3**a)* (from catalytic hydrogenation of **5***c*) was recrystallized twice from ethanol to yield colourless needles, mp 89–90°C. ^{1}H nmr: δ 1.40(m, 5H), 1.84(m, 5H), 2.43(m, 1H), 3.12(m, 4H), 3.84(s, 3H), 6.91(d, 2H), 7.17(s, 4H), 7.96(d, 2H). Ir (CCl_4): 3080(w), 2925(s), 2851(s), 1683(s), 1594(m, sh), 1530(s, br), 1241(s), 1201(w), 1165(s), 1300(m), 966(w), 709(s, br). Mass: calcd. for $C_{22}H_{26}O_2$, 322.1933; found, 322.1918.

*3-(4-Cyclohexylphenyl)-1-(4-pentoxyphenyl)propan-1-one (**3**b)* (from **6***c* and 1-bromopentane) was recrystallized twice from ethanol to yield colourless plates, mp 70–71°C. ^{1}H nmr: δ 0.92(t, 3H), 1.38(m, 9H), 1.81(m, 7H), 2.43(m, 1H), 3.13(m, 4H), 4.01(t, 2H), 6.92(d, 2H), 7.17(s, 4H), 7.94(d, 2H). The ir spectrum was similar to that of **3***a* except for minor differences in the 2800–3100 and 950–1050 cm^{-1} regions. Mass: calcd. for $C_{26}H_{34}O_2$, 378.2558; found, 378.2560.

*3-(4-Cyclohexylphenyl)-1-(4-octoxyphenyl)propan-1-one (**3**c)* (from **6***c* and 1-bromooctane) was recrystallized twice from ethanol to yield colourless plates, mp 63–64°C. ^{1}H nmr: δ 0.90(t, 3H), 1.32(m, 15H), 1.84(m, 7H), 2.47(m, 1H), 3.13(m, 4H), 4.02(t, 2H), 6.92(d, 2H), 7.18(s, 4H), 7.94(d, 2H). The ir spectrum was similar to those of **3***a*, *b* except for minor differences in the 2800–3100 and 950–1050 cm^{-1} regions. Mass: calcd. for $C_{29}H_{40}O_2$, 420.3028; found, 420.3037.

Acknowledgements

I wish to express my gratitude to Dr. J. C. Scaiano and the National Research Council of Canada for the use of the laser flash photolysis facility, Mr. H. Ladendorff, BDH Canada, for generous gifts of BCCN and ECCN, Dr. J. J. McCullough for the use of the thermal microscope, and Mr. J. Chan for technical assistance. Financial support of this work by the Natural Sciences and Engineering Research Council of Canada and the Research Corporation is gratefully acknowledged.

1. Aldrich catalog handbook of fine chemicals. Aldrich Chemical Co. Milwaukee. 1985. p. 702.
2. (*a*) W. E. Bacon and G. H. Brown. Mol. Cryst. Liq. Cryst. **12**, 229 (1971); (*b*) W. E. Barnett and W. H. Sohn. J. Chem. Soc. Chem. Commun. 1002 (1971); (*c*) M. J. S. Dewar and B. D. Nahlovsky. J. Am. Chem. Soc. **96**, 460 (1974); (*d*) F. D. Saeva, P. E. Sharpe, and G. R. Olin. J. Am. Chem. Soc. **97**, 204 (1975); (*e*) J. P. Otruba III and R. G. Weiss. Mol. Cryst. Liq. Cryst. **80**, 165 (1982); (*f*) S. Melone, V. Mosini, R. Nicoletti, B. Samori, and G. Torquati. Mol. Cryst. Liq. Cryst. **98**, 399 (1983).
3. (*a*) J. M. Nerbonne and R. G. Weiss. Isr. J. Chem. **18**, 266 (1979); (*b*) E. G. Cassis, Jr. and R. G. Weiss. Photochem. Photobiol. **35**, 439 (1982); (*c*) V. C. Anderson, B. B. Craig,

and R. G. WEISS. J. Phys. Chem. **86**, 4642 (1982); (*d*) V. C. ANDERSON, B. B. CRAIG, and R. G. WEISS. Mol. Cryst. Liq. Cryst. **97**, 351 (1983); (*e*) V. C. ANDERSON and R. G. WEISS. J. Am. Chem. Soc. **106**, 6628 (1984); (*f*) D. A. HROVAT, J. H. LIU, N. J. TURRO, and R. G. WEISS. J. Am. Chem. Soc. **106**, 7033 (1984).

4. (*a*) F. D. SAEVA (*Editor*). Liquid crystals. The fourth state of matter. Marcel Dekker Inc., New York. 1979; (*b*) H. KELKER and R. HATZ. Handbook of liquid crystals. Verlag Chemie, Weinheim, Deerfield. 1980.
5. W. J. LEIGH, D. T. FRENDO, and P. J. KLAWUNN. Can. J. Chem. **63**, 2131 (1985).
6. (*a*) J. M. SCHNUR and D. E. MARTIRE. Mol. Cryst. Liq. Cryst. **26**, 213 (1974); (*b*) G. A. OWEIMREEN, G. C. LIN, and D. E. MARTIRE. J. Phys. Chem. **83**, 2111 (1979); (*c*) D. E. MARTIRE. *In* The molecular physics of liquid crystals. *Edited by* G. R. Luckhurst and G. W. Gray. Academic Press, New York. 1979. Chapt. 11; (*d*) G. A. OWEIMREEN and D. E. MARTIRE. J. Chem. Phys. **72**, 2500 (1980); (*e*) P. J. PORCARO and P. SHUBIAK. J. Chromatogr. Sci. **9**, 690 (1971).
7. W. J. LEIGH. J. Am. Chem. Soc. **107**, 6114 (1985).
8. (*a*) R. S. PORTER, C. GRIFFIN, and J. F. JOHNSON. Mol. Cryst. Liq. Cryst. **25**, 131 (1974); (*b*) A. E. WHITE, P. E. CLADIS, and S. TORZA. Mol. Cryst. Liq. Cryst. **43**, 13 (1977).
9. (*a*) Z. LUZ. *In* Nuclear magnetic resonance of liquid crystals. NATO ASI Series, Ser. C. Vol. 141. *Edited by* J. W. Emsley. D. Reidel Publishing Co., Dordrecht. 1985. Chapt. 13; (*b*) N. A. P. VAZ and J. W. DOANE. J. Chem. Phys. **79**, 2470 (1983); (*c*) A. G. AVENT, J. W. EMSLEY, S. NG, and S. M. VENABLES. J. Chem. Soc. Perkin Trans. II, 1855 (1984); (*d*) B. M. FUNG, R. V. SIGH, and M. M. ALCOCK. J. Am. Chem. Soc. **106**, 7301 (1984); (*e*) R. R. VOLD and R. L. VOLD. *In* Liquid crystals and ordered fluids. Vol. 4. *Edited by* A. C. Giffin and J. F. Johnson. Plenum Publishing Corp. 1984. p. 561; (*f*) R. BLINC, B. MARIN, J. PIRS, and J. W. DOANE. Phys. Rev. Lett. **54**, 438 (1985); (*g*) E. T. SAMULSKI. Polymer, **26**, 177 (1985).
10. (*a*) K. V. S. RAO, C. F. POLNASZEK, and J. H. FREED. J. Phys. Chem. **81**, 449 (1977); (*b*) W. LIN and J. H. FREED. J. Phys. Chem. **83**, 379 (1979); (*c*) E. MEIROVITCH, D. IGNER, E. IGNER, G. MORO, and J. H. FREED. J. Chem. Phys. **77**, 3915 (1982); (*d*) M. S. BROIDO, I. BELSKY, and E. MEIROVITCH. J. Phys. Chem. **86**, 4197 (1982); (*e*) E. MEIROVITCH and M. S. BROIDO. J. Phys. Chem. **88**, 4316 (1984); (*f*) E. MEIROVITCH and J. H. FREED. J. Phys. Chem. **88**, 4995 (1984).
11. V. C. ANDERSON, B. B. CRAIG, and R. G. WEISS. J. Am. Chem. Soc. **103**, 7169 (1981); **104**, 2972 (1982).
12. (*a*) F. BERGMANN and Y. HIRSHBERG. J. Am. Chem. Soc. **65**, 1429 (1943); (*b*) F. R. STERMITZ, D. E. NICODEM, V. P. MURALIDHARAN, and C. M. O'DONNELL. Mol. Photochem. **2**, 87 (1970).
13. (*a*) D. G. WHITTEN and W. E. PUNCH. Mol. Photochem. **2**, 77 (1970); (*b*) P. J. WAGNER, P. A. KELSO, A. E. KEMPPAINEN, A. HAUG, and D. R. GRABER. Mol. Photochem. **2**, 81 (1970); (*c*) G. L. B. CARLSON, F. H. QUINA, B. M. ZARNEGAR, and D. G. WHITTEN. J. Am. Chem. Soc. **97**, 347 (1975).
14. J. C. SCAIANO, M. J. PERKINS, J. W. SHEPPARD, M. S. PLATZ, and R. L. BARCUS. J. Photochem. **21**, 137 (1983).
15. T. WILSON and A. M. HALPERN. J. Am. Chem. Soc. **103**, 2412 (1981).
16. (*a*) H. L. CASAL and J. C. SCAIANO. Can. J. Chem. **62**, 628 (1984); (*b*) J. C. SCAIANO, H. L. CASAL, and J. C. NETTO-FERREIRA. *In* Organic phototransformations in nonhomogeneous media. *Edited by* M. A. Fox. Am. Chem. Soc. Symp. Ser. No. 278. 1985. Chapt. 13.
17. (*a*) J. C. NETTO-FERREIRA, W. J. LEIGH, and J. C. SCAIANO. J. Am. Chem. Soc. **107**, 2617 (1985); (*b*) W. J. LEIGH, J. C. SCAIANO, C. I. PARASKEVOPOULOS, G. M. CHARETTE, and S. E. SUGAMORI. Macromolecules, **18**, 2148 (1985).
18. (*a*) Org. Synth. Coll. Vol. I, 78; (*b*) Y. A. ZASASOV, E. I. MITEL'KOVA, and S. N. MILANOVA. Zh. Obs. Khim. **26**, 2499 (1957); Chem. Abstr. **51**, 4994*d* (1957).
19. J. C. SCAIANO. J. Am. Chem. Soc. **102**, 7747 (1980).
20. T. WISMONTSKI-KNITTEL and T. KILP. J. Phys. Chem. **88**, 110 (1984).
21. J. E. PIERCEY and M. G. RAO. J. Chem. Phys. **46**, 3951 (1967).
22. (*a*) M. V. ENCINA, E. A. LISSI, E. LEMP, A. ZANOCCO, and J. C. SCAIANO. J. Am. Chem. Soc. **105**, 1856 (1983). (*b*) P. J. WAGNER, A. E. KEMPPAINEN, and H. N. SCHOTT. J. Am. Chem. Soc. **95**, 5604 (1973); **92**, 5280 (1970).
23. J. BILLARD. *In* Liquid crystals of one and two dimensional order. *Edited by* W. Helfrich and G. Heppke. Springer Verlag, Berlin. 1980. p. 383.
24. A. DE VRIES. J. Phys. Paris, **36**, C1-1 (1975).
25. (*a*) A. DE VRIES. *In* Liquid crystals. The fourth state of matter. *Edited by* F. D. Saeva. Marcel Dekker Inc., New York. 1979. Chapt. 1; (*b*) H. SACKMANN and D. DEMUS. Mol. Cryst. Liq. Cryst. **21**, 239 (1973).
26. Licristal liquid crystals. EM Chemicals. Hawthorne, New York. 1984.
27. G. J. BROWNSEY and A. J. LEADBETTER. J. Phys. (Paris), **42**, L135 (1981).
28. D. S. MITCHELL and W. J. LEIGH. To be published.
29. (*a*) D. COATES and G. W. GRAY. Microscope, **24**, 117 (1976); (*b*) D. DEMUS and L. RICHTER. Textures of liquid crystals. Verlag Chemie, Weinheim. 1978.
30. J. M. NERBONNE and R. G. WEISS. J. Am. Chem. Soc. **101**, 402 (1979).
31. (*a*) E. SACKMANN, P. KREBS, H. U. REGA, J. VOSS, and H. MOHWALD. Mol. Cryst. Liq. Cryst. **24**, 283 (1973); (*b*) F. D. SAEVA. Pure Appl. Chem. **38**, 25 (1974).
32. J. SALTIEL, G. R. MARCHAND, E. KIRKOR-KAMINSKA, W. K. SMOTHERS, W. B. MUELLER, and J. L. CHARLTON. J. Am. Chem. Soc. **106**, 3144 (1984).
33. W. E. SMITH. J. Org. Chem. **37**, 3972 (1972).
34. C. F. H. ALLEN and J. H. GATES, JR. Org. Synth. Coll. Vol. 3. p. 418.

Activation volumes for ester hydrolysis via elimination–addition

NEIL S. ISAACS[1] AND TARIQ S. NAJEM
Department of Chemistry, University of Reading, Whiteknights, Reading, Berks, England

Received October 29, 1985

This paper is dedicated to Professor Arthur N. Bourns

NEIL S. ISAACS and TARIQ S. NAJEM. Can. J. Chem. **64**, 1140 (1986).

Esters that have an acidic proton α to the carboxyl group (or in a vinylogous situation) and a good leaving group may undergo hydrolysis by elimination to an intermediate ketene, which rapidly hydrates. Examples are found in *p*-hydroxybenzoate, malonate, and acetoacetate esters of nitrophenols. The evidence for this mechanism (E1cb type) includes the independence of rate with pH in the region of dissociation of the acidic proton and, in particular, positive volumes of activation that contrast sharply with negative values typical of the more usual $B_{Ac}2$ mechanism of hydrolysis.

NEIL S. ISAACS et TARIQ S. NAJEM. Can. J. Chem. **64**, 1140 (1986).

Les esters qui possèdent un proton acide dans la position en α du groupement carbonyle (ou dans une position vinylique) et un bon groupement nucléofuge peuvent subir une hydrolyse impliquant une élimination conduisant à un cétène intermédiaire qui s'hydrate rapidement. Les *p*-hydroxybenzoate, malonate et acétoacétate des nitrophénols constituent de bons exemples de ce type de réaction. Les données qui laissent croire en ce mécanisme (du type E1cb) impliquent le fait que la vitesse de réaction est indépendante du pH, dans la région de dissociation du proton acide, et, en particulier, sur le fait que les volumes d'activation positifs contrastent nettement avec les valeurs négatives qui sont caractéristiques du mécanisme plus courant d'hydrolyse du type $B_{Ac}2$.

[Traduit par la revue]

Alkene-forming eliminations via the conjugate base of the substrate, the E1cb mechanism, have been conclusively demonstrated to take place in competition with the synchronous E2 route when the α-proton is of high acidity and the leaving group has a rather low nucleofugacity:

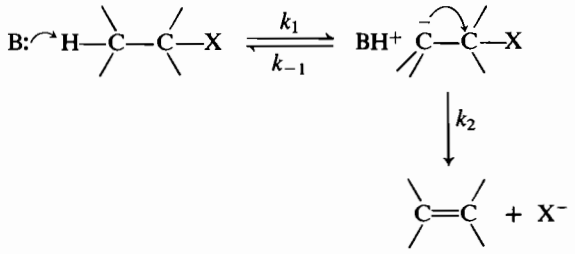

Several variants of this mechanism have been identified according to whether step 1 is reversible or not and whether k_1 or k_2 is rate determining ($E1cb_{re}$, $E1cb_{irr}$, $E1cb_{anion}$, respectively).

The E1cb mechanism of hydrolysis of esters, Scheme 1, was proposed by Holmquist and Bruice in 1969 (1, 2) to account for the kinetics of hydrolysis of certain malonate esters possessing at least one acidic α-hydrogen. Since that study, many esters have been inferred to hydrolyse in an analogous manner, the structural requirement in all cases being the availability of a stabilized carbanion or oxyanion α to the carboxyl group or in a vinylogous position such that $pK_A < pK_w$. Usually, a leaving group of high nucleofugacity such as a nitrophenolate is also required so that the more usual $B_{Ac}2$ mechanism should not supervene. In addition to the obvious candidates such as malonate and β-ketoesters (3) (and their thio-analogues (4, 5)), Williams, Thea, and co-workers (6–8) have supplied evidence that the hydrolyses of *p*-hydroxybenzoates and of *p*-hydroxybenzenesulphonates also occur by an E1cb route. In all the cases cited, the main body of evidence leading to these mechanistic proposals was the observation of anomalous pH–rate profiles. Typically, rates of hydrolysis in buffered solution were found to be abnormally high in the region of dissociation of the acidic hydrogen and to exhibit a plateau indicative of rate-determining proton removal by general base catalysis with a sharp discontinuity indicative of a mechanistic change. At a pH below the plateau, the mechanism is $B_{Ac}2$ since the substrate is not appreciably dissociated, and similarly above, where $[OH^-]$ is high enough for $B_{Ac}2$ hydrolysis of the conjugate base to compete with the E1cb pathway. In each of these regions, a linear relationship between log *k* and pOH (or a suitable acidity function at high basicity) is required and is observed. Also, deviations from linear free energy relationships have been observed, rates of hydrolysis of *o*-nitrophenyl malonates being 10^2–10^3 times greater than predicted from those of other substituted acetates with less acidic α-hydrogens. We considered it likely that there would be a significant difference between volumes of activation for $B_{Ac}2$ and E1cb routes. The former are known to have small, negative values ($\Delta V^{\ddagger}$ −10 to −20 $cm^3\ mol^{-1}$ (9)), rates being mildly increased by pressure, consistent with an associative activation step. E1cb mechanisms in olefin formation have been found (10) to be characterized by positive values of $\Delta V^{\ddagger}$ (the rate diminished by pressure), which would be expected for an activation step in which an intermediate carbanion dissociates into two fragments, i.e. k_2. This would apply to the E1cb (anion) mechanism for which k_2 is rate-determining and $\Delta V^{\ddagger}_{obs} = \Delta V^{\ddagger}_2$. Predictions concerning the other variants of the mechanism may depend upon the charge state of the base. If neutral, then $\Delta V^{\ddagger}_1$ will be strongly negative due to solvent electrostriction around the developing charges and $\Delta V^{\ddagger}_2$ correspondingly positive, making the reaction volume for the pre-equilibrium, ΔV_e ($= \Delta V^{\ddagger}_1/\Delta V^{\ddagger}_2$) large and positive. If the base is an anion such that there is no net change in charge during the pre-equilibrium, then $\Delta V^{\ddagger}_1$ and ΔV_e will be small and probably negative. The following mechanistic relationships with observed activation volumes may be made:

[1]Author to whom correspondence may be addressed.

Printed in Canada / Imprimé au Canada

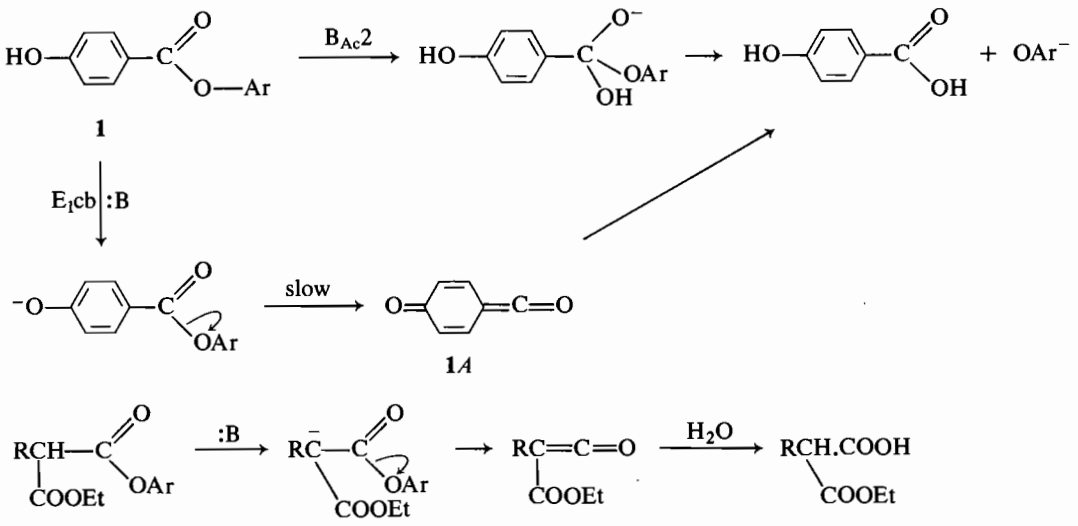

SCHEME 1

	E1cb type				
	Anion	Reversible		Irreversible	
$\Delta V^{\ddagger}_{obs}$	$\Delta V^{\ddagger}_2$	$\Delta V^{\ddagger}_e + \Delta V^{\ddagger}_2$		$\Delta V^{\ddagger}_1$	
Base charge	0 or −	0	−	0	−
Magnitude of $\Delta V^{\ddagger}_{obs}$	Moderate positive	Large negative	Moderate positive	Large negative	Small

Similar predictions may be made for ester hydrolyses by this group of mechanisms. The examples that we have studied are of the E1cb (anion) or possibly E1cb (rev) with an anionic base and therefore we would expect to have an especially favourable situation for the application of high pressures to this mechanistic problem, since the two possible pathways to be considered, E1cb or $B_{Ac}2$, would be characterized by activation volumes of opposite sign. This paper reports that this expectation has been borne out and concludes that the measurement of activation volumes is diagnostically appropriate to distinguish between these mechanisms.

Experimental

Nitrophenyl esters of aromatic carboxylic acids were prepared by the following general method (11); carboxylic acid (100 mmol) and nitrophenol (100 mmol) were dissolved in dry ether or tetrahydrofuran and dicyclohexylcarbodiimide (110 mmol) was added. The mixture was stirred at room temperature for several hours or until the precipitation of dicyclohexylurea was complete. After filtration, the product was isolated by evaporation of the solvent and purified by recrystallization.

Nitrophenyl esters of malonic acids were prepared by an analogous method, starting with the potassium salt of ethyl hydrogen malonate (methylmalonate or dimethylmalonate), while nitrophenyl acetoacetates were prepared by reaction between the nitrophenol and diketene in dichloromethane (12).

Melting points in all cases corresponded with published values and nmr spectra were in accordance with the expected structures, as follows.

2,4-Dinitrophenyl 4-hydroxybenzoate: mp 160–161°C. *Anal.* calcd. for $C_{13}H_8N_2O_7$: C 51.3, H 2.65, N 9.2%; found: C 51.5, H 2.63, N 9.52%.

2,4-Dinitrophenyl 3-hydroxybenzoate: mp 180°C. *Anal.* calcd. for $C_{13}H_8N_2O_7$: C 51.3, H 2.65, N 9.2%; found: C 51.27, H 2.51, N 9.4%.

2,4-Dinitrophenyl 4-methoxybenzoate: mp 134°C. *Anal.* calcd. for $C_{14}H_{10}N_2O_7$: C 52.8, H 3.14, N 8.8%; found: C 54.2, H 3.3, N 8.8%.

2,4-Dinitrophenyl 4-acetamidobenzoate: mp 170°C. *Anal.* calcd. for $C_{15}H_{11}N_3O_8$: C 52.2, H 3.21, N 12.1%; found: C 51.9, H 3.03, N 12.1%.

4-Nitrophenyl benzoate: mp 142°C. *Anal.* calcd. for $C_{13}H_9NO_4$: C 64.5, H 3.3, N 5.7%; found: C 63.5, H 3.51, N 5.7%.

Ethyl 4-nitrophenyl malonate: mp 62°C. *Anal.* calcd. for $C_{10}H_9NO_5$: C 52.2, H 4.4, N 5.5%; found: C 52.2, H 4.4, N 5.5%.

2-Nitrophenyl acetoacetate: mp 73°C. *Anal.* calcd. for $C_{10}H_9NO_5$: C 53.8, H 4.1, N 6.3%; found: C 53.9, H 4.3, N 6.3%.

Kinetic measurements were carried out in water or in aqueous acetone or methanol, buffered between pH 7 and 12, at concentrations around 10^{-4} *M*. The particular choice of conditions was governed by the reactivities of the substrates but the pH at which measurements were made corresponded to the plateau region for E1cb reactions. The reaction solution was placed within a 1-cm cuvette ("Spectrosil"), closed with a stopper fitted with a rubber bulb for equalization of pressure and enclosed within a high pressure optical cell, thermostatted to ±0.5°C in a spectrophotometer as previously described (13). The progress of reaction was monitored by following the absorption of the nitrophenol produced at wavelengths around 400 nm. Reactions were all of first order and rate constants were evaluated using the Guggenheim procedure. Volumes of activation were calculated from eq. [1], the constant *B* being calculated by a computed fit to a plot of ln *k* against pressure.

$$[1] \quad RT\,\mathrm{d}\ln k/\mathrm{d}p = -\Delta V^{\ddagger} = RT(A + Bp + Cp^2)$$
$$B = -\Delta V^{\ddagger}/RT$$

Results are summarized in Tables 1 and 2 and Figs. 1–3.

Discussion

Volumes of activation for nitrophenyl esters of *p*-nitrophenylacetic acid were, as expected, negative, as were those for hydrolyses of the *p*-methoxybenzoate. This is a consequence of the $B_{Ac}2$ mechanism and the rate-determining association between ester and base, in this case water. The values of the activation volumes, −21 and −19 $cm^3\,mol^{-1}$, respectively, are comparable with that for uncatalysed hydrolysis of ethyl acetate

TABLE 1. Rates of hydrolysis of nitrophenyl esters as a function of pressure

		p (bar)						
		1	300	600	90	pH	*T* (°C)	Solvent[a]
1. *2,4-Dinitrophenyl 4-hydroxybenzoate*								
$10^4 k(s^{-1})$	A.	8.70	7.35	6.70	6.24	8.00	28.9	a
	B.	9.30	8.76	7.95	7.24	10.1	29.8	b
	C.	18.9	22.8	25.9	29.1	12.5	29.8	b
2. *2,4-Dinitrophenyl 4-methoxybenzoate*								
$10^4 k(s^{-1})$		8.38	10.15	12.05	13.2	10.3	29.8	b
3. *4-Nitrophenyl benzote*								
$10^4 k(s^{-1})$		5.84	7.45	8.71	9.97	10.1	29.8	b
4. *2,4-Dinitrophenyl 3-hydroxybenzoate*								
$10^4 k(s^{-1})$		6.81	8.47	9.83	11.9	10.7	29.0	b
6. *Ethyl 4-nitrophenyl malonate*								
$10^4 k(s^{-1})$		8.82	7.85	7.07	6.15	5.8	30.6	a
7. *Ethyl 2-nitrophenyl methylmalonate*								
$10^4 k(s^{-1})$		19.1	17.0	15.1	13.3	8.00	23	a
8. *Ethyl 2-nitrophenyl dimethylmalonate*								
$10^4 k(s^{-1})$		6.43	8.49	10.5	13.0	11.3	29.7	b
12. *2,4-Dinitrophenyl acetate*								
$10 k(s^{-1})$		2.05	3.08	3.51	4.30	4.75	28.0	a

	p (bar)						
	1	300	500	700	pH	*T* (°C)	Solvent
5. *2,4-Dinitro 4-acetylaminobenzoate*							
$10^4 k(s)$	6.16	7.32	8.35	8.92	9.8	27	b
10. *2-Nitrophenyl 4-nitrophenylacetate*							
$10^4 k(s)$	5.49	6.71	7.40	7.68	7.5	24	b
11. *3-Nitrophenyl acetoacetate*							
$10^4 k(s)$	9.80	8.87	8.49	8.06	4.58	30.0	c

	p (bar)						
	1	200	400	600	pH	*T* (°C)	Solvent
9. *Ethyl 2,4-dinitrophenyl dimethylmalonate*							
$10^4 k(s)$	12.8	15.9	18.7	21.7	—	23	—

[a]Solvents: a, water; b, acetone–water 43:57 v:v%; c, acetone–water 86:14 v:v%.

in aqueous ethanol (-31 cm^3 mol^{-1} (12)), the difference being attributable to the less polar solvent in the latter case and the greater degree of electrostriction. These activation volumes are considerably more negative than those for hydrolyses promoted by either H^+ or OH^-, for both of which $\Delta V^{\neq}$ is around -5 to -10 cm^3 mol^{-1}.

The *p*-hydroxybenzoate ester, in contrast, hydrolyses at around pH 8, where the phenolic group is substantially dissociated, at a rate which decreases with pressure and in consequence has a positive volume of activation, $+16$ cm^3 mol^{-1}. This points to the operation of a different mechanism and is in accordance with a rate-determining fission of the conjugate base of the ester, the E1cb process. As a reactive intermediate, the ketenoid species, **1***A*, is presumed to be formed, which would rapidly hydrolyse to *p*-hydroxybenzoic acid. This interpretation is given more force by the observation that $\Delta V^{\neq}$ changes with increasing pH, becoming $+7$ at pH 10.1, in the intermediate region, and finally negative, -18 at pH 12.5, where the $B_{Ac}2$ pathway is reestablished due to the increase in $[OH^-]$. The behaviour of *p*-methoxybenzoate and *m*-hydroxybenzoate, neither of which are capable of producing an intermediate analogous to **1***A*, is understandable: hydrolyses of these esters are characterized by the negative volumes of activation typical of the $B_{Ac}2$ mechanism.

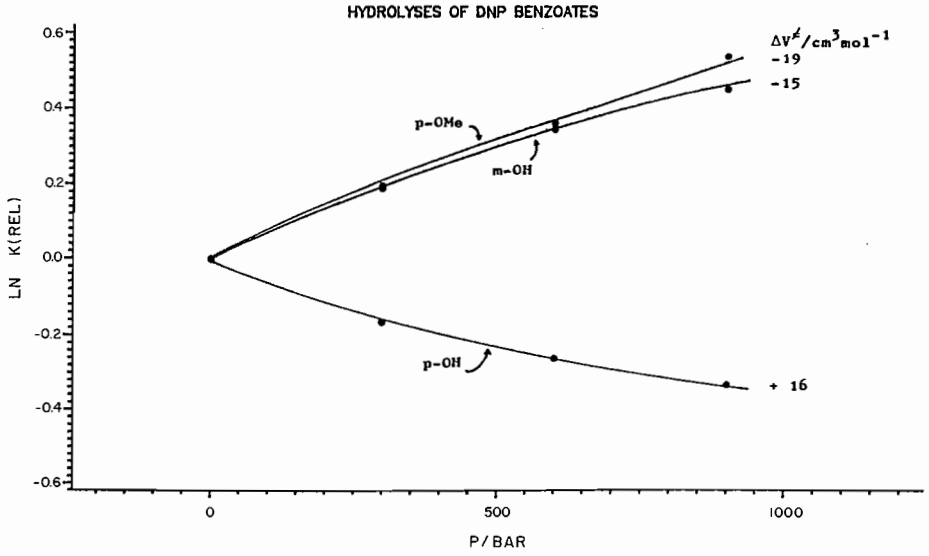

FIG. 1. Hydrolyses of DNP benzoates.

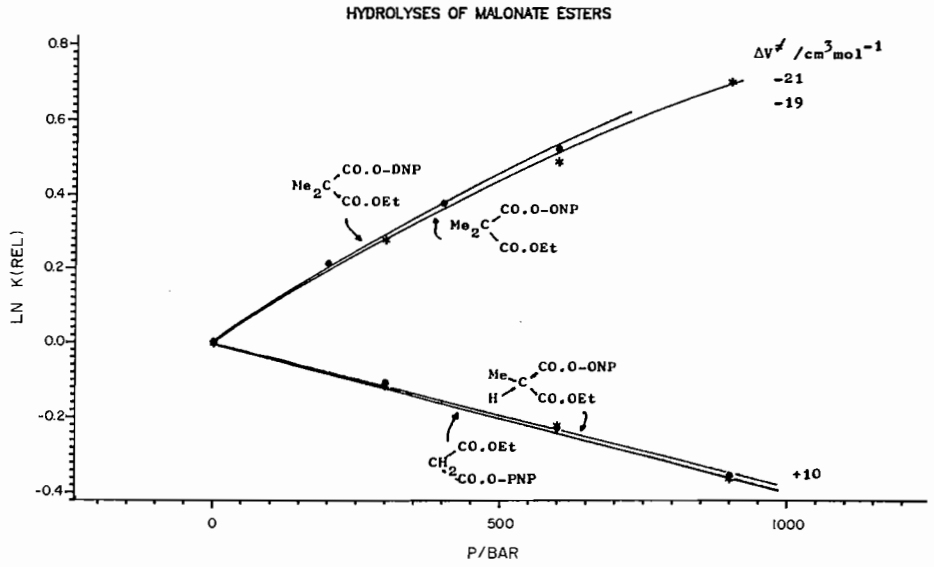

FIG. 2. Hydrolyses of malonate esters.

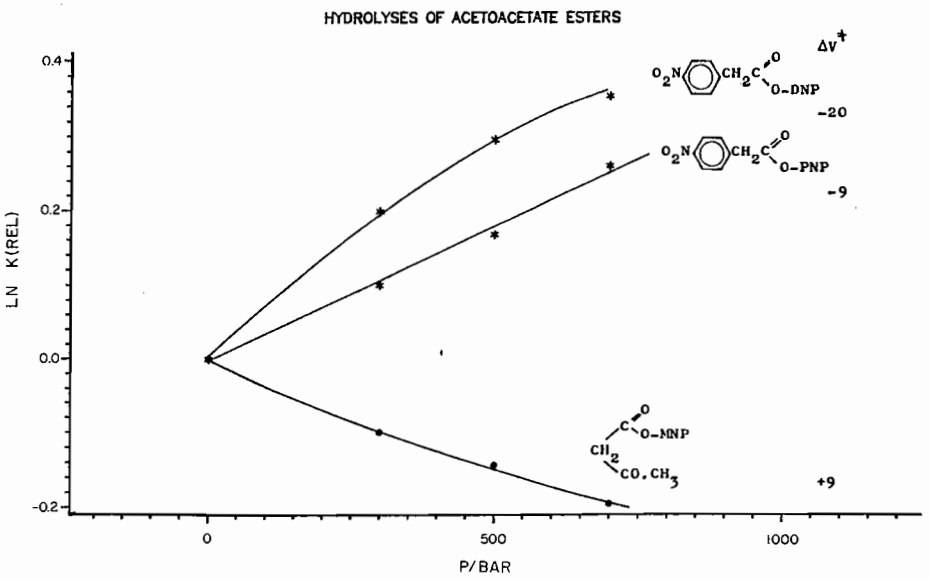

FIG. 3. Hydrolyses of acetoacetate esters.

TABLE 2. Volumes of activation for hydrolyses of nitrophenyl esters

Ester[a]	$\Delta V^{\neq}$ (cm^3 mol^{-1}) $B_{Ac}2$	$\Delta V^{\neq}$ (cm^3 mol^{-1}) E1cb
1 (pH 12.5)	−17.9	
1 (pH 8.0)		+16.5
1 (pH 10.1)		+7.1
2	−19.2	—
3	−21.4	—
4	−14.8	—
5	−17.3	—
6	—	+10.0
7	—	+9.7
8	−19.6	—
9	−21.4	—
10	−20.7	—
11	—	+8.7
12	−19.7	—

[a]The esters correspond to the numbering in Table 1.

Malonate esters with at least one α-hydrogen are also potentially able to partake of the E1cb mechanism and accordingly it was observed that hydrolyses of both the malonate and monomethylmalonate esters had positive volumes of activation, as also had nitrophenyl acetoacetate. The dimethylmalonate with no remaining acidic protons must of necessity hydrolyse by the $B_{Ac}2$ route and is indeed found to have $\Delta V^{\neq}$ negative.

The examples studied therefore show a clear distinction in their response to pressure between, on the one hand, those esters which possess a proton on the α-carbon or a vinylogous position that has $pK <$ ca. 10 and those which do not, and we take this as convincing evidence of the availability of the E1cb mechanism in the former case and the $B_{Ac}2$ mechanism in the latter.

1. B. HOLMQUIST and T. C. BRUICE. J. Am. Chem. Soc. **91**, 2113 (1969).
2. B. HOLMQUIST and T. C. BRUICE. J. Am. Chem. Soc. **91**, 3003 (1969).
3. R. F. PRATT and T. C. BRUICE. J. Am. Chem. Soc. **92**, 5956 (1970).
4. K. T. DOUGLAS and N. F. YAGGI. J. Chem. Soc. Perkin Trans. **2**, 1037 (1980).
5. K. T. DOUGLAS, M. ALBORZ, G. R. RULLO, and N. F. YAGGI. J. Chem. Soc. Chem. Commun. 245 (1982); S. THEA, G. CEVASCO, G. GUANTI, A. HOPKINS, N. KASHEFI-NAINI, and A. WILLIAMS. J. Org. Chem. **50**, 2158 (1985); A. WILLIAMS and K. T. DOUGLAS. Chem. Rev. **75**, 627 (1975).
6. S. THEA, G. GUANTI, G. PETRILLO, A. HOPKINS, and A. WILLIAMS. J. Chem. Soc. Chem. Commun. 577 (1982).
7. S. THEA, G. GUANTI, N. KASHEFI-NAINI, and A. WILLIAMS. J. Chem. Soc. Chem. Commun. 529 (1983).
8. G. CAVASCO, G. GUANTI, S. THEA, and A. WILLIAMS. J. Chem. Soc. Chem. Commun. 783 (1984).
9. H. ITSUKI, B. MATSUDA, and S. TERASAWA. Nippon Kagaku Zasshi, **90**, 1016 (1969).
10. K. R. BROWER, M. MUHSIN, and H. E. BROWER. J. Am. Chem. Soc. **98**, 779 (1976).
11. D. M. BROWN. Adv. Org. Chem. **3**, 115 (1963).
12. N. S. ISAACS and P. VAN DER BEEKE. J. Chem. Soc. Perkin Trans. **2**, 1205 (1982).
13. T. ASANO and W. J. LENOBLE. Chem. Rev. **78**, 407 (1978); see ref. 198 therein.

Inner shell electron energy loss spectroscopy of some heterocyclic molecules

D. C. NEWBURY, I. ISHII, AND A. P. HITCHCOCK
Department of Chemistry, McMaster University, Hamilton, Ont., Canada L8S 4M1

Received October 18, 1985

This paper is dedicated to Professor Arthur N. Bourns

D. C. NEWBURY, I. ISHII, and A. P. HITCHCOCK. Can. J. Chem. **64**, 1145 (1986).

The carbon K-shell spectra of gaseous furan, pyrrole, tetrahydrofuran, pyrrolidine, tetrahydropyran, and piperidine have been recorded by electron energy loss spectroscopy (ISEELS) under electric dipole scattering conditions (2.5 keV impact, small angle). The spectra are dominated by transitions to unoccupied valence states of π and σ symmetry. Features attributed to transitions to $\pi^*(CH_2)$ levels are consistently observed below the ionization threshold in the spectra of the saturated species. The positions of continuum features are generally in agreement with a previously documented correlation with bond lengths. Additional weak continuum features are observed in the smaller saturated heterocyclic species which are ascribed to delocalized σ^* states.

D. C. NEWBURY, I. ISHII et A. P. HITCHCOCK. Can. J. Chem. **64**, 1145 (1986).

Faisant appel à la spectroscopie par perte d'énergie électronique (ISEELS) dans des conditions de diffusion des dipôles électriques (impact de 2,5 keV, petit angle), on a déterminé les spectres de la couche K du carbone du furanne, du pyrrole, du tétrahydrofuranne, de la pyrrolidine, du tétrahydropyranne et de la pipéridine à l'état gazeux. Les spectres sont dominés par des transitions vers des états de valence non-occupés de symétrie π ou σ. Dans les spectres des espèces saturées, on observe d'une façon systématique que les caractéristiques attribuables aux transitions vers les niveaux $\pi^*(CH_2)$ apparaissent à des niveaux inférieurs à ceux du seuil d'ionisation. Les caractéristiques continues apparaissent généralement à des positions qui sont en accord avec les relations qui ont été observées antérieurement avec les longueurs des liaisons. Dans les espèces hétérocycliques saturées plus petites, on a observé des caractéristiques additionnelles continues faibles que l'on attribue à des états σ^* délocalisés.
[Traduit par la revue]

Introduction

Over the last few years K-shell excitation studies by Inner Shell Electron Energy Loss (ISEELS) spectroscopy have proven to be particularly useful in examining the unoccupied energy levels of molecules containing the second row elements C, N, O, and F (1). The features present in the K-shell spectra of free molecules can be classified as transitions either to Rydberg orbitals or to unoccupied molecular orbitals of σ^* or π^* character. In contrast to valence shell excitation spectroscopy the latter dominate when the highly localized K-shell electrons are excited. An intriguing development in K-shell excitation is the evidence recently presented for an empirical relationship between bond length and σ shape resonance position (2, 3). According to this simple picture the K-shell spectrum of a molecule containing 2 or more second row atoms will exhibit a σ shape resonance associated with each bond. The position of this resonance relative to the core ionisation potential (IP) can be related to the bond length through a correlation among all bonds of the same class defined by a parameter Z, the sum of the atomic numbers of the two bonded atoms. The correlation was developed from the spectra of diatomic and "pseudo-diatomic" molecules (e.g. C_2H_2, C_2H_4, HCN, H_2CO etc.). A general goal of our research is to test the utility of the empirical relationship in larger molecules, both for bond length determination and spectral interpretation.

Recently studies have been reported on K-shell excitation in gas phase non-cyclic aliphatic hydrocarbons (2–4), cyclic aliphatics (5), and cyclic aromatics (6). In order to provide further understanding of inner shell excitation in different environments we have carried out an investigation of some saturated and unsaturated heterocyclic hydrocarbons, in particular furan (C_4H_4O), pyrrole (C_4H_4NH), tetrahydrofuran (C_4H_8O or THF), pyrrolidine (C_4H_8NH), tetrahydropyran ($C_5H_{10}O$ or THP), and piperidine ($C_5H_{10}NH$). Heterocyclic molecules such as these are important in many organic and biochemical reactions. Furan and pyrrole in particular, have been the topics of extensive study (7). The ISEELS spectra of all of these molecules are compared to their cyclic hydrocarbon analogs (5) to explore the effect of the heteroatom on the electronic structure of the ring. The continuum features are interpreted in comparison with the results predicted from the previously documented correlation between the position of σ shape resonances and bond lengths (3).

Experimental

The experimental apparatus and techniques used to acquire the ISEELS spectra have been described in detail elsewhere (2, 5). Briefly, the spectra are produced by inelastic scattering of energetic electrons by gases at ca. 10^{-4} Torr (10^{-2} Pa). The spectrometer is operated with scattering angles of 1–2° and a final electron energy (2) of 2.5 keV. The spectral resolution is limited to 0.7 eV, largely determined by the thermal spread of electron energies in the unmonochromated incident electron beam. The gases used were obtained from the vapours of high purity liquid samples, which, except for the THF and THP, were obtained commercially and used without further purification. THF was vacuum distilled to remove impurities (probably peroxides) detected in spectra recorded prior to distillation. A distilled THP sample was also studied to check for possible peroxide contamination. No changes were observed between the spectra of the distilled and undistilled THP samples. Air and volatile impurities in the liquids were removed by a series of freeze–pump–thaw cycles. The absolute energy scales were determined by calibrating the spectra relative to the C $1s \rightarrow \pi^*$ transition in CO (287.40(2) eV (8)), C_2H_4 (284.7(1) eV (4)) or CO_2 (290.7(1) eV (9)); the N $1s \rightarrow \pi^*$ transition in N_2 (401.10(2) eV (8)); or the O $1s \rightarrow \pi^*$ transition in CO (534.21(9) eV (8)). The calibrant gas was chosen for minimum overlap between the calibrant feature and the sharpest feature in the heterocyclic spectrum. In all cases the spectrum of a mixture of the two gases was recorded with each gas being let into the collision region through a separate leak vale to ensure a constant composition mixture. This approach is desirable since the spectrometer energy scale shifts slightly with changes in sample gas pressure or composition because of changes in the work function of the electron emitting surface and of surface potentials throughout the spectrometer.

Results and discussion

Knowledge of the core ionization threshold (IP) aids spectral analysis both through identification of Rydberg states through term values (10) and alignment of corresponding features in

different core edge spectra. In addition the correlation between shape resonance position and bond length (3) uses the IP as a reference level. Where available (11), gas phase ionization potentials measured by X-ray photoelectron spectroscopy (XPS) have been used for the carbon and heteroatom 1*s* IP's. However, XPS data was not available for the C 1*s* and O 1*s* IP's of THF and tetrahydropyran (THP) and the C 1*s* IP's of pyrrolidine and piperidine. For these molecules the IP's were estimated from literature values of similar molecules. For THF and THP the IP's were estimated from the gas phase XPS IP's of furan, dimethyl ether, and ethanol. The 1*s* IP's of the carbon nearest the oxygen in these molecules are 291.6, 292.3, and 292.5 eV, respectively (11), while the more distant carbons of furan and ethanol have IP's of 290.4 and 291.1 eV. The values of THF should be similar to these and thus the C 1*s* IP's for the two distinguishable C 1*s* environments in THF and THP are estimated to be 292.0 and 290.8 eV. (Note that all carbons more than one position away from the heteroatom are expected to have IP's within 0.5 eV of each other and are essentially indistinguishable in unmonochromated XPS and in ISEELS with the present resolution. For this reason in all of the molecules studied carbons more than one position away from the heteroatom are labelled C_1 while those adjacent to the heteroatom are labelled C_2.) The O 1*s* IP of furan is 540.0 eV while that of both dimethyl ether and ethanol is 538.6 eV (11). The O 1*s* IP of THF is estimated to be 539.0(5) eV, closer to the value for the non-aromatic species. The gas phase C 1*s* IP's were also unavailable for both pyrrolidine and piperidine. The C 1*s* IP's of CH_3NH_2 and $N(CH_3)_3$ are 291.6 and 291.3 eV while that of pyrrole is 290.8 eV. The C_2 IP of pyrrolidine and piperidine is expected to be similar to these and is given a value of 291.0 eV. The effect of the nitrogen is expected to disturb the ring less than the oxygen in THF so the C_1 IP is estimated to be 290.3 eV, close to that for cyclic hydrocarbons. In all cases the deviation between the estimated and actual IP's is expected to be less than 0.5 eV.

1.1. Carbon K-shell spectrum of furan

Furan, an aromatic five-membered ring with C_{2v} symmetry, is isoelectronic with the cyclopentadienyl anion. Since the carbon K-shell spectrum of the cyclopentadienyl anion has not been studied yet a direct comparison between furan and its closest hydrocarbon analog is not possible. However, comparisons to benzene or pyridine are appropriate. The carbon K-shell electron energy loss spectrum of furan is shown in Fig. 1 while the energies and assignments of the features in the spectra are listed in Table 1.

The first four features in the carbon K-shell electron energy loss spectrum of furan are attributed to $1s \rightarrow \pi^*$ transitions. There are two distinguishable carbon 1*s* environments and two unoccupied π^* levels which leads to four possible C $1s \rightarrow \pi^*$ transitions, all of which are electric-dipole allowed. The 0.86(6) eV separation of features 1 and 2 and the 0.80(4) eV separation of features 3 and 4 could represent the separation of either the C 1*s* levels (1.2 eV (11)) or that of the $3b_1$ and $2a_2$ π^* levels. Optical and valence electron energy loss spectra (7, 12) and a number of theoretical calculations (13, 14) indicate that the two π^* levels are separated by about 1.8 eV with the $3b_1$ orbital at lower energy. This suggests that the separation of features 1 and 2 reflects the separation of the core levels rather than the π^* levels. Thus the first shoulder (#1) is assigned to the C_1 $1s \rightarrow \pi^*(3b_1)$ transition while the more intense feature 2 is attributed to the C_2 $1s \rightarrow \pi^*(3b_1)$ transition. Features 3 and 4

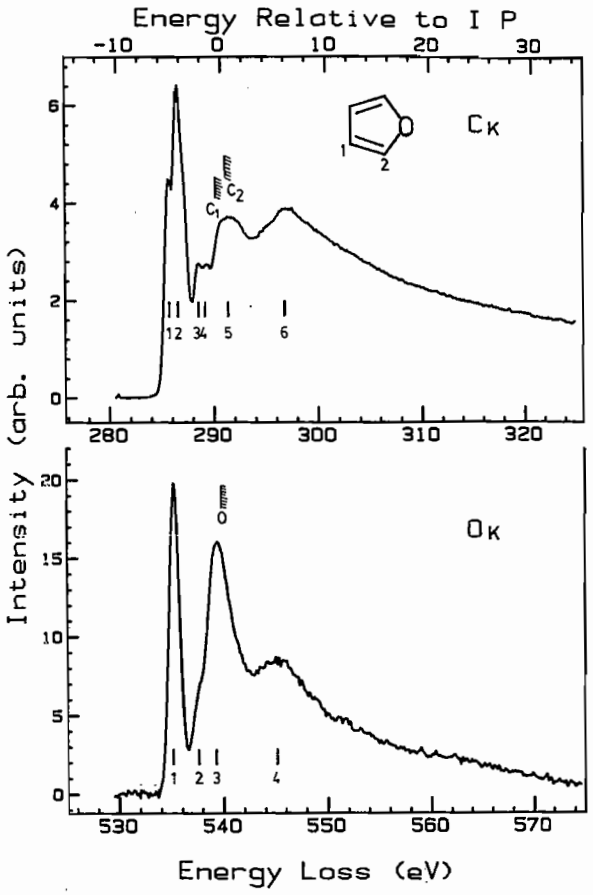

FIG. 1. The carbon and oxygen K-shell ISEELS spectra of gaseous furan recorded at 0.7 eV FWHM resolution by electron energy loss with 2.5 keV final electron energy. The hatched lines indicate the locations of the IP's as determined by XPS. A (linear) background following the shape of the underlying continuum was subtracted prior to plotting each of the spectra.

are then assigned to the C_1 $1s \rightarrow \pi^*(2a_2)$ and C_2 $1s \rightarrow \pi^*(2a_2)$ transitions. These assignments are consistent with the similarity of the 1–2 and 3–4 separations. The average separation (0.83(5) eV) is an ISEELS measure of the difference in the IP's of the two distinguishable carbon environments. This estimate is significantly lower than the measured C_1—C_2 splitting reported by two independent XPS measurements (15, 16). We have re-examined the published XPS spectrum (16) and measure a separation of 1.0 ± 0.2 eV, somewhat lower than the reported values and in better agreement with our results. If there is a smaller C_1—C_2 separation in excitation (ISEELS) rather than ionization (XPS), the electron in the π^*(C=C) level is having a different influence on the (C_1^{-1}, π^*) than on the (C_2^{-1}, π^*) state. Previously the carbon 1*s* core level separation in the monohalobenzenes was found to be essentially the same whether measured directly by XPS or indirectly by ISEELS in terms of the separation of transitions from the different core levels to the same π^* level (17).

The relative intensities of features 1 to 4 in furan provide strong support for our assignments since the $3b_1$ orbital has greater density on the C_1 and O atoms while the $2a_2$ orbital has roughly equal density on the C_1 and C_2 atoms (18). This matches the experimental observations of greatly differing intensities of the transitions from C_1 and C_2 to the $3b_1$ (#1 and #2) but very similar intensities to the $2a_2$ level (#3 and #4). The possibility that features 3 and 4 are 3*p* Rydberg transitions

TABLE 1. Energies, term values, and proposed assignments for features observed in the K-shell spectra of furan

(*a*) Carbon 1*s*

Feature	Energy (±0.1 eV)	Term value (eV) C_1	Term value (eV) C_2	Assignment[a] C_1	Assignment[a] C_2
1	285.6	4.8		$\pi^*(3b_1)$	
2	286.5[b]		5.1		$\pi^*(3b_1)$
3	288.5	1.9		$\pi^*(2a_2)$	
4	289.3		2.3		$\pi^*(2a_2)$
C_1 IP	290.4[c]				
C_2 IP	291.6[c]				
5	291.4	−0.4[d]		σ*(C—O)	
6	297.0	−6.0[d]		σ*(C—C)	

(*b*) Oxygen 1*s*

Feature	Energy (±0.1 eV)	Term value (eV)	Assignment[a]
1	535.3[e]	4.7	$\pi^*(3b_1)$
2	537.6	2.4	$3p$ or $\pi(2a_2)$
O IP	540.0[c]		
3	539.4	0.6	σ*(C—O)
4	545.3	−5.3	σ*(C—C)

[a]Transitions occur from the indicated core level to the final orbital listed.
[b]This feature is located 4.3(1) eV below the C $1s \rightarrow \pi^*$ transition in CO_2 (290.7 eV (9)).
[c]Average of two XPS determinations (15, 16).
[d]Determined relative to the average C 1*s* IP.
[e]This feature is located 1.1(1) eV above the O $1s \rightarrow \pi^*$ transition in CO (534.21(9) eV (8)).

was also considered but the indicated assignments are preferred because of the relative intensity evidence and also because the transitions to the second π^* level in benzene and pyridine (6) have appreciable intensity and similar term values to those of features 3 and 4 in the carbon K-shell spectrum of furan. The presence of these features at similar intensity in the spectrum of condensed furan would confirm our assignment.

The two remaining features (5 and 6) present an interesting dilemma. They are assigned to C $1s \rightarrow \sigma^*$ transitions or σ shape resonances which should correlate with bond lengths according to the empirical analysis of σ shape resonances by Sette *et al.* (3). Furan contains two different carbon–carbon bond lengths (136.1 and 143.1 pm) and one carbon–oxygen bond length (136.2 pm) (19). Thus the bond length correlation predicts three resonances in the carbon K-shell spectrum of furan around 10.6, 6.8, and 2.5 eV above the IP, corresponding to the three different bond lengths. However, only two continuum resonances are observed and they are located 0.4 and 6.0 eV above the average C 1*s* IP, not in the positions predicted by the simple correlation. The aromatic character of furan suggests that its resonances should be treated in a manner similar to those of benzene and pyridine (6). Further discussion of the continuum resonances (features 5 and 6) is given in section 7 in comparison to analogous features in the spectra of the other heterocyclic molecules studied.

1.2. Oxygen K-shell spectrum of furan

The oxygen K-shell electron energy loss spectrum of furan is shown in the lower panel of Fig. 1 while the energies and assignments of the observed features are listed in Table 1. Four features can be distinguished in the oxygen K-shell spectrum of furan. The first feature is assigned to the O $1s(a_1) \rightarrow \pi^*(3b_1)$ transition. This feature is appreciably narrower than the corresponding C $1s \rightarrow \pi^*(3b_1)$ features (1 and 2) in the upper panel of Fig. 1. It is clearly a single transition. In general excitations from different core levels in a molecule occur to the same set of valence antibonding orbitals with the intensities determined by dipole selection rules and overlap considerations. In oxygen 1*s* excitation the symmetry of furan remains C_{2v} and only the O $1s \rightarrow \pi^*(3b_1)$ transition is allowed by dipole selection rules. Thus only one O $1s \rightarrow \pi^*$ feature is expected. The shoulder (#2) on the low energy side of feature 3 is assigned to a $3p$ Rydberg transition based on its term value of 2.4 eV (10). It is possible that this feature is the O $1s \rightarrow \pi^*(2a_2)$ transition observed either because of vibronic coupling or as a quadrupole transition due to the finite momentum transfer under our experimental conditions. The X-ray photoabsorption spectrum of gaseous or solid furan would clarify the origin of this feature. Peaks 3 and 4 are analogous to features 5 and 6 in the carbon K-shell spectrum and are also assigned to σ shape resonances. Within the simple bond length correlation (3) only a single resonance associated with the C—O bond is expected while transitions to σ* states associated with carbon–carbon bonds should not be observed. The presence of an additional σ resonance in the oxygen K-shell spectrum suggests that there are interacting σ* levels in furan which produce delocalized σ* states similar to those in benzene and pyridine (6).

2.1. Carbon K-shell spectrum of pyrrole

Pyrrole is an aromatic five-membered ring, isoelectronic with furan with the oxygen replaced by an NH group. The spectrum of pyrrole might then be expected to resemble those of furan and pyridine. The carbon K-shell electron energy loss spectrum of pyrrole and the energies and proposed assignments of the observed features are presented in Fig. 2 and Table 2 respectively. As with furan there are four possible dipole-allowed $1s \rightarrow \pi^*$ transitions. According to XPS (15, 16) the carbon 1*s* IP's are separated by 1.0 eV. Valence shell studies (20) and *ab initio* calculations (21) indicate that the $3b_1$ and $2a_2$ π^* levels are separated by about 0.9 eV. The splittings of both the carbon 1*s* and π^* levels are considerably smaller in pyrrole than in furan so the four separate transitions will not be as well resolved as in furan. The fwhm of the broad feature centered at 286.3 is 1.8 eV, considerably greater than the instrumental resolution (0.7 eV as measured on the C $1s \rightarrow \pi^*$ transition in CO or on the main beam). Close inspection of its lineshape (see insert to Fig. 2) shows a shoulder on the low energy side around 285.6 eV. Thus the low energy shoulder (#1) is assigned to the C_1 $1s \rightarrow \pi^*(3b_1)$ transition and the main intensity of the peak (#2) to the C_2 $1s \rightarrow \pi^*(3b_1)$ transition. As with furan the C_1 $1s \rightarrow \pi^*(3b_1)$ transition is weaker than the C_2 $1s \rightarrow \pi^*(3b_1)$, consistent with the lower density of the $3b_1$ orbital on the carbons farthest from the nitrogen (18). A shoulder is not observed on feature 3, which is not unexpected at our experimental resolution from two equal intensity transitions to the $\pi^*(2a_2)$ level. Higher resolution spectra would be very desirable to confirm our spectral interpretation and to provide more accurate transition energies.

Peaks 4, 5, and 6 in the carbon K-shell spectrum of pyrrole are assigned to σ shape resonances similar to those in furan and pyridine. Again, as in furan, the simple relationship (3) predicts three resonances at 3.9, 7.4, and 9.6 eV above the IP in the carbon K-shell spectrum corresponding to the carbon–nitrogen (137 pm) and carbon–carbon (142, 138 pm) bond lengths (19).

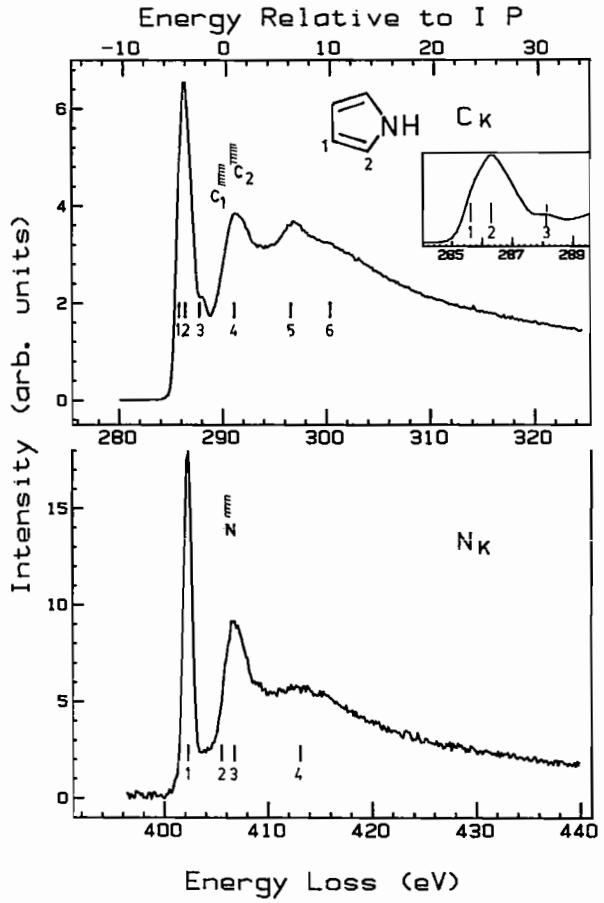

FIG. 2. The carbon and nitrogen K-shell ISEELS spectra of gaseous pyrrole recorded by electron energy loss. The hatched lines indicate the locations of the IP's as determined by XPS. The insert in the upper panel is an expansion of the spectrum in the region of the first three features.

Three resonances are observed at 1, 6.5, and 11 eV above the average C 1*s* IP. In contrast to furan the simple predictions seem to be in fair agreement with the experimental spectrum. However, the highest energy continuum feature is very broad and weak relative to the other two. While this feature may be a σ shape resonance, its absence in the furan spectrum suggests an alternate assignment such as a multielectron process (shake-up). The XPS satellite spectrum shows a prominent feature 7.6 eV above the main line (16) which is in reasonable agreement with the onset of feature 6 at 298 eV, about 8 eV above threshold. K-shell excitation features previously identified as shake-up onsets (22) have generally been weaker and more rapidly damped than feature 6 in pyrrole. Another possibility is a weak splitting of the σ shape resonances as suggested by MSXα calculations for benzene (6). From the studies of benzene and pyridine (6) one expects greatest deviation from the simple correlation in delocalized aromatic molecules. Since pyrrole is more aromatic than furan (23) we have also considered the intensity weighted average interpretation for the pyrrole continuum features (see section 7).

2.2. *Nitrogen K-shell spectrum of pyrrole*

The nitrogen K-shell electron energy loss spectrum of pyrrole is presented in the lower panel of Fig. 2 while the energies of the features and proposed assignments are listed in Table 2. To an even greater extent than the carbon K-shell spectra, the heteroatom core spectra of pyrrole and furan are similar. As

TABLE 2. Energies, term values, and proposed assignments for features observed in the K-shell spectra of pyrrole

(*a*) Carbon 1*s*

Feature	Energy (±0.1 eV)	Term value (eV) C_1	Term value (eV) C_2	Assignment[a] C_1	Assignment[a] C_2
1	285.6	4.2		$\pi^*(3b_1)$	
2	286.3[b]		4.5		$\pi^*(3b_1)$
3	288.1		2.2[c]	$\pi^*(2a_2)$	$\pi^*(2a_2)$[d]
C_1 IP	289.8[e]				
C_2 IP	290.8[e]				
4	291.3		−1.0[c]	σ*(C—N)	
5	296.8		−6.5[c]	σ*(C—C)	
6	300.5(8)		−10[c]	σ*(C═C)	

(*b*) Nitrogen 1*s*

Feature	Energy (±0.1 eV)	Term value (eV)	Assignment[a]
1	402.3[f]	3.8	$\pi^*(3b_1)$
2	405.9	0.2	4*p*
N IP	406.1[e]		
3	406.7	−0.6	σ*(C—N)
4	413.4	−7.3	σ*(C—C)

[a]Transitions occur from the indicated core level to the final orbital listed.
[b]This feature is located 4.4(1) eV below the C 1*s* → π* transition in CO_2 (290.7 eV (9)).
[c]Determined relative to the average C 1*s* IP.
[d]Not resolved as separate features.
[e]From XPS (11).
[f]This feature is located 1.2(1) eV above the N 1*s* → π* transition in N_2 (401.1(1) eV (8)).

with furan, dipole selection rules identify the first feature as the N $1s(a_1) \rightarrow \pi^*(3b_1)$ transition. A peak attributable to the N $1s \rightarrow \pi^*(2a_2)$ transition is not observed, as expected from its dipole-forbidden character. However, the valley between the first and second features is not baseline resolved suggesting some transition intensity which could be the dipole-forbidden $2a_2$ transition. Feature 2, a shoulder on #3, probably arises from Rydberg transitions. The two continuum features (3 and 4) are similar in appearance to those found in the oxygen K-shell spectrum of furan and are assigned correspondingly to σ shape resonances with the one at lower energy being closely associated with the C—N bond. The higher energy feature (#4) could arise from shake-up. However shake-up satellites are observed only at 8.7 and 15.1 eV above the N 1*s* IP in pyrrole (16), neither of which correlate with the onset of feature 4 around 411 eV, about 5 eV above threshold. The presence of two resonances where only the σ*(C—N) feature might be expected indicates that the σ*(C—C) levels are delocalized and have some density at the nitrogen atom.

3.1. *Carbon K-shell spectrum of tetrahydrofuran*

The carbon K-shell electron energy loss spectrum of tetrahydrofuran (THF) is shown in Fig. 3 while the energies and proposed assignments of the observed features are listed in Table 3. Tetrahydrofuran is the oxygen heterocyclic analog of cyclopentane and thus the carbon K shell spectrum of THF might be expected to be similar to that of cyclopentane (5). While the spectra are not precisely the same, some similarities can be noted. In cyclopentane, as in cyclohexane, a sharp

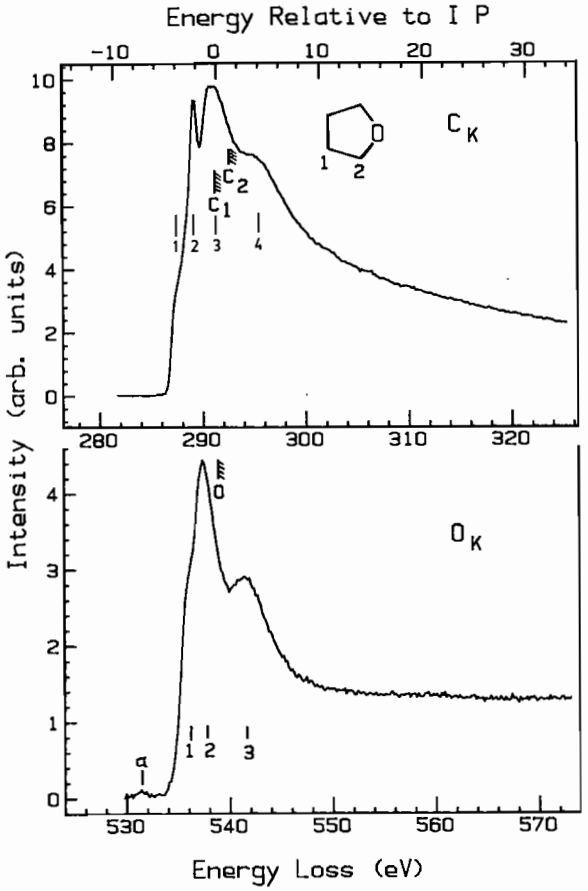

FIG. 3. The carbon and oxygen K-shell ISEELS spectra of gaseous tetrahydrofuran recorded by electron energy loss. The hatched lines indicate the estimated locations of the IP's.

TABLE 3. Energies, term values, and proposed assignments for features observed in the K-shell spectra of tetrahydrofuran

(*a*) Carbon 1*s*

Feature	Energy (±0.1 eV)	Term value (eV) C_1	Term value (eV) C_2	Assignment[a] C_1	Assignment[a] C_2
1	287.6(2)	3.2		$\pi^*(CH_2)$	
2	289.2		2.8		$\pi^*(CH_2)$
C_1 IP	290.8(5)[b]				
C_2 IP	292.0(5)[b]				
3	291.0[c]	0.5[d]		σ^*(C—O), σ^*(C—C)	
4	294.9	−3.6[d]		σ^*(in-ring)	

(*b*) Oxygen 1*s*

Feature	Energy (±0.1 eV)	Term value (eV)	Assignment[a]
a	531	—	(peroxide)
1	536.0	3.0	$\pi^*(CH_2)$
O IP	539.0(5)[b]		
2	537.4[e]	1.6	σ^*(C—O)
3	541.4	−2.4	σ^*(in-ring)

[a]Transitions occur from the indicated core level to the final orbital listed.
[b]Estimated from the XPS IP's of furan and ethanol (11).
[c]This feature is located 3.6(1) eV below the C 1*s* → π^* transition in CO (287.40 eV (8)).
[d]Determined relative to the average C 1*s* IP.
[e]This feature is located 3.2(1) eV above the O 1*s* → π^* transition in CO (534.2 eV (8)).

feature below the IP has been assigned to transitions to a $\pi^*(CH_2)$ level (5). This assignment was based on the observation of a corresponding feature in the C 1*s* spectra of both solid and chemisorbed cyclohexane recorded by partial photoelectron yield (near edge X-ray absorption fine structure, NEXAFS). A strong polarization dependence of the NEXAFS feature was observed, consistent with transitions to a state of π symmetry with respect to the C—H bond. Both its observation in the condensed phase spectrum and the strong polarisation dependence rule out a Rydberg assignment for this feature. The existence of unoccupied $\pi^*(CH_2)$ levels, their spatial distribution and their importance in descriptions of the electronic structure of saturated organic molecules has been noted by Jorgensen and Salem (18). Based on comparison to cyclopentane and cyclohexane features 1 and 2 in THF are also assigned to $\pi^*(CH_2)$ states corresponding to transitions from the C_1 and C_2 levels, respectively.

The third feature in the C 1*s* spectrum of THF is a σ shape resonance associated with the carbon–carbon and carbon–oxygen bonds. All of the carbon–carbon bond lengths in THF are very similar (19) and therefore only one σ(C—C) resonance is expected at 1.1 eV above the IP. In addition the bond length correlation predicts a σ shape resonance for the C—O bond at 0.6 eV above the IP which should be roughly 40% as intense as the σ(C—C) feature. Close examination of feature 3 in Fig. 3 reveals indications of two maxima (at 290.7 and 291.2 eV) at the top of this broad peak. The 0.5 eV separation of these maxima is in good agreement with the predicted separation of the σ(C—O) and σ(C—C) resonances. Feature 3 is significantly broader than the σ(C—O) resonance in the O 1*s* spectrum (feature 2 in the lower panel of Fig. 3). The increased width of this feature in the C 1*s* spectrum is likely associated with the overlap of the lower energy σ(C—O) resonance with two σ^*(C—C) features at higher energy separated by the 1.2 eV spacing of the two C 1*s* levels. According to the simple correlation (3) feature 4 is too high in energy to correlate directly with any of the bond lengths in THF. A continuum feature similar to peak 4 in THF was also observed in cyclopentane (5) and was assigned to transitions to a second σ^* state, possibly arising from the overlap of in-ring orbitals. A similar assignment is proposed for feature 4 in THF (see section 7 for further discussion).

3.2. Oxygen K-shell spectrum of tetrahydrofuran

The oxygen K-shell electron energy loss spectrum for THF is shown in the lower panel of Fig. 3 while the energies and proposed assignments of the observed features are listed in Table 3. The oxygen K-shell spectrum is quite similar to the carbon K-shell spectrum, indicating that the unoccupied levels are substantially delocalized. A weak peak, observed at 531 eV, is attributed to residual peroxide since a much more intense peak was observed at exactly the same energy in the undistilled sample. The first THF feature, which appears only as a shoulder, is assigned to transitions to the $\pi^*(CH_2)$ level as in the carbon K-shell spectrum. This indicates that these levels are not localized on the carbon atoms but can be reached by a 1*s* excitation from any atom provided it is dipole-allowed. The second feature is assigned to a σ shape resonance associated with the C—O bond. The final feature in the oxygen K-shell

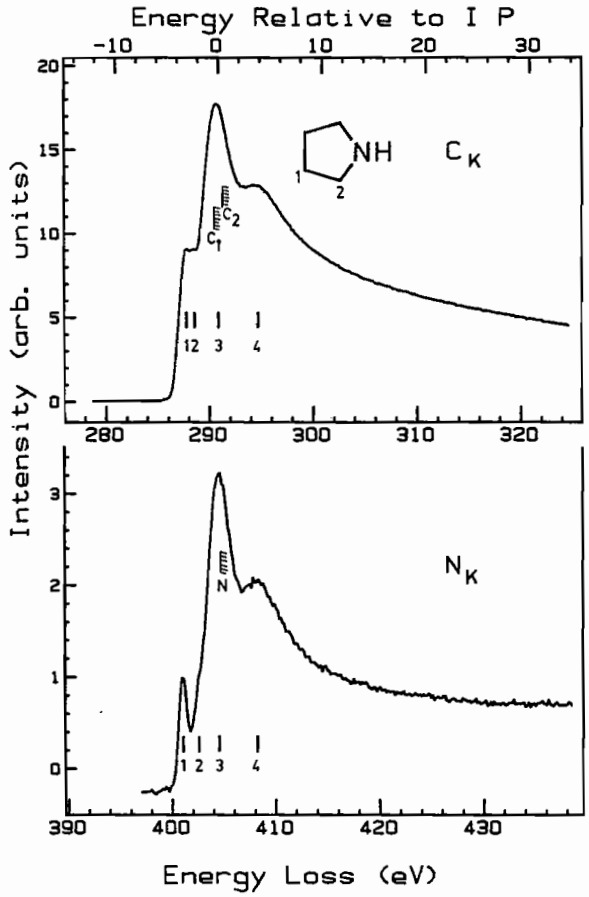

FIG. 4. The carbon and nitrogen K-shell ISEELS spectra of gaseous pyrrolidine recorded by electron energy loss. The hatched lines indicate the locations of the IP's as determined either by XPS (N_K) or by estimates from the IP's of similar compounds.

TABLE 4. Energies, term values, and proposed assignments for features observed in the K-shell spectra of pyrrolidine

(*a*) Carbon 1*s*

Feature	Energy (±0.1 eV)	Term value (eV) C_1	Term value (eV) C_2	Assignment[a] C_1	Assignment[a] C_2
1	287.7	2.6		$\pi^*(CH_2)$	
2	288.4		2.6		$\pi^*(CH_2)$
C_1 IP	290.3(5)[b]				
C_2 IP	291.0(5)[b]				
3	290.7[c]	0[d]		σ*(C—N), σ*(C—C)	
4	294.6(6)	−4[d]		σ*(in-ring)	

(*b*) Nitrogen 1*s*

Feature	Energy (±0.1 eV)	Term value (eV)	Assignment[a]
1	401	3.6	$\pi^*(CH_2)$
2 (sh)	402.5	2.1	3*p*
N IP	404.6[e]		
3	404.5[f]	0.1	σ*(C—N)
4	408.0	−3.4	σ*(in-ring)

[a]Transitions occur from the indicated core level to the final orbital listed.
[b]Estimated from the XPS IP's of pyrrole and amines (11).
[c]This feature is located 3.3(1) eV below the C 1*s* → π* transition in CO (287.40 eV (8)).
[d]Determined relative to the average C 1*s* IP.
[e]From XPS (11).
[f]This feature is located 3.40(6) eV above the N 1*s* → π* transition in N_2 (401.1(1) eV (8)).

spectrum is a transition to a second σ shape resonance analogous to feature 4 in the carbon K-shell spectrum.

4.1. Carbon K-shell spectrum of pyrrolidine

Pyrrolidine, C_4H_8NH, is the nitrogen heterocyclic analog of cyclopentane. Since nitrogen is not as electronegative as oxygen, the perturbation of the ring electronic structure is expected to be less and the carbon K-shell spectrum of pyrrolidine, shown in Fig. 4, should and does resemble that of cyclopentane more closely than does that of THF. The energies and assignments of spectral features are listed in Table 4. There are four identifiable features in the spectrum. The first and second features occur at an energy and intensity similar to the features assigned to the C 1*s* → $\pi^*(CH_2)$ transitions in cyclopentane and THF (see Fig. 7). The two C 1*s* → $\pi^*(CH_2)$ transitions in pyrrolidine are closely spaced because of the small separation of the C_1 and C_2 carbon 1*s* levels. The separation of features 1 and 2 (0.7(1) eV) is in good agreement with that of the two C 1*s* IP's estimated from the IP's of similar molecules. The $\pi^*(CH_2)$ transitions in pyrrolidine are less distinct than those in THF because the separation of the two C 1*s* levels is considerably smaller.

The major feature (#3) is assigned to the σ shape resonance associated with the carbon–carbon bond. There should also be a resonance associated with the carbon–nitrogen bond. However, the σ(C—N) transition does not appear as a distinct feature because of overlap with the σ(C—C) resonance. Feature 4 is assigned to a second σ transition, possibly associated with an in-ring σ* state, similar to those seen in cyclopentane and THF. These features are discussed in more detail in section 7.

4.2. Nitrogen K-shell spectrum of pyrrolidine

The nitrogen K-shell spectrum of pyrrolidine is shown in the lower panel of Fig. 4 while the energies and proposed assignments of the observed features are listed in Table 4. The nitrogen K-shell spectrum shows four features and bears a strong resemblance to the carbon K-shell spectrum of pyrrolidine. The first feature is at essentially the same energy as the intense N 1*s* → π* transition in N_2 and was originally suspected to arise from nitrogen impurity or an air leak. However, the absence of signal in the oxygen K-shell region eliminated the air leak explanation. Extensive degassing was done to remove any N_2 trapped in the liquid. The intensity of feature 1 with respect to the rest of the spectrum remained constant throughout successive degassings. Thus we are convinced that this is a true spectral feature of pyrrolidine. In analogy with features 1 and 2 in the C 1*s* spectrum it is assigned to transitions to a delocalized $\pi^*(CH_2)$ level. The shoulder 2, on the low energy side of the third feature, is assigned to a 3*p* Rydberg transition based on its term value of 2.1 eV. The largest feature in the spectrum is the σ shape resonance associated with the carbon–nitrogen bond. Feature 4 is assigned to a second σ shape resonance analogous to that observed in the C 1*s* spectra of pyrrolidine, THF, and cyclopentane (see Fig. 7). The $\pi^*(CH_2)$ and continuum features are discussed further in section 7.

5.1. Carbon K-shell spectrum of tetrahydropyran

The carbon K-shell spectrum of tetrahydropyran (THP) is

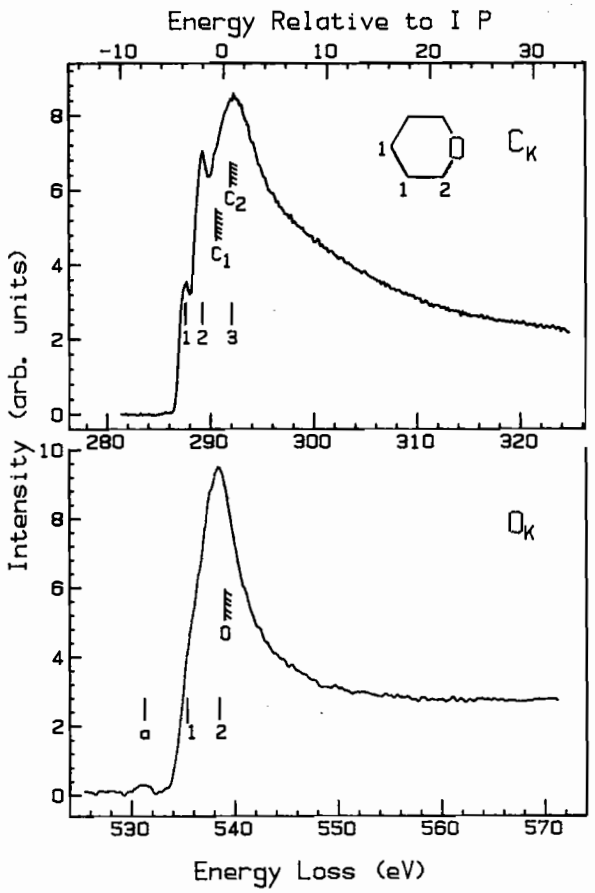

FIG. 5. The carbon and oxygen K-shell ISEELS spectra of gaseous tetrahydropyran recorded by electron energy loss. The hatched lines indicate the estimated locations of the IP's.

TABLE 5. Energies, term values, and proposed assignments for features observed in the K-shell spectra of tetrahydropyran

(*a*) Carbon 1*s*

Feature	Energy (±0.1 eV)	Term value (eV) C_1	Term value (eV) C_2	Assignment[a] C_1	Assignment[a] C_2
1	287.7	3.1		$\pi^*(CH_2)$	
2	289.3[b]		2.7		$\pi^*(CH_2)$
C_1 IP	290.8(5)[c]				
C_2 IP	292.0(5)[b]				
3	292.3	−0.9[d]		σ^*(C—O), σ^*(C—C)	

(*b*) Oxygen 1*s*

Feature	Energy (±0.1 eV)	Term value (eV)	Assignment[a]
a	531		π^*(in O_2)[e]
1 (sh)	536.6	3.4	$\pi^*(CH_2)$
O IP	539.0(5)[c]		
2	538.3[f]	0.7	σ^*(C—O)

[a]Transitions occur from the indicated core level to the final orbital listed.
[b]This feature is located 4.6(1) eV above the C 1*s* → π^* transition in C_2H_4 (284.7(1) eV (4)).
[c]Estimated from the XPS IP's of furan and ethanol (11).
[d]Determined relative to the average C 1*s* IP.
[e]The O 1*s* → π^* transition in O_2 occurs at 530.6 eV (25).
[f]This feature is located 4.1(1) eV above the O 1*s* → π^* transition in CO (534.2(1) eV (8)).

presented in Fig. 5 while the energies and proposed assignments are listed in Table 5. The spectrum is similar to those of cyclohexane (5) and piperidine (section 6.1) and resembles that of THF. According to our estimates the C 1*s* IP's of the two distinguishable carbon environments differ by about 1.2(7) eV. Thus transitions from these two levels to a common unoccupied level should be clearly resolved with our apparatus. On this basis the first two features are assigned to C_1 1*s* → $\pi^*(CH_2)$ and C_2 1*s* → $\pi^*(CH_2)$ transitions, respectively, analogous to the assignments of the first features in the carbon K-shell spectra of both cyclohexane and piperidine. The measured separation of features 1 and 2 (1.64(1) eV) suggests that the separation of the estimated C 1*s* IP's of THP may be too small. The total intensity of the C 1*s* → $\pi^*(CH_2)$ transitions increases as heavier heteroatoms are substituted for carbon (see Fig. 7). The explanation for this is not clear although the shift in intensity from C_1 to C_2 excitation in the CH_2 → NH → O sequence indicates that the electron density in the $\pi^*(CH_2)$ orbital shifts systematically towards the heteroatom end of the molecule. Further discussion of the $\pi^*(CH_2)$ transitions is given in section 7.

The third feature is assigned to the σ(C—C) shape resonance. There is no distinguishable feature from the σ(C—O) presumably since it overlaps the σ(C—C) resonance. The predicted σ(C—C) and σ(C—O) resonance positions are 0.9 and 0.5 eV above the edge while feature 3 has a width of at least 4 eV. This is noticeably wider than the continuum resonance in the oxygen K-shell spectrum of THP (feature 2 in the lower panel of Fig. 5) because of overlapping transitions from the C_1 and C_2 levels to both the σ(C—C) and σ(C—O) levels. As with piperidine (section 6.1) the σ resonance region is in good accord with the expectations from the simple correlation, in contrast to the situation in the spectra of the five-membered ring heterocyclics.

5.2. *Oxygen K-shell spectrum of tetrahydropyran*

The oxygen K-shell spectrum of THP is shown in the lower panel of Fig. 5 while the energies and proposed assignments are listed in Table 5. A weak feature is observed around 531 eV from the O 1*s* → π^* transition in impurity O_2 or possibly peroxide contamination. The THP oxygen K-shell spectrum is dominated by one intense broad feature which is attributed to the σ shape resonance associated with the C—O bond. There is a relatively intense shoulder on the low energy side of the σ^*(C—O) feature which likely arises from transitions to the $\sigma^*(CH_2)$ level. As with the nitrogen K-shell spectrum of piperidine (section 6.2) the simple one bond, one resonance picture (3) is in good agreement with the observed spectrum.

6.1. *Carbon K-shell spectrum of piperidine*

The carbon K-shell electron energy loss spectrum of piperidine, $C_5H_{10}NH$, is shown in Fig. 6 while the energies and proposed assignments of the observed features are listed in Table 6. The carbon K-shell spectrum of piperidine should and does closely resemble that of cyclohexane since the replacement of a CH_2 with an NH group should have even less effect in a six- than a five-membered ring. The first and second features in the carbon K-shell spectrum of piperidine are assigned to the C_1 1*s* → $\pi^*(CH_2)$ and C_2 1*s* → $\pi^*(CH_2)$ transitions, respectively. The separation of 0.82(4) eV between these two features is an ISEELS estimate of the splitting of the C_1 and C_2 levels. In

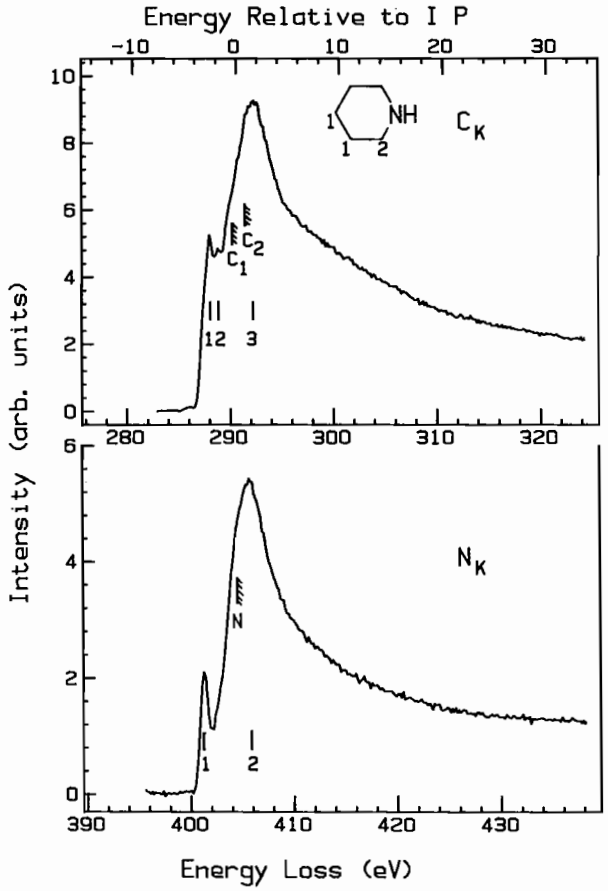

FIG. 6. The carbon and nitrogen K-shell ISEELS spectra of gaseous piperidine recorded by electron energy loss. The hatched lines indicate the locations of the IP's as determined either by XPS (N_K) or by estimates from the IP's of similar compounds.

contrast to the C_1—C_2 separation of the π^*(C=C) transitions in furan and pyrrole, it is in good agreement with that of the estimated C 1*s* IP's.

The third feature is assigned to overlapping σ(C—C) and σ(C—N) shape resonances. Interestingly a peak analogous to peak 4 in the carbon K-shell spectrum of pyrrolidine is not observed in piperidine. This feature was also less intense in cyclohexane than in cyclopentane (5). This suggests that the positions and intensities of continuum excitations depend on ring geometry as well as on the type of heteroatom and the bond lengths (see section 7).

6.2. *Nitrogen K-shell spectrum of piperidine*

The nitrogen K-shell electron energy loss spectrum of piperidine is shown in the lower panel of Fig. 6 while the energies and proposed assignments of the observed features are listed in Table 6. The N 1*s* and C 1*s* spectra of piperidine are very similar indicating that transitions are occurring to a common set of delocalized levels. The first feature, a sharp, well-resolved peak, is quite intense and is likely due to a N $1s \rightarrow \pi^*(CH_2)$ transition as in pyrrolidine. Observation of an unchanging intensity with successive degassings ruled out the possibility of impurity N_2 in the sample. The presence of this transition in the heteroatom core edge spectrum of each of the saturated heterocyclic molecules is an indication that the $\pi^*(CH_2)$ orbital is not highly localized on the carbon atoms. The second feature is the σ shape resonance from the carbon–nitrogen bond. There are no features beyond this peak again

TABLE 6. Energies, term values, and proposed assignments for features observed in the K-shell spectra of piperidine

(*a*) Carbon 1*s*

Feature	Energy (±0.1 eV)	Term value (eV) C_1	Term value (eV) C_2	Assignment[a] C_1	Assignment[a] C_2
1	288.0	2.3		$\pi^*(CH_2)$	
2	288.8		2.2		$\pi^*(CH_2)$
C_1 IP	290.3(5)[b]				
C_2 IP	291.0(5)				
3	292.2[c]	−1.2[d]		σ^*(C—N), σ^*(C—C)	

(*b*) Nitrogen 1*s*

Feature	Energy (±0.1 eV)	Term value (eV)	Assignment[a]
1	401.2	3.4	$\pi^*(CH_2)$
N IP	404.6[b]		
2	405.6[f]	−1.0	σ^*(C—N)

[a]Transitions occur from the indicated core level to the final orbital listed.
[b]Estimated from the XPS IP's of pyrrole and amines (11).
[c]This feature is located 4.8(1) eV above the C $1s \rightarrow \pi^*$ transition in CO (287.40 eV (8)).
[d]Determined relative to the average C 1*s* IP.
[e]From XPS (11).
[f]This feature is located 4.5(1) eV above the N $1s \rightarrow \pi^*$ transition in N_2 (401.1(1) eV (8)).

suggesting that the intensity of the second σ shape resonance which was present in the five-membered saturated rings is strongly geometry dependent. Since the feature is present at a low intensity in cyclohexane but absent in piperidine, a dependence on the heteroatom also exists.

7. *Systematics of π^* intensities and the positions of K-shell continuum resonances*

A comparison of the carbon K-shell spectra of the CH_2, NH, and O five- and six-membered rings is presented in Fig. 7. There are interesting trends in the intensities of the discrete features attributed to the $\pi^*(CH_2)$ states. The NH and O heterocyclics each have two distinguishable C 1*s* environments and a splitting of the $\pi^*(CH_2)$ features is observed, as expected. Because of the 50% increase in number of C_1 carbons one might expect a large increase in the $C_1 \rightarrow \pi^*(CH_2)$ transition relative to that from C_2 as the ring size increases from 5 to 6. Although an increase is observed it is much smaller than expected. A more dramatic effect is observed in the comparison of the NH and O species. The $C_2 \rightarrow \pi^*(CH_2)$ feature is substantially more intense in THF or THP than it is in pyrrolidine or piperidine. This suggests that the $\pi^*(CH_2)$ level has considerably greater density at the heteroatom end of the molecule and that the electron density shifts towards the heteroatom as the heteroatom electronegativity increases. This is also consistent with the increased intensity of the $\pi^*(CH_2)$ features in the O K-shell spectra of THF and THP relative to those in the N K-shell spectra of pyrrolidine or piperidine (see Figs. 3–6) (although the shift to higher energy caused by the more electronegative O results in greater overlap with higher energy features in the O 1*s* spectra). Finally there is an obvious increase in the width of the first *continuum* feature through the $CH_2 \rightarrow NH \rightarrow O$ sequence in both the five- and six-membered ring series. This increased width is partially due to overlap of the σ(C—C) and σ(C—O)

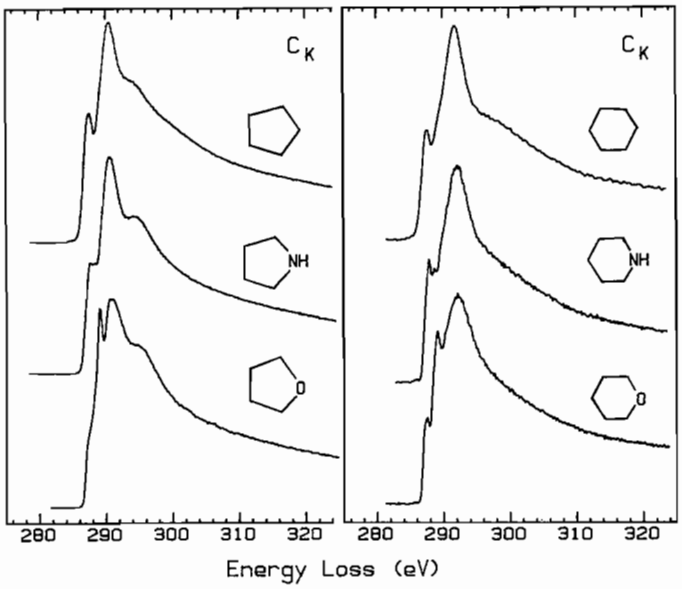

FIG. 7. Comparison of the carbon K-shell spectra of the five- and six-membered (CH_2, NH, O) saturated rings.

resonances in the heterocyclics but it is also indicative of the occurrence of transitions to both σ* levels from each of the two distinguishable C 1*s* levels which are separated by increasing amounts in the NH (0.7 eV) and O (1.2 eV) cases. This same trend of increasing widths of σ resonances is apparent also in the series cyclopentene (5), pyrrole (Fig. 2), and furan (Fig. 1), again in good agreement with contributions of transitions from two separate C 1*s* levels.

Turning now to the positions of continuum features, the correlation between δ, the shape resonance position relative to the IP, and *R*, the bond length, gives reasonable results for the ISEELS spectra of many molecules (2, 3, 5). Among the heterocyclic molecules studied in this work, those with simple bonding generally show good agreement between predicted and experimental results. However, although there is a continuum feature in each of the saturated molecules which correlates well with bond length, an additional continuum feature is also observed, in some cases with appreciable intensity. The second continuum feature in THF and pyrrolidine is similar to that seen in cyclopentane (5) and is similarly assigned to in-ring σ* states. This feature appears to decrease in intensity from THF to pyrrolidine and then to cyclopentane (see Fig. 7). This is consistent with shorter C—O and C—N bonds. The more constrained geometry should increase the overlap of the in-ring σ* orbitals and thus the splitting of the derived states. It is interesting to note that compared to the five-membered rings, the spectra of the six-membered rings are all in much better agreement with the one bond, one resonance picture. A second continuum feature is observed weakly only in the spectrum of cyclohexane (see Fig. 7). This suggests that the overlap of σ* states is less in the larger rings so that delocalization and splittings are greatly reduced compared to smaller rings. Note however that the continuum resonances in the C 1*s* spectra of the six-membered rings are significantly wider than the first continuum resonances in the corresponding five-membered ring. The increased width suggests that there may be overlap with a second resonance.

In the two aromatic molecules, furan and pyrrole, the number and positions of the observed resonance features are not fully

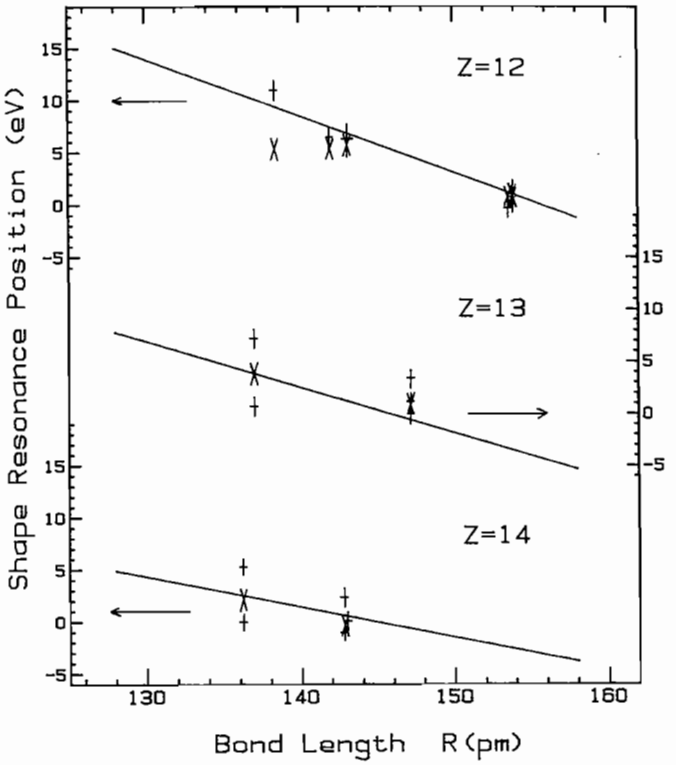

FIG. 8. Plots of the bond length versus resonance position for Z = 12 (C—C), Z = 13 (C—N), and Z = 14 (C—O) bonds in the heterocyclic molecules studied in this work. The daggers indicate the positions of individual spectral features while the X's indicate intensity weighted average positions of several continuum features. The straight lines are the correlation lines derived earlier from the spectra of other molecules (3). The data used for this figure are listed in Table 7.

consistent with the simple correlation suggesting that a different interpretation may be required. In the K-shell continua of benzene, pyridine (6), and borazine (24) two resonances are observed whereas only one is expected (2, 3). Based on the correlation derived from smaller molecules the intensity-weighted average (IWA) positions of the experimentally observed resonances give much better estimates of the C—C, C—N, and B—N bond lengths than the positions of any single resonance feature (6, 24). The merits of a similar approach for the spectra of furan and pyrrole have been investigated. The intensity weighted average positions were determined by first subtracting an estimation of the smooth continuum upon which the resonances are located. The position and area of each background-subtracted peak were then measured and the IWA calculated. The relevant data for all of the molecules studied in this work are listed in Table 7 while the observed resonance positions and their intensity weighted averages are plotted against bond length in Fig. 8. For both furan and pyrrole, the intensity weighted averages of the two heteroatom continuum resonances gives better agreement with the correlation than does the position of either of the individual features. The continuum resonances in the carbon K-shell spectrum of pyrrole are well interpreted within the simple correlation. For the carbon–carbon distances in furan, if peak 5 is assigned to overlapping σ(C—O) and σ(C—C) and peak 6 to σ(C=C), the IWA improves the situation relative to this one-bond one-resonance assignment although the fit is not spectacular. This may be a reflection of the lesser degree of aromaticity in pyrrole or furan with respect to benzene and pyridine. The decrease in π delocalization appears

TABLE 7. Bond lengths and continuum resonance positions for heterocyclic molecules

Molecule	Edge	E_σ	IP[a]	Resonance position (eV) δ	Direct[b]	IWA[c]	Pred[d]	Bond length[e]
$Z = 12$								
C_4H_4O	C1*s*	297.0	291.0		—	—	10.6	136.1
	C1*s*	291.4	291.0		6.0	5.5	6.8	143.1
C_4H_4NH	C1*s*	296.8	290.3		11.0	5.2	9.6	138.4
	C1*s*	291.3	290.3		6.5	5.2	7.4	142.0
C_4H_8O	C1*s*	291.0	291.4[f]		−0.4	0.5	1.1	153.6
C_4H_8NH	C1*s*	290.7	290.7[f]		0.0	0.5	0.9	153.9[g]
$C_5H_{10}O$	C1*s*	292.3	291.4[f]		1.0	—	0.9	153.9[g]
$C_5H_{10}NH$	C1*s*	292.2	290.7[f]		1.5	—	0.9	153.9[g]
$Z = 13$								
C_4H_4NH	C1*s*	291.3	290.3	1.0	0.8	3.6	3.9	137.0
	N1*s*	406.7	406.1	0.6				
C_4H_8NH	C1*s*	290.7	290.7[f]	0.0	0.0	0.7	−0.6	147.2[h]
	N1*s*	404.5	404.6	−0.1				
$C_5H_{10}NH$	C1*s*	292.2	290.7[f]	1.5	1.2	—	−0.6	147.2[h]
	N1*s*	405.6	404.6	1.0				
$Z = 14$								
C_4H_4O	C1*s*	291.4	290.9	0.4	−0.1	1.9	2.5	136.2
	O1*s*	539.4	540.0	−0.6				
C_4H_8O	C1*s*	291.0	291.4[f]	−0.4	−1.0	−0.6	0.6	142.8
	O1*s*	537.4	539.0	−1.6				
$C_5H_{10}O$	C1*s*	292.3	291.4[f]	0.9	0.1	—	0.5	143.0[h]
	O1*s*	538.3	539.0	−0.7				

[a]From XPS (11) except where noted. For those core edges with distinguishable environments the average of the two C 1*s* IP's has been used.

[b]Determined as $\delta = E_\sigma - IP$ from the values listed. For the $Z = 13$ and $Z = 14$ data the average of the δ values from the carbon and heteroatom spectra is listed.

[c]Position (±0.8 eV) determined from the intensity weighted average of the continuum features observed in the same core edge spectrum. The IWA was determined by subtracting an estimated background representing the underlying non-resonant continuum, measuring the position (E) and area (A) and calculating: $IWA = (E_1A_1 + E_2A_2)/(A_1 + A_2)$.

[d]Predicted from the previously reported correlation (3) according to the linear relationship: $\delta = m - n \times R$, with [m (eV), n (eV pm^{-1})] values of: (84.73, 0.5445) for $Z = 12$; (64.15, 0.4401) for $Z = 13$; and (42.19, 0.2913) for $Z = 14$.

[e]Bond lengths (pm) are from (19) except where noted.

[f]Estimated from the IP's of similar molecules (11) (see text).

[g]Estimated from Stoicheff rules (26).

[h]Estimated from average C—N and C—O bond lengths (27).

to be accompanied by a decrease in σ delocalization which results in a situation intermediate between benzene and the more localized aliphatic molecules. An alternate assignment of furan gives good agreement with the bond length correlation within the simple one bond one-resonance picture. This occurs if peak 5 in the C K-shell spectrum of furan is assigned to σ(C—O) and peak 6 to σ(C—C), with no feature in the spectrum being explicitly associated with σ(C=C). A high energy tail on peak 6 can be discerned by comparison to the O K-shell spectrum which may be how the σ(C=C) intensity appears in furan. This interpretation is the one presented in Tables 1 and 7. Calculations of the continuum cross-sections in furan and pyrrole would be helpful in evaluating these alternate interpretations.

For all of the heterocyclic molecules the heteroatom core spectrum resembled the C 1*s* spectrum of the same molecule quite closely. This indicates that the unoccupied levels in these molecules are extensively delocalized so that, within symmetry restrictions, transitions to all antibonding orbitals occur from any site with finite intensity. In the heteroatom spectra of furan and pyrrole, the first σ shape resonance is more intense, relative to the higher energy resonance, than it is in the corresponding carbon 1*s* spectrum. This resonance is approximately where the σ(C—O) or σ(C—N) shape resonances would be expected in a localized picture. The increased intensity of this feature, relative to its counterpart in the carbon spectrum, appears to be a further reflection of the decrease in aromaticity of furan and pyrrole relative to pyridine and benzene, where the two continuum resonances are more similar in intensity (6).

Conclusions

The core excitation spectra of furan, pyrrole, tetrahydrofuran, pyrrolidine, tetrahydropyran, and piperidine have been recorded by gas phase ISEELS spectroscopy and assignments have been proposed for all observed features. To our knowledge none of these spectra have been reported previously. The spectra of the saturated heterocyclic molecules are similar to those of their cyclic hydrocarbon analogs. In all cases the carbon and heteroatom K-shell spectra are generally similar indicating that transitions occur to a common set of extensively delocalized unoccupied levels. Features attributed to a $\pi^*(CH_2)$ state were observed about 3 eV below the IP in both the carbon and heteroatom spectra of all of the saturated heterocyclics studied.

The correlation of experimental σ shape resonance positions with bond lengths shows reasonable agreement with earlier results. This is further indication that the empirical approach developed by Sette *et al.* (3) can be useful for a wide variety of molecules. However the complications of additional continuum features and the somewhat greater scatter in the correlation for more complex molecules appears to limit the accuracy of the structural information obtainable. The greatest accuracy is expected from shifts in resonance position in the same molecule in different environments, as in geometry changes of a surface adsorbed molecule. From the viewpoint of gas phase K-shell spectroscopy the correlation between resonance position and bond length provides a useful framework for spectral interpretation.

Acknowledgements

This research was supported by grants from the Natural Sciences and Engineering Research Council of Canada (NSERC) and the Exxon Research and Engineering Co. (New Jersey). A. P. Hitchcock acknowledges the support of an NSERC University Research Fellowship.

1. C. E. Brion, S. Daviel, R. N. S. Sodhi, and A. P. Hitchcock. AIP Conference Proceedings, **94**, 426 (1982); A. P. Hitchcock. J. Electron Spectrosc. **25**, 245 (1982).
2. A. P. Hitchcock, S. Beaulieu, T. Steel, J. Stöhr, and F. Sette. J. Chem. Phys. **80**, 3927 (1984).
3. F. Sette, J. Stöhr, and A. P. Hitchcock. J. Chem. Phys. **81**, 4906 (1984).
4. A. P. Hitchcock and C. E. Brion. J. Electron. Spectrosc. **10**, 317 (1977).
5. A. P. Hitchcock, D. C. Newbury, I. Ishii, J. Stöhr, A. L. Johnson, R. D. Redwing, and J. A. Horsley. To be published.
6. J. A. Horsley, J. Stöhr, A. P. Hitchcock, D. C. Newbury, A. L. Johnson, and F. Sette. J. Chem. Phys. **83**, 6099 (1985).
7. W. M. Flicker, O. A. Mosher, and A. Kupperman. J. Chem. Phys. **64**, 1315 (1976).
8. R. N. S. Sodhi and C. E. Brion. J. Electron Spectrosc. **34**, 363 (1984).
9. G. R. Wight and C. E. Brion. J. Electron Spectrosc. **3**, 191 (1974).
10. M. B. Robin. Higher excited states of polyatomic molecules. Vol. 1. Academic Press, New York. 1974.
11. A. A. Bakke, H. W. Chen, and W. J. Jolly. J. Electron Spectrosc. **20**, 333 (1980); K. D. Bomben, C. J. Eyermann, and W. L. Jolly. (Jan. 1985) updated list of XPS IP's.
12. L. W. Pickett. J. Chem. Phys. **8**, 293 (1940).
13. C. A. Coulson and A. Streitweiser. Dictionary of π-electron calculations. W. H. Freeman Co., San Francisco. 1965.
14. L. Asbrink, C. Fridh, and E. Lindholm. J. Electron Spectrosc. **16**, 65 (1979).
15. U. Gelius, C. J. Allan, G. Johansson, H. Siegbahn, D. A. Allison, and K. Siegbahn. Phys. Scr. **3**, 237 (1971).
16. S. A. Chambers and T. D. Thomas. J. Chem. Phys. **67**, 2596 (1977).
17. A. P. Hitchcock, M. Pocock, C. E. Brion, M. S. Banna, D. C. Frost, C. A. McDowell, and B. Wallbank. J. Electron Spectrosc. **13**, 345 (1978).
18. L. Jorgensen and L. Salem. The organic chemists book of orbitals. Academic Press, New York. 1973.
19. Landolt and Bornstein (*Editor*). Structure data of free polyatomic molecules. New Ser. II. Vol. 7. Springer, Berlin. 1976.
20. L. W. Pickett, M. E. Corning, G. H. Wieder, D. A. Semenow, and J. A. Buckley. J. Am. Chem. Soc. **75**, 1618 (1953).
21. K. Tanaka, T. Nakamura, T. Noro, H. Takewaki, T. Takada, H. Kashiwagi, F. Sasaki, and K. Ohno. J. Chem. Phys. **67**, 5738 (1977).
22. G. R. Wight and C. E. Brion. J. Electron Spectrosc. **4**, 25 (1974); R. N. S. Sodhi and C. E. Brion. J. Electron Spectrosc. **34**, 373 (1984).
23. J. March. Advanced organic chemistry: reactions, mechanism and structure. 3rd ed. Wiley-Interscience, New York. 1985. p. 42.
24. J. P. Doering, A. Gedanken, A. P. Hitchcock, P. Fischer, J. Moore, J. K. Olthoff, J. Tossell, K. Raghavachari, and M. B. Robin. J. Am. Chem. Soc. In press.
25. A. P. Hitchcock and C. E. Brion. J. Electron Spectrosc. **18**, 1 (1980); G. R. Wight and C. E. Brion. J. Electron Spectrosc. **4**, 313 (1974).
26. B. P. Stoicheff. Tetrahedron, **17**, 135 (1962).
27. R. C. Weast (*Editor*). CRC handbook of chemistry and physics. 64th ed. CRC Press, Florida. 1983.

Alkoxyphosphonium ions. 5. Kinetics of the Michaelis–Arbuzov intermediate

EDWARD S. LEWIS AND BRIDGET A. MCCORTNEY[1]

Department of Chemistry, Rice University, P.O. Box 1892, Houston, TX 77251, U.S.A.

Received October 21, 1985

This paper is dedicated to Professor Arthur N. Bourns

EDWARD S. LEWIS and BRIDGET A. MCCORTNEY. Can. J. Chem. **64**, 1156 (1986).

Rates of formation and destruction of the alkoxyphosphonium ion, the intermediate in the Michaelis–Arbuzov reactions of some methyl esters of trivalent phosphorus acids with methyl iodide, are followed by a conductivity method in the solvent propylene carbonate. Specific conductances of the unstable intermediates are well estimated through stable model salts. Rate constants for both the alkylation of the reagent and the dealkylation of the intermediate are obtained. The conductivity time curves are simulated by adjusting rate constants for two sequential second order reactions, assuming no ion pairing at the concentrations used. In these measurements of the intermediate only, there is no rate-determining step; for the overall reaction the first step is in most cases rate-determining.

EDWARD S. LEWIS et BRIDGET A. MCCORTNEY. Can. J. Chem. **64**, 1156 (1986).

Opérant dans le carbonate de propylène comme solvant et faisant appel à une méthode de conductivité, on a déterminé les vitesses de formation et de destruction de l'ion alkylphosphonium, l'intermédiaire dans les réactions de Michaelis–Arbuzov de quelques esters méthyliques d'acides phosphoreux trivalents avec l'iodure de méthyle. En se basant sur des sels modèles stables, on a pu bien évalué les conductivités spécifiques des intermédiaires instables. On a pu déterminer les constantes de vitesse tant de l'alkylation du réactif que de la déalkylation de l'intermédiaire. Faisant l'hypothèse qu'il n'y a pas de couplage d'ions ux concentrations utilisées, on a simulé les courbes de conductivité vs. temps en ajustant les constantes de vitesse pour deux réactions du deuxième ordre qui se suivent. Dans ces mesures qui n'impliquent que l'intermédiaire, il n'y a pas d'étape déterminante; pour l'ensemble de la réaction, la première étape est généralement l'étape qui détermine la vitesse.

[Traduit par la revue]

Introduction

Up to now, kinetic studies of the Arbuzov reaction have not provided the precision needed to uncover the possible mechanistic complexities, and to allow studies of structure–reactivity relations. This interesting reaction has been neglected quantitatively, in part because many potential analyses such as absorption or titration for the reagents or products are inapplicable or undeveloped.

The first reasonably successful method, by Aksnes and Aksnes (1), used an infrared analysis based upon the formation of the characteristic P=O bond in the product, leading to the still accepted conclusion that in that case the first alkylation step was rate-determining. This analysis is cumbersome, slow, and of limited precision; we have not found it attractive for our studies. Our attempts to substitute a gas chromatographic analysis did not overcome these problems, but a nmr method showed promise as a highly compound-specific method. This was in fact successful at the level of seeing compounds at fairly high concentrations and it allowed the observation of the intermediate alkoxyphosphonium salt and rough rate studies using both proton and phosphorus nmr (2). Studies of structure reactivity relations were unconvincing. Nevertheless, the mechanisms were clearly delineated as a combination of reactions [1] and [2], with in some cases a contribution of reaction [3]. Reaction [3] was not identified as an important contributor in the case of the iodide counter ion; it was observed only with less nucleophilic anions.

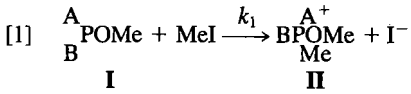

[1] $\underset{\mathbf{I}}{\overset{A}{\underset{B}{P}}OMe} + MeI \xrightarrow{k_1} \underset{\mathbf{II}}{BP^{+}(A)OMe} + I^-$

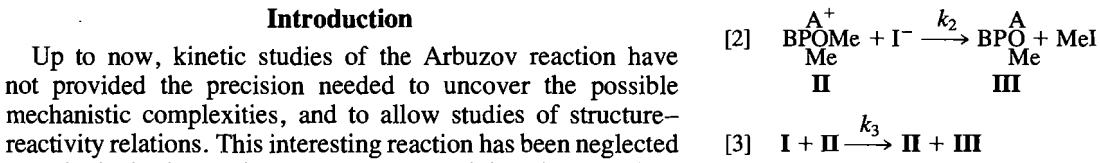

[2] $\underset{\mathbf{II}}{BP^{+}(A)OMe} + I^- \xrightarrow{k_2} \underset{\mathbf{III}}{BP(A)O} + MeI$

[3] $\mathbf{I} + \mathbf{II} \xrightarrow{k_3} \mathbf{II} + \mathbf{III}$

Earlier studies (3, 4), in which the intermediate salt is detected quantitatively by its electrical conductivity tempted us to revive this method. Although these earlier studies succeeded in detecting the intermediate and observing its concentration rise and fall, they failed to establish the relation between conductivity and concentration and were led into some incorrect assumptions and hence unjustifiable mechanistic conclusions. The further conclusion that in acetonitrile there is extensive ion pairing is now suspect.

Results

The alkoxyphosphonium iodides are unstable; it is thus not possible to measure directly the conductivities of solutions of known concentration. Alkoxyphosphonium trifluoromethanesulfonates are stable, as are ordinary phosphonium iodides. The strategy was therefore to substitute for the methoxy groups of the unstable salts ethyl groups which have a similar size. The results of these measurements are shown in Table 1. The conductivity data are presented as the slopes of the conductivity–concentration plots corrected for the cell constant. Conductivities of triflate salts with ethyl groups substituted for the methoxy groups showed that indeed this substitution had only a minor effect on the conductivity, as shown by the last two entries in Table 1. It was then assumed that the concentration of the methoxyphosphonium iodide was the same as that of the corresponding ethylphosphonium iodide of the same conductivity.

The same measurements showed that, for the stable salts, the conductivity was with good precision proportional to the

[1]National Science Foundation Predoctoral Fellow.

TABLE 1. Concentration dependence of the conductivity of salts $ABCP^+Me\ X^-$ at 25°C in propylene carbonate

A	B	C	X	Specific conductance (mho cm^{-1})/M^a	Melting point (°C)
OCH_3	OCH_3	OCH_3	OTf	0.0229 ± 0.0009	49–50[c]
CH_3CH_2	CH_3CH_2	CH_3CH_2	OTf	0.0238 ± 0.0001	87–90
CH_3CH_2	CH_3CH_2	CH_3CH_2	I	0.0296 ± 0.0002	307–311 (lit.[d] 300–302)
CH_3CH_2	CH_3CH_2	Ph	I	0.0248 ± 0.0003	110–112 (lit.[e] 110)
CH_3CH_2	Ph	Ph	I	0.0256 ± 0.0003	188–190 (lit.[f] 183)
CH_3CH_2	Ph	Ph	OTf	0.0237 ± 0.0005	~22
OCH_3	Ph	Ph	OTf	0.0244 ± 0.0005	34–36 (lit.[g] 34–37)

[a]Values reported are the slope ± s.d. of the specific conductivity vs. concentration plot.
[b]Data on this compound were much more scattered than with the other compounds. The salt is very sensitive and possible water contamination may be the source of error.
[c]This melting point was taken in a capillary sealed under N_2. The earlier reported value (28–32°C), ref. 7, did not take this precaution.
[d]Reference 11.
[e]Reference 12.
[f]Reference 13.
[g]Reference 7.

concentration. This gave assurance that there was no significant ion pairing or covalent phosphorane formation, at least in the concentration range (up to about 0.01 *M*). The data for concentration vs. conductivity were subject to a linear least-square fit, and in every case the calculated intercept at zero concentration was so small that assuming it to be zero introduced no significant error, as long as concentrations in the kinetic runs did not exceed those in these calibrations. Parenthetically, we may note that very little error in concentrations would have resulted if we had assumed that the slopes of all these plots had been the same.

The experiments on reacting systems showed usually an initial rise followed by a slow fall in conductivity. These data, converted to concentration time dependencies using Table 1, were then compared to the computed values of the salt concentration from the numerical integration of eqs. [4], [5], and [6], with plausibly guessed values of k_1 and k_2.

$$[4]\quad -\mathrm{d(ABPOMe)}/\mathrm{d}t = k_1(\mathrm{ABPOMe})(\mathrm{MeI})$$

$$[5]\quad \mathrm{d(MeABPO)}/\mathrm{d}t = k_2(\mathrm{MeABPOMe^+})(\mathrm{I^-})$$

$$[6]\quad \mathrm{d(MeABPOMe^+)}/\mathrm{d}t = k_1(\mathrm{ABPOMe})(\mathrm{MeI}) - k_2(\mathrm{MeABPOMe^+})(\mathrm{I^-})$$

Then the two rate constants were adjusted for a good fit to the experimental data. Figure 1 shows this plot for trimethyl phosphite, the only case where the rise in conductivity was too fast to follow by our manual conductivity bridge. For methyl diethylphosphinite, the curve could not be even remotely well fitted by adjustment of only two rate constants. The inclusion of reaction [3] resulted in the fit shown in Fig. 2.[2] There is a wide variation in the maximum concentration of the salt, with the two extremes shown in Figs. 1 and 2, about 0.2% of the starting ester concentration in the first case and about 60% in the second.

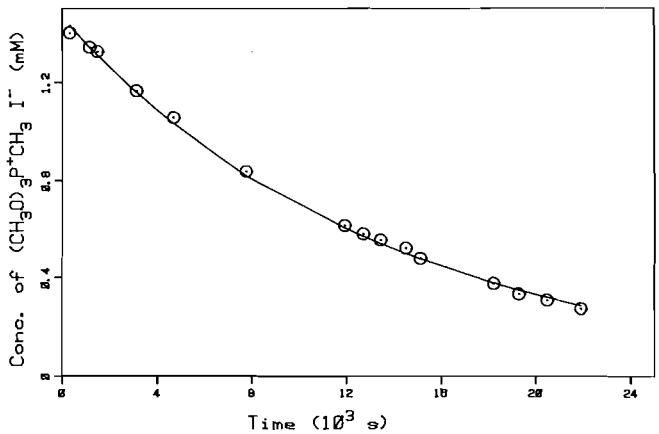

FIG. 1. Plot of methyltrimethoxyphosphonium iodide concentration vs. time with initial concentrations for this run of 0.7119 molar in trimethyl phosphite and 2.068 molar in methyl iodide. The circles represent experimental data points; the solid curve is that calculated from numerical integration of the rate law.

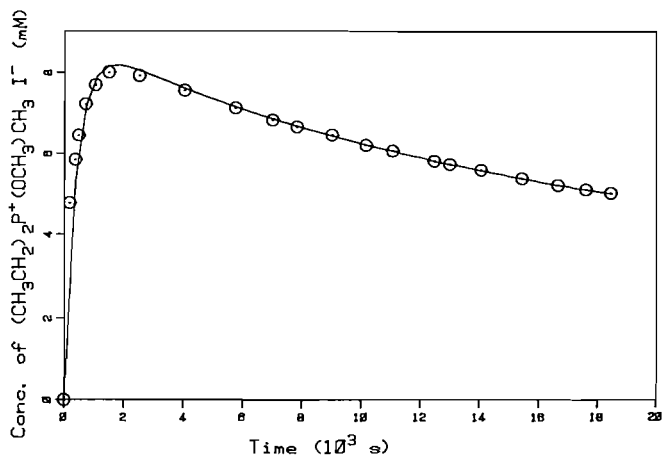

FIG. 2. Plot of diethylmethoxymethylphosphonium iodide concentration vs. time with initial concentrations for this run of 1.28×10^{-2} molar in methyl diethylphosphinite and 2.165×10^{-2} molar in methyl iodide. The circles represent experimental data points; every third point up to 12 000 s and every point thereafter is shown. The solid curve is that calculated from numerical integration of the rate law.

[2]ADDED IN PROOF: Later direct measurement of k_3 has shown that the value given here in Table 2 is more than an order of magnitude too large. The fit in Fig. 2 is at least as good with only k_1 and k_2, having the values 1.75×10^{-1} and 4.7×10^{-3}, respectively. The discrepancy arises from loss of some of the reagent by oxidation prior to conductivity measurements, which makes the apparent extent of conversion of the reagent to the intermediate salt far too small. In fact, in this case the conversion is almost quantitative before much decay has occurred.

TABLE 2. Rate constants for reactions [1], [2], and [3] of $ABPOCH_3$ at 25°C in propylene carbonate

A	B	k_1, M^{-1} s^{-1} [a]	k_2, M^{-1} s^{-1} [a]	k_3, M^{-1} s^{-1} [a,b]
OCH_3	OCH_3	$(8.25 \pm 2.32) \times 10^{-5}$ [c]	52.5 ± 6.7	—
OCH_3	Ph	$(1.86 \pm 0.10) \times 10^{-3}$	4.17 ± 0.25	—
Ph	Ph	$(5.68 \pm 0.36) \times 10^{-3}$	0.217 ± 0.008	—
CH_3CH_2	CH_3CH_2	$(6.61 \pm 1.77) \times 10^{-2}$	$(4.62 \pm 0.30) \times 10^{-3}$	0.142 ± 0.004

[a]Values reported are the mean ± s.d. for three independent runs of the same reaction. The effect of ionic strength variations is neglected.

[b]Not required for fit except in last compound. The value is presumed small enough in the other cases that its contribution is unimportant. However, see footnote 2 for more details.

[c]^{31}P nmr kinetic result: $1.18 \pm 0.04 \times 10^{-4}$ M^{-1} s^{-1} at 26.4°C. A few other less satisfactory nmr runs scattered badly, but agreed within their own rather large error limits.

The rate constants determined are presented in Table 2. A rate constant measured by observing the loss of trimethyl phosphite as shown by its ^{31}P nmr signal at an estimated temperature of 26.4°C is also included to show that within that rather substantial experimental error, especially of the nmr rate, the rate constant k_1 calculated by fitting procedure is indeed the rate of the first and rate determining step (Table 3). It is note-worthy that the intermediate treated quantitatively by the conductivity studies in this case is completely invisible in the nmr.

Discussion

In a case such as this in which neither the reagents nor the products of a reaction are observed, it is absolutely necessary to show that the reaction being followed is in fact the correct one. The fact that the reagents are those well known to undergo the Arbuzov reaction is useful. The identification of the reaction products by nmr as the only detected phosphorus containing material adds further evidence. The accepted mechanism requires the intermediacy of an electrolyte, which is detected. Finally, the similarity of the rate constants postulated to account for the conductivity and that measured by an nmr method, which observes the reagent and the product, but not the intermediate, makes the identification of the two processes very convincing.

The identification of the conducting species as the alkoxyphosphonium iodide rests not only on the mechanism, but also on the isolation of such salts in related reactions where the lower reactivity is understood; examples are phenyl esters (5), neopentyl esters (6), many of these alkoxyphosphonium salts as their triflates (7) and fluoborates (8), and even one quite unstable iodide salt of a methyl ester (7, 9). The concentrations of the salts are determined plausibly by the relation to the stable salts described above. These concentration determinations probably do not have errors exceeding a few percent, but also are not much more precise than that either. The assumption of linearity of the concentration–conductivity plots cannot be correct (10), but concentration errors of this sort are very small, as are random errors in the conductivity measurements, because the conductivity–time curves are very smooth.

This method still does not answer the question of a highly precise method for following the Arbuzov kinetics. Almost certainly, this is due to the fact that only the small difference between the rates of the two important steps is measured, the actual rate constants are subject to an amplification of errors more or less related to the concentration ratio of the major species to the measured intermediate, a factor between 2 and 500. It appears to provide data of an extremely exacting nature that, when the good analysis becomes available, will have to be fitted.

We can check on the plausibility of the results by looking at the substituent effects on the rate. If log k_1 is plotted in a Taft plot against $\Sigma\sigma_1$, a rather poor line results ($\rho_1 = -4.1$, $r = 0.97$), a line which includes a rate for the methylation of triphenylphosphine, measured independently in this solvent by conductivity.[3] The sign is reasonable; the less than perfect fit is expected for a reaction so close to the substituents.

The same plot for k_2 is much better ($\rho_1 = +6.4$, $r = 0.99$), again with the expected sign of ρ_1. The greater distance from the site of substitution is probably the reason for the better fit; there is no reason to expect one rate constant to be better than another.

In the previous nmr study no intermediate was observed even with methyl dialkylphosphinite, although here it builds up to as high as 60% of the starting material concentration, which should be conspicuous by nmr. The discrepancy is probably a solvent effect; the salt should be formed less rapidly and be decomposed more rapidly in chloroform than in propylene carbonate.

These results differ greatly from those of Buck and Yoke (3) and of Cachaza, Casado, and Varela (4). The major difference is that they all assumed that the intermediate was formed quantitatively; thus the rise in concentration was interpreted as a measured k_1 and the subsequent fall as a measure only of k_2.

In fact, the two rate constants are combined in both the rise and the fall; the fall does nearly follow a first order course, as observed by Buck and Yoke, but the apparent rate constant is closer to k_1 than to k_2! A manifestation of this aspect is that the fastest rise to the maximum was observed with trimethyl phosphite, which has the smallest value of k_1. Both the conductivities and the rate measurements show that in this solvent ion-pairs are insignificant.

In conclusion, the kinetics of the Arbuzov reaction are followed in a consistent way by measuring the conductivity of the alkoxyphosphonium iodide intermediate. The fallacies of earlier measurements by this method are now understood. Rather precise determination of the time dependence of the concentration of the intermediate provides new kinetic data of good precision, but translates into much less precise rates for the overall reaction. Nevertheless, significant new structure reactivity data on the formation and destruction of the intermediate are presented, and the previously confusing conduc-

[3]B. A. McCortney. Unpublished result.

TABLE 3. ^{31}P Chemical shifts[f]

Compound	δ (ppm)
$MeOPEt_2$	142[a] (lit.[d] 139.4)
$MeOP(Ph)_2$	117[a] (lit.[c] 115)
$(MeO)_2P(Ph)$	160[a] (lit.[c] 159)
$(MeO)_3P$	138[b] (lit.[c] 141)
$(Ph)_2P^+EtMe$	26[a]
$(Ph)_2P^+(OMe)Me$	75[a] (lit.[d] 78.5)
$(Ph)P^+Et_2Me$	33[a]
Et_3P^+Me	37[a] (lit.[c] 37)
$(MeO)_3P^+Me$	53[b] (lit.[d] 53.1)
$Et_2P^+(OMe)Me$	101[b] (lit.[d] 99.0)
$Et_2P(O)Me$	46[b] (lit.[e] 37)
$(Ph)_2P(O)Me$	27[b] (lit.[e] 31)
$(Ph)(MeO)P(O)Me$	41[b] (lit.[e] 45)
$(MeO)_2P(O)Me$	33[b] (lit.[c] 32.6)

[a]Solvent is $CDCl_3$, reference is 85% H_3PO_4/H_2O.
[b]Solvent is propylene carbonate, reference is $(MeO)_3P(O)$ in d_6 acetone. The chemical shift of $(MeO)_3P(O)$ relative to 85% H_3PO_4/H_2O is +1.9 ppm. This was used because 85% D_3PO_4/D_2O did not provide a suitable lock for the nmr.
[c]Reference 14.
[d]Reference 7.
[e]Reference 15.
[f]Positive chemical shifts refer to peaks downfield from 85% H_3PO_4/H_2O.

tivity measurements are explained. A precise measurement of overall rates of this reaction is not yet available. The substituent dependence of the autocatalytic rate constant is small, as observed before (2), but there is no evidence even on the sign of ρ_I for this reaction.

Experimental section

Materials

Methyl diethylphosphinite, methyl diphenylphosphinite, and dimethyl phenylphosphonite were obtained commercially (Strem Chemical) and used without further purification. The identity and purity of each was checked by ^{31}P nmr before use. Trimethyl phosphite (Aldrich) was treated with sodium followed by distillation under nitrogen: bp 112°C. Propylene carbonate (99% from Aldrich Chemical Co.) was twice vacuum distilled at 8–10 Torr and stored under nitrogen until used. This procedure was sufficient to give propylene carbonate with undetectable conductivity on the system described below. Methyl iodide was distilled under nitrogen from P_2O_5. The methoxyphosphonium trifluoromethanesulfonate (triflate) salts were prepared following the procedure of Lewis and Colle (7). The four triflate salts prepared were oils which, after removal of the solvent under vacuum, solidified upon storage at 0°C. The phosphonium iodides (triethylmethyl, diethylmethylphenyl, diphenylethylmethyl) were prepared by methylation of the commercial phosphines with methyl iodide in the same manner as the triflates. These salts were obtained as fine white precipitates which were recrystallized from EtOH/Ether (diphenylethylmethylphosphonium iodide, diethylmethylphenylphosphonium iodide) or isopropanol (methyltriethylphosphonium iodide). The purity of the phosphonium salts was determined by their melting points and ^{31}P nmr spectra. The ^{31}P chemical shifts of the reagents, intermediates, and products of the reactions studied are reported in Table 3.

Conductivity measurements

Conductivities were measured using a Fisher brand enclosed conductivity cell with platinized electrodes (cell constant 0.250 ± 0.003 cm^{-1}), a General Radio conductivity bridge (Model 1603-A), an oscillator operated at 1000 Hz with an applied voltage of 0.50 V across the bridge with the bridge imbalance detected with an oscilloscope. The cell was immersed in a 25.0°C thermostat; all conductivity measurements were taken at this temperature. Propylene carbonate was chosen as a solvent only because it is the solvent we found with minimal reaction with methyl iodide, a reaction which turned out to be a consequence of using too high a voltage and too low a frequency on a different bridge, and not a property of the solvent. Thus, there is no reason to believe that several other aprotic solvents rejected earlier would not have worked well with the proper bridge. The electrodes also were platinized during this preliminary bridge problem; there is no reason to believe that it is necessary. To obtain the concentration dependence of the conductivity for the phosphonium iodides and triflates, an approximately 0.01 *M* solution of each salt in propylene carbonate was prepared; this was diluted to obtain solutions of approximately 0.001, 0.003, 0.005, 0.007, and 0.009 molar concentration. The conductivities of the solutions were measured and plotted as a function of the concentration.

Kinetic experiments

The reaction mixtures were prepared at room temperature by mixing the two reagents (either as stock solutions in propylene carbonate or by addition of the neat compounds) in propylene carbonate in a 25 mL volumetric flask. After mixing, approximately 15 mL of the solution were transferred to the conductivity cell. All transfers were performed under nitrogen, and the cell was kept under nitrogen and away from light during the course of the experiments. Measurements were made at frequent intervals. The possibility of a reaction occurring at the cell electrodes was ruled out by adding a few millilitres of the starting reaction solution to the conductivity cell after the reaction was nearly complete. In all cases, the conductivity changed by a negligible amount. Each reaction solution was allowed to remain in the cell until the conductivity no longer changed (in each case the final conductivity was less than 10% of the maximum conductivity for that run, except in the case of trimethyl phosphite which had a very low conductivity), and at that point a ^{31}P nmr was taken. In each case, only one phosphorus-containing compound was detected. It had an appropriate chemical shift for the product.

Two programs were used to integrate the concentration as a function of time data for chosen rate constants, one that was used by Lewis and Hamp (2), and one kindly provided by Professor David Stanbury of Rice University (used only for trimethyl phosphite, except on a few other runs to show that the results are the same). The iteration to find the best rate constant to fit the experimental data was done by hand (manually adjusting the guessed rate constants and evaluating the resulting fit); the least-squares method described by Lewis and Hamp was time consuming and did not always converge. The error of the rate constants is mostly derived from agreement between different runs; the sensitivity of the fit to the chosen rate constants was usually somewhat better than the reproducibility.

^{31}P nmr kinetics

All ^{31}P FT nmr spectra were obtained on a Jeolco FX-90Q instrument. The reaction solution was prepared at room temperature under nitrogen by addition of trimethyl phosphite and methyl iodide to propylene carbonate in a 10 mL volumetric flask. The solution was transferred under nitrogen to a 10 mm nmr tube containing a concentric capillary tube containing $(CH_3O)_3P(O)$ (as an external reference and standard for concentration determination) in *d*-6 acetone (as an external deuterium lock). A total of 15 spectra were obtained at intervals of 2000 s between the first six and 2500 s between the remaining nine. Each spectra contains 15 pulses (interpulse delay of 5 s). The reaction was followed by observing the increase in the dimethyl methyl phosphonate(III) peak with time. The second order rate constant for reaction [1] of trimethyl phosphite was obtained by dividing the slope of the plot of $\ln[(\mathbf{III})_\infty - (\mathbf{III})_t]$ vs. time by the methyl iodide concentration which remains essentially constant.

Acknowledgement

This material is based upon work supported under a National Science Foundation Graduate Fellowship awarded to Bridget A. McCortney. We would also like to gratefully acknowledge support of this work by a grant from The Robert A. Welch Foundation, and the technical assistance of Ms. Sharon R. Hoffman in obtaining some of the conductivity vs. concentration data.

1. G. Aksnes and D. Aksnes. Acta Chem. Scand. **18**, 38 (1969).
2. E. S. Lewis and D. W. Hamp. J. Org. Chem. **48**, 2025 (1983).
3. F. C. Buck and J. T. Yoke, III. J. Org. Chem. **27**, 3675 (1962).
4. J. M. Cachaza, J. Casado, and A. Varela. Rev. Roum. Chim. **22**, 2, 213 (1977); **23**, 2, 233 (1978).
5. S. R. Landauer and H. N. Rydon. J. Chem. Soc. 224 (1953).
6. H. R. Hudson, R. G. Rees, and J. E. Weekes. Chem. Commun. 1297 (1971).
7. E. S. Lewis and K. Colle. J. Org. Chem. **43**, 571 (1978).
8. K. Dimroth and A. Nurrenbach. Angew. Chem. **70**, 26 (1958).
9. A. I. Razumov and N. N. Bankovskaya. J. Gen. Chem. USSR (Engl. Transl.) **34**, 1871 (1964).
10. P. W. Atkins. Physical chemistry. W. H. Freeman, San Francisco. 1978. p. 822.
11. V. Akamsin and N. Rizpolozhensky. Dokl. Akad. Nauk SSSR, **168**, 807 (1966).
12. J. Meisenheimer and L. Lichtenstadt. Ann. **449**, 213 (1926).
13. S. Gough and B. Tripett. J. Chem. Soc. 4263 (1951).
14. M. Grayson and E. J. Griffith (*Editors*). Topics in phosphorus chemistry. Vol. 5. ^{31}P nuclear magnetic resonance. pp. 227–997.
15. D. W. Hamp. Ph.D. Thesis. Rice University, Houston, TX. 1982.

Kinetics and mechanism of nucleophilic displacements with heterocycles as leaving groups. Part 23.[1] Studies at the borderlines between reactions proceeding (*i*) via free carbocations, (*ii*) via rate-determining formation of ion–molecule pairs, and (*iii*) via rate-determining nucleophilic attack on ion–molecule pairs

ALAN R. KATRITZKY[2] AND BOGUMIL BRYCKI
Department of Chemistry, University of Florida, Gainesville, FL 32611, U.S.A.

Received August 9, 1985

This paper is dedicated to Professor Arthur N. Bourns

ALAN R. KATRITZKY and BOGUMIL BRYCKI. Can. J. Chem. **64**, 1161 (1986).

Evidence is presented to demonstrate that at the borderline between first-order reaction via nucleophilic trapping of intimate ion–molecule pairs and first-order reaction via the formation of free carbocations, both mechanisms proceed independently, without merging. Similarly at the borderline between first-order (rate-determining formation) and second-order (rate-determining nucleophilic attack) reactions of intimate ion–molecule pairs, both reactions again proceed independently.

ALAN R. KATRITZKY et BOGUMIL BRYCKI. Can. J. Chem. **64**, 1161 (1986).

On présente des données qui démontrent que, à la limite entre la réaction du premier ordre se produisant par le piégeage nucléophile de paires intimes ion–molécule et la réaction du premier ordre se produisant par le biais de la formation de carbocations libres, les deux mécanismes se produisent d'une façon indépendante, sans se confondre. De la même manière, à la limite entre les réactions du premier ordre (la formation est l'étape déterminante) et du deuxième ordre (l'attaque nucléophile est l'étape déterminante) des paires intimes ion–molécule, chacune des réactions se produit encore une fois d'une façon indépendante.

[Traduit par la revue]

Introduction

Nucleophilic displacements of the N-substituents in pyridinium cations have been shown to proceed by each of the five mechanisms of Scheme 1 (1). In solvents of low nucleophilicity solvolyses of *N*-(primary alkyl)pyridiniums occur via ion-pair intermediates formed without anchimeric assistance by synchronous rate-enhancing H^+ or R^+ migration (2). Nucleophilic displacement of *N*-(secondary alkyl)pyridiniums can occur by the classical S_N2 reaction, by rate-determining ion-pair formation, or by rate-determining ion-pair dissociation, depending on the conditions (3). In particular, no evidence was found in these systems for any "merging" of S_N1–S_N2 reaction type or for the "S_N2 intermediate" mechanism which has been advocated by Bentley and Schleyer (4). We have recently confirmed that the nature of the gegen ion, or the presence of small quantities of water, have no significant effect on the rate.[3]

Studies of tertiary alkyl halides and sulfonates have usually been interpreted to demonstrate that nucleophilic displacement occurs exclusively by unimolecular S_N1 type mechanism: with (5) or without (6) the intermediacy of ion-pairs. Although Bentley and co-workers have recently advocated nucleophilic solvent assistance in the solvolysis reactions of such *t*-alkyl substrates (7, 8) our own detailed studies of *N*-(*t*-alkyl)pyridinium salts[4] have shown solvolysis rates almost independent of solvent, and with less variation with the substrate structure than found for analogs with anionic leaving groups: specifically, no evidence was found for nucleophilic assistance by solvent.

The use of positively charged substrates and neutral leaving groups has several advantages for the study of nucleophilic substitution mechanisms (1). Unimolecular reactions of a neutral substrate involve charge creation: such reactions require media of high dielectric constant, where the role of the medium as solvent and as nucleophile is not easily disentangled. Substrates with neutral leaving groups can undergo unimolecular reactions in media of low dielectric constant. Furthermore, the reaction scheme is less complex in that the distinction (caused by strong electrostatic attraction) between a solvent-separated ion pair and a free carbocation disappears: for positively charged substrates we simply have intimate ion–molecular pairs and free carbocations.

To better understand the detailed mechanism of nucleophilic substitution at sp^3-hybridised carbon atoms, we wished to investigate four mechanistic borderlines utilizing pyridines as leaving groups (Scheme 1). These borderlines comprise: (*1*) that between first-order reactions involving ion-molecule pairs and first-order reactions proceeding via dissociation into free carbocations; (*2*) that between first-order and second-order reactions of nucleophiles with ion–molecule pairs; (*3*) that between second-order attack on ion–molecule pairs and second-order mechanism proceeding by direct displacement; (*4*) that between classical second-order displacements and second-order displacements involving previous electron transfer.

The present paper describes the results of investigations aimed at the further clarification of borderlines (*1*) and (*2*). In particular, we wished to investigate whether it was possible to explain the results at the borderlines by the simultaneous operation of the two appropriate independent reaction mechanisms, or whether "merging" occurred between them so that a reaction occurred by a single mechanism of intermediate type. In other words, do the two mechanisms remain distinct and competitive with dominance passing gradually from one to the other or does a single mechanism always operate with gradual change over?[5]

[1]Part 22. A. R. Katritzky and B. Brycki. To be published.

[2]To whom all correspondence should be addressed.

[3]A. R. Katritzky, H. Schultz, M. L. Lopez-Rodriguez, G. Musumarra, and G. Cirma. To be published.

[4]A. R. Katritzky and B. Brycki. To be published.

[5]Opposing views on this general and fundamental question complicate the teaching of this subject, see ref. 19.

Printed in Canada / Imprimé au Canada

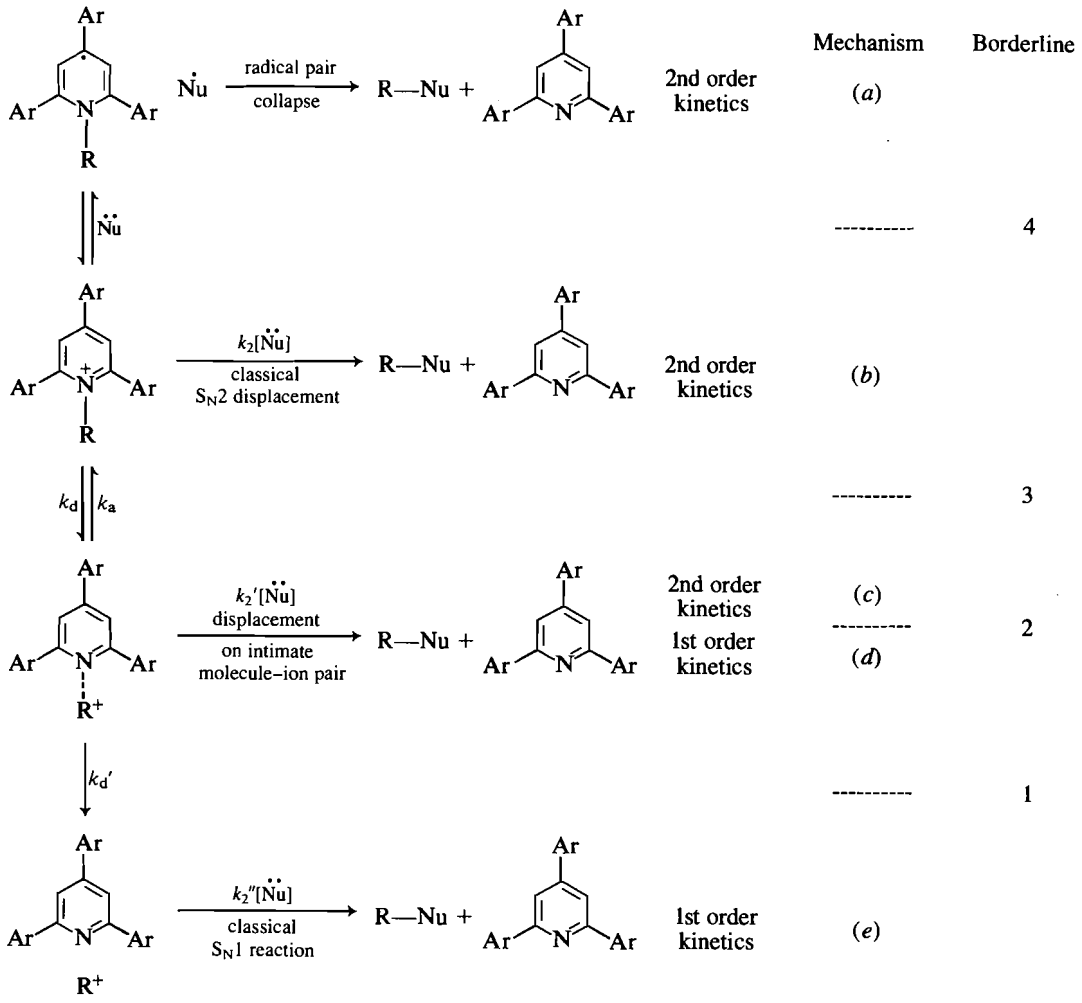

SCHEME 1. Nucleophilic substitutions with pyridine-leaving group

Borderline (*1*) between classical S_N1 and S_N1 by nucleophilic capture of an ion–molecule pair

In the region of this borderline, competition between two alternative first-order reactions occurs: (*i*) mechanism *d*; capture by solvent or nucleophile at the ion–molecule pair stage (i.e. rate-determining formation of the ion–molecule pair) and (*ii*) mechanism *e*; dissociation of the ion–molecule pair to give a free carbocation followed by further reactions with solvent or nucleophile (here the rate-determining step could be either formation of a ion–molecule pair or its dissociation to a carbocation).

Some results for solvolyses of secondary alkyl substrates indicating that reaction can occur either via free carbocations or via solvent capture of an ion–molecule pair (the first borderline region) have already been reported (3). The present experiments were based on the expectation that secondary substrates in non- or very weakly nucleophilic solvents with small amounts of strong nucleophiles (piperidine or morpholine) should give first-order kinetics (no dependence of nucleophile concentration) but undergo reaction via ion–molecule pairs, i.e. without any rearrangement of the secondary substrates. By contrast, weak nucleophiles such as 1,1,1,3,3,3-hexafluoropropan-2-ol or trifluoroacetic acid should give classical unimolecular reaction via free carbocations, and carbocation rearrangements should occur.

Solvolyses[6] of 1-(2-pentyl)-5,6-dihydro-2,4-diphenylbenzo[*h*]quinolinium trifluoromethanesulphonate (**2***c*) and 1-(3-pentyl)-5,6-dihydro-2,4-diphenylbenzo[*h*]quinolinium tetrafluoroborate (**2***e*) in chlorobenzene occur at convenient rates at 65.0°C. The kinetics of these solvolyses were followed spectrophotometrically at 345 nm. In pure, unbuffered solvent an initial decrease in absorption followed by an increase is due to acid–base equilibria (cf. footnote 4). These equilibria were suppressed *either* by carrying out the reaction in the presence of triethylamine, *or* by diluting the kinetic solutions with chlorobenzene containing trifluoroacetic acid prior to measurement of the absorbance. With this precaution, all reactions showed good pseudo-first-order behaviour. Reactions carried out in the presence of a nucleophile (piperidine, morpholine, pyridine, lutidine, anisole, *p*-chlorophenol, acetic acid, or trifluoroacetic acid) were measured under pseudo-first-order conditions: good straight lines were obtained to at least 70% completion. The observed rate constants (k_{obs}) (Tables 1 and 2) plotted against

[6]Here and elsewhere the word "solvolysis" is used to denote a reaction which is induced by the fact that a substrate is dissolved in a solvent. In a solvolysis, a solvent molecule need not be involved in the rate-determining stage. Solvolyses of some of the present and other similar substrates, in the absence of added nucleophiles has been shown to give various products of carbocation attack on solvent or product molecules (unpublished work) when elimination is not possible.

TABLE 1. Pseudo-first-order rate constants for the reactions of 1-(2-pentyl)-5,6-dihydro-2,4-diphenylbenzo[*h*]quinolinium trifluoromethanesulphonate **2***c* with nucleophiles in chlorobenzene at 65.0°C[a]

Entry No.	Nucleophile (mol L^{-1})	$10^5 k_{obs}$ (s^{-1})	Error (%)	*r*	React. (%)
1	None	18.75 ± 0.19	1.00	0.9998	86.8
	Piperidine				
2	0.0005[b]	18.94 ± 0.08	0.44	0.99998	81.8
3	0.0010[b]	18.96 ± 0.07	0.38	0.99998	81.8
4	0.0100[b]	19.12 ± 0.11	0.56	0.99997	82.2
5	0.1000[b]	22.51 ± 0.09	0.38	0.99998	80.3
6	1.000[b]	50.29 ± 0.23	0.45	0.99997	85.8
	Morpholine				
7	0.005	16.85 ± 0.15	0.92	0.99985	78.1
8	0.010	17.33 ± 0.21	1.19	0.99975	79.0
9	0.050	17.87 ± 0.52	0.52	0.99995	80.0
10	0.100	18.65 ± 0.16	0.85	0.99987	81.5
11	0.200	19.36 ± 0.11	0.55	0.99995	82.5
12	0.400	22.25 ± 0.21	0.96	0.99984	86.5
13	0.600	27.25 ± 0.37	1.35	0.99968	91.5
	Pyridine				
14	0.005	18.62 ± 0.04	0.23	0.99999	81.3
15	0.010	18.75 ± 0.06	0.31	0.99998	81.5
16	0.050	18.50 ± 0.07	0.36	0.99998	81.5
17	0.100	18.57 ± 0.09	0.46	0.99996	81.0
18	0.200	18.67 ± 0.11	0.60	0.99994	81.4
19	0.400	18.65 ± 0.11	0.61	0.99993	81.3
	2,6-Lutidine				
20	0.001	18.78 ± 0.10	0.52	0.99997	78.1
21	0.010	18.84 ± 0.23	1.26	0.99982	81.7
22	0.050	18.98 ± 0.09	0.47	0.99997	81.9
23	0.100	18.86 ± 0.10	0.52	0.99997	81.7
24	0.400	19.01 ± 0.15	0.81	0.99993	81.9
	Isopropylamine				
25	0.005	17.97 ± 0.10	0.57	0.99994	80.1
26	0.010	18.37 ± 0.12	0.66	0.99993	80.8
27	0.050	19.53 ± 0.27	0.27	0.99999	82.7
28	0.100	19.89 ± 0.18	0.93	0.99987	78.7
29	0.400	25.50 ± 0.32	1.26	0.99982	78.7
30	1.000	31.32 ± 0.94	2.99	0.9984	76.3
	p-*Chlorophenol*				
31	0.001[c]	18.89 ± 0.96	5.10	0.9989	78.5
32	0.050[c]	18.78 ± 0.93	4.95	0.9990	77.6
33	0.010[c]	18.76 ± 0.92	4.80	0.9990	76.5
34	0.100[c]	18.81 ± 0.88	4.68	0.9991	75.2
35	1.000[c]	18.93 ± 1.00	5.28	0.9989	76.9
	Anisole				
36	0.001[d]	18.90 ± 0.09	0.47	0.9999	81.7
37	0.010[d]	19.30 ± 0.15	0.78	0.9999	82.2
38	0.100[d]	18.84 ± 0.09	0.50	0.9999	81.7
39	1.000[d]	18.94 ± 0.12	0.62	0.9999	81.9
	Acetic acid				
40	0.1[e]	18.07 ± 0.93	5.15	0.9987	66.3
41	1.0[e]	18.18 ± 0.96	5.24	0.9986	66.3
	Trifluoroacetic acid				
42	0.1[e]	17.95 ± 1.40	7.78	0.9970	65.7
43	1.0[e]	17.49 ± 1.15	6.57	0.9978	64.0

[a]Concentration of pyridinium salt 2.8×10^{-5} (mol L^{-1}); measured at 345 nm.
[b]Concentration of pyridinium salt 1×10^{-4} (mol L^{-1}); measured at 345 nm.
[c]Kinetic solutions of the pyridinium salt (2.8×10^{-5} mol L^{-1}) were diluted to uv concentration (1.4×10^{-5} mol L^{-1}) using 8% (v/v) solution of trifluoroacetic acid in chlorobenzene; measured at 360 nm.
[d]Solvent contained triethylamine, 2.8×10^{-4} (mol L^{-1}).
[e]Kinetic solutions of the pyridinium salt (1.4×10^{-4} mol L^{-1}) were diluted to uv concentration (2.8×10^{-5} mol L^{-1}) using 5% (v/v) solution of triethylamine in chlorobenzene; measured at 345 nm.

TABLE 2. Pseudo-first-order rate constants for the reactions of 1-(3-pentyl)-5,6-dihydro-2,4-diphenylbenzo[*h*]quinolinium tetrafluoroborate **2***e* with nucleophiles in chlorobenzene at 65.0°C[a]

Entry No.	Nucleophile (mol L^{-1})	$10^5 k_{obs}$ (s^{-1})	Error (%)	*r*	React. (%)
1	None	15.93 ± 0.09	0.61	0.9999	86.1
	Morpholine				
2	0.001	16.03 ± 0.15	0.95	0.9999	79.6
3	0.010	16.49 ± 0.15	0.91	0.9999	80.6
4	0.100	17.63 ± 0.31	1.76	0.9994	81.7
5	1.000	29.02 ± 0.58	2.00	0.9995	82.7
	Pyridine				
6	0.001	16.26 ± 0.06	0.38	0.99997	76.9
7	0.010	16.31 ± 0.09	0.55	0.99995	77.0
8	0.100	16.38 ± 0.03	0.16	0.99999	77.1
9	0.500	16.51 ± 0.05	0.29	0.99999	77.4
	2,6-Lutidine				
10	0.001	15.59 ± 0.11	0.74	0.9999	81.5
11	0.010	15.75 ± 0.13	0.83	0.9999	81.9
12	0.100	16.31 ± 0.11	0.69	0.9999	81.0
13	1.000	16.82 ± 0.09	0.55	0.9999	80.1
	Anisole				
14	0.001[b]	18.72 ± 0.08	0.43	0.9999	79.1
15	0.010[b]	18.51 ± 0.11	0.62	0.9999	78.9
16	0.100[b]	19.54 ± 0.14	0.71	0.9999	80.5
17	1.000[b]	20.93 ± 0.12	0.57	0.9999	80.4
	Acetic acid				
18	0.1[c]	16.52 ± 0.82	4.98	0.9988	61.9
19	1.0[c]	16.68 ± 1.09	6.51	0.9979	62.7
	Trifluoroacetic acid				
20	0.1[c]	17.67 ± 0.87	4.91	0.9988	65.3
21	1.0[c]	16.86 ± 1.47	8.72	0.9962	62.5

[a]Concentration of pyridinium salt 2.8×10^{-5} (mol L^{-1}); measured at 345 nm.
[b]Solvent contained triethylamine, 2.8×10^{-4} (mol L^{-1}).
[c]Kinetic solutions of pyridinium salt (1.4×10^{-4} mol L^{-1}) were diluted to uv concentration (2.8×10^{-5} mol L^{-1}) using 5% (v/v) solution of triethylamine in chlorobenzene; measured at 345 nm.

concentration of nucleophile gave straight lines (Figs. 1 and 2). The derived first order rate constants (intercepts) are given in Table 3. Weak nucleophiles such as *p*-chlorophenol, anisole, or acetic acid have negligible effects on the rate: strong nucleophiles (piperidine, morpholine) show only small rate accelerations, i.e. first-order predominates over second-order reaction. Similar results were previously obtained (3*b*) for the solvolyses of a series of 1-(s-alkyl)pyridinium cations in $CHCl_3$, CH_3CN, TFE, and $(CF_3)_2CHOH$ as solvents, and with pyridine, piperidine, or morpholine as added nucleophiles.

Product analyses were carried out by gc/ms. The solvolysis of 2-pentyl derivative **2***c*, in chlorobenzene at 65°C containing morpholine (0.1 *M*) (i.e. under conditions where over 91% of the reaction is kinetically of first-order) gave: pentene (14%) and *N*-2-pentylmorpholine (86%) (Table 7).[7] The mass spectrum of pentene shows three peaks at *m/z* 70 (M^+), 55 ($C_4H_7^+$, the base peak), and 42 ($C_3H_6^+$), the two latter correspond to $M^+ - CH_3$ and to $M^+ - CH_2{=}CH_2$, respectively (9), and clearly show the pent-2-ene structure (10). *N*-2-Pentylmorpholine shows three major peaks at *m/z* 157, 142, and 114 which correspond to molecular ion, to $M^+ - CH_3$, and to $M^+ - C_3H_7$, respectively (Table 7). In tertiary amines, loss of the largest branch from the α-C atom is preferred. Since the peak at *m/z* 114 is the base peak, the fragmentation pattern corresponds to the *N*-(2-pentyl)morpholine structure. Thus, the solvolysis of **2***c* in chlorobenzene in the presence of morpholine gave mixtures of pent-2-ene (14.4 ± 2.0%; elimination product) and *N*-2-pentylmorpholine (85.6 ± 2.0%; nonrearrangement product): specifically no *N*-3-pentylmorpholine could be detected. Similarly, solvolysis of **2***c* in the presence of acetic acid (1 *M*) gave only 2-pentyl acetate, the fragmentation pattern of which exhibited a characteristic fragment ion at *m/z* 87 corresponding to $M^+ - 43$. No peak at *m/z* 101 for 3-pentyl acetate (rearranged product) was found.

Gas chromatography/mass spectral analysis of the products from solvolyses of the 2-pentyl derivative **2***c* in chlorobenzene in the presence of *p*-chlorophenol gave pent-2-ene (72.7%) and *p*-chlorophenyl-2-pentyl ether (27.3%) which showed five significant peaks (Table 9). The structure of the ether is supported by the base peak at *m/z* 128 and the peak at *m/z* 111 corresponding respectively to cleavage β and α to the ring, with hydrogen migration. β-Cleavage of aromatic ethers is dominant; therefore the peak at *m/z* 128 is the base peak. The peaks at *m/z* 155 ($M^+ - 43$) and *m/z* 43 ($C_3H_7^+$) prove the 2-pentyl structure. Solvolysis of 2-pentyl derivative **2***c* in chlorobenzene in the presence of anisole gave only pent-2-ene.

The fact that the rate constants, and specifically the inter-

[7]Tables 7 to 9 have been deposited. Complete set of material may be obtained, at a nominal charge, from the Depository of Unpublished Data, CISTI, National Research Council of Canada, Ottawa, Ont., Canada K1A 0S2.

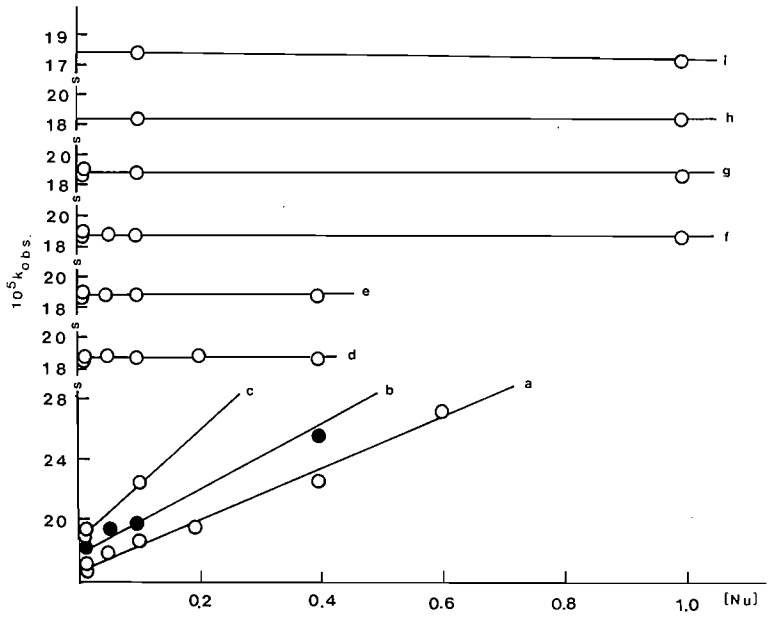

FIG. 1. Plots of observed rate constants for the solvolyses of 1-(2-pentyl)-5,6-dihydro-2,4-diphenylbenzo[*h*]quinolinium trifluoromethanesulphonate **2***c* in chlorobenzene at 65.0°C vs. nucleophilic concentration; *a*, morpholine; *b*, isopropylamine; *c*, piperidine; *d*, pyridine; *e*, 2,6-lutidine; *f*, *p*-chlorophenol; *g*, anisole; *h*, acetic acid; *i*, trifluoroacetic acid.

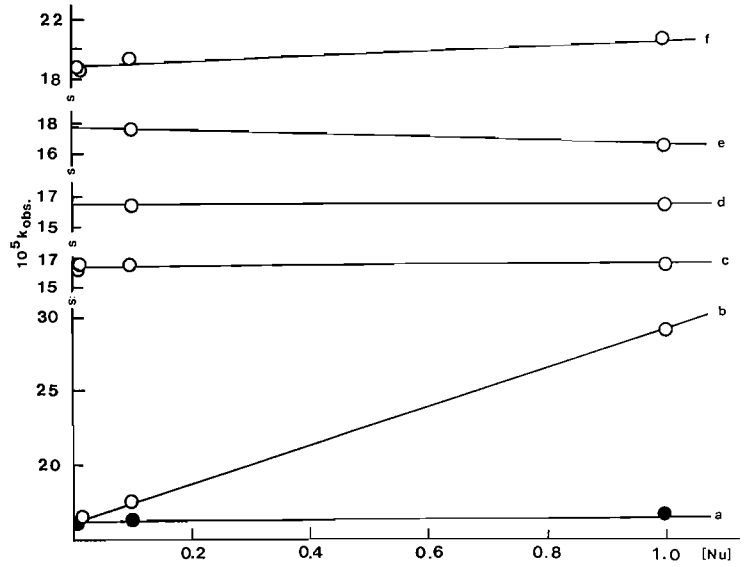

FIG. 2. Plots of observed rate constants for the solvolyses of 1-(3-pentyl)-5,6-dihydro-2,4-diphenylbenzo[*h*]quinolinium tetrafluoroborate **2***e* in chlorobenzene at 65.0°C vs. nucleophilic concentration; *a*, 2,6-lutidine; *b*, morpholine; *c*, pyridine; *d*, acetic acid; *e*, trifluoroacetic acid; *f*, anisole.

cepts, for the reaction of the 2-pentyl derivative **2***c* in chlorobenzene containing morpholine, *p*-chlorophenol, and anisole are so similar, whereas the proportion of elimination varies from 14–100%, confirms that the rate-determining step occurs before elimination.

Solvolysis of 3-pentyl derivative **2***e* in chlorobenzene containing morpholine (0.1 *M*) gave 2-pentene (88%) (identified as above) and *N*-3-pentylmorpholine (12%) (Table 8) for which the only two peaks above *m/z* 100 at *m/z* 157 (1.67%) and *m/z* 128 (100%) correspond to M^+ and to $M^+ - C_2H_5$, respectively, and prove the structure. No *N*-2-pentylmorpholine was detected. Likewise solvolysis of **3***a* in chlorobenzene containing acetic acid gave only the 3-pentyl acetate which showed a fragment ion at *m/z* 101 which corresponds to $M^+ - 29$, and no peak at *m/z* 87 (for rearranged 2-pentyl acetate) was detected.

The kinetic results discussed above show that there is no large rate acceleration in the reactions of **2***c* and **2***e* when 0.1 *M* morpholine or 1 *M* acetic acid is added to chlorobenzene. However, morpholine or acetic acid is able to intercept the incipient 2- or 3-pentyl carbocations before rearrangement to give only the 2-pentyl or only the 3-pentyl products, respectively, which strongly suggests that the solvolyses of **2***c* and **2***e* occur through intimate ion–molecule pairs. This supports the conclusions drawn from our earlier work with 1,1,1,3,3,3-hexafluoropropan-2-ol (3): solvolyses of **2***c* and **2***e* in this solvent gave identical mixtures of rearranged and non-rearranged ether

TABLE 3. First-order (k_1) and second-order (k_2) rate constants for the reactions of 1-substituted pyridinium salts (**2c**, **2e**) with nucleophiles in chlorobenzene

Compound	Nucleophile	N^a	R^b	Slope		Intercept		$10^3 k_1{}^f$
				$10^3 k_2{}^{c,d}$	% Error	$10^5 k_1{}^{d,e}$	% Error	$k_2 + 10k_1$
2c	Piperidine	5	0.9999	0.313 ± 0.009	2.8	19.00 ± 0.40	2.1	85
2c	Morpholine	5	0.9995	0.171 ± 0.01	5.8	16.97 ± 0.27	1.6	>91
2c	Pyridine	6		(0.62 ± 5.3) × 10^{-3}		18.62 ± 0.10	0.5	>99.9
2c	Lutidine	5		(0.43 ± 0.72) × 10^{-3}		18.83 ± 0.13	0.7	>99.9
2c	Isopropylamine	6	0.9872	0.133 ± 0.02	15.2	18.62 ± 0.89	4.8	93
2c	*p*-Chlorophenol	5		(0.12 ± 0.21) × 10^{-2}		18.80 ± 0.09	0.5	>99.9
2c	Anisole	4		(0.963 ± 1.210) × 10^{-3}		19.02 ± 0.09	0.5	>99.9
2c	Acetic acid	2		0.002 ± 0.021		18.05 ± 1.14	6.3	>99.9
2c	Trifluoroacetic acid	2		−0.005 ± 0.028		18.06 ± 1.62	9.0	>99.9
2e	Morpholine	4	0.997	0.13 ± 0.01	7.7	16.24 ± 0.11	0.7	93
2e	Pyridine	4	0.9963	0.004 ± 0.001	25.0	16.30 ± 0.41	2.5	99
2e	Lutidine	4		0.010 ± 0.001	10.0	15.83 ± 1.35	8.5	99
2e	Anisole	4	0.95	0.021 ± 0.004	19.0	18.83 ± 1.23	6.5	99
2e	Acetic acid	2		0.002 ± 0.021		16.50 ± 1.03	6.2	>99.9
2e	Trifluoroacetic acid	2		−0.009 ± 0.026		17.76 ± 1.13	6.3	>99.9

[a]Numbers of runs.
[b]Correlation coefficient.
[c]L mol^{-1} s^{-1}.
[d]90% confidence limit.
[e]s^{-1}.
[f]Percentage reaction by unimolecular route at [nucleophile] 10^{-1} mol L^{-1}.

TABLE 4. Pseudo-first-order rate constants for the reactions of 1-benzyl-5,6,8,9-tetrahydro-7-phenyldibenzo[*c*,*h*]acridinium trifluoromethanesulphonate **3b** with nucleophiles in chlorobenzene[a]

Entry No.	Temperature (°C)	Nucleophile (mol L^{-1})	$10^5 k_{obs}$ (s^{-1})	Error (%)	*r*	React. (%)
1	60	None[b]	3.98 ± 0.09	2.26	0.9996	70.1
		Morpholine				
2	65	0.00005	8.75 ± 0.10	1.16	0.9998	69.7
3	65	0.00010	11.25 ± 0.10	0.92	0.9999	80.5
4	65	0.00050	26.37 ± 0.30	1.15	0.9999	88.3
5	65	0.00100	50.25 ± 0.79	1.57	0.9999	89.7
6	65	0.00500	221.75 ± 2.46	1.11	0.9999	93.0
		Pyridine				
7	65	0.0001	7.44 ± 0.04	0.60	0.9999	73.9
8	65	0.0010	7.69 ± 0.05	0.69	0.9999	75.2
9	65	0.0100	11.47 ± 0.05	0.46	0.9999	74.8
10	65	0.0500	28.80 ± 0.23	0.80	0.9999	79.1
11	65	0.1000	49.74 ± 0.48	0.97	0.9999	83.4
		Pyridine				
12	60	0.0001	4.15 ± 0.03	0.70	0.9999	77.5
13	60	0.0010	4.28 ± 0.05	1.19	0.9999	75.2
14	60	0.0050	5.20 ± 0.08	1.51	0.9998	81.7
15	60	0.0100	6.85 ± 0.20	2.88	0.9998	81.0
16	60	0.0500	17.83 ± 0.05	0.29	1.0000	61.8
		2,6-Lutidine				
17	60	0.0001	4.03 ± 0.04	1.01	0.9999	76.9
18	60	0.0010	4.02 ± 0.03	0.70	0.9999	66.4
19	60	0.0050	4.07 ± 0.02	0.52	0.9999	66.6
20	60	0.0100	4.11 ± 0.02	0.60	0.9999	64.6
21	60	0.0500	4.41 ± 0.04	0.99	0.9998	69.9
		Isopropylamine				
22	60	0.0001	3.99 ± 0.04	1.09	0.9998	88.7
23	60	0.0050	15.01 ± 0.12	0.78	0.9999	88.6
24	60	0.0500	120.84 ± 3.02	2.50	0.9998	88.6

[a]Concentration of pyridinium salt 2.0 × 10^{-5} (mol L^{-1}); measured at 399 nm.
[b]Solvent contained triethylamine, 2.0 × 10^{-4} (mol L^{-1}); measured at 399 nm.

TABLE 5. Pseudo-first-order rate constants for the reactions of 1-(*p*-methoxybenzyl)-2,4,6-triphenylpyridinium tetrafluoroborate **1***b* with anisole in chlorobenzene at 65.0°C[a]

Entry No.	Anisole (mol L^{-1})	$10^5 k_{obs}$ (s^{-1})	Error (%)	*r*	React. (%)
1	0.000[b]	96.49 ± 0.53	0.55	0.99999	90.1
2	0.100[b]	97.10 ± 0.60	0.62	0.99998	87.7
3	0.500[b]	99.46 ± 0.58	0.58	0.99997	87.5
4	1.000[b]	101.71 ± 0.55	0.55	0.99998	88.1

[a]Concentration of pyridinium salt 9×10^{-5} (mol L^{-1}), measured at 312 nm.
[b]Solvent contained triethylamine, 1×10^{-3} (mol L^{-1}).

products, evidently by a carbocation mechanism; however, solvolysis of **2***c* and **2***e* in 1,1,1,3,3,3-hexafluoropropan-2-ol in the presence of morpholine as nucleophile, gave the non-rearranged *N*-(2-pentyl)- and *N*-(3-pentyl)-morpholine products, respectively, just as we have now observed (3*b*).

We showed previously (3*b*) that both the 2-pentyl and the 3-pentyl substrates underwent solvolysis in trifluoroacetic acid to give the same mixture of 2-pentyl and 3-pentyl trifluoroacetates. We have now carried out solvolysis of **2***c* and **2***e* in chlorobenzene in the presence of trifluoroacetic acid (1 *M*): in further confirmation of our previous work, in each case a mixture of *both* the 2-pentyl and 3-pentyl trifluoroacetates was obtained. Although the trifluoroacetates were not separable under gc condition used,[8] the fragmentation pattern of the isomeric mixture obtained from the solvolysis of the 2-pentyl derivative **2***c* on gc/ms analysis exhibited characteristic fragment ions for both *m/z* 155 and 141, which correspond to the rearranged product (3-pentyl trifluoroacetate *m/z* 155, i.e. $M^+ - 29$) and the non-rearranged product (2-pentyl trifluoroacetate *m/z* 141, i.e. $M^+ - 43$, respectively). The same fragmentation pattern was obtained on analysis of the mixture obtained from the 3-pentyl derivative.

Borderline (*2*): reactions by rate-determining formation of an ion–molecule pair and by rate-determining attack by nucleophile

In this region, reactions proceed by capture of an ion–molecule pair by the solvent or added nucleophile, and competition occurs between two different mechanisms: (*i*) mechanism *d* or *e*; rate-determining formation of the ion–molecule pair, or of the free carbocation, i.e. unimolecular reaction mode and (*ii*) mechanism *b* or *c*; rate-determining nucleophilic attack, i.e. bimolecular reaction mode. Here, we have studied the behaviour of the *N*-benzylpentacyclic pyridinium cation in chlorobenzene containing small amounts of nucleophiles, i.e. under conditions where both mechanisms should be of comparable importance.

Solvolyses of 1-benzyl-5,6,8,9-tetrahydro-7-phenyldibenzo[*c*,*h*]acridinium trifluoromethanesulphonate (**3***b*) and 1-(*p*-methoxybenzyl)-2,4,6-triphenylpyridinium tetrafluoroborate **1***b* in chlorobenzene occur at convenient rates at 65.0°C and were followed spectrophotometrically at 399 and 312 nm, respectively. In pure solvent an initial decrease in absorption is followed by an increase due to acid–base equilibria; this was avoided by the addition of small amounts of NEt_3 (see experimental section). Reactions carried out in the presence of morpholine, pyridine, lutidine, isopropylamine, and anisole, measured under pseudo-first-order conditions, gave good straight lines to at least 62% completion. The observed rate constants (k_{obs}) (Tables 4 and 5) for these reactions plotted against concentration of nucleophile gave straight lines (Fig. 3). The first order rate constants (intercepts) are given in Table 6.

[8]Conditions: 3% SP 2100 on 100/120 Supelcoport, flow rate 30 mL/min, helium carrier gas, 40–200 deg at 10 deg/min.

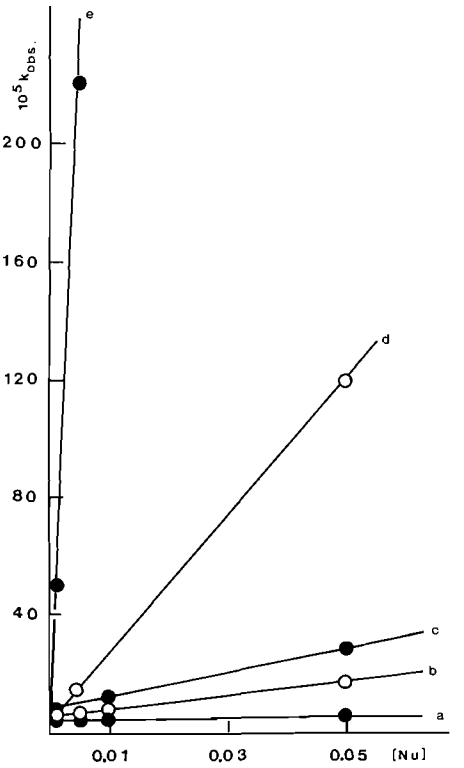

FIG. 3. Plots of observed rate constants for the solvolyses of 1-benzyl-5,6,8,8-tetrahydro-7-phenyldibenzo[*c*,*h*]acridiniumtrifluoromethanesulphonate **3***b* in chlorobenzene vs. nucleophilic concentration; *a*, 2,6-lutidine (60°C); *b*, pyridine (60°C); *c*, pyridine (65.0°C); *d*, isopropylamine (60°C); *e*, morpholine.

The *N*-benzylpentacyclic derivative **3***b* reacts with morpholine almost exclusively via a bimolecular route (Table 6). Dramatically different is the reaction of **3***b* with lutidine; for this much less powerful nucleophile the second-order component is insignificant and the substrate undergoes solvolysis almost entirely via a unimolecular route. For solvolysis in the presence of pyridine, the percentage reaction by the unimolecular route is found to be 15% at 65.0°C and 13% at 60.0°C for 0.1 *M* nucleophile. It has been demonstrated that *N*-benzylpentacyclic derivative **3***b* reacts with piperidine predominantly through the second-order reaction of the intimate ion–molecule pair with the nucleophile at normal and fairly low pressures, but that at higher pressures reaction by the classical S_N2 process takes over (11). We therefore believe that at normal pressures the dominant second-order reaction of **3***b* with morpholine is also via the intimate ion–molecule pair. The first-order rates at 65°C for the *N*-benzylpentacyclic derivative **3***b* do not change appreciably on changing the nucleophile: morpholine $6.38 \times 10^{-2}\ s^{-1}$, pyridine $7.33 \times 10^{-5}\ s^{-1}$. Similarly, first-order rates for **3***b* at 60°C are likewise constant: pyridine $4.01 \times 10^{-5}\ s^{-1}$, lutidine $4.03 \times 10^{-5}\ s^{-1}$, isopropylamine $3.53 \times 10^{-5}\ s^{-1}$. The solvolysis rate of **3***b* in the absence of nucleophile is $(3.98 \pm 0.09) \times 10^{-5}\ s^{-1}$ at 60.0°C. We interpret this invariance as evidence that there is no merging of the unimolecular (S_N1 type) and bimolecular (S_N2 type) mechanisms; rather two mechanisms can and do proceed independently. If the bimolecular mode is the reaction of nucleophile with the ion–molecular

TABLE 6. First-order (k_1) and second-order (k_2) rate constants for the reactions of 1-substituted pyridinium salts with nucleophiles in chlorobenzene

Compound	Nucleophile	Temperature (°C)	N^a	R^b	Slope		Intercept		$10^3 k_1{}^f$
					$10^3 k2^{c,d}$	% Error	$10^5 k_1{}^{d,e}$	% Error	$k_2 + 10k_1$
1*b*	Anisole	65	3	0.997	0.05 ± 0.01	20.0	96.70 ± 0.99	1.0	>99
3*b*	Pyridine	65	5	0.9999	4.25 ± 0.06	1.3	7.33 ± 0.29	3.9	15
3*b*	Pyridine	60	5	0.9998	2.76 ± 0.10	3.6	4.01 ± 0.22	5.7	13
3*b*	Lutidine	60	5	0.9986	0.077 ± 0.07	9.3	4.03 ± 0.02	0.5	>99
3*b*	*i*-$PrNH_2$	60	3	1.000	23.40 ± 0.06	0.3	3.53 ± 0.01	0.3	<1
3*b*	Morpholine	65	5	0.9999	430.77 ± 7.84	1.8	6.38 ± 1.80	28.1	<0.1

[a]Number of runs.
[b]Correlation coefficient.
[c]L mol^{-1} s^{-1}.
[d]90% confidence limit.
[e]s^{-1}.
[f]Percentage reaction by S_N1 route at [nucleophile] 10^{-1} mol L^{-1}.

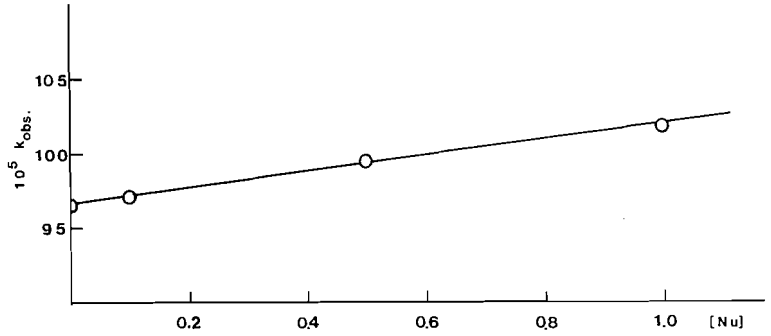

FIG. 4. Plot of observed rate constants for the solvolyses of 1-(*p*-methoxybenzyl)-2,4,6-triphenylpyridinium tetrafluoroborate **1***b* in chlorobenzene at 65.0°C vs. anisole concentration.

pair (mechanism *c*), then the unimolecular modes must in this case be the dissociation of the ion-molecular pair to the free carbocation (mechanism *e*).

Solvolysis of 1-(*p*-methoxybenzyl)-2,4,6-triphenylpyridinium tetrafluoroborate **1***b* was carried out at 65.0°C in chlorobenzene with anisole as nucleophile. As can be seen from Table 6 nucleophilic displacement in this case occurs almost exclusively by an unimolecular S_N1 type mechanism. There is no large rate acceleration when some anisole is added to chlorobenzene solvent. The calculated first-order component (k_1) is the same as that observed for the reaction without the nucleophile.

Conclusions

From Scheme 1, rates for mechanisms (*c*) and (*d*) are proportional to $k'_2[Nu]k_d/(k'_2[Nu] + k_a)$. For mechanism (*c*), $k_a \gg k'_2[Nu]$ and thus the rate is proportional to $k'_2[Nu]k_a/k_d$. For mechanism (*d*), $k'_2[Nu] \gg k_a$ and thus the rate is proportional to k_d. For mechanism (*e*), k''_2 is fast and the rate is proportional to $k_d k'_d/(k_a + k'_d)$. The results presented in this paper are entirely consistent with this scheme and with the operation of two distinct mechanisms at the appropriate borderlines.

Experimental

Ultraviolet spectra of reactants and products were measured on Pye Unicam PU 8800 and Pye Unicam SP6-550 uv–visible spectrophotometers. ^1H nmr spectra were obtained with a Varian Model EM 3604 spectrometer (Me_4Si as internal standard). Infrared spectra were recorded with a Perkin-Elmer Model 283 B spectrophotometer. Melting points (mp) were determined with a Reichart hot stage microscope.

Gas chromatography/mass spectra analysis utilized an AEI MS-30 mass spectrometer (using a Kratos DS-55 data system) interfaced to a Pye 104 gas chromatograph. The column packings employed were 3% SP2100 on 100/120 Supelcoport, 10% Carbowax — 20M/2%KOH (5 or 6 ft × 4 mm) in glass columns, 30 mL/min helium as the carrier gas at flow rates and temperatures specified (Tables 7, 8, 9).

Preparation of compounds

The following were prepared by the literature method quoted: 2,4,6-triphenylpyrylium tetrafluoroborate **1***a*, mp 257°C (lit. (12): 251–257°C); 5,6-dihydro-2,4-diphenylnaphtho[1,2-*b*]pyrylium trifluoromethanesulphonate **2***a*, mp 276°C (lit. (13): 276°C); 5,6-dihydro-2,4-diphenylnaphtho[1,2-*b*]pyrylium tetrafluoroborate **2***b*, mp 268–271°C (lit. (14): 270°C); 5,6,8,9-tetrahydro-7-phenyldibenzo[*c*,*h*]xanthylium trifluoromethanesulphonate **3***a*, mp 304 (lit. (15): 304°C).

General procedure for preparation of pyridinium salts (Scheme 2)

Equimolar quantities of the pyrylium salt, the amine and triethylamine were stirred in dichloromethane (5 mL/g of pyrylium salt) for 2 h. Glacial acetic acid (double molar quantity) was added and the mixture stirred for 24 h. After washing the solution with water, precipitation with ethyl ether gave the products: 1-(*p*-methoxybenzyl)-2,4,6-triphenylpyridinium tetrafluoroborate **1***b*, mp 138–139°C; 1-(2-pentyl)-5,6-dihydro-2,4-diphenylbenzo[*h*]quinolinium trifluoromethanesulphonate **2***c*, mp 141–144°C; 1-(3-pentyl)-5,6-dihydro-2,4-diphenylbenzo[*h*]quinolinium tetrafluoroborate **2***e*, mp 153–154°C (lit. (3*a*): 147–150°C); 1-benzyl-5,6,8,9-tetrahydro-7-phenyldibenzo[*c*,*h*]acridinium trifluoromethanesulphonate **3***b*, mp 170–171°C (lit. (16): 170–171°C).

Kinetic measurements

Kinetics were followed by uv spectrophotometry by monitoring the decrease or the increase of absorbance of the pyridinium salts at fixed wavelengths using the procedure already described (17). Ultraviolet

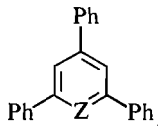

1

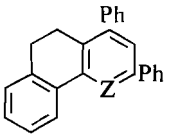

2

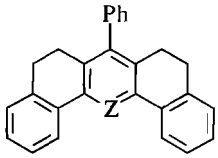

3

1*a*: Z = O^+, (BF_4^-)
1*b*: Z = N^+—$CH_2C_6H_4OCH_3$-*p*, (BF_4^-)
2*a*: Z = O^+, ($CF_3SO_3^-$)
2*b*: Z = O^+, (BF_4^-)
2*c*: Z = N^+—2-pentyl, ($CF_3SO_3^-$)
2*e*: Z = N^+—3-pentyl, (BF_4^-)
3*a*: Z = O^+, ($CF_3SO_3^-$)
3*b*: Z = N^+—$CH_2C_6H_5$, ($CF_3SO_3^-$)

SCHEME 2. Pyrylium and pyridinium salts

cells and sealed glass tubes of 28 cm × 14 mm diameter were used as reaction vessels. Ultraviolet cells were controlled to ±0.5°C in a cell basket inside the uv spectrophotometer by the Pye Unicam Cell Temperature Controller. Glass tubes were controlled to ±1°C in hot blocks (Statim Model 252). For kinetic runs in which the solvent did not contain a basic nucleophile, either small amounts of Et_3N (1×10^{-3} mol L^{-1}) were added, or the kinetic solutions of the pyridinium compounds were diluted to uv concentration (1.4×10^{-5} mol L^{-1}) using an 8% solution of trifluoroacetic acid in chlorobenzene before uv measurement. For solvolyses in the presence of acetic acid and trifluoroacetic acid as nucleophiles, the kinetic solutions of the pyridiniums (1.4×10^{-4} mol L^{-1}) were diluted to uv concentration (2.8×10^{-5} m L^{-1}) using 5% (v/v) solution of triethylamine in chlorobenzene before uv measurement. These procedures converted acid–base equilibrium mixtures into free base or protonated pyridine, respectively (see footnotes to Tables). Pseudo-first-order rate constants were calculated from the slopes of conventional plots of ln $(\epsilon - \epsilon_2)/(\epsilon - \epsilon_2)$ vs. time (18). Such plots were linear to at least 70% completion, and k_{obs} values were reproducible to ca. 2%.

Solvolysis procedure for gc/ms study

The pyridinium salt in 1.0 mL of solvent was heated with the nucleophile in a sealed glass tube at 65°C for 24 h. The tube was opened immediately before the gc/ms study.

1. A. R. KATRITZKY and G. MUSUMARRA. Chem. Soc. Rev. **13**, 47 (1984).
2. A. R. KATRITZKY, Z. DEGA-SZAFRAN, M. L. LOPEZ-RODRIGUEZ, and R. W. KING. J. Am. Chem. Soc. **106**, 5577 (1984).
3. (*a*) A. R. KATRITZKY, J. MARQUET, and M. L. LOPEZ-RODRIGUEZ. J. Chem. Soc. Perkin II, 1443 (1983); (*b*) A. R. KATRITZKY, M. L. LOPEZ-RODRIGUEZ, and J. MARQUET. J. Chem. Soc. Perkin II, 349 (1984).
4. T. W. BENTLEY and P. v. R. SCHLEYER. (*a*) J. Am. Chem. Soc. **98**, 7658 (1976); (*b*) Adv. Phys. Org. Chem. **14**, 1 (1977).
5. C. K. INGOLD. Structure and mechanism in organic chemistry. 2nd ed. Cornell Univer. Press, New York. 1969. p. 460.
6. J. M. HARRIS. Prog. Phys. Org. Chem. **11**, 89 (1974).
7. T. W. BENTLEY, C. T. BOWEN, W. PARKER, and C. I. F. WATT. J. Am. Chem. Soc. **101**, 2486 (1979).
8. T. W. BENTLEY and G. E. CARTER. J. Am. Chem. Soc. **104**, 5741 (1982).
9. F. W. MCLAFFERTY. Interpretation of mass spectra. 3rd ed. W. A. Benjamin, New York. 1980. p. 179.
10. S. R. HELLER and G. W. A. MILNE. EPA/NIH mass spectral data base. Vol. I. Molecular weights 30-186, NSRDS, Washington. 1978. p. 16.
11. A. R. KATRITZKY, K. SAKIZADEH, W. J. LE NOBLE, and B. GABRIELSEN. J. Am. Chem. Soc. **106**, 1879 (1984).
12. K. DIMROTH, C. REICHARDT, and K. VOGEL. Org. Synth. Coll. Vol. V, 1135 (1973).
13. A. R. KATRITZKY, F. AL-OMRAN, R. C. PATEL, and S. S. THIND. J. Chem. Soc. Perkin I, 1890 (1980).
14. A. R. KATRITZKY and S. S. THIND. J. Chem. Soc. Perkin I, 1895 (1980).
15. A. R. KATRITZKY and S. S. THIND. J. Chem. Soc. Perkin I, 661 (1981).
16. A. A. KATRITZKY, A. M. EL-MOWAFY, L. MARZORATI, R. C. PATEL, and S. S. THIND. J. Chem. Res. (S) 310 (1980); (M) 4001 (1980).
17. A. R. KATRITZKY, G. MUSUMARRA, K. SAKIZADEH, and M. MISIC-VUKOVIC. J. Org. Chem. **46**, 3820 (1981).
18. J. L. LATHAM. Elementary reaction kinetics. Buttersworths, London. 1969. p. 12.
19. J. MARCH. Advanced organic chemistry. 3rd ed. J. Wiley, New York. 1985. p. 265–268.

The hydrolysis of $(\pi\text{-}C_6H_6)Cr(\pi\text{-}C_6F_5CO_2C_2H_5)$: an unexpected decarboxylation

MICHAEL J. MCGLINCHEY AND HAO NGUYEN
Department of Chemistry, McMaster University, Hamilton, Ont., Canada L8S 4M1

Received November 5, 1985

This paper is dedicated to Professor Arthur N. Bourns

MICHAEL J. MCGLINCHEY and HAO NGUYEN. Can. J. Chem. **64**, 1170 (1986).

The attempted basic hydrolysis of the ester sandwich compound $(C_6H_6)Cr(C_6F_5CO_2Et)$ did not yield the expected carboxylic acid but instead produced $(C_6H_6)Cr(C_6F_5H)$ in good yield together with traces of $(C_6H_6)Cr(C_6HF_4OMe)$. Attempts to trap a benzyne intermediate were unsuccessful and the mechanism of decarboxylation is discussed in terms of internal chelation at the chromium centre.

MICHAEL J. MCGLINCHEY et HAO NGUYEN. Can. J. Chem. **64**, 1170 (1986).

On a tenté une hydrolysé en milieu basique de composé ester sandwinch $(C_6H_6)Cr(C_6F_5CO_2Et)$; toutefois, au lieu d'obtenir l'acide carboxylique attendu, il y a eu formation du $(C_6H_6)Cr(C_6F_5H)$, avec un bon rendement, ainsi que des traces du $(C_6H_6)Cr(C_6HF_4OMe)$. On a tenté sans succès de piéger l'intermédiaire benzynique et on discute du mécanisme de décarboxylation en fonction d'une chélation interne au niveau du chrome central.

[Traduit par la revue]

Introduction

While the ferrocenyl moiety has now become a standard organic functional group (1) and the $(C_5H_5)Fe$ fragment has been exploited for synthetic purposes (2, 3), the chemistry of the analogous bis(arene)chromium complexes (chromarenes) (4) is much less understood. Initially, the problems were synthetic in that the Friedel–Crafts route (5) to $(C_6H_6)_2Cr$ — viz., $CrCl_3/C_6H_6/AlCl_3/Al$ — would not tolerate functional groups on the arene. Thus, arenes such as chlorobenzene or anisole, which possess non-bonding electron pairs, react with the Lewis acid catalyst ($AlCl_3$) and undergo side reactions which do not yield the desired sandwich compounds (6). This problem has been largely circumvented by the metal atom vapour technique (7–10) whereby the gaseous metal and the ligand vapour are cocondensed onto a cold (77 K) surface and direct combination occurs to give the required products. By this means, a wide variety of organic functional groups can be incorporated into the chromarene system (11).

A further development was the discovery that in the mixed sandwich compound 1,2,3,4,5-pentafluorochromarene, **1**, the unique hydrogen was readily removable using an alkyl lithium (12) and the corresponding anion **2** reacted with a variety of electrophiles (4). In particular, one can produce the ester **3** in high yields (13). It therefore seemed not unreasonable that one could hydrolyze the ester to the corresponding carboxylic acid **4**; subsequent measurement of the pK_a of **4** and also of $C_6F_5CO_2H$ should allow a direct evaluation of the electronic effect of the $(C_6H_6)Cr$ moiety on another arene ring.

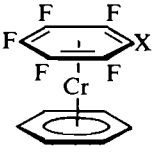

1: X = H
2: X = Li
3: X = $COOC_2H_5$
4: X = COOH

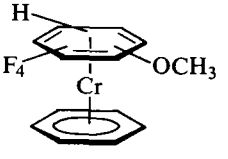

5

Results and discussion

The electronic effect of an organometallic fragment on an organic molecule was probably first studied by Nicholls and Whiting (14) who noted that the pK_a of $(C_6H_5CO_2H)Cr(CO)_3$ was similar to that of *para*-nitrobenzoic acid. He proposed that the tricarbonylchromium moiety was strongly electron-withdrawing and should hence facilitate nucleophilic attack on aromatic rings. This perceptive prediction has since been amply verified and much elegant chemistry has resulted (15). Owing to the non-availability of chromarenyl carboxylic acids, such an approach has not been possible and so more indirect probes have been used. Typically, a comparison of the ν_{CO} values for $C_6F_5M(CO)_x$ and the corresponding chromarenes $(C_6H_6)Cr(C_6F_5M(CO)_x)$ indicated that the $(C_6H_6)Cr$ moiety was a net donor of electron density to the fluorinated ring (4).

For these reasons, we attempted a standard basic hydrolysis of **3** using methanolic KOH. To our surprise, the product after neutralization and extraction was not the anticipated acid but rather pentafluorochromarene, **1**, with traces of a methoxytetrafluorochromarene, **5**, which was identified mass spectroscopically.

Our initial thoughts focussed on the possibility of a benzyne intermediate, **6**, produced via decarboxylation and elimination of fluoride ion. Subsequent attack by methanol should then yield the ortho isomer **5***a*, as in Scheme 1. Indeed, it is well established that pentafluorophenyl lithium is an excellent precursor for tetrafluorobenzyne (16) which undergoes Diels–Alder reactions with thiophene and benzene (17, 18). However, in our hands, repeated attempts to trap **6** as its furan adduct **7** were unsuccessful and we are not of the opinion that a benzyne intermediate is formed. We note that other attempts to detect π-complexed arynes have not been successful (19–21) except where the aryne binds to a metal triangle as in **8** (22). In these latter molecules the ligand functions as a cycloalkyne rather than as an aryne. Recently, however, it has been shown that a benzyne–zirconocene adduct has a transient existence (23) and can be used in synthesis (24).

Eventually, after numerous reactions, the available quantities of **5** were such as to allow the measurement of its ^{19}F nmr spectrum which showed only two fluorine environments. We thus assign **5** as the *para* isomer since the other possibilities would exhibit four fluorine resonances. As we have noted previously (25–27), the fluorine chemical shifts of π-complexed fluoroarenes are very markedly shielded relative to those of the free arenes themselves. It seems most likely that **5** arises via a nucleophilic attack on the complexed fluoroarene and is probably unrelated to the mechanism of decarboxylation. As

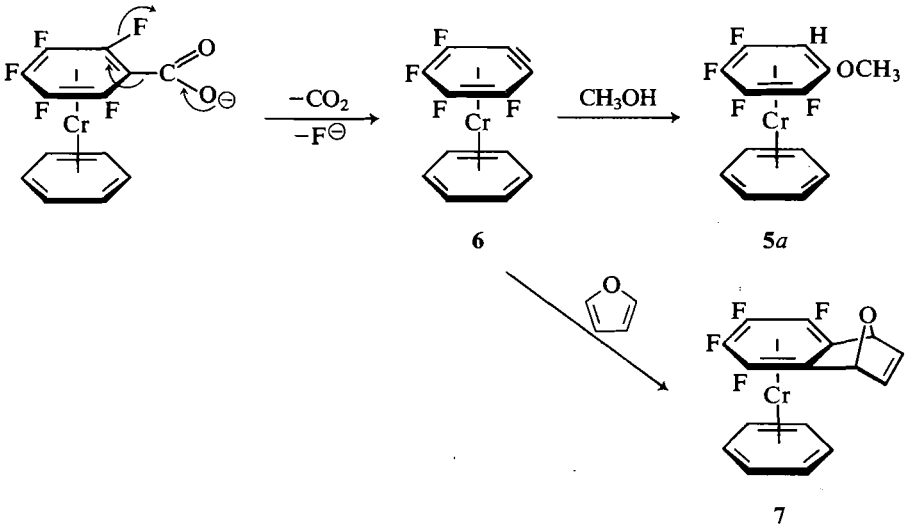

SCHEME 1

with their non-complexed analogues (28), nucleophilic attack to displace fluoride from pentafluorochromarenes occurs predominantly at the *para* position (29).

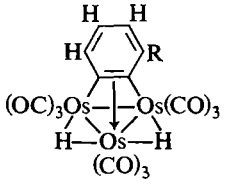

8

Finally, one might speculate as to the reason for the unexpectedly facile decarboxylation during ester hydrolysis. Clearly, since this process is not observed with the free arene, the metal must be implicated either directly or indirectly in the elimination of carbon dioxide. We note that decarboxylation processes are sometimes catalyzed by the presence of transition metal ions, such as Cu^+ or Mn^{2+}, and chelate formation is almost invariably invoked (30). In fluorochromarene sandwiches, such as those discussed here, the chromium is generally considered to be rather more positive than its formal zero oxidation state would indicate. Thus, the relative difficulty of oxidizing the chromium (31), the decreased infrared frequency of the ring-breathing mode of the fluorinated ring (32), as well as ESCA data (unpublished data from this laboratory), all indicate that there is a net transfer of electron density into the fluorinated ring and that the chromium atom bears a partial positive charge. It is then reasonable to visualize chelation by the carboxylate oxygen, thus placing a formal negative charge on the fluorinated ring as in **9**. Subsequent protonation and elimination of CO_2 from the cyclohexadienyl complex **10** would lead directly to the observed product. A tentative mechanism is presented in Scheme 2.

To conclude, complexation of $C_6F_5CO_2Et$ to a π-$(C_6H_6)Cr$ moiety reduces its susceptibility towards nucleophilic displacement of fluoride. However, upon hydrolysis to the corresponding carboxylate, loss of CO_2 is greatly facilitated. There is no evidence in favour of a π-complexed benzyne intermediate.

Experimental section

All reactions were carried out under an atomosphere of nitrogen. Mass spectra were obtained using a VG-7070F mass spectrometer fitted with a VG 2035 data system. ^{19}F nmr spectra were obtained on a Bruker WH90 spectrometer operating at 84.66 MHz using $CFCl_3$ as an external reference.

Using the metal atom vapour apparatus previously described (25), pentafluorobenzene, benzene and chromium vapour were cocondensed at −196°C to yield **1** which was purified by repeated sublimations.

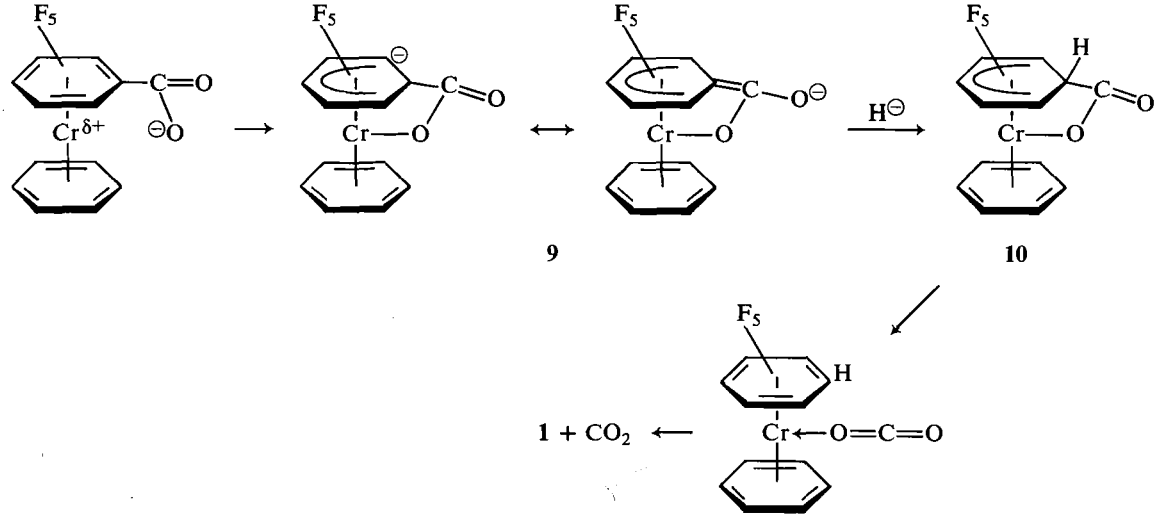

SCHEME 2

As described elsewhere (4), treatment of **1** with *tert*-butyl lithium at −78°C and subsequently with an excess of ethyl chloroformate yielded ethyl pentafluorochromarenoate, **3**. Attempted hydrolysis of **3** (500 mg, 1.35 mmol) with a six-fold excess of KOH in methanol gave a slightly greenish coloured solution. After neutralisation with HCl, filtration and ether extraction, the products were chromatographed on alumina and eluted with benzene to give **1** (221 mg, 0.76 mmol; 55%), identical in all respects with an authentic sample, and traces of a yellow compound **5** showing mass spectral peaks at m/z 310, $C_{13}H_{10}F_4OCr^+$; 279, $C_{12}H_7F_4Cr^+$; 261, $C_{12}H_8F_3Cr^+$; 242, $C_{12}H_8F_2Cr^+$; 180, $C_7H_4F_4O^+$; 149, $C_6HF_4^+$; 131, $C_6H_2F_3^+$; 130, $C_6H_6Cr^+$; 78, $C_6H_6^+$; 52, Cr^+. The accumulated samples of **5** from six experiments gave multiplets in the ^{19}F nmr spectrum at −173 and −178 ppm (i.e., to high field of $CFCl_3$).

When the hydrolysis was repeated in a ten-fold excess of furan, the same products were obtained and no evidence for the production of **7** could be obtained.

Acknowledgements

We thank the Natural Sciences and Engineering Research Council of Canada for financial support and Professor G. Jaouen (Univ. de Paris) for helpful discussions.

1. M. Rosenblum. Chemistry of the iron group metallocenes. Interscience, New York, NY. 1965.
2. R. G. Sutherland, A. Piorko, U. S. Gill, and C. C. Lee. J. Heterocyclic Chem. **19**, 801 (1982) and references therein.
3. J.-R. Hamon, J.-Y. Saillard, A. Le Beuze, M. J. McGlinchey, and D. Astruc. J. Am. Chem. Soc. **104**, 7549 (1982), and releated papers in this series.
4. A. Agarwal, M. J. McGlinchey, and T.-S. Tan. J. Organomet. Chem. **141**, 85 (1977).
5. E. O. Fischer and W. Hafner. Z. Naturforsch. B, **10**, 665 (1955).
6. R. W. Bush and H. R. Snyder. J. Org. Chem. **25**, 1240 (1960).
7. P. L. Timms and T. W. Turney. Adv. Organomet. Chem. **15**, 53 (1977).
8. P. S. Skell and M. J. McGlinchey. Angew. Chem. Int. Ed. Engl. **14**, 195 (1975).
9. K. J. Klabunde. Acc. Chem. Res. **8**, 393 (1975).
10. M. J. McGlinchey. *In* The chemistry of the metal–carbon bond. *Edited by* F. R. Hartley and S. Patai. John Wiley and Sons, New York, NY. pp. 539–574.
11. R. Davis and L. A. P. Kane-Maguire. *In* Comprehensive organometallic chemistry. Vol. 3. *Edited by* G. Wilkinson, F. G. A. Stone, and E. W. Abel. Pergamon Press, Oxford. 1982. pp. 979–981.
12. T.-S. Tan and M. J. McGlinchey. J. Chem. Soc. Chem. Commun. 155 (1976).
13. Nguyen Hao and M. J. McGlinchey. J. Organomet. Chem. **165**, 225 (1979).
14. B. Nicholls and M. C. Whiting. J. Chem. Soc. 551 (1959).
15. G. Jaouen. *In* Transition metal organometallics in organic synthesis. *Edited by* H. Alper. Academic Press, New York, NY. 1978. pp. 65–120, and references therein.
16. S. C. Cohen, A. J. Tomlinson, M. R. Wiles, and A. G. Massey. J. Organomet. Chem. **11**, 385 (1968).
17. A. J. Tomlinson and A. G. Massey. J. Organomet. Chem. **8**, 321 (1967).
18. D. D. Callender, P. L. Coe, J. C. Tatlow, and A. J. Uff. Tetrahedron, **25**, 25 (1969).
19. D. A. Brown and J. R. Raju. J. Chem. Soc. A, 40 (1966).
20. J. F. Bunnett and H. Herrmann. J. Org. Chem. **36**, 4081 (1971).
21. M. F. Semmelhack. J. Organomet. Chem. Libr. **1**, 361 (1976).
22. A. J. Deeming. J. Organomet. Chem. **150**, 123 (1978).
23. G. Erker. J. Organomet. Chem. **134**, 189 (1977).
24. G. Erker, U. Dorf, R. Mynott, Y.-H. Tsay, and C. Krüger. Angew. Chem. Int. Ed. Engl. **24**, 584 (1985).
25. M. J. McGlinchey and T.-S. Tan. Can. J. Chem. **52**, 2439 (1974).
26. M. J. McGlinchey, H. Nguyen, B. G. Sayer, and T.-S. Tan. J. Organomet. Chem. **194**, 325 (1980).
27. R. Faggiani, H. Nguyen, C. J. L. Lock, B. G. Sayer, and M. J. McGlinchey. Organometallics, **2**, 96 (1983).
28. R. E. Banks. Fluorocarbons and their derivatives. Oldbourne Press, London. 1964. p. 140.
29. M. J. McGlinchey and T.-S. Tan. J. Am. Chem. Soc. **98**, 2271 (1976).
30. E. S. Gould. Mechanism and structure in organic chemistry. Holt, Rinehart and Winston, New York, NY. 1959. p. 351 and references therein.
31. H. Nguyen and M. J. McGlinchey. J. Organomet. Chem. **161**, 381 (1979).
32. J. D. Laposa, H. Nguyen, B. G. Sayer, and M. J. McGlinchey. J. Organomet. Chem. **195**, 193 (1980).

An MNDO SCF-MO study of proton transfer from fluoroethanols

BO ANHEDE AND NILS-ÅKE BERGMAN[1]

Department of Organic Chemistry, University of Göteborg and Chalmers University of Technology, S-412 96 Göteborg, Sweden

AND

A. JERRY KRESGE

Department of Chemistry, University of Toronto, Scarborough College, Scarborough, Ont., Canada M1C 1A4

Received October 7, 1985

This paper is dedicated to Professor Arthur N. Bourns

BO ANHEDE, NILS-ÅKE BERGMAN, and A. JERRY KRESGE. Can. J. Chem. **64**, 1173 (1986).

Proton exchange between β-fluorinated ethanols and ethoxide ions has been studied using the MNDO SCF-MO method. Calculations were performed on reactions of ethoxide ion with ethanols substituted in the β-position with 0, 1, 2, and 3 fluorine atoms as well as on reactions where both the ethanol and the ethoxide ion were substituted with the same number (1, 2, 3) of fluorine atoms in the β-position. The energies obtained for the ion–molecule reactant complexes and the transition states from these reactions have been analyzed using the Marcus equation. Through the calculated force-constant matrices of reactants and transition states we also calculated the kinetic isotope effects for the proton-transfer reactions. The semiclassical isotopic rate constant ratios $(k_H/k_D)_s$ were found to be of rather normal magnitude and showed a variation with the energy of reaction. The calculated ratios of tunnel correction factors, Q_{tH}/Q_{tD}, proved to be unrealistically high. These factors were also calculated with the frequencies scaled down by 10% and this was found to reduce the Q_{tH}/Q_{tD} ratios to more realistic values.

BO ANHEDE, NILS-ÅKE BERGMAN et A. JERRY KRESGE. Can. J. Chem. **64**, 1173 (1986).

Utilisant la méthode MNDO d'orbitales moléculaires en champ auto-cohérent, on a étudié l'échange protonique entre des éthanols β-fluorés et des ions éthylates. On a effectué des calculs sur les réactions de l'ion éthylate avec des éthanols substitués par 0, 1, 2 et 3 atomes de fluor en position β ainsi que sur les réactions dans lesquelles tant l'éthanol que l'éthylate étaient substitués par le même nombre (1, 2 ou 3) d'atomes de fluor en positions β. Faisant appel à l'équation de Marcus, on a analysé les énergies obtenues pour les complexes ion–molécule qui réagit ainsi que pour les états de transition de ces réactions. À l'aide des matrices des constantes de force calculées pour les réactifs et pour les états de transition, on a aussi calculé les effets isotopiques cinétiques pour les réactions de transfert de protons. On a trouvé que les rapports (k_H/k_D) des constantes de vitesse isotopiques semi-classiques sont d'une amplitude assez normale et on a trouvé qu'elles varient avec l'énergie de la réaction. Il appert que les rapports calculés pour les facteurs de correction pour l'effet tunnel, Q_{tH}/Q_{tD}, sont trop élevés et non réalistes. On a aussi calculé ces facteurs en se basant sur les fréquences réduites par 10% et on a ainsi trouvé que les valeurs des rapports Q_{tH}/Q_{tD} sont beaucoup plus réalistes.

[Traduit par la revue]

Proton-transfer reactions have been extensively studied from an experimental point of view (1). In such investigations isotope effects and linear free-energy relationships have often been employed. These methods have generated parameters that the investigators have interpreted in terms of the transition-state theory. This approach has proved successful in gaining knowledge usable in predicting the behaviour of many reactions. However, in order to use the transition-state theory one has to make assumptions regarding the reaction step studied, not always easily done in an unambiguous way.

Modern quantum-mechanical methods and powerful computers have made it possible to calculate the stationary points on the potential-energy surface for simple reactions, and thus calculated quantities, e.g., isotope effects, can be compared with experimental data. Even though other assumptions are introduced by the quantum-mechanical methods the two approaches may complement each other. A successful application of this to proton-transfer reactions would contribute to our understanding of such reactions.

In an earlier study we investigated the proton transfers between some carbon acids (CH_3CN and HCCH) and bases (OH^-, CH_3O^-, and CH_2CN^-), utilizing MNDO computations (2). We have now extended our tests of this method and have investigated a series of proton-transfer systems where the immediate vicinity of the reaction centre is unchanged while a perturbation is introduced at some distance from the proton to be transferred. Our choice of system fell on ethanols fluorinated in the β position with 0, 1, 2, and 3 fluorine atoms. This series shows an increasing gas-phase acidity, according to ion cyclotron resonance spectroscopy (3). We employed ethoxide as the base in our simulation of proton abstraction from these substances. In order to have the symmetrical reaction parameters available we also made calculations on the proton transfers with β-fluorinated ethoxides as bases.

Method

The calculations were performed according to the semiempirical scheme devised by Dewar and Thiel (4). During the present investigation different versions of the MNDO computer program have been used. In the first preliminary computations we used the MNDO program by Thiel (5), installed on an IBM 3030 N computer at the Gothenburg University Computing Centre. This program was later transferred and adapted to the VAX 11/730 computer at the Department of Organic Chemistry, University of Gothenburg and Chalmers University of Technology. Later the VAX version of the program package, MOPAC (6), was acquired and used for most of the calculations.

Computational aspects

The energy of each stable species was computed separately with optimization of all geometric parameters (bond lengths, bond angles, and dihedral angles). The species considered as reactants and products on our energy profiles were the stable ion–molecule complexes found by complete optimization of an alcohol molecule and alkoxide ion. See for example, Fig. 1.

The transition states were located as described earlier (2). The

[1]Author to whom correspondence may be addressed.

Printed in Canada / Imprimé au Canada

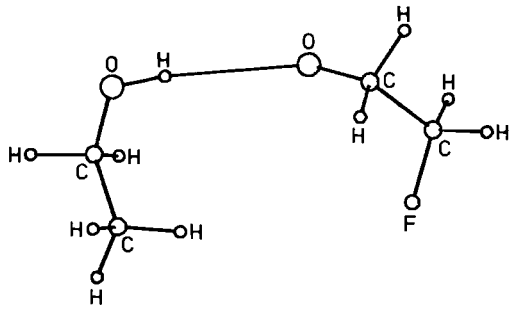

FIG. 1. Optimized reaction complex between 2-fluoroethanol and ethoxide ion.

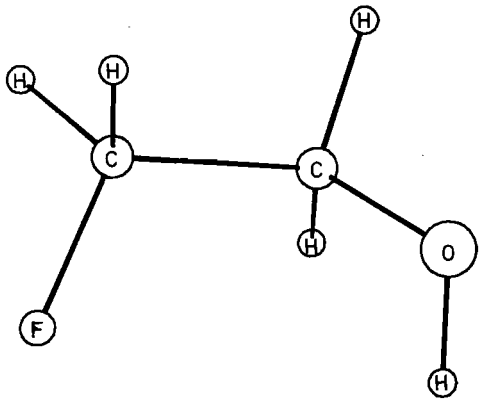

FIG. 2. Optimized geometry for 2-fluoroethanol when the calculation was started from a *gauche*-type geometry.

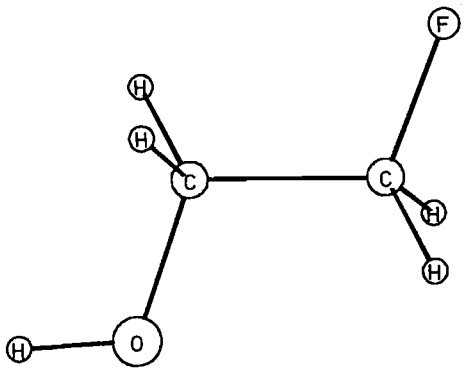

FIG. 3. Optimized geometry for 2-fluoroethanol when the calculation was started from a *trans* geometry with O—H pointing away from C—C.

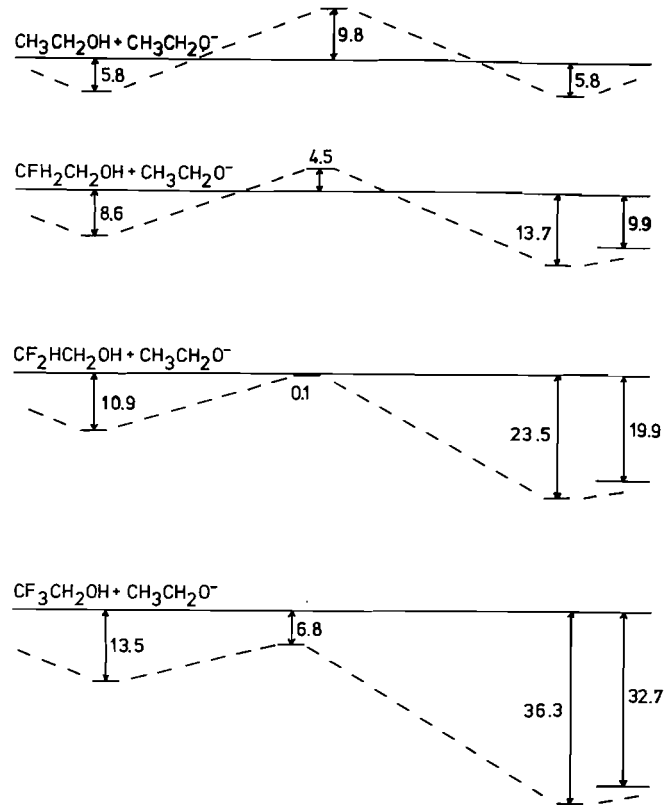

FIG. 4. Energy profiles for some proton-transfer reactions calculated by the MNDO method. Energies in kcal/mol.

semiclassical isotopic rate constant ratios were calculated according to ref. 7*a* using frequencies taken from a FORCE calculation within MOPAC. The tunnel correction factors were calculated from the Bell formula (7*b*). The summation was carried out until Q_t changed by less than 10^{-6} when adding a new term.

Conformational aspects

A number of investigations (microwave, ir, and *ab initio* calculations) (8) have revealed the most stable conformers of the 2-fluoroalcohols to be the *gauche* (G'g), with an intramolecular hydrogen bond between the alcohol hydrogen and a fluorine atom (Fig. 2).

If we started our calculations with a *gauche*-type geometry, the MNDO optimization facility ended up with a minimum-energy geometry for a *gauche* conformer. However, if the starting geometry was given as a conformer close to one with the O—H bond pointing away from the atoms on carbon 2, the optimization resulted in a geometry that retained this feature (Fig. 3). This latter conformer showed a little higher energy (ca. 0.6 kcal/mol) than the one obtained in the preceding procedure.

These findings show that actual proton transfers from fluoroalcohols certainly are more complex than the model we utilize in our computations. However, our reasoning concerns the pure proton-transfer steps of the reactions, and the stable complexes could be considered as the starting species for these steps. All the systems gave such complexes with the O—H pointing more or less away from the C—C bond (see Fig. 1).

Our aim has been to investigate a relatively simple system where a perturbation some distance away from the reaction centre could be introduced stepwise. This was done in such a manner that the overall equilibrium of the reaction could be varied from balanced to more and more unbalanced.

Energy relationships

The computations refer to the gas phase since no solvent molecules are included. A simplified picture of the energy profiles for all the systems calculated in this investigation is given in Figs. 4 and 5.

The supply of experimental data pertinent to the present systems is not overwhelming. However, some gas phase measurements have been made on ethanol and β-fluoro-substituted ethanols (3). From these measurements the ΔH^0 values for the two last reactions in Fig. 4 can be calculated to be −9.1 kcal/mol and −11.7 kcal/mol, respectively. The corresponding ΔE values (−19.9 kcal/mol and −32.7 kcal/mol) obtained in the present investigation are thus too large in both cases. In order to see whether this is a result of computational difficulties connected with the anions, the experimental and the calculated heats of formation (Table 1) for the molecules treated in the present investigation have to be compared.

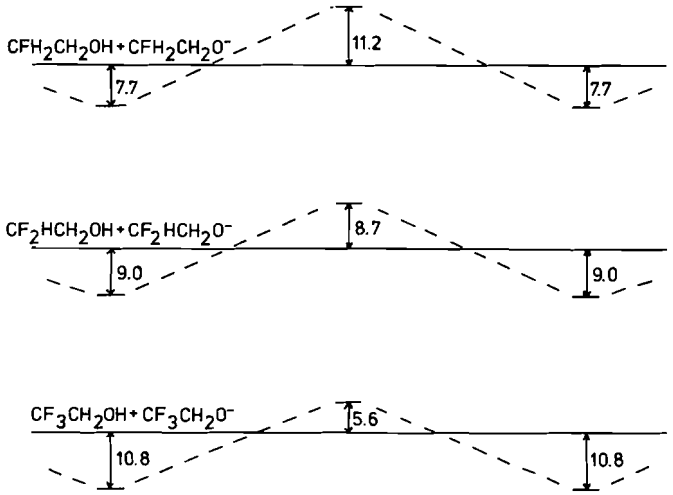

FIG. 5. Energy profiles for some thermoneutral proton transfers calculated by MNDO. Energy in kcal/mol.

TABLE 1. Experimental and calculated heats of formation of ethanol and β-fluoro-substituted ethanols and the corresponding anions

	ΔH_f(ROH) (kcal/mol)		ΔH_f(RO^-) (kcal/mol)	
R in ROH	Experimental[a]	MNDO	Experimental[b]	MNDO
CH_3CH_2—	−56.2	−63.0	−47.5	−45.3
CFH_2CH_2—	—	−108.3	—	−100.5
CF_2HCH_2—	−148.3[c]	−156.9	−148.5	−159.1
CF_3CH_2—	−207.0[c]	−208.4	−209.8	−223.4

[a]Cited in ref. 3.
[b]Derived values according to ref. 3.
[c]Estimated values, see ref. 3.

As can be seen in Table 1, the calculated value for ethoxide ion is in better agreement with the experimental value than is the value for ethanol. The reverse seems to be true for the alcohols substituted with fluorine atoms in the β-position. However, a general trend is not easily discernible.

The energies of the ion–molecule complexes could be compared with experimental data in one case. In a recent paper (9) dealing with anion–alcohol hydrogen bond strengths in the gas phase, the stability of EtO^-—HOEt compared to EtO^- + HOEt is determined to be −20.6 kcal/mol. The ion–molecule complex is thus far more stable than indicated by the present calculation. Comparable data for the β-fluoro-substituted reactions are not accessible.

From Fig. 4 it can be seen, in a qualitative way, that the activation barrier decreases as the reaction becomes more exoenergetic and, from the other direction of reaction, the barrier grows higher the more endoenergetic the calculated reaction becomes. To test if this qualitatively recognisable pattern could be tied to a quantitative relationship, we plotted the calculated barrier heights (calculated from ion–molecule complexes) against the energies of reaction (Fig. 6).

A number of equations of different mathematical form have been considered in the examination of a possible relationship between the activation energy $\Delta E^{\ddagger}$ and the energy of reaction ΔE (10). Among those, the Marcus equation is the one most used (see ref. 10 for references).

According to that:

$$\Delta E^{\ddagger} = \Delta E_0^{\ddagger} + \Delta E/2 + [\Delta E^2/16\Delta E_0^{\ddagger}]$$

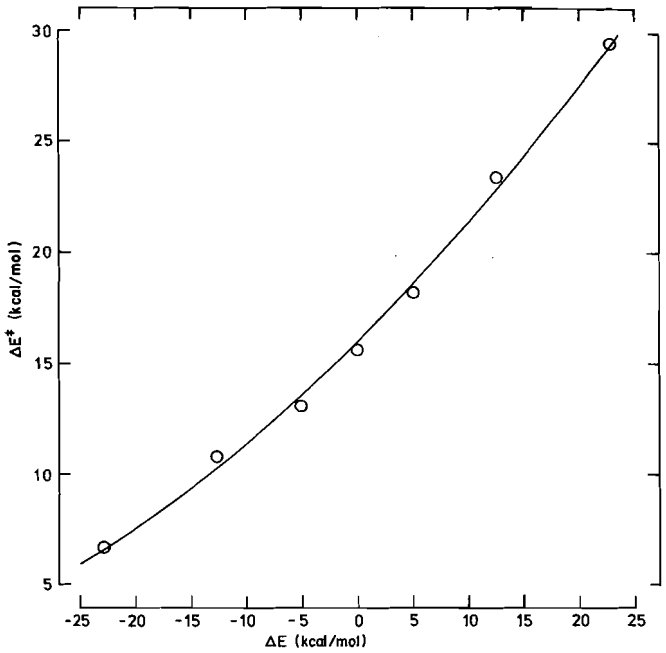

FIG. 6. Plot of $\Delta E^{\ddagger}$ versus ΔE for the MNDO calculated proton transfers in forward and reverse direction of reaction. The solid curve is a nonlinear least-squares fit of the points to the Marcus equation with $\Delta E_0^{\ddagger}$ = 15.96 kcal/mol.

where $\Delta E_0^{\ddagger}$ is the intrinsic barrier, i.e., the formal barrier when $\Delta E = 0$. The fulldrawn curve in Fig. 6 represents the Marcus expression with $\Delta E_0^{\ddagger}$ = 15.96 kcal/mol as determined from a nonlinear least-squares fit of ΔE and $\Delta E^{\ddagger}$ to the Marcus equation, treating $\Delta E_0^{\ddagger}$ as an adjustable parameter.

The Marcus relation could be used to find predictions for the barrier heights of the unsymmetrical reactions in an indirect way by using the additivity assumption:

$$\Delta E_0^{\ddagger} = (\Delta E_{AA}^{\ddagger} + \Delta E_{CC}^{\ddagger})/2$$

where $\Delta E_{AA}^{\ddagger}$ and $\Delta E_{CC}^{\ddagger}$ are the activation energies for the identity reactions (10, 11). The activation energies so calculated are included in Table 2 under the heading $\Delta E_{(Marcus)}^{\ddagger}$ and are seen to deviate only slightly from the directly computed values under the heading $\Delta E^{\ddagger}$. The significance of the found conformity with the Marcus equation should not be overestimated. However, it is gratifying to find that the MNDO method, as well as other SCF (self-consistent field) methods (11), give results which could be interpreted using this formalism.

The barriers for our symmetric reactions all fall in the region of 15–19 kcal/mol (Table 3). The term in the Marcus formula responsible for nonlinearity, i.e. $\Delta E^2/16\Delta E_0^{\ddagger}$, will thus be small compared to the terms corresponding to the kinetic ($\Delta E_0^{\ddagger}$) and thermodynamic ($\Delta E/2$) contributions to $\Delta E^{\ddagger}$. The very slight curvature in Fig. 6 is an indication of this.

Isotope effects

The calculated primary kinetic deuterium isotope effects are listed in Tables 3 and 4.

In Table 3 the symmetric reactions are given and the semi-classical isotopic rate constant ratios for these systems are all between 8.04 and 8.44, i.e., of rather normal magnitude.

The tunneling factors are calculated from the absolute values of the imaginary frequencies and the barrier heights above the most energetic complex. For the symmetric systems the hydrogen tunneling factors Q_{tH} are all very high, due to the high

TABLE 2. Calculated reaction and activation energies for some proton transfer reactions

Reactant	ΔE^a (kcal/mol)	$\Delta E^{\ddagger a}$ (kcal/mol)	$\Delta E^{\ddagger}_{(\text{Marcus})}{}^b$ (kcal/mol)
$[CH_2FCH_2OH—OCH_2CH_3]^-$	−5.1	13.1	14.8
$[CH_2FCH_2O—HOCH_2CH_3]^-$	5.1	18.2	19.9
$[CHF_2CH_2OH—OCH_2CH_3]^-$	−12.6	10.8	11.0
$[CHF_2CH_2O—HOCH_2CH_3]^-$	12.6	23.4	23.6
$[CF_3CH_2OH—OCH_2CH_3]^-$	−22.8	6.7	6.6
$[CF_3CH_2O—HOCH_2CH_3]^-$	22.8	29.5	29.4

[a]MNDO values.
[b]Calculated according to the Marcus equation, see text.

TABLE 3. Calculated activation energies, isotope effects (25°C) and reaction coordinate frequencies for some symmetric proton-transfer reactions

Reactant	$\Delta E^{\ddagger}$ (kcal/mol)	$(k_H/k_D)_s$	$\upsilon^{\ddagger}_H$ (cm^{-1})	$\upsilon^{\ddagger}_D$ (cm^{-1})	Q_{tH}	Q_{tD}	Q_{tH}/Q_{tD}	k_H/k_D
$[CH_3CH_2OH—OCH_2CH_3]^-$	15.6	8.32	1431i	1046i	107.9	4.35	24.8	207
$[CH_2FCH_2OH—OCH_2CH_2F]^-$	18.9	8.44	1441i	1055i	215.1	4.53	47.5	403
$[CHF_2CH_2OH—OCH_2CHF_2]^-$	17.7	8.06	1447i	1060i	166.4	4.64	35.9	289
$[CF_3CH_2OH—OCH_2CF_3]^-$	16.4	8.04	1409i	1035i	94.2	4.16	22.7	182

TABLE 4. Calculated isotope effects (25°C) and reaction coordinate frequencies for some proton-transfer reactions

Reactant	$(k_H/k_D)_s$	$\upsilon^{\ddagger}_H$ (cm^{-1})	$\upsilon^{\ddagger}_D$ (cm^{-1})	Q_{tH}	Q_{tD}	Q_{tH}/Q_{tD}	k_H/k_D
$[CH_2FCH_2OH—OCH_2CH_3]^-$	8.2	1296.5i	957.1i	21.11	3.12	6.76	56
$[CH_2FCH_2O—HOCH_2CH_3]^-$	8.2	1296.5i	957.1i	21.11	3.12	6.76	55
$[CHF_2CH_2OH—OCH_2CH_3]^-$	7.6	1064.1i	816.6i	4.65	2.14	2.17	16.5
$[CHF_2CH_2O—HOCH_2CH_3]^-$	7.7	1064.1i	816.6i	4.65	2.14	2.17	16.8
$[CF_3CH_2OH—OCH_2CH_3]^-$	4.6	548.3i	484.8i	1.37	1.27	1.07	4.92
$[CF_3CH_2O—HOCH_2CH_3]^-$	4.7	548.3i	484.8i	1.37	1.27	1.07	5.03

imaginary frequencies (1409i–1447i cm^{-1}). The deuterium tunneling factors Q_{tD} are more reasonable (imaginary frequencies in the range 1035i–1060i cm^{-1}). However, the ratios of tunneling factors Q_{tH}/Q_{tH} give an unrealistically large contribution to the overall isotope effects for all of the symmetric systems. The reason for this will be discussed below.

Table 4 lists the unsymmetrical reactions. For these the tunnel correction factor for the direction of highest activation is taken from the direction of least activation, since no tunneling can occur from a lower level than the most energetic one of the reactants and products (*7c*).

Also here the semiclassical effects come out as expected and the tunnel effect ratios are of a more realistic magnitude, possibly with the exception of the two first entries due to high imaginary frequencies for the hydrogen cases.

As the reaction becomes more exoenergetic the barrier in the forward direction decreases and the decomposition frequency drops, signifying a broader barrier. The reason for this is not easily visualized in a complicated case like the present one. However, it could be illustrated in a qualitative way using a simple truncated parabola model for the activation barrier (12).

These facts should lead to a weaker semiclassical isotope effect as well as a smaller tunnel correction factor (*7c*). The trend in a series of progressively more perturbed reactions (0, 1, 2, 3 fluorine atoms) seems to come out as expected for increasingly unsymmetric reactions. The same trend was found in ref. 2 even though the proton transfers investigated there were more disparate than the present ones.

The calculated isotopic rate constant ratios may also be subjected to an analysis according to an expression derived from the Marcus relation (13). A nonlinear least-squares fit of

$$\ln (k_H/k_D) = \ln (k_H/k_D)_{max}[1 - (\Delta E/4\Delta E^{\ddagger}_0)^2]$$

to the semiclassical isotopic rate constant ratios and reaction energies for all the unsymmetric reactions in forward and reverse direction of reaction was carried out. With $(k_H/k_D)_{max}$ and $\Delta E^{\ddagger}_0$ treated as adjustable parameters, an acceptable fit was reached when $(k_H/k_D)_{max} = 8.8$ and $\Delta E^{\ddagger}_0 = 10.7$. The same procedure without the two points for the trifluorinated species yielded $(k_H/k_D)_{max} = 8.3$ and $\Delta E^{\ddagger}_0 = 15.9$. As can be seen from Fig. 7 this latter procedure gives a better fit to the remaining four points. The values are also in better agreement with the ones in Table 3. The reaction involving the trifluorinated species represents a relatively larger perturbation than the other reactions and this may cause the relation to break down.

The reason for the unrealistic outcome of the ratio of tunneling factors probably stems from MNDO's known weakness to overestimate frequencies (14, 2) (a weakness shared with simple *ab initio* calculations also, ref. 15). Another contribution to the large tunneling factors may be too high $\Delta E^{\ddagger}$ values calculated by the MNDO method (16). The tunnel factors for the hydrogen species of the symmetric reactions are especially

TABLE 5. Tunnel correction factors calculated for downscaled imaginary frequencies

Reactant	$0.9\upsilon_H^{\ddagger}$ (cm^{-1})	$0.9\upsilon_D^{\ddagger}$ (cm^{-1})	Q_{tH}	Q_{tD}	Q_{tH}/Q_{tD}
$[CH_3CH_2OH—OCH_2CH_3]^-$	1288i	941i	22.9	2.97	7.70
$[CH_2FCH_2OH—OCH_2CH_2F]^-$	1297i	950i	30.0	3.05	9.82
$[CHF_2CH_2OH—OCH_2CHF_2]^-$	1302i	954i	30.5	3.09	9.88
$[CF_3CH_2OH—OCH_2CF_3]^-$	1268i	932i	19.6	2.88	6.80
$[CH_2FCH_2OH—OCH_2CH_3]^-$	1167i	861i	8.12	2.38	3.41
$[CHF_2CH_2OH—OCH_2CH_3]^-$	958i	735i	3.13	1.81	1.73
$[CF_3CH_2OH—OCH_2CH_3]^-$	494i	436i	1.28	1.21	1.06

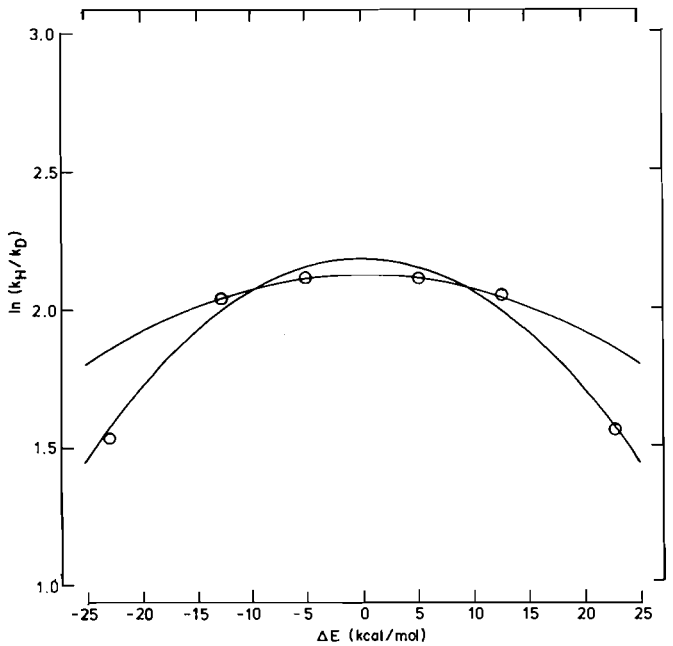

FIG. 7. Plot of ln (k_H/k_D) versus ΔE for the calculated semiclassical isotopic rate constant ratios. Included are two curves representing nonlinear least-squares fits of all six points and of the four points excluding the trifluorinated species.

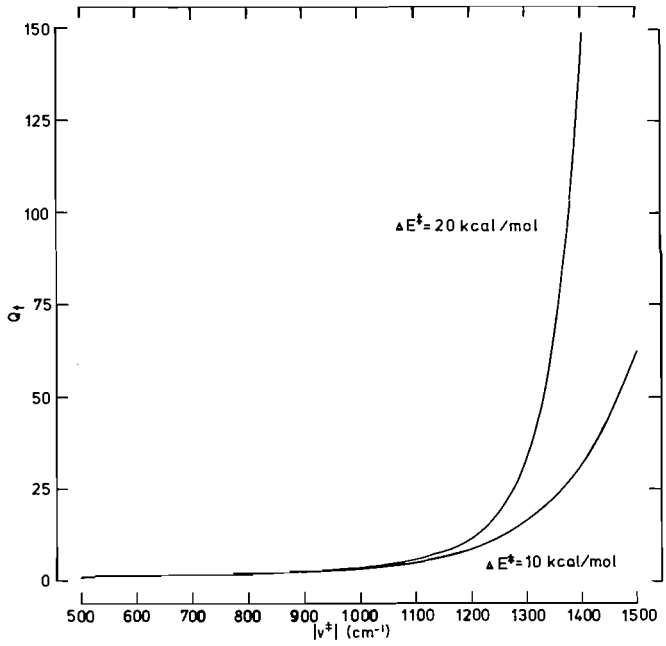

FIG. 8. The shape of the tunnel correction factor function for two barrier heights.

large. When frequencies higher than ca. 1000i cm^{-1} are involved and the barrier heights are of reasonable magnitude (<25 kcal/mol), the tunnel correction factor starts to increase rather rapidly so that an overestimated frequency leads to a still more overestimated tunnel factor. This tendency is amplified the higher the frequency for a given barrier height.

For *ab initio* calculations it has been found that an empirical scaling factor for force constants should be introduced in order to obtain agreement with experiment (17). As a test on the effect of scaling of the frequencies in the present case, we have calculated tunnel correction factors with the absolute values of the imaginary frequencies scaled down by 10% (a rough estimation of the mean value of the deviation for all types of vibrations from experimentally determined values according to ref. 14), see Table 5. The scaling is seen to have most effect on reactions with high imaginary frequencies. In the first row Q_{tH}/Q_{tD} is 7.70 compared to 24.8 without scaling (Table 3), and in the last row the corresponding value is 1.06 compared to 1.07 (Table 4).

Scaling of the frequencies might also influence the semiclassical isotope effect. As an example we calculated the semiclassical isotope effect for the proton transfer from trifluoroethanol to trifluoroethoxide with all the frequencies (both in the reactant complex and transition state) reduced by 10%. The effect turned out to be a reduction of the calculated $(k_H/k_D)_s$ from 8.04 to 6.68, which is a very slight change.

Conclusions

In some aspects the calculation of proton transfer reactions by the MNDO method turns out to give results that qualitatively agree well with notions commonly used by physical organic chemists. We now have confirmed that a quantitative analysis (according to the Marcus equation) of some MNDO calculated proton transfers turns out in a reasonable way.

The results of our isotope effect calculations, however, are rather unexpected, at least if the tunnel corrections are included. The reason for this stems from MNDO's known overestimation of frequencies and from the overestimation of $\Delta E^{\ddagger}$. The tunnel correction function turns out to be especially sensitive to changes in the frequencies in the region of interest in this investigation.

In order to make the MNDO method usable for quantitative isotope effect calculations, either the program should be modified to give frequencies very close to experimental ones, or a separate function for correction of frequencies should be determined and applied to the MNDO-calculated frequencies.

Acknowledgements

We thank Professor Lars Melander for valuable suggestions during the planning of this work. Financial support from the Swedish Natural Science Research Council is gratefully acknowledged. The calculations were carried out on a DEC VAX 11-730 computer purchased with funds kindly provided by the Knut and Alice Wallenberg foundation.

1. R. P. BELL. The proton in chemistry. Chapman and Hall, London. 1973.
2. B. ANHEDE, N.-Å. BERGMAN, and L. MELANDER. Acta Chem. Scand. A, **37**, 843 (1983).
3. J. E. BARTMESS, J. A. SCOTT, and R. T. MCIVER, JR. J. Am. Chem. Soc. **101**, 6046 (1979); **101**, 6056 (1979).
4. M. J. S. DEWAR and W. THIEL. J. Am. Chem. Soc. **99**, 4907 (1977).
5. W. THIEL. QCPE, **11**, 353 (1978).
6. W. THIEL, P. WEINER, J. STEWART, and M. J. S. DEWAR. QCPE, **15**, 455 (1983).
7. L. MELANDER and W. H. SAUNDERS, JR. Reaction rates of isotopic molecules. Wiley, New York. 1980. (*a*) Section 2.1.2; (*b*) Section 2.1.1; (*c*) Section 2.2.3.
8. (*a*) J. MURTO, A. RASANEN, A. ASPIALA, and T. LOTTA. J. Mol. Struct. THEOCHEM, **108**, 99 (1984); (*b*) K.-M. MARSTOCK and H. MOLLENDAL. Acta Chem. Scand. A, **34**, 765 (1980).
9. G. CALDWELL, M. D. ROZEBOOM, J. P. KIPLINGER, and J. E. BARTMESS. J. Am. Chem. Soc. **106**, 4660 (1984).
10. J. R. MURDOCH. J. Am. Chem. Soc. **105**, 2159 (1983), and references therein.
11. J. DONNELLA and J. R. MURDOCH. J. Am. Chem. Soc. **106**, 4724 (1984), and references therein.
12. R. P. BELL. The tunnel effect in chemistry. Chapman and Hall, London. 1980.
13. (*a*) A. J. KRESGE, D. S. SAGATYS, and H. L. CHEN. J. Am. Chem. Soc. **99**, 7228 (1977); (*b*) A. J. KRESGE. J. Am. Chem. Soc. **102**, 7797 (1980).
14. M. J. S. DEWAR, G. P. FORD, M. L. MCKEE, H. S. RZEPA, W. THIEL, and Y. M. YAMAGUCHI. J. Mol. Struct. **43**, 135 (1978).
15. J. A. POPLE, H. B. SCHLEGEL, R. KRISHNAN, D. J. DEFREES, J. S. BINKLEY, M. J. FRISCH, R. A. WHITESIDE, R. F. HOUT, and W. J. HEHRE. Int. J. Quantum Chem. Quantum Chem. Symp. **15**, 269 (1981).
16. S. SCHRÖDER and W. THIEL. J. Am. Chem. Soc. **107**, 4422 (1985).
17. I. H. WILLIAMS. J. Mol. Struct. THEOCHEM, **105**, 105 (1983).

Micellar effects upon reactions of the 2,2′,4,4′,4″-pentamethoxytrityl cation with nucleophiles

CLIFFORD A. BUNTON AND ANGELA CUENCA[1]

Department of Chemistry, University of California, Santa Barbara, CA 93106, U.S.A.

Received September 17, 1985

This paper is dedicated to Professor Arthur N. Bourns

CLIFFORD A. BUNTON and ANGELA CUENCA. Can. J. Chem. **64**, 1179 (1986).

Cationic micelles of cetyltrimethylammonium chloride and bromide (CTACl and CTABr) speed attack of water upon the 2,2′,4,4′,4″-pentamethoxytrityl cation by a factor of ca. 5. The first-order rate constant in water is 5.51 s^{-1} at 25.0°C. Anionic micelles of sodium dodecyl sulfate (SDS) have little effect on this reaction, but they strongly inhibit attack of OH^-. In water, second-order rate constants for attack of OH^-, CN^-, and N_3^- are, respectively, 235, 177, and 2.8 × 10^5 M^{-1} s^{-1}. Rate constants of reaction in CTACl go through maxima with increasing [surfactant] and analysis of the data shows that second-order rate constants at the micellar surface are similar to those in water.

CLIFFORD A. BUNTON et ANGELA CUENCA. Can. J. Chem. **64**, 1179 (1986).

L'addition de micelles cationiques des chlorure ou bromure de cétyltriméthylammonium (ClCTA et BrCTA) augmente la vitesse d'attaque de l'eau sur le cation pentaméthoxy-2,2′,4,4′,4″ trityle par un facteur d'environ 5. Dans l'eau, à 25,0°C, la constante de vitesse du premier ordre est égale à 5,51 s^{-1}. Les micelles anioniques du dodécylsulfate de sodium (DSS) n'ont que peu d'effet sur cette réaction; toutefois, elles inhibent fortement l'attaque par OH^-. Dans l'eau, les constantes de vitesse pour les attaques par OH^-, CN^- et N_3^- sont respectivement 235, 177 et 2,8 × 10^5 M^{-1} s^{-1}. Les constantes de vitesse pour les réactions du ClCTA passent par un maximum lorsqu'on augmente la quantité d'agent de surface et l'analyse des données démontre que les constantes du deuxième ordre à la surface micellaire sont semblables à celles dans l'eau.

[Traduit par la revue]

Introduction

Aqueous ionic micelles speed bimolecular reactions of counterions by bringing substrate and ionic reagent together in the small volume of the micelles (1–6). The dependence of rate on [surfactant] can be treated quantitatively assuming that reactants are distributed between aqueous and micellar pseudophases, which are treated as distinct reaction media. Second-order rate constants can be calculated for reaction in the micellar pseudophases, and for many bimolecular ionic reactions these second-order rate constants are similar to those in water. Thus the micellar rate enhancements are due largely to concentration of reactants in the micellar pseudophase.

Reactions of dinitrohaloarenes with azide ion are major exceptions to this generalization, and second-order rate constants in cationic micelles are greater than those in water by factors of 10^2–10^3 (7). We found similar large micellar effects for reactions of azide ion with hydrophobic *N*-alkyl-2-bromopyridinium ions. However, rate constants of deacylation and S_N2 displacements by azide ion are similar in micellar and aqueous pseudophases (7), so that these unusual rate effects are not simply characteristic of azide ion as a nucleophile.

Azide ion is very reactive towards carbocations, either preformed (8, 9) or generated in S_N1 solvolyses (10, 11). The present investigation had the aim of comparing second-order rate constants for reaction of azide ion with a carbocation in water and micelles. Micellar effects upon nucleophilic addition to triarylmethyl dye cations have been well studied (12, 13), but we could not use such cations as Malachite Green or Crystal Violet because of the unfavorable equilibria with azide ion (14). The tri-*p*-anisylmethyl cation is also unsatisfactory, because it binds weakly to cationic micelles (13) and even in water the reaction is so fast that it can only be followed in very dilute azide ion (9). However, the 2,2′,4,4′,4″-pentamethoxytrityl cation, **1**, reacts at a convenient rate with azide ion and other nucleophiles (Scheme 1).

The surfactants were cetyltrimethylammonium chloride and bromide (CTACl and CTABr). The chloride was generally used because of the relatively low solubility of CTABr. Reactions of water and OH^- were also followed in solutions of sodium dodecyl sulfate (SDS).

Results

Rate constants for reactions of **1** in the absence of surfactants are given in Table 1. Reaction with N_3^- does not go to completion in water because the alkyl azide dissociates, c.f. ref. 14. Reaction goes to completion in aqueous MeCN, and second-order rate constants are 10^{-5} k_2 = 2.6, 2.4, 2.1, and 1.7 M^{-1} s^{-1} in 90, 80, 70, and 60 wt% H_2O, respectively, and the reaction is first order in [N_3^-]. Linear extrapolation of k_2 against mole fraction of H_2O or log k_2 against Y (15) gave k_2 = 2.8 × 10^5 M^{-1} s^{-1}.

The decrease of k_2 with decrease of water content was unexpected for a reaction between oppositely charged anions (10, 16), but reactions of **1** with OH^- and CN^- are also slowed by addition of MeCN to H_2O.

Micellar effects upon the spontaneous reactions are shown in Tables 2 and 3, and for reactions of anions are shown in Fig. 1.

Discussion

Micellar effects upon spontaneous reactions can be analyzed using eq. [1] as applied to the reactions of Scheme 2 (1–7, 17), where water is the nucleophile, Nu.

Scheme 2 gives:

$$[1] \quad k_\psi = \frac{k'_W + k'_M K_s([D] - cmc)}{1 + K_s([D] - cmc)}$$

where k'_W and k'_M are first-order rate constants in aqueous and micellar pseudophases respectively, K_s is the substrate binding

[1]On leave from the Department of Chemistry, Simon Bolivar University, Caracas, Venezuela. This paper is abstracted in part from the thesis submitted as partial requirements of the Ph.D. degree of the University of California, Santa Barbara.

Printed in Canada / Imprimé au Canada

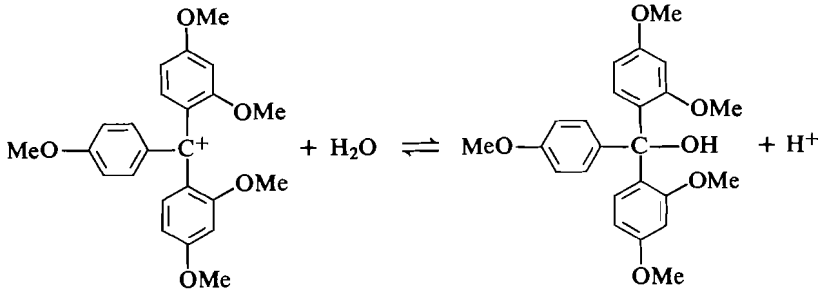

1

SCHEME 1

TABLE 1. Rate constants in water

Nucleophile	k_W, M^{-1} s^{-1}
H_2O	5.52[a,b]
H_2O	5.51[a,c]
OH^-	235
CN^-	177
N_3^-	2.8×10^5[d]

[a]First-order rate constants, s^{-1}; mean of two values; the other values are for second-order rate constants; in water, $pK_{R+} = 2.02$.
[b]Excess of NaOAc.
[c]Neutralization with NaOH.
[d]By extrapolation.

TABLE 2. Effects of cationic micelles upon reaction with water[a]

	Condition		
[D], M	CTACl[b]	CTACl + NaCl[a]	CTABr
0.005		10.0	5.96
0.007			6.11
0.01	6.02 (6.05)	11.2	6.88
0.03	8.09 (8.30)		8.94
0.05	10.5 (10.5)		11.1
0.07	12.3 (12.2)		12.3
0.10	14.7 (14.2)	18.3	16.3
0.15		19.6	
0.20	18.7 (18.0)		
0.30	20.5 (20.2)	25.0	

[a]Values of k_ψ, s^{-1} at 25.0°C; in the absence of surfactant, $k_\psi = 5.15$ s^{-1}; solutions in 0.01 M HCl and 0.01 M NaOH were mixed.
[b]Values in parentheses are calculated using eq. [1].
[c]0.5 M total Cl^-.

TABLE 3. Effects of SDS on reaction with H_2O and OH^-[a]

10^4 [SDS], M	k_ψ, s^{-1}	10^4 [SDS], M	k_ψ, s^{-1}
1.0	27.1 (5.06)	15.0	4.17
3.0	25.2 (5.01)	20.0	4.36
5.0	10.2 (5.16)	30.0	4.01
7.0	6.66 (5.01)	40.0	4.07
10.0	4.93 (5.42)	50.0	3.91

[a]At 25.0°C with 10^{-5} M **1**; 0.21 M NaOH was mixed with 0.01 M HCl. In absence of SDS $k_\psi = 29$ s^{-1}. Values in parentheses are for the water reaction using NaOAc.

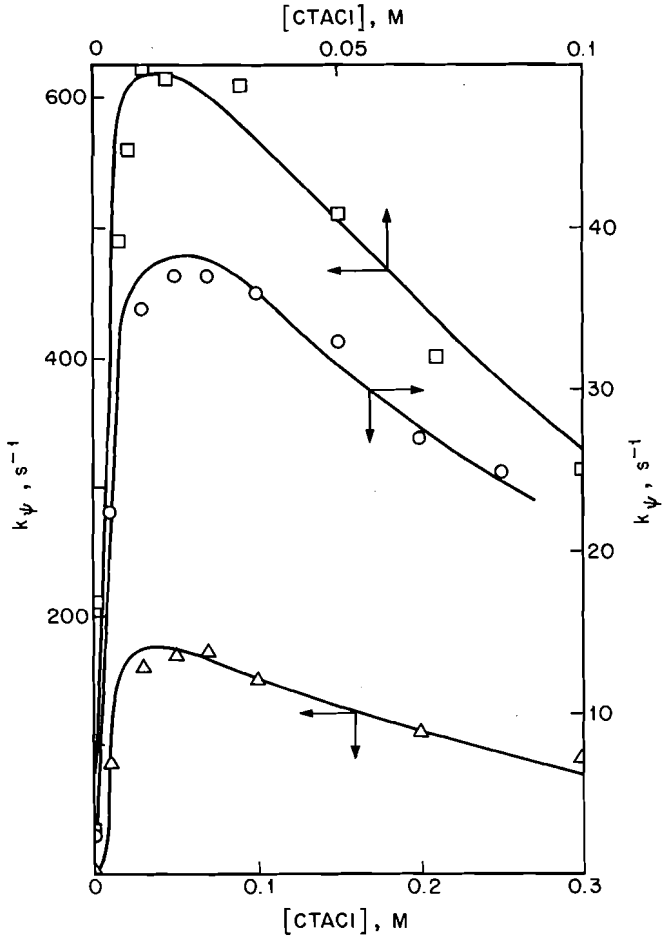

FIG. 1. Reactions of 2,2′,4,4′,4″-pentamethoxy trityl cation with nucleophilic anions in CTACl. ○, 0.01 M NaOH; △, 0.01 M NaCN; □, 10^{-4} M NaN_3. The curves are predicted from the parameters in Table 4 and eqs. [1]–[5].

constant, written in terms of micellized surfactant, [D] − cmc, where D is total surfactant and cmc is the critical micelle concentration.

The value of K_s is assumed to be independent of [surfactant] and [salt]. This assumption is reasonably satisfactory for dilute surfactant and salt, but K_s is expected to increase with increasing [salt] (13, 18).

Values of k'_M and K_s (eq. [1]) can be calculated by simulation or by rearranging eq. [1] into a reciprocal form. We calculated values of K_s and k'_M of 7 M^{-1} and 27 s^{-1}, respectively, for reaction in CTACl using the reciprocal form (17) and the fit is illustrated in Table 2.

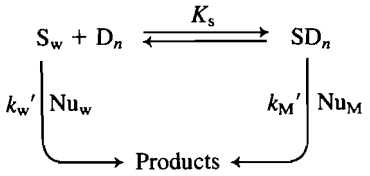

SCHEME 2

The kinetic data were not fitted for reaction in CTABr, because of the limited concentration range. However, reaction is slightly faster in CTABr than in CTACl (Table 2) probably because ion pairing slightly increases substrate binding, and Br^- should be more effective than Cl^- in this regard (13, 18). Consistently, addition of 0.5 *M* NaCl to CTACl also modestly speeds reaction (Table 2).

Rates of bimolecular attack by water are generally unaffected or slightly reduced by ionic micelles, and micelles of SDS have no effect on rates of water addition to **1** (Table 3) or to other carbocations (13). Consistently, bimolecular water additions to nonionic substrates are faster in cationic than in anionic micelles, although generally both give overall inhibition (19–21).

It has been pointed out elsewhere that spontaneous hydrolyses in which bond making predominates are faster in cationic than in anionic molecules, whereas the opposite is true when bond breaking predominates (19). For example, in spontaneous hydrolyses of 4-nitrophenyl chloroformate and 3,5-dinitrobenzoyl chloride, where bond making predominates, reaction in cationic micelles is faster than in water, whereas reaction is slower in anionic micelles (19, 20). In these reactions there is a partial compensation between bond making and breaking, whereas only bond making at the reaction center is involved in water addition to **1**, and the rate enhancement by micellized CTACl is larger than those with the acid chlorides (19, 20). Thus, the results for water addition to **1** (Table 2 and 3) support the generalization that the water addition step is assisted by cationic micelles.

Reaction occurs in the water-rich region at the micellar surface (1–7, 22) and involves a transfer of positive charge from the reaction center, in the micelle, to water molecules adjacent to its surface. This transfer should be more favorable in a cationic than in an anionic micelle. The overall effect of the micelle will depend upon this "charge effect" and also upon effects due to a lowered polarity at the micellar surface to that of water.[2] Micelles may lower the activity of bound water, but the effects are small at most, and there is no evidence for lowered nucleophilicity (20). These "solvent" and "polarity" effects of the micelle are probably not large and, in the absence of surfactant organic solvents (e.g. MeCN), inhibit water addition to cation **1**.[3]

Quantitative analysis of micellar rate enhancements for reactions of ionic nucleophiles, Nu^-, involves modification of eq. [1]. The first-order rate constants are written as:

$$[2] \quad k_w' = k_W[Nu_W^-]$$

$$[3] \quad k_M' = k_M m_{Nu}^s = k_M[Nu_M^-]/([D] - cmc)$$

where m_{Nu}^s is the mole ratio of micellar-bound nucleophile to micellized surfactant (1, 3). Reaction with water is sufficiently slow to be neglected.

These equations give:

$$[4] \quad k_\psi = \frac{k_W[Nu_W^-] + k_M K_s[Nu_M^-]}{1 + K_s([D] - cmc)}$$

The competition between Nu^- and the inert counterion, X^-, is written as (1, 3, 6):

$$[5] \quad K_X^{Nu} = \frac{[Nu_W^-][X_M^-]}{[Nu_M^-][X_W^-]}$$

Values of K_{Cl}^{Nu} are known or can be estimated (1, 3–7, 24, 25) and, provided that the micellar fractional charge, α, is independent of [surfactant] and the nature or concentration of the ions, values of k_M (eq. [4]) can be calculated by computer simulation of the data. The procedure and assumptions in the treatment have been discussed (1, 3, 6, 25). We write binding of the carbocation, neglecting its charge–charge interaction with the micelle and the effect of added salts on this interaction, and to this extent we probably underestimate the extent of micellar binding. However, this approximation has not caused serious problems in micellar reactions of other ionic substrates in the presence of dilute salt (13, 25).

Values of k_M and K_s are given in Table 4. There is uncertainty in k_M, because reasonably good fits can be obtained with a range of values of k_M, K_s, and α. This problem has been discussed (1, 3), but the uncertainties in k_M do not affect our overall conclusions. In addition, k_ψ for reaction with N_3^- is close to the limit of the stopped-flow spectrophotometer.

The rate constants, k_W and k_M, cannot be compared directly because of the difference in dimensions, but k_M can be converted into k_2^m, $M^{-1}\,s^{-1}$, using eq. [6] (3, 13):

$$[6] \quad k_2^m = 0.14\, k_M$$

where 0.14 is the assumed molar volume (L) of the region at the micellar surface in which reaction takes place. Other estimates of the molar volume range up to ca. 0.37 L, which would give an approximately two-fold increase of k_2^m (2, 4–6).

Values of k_2^m/k_W are given in Table 4. Despite the uncertainties in k_2^m, the micellar rate enhancements are clearly due largely to increased reactant concentrations in the micelles. There seems to be a slight dependence of K_s upon the nucleophilic ion, which may be due to ion pairing assisting substrate binding. Second-order rate constants for reactions of OH^- and N_3^- are lower in micelles than in water, but that for reaction of CN^- appears to be higher. This behavior is not observed in other reactions of CN^- (25) and our tentative explanation is that it interacts preferentially by ion pairing with cation **1** in the micelle.

There is no unusual micellar effect upon reaction of azide ion (Table 4). Very large second-order rate constants in the micelles have been observed only for reactions of 2,4-dinitrochlorobenzene and naphthalene (7) and of *N*-alkyl-2-bromopyridinium ions. We have no simple explanation for this behavior, although second-order rate constants for several aromatic nucleophilic substitutions are slightly higher in micelles than in water, whereas for deacylations and dephosphorylations rate constants are often slightly lower in micelles than in water (1–7).

Aromatic substitution by azide ion is faster in cationic micelles than in water, but this result may be due to this reaction

[2] Mukerjee and co-workers have observed a dependence of micellar polarity, or effective dielectric constant, upon micellar charge (23).

[3] This solvent effect is opposite to that upon water addition to tri-*p*-anisylmethyl cation (16).

TABLE 4. Rate constants for reactions in cationic micelles[a]

Nucleophile	K_s, M	K^X_{Cl}	k^m_2 M^{-1} s^{-1}	k^m_2/k_W
H_2O	7		27[b]	5[b]
OH^-	7	3.5	33	0.15
CN^-	7	0.5	ca. 600	3
N_3^-	10	1.3	4×10^4	0.15

[a]In CTACl; calculated with $\alpha = 0.2$ and cmc $= 10^{-3}$ M.
[b]Rate constants for reactions in H_2O are in Table 1.

being unusually slow in water, rather than fast in micelles. Ritchie and Sawada (26) have compared nucleophilicities for several reactions in terms of the N_+ scale, which was initially based on rates of addition to preformed carbocations. They found that the scale applied reasonably well to aromatic nucleophilic substitution, except that azide ion was much less reactive than predicted from its N_+ value. Thus, unusual micellar effects in aromatic nucleophilic substitution may be due to azide ion being abnormally unreactive in the absence of micelles.

Anionic micelles suppress attack of OH^- upon **1**. The inhibition is observed with [SDS] much lower than its cmc of ca. 8×10^{-3} M (Table 3), suggesting that the cation induces formation of anionic aggregates that exclude OH^- (27). The value of k_ψ becomes constant at high [SDS] and is slightly lower than that for reaction with water. The differences are probably due to differences in [electrolyte] in the two reaction systems.

Ritchie *et al.* (28) found that 2,2′,2″,4,4′,4″-hexamethoxytrityl cation was unusually reactive towards H_2O, relative to such anions as OH^-, and that CN^- was more reactive than OH^-. These rate differences are unusual, and we observe qualitatively similar behavior in reactions of **1** in water (Table 1). The introduction of *o*-methoxy groups seems to be affecting relative reactivities towards nucleophiles and an effect of *o*-methoxy groups on the local structure of water has been suggested (28). The *ortho* groups could also affect reactivity of a carbocation by increasing the out-of-plane twisting of the aryl groups, which will reduce their electron-donating ability. There will then be steric effects upon attack of the nucleophile and hybridization at the reaction center will change from sp^2 towards sp^3. There is thus considerable interplay between steric and electronic effects, and *p*-methoxy groups very sharply retard attack of H_2O upon trityl cations. *o*-Methoxy groups have much less effect, although they have a larger effect upon the stability of the carbocation relative to that of the alcohol (9, 16, 28, 29). For example, the first-order rate constants for reactions of H_2O with the 4-methoxy trityl, tri-*p*-anisylmethyl, 2,2′,4,4′,4″-pentamethoxy trityl, and 2,2′,2″,4,4′,4″-hexamethoxy trityl cations are ca. 10^3, 12, 5.51, and 2.00 s^{-1}, respectively. But values of pK_{R+} are −3.4, +0.82, +2.02, and +3.80[4] (refs. 9, 16, 28, 29), respectively, and this sequence is consistent with electron release by both *ortho* and *para* methoxy groups stabilizing the cation, relative to the alcohol. Carbocation stability is not closely related to its reactivity towards water, which appears to be governed largely by electron release from the *para* methoxy groups.

Experimental

Materials

The preparation or purification of the surfactants has been described (13) and the cmc values agreed with those in the literature (30). 2,2′,4,4′,4″-Pentamethoxytriphenyl methanol was from Aldrich. All solutions were made up using redistilled, deionized water.

Kinetics

Reactions were followed spectrophotometrically at 474 nm and 25.0°C using a Durrum stopped-flow spectrophotometer. The carbocation, in dilute HCl (0.05–0.01 M) was in one drive syringe and the nucleophile in the other. For the water reaction, HCl was neutralized with an equivalent amount of NaOH, or with excess NaOAc, which does not affect reaction, cf. refs. 13 and 16. An equivalent amount of NaOH was used for reaction of N_3^-, but excess NaCN was used for reaction of CN^-.

Reaction of N_3^- could not be followed to completion in water because of its reversibility, and the rate constant was obtained by extrapolation from data in aqueous MeCN; however, reaction goes to completion in aqueous surfactant. Reactions of OH^- and CN^- in water were second order: the concentration ranges were up to 0.1 and 0.15 M for OH^- and CN^-, respectively.

The first-order rate constants, k_ψ, are in reciprocal seconds (s^{-1}).

Acknowledgements

Support of this work by the National Science Foundation (Chemical Dynamics) and the Consejo Nacional de Investigaciones Cientificas y Tecnologicas, Caracas, Venezuela, is gratefully acknowledged.

1. L. S. ROMSTED. *In* Micellization, solubilization and microemulsions. Vol. 2. *Edited by* K. L. Mittal. Plenum Press, New York. 1977. p. 509; L. S. ROMSTED. *In* Surfactants in solution. Vol. 2. *Edited by* K. L. Mittal and B. Lindman. Plenum Press, New York. 1985. p. 1015.
2. K. MARTINEK, A. K. YATSIMIRSKI, A. V. LEVASHOV, and I. V. BEREZIN. *In* Micellization, solubilization and microemulsions. Vol. 2. *Edited by* K. L. Mittal. Plenum Press, New York. 1977. p. 489.
3. C. A. BUNTON. Catal. Rev.-Sci. Eng. **20**, 1 (1979).
4. E. J. R. SUDHOLTER, G. B. VAN DER LANGKRUIS, and J. B. F. N. ENGBERTS. Recl. Trav. Chim. Pays-Bas, **99**, 73 (1980).
5. I. M. CUCCOVIA, E. M. SCHROTER, P. M. MONTEIRO, and H. CHAIMOVICH. J. Org. Chem. **43**, 2248 (1978).
6. F. H. QUINA and H. CHAIMOVICH. J. Phys. Chem. **83**, 1844 (1979); H. CHAIMOVICH, J. B. S. BONILHA, M. J. POLITI, and F. H. QUINA. J. Phys. Chem. **83**, 1851 (1979).
7. C. A. BUNTON, J. R. MOFFATT, and E. RODENAS. J. Am. Chem. Soc. **104**, 2653 (1982).
8. C. D. RITCHIE. J. Am. Chem. Soc. **97**, 1170 (1975).
9. C. A. BUNTON and S. K. HUANG. J. Am. Chem. Soc. **94**, 3536 (1972).
10. C. K. INGOLD. Structure and mechanism in organic chemistry. 2nd ed. Cornell University Press, Ithaca, NY. 1969. Chapt. 7.
11. R. TA-SHMA and Z. RAPPOPORT. J. Am. Chem. Soc. **105**, 6082 (1983).
12. G. S. HARTLEY. Trans. Faraday Soc. **30**, 444 (1934); G. S. HARTLEY and J. W. ROE. Trans. Faraday Soc. **36**, 101 (1940); A. J. ALBRIZZIO, A. ARCHILA, T. RODULFO, and E. H. CORDES. J. Org. Chem. **37**, 871 (1972).
13. C. A. BUNTON and S. K. HUANG. J. Org. Chem. **37**, 1790 (1972); C. A. BUNTON, N. CARRASCO, S. K. HUANG, C. H. PAIK, and L. S. ROMSTED. J. Am. Chem. Soc. **100**, 5420 (1978).
14. C. D. RITCHIE, G. A. SKINNER, and G. BADDING. J. Am. Chem. Soc. **89**, 2063 (1967).
15. C. A. BUNTON, M. M. MHALA, and J. R. MOFFATT. J. Org. Chem. **49**, 3637 (1984).
16. E. A. HILL and W. J. MUELLER. Tetrahedron Lett. 2565 (1968); H. NICHOLSON and P. A. H. WYATT. J. Chem. Soc. (B), 198 (1968); J. M. RIDE and P. A. H. WYATT. J. Chem. Soc. Perkin Trans. **2**, 1188 (1974).
17. F. M. MENGER and C. E. PORTNOY. J. Am. Chem. Soc. **89**, 4698 (1967).

[4]A value of $pK_{R+} = 3.28$ is quoted in ref. 29.

18. S. MALAVIYA and S. S. KATIYAR. Z. Phys. Chem. (Leipzig), **265**, 26 (1984).
19. H. AL-LOHEDAN, C. A. BUNTON, and M. M. MHALA. J. Am. Chem. Soc. **104**, 6654 (1982); C. A. BUNTON and S. LJUNGGREN. J. Chem. Soc. Perkin Trans. **2**, 355 (1984).
20. C. A. BUNTON, M. M. MHALA, and J. R. MOFFATT. *In* Surfactants in solution. *Edited by* K. L. Mittal. Plenum Press, New York. 1985. In press.
21. N. FADNAVIS and J. B. F. N. ENGBERTS. J. Org. Chem. **47**, 415 (1982).
22. F. M. MENGER. Acc. Chem. Res. **12**, 111 (1979).
23. C. RAMACHANDRAN, R. A. PYTER, and P. MUKERJEE. J. Phys. Chem. **86**, 3198 (1982).
24. N. FUNASAKI and A. MURATA. Chem. Pharm. Bull. **28**, 805 (1980); D. BARTET, G. GAMBOA, and L. SEPULVEDA. J. Phys. Chem. **84**, 272 (1980); C. GAMBOA, L. SEPULVEDA, and R. SOTO. J. Phys. Chem. **85**, 1429 (1981).
25. C. A. BUNTON, L. S. ROMSTED, and C. THAMAVIT. J. Am. Chem. Soc. **102**, 3900 (1980).
26. C. D. RITCHIE and M. SAWADA. J. Am. Chem. Soc. **99**, 3754 (1977).
27. J. H. BAXENDALE and M. A. J. RODGERS. J. Phys. Chem. **86**, 4906 (1982).
28. C. D. RITCHIE, A. A. KAMEGO, P. O. I. VIRTANEN, and C. KUBISTY. J. Org. Chem. **46**, 1957 (1981).
29. R. A. DIFFENBACH, K. SANO, and R. W. TAFT. J. Am. Chem. Soc. **88**, 4747 (1966).
30. P. MUKERJEE and K. J. MYSELS. Critical micelle concentrations of aqueous surfactant systems. Natl. Bur. Standards, U.S. Govt. Printing Office, Washington, DC. 1970.

Importance of repulsion of lone electron pairs in the enhanced reactivity of 1,8-naphthyridine and the large α-effect of hydrazine in the aminolyses of *p*-toluenesulfonyl chloride[1]

SHIGERU OAE[2]
Okayama University of Science, 1-1 Ridai-cho, Okayama 700, Japan
AND
YOSHIHITO KADOMA[3]
Department of Applied Chemistry, Osaka City University, Sumiyoshi-ku, Osaka 558, Japan
Received October 7, 1985
This paper is dedicated to Professor Arthur N. Bourns

SHIGERU OAE and YOSHIHITO KADOMA. Can. J. Chem. **64**, 1184 (1986).

The rates of aminolyses of *p*-toluenesulfonyl chloride with primary and tertiary amines have been determined both in acetonitrile and in ethanol. The Brönsted plots of log k_{rel} again $pK_{a'}$ values of amines (except hydrazine and 1,8-naphthyridine in acetonitrile) gave a good correlation when the aminolyses were carried out in acetonitrile. In ethanol, however, although Brönsted plots with all tertiary amines show a good correlation, less basic hydrazine shows a higher reactivity than *n*-butylamine. The abnormal rate enhancement found with hydrazine is undoubtedly due to the α-effect, while that with 1,8-naphthyridine in acetonitrile is considered to be due to the repulsion of two lone electron pairs on the two nitrogen atoms in 1,8-naphthyridine.

SHIGERU OAE et YOSHIHITO KADOMA. Can. J. Chem. **64**, 1184 (1986).

On a déterminé les vitesses d'aminolyse du chlorure de *p*-toluènesulfonyle par des amines primaires ainsi que tertiaires, tant dans l'acétonitrile que dans l'éthanol. Lorsque les aminolyses sont effectuées dans l'acétonitrile, il existe une bonne corrélation pour les courbes de Brönsted du log k_{rel} vs. les valeurs de $pK_{a'}$ des amines (excepté dans les cas de l'hydrazine et de la naphtyridine-1,8 dans l'acétonitrile). Dans l'éthanol, les courbes de Brönsted des amines tertiaires présentent toutes une bonne corrélation; toutefois, l'hydrazine qui est moins basique présente une réactivité qui est supérieure à celle de la *n*-butylamine. La vitesse de réaction anormalement élevée qui a été observée avec l'hydrazine est sans doute due à un effet α, alors que l'on considère celle de la naphtyridine dans l'acétonitrile comme étant due à une répulsion des deux paires libres d'électrons des deux azotes de la naphtyridine-1,8.

[Traduit par la revue]

The enhanced reactivity of nucleophiles containing one or more lone electron pairs adjacent to the reacting center has been known as the α-effect (2–4). Among the following three major factors responsible for the α-effect, namely, (*1*) destabilization of the ground state of the α-nucleophile by repulsion between the adjacent lone electron pairs (5), (*2*) stabilization of the transition state by the extra pair of electrons, and (*3*) reduced solvation of the α-nucleophile by the adjacent lone electron pair, the last two factors have been fairly well substantiated by both theoretical (6–9) and experimental studies (10–13). Stabilization of the transition state by the α-nucleophile, namely the second factor, has recently been considered quite important and possibly the major factor for the enhanced reactivity in the nucleophilic attack of the α-nucleophile on the electropositive reacting center, especially in solution. Evidence supporting the third factor has become especially convincing now, since no α-effect was observed in the reaction of HOO^- with methyl formate in the gas phase (13), where HOO^- shows a strong α-effect in solution.

Not much significance has been given to the first factor, i.e., destabilization of the ground state of the α-nucleophile by repulsion between the lone pairs on adjacent atoms, and practically no convincing evidence has yet been shown, although repulsion between lone electron pairs on adjacent heteroatoms is considered to be quite substantial in view of the well-known "rabbit ear effect" (14) of lone electron pairs on nonadjacent atoms.

A nonbonding unshared electron pair, namely, a lone electron pair, is large and takes up more space than a bonding pair (15). Therefore, if there is no electron pair other than a lone electron pair, the unshared pair of electrons would occupy a "*s*" type spherical orbital, spreading widely on the surface of the particular heteroatom (16). Even when the central heteroatom is bound to other atoms, the lone electron pair on the heteroatom tends to spread out, as exemplified by the decrease in the bond angle in the following three representative compounds: CH_4, which has no lone electron pair on the central atom, has a bond angle, $<\mathrm{C}\begin{smallmatrix}\diagup\mathrm{H}\\ \diagdown\mathrm{H}\end{smallmatrix} = 109.5°$; NH_3, in which there is one lone electron pair on the central atom, has $<\mathrm{N}\begin{smallmatrix}\diagup\mathrm{H}\\ \diagdown\mathrm{H}\end{smallmatrix} = 107.3°$; while H_2O, which has two lone electron pairs, is more angular, i.e., $<\mathrm{O}\begin{smallmatrix}\diagup\mathrm{H}\\ \diagdown\mathrm{H}\end{smallmatrix} = 104.7°$. When bonding pairs are replaced successively by a lone electron pair, the bond angle between the bonding pairs decreases, since the lone electron pair takes up more space than the bonding electron pair. Since the lone electron pair engenders an electronic dipole, two lone electron pairs placed in proximity or in parallel must create a considerable electrostatic, and also even some steric, repulsion. The "rabbit ear effect" is caused by such a repulsion between two vicinal lone electron pairs on heteroatoms placed at the β-position to disfavor the conformations in which lone electron pairs on nonadjacent atoms are placed at parallel or at the *syn-axial* position (14), as shown below.

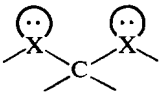

[1]Taken in part from ref. 1.
[2]Author to whom correspondence may be addressed.
[3]Present address: Nippon Oil & Fats Co., 1-56 Ohama-cho, Amagasaki, Hyogo-ken 660, Japan.

Printed in Canada / Imprimé au Canada

In 1,8-naphthyridine two lone electon pairs on the two nitrogen atoms of the heterocyclic compound are placed in parallel, as shown below.

Therefore, due to the repulsion, this compound should have a considerable internal strain. However, if one of the nonbonding lone electron pairs is used for bonding, such a repulsion would be released, since one of repulsive dipoles would disappear and the steric requirement of a bonding electron pair is less than that of a nonbonding electron pair. Hence, if 1,8-naphthyridine is used as a nucleophile in the nucleophilic reaction and the conventional Brönsted plot of logarithm of rate constant against $pK_{a'}$s of attacking nucleophiles, 1,8-naphthyridine would show a positive deviation from the plotted line, since the release of repulsion between the two lone electron pairs would occur in the transition state by forming a new σ-bond between the nucleophile and the substrate, thus lowering the energy of activation. One earlier report (5*b*) suggested, based on others' work, that 1,8-naphthyridine would show fourfold rate acceleration in the reaction with methyl iodide. One might propose, however, that protonation of one of the two lone electron pairs would result in the release of this unfavorable repulsion, which in turn would result in the increase of the $pK_{a'}$ value of 1,8-naphthyridine. These two opposing effects, i.e., lowering of the activation energy and increasing $pK_{a'}$ value, should cancel out much of the anticipated positive deviation from the Brönsted slope. However, this consideration has been suggested to be not very significant in nucleophilic displacements (17), since the lone electron pairs are more fully removed in the transition state than when perturbed by protonation. The result of our SCF MO calculation also supports this argument (6).

Therefore, if one finds a substantial positive deviation from the Brönsted slope for 1,8-naphthyridine, similar to that for some α-nucleophiles, e.g., hydrazine, it may serve as supporting evidence that repulsion between lone electron pairs is at least partially responsible for the rate enhancement in the nucleophilic reactions. An observation by Zoltewicz and Deady (5*b*) seems to show the possibility of the above argument. However, in order to substantiate the argument, further data such as the solvent effect on the α-nucleophile and 1,8-naphthyridine, as well as quantitative measurements of deviations of both nucleophiles from the slope, should be necessary. Meanwhile, since 1,8-naphthyridine has a low $pK_{a'}$ value, it does not react readily with ordinary esters and hence a more reactive *p*-toluenesulfonyl chloride was used as substrate for the nucleophilic reaction. Thus, we have carried out a kinetic study on the reaction of *p*-toluenesulfonyl chloride with 1,8-naphthyridine, its isomer, 1,5-naphthyridine, hydrazine, and other amines in both ethanol and acetonitrile, observing substantial rate enhancements with both 1,8-naphthyridine and hydrazine in acetonitrile.

Results and discussion

In the reaction of *p*-toluenesulfonyl chloride with amines, the following two reaction paths, i.e., (a) and (b), are conceivable. However, the product analysis indicates the absence of *p*-toluenesulfinate ion and only the presence of the sulfonate ion in the reaction mixture. Thus, path (b) has been ruled out and the reaction is purely a nucleophilic substitution on the sulfonyl S atom.

Earlier, Kice and Legan (18) observed a marked α-effect in the nucleophilic substitution on the sulfonyl sulfur atom with hydroperoxide ion, and hence a substantial rate enhancement has been expected in the nucleophilic substitution of arenesulfonyl chloride with the α-nucleophile. Thus, we have carried out a kinetic study on the nucleophilic substitution of *p*-toluenesulfonyl chloride with various amines.

Although *p*-toluenesulfonyl chloride is quite reactive as compared to ordinary esters, the amines used for this study have a wide range of basicity from low basic 1,5-naphthyridine to highly basic piperidine, the rate of the reaction was found to vary widely in the range of $10^{7.5}$. Therefore, two different analytical procedures were necessary for kinetic measurements in order to compare all the rates. For the reaction with amines of low basicities, such as naphthyridines, quinolines, and pyridine, the reactions were carried out so that the amine concentration was maintained usually 100 times higher than that of the substrate in the reaction cell, and pseudo-first-order rate constants thus obtained were divided by the amine concentration to obtain bimolecular rate constants. In this case, the rate measurement was followed by monitoring the amount of chloride ion liberated in the reaction by conductometry. In the reactions with amines of high basicities from pyridine to piperidine, the conventional uv measurement of the absorption of *p*-toluenesulfonyl chloride was quite applicable, and concentrations of both the amine and the substrate can be kept nearly equal in this procedure. In both procedures, pyridine was used as the reference base and practically identical rate constants were obtained.

Since the repulsion between the vicinally situated lone electron pairs is expected to change considerably, both sterically and in dipole interaction, due to the possible change of solvation, the reaction was carried out in both protic and polar aprotic solvents, i.e., ethanol and acetonitrile. *p*-Toluenesulfonyl chloride is stable in both solvents at these kinetic temperatures and kinetic concentrations for over 10 days, while the concentrations of amines were not affected by these solvents. Thus, the rate constants obtained in acetonitrile are listed in Table 1.

In Fig. 1, the values of log k_{rel} in Table 1 were plotted against the $pK_{a'}$ values of amines used. Apparently, there is a good correlation and the β-value, 0.89, obtained from the Brönsted slope seems to suggest that the reaction is highly dependent on basicity, while there is a high degree of bond formation in the transition state.

The rate constants obtained with 1,8- and 1,5-naphthyridines

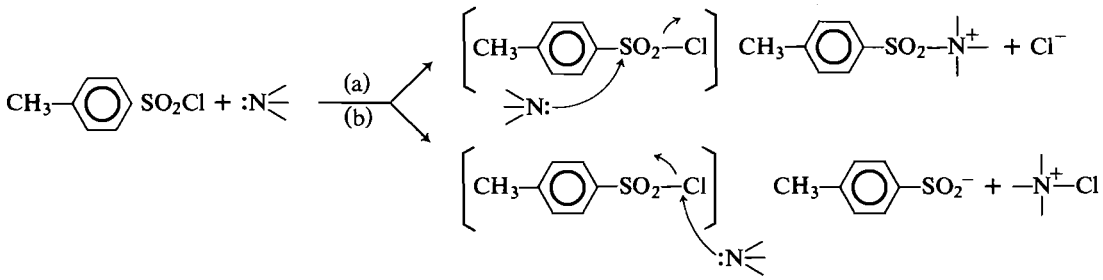

TABLE 1. Second-order rate constants for the reaction of *p*-toluenesulfonyl chloride with amines in acetonitrile at 20°C

Amine	k_2	log k_{rel}	$pK_{a'}$[a]
Piperidine[b]	101 ± 3	7.69	18.92
n-Butylamine[b]	64.4 ± 0.5	7.49	18.26
Monoethanolamine[b]	20.4 ± 0.3	6.99	17.53
Hydrazine[b]	74.0 ± 0.5[c]	7.55	16.61
Ammonia[b]	$(8.73 \pm 0.1) \times 10^{-1}$	5.62	16.46
Isoquinoline[d]	$4.3–2.0 \times 10^{-4}$	2.0–2.35	12.50[e]
Pyridine[b,d]	$(2.34 \pm 0.06) \times 10^{-4}$	1.20	11.98[e]
1,8-Naphythyridine[d]	$(2.08–7.04) \times 10^{-4}$[c]	2.5–3.0	10.44[e]
1,5-Naphythyridine[d]	$(2.08 \pm 0.3) \times 10^{-6}$	0.0	9.92[e]

[a]$pK_{a'}$ values are taken from Coetzee and Padmanabhan (19).
[b]Rate constant was obtained by conductometry.
[c]Obtained rate constant was divided by 2 because these amines have two nucleophilic centers.
[d]Rate constant was obtained by uv spectrophotometry.
[e]Estimated value from a linear plot of $pK_{a'}$ in water vs. $pK_{a'}$ in acetonitrile.

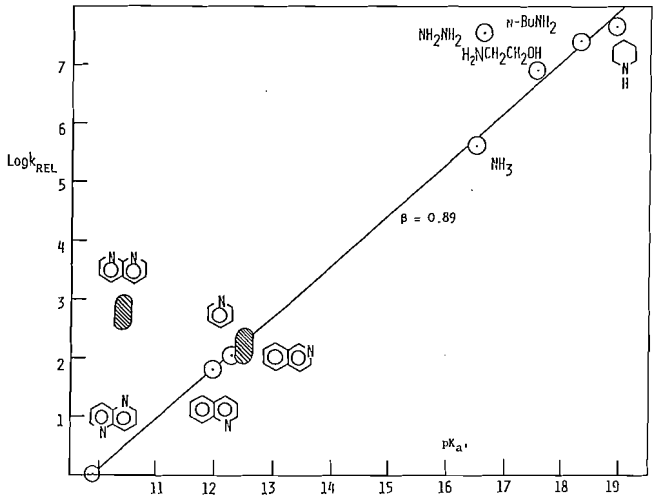

FIG. 1. Brönsted plot for the reaction of *p*-toluenesulfonyl chloride with amines in acetonitrile.

are divided by 2, since these amines have two nucleophilic centers (20). The plot for 1,5-naphthyridine lies well on the slope; however, hydrazine and 1,8-naphthyridine exhibit considerable deviations from the slope. The deviation of the plot with hydrazine is undoubtedly due to the α-effect, while that with 1,8-naphthyridine cannot be assigned to the α-effect but is obviously due to the repulsion of the two lone electron pairs, very likely in the ground state, since vicinally situated lone electron pairs, particularly in parallel positions, would result in a considerable repulsion. In this connecton, it is interesting to see the first $pK_{a'}$ values of substituted diaminonaphthalenes (21); namely, 4.61 for 1,8-diaminonaphthalene, 5.6 for 1,8-bis(monomethylamino)naphthalene, 6.43 for 1-dimethylamino-8-monomethylaminonaphthalene, and 12.34 for 1,8-bis(dimethylamino)naphthalene. The first $pK_{a'}$ value for 1,8-bis(dimethylamino)naphthalene is thus higher than those of normal aliphatic amines. This compound is apparently a highly strained molecule in which the conjugative resonance between the amino group and the naphthalene ring is considerably inhibited and, despite the high van der Waals repulsion, both dipolar repulsion and the strain would be effectively relieved by protonation. Since the unfavorable strain produced by repulsion is expected to be relieved more by forming a σ-bond at the transition state of

TABLE 2. Second-order rate constants for the reaction of *p*-toluenesulfonyl chloride with tertiary amines in absolute ethanol at 21°C, by conductometry

Amine	k_2 (L mol^{-1} s^{-1})	log k_{rel}	$pK_{a'}$[a] in water
Pyridine	$(4.88 \pm 0.04) \times 10^{-3}$	2.58	5.25
Isoquinoline	$(1.14 \pm 0.04) \times 10^{-2}$	2.95	5.42
Quinoline	$(5.84 \pm 0.06) \times 10^{-4}$	1.64	4.90
1,8-Naphthyridine[b]	$(7.83 \pm 0.07) \times 10^{-5}$	0.79	3.36
1,5-Naphthyridine[b]	$(1.27 \pm 0.15) \times 10^{-5}$	0.00	2.84

[a]$pK_{a'}$ values are taken from Perrin (23).
[b]Obtained rate constants were divided by 2 because these amines have two nucleophilic centers.

TABLE 3. Second-order rate constants for the reaction of *p*-toluenesulfonyl chloride with primary amines in absolute ethanol at 21°C, by ultraviolet spectrophotometry

Amine	k_2 (L mol^{-1} s^{-1})	log k_{rel}	$pK_{a'}$[a] in water
Hydrazine[b]	1.63 ± 0.05	1.89	7.96
n-Butylamine	0.860 ± 0.03	1.61	10.59
Monoethanolamine	0.605 ± 0.03	1.46	9.50

[a]$pK_{a'}$ values are taken from Perrin (23).
[b]Obtained rate constant was divided by 2 because these amines have two nucleophilic centers.

nucleophilic substitution than when perturbed by protonation, 1,8-bis(dimethylamino)naphthalene is considered to be more reactive than anticipated from its basicity. However, because of the sterically crowded center of the amino groups, it is not a good nucleophile for substitution.

As for 1,8-naphthyridine, the repulsion of lone electron pairs is considered to be effectively reduced at the transition state; thus the compound is 100-fold more reactive than anticipated from its basicity. The rate enhancement observed with 1,8-naphthyridine seems to indicate that the σ-bond formation is nearly complete at the transition state. This is also a favorable condition for hydrazine to exhibit its α-effect, as observed by the markedly positive deviation from the Brönsted slope, the rate enhancement being 40-fold (see Fig. 1).

Our earlier data (22)[4] revealed that the α-effect was not observed in the aminolyses of alkyl, allyl, and benzyl iodides, nor in the hydrolyses of benzylic bromides with hydroperoxide ion, although the aminolyses of allyl and benzyl iodides give nearly identical Brönsted values (0.60 and 0.55, respectively) to that (0.54) obtained with *p*-nitrophenyl acetate. This lack of α-effect in the aminolyses on the sp^3 carbon atom and also in the S_N2 reaction of benzylic bromides with hydroperoxide ion may be explained on the basis of the inability to form tight σ-bonds at the transition state of these S_N2 processes. The tight σ-bond formation, as observed in the formation of a tight tetrahedral intermediate in the ester hydrolysis, seems to be quite essential in releasing repulsion between lone electron pairs, thus enhancing the rate and exhibiting a marked α-effect.

Since large rate enhancements can be observed in the aminolyses of *p*-toluenesulfonyl chloride with 1,8-naphthyridine and hydrazine in such an aprotic solvent as acetonitrile, it is interesting to see how the change of solvent from acetonitrile to

[4]Also, S. Oae and Y. Kadoma, unpublished results.

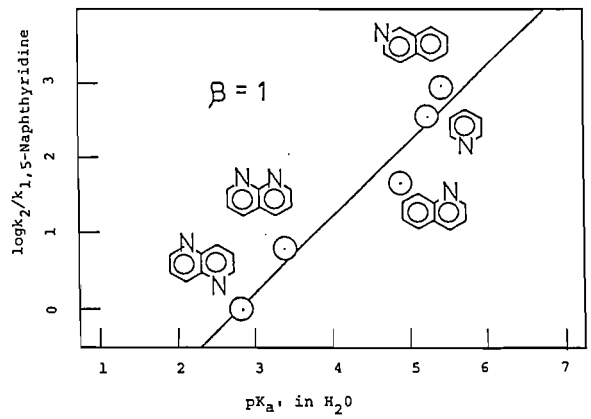

FIG. 2. Brönsted plot for the reaction of tertiary amines to *p*-toluenesulfonyl chloride in ethanol.

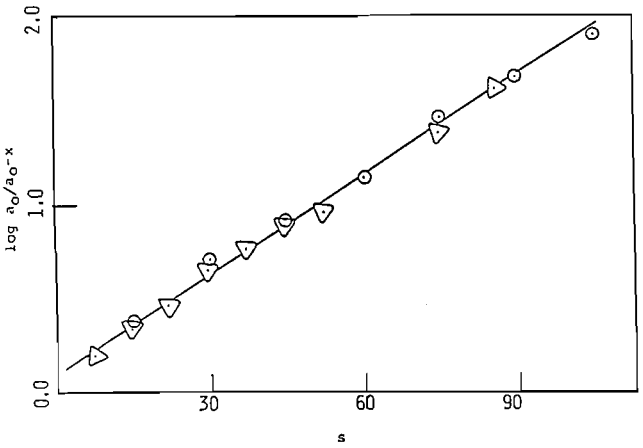

FIG. 3. Kinetic plots of the rates of aminolysis of *p*-toluenesulfonyl chloride with pyridine in ethanol. The log $a_0(a_0 - x)$ values are obtained by the plot of $[Cl^-]$ vs. conductivity of the reaction cell; ⊙ by uv spectrophotometry; △ by conductivity.

a protic solvent such as ethanol would affect the rate of the reaction. Thus, a kinetic study on the aminolyses of *p*-toluenesulfonyl chloride with tertiary as well as primary and secondary amines has been carried out and the results are summarized in Tables 2 and 3, respectively. The Brönsted plot for aminolysis with tertiary amines is also illustrated in Fig. 2. Since it has been known that the relative basicities are little affected by the change of solvent from water to alcohol (24), the rate constants are plotted against $pK_{a'}$ values of amines used in water.

In the aminolyses of *p*-toluenesulfonyl chloride with tertiary amines in ethanol (see Table 2 and Fig. 2), there is also a good correlation between the rate constants and $pK_{a'}$ values of amines used, and the Brönsted β-value of $\simeq 1$ indicates that the bond formation between the nucleophile and the substrate is nearly complete at the transition state, very likely expanding the valence shell of the central sulfur atom. However, in the aminolyses in ethanol, 1,8-naphthyridine does not show any positive deviation from the Brönsted slope, due mainly to solvation, since the lone electron pairs on two nitrogen atoms in the heterocycle are substantially solvated in ethanol by strong hydrogen bonding. Because of this solvation, orbitals of the lone electron pairs would be so contracted that the size of lone electron pairs would be reduced, thus reducing the unfavorable steric interaction, while the unfavorable dipolar repulsion would also be reduced substantially. These repulsive interactions are considered to be removed by formation of a σ-bond between the sulfur atom and the nucleophile. However, the reacting center of 1,8-naphthyridine has vicinally situated lone electron pairs on the two nitrogen atoms, which would be solvated by ethanol molecules, far more in number than in the aminolyses with other tertiary amines. Hence this sterically unfavorable condition created by the strong hydrogen bonding would cancel out any positive deviation from the slope.

In general, the α-effect seems to be somewhat larger in protic solvents than in aprotic media, while it is also considered to be affected markedly by the change of solvent (20). However, there are not many data to substantiate the argument. Therefore, aminolyses of *p*-toluenesulfonyl chloride with primary amines have been carried out, just to see if the α-effect would depend on the solvent change as was observed with 1,8-naphthyridine. The results are shown in Table 3.

One finds in Table 3 that hydrazine reacts faster than other more basic primary amines, due obviously to the α-effect. In the reaction in ethanol the transition state would be well solvated by the solvent ethanol, and further solvation by the vicinally situated lone electron pair will not increase the stability, whereas the presence of the vicinial lone electron pair would rather decrease the solvation at the transition state by repelling some ethanol molecules. Thus in ethanol the ground state destabilization would be cancelled out by the transition state destabilization; the net result is no rate enhancement. The α-effect is solvent independent, while the lone pair – lone pair repulsion is solvent dependent. These observations suggest that while the lone pair – lone pair repulsion is an important factor, it is not the sole cause of the α-effect.

Experimental

Preparation of materials

1,8-Naphthyridine was prepared by the Skraup reaction (25). Five repeated sublimations at 80°C (0.2 Torr; 1 Torr = 133.3 Pa) gave glassy colorless needles, mp 99.5°C (lit. (25) mp 98–99°C). 1,5-Naphthyridine was prepared similarly (26); mp 75°C (lit. (26) mp 75°C). Other amines were prepared by distillation (19), or by recrystallization.

Product analysis

One gram of a given amine (pyridine or 1,8-naphthyridine) was added into the solution containing 1 g of *p*-toluenesulfonyl chloride in 20 g of acetonitrile. After keeping the solution for 5–30 min at room temperature, the reaction mixture was poured onto ice-water, acidified with HCl, and extracted with ether. In the ether solution, there was no *p*-toluenesulfinic acid present and only a trace of the unreacted sulfonyl chloride was detected. *p*-Toluenesulfonic acid in the remaining water layer was identified by adding a solution of *S*-benzylthiouronium chloride to obtain the crystalline *S*-benzylthiouronium salt of *p*-toluenesulfonic acid. After recrystallization from ethanol, the salt gave mp 178°C (lit. (27) mp 178°C).

Product analyses for the reaction of *p*-toluenesulfonyl chloride with primary and secondary amines in ethanol were also carried out using the same method as described above. In the case of a primary amine, the corresponding sulfonamide was isolated quantitatively, while the reaction product with a tertiary amine was the *p*-toluenesulfonic acid ester, which was also obtained quantitatively. The lack of the sulfonic acid ester among the products in the reaction with primary amines in ethanol suggests that at the rate-determining step the unfavorable influence of ethoxide anion can be neglected.

Kinetic measurements

Since a wide variety of amines were used, the rate constant changed widely over the range of $10^{7.5}$. Therefore, two kinetic procedures have

been applied. For the aminolyses with reactive primary and secondary amines, the reactions have been followed by uv spectrophotometry using the absorption of *p*-toluenesulfonyl chloride at 245 nm, while for the tertiary amines, the rates of the reactions have been followed by conductometry, by monitoring the conductivity change in the reaction cell that is caused by the change of chloride ion, liberated during the aminolysis. In the latter method, the concentration of the amine was usually maintained 100 times higher than that of the sulfonyl chloride. Thus, the pseudo-first-order rate constants obtained were divided by the concentration of the amine used, to estimate the second-order rate constant of the aminolysis. For all the kinetic measurements both in ethanol and in acetonitrile, the concentration range of the amine for conductometry was in the range of 1–0.5 mol/L, while *p*-toluenesulfonyl chloride was kept between 0.01 mol/L and 0.005 mol/L; also for the uv spectrophotometry the concentration of amine was between 0.5 mol/L and 5×10^{-4} mol/L, while the concentraton of *p*-toluenesulfonyl chloride was between 0.2 mol/L and 1×10^{-4} mol/L. A typical run is shown in Fig. 3. The apparatus used for the conductivity is the same as that used previously (28). Meanwhile, the rate of the reaction with pyridine was measured by both uv spectrophotometry and conductometry and there was a good agreement in both.

In the aminolysis of sulfonyl chloride with pyridine in ethanol, $\Delta E^{\neq}$ and $\Delta S^{\neq}$ values are calculated to be 14.7 kcal/mol (61.61 kJ) and −15.9 eu, respectively, while $\Delta E^{\neq}$ and $\Delta S^{\neq}$ for the reaction with 1,8-naphthyridine are 17.2 kcal/mol (72.2 kJ) and −15.6 eu, respectively.

1. Y. KADOMA. Ph.D. Thesis, Osaka City University. 1972.
2. J. O. EDWARDS and R. PEARSON. J. Am. Chem. Soc. **84**, 16 (1962).
3. A. P. GREKOV and V. Y. VESELOV. Russ. Chem. Rev. **47**, 631–648 (1978).
4. S. OAE and Y. KADOMA. Kagaku (Kyoto), **27**, 1045 (1972).
5. (*a*) J. D. AUBORT and R. F. HUDSON. Chem. Commun. 937 (1970); (*b*) J. A. ZOLTEWICZ and L. W. DEADY. J. Am. Chem. Soc. **44**, 2765 (1972).
6. Y. KADOMA, S. TAMAGAKI, and S. OAE. Chem. Commun. 1155 (1972).
7. E. BUNCEL and S. HOZ. Tetrahedron Lett. **24**, 4777 (1983).
8. S. HOZ. J. Org. Chem. **47**, 3545 (1982).
9. S. WOLFE, D. J. MITCHELL, H. S. SCHLEGEL, C. MINOT, and O. EINSTEIN. Tetrahedron Lett. **23**, 615 (1982).
10. E. BUNCEL, C. CHUAQUI, and H. WILSON. J. Org. Chem. **45**, 3621 (1980).
11. E. BUNCEL, H. WILSON, and C. CHUAQUI. J. Am. Chem. Soc. **104**, 4896 (1982).
12. M. LALOI-DIARD, J.-F. VERCHERE, P. GOSSELIN, and F. TERRIER. Tetrahedron Lett. **25**, 1267 (1984).
13. C. H. DEPUY, E. W. DELLA, J. FILLEY, J. J. GRABOWSKI, and V. M. BIERBAUM. J. Am. Chem. Soc. **105**, 2481 (1983).
14. R. HUTCHINS, L. D. KOPPER, and E. ELIEL. J. Am. Chem. Soc. **90**, 7174 (1968).
15. S. OAE. Historical development of sulfur bonding. *In* Organic sulfur chemistry. *Edited by* F. Bernardi, I. G. Csizmadia, and A. Mangini. Elsevier, Amsterdam. 1985. Chapt. 1.
16. R. J. GILLESPIE. J. Chem. Educ. **47**, 18 (1970).
17. (*a*) J. E. DIXON and T. C. BRUICE. J. Am. Chem. Soc. **93**, 3248 (1971); (*b*) K. TSUDA, J. B. LOUIS, and R. E. DAVIS. Tetrahedron, **26**, 4549 (1970).
18. J. L. KICE and E. LEGAN. J. Am. Chem. Soc. **95**, 3912 (1973).
19. J. F. COETZEE and G. R. PADMANABHAN. J. Am. Chem. Soc. **87**, 5005 (1968).
20. M. J. GREGORY and T. C. BRUICE. J. Am. Chem. Soc. **89**, 4400 (1967).
21. R. W. ALDER, P. S. BOWMAN, W. R. S. STEELE, and D. R. WINTERMAN. Chem. Commun. 723 (1968).
22. S. OAE, Y. KADOMA, AND Y. YANO. Bull. Chem. Soc. Jpn. **42**, 1110 (1969).
23. D. D. PERRIN. Dissociation constants of organic bases in aqueous solution. Butterworths, London. 1965.
24. H. K. HALL. J. Phys. Chem. **60**, 63 (1956).
25. W. W. PAUDLER and T. J. KRESS. J. Org. Chem. **32**, 832 (1967).
26. H. RAPAPORT and A. D. BATCHO. J. Org. Chem. **28**, 1753 (1963).
27. J. DONLEAVY. J. Am. Chem. Soc. **78**, 1005 (1956).
28. HIROYUKI MORITA. Ph.D. Thesis, Tokyo Kyoiku Daigaku – The University of Tsukuba. 1977.

Metal catalysis in oxidation by peroxides. 24.[1] Extraction of aqueous peroxomolybdenum species into organic media and their reactivity

OLGA BORTOLINI, LETANZIO BRAGANTE, FULVIO DI FURIA, AND GIORGIO MODENA

Centro C.N.R. di Studio sui Meccanismi di Reazioni Organiche, Dipartimento di Chimica Organica, Via Marzolo 1, 35131 Padova, Italy

Received October 18, 1985

This paper is dedicated to Professor Arthur N. Bourns

OLGA BORTOLINI, LETANZIO BRAGANTE, FULVIO DI FURIA, and GIORGIO MODENA. Can. J. Chem. **64**, 1189 (1986).

The effect of the lipophilicity and coordinating ability of neutral ligands, belonging to the classes of phosphoric amides and pyridine oxides, on the extraction of the neutral oxidants molybdenum(VI)–peroxo complexes from an aqueous acidic phase to an organic one, has been studied. The nature of the Mo(VI)–peroxo species present both in aqueous and organic phase has also been investigated. Sizable amounts of mineral acid, added to adjust pH, may be extracted into the organic phase. The various factors affecting this process such as the nature of the acid added, the organic solvent and the neutral ligand, as well as the effect of this feature on the partition of the oxidant between the two phases are briefly discussed.

OLGA BORTOLINI, LETANZIO BRAGANTE, FULVIO DI FURIA et GIORGIO MODENA. Can. J. Chem. **64**, 1189 (1986).

On a étudié les effects, sur l'extraction d'oxydants neutres comme les complexes peroxo–molybdène(VI), du caractère lipophile et de l'habilité à coordonner des ligands neutres que possèdent les phosphoramides et les oxydes de pyridine. On a aussi examiné la nature des espèces peroxo-molybdène(VI) tant dans la phase aqueuse que dans la phase organique. De grandes quantités d'acides minéraux, qui sont ajoutés pour ajuster le pH, peuvent être extraites dans la phase organique. On discute brièvement des divers facteurs qui affectent ce processus, tel que la nature de l'acide qui est ajouté, la nature du solvant organique et du ligand neutre ainsi que l'effet de cette caractéristique sur la répartition de l'oxydant entre les deux phases.

[Traduit par la revue]

Introduction

Selective oxidations by dilute hydrogen peroxide, catalyzed by transition metal derivatives, present several attractive features (1). In fact, aqueous hydrogen peroxide is a readily available and safe oxidant which has the additional advantage of producing no other by-products than water. Moreover, novel procedures recently proposed, based on biphasic systems (2, 3), allow to overcome the main drawback encountered in the homogeneous catalytic reactions, that is the need of using polar solvents such as water, alcohols, or ethers where the oxidation rates by peroxometal complexes are usually much slower than those in non-polar media (1).

Two main approaches to the development of biphasic systems have been used (2, 3), both based on the acid–base properties of some peroxometal species, namely peroxomolybdenum and peroxotungsten complexes, formed by addition of hydrogen peroxide to Mo(VI) or W(VI) derivatives in protic solvents. In fact, both Mo(VI) and W(VI) peroxo complexes are fairly acidic (4). Thus, it is possible to transfer, by means of a lipophilic quaternary ammonium cation or similar cationic phase-transfer agents, the peroxo anions from the aqueous to the organic phase (2) where the oxidation of the substrate takes place.[2] Alternatively, we have proposed (3) the transfer of neutral peroxo complexes to the organic phase, generally a chlorinated hydrocarbon, by employing neutral lipophilic ligands such as phosphoric amides or pyridine oxides.

Our system has been tested in two model reactions (3), the oxidation of organic sulfides and the epoxidation of olefins. This system exhibits fairly good rates and selectivities under the appropriate experimental conditions, particularly with a Mo(VI) catalyst. Clearly, the efficiency of the oxidation was found to depend on several factors, a very important one of which is the nature of the ligand employed.

We have therefore deemed worthwhile to extend our study by examining in greater detail the chemistry of the peroxo-species formed and transferred. We limited ourselves to Mo(VI) derivatives, and the interactions of such species with the extracting ligands. It may be anticipated that the results reported in the present paper confirm more quantitatively the relevance of both the lipophilicity and the coordinating ability of a ligand in determining the success of the oxidation procedures. Moreover, this study provided evidence of a less known process, *i.e.* the extraction of the mineral acid in the organic phase by the ligand, which affects both the partition of the peroxo complexes and the reactivity of the system.

Results and discussion

Peroxomolybdenum(VI) species in acid aqueous solutions

Early results reviewed by Connor and Ebsworth in 1964 (5) provided evidence that in acid aqueous solutions containing alkali metal molybdates and an excess of hydrogen peroxide, peroxomolybdenum compounds containing two peroxo groups per molybdenum atom are formed. However, no detailed information on the structure and the chemistry of such species was available at that time. Since then, a variety of well characterized peroxomolybdenum complexes has been prepared (6). Among these, we selected, for the purposes of this investigation, the oxo–diperoxo–phosphoro–amido–aquo complex $MoO(O_2)_2.HMPT.H_2O$, **1** (4*c*):

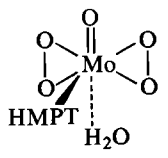

1

In protic solvents, the organic ligand HMPT may be displaced by the solvent itself (4*c*, 7). The displacement

[1]Part 23. O. Bortolini, F. Di Furia, G. Modena, and A. Schionato. J. Mol. Catal. In press.

[2]Addition of phosphoric or arsenic acids in the aqueous phase is essential in this procedure (2) thus suggesting the formation and subsequent extraction of peroxo-heteropolyanions.

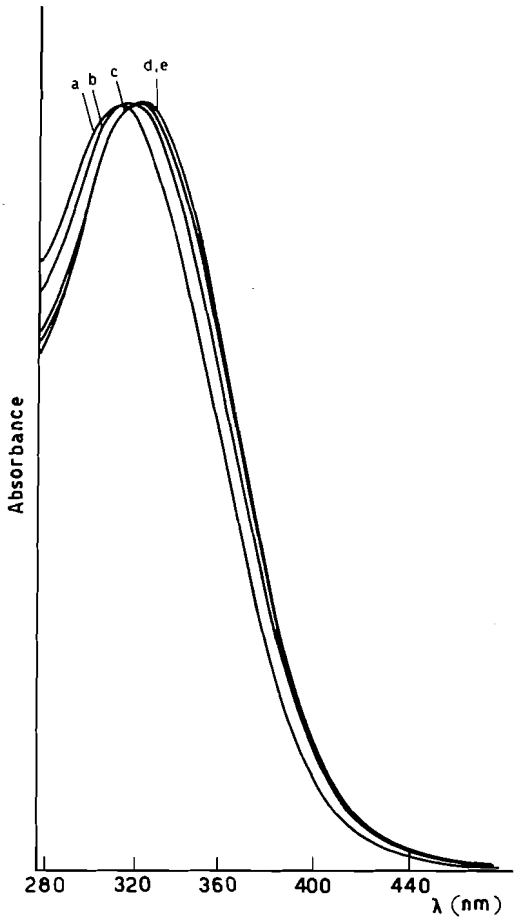

FIG. 1. Electronic spectra of $MoO_5HMPT.H_2O$ (2×10^{-2} *M*) in H_2O at different acidities (H_2SO_4): pH 2.06 (*a*), 1.66 (*b*), 1.24 *c*, 1.17 (*d*), 1.00 (*e*).

equilibrium is easily monitored by ^1H nmr spectroscopy because of the different chemical shifts of the CH_3 group in coordinated and free HMPT, respectively (7). Moreover, the equilibrium is sufficiently slow at room temperature to give two separate signals.

We first determined that in D_2O, 2×10^{-3} *M* solutions of **1** only gave signals (doublet) corresponding to free HMPT. In other words, the ligand was completely displaced. We then measured the electronic spectra of a 2×10^{-3} *M* aqueous solution of **1** at different acidities (H_2SO_4). The pertinent spectra are shown in Fig. 1.

The absorption at ca. 310–320 nm is typical of oxodiperoxomolybdenum complexes (8). Similar features are observed in a series of solvents ranging from protic to hydrocarbon ones (see the following for an example). Moreover, no absorption due to HMPT is observed in this region of the spectrum, as expected. Inspection of the spectra of Fig. 1 indicates that an increase in the acidity of the aqueous solution causes a shift of the peroxide absorption at lower energies, showing acid–base equilibria above pH ~1.2. At higher acidity, on the other hand, no appreciable variation of the band is observed.

It is also observed that in the presence of H_2O_2, at pH values below 1.2, aqueous solutions of H_2MoO_4 or MoO_3 exhibit an absorption spectra which are identical to those shown in Fig. 1, within experimental error. $\lambda_{max} = 324$ nm, $\epsilon_{max} = 1060\,cm^{-1}\,M^{-1}$.

From these data we conclude that the same peroxomolybdenum species occur in solutions, whatever the precursor, provided that the pH values are sufficiently low. The species is most likely an aquo–oxo–diperoxo complex $MoO(O_2)_2(H_2O)_n$.

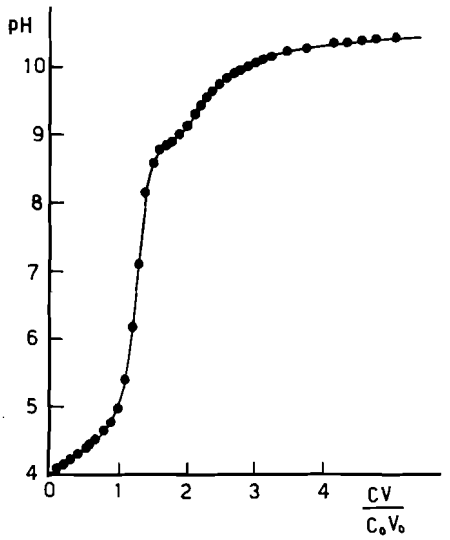

FIG. 2. Potentiometric titration of $MoO_5HMPT.H_2O$ (1×10^{-4} *M*) with NaOH (1×10^{-2} *M*) in H_2O at 25°C, under argon.

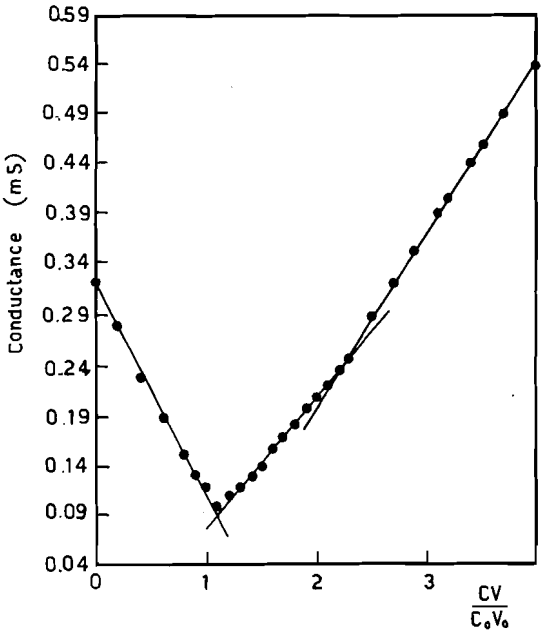

FIG. 3. Conductometric titration of $MoO_5HMPT.H_2O$ (1.25×10^{-4} *M*) with NaOH (1×10^{-2} *M*) in H_2O at 25°C, under argon.

Again using $MoO_5HMPT.H_2O$ as a precursor, we then examined the acid–base behavior of such peroxo complex in aqueous solutions. Figures 2 and 3 show the results of the potentiometric and conductometric titrations of **1**, 1×10^{-4} *M*, with NaOH in aqueous solution. The concentration of **1** in these experiments was such that no HMPT bound to the metal was observed. In both titrations two equivalent points, at [NaOH]/[Mo] ratios of 1 and 2, respectively, are found, in agreement with previous results obtained in very similar systems (4*c*).

The acidic character of Mo(VI)–peroxo species in other protic solvents such as alcohols has been also observed (4*a*, *b*). For comparative purposes, Fig. 4 shows the potentiometric titration of a 1×10^{-4} *M* solution in *i*-PrOH (no HMPT bound to

the metal) with *i*-PrONa. Interestingly, in alcoholic solution only one, fairly acidic, titratable proton is found.

Therefore, the acidity of the peroxo–molybdenum species should not be related to the opening up of the peroxo bridges yielding peracid-like derivatives since such a process should be equally possible in water and in alcoholic solvents.

On the other hand, the titration curve in Fig. 2 clearly shows that the presence of dianionic molybdenum(VI) species in water is confined to basic solution where complicated equilibria involving dimerization and dissociation of hydrogen peroxide are likely to occur (4*c*, 5). Therefore, in aqueous acid solution, where our experiments have been carried out, the only acid–base equilibrium which needs to be considered is that occurring between the neutral peroxomolybdenum species and the mono-anionic one. This might be envisaged as:

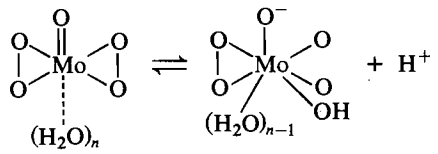

Extraction of neutral peroxomolybdenum(VI) species from water to DCE by neutral lipophilic ligands

The experiments reported here were carried out under the following experimental conditions: 2.5 mL of an aqueous solution containing respectively the molybdenum precursor, typically Na_2MoO_4, in the presence of an excess of H_2O_2, at a fixed pH value (obtained by addition of a strong acid) and an equal volume of an organic phase, containing the neutral lipophilic ligand, were mixed together under controlled stirring for 3 min. After this time the stirring was suspended, the two phases were separated, and the peroxomolybdenum complex remaining in the aqueous solution was determined by uv spectroscopy (absorption at ca. 310–320 nm depending on the pH, see preceding paragraph).[3] Control experiments confirmed that, in the absence of the ligand in the organic phase, no appreciable decrease of the concentration of Mo(VI)–peroxo complex in the aqueous phase, after the experiments run under otherwise identical conditions, was observed.

First we examined the yields of extraction as a function of the pH of the aqueous phase, taking two representative neutral ligands, hexaethylphosphoric triamide, HEPT, and phenylpropylpyridine *N*-oxide, RPyNO. (RPy = 4-(C_6H_5—$(CH_2)_3$—C_5H_4N). The pertinent results, concerning aqueous solution of H_2SO_4 and $HClO_4$, are shown in Figs. 5 and 6. A 2-fold excess of the ligand over the peroxomolybdenum complex, under the condition of a 40-fold excess of H_2O_2 over molybdenum, has been used. The curves of Figs. 5 and 6, referring to the extraction from H_2SO_4 aqueous solutions, are in very good agreement with the results reported in the previous paragraph. In fact, the maximum extraction is obtained at a pH value *ca.* 1.5–1.0, roughly corresponding to the invariance of the absorption at 324 nm, see Fig. 1, which has been attributed to the complete neutralization of the anionic peroxomolybdenum species. We observe also that the yields of extraction are larger for RPyNO than for HEPT. This point will be discussed in

[3]It has been confirmed directly that the peroxomolybdenum species in the aqueous phase plus that extracted into the organic one, also determined by uv spectroscopy, as discussed in the next paragraph, correspond to the stoichiometric concentration of molybdenum initially added. Furthermore, under identical conditions, but in the absence of metal derivatives, only negligible amounts of hydrogen peroxide, as determined by iodometric titre, are extracted into the organic phase.

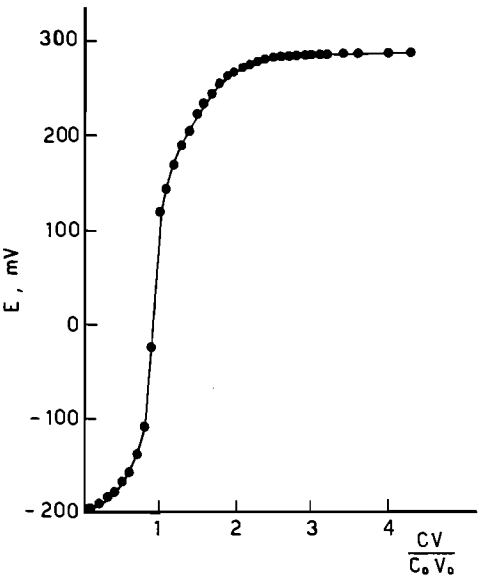

FIG. 4. Potentiometric titration of $MoO_5HMPT.H_2O$ (1×10^{-4} *M*) with $NaOPr^i$ (1×10^{-2} *M*) in Pr^iOH at 25°C, under argon.

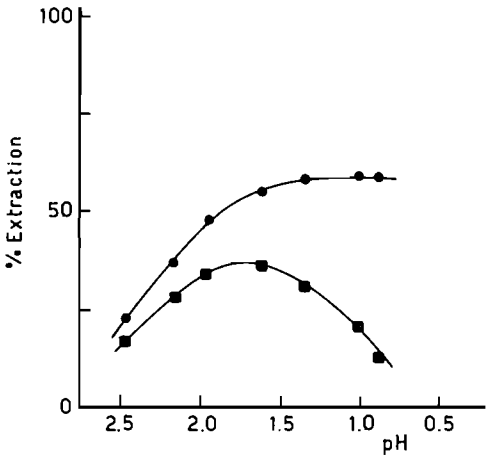

FIG. 5. Extraction (%) of Mo(VI)–peroxo compound in organic phase as a function of pH and the type of acid used: H_2SO_4 (●) or $HClO_4$ (■). $[Mo]_{st} = 2 \times 10^{-2}$ *M*, $[H_2O_2] = 0.8$ *M*, [HEPT] = 4×10^{-2} *M* DCE/H_2O 2.5/2.5 mL at 25°C.

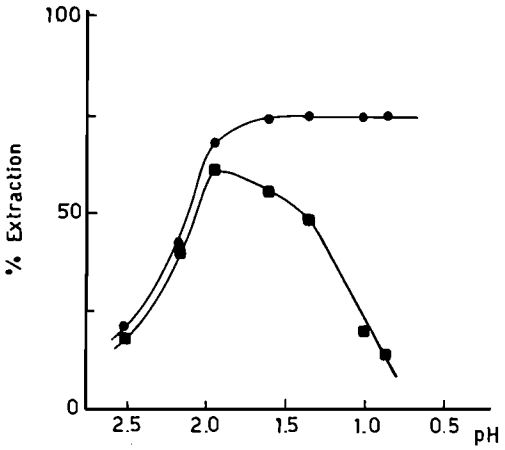

FIG. 6. Extraction (%) of Mo(VI)–peroxo compound in the organic phase as a function of pH and the type of acid used: H_2SO_4 (●) or $HClO_4$ (■). $[Mo]_{st} = 2 \times 10^{-2}$ *M*, $[H_2O_2] = 0.8$ *M*, [RPyO] = 4×10^{-2} *M* DCE/H_2O 2.5/2.5 mL at 25°C.

TABLE 1. Percentage of mineral acid extracted from the aqueous into the organic phase (DCE) $[H_2SO_4]_0 = 7.9 \times 10^{-2}$ mmol, $[HClO_4]_0 = 0.158$ mmol in 2.5 mL of H_2O (pH ~ 1.2)[a]

Ligand	Solvent	% $HClO_4$ in the organic phase		% H_2SO_4 in the organic phase	
		No ligand added	Ligand added	No ligand added	Ligand added
HEPT	DCE	~0.1	14.0	~0.1	0.3
RPyNO	DCE	~0.1	15.4	~0.1	0.6
HEPT	$CHCl_3$	~0.1	1.5	~0.1	~0.1
RPyNO	$CHCl_3$	~0.1	0.5	~0.1	~0.1
HEPT	CH_2Cl_2	<0.1	15.9	~0.1	0.2
RPyNO	CH_2Cl_2	<0.1	17.5	~0.1	0.5
HEPT	Chlorobenzene	~0.1	9.7	~0.1	~0.1
RPyNO	Chlorobenzene	~0.1	17.5	~0.1	0.2

[a]The experiments were carried out under standard conditions (see text) at a fixed (4×10^{-2} *M*) concentration of ligand in DCE. The concentration of the mineral acid in the organic phase was determined by titration (NaOH) after pouring the DCE solution in water.

more detail later on. The shape of the curves of Figs. 4 and 5 concerning extractions from $HClO_4$ solutions is, at first glance, rather puzzling. Also in this case, an increase of the extraction yields is observed upon neutralization of the anionic peroxomolybdenum species. However, at higher acidity of the medium, the yields of extraction sharply decrease. The data reported in Table 1 clearly indicate that in the presence of both ligands HEPT and RPyNO, the concentration of $HClO_4$ in the organic phase is 30- to 40-fold that of H_2SO_4, whereas, in the absence of the ligand, the acid concentration in the organic phase is similar for the two acids and much lower in value. Therefore, it appears that the basic ligands are also able to extract the mineral acids in the organic phase, likely *via* hydrogen bonding or true protonation equilibria (9). Moreover, $HClO_4$ is much more easily extracted than H_2SO_4, possibly because of the known higher solubility of the anion ClO_4^- in organic media. The presence of acid in the organic phase clearly reduces the extracting ability of the ligand toward the peroxomolybdenum species.

For comparative purposes, in Table 1 are reported data referring to other chlorinated solvents. Although the qualitative behavior is the same as that observed for DCE, it may be interesting to note that chloroform appears to be the solvent where less acid is extracted. This feature might be relevant as far as the search for a more efficient oxidizing system is concerned (3). However, we have directly confirmed that, in general, the yields of extraction of Mo(VI)–peroxo complexes are much lower in chloroform compared to other chlorinated hydrocarbons.

Under the best conditions of acidity in the aqueous phase determined by the above experiments, *i.e.* pH 1.2, H_2SO_4, we have studied the increase of extraction yields as a function of the neutral ligand concentration. The pertinent results are shown in Fig. 7 where four different ligands are considered. Beside the two ligands previously employed, HEPT and RPyNO, we have also examined hexabutylphosphoric triamide, HBPT, and tridodecylphosphoric triamide, TDPT. The comparison of the behavior of HEPT and HBPT may give an estimate of the relevance of the lipophilicity of the ligands on their extracting ability. Thus, the similarity of the two curves in Fig. 7 indicates that the efficiency of the two species is largely dominated by the coordinating ability of the oxygen of the P=O group provided that the ligands are sufficiently lipophilic. In fact, control experiments indicate that the water-soluble HMPT is much less effective.

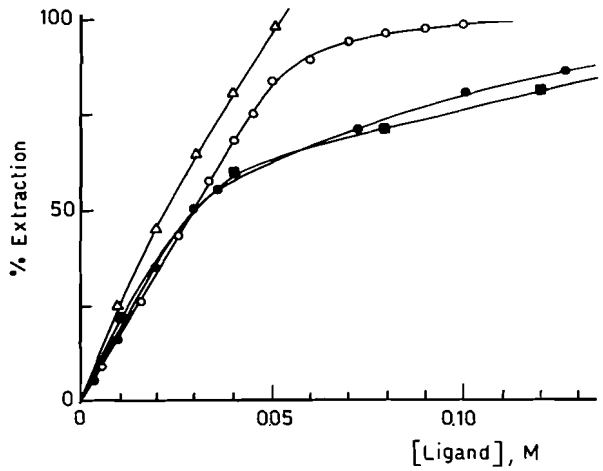

FIG. 7. Effect of increasing concentration of added ligands HBPT (■), HEPT (●), RPyO (○), TDPT (△) on the % extraction of the Mo(VI)–peroxo compound in the organic phase. $[Mo]_{st} = 2 \times 10^{-2}$ *M*, $[H_2O_2] = 0.8$ *M*, pH = 1.2 (H_2SO_4), DCE/H_2O 2.5/2.5 mL at 25°C.

As observed previously, the N-oxide derivative is a better extracting agent than either HEPT or HBPT. Interestingly, TDPT gives the best results under the adopted conditions.

In an attempt to correlate the extraction behavior observed with the coordinating ability of the various classes of ligands we have synthesized two novel model peroxo complexes, $MoO_5(PyNO).H_2O$ (PyNO ≡ 4—CH_3—C_5H_4N → O) and $MoO_5TEPT.H_2O$ (TEPT ≡ $(CH_3CH_2NH)_3P$=O), characterized by a fairly good solubility in alcoholic solvents. We have then studied the displacement equilibria of the ligands for the two complexes, and for $MoO_5HMPT.H_2O$, in the solvent CD_3OD, determining the values of K_{DISS} at 25°C by ^1H nmr technique and standard calculation methods. It should be mentioned that, at variance with $MoO_5HMPT.H_2O$ complex for which, as previously mentioned, two separate signals of the CH_3-group of the coordinated and free HMPT are observed (7), the rates of ligands exchange of the other two complexes are, at 25°C, relatively fast so that a single average signal is observed for the CH_3-group both in $MoO_5(PyNO).H_2O$ and $MoO_5TERP.H_2O$.

$$MoO_5L.H_2O \xrightarrow{CD_3OD} MoO_5L.CD_3OD + H_2O$$

$$MoO_5L.CD_3OD + CD_3OD \rightleftharpoons MoO_5(CD_3OD)_2 + L \qquad K_{DISS}$$

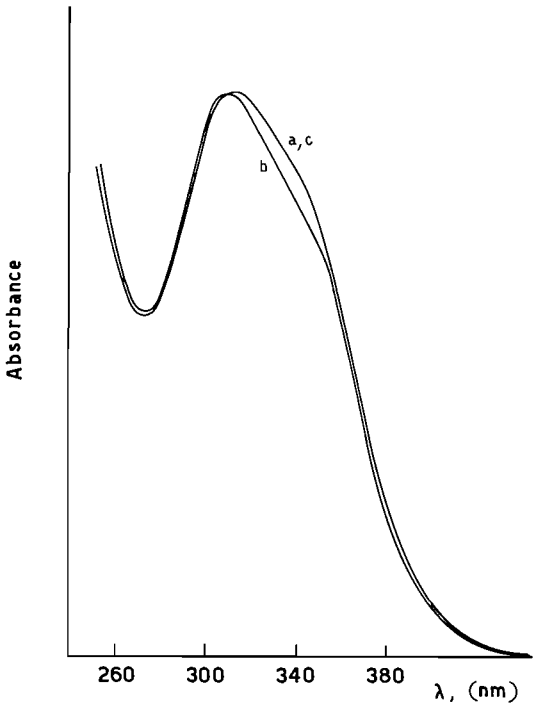

FIG. 8. Electronic spectra of: (*a*) Mo(VI) peroxocompound in DCE extracted from the aqueous phase under standard conditions: $[Mo]_{st} = 2 \times 10^{-2} M$, $[H_2O_2] = 0.8 M$ pH = 1.2 (H_2SO_4); (*b*) $MoO_5HMPT.H_2O$ $1.5 \times 10^{-2} M$ in DCE; (*c*) $MoO_5HMPT.H_2O$ $1.5 \times 10^{-2} M$ in DCE in the presence of acid (H_2SO_4).

The K_{DISS} values thus obtained, $MoO_5(PyNO).H_2O$ (1×10^{-4}), $MoO_5HMPT.H_2O$ (2.4×10^{-4}), and $MoO_5TEPT.H_2O$ (3.7×10^{-4}) follow an order which does not parallel the order of extraction efficiency of the liphophilic ligands containing the same coordinating group. Indeed, the trialkylphosphoric amide ligand TEPT is more easily displaced than PyNO, whereas lipophilic *N*-oxides appear to be less effective as extracting agents than trialkylphosphoric amides. These findings underline the complexity of the biphasic systems where equilibrium processes, other than the partition of the ligands and their coordination to the metal, need to be considered. Among these, an important role is likely played by the interaction between the ligands and the acid in both the organic phase and aqueous phase (9).

Peroxomolybdenum(VI) species extracted into the organic phase

In this part of our investigation we looked for direct evidence that the peroxomolybdenum(VI) complex extracted into the organic phase, independent of the molybdenum precursor present in the aqueous solution, belongs to the well-known family of compounds of the general formula $MoO(O_2)_2L_1L_2$ which were isolated and characterized by Mimoun *et al.* (4*c*). We proceeded by doing spectroscopic and kinetic experiments. We first measured the uv spectrum of the DCE solution after the extraction, using the same conditions as described in the preceding paragraph, from an acidic (pH 1.2) solution of Na_2MoO_4 containing an excess (40-fold) of hydrogen peroxide, employing HEPT as the extracting agent. We then registered the uv spectrum of a DCE solution of $MoO_5HEPT.H_2O$. As shown in Fig. 8, the two spectra are very similar, except for a small red-shift in the extracted peroxo complex. Control experiments have shown that this shift is attributable to a kind of solvent effect caused by the presence of acid in the DCE solution of the extracted peroxo complex.

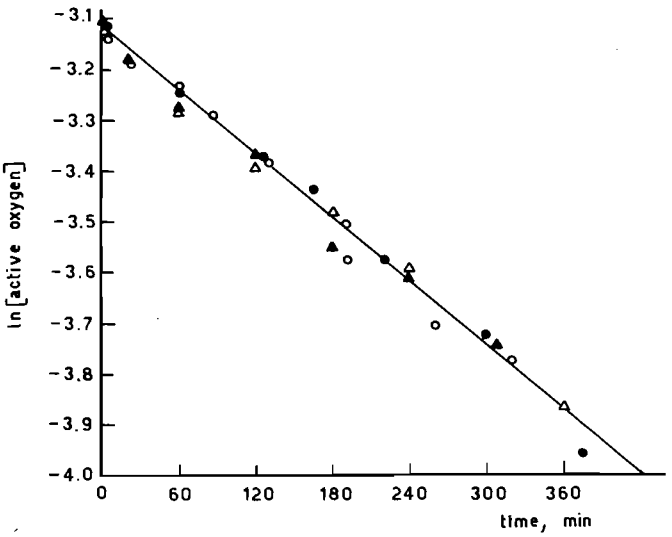

FIG. 9. Rate of disappearance of active oxygen in the oxidation of cyclohexene (0.2 *M*) by Mo(VI)–peroxo compound extracted from the aqueous phase (▲), duplicated reaction (△), or by $MoO_5HMPT.H_2O$ (●), duplicated reaction (○), in DCE in the presence of HEPT $5.76 \times 10^{-2} M$, at 25°C.

Finally, we have tested the oxidizing ability of a solution of the extracted peroxomolybdenum complex by comparing it with that of $MoO_5HEPT.H_2O$ in a model reaction, *i.e.* the epoxidation of cyclohexene. We used identical experimental conditions, particularly the excess of the free ligand over the oxidant since it is known that added ligand reduces the oxidation rates. The results are shown in Fig. 9. Within experimental error, the oxidizing ability of the two systems appears identical thus confirming that the same oxidant is present in solution.

Conclusions

We have shown that the efficiency of the two-phase oxidizing system comprising dilute hydrogen peroxide, Mo(VI) derivatives, and neutral phase-transfer agent depends on several, sometime conflicting, factors. Our results indicate that an increase of the acidity of the aqueous solution is beneficial as far as the neutralization of the anionic peroxo complexes is concerned. On the other hand, the mineral acid, particularly $HClO_4$, may also be transferred into the organic phase. This results in a decrease in the extracting capability of the ligand. Moreover, the presence of an acid in DCE may lower the yields of acid-sensitive products such as some of the epoxides obtained by oxidation of the olefin (3). Although the lipophilicity of the neutral ligands plays a role in the sense that its insolubility in water is a necessary requisite, our studies indicate that the nature of the coordinating group in the ligand itself is more important. On the other hand, the fact that the extraction ability increases in the order hexaalkylphosphoric triamides < *N*-oxides < trialkylphosphoric triamides which is also the order of increasing oxidizing ability of the two-phase systems (3), but is not the order of increasing coordinating ability of the ligands, suggests that other factors, such as the interaction with the acid extracted in the organic phase, may play a relevant role.

Experimental section

Reagents and solvents

Reagent grade MoO_3, Na_2MoO_4, H_2O_2 (36% w/v) were used without further purification. Aqueous solution of peroxo–Mo(VI) complex were prepared by dissolving MoO_3 (10 g, 0.069 mol) in H_2O_2 (100 mL) in the dark at 20°C. Complete dissolution is usually achieved in 4–5 days. DCE, CH_2Cl_2, $CHCl_3$, and chlorobenzene were purified

by standard procedures from highly pure commercial samples. All other chemicals were used as received.

Preparation of the ligands

Hexabutylphosphoric triamide (HBPT). An ethereal solution of PCl_3 (55 g, 0.4 mol) was dropwise added, over a 2-h period, to a solution of dibutyl amine (350 g, 2.71 mol) in 500 mL of anhydrous diethyl ether under vigorous stirring (10). After this time the mixture was allowed to return to room temperature and then refluxed for 6 h. The precipitated amine hydrochloride was filtered off, and carefully washed with ether. From the combined ethereal solutions the solvent was removed in a rotating evaporator. The crude product was dissolved in 200 mL of acetone and oxidized with an excess (ca. 20%) of hydrogen peroxide (36% w/v) slowly added to the reaction mixture maintained at 0°C. The resulting solution was then stirred for 3 h at 40–50°C, cooled, poured into an equal volume of water, and extracted with diethyl ether. The ethereal solution was washed with water, dried over $MgSO_4$, and the solvent removed *in vacuo*. The product was purified by low pressure (4–5 atm) liquid chromatography (11) (silica gel (>0.063 mm), petroleum ether – acetone 90–10) and by subsequent distillation, bp 153°C 0.06 mm Hg, yield 40%. ^{1}H nmr δ 0.93 (t, 18H), 1.28 (m, 12H), 1.49 (m, 12H), 2.90 (m, 12H); ^{31}P nmr δ 23.98 (s) H_3PO_4 30% in D_2O as external reference, broad-band proton-decoupled spectra. *Anal.* calcd. for $C_{24}H_{54}N_3OP$: C 66.77, H 12.61, N 9.73; found: C 66.15, H 12.43, N 9.51.

Hexaethylphosphoric triamide (HEPT). It was obtained in a similar manner from the di-*n*-ethyl amine (10). The product was purified by low pressure liquid chromatography (11) (silica gel > 0.063 mm, petroleum ether – acetone 70–30) followed by distillation bp 107°C 0.3 mm Hg; yield 30%. ^{1}H nmr δ 1.10 (t, 18H) 3.05 (qd, J = 7.2 Hz, J_{P-H} = 10.0 Hz, 12H); ^{31}P nmr δ 23.90 (s) H_3PO_4 30% in D_2O as external reference, broad-band proton-decoupled spectra. *Anal.* calcd. for $C_{12}H_{30}N_3OP$: C 54.70, H 11.50, N 15.90; found: C 54.25, H 11.25, N 15.23.

Triethylphosphoric triamide (TEPT). Precooled $CH_3CH_2NH_2$ (150 mL, 2.29 mol) was rapidly transferred, under stirring, into a round-bottomed flask containing 300 mL of *t*-butyl methyl ether, equipped with a cold-finger condenser and maintained at −10°C. $POCl_3$ (43 mL, 0.17 mol) dissolved in 50 mL of ether was added slowly and the flask allowed to warm at room temperature (12). The reaction was then refluxed for 4 h under stirring. When cooled at room temperature two phases separated spontaneously. The lower layer containing the product was separated and diluted with a 25–30-fold volume of ethylic ether. The amine hydrochloride precipitated and was filtered off. The ethereal solution was concentrated under reduced pressure and the crude product purified by liquid chromatography (silica gel CH_2Cl_2–CH_3OH 97–3), mp 28–29°C, yield 30%. ^{1}H nmr δ 1.15 (t, 9H), 3.05 (m, 6H) 2.35 (s, broad, 3H); ^{31}P nmr δ 19.60 (s) H_3PO_4 30% D_2O reference, proton decoupled. *Anal.* calcd. for $C_6H_{18}N_3OP$: C 40.22, H 10.12, N 23.45; found: C 39.69, H 10.19, N 23.31.

Tridodecylphosphoric triamide (TDPT). $POCl_3$ (11.8 g, 0.078 mol) dissolved in 60 mL of *t*-butyl methyl ether was slowly added, under stirring, to a solution of dodecylamine (93.3 g, 0.05 mol) in 250 mL of ether at 0°C (12).

The temperature was raised to 25°C and the reaction refluxed overnight. The white precipitate formed contained both the amine hydrochloride and the product. The solid was dissolved in hot water and the product separated as an insoluble layer, which was recovered. Recrystallization from ethanol gave a white solid; mp 71–72°C, yield 42%. ^{1}H nmr δ 0.95 (t, 9H), 1.35 (s, 54H), 1.55 (m, 6H), 2.27 (m, 3H) 3.05 (m, 6H); ^{31}P nmr δ 18.01 (s) H_3PO_4 30% D_2O reference, proton decoupled. *Anal.* calcd. for $C_{36}H_{78}N_3OP$: C 72.10, H 13.10, N 7.03; found: C 72.37, H 13.43, N 7.16

CAUTION: HMPT has been proved to be carcinogenic; therefore caution has to be used in handling this and other phosphoric amides.

Preparation of the Mo(VI)–peroxo complexes

$MoO_5.HMPT.H_2O$. The procedure adopted is essentially that reported by Mimoun *et al.* (4*c*). Na_2MoO_4 (8.5 g, 35 mmol) was dissolved in a minimum volume of water and the pH of the solution adjusted with H_2SO_4 (30% w/w) to ca. 2. Then 25 mL of H_2O_2 (0.3 mol) were added at 0°C. To this solution, under stirring, 6.08 mL (35 mmol) of HMPT were added and a yellow precipitate was immediately formed. The product was recrystallized from methanol. If needed, water molecule may be removed by keeping the complex over P_2O_5 under vacuum for one night. The properties of the complex are in agreement with the previously reported data.

$MoO_5.HEPT.H_2O$. HEPT (0.58 g, 2.2 mmol) was slowly added, under stirring at 0°C, to an aqueous solution of MoO_3 dissolved in H_2O_2 (see preceding paragraph). A yellow precipitate was formed immediately, and was stirred for an additional 30 min, then filtered off. The filtrate was washed several times with water and ethylic ether (80% yield). The complex may be dehydrated as previously described; ir (KBr) ν(Mo=O) 950, ν (Mo<O,O>) 542, 590, ν(P=O) 1212 cm^{-1}. *Anal.* calcd. for $C_{12}H_{30}N_3O_6MoP$: C 32.80, H 6.90, N 9.60; found: C 32.93, H 7.07, N 9.59.

$MoO_5.p\text{-}MePyO.H_2O$. A solution of *para*-methyl pyridine *N*-oxide (10.9 g, 0.1 mol) in 5 mL of water was added to a solution of MoO_3 (15 g, 0.1 mol) dissolved in H_2O_2, in an ice-cold bath. A bright yellow precipitate was formed. It was filtered off and washed well with water and ether (70% yield); ir (KBr) ν(Mo=O) 965, ν(Mo<O,O>) 540, 583 cm^{-1}. *Anal.* calcd. for $C_6H_9NO_7Mo$: C 23.78, H 2.99, N 4.62; found: C 23.56, H 2.99, N 4.63.

$MoO_5.TEPT.H_2O$. To a solution of MoO_3 dissolved in H_2O_2 1 equiv. of TEPT was added in a minimum volume of water at 0°C. A pale yellow precipitate was immediately formed. It was filtered off and washed with ether (40% yield). Iodometric titration of active oxygen indicated a purity of 95% based on a molecular weight of 372.99 corresponding to $C_6H_{20}N_3O_7MoP$. Contrary to previously reported compounds this complex decomposes rapidly.

It may be stored at −23°C for 3–4 days.

CAUTION: Dehydration of $MoO_5.TEPT.H_2O$ under vacuum has resulted in a violent decomposition. Such procedure should be avoided. Concentration of the organic phase containing the peroxometal complexes during work-up may also be dangerous.

Apparatus and standard procedures

^{1}H nmr spectra were recorded on a Bruker WP 200 ST, TMS as internal reference; ^{31}P nmr spectra were obtained on a Bruker WP60, H_3PO_4 30% in D_2O as external reference. Ultraviolet–visible spectra were recorded using a Varian Cary 219 or a Perkin-Elmer Lambda 5 spectrophotometer. Infrared spectra were recorded on a Perkin-Elmer PE 580 B in KBr pellets.

The pH values of the solutions were controlled and the potentiometric measurements were carried out on a Metrohm 632, using a standard glass electrode. Conductometric measurements were obtained on RADIOMETER CDM 3. Potentiometric and conductometric acid–base titrations were performed by stepwise addition of freshly prepared 0.01 *M* solutions of NaOH (Normex) or $NaOPr^i$, under argon. Acid–base titrations were carried out using phenolphthalein as indicator. Melting and boiling points are uncorrected. The extraction experiments were carried out as follows: 2.5 mL of an aqueous solution containing Na_2MoO_4 (0.02 *M*) and H_2O_2 (0.8 *M*) at a fixed pH value, obtained by the addition of a strong acid and 2.5 mL of organic phase containing the lipophilic ligand, usually 0.04 *M*, were stirred together for 3 min. After this time the stirring was suspended and the two phases separated. The amount of peroxomolybdenum complex remaining in the aqueous solution was determined by uv spectroscopy using the appropriate λ_{max}, depending on the pH.

Acknowledgment

We thank the Ministry of Public Education, Italy, for financial support.

1. M. PRALUS, J. C. LECOQ, and J. P. SCHIRMANN. Fundamental research in homogeneous catalysis. Vol. 3. *Edited by* M. Tsutsui. Plenum Press, New York. 1979 and references therein. p. 327.
2. C. VENTURELLO, E. ALNERI, and M. RICCI. J. Org. Chem. **48**, 3831 (1983).
3. (*a*) O. BORTOLINI, F. DI FURIA, and G. MODENA. Ital. Patent Appl. 25720 A (1981), 25721 A (1981); (*b*) O. BORTOLINI, F. DI FURIA, G. MODENA, and R. SERAGLIA. J. Org. Chem. **50**, 2688 (1985).
4. (*a*) A. ARCORIA, F. P. BALLISTRERI, G. A. TOMASELLI, F. DI FURIA, and G. MODENA. J. Mol. Catal. **14**, 53 (1982); (*b*) A. ARCORIA, F. P. BALLISTRERI, G. A. TOMASELLI, F. DI FURIA, and G. MODENA. J. Mol. Catal. **24**, 189 (1984); (*c*) H. MIMOUN, I. SERRE DE ROCH, and L. SAJUS. Bull. Soc. Chim. Fr. 1481 (1969); (*d*) Z. RACISZEWSKI. J. Am. Chem. Soc. **82**, 1267 (1960).
5. J. A. CONNOR and E. A. V. EBSWORTH. Adv. Inorg. Chem. Radiochem. **6**, 279 (1964).
6. F. DI FURIA and G. MODENA. Rev. Chem. Interm. **6**, 51 (1985).
7. H. MIMOUN, I. SEREE DE ROCH, and L. SAJUS. Tetrahedron, **26**, 37 (1970).
8. S. E. JACOBSON, R. TANG, and F. MARES. Inorg. Chem. **17**, 3055 (1978).
9. H. A. ZAHALKA and Y. SASSON. J. Chem. Soc. Chem. Commun. 1581 (1984).
10. C. STUEBE and H. P. LANKELMA. J. Am. Chem. Soc. **78**, 976 (1956).
11. J. C. MAGAND, C. GONNET, and A. LAMOTTE. J. Chromatogr. **76**, 496 (1973).
12. B. BOCH and W. H. WIEGRABE. Chem. Ber. **99**, 377 (1966).

Kinetics of the equilibration of 3-hydroxyphthalide and *o*-formylbenzoic acid. Hemiacetal breakdown with a carboxylic acid leaving group

ROBERT A. MCCLELLAND
Department of Chemistry, Scarborough Campus, University of Toronto, Toronto, Ont., Canada M1C 1A4
AND
POUL E. SØRENSEN
Chemistry Department A, Building 207, The Technical University of Denmark, DK-2800, Lyngby, Denmark
Received October 15, 1985

This paper is dedicated to Professor Arthur N. Bourns

ROBERT A. MCCLELLAND and POUL E. SØRENSEN. Can. J. Chem. **64**, 1196 (1986).

A temperature-jump relaxation study is reported for the equilibration: 3-hydroxyphthalide (SH) ⇄ *o*-formylbenzoate (R^-) ⇄ *o*-formylbenzoic acid (RH). A kinetic analysis is carried out in which SH and R^- interconvert with catalysis in the ring opening direction by water and by added general bases. Excellent Brønsted plots based upon a series of oxyacid buffer catalysts are obtained. These have slopes β for the base-catalyzed ring opening of 0.81 and α for the reverse acid-catalyzed ring closing of 0.19. A mechanism where S^-, the conjugate base of SH, is a discrete intermediate can be ruled out on the basis of the Brønsted values and the magnitudes of the rate constants. The lifetime of S^- is estimated to lie in the range 10^{-11}–10^{-15} s. Two mechanisms can be proposed. A fully concerted mechanism "enforced" by lifetimes less than 10^{-13} s involves direct interconversion of SH and R^- with no intermediate. A preassociated mechanism "enforced" by lifetimes in the 10^{-11}–10^{-12} s range requires, in the ring closing direction, that an acid catalyst be hydrogen bonded to the carbonyl in R^-.

ROBERT A. MCCLELLAND et POUL E. SØRENSEN. Can. J. Chem. **64**, 1196 (1986).

On rapporte une étude sur la relaxation par saut de température de l'équilibre hydroxy-3 phtalide (SH) ⇄ *o*-formylbenzoate (R^-) ⇄ acide *o*-formylbenzoïque (RH). On a effectué une analyse cinétique dans laquelle SH et R^- se transforment l'un dans l'autre sous l'influence d'une catalyse par l'eau et les bases générales qui favorise l'ouverture du cycle. On a obtenu d'excellentes corrélations de Brønsted qui sont basées sur une série de catalyseurs de tampons d'oxyacides. Les pentes, β pour l'ouverture du cycle qui est catalysée par les bases et α pour la réaction inverse de fermeture du cycle sous l'influence des acides, sont respectivement 0,81 et 0,19. En se basant sur les valeurs de Brønsted et sur les amplitudes des constantes de vitesse, on peut éliminer le mécanisme impliquant S^-, la base conjuguée de SH, comme intermédiaire identifiable. On estime que le temps de vie de S^- se situe entre 10^{-11} et 10^{-15} s. On propose deux mécanismes. Un mécanisme complètement concerté et maintenu par des temps de vie de moins de 10^{-13} s implique une interconversion directe de SH et R^-, sans intermédiaire. Un mécanisme pré-associé maintenu par des temps de vie de 10^{-11} à 10^{-12} s nécessite, lors de la fermeture du cycle, qu'un catalyseur acide forme une liaison hydrogène avec le groupement carbonyle de R^-.

[Traduit par la revue]

Structure–reactivity correlations have provided recent evidence (1–4) that the general acid-catalyzed breakdown of hemiacetals follows the class "e" mechanism (5) of eq. [1] while the general base-catalyzed breakdown follows the class "n" mechanism of eq. [2]. The overall reaction involves three

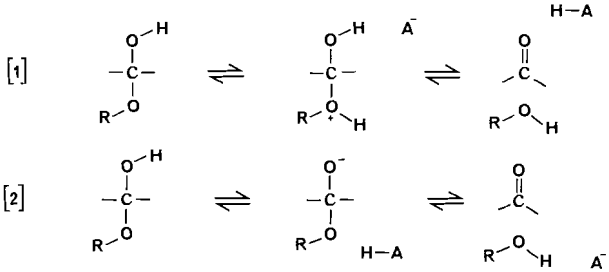

bonding changes, C—O bond breaking and two proton transfers, and in each of the two reactions one of the proton transfers is usually written coupled with the heavy atom reorganization. A simple explanation as to why the two reactions follow their particular courses is that in so doing they avoid a less stable intermediate, a protonated aldehyde in the case of the acid reaction and an alkoxide ion in the case of the base reaction.

We recently analyzed the base catalysis of the equilibration of the cyclic hemiacetal B (Ar = 4-methoxyphenyl) with its *cis*-chalcone isomer C (6). This system has a phenol leaving

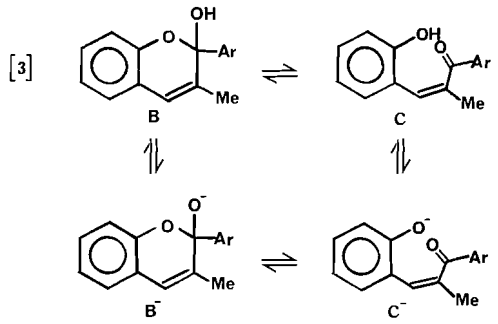

group and thus represents the situation where the anion derived from the leaving group is more stable. Indeed the evidence supported a different mechanism, one in which all three bonding changes were uncoupled and both the hemiacetal anion B^- and the phenolate anion C^- were formed as intermediates. Also of interest were the enormous rates associated with the interconversion of the two anions, ring opening of B^- to C^- for example having a rate constant of 10^9 s^{-1}. The lifetime of the hemiacetal anion is therefore extremely short, and one can imagine a situation with even more stable leaving anions where the lifetime might become so short that the hemiacetal anion could not exist. In this case the reaction would become two steps again, but now as a class "e" mechanism (eq. [4]).

In this paper we present kinetic results pertaining to the buffer

[4] 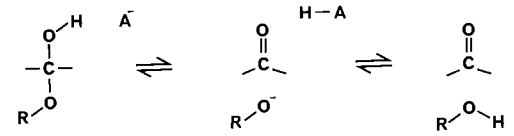

catalysis of the reversible ring opening of the hemiacylal 3-hydroxyphthalide, a system with a carboxylate leaving group. Although the equilibration in question is very rapid, it can be studied by the temperature-jump relaxation method (7). A previous study (7) has demonstrated buffer catalysis, but only two buffers, the substrate itself and HF, were investigated. In order to more fully establish mechanistic details we have now looked at a series of carboxylic acid and other oxyacid catalysts.

Experimental

o-Formylbenzoic acid (Aldrich) was recrystallized from water–benzene. Other materials were of Analar grade and were used without further purification. Phosphonic acids were the gifts of A. J. Kresge (8).

The equilibration was studied by use of the temperature-jump method, on a Messanlagen-Studiengesellschaft spectrophotometer. Solutions of the substrate ($(1–6) \times 10^{-4}$ *M*) were prepared in the appropriate buffer, the pH recorded, and the solution placed in the T-jump cell. The spectrophotometer was thermostatted at 21.5°C and a 3.5°C temperature jump applied. The relaxation was observed at 255 nm. The photomultiplier output was digitized (380 points per run), and the digital data transferred to an IBM 3033 computer (NEUCC, Copenhagen), where relaxation constants (τ^{-1}) were evaluated by least-squares fitting. Four to six kinetic runs were carried out for each solution.

Results and discussion

The system in question consists of three species (eq. [5]),

[5] 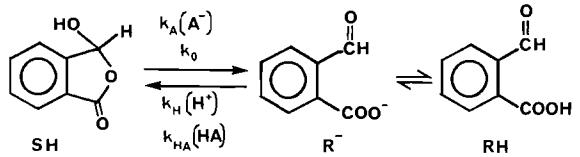

whose equilibrium relationships are known (7).

$$[6] \qquad \frac{[SH]}{[RH]} = K_0 = 14.8$$

$$[7] \qquad \frac{[R^-][H^+]}{[RH]} = K_{RH} = 10^{-3.36}\,M$$

$$[8] \qquad \frac{[R^-][H^+]}{[SH]} = \frac{K_{RH}}{K_o} = 10^{-4.55}\,M = \frac{k_0}{k_{H+}} = \frac{k_A K_{HA}}{k_{HA}}$$

Equilibration kinetics were investigated by the T-jump method (7), monitoring changes in absorbance at 255 nm due to the *o*-formylbenzoate ion. Relaxations were observed in a variety of oxyacid buffers; conditions and relaxation constants τ^{-1} are given as supplementary material (see Appendix, Table A1). Data for acetate buffers are plotted in Fig. 1.

Analysis is carried out through the mechanism of eq. [5], where ring opening of SH occurs with general base catalysis to give directly R^- (7). Bases involved are the solvent and the base component of the buffer. R^- itself can also function as a base, and its catalytic coefficient was determined in the previous study with unbuffered solutions (7). At the concentrations employed here, however, its contribution is small. A similar argument applies to hydroxide ion, another possible base catalyst. The assumption is made that simple proton transfers are fast on the time scale of the observed relaxation, so that

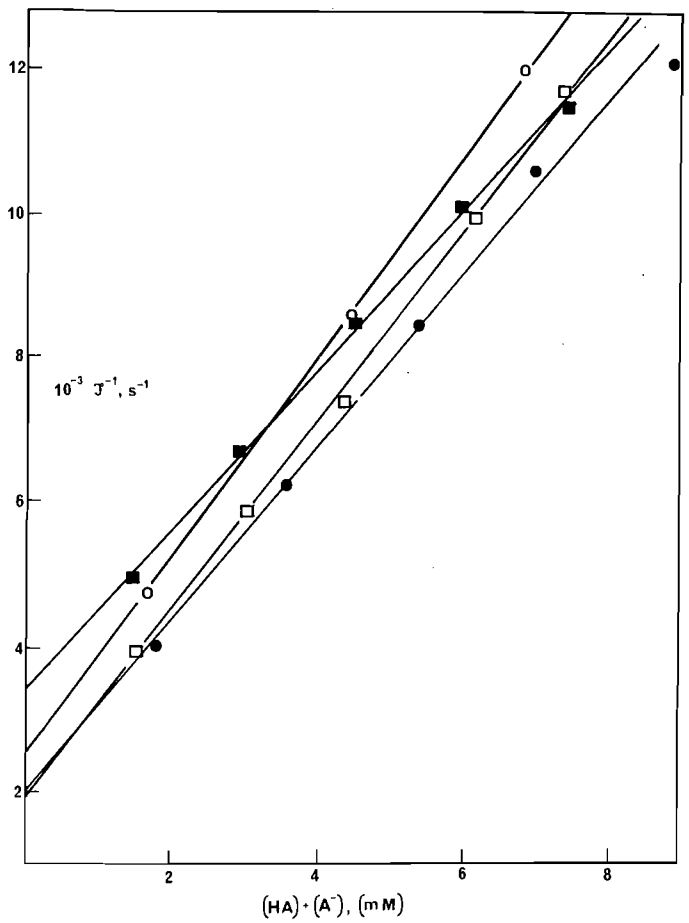

FIG. 1. Relaxation constants as a function of total buffer concentration in acetate buffers. (□), pH = 4.94, [S] = total substrate concentration = 0.155 m*M*; (○), pH = 4.50, [S] = 0.31 m*M*; (●), pH = 4.50, [S] = 0.155 m*M*; (■), pH = 4.22, [S] = 0.31 m*M*.

$$[9] \qquad K_{RH} = \frac{(\bar{H} + \delta_H)(\bar{R} + \delta_R)}{(\overline{RH} + \delta_{RH})}$$

$$[10] \qquad K_{HA} = \frac{(\bar{H} + \delta_H)(\bar{A} + \delta_A)}{(\overline{HA} + \delta_{HA})}$$

where $\bar{X}$ = concentration at equilibrium after the T-jump, δ_X = displacement from equilibrium at any time, and K_{HA} = dissociation constant of buffer. Noting that the following conditions apply: $\delta_{HA} + \delta_A = 0$, $\delta_{SH} + \delta_{RH} + \delta_R = 0$, and $\delta_R + \delta_A = \delta_H$, expressions can then be derived relating all displacements to δ_{SH}. The forward and reverse rate constants are also related (eq. [8]). The appropriate equation is then written for $d\delta_{SH}/dt$, and after some algebra, the following is obtained,

$$[11] \qquad \tau^{-1} = (k_0 + k_A[A^+])\left(1 + \frac{K_0([H^+] + [R^-]X)}{(K_{RH} + [H^+] + [R^-]X)}\right)$$

where $X = (K_{HA} + [H^+])/(K_{HA} + [H^+] + [A^-])$. We define the second term in brackets as C, and plot τ^{-1}/C versus $[A^-]$ (Fig. 2). The validity of this analysis is established by the observation of a common line for the various sets of relaxations obtained in acetate buffers. In addition, a common intercept (k_0)

TABLE 1. Catalytic constants for the general base-catalyzed ring opening of 3-hydroxyphthalide, general acid-catalyzed ring closing of 2-formylbenzoate

Catalyst (acid form)	pK_a	k_A, M^{-1} s^{-1}	k_{HA},[a] M^{-1} s^{-1}
1. H_3O^+	−1.74	19[b]	3.2×10^7[c]
		23[d]	2.5×10^7[d]
2. $CH_2ClCOOH$	2.76	5.0×10^4	2.3×10^6
3. RH	3.25	2.2×10^5[d]	3.3×10^6[d]
4. HF	3.02	1.4×10^5[d]	3.5×10^6[d]
5. $MeOCH_2COOH$	3.33	1.3×10^5	1.6×10^6
6. $Cl(CH_2)_2COOH$	3.95	3.8×10^5	1.12×10^6
7. $CCl_3PO_3H^-$	4.54	1.2×10^6	9.1×10^5
8. CH_3COOH	4.65	1.8×10^6	1.1×10^6
9. $CHCl_2PO_3H^-$	5.23	4.4×10^6	6.8×10^5
10. $(CH_3)_2AsO_2H$	6.11	5.1×10^7	1.04×10^6

[a] $k_{HA} = k_A K_{HA} K_0 / K_{RH}$.
[b] $k_0/55.5$.
[c] $k_{H_3O^+} = k_0 K_0 / K_{RH}$.
[d] From ref. 7.

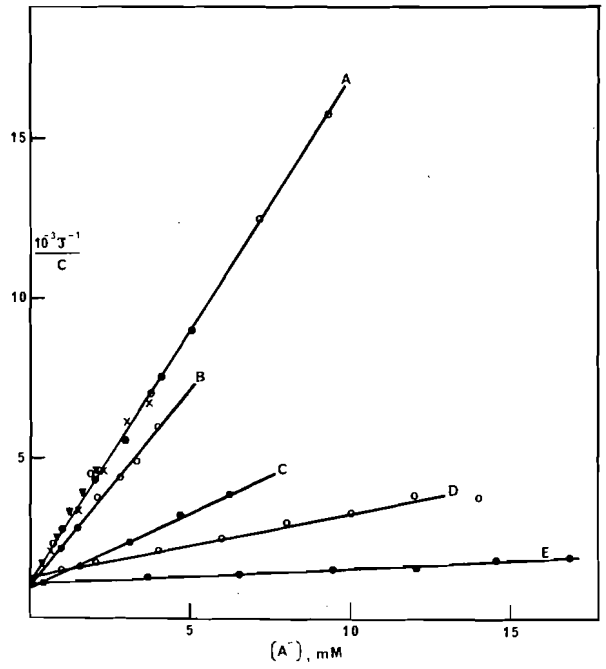

FIG. 2. Corrected relaxation constants (τ^{-1}/C) as a function of the concentration of the base component of the buffer. A: acetate, ●, pH 4.94, [S] = 0.155 mM; ○, pH = 4.50, [S] = 0.31 mM; X, pH = 4.50, [S] = 0.155 mM; ▼, pH = 4.22, [S] = 0.31 mM. B: trichloromethylphosphonate, pH = 4.45, [S] = 0.31 mM. D: methoxyacetate, pH = 4.04, [S] = 0.62 mM. E: chloroacetate, pH = 3.60, [S] = 0.62 mM.

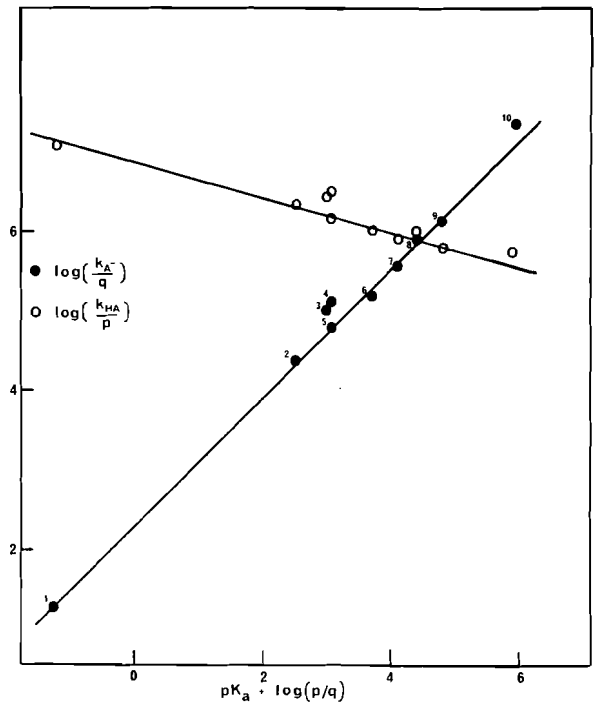

FIG. 3. Brønsted plots for the general base-catalyzed ring opening and microscopic reverse general acid-catalyzed ring closing of the equilibration 3-hydroxyphthalide ⇄ *o*-formylbenzoate. For catalysts see Table 1. Lines drawn are based on linear regression, excluding points 3, 4, and 10.

is found for the data in the different buffers. The slopes of the various lines provide the catalytic coefficients k_A. These and values of k_{HA} calculated using the relationship noted in eq. [8] are listed in Table 1.

Brønsted plots based on the catalytic coefficients are shown in Fig. 3. The cacodylic acid points deviate somewhat, as do the rates obtained previously (7) for HF/F^- and the substrate itself. Otherwise excellent linearity is observed, with the points for RPO_3H^-/RPO_3^{-2}, $RCOOH/RCO_2^-$, and H_3O^+/H_2O falling on a common line. The Brønsted β value for the base plot is 0.81 (correlation coefficient (cc) = 0.9996), ignoring the three deviating points, and shows an insignificant change (0.82, cc = 0.998) if the H_2O point is omitted. Considering all the data, β = 0.83 (cc = 0.994). The Brønsted α value is, as expected, 1−β or 0.19 (ignoring the three points). There is no apparent curvature in these plots. The base rates are becoming extremely fast with the stronger bases, and must soon plateau at the diffusion limit of $\approx 10^{10}$ M^{-1} s^{-1}. Hydroxide presumably would react with a rate constant near this limit, but its catalytic coefficient cannot be measured since at the acidity where the equilibration can be studied (pH 3.5–5) it cannot compete even with the solvent. (With $k_0 = 10^3$ s^{-1}, the value of k_{OH} would have to be 10^{12} M^{-1} s^{-1} or greater for the hydroxide reaction to be important at pH 5.)

In terms of a detailed mechanism we can note first that the class "n" mechanism of eq. [2] is highly improbable, since there

is no need to protonate the carboxylate leaving group. A second possibility is a step-wise mechanism with a discrete hemiacylal anion S^- as an intermediate and, in order to account for the general acid–base catalysis, the proton transfer step rate limiting. This situation will arise if the ring opening of S^- (k_3) occurs faster than its reprotonation, as has now been observed in two cases (6, 9) including that described by eq. [3]. This mechanism can also be rejected. It requires that the observed rate constants k_0 and k_A be equal to k_1 and k_2 of eq. [12],

[12] 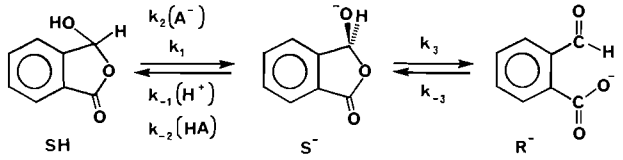

respectively. This, however, predicts a Brønsted β value of 1, since k_1 and k_2 represent proton transfers in the thermodynamically unfavorable direction. The observed β is significantly less than this. Moreover, the observed k_0, k_A values predict an acidity constant for SH ⇄ S^- + H^+ of 7–8 (as pK_{SH}) using the relationship $K_{SH} = k_1/k_{-1} = k_2K_{HA}/k_{-2}$, with k_{-1}, k_{-2} having values near 10^{10} M^{-1} s^{-1}. As discussed in the next paragraph, pK_{SH} is likely considerably greater.

Some idea of the magnitude of pK_{SH} is important for future considerations. A value of 12.3 has been obtained for the hemiacetal AH (10). *Ortho* carbonyl groups are acid strengthening towards a neighbouring carboxylic acid group, decreasing the dissociation constant by about one pK unit, as for example in phthalic acid or RH. Since ρ values for Ar-CRR′ (OH) are close to unity (11), the effect on an alcohol dissociation should be similar, and thus an initial estimate for pK_{SH} is 11.3. For two reasons this may underestimate the effect. Firstly, in SH there is additional inductive transmission through the ring oxygen (12). The magnitude of this effect is difficult to determine; current thinking is that inductive effects are relatively unimportant (12). A second and perhaps more significant effect is a polar one arising from the placement of a partial positive charge on the ring oxygen through its conjugation with the carbonyl. This effect is also difficult to estimate but it should also result in acid strengthening. Considering these uncertainties, we predict that pK_{SH} lies in the range 10.5–11.0.

A further important consideration is the rate constant expected for ring opening of the hemiacylal anion S^- (k_3 of eq. [12]). A rate constant (k_{op} of eq. [13]) of 6×10^5 s^{-1} can be calculated

[13] 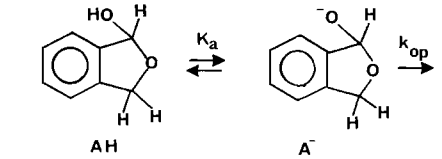

for the hemiacetal anion A^-. This is based upon an observed rate constant of 1.4×10^7 M^{-1} s^{-1} for hydroxide ion catalyzed opening of AH and the pK_a value of 12.3 (10), since $k_{OH} = k_{op}K_a/K_w$. For hydroxide ion catalyzed breakdown of formaldehyde hemiacetals (1) and acetaldehyde hemiacetals (14), β_{1g} values are −1.1 and −0.9, respectively. These contain a contribution from deprotonation of about −0.2 (1), so that β_{1g} values for hemiacetal anion breakdown are −0.9 and −0.7. Such values will obviously depend on the "push" due to the developing carbonyl, more stable carbonyls resulting in an earlier transition state and less negative β_{1g}. For example, for the tetrahedral intermediate $CH_3C(O^-)(SAr)(OAr)$ β_{1g} for aryloxide expulsion is only −0.3 (13). Acetaldehyde provides a better model for the carbonyl group in question here, although it can be noted that geometrical constraints are such that in the ring opening of S^- the developing carbonyl and benzene are not conjugated in the transition state so that the actual "push" may be more like that in a formaldehyde system. The pK_a of the carboxylic acid leaving group in S^- is 11 log units smaller than that of the benzyl alcohol in A^-. The two hemiacetal values then predict ring opening rate constants of 5×10^{15} s^{-1} (−0.9) and 3×10^{13} s^{-1} (−0.7). Both numbers are such that S^- could not exist (14). Considering that there is some uncertainty in β_{1g} and, perhaps more importantly, a rather lengthy extrapolation is involved, the actual number could be smaller. It is, however, difficult to see how it could be much less than 10^{11} s^{-1}.

[14] 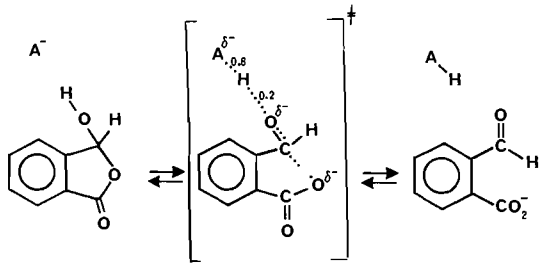

With these considerations two mechanisms can be proposed. One is fully concerted with proton transfer and CO bond making/breaking occurring at the same time, and with no intermediate between SH and R^-. For such a mechanism the position of the transition state with respect to proton transfer is defined by the Brønsted values. In the ring opening direction, proton transfer to the catalyzing base is 8/10 complete. A concerted mechanism would be "enforced" (14) by rate constants for S^- breakdown greater than 10^{13} s^{-1}.

The second possibility is a preassociation mechanism (14, 15). Viewed in the direction of the ring closure, the catalyzing acid is present in the rate-limiting C—O bond-forming step hydrogen bonded to the carbonyl oxygen, and is therefore available to convert the hemiacylal anion into neutral hemiacylal as soon as the anion is formed. This mechanism would also be "enforced", this time by rate constants for S^- breakdown in the range 10^{11}–10^{12} s^{-1}, such that ring opening occurs before diffusional separation. Such a mechanism does fit with the Brønsted data. Previous examples have had α values near 0.15 (13), attributable to a small stabilization of the transition state with increased acidity because of the hydrogen bonding to the developing negative charge.

It is also instructive to consider what the last mechanism requires to explain the observed rate constants. The equilibrium constant $[S^-]/[R^-]$ is equal to $K_{SH}K_0K_{RH}$, and a value of 10^{-6}–10^{-7} is calculated with the known K_0 and K_{RH} and the K_{SH} estimate noted previously. The equilibrium in eq. [15] involves hydrogen bonded anions ($[S^- \ldots HA]/[R^- \ldots HA]$) and will be more favorable towards the stronger base S^-. It seems unlikely, however, that the equilibrium constant can be greater than 10^{-5}. The rate constant k_{-4} cannot be greater than 10^{12} s^{-1}, or otherwise $S^- \ldots$ HA would not exist. Coupling this with the equilibrium constant, k_4 must be less than 10^7. For this mechanism the observed k_{HA} is equal to $K_{as}k_4$, and thus even for the weakest acid, cacodylic acid ($k_{HA} = 1 \times 10^6$ M^{-1} s^{-1}, K_{as} must be greater than 0.1 M^{-1}. Hydrogen bonding association constants for aldehydes are unknown, but since they are weakly basic, it seems unlikely that the value can be much larger than this. The more basic formate ion associates with its conjugate acid $(HCOOH{\cdot}OOCH)^-$, and even here K_{as} is only 0.25 M^{-1}

[15] 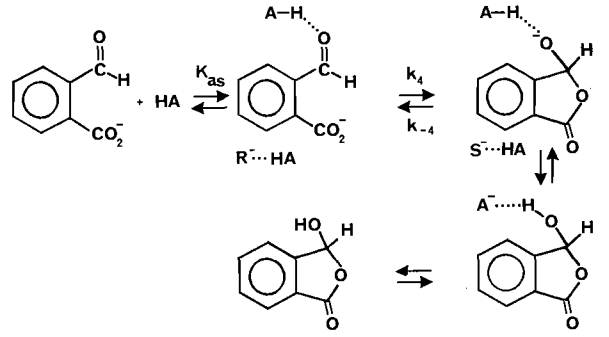

(16). A value of 1/55.5 or 0.02 would pertain to a situation with random encounter.

[16] 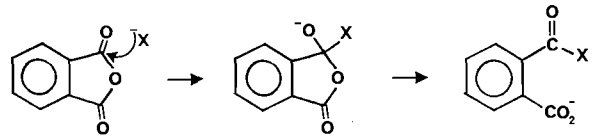

In summary, both the S^- life-time estimate and the requirements for k_4, K_{as} in the preassociation mechanism provide some support for a fully concerted mechanism. However, the uncertainties in the various analyses are such that preassociation cannot be rigorously excluded. The lifetime of S^-, however, must be extremely short, and whichever is the mechanism, it is different from those previously observed. Finally, it can be noted that an anion like S^- is the tetrahedral intermediate of a nucleophilic substitution of a phthalic anhydride. (If $X^- = H^-$, the intermediate is S^-.) If this anion has a lifetime such that it cannot exist, it is not an intermediate but has been transformed into a transition state for a concerted reaction.

Acknowledgements

The financial support of the Natural Sciences and Engineering Research Council of Canada is gratefully acknowledged. We wish to also thank Statens Naturvidenskabelige Forskningsraad for an equipment grant.

1. L. H. Funderburk, L. Aldwin, and W. P. Jencks. J. Am. Chem. Soc. **100**, 5444 (1978).
2. R. A. McClelland and M. Coe. J. Am. Chem. Soc. **105**, 2719 (1983).
3. E. Grunwald. J. Am. Chem. Soc. **107**, 4710 (1985); **107**, 4715 (1985).
4. P. E. Sørensen and W. P. Jencks. J. Am. Chem. Soc. Submitted.
5. W. P. Jencks. Acc. Chem. Res. **9**, 425 (1976).
6. R. A. McClelland, D. B. Devine, and P. E. Sørensen. J. Am. Chem. Soc. **107**, 5459 (1985).
7. R. P. Bell, B. G. Cox, and B. A. Timimi. J. Chem. Soc. B, 2247 (1971).
8. A. J. Kresge and Y. Chiang. J. Am. Chem. Soc. **95**, 803 (1975).
9. R. A. McClelland. J. Am. Chem. Soc. **106**, 7579 (1984).
10. J. Harron, R. A. McClelland, C. Thankachan, and T. T. Tidwell. J. Org. Chem. **46**, 903 (1981).
11. R. Stewart and R. Van der Linden. Can. J. Chem. **38**, 400 (1960).
12. J. Hine. Structural effects on equilibria in organic chemistry. John Wiley and Sons, New York. 1975. p. 40.
13. D. J. Hupe and W. P. Jencks. J. Am. Chem. Soc. **99**, 451 (1977).
14. W. P. Jencks. Acc. Chem. Res. **13**, 161 (1980).
15. M. M. Cox and W. P. Jencks. J. Am. Chem. Soc. **103**, 572 (1981), and references therein.
16. E. S. Hand and W. P. Jencks. J. Am. Chem. Soc. **97**, 6221 (1975).

Appendix

TABLE A1. Relaxation constants τ^{-1} (s^{-1}), 25°C, ionic strength = 0.2

Buffer base[a]	Buffer acid[b]	Total substrate[c]	pH[d]	$10^{-3}\tau^{-1}$
		Acetic acid		
5.00	2.50	0.155	4.95	11.8 ± 0.5[e]
4.10	2.05	0.155	4.95	10.0 ± 0.9
3.10	1.50	0.155	4.94	7.4 ± 0.7
2.00	1.00	0.155	4.94	5.9 ± 0.3
1.10	0.50	0.155	4.94	3.9 ± 0.4
5.63	7.88	0.310	4.50	22.9 ± 1.9
3.70	5.22	0.310	4.51	12.9 ± 0.8
1.88	2.63	0.310	4.50	8.6 ± 0.3
0.75	1.05	0.310	4.51	4.7 ± 0.3
3.70	5.22	0.155	4.51	12.1 ± 0.7
2.96	4.18	0.155	4.50	11.3 ± 0.9
2.22	3.13	0.155	4.50	8.4 ± 1.2
1.48	2.09	0.155	4.50	6.2 ± 0.5
0.74	1.04	0.155	4.51	4.0 ± 0.3
2.00	5.50	0.310	4.23	11.5 ± 0.6
1.60	4.40	0.310	4.22	10.1 ± 0.3
1.20	3.30	0.310	4.22	8.7 ± 0.8
0.80	2.20	0.310	4.23	6.7 ± 0.4
0.40	1.10	0.310	4.21	4.9 ± 0.2
		3-Chloropropionic acid		
7.60	3.80	0.310	4.26	11.1 ± 0.7
6.20	3.12	0.310	4.25	9.4 ± 0.5
4.65	2.34	0.310	4.26	7.8 ± 0.7
3.10	1.56	0.310	4.27	5.8 ± 0.3
1.55	0.78	0.310	4.27	4.0 ± 0.2
		Methoxyacetic acid		
32.0	6.4	0.620	4.03	16.3 ± 0.5
28.0	5.6	0.620	4.04	14.8 ± 0.7
23.6	4.7	0.620	4.03	13.3 ± 1.0
20.0	3.9	0.620	4.04	11.9 ± 0.5
16.1	3.1	0.620	4.05	10.6 ± 0.3
12.1	2.3	0.620	4.07	9.3 ± 0.6
8.2	1.4	0.620	4.09	7.8 ± 0.4
		Chloroacetic acid		
16.80	2.70	0.620	3.56	11.6 ± 0.5
14.50	2.20	0.620	3.57	10.6 ± 0.7
12.10	1.80	0.620	3.59	9.3 ± 0.3
9.46	1.24	0.620	3.64	8.5 ± 0.3
6.61	0.88	0.620	3.64	7.5 ± 0.7
3.77	0.51	0.620	3.63	7.5 ± 0.1
		Cacodylic acid		
1.00	22.0	0.310	4.77	77.9 ± 0.7
0.40	8.0	0.310	4.76	39.3 ± 4.0
0.30	6.6	0.310	4.76	26.6 ± 5.0
0.20	4.4	0.310	4.75	21.4 ± 3.6
0.10	2.2	0.310	4.75	10.2 ± 1.1
		$CHCl_2PO_3H^-$		
1.20	12.2	0.620	4.22	19.3 ± 0.9
1.00	9.7	0.620	4.24	15.2 ± 0.9
0.80	7.7	0.620	4.27	11.5 ± 0.8
0.60	4.9	0.620	4.31	0.5 ± 0.5
		$CCl_3PO_3^-$		
3.96	4.90	0.620	4.44	12.3 ± 0.7
3.32	4.31	0.620	4.43	10.1 ± 0.4
2.78	3.51	0.620	4.44	9.1 ± 0.3
2.03	2.46	0.620	4.46	8.0 ± 0.2
1.44	1.68	0.620	4.48	5.9 ± 0.2
0.87	0.924	0.620	4.52	5.1 ± 0.5

[a]Millimolar concentration of base component of buffer.
[b]Millimolar concentration of acid component of buffer.
[c]Millimolar concentration of total substrate (R^- + RH + SH).
[d]Measured pH.
[e]Standard deviation of 4–5 determinations.

Chlorine isotope effects in the solvolysis of substituted 1-phenylethyl chlorides

DUNCAN J. MCLENNAN, ALLAN R. STEIN,[1] AND BRIAN DOBSON
Department of Chemistry, University of Auckland, Auckland, New Zealand
Received October 21, 1985

This paper is dedicated to Professor Arthur N. Bourns

D. J. MCLENNAN, A. R. STEIN, and B. DOBSON. Can. J. Chem. **64**, 1201 (1986).

Kinetic chlorine isotope effects attending the solvolysis of several ring-substituted 1-phenylethyl chlorides in alcohol–water solvent mixtures are reported. The k_{35}/k_{37} values are insensitive to the identity of ring substituents and to solvent composition. Results are interpreted in terms of an S_N1 heterolytic process incorporating a significant amount of internal return. Theoretical calculations suggest that the incipient chloride ion in the transition state may be strongly hydrogen-bonded.

D. J. MCLENNAN, A. R. STEIN et B. DOBSON. Can. J. Chem. **64**, 1201 (1986).

On a mesuré les effets isotopiques cinétiques du chlore qui accompagnent les solvolyses de plusieurs chlorures de phényl-1 éthyle substitués sur le cycle. Les valeurs de k_{35}/k_{37} sont insensibles à la nature des substituants sur le cycle ainsi qu'à la composition du solvant. On interprète les résultats en fonction d'un processus hétérolytique S_N1 incorporant une part importante de retour interne. Des calcultes théoriques suggèrent que l'ion chlorure qui attaque dans l'état de transition pourrait être fortement lié par des liaisons hydrogènes.

[Traduit par la revue]

Introduction

Much insight into the nature of S_N1 solvolysis has come from studies on 1-phenylethyl halides. Kinetic (1), stereochemical (2), secondary α- and β-deuterium isotope effect (3, 4), and carbon isotope effect (5–8) studies have been reported. Recent work has focussed on the generation and the fate of substituted 1-phenylethyl cations in solution as a function of their lifetimes (9–11).

Leaving group kinetic isotope effects have not been as widely exploited in solvolysis reactions as in other systems. Chlorine isotope effects in the solvolysis of *tert*-butyl chloride (12) and substituted benzyl chlorides (13), and sulfur isotope effects in the solvolysis of the *tert*-butyldimethylsulfonium (14) and benzyldimethylsulfonium (15) cations appear to be the only available examples. In view of our interests in the reactions of 1-phenylethyl derivatives (16–18), in chlorine isotope effects (19, 20), and in isotope effects in general solvolytic processes (21, 22), we decided to measure chlorine isotope effects in the solvolysis of ring-substituted 1-phenylethyl chlorides.

Results

The reactions exemplified by reaction [1] were investigated.

[1] $$\mathrm{Ar{-}\underset{\displaystyle CH_3}{\underset{|}{CH}}{-}Cl + SOH \rightarrow Ar{-}\underset{\displaystyle CH_3}{\underset{|}{CH}}{-}OS + H^+ + Cl^-}$$

Ar = 3,4-$Me_2C_6H_3$, 4-MeC_6H_4, C_6H_5, 4-BrC_6H_4 S = H, Et, CF_3CH_2

Previous investigations have shown that styrene formation is never greater than 3% (3, 5, 18); hence it was neglected. Chloride ion released after partial and complete reaction was quantitatively converted to methyl chloride, and the $^{35}Cl/^{37}Cl$ ratio was assessed in the usual way using an isotope ratio mass spectrometer. Results obtained are shown in Table 1 (for EtOH–H_2O solvents) and Table 2 (for 97% TFE – H_2O solvent). Comment on the accuracy and reproducibility of the isotope effects is in order. The sample 52/50 mass ratios, R, and those for the standard methyl chloride, R_0, are commonly expressed as δ values via eq. [2]. As calculated by repetitive

[2] $$\delta = 1000(R/R_0 - 1)$$

sample/reference comparisons on a single gas sample, δ values were as constant as those previously reported from our laboratory, and varied by no more than 0.5% (19, 20). However, day-to-day variations in δ for the same sample of methyl chloride were of the order of ±2–3%, when compared with the same reference gas. Variations of this nature are not unusual (15) and, so as far as was possible, partial reaction samples and infinity samples were analysed on the same day. Furthermore, samples of methyl chloride independently prepared from the same original sample of AgCl and analysed on different days exhibited variations in δ of up to ±5%, whereas in our previous studies (19, 20), these variations were no greater than ±1%. Limited access to the mass spectrometer precluded a systematic and detailed examination of reasons for this loss of reproducibility under conditions of apparently equal precision.

Constraints of access prevented our analysing all partial reaction and infinity samples of methyl chloride on the same day. Since all infinities were generated from the same sample of 1-arylethyl chloride, it seemed in order to use a mean value obtained from measurements on different days, since δ_∞ values showed no temporal trend. To illustrate the effect of this we recalculated the results for 1-phenylethyl chloride itself, using the individual δ values from Table 1 and mean of the six δ_∞ values, which themselves were calculated from 17 separate 6-fold cycles (see Experimental). In Table 3 we show that the ultimate effect on k_{35}/k_{37} is almost inconsequential. We therefore estimate that the k_{35}/k_{37} values in Tables 1 and 2 are uncertain to the extent of around ±0.0005, which is some ten times the uncertainty established in our earlier work. For this reason we were unable to detect any real variation in k_{35}/k_{37} as (*i*) ring substituents, (*ii*) solvent compositions in EtOH–H_2O, and (*iii*) temperatures, were varied. Within 95% confidence limits, there is no substrate or solvent variation of k_{35}/k_{37}. The same applies to reactions in TFE–H_2O (Table 2) but, when

[1]On leave from the Department of Chemistry, Memorial University of Newfoundland, St. John's, Nfld, Canada A1B 3X7.

Printed in Canada / Imprimé au Canada

TABLE 1. Chlorine isotope effects in the solvolysis of $ArCH(CH_3)Cl$ compounds in ethanol–water solvent mixtures

Ar	Vol % EtOH	T (°C)	δ^a	$\delta_\infty{}^a$	f^b	k_{35}/k_{37}
$3,4\text{-}Me_2C_6H_3$	95	25	−17.66±0.05	−10.62±0.51	0.226	1.0082
$3,4\text{-}Me_2C_6H_3$	90	0	−17.32±0.24	−10.64±0.39	0.141	1.0073
$3,4\text{-}Me_2C_6H_3$	80	0	−17.55±0.01	−10.62±0.51	0.169	1.0078
$3,4\text{-}Me_2C_6H_3$	70	0	−17.54±0.24	−10.62±0.51	0.132	1.0076
$4\text{-}MeC_6H_4$	95	25	−17.83±0.35	−11.71±0.32	0.359	1.0078
$4\text{-}MeC_6H_4$	90	25	−18.99±0.33	−12.41±0.13	0.329	1.0082
$4\text{-}MeC_6H_4$	80	25	−17.88±0.03	−12.41±0.13	0.416	1.0074
$4\text{-}MeC_6H_4$	70	25	−18.05±0.01	−12.41±0.13	0.424	1.0077
$4\text{-}MeC_6H_4$	70	0	−19.58±0.26	−12.41±0.13	0.231	1.0084
$4\text{-}MeC_6H_4$	50	0	−18.23±0.49	−11.71±0.32	0.223	1.0076
C_6H_5	95	50	−13.38±0.13	−8.91±0.28	0.675	1.0084
C_6H_5	90	50	−15.47±0.40	−9.31±0.22	0.368	1.0079
C_6H_5	80	50	−15.19±0.63	−9.26±0.04	0.422	1.0080
C_6H_5	80	25	−15.36±0.49	−9.20±0.02	0.411	1.0083
C_6H_5	70	25	−15.90±0.30	−9.27±0.17	0.356	1.0085
C_6H_5	50	25	−15.81±0.35	−9.75±0.01	0.318	1.0076
$4\text{-}BrC_6H_4$	95	50	−12.73±0.10	−5.84±0.46	0.314	1.0085
$4\text{-}BrC_6H_4$	90	50	−11.52±0.35	−5.84±0.46	0.475	1.0081
$4\text{-}BrC_6H_4$	80	50	−11.83±0.21	−5.84±0.46	0.367	1.0077
$4\text{-}BrC_6H_4$	70	50	−9.49±0.08	−5.43±0.01	0.672	1.0075
$4\text{-}BrC_6H_4$	50	50	−11.30±0.06	−5.68±0.16	0.406	1.0075

[a]See text for explanation of uncertainties.
[b]Fraction of reaction at which δ value was measured.

TABLE 2. Chlorine isotope effects in the solvolysis of $ArCH(CH_3)Cl$ compounds in 97% (w/w) trifluoroethanol–water solvent[a]

Ar	T (°C)	δ	$\delta_\infty{}^a$	f	k_{35}/k_{37}
$3,4\text{-}Me_2C_6H_3$	−23	−13.66±0.28	−10.71±0.02	0.686	1.0056
$4\text{-}MeC_6H_4$	−23	−16.31±0.27	−12.41±0.13	0.514	1.0058
$C_6H_5{}^a$	25	−12.70±0.02	−10.39±0.03	0.690	1.0045
$C_6H_5{}^a$	25	−14.53±0.17	−10.39±0.03	0.422	1.0056
$4\text{-}BrC_6H_4$	25	−10.72±0.05	−5.43±0.01	0.277	1.0063

[a]These represent completely independent solvolyses. A common δ_∞ only was used to calculate k_{35}/k_{37}.

standard deviations are taken into account, k_{35}/k_{37} is significantly larger for the EtOH–H_2O solvent system than for reactions conducted in TFE–H_2O.

Discussion

Transition state variation

If all solvolyses are k_C processes, represented by reaction [3]

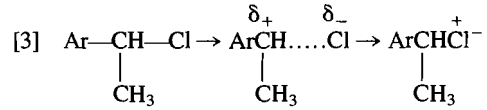

as the rate-limiting step, then the results suggest that neither ring substituents nor solvent composition (in EtOH–H_2O) affect the degree of bond-breaking and charge development in the transition state (TS). Both ρ^+ (3) and Grunwald–Winstein m values (23) are numerically large for the 1-phenylethyl halide solvolysis system, suggesting that bond rupture and charge transfer are well advanced at the TS. Theory decrees that if simple carbon–chlorine stretching comprises the reaction coordinate the TS should become more reactant-like as electron-donating groups stabilize the carbocationic portion of the ion pair (24, 25) and if such a variation is significant the chlorine isotope effect should become smaller (20, 26, 27). It does not.[2]

Similarly, if C—Cl heterolysis is nucleophilically solvent-assisted (S_N2-like ion pair formation) the same should apply (24, 28). We are therefore left with the alternatives that either the theory is wrong, or that the mechanism is more complex than has been supposed.

Two earlier reports concur. Hill and Fry (13) find that k_{35}/k_{37} for solvolyses in the $ArCH_2Cl$ system is substituent-insensitive. Friedburger and Thornton find the same pattern for sulfur isotope effects in the hydrolysis of $ArCH_2SMe_2^+$ ions. The latter authors have made a detailed enquiry into mechanistic alternatives, and have somewhat tentatively suggested that S_N2 water attack, with TS insensitivity in the tight–loose dimension to substituent changes, may cause constant leaving-group isotope effects. They dismiss the possibility of rate-limiting water

[2]The relationship between chlorine isotope effects and transition state structure in bimolecular S_N2 reactions has recently been examined in detail. See ref. 46. It is not yet certain that all their conclusions can be extrapolated to solvolytic S_N1 reactions, and some of the present results suggest that there may be some differences.

TABLE 3. Chlorine isotope effects in the solvolysis of $C_6H_5CH(CH_3)Cl$ compounds in ethanol–water solvent mixtures, based on a mean δ_∞[a]

Vol % EtOH	T (°C)	δ	δ_∞[a]	f	k_{35}/k_{37}
95	50	−13.38±0.13	−9.28±0.16	0.675	1.0078
90	50	−15.47±0.40	−9.28±0.16	0.368	1.0080
80	50	−15.19±0.63	−9.28±0.16	0.422	1.0080
80	25	−15.36±0.49	−9.28±0.16	0.411	1.0079
70	25	−15.90±0.30	−9.28±0.16	0.356	1.0085
50	25	−15.81±0.35	−9.28±0.16	0.318	1.0081

[a]See footnotes to Table 1.

attack on a preformed ion–molecule pair (29). This may indeed be the case for a primary benzylic system, but we will show later that an S_N2 explanation is untenable for our secondary substrates. We recognise that the primary vs. secondary comparison is not in itself sufficient reason to reject nucleophilic solvent assistance to ion pair formation in our system (30).

The suggestion that TS structure (whatever it may be) is insensitive both to substituent and to solvent polarity (EtOH and H_2O have similar nucleophilicities (31)) has a parallel in findings on solvolysis of benzhydryl *p*-nitrobenzoates (32). However, the latter results were eventually interpreted in terms of a multistep mechanism, to which we will later return. In the meantime we recall the rejection by Jencks and Richard (32) of a significant degree of nucleophilic solvent assistance in the solvolysis of mildly activated 1-arylethyl chlorides.

It is of interest to note that the chlorine isotope effect is significantly lower when TFE–H_2O is the solvent (compare Tables 1 and 2). Trifluoroethanol is more electrophilic than EtOH and H_2O (33) and so will hydrogen bond more strongly to an incipient chloride ion in the TS than will the latter. If the degree of negative change development on chlorine is about the same in both solvent systems (and this does not necessarily mean that the solvolysis mechanisms need be identical) one would expect that k_{35}/k_{37} would be diminished by increasingly strong solvent coordination (26, 27). An alternative viewpoint is that the TS is earlier in the "faster" TFE–H_2O solvent, but there is no independent evidence for this. Calculations in the following section and others already reported (26) show that solvent coordination is necessary to obtain reasonable theoretical k_{35}/k_{37} values in the first place, and so an explanation based on relative electrophilicities would appear to be more reasonable.

Model calculations of chlorine isotope effects

Model calculations based on assumed TS structures and force constants for an ionization (k_C) model have been performed in an effort to understand the pattern of chlorine isotope effects. The basic model was as described for *iso*propyl chloride solvolysis (22) except that a point mass of 27 amu replaced a methyl group, and effectively simulated a phenyl group. The possibility that the positive charge on C_α in the TS is not fully delocalized by the phenyl group was simulated by assuming that the charge, equal to $1 - n_1$ in the *i*-PrCl case (22) where n_1 is the C_α....Cl TS bond order, could be replaced by $F(1 - n_1)$, where F is the fraction of charge not delocalized by the phenyl. The phenyl–C_α bond order then becomes $1 + (1 - F)(1 - n_1)$, which simulates partial double bond character for $F \neq 1.0$. Nucleophilic participation by π electrons in 1-phenylethyl halide solvolysis was first proposed by Bourns and Stothers (5) to explain an anomalously low carbon isotope effect, and the idea has re-emerged in more recent isotope effect calculations (34).

In order to obtain chlorine isotope effects of reasonable magnitude, it was necessary to simulate solvation of the incipent chloride ion in the TS, and this was done following the format established for *tert*-butyl chloride isotope effects (27). Three tetrahedrally-disposed HO groups were placed in proximity to the chlorine. The Cl....HO bond was assigned bond orders in the range $0.05(1 - n_1)$ to $0.3(1 - n_1)$, which are somewhat larger than those orginally specified (27, 35).

The reaction coordinate motion for the simple k_C model was visualized as chloride transfer from C_α to the solvent hydrogens:

$$\overset{\qquad f_{11} \qquad f_{22}}{C_\alpha \cdots\cdots Cl \cdots\cdots (HO)_3}$$
$$\leftarrow \qquad \rightarrow \qquad \leftarrow$$

by appropriate formulation of an off-diagonal force constant f_{12} based on the diagonal constants f_{11} and f_{22} (36). A solvent-assistance model was also used, similar to that employed for *i*-PrCl (22). Here the nucleophilic H_2O was viewed either as an entering nucleophile so that O....C_α shortening accompanied C_α....Cl stretching in the TS, or as a solvating spectator. Similar results were obtained for both cases and, since only weak solvent assistance was simulated ($n_{OC} < 0.2$), the inclusion of assistance had little effect on the calculated values of k_{35}/k_{37}. Values of α-k_H/k_D, β-k_{CH_3}/k_{CD_3}, and k_{12}/k_{13} for the central carbon were calculated as well. Details and results will be presented in a forthcoming publication.

It is necessary only to contrast two extreme cases for k_{35}/k_{37}. The first line of Table 4 shows the dependence of k_{35}/k_{37} on n_1 as the TS structure is changed from reactant-like to product-like in a case where (*i*) the choice of parameters for formulation of f_{12} keeps $\nu_L^\pm$, the reaction coordinate frequencies, at low absolute values and (*ii*) only weak hydrogen bonding of the chlorine is similated. The k_{35}/k_{37} values are seen to increase as the TS C_α....Cl bond is made weaker, as expected (20, 22, 26, 27). The second line refers to a case where (*i*) higher absolute values of $\nu_L^\pm$, corresponding to higher barrier curvature, are generated and (*ii*) stronger hydrogen bonding of the chlorine is simulated. The k_{35}/k_{37} values now pass through a flat maximum. Between n_1 values of 0.7 and 0.1 k_{35}/k_{37} is almost constant.

This is then the chlorine analogue of the Westheimer–Melander maximum for proton transfer (37). This is the first theoretical report of such a phenomenon for a leaving group isotope effect; maximal carbon isotope effects in S_N2 alkyl transfers have already been experimentally (38) and theoretically (39) described. It provides a rationale of our results within the framework of substituent-induced TS variation according to the

TABLE 4. Calculated chlorine isotope effects at 25.0°C for two TS models for the unassisted solvolysis of 1-phenylethyl chloride

	k_{35}/k_{37} for n_1 =					
	0.9	0.7	0.5	0.3	0.1	0.05
Model 1[a]	1.00519	1.00870	1.01111	1.01300	1.01494	—
Model 2[b]	1.00841	1.00968	1.00985	1.00982	1.00981	1.00889

[a] $F = 1.00$, average $\nu_L^{\ddagger}$ 200i cm^{-1}, Cl....HO bond order 0.1 $(1 - n_1)$.
[b] $F = 1.00$, average $\nu_L^{\ddagger}$ 365i cm^{-1}, Cl....HO bond order 0.3 $(1 - n_1)$. Note that k_{35}/k_{37} is relatively insensitive to the value chosen for F over the range 1.00–0.4.

rules (24, 25, 28). The effect of strengthening the hydrogen bonds to chlorine is to lower k_{35}/k_{37} overall; this provides a rationale for the lower isotope effects observed for solvolysis in the more electrophilic TFE–H_2O solvent (Tables 1 and 2). The model also yields values of α-k_H/k_D and β-k_{CH_3}/k_{CD_3} in reasonable agreement with experiment (3). Yet it may well be wrong, for two reasons.

Firstly, the degree of hydrogen bonding needed to generate a maximum without resorting to reaction coordinate formulations which generate unrealistically high absolute values of $\nu_L^{\ddagger}$ is unreasonably high. It is in fact higher than the amount of hydrogen bonding (in bond order terms) estimated for a fully-developed, solvated chloride ion (26, 35).

Secondly, the model fails to reproduce the low carbon isotope effect reported by Bourns and Stothers (5) and the anomalous temperature dependence of this isotope effect reported by Bron and Stothers (7, 8), even when small values of F are employed.

Admittedly, the experimental work pertains to 1-phenylethyl bromide solvolysis, but model calculations on the bromide also yielded larger carbon isotope effects having a normal temperature dependence. We must therefore reject the simple k_C and solvent-assistance models despite the attraction of their reproducing the observed patterns of k_{35}/k_{37} behaviour.

We also note that while theory predicts the possibility of obtaining a maximum in k_{35}/k_{37} as TS symmetry is varied, the impractical parameters needed to force this result mean that experimental demonstration of this effect is unlikely.

Isotope effects in multistep mechanisms

Apparent lack of reactivity-selectivity behaviour in the benzhydryl-*p*-nitrobenzoate reaction series was explained in terms of a multistep mechanism in which opposing effects cancelled (40). We adopt the same approach here in following a treatment proposed by Murr and Donnelly (41). Assume that a stepwise mechanism of minimal complexity can be represented by reaction [4]. If intimate ion pair **2** partitions between internal

$$[4]\quad \underset{\mathbf{1}}{RCl} \underset{k_{-1}}{\overset{k_1}{\rightleftharpoons}} \underset{\mathbf{2}}{R^+Cl^-} \underset{k_{-2}}{\overset{k_2}{\rightleftharpoons}} \underset{\mathbf{3}}{R^+ \parallel Cl^-} \xrightarrow[SOH]{k_3} ROS$$

return to **1** and irreversible dissociation to loose ion pair **3**, such that $k_3 \gg k_{-2}$, then the observed chlorine isotope effect is given by eqs. [5] and [6] (41). In these, k_1^{35}/k_1^{37} is the

$$[5]\quad k_{obs}^{35}/k_{obs}^{37} = (k_1^{35}/k_1^{37})(F_2^{35}/F_2^{37})$$

$$[6]\quad F_2^{35}/F_2^{37} = \frac{(k_2^{35}/k_{-1}^{35}) + (k_{-1}^{37}/k_2^{37})/(k_{-1}^{35}/k_2^{35})}{1 + (k_2^{35}/k_{-1}^{35})}$$

ionization isotope effect to which the models in the previous section pertained, and F_2^{35}/F_2^{37} is the partitioning isotope effect for partitioning of **2**. Thus *two* transition states need to be considered: TS(**1** → **2**) for ionization and TS(**2** → **3**) for ion pair interchange. The carbon–chlorine bond should become progressively looser as one proceeds from **1** to **3**.

The introduction of electron-donating substituents into the ring should cause k_1^{35}/k_1^{37} to decrease as TS(**1** → **2**) becomes more reactant-like if theory is correct, and if the more normal of the two models of Table 3 applies. On the other hand, k_2^{35}/k_2^{37} (which should be greater than unity (41)) may well increase in compensation, and the following reason can be advanced. Electron donation will stabilize the carbocationic portion of ion pair **2**, which should increase its selectivity. A stereochemical study suggests that k_2/k_{-1} is less than unity for the unsubstituted ion pair (2*d*) so k_2^{35}/k_{-1}^{35} could decrease further as electron donation renders the ion pair more selective (40). If then the second term in the numerator of eq. [6] is relatively insensitive to ion pair stability, being the quotient of isotope effects for the k_2 and k_{-1} steps, it is easily shown that F_2^{35}/F_2^{37} increases as k_2^{35}/k_{-1}^{35} decreases. Thus the compensating effect sought in eq. [5] can be realised. It is therefore possible that $k_{obs}^{35}/k_{obs}^{37}$ is insensitive to substituents even though chlorine isotope effects on the individual k_1, k_{-1}, and k_2 steps are sensitive because of substituent-induced changes in the character of TS(**1** → **2**) and TS(**2** → **3**).

This argument, insofar as it relates only to $k_{obs}^{35}/k_{obs}^{37}$, is speculative. However, similar considerations based on the same partitioning mechanism allow quantitative rationalization of α-k_H/k_D, β-k_{CH_3}/k_{CD_3}, and both k_{12}/k_{13} and its abnormal temperature dependence, as a forthcoming publication will reveal. A necessary condition is that K_1^{12}/K_1^{13} ($K_1 = k_1/k_{-1}$), the equilibrium carbon isotope effect for **1** ⇌ **2**, is less than unity, and this can be achieved either by using values of F less than unity (nucleophilic donation of π electrons to C_α of the carbocation as originally proposed by Bourns and Stothers (6)), or by nucleophilically solvating the carbocation (the S_N2 (int) mechanism (31)), or both. Thus the present results support the mechanistic arguments advanced by Shiner and co-workers on isotope effect (3) and stereochemical (2*d*) grounds in emphasizing the necessity for an element of internal return in 1-phenylethyl halide solvolysis. We note that competitive internal return is not incompatible with weak nucleophilic solvent assistance (42), nor alternatively with the presence of a pre-associating solvent molecule as a spectator (32).

It must also be mentioned that isotope effect anomalies frequently arise in multistep reactions where no single step is clearly rate-limiting. The present case thus complements a recently reported example from the elimination field, where internal return in a hydrogen-bonded carbanion gives rise to unusual chlorine isotope effects (20). On the other hand, stereochemical results for 1-arylethyl tosylate solvolysis in a variety of solvents have been interpreted in terms of an ion pair

mechanism where one step is clearly rate-limiting in a given solvent (43). It would be interesting to see if the primary carbon isotope effect in this system behaved normally.

Experimental

Substrates and solvents

The 1-phenylethyl chlorides were prepared by standard methods (3) from the corresponding alcohols, which were in turn afforded by reduction of substituted acetophenones. Solvolysis for 10 or more half-lives afforded yields of Cl^- in the 99–101% range, as assessed by precipitation with $AgNO_3$ and weighing. Ethanol was purified by a standard method and TFE as described by Sinnott and Jencks (44).

Isotope effect studies

Chloride ion released after partial and complete reaction was precipitated as AgCl and converted quantitatively to CH_3Cl. The isotope ratio was measured using a Varian-MAT CH7 mass spectrometer operating in the isotope ratio mode. Details are as earlier described in accounts from these (19, 20) and other (12, 13, 45) laboratories. One-point "rate coefficients" could be calculated from the weights of AgCl collected after partial and complete reaction. Where comparison was possible, these were in good agreement with published values of accurate rate constants (3, 23).

In each mass spectrometer measurement, a sample of gas was admitted to the sample inlet reservoir. Gas from a cylinder of methyl chloride was admitted to the reference reservoir and the pressures were equalized. A cycle: sample/purge/reference: (1 min each) was run at least six times and δ values were calculated using eq. [2]. These were concordant to within 0.5%, and a mean was taken. Both sample and reference reservoirs were then evacuated and fresh portions of gas were admitted to each side. The 6-fold cycle was repeated. In most cases two further repeats of the same gas sample were run. Where possible the same sequence was run, on the same day, for the infinity sample from the same reaction.

The uncertainties in δ and δ_∞ shown in Tables 1 and 2 are the mean deviations based on the two or four complete cycles run for the same methyl chloride sample. They are larger than the uncertainties calculated from individual δ values in a single cycle, and day-to-day variations in δ based on methyl chloride generated independently from the same AgCl sample varied more, up to ±5% from the mean. On the basis of the uncertainties in δ and δ_∞ in Tables 1 and 2, and an estimated 1% uncertainty in values of f, we calculate that the maximum experimental error in the derived k_{35}/k_{37} values is ±0.0005, or 0.05%.

1. C. K. INGOLD. Structure and mechanism in organic chemistry. 2nd ed. G. Bell and Sons, London. 1969. Chapt. 7.
2. (*a*) E. D. HUGHES, C. K. INGOLD, and A. D. SCOTT. J. Chem. Soc. 1201 (1937); (*b*) E. D. HUGHES, C. K. INGOLD, and S. MASTERMAN. J. Chem. Soc. 1236 (1937); (*c*) P. B. D. DE LA MARE, D. M. HALL, and E. MANGER. Rec. Trav. Chim. **74**, 1394 (1968); (*d*) V. J. SHINER, S. R. HARTSHORN, and P. C. VOGEL. J. Org. Chem. **38**, 3604 (1973); (*e*) K. OKAMOTO, K. KOMATSU, and H. SHINGU. Bull. Chem. Soc. Jpn. **40**, 1677 (1967).
3. V. J. SHINER, W. E. BUDDENBAUM, B. L. MURR, and G. LAMATY. J. Am. Chem. Soc. **90**, 418 (1968).
4. V. J. SHINER, W. DOWD, R. D. FISHER, S. R. HARTSHORN, M. A. KESSICK, L. MILANOVSKI, and M. W. RAPP. J. Am. Chem. Soc. **91**, 4838 (1969); A. TRAN. Tetrahedron, **32**, 1903 (1976).
5. J. B. STOTHERS and A. N. BOURNS. Can. J. Chem. **38**, 923 (1960).
6. J. B. STOTHERS and A. N. BOURNS. Can. J. Chem. **40**, 2007 (1972).
7. J. BRON and J. B. STOTHERS. Can. J. Chem. **46**, 1435 (1968).
8. J. BRON and J. B. STOTHERS. Can. J. Chem. **47**, 2506 (1969).
9. J. P. RICHARD, M. E. ROTHENBERG, and W. P. JENCKS. J. Am. Chem. Soc. **106**, 1361 (1984).
10. J. P. RICHARD and W. P. JENCKS. J. Am. Chem. Soc. **106**, 1373 (1984); **106**, 1396 (1984).
11. M. E. ROTHENBERG, J. P. RICHARD, and W. P. JENCKS. J. Am. Chem. Soc. **107**, 1340 (1985).
12. C. R. TURNQUIST, J. W. TAYLOR, E. P. GRIMSRUD, and R. C. WILLIAMS. J. Am. Chem. Soc. **95**, 4133 (1973).
13. J. W. HILL and A. FRY. J. Am. Chem. Soc. **84**, 2763 (1962).
14. W. H. SAUNDERS and S. AŠPERGER. J. Am. Chem. Soc. **79**, 1612 (1957); W. H. SAUNDERS and S. E. ZIMMERMAN. J. Am. Chem. Soc. **86**, 3789 (1964).
15. M. P. FRIEDBERGER and E. R. THORNTON. J. Am. Chem. Soc. **98**, 2861 (1976).
16. A. R. STEIN. J. Org. Chem. **38**, 4022 (1973).
17. A. R. STEIN, M. TENCER, E. A. MOFFATT, R. DAWE, and J. SWEET. J. Org. Chem. **45**, 3539 (1980).
18. D. J. MCLENNAN. J. Chem. Soc. Perkin Trans. 2, 1577 (1972).
19. A. GROUT, D. J. MCLENNAN, and I. H. SPACKMAN. J. Chem. Soc. Perkin Trans. 2, 1758 (1977).
20. H. F. KOCH, D. J. MCLENNAN, J. G. KOCH, W. TUMAS, B. DOBSON, and N. H. KOCH. J. Am. Chem. Soc. **105**, 1930 (1983).
21. M. H. ABRAHAM and D. J. MCLENNAN. J. Chem. Soc. Perkin Trans. 2, 873 (1977).
22. D. J. MCLENNAN. J. Chem. Soc. Perkin Trans. 2, 1316 (1981).
23. A. H. FAINBERG and S. WINSTEIN. J. Am. Chem. Soc. **79**, 1597 (1957).
24. E. R. THORNTON. J. Am. Chem. Soc. **89**, 2915 (1967); G. S. HAMMOND. J. Am. Chem. Soc. **77**, 334 (1955).
25. A. PROSS. Adv. Phys. Org. Chem. **14**, 69 (1977).
26. G. W. BURTON, L. B. SIMS, J. C. WILSON, and A. FRY. J. Am. Chem. Soc. **99**, 3371 (1977).
27. G. W. BURTON, L. B. SIMS, and D. J. MCLENNAN. J. Chem. Soc. Perkin Trans. 2, 1847 (1977).
28. A. PROSS and S. S. SHAIK. J. Am. Chem. Soc. **103**, 37092 (1981); S. G. SHAFER and J. M. HARRIS. J. Org. Chem. **46**, 2164 (1981).
29. R. A. SNEEN. Acc. Chem. Res. **6**, 46 (1973).
30. T. W. BENTLEY and G. E. CARTER. J. Am. Chem. Soc. **104**, 5741 (1982).
31. F. L. SCHADT, T. W. BENTLEY, and P. VON R. SCHLEYER. J. Am. Chem. Soc. **98**, 7667 (1976).
32. J. P. RICHARD and W. P. JENCKS. J. Am. Chem. Soc. **106**, 1383 (1984).
33. D. FĂRCAŞIU, J. JÄHME, and C. RÜCHARDT. J. Am. Chem. Soc. **107**, 5717 (1985).
34. T. ANDO, S.-G. KIM, K. MATSUDA, H. YAMATAKA, Y. YUKAWA, A. FRY, D. E. LEWIS, L. B. SIMS, and J. C. WILSON. J. Am. Chem. Soc. **103**, 3505 (1981); H. YAMATAKA and T. ANDO. J. Phys. Chem. **85**, 2281 (1981); T. HASAN, L. B. SIMS, and A. FRY. J. Am. Chem. Soc. **105**, 3967 (1983).
35. L. B. SIMS and D. E. LEWIS. *In* Isotopes in organic chemistry. Vol. 6. *Edited by* E. Buncel and C. C. Lee. Elsevier, Amsterdam. 1984. p. 211.
36. L. MELANDER and W. H. SAUNDERS. Reaction rates of isotopic molecules. Wiley-Interscience, New York. 1980. pp. 64–67.
37. F. H. WESTHEIMER. Chem. Rev. **61**, 265 (1961); L. MELANDER. Isotope effects on reaction rates. Ronald Press Co., New York. 1960. pp. 24–32.
38. T. ANDO, H. TANABE, and Y. YAMATAKA. J. Am. Chem. Soc. **106**, 2084 (1984).
39. L. B. SIMS, A. FRY, L. T. NETHERTON, J. C. WILSON, K. D. REPPOND, and S. W. CROOK. J. Am. Chem. Soc. **94**, 1364 (1972).
40. D. J. MCLENNAN and P. L. MARTIN. J. Chem. Soc. Perkin Trans. 2, 1091 (1982).
41. B. L. MURR and M. F. DONNELLY. J. Am. Chem. Soc. **92**, 6686 (1970); **92**, 6688 (1970).
42. T. W. BENTLEY, C. T. BOWEN, D. H. MORTEN, and P. VON R. SCHLEYER. J. Am. Chem. Soc. **103**, 5466 (1981).
43. A. D. ALLEN, V. M. KANAGASABAPATHY, and T. T. TIDWELL. J. Am. Chem. Soc. **107**, 4513 (1985).
44. M. L. SINNOTT and W. P. JENCKS. J. Am. Chem. Soc. **102**, 2026 (1980).
45. J. W. TAYLOR and E. P. GRIMSRUD. Anal. Chem. **41**, 805 (1969).
46. K. C. WESTAWAY and Z. WASZCZYLO. Can. J. Chem. **60**, 2500 (1982).

Isotope effects in nucleophilic substitution reactions. V. The mechanism of the decomposition of 1-phenylethyldimethylphenylammonium halides in chloroform

HELEN ALMA JOLY AND KENNETH CHARLES WESTAWAY[1]
Chemistry Department, Laurentian University, Sudbury, Ont., Canada P3E 2C6
Received November 1, 1985
This paper is dedicated to Professor Arthur N. Bourns

HELEN ALMA JOLY and KENNETH CHARLES WESTAWAY. Can. J. Chem. **64**, 1206 (1986).

Secondary α and β hydrogen–deuterium kinetic isotope effects have been used together to show that the S_N reaction between 1-phenylethyldimethylphenylammonium ion and bromide or iodide ion in chloroform occurs by way of an S_N2 mechanism within a triple ion in spite of the fact that it reacts faster than the primary substrate, benzyldimethylphenylammonium bromide. The very loose transition state and steric effects in the ground state appear to be responsible for the unusually fast S_N2 reactions between 1-phenylethyldimethylphenylammonium ion and halide ions in chloroform.

HELEN ALMA JOLY et KENNETH CHARLES WESTAWAY. Can. J. Chem. **64**, 1206 (1986).

On a fait appel à une combinaison des effets isotopiques cinétiques secondaires des hydrogènes et (ou) deutériums en α ainsi qu'en β pour montrer que le mécanisme de la réaction S_N qui se produit dans le chloroforme entre l'ion diméthyl phényl-1 éthyl phénylammonium et les ions bromure ou iodure est S_N2, dans un ion triple, et ce en dépit du fait que cette réaction soit plus rapide que celle du substrat primaire, le bromure de benzyl diméthyl phénylammonium. Il semble que l'état de transition très lâche et que les effets stériques dans l'état fondamental soient responsables pour la réaction S_N2 exceptionnellement rapide des halogénures de diméthyl phényl-1 éthyl phénylammonium dans le chloroforme.

[Traduit par la revue]

Introduction

Leffek and co-workers have extensively studied the decomposition of aralkyldimethylphenylammonium halides to aralkyl halides and dimethylaniline (the reverse of the Menschutkin reaction) in chloroform (1–5), eq. [1].

[1] $$Ar{-}\overset{|}{\underset{|}{C}}{-}\overset{+}{N}(CH_3)_2C_6H_5\ X^- \xrightarrow{CHCl_3} Ar{-}\overset{|}{\underset{|}{C}}{-}X + (CH_3)_2NC_6H_5$$

These workers concluded that the rate-determining step of the decomposition was the conversion of a quaternary ammonium ion into a carbocation and dimethylaniline inside a positively charged triple ion consisting of the two quaternary ammonium ions and one halide ion, eq. [2] (1–6).

[2] $$3\ ArCH_2\overset{+}{N}(CH_3)_2C_6H_5\ X^- \rightleftarrows [(ArCH_2\overset{+}{N}(CH_3)_2C_6H_5)_2\ X^-]^+ + [ArCH_2\overset{+}{N}(CH_3)_2C_6H_5\ X^-{}_2]^-$$

$$[(ArCH_2\overset{+}{N}(CH_3)_2C_6H_5)_2\ X^-]^+ \xrightarrow{slow} [ArCH_2\overset{+}{N}(CH_3)_2C_6H_5\ X^- + Ar{-}CH_2{}^+ + (CH_3)_2NC_6H_5]^+$$

$$\xrightarrow{fast} ArCH_2N(CH_3)_2C_6H_5 + ArCH_2{-}X + (CH_3)_2NC_6H_5$$

This mechanism was suggested for two reasons, i.e., because (*i*) very large secondary α-deuterium kinetic isotope effects of 1.25 (1.12 per α-D) and 1.20 (1.10 per α-D) were found for the decomposition of benzyldimethylphenylammonium bromide in chloroform and acetone, respectively (3) (the maximum value expected for a secondary α-deuterium kinetic isotope effect in an S_N2 reaction at this time was 1.04 per α-D or 1.08 per CD_2 group (7)), and (*ii*) because the reactivity of these salts was that observed for carbocation ion S_N reactions, i.e., the secondary substrate, 1-phenylethyldimethylphenylammonium bromide, reacted 22.5 times faster than the primary substrate, benzyldimethylphenylammonium bromide in chloroform.

More recent work, however, has shown that the benzyldimethylphenylammonium salts decompose by an S_N2 mechanism in dipolar aprotic solvents (8) and that unusually large secondary α-deuterium kinetic isotope effects are observed in the S_N2 reactions of benzyldimethylphenylammonium ions. In fact, Westaway *et al.* (9, 10) observed a secondary α-deuterium isotope effect of 1.18 (1.09 per α-D) in the S_N2 reaction with thiophenoxide ion in the dipolar aprotic solvent, DMF, eq. [3].

[3] $$C_6H_5S^- + C_6H_5CH_2\overset{+}{N}(CH_3)_2C_6H_5 \xrightarrow[DMF]{0°C} C_6H_5SCH_2C_6H_5 + (CH_3)_2NC_6H_5$$

Thus, the isotope effects for the S_N reactions of benzyldimethylphenylammonium ion in DMF, chloroform, and acetone are very similar, i.e., they vary from 1.09 to 1.12 per α-D and suggest that all three S_N reactions occur by the same mechanism, i.e., an S_N2 mechanism.

Theoretical calculations by Hartshorn and Shiner (11) support this conclusion. Their calculations predict that the maximum secondary α-deuterium kinetic isotope effect for the ionization of the methylammonium ion to a methyl carbocation and ammonia should be 1.19 per α-D (1.42 per CD_2 group). This means the minimum isotope effect for the formation of the methyl carbocation would be $(1.19)^{0.75} = 1.14$ per α-D or 1.30 per CD_2 group (10, 12). In the light of these facts, Westaway and Ali concluded that the substitution reaction in the decomposition of the benzyldimethylphenylammonium bromide in chloroform occurs by a simple S_N2

[1]Author to whom correspondence may be addressed.

reaction within the triple ion (10), eq. [4].

[4] $[(C_6H_5CH_2\overset{+}{N}(CH_3)_2C_6H_5)_2Br^-]^+ \longrightarrow$ 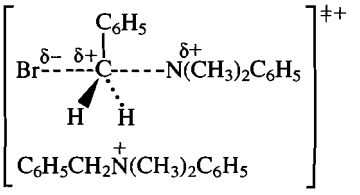

$\longrightarrow C_6H_5CH_2Br + (CH_3)_2NC_6H_5 + C_6H_5CH_2\overset{+}{N}(CH_3)_2C_6H_5$

Finally, Islam and Leffek in a later publication (5) indicated that they believe the benzyl substrate reacts by the mechanism shown in eq. [4].

If the substitution reaction in the decomposition of benzyldimethylphenylammonium halides in chloroform occurs by an S_N2 mechanism within the triple ion, the observation that the secondary substrate, 1-phenylethyldimethylphenylammonium bromide reacts 22.5 times faster than the primary compound, benzyldimethylphenylammonium bromide, is surprising. This study was undertaken in an effort to determine the mechanism of the faster reaction and to learn why the rate of reaction is greater for the more highly substituted quaternary ammonium salt.

Results and discussion

Four different mechanisms, all occurring within the triple ion, could account for the surprisingly fast rate of decomposition found for the 1-phenylethyldimethylphenylammonium bromide in chloroform, Scheme 1. The first possibility is that this reaction occurs by the same S_N2 mechanism as the benzyldimethylphenylammonium bromide but that there is some factor that makes it faster than expected. The second possibility is that the substitution reaction in the decomposition of the 1-phenylethyldimethylphenylammonium bromide occurs via the carbocation S_N mechanism originally suggested by Leffek and co-workers. If this were the case, the carbocation S_N reaction would simply occur faster than the S_N2 reaction of the benzyldimethylphenylammonium bromide.

The rate constant could also be larger for the 1-phenylethyl compound if the only products of the reaction, 1-phenylethylbromide and dimethylaniline, were produced in a two-step elimination–addition reaction. In the first step, the bromide ion would act as the base and abstract a β-hydrogen from the substrate in an E2 elimination reaction to give styrene, hydrobromic acid, and *N,N*-dimethylaniline in the triple ion complex. In the second step, the hydrobromic acid would add across the π bond of the styrene in a Markovnikov addition to give the observed product, 1-phenylethyl bromide. If the reaction occurred via the elimination–addition mechanism, the first (elimination) step of the reaction would have to be rate determining for several reasons. First, no elimination product (styrene) could be found either during or after the reaction. This means that any hydrobromic acid that formed during the reaction must add quantitatively to the styrene. Since the acid could also react with the other elimination product, dimethylaniline, to form dimethylanilinium bromide in a fast acid–base reaction, the hydrobromic acid would have to react instantaneously with the styrene. Although this might seem unlikely, a simple experiment showed that hydrobromic acid does add instantaneously to styrene in chloroform at room temperature.[2] The addition reaction would be expected to be especially fast in the elimination–addition mechanism because the hydrobromic acid is formed immediately beside the π bond of the styrene and, in fact, the proton of hydrobromic acid is removed from the carbon that accepts the proton in the addition step. Finally, the reaction between hydrobromic acid and dimethylaniline might not occur because the hydrobromic acid is released on the opposite side of the π bond from the dimethylaniline in a *trans*, coplanar E2 elimination reaction.

The last possibility is that the observed rate of decomposition is the sum of the rate constants for the elimination–addition and the substitution reaction. If this was the case, the rate constant for the S_N reaction of the 1-phenylethyldimethylphenylammonium bromide might even be smaller than that found for the S_N2 reaction of the benzyl substrate.

Normally, a kinetic study would distinguish between most of the mechanistic alternatives for this reaction. However, because the reaction occurs within the triple ion, the same kinetic expression would be obtained for all of the mechanisms. As a result, the problem had to be resolved with other mechanistic criteria.

The initial attempt to distinguish between these four mechanisms involved determining the β-deuterium kinetic isotope effect for the reaction. If the substitution reaction occurred via an S_N2 mechanism within the triple ion, a small secondary β-deuterium kinetic isotope effect of between 1.02 and 1.10 would be expected,[3] Table 1. If the substitution reaction involved the formation of a carbocation triple ion intermediate, a large, hyperconjugative secondary β-deuterium isotope effect of between 1.15 and 2.5 should be observed.[3] If the elimination–addition mechanism is followed, the β-hydrogen (deuterium) is removed in the rate-determining step of the overall reaction and a large primary hydrogen–deuterium kinetic isotope effect of between three and ten would be expected (13). Finally, even if a small percentage of the reaction were to proceed via the elimination–addition pathway with a very small primary deuterium kinetic isotope effect of 3.0, a significant β-deuterium kinetic isotope effect would be observed.

The observed β-deuterium kinetic isotope effect for the reaction of the 1-phenylethyldimethylphenylammonium bromide in chloroform at 25°C was 1.144 ± 0.0097 per CD_3 (1.046/β-D), Table 2. This small isotope effect clearly eliminates any appreciable contribution from the elimination–addition mechanism, which would have a primary isotope effect of at least 3.0, Table 1. If one assumes the average secondary β-deuterium kinetic isotope effect found for an S_N2 reaction (1.06/CD_3 group) and an average primary isotope effect of 5.0 for the E2 elimination reaction, the isotope effect would be 1.14 when 9% of the reaction occurred via this route. Even if one uses the minimum secondary β-deuterium isotope effect of 1.02/CD_3 group for the S_N2 reaction and a minimum primary isotope

[2]K. C. Westaway. Unpublished results.

[3]See ref. 12, pp. 122–126.

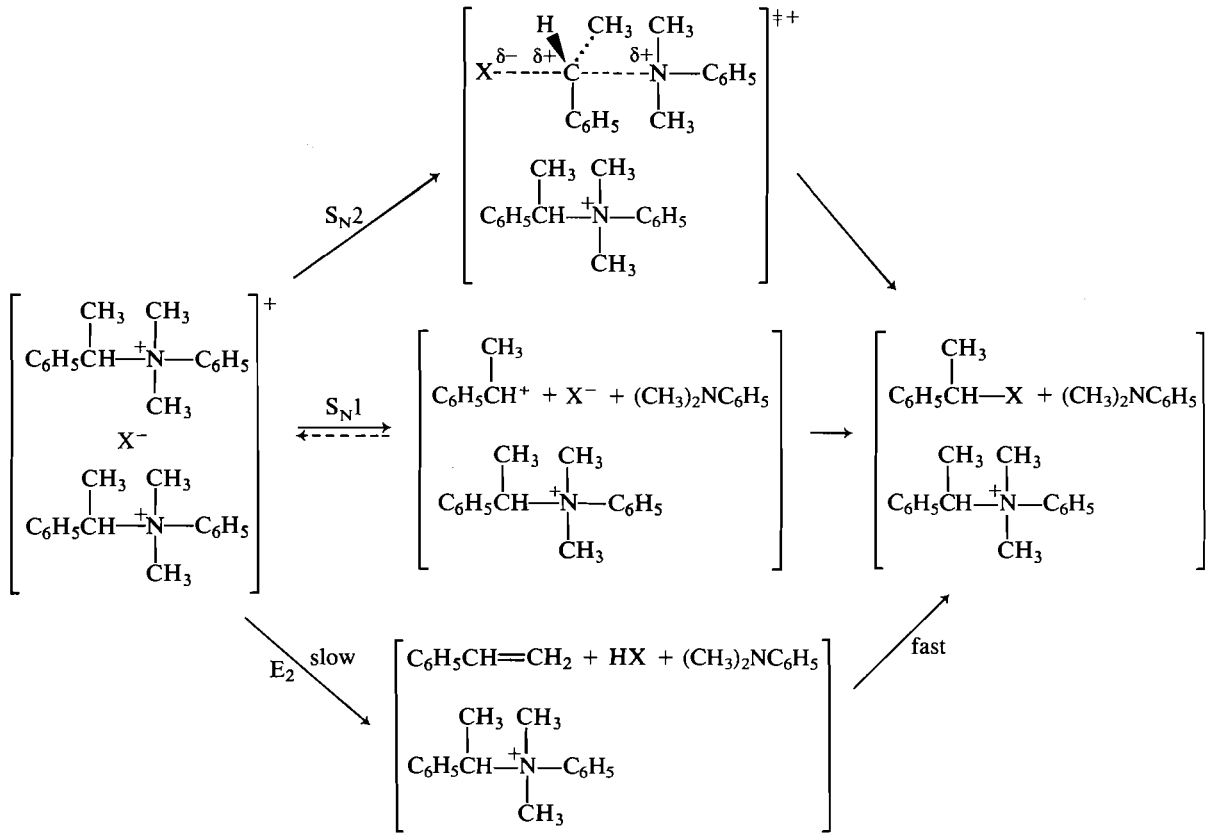

SCHEME 1

TABLE 1. The β-deuterium kinetic isotope effects expected for the different decomposition mechanisms of 1-phenylethyldimethylphenylammonium bromide in chloroform at 25°C.

Decomposition mechanism within the triple ion	Expected $(k_H/k_D)/\beta\text{-}D_3$
S_N2	1.02–1.11
Carbocation S_N	
with k_2 rate determining	1.34–1.52
with k_1, k_3, or k_4 rate determining	1.16–1.34
Elimination–addition	3.0–10
Elimination–addition–substitution with[a]	
$(k_H/k_D)_{\beta S} = 1.02$ and $(k_H/k_D)_{\beta E} = 3.0$ and $P_{HE} = 16\%$	1.14[b]
$(k_H/k_D)_{\beta S} = 1.06$ and $(k_H/k_D)_{\beta E} = 5.0$ and $P_{HE} = 9\%$	1.14[b]

[a] P_{HE} is the percent elimination–addition mechanism for the undeuterated substrate, $(k_H/k_D)_{\beta S}$ and $(k_H/k_D)_{\beta E}$ are the β-deuterium kinetic isotope effects for the substitution and elimination reactions, respectively.

[b] The observed isotope effect is calculated from

$$k_H/k_D = 100[(k_H/k_D)_{\beta S}(k_H/k_D)_{\beta E}]/[(k_H/k_D)_{\beta S} \times P_{HE} + (k_H/k_D)_{\beta E} \times (100 - P_{HE})]$$

effect of 3.0 for the E2 elimination reaction, the observed isotope effect is 1.14 when 16% of the reaction occurs via the elimination–addition pathway. Thus, the β-deuterium isotope effect indicates that less than 16% of the reaction occurs via the elimination–addition pathway and suggests that less than 9% of the reaction occurs via this route if the S_N reaction occurs via an S_N2 mechanism within the triple ion. If the S_N reaction occurs via a carbocation – triple ion intermediate, on the other hand, none of the product forms in an elimination–addition reaction because the secondary β-deuterium isotope effects for carbocation S_N reactions range from 1.05–1.15/β-D (1.16–1.52/CD_3 group),[3] i.e., are larger than the isotope effect observed in this reaction. Thus, the β-deuterium isotope effect demonstrates that the decomposition must occur via one of the S_N mechanisms.

The maximum kinetic isotope effect for a particular leaving group is observed in normal (not occurring in a triple ion) carbocation S_N reactions when the slow step is the formation of the solvent-separated ion pair or the free carbonium ion and hyperconjugation is a maximum (ref. 10 and footnote 3). Smaller isotope effects are found when formation of the intimate ion pair or the destruction of a carbocation intermediate is rate determining. The smaller isotope effect is presumably found in these reactions because the positive charge has not been developed fully or has been partially destroyed in the transition state of the rate-determining step of the reaction and hyperconjugation is not a maximum.[3]

Although a carbocation intermediate in a triple ion cannot exist as a solvent-separated ion pair, the carbocation could react either as an intimate ion–molecule pair or as a free carbocation. Thus, a carbocation S_N reaction occurring within the triple ion, Scheme 2, could have any of the k_1, the k_2, the k_3, or the k_4 steps rate-determining.

In fact, the secondary β-deuterium kinetic isotope effect found when the k_1, the k_3, or the k_4 step of a carbocation reaction is rate determining is only about 1.05/β-D (1.16/CD_3 group) or 60% of the isotope effect found when the k_2 step is rate determining.[3] Since the observed isotope effect of 1.144 is within experimental error of the minimum value expected for a carbocation S_N reaction, one cannot eliminate a carbocation mechanism where the rate-determining step is the formation of

TABLE 2. The α- and β-deuterium kinetic isotope effects for the decomposition of 1-phenylethyldimethylphenylammonium bromide in chloroform at 25°C

$k_H \times 10^4$, s^{-1}	$k_{D_\beta} \times 10^4$, s^{-1}	(k_H/k_D)/β-D_3	$k_{D_\alpha} \times 10^4$, s^{-1}	(k_H/k_D)/α-D
1.164	1.022		9.872	
1.153	1.007		9.852	
1.166	1.016		9.857	
1.161±0.007[a]	1.015±0.008[a]	1.144±0.0097[b] (1.046/β-D)	9.857±0.010[a]	1.178±0.006[b]

[a]The error limits are the standard deviation.
[b]The error limits were calculated using the equation
Error = $1/k_D[(\Delta k_H)^2 + (k_H/k_D)^2(\Delta k_D)^2]^{1/2}$
where Δk_H and Δk_D are the standard deviations for the rate constants of the undeuterated and deuterated substrate, respectively.

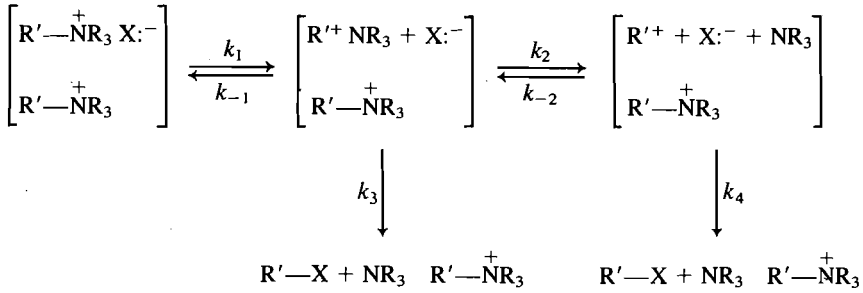

SCHEME 2

the intimate ion–molecule pair or the destruction of a carbocation intermediate.

The secondary β-deuterium isotope effects for S_N2 reactions normally range from 1.01 to 1.03/β-D (1.03–1.09/CD_3 group). However, much larger secondary β-deuterium isotope effects have been found in some S_N2 reactons. For example, an isotope effect of 1.13/CD_3 group was reported for the ethanolysis of isopropyl brosylate[3] and an isotope effect of 1.16/CD_3 group was found in the acetolysis of ethyl triflate at 25°C (14). Although the observed isotope effect of 1.14 is larger than those found in most normal S_N2 reactions, it is smaller than the largest isotope effects that have been found and one cannot rule out the S_N2 mechanism for the reaction within the triple ion. Thus, the β-deuterium kinetic isotope effect eliminates the elimination–addition mechanism as a significant pathway for the reaction and reduces the problem to distinguishing between an S_N2 mechanism and a carbocation S_N mechanism with the k_1 (an S_N1_{lim} mechanism), or the k_3 or k_4 step (S_N2C^+ mechanisms), rate determining.

The second criterion of mechanism that was used to distinguish between the carbocation and the S_N2 mechanisms for the S_N reaction between 1-phenylethyldimethylphenylammonium ion and bromide ion in the triple ion was the secondary α-deuterium kinetic isotope effect. The large isotope effect of 1.178 ± 0.006/α-D found for this reaction, Table 2, is significantly larger than the isotope effect of 1.12 found for the S_N2 reaction of the benzyl derivative in chloroform. In spite of this, the S_N2 mechanism cannot be ruled out for several reasons. Adding a methyl group to the α-carbon of primary substrates that react via S_N2 mechanisms increases the secondary α-deuterium kinetic isotope effect by 1.036 ± 0.003 (15). Adding a methyl group to the α-carbon of the benzyldimethylphenylammonium ion should, therefore, raise the isotope effect for an S_N2 reaction of the 1-phenylethyldimethylphenylammonium bromide from 1.12 to 1.16. Since one would expect the increase in isotope effect to be greater when the substrate is more sterically crowded, i.e., adding a methyl group to the α-carbon of a more crowded substrate would increase the frequency of the out-of-plane C_α—H(D) ground state bending vibrations and the zero-point energy difference more than adding a methyl group to a less crowded substrate, one would expect an even larger isotope effect than 1.16 for the 1-phenylethyl compound. Thus, the expected ($k_H/k_D > 1.16$) and the observed isotope effect ($k_H/k_D = 1.178$) are close enough so that one cannot rule out the S_N2 mechanism. This conclusion is supported by the large secondary α-deuterium isotope effects found in S_N2 reactions by Craze *et al.* (16) and by Knier and Jencks (17). Craze *et al.* reported secondary α-deuterium kinetic isotope effects as large as 1.16/α-D in the S_N2 reactions of 1-methoxymethoxy-2,4-dinitrobenzene and Knier and Jencks found isotope effects as large as 1.18/α-D in the S_N2 reactions of the quaternary ammonium ion, methoxymethyldimethyl-*m*-nitroanilinium ion.

Large secondary α-deuterium kinetic isotope effects at or near the maximum are found in carbocation S_N reactions where the formation of the solvent-separated or the free carbonium ion is rate determining, whereas smaller isotope effects, approximately 75% of the maximum, are found in carbonium ion S_N reactions where the k_1 step is rate-determining (12). The maximum and minimum isotope effect for a carbonium ion mechanism of a primary ammonium salt is 1.19/α-D (11) and $1.19^{0.75} = 1.14$/α-D. The maximum and minimum isotope effects for a secondary substrate would be approximately 1.04 times greater, i.e., 1.24 and 1.17/α-D, respectively. Thus, although the isotope effect of 1.178 is too small to be indicative of a carbocation mechanism where the formation of the free carbocation within the triple ion is rate determining, it is

TABLE 3. The rate constants and Hammett ρ value for a series of *para*-substituted phenyl-1-phenylethyldimethylammonium bromides in chloroform at 34.88°C

para-Substituent in the leaving group	$k \times 10^5$, s^{-1}	ρ (leaving group)
CH_3O	7.681±0.0004[a]	
CH_3	17.36±0.007	
H	41.49±0.15	
Cl	103.4±0.1	2.20±0.07[a] Corr. coeff. = 0.989

[a]The error limits are the standard deviation.

consistent with a carbocation mechanism where the k_1, the k_3, or the k_4 step is rate determining. Unfortunately, both the secondary α- and β-deuterium kinetic isotope effects are at the borderline between the values expected for an S_N2 and a carbocation S_N reaction, with the formation of the intimate ion–molecule pair or the destruction of a carbocation intermediate rate determining. Thus, while measuring these isotope effects limited the mechanistic options to three S_N mechanisms, they did not distinguish between a simple S_N2, an S_N1_{lim}, and an S_N2C^+ mechanism for the triple ion substitution reaction.

The next criterion that was used to determine the mechanism of the triple ion S_N reaction between 1-phenylethyldimethylphenylammonium ion and bromide ion was the Hammett ρ value found by changing the *para* substituent on the benzene ring of the leaving group. If the reaction occurs via an S_N2 or a carbocation mechanism with the k_1 step rate determining, the C—N bond breaks in the slow step of the reaction and a small Hammett ρ value would be observed. If the reaction occurs via a carbocation mechanism with the k_1 step reversible and the k_3 or the k_4 step rate determining, the C—N bond is broken in a fast, reversible step and a large, equilibrium ρ value would be observed. The Hammett ρ value of +2.20, Table 3, is significantly smaller than the ρ values found for the complete destruction of a positive charge on a nitrogen atom. In fact, the ρ values found for the equilibrium dissociation of *para*-substituted *N,N*-dimethylanilinium ions to dimethylanilines and a proton, i.e., for the complete destruction of a positive charge on nitrogen, range from +3.43 to +4.19 in various solvents (8). Thus, one would expect a ρ value of at least 3.4 if the positive charge had been completely destroyed in the transition state of the rate-determining step of the S_N reaction between 1-phenylethyldimethylphenylammonium ion and bromide ion. The much smaller ρ value of +2.20 indicates that the C_α—N^+ bond is breaking in the rate-determining step of the reaction and rules out a carbocation mechanism where the k_3 or the k_4 step is rate determining. Thus, the S_N reaction between the 1-phenylethyldimethylphenylammonium ion and bromide ion in the triple ion must proceed by way of an S_N2 mechanism or a S_N1_{lim} mechanism with the k_1 step rate determining.

The mechanism for the reaction was finally determined by comparing the secondary α- and secondary β-deuterium kinetic isotope effects for the bromide ion reaction with those found when the nucleophile was iodide ion. If the S_N reaction within the triple ion occurred via the rate-determining formation of the intimate ion–molecule pair, the transition state would be independent of the nucleophile and one would find the same α- and β-deuterium isotope effects in both reactions. If the reaction proceeded via an S_N2 mechanism on the other hand, the nucleophiles are a part of the transition states, the transition states would be different, and the magnitude of both the secondary α- and secondary β-deuterium kinetic isotope effects would be different in the two reactions. A comparison of the secondary α- and β-deuterium kinetic isotope effects for the bromide ion (Table 2) and iodide ion reactions, Table 4, show that the isotope effects do change when the nucleophile is changed. In fact, a Wilcoxin test and the Student's *t* test (18, 19) show that the secondary α-deuterium kinetic isotope effects of 1.178 ± 0.006 for the bromide ion reaction and 1.184 ± 0.0077 for the iodide ion reaction, respectively, are significantly different at the 92% confidence level if one uses the average isotope effects obtained by combining each k_H value with each k_D value, and are significantly different at the 53–81% confidence level if one uses the worst and best combinations of the three isotope effects, respectively, in the statistical analysis. While the α-deuterium kinetic isotope effects are not significantly different at a high confidence level, the same two statistical tests indicate that the secondary β-deuterium kinetic isotope effects of 1.144 ± 0.0097 for the bromide ion reaction and 1.172 ± 0.0072 for the iodide ion reaction are significantly different at the 99.9% confidence level. The different isotope effects for these two reactions clearly demonstrate that the nucleophile is in the transition state of the rate-determining step of these reactions and it has been concluded that the decomposition of the 1-phenyldimethylphenylammonium halides in chloroform occurs via an S_N2 mechanism within a triple ion.

Once it had been established that the S_N reaction of both the benzyl- and the 1-phenylethyldimethylphenylammonium bromides in chloroform occurred by an S_N2 mechanism within a triple ion, attention was turned to determining the relative structures of the transition states for these two reactions. The transition states for these two reactions were estimated in two ways. First, the relative lengths of the α-carbon-leaving group transition state bonds were determined by comparing the Hammett ρ values found by changing the substituent in the leaving group. The results in Tables 3 and 5 show that the Hammett ρ values for these two reactions are very different. In fact, the ρ value for the 1-phenylethyl reaction is more than twice that found for the reaction of the benzyl substrate. This clearly indicates that there is a greater change in electron density on the nitrogen atom in going from the reactant to the transition state of the 1-phenylethyldimethylphenylammonium ion reaction and that the α-carbon–nitrogen bond is significantly longer in the 1-phenylethyldimethylphenylammonium bromide transition state.

Next, the relative lengths of the nucleophile–α-carbon bonds in the two transition states were estimated by determining the selectivity of the reactions to a change in nucleophile. Both we (20) and Harris *et al.* (21) have used the selectivity of a reaction to a change in nucleophile to estimate the lengths of nucleophile–α-carbon bonds in S_N reactions. In fact, it is believed that the

TABLE 4. The secondary α- and β-deuterium kinetic isotope effects for the decomposition of 1-phenylethyldimethylphenylammonium iodide in chloroform at 25°C

$k_H \times 10^4$, s^{-1}	$k_{D_\alpha} \times 10^4$, s^{-1}	$(k_H/k_D)/\alpha$-D	$k_{D_\beta} \times 10^4$, s^{-1}	$(k_H/k_D)/\beta$-D_3
2.752	2.317		2.336	
2.762	2.315		2.335	
2.739	2.337		2.353	
2.751±0.012[a]	2.323±0.012[a]	1.184±0.0077[b]	2.348±0.010[a]	1.172±0.0072[b]

[a]The error limits are the standard deviation.
[b]The error limits were calculated using the equation
Error = $1/k_D[(\Delta k_H)^2 + (k_H/k_D)^2(\Delta k_D)^2]^{1/2}$
where Δk_H and Δk_D are the standard deviations for the rate constants of the undeuterated and deuterated substrate, respectively.

TABLE 5. The rate constants and Hammett ρ value for a series of *para*-substituted phenylbenzyldimethylammonium bromides in chloroform at 34.88°C

para-Substituent in the leaving group	$k \times 10^5$, s^{-1}	ρ (leaving group)
CH_3O	1.958±0.006[a]	
CH_3	2.166±0.048	
H	2.870±0.011	
Cl	5.576±0.021	0.918±0.04[a] Corr. coeff. = 0.982

[a]The error limits are the standard deviation.

TABLE 6. The rate constants and selectivity for the decomposition of benzyl and 1-phenylethyldimethylphenylammonium bromides and iodides in chloroform

	Substrate	
Parameter	$C_6H_5CH_2\text{—}\overset{+}{N}(CH_3)_2C_6H_5$[a]	$C_6H_5\underset{\displaystyle CH_3}{\underset{\vert}{CH}}\text{—}\overset{+}{N}(CH_3)_2C_6H_5$
$k_I \times 10^5$, s^{-1}	47.7 at 40°C 93.2 at 45°C	27.53 at 25°C
$k_{Br} \times 10^5$, s^{-1}	6.1 at 40°C 12.3 at 45°C	11.61 at 25°C
k_I/k_{Br}	7.8 at 40°C 7.6 at 45°C	2.4 at 25°C

[a]The rate constants are from ref. 5.

selectivity does not indicate the total structure of the transition state but is related to the length of the bond nearest to the point of structural change. The rate constants for the S_N2 reactions of the benzyl and 1-phenylethyl substrates with bromide ion and iodide ion, Table 6, give the selectivity of each reaction to a change in nucleophile. Although the rate constants for the two reactions were measured at different temperatures, the temperature effect on the selectivity (k_I/k_{Br}) for the benzyldimethylphenylammonium ion reaction is small and it is clear that the 1-phenylethyldimethylphenylammonium ion reaction is much less sensitive to change in nucleophile than the benzyldimethylphenylammonium ion reaction. A greater selectivity is indicative of a shorter nucleophile–α-carbon transition state bond because the difference in energy of the two transition states (the rate constants) will be greater when the nucleophile–α-carbon bonds are more complete in the transition state. Thus, the selectivities indicate that the nucelophile–α-carbon transition state bond is significantly longer in the 1-phenylethyldimethylphenylammonium ion transition state than in the benzyldimethylphenylammonium ion transition state.

The selectivities and the Hammett ρ values indicate that the 1-phenylethyldimethylphenylammonium ion reaction has a much looser transition state with longer nucleophile–α-carbon *and* α-carbon-leaving group bonds than the corresponding benzyl salt. In fact, Schowen and co-workers (22) had indicated that adding a methyl group to the α-carbon of the substrate in an S_N2 reaction would lead to a looser transition state and this is what has been found. However, this study has gone further by demonstrating that both of the reacting bonds in the S_N2 transition state become longer when a methyl group is added to the α-carbon.

Finally, it is interesting to speculate on the reason the 1-phenylethyldimethylphenylammonium ion reacts faster than the corresponding primary benzyl substrate. This is unusual because secondary compounds normally react from 25 to 150 times slower than primary compounds in S_N2 reactions (23) because the S_N2 transition state for a secondary substrate is more sterically crowded. It would appear that the 1-phenylethyldimethylphenylammonium ion reacts faster than the benzyl substrate for two reasons. One contributing factor is undoubtedly

that the transition state is very loose. In fact, both the secondary α- and β-deuterium kinetic isotope effects are unusually large for an S_N2 reaction, i.e., they are almost in the range expected for a carbocation S_N reaction and confirm that the transition state for this reaction is very loose. Thus, the steric crowding that is present in the S_N2 transition states of most secondary substrates is not present in the 1-phenylethyldimethylphenylammonium ion S_N2 transition state; the transition state will be lower in free energy and the reaction will be faster than expected. Another factor contributing to the faster rate of reaction is steric crowding in the initial state. Westaway and Ali attributed the very large secondary α-deuterium kinetic isotope effects in the S_N2 reactions of benzyldimethylphenylammonium ions to steric hindrance of the C_α—H(D) out-of-plane bending vibrations in the initial state (10). Obviously, the steric crowding would be greater in the initial state of the 1-phenyl substrate. This would increase the ground state energy of the 1-phenylethyldimethylphenylammonium ion, further reducing the free energy of activation. Thus, the reaction is probably faster than expected for two reasons, steric acceleration due to steric crowding in the initial state and a looser (less sterically crowded) S_N2 transition state within the triple ion.

Experimental

Preparation of reagents

Preparation of 1-phenylethyldimethylphenylammonium bromide

Anhydrous hydrogen bromide gas (Matheson) was bubbled with occasional cooling into 56.80 g (0.546 mol) of styrene for approximately 3 h at room temperature. The product, 1-phenylethyl bromide, was washed several times with distilled water, dried over magnesium sulfate, and distilled, bp 55.5–56.0°C at 3.5 Torr (1 Torr = 133.3 Pa) (lit. (24) bp, 202–203°C). The yield was 91.2 g (90%).

Twenty-five grams (0.135 mol) of 1-phenylethyl bromide was added to 18.2 g (0.150 mol) of freshly distilled *N,N*-dimethylaniline and left under dry nitrogen in the dark for four days. Then the solid product was filtered and washed with anhydrous ether. The crude product (35.4 g (86%)) was recrystallized to a constant melting point of 119.5–120.5°C (lit. (4) mp 125–126°C) by dissolving it in a minimum of acetonitrile at room temperature and precipitating the salt with ether. The discrepancy between the reported and experimental melting point arose because a change in the heating rate of the melting point apparatus altered the melting point markedly. For example, a sample melting between 119.5 and 120.5°C melted at 129–130°C when the heating rate was higher. As a result all of the melting points were determined on the same melting point apparatus at the same heating rate. Finally, all of the quaternary ammonium salts used in this study were stored in a desiccator in the dark until they were used in a kinetic run.

Preparation of 1-phenylethyl-2,2,2-d$_3$-dimethylphenylammonium bromide

This compound was synthesized by adding a mixture of 12.5 g (0.0862 mol) of iodomethane-d_3 (Merck, Sharp and Dohme) in 20 mL of sodium-dried ether, dropwise, to 2.72 g (0.0112 mol) of clean magnesium and 10 mL of sodium-dried ether in a dry, 250-mL three-necked round-bottom flask fitted with a condenser and a dropping funnel. When the addition was complete, the mixture was refluxed for 30 min, cooled to below −5°C with an ice–salt bath, and a solution of 8.74 g (0.0824 mol) of "purified" benzaldehyde (25) in 25 mL of sodium-dried ether was added so that the temperature did not exceed −5°C. When the addition was complete, the reaction mixture was stirred for 30 min and then decanted onto 38 g of crushed ice. After acidification with 10% sulfuric acid, the ether layer was separated. The aqueous layer was extracted with three 20-mL portions of anhydrous ether. Then, the combined ether extracts were washed three times with 10% sodium hydroxide, once with distilled water, and dried with anhydrous magnesium sulfate. A distillation gave 5.38 g (52%) of 1-phenylethyl-2,2,2-d_3 alcohol, bp 62°C at 3 Torr (lit. (26) bp 71–72°C at 2 Torr). The nmr spectrum was identical to that reported for the product (27).

After anhydrous hydrogen bromide (Matheson) had been bubbled through a solution of 5.38 g (0.0423 mol) of 1-phenylethyl-2,2,2-d_3 alcohol in 10 mL of benzene for 90 min, the benzene-1-phenylethyl-2,2,2-d_3 bromide solution was washed several times with water and dried with anhydrous magnesium sulfate. After the benzene had been removed on the rotary evaporator, a distillation gave 3.70 g (69%) 1-phenylethyl-2,2,2-d_3 bromide, bp 50.5°C at 3 Torr (lit. (24) bp 202–203°C at 760 Torr). An analysis of the nmr spectrum indicated that the product was 99% deuterated at the 2 position.

In the third step, 2.93 g (0.0155 mol) of 1-phenylethyl-2,2,2-d_3 bromide was added to 1.65 g (0.0136 mol) of freshly distilled *N,N*-dimethylaniline and left for several days in a dry, nitrogen atmosphere. The product was filtered, washed with several portions of anhydrous ether, and crystallized from a mixture of acetonitrile – anhydrous ether, *vide supra*. This gave 2.59 g (63%) of 1-phenylethyl-2,2,2-d_3-dimethylphenylammonium bromide, mp 119.5–120.5°C.

Preparation of 1-phenylethyl-1-d$_1$-dimethylphenylammonium bromide

A solution containing 15.07 g (0.126 mol) of acetophenone and 150 mL of sodium-dried ether was added dropwise to a mixture of 3 g (0.07 mol) of lithium aluminium deuteride in 200 mL of sodium-dried ether. After refluxing overnight, the reaction mixture was slowly poured onto crushed ice. The solution was made basic by adding sodium hydroxide pellets and the ether layer separated. The aqueous phase was extracted twice with 50-mL portions of ether. Then the ether layers were combined and dried over anhydrous magnesium sulfate. After the ether had been removed on a rotary evaporator, distillation gave 13.31 g (0.1081 mol) of pure 1-phenylethyl-1-d_1 alcohol, bp 66°C at 2 Torr (lit. (26) bp 71–72°C at 2 Torr).

Anhydrous hydrogen bromide was bubbled through 13.31 g (0.1081 mol) of 1-phenylethyl-1-d_1 alcohol for 3 h. The two phases were separated and the organic layer was washed several times with distilled water, dried with anhydrous magnesium sulfate, and then distilled to give 18.5 g (92%) of 1-phenylethyl-1-d_1 bromide, bp 60°C at 2 Torr. An analysis of the C_α-H absorption at 4.56 ppm in the nmr spectrum suggested that the 1-phenylethyl-1-d_1 bromide was 99.4% deuterated.

Finally, 18.03 g (0.0969 mol) of 1-phenylethyl-1-d_1 bromide and 13.29 g (0.109 mol) of freshly distilled *N,N*-dimethylaniline were mixed in a dry nitrogen atmosphere and left at room temperature for 1 week. The solid product was filtered, then washed several times with anhydrous ether. The 25.43 g (85.4%) of crude 1-phenylethyl-1-d_1-dimethylphenylammonium bromide was recrystallized from acetonitrrile – anhydrous ether to a constant melting point of 120–120.5°C.

Preparation of the α-deuterated, β-deuterated, and undeuterated 1-phenylethyldimethylphenylammonium iodides

The α-deuterated, β-deuterated, and undeuterated quaternary ammonium iodides were obtained by converting the appropriate quaternary ammonium bromides into the quaternary ammonium hydroxides with silver oxide and then titrating the hydroxides with hydriodic acid.

Preparation of 1-phenylethyldimethylphenylammonium iodide

A 99% excess (3.255 g, 0.01403 mol) of nitrate-free silver oxide (28) was stirred with a solution of 2.15 g (7.03×10^{-3} mol) of 1-phenylethyldimethylphenylammonium bromide in 60 mL of distilled water for 3.5 h. After the solution was filtered through a 934 AH Reeve Angel glass fiber filter, the filtrate was taken to a pH of 3.9 by adding hydriodic acid and left overnight in the dark. After the solution was filtered through another 934 AH Reeve Angel glass fiber filter, the filtrate was taken to dryness on the rotary evaporator. The crude product (18 g, 74%) was dried in an evacuated desiccator overnight and then recrystallized from an acetonitrile–ether mixture, mp 101–102°C. All of the quaternary ammonium iodides were stored in the dark (28) in a vacuum desiccator until they were used for kinetics.

Preparation of 1-phenylethyl-2,2,2,-d_3-dimethylphenylammonium iodide

1-Phenylethyl-2,2,2-d_3-dimethylphenylammonium bromide, 2.352 g (7.61×10^{-3} mol) was dissolved in approximately 50 mL of distilled water and stirred with 3.53 g (0.0152 mol) of nitrate-free silver oxide for 6 h. Then the solution was filtered through a 934 AH Reeve Angel glass fiber filter and the filtrate acidified to a pH of 3.04 with hydriodic acid. The next day, the solution was filtered through a 934 AH glass fiber filter and the filtrate taken to dryness on the rotary evaporator. The crude product (18 g, 65%) was dried in a vacuum desiccator and recrystallized from acetonitrile–ether, mp 101–102°C.

Preparation of 1-phenylethyl-1-d_1-dimethylphenylammonium iodide

1-Phenylethyl-1-d_1-ammonium bromide, 6.02 g (0.0196 mol), was stirred with 120 mL of distilled water and 9.08 g (0.0391 mol) of silver oxide for 3.5 h, filtered through a 934 AH Reeve Angel glass fiber filter, and the filtrate taken to a pH of 5.40 with hydriodic acid. After the solution had been stored overnight, it was filtered through a 934 AH Reeve Angel glass filter and the water removed on the rotary evaporator. The resulting solid (6.0 g, (86%)) was dried overnight in an evacuated desiccator and recrystallized from acetonitrile–ether, mp 101.5–103°C.

Preparation of a series of 4-substituted phenyl-1-phenylethyldimethylammonium bromides

The 4-methoxy-, the 4-chloro-, and the 4-methylphenyl-1-phenylethyldimethylammonium bromides were prepared by reacting 1-phenylethyl bromide with an excess of 4-methoxy-, 4-chloro-, and 4-methyl-*N,N*-dimethylanilines, respectively. The *N,N*-dimethyl-4-methylaniline (Aldrich) was purified by distillation under reduced pressure. The synthesis of the *N,N*-dimethyl-4-methoxy- and *N,N*-dimethyl-4-chloroanilines are described elsewhere (8).

Preparation of 4-methoxyphenyl-1-phenylethyldimethylphenylammonium bromide

N,N-dimethyl-4-methoxyaniline (4.24 g, 0.280 mol) and 5.31 g (0.0287 mol) of 1-phenylethyl bromide were sealed in an Erlenmeyer flask that had been flushed with dry nitrogen, and stirred overnight. The solid product was filtered, washed several times with anhydrous ether, and dried in an evacuated desiccator. The 9.3 g (99%) of crude 4-methoxyphenyl-1-phenylethyldimethylphenylammonium bromide was recrystallized by dissolving it in a minimum of acetonitrile, placing 4-mL portions into 25 mm × 150 mm test tubes, filling the tubes with anhydrous ether, and allowing the salt to precipitate overnight (recrystallization on a larger scale yielded a sticky oil). Repeated recrystallizations gave a product with a melting point of 107–109°C. The nmr spectrum was consistent with that expected for 4-methoxyphenyl-1-phenylethyldimethylphenylammonium bromide.

Preparation of 4-chlorophenyl-1-phenylethyldimethylphenylammonium bromide

N,N-dimethyl-4-chloroaniline (4.25 g, 0.0273 mol) and 5.04 g (0.0272 mol) of 1-phenylethyl bromide were mixed and left sealed in a dry nitrogen atmosphere overnight. Then the product was filtered, washed with anhydrous ether, and dried in an evacuated desiccator. The 8.88 g (96%) of crude 4-chlorophenyl-1-phenylethyldimethylammonium bromide was recrystallized with acetonitrile – anhydrous ether to a constant melting point of 112.5–113.5°C. The nmr spectrum of the solid was consistent with that expected for the product.

Preparation of 4-methylphenyl-1-phenylethyldimethylphenylammonium bromide

The reactants, 5.06 g (0.0273 mol) of 1-phenylethyl bromide and 4.74 g (0.035 mol) of freshly distilled *N,N*-dimethyl-4-methylaniline were mixed together in a nitrogen atmosphere. The solid that formed in one day was filtered, washed with anhydrous ether, and dried in an evacuated desiccator. Finally, the 6.3 g (72%) of 4-methylphenyl-1-phenylethyldimethylphenylammonium bromide was recrystallized using the method described for the 4-methoxyphenyl-1-phenylethyldimethylphenylammonium bromide. The mp of the pure product was 101–102°C. The chemical shifts and the integration of the peaks in the nmr spectrum were consistent with the structure 4-methylphenyl-1-phenylethyldimethylphenylammonium bromide.

Kinetic measurements

The electrolytic conductivity apparatus used to measure the rate constants for the decomposition of the quaternary ammonium salts consisted of three units, a 1-kHz/s sine wave oscillator (Heath Kit IG-72), a conductivity bridge capable of measuring resistances ranging from 0.1 to 110 000 ohms, and a detector consisting of a 1-kHz low noise, transistorized amplifier and an *X–Y* oscilloscope. The decade resistance of the measuring arm, which was in parallel with variable capacitors to obtain a sharp balance point, measured the resistance to within 0.1%. The conductivity dip cell (cell constant of 0.1) that was used as the unknown arm of the conductivity bridge was equipped with a thermometer adapter and a bushing adapter so that the cell could be sealed completely into the 25 mm × 150 mm ground glass topped test tube that was used as the reaction vessel. These precautions were taken to minimize evaporation of the solvent because the reactions were followed for several hours.

In a typical reaction, approximately 15 mL of distilled chloroform was placed in the reaction vessel. The reaction vessel was sealed with the conductivity dip cell and temperature equilibrated for 30 min at 25.00 ± 0.02°C. Then, a weighed amount (between 0.22 and 0.25 g) of quaternary ammonium salt was dissolved in the temperature equilibrated chloroform. After waiting at least 10 min for the quaternary ammonium salt – chloroform solution to equilibrate, the bridge was balanced and the timer started. Resistance measurements were made every "*x*" minutes according to the Guggenheim method (6, 29). The first-order rate constants were determined from the linear least-squares slope of the Guggenheim plot (6). Care was taken to collect the resistance measurements for each bromide salt over the same range of resistances (concentrations), i.e., from 2747 ± 6 ohms to 44518 ± 1981 ohms, to eliminate any ionic strength effects on the rate constants.

The procedure used to measure the rate constants that were required for determining the Hammett ρ value for the 4-substituted phenyl-1-phenylethyldimethylphenylammonium bromides was slightly different. The changes were (*i*) that 20 mL of distilled chloroform was placed in the reaction vessel, (*ii*) that the temperature was 34.88 ± 0.02°C, (*iii*) that between 0.31 and 0.39 g for the 4-substituted phenyl-1-phenylethyldimethylphenylammonium bromides was used in these runs, and (*iv*) that the time and resistance readings were begun when the quaternary ammonium salt was added to the chloroform and continued every "*x*" minutes until the capacity of the bridge (110 000 ohms) was exceeded or until the concentration of the substrate was less than 0.0246 mol/L. The rate constants for these reactions were obtained by applying the Guggenheim method to the resistances found over the concentrations ranges 0.0508–0.0379 mol/L and from 0.0329–0.0246 mol/L.

Acknowledgements

The authors thank the Natural Sciences and Engineering Research Council of Canada for the financial support required to complete this study and for providing a scholarship to H.A.J.

1. J. T. Burns and K. T. Leffek. Can. J. Chem. **47**, 3725 (1969).
2. E. C. F. Ko and K. T. Leffek. Can. J. Chem. **48**, 1865 (1970).
3. E. C. F. Ko and K. T. Leffek. Can. J. Chem. **49**, 129 (1971).
4. E. C. F. Ko and K. T. Leffek. Can. J. Chem. **50**, 1297 (1972).
5. M. N. Islam and K. T. Leffek. J. Chem. Soc. Perkin Trans. **2**, 952 (1977).
6. K. T. Leffek and F. H. C. Tsao. Can. J. Chem. **46**, 1215 (1968).
7. K. Humski, V. Sendijarevic, and V. J. Shiner, Jr. J. Am. Chem. Soc. **96**, 6187 (1974).
8. K. C. Westaway and R. A. Poirier. Can. J. Chem. **53**, 3216 (1975).
9. K. C. Westaway and R. A. Poirier. 58th Canadian Chemical Conference, Toronto, Ont. 1975.

10. K. C. WESTAWAY and S. F. ALI. Can. J. Chem. **57**, 1089 (1979).
11. S. R. HARTSHORN and V. J. SHINER, JR. J. Am. Chem. Soc. **94**, 9002 (1972).
12. V. J. SHINER, JR. *In* Isotope effects in chemical reactions. Am. Chem. Soc. Monograph 166. *Edited by* C. J. Collins and N. S. Bowman. Van Nostrand – Reinhold, New York. 1971. p. 137.
13. P. J. SMITH. *In* Isotopes in hydrogen transfer processes. Vol. 2 of the Isotopes in Organic Chemistry series. *Edited by* E. Buncel and C. C. Lee. Elsevier, Amsterdam. 1976. pp. 231–237.
14. J. M. HARRIS. Prog. Phys. Org. Chem. Vol. 11. *Edited by* A. Streitwieser, Jr. and R. W. Taft. J. Wiley and Sons, Toronto. 1974. pp. 89–168.
15. K. C. WESTAWAY. *In* Isotopes in chemistry. Vol. 7. *Edited by* C. C. Lee and E. Buncel. Elsevier, Amsterdam. In press.
16. G. A. CRAZE, A. J. KIRBY, and R. OSBORNE. J. Chem. Soc. Perkin Trans. **2**, 357 (1978).
17. B. L. KNIER and W. P. JENCKS. J. Am. Chem. Soc., **102**, 6789 (1980).
18. R. D. G. STEEL and J. H. TORRIE. Principles and procedures of statistics with special reference to biological sciences. McGraw–Hill, Toronto. 1960. pp. 404 and 470.
19. C. WHITE. Biometrics, **8**, 33 (1950).
20. K. C. WESTAWAY and H. A. JOLY. 63rd Canadian Chemical Conference, Ottawa, Ont. 1980.
21. J. M. HARRIS, S. G. SHAFER, J. R. MOFFAT, and A. R. BECKER.. J. Am. Chem. Soc. **101**, 3295 (1979).
22. C. H. GRAY, J. K. COWARD, K. B. SCHOWEN, and R. L. SCHOWEN. J. Am. Chem. Soc. **101**, 4351 (1979).
23. A. STREITWEISER, JR. Solvolytic displacement reactions. McGraw–Hill Co., Toronto. 1962. p. 12.
24. R. C. WEAST (*Editor*). Handbook of chemistry and physics. 48th ed. CRC Press, Boca Raton, Florida 1967–1968. p. 196.
25. A. I. VOGEL. Practical organic chemistry. 3rd ed. Longmans, Green and Co., Toronto. 1954. p. 694.
26. V. J. SHINER, JR., W. E. BUDDENBAUM, B. L. MURR, and G. LAMATY. J. Am. Chem. Soc. **90**, 418 (1968).
27. C. J. POUCHERT. The Aldrich library of NMR spectra. 2nd ed. Aldrich Chemical Co., Milwaukee, WI. 1983. p. 921.
28. K. C. WESTAWAY and A. N. BOURNS. Can. J. Chem. **50**, 2332 (1972).
29. A. A. FROST and R. G. PEARSON. Kinetics and mechanism. 2nd ed. J. Wiley and Sons, New York. 1961. pp. 49–50.

Amino-acid zwitterion equilibria: vibrational and nuclear magnetic resonance studies of methyl-substituted thiazolidine-4-carboxylic acids

H. E. HOWARD-LOCK, C. J. L. LOCK, M. L. MARTINS, P. S. SMALLEY, AND R. A. BELL
Institute for Materials Research and the Department of Chemistry, McMaster University, Hamilton, Ont., Canada L8S 4M1
Received September 23, 1985
This paper is dedicated to Professor Arthur N. Bourns

H. E. HOWARD-LOCK, C. J. L. LOCK, M. L. MARTINS, P. S. SMALLEY, and R. A. BELL. Can. J. Chem. **64**, 1215 (1986).
Infrared and Raman spectra (4000–100 cm^{-1}) of solid samples of six different methyl substituted thiazolidine products of D-penicillamine and L-cysteine hydrochloride have been observed and assigned. Infrared spectra in D_2O solutions have been obtained for comparison in order to study the amino-acid zwitterion equilibria. Proton and ^{13}C nmr spectra for the compounds have also been measured.

H. E. HOWARD-LOCK, C. J. L. LOCK, M. L. MARTINS, P. S. SMALLEY et R. A. BELL. Can. J. Chem. **64**, 1215 (1986).
On a déterminé et interprété les spectres infrarouges et Raman (4000–100 cm^{-1}) d'échantillons solides de six produits différents de la D-pénicillamine et du chlorhydrate de la L-cystéine avec des thiazolidines substituées par des groupements méthyles. Dans le but d'examiner l'équilibre acide aminé zwitterion, on a mesuré les spectres infrarouges dans le D_2O. On a aussi mesuré les spectres rmn du ^1H et du ^{13}C de ces composés.

[Traduit par le revue]

Introduction

The modes of therapeutic action and adverse side effects of the drug D-penicillamine depend on several biochemical reactions, an important one being the ability to form thiazolidine rings with aldehydes and ketones. Thiazolidine-4-carboxylic acid has also been found to act on the cell membrane of tumour cells, possibly causing a reverse transformation to normal cells through restoration of contact inhibition (1). Therefore, we have been investigating thiazolidine-4-carboxylic acids, and in particular measuring their physical, chemical, and spectroscopic properties, as part of our overall program of studying reactions having biological significance or potential medical applications.

The essential amino acids normally exist in the zwitterion form both in the solid state and in aqueous solutions. Recently, we have shown by vibrational spectroscopy and single crystal X-ray diffraction that (*S*)-2,2,5,5-tetramethylthiazolidine-4-carboxylic acid exists in the amino acid form in the solid state and to a minor extent in aqueous solution (2). The unsubstituted thiazolidine-4-carboxylic acid, however, exists in the zwitterion form (2–4). In this work, we attempt to establish by vibrational spectroscopic studies whether methyl substitution at the C2 and C5 positions of the thiazolidine ring affects the amino-acid zwitterion equilibrium. In addition, we have characterized the various species by ^1H and ^{13}C nmr spectroscopy.

Materials and methods

The D-(−)-penicillamine (free base) and L-(+)-cysteine hydrochloride were of reagent grade, as supplied by Sigma Chemical Co., St. Louis, MS. Formaldehyde, 37%, reagent grade was supplied by Sargent Welch Scientific Co., Skokie, IL. Acetaldehyde was distilled from paraldehyde, reagent grade, supplied by BDH; acetone, reagent grade, was supplied by BDH Chemicals, Toronto, Ont. The preparation of the several thiazolidine-4-carboxylic acids was carried out as indicated schematically in Table 1 and outlined in detail as follows:

Thiazolidine-4-carboxylic acid, I

The method of Ratner and Clarke (5) was followed with modification. L-Cysteine hydrochloride hydrate, **A**, 0.5 g (0.003 mol) was dissolved in 2 mL H_2O to which 0.4 ml (0.4 g or 0.003 mol) of 37% (w/w) formaldehyde was added; the mixture was left to react for 15 h at room temperature. Then 0.5 mL pyridine was added. In 30 min, a white solid started separating slowly. Ethanol, 1 mL, was added and the mixture was placed in the refrigerator. Prismatic crystals were separated from the pyridine ethanol mixture by filtration. The compound was recrystallized from ~10 mL hot H_2O to give 0.3 g (0.002 mol, 70%) of a white, crystalline product, mp 185–187°C (dec.), lit. 184–185°C (dec.) (5).

2-Methylthiazolidine-4-carboxylic acid, II

The method of Riemschneider and Hoyle (6) was followed with modification. To 1.4 mL H_2O was added 2.0 g **A** (0.01 mol) 1 mL, glacial acetic acid, followed by 20 mL EtOH. The solution was placed on ice and after 30 min the solid hydroacetate precipitated. This was filtered out, dissolved in water, and the solution placed on ice. Freshly prepared acetaldehyde, 0.5 g (0.013 mol), was added. The clear mixture was allowed to stand in the refrigerator 48 h; then 0.5 mL pyridine was added. A few days later a thick white precipitate was filtered out and air-dried. Weight 1.0 g (yield 60%); mp 153–155°C (dec.), lit. 161–163°C (6).

2,2-Dimethylthiazolidine-4-carboxylic acid, III

The method of Sheehan and Yang (7) was followed with modification. **A**, 0.7 g (0.0057 mol), was added to 180 mL freshly distilled acetone in a 250 mL round bottom flask. The mixture was refluxed for 7 h and then allowed to cool. The undissolved material (0.5 g unreacted cysteine) was removed by filtration. Acetone was removed by distillation and the remaining 10 mL solution was allowed to stand in the refrigerator. Within a few days a cluster of long thin crystals formed in the acetone solution. These were recrystallized from hot acetone to give 0.1 g product, (62% based on the 0.2 g L-cysteine which reacted, 11% based on the initial 0.7 g); mp 163–165°C, lit. 163–165°C (7).

5,5-Dimethylthiazolidine-4-carboxylic acid, IV

The method of Nagasawa *et al.* (8) was followed with modification for **IV** and **V**. D-Penicillamine, **B**, 0.50 mg (0.0034 mol), was mixed with 10 mL EtOH and 2.5 mL H_2O, resulting in a white suspension. Formaldehyde, (37% w/w), 0.5 mL (0.004 mol), was added with stirring and within 30 min the mixture was clear. In 1 h the mixture turned into a white jelly-like solid suspension. This was left at room temperature for approximately 15 h, and then a few drops of pyridine were added. There was no apparent change in the reaction mixture. The white suspension was filtered off and dried in a desiccator for several days. Yield 0.285 g product (0.0018 mol, 53%); mp 194–196°C, lit. 196–197°C (dec.) (8).

2,5,5-Trimethylthiazolidine-4-carboxylic acid, V

B, 1.55 g (0.01 mol), was dissolved in 15 mL H_2O and the mixture was filtered to remove a small amount of undissolved material. The solution was cooled in an ice bath and 1.2 mL (0.02 mol) acetaldehyde was added with stirring; the flask was then sealed with parafilm. In

TABLE 1. Nomenclature and preparation scheme for the thiazolidine-4-carboxylic acids[a]

Reactants	Formaldehyde	Acetaldehyde	Acetone
A, L-cysteine	**I**, thiazolidine-4-COOH	**II**, 2-monomethyl-	**III**, 2-dimethyl-
B, D-penicillamine	**IV**, 5,5-dimethyl-	**V**, 2,5,5-trimethyl-	**VI**, 2,2,5,5-tetramethyl-

Nomenclature: The products are secondary amino acids which are 5-membered heterocyclic rings containing sulfur at atom position 1, nitrogen at position 3, carbons at 2, 4, and 5, and the COOH group attached to the carbon at 4.

[a]Reflux overnight at room temperature or gentle heat (~80°C).

~1½ h a white precipitate started to form and the cold bath was removed. After 3 h stirring at room temperature the mixture became clear. The solvent was evaporated in a Buchi rotoevaporator and the white residue was recrystallized from hot ethyl acetate to give 0.721 g of product (0.004 mol, 40%); mp 161–162°C, lit. 165.5–167.5°C (8).

2,2,5,5-Tetramethylthiazolidine-4-carboxylic acid, VI

The method of Howard-Lock *et al.* (2) was followed: **B**, 3.0 g (0.02 mol), was dissolved in 20 mL H_2O and excess acetone (40 mL) was added. The mixture was stirred for 15 h at room temperature. The solvent was evaporated under N_2 to near dryness, and the resulting solid was filtered off and recrystallized from hot acetone. Yield: 2.70 g product (0.014 mol, 70%).

Spectral measurements

Infrared spectra were recorded on both Nicolet 7199 FT-IR and Perkin-Elmer Model 283 spectrophotometers. The samples were ground with KBr at a concentration of approximately 1% by weight and then pressed into pellets. To confirm that certain peaks were real, and not manifestations of the pelleting procedure, the spectra of certain samples were also run in Nujol and again in hexachlorobutadiene. D_2O solution spectra were run with AgCl windows. Spectra were calibrated with polystyrene. Raman spectra were excited by means of the λ5145 Å radiation from a Spectra-Physics Model 164-02 argon ion laser and recorded on a Spex 14018 double monochromator. Solid samples were contained in glass melting point tubes, and solutions in nmr tubes. The spectrometer was calibrated regularly against an indene standard and had previously been calibrated with a neon lamp; the wavelength readout scale was found not to change (± 1–2 cm^{-1}).

Solutions for nmr studies were prepared in D_2O and concentrations were about 100 mg (solid) mL^{-1} of solvent. Internal TSP (trimethylsilylpropionic acid) was used as the reference. Proton nmr spectra were recorded on a Varian T60 spectrometer, and ^{13}C nmr spectra were recorded on a Bruker WP-80 spectrometer operating at 20.115 MHz.

The p*K*'s of the various thiazolidine-4-carboxylic acids were obtained by titration of an aqueous solution with 0.01 *N* NaOH and 0.01 *N* HCl. The pH's were measured with a Corning Model 130 pH meter which was standardized with Scientific Products potassium hydrogen phthalate pH 4.00 buffer, BDH pH 7.00 buffer, and Scientific Products boric acid/potassium hydroxide pH 10.00 buffer. The pH measurements are reliable to ±0.03.

Results and discussion

The vibrational spectra

The thiazolidine-4-carboxylic acids are secondary α-amino acids which are five-membered heterocyclic molecules having no symmetry elements. There is very little published work relating to the vibrational spectra of thiazolidine-4-carboxylic acids. Some isolated C—S bond frequencies are listed by Freeman (9) for various cyclic sulfides. A study of the vibrational spectra of thiazolidine and ND thiazolidine has been reported, followed by a similar study of three monomethyl thiazolidines (substituted at the C(2), C(4), and C(5) positions (10). These studies did not include work on the 4-carboxylic acids. The infrared spectra of some chelates of thiazolidine acids, including the spectra of free ligands 2-methyl-, 2,2-dimethyl-, 2,2,5,5-tetramethyl- and 2-benzylthiazolidine-4-carboxylic acids have been reported, for the range 4000–400 cm^{-1} (11). Our spectra of these ligands cover a greater cm^{-1} range, and they differ in many details. Detailed spectroscopic studies of D-(−)-penicillamine and its deuterated derivatives, in solid solution, both acid and zwitterion forms (12) and of (*S*)-2,2,5,5-tetramethylthiazolidine-4-carboxylic acid and several deuterated species (2) have been reported recently by us.

The spectra of the thiazolidines show many similarities to those of D-penicillamine and its deuterated derivatives, both ref. 12 and this work, and to those for L-cysteine, the main differences being (*i*) the absence of νS—H and δS—H bands; (*ii*) the replacement of bands of the NH_3^+ group by those of the NH group; and (*iii*) the presence of the three unique ring deformations δCSC, δCNC, and δNCS, which are not present in D-penicillamine or L-cysteine.[1]

We discuss here only those features of the spectra which pertain to the CO_2^- (or COOH) and NH_2^+ (or NH) groups; that is, the features relevant to the amino-acid zwitterion equilibria (see Table 2). Strong, broad bands in the infrared spectrum at about 2500 and 1950 cm^{-1}, compounds **IV**, **V** and **VI**, (slightly higher for compounds **I**, **II**, **III**) are typical of fairly strong O—H···N bonding. These bands appear only in the infrared, and not in the Raman spectra for compounds **IV–VI**. They are present in all samples, whether prepared as KBr discs or Nujol or hexachlorobutadiene mulls (and thus are not spurious bands from moisture in KBr). These bands are less consistent in the L-cysteine based compounds, with compounds **I** and **II** showing a single broad band at 2330 and 2630 cm^{-1} and **III** showing bands at 2528 cm^{-1} (ir, Raman) and 2075 cm^{-1} (ir alone).

Bands attributed to the COOH group: The strong infrared bands at 1744–1715, 1330, and 1190–1215 cm^{-1} are assigned as νC=O, δOH, and νC—O, respectively, in **III**, **V**, and **VI**, having mainly the amino-acid form. These assignments are consistent with the findings of the X-ray work for (*S*)-2,2,5,5-tetramethylthiazolidine-4-carboxylic acid, a compound which exists in the solid in the strongly hydrogen-bonded acid form (2). Bands attributable to the CO_2^- and NH_2^+ groups help identify compounds in the zwitterion form, **I** and **IV**. The specific assignments are in the regions 1620–1555 and 1425–1393 cm^{-1} for $\nu_a CO_2^-$ and $\nu_s CO_2^-$, and 1550–1585 cm^{-1} for δNH_2^+. The spectra of **II** show bands for both forms.

Nuclear magnetic resonance spectra

The ^1H nmr spectra and assignments of the methyl-substituted thiazolidine-4-carboxylic acids are given in Table 3. The

[1]Tables containing the complete listing of infrared and Raman frequencies and the approximate mode descriptions and assignments for compounds **A**, **B**, **I–VI** (6 pages) may be purchased from the Depository of Unpublished Data, CISTI, National Research Council of Canada, Ottawa, Ont., Canada K1A 0S7.

TABLE 2. Selected vibrational bands[a]

I[b] Z[d] *R*[e]	II AA and Z *RR, SR*	III AA *R*	IV Z *S*	V AA, A* *RS, SS*	VI AA, Z* *S*	Assignment[c]
2330, ir	2630, ir	2528, ir	2435, ir	2450, ir	2470, ir	O—H...N
2320, R		2075, ir				
—	1732, ir	1745, ir⎫	—	1732, ir⎫	1728, ir	ν C═O
		1740, R⎭		1730, R⎭		
1628, ir⎫	1610, ir	—		1634, ir*		
1630, R⎭			1598, ir⎫		1612, ir*	$\nu_a CO_2^-$
1552, ir	1536, ir	—	1598, ir⎭			δNH_2^+
1380, ir⎫	1388, ir	—	1385, ir	1400, R*	—	$\nu_s CO_2^-$
1388, R⎭						
1340, ir	—	1335, ir	—	1322, ir	1329, ir	δ OH
—	1218, ir	1200, ir	—	1227, ir	1216, ir	ν C—O

[a]Infrared and Raman bands, cm^{-1}, relevant to the amino acid and zwitterion equilibria.
[b]Compounds **I–VI** as defined in Table 1.
[c]ν = stretch frequency, a = antisymmetric, s = symmetric, δ = deformation.
[d]Forms present in the solid state: Z, zwitterion; AA, amino acid; Z*, zwitterion detected by ir bands in D_2O solution.
[e]Enantiomers and diastereomers present.

TABLE 3. ^1H nmr spectra of methyl-substituted thiazolidine-4-carboxylic acids[a,b]

Compound	H(C-2)	H(C-4)	H(C-5)	CH_3(C-2)	CH_3(C-5)
Thiazolidine	4.35, s, 10	4.40, dt, 5	3.32, m, 10	—	—
2-Methyl-	4.60, q, 6	5.05, t, 6	3.50, m, 12	1.73, d, 18	—
				1.76, d	
2,2-Dimethyl-	—	4.77, t, 3	3.45, d, 8	1.70, s, 18	
			3.50, d		
5,5-Dimethyl-	4.45, s 12	3.95, s, 7	—	—	1.42, s, 21
	4.50, s				1.68, s, 21
2,5,5-Trimethyl-	4.90, q, 5	3.94, s, 5	—	1.58, d, 14	1.37, s, 28
		4.02, s			1.63, s
2,2,5,5-Tetramethyl-	—	4.2, s, 44	—	1.76, s, 16	1.43, s, 18
				1.94, s, 18	1.68, s, 17

[a]Solutions in D_2O, TSP used as internal standard.
[b]The chemical shift in ppm is followed by peak multiplicity (s = singlet, d = doublet, t = triplet, q = quartet, m = multiplet) and by the integrated peak area.

non-methylated compound has the simplest spectrum with the C2 hydrogens giving rise to a singlet which indicated both protons have the same average chemical environment. The downfield signal is the hydrogen at C4, which is next to an electron-withdrawing carboxyl group having a deshielding effect; the signal is split into a triplet by the two neighbouring protons on C5. The signal of the C5 protons is upfield; these protons have slightly different chemical environments because of their proximity to the carboxyl group; each proton gives rise to a doublet as a result of splitting by the vicinal proton on C4.

2-Methylthiazolidine-4-carboxylic acid, **II**, is a mixture of two stereoisomers: C4 is a fixed chiral center, derived from L-cysteine in this case and with the same *R* conformation, but there is a new chiral carbon, C2, which can be *R* or *S*. The lowest field triplet is the C4 hydrogen. C2-H is split into a quartet by the methyl group attached to the same carbon. The C5 proton signal, of chemical shift 3.5 ppm, is a multiplet because it results from two overlapping doublets of doublets. The doublet of doublets of each proton arises from it being split by the C4 proton and by the geminal proton. The methyl group on C2 gives a doublet and there are two such signals because the methyl group can be on the same side of the ring as the carboxyl group or on the opposite side, because both *R* and *S* isomers are present.

The two methyl groups of the 2,2-dimethyl compound, **III**, give only one singlet in the spectrum, and therefore, they have equivalent chemical environments. They are situated far enough away not to be affected by the carboxyl group, but the two C5 protons, both doublets of doublets, give rise to two distinct signals, split by the C4 proton and in turn by each of the C5 protons, resulting in a quartet of peaks of equal intensity. For the C4 proton, a triplet is observed.

For the 5,5-dimethyl- compound, **IV**, it is somewhat surprising that there are two different C2 proton signals in the spectrum. The two methyl groups appear as two singlets, because there is no plane of symmetry in the molecule.

2,5,5-Trimethylthiazolidine-4-carboxylic acid, compound **V**, also has two chiral centers, and can exist as two diastereomers (*S*,*R* or *R*,*R*) in any proportion. Two sets of resonance signals for each type of proton in the molecule are expected; only one signal was observed for the C2 proton and another one for the methyl group, but the presence of the two diastereomers is shown by the signals for C4.

2,2,5,5-Tetramethylthiazolidine-4-carboxylic acid, compound **VI**, exhibits the expected nmr spectrum. It consists of five singlets, one for each methyl group and one for the single proton bonded to C4. The methyls on C2 are the downfield singlets because they are more deshielded by S and N, both of which are

TABLE 4. Carbon-13 chemical shifts of methyl-substituted thiazolidine-4-carboxylic acids[a]

Compound	C-2	C-4	C-5	C(OOH)	CH_3(C-2)	CH_3(C-5)
Thiazolidine	50.00	65.30	34.29	173.14	—	—
2-Methyl-	62.04	64.84	33.99	172.89	19.80	—
	62.57	65.60	34.20		18.85	
2,2-Dimethyl-	63.52	55.63	32.81	171.36	25.04	—
					27.85	
5,5-Dimethyl-	53.84	73.08	46.87	170.16	—	26.45
						28.26
2,5,5-Trimethyl-	58.38	73.29	54.18	170.86	28.49	26.79
	58.83	74.51	54.84		30.94	28.14
2,2,5,5-Tetramethyl-	73.46	73.46	61.62	171.31	32.24	28.52
					34.36	29.61

[a]Solutions in D_2O.

TABLE 5. pK values of L-cysteine, D-penicillamine and related thiazolidine-4-carboxylic acids

Compound	pK_1[a]	pK_2[b]	$\Delta G°$	Isoelectric point[c]
L-Cysteine	1.96[d]	8.18[d]	−4.23[e]	5.07
D-Pencillamine	1.8	7.9	−4.14	4.85
Thiazolidine-4-carboxylic acid	1.51[d]	6.21[d]	−3.19	3.86
2-Methyl-4-carboxylic acid	2.8	6.0	−2.17	4.4
2,2-Dimethyl-4-carboxylic acid	2.7	5.7	−2.04	4.2
5,5-Dimethyl-4-carboxylic acid	2.7	5.8	−2.11	4.25
2,5,5-Trimethyl-4-carboxylic acid	2.6	5.6	−2.04	4.1
2,2,5,5-Tetramethyl-4-carboxylic acid	2.8	5.5	−1.83	4.35

[a]pK_1 is pK of COOH group.
[b]pK_2 is pK of amino group.
[c](1/2) (pK_1 + pK_2).
[d]Ratner and Clarke, ref. 5.
[e]Calculated in kcal mol^{-1}, from $\Delta G = -RT \ln (K_2/K_1)^{1/2}$.

electron withdrawing. This assignment was confirmed previously by deuteration of the C2 methyl groups (2).

All the C5 methyl groups in Table 2 have very consistent chemical shifts, generally to high field of the C2 methyl groups.

NOE experiments have been carried out with derivatives of penicillin to study thiazolidine ring conformation (13), and have shown that the signals of pro-*R* methyl hydrogens are always at higher field than the hydrogens of pro-*S* methyl groups. By analogy, the 1.68 ppm peak in the spectrum of the 2,2,5,5-tetramethyl compound **VI**, spectrum is assigned to the pro-*R* methyl protons of C5 and the 1.43 singlet to the pro-*S* methyl protons. A study of *erythro* and *threo* sterochemistry of five-membered rings by proton nmr lists also the spectra of tetramethylthiazolidine-4-carboxylic acid, and the assignments agree with those above (14).

Table 4 lists the carbon-13 shifts observed.

The carboxyl carbon is highly deshielded by the two oxygens, and its signal is well downfield, always 170–174 ppm. C4 is expected to be the next most deshielded carbon. As previously discussed with respect to the ^{1}H nmr spectra, the proton on C4 is also the most deshielded because of the proximity to the carboxyl group. C5 is more deshielded than C2 as illustrated by compound **I**, with C2 assigned a chemical shift of 50, and C5, 34.29. This trend continues down the table, although peaks are quite close.

The carbon-13 chemical shifts of compounds **II** and **I** are very similar. C4 and C5 are deshielded to nearly the same extent. The greatest change was observed with C2, with the CH_3 group on C2 causing increased chemical shift, as expected.

In compound **III**, the value of C2 increased only slightly, compared to the same carbon in the 2-methyl compound. C4 has decreased, which cannot be easily explained because the two methyl groups on C2 appear to be too far away from C4 to cause an alteration in the chemical shift unless the conformation of the ring was changed. The carboxyl carbon has its chemical shift lowered by >1 ppm. The methyl carbon on C2 was shifted downfield considerably compared with 2-methylthiazolidine.

For compound **IV**, an increase in the chemical shift of C5 was observed, compared to the values for compounds **I–III** derived from L-cysteine. There is also a large increase in the value for C4; it appears that these methyl groups are close enough to C4 to have an effect similar to that observed for the C5 carbon to which the methyls are directly bound. The chemical shift of C2 has reverted to nearly the same value as in the non-methylated thiazolidine compounds. The C5 methyl groups always occur to slightly higher field than the C2 methyl groups, presumably because of the γ-shielding of the COOH group. This is a general trend which becomes more apparent as more methyl groups are introduced into the molecule.

With compound **V**, C2 again showed an increase in chemical shift relative to compound **IV**. This molecule, **V**, like the 2-methyl compound, **II**, contains two chiral centers, the one at C4 being always *S*, and it can occur in *R*,*S* and *S*,*S* configurations. The compounds are probably about 50:50 mixtures of the two diastereomers, judging from the heights of the duplicated proton nmr signals. The increased chemical shift of C2 relative to that for the compound **IV** reflects the presence of a new methyl group on that carbon. C4 also increased

slightly, which is consistent with the trend previously noted of increasing chemical shifts with every new methyl group added to the thiazolidine ring. The chemical shift of C5 has increased by almost 8 ppm; the presence of one more methyl group on another carbon in the molecule is not a sufficient reason to explain such a large effect, unless the stereochemistry of the ring has changed in such a way as to bring the new methyl spatially close the C5 atom so that the nuclear shielding is altered.

In the compound **VI**, C2 again has a higher value than in the previous compound which only had one C2 methyl group. It should be noted that since there is peak overlap in this compound, either of 61.62 or 76.46 could be assigned to C2 and it is arguable which of the assignments is correct. The chemical shift of C2 is more likely to be 73.46 since it is expected to be higher than that of C5, because of the higher deshielding effects of the N and S atoms around C2 in the ring. For this compound, the methyl group chemical shifts have been assigned previously to C2 and C5 methyl carbons by deuteration of the C2 methyls (2). The 61.62 ppm peak assigned to C5 is of higher chemical shift than expected from the values in ppm assigned to C5 of the other thiazolidine molecules listed in Table 3. Previosly published spectra of *N*-formyl-2,2,5,5-tetramethylthiazolidine compounds (15) helped in the assignment of peaks, as well as the recording of "spin-sort" spectra in which the peaks arising from carbons with an odd number of protons show up below the baseline while carbons with an even number of protons give rise to peaks above the baseline. The methyl group carbons deserve a reference. In thiazolidines that have both C2 and C5 methyl substituents, the methyls on C2 have higher chemical shifts than the C5 methyls, probably because of the proximity of the electronegative N and S. In substituted penicillins the relative shifts were C2 > C5, pro *S* CH_3(C5) > pro *R* (16). If 2,2,5,5-tetramethylthiazolidine-4-carboxylic acid can be considered analogous, the assignments have the same order.

The amino-acid zwitterion equilibria

The p*K* values represent the extent of protonation of ionizable groups, and are presented in Table 5. There is a downward shift of amino group p*K* with increasing CH_3 substitution, especially C2. Increase of COOH group p*K* with methyl substitution is partly caused by inductive effects of the methyl group. Also the anion cannot be solvated so effectively, so that the equilibrium $AH \rightleftarrows A^- + H^+$ is shifted to the left hand side.

From the usual relationship of the Gibbs standard free energy to the equilibrium constant associated with a given reaction in solution, we have calculated the free energy of conversion from the amino acid to the zwitterion form. The values of ΔG^0, also shown in Table 5, vary between -4.2 and -1.8 kcal mol^{-1} for L-cysteine and tetramethylthiazolidine-4-carboxylic acid. If the compounds were tabulated in order of ΔG°, the 2,2-dimethyl-compound, **III**, would be placed below the 5,5-dimethyl compound, **IV**.

Compounds which exist in the amino-acid form in the solid include 2,5,5-trimethyl- and 2,2,5,5-tetramethylthiazolidine-4-carboxylic acid, **V** and **VI**, both derived from D-penicillamine, and the 2,2-dimethyl species, **III**, derived from L-cysteine. When **V** is crystallized from D_2O, howver, it occurs as the zwitterion in the solid state. In D_2O solutions, zwitterion forms are present for all three compounds, although compound **VI** still has a significant concentration of the acid form, as shown by the infrared spectra.

We have shown that methyl substitution at the C2 and C5 positions of the thiazolidine ring does indeed affect the amino-acid zwitterion equilibrium. It was originally assumed that the acidity mght be proportional to the number of CH_3 groups. The shift in equilibrium did not follow this simple relationship, however, since from the infrared spectra the 5,5-dimethyl compound, **IV**, showed no amino acid form in the solid, while the 2-methyl and 2,2-methyl compounds, **II** and **III**, showed evidence for both amino acid and zwitterion forms in the solid. It seems likely that both the number and position of the methyl groups affect the ring conformation and the hydrogen bonding patterns in ways which result in stabilization of either the amino acid or the zwitterion.

The 2-methyl and 2,5,5-trimethyl compounds, **II** and **V**, do have one other feature in common; namely, they can exist as two diastereomers, *RR*, *SR* and *RS*, *SS* respectively. The vibrational spectra of these two compounds show many extra bands, a fact which is consistent with both diastereomers being present. There is, however, no evidence that this factor alone is sufficient to explain the change in the amino acid zwitterion equilibria, although it would mean different entropy values.

Acknowledgement

We thank the Natural Sciences and Engineering Research Council of Canada for financial support of this work.

1. A. BRUGAROLAS and M. GOSALVEZ. Lancet, **1**, 68 (1980).
2. H. E. HOWARD-LOCK, C. J. L. LOCK, and P. S. SMALLEY. Can. J. Chem. **63**, 2411 (1985).
3. J. LOSCALZO, R. G. KALLEN, and D. VOET. Arch. Biochem. Biophys. **157**, 426 (1973).
4. M. GOODMAN, V. CHEN, L. BENEDETTI, C. PEDONE, and P. CORRADINI. Biopolymers, **11**, 1779 (1972).
5. S. RATNER and H. T. CLARKE. J. Am. Chem. Soc. **59**, 200 (1937).
6. V. R. RIEMSCHNEIDER and G. A. HOYER. Z. Naturforsch. **17***b*, 765 (1962).
7. J. C. SHEEHAN and D. D. H. YANG. J. Am. Chem. Soc. **80**, 1158 (1957).
8. N. T. NAGASAWA, D. J. GOON, and E. G. DEMASTER. J. Med. Chem. **21**, 1274 (1978).
9. S. K. FREEMAN. Applications of laser Raman spectroscopy. John Wiley and Sons, New York. 1974.
10. M. GUILIANO, G. DAVIDOVICS, J. CHOUTEAU, J. L. LARICE, and J. P. ROGGERO. (*i*) J. Mol. Struct. **25**, 329 (1975); (*ii*) J. Mol. Struct. **25**, 343 (1975).
11. E. CATRINA. Rev. Roumaine Chim. **21**, 81 (1976).
12. H. E. HOWARD-LOCK, C. J. L. LOCK, and P. S. SMALLEY. J. Cryst. Spectrosc. Res. **13**, 333 (1983).
13. R. D. G. COOPER, P. V. DEMARIO, J. C. CHENG, and N. D. JONAS. J. Am. Chem. Soc. **91**(6) 1408 (1969).
14. K. NAKANISHI, D. A. SCHOOLEY, M. KOREEDA, and I. MIURA. J. Am. Chem. Soc. **94**, 2865 (1972).
15. S. TOPPET, P. CLAES, and J. HOOGMARTENS. Org. Magn. Res. **6**, 48 (1974).
16. R. A. ARCHER, R. D. G. COOPER, P. V. DEMARCO, and L. F. JOHNSON. Chem. Commun. 1291 (1970).

Photoisomerization of the $AlEtCl_2$ complex of *endo*-tricyclo[5.2.1.$0^{2,6}$]deca-4,8-dien-3-one

RONALD F. CHILDS,[1] BARRY M. DUFFEY, AND MAILVAGANAM MAHENDRAN
Department of Chemistry, McMaster University, Hamilton, Ont., Canada L8S 4M1
Received October 17, 1985
This paper is dedicated to Professor Arthur N. Bourns

RONALD F. CHILDS, BARRY M. DUFFEY, and MAILVAGANAM MAHENDRAN. Can. J. Chem. **64**, 1220 (1986).

Irradiation of the $AlEtCl_2$ complex of *endo*-tricyclo[5.2.1.$0^{2,6}$]deca-4,8-dien-3-one (**1AL**) yielded the $AlEtCl_2$ complex of *exo*-tricyclo[5.3.0.$0^{2,6}$]deca-4,8-dien-3-one (**3AL**). The structure of **3**, which was obtained on treatment of the irradiated solution with water, was established by its reduction to give the known *exo*-tricyclo[5.3.0.$0^{2,6}$]decan-3-one. The photoisomerization of **1AL** could not be driven to completion as **3AL** underwent a photoisomerization to regenerate **1AL**. Control experiments showed that the interconversions of **1AL** and **3AL** were photochemically and not thermally induced. Irradiation of $AlEtCl_2$ complex of trideutero derivative **6** did not lead to any deuterium scrambling in the starting material, indicating that no hidden skeletal isomerization such as a 2-carbon plus 3-carbon cycloaddition is taking place during this isomerization. The mechanisms of the photoisomerizations are discussed.

RONALD F. CHILDS, BARRY M. DUFFEY et MAILVAGANAM MAHENDRAN. Can. J. Chem. **64**, 1220 (1986).

L'irradiation d'un complexe formé de $AlEtCl_2$ et de la tricyclo[5.2.1.$0^{2,6}$] décadiène-4,8 one-3-*endo* (**1AL**) conduit à un complexe du $AlEtCl_2$ avec de la tricyclo[5.3.0.$0^{2,6}$] décadiène-4,8 one-3-*exo* (**3AL**). Le composé **3** est obtenu par traitement de solution irradiée avec de l'eau et sa structure a été déterminée à la suite de sa réduction en tricyclo[5.3.0.$0^{2,6}$] décanone-3-*exo* qui était déjà connue. Le composé **3AL** subissant une photo-isomérisation qui regénère le composé **1AL**, la photo-isomérisation du composé **1AL** ne peut donc jamais être complète. Des expériences de contrôle ont permis de montrer que les interconversions entre les composés **1AL** et **3AL** sont induites photochimiquement et non pas thermiquement. L'irradiation du complexe formé par le $AlEtCl_2$ et le dérivé trideutéré **6** conduit pas à une répartition au hasard des deutérium présents dans le produit de départ; ce résultat suggère que cette isomérisation n'est pas accompagnée d'isomérisations cachées du squelette, comme des cycloadditions de 2 carbones avec 3 carbones. On discute des mécanismes des photo-isomérisations.

[Traduit par le revue]

In a continuation of our studies on the photochemistry of oxygen protonated or complexed enones (1) we have examined the effect of Lewis acids on the photochemistry of **1**. Irradiation of **1** under conventional conditions leads to an intramolecular [2 + 2] cycloaddition and the formation of **2** in high chemical and photochemical yield (2). Complexation of the carbonyl oxygen of **1** with a Lewis acid will cause the lowest excited states to be of π,π^* character and we were interested in seeing if the cycloaddition reaction would still occur under these conditions. In addition there is the possibility that a further [2 + 2] cyloaddition could occur with bonding from C_3 and C_5 of the complexed cyclopentenone with the double bond. Such a reaction would correspond to the photoaddition of an allyl cation to a double bond and would extend the range of known photochemical cycloadditions.

Results and discussion

The reaction of **1** with several Lewis acids was examined in $CDCl_3$ solution using ^1H nmr spectroscopy. The changes observed in the nmr spectra of **1** at room temperature in the presence of $[AlEtCl_2]_2$ were consistent with the formation of an oxygen bound complex, Table 1. Spectra obtained at low temperature indicated that the seemingly simple room temperature spectrum was due to a rapid exchange between several closely related complexes resulting from the disproportionation of the aluminum species (3). The uv spectrum of this mixture of complexes showed a strong absorption at 258 nm. The $AlEtCl_2$ complex of **1** was thermally stable at room temperature and **1** could be recovered unchanged on neutralization of the Lewis acid.

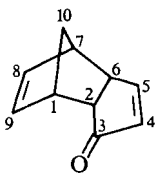

1

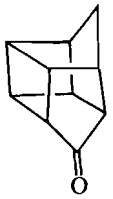

2

Other Lewis acid complexes of **1** were not so suitable for photochemical studies. The $SnCl_4$ complexes were found to be very insoluble and unsuitable for photochemical work. The $SbCl_5$ complexes were soluble but their uv spectra were complicated by the presence of a strong absorption band due to the Lewis acid (4). In view of the well behaved nature of the $AlEtCl_2$ complexes, it was decided to use these for the photochemical studies.

Irradiation of a $CHCl_3$ solution of complex **1AL** at −50°C led to the formation of a new product. The course of the photoreaction was monitored by ^1H nmr spectroscopy directly on the irradiated solution and by glc after the Lewis acid had been removed. Neutralization of the reaction mixture and separation of the product yielded a new compound, **3**, which was isomeric with the starting material.

The carbon skeleton of **3** and position of the carbonyl group were established by its reduction to **4** which was shown to be identical to authentic material prepared by an independent route (5). The presence of one double bond conjugated to the carbonyl group in **3** was clearly shown by the characteristic chemical shifts of the two vinyl protons (δ 7.71 and 6.29) and their downfield shift when **3** was complexed with $AlEtCl_2$ (δ 8.75 and 7.00). The position of the second double bond was shown by examination of high field ^1H nmr spectra of **3** and shift reagent experiments. At 500 MHz it was possible to resolve all the proton resonances of **3** and with the use of a homonuclear 2D ^1H nmr spectrum completely assign all the signals, Table 2. It was thus shown that the two methylene protons at δ 2.33 and 2.59 were coupled to H(1) (δ 3.04) and not to H(7) (δ 2.36). The

TABLE 1. ^{1}H nmr[a] and uv[b] data for ketones

Compound[e]	Chemical shift[c,d], ppm				λ_{max} (nm)	ϵ
	H_4	H_5	viny H	Other		
1		7.38dd	5.88m	3.40m, 3.14m, 2.96m, 2.75m, 1.67m	225	6.6×10
1AL	6.63d	8.30dd	5.91m	3.80m, 3.51m, 3.19m, 1.94m	258	9.0×10^3
2				2.98m, 2.40bt, 2.02m, 1.61m		
2AL				2.4–3.4m, 1.8m		
3	6.29d	7.71dd	5.82m	3.18m, 3.12m, 2.4–2.7m	229	8.4×10^3
3AL	7.00d	8.75dd	5.92m	3.55m, 3.43m, 2.4–2.9m	261	1.2×10^4
Trideuterio Compounds						
6		7.39s	5.89m	3.15bs, 2.90bs, 1.63m		
6AL		8.26s	5.92m	3.50m, 3.16m, 1.90m		
7		7.69s	5.80m	2.5–2.7m, 3.10m		
7AL		8.71s	5.92m	2.6–2.8m, 3.43m		

[a]In $CDCl_3$, 35°C.
[b]In $CHCl_3$, 25°C.
[c]In ppm from CH_2Cl_2 (5.336, 35°C) or $CHCl_3$ (7.249, 35°C).
[d]d = doublet, m = multiplet, bt = broad triplet, s = singlet, bs = broad singlet.
[e]1.1–1.2 mol. equiv. $[AlEtCl_2]_2$ was used. This gave rise to (an additional) two signals of lesser intensity for H_4, indicating the occurrence of disproportionation.

addition of shift reagent ($Eu(TFC)_3$) to a solution of **3** caused the resonances of the two methylene protons to be shifted downfield whereas those of the two vinyl protons of the second double bond remained essentially unaffected. The results of both the high field ^{1}H nmr study and the shift reagent experiment show that the second double bond is between C_8 and C_9.

The photoisomerization of **1AL** could not be driven to completion with extended periods of irradiation and it appeared that a photostationary state was being established. This was confirmed by irradiation of a solution of **3AL** when it was found to be converted back to **1AL**. The limiting amount of **3AL** present at the photostationary state was ca. 36% using either 254 nm or 300 nm light sources.

The same interconversion of **1AL** and **3AL** occurred on irradiation at room temperature, however, more material was lost as an insoluble polymer under these conditions. At the lower temperatures typically >85% of the starting ketone could be accounted for in terms of volatile products.

Several control experiments were run. Complexes **1AL** and **3AL** were stable at room temperature and did not interconvert showing that the interconversions of the complexes **1AL** and **3AL** were photochemical and not thermally initiated. It was further shown that the $AlEtCl_2$ complex of **2**, a potential photoproduct in the reaction, was also photochemically and thermally stable under the conditions used for the photochemical reactions of the complexes **1AL** and **3AL**. The cage compound **2** in the absence of the Lewis acid was shown to be inert when irradiated at 254 nm under the conditions used here. It is clear that **2** is not produced under the photochemical conditions used in this work. The irradiation of **1** in the absence of the Lewis acid at 254 nm led only to the formation of **2**.

From the results given above it is clear that the interconversion of **1AL** and **3AL** is a photochemical reaction involving the complexed ketones and that the $AlEtCl_2$ complex of **2** is not an intermediate in these reactions. The isomerizations observed are quite different from those of the neutral ketones when irradiated under the same conditions in the absence of $AlEtCl_2$. The chromophore absorbing the photon in the cases presented here is a complexed cyclopentenone and the lowest energy excited states will be of π,π^* character (6). A further possible difference between the photoisomerizations **1** and **1AL** is the multiplicity of the excited states involved. The conversion of **1** to **2** is known to involve a triplet state (2).

The question arises as to whether a 3-carbon plus 2-carbon (3C + 2C) closure is occurring in **1AL**. The product of such a reaction would be **5** which could reopen to yield **1AL**. Owing to

[1]

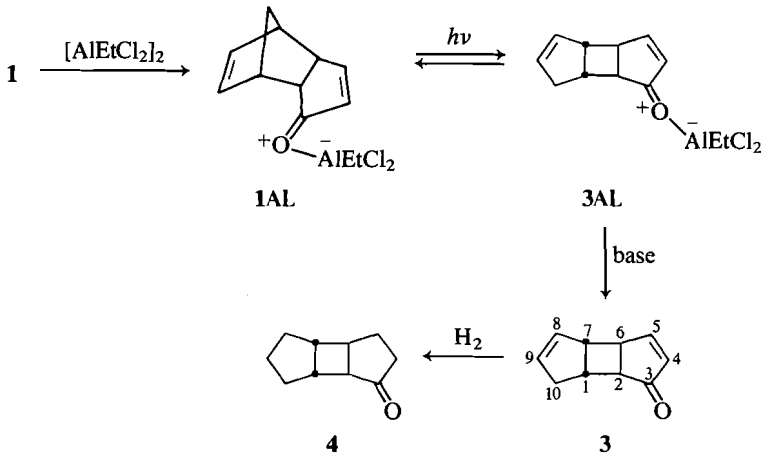

TABLE 2. Highfield nmr of **3** and **7**[a]

Compound		^{1}H or ^{13}C chemical shift, ppm									
		3	4	5	8	9	10	1	2	6	7
3	^{1}H nmr	—	6.20d $J_{4,5}$ = 5.6 Hz	7.64dd $J_{5,6}$ = 3.0 Hz	5.75m	5.71m	2.33dm 2.59dm	3.04m	2.55m	3.10m $J_{6,7}$ = 4.6 Hz	2.36t
3	^{13}C nmr	212.0	135.50	165.20	131.70	131.50	39.50	37.20[b]	50.72[b]	49.70[b]	49.54[b]
7	^{1}H nmr	—	—	7.66s	5.77m	5.75m	2.35dm 2.60dm	3.05m	—	—	2.40m

[a]In $CDCl_3$; d = doublet, m = multiplet, dm = doublet of multiplet, t = triplet, s = singlet.
[b]Assignment may be interchanged.

the symmetrical nature of **5**, there are two possible ways it can reopen to yield **1AL**.

To test for the occurrence of this 3C + 2C cycloaddition and subsequent ring opening to give **1AL**, the trideutero derivative **6** was prepared by reacting **1** with $NaOD/D_2O$ in dioxane. It was shown that three deuteriums were incorporated into **6** by mass spectrometric analysis. The ^{1}H nmr spectrum of this compound showed that the resonances attributable to H(2), H(4), and H(6) in **1** were absent.

Irradiation of the $AlEtCl_2$ complex of **6** under the same conditions used previously led to the formation of the $AlEtCl_2$ complex of **7**. Ketones **6** and **7** were recovered and separated after neutralization of the irradiated solution and examined by ^{1}H nmr spectroscopy. No scrambling or loss of deuterium was found for **6**. In the case of **7**, deuterium was shown to be at C_2, C_4, and C_6 by the absence of signals corresponding to the proton resonances of the corresponding protio material, Table 2. These results show that there is no reversible formation of the intermediate **5** by a 3C + 2C cycloaddition occurring in these reactions.

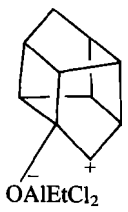

5

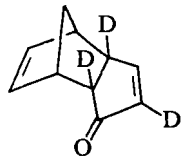

6

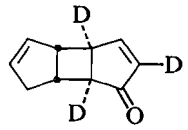

7

The interconversion of **1AL** and **3AL** can formally be regarded as a suprafacial 1,3-sigmatropic shift as shown in reaction [1]. It is not clear whether this reaction is concerted or whether it involves an intermediate such as **8**. It has been suggested that twisting about the C_2,C_3 bond of the excited state of the protonated enone leads to a build up of a positive charge at C_3 (7). Cyclopentenone is a fairly rigid system, so that only a partial rotation about the C_2,C_3 bond is possible. Such partial rotation could lead to charge localization at C_3, and a subsequent β-cleavage reaction. The intermediate **8**, which can also be formed by a comparable sequence of events from **3AL**, would be able to revert to **1AL** or close to **3AL**. Comparable thermal interconversions of other substituted derivatives of ring systems corresponding to **1** and **3** have been described (8). The alternative cleavage of the C_1,C_2 bond in a 1,3-sigmatropic shift does not lead to the formation of **3AL**.

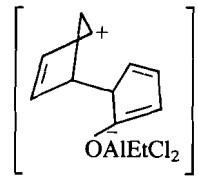

8

Overall these results show that the presence of a Lewis acid in solution on irradiation of **1** produces a remarkable change in the course of the photoreaction. It remains to be seen how general this type of Lewis acid catalyzed photorearrangement will be with other cyclic enones.

Experimental

General

^{1}H nmr spectra were obtained on Varian EM-390 or Bruker WM-250 and AM-500 instruments. Gas chromatographic analyses were per-

formed on a Hewlett-Packard 5790A gas chromatograph, using 10% Flourad FC 431 on Chromosorb W-HP 80/100 mesh, packed in a (1 m × 3 mm) stainless steel column. Ultraviolet spectra were measured on Pye Unicam instruments.

Ketone **1** was prepared in 45% yield from dicyclopentadiene according to the method of Woodward and Katz (9). Ethylaluminumdichloride (Ethyl Corporation) was distilled before use and stored under nitrogen in sealed glass ampules. All manipulations were carried out in a nitrogen glove box, using an SMI digital micropipette which was calibrated by weight. Chloroform was used as the solvent, and was dried by storing in a sealed container over activated Linde 4 Å molecular sieves. Irradiations were carried out in quartz apparatus at −50°C using a Rayonet Photoreactor (Southern New England Company) equipped with a magnetic stirrer, and RPR 2540 or 3000 Å lamps.

Preparation of ***3***

The ketone **1** (1.3 g) was added to a solution of $AlEtCl_2$ (1.2 g, 1 mol equiv.) in $CHCl_3$ (50 mL). The solution was cooled to −50°C, and irradiated until a photostationary state was reached (typically 24 h). (The course of the reaction was monitored at regular intervals by gc analysis of quenched aliquots). The solution was then poured into water (5 mL), the organic layer was separated, and the aqueous layer further extracted with $CHCl_3$. The combined organic layers were dried (anhydrous $MgSO_4$), the solvent was removed under reduced pressure, and the resulting residue distilled (120°C, 1 mm Hg) to yield a mixture (1.1 g) containing 64% **1**, and 36% **3**. The latter was separated from the mixture by column chromatography using a 10 cm × 2 cm column packed with tlc grade silica with a petroleum ether/ether mixture as eluent. The product **3** eluted before **1**. The solvent was removed and the product distilled (120°C, 1 mm Hg) to yield **3** (300 mg). Mol. wt. calcd. for $C_{10}H_{10}O$: 146.0732; found (high resolution ms): 146.0732 (Ir (film) ν_{max} 2930, 2850, 1701, 1580, 1350, 1170, 790, 720, and 700 cm^{-1}.

Hydrogenation of ***3***

The ketone **3** (10 mg) was dissolved in methanol (3 mL) containing palladium, 5% on $BaSO_4$ (Koch Light Laboratories) (5 mg). The suspension was stirred under H_2, until 2 mol. equiv. of H_2 was consumed. The suspension was filtered and the catalyst rinsed with methanol. The combined solvents were removed under reduced pressure and the residue distilled (120°C, 1 mm Hg) to yield a clear liquid (8 mg), which was subsequently shown to be tricyclo[5.3.0.$0^{2,6}$]decan-3-one by comparison with an authentic sample prepared by a standard procedure (5).

Preparation of ***6***

D_2O (12 mL) was slowly added to sodium wire (0.6 g) in dioxane (35 mL) under nitrogen atmosphere. A solution of **1** (250 mg) in dioxane (2 mL) was added and the mixture refluxed for 5 days. The mixture was neutralized to pH = 7 with 25% D_2SO_4 in D_2O. The resultant mxture was extracted three times with ether (25 mL) and the combined organic layers dried over anhydrous $MgSO_4$. The solvent was removed under reduced pressure and the residue distilled (120°C, 1 mm Hg), to yield **6** (150 mg) as a clear liquid which slowly turned into white waxy solid upon standing.

Acknowledgment

The financial support of the Natural Sciences and Engineering Research Council of Canada is gratefully acknowledged.

1. (*a*) R. F. Childs, B. Duffey, and A. Mika-Gibala. J. Org. Chem. **49**, 4352 (1984); (*b*) R. F. Childs. Rev. Chem. Intermed. 285 (1980).
2. G. Jones and B. R. Ramachandran. J. Org. Chem. **41**, 798 (1976).
3. R. F. Childs and A. Nixon. J. Polym. Sci. Polym. Ed. **18**, 1499 (1980).
4. L. Gmelin. Gmelins Handbuch Der Anorganischen Chemie No. 18, **2**, 442, Verlag chemie (1943).
5. P. E. Eaton. J. Am. Chem. Soc. **84**, 2344 (1962).
6. R. Rusakowicz, G. W. Byers, and P. A. Leermakers. J. Am. Chem. Soc. **93**, 3263 (1971).
7. R. F. Childs and G. S. Shaw. J. Chem. Soc. Chem. Commun. 261 (1983).
8. von B. Vebersax, M. Neuenschwander, and H.-P. Kellerhals. Helv. Chim. Acta, **65**, 74 (1982); U. Klinsmann, J. Gauthier, K. Schaffner, M. Pasternak, and B. Fuchs. Helv. Chim. Acta, **55**, 2643 (1972).
9. R. B. Woodward and T. J. Katz. Tetrahedron, **5**, 70 (1959).

Acid-catalyzed enolization of acetophenone: catalysis by bisulfate ion in sulfuric acid solutions

J. R. KEEFFE[1] AND A. J. KRESGE[2]
Department of Chemistry, University of Toronto, Toronto, Ont., Canada M5S 1A1
AND
J. TOULLEC
Institut de topologie et de dynamique des systèmes, Université Paris VII, associé au Centre national de la recherche scientifique, 75005 Paris, France
Received November 4, 1985
This paper is dedicted to Professor Arthur N. Bourns

J. R. KEEFFE, A. J. KRESGE, and J. TOULLEC. Can. J. Chem. **64**, 1224 (1986).

Rates of acid-catalyzed enolization of acetophenone in dilute aqueous solution, measured under conditions where the solvated proton is the only acidic species present, give a hydrogen ion catalytic coefficient, $k^E_{H+} = (1.21 \pm 0.01) \times 10^{-5}\ M^{-1}\ s^{-1}$, that is 35% smaller than the value obtained by X acidity function extrapolation of measurements made in moderately concentrated sulfuric acid solutions. The difference may be attributed to catalysis by bisulfate ion in the sulfuric acid solutions; this is supported by direct measurement of the bisulfate ion catalytic coefficient in dilute sulfuric acid. This revised value of k^E_{H+} leads to new, but only slightly different, values of the keto–enol equilibrium constant for acetophenone in aqueous solution, $pK_E = 7.96 \pm 0.04$, the acidity constant for acetophenone ionizing as a carbon acid, $pK^K_a = 18.31 \pm 0.05$, and the encounter-controlled rate constant for the reaction of acetophenone enol with molecular bromine, $k = (3.2 \pm 0.4) \times 10^9\ M^{-1}\ s^{-1}$.

J. R. KEEFFE, A. J. KRESGE et J. TOULLEC. Can. J. Chem. **64**, 1224 (1986).

Les vitesses pour les réactions d'énolisations acido-catalysées de l'acétophénone, mesurées en solution aqueuses diluées dans des conditions sous lesquelles le proton solvaté est la seule espèce acide présente, conduisent à une coefficient catalytique de l'ion hydrogène, $k^E_{H+} = (1{,}21 \pm 0.01) \times 10^{-5}\ M^{-1}\ s^{-1}$ qui est environ 35% plus faible que la valeur obtenue à l'aide de l'extrapolation de mesures de la fonction d'acidité X qui ont été faites dans des solutions d'acide sulfurique modérément concentrées. On peut attribuer cette différence à la catalyse de l'ion bisulfate qui est présent dans les solutions d'acide sulfurique; cette conclusion est supportée par des mesures directes du coefficient catalytique de l'ion bisulfate dans des solutions diluées d'acide sulfurique. Cette valeur revisée de k^E_{H+} conduit à de nouvelles, mais que légèrement différentes, valeurs pour: (*a*) la constante céto-énolique de l'acétophénone en solution aqueuse, $pK_E = 7{,}96 \pm 0.04$; (*b*) la constante d'acidité de l'acétophénone qui s'ionise sous forme d'acide du carbone, $pK^K_a = 18{,}31 \pm 0{,}05$ et (*c*) la constante de vitesse contrôlée par les rencontres pour la réaction de l'énol de l'acétophénone avec le brome moléculaire, $k = (3{,}2 \pm 0{,}4) \times 10^9\ M^{-1}\ s^{-1}$.

[Traduit par la revue]

The equilibrium constant for the enolization of acetophenone, eq. [1], was determined recently for dilute aqueous

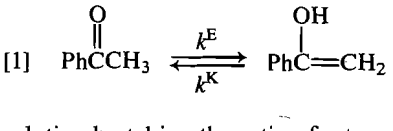

[1] $PhCCH_3 \underset{k^K}{\overset{k^E}{\rightleftharpoons}} PhC{=}CH_2$ (OH)

solution by taking the ratio of rate constants for this reaction in the forward (enolization) and reverse (ketonization) directions: $K_E = k^E/k^K$ (1). One set of rate constants used for this purpose referred to measurements made in acid solution. The ketonization rate constant was a value determined directy in dilute hydrochloric acid solutions; it was therefore a true hydrogen ion catalytic coefficient, k^E_{H+}. The enolization rate constant, on the other hand, was based upon measurements made in moderately concentrated sulfuric acid; these data were then extrapolated down to dilute solution by using the X acidity function (2). Sulfuric acid of the concentrations used for the rate measurements, however, contains appreciable quantities of bisulfate ion (3), and bisulfate ion in such solutions is known to be a kinetically active proton transfer agent in general acid catalyzed processes such as the enolization of acetophenone (4). The possibility existed, therefore, that the extrapolated rate constant did not represent reaction through H^+ alone, but that it was a combination of H^+ and HSO_4^- catalytic coefficients, and that the keto–enol equilibrium constant based upon it was in error.

To investigate this matter, we have measured the rate of enolization of acetophenone directly in dilute solution under conditions where H^+ is the only acidic species present. The value of k^E_{H+} so obtained is indeed significantly less than the rate constant produced by extrapolating the concentrated sulfuric acid data. We have also measured the rate of enolization of acetophenone in dilute sulfuric acid solutions and from these data have evaluated the HSO_4^- catalytic coefficient for this reaction.

Experimental

Materials

Acetophenone (Fisher, certified reagent) was dried over molecular sieves and then fractionally distilled at reduced pressure through an efficient column. All other substances were best available commercial grades and were used as received. Solutions were made with deionized water that had been purified further by distillation.

Kinetics

Rates of enolization were measured by bromine scavenging in the presence of bromide ion using the absorbance of Br_3^- at 320 nm to monitor the reaction. Runs were performed under zero-order conditions with acetophenone concentrations of ca. $10^{-2}\ M$ and stoichiometric bromine concentrations of ca. $10^{-4}\ M$. Bromide ion was 0.10 M; it was supplied either as HBr, to provide a variable acidity, or as NaBr, to keep ionic strength constant at 0.10 M. Absorbance measurements were made using a Cary Model 118C spectrometer with cell compartment thermostatted at 25.0 ± 0.02°C.

In a typical experiment, 3.0 mL of acid solution contained in a cuvette was brought to temperature equilibrium with the spectrometer

[1]American Chemical Society – Petroleum Research Fund Summer Research Fellow; permanent address: Department of Chemistry, San Francisco State University, 1600 Holloway Avenue, San Francisco, CA 94132, U.S.A.

[2]Author to whom correspondence may be addressed.

cell compartment. Acetophenone (3.5–4.0 μL) was then added, the mixture was shaken thoroughly to effect solution, and the absorbance at 320 nm was recorded (for the purpose of determining the acetophenone concentration). Saturated bromine water (15–20 μL) was then added to start the reaction. The disappearance of Br_3^- was accurately zero order for ca. 70% of the total absorbance change; this corresponds to 0.8–1.0% consumption of acetophenone on the basis of 1:1 stoichiometry. The rate of change of absorbance was converted to $\Delta[Br_3^-]/\Delta t$ using a value of $\epsilon_{Br_3^-}$ determined here, and thence to $\Delta[Br_2]_{st}/\Delta t$ through the factor $(1 + K_{ass}^{-1}[Br^-]^{-1})$ where $K_{ass} = 16.7\ M^{-1}$ is the equilibrium constant for $Br_2 + Br^- = Br_3^-$.[3] Zero-order rates of disappearance of bromine were then converted to first-order enolization rate constants by dividing by the acetophenone concentration.

Results and discussion

The acid-catalyzed bromination of a ketone such as acetophenone in aqueous solution is known to occur in two stages: formation of the enol, eq. [2], followed by reaction of this intermediate with bromine, eq. [3] (6*a*, 7). Formation of the

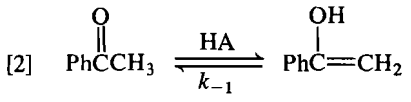

[2] $PhCCH_3 \underset{k_{-1}}{\overset{HA}{\rightleftharpoons}} PhC{=}CH_2$ (O over C; OH over C)

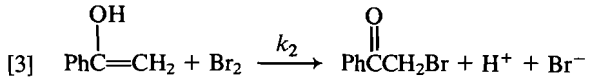

[3] $PhC{=}CH_2 + Br_2 \xrightarrow{k_2} PhCCH_2Br + H^+ + Br^-$ (OH over C; O over C)

enol will be the rate-determining stage, and the rate of bromine consumption will consequently measure the rate of the enolization reaction, when the enol reacts with bromine sufficiently more rapidly (say by a factor of 10^2) than it undergoes acid-catalyzed reversion to ketone. This was easily the case in the present study. There is good evidence that the reaction of acetophenone enol with bromine, eq. [3], is an encounter-controlled process (8) whose rate constant is $3 \times 10^9\ M^{-1}\ s^{-1}$ (1), and that the rate constant for the corresponding reaction with Br_3^- as the brominating agent is only a factor of two smaller (8). These values lead to $2 \times 10^5\ s^{-1}$ as the first-order specific rate of bromination of acetophenone enol at the stoichiometric bromine concentration used here, $10^{-4}\ M$. The rate constant for the reketonization of acetophenone enol, k_{-1}, is also known for the case of catalysis by H^+: $k_{H^+} = 1.25 \times 10^3\ M^{-1}\ s^{-1}$ (1), and that value coupled with the highest acidity used in the present study, $[H^+] = 0.1\ M$, leads to $1 \times 10^2\ s^{-1}$ as the maximum first-order specific rate of reversion of the enol to ketone. Bromination of the enol thus occurs at least 2×10^3 times faster than reketonization under the conditions used here.

Although the base-catalyzed halogenation of carbonyl compounds commonly gives polyhalogenated products, only monosubstituted products are generally found in the acid-catalyzed reaction (6*a*). There is direct evidence that this was the case in the present study and that the stoichiometry of the reaction was indeed 1:1 as indicated in eq. [3]. In an early investigation of the acid-catalyzed bromination of acetophenone, phenacyl bromide was the only product isolated (9), and a more recent examination of the reaction product by proton nmr failed to reveal any dibrominated material under circumstances where 4% could have been detected (2, 10). This nmr analysis was carried out on product formed from reaction of roughly equimolar amounts of acetophenone and bromine. Since in the present study acetophenone was always supplied in 100-fold excess over stoichiometric bromine, it seems safe to conclude that under our conditions only one equivalent of bromine was consumed per equivalent of enol formed, and that rates of bromine consumption can therefore be taken to be exactly equal to rates of enolization.

[3]This value of K_{ass} refers to 25°C and ionic strength $\mu = 0.10\ M$; it was obtained by extrapolating determinations reported for 16.5 and 21.5°C (5). Because K_{ass} entered into our data analysis as the factor $(1 + K_{ass}^{-1}[Br^-]^{-1})$, exact knowledge of its value was not critical.

TABLE 1. Rate data for the enolization of acetophenone in aqueous hydrobromic acid solutions at 25°C, ionic strength = 0.100 M[a]

$[HBr]/10^{-2}\ M$	$k_{obs}/10^{-7}\ s^{-1}$
1.97	2.62, 2.72
3.93	5.14, 5.17, 5.18, 5.34
4.72	5.98, 6.11
5.90	7.28
6.68	8.35, 8.37
7.86	9.78, 9.90
8.65	10.7, 11.1
9.83	12.3

$k_{obs} = (3.51 \pm 0.86) \times 10^{-8} + (1.21 \pm 0.01) \times 10^{-5}\ [HBr]$

[a]Ionic strength maintained constant with NaBr.

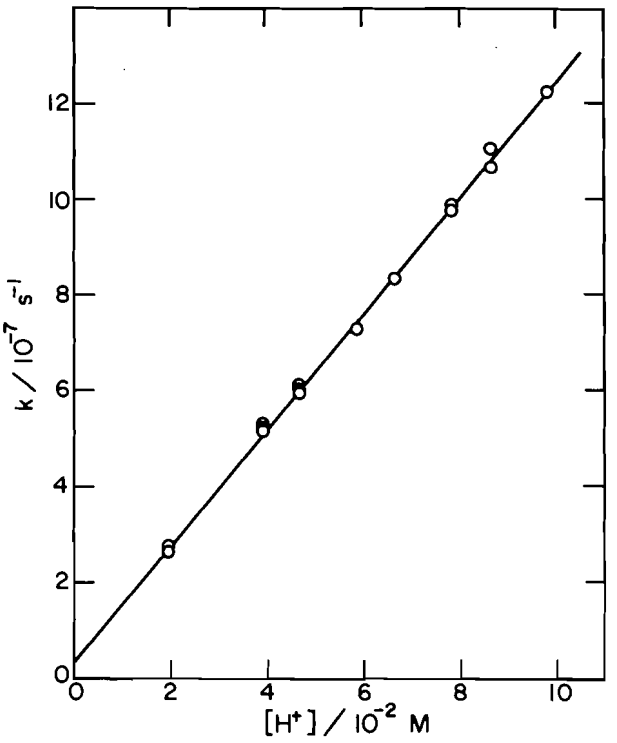

FIG. 1. Relationship between hydrogen ion concentration and observed first-order rate constants for the enolization of acetophenone in aqueous hydrobromic acid solutions at 25°C.

First-order rates of enolization determined in this way were measured in hydrobromic acid solutions over the concentration range $[HBr] = 0.02–0.10\ M$. The data are summarized in Table 1 and are displayed in Fig. 1. It may be seen that these rate constants are accurately proportional to acid concentration; least-squares analysis gives the relationship $k_{obs} = (3.51 \pm 0.86) \times 10^{-8} + (1.21 \pm 0.01) \times 10^{-5}\ [HBr]$. Since hydrobromic acid is completely ionized in dilute aqueous solution (6*b*), the only acidic species present in these solutions is the solvated proton; the bimolecular rate constant determined here is therefore a true hydrogen ion catalytic coefficient.

TABLE 2. Rate data for the enolization of acetophenone in aqueous bisulfate solutions at 25°C[a]

$[H_2SO_4]_{St}/10^{-2}\,M$	$[HBr]_{St}/10^{-2}\,M$	$[Na_2SO_4]_{St}/10^{-2}\,M$	$[NaBr]_{St}/10^{-2}\,M$	$[H^+]/10^{-2}\,M$	$[HSO_4^-]/10^{-2}\,M$	$\mu/10^{-2}\,M$[b]	$k_{obs}/10^{-7}\,s^{-1}$
0.92	—	—	8.50	1.52	0.32	10.6	2.26
1.84	—	—	7.01	2.77	0.91	10.6	4.40
2.76	—	—	5.51	3.92	1.60	10.6	6.26
4.60	—	—	2.52	6.04	3.16	10.0	11.26
0.92	—	2.73	0.86	0.92	0.92	9.98	2.68
0.92	0.46	1.84	2.89	1.38	0.92	9.56	2.63
0.92	0.92	1.39	3.64	1.84	0.93	9.18	2.60
0.92	1.38	1.10	3.74	2.30	0.93	8.66	3.89
0.92	1.82	0.91	3.58	2.74	0.95	8.20	4.46

$k_{obs}/s^{-1} = -(0.57 \pm 2.54) \times 10^{-8} + (1.07 \pm 0.20) \times 10^{-5}\,[H^+] + (1.49 \pm 0.40) \times 10^{-5}\,[HSO_4^-]$

[a]Stoichiometric concentrations are denoted by the subscript "St"; others are actual (calculated) concentrations. The latter were obtained from the thermodynamic dissociation constant for HSO_4^-, $K_a = 1.05 \times 10^{-2}\,M$ (20), using activity coefficients determined by the Debye–Huckel equation with ion-size parameters of Bates (21); for HSO_4^- this quantity (4.0 Å) was estimated as the average of values for similarily sized and charged ions. This procedure produced the following concentration quotients for HSO_4^- at our experimental ionic strengths: $Q_a = 2.62 \times 10^{-2}\,M$ ($\mu = 0.082\,M$), $2.74 \times 10^{-2}\,M$ ($\mu = 0.100\,M$), and $2.85 \times 10^{-2}\,M$ ($\mu = 0.106\,M$); this spread in Q_a had little effect on the calculated concentrations.
[b]μ = ionic strength.

This result, $k^E_{H+} = 1.21 \times 10^{-5}\,M^{-1}\,s^{-1}$, is 35% less than the rate constant obtained by extrapolation of measurements made in moderately concentrated sulfuric acid solutions, $k = (1.63 \pm 0.03) \times 10^{-5}\,M^{-1}\,s^{-1}$ (2). This suggests that additional catalysis of the enolization reaction by bisulfate ion was indeed taking place in these sulfuric acid solutions, and that extrapolation of the data down the X function did not remove this extra catalysis. Additional evidence in support of this hypothesis may be obtained from some measurements of the enolization of acetophenone made in moderately concentrated perchloric acid solutions (11). This acid is monobasic and fully ionized at the concentrations used, and therefore only catalysis by H^+ is possible. It is thus significant that extrapolation of these data down the X_0 function (12) gives a dilute solution rate constant whose value, $k^E_{H+} = (1.21 \pm 0.01) \times 10^{-5}\,M^{-1}\,s^{-1}$, is identical with the result obtained here by direct measurement in dilute solution.

When this revised value of k^E_{H+} is used to determine the keto–enol equilibrium constant for acetophenone in aqueous solution, the result obtained, $K_E = (9.71 \pm 0.21) \times 10^{-9}$, is still in reasonable agreement with an independently determined value based upon a set of hydroxide ion catalytic coefficients for the enolization and ketonization reactions, $K_E = (1.20 \pm 0.07) \times 10^{-8}$ (1). The current best value of this constant is then the average of these two results, $K_E = (1.08 \pm 0.11) \times 10^{-8}$, $pK_E = 7.96 \pm 0.04$; this differs only marginally from our previous best estimate, $pK_E = 7.90 \pm 0.02$ (1). This change also requires revision of our previous estimate of the equilibrium constant for the ionization of acetophenone as a carbon acid, eq. [4], which

$$[4]\quad \underset{\text{O}}{\overset{\|}{\text{PhCCH}_3}} \overset{K^K_a}{\rightleftharpoons} \underset{\text{O}^-}{\overset{|}{\text{PhC}{=}\text{CH}_2}} + H^+$$

is the product of K_E and the known (13) equilibrium constant for ionization of acetophenone enol as an oxygen acid, K^E_a: $K^K_a = K_E K^E_a$. The new value, $K^K_a = (4.96 \pm 0.59) \times 10^{-19}\,M$, $pK^K_a = 18.31 \pm 0.05$,[4] is again only marginally different from the old: $pK^K_a = 18.24 \pm 0.03$ (1). Another quantity which can be derived from K_E is the rate constant for the encounter-controlled reaction of acetophenone enol with molecular bromine; the new value of this constant, based upon our revised K_E, is $k = (3.2 \pm 0.4) \times 10^9\,M^{-1}\,s^{-1}$, up from the $k = (2.8 \pm 0.02) \times 10^9\,M^{-1}\,s^{-1}$ we had estimated before (1).

In addition to these determinations of the rate of enolization of acetophenone in hydrobromic acid solutions, we also made some measurements of the rate of this reaction in dilute sulfuric acid, at various stoichiometric acid concentrations and with various additions of HBr and Na_2SO_4, to get further variation in the concentrations of solution species. The data are summarized in Table 2. The only acids present in these solutions were H^+ and HSO_4^- (3), and we therefore fitted the data to the rate law shown in eq. [5]. The concentrations of H^+ and HSO_4^- required for this purpose were obtained by calculation, using $K_a = 1.05 \times 10^{-2}\,M$ for the acidity constant of HSO_4^- (14) and activity coefficients determined by the Debye–Hückel equation with ion-size parameters of 9 Å for H^+, and 4 Å for HSO_4^- and SO_4^{2-} (15).

$$[5]\quad k_{obs} = k_0 + k_{H+}[H^+] + k_{HSO_4}[HSO_4^-]$$

We sought to keep ionic strength constant in these sulfuric acid solutions, but this goal was unfortunately incompletely realized: ionic strength varied from $\mu = 0.082$–$0.106\,M$. To determine whether this spread would have a significant effect on the rate of enolization, we performed another series of rate measurements varying ionic strength from $\mu = 0.06$–$0.14\,M$ at a fixed acid concentration, $[HBr] = 0.059\,M$. These data, summarized in Table 3, show no systematic dependence of observed rate constant upon ionic strength: linear least-squares analysis gives a relationship, $k_{obs} = (7.61 \pm 0.11) \times 10^{-7} - (0.04 \pm 1.08) \times 10^{-7}\,\mu$, with zero slope and a predicted value for $\mu = 0.10\,M$, $k = (7.61 \pm 0.03) \times 10^{-7}\,M^{-1}\,s^{-1}$, which is consistent with the rate constant, $k = (7.49 \pm 0.03) \times 10^{-7}\,M^{-1}\,s^{-1}$ predicted for $[H^+] = 0.059\,M$ from the correlation of rate measurements made at variable [HBr] and $\mu = 0.10\,M$.

This result indicates that the variation in ionic strength of our sulfuric acid solutions will have no significant effect on the rate measurements performed in these media. We therefore fit the data to the rate law of eq. [5] with no further adjustment. The result, $k_{obs} = -(0.57 \pm 2.54) \times 10^{-8} + (1.07 \pm 0.20) \times 10^{-5}\,[H^+] + (1.49 \pm 0.40) \times 10^{-5}\,[HSO_4^-]$, gives a hydrogen ion catalytic coefficient in good agreement with the value deter-

[4]This equilibrium constant is a *concentration quotient* which refers specifically to an ionic strength of 0.10 M.

TABLE 3. Rate data for the enolization of acetophenone in aqueous hydrobromic acid solution at 25°C at variable ionic strength[a]

Ionic strength/10^{-2} M	$k_{obs}/10^{-7}$ s^{-1}
5.90	7.56
7.55	7.70
9.45	7.56
12.3	7.65
14.0	7.58

$k_{obs} = (7.61 \pm 0.11) \times 10^{-7} - (0.04 \pm 1.08) \times 10^{-7}\ \mu$

[a][HBr] = 5.9×10^{-2} M; ionic strength varied with $NaClO_4$.

mined more precisely in HBr solutions: $k^E_{H+} = (1.21 \pm 0.01) \times 10^{-5}\ M^{-1}\ s^{-1}$. It also gives a bisulfate ion catalytic coefficient that is very similar in magnitude to k^E_{H+}; this shows that appreciable catalysis of the enolization reaction by bisulfate ion can be expected to occur in moderately concentrated sulfuric acid solutions where the concentrations of this ion are large (3).

Such similarity of bisulfate and hydrogen ion catalytic coefficients is unexpected because of the considerable difference in acid strength of these two catalytic species. As the basis for a molecular explanation we can consider two reaction mechanisms. The conventional scheme for acid catalyzed enolization consists of two steps: equilibrium protonation of the carbonyl group followed by rate controlling deprotonation at carbon (6*c*, 7, 16). The other mechanism, alternative or concurrent, is a termolecular reaction in which protonation at oxygen is concerted with deprotonation at carbon (17). The acid–base pair responsible for bisulfate catalysis by this termolecular mechanism could be either H^+/SO_4^{2-} or HSO_4^-/H_2O.[5]

In the two-step mechanism we can account for the surprising catalytic effectiveness of bisulfate by postulating an electrostatic effect (18). The rate controlling transition state is formed from an oxonium ion and a base. For hydrogen ion catalysis the base is water, but for bisulfate ion catalysis the transition state brings together positive oxonium ion and doubly negative sulfate ion. Electrostatic effects on the rates of deprotonation at carbon have been documented (18).

In the termolecular mechanism the transition state for bisulfate catalysis is composed of ketone, hydrogen ion, and sulfate ion, or of ketone, bisulfate, and water. For the former case we note the electrostatic analogy with the transition state of the two-step mechanism. For the latter case the comparison to be made is between the protonation of ketone by hydrogen ion and the protonation of ketone by bisulfate, in both cases with concurrent deprotonation at carbon by water. An unusually high kinetic acidity of bisulfate in proton transfer reactions has been observed before, notably in the acid cleavage of allylmercuric iodide (19) and isobutenylmercuric bromide (20), in the detritiation of 1,3,5-trimethoxybenzene (21), and in the hydrolysis of ethyl vinyl ether (22). The speculation has been advanced that bisulfate ion might be unusually effective in these reactions because the configuration of the solvent molecules in its initial state solvation shell is similar to that required in the transition state, and the need for solvent reorganization during the proton transfer process is thereby minimized.

[5]The first of these pairs consists of the stronger acid and the stronger base; it should therefore be the more effective. In that case the bisulfate-ion catalytic coefficient would be equivalent to a third-order rate constant having the value $(5.6 \pm 1.5) \times 10^{-4}\ M^{-2}\ s^{-1}$.

Acknowledgements

We wish to thank Dr. R. A. Cox for helpful discussion; we are grateful as well to the Natural Sciences and Engineering Research Council of Canada and the Donors of the Petroleum Research Fund, administered by the American Chemical Society, for financial support of this work.

1. Y. CHIANG, A. J. KRESGE, and J. WIRZ. J. Am. Chem. Soc. **106**, 6392 (1984).
2. R. A. COX, C. R. SMITH, and K. YATES. Can. J. Chem. **57**, 2952 (1979).
3. E. B. ROBERTSON and H. B. DUNFORD. J. Am. Chem. Soc. **86**, 5080 (1964).
4. W. M. SCHUBERT and P. C. MYHRE. J. Am. Chem. Soc. **80**, 1755 (1958); A. J. KRESGE, L. E. HAKKA, S. MYLONAKIS, and Y. SATO. Disc. Faraday Soc. **39**, 75 (1965); A. J. KRESGE, Y. CHIANG, P. H. FITZGERALD, R. S. MCDONALD, and G. H. SCHMID. J. Am. Chem. Soc. **93**, 4907 (1971); A. J. KRESGE, S. MYLONAKIS, and L. E. HAKKA. J. Am. Chem. Soc. **94**, 4197 (1972); Y. CHIANG and A. J. KRESGE. J. Am. Chem. Soc. Submitted.
5. R. O. GRIFFITH, A. MCKEOWN, and A. G. WINN. Trans. Faraday Soc. **28**, 101 (1932).
6. R. P. BELL. The proton in chemistry. 2nd ed. Cornell Univ. Press, Ithaca, NY 1973. (*a*) pp. 171–181; (*b*) pp. 88–91; (*c*) p. 177.
7. J. TOULLEC. Adv. Phys. Org. Chem. **18**, 1 (1982).
8. J. E. DUBOIS, M. EL-ALAOUI, and J. TOULLEC. J. Am. Chem. Soc. **103**, 5393 (1981).
9. L. ZUCKER and L. P. HAMMETT. J. Am. Chem. Soc. **61**, 2785 (1939).
10. C. R. SMITH. M.Sc. Thesis, University of Toronto, 1968.
11. L. ZUCKER and L. P. HAMMETT. J. Am. Chem. Soc. **61**, 2791 (1939).
12. R. A. COX and K. YATES. Can. J. Chem. **59**, 2116 (1981).
13. P. HASPRA, A. SUTTER, and J. WIRZ. Angew. Chem. **91**, 652 (1979); Angew. Chem. Int. Ed. Engl. **18**, 617 (1979).
14. K. S. PITZER, R. N. ROY, and L. F. SILVESTER. J. Am. Chem. Soc. **99**, 4930 (1977).
15. R. G. BATES. Determination of pH; theory and practice. Wiley, New York. 1973. p. 49.
16. K. J. PEDERSEN. J. Phys. Chem. **38**, 581 (1934); T. H. LOWRY and K. S. RICHARDSON. Mechanism and structure in organic chemistry. 2nd ed. Harper and Row, New York. 1981. p. 657.
17. A. F. HEGARTY and W. P. JENCKS. J. Am. Chem. Soc. **97**, 7188 (1975).
18. A. J. KRESGE and Y. CHIANG. J. Am. Chem. Soc. **95**, 803 (1973); W. K. CHWANG, R. ELIASON, and A. J. KRESGE. J. Am. Chem. Soc. **99**, 805 (1977); D. B. DAHLBERG, M. A. KUZEMKO, Y. CHIANG, A. J. KRESGE, and M. F. POWELL. J. Am. Chem. Soc. **105**, 5387 (1983).
19. M. M. KREEVOY, T. S. STRAUB, W. V. KAYSER, and J. L. MELQUIST. J. Am. Chem. Soc. **89**, 1201 (1967).
20. M. M. KREEVOY and R. A. LANDHOLM. Int. J. Chem. Kinet. **1**, 157 (1969).
21. A. J. KRESGE, S. SLAE, and D. W. TAYLOR. J. Am. Chem. Soc. **92**, 6309 (1970).
22. A. J. KRESGE and Y. CHIANG. J. Am. Chem. Soc. **95**, 803 (1973).

A fast atom bombardment mass spectrometry study of H-bonded complexes of imidazole with various electron donors

STEPHEN J. BROWN, JACK M. MILLER,[1] AND ROGER THEBERGE
Department of Chemistry, Brock University, St. Catharines, Ont., Canada L2S 3A1

AND

JAMES H. CLARK
Department of Chemistry, University of York, Heslington, York, YO1 5DD England

Received October 21, 1985

STEPHEN J. BROWN, JACK M. MILLER, ROGER THEBERGE, and JAMES H. CLARK. Can. J. Chem. **64**, 1277 (1986).

Fast Atom Bombardment mass spectrometry is shown to be a useful tool in the investigation of strongly hydrogen bonded complexes of imidazole with various electron donors.

STEPHEN J. BROWN, JACK M. MILLER, ROGER THEBERGE et JAMES H. CLARK. Can. J. Chem. **64**, 1277 (1986).

On démontre que la spectrométrie de masse par bombardement avec des atomes rapides est un outil utile pour étudier les complexes, contenant de fortes liaisons hydrogènes, de l'imidazole avec divers donneurs électroniques.

[Traduit par la revue]

Introduction

The hydrogen-bonding properties of imidazole and its derivatives are of considerable importance in biochemistry (1). Of particular interest is the ability of imidazole to form strong, easily polarizable hydrogen bonds that may play an important role in many biochemical functions (1, 2).

Both nonspectroscopic and spectroscopic techniques have been used for the detection of hydrogen bonds (3). Since the emphasis in recent years has shifted to the use of spectroscopic techniques, a remarkable variety of such methods including infrared, nuclear magnetic resonance, visible, and photoelectron spectroscopy have been successfully applied to the study of hydrogen bonding.

The use of mass spectrometry as a technique for the study of hydrogen bonding has received little attention. The traditional method of electron impact mass spectrometry (EIMS) requires thermal volatilization of the sample and then subjects it to bombardment with electrons, the combination of which effectively precludes the use of EIMS for the study of hydrogen bonding. On the other hand, fast atom bombardment mass spectrometry (FABMS) is a "soft ionization" technique that does not require sample heating (4). In the case of the FABMS experiment the sample is dissolved in a matrix liquid that is relatively involatile under the high vacuum conditions present in the source of the mass spectrometer. The sample is then subjected to bombardment with energetic (6–8 keV) "fast atoms" and by this means both ionization and volatilization of the sample is achieved. Many different matrix liquids may be used in the FABMS experiment and a matrix of the "correct chemistry" is often needed to obtain useful spectra, which in turn can require considerable experimentation. The most commonly used FABMS matrix liquid is glycerol.

Those familiar with the FABMS technique have long known that ions corresponding to protonated dimers and trimers of the matrix liquid are often seen, particularly when using glycerol as the matrix liquid. These ions, containing clusters of molecules, are presumably held together by hydrogen bonding. Despite these observations, FABMS has never been used to systematically study hydrogen bonding *per se*.

Recently, the FABMS of the strongly hydrogen-bonded complex formed between imidazole and trimethylphosphate was reported (5) and an ion corresponding to the hydrogen-bonded complex was observed for this system. We have carried out a further study of hydrogen bonding to imidazole using FABMS with a range of electron donors of varying strength. With the FABMS method, we have studied the effect of the matrix liquid, concentration, and water content on the hydrogen bonding to imidazole. With FABMS the question of how representative of solution behavior the spectrum is must always be considered. Our experiments lead us to conclude that FABMS does indeed give an accurate picture of the hydrogen bonding between the various substrates in the matrix liquid and that FABMS may become a routine method for the analysis of some hydrogen bonded systems.

Experimental

FAB spectra were obtained using an AEI MS-30 (Kratos Ltd., Manchester U.K.) retrofitted with a saddle-field FAB gun (Ion tech, Teddington, U.K.) and a Kratos FAB source in beam 1. Xenon was used as the bombarding atom, the energy of the beam being 6–8 keV and a stainless steel probe tip being used. All the spectra were peak averaged from a minimum of 8 scans using a DS-55 data system. Mass conversion was done off-line based on a tris-perfluoroheptyl-*s*-triazine calibration. Infrared spectra were recorded as hexachlorobutadiene mulls using an Analect FX 6260 FT-IR at 4 wavenumber resolution. The ^{1}H nmr spectra were recorded on a Brüker WP-80 in $CDCl_3$ solution.

meta-Nitrobenzyl alcohol (NBA), imidazole, triphenylphosphine oxide, diphenyl sulphoxide, acetophenone, diphenyl ether, and triphenyl methanol were obtained from BDH and Aldrich (reagent grade), and were used unpurified. Dry *meta*-nitrobenzyl alcohol was obtained by storing NBA over type 4 angstrom molecular sieves activated at 400°C. The hydrogen-bonded complexes were prepared by dissolving 1 g (14.7 mmol) of imidazole in 200 cm^3 of diethyl ether followed by the addition of an equimolar amount of the electron donor. The bulk of the diethyl ether was removed by rotary evaporation to leave an oil. The oil was then pumped dry under vacuum (0.1 Torr; 1 Torr = 133.3 Pa) to leave the solid complex.

Deuteroimidazole was prepared by warming imidazole in D_2O followed by the removal of the water under vacuum. The deuteroimidazole – diphenyl sulphoxide complex was prepared as above, the ^{1}H nmr showing in excess of 90% deuterium incorporation.

Complexes containing a 2:1 electron donor-to-imidazole ratio were prepared as follows. Imidazole (1 g, 14.7 mmol) was dissolved in

[1]Author to whom correspondence may be addressed.

acetonitrile. Concentrated hydrobromic acid (14.7 mmol) was added, generating the protonated imidazole species. Two equivalents of the electron donor were next added, and the acetonitrile was then removed to leave a white crystalline solid in every case.

Results and discussion

Imidazole – electron donor complexes are ideal candidates for the study of hydrogen bonding by FABMS since the complex can be protonated (at N3) without breaking the hydrogen bond. Thus the complex may be easily protonated, generating the quasi-molecular ion observed in the FABMS spectrum. In comparison, we have been unable to observe the H-bonded dimer of benzoic acid by FABMS, presumably because there is no site at which protonation of this species may occur without breakdown of the dimer itself.

We have been able to observe hydrogen-bonded complexes formed between trialkylammonium ions, pyridinium ion, and substituted pyridinium ions with a range of electron donors. These hydrogen-bonded ions, which show 1:1 complex formation, are clearly distinct from clustering caused by electrostatic interaction, which gives rise to ions of the general formula $[\text{cation}(\text{cation}/\text{anion})_n]^+$ where $n = 1, 2, 3 \ldots$.[2]

The choice of the matrix liquid is obviously going to be critical in a hydrogen-bonding FABMS study. Weakly hydrogen-bonded species would not be expected to be observed in a strong H-bonding matrix such as glycerol. The water content of the matrix may also play a critical role in the observation of many H-bonded species by FABMS. Trace amounts of water may be necessary for the generation of protonated species, yet too high a water content may result in breakdown of the complex.

We have found through considerable experimentation that *meta*-nitrobenzyl alcohol (NBA) is the best matrix for the study of hydrogen bonding to imidazole (IM). We were able to obtain spectra over a period of 15 min with no loss in ion current. Cross-scan reports of the spectra showed the very stable nature of the ion current arising from the H-bonded complexes (see Fig. 1).

Preliminary work using glycerol as the matrix liquid showed that only the strongest hydrogen bonds to imidazole were able to survive in this medium, such as those formed with trimethylphosphate and triphenylphosphine oxide. Ions corresponding to glycerol and imidazole or glycerol and electron donor complexes were also observed.[2]

Nitrophenyl octyl ether (NPOE) is another commonly used matrix liquid, but the complexes were found to have low solubility in this matrix. Because of the low solubility only the stronger hydrogen-bonded complex between imidazole and triphenylphosphine oxide was observed. With other electron donors the low concentration of the species present in the matrix resulted in dissociation of the complex, as could be expected. The use of a polyphenyl ether as the matrix liquid was also limited by poor solubility of the complexes.

Sulpholane also proved to be a useful matrix for higher concentrations of the complexes. At low concentration the sulpholane proved to be too volatile in the mass spectrometer and we were only able to obtain spectra over a period of a few minutes (2–3 scans). Because of the transient nature of sulpholane we were unable to obtain quantitative data using this matrix even though peaks due to the H-bonded complexes were in general more intense using sulpholane rather than NBA as the matrix liquid.

[2]Work in progress.

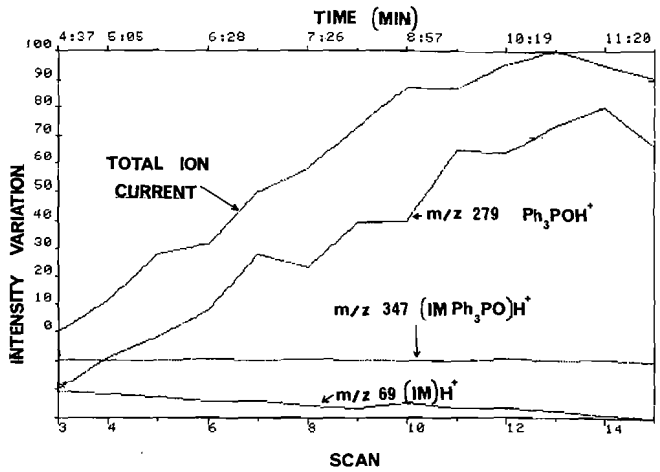

FIG. 1. Cross-scan report of imidazole – triphenylphosphine oxide complex in NBA.

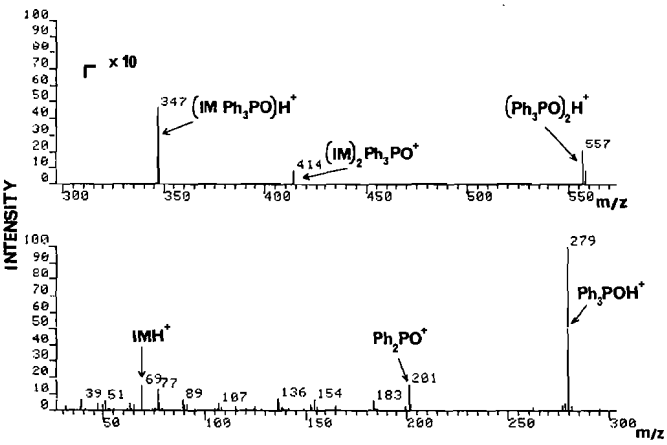

FIG. 2. FABMS of imidazole – triphenylphosphine oxide complex in NBA.

The FABMS of imidazole in NBA at a concentration of approximately 1.3 *M* showed a base peak at m/z 69 corresponding to the quasi-molecular ion $(\text{IM} + \text{H})^+$ for imidazole. Other significant peaks in the spectra included the imidazole dimer (m/z 137, 13% of base) and a peak at m/z 222 (2% of base) corresponding to the imidazole–NBA complex. At this concentration the spectrum due to NBA was relatively weak; the NBA $M + 1$ ion at m/z 154 amounted to only 11% of the base peak. The FABMS spectra of the complexes typically showed peaks at masses corresponding to the H-bonded complex, free imidazole (as an $M + 1$ peak), and the free electron donor (as $M + 1$ peak), except in the case of triphenyl methanol where the base peak corresponds to the Ph_3C^+ ion at m/z 243. In every case H-bond formation was confirmed by ir spectroscopy and the 1:1 ratio of imidazole to electron donor by ^1H nmr. A typical FABMS spectrum is shown in Fig. 2.

Since observation of the imidazole H-bonded complexes by FABMS involves protonation of the imidazole, likely at the N3 position, generating two equivalent H-bonding sites, we have also studied the complexes formed between protonated imidazole and two equivalents of the electron donors triphenylphosphine oxide and diphenyl sulphoxide. In these systems, in addition to the 1:1 complexes in the NBA matrix, we were able to observe the 2:1 donor-to-imidazole H-bonded complexes at low intensity.

TABLE 1. The effect of concentration on the intensity of the H-bonded complex peak relative to that of free imidazole

Complex	Concentration*	Complex/free IM†
$Ph_3P{=}O$/IM	0.08 *M*	0.17
$Ph_3P{=}O$/IM	0.42 *M*	0.20
$Ph_3P{=}O$/IM	0.84 *M*	0.26
$Ph_3P{=}O$/IM	1.26 *M*	0.28
$Ph_2S{=}O$/IM	1.26 *M*	0.15
$Ph_2S{=}O$/IM	2.14 *M*	0.17

*In NBA matrix.
†Ratio in terms of absolute intensity of peaks.

TABLE 2. H-bond strength of imidazole complexes by FABMS*

Complex	Concentration	Complex/free IM
$Ph_3P{=}O$/IM	1.26 *M*	0.28
$Ph_2S{=}O$/IM	1.26 *M*	0.15
$Ph_2C{=}O$/IM	1.26 *M*	0.02
Ph_3COH/IM	<1.00 *M*†	trace
Ph_2O/IM	1.26 *M*	0.00

*Ratios in terms of absolute intensities of peaks.
†Ph_3COH/IM limited by lower solubility, but H-bonded complex was observed.

The effect of concentration on the intensity of the H-bonded complex peak relative to that of the free imidazole was studied for the triphenylphosphine oxide – imidazole complex and for the diphenyl sulphoxide – imidazole complex, the results of which are shown in Table 1. As expected, we observed a decrease in the intensity of the complex peak relative to that of free imidazole, with decreasing concentration of the complex for both the triphenylphosphine oxide – imidazole and the diphenyl sulphoxide – imidazole complexes. The imidazole peak at m/z 69 was used for the ratio calculation even though the base peak in each case was the quasi-molecular ion from the electron donor, as the ionization efficiency for imidazole was assumed to be closer to that of the complex. The ionization of imidazole and the complex involves protonation at N3 whereas, in the case of the electron donor, ionization involves protonation of a P=O, S=O, or other functional group.

Comparison of the intensity of the H-bonded complex peak relative to that of free imidazole (in terms of absolute intensity) for the range of complexes prepared (at the same concentration) yielded the expected order of H-bond strength (see Table 2), i.e.

$$Ph_3P{=}O/IM > Ph_2S{=}O/IM > Ph_2C{=}O/IM > Ph_3COH/IM > Ph_2O/IM$$

Preparation of a deuterated imidazole – dimethyl sulphoxide complex showed rapid exchange of the deuterium atom involved in the hydrogen bond. This exchange was rapid in both dried and undried NBA. The ^1H nmr of the deuterated complex showed greater than 90% deuteration at the N1 position of imidazole (dissolved in $CDCl_3$). However, FABMS showed approximately 9% deuterium in the complex, using both dried and undried NBA. The $M + 2$ peak of NBA was also larger than the calculated ^{13}C contribution, demonstrating deuterium incorporation in the matrix. Removal of the water from the matrix also resulted in a 23% decrease in the total ion current of the imidazole – diphenyl sulphoxide complex, showing that water plays some part in the generation of the quasi-molecular ions observed by FABMS in these systems.

In conclusion, we believe that FABMS is a promising new technique for the study of hydrogen bonding although the range of complexes that can be studied is clearly limited. The study of hydrogen bonding to preformed anions or cations, which are especially susceptible to FABMS study, should be straightforward. However, the neutral complexes would seem to need to be resistant to protonation if confusion between bonding to the neutral or protonated species is to be avoided. Our studies indicate that semiquantitative information on hydrogen–deuterium exchange and the relative strengths of hydrogen bonds can also be obtained.

Acknowledgements

The authors wish to thank NSERC (Canada) for an operating and equipment grant (J.M.M.), the Joseph H. DeFrees Grant of the Research Corporation and the Shaver Research Foundation for aid in acquiring the FAB facilities (J.M.M.), and the SERC (UK) for a travel grant (J.H.C.).

1. G. ZUNDEL. *In* The hydrogen bond, recent developments in theory and experiment. *Edited by* P. Schuster, G. Zundel, and C. Sandorfy. North Holland, Amsterdam. 1976. Chapt. 15.
2. B. SHAANAN. Nature (London), **296**, 682 (1982); S. E. V. PHILLIPS and B. P. SCHOENHORN. Nature (London), **292**, 81 (1981); R. QUINN, M. NAPPA, and J. S. VALENTINE. J. Am. Chem. Soc. **104**, 2588 (1982).
3. M. D. JOESTEN and L. J. SCHAAD. Hydrogen bonding. Marcel Dekker Inc., New York. 1974, and references therein.
4. J. M. MILLER. Adv. Inorg. Chem. radiochem. **28**, 1 (1984).
5. J. H. CLARK, M. GREEN, R. MADDEN, C. D. REYNOLDS, Z. DAUTER, J. M. MILLER, and T. JONES. J. Am. Chem. Soc. **106**, 4056 (1984).

Solvolytic rearrangement studies with ^{14}C or ^{13}C labeled (*E*)- and (*Z*)-1,2-diphenyl-2-tolylvinyl bromides[1]

CHOI CHUCK LEE AND DAVE WANIGASEKERA
Department of Chemistry, University of Saskatchewan, Saskatoon, Sask., Canada S7N 0W0
Received October 4, 1985
This paper is dedicated to Professor Arthur N. Bourns

CHOI CHUCK LEE and DAVE WANIGASEKERA. Can. J. Chem. **64**, 1228 (1986).

The reaction of (*E*)-, (*Z*)-, or a 2:3 mixture of (*E*)- and (*Z*)-1,2-diphenyl-2-tolyl[2-^{14}C]vinyl bromide ((*E*)-, (*Z*)-, or (*E*,*Z*)-**3**-Br-2-^{14}C) in HOAc–AgOAc gave a 1:1 mixture of the structurally unrearranged but isotopically scrambled (*E*)- and (*Z*)-1,2-diphenyl-2-tolyl[1,2-^{14}C]vinyl acetates ((*E*,*Z*)-**3**-OAc-1,2-^{14}C), with an average of 18.3% scrambling of the ^{14}C label from C-2 to C-1 arising from 1,2-tolyl shifts in the 1,2-diphenyl-2-tolylvinyl cation (**3**). No detectable amount of the structurally rearranged 2,2-diphenyl-1-tolylvinyl acetate (**4**-OAc) was formed. Solvolysis of (*E*,*Z*)-**3**-Br-2-^{14}C in TFE-2,6-lutidine gave as products 62% **4**-OTFE-1,2-^{14}C and 38% of a 1:1 mixture of (*E*)- and (*Z*)-**3**-OTFE-1,2^{14}C. Only (*Z*)-**3**-OTFE-1,2-^{14}C could be isolated as a pure product and it showed an average of 44.7% scrambling of the label from C-2 to C-1. Similar trifluoroethanolyses of (*E*,*Z*)-**3**-Br-2-^{13}C coupled with gas chromatographic – mass spectral analyses of the diphenyl and phenyl tolyl ketones from ozonolysis of the product mixture showed 44.6% scrambling in the (*E*,*Z*)-**3**-OTFE-1,2-^{13}C, confirming the ^{14}C results for the (*Z*) isomer. Nondegenerate rearrangements from 1,2-phenyl shifts before and after the degenerate 1,2-tolyl shifts to give **4**-OTFE-1-^{13}C and **4**-OTFE-2-^{13}C were also observed, demonstrating the occurrence of successive 1,2-aryl shifts in these triarylvinyl cations.

CHOI CHUCK LEE et DAVE WANIGASEKERA. Can. J. Chem. **64**, 1228 (1986).

La réaction du bromure de diphényl-1,2 tolyl-2 vinyle [^{14}C-2]-(*E*), -(*Z*) ou sous la forme d'un mélange 2:3 de -(*E*) et -(*Z*) (**3**-Br ^{14}C-2-(*E*), -(*Z*) ou -(*E*,*Z*)) avec du AgOAc en solution dans de l'acide acétique conduit à un mélange 1:1 des acétates de diphényl-1,2 tolyl-2 vinyle [^{14}C-1,2]-(*E*) et -(*Z*) qui ne sont pas transposés du point de vue de la structure, mais dont le taux moyen de répartition au hasard du marqueur ^{14}C, provenant de glissements-1,2 du groupement tolyle dans le cation diphényl-1,2 tolyl-2 vinyle (**3**), est de 18.3%. Il ne se forme pas de quantités détectables d'acétate de diphényl-2,2 tolyl-1 vinyle (**4**-OAc) qui serait structuralement transposé. La solvolyse du **3**-Br ^{14}C-2-(*E*,*Z*), dans un mélange de TFE–lutidine-2,6, conduit à 62% de **4**-OTFE ^{14}C-1,2 et à 38% d'un mélange 1:1 des isomères (*E*) et (*Z*) du **3**-OTFE ^{14}C-1,2. Seul le **3**-OTFE ^{14}C-1,2-(*Z*) a pu être isolé à l'état pur et, en moyenne, il comportait 44,7% de répartition au hasard du marqueur dans les positions C-2 et C-1. Des trifluoroéthanolyses analogues du composé **3**-Br ^{13}C-2-(*E*,*Z*), couplées à des analyses par spectre de masse/chromatographie en phase gaseuse de la diphénylcétone et de la phényl-tolylcétone qui résultent de l'ozonolyse du mélange, mettent en évidence qu'il s'est produit 44,6% de répartition au hasard du marqueur dans le composé **3**-OTFE ^{13}C-1,2-(*E*,*Z*); ces résultats confirment les résultats de ^{14}C obenus avec l'isomère (*Z*). On a également observé des transpositions non dégénérées provenant de glissements-1,2 de groupements phényles avant et après les glissements-1,2 dégénérés des groupements tolyles qui conduisent aux composés **4**-OTFE ^{13}C-1 et **4**-OTFE ^{13}C-2; ces résultats démontrent l'existence de déplacements-1,2 de groupements aryles dans ces cations triarylvinyles.

[Traduit par la revue]

Introduction

Rearrangements arising from 1,2-aryl shifts across the double bond in triarylvinyl cations have been studied with various combinations of phenyl (Ph), *p*-tolyl (Tol), and *p*-anisyl (An) groups as the three aryl substituents (2–4). Only one of these triarylvinyl cationic systems that have been investigated so far, namely, the 2-anisyl-1,2-diphenylvinyl cation (**1**), was capable of giving rise to both nondegenerate and degenerate rearrangements (5, 6). Thus, for example, the reaction of (*E*)- or (*Z*)-2-anisyl-1,2-diphenylvinyl bromide ((*E*)- or (*Z*)-**1**-Br) in 2,2,2-trifluoroethanol (TFE) – 2,6-lutidine gave, as major product, the structurally rearranged 1-anisyl-2,2-diphenylvinyl 2,2,2-trifluoroethyl ether (**2**-OTFE), arising from nondegenerate 1,2-phenyl shifts in cation **1** to the more stable 1-anisyl-2,2-diphenylvinyl cation (**2**), and a 1:1 mixture of the structurally unrearranged (*E*)- and (*Z*)-2-anisyl-1,2-diphenylvinyl 2,2,2-trifluoroethyl ethers ((*E*)- and (*Z*)-**1**-OTFE) as minor products (5). Using the pentadeuteriophenyl group as label and analysis by ^1H nmr and mass spectrometry, the trifluoroethanolysis of (*E*)-2-anisyl-1-phenyl-2-($^2H_5$)phenylvinyl bromide ((*E*)-**1**-Br-2-Ph-d_5) was found to give essentially complete scrambling of the label between C-2 and C-1 in the minor products, (*E*)- and (*Z*)-**1**-OTFE-1,2-Ph-d_5, arising from degenerate 1,2-anisyl shifts in the labeled cation **1**, the various rearrangement processes being summarized in Scheme 1.

It may be noted from Scheme 1 that if the nondegenerate 1,2-phenyl shift in cation **1**-1-Ph-d_5, obtained after the degenerate rearrangement, were to take place, cation **2**-2-Ph-d_5 would also be formed. Thus with Ph-d_5 as label, this process could not be demonstrated and was not considered (6). It is also of interest to note that in the reaction of (*E*)-**1**-Br-2-Ph-d_5 with HOAc–AgOAc, only degenerate rearrangement to give (*E*,*Z*)-**1**-OAc-1,2-Ph-d_5 was observed, with no product derived from the more stable cation **2**-2-Ph-d_5 (6). In the present work, we have studied another triarylvinyl cationic system that is capable of giving rise to both nondegenerate and degenerate rearrangements, i.e. the various rearrangement and isotopic scrambling processes in the 1,2-diphenyl-2-tolylvinyl cation (**3**) derived from solvolyses of (*E*)- and (*Z*)-1,2-diphenyl-2-tolyl[2-^{14}C]-vinyl or (*E*)- and (*Z*)-1,2-diphenyl-2-tolyl[2-^{13}C]vinyl bromides ((*E*)- and (*Z*)-**3**-Br-2-^{14}C or (*E*)- and (*Z*)-**3**-Br-2-^{13}C) in TFE–2,6-lutidine or in HOAc–AgOAc. The results are compared with those obtained from analogous studies with (*E*)-**1**-Br-2-Ph-d_5 and other triarylvinyl cationic systems to show the

[1]Rearrangement studies with ^{14}C. L; for part XLIX, see ref. 1.

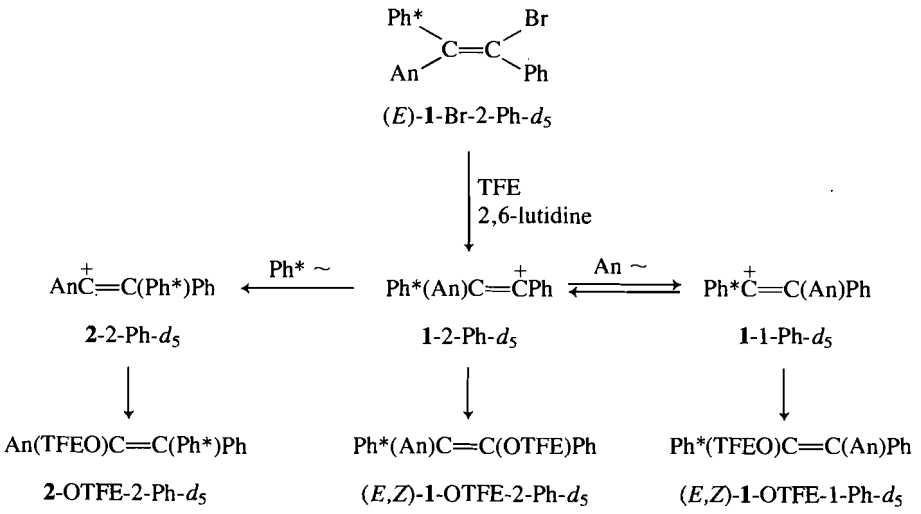

SCHEME 1

possibility of successive 1,2-aryl shifts (1,2-tolyl shift followed by 1,2-phenyl shift in cation **3**) and to give information on migratory aptitudes. Moreover, a method of analysis using a gc–ms technique in studies with (*E*)- and (*Z*)-**3**-Br-2-^{13}C has also been developed in the present work.

$Ph(Tol)C=\overset{+}{C}Ph$	$Ph(Tol)C^*=C(Br)Ph$
3	(*E*)- and (*Z*)-**3**-Br-2-^{14}C
	or (*E*)- and (*Z*)-**3**-Br-2-^{13}C

Results and discussion

Synthesis of (E,Z)-**3**-*Br-2-*^{14}*C and* (E,Z)-**3**-*Br-2-*^{13}*C*

The synthesis of (*E*)- and (*Z*)-**3**-Br-2-^{14}C was carried out via a series of reactions analogous to those utilized in previous preparations of (*E*,*Z*)-1,2-dianisyl-2-phenyl[2-^{13}C]vinyl (7), (*E*,*Z*)-2-phenyl-1,2-ditolyl[2-^{13}C]vinyl (8), and (*E*,*Z*)-1,2-dianisyl-2-tolyl[2-^{14}C]vinyl (9) bromides. Starting with [^{14}C]-$BaCO_3$, 1,2-diphenyl[1-^{14}C]ethanone (carbonyl labeled desoxybenzoin) was prepared as previously described (10). Treatment of this ketone with TolMgBr gave 1,2-diphenyl-1-tolyl[1-^{14}C]ethanol which, upon reaction with Br_2 in HOAc, gave a 2:3 mixture of (*E*)- and (*Z*)-1,2-diphenyl-2-tolyl[2-^{14}C]-vinyl bromides (to be designated (*E*,*Z*)-**3**-Br-2-^{14}C). The pure (*E*) and (*Z*) isomers were then obtained by fractional crystallization from acetone–methanol. In the same way, starting from 1,2-diphenyl[1-^{13}C]ethanone (10), (*E*,*Z*)-**3**-Br-2-^{13}C was also prepared.

Reactions in HOAc–AgOAc

In preliminary work using unlabeled material, reaction of (*E*)- or (*Z*)-**3**-Br in HOAc containing a small amount of Ac_2O to eliminate any moisture, and with the presence of 1.1 molar equivalents of AgOAc under reflux for 24 h, gave an essentially 1:1 mixture of (*E*)- and (*Z*)-1,2-diphenyl-2-tolylvinyl acetates ((*E*,*Z*)-**3**-OAc). No 2,2-diphenyl-1-tolylvinyl acetate (**4**-OAc) was formed, in agreement with the finding that no **2**-OAc-2-Ph-d_5 was obtained in the reaction of (*E*)-**1**-Br-2-Ph-d_5 with HOAc–AgOAc (6).

In similar reactions of (*E*)-**3**-Br-2-^{14}C, (*Z*)-**3**-Br-2-^{14}C, or (*E*,*Z*)-**3**-Br-2-^{14}C in HOAc–AgOAc, the (*E*,*Z*)-**3**-OAc-1,2-^{14}C product was degraded by ozonolysis to give phenyl tolyl[^{14}C]-ketone (**5**-^{14}C), and the difference between the specific activities of the (*E*,*Z*)-**3**-OAc-1,2-^{14}C and the corresponding **5**-^{14}C gave the extent of scrambling of the label from C-2 to C-1. The results are summarized in Table 1, showing a mean scrambling value of 18.3%. The formation of the same 1:1 mixture of (*E*)- and (*Z*)-**3**-OAc-1,2-^{14}C with essentially the same extent of scrambling in the reaction of (*E*)-, (*Z*)-, or (*E*,*Z*)-**3**-Br-2-^{14}C in HOAc–AgOAc would support the dissociated, linear 1,2-diphenyl-2-tolylvinyl cation (**3**) as intermediate in these reactions, with the isotopic scrambling arising from degenerate 1,2-tolyl shifts across the double bond in cation **3** (Scheme 2). Moreover, it is seen from Table 1 that extending the reaction time from 1 day to 2 days for the reaction in HOAc–AgOAc did not affect the extent of scrambling, indicating that the product, (*E*,*Z*)-**3**-OAc-1,2-^{14}C, was stable in the reaction medium.

For the processes depicted in Scheme 2, eq. [1] holds (11), and for a mean scrambling value of 18.3%, from eq. [1], $k_{SOH}/k_r^{Tol} = 3.5$.

$$[1]\quad [(E,Z)\text{-}3\text{-OAc-2-}^{14}C]/[(E,Z)\text{-}3\text{-OAc-1-}^{14}C] = 1 + (k_{SOH}/k_r^{Tol})$$

In the analogous reaction of (*E*)-**1**-Br-2-Ph-d_5 in HOAc–AgOAc, 90.0–94.6% β-anisyl rearrangement (45.0–47.3% scrambling) was reported (6). Using a mean scrambling value of 46.2% and applying eq. [1] to this system, $k'_{SOH}/k_r^{An} = 0.16$. Assuming that k_{SOH} and k'_{SOH} are about the same for the product-forming capture of the 1,2-diphenyl-2-tolylvinyl cation (**3**) and the 2-anisyl-1,2-diphenylvinyl cation (**1**), then the migratory aptitude of An:Tol can be calculated:

$$(k_{SOH}/k_r^{Tol})/(k'_{SOH}/k_r^{An}) = k_r^{An}/k_r^{Tol} = 3.5/0.16 = 22$$

This k_r^{An}/k_r^{Tol} value of 22 may be compared with a similar migratory ratio for An:Tol of 33 obtained from a comparison of data derived from reactions of labeled 1,2-dianisyl-2-tolylvinyl and trianisylvinyl bromides in HOAc–AgOAc (9). While these values differ by 50%, considering the errors that may be involved, the agreement obtained from the two sets of experiments may be considered to be reasonably good. For systems showing very large extents of scrambling, such as the reaction of (*E*)-**1**-Br-2-Ph-d_5 with HOAc–AgOAc, small changes in the extent of scrambling will lead to relatively large variations in k_{SOH}/k_r. For example, if the higher observed value of 47.3% scrambling as reported by Rappoport *et al.* (6) instead of the mean value of 46.2% scrambling were employed in the calculations, k'_{SOH}/k_r^{An} would be 0.11 (instead of 0.16), and

TABLE 1. Isotopic scrambling data in solvolyses of (*E*)-, (*Z*)-, or (*E*,*Z*)-**3**-Br-2-^{14}C in HOAc–AgOAc or TFE–2,6-lutidine

		Specific activity, 10^{-5} dpm/mmol				Scrambling from C-2 to C-1, %[e]	
		Reaction product[c]		Degradation product[d]			
Substrate[a]	Reaction medium[b]	Run 1	Run 2	Run 1	Run 2	Run 1	Run 2
(*E*)-**3**-Br-2-^{14}C	HOAc–AgOAc	26.8	19.7	21.9	16.0	18.2	18.7
(*Z*)-**3**-Br-2-^{14}C	HOAc–AgOAc	7.46	5.00	6.11	4.10	18.1	18.0
(*E*,*Z*)-**3**-Br-2-^{14}C	HOAc–AgOAc	5.10	11.6	4.10	9.48	18.1	18.3
(*E*,*Z*)-**3**-Br-2-^{14}C	HOAc–AgOAc[f]	9.96	6.96	8.15	5.64	18.1	18.9
(*E*,*Z*)-**3**-Br-2-^{14}C	TFE–2,6-lutidine	7.10	1.36	3.89	0.75	44.5	44.9

[a]The substrate was pure (*E*)-, pure (*Z*)-, or a 2:3 mixture of (*E*)- and (*Z*)-1,2-diphenyl-2-tolyl[2-^{14}C]vinyl bromides.
[b]The acetolyses were carried out with 0.15 molar concentration of substrate in HOAc containing about 5% Ac_2O and 1.1 equivalents of AgOAc at reflux temperature for 1 day; the trifluoroethanolyses were carried out with 0.15 molar concentration of substrate in TFE containing 1.1 equivalents of 2,6-lutidine in sealed ampoules at 150 ± 2°C for 10 days.
[c]The products analyzed were the 1:1 mixture of (*E*)- and (*Z*)-acetates, (*E*,*Z*)-**3**-OAc-1,2-^{14}C, for the acetolyses, and the pure *Z*-trifluoroethyl ether, (*Z*)-3-OTFE-1,2-^{14}C, for the trifluoroethanolyses.
[d]The degradation product was phenyl tolyl [^{14}C]ketone.
[e]The mean scrambling value is 18.3% for the reactions in HOAc–AgOAc, and 44.7% for the reactions in TFE–2,6-lutidine.
[f]The reaction time was extended to 2 days.

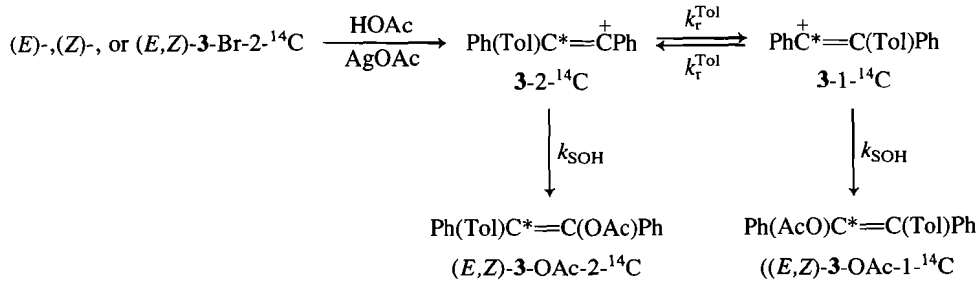

SCHEME 2

k_r^{An}/k_r^{Tol} would be 3.5/0.11 = 32, in almost exact agreement with the previous value of 33 (9).

In another comparison, the 18.3% scrambling arising from 1,2-tolyl shifts in the reaction of *E*,*Z*-**3**-Br-2-^{14}C in HOAc–AgOAc may be considered in conjunction with the 6–7% scrambling observed for the reaction of triphenyl[2-^{14}C]vinyl bromide (**6**-Br-2^{14}C) with HOAc–AgOAc (12). Taking into account the statistical factor of 2 for the 1,2-phenyl shift in the triphenylvinyl cationic system, eq. [2] applies for the reaction of **6**-Br-2-^{14}C in HOAc–AgOAc (11).

$$[2] \quad [\mathbf{6}\text{-OAc-2-}^{14}\text{C}]/[\mathbf{6}\text{-OAc-1-}^{14}\text{C}] = 1 + (k'_{SOH}/2k_r^{Ph})$$

For a mean value of 6.5% scrambling, $k'_{SOH}/k_r^{Ph} = 26$. Again assuming that $k_{SOH} = k'_{SOH}$, $k_r^{Tol}/k_r^{Ph} = 26/3.5$ or about 7, in fairly good agreement with the previously reported value of about 5 (11).

Reactions in TFE–2,6-lutidine

The trifluoroethanolysis of (*E*,*Z*)-**3**-Br-2-^{14}C in the presence of 1.1 equivalents of 2,6-lutidine was carried out in sealed ampoules at 150 ± 2°C for 10 days. In preliminary work with nonlabeled material, such a reaction gave 3 products as identified by ^{1}H nmr. The major product was 2,2-diphenyl-1-tolylvinyl 2,2,2-trifluoroethyl ether (**4**-OTFE, 62%) and the minor component was a 1:1 mixture of the (*E*) and (*Z*) isomers of 1,2-diphenyl-2-tolylvinyl 2,2,2-trifluoroethyl ethers ((*E*)-**3**-OTFE, 38%). The major product, **4**-OTFE, was derived from a nondegenerate 1,2-phenyl shift in cation **3**, while in the structurally unrearranged (*E*)-**3**-OTFE, a degenerate 1,2-tolyl shift may occur and this would be detectable from studies with a labeled substrate.

When the mixture of products, **4**-OTFE and the 1:1 mixture of (*E*,*Z*)-**3**-OTFE, was subjected to fractional crystallization, only the pure (*Z*)-**3**-OTFE could be isolated. Thus in the trifluoroethanolysis of (*E*,*Z*)-**3**-Br-2-^{14}C, the only isolable pure product, (*Z*)-**3**-OTFE-1,2-^{14}C, was degraded by ozonolysis to give phenyl tolyl [^{14}C]ketone (**5**-^{14}C) and, from the specific activities of this (*Z*) isomer and its degradation product, the extent of scrambling of the label from C-2 to C-1 was obtained. The results, as summarized in Table 1, show an average of 44.7% scrambling arising from 1,2-tolyl shifts across the double bond in the 1,2-diphenyl-2-tolylvinyl cation (**3**).

Since only one of three products obtained in the trifluoroethanolysis of (*E*,*Z*)-**3**-Br-2-^{14}C was analyzed for isotopic scrambling, the experiments were repeated using (*E*,*Z*)-**3**-Br-2-^{13}C as substrate with the object of analyzing the extents of possible isotopic scramblings in both the major nondegenerate rearrangement product, **4**-OTFE-1,2-^{13}C, and in the minor products (*E*,*Z*)-**3**-OTFE-1,2-^{13}C. This mixture of products was degraded by ozonolysis to give a mixture of labeled and unlabeled diphenyl and phenyl tolyl ketones which were analyzed by gas chromotography – mass spectrometry (gc–ms), with the mass spectra of the separated ketones obtained by the electron impact method. The extents of scrambling were then evaluated by comparing the relative intensities of the base peaks and the molecular ions of the respective labeled and unlabeled ketones,

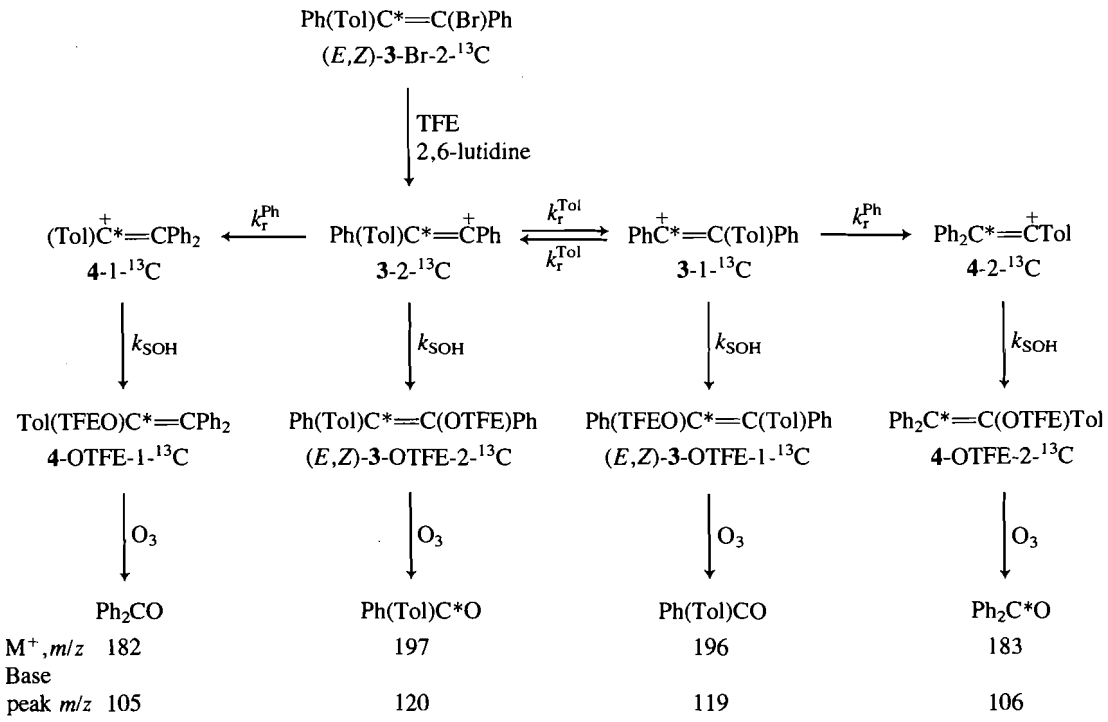

SCHEME 3

TABLE 2. Data from the mass spectra of PhCOTol and Ph^{13}CTol

	Observed intensity		Corrected for $(M+1)^+$		Corrected for 90% ^{13}C enrichment		% Distribution[b]	
m/z[a]	Run 1	Run 2	Run 1	Run 2	Run 1	Run 2	Run 1	Run 2
195	2.01	2.03						
196	32.35	30.97	32.09	30.71	25.76	24.55	45.2	44.3
197	35.39	34.87	31.22	30.91	31.22	30.91	54.8	55.7
198	4.57	4.46						
118	—	0.02						
119	93.58	93.02	93.58	93.02	74.93	74.42	44.6	44.4
120	100.00	100.00	92.93	93.01	92.93	93.01	55.4	55.6
121	7.41	7.51						

[a]Molecular ions for [TolCOPh]$^+$ and [Tol^{13}COPh]$^+$ at m/z 196 and 197, respectively; the base peak is [Tol^{13}CO]$^+$ at m/z 120.

[b]Percentages for m/z 196 ([TolCOPh]$^+$) and for m/z 119 ([TolCO]$^+$) correspond to % scrambling from C-2 to C-1 in the (*E*,*Z*)-3-OTFE-1,2-^{13}C (see Scheme 3); mean value = (45.2 + 44.3 + 44.6 + 44.4)/4 = 44.6 ± 0.3%.

the relative intensities being correted for $(M+1)^+$ absorption and for the fact that the ^{13}C enrichment was 90%. The processes involved in the trifluoroethanolysis of (*E*,*Z*)-3-Br-2-^{13}C are summarized in Scheme 3. The results from the mass spectral analyses of the degradation products, diphenyl and phenyl tolyl ketones, are given in Tables 2 and 3.

As an illustration of the calculations, consider, for example, the relative intensities of the peaks in the molecular ion region of run 1 for the phenyl tolyl ketones (Table 2). Since the intensity of m/z 198 is 12.9% of the intensity of m/z 197, the $(M+1)^+$ correction should be 12.9% of the intensity of the M^+ ion. Thus correcting for $(M+1)^+$, the intensities of m/z 196 and 197 should be $(32.35 - 0.129 \times 2.01) = 32.09$ and $(35.39 - 0.129 \times 32.35) = 31.22$, respectively.

Since the reaction was carried out using materials with 90% ^{13}C enrichment, 10% of the total reaction would only give rise to TolCOPh (m/z 196) and 90% would give Tol^{13}COPh (m/z 197) and TolCOPh (m/z 196). Therefore, 10% of the total intensity should be subtracted from the m/z 196 peak to give the actual intensity of m/z 196 derived from the 90% enriched reactant. Thus, correcting for the 90% enrichment, the m/z 196 intensity should be $32.09 - [0.1(32.09 + 31.22) = 25.76$.

Since TolCOPh (m/z 196) was derived from the rearranged (*E*,*Z*)-3-OTFE-1-^{13}C, the percentage scrambling of the label from C-2 to C-1, as given in Table 2, would be $(100 \times 25.76)/(25.76 + 31.22) = 45.2\%$.

It is of interest to note that the mean value of 44.6% scrambling of the ^{13}C label from C-2 to C-1 arising from degenerate 1,2-tolyl shifts (Table 2) is in very good agreement with the mean value of 44.7% scrambling (Table 1) obtained from the use of ^{14}C labelling. The formation of unrearranged and rearranged products given in Scheme 3 is summarized again

TABLE 3. Data from the mass spectra of PhCOPh and Ph^{13}COPh

	Observed intensity		Corrected for $(M+1)^+$		Corrected for 90% ^{13}C enrichment		% Distribution[b]	
m/z[a]	Run 1	Run 2	Run 1	Run 2	Run 1	Run 2	Run 1	Run 2
181	5.64	5.06						
182	31.24	29.33	30.57	28.74	25.49	23.96	55.7	55.7
183	23.96	22.51	20.27	19.08	20.27	19.08	44.3	44.3
184	2.82	2.63						
104	0.06	0.02						
105	85.80	81.25	85.80	81.25	71.28	67.49	54.6	54.5
106	64.87	61.43	59.38	56.33	59.38	56.33	45.4	45.5
107	4.15	3.86						

[a]Molecular ions for $[PhCOPh]^+$ and $[Ph^{13}COPh]^+$ at m/z 182 and 183, respectively; the base peak is Ph^+ at m/z 77, although for the unlabeled pure sample of PhCOPh, the base peak was $[PhCO]^+$ at m/z 105. Presumably, in the labeled system, the benzoyl ions appear as 2 peaks at m/z 105 and 106, each of which showed a relative intensity of less than that at m/z 77.

[b]Percentages for m/z 183 ($[Ph^{13}COPh]^+$) and for m/z 106 ($[Ph^{13}CO]^+$) correspond to % of the isotopically rearranged product, **4**-OTFE-2-^{13}C (see Scheme 3); mean value = (44.3 + 44.3 + 45.4 + 45.5)/4 = 44.9 ± 0.5%.

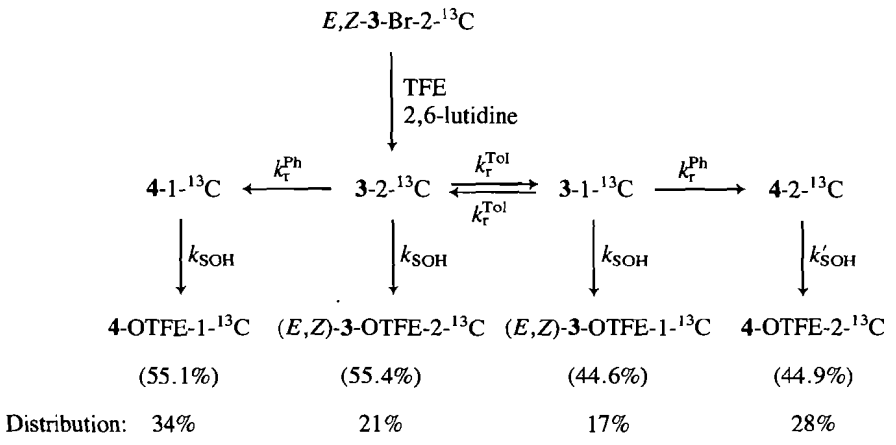

SCHEME 4

in Scheme 4, with the extents of scrambling of the isotopic label in (*E*,*Z*)-**3**-OTFE-1,2-^{13}C and **4**-OTFE-1,2-^{13}C shown in parentheses. It was indicated earlier that from ^{1}H nmr, the major product (62%) was **4**-OTFE-1,2-^{13}C and the minor product (38%) was (*E*,*Z*)-**3**-OTFE-1,2-^{13}C. Using this 62:38 product ratio and the observed extents of scrambling, a percentage distribution of the products can be calculated. Thus, of the product mixture, the distribution for the unrearranged **4**-OTFE-1-^{13}C and the rearranged **4**-OTFE-2-^{13}C would be 0.551 × 62 = 34% and 0.449 × 62 = 28%, respectively. Similarly, the distribution for (*E*,*Z*)-**3**-OTFE-2-^{13}C and (*E*,*Z*)-**3**-OTFE-1-^{13}C would be 0.554 × 38 = 21% and 0.446 × 38 = 17%. These values are also shown in Scheme 4. Interestingly, the ratios of **4**-OTFE-1-^{13}C/ (*E*,*Z*)-**3**-OTFE-2-^{13}C and **4**-OTFE-2-^{13}C/(*E*,*Z*)-**3**-OTFE-1-^{13}C, or 34/21 = 1.6 and 28/17 = 1.6, are the same, indicating the same extent of rearrangement from the 1,2-diphenyl-2-tolylvinyl cation (**3**) to the more stable 2,2-diphenyl-1-tolylvinyl cation (**4**) before or after the degenerate 1,2-tolyl shift in **3**-2-^{13}C and **3**-1-^{13}C.

From a steady state treatment or with the use of the method of Bonner and Collins (13), it can be shown that eq. [3] applies to the processes given in Scheme 4. The observed results are in agreement with this prediction since the 44.6% scrambling to cation **3**-1-^{13}C is essentially equal to the 44.9% scrambling to cation **4**-2-^{13}C, or 55.4/44.6 = 1.2 and 55.1/44.9 = 1.2 are the same.

$$[3]\quad [(E,Z)\text{-}\mathbf{3}\text{-OTFE-2-}^{13}\text{C}]/[(E,Z)\text{-}\mathbf{3}\text{-OTFE-1-}^{13}\text{C}] = [\mathbf{4}\text{-OTFE-1-}^{13}\text{C}]/[\mathbf{4}\text{-OTFE-2-}^{13}\text{C}]$$

The formation of **4**-OTFE-2-^{13}C, as indicated in Schemes 3 or 4, clearly demonstrated the occurrence of 1,2-phenyl shifts after 1,2-tolyl shifts have taken place. Such successive 1,2-aryl shifts in triarylvinyl cationic systems have recently been shown to occur by the use of doubly labeled triarylvinyl substrates (14, 15). In the present work, the occurrence of both degenerate and nondegenerate rearrangements also provides another route in demonstrating such successive 1,2-shifts.

It has already been noted that in the reaction of (*E*,*Z*)-**3**-Br-2-^{13}C with HOAc–AgOAc, only degenerate rearrangements to give (*E*,*Z*)-**3**-OAc-2-^{14}C and (*E*,*Z*)-**3**-OAc-1-^{14}C were observed, with no detectable amount of nondegenerate 1,2-phenyl shifts to give **4**-OAc-1,2-^{14}C. For a possible explanation of these results, let us consider the transition states involved in these 1,2-aryl shifts. For the degenerate rearrangement, the tolyl bridged transition state **7** may be more stable than the phenyl bridged transition state **8** for the nondegenerate rearrangement. Apparently, in a medium of low nucleophilic

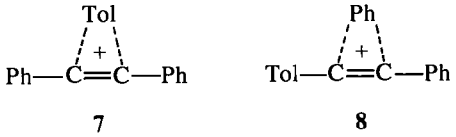

7 8

character such as TFE (16), the lifetime of the cations is sufficiently long for the nondegenerate rearrangement of **3**-2-^{13}C → **4**-1-^{13}C and **3**-1-^{13}C → **4**-2-^{13}C to proceed, overcoming the higher energy barrier via transition state **8**. In HOAc–AgOAc, the lifetime of the cations is shorter and only degenerate rearrangements through the lower energy barrier of **7** could take place.

Experimental

1,2-Diphenyl-1-tolyl[1-^{14}C]ethanol

To a Grignard solution prepared from 8.0 g (47 mmol) of *p*-bromotoluene and 2.0 g (82 mmol) of Mg in 250 mL of dry tetrahydrofuran (THF), and cooled in an ice bath, was added dropwise and with stirring over a period of 1 h a solution of 4.5 g (23 mmol) of 1,2-diphenyl-[1-^{14}C]ethanone (10) in 100 mL of dry THF. The resulting solution was stirred at room temperature for 1 h, refluxed for 2 h, and then poured into 200 mL of H_2O containing 25 g of NH_4Cl and 5 mL of NH_4OH. The organic layer was washed with H_2O (3 × 25 mL) and, after drying over $MgSO_4$, the solvent was evaporated to give 4.1 g (66%) of 1,2-diphenyl-1-tolyl[1-^{14}C]ethanol, which was recrystallized from acetone–methanol. The unlabeled alcohol was prepared in the same way using ordinary desoxybenzoin, mp 87–88°C; ^{1}H nmr ($CDCl_3$) δ: 2.25 (4H, s, CH_3 + OH), 2.29 (sh, OH), 3.57 (2H, s, CH_2), 6.78–7.53 (14H, m, Ar). *Anal.* calcd. for $C_{21}H_{20}O$: C 87.46, H 6.99; found: C 87.17, H 7.04.

(E)- and (Z)-1,2-diphenyl-2-tolyl[2-^{14}C]vinyl bromides

To a solution of 5.00 g (17.4 mmol) of 1,2-diphenyl-1-tolyl[1-^{14}C]-ethanol in 50 mL of HOAc was added dropwise with stirring 3.0 g (19 mmol) of bromine in 20 mL of HOAc over a period of 0.5 h. During this period the temperature of the reaction mixture was maintained below 50°C and any HBr that was produced was flushed out with N_2. The resulting mixture was stirred overnight and the bright yellow solid that was formed was filtered, and washed with 10% $Na_2S_2O_3$ solution and with H_2O. The yield of the dried product was 4.8 g (79%), consisting of an approximately 2:3 mixture of (*E*)-:(*Z*)-1,2-diphenyl-2-tolyl[2-^{14}C]vinyl bromides ((*E*,*Z*)-**3**-Br-2-^{14}C). Degradation of a sample of this (*E*,*Z*)-**3**-Br-2-^{14}C by ozonolysis gave phenyl tolyl [^{14}C]-ketone with the same specific activity, indicating that all the ^{14}C label was located at the C-2 position.

In the same way, (*E*,*Z*)-**3**-Br or (*E*,*Z*)-**3**-Br-2-^{13}C was synthesized from ordinary desoxybenzoin or from 1,2-diphenyl[1-^{13}C]ethanone prepared from 90% enriched [^{13}C]$BaCO_3$. These (*E*,*Z*) isomers could be separated by fractional crystallization from 10% acetone – 90% methanol at room temperature and their (*E*) and (*Z*) structures were assigned based on preliminary crystallographic studies by Professor B. E. Robertson of the University of Regina. The (*Z*) isomer crystallized out first as fluffy colorless crystals, followed by the (*E*) isomer as bright yellow octagons. After further purification by recrystallization from acetone–methanol, the pure (*E*) isomer melted at 131–133°C; ^{1}H nmr ($CDCl_3$) δ: 2.39 (3H, s, CH_3), 7.03–7.51 (14H, m, Ar). *Anal.* calcd. for $C_{21}H_{17}Br$: C 72.21, H 4.91, Br 22.88; found: C 72.04, H 4.92, Br 22.83. The pure (*Z*) isomer melted at 141–143°C; ^{1}H nmr ($CDCl_3$) δ: 2.20 (3H, s, CH_3), 6.87–7.37 (14H, m, Ar). *Anal.* calcd. for $C_{21}H_{17}Br$: C 72.21, H 4.91, Br 22.88; found: C 72.02, H 4.89, Br 23.38.

Reaction of (E)-, (Z)-, or (E,Z)-3-Br-2-^{14}C in HOAc–AgOAc

In a typical experiment, 733 mg (2.10 mmol) of (*E*,*Z*)-**3**-Br-2-^{14}C and 386 mg (2.30 mmol) of AgOAc in 14 mL of HOAc containing about 5% Ac_2O was heated under reflux for 24 h. The excess solvent was then evaporated off under reduced pressure in a rotary evaporator. The residue was disolved in 100 mL of CH_2Cl_2 and washed successively with water (2 × 20 mL), 3% $NaHCO_3$ (2 × 20 mL), and again with water (1 × 10 mL). After drying over $MgSO_4$, the solvent was removed, giving an oil that was purified through an alumina column with elution by 20:80 CH_2Cl_2 – petroleum ether (bp 40–60°C). The first fraction eluted contained some unreacted bromide and the second fraction contained the acetate product. Removal of the solvent gave a white solid, the ^{1}H nmr spectrum of which showed that it was a 1:1 mixture of (*E*)- and (*Z*)-**3**-OAc-1,2-^{14}C on the basis of the tolyl-CH_3 absorptions at 2.27 and 2.35 ppm. Degradation of this product mixture by ozonolysis (17) gave phenyl tolyl [^{14}C]ketone for the determination of the extent of scrambling.

The mixture of (*E*)- and (*Z*)-**3**-OAc could be separated by fractional crystallization from methanol. The first to crystallize and presumably the (*Z*) isomer melted at 91–93°C; ^{1}H nmr ($CDCl_3$) δ: 2.00 (3H, s, OAc), 2.35 (3H, s, CH_3), 7.18–7.31 (14H, m, Ar). *Anal.* calcd. for $C_{23}H_{20}O_2$: C 84.12, H 6.14; found: C 84.30, H 6.11. The other and presumably (*E*) isomer melted at 165–167°C; ^{1}H nmr ($CDCl_3$) δ: 1.95 (3H, s, OAc), 2.27 (3H, s, CH_3), 7.01–7.33 (14H, m, Ar). *Anal.* calcd. for $C_{23}H_{20}O_2$: C 84.12, H 6.14; found: C 84.08, H 6.18.

Reaction of (E,Z)-3-Br-2-^{14}C or (E,Z)-3-Br-2-^{13}C in TFE–2,6-lutidine

In a typical experiment, 800 mg (2.29 mmol) of (*E*,*Z*)-**3**-Br-2-^{14}C in 15 mL of TFE containing 290 mg (2.52 mmol) of 2,6-lutidine in a sealed glass ampoule was heated in an oil bath at 150 ± 2°C for 10 days. After cooling, the dark brown solution was transferred into a round-bottom flask and the excess solvent was distilled off under reduced pressure. The residue was dissolved in 100 mL of ether and the solution was washed successively with H_2O, 1 *M* HCl, and water, and then dried over $MgSO_4$. The excess solvent was removed, giving a brown oil that was passed through an alumina column and eluted with a 20:80 mixture of CH_2Cl_2 – petroleum ether (bp 40–60°C). Removal of the solvent from the eluate under reduced pressure gave 548 mg (65%) of products as a yellow oil. The distribution of products in this oil was estimated from the relative intensities of the tolyl-CH_3 peaks in its ^{1}H nmr spectrum. The two smaller peaks of similar intensity at 2.20 and 2.33 ppm were assigned to the (*E*)- and (*Z*)-1,2-diphenyl-2-tolyl[1,2-^{14}C]vinyl 2,2,2-trifluoroethyl ethers ((*E*,*Z*)-**3**-OTFE-1,2-^{14}C) as minor products. The more intense peak at 2.25 ppm was assigned to the structurally rearranged 2,2-diphenyl-1-tolyl[1,2-^{14}C]vinyl 2,2,2-trifluoroethyl ether (**4**-OTFE-1,2-^{14}C), the ratio of **4**-OTFE-1,2-^{14}C to (*E*,*Z*)-**3**-OTFE-1,2-^{14}C being about 62 to 38.

From a similar solvolysis with unlabeled (*E*,*Z*)-**3**-Br in TFE–2,6-lutidine, the mixture of products as a yellow oil was crystallized from a dilute solution in 95% ethanol. Bright yellow and colorless crystals were formed and these were physically separated. The yellow crystals were recrystallized from 95% ethanol to give pale yellow hexagons, mp 90–91°C; ^{1}H nmr ($CDCl_3$) δ: 2.33 (3H, s, CH_3), 3.73–4.17 (2H, q, CH_2), 7.10–7.37 (14H, m, Ar). *Anal.* calcd. for $C_{23}H_{19}OF_3$: C 74.99, H 5.20; found: C 74.57, H 5.37. This product was assigned the (*Z*) structure based on preliminary crystallographic work by Prof. B. E. Robertson. The major portion of the white crystalline product from the original crystallization was repeatedly recrystallized from 95% ethanol, and the product obtained was **4**-OTFE contaminated by about 10% (*E*)-**3**-OTFE. This mixture melted at 72–74°C, ^{1}H nmr ($CDCl_3$) δ: 2.20 (trace, CH_3, (*E*) isomer), 2.25 (3H, s, CH_3), 3.62–4.06 (2H, q, CH_2), 6.79–7.33 (14H, m, Ar). *Anal.* calcd. for $C_{23}H_{19}OF_3$: C 74.99, H 5.20; found: C 74.51, H 5.26.

In similar reactions of (*E*,*Z*)-**3**-Br-2-^{13}C with TFE-2,6-lutidine, the mixture of products containing (*E*,*Z*)-**3**-OTFE-1,2-^{13}C and **4**-OTFE-1,2-^{13}C, as an oil, was subjected to ozonolysis (17) to give a mixture of unlabeled and labeled diphenyl and phenyl tolyl ketones, which were analyzed by a Model 4000 Finnigan gc–ms system.

Acknowledgement

The financial support given by the Natural Sciences and Engineering Research Council of Canada is sincerely acknowledged.

1. C. C. LEE and C. Y. FIAKPUI. Can. J. Chem. **63**, 681 (1985).
2. P. J. STANG, Z. RAPPOPORT, M. HANACK, and L. R. SUBRAMANIAN. Vinyl cations. Academic Press, New York. 1979. pp. 395–432.
3. C. C. LEE. *In* Isotopes in organic chemistry. Vol. 5. Isotopes in cationic reactions. *Edited by* E. Buncel and C. C. Lee. Elsevier, Amsterdam. 1980. pp. 1–44.
4. A. A. SHCHEGALEV and M. KANISHCHEV. Russ. Chem. Revs. **50**, 553 (1981).
5. Z. RAPPOPORT and Y. HOUMINER. J. Chem. Soc. Perkin Trans. **2**, 1506 (1973).
6. Z. RAPPOPORT, E. NOY, and Y. HOUMINER. J. Am. Chem. Soc. **98**, 2238 (1976).
7. C. C. LEE and M. OKA. Can. J. Chem. **54**, 604 (1976).
8. C. C. LEE, A. J. PAINE, and E. C. F. KO. J. Am. Chem. Soc. **99**, 7267 (1977).
9. D. WANIGASEKERA, C. C. LEE, Y. HOUMINER, M. AVIV, and Z. RAPPOPORT. J. Org. Chem. **49**, 4367 (1984).
10. C. C. LEE, C. Y. FIAKPUI, and J. W. QUAIL. Can. J. Chem. **60**, 735 (1982).
11. C. C. LEE, E. C. F. KO, and Z. RAPPOPORT. Can. J. Chem. **58**, 884 (1980).
12. F. H. A. RUMENS, R. D. GREEN, A. J. CESSNA, M. OKA, and C. C. LEE. Can. J. Chem. **53**, 314 (1975).
13. W. A. BONNER and C. J. COLLINS. J. Am. Chem. Soc. **78**, 5587 (1965).
14. C. C. LEE, C. Y. FIAKPUI, and K. K. MIDHA. J. Org. Chem. **48**, 1025 (1983).
15. Z. RAPPOPORT, C. Y. FIAKPUI, X.-D. YU, and C. C. LEE. J. Org. Chem. **49**, 570 (1984).
16. F. L. SCHADT, T. W. BENTLEY, and P. v. R. SCHLEYER. J. Am. Chem. Soc. **98**, 7667 (1976).
17. J. J. PAPAS, W. P. KEAVENEY, E. GANCHER, and M. BERGER. Tetrahedron Lett. 4273 (1966).

Electron transfer and autoxidation kinetics of the bis(imidazole)bis(dimethylglyoximato)iron(II) complex

HENRIQUE E. TOMA[1] AND ANTONIO CARLOS C. SILVA

Instituto de Quimica, Universidade de Sao Paulo, Caixa Postal 20780, Sao Paulo, SP, Brazil

Received October 23, 1985

HENRIQUE E. TOMA and ANTONIO CARLOS C. SILVA. Can. J. Chem. **64**, 1280 (1986).

The properties and reactivity of the bis(imidazole)bis-(dimethylglyoximato)iron(II) complex have been studied based on spectroelectrochemistry, cyclic voltammetry, and stopped-flow kinetics in aqueous solution. The autoxidation reaction was found to be inhibited by the imidazole ligand in excess but susceptible to copper(II) catalysis. In this case a mechanism has been proposed, consisting of a rapid electron transfer followed by the reoxidation of the resulting Cu(I) species by O_2.

HENRIQUE E. TOMA et ANTONIO CARLOS C. SILVA. Can. J. Chem. **64**, 1280 (1986).

Opérant en solution aqueuse et faisant appel à la spectroélectrochimie, à la voltamétrie cyclique et à la cinétique par flux stoppé, on a étudié les propriétés et la réactivité du complexe bis(imidazole) bis(diméthyglyoximato) fer(II). On a trouvé que la réaction d'auto-oxydation est inhibée par le ligand imidazole qui est présent en excès, alors qu'elle est susceptible à la catalyse par le cuivre(II). Dans ce cas, on propose un mécanisme d'après lequel il se produit une transfert rapide d'électron qui est suivi d'une réoxydation, par le O_2, de l'espèce Cu(I) qui résulte.

[Traduit par la revue]

Introduction

Dioxime complexes of iron(II) are interesting examples of coordination compounds which mimic hemoglobin and mioglobin in their ability to reversibly bind carbon monoxide (1–4). Among the several dioxime complexes, the bis(dimethylglyoximato)bis(imidazole)iron(II) complex $[Fe(Hdmg)_2(Him)_2]$, because of its well known molecular structure (5) which resembles the porphyrin species with biologically important ligands, has attracted our attention. On the other hand, in contrast with the pyridine analogues, the imidazole complex is soluble enough in water for comparative studies with the biological hemes.

In this work we have studied the properties and reactivity of the $[Fe(Hdmg)_2(Him)_2]$ complex, with particular emphasis on the electrochemistry and redox kinetics in aqueous solution. We have also investigated the autoxidation mechanisms, including the copper-catalyzed reaction, because of their possible relevance to the understanding of the biological oxidation processes (6–8).

Experimental

The complex $[Fe(Hdmg)_2(Him)_2]$ was synthesized from iron(II) acetate and the corresponding ligands (Aldrich) by the method of Pang and Stynes (3). *Anal.* calcd. for C 39.75, N 26.48, H 5.20; found: C 38.9, N 26.4, H 5.0. $[Co(phen)_3](ClO_4)_3$ dihydrate (phen = *o*-phenanthroline) was prepared according to the procedure of Schilt and Taylor (9). *Anal.* calcd. for C 46.41, N 9.0, H 3.0; found: C 46.4, N 8.8, H 2.7. Imidazole, *o*-phenantroline, $CuSO_4 \cdot 5H_2O$ and other reagent grade chemicals were used as supplied.

The electronic spectra of the complexes in the visible and uv region were recorded on a Cary 17 or a Hewlett-Packard 8451 diode-array spectrophotometer fitted with thermostatted cell compartments. Cyclic voltammetry measurements were carried out with a Princeton Applied Research instrument, consisting of a 173 potentiostat and a 175 universal programmer. A platinum electrode was employed for the measurements, using the conventional Luggin capillary with the Ag/AgCl(1 *M* KCl) reference electrode in a non-isothermic arrangement. A platinum wire was used as the auxiliary electrode.

Spectroelectrochemical measurements were carried out using the diode-array spectrophotometer and the 173 potentiostat, with a transparent electrochemical cell of 0.03 cm internal optical pathlength. A gold minigrid was employed as the working electrode, in the presence of a small Ag/AgCl (1 *M* KCl) reference electrode, and of a platinum auxiliary electrode. The experiments were carried out at 25°C, under semi-infinite diffusion conditions, as described by Kuwana and Winograd (10).

The kinetics of the substitution and electron transfer reactions were investigated with the diode-array spectrophotometer, using a flow cell attached to a rapid mixing system, or with a Durrum D-110 stopped flow apparatus, equipped with a Kel-F flow system.

The $[Fe(Hdmg)_2(Him)_2]$ solutions were freshly prepared under argon atmosphere, by dissolving the solid complex in water, in the presence of an excess of imidazole.

The reactions were followed spectrophotometrically, by monitoring the decay of the absorption band of the $[Fe(Hdmg)_2(Him)_2]$ complex at 530 nm. Pseudo first order rate constants were evaluated from the linear logarithmic plots of absorbance versus time. The reversible reaction between $[Fe(Hdmg)_2(Him)_2]$ or A, and $[Cu(Him)_4]^{2+}$ or B, was analysed according to the following scheme:

$$[1] \qquad A + B \underset{k_r}{\overset{k_f}{\rightleftharpoons}} C + D$$

where

$$[2] \qquad K = \frac{k_f}{k_r} = \frac{[C][D]}{[A][B]}$$

The kinetic constant k_f was evaluated from the plots of eq. [3] versus time (11), for an initial concentration $[B]_0 > [A]_0$, and $[C]_0 = [D]_0 = 0$.

$$[3] \qquad R = \frac{K}{2(K-1)[A]_\infty + \Delta K + 2[A]_0} \times \ln \frac{([A]_0 - [A]_\infty)\{[A] + [A]_\infty + (\Delta K + 2[A]_0)/(K-1)\}}{([A] - [A]_\infty)\{[A]_0 + [A]_\infty + (\Delta K + 2[A]_0)/(K-1)\}}$$

$$\Delta = [B]_0 - [A]_0,$$

$$[A]_\infty = \frac{1}{2(K-1)}\{[(\Delta K + 2[A]_0)^2 + 4[A]_0^2(K-1)]^{1/2} - (\Delta K + 2[A]_0)\}$$

In the case of the copper-catalysed autoxidation reaction, the kinetics were analyzed based on a second order rate law of the type:

$$[4] \qquad -\frac{d[Fe^{II}]}{dt} = k_{obs}\frac{[Fe^{II}]^2}{[Fe^{III}]}$$

where $[Fe^{III}] = [Fe]_0 - [Fe^{II}]$.

[1]To whom all correspondence should be addressed.

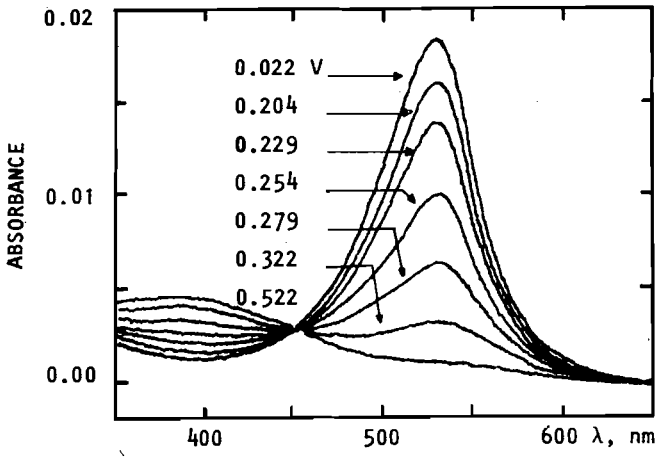

FIG. 1. Absorption spectra of the $[Fe(Hdmg)_2(Him)_2]$ complex (1×10^{-4} *M*) obtained with a spectroelectrochemical cell at several applied potentials versus NHE, [Him] = 0.200 *M*, *I* = 0.100 *M* KCl, 25°C.

The observed rate constant was obtained from the linear plots of eq. [5] versus time.

$$[5] \quad S = \ln [Fe^{II}] + \frac{[Fe]_0}{[Fe^{II}]} = kt + \text{constant}$$

Calculations of kinetic constants and of Marcus theory were carried out using a Microdigital computer.

Results and discussion

The electronic spectrum of the $[Fe(Hdmg)_2(Him)_2]$ complex is characterized by a strong absorption band in the visible (λ_{max} = 530 nm, $\epsilon_{max} = 7.6 \times 10^3\ M^{-1}\ cm^{-1}$) which has been assigned to the Fe-to-Hdmg charge-transfer (CT) transition (12). The spectroelectrochemistry was typically reversible, as shown in Fig. 1. By increasing the applied potential, we observed a systematic decay of the CT band at 530 nm, forming a product which absorbed at 400 nm with an isosbestic point at 445 nm. The measurements led to a Nernst plot with a slope (60 mV) characteristic of a monoelectronic process, and a formal potential of 0.265 V versus NHE (25°C, *I* = 0.10 *M* KCl).

Cyclic voltammograms of the imidazole complex are shown in Fig. 2. The voltammograms of the starting solutions around pH 7 were consistent with the reversibility criteria (13) for a monoelectronic process, with $E_{1/2}$ = 0.268 V versus NHE and $D = 4 \times 10^{-6}\ cm^2\ s^{-1}$, at 25°C and *I* = 0.10 *M* KCl. Above pH 9, however, a systematic cathodic shift was observed in the cyclic voltammograms, with two successive breakpoints in the linear plots of $E_{1/2}$ versus pH, as illustrated in Fig. 2. The observed slopes of 0.058 and 0.110 V/pH were consistent with two successive acid–base equilibria, with pK_a of 9.30 and 10.50, respectively. The assignment of the equilibria involved in the complex was not simple, in view of the following possible reactions:

$$[6] \quad [Fe(Hdmg)_2(Him)_2] = [Fe(Hdmg)(dmg)(Him)_2] + H^+ + e$$

$$[7] \quad [Fe(Hdmg)_2(Him)_2] = [Fe(Hdmg)_2(Him)(im)] + H^+ + e$$

$$[8] \quad [Fe(Hdmg)_2(Him)_2] = [Fe(Hdmg)_2(dmg)(Him)(im)]^- + 2H^+ + e$$

$$[9] \quad [Fe(Hdmg)_2(Him)_2] = [Fe(Hdmg)_2(im)_2]^- + 2H^+ + e$$

$$[10] \quad [Fe(Hdmg)_2(Him)_2] = [Fe(dmg)_2(Him)_2]^- + 2H^+ + e$$

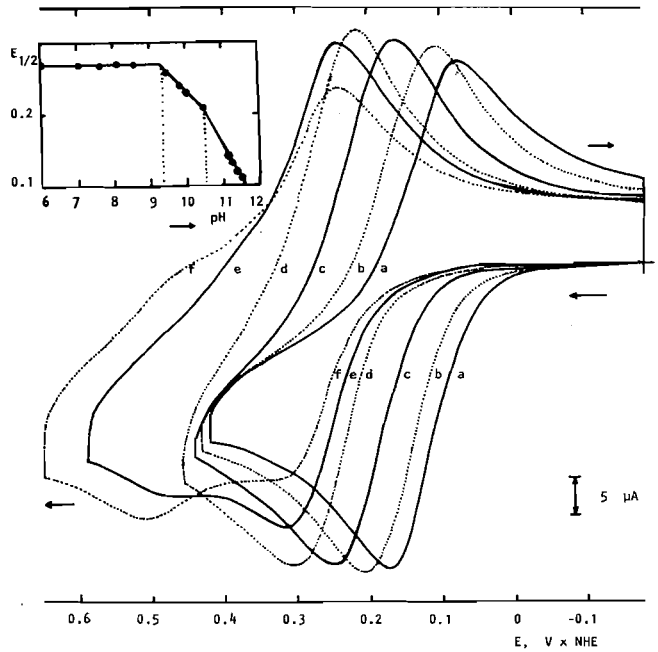

FIG. 2. Cyclic voltammograms of the $[Fe(Hdmg)_2(Him)_2]$ complex (1.8×10^{-4} *M*) in the presence of Him (0.20 *M*), 25°C, *I* = 0.100 *M* KCl, at pH (*a*) 12.08, (*b*) 11.68, (*c*) 11.0, (*d*) 9.65, (*e*) 7.96, and (*f*) 5.94. The dependence of $E_{1/2}$ versus pH is shown in the inset.

It is known that the pK_a of imidazole decreases from 14.2 in the free ligand to 11.0 and 8.9 in the $[Fe(CN)_5(Him)]^{2-}$ and $[(NH_3)_5Ru(Him)]^{3+}$ complexes, respectively (14, 15). On the other hand, pK_a values in the range of 11 to 13 have been reported for the ionization of the hydrogen bonded proton in the O—H···O unit of several bis(dimethylglyoximato)cobalt(III) complexes (16, 17).

Based on these examples, the pK_a of 9.30 would be better ascribed to the deprotonation of the coordinated imidazole ligand in the iron(III)–dioxime complex. However, parallel measurements carried out in this laboratory (18) for the N-methyl imidazole (NMIm) complex led to a single dependence of $E_{1/2}$ versus pH, with a slope of 0.055 V/pH and a pK_a = 9.20 ($E_{1/2}$ = 0.266 V). Since the N-methyl imidazole complexes do not undergo deprotonation reactions below pH 11 (15), we concluded that the observed pK_a in the $[Fe(Hdmg)_2)(Him)_2]^+$ and $[Fe(Hdmg)_2(NMim)_2]^+$ complex should be ascribed to the ionization of the hydrogen bonded proton of the oxyme groups, as in eq. [16]. Analogously, we assigned the pK_a of 10.5 to the deprotonation of the coordinated imidazole ligand in the $[Fe(Hdmg)(dmg)(Him)_2]$ complex, in agreement with the pK_a of 10.3 and 10.45 previously reported for imidazole complexed to Fe(III) porphyrin systems (19, 20).

Below pH 6, a second wave appeared at 0.45 V with a corresponding decrease of the characteristic peaks of the $[Fe(Hdmg)_2(Him)_2]^+$ complex at 0.3 V, as shown in Fig. 2. The intensity of this new wave decreased with the concentration of the imidazole ligand, and was consistent with the presence of $[Fe(Hdmg)_2(Him)(H_2O)]$ species produced in the dissociation equilibrium:

$$[11] \quad [Fe(Hdmg)_2(Him)_2] + H_3O^+ \overset{K}{\rightleftharpoons} [Fe(Hdmg)_2(Him)(H_2O)] + H_2im^+$$

From the relative peak heights we estimated the equilibrium constant *K* as $3 \pm 1 \times 10^4$.

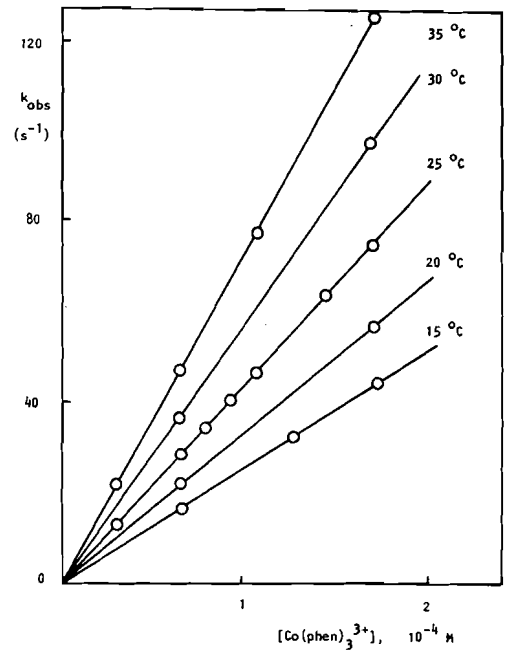

FIG. 3. Plots of the observed rate constants for the electron transfer reaction between $[Fe(Hdmg)_2(Him)_2]$ and $[Co(phen)_3]^{3+}$ at several temperatures, versus the concentation of the cobalt(III) complex (I = 0.100 M KCl, [Him] = 0.20 M).

Electron transfer kinetics

The reaction between $[Fe(Hdmg)_2(Him)_2]$ and $[Co(phen)_3]^{3+}$ followed a first order kinetics, in the presence of an excess of the cobalt complex. The observed rate constants were proportional to the concentration of the reactants, as shown in Fig. 3.

[12] $[Fe(Hdmg)_2(Him)_2] + [Co(phen)_3]^{3+} \rightarrow [Fe(Hdmg)_2(Him)_2]^{+} + (Co(phen)_3]^{2+}$

[13] $$-\frac{d[Fe(Hdmg)_2(Him)_2]}{dt} = k_{12}[Fe(Hdmg)_2(Him)_2] \times [Co(phen)_3^{3+}]$$

The second order rate constant k_{12} measured at 25°C and I = 0.10 M KCl was 4.4 × 10^5 M^{-1} s^{-1}. The activation parameters for the electron transfer reaction were $\Delta H^{\neq}$ = 40 kJ mol^{-1} and $\Delta S^{\neq} = -0.4$ J mol^{-1} K^{-1}.

To evaluate the self-exchange rate constants of the imidazole complex we have performed Marcus theory calculations based on eq. [14] with a pre-exponential factor of 6 × 10^{12} M^{-1} s^{-1}, and using the Wherland-Gray formalism (21) for the work terms W_{ij}.

[14] $$k_{ij} = \kappa_{el}\Gamma_n V\nu_n \exp - (W_{ij}/RT) \exp - (\Delta G_{ij}^{**}/RT)$$

In eq. [14] the product of the electronic and nuclear tunneling factors $\kappa_{el}\nu_n$ is close to unity, $V = 4\pi Nr^3/3000$; ν_n is the nuclear vibration frequency, and $V\nu_n \simeq kTh$.

The self exchange rate constant k_{22} for the $[Co(phen)_3]^{3+}$ complex was measured by Baker *et al.* (22) as 5.5 M^{-1} s^{-1}, at 0°C, and I = 0.10 M KNO_3. The calculated value at 25°C was 45 M^{-1} s^{-1}. The reorganization free energies ΔG_{11}^{**} are given by eq. [15]:

[15] $$\Delta G_{11}^{**} = 2\Delta G_{12}^{**} - \Delta G_{22}^{**} - \Delta G_r^0(1 + \alpha_{12})$$

where

$$\alpha_{12} = \frac{\Delta G_r^0}{4(\Delta G_{11}^{**} + \Delta G_{22}^{**})}$$

and

$$\Delta G_r^0 = -nF\Delta E_{12}^0 - W_{12} + W_{21}$$

The input and output parameters are given in Table 1. The calculated self-exchange rate constant for the $[Fe(Hdmg)_2(Him)_2]$ complex (k_{11} = 5.9 × 10^7 M^{-1} s^{-1}) is similar to those recently reported for several dicyanoiron porphyrins (10^7 M^{-1} s^{-1}) and $[Fe(TPP)(RIm)_2]^{+/0}$ (10^7–10^8 M^{-1} s^{-1}, TPP = tetraphenyl porphyrin). This self exchange rate constant is related to a free energy barrier of 28 kJ mol^{-1}, which is made up of two parts, the inner-sphere and the outer-sphere reorganization energy:

[16] $$\Delta G^{**} = \Delta G_{in}^{**} + \Delta G_{out}^{**}$$

Calculations of the outer-sphere reorganization energy can be made based on eq. [17]:

[17] $$\Delta G_{out}^{**} = \frac{1}{4}\left(\frac{e^2}{2r}\right)\left(\frac{1}{D_{op}} - \frac{1}{D_s}\right)$$

where e is the electronic charge, r is the radius of the complex, D_{op} is the optical dielectric constant, and D_s is the static dielectric constant. Using an average radius of 0.51 nm for the imidazole complex, we obtained ΔG_{out}^{**} = 19 kJ mol^{-1}. The inner sphere reorganization energy was estimated from eq. [16] as 9 kJ mol^{-1}. This value reflects a small change in the equilibrium bond distances, $\Delta r_0 = r_2 - r_1$, as expressed by eq. [18], where f_1 and f_2 are the force constants for the metal–ligand breathing vibrations:

[18] $$\Delta G_{in}^{**} = \frac{3f_1f_2}{f_1 + f_2}(\Delta r_0)^2$$

The estimated value of Δr_0 was 0.007 nm, using an average force constant of 2.0 × 10^5 dyn cm^{-1} taken from the literature (23) for a series of first row transition metal glyoximato complexes.

The reorganization entropy associated with the self-exchange reaction can be calculated from eq. [19],

[19] $$\Delta S_{11}^{**} = \frac{2\Delta S_{12}^{**}}{(1 - 4\alpha_{12}^2)} - \Delta S_{22}^{**} - \frac{\Delta S_r^0(1 + 2\alpha_{12})}{(1 - 4\alpha_{12}^2)}$$

where

$$\Delta S_{ij}^{**} = \Delta S_{ij}^{*} + \frac{dW_{ij}}{dT} + R$$

and

$$\Delta S_r^0 = \Delta S_{rc(Co)}^0 - \Delta S_{rc(Fe)}^0 + \frac{dW_{12}}{dT} - \frac{dW_{21}}{dT}$$

The activation entropy $\Delta S_{22}^{\neq}$ for the $[Co(phen)_3]^{3+/2+}$ system has been reported (22) as 14 J mol^{-1} K^{-1} at I = 0.002 M. Derivation of the work terms dW/dT was carried out as previously described in the literature (24–27). The entropy of the $[Fe(Hdmg)_2(Him)_2]^{+/0}$ redox couple was obtained as 71 J mol^{-1} K^{-1} from careful measurements of $E_{1/2}$ at several temperatures. The corresponding value for the $[Cu(phen)_3]^{3+/2+}$ complex was 92 J mol^{-1} K^{-1}, at I = 0.10 M KCl (28). From these data we calculated the activation parameters shown in Table 1.

These results may involve an appreciable error, due to the uncertainty in the evaluation of the entropy terms and of dW/dT (24). Nevertheless, it is interesting to note that the reorganization entropy for the $[Fe(Hdmg)_2(Him)_2]$ complex, ΔS_{11}^{**} = −50 J mol^{-1} K^{-1}, is similar to those reported for

TABLE 1. Self-exchange rate constants and activation parameters for the $[Fe(Hdmg)_2(Him)_2]$–$[Co(phen)_3^{3+}]$ electron transfer reaction[a]

Parameter	Fe(II)/Co(III)	Co(III)/Co(II)	Fe(III)/Fe(II)
Z	0/3	3/2	1/0
r (nm)	0.52/0.70	0.70/0.71	0.51/0.52
W_{ij}, W_{ii} (kJ mol^{-1})	0	2.0	0
W_{ji} (kJ mol^{-1})	0.92		
ΔE^0, E^0_{rc} (V vs. NHE)	0.102	0.370	0.268
k_{ij}, k_{ii} (M^{-1} s^{-1})	4.4×10^5	45	5.8×10^7
ΔG^{*}_{ij}, ΔG^{*}_{ii} (kJ mol^{-1})	40	61	28
$\frac{\partial W_{ij}}{\partial T}$, $\frac{\partial W_{ii}}{\partial T}$ (J mol^{-1} K^{-1})	0	9.4	0
$\frac{\partial W_{ji}}{\partial T}$ (J mol^{-1} K^{-1})		4.3	
ΔS^0_{12}, ΔS^0_{rc} (J mol^{-} K^{-1})	21	92	71
ΔS^{*}_{ij}, ΔS^{*}_{ii} (J mol^{-1} K^{-1})	8	51	−49
$\Delta S^{\ddagger}_{ij}$, $\Delta S^{\ddagger}_{ii}$ (J mol^{-1} K^{-1})	−0.4	14[b]	−58
$\Delta H^{\ddagger}_{ij}$, $\Delta H^{\ddagger}_{ii}$ (J mol^{-1} K^{-1})	40	70[b]	13

[a] I = 0.100 M, 25°C.
[b] I = 0.002 M, 25°C.

TABLE 2. Kinetic constants for the autoxidation of $[Fe(Hdmg)_2(Him)_2]$ at 25°C, and I = 0.10 M KCl[a]

Exp. no.	[Him] (M)	$10^4[O_2]$ (M)	[Cu(II)] (M)	10^5[Fe] (M)	k_{obs} (s^{-1})	k_f (M^{-1}s^{-1})
1	2.98×10^{-4}	5.0	—	0.70	8.2×10^{-3}	
2	1.10×10^{-3}	5.0	—	2.0	7.0×10^{-3}	
3	2.78×10^{-3}	5.0	—	2.1	5.1×10^{-3}	
4	2.78×10^{-3}	3.7	—	1.1	3.8×10^{-3}	
5	2.78×10^{-3}	2.5	—	2.2	2.7×10^{-3}	
6	2.78×10^{-3}	6.7	6.7×10^{-6}	1.5	1.0×10^{-2}	
7	2.78×10^{-3}	6.7	8.6×10^{-6}	1.5	1.1×10^{-2}	
8	2.78×10^{-3}	6.7	1.3×10^{-5}	1.5	1.3×10^{-2}	
9	0.97×10^{-2}	6.7	6.7×10^{-6}	1.5	1.3×10^{-2}	
10	1.37×10^{-2}	6.7	6.7×10^{-6}	1.5	1.6×10^{-2}	
11	2.02×10^{-2}	6.7	6.7×10^{-6}	1.5	1.9×10^{-2}	
12	2.00×10^{-1}	5.0	4.9×10^{-5}	1.8	0.28	1.3×10^6
13	2.00×10^{-1}	5.0	7.3×10^{-5}	2.4	0.67	1.4×10^6
14	2.00×10^{-1}	5.0	9.8×10^{-5}	1.8	0.90	1.2×10^6
15	2.00×10^{-1}	5.0	1.2×10^{-4}	2.4	1.15	1.2×10^6
16	2.00×10^{-1}	3.7	9.8×10^{-5}	1.8	0.67	1.2×10^6
17	2.00×10^{-1}	2.5	9.8×10^{-5}	1.8	0.45	1.2×10^6
18	2.00×10^{-1}	1.2	9.8×10^{-5}	1.8	0.28	1.2×10^6

[a] Selected data, for comparison purposes. Additional data are available under request.

typical transition metal complexes (27, 29). The contribution of ΔH^{*}_{i} = 14 kJ mol^{-1} to the free reorganization energy is comparable to that of the ΔS^{*}_{i} term. Based on the calculations shown in Table 1, we concluded that the null activation entropy for the cross reaction, $\Delta S^{\ddagger}_{12}$, arises from the compensation of the reorganization entropies of the two complexes.

Autoxidation kinetics

The $[Fe(Hdmg)_2(Him)_2]$ complex is autoxidized in air very rapidly, in the absence of an excess of the imidazole ligand. The rates were proportional to the concentration of O_2, but inversely proportional to the concentration of imidazole, as shown in Table 2 (exps. 1–5).

This inhibiting effect associated with the imidazole ligand was indicative of a dissociative equilibrium, as expressed by reaction [20].

[20] $$[Fe(Hdmg)_2(Him)_2] + H_2O \underset{k_L}{\overset{k_{-L}}{\rightleftharpoons}} [Fe(Hdmg)_2(Him)(H_2O)] + Him$$

Because of the presence of a labile water ligand in the axial position, the $[Fe(Hdmg)_2(Him)(H_2O)]$ intermediate was expected to have pronounced reactivity toward substitution and oxidation by dioxygen. As a matter of fact, the dissociation reaction can be quantitatively reversed by reacting the product with an excess of the imidazole ligand, under argon atmosphere.

In order to evaluate k_L, we have investigated the kinetics of the reverse step, using the stopped-flow technique. The observed rate constants in this case were proportional to the concentration of the imidazole ligand, in the range of 0.02 to 0.20 M. From these experiments we obtained $k_L = 1.7 \pm 0.1 \times 10^2$ M^{-1} s^{-1} (25°C, I = 0.10 M).

The $[Fe(Hdmg)_2(Him)(H_2O)]$ complex produced in the dissociation equilibrium can react with dioxygen via inner-sphere or outer-sphere mechanisms, yielding $[Fe(Hdmg)_2(Him)(O_2)]$ or $[Fe(Hdmg)_2(Him)(H_2O)]^+$ and O_2^- species.

$$[21] \quad [Fe(Hdmg)_2(Him)(H_2O)] + O_2 \xrightarrow{k_{ox}} \text{oxidation products}$$

the superoxide species would then react with the bis-imidazole complex, forming $[Fe(Hdmg)_2(Him)_2]^+$ and H_2O_2.

The derived rate law for the mechanism described by reactions [20]–[21], assuming a steady-state approximation for $[Fe(Hdmg)_2(Him)(H_2O)]$, is given by eq. [22],

$$[22] \quad -\frac{d[Fe(Hdmg)_2(Him)_2]}{dt} = k_{obs}[Fe(Hdmg)_2(Him)_2]$$

where

$$k_{obs} = \frac{k_{ox}k_{-L}[O_2]}{k_{-L} + k_L[Him] + k_{ox}[O_2]}$$

In agreement with eq. [22], the plots of k_{obs}^{-1} versus [Him] were linear, leading to the following parameters, calculated from the slope and intercept, respectively.

$$[23] \quad \frac{k_L}{k_{-L}k_{ox}[O_2]} = 5.0 \times 10^4\ M^{-1}\ s$$

$$[24] \quad \frac{k_{-L} + k_{ox}[O_2]}{k_{-L}k_{ox}[O_2]} = 110\ s$$

By substituting $k_L = 170\ M^{-1}\ s^{-1}$ and $[O_2] = 5.0 \times 10^4\ M$ into eqs. [23] and [24], we obtained $k_{-L} = 0.36\ s^{-1}$ and $k_{ox} = 20\ M^{-1}\ s^{-1}$.

The plots of k_{obs}^{-1} versus $[O_2]^{-1}$ were also linear, with an intercept of 3 ± 2 s, and a slope of $0.093 \pm 0.005\ M$ s. The calculated values were 3 s and 0.097 M s, respectively, in excellent agreement with the experimental results.

From the values of k_{-L} and k_L we have evaluated the dissociation constant $K = k_{-L}/k_L = 2.1 \times 10^{-3}\ M$.

The fact that k_{ox} is one order of magnitude smaller than k_L implies that the electron transfer reaction can be preceded by substitution, as in a typical inner sphere mechanism. Although we can not exclude an outer-sphere mechanism, it seems much less probable to occur in the present case. According to the cyclic voltammograms of Fig. 2, the bis-substituted complex would be more easily oxidized than the dissociated product, which has a high E^0 value. Consequently, electron transfer would be faster in the presence of an excess of the imidazole ligand, in contrast to the results observed in this work.

The autoxidation of the $[Fe(Hdmg)_2(Him)_2]$ complex is accelerated in the presence of copper(II) ions, with a complex kinetic behavior as a function of the concentration of the reactants. At low concentrations of imidazole and of copper(II) ions, the autoxidation reaction proceeds according to a first order kinetics. The observed rate constants increase with the concentration of Him and Cu(II), as shown in Table 2 (exps. 6–11). The mechanism, however, is complicated by the dissociative equilibrium in the $[Fe(Hdmg)_2(Him)_2]$ system, and by the presence of several copper(II) species, e.g., Cu^{2+} (aq), $Cu(Him)^{2+}$, $Cu(Him)_2^{2+}$, and $Cu(Him)_3^{2+}$.

At a high imidazole concentration, e.g. 0.20 M, the only relevant species are the $[Fe(Hdmg)_2(Him)_2]$ and $[Cu(Him)_4]^{2+}$ complexes. In this case, two successive reactions have been observed, as shown in Fig. 4. The first reaction occurs within a millisecond time scale, producing only a partial decay of the $[Fe(Hdmg)_2(Him)_2]$ complex. The second reaction is a thousand times slower and leads the oxidation reaction to completion.

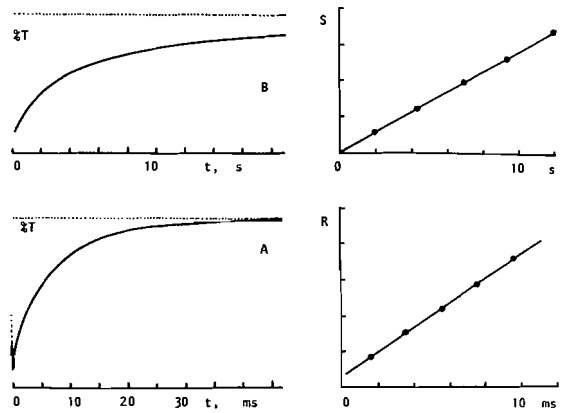

FIG. 4. Oscilloscope traces for the reversible electron transfer reaction (A) and the copper(II) catalyzed autoxidation of the $[Fe(Hdmg)_2(Him)_2]$ complex (B). The plots refer to the analysis described in the Experimental section ($[Fe(II)] = 2.4 \times 10^{-5}\ M$, $[Him] = 0.20\ M$, $[O_2] = 5.0 \times 10^{-4}\ M$, $[Cu(II)] = 7.3 \times 10^{-5}\ M$, 25°C, $I = 0.100\ M$ KCl).

The first rapid reaction was also observed under argon atmosphere, and was assigned to the reversible electron transfer process:

$$[25] \quad [Fe(Hdmg)_2(Him)_2] + [Cu(Him)_4]^{2+} \underset{k_r}{\overset{k_f}{\rightleftharpoons}} [Fe(Hdmg)_2(Him)_2]^+ + [Cu(Him)_4]^+$$

Based on the initial (Fe_T, Cu_T) and equilibrium concentrations (x) measured after 40 ms (Fig. 4), we evaluated $K_1 = k_f/k_r$ as

$$[26] \quad K_1 = \frac{x^2}{[Fe_T - x][Cu_T - x]} = 0.33 \pm 0.01$$

In order to calculate the kinetic constant k_f, we performed a rigorous analysis of the reversible scheme, as described in the Experimental section. The results are shown in Table 2 (exps. 12–18). Based on the calculated second order rate constant $k_f = 1.2 \pm 0.1 \times 10^6\ M^{-1}\ s^{-1}$, and on the calculated work terms, $W_{11} = 1.93$, $W_{21} = 0.79$, $W_{12} = W_{22} = 0$ kJ mol^{-1} ($R_{Cu} = 0.42$ nm, $I = 0.10\ M$, 25°C), we estimated the self exchange rate constant for the $[Cu(Him)_4]^{2+}$ complex as $k_{11} = 4.8 \times 10^4\ M^{-1}\ s^{-1}$.

Preliminary analysis of the second order reaction results in systematic deviations from the first order kinetics. In contrast, the observed pattern was typical of a second order process. Starting from the reversible electron transfer reaction [25], we considered as the next step of the mechanism, the reaction of the Cu(I) species with O_2 leading to superoxide species, as previously described in the literature (30–32). Under the conditions of this work, the $[Cu(Him)_4]^+$ ion dissociates rapidly, producing the catalytically active $[Cu(Him)_2]^+$ complex (30).[2]

$$[27] \quad [Cu(Him)_4]^+ \overset{K_2}{\rightleftharpoons} [Cu(Him)_2]^+ + 2\,Him$$

$$[28] \quad [Cu(Him)_2]^+ + O_2 \overset{K_3}{\rightleftharpoons} [Cu(Him)_2(O_2)]^+$$

Electron transfer between $[Cu(Him)_2(O_2)]^+$ and $[Fe(Hdmg)_2(Him)_2]$ leads the autoxidation reaction to completion, producing H_2O_2 and regenerating the catalyst.

[2]Reversible cyclic voltammograms were obtained for the $[Cu(Him)_4]^{2+}$ complex in the presence of [Him] = 0.1–2.0 M. The half wave potentials varied according to the equation $E_{1/2} = 0.065 - 0.120 \times \log [Him]$. The Nernst slope is consistent with the dissociation of two imidazole ligands from the Cu(I) complex, as expressed by reaction [29].

[29] $[Cu(Him)_2(O_2)]^+ + [Fe(Hdmg)_2(Him)_2] \xrightarrow[2H^+]{k_4} [Cu(Him)_2]^{2+} + [Fe(Hdmg)_2(Him)_2]^+ + H_2O_2$

It should be noted that the reaction of hydrogen peroxide with Cu(I) and Fe(II) species is slower than the corresponding reaction of dioxygen and does not contribute to the derived rate law:

[30] $$-d[Fe^{II}] = k_{obs}\frac{[Fe^{II}]^2}{[Fe^{III}]}$$

where

$$k_{obs} = K_1K_2K_3K_4\frac{[Cu(Him)_4][O_2]}{[Him]^2}$$

The analysis based on eq. [30] was described in the Experimental section, and is illustrated in Fig. 4. The observed rate constants were obtained from the slopes of the second order plots, and incorporate the concentration of the Cu(II), O_2 and Him species used in large excess over the Fe(II) complex. As a matter of fact, the observed rate constants increased linearly with the concentration of the Cu(II) ions and O_2, as shown in Table 2, in agreement with the proposed mechanism.[3]

Another possible reaction to be considered is the oxidation of the $[Cu(Him)_4]^+$ complex by the superoxide species, as in reaction [31].

[31] $[Cu(Him)_4(O_2)]^+ + [Cu(Him)_2]^+ \xrightarrow{k_8} 2[Cu(Him)_2]^{2+} + H_2O_2$

This reaction provides an additional pathway for the regeneration of the Cu(II) species, and has been postulated in the autoxidation of a number of Cu(I) complexes. In the present case, however, it would lead to a quadratic dependence of k_{obs} with respect to the concentration of the Cu(II) ion. Therefore, according to the experimental rate law, reaction [29] should predominate over reaction [31].

It is interesting to compare the mechanism proposed here for the copper catalyzed autoxidation of the $[Fe(Hdmg)_2(Him)_2]$ complex with those previously reported for metalloproteins such as the cytochrome-c (6–8). In the case of the metalloproteins, the rate-determining step is the one electron oxidation of the biomolecule by the copper(II) species. This step is followed by the rapid reoxidation of the resulting Cu(I) products by molecular oxygen. The redox potential of the reacting species becomes the dominant factor in determining the relative rates of the electron transfer reactions (8). In the case of the heme model compounds, the absence of the protein chain facilitates the necessary approach for electron transfer. The reactions are typically adiabatic, with a unity probability factor. For this reason, in contrast with the biological molecules, the electron transfer reaction proceeds very rapidly, and the reoxidation of the resulting Cu(I) species by O_2 becomes the rate-determining step.

[3] An alternative outer-sphere mechanism would lead to the following rate law, assuming a steady state approximation for the concentration of O_2^-:

$$[Cu(Him)_2]^+ + O_2 \underset{k_6}{\overset{k_5}{\rightleftharpoons}} [Cu(Him)_2]^{2+} + O_2^-$$

$$O_2^- + [Fe(Hdmg)_2(Him)_2] \xrightarrow[2H^+]{k_7} [Fe(Hdmg)_2(Him)_2]^+ + H_2O_2$$

$$\frac{-d[Fe^{II}]}{dt} = \frac{KK_2K_5k_7[Fe^{II}]^2[O_2][Cu(Him)_4{}^{2+}]}{[Fe^{III}](k_7[Fe^{II}][Him]^2 + k_6K_2[Cu(Him)_4{}^{2+}])}$$

In order to explain the first order dependence of k_{obs} on the concentration of the $[Cu(Him)_4{}^{2+}]$ complex, the product $k_6K_2[Cu(Him)_4{}^{2+}]$ should be smaller than $k_7[Fe^{II}][Him]^2$. However, in this case, the second order dependence on the concentration of the Fe(II) complex would be reduced to a first order dependence. Therefore, the outer-sphere mechanism is not consistent with the rate law (eq. [30]) observed in this work.

Acknowledgements

We thank the FAPESP, CNPq, and FINEP agencies for their invaluable support.

1. B. J. JILLOT and R. J. P. WILLIAMS. J. Chem. Soc. 462 (1958).
2. L. VASKA and T. YAMAJI. J. Am. Chem. Soc. **93**, 6673 (1971).
3. I. W. PANG and D. V. STYNES. Inorg. Chem. **16**, 590 (1977).
4. F. POMPOSO and D. V. STYNES. Inorg. Chem. **22**, 569 (1983).
5. K. BOWMAN, A. P. GAUGHAN, and Z. DORI. J. Am. Chem. Soc. **94**, 727 (1972).
6. C. C. WINTERBOURN and R. W. CARRELL. Biochem. J. **165**, 141 (1977).
7. J. M. RIFKIND, L. D. LAUER, S. H. CHIANG, and N. C. LI. Biochemistry, **15**, 5337 (1976).
8. M. A. AUGUSTIN and J. K. YANDELL. Inorg. Chim. Acta, **37**, 11 (1979).
9. A. A. SCHILT and R. C. TAYLOR. J. Inorg. Nucl. Chem. **9**, 211 (1959).
10. T. KUWANA and N. WINOGRAD. *In* Electroanalytical chemistry. Vol. 7. *Edited by* A. J. Bard. Marcel Dekker, New York. 1974. pp. 1–78.
11. J. H. ESPENSON. Chemical kinetics and reaction mechanisms. McGraw-Hill, New York. 1981. p. 46.
12. N. SANDERS and P. DAY. J. Chem. Soc. A, 2303 (1969).
13. R. S. NICHOLSON and I. SHAIN. Anal. Chem. **36**, 706 (1964).
14. C. R. JOHNSON, R. E. SHEPHERD, B. MARR, S. O'DONNELL, and W. DRESSIK. J. Am. Chem. Soc. **102**, 6227 (1980).
15. R. J. SUNDBERG, F. BRIAN, I. F. TAYLOR, and H. TAUBE. J. Am. Chem. Soc. **96**, 381 (1974).
16. K. L. BROWN, D. CHERNOFF, D. J. KELJO, and R. G. KALLEN. J. Am. Chem. Soc. **94**, 6697 (1972).
17. J. P. BIRK, P. B. CHOCK, and J. HALPERN. J. Am. Chem. Soc. **90**, 6959 (1968).
18. A. C. C. SILVA. Thesis, University of S. Paulo. 1985.
19. P. GEORGE, G. I. HANANIA, D. H. IRVINE, and I. ABU-ISSA. J. Chem. Soc. 5689 (1964).
20. P. MOHR, W. CHELER, H. SCHUMANN, and K. MULLER. Eur. J. Biochem. **3**, 158 (1967).
21. S. WHERLAND and H. B. GRAY. *In* Biological aspects of inorganic chemistry. *Edited by* D. Dolphin *et al.* Wiley, New York. 1977. pp. 289–368.
22. B. R. BAKER, F. BASOLO, and H. M. NEUMANN. J. Phys. Chem. **63**, 371 (1959).
23. A. BIGOTTO, G. COSTA, V. GALASSO, and G. DE ALTI. Spectrochim. Acta, **26A**, 1939 (1970).
24. N. SUTIN. *In* Tunneling in biological systems. *Edited by* B. Chance *et al.* Academic Press, New York. 1979. p. 210.
25. F. MOATTAR, J. R. WALTON, and L. R. BENNETT. Inorg. Chem. **22**, 550 (1983).
26. H. E. TOMA and R. A. MURAKAMI. Inorg. Chim. Acta, **93**, L33 (1984).
27. H. E. TOMA and F. T. P. LELLIS. Polyhedron, **4**, 993 (1985).
28. S. SAHAMI and M. J. WEAVER. J. Electroanal. Chem. **122**, 155 (1981).
29. E. WAISMAN, G. WORRY, and R. A. MARCUS. J. Electroanal. Chem. **82**, 9 (1977).
30. A. ZUBERBUHLER. Helv. Chim. Acta, **54**, 466 (1967).
31. I. PECHT and M. AMBAR. J. Chem. Soc. A, 1902 (1968).
32. S. GOLDSTEIN and G. CZAPSKI. Inorg. Chem. **24**, 1087 (1985).

Solvolyses of some ^{13}C- or ^{14}C-labeled triarylvinyl bromides in aqueous acetic acid[1]

CHOI CHUCK LEE, DAVE WANIGASEKERA, AND CHARLES Y. FIAKPUI
Department of Chemistry, University of Saskatchewan, Saskatoon, Sask., Canada S7N 0W0
Received October 4, 1985
This paper is dedicated to Professor Arthur N. Bourns

CHOI CHUCK LEE, DAVE WANIGASEKERA, and CHARLES Y. FIAKPUI. Can. J. Chem. **64**, 1235 (1986).

The presence of different amounts of added $LiClO_4$ in the solvolysis of triphenyl[2-^{14}C]vinyl bromide (**1**-Br-2-^{14}C) or trianisyl[2-^{14}C]vinyl bromide (**2**-Br-2-^{14}C) in 70% HOAc did not materially affect the extent of scrambling of the label arising from 1,2-aryl shifts in the triarylvinyl cation or k_r, the rate constant for the 1,2-aryl shift. Solvolysis of a 2:3 mixture of (*E*)- and (*Z*)-1,2-diphenyl-2-tolylvinyl bromide ((*E*,*Z*)-**3**-Br) in 70% HOAc gave an 85:15 mixture of 1,2-diphenyl-2-tolylethanone (**5**) and 2,2-diphenyl-1-tolylethanone (**6**), the latter product, **6**, being derived from a 1,2-phenyl shift in the 1,2-diphenyl-2-tolylvinyl cation to the more stable 2,2-diphenyl-1-tolylvinyl cation. With (*E*,*Z*)-**3**-Br-2-^{13}C as substrate and analysis by gc–ms, about 26–27% scrambling of the ^{13}C label was found in both products, **5**-1,2-^{13}C and **6**-1,2-^{13}C. Solvolyses of (*E*,*Z*)-**3**-Br-2-^{13}C in 50% and 70% HOAc showed that the extent of scrambling in the major products, **5**-1,2-^{13}C, was lower in 50% HOAc than in 70% HOAc, similar to a trend previously observed for solvolyses of **1**-Br-2-^{14}C. In contrast, solvolyses of **2**-Br-2-^{14}C in 50, 70, or 90% HOAc gave essentially the same extent of scrambling. Mechanistic implications of these results are discussed.

CHOI CHUCK LEE, DAVE WANIGASEKERA et CHARLES Y. FIAKPUI. Can. J. Chem. **64**, 1235 (1986).

L'addition de diverses quantités de $LiClO_4$ lors de la solvolyse du bromure de triphénylvinyle [^{14}C-2] (**1**-Br-^{14}C-2) ou du bromure de trianysylvinyle [^{14}C-2] (**2**-Br-^{14}C-2) dans de l'acide acétique à 70% n'affecte pas matériellement le taux de répartition au hasard du marqueur provenant de glissements-1,2 des groupements aryles dans le cation triarylvinyle ou la constante de vitesse, k_r, des glissements-1,2 des groupements aryles. La solvolyse d'un mélange 2:3 des bromures (*E*) et (*Z*) de diphényl-1,2 tolyl-2 vinyle (**3**-Br-(*E*,*Z*)), dans de l'acide acétique à 70%, conduit à un mélange 85:15 de diphényl-1,2 tolyl-2 éthanone (**5**) et de diphényl-2,2 tolyl-1 éthanone (**6**). Ce dernier composé (**6**) provient d'un glissement-1,2 du groupement phényle dans le cation diphényl-1,2 vinyle pour donner le cation diphényl-2,2 tolyl-1 vinyle qui est plus stable. Dans le cas du **3**-Br-^{13}C-2-(*E*,*Z*), et sur la base d'une analyse par sm/cpg, on note la présence d'un mélange correspondant à environ 26–27% de répartition au hasard du marqueur ^{13}C dans les 2 produits **5**-^{13}C-1,2 et **6**-^{13}C-1,2. Le taux de répartition au hasard du marqueur dans les produits majoritaires, **5**-^{13}C-1,2, qui est obtenu lors de la solvolyse du composé **3**-Br-^{13}C-2-(*E*,*Z*) dans de l'acide acétique à 50% est inférieur à celui observé lors de la même réaction dans de l'acide acétique à 70%; cette tendance est analogue à celle observée antérieurement lors des solvolyses du **1**-Br-^{14}C-2. Par ailleurs, les solvolyses du **2**-Br-^{14}C-2 dans de l'acide acétique à 50, 70 ou 90% donnent essentiellement le même taux de répartition au hasard du marqueur. On discute des implications mécanistiques de ces résultats.

[Traduit par la revue]

α-Arylvinyl cations derived from solvolytic reactions have been extensively discussed (2). Because the solvolysis of triphenylvinyl bromide (**1**-Br) in glacial HOAc without the presence of AgOAc was found to be too slow, isotopic scrambling studies with triphenyl[2-^{14}C]vinyl bromide (**1**-Br-2-^{14}C) have been carried out in aqueous acetic acid containing different proportions of HOAc and H_2O as solvent (3). Subsequently, a mixture of 70% HOAc – 30% H_2O (by volume) (to be designated as 70% HOAc) was arbitrarily chosen as solvent in other solvolytic studies on systems such as **1**-Br or **1**-Br-2-^{14}C and trianisylvinyl bromide (**2**-Br) or trianisyl[2-^{14}C]vinyl bromide (**2**-Br-2-^{14}C) (4, 5). In the present paper, further observations on isotopic scramblings are reported for solvolyses in aqueous HOAc of ^{14}C- or ^{13}C-labeled triphenylvinyl, trianisylvinyl, and (*E*,*Z*)-1,2-diphenyl-2-tolylvinyl bromides.

In a previous study (5), the solvolysis of **1**-Br or **2**-Br in 70% HOAc in the presence of $LiClO_4$ was found to give a normal salt effect (6), with the specific rate constant increasing linearly with increasing concentrations of the added salt. In the initial part of the present work, the effect of added $LiClO_4$ on the extent of isotopic scrambling arising from 1,2-aryl shifts in a triarylvinyl cation was investigated. When **1**-Br-2-^{14}C or **2**-Br-2-^{14}C was solvolyzed in 70% HOAc in the presence of different concentrations of added $LiClO_4$, the product, 1,2,2-triphenyl[1,2-^{14}C]-ethanone or 1,2,2-trianisyl[1,2-^{14}C]ethanone, degraded to give the extent of isotopic scrambling (3, 4), showed that the added $LiClO_4$ did not significantly affect the extent of scrambling of the ^{14}C-label from C-2 to C-1 (Table 1).

For the scrambling processes as depicted in Scheme 1, it has been shown that eq. [1] holds (7). When Ar and Ar′ are the same, e.g., with **1**-Br-2-^{14}C or **2**-Br-2-^{14}C, a statistical factor of 2 applies and eq. [1] is modified to eq. [2] (8). While $LiClO_4$ could affect the rate-determining ionization step and gave rise to a normal salt effect, the finding that it did not influence the extent of scrambling indicated that k_{SOH}/k_r did not change significantly in the presence of added $LiClO_4$. Since the medium in all of these experiments is 70% HOAc, k_{SOH} is not expected to vary. A model of the transition state for the 1,2-aryl shift process is an aryl-bridged vinyl cation with dispersal of the positive charge, and hence k_r might be expected to show a decrease with increasing polarity of the medium (9). However, this effect is apparently very small since k_{SOH}/k_r remained essentially constant in the presence of different concentrations of $LiClO_4$.

$$[1] \quad [RY]/[R'Y] = 1 + (k_{SOH}/k_r)$$

$$[2] \quad [RY]/[R'Y] = 1 + (k_{SOH}/2k_r)$$

In the preceding paper of this series (1), we studied the solvolysis of a 2:3 mixture of C-2 labeled (*E*)- and (*Z*)-1,2-diphenyl-2-tolylvinyl bromides (to be designated as (*E*,*Z*)-**3**-Br) in HOAc–AgOAc and in 2,2,2-trifluoroethanol (TFE)–

[1]Rearrangement studies with ^{14}C, LI; for part L, see ref. 1.

TABLE 1. Isotopic scrambling data from solvolyses of triphenyl[2-^{14}C]vinyl bromide (**1**-Br-1-^{14}C) or trianisyl[2-^{14}C]vinyl bromide (**2**-Br-1-^{14}C) in 70% HOAc in the presence of added $LiClO_4$

RX	[RX] (mmolar)	[$LiClO_4$] (mmolar)	Scrambling from C-2 to C-1 (%) Run 1	Run 2	k_{SOH}/k_r[a]
1-Br-1-^{14}C[b]	15	0	15.8[c]	15.3[c]	8.8
	15	15	15.2	15.8	8.9
	15	75	15.7	15.7	8.7
	15	150	15.8	15.1	8.9
2-Br-1-^{14}C[d]	6	0	29.5[e]	30.5[e]	2.7
	6	30	29.5	30.8	2.6
	6	60	30.0	30.9	2.6
	6	100	30.7	30.9	2.5

[a]Calculated from eq. [2] using the average scrambling values for the duplicate runs.
[b]Solvolyses of **1**-Br-1-^{14}C were carried out at 150 ± 2°C for 10 days, giving essentially complete reaction.
[c]Previously reported (3) mean scrambling value for similar reactions was 15.3%.
[d]Solvolyses of **2**-Br-2-^{14}C were carried out at 120 ± 2°C for 3 days, giving essentially complete reaction.
[e]A previously reported (4) mean scrambling value for similar reactions was somewhat lower at 27.7%.

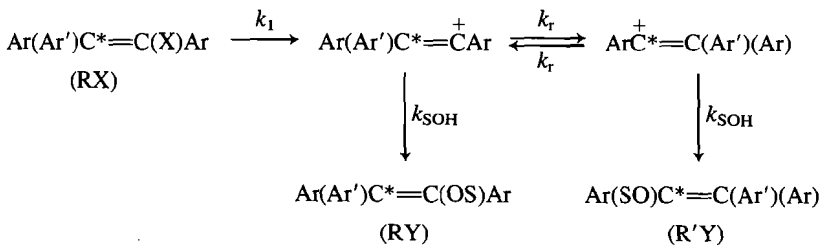

SCHEME 1

2,6-lutidine. In the present work, the solvolysis of (*E,Z*)-**3**-Br-2-^{13}C in aqueous HOAc was investigated. In preliminary work with nonlabeled (*E,Z*)-**3**-Br, solvolysis in 70% HOAc was found to give, according to ^{1}H nmr, a mixture of 85% 1,2-diphenyl-1-tolylethanone (**5**) and 15% 2,2-diphenyl-1-tolylethanone (**6**), the latter product, **6**, being derived from a 1,2-phenyl shift in the 1,2-diphenyl-2-tolylvinyl cation (**3**) to the more stable 2,2-diphenyl-1-tolylvinyl cation (**4**). An analogous reaction of (*E,Z*)-**3**-Br-2-^{13}C in 70% HOAc gave a mixture of isotopically scrambled products, **5**-1,2-^{13}C and **6**-1,2-^{13}C. Oxidation of this product mixture to give nonlabeled and labeled diphenyl and phenyl tolyl ketones, followed by gc–ms analyses as described previously for the solvolysis of (*E,Z*)-**3**-Br-2-^{13}C in TFE–2,6-lutidine (1), gave the extents of scrambling of the ^{13}C-label between C-1 and C-2 in **5**-1,2-^{13}C arising from degenerate 1,2-tolyl shifts in the 1,2-diphenyl-2-tolylvinyl cation (**3**), and in **6**-1,2-^{13}C arising from nondegenerate 1,2-phenyl shifts in cation **3** before and after the degenerate 1,2-tolyl shifts. The processes involved are depicted in Scheme 2.

The extents of scrambling were calculated from the intensities of the ms absorptions in the molecular ion region and in the base peak region. The observed data are summarized in Tables 2 and 3, and the method of calculation has been described previously (1). A steady-state treatment of the scrambling processes in Scheme 2 gives eq. [3], an equation analogous to that used previously for the reaction of (*E,Z*)-**3**-Br-2-^{13}C with TFE–2,6-lutidine (1).

[3] [**5**-2-^{13}C]/[**5**-1-^{13}C] = [**6**-1-^{13}C]/[**6**-2-^{13}C]

From Tables 2 and 3, it is seen that the mean scramblings in **5**-1,2-^{13}C and **6**-1,2-^{13}C are 26.3 ± 0.9% and 27.5 ± 0.5%, respectively, and these values are identical within experimental errors, in agreement with eq. [3]. Again, analogous to the treatment of data from trifluoroethanolysis (1), the distribution of unrearranged and rearranged products **5**-2-^{13}C, **5**-1-^{13}C, **6**-1-^{13}C, and **6**-2-^{13}C (Scheme 2) can be calculated. Since the ratio of **5** to **6** was 85:15, and since the mean scrambling values were 26.3% from **5**-2-^{13}C to **5**-1-^{13}C and 27.5% from **6**-1-^{13}C to **6**-2-^{13}C, in the product mixture, there would be 85 × 0.263 = 22% **5**-1-^{13}C, 85 × 0.737 = 63% **5**-2-^{13}C, 15 × 0.275 = 4% **6**-2-^{13}C, and 15 × 0.725 = 11% **6**-1-^{13}C. As depicted in Scheme 2, nondegenerate 1,2-phenyl shifts gave **4**-1-^{13}C from **3**-2-^{13}C and **4**-2-^{13}C from **3**-1-^{13}C, respectively, before and after the degenerate 1,2-tolyl shifts in cation **3**. since the ratios of [**6**-1-^{13}C]/[**5**-2-^{13}C] = 11/63 = 0.17 and [**6**-2-^{13}C]/[**5**-1-^{13}C] = 4/22 = 0.18 are essentially the same, the product distribution observed thus indicated that in cation **3**, the same extent of nondegenerate 1,2-phenyl shifts occurred before or after the degenerate 1,2-tolyl shifts, a conclusion that was also reached in the previous study on the trifluoroethanolyis of (*E,Z*)-**3**-Br-2-^{13}C (1).

It is of interest to note that from the present work, reaction of (*E,Z*)-**3**-Br in 70% HOAc gave, as major product, ketone **5** derived from the less stable cation **3**, while the minor product, ketone **6**, was derived from the more stable cation **4**. In contrast, for the trifluoroethanolysis of (*E,Z*)-**3**-Br (1), the major product was derived from the more stable cation **4** while the minor product was derived from the less stable cation **3**. Moreover, in the reaction of (*E,Z*)-**3**-Br with HOAc–AgOAc, the only

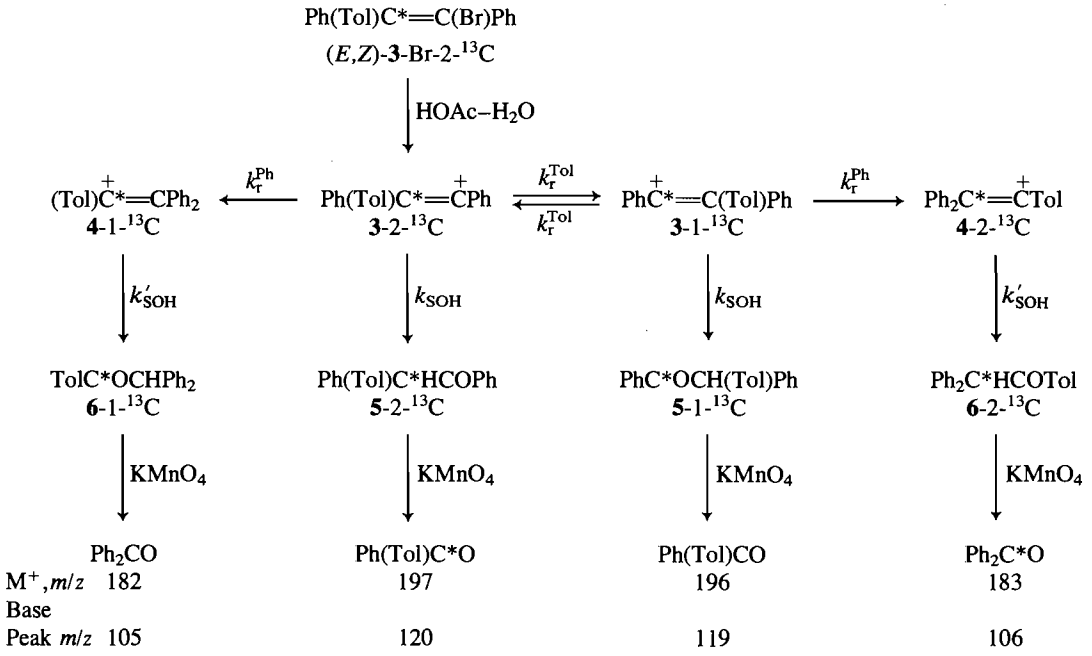

SCHEME 2

product was derived from cation **3**, with no detectable amount of product derived from the more stable cation **4**. As was suggested (1), the nucleophilic character of the reaction medium and the lifetime of the vinyl cations may play a role in determining these variations. In TFE with its low nucleophilic character and long cationic lifetime, the nondegenerate 1,2-phenyl shifts from **3** to **4** could be extensive, while in HOAc–AgOAc, the cationic lifetime was short and there was no detectable amount of rearrangement from **3** to **4**. In 70% HOAc, the cationic lifetime would be intermediate between HOAc–AgOAc and TFE and only a small extent of rearrangement from **3** to **4** could take place, resulting in the formation of a minor amount of product derived from **4**.

Another method, involving analysis by ^{13}C nmr, may also be utilized to determine the extent of scrambling arising from degenerate 1,2-tolyl shifts in the solvolysis of (*E,Z*)-**3**-Br-2-^{13}C. Experiments were carried out in 70% and in 50% aqueous HOAc. The major product, **5**-1,2-^{13}C, was recovered after separation by thin-layer chromatography and then reduced with $LiAlH_4$ to give a mixture of *erythro*- and *threo*-1,2-diphenyl-2-tolyl[1,2-^{13}C]ethanol (**7**-1,2-^{13}C). The ^{13}C enrichments at C-2 and C-1, and hence the extent of scrambling, were determined from the ^{13}C nmr spectrum of **7**-1,2-^{13}C by the intensity ratio method as previously described (10, 11). From duplicate solvolyses of (*E,Z*)-**3**-Br-2-^{13}C in 70% HOAc, the scramblings from C-2 to C-1 in **5**-1,2-^{13}C, as measured by ^{13}C nmr, were 26.1 and 27.0%, in good agreement with the data obtained from gc–ms analyses given in Tables 2 and 3. In similar solvolyses in 50% HOAc, 22.3 and 23.2% scramblings from C-2 to C-1 were observed for duplicate runs. It is seen that a higher proportion of H_2O in the HOAc–H_2O solvent mixture gave rise to a lower extent of scrambling (mean scrambling values of 26.6% and 22.8%, respectively, in 70% and 50% HOAc). This trend was also observed in the earlier study on the solvolysis of triphenyl[2-^{14}C]vinyl bromide (**1**-Br-2-^{14}C) in different mixtures of HOAc and H_2O (3). For comparison, some of the data from the earlier work with **1**-Br-2-^{14}C (3) and the present results from reactions of (*E,Z*)-**3**-Br-2-^{13}C in 50% and 70% HOAc are summarized in Table 4.

In Table 1, it is shown that solvolysis of trianisyl[2-^{14}C]vinyl bromide (**2**-Br-2-^{14}C) in 70% HOAc gave a product with 29.5 and 30.5% scrambling in duplicate runs. It is of interest to note that similar reactions of **2**-Br-2-^{14}C in 50% or 90% HOAc also gave essentially the same extent of about 30% scrambling, the results being included in Table 4. These results for **2**-Br-2-^{14}C, therefore, do not follow the same trend of decreasing amounts of scrambling with increasing proportions of H_2O in the HOAc–H_2O solvent mixture that was observed with **1**-Br-2-^{14}C or (*E,Z*)-**3**-Br-2-^{13}C. Recently, isotopic scramblings from reactions of C-2 labeled (*E,Z*)-1,2-dianisyl-2-tolylvinyl bromides ((*E,Z*)-**8**-Br) with HOAc–AgOAc or with TFE–2,6-lutidine have been reported (12). It may also be of interest to note that preliminary work on the solvolysis of (*E,Z*)-**8**-Br-2-^{13}C in aqueous HOAc also indicates no significant changes in the extent of scrambling for different proportions of HOAc and H_2O.

To account for the difference in behavior for the solvolysis of **1**-Br-2-^{14}C, (*E,Z*)-**3**-Br-2-^{13}C, and **2**-Br-2-^{14}C in aqueous HOAc containing different amounts of H_2O, the nature of the triarylvinyl cations involved may be considered. As given in Table 4, a lower extent of scrambling corresponds to a higher value for k_{SOH}/k_r. For the α-phenyl substituted triarylvinyl cations generated from **1**-Br-2-^{14}C or (*E,Z*)-**3**-Br-2-^{13}C, a higher H_2O content in the solvent would increase the nucleophilic character of the reaction medium and would give a higher value for k_{SOH}. As well, a higher H_2O content would also increase the polar character of the solvent and may give rise to a lower k_r, although this effect may be small since it was shown earlier that the presence of $LiClO_4$ in 70% HOAc did not materially influence k_{SOH}/k_r. Thus for solvolyses of **1**-Br-2-^{14}C or (*E,Z*)-**3**-Br-2-^{13}C in HOAc–H_2O, a higher proportion of H_2O in the solvent would increase k_{SOH}/k_r and hence decrease the extent of scrambling as observed. For the reaction of **2**-Br-2-^{14}C, however, the α-anisyl substituted triarylvinyl cation that is generated is more stable than an α-phenyl substituted triarylvinyl cation and would have a longer lifetime and a lower value for k_{SOH}. Apparently, changes in H_2O content in the HOAc–H_2O solvent did not greatly affect the relatively low value of k_{SOH} and since the effect of k_r would also be small,

TABLE 2. Data from the mass spectra of PhCOTol and Ph^{13}COTol

	Observed intensity		Corrected for $(M+1)^+$		Corrected for 90% ^{13}C enrichment		% Distribution[b]	
m/z[a]	Run 1	Run 2	Run 1	Run 2	Run 1	Run 2	Run 1	Run 2
195	0.86	0.85						
196	24.88	27.54	24.76	27.42	17.54	19.19	27.0	25.9
197	51.03	58.85	47.47	54.91	47.47	54.91	73.0	74.1
198	7.28	8.42						
118	0.12	0.03						
119	49.95	46.59	49.94	46.59	35.38	32.33	27.0	25.2
120	100.00	100.00	95.65	95.96	95.65	95.96	73.0	74.8
121	8.70	8.68						

[a]Molecular ions for [TolCOPh]$^+$ and [Tol^{13}COPh]$^+$ at m/z 196 and 197, respectively; the base peak is [Tol^{13}CO]$^+$ at m/z 120.
[b]Percentages for m/z 196 [TolCOPh]$^+$ and for m/z 119 ([TolCO]$^+$ correspond to % scrambling from C-2 to C-1 in **4**-1,2-^{13}C (see Scheme 2); mean value = (27.0 + 25.9 + 27.0 + 25.2)/4 = 26.3 ± 0.9%.

TABLE 3. Data from the mass spectra of PhCOPh and Ph^{13}COPh

	Observed intensity		Corrected for $(M+1)^+$		Corrected for 90% ^{13}C enrichment		% Distribution	
m/z[a]	Run 1	Run 2	Run 1	Run 2	Run 1	Run 2	Run 1	Run 2
181	8.70	7.40						
182	64.26	44.05	63.28	54.39	54.71	47.17	72.8	72.6
183	27.69	24.05	20.43	17.81	20.43	7.81	27.2	27.4
184	3.12	2.27						
104	—	0.25						
105	100.00	100.00	100.00	100.00	86.76	86.60	72.8	71.8
106	38.51	40.30	32.38	34.03	32.38	34.03	27.2	28.2
107	2.36	2.59						

[a]Molecular ions from [PhCOPh]$^+$ and [Ph^{13}COPh]$^+$ at m/z 182 and 183, respectively; the base peak is [PhCO]$^+$ at m/z 105.
[b]Percentages for m/z 183 ([Ph^{13}COPh]$^+$) and ([Ph^{13}CO]$^+$) correspond to % of the isotopically rearranged product, **6**-2-^{13}C (see Scheme 2); mean value = (27.2 + 27.4 + 27.2 + 28.2)/4 = 27.5 ± 0.5%.

TABLE 4. Isotopic scrambling data from solvolyses in HOAc–H_2O

	Reaction with **1**-Br-2-^{14}C[b]		Reaction with (*E*,*Z*)-**3**-Br-2-^{13}C[c]		Reaction with **2**-Br-2-^{14}C[d]	
Solvent (% HOAc)[a]	Scrambling from C-2 to C-1 (%)[e]	k_{SOH}/k_r[f]	Scrambling from C-2 to C-1 (%)[g]	k_{SOH}/k_r[f]	Scrambling from C-2 to C-1 (%)[h]	k_{SOH}/k_r[f]
50	9.6	17.0	22.2; 23.2	2.4	31.2; 30.2	2.5
70	15.3	8.8	26.1; 27.0	1.8	29.5; 30.5	2.7
90	18.4	6.8			29.8; 31.0	2.6

[a]Proportion of HOAc by volume in mixtures of HOAc and H_2O.
[b]Reaction of triphenyl[2-^{14}C]vinyl bromide (**1**-Br-2-^{14}C) in HOAc–H_2O at 150 ± 2°C.
[c]Reaction of (*E*,*Z*)-1,2-diphenyl-2-tolyl[2-^{13}C]vinyl bromides ((*E*,*Z*)-**3**-Br-2-^{13}C) in HOAc–H_2O at 150 ± 2°C.
[d]Reaction of trianisyl[2-^{14}C]vinyl bromide (**2**-Br-1-^{14}C) in HOAc–H_2O at 120 ± 2°C.
[e]Mean scrambling values from ref. 3.
[f]Calculated from eq. [1] or eq. [2] using the mean scrambling values. For (*E*,*Z*)-**3**-Br-2-^{13}C, steady-state treatment of Scheme 2 gave $k_{SOH}/k_r = [RY]/[R'Y] - 1 - k_{Ph}/k_{Tol}$, but eq. [1] is used since k_{Ph}/k_{Tol} may be quite small.
[g]Scramblings for duplicate runs in the major product, 1,2-diphenyl-2-tolyl[1,2-^{13}C]ethanone (**5**-1,2-^{13}C).
[h]Scramblings for duplicate runs in the product, trianisyl[1,2-^{14}C]ethanone.

the net result is a relatively constant k_{SOH}/k_r, giving rise to about the same extent of scrambling for solvolyses in HOAc–H_2O of α-anisyl substituted triarylvinyl systems such as the trianisylvinyl and (*E*,*Z*)-1,2-dianisyl-2-tolylvinyl bromides.

Since the degenerate rearrangement processes in the triphenylvinyl and 1,2-diphenyl-2-tolylvinyl cations differ only in the migrating phenyl and tolyl groups, a comparison of the data from **1**-Br-2-^{14}C and (*E*,*Z*)-**3**-Br-2-^{13}C in Table 4 would give a measure of the Tol:Ph migratory aptitude. The k_{SOH}/k_r values in Table 4 may be more specifically designated as k_{SOH}/k_r^{Ph} and k'_{SOH}/k_r^{Tol}, respectively, for the triphenylvinyl and 1,2-diphenyl-2-tolylvinyl systems. If k_{SOH} and k'_{SOH} for the capture of the two ions in a given solvent system were assumed to be about the same, then $(k_{SOH}/k_r^{Ph})/(k'_{SOH}/k_r^{Tol}) =$

k_r^{Tol}/k_r^{Ph} would be 17.0/2.4 or about 7 and 8.8/1.8 or about 5, respectively, for solvolyses in 50% and 70% HOAc. These values of about 5–7 are of the same magnitude as previously reported Tol:Ph migratory ratios of 4–5 from comparisons of scrambling data for the tritolyvinyl and 2-phenyl-1,2-ditolylvinyl cations (8), and a k_r^{Tol}/k_r^{Ph} ratio of about 7 from comparisons of the scramblings observed in reactions of **1**-Br-1-^{14}C and (*E,Z*)-**3**-Br-2-^{14}C with HOAc–AgOAc (1).

Experimental

*Solvolyses with triphenyl[2-^{14}C]vinyl bromide (**1**-Br-2-^{14}C)*

Solutions of **1**-Br-2-^{14}C (15 mmolar) in 70% HOAc containing different amounts of $LiClO_4$ (Table 1) were heated in sealed tubes at 150 ± 2°C for 10 days. Each reaction mixture was worked up to give 1,2,2-triphenyl[1,2-^{14}C]ethanone (α,α-diphenylacetophenone), which was in turn degraded to diphenyl [^{14}C]ketone, using procedures previously described (3). The difference in specific activities between each sample of 1,2,2-triphenyl[1,2-^{14}C]ethanone and the corresponding diphenyl [^{14}C]ketone gave the extents of scrambling of the ^{14}C label from C-2 to C-1.

*Solvolyses with trianisyl[2-^{14}C]vinyl bromide (**2**-Br-2-^{14}C)*

Solutions of **2**-Br-2-^{14}C (6.0 mmolar) in 50, 70, or 90% HOAc or in 70% HOAc containing different amounts of $LiClO_4$ (Table 1) were heated in sealed tubes at 120 ± 2°C for 3 days. Each reaction mixture was worked up to give 1,2,2-trianisyl[1,2-^{14}C]ethanone, which was subsequently degraded to give dianisyl [^{14}C]ketone using procedures reported previously (4). The difference in specific activities between each sample of 1,2,2-trianisyl[1,2-^{14}C]ethanone and its degradation product, dianisyl [^{14}C]ketone, gave the extents of scrambling of the ^{14}C label from C-2 to C-1.

*Solvolyses with (E,Z)-1,2-diphenyl-2-tolyl[2-^{13}C]vinyl bromide ((E,Z)-**3**-Br-2-^{13}C)*

The substrate, (*E,Z*)-**3**-Br or (*E,Z*)-**3**-Br-2-^{13}C, consisting of an approximately 2:3 mixture of the (*E*) and (*Z*) isomers, was prepared as described in the preceding paper (1).

A solution of 1.00 g (2.86 mmol) of (*E,Z*)-**3**-Br in 100 mL of 70% HOAc in a sealed tube was heated in an oil bath at 150 ± 2°C for 10 days. After cooling, the tube was opened and the contents extracted 3 times with ether. The extract was washed with H_2O and dried over $MgSO_4$. Removal of the ether under reduced pressure gave about 700 mg of a mixture of 1,2-diphenyl-2-tolylethanone (**5**) and 2,2-diphenyl-1-tolylethanone (**6**) as an oil. Its ^{1}H nmr spectrum indicated that the ratio of **5**:**6** was about 85:15 based on the relative area of the tolyl-CH_3 peaks at δ 2.24 and 2.33 ppm and the CH peaks at δ 6.06 and 6.40 ppm, respectively, for **5** and **6**. The major product, **5**, was purified by preparative thin-layer chromatography using silica gel G/UV_{254} (Brinkmann Instruments (Canada) Ltd.) as the stationary phase and 80% $CHCl_3$ – 20% petroleum ether (bp 40–60°C) as the moving phase. The major band was scraped off, thoroughly washed with 300 mL of $CHCl_3$, and filtered. After removal of the $CHCl_3$ from the filtrate, the colorless residue was recrystallized from methanol to give 320 mg (overall yield of 46% based on a product ratio of 85:15 for **5**:**6**) of **5**, mp 94–95°C; ^{1}H nmr ($CDCl_3$) δ: 2.24 (s, 3H, CH_3), 6.06 (s, 1H, CH), 7.2–8.1 (m, 14H, Ar). *Anal.* calcd. for $C_{21}H_{18}O$: C 88.07, H 6.34; found: C 88.58, H 6.58. Oxidation of a sample of this product gave phenyl tolyl ketone, confirming its structure as **5**. If the product were **6**, its oxidation would give rise to diphenyl ketone.

In analogous solvolyses in 70% HOAc of (*E,Z*)-**3**-Br-2-^{13}C, prepared from 90% enriched [^{13}C]$BaCO_3$, the mixture of products, **5**-1,2-^{13}C and **6**-1,2-^{13}C, was oxidized without prior separation to give a mixture of phenyl tolyl ketone, phenyl tolyl [^{13}C]ketone, diphenyl ketone, and diphenyl [^{13}C]ketone for analysis using a Model 4000 Finnigan gc–ms system. In contrast to the degradation of 1,2,2-triphenyl[1,2-^{14}C]ethanone and 1,2,2-trianisyl[1,2-^{14}C]ethanone, which involved reduction with $LiAlH_4$ to the corresponding ethanol followed by oxidation with alkaline $KMnO_4$ (3, 4), the mixtures of **5**-1,2-^{13}C and **6**-1,2-^{13}C were oxidized directly by $KMnO_4$ in the presence of H_2SO_4 to give the unlabeled and labeled phenyl tolyl and diphenyl ketones for gc–ms analyses.

In another set of experiments, (*E,Z*)-**3**-Br-2-^{13}C, with 45% ^{13}C enrichment, was solvolyzed in 50, 70, or 90% HOAc at 150 ± 2°C for 10 days. From each run, the major product, **5**-1,2-^{13}C, was recovered after separation by thin-layer chromatography and then reduced with $LiAlH_4$ (3, 4) to give a mixture of *erythro*- and *threo*-1,2-diphenyl-2-tolyl[1,2-^{13}C]ethanol (**7**-1,2-^{13}C), which, after crystallization from 95% ethanol, melted at 87–88°C; ^{1}H nmr ($CDCl_3$) δ: 2.17, 2.28 (4H, two s, CH_3 + OH), 2.21 (shr, OH), 4.10, 4.25 (1H, two d, C-2 CH), 5.23, 5.38 (1H, two d, C-1 CH), 6.97–7.35 (14H, m, Ar). *Anal.* calcd. for $C_{21}H_{20}O$: C 87.46, H 6.99; found: C 87.17, H 7.04. Determinations of the ^{13}C enrichments at C-2 and C-1 of **7**-1,2-^{13}C, and hence the extents of scrambling from C-2 to C-1 as recorded in Table 4, were carried out using the ^{13}C nmr spectrum of **7**-1,2-^{13}C by the intensity ratio method as previously described (10, 11). Although the ^{1}H nmr of **7**-1,2-^{13}C gave separate peaks for the *erythro* and *threo* diastereomers, the peaks of interest in the ^{1}H-decoupled ^{13}C nmr spectrum of **7**-1,2-^{13}C, in a 60-MHz instrument, appear as nearly overlapping doublets at 21.0, 60.6, and 76.9 ppm, respectively, for tolyl-CH_3, C-2, and C-1. Ratios of the integrated intensities for C-2 or C-1 relative to the integrated intensity of tolyl-CH_3 containing ^{13}C in its natural abundance as internal reference standard are utilized in the calculations (10, 11).

Acknowledgement

The financial support given by the Natural Sciences and Engineering Research Council of Canada is sincerely acknowledged.

1. C. C. Lee and D. Wanigasekera. Can. J. Chem. **64**, 1228 (1986).
2. P. J. Stang, Z. Rappoport, M. Hanack, and L. R. Subramanian. Vinyl cations. Academic Press, New York. 1979. Chapt. 6.
3. C. C. Lee and E. C. F. Ko. Can. J. Chem. **56**, 2459 (1978).
4. C. C. Lee, E. C. F. Ko, and Z. Rappoport. Can. J. Chem. **58**, 2369 (1980).
5. C. C. Lee, C. A. Obafemi, and Z. Rappoport. Can. J. Chem. **60**, 3019 (1982).
6. A. H. Fainberg and S. Winstein. J. Am. Chem. Soc. **78**, 2763 (1956).
7. Y. Houminer, E. Noy, and Z. Rappoport. J. Am. Chem. Soc. **98**, 5632 (1976).
8. C. C. Lee, E. C. F. Ko, and Z. Rappoport. Can. J. Chem. **58**, 884 (1980).
9. C. K. Ingold. Structure and mechanism in organic chemistry. 2nd ed. Cornell University Press, Ithaca, NY. 1969. pp. 457–463.
10. M. Oka and C. C. Lee. Can. J. Chem. **53**, 320 (1975).
11. C. C. Lee, A. J. Paine, and E. C. F. Ko. J. Am. Chem. Soc. **99**, 7267 (1977).
12. D. Wanigasekera, C. C. Lee, Y. Houminer, M. Aviv, and Z. Rappoport. J. Org. Chem. **49**, 4367 (1984).

Dipole interactions in models of the dense part of the electrical double layer

PANAGHIOTIS NIKITAS[1]

Laboratory of Physical Chemistry, Department of Chemistry, University of Thessaloniki, Thessaloniki, Greece

Received September 30, 1985

PANAGHIOTIS NIKITAS. Can. J. Chem. **64**, 1286 (1986).

Since Monte-Carlo studies on freely oriented dipoles suggest that at zero external field the dipoles are oriented preferentially in-plane in ordered configurations, an attempt is made here to incorporate dipole in-plane interactions in the multi-state model of the inner layer. It is found that the predictions of the model become unsatisfactory as ordered structures are taken into consideration. Polarization catastrophe and concentration dependent adsorption maxima are the main problems. Analysis of the polarization behaviour of the inner layer at the adsorption maximum of an adsorbate suggests that in aqueous interfaces and possibly in other real interfaces the dipole in-plane interactions should be quite weak. This is attributed to rotational barriers leading to an almost random distribution of the dipoles in the monolayer.

PANAGHIOTIS NIKITAS. Can. J. Chem. **64**, 1286 (1986).

Des études effectuées par la méthode de Monte Carlo sur des dipôles d'orientation libre suggère que, à un champ externe qui est nul, les dipôles s'orientent d'une façon préférentielle dans des configurations ordonnées; on a donc fait un essai dans le but d'incorporer le dipôle dans les interactions planes d'un modèle à plusieurs états de la couche interne. On a trouvé que les prédictions du modèle deviennent insatisfaisantes lorsqu'on prend des structures ordonnées en considération. Les principaux problèmes sont la catastrophe de la polarisation et les maxima d'absorption qui dépendent de la concentration. Une analyse du comportement de la substance adsorbée, sous polarisation de la couche interne et à un degré maximal d'adsorption, suggère que, dans les interfaces aqueux et possiblement dans d'autres interfaces réelles, le dipôle dans les interactions planes doit être très faible. On attribue cette propriété à des barrières à la rotation qui font que les dipôles de la mononcouche sont pratiquement distribués au hasard.

[Traduit par la revue]

I. Introduction

The conventional methodology followed for the microscopic modelling of the electrical double layer is characterized by the formal division of the double layer into a dense part and a diffuse layer. The former is modelled as a two-dimensional monolayer of dipoles which can take up only a finite number of orientations. In the first molecular treatments the solvent dipoles may have two positions normal to the adsorbing surface (1–5). The multi-state models are reasonable developments of this approach (6–8).

In all these models the dipole–dipole interactions, which predominately determine the properties of the inner layer, are considered as limiting only perpendicular to the electrode surface. Non-nearest-neighbour interactions as well as effects of imaging are incorporated indirectly by introducing an effective coordination number. Dipole interactions parallel to the electrode surface are neglected in all cases. This interpretation overlooks the dipole interaction energy arising from the parallel component of the dipoles and it can be considered a reasonable approximation only if the dipole components in-plane are randomly oriented. However, Monte-Carlo studies (9) clearly indicate that freely oriented dipoles are oriented preferentially parallel to the plane, showing a definite structure when the external field is zero. Therefore, for freely oriented dipoles the in-plane interaction energy cannot be considered negligible. This interaction energy, its incorporation in molecular models for the inner part of the electrical double layer, the problems arising, and their origin are the object of the present paper.

II. Dipole interactions

The dipole–dipole interactions have been made the subject of a number of publications (4, 10–14). However, many problems are still unsolved. There is no work on the effect of imaging on in-plane interactions and, as we show below, the contribution from imaging in interactions normal to the electrode surface is taken erroneously. Here, for reasons of simplicity and continuity with the inner layer models, we consider only point dipoles. The dipoles are arranged on a planar regular lattice with coordination number c and lattice constant d.

The field strength $\mathbf{E}$ caused by an ideal dipole $\mathbf{P}$ at $\mathbf{r}$ is given by (15).

$$[1] \quad \mathbf{E} = \frac{3\mathbf{P}\cdot\mathbf{r}}{r^5}\mathbf{r} - \frac{\mathbf{P}}{r^3}$$

Since the dipole moment $\mathbf{P}$ can be split in a perpendicular and a planar component, relatively to the plane of the dipoles, we examine these two cases separately.

(a) Interactions normal to the plane

The electric field $\mathbf{E}$ caused by an hexagonal array of infinite extent of ideal dipoles at any position (x, y, z) along an outward perpendicular to the surface can be calculated from the work of MacDonald and Barlow (11). Alternatively one may use eq. [1] which results in

$$[2] \quad E = c_e P/d^3$$

where

$$[3] \quad c_e = \sum_{n=m=-\infty}^{\infty} \left(\frac{3\xi^2}{m^2 + n^2 + \xi^2 - nm} - 1\right) \times (m^2 + n^2 + \xi^2 - nm)^{-3/2}$$

for an hexagonal array of dipoles and

$$[4] \quad c_e = \sum_{n=m=-\infty}^{\infty} \left(\frac{3\xi^2}{n^2 + m^2 + \xi^2} - 1\right)(n^2 + m^2 + \xi^2)^{-3/2}$$

in a square plane. $\xi = z/d$. n and m take all negative, zero, and positive integer values except the values $m = n = \xi = 0$.

[1]This work was carried out at the Electrochemistry Research Laboratories, Department of Physical Chemistry, University of Newcastle-upon-Tyne, Newcastle-upon-Tyne, NE1 7RU, England.

Printed in Canada / Imprimé au Canada

Here we should note that the work of MacDonald and Barlow concerns the electrostatic properties of an hexagonal array with a single vacancy. The electric field and the electrostatic potential are calculated along a perpendicular axis to the surface taken through the position of a missing array element. Therefore, to calculate the field strength at any position outside the plane we have to add the contribution arising from the missing element. This detail, unfortunately, has been overlooked by Levine *et al.* (4, 16) in their calculation of the effective coordination number, z_e. In the LBS theory (4) the dipole–dipole interactions between non-nearest neighbouring pairs as well as interactions arising from dipole images are incorporated indirectly into the model by increasing the coordination number of the lattice, c, to an effective value z_e. For the calculation of z_e Levine *et al.* (4, 16) take into account all the interactions arising from the surrounding dipoles and their images on both sides of the interface, but they ignore the contribution from the images of the test dipole. Thus, a number of papers appeared in the literature (4, 6–8, 17–26) make use of an incorrect value of z_e.

Table 1 shows the obtained values of c_e. To calculate c_e with eqs. [2] and [3] the first $n = m = 500$ nearest-neighbours are summed in an IBM 370-168 computer and the remainder of the sum replaced by an integral. It is seen that the field strength falls rapidly out of the plane and dipoles outwards the monolayer, only adjacent to it, can feel very weak repulsive interactions.

The effective coordination number for lateral dipole–dipole interactions due to dipole imaging at an interface formed by a conductor and an electrolyte solution can now be calculated from

$$[5] \quad z_e = 11.034 - 0.226(1 + f)$$

for an hexagonal lattice and

$$[6] \quad z_e = 9.034 - 0.326(1 + f)$$

for a square one. $f = (\epsilon - 1)/(\epsilon + 1)$, ϵ being the dielectric constant of the bulk electrolyte solution. For aqueous electrolyte solutions we have $\epsilon = 78.3$ (at 25°C) and eqs. [5], [6] give $z_e \approx 10.6$ and 8.4 for an hexagonal and a square lattice, respectively. We see that the effective coordination number is smaller than the Topping's values of 11.03 and 9.03 in the two lattice, as first noticed by Guidelli (5). However, he used different arguments.

(b) Interactions in plane

The interpretation of the dipole in plane interactions is the most difficult task, since we can hardly accept that the parallel component takes up few orientations. Here we make use of the Monte-Carlo results (9). It has been found that for freely oriented dipoles and in the configuration with minimum energy the dipoles line up head-to-tail in rows of opposite orientation. Configurations of rows of dipoles with the same orientation should be considered possible, since such configurations present minimum energy as well (12, 13). For these configurations the field strength parallel to the dipoles at the position (x, y, z) can be calculated from eq. [2] with

$$[7] \quad c_e = \sum_{n=m=-\infty}^{\infty} (-1)^{|m|} \left(1 - \frac{3}{4} \cdot \frac{(2n - m)^2}{n^2 + m^2 + \xi^2 - nm}\right) \times (n^2 + m^2 + \xi^2 - nm)^{-3/2}$$

in an hexagonal lattice, whereas in a square one we have

$$[8] \quad c_e = \sum_{n=m=-\infty}^{\infty} (-1)^{|m|} \left(1 - \frac{3n^2}{n^2 + m^2 + \xi^2}\right) \times (n^2 + m^2 + \xi^2)^{-3/2}$$

TABLE 1. Values of c_e calculated from eqs. [3] and [4]

ξ	c_e ($c = 4$)	c_e ($c = 6$)	c_e ($c = 6$)*
0	−9.034	−11.032	−11.034
1	+0.326	+0.226	+0.224
2	-7×10^{-4}	+0.002	$+7 \times 10^{-4}$
3	−0.001	+0.002	-2×10^{-4}

*Calculated from the work of Macdonald-Barlow (11).

Equations [7] and [8] hold for "anti-parallel" configurations, i.e. when the rows of the oriented dipoles have opposite orientations. For "parallel" configurations the term $(-1)^{|m|}$ should be omitted.

The values of c_e obtained from eqs. [7] and [8] are summarized in Table 2. The minus sign indicates that the field E parallel to a row of oriented dipoles is in an opposite direction to that of the dipoles leading to attractive interactions. To calculate the sums we used the same method as previously except for the parallel configurations where the long distance effect is small and estimated by a least-squares procedure. It is seen that the field drops rapidly out of the dipole layer and practically becomes zero after one molecular diameter. Therefore, dipole imaging effects should have a small contribution. This becomes apparent if we calculate the effective coordination number. For aqueous electrolyte solutions in the hexagonal lattice with parallel orientation we have

$$[9] \quad z_e^{\uparrow\uparrow} = -5.516 - 0.114(1 + f) = -5.74$$

and with anti-parallel

$$[10] \quad z_e^{\uparrow\downarrow} = -4.095 - 0.179(1 + f) = -4.45$$

In a square lattice we have, correspondingly

$$[11] \quad z_e^{\uparrow\uparrow} = -4.158 - 0.163(1 + f) = -4.84$$

$$[12] \quad z_e^{\uparrow\downarrow} = -5.099 - 0.127(1 + f) = -5.35$$

Therefore, a value of $z_e \approx -5$ for well oriented in-plane configurations seems appropriate. However, in real interfaces the thermal motion and rotational barriers should increase its value.

An alternative approach to treat in-plane dipole interactions is to evaluate the average dipole–dipole interaction energy from

$$[13] \quad \langle w_{12} \rangle = \frac{\int_0^{2\pi} w_{12} \exp(-w_{12}/kT) d\varphi_1 d\varphi_2}{\int_0^{2\pi} \exp(-w_{12}/kT) d\varphi_1 d\varphi_2}$$

where

$$[14] \quad w_{12} = -\frac{P_1 P_2}{d^3} (2 \cos \varphi_1 \cos \varphi_2 - \sin \varphi_1 \sin \varphi_2)$$

φ_1, φ_2 being the angles of the dipoles in the plane containing the line joining them.

If $|w_{12}| \ll kT$ then eq. [13] results in a two-dimensional Keesom equation (27, 28)

$$[15] \quad \langle w_{12} \rangle = -\frac{5}{4} \cdot \frac{P_1^2 P_2^2}{d^6 kT}$$

However, for an aqueous solution interface we have $d = 3 \times 10^{-10}$ m, $P_1 = P_2 = 6.12 \times 10^{-30}$ Cm and therefore $\langle w_{12} \rangle = -11.5kT$. In this case the numerical evaluation of the integrals in eq. [13] gives

TABLE 2. Values of c_e calculated from eqs. [7] and [8]

	c_e			
	$c = 4$		$c = 6$	
ξ	Parallel	Anti-parallel	Parallel	Anti-parallel
0	−4.518	−5.099	−5.516	−4.095
1	+0.163	+0.127	+0.114	+0.179
2	-7×10^{-4}	$+1 \times 10^{-4}$	+0.001	$+2 \times 10^{-4}$
3	−0.001	-1×10^{-4}	+0.001	-1×10^{-4}

[16] $\langle w_{12} \rangle = -1.62P^2/d^3$

which, for an hexagonal lattice without imaging effects, results in an effective coordination number equal to $z_e \approx -9.7$. This value should be considered high enough, probably because this approach emphasizes the interactions of the central dipole with its neighbours while it ignores the interactions of the neighbouring dipoles with each other.

III. Application to inner layer models

The above results can be easily incorporated in the multistate models of the inner layer (7, 26). Here we consider site-parity for the solvent molecules, i.e. we restrict our treatment in unassociated solvents. Fawcett (6, 8) claims that such behaviour is evident in certain solvents like alcohols, formic acid, and dimethylformamide, whereas water and *N*-methylformamide should be described in terms of clusters. However, in one of our previous publications (26) we have shown that the lattice models and possibly every model of the inner layer is not compatible with the existence of clusters, since their presence as definite units leads to models which predict a concentration-dependent adsorption maximum, in disagreement with most experimental data. For this reason we modelled the inner part of the electrical double layer as a planar monolayer of solvent dipoles, each of them occupying one lattice site. The dipole vector may take a finite number of orientations. If P_s is the absolute value of the solvent dipole moment, then we have

[17] $P_{jn} = P_s \cos \varphi_j \qquad \text{and} \qquad P_{jp} = P_s \sin \varphi_j$

where the subscripts n and p denote the normal and the parallel component of P_s. This notation will be used throughout this paper. φ_j is the angle formed between the dipole vector and a vector normal to the electrode surface. Adsorbate molecules with dipole moment P_A may be present in the lattice occupying r sites.

In a site-parity model the in-plane dipole–dipole interaction energy, under mean field approximation, may be calculated from

[18] $$U_p^{d-d} = \frac{z_{ep}}{2Nd^3}\left(\sum_{i=1}^{N} P_{ip}^t N_i\right)^2 = \frac{1}{2} Y_m \sum_{i=1}^{N} P_{ip}^t N_i$$

where Y_m is the electric field parallel to the adsorbing surface in a site occupied by a monomer dipole, N_i the number of dipoles of type i, N the total number of dipoles equal to the number of the lattice sites, and P_{ip}^t the total (permanent plus induced) in-plane dipole moment of the ith dipole. Note that eq. [18] may include adsorbate molecules with $r = 1$ and dipole moment P_{Ap}. If a_i is the polarizability of the ith type dipoles we have

[19] $P_{ip}^t = P_{ip} - a_i Y_m$

In site-disparity models (say due to absorbate molecules with $r \neq 1$) eq. [18] is easily generalized to

[20] $$U_p^{d-d} = \frac{z_{ep}}{2N_q d^3}\left(\sum_{i=1}^{N} q_i P_{ip}^t N_i/n_i\right)^2 = \frac{1}{2}\sum_{i=1}^{N} P_{ip}^t N_i Y_i$$

where

[21] $Y_i = q_i Y_m/n_i$

[22] $$N_q = \sum_{i=1}^{N} q_i N_i$$

n_i is the number of sites occupied by one dipole of ith type and q_i is defined so that the product $q_i c$ is the number of first neighbour sites surrounding each ith dipole.

Equation [20] results in

[23] $$Y_m = \frac{\sum_{i=1}^{N} q_i P_{ip}\vartheta_i/n_i^2}{\sum_{i=1}^{N} q_i\left(\frac{d^3}{z_{ep}} + a_i q_i/n_i^2\right)\vartheta_i/n_i}$$

where

[24] $$\vartheta_i = n_i N_i \Big/ \left(\sum_{i=1}^{N} n_i N_i\right)$$

Also, by differentiating eq. [20] with respect to N_1 we can obtain the contributions of in-plane interactions to the chemical potentials of the absorbed molecules. We have

[25] $$\mu_{ip}^{el} = P_{1p}Y_1 - \frac{1}{2} Y_1^2(a_1 + d^3 n_1^2/q_1 z_{ep})$$

The contribution to the chemical potentials from all the other sources, i.e. dipole interactions normal to the adsorbing surface, short-range interactions, interactions with the boundaries of the interface and entropy effects have been calculated in an earlier paper (26). The result, for the ith type solvent dipoles, is

[26] $$\mu_{is}/kT = \ln \vartheta_i - \vartheta/r - (1/r)\sum_{i=0}^{r-1}(1/b_i')\ln(1 - b_i'\vartheta) + \frac{A^{AS}(q/r)^2\vartheta^2}{(1 - \vartheta + q\vartheta/r)^2} + \left\{(4\pi\sigma^M + X_m)P_{in} - 4\pi\sigma^M a_{in}X_m - \frac{1}{2}a_{in}(4\pi\sigma^M)^2 - \frac{1}{2}X_m^2\left(\frac{d^3}{z_{en}} + a_{in}\right)\right\}\Big/ kT + U_{is}/kT$$

For the adsorbate molecules we have

[27] $$\mu_A/kT = \ln\vartheta + 1 - \vartheta - \sum_{i=0}^{r-1}\frac{1 - b_i'}{b_i'}\ln\frac{1 - b_i'\vartheta}{1 - b_i'} + \frac{A^{AS}q(1 - \vartheta)^2}{(1 - \vartheta + q\vartheta/r)^2} + U_A/kT + \left\{(4\pi\sigma^M + qX_m/r)P_{An} - 4\pi\sigma^M a_{An}qX_m/r - \frac{1}{2}a_{An}(4\pi\sigma^M)^2 - \frac{1}{2}X_m^2\left(\frac{d^3q}{z_{en}} + a_{An}q^2/r^2\right)\right\}\Big/ kT$$

Here, ϑ_i, ϑ are the surface coverages of the solvent ith state and the adsorbate, respectively; b_i' are lattice constants depending on the geometrical characteristics of the adsorbate; A^{AS} is a constant related to the short-range interactions; σ^M is the electrode charge density; and X_m is the electric field normal to the adsorbing surface at every solvent site. It is given by

$$[28]\quad X_m = \frac{\sum_{i=1}^{N} (P_{in} - a_{in}4\pi\sigma^M)q_i\vartheta_i/n_i^2}{\sum_{i=1}^{N}\left(\frac{d^3}{z_{en}} + a_{in}q_i/n_i^2\right)q_i\vartheta_i/n_i}$$

Finally, U_{is} and U_A are residual energies of the solvent in the ith state and the adsorbate, respectively, at the interface.

Equations [26] and [27] enable us to calculate the equilibrium properties of the model. First we examine the case where there are no adsorbate molecules in the lattice ($\vartheta = 0$). The equilibrium relationships may be written as

$$[29]\quad kT\ln\frac{\vartheta_1}{\vartheta_k} = U_k - U_1 + (P_{kn} - P_{1n})(4\pi\sigma^M + X_m) + (P_{kp} - P_{1p})Y_m$$

From these equations we can obtain

$$[30]\quad \vartheta_1 = (1/q_0)\exp\{-(U_1 + P_{1n}\epsilon + P_{1p}Y_m)/kT\}$$

where

$$[31]\quad \epsilon = 4\pi\sigma^M + X_m$$

$$[32]\quad q_0 = \sum_{i=1}^{N}\exp\{-(U_i + P_{in}\epsilon + P_{ip}Y_m)/kT\}$$

Equation [30], in combination with eqs. [23] and [28], gives

$$[33]\quad q_0Y_m(a_s + d^3/z_{ep}) = \sum_{i=1}^{N} P_{ip}\exp\{-(U_i + P_{in}\epsilon + P_{ip}Y_m)/kT\}$$

$$[34]\quad \epsilon = \frac{d^3 4\pi\sigma^M/z_{en}}{a_s + d^3/z_{en}} + \frac{\sum_{i=1}^{N} P_{in}\exp\{-(U_i + P_{in}\epsilon + P_{ip}Y_m)/kT\}}{q_0(a_s + d^3/z_{en})}$$

where a mean polarizability, a_s, for all solvent states, is assumed. At every σ^M value eqs. [33], [34] can be solved numerically for ϵ and Y_m. Then the surface composition can be calculated by means of eq. [30].

The inner layer differential capacity may be calculated from (6, 8)

$$[35]\quad C_i^{-1} = 4\pi\left(\alpha + \frac{2d}{z_{en}\sqrt{3}}\cdot\frac{\partial X_m}{\partial\sigma^M}\right)$$

where we have accepted that the inner layer thickness, α, is different from the lattice constant, d. Equation [35] after some algebra results in

$$[36]\quad C_i^{-1} = 4\pi\left\{\alpha - \frac{8\pi d}{z_{en}\sqrt{3}}(1 + d^3/\Phi z_{en})^{-1}\right\}$$

where

$$[37]\quad \Phi = a_s + P_s^2 f_1/kT - (P_s^2 f_{12}/kT)^2/(d^3/z_{ep} + a_s - P_s^2 f_2/kT)$$

$$[38]\quad f_1 = \left(\sum_{i=1}^{N}\vartheta_i\cos\varphi_i\right)^2 - \sum_{i=1}^{N}\vartheta_i\cos^2\varphi_i$$

$$[39]\quad f_2 = \left(\sum_{i=1}^{N}\vartheta_i\sin\varphi_i\right)^2 - \sum_{i=1}^{N}\vartheta_i\sin^2\varphi_i$$

$$[40]\quad f_{12} = \left(\sum_{i=1}^{N}\vartheta_i\cos\varphi_i\right)\left(\sum_{i=1}^{N}\vartheta_i\sin\varphi_i\right) - \sum_{i=1}^{N}\vartheta_i\cos\varphi_i\sin\varphi_i$$

When adsorbate molecules are present at the interface the equilibrium equations [29] are still valid. The adsorption isotherm may be calculated from eqs. [25]–[27] and it is given by

$$[41]\quad \ln(\vartheta/\vartheta_{\uparrow}^r) + \sum_{i=0}^{r-1}\ln(1 - b_i'\vartheta) + A_nX_m + B_nX_m^2 + A_pY_m + B_pY_m^2 + A^{AS}q \times \frac{(1-\vartheta)^2 - q\vartheta^2/r}{(1 - \vartheta + q\vartheta/r)^2} = \ln(\beta c_A) + \ln\beta^{el}$$

$$[42]\quad A_n = \{P_{An}q/r - 4\pi\sigma^M a_A q/r - rP_{\uparrow n} + r4\pi\sigma^M a_s\}/kT$$

$$[43]\quad A_p = \{P_{Ap}q/r\}/kT$$

$$[44]\quad B_n = \{r(a_s + d^3/z_{en}) - q^2(a_A + d^3r^2/qz_{en})/r^2\}/2kT$$

$$[45]\quad B_p = \{r(a_s + d^3/z_{ep}) - q^2(a_A + d^3r^2/qz_{ep})/r^2\}/2kT$$

$$[46]\quad \ln\beta = \{\mu_A^0 - r\mu_s^0 + r\mu_{\uparrow}^{0,sr} + r\mu_{\uparrow}^{0,ent} - \mu_A^{0,sr} - \mu_A^{0,ent} + rU_{\uparrow} - U_A\}/kT - \ln c_s - 1 - \sum_{i=0}^{r-1}\frac{1 - b_i'}{b_i'} \times \ln(1 - b_i')$$

$$[47]\quad \ln\beta^{el} = -4\pi\sigma^M\{P_{An} - rP_{\uparrow n} - 4\pi\sigma^M(a_A - ra_s)/2\}/kT$$

Here c_j (j = A, S) is the bulk concentration of the jth component, ($\uparrow$) denotes the solvent state with dipole vector pointing to the solution, and $\mu_j^{0,1}$ represents chemical potentials of the j component in their standard states (26).

Numerical examples were performed for the three-state model (6) only. Here we used for z_{en} the corrected value 10.6. However, as is also expected from the work of Borkowska and Stafiej (29), this value causes polarization catastrophe problems. The polarization catastrophe can be avoided, at least for values of z_{ep} close to zero, if we assume that the thickness of the inner layer is greater than the lattice constant. This is a reasonable assumption, since the plate separation should be equal to one solvent diameter plus one radius of the electrolyte ion and possibly one atomic radius of the metal electrode (30). For an aqueous electrolyte interface the thickness of the inner layer should range from 4×10^{-10} to 4.5×10^{-10} m. Figures 1–4 show some of the obtained results. It is seen that the inclusion of in-plane dipole interactions results in the considerable increase of the parallel state, around the pzc, even at no highly ordered structures. For intermediate z_{ep} values this configuration breaks at relatively high fields and causes polarization catastrophe problems.

Problems appear also when adsorbate molecules are present at the inner layer. At the adsorption maximum the total dipole moment, P, normal to the adsorbing surface, should be independent of the adsorbate surface concentration (26). Since

$$[48]\quad P/M = P_{An}\vartheta/r + (1 - \vartheta)\sum_{i=1}^{N_s}P_{in}g_i - a_A\vartheta(4\pi\sigma^M + X_A)/r - (1 - \vartheta)\sum_{i=1}^{N_s}a_ig_i(4\pi\sigma^M + X_m)$$

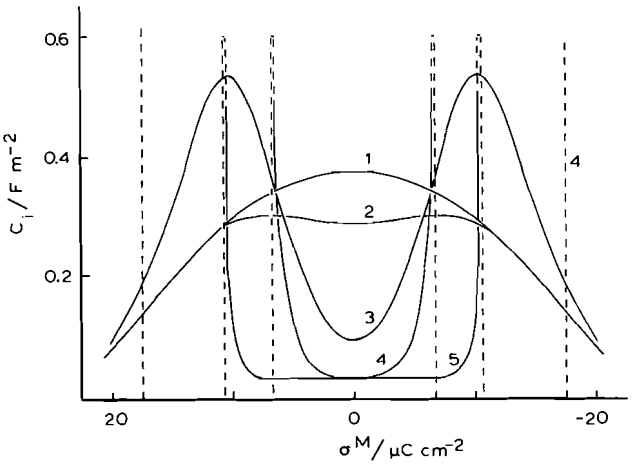

FIG. 1. Plots of the inner-layer capacity C_i against electrode charge density σ^M according to the three-state model. The parameters used were $T = 298$, $P_s = 6.12 \times 10^{-30}$ Cm, $a_s = 1.5 \times 10^{-30}$ m^3, $\alpha = 4.2 \times 10^{-10}$ m, $d = 3 \times 10^{-10}$ m, $U_\uparrow = U_\downarrow = U_\rightarrow$. Values of z_{ep}: (*1*) 0; (*2*) −0.5; (*3*) −1; (*4*) −2; (*5*) −5.

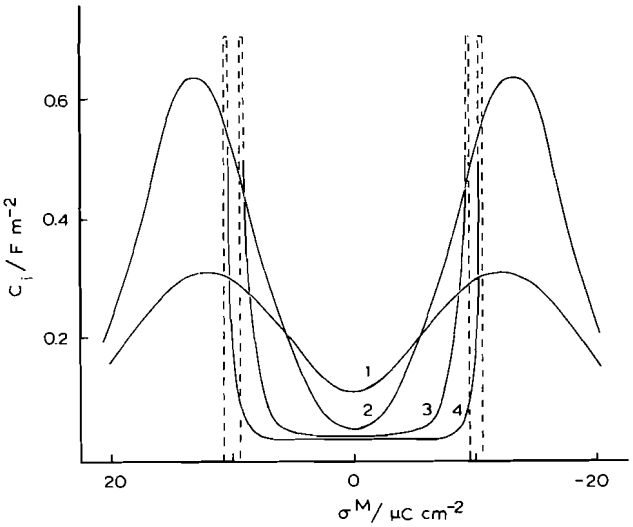

FIG. 2. Plots of the inner-layer capacity C_i against electrode charge density σ^M according to the three-state model. Parameters as in Fig. 1 except $\alpha = 4 \times 10^{-10}$ m and $U_\downarrow - U_\rightarrow = 3kT$. Values of z_{ep}: (*1*) 0; (*2*) −0.5; (*3*) −2; (*4*) −5.

where

$$[49] \quad M = \sum_{i=1}^{N} n_i N_i$$

$$[50] \quad g_i = \vartheta_i/(1 - \vartheta)$$

the condition

$$[51] \quad \left(\frac{\partial P/M}{\partial \vartheta^M}\right)_{\sigma^M_{max}} = 0$$

results in

$$[52] \quad P_{An}/r - \sum_{i=1}^{N_s} P_{in} g_i - a_A(4\pi\sigma^M + X_A)/r + a_s(4\pi\sigma^M + X_m) = 0$$

$$[53] \quad (\partial g_i/\partial\vartheta) = 0$$

$$[54] \quad (\partial X_m/\partial\vartheta) = 0$$

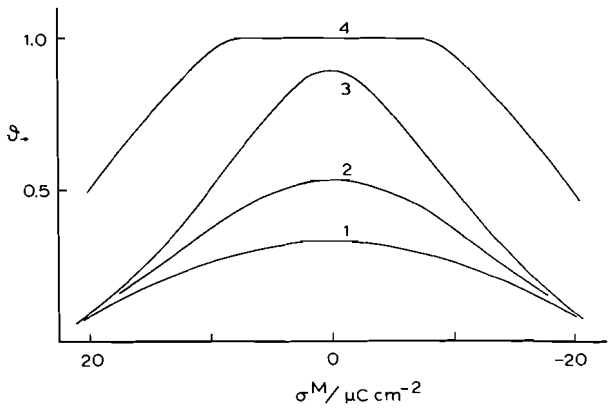

FIG. 3. Plots of the surface coverage of the parallel (→) state against electrode charge density. Parameters as in Fig. 1. Values of z_{ep}: (*1*) 0; (*2*) −0.5; (*3*) −1; (*4*) −5.

However, eqs. [53] and [54] are compatible with the equilibrium equations [29] only when

$$[55] \quad (\partial Y_m/\partial\vartheta) = 0$$

Equations [29], [52]–[55] and the obvious one

$$[56] \quad \sum_{i=1}^{N} \vartheta_i = 1$$

constitute a system of $N_s + 3$ equations, N_s being the number of solvent states. However, there are only $N_s + 2$ unknowns, namely $\vartheta_1, \vartheta_2, \ldots, \vartheta_{N_s}, \vartheta, \sigma^M_{max}$. Therefore, in general, it is impossible to find a solution which would give σ^M_{max} independent of ϑ. Figure 5 shows that the dependence of σ^M_{max} on ϑ is strong even for values of z_{ep} close to zero. Moreover as z_{ep} decreases phase transitions appear in all cases (Fig. 5).

IV. Discussion and conclusions

The above results show that the agreement between the predictions of the model and experimental behaviour is unsatisfactory when ordered in-plane configurations are taken into consideration. This disagreement could be attributed to the following two points of the present treatment:

(*1*) The increase of solvent states with dipoles normal to the adsorbing surface (at intermediate and high fields) as well as adsorbate molecules with small or zero parallel dipole component is expected to unfavour ordered in-plane configurations. Therefore z_{ep} should be a function of both ϑ and σ^M. However, it can hardly be accepted that the use of a variable z_{ep} would improve the results. In this case it is expected that a more pronounced dependence of the parallel state population on σ^M results in polarization catastrophe problems. In the case of σ^M_{max}, a more rapid convocation of σ^M_{max} to its value corresponding to $z_{ep} = 0$ as $\vartheta \rightarrow 1$ would be expected. But at low ϑ values σ^M_{max} would be close to the values of the present treatment. Therefore, a strong dependence of σ^M_{max} on ϑ would also be expected.

(*2*) From a strict theoretical point of view the treatment presented here lacks self-consistency. If we accept a random distribution for the dipoles normal to the electrode it is reasonable to accept the same random distribution for the parallel dipoles as well. However, such an approach is in disagreement with the Monte-Carlo results (9). Therefore, the present results seem to point out the failure of the mean field approximation and the need to find more realistic models.

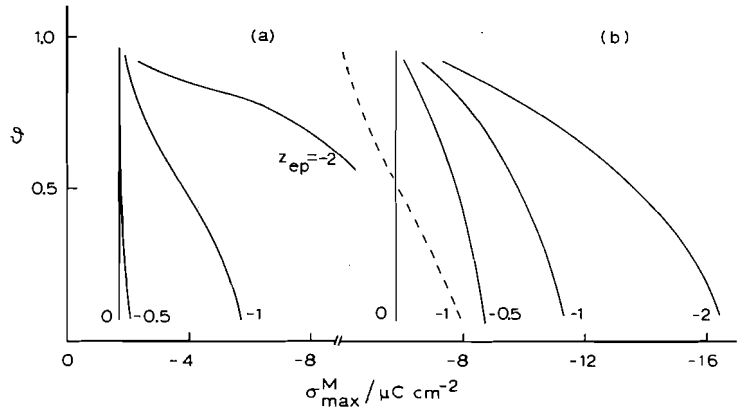

FIG. 4. Dependence of adsorption maximum, σ^{M}_{max}, on ϑ. Parameters used: $T = 298$; $r = 3$; $b'_0 = 0$; $b'_1 = 0.333$; $b'_2 = 0.5$; $A^{AS} = 0$; $P_s = 6.12 \times 10^{-30}$ Cm; $a_s = 1.5 \times 10^{-30}$ m^3; $a_A = 5 \times 10^{-30}$ m^3; $d = 3 \times 10^{-10}$ m; $\alpha = 4 \times 10^{-10}$ m and for (*a*) $P_{Ap} = 5 \times 10^{-30}$ Cm; $P_{An} = 0$; $U_\downarrow - U_\uparrow = U_\downarrow - U_\rightarrow = 3kT$; for (*b*) $P_{Ap} = 0$; $P_{An} = 3 \times 10^{-30}$ Cm; $U_\uparrow = U_\downarrow$; $U_\downarrow - U_\rightarrow = 3kT$. The broken line corresponds to $\alpha = 4.2 \times 10^{-10}$ m, $P_{Ap} = 0$, $P_{An} = 3 \times 10^{-30}$ Cm, $U_\uparrow = U_\downarrow = U_\rightarrow$.

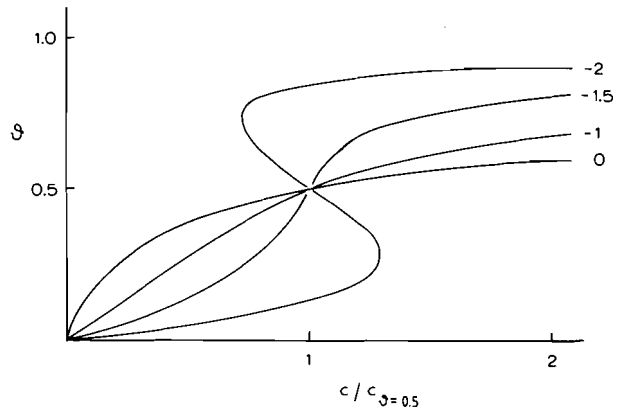

FIG. 5. Dependence of the surface coverage ϑ on the relative concentration at $\sigma^M = -2\,\mu C\,cm^{-2}$ calculated from eq. [41] for different values of z_{ep} indicated by the lines. Other parameters as in Fig. 4 (*a*).

Let us now concentrate our attention on two points; the dependence of σ^{M}_{max} on ϑ and the Monte Carlo results. We have proved that the model predicts a concentration-dependent σ^{M}_{max} even for z_{ep} values close to zero. We can easily extend the above results for every model of the inner layer which assumes ordered in-plane configurations. At the adsorption maximum the total dipole moment normal to the adsorbing surface should be independent of ϑ. That is, the order parameters g_i for the solvent states with perpendicular dipole component should be constant at σ^{M}_{max}. Now, if we assume a Y field parallel to the electrode, having a detectable effect on the population of the various solvent states in the inner layer, then the constancy of g_i should lead to the constancy of Y. However, this is impossible in general. For example, if the dipole moment vector of the adsorbate is oriented normal to the electrode then $Y \rightarrow 0$ as $\vartheta \rightarrow 1$. Perhaps the dependence of σ^{M}_{max} on ϑ would not be as strong as in the model examined, but it should be experimentally detectable. Therefore, at least for the Hg/aq. solution interface, where we have the most accurate data, the constancy of σ^{M}_{max} from ϑ should indicate very weak Y interactions.

The Monte–Carlo treatment of Schmickler (9) deals with freely oriented dipoles. It has been found that at zero external field the dipoles are oriented preferentially in-plane. This means that, at the pzc or around it, the differential capacity of a monolayer of freely oriented dipoles should present a minimum. However, this behaviour does not characterize the Hg/water interface and it further supports the view that at this interface there are no freely oriented dipoles, probably because of the presence of hydrogen bonds. A shallow minimum in the capacity vs. charge curves is the principal feature of alcohols, formic acid, ammonia, and dimethylformamide (6). However, this does not in itself prove the existence of freely oriented dipoles or strong Y fields at the interfaces. Theoretically a minimum in the capacity curves can be predicted even by using the mean field approximation without assuming ordered in-plane structures (6–8). Moreover, adsorption studies at the mercury–methanol interface carried out in our laboratory show a concentration independent adsorption maximum (31–35). Consequently, at this interface Y dipole interactions should not predominate. However, more precise data are needed to clarify the behaviour of non-aqueous solvents at charged interfaces.

The final problem arising from the above discussion is whether the existence of rotational barriers can lead to a random (or an almost random) distribution of the dipoles. It is easily seen from the results of the dipole interactions in section II that a monolayer of dipoles, oriented or not, does not interact or interacts very weakly with a dipole outside the layer. Therefore, a dipole, even near a dipole layer, does not feel strong directional interactions. Now if we take into account that the inner layer of real interfaces is not an isolate system but in continuous competition with the solvent dipoles in the bulk of the electrolyte solution, then it is very likely for the dipoles to enter almost in random the inner layer and the existence of barriers to stabilize such random configurations.

1. N. F. MOTT and R. J. WATTS-TOBIN. Electrochim. Acta, **4**, 79 (1961).
2. R. J. WATTS-TOBIN. Philos. Mag. **6**, 133 (1961).
3. J. O'M. BROCKRIS, M. A. V. DEVANATHAN, and K. MÜLLER. Proc. R. Soc. A**274**, 55 (1963).
4. S. LEVINE, G. M. BELL, and A. L. SMITH. J. Phys. Chem. **73**, 3534 (1969).
5. R. GUIDELLI. J. Electroanal. Chem. **110**, 205 (1980).
6. W. R. FAWCETT. J. Phys. Chem. **82**, 1385 (1978).
7. W. R. FAWCETT and R. M. DE NOBRIGA. J. Phys. Chem. **86**, 371 (1982).
8. W. R. FAWCETT. Isr. J. Chem. **18**, 3 (1979).
9. W. SCHMICKLER. J. Electroanal. Chem. **157**, 1 (1983).

10. J. TOPPING. Proc. R. Soc. A**113**, 67 (1927).
11. J. R. MACDONALD and C. A. BARLOW. Surface Sci. **4**, 381 (1966).
12. M. C. PHILLIPS, D. A. CADENHEAD, R. J. GOOD, and H. F. KING. J. Colloid. Interface Sci. **38**, 437 (1971).
13. R. PARSON and R. M. REEVES. J. Electroanal. Chem. **123**, 141 (1981).
14. W. SCHMICKLER. J. Electroanal. Chem. **149**, 15 (1983).
15. C. BÖTTCHER. Theory of electric polarization. Vol. 1. Elsevier, Amsterdam. 1973.
16. S. LEVINE, A. L. SMITH, and E. MATIJEVIC. J. Colloid. Interface Sci. **39**, 409 (1969).
17. S. LEVINE, K. ROBINSON, A. L. SMITH, and A. C. BRETT. Discuss. Faraday Soc. **59**, 133 (1975).
18. W. R. FAWCETT, B. M. IKEDA, and J. B. SELLAN. Can. J. Chem. **57**, 2269 (1979).
19. W. R. FAWCETT, S. LEVINE, R. M. DE NOBRIGA, and A. C. MACDONALD. J. Electroanal. Chem. **111**, 163 (1980).
20. Z. BORKOWSKA and W. R. FAWCETT. Can. J. Chem. **59**, 710 (1981).
21. Z. BORKOWSKA and W. R. FAWCETT. Can. J. Chem. **60**, 1787 (1982).
22. W. R. FAWCETT and Z. BORKOWSKA. J. Phys. Chem. **87**, 4861 (1983).
23. M. V. SANGARANARAYANAN and S. K. RANGARAJAN. J. Electroanal. Chem. **176**, 1 (1984).
24. M. V. SANGARANARAYANAN and S. K. RANGARAJAN. J. Electroanal. Chem. **176**, 45 (1984).
25. P. NIKITAS. Electrochim. Acta, **30**, 1513 (1985).
26. P. NIKITAS. J. Chem.Soc. Faraday Trans. 1, In press.
27. J. O. HIRSCHFELDER, C. F. CURTISS, and R. B. BIRD. Molecular theory of gases and liquids. Wiley, New York. 1954.
28. W. H. KEESOM. Physik. Z. **22**, 129 (1921).
29. Z. BORKOWSKA and J. STAFIEJ. J. Electroanal. Chem. **182**, 253 (1985).
30. J. R. MACDONALD and C. A. BARLOW, JR. J. Chem. Phys. **36**, 3062 (1962).
31. P. NIKITAS, A. ANASTOPOULOS, and D. JANNAKOUDAKIS. J. Electroanal. Chem. **143**, 361 (1983).
32. A. PAPPA-LOUISI, P. NIKITAS, and D. JANNAKOUDAKIS. Electrochim. Acta, **29**, 515 (1984).
33. P. NIKITAS, A. PAPPA-LOUISI, and D. JANNAKOUDAKIS. J. Electroanal. Chem. **162**, 175 (1984).
34. P. NIKITAS, A. ANASTOPOULOS, and D. JANNAKOUDAKIS. J. Electroanal. Chem. **145**, 407 (1983).
35. P. NIKITAS, A. PAPPA-LOUISI, and D. JANNAKOUDAKIS. J. Electroanal. Chem. **184**, 109 (1985).

Proton transfer from imidazole, benzimidazole, and their 1-alkyl derivatives. FMO analysis of the effect of methyl and benzo substitution[1]

ERWIN BUNCEL AND HELEN A. JOLY
Department of Chemistry, Queen's University, Kingston, Ont., Canada K7L 3N6
AND
JOHN R. JONES
Department of Chemistry, University of Surrey, Guildford, GU2 5XH, U.K.
Received October 31, 1985
This paper is dedicated to Professor Arthur N. Bourns

ERWIN BUNCEL, HELEN A. JOLY, and JOHN R. JONES. Can. J. Chem. **64**, 1240 (1986).

The rate–pH profile for detritiation from the C-2 position of 1-methylimidazole has been determined in aqueous solution at 85°C. The profile is consistent with a mechanism involving attack by hydroxide ion on the conjugate acid of the substrate to give an ylid intermediate in the rate-determining step. At higher pH, hydroxide-catalyzed exchange of the neutral species becomes increasingly important. Comparison of the second-order rate constants derived from the rate–pH profiles of imidazole, 1-methylimidazole, benzimidazole, and 1-methylbenzimidazole showed that methyl substitution caused the rate to increase by 2- to 3-fold while benzo annelation increased the rate by 10- to 20-fold. Frontier molecular orbital (FMO) analysis of the reaction scheme for proton transfer from imidazole, benzimidazole, and their 1-alkyl derivatives has been used to explain the rate-accelerating effect of methyl substitution and benzo annelation in these processes.

ERWIN BUNCEL, HELEN A. JOLY et JOHN R. JONES. Can. J. Chem. **64**, 1240 (1986).

Opérant à 85°C et dans une solution aqueuse, on a déterminé un profil de la vitesse/pH pour la réaction de détritiation de la position C-2 du méthyl-1 imidazole. Le profil est en accord avec un mécanisme impliquant une étape déterminante dans laquelle un ion hydroxyde attaque l'acide conjugué du substrat pour conduire à un ylide intermédiaire. A des pH plus élevés, l'échange catalysé par des bases des espèces neutres devient de plus en plus important. Une comparaison des constantes de vitesse du deuxième ordre, obtenues à partir des profils de vitesse/pH, des imidazole, méthyl-1 imidazole, benzimidazole et méthyl-1 benzimidazole a permis de montrer que la substitution par des groupements méthyles multiplie la vitesse par 2 à 3 alors que l'annelation par un noyau benzénique multiplie les vitesses par 10 à 20. Dans le but d'expliquer l'accélération de la vitesse lors de substitutions par des groupements méthyles et lors de l'annelation par des cycles benzéniques, on a utilisé une analyse, par les orbitales moléculaires frontières, du schéma réactionnel des transferts protoniques de l'imidazole, du benzimidazole et de leurs dérivés substitués par un groupement méthyle en position 1.

[Traduit par la revue]

The rate of hydrogen isotope exchange from the C-2 position of the imidazole ring is of interest, in part because of its presence in biologically important systems such as adenine and guanine, fundamental components of nucleic acids, and in drugs such as puromycin. Imidazole is also the primary component of histidine which is present at the active site of many enzymes. The importance of the imidazole ring can be coupled with the use of deuterium and tritium labels as probes in the investigation of chemical and biochemical processes. For instance, the rate of hydrogen isotope exchange from the C-2 position of the imidazole nucleus present in the histidine residues of the enzymes β-lactamase II and superoxide dismutase has been used to identify the specific histidine residues which act as ligands towards metal ions (1, 2). It is useful therefore to have some knowledge of the factors which can influence the rates of deuterium or tritium loss from the imidazole moiety in different structural environments.

Past studies (3) of proton abstraction from compounds containing the imidazole nucleus suggest that reaction occurs via rate-determining hydroxide attack on either the protonated or the neutral forms of the substrate to form an ylid intermediate. On the basis of such a mechanism one would expect the rate of isotopic hydrogen exchange to be dramatically increased on introduction of a positive charge at sites adjacent to the exchanging hydrogen.

Isotopic exchange involving 1-methylimidazole has previously been studied by two groups of workers but the results obtained are at variance. Harris and Randall (4) reported that the rate–pH profile for deuteration of the C-2 position of 1-methylimidazole at 26°C in the pH region 0–14 was sigmoid. Between pH values 0–4 the rate was undetectable but increased sharply between pH 4–8, beyond which the rate leveled off. This study was qualitative in the sense that the overall rate was not dissected into constituent second order rate constants. Wong and Keck (5) also determined a rate–pH profile for C-2 hydrogen/deuterium exchange between pH 0–14 at 81°C. This study showed some discrepancy with the findings of the previous workers in that the rate increased from pH 2 until pH 8.

The rate–pH profiles obtained for detritiation of 9-alkylpurines (6), 1-methylguanosine (7), and 1-methylinosine (7), which are structurally similar to 1-methylimidazole in that they possess the imidazole nucleus and the pyrrole nitrogen adjacent to C-2 is substituted by an alkyl group, show some deviation in highly basic media from the profile reported for 1-methylimidazole (4, 5), since the rates of proton exchange for the former compounds increase with pH in this region. A re-investigation of the 1-methylimidazole system using a more sensitive means of obtaining rate data was desirable and the results of the detritiation study are reported herein. The resulting reactivity relationships involving imidazole (**1**, R = H), 1-methylimidazole (**1**, R = Me) and the corresponding benzimidazole derivatives (**2**, R = H or Me) which have come to light in

[1]Hydrogen exchange studies, Part 15; for Part 14, see ref. 23.

Printed in Canada / Imprimé au Canada

this work are unusual in terms of qualitative electronic considerations, but can be explained using frontier molecular orbital theory.

R = H or Me

1 2

Experimental

Preparation of [2-^{3}H]-1-methylimidazole

Tritiated water (5 μL, 50 Ci/mL) was added to freshly distilled 1-methylimidazole (100 μL) in a small glass ampoule. After sealing, the ampoule was submerged in an oil bath at 85°C for 72 h. The ampoule was then opened, 1 mL of methanol was added to exchange labile tritium and the solvent was removed by lyophilization. Addition of 1 mL portions of methanol was continued until the activity of the lyophilized methanol was found to be insignificant. The purity of the [2-^{3}H]-1-methylimidazole as well as the specificity of labelling of the tritium in the C2 position was checked by ^{1}H and ^{3}H nmr.

Kinetics

The rates of detritiation of [2-^{3}H]-1-methylimidazole in a series of aqueous buffer solutions of known pH – temperature dependence (8) were determined by measuring the increase in the radioactivity of the reaction medium with time in a fashion similar to that used for imidazole (9) and benzimidazole (10). [2-^{3}H]-1-methylimidazole (10 μL) was dissolved in 20 mL of an aqueous buffer solution previously thermostatted at 85.0 ± 0.2°C. Ten 0.5 mL aliquots of the reaction mixture were withdrawn individually at specific time intervals, placed into small round bottom flasks and cooled in liquid nitrogen. Lyophilization of the quenched samples enabled separation of the water from the substrate. A 0.1 mL aliquot of the water collected was placed in 6 mL of Unisolve E liquid scintillator and assayed for tritium (C_t) on a Beckman 100 liquid scintillation counter. The exchange reaction was generally followed for at least two half-lives. The infinity reading (C_∞), i.e., the activity of the water after complete exchange, was obtained by counting the activity of 0.1 mL of the original reaction mixture. All samples were counted for 2 min to ensure statistical accuracy. The pseudo first order rate constant, k_{obs}, was obtained from the slope ($-2.303k_{obs}$) of the plot of log ($C_\infty - C_t$) as a function of time t. The rate constant data in Table 1 are average values of two or more determinations which generally agreed to within 2–3%. For very slow reactions an initial rate method was employed wherein the tritium content of the water (C_t) was measured for only the first 3–5% of the reaction. A linear plot of C_t vs. t is obtained with slope equal to the zero-order rate constant (k_0). The first order rate constant k_{obs} for the slow reactions was obtained by dividing k_0 by the total radioactivity of the substrate (C_∞) obtained as before.

Potassium hydrogen phthalate and sodium borate buffers were used for kinetic measurements carried out at low and intermediate pH ranges, respectively, while sodium hydroxide solutions were used for measurements at higher pH values.

Results and discussion

Kinetic analysis and reaction mechanism

The results obtained for detritiation of [2-^{3}H]-1-methylimidazole in aqueous buffers at 85°C are listed in Table 1 and shown graphically in Fig. 1 in the form of a rate–pH profile for the pH range 2.5–11.5. Exchange rates in more basic media (pH > 11.5) were too fast to be reliably determined by the kinetic technique used.

The rate profile for 1-methylimidazole is similar to that obtained (10) for 1-methylbenzimidazole (Fig. 1) as well as for

TABLE 1. Rates of detritiation of [2-^{3}H]-1-methylimidazole as function of pH at 85.0 ± 0.2°C

pH at 85.0°C	$k_{obs} \times 10^4$ (s^{-1})	pH at 85.0°C	$k_{obs} \times 10^4$ (s^{-1})
2.56	0.0204	9.18	29.6
3.77	0.248	10.52	28.5
4.94	2.80	10.82	28.4
6.25	21.2	11.20	34.7
7.70	30.3	11.51	34.5

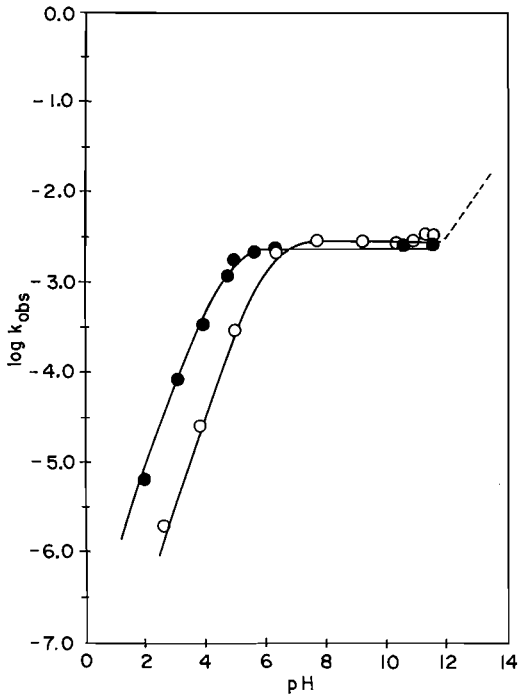

FIG. 1. Rate–pH profiles for the detritiation of [2-^{3}H]-1-methylimidazole ○ and [2-^{3}H]-1-methylbenzimidazole ●. The solid lines represent the theoretical profiles calculated from eq. [9] using the values from the text and the dashed line is the theoretical behaviour expected on the basis of eq. [5].

1-methylguanosine, 1-methylinosine (7), and 9-alkylpurines. Initially the rate increases with increasing pH until a pH-independent region is obtained, extending between pH 7 and 10. Such behaviour is consistent with a mechanism in which the conjugate acid of the substrate is being attacked by hydroxide ion in the rate determining step. At pH > 11 the rate increases again with increasing pH. This has been attributed to rate-determining attack by hydroxide ion on the neutral form of the substrate (Scheme 1). Though the rate of tritium exchange in more highly basic media (pH > 11.5) could not be determined, one would expect 1-methylimidazole to behave in a manner similar to that of the 9-alkylpurines (6), namely that the rate would increase with increasing pH. The expected behaviour is indicated by a dashed line in Fig. 1.

The rate expression for the isotopic exchange reaction over the entire pH region is given by eq. [1] from which eq. [2] follows,

$$[1] \quad \text{Rate} = k[\text{ImH}^+][\text{OH}^-] + k'[\text{Im}][\text{OH}^-] = k_{obs}[\text{Im}]_T$$

$$[2] \quad k_{obs} = (k[\text{ImH}^+] + k'[\text{Im}])[\text{OH}^-]/[\text{Im}]_T$$

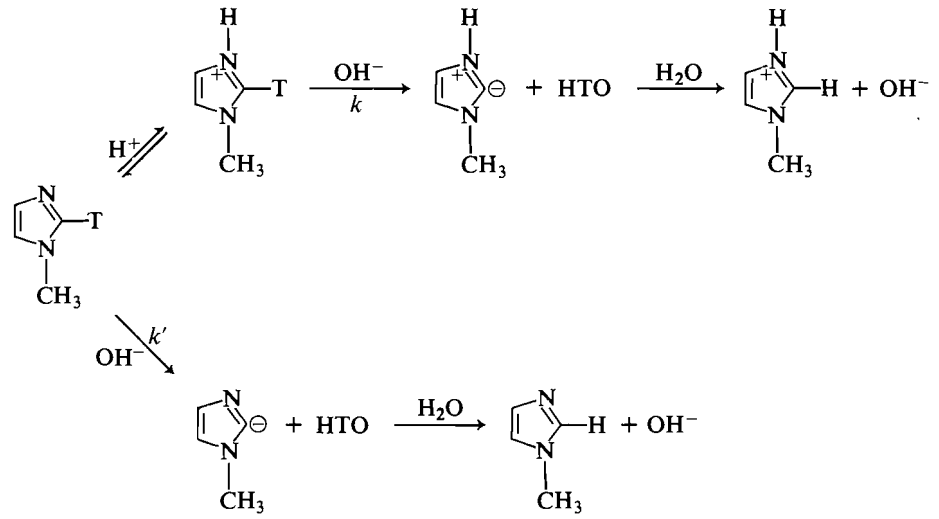

SCHEME 1

where $[ImH^+]$ and [Im] represent the concentration of the protonated and neutral forms of 1-methylimidazole, respectively, k and k' are the corresponding second order rate constants, and k_{obs} is the pseudo-first order rate constant for the detritiation of [2-^{3}H]-1-methylimidazole. The $[ImH^+]$ and [Im] terms can be expressed by means of experimentally measurable quantities, i.e.

$$[3] \quad [ImH^+] = [Im]_T/(1 + K_a/[H^+])$$

$$[4] \quad [Im] = [Im]_T/(1 + [H^+]/K_a)$$

Now $[Im]_T = [ImH^+] + [Im]$, where $[Im]_T$ is the total concentration of 1-methylimidazole in solution. Also, the acid association constant of protonated 1-methylimidazole is given by $K_a = [Im][H^+]/[ImH^+]$. Substitution of eqs. [3] and [4] into [1] gives

$$[5] \quad k_{obs} = \frac{k[H^+][OH^-]}{K_a + [H^+]} + \frac{k'K_a[OH^-]}{K_a + [H^+]}$$

At low pH, $[H^+] \gg K_a$ and eq. [5] reduces to

$$[6] \quad k_{obs} = k[OH^-] + \frac{k'K_a[OH^-]}{[H^+]}$$

Since K_a is small, and at low pH, [OH] is small while $[H^+]$ is large, the second term can be neglected and eq. [7] follows.

$$[7] \quad k_{obs} = k[OH^-]$$

In accord with eq. [7], plotting k_{obs} versus $[OH^-]$ for the first three data points in Table 1 (pH 2.56–4.94) gave an excellent linear plot which yielded $k = 1.01 \times 10^4\ L\ mol^{-1}\ s^{-1}$ as the rate constant for deprotonation of the conjugate acid (Scheme 1). The rate constant k' corresponding to deprotonation of the neutral substrate is usually derived by plotting data in the high pH region (see eq. [5]) but this could not be evaluated in the present study as noted above.

At the intermediate pH values, corresponding to the plateau region in Fig. 1, $K_a \gg [H^+]$ and eq. [5] reduces to eq. [8], neglecting the second term.

$$[8] \quad k_{obs} = kK_w/K_a$$

Using the values of k ($1.01 \times 10^4\ L\ mol^{-1}\ s^{-1}$), k_{obs} for the pH-independent region ($2.95 \times 10^{-3}\ s^{-1}$) and K_w at 85°C (3.16×10^{-13}) (11), enables K_a for 1-methylimidazole to be estimated as $1.08 \times 10^{-6}\ mol\ L^{-1}$, i.e. $pK_a = 5.96$ at 85°C. The experimentally (12) determined pK_a value is ca. 7.2 at 25°C. Typical temperature coefficients (13) for nitrogen acids of similar acidities are $-0.022\ pK_a$ units per °C rise, and hence the experimental pK_a at 85°C should be 5.88. Extrapolation of pK_a versus temperature data (12) collected for 1-methylimidazole between 10 and 45°C suggests that the pK_a at 85°C for 1-methylimidazole is 6.09. These values are in good agreement with the calculated value from the rate data as given above.

The solid curve drawn for the 1-methylimidazole rate data in Fig. 1 is the result of calculating, for various $[H^+]$ values, theoretical k_{obs} values by means of eq. [9], using $k = 1.01 \times 10^4\ L\ mol^{-1}\ s^{-1}$, $K_w = 3.16 \times 10^{-13}$, and $K_a = 1.08 \times 10^{-6}\ mol\ L^{-1}$.

$$[9] \quad k_{obs} = kK_w/(K_a + [H^+])$$

Equation [9] is obtained from [5] assuming that the contribution from the hydroxide-catalyzed exchange of the neutral species is small and that the second term can hence be neglected. The agreement with the experimental data is satisfactory.

Reactivity relationships

One can compare the second order rate constant corresponding to the rate-determining attack of hydroxide ion on the conjugate acid of 1-methylimidazole with the corresponding rate constants previously reported for imidazole (9), benzimidazole (9, 10), and 1-methylbenzimidazole (9), Table 2. Thus inclusion of the results for 1-methylimidazole allows for a more complete discussion of the effect of methyl substitution and benzo annelation on proton transfer from heterocycles containing an imidazole nucleus. Substitution of N-1 of imidazole and benzimidazole with a methyl group causes the rate of proton transfer to increase by a factor of 2 and 3 respectively, while annelation of a benzo group to the imidazole and 1-methylimidazole nucleus results in a 10- or 20-fold rate increase, respectively (Table 2).

It is also noteworthy that substitution by a methyl group at the N-1 position of imidazole and benzimidazole has no effect on the magnitude of the pK_a for N_3-protonation, i.e. a pK_a value of 6.0 was found for both imidazole and 1-methylimidazole, while a pK_a value of 4.6 was found for both benzimidazole and 1-methylbenzimidazole. On the other hand, benzo annelation

TABLE 2. Comparison of pK_a and rate constants derived from rate–pH profiles for imidazole (Im); benzimidazole (ϕIm) and their 1-methyl derivatives

Compound	pK_a	k ($L\ mol^{-1}\ s^{-1}$)	k_{Me}/k_H	$k_{\phi Im-X}/k_{Im-X}$ (X = Me or H)
Imidazole (**1**, H)	5.9	6.0×10^3	2	10 (X = H)
1-Methylimidazole (**1**, Me)	6.0	1.0×10^4		20 (X = Me)
Benzimidazole (**2**, H)	4.6	6.2×10^4	3	
1-Methylbenzimidazole (**2**, Me)	4.6	2.0×10^5		

does have a substantial effect on the pK_a, which decreases by 1.3 pK units for both imidazole and 1-methylimidazole.

An interesting point in these systems is that they lack a saturation effect, that is, the effect of methyl substitution on the rate of C(2)–H exchange, is not diminished by benzo annelation ($k_{MeIm}/k_{Im} = 2$ and $k_{Me\phi Im}/k_{\phi Im} = 3$). Conversely the effect of benzo annelation on the rate of C(2)–H exchange is not reduced by methyl substitution ($k_{\phi Im}/k_{Im} = 10$ and $k_{Me\phi Im}/k_{MeIm} = 20$).

Conventional arguments, such as those based on the inductive effect of the methyl substituent, do not suffice to explain reactivity diferences in these systems. For example, a methyl group acting as an inductively electron-releasing substituent would be expected to destabilize the ylid intermediate and thereby lead to a rate decrease, whereas the opposite is found to be the case. However, Jones and co-workers (3*a*, 11) showed that there is a linear correlation between log k, the second order rate constant for C-2 proton exchange in azoles, and pK_a for N_3-protonation, which is adhered to by imidazole and benzimidazole. We have found that frontier molecular orbital (FMO) theory provides an explanation of reactivity in the series imidazole, benzimidazole and their 1-methylated analogs, as described below.

FMO analysis of reactivities

The effect of benzo annelation and methyl substitution on the rate of proton transfer from these imidazole derivatives can be rationalized by means of the FMO approach (14, 15). We consider the rate-determining step of the reaction and apply FMO theory to obtain the relative energies of the reacting species and of the intermediates involved, as a result of the structural change which is effected.

Thus considering the exchange process as involving abstraction of the C(2)-hydrogen from the reactant species (R), i.e., the protonated substrate, to form the ylid intermediate (I), one can dissect the reactant and intermediate into fragments whose FMOs are known and estimate the relative intramolecular stabilization energies resulting from interaction of the LUMO of one fragment with the HOMO of the other. The magnitude of the stabilization energy (SE) is dependent on the difference in energy between the HOMO and LUMO of the respective fragments; the smaller the energy gap, the greater the orbital overlap and the greater the stabilization energy. In this system, the degree of stabilization increases significantly in going from the reactant to the intermediate, because of the much smaller energy gap and the consequent enhanced LUMO/HOMO interaction present in the latter. If a structural change results in greater stabilization of the intermediates as compared to the reactants, then an increase in rate is expected since the transition state should also be stabilized on effecting the structural change.

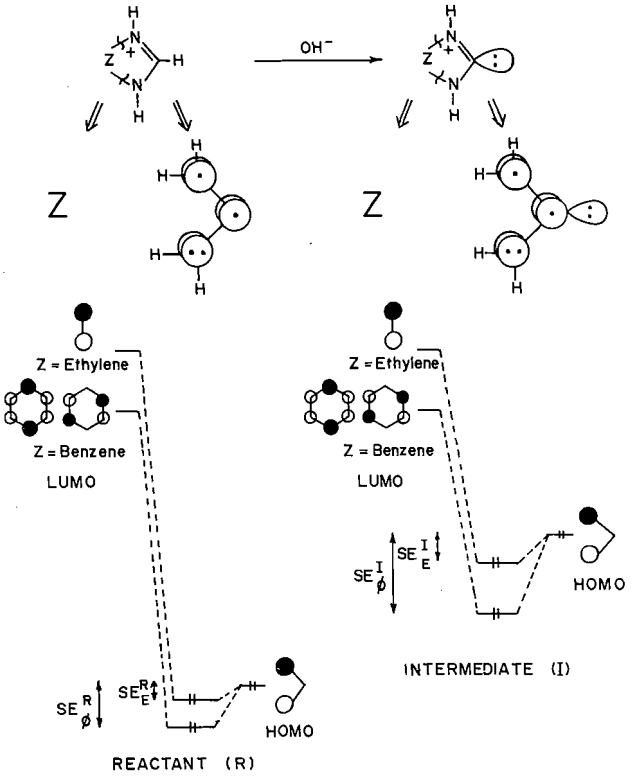

FIG. 2. FMO analysis of the effect of benzo annelation on proton transfer from imidazole showing the interaction between the HOMO of the allyl fragment and the LUMO of ethylene or benzene fragments for the reactant (R) and intermediate (I).

1. Effect of benzo annelation

The FMO analysis of the reaction scheme for benzimidazole and imidazole is shown in Fig. 2. The relative energies of the FMOs of the two reactant species and their corresponding intermediate structures can be estimated by fragmenting the molecules into two moieties whose FMOs are known. Thus benzimidazole is dissected into a benzene and a pseudo allyl fragment;

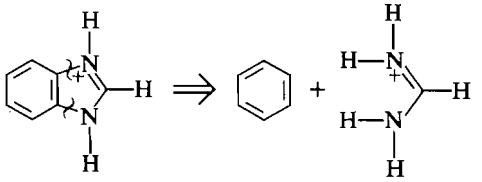

while imidazole is fragmented into an ethylene and the pseudo allyl fragment:

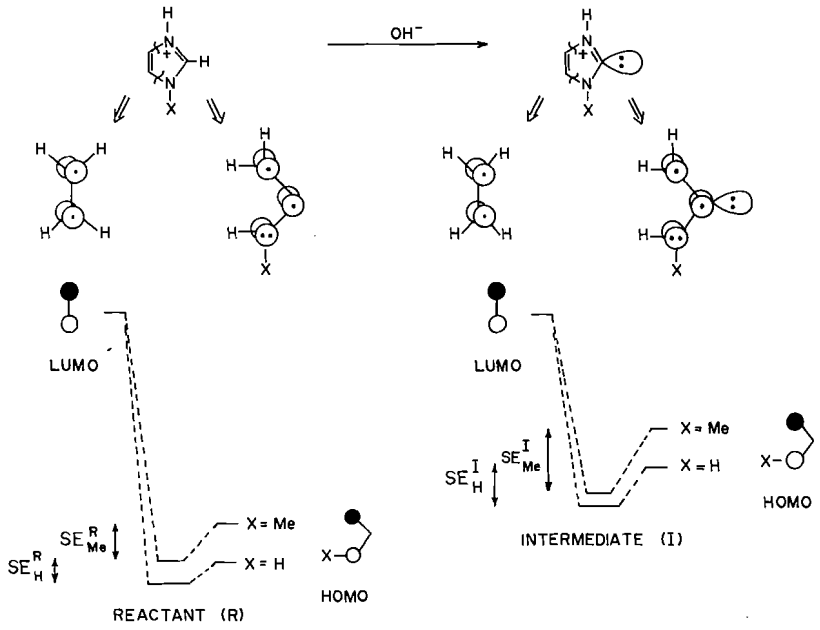

FIG. 3. FMO analysis of the effect of 1-methylation on proton transfer from imidazole.

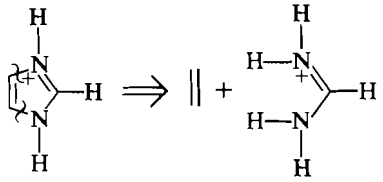

The same procedure is followed for the intermediate structures. This is shown in Fig. 2 with Z corresponding to benzene or ethylene.

The LUMOs of benzene and of ethylene are allowed to interact with the HOMO of the allyl fragment, resulting in molecular orbitals for the benzimidazole and imidazole reacting species, and similarly for the intermediate structures. The relative energies of the LUMOs of ethylene and of benzene can be estimated from the respective electron affinities ($E_{LUMO} = -EA$), which have the values -1.78 and -1.15 eV as determined from electron transmission spectroscopy (16, 17). It follows that greater orbital interaction results between the LUMO of benzene and the HOMO of the allyl fragment, as compared with the corresponding interaction between the ethylene (LUMO) and allyl (HOMO) fragments. The differential stabilization energy for the two reactant species is $\delta SE^R = SE^R_\phi - SE^R_E$, where SE^R_ϕ and SE^R_E are the stabilization energies for the benzene and ethylene cases.

Considering the intermediate structures, the energies of the HOMOs can be taken as corresponding to the ionization potentials (15), i.e. $E_{HOMO} = -IP$. One would expect the energy required to remove an electron from a molecule RH to be much greater than that from the deprotonated species R^-. For example, the first ionization potentials of CH_4 and $CH_3{:}^-$ are 12.99 and 1.08 eV, respectively (18, 19). This would imply that the HOMO of the deprotonated fragment must be significantly higher in energy than that of the parent allyl fragment. The consequent smaller energy gap between the HOMO of the deprotonated allyl fragment and the LUMO of ethylene, or the LUMO of benzene, leads to greater orbital interaction and thus enhanced stabilization in the intermediate structures relative to the reactants. The differential stabilization energy for the two intermediate structures, $\delta SE^I = SE^I_\phi - SE^I_E$, is thus greater than for the reactant species, i.e. $\delta SE^I > \delta SE^R$.

It follows from the above that the transition state for reaction of the benzo annelated reactant will be of lower energy compared to the parent imidazole, thus accounting for the increased reaction rate. A similar analysis can be performed for 1-methylimidazole vs. 1-methylbenzimidazole, which would account for the reactivity difference between these two substrates in an analogous fashion.

2. Effect of methyl substitution

To account for the effect of methylation at N-1 of imidazole and benzimidazole on the rate of C(2)–H exchange, we examine the effect of methyl substitution on the energy of the HOMO of the allyl and the deprotonated allyl fragment. The relative energies of the HOMOs of the allyl and 1-methylallyl fragments is afforded through comparison of the ionization potentials (20) of methylamine (8.97 eV) and dimethylamine (8.24 eV), as well as of methyl (9.95 eV) and ethyl (8.78 eV) radicals (21, 22). Thus the introduction of a methyl group is associated with a decrease in ionization potential, which indicates that the energy of the HOMO for the 1-methylallyl fragment in our system is higher than that for the unsubstituted allyl fragment, in both the reactant and the intermediate.

The FMO analysis for methyl substitution in imidazole is shown in Fig. 3. For the reactants, the orbital interaction is between the ethylene (LUMO) and the allyl (HOMO) fragment for imidazole, as compared with the corresponding interaction between the ethylene (LUMO) and the 1-methylallyl (HOMO) fragments for 1-methylimidazole. The energy of the HOMO for X = Me is greater than for X = H, which results in a greater stabilization energy for the methyl case. The differential stabilization energy for the two reactants is given by $\delta SE^R = SE^R_{Me} - SE^R_H$.

In the intermediate structures, the orbital interactions are now between an ethylene (LUMO) fragment and the deprotonated allyl (HOMO) fragment for imidazole, and between ethylene and deprotonated 1-methylallyl for 1-methylimidazole. The HOMO energies in the intermediates will be significantly higher

than in the reactants, following the argument as applied in Fig. 2. The differential stabilization energy for the intermediates, $\delta SE^I = SE^I_{Me} - SE^I_H$, is hence greater than in the reactants, i.e. $\delta SE^I > \delta SE^R$. The change in structure from X = H to X = Me will hence lead to an intermediate of lower energy. The transition state for the process should thus be stabilized, accounting for the increase in rate on methyl substitution. A similar argument would apply to the case of benzimidazole versus 1-methylbenzimidazole.

Thus FMO analysis provides a satisfactory explanation of relative reactivities in these series of substrates. To our knowledge, this is the first application of FMO theory to reactivity differences in such processes.

Acknowledgements

We thank NATO, NSERC, and SRC for financial support of this research. Discussions with Professor S. Shaik are also warmly acknowledged.

1. G. S. Baldwin, S. G. Waley, and E. P. Abraham. Biochem. J. **179**, 459 (1979).
2. A. E. G. Cass, H. A. O. Hill, J. V. Bannister, and W. H. Bannister. Biochem. J. **183**, 127 (1979).
3. (*a*) J. R. Jones and S. E. Taylor. Chem. Soc. Rev. **10**, 329 (1981); (*b*) E. Buncel, A. R. Norris, W. J. Racz, and S. E. Taylor. J. Chem. Soc. Chem. Commun. 562 (1979); (*c*) E. Buncel, A. R. Norris, W. J. Racz, and S. E. Taylor. Inorg. Chem. **20**, 98 (1981); (*d*) E. Buncel, B. K. Hunter, R. Kumar and A. R. Norris. J. Inorg. Biochem. **20**, 171 (1984); (*e*) E. Buncel, R. Kumar, and A. R. Norris. Can. J. Chem. In press.
4. T. M. Harris and J. C. Randall. Chem. Ind. (London), 1728 (1965).
5. J. L. Wong and J. H. Keck, Jr. J. Org. Chem. **39**, 2398 (1974).
6. J. A. Elvidge, J. R. Jones, C. O'Brien, E. A. Evans, and H. C. Sheppard. J. Chem. Soc. Perkin II, 1889 (1973).
7. J. R. Jones and S. E. Taylor. J. Chem. Soc. Perkin II, 1587 (1979).
8. D. D. Perrin and B. Dempsey. Buffers for pH and metal ion control. Chapman and Hall, London. 1974. pp. 134–150.
9. J. A. Elvidge, J. R. Jones, R. Salih, M. Shandala, and S. E. Taylor. J. Chem. Research. [M] 2373 (1980).
10. J. A. Elvidge, J. R. Jones, C. O'Brien, E. A. Evans, and J. C. Turner. J. Chem. Soc. Perkin II, 432 (1973).
11. H. L. Clever. J. Chem. Educ. **45**, 231 (1968).
12. A. C. M. Paiva, L. Juliano and P. Boschcov. J. Am. Chem. Soc. **98**, 7645 (1976).
13. D. D. Perrin. Austral. J. Chem. **17**, 484 (1964).
14. (*a*) R. B. Woodward and R. Hoffman. The conservation of orbital symmetry. Verlag Chemie, Weinheim. 1970; (*b*) K. Fukui. Acc. Chem. Res. **4**, 57 (1971); (*c*) K. N. Houk. Top. Curr. Chem. **79**, 1 (1979).
15. A. Steitwieser. Molecular orbital theory for organic chemists. Wiley, New York. 1961.
16. K. D. Jordan and P. D. Burrow. Acc. Chem. Res. **11**, 341 (1978).
17. P. D. Burrow, J. A. Michejda, and K. D. Jordan. J. Am. Chem. Soc. **98**, 6392 (1976).
18. K. Watanabe. J. Chem. Phys. **26**, 542 (1957).
19. H. O. Pritchard. Chem. Rev. **52**, 529 (1953).
20. K. Watanabe and J. R. Mottl. J. Chem. Phys. **26**, 1773 (1957).
21. F. P. Lossing, K. U. Ingold, and I. H. S. Henderson. J. Chem. Phys. **22**, 621 (1954).
22. J. B. Farmer and F. P. Lossing. Can. J. Chem. **33**, 861 (1955).
23. E. Buncel and A. W. Zabel. Can. J. Chem. **59**, 3177 (1981).

Surface photochemistry: the photolysis of α-methoxy acetophenones on silica gel[1]

PAUL DE MAYO AND N. RAMNATH
Photochemistry Unit, Department of Chemistry, The University of Western Ontario, London, Ont., Canada N6A 5B7

Received January 22, 1986

PAUL DE MAYO and N. RAMNATH. Can. J. Chem. **64**, 1293 (1986).

The photolysis of α-methoxy acetophenones **1***a*–**1***e* adsorbed on silica gel show a significant deviation from the course of reaction in methanol. The results are discussed in terms of conformational control and restricted movement of the radical through adsorption on silica gel. Factors affecting the efficiency of modification of photochemical reactivity on silica gel surface have been examined.

PAUL DE MAYO et N. RAMNATH. Can. J. Chem. **64**, 1293 (1986).

On a effectué la photolyse des α-méthoxy acétophénones **1***a*–**1***e* adsorbées sur du gel de silice; les résultats obtenus diffèrent grandement de ceux obtenus lorsque la même réaction a été réalisée dans du méthanol. On discute des résultats en fonction du contrôle conformationnel et de la restriction du mouvement des radicaux par adsorbtion sur le gel de silice. On discute des facteurs affectant l'efficacité de la modification de la réactivité photochimique sur une surface de gel de silice.

[Traduit par la revue]

Introduction

Specificity in organic reactions is of considerable interest to the synthetic chemist and any general technique by which the course of a reaction may be modified is worthy of attention. We have examined, with this purpose in mind, the way the fact of adsorption of a molecule on a silica gel surface may alter its photochemistry (1–5).

The silica gel surface is composed of siloxane and silanol functional groups. The silanol groups, which may be isolated, vicinal or geminal, are not uniformly distributed. These groups constitute the principal sites for the adsorption of organic molecules on the silica gel surface (6, 7). Electrostatic interactions (8), dispersion forces (11), and hydrogen bonding (8–10) which result in heats of adsorption of 8–40 kJ/mol are assumed to be the forces responsible for the adsorption. In general, the degree of adsorption is a function of the polarity of the organic molecule as well as the activity of the silica gel (12).

It has been shown earlier that adsorption on silica gel imposes constraints on the movement of both closed-shell molecules (1, 13) and radical pairs (14–18). That such constraints lead to a significant deviation of the course of benzoin methyl ether, **1***d*, when adsorbed on a silica gel surface has also been demonstrated (3). In this paper we describe the Norrish type I and II photochemical reactions of variously substituted α-methoxy acetophenones **1***a*–**1***e*. The choice of the substrates was motivated by the desire to study the generality and degree of conformational control and restricted movement that can be brought about through the use of silica gel.

Results

Silica gel irradiations were carried out by tumbling degassed samples in Pyrex tubes before a 450-W medium pressure mercury lamp. The results from silica gel irradiations were compared with the photochemical behaviour of the corresponding ketones in a hydroxylated solvent, viz. methanol, chosen because its polarity approaches that of silica gel (19, 20). The product distributions are shown in Table 1.

Scheme 1 outlines the possible reaction pathways and products thereof. The ketones react by way of a triplet excited $n\pi^*$ state which leads to a triplet radical pair (Norrish type I) to give type I products **4**–**8** and/or a 1,4-biradical intermediate by virtue of a γ-hydrogen abstraction (Norrish type II) to give products **9** and **10**.

Compounds **1***a* and **1***b* react exclusively via the type II pathway in solution and give the corresponding products **9** and **10**. Irradiation on silica gel does not lead to any significant change in the nature of products other than a marginal decrease in percentage cyclization. On the other hand α-disubstituted ketones **1***c*–**1***e* react primarily via the type I pathway. Irradiation in methanol leads almost exclusively to type I products with a very small percentage of type II products ($< 4\%$) which decreases even further at lower temperatures. Photolysis on silica gel leads to a pronounced change in the course of the reaction.

Irradiation of **1***c* in methanol yields type I products, benzaldehyde and benzil. Other products with very low retention times, presumably derived from the 2-methoxy propyl radical, were also observed. Type II products isobutyrophenone and the oxetanol are formed to the extent of $\sim 1\%$. On silica gel, type II products rise nearly ten-fold at 25°C and to nearly 17% at −50°C.

Irradiation of **1***d* and **1***e* in methanol leads to a number of α-cleavage products with a small percentage of products contributed to by the type II process. The major product in either case is the corresponding pinacol ether (*dl* and *meso*) derived from geminate pair escape and combination. Benzaldehyde and benzyl methyl ethers are formed in varying amounts. Rearrangement of the radical pair gives **8**, **1***d*, and **1***e* although the amount formed in solution is very small for the latter. Photolysis on silica gel leads to a significant difference. The amount of type II reaction increases to approximately 10% and the rearranged radical pair combination products **8***d* and **8***e*, respectively, are formed more efficiently, especially in the latter case.

The mass balance in all the above cases is not entirely satisfactory. Reasons for this have been described in the Experimental section.

Discussion

The results obtained bring out the generality of conformational reactions and constraints imposed on adsorbates/radical intermediates upon adsorption on silica gel, albeit in a limited way.

Based on earlier studies (3) this work was aimed at testing the generality of two main features of the consequences of

[1]Publication No. 360 from the Photochemistry Unit, University of Western Ontario.

TABLE 1. Product distribution of photolysis of **1***a*–**1***e* in MeOH and on silica gel (mol% of product based on starting material consumed)[a]

System	T °C	Type I 4	6	7[d]	8	Type II 9	10	Other products
1*a*: MeOH	25					60	25[b]	
Silica gel	25					55	18	
1*b*: MeOH	25	3	2			16	53	
Silica gel	25	3	3			16	23	
1*c*: MeOH	25	21	6			0.5	0.5	Low glc retention
	−50	20	8			0.3	0.4	time products
Silica gel	25	33	8			6.0	2.5	~25%
	−50	21.2	5			14.2	3.0	
1*d*: MeOH	25[c]	1	15	40	4[e]	1.0	2.0[e]	**5***d*: trace amounts
	−50		20	38	3.6	0.4	0.7	
Silica gel	25		3	35	7.0	9.0	3.0	
	−50		7.2	25.7	38.3	9.8	8.9	
1*e*: MeOH	25	20	4.0	25	0.2	0.2		**5***e*: ~25%
Silica gel	25	25	6.0	20	15.0	6.0		

[a]Estimated by gc with internal standards.
[b]See ref. 22 for nmr chemical shifts.
[c]Interpolated from values obtained at 56°C and 4°C; see ref. 3.
[d]Products identical to those reported in ref. 26.
[e]Synthesized by Akira Nakamura.

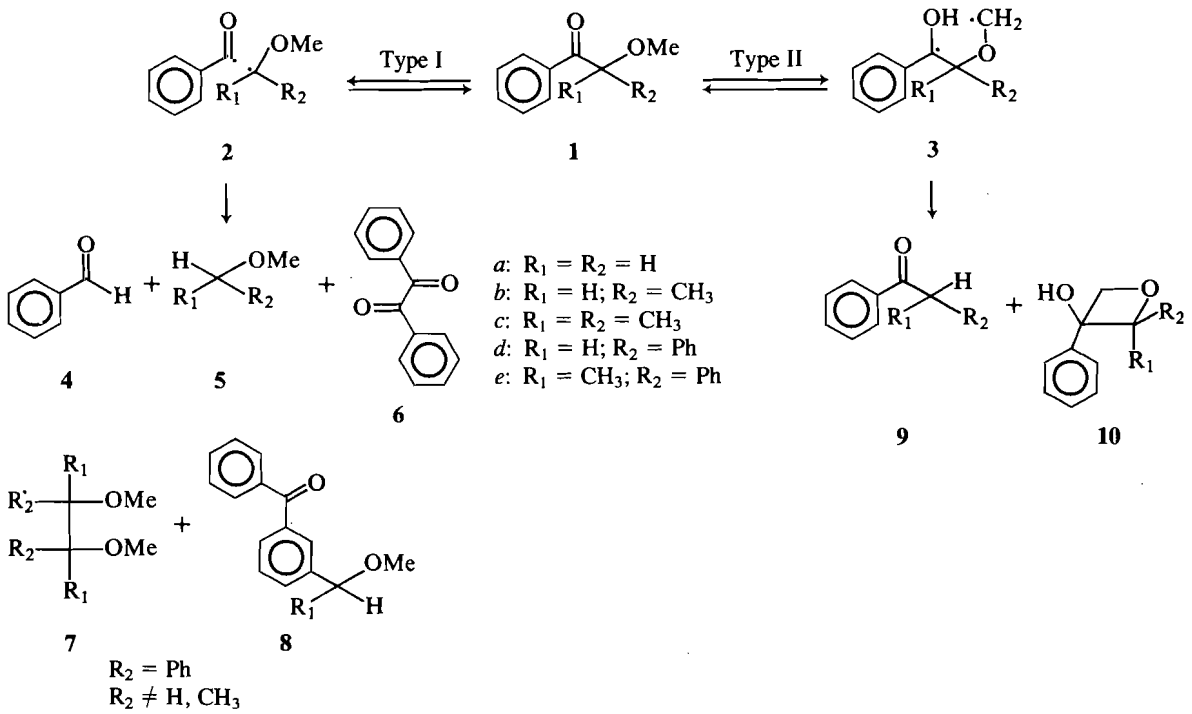

SCHEME I

adsorption on silica gel. (*i*) Restriction of translational movement in radical pairs to permit other forms of recombination. (*ii*) Modification of photochemical reactivity by bringing about a change in conformation through hydrogen bonding forces.

Restriction in translational movement of radical pairs is evident in the reaction of **1***d* and **1***e* with the increased formation of the rearranged product **8***d* and **8***e*, respectively, and a decrease in the formation of the pinacol ethers. In **1***d*, at lower temperatures, the pinacol ethers become minor products while **8***d* is the major rearranged product (3). This has been interpreted as an indication of the suppression of translational motion in the radical pair **2***d*, but not of their rotational motion.

The ketones **1***a*–**1***e* were chosen by virtue of their ability to exist as, at least, two possible conformers. Owing to nonbonded interactions of the electron pairs on the oxygen atoms, the ketones may undergo anomerization (21) in solution so as to

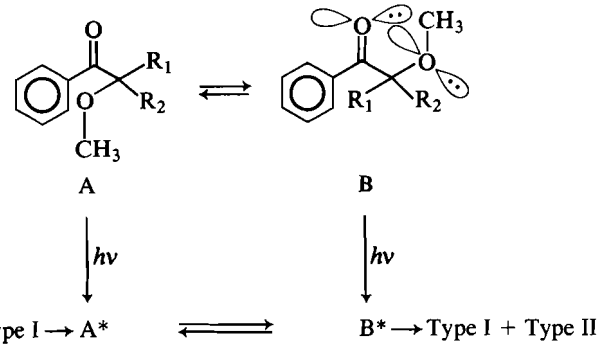

SCHEME 2

exist in the transoid form **A** rather than the cisoid form **B** (Scheme 2).

Lewis and co-workers (22) have examined aspects of conformational control on the photochemical behaviour of α,α-dimethylvalerophenone, α-methyl cyclopentyl- and cyclohexylphenyl ketone. They found that photochemical reactions of cyclohexyl phenyl ketone are more rapid than ring inversion and as a consequence, product compositions are determined by ground state conformational populations (Case I). On the other hand, bond rotations in acyclic ketones are more rapid than photochemical reactions, in which case product compositions are determined by relative rates of the competitive photoprocesses rather than conformational populations (Case II). In the present investigation, adsorption of ketones **1***a*–**1***e* on silica gel could shift the equilibrium in favor of **B** (Scheme 2) owing to hydrogen bonding to the oxygen atoms and the phenyl groups. In such a case an increase in type II products would be expected. The extent of deviation of the course of reaction may depend on whether Case I or Case II operates on the adsorbed ketones.

Results show an encouraging increase in type II products on silica gel in the case of compounds **1***c*–**1***e*. However, type I α-cleavage reactions continue to be more efficient than the type II reactions for these compounds. This indicates that, conformational changes notwithstanding, product compositions are still determined by relative rates of the competitive α-cleavage and γ-hydrogen abstraction processes (Case II) as in solution. Compounds **1***a* and **1***b* react almost exclusively via the type II pathway whereas **1***c*–**1***e* undergo efficient α-cleavage. The rate of α-cleavage is related to the stability of the radicals produced. For different molecules of similar structure, the more stable the radical pair produced by α-cleavage, the faster is the absolute rate constant for reaction (23). Since stability of radicals increases with substitution, the rates for α-cleavage increase with increasing α-substituents. Thus, in solution, the rate constants for α-cleavage should increase from **1***a*–**1***e* with a net decrease in type II reaction. Rate constants for type II reactions of **1***a* and **1***b* are in the order of $10^9\ s^{-1}$ (24). Exclusive type II reaction in these cases has been attributed to the absence of α-methylphenyl eclipsing interactions which permits a favorable conformation for γ-hydrogen abstraction (25). Similarly, it has been observed in the case of *exo*-2-benzoyl-2-norbornane and *exo*-2-benzoyl-2-methylnorbornane that the former undergoes γ-hydrogen abstraction to undergo photoelimination while the latter undergoes efficient α-cleavage (26). This has also been attributed to the presence of eclipsing 1,2-methylphenyl interactions that retard γ-hydrogen abstraction. Thus radical stability as well as 1,2-eclipsing interactions may influence competitive α-cleavage and γ-hydrogen abstractions in solution.

1*d* and **1***e* undergo very efficient α-cleavage. Lewis *et al.* (24) have found that α-cleavage of **1***d* is a rapid process with a rate constant $\sim 10^{10}\ s^{-1}$. Type II reactions for these ketones have not been observed in solution before and were not expected to compete with the α-cleavage of benzoin ethers (24). However, we have observed type II products in solution to the extent of ~4% thus suggesting that rates of type II reaction must be smaller than that of **1***a* ($\sim 10^9\ s^{-1}$). The increase in type II products of **1***c*–**1***e* on silica gel indicates the influence exerted on the competitive α-cleavage and γ-hydrogen abstraction as a consequence of adsorption on silica gel.

Reasons for this change could be partly attributable to a change in the conformation of the ketone to one more favorable for γ-hydrogen abstraction and/or greater stabilization of the 1,4-biradical on silica gel as compared to conditions in solution. The increase in type II products could thus be due to an increase in the efficiency of type II product formation. Conversely, increased formation of type II products may occur because of a decrease in the efficiency of α-cleavage product formation. This decrease could arise because of the restrictions imposed on the translational motion of radicals on silica gel leading to more efficient cage recombination of the radicals resulting from α-cleavage. This increase in cage recombination is shown by the increasing amounts of the rearranged product **8**. This process will not affect the efficiency of α-cleavage or the rate of α-cleavage but merely decreases the efficiency of formation of geminate pair escape products, thus increasing the probability for type II reaction. In the absence of any kinetic parameters and quantum yields of these processes on silica gel (because of the experimental problems involved in devising methods for such measurements under the conditions involved), it is not possible to distinguish clearly between the factors that affect the reactivity of these ketones. For these reasons, this phenomena remains far from predictable. Turro *et al.* (27) have recently described the elegant use of diffuse reflectance laser flash photolysis to measure the lifetimes of some aryl alkyl ketones adsorbed on silica gel. These measurements reveal an increase in the lifetimes of these ketone triplets and has been attributed to restrictions in the accessibility of the conformations required for intramolecular hydrogen abstraction as a result of binding to the silica gel surface. Such measurements for the ketones described in this paper may shed valuable information on the phenomena described here.

Experimental

Silica gel (Merck 60, 35–70 mesh) was used for all experiments. Baker analyzed spectrograde solvents were used. Infrared spectra were recorded on a Beckman IR 4250 and proton nmr spectra were recorded on a Varian XL-200 (MHz) spectrophotometer. Gas chromatography was carried out on Varian 3700 (2 m × 2 mm glass column packed with 3% OV-101 on 80/100 mesh Chromosorb W-HP) fitted with flame ionization detectors and using a Hewlett-Packard 5890 A integrator. Irradiations were carried out with a 450-W medium pressure mercury lamp housed in a Pyrex sleeve.

Preparation of ketones

Compound **1***a* was obtained commercially (Aldrich, 95%) and purified to ~99% purity by fractional distillation. Compounds **1***b* (28) and **1***c* (29) were prepared by the reaction of 2-methoxypropionitrile (28) and 2-methoxyisobutyronitrile (30), respectively, with phenylmagnesium bromide. Compounds **1***d* and **1***e* were prepared by the method of Fisher (31) and Heine (32), respectively. All ketones were purified by column chromatography on silica gel and (or) vacuum distillation prior to use. **1***d* was purified by recrystallization from benzene–ether. All the synthesized compounds had ir, nmr, and uv spectra consistent with the assigned structures.

Irradiations

Photolysis in solution: 0.05 *M* methanolic solutions of the ketones were purged with nitrogen and irradiated to 20–35% conversion of the starting material. Larger conversions did not affect the product ratios significantly. The products of the reaction were estimated by gas chromatography using the appropriate internal standards (C_{11}–C_{16} *n*-alkanes).

Photolysis of silica gel samples: Silica gel samples containing, typically, 20 mg per g of silica gel (5–10% coverage) and were prepared as described in earlier reports (1, 4) in Pyrex cylinders. The cylinders were rotated horizonally on their long axis during irradiations. Conversions were held at 20–35%. After completion of irradiation the products were extracted with 5% methanol in chloroform and estimated by gas chromatography as before.

Identification of products

The identity of all compounds other than **10***a*–**10***e* was confirmed by coinjection with authentic samples that were either obtained commercially (**4**, **6**, **5***d*, and **9***a*–**9***c*) or synthesized (**5***e*, **8***d*, **9***d*, **9***e*, and **10***d*) or isolated from the reaction mixture (**7***d*, **7***e*, **8***e*, and **10***a*). The oxetanols were formed in very small yields and were tentatively identified by comparing the glc retention time patterns with those of the isolated **10***a* and synthesized **10***d*, respectively. Although this may lead to a degree of error, it is not likely to affect the conclusions darwn by virtue of their low yields.

Material balance

As mentioned earlier, the mass balances are not entirely satisfactory. Undetected low molecular weight compounds resulting from α-cleavage and subsequent radical termination reactions, combination or cleavage reactions to form low boiling ethers, alkanes, and alkenes could be a major reason. Although formation of other compounds could be detected by low temperature glc, their estimation and identification proved to be inconsistent and cumbersome and were therefore not attempted.

1. R. K. Bauer, R. Borenstein, P. de Mayo, K. Okada, M. Rafalska, W. R. Ware, and K. C. Wu. J. Am. Chem. Soc. **104**, 4635 (1982).
2. P. de Mayo. Pure Appl. Chem. **54**, 1623 (1982).
3. P. de Mayo, A. Nakamura, P. W. K. Tsang, and S. K. Wong. J. Am. Chem. Soc. **104**, 6824 (1982).
4. M. M. Abdel-Malik and P. de Mayo. Can. J. Chem. **62**, 1275 (1985).
5. V. Dave, R. Farwaha, P. de Mayo, and J. B. Stothers. Can. J. Chem. **63**, 2401 (1985).
6. H. P. Boehm. Adv. Cat. **16**, 179 (1966).
7. R. K. Iler. The chemistry of silica. Wiley-Interscience, New York. 1979. Chapt. 6.
8. L. R. Snyder. J. Phys. Chem. **67**, 2622 (1963).
9. A. V. Kisielev. Structure and properties of porous materials. Academic Press, New York. 1958.
10. A. V. Kisielev and V. I. Lygnin. Infrared spectra of surface compounds. Keterpress enterprises, Jerusalem. 1975.
11. C. H. Nichols and P. A. Lermakers. Adv. Photochem. **8**, 315 (1971).
12. D. Oelkrug, M. Radjaipour, and H. Erbse. Z. Phys. Chem. 23 (1974).
13. P. de Mayo, K. Okada, M. Rafalska, A. C. Weedon, and G. S. K. Wong. J. Chem. Soc. Chem. Commun. 820 (1981).
14. D. Avnir, P. de Mayo, and I. Ono. J. Chem. Soc. Chem. Commun. 1109 (1978).
15. D. Avnir, L. J. Johnston, P. de Mayo, and S. K. Wong. J. Chem. Soc. Chem. Commun. 958 (1981).
16. B. Frederick, L. J. Johnston, P. de Mayo, and S. K. Wong. Can. J. Chem. **62**, 403 (1984).
17. J. E. Leffler and J. E. Zupancic. J. Am. Chem. Soc. **102**, 259 (1980).
18. J. E. Leffler and J. T. Barbas. J. Am. Chem. Soc. **103**, 7768 (1981).
19. P. A. Leermakers, H. T. Thomas, L. D. Weiss, and F. C. James. J. Am. Chem. Soc. **88**, 5085 (1966).
20. P. de Mayo, A. Safarzadeh-Amiri, and S. K. Wong. Can. J. Chem. **62**, 1001 (1984).
21. V. M. Gittins, E. Wyn-Jones, and R. F. M. White. Internal rotations in organic molecules. *Edited by* P. de Mayo. Wiley-Interscience, New York. 1974. p. 448.
22. F. D. Lewis, R. W. Johnson, and D. E. Johnson. J. Am. Chem. Soc. **96**, 6090 (1974).
23. N. J. Turro. Modern molecular photochemistry. Benjamin/Cummings, California. 1978. Chapt. 13.
24. F. D. Lewis and N. J. Turro. J. Am. Chem. Soc. **92**, 311 (1970).
25. F. D. Lewis, R. W. Johnson, and D. E. Johnson. J. Am. Chem. Soc. **94**, 4292 (1972).
26. F. D. Lewis, R. T. Lauterebach, H.-G. Heine, W. Hartman, and H. Rudolph. J. Am. Chem. Soc. **97**, 1519 (1975).
27. N. J. Turro, I. R. Gould, M. B. Zimmt, and C.-C. Cheng. Chem. Phys. Lett. **119**, 484 (1985).
28. C. L. Stevens, W. Malik, and R. Pratti. J. Am. Chem. Soc. **72**, 4758 (1950).
29. H. O. House, A. V. Prabhu, J. M. Wilkins, and L. F. Lee. J. Org. Chem. **41**, 3067 (1976).
30. R. A. Navolokina and E. N. Zil'berman. J. Org. Chem. USSR. **16**, 1382 (1980).
31. E. Fischer. Ber. **26**, 2412 (1893).
32. H.-G. Heine. Justus Liebigs Ann. Chem. **735**, 56 (1970).

Kinetics of ionisation of carbon acids in non-aqueous media: detritiation of [2-$^3H_1$]diethyl malonate by heterocyclic bases[1]

JOHN P. DAVEY AND JOHN R. JONES
Department of Chemistry, University of Surrey, Guildford GU2 5XH, U.K.
AND
ERWIN BUNCEL
Department of Chemistry, Queen's University, Kingston, Ont., Canada K7L 3N6
Received October 31, 1985
This paper is dedicated to Professor Arthur N. Bourns

J. P. DAVEY, J. R. JONES, and E. BUNCEL. Can. J. Chem. **64**, 1246 (1986).

To investigate proton transfer processes in non-aqueous media, two procedures have been developed of general applicability for the measurement of detritiation rates of carbon acids. One method is a variation of an existing solvent extraction procedure but with inclusion of a trace of trifluoroacetic acid, while the other involves the simple modification of a gas chromatograph so as to function as a radio-gas chromatograph. They have been established by studying the detritiation of [2-$^3H_1$]diethyl malonate in six different solvents (dimethylformamide, dimethyl sulfoxide, sulfolane, hexamethylphosphortriamide, tetrahydrofuran, ethanol) as catalyzed by various heterocyclic bases (substituted pyridines, imidazoles, benzimidazoles, pyrrole, pyrazole, purine, adenosine). The results are discussed in terms of solvation effects and catalyst structure. An approximate Brønsted correlation is found to exist between log k_B^T for detritiation determined in DMSO and the pK_a of the conjugate base measured in water at 25°C.

J. P. DAVEY, J. R. JONES et E. BUNCEL. Can. J. Chem. **64**, 1246 (1986).

Dans le but d'étudier les processus de transferts protoniques dans des milieux non-aqueux, on a développer deux méthodes d'application générale pour mesurer les vitesses de détritiation d'acides carboniques. Une des méthodes est une variation d'une procédure existante d'extraction par les solvants impliquant l'inclusion d'une trace d'acide trifluoroacétique; par ailleurs, l'autre implique une modification simple d'un chromatographe en phase gazeuse de façon à le faire fonctionner comme une chromatographe en phase gazeuse radio. On a établi la validité de ces méthodes en étudiant la réaction de détritiation du malonate de diéthyle [$^3H_1$-2] qui a été effectuée dans six solvants différents (diméthylformamide, diméthylsulfoxyde, sulfolane, hexaméthylphosphoretriamide, tétrahydrofuranne et éthanol) et catalysée par diverses bases hétérocycliques (pyridines substituées, imidazoles, benzimidazoles, pyrrole, pyrazole, purine, adénosine). On discute des résultats en fonction d'effets de solvatation et de structure du catalyseur. On a trouvé qu'il existe un corrélation approximative de Brønsted entre le log k_B^T pour la réaction de détritiation effectuée dans le DMSO et le pK_a de la base conjugée, mesuré dans l'eau, à 25°C.
[Traduit par la revue]

Proton transfer from one atom to another is a fundamental process in chemistry, present in the elementary steps of many reactions (1). In acid, base and enzyme catalyzed reactions, proton transfer between catalyst and substrate is often a key step in the mechanism (2, 3). In many organic reactions in particular, proton transfer from carbon plays a central role and has led to an appreciation of the factors governing the kinetic and thermodynamic properties of carbon acids (4, 5). However, despite an awareness of the importance of the solvent in proton transfer reactions (6) this is a relatively unexplored area. This may be due in part to the fact that the most widely used method of measuring the rates of such reactions, namely halogenation, cannot be readily adapted to non-aqueous conditions.

Hydrogen isotope exchange is particularly suited for studying proton transfer from carbon acids under a variety of conditions, for example as catalyzed by acids, bases and metal ions (7–12), but in the past such investigations have also been largely limited to aqueous media. In this paper we report on the development of two procedures which have general applicability for measurement of detritiation rates of carbon acids in non-aqueous media.

The first method is a variation of an existing extraction procedure with the difference that the exchange is carried out in the presence of a trace amount (0.01% v/v) of trifluoroacetic acid. This addend serves as a source of exchangeable protium in the system (*vide infra*), but does not alter the properties of the solvent to a measurable degree.

[1]Hydrogen exchange studies, Part 16: for Part 15, see ref. 12.

The second procedure takes advantage of the fact that commercial gas chromatographs usually have two flame ionisation detectors, a variable post-column splitter and dual pen recorder, and by attaching a second electrometer capable of measuring currents down to 10^{-12}–10^{-14} A, it is possible to use the second ionisation chamber as a radiation detector (13). Such a simple modification converts the instrument to a radio-gas chromatograph with good sample throughput, ideal for measuring the decrease in the tritium radioactivity of a labelled carbon acid. This method is particularly useful when no satisfactory solvent extraction procedure is available.

Both procedures have been established through investigating the detritiation of [2-$^3H_1$]diethyl malonate, which was previously studied only in aqueous media. In the present study, six different solvents have been employed, namely dimethylformamide (DMF), dimethyl sulfoxide (DMSO), sulfolane, hexamethylphosphortriamide (HMPT), tetrahydrofuran (THF), and ethanol. The catalysts used are heterocyclic nitrogen bases, namely substituted pyridines, imidazoles, benzimidazoles, pyrrole, pyrazole, purines, and adenosine. Because a solvent extraction procedure could be established for all the different solvent systems, the large majority of the experimental results were obtained using the first procedure.

Experimental

Materials

Stringent precautions were employed to ensure high solvent purity and the elimination of water from the experimental systems. Sulfolane

Printed in Canada / Imprimé au Canada

was purified by heating the solvent (2 L) to 210°C in the presence of polyethylene sulfone (20 g) and anhydrous potassium fluoride (10 g); the mixture was then stirred for 24 h under a constant stream of dry nitrogen so as to remove any volatile impurities prior to distillation under reduced pressure. Dimethyl sulfoxide was partially frozen, the remaining liquid decanted off, and the solvent distilled under reduced pressure before storing over Linde type 4A molecular sieve. Dimethylformamide was stored in a similar manner prior to distillation under reduced pressure. Tetrahydrofuran was refluxed over lithium aluminum hydride prior to distillation and storing over calcium hydride. Ethanol was refluxed in the presence of magnesium turnings and iodine for 3 h before the fraction that distilled at 78.4°C/760 mm was collected.

All the organic bases used, with the exception of 6-aminobenzimidazole, were obtained commercially and their purity checked prior to use; this compound was prepared by the catalytic hydrogenation of 6-nitrobenzimidazole using a 5% Pd/C catalyst in methanol.

Tritiation procedure

Diethyl malonate was tritiated by adding freshly distilled material (1 mL) to a small ampoule containing sodium carbonate (0.3 g) and dioxane (0.5 mL); after adding tritiated water (5 μL, 50 Ci mL^{-1}) the ampoule was sealed and left at room temperature for 72 h. The tritiated substrate was isolated by extraction into chloroform (10 mL), which was washed with water (10 mL) and dried over anhydrous Na_2SO_4. After removing the solvent by carefully passing N_2, the tritiated product was taken up in a small volume (100 μL) of $CDCl_3$, a trace of internal standard (TMS) was added and the sample subjected to both ^1H and ^3H nmr analysis.

Kinetic measurements

Method 1

To a known volume (usually 50 mL) of the base solution thermostatted in a constant temperature bath at 50.0°C was added 5 μL of trifluoroacetic acid followed by 10 μL of a stock solution of the labelled diethyl malonate. At given time intervals, aliquots (2 mL) of the solution were withdrawn and injected into tubes containing 10 mL of 0.1 *M* hydrochloric acid and 10 mL of liquid scintillator (3.4 gL^{-1} of 2,5-diphenyl oxazole in toluene). After shaking, most of the toluene layer was extracted and dried over anhydrous Na_2SO_4 before counting 5 mL samples on a Beckman LS 100 scintillation counter. Normally the reaction was followed to more than 90% completion. The rate constants k^T obtained from the plots of $\log_{10}$ (radioactivity) against time (slope = $-2.303k^T$) agreed to within ± 2–3%; dividing k^T by the base concentration (usually in the range 10^{-1}–10^{-3} *M*) gave the second-order rate constant (k_B^T).

In the case of hexamethylphosphortriamide at 50°C there was evidence of catalysis by the solvent. For this reason the results reported for this solvent are limited to 25.0°C.

Method 2

For the radio-gas chromatography procedure (13) the main differences were that the radioactivity of the diethyl malonate was some 10–100 times higher and that the volume of reaction mixture was some ten times smaller than in the solvent extraction method. As mentioned previously the advantage of the method is that it is no longer dependent on our ability of achieving a satisfactory extraction procedure; it is only required to quench the reaction (using 0.1 *M* HCl), inject a sample into the radio-gas chromatograph, and integrate the diethyl malonate radioactivity signal. In the present investigation a 10% OV17 on chromosorb 80–100 mesh column at an oven temperature of 145°C was employed.

In both methods 1 and 2 the base concentration was varied at least ten-fold. In the case of imidazole catalysis where both methods were used the k_B^T values were 0.0224 ± 0.0005 for the solvent extraction procedure and 0.0220 ± 0.001 for the radio-gas chromatographic method.

Results and discussion

Investigation of proton transfer processes in non-aqueous media, while offering insight on solvation effects, also brings into focus the nature of the base to be used for proton abstraction. There is clearly less emphasis on the use of the lyate ion of the solvent compared with hydroxylic media, although work by Bordwell (14, 15), Ritchie (16), and Streitwieser (17, 18) in particular, has shown that the use of the methylsulfinyl anion and the cyclohexylamide anion in dimethyl sulfoxide and cyclohexylamine, respectively, has given forth a wealth of information on kinetic and thermodynamic acidities of carbon acids. However, it appears much less probable that comparable investigations would be undertaken in solvents such as DMF, HMPT, or THF with their lyate ion counterparts. One is hence led to investigate the efficacy of all types of bases when studying proton transfer in non-aqueous media. The goals of such studies will be to determine kinetic and thermodynamic acidities of carbon acids in different media, and to obtain information on inherent properties of the bases, unmasked by solvent effects, thus to improve the understanding of solvent effects on proton transfer processes.

In this first study, we have chosen to investigate the catalytic properties of a range of heterocyclic nitrogen bases, in various solvents, for the abstraction of the acidic proton from diethyl malonate.

The heterocyclic bases were chosen partly as a result of a parallel interest in the kinetic acidities of the C-2(H) proton in compounds such as the imidazoles and benzimidazoles (12, 19) and the equivalent C-8(H) position in purines, and partly because of the opportunity they afforded of investigating structural factors not frequently made available in this kind of study. Thus imidazole, benzimidazole, purine, and pyrrole are all examples of π-excessive N-heteroatoms where the nitrogen is in an electron releasing environment (=CH—NH—CH=). In pyrrole, however, the nitrogen atom contributes its lone pair of electrons to the π-system, completing an aromatic sextet, and

TABLE 1. Rates of detritiation of [2-$^3H_1$]diethyl malonate in dimethyl sulfoxide at 50°C by heterocyclic bases

Base	pK_a (H_2O, 25°C)	Ref.	$10^4k_B^T$ (M^{-1} s^{-1})
1. Imidazole	7.18	20	224
2. 1-Me imidazole			119
3. 2-Me imidazole	8.13	21	1680
4. 1,2-diMe imidazole			1140
5. 2-Et, 4-Me imidazole	8.57[a]	21	4390
6. 1-Benzyl, 2-Me imidazole			495
7. 2,4,5-Triphenyl imidazole			0.36
8. 4-NO_2 imidazole			No detritiation
9. Benzimidazole	5.53	22	22.3
10. 2-Me benzimidazole			130
11. 2-Phenyl benzimidazole			3.7
12. 2-NH_2 benzimidazole			1470
13. 6-NH_2 benzimidazole			158
14. 6-NO_2 benzimidazole			0.37
15. Pyridine	5.47	23	2.14
16. 2-Me pyridine	6.07	24	6.80
17. 3-Me pyridine	5.80	24	3.54
18. 4-Me pyridine	6.10	24	7.48
19. 4-Benzyl pyridine			3.74
20. 2-Acetyl pyridine			No detritiation
21. Adenine	4.20	25	13.8
22. Adenosine	3.50	25	2.88
23. Pyrazole	2.57	26	0.037
24. Pyrrole			No detritiation
25. Purine	2.60	27	No detritiation

[a]Refers to the structurally similar 2,4-dimethylimidazole.

thus rendering the substance only very weakly basic. The pyridines, on the other hand, are examples of π-deficient heterocycles; here nitrogen has dual character, attracting π-electron density from the ring while making available an unshared electron pair towards a proton.

The results on the detritiation of [2-$^3H_1$]diethyl malonate in DMSO are given in Table 1. Analysis of these results reveals the following trend in kinetic basicities: imidazole > benzimidazole > pyridine > pyrazole > pyrrole, purine. However, within each group there are considerable rate variations. Thus in imidazole itself methyl substitution can lead to both rate retardation and rate acceleration, an observation that can be accounted for in the following way. In dimethyl sulfoxide the protonated base formed will be highly solvated and the insertion of electron donating groups X and Y at C-2 and C-4 will stabilise the charge to some degree via the resonance contributions **1***b* and **1***c*:

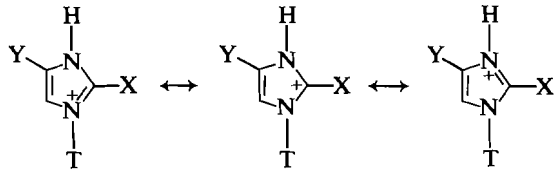

1*a* **1***b* **1***c*

This would lower the transition state energy for proton abstraction, leading to an increase in reaction rate. On the other hand, bases containing an —N—H group will be highly coordinated to the sulfoxide oxygen, so that N-alkylation will remove this mode of stabilisation, leading to a rate reduction even though the substituent may be electron donating. This would explain why the rate for 1-methylimidazole is lower than that for the parent compound, opposite to what is expected on the basis of pK_a data in water. It would also explain the less than expected rate enhancement for 1,2-dimethylimidazole as well as for 1-benzyl-2-methylimidazole compared with 2-methylimidazole. Steric hindrance in approach of the base (F-strain) is probably the main factor causing the slow rate for 2,4,5-triphenylimidazole.

Introduction of an amino group in both benzimidazole and purine has an accelerating effect, possibly because the amino group is itself able to act as the base in proton abstraction. An alternative possibility[2] is that of a guanidine-like structure whose high basicity is the result of a stabilized conjugate acid, i.e.,

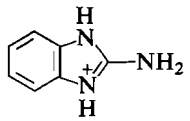

2

No detritiation of the substrate was observed with the π-excessive bases pyrrole and purine, and to this list can be added indole, thymidine, and uridine.

It is interesting that an approximate Brønsted correlation exists between log k_B^T and pK_a (H_2O, 25°C) for the twelve bases for which pK_a data are available, despite the fact that k_B^T refers to DMSO and K_a to the aqueous state. The graph (Fig. 1) covers some 5 pK_a units and only the points for adenine and adenosine deviate significantly. This suggests that any solvation

[2]The authors thank a referee for this suggestion.

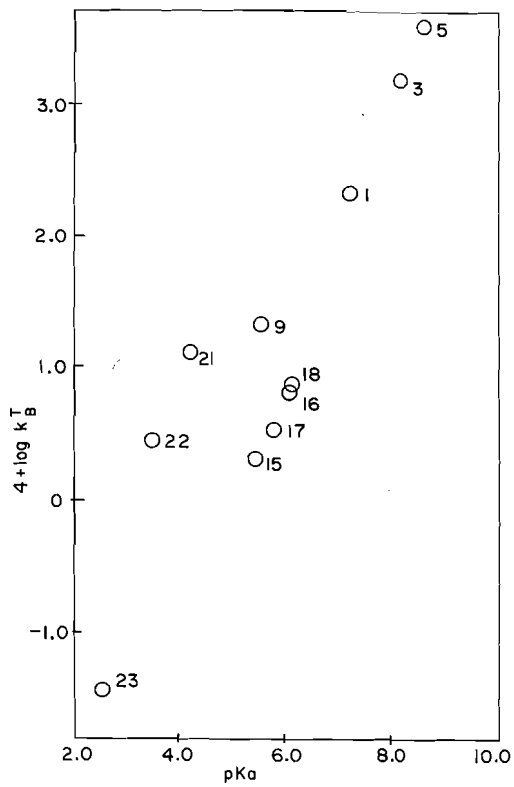

FIG. 1. Brønsted plot for detritiation of [2-$^3H_1$]diethyl malonate by heterocyclic bases: k_B^T values in DMSO at 50°C, K_a values in H_2O at 25°C (Table 1).

type arguments will hold for both media. More importantly, the observation of a Brønsted correlation is in accordance with the proposal that proton transfer is the rate-determining step.

Results on the variation of solvent in detritiation of diethyl malonate using the four imidazole-type bases are given in Table 2. It is seen that the rates vary within relatively narrow limits on solvent change, though the highest rate is generally observed in DMSO. Also noticeable is the regular trend observed for each catalyst, with the possible exception of 1-methylimidazole in tetrahydrofuran, the solvent with the lowest dielectric constant. In this case the possibility of some kind of association causing the unusually low rate cannot be ruled out.

The detritiation of diethyl malonate by the heterocyclic bases represents a reaction between two neutral molecules and hence differential effects of solvents would be expected to be at a minimum, as is borne out in the present investigation. Nevertheless it is somewhat surprising that the vastly different properties of some of the solvents, such as dimethyl sulfoxide, tetrahydrofuran, and ethanol, is not reflected in a wider range of rates.

The reaction mechanism followed in this hydrogen isotope exchange must differ from what operates in hydroxylic media leading to regeneration of base and unlabelled carbon acid, since solvents such as THF contain no exchangeable hydrogen. Radio-gas chromatographic analysis of a reaction mixture showed that the only radioactive peak present not arising from the diethyl malonate originated from the trifluoroacetic acid. Consequently we favour the following scheme in which the trifluoroacetic acid acts as the proton donor towards the carbanion formed on triton abstraction, generating unlabelled carbon acid and the neutral base via the equilibria in reactions [2] and [3]:

TABLE 2. Rate data for detritiation of [2-$^3H_1$]diethyl malonate with imidazole-type catalysts in various solvents at 50.0°C[a]

Base	Solvent					
	DMSO	DMF	Sulfolane	HMPT[b]	THF	EtOH
Imidazole	(224)[a]	(132)[a]	(89.8)[a]	(48.1)[a]	(108)[a]	(145)[a]
	1.00	1.00	1.00	1.00	1.00	1.00
1-Me imidazole	0.53	0.40	0.18	0.20	.057	0.46
2-Me imidazole	7.5	6.68	7.10	8.11	7.43	4.50
2-Et, 4-Me imidazole	19.6	15.0	13.4	15.8	8.44	8.14

[a]The data given in parentheses are the actual $10^4 k_B^T$ values (M^{-1} s^{-1}) for imidazole catalysis at 50°C (25°C for HMPT). The remaining data are the relative rate constants with respect to imidazole as the reference standard.
[b]At 25.0°C, the extrapolated rate constant for imidazole catalysis at 50°C being 164×10^{-4} M^{-1} s^{-1}.

[1] $RT + B \rightarrow R^- + BT^+$

[2] $R^- + CF_3COOH \rightleftharpoons RH + CF_3COO^-$

[3] $CF_3COO^- + BT^+ \rightleftharpoons CF_3COOT + B$

It is emphasized that the addition of only a trace quantity of trifluoroacetic acid (0.01% v/v) is required, since the substrate is present in extremely small concentration and the properties of the solvent medium are thereby unchanged. The kinetic data thus provide a valid measure of the solvent effect on the proton transfer (10, 13).

Acknowledgements

We are grateful to NATO, NSERC, and SRC for funding of this study.

1. R. P. BELL. The proton in chemistry. 2nd ed. Chapman and Hall, London. 1973.
2. W. P. JENCKS. Catalysis in chemistry and enzymology. McGraw Hill, New York. 1969.
3. M. L. BENDER. Mechanisms of homogenous catalysis from protons to proteins. Wiley, New York. 1971.
4. J. R. JONES. The ionization of carbon acids. Academic Press, London 1973.
5. E. BUNCEL. Carbanions. Mechanistic and isotopic aspects. Elsevier, Amsterdam 1975.
6. W. J. ALBERY. Ann. Rev. Phys. Chem. **31**, 227 (1980).
7. A. F. THOMAS. Deuterium labelling in organic chemistry. Appleton–Century–Crofts, New York. 1971.
8. E. A. EVANS. Tritium and its compounds. 2nd ed. Butterworths, London. 1974.
9. M. A. LONG and J. R. JONES. J. Chromatogr. **287**, 381 (1984).
10. E. BUNCEL and H. WILSON. Adv. Phys. Org. Chem. **14**, 133 (1977).
11. (*a*) E. BUNCEL and W. A. ZABEL. Can. J. Chem. **59**, 3177 (1981); (*b*) E. BUNCEL and E. A. SYMONS. J. Am. Chem. Soc. **98**, 656 (1976); (*c*) E. BUNCEL, J. A. ELVIDGE, J. R. JONES, and K. T. WALKIN. J. Chem. Res. (S). **272** (1980).
12. E. BUNCEL, H. A. JOLY, and J. R. JONES. Can. J. Chem. **64**, 1240 (1986).
13. J. R. JONES. Q. Rev. Chem. Soc. **25**, 365 (1971).
14. W. S. MATTHEWS, J. E. BARES, J. E. BARTMESS, F. G. BORDWELL, F. J. CORNFORTH, G. E. DRUCKER, Z. MARGOLIN, R. J. MCCALLUM, G. J. MCCOLLUM, and N. R. VANIER. J. Am. Chem. Soc. **97**, 7006 (1975).
15. F. G. BORDWELL, R. J. MCCALLUM, and W. N. OLMSTEAD. J. Org. Chem. **49**, 1424 (1984).
16. C. D. RITCHIE and R. E. USCHOLD. J. Am. Chem. Soc. **90**, 3415 (1968).
17. A. STREITWIESER, JR., E. JUARISTI, and L. L. NEBENZAHL. *In* Comprehensive carbanion chemistry. Vol. 1. *Edited by* E. Buncel and T. Durst. Elsevier, Amsterdam. 1980.
18. A. STREITWIESER, JR., D. A. BORS, and M. J. KAUFMAN. J. Chem. Soc. Chem. Commun. 1394 (1983).
19. J. R. JONES and S. E. TAYLOR. Chem. Soc. Rev. **10**, 329 (1981).
20. H. REINERT and R. WEISS. Z. Physiol. Chem. **350**, 1310 (1969).
21. S. NAKATSUJI, R. NAKAJIMA, and T. HARA. Bull. Chem. Soc. Jpn. **42**, 3598 (1969).
22. J. A. ELVIDGE, J. R. JONES, C. O'BRIEN, E. A. EVANS, and J. C. TURNER. J. Chem. Soc. Perkin II, 432 (1973).
23. G. FARAGLIA, F. J. C. ROSSOTTI, and H. S. ROSSOTTI. Inorg. Chim. Acta, **4**, 488 (1970).
24. YA. I. TUR'YAN, M. I. PERSHAKOVA, and O. E. RUVINSKII. Zhur. Obshchev Khim. **42**, 1198 (1972).
25. J. J. CHRISTENSEN, J. H. RYTTING, and R. M. IZATT. Biochemistry, **9**, 4907 (1970).
26. T. R. MUSGRAVE and E. R. HUMBURG, JR. J. Inorg. Nucl. Chem. **32**, 2229 (1970).
27. T. M. MARSHALL and E. GRUNWALD. J. Am. Chem. Soc. **91**, 4541 (1969).

Controlled oxidations of benzo[*a*]pyrene

E. LEE-RUFF,[1] H. KAZARIANS-MOGHADDAM, AND M. KATZ
Department of Chemistry, York University, 4700 Keele Street, North York, Ont., Canada M3J 1P3

Received July 19, 1985[2]

E. LEE-RUFF, H. KAZARIANS-MOGHADDAM, and M. KATZ. Can. J. Chem. **64**, 1297 (1986).

The four diones derived from benzo[*a*]pyrene oxidation have been characterized by high-field nuclear magnetic resonance techniques including 2-D COSY and selective nuclear Overhauser enhancement. All the proton chemical shifts for these four quinones have been uneqivocally assigned. The direct photoxidation of benzo[*a*]pyrene gives a product distribution very similar to the TPP photosensitized oxygenation, suggesting singlet oxygen is involved in the former. A major product, which was characterized as the 6-seco derivative **6** and not previously reported, was detected in the singlet oxygen reaction. The presence of this product suggests a possible mechanism for quinone formation in the singlet oxygen reaction. One-electron oxidations of benzo[*a*]pyrene were carried out using tris(*p*-bromophenyl)aminium hexachloroantimonate and quenching of the radical cation with superoxide or water. The product distribution in this case was quite different from that obtained in the direct photooxidation.

E. LEE-RUFF, H. KAZARIANS-MOGHADDAM et M. KATZ. Can. J. Chem. **64**, 1297 (1986).

Utilisant des techniques de résonance magnétique nucléaire à haut champ, y compris des techniques de COSY en 2D et d'effet Overhauser nucléaire sélectif, on a caractérisé les quatre diones qui sont obtenues par oxydation du benzo[*a*]pyrène. On a pu attribuer sans équivoque les déplacements chimiques de tous les protons de ces quatre quinones. La photo-oxydation directe du benzo[*a*]pyrène conduit à une distribution de produits qui est très semblable à celle qui est obtenue par oxygénation photo-sensibilisée par le TPP; ceci suggère qu'un oxygène singulet est impliqué dans le premier cas. Lors de la réaction effectuée sous l'influence de l'oxygène singulet, un produit majeur est le dérivé séco-6 **6** qui n'avait pas été rapporté antérieurement. La présence de ce produit suggère un mécanisme possible pour la formation de la quinone lors de la réaction effectuée sous l'influence de l'oxygène singulet. On a effectué des oxydations mono-électroniques du benzo[*a*]pyrène en faisant appel à l'aminiumhexchloroantimonate de tris(*p*-bromophényle) et en piégeant le radical cation par du superoxyde ou de l'eau. La distribution des produits qui résultent de cette réaction est très différente de celle qui est obtenue par photo-oxydation directe.

[Traduit par la revue]

Introduction

The presence of environmental polynuclear aromatic hydrocarbons (PAH) has been of great concern due to the toxicities as carcinogenic initiators exhibited by a number of these derivatives (1). Various oxidized species have been implicated as being responsible in the molecular binding with vital biopolymers such as DNA, proteins, and polysaccharides (2). Benzo[*a*]pyrene (BaP) (**1**) is a classical example of such PAHs. It has been well established that epoxides and diol epoxides, metabolites of this derivative, bind with DNA to form stable adducts and are responsible for the mutagenic activity. Certain peroxidase systems are also known to catalyze the oxygenation of BaP to a mixture of quinones. Whereas most of the metabolic studies on BaP have focussed on the 7,8-epoxide and 7,8-diol-9,10-epoxide, interest in the oxidation to the 1,6- 3,6- and 6,12-quinones has recently picked up (3) as the result of the observation that these quinones themselves exhibit moderate mutagenic activity (4). The 3,6- and 6,12-benzo[*a*]pyrene quinones are as active as the classical mutagen 3-methylcholanthrene and a little less active than the parent BaP. Recently, Tso and co-workers (5) have shown that all three quinones caused degradation of DNA and that this process is oxygen dependent. Electron spin resonance (esr) studies have shown that the semiquinones of these derivatives covalently bind to DNA and polyglutamic acid (6). Katz and co-workers have shown that the three benzo[*a*]pyrene quinones are also produced by oxidation of BaP adsorbed on cellulose acetate plates and on glass under simulated environmental conditions (7, 8) involving a high-intensity visible light source. In these studies, the half-life of BaP was found to be 5 h, significantly more inert than benzo[*a*]anthracene.

Introduction of ozone to the system led to a marked rate enhancement of BaP decomposition, leading to the same mixture of quinones. Recently, Eisenberg *et al.* (9) have obtained evidence that certain PAHs sensitize production of singlet oxygen under environmental conditions and that the oxidation of these PAHs, including BaP, involves the self-sensitized singlet oxygenation of these compounds (10). However, to our knowledge, no systematic study of the singlet oxygen reaction of BAP has been reported. We undertook a study of the oxidation of benzo[*a*]pyrene, under photosensitized singlet oxygen production as well as the use of one-electron oxidations, to establish whether singlet oxygen is responsible for the photooxidation process. Furthermore, we report that the photooxidation and photosensitized singlet oxygenation of BaP produces a major product that has not been previously reported, and which suggests a possible mechanism for quinone production by singlet oxygen reaction. Heretofore, the structures of three isomeric 1,6-, 3,6-, and 6,12-benzo[*a*]pyrene diones **2–4** were all assigned by comparison of uv and mass spectra with "authentic" material obtained from chromium trioxide oxidation of BaP based on an early literature report (11) that predates nmr spectroscopy. Neither uv nor mass spectrometry represent absolute molecular structure characterization methods and, in order to confirm the original structural assignments, we carried out a detailed structural analysis of the above-mentioned three quinones, as well as 4,5 BaP quinone, based on ^{1}H 2-D COSY and selective nOe (nuclear Overhauser enhancement) nmr studies.

Results

Confirmation of benzo[a]pyrene quinone structures by high-field nuclear magnetic resonance studies

The mixture of 6,12-, 1,6-, and 3,6-benzo[*a*]pyrene diones (**2–4**) was prepared according to an early literature procedure (11). The mixture was separated on a dry column of flash-grade silica gel. The order of elution according to previous reports is

[1]Author to whom correspondence may be addressed.

[2]Revision received January 20, 1986.

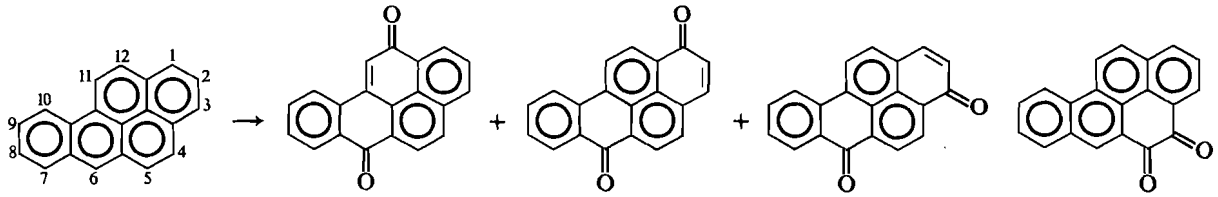

1 2 3 4 5

2, followed by **3** and **4**. All three compounds were obtained as crystalline materials with identical melting points, as reported. Of the three quinones, only the 6,12-dione **2** had been prepared by independent synthesis (12). We have repeated this synthesis and the product obtained was identical in all respects with the faster eluting component in the dione mixture. Benzo[*a*]pyrene-4,5-dione **5** was also prepared by literature methods (13, 14) for comparison with products obtained in the oxidation studies of BaP. The confirmation of structures of all four benzo[*a*]pyrene diones **2–5** was established by the mapping of all vicinally coupled and proximal protons by a combination of the 2-D COSY and selective nOe difference spectroscopy methods (15) and checking for self-consistency. In this manner, all of the proton nmr chemical shifts for each of the isomers **2–5** have been unequivocally established and listed in Table 1 and the original structural assignments have now been confirmed. One feature of note is that bay-region hydrogen signals (H-11, H-10), which appear at lowest field in benzo[*a*]pyrene **1**, are shifted to higher fields by about 0.5–0.7 ppm in the four quinones. This can be rationalized in terms of decreasing ring current effects brought about by the decrease in π-electron density in the quinones. The lowest-field signals in the nmr spectra appear to be for those protons at the *peri* position relative to the carbonyl groups. The sensitivity of the high-field nmr method now permits analysis of trace photooxidation products of PAHs by an absolute method. (The sensitivity of the uv–visible spectrometric analysis still exceeds the nmr method by at least two orders of magnitude; however, the latter is limited by the reliance of authentic material for comparison purposes.)

Oxidation studies of benzo[a]pyrene

It has been suggested that the environmental oxidation of PAHs proceeds via self-sensitized singlet oxygen reaction (16). Evidence for gas-phase singlet oxygen formation using heterogeneous gas-phase photosensitization involving PAHs has been obtained from trapping experiments with known singlet oxygen scavengers such as 9,10-diphenylanthracene (9). To establish that singlet oxygen is involved in the direct photooxidation reaction and to elucidate the mechanism of quinone formation, we analyzed and compared the product distribution of the direct photooxidation with those derived from photosensitized singlet oxygen reaction using the common sensitizers, tetraphenylporphyrin (TPP) and methylene blue. Furthermore, it has been suggested that certain reactions involving singlet oxygen proceed via electron transfer processes involving superoxide O^-_2. To establish whether such a mechanism operates in the photooxidation of benzo[*a*]pyrene, we prepared the benzo[*a*]pyrene radical cation by reaction of BaP with tris(4-bromophenyl)aminium hexachloroantimonate and subjected the radical cation to reaction with potassium superoxide. The product distribution was compared with those of the direct photooxidation and photo-sensitized singlet oxygen reaction.

The direct photooxidations of BaP were carried out in one of two ways: aerated benzene solutions of **1** (10^{-3} *M*) were irradiated with an uv source (450-W medium-pressure Hg lamp) using a Pyrex filter (>300 nm). Alternatively, aerated solutions of **1** (10^{-3} *M*) in $CHCl_3$ were irradiated using a visible light source (500 W) with a Pyrex filter. The only products in the uv irradiations are the diones **2–4** with a small amount of product having the identical hplc (high performance liquid chromatography) retention time as the 4,5-dione (**5**). Infrared and nmr spectral comparisons of this minor product with authentic 4,5-dione **5** showed that the two were not identical. The uv data of this minor product were also not compatible with those of an 11,12-benzo[*a*]pyrene dione (17) and no further attempts at identifying this compound were made. The product mixture obtained from irradiation with visible light consisted of the three quinones **2–4** and a *major product that constituted 48% of this mixture*. This product was identified as the 6-seco-benzo[*a*]pyrene derivative **6** and has not been previously

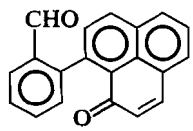

6

$(4\text{-}BrC_6H_4)_3N^{\cdot+}SbCl_6^-$

7

reported in benzo[*a*]pyrene photooxidations. This assignment was based on high-field nmr 2-D COSY correlations, which indicate a vicinal proton coupling system very similar to benzo[*a*]pyrene; however, a low-field proton at 9.7 ppm assigned to the aldehydic C-6 proton was found to be long-range coupled to the C-7 proton. Furthermore, the unusually shielded C-5 proton at 6.5 ppm is characteristic of the α-proton (next to carbonyl) in phenalenones (18). The uv spectrum of this compound was similar to that of phenalenone. Further confirmation of this assignment was obtained from comparison of spectral data with those reported for the same compound obtained in 0.03% yield from the oxidative γ-radiolysis of benzo[*a*]pyrene (19).

In addition, the hplc chromatogram showed the presence of nonpolar components (20%) that could not be resolved. This nonpolar fraction was analyzed by mass spectrometry and showed parent ions corresponding to dimethylbenzo[*a*]pyrenes. Evidence for this suggestion was obtained from experiments in which the photooxidation was performed in CH_2Cl_2 in place of $CHCl_3$ and noticing the absence of this nonpolar fraction. The use of chloroform as a photolysis medium could result in methylation of PAHs by free-radical or cationic pathways. Up to 65% quenching of the oxidation occurred in the presence of 1 equiv. of DABCO (1,4-diazabicyclo[2.2.2]octane), implying presence of $^1O_2$ as the reactive species. The photosensitized oxidation was carried out using either TPP or methylene blue. A filter had to be used for selective excitation of the sensitizer. The filter chosen was a chemical filter solution (21) consisting of $CuSO_4$ and $NaNO_3$ in ammonium hydroxide with a transparent window between 405 and 520 mm. Benzo[*a*]pyrene **1** showed a weak tail-end absorption in this region. Using a 2-cm path width of filter solution, the direct photooxidation of **1** proceeds at 1/20

TABLE 1. ^{1}H chemical shift assignments of BaP oxidation products

Compound	H-1	H-2	H-3	H-4	H-5	H-6	H-7	H-8	H-9	H-10	H-11	H-12
BaP* (**1**)	8.26	8.00	8.11	7.94	8.01	8.54	8.31	7.79	7.84	9.06	9.07	8.35
4,5-Dione (**5**)	8.26	7.76	8.55	—	—	8.88	8.10	7.71	7.86	8.69	8.67	8.07
6,12-Dione (**2**)	8.63	7.85	8.22	8.17	8.47	—	8.46	7.68	7.77	8.19	7.58	—
3,6-Dione (**4**)	7.73	6.71	—	8.82	8.72	—	8.45	7.59	7.77	8.28	8.37	7.80
1,6-Dione (**3**)	—	6.76	7.74	7.91	8.68	—	8.47	7.79	7.63	8.35	8.57	8.67
seco BaP (**6**)	7.25	7.70	7.86	7.77	6.51	9.72	8.00	7.57	7.70	8.13	8.26	7.55

*Reference 31.

TABLE 2. Relative yields* of the major BaP oxidation products

Type of oxidation	6,12-Dione **2**	6,1-Dione **3**	3,6-Dione **4**	Seco BaP **6**	Overall conversion
Ultraviolet radiation (benzene)	43.3	26.7	30.0	—	60
Visible light radiation ($CHCl_3$)	22.0	18.8	11.0	48.1	64
Visible light radiation (CH_2Cl_2)	25.9	26.4	25.5	22.2	27
Photosensitized oxygenation (TPP sensitizer)	13.8	10.3	11.9	54	20
Photosensitized oxygenation (methylene blue)	13.0	27.3	23.9	36	17
BaP radical cation quenched with O^-_2	3.4	54.3	42.3	—	57†
BaP radical cation quenched with H_2O	13.1	37.6	49.3	—	13†

*The yields are reproducible to within 10% of their absolute values.
†Balance consisted of only unreacted BaP.

of the rate in the absence of the filter. This was used as the control for the photosensitized oxygenation experiments. TPP exhibits strong absorption at 416 mm so that, using the filter assembly, the sensitizer (TPP) absorbs greater than 95% of the light. Methylene blue, on the other hand, has a maximum absorption at 610 mm; however, this band extends into the filter window. In both instances the photosensitized oxygenation rate was at least twice as fast as that in the absence of photosensitizer. The product mixture consisted of the nonpolar fraction obtained in the direct photooxidation, a mixture of the diones **2**–**4**, and the seco product **6**. The relative yields of the products are listed in Table 2.

The one-electron oxidation of benzo[*a*]pyrene was carried out using the oxidant tris(4-bromophenyl)aminium hexachloroantimonate **7**. When a chloroform solution of benzo[*a*]pyrene **1** was added to a solution of **7**, an instant rose-coloured mixture was developed. This species was attributed to the radical cation of **1**. The uv–visible spectrum exhibited peaks at 450 and 560 mm. The radical cation of **1** was reported to show a peak at 450 mm (20). In air, the coloured solution faded after a few minutes. The coloured species was instantly quenched with water. It was also quenched by addition of powdered potassium superoxide. In each case, the reaction mixture consisted of the three quinones, with no detectable trace of the seco product **6**. The product distributions of the quinone mixture obtained in all of the oxidations are listed in Table 2.

Discussion

The possibility that PAHs can sensitize singlet oxygen formation has been aptly demonstrated by Eisenberg *et al.* (9). On energetic grounds (see Fig. 1) both the first excited singlet as well as the triplet states of benzo[*a*]pyrene **1** can result in singlet oxygen formation by energy transfer by mechanisms shown in Scheme 1. The lifetimes of both excited states of **1** permit bimolecular collisions with oxygen to take place for energy transfer and it has been shown for other PAHs that fluorescence and phosphorescence can be quenched by oxygen.

In other readily reducing aromatic derivatives, it has been suggested that singlet oxygen reactions occur by way of single electron transfer processes involving PAH radical cation formation (22). Electron transfer from BaP to either singlet (Δg) or ground state oxygen would be endoergonic and not likely to

$$\mathrm{BaP} \xrightarrow{h\nu} \mathrm{BaP}^1$$

$$\mathrm{BaP}^1 + {}^3\mathrm{O}_2 \longrightarrow \mathrm{BaP}^3 + {}^1\mathrm{O}_2$$

$$\mathrm{BaP}^1 \longrightarrow \mathrm{BaP}^3$$

$$\mathrm{BaP}^3 + {}^3\mathrm{O}_2 \longrightarrow {}^1\mathrm{O}_2 + \mathrm{BaP}^1$$

$$\mathrm{BaP} + {}^1\mathrm{O}_2 \longrightarrow \text{reaction products}$$

SCHEME 1

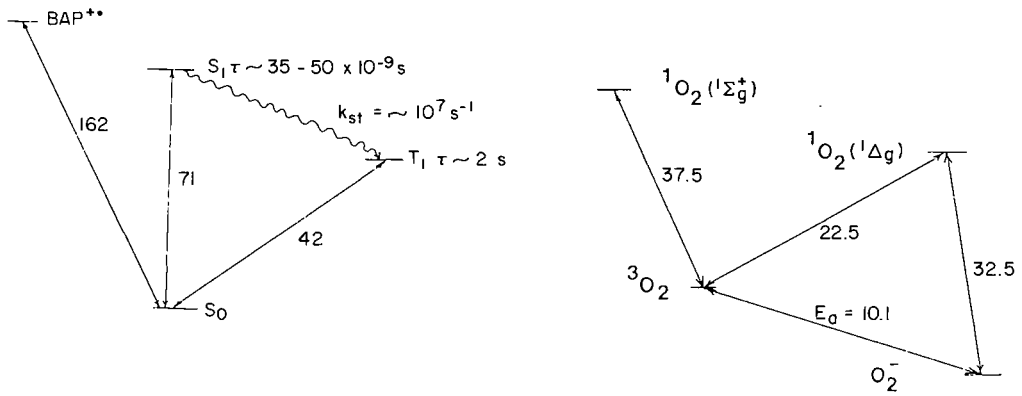

FIG. 1. Excited states of BaP and O_2 (29, 30; see also ref. 26); numbers are in kcal/mol.

occur on the basis of the high ionization potential of BaP (162 kcal/mol) (23). Similar consideration even for the excited states of BaP would preclude electron transfer to oxygen. To test this, we have shown that the *BaP radical cation, generated independently, reacts with superoxide or water to give a significantly different product distribution* (see Table 2). The 6,12-dione in this case is formed only as a minor product. These relative yields are very similar to ones reported for the electrochemical oxidation of BaP (24). Greenstock and Ruddock have reported that neutral BaP reacts with superoxide generated by pulse radiolysis (25). In our hands, mixtures of BaP with KO_2 were found to be stable indefinitely. It is likely that under conditions of pulse radiolysis, ionization of **1** to the radical cation takes place and that the decomposition of BaP with O_2 takes place by way of this radical cation. The direct photooxidation of BaP **1** produces a mixture that is similar to one obtained from the TPP sensitized oxidations in which the 6,12-dione **2** and seco product **6** predominate. Evidence that the direct photooxidation proceeds via singlet oxygen was shown from DABCO quenching and the trapping of diphenylanthracene-9,10-peroxide when diphenylanthracene, a known singlet oxygen quencher, was added to the photomixture.

The different product distributions observed in the one-electron and photooxidations of BaP suggest that two fundamentally different mechanisms operate in quinone formation in the two reactions. Adams has suggested (24) that quinone formation by way of electrochemical oxidation proceeds through the intermediacy of the radical cation **8**, which, in aqueous solution, is trapped by water leading to 6-hydroxy BaP **9**. Further oxidation by way of the corresponding oxyradical leads to the mixture of quinones (Scheme 2). Formation of the quinones from reaction of the radical cation with superoxide could proceed by nucleophilic trapping at position 6 and formation of dihydroperoxides. These dihydroperoxides, under basic conditions, could conceivably rearrange to the diones.

It is interesting that the enzymatic oxidation of 6-hydroxybenzo[*a*]pyrene using rat liver homogenates has been reported to produce a mixture of diones **2–4** with a distribution almost identical to one we obtained from the one-electron oxidation of **1** and subsequent quenching with water (28).

The formation of diones from singlet reaction of arenes is believed to proceed via the intermediacy of *meso*-endoperoxides, which represent Diels–Alder adducts of singlet oxygen (26). This is illustrated by the example of anthracene, which undergoes cycloaddition with singlet oxygen to produce the *meso*-peroxide **10**. Formation of 9,10-anthraquinone from the peroxide could involve homolytic O—O bond cleavage and subsequent rearrangement to the half-oxidized hydroquinone **11**. Further oxidation to the dione could be initiated either by ground state or singlet oxygen. The formation of diones **2–4** from benzo[*a*]pyrene is unlikely to involve a mechanism as described above. It would be unlikely for a peroxo bridge to span the 6,12, 1,6, and 3,6 centers. The formation of the seco derivative **6** as the major product in the singlet oxygen reaction of benzo[*a*]pyrene suggests that a dioxetan **12** or perepoxide **13** is involved in the formation of this product. Such an intermediate may also be responsible for quinone formation. It is conceivable that these intermediates could lead to the zwitterion

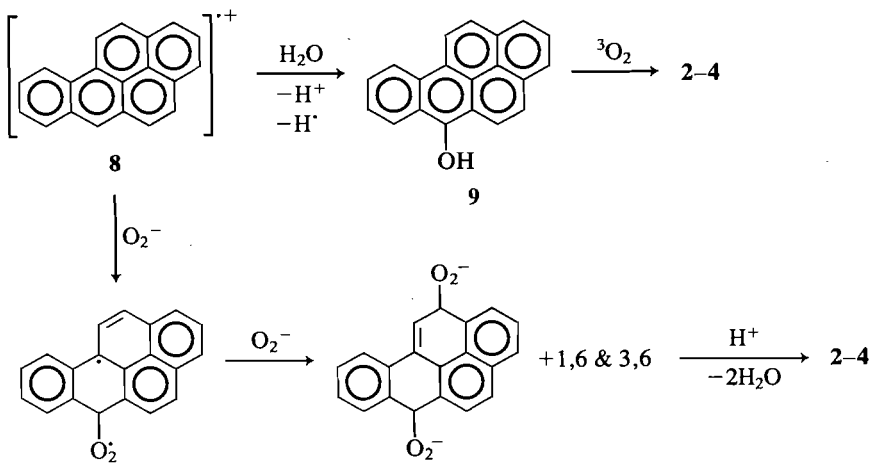

SCHEME 2

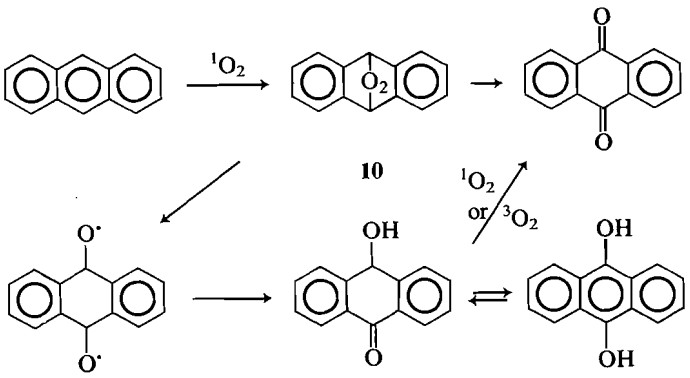

SCHEME 3

13. Subsequent trapping of this species by water and further oxidation could lead to the observed quinones. It is interesting that the relative amount of seco derivative **6** and the quinones is dependent on the rigour to which the solvent has been subjected in drying.

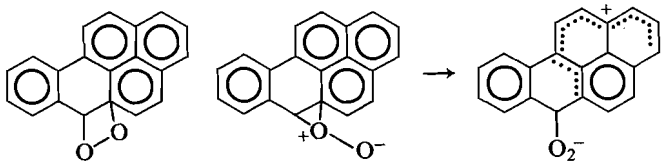

Conclusion

Structures of the three major isomeric diones **2–4** formed from benzo[*a*]pyrene **1** oxidation have been confirmed by 2-D COSY and selective nOe nmr techniques. The relative distribution of diones is markedly dependent on the nature of the oxidation. One-electron oxidation of benzo[*a*]pyrene using tris(4-bromophenyl)aminium hexachloroantimonate as a one-electron oxidant produces exclusively a mixture of diones **2–4** with **3** predominating and **2** present as a minor component. On the other hand, direct photooxidation or photosensitized oxgenation of **1** produces a mixture of diones with dione **2** as the major product. Another major product identified as the seco derivative **6** was isolated in these reactions. The presence of **6** suggests a mechanism involving a dioxetan or perepoxide as the probable precursor to diones **2–4** under conditions of singlet oxygen reaction. It is interesting to note that biochemical systems in which singlet oxygen has been implicated catalyze the oxidation of BaP to give a similar mixture of diones as reported by us for the direct or photosensitized oxidations. Marnett *et al.* (27) have reported that **1** is oxidized by sheep seminal vesicals arichodonate-dependent system to a mixture of diones **2–4** with a relative distribution of 45:25:35. On the other hand, oxidation of **1** by rat-liver homogenate (28) (cytochrome dependent) produces a dione mixture **2–4** with relative yields 5:41:44, which is similar to our observed product distribution from the one-electron oxidation. Oxidized cytochromes contain complexed ferric ions that would initiate one-electron oxidation processes with aromatic derivatives with sufficiently low oxidation potentials.

The environmental analysis of benzo[*a*]pyrene is complicated by its oxidation to the diones **2–4** during sampling. In our study we find that a new major product **6** is also present in simulated environmental oxidations. Thus a complete analysis of environmental benzo[*a*]pyrene would have to include analysis of diones **2–4** as well as aldehyde **6**.

Experimental

Benzo[*a*]pyrene and tris(4-bromophenyl)aminium hexachloroantimonate were obtained from Aldrich.

Dry column chromatography was performed with silica gel, Merck Kieselgel 60, 230–400 mesh ASTM, deactivated with water (15% w/w). High performance liquid chromatography (hplc) was carried out with a Waters Associate chromatography equipped with a Model 6000A pump, a model U6K injector, and a model 440 absorbance detector set at 254 nm. A Waters straight-phase μ-Porasil column (3.9 mm × 30 cm/10 μm) was used with a mixture of hexane and chloroform as the mobile phase.

The diones **2–4** were prepared according to the literature and their separation was carried out using dry column chromatography with chloroform as the eluant. The 6,12-dione **2** was first to elute, followed by the 1,6 and 3,6 isomers **3** and **4**, respectively. The purity of the individual fractions was tested by hplc and their retention times are: 6,12-dione **2**, 8.78 min; 1,6-dione **3**, 13.43 min; 3,6-dione **4**, 15.21 min.[3]

Benzo[*a*]pyrene-4,5-dione (**5**) was synthesized according to literature methods (13, 14). The uv and mass spectra data of **2–5** were in good agreement with those reported in the literature.

The nmr acquisitions were performed on a Brüker AM-300 spectrometer.

Selective nOe and 2-D COSY acquisitions

The Brüker pulse sequence 90_{PH1}–t_1–90_{PH2}–F1D(t_2) was used for the 2-D COSY experiment with a 1K × 1K array of data points. The sweepwidth was restricted to the aromatic region 900 Hz. The 2-D plot allows the correlation of vicinally coupled protons. The selective nOe experiments were carried out using a decoupler power of 45–50 L and a decoupler pulse approximately equal to the longest proton T_1 (7 s) to ensure maximum saturation and polarization transfer. The nOe enhancements ranged from 3–15% with bay-region protons exhibiting the largest effects. In all cases a marker proton was established (H-11 in **2**, H-2 in **3**, H-2 in **4**, and H-6 in **5**) and bay-region as well as *peri* relationships of protons determined by this method.

Photooxidation reactions

General: All photooxidations were performed in glass-distilled solvents in Pyrex tubes equipped with a gas purger.

For the uv radiations, the tube was strapped around a quartz cooling well and the assembly was placed in an ice-water bath. A Pyrex inner filter was used and a Hanovia 450-W medium-pressure lamp served as the light source. Dry oxygen was bubbled through the solution during the photolysis.

For the visible light irradiation, the sample tube was placed in the inner well of the cooling vessel. A GE 500-W quartzline lamp was used as the light source and placed exterior to the photolysis assembly. Irradiations with a chemical filter solution were run using a concentric tube placed in the interior of the cooling well, which was filled with a Cu^{+2} ammonia complex solution (21).

Ultraviolet irradiation of benzo[a]pyrene (1)

A solution of 30 mg (0.12 mmol) of **1** in 120 mL AnalaR benzene was irradiated for 16 h with the uv assembly. The solvent was removed under reduced pressure and unreacted **1** was separated using a silica gel column, employing a 50:50 mixture of hexane:benzene as the eluant. The reaction was 60% complete based on the recovery of unreacted benzo[*a*]pyrene. The photomixture was eluted off the column (18 mg) and reapplied on another silica gel column. The quinone mixture of **2–4** (16 mg) was separated and characterized by uv, mass spectroscopy, and 1H nmr, which were identical with authentic samples. The hplc analysis of the product mixture gave the following distribution: 34.6% 6,12-dione **2**, 8% of yellow crystalline material, 21.4% of 6,1-dione **3**, and 24.0% of 3,6-dione **4**. The remaining 11.4% consisted of thirteen

[3]The response of all four diones was identical to within 2% when standard solutions were analysed.

minor components. The unidentified crystalline material, which had the same retention time as the 4,5-dione **5**, exhibited different ^1H nmr and mass spectra. No further attempt was made to characterize this compound.

Visible light irradiation of 1

A solution of 10 mg of **1** (0.039 mmol) in 80 mL of chloroform was photolyzed using a visible light source for 48 h. The solvent was removed and the residue applied to a dry column of silica gel. The unreacted **1** (3.5 mg) was eluted with 50:50 hexane:benzene mixture and the photomixture was eluted with chloroform (6.4 mg). The hplc analysis (90:10 *n*-hexane:chloroform; 1.3 mL/min) indicated the following distribution: 25% of nonpolar unidentified material (ms, $M^+ + 2CH_2$), 11% of **2**, 9.4% of **3**, 5.5% of **4**, and 24.0% of secobenzo[*a*]pyrene derivative **6**. The remaining 23.7% consisted of fourteen minor components. The isomeric quinones **2–4** and seco derivative **6** were separated by dry column chromatography, further purified by hplc, and subjected to spectral analysis. The ir, uv, and ^1H nmr data for **6** were identical to those reported by Gibson and Smith (19). The quinones exhibited identical spectral data with those of the authentic samples.

When the photolysis was carried out in CH_2Cl_2 under identical conditions as above, the nonpolar fraction was absent as evident by hplc. The reaction mixture consisted of 15.8% of **2**, 16.1% of **3**, 15.5% of **4**, and 13.5% of **6**. The remaining 39.1% consisted of at least ten minor components.

Triethylene diamine (DABCO) quenching studies

A solution of 10 mg of **1** in 80 mL of $CHCl_3$ containing 10 mg of DABCO was irradiated with the visible light source for 48 h. The usual work-up yielded 2.7 mg of photooxidized products and hplc analysis showed a reduction of 50% of each of the quinones **2–4** and 60% of the seco product **6**.

9,10-Diphenylanthracene trapping experiment

A solution of 20 mg of diphenylanthracene and 5 mg of **1** in 80 mL of $CHCl_3$ was irradiated for 24 h using the visible light source and the inorganic filter solution. In addition to quinone **2–4** formation, a new product identified as the 9,10-diphenylanthracene peroxide was isolated and its structure confirmed by comparison of its ir spectrum with that of an authentic sample. A control experiment without benzo[*a*]pyrene present was carried out under identical conditions and, in this case, no detectable amount of the peroxide was obtained. The photomixture consisted only of unreacted starting material, by tlc analysis.

Photosensitized oxidation of benzo[a]pyrene (1)

A solution of 10 mg of **1** and 5 mg of methylene blue in 80 mL of $CHCl_3$ was irradiated with the visible light source for 48 h using the inorganic filter solution. After separating unreacted **1** from the photomixture, continued elution with $CHCl_3$ on a silica gel column gave a mixture which was analyzed by hplc (60:40 hexane:$CHCl_3$; 1 mL/min). The following distribution of products was observed: 11.6% (4.45 min) unidentified, 9.5% (4.64 min) unidentified, 7.2% 6,12-dione **2** (8.78 min), 15.1% 1,6-dione **3** (12.97 min), 13.2% 3,6-dione **4** (14.34 min), and 19.8% 9-(2-formylphenyl)phenalenone **6** (18.78 min). The remaining 23.6% consisted of ten minor components.

In a control experiment, in the absence of methylene blue, no seco derivative **6** was detected. Only trace amounts of **2–4** were detected, along with the two less polar components.

The above experiment was repeated with tetraphenylporphyrin as the photosensitizer under identical conditions. A 20% conversion to photooxygenated products was observed by hplc analysis, with the following distribution: 40% nonpolar dimethylated material, 7.5% 6,12-dione **2**, 5.6% 1,6-dione **3**, 6.5% of 3,6-dione **4**, and 35% of seco derivative **6**.

Oxidation of benzo[a]pyrene (1) with tris(4-bromophenyl)aminium hexachloroantimonate and quenching with O_2^-

To a solution of 20 mg of benzo[*a*]pyrene in 50 mL of dry CH_2Cl_2 was added slowly a solution of 65.2 mg of tris(4-bromophenyl)aminium hexachloroantimonate in 50 mL of dry CH_2Cl_2. The solution turned to a rose-purple colour. To this solution was added a suspension of KO_2 in dry CH_2Cl_2, at which point the colour changed to a yellow solution. The solution was stirred for 3 min and poured over crushed ice. The organic layer was separated and washed with 3 × 30 mL of 10% HCl, followed by 3 × 30 mL of water, and dried over magnesium sulphate. The solvent was removed under reduced pressure and the residue was applied to a dry silica gel column. The unreacted benzo[*a*]pyrene (5 mg) was eluted with 50:50 hexane:benzene mixture. Following elution with $CHCl_3$ the quinone fraction **2–4** (15 mg) was obtained; hplc analysis showed the following distribution: 3.4% of 6,12-dione **2**, 54.3% of 1,6-dione **3**, and 42.3% and 3,6-dione **4**. No other peaks were observed by hplc.

In a control experiment, no reaction was observed between KO_2 and benzo[*a*]pyrene in the absence of tris(4-bromophenyl)aminium hexachloroantimonate.

Repetition of the above experiment, using water instead of KO_2 as the quenching agent, led to 2.85 mg (12.6%) conversion to quinones **2–4**. The balance of the mixture was unreacted **1**. The hplc of the oxidation mixture showed the following distribution of products: 13.1% of 6,12-dione **2**, 37.6% of 1,6-dione **3**, and 49.3% of 3,6-dione **4**.

Acknowledgements

We would like to thank the Natural Sciences and Engineering Research Council of Canada for their generous support of a strategic grant in environmental toxicology. One of us (E. Lee-Ruff) would like to acknowledge the support of an Environment Canada Atmospheric Environment Services (AES) grant.

1. (*a*) E. Cavalieri, E. Rogan, and R. Roth. *In* Free radicals and cancer. *Edited by* R. A. Floyd. Dekker, New York. 1982. pp. 117–158. (*b*) W. Levin, A. Wood, A. Chang, D. Ryan, P. Thomas, H. Yagi, D. Thakker, K. Vyas, and C. Boyd. Drug Metab. Rev. **13**, 555 (1982).
2. A. W. Wood, W. Levin, R. L. Chang, H. Yagi, D. R. Thakker, R. E. Lehr, D. M. Jerina, and A. H. Conney. *In* Polynuclear aromatic hydrocarbons. Third International symposium on Chemistry and Biology – Carcinogenesis and Mutagenesis. *Edited by* P. W. Jones and P. Leber. Ann Arbor Science Publishers, Ann Arbor, Michigan. 1979. pp. 531–551.
3. R. Morgenstern, C. Guthenberg, B. Mannervik, J. W. De Pierre, and L. Ernster. Cancer Res. **42**, 4215 (1982).
4. M. F. Salamone, J. A. Heddle, and M. Katz. Environ. Int. **2**, 37 (1979).
5. S. A. Lesko, R. J. Lorentzen, and P. O. P. Tso. *In* Polycyclic hydrocarbons and cancer. *Edited by* P. O. P. Tso and H. V. Gelboin. Academic Press, New York. 1978. pp. 261–269.
6. C. Nagata, M. Kodama, and Y. Ioki. *In* Polycyclic hydrocarbons and cancer. *Edited by* P. O. P. Tso and H. V. Gelboin. Academic Press, New York. 1978. pp. 247–260.
7. D. A. Lane and M. Katz. *In* Advances in environmental science and technology, fate of pollutants in air and water environments. Vol. 9. *Edited by* I. H. Suffet. Wiley–Interscience, New York. 1978. pp. 137–154.
8. M. Katz, C. Chan, H. Tosine, and T. Sakuma. *In* Polynuclear aromatic hydrocarbons. *Edited by* P. W. Jones and P. Leber. Ann Arbor Science Publishers, Ann Arbor, Michigan 1980. pp. 171–189.
9. W. C. Eisenberg, K. Taylor, D. L. B. Cunningham, and R. W. Murray. *In* Eighth International Symposium on Polynuclear Aromatic Hydrocarbons, Columbus, Ohio. Battelle Press, Columbus. 1984.
10. W. C. Eisenberg, K. Taylor, and R. W. Murray. Carcinogenesis, **5**, 1095 (1984).
11. H. Vollmann, H. Becker, M. Corell, and H. Streeck. Ann. **531**, 2 (1937).
12. H. E. Schroeder, F. B. Stilmar, and F. S. Palmer. J. Am. Chem. Soc. **78**, 446 (1956).
13. R. G. Harvey, S. H. Goh, and C. Cortez. J. Am. Chem. Soc. **97**, 3468 (1975).

14. C. R. RAHA, L. K. KEEFER, and J. LOO. J. Chem. Eng. Data, **18**, 332 (1973).
15. A. BAX and R. FREEMAN. J. Magn. Reson. **43**, 259 (1981); Two-dimensional NMR, Aspect 2000, 3000. Brüker publication. 1982.
16. M. ZANDER. *In* Environmental chemistry: anthropogenic compounds. Vol. 3. Pt. A. Springer Verlag. 1980. p. 121.
17. R. S. BODINE, M. HYLARIDES, G. DAUB, and D. L. VANDER-JAGT. J. Org. Chem. **43**, 4025 (1978).
18. H. PRINZBACH, V. FREUDENBERGER, and V. SCHEIDEGGER. Helv. Chim. Acta, **50**, 1087 (1971).
19. T. L. GIBSON and L. L. SMITH. J. Org. Chem. **44**, 1842 (1979).
20. W. CASPARY, B. COHEN, S. LESKO, and P. O. P. TSO. Biochemistry, **12**, 2649 (1973).
21. K. GOLLNICK and A. SCHNATTERER. Tetrahedron Lett. 185 (1984).
22. A. P. SCHAAP, K. A. ZAKLIKR, B. KASHAR, and L. W. H. FUNG. J. Am. Chem. Soc. **102**, 389 (1980).
23. E. L. CAVALIERI, E. G. ROGAN, R. W. ROTH, R. K. SAUGIER, and A. HAKAM. Chem.-Biol. Interact. **47**, 87 (1983).
24. L. JEFTIC and R. N. ADAMS. J. Am. Chem. Soc. **92**, 1332 (1970).
25. C. L. GREENSTOCK and G. W. RUDDOCK. Photochem. Photobiol. **28**, 887 (1978).
26. A. A. FRIMER. Singlet oxygen in peroxide chemistry. *In* The chemistry of functional groups. *Edited by* John Wiley and Sons, Ltd., New York. 1983.
27. L. J. MARNETT, G. A. REED, and J. T. JOHNSON. Biochem. Biophys. Res. Commun. **79**, 569 (1977).
28. S. LESKO, W. CASPARY, and R. LORENTZEN. Biochemistry, **14**, 3978 (1978).
29. J. B. BIRKS. Photophysics of aromatic molecules. Wiley–Interscience, New York. 1976.
30. A. A. FRIMER. The organic chemistry of superoxide anion radical. In Superoxide dismutase. *Edited by* L. W. Oberley. CRC Press, Boca Raton, Florida. 1984.
31. C. J. UNKEFER, R. E. LONDON, T. W. WHALEY, and G. H. DAUB. J. Am. Chem. Soc. **105**, 733 (1983).

The chlorination of acetone: a complete kinetic analysis

J. Peter Guthrie[1] and John Cossar
Department of Chemistry, University of Western Ontario, London, Ont., Canada N6A 5B7

Received October 25, 1985

This paper is dedicated to Professor Arthur N. Bourns

J. Peter Guthrie and John Cossar. Can. J. Chem. **64**, 1250 (1986).

Rate constants are reported for all of the major steps followed in the chlorination of acetone, including the chlorination of mono- and 1,1-dichloroacetone, the chlorination of hydroxyacetone, the chlorination and hydroxide-catalyzed rearrangement of 1,1-dihydroxyacetone, and the haloform cleavage of trichloroacetone. pK_a values are reported for hydroxyacetone and monochloroacetone. Rate constants for the hydrolyses of chloroacetone and 1,1-dichloroacetone are reported; these reactions are probably not S_N2 displacements but proceed by addition of hydroxide and intramolecular displacement.

J. Peter Guthrie et John Cossar. Can. J. Chem. **64**, 1250 (1986).

On a déterminé les constantes de vitesses pour chacune des étapes principales de la chloration de l'acétone, y compris la chloration des mono- et dichloro-1,1 acétones, la chloration de l'hydroxyacétone, la chloration et la transposition catalysée par les bases de la dihydroxy-1,1 acétone ainsi que le clivage haloformique de la trichloroacétone. On rapporte aussi les valeurs de pK_a de l'hydroxyacétone et de la monochloroacétone. On rapporte aussi les constantes de vitesse pour l'hydrolyse de la chloroacétone et de la dichloro-1,1 acétone. Ces réactions ne sont probablement des substitutions S_N2 et elles se produisent probablement par une addition d'hydroxyde qui est suivie d'une substitution intramoléculaire.

[Traduit par le revue]

Introduction

The haloform reaction has long been used both as an analytical procedure (1–3) and as a synthetic method (3–8). Despite this long history of its use we were surprised to discover that the major product from the room temperature reaction of acetone with hypochlorite was lactate and not acetate (9). Clearly this familiar reaction was imperfectly understood. We have now carried out a detailed study of the course of the reactions which occur when acetone reacts with alkaline hypochlorite solutions. It has become clear that at several points the course of the reaction depends on a delicate balance between competing paths, so that minor changes in structure can alter the qualitative outcome of the reaction.

Results

The reactions which we have found to be significant in the chlorination of acetone are shown in Scheme 1. We will now describe experiments leading to rate or equilibrium constants for almost every step in the scheme. In the case of acetone itself the results of earlier work (9, 10) are summarized.

Chlorination of acetone

The rate constant[2] for hydroxide-catalyzed enolization of acetone is $k_{12} = 0.173\ M^{-1}\ s^{-1}$ (10). The equilibrium constant for the reaction of hydroxide with acetone to give the enolate may be calculated from the pK_a of acetone, 19.37 ± 0.51 (9). This allows calculation of the rate constants for the reaction of water with the enolate as $k_{21} = 4.1 \times 10^4\ s^{-1}$. The rate constant for the reaction of the enolate with OCl^- is $k_{23}^- = 2.0 \times 10^4\ M^{-1}\ s^{-1}$ and that for reaction with HOCl is $k_{23}^0 = 1.7 \times 10^9\ M^{-1}\ s^{-1}$, i.e. diffusion controlled (9).

Hydrolysis of monochloroacetone and 1,1-dichloroacetone

The hydrolysis reactions of haloacetones could be studied by the pH stat technique, measuring the consumption of hydroxide ion. The experimental data are given in Tables 1 and 2.[3] From these results we obtain the second order rate constants for reaction with hydroxide ion given in Tables 1 and 2. The kinetics were studied over a range of one pH unit; the range was restricted by the need for a reasonably slow reaction in order to be able to monitor it conveniently, and for a reasonably fast reaction in order to avoid confusion with the continual drift from uptake of atmospheric CO_2. Over the range studied the rates of these reactions were linearly dependent on hydroxide ion concentration. We anticipate that there could be a second order dependence on hydroxide at some higher hydroxide concentration, but saw no evidence for it in these experiments.

Chlorination of monochloroacetone

The chlorination of monochloroacetone was inevitably accompanied by hydrolysis leading to the more slowly reacting hydroxyacetone. This led to biphasic kinetics (Table 3) with the faster phase reflecting hydrolysis plus halogenation, and the slower phase reflecting halogenation of hydroxyacetone. For the faster phase, graphical analysis suggested that there were the following terms in the rate law: zero order in hypochlorite and first order in hydroxide (corresponding to hydrolysis); and first order in hypochlorite, zero or first order in hydroxide (corresponding to halogenation). Since the concentrations of both hydroxide and hypochlorite were low, it was difficult to make up solutions with fixed values of one concentration while the other was varied; this meant that both variables changed from experiment to experiment. The hydroxide concentration was determined by titration for each run. The hypochlorite concentration was determined from the initial absorbance; comparison with direct titration showed that this is a reliable measure. To perform a graphical analysis it was necessary to use data where the hydroxide or hypochlorite concentration, although nominally fixed, actually varied considerably. This meant that the simple graphical analysis could only provide rough approximation to the desired rate constants. To extract rate constants we used a non-linear least-squares treatment with two independent variables and one dependent variable (11), fitting to the three parameter equation [1].

$$[1] \quad k_{obs} = (a + b[OH^-])[OCl^-] + c[OH^-]$$

In addition to the data for chlorination in hydroxide/hypo-

[1]Author to whom correspondence should be addressed.

[2]All rate constants are defined in Scheme 1.

[3]Tables 1–8, containing the experimental rate constants, may be purchased from the Depository of Unpublished Data, CISTI, National Research Council of Canada, Ottawa, Ont., Canada K1A 0S2.

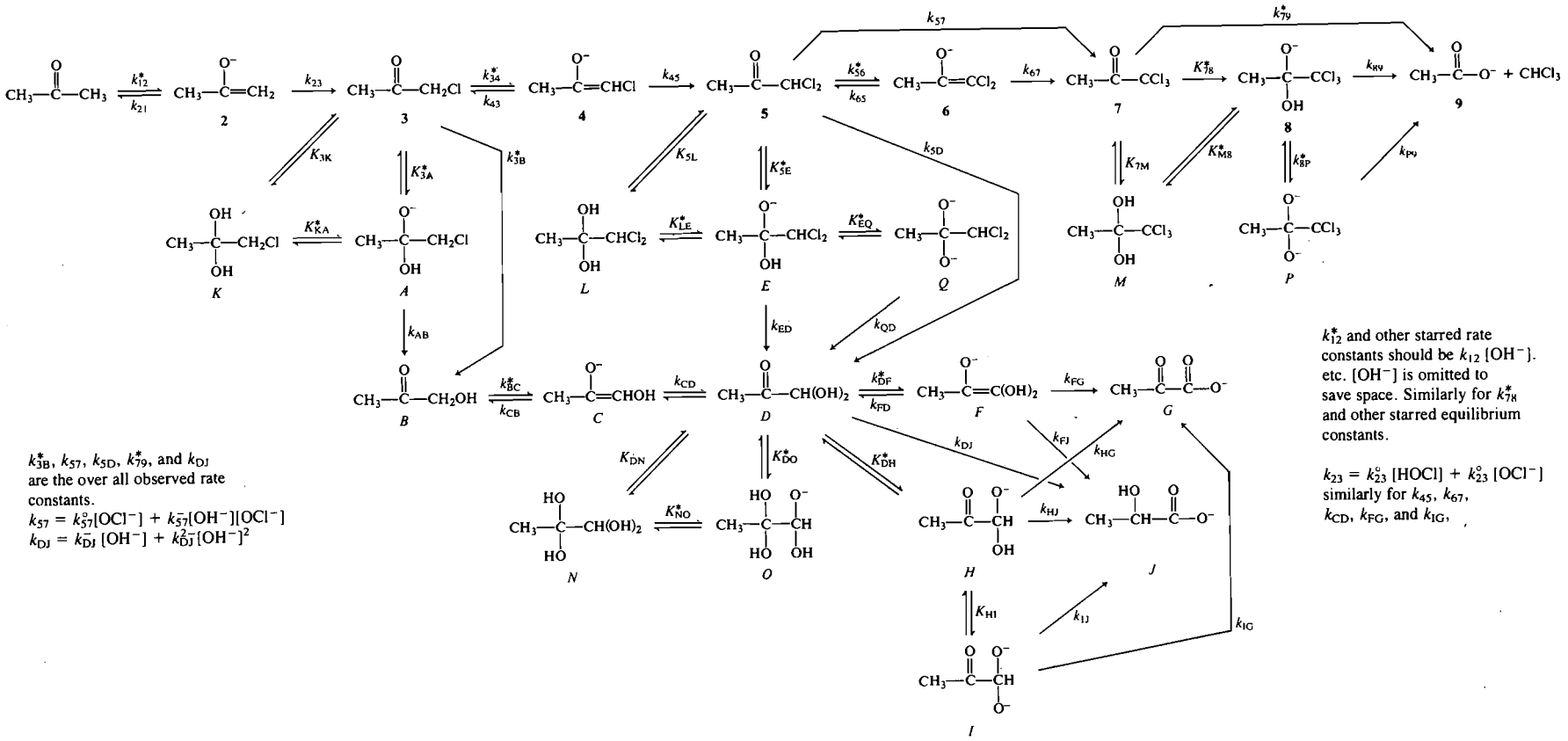

SCHEME 1.

chlorite solutions we used the data for chlorination in pH 10.3 buffers and for hydrolysis of monochloroacetone. With the full data set of 31 points the rate constant for the term first order in both hydroxide and hypochlorite was not well defined; the error limits calculated by the least-squares program were larger than the value:

$$a = 10.1 \pm 1.76$$
$$b = 261 \pm 524$$
$$c = 1.14 \pm 0.94$$

where

$$a = k_{34}k_{45}{}^{0}K_w/k_{43}K_a{}^{HOCl}$$
$$b = k_{34}k_{45}{}^{-}/k_{43}$$
$$c = K_{3A}k_{AB}/(1 + K_{3K})$$

If points deviating by more than 20% were deleted from the data set, one could end up with a set of 22 points for which all three parameters were well defined, and agreed with the parameters defined by the full set within the uncertainty limits calculated by the least-squares program:

$$a = 10.0 \pm 0.64$$
$$b = 224 \pm 179$$
$$c = 1.32 \pm 0.43$$

Alternatively we could try fitting the data to a two-parameter equation, [2], with the same interpretations for the parameters:

[2] $$k_{obs} = a[OCl^-] + b[OH^-]$$

Using the full data set we obtained:

$$a = 10.5 \pm 1.86$$
$$b = 1.41 \pm 0.87$$

Using the reduced data set which allowed the three parameters of eq. [1] to be determined we obtained:

$$a = 10.3 \pm 1.12$$
$$b = 1.65 \pm 0.62$$

Although the parameters are well defined in both cases, the fits are inferior to those obtained with eq. [1]. For the full data set, fitting with eq. [2], there were 10 points deviating by more than 20%; for the reduced data set there were three points deviating by more than 20%. The corresponding values for fits to eq. [1] were eight points deviating by more than 20% for the full data set, and none deviating by more than 20% for the reduced set. The quality of the fit is shown in Fig. 1.[4]

Since other compounds have normally shown hydroxide-dependent as well as hydroxide-independent chlorination we conclude that the corresponding term in the rate law is probably real. Although the data set obtained by discarding deviant points does define the rate constant we have no independent basis for discarding these points, and it seems ill advised to do so. Accordingly we conclude that although the term is real it is ill defined by our data, and we will use the value suggested by the full data set.

Experiments involving the chlorination of monochloroacetone at pH 10.33–10.55 led to rate constants which were first order in hypochlorite; the corresponding second order rate constant was 9.80 ± 0.89 which is indistinguishable from the value obtained above from the full data set. These experiments were unbuffered to avoid possible complications from interactions of buffer and hypochlorite, but as a consequence the pH changed during a set of runs as successive portions of ketone were added. The hydroxide concentration was calculated by interpolation between the initial and final values.

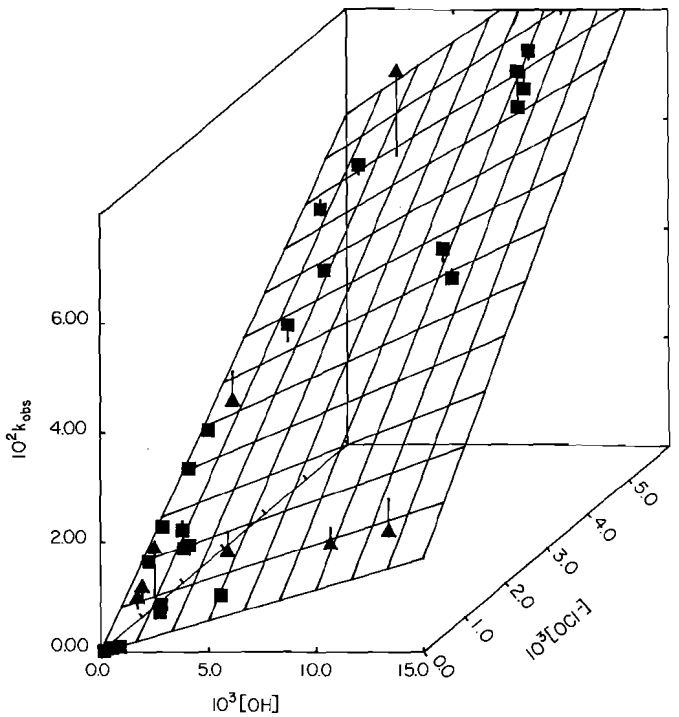

FIG. 1. Rate constants for the combined chlorination and hydrolysis of monochloroacetone, fitted to $k = \{(10.1 \pm 1.76) + (261 \pm 524)[OH^-]\}[OCl^-] + (1.14 \pm 0.94)[OH^-]$. (■) points falling within 20% of the calculated surface; (▲) points falling more than 20% off the calculated surface.

Experiments involving the bromination of monochloroacetone in carbonate buffers at pH 8.82 led to rate constants which were zero order in hypobromite and first order in hydroxide and in carbonate. The corresponding second order rate constants were 0.25 $M^{-1}s^{-1}$ for carbonate and $k_{34} = 136\ M^{-1}s^{-1}$ for hydroxide. These were taken as the rate constants for enolization. From experiments in buffered solutions at lower pH Bell had reported a value of 9.3 $M^{-1}s^{-1}$ (12). We were surprised at the discrepancy, but note that Bell's value is based on experiments in buffer solutions of pH less than 7.

From the rate constant for hydroxide-independent chlorination we can calculate the pK_a of monochloroacetone (subject to the assumption that the halogenation of the enolate of monochloroacetone by hypochlorous acid is diffusion controlled (9)) as 15.76 ± 0.51. We then calculate the rate constant for protonation of the enolate by water, from the rate constant for hydroxide-catalyzed enolate formation and the pK_a, as $k_{43} = 7.8 \times 10^3 s^{-1}$. Finally we estimate $k_{45}{}^-$, the rate constant for the reaction of the enolate with hypochlorite ion, from the value of the rate constant for hydroxide dependent chlorination, as ca. $2 \times 10^4\ M^{-1}s^{-1}$.

Chlorination of hydroxyacetone

The halogenation of hydroxyacetone was, as reported previously (9), faster than the halogenation of acetone. We have

[4]For the cases where we have fitted k_{obs} simultaneously as a function of $[OH^-]$ and $[OCl^-]$, we present three dimensional graphs, with a grid showing the calculated surface and a perpendicular line from the center of each point to the surface, to make clear which points deviate significantly.

extended the range of the kinetics over that previously reported in an attempt to evaluate the rate constant for the term in the rate law first order in hypochlorite and zero order in hydroxide with sufficient accuracy to calculate the pK_a. These additional rate constants are found in Table 4.

The data, including the rate constants reported previously, were subjected to a graphical analysis based on the use of Eadie–Hofstee (13, 14) type plots to analyze the $[OCl^-]$ dependence of k_{obs} at "fixed" $[OH^-]$. The approach is based on the assumed mechanism shown in Scheme 1, which leads to the following expression for the observed rate constant:

$$k = a[OH^-](b/[OH^-] + c)[OCl^-]/\{d + (b/[OH^-] + c)[OCl^-]\}$$
$$= a[OH^-]/\{d/(b/[OH^-] + c)/[OCl^-] + 1\}$$

with

$$a = k_{BC}$$
$$b = k_{CD}{}^0K_w/K_a{}^{HOCl}$$
$$c = k_{CD}{}^-$$
$$d = k_{CB}$$

and at fixed $[OH^-]$ this can be simplified to:

$$k = A/(1 + B/[OCl^-])$$

Then $k + kB/[OCl^-] = A$, $k = A - B\{k/[OCl^-]\}$, and a plot of k_{obs} vs. $k_2 = k_{obs}/[OCl^-]$ will give A and A/B as the y- and x-intercepts.

When the analysis was carried out, the data showed considerable scatter, but were in rough accord with the mechanism of Scheme 1.

The data could also be analyzed directly by least squares, determining all three parameters at once by fitting to the equation:

[3] $$k_{obs} = (e + f[OH^-])/(1/[OCl^-] + e/g[OH^-] + f/g)$$

with

$$e = k_{BC}k_{CD}{}^0K_w/k_{CB}K_a{}^{HOCl}$$
$$f = k_{BC}k_{CD}{}^-/k_{CB}$$
$$g = k_{BC}$$

With the full set of 28 points we found that the parameter "e" was not well defined. If seven points deviating from the curve by more than 20% were deleted from the set, all three parameters were better defined, but the "e" parameter still had errors larger than its value. The values for the parameters obtained by least squares are:

	Full set	Truncated set
e	0.210 ± 0.274	0.176 ± 0.191
f	19.9 ± 6.70	20.8 ± 3.67
g	0.0480 ± 0.0258	0.0473 ± 0.0117

We conclude that although the data almost define the "intercept" parameter, this parameter is really not yet properly defined and little confidence can be placed in it. It is at best a limit, since it might be smaller, but would be readily determined if it were larger.

Since the three-parameter equation was not well defined by the data, attempts were made to fit the data using a simpler equation, corresponding to negligible reaction of the enolate with hypochlorous acid.

$$k = f[OH^-]/(1/[OCl^-] + f/g)$$

A reasonable fit was obtained with the full data set and a better fit was obtained if eight points deviating by more than 20% from the curve were deleted:

	Full set	Truncated set
f	22.5 ± 9.19	22.4 ± 4.06
g	0.0467 ± 0.035	0.0462 ± 0.01371

The three parameter equation gives a better fit, and there is adequate justification for using it based on the results obtained with other ketones, even though one parameter is not well defined.

We can calculate the pK_a on the assumption that the intercept has been determined. As has been previously shown (9):

$$pK_a = \log k_{diffusion} + pK_a^{HOCl} - \log (k^0) \geqslant 17.61$$

k^0 might be smaller, in which case pK_a would be higher; we can only put a lower limit on it. It seems certain that hydroxyacetone will be more acidic than acetone because of the electron-withdrawing effect of the hydroxyl group. This puts an upper limit on pK_a, namely, that of acetone.

Since $k_{BC} = 0.0473 \pm 0.0117\ M^{-1}\,s^{-1}$, we may calculate from the pK_a of the ketone that $k_{CB} \geqslant 190\ s^{-1}$, and that $k_{CD}{}^- \geqslant 8.55 \times 10^4\ M^{-1}\,s^{-1}$.

The values for the rate constants for the second phase of the kinetics measured starting with monochloroacetone are also in qualitative agreement with values calculated from eq. [3]. The second phase rate constants were of low precision because they are based on a small absorbance change and may be accompanied by other side reactions, including the slow decomposition of hypochlorite. In some cases the reactions were not followed long enough to determine the rate constant very well. Accordingly rate constants from these experiments were not included in the least-squares fit. Figure 2 shows a three-dimensional representation of the dependence of k_{obs} on $[OH^-]$ and $[OCl^-]$.

Chlorination of dichloroacetone

The halogenation of 1,1-dichloroacetone was also studied. It was possible to determine the stoichiometry of the reaction and show that it was often close to unity. From the absorbance change accompanying reaction we could determine the amount of OCl^- consumed by a known amount of dichloroacetone. The data in Table 5 show that for low concentrations of hydroxide the stoichiometry was very close to one OCl^- consumed per mole of ketone, consistent with almost complete conversion to acetate by way of trichloroacetone.

At pH 10 reaction with hypobromite was very fast. The amount of bromine consumed (Table 5) was 1.12 moles per mole of ketone, based on the change in absorbance. Except for a small absorbance change with a rate constant of around $3 \times 10^{-2}\ s^{-1}$, attributed to impurities, the consumption of bromine was complete within the time of mixing. This implies a pseudo-first order rate constant greater than $0.1\ s^{-1}$, and a second order rate constant for hydroxide catalyzed enolization greater than $1000\ M^{-1}\,s^{-1}$.

Enolization rates were determined by measuring the rate of bromination in phosphate and acetate buffers as well as $10^{-3}\ M$ HCl; these data are also found in Table 5. The reactions were

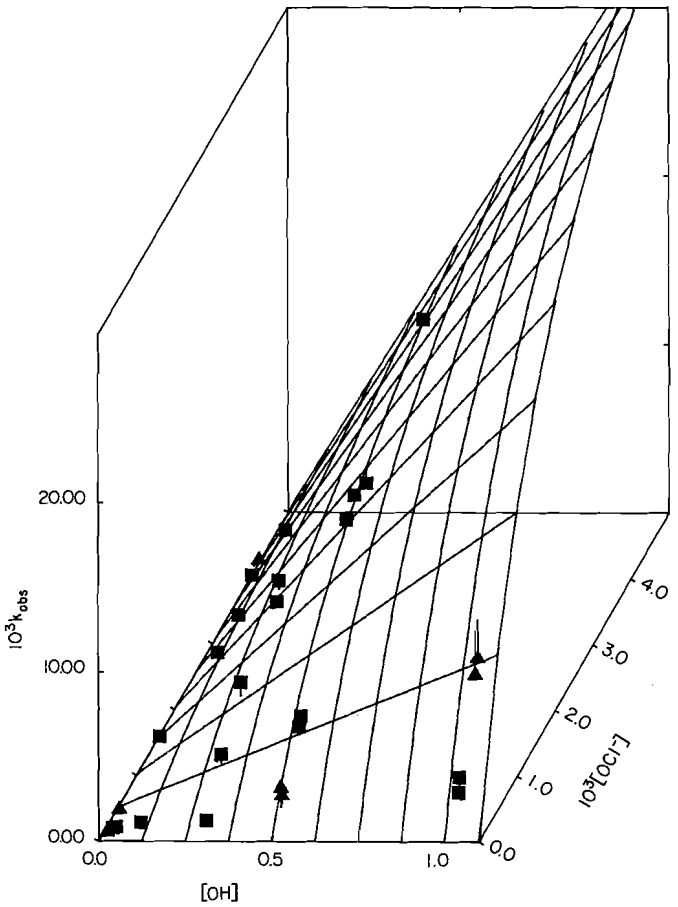

FIG. 2. Rate constants for the chlorination of monohydroxyacetone, fitted to $k = \{(0.210 \pm 0.274) + (19.9 \pm 6.70)[OH^-]\}/\{1/[OCl^-] + (0.210 \pm 0.274)/(0.0480 \pm 0.0258)[OH^-] + (19.9 \pm 6.70)/(0.0480 \pm 0.0258)\}$. (■) points falling within 20% of the calculated surface; (▲) points falling more than 20% off the calculated surface.

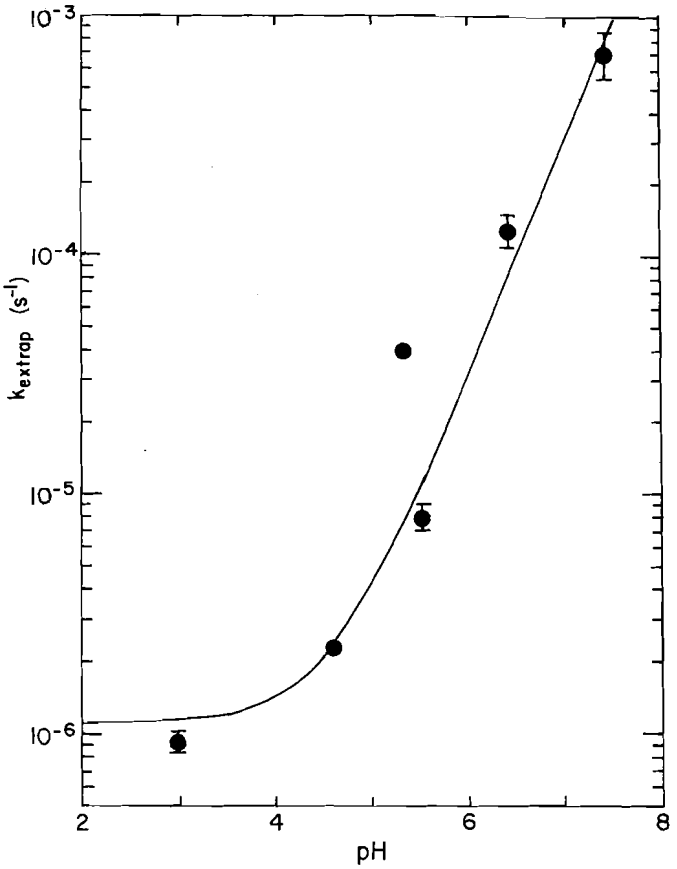

FIG. 3. pH rate profile for the enolization of dichloroacetone; all rate constants extrapolated to zero buffer concentration. The calculated line is based on $k = 1.11 \pm 0.20 \times 10^{-6} + (3010 \pm 514)[OH^-]$.

initially zero order in bromine, but at long times became first order in bromine. The initial slopes were used as a measure of the enolization rate, and were first order in buffer. Extrapolation to zero buffer gave rate constants which contained only the water and hydroxide rates, from which we determined by weighted least squares

$$k_{extrap} = \{(1.1 \pm 0.2) \times 10^{-6} + (3010 \pm 514)[OH^-]\}\ s^{-1}$$

The phosphate catalyzed enolizations at pH 5.33 were anomalous, in that both slope and intercept were out of line with the results of phosphate-catalyzed reactions at higher pH. Since we had only three runs at pH 5.33 and these happened to fall very close to a straight line, the weights based on least-squares fitting were very high. Results at pH 5.33 were not used for further calculations. Figure 3 shows the corresponding pH rate profile.

Our value for the rate constant for uncatalyzed reaction (the water rate) is $(1.1 \pm 0.2) \times 10^{-6}\ s^{-1}$ where Bell reported $7.3 \times 10^{-7}\ s^{-1}$ (12). Our value for the rate constant for acetate-catalyzed enolization is $(5.3 \pm 0.2) \times 10^{-4}\ M^{-1}\ s^{-1}$ where Bell reported $5.7 \times 10^{-4}\ M^{-1}\ s^{-1}$ (12). Our value for the phosphate dianion rate constant is $0.018 \pm 0.005\ M^{-1}\ s^{-1}$; a value of $0.0122\ M^{-1}\ s^{-1}$ can be estimated from the Bell's (12) Brønsted equation using a pK_a of 6.42 for phosphate. For all of these rate constants the agreement is reasonable considering that it was necessary to use initial slopes, and that lines were fitted to limited numbers of points. For the hydroxide-catalyzed reaction, our value for the rate constant is $3010\ M^{-1}\ s^{-1}$ where Bell reported $450\ M^{-1}\ s^{-1}$; here the disagreement is more serious, and again we have no satisfactory explanation for the anomaly.

Product ratios were determined by ^{1}H-nmr analysis of product solutions. The results of these experiments are summarized in Table 6. The only products seen were acetate and lactate.

Graphical analysis showed that the product ratio, r = [acetate]/[lactate], was roughly linear in [OCl$^-$] (lines passing through the origin) for fixed [OH$^-$], and $1/r$ was linear in [OH$^-$] (lines passing through the origin) for fixed [OCl$^-$]. When r was plotted as a function of [OCl$^-$]/[OH$^-$], a line passing through the origin with slope 156 was obtained. The only serious deviation was for the point at [OH$^-$] = 0.049 and [OCl$^-$] = 0.0071, which is also the point with the largest value of r, based on the most dissimilar peak areas.

The rate of the combined halogenation/hydrolysis could be followed by monitoring the uv absorption of hypochlorite. The rate constants so obtained are listed in Table 5. These rate constants could be fitted to:

$$k_{obs} = a + b[OH^-] + c[OCl^-]$$

where, in terms of Scheme 1,

$$a = k_{ED}$$
$$b = k_{QD}K_{EQ}$$
$$c = k_{57}^-/K_{5E} = k_{67}^-k_{56}/k_{65}K_{5E}$$

with

$a = 0.00445 \pm 0.00535$

$b = 0.0333 \pm 0.0134$

$c = 3.33 \pm 1.74$

Figure 4 shows the quality of the fit. The terms a and b are identified with hydrolysis of dichloroacetone. At the hydroxide concentrations used the ketone is entirely converted to the anionic hydroxide adduct, so that the "a" term corresponds to the hydroxide-catalyzed hydrolysis observed at low pH while the "b" term corresponds to hydrolysis via the dianion. In order to fit the entire pH rate profile for hydrolysis we calculated the contribution for hydrolysis alone for each of the observed rate constants by subtracting $c[OCl^-]$. We then fitted all the data to:

$$\frac{k_{obs}}{[OH^-]} = \frac{d + e[OH^-]}{1 + f[OH^-]}$$

where in terms of Scheme 1,

$d = k_{ED}K_{5E}/(1 + K_{5L})$

$e = k_{QD}K_{EQ}K_{5E}/(1 + K_{5L})$

$f = K_{5E}/(1 + K_{5L})$

with

$d = 4.77 \pm 0.60$

$e = 25.3 \pm 15.8$

$f = 992 \pm 216$

The quality of this fit is shown in Fig. 5.

The corresponding values from these two equations are:

$a = d/f$ and $b = e/f$

$a = 0.00445 \pm 0.0054$

$d/f = 0.0048 \pm 0.0034$

$b = 0.0333 \pm 0.0134$

$e/f = 0.0255 \pm 0.0114$

The agreement is satisfactory. Although we have not been able to determine precise values for the parameters, we have a consistent picture fitting the data in hand. From the parameters we can calculate the microscopic rate and equilibrium constants. From $f = 992$, we calculate $K_{5E} = 3.8 \times 10^3\ M^{-1}$. The value which we had estimated is $670\ M^{-1}$, which differs by 0.8 pK units. The difference is larger than one would wish but not outside the range to be expected for estimation procedures. Since $d/f = k_{ED}$, the latter is taken as $0.0048 \pm 0.0034\ s^{-1}$. From $e/f = k_{QD}K_{EQ} = 0.0255 \pm 0.0114$, we can calculate k_{QD} by using an estimated K_{EQ}, which we obtained using Pauling's rule (15) to estimate the second pK_a of 1,1-dichloro-2,2-dihydroxypropane. The value so obtained is $k_{QD} \cong 2.6\ s^{-1}$.

The product ratio, r = [acetate]/[lactate], could be calculated from the absorbance change, ΔA, assuming that the absorbance change represented reaction of part of the dichloroacetone with one equivalent of hypochlorite to give acetate, while the rest underwent hydrolysis followed by rearrangement to give lactate.

The product ratios, r, calculated from the values of ΔA determined by least squares are not in good agreement with those determined by nmr for experiments at low $[OH^-]$. If r values are calculated from the total absorbance change calculated from the infinity value and the absorbance before addition of ketone (corrected for dilution) then the agreement is much better. This suggests that an important amount of reaction

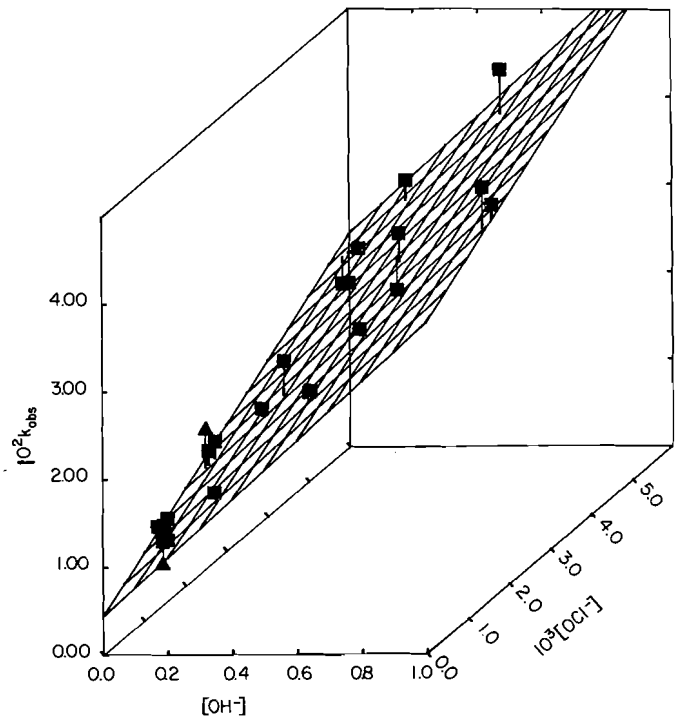

FIG. 4. Rate constants for the combined chlorination and hydrolysis of 1,1-dichloroacetone, fitted to $k = (0.00445 \pm 0.00536) + (0.0333 \pm 0.0134)[OH^-] + (3.33 \pm 1.74)[OCl^-]$. (■) points falling within 20% of the calculated surface; (▲) points falling more than 20% off the calculated surface.

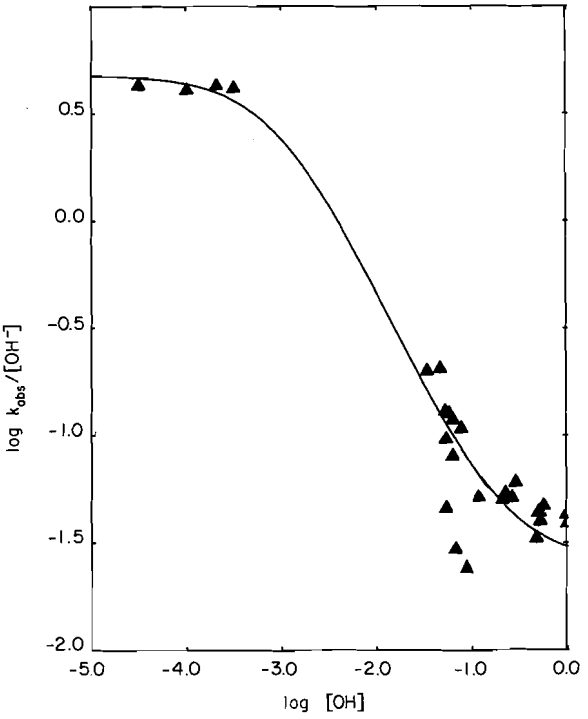

FIG. 5. Rate constants for the hydrolysis of 1,1-dichloroacetone. Values at low $[OH^-]$ by direct measurement, values at higher $[OH^-]$ calculated from rate constants for combined hydrolysis and chlorination by subtracting the contribution from chlorination. The data were fitted to $k_{obs}/[OH^-] = \{(4.77 \pm 0.60) + (25.3 \pm 15.8)[OH^-]\}/\{1 + (992 \pm 216)[OH^-]\}$.

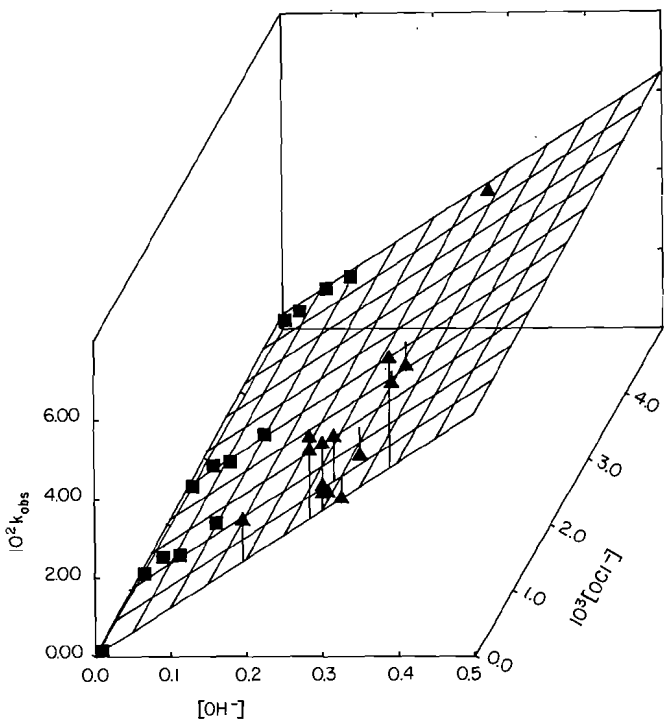

FIG. 6. Rate constants for the combined chlorination and rearrangement of 1,1-dihydroxyacetone, fitted to $k = (0.00034 \pm 0.00027) + (0.673 \pm 0.151)[OCl^-] + (0.122 \pm 0.0155)[OH^-]$. (■) points included in the least squares fit; (▲) points which were not included in the least squares fit, and which fall off the calculated surface.

occurs before measurements begin. This could be the result of the reaction of the keto form of dichloroacetone with hypochlorite before there was time for keto–hydrate anion equilibrium to be established. The phenomenon, a total absorbance change corresponding to the expected stoichiometry, while the measurable kinetic process corresponds to a smaller amount of reaction, has been seen repeatedly in these experiments.

One explanation which must be considered immediately is that the fast reaction, completed before the recording of absorbance time data begins, is the actual reaction of dichloroacetone, while the measurable process is some subsequent reaction. We reject this explanation because the reaction subsequent to chlorination of dichloroacetone, namely haloform cleavage, is rapid and is not expected to lead to any absorbance change, and the reaction subsequent to hydrolysis, namely the chlorination/rearrangement of dihydroxyacetone, shows quite different kinetics and very small consumption of hypochlorite.

There is clearly something complicated going on which will reveal further details of the reaction upon suitable investigation. For the purpose of defining the behaviour of fully equilibrated dichloroacetone the kinetic parameters are adequate. For the immediate purpose of defining the behavior of dichloroacetone generated in situ in the course of the chlorination of acetone, the rate ratio implied by the nmr studies, and the total absorbance changes, is a better guide to the partitioning of this intermediate.

The clear implication of this work is that the major form of dichloroacetone in solution in dilute hydroxide is the hydrate monoanion, and that halogenation will occur at a rate inversely proportional to $[OH^-]$.

Chlorination and rearrangement of 1,1-dihydroxyacetone

2-Oxopropanal (pyruvaldehyde, methylglyoxal) is shown by ^{1}H-nmr to be a mixture of two species in aqueous solution. The major species has a signal at 2.30 attributed to the methyl of 1,1-dihydroxyacetone, and the minor species has a signal at 1.37 attributed to 1,1,2,2-tetrahydroxypropane. Form the areas of the peaks we calculate that the dimensionless equilibrium constant for hydration of 1,1-dihydroxyacetone is 0.61. The chlorination of 1,1-dihydroxyacetone was studied in order to determine the rates of its reaction, the stoichiometry, and the rate of the rearrangement to lactate. These kinetics results are found in Table 7. This latter reaction was difficult to study directly because the absorbance change accompanying rearrangement is small, making it difficult to perform studies at low concentrations. Unfortunately kinetics at higher values of $[OH^-]$, greater than $0.2\,M$, with or without hypochlorite present, gave fast and irreproducible kinetics, with $k_{obs} > 0.04\,s^{-1}$. These kinetics did not fit the general pattern seen at lower hydroxide concentrations, and were subject to a scatter of 25–30%. The data for $[OH^-] < 0.2\,M$ were fitted to:

$$[4] \quad k = a + b[OCl^-] + c[OH^-]$$

where, in terms of Scheme 1,

$$a = k_{HJ}$$
$$b = k_{HG}$$
$$c = k_{IJ}K_{HI}$$

This gave a very good fit; the parameters determined by least squares were:

$$a = 0.00034 \pm 0.00027$$
$$b = 0.673 \pm 0.151$$
$$c = 0.122 \pm 0.0155$$

It should be noted that eq. [4] assumes that the major substrate species in solution is the anionic form of methylglyoxal hydrate, either rearranging with or without hydroxide catalysis or else reacting with ClO^-. Under most conditions relevant to the present study, halogenation is a minor side reaction. The quality of the fit is shown in Fig. 6.

Haloform cleavage of trichloroacetone

The kinetics of this reaction were followed by the pH-stat technique. The data are found in Table 8. These values led to a second order rate constant for hydroxide-catalyzed breakdown of $48.2\,M^{-1}\,s^{-1}$.

Summary of rate constants

All of the rate and equilibrium constants for processes shown in Scheme 1 which are currently known or estimated are given in Table 9.

Discussion

Hydrolysis of chloroacetone

The hydrolysis of chloroacetone is a rapid reaction. Although substitution reactions of powerful nucleophiles with α-halo ketones are normally considered to occur by the S_N2 mechanism (16, 17) with some special accelerating effects attributed to the carbonyl group (18–21), it seemed worthwhile to test whether the present reaction was occurring at a rate which was plausible for the classical mechanism. To do this we endeavored to estimate the rate of the substitution from rates of reaction of other nucleophiles which must react by direct displacement.

The closest available data to the rate constants we wish to estimate are for reactions of nucleophiles with α-halo ketones in aqueous dimethyoxyethane at 54.8°C (16). No temperature

TABLE 9. Rate and equilibrim constants for individual steps in Scheme 1

k_{12}	$= 0.173\ M^{-1}\ s^{-1}$
k_{21}	$= 4.1 \times 10^4\ s^{-1}$
k_{23}^0	$= 1.7 \times 10^9\ M^{-1}\ s^{-1}$
k_{23}^-	$= 2.0 \times 10^4\ M^{-1}\ s^{-1}$
k_{34}	$= 136\ M^{-1}\ s^{-1}$
k_{43}	$= 7.8 \times 10^3\ s^{-1}$
k_{45}^0	$= 1.7 \times 10^9\ M^{-1}\ s^{-1}$
k_{45}^-	$= 2 \times 10^4\ M^{-1}\ s^{-1}$
k_{56}	$= 3010\ M^{-1}\ s^{-1}$
k_{57}^-	$= 1.3 \times 10^4\ M^{-2}\ s^{-1}$
k_{65}	= unknown
k_{67}^0	= unknown
k_{67}^-	= unknown
k_{79}	$= 48.2\ M^{-1}\ s^{-1}$
K_{78}	$= 1.0 \times 10^5\ M^{-1}$
K_{7M}	= 50.
K_{M8}	$= 2.0 \times 10^3\ M^{-1}$
k_{89}	$= 0.023\ s^{-1}$
K_{8P}	$= 0.02\ M^{-1}$
k_{P9}	= unknown, but $< 4.5 \times 10^5\ s^{-1}$; estimated value $3000\ s^{-1}$
k_{3B}	$= 1.19\ M^{-1}\ s^{-1}$
K_{3K}	= 0.11
K_{3A}	$= 1.7\ M^{-1}$
k_{AB}	$= 0.78\ s^{-1}$
k_{BC}	$= 0.047\ M^{-1}\ s^{-1}$
k_{CB}	$\geq 190\ s^{-1}$
k_{CD}^0	$= 1.7 \times 10^9\ M^{-1}\ s^{-1}$
k_{CD}^-	$\geq 8.6 \times 10^4\ M^{-1}\ s^{-1}$
k_{5D}	$= 4.27\ M^{-1}\ s^{-1}$
K_{5L}	= 2.86
K_{5E}	$= 670\ M^{-1}$ (estimated)
	$= 3.8 \times 10^3\ M^{-1}$ (determined from our kinetics)
K_{EQ}	$= 0.002\ M^{-1}$ (estimated)
k_{ED}	$= 0.0048\ s^{-1}$
k_{QD}	$= 2.6\ s^{-1}$
k_{DJ}^-	$= 0.15\ M^{-1}\ s^{-1}$
k_{DJ}^{2-}	$= 54\ M^{-2}\ s^{-1}$
K_{DH}	$= 708\ M^{-1}$
K_{DN}	= 0.61
K_{DO}	$= 17\ M^{-1}$
K_{NO}	$= 28\ M^{-1}$
K_{HI}	$= 0.007\ M^{-1}$
k_{IJ}	$= 17\ s^{-1}$
k_{HJ}	$= 0.00034\ s^{-1}$
k_{HG}	$= 0.67\ M^{-1}\ s^{-1}$
k_{IG}	= unknown
k_{DF}	= unknown; estimated value $0.02\ M^{-1}\ s^{-1}$
k_{FD}	= unknown
k_{FG}	= unknown
k_{FJ}	= unknown
K_{KA}	= 16.
K_{LE}	= 234.

dependence studies were done for chloroacetone itself; the closest model is the reaction of AcO^- with 1-bromo-2-butanone for which the $\Delta S^{\ddagger}$ is -5. We will assume that $\Delta S^{\ddagger}$ is the same for the reactions of simple ionic nucleophiles with chloroacetone. The rate constant for the reaction of acetate with chloroacetone is $1.14 \times 10^{-3}\ M^{-1}\ s^{-1}$ (16). For bromoacetone, rate constants for acetate ($1.46 \times 10^{-3}\ M^{-1}\ s^{-1}$) and azide ($94.8 \times 10^{-3}\ M^{-1}\ s^{-1}$) were reported (16). We will assume that the rate ratio is the same, and so estimate a rate constant for the reaction of chloroacetone and azide as $7.4 \times 10^{-2}\ M^{-1}\ s^{-1}$. We then correct to 25°C and get rate constants for acetate ($3.78 \times 10^{-5}\ M^{-1}\ s^{-1}$) and azide ($3.74 \times 10^{-3}\ M^{-1}\ s^{-1}$). Then using Swain–Scott n values (acetate, 2.72; azide, 4.00; hydroxide, 4.20; all from Wiberg (22) we get $k = 0.0077\ M^{-1}\ s^{-1}$ for hydroxide. This is clearly slower than the observed value ($1.19\ M^{-1}\ s^{-1}$). Unfortunately there are a number of weak points in the estimation procedure which we had to use, and so we cannot have high confidence that the mechanism is not S_N2, although there is a basis for very strong doubt.

The observed rate constant for the reaction of hydroxide with chloroacetone to give hydroxyacetone presumably represents the reaction of the hydroxide adduct, so it is the product of a rate and an equilibrium constant. The equilibrium constant can be estimated as $1.7\ M^{-1}$. The equilibrium constants for hydration of mono- and dichloroacetone have been reported (23); the pK_a's for the hydrates can be calculated using Hine's equation ($pK_a = 14.19 - 1.32\Sigma\sigma^*$) (24); the equilibrium constants for addition of hydroxide then come from a simple cycle; see Table 10.

The rate constant for the intramolecular reaction can now be calculated to be $0.78\ s^{-1}$. This is somewhat faster than what might have naïvely been expected. For $^-O—CH_2—CH_2—Cl$, the rate constant is $0.022\ s^{-1}$ (25). One can, however, anticipate that the cyclization should be favored by the additional substituents present in $^-O—C(OH)(CH_3)—CH_2—Cl$ (26), so that a rate constant greater than $0.022\ s^{-1}$ is to be expected, although it is not clear how much greater. Base-catalyzed cyclization of $HOC(CH_3)_2—CH_2—Cl$ is 252 times faster than that of $HO—CH_2—CH_2—Cl$ (26, 27). Once again the arguments are suggestive but not compelling.

TABLE 10. Equilibrium constants for addition of water and hydroxide to mono-, di-, and trichloroacetone[a]

Ketone	K_{hyd}[b]	K_a[c]	K_{OH}
$MeCOCH_2Cl$	0.11	12.80	1.7
$MeCOCHCl_2$	2.86	11.63	670
$MeCOCCl_3$	50	10.69	1.0×10^5

[a]In water at 25°C.
[b]Values from ref. 23; value for trichloroacetone estimated after ref. 23.
[c]$pK_a = 14.19 - 1.32\Sigma\sigma^*$ (24).

Thus for chloroacetone a plausible case can be made for reaction by an addition–intramolecular displacement mechanism, rather than direct S_N2 attack, but the case cannot be considered proven.

Other, closely related, reactions have been attributed to the addition-intramolecular displacement mechanism. Addition of alkoxide and formation of an alkoxy-oxirane (or products derived from it) is a well-known side reaction in the Favorskii rearrangement (28–31). For secondary α-halo ketones (but not primary) an alternative mechanistic path is available for hydrolysis, namely, solvolysis of the α′-enol (32). Fortunately this additional path is unlikely (32) for the present system, which is already sufficiently complicated.

We may estimate rate constants for the addition of hydroxide to the carbonyl groups of mono- and dichloroacetone from the

TABLE 11. Rate constants for addition of hydroxide to mono-, di-, and trichloroacetone[a]

Compound	K^b (M^{-1})	$k_{on}{}^c$ ($M^{-1}\,s^{-1}$)	k_{off} (s^{-1})
$MeCOCH_2Cl$	1.7	1.3×10^4	7.6×10^3
$MeCOCHCl_2$	470	2.0×10^5	4.3×10^2
$MeCOCCl_3$	1.0×10^5	1.7×10^6	1.7×10^1

[a]In water at 25°C.

[b]Equilibrium constant for the addition of hydroxide to ketone, producing an anionic adduct; values from Table 10.

[c]k_{on} is the rate constant for the addition of hydroxide to carbonyl; k_{off} is the rate constant for the expulsion of hydroxide from the anionic adduct. Values were calculated using the appropriate Marcus equation (33), for which $b = 6$. b is the "intrinsic barrier" expressed in units of log k.

equilibrium constants calculated above and the Marcus correlation for rate and equilibrium constants for addition of hydroxide to carbonyl compounds (33) (see Table 11):

$$\log k = 10 - b(1 - \log K/4b)^2$$

Note that these rates make the addition reaction the fastest reaction channel available. The peculiar behavior observed in the kinetics of halogenation/hydrolysis of dichloroacetone suggest that for dichloroacetone there may be steric hindrance to the addition of hydroxide, leading to slower reaction than predicted in Table 11.

Hydrolysis of dichloroacetone

Although we could not find any information allowing an estimation of the rate constant to be expected for simple S_N2 attack of hydroxide on 1,1-dichloroacetone, we can state that this reaction would be expected to be considerably slower than the S_N2 attack of hydroxide on monochloroacetone. Streitwieser (34) gives relative rate data for the reactions of methoxide ion in methanol at 50°C with dibromomethane and bromoethane; the rates are in the ratio 0.0078:1. This comparison is for the effect of the second halogen atom with steric effects roughly compensated; since methyl bromide reacts 23 times faster than ethyl bromide with ethoxide in ethanol the rate ratio for dibromomethane and monobromomethane would be more like 0.0003:1. Although these data represent an imperfect model for the case of 1,1-dichloroacetone vs. monochloroacetone, it is clear that for the S_N2 mechanism the former must be much slower. In fact, as was shown above, 1,1-dichloroacetone is somewhat *more* reactive; this demands the conclusion that it does not react by the S_N2 pathway. If, as we suggested was likely, monochloroacetone does not react by the S_N2 pathway either, this conclusion becomes even stronger.

From the fit of the experimental rate constants to the appropriate portions of the mechanism in Scheme 1, we obtained $k_{ED} = 0.0048\ s^{-1}$. It should be noted that this is almost 1000 times slower than the analogous rate constant for monochloroacetone. As shown above, one expects approximately this ratio based on the analogy with mono- and dibromomethane. Thus the proposal that both reactions proceed by the addition–intramolecular displacement mechanism is consistent with the facts.

Chlorination of chloroacetone

From the total change in absorbance due to hypochlorite ion accompanying reaction of monochloroacetone it is possible to calculate the stoichiometry. These measurements are complicated by the slow second phase of the reaction representing halogenation of the hydroxyacetone produced as a byproduct in the fast phase of halogenation. Furthermore there is a very slow pseudo-zero order decrease in absorbance, probably due to decomposition of the hypochlorite ion. For experiments where reaction was relatively rapid the stoichiometry was in the range of 1.5–2.0 moles of OCl^- per mole of monochloroacetone. This is consistent with competing chlorination and hydrolysis, since hydrolysis to hydroxyacetone is followed by consumption of a single mole of OCl^- and then rearrangement to lactate.

The stoichiometry for the initial rapid phase can be estimated from the absorbance change for this phase alone. Values so calculated show considerable scatter, but a plot of n (moles of OCl^- consumed per mole of ketone reacting) vs. $[OCl^-]/[OH^-]$ is in approximate accord with a line calculated from the rate law for the reactions of monochloroacetone, making the simplifying assumption that all dichloroacetone formed consumes another mole of OCl^-.

The equilibrium constant estimated for the addition of OH^- to monochloroacetone implies that for $[OH^-]$ less than 1 M, the anionic adduct is not present as a significant fraction of the total ketone.

Although no products attributable to Favorskii rearrangement were observed, it seems worthwhile to examine the question of why this common reaction of α-haloketones is not a competing side reaction accompanying the halogenation in alkaline solution.

We will first estimate rates of enolization at the α and α′ carbons. The pK_a for chloroacetone at the carbon bearing a chlorine has been calculated above as 15.8 (subject to the assumption that the enolate of chloroacetone reacts with hypochlorous acid at a diffusion-controlled rate). To estimate the pK_a at the other α′ carbon we need an estimate for the effect of a chlorine on the other side. The only available data are rate constants for enolization of 1,3-dichloroacetone from Bell's study (12), which led (35) to a pK_a of 11.04 ± 0.20, based on four carboxylic acids. The same pK_a estimation procedure applied to Bell's data for monochloroacetone led to a pK_a of 14.1 (35), which is quite different from the value calculated in this work. One possible explanation is that there is a different intrinsic barrier associated with deprotonation of a chloromethyl ketone than for a methyl ketone. If one determines a b value (intrinsic barrier in log k units) from the rate constants for carboxylate-catalyzed enolization of chloroacetone using the pK_a derived from the present work, one obtains a value of 7.4 (as opposed to the value of 9.9 for simple alkyl ketones (35)). If this new b value is used for the data for 1,3-dichloroacetone, one estimates a pK_a of 12.7. This means that there is a 3.1 pK_a unit effect of a chlorine on the opposite side of the carbonyl. The effect of a chlorine at the α carbon is 3.3 units (pK_a acetone = 19.1 (9)). We now estimate the pK_a at the α′-carbon of monochloroacetone to be 16.0.

The rate constant for reaction at the α-carbon has been determined in this work as $367\ M^{-1}\,s^{-1}$. For the α′-carbon, using the Marcus relation from ref. 35, with $b = 9.9$ (since there is no chlorine on the carbon bearing the enolizable hydrogen) and a pK_a for H_2O of 15.74, we get $k_{cor} = 0.89\ M^{-1}\,s^{-1}$, which leds to $k_{obs} = 2.7\ M^{-1}\,s^{-1}$, and a rate constant for reprotonation of $270\ s^{-1}$.

For use with Bordwell's results (29, 36), we will do the same for 1-chloro-3-phenylacetone. For phenylacetone the pK_a values are α-, 15.91; α′-, 18.27 (35). Then for the chloro compound, C-1, $pK_a = 18.27 - 3.3 = 15.0$; C-3, $pK_a = 15.91 - 3.1 = 12.8$. When rate constants for hydroxide-catalyzed

enolization are estimated using the appropriate b values in each case, we estimate them as C-1, $k_{OH} = 1200\,M^{-1}\,s^{-}$; C-3, $k_{OH} = 45\,M^{-1}\,s^{-}$. These are necessarily quite approximate estimates, but in fact the exchange results say that they are in the correct order because there is more exchange next to the chlorine, although the two exchange rates are close. The reverse rate constants can be estimated as C-1, $k_w = 1.2 \times 10^4\,s^{-1}$; C-3, $k_w = 2.8\,s^{-1}$.

In order to estimate rate constants for the Favorskii rearrangement, we start with the studies of Bordwell *et al.* (29), (36). Bordwell gives rate constants for the rearrangement of 1-chloro-3-phenylacetone in water–methanol mixtures with up to 50% water present (29). The rate-determining step is changing as the solvent changes because the fraction of exchange is varying. We will correct for this solvent effect by using a log k vs. Y correlation to extrapolate to water; the data employed are given in Table 12. We then use the fraction of exchange to determine the partitioning ratio between reprotonation and rearrangement, and assume that this rate ratio follows Y as well, to extrapolate to water. Then in water, using our estimated rate constant for reprotonation, we calculate a rate constant for the Favorskii step in water. We then consider the probable magnitude of the effect of the phenyl substituent on the rate constant for the ionization step, in order to calculate a rate constant for the reaction of chloroacetone from the rate constant for 1-chloro-3-phenyl-2-propanone.

A plot of log k for the rearrangement vs. Y gives log $k = -0.775 + 0.648Y$, $r = 0.995$, which leads to $k = 31.7\,M^{-1}\,s^{-1}$ in water at 0°C. In pure methanol the temperature effect is such that the rate at 25°C is 34 times the rate at 0°C. This rate ratio leads to a value of the apparent rate constant for the Favorskii rearrangement of 1-chloro-3-phenylacetone in water at 25°C of $1080\,M^{-1}\,s^{-1}$. It is subject to the assumption that the rate-determining step is the same in methanol as in water, and that the partitioning of the intermediate is not a function of temperature. Both assumptions are questionable. The value estimated is the overall rate constant $= k_{deprot}/[1 + (k_{reprot}/k_{ion})]$. As we will see k_{reprot}/k_{ion} is likely to be less than 1 in water so that the overall rate constant should be essentially the rate of deprotonation, for which the temperature coefficient k_{25}/k_0 is likely to be small; a value of $k_{25}/k_0 = 7.67$ is reported for acetone in water (10). Using this value as an estimate of the effect of temperature on the overall rate of the Favorskii rearrangement in water would lead to $k_{observed} = 243\,M^{-1}\,s^{-1}$; we had estimated above that k_{deprot} would be $45\,s^{-1}$.

We next consider the partitioning of the intermediate. We assume that α′ deuterium exchange represents reprotonation of the enolate, which partitions between reprotonation and solvolysis, and that reprotonation in deuterated medium leads to deuterated product. Then from the observed percent exchange (29) we can calculate the rate ratio, $r = k_{reprot}/k_{Fav}$, and extrapolate to water assuming log (r) is linear in Y, as shown in Table 13; since only two exchange experiments were done the assumption cannot be tested.

We can estimate the rate constant for the Favorskii step, based on the partitioning ratio, which is for the moment assumed to be temperature independent. If the rate constant for the reprotonation step is $2.8\,s^{-1}$ in water (*vide supra*) and the rate ratio is 0.102, then the microscopic rate constant for the Favorskii ionization is $27\,s^{-1}$.

One must now consider the effect of the phenyl group in 1-chloro-3-phenylpropanone on the rate of the Favorskii ionization. Streitwieser (37) gives rates for phenylallyl chloride relative to allyl chloride. The rate ratio is solvent dependent, being 139:1 at 100% EtOH at 44.6°C and 7700:1 in 50% EtOH at 44.6°C. Once again we must do an extrapolation making the untested assumption that the rate ratio is linear in Y; see Table 14. The extrapolated value for water is 58000:1.

If we use this rate ratio, and assume that it is insensitive to temperature, we predict that the rate of the Favorskii ionization for the enolate of chloroacetone would be $27/58\,000 = 5 \times 10^{-4}\,s^{-1}$. An argument in favor of this rate ratio is that ρ for 1-aryl-3-chloroacetones is −5. Nevertheless it is very possible that the rate ratio overestimates the effect of the phenyl substituent, because an oxyallyl cation should be sufficiently much more stable than an allyl cation to make less demand upon the substituents for stabilization. It is known that solvolysis of the enol of 3-chloro-1-phenyl-2-butanone readily leads to methoxyketone products, while analogous products are not seen in the reactions of 1-chloro-3-phenyl-2-propanone (32); clearly stabilization of the "carbocation" is still very important at least in the enol. Since 1-chloro-3-phenyl-2-propanone undergoes Favorskii rearrangement, ionization of the enolate is facile in

TABLE 12. Extrapolation of the rate constant for the Favorskii rearrangement of 1-chloro-3-phenylpropanone to aqueous solution[a]

Volume % H_2O	Y[b]	k ($M^{-1}\,s^{-1}$)	log k
0	−1.079	0.0263	−1.58
5	−0.699	0.0623	−1.21
10	−0.327	0.131	−0.88
25	0.689	0.503	−0.30
50	1.970	2.89	0.46
100	3.512	(31.7	1.50)[c]

[a]Data from ref. 29; kinetics at 0°C.
[b]Estimated Y values for Bordwell's solvent mixtures. He reported vol.% which we will assume follows the Winstein convention and means x% of A and 100 − x% of B. Then the mole fraction, N, can be calculated directly. Fainberg and Winstein (49) report values of Y for various solvent water mixtures, and give polynomials relating Y to N. We used the polynomial to calculate Y for Bordwell's mixtures.
[c]Estimated by linear extrapolation of a plot of log k vs. Y.

TABLE 13. Solvent effect on the partitioning of the α′-enolate from 1-chloro-3-phenylpropanone[a]

%MeOH	%exchange	r	log r	Y
100	86	6.14	0.79	−1.079
50	29	0.408	−0.39	1.970
(0		0.102	−0.99[b]	3.512)

[a]Data from ref. 29; kinetics at 0°C.
[b]Extrapolated assuming a linear relation between log r and Y.

TABLE 14. Solvent effect on the rate ratio for ionization of phenylallyl chloride relative to allyl chloride[a]

Vol.% EtOH	Y	Ratio	log ratio
100	−2.033	139	2.14
50	1.655	7700	3.89
(0	3.493	58000[b]	4.76)

[a]Relative rates from ref. 37.
[b]Extrapolated assuming a linear relation between log ratio and Y.

this system. Thus we can only estimate upper and lower limits on the rate of Favorskii ionization for the α′-enolate of monochloroacetone, and the pattern is:

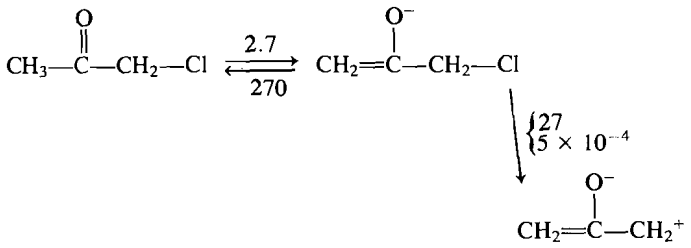

with an overall rate constant, $k_1k_2/(k_{-1} + k_2)$, of $0.27[OH^-]$ s^{-1} estimated if the effect of the phenyl substituent in 1-chloro-3-phenyl-2-propanone is negligible, and $5 \times 10^{-6}[OH^-]\,s^{-1}$ using the large effect of the phenyl substituent estimated using the allyl system as a model. Both of these estimates are smaller than the observed rate constant for hydrolysis, namely, $1.19\ [OH^-]\,s^{-1}$.

The facts of the matter are clearly that the Favorskii rearrangement does not happen, because the nmr shows no sign of propionate, which would be clearly detectable if it were 10% of the total, and probably so even if it were less. The competing reactions are trapping of the α-enolate by halogen and intramolecular displacement by the hydroxide adduct, with the latter often being the dominant reaction. This suggests that the estimation procedure which we used for the upper limit on the rate of the Favorskii rearrangement has led to too high a value. Unfortunately there does not seem to be information available which would permit a better estimate of the value to be expected for our system.

Chlorination of hydroxyacetone

The stoichiometry of the hydroxyacetone reaction appears to be a function of $[OH^-]$; at $0.486\,M$ $[OH^-]$ it is 1.25 while at $0.0129\,M$ $[OH^-]$ it is 1.85 (9). This suggested that there is a competition between rearrangement, which is hydroxide-dependent and leads to a stoichiometry of 1, and a hydroxide-independent second halogenation which leads to a stoichiometry of 2. One must be cautious because the lower hydroxide concentrations lead to slower reactions which may also have more drift, giving spuriously high stoichiometries. Product studies (9) revealed only lactate as a detectable product in the nmr, but the intensity of the peaks was less than expected. There was no acetate.

A plot of n_{app} vs. $[OCl^-]/[OH^-]$, using data from Table 4, showed a possible tendency to increase with increasing $[OCl^-]/[OH^-]$ masked by very considerable scatter. A line calculated on the basis of the observed rate law for the reaction of 1,1-dihydroxyacetone was consistently too low.

One possible explanation would be competing reaction at the methyl group. The proportions of reaction of the methyl and methylene of hydroxyacetone will depend upon the hypochlorite concentration, because at high concentration only the relative rates of ionization matter, and at low concentration only the rates of trapping of the enolate by hypochlorite matter. Using the rate constant for hydroxyacetone enolization evaluated above, i.e. $0.048\,M^{-1}\,s^{-1}$ as the value for the methylene group, and taking the value for acetone (corrected for the number of hydrogens) as an estimate for the methyl group, i.e. $0.087\,M^{-1}\,s^{-1}$, we calculate that at high hypochlorite, reaction would be 64% at the methyl and 36% at the methylene. However, these values are of purely theoretical interest because from the values of the microscopic rate constants for acetone in Table 9 we can calculate that "high hypochlorite" for reaction at the methyl group would be in excess of $20\,M$. At low hypochlorite concentration, and high enough $[OH^-]$ that the reaction of hypochlorite ion dominates, the rate constant for halogenation involving the enolate derived from the hydroxymethylene is $19.2\,M^{-1}\,s^{-1}$ (9), and half the rate constant for acetone, taken as an estimate for the value for reaction involving the enolate derived from the methyl of hydroxyacetone, is $0.044\,M^{-1}\,s^{-1}$. Thus at low hypochlorite less than 0.5% of the reaction is by way of the methyl group.

Chlorination of dichloroacetone

We found that the rate law for the chlorination/hydrolysis kinetics required terms for intramolecular nucleophilic attack by both the mono- and dianionic hydrates of dichloroacetone. The results described above led to a rate constant for the intramolecular reaction of the monoanion of $0.0048\,s^{-1}$, while the intramolecular reaction of the dianion had a rate constant of $2.6\,s^{-1}$. The rate ratio is 531, although it should be borne in mind that the ratio is dependent upon a quite uncertain estimate for the second pK_a of 1,1-dichloroacetone hydrate. For the, admittedly quite different, rearrangement of phenylglyoxal to mandelate, the rate ratio can be estimated as 2000 (*vide infra*).

We did not detect a term in the rate law corresponding to reaction of the enolate of dichloroacetone with hypochlorous acid. Consequently we cannot make any estimate of the pK_a of the ketone. In any case such an estimate would be of doubtful validity, because it is by no means certain that the reaction would be diffusion-controlled (9). The equilibrium constant estimated for the halogenation reaction is distinctly smaller than for the earlier halogenations (9), even though it is still 10^{24}. Thus even if we had a rate constant permitting an estimation of the pK_a, the value so estimated would only be an upper limit.

The rate constants for hydroxide catalyzed enolization of acetone, monochloroacetone, and dichloroacetone are $0.173\,M^{-1}\,s^{-1}$ (10), $136\,M^{-1}\,s^{-1}$, and $3800\,M^{-1}\,s^{-1}$, respectively. These should be corrected for the number of reactive hydrogens in order to compare reactivity; the corrected values are $0.0288\,M^{-1}\,s^{-1}$, $68\,M^{-1}\,s^{-1}$, and $3800\,M^{-1}\,s^{-1}$, respectivley, for relative rates of $1{:}2.4 \times 10^3{:}1.3 \times 10^5$. For comparison Cox and Warkentin (38) report rate constants for acetate-catalyzed enolization of acetone, monobromoacetone, and dibromoacetone at 30°C in aqueous solution as 7.38×10^{-8}, 3.27×10^{-4}, and 5.05×10^{-3} respectively (all $M^{-1}\,s^{-1}$, and corrected for the number of reactive hydrogens). The relative rates are $1{:}4.4 \times 10^3{:}6.8 \times 10^4$. The relative rates are similar to those we found for the chloro ketones. In contrast Bell and Lidwell reported rate constants for acetone, monochloroacetone, and dichloroacetone of 0.042, 4.7, and 450, respectively (all converted to $M^{-1}\,s^{-1}$ and corrected for the number of reactive hydrogens). The corresponding relative rates are $1{:}1.1 \times 10^2{:}1.1 \times 10^4$. These relative rates suggest a distinctly smaller effect for replacement of hydrogen by halogen than what we found or what Cox and Warkentin found for bromine.

For dichloroacetone, the rate constant for phosphate dianion catalyzed enolization which we determined is very close to the value predicted by Bell's Brønsted correlation (12): observed, $0.018\,M^{-1}\,s^{-1}$; predicted $0.0122\,M^{-1}\,s^{-1}$. For monochloroacetone, the rate constant for carbonate anion catalyzed enolization which we determined is actually somewhat slower than the value predicted by Bell's Brønsted correlation (12) (although this represents a much longer extrapolation than for phosphate

and dichloroacetone): observed, $0.25\,M^{-1}\,s^{-1}$; predicted 1.5 $M^{-1}\,s^{-1}$.

Rearrangement of 1,1-dihydroxyacetone

We may estimate pK_a values for dihydroxyacetone and tetrahydroxypropane using the Hine equation (24):

$$pK_a = 14.19 - 1.32\Sigma\sigma^*$$

For dihydroxyacetone we use $\sigma^*_{MeCO} = 1.81$ and $\sigma^*_H = 0.49$. For tetrahydroxypropane we use $\sigma^*_{MeC(OH)2} = 2 \times \sigma^*_{CH2OH} = 2 \times 0.62 = 1.24$. With these σ^* values, and the experimental value for hydration of neutral dihydroxyacetone, we estimate the equilibrium constants for the reaction cycle:

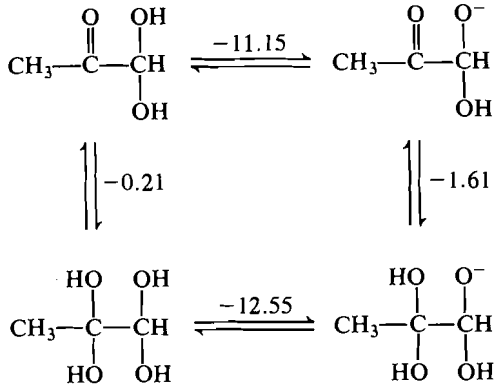

We also tried estimating the equilibrium constants for hydration of methylglyoxal and dihydroxyacetone, using the Greenzaid equation (23), $\log K_{hydration} = 1.70\Sigma\sigma^* + 2.03\Delta - 2.81$. For methylglyoxal this leads to $K_{hydration} = 1350$. For dihydroxyacetone the equation leads to $K_{hydration} = 0.198$; this is somewhat smaller than the observed value of 0.61 but is not bad, especially considering that the σ^* value had to be estimated.

The empirical rate law, expressed in terms of Scheme 1, gives $k_{IJ}K_{HI} = 0.122\,M^{-1}\,s^{-1}$ and $k_{HJ} = 0.00034$. The pK_a value of 11.15 estimated above leads to $K_{DH} = 708\,M^{-1}$. We may make a crude estimate of the second pK_a using Pauling's rules (15) as 16.2, and hence calculate $K_{HI} = 0.007$, and $k_{IJ} = 17\,s^{-1}$. At low pH, the apparent rate constants will be $k_{DJ} = k_{HJ}K_{DH}/(1 + K_{DN}) = 0.15\,M^{-1}\,s^{-1}$ and $k_{DJ}^- = k_{IJ}K_{HI}K_{DH}/(1 + K_{DN}) = 54\,M^{-2}\,s^{-1}$.

For 1,1-dihydroxyacetone rate constants at 37.5°C are available from the work of Ariyama (39). His values are given in Table 15. For 25°C we estimate that the rate constant will be 0.7 ± 0.4; this estimate was obtained using a factor of 2 in rate for a 12.5°C decrease in temperature, while giving error limits large enough to allow for the possiblity that the temperature effect is small; see below for phenyl glyoxal.

For phenyl glyoxal, a careful study at 35°C by Hine and Koser (40) is available. The apparent rate constant depends on the fraction of substrate which has ionized (K_1 (expressed as K_b) = 247 ± 17 M^{-1}) and is the sum of contributions for reaction of the monoanion and the dianion. The acid dissociation constant for the monoanion to give the dianion could not be determined. For conditions where the monoanion is the major species,

$$k_{app} = 2.95 \times 10^{-4} + 9.14 \times 10^{-2}[OH^-]\,s^{-1}$$

At pH 12, these values lead to a fraction of monoanion = 0.71, and an overall pseudo-first order rate constant = $8.61 \times 10^{-4}\,s^{-1}$.

A study of substituent effects at pH 12 was reported by Vanderjagt *et al.* (41). It should be noted that at pH 12 both monanion and dianion pathways are important, and that the proportions of these paths may depend on the substituent. For phenyl glyoxal itself a rate constant at pH 12, 25°C, of $7.6 \times 10^{-4}\,s^{-1}$ was reported. This is only slightly smaller than the value calculated from data (40) at 35°C, suggesting that the temperature dependence for this reaction may be small.

Our results lead to a predicted second order rate constant at low pH of $0.24\,M^{-1}\,s^{-1}$. This is somewhat smaller than the value estimated from the results of Ariyama, but depends on an estimated pK_a. For our rate constant from experiments at $[OH^-] > 0.01\,M$ to be consistent with the value calculated from Ariyama's data, i.e. $0.7\,M^{-1}\,s^{-1}$ the pK_a of dihydroxyacetone would have to be 10.3 and not 11.15. The difference is disturbing, but not impossible, especially when the acid strengthening substituent is a directly bonded carbonyl group which might exert a direct inductive effect as well as the field effect allowed for by a σ^* treatment.

There is a serious interpretational problem for the kinetics, because an alternative mechanism for the rearrangement of 1,1-dihydroxyacetone to lactate is enolization followed by reprotonation. The question is then whether this is competitive with intramolecular hydride transfer. If this were the mechanism, then the hydroxide-independent rate of rearrangement observed in dilute hydroxide solutions would represent enolization and not hydride transfer in the monoanion. The enolization would have to be a hydroxide-catalyzed reaction of the unionized substrate, with

$$k_{obs} = k_{enolization}[OH^-]/K_{DH}[OH^-]$$
$$k_{enolization} = 0.00034 \times 708 = 0.21 \text{ (using } pK_a = 11.15)$$
$$= 0.00034 \times 5000 = 1.5 \text{ (using } pK_a = 10.3)$$

In either case the rate constant for enolization seems far too large compared to the trend observed for acetone and hydroxyacetone ($k_{enolization} = 0.0288\,M^{-1}\,s^{-1}$ and $0.0235\,M^{-1}\,s^{-1}$, respectively, on a per hydrogen basis). One would expect a rate constant of about $0.02\,M^{-1}\,s^{-1}$ for dihydroxyacetone as well. Since the pK_a value is likely to be less than 11.15 rather than greater, it seems improbable that the enolization mechanism is of major importance.

This has immediate consequences for the halogenation path; it clearly cannot involve enolization because in that case the observed halogen dependence of the rate constant would imply preequilibrium proton transfer. If the enolate formed, it would rapidly and irreversibly be converted to lactate (which is known to be inert under our conditions.) The hypochlorite-dependent reacton must then represent some other process; one could imagine either fragmentation of a hypochlorite adduct:

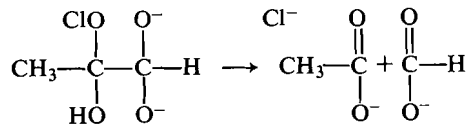

or hydride transfer from the monoanion to hypochlorite or from the dianion to hypochlorous acid:

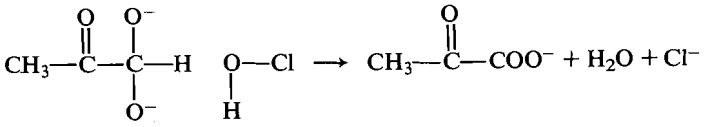

A product study by nmr showed only lactate; acetate would be inert and should have persisted, but pyruvate would be expected

TABLE 15. Rate constants for rearrangement of methyl glyoxal[a]

pH	k (min^{-1})	k_2 ($M^{-1}\,s^{-1}$)
8.5	2.4×10^{-4}	1.27
9.5	3.22×10^{-3}	1.70
10.5	1.77×10^{-2}	0.93
		Av. 1.3 ± 0.4

[a]Rate constants from ref. 39; kinetics in water at 37.5°C.

to react further by halogenation on the methyl. Thus a hydride transfer mechanism looks more likely at this time.

Cleavage of trichloroacetone

The observed rate constant for the cleavage of trichloroacetone can be expressed in terms of the mechanism shown in Scheme 1 as:

$$k_{obs} = \frac{(k_{89}K_{78}[OH^-] + K_{78}K_{8N}k_{N9}[OH^-]^2)}{(1 + K_{7M} + K_{78}[OH^-] + K_{78}K_{8N}[OH^-]^2)}$$

At low hydroxide concentrations, where the anionic adduct is present in small amounts, and the dianionic adduct is not kinetically important, this can be simplified to

$$k_{obs} = (k_{89}K_{78}[OH^-])/(1 + K_{7M})$$

Using the equilibium constants from Table 10, we can calculate that $k_{89} = 0.023\ s^{-1}$. This value may be somewhat low because it implies that some signs of levelling off should have been observable in the measured portion of the pH rate profile for the reaction, while in fact there was no levelling off seen. The pK_a estimation may be imperfect because of steric effects of the bulky trichloromethyl group.

It seems distinctly possible that cleavage reactions involving the dianion will be significant in dilute hydroxide solutions, but we have not yet devised a way to follow the cleavage reaction under such conditions.

For chloral the reaction is distinctly slower (42); this probably reflects the smaller driving force for generating a formate rather than an acetate anion. For the monoanion $k = 1.29 \times 10^{-4}\ s^{-1}$. The p$K_a$ of the hydrate is 9.76; estimating the second pK_a of the hydrate as 14.8 (using Pauling's rule of 5 pK_a units for successive pK_a's (15)) we estimate that for the dianion $k = 18\ s^{-1}$, which is 1.4×10^5 faster than for the monoanion.

The monoanion reaction of trichloroacetone hydrate has $k_{89} = 0.023\ s^{-1}$ which is 178 times faster than the corresponding rate constant for chloral hydrate. If the same ratio holds for the rate constant for the dianions, we would expect that for trichloroacetone the dianion would react with a rate constant of $k_{P9} = 3000\ s^{-1}$. All we can say on the basis of our results is that this rate constant is less than $4.2 \times 10^5\ s^{-1}$, assuming that a 20% increase would have been visible.

Stoichiometry of the reactions

The overall stoichiometry, $n_{acetone}$, i.e., the number of moles of OCl^- consumed per mole of acetone reacting, can be expressed in terms of partitioning fractions as:

$$n_{acetone} = 1 + f_1(1 + f_2) + [(1 - f_1) + (1 - f_2)]f_3$$

where

f_1 = partitioning fraction for monochloroacetone
= halogenation/(hydrolysis + halogenation)

f_2 = partitioning ratio for dichloroacetone
= halogenation/(hydrolysis + halogenation)

f_3 = partitioning ratio for dihydroxyacetone
= halogenation/(hydrolysis + halogenation)

A similar expression can be derived for n_{mono}, the stoichiometry number for reaction of monochloroacetone, with the complicating factor that the reaction occurs in two phases; rapid reaction involving halogenation of monochloroacetone, and slower reaction of the hydroxyacetone formed by hydrolysis.

$$n_{mono} = f_1(1 + f_2) + (1 - f_1) + [(1 - f_1) + f_1(1 - f_2)]f_3$$

The same complication applies to n_{di}, the stoichiometry number for reaction of dichloroacetone.

$$n_{di} = f_2 + (1 - f_2)f_3$$

The stoichiometry numbers for hydroxyacetone, $n_{hydroxy}$, and dihydroxyacetone, n_{glyox}, are quite simple.

$$n_{hydroxy} = 1 + f_3$$

$$n_{glyox} = f_3$$

The three partitioning fractions may be expressed in terms of the mechanism in Scheme 1 as:

$$f_1 = \frac{\dfrac{k_{34}[OH^-]\{(k_{45}^{0}K_w/K_a^{HOCl}[OH^-]) + k_{45}^{-}\}[OCl^-]}{\{(k_{45}^{0}K_w/K_a^{HOCl}[OH^-]) + k_{45}^{-}\}[OCl^-] + k_{43}}}{\dfrac{k_{34}[OH^-]\{(k_{45}^{0}K_w/K_a^{HOCl}[OH^-]) + k_{45}^{-}\}[OCl^-]}{\{(k_{45}^{0}K_w/K_a^{HOCl}[OH^-]) + k_{45}^{-}\}[OCl^-] + k_{43}} + k_{AB}K_{3A}[OH^-]}$$

$$= \frac{1}{1 + \dfrac{k_{AB}K_{3A}[OH^-]\{1 + \{(k_{45}^{0}K_w/K_a^{HOCl}[OH^-]) + k_{45}^{-}\}[OCl^-]/k_{43}\}}{(k_{34}/k_{43})\{(k_{45}^{0}K_w/K_a^{HOCl}[OH^-]) + k_{45}^{-}\}[OCl^-]}}$$

$$f_2 = \frac{\dfrac{k_{56}[OH^-]\{(k_{67}^{0}K_w/K_a^{HOCl}[OH^-]) + k_{67}^{-}\}[OCl^-]}{\{(k_{67}^{0}K_w/K_a^{HOCl}[OH^-]) + k_{67}^{-}\}[OCl^-] + k_{65}}}{\dfrac{k_{56}[OH^-]\{(k_{67}^{0}K_w/K_a^{HOCl}[OH^-]) + k_{67}^{-}\}[OCl^-]}{\{(k_{67}^{0}K_w/K_a^{HOCl}[OH^-]) + k_{67}^{-}\}[OCl^-] + k_{65}} + k_{ED}K_{5E}[OH^-]}$$

$$= \frac{1}{1 + \dfrac{k_{ED}K_{5E}[OH^-]\{1 + \{(k_{67}^{0}K_w/K_a^{HOCl}[OH^-]) + k_{67}^{-}\}[OCl^-]/k_{65}\}}{(k_{56}/k_{65})\{(k_{67}^{0}K_w/K_a^{HOCl}[OH^-]) + k_{67}^{-}\}[OCl^-]}}$$

$$f_3 = \frac{k_{HG}[OCl^-]}{k_{HG}[OCl^-] + K_{DH}[OH^-]\{k_{HJ} + k_{IJ}K_{HI}[OH^-]\}} = \frac{1}{1 + \dfrac{\{k_{HJ} + k_{IJ}K_{HI}[OH^-]\}K_{DH}[OH^-]}{k_{HG}[OCl^-]}}$$

The product ratios, [acetate]/[lactate], may be expressed in terms of the same partitioning fractions as:

$$([Acetate]/[lactate]_{acetone} = f_1f_2/\{[(1 - f_1) + f_1(1 - f_2)](1 - f_3)$$
$$= ([Acetate]/[lactate])_{monochloro}$$
$$([Acetate]/[lactate]_{dichloro} = f_2/[(1 - f_2)(1 - f_3)]$$

Figures 7–9 show the dependence of the stoichiometry numbers upon the concentrations of hydroxide and hypochlorite calculated using the rate and equilibrium constants in Table 9. The major uncertainty in these stoichiometry numbers is probably our uncertain knowledge of f_3, since the kinetics of the dihydroxyacetone reaction were less thoroughly explored. However, for most conditions this reaction is almost entirely rearrangement. There is also an uncertainty in f_2 at low $[OH^-]$ because we were not able to determine the rate constant for the term in the rate law corresponding to reaction of hypochlorous acid with the enolate of dichloroacetone.

When the ketone is in excess, one of the competitions which governs the stoichiometry is the competition for halogenating agent among the unhalogenated ketone, less reactive but at higher concentration, and the halogenated intermediates, more reactive, but present at low concentrations. This question may be addressed in terms of the steady-state concentrations of the halogenated ketone intermediates, because if the ratio of concentrations of two ketones becomes less than the reciprocal of the ratio of their reactivities under the same conditions, then the less abundant though more reactive ketone will lose out, and will undergo reactions other than halogenation, or simply accumulate if there is no facile reaction path other than halogenation. The steady-state concentrations of monochloroacetone and dichloroacetone may be expressed as:

$$[mono]_{ss} = \frac{\dfrac{k_{12}[OH^-]\{(k_{23}{}^0K_w/K_a{}^{HOCl}[OH^-]) + k_{23}{}^-\}[OCl^-]}{\{(k_{23}{}^0K_w/K_a{}^{HOCl}[OH^-]) + k_{23}{}^-\}[OCl^-] + k_{21}}}{\dfrac{k_{34}[OH^-]\{(k_{45}{}^0K_w/K_a{}^{HOCl}[OH^-]) + k_{45}{}^-\}[OCl^-]}{\{(k_{45}{}^0K_w/K_a{}^{HOCl}[OH^-]) + k_{45}{}^-\}[OCl^-] + k_{43}} + k_{AB}K_{3A}[OH^-]}$$

$$[di]_{ss} = \left\{\frac{k_{34}[OH^-]\{(k_{45}{}^0K_w/K_a{}^{HOCl}[OH^-]) + k_{45}{}^-\}[OCl^-]}{\{(k_{45}{}^0K_w/K_a{}^{HOCl}[OH^-]) + k_{45}{}^-\}[OCl^-] + k_{43}}\right\} \Bigg/ \left\{\frac{k_{56}[OH^-]\{(k_{67}{}^0K_w/K_a{}^{HOCl}[OH^-]) + k_{67}{}^-\}[OCl^-]}{\{\{(k_{67}{}^0K_w/K_a{}^{HOCl}[OH^-]) + k_{67}{}^-\}[OCl^-] + k_{65}\}\{1 + K_{5L} + K_{5E}[OH^-]\}} + \frac{k_{ED}K_{5E}[OCl^-]}{\{1 + 1/K_{5L} + 1/(K_{5E}[OH^-])\}}\right\}$$

Now we derive expressions for the relative rates of halogenation

$$k_{acetone}/k_{mono} = \frac{\dfrac{k_{12}[OH^-]\{(k_{23}{}^0K_w/K_a{}^{HOCl}[OH^-]) + k_{23}{}^-\}[OCl^-]}{\{(k_{23}{}^0K_w/K_a{}^{HOCl}[OH^-] + k_{23}{}^-\}[OCl^-] + k_{21}}}{\dfrac{k_{34}[OH^-]\{(k_{45}{}^0K_w/K_a{}^{HOCl}[OH^-]) + k_{45}{}^-\}[OCl^-]}{\{(k_{45}{}^0K_w/K_a{}^{HOCl}[OH^-] + k_{45}{}^-\}[OCl^-] + k_{43}}}$$

$$k_{acetone}/k_{di} = \frac{\dfrac{k_{12}[OH^-]\{(k_{23}{}^0K_w/K_a{}^{HOCl}[OH^-]) + k_{23}{}^-\}[OCl^-]}{\{(k_{23}{}^0K_w/K_a{}^{HOCl}[OH^-] + k_{23}{}^-\}[OCl^-] + k_{21}}}{\dfrac{k_{56}[OH^-]\{(k_{67}{}^0K_w/K_a{}^{HOCl}[OH^-]) + k_{67}{}^-\}[OCl^-]}{\{\{(k_{67}{}^0K_w/K_a{}^{HOCl}[OH^-] + k_{67}{}^-\}[OCl^-] + k_{65}\}\{1 + K_{5L} + K_{5E}[OH^-]\}}}$$

$$k_{mono}/k_{di} = \frac{\dfrac{k_{34}[OH^-]\{(k_{45}{}^0K_w/K_a{}^{HOCl}[OH^-]) + k_{45}{}^-\}[OCl^-]}{\{(k_{45}{}^0K_w/K_a{}^{HOCl}[OH^-] + k_{45}{}^-\}[OCl^-] + k_{43}}}{\dfrac{k_{56}[OH^-]\{(k_{67}{}^0K_w/K_a{}^{HOCl}[OH^-]) + k_{67}{}^-\}[OCl^-]}{\{\{(k_{67}{}^0K_w/K_a{}^{HOCl}[OH^-] + k_{67}{}^-\}[OCl^-] + k_{65}\}\{1 + K_{5L} + K_{5E}[OH^-]\}}}$$

Examination of these expressions shows that the problem was incorrectly phrased; the steady-state concentration is that concentration at which the intermediate *does* compete effectively for the halogenating agent, unless other reactions provide the major channel for consumption of the intermediate. Thus in assessing the partitioning of the intermediate with ketone in excess only the partitioning fractions matter.

Conclusions

Although some of the component reactions are not yet completely understood, and some terms in the rate law have not yet been detected, we have now a far more detailed picture of the overall kinetics of the alkaline chlorination of acetone. The most striking conclusion is that for this "well-known" reaction there are numerous competing paths with closely similar activation

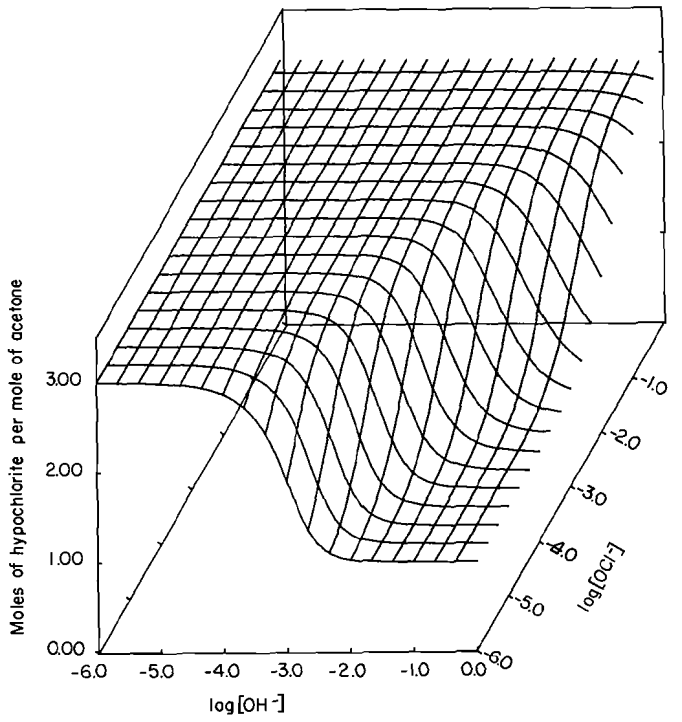

FIG. 7. Stoichiometry for chlorination of acetone in aqueous alkali. Number of moles of hypochlorite consumed per mole of acetone reacting, as a function of hydroxide and hypochlorite concentrations.

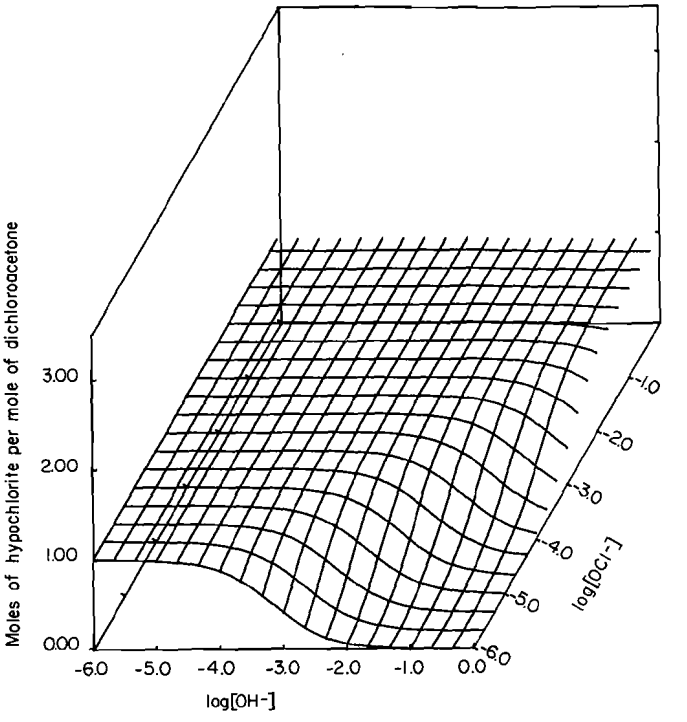

FIG. 9. Stoichiometry for chlorination of 1,1-dichloroacetone in aqueous alkali. Number of moles of hypochlorite consumed per mole of 1,1-dichloroacetone reacting, as a function of hydroxide and hypochlorite concentrations.

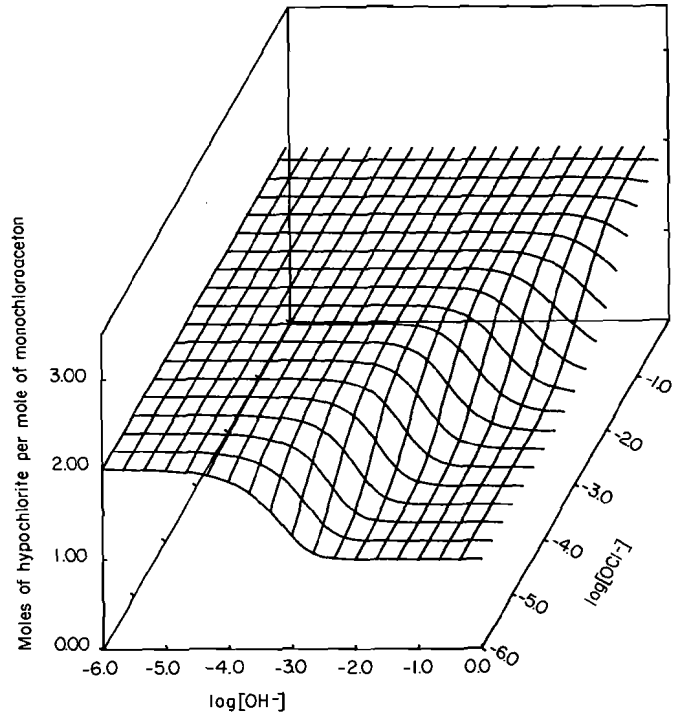

FIG. 8. Stoichiometry for chlorination of monochloroacetone in aqueous alkali. Number of moles of hypochlorite consumed per mole of monochloroacetone reacting, as a function of hydroxide and hypochlorite concentrations.

energies, so that small changes in conditions can lead to new and unexpected products.

Experimental

Materials

1-Chloro-2-propanone (Eastman practical grade) was shown by proton nmr to be 93 mol% monochloroacetone, 5 mol% 1,1-dichloroacetone, and 1–2 mol% acetone. As these were not separable by fractional distillation, the impure compound was used for the initial kinetics. A 0.10 *M* stock solution was made up in 1 *M* KCl containing 0.00001 *M* HCl and stored in a refrigerator; fresh stock solutions were made up every 2–3 weeks. For each run, 2.0 mL of the stock solution was made up to 50 mL with 1 *M* KCl to make 0.004 *M* chloroacetone.

Chloroacetone dimethyl ketal. 1-Chloro-2-propanone (Eastman practical grade), 30.3 g (0.3 mol), trimethyl orthoformate, 35 mL (34.1 g, 0.3 mol), methanesulphonic acid, 0.5 mL, and methanol, 1 mL, were refluxed for ½ h. Distillation yielded 20 mL of methyl formate, bp 32–34°C and 20 mL of a mixture, bp 102–112°C, found by ^{1}H-nmr analysis to contain chloroacetone, chloroacetone dimethyl ketal, and methanol as well as other unidentified impurities. This mixture was stirred overnight with 20% aqueous Na_2CO_3, 40 mL, and extracted with ether, 3 × 10 mL. The extracts were dried, Na_2CO_3, and distilled at atmospheric pressure, yielding 3 mL of material with bp 132–134°C, and 3 mL with bp 134–136°C; higher boiling residues began to decompose before distilling and were discarded. ^{1}H-nmr analysis of these distillates showed that the fraction boiling at 132–134°C was about 90% ketal, with about 3% chloroacetone, and the fraction boiling at 134–136 was about 80% ketal with about 1–2% chloroacetone. The ketal fraction boiling at 132–134°C was purified by preparative gas chromatography using a 20′ by ⅜″ od column of 20% SE-30 on chromosorb A and a helium flow rate of 135 mL/min. A total of six injections, 200–300 μL each, yielded about 1 mL of product. ^{1}H-nmr analysis showed that the peaks assigned to the ketal accounted for 95% of the total protons. This material was redistilled, bp 50°C/15 Torr, yielding about 0.75 g of colorless product. Literautre bp: 132–134°C (43).

Stock solutions of monochloroacetone prepared from the ketal. For all of the later kinetics of chlorination of monochloroacetone, chloroacetone dimethyl ketal was used as the source of chloroacetone. Stock solutions prepared from the ketal were made 0.002 *M* in HCl and were allowed to stand for 24 h at room temperature to hydrolyze. ^{1}H-nmr showed that hydrolysis was complete after this period. The stock solutions were then neutralized (1 *M* NaOH) to pH 5. The ^{1}H-nmr spectra subsequently remained unchanged after 3 days at room temperature. The stock solutions were stored in a refrigerator.

Bromoacetone stock solutions were made in a similar manner from the dimethyl ketal (Aldrich 97% 1-bromo-2,2-dimethyoxypropane).

1,1-Dichloroacetone (Aldrich 98%) was used without purification. The proton nmr in chloroform was clean except for a small (less than 3%) extra signal at 2.6 ppm, 0.2 ppm downfield from the methyl signal at 2.4 ppm. The stock solution (0.116 *M* in 1 *M* KCl) had a pH of 3.2 immediately after preparation. The stock solution was stored in a refrigerator when not in use. For each run, 1.0 mL of stock was diluted to 50 mL with 1 *M* KCl, making 0.0023 *M* ketone.

1,1,1-Trichloroacetone was prepared according to the method of Winston *et al.* (44) in 10% yield from sodium trichloroacetate and acetic anhydride, and purified by column chromatography on silica gel with 20:80 ether/petroleum ether as eluant, followed by distillation at 60°C/40 Torr. The proton spectrum in water showed two signals assigned to methyl groups, a larger one at 1.9 ppm for the hydrate, and a much smaller one at 2.6 ppm for the ketone. The stock solution (0.345 *M* in water) was made 0.0005 *M* in HCl as a protection against premature hydrolysis. For each titration, 0.50 mL of the stock was diluted to 50 mL with 1 *M* KCl, making 0.00345 *M* ketone.

All the stock solutions in water appeared to be stable for up to two months at room temperature, as their proton nmr spectra did not change.

Methods

pH-state kinetics with mono-, di-, and trichloroacetone. The reactions were followed for 50 mL portions of substrate solution in 1 *M* aqueous KCl made from freshly degassed water. The reaction vessel was a water-jacketed beaker kept at 25.0°C by a circulating water bath. Standardized 0.102, 0.512, or 1.027 *M* NaOH was used as titrant. The apparatus used consisted of a Radiometer pH meter 25, titrator 11, and glass electrode GK2301C, standardized with Fisher buffers at pH 4, 7, and 10 (±0.02) Points were taken manually and then typed into a computer file which was fitted by least squares to a single exponential with a linear term to accommodate CO_2 uptake. The pH was maintained constant to within 0.03 pH units during a run. Runs were followed to at least 10 half-lives, often 20 or more, except for one of the trichloroacetone runs, which was stopped because of leakage in the system; for this run a calculated infinity parameter was used.

Chloroacetone and dichloroacetone kinetics with OCl^- and OBr^-. All hypochlorite and hypobromite solutions were made using water redistilled from permanganate, reagent grade NaOH and chlorine or bromine, and were made up to 1 *M* ionic strength with KCl and KBr, respectively. All values of hydroxide concentrations were obtained by titration against aqueous HCl standardized with vacuum-dried TRIS. Hypochlorite concentrations were determined by absorbance measurements at the uv maximum, 292 nm, using an extinction coefficient of 352 (45). Some OCl^- concentrations were determined by titration using thiosulfate solution standardized against KIO_3. For 22 solutions where comparisons of titration values with absorbance values were made (concentrations 0.0005 *M* – 0.005 *M*), the discrepancy was always less than 2%, with an average of 0.7%. Hypobromite concentration were determined by absorbance at 331 nm using the published (46) extinction coefficient of 326.

Buffers. Carbonate buffers (ionic strength 1 *M*) were prepared from $KHCO_3$ (Fisher A.C.S. Reagent), KBr (Baker reagent), NaOH (Baker reagent), and redistilled water. Phosphate buffers (ionic strength 1 *M*) were prepared from KH_2PO_4 (Baker analytical reagent), KBr (Baker reagent), NaOH (Baker reagent), and redistilled water. Acetate buffers (ionic strength 1 *M*) were prepared from glacial acetic acid (Baker reagent), NaOAc (Fisher certified reagent), and KBr (Baker reagent). Less concentrated buffers in a buffer-dilution series were made by diluting the more concentrated buffer with 1 *M* KBr and making fine adjustments with 1 *M* NaOH and 1 *M* HCl (pH meter) if necessary to keep the pH constant. Such adjustments were not usually necessary.

Bromination of mono- and 1,1-dichloroacetone. A solution of KBr in redistilled water was made approximately 0.025 *M* in bromine (Merck ultra-pure). For runs involving the most dilute carbonate buffers (0.001 *M* CO_3^{2-}), the 0.025 *M* bromine was adjusted to the pH of the buffer being used by adding 0.05 *M* NaOH. This was done so that the bromine addition would not alter the buffer ratio. Measured volumes of buffer in 1- or 2-cm uv cells were brought to temperature equilibrium in the thermostatted cell holder of a Cary-210 spectrophotometer and the balance control brought to zero absorbance at 267 nm. A small volume (less than 1.5% of total volume) of 0.025 *M* bromine was added and the absorbance at 267 nm recorded. Reactions were initiated by injecting a portion (less than 1% of the total volume) of an aqueous stock solution of ketone and shaking the cell for 2–3 s before returning it to the cell compartment. The absorbance was followed at 267 nm. Bromine was present in 5- to 10-fold excess over ketone.

The apparent extinction coefficient of bromine in 1 *M* KBr or in 1 *M* KBr buffered at pH 8.82 (0.015 *M* CO_3^{2-}) was determined using solutions of ca. 1×10^{-4} *M* bromine which had been allowed to stand for several days and then titrated against freshly standardized 0.01 *N* thiosulphate solution. For pH 8.82 buffer the concentration of the solution was 1.57×10^{-4} *M*, the absorbance was 2.999 at 267 nm and the extinction coefficient was 19 000 M^{-1} cm^{-1}. For 1 *M* KBr the total bromine concentration was 6.16×10^{-5} *M*, the absorbance was 2.396 at 267 nm and the extinction coefficient was 38 900 M^{-1} cm^{-1}. In the same way apparent extinction coefficients were determined for phosphate buffers at each pH and for acetate buffers at pH 5.53 at least at the highest and lowest buffer concentrations; the main factor influencing the apparent extinction coefficient is presumed to be the bromide ion concentration. The values found are given in the footnotes to Table 5.

Dihydroxyacetone kinetics. Stock solutions for kinetics were prepared from pyruvic aldehyde dimethyl acetal (Aldrich 99%). A 60 MHz proton spectrum of the acetal in chloroform showed only three singlets: δ 4.6 (1H), 3.6 (6H) and 2.3 (3H). The acetal (0.900 g, 0.0076 mol) was dissolved in 1 *M* HCl, 250 mL, and heated on a steam bath for 3 h. 1 *M* NaOH was then added, with efficient stirring, until the pH reached 6.8. The resulting solution, made up to 500 mL, was 0.0152 *M* in product and did not decolorize bromine water. A ^{1}H-nmr spectrum showed three singlets: δ 3.49 (6H), MeOH; 2.67 and 1.75 (3H for the two together), MeCO- and $MeC(OH)_2$- in a ratio of 1.63:1. UV (water) $\lambda_{max} = 282.5$, $\epsilon = 15$; Lit $\lambda_{max} = 282.5$ $\epsilon = 27.5$ (47). All hydroxide concentrations were determined by titration. Cells were filled with the hydroxide solution, a base line recorded on the Cary, adjusted to zero absorbance and then injected with concentrated NaOCl. The volume of added hypochlorite was small compared to the cell volume (maximum 1.3% volume change). The hypochlorite concentration was taken as absorbance at 292 just before the reaction divided by the extinction coefficient, 352. Reactions were initiated by injecting ketone stock solutions: 40–100 μL with a 100 μL syringe into 3 mL of base-hypochlorite solution or 400 μL with a 500 μL syringe into 25 mL. Concentrations of OH^- and OCl^- were corrected for the volume change accompanying injections.

Product studies on dihydroxyacetone. (*i*) Stock dihydroxyacetone, 1 mL, was added to 0.294 *M* NaOH, 34 mL, stirred for 200 s and then neutralized to pH 7 with HCl containing a small proportion of phosphate. Initial concentrations: $[OH^-]$ 0.285; [ketone] 4.34×10^{-4} *M*. (*ii*) Stock dihydroxyacetone, 1 mL, was added to a solution 0.294 *M* in NaOH and 0.0018 *M* in NaOCl, 34 mL, stirred for 300 s, then hypochlorite was destroyed by adding sodium bisulphite, 7 mg, and the solution neutralized as before. Initial concentrations: $[OH^-]$, 0.285 *M*; $[OCl^-]$, 0.0017 *M*; [ketone], 4.34×10^{-4} *M*. The second procedure was repeated using lithium lactate, 1.45 mg, instead of dihydroxyacetone. Initial concentration: [lactate] 4.32×10^{-4} *M*. When the solutions were evaporated to dryness, the salts could not be dissolved by adding less than 2 mL of water. The resulting product concentration, less than 0.01 *M*, could not be seen by ^{1}H nmr at

TABLE 16. Product studies with dihydroxyacetone

$[OH^-]$ (M)	$[OCl^-]$ (M)	[Substrate] (10^4 M)	%lactate found
0.285	0.0	4.34[a]	87
0.285	0.0018	4.34[a]	78
0.285	0.0018	4.32[b]	85

[a]Dihydroxyacetone as substrate.
[b]Lactate as substrate.

60 MHz. The product solutions were made up to 2.0 mL and subjected to lactate enzyme assays using the Sigma diagnostic kit (9, 48). The results obtained are found in Table 16.

Acknowledgements

We thank the Natural Sciences and Engineering Research Council of Canada and the Academic Development Fund of the University of Western Ontario for financial support of this work.

1. G. KRAMER. Chem. Ber. **13**, 1000 (1880).
2. J. MESSINGER. Chem. Ber. **21**, 3366 (1888).
3. R. C. FUSON and B. A. BULL. Chem. Rev. **15**, 275 (1934).
4. L. T. SANDBORN and E. W. BOUSQUET. Org. Synth. Coll. Vol. I, 526 (1932).
5. M. S. NEWMAN and H. L. HOLMES. Org. Synth. Coll. Vol. II, 428 (1943).
6. L. I. SMITH, W. W. PRICHARD, and L. J. SPILLANE. Org. Synth. Coll. Vol. III, 302 (1955).
7. W. T. SMITH and G. L. MCLEOD. Org. Synth. Coll. Vol. IV, 345 (1963).
8. J. STAUNTON and E. J. EISENBRAUN. Org. Synth. Coll. Vol. V, 8 (1973).
9. J. P. GUTHRIE, J. COSSAR, and A. KLYM. J. Am. Chem. Soc. **106**, 1351 (1984).
10. R. P. BELL and H. C. LONGUET-HIGGINS. J. Chem. Soc. 636 (1946).
11. W. E. DEMING. Statistical adjustment of data. Dover, New York. 1964.
12. R. P. BELL and O. M. LIDWELL. Proc. R. Soc. A**176**, 88 (1940).
13. S. S. EADIE. J. Biol. Chem. **146**, 85 (1942).
14. B. H. J. HOFSTEE. Nature, **184**, 1296 (1959).
15. B. E. DOUGLAS and D. H. MCDANIEL. Concepts and models of inorganic chemistry. Blaisdell Publishing Co; New York. 1965. p. 191. L. PAULING. College chemistry. 3rd ed. W. H. Freeman and Co., San Francisco. 1964. p. 540.
16. J. W. THORPE and J. WARKENTIN. Can. J. Chem. **51**, 927 (1973).
17. J. MARCH. Advanced organic chemistry. 3rd ed. Wiley, New York. 1985. p. 302.
18. A. STREITWIESER, JR. Solvolytic displacement reactions. McGraw-Hill, New York. 1962. p. 28.
19. P. D. BARTLETT and E. N. TRACHTENBERG. J. Am. Chem. Soc. **80**, 5808 (1958).
20. W. FORSTER and R. M. LAIRD. J. Chem. Soc. Perkin II, 135 (1982).
21. A. PROSS, K. AVIRAM, R. C. KLIX, D. KOST, and R. D. BACH. Nouv. J. Chim. **8**, 711 (1984).
22. K. B. WIBERG. Physical organic chemistry. Wiley, New York. 1964.
23. P. GREENZAID, Z. LUZ, and D. SAMUEL. J. Am. Chem. Soc. **89**, 749 (1967).
24. J. HINE and G. F. KOSER. J. Org. Chem. **36**, 1348 (1971).
25. J. P. GUTHRIE. Enzyme models and related topics. *In* Applications of biochemical systems in organic chemistry. *Edited by* J. B. Jones, C. J. Sih, and D. Perlman. Wiley, New York. 1976.
26. E. L. ELIEL. Stereochemistry of carbon compounds. McGraw-Hill, New York. 1962. pp. 197–202.
27. H. NILSSON and L. SMITH. Z. physik. Chem. **166**A, 136 (1933).
28. F. G. BORDWELL and R. G. SCAMEHORN. J. Am. Chem. Soc. **90**, 6751 (1968).
29. F. G. BORWELL, R. G. SCAMEHORN, and W. R. SPRINGER. J. Am. Chem. Soc. **91**, 2087 (1969).
30. A. KENDE. Org. React. **11**, 261 (1960).
31. A. T. ROWLAND. J. Org. Chem. **27**, 1135 (1962).
32. F. G. BORDWELL and M. W. CARLSON. J. Am. Chem. Soc. **92**, 3377 (1970).
33. J. P. GUTHRIE. J. Am. Chem. Soc. **100**, 5892 (1978).
34. A. STEITWIESER, JR. Solvolytic displacement reactions. McGraw-Hill, New York. 1962. pp. 25, 26.
35. J. P. GUTHRIE. Can. J. Chem. **57**, 1177 (1979).
36. F. G. BORDWELL, R. R. FRAME, R. G. SCAMEHORN, J. G. STRONG, and S. MEYERSON. J. Am. Chem. Soc. **89**, 6704 (1967).
37. A. STREITWIESER, JR. Solvolytic displacement reactions, McGraw-Hill, New York. 1962. p. 78.
38. R. A. COX and J. WARKENTIN. Can. J. Chem. **50**, 3233 (1972).
39. N. ARIYAMA. J. Biol. Chem. **77**, 359 (1928).
40. J. HINE and G. F. KOSER. J. Org. Chem. **36**, 3591 (1971).
41. D. L. VANDERJAGT, L.-P. B. HAN, and C. H. LEHMAN. J. Org. Chem. **37**, 4100 (1978).
42. C. GUSTAFSSON and M. JOHANSON. Acta Chem. Scand. **2**, 42 (1948).
43. Beilstein's Handbuch der organischen chemie. Vol. 1, III, Springer, Berlin, 1959. p. 2746.
44. A. WINSTON, J. P. M. BEDERKA, W. G. ISNER, P. C. JULIANO, and J. C. SHARP. J. Org. Chem. **30**, 2784 (1965).
45. J. C. MORRIS. J. Phys. Chem. **70**, 3798 (1966).
46. C. H. CHEEK and V. J. LINNENBOM. J. Phys. Chem. **67**, 1856 (1963).
47. G. MACKINNEY and O. TEMMER. J. Am. Chem. Soc. **70**, 3586 (1948).
48. Sigma Technical Bulletin No. 726-UV/826-UV. Sigma Chemical Co., P.O. Box 14508, St. Louis, MO.
49. A. H. FAINBERG and S. WINSTEIN. J. Am. Chem. Soc. **78**, 2770 (1956).

Pyrrolyl complexes of the early transition metals. 3. Preparation and crystal structure of $(\eta^5\text{-}C_5H_5)_2Zr(\eta^1\text{-}NC_4H_2Me_2)_2$ and $Zr(\eta^1\text{-}NC_4H_2Me_2)_4$

R. VANN BYNUM, H.-M. ZHANG, WILLIAM E. HUNTER, AND JERRY L. ATWOOD[1]
Department of Chemistry, University of Alabama, University, AL, U.S.A. 35486

Received February 24, 1984[2]

R. VANN BYNUM, H.-M. ZHANG, WILLIAM E. HUNTER, and JERRY L. ATWOOD. Can. J. Chem. **64**, 1304 (1986).

The title compounds were synthesized by the reactions of $NaNC_4H_2Me_2$ with the appropriate complex metal chloride in THF. The crystal structures have been determined from X-ray data measured by counter methods. $(\eta^5\text{-}C_5H_5)_2Zr(\eta^1\text{-}NC_4H_2Me_2)_2$ crystallizes in the orthorhombic space group Pbca with cell dimensions $a = 15.797(6)$, $b = 14.327(5)$, $c = 16.417(6)$ Å, and $\rho_{calcd} = 1.46$ g cm^{-3} for $Z = 8$. Full-matrix least-squares refinement led to a final R factor of 0.041 based on 536 observed reflections. $Zr(\eta^1\text{-}NC_4H_2Me_2)_4$ belongs to the monoclinic space group $P2_1/n$ with $a = 14.065(5)$, $b = 10.717(4)$, $c = 15.733(6)$ Å, $\beta = 90.61(4)°$, and $\rho_{calcd} = 1.31$ g cm^{-3} for $Z = 4$. A final R value of 0.029 resulted from the refinement on the basis of 2649 observed reflections. The dicyclopentadienyl derivative exhibits two features of importance. The Zr—N—centroid angles are 159 and 168°, and the Zr—N bond lengths are 2.24(2) Å. In the homoleptic complex the corresponding values are 164–169° and 2.069(3)–2.090(3) Å. In both cases the bonding parameters are indicative of a substantial amount of π overlap between the zirconium atom and the pyrrolyl nitrogen atom.

R. VANN BYNUM, H.-M. ZHANG, WILLIAM E. HUNTER et JERRY L. ATWOOD. Can. J. Chem. **64**, 1304 (1986).

On a synthétisé les composés mentionnés dans le titre par réaction, dans du THF, du $NaNC_4H_2Me_2$ avec le complexe du chlorure métallique approprié. On a déterminé les structures cristallines à partir de données de diffraction de rayons x obtenues par les méthodes des compteurs. Le $(\eta^5\text{-}C_5H_5)_2Zr(\eta^1\text{-}NC_4H_2Me_2)_2$ cristallise dans le groupe d'espace orthorhombique Pbca avec $a = 15,797(6)$, $b = 14,327(5)$ et $c = 16,417(6)$ Å et $\rho_{calcd} = 1,46$ g cm^{-3} pour $Z = 8$. On a affiné la structure par la méthode des moindres carrés (matrice entière) jusqu'à une valeur finale de R de 0,041 pour 536 réflexions observées. Le $Zr(\eta^1\text{-}NC_4H_2Me_2)_4$ cristallise dans le groupe d'espace monoclinique $P2_1/n$ avec $a = 14,065(5)$, $b = 10,717(4)$, $c = 15,733(6)$ Å, $\beta = 90,61(4)°$ et $\rho_{calcd} = 1,31$ g cm^{-3} pour $Z = 4$. On a affiné la structure jusqu'à une valeur finale de R égale à 0,029 pour 2649 réflexions observées. Le dérivé dicyclopentaniényle présente deux caractéristiques importantes. Les angles 2r—N—centroïdes sont égaux à 159 et 168° alors que les longueurs des liaisons Zr—N sont égales à 2,24(2) Å. Dans le complexe homoleptique, les valeurs correspondantes sont de 164–169° et 2,069(3)–2,090(3) Å. Dans les deux cas, les paramètres de liaison sont une indication d'une quantité importante de recouvrement π entre l'atome de zirconium et l'azote du cycle pyrrolyle.

[Traduit par la revue]

Introduction

The pyrrolyl anion can interact with a metal ion in three different ways, **1**–**3**. Compared to the isoelectronic cyclopenta-

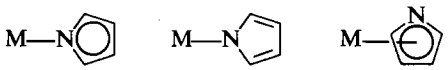

1 **2** **3**

dienyl ion, the σ bonding modes are expected to be preferred. However, under an appropriate combination of steric and electronic environments the π-attachment should be accessible to early transition metals. We have previously characterized several Group IVb pyrrolyl complexes: $(\eta^5\text{-}C_5H_5)_2M(\eta^1\text{-}NC_4H_4)_2$ (M = Ti (1), Zr (1), and Hf (2)), $[Na(THF)_6]_2[Zr(\eta^1\text{-}NC_4H_4)_6]$, and $[Li(DME)_3][(\mu\text{-}Cl)(\mu\text{-}O)\{(\eta^5\text{-}C_5Me_5)Zr(\eta^1\text{-}NC_4H_4)(Cl)\}_2]$ (3). In each case the σ interaction, **1**, was found. Since the existence of four cyclopentadienyl-like ligands about Zr or Hf clearly presents a delicate balance of steric and electronic effects,[3] we have undertaken a study of several hindered pyrrolyl anions. Specifically, substitution of bulky groups for the hydrogen atoms in the 2- and 5-positions on the parent molecule should make a π-bonding mode more attractive. Herein we present work with the 2,5-dimethylpyrrolyl anion,

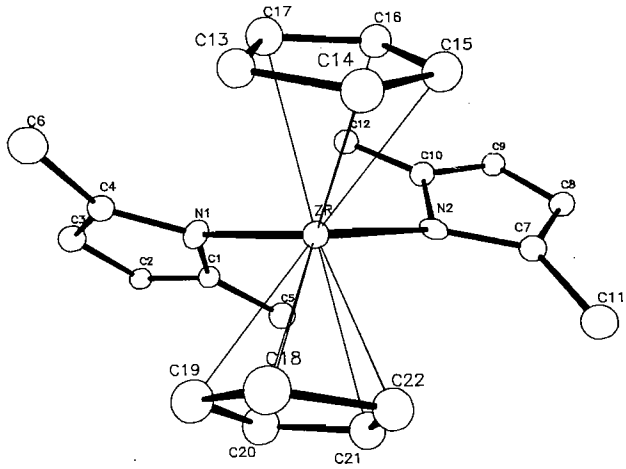

FIG. 1. Molecular structure and atom numbering scheme for $(\eta^5\text{-}C_5H_5)_2Zr(\eta^1\text{-}NC_4H_2Me_2)_2$.

and show that under the conditions employed bond type **1** is again dominant.

Results and discussion

Dicyclopentadienylbis(2,5-dimethylpyrrolyl)zirconium(IV) was prepared by the straightforward addition of $NaNC_4H_2Me_2$ to $(\eta^5\text{-}C_5H_5)_2ZrCl_2$ in THF. The deep red complex was obtained by extraction with and recrystallization from benzene. The structure presented in Fig. 1 illustrates the σ bonding mode of the pyrrolyl ligand. **1** rather than **2** is designated by the

[1]To whom all correspondence should be addressed.

[2]Revision received February 3, 1986.

[3]The tetracyclopentadienyls of Zr and Hf possess different structures even though the two metals differ by only *ca.* 0.01 Å in atomic or ionic radius: $(\eta^5\text{–}C_5H_5)_3Zr(\eta^1\text{–}C_5H_5)$, see ref. 4*a*; $(\eta^5\text{–}C_5H_5)_2Hf(\eta^1\text{–}C_5H_5)_2$, see ref. 4*b*.

Printed in Canada / Imprimé au Canada

TABLE 1. Bond lengths (Å) and angles (deg)

(*A*) $(\eta^5\text{-}C_5H_5)_2Zr(\eta^1\text{-}NC_4H_2Me_2)_2$

Atoms	Distance	Atoms	Distance
Zr---N(1)	2.22(2)	Zr---N(2)	2.25(2)
Zr---C(13)	2.49(2)	Zr---C(14)	2.54(2)
Zr---C(15)	2.56(2)	Zr---C(16)	2.59(2)
Zr---C(17)	2.55(3)	Zr---C(18)	2.56(2)
Zr---C(19)	2.56(2)	Zr---C(20)	2.58(2)
Zr---C(21)	2.55(2)	Zr---C(22)	2.50(2)
Zr---Cnt(3)	2.249	Zr---Cnt(4)	2.251
Zr---Ave(1)	2.55(3)	Zr---Ave(2)	2.55(3)

Atoms	Angle	Atoms	Angle
N(1)---Zr---N(2)	106.4(6)	N(1)---Zr---Cnt(3)	110.9
N(2)---Zr---Cnt(3)	99.9	N(2)---Zr---Cnt(4)	111.7
N(1)---Zr---Cnt(4)	99.6	Cnt(3)---Zr---Cnt(4)	127.0
Zr---N(1)---Cnt(1)	168.2	Zr---N(2)---Cnt(2)	159.2

(*B*) $Zr(\eta^1\text{-}NC_4H_2Me_2)_4$

Atoms	Distance	Atoms	Distance
Zr---N(1)	2.090(3)	Zr---N(2)	2.069(3)
Zr---N(3)	2.080(3)	Zr---N(4)	2.076(3)
N(1)---C(1)	1.404(4)	N(1)---C(4)	1.409(4)
N(2)---C(7)	1.408(5)	N(2)---C(10)	1.404(5)
N(3)---C(13)	1.401(4)	N(3)---C(16)	1.417(4)
N(4)---C(19)	1.410(4)	N(4)---C(22)	1.396(4)
C(1)---C(2)	1.347(5)	C(1)---C(5)	1.492(5)
C(2)---C(3)	1.415(5)	C(3)---C(4)	1.348(5)
C(4)---C(6)	1.493(5)	C(7)---C(8)	1.344(5)
C(7)---C(11)	1.490(6)	C(8)---C(9)	1.395(6)
C(9)---C(10)	1.338(6)	C(10)---C(12)	1.478(6)
C(13)---C(14)	1.353(5)	C(13)---C(17)	1.494(5)
C(14)---C(15)	1.409(6)	C(15)---C(16)	1.344(5)
C(16)---C(18)	1.492(5)	C(19)---C(20)	1.330(5)
C(19)---C(23)	1.487(5)	C(20)---C(21)	1.412(6)
C(20)---C(22)	1.335(6)	C(22)---C(24)	1.490(6)

Atoms	Angle	Atoms	Angle
N(1)---Zr---N(2)	104.3(1)	N(1)---Zr---N(3)	110.4(1)
N(2)---Zr---N(3)	113.4(1)	N(1)---Zr---N(4)	114.6(1)
N(2)---Zr---N(4)	111.1(1)	N(3)---Zr---N(4)	103.4(1)
Zr---N(1)---Cnt(1)	164.1	Zr---N(3)---Cnt(3)	165.9
Zr---N(2)---Cnt(2)	1667.	Zr---N(4)---Cnt(4)	169.4

Zr—N—centroid angles of 159 and 168°. The average is virtually identical to that found for $(\eta^5\text{-}C_5H_5)_2Zr(\eta^1\text{-}NC_4H_4)_2$, 164° (1). The presence of the methyl substituents on the ligand apparently serve to weaken the Zr—N bond. The length is 2.169(3) Å in the dipyrrolyl complex, but 2.24(2) Å in $(\eta^5\text{-}C_5H_5)_2Zr(\eta^1\text{-}NC_4H_2Me_2)_2$. Other bond lengths and angles are given in Table 1.

Encouraged by the evidence of a weaker Zr—N σ bond in $(\eta^5\text{-}C_5H_5)_2Zr(\eta^1\text{-}NC_4H_2Me_2)_2$, we sought tetrakis(2,5-dimethylpyrrolyl)zirconium(IV). Perhaps here the need for coordinative saturation would force one or more π-bonded pyrrolyl groups on the metal. The complex was prepared by the reaction of THF-free $NaNC_4H_2Me_2$ with $ZrCl_4$ in benzene. The structure of the red–orange air-sensitive compound is shown in Fig. 2. The ligand obviously has the bulk to prevent the formation of an anion such as that found for $NC_4H_4^-$ itself, $Zr(\eta^1\text{-}NC_4H_4)_6^{2-}$, but the nitrogen atom is still available for the formation of Zr—N σ bonds. Indeed, the Zr—N lengths of 2.069(3) → 2.090(3) Å are among the shortest yet reported.[4]

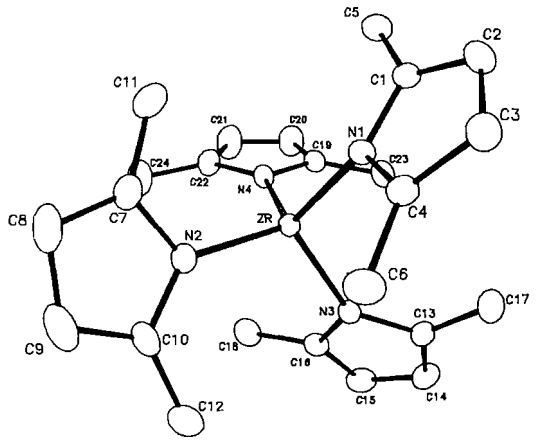

FIG. 2. Molecular structure of $Zr(\eta^1\text{-}NC_4H_2Me_2)_4$.

Before a comparison is made between the Zr—N distances in $(\eta^5\text{-}C_5H_5)_2Zr(\eta^1\text{-}NC_4H_2Me_2)_2$ and $Zr(\eta^1\text{-}NC_4H_2Me_2)_4$, a few general comments on metal–ligand σ bond lengths are in order. Over the past several years our group has studied a large number of compounds which contain M—C(σ) bonds. Of the many factors governing bond lengths one seems dominant: the electronic environment at the metal as simply evidenced by the electron count. For example, Mo—C(σ) bond lengths range from 2.291(5) Å in $(\eta^6\text{-}C_6H_5Me)MoMe_2(PPhMe_2)_2$ (6) to 2.397(19) Å in $(\eta^5\text{-}C_5H_5)MoEt(CO)_3$ (7) for 18-electron situations. However, typical 12-electron cases reveal much shorter bond distances: 2.110(16) Å in $Mo(CH_2SiMe_3)_3(PMe_3)(Cl)$ (8) and 2.131 Å in $Mo_2(CH_2SiMe_3)_6$ (9). There exists a large body of data to support this view, and the examples given above are simply representative. One should expect a shorter Zn—N length in the formally 8-electron situation, $Zr(\eta^1\text{-}NC_4H_2Me_2)_4$, relative to the 16-electron $(\eta^5\text{-}C_5H_5)_2Zr(\eta^1\text{-}NC_4H_2Me_2)_2$. One finds average values of 2.079(8) and 2.24(2) Å, respectively.

The Zr—N distance of 2.079(8) Å (or even the one at 2.24(2) Å is indicative of a substantial d_π–p_π interaction. The value is one of the shortest reported for a Zr^{4+} complex (5), and is significantly shorter than the Zr—C(carbonyl) distance of 2.187(4) Å in $(\eta^5\text{-}C_5H_5)_2Zr(CO)_2$ (10). Further evidence for π overlap is found in the Zr—N—centroid angles which range from 164 to 169° and average 167°. Table 1 contains additional bond lengths and angles.

Present work centers on the 2,5-di-*t*-butylpyrrolyl ligand, and the elusive η^5-attachment may soon be available.

Experimental

All reactions were carried out by Schlenk techniques under argon or in a Vacuum Atmospheres drybox. Solvents were distilled from $LiAlH_4$ (tetrahydrofuran, THF) or sodium and degassed before use. $(\eta^5\text{-}C_5H_5)_2ZrCl_2$ and purchased from Alfa Inorganics and used without further purification. 2,5-Dimethylpyrrolyl was purchased from Aldrich and distilled prior to use.

Synthesis of 2,5-dimethylpyrrolylsodium

Excess sodium hydride and THF (*ca.* 500 mL) were placed in a Schlenk flask fitted with an overhead stirrer and a dropping funnel.

[4]The literature contains a Zr—N length of 2.081(4) Å in the Zr^{2+} compound $[(\eta^5\text{–}C_5Me_5)_2ZrN_2]_2N_2$ (5*a*). We have recently characterized $(\eta^5\text{–}C_5H_5)_2Zr(Cl)$ (N=CHPh) in which the Zr=N distance, 2.013(5) Å, implies the existence of a Zr=N linkage (5*b*).

Freshly redistilled 2,5-dimethylpyrrole (95 g, 1 mol) as a 50% solution in THF was then added dropwise over several hours. Gas evolution was noted, and heat was given off. After the mixture was stirred overnight, the excess sodium hydride was removed by filtration and the solution diluted to 1.0 L with THF. Aliquots were hydrolyzed and titrated with standardized HCl to confirm a 1.0 *M* solution.

Synthesis of dicyclopentadienylbis(2,5-dimethylpyrrolyl)zirconium(IV)

$(\eta^5\text{-}C_5H_5)_2ZrCl_2$ (1.46 g, 5 mmol) was dissolved in *ca.* 100 mL of THF. 2,5-Dimethylpyrrolylsodium (1.17 g, 10 mmol) was added via syringe. The solution immediately changed from colorless to red–orange. After 24 h, the solvent was removed under vacuum and the residue extracted with benzene. The solution thus obtained was filtered and on cooling produced deep red, mildly air-sensitive crystals (1.25 g, 61%).

Synthesis of tetrakis(2,5-dimethylpyrrolyl)zirconium(IV)

2,5-Dimethylpyrrolylsodium (2.34 g, 20 mmol) was syringed into a Schlenk flask and the THF removed under vacuum. The flask was then warmed under vacuum overnight to ensure complete removal of the THF. Benzene (*ca.* 100 mL) and $ZrCl_4$ (1.16 g, 5 mmol) were added and the solution brought to reflux. After 24 h, the resulting orange solution was filtered and cooled, and the red–orange air-sensitive crystals were collected (1.14 g, 49%).

X-ray data collection, structure determination, and refinement for $(\eta^5\text{-}C_5H_5)_2Zr(\eta^1\text{-}NC_4H_2Me_2)_2$

Single crystals of the compound were sealed under N_2 in thin-walled glass capillaries. A well-formed crystal of dimensions 0.10 × 0.10 × 0.20 mm was selected. Final lattice parameters were determined from a least-squares refinement of $(\sin\theta/\lambda)^2$ values for 15 reflections ($\theta > 15°$) accurately centered on the diffractometer.

Data were collected on an Enraf-Nonius CAD-4 diffractometer by the θ–2θ scan technique. The method has been previously described (11). Three check reflections were measured after every 297 reflections and they showed only random fluctuations. A total of 1504 reflections were measured of which 536 were deemed observed ($I/\sigma(I) \geq 3.0$). The intensities were corrected for Lorentz and polarization effects, but not for absorption.

Calculations were carried out with the SHELX system of computer programs (12). Neutral atom scattering factors for Zr, N, and C were taken from Cromer and Waber (13). Scattering factors for H were from ref. 14.

The structure was solved by the application of the direct methods program MULTAN (15). Least-squares refinement with isotropic thermal parameters led to $R = \Sigma||F_o| - |F_c||/\Sigma|F_o| = 0.092$. Hydrogen atoms on the cyclopentadienyl rings were placed in calculated positions and not refined. At this point it should be noted that only very small crystals could be grown. The data were therefore quite limited: only 36% of the measured reflections were considered observed, and virtually no data could be obtained beyond $2\theta = 36°$. While the small data set was good (as evidenced by the *R* factors), it would support only a limited refinement, and high standard deviations for the derived parameters were obtained. Only the Zr and N atoms were refined with anisotropic thermal parameters. The value of *R* was 0.041 and $R_w = \{\Sigma(|F_o| - |F_c|)^2/\Sigma w(F_o)^2\}^{1/2}$, 0.049. A final difference Fourier map showed no significant feature. Unit weights were used at all stages of refinement. The positional parameters are given in Table 2.[5]

Crystal data

$C_{22}H_{26}N_2Zr$ $M = 409.7$

Orthorhombic, space group *Pbca*, $a = 15.797(6)$, $b = 14.327(5)$, $c = 16.471(6)$ Å, $U = 3727.8$ Å^3, $Z = 8$, $D_c = 1.46$ g cm^{-3}, MoK_α radiation, $\lambda = 0.71069$ Å, $\mu(MoK_\alpha) = 5.89$ cm^{-1}, $F(000) = 1696$.

[5]The tables of structure factors, anisotropic thermal parameters, hydrogen atom coordinates, and complete bond lengths and angles for both compounds are available, at a nominal charge, from the Depository of Unpublished Data, CISTI, National Research Council of Canada, Ottawa, Ont., Canada K1A 0S2.

TABLE 2. Final fractional coordinates for $(\eta^5\text{-}C_5H_5)_2Zr(\eta^1\text{-}NC_4H_2Me_2)_2$

Atom	*x/a*	*y/b*	*z/c*	$U_{eqv.}$
Zr	0.4300(1)	0.2810(1)	0.1783(1)	0.031
N(1)	0.449(1)	0.371(1)	0.2864(9)	0.036
N(2)	0.336(1)	0.355(1)	0.099(1)	0.035
C(1)	0.381(1)	0.418(1)	0.321(1)	0.032
C(2)	0.405(1)	0.455(1)	0.396(1)	0.034
C(3)	0.492(1)	0.430(2)	0.410(1)	0.045
C(4)	0.517(1)	0.379(1)	0.343(1)	0.035
C(5)	0.289(1)	0.426(2)	0.289(1)	0.054
C(6)	0.603(1)	0.333(1)	0.332(2)	0.054
C(7)	0.287(1)	0.319(1)	0.031(1)	0.036
C(8)	0.268(1)	0.390(2)	−0.018(1)	0.037
C(9)	0.303(1)	0.475(2)	0.014(1)	0.039
C(10)	0.347(1)	0.451(2)	0.083(1)	0.040
C(11)	0.263(1)	0.217(2)	0.021(1)	0.048
C(12)	0.396(1)	0.521(1)	0.137(1)	0.046
C(13)	0.583(1)	0.251(1)	0.153(1)	0.040
C(14)	0.541(1)	0.201(2)	0.091(1)	0.044
C(15)	0.502(1)	0.266(2)	0.039(1)	0.047
C(16)	0.521(1)	0.357(2)	0.065(1)	0.041
C(17)	0.574(2)	0.346(2)	0.135(1)	0.051
C(18)	0.436(2)	0.111(2)	0.224(1)	0.054
C(19)	0.420(2)	0.162(2)	0.294(1)	0.056
C(20)	0.339(1)	0.202(2)	0.289(1)	0.058
C(21)	0.304(1)	0.178(2)	0.214(1)	0.051
C(22)	0.364(1)	0.122(1)	0.173(2)	0.048

TABLE 3. Final fractional coordinates for $Zr(\eta^1\text{-}NC_4H_2Me_2)_4$

Atom	*x/a*	*y/b*	*z/c*	$U_{eqv.}$
Zr	0.24927(2)	0.21615(3)	0.98949(2)	0.040
N(1)	0.2432(2)	0.0329(3)	0.9444(2)	0.045
C(1)	0.2818(2)	−0.0823(3)	0.9694(2)	0.047
C(2)	0.2769(3)	−0.1609(4)	0.9028(2)	0.059
C(3)	0.2327(3)	−0.0986(4)	0.8338(2)	0.059
C(4)	0.2114(3)	0.0177(3)	0.8600(3)	0.048
C(5)	0.3113(3)	−0.1070(4)	1.0589(2)	0.065
C(6)	0.1607(3)	0.1181(4)	0.8119(2)	0.069
N(2)	0.1099(2)	0.2776(3)	0.9832(2)	0.051
C(7)	0.0414(3)	0.2054(4)	1.0254(2)	0.060
C(8)	−0.0453(3)	0.2475(5)	1.0030(3)	0.082
C(9)	−0.0334(3)	0.3447(5)	0.9453(3)	0.082
C(10)	0.0595(3)	0.3640(4)	0.9332(2)	0.058
C(11)	0.0677(3)	0.0988(4)	1.0816(3)	0.081
C(12)	0.1061(3)	0.4545(4)	0.8765(3)	0.082
N(3)	0.3417(2)	0.3220(3)	0.9167(2)	0.050
C(13)	0.4084(2)	0.2956(4)	0.8538(2)	0.053
C(14)	0.4645(3)	0.3968(4)	0.8431(3)	0.067
C(15)	0.4347(3)	0.4902(4)	0.8999(3)	0.069
C(16)	0.3612(3)	0.4453(4)	0.9443(2)	0.055
C(17)	0.4135(3)	0.1721(4)	0.8101(3)	0.073
C(18)	0.3091(3)	0.5046(4)	1.0157(3)	0.081
N(4)	0.3044(2)	0.2341(3)	1.1115(2)	0.049
C(19)	0.4000(2)	0.1985(4)	1.1243(2)	0.053
C(20)	0.4244(3)	0.2201(5)	1.2047(3)	0.090
C(21)	0.3450(4)	0.2734(6)	1.2450(3)	0.102
C(22)	0.2735(3)	0.2811(4)	1.1890(2)	0.066
C(23)	0.4607(3)	0.1537(4)	1.0540(3)	0.067
C(24)	0.1776(3)	0.3379(5)	1.1994(3)	0.093

X-ray data collection, structure determination, and refinement for $Zr(\eta^1\text{-}NC_4H_2Me_2)^4$

The compound was manipulated and data collected in the same manner as for $(\eta^5\text{-}C_5H_5)_2Zr(\eta^1\text{-}NC_4H_2Me_2)_2$. However, an excellent crystal gave rise to a superb data set, and faith can be placed in the derived parameters. The crystal of dimension 0.20 × 0.30 × 0.40 mm gave 2649 observed reflections out of a total of 3100 measured to 2θ cut-off of 46°. Three check reflections were measured after 297 reflections and only random fluctuations were noted. All hydrogen atoms were located with the aid of a difference Fourier map, but the coordinates were not refined. The nonhydrogen atoms were refined with anisotropic thermal parameters. The final reliability factors were $R = 0.029$ and $R_w = 0.031$. A final difference Fourier showed no feature greater than $0.3\ e^-/Å^3$. Unit weights were used at all stages of refinement. The atomic coordinates are given in Table 3.[3]

Crystal data

$C_{24}H_{32}N_4Zr$ $M = 467.8$

Monoclinic, space group $P2_1/n$, $a = 14.065(5)$, $b = 10.717(4)$, $c = 15.773(6)$ Å, $\beta = 90.61(4)°$, $U = 2377.4$ Å^3, $Z = 4$, $D_c = 1.31\ g\ cm^{-3}$, MoK_α radiation, $\lambda = 0.71069$ Å, $\mu(MoK_\alpha) = 4.74\ cm^{-1}$, $F(000) = 976$.

Acknowledgement

We are grateful to the National Science Foundation for support of this work.

1. R. V. Bynum, W. E. Hunter, R. D. Rogers, and J. L. Atwood. Inorg. Chem. **19**, 2368 (1980).
2. R. D. Rogers, R. V. Bynum, and J. L. Atwood. J. Cryst. Spec. Res. **14**, 21 (1984).
3. J. L. Atwood, R. D. Rogers, and R. V. Bynum. Acta Crystallogr. C**40**, 1812 (1984).
4. (*a*) R. D. Rogers, R. V. Bynum, and J. L. Atwood. J. Am. Chem. Soc. **100**, 5238 (1978); (*b*) R. D. Rogers, R. V. Bynum, and J. L. Atwood. J. Am. Chem. Soc. **103**, 692 (1981).
5. (*a*) R. D. Sanner, J. M. Manriquez, R. E. Marsh, and J. E. Bercaw. J. Am. Chem. Soc. **98**, 8351 (1976); (*b*) G. Erker, W. Fromberg, W. E. Hunter, and J. L. Atwood. Angew. Chem. Int. Ed. Engl. **23**, 68 (1984).
6. J. L. Atwood, W. E. Hunter, R. D. Rogers, E. Carmona-Guzman, and G. Wilkinson. J. Chem. Soc. Dalton Trans. 1519 (1979).
7. M. J. Bennett. Ph.D. Thesis, Sheffield. 1965.
8. E. Carmona-Guzman, G. Wilkinson, R. D. Rogers, W. E. Hunter, and J. L. Atwood. J. Chem. Soc. Dalton Trans. 229 (1980).
9. F. Huq, W. Mowat, A. Shortland, A. C. Skapski, and G. Wilkinson. Chem. Commun. 1079 (1971).
10. J. L. Atwood, R. D. Rogers, W. E. Hunter, C. Floriani, G. Fachinetti, and A. Chiesi-Villa. Inorg. Chem. **19**, 3812 (1980).
11. J. Holton, M. F. Lappert, D. G. H. Ballard, R. Pearce, J. L. Atwood, and W. E. Hunter. J. Chem. Soc. Dalton Trans. 46 (1979).
12. SHELX. A system of computer programs for X-ray structure determination by G. M. Sheldrick. 1976.
13. D. T. Cromer and J. T. Waber. Acta Crystallogr. **18**, 104 (1965).
14. International tables for X-ray crystallography. Vol. IV. Kynoch Press. Birmingham, England. 1974. p. 72.
15. G. Germain, P. Main, and M. M. Woolfson. Acta Crystallogr. A**27**, 368 (1971).

The structure of fusarochromanone: new mycotoxin from *Fusarium roseum*, "Graminearum"

SADANAND V. PATHRE AND WILLIAM B. GLEASON
Central Research Laboratories, 3M Company, 3M Center, St. Paul, Minnesota 55144, U.S.A.

AND

YIN-WAN LEE AND CHESTER J. MIROCHA
Department of Plant Pathology, University of Minnesota, St. Paul, Minnesota 55101, U.S.A.

Received July 10, 1985[1]

SADANAND V. PATHRE, WILLIAM B. GLEASON, YIN-WAN LEE, and CHESTER J. MIROCHA. Can. J. Chem. **64**, 1308 (1986).

An isolate of *Fusarium roseum* "Graminearum" obtained from overwintered oats in Alaska produced toxic cultures when grown on rice. The toxic principle called fusarochromanone isolated from these cultures reproduced the signs of tibial dyschondroplasia in poultry and also reduced hatchability of fertile eggs. Spectroscopic data (nmr, ir, and ms) indicated the mycotoxin to be a chromanone derivative. The chromanone ring structure was also confirmed by single crystal X-ray.

SADANAND V. PATHRE, WILLIAM B. GLEASON, YIN-WAN LEE et CHESTER J. MIROCHA. Can. J. Chem. **64**, 1308 (1986).

Un produit, isolé du *Fusarium roseum* "Graminearum" et qui a été obtenu à partir d'avoine de l'Alaska gardée pour l'hiver, a donné lieu à des cultures toxiques lorsqu'on l'a fait croître sur du riz. Le principe toxique, qui se nomme fusarochromanone et qui a été isolé de ces cultures, permet de reproduire la dyschondroplasie tibiale chez les poules et a aussi réduit la possibilité d'éclosion des oeufs fertiles. Les données spectroscopiques (rmn, ir et sm) indiquent que la mycotoxine est un dérivé de la chromanone. La structure du cycle chromanone a aussi été confirmée par diffraction des rayons X par un cristal unique.
[Traduit par la revue]

Introduction

Species of *Fusarium* are worldwide in distribution and are capable of causing plant disease such as wilt, scab, and rot in the field (1). They also produce a wide variety of mycotoxins such as zearalenone (2), an estrogen, and the trichothecenes. The latter cause complications to farm animals when ingested in animal feeds and have been also found in "Yellow rain" (3).

Since *Fusarium* fungi infect important agricultural plants and products, they have been associated with human and animal intoxications (4). Notable among these reports are bone malformation (tibial dyschondroplasia) in poultry and the incidence of low hatchability of fertile eggs when birds were fed diets containing *Fusarium* infected feed (5, 6). Tibial dyschondroplasia (TDP) is characterized by the presence of a cone of cartilage which extends distally from the proximal tibiotarsal physis (7, 8). Similar lesions occur in swine, horses, bulls, and dogs (9).

Recently we isolated a mycotoxin (herein called fusarochromanone) from rice cultures of *Fusarium* grown in the laboratory. Purified fusarochromanone reproduced the signs of TDP in chicks and also reduced hatchability of fertile eggs (10). This report describes the elucidation of the structure of this mycotoxin.

Results and discussion

Several isolates of *Fusarium roseum* "Graminearum" were collected from the overwintered oats in Fairbanks, Alaska, during 1978. All these isolates were screened for the toxicity by growing them on rice. Rice cultures of one of the isolates were found to be toxic to chickens and elaborated lesions of TDP. Several kilograms of rice cultures were extracted with chloroform–methanol – ammonium hydroxide (90:10:1, vol/vol/vol). The extract was subsequently chromatographed to give pure toxin as shown in Scheme 1.

Mass spectral analyses of fusarochromanone (**1**) yielded an ion at nominal mass of 292 (measured at 292.1421 to fit $C_{15}H_{20}N_2O_4$ within 1 ppm). Fast atom bombardment (FAB) mass spectrometry indicated a protonated species at m/z 293, which was peak matched to 293.1524 to fit a composition of $C_{15}H_{21}N_2O_4$ within 7.8 ppm. The FAB also showed an ion at m/z 558.2960, which fitted to within 6.3 ppm for a composition of $C_{30}H_{41}N_4O_8$, presumably due to a dimer.

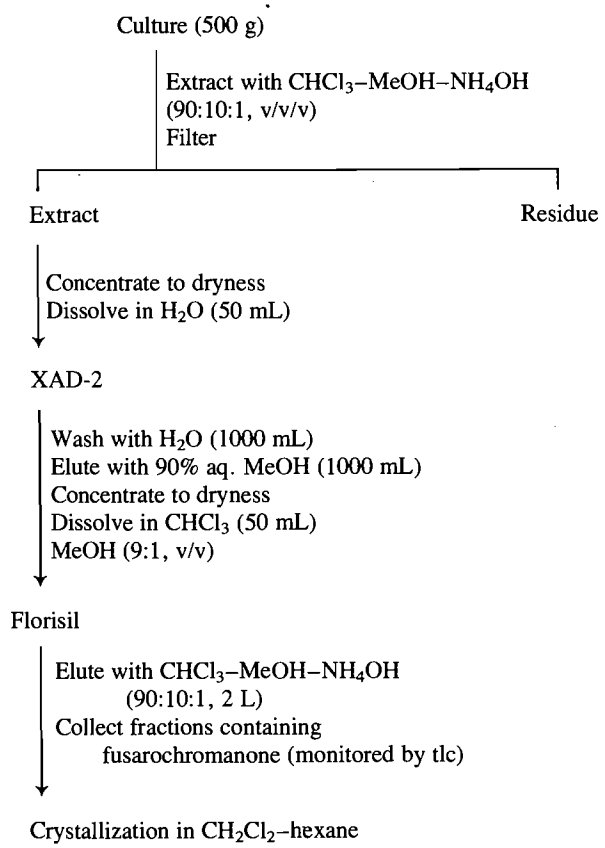

SCHEME 1. Isolation and purification of fusarochromanone.

[1]Revision received February 7, 1986.

TABLE 1. ^{1}H nuclear magnetic resonance assignment for fusarochromanone and its derivatives

	Chemical shifts (ppm)					Coupling constants (Hz)			
	1	**2**	**3**	**4**	Multiplicity	**1**	**2**	**3**	**4**
H-3	2.7	2.7	2.7	2.7					
H-7	7.86	7.94	7.85	7.87	d	8	8	8	8
H-8	6.08	6.08	6.09	6.06	d	8	8	8	8
H-2′	3.03	3.08	3.04	3.01	ddd	15,7.5,4	6,6,16	16,4,6	dd,16,8
	3.88	3.27	3.26	2.92					
H-3′	3.50	4.30	4.50	3.93	m				quint, 6
H-4′	3.60	3.76	4.18	4.16	m		d, 6	11,6,6	t, 6
			4.33	3.62					
CMe_2	1.26	1.46	1.46	1.46					
$ArNH_2$	9.46	9.48	9.47	9.46					
	9.60								
OAc		1.98	2.06						
			1.98						
N*H*Ac		6.42	6.40				d, 6	d, 6	

The ^{1}H nmr spectrum of **1** (Table 1) shows two aromatic *ortho* protons (J = 8 Hz), a *gem*-dimethyl, an isolated methylene, and five exchangeable protons, three of which were readily exchanged with D_2O in $CDCl_3$. The remaining two are those observed near 9 ppm as broad singlets. In addition, the spectrum displayed several multiplets between 2.8 and 3.8 ppm representing five protons. This five-proton multiplicity pattern

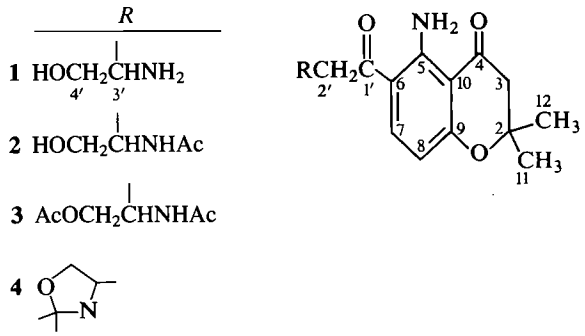

was assigned to a three-carbon unit **A** consisting of a methine flanked by two methylenes.

OH—CH_2—$CH(NH_2)CH_2$—

A

This assignment was deduced by acetylation of **1** with *N*-acetylimidazole, which afforded two major products identified as mono (**2**) and di (**3**) acetates of **1** by ^{1}nmr (Table 1).

The ^{13}C nmr spectrum of fusarochromanone (Table 2) exhibits 14 carbon signals including a single resonance for *gem*-dimethyl carbons, three methylenes, one aliphatic methine, two aromatic methines, and seven quaternaries. The two-dimensional carbon–proton correlation (HETCOR) spectrum of the toxin established the attachment of protons at 3.5 (isolated methylene singlet), 6.08, and 7.86 ppm to the carbons at 48.96, 104.10, and 140.16 ppm, respectively. The methylene (42.44 ppm) and methine (49.71 ppm) carbons were correlated to the proton multiplets near 3.0 and 3.5 ppm, respectively. Among the quaternaries, two of them were carbonyls. Chemical shifts and ir data indicate these carbonyls are conjugated. One of the carbonyls (193.70 ppm) gave a 3-Hz triplet in the proton-coupled carbon spectrum; this triplet was collapsed to a singlet when the isolated methylene proton singlet was selectively

TABLE 2. ^{13}C nuclear magnetic resonance assignment for fusarochromanone

Carbon	Chemical shift (ppm)	Multiplicity
2	79.32	s
3	48.96	t
4	193.70	s
5	154.71	s
6	111.71	s
7	140.16	d
8	104.10	d
9	165.99	s
10	104.10	s
1′	198.80	s
2′	42.44	t
3′	49.71	d
4′	65.82	t
11 and 12	26.28	q

decoupled. Since no other changes in the carbonyl triplet were observed during coherent low-power irradiation of other protons, this carbonyl should be adjacent to the isolated methylene carbon and well removed from the other protonated carbons. Single frequency low-power irradiation also permitted assignment of most of the quaternary carbons by virtue of their long range coupling with protons. For instance, the resonance at 165.99 ppm was observed as a doublet of doublets (J = 10 and 2.5 Hz) in the undecoupled spectrum. Irradiation of the 6.08-ppm proton resulted in the collapse of the smaller couplings to give a 10-Hz doublet, whereas the 7.86-ppm proton irradiation caused the 10-Hz doublet to collapse to yield a broad singlet. The magnitude of coupling constants indicates that the aromatic protons at 6.08 and 7.86 ppm must be situated *ortho* and *meta*, respectively, to this quaternary carbon. The aliphatic quaternary carbon at 79.32 ppm exhibited a complex multiplet, which reduced to a 2.5-Hz triplet upon irradiation of the *gem*-dimethyl proton singlet. This observation, together with the fact that the decoupling of the dimethyl resonance also caused removal of the long range couplings observed for the isolated methylene carbon, provided a contiguous arrangement of the isopropyl carbon, isolated methylene, and the 193.70-

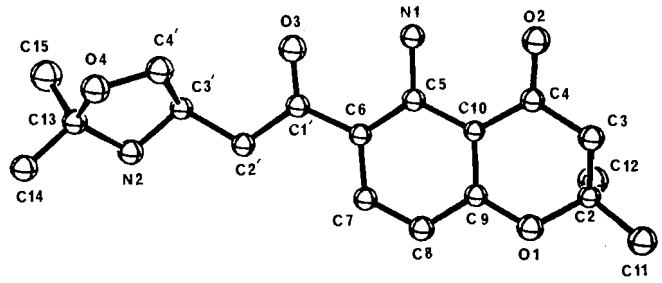

FIG. 1. Labelled drawing of **4** (50% probability).

ppm carbonyl. The chemical shift of the isopropyl quaternary carbon indicated it to be an ether carbon. The other end of this ether substituent was readily deduced to be the 165.99-ppm quaternary carbon since there was only one oxygen left to be accounted for (*vide infra*); the arrangement also provided a clue to the chromanone (3,4-dihydro-4*H*-1-benzopyra-4-one) system. Bookkeeping of all hetero atoms considered so far showed that $-NH_2$ should be one of the substituents, which was assigned to the 154.71-ppm quaternary carbon. The remaining quaternary carbons at 111.71 and 104.16 ppm were identified with the 198.80-ppm carbonyl bearing the three-carbon unit **A** and the γ-pyrone carbonyl, respectively, as substituents.

The substitution pattern in fusarochromanone is unique. A naturally occurring chromanone with an amino substituent at C6 has not been reported in the literature. The placement of the side chain at C7 is also unique. Although the nmr data is quite convincing in proving the structure of fusarochromanone, it was desirable to obtain a single crystal X-ray analysis of fusarochromanone.

Many solvents were used in an attempt to grow crystals of **1** suitable for the analysis, without any success. Finally, an acetone solution of **1** yielded pale yellow needle-shaped crystals. Unfortunately, these crystals were very thin and the best crystal that could be obtained was $0.18 \times 0.26 \times 0.05$ mm. Data of sufficient quality to solve the structure could not be obtained except at low temperature. Further, the ^1H nmr spectrum of these crystals in $CDCl_3$ indicated incorporation of acetone; however, there was no evidence of modification of the ring structure. Since our objective was to confirm the chromanone ring system, no further attempts were made to produce a more accurate structure.

Crystal data

$C_{18}H_{24}N_2O_4$ fw = 332.39

Orthorhombic, $P2_12_12$ (#18), $a = 11.282(4)$, $b = 23.265(6)$, $c = 6.246(4)$ Å^3, $Z = 4$, $V = 1639.4$ Å^3, $\mu = 0.89$ cm^{-1}, $\rho = 1.35$ g cm^{-1} (−100°C, Mo K_α, $\lambda = 0.71073$ Å, graphite monochromator). A labeled drawing of the molecule is given in Fig. 1. Atomic coordinates for non-hydrogen atoms are given in Table A, bond lengths and angles are summarized in Table B, and bond angles in Table C.[2]

Experimental

Infrared spectra were recorded on a Perkin Elmer 283 spectrophotometer. Proton nmr spectra were obtained on Varian XL-100 and XL-200 nmr spectrometers operating at 100 MHz and 200 MHz, respectively, using chloroform-*d* solutions. Carbon-13 nmr spectra were recorded on the Varian XL-200 spectrometer operating at 50.306 MHz using standard acquisition parameters. To obtain undecoupled carbon spectra the decoupler was kept on during a delay of 1 s and was gated off during acquisition to maintain maximum nOe (nuclear Overhauser enhancement). The 2D-nmr experiment was run using the pulse sequence HETCOR resident in the spectrometer system. Ultraviolet spectra were recorded on a Perkin Elmer 554 spectrophotometer in MeOH solutions. Mass spectra were obtained on a Kratos MS-50 high resolution mass spectrometer operating at 10 000 resolution. The standard Kratos FAB source were used. Thin-layer chromatographic analyses were carried out on precoated silica gel-254 (EM Reagents) and KC_{18} (Whatman) glass plates; components were visualized under uv light (either 254 or 356 nm).

For single crystal X-ray analysis, a crystal (obtained by slow evaporation of solvent from an acetone solution) was mounted on an Enraf–Nonius CAD4 diffractometer. Intensity data were collected at low temperature (−100°C) using an ω–2θ scan. Data were collected in the $+h, k, l$ octant to a maximum 2θ value of 48.0°. Three standard reflections measured every two hours during data collection showed a total loss of intensity of 10.3%. A linear decay correction was applied. Lorentz and polarization corrections were applied to the data. Since the linear absorption coefficient is small, an absorption correction was not made.

A total of 1662 reflections were collected (1608 unique and not systematically absent) and the space group of the crystal was determined to be $P2_12_12$ (#18 International Tables) from the systematic absences $h00$: $h = 2n$, and $0k0$: $k = 2n$ and subsequent least-squares refinement. The structure (**4**) was solved by direct methods (11). A total of 19 atoms were located from an *E*-map and the remaining atoms located in succeeding difference Fourier syntheses. Because of a paucity of data, isotropic temperature factors were used for C, O, and N. It was not possible to locate a hydrogen on N2 in difference maps although N1 had two peaks of reasonable intensity (0.4 e/Å^3) and distances (0.6, 1.2 Å). Therefore, hydrogen atoms were included at calculated positions (C—H bond length = 0.95 Å and N—H = 0.90 Å) but their positions were not refined. Hydrogen atoms were assigned fixed isotropic *B* values approximately equal to the *B* value of the atom to which they were attached. The structure was refined using full-matrix least-squares techniques where the function minimized was:

$$\sum w(|F_o| - |F_c|)^2$$

and the weight, w, is defined as:

$$w = 4F_o^2/\sigma^2(F_o^2)$$

All calculations were carried out on Digital Equipment Corporation PDP 8A and 11/34 computers using the Enraf–Nonius CAD4-SDP programs (12). The values of the atomic scattering factors were taken from the International Tables and effects of anomalous scattering were included (13). The model converged for 912 reflections $F_o^2 > 3.0\sigma(F_o^2)$ and 97 variables with agreement factor:

$$R = \sum||F_o| - |F_c|/\sum|F_o| = 0.093$$

$$R_w = \{\sum w(|F_o| - |F_c|)^2/\sum w|F_o|^2\}^{\frac{1}{2}} = 0.108$$

In the final cycle, the maximum shift/error was 0.01, the goodness of fit 2.45, and the largest peak in the difference map 0.5 e/Å^3.

Isolation and purification of fusarochromanone (1)

Five hundred grams of crude cultures (10) was extracted 5 times with the solvent system described in the scheme. The extracts were pooled and concentrated *in vacuo* at 40°C to give an oily residue, which was dissolved in 50 mL methanol in 200 mL of distilled water. This mixture was further concentrated to approximately 150 mL of solution and applied to an XAD-2 column (3.5 × 60 cm), rinsed with 1 L of distilled water, and eluted with 1 L of 90% methanol. The methanol fraction was concentrated *in vacuo* at 40°C, and reconstituted in 50 mL $CHCl_3$–MeOH (9:1, v/v). This solution was mixed with 50 g of

[2]A complete set of structure factor listings, thermal parameters, atomic coordinates including hydrogen atom positions, bond distances, bond angles, and torsional angles may be purchased from the Depository of Unpublished Data, CISTI, National Research Council of Canada, Ottawa, Ont., Canada K1A 0S2.

anhydrous sodium sulfate and the mixture was dried at room temperature. The dry yellow powder was then packed on the top of a column (3.5 × 60 cm) containing 150 g of Florisil, and eluted with 2 L of $CHCl_3$–MeOH (9:1, v/v) followed by 2 L of $CHCl_3$–MeOH–NH_4OH (90:10:1, v/v/v). Fusarochromanone was detected by irradiating the column with long-wave uv (365 nm) light since the toxin produces an intense blue fluorescence under the uv light. The fractions containing fusarochromanone were concentrated (40°C) and subsequently purified by tlc using $CHCl_3$–MeOH–NH_4OH (80:20:2, v/v/v).

Fusarochromanone (**1**): mp 132–134°C; uv λ_{max} (MeOH) (nm): 248 (ε 21 800), 277 (ε 8 800), 383 (ε 11 700); ir λ_{max} (KBr) (cm^{-1}): 3373, 3267, 3160 (NH_2, OH), 1655 (CO), 1562 (CO, -H bonded); nmr ($CDCl_3$) (see Tables 1 and 2); ms (M^+ 292.1421 calcd. for $C_{15}H_{20}N_2O_4$).

Acetylation of ***1***

Fifty milligrams of 1-acetylimidazole was added to a solution of **1** (50 mg) in $CHCl_3$ (2 mL). The reaction mixture was kept at room temperature for 2 h. The mixture was then chromatographed on preparative tlc ($CHCl_3$–MeOH; 9:1). Two major bands corresponding to R_f of 0.7 and 0.4 were scraped and eluted with $CHCl_3$; removal of solvent gave gummy solids.

*Monoacetate (**2**)*: ir λ_{max} (KBr) (cm^{-1}): 3380, 3280 (NH, OH), 1660 (CO), 1560 (amide II); nmr ($CDCl_3$) (see Table 1); ms (M^+ 334, M − AcO 275).

*Diacetate (**3**)*: ir λ_{max} (KBr) (cm^{-1}): 3382, 3322, 3275 (NH_2, NH), 1728 (CO ester), 1650 (CO), 1590, 1572, 1545 (CO -H bonded, amide II, Ar); nmr ($CDCl_3$) (see Table 1); ms (M^+ 376, M − AcO 317).

(**4**): A solution of **1** (50 mg) in acetone (15 mL) was kept at room temperature in a test tube and acetone was allowed to evaporate slowly to give needle-shaped crystals of **4**, mp 118–119°C; ir λ_{max} (KBr) (cm^{-1}): 3413, 3300, 3275 (NH_2, OH), 1650 (CO); nmr ($CDCl_3$) (see Table 1); ms (M + 1 333).

1. C. M. Christensen, and H. H. Kaufmann. *In* Grain storage: The role of fungi in quality loss. University of Minnesota Press, Minneapolis. 1969.
2. C. J. Mirocha, S. V. Pathre, and C. M. Christensen. *In* Mycotoxic fungi and mycotoxins. Vol. 2. *Edited by* T. D. Wyllie and L. G. Morehouse. Marcel Dekker Inc., New York. 1977. pp. 365–420.
3. S. A. Watson, C. J. Mirocha, and A. W. Hayes. Fundam. Appl. Toxicol. **4**, 700 (1984).
4. S. V. Pathre and C. J. Mirocha. J. Am. Oil Chem. Soc. **56**, 820 (1979).
5. T. F. Sharby, G. E. Templeton, J. N. Beasley, and E. L. Stephenson. Poult. Sci. **52**, 1007 (1973).
6. M. M. Walser, N. K. Allen, C. J. Mirocha, G. F. Hanlon, and J. A. Newman. Vet. Pathol. **19**, 544 (1982).
7. C. Itakura, and M. Goto. Jpn. J. Vet. Sci. **35**, 289 (1972).
8. P. W. Poulos, S. Reiland, K. Elwinger, and S. E. Olsson. Acta Radiol. Suppl. **358**, 229 (1978).
9. S. E. Olsson. Acta Radiol. Suppl. **358**, 9 (1978).
10. Y. W. Lee, and C. J. Mirocha. Appl. Environ. Microbiol. **50**, 102 (1985).
11. G. Germain, P. Main, and M. M. Woolfson. Acta Crystallogr. Sect. A, **27**, 368 (1971).
12. B. A. Frenz. *In* Computing in crystallography. *Edited by* H. Schenk, R. Olthof-Hazekamp, H. van Koningsveld, and G. C. Bussi. Delft University Press, Delft, Holland. 1978. pp. 64–71.
13. International tables for X-ray crystallography. Vol. IV. Kynoch Press, Birmingham, England. 1974. Tables 2.2A, 2.2C, Table 2.3.1.

New physostigmine related bromoalkaloids from the marine bryozoan *Flustra foliacea*[1]

MAURICE V. LAYCOCK AND JEFFREY L. C. WRIGHT[2]
National Research Council of Canada, Atlantic Research Laboratory, 1411 Oxford Street, Halifax, N.S., Canada B3H 3Z1

AND

JOHN A. FINDLAY AND ASHOK D. PATIL
Department of Chemistry, University of New Brunswick, Fredericton, N.B., Canada E3B 6E2

Received December 4, 1985

MAURICE V. LAYCOCK, JEFFREY L. C. WRIGHT, JOHN A. FINDLAY, and ASHOK D. PATIL. Can. J. Chem. **64**, 1312 (1986).

Methylene chloride extracts of the bryozoan *Flustra foliaceae* show strong antimicrobial activity. Chemical investigation of the metabolites has led to the identification of a series of new bromoalkaloids belonging to the physostigmine class, which are responsible for this activity.

MAURICE V. LAYCOCK, JEFFREY L. C. WRIGHT, JOHN A. FINDLAY et ASHOK D. PATIL. Can. J. Chem. **64**, 1312 (1986).

L'extraction du bryozoaire *Flustra foliaceae* par du chlorure de méthylène fournit des produits qui présentent une activité antimicrobienne très forte. Une étude chimique des métabolites a conduit à l'identification d'une série de nouveaux bromoalcaloïdes de la classe de la physostigmine, qui sont responsables de cette activité.

[Traduit par la revue]

Introduction

A few of the marine invertebrates belonging to the phylum Bryozoa have been the subject of chemical investigations (1) and these studies have revealed several unusual compounds, most of which display interesting biological activity. A chemical study of the bryozoan *Flustra foliacea L.* from Scandinavian waters revealed the presence of a remarkable variety of bromine-containing metabolites representing the physostigmine (2), tryptamine (3), and quinoline (4) alkaloid types. The bryozoan *F. foliacea* also grows abundantly in several areas of the Bay of Fundy and the methylene chloride extract of this organism showed strong antibacterial activity against an indicator bacterium, *Bacillus subtilis*. Assay-guided fractionation of this crude extract has led to a series of bromoalkaloids and we now wish to report in detail the isolation and structure elucidation of these compounds, two of which occur as N-oxides.

Results and discussion

The methylene chloride fraction of the aqueous methanol extract of fresh or frozen *Flustra foliacea* showed significant antibacterial activity against the indicator bacterium *Bacillus subtilis* in a disc diffusion assay (0.5 mg/disc). Large-scale reversed-phase separation (Waters Prep Pak) of the partially purified extract yielded several early fractions displaying antibacterial activity and containing uv-active compounds. Further adsorption chromatography of these active fractions, followed by a final reversed-phase hplc step, yielded the following series of related physostigmine bromoalkaloids.

Dihydroflustramine C, 1

Details of the structure analysis of dihydroflustramine C have already been published (5) but the nmr data are reproduced here for comparison (Tables 1 and 2). This metabolite was the major bromoalkaloid and consistently accounted for at least 60% of the alkaloid mixture. It is very closely related to flustramine C, **6**, obtained as a minor component from the Scandinavian strain, but remarkably we have not identified this latter compound in any of the Fundy samples.

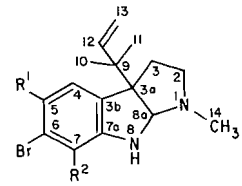

1 R^1, R^2 = H

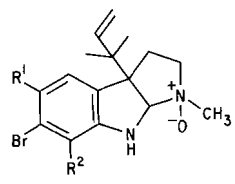

2 R^1, R^2 = H

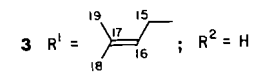

3 R^1 = ; R^2 = H

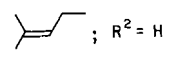

4 R^1 = ; R^2 = H

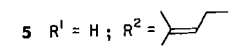

5 R^1 = H; R^2 =

Flustramine D, 3

This metabolite was the next most abundant component (ca. 40%) of the alkaloid mixture. The general shape of the uv spectrum (λ 231, 292 nm) was similar to that of dihydroflustramine C. The mass spectrum of flustramine D showed parent ions at *m/z* 390 and 388 ($C_{21}H_{29}N_2Br$). The base peaks at *m/z* 321 and 319 arise by a loss of 69 mass units from the parent ions and correspond to the loss of an isoprene unit. This is followed by a further loss of 68 mass units from the base peaks corresponding to cleavage of a second isoprene unit. The peaks at *m/z* 347 and *m/z* 345 arise by the loss of 43 mass units from the corresponding parent ions. A similar loss was observed in the mass spectrum of dihydroflustramine C and is accounted for by ejection of a CH_3—N=CH_2 fragment following partial cleavage of the pyrrole ring.

The ^{1}H nmr data for flustramine D are presented in Table 1. By comparison with dihydroflustramine C, **1**, and other related alkaloids (2) the 1H singlet at δ_H 4.39 ppm and the 3H singlet at δ_H 2.38 ppm were assigned to H-8a and the N-methyl group respectively. Irradiation of the N-methyl group resulted in nuclear Overhauser enhancement (nOe) of H-8a. The resonance for H-2 appeared as a 2H multiplet at δ_H 2.56 and the two H-3 protons resonated at δ_H 2.28 and 1.81 ppm. These latter assignments were confirmed by decoupling experiments. After irradiation of the H-2 protons the resonance for each H-3 proton appeared as a doublet due to geminal coupling (^2J = 12 Hz). Irradiation of either H-3 proton caused the H-2 multiplet to collapse to an ill-defined doublet. The spectrum of this second

[1]NRCC No. 25516.

[2]Author to whom correspondence should be addressed.

alkaloid also displayed the characteristic resonances for a "reversed" γ,γ-dimethylallyl group (2, 6): two 3H singlets at δ_H 0.98 and 1.02 ppm and the easily recognised ABM pattern at δ_H 4.99, 5.06, and 5.95 ppm. Methyl singlets at δ_H 1.70 and 1.73 ppm together with a methylene doublet at δ_H 3.31 (J = 7.1 Hz) and an olefinic methine at δ_H 5.22 (J = 7.1 Hz) revealed the presence of a second "regular" isoprene unit. The aromatic region contained only two proton resonances and both appeared as singlets, δ_H 6.74 and 6.93 ppm.

All twenty-one carbons of flustramine D, **3**, could be accounted for in the ^{13}C nmr spectrum (Table 2). In many respects the ^{13}C spectrum was very similar to that of **1** except for the five additional resonances (δ_c 17.97, 25.72, 34.26, 122.63, and 132.80 ppm) due to the second isoprene unit. The signals for C-2, C-3, and C-14 could be assigned by comparison of the chemical shift data with model and related compounds. The characteristically large coupling constant ($^1J_{CH}$ = 152.7 Hz) defined the resonance for the methine carbon C-8a. The quaternary carbon C-3a resonates at δ_c 64.12 ppm and must be substituted with a "reversed" γ,γ-dimethylallyl group; the resonance for C-3a is more shielded (ca. 56 ppm) when substituted with a regular γ,γ-dimethylallyl group. The position of this isoprene unit was further established upon irradiation of the methyl resonances H-10 and H-11, which resulted in nOe of H-8a, confirming *cis* fusion of the two heterocyclic rings. The same experiment also resulted in nOe of the H-3 proton resonating at δ_H 2.28 ppm; hence this proton is located on the same side of the pyrrole ring as H-8a and the "reversed" isoprene unit.

The second isoprene unit could be located by consideration of the ^1H and ^{13}C nmr data, and by a series of long-range heteronuclear decoupling experiments that unequivocally assigned the aromatic resonances. The ^1H chemical shift (δ_H 3.31 ppm) of the allylic methylene group H-15 precludes attachment of the C-5 unit at N-1. Because C-3a is already substituted and C-2, C-3, and C-8a all carry the requisite number of hydrogens, the second isoprene unit must be attached to the aromatic ring. Since there is no evidence in the ^1H spectrum of coupling between the aromatic protons, the isoprene unit was placed at C-5. This was consistent with the undecoupled ^{13}C nmr spectrum. The aromatic methine at C-7 (δ_c 112.62) appeared as a clean doublet (J = 164.07 Hz), whereas the resonance for C-4 (δ_c 126.34) appeared as a doublet of triplets (^1J = 157 Hz; ^3J = 4.8 Hz) through long-range coupling with the methylene protons at C-15. This was confirmed by single frequency irradiation of H-15, which removed the long-range coupling to C-4. The same decoupling experiment removed the two-bond coupling to C-5, which now appeared as a narrow doublet ($^3J \approx$ 4.0 Hz) due to coupling with H-7. Conversely, irradiation of

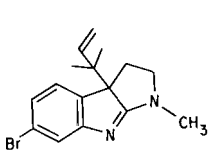

6

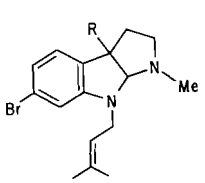

7 R =

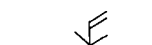

8 R =

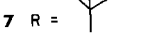

H-7 reduced the resonance for C-5 to a triplet ($^2J \approx$ 5.0 Hz) due to coupling with H-15. The same decoupling experiments indicated long-range coupling to C-6 but this was harder to interpret due to overlap with the resonance for C-16.

Dihydroflustramine C N-oxide, 2

This minor and somewhat unstable component was isolated from the more polar bromoalkaloid fractions. Both it and the other N-oxide, **4**, were present in the initial MeOH extract. The ^1H spectrum of **2** was very similar in overall appearance to that of **1** except for certain chemical shift differences (Table 1). Thus the spectrum displayed two aromatic resonances that integrated for three protons, as well as all the resonances associated with the inverted γ,γ-dimethylallyl group. However, the resonance assigned to H-8a in dihydroflustramine C, **1**, was now considerably deshielded (Δ 0.86 ppm) in this minor component, as was the resonance for the N-methyl group (Δ 0.1 ppm). Furthermore, one H-2 proton was deshielded (Δ 0.17 ppm) and the second one was shielded (Δ 0.18 ppm), whereas both H-3 proton resonances were deshielded by smaller amounts. These assignments were confirmed by a series of decoupling experiments. Irradiation of the 1H multiplet at δ_H 2.0 ppm assigned to H-3 removed a small vicinal coupling to the low-field H-2 resonance at δ_H 2.70 ppm, which now appeared as a clean doublet of doublets due to residual geminal (^2J = 11 Hz) and vicinal (^3J = 6.4 Hz) coupling. Similarly, irradiation at δ_H 2.70 ppm reduced the broadened multiplet at δ_H 2.00 ppm to a doublet of doublets (^2J = 13.1 Hz; ^3J = 4 Hz). Finally, irradiation of the 2H multiplet at δ_H 2.35 ppm collapsed the two resonances at δ_H 2.00 and 2.70 ppm to broad singlets.

In the ^{13}C nmr spectrum the chemical shifts of most resonances of the minor component were essentially the same as those for **1** except for marked shifts of certain resonances associated with the second pyrrole ring (Table 2). In particular, the resonances for C-3, C-8a, and C-14 were considerably deshielded (ca. 11.5, 8, and 9.5 ppm respectively), whereas the signal for C-3a was shielded (Δ ca. 13 ppm).

The mass spectrum showed parent ions at m/z 336 and 338, 16 mass units higher than the corresponding peaks for dihydroflustramine C, **1**. The hrms data established a molecular formula with an extra oxygen, and the fragmentation pathway was characterized by a strong $M - 16$ ion, a feature of amine oxides (7). This characteristic loss of 16 mass units from the parent ion was confirmed in a series of daughter-ion experiments. Thus the accumulated evidence suggests this new compound is an N-oxide of dihydroflustramine C but does not unequivocally discriminate between an N-1 oxide or an N-8 hydroxy function. The evidence favours N-1 substitution since H-8a, H-3, and the N-methyl protons are deshielded and there is little or no perturbation of the aromatic resonances in the ^1H and ^{13}C spectra. Placement of the oxide grouping at N-1 was confirmed by reinspection of the daughter-ion experiments, which showed that in addition to the characteristic loss of 16 mass units from the molecular ions, there is also a loss of 59 mass units from the molecular ions, giving rise to ions at m/z 277 and 279. This corresponds to elimination of a [CH_3—$N^+(O^-)$=CH_2] fragment arising by a fragmentation pathway analogous to the expulsion of [CH_3—N=CH_2] in dihydroflustramine C, **1**, and flustramine D, **3**. This fact also precludes an alternate structure for this minor component based on the structure of geneserine, **9**, a plant alkaloid isolated from *Physostigma venenosum* (8). Long believed to be the N-8 oxide of physostigmine, the structure of geneserine was revised to **9** following the observation that the mass spectrum of the alkaloid did not display a characteristic $M - 16$ loss. Instead, one of the major frag-

TABLE 1. ^{1}H nuclear magnetic resonance data

Compounds	H-2	H-3	H-4	H-5	H-7	H-8a	10-CH_3	11-CH_3
1	2.53	1.77	6.94 ^3J = 8.0 Hz	6.76 ^3J = 8.0 Hz ^4J = 1.8 Hz	6.66 ^4J = 1.8 Hz	4.37	1.02	0.96
2	2.35 2.70	2.0 2.35	6.88	6.88	6.75	5.23	0.97	0.93
3	2.56	1.81 2.28	6.93	—	6.74	4.39	1.02	0.98
4	2.33 2.69	2.0 2.69	6.84	—	6.80	5.23	0.95	0.98
5	2.56	1.81 2.28	6.9 d ^3J = 8.4 Hz	6.83 d ^3J = 8.4 Hz	—	4.44	1.04	0.98

*Chemical shifts in ppm relative to TMS as internal standard. Solvent $CDCl_3$. Shifts and coupling constants for coupled protons were, where possible,

TABLE 2. ^{13}C nuclear magnetic resonance

	C-2	C-3	C-3a	C-3b	C-4	C-5	C-6	C-7	C-7a	C-8a
1	53.1	34.78	64.0	132.53	126.3	120.8	121.4	111.6	152.1	84.5
2	53.8	46.35	50.9	129.37	125.78	120.97	121.26	111.79	152.51	92.62
3	53.12	34.57	64.12	133.46	126.34	129.98	122.97	112.62	149.82	84.76
4	53.95	46.39	51.17	130.88	126.01	130.21	122.93	112.69	152.23	92.90

*Chemical shifts in ppm relative to TMS as internal standard. Solvent $CDCl_3$.

mentations is a loss of 45 mass units corresponding to ejection of [CH_3—N═O]. No such loss is observed for the bryozoan alkaloid. Final structural proof was obtained by oxidation of **1** with *m*-chloroperoxybenzoic acid to yield a product with identical chromatographic (tlc and hplc) and spectroscopic properties (uv and ^{1}H nmr) to the naturally occurring N-oxide.

*Flustramine D N-oxide, **4***

This unstable compound was isolated as a very minor constituent of the alkaloid mixture. Except for a few resonances, the ^{1}H nmr spectrum of this material was very similar to that of flustramine D, **3** (Table 1). In particular, the resonance for H-2 now appeared as two 1H doublets (δ_H 2.33 and 2.69) and the signals for H-3 were deshielded (δ_H 2.0 and 2.69 ppm), as was C-8a (δ_H 5.23 ppm) and the N-methyl group (δ_H 2.46 ppm). Since these chemical differences between **3** and **4** were the same as those observed between **1** and **2** it appeared that this minor component was the N-oxide of flustramine D. This was substantiated by the mass spectral data, which displayed molecular ions at *m/z* 406 and *m/z* 404, 16 mass units higher than those for flustramine D. More significantly, the mass

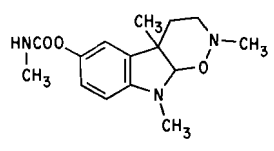

9

spectrum of this minor component displayed the characteristic losses of 16 mass units and 59 mass units from the molecular ions confirmed in a series of daughter-ion experiments and previously observed in the mass spectrum of dihydroflustramine C N-oxide, **2**.

This N-oxide could be prepared by oxidation of flustramine D with *m*-chloroperoxybenzoic acid. The synthetic material was identical by chromatographic (tlc and hplc) and spectroscopic (uv and ^{1}H nmr) comparisons.

*Isoflustramine D, **5***

One fraction was obtained that was an inseparable mixture of flustramine D, **3**, and another minor related component. The ^{1}H nmr spectrum of the mixture was almost identical with that of **3**, except for several additional resonances that suggested that the second minor component possessed the same basic skeleton as **3**, but that the C_5 isoprene unit was repositioned on the benzene ring. This followed from the observation that the two aromatic resonances of the minor component now appeared as an AB quartet due to *ortho* coupling (J = 8.4 Hz), the allylic methylene protons H-15 were somewhat deshielded (δ_H 3.40; J = 6.7 Hz), and the olefinic methyl protons were shifted to δ_H 1.72 and 1.81 ppm. In addition, the N-methyl, H-8a, and the methyl resonance H-10 were slightly shifted (see Table 1) but the remaining proton resonances for both isoprene units and the multiplets for H-2 and H-3 were unchanged. Based on this evidence and the similarity of the mass spectral data between flustramine D and the mixture, which was obtained over a wide temperature range, the structure of this minor component is tentatively proposed as **5**, a positional isomer of **3**.

Flustrabromine A, **7**, and B, **8**, were reported as the two main physostigmine alkaloids from *F. foliacea* collected from the North Sea (2). In our studies with *F. foliacea* collected from around the Bay of Fundy we did not detect these physostigmine derivatives. Instead our investigations serve to underscore the ability of *F. foliacea* to produce a variety of brominated alkaloids. It is not uncommon to find bromoalkaloids from marine invertebrates, though they appear to occur more frequently among sponges and tunicates (1), two of the most widely

of bromoalkaloids from *Flustra foliacea**

H-12	H-13 *cis*	H-13 *trans*	N-CH_3	H-15	H-16	18,19-CH_3
5.94 m $^3J_{cis}$ = 10.8 Hz $^3J_{trans}$ = 17.3 Hz	5.05 d ^3J = 10.8 Hz	4.99 d ^3J = 17.3 Hz	2.36			
5.98 m $^3J_{cis}$ = 10.0 Hz $^3J_{trans}$ = 17.1 Hz	5.07 d ^3J = 10.0 Hz	4.97 d ^3J = 17.1 Hz	2.46			
5.95	5.06	4.99	2.38	3.31 d ^3J = 7.1 Hz	5.22 d ^3J = 7.1 Hz	1.70 1.73
5.98	5.06	4.96	2.46	3.35	5.25	1.72 1.75
5.97	5.06	5.02	2.37	3.40 d ^3J = 6.7 Hz	5.22	1.72 1.81

derived by first-order analysis of the sub-spectra.

data of bromoalkaloids from *Flustra foliacea**

C-9	C-10	C-11	C-12	C-13	C-14	C-15	C-16	C-17	C-18	C-19
41.3	23.2	22.4	144.6	113.2	36.89					
41.8	22.73	22.3	144.44	113.28	46.36					
41.25	23.26	22.4	144.68	113.07	36.95	34.26	122.63	132.8	25.72	17.97
41.87	22.91	22.31	144.74	113.20	46.39	34.45	122.74	132.54	25.73	18.08

studied phyla. Studies with bryozoans are less common, mainly due to the difficulty in collecting enough material for analysis. However, of the marine bryozoans that have been investigated, a member of the genus *Zoobotryon*, which belongs to the family Flustridae, contains the brominated gramine derivative **10** as well as the N-oxide **11** (9). Thus, the discovery of **2** and **4** from *F. foliacea* is, to our knowledge, only the second time N-oxides have been isolated from marine sources. It will be interesting to learn if other members of the family Flustridae contain further variants of these unusual bromoalkaloids.

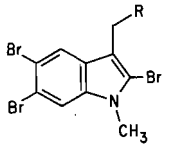

10 R = $N(CH_3)_2$

11 R = $\overset{+}{N}(CH_3)_2\ \overset{-}{O}$

The alkaloids from our local *F. foliacea* also display a wide antibacterial spectrum. The alkaloid fraction containing mainly **1** and **3** showed activity against *Enterobacter cloacea*, *Escherichia coli*, *Klebsiella pneumoniae*, *Proteus vulgaris*, *Pseudomonas aeruginosa*, *Salmonella typhimurium*, *Serratia marcescens*, *Staphylococcus aureus* and *Staphylococcus epidermidis* in disc diffusion assays (0.5 mg/disc) using procedures already described (10).

Experimental

Optical rotations were measured with a Perkin–Elmer polarimeter. Ultraviolet and infrared spectra were recorded with a GCA-MacPherson Series 700 and a Perkin–Elmer 283B spectrophotometer. ^1H and ^{13}C nuclear magnetic resonance spectra were all recorded in $CDCl_3$ with TMS as internal standard on the Nicolet 360 NB spectrometer of the Atlantic Region Magnetic Resonance Centre. Mass spectra were obtained with a Dupont model 21-110B double-focussing spectrometer used in the electrical detection mode (8 kV accelerating voltage, 70 eV ionizing energy). Accurate mass measurements were made by peak matching against a perfluorokerosene reference. Large scale hplc was performed with a Waters Associates Prep System 500 and semi-preparative hplc was carried out using Waters Associates model 6000 pumps, U6K injector, and a model 450 variable wavelength detector. Rotating-disc chromatography was performed using a Chromatotron model 7924.

The bryozoan *Flustra foliacea* was collected in the Bay of Fundy off the New Brunswick and Nova Scotian shores. A voucher specimen is on deposit at the Department of Biology, Acadia University, Wolfville, N.S.

Isolation of flustramine alkaloids

The bryozoan (3 kg), either fresh or frozen material, was extracted with methanol at room temperature for 3 days. The methanolic extract (18 L) was concentrated under reduced pressure until most of the methanol was removed and the residue was shaken against methylene chloride. The methylene chloride soluble fraction (12.8 g) was divided into 4 equal portions and each one was chromatographed on a pad ($1\frac{3}{4}$ in. × $3\frac{3}{4}$ in. diam.) of silica gel (Merck, Kieselgel GF_{254}, Type 60) and eluted with a solvent gradient system from hexane through ether, methylene chloride, ethyl acetate, and methanol. Several fractions (2.8 g) displaying antibacterial activity were combined and subjected to large-scale reversed-phase liquid chromatography. The bioactive fractions, eluted with 15% aqueous methanol, all contained uv-active (254 nm) spots and these were further separated by rotating-disc adsorption chromatography on silica gel using solvent mixtures of methylene chloride, methanol, and acetone. The uv-active bands were collected as they were eluted from the disc and from these fractions the individual bromoalkaloids were obtained in a final hplc purification step using Spherisorb ODSII (5μ; Regis, 10 mm × 25 cm) with 10% aqueous methanol containing 0.1% triethylamine.

Dihydroflustramine C, 1

Crystallized from ether – petroleum ether mixtures, mp 82–84°C; $[\alpha]_D^{25}$ −110° (c = 1.5, CH_2Cl_2); λ_{max} (MeOH): 213 (ε 2 × 10^4), 250 (ε 5.6 × 10^3), 309 (ε 3.4 × 10^3) nm; ν_{max} (KBr): 3200, 1600, 1590, 1475, 1350, 1150, 1050 cm^{-1}; ^1H (360 MHz) and ^{13}C (98.2 MHz) nmr data in Tables 1 and 2; m/z (rel. int.): 320/322 (M^+, 50%), 305/307 (8%), 227/229 (15%), 251/253 (100%), 208/210 (66%), 172 (90%), 129 (40%). Accurate mass measurement M^+ at m/z 322.0875 (calcd. for $C_{16}H_{21}N_2{}^{81}Br$: 322.0869).

Dihydroflustramine C N-oxide, 2

Obtained as an oil; $[\alpha]_D^{25}$ −67.1° (c = 0.38, CH_2Cl_2); λ_{max} (MeOH): 226 (ε 3.8 × 10^3), 283 (ε 2 × 10^3) nm; ν_{max} (thin film): 3400–3200 br, 1610, 1460, 1270, 1120, 1010 cm^{-1}; ^1H and ^{13}C nmr data in Tables 1 and 2; m/z (rel. int.): 336/338 (M^+, 17%), 320/322 (34%), 277/279 (44%), 268/270 (17%), 251/253 (100%), 209/211 (76%). Accurate mass measurement M^+ at m/z 336.0843 (calcd. for $C_{16}H_{21}N_2O^{79}Br$: 336.083).

Flustramine D, 3

Obtained as an oil; $[\alpha]_D^{25}$ −86.5° (c = 1.03, CH_2Cl_2); λ_{max} (MeOH): 231 (ε 7.1 × 10^3), 292 (ε 3.1 × 10^3) nm; ν_{max} (thin film): 3180, 1610, 1475, 1355, 1240, 1140, 1010 cm^{-1}; ^1H and ^{13}C nmr data in Tables 1 and 2; m/z (rel. int.): 388/390 (M^+, 26%), 373/375 (2%), 345/347 (4%), 319/321 (100%), 276/278 (7%), 251/253 (14%). Accurate mass measurement M^+ at m/z 390.1498 (calcd. for $C_{21}H_{29}N_2{}^{81}Br$: 390.1494).

Flustramine D N-oxide, 4

Obtained as an oil; λ_{max} (MeOH): 224 (ε 7.1 × 10^3) and 285 (ε 3.1 × 10^3) nm; ν_{max} (thin film): 3400, 1610, 1485, 1467, 1383, 1285, 1127, 1075 cm^{-1}; ^1H nmr data listed in Table 1. The ^{13}C nmr data in Table 2 were obtained on the synthetic material; m/z (rel. int.): 404/406 (M^+, 2%), 388/390 (26%), 373/375 (2%), 345/347 (10%), 319/321 (100%), 277/279 (15%). Accurate mass measurement M^+ at m/z 404.1286 (calcd. for $C_{21}H_{29}N_2O^{79}Br$: 404.12873).

Isoflustramine D, 5

Obtained as a 65:35 mixture with **3**; $[\alpha]_D^{25}$ −14.6° (c = 0.07, CH_2Cl_2); λ_{max} (MeOH): 230 and 290 nm; ν_{max} (thin film): 3400, 1610, 1490, 1450, 1380, 1255, 1160, 1010 cm^{-1}; ^1H nmr data in Table 1; m/z (rel. int.): 388/389 (M^+, 39%), 319/321 (100%), 276/278 (5%), 263/265 (22%), 251/253 (2%), 241 (9%).

Preparation of N-oxides

Dihydroflustramine C (32 mg; 0.01 mmol) or flustramine D (39 mg; 0.01 mmol) in CH_2Cl_2 (5 mL) was stirred and cooled on ice for several minutes preceding addition of an equimolar amount of *m*-chloroperoxybenzoic acid in CH_2Cl_2 (2.5 mL). Stirring was continued until oxidation was complete (1–2 h). The reaction mixture was partially purified by flash chromatography followed by further purification by reversed phase hplc using Spherisorb ODS II (5μ; Regis; 10 mm × 25 cm) and elution with 10% aqueous MeOH containing 0.1% triethylamine.

Acknowledgements

The authors acknowledge the technical assistance of Cheryl Craft and Brigitte Tremblay, and thank Professor Sherman Blakeney, Acadeia University, Wolfville, N.S., for his assistance and identification of the bryozoan. Two of us (J.A.F. and A.D.P.) are grateful to the Natural Sciences and Engineering Research Council of Canada for financial assistance and to Barry Hill (St. Andrews, N.B.) for collection and identification of material from Passamaquoddy Bay.

1. D. J. FAULKNER. Nat. Prod. Rep. **1**, 551 (1984).
2. (*a*) J. S. CARLÉ and C. CHRISTOPHERSEN. J. Org. Chem. **45**, 1586 (1980); (*b*) J. Org. Chem. **46**, 3439 (1981).
3. P. WULFF, J. S. CARLÉ, and C. CHRISTOPHERSEN. J. Chem. Soc. Perkin Trans. 1, 2895 (1981).
4. P. WULFF, J. S. CARLÉ, and C. CHRISTOPHERSEN. Comp. Biochem. Physiol. B, **71**, 525 (1982).
5. J. L. C. WRIGHT. J. Nat. Prod. **47**, 893 (1984).
6. P. M. SCOTT, M. A. MERRIEN, and J. POLANSKY. Experientia, **32**, 140 (1976).
7. N. BILD and M. HESSE. Helv. Chim. Acta, **50**, 1885 (1967).
8. C. HOOTELÉ. Tetrahedron Let. 2713 (1969).
9. A. SATO and W. FENICAL. Tetrahedron Lett. **24**, 481 (1983).
10. J. A. FINDLAY and A. D. PATIL. J. Nat. Prod. **47**, 815 (1984).

Rates and equilibrium constants for the covalent hydration of 5-bromo-2(1*H*)-pyrimidinone in aqueous solution

OSWALD S. TEE,[1] JANA PIKA, M. JUDITH KORNBLATT, AND MICHAEL TRANI
Department of Chemistry, Concordia University, 1455 Boulevard de Maisonneuve, Montréal, Qué., Canada H3G 1M8
Received December 24, 1985
This paper is dedicated to Professor Arthur N. Bourns

OSWALD S. TEE, JANA PIKA, M. JUDITH KORNBLATT, and MICHAEL TRANI. Can. J. Chem. **64**, 1267 (1986).

The kinetics of bromination of the title compound (**1**) have been measured in aqueous solutions of pH 0–6. The change in the order of reaction which occurs around pH 2.5 is explained by **1** reacting via its covalent hydrate, **3**. Furthermore, there is sufficient **3** present at equilibrium that the kinetics of its equilibration with **1** were also measured. From these two studies the extent of covalent hydration of **1** is estimated to be 5%.

Kinetic studies of the bromination of the dimethyl cation **5** and of its equilibration with the pseudobase **6** were also carried out for the purposes of comparison.

The present results for **1**, **3**, **5**, and **6** are compared to earlier results for 2-pyrimidinone and analogous derivatives.

OSWALD S. TEE, JANA PIKA, M. JUDITH KORNBLATT et MICHAEL TRANI. Can. J. Chem. **64**, 1267 (1986).

Opérant en solutions aqueuses et à des pH allant de 0 à 6, on a mesuré les cinétiques de bromation du composé (**1**) mentionné dans le titre. A un pH de 2,5, il se produit un changement dans l'ordre de la réaction qui est expliqué par le fait que le composé **1** réagit alors par le biais de son hydrate covalent, **3**. De plus, la concentration à l'équilibre du composé **3** est telle que l'on peut aussi mesurer la cinétique de son équilibre. Sur la base des résultats obtenus au cours de ces deux études, on peut évaluer à 5% le taux d'hydratation covalente du composé **1**.

Pour fins de comparaison, on a aussi effectué des études cinétiques de la bromation du cation diméthylé **5** et de son équilibre avec la pseudobase **6**.

On compare les résultats obtenus avec les composés **1**, **3**, **5** et **6** avec ceux obtenus antérieurement avec la pyrimidinone-2 et ses dérivés analogues.

[Traduit par la revue]

Previous studies from this laboratory have shown that covalent hydrates are involved in the aqueous bromination of 2-pyrimidinone (1, 2), 4-pyrimidinone (3), and 4-quinazolinone (4). In contrast, evidence against their involvement was adduced for the bromination of the closely related pyrimidines: uracil (5) and cytosine (6).

From kinetic and equilibrium measurements on the parents and on their *N*-methyl derivatives it was estimated that the extent of hydration of 2-pyrimidinone is ~0.05% (2) and that of 4-pyrimidinone is ~0.0003% (3). The hydrates are involved in the bromination because they are enamines and as such they are very reactive towards bromine ($k_2 \sim 10^9 M^{-1} s^{-1}$) (2, 3, 7).

Since these covalent hydrates are only present at very low levels, they are not observable by normal spectroscopic means (8). However, from the earlier work on 5-bromo-2-pyrimidinone (**1**) and its *N*-methyl derivatives (1) it is possible to estimate[2] that its covalent hydrate (**3**) is present to the level of a few percent and so it might be observable.

The previous study of the bromination of **1** (Scheme 1) was carried out in strong aqueous acid in which the reaction is slow enough to be followed by conventional spectrophotometry (1). In such media **1** is almost solely present as its conjugate acid, **2**, and it shows a reactivity towards bromine which is very similar to that of the related *N*,*N*′-dimethyl cation, **5**. Since the quaternary ion **5** reacts via its pseudobase **6**, it was concluded that **1** reacts as its covalent hydrate **3** (1).

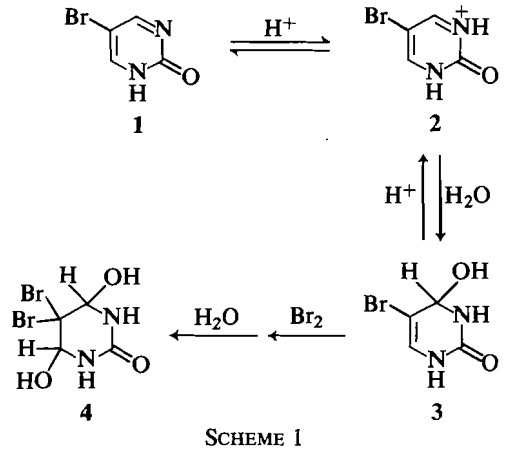

SCHEME 1

Subsequently much stronger evidence for this type of mechanism was obtained for 2- and 4-pyrimidinones by carrying out stopped-flow kinetic studies in the pH region (2, 3). In particular, it was found that the order of the reaction changes with pH (2, 3, 7). At low pH bromine attack on the hydrate is rate-limiting and so the reaction is first order in substrate and in bromine. However, at intermediate pH the formation of the hydrate is the slow step and consequently the reaction is zero order in bromine (2, 3).

The present paper reports a similar study of the bromination of **1** carried out in the pH region which corroborates the earlier conclusions derived from the study in strong acid (1). More-

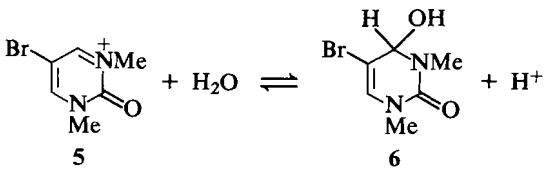

[1]To whom correspondence should be addressed.

[2]For the reaction of the pseudobase **6** with bromine the previous work in strong acid at 30°C gave $k_2 \sim 4 \times 10^6 M^{-1} s^{-1}$ (1). *If* one assumes that the same value applies to reaction of the covalent hydrate **3** then the equilibrium constant K_2 (defined later) = 0.012 *M*. However, the literature value of the acid dissociation constant (20°C) of **1** is K_1 = 0.36 *M*. Therefore, the hydration ratio K_h = [**3**]/[**1**] = $K_2/K_1 \sim 0.03$.

over, we have been able to observe the small percentage of the covalent hydrate **3** and to measure its equilibration with **1**. For comparison we have also studied the equilibration of the dimethyl cation **5** with its pseudobase **6**. These studies became necessary because of work in this laboratory in which it has been found that **1** and **3** are inhibitors of the enzyme, cytosine deaminase (9). In particular, we needed to know the equilibrium constant between **1** and **3** and the rate constants for their interconversion as a function of pH.

Results

For the most part the approach taken was as in our earlier studies on 2-pyrimidinones (2, 7) and similar results have been obtained. Accordingly, the present study will not be described in the same detail, except where necessary. The covalent hydrate **3** was detected using uv spectrophotometry and so its equilibration with **1** was studied. Attempts to observe **3** using nmr spectroscopy were thwarted by the low solubility of **1** in water and even in 50% aqueous DMSO.

Bromination studies

The rates of bromination of **1** and of its dimethyl cation **5** were measured by stopped-flow methods (2, 3, 5–7). The results resemble those obtained for 2-pyrimidinone (2) in that there is a change of kinetic order with pH. For **1** they can be explained by Scheme 1 and using a rate expression based on the constants in eq. [1]. Assuming that the covalent hydrate **3** is present in steady

$$[1]\quad \mathbf{1} \underset{K_1}{\overset{H^+}{\rightleftharpoons}} \mathbf{2} \underset{k_H, H^+}{\overset{k_1}{\rightleftharpoons}} \mathbf{3} \xrightarrow[Br_2]{k_2}$$

state amounts[3] leads to eq. [2] for the rate of disappearance of bromine:

$$[2]\quad \text{Rate} = \frac{k_1 k_2[Br_2]}{(k_H[H^+] + k_2[Br_2])} \cdot \frac{[\mathbf{1}]_t[H^+]}{(K_1 + [H^+])}$$

where $[\mathbf{1}]_t = [\mathbf{1}] + [\mathbf{2}]$ and $K_1 = [\mathbf{1}][H^+]/[\mathbf{2}]$. Obviously, the observed kinetic order and the variation of rate with pH will depend on the dominant terms in each of the two bracketed parts of the denominator of eq. [2].

In the pH range 0–2 the bromination of **1** and its dimethyl cation **5** both exhibit second-order kinetics. For **5** the values of k_2^{obs} (Table 1) increase regularly[4] with pH whereas for **1** they give a curved rate profile (see Fig. 1). As previously (1), the results for **5** are attributed to rate-limiting attack of bromine on its pseudobase **6**:

$$[3]\quad \mathbf{5} \underset{H^+}{\overset{K_2}{\rightleftharpoons}} \mathbf{6} \xrightarrow[Br_2]{k_2}$$

For this reaction scheme $k_2^{obs} = k_2K_2/[H^+]$ and from the data we estimate[5] that $k_2K_2 = 9400\ s^{-1}$. From equilibrium measurements we have $pK_a = 3.47$ and so $k_2 = 2.8 \times 10^7\ M^{-1}\ s^{-1}$.

The curved rate profile for **1** is expected since the literature value of $pK_a = 0.44$ (10). The data can be explained by eq. [2] with the condition that $k_H[H^+] \gg k_2[Br_2]$. In this case eq. [2] simplifies to a second-order rate expression (at fixed pH) and the form of the rate constant is:

$$[4]\quad k_2^{obs} = k_2k_2/k_H(K_1 + [H^+]) = k_2K_2/(K_1 + [H^+])$$

TABLE 1. Rate constants for the reaction of bromine with **1** and **5** (bromide salt) at low pH[a]

S	pH	k_1^{obs} (s^{-1})	$k_2^{obs} \times 10^{-3}$ ($M^{-1}\ s^{-1}$)
1	0.13	2.41	14.9
	0.59	8.96	55.3
	0.94	15.4	95.1
	1.20	21.0	130
	1.32	21.2	131
	1.39	21.8	135
	1.79	9.54[b]	140
5(Br^-)[c]	0.13	0.57	4.23
	0.34	1.47	11.0
	0.64	4.03	30.0
	0.81	7.26	54.1
	1.10	15.5	115
	1.39	34.3	256
	1.61	53.6	399

[a]At 25°C, I = [HCl] + 0.1 M (KBr), $[S]_0$ = 0.5 mM, $[Br_2]_0$ = 0.05 mM.
[b]$[S]_0$ = 0.2 mM, $[Br_2]_0$ = 0.01 mM.
[c]$[S]_0$ = 0.422 mM.

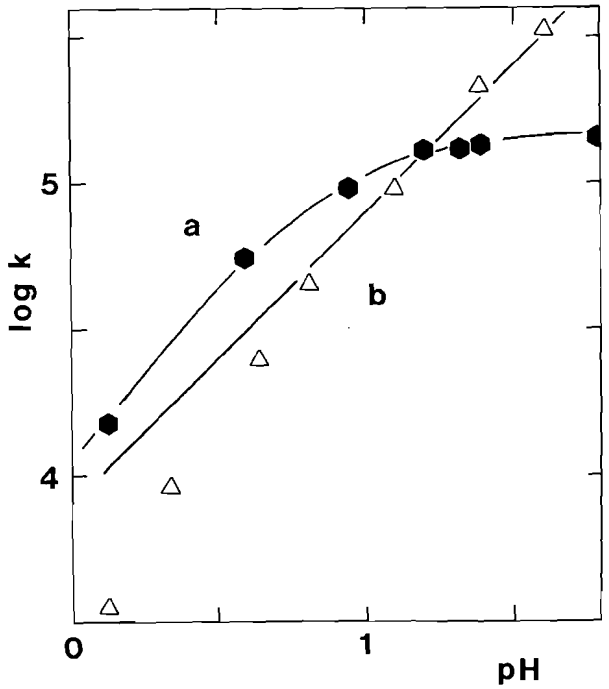

FIG. 1. Second-order rate constants for the bromination of: (*a*) **1**; (*b*) **5** (as bromide ion salt). Conditions are given in Table 1.

[3]This is not strictly true in that **3** is not always present at very low levels. However, at low pH as **3** is consumed by bromine more **1** (present in large excess) is converted to **3** and so its level remains relatively constant. At higher pH values, the initial amount of **3** is consumed rapidly (see later, Fig. 2*a*) and then its formation becomes rate-limiting, as described later. Furthermore, most of the experiments at higher pH values were carried out in such a way that *no* **3** was present initially. In view of the foregoing, we retain eqs. [1] and [2] for the convenience of their use, rather than using a more rigorous (and more abstruse) treatment which takes account of the fact that **3** is present to the level of a few percent at equilibrium.

[4]The pH–rate profile deviates from ideality (slope = 1) as the pH decreases to 0. This is due to the increase in ionic strength which accrues from the higher concentrations of HCl.

[5]The value of k_2K_2 is estimated from the four higher pH values where the ionic strength is reasonably constant (see footnote 4).

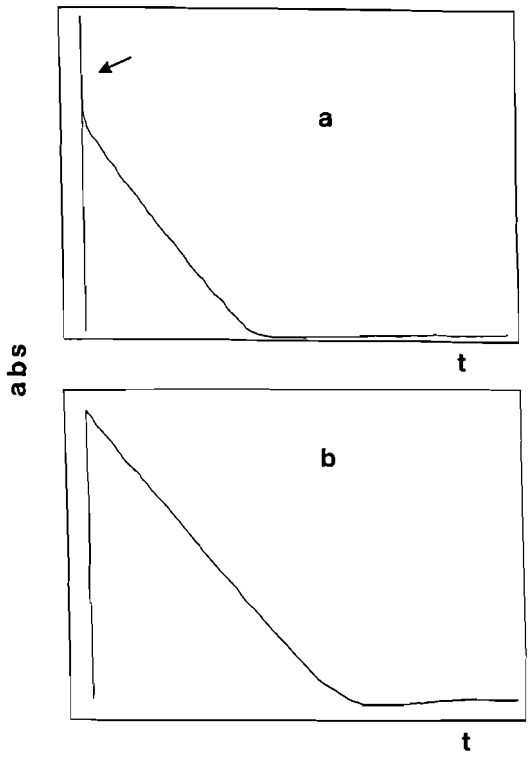

FIG. 2. Sketches of typical absorbance-time traces obtained for the reaction of bromine with **1** in the pH range 3.5–6.0. (*a*) When **1**, at equilibrium in acidic buffer, is mixed with bromine in the same buffer. (*b*) When **1** is generated *in situ* by mixing the anion $\mathbf{1}^-$ with acidic buffer containing bromine. Conditions are given in Table 2.

where $K_2 = k_1/k_H = [\mathbf{3}][H^+]/[\mathbf{2}]$ is the equilibrium constant relating the cation **2** and the hydrate **3**. From the plateau in the rate profile $k_2K_2/K_1 = 1.4 \times 10^5\ M^{-1}\,s^{-1}$. Taking a value of $pK_1 = 0.70$[6] leads to $k_2K_2 = 28\,000\ s^{-1}$.

Above pH 2 the rate of bromination of **5** is too fast to follow by the stopped–flow method. This arises because the increase in the amount of **6** does not level off until after pH 3.5 ($\simeq pK_2$). In the pH range 2–3 the bromination of **1** shows mixed-order kinetics, as was found earlier for the parent, 2-pyrimidinone (**2**). Above pH 3.5 the kinetics are more straightforward and, for an excess of the substrate **1**, the disappearance of bromine follows zero-order kinetics but with an illuminating complication.

When a solution of bromine is mixed with a ten-fold excess of **1** *two* distinct kinetic phases are seen in the absorbance decay curve (Fig. 2*a*). There is an initial rapid phase during which about 30% of the starting absorbance disappears followed by a slower phase which is clearly zero-order. This behaviour we take as direct evidence for the presence of the covalent hydrate **3** and that it is present to a level of *approximately*[7] 3% (since [**1**] is 10× that of Br_2). We argue that when the solution of **1** is mixed with a bromine solution there is a fast initial phase during which the equilibrium amount of the hydrate **3** is consumed. Thereafter, the rate of reaction is determined by the rate of formation of more **3** from **1** and so zero-order behaviour (with respect to bromine) is observed.

TABLE 2. Rate constants for the reaction of bromine with **1** at intermediate pH values[a]

pH	$k_0^{obs} \times 10^5$ ($M\,s^{-1}$)	$k_1^{obs} \times 10^2$ (s^{-1})
3.67	12.2	24.4
4.17	4.33	8.66
4.73	1.55	3.10
5.10	0.764	1.53
6.17	[b]	0.091[b]

[a]At 25°C, $I = 0.11\ M$ (KBr + buffer), $[\mathbf{1}]_0 = 0.5\ mM$, $[Br_2]_0 = 0.05\ mM$. Solutions of $\mathbf{1}^-$ at pH 9–10 were mixed with acidic buffers containing bromine (see text).
[b]See footnote 8.

Confirmation of this interpretation was obtained by carrying out experiments in which *no* hydrate was present initially and so the initial fast phase was absent. Substrate solutions were prepared at pH 9–10 so that **1** was present as its anion $\mathbf{1}^-$, the deprotonation pK_a of **1** being 7.36 (10). Such solutions were then mixed with acidic buffers (pH 3.5–6.5) containing bromine. Upon mixing, the anion $\mathbf{1}^-$ is rapidly protonated (within the dead-time of the instrument) to give **1** in the absence of any of its hydrate **3**. Consequently, no initial fast phase is seen and one simply observes the zero-order disappearance of bromine (Fig. 2*b*) corresponding to rate-limiting formation of the covalent hydrate **3**:

$$[5] \quad (\mathbf{1}^- \xrightarrow[\text{fast}]{H^+})\,\mathbf{1} \xrightarrow[\text{slow}]{} \mathbf{3} \xrightarrow[\text{fast}]{Br_2}$$

Analysis of the absorbance traces obtained at various pHs yielded the zero-order rate constants given in Table 2.[8]

The kinetic behaviour described above and the pH dependence of the rate constants are accommodated by eq. [2] with the conditions that $k_2\,[Br_2] \gg k_H[H^+]$ and $K_1 \gg [H^+]$ ($pH > pK_1$), both of which are reasonable. With these conditions imposed eq. [2] simplifies to an expression which is zero-order in bromine when the substrate **1** is in large excess and constant:

$$[6] \quad \text{Rate} = k_0^{obs} = k_1[\mathbf{1}]_t[H^+]/K_1$$

Accordingly, the expected form of the pH dependence of the first-order rate constant (with respect to **1**) is given by:

$$[7] \quad k_1^{obs} = k_0^{obs}/[\mathbf{1}]_t = k_1[H^+]/K_1$$

As shown by Fig. 3*a* (data from Table 2) the observed values of k_1^{obs} vary with pH in the manner prescribed by eq. [7]. The decrease in rate with increasing pH arises because the rate-limiting step of the formation of the hydrate **3** involves the attack of water (k_1) on the protonated form of the substrate (see **2** → **3**,

[6]The literature value of $pK_1 = 0.44$ is for 20°C at low ionic strength (10). A value of 0.70 is more appropriate for the present work at 25°C and $I = 0.1\ M$. It is derived from the pH at which the observed rate is half of the plateau rate.

[7]The estimate is only approximate since the apparent extinction coefficients for the two phases of the reaction are not the same. The initial fast decrease in absorbance is due to the consumption of **3** and bromine whereas the second is due to the disappearance of **1** and bromine. Furthermore, because of the speed of the first phase it is difficult to accurately measure the absorbance value at time zero.

[8]Around pH 6 the absorbance changes again start to show mixed-order behaviour. This is most probably due to the onset of reaction of bromine with the anion $\mathbf{1}^-$. The absorbance–time data can be analyzed in terms of a combination of pseudo-zero- and pseudo-first-order processes in the manner described by Paventi (19). He found similar behaviour in the bromination of 2- and 4-pyrimidinone, both of which react via their anions at pH > 5.

TABLE 3. Rate constants for the equilibration of the cation **5** with its pseudobase **6**[a]

pH	k_{obs} (s^{-1})	k_f (s^{-1})	k_d (s^{-1})
3.29	158	62.9	95.1
3.60	121	69.5	51.5
3.78	107	69.1	33.9
4.13	102	87.0	19.0
4.41	85.2	76.4	8.77
4.97	79.3	76.9	2.43
5.29	81.2	80.0	1.21
5.58	81.5	80.9	0.628
5.89	82.8	82.5	0.314
6.06	80.9	80.7	0.207
6.50	81.2	81.1	0.0757
6.75	76.3	76.3	0.0400
6.95	80.2	80.2	0.0265
7.90	101	101	0.00375
8.25	123	123	0.00204
8.52	149	149	0.00133

[a]At 25°C, $I = 0.11\,M$ (NaCl + buffer). Values of k_f and k_d were calculated from k_{obs} and K_2 as described in the text.

Scheme 1). Analysis of the data in Table 2 in terms of eq. [7] gives $k_1/K_1 = 1\,500\,M^{-1}\,s^{-1}$, from which $k_1 = 300\,s^{-1}$ for $pK_1 = 0.70$.[6]

Overall, the kinetic behaviour displayed by the bromination of the 5-bromo compound **1** is very similar to that observed previously for its parent, 2-pyrimidinone (2): (*a*) at low pH bromine attack on the covalent hydrate **3**, in equilibrium with **1**, is rate-limiting; (*b*) at higher pH, where dehydration of **3** is slow relative to bromine attack, the formation of **3** from **1** is rate-limiting. However, in the present case of **1** there is sufficient of the hydrate **3** present at equilibrium that its rapid consumption by bromine can be observed (Fig. 2*a*) prior to the zero-order disappearance of bromine due to (*b*).

Equilibration studies

The equilibration of the cation **5** with its pseudobase **6** was studied using established procedures (7, 11). The reaction is quite fast and the observed first-order rate constants (k_{obs}, Table 3) are only just within the range accessible by the stopped–flow method. Between pH 4.5 and 7.0 values of k_{obs} are invariant with pH but at lower and higher pHs they rise beyond the limits of the apparatus.

For such an equilibration (11) the observed rate constant is the sum of the forward and backward rate constants (12), $k_{obs} = k_f + k_d$:

$$[8]\quad \mathbf{5} \underset{k_d}{\overset{k_f}{\rightleftarrows}} \mathbf{6}$$

Using the measured equilibrium constant $K_2 = 3.4 \times 10^{-4}\,M$ ($pK_2 = 3.47$) these contributions are accessible through the expressions derived by Bunting (11): $k_f = k_{obs}K_2/(K_2 + [H^+])$ and $k_d = k_{obs}[H^+]/(K_2 + [H^+])$. Table 3 lists values of k_f and k_d obtained in this way for the pH range 3–9. As expected from previous studies of pseudobase formation (3, 7, 11), they have pH-dependent and pH-independent components which may be described by the following equations:

$$[9]\quad k_f = k_1 + k_{OH}[OH^-]$$

$$[10]\quad k_d = k_H[H^+] + k_0$$

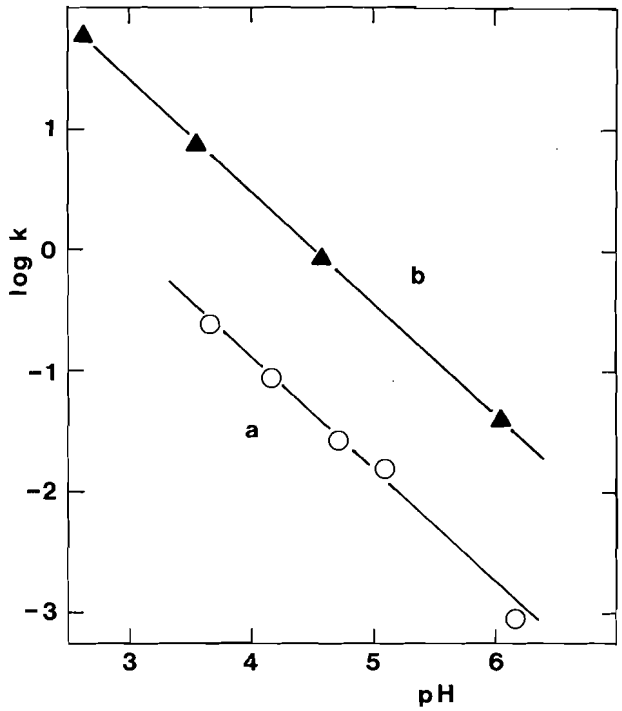

FIG. 3. First-order rate constants for: (*a*) rate-limiting formation of **3** from **1**. Obtained from zero-order bromination studies (see Table 2); (*b*) equilibration of **1** with **3**. The substrate **1** was generated *in situ* in the absence of **3** by mixing solutions of the anion $\mathbf{1}^-$ with acidic buffers. Conditions as in Table 2 except that no bromine was present in the acidic buffer.

In these equations the rate constants on the right-hand side refer to the processes depicted below:

$$[11]\quad \mathbf{5}\ (+\ H_2O) \underset{k_H}{\overset{k_1}{\rightleftarrows}} \mathbf{6} + H^+$$

$$[12]\quad \mathbf{5} + OH^- \underset{k_0}{\overset{k_{OH}}{\rightleftarrows}} \mathbf{6}$$

Appropriate values[9] of these rate constants obtained by fitting eqs. [9] and [10] to the observed values of k_f and k_d are presented later.

From the bromination studies described above it appeared that sufficient of the covalent hydrate **3** is present at equilibrium that a study of its equilibration with **1** might be possible and, fortunately, such was the case. The pseudobase **6** has a uv absorption maximum at 252 nm (ϵ = 7 600) (13) and so the covalent hydrate was anticipated to have a similar absorption in the same region. In contrast, the parent **1** has its long wavelength maximum at 322 nm (ϵ = 3 470) (10, 13) and a *minimum* at 259 nm ($\epsilon \sim 370$). Thus, it appeared quite feasible to observe the formation of **3** in the region of 250 nm.

Solutions of $\mathbf{1}^-$, the anion of **1**, at pH 9–10 were mixed with strong buffers of pH < 7.5. Immediately after mixing, the uv spectrum obtained closely resembles that of **1** at equilibrium, as one expects for the rapid protonation of the anion (14). However, with time there is a modest increase in absorbance at 250 nm and a concomitant small decrease in the 322 nm maximum of **1**. These spectral changes are consistent with the relatively slow formation of a small percentage of the covalent hydrate **3** following the rapid protonation of $\mathbf{1}^-$.

[9]These constants are, of course, interdependent since $k_1 = k_HK_2$ and $k_{OH} = k_0K_2/K_w$ (11).

Figure 3*b* shows the pH dependence[10] of the pseudo-first-order rate constants (k_{obs}) obtained by monitoring the increase at 250 nm. Note well that these rate constants are *not* simply due to the slow formation of **3** from **1**, being substantially faster than the values measured for this process in the bromination studies (Fig. 3*a*). Rather, they are for the equilibration of **1** and **3**:

$$[13]\quad \mathbf{1} \overset{H^+}{\underset{K_1}{\rightleftharpoons}} \mathbf{2} \overset{k_1}{\underset{k_H[H^+]}{\rightleftharpoons}} \mathbf{3}$$

and so k_{obs} is the sum of the forward and backward rate constants (12). For the situation depicted above this means that:

$$[14]\quad k_{obs} = k_1[H^+]/K_1 + k_H[H^+]$$

(since $K_1 \gg [H^+]$, $pK_1 = 0.70$). Of the two contributing terms in this equation, the second one due to the back reaction of **3** to **2** is dominant, as will be made apparent below.

Obviously, the two terms in eq. [14] are not immediately separable since they have the same dependence on acidity. However, the constants k_1 and k_H are related through the constant K_2 ($= k_1/k_H$). To aid subsequent discussion we define the covalent hydrate/parent ratio as $K_h = [\mathbf{3}]/[\mathbf{1}] = K_2/K_1 = k_1/k_HK_1$. With this definition eq. [14] can be rewritten as:

$$[15]\quad k_{obs} = k_H(K_h + 1)[H^+]$$

Again, as with eq. [14], it is the second term which is dominant since $K_h \ll 1$ as $[\mathbf{3}] \ll [\mathbf{1}]$, at equilibrium.

Fitting eq. [14] to the equilibration data gives $(k_1/K_1 + k_H) = 31\,000\ M^{-1}\,s^{-1}$. From the zero-order bromination results we have a value of k_1/K_1, whence $k_H = 29\,500\ M^{-1}\,s^{-1}$ and so $K_h = 0.051$. This value means that at equilibrium in water 4.9% of **1** is present as its covalent hydrate **3**.

Discussion

The present studies of the bromination of **1** and **5** extend into the pH region the behaviour previously observed in strong acid (1). Moreover, the change to a different kinetic order which occurs around pH 2.5 is consistent with earlier proposals (1, 13) that **1** reacts via its covalent hydrate **3**. The direct observation of **3** and the study of its equilibration with **1** further consolidates this mechanism. Combining results from the bromination and equilibration studies provides a fairly reliable estimate of the proportion of **3** present at equilibrium in aqueous solution.

Taken as a whole, the behaviours exhibited by **1** and its dimethyl cation **5** are qualitatively similar to those observed for 2-pyrimidinone (**7**) and its dimethyl cation (**8**) (2, 7). This is

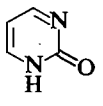

7

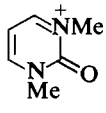

8

most clearly seen by reference to Table 4 in which are collected various constants for the two systems. Table 4 also serves to show the quantitative differences between them.

Firstly, it is noted that the 5-bromo substituent of **1** results in a 100-fold increase in the extent of covalent hydration. In a sense this arises from destabilization in the cation **2** (Scheme 1). This cation is more difficult to form ($\Delta pK_1 = 1.74$) but is much more easily attacked by water ($\Delta pK_2 = 3.70$). Comparable behaviour is displayed by the dimethyl cations for which $\Delta pK_2 = 3.69$.

[10]Beyond pH 6.1 we have not studied the kinetics of equilibration of **1** and **3** in detail because of the complications due to the deprotonation of **1** ($pK_a = 7.36$). At pH 7.5, $k_{obs} \simeq 1.9 \times 10^{-3}\,s^{-1}$.

TABLE 4. Summary of rate and equilibrium constants for 2-pyrimidinone (**7**), 5-bromo-2-pyrimidinone (**1**), and their respective *N*,*N*′-dimethyl cations (**8** and **5**)[a]

Constant	**1**	**5**	**7**[b]	**8**
k_1 (s^{-1})	300	77	10	1.3
k_H ($M^{-1}\,s^{-1}$)	3×10^4	2.3×10^5	5×10^6	2×10^7
k_0 (s^{-1})		7×10^{-4}		0.31
k_{OH} ($M^{-1}\,s^{-1}$)		2.4×10^7		2.1×10^6
k_2K_2 (s^{-1})	28000	9400	1900	135
k_2K_h ($M^{-1}\,s^{-1}$)	1.4×10^5	n.a.	5.2×10^5	n.a.
k_2 ($M^{-1}\,s^{-1}$)	2.8×10^7	2.8×10^7	10^9	2×10^9
pK_1	0.70[c]	n.a.	2.44[c]	n.a.
pK_2	2.00	3.47[d]	5.70	7.16[d]
K_h	0.05	n.a.	0.0005	n.a.

[a]The value for **1** and **5** are from the present work, at 25°C, $I = 0.1\ M$. Those for **7** and **8** are from earlier work at 30°C (2, 7).

[b]Some of the constants in this column are based on an assumed value of k_2 (2).

[c]Obtained from the kinetics. Literature values measured at 20°C and at weaker ionic strengths are lower (2, 10).

[d]Measured spectrophotometrically.

The actual rate of bromine attack (k_2) is about 100 times slower for **1** and **5** where this attack (on **3** and **6**) is occurring *ipso* to the 5-bromo group (Scheme 1). Nevertheless, the *apparent* reactivity of **1** towards bromine is about the same as that for **7** since the former is 100 times more hydrated. Furthermore, this apparent reactivity of **1** ($k_2K_h \sim 10^5\ M^{-1}\,s^{-1}$), which is perfectly reasonable for reaction via its covalent hydrate **3**, is not explicable by a conventional mechanism involving direct bromine attack. Such attack on **1** should be slower than that for 5-bromo-2-pyridinone, for which $k_2 = 380\ M^{-1}\,s^{-1}$ (15).

The effect of *N*-methylation on the protonated forms of **1** and **7** is much the same. In both cases it reduces the rate of water attack (k_0) and increases the rate of proton-catalyzed loss of hydroxyl (k_H) (Table 4). As a result, the pK_2 values are higher for the dimethyl cations **5** and **8**. These effects are probably as much steric as electronic in origin (2).

The present work shows that the rates of bromine attack (k_2) on the hydrate **3** and the pseudobase **6** are the same (Table 4). In other words, the effect of *N*-methylation on the reactivity of **3** is negligible. This is reasonable since *N*-methylation likewise has very little effect on the rates of bromination of pyridinones (15, 16), uracils (5), cytosines (6), and their 5-bromo derivatives. Moreover, the fact that k_2 comes out to be the same for the covalent hydrate **3** as for the pseudobase **6** is excellent evidence that **1** reacts via **3**.

In the case of 2-pyrimidinone (**7**), k_2 was not directly available since K_h was not measurable as here. Accordingly, a value half that for the pseudobase **8** was assumed which allowed us to estimate $K_h \simeq 0.0005$ for **7**. If, as in the present work, k_2 is the same for the hydrate of **7** and the pseudobase of **8**, then this estimate of K_h should be reduced by a factor of 2.

The results summarized in Table 4 are perfectly reasonable, then, for both the effects of 5-bromo substitution and *N*-methylation. More importantly, the overall consistency which is seen there means that the bromination of 2-pyrimidinones via covalent hydrates is now firmly established. As required also, the present study provided valuable information for our study of **1** and **3** as inhibitors of the enzyme, cytosine deaminase (20).

Experimental

The substrates **1** and **5** (bromide ion salt) were synthesized as previously (13). Buffer solutions and bromine solutions were made up

according to standard practice in this laboratory (5–7). For the bromination studies all of the aqueous solutions contained a fixed concentration of KBr for reasons given earlier (5). In the equilibration studies ionic strength was maintained with NaCl.

Kinetics were followed using the stopped–flow apparatus (7) and data acquisition system (17) described elsewhere. The observation cell was thermostatted at 25.0 ± 0.1°C. Bromination reactions were monitored at 267 nm (Br_3^- maximum) and analysis of the absorbance/time data was as in previous studies (5–7). The values of k_2^{obs} given in the text are corrected for the formation of tribromide ion (5). The equilibration of **5** with **6** was monitored as decreases in the long wavelength bands of **5** or of **6**, depending on the pH. The equilibration of **1** with its hydrate **3** was measured as an increase at 250 nm, in the region where **3** should have a maximum (see text). Solutions of **1**, present as its anion, at pH 9–10 were mixed in the stopped–flow apparatus with acidic buffers. For the measurement of zero-order kinetics similar solutions were mixed with acidic buffers containing bromine (see text). Note that this technique would not work if the anion of **1** was more reactive towards bromine. That it does not interfere over most of the pH range studied[8] is evidenced by the order of the reaction and the pH dependence of the rate constants.

The determination of pK_2 for **5** was carried out by making spectrophotometric measurements in 9 buffers spanning pH 2.5–4.5. Analysis of the data obtained at 250 nm (pseudobase maximum) and 345 nm (cation maximum) by standard means (18) gave $pK_2 = 3.47 \pm 0.10$ in both cases.

Acknowledgements

This work was made possible by operating grants to O.S.T. and M.J.K. from the Natural Sciences and Engineering Research Council of Canada and a joint grant from the F.C.A.C. program of the Ministère de l'Education du Québec. One of us (O.S.T.) also thanks Professors J-M. Lehn and J. A. Osborn (Université Louis Pasteur, Strasbourg) for their hospitality and the use of facilities during a sabbatical leave.

1. S. Banerjee, O. S. Tee, and K. D. Wood. J. Org. Chem. **42**, 3670 (1977).
2. O. S. Tee and M. Paventi. J. Org. Chem. **45**, 2072 (1980).
3. O. S. Tee and M. Paventi. J. Org. Chem. **46**, 4172 (1981).
4. O. S. Tee and G. V. Patil. J. Org. Chem. **41**, 838 (1976).
5. O. S. Tee and C. G. Berks. J. Org. Chem. **45**, 830 (1980).
6. O. S. Tee, M. J. Kornblatt, and C. G. Berks. J. Org. Chem. **47**, 1018 (1982).
7. O. S. Tee, D. C. Thackray, and C. G. Berks. Can. J. Chem. **56**, 2970 (1978).
8. A. Albert and W. L. F. Armarego. Adv. Heterocycl. Chem. **4**, 1 (1965); D. D. Perrin. Adv. Heterocycl. Chem. **4**, 43 (1965); A. Albert. Angew. Chem. Int. Ed. Engl. **6**, 919 (1967); A. Albert. Adv. Heterocycl. Chem. **20**, 117 (1976).
9. G. A. O'Donovan and J. Neuhard. Bact. Rev. **34**, 278 (1970); J. Kream and E. Chargaff. J. Am. Chem. Soc. **74**, 5157 (1950); P. L. Ipata, G. Cercignani, and E. Balestreri. Biochemistry, **9**, 339 (1970).
10. D. J. Brown and T. C. Lee. Aust. J. Chem. **21**, 243 (1963); D. J. Brown and J. S. Harper. J. Chem. Soc. 1276 (1963).
11. J. W. Bunting. Adv. Heterocycl. Chem. **25**, 1 (1979).
12. A. A. Frost and R. G. Pearson. Kinetics and mechanism. Wiley, New York. 1961. p. 186.
13. O. S. Tee and S. Banerjee. Can. J. Chem. **52**, 451 (1974).
14. M. Eigen. Angew. Chem. Int. Ed. Engl. **3**, 1 (1964).
15. O. S. Tee and M. Paventi. J. Am. Chem. Soc. **104**, 4142 (1982).
16. O. S. Tee and M. Paventi. Can. J. Chem. **61**, 2556 (1983).
17. O. S. Tee, M. Trani, R. A. McClelland, and N. E. Seaman. J. Am. Chem. Soc. **104**, 7219 (1982).
18. A. Albert and E. P. Serjeant. Ionization constants of acids and bases. Methuen, London. 1962.
19. M. Paventi. Ph.D. Thesis. Concordia University, Montreal. 1984.
20. M. J. Kornblatt and O. S. Tee. Eur. J. Biochem. In press.

Structure et conformation du complexe du *N*-acétyl-aspartate avec un cation lanthanide. Étude par résonance magnétique nucléaire du ^{1}H et du ^{13}C

DANIEL BARON ET NICOLE LUMBROSO-BADER

Laboratoire de spectrochimie infrarouge et Raman, Centre national de la recherche scientifique, 2, rue Henri Dunant, 94320 Thiais, France[1] et Université Pierre et Marie Curie, 4, place Jussieu, 75230 Paris 05, France

Reçu le 5 novembre 1985

D. BARON et N. LUMBROSO-BADER. Can. J. Chem. **64**, 1317 (1986).

Les déplacements induits dans les complexes 1:1 de NAcAsp (0,14 *M*) avec Lu^{3+}, Yb^{3+}, Tm^{3+}, Er^{3+}, Ho^{3+} et Dy^{3+} sont déterminés dans du D_2O à un pH 5 pour 10 sites ^{1}H et ^{13}C. La constante de complexation moyenne (pour une concentration en chlorure d'environ 0,05 *M*) est 72 M^{-1}. La détermination du facteur géométrique du terme de pseudo-contact de chaque site (approximation d'une symétrie axiale) nécessite de tenir compte d'un terme de contact et d'écarter les données concernant Tm^{3+}.

Six structures du résidu Asp correspondant à une chélation par les deux carboxylates sont compatibles avec les données obtenues pour ce résidu; la distance $O_\beta^- \ldots C_\alpha'$ semble être critique tandis que l'orientation du COO_α^- est secondaire. L'analyse utilisant tous les sites étudiés permet de sélectionner les trois structures du résidu pour lesquelles l'azote est éloigné au maximum de l'interaction et, parmi les rotamères autour de la liaison C_α—N, ceux qui favorisent les conformations les plus étendues. La chélation implique trois oxygènes dont deux appartiennent au COO_β^-. L'existence d'un équilibre avec un autre complexe minoritaire ne peut cependant pas être totalement exclue.

D. BARON and N. LUMBROSO-BADER. Can. J. Chem. **64**, 1317 (1986).

Lanthanide induced shifts by Lu^{3+}, Yb^{3+}, Tm^{3+}, Er^{3+}, Ho^{3+}, and Dy^{3+} in NAcAsp (0.14 *M* in D_2O, pH 5) are observed for ten magnetic sites (^{1}H and ^{13}C). The averaged binding constant for 1:1 complexes is 72 M^{-1} (for chloride solutions of ca. 0.05 *M*). Determination of the pseudo-contact geometrical factors (under axial symmetry approximation) requires taking into account a contact term and discarding the Tm^{3+} results. Data from the Asp residue are in agreement with 6 structures of this residue such that chelation occurs through the two carboxylates. $O_\beta^- \ldots C_\alpha'$ length seems to be the main factor while COO_α^- orientation is a minor one. The entire set of results is consistent with only three structures where the nitrogen atom is far from the carboxylates, and the C_α—N rotamers have extended conformations. Three oxygen atoms (two from the COO_β^- group) appear to be involved in the chelation. However, the data do not exclude another minor conformational species.

Introduction

La détermination des conformations adoptées préférentiellement par les résidus aspartate ou glutamate en interaction avec un cation est une étape nécessaire pour analyser la structure locale du peptide ou de la protéine complexée par ces ions, qu'il s'agisse d'expliquer les structures obtenues par radiocristallographie ou, éventuellement, de faciliter l'interprétation des cartes de densité électronique. Dans le cas des polypeptides naturels, les cations étant généralement complexés par des chélations impliquant plusieurs groupements carboxylates et des ligandes non chargés (1), il paraît a priori difficile d'analyser ce type d'interaction à partir des contributions individuelles de chaque résidu. Il faut cependant rappeler que les calculs conformationnels peuvent conduire à des résultats très intéressants (2). Par exemple, dans le cas de l'inhibiteur trypsique BPTI, petite protéine fréquemment étudiée dans le domaine de la physicochimie biologique, les résultats obtenus par Levitt, à partir d'un modèle relativement simplifié (3), ont pu être raffinés en prenant en compte de façon plus précise des propriétés des chaînes latérales, notamment la possibilité de formation des ponts disulfures, ce qui a récemment conduit à des structures très proches de celle du cristal (4).

Le but de ce travail est donc d'obtenir des données expérimentales fiables, utilisables, le cas échéant, dans des calculs théoriques, sur la répercussion d'une interaction carboxylate–cation, tant au niveau de la chaîne latérale du résidu, Asp ou Glu, qu'à celui du squelette peptidique. Dans une première étude (5), certaines caractéristiques de la monocomplexation du carboxylate de la chaîne latérale avaient été dégagées, notamment la structure étendue du résidu et l'absence de chélation avec le squelette peptidique, du moins en ce qui concerne les deux carbonyles adjacents à la chaîne latérale. Le présent travail a pour objet l'étude d'une chélation par deux groupements carboxylates proches. Le choix du composé dérivé N-acétyl-aspartate est justifié par le fait que l'amino-acide non bloqué aurait présenté les inconvénients d'avoir un groupe NH_3^+ trop proche du COO_α^- et de ne pas posséder de liaison peptidique. En outre, NAcAsp semble jouer un rôle dans le métabolisme du cerveau (6, 7).

La méthode utilisée est basée sur l'interprétation des déplacements chimiques induits sur les sites ^{1}H et ^{13}C dans les complexes formés par des ions lanthanides paramagnétiques en solution aqueuse. L'étude précédente sur des dérivés monocarboxylates (5) avait montré que les données ^{1}H et ^{13}C obtenues avec l'ytterbium (Yb^{3+}), corrigées des termes diamagnétiques déterminés à l'aide du lutétium (Lu^{3+}), permettaient l'analyse structurale du résidu complexé en se basant sur un modèle de pseudo-contact. En effet, bien que des contributions de contact aient été systématiquement décelées pour les deux carbones proches de Yb^{3+} (COO_β^- et C_β), l'utilisation, ou non, de leurs déplacements induits ne modifiait pas les résultats concernant la conformation moyenne du résidu dans le complexe ni la distance oxygène–lanthanide; elle influait par contre sur la détermination de l'ange $\widehat{C—O—Yb}$ et la qualité du paramétrage.

Dans le présent travail, l'analyse structurale devait s'avérer plus délicate en raison de deux nouveaux éléments : (a) l'axe magnétique principal du complexe ne peut plus être assimilé à une direction $Yb^{3+} \ldots COO^-$ puisque deux groupements carboxylates sont impliqués dans le chélate; (b) un équilibre est possible entre le chélate et un complexe monodentate ne mettant en jeu qu'un seul COO^-. En conséquence, il était indispensable que les données de tous les sites ^{1}H et ^{13}C du résidu puissent être

1. Adresse pour la correspondance.

Printed in Canada / Imprimé au Canada

TABLEAU 1. Déplacements chimiques : systèmes avec Lu^{3+}, Yb^{3+}, Tm^{3+}, Er^{3+} [a]

[P][b]	ρ[c]	C_{Me}	C_β	C_α	CO_{NH}	COO_β	COO_α	H_{Me}	$H_{\beta1}$	$H_{\beta2}$	H_α
		δ									
136	0,000	24,67	41,72	55,36	176,34	180,90	181,05	2,012	2,559	2,722	4,423
	(Lu^{3+})	Δδ									
137	0,037	0,01	0,00	−0,04	0,00	0,24	0.09	0,001	0,004[d]		0,005
130	0,139	0,01	0,11	−0,12	0,00	0,91	0,36	0,004	0,007[d]		0,012
129	0,250	0,04	0,22	−0,20	0,05	1,56	0,65	0,008	0,015[d]		0,022
126	0,389	0,04	0,22	−0,39	0,05	2,21	0,90	0,011	0,027[d]		0,033
133	0,531	0,04	0,11	−0,61	0,08	2,56	1,08	0,017	0,048[d]		0,054
	(Yb^{3+})	Δδ									
142	0,141	0,01	−4,34	−3,49	−0,65	−7,02	−5,23	0,083	−2,24	−2,44	−1,59
140	0,233	0,01	−7,01	−5,71	−1,03	−11,25	−8,49	0,138	−3,57	−3,90	−2,50
135	0,348	0,01	−9,89	−8,11	−1,49	−15,89	−12,00	0,211	−4,94	−5,44	−3,42
131	0,462	0,04	−12,02	−9,94	−1,73	−19,05	−14,75	0,280	−5,97	−6,60	−4,04
132	0,578	0,09	−13,45	−11,13	−1,89	−21,15	−16,39	0,349	−6,63	−7,36	−4,34
	(Tm^{3+})	Δδ									
134	0,093							0,39	−2,25	−2,62	−0,35
139	0,125	0,41	−8,22	−5,68	−0,60	−10,12	−8,33	0,51	−2,98	−3,56	−0,50
135	0,220							0,90	−4,90	−5,89	−0,64
138	0,252	0,84	−15,34	−10,75	−1,03	−18,75	−15,39	1,03	−5,52	−6,66	−0,65
138	0,377	1,22	−21,44	−15,07	−1,41	−25,76	−21,33	1,52	−7,51	−9,16	[e]
137	0,509	1,71	−25,65	−17,98	−1,51	−30,24	−25,10	1,99	−8,66	−10,75	[e]
	(Er^{3+})	Δδ									
141	0,304	0,41	−20,57	−13,66	−1,95	−6,99	−7,68	0,470	−3,89	−4,53	[e]
141	0,351	0,47	−22,89	−15,50	−2,22	−7,68	−8,44	0,533	−4,28	−5,08	[e]
142	0,398	0,52	−25,05	−17,22	−2,49	−7,85	−9,25	0,593	−4,63	−5,47	[e]

[a] δ/DSS ou Δδ/solution sans Ln^{3+}; en ppm; positif pour un déplacement à champ faible.
[b] [P] = [NAcAsp] en m*M*.
[c] ρ = [Ln]/[P].
[d] Par rapport à la moyenne $H_{\beta1}$, $H_{\beta2}$.
[e] Signal trop large.

utilisées sans réserves dans une analyse structurale basée sur un modèle de pseudo-contact. La détermination des déplacements induits par plusieurs lanthanides permet, en appliquant les méthodes proposées par Reilley *et al.* (8, 9), de calculer les termes de contact affectant chaque site. Outre les effets dus à Yb^{3+} et du Lu^{3+}, ceux du thullium (Tm^{3+}), de l'erbium (Er^{3+}), de l'holmium (Ho^{3+}) et du dysprosium (Dy^{3+}) ont donc été déterminés.

Récemment, Shelling *et al.* (10) ont publiés les déplacements induits des protons dans les complexes de NAcAsp avec ces mêmes ions lanthanides, mais d'une part ces données étaient en nombre insuffisant (4 sites) pour tenter une analyse structurale et d'autre part nos résultats expérimentaux diffèrent sensiblement en ce qui concerne H_α.

Partie expérimentale

Systèmes

Produits

Origine commerciale : NAcAsp (Sigma); $LnCl_3$, *x* H_2O (Johnson et Mathey); D_2O deutérié à 99,8% (CEA, France).

Teneur des chlorures de lanthanide en $LnCl_3,6H_2O$

Dosage par NaOH des acidités fortes libérées par $EDTAH_2^{2-}$ (en excès) lors de la complexation avec Ln^{3+} (Ln^{3+} + $EDTAH_2^{2-}$ → $LnEDTA^-$ + 2 H^+); teneurs obtenues : Lu^{3+} (93,5%), Yb^{3+} (93,2%), Tm^{3+} (95,3%), Er^{3+} (97,4%), Ho^{3+} (97,6%), Dy^{3+} (97,4%).

Solutions

NAcAsp : ≃ 0,14 *M*; DSS (référence rmn : diméthyl 4,4-silapentane 4-sulfonate de sodium) : ≃ 0,02 *M*; pH : ajusté à 5,0 (±0,1), à l'aide de NaOD, valeur brute non corrigée de l'effet isotopique (11); Ln^{3+} : concentration variable jusqu'à ρ = $[Ln^{3+}]/[NAcAsp]$ ≃ 0,5 (cf. tableau 1); pour les systèmes tamponnés par Lu^{3+}, $\rho_{tot} = \rho_{Lu} + \rho_{para} \simeq$ 0,35 avec $\rho_{para} \leqslant 0{,}15$ (cf. tableau 2).

Résonance magnétique nucléaire

Spectromètre Brüker WH 90 (^1H : 90 MHz; ^{13}C : 22,63 MHz); température 303 K; référence DSS, les variations à champ faible sont comptées positives; résultats : tableaux 1 et 2.

Attribution des spectres ^1H

Deux problèmes principaux ont été rencontrés :

(a) H_β. Impossibilité d'attribuer de façon univoque les sites $H_{\beta1}$ et $H_{\beta2}$ aux protons $H_{\beta R}$ et $H_{\beta S}$ (ou réciproquement); cependant, ce problème n'a d'incidence que dans les modèles d'analyse structurale basés sur plusieurs complexes 1:1. Par ailleurs, on observe une coalescence des signaux de ces deux sites dans le cas de Lu^{3+} et dans ceux des ions paramagnétiques Ho^{3+} et Dy^{3+}, coalescence partiellement due, pour ces derniers, à l'élargissement des signaux.

(b) H_α. Disparition du signal (largeur trop importante) avec Tm^{3+} (à partir de ρ = 0,38) et avec Er^{3+} (à partir de 0,30); malgré ce problème, nous attribuons sans ambiguïté H_α à un signal se déplaçant à champ fort avec ces deux ions, contrairement à d'autres auteurs (10).

Attribution des ^{13}COO (faible différence de déplacements chimiques dans la solution sans lanthanide : 0,15 ppm)

TABLEAU 2. Déplacements chimiques : systèmes Er^{3+}–Lu^{3+}, Ho^{3+}–Lu^{3+}, Dy^{3+}–Lu^{3+} [a]

[P][b]	ρ_{para}[c]	ρ_{tot}[c]	C_{Me}	C_β	C_α	CO_{NH}	COO_β	COO_α	H_{Me}	$H_{\beta1}$	$H_{\beta2}$	H_α
	(Er^{3+})											
145	0,049	0,340	0,09	−3,21	−2,63	−0,27	0,53	−0,64	0,087	[d]	[d]	−0,171
145	0,072	0,341							0,121	−0,89	−1,01	−0,284
145	0,098	0,342	0,14	−6,52	−4,82	−0,62	−0,71	−1,96	0,165	−1,22	−1,39	−0,394
144	0,121	0,342							0,194	−1,52	−1,73	−0,510
144	0,148	0,344	0,20	−9,79	−6,97	−0,92	−1,95	−3,31	0,235	[e]	[e]	−0,658
	(Ho^{3+})											
141	0,050	0,393	0,12	−0,33	−0,02	0,24	10,22	6,13	−0,021	[f]		1,43
140	0,099	0,389	0,20	−0,76	0,47	0,40	18,05	11,28	−0,051	3,71[g]		2,79
140	0,120	0,387							−0,068	4,53[g]		3,41
139	0,141	0,386	0,28	−1,13	0,98	0,59	24,96	15,57	−0,079	5,30[g]		[h]
	(Dy^{3+})											
141	0,035	0,361	0,27	1,79	1,84	0,65	14,32	9,24	0,067	3,30[g]		3,01
141	0,062	0,363							0,114	5,80[g]		5,29
142	0,089	0,364	0,74	4,56	5,92	1,88	34,33	22,58	0,158	8,38[g]		7,72
157	0,106	0,370							0,171	10,10[g]		9,03
144	0,146	0,367	1,07	7,19	9,88	3,02	55,11	36,67	0,250	13,06[g]		12,44

[a] $\Delta\delta$/solution sans Ln^{3+}; en ppm; positif pour un déplacement à champ faible.
[b] [P] = [NAcAsp] en m*M*.
[c] ρ = [Ln]/[NAcAsp]; $\rho_{tot} = \rho_{para} + \rho_{Lu}$.
[d] Signal sous H_{Me}.
[e] Signal sous CH_2 du DSS.
[f] Signal sous HDO.
[g] Par rapport à la moyenne $H_{\beta1}$, $H_{\beta2}$.
[h] Signal sur le flanc du $CH_{2\beta}$.

L'attribution est d'abord basée sur les résultats obtenus avec NAcGlu[2] pour lequel les signaux COO_α et COO_γ sont suffisamment distincts ($\Delta\delta$ = 2,15 ppm) et attribués sans ambiguïté. Avec NAcGlu, on observe systématiquement, pour une même variations de ρ, $|\Delta\delta_\gamma| > |\Delta\delta_\alpha|$, sauf dans le cas de Er^{3+}. Compte tenu des résultats obtenus avec les dérivés monocarboxylates (5), la relation précédente semble pouvoir être valablement appliquée au problème de NAcAsp. Dans le système NAcAsp–Lu^{3+}, les signaux des deux carboxylates se déplacent à champ faible en se croisant pour ρ = 0,04, ce qui permet d'attribuer le pic à champ fort dans la solution sans lanthanide au COO_β.

Calculs

Programmes d'analyse conçus et exploités au laboratoire (Digital PDP 11/34).

Analyse thermodynamique (systèmes avec Lu^{3+}, Yb^{3+} ou Tm^{3+})

(a) Normalisation des variations de déplacements chimiques, site par site et cation par cation, par rapport à la variation maximale observée pour $\rho \simeq 0,5$: $\Delta\delta_{ij(norm)} = \Delta\delta_{ij(exp)}/\Delta\delta_{ij(\rho\simeq0,5)}$. Quand $\Delta\delta_{ij(\rho\simeq0,5)}$ n'a pas été obtenu, une valeur approchée est définie à l'aide des données du carboxylate β :

$$\Delta\delta_{ij(\rho\simeq0,5)} = \Delta\delta_{ij(\rho)} \cdot \Delta\delta_{COO\beta,j(\rho\simeq0,5)}/\Delta\delta_{COO\beta,j(\rho)}.$$

(b) Minimisation de la variance V pour l'ensemble des 10 sites et des 3 cations, $V = \Sigma_i \Sigma_j p_{ij} (\Delta\delta_{ij(norm)} - \Delta\delta_{ij(calc)})^2$, en fonction de la valeur de K, constante de complexation 1:1; p_{ij} est un facteur de poids, dépendant de la déviation standard σ_{ij}.

(c) Pondération $(p_{ij}) \cdot \sigma_{moy} = \Sigma \sigma_{ij}/n$ (n étant le nombre de déplacements induits calculés); $p_{ij} = 1$ si $\sigma_{ij} \leq \sigma_{moy}$ et $p_{ij} = \sigma_{moy}/\sigma_{ij}$ si $\sigma_{ij} > \sigma_{moy}$.

(d) Elimination des données si $\sqrt{p_{ij}}(\Delta\delta_{ij(norm)} - \Delta\delta_{ij(calc)}) > 2\,\sigma_{ij}$ (dans la limite de 10% du nombre total de données).

2. Étude en cours.

Vérification de l'additivité des effets dans les systèmes comportant un tampon de Lu^{3+}

Pour Er^{3+}, à partir des données pour lesquelles $0,3 < \rho < 0,4$, calcul des moyennes $\Delta\delta_{iEr}/\rho_{Er}$ et des gradients moyens $\Delta(\Delta\delta_{iEr})/\Delta\rho_{Er}$, ce qui permet d'estimer $(\Delta\delta_{iEr}/\rho_{Er})$ pour toute valeur autour de ρ = 0,351; pour Lu^{3+}, calcul des moyennes $\Delta\delta_{iLu}/\rho_{Lu}$ dans le domaine $0,25 \leq \rho \leq 0,53$ (les gradients ne sont pas significatifs pour cet ion); pour une solution mixte Lu^{3+}–Er^{3+}, avec $\rho_{tot} = \rho_{Lu} + \rho_{Er}$:

$$\Delta\delta_{i(calc)} = \rho_{Er} \cdot (\Delta\delta_{iEr}/\rho_{Er})_{\rho tot} + \rho_{Lu} \cdot (\Delta\delta_{iLu}/\rho_{Lu})$$

Facteur d'accord (12)

$$[1] \quad R = \Sigma\,(\Delta\delta_{exp} - \Delta\delta_{calc})^2/\Sigma\,\Delta\delta^2_{exp}$$

Symétrie non axiale du tenseur d'anisotropie magnétique du complexe

Le système d'équations (10, 13)

$$[2] \quad \Delta\delta_{Pij}/D_j = F \cdot G_i + F \cdot G_i'(D_j'/D_j) + F \cdot A_i(\langle S_z\rangle_j/D_j)$$

est résolu par une méthode de moindres carrés en fonction des paramètres D_j', avec itérations sur les termes D_j' supposés non nuls et recherche du minimum de la variance.

Remarques : (a) tous les calculs ont été effectués avec au départ $D_j' = 0$ pour tous les cations; (b) les estimations de D_j' (13) n'ont pas été utilisées.

Déplacements induits dans les complexes

Méthode

L'analyse des résultats expérimentaux (variations des déplacements chimiques des 10 sites magnétiques de NAcAsp en fonction de la concentration en lanthanide) est basée sur l'égalité des constantes de complexation ligande –Ln^{3+} pour les différents lanthanides utilisés dans cette étude. Cette approxima-

TABLEAU 3. Déplacements induits dans les complexes $\Delta\delta_{Cij}$ [a]

	C_{Me}	C_β	C_α	CO_{NH}	COO_β	COO_α	H_{Me}	$H_{\beta 1}$	$H_{\beta 2}$	H_α
Lu	0,07	0,44	−0,69	0,12	4,20*	1,74*	0,02	0,05[b]		0,06
Yb	0,03[c]	−20,71*	−17,06*	−2,99*	−32,88*	−25,24*	0,48	−10,31*	−11,39*	−6,96
Tm	2,52	−41,49*	−29,09*	−2,62	−49,61*	−41,05*	2,99*	−14,49*	−17,71*	−2,00
Er	0,94	−46,51	−31,56	−4,53	−15,19	−17,27	1,09	−8,68	−10,20	−3,08
Ho	1,30	−6,71	5,79	2,75	120,88*	77,28	−0,44	27,15[b]		20,29
Dy	5,26	34,52	48,99	14,48	262,01	175,82	1,17	66,41[b]		60,41

*Données ayant un poids égal à 1 dans l'analyse thermodynamique.
[a]En ppm; positif pour un déplacement à champ faible.
[b]Par rapport à la moyenne $H_{\beta 1}$, $H_{\beta 2}$.
[c]Série de données non utilisée dans l'analyse thermodynamique (Lu, Yb, Tm).

tion (14–16) a été fréquemment vérifiée et utilisée dans des travaux de rmn (10, 17–20); elle semble particulièrement justifiée lorsqu'il s'agit, comme ici, de chélates de lanthanides lourds (21).

Trois systèmes pour lesquels les variations de déplacements chimiques ont été étudiées dans le domaine $0 < \rho = [Ln]/[NAcAsp] \leqslant 0{,}5$ (Lu^{3+}, Yb^{3+}, Tm^{3+}; cf. tableau 1) sont analysés simultanément, c'est-à-dire en recherchant la constante K_1 qui minimise la variance pour l'ensemble des séries de données $\Delta\delta_{ij}$ (i: site magnétique; j: cation) pour lesquelles on calculera un déplacement chimique induit dans le complexe $\Delta\delta_{Cij}$. Les avantages d'une analyse simultanée ont déjà été discutés (5) : prise en compte effective d'un plus grand nombre de données pour la détermination de K_1 et meilleure cohérence des valeurs de Δ_{Cij}, ce qui est particulièrement important pour l'analyse structurale. Pour cela, il est nécessaire de normaliser les résultats expérimentaux et de tenir compte des différences de précision entre les séries de données $\Delta\delta_{ij}$ en introduisant des facteurs de poids p_{ij} en fonction des déviations standards σ_{ij} (cf. Partie expérimentale, § Calculs).

Les résultats sont interprétés en utilisant le modèle qui s'était avéré valable dans l'étude des dérivés monocarboxylates (5) : complexes 1:1 et 2:1 (peptide:lanthanide). En effet, il n'est pas possible, à partir de données obtenues à une seule concentration en peptide (0,14 M), de discriminer efficacement divers modèles de solution. Mais il faut remarquer que les données ^1H et ^{13}C proviennent des mêmes solutions et qu'en conséquence les valeurs de $\Delta\delta_{Cij}$, calculées pour différents modèles thermodynamiques vraisemblables, restent pratiquement proportionnelles pour les divers sites. Ce mode d'analyse simplifié ne peut donc, en principe, perturber les conditions de l'analyse structurale; il en est de même de l'utilisation des approximations $\delta(P_2Ln) = \delta(PLn)$, égalité des déplacements chimiques dans les deux types de complexes, et $K_1 = 4\ K_2$ (K_2, constante de l'équilibre $P + PLn \rightleftarrows P_2Ln$). Bien qu'inattendues dans un problème d'interaction entre cations et ligandes, de telles relations ont déjà été observées dans certains travaux sur la complexation d'ions lanthanides par des acides aminés (20, 22).

Compte tenu des approximations du modèle, les valeurs de K_1 et des $\Delta\delta_{Cij}$ doivent être considérées comme des moyennes, d'autant plus valables que l'on se rapproche de $\rho \simeq 0{,}34$, ceci dû au fait que le processus de minimisation est basé sur la somme des carrés des déviations. Or, pour les besoins de l'analyse structurale, les déplacements induits par les différents lanthanides doivent être obtenus à partir de domaines d'étude comparables, ce qui n'est pas possible avec Ho^{3+} et Dy^{3+} pour lesquels de nombreux signaux disparaissent pour des valeurs de ρ inférieures à 0,3. On peut alors utiliser un tampon de Lu^{3+} qui permet de ne pas restreindre l'étude au domaine des faibles concentrations en lanthanide paramagnétique : $\rho_{tot} = \rho_{Lu} + \rho_{para}$. Pour déterminer $\Delta\delta_{Ci,para}$, K_1 et $\Delta\delta_{Ci,Lu}$ étant par ailleurs connus, il suffit de faire varier ρ_{para} jusqu'à 0,15 par exemple tout en maintenant ρ_{tot} à environ 0,34. L'emploi de tampon de lanthanides diamagnétiques est une méthode qui a déjà été utilisée pour maintenir la force ionique constante (23).

Résultats et discussion

Les résultats finaux, K_1 et $\Delta\delta_{Cij}$ (j = Lu^{3+}, Yb^{3+}, Tm^{3+}) sont obtenus à partir de 135 données, certaines d'entre elles ayant été éliminées (voir Partie expérimentale, § Calculs). La déviation standard moyenne, relative aux données normalisées et pondérées, est très satisfaisante (4,1%) compte tenu de la simplicité du modèle. En ce qui concerne la pondération des résultats expérimentaux, on remarque une certaine corrélation entre p_{ij} et $\Delta\delta_{Cij}$ (dans le tableau 3, on a signalé les sites pour lesquels p_{ij} est maximum), mais les exceptions sont trop nombreuses (cas de Lu^{3+} notamment) pour que cette pondération puisse être liée a priori aux valeurs maximales de $\Delta\delta_{ij}$; d'autres facteurs interviennent, dont, en particulier, l'élargissement des signaux dû à l'ion paramagnétique, ce qui justifie un mode de calcul de facteurs de poids basé sur la précision effective des paramétrages. Par ailleurs, signalons que les données relatives à C_{Me}—Yb ayant dû être écartées de l'analyse générale, le déplacement induit, dans ce cas, a été calculé de façon indépendante, en utilisant la valeur de K_1 précédemment déterminée.

Les valeurs de $\Delta\delta_{Cij}$ (tableau 3) peuvent être comparées, pour Lu^{3+} et Yb^{3+} du moins, à celles des dérivés monocarboxylates de Asp (5) : apparemment, la chélation augmente d'environ 50% les effets de Yb^{3+} sur les sites COO_β, C_β et H_β. Précisons qu'une analyse de nos résultats, basée sur un modèle de solution à un seul complexe (PLn ou P_2Ln), conduirait à des valeurs de déplacements induits anormalement élevées (par exemple, $|\Delta\delta_C| \simeq 88$ ppm pour COO_β avec Yb^{3+}) et, on le verra, incompatibles avec la plupart des résultats de Shelling *et al.* (10). Enfin, la nette différence entre les effets de Lu^{3+} sur les deux carboxylates montre que les forces d'interaction ne sont pas identiques et reflètent sans doute les pK des fonctions ($COO_\alpha \simeq 2$ et $COO_\beta \simeq 4$).

La constante moyenne K_1, déterminée à partir des données relatives aux ions Lu^{3+}, Yb^{3+} et Tm^{3+} est de 72 M^{-1}; pour la comparer avec la valeur obtenue dans le système NAcAspOMe $-Yb^{3+}$, 70 M^{-1} (5), il faudrait pouvoir effectuer des corrections qui concourraient toutes à augmenter le rapport K_1 (NAcAsp)/

K_1 (NAcAspOMe) : corrections de méthode d'analyse (K_1/K_2 a été fixé à 4 dans ce travail, alors qu'il était de 11 pour NAcAspOMe), d'anion (Cl^- pour ce travail, ClO_4^- précédemment) et de force ionique, la majeure partie des déplacements chimiques du proton du système NAcAspOMe–Yb^{3+} ayant été obtenue à la concentration de 10^{-2} *M* en acide aminé. Récemment d'ailleurs, pour des concentrations en lanthanide de 10 à 20 m*M* (soit une cinquantaine de fois plus faibles que dans cette étude), Shelling *et al.* (10) obtenaient, pour la complexation de NAcAsp avec des lanthanides lourds, une valeur moyenne de K_1 d'environ 5000 M^{-1}. Cette variation de la valeur du quotient de complexation devrait pouvoir être attribuée, pour l'essentiel, à un effet de la force ionique sur les coefficients d'activité des ions impliqués dans le complexe. Ainsi, d'après les résultats de Hurlen (24), en passant du domaine moyen de concentration utilisé par Shelling *et al.* au nôtre, le coefficient d'activité du seul ion lanthanide serait divisé par un facteur 30, ce qui expliquerait l'essentiel de la divergence des résultats thermodynamiques. L'incidence éventuelle du domaine de concentration en lanthanide sur les valeurs de $\Delta\delta_{Cij}$ sera examinée après avoir discuté de la détermination des grandeurs relatives à Er^{3+}, Ho^{3+} et Dy^{3+}.

Pour tester la validité de la méthode utilisant des solutions tamponnées par le lutétium, on a comparé les résultats expérimentaux obtenus avec l'erbium seul (domaine $0{,}3 < \rho < 0{,}4$; tableau 1) et le système mixte Lu^{3+}–Er^{3+} ($\rho_{tot} \simeq 0{,}35$; $\rho_{Er} < 0{,}15$; tableau 2); voir Partie expérimentale, § Calculs. L'erbium a été choisi car il permettait d'obtenir (sauf cas du H_α déjà signalé) des spectres rmn exploitables jusque vers $\rho = 0{,}4$. La comparaison entre les valeurs expérimentales et calculées est très satisfaisante, le facteur d'accord de Wilcott (cf. éq. [1]) étant de 3,6%. Par ailleurs, incidemment, cette étude a permis de confirmer l'attribution des variations de déplacements chimiques des carboxylates par effet des ions Er^{3+} (dans ce cas particulier, l'effet à champ fort est plus important sur le COO_α que sur le COO_β). Précisons encore qu'une vérification similaire de la validité de la méthode a été effectuée avec les systèmes NAcGlu–Tm^{3+} et Lu^{3+}–Tm^{3+}.[3] Finalement, le procédé a été appliqué à Ho^{3+} et Dy^{3+} (tableau 2). Le calcul des valeurs de $\Delta\delta_{Cij}$ pour les complexes de Er^{3+}, Ho^{3+} et Dy^{3+} est effectué en utilisant les valeurs de K_1 et des $\Delta\delta_{CiLu}$ précédemment obtenues (tableau 3). Aucune déviation significative n'est observée lors de ces déterminations de déplacements induits.

Nos valeurs de $\Delta\delta_{Cij}$ sont comparables à celles de Shelling *et al.* (10) pour les sites H_{Me}, $H_{\beta 1}$ et $H_{\beta 2}$ en dépit de la différence des domaines de concentrations en lanthanides (cf. *supra*); par contre le désaccord est très important pour H_α, tant en grandeur qu'en signe (cas de Tm^{3+} et de Er^{3+}); voir Partie expérimentale, § Résonance magnétique nucléaire. Il parait improbable que notre modèle d'analyse des données soit en cause puisque pour 3 des 4 sites ^1H, l'accord entre les déplacements induits déterminés dans les deux travaux est en moyenne de 7%. Enfin, il est possible de vérifier que, dans les conditions expérimentales utilisées, l'influence du pH sur ces grandeurs est négligeable (cf. Appendice).

Facteurs géometriques

Principe

La détermination des déplacements induits dans les complexes pour une série de lanthanides paramagnétiques doit permettre de calculer, pour chaque site, le facteur géométrique de l'équation de McConnell et Robertson (25), ($3\cos^3\theta_i - 1)/r_i^3$, θ_i et r_i se référant aux coordonnées du site *i* de la molécule, par rapport à la position de l'ion lanthanide et à la direction de l'axe magnétique principal du complexe; à partir d'un ensemble suffisant de valeurs de facteurs géométriques, on peut entreprendre une analyse structurale de ce complexe. Les grandeurs utilisées dans les calculs sont les termes paramagnétiques $\Delta\delta_{Pij}$ (déplacements induits corrigés de l'effet diamagnétique du lutétium) :

$$[3] \quad \Delta\delta_{Pij} = \Delta\delta_{Cij} - \Delta\delta_{CiLu}$$

La prise en compte d'un effet de contact étant indispensable pour disposer d'un maximum de valeurs fiables des facteurs géométriques (cf. Introduction), les termes paramagnétiques sont analysés suivant (8–10, 13) :

$$[4] \quad \Delta\delta_{Pij} = F(G_i \cdot D_j + A_i\langle S_z\rangle_j)$$

$G_i \cdot D_j$ est le terme de pseudo-contact, $A_i\langle S_z\rangle_j$ celui de contact, G_i le facteur géométrique recherché, A_i la constante hyperfine de contact du site (ou sa valeur relative), D_j et $\langle S_z\rangle_j$ des paramètres calculés théoriquement (26–29) et fréquemment utilisés dans ce type d'analyse (8–10, 13, 20); enfin F est un facteur d'échelle tenant compte de la normalisation des valeurs de D_j et $\langle S_z\rangle_j$ à $D_{Dy} = 100$. On rappelle que cette méthode est basée d'une part sur l'isostructuralité des complexes et la constance de A_i à l'intérieur de la série d'ions considérés (9) et d'autre part sur la symétrie axiale du tenseur de susceptibilité magnétique dans le complexe. Lorsque cette dernière approximation est discutable (13, 30), il convient d'utiliser la relation (10, 13) :

$$[5] \quad \Delta\delta_{Pij} = F(G_i \cdot D_j + G_i' \cdot D_j' + A_i\langle S_z\rangle_j)$$

G_i' est un second facteur géométrique qui dépend de θ_i et de r_i mais également de l'angle entre la direction Ln^{3+} – site *i* et l'un des axes secondaires du tenseur d'anisotropie magnétique (31). Des valeurs de D_j' ont été évaluées pour les ions lanthanides (13).

Résultats et discussion

En premier lieu, il faut remarquer que les termes paramagnétiques ne peuvent être expliqués par un seul effet de pseudocontact axial, l'incertitude moyenne sur les facteurs géométriques G_i étant nettement trop importante (tableau 4).

TABLEAU 4. Comparaison des méthodes de détermination des facteurs géométriques : facteur d'accord R^a et incertidue moyenne $\overline{dG_i}^{b,c}$

Contact ($A_i \neq 0$)	Pseudo-contact non axial ($D_j' \neq 0$)	No. de cations	R(%)	$\overline{dG_i}$(%)
—	—	5	45,3	22,6
—	—	4	38,1	28,9
+	—	5	11,8	9,2
+	—	4(sans Tm)	7,3	9,4
+	1(Tm)[d]	5	7,3	9,4
+	2(Tm, Ho)[d]	5	3,4	5,5
+	3 cations dont Tm[e]	5	2,0[f]	5,1[f]

[a]Facteur d'accord de Wilcott (12).
[b]Niveau de confiance 90%.
[c]Équation : $\Delta\delta_{Pij}/D_j = F\cdot G_i + F\cdot G_i'\ (D_j'/D_j) + F\cdot A_i(\langle S_z\rangle_j/D_j)$; ($\langle S_z\rangle_j$: valeurs de Golding et Halton (27)).
[d]Meilleure combinaison.
[e]Six combinaisons quasi-équivalentes en *R*.
[f]Moyenne.

3. Étude en cours.

TABLEAU 5. Facteurs géométriques[a]

No. de cations	Symétrie non axiale			Symétrie axiale		
	5	5	5	5	2	1
$D_j' \neq 0$	3[c]	Tm—Ho	Tm[d]		(Yb—Dy)	(Yb)[b]
C_{Me}	1,01	1,04	0,56	0,03	0,85	−0,11
C_β	40,82	40,95	41,34	41,18	40,10	57,04
C_α	35,47	35,68	35,36	34,64	34,53	44,15
CO_{NH}	7,57	7,61	7,09	6,43	6,90	7,74
COO_α	70,81	70,90	71,05	71,48	70,74	72,76
H_{Me}	−0,45	−0,42	−0,86	−1,34	−0,59	−1,24
$H_{\beta 1}$	27,58	27,69	27,44	27,00	27,09	27,94
$H_{\beta 2}$	28,97	28,99	28,98	28,92	28,87	30,85
H_α	21,37	21,55	19,59	17,66	20,66	18,93
Ecart moyen[e]	0,59[f]	0,09	0,46	1,02	0,44	3,73

[a]Normalisés par rapport au COO_β (%).
[b]Contact négligé.
[c]Moyenne des 6 meilleures combinaisons.
[d]Résultats équivalents à ceux de l'analyse des données de 4 cations (sans Tm^{3+}) sur la base d'un modèle de symétrie axiale.
[e]Par rapport à la moyenne des 6 meilleures combinaisons impliquant 3 cations non axiaux.
[f]Écart moyen interne aux 6 combinaisons.

TABLEAU 6. Valeurs relatives des constantes hyperfines de contact (A_i) [a,b]

C_{Me}	C_β	C_α	CO_{NH}	COO_β	COO_α	H_{Me}	$H_{\beta 1}$	$H_{\beta 2}$	H_α
0,07	−1,55	−0,73	−0,06	2,25	1,27	0,03	0,41	0,36	0,44

[a]$A_i = 1$ entraine un effet, à champ faible, de 28,54 ppm avec Dy^{3+} (2,59 ppm avec Yb^{3+}).
[b]Calculées pour le modèle symétrie axiale, analyse avec 4 cations (sans Tm).

Par contre, lorsque l'analyse tient compte de l'effet de contact (éq. [4]), la précision est fortement améliorée bien qu'une déviation systématique soit encore observée, au niveau de chaque site, dans le cas de l'ion Tm^{3+}. Ces déviations peuvent être dues à une absence de symétrie axiale du tenseur d'anisotropie magnétique, comme cela avait déjà été suggéré pour cet ion (10, 30). On a essayé de vérifier cette hypothèse en supposant que pour un ou plusieurs cations l'approximation de la symétrie axiale ne soit pas valable. Les termes paramagnétiques sont alors analysés suivant l'éq. [5] (cf. Partie expérimentale pour la méthode de calculs) en postulant que seuls certains cations entrainent un effet non-axial important et que pour les autres on a $D_j' \simeq 0$. Dans chacun des groupes de combinaisons avec 1, 2 ou 3 cations pour lesquels $D_j' \neq 0$, les meilleurs résultats (plus faible incertitue moyenne sur les facteurs géométriques, par exemple) impliquent toujours l'ion Tm^{3+} (cf. tableau 4).

Il faut remarquer que lorsque $D_j' \neq 0$ pour un seul cation k les résultats obtenus avec l'éq. [5] sont équivalents à ceux de l'analyse basée sur l'éq. [4] dans un système n'incluant pas les données du cation k; c'est en particulier le cas pour Tm^{3+} (tableau 4). Par ailleurs, toutes les combinaisons de 3 cations à symétrie non-axiale qui impliquent l'ion Tm^{3+} conduisent à des variances très proches, ce qui semble indiquer que l'on atteint, à ce niveau, la limite des possibilités d'une telle analyse de nos données. Pour discuter des différents modes d'interprétation des termes paramagnétiques, on a choisi de se référer à la moyenne des facteurs géométriques obtenus à partir de ces 6 combinaisons avec Tm^{3+} et deux autres cations non-axiaux; cf. tableau 5. On constate le très bon accord entre ces moyennes de référence et les valeurs obtenues avec l'éq. [4], à partir d'un système à 4 cations (sans Tm^{3+}); ces derniers résultats ont donc été utilisés dans l'analyse structurale.

Il faut également noter que les facteurs géométriques calculés à partir des seules données de Yb^{3+} et Dy^{3+} et du modèle à symétrie axiale et effet de contact (éq. [4]) sont également très cohérents avec les résultats précédents (tableau 5). Si ce résultat peut être corroboré par des études ultérieures, sur des dérivés du glutamate notamment,[4] on disposerait d'une méthode beaucoup plus rapide pour la détermination des facteurs géométriques. Par contre, les termes paramagnétiques relatifs à Yb^{3+} ne sont pas exempts d'effets de contact et d'importantes déviations apparaissent sur les valeurs de G_i calculées à partir de ces seules données, particulièrement au niveau des carbones adjacents aux carboxylates, ce que l'on peut expliquer par les valeurs relatives des constantes hyperfines de contact.

Les variations de A_i sont relativement cohérentes (tableau 6), ce qui valide, a posteriori, le modèle : les effets sont d'autant plus importants que le site est proche du lanthanide et on observe l'alternance de signe attendue lorsque le phénomène de polarisation de spin est prépondérant : 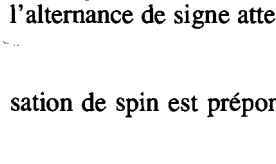 (réf. 9); par ailleurs, le contact est apparemment négligeable pour les noyaux du groupement N-acétyle. Enfin, deux observations importantes sont à souligner : les effets de contact sont plus grands du côté du carboxylate β que du COO_α et, par ailleurs, la proportion de contact dans le terme paramagnétique est relative-

4. Étude en cours.

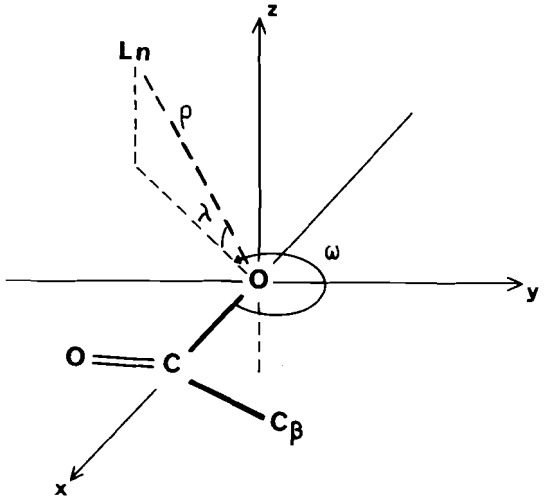

FIG. 1. Définition des coordonnées du lanthanide (ρ, ω, λ) par rapport au carboxylate.

ment plus importante pour les carbones β et α que pour les carboxylates eux-mêmes, ce qui explique que, dans une étude antérieure basée sur les seules données de Yb^{3+}, les déviations les plus importantes provenaient justement des C_β (5).

Structure et conformation du complexe

Les facteurs géométriques précédemment déterminés (tableau 5), ainsi que les constantes hyperfines relatives à l'effet de contact (tableau 6), montrent clairement que les deux carboxylates sont impliqués dans l'interaction mais que les effets sont plus importants au niveau du COO_β que du COO_α; il peut donc s'agir d'un chélate dissymétrique.

La méthode générale de calcul, ainsi que les longueurs et angles de liaison utilisés, ont été détaillés dans un travail antérieur (5). En ce qui concerne les rotamères, nous avons conservé également les approximations suivantes: rotations d'ordre 3 autour des liaisons C_{sp^3}—C_{sp^3} (positions alternées), C_{sp^3}—COO^- (avec éclipse du C=O); rotation d'ordre 6 autour de C_α—N. La position de l'ion Ln^{3+} (ρ, ω, λ) est définie dans le chélate par rapport au COO_β (fig. 1) et la direction de l'axe magnétique principal est déterminée en fonction de l'inverse du carré des distances Ln^{3+} ... O_α^- et Ln^{3+} ... O_β^-, ce que nous discuterons ultérieurement. Enfin, la variance est exprimée sous la forme du facteur d'accord R (éq. [1]).

Résultats

Dans un premier temps, l'analyse a été limitée aux noyaux proches des interactions avec le lanthanide (les 7 sites du résidu Asp) dans le but de préciser les structures possibles parmi les 27 conformations du résidu. Seules 6 structures (tableau 7) permettent d'obtenir des valeurs acceptables de R (entre 9,8 et 12,7%) et de ρ (entre 2,45 et 3,15 Å). Dans tous les autres cas R est supérieur à 14% (ρ étant limité à 3,2 Å) et il paraît statistiquement impossible que ces autres structures aient une quelconque importance dans le complexe.

La distance O_β^- ... C_α' semble le facteur essentiel de discrimination entre ces conformations: les arrangements correspondant aux deux carboxylates en position *anti* par rapport à la liaison C_β—C_α sont évidemment défavorisés (fig. 2c), mais ceux pour lesquels le C—O_β^- ne pointe pas directement vers le carboxylate α le sont également (fig. 2a, e, f). Par contre, on observe peu de différence pour les 3 rotamères autour de C_α—C', ce qui peut s'interpréter par une quasi-équivalence des

TABLEAU 7. Conformations du résidu Asp dans le chélate

	Structure					
Angle[a]	**4**	**5**	**6**	**10**	**11**	**12**
C_α—C_β/C_γ—O^-	+60°	+60°	+60°	−60°	−60°	−60°
C'_α—C_α/C_β—C_γ	−60°	−60°	−60°	+60°	+60°	+60°
O^-—C'_α/C_α—C_β	+60°	−60°	180°	+60°	−60°	180°
R(%)[b]	9,8	11,6	11,8	11,6	11,3	12,7

[a]Angle A—B/C—D: rotation pour amener DC sur BA, comptée >0 dans le sens des aiguilles d'une montre (vue de C vers B); (voir réf. 33).

[b]Facteur d'accord pour le modèle «chélate» (analyse sur 7 sites: sans le groupement N-acétyle).

deux oxygènes du carboxylate α, en relation peut-être avec la faible basicité de ce groupement ($pK \simeq 2$).

L'analyse finale peut donc être restreinte aux conformères dérivés, par rotation d'ordre 6 autour de C_α—N, des 6 structures possibles du résidu, soit 36 conformères sur les 162 théoriques. Une exploration préalable a été effectuée avec des pas de 0,2 Å pour ρ ($2,2 \leqslant \rho \leqslant 3,0$ Å) et des pas de 10° pour les angles ω et λ; les résultats sont alors affinés pour chaque sous minimum obtenu (résolution finale: 0,05 Å et 2,5°). Le meilleur résultat est relatif à des conformères de structure **10** ou **11** pour lesquels R = 11,7% (respectivement 11,6 et 11,3% lors de l'analyse à 7 sites). Cette légère augmentation du facteur d'accord R n'est pas surprenante: les sites du N-acétyl ont des déplacements induits faibles et les répercussions des incertitudes du modèle y seront relativement plus importantes.

L'analyse permet de déterminer le conformère prédominant, les 3 coordonnées du lanthanide (ρ, ω, λ) et le facteur d'échelle de l'équation de McConnell et Robertson (25). Compte-tenu des 10 sites considérés, on peut admettre qu'il reste 5 degrés de liberté et que la valeur maximale admissible pour R est (32) $R_{max} = R_{mini}(1 + 1/5)^{1/2}$ soit 12,8%. Quatorze conformères (sur 36) répondent à cette condition (tableau 8) et ne diffèrent que par des rotations autour de C_α—C' (tableau 7) et de C_α—N (angle ϕ). Ils correspondent donc au même squelette $^-$O—C—C_β—C_α—C' et sont issus des structures **10**, **11** et **12** du résidu, le groupement N-acétyle étant en position *anti* par rapport au COO_β (fig. 2d), donc éloigné au maximum des deux carboxylates en interaction avec le cation, contrairement à leur situation dans les structures **4**–**6** (fig. 2b). Ainsi, l'introduction des données du N—Ac permet une sélection parmi les précédentes conformations du résidu et montre, comme dans les complexes de monocarboxylates (5), la tendance à l'extension des groupements de la molécule ne participant pas à l'interaction.

L'orientation du lanthanide par rapport au carboxylate β est pratiquement constante dans cette série de 14 conformères: ω = 256° (±7°), λ = −67° (±4°); par contre ρ varie de 2,6 à 3,2 Å avec une valeur moyenne de 2,95 Å (±0,19). Les meilleurs résultats sont obtenus avec les structures **10** et **11** où deux oxygènes sont à des distances de 2,9 à 3,2 Å du lanthanide (l'un est le O^- du COO_β, l'autre appartient au COO_α); un troisième oxygène, le C=O du COO_β, est à environ 3,4 Å (**11**) ou 3,8 Å (**10**). Dans les structures **12**, la distance moyenne du lanthanide aux 3 oxygènes les plus proches est comparable aux cas précédents mais par contre l'interaction se fait préférentiellement avec le COO_β (2,6 et 3,2 Å) tandis que le plus proche oxygène du COO_α est à environ 3,7 Å. Cette structure moins chélatée semble être défavorisée puisque 3 conformères seule-

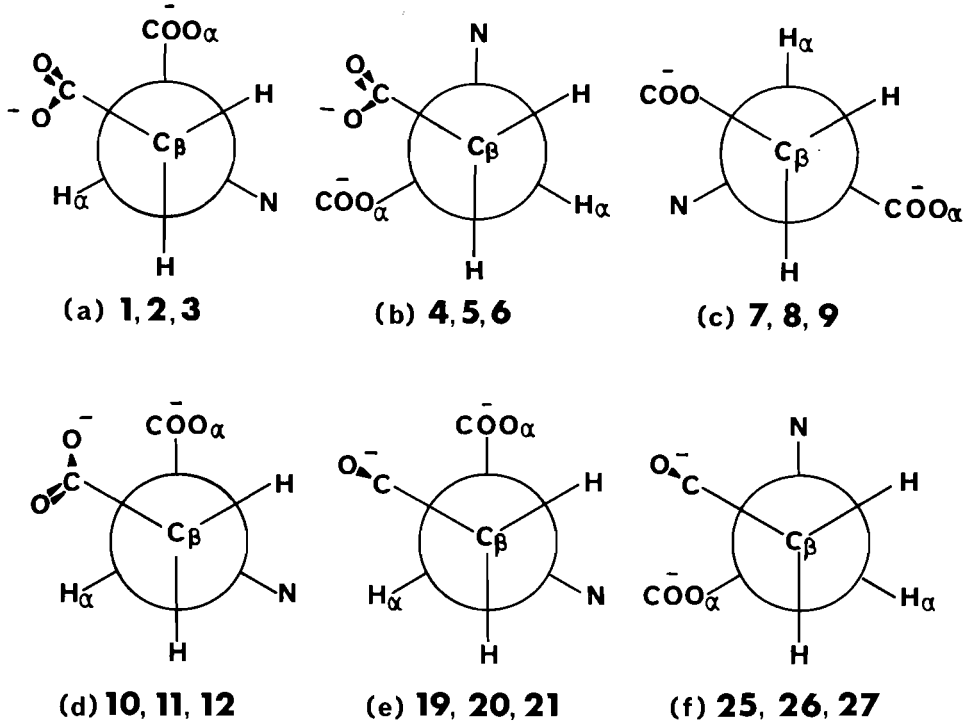

FIG. 2. Types de conformations du résidu Asp.

TABLEAU 8. Conformations de NAcAsp dans le chélate[a]

Conformère					Distances Ln ... O (Å)				
Résidu[b]	ϕ[c]	R (%)	ω (°)	λ (°)	$O_{\beta}^{-}(\rho)$	O_{β}=C	O_{α}^{-}	O_{α}=C	O=C—N
10	−150°	12,0	235	−70	3,10	3,90	4,80	3,10	6,10
10	+150°	11,8	245	−72,5	3,15	3,80	4,85	3,15	6,50
10	+90°	12,4	257,5	−75	3,20	3,75	4,85	3,15	6,60
10	+30°	12,3	257,5	−75	3,20	3,75	4,85	3,15	6,35
10	−30°	11,7	245	−72,5	3,15	3,80	4,85	3,15	5,80
10	−90°	12,2	235	−70	3,10	3,90	4,80	3,15	5,70
11	−150°	11,7	257,5	−62,5	2.90	3,40	3,15	5,25	6,10
11	+150°	11,9	257,5	−62,5	2,85	3,40	3,10	5,20	6,40
11	+90°	12,6	270	−65	3,05	3,40	3,25	5,30	6,65
11	−30°	12,1	257,5	−62,5	2,85	3,40	3,10	5,20	6,15
11	−90°	11,7	260	−62,5	2,90	3,40	3,15	5,25	5,95
12	−150°	12,5	257,5	−65	2,60	3,20	4,35	3,70	5,90
12	+150°	12,8	260	−65	2,60	3,20	4,35	3,75	6,20
12	−90°	12,5	257,5	−65	2,60	3,20	4,35	3,70	5,75

[a]Dont le facteur d'accord est $R \leq 12{,}8\%$.
[b]Voir tableau 7.
[c]Angle C′—C_{α}/N—C(O); voir (*a*), tableau 7 et réf. 33.

ment ont un facteur $R \leq 12{,}8\%$. La figure 3 illustre ces 3 types de structures.

Par rapport à la complexation monodentate du carboxylate d'un résidu aspartate (5), on observe donc dans le chélate, outre la structure repliée du résidu, deux modifications significatives qui favorisent l'interaction avec 3 oxygènes : l'allongement de la distance O_{β}^{-} ... Ln^{3+} et le positionnement du cation à proximité du plan bissecteur du COO_{β} et nettement en dehors du plan du carboxylate.

Enfin, en ce qui concerne le groupement N-acétyle, l'oxygène de l'amide étant toujours à plus de 5,7 Å du lanthanide (tableau 8), les rotamères les moins étendus (ϕ = 90° et +30°) semblent légèrement moins stables, comme le suggère les facteurs d'accord (tableau 8). Pour ces conformères défavorisés, le groupe CH_3CO est proche à la fois du C′ et du C_{β} (fig. 4); ces résultats, s'ils sont significatifs, sont en accord avec les valeurs théoriques ou expérimentales de l'angle ϕ dans les protéines (2).

Discussion

Le facteur d'acord, près de 12%, peut sembler relativement élevé pour ce type d'analyse et rappelle les valeurs obtenues pour les complexes monocarboxylates–Yb^{3+} lorsque tous les sites, y compris le carboxylate et son carbone adjacent, étaient

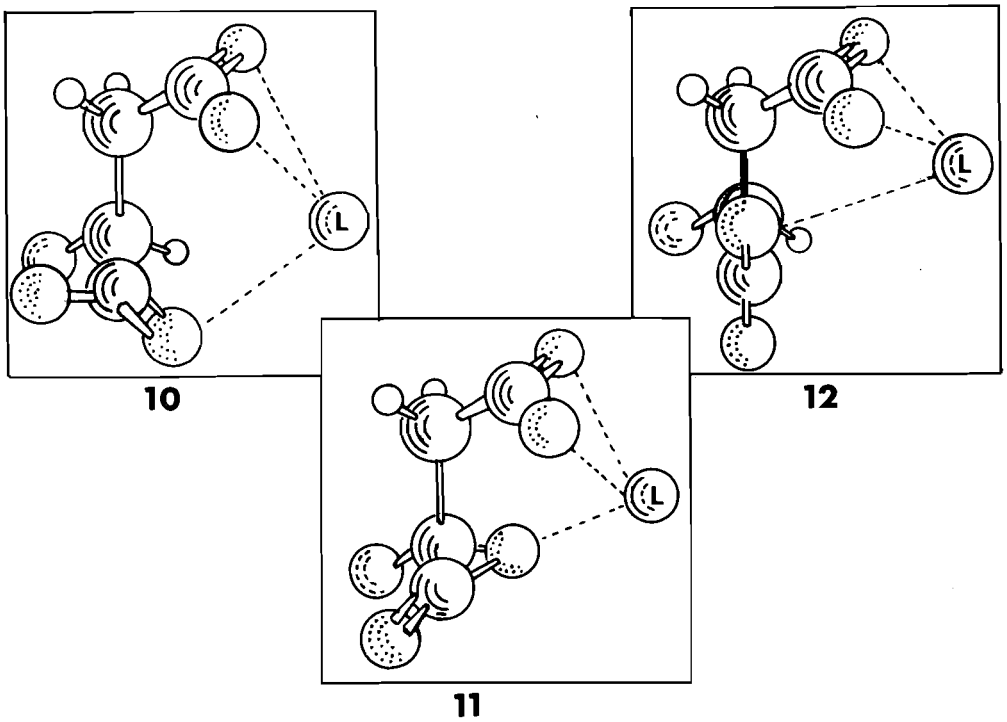

FIG. 3. Structures du chélate (le groupement acétyle n'est pas représenté).

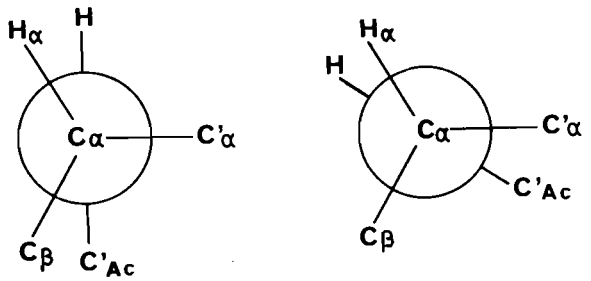

FIG. 4. Conformères défavorisés (rotamères autour de C_α—N).

inclus dans l'analyse (5). Toutefois, la détermination des facteurs géométriques du NAcAsp a été effectuée en tenant compte, pour l'essentiel, des effets de contact et d'ailleurs les déviations les plus importantes observées dans l'analyse structurale concernent les sites $H_{\beta 1}$ et $H_{\beta 2}$ et non les carbones proches du lanthanide. Nous avons donc recherché d'autres causes possibles de ces déviations et, en particulier, examiné successivement l'influence d'une variation sensible de la direction de l'axe magnétique et celle d'un équilibre entre plusieurs types de complexes 1:1.

Dans les analyses précédentes, la direction de l'axe magnétique principal du complexe avait été déterminée par une pondération en fonction de l'inverse du carré des distances entre le cation et les deux oxygènes O_α^- et O_β^-. On pouvait penser qu'un paramétrage de la direction de cet axe permettrait de tenir compte de l'intervention des 3 oxygènes les plus proches du cation. En fait, les calculs montrent que l'amélioration du facteur d'accord est relativement négligeable ($R \simeq 11\%$) et statistiquement insuffisante. Il ne faut cependant pas en déduire que la direction de l'axe magnétique ne soit pas un élément important pour l'analyse : en fixant par exemple l'axe dans la direction $Ln^{3+} \ldots O_\beta^-$, ce qui correspondrait à un complexe monodentate, le facteur d'accord minimum atteindrait 27%.

En ce qui concerne l'existence de complexes secondaires, plusieurs modèles ont été testés : deux complexes monodentates (« α » et « β »), un équilibre entre un chélate et un monodentate « β » et enfin un équilibre entre conformations du chélate. Précisons que lorsqu'un complexe monodentate est impliqué, on a fait l'hypothèse que l'ion Ln^{3+} était sur l'axe C—O^- (5). Il est facile d'éliminer le modèle avec deux complexes monodentates : la variance décroit régulièrement lorsque les distances ρ_α et ρ_β tendent vers des valeurs inférieures à 2,0 Å; les calculs ont été effectués avec les 7 données relatives au résidu Asp, pour les 81 combinaisons possibles (9 conformères « α » et 9 conformères « β »).

Dans le cas d'un équilibre chélate – monodentate β, l'analyse préliminaire limitée aux 7 sites du résidu Asp montre encore que seules les 6 structures du chélate précédemment évoquées (**4–6** et **10–12**) sont compatibles avec nos résultats. Les calculs finaux ont donc été restreints aux combinatisons entre 36 conformères du chélate et 54 du monodentate « β » pour lequel on a fixé ρ à 2,7 Å, valeur obtenue pour les complexes de la chaîne latérale de Asp (5). Dans ces conditions, la meilleure combinaison conduit à $R = 5{,}1\%$. Ce résultat n'est pourtant pas réellement significatif étant donné la réduction du degré de liberté du système due aux déterminations du type de conformère pour le monodentate « β » et du poids relatif de ce complexe ouvert. La valeur du test statistique F (34) n'est que de 4,2 alors qu'un seuil de 9,0 est nécessaire pour que ce modèle soit probablement significatif (niveau de confiance de 90%) par rapport à celui n'impliquant que le chélate. D'autres arguments (nombre de sous-minima apparus lors de l'analyse, poids de chacun des complexes) concourrent également à ne pas retenir ce modèle.

Enfin, deux conformères du chélate pourraient être en équilibre, mais, comme dans le cas précédent, il est actuellement difficile d'effectuer une analyse quantitative significative, même en imposant, par exemple, des valeurs identiques de ρ et de ω dans les deux conformères. Pourtant, un équilibre

conformationnel de ce type permettrait d'expliquer les déviations observées pour les sites $H_{\beta 1}$ et $H_{\beta 2}$ lorsqu'on ne considère qu'un seul conformère. En effet, si les variations d'angle ϕ et les rotations autour de la liaison C_α—C′ sont apparemment sans effet important sur la valeur des facteurs géométriques de ces deux protons, par contre leur ordre est inversé lorsque l'on passe d'une structure de type **10–12** à une autre de type **4–6** et, compte tenu des signes des déviations pour ces deux sites proton, un tel équilibre conformationnel devrait améliorer le facteur d'accord. En considérant un modèle de 2 conformères (**4–6**, **10–12**) pour lesquels ρ et ω sont supposés identiques, il est possible d'abaisser R en dessous de 8%.

Conclusion

Un modèle de solution simplifié, n'impliquant que deux complexes, PLn et P_2Ln, est suffisant pour interpréter les résultats obtenus pour des solutions relativement concentrées en NAcAsp (0,14 *M*) et en sel de lanthanide (0,05 *M* en moyenne) et déterminer les déplacements induits dans le complexe 1:1. Une plus grande cohérence des résultats est obtenue à l'aide d'une méthode de pondération des données dans laquelle intervient la déviation standard de chaque série de résultats expérimentaux. Enfin, l'utilisation de solutions tamponnées par les ions Lu^{3+} résoud les problèmes posés par l'élargissement des signaux dans le cas de certains lanthanides.

Pour la détermination des facteurs géométriques, il est nécessaire de ne pas utiliser les données relatives au thullium, en raison sans doute d'une forte déviation par rapport au modèle à symétrie axiale en ce qui concerne le terme de pseudo-contact. Pour certains sites, l'effet de contact n'est jamais négligeable, même avec l'ytterbium; par contre, il semble suffisant de combiner les données relatives à Yb^{3+} et à Dy^{3+} pour obtenir les facteurs géométriques avec une bonne approximation.

D'après les données du seul résidu Asp, les deux carboxylates du chélate sont en conformation *gauche* par rapport à la liaison C_α—C_β et O_β^- est dirigé vers COO_α. Les résultats relatifs au N-acétyle introduisent une condition supplémentaire, ce groupement devant être éloigné au maximum du cation et des carboxylates. Les conformères finalement retenus ne diffèrent que par des rotations autour de C_α—C′ et C_α—N; la chélation implique toujours 3 oxygènes (un pour le COO_α à 3,25 Å du cation en moyenne, deux pour le COO_β à environ 2,95 et 3,55 Å), le cation se rapprochant du plan bissecteur du carboxylate β par rapport à la situation observée dans les complexes de monocarboxylates. Ces conformères pourraient cependant ne correspondre qu'à l'espèce majoritaire d'un équilibre conformationnel; dans l'autre forme le groupement N-acétyle serait alors en conformation *gauche* par rapport au carboxylate β.

1. R. H. Kretsinger. Annu. Rev. Biochem. **45**, 239 (1976).
2. G. E. Schulz et R. H. Schirmer. Principles of protein structure. Springer Verlag, New York. 1979. p. 162.
3. M. Levitt. J. Mol. Biol. **104**, 59 (1976).
4. M. Levitt. J. Mol. Biol. **170**, 723 (1983).
5. N. Jamin, D. Baron et N. Lumbroso-Bader. J. Chem. Soc. Perkin Trans. 2, 1 (1985).
6. H. Shigematsu, N. Okamura, H. Shimeno, Y. Kishimoto, L. S. Kan et C. Fenselau. J. Neurochem. **40**, 814 (1983).
7. M. Burgal, J. Lizondo, A. Jorda et S. Grisolia. Neurochem. Res. **9**, 219 (1984).
8. C. N. Reilley, B. W. Good et J. F. Desreux. Anal. Chem. **47**, 2110 (1975).
9. C. N. Reilley, B. W. Good et R. D. Allendoerfer. Anal. Chem. **48**, 1446 (1976).
10. J. G. Shelling, M. E. Bjornson, R. S. Hodges, A. K. Taneja et B. D. Sykes. J. Magn. Reson. **57**, 99 (1984).
11. P. K. Glasoe et F. A. Long. J. Phys. Chem. **64**, 188 (1960).
12. M. R. Wilcott III, R. E. Lenkinski et R. E. Davis. J. Am. Chem. Soc. **94**, 1742 (1972).
13. J. Reuben et G. A. Elgavish. J. Magn. Reson. **39**, 421 (1980).
14. R. S. Kolat et J. E. Powell. Inorg. Chem. **1**, 293 (1962).
15. G. R. Choppin et A. J. Graffeo. Inorg. Chem. **4**, 1254 (1965).
16. E. Nieboer. Struct. Bonding (Berlin), **22**, 1 (1975).
17. C. M. Dobson, R. J. P. Williams et A. V. Xavier. J. Chem. Soc. Dalton Trans. 2662 (1973).
18. C. D. Barry, C. M. Dobson, R. J. P. Williams et A. V. Xavier. J. Chem. Soc. Dalton Trans. 1765 (1974).
19. A. D. Sherry et E. Pascual. J. Am. Chem. Soc. **99**, 5871 (1977).
20. G. A. Elgavish et J. Reuben. J. Magn. Reson. **42**, 242 (1981).
21. G. R. Choppin et H. G. Friedman, Jr. Inorg. Chem. **5**, 1599 (1966).
22. B. T. Pennington et J. R. Cavanaugh. J. Magn. Reson. **29**, 483 (1978).
23. C. M. Dobson, L. O. Ford, S. E. Summers et R. J. P. Williams. J. Chem. Soc. Faraday Trans. 2, **71**, 1145 (1975).
24. T. Hurlen. Acta Chem. Scand. A, **37**, 803 (1983).
25. H. M. McConnell et R. E. Robertson. J. Chem. Phys. **29**, 1361 (1958).
26. B. Bleaney. J. Magn. Reson. **8**, 91 (1972).
27. R. M. Golding et M. P. Halton. Aust. J. Chem. **25**, 2577 (1972).
28. B. Bleaney, C. M. Dobson, B. A. Levine, R. B. Martin, R. J. P. Williams et A. V. Xavier. J. Chem. Soc. Chem. Commun. 791 (1973).
29. R. M. Golding et P. Pyykko. Mol. Phys. **26**, 1389 (1973).
30. M. Delepierre, C. M. Dobson et S. L. Menear. J. Chem. Soc. Dalton Trans. 678 (1980).
31. R. J. Kurland et B. R. McGarvey. J. Magn. Reson. **2**, 286 (1970).
32. L. G. Sillen. Acta Chem. Scand. **16**, 159 (1962).
33. IUPAC-IUB Commission on Biochemical Nomenclature 1969. Biochemistry, **9**, 3471 (1970).
34. E. J. Middlebrooks. Statistical calculations. Ann Arbor Science, Ann Arbor, Michigan. 1976.

Appendice

Variation de la constante de complexation apparente et du déplacement induit en fonction du pH

On considère un système constitué par 2 espèces acido-basiques AH^- et A^{2-} (cette dernière étant prédominante) et les 2 complexes $(AHLn)^{2+}$ et $(ALn)^+$.

$$AH^- \rightleftarrows A^{2-} + H^+ \qquad [AH^-]/[A^{2-}] = [H^+]/K_A = h$$

$$AH^- + Ln^{3+} \rightleftarrows (AHLn)^{2+} \qquad [(AHLn)^{2+}]/[AH^-] = K_1\,[Ln^{3+}]$$

$$[(AHLn)^{2+}]/[A^{2-}] = K_1 h\,[Ln^{3+}]$$

$$A^{2-} + Ln^{3+} \rightleftarrows (ALn)^+ \qquad [(ALn)^+]/[A^{2-}] = K_2\,[Ln^{3+}]$$

Déplacements chimiques

$AH^- : (\delta_1)$ $\quad A^{2-} : (\delta_2)$ $\quad (AHLn)^{2+} : (\delta_{C_1})$ $\quad (ALn)^+ : (\delta_{C_2})$

$$\delta = \Sigma(C_i\delta_i)/\Sigma C_i = \Sigma(C_i\delta_i/[A^{2-}])/\Sigma(C_i/[A^{2-}])$$

$$\delta = \{h\delta_1 + \delta_2 + (K_1 h\delta_{C_1} + K_2\delta_{C_2})[Ln^{3+}]\}/\{h + 1 + (K_1 h + K_2)[Ln^{3+}]\}$$

pour $[Ln^{3+}] = 0$

$$\delta = (h\delta_1 + \delta_2)/(h + 1)$$

$$\Delta\delta = \delta_{[Ln^{3+}]\neq 0} - \delta_{[Ln^{3+}]=0} = \frac{K'\cdot\Delta\delta'_C\cdot[Ln^{3+}]}{1 + K'\cdot[Ln^{3+}]}$$

avec

$$K' = K_2(1 + hK_1/K_2)/(1 + h)$$

$$\Delta\delta'_C = (K_1 h\delta_{C_1} + K_2\delta_{C_2})/(K_1 h + K_2) - (h\delta_1 + \delta_2)/(h + 1)$$

Déplacement paramagnétique :

$$\Delta\delta'_P = \Delta\delta'_{C(Ln\ para)} - \Delta\delta'_{C(Ln\ dia)}$$

avec

$$\Delta\delta'_{C(Ln\ dia)} = \Delta\delta'_{C(Lu^{3+})}$$

$$\Delta\delta'_P = \frac{(\delta_{C2P} - \delta_{C2D})\{1 + [(\delta_{C1P} - \delta_{C1D})/(\delta_{D2P} - \delta_{C2D})] \cdot (K_1 h/K_2)\}}{1 + K_1 h/K_2}$$

Remarques :

(a) K' dépend du pH même si $K_1 = 0$

(b) $\Delta\delta'_P$ dépend du pH si $K_1 \neq 0$ *et* si $(\delta_{C1P} - \delta_{C1D}) \neq (\delta_{C2P} - \delta_{C2D})$

Cas de NAcAsp à pH 5 : $h \simeq 0{,}1$ ($pK_2 \simeq 4$)

Situation la plus défavorable : les 2 carboxylates complexent le cation de façon équivalente : $K_1/K_2 = 0{,}5$ et $0 \leqslant (\delta_{C1P} - \delta_{C1D})/(\delta_{C2P} - \delta_{C2D}) \leqslant 2$ (suivant les sites). Dans le pire des cas, l'incertitude introduite en assimilant $\Delta\delta'_P$ à $\delta_{C2P} - \delta_{C2D}$ est de 4,8%. En réalité l'importance du chélate dans les complexes $(ALn)^+$ doit abaisser l'incertidue maximale aux environs de 1%.

COMMUNICATION

Ionization of 9-cyanofluorene in Me_2SO–water mixtures. The role of solvent reorientation in proton tranfers

CLAUDE F. BERNASCONI AND FRANÇOIS TERRIER[1]

Thimann Laboratories of the University of California, Santa Cruz, CA 95064, U.S.A.

Received October 23, 1985

This paper is dedicated to Professor Arthur N. Bourns

CLAUDE F. BERNASCONI and FRANÇOIS TERRIER. Can. J. Chem. **64**, 1273 (1986).

Rate constants of the reversible deprotonation of 9-cyanofluorene by primary aliphatic amines were measured in 10%, 50%, and 90% aqueous Me_2SO (v/v) by the stopped-flow method. Intrinsic rate constants defined as $k_0 = k_1^B/q = k_{-1}^{BH+}/p$ at $\Delta pK + \log(p/q) = 0$ were obtained from Brønsted plots. The values for $\log k_0$ are 3.60 ± 0.15 in 10%, 3.81 ± 0.10 in 50%, and 3.61 ± 0.05 in 90% Me_2SO. The constancy of k_0 with increasing Me_2SO content of the solvent contrasts with results obtained by Ritchie (C. D. Ritchie, J. Am. Chem. Soc. **91**, 6749 (1969)) who found that k_0 for the ionization of 9-carbomethoxyfluorene by carboxylate ions in Me_2SO is much higher than for the ionization of the same carbon acid by methoxide ion in methanol. Our findings suggest that it is mainly early desolvation of the oxyanions in the hydroxylic solvent which accounts for Ritchie's results.

CLAUDE F. BERNASCONI et FRANÇOIS TERRIER. Can. J. Chem. **64**, 1273 (1986).

Faisant appel à une méthode par flux stoppé et opérant dans des solutions aqueuses à 10, 50 et 90% (v/v) de DMSO, on a mesuré les constantes de vitesse pour la déprotonation réversible du cyano-9 fluorène par des amines primaires. En se basant sur des courbes de Brønsted, on a pu évaluer les constantes de vitesse intrinsèque qui sont définies par l'équation $k_0 = k_1^B/q = k_{-1}^{BH+}/p$ lorsque $\Delta pK + \log(p/q) = 0$. A 10, 50 et 90% de DMSO, les valeurs de $\log k_0$ sont respectivement $3{,}60 \pm 0{,}15$, $3{,}81 \pm 0{,}10$ et $3{,}61 \pm 0{,}05$. La relative constance de k_0 avec une augmentation de la concentration en DMSO est en opposition avec les résultats obtenus par Ritchie (C. D. Ritchie, J. Am. Chem. Soc. **91**, 6749 (1969)) qui a trouvé que le k_0, dans le DMSO, de l'ionisation du carbométhoxy-9 fluorène en ions carboxylates est beaucoup plus élevé que pour l'ionisation du même acide carboné sous l'influence de l'ion méthylate dans le méthanol. Nos observations suggèrent que les résultats de Ritchie sont principalement expliqués par une désolvatation précoce des oxyanions dans le solvant hydroxylique.

[Traduit par la revue]

The study of solvent effects on the rates of proton transfer between aromatic hydrocarbons and oxyanions has led to some unorthodox notions about the role played by the solvent in these reactions. In 1968 and 1969 Ritchie (1, 2) reported that, for a given ΔpK, the rates in Me_2SO were substantially higher than in methanol. If one defines k at $\Delta pK = 0$ as the *intrinsic* rate constant, k_0, it appeared that in Me_2SO k_0 was approximately 10^2 fold higher than in methanol, based on the deprotonation of 9-carbomethoxyfluorene for which the most accurate data were available (2).

Ritchie (1, 2) interpreted these results in terms of a rate retarding effect of solvent reorientation in methanol. The basic idea was that the amount of energy required to reorganize methanol (or hydroxylic solvents in general) around reactants and products, as they interconvert, is greater than in Me_2SO, because of the presence of strong oriented hydrogen bonds.

The notion that solvent reorganization or reorientation may affect intrinsic rates in the manner envisioned by Ritchie is an intriguing one.[2] Similar ideas had been expressed earlier by Caldin (4) and by Ogg and Polanyi (5). In the intervening years since Ritchie's proposal, a number of workers have reported results that confirm the importance of solvent reorganization effects (6–17). Many of these studies have shown that at least part of the rate retarding effects of solvent reorientation can be understood as a consequence of early desolvation of reactant ions and/or late solvation of product ions. For example, in reactions of oxyanions acting as bases or nucleophiles, strongly basic ions show marked negative deviations from Brønsted plots. These deviations, which are tantamount to a lowering of k_0, have been attributed to the strong solvation of these ions, coupled with the requirement that their desolvation is ahead of bond formation in the transition state[3] (11, 12, 16, 17). In reactions that lead to resonance stabilized carbanions, with the negative charge localized on oxygen as in nitronate (14, 15) and enolate ions (16, 17), the late development of the solvation of the negative charge, for which there is independent evidence (10, 13, 15), leads to a lowering of k_0 (10, 13–17).[3]

The ionization of 9-substituted fluorenes provides a particularly nice system in which to demonstrate the effect on k_0 of early desolvation of the oxyanion. This is because, in contrast to nitronate and enolate ions, the negative charge in the carbanion is highly dispersed and thus is only subject to small solvation effects of its own. In other words, most of the observed solvent effect on k_0 should come from the early desolvation of the oxyanion. We have tested this idea by studying the solvent effect on the ionization of 9-cyanofluorene by primary aliphatic amines, a series of bases that are much less strongly solvated than oxyanions.

Our results in 10%, 50%, and 90% aqueous Me_2SO (v/v), obtained by the stopped-flow method, are summarized in Table 1. In 10% Me_2SO only two amines were amenable to study, because the rates with the other amines were too fast for the

[1]On leave from Département de Chimie, Faculté des Sciences de Rouen, 76130 Mont Saint Aignan, France.

[2]There is a distinct analogy between this proposal and current notions about how outer sphere electron transfer reactions occur (3).

[3]This lowering of k_0 is the consequence of a general principle that we have called the Principle of Imperfect Synchronization (13).

Printed in Canada / Imprimé au Canada

TABLE 1. Rate constants, pK_a and log k_0 values for the ionization of 9-cyanofluorene in Me_2SO–water mixtures at 20°C

Amine	$pK^{RNH_3^+}$	k_B (M^{-1} s^{-1})	k_{BH} (M^{-1} s^{-1})
10% Me_2SO – 90% water[a] (pK_a^{CH} = 10.71, log k_0 = 3.60 ± 0.15)			
n-$BuNH_2$	10.98	1.07×10^4	6.90×10^3
$MeOCH_2CH_2NH_2$	9.73	2.75×10^3	2.64×10^4
50% Me_2SO – 50% water[a] (pK_a^{CH} = 9.53, log k_0 = 3.81 ± 0.10)			
n-$BuNH_2$	10.65	4.46×10^4	3.39×10^3
$MeOCH_2CH_2NH_2$	9.62	9.60×10^3	7.80×10^3
$EtOOCCH_2NH_2$	7.87	1.90×10^3	8.61×10^4
90% Me_2SO – 10% water[a] (pK_a^{CH} = 8.01, log k_0 = 3.61 ± 0.05)			
n-$BuNH_2$	10.96	4.10×10^5	4.60×10^2
$MeOCH_2CH_2NH_2$	10.16	1.22×10^5	8.66×10^2
$EtOOCCH_2NH_2$	8.22	1.26×10^4	7.78×10^3
$NCCH_2NH_2$	5.94	4.50×10^2	5.37×10^4

[a](v/v).

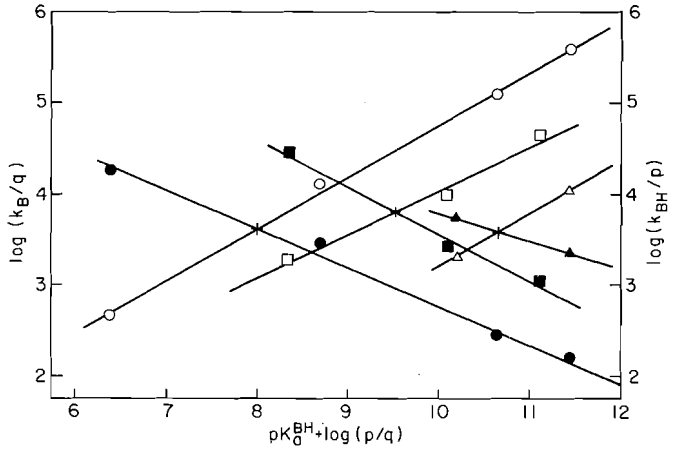

FIG. 1. Brønsted plots for the ionization of 9-cyanofluorene by amines in aqueous Me_2SO at 20°C. Open symbols: k_B; filled symbols: k_{BH}. Circles: 90% Me_2SO; squares: 50% Me_2SO; triangles: 10% Me_2SO. log k_0 is obtained where log (k_B/q) = log (k_{BH}/p) indicated by crosses.

stopped-flow technique; the same is true for oxyanions in all solvents.[4]

Figure 1 shows the Brønsted plots from which the following log k_0 values[5] were obtained: 3.60 ± 0.15 in 10% Me_2SO, 3.81 ± 0.10 in 50% Me_2SO, 3.61 ± 0.05 in 90% Me_2SO. It is quite apparent that, within experimental error, k_0 is solvent independent. These results contrast with Ritchie's finding of an approximately 100-fold increase in k_0 upon transferring the reaction of 9-carbomethoxyfluorene with oxyanions from methanol to Me_2SO. This difference between amine and oxyanion reactions is reminiscent of recent results with 1,3-indandione (17) and acetylacetone (16): log k_0 for the deprotonation of the former by carboxylate ions increases from 2.64 in 10% aqueous Me_2SO to 4.53 in 90% Me_2SO, while for the deprotonation by primary aliphatic amines the increase is only from 2.27 to 2.97; similar results were obtained for acetylacetone. Note that in these examples there is still some increase in k_0 for the amine reactions because of the effect of late solvation of the enolate ions.

It would appear then that the major conclusion to be drawn from the present study is that a large fraction, and perhaps most of the solvent effect observed by Ritchie, is caused by the requirement of early oxyanion desolvation. But closer scrutiny of our results suggests an additional solvent reorientation factor may be present, one that is more in keeping with Ritchie's original formulation[6] and related to what has been called "dynamic solvent effects" (18). The reason why this additional factor does not manifest itself as a modest increase in k_0 for the amine reactions in the Me_2SO-rich solvents, is that it is masked by other effects of nonsynchronous solvation/desolvation that tend to depress k_0 in Me_2SO. One such effect is the solvation of the developing ammonium ion that probably lags behind proton transfer, as has been suggested by Bell (19) and Jencks (20). This should lead to a lowering of k_0 which is expected to be somewhat more pronounced in the Me_2SO-rich solvents, due to the stronger solvation of ammonium ions by Me_2SO than by water (21, 22).[3]

If solvation of the developing carbanion is also retarded in the transition state,[7] this, too, would lower k_0 in both solvents. But because of the somewhat stronger solvation of fluorenyl ions in Me_2SO compared to water or methanol (2), this decrease in k_0 would again be somewhat more pronounced in the Me_2SO-rich mixtures. Finally, early desolvation of the carbon acid could also lower k_0 (17). Work is in progress to develop a more quantitative assessment of all these factors along lines suggested elsewhere (13, 17).

Acknowledgements

Support by Grant No. CHE-8315374 from the National Science Foundation is gratefully acknowledged.

1. C. D. RITCHIE and R. E. USCHOLD. J. Am. Chem. Soc. **90**, 3415 (1968).
2. C. D. RITCHIE. J. Am. Chem. Soc. **91**, 6749 (1969).
3. (*a*) R. A. MARCUS. J. Chem. Phys. **24**, 966 (1956); **43**, 679 (1965); **43**, 3477 (1965); (*b*) J. Phys. Chem. **67**, 853 (1963); (*c*) W. J. ALBERY. Ann. Rev. Phys. Chem. **31**, 227 (1980).
4. E. F. CALDIN. J. Chem. Soc. 3345 (1959).
5. R. A. OGG and M. POLANYI. Trans. Faraday Soc. **31**, 604 (1935).
6. (*a*) M. M. KREEVOY and S.-W. OH. J. Am. Chem. Soc. **95**, 4805 (1973); (*b*) A. I. HASSID, M. M. KREEVOY, and T. M. LAING. Symp. Faraday Soc. **10**, 69 (1975).
7. W. J. ALBERY, A. N. CAMPBELL-CRAWFORD, and J. S. CURRAN. J. Chem. Soc. Perkin Trans. 2, 2206 (1972).
8. A. J. KRESGE. Acc. Chem. Res. **8**, 354 (1975).
9. J. R. MURDOCH, J. A. BRYSON, D. F. MCMILLEN, and J. I. BRAUMAN. J. Am. Chem. Soc. **104**, 600 (1982).
10. C. F. BERNASCONI. Pure Appl. Chem. **54**, 2335 (1982).
11. (*a*) D. J. HUPE and D. WU. J. Am. Chem. Soc. **99**, 7653 (1977); (*b*) D. J. HUPE, D. WU, and P. SHEPPERD. J. Am. Chem. Soc. **99**, 7659 (1977).
12. W. P. JENCKS, S. R. BRANT, J. R. GANDLER, G. FENDRICH, and C. NAKAMURA. J. Am. Chem. Soc. **104**, 7045 (1982).
13. C. F. BERNASCONI. Tetrahedron, **41**, 3219 (1985).

[4]In Me_2SO-rich solvents ionizations of carbon acids by oxyanions are generally substantially faster than ionizations by amines (16, 17).

[5]Since our Brønsted plots are statistically corrected, k_0 is defined as $k_B/q = k_{BH}/p$ at $pK_a^{BH} - pK_a^{CH} + \log(p/q) = 0$.

[6]In the original formulation there was more emphasis on solvent–solvent as contrasted to solvent–solute interactions.

[7]Work by Murdoch *et al.* (9) suggests that this is the case for fluorenyl ions just as for nitronate and enolate ions.

14. F. G. BORDWELL and W. J. BOYLE, JR. J. Am. Chem. Soc. **94**, 3907 (1972); **97**, 3447 (1975).
15. J. R. KEEFFE, J. MOREY, C. A. PALMER, and J. C. LEE. J. Am. Chem. Soc. **101**, 1295 (1979).
16. C. F. BERNASCONI and R. D. BUNNELL. Isr. J. Chem. **26**, 420 (1985).
17. C. F. BERNASCONI and P. PASCHALIS. J. Am. Chem. Soc. **108**, 2969 (1986).
18. (*a*) J. L. KURZ and L. C. KURZ. J. Am. Chem. Soc. **106**, 1373 (1984); (*b*) G. VAN DER ZWAN and J. T. HYNES. J. Chem. Phys. **76**, 2993 (1982); (*c*) D. G. TRUHLAR, W. L. HASE, and J. T. HYNES. J. Phys. Chem. **87**, 2664 (1983).
19. R. P. BELL. The proton in chemistry. 2nd ed. Cornell University Press, Ithaca, NY. 1973. Chapt. 10.
20. W. P. JENCKS. Catalysis in chemistry and enzymology. McGraw-Hill, New York. 1969. p. 178.
21. A. J. PARKER. Chem. Rev. **69**, 1 (1969).
22. C. F. WELLS. *In* Thermodynamic behavior of electrolytes in mixed solvents. II. *Edited by* W. F. Furter. Advance Chemical Series. Vol. 177. 1977. p. 53.

High-temperature thermodynamic properties of several 1:1 electrolytes[1]

PREET P. S. SALUJA
Atomic Energy of Canada Limited, Whiteshell Nuclear Research Establishment, Pinawa, Man., Canada R0E 1K0
AND
KENNETH S. PITZER AND RAMESH C. PHUTELA
Department of Chemistry and Lawrence Berkeley Laboratory, University of California, Berkeley, California 94720, U.S.A.
Received November 20, 1985

PREET P. S. SALUJA, KENNETH S. PITZER, and RAMESH C. PHUTELA. Can. J. Chem. **64**, 1328 (1986).

Comprehensive equations for the thermodynamic properties of aqueous NaI, CsF, CsCl, CsI, $NaIO_3$, KIO_3, $CsIO_3$, $KClO_4$, and HCl are generated by combining the heat capacity and density measurements reported by the first author with literature data for the enthalpy and Gibbs energy, or activity, as a function of molality at 298 K. The composition dependence is represented by the equations of Pitzer, which combine a theoretical form and Debye–Hückel terms with empirically evaluated parameters for short-range ion interactions. Temperature dependencies are represented by simple empirical equations, which should be reliable to 413 K or a little higher.

PREET P. S. SALUJA, KENNETH S. PITZER et RAMESH C. PHUTELA. Can. J. Chem. **64**, 1328 (1986).

Si l'on combine les données de capacité calorifique et de densité, qui sont rapportées par le premier auteur, avec les données rapportées dans la littérature pour l'enthalpie et l'énergie de Gibbs, ou l'activité en fonction de la molalité à 298 K, on peut générer des équations étendues pour les propriétés thermodynamiques de solutions aqueuses de NaI, de CsF, de CsCl, de CsI, de $NaIO_3$, de KIO_3, de $CsIO_3$, de $KClO_4$ et de HCl. On peut représenter la dépendance sur la composition par les équations de Pitzer qui combinent une forme théorique et des termes de Debye–Hückel avec des paramètres évalués d'une façon empirique pour les interactions ioniques à courte distance. On représente la dépendance sur la température à l'aide d'équations empiriques simples qui devraient être fiables au moins jusqu'à 413 K.

[Traduit par la revue]

Introduction

Thermodynamic properties of various mixed aqueous electrolytes are of great practical interest in a number of engineering and geological situations. It has been shown (1–4) that a good estimate of the properties of a mixed electrolyte can be obtained from knowledge for each cation–anion interaction present and this is given in turn from the properties of the various pure electrolytes. Small terms for the mixing of ions of the same sign, if available, should be added to obtain more accurate prediction of the properties of mixtures.

Preliminary analysis of the various chemical processes in the vicinity of a deep underground nuclear fuel waste-disposal vault (5) has shown the radiological importance of ^{129}I, ^{135}Cs, ^{99}Tc, and ^{90}Sr. Thus, our current interest lies in understanding the interactions of several singly charged ions, including the fission products I^- (or IO_3^-) and Cs^+ with the major constituents of ground water.

While the thermodynamic properties of aqueous electrolytes have been studied extensively at room temperature and low pressure, only recently have a few electrolytes been investigated at higher temperature and pressure. For the most abundant components of most natural waters, there are comprehensive and accurate data through 473 K or higher temperature for NaCl (6, 7), KCl (8), and Na_2SO_4 (9). For $MgCl_2$ there are excellent isopiestic data (10) and further studies are now in progress. Measurements at Berkeley have been completed and a paper is (33) for $MgSO_4$. Thus, information is now, or soon will be, available for the most abundant ions in ground water, and the present paper presents data for other singly charged ions important for radio-active waste disposal studies. Similar studies for multiple charged ions are in preparation.

In addition to the practical interest in these particular ionic species, it is of interest to compare the thermodynamic properties of various ions from a theoretical viewpoint.

Since the Gibbs energy (and activity) and the enthalpy are known as a function of molality for most aqueous electrolytes at room temperature (298.15 K), it is an efficient procedure to measure the apparent molar heat capacity as a function of temperature, ${}^{\phi}C_p(T, m)$. Then the apparent molar enthalpy ${}^{\phi}L$ is found by integration

$$[1] \quad {}^{\phi}L(T, m) = \int_{298}^{T} [{}^{\phi}C_p(T', m) - {}^{\phi}C_p(T', 0)]\, dT' + {}^{\phi}L(298, m)$$

where 298 is an abbreviation of 298.15 K. The total excess enthalpy $H^{EX} = L = n_2{}^{\phi}L$ with

$$[2] \quad L = H - n_1H_1^0 - n_2\bar{H}_2^0$$

Here n_1 and n_2 are numbers of moles of components 1 and 2 (H_2O and salt, respectively) with standard molar enthalpies H_1^0 for pure water and $\bar{H}_2^0$ for the salt at infinite dilution.

A second integration yields the excess Gibbs energy per mole of solute G^{EX}/n_2.

$$[3] \quad G^{EX}(T, m)/n_2T = -\int_{298}^{T} [{}^{\phi}L(T', m)/(T')^2]\, dT' + G^{EX}(298, m)/298n_2$$

Appropriate derivatives of G^{EX} with respect to m yield the activity and osmotic coefficients. The treatment of aqueous Na_2SO_4 by Rogers and Pitzer (9) is a prototype investigation of this type in which heat capacities were integrated twice to yield Gibbs energy data.

The equations of Pitzer (2, 11) give an accurate and concise representation of the molality dependence, and the ion-interaction parameters for those equations are now available for several electrolytes as a function of temperature (2, 6–10). Furthermore, these equations have proved to be quite accurate in predicting the properties of complex mixed electrolytes (3, 4).

[1]Issued as AECL-8932 and as LBL-20208.

Printed in Canada / Imprimé au Canada

TABLE 1. General definitions[a] and composition-dependent (Pitzer) equations for a 1:1 electrolyte[b]

Gibbs energy functions

[5] $G^{EX} = G - n_1G_1^0 - n_2\tilde{G}_2^0 + 2n_2RT(1 - \ln m)$
$= 2n_2RT(\ln \gamma_\pm + 1 - \phi)$

[6] $1 - \phi = (\partial G^{EX}/\partial n_w)_{T,P,n_2}/RTm$

[7] $\ln \gamma_\pm = (\partial G^{EX}/\partial n_2)_{T,P,n_1}/2RT$

[8] $G^{EX}/n_wRT = -A_\phi(4m/b) \ln (1 + bm^{1/2}) + 2m^2(B_{MX} + mC_{MX})$

[9] $B_{MX} = \beta_{MX}^{(0)} + 2\beta_{MX}^{(1)}g(\alpha m^{1/2})$, $C_{MX} = C_{MX}^{\phi}/2$

[10] $g(x) = [1 - (1 + x) \exp (-x)]/x^2$

[11] $\phi - 1 = -A_\phi m^{1/2}/(1 + bm^{1/2}) + m[\beta_{MX}^{(0)} + \beta_{MX}^{(1)} \exp (-\alpha m^{1/2})] + m^2C_{MX}^{\phi}$

[12] $\ln \gamma_\pm = -A_\phi[(2/b) \ln (1 + bm^{1/2}) + m^{1/2}/(1 + bm^{1/2})]$
$+ m\{2\beta_{MX}^{(0)} + 2\beta_{MX}^{(1)}[1 - (1 + \alpha m^{1/2} - \alpha^2 m/2) \exp (-\alpha m^{1/2})]/\alpha^2 m\} + 3m^2C_{MX}$

Apparent molar enthalpy

[13] ${}^{\phi}L = (A_H/b) \ln (1 + bm^{1/2}) - 2RT^2(mB_{MX}^L + m^2C_{MX}^L)$

[14] $B_{MX}^L = \beta_{MX}^{(0)L} + 2\beta_{MX}^{(1)L}g(\alpha m^{1/2})$

[15] $\beta_{MX}^{(0)L} = (\partial\beta_{MX}^{(0)}/\partial T)_P$, $\beta_{MX}^{(1)L} = (\partial\beta_{MX}^{(1)}/\partial T)_P$
$C_{MX}^L = (\partial C_{MX}/\partial T)_P$

Apparent molar heat capacity

[16] ${}^{\phi}C_p = \tilde{C}_{p,2}^0 + (A_J/b) \ln (1 + bm^{1/2}) - 2RT^2(mB_{MX}^J + m^2C_{MX}^J)$

[17] $B_{MX}^J = \beta_{MX}^{(0)J} + 2\beta_{MX}^{(1)J}g(\alpha m^{1/2})$

[18] $\beta_{MX}^{(0)J} = (\partial\beta_{MX}^{(0)L}/\partial T)_P + (2/T)\beta_{MX}^{(0)L}$
$\beta_{MX}^{(1)J} = (\partial\beta_{MX}^{(1)L}/\partial T)_P + (2/T)\beta_{MX}^{(1)L}$
$C_{MX}^J = (\partial C_{MX}^L/\partial T)_P + (2/T)C_{MX}^L$

Apparent molar volume

[19] ${}^{\phi}V = \tilde{V}_2^0 + (\partial G^{EX}/\partial P)_{T,n_1,n_2}/n_2$

[20] ${}^{\phi}V = \tilde{V}_2^0 + (A_V/b) \ln (1 + bm^{1/2}) + 2RT(mB_{MX}^V + m^2C_{MX}^V)$

[21] $B_{MX}^V = \beta_{MX}^{(0)V} + 2\beta_{MX}^{(1)V}g(\alpha m^{1/2})$

[22] $\beta_{MX}^{(0)V} = (\partial\beta_{MX}^{(0)}/\partial P)_T$, $\beta_{MX}^{(1)V} = (\partial\beta_{MX}^{(1)}/\partial P)_T$
$C_{MX}^V = (\partial C_{MX}/\partial P)_T$

Debye-Hückel slopes

[23] $A_\phi = (2\pi N_0d_1/1000)^{1/2}(e^2/4\pi\epsilon_0DkT)^{3/2}/3$

[24] $A_H = 4RT^2(\partial A_\phi/\partial T)_P$

[25] $A_J = (\partial A_H/\partial T)_P$

[26] $A_V = -4RT(\partial A_\phi/\partial P)_T$

[a]Definitions of symbols: n_w = No. of kg of water ($n_w = n_1/M_1$), $b = 1.2$ kg$^{1/2}$ mol$^{-1/2}$ and $\alpha = 2.0$ kg$^{1/2}$ mol$^{-1/2}$ are parameters which are constant for all 1:1 electrolytes (and more generally), m is molality (which is equal to ionic strength for a 1:1 electrolyte), $\beta_{MX}^{(0)}$, $\beta_{MX}^{(1)}$, C_{MX} are fitting parameters specific to the salt MX, $\tilde{C}_{p,2}^0$ and $\tilde{V}_2^0$ are the apparent or partial molar heat capacity and volume, respectively, of the solute at infinite dilution.
[b]See ref. 7 or 9 for the more general equations for other charge types.

Hence these equations are used for the present research. Table 1 presents the equations in the form simplified for pure 1:1 electrolytes. Equations for mixed electrolytes were derived by Pitzer and Kim (1) and are now available from several sources (2–4).

Somewhat similarly, the apparent molar volume is related to the pressure dependence of the Gibbs energy. Thus

$$[4] \quad G^{EX}(T, P, m)/n_2 = \int_{P_0}^{P} {}^{\phi}V(T, P', m)\, dP' + G^{EX}(T, P_0, m)/n_2$$

In general, the apparent molar volume should be known as a function of pressure, but at moderate pressures it is a satisfactory approximation to neglect the pressure dependency and to measure the volume or density at any convenient and moderate pressure.

Review of available data

Heat capacity data

The development of flow microcalorimeters has made heat capacity measurements easier and more accurate for aqueous solutions at room temperature and more recently at high temperature. For aqueous NaCl and Na_2SO_4 measurements have been reported to 473 K or higher temperature (9, 12, 13). For the electrolytes discussed in this paper, measurements through 373 K are reported in reference 14. In addition there are published data, primarily near room temperature, for several of these systems (15–20). Table 2 gives the references for the literature data actually used in our calculations and the ranges of temperature, pressure, and concentration.

Literature data reported for other pressures, usually 0.1 MPa, were converted to 0.6 MPa for the present calculations by use of the available volumetric data for these systems. The change in heat capacity is very small for this pressure change.

Since the primary purpose of this research concerned proper-

TABLE 2. Literature heat capacity data for aqueous 1:1 electrolytes

Electrolyte	Reference	Temperature range (K)	Pressure (MPa)	Concentration range (Molal)	Standard deviation of fit ($J K^{-1} mol^{-1}$)
NaI	15	298	0.1	0.06–1.0	1.4
	14	323–373	0.6	0.05–2.0	
CsF	15	298	0.1	0.02–1.1	2.4
	14	298–373	0.6	0.03–1.1	
CsCl	15	298	0.1	0.01–0.8	1.0
	14	298–373	0.6	0.04–1.0	
CsI	15	298	0.1	0.02–0.7	1.8
	14	298–373	0.6	0.09–1.0	
$NaIO_3$	14	298–373	0.6	0.05–0.52	2.1
KIO_3	14	298–373	0.6	0.02–0.4	1.8
$CsIO_3$	14	298–373	0.6	0.01–0.06	1.8
$KClO_4$	14	298–373	0.6	0.01–1.12	2.1
HCl	15	298	0.1		2.2
	14	323–373	0.6	0.03–0.20	
	16	283–313[a]	0.1	0.05–0.40	

[a]Data for temperatures below 298 K were not used in our final calculations.

ties at higher temperatures, we did not burden our calculations with the very large number of room-temperature measurements of varying precision which were available in some cases. One or two of the best sets of measurements sufficed to determine the properties at 298 K.

Of the literature data for temperatures higher than 298 K, only those of Allred and Woolley (16) for HCl were included in the final calculations.

Other sets of measurements (17–19) were considered carefully, but it was concluded that their inclusion with more than negligible weight would only distort the results from the recent measurements (14–16).

After the present calculations were essentially complete, we became aware of the very recent measurements extending to 413 K for HCl by Tremaine *et al.* (21) which have subsequently been published. Since these authors offer an excellent treatment for HCl in terms of the same (Pitzer) equations used here, there seemed to be little reason to repeat our calculations with the addition of their data. As indicated below, there is good agreement between the two investigations.

Volumetric data

In comparison with heat capacity, there are even fewer investigations of the volumetric properties of the systems of present interest at high temperature. Again, we used enough of the best measurements at room temperature to be sure the properties at 298 K were accurately determined without including all data in all cases. In addition to the measurements reported in ref. 14, the data of Allred and Woolley (16) for HCl at several temperatures and of Fortier *et al.* (15) for NaI, CsCl, and HCl at 298 K were included in the present calculations. All these data arise from modern instruments and have comparable precision.

Calculations and results

Heat capacity

Equation [16] (see Table 1) was fitted to the measured values of the apparent molar heat capacity. The Debye–Hückel parameters for various functions, including A_J, were calculated from the equation of Bradley and Pitzer (22) for the dielectric constant of water as a function of T and P and from the equations in Table 1. The other properties of water were taken from the equation of Haar *et al.* (23).

Exploratory calculations were made of the data at a single temperature to assure that the composition dependence was accurately reproduced by eq. [16]. Indeed, it was found that, for the limited range of molality of measurement, the third virial coefficient C^J_{MX} was not needed. Also the precision at very low molality was not high enough to justify inclusion of the term in $\beta^{(1)J}_{MX}$. Thus, equation [16] was reduced in practice to

$$[27]\quad {}^{\phi}C_p = \tilde{C}^0_{p,2} + (A_J/b)\ln(1 + bm^{1/2}) - 2mRT^2\beta^{(0)J}_{MX}$$

Next, the temperature dependence of $\tilde{C}^0_{p,2}$ and $\beta^{(0)J}_{MX}$ were considered. Three-term expressions were found to be adequate:

$$[28]\quad \tilde{C}^0_{p,2}(T) = A^C_c/T + B^C_c + C^C_c T$$

$$[29]\quad \beta^{(0)J}_{MX}(T) = A^C_\beta/T + B^C_\beta + C^C_\beta T$$

The entire array of data at all temperatures was then fitted in a single least-squares calculation adjusting the six parameters in eqs. [28] and [29].

Initially, all data were given equal weight. With the guidance of the calculations at a single temperature, it was then decided whether certain literature data were accurate enough to be retained. Also, a very few individual values were sufficiently deviant as to suggest error, and these were assigned greatly reduced weights. While the precision of apparent molar quantities decreases at low molality, we did not generally reduce weight with molality because we wanted to maintain as high accuracy as possible for the limiting $\tilde{C}^0_{p,2}$. Also, we found that the resulting function usually agreed very well with the measurements at high molality, even with full weight for the low-molality data. The exception was $CsIO_3$, where the data at very low molalities showed substantial deviations. In this case the weight was greatly reduced for all measurements below 0.016 mol kg^{-1}. The resulting equation for $CsIO_3$ then fitted quite accurately all of the measurements above 0.016 mol kg^{-1}.

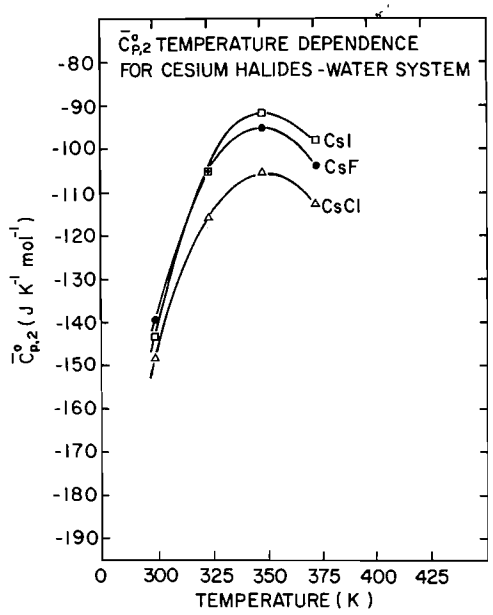

FIG. 1. Temperature dependence of the partial molar heat capacities, $\bar{C}^0_{p,2}(T)$, of cesium halides in water at 0.6 MPa. ●, △, and □ are isothermal $\bar{C}^0_{p,2}$ values from present work.

TABLE 3. Coefficients for eq. [28] for the partial molar heat capacity function, $\bar{C}^0_{p,2}(T)$, at 0.6 MPa

System	$A^C_c \times 10^{-5}$ / J mol^{-1}	$B^C_c \times 10^{-3}$ / J mol^{-1} K^{-1}	C^C_c / J mol^{-1} K^{-2}
NaI–H_2O	−6.3812	3.71181	−5.5301
CsF–H_2O	−6.4956	3.63455	−5.3536
CsCl–H_2O	−6.0076	3.33271	−4.9190
CsI–H_2O	−6.8489	3.80083	−5.5296
$NaIO_3$–H_2O	−10.1759	5.83106	−8.2159
KIO_3–H_2O	−10.3330	5.89793	−8.3571
$CsIO_3$–H_2O	−11.4674	6.43049	−9.0063
$KClO_4$–H_2O	−6.4708	3.81151	−5.5555
HCl–H_2O	−2.8802	1.61240	−2.5884

Figure 1 shows the resulting curves for $\bar{C}^0_{p,2}$ for the cesium halides as typical examples of the results. The points on Fig. 1 are the values arising from separate fits of the data at each temperature. It is evident that the three terms of eq. [28] are adequate to express the temperature dependence of $\bar{C}^0_{p,2}$.

The resulting values for these parameters for each system are given in Table 3 for the $\bar{C}^0_{p,2}$ function and in Table 4 for the $\beta^{(0)V}_{MX}$ function. The standard deviation of fit in each case is given in Table 2.

Although there are measurements for HCl below 298 K, these were not included in our calculations. The rapid change in heat capacity near 273 K is well-known. It did not seem worthwhile to complicate the present equations in order to represent exactly this effect below 298 K. Thus the present equations for HCl and for all of the various salts apply with full accuracy only from 298 to 373 K. As indicated below, the integrated functions of enthalpy and Gibbs energy will be quite accurate over an extended range.

Volumetric properties

The treatment of the data for the apparent molar volume was similar in every respect to that for the heat capacity. The terms in C^V_{MX} and $\beta^{(1)V}_{MX}$ in eqs. [20] and [21] were not needed. The

TABLE 4. Coefficients for eq. [29] for the ion-interaction parameter $\beta^{(0)V}_{MX}(T)$ at 0.6 MPa

System	$A^C_\beta \times 10$ / kg mol^{-1} K^{-1}	$B^C_\beta \times 10^4$ / kg mol^{-1} K^{-2}	$C^C_\beta \times 10^6$ / kg mol^{-1} K^{-3}
NaI–H_2O	−1.552	8.422	−1.134
CsF–H_2O	−1.347	7.455	−1.035
CsCl–H_2O	−1.392	7.700	−1.068
CsI–H_2O	−2.057	11.253	−1.541
$NaIO_3$–H_2O	−7.690	42.658	−5.951
KIO_3–H_2O	−6.071	33.617	−4.677
$CsIO_3$–H_2O	−17.066	98.489	−14.403
$KClO_4$–H_2O	−6.344	35.707	−5.125
HCl–H_2O	4.939	−30.956	4.825

TABLE 5. Coefficients for eq. [30] for the partial molar volumes, $\bar{V}^0_2(T)$, at 0.6 MPa

System	$A^V_v \times 10^{-4}$ / cm^3 K mol^{-1}	$B^V_v \times 10^{-2}$ / cm^3 mol^{-1}	$C^V_v \times 10$ / cm^3 mol^{-1} K^{-1}
NaI–H_2O	−4.4628	2.9548	−3.718
CsF–H_2O	−3.3511	2.2740	−3.184
CsCl–H_2O	−2.8035	2.0855	−2.525
CsI–H_2O	−2.8844	2.1904	−2.179
$NaIO_3$–H_2O	−4.7505	2.8997	−3.532
KIO_3–H_2O	−5.2419	3.2927	−3.982
$CsIO_3$–H_2O	−4.0960	2.6899	−2.852
$KClO_4$–H_2O	−3.6628	2.4669	−2.375
HCl–H_2O	−3.7806	2.6361	−3.992

temperature dependencies of $\bar{V}^0_2$ and $\beta^{(0)V}_{MX}$ were represented by the following three-term expressions:

$$[30]\quad \bar{V}^0_2(T) = A^V_v/T + B^V_v + C^V_v T$$

$$[31]\quad \beta^{(0)V}_{MX}(T) = A^V_\beta/T + B^V_\beta + C^V_\beta T$$

The resulting values of the parameters for each system are given in Table 5 for $\bar{V}^0_2$ and in Table 6 for $\beta^{(0)V}_{MX}$. For the four cesium salts, the C^V_β term was not needed, while for $NaIO_3$ and $KClO_4$ only one term was required for $\beta^{(0)V}_{MX}$. The standard deviations of fit for the apparent molar volume range from 0.06 to 0.38 cm^3 mol^{-1}. The highest value, 0.38, is for CsF. In this case there is a systematic deviation at all temperatures between the measurements for 0.658 and those for 1.06 mol kg^{-1}. The inclusion of the third virial coefficient term in C^V_{MX} would substantially reduce this deviation, but we are reluctant to introduce this term for data extending only to 1.06 mol kg^{-1} and for just the one salt. For most of the other salts, the standard deviation is 0.2 cm^3 mol^{-1} or less.

Pressure dependence of thermodynamic properties

From the volumetric results one has a measure of the pressure dependency of various thermodynamic properties through the relationships:

$$[32]\quad (\partial G/\partial P)_T = V$$

$$[33]\quad (\partial H/\partial P)_T = V - T(\partial V/\partial T)_P$$

$$[34]\quad (\partial C_p/\partial P)_T = -T(\partial^2 V/\partial T^2)_P$$

$$[35]\quad (\partial \beta^{(0)V}_{MX}/\partial P)_T = (\partial^2 \beta^{(0)V}_{MX}/\partial T^2)_P + (2/T)(\partial \beta^{(0)V}_{MX}/\partial T)_P = 2C^V_\beta/T$$

TABLE 6. Coefficients for eq. [31] for the interaction parameter $\beta_{MX}^{(0)V}(T)$ at 0.6 MPa

System	$A_\beta^V \times 10$ kg K mol^{-1} MPa^{-1}	$B_\beta^V \times 10^4$ kg mol^{-1} MPa^{-1}	$C_\beta^V \times 10^5$ kg mol^{-1} MPa^{-1} K^{-1}
NaI–H_2O	27.291	−164.98	2.4788
CsF–H_2O	2.526	−5.603	—
CsCl–H_2O	1.068	−2.231	—
CsI–H_2O	2.562	−7.550	—
$NaIO_3$–H_2O	1.733	—	—
KIO_3–H_2O	28.698	−143.43	1.8012
$CsIO_3$–H_2O	7.977	—	—
$KClO_4$–H_2O	—	6.034	—
HCl–H_2O	192.58	−1284.2	21.401

TABLE 7. Typical pressure coefficients of $\bar{C}_{p,2}^0$ at 298.15 K

System	$\partial\bar{C}_{p,2}^0/\partial P$ J K^{-1} mol^{-1} MPa^{-1}
NaI–H_2O	1.00
CsF–H_2O	0.75
CsCl–H_2O	0.63
CsI–H_2O	0.65
$NaIO_3$–H_2O	1.07
KIO_3–H_2O	1.18
$CsIO_3$–H_2O	0.92
$KClO_4$–H_2O	0.82
HCl–H_2O	0.85

Equation [34] may be used to obtain the effect of pressure on the standard-state heat capacity at infinite dilution $\partial\bar{C}_{p,2}^0/\partial P$. The results, which are given in Table 7, are subject to considerable uncertainty since they arise from the second temperature derivative of $\bar{V}_2^0$ as expressed by eq. [30]. It is clear that pressures of several MPa (or several tens of bar) will have a significant effect on heat capacity, but that a few tenths of MPa will have only a very small effect. At very high pressures, the pressure coefficient will decrease significantly and the present treatment is no longer adequate.

Enthalpy and Gibbs energy

The enthalpy is obtained by integration of the heat capacity, eq. [1]. In terms of the ion-interaction parameters, one has

$$[36]\quad T^2\beta_{MX}^{(0)L}(T) = \int_{298}^{T} (T')^2\beta_{MX}^{(0)L}dT' + 298^2\beta_{MX}^{(0)L}(298)$$

where the last term is the value of the enthalpy parameter at 298.15 K. The pressure dependency may also be introduced by the relationship

$$[37]\quad \beta_{MX}^{(0)L}(P) = \int_{P_0}^{P} (\partial\beta_{MX}^{(0)V}/\partial T)_P dP' + \beta_{MX}^{(0)L}(P_0)$$

where P_0 is the pressure at which $\beta_{MX}^{(0)L}$ is known. Similar equations apply for $\beta_{MX}^{(1)L}$ and C_{MX}^L, but we have found those terms unnecessary for the heat capacity or the volume. If we substitute eqs. [29] and [31] and integrate, we obtain

$$[38]\quad \beta_{MX}^{(0)L} = [(T^2 - 298^2)A_\beta^C/2 + (T^3 - 298^3)B_\beta^C/3 + (T^4 - 298^4)C_\beta^C/4 + 298^2\beta_{MX}^{(0)L}(298, P_0) - A_\beta^V(P - P_0)]/T^2 + C_\beta^V(P - P_0)$$

A second integration yields the excess Gibbs energy as given in eq. [3]. Again, for the ion-interaction parameter, this yields

$$[39]\quad \beta_{MX}^{(0)}(T) = \int_{298}^{T} \beta_{MX}^{(0)L}dT' + \beta_{MX}^{(0)}(298)$$

and for the particular temperature dependency of eqs. [29] and [38]

$$[40]\quad \beta_{MX}^{(0)} = A_\beta^C(T/2 + 298^2/2T - 298) + B_\beta^C(T^2/6 + 298^3/3T - 298^2/2) + C_\beta^C(T^3/12 + 298^4/4T - 298^3/3) + [A_\beta^V/T + B_\beta^V + C_\beta^V T](P - P_0) + (298 - 298^2/T)\beta_{MX}^{(0)L}(298, P_0) + \beta_{MX}^{(0)}(298, P_0)$$

Strictly, the pressure for the heat capacity equation should be the same as that for the integration constants $\beta_{MX}^{(0)L}(298, P_0)$ and $\beta_{MX}^{(0)}(298, P_0)$. The effect of pressure differences of a fraction of one MPa, however, will be negligible. Hence, values for one bar or another low pressure can be used without significant error. Again, for $\beta_{MX}^{(1)}$ and C_{MX}, only the last two terms remain, i.e., $\beta_{MX}^{(1)}(298)$ and $(298 - 298^2/T)\,\beta_{MX}^{(1)L}(298)$, and similarly for C_{MX}.

The integrations of $\bar{C}_{p,2}^0$ to yield the enthalpy and Gibbs energy as a function of temperature and pressure for the salt in its standard state are similar and yield

$$[41]\quad \bar{H}_2^0(T, P) = A_c^C \ln(T/298) + B_c^C(T - 298) + (C_c^C/2)(T^2 - 298^2) + (P - P_0)[-A_v^V/T^2 + C_v^V] + \bar{H}_2^0(298, P_0)$$

$$[42]\quad \bar{G}_2^0(T, P)/T = A_c^C\left[\frac{\ln T}{T} + \frac{1}{T} - \frac{1}{298} - \frac{\ln 298}{T}\right] + B_c^C\left[1 - \frac{298}{T} - \ln\left(\frac{T}{298}\right)\right] + \frac{C_c^C}{2}\left[596 - T - \frac{298^2}{T}\right] + (P - P_0)\left[\frac{A_v^V}{T^2} + \frac{B_v^V}{T} + C_v^V\right] + \bar{H}_2^0(298, P_0)\left[\frac{1}{T} - \frac{1}{298}\right] + \bar{G}_2^0(298, P_0)/298$$

TABLE 8. Values for the ion-interaction parameters and their temperature derivatives at 298.15 K

System	$\beta^{(0)}_{MX}$	$\beta^{(1)}_{MX}$	$10^3 C_{MX}$	$10^4\beta^{(0)L}_{MX}$	$10^4\beta^{(1)L}_{MX}$	$10^5 C^L_{MX}$
NaI–H_2O	0.1195[a]	0.3439[a]	0.9_0[b]	9.16_3[c]	9.96_4[c]	-5.5_8[d]
CsF–H_2O	0.1306	0.2570	-2.1_5	0.95	5.9_7	—
CsCl–H_2O	0.0300	0.0558	0.1_9	7.03_0	21.0_7	-4.0_6
CsI–H_2O	0.0244	0.0262	-1.8_2	9.75	34.7_7	—
$NaIO_3$–H_2O	—	—	—	11.7_9	59.3_8	—
KIO_3–H_2O	—	—	—	27.1_0	45.3_6	—
$KClO_4$–H_2O	—	—	—	4.9_8	95.1_9	—
HCl–H_2O	0.1775	0.2945	0.4_0	-3.08_1	1.41_9	3.10_6

[a]In kg mol^{-1}.
[b]In kg^2 mol^{-2}, note that $C^{\phi}_{MX} = 2C_{MX}$.
[c]In kg mol^{-1} K^{-1}.
[d]In kg^2 mol^{-2} K^{-1}.

TABLE 9. Standard state volumes and heat capacities at 298.15 K

	$\tilde{V}^0_2$/cm^3 mol^{-1}		$\tilde{C}^0_{p,2}$/J K^{-1} mol^{-1}	
Salt	This research (0.6 MPa)	Literature[a] (0.1 MPa)	This research (0.6 MPa)	Literature[b] (0.1 MPa)
NaI	34.9_6	35.0_1	−77	-78.5
CsF	20.0_7	20.1_8	−140	−140
CsCl	39.2_4	39.1_7	−149	−150
CsI	57.3_3	57.5_6	−145	-144.5
$NaIO_3$	25.3_3	24.8	−32	−31
KIO_3	34.7_4	35.0	−59	−61
$CsIO_3$	46.5_8	47.3_4	−101	−97
$KClO_4$	53.0_3	53.2	−15	−12
HCl	17.7_9	18.1	−125	−126

[a]From refs. 31 and 32.
[b]From refs. 30 and 32.

where again the P_0 of the integration constants and that of the heat capacity and volume measurements should be the same. But again the effects of small differences will be negligible.

Table 8 gives the enthalpy and Gibbs energy parameters at 298 K, which are needed as integration constants in eqs. [36] and [38]. All values for $\beta^{(0)}_{MX}$, $\beta^{(1)}_{MX}$, and C_{MX} were obtained from Pitzer and Mayorga (24). The enthalpy parameters for CsF, CsI, and HCl were taken from Silvester and Pitzer (25) while the remaining enthalpy parameters were obtained in the present work – NaI, CsCl, and $NaIO_3$ from the NBS tables (26); $KClO_4$ from the NBS report (27); and KIO_3 from the recent work of Vanderzee *et al.* (28). Unfortunately, there appear to be no measurements from which the Gibbs-energy parameters can be calculated for $NaIO_3$, KIO_3, or $KClO_4$. For $CsIO_3$ neither type of parameter is available. Appropriate heat-of-dilution and activity or osmotic measurements should be made to provide this information.

Except for the cases with missing values for the integration constants, the tables of this paper provide comprehensive equations for the various thermodynamic properties over the temperature range 298–373 K and for pressure variation in the low-pressure range where such effects are linear.

Since this treatment gives the second temperature derivative up to 373 K, one expects the equations to extrapolate upward in temperature with considerable accuracy for the enthalpy and especially for the Gibbs energy. This accuracy of extrapolation was demonstrated for the activity coefficients of Na_2SO_4 by comparison with the solid solubility (29). Tremaine *et al.* (21) discuss this type of extrapolation for HCl.

Single ion and standard state properties

Since the standard state properties at infinite dilution must be additive for the ions present, it is convenient to assign the value zero to the H^+ ion and give relative values for the other ions. For $\tilde{C}^0_{p,2}$ and $\tilde{V}^0_2$ at 298 K, this has been done recently by Desnoyers *et al.* (30) and by Millero (31), respectively. Roux *et al.* (32) added values for several additional ions. Table 9 compares our results with the values calculated from these tables of individual ion values (30–32).

Since the literature values are for a pressure of 0.1 MPa whereas ours are for 0.6 MPa, exact agreement is not expected, but the difference from this source is very small. The agreement in Table 9 is excellent for the volumes and as good as reasonably expected for the heat capacities. Thus the published values of single ion properties at 298 K are confirmed by the present research.

At higher temperatures, our results can be compared with those of Holmes and Mesmer (8) for CsCl and those of Tremaine *et al.* (21) for HCl. For CsCl, Holmes and Mesmer (8) carried out a comprehensive treatment of various types of thermodynamic data, including the high-temperature heat capacity measurements of Rüterjans *et al.* (17). Their values of $\tilde{C}^0_{p,2}$ at 298 and 373 K are −145 and −114 J K^{-1} mol^{-1}, respectively, compared to our values of −149 and −113. Thus, the agreement is essentially perfect at 373 K and quite good at 298 K where one also has the value −150 from Desnoyers *et al.* (30). For HCl, Tremaine *et al.* (21) report -118.7 ± 3.3 from a series of measurements at 349.43 K and −114.5 J K^{-1} mol^{-1} from their general equation fitted over their range of temperature. The

TABLE 10. Calculated maxima in volume and heat capacity

	Volume		Heat capacity	
	T_{max}	$\tilde{V}^0_{2,max}$	T_{max}	$\tilde{C}^0_{2p,2,max}$
System	K	$cm^3\ mol^{-1}$	K	$J\ K^{-1}\ mol^{-1}$
$NaI-H_2O$	346	37.9	340	−45
$CsF-H_2O$	324	20.8	348	−95
$CsCl-H_2O$	333	40.3	349	−105
$CsI-H_2O$	364	60.5	352	−91
$NaIO_3-H_2O$	367	30.9	352	48
KIO_3-H_2O	363	40.3	352	21
$CsIO_3-H_2O$	(379)	(52.8)	357	3
$KClO_4-H_2O$	(393)	(60.2)	341	20
$HCl-H_2O$	308	17.9	334	−114

value from our equation at that temperature is $-116.3\ J\ K^{-1}\ mol^{-1}$, in excellent agreement. Even at 412.61 K our extrapolated value of −154 agrees reasonably well with Tremaine's results of -149.2 ± 0.8 and $-150.4\ J\ K^{-1}\ mol^{-1}$.

Discussion

While the primary value of these results will lie in their use in various applications, it is of interest to consider briefly the pattern of behavior displayed. The three curves on Fig. 1 for $\tilde{C}^0_{p,2}$ for the cesium halides are typical of all of the systems studied in that they show maxima near 353 K. Indeed, the standard state volumes $\tilde{V}^0_2$ also show similar curves with maxima. Clearly, this similarity of behavior must arise from the properties of ions in water without regard to the details of the ionic structure. It is the effect of the ionic charge on the water structure that yields this similarity.

Table 10 lists the temperatures for these maxima and the maximum values of $\tilde{C}^0_{p,2}$ and $\tilde{V}^0_2$ for each of the solutes measured. The temperatures for the maxima for HCl are somewhat lower than those for the various salts where there appears to be a slight upward trend with ion size. But there is considerable uncertainty in these temperatures and the differences are rather small, hence one should be cautious in more detailed interpretation. The relative values of the volumes and heat capacities at their maxima follow essentially the same pattern as that for values at 298 K. The 298 K values have been available for some time, although we are not aware of any very detailed theory that yields good agreement. The Born theory for an ion in a dielectric gives the sign and magnitude of the effects correctly. While the aqueous standard-state volumes generally increase with the intrinsic ion size, the behavior of the heat capacities is more compex. The large decrease of about $45\ J\ K^{-1}\ mol^{-1}$ from Na^+ to Cs^+ is striking as is the large negative value for any halide. The complex anions have internal heat capacity which probably accounts for the positive values for salts containing these ions. More detailed discussion of these aspects is beyond the scope of this paper.

Acknowledgements

We thank Dr. Peter Tremaine for providing a copy of his paper on HCl in advance of publication and Drs. A. C. Vikis, N. H. Sagert, P. Taylor, and F. Garisto for their comments on this paper. The work at Berkeley was supported by the Director, Office of Energy Research, Office of Basic Energy Sciences, Division of Engineering, Mathematics, and Geosciences of the U.S. Department of Energy under Contract No. DE-AC03-76SF00098.

1. K. S. PITZER and J. J. KIM. J. Am. Chem. Soc. **96**, 5701 (1974).
2. K. S. PITZER. Theory: ion interaction approach. *In* Activity coefficients in electrolyte solutions. Vol. 1. *Edited by* R. M. Pytkowicz. CRC Press, Boca Raton, FL. 1979. pp. 157–208.
3. C. E. HARVIE and J. H. WEARE. Geochim. Cosmochim. Acta, **44**, 981 (1980).
4. C. E. HARVIE, N. MOLLER, and J. H. WEARE. Geochim. Cosmochim. Acta, **48**, 723 (1984).
5. P. P. S. SALUJA. J. Nucl. Mater. **130**, 329 (1985).
6. P. S. Z. ROGERS and K. S. PITZER. J. Phys. Chem. Ref. Data, **11**, 15 (1982).
7. K. S. PITZER, J. C. PEIPER, and R. H. BUSEY. J. Phys. Chem. Ref. Data, **13**, 1 (1984).
8. H. F. HOLMES and R. E. MESMER. J. Phys. Chem. **87**, 1242 (1983).
9. P. S. Z. ROGERS and K. S. PITZER. J. Phys. Chem. **85**, 2886 (1981); **86**, 2110 (1982).
10. H. F. HOLMES, C. F. BAES, and R. E. MESMER. J. Chem. Thermodyn. **10**, 983 (1978).
11. K. S. PITZER. J. Phys. Chem. **77**, 268 (1973).
12. D. SMITH-MAGOWAN and R. H. WOOD. J. Chem. Thermodyn. **13**, 1047 (1981).
13. D. E. WHITE and R. H. WOOD. J. Solution Chem. **11**, 223 (1982).
14. P. P. S. SALUJA, J. C. LEBLANC, and H. B. HUME. Can. J. Chem. **64**, 926 (1986).
15. J.-L. FORTIER, P.-A. LEDUC, and J. E. DESNOYERS. J. Solution Chem. **3**, 323 (1974); **5**, 605 (1976).
16. G. C. ALLRED and E. M. WOOLLEY. J. Chem. Thermodyn. **13**, 147 (1981).
17. H. RÜTERJANS, F. SCHREINER, U. SAGE, AND TH. ACKERMANN. J. Phys. Chem. **73**, 986 (1969).
18. TH. ACKERMANN. Z. Elektrochem. **62**, 411 (1958).
19. R. E. MITCHELL and J. W. COBBLE. J. Am. Chem. Soc. **86**, 5401 (1964).
20. P. P. SINGH, E. M. WOOLLEY, K. G. MCCURDY, and L. G. HEPLER. Can. J. Chem. **54**, 3315 (1976).
21. P. R. TREMAINE, K. SWAY, and J. A. BARBERO. J. Solution Chem. **15**, 1 (1986).
22. D. J. BRADLEY and K. S. PITZER. J. Phys. Chem. **83**, 1599 (1979); **87**, 3798 (1983).
23. L. HAAR, J. S. GALLAGHER, and G. S. KELL. NBS/NRC Steam Tables, Appendix A. Hemisphere Pub. Co. Washington 1984.
24. K. S. PITZER and G. MAYORGA. J. Phys. Chem. **77**, 2300 (1973).
25. L. F. SILVESTER and K. S. PITZER. J. Solution Chem. **7**, 327 (1978).
26. D. D. WAGMAN, W. H. EVANS, V. B. PARKER, R. H. SCHUMM, I.

HALOW, S. M. BAILEY, K. L. CHURNEY, and R. L. NUTTAL. J. Phys. Chem. Ref. Data, **11**, supplement No. 2 (1982).
27. V. B. PARKER. Thermal properties of aqueous uni-univalent electrolytes. Nat. Stand. Ref. Data Ser. Nat. Bur. Stand. Washington. 1965.
28. C. E. VANDERZEE, D. H. WAUGH, N. C. HAAS, and D. D. CLYDE. J. Chem. Thermodyn. **12**, 737 (1980).
29. K. S. PITZER and JOHN S. MURDZEK. J. Solution Chem. **11**, 409 (1982).
30. J. E. DESNOYERS, C. DE VISSER, G. PERRON, and P. PICKER. J. Solution Chem. **5**, 605 (1976).
31. F. J. MILLERO. *In Water and aqueous solutions. Edited by* R. A. Horne. Wiley-Interscience, New York, NY. 1972. Chapt. 13.
32. A. ROUX, G. M. MUSBALLY, G. PERRON, J. E. DESNOYERS, P. P. SINGH, E. M. WOOLLEY, and L. G. HEPLER. Can. J. Chem. **56**, 24 (1978).
33. R. C. PHUTELA and K. S. PITZER. J. Phys. Chem. **90**, 895 (1986).

Sulphite-promoted delignification of wood: identification of paucidisperse lignosulphonates

ALEC M. BIALSKI AND CORINNE E. LUTHE
Temfibre Inc., Temiscaming, P.Q., Canada J0Z 3R0
AND
JENNY L. FONG AND NORMAN G. LEWIS[1]
Pulp and Paper Research Institute of Canada, 3420 University Street, Montreal, P.Q., Canada H3A 2A7
Received November 4, 1985

ALEC M. BIALSKI, CORINNE E. LUTHE, JENNY L. FONG, and NORMAN G. LEWIS. Can. J. Chem. **64**, 1336 (1986).

Paucidisperse lignosulphonates, previously described as a distinct group of compounds called "hemilignins" ($\bar{M}_w \sim 2\,000$), were conclusively shown to be a complex mixture of monomeric (C_9) sulphonic acids. Since these compounds are rapidly solubilized only during the early stages of delignification from softwoods (≤30% lignin removal), it can be concluded that they are selectively removed from the secondary wall and not from the middle lamella. This result gives chemical support to the hypothesis that morphological differences in lignin structure exist. It is proposed that the generation of monolignols and their sulphonated derivatives may occur via an α-O-aryl bond cleavage rather than β-O-aryl cleavage as previously suggested. For softwoods, several other major constituents were isolated, which may be derived from sulphonation of a β-hydroxylated form of coniferyl alcohol.

ALEC M. BIALSKI, CORINNE E. LUTHE, JENNY L. FONG et NORMAN G. LEWIS. Can. J. Chem. **64**, 1336 (1986).

Les lignosulfonates, mélange de macromolécules monodispersées, ont été préalablement décrit. Ils sont formés de groupes de composés séparables appelés "hémilignines" ($\bar{M}_w \sim 2\,000$); on démontre sans ambiguïté qu'il s'agit d'un mélange complexe d'unités (C_9) d'acides sulphoniques monomères. Puisque ces composés ne se solubilisent rapidement que lors des premières étapes de la delignification du conifère (au plus 30% de la lignine est eliminée), on en conclut qu'ils sont selectivement éliminés de la paroi secondaire et non de la lamelle centrale. Ce résultat fournit un support chimique à l'hypothèse selon laquelle des différences morphologiques existent au sein de la structure de la lignine. Le méchanisme suivant a été proposé: la génération des monolignols et de leur derivés sulfonés serait préférentielle lors de la coupure de la liaison α-O-aryl et non lors de la coupure de la liaison β-O-aryl comme ce fut préalablement suggéré. Chez les conifères, plusieurs autres constituents ont été isolés, ce qui pourrait provenir de la sulfonation de l'alcool conifèrylique hydroxylé en β.

Introduction

The structure and biosynthesis of the terrestrial plant polymer, lignin, is not well understood because of its molecular complexity and intractable nature. The most widely held view of lignin, as it exists in nature, is that of a random, three-dimensional, infinite polymeric network (1–7) derived from the three basic monomeric building blocks, *p*-coumaryl alcohol **1**, coniferyl alcohol **2**, and sinapyl alcohol **3**.

This concept has been directly challenged by the reported finding that sulphonated lignin from softwoods is composed (~80%) mainly of an homologous series of lignin sulphonates having *identical* repeating units, with the remainder (~20%) being described as a distinct group of compounds, called "hemilignins," of weight-average molecular weight $\bar{M}_w \sim 2\,000$ (8).

Clearly, these two postulates, i.e., random versus regular structure, are incompatible.

In our recent studies (9), we reported that during the sulphite-promoted delignification of the softwood, black spruce (*Picea mariana*), two broad classes of sulphonated lignins appeared to be formed: Type I (paucidisperse) and Type II (widely polydisperse). Lignin heterogeneity has also been reported for the acidolysis products from poplar (*Populus euramericana*) obtained under lengthy isolation conditions (10).

We now wish to extend our observations regarding Type I lignosulphonates and "hemilignins" in terms of their chemical structures, point of formation, and anatomical origin.

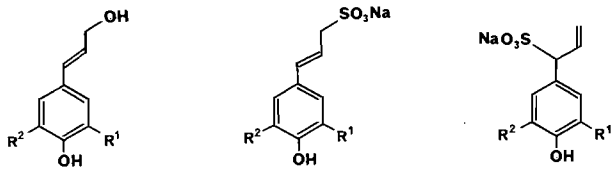

1, $R^1, R^2 = H$ **4**, $R^1, R^2 = H$ **7**, $R^1, R^2 = H$
2, $R^1 = OCH_3, R^2 = H$ **5**, $R^1 = OCH_3, R^2 = H$ **8**, $R^1 = OCH_3, R^2 = H$
3, $R^1, R^2 = OCH_3$ **6**, $R^1, R^2 = OCH_3$ **9**, $R^1, R^2 = OCH_3$

Results

The hplc (high performance liquid chromatographic) separation of paucidisperse lignin sulphonates for both the softwood, black spruce (*Picea mariana*), and the hardwood, poplar (*Populus tremuloides*), can be seen in Figs. 1A and 1B. These samples were produced by mild sulphonation of each species under conditions which effect ~30% and 45% delignification, respectively. Following isolation by chromatography, it was established that H, I, and J (see Fig. 1A) from black spruce corresponded to the sulphonates **8**, **4**, and **5**, respectively. The structural elements of these monomers contribute to about 4–5% of the total lignin in wood. Structural confirmation of **5** and **8** was achieved by total synthesis from eugenol **10** (Scheme 1), via a combination and modification of previously reported routes (11, 12). For the hardwood lignin sulphonates, compo-

[1]Author to whom correspondence should be addressed. New address: Department of Forest Products, Virginia Polytechnic Institute and State University, Blacksburg, VA 24061, U.S.A.

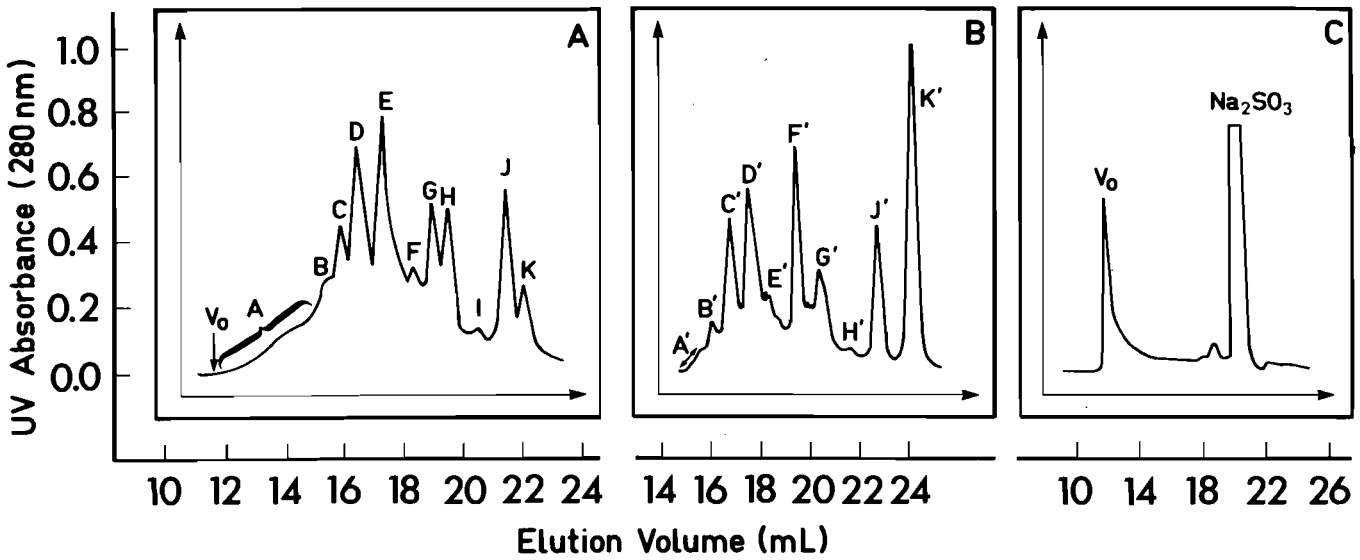

FIG. 1. Chromatograms of dissolved uv-absorbing paucidisperse lignosulphonates from (A) black spruce (*Picea mariana*) and (B) poplar (*Populus tremuloides*). Fig. 1C is an hplc trace of spruce polydisperse lignosulphonates produced during continuous flow experiments (see experimental section). Elution details: Waters I-125 and I-60 protein columns in series eluted with 50 m*M* citric acid/Na_2HPO_4 buffer, pH 3.0. Flow = 1 mL/min, V_0 = void volume. (Note: retention times in Fig. 1B are slightly longer due to the use of a guard column.)

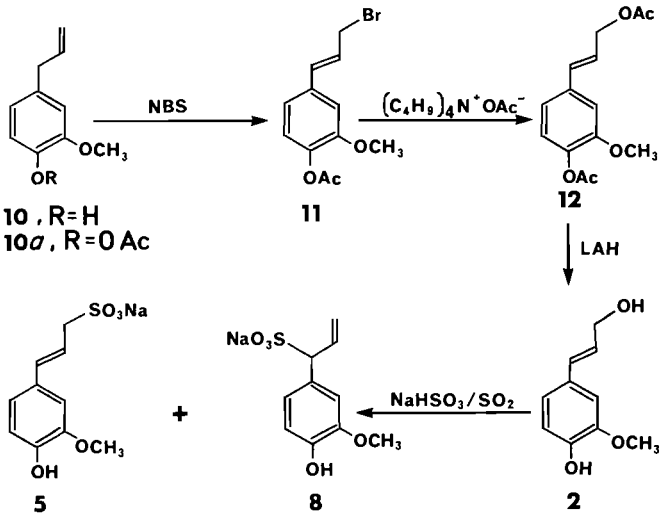

SCHEME 1. Synthesis of sulphonates **5** and **8** from eugenol **10**.

nents G′, H′, and J′ (Fig. 1B) were also shown to be the sulphonates **8**, **4**, and **5**. In addition, the corresponding sinapate sulphonates **6** and **9** were also isolated (same peak *K*′) reflecting the known differences in hardwood lignin composition (13). Structural proof was achieved by comparison with synthetic material produced from *E*-sinapic acid **13** (Scheme 2).

It was of interest to establish whether these monomers were produced continuously or only at specific stages of delignification. To resolve this particular point, black spruce wood was delignified at pH 3.0 in a "continuous-flow" reactor (14) scaled down for micropulping experiments (15). In this experiment, any soluble sulphonated lignin is removed almost immediately, thus reducing the possibility of further degradation/condensation reactions. These soluble materials were then collected at various time intervals and analysed following separation on high performance liquid chromatographic columns (9), previously calibrated with lignosulphonates of known $\bar{M}_w$ (16). Using this approach, it could be concluded that essentially only Type I (paucidisperse) lignin sulphonates, with a $\bar{M}_w \leq 3\,300$, were solubilized during the early stages of delignification (<30–40% lignin removal) (cf. Fig. 1A). Beyond this point only widely polydisperse (Type II) lignin sulphonates ($\bar{M}_w > 3\,300$) of increasing $\bar{M}_w$ (Fig. 1C) were removed, i.e., the monomeric moieties **4**, **5**, and **8** were produced just during the release of the paucidisperse lignin sulphonates. Similar findings were also noted at pH 2, 5, and 7, the only observable difference being the rate at which delignification took place. These findings were also true for hardwoods, i.e., monomers were removed only during the initial stages of delignification.

One severe drawback to the handling of paucidisperse lignosulphonates is that all manipulations are performed in aqueous media. We have therefore developed methodology for their derivatization into organic soluble compounds. To date, the most frequently used method was to prepare the corresponding acetyl lignin sulphonic acid methyl esters (17). However, we found this procedure to be cumbersome and consequently developed alternate strategies. Sulphonic acids were thus converted specifically to their methyl or ethyl esters using methyl or ethyl orthoformate, respectively (18), or treated with ethereal diazomethane, thereby alkylating both phenolic and sulphonic acid moieties directly. Surprisingly, diazomethane has been reported to only incompletely methylate lignosulphonates (19). However, no such difficulties were experienced in this study.

Prior to methylation, paucidisperse lignosulphonates from either softwoods (Fig. 1A) or hardwoods (Fig. 1B) were *exhaustively* extracted with *n*-butanol to remove the monomeric sulphonic acids (12, 20). These monomers were converted to their free acid (H) form using Amberlite IR-120 (H) resin and then methylated with ethereal diazomethane. Figure 2A and 2B show the hplc profile of these methylated monomers from both softwoods and hardwoods, respectively. Monomers **16**–**22** were then each isolated following separation on a semi-preparative hplc column and their structures determined using

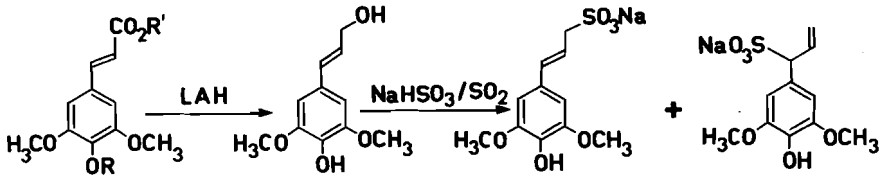

13, R=R'=H
14, R=OAc, R'=H
15, R=OAc, R'=CH_2CH_3

3 **6** **9**

SCHEME 2. Synthesis of sulphonates **6** and **9** from sinapic acid **13**.

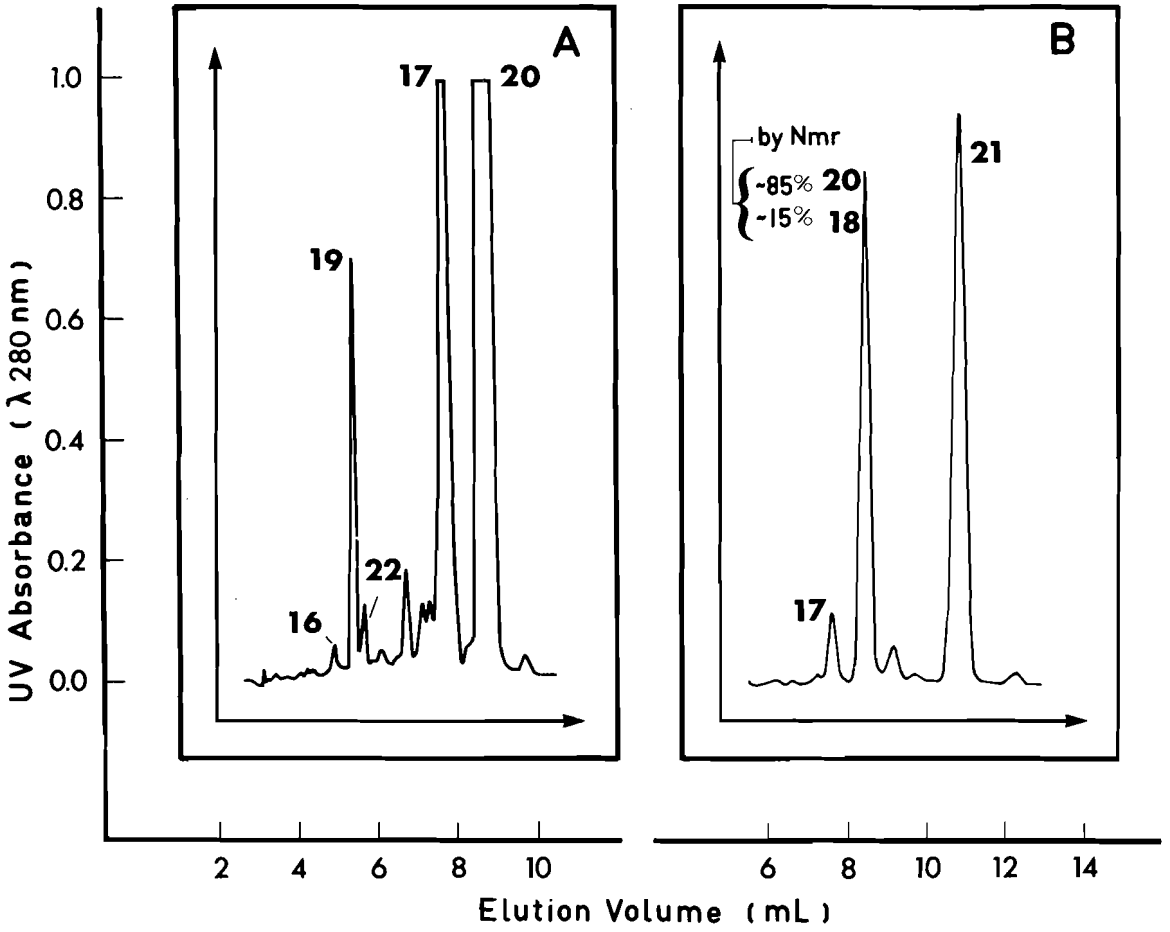

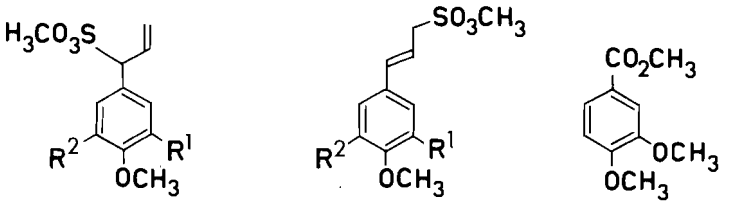

16, R^1,R^2 = H
17, R^1=OCH_3, R^2=H
18, R^1,R^2=OCH_3

19, R^1,R^2=H
20, R^1=OCH_3, R^2=H
21, R^1,R^2=OCH_3

22

FIG. 2. Chromatograms of fully methylated butanol soluble lignosulphonates of SSL from a softwood (A) and hardwood (B) bisulphite cook, using a Waters μ-Porasil column with 59% hexanes/41%CH_2Cl_2:MeOH (99.1:0.9) as eluant, and the flow set at 1 mL/min.

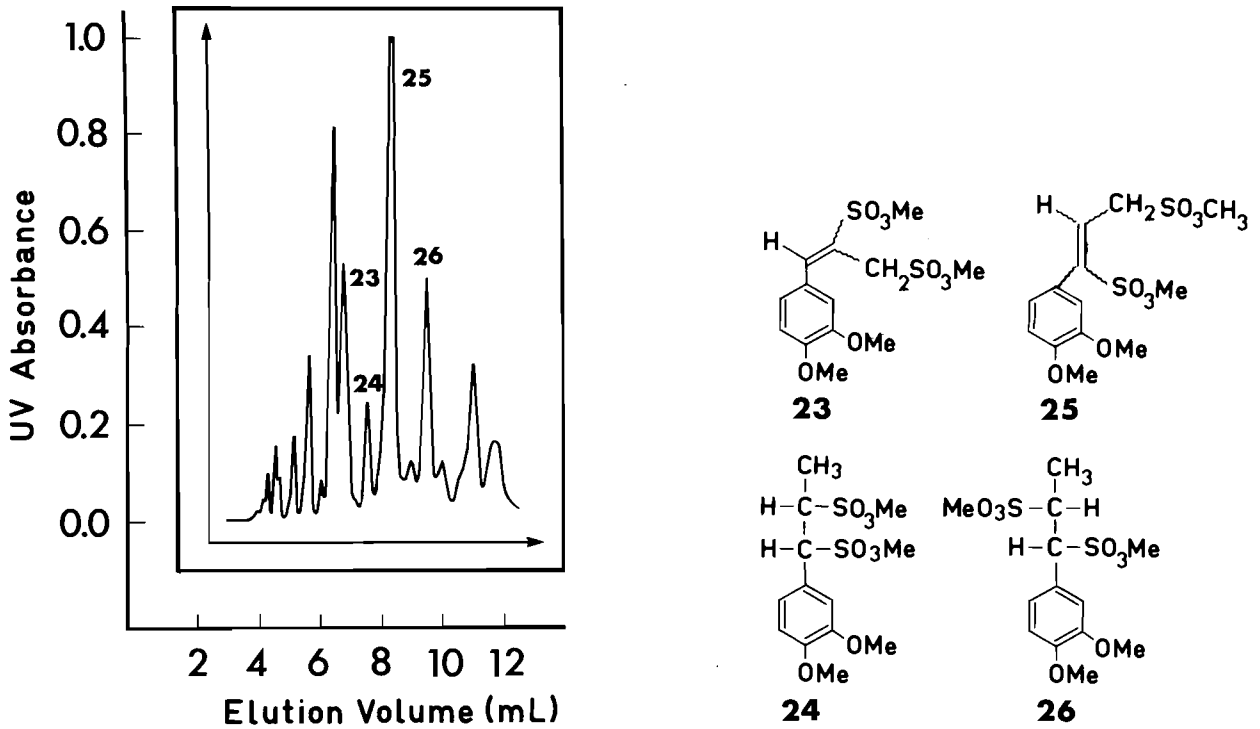

FIG. 3. Chromatogram of methylated uv-absorbing paucidisperse lignosulphonates from a softwood bisulphite cook, using a Waters μ-Porasil column with 5% hexanes/95%CH_2Cl_2:MeOH (99.75:0.25) as eluant, and the flow set at 1 mL/min.

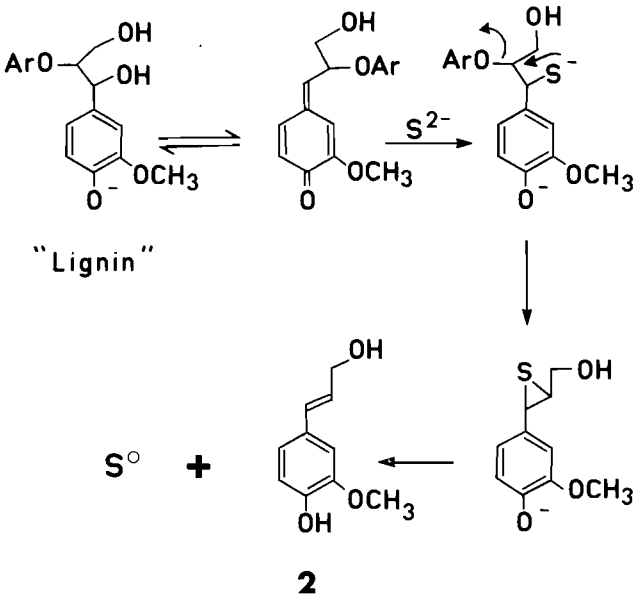

SCHEME 3. Gierer's mechanism for the formation of coniferyl alcohol **2** formed during alkaline (kraft) pulping.

standard spectroscopic techniques (see Experimental). In particular, ^{13}C DEPT analysis (21) of these monomers was most useful.[2] The unambiguous assignment of near or overlapping carbon signals containing different numbers of hydrogen atoms (e.g., CH_2SO_3H vs. OCH_3, etc.) is exactly the type of precise information required for assigning signals in the more complex polydisperse lignosulphonates.

[2]Preliminary findings using DEPT ^{13}C nmr for the analysis of sulphonated lignins were presented at the ACS Chemistry Meeting, Philadelphia, September 1984 (ref. 21*b*).

The remaining paucidisperse lignosulphonates from the spent softwood pulping liquors were further purified by a complexation/decomplexation procedure using dicyclohexylamine as previously described (9). We then converted these substances to their fully methylated derivatives and separated them by hplc (as before). The major components in these mixtures have now been isolated (see Fig. 3) and their structures determined by spectroscopic techniques (see Experimental). It is important to note that all of the substances identified to date in this category are disulphonic acids of lignin-derived monomers (i.e., **23–26**). The other remaining uncharacterized substances are also monomeric in character, having molecular weights <450. Additional work is in progress to establish their structures.

Discussion

It is well known that the monomers (**5**, **6**, **8**, and **9**) are produced in minute quantities during the extensive delignification (~95%) of wood, carried out under strongly acidic sulphonation conditions (12, 20, 22).

There appears to be a striking correlation between their formation and the presence of minute quantities of the monolignols **2** and **3** in soluble lignin fractions obtained by treatment of wood at elevated temperatures with either THF/H_2O (23–25), dioxane/H_2O (24), or sodium sulphide/H_2O solutions (kraft) (26–30). With the exception of kraft lignin, which is removed under strongly alkaline treatment, these preparations are all produced under mildly acidic conditions. A feature common to all, however, is the fact that these monolignols are liberated during the early stages of delignification. This suggests that their genesis might be the consequence of a common bond-breaking process. For kraft lignin, coniferyl alcohol **2** is considered to be formed only via β-O-aryl cleavage as shown in Scheme 3 (31, 32). However, since such cleavages are less likely under sulphonation conditions (32), it seems more

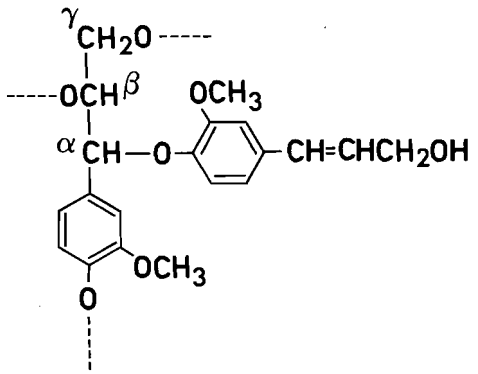

FIG. 4. Possible bonding pattern of coniferyl alcohol **2** to the lignin macromolecule.

reasonable that, during the early stages of delignification, the formation of these monolignols is, instead, a consequence of α-O-aryl bond cleavage (Fig. 4). This interpretation would unify the various experimental observations, and would be consistent with the known lability of α-O-aryl bonds.

It was also interesting to note that the monolignols **1–3** were essentially absent from the side-chain oxygenated monomeric products produced following lengthy acidolysis of poplar (10). This can simply be attributed to the instability of compounds **1–3** under these conditions.

It is now also clear that Forss' "hemilignins" ($\bar{M}_w \sim 2\,000$) are in fact monomeric sulphonic acids of the type **22–26**. The high $\bar{M}_w$ values previously reported for these hemilignins (8, 16) may be due to a limitation of the ultracentrifugation technique used, and (or) simply nonideal chromatographic behaviour of these substances.

From a wood anatomical viewpoint, it is well documented that earlywood tracheids from black spruce contain 72% of the *total lignin* in the secondary wall versus 28% in the compound middle lamella (33). (It should be noted, though, that the *concentration of lignin* is much higher in the middle lamella (~50–85%) than in the secondary wall (22%).)

Of importance, however, was the observation that the rates of acid-sulphite promoted delignification of the secondary wall and middle lamella were different (34); e.g., by 30% total delignification of spruce wood, the total lignin content of the secondary wall was reduced from 72 to 45% whereas the middle lamella was almost the same (from 28 to 25.5%). This clearly suggests that softwood paucidisperse lignosulphonates, including the monomers, are removed from the secondary wall. A similar proposal has been made by Forss for hemilignins ($\bar{M}_w \sim 2\,000$) (8). If this morphological observation is correct, then our results clearly show that secondary wall lignin contains more easily hydrolysable linkages. This further supports the contention that lignin in black spruce is heterogeneous (8, 9). Additional support for this hypothesis can also be found from the results obtained from the alkaline (kraft) pulping of black spruce wood tissue fractions *enriched* in either secondary wall or middle lamella material respectively (29). In that particular study, it was clearly demonstrated that, following correction for lignin contents, 14–16 times more coniferyl alcohol **2** was liberated from the secondary wall tissue than from the middle lamella.

These findings not only support the concept of heterogeneity but again appear to mitigate against coniferyl alcohol **2** formation being simply the consequence of β-O-aryl bond cleavage (31, 32). In addition, these results with isolated tissue fractions are also important in addressing discussions concerning diffusion through the cell wall. For example, it has been argued that the differences in the rate of delignification from the secondary wall and middle lamella may be due to differences in diffusion of the pulping chemicals into, or diffusion of the lignin degradation products out of, the wood cell (35). Such penetration problems are likely to be substantially reduced with isolated tissue fractions.

The steps involved in lignification beyond the monolignols, e.g., coniferyl alcohol **2**, are poorly understood (36). However, speculation as to the nature of the precursors that, after sulphonation, lead to the disulphonic acids **23–26** is important. This is because it may provide some insight into the biosynthetic conversions beyond **2**.

Hibbert originally suggested (37) that the first biosynthetic step beyond coniferyl alcohol **2** occurred via a free radical β-hydroxylation to give ketone **27** (Scheme 4). According to this hypothesis, the genesis of compound **23** could be envisaged via sulphonation, dehydration, and methylation. Hibbert's proposal was, however, subsequently modified (38, 39) to include results from the acidolysis of the lignin model compound, guaiacyl glycerol β-guaiacyl ether. In those experiments, it was demonstrated that phenyl glycerol type compounds could afford a series of keto and hydroxyketo compounds (38, 39). Presumably ketone **27** is formed as an acidolytic intermediate. Thus, by means of this modified route, the precursors of compounds **24–27** could be produced.

There are, however, additional experiments that do not appear to be in agreement with this latter hypothesis: (*i*) the acidolysis pathway is *not* considered to be important under the conditions of sulphonation (31, 32) and (*ii*) sulphite-promoted delignificaton of *borohydride*-reduced wood meal (40, 41) proceeds at a considerably slower rate, suggesting the involvement of ketonic functionalities during delignification.

It is therefore clear that these inconsistencies require further examination in order to fully understand the pathway of sulphite-promoted delignification.

In closing, it should also be mentioned that while the purported existence of an identical repeating unit in the high molecular weight (Type II) polydisperse material (8) is appealing, we have to date found no evidence supporting that statement. This hypothesis will be investigated more deeply.

Conclusions

We have investigated the sulphite-promoted delignification of the softwood, black spruce (*Picea mariana*), and the hardwood, poplar (*Populus tremuloides*), and have concluded that:

(*i*) Paucidisperse lignosulphonates (Type I), previously called "hemilignins," are only solubilized during the initial stages of delignification. These materials have been characterized and have been shown to be either monomeric or disulphonic acids of lignin monomers. No oligomeric material with M_w approaching 2 000 has been isolated.

(*ii*) A unified hypothesis for the hydrolytic removal of *p*-hydroxycinnamyl alcohols **1–3** during the initial stages of delignification can now be made. This uses simple α-O-C cleavage (Fig. 4) of the lignin macromolecule and removes the necessity to involve β-O-cleavages (Scheme 3), which are less likely under the conditions employed.

(*iii*) The acidolysis products from poplar (10) bear certain similarities to our findings in the sense that the substances removed are mainly monomeric. One major difference noted,

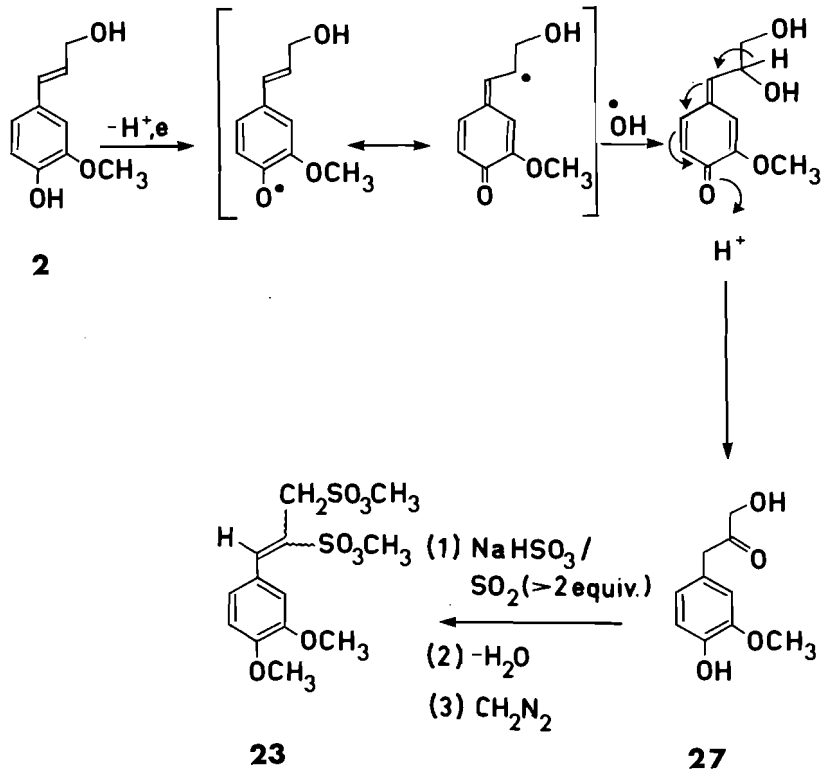

SCHEME 4. Postulated formation of disulphonic acids from coniferyl alcohol **2**.

however, was the essential absence of the *p*-hydroxycinnamyl alcohols **1**–**3**. These substances are significant delignification products and are stabilized in solution by sulphonation.

(*iv*) Based upon previous studies, it can be concluded that these soluble paucidisperse substances are removed exclusively from the secondary wall and not the middle lamella. It therefore follows that softwood lignin is chemically heterogeneous. This places a substantial constraint on the random, infinite polymeric network theories (1–7).

(*v*) To account for the formation of the disulphonic acids **23**–**26**, it appears that no hypothesis can be presented that is in agreement with all of the experimental observations accumulated to date.

Experimental

The hplc analyses and separations were carried out using a Hewlett–Packard or a Waters liquid chromatograph equipped with a variable wavelength detector set at 280 nm. Columns used were of the protein I-125 and I-60, as well as μ-Porasil types, purchased from Waters Associates. Nuclear magnetic resonance spectra were obtained on Varian XL-200 or XL-300 instruments. Carbon-13 assignments are tentative unless unambiguously determined using ^{13}C-DEPT techniques. Low and high resolution mass spectra were run on Hewlett–Packard 5984 and Dupont 21-492B instruments, respectively. Ultraviolet analyses were carried out using a Unicam SP-800 spectrophotometer. All solvents (and dicyclohexylamine) were distilled prior to use.

trans-*3-(4-Acetoxy-3-methoxyphenyl)-2-propenyl acetate (12)*

Bromide **11** was prepared from **10***a* exactly as described (11) in 65% yield and used without further purification. A solution of crude bromide **11** (57 g, 0.2 mol) and tetra-*n*-butylammonium acetate (72.2 g, 0.24 mol) (42) in chloroform (300 mL) was stirred at reflux temperature for 0.5 h. The chloroform was then removed under reduced pressure and the residual oil extracted (magnetic stirring) with diethyl ether (3 × 500 mL). The combined ether extracts were washed with water (3 × 500 mL), each water wash being reextracted with ether (450 mL). The ether fractions were then dried over magnesium sulphate and evaporated to afford, as an oil, the desired acetate **12** (44.9 g, 85%).

trans-*3-(4-Hydroxy-3-methoxyphenyl)-2-propenol (2)*

Diacetate **12** (26.4 g, 100 mmol) was reduced with lithium aluminium hydride (7.6 g, 200 mmol) exactly as described (11). Immediate flash chromatography (43) of the crude product on silica eluted with EtOAc–hexane (1:1) gave fractions containing pure coniferyl alcohol **2**. Recrystallization from diethyl ether – petroleum ether afforded pure alcohol **2** (11.7 g, 65%), mp 74–75°C (lit. (44) mp 74–76°C).

*Sodium-1-(4-hydroxy-3-methoxyphenyl)-2-propene-1-sulphonate 8 and sodium-*trans*-3-(4-hydroxy-3-methoxyphenyl)-2-propene-1-sulphonate 5*

The sulphonation procedure used was based upon previously reported work (12, 20), and the crude mixture of sulphonates **8** and **5** recovered as described.

Sulphonates **8** and **5** (200 mg) were dissolved in 50 m*M* citric acid/Na_2HPO_4 (4 mL, pH 3.0). This solution was applied to two preparative liquid chromatographic columns (Waters I-125) in series, and then eluted with 50 m*M* citric acid/Na_2HPO_4 buffer solution (pH 3.0) at 50 mL min^{-1}. Fractions containing either pure **5** or **8** were combined, neutralized (1.0 *M* NaOH), and freeze-dried. The resulting material (~3–4 g for each isomer), was then dissolved in water (~52 mL) and subsequently extracted with *n*-butanol (6 × 30 mL). The *n*-butanol extracts for each isomer were combined and azeotroped as before to yield a white amorphous material. Each was then applied to 20 × 20 cm silica plates eluted with *n*-butanol to afford the sulphonates **5** (35 mg, 16.6%) and **8** (27 mg, 12.8%).

3-(4'-Acetoxy-3',5'-dimethyoxyphenyl)-prop-2-enoic acid (14)

Sinapic acid **13** (5 g, 22.32 mmol) was converted to its corresponding acetate **14** as before (5.58 g, 94%), mp 202–203°C.

Ethyl-(4'-acetoxy-3',5'-dimethoxyphenyl)-prop-2-enoate (15)

Acetate **14** (5.498 g, 20.67 mmol) was taken and placed in a 250-mL round-bottomed flask under an atmosphere of nitrogen. Dry thionyl chloride (~55 mL, 0.765 mol) was added and the resulting solution heated until reflux began. This was maintained for 1 h, following which

the solution was cooled (to 20°C) and the excess thionyl chloride removed under reduced pressure. Dry redistilled ethanol (125 mL, 2.14 mol) was added and the solution then allowed to stir at room temperature for 1.25 h, following which the solvent was removed. Recrystallization of the product from CH_3OH–H_2O afforded the required ethyl ester **15** (4.31 g, 71%), mp 120–121°C (lit. (44) mp (120–121°C).

trans-*3-(4'-Hydroxy-3',5'-dimethoxyphenyl)-2-propenol (3) (44)*

Starting from ethyl ester **15** (8 g, 27.2 mmol), sinapyl alcohol (2.95 mg, 51.7%) was prepared exactly as described (44), mp 66–67°C (lit. (44) mp 66–67°C).

*Sodium-*trans*-1-(3,5-dimethoxy-4-hydroxyphenyl)-2-propene-1-sulphonate (6) and sodium-3-(3,5-dimethoxy-4-hydroxyphenyl)-2-propene-1-sulphonate (9)*

Sinapyl alcohol **3** (144 mg, 0.686 mmol) was converted to the corresponding sulphonates **6** and **9** exactly as previously described for coniferyl alcohol **2**. An aliquot (20 mg) of the resulting butanol soluble material (156 mg) was then applied to silica gel plates (20 × 20 cm) and eluted with *n*-butanol to afford **6** (3 mg); ^{1}H nmr (D_2O) δ: 3.57 (2H, d, $J \sim 7$ Hz, CH_2), 3.61 (3H, s, OCH_3), 6.05–6.23 (1H, m, CH=CH_2), 6.43 (1H, $J = 21.6$ Hz, CH=CH—CH_2), 6.64 (2H, s, ArH), and **9** (2 mg); ^{1}H nmr (D_2O) δ: 3.57 (3H, s, OCH_3), 4.51 (1H, d, $J = 9$ Hz, $CHSO_3Na$), 5.18–5.26 (2H, m, CH_2), 6.05–6.23 (1H, m, CH=CH_2), 6.64 (2H, m, ArH).

*Lignosulphonates from black spruce (*Picea mariana*)*

Black spruce chips were delignified as described previously (9). The lignosulphonates so obtained were freeze-dried as described below.

*Lignosulphonates from Poplar (*Populus tremuloides*)*

Poplar chips (5.0 kg dry weight, Klason lignin = 22.1 g/100 g) were steam-pretreated (pressure = 138 kPa, 3 min, 3 cycles) in a 56-L batch digester. The wood was then exposed to a sodium-based bisulphite solution (27.5 L; total SO_2 = 4.99%, free SO_2 = 2.48; pH = 3.91). Pulping conditions were as follows: temperature raised from 20 to 160°C over 120 min and then held for 45 min at 160°C with a maximum pressure of 627 kPa. The resulting pulp (3.85 kg, 77% yield), with a Klason lignin content of 16 g/100 g, was then removed by filtration to recover the crude lignosulphonate solution. The solution was then concentrated to half-volume, neutralized (1 *N* NaOH), and freeze-dried.

General experimental procedure to remove lignin-derived butanol solubles

A solution of crude freeze-dried spent sulphite liquor (50 g/225 mL H_2O) was extracted with *n*-butanol (5 × 200 mL). Following removal of the butanol by azeotroping with water, the organic extracts were freeze-dried. The butanol soluble lignosulphonates were further purified by modification of a complexation/decomplexation procedure with dicyclohexylamine (DCHA), previously described (9). Thus an aqueous solution of butanol solubles (1.5 g/20 mL H_2O) adjusted to pH 2.0 with 18 *M* H_2SO_4 was extracted with CH_2Cl_2–*n*BuOH–DCHA (25:1.3:0.5, 25 mL) and the organic layer separated (Fraction 1); three additional fractions were obtained in an analogous manner. In order to effect decomplexation of the various fractions, water (20 mL) was added and the pH adjusted to 11 with 1 *N* NaOH; the mixture was washed with ether (5 × 100 mL) and the aqueous layer was then freeze-dried after neutralization with Amberlite IR-120 (H^+) resin.

Sulphonates 8 and 5 from black spruce butanol solubles

An aliquot (304 mg) of butanol solubles from black spruce was taken and dissolved in a minimum amount of 50 m*M* citric acid/Na_2HPO_4 buffer at pH = 3.0. Separation and purification as described previously afforded sulphonate **8** (29 mg) and sulphonate **5** (37 mg), identical to synthetic material in all respects.

Sulphonates 5, 6, 8, and 9 from poplar butanol solubles

An aliquot (353 mg) of butanol solubles separated as before from poplar was taken and sulphonates **5** (11 mg), **8** (15 mg), **6** (16 mg), and **9** (14 mg) were isolated as described above.

Note: In all cases, extensive losses were experienced using this procedure. Consequently, methylation was chosen instead.

General experimental procedure for methylating butanol-soluble lignosulphonates

To a suspension of lignosulphonates – sodium sulphate (100 mg) in MeOH (4 mL) was added Amberlite-120 (H^+) resin (2 g, prewashed with MeOH). The lignosulphonates were thus rendered MeOH soluble, and the solution was stirred at room temperature for 10 min. After this time, the resin was filtered off and washed with MeOH (2 × 1 mL); to the combined filtrate and washings was added freshly distilled ethereal diazomethane (25 mL). After 2 h, the excess diazomethane and solvents were removed under reduced pressure. The methylated adducts were redissolved in CH_2Cl_2 and filtered; solvent removal afforded CH_2Cl_2-soluble material in yields ranging from ~50–90%. The major components were separated by hplc, on a Waters μ-Porasil column (7.8 mm × 30 cm) using 60% hexanes:40% (0.90% MeOH/CH_2Cl_2) as eluant.

Methylated butanol-soluble lignosulphonates from black spruce

Characterization data for each compound is given below:

*Methyl-*trans*-3-(4'-methoxyphenyl)-2-propene-1-sulphonate (19)*, uv λ_{max}(MeOH): 267, 215 nm; ^{1}H nmr ($CDCl_3$) δ: 3.77 (3H, s, OCH_3), 3.88 (3H, s, OCH_3), 3.94 (2H, dd, $J_{1,2} = 7.5$ Hz, $J_{1,3} = 1.2$ Hz, $CH_2SO_3CH_3$), 6.03 (1H, dt, $J_{1,2} = 7.5$ Hz, $J_{2,3} = 15.7$ Hz, CH=$CHCH_2$), 6.64 (1H, bd, $J_{2,3} = 15.7$ Hz, CH=$CHCH_2$), 6.82–7.36 (4H, bABq, $J = 8.8$ Hz, ArH); ms (*m/e*): 242 (M^+, 13%), 147 ($M^+ - SO_3CH_3$, 100%), 132 ($M^+ - SO_3CH_3$, —CH_3, 6.8%), 91 ($M^+ - CH_2$=CH—$CH_2SO_3CH_3$, —CH_3, 18.9%). *Exact Mass* calcd. for $C_{11}H_{14}SO_4$: 242.0613; found; 242.0611.

Methyl-1-(4'-methoxyphenyl)-2-propene-1-sulphonate (16), uv λ_{max}(MeOH): 231, 207 nm; ^{1}H nmr ($CDCl_3$) δ: 3.70 (3H, s, OCH_3), 3.77 (3H, s, OCH_3), 4.83 (1H, bd, $J_{1,2} = 8.3$ Hz, $CHSO_3CH_3$), 5.38–5.48 (2H, m, CH=CH_2), 6.12–6.35 (1H, m, CH=CH_2), 6.88–7.36 (4H, ABq, $J = 8.7$ Hz, ArH); ms (*m/e*): 242 (M^+, 5%), 178 (35.9%), 147 ($M^+ - SO_3CH_3$, 100%), 91 ($M^+ - CH_2$=CH—CH—SO_3CH_3, —CH_3, 32%). *Exact Mass* calcd. for $C_{11}H_{14}SO_4$: 242.0612; found: 242.0621.

*Methyl-*trans*-3-(3',4'-dimethoxyphenyl)-2-propene-1-sulphonate (20)*, uv λ_{max}(MeOH): 269, 220 nm; ^{1}H nmr (CD_2Cl_2) δ: 3.80 (3H, s, OCH_3), 3.82 (3H, s, OCH_3), 3.88 (3H, s, OCH_3), 3.94 (2H, dd, $J_{1,2} = 7.4$ Hz, $J_{1,3} = 1.2$ Hz, $CH_2SO_3CH_3$), 6.04 (1H, dt, $J_{1,2} = 7.5$ Hz, $J_{2,3} = 15.8$ Hz, CH=CH—CH_2), 6.63 (1H, dd, $J_{1,3} = 1.2$ Hz, $J_{2,3} = 15.7$ Hz, CH=$CHCH_2$), 6.78–6.96 (3H, m, ArH); ^{13}C nmr (CD_2Cl_2) δ: 54.16 (CH_2), 56.13 (2 × OCH_3), 56.94 (SO_3CH_3), 109.42 (C-2'), 111.62 (C-6'), 112.90 (C-5'), 120.60 (C-2), 128.92 (C-1'), 138.86 (C-3), 149.69 (C-3'), 150.28 (C-4'); ms (*m/e*): 272 (M^+, 21.9%), 177 ($M^+ - SO_3CH_3$, 100%), 162 ($M^+ - SO_3CH_3$, —CH_3, 3.5%), 146 ($M^+ - SO_3CH_3$, —OCH_3, 27.5%), 131 ($M^+ - SO_3CH_3$, —OCH_3, —CH_3, 7%), 119 ($M^+ - SO_3CH_3$, —OCH_3, —CH=CH_2, 3.4%), 115 ($M^+ - SO_3CH_3$), −2 × OCH_3, 3.9%). *Exact Mass* calcd. for $C_{12}H_{16}SO_5$: 272.0718; found: 272.0706.

Methyl-1-(3',4'-dimethyoxyphenyl)-2-propene-1-sulphonate (17), uv λ_{max}(MeOH): 278, 235, 213 nm; ^{1}H nmr (CD_2Cl_2) δ: 3.72 (3H, s, SO_3CH_3), 3.81 (3H, s, OCH_3), 3.82 (3H, s, OCH_3), 4.82 (1H, bd, $J_{1,2} = 8.6$ Hz, CH—SO_3CH_3), 5.43 (1H, ddd, $J_{2,3_{trans}} = 16.7$ Hz, $J_{1,3_{trans}} \sim J_{3,3} = 0.9$ Hz, H_3-*trans*), 5.46 (1H, ddd, $J_{2,3_{cis}} = 10.3$ Hz, $J_{1,3_{cis}} \sim J_{3,3} = 0.8$ Hz, H_3-*cis*), 6.25 (1H, ddd, $J_{2,3_{trans}} = 16.7$ Hz, $J_{2,3_{cis}} = 10.4$ Hz, $J_{1,2} = 8.6$ Hz, CH=CH_2), 6.84–7.00 (3H, m, ArH); ^{13}C nmr (CD_2Cl_2) δ: 56.13 (OCH_3), 56.25 (OCH_3), 58.01 (SO_3CH_3), 70.65 (C-1), 111.80 (C-2'), 112.76 (C-6'), 122.25 (C-5'), 122.71 (CH_2), 124.74 (C-2), 130.57 (C-1'), 149.71 (C-3'), 150.31 (C-4'); ms (*m/e*): 272 (M^+, 0.52%), 177 ($M^+ - SO_3CH_3$, 8.5%), 162 ($M^+ - SO_3CH_3$, —CH_3, 1.8%), 146 ($M^+ - SO_3CH_3$, —OCH_3, 3.76%), 131 ($M^+ - SO_3CH_3$, —OCH_3, —CH_3, 3.5%), 119 ($M^+ - SO_3CH_3$, —OCH_3, —CH=CH_2, 2.9%), 115 ($M^+ - SO_3CH_3$, −2 × OCH_3, 2.4%). *Exact Mass* calcd. for $C_{12}H_{16}SO_5$: 272.0718; found: 272.0720.

Methyl-(3,4-dimethoxy)-benzoate (22), uv λ_{max}(MeOH): 260, 292 nm; ^{1}H nmr (CD_2Cl_2) δ: 3.85 (3H, s, OCH_3), 3.87 (3H, s, OCH_3),

3.88 (3H, s, OCH_3), 6.89 (1H, d, $J_{5,6}$ = 8.4 Hz, C_5H), 7.51 (1H, d, $J_{2,6}$ = 2.0 Hz, C_2H), 7.64 (1H, dd, $J_{5,6}$ = 8.4 Hz, $J_{2,6}$ = 2.0 Hz, C_6H); ^{13}C nmr (CD_2Cl_2) δ: 51.39 (CO_2CH_3), 55.41 (2 × OCH_3), 110.15 (C-2), 111.76 (C-5), 122.35 (C-6), 123.09 (C-1), 148.59 (C-4), 152.97 (C-3), 166.27 (CO); ms (*m/e*): 196 (M^+, 100%), 165 ($M^+ - OCH_3$, 96%), 137 ($M^+ - CO_2CH_3$, 12%). *Exact Mass* calcd. for $C_{10}H_{12}O_4$: 196.0735; found: 196.0656.

Methylated butanol solubles from poplar

Characterization data for compounds **16**, **17**, **19**, **20**, and **22** have already been given in the preceding section.

Methyl-3-(3',4',5'-trimethoxyphenyl)-2-propene-1-sulphonate (21), uv λ_{max}(MeOH): 273, 222 nm; ^1H nmr (CD_2Cl_2) δ: 3.74 (3H, s, OCH_3), 3.82 (6H, s, 2 × OCH_3), 3.89 (3H, s, OCH_3), 3.96 (2H, dd, $J_{1,2}$ = 7.5 Hz, $J_{1,3}$ = 1.2 Hz, $CH_2SO_3CH_3$), 6.10 (1H, dt, $J_{1,2}$ = 7.5 Hz, $J_{2,3}$ = 15.8 Hz, CH=C*H*—CH_2), 6.62 (2H, s, ArH), 6.62 (1H, d, $J_{2,3}$ = 15.8 Hz, C*H*=CH—CH_2); ^{13}C nmr (CD_2Cl_2) δ: 53.99 (CH_2), 56.40 (2 × OCH_3), 57.00 (OCH_3), 60.85 (SO_3CH_3), 104.19 (C-2', C-6'), 114.50 (*C*H—CH_2), 131.49 (C-1'), 139.07 (*C*H=CH—CH_2), 153.80 (3 × C—OCH_3); ms (*m/e*): 302 (M^+, 38%), 207 ($M^+ - SO_3CH_3$, 100%), 176 ($M^+ - SO_3CH_3$, —OCH_3, 80%), 161 ($M^+ - SO_3CH_3$, —OCH_3, —CH_3, 21.7%), 149 ($M^+ - SO_3CH_3$, —OCH_2, —CH=CH_2, 10.4%). *Exact Mass* calcd. for $C_{13}H_{18}SO_6$: 302.0824; found: 302.0762.

General experimental procedure to isolate paucidisperse lignosulphonates

Freeze-dried spent sulphite liquor (20 g) from a high yield bisulphite cook was dissolved in H_2O (100 mL) and washed with *n*-BuOH (5 × 200 mL; 125 mL H_2O added during extraction). The volume of the aqueous layer was then adjusted to 300 mL and its pH adjusted to 6.3 with 18 *M* H_2SO_4. Dicyclohexylamine (20 mL) and CH_2Cl_2–BuOH (5:1; 200 mL) were added, and the resultant mixture was shaken very gently for 5 min. After separation of the organic layer, the aqueous fraction was readjusted to pH 6.3 and an analogous extraction was performed. To the combined organic layers were added H_2O (150 mL) and 1 *N* NaOH (~30 mL; pH of aqueous layer ~11). After vigorous shaking, the aqueous layer was separated, washed with diethyl ether (5 × 100 mL), neutralized with Amberlite-120 (H^+) resin, and freeze-dried. The solid thus obtained was redissolved in H_2O (10 mL), washed with BuOH (7 × 20 mL), neutralized, and freeze-dried to afford ~2.5 g of material.

General experimental procedure for methylating paucidisperse lignosulphonates

This methylation procedure is analogous to that described for the corresponding BuOH-soluble lignosulphonates and afforded CH_2Cl_2-soluble material in ~70% yield. The major components were separated by hplc, on a Waters μ-Porasil column (7.8 mm × 30 cm) using 5% hexanes:95% (0.35% MeOH/CH_2Cl_2) as eluant. The solvent polarity was adjusted slightly from the above value, depending on the age and activity of the silica gel.

1,2-Disulphonomethyl-3-(3',4'-dimethoxyphenyl)-prop-2-ene (23), uv λ_{max}(MeOH): 290, 232, 212 nm; ^1H nmr (CD_2Cl_2) δ: 3.86 (3H, s, OCH_3), 3.88 (3H, s, OCH_3), 3.90 (3H, s, OCH_3), 4.00 (3H, s, OCH_3), 4.54 (2H, s, $CH_2SO_3CH_3$), 6.96–7.27 (3H, m, ArH), 7.98 (1H, s, C*H*=CSO_3CH_3); ms (*m/e*): 366 (M^+, 36.9%), 271 ($M^+ - SO_3CH_3$, 35.8%), 175 ($M^+ - HSO_3CH_3$, —SO_3CH_3, —H, 100%), 161 ($M^+ - 2 \times SO_3CH_3$, —CH_3, 29.1%), 145 ($M^+ - 2SO_3CH_3$, —OCH_3, 13.4%). *Exact Mass* calcd. for $C_{13}H_{18}O_8S_2$: 366.0443; found: 366.0382.

1,2-Disulphonomethyl-1-(3',4'-dimethoxyphenyl)-propane (24), uv λ_{max}(MeOH): 276, 233 nm; ^1H nmr (CD_2Cl_2) δ: 1.61 (3H, d, $J_{2,3}$ = 7.2 Hz, CH_3), 3.79 (3H, s, OCH_3), 3.82 (3H, s, OCH_3), 3.85 (3H, s, OCH_3), 3.86 (3H, s, OCH_3), 4.18 (1H, dt, $J_{2,3}$ = 7.2 Hz, $J_{1,2}$ = 2.1 Hz, $HCSO_3CH_3$), 5.03 (1H, d, $J_{1,2}$ = 2.1 Hz, $HCSO_3CH_3$), 6.89–7.11 (3H, m, ArH); ms (*m/e*): 368 (M^+, 7.8%), 273 ($M^+ - SO_3CH_3$, 15.1%), 178 ($M^+ - 2SO_3CH_3$, 100%), 163 ($M^+ - 2SO_3CH_3$, —CH_3, 8.9%), 147 ($M^+ - 2SO_3CH_3$, —OCH_3, 2.3%). *Exact Mass* calcd. for $C_{13}H_{20}O_8S_2$: 368.0599; found: 368.0518.

trans-*1,3-Disulphonomethyl-1-(3',4'-dimethoxyphenyl)-1-propene (25)*, uv λ_{max}(MeOH): 284, 230, 208 nm; ^1H nmr (CD_2Cl_2) δ: 3.78 (3H, s, OCH_3), 3.85 (3H, s, OCH_3), 3.88 (3H, s, OCH_3), 3.88 (3H, s, OCH_3), 3.93 (2H, d, $J_{2,3}$ = 7.8 Hz, $CH_2SO_3CH_3$), 6.94–6.96 (3H, m, ArH), 7.02 (1H, t, $J_{2,3}$ = 7.8 Hz, SO_3CH_3C=C*H*$CH_2SO_3CH_3$); ms (*m/e*): 366 (M^+, 68.7%), 271 ($M^+ - SO_3CH_3$, 8.9%), 175 ($M^+ - HSO_3CH_3$, —SO_3CH_3, —H, 100%), 161 ($M^+ - HSO_3CH_3$, —SO_3CH_3, —CH_3, 20.6%). *Exact Mass* calcd. for $C_{13}H_{18}O_8S_2$: 366.0443; found: 366.0443.

1,2-Disulphonomethyl-1-(3',4'-dimethoxyphenyl)-propane (26), uv λ_{max}(MeOH): 280, 238, 210 nm; ^1H nmr (CD_2Cl_2) δ: 1.88 (3H, d, $J_{2,3}$ = 7.1 Hz, CH_3), 3.50 (3H, s, OCH_3), 3.62 (3H, s, OCH_3, 3.86 (6H, s, 2 × OCH_3), 4.00 (1H, dq, $J_{2,3}$ = 7.1 Hz, $J_{1,2}$ = 9.4 Hz, $HC(SO_3CH_3)CH_3$), 4.61 (1H, d, $J_{1,2}$ = 9.4 Hz, $HCSO_3CH_3$), 6.89–7.07 (3H, m, ArH); ms (*m/e*): 368 (M^+, 4.8%), 273 ($M^+ - SO_3CH_3$, 21.1%), 178 ($M^+ - 2SO_3CH_3$, 100%), 163 ($M^+ - 2SO_3CH_3$, —CH_3, 8.9%), 147 ($M^+ - 2SO_3CH_3$, —OCH_3, 2.5%). *Exact Mass* calcd. for $C_{13}H_{20}O_8S_2$; 368.0599; found: 368.0614.

Continuous flow micropulping

The apparatus used was based upon a previous report (14) and scaled down for our purposes (15). Black spruce wood (500 mg) was taken and allowed to sit in water under vacuum for 1 h. The resulting material was then packed into a cylindrical stainless-steel tube (80 × 5 mm). A solution of sodium sulphite (250 mL, 13.6 g/L Na_2SO_3, 0.5% Na^+) in nitrogen-sparged water, previously adjusted to pH 3.0 with gaseous sulphur dioxide, was placed in the reservoir. The micropulping apparatus was then flushed with nitrogen gas and assembled. The flow of the pulping solution was adjusted to 1 mL min^{-1} after which the digester and coils were immersed in the heating bath oil at 155°C for 4 h. Fractions (1.5–2 mL) were collected and analysed by hplc. After 4 h, the bomb was removed, cooled, and the resulting pulp washed, filtered, and freeze-dried. Weight of pulp = 222 mg, 44%. (Pulping experiments were also repeated at pH 2, 5, and 7 and with poplar.) Micro-Klason determinations were carried out according to the described method (45).

Acknowledgements

The authors thank Harold Bradford for technical assistance, the Natural Sciences and Engineering Research Council of Canada for financial support, and R. D. Mortimer for an authentic sample of ester **15**.

1. E. Nokihara, M. J. Tuttle, V. F. Felicetta, and J. L. McCarthy. J. Am. Chem. Soc. **79**, 4495 (1957).
2. D. A. I. Goring, A. Procter, and W. Q. Yean. Pulp Pap. Can. **68**, T445 (1967).
3. D. A. I. Goring and A. Szabo. Tappi, **51**, 440 (1968).
4. H. I. Bolker and H. S. Brenner. Science, **170**, 173 (1970).
5. (*a*) D. C. Johnson and J. F. Yan. J. Appl. Polym. Sci. **26**, 1623 (1981); (*b*) J. F. Yan. Macromolecules, **14**, 1438 (1981).
6. D. A. I. Goring. Polymer properties of lignin and lignin derivatives from lignins. *Edited by* K. V. Sarkanen and C. H. Ludwig. J. Wiley and Sons Ltd., New York. 1971. pp. 695–768.
7. D. A. I. Goring. Am. Chem. Soc. Symp. Ser. **48**, 273 (1977).
8. K. Forss and K.-E. Fremer. J. Appl. Polym. Sci. Appl. Polym. Symp. **37**, 531 (1983), and references therein.
9. N. G. Lewis, D. A. I. Goring, and A. Wong. Can. J. Chem. **61**, 416 (1983).
10. C. Lapierre, C. Rolando, and B. Monties. Holzforschung, **37**, 189 (1983).
11. O. Lindeberg. Acta Chem. Scand. Ser. B, **34**, 15 (1980).
12. S. W. Schubert, M. G. Andrus, C. Ludwig, D. Glennie, and J. L. McCarthy. Tappi, **50**, 186 (1967).
13. O. Faix. Das Papier, **30**: V, 1 (1982).
14. W. Q. Yean and D. A. I. Goring. Pulp Pap. Can. **65**, T127 (1964).
15. J. L. Fong. Studies on lignin heterogeneity and removal. Honours Thesis, McGill University. April 6, 1983.

16. N. G. LEWIS and W. Q. YEAN. J. Chromatogr. **331**, 419 (1985).
17. J. J. COLLINS, K. FORSS, W. G. GLASSER, J. S. GRATZL, and J. L. MCCARTHY. Macromolecules, **8**, 565 (1975).
18. A. A. PADMAPRIYA, G. JUST, and N. G. LEWIS. Synth. Commun. **15**, 1057 (1985).
19. E. G. KING, F. BRAUNS, and H. HIBBERT. Can. J. Res. **13**, 88, (1935).
20. V. F. FELICETTA, D. GLENNIE, and J. L. MCCARTHY. Tappi, **50**, 170 (1967).
21. (*a*) R. BENN and H. GÜNTHER. Angew. Chem. Int. Ed. Engl. **22**, 350 (1983); (*b*) A. M. BIALSKI, N. G. LEWIS, and C. E. LUTHE. ACS Chemistry Meeting, Philadelphia. September 1984.
22. (*a*) J. R. PARRISH. J. Chem. Soc. C, 1145 (1967); (*b*) Tetrahedron Lett. **11**, 555 (1964).
23. A. SAKAKIBARA and N. NAKAYAMA. J. Jpn. Wood Res. Soc. **7**, 13 (1961).
24. A. SAKAKIBARA and N. NAKAYAMA. J. Jpn. Wood Res. Soc., **8**, 153 (1962).
25. E. MORELLI, R. N. REJ, N. G. LEWIS, G. JUST, and G. H. N. TOWERS. Phytochemistry. In press.
26. S. RAISANEN. Suom. Kemistil. B, **40**, 35 (1967).
27. T. ASHORN. Soc. Sci. Fenn. Commentat. Phys.-Math. **25**, 8 (1961).
28. R. D. MORTIMER. J. Wood Chem. Tech. **2**, 383 (1982).
29. R. D. MORTIMER and B. I. FLEMING. J. Wood Chem. Tech. In press.
30. R. KONDO and J. L. MCCARTHY. J. Wood Chem. Tech. **3**, 37 (1985).
31. J. GIERER. Svensk Papperstidn. **74**, 571 (1970).
32. J. GIERER. Holzforschung, **36**, 43 (1982).
33. B. J. FERGUS, A. R. PROCTER, J. A. N. SCOTT, and D. A. I. GORING. Wood Sci. Tech. **3**, 117 (1969).
34. J. R. WOOD and D. A. I. GORING. Pulp Pap. Mag. Can. **74**, , T309 (1979).
35. A. R. PROCTER, W. Q. YEAN, and D. A. I. GORING. Pulp Pap. Mag. Can. **68**, T445 (1967), and references therein.
36. H. GRISEBACH. *In* The biochemistry of plants. Secondary plant products. Vol. 7. *Edited by* by P. K. Stumpf and E. E. Conn. Academic Press, New York. 1981. Chapt. 15. p. 474.
37. H. HIBBERT. Ann. Rev. Biochem. **11**, 183 (1942).
38. E. ADLER, J. M. PEPPER, and E. ERIKSOO. Ind. Eng. Chem. **49**, 1391 (1957).
39. E. ADLER, B. O. LINDGREN, and U. SAEDEN. Svensk Papperstidn. **55**, 245 (1952).
40. J. GIERER. Svensk Papperstidn. **61**, 648 (1958).
41. N. SANYER, T. ITOH, and E. L. KELLER. Tappi **47**, 323 (1964).
42. (*a*) S. WINSTEIN, E. C. FRIEDRICH, R. BAKER, and Y. LIN. Tetrahedron, **22**, Suppl. 8, 621 (1966); (*b*) R. BAKER, J. HUDEC, and K. L. RABONE. J. Chem. Soc. C, 1605 (1969).
43. W. C. STILL, M. KAHN, and A. MITRA. J. Am. Chem. Soc. **43**, 2923 (1978).
44. K. FREUDENBERG and H. H. HÜBNER. Chem. Ber. **85**, 1181 (1952).
45. P. WHITING, B. D. FAVIS, F. G. T. ST.-GERMAIN, and D. A. I. GORING. J. Wood Chem. Tech. **1**, 29 (1981).

Gas phase basicity of dihydropyran and dihydro-1,4-dioxin

G. BOUCHOUX AND I. HANNA
Laboratoire de Synthèse Organique, Ecole Polytechnique, 91128 Palaiseau Cedex France
AND
R. HOURIET AND E. ROLLI
Institute de Chimie Physique, E. P. F. L., Ch 1015 Lausanne, Switzerland
Received December 19, 1985

G. BOUCHOUX, I. HANNA, R. HOURIET, and E. ROLLI. Can. J. Chem. **64**, 1345 (1986).

The gas phase basicity (GB) of dihydropyran **1** and dihydro-1,4-dioxin **2** is measured in equilibrium proton transfer reactions conducted in an ion cyclotron resonance spectrometer. GB(**1**) is found to be greater than GB(**2**) by 37 kJ mol^{-1}, this difference parallels the lower reactivity of **2** observed in solution under acidic condition. Conclusion as to the favoured protonation of the C—C double bond, giving rise for both **1** and **2** to oxycarbonium cations, is drawn from comparison with analogous compounds and substantiated by molecular orbital calculations (MNDO) on the protonated structures.

G. BOUCHOUX, I. HANNA, R. HOURIET et E. ROLLI. Can. J. Chem. **64**, 1345 (1986).

Les basicités gazeuses (BG) du dihydropyrane **1** et de la dihydrodioxine-1,4 **2** ont été mesurées à partir d'équilibres de transferts de protons dans un spectromètre à résonance cyclotronique ionique. BG(**1**) est supérieure à BG(**2**) de 37 kJ mol^{-1}, cet écart est à comparer à la plus faible réactivité de **2** en solution acide. Pour les deux composés, le site de protonation est la double liaison C=C, l'ion résultant possède une structure oxycarbonium. Ceci est établi par comparaison avec des composés voisins et par des calculs d'orbitales moléculaires (méthode MNDO).

Introduction

Dihydropyran **1** and dihydro-1,4-dioxin **2** undergo acid-catalyzed addition of alcohols affording 2-tetrahydropyranyl (THP) **3** and 1,4-dioxan-2-yl **4** ethers, respectively. However, whereas tetrahydropyranylation of alcohols readily occurs under very mild conditions (pyridinium *p*-toluenesulfonate (1) or iodotrimethylsilane (2)), more acidic catalysis (TsOH or $CuBr_2$) (3) are necessary for the preparation of **4**:

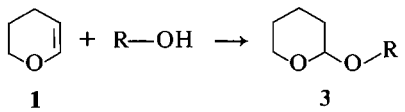

1 **3**

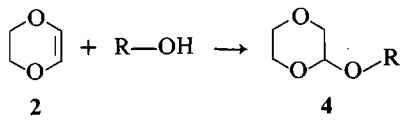

2 **4**

In order to account for this unexpected observation, we have examined the intrinsic basicity of compounds **1** and **2** by the method of equilibrium proton-transfer reaction in an ion cyclotron resonance (ICR) spectrometer.

For each molecule the favoured site of protonation was unambiguously determined by comparison with the basicity data of molecules containing closely analogous substructures (4). The conclusions were strengthened by molecular orbital calculations on the five possible protonated forms of **1** and **2**, i.e. cations *a*–*c* and *d*, *e*, respectively.

Results

Experimental

Determination of the equilibrium constant K for the proton transfer reaction:

[1] $[MH]^+ + B \rightleftarrows [BH]^+ + M$

was carried out for M = **1** and **2** and several reference bases B in the ICR cell. The latter was operated in the trapped mode under a total pressure of ca. 10^{-6} Torr and at a temperature of 313 K (5). The gas phase basicity of M is given by GB(M) = GB(B) − RT ln K where K is the equilibrium constant for reaction [1], with an accuracy better than 1 kJ mol^{-1}. Experimental data are given in Table 1.

TABLE 1. Experimental ΔG_r^0 for reaction $[MH]^+ + B \rightleftarrows M + [BH]^+$ and related gas phase basicities GB (kJ mol^{-1})

M	Reference base B	ΔG_r^0	GB(B)	GB(M)[a]
1	2,4-Pentanedione	−0.4	837[b]	
	Diisopropyl ether	+4.2	831[b]	836±1
	3,4-Dimethylfuran	−3.8	839[c]	
2	Methyl acetate	+2.1	797[b]	799±1
	para-Nitrotoluene	+3.3	795[d]	

[a]Standard experimental deviation 0.8 kJ mol^{-1}.
[b]From ref. 12.
[c]From ref. 9*b*.
[d]A revised value, ref. 15.

The corresponding proton affinity, PA(M) is obtained after introduction of the appropriate entropic term:

$$PA(M) = GB(M) + T\Delta S^0$$

For the first molecule **1**, ΔS^0 may be satisfactorily approximated by the translational entropy for the isolated proton ($T\Delta S^0$ = 33 kJ mol^{-1} at 313 K) if structures *a* or *b* are produced.

Conversely $T\Delta S^0$ should be reduced by RT ln 2 for the symmetrical molecule **2** yielding *d* or *e*. The PA values deduced this way from the experimental GB are collected in Table 2. The heats of formation of $[MH]^+$ are estimated using $\Delta H_f^0[H]^+$ = 1530 kJ mol^{-1} and experimental heat of formation for **1**, an additivity method was used in order to determine ΔH_f^0(**2**) (Table 2).

Molecular orbital calculation

The five possible structures *a*–*e* resulting from protonation of dihydropyran **1** and dihydro-1,4-dioxin **2** were examined using the semiempirical MNDO method (8). This calculation procedure gives satisfactory estimates of relative heats of formation for isomeric oxygenated closed-shell cations (9). Thus it can be

TABLE 2. Experimental proton affinities PA(M) and heats of formation of M and $[MH]^+$ for dihydropyran and dihydro-1,4-dioxin

M	PA(M)	$\Delta H_f^0(M)$	$\Delta H_f^0[MH]^+$
1	870[a]	−125[c]	535
2	829[b]	−234[d]	467

[a] $T\Delta S^0 = 33\,kJ\,mol^{-1}$, see text.
[b] $T\Delta S^0 = 30\,kJ\,mol^{-1}$, see text.
[c] Reference 6.
[d] Reference 7. A ring correction of $17\,kJ\,mol^{-1}$ was applied. This value is estimated using the ring correction term associated to 1,4-dioxan (i.e. $14\,kJ\,mol^{-1}$) and taking into account a strain energy of $3\,kJ\,mol^{-1}$ due to the C=C double bond. This latter value is obtained by comparison with the ring correction terms of tetrahydropyran ($2\,kJ\,mol^{-1}$) and 2,3-dihydropyran ($5\,kJ\,mol^{-1}$).

TABLE 3. Calculated (MNDO) heats of formation of protonated dihydropyran and dihydro-1,4-dioxin

$[MH]^+$ structure	ΔH_f^0	$\Delta\Delta H_f^0$
a	699	143
b	553	0
c	628	75
d	474	0
e	528	54

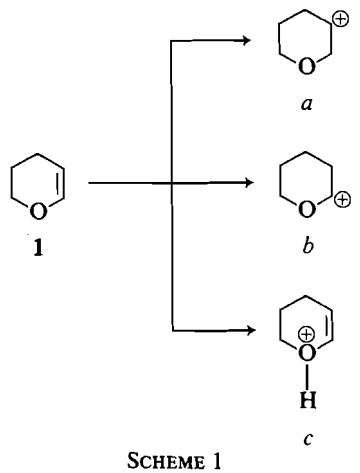

SCHEME 1

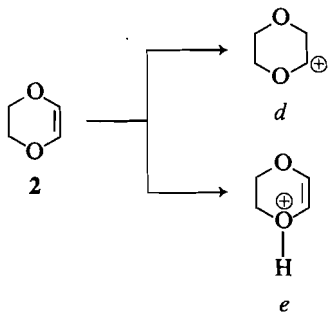

SCHEME 2

used for predicting the most favoured protonation site on **1** and **2**.

The heats of formation presented in Table 3 were obtained after complete geometry optimisation of the corresponding species *a*–*e* (optimized geometrical parameters are available upon request to the authors).

Discussion

Protonation of dihydropyran **1** and dihydro-1,4-dioxin **2** may occur either on an unsaturated carbon atom or on conjugated oxygen atom as illustrated by Schemes 1 and 2.

The assignment of the protonation site under equilibrium proton transfer conditions can be made using the following arguments.

Firstly, the gas phase basicities of **1** and **2** are greater than those of their saturated analogs:[1]

$$GB(\mathbf{1}) - GB(\text{tetrahydropyran})\ (10) = 34\,kJ\,mol^{-1}$$

$$GB(\mathbf{2}) - GB(\text{1,4-dioxane})\ (10, 11) = 19\,kJ\,mol^{-1}$$

It is well known that the introduction of a conjugated carbon–carbon double bond tends to lower the basicity of an oxygen atom (4, 12). Since protonation of tetrahydropyrane and 1,4-dioxane certainly occurs on one oxygen atom, the present results dismiss protonation on the oxygen atom both in **1** and **2**.

Thus we conclude that formation of ions *c* and *e* by protonation of **1** and **2** can be excluded under our experimental conditions.

Secondly, the experimentally determined GB values for 2,3-dihydrofuran and ethyl-vinyl ether (4) are exactly the same as GB(**1**), i.e. $836\,kJ\,mol^{-1}$ (Table 1). This observation constitutes a strong support in favour of the same protonation site for the three afore-cited compounds which contain the same α,β-unsaturated ether moiety. Owing to earlier conclusions (4) protonation on the β carbon is thermodynamically favoured. This leaves little doubt that *b* is obtained from **1** during equilibrium proton transfer.

A *third* indication confirms that oxygens are not involved in the low energy protonation process of **1** and **2**. Bloch *et al.* (13) have demonstrated that the highest occupied molecular orbital (HOMO) in neutral molecules **1** and **2** is a π-orbital mainly centred on the CC double bond. Approximately 2.5 eV above, the second band of the photoelectron spectra is due to ejection of an electron from a delocalized σ-orbital involving mainly the in-plane oxygen lone pair.

The final arguments will be given by molecular orbital calculations. In agreement with the preceding indications, MNDO calculation predict that structures *b* and *d* are the most stable protonated forms of **1** and **2**.

One may note that the corresponding oxygen protonated form *c* and *e* are less stable by 75 and $54\,kJ\,mol^{-1}$, respectively. The difference between these two values constitutes an illustration of the withdrawing effect of the second oxygen atom destabilizing the positive charge in *d* with respect to *b*. Experimentally, GB(**2**) is lower than GB(**1**) by $37\,kJ\,mol^{-1}$ (Table 1) in agreement with the lower ability of *d* to bear the positive charge. Moreover the relative proximity in energy of *d* and *e* is in keeping with the participation of this latter ion in the acid-catalyzed hydrolysis of **2** in solution (14).

Conclusion

The most thermodynamically favoured protonated forms of dihydropyran **1** and dihydro-1,4-dioxin **2** are the oxycarbonium ions *b* and *d*. This fact is established from experimental as well

[1] Using $PA(NH_3) = 205.0\,kcal\,mol^{-1}$, one obtained a revised PA value of $193.6\,kcal\,mol^{-1}$ for 1,4-dioxane.

as theoretical arguments. In addition, the lower basicity of dihydro-1,4-dioxin **2** with respect to dihydropyran **1** in the gas phase is clearly established. This inherent property attributed to the base-weakening effect of the second oxygen atom in **2** is probably also operative in solution.

1. M. MIGASHITA, A. YOSHIKOSHI, and P. GRIECO. J. Org. Chem. **42**, 3772 (1977).
2. G. A. OLAH, A. HUSAN, and B. P. SINGH. Synthesis, 703 (1985).
3. M. FETIZON and I. HANNA. Synthesis, 806 (1985).
4. G. BOUCHOUX, F. DJAZI, Y. HOPPILLIARD, R. HOURIET, and E. ROLLI. Org. Mass Spectrom. **21**, 209 (1986).
5. R. HOURIET, H. RÜFENACHT, P. A. CARRUPT, P. VOGEL, and M. TICHY. J. Am. Chem. Soc. **105**, 3417 (1983).
6. J. D. COX and G. PILCHER. Thermochemistry of organic and organometallic compounds. Academic Press, New York. 1970.
7. S. W. BENSON. Thermochemical kinetics. John Wiley, New York. 1976.
8. M. J. S. DEWAR and W. THIEL. J. Am. Chem. Soc. **99**, 4899 (1977).
9. (*a*) R. HOURIET, H. SCHWARZ, Z. ZUMMACK, J. G. ANDRADE, and P. VON R. SCHLEYER. Nouv. J. Chim. **5**, 505 (1981); (*b*) R. HOURIET, E. ROLLI, G. BOUCHOUX, and Y. HOPPILLIARD. Helv. Chim. Acta, **68**, 2037 (1985); (*c*) G. BOUCHOUX and Y. HOPPILLIARD. J. Mol. Struct. Theochem, **104**, 365 (1983); (*d*) G. BOUCHOUX, Y. HOPPILLIARD, and J. P. FLAMENT. Org. Mass Spectrom. In press.
10. J. F. WOLF, R. H. STALEY, I. KOPPEL, M. TAAGEPEPA, R. T. MCIVER, JR., J. L BEAUCHAMP, and R. W. TAFT. J. Am. Chem. Soc. **99**, 5417 (1977).
11. M. MAUTNER. J. Am. Chem. Soc. **105**, 4906 (1983).
12. D. H. AUE and M. T. BOWERS. *In* Gas phase ion chemistry. Vol. 2. Academic Press, New York. 1979. Chapt. 9.
13. M. BLOCH, F. BRIOGLI, E. HEILBRONNER, T. B. JONES, H. PRINZBACH, and O. SCHWEINERT. Helv. Chim. Acta, **61**, 1388 (1978).
14. V. S. TSIVUNIN, V. G. ZARIPOVA, I. N. ZARIPOV, and S. A. NASYBULLIN. Chem. Abstr. **95**, 96435f (1981); Z. Obshch. Khim, **51**, 318 (1981).
15. E. ROLLI and R. HOURIET. Specrosc. Int. J. **3**, 177 (1984).

^{2}H nuclear magnetic resonance studies of motions in tetramethylammonium salts: the question of methyl reorientation[1]

CHRISTOPHER I. RATCLIFFE AND JOHN A. RIPMEESTER
Division of Chemistry, National Research Council of Canada, Ottawa, Ont., Canada K1A 0R9
Received November 28, 1985

CHRISTOPHER I. RATCLIFFE and JOHN A. RIPMEESTER. Can. J. Chem. **64**, 1348 (1986).

The ^{2}H nmr lineshapes of a number of tetramethylammonium salts have been studied as a function of temperature. It is shown from this and previous evidence that in certain cases the lowest temperature motions should be assigned to whole ion C_3' or pseudo-isotropic motion, rather than to methyl group motions as has been assumed in previous ^{1}H nmr studies. Steric potential calculations have been used to investigate a previously suggested model of concerted partial reorientations of methyl groups.

CHRISTOPHER I. RATCLIFFE et JOHN A. RIPMEESTER. Can. J. Chem. **64**, 1348 (1986).

On a déterminé les spectres rmn du ^{2}H d'un certain nombre de sels de tétraméthylammonium et on a étudié la forme des raies en fonction de la température. En se basant sur ces données et sur des données antérieures, on tire des conclusions relativement à la nature des mouvements se produisant aux températures les plus basses; alors que des études antérieures basées sur la rmn du ^{1}H laissaient croire que ces mouvements devraient être attribues à des mouvements des groupements méthyles, on doit plutôt les attribuer à l'ion global C_3' ou à un mouvement pseudo-isotrope. On a utilisé des calculs de potentiels stériques pour étudier un modèle qui avait été suggéré antérieurement et qui implique des réorientations partielles concertées des groupements méthyles.
[Traduit par la revue]

Introduction

In a recent study of deuterated *tert*-butyl compounds (1) we demonstrated the utility of ^{2}H nmr in discriminating between C_3 methyl group reorientation, and reorientation of the *tert*-butyl group about its principal C_3' axis when the methyls do not rotate internally. ^{1}H spin-lattice relaxation time (T_1) and second moments (M_2) measurements cannot distinguish between the two and, although this was known, it had generally been assumed that C_3 methyl motion always occurred at lower temperatures than C_3'. Using ^{2}H nmr we were able to show, in agreement with recent neutron scattering results (2), that this is not true in all cases.

Numerous ^{1}H nmr T_1 and M_2 studies of $(CH_3)_4N^+$, tetramethylammonium (TMA), salts have appeared in the past (3–21). In almost all of the T_1 studies it has again been *assumed* that C_3 methyl reorientation is always responsible for the relaxation at the lowest temperatures, followed by pseudo-isotropic motion at higher temperatures, or in some cases at about the same temperature as the methyl motion. (Since isotropic motion strictly implies random reorientation among all directions in space of any vector within the molecule, the term pseudo-isotropic motion is used here to imply rapid reorientation between specific equilibrium positions about many or all of the threefold and twofold axes of the $(CH_3)_4N^+$. ion. In either case the lineshape is narrowed to a single sharp line.) Through a number of arguments, which we discuss later, it became apparent to us that some of the activation energies claimed for the methyl C_3 reorientation are *much lower* than should be anticipated. This suggested that in some cases (just as in some of the *tert*-butyl compounds) the lower temperature T_1 behaviour might be explained better by whole ion C_3', C_2', or pseudo-isotropic motions, occurring before any methyl C_3 motion begins. There are similar complications in the interpretation of the ^{1}H nmr results for the lowest temperature phase of neopentane (5, 22–24). Results for this material will be presented elsewhere.

Another novel reorientation process has recently been proposed to account for an unusually shallow T_1 minimum that has been observed only in the $PtBr_6^{2-}$, $TeBr_6^{2-}$, $SnBr_6^{2-}$, and $TeCl_6^{2-}$ salts of TMA (18, 19) at low temperatures; the model interprets this minimum in terms of a partial and symmetrical rotation of all the methyl groups around their C_3 axes between two positions about 15° on either side of the all-staggered configuration of the ion. While this model (which we will refer to from here on as the "twisted methyls" model) is interesting and worthy of consideration, we felt that there may be another simpler explanation of the T_1 results. Furthermore, one might question the existence of the two equilibrium positions necessary for this model.

All these motions should give different characteristic ^{2}H nmr powder lineshapes (in the fast motion limit), so this seemed to be an ideal method for attempting to sort out exactly which motions do occur in several selected TMA salts.

Experimental

TMA-d_{12} chloride was obtained from M.S.D. isotopes. TMA-d_9 iodide was prepared by condensing $(CD_3)_3N$ (MSD isotopes) into a tube containing an ethanol solution of methyl iodide at liquid nitrogen temperatures (by means of a vacuum line). The tube was sealed and allowed to warm up to room temperature, by which time the solids had melted, mixed, and reacted. The ethanol was then removed. TMA-d_9 OH·5H_2O was prepared from TMA-d_9I as follows: An excess of a freshly prepared suspension of silver oxide was stirred into a solution of TMA-d_9I. The silver iodide and excess silver oxide were filtered off. The resulting solution of TMA-d_9 hydroxide was then concentrated and left in a desiccator until crystals of the pentahydrate had formed. This hydroxide was later neutralized with HBr solution to give TMA-d_9Br, which was used to prepare the $SnBr_6^{2-}$ and $TeBr_6^{2-}$ salts. [TMA-d_9]$_2$$SnBr_6$ was prepared by mixing the appropriate amounts of TMA-d_9Br (dissolved in a minimum amount of water at 80°C) and $SnBr_4$ (in a small amount of concentrated hydrobromic acid at 80°C). The yellow precipitate was cooled, filtered, and washed with absolute ethanol (19).[TMA-d_9]$_2$$TeBr_6$ was prepared in a similar manner, except TeO_2 was substituted in the place of $SnBr_4$ (19). [TMA-d_{12}]$_2$$ZnCl_4$ was prepared by mixing concentrated solutions of the appropriate amounts of dried TMA-d_{12}Cl and $ZnCl_2$. The resulting precipitate was filtered and dried. A second sample of $(CD_3)_4$NOH·5-H_2O was prepared at a later date from a sample of perdeuterated TMAOD hydrate obtained from Cambridge Isotopes Ltd.

The ^{2}H nmr powder lineshapes were obtained at 27.63 MHz using a

[1]NRCC No. 25524.

TABLE 1. Claimed activation energies for methyl group rotation in TMA from ^1H T_1 studies (kcal/mol)

Anion	Ref.	E_a	Anion	Ref.	E_a
Cl^-	7	6.8	ClO_4^-	21	4.4
NO_3^-	20	6.5	$PtBr_6^{2-}$	19	4.4
Br^-	7	6.4	$TeBr_6^{2-}$	19	4.3
SiF_6^{2-}	14	6.0	$SnBr_6^{2-}$	19	3.7
I^-	7	5.5	δ-$PtCl_6^{2-}$	18	3.6[a]
α-$PtCl_6^{2-}$	18	5.5[a]	$ZnCl_4^{2-}$	17	3.8[b] 2.8
SO_4^{2-}	20	5.4			
			$B_3H_8^-$	16	2.3
ClO_3^-	13	5.1			
			$CdCl_3^-$	12	2.0[c] 1.6
$TeCl_6^{2-}$	18	4.9[a]			
$SnCl_6^{2-}$	18	4.6[a]			

[a]Authors (18) suggest alternatively that this is overall reorientation.
[b]Two types of TMA ion in unit cell, *assumed* (17).
[c]Assumes one methyl (E_a = 1.6 kcal/mol) is unique (12).

Brüker CXP 180 spectrometer, a Brüker/Oxford Instruments cryomagnet, and a variable temperature N_2 gas-flow probe with a Brüker B-VT-1000 temperature controller. Spectra at liquid nitrogen temperature were obtained with a separate probe designed to hold liquid nitrogen around the coil and sample. A quadrupole echo pulse sequence (25) was used, with a delay time of 35 μs between X and Y pulses of 2.5 μs, and phase alternation. The cycle repetition times varied from 0.4–20 s depending on T_1. The second sample of TMA-d_{12} hydroxide was investigated below 77 K using liquid helium coolant in an Andonian cryostat, with a different probe and a Brüker 1.41 Tesla electromagnet. Spectra were then obtained at 9.2 MHz using the CXP spectrometer.

Discussion

Previously determined methyl rotation barriers

Table 1 lists all the claimed activation energies for methyl reorientation in TMA obtained from T_1 versus temperature studies. The values range widely from 1.6 to 6.8 kcal/mol, which itself seems rather unusual. Inelastic neutron scattering (INS) studies of the methyl torsional modes in the TMA halide salts (26) indicate threefold barriers of 7.9, 7.5, and 6.7 kcal/mol for the chloride, bromide, and iodide respectively. Allowing for the zero point energies, the INS barriers correspond quite well with the activation energies (7) given in Table 1, and help to substantiate the interpretation of those nmr results. Methyl torsional mode assignments in the infrared and Raman spectra of the $PtCl_6^{2-}$, $PtBr_6^{2-}$, $TeBr_6^{2-}$, and $NiCl_3^-$ salts (27) also lead to barrier values of the order of 5 kcal/mol. Now, there is no reason why the *internal* barrier to methyl reorientation should change drastically from one salt to another, though small changes in the total methyl barrier would be expected to arise from differences in the external barriers, as indicated by the halide salts. This cannot account, however, for the large range of claimed methyl activation energies. The barrier to methyl rotation in $(CH_3)_3N$ in its clathrate hydrate has been determined from ^1H nmr tunnelling lineshapes to be 4.17 kcal/mol (28). Any external contribution to the barrier in this hydrate should be extremely small, and the internal barrier would be lower than that in $(CH_3)_4N^+$ since there is less steric crowding. Furthermore, since the barriers to methyl reorientation in $(CH_3)_4X$ species increase with decreasing C—X distance (29, 30), the barrier in TMA^+ should be higher than that in neopentane, $(CH_3)_4C$, for which the barrier has been determined by infrared, INS, and thermodynamics studies (summarized in ref. 29) to be no lower than 4.3 kcal/mol. The barrier determined from the tunnelling lineshape of neopentane clathrate hydrate is also 4.26 kcal/mol (28). The implication is that the values lower than this for TMA salts, obtained from ^1H T_1 studies, do not represent methyl reorientation. Consequently those values in the right hand column of Table 1 probably represent either pseudo-isotropic reorientation or preferred reorientation about specific axes (C_3' or C_2') of internally rigid TMA ions.

Second moment discrepancies

When methyl groups have barriers of ~4.5–3.5 kcal/mol, tunnelling processes produce lineshapes, at low temperatures, that are quite distinct from the rigid lattice lineshape, and for barriers lower than 3.5 kcal/mol the lineshapes are the same as for the classical rotor. Consequently the observed ^1H second moments may never reach their anticipated rigid lattice values (31). This being the case, there are obvious discrepancies between the low activation energies claimed for methyl rotation from T_1 results and the observation of rigid lattice lineshapes and second moments: this is particularly clear in the case of TMA $CdCl_3$ (12). In fact all the second moment values reported at sufficiently low temperatures are very close to the expected rigid lattice values (4, 6, 9, 10, 18, 19), though most of these studies do not go right down to liquid helium temperatures.

For whole ion motions the moments of inertia are *much* higher than for methyl reorientation. Consequently energy level splittings due to barrier tunnelling are very much smaller than for methyl and hence have no observable effect on the lineshape.

Considerations of the "twisted methyls" model

The model involving the "twisted methyls" appears to have originated with Lassettre and Dean (32), who calculated potentials using semi-empirical bond dipole and quadrupole interactions. Their calculations for neopentane suggested that the minimum energy configuration occurs when the methyls are all twisted symmetrically away from the all-staggered configuration by an angle between 0 and 30°. However, it has been suggested from the analysis of the different energy contributions, calculated more recently by *ab initio* methods, that internal barriers are not simply due to bond dipole–quadrupole interactions (33); the similarity between observed barriers and those calculated using the bond dipole–quadrupole interactions may therefore be more fortuitous than realistic.

Berg (27) revived the model to attempt to explain some features of his infrared and Raman spectra of the hexahalometallate salts of TMA, and following this the model seemed to provide a plausible explanation of the corresponding ^1H T_1 results (18, 19). Berg's statements (27) are misleading, however, in that they imply that the torsional barriers in the isolated TMA ion are due entirely to electrostatic repulsions between the protons. In fact, although H–H interactions must certainly play a part, they are only one contributor to the total torsional potential.

We considered it worthwhile doing some simple empirical calculations for TMA to attempt to clarify the situation. We used the following potential and empirical parameters (34, 35).

$$V(r) = a \exp(-br) - c/r^6$$

for	H—H	a = 2171	b = 3.74	c = 24.39
	C—H	a = 8503	b = 3.67	c = 111.82

TABLE 2. Calculated frequency separations of the pairs of discontinuities (kHz) for various reorientations in the fast motion limit based on the rigid parameters given in the first row

	q_{zz}	q_{yy}	q_{xx}	η	e^2qQ/h (kHz)
Rigid	252	134	118	0.0635	168.0
C_3, C_3' inner doublet	76.89	38.44	38.44	0	51.26
C_3' outer doublet	252	126	126	0	168.0
C_2' (2-fold)	134	128.67	5.33	0.9204	89.33
C_2' (4-fold)	5.33	2.67	2.67	0	3.55
Twisted Methyls 30°	229	118.1	110.9	0.03144	152.67
Twisted Methyls 20°	241.7	123.6	118.0	0.02317	161.13

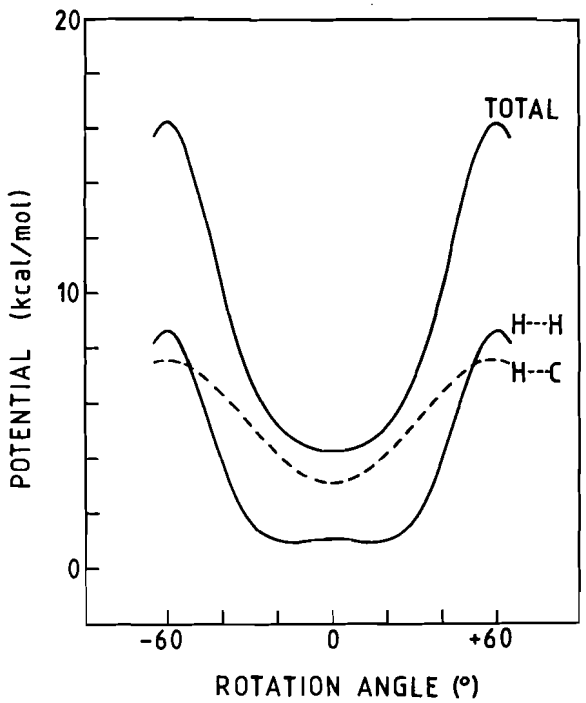

FIG. 1. Steric potential contributions for $(CH_3)_4N^+$ when *all* CH_3 groups are rotated simultaneously in the same direction with respect to their C—N axes. (Angle 0° = all-staggered configuration.)

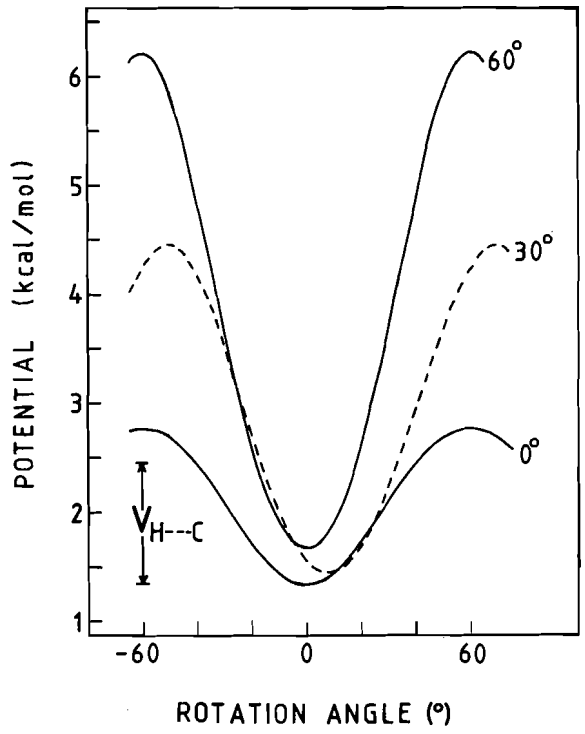

FIG. 2. Steric potential for one CH_3 group of $(CH_3)_4N^+$ when the three other CH_3 groups have all been rotated, in the same direction with respect to their C—N axes, to 0, 30, or 60° from the all-staggered configuration.

(The potential is in kcal/mol if r is in Å, using these parameters.) We assumed C—H = 1.09 Å, C—N = 1.5 Å, and all bond angles to be tetrahedral.

We first calculated the *total* steric interaction potential for the whole molecule as *all* 4 methyls are rotated by the same angle, Fig. 1. The H—H interactions do indeed produce potential minima at about ±16° on each side of the all-staggered configuration, but note that the barrier between the two positions is *very* small. The C—H interactions, however, produce a symmetrical 3-fold potential with its minimum at the all-staggered configuration (indeed because of symmetry this must occur). The *total* potential then has only one broadened minimum (in a 120° rotation) at the all-staggered configuration. It should also be pointed out that the C—H interactions may be underestimated by this kind of interaction potential, because the internal barrier involves the electron distributions in the C—H and N—C bonds as well as the interatomic interactions.

Secondly we calculated the steric potential for reorientation of *one* methyl group with the other 3 groups all rotated by angle α, for a range of values of α, Fig.2. The H—C term is again a constant 3-fold potential with a minimum at the all-staggered configuration. The H—H term is a 3-fold potential with a minimum at the all-staggered configuration only for α = 0 or 60°; for $0 < \alpha < 60$ the minimum shifts first away from and then back to the all-staggered configuration. Note that the height of the barrier increases as α increases. Perhaps the most significant aspect of this second set of calculations is that the minimum is always single, and hence it appears that the double minimum will only appear in the total H—H potential when there are simultaneous symmetric twists of all 4 methyl groups.

Obviously these calculations are very simplistic and depend both on the molecular dimensions and the potential function and parameter set chosen. They do indicate, however, that even if the parameters were chosen (and weighted in favour of the H—H interactions) so as to produce a double minimum in the total potential, then the barrier between the two would likely be

much smaller than the 7.7–12.8 kJ/mol (1.83–3.05 kcal/mol) assigned to the "twisted methyls" motion in the earlier nmr studies (18,19). We thus have good reason for investigating alternative explanations of the low temperature relaxation minimum for those hexahalometallate salts concerned.

^2H lineshape calculations

Values for the rigid lineshape quadrupole coupling constant $e^2qQ/h = 168$ kHz and asymmetry parameter $\eta = 0.0635$ were used in calculating the motionally averaged lineshapes for a number of cases. The results are given in Table 2 and shown in Fig. 3. All bond angles were assumed to be tetrahedral and the rigid lattice q_{zz} tensor component was assumed to be along the C—D bond axis. The narrowed lineshapes were calculated by averaging the tensor components at all the equilibrium positions sampled by a deuteron during the motion (see ref. 36). The calculations apply to the fast motion limit, i.e. when the reorientation rate is much faster than the reciprocal of the quadrupole coupling constant of the unnarrowed lineshape.

For the "twisted methyls" model we calculated the motional averaging for in-plane flips between two sites for two cases, where the sites are separated by angles of 20 and 30° respectively. Translated into methyl torsional angles these correspond to 21.2 and 31.9°. The larger angle is closer to the values suggested by the ^1H nmr study (19), but we wished to see whether the reduced effect of the smaller angle on the lineshape would still be detectable if it occurred. (Other angles were considered but are not shown here.) It was found that q_{zz} changes the most rapidly at low flip angles. The lineshape for most flip angles retains a non-zero asymmetry parameter but the overall width is reduced.

For the C_3' motion, 9 of the deuterons are averaged in exactly the same way as the deuterons in a C_3 methyl rotation would be, i.e. the lineshape is narrowed by a factor of about 1/3 to give the inner doublet of Fig. 3(d). However, the 3 deuterons whose C—D axes lie parallel to the C_3' axis show very little narrowing, since q_{zz} remains unchanged and q_{xx}, q_{yy} are averaged. Note that the two sets of doublets that thus make up the total lineshape for this motion both have $\eta = 0$. For TMA-d_9 ions $(CD_3)_3CH_3N^+$ the result will be exactly the same as for $(CD_3)_4N^+$; even the intensity ratio of 3:1 of inner:outer doublet is unchanged (consider the average of the four possible C_3' axes of the ion).

The C_2' twofold reorientation produces an unmistakable averaged lineshape with a very large η. Perhaps of more interest is the lineshape produced when reorientation occurs about C_2' among more than the 2-fold positions (e.g. 4-fold is plausible). The line in this case is almost completely narrowed, a result which arises because all the C—D bonds are oriented at the magic angle with respect to the C_2' axis. (In fact if the rigid lattice η were zero then the narrowing *would* be complete.)

Observed ^2H lineshapes

The experimental ^2H lineshapes at various temperatures are shown in Figs. 4–8. Our efforts to determine which motion occurs first at low temperatures are generally hampered because of (*1*) dynamic effects on the lineshape, and (*2*) the overlap of other line-narrowing processes at higher temperature, i.e. the pure lineshape as calculated for the fast motion limit above may not necessarily be seen. Fortunately the lineshape changes occurring are sufficiently well defined in most cases that we may be unambiguous in assigning the motions.

We can briefly summarize some general observations before considering each case in more detail:

TABLE 3. Observed ^2H nmr lineshapes: estimated quadrupole coupling constants and asymmetry parameters

TMA salt	e^2qQ/h (kHz)	η	T (K)
Rigid lineshape components:			
Cl	169	0.0512	77
I	165	0.0484	77
$ZnCl_4$	167	0.0637	77
$OH{\cdot}5H_2O$	165	0.0687	69
$TeBr_6$	169	0.0630	77
$SnBr_6$	170	0.0706	77
C_3 or C_3' reduced doublet components			
Cl	49	0	270
I	51	0	170
$ZnCl_4$	53	0	100
$OH{\cdot}5H_2O$	54	0	69

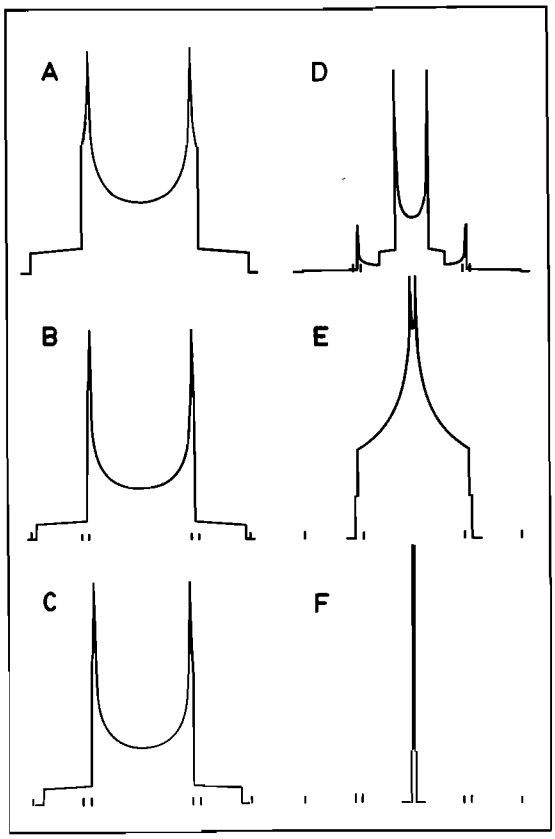

FIG. 3. Calculated ^2H nmr lineshapes. A, rigid lattice; B, C, "twisted methyls" model, rotation angle between 2 sites 20° and 30° respectively; D, C_3' motion; E, C_2' 2-fold motion; F, C_2' n-fold motion ($n > 2$). The short vertical marks indicate the positions of the rigid lineshape singularities. (Note: the inner singularities of the doublets have been truncated, since no broadening functions have been convoluted with the pure lineshapes.) All lineshapes (except rigid) in the fast motion limit.

1. In most of the cases studied (except for the OH^- salt) we have largely the rigid lattice lineshape at 77 K. This is basically the same in all the salts, though it may be significant that for the Cl and I salts, where motional barriers are highest, the asymmetry parameters are lower. Values of e^2qQ/h and η are given in Table 3.

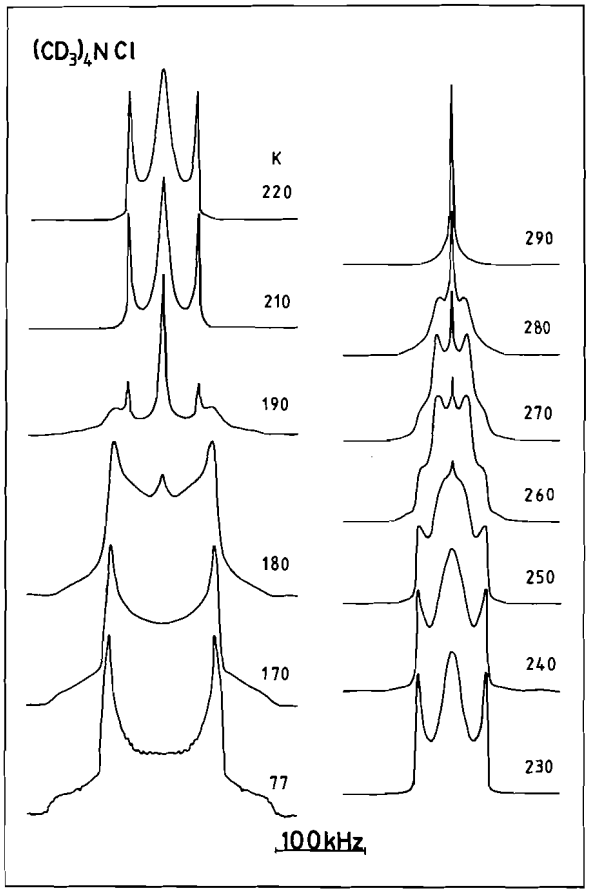

FIG. 4. The ^2H nmr lineshapes of (TMA)Cl as a function of temperature. Note there is a phase change between the lineshapes at 180 and 190 K.

2. There is no evidence in any of the spectra of the C_2' 2-fold rotation lineshape.

3. Features due to the roughly 1/3 reduced doublet characteristic of C_3 or C_3' appear in the spectra of the Cl^-, I^-, $ZnCl_4^-$, and OH^- salts.

4. In all cases as temperature increases we see the development of the pseudo-isotropic lineshape. (Note this could include C_2' 4-fold reorientation.)

5. There is no evidence for the reduced lineshape for 20–30° "twisted methyls" flipping in the $TeBr_6^{2-}$ and $SnBr_6^{2-}$ salts.

TMA Cl and I

In the ^2H lineshapes of both these salts (Figs. 4 and 5) we can observe the appearance of the features of the reduced lineshape due to C_3 methyl reorientation (see Table 3), over a wide temperature range, as the rigid lattice features become less well defined and eventually disappear. It is perhaps here where we can distinguish between C_3 and C_3' motion, since for C_3' we should retain a well-defined outer doublet (cf. C_3' motion in certain *tert*-butyl compounds and $(CD_3)_3N$ (ref. 1). Of course for these two salts we do not question the previous studies, which show that C_3 motion is the first to occur (7). In both salts the C_3 fast motion limit lineshape is never attained, since the pseudo-isotropic lineshape begins to develop before this occurs. Another feature that distinguishes these halide salts is that the pseudo-isotropic lineshape begins to appear, and finally becomes the only lineshape, at much higher temperatures than in the other salts.

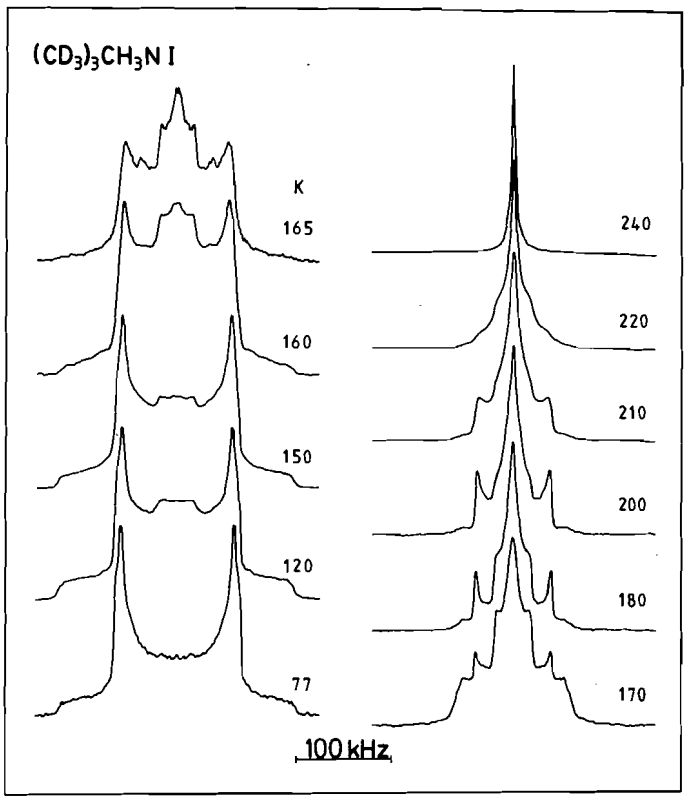

FIG. 5. The ^2H nmr lineshapes of (TMA)I as a function of temperature.

$(TMA)_2$ $ZnCl_4$

All the lineshapes we are concerned with for this salt are for the lowest temperature phase VI, which is stable below 161 K (37). The lineshape is almost completely rigid at 77 K, by 90 K we can see features due to both pseudo-isotropic and C_3 or C_3' motions, but by 120 K virtually all the intensity is in the sharp central pseudo-isotropic line, Fig. 6. Ignoring the central line, if we focus on the spectra above 100 K where the inner doublet has more intensity than the outer doublet, the outer doublet now appears to have $\eta = 0$. Whether this is simply a dynamic effect in the narrowing region or the expected effect due to C_3' motion (see calculations) cannot be resolved. However, since we have already argued that the activation energies derived from the ^1H T_1 results for this salt are too low for methyl $C3$ reorientation, it is quite clear from the ^2H lineshapes that the motions involved are C_3' reorientation about one axis followed very closely by pseudo-isotropic reorientation.

The crystal structure of phase VI is not known so one should also consider the possibility of having inequivalent TMA ions. Some ions may reorient by C_3' followed by pseudo-isotropic motion and others might go straight to pseudo-isotropic motion. This would be reflected in the relative line intensities and the depths of the two observed T_1 minima (17).

$(TMA)\,OH{\cdot}5H_2O$

The lineshapes shown in Fig. 7 were all obtained at 9.2 MHz. The one spectrum of $(CD_3)_3CH_3NOH{\cdot}5H_2O$ that was obtained at 77 K and 27.63 MHz was virtually identical to that at 9.2 MHz except it showed the outer singularities of the broad doublet more clearly. (This is on account of the higher pulse power attainable in the 27.63 MHz probe.)

Even at 69 K the ^2H lineshape of this material clearly shows evidence of a great deal of motion. Again there are features due

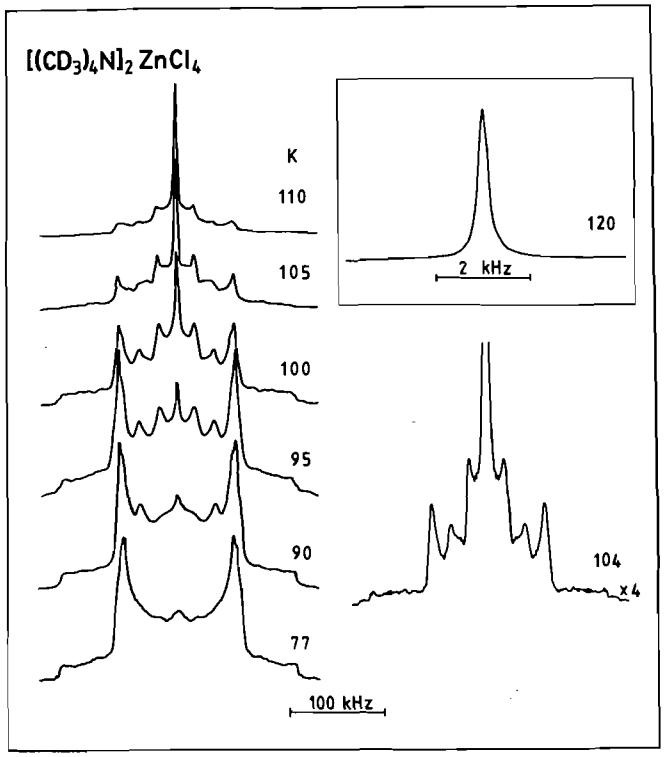

FIG. 6. The ^2H nmr lineshapes of $(TMA)_2ZnCl_4$, phase IV, as a function of temperature.

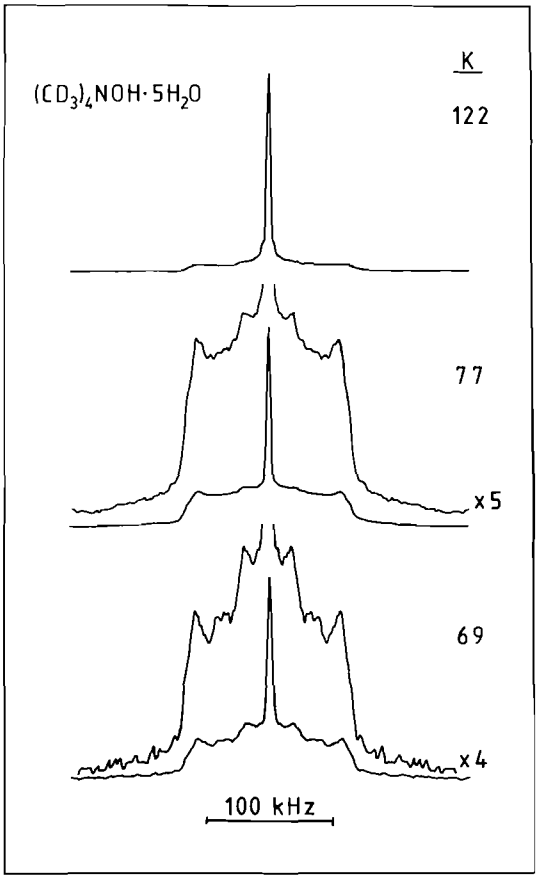

FIG. 7. The ^2H nmr lineshapes of $(TMA)OH\cdot 5H_2O$ at low temperatures (9.2 mHz).

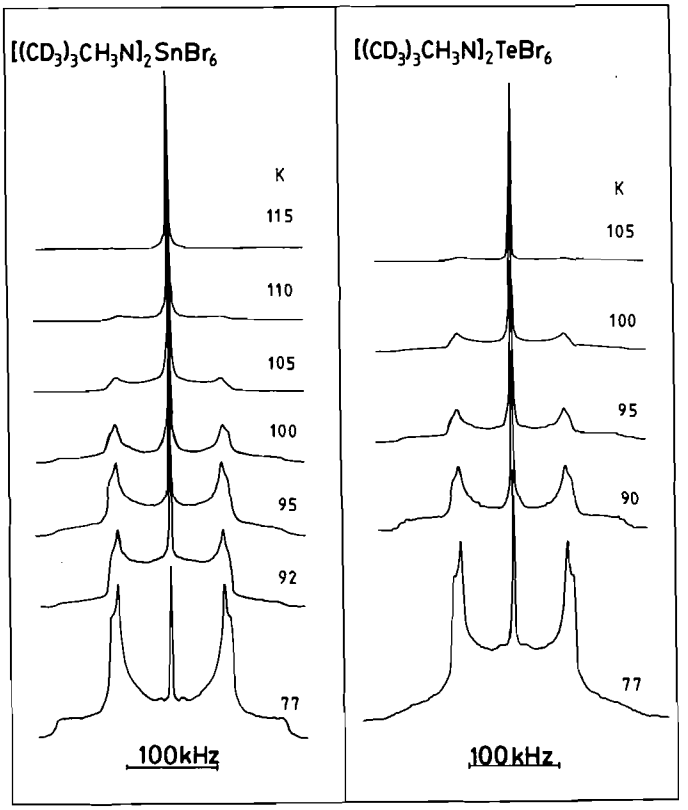

FIG. 8. The ^2H nmr lineshapes of $(TMA)_2SnBr_6$ and $(TMA)_2TeBr_6$ below 120 K.

to C_3' and pseudo-isotropic motions. The broad outer doublet must consist of a small contribution from the broad component of the C_3' lineshape, but it can be largely attributed to the rigid lattice lineshape (showing dynamic effects). Note that the C_3' lineshape is most prominent at the lowest temperature and together with the rigid lineshape loses intensity to the pseudo-isotropic line as the temperature increases. This suggests that although C_3' motion may occur first it is closely followed by pseudo-isotropic motion.

In this particular case one would anticipate a C_3' motion based on X-ray structure information (38); the TMA ion is enclathrated in a cage consisting of water molecules incorporating the OH^- ion and it has a unique C_3' symmetry axis. Also, as with most clathrate hydrates (39), reorientation of the ion within the cage would be expected to have a very small barrier, and it is quite possible that there is disorder of the protons of the cage structure at low temperatures. This latter feature can lead to a distribution of cage potentials and reorientational correlation times. From ^1H T_1 and second moments studies (in progress in this laboratory) it is also clear that C_3 methyl motion is not observed (i.e. (*1*) motional narrowing gives the second moment values expected for pseudo-isotropic motion, below 110 K; (*2*) at 4 K one obtains a rigid lattice lineshape (no methyl tunnelling effects); and (*3*) the activation energy obtained from T_1 for the lowest temperature motion is too low for methyl reorientation).

$(TMA)_2SnBr_6$ and $TeBr_6$

The ^2H lineshape changes for these two salts are very similar, Fig. 8, and are quite distinct from the others we have considered so far. In both salts the rigid lattice lineshape simply seems to diminish in intensity while a sharp central line grows, as the temperature is increased. In fact there is a trace of the central

line even at 77 K. Note that phase transitions have been detected at 84 K ($TeBr_6^{2-}$ salt) and 90 K ($SnBr_6^{2-}$ salt) (19), so that except for the 77 K spectra all the lineshapes shown belong to the phase which is also stable at room temperature. There is obviously no evidence for C_3, C_3', or C_2' (2-fold) reorientation in these lineshapes. It is also clear that the broad doublet of the rigid lattice does not show any significant narrowing as temperature increases, and certainly not to the degree expected for the "twisted methyls" flipping motion.

Since the only motion indicated is pseudo-isotropic (or perhaps C_2' (4-fold)), we must now find an alternative explanation for the observed T_1 minima. At room temperature all the $(TMA)_2MX_6$ salts, where M = Pt, Te, Sn and X = Cl, Br, belong to space group $Fd3c$ (19, 40, 41), and whenever this phase is stable down to low enough temperatures the shallow ^1H T_1 minimum appears (previously ascribed to "twisted methyls" motion), i.e. in $TeCl_6^{2-}$, $PtBr_6^{2-}$, $TeBr_6^{2-}$, and $SnBr_6^{2-}$. (In the $TeCl_6^{2-}$ case the phase appears to be metastable in the temperature range of the shallow T_1 minimum, and the lower temperature phase does not show this minimum (18).) In general, the shallow minimum does not appear in the other solid phases.

The detailed $Fd3c$ structure of the $TeBr_6^{2-}$ salt (41) shows two crystallographically inequivalent types of TMA ion in the ratio 3:1. We propose that the most plausible reinterpretation of the T_1 behaviour for these salts is that both observed minima are due to pseudo-isotropic reorientation, but with motion of the rarer type of TMA ion occurring at lower temperature and hence producing a separate shallow minimum. In fact the ratio of the two T_1 minima roughly fits a 1:3 ratio. The observation that the deeper minimum is not very symmetrical is most probably due to the *pseudo*-isotropic nature of the motion. Pseudo-isotropic motion for this ion really implies a combination of C_3' and C_2' motions about all such axes, and some of these motions may have slightly different rates (though insufficiently distinct to separate them).

In conclusion, we have demonstrated by way of old and new results that methyl group reorientation is not the lowest temperature motion occurring in a number of TMA salts. This once again shows that careful consideration must be given to all the known results concerning structure and motion for any case before a complete understanding can be attained.

1. J. A. Ripmeester and C. I. Ratcliffe. J. Chem. Phys. **82**, 1053 (1985).
2. J. C. Frost, A. J. Leadbetter, and R. M. Richardson. Philos. Trans. R. Soc. London B, **290**, 567 (1980); J. Chem. Soc. Faraday Trans. 2, **78**, 2139 (1982).
3. D. J. Blears, S. S. Danyluk, and E. Bock. J. Phys. Chem. **72**, 2269 (1968).
4. J. Dufourq and B. Lemanceau. J. Chim. Phys. **67**, 9 (1970).
5. S. B. W. Roeder and D. C. Douglass. J. Chem. Phys. **52**, 5525 (1970).
6. M. Mahajan and B. D. Nageswara Rao. J. Phys. Chem. Solids, **33**, 2191 (1972).
7. S. Albert, H. S. Gutowsky, and J. A. Ripmeester. J. Chem. Phys. **56**, 3672 (1972).
8. E. R. Andrew and P. C. Canepa. J. Magn. Reson. **7**, 429 (1972).
9. M. Polak and M. Scheinblatt. J. Magn. Reson. **12**, 261 (1973).
10. M. Mahajan and B. D. Nageswara Rao. J. Phys. C: Solid State Phys. **7**, 995 (1974).
11. H. Rager and A. Weiss. Z. Phys. Chem. **93**, 299 (1974).
12. T. Tsang and D. B. Utton. J. Chem. Phys. **64**, 3780 (1976).
13. T. Tsuneyoshi, N. Nakamura, and H. Chihara. J. Magn. Reson. **27**, 191 (1977).
14. H. Rager and A. Weiss. Ber. Bunsenges. Phys. Chem. **82**, 535 (1978).
15. R. Blinc, M. Burgar, J. Slak, V. Rutar, and F. Milia. Phys. Status Solidi A, **56**, K65 (1979).
16. E. C. Reynhardt. J. Phys. C: Solid State Phys. **13**, 4109 (1980).
17. L. K. E. Niemelä and J. E. Heinilä. Chem. Phys. Lett. **82**, 182 (1981).
18. L. S. Prabhumirashi, R. Ikeda, and D. Nakamura. Ber. Bunsenges. Phys. Chem. **85**, 1142 (1981).
19. S. Sato, R. Ikeda, and D. Nakamura. Ber. Bunsenges. Phys. Chem. **86**, 936 (1982).
20. S. Jurga, J. Depireux and Z. Pajak. *In* Magnetic resonance and related Phenomena. Vol. 2. Proc. 18th Ampère Congress, Nottingham, 1974. *Edited by* P. S. Allen, E. R. Andrew, and C. A. Bates. North-Holland, Amsterdam. 1975. p. 403.
21. S. Jurga. Phys. Status. Solidi A, **81**, 77 (1984).
22. J. G. Powles and H. S. Gutowsky. J. Chem. Phys. **21**, 1695 (1953).
23. E. O. Stejskal, D. E. Woessner, T. C. Farrar, and H. S. Gutowsky. J. Chem. Phys. **31**, 55 (1959).
24. S. Takeda, G. Soda, and H. Chihara. Mol. Phys. **47**, 501 (1982).
25. J. H. Davis, K. R. Jeffrey, M. Bloom, M. I. Valic, and T. P. Higgs. Chem. Phys. Lett. **42**, 390 (1976).
26. C. I. Ratcliffe and T. C. Waddington. J. Chem. Soc. Faraday Trans. 2, **72**, 1935 (1976).
27. R. W. Berg. J. Chem. Phys. **71**, 2531 (1979).
28. J. A. Ripmeester. Can. J. Chem. **60**, 1702 (1982).
29. C. I. Ratcliffe and T. C. Waddington. J. Chem. Soc. Faraday Trans. 2, **72**, 1840 (1976).
30. T. T. Ang and B. A. Dunell. J. Chem. Soc. Faraday Trans. 2, **75**, 169 (1979).
31. P. S. Allen and D. G. Taylor. J. Phys. C: Solid State Phys. **8**, 3036 (1975); Chem. Phys. **31**, 197 (1978).
32. E. N. Lassettre and L. B. Dean, Jr. J. Chem. Phys. **17**, 317 (1949).
33. D. G. Lister, J. N. Macdonald, and N. L. Owen. *In* Internal rotation and inversion. Academic Press, London. 1978. p. 99.
34. U. Shmueli and I. Goldberg. Acta Crystallogr. Sect. B, **29**, 2466 (1973).
35. D. E. Williams. Acta Crystallogr. Sect. A, **28**, 84 (1972).
36. R. G. Barnes. Adv. Nucl. Quadrupole Reson. **1**, 335 (1974).
37. S. Sawada, Y. Shiroishi, A. Yamamoto, M. Takashige, and M. Matsuo. J. Phys. Soc. Jpn. **44**, 687 (1978).
38. R. K. McMullan, T. C. W. Mak, and G. A. Jeffrey. J. Chem. Phys. **44**, 2338 (1966).
39. D. W. Davidson and J. A. Ripmeester. *In* Inclusion compounds. Vol. 3. *Edited by* J. L. Atwood, J. E. D. Davies, and D. D. MacNicol. Academic Press, London. 1984. Chapt. 3.
40. Y. Furukawa, L. S. Prabhumirashi, R. Ikeda, and D. Nakamura. Bull. Chem. Soc. Jpn. **55**, 995 (1982).
41. R. W. Berg and K. Nielsen. Acta Chem. Scand. Ser. A, **33**, 157 (1979).

Structure and conformation of 5-methoxymethyl-1-(2′-deoxy-β-D-lyxofuranosyl)uracil

J. WILSON QUAIL
Department of Chemistry, University of Saskatchewan, Saskatoon, Saskatchewan, Canada S7N 0W0
IRENA EKIEL
Division of Biological Sciences, National Research Council of Canada, Ottawa, Ont., Canada K1A 0R6
OSSAMA A. L. EL-KABBANI
Department of Biochemistry, University of Saskatchewan, Saskatoon, Sask., Canada S7N 0W0
GUY TOURIGNY
Department of Chemistry, University of Saskatchewan, Saskatoon, Sask., Canada S7N 0W0
LOUIS T. J. DELBAERE
Department of Biochemistry, University of Saskatchewan, Saskatoon, Sask., Canada S7N 0W0
AND
ALLAN L. STUART AND SAGAR V. GUPTA[1]
Department of Veterinary Physiological Sciences, University of Saskatchewan, Saskatoon, Sask., Canada S7N 0W0
Received September 26, 1985

J. WILSON QUAIL, IRENA EKIEL, OSSAMA A. L. EL-KABBANI, GUY TOURIGNY, LOUIS T. J. DELBAERE, ALLAN L. STUART, and SAGAR V. GUPTA. Can. J. Chem. **64**, 1355 (1986).

The structure of the nucleoside 5-methoxymethyl-1-(2′-deoxy-β-D-lyxofuranosyl)uracil (MMdLU) was deduced by X-ray crystallographic analysis. MMdLU crystallized in space group $P2_1$ with a = 8.719(4), b = 13.188(3), c = 5.701(3) Å, β = 109.56(2)° and Z = 2; R = 0.040 for 1208 unique reflections with net $I > 2\sigma(I)$. The furanose ring adopts the rare C(4′)—*exo* envelope conformation ($_4E$). The glycosyl linkage is *anti* (χ = 243.5°) and the C(5′) side chain has the *t* conformation. The conformation was also determined in solution by nmr analysis. The sugar ring exists in the *N*-conformation (97 ± 5%), the populations of the three rotamers about the exocyclic C(4′)—C(5′) bond were estimated to be $g^+:t:g^-$ = 23%:59%:18% and the glycosidic conformation is predominantly *anti*.

J. WILSON QUAIL, IRENA EKIEL, OSSAMA A. L. EL-KABBANI, GUY TOURIGNY, LOUIS T. J. DELBAERE, ALLAN L. STUART et SAGAR V. GUPTA. Can. J. Chem. **64**, 1355 (1986).

Faisant appel à la diffraction des rayons X, on a déterminé la structure du nucléoside méthoxyméthyl-5 (déoxy-2′ β-D-lyxo-furannosyl)-1 uracil (MMdLU). Le MMdLU cristallise dans le groupe d'espace $P2_1$ avec a = 8,719(4), b = 13,188(3) et c = 5,701(3) Å. β = 109,56(2)° et Z = 2; R = 0,040 pour 1208 réflexions uniques avec $I > 2\sigma(I)$. Le cycle furannose adopte la configuration enveloppe C(4′)-*exo* ($_4E$) qui est rare. La liaison glycosidique est *anti* (χ = 243,5°) alors que la chaîne latérale C(5′) adopte une conformation *t*. On a aussi déterminé la conformation en solution en se basant sur une analyse par rmn. Le cycle du sucre existe dans la conformation-*N* (97 ± 5%) et on a évalué que les populations des trois rotamères autour de la liaison exocyclique C(4′)—C(5′) sont $g^+:t:g^-$ = 23%:59%:18% et la conformation glycosidique est principalement *anti*.
[Traduit par la revue]

Introduction

Our laboratory has been interested in viral chemotherapy, and, more specifically, the effect of nucleoside analogs on herpes simplex virus infections (1–8). The nucleoside, 5-methoxymethyl-2′-deoxyuridine (MMdUrd), was synthesized (9) and its selective activity against herpes simplex virus was discovered in the early seventies (2). In order to understand the molecular basis for selective action of antiherpes drugs, analogs of MMdUrd were synthesized and the structural modifications were related to the antiviral activity (7, 10). The 3′-epimer of MMdUrd, *5-methoxymethyl-1-(2′-deoxy-β-D-lyxofuranosyl)uracil* (MMdLU), which has the 3′-OH group in the *endo* position (1′*R*,3′*R*,4′*R*-configuration), was synthesized. MMdLU was essentially devoid of activity against herpes simplex virus (11). The selective activity of MMdUrd is due to preferential phosphorylation by virus-induced pyrimidine deoxyribose kinase (viral-K). The nucleotide, after conversion to its triphosphate, is a competitive inhibitor of viral DNA-dependent DNA polymerase (12). The substrate specificity of MMdUrd is most likely a reflection of the amino acids at the active center of the viral-K enzyme and the lack of activity of MMdLU is related to differences in the stereochemistry of the two analogs. Furthermore, since no 2′-deoxy*lyxo*nucleoside (or 2′-deoxy*xylo*nucleoside) has been subjected to X-ray analysis, the crystal structure determination of MMdLU was considered to be relevant. In order to compare the conformation in solution with that found in the solid state, the structure of MMdLU was also determined in D_2O by nmr spectroscopy.

[1]Author to whom all correspondence should be addressed.

Results and discussion

The synthesis of MMdLU was accomplished by a four-step reaction sequence. The 5′-OH group of MMdUrd was protected by tritylation (7). Treatment of the triphenylmethyl derivative with methanesulfonyl chloride in pyridine at 4°C gave the 3′-mesyl ester, which upon hydrolysis in base yielded 5′-tritylated MMdLU. Detritylation was done in 80% acetic acid at 50°C. The structural formula with atomic numbering for MMdLU is shown in Fig. 1.

X-ray analysis.

The bond lengths and angles determined for MMdLU are given in Tables 1 and 2, respectively, and a stereoscopic view of the molecule is shown in Fig. 2. The bond distances in MMdLU and most of the bond angles are very similar to those in MMdUrd. However, the bond angles involving C(3′) differ considerably due to the difference in configuration. The

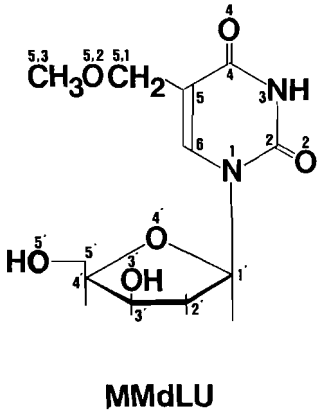

FIG. 1. Structure and atomic numbering of MMdLU.

respective values for MMdLU and MMdUrd are C(1′)—C(2′)—C(3′) 104.0(3)° and 101.4(2)°, C(2′)—C(3′)—O(3′) 112.0(3)° and 106.8(2)°, O(3′)—C(3′)—C(4′) 108.1(3)° and 111.6(2)°, O(4′)—C(4′)—C(3′) 103.6(3)° and 106.2(2)°. Selected torsion angles are shown in Table 3. The glycosidic torsion angle χ, O(4′)—C(1′)—N(1)—C(2), is 243.5° which is within the usual range of pyrimidine nucleosides that have the *anti* configuration (13). The χ values found in MMdUrd and in 5-hydroxymethyl-2′-deoxyuridine (HMdUrd) were 233.3° and 236.4°, respectively (14, 15). Torsion angles for the 5-methoxymethyl group C(5)—C(5,1)—O(5,2)—C(5,3) and C(6)—C(5)—C(5,1)—O(5,2) are 170.7° and −2.7° for MMdLU. The corresponding values are −114.2° and −99.2° in MMdUrd (14). The change in these torsion angles reflect the relatively flexible nature of the 5-methoxymethyl group and differences in intermolecular hydrogen bonding.

The values calculated for the two pseudorotational parameters (16) of the furanose ring are $P = 55.8°$ and $\tau_m = 41.8°$ for the phase angle of pseudorotation and the amplitude of puckering, respectively. Each of the deoxyribose rings of MMdLU, MMdUrd, HMdUrd, and 2′-deoxythymidine (dThd) in the crystalline state exhibit differences in their envelope conformation. The conformations and corresponding displacements from the mean plane through the other four ring atoms are C(4′)—*exo*, 0.76 Å for MMdLU; C(2′)—*endo*, 0.58 Å for MMdUrd (14); C(1′)—*exo*, 0.42 Å for HMdUrd (15); C(3′)—*exo*, 0.57 Å for dThd (17). It is interesting to note that the C(4′)—*exo* conformation observed has not been reported previously for pyrimidine nucleosides.

The crystal structure is stabilized by three intermolecular hydrogen bonds. The first one is O(5′)—H(05′) ... O(4) [2 − x, 1/2 + y, 2 − z] with distances O(5′) ... O(4) 2.655(4) Å, H(05′) ... O(4) 1.74(8) Å, O(5′)—H(05′) 1.04(6) Å, and angle O(5′)—H(05′) ... O(4) of 144(7)°; the second one is O(3′)—H(03′) ... O(5′) [1 − x, 1/2 − y, 1 − z] with distances O(3′) ... O(5′) 2.649(5) Å, H(03′) ... O(5′) 1.80(9) Å, O(3′)—H(03′) 0.93(9) Å, and angle O(3′)—H(03′) ... O(5′) 150(7)°; the third one is N(3)—H(3) ... O(3′) [1 + x, y, z] with distances N(3) ... O(3′) 2.878(4) Å, H(3) ... O(3′) 2.01(5) Å, N(3)—H(3) 0.87(5) Å, and angle N(3)—H(3) ... O(3′) of 174(4)°.

Nuclear magnetic resonance analysis

The ^1H and ^{13}C parameters are summarized in Tables 4 and 5, respectively. The conformation of the sugar ring was obtained from the relationship between the proton–proton coupling constants and the pseudorotational properties of the ring using a computer program (SPACEJ) based on the method described by Haasnoot *et al.* (18). The calculated coupling constants for the full pseudorotational circuit ($P = 0°$ to 360°) at a puckering amplitude (τ_m) of 39° are shown in Fig. 3. Based on nmr and X-ray evidence (13, 16) as well as theoretical calculations (19), the furanose ring in nucleosides exists in solution in a dynamic equilibrium between two puckered conformations centered around $P = 18°$ (*N*-conformer) and $P = 162°$ (*S*-conformer). The observed vicinal coupling constants represent time-averaged coupling which are linearly related to the couplings of the two conformers and their relative populations by eq. [1], where X_N is the mole fraction of the *N*-conformer.

$$[1] \quad J_{obs} = X_N J_N + (1 - X_n) J_S$$

Using this model, it was calculated that in solution, MMdLU exists in the *N*-conformation (97 ± 5%). Similarly, a strong preference for *N*-type puckering has been reported for 2′-deoxy-*lyxo*-furanosyladenine (20). A shift of the conformational equilibrium toward the C(3′)—*endo* conformer (*N*-type) was also reported for lyxonucleosides (16, 21) and xylonucleosides (22–24). These results suggest that the 2′-OH group in lyxo- and xylonucleosides is much less important than 3′-OH in determining the conformation of the furanose ring. The cisoidal relationship between the 3′-OH and 5′-CH_2OH groups shifts the equilibrium towards the *N*-type conformation. Since the X-ray crystallographic analysis showed an unusual C(4′)—*exo* envelope conformation ($P = 55.8°$), the possibility of such a conformation in the solution was also considered. There is a greater difference between observed and calculated coupling constants when a τ_m value of 39° (the average value reported for nucleosides (16, 25)) is used. However, if the value of $\tau_m = 41.8°$, found in the solid state, is used for these calculations the correlation between experimental and calculated values is improved for the C(4′)—*exo* conformation.

The population of the three rotamers about the exocyclic C(4′)—C(5′) bond was estimated from the $J_{4',5'}$ and $J_{4',5''}$ coupling constants using the method of Haasnoot *et al.* (26). The weighted time-averaged nmr couplings are related to the couplings of the individual conformers and their relative populations by eqs. [2] and [3] where x denotes the mole fraction of each conformer present.

$$[2] \quad {}^3J_{4'5'} = X_{g^+} J'_{g^+} + X_{g^-} J'_{g^-} + X_t J'_t$$

$$[3] \quad {}^3J_{4'5''} = X_{g^+} J''_{g^+} + X_{g^-} J''_{g^-} + X_t J''_t$$

The relative populations for the g^+, t, and g^- modes are 23%, 59%, and 18%, respectively. Assignment of protons H(5′) and

TABLE 1. Bond distances (Å, estimated standard deviation of the last digit is given in parentheses)

Bond	Distance	Bond	Distance
N(1)—C(2)	1.379(5)	C(5, 1)—O(5, 2)	1.400(5)
N(1)—C(6)	1.382(5)	O(5, 2)—C(5, 3)	1.413(7)
N(1)—C(1′)	1.461(4)	C(1′)—C(2′)	1.540(5)
C(2)—O(2)	1.205(5)	C(1′)—O(4′)	1.422(5)
C(2)—N(3)	1.382(4)	C(2′)—C(3′)	1.524(5)
N(3)—C(4)	1.373(5)	C(3′)—C(4′)	1.527(5)
C(4)—O(4)	1.227(4)	C(3′)—O(3′)	1.430(5)
C(4)—C(5)	1.448(5)	C(4′)—O(4′)	1.431(3)
C(5)—C(5, 1)	1.496(5)	C(4′)—C(5′)	1.505(6)
C(5)—C(6)	1.340(5)	C(5′)—O(5′)	1.414(6)

TABLE 2. Bond angles (degrees, estimated standard deviation of the last digit is given in parentheses)

Bonds	Angle	Bonds	Angle
C(2)—N(1)—C(6)	121.6(2)	C(5)—C(5, 1)—O(5, 2)	109.0(3)
C(2)—N(1)—C(1′)	119.0(3)	C(5, 1)—O(5, 2)—C(5, 3)	111.6(4)
C(6)—N(1)—C(1′)	119.3(3)	N(1)—C(1′)—O(4′)	107.7(2)
N(1)—C(2)—O(2)	124.4(3)	N(1)—C(1′)—C(2′)	114.2(3)
N(1)—C(2)—N(3)	114.1(3)	O(4′)—C(1′)—C(2′)	106.9(3)
O(2)—C(2)—N(3)	121.5(3)	C(1′)—C(2′)—C(3′)	104.0(3)
C(2)—N(3)—C(4)	127.4(3)	C(2′)—C(3′)—O(3′)	112.0(3)
N(3)—C(4)—O(4)	119.4(3)	C(2′)—C(3′)—C(4′)	101.7(3)
N(3)—C(4)—C(5)	115.3(3)	O(3′)—C(3′)—C(4′)	108.1(3)
O(4)—C(4)—C(5)	125.3(3)	O(4′)—C(4′)—C(3′)	103.6(3)
C(4)—C(5)—C(5, 1)	117.9(3)	O(4′)—C(4′)—C(5′)	110.8(2)
C(4)—C(5)—C(6)	118.2(3)	C(3′)—C(4′)—C(5′)	114.3(3)
C(5, 1)—C(5)—C(6)	123.8(3)	C(4′)—C(5′)—O(5′)	111.3(4)
N(1)—C(6)—C(5)	123.3(3)	C(1′)—O(4′)—C(4′)	106.6(2)

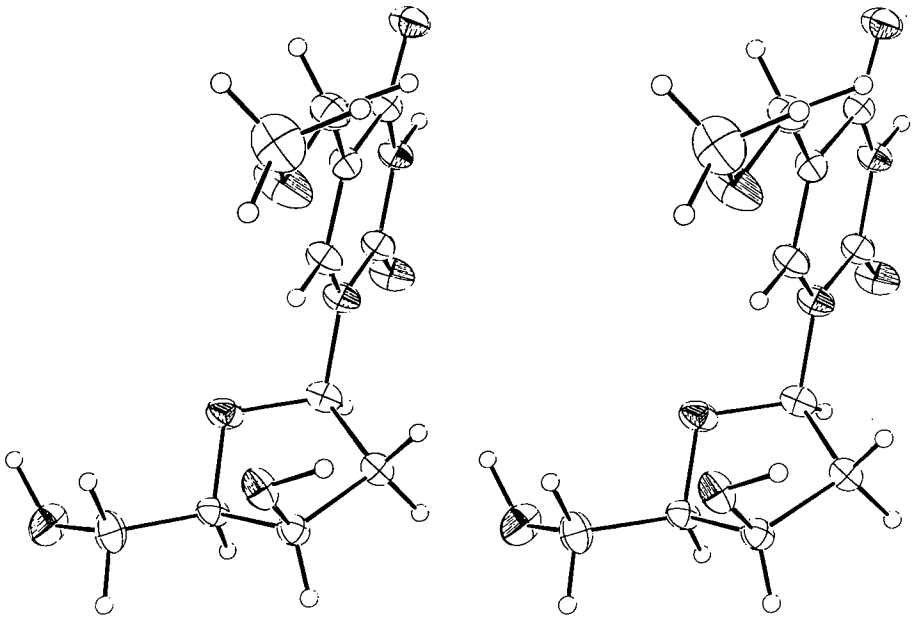

FIG. 2. Stereoscopic view of MMdLU.

H(5″) was done according to Remin and Shugar (27). The reverse assignment leads to values of 29%, 13%, and 58%, respectively. In contrast, the biologically active epimer MMdUrd exists predominantly in the g^+ mode (14). The strong destabilization of the g^+ mode in MMdLU is typical for nucleosides having the 3′-OH group cisoidal to the exocyclic C(5′) group (27). Most likely this is due to the steric and/or electrostatic effects of the cisoidal configuration.

The nmr signal for C(2) is a form of a doublet with $J_{C(2),H(6)}$ = 8.8 Hz but $^3J_{C(2),H(1')}$ is not resolved. The value of the latter coupling constant can be estimated to be less than 2 Hz which is consistent with an *anti* conformation about the glycosidic bond. The relationship between the 5-methoxymethyluracil and furanose rings seems to be independent of whether the 3′-OH group is *endo* or *exo*.

The two hydrogens of the methylene in the 5-methoxymethyl substituent have different chemical shifts. However, since both protons of the methylene group have the same coupling constant with H(6), the methoxy group does not seem to have any preference to be on one particular side of the pyrimidine ring. The anisotropic effects are stronger in MMdLU than in its epimer because the methoxy group is closer to the sugar moiety in MMdLU.

Experimental

5-Methoxymethyl-1-(2′-deoxy-β-D-lyxofuranosyl)uracil

Epimerization at the 3′-carbon was accomplished using the procedure described previously for thymidine (28, 29). Methanesulfonyl chloride (0.94 mL, 12.4 mmol) was added to a cooled solution of 2.0 g (3.4 mmol) of 5-methoxymethyl-5′-triphenylmethyl-2′-deoxyuridine (7) in 20 mL of pyridine at 4°C and the solution was stirred for 16 h. Water (0.4 mL) was added and after stirring for 1 h, the reaction mixture was added dropwise to ice-water. The precipitate was dissolved in 70 mL of $CHCl_3$, washed successively with 0.1 *M* HCl, 5% $NaHCO_3$, and dried over Na_2SO_4. The solvent was removed *in vacuo* and the amorphous powder (2.2 g) was dissolved in a solution of 60% ethanol–water containing 1 equiv. of NaOH. The reaction mixture was stirred at room temperature for 16 h to yield the O^2,3′-cyclic intermediate monitored by the disappearance of the 265

TABLE 3. Selected torsion angles (degrees, estimated standard deviation of the last digit is given in parentheses)

Bonds	Torsion angle
O(4′)—C(1′)—N(1)—C(2)	243.5(4)*
O(4′)—C(1′)—C(2′)—C(3′)	+0.1(3)
C(1′)—C(2′)—C(3′)—C(4′)	+23.2(3)
C(2′)—C(3′)—C(4′)—O(4′)	−39.2(3)
C(3′)—C(4′)—O(4′)—C(1′)	+41.0(3)
C(4′)—O(4′)—C(1′)—C(2′)	−25.6(4)
C(1′)—C(2′)—C(3′)—O(3′)	−91.9(3)
C(3′)—C(4′)—C(5′)—O(5′)	−173.4(2)
O(4′)—C(4′)—C(5′)—O(5′)	+70.1(4)
N(1)—C(1′)—C(2′)—C(3′)	+119.1(3)
C(5)—C(5, 1)—O(5, 2)—C(5, 3)	+170.7(3)
C(6)—C(5)—C(5, 1)—O(5, 2)	−2.7(5)
H(1′)—C(1′)—C(2′)—H(2′)	+117(5)
H(1′)—C(1′)—C(2′)—H(2″)	−4(4)
H(2′)—C(2′)—C(3′)—H(3′)	−98(4)
H(2″)—C(2′)—C(3′)—H(3′)	+29(4)
H(3′)—C(3′)—C(4′)—H(4′)	−47(4)
H(4′)—C(4′)—C(5′)—H(5′)	+67(3)
H(4′)—C(4′)—C(5′)—H(5″)	−170(4)

*The convention (15), based on accepted chemical nomenclature, differs from the one frequently used where χ_{CN} was defined by O(4′)—C(1′)—N(1)—C(6). $\chi = \chi_{CN} \pm 180$, vis. *syn* = 0 ± 90° and *anti* = 180 ± 90°.

TABLE 4. Chemical shifts (ppm)

Proton	Chemical shift	Carbon-13	Chemical shift
H(1′)	6.15	C(1′)	85.83
H(2′)	2.17	C(2′)	40.43
H(2″)	2.74	C(3′)	69.50
H(3′)	4.52	C(4′)	85.15
H(4′)	4.16	C(5′)	60.00
H(5′)	4.00	C(2)	151.58
H(5″)	3.96	C(4)	165.25
H(6)	8.10	C(5)	109.58
CH_2	4.22, 4.29	C(6)	141.96
CH_3	3.35	C(5, 1)	66.66
		C(5, 3)	57.12

nm peak and the appearance of shoulders at 231 and 255 nm (29). After addition of 2 equiv. of NaOH, the mixture was refluxed for 5 h, cooled, the pH adjusted to 5 with HCl, and the solvent was evaporated *in vacuo*. The gummy residue was triturated with water and filtered. The amorphous power was added to 20 mL of 80% acetic acid and incubated at 50°C for 2 h to remove the trityl group. After chilling, triphenylmethanol was removed by filtration. The solvent was evaporated and crystallization from absolute ethanol gave 0.7 g of *5-methoxy-1-(2′-deoxy-β-D-lyxofuranosyl)uracil* (yield 75%); mp 155–156°C; uv (0.1 *M*, phosphate buffer, pH 7.0) λ_{max} 264 nm (10,300). *Anal.* calcd. for $C_{11}H_{16}O_6N_2$: C 48.52, H 5.93, N 10.29; found: C 49.15, H 6.10, N 10.36.

X-ray crystallography

Suitable crystals were obtained from a saturated solution of MMdLU in methanol/ethyl acetate over a period of one month. The colorless crystals of MMdLU, empirical formula $C_{11}H_{16}O_6N_2$ have the space group $P2_1$ with a = 8.719(4), b = 13.188(3), c = 5.701(3) Å, β = 109.56(2)°, V = 6.77 Å^3, Z = 2, μ = 10.4 cm^{-1}, observed density = 1.44 g cm^{-3}, calculated density = 1.46 g cm^{-3}. Quantitative data collection was done on an ENRAF-NONIUS CAD4F Diffractometer with an ω/2θ scan and Ni-filtered copper radiation (λ = 1.5418 Å). Three standard reflections were checked every 5000 s for intensity variations and every 100 reflections for orientation. The maximum variation of the intensity standard was 3.1%. There was no significant decay of the crystal over the entire data collection. The octants ±*h*, *k*, *l* were measured. Observational weights for the reflections were derived from

[4] $w = 1/\sigma((F_0))^2$.

The crystal was 0.825 × 0.375 × 0.150 mm in size and exhibited the forms (101), (010), (001), (031), and (100). A total of 2768 reflections were collected out to θ = 70°; of 1224 unique reflections, 1208 had net $I > 2\sigma(I)$. X-ray data were processed and the structure was solved using the XTAL83 system (30) using atomic scattering factors from Cromer and Mann (31). All four figures of merit by GENTAN were used to choose the best set of phases in the structure determination (RFOM = 1.04, RFAC = 0.12, PSIO = 0.79, NEGQ = 96, and CFOM = 0.83). All 19 nonhydrogen atoms in the molecule were found on the *E* map.

Least-squares isotropic refinement gave an *R* value of 0.117. Anisotropic refinement was then carried out and gave an *R* value of 0.068. The positions of the hydrogen atoms were located by using a difference Fourier map. Finally, full-matrix least-square refinement of anisotropic temperature factors for the non-hydrogen atoms and isotropic refinement for the hydrogen atoms converged to an *R* index of 0.040. The quantity minimized in refinement was $\Sigma W\Delta F^2$.

[5] $R = \Sigma||F_0| - |F_c||/\Sigma|F_0|$

[6] $R_w = [\Sigma w\Delta F^2/\Sigma wF_0^2]^{1/2}$

[7] $S = [\Sigma w\Delta F^2/(m - n)]^{1/2}$

R_w was 0.059 and S was 4.1. The largest and average shift/error ratios

TABLE 5. Observed and calculated (17) coupling constants (Hz)

	J_{obsd}	J_{calcd} for P = 18° τ_m = 39°	J_{calcd} for P = 162° τ_m = 39°	Population of *N*-state (%)
$J_{1'2'}$	2.0	1.9	10.2	99
$J_{1'2''}$	7.8	8.1	5.6	88
$J_{2'3'}$	1.1	1.4	9.3	103
$J_{2''3'}$	5.2	5.1	7.6	96
$J_{3'4'}$	3.2	3.1	7.7	98
				97±5%
$J_{2'2''}$	−15.0			
$J_{4'5'}$	4.0			
$J_{4'5''}$	7.3			
$J_{5'5''}$	−11.9			

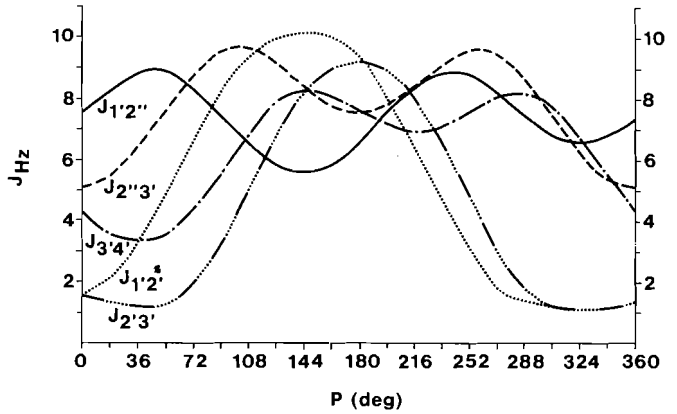

FIG. 3. Coupling constants $^3J_{HH}$ (Hz) for deox*ylyxo*furanose as a function of pseudorotation phase angle P, assuming a puckering amplitude, τ_m = 39°, calculated by SPACEJ, a program based on the method of Haasnoot *et al.* (17).

TABLE 6. Fractional coordinates and average thermal parameters for MMdLU (estimated standard deviation of the last digit is given in parentheses; nonhydrogen atom positions × 10^4, hydrogen atom positions × 10^3; $U_{eq} = (U_{11} + U_{22} + U_{33})/3$; U_{iso} or $U_{eq} \times 10^3$)

Atom	x/a	y/b	z/c	U_{iso} or U_{eq} (Å^2)
N(1)	9342(3)	7122	5008(5)	31
C(2)	10793(4)	7228(3)	4560(6)	32
O(2)	10996(3)	7790(3)	3022(6)	40
N(3)	12039(3)	6630(3)	6051(5)	30
C(4)	11955(4)	5930(3)	7786(5)	32
O(4)	13164(3)	5427(3)	8895(5)	39
C(5)	10398(4)	5866(3)	8172(5)	35
C(5, 1)	10227(4)	5116(3)	10036(6)	43
O(5, 2)	8653(4)	5184(3)	10156(6)	61
C(5, 3)	8331(7)	4389(4)	11587(10)	76
C(6)	9186(4)	6461(3)	6796(6)	32
C(1′)	7918(4)	7686(3)	3473(6)	32
C(2′)	6447(4)	7015(3)	2091(6)	35
C(3′)	5119(3)	7364(3)	3094(5)	30
O(3′)	5103(3)	6779(3)	5199(5)	43
C(4′)	5687(3)	8435(3)	3992(5)	29
O(4′)	7416(2)	8334(3)	5073(5)	29
C(5′)	4972(5)	8853(3)	5833(7)	57
O(5′)	5400(4)	9882(3)	6393(5)	82
H(3)	1298(6)	663(3)	584(7)	40(10)
H1(5, 1)	1110(6)	515(4)	1155(8)	45(10)
H2(5, 1)	1044(5)	433(4)	947(8)	47(11)
H1(5, 3)	897(7)	452(5)	1333(12)	76(16)
H2(5, 3)	866(6)	367(4)	1104(9)	57(13)
H3(5, 3)	712(9)	448(7)	1133(13)	101(23)
H(6)	820(5)	641(3)	705(7)	34(9)
H(1′)	823(6)	803(4)	228(8)	43(11)
H(2′)	673(7)	630(4)	247(10)	66(14)
H(2″)	614(6)	717(4)	13(9)	57(12)
H(3′)	410(5)	735(3)	191(7)	36(9)
H(03′)	531(9)	612(7)	476(14)	99(22)
H(4′)	546(4)	890(3)	250(6)	23(7)

for the parameters in the final cycle of refinement were 0.47 and 0.014, respectively. A final difference Fourier map showed a largest peak of 0.23e. A stereoscopic representation of the molecule is shown in Fig. 2 and all final coordinates are given in Table 6.* A VAX 11/780 computer at the University of Saskatchewan was used to carry out all crystallographic computations.[2]

Nuclear magnetic resonance spectroscopy

The nmr experiments were carried out using a Brucker CXP300 spectrometer. Spectra were recorded in the Fourier transform mode at 26°C. Solutions were made to a concentration of 0.2 M in D_2O. Chemical shifts were measured relative to internal trimethylsilyl propanesulfonic acid, sodium salt (TSP) for ^1H and relative to tetramethylsilane (TMS) in a concentric capillary for ^{13}C. ^1H nmr spectra were simulated with the aid of the LAOCOON III program and final coupling constants have a precision of 0.1–0.2 Hz.

Acknowledgements

This research was funded by grants from the Medical Research Council of Canada (to V.S.G. and L.T.J.D.). O.A.L. El-K. is the recipient of a Saskatchewan Health Research Board Training Fellowship.

[2]Tables of anisotropic thermal parameters and structure factors are available may be purchased from the Depository of Unpublished Data, CISTI, National Research Council of Canada, Ottawa, Ont., Canada K1A 0S2.

1. V. S. GUPTA. Drugs of the Future, **6**, 32 (1981).
2. L. A. BABIUK, J. B. MELDRUM, V. S. GUPTA, and B. T. ROUSE. Antimicrob. Agents Chemother. **8**, 643 (1975).
3. N. K. AYISI, V. S. GUPTA, J. B. MELDRUM, A. K. TANEJA, and L. A. BABIUK. Antimicrob. Agents Chemother. **17**, 558 (1980).
4. J. B. MELDRUM, V. S. GUPTA, and L. A. BABIUK. Chemotherapy, **26**, 54 (1980).
5. N. K. AYISI, J. B. MELDRUM, A. L. STUART, and V. S. GUPTA. Antiviral Res. **3**, 161 (1983).
6. N. K. AYISI, V. S. GUPTA, and L. A. BABIUK. Antiviral Res. **5**, 13 (1985).
7. A. L. STUART, N. K. AYISI, G. TOURIGNY, and V. S. GUPTA. J. Pharm. Sci. **74**, 246 (1985).
8. N. K. AYISI, V. S. GUPTA, and L. A. BABIUK. Antiviral Res. **6**, 33 (1986).
9. G. L. BUBBAR and V. S. GUPTA. Can. J. Chem. **48**, 3147 (1970).
10. A. L. STUART, G. TOURIGNY, and V. S. GUPTA. Proc. Can. Fed. Biol. Soc. **26**, 105 (1983).
11. V. S. GUPTA, G. TOURIGNY, A. L. STUART, J. W. QUAIL, I. EKIEL, O. A. L. EL-KABBANI, and L. T. J. DELBAERE. Antiviral Res. To be published.
12. G. A. WEINMASTER. M.Sc. thesis. University of Saskatchewan, Saskatoon. 1981.
13. D. B. DAVIES. Prog. Nucl. Magn. Reson. Spectrosc. **12**, 136 (1978).
14. O. A. L. EL-KABBANI, I. EKIEL, L. T. J. DELBAERE, G. TOURIGNY, A. L. STUART, and V. S. GUPTA. Nucleos. Nucleot. **5**, 95 (1986).
15. G. I. BIRNBAUM, R. DESLAURIERS, T. S. LIN, G. T. SHIAU, and W. H. PRUSOFF. J. Am. Chem. Soc. **102**, 4236 (1980).
16. C. ALTONA and M. SUNDARALINGAM. J. Am. Chem. Soc. **94**, 8205 (1972).
17. D. W. YOUNG, P. TOLLIN, and H. R. WILSON. Acta Crystallogr. Sect. B, **25**, 1423 (1969).
18. C. A. G. HAASNOOT, F. A. A. M. DE LEEUW, H. P. M. DE LEEUW, and C. ALTONA. Org. Magn. Reson. **15**, 43 (1981).
19. B. PULLMAN and A. SARAN. *In* Progress in nucleic acid research and molecular biology. Vol. 18. *Edited by* W. E. Cohn. Academic Press, N.Y. 1976, p. 215.
20. H. D. LUDEMAN, G. KNOPP, F. HANSSKE, and M. J. ROBINS. *In* Nucleic acids: the vectors of life. *Edited by* B. Pullman and J. Jortner. D. Reidel Publishing Co., Dordrect. 1983. p. 537.
21. I. EKIEL, E. DARZYNKIEWICZ, G. I. BIRNBAUM, and D. SHUGAR. J. Am. Chem. Soc. **101**, 4724 (1979).
22. I. EKIEL and D. SHUGAR. Acta Biochem. Polon. **26**, 435 (1979).
23. I. EKIEL, E. DARZYNKIEWICZ and D. SHUGAR. Biochem. **17**, 1530 (1978).
24. I. EKIEL, J. GIZIEWICZ and D. SHUGAR. J. Carbohydr. Nucleos. Nucleot. **8**, 279 (1981).
25. H. P. M. DE LEEUW, C. A. G. HAASNOOT, and C. ALTONA. Isr. J. Chem. **20**, 108 (1980).
26. C. A. G. HAASNOOT, F. A. A. M. DE LEEUW, H. P. M. DE LEEUW, and C. ALTONA. Rec. Trav. Chim. Phys. Bas. **98**, 576 (1979).
27. M. REMIN and D. SHUGAR. Biochem. Biophys. Res. Commun. **48**, 636 (1972).
28. A. M. MICHELSON and A. R. TODD. J. Chem. Soc. 816 (1955).
29. J. J. FOX and N. C. MILLER. J. Org. Chem. **28**, 936 (1963).
30. J. M. STEWART, S. R. HALL, R. A. ALDEN, R. OLTHOF-HAZENKAMP, and R. M. DOHERTY. The XTAL system of crystallographic programs. Computer Science Center, University of Maryland, College Park, MD. 1983.
31. D. T. CROMER and J. B. MANN. Acta. Crystallogr. A**24**, 321 (1968).

Synthèses, réactivité et études structurales en série thiophéno[*b*]homotroponique

BERNARD HANQUET ET ROGER GUILARD[1]

Laboratoire de synthèse et d'électrosynthèse organométallique associé au Centre national de la recherche scientifique (Unité associée 33), Faculté des sciences « Gabriel », 6, Boulevard Gabriel, 21100 Dijon, France

Recù le 26 avril 1985[2]

B. HANQUET et R. GUILARD. Can. J. Chem. **64**, 1360 (1986).

Les thiophéno[*b*]mono et bishomotropones sont préparées par action du méthylure de diméthylsulfoxonium sur les thiophéno[*b*]tropones. La position, la nature des substituants du carbocycle et le solvant réactionnel sont les paramètres qui gouvernent l'évolution de la réaction de cyclopropanation. La structure des monohomotropones obtenues est établie en mettant en oeuvre des analogues deutériés et l'analyse des spectres rmn des thiophéno[*b*]bishomotropones permet de préciser la configuration *cis* ou *trans* des composés bishomotroponiques. La réduction, selon Clemmensen, de ces dérivés livre des cycloocta et cyclonona[*b*]thiophénones dont la structure est déterminée par rmn à deux dimensions.

B. HANQUET and R. GUILARD. Can. J. Chem. **64**, 1360 (1986).

Thiopheno[*b*]mono and bishomotropones are readily synthesized from thiopheno[*b*]tropones and dimethyloxosulfonium methylide. The position, the nature of the seven-membered ring substituents, and the reaction medium are the most important parameters of the cyclopropanation reaction. The structure of the monohomotropones is established by comparison with deuteriated analogues. The *cis* or *trans* configuration of the bishomotropones is determined by nmr data analysis of the corresponding alcohols. Clemmensen reduction leads to cycloocta or cyclonona[*b*]thiophenones. The structure of the latter is proved by 2D nmr.

Introduction

Dans un mémoire précédent (1), nous avons décrit les modalités d'accès aux thiophéno[*c*]mono et bishomotropones et examiné les problèmes liés à la détermination de leur structure. La préparation de ces composés est réalisée avec de bons rendements (jusqu'à 87%) par condensation du méthylure de diméthylsulfoxonium sur les thiophéno[*c*]tropones. Le bilan réactionnel peut être résumé selon le schéma suivant :

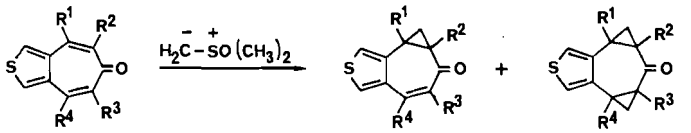

cis/trans

Lors des recherches effectuées dans cette série nous avons montré que le nombre et la nature des thiophéno[*c*]homotropones obtenues dépendaient pour l'essentiel du nombre, de la nature et de la position des substituants présents sur le carbocycle. Nous avons voulu étendre les résultats obtenus en série [*c*] à la série des thiophéno[*b*]homotropones pour laquelle l'asymétrie introduite par la position de l'atome de soufre entraîne, *a priori*, l'existence de deux thiophéno[*b*]monohomotropones isomères et pour laquelle subsistent les problèmes structuraux liés à l'isomérie *cis/trans* des systèmes bishomotroponiques.

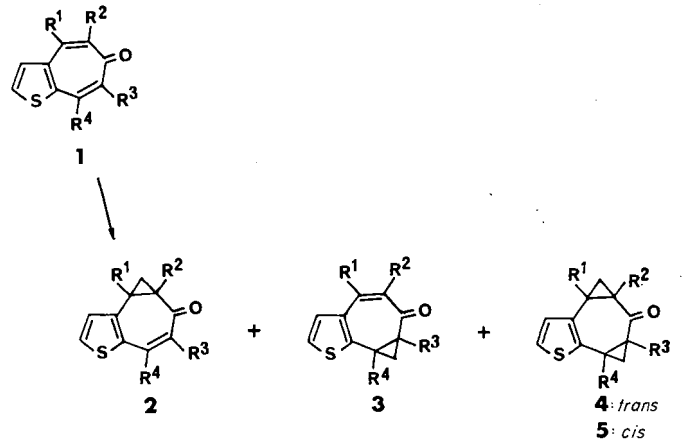

Ce mémoire sera donc consacré à la synthèse, l'étude de la réactivité et la détermination structurale des thiophéno[*b*]homotropones. Nous montrerons que trois paramètres ont une incidence sur l'évolution de la réaction : la nature et la position des substituants présents sur le carbocycle, le rapport agent de cyclopropanation/substrat et le solvant réactionnel. Nous aborderons enfin quelques aspects de la réactivité des thiophénohomotropones synthétisées ayant trait à la présence du groupement carbonyle en envisageant l'action de réducteurs tels que l'hydrure double de lithium et d'aluminium et l'amalgame de zinc. Ces derniers résultats complètent ceux que nous avons publiés par ailleurs (2, 3) concernant l'action des agents protecteurs de la fonction carbonyle.

Synthèses

Le nombre et la structure des composés obtenus dépendent de la structure des thiophéno[*b*]tropones mises en oeuvre et des conditions opératoires. Les transformations sont conduites, sauf indication contraire, dans le *N,N*-diméthylformamide (DMF) à la température ambiante.

(1) *Influence des substituants du carbocycle*

Au départ de la thiophéno[*b*]tropone non substituée **1***a* il ne nous a pas été possible d'isoler d'homotropones, quelles que soient les conditions de température et de solvant. En revanche la thiophéno[*b*]tropone diméthylée **1***b* conduit à deux thiophéno[*b*]monohomotropones isomères **2***b* et **3***b*. Un analogue deutérié **1'***b* de **1***b* a été mis en oeuvre pour démontrer la structure des deux isomères. Lors de la réaction de cyclopropanation, aucun phénomène d'échange isotopique n'intervient.

Au départ des thiophéno[*b*]tropones triméthylées **1***c* et **1***d* une seule monohomotropone est obtenue. On retrouve ici un résultat déjà observé en série [*c*] : l'encombrement stérique de deux groupements méthyle vicinaux induit la formation de la monohomotropone la moins encombrée.

De même qu'en série [*c*] la présence de substituants électroattracteurs identiques sur le reste troponique ($R^2 = R^3 = CO_2C_2H_5$ ou Ph) conduit simultanément aux deux monohomo-

1. Auteur à qui adresser toute correspondance.
2. Révision reçue le 16 janvier 1986.

Printed in Canada / Imprimé au Canada

TABLEAU 1. Thiophéno[*b*] mono et bishomotropones synthétisées par action du méthylure de diméthylsulfoxonium sur les thiophéno[*b*]tropones

R^1	R^2	R^3	R^4	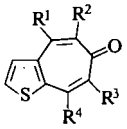	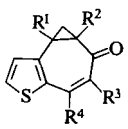		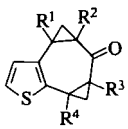
H	H	H	H	**1***a*	—	—	—
H	CH_3	CH_3	H	**1***b*	**2***b*	**3***b*	—
H	CH_3	CH_3	D	**1′***b*	**2′***b*	**3′***b*	—
H	CH_3	CH_3	CH_3	**1***c*	**2***c*	—	—
CH_3	CH_3	CH_3	H	**1***d*	—	**3***d*	—
H	CO_2Et	CO_2Et	H	**1***e*	**2***e*	**3***e*	**4***e*
H	CO_2Et	CO_2Et	D	**1′***e*	**2′***e*	**3′***e*	**4′***e*
H	Ph	Ph	H	**1***f*	**2***f*	**3***f*	**4***f* (**5***f*)[a]
H	Ph	Ph	D	**1′***f*	**2′***f*	**3′***f*	**4′***f*
D	Ph	Ph	H	**1″***f*	**2″***f*	**3″***f*	**4″***f*

a. **5***f*: composé *cis*.

tropones isomères et à une bishomotropone de configuration *trans*. La cyclopropanation des analogues deutériés **1′***e*, **1′***f* et **1″***f* a été également réalisée.

Même si la température de la réaction est abaissée, les rendements en thiophéno[*b*]homotropones diester restent faibles (~33%) alors que la transformation des dérivés diphénylés s'effectue avec des rendements comparables à ceux obtenus en série [*c*] (~77%). Lorsque les deux thiophéno[*b*]monohomotropones sont obtenues, le composé **2** est souvent en quantité plus importante que son isomère **3**. La cyclopropanation de la double liaison située du côté de l'atome de soufre semble donc moins aisée. Les résultats sont en accord avec les caractéristiques rmn ^{13}C du substrat de départ. Ainsi dans le cas de la thiophéno[*b*]tropone **1***f* le déblindage plus important de C_4 (132,5 ppm) par rapport à C_8 (130,6 ppm) privilégie l'attaque du réactif sur ce sommet. Cependant la valeur faible de cette différence des glissements chimiques explique que les proportions relatives des isomères **2** et **3** sont parfois très voisines.[3] Le tableau 1 indique les différentes thiophéno[*b*]homotropones synthétisées (le tableau 5 de la partie expérimentale précise leurs proportions relatives).

Bien que la thiophéno[*b*]tropone **1***a* n'ait pu subir avec succès l'addition d'ylure de diméthylsulfoxonium, nous avons accédé à certaines thiophéno[*b*]homotropones non substituées au départ des homotropones diester. Ainsi, en présence d'un sel alcalin, le dérivé **2***e* livre la monohomotropone non substituée **2***a*. En revanche, et dans les mêmes conditions expérimentales, **3***e* conserve un groupement ester pour donner **3***g* :

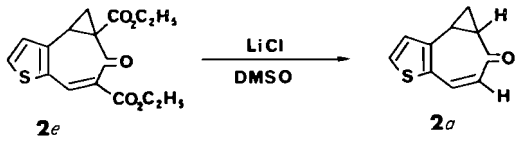

2*e* **2***a*

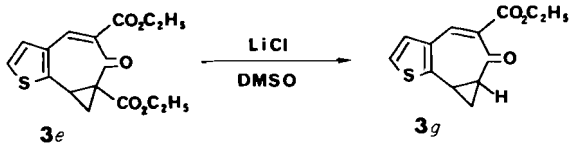

3*e* **3***g*

3. Une étude théorique par les méthodes de Hückel étendu et CNDO/4 est en cours. Les calculs portent essentiellement sur les intermédiaires résultant de l'addition de l'ylure sur les thiophéno[*b*]tropones et conduisant aux composés **2** et **3**.

La thiophéno[*b*]bishomotropone **4***e* conduit avec un bon rendement (61%) au dérivé non substitué **4***a* :

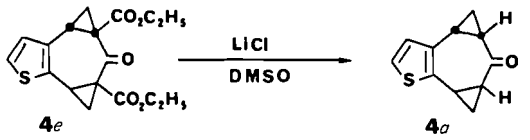

4*e* **4***a*

(2) *Influence du rapport ylure/tropone et du solvant réactionnel*

Le tableau 2 regroupe les résultats observés en faisant varier la quantité relative d'ylure mise en oeuvre et le solvant. Le substrat mis en jeu est la thiophéno[*b*]tropone diphénylée **1***f*.

Lorsque la réaction est effectuée dans le DMF et sur des quantités équimoléculaires (exp. 1), la transformation n'est pas totale et seules les deux monohomotropones isomères apparaissent. Lorsque la proportion d'ylure augmente (exp. 2), le dérivé bishomotroponique *trans* est obtenu simultanément avec les deux composés monohomotroponiques et le rendement global de la réaction est très voisin du précédent (76%). Si le solvant réactionnel est le DMSO (exp. 3), le mélange des monohomotropones n'apparaît qu'avec un rendement de 4% et le produit majoritaire est la bishomotropone *trans*. Il convient également de souligner que l'isomère *cis* apparaît simultanément (2%). Enfin, si la proportion d'ylure est plus importante (exp. 4), le rendement global diminue car l'on observe une dégradation partielle des produits de la réaction.

Ces constatations expérimentales suggèrent que la monohomotropone ne subit que difficilement une nouvelle attaque d'ylure de diméthylsulfoxonium dans le DMF même avec un rapport élevé de réactif. Un effet cinétique important est mis en évidence en substituant le DMSO au DMF. Dans ce cas la transformation est, pour des rapports de réactif comparables, beaucoup plus importante.

Action des reducteurs

Les réactions de réduction des thiophéno[*b*]homotropones ont été essentiellement étudiées au départ des composés diphénylés pour lesquels nous disposions du plus grand nombre de représentants. Deux types de réducteurs ont été mis en oeuvre : l'hydrure double de lithium et d'aluminium et l'amalgame de zinc en milieu chlorohydrique.

(1) *Hydrure double de lithium et d'aluminium*

Comme en série thiophéno[*c*]homotroponique, opposé à

TABLEAU 2. Influence du rapport ylure/tropone et rôle du solvant

Exp.	Solvant réactionnel	Rapport ylure/tropone	Rendements en produits formés (ou récupérés) Tropone 1*f*	Monohomos 2*f* + 3*f*	Bishomo *trans* 4*f*	Bishomo *cis* 5*f*
1	DMF	1:1	8	75	0	0
2	DMF	5:1	0	51	25	0
3	DMSO	4:1	0	4	71	2
4	DMSO	5:1	0	0	74	0

l'hydrure double de lithium et d'aluminium, le mélange des thiophéno[*b*]monohomotropones, non séparées, conduit au mélange d'alcools attendus. Seuls les dérivés d'addition-1,2 sont obtenus :

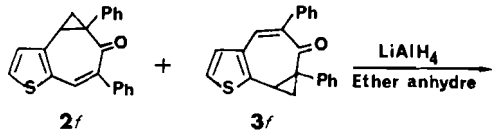

2*f* **3***f*

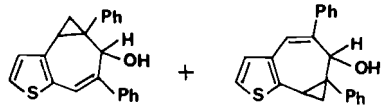

6*f* **7***f*

La réduction des thiophéno[*b*]bishomotropones procède également d'une addition-1,2. Mais au départ du composé **5***f* un seul alcool est obtenu, alors que deux alcools isomères en proportions voisines sont isolés au départ de **4***f*.

Nous avons déjà signalé dans un précédent mémoire (1) que l'on observait lors de la réduction des thiophéno[*c*]bishomotropones une très grande stéréosélectivité, un seul alcool étant obtenu au départ de chacune des thiophéno[*c*]bishomotropones *cis* et *trans*. Cette même stéréosélectivité conduit à un seul alcool au départ du composé *cis* **5***f* alors que deux alcools diastéréoisomères sont produits au départ de **4***f*.

5*f* **9***f*

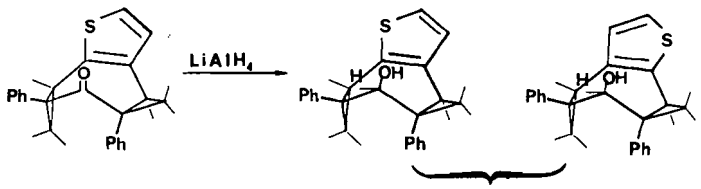

4*f* **8***f*

(2) *Amalgame de zinc*

La réduction selon Clemmensen (4) de la thiophéno[*b*]homotropone **4***f* conduit aux deux composés isomères **10** et **11** (non séparés) dans les proportions relatives de 40 et 60%. Ce résultat est observé pour un rapport zinc/substrat voisin de 40:1 mais si la quantité de réducteur est augmentée (100:1) on note également l'apparition d'une cyclonona[*b*]thiophénone **12**, dérivé ultime de la réaction de réduction.

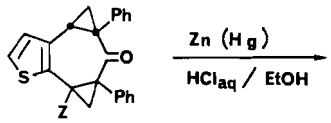

4*f*: Z=H
4*f'*: Z=D

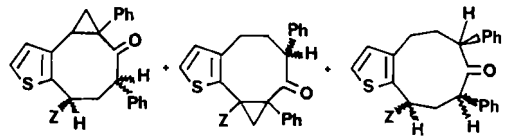

10 **11** **12**
10' **11'** **12'**

Ces résultats font clairement apparaître que pour la série de composés étudiés, l'hydrure double de lithium et d'aluminium ne conduit qu'à des dérivés d'addition-1,2 alors que par réduction selon Clemmensen seuls les produits d'addition-1,4 sont obtenus. Enfin, pour aucun des systèmes étudiés nous n'avons pu mettre en évidence la formation de thiophénohomotropilidènes.

Détermination des structures

La détermination de la structure des thiophéno[*b*]homotropones ou de leurs dérivés est rendue délicate en raison de l'absence de symétrie du substrat de départ. Ainsi pour les monohomotropones la position du cycle à trois chaînons ne peut généralement être établie que par comparaison du spectre du composé avec celui de son analogue deutérié. Pour les bishomotropones le recours à l'examen radiocristallographique a été nécessaire (5). L'analyse des spectres rmn à haut champ a permis de lever certaines incertitudes structurales.

(1) *Thiophéno[*b*]monohomotropones*

Les caractéristiques rmn de ces dérivés apparaissent dans le tableau 3. L'analyse des spectres de rmn protonique des deux thiophéno[*b*]monohomotropones triméthylées **2***c* et **3***d* (fig. 1) est très aisée : pour chaque composé les protons du motif cyclopropanique apparaissent sous la forme d'un système ABX. Il s'ensuit que le cycle à trois chaînons a été introduit au niveau de la double liaison la moins encombrée. Les deux spectres présentent par ailleurs des caractéristiques très proches tant pour les déplacements chimiques que pour les constantes de couplage. Les deux protons thiophéniques de **2***c* donnent un système AB classique alors que ces mêmes protons sont équivalents dans **3***d*.

L'analyse comparative des spectres de **2***b* et de son analogue deutérié **2'***b* (fig. 2) permet d'établir sans ambiguïté la structure de **2***b*. L'absence de proton éthylénique sur le spectre de **2'***b* et la disparition simultanée du couplage avec les protons du

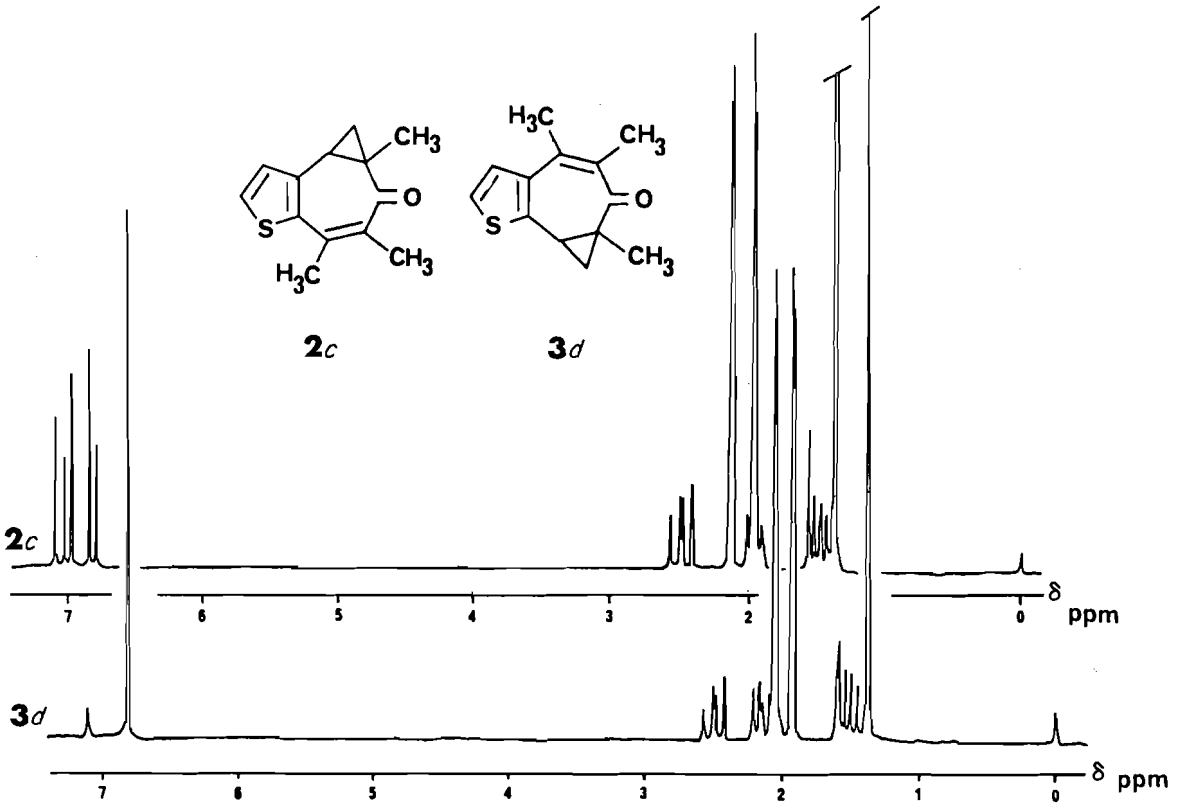

FIG. 1. Spectre rmn ^1H (100 MHz, $CDCl_3$) des thiophéno[*b*]monohomotropones **2***c* et **3***d*.

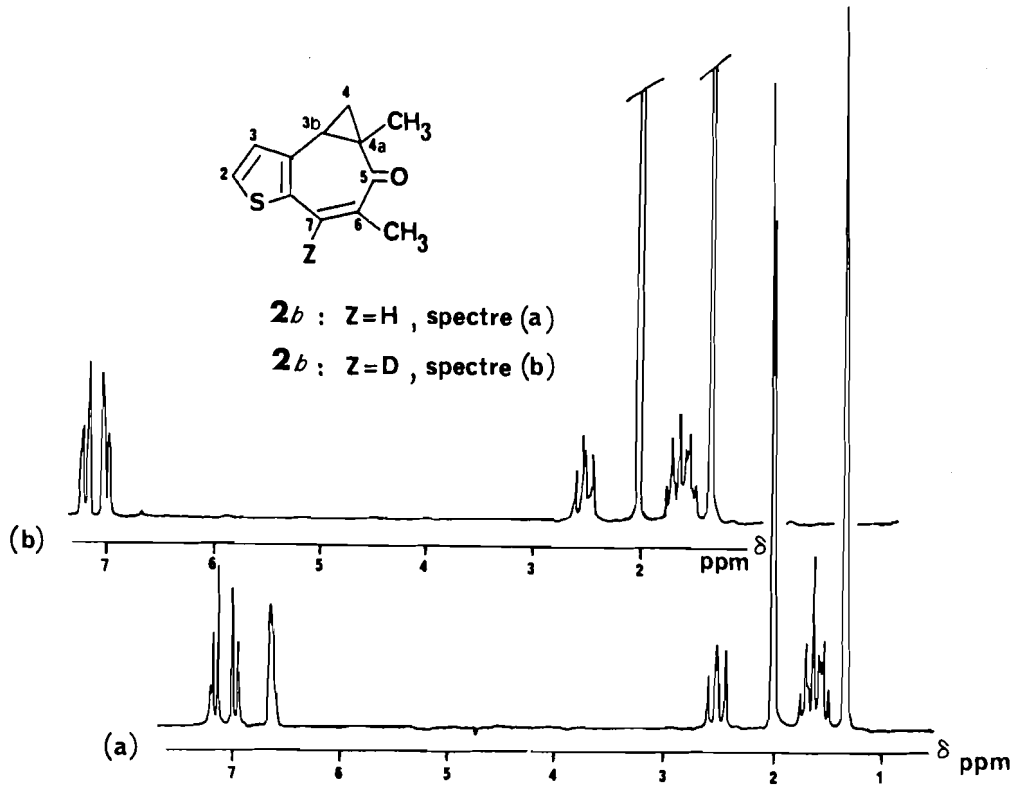

FIG. 2. Spectres rmn ^1H (100 MHz, $CDCl_3$) de **2***b* et de son analogue deutérié **2′***b*.

TABLEAU 3. Caractéristiques rmn des dihydro-4,4 3b*H*-cyclopropa[3,4]cyclohepta[1,2-*b*]thiophénones-5, **2**,

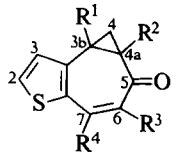

2

Protons

					Thiophéniques						Exocycliques							
					H_1		H_2		H_3		de R^1		de R^2		de R^3		de R^4	
Composé	R^1	R^2	R^3	R^4	m/i	δ	m/i	δ	m/i	δ	m/i	δ	m/i	δ	m/i	δ	m/i	δ
2*a*	H	H	H	H	—	—	d/1	7,35	2d/1[a]	7,13	—	—	—	—	—	—	—	—
2*b*	H	CH_3	CH_3	H	—	—	d/1	7,20	2d/1[f]	7,03	—	—	s/3	1,41	d/3	2,05	—	—
2′*b*	H	CH_3	CH_3	D	—	—	d/1	7,20	d/1	7,04	—	—	s/3	1,41	s/3	2,04	—	—
2*c*	H	CH_3	CH_3	CH_3	—	—	d/1	7,16	d/1	6,98	—	—	s/3	1,41	q/3[c]	2,00	q/3[c]	2,16
2*e*	H	E[e]	E	H	—	—	d/1	7,49	2d/1[d]	7,18	—	—	q/2	4,28	q/2	4,30	—	—
													t/3	1,33	t/3	1,34		
2′*e*	H	E	E	D	—	—	d/1	7,49	d/1	7,18	—		q/2	4,28	q/2	4,30	—	—
													t/3	1,33	t/3	1,34		
2*f*	H	Ph[e]	Ph	H	—	—	M/11	7,30–7,60	2d/1	7,11	—	—	M/11	7,30–7,60	M/11	7,30–7,60	—	—
2′*f*	H	Ph	Ph	D	—	—	M/11	7,30–7,60	d/1	7,11	—	—	M/11	7,30–7,60	M/11	7,30–7,60	—	—
2″*f*	D	Ph	Ph	H	—	—	M/11	7,30–7,60	2d/1	7,11	—	—	M/11	7,30–7,60	M/11	7,30–7,60	—	—
3*b*	H	CH_3	CH_3	H	d/1	6,79	d/1	6,96	—	—	—	—	d/3	2,04	s/3	1,40	—	—
3′*b*	H	CH_3	CH_3	D	d/1	6,79	d/1	6,96	—	—	—	—	d/3	2,04	s/3	1,39	—	—
3*d*	CH_3	CH_3	CH_3	H	s/2	6,96	s/2	6,96	—	—	q/3	2,09	q/3	1,96	s/3	1,41	—	—
3*e*	H	E	E	H	d/1	6,98	d/1	7,13	—	—	—	—	q/2	4,30	q/2	4,28	—	—
													t/3	1,34	t/3	1,33		
3′*e*	H	E	E	D	d/1	6,98	d/1	7,13	—	—	—	—	q/2	4,30	q/2	4,28	—	—
													t/3	1,34	t/3	1,33		
3*g*	H	E	H	H	d/1	7,00	d/1	7,07	—	—	—	—	q/2	4,29	—	—	—	—
													t/3	1,34				
3*f*	H	Ph	Ph	H	d/1	6,98	d/1	7,07	—	—	—	—	M/10	7,30–7,60	M/10	7,30–7,60	—	—
3′*f*	H	Ph	Ph	D	d/1	6,98	d/1	7,07	—	—	—	—	M/10	7,30–7,60	M/10	7,30–7,60	—	—
3″*f*	D	Ph	Ph	H	d/1	6,98	d/1	7,07	—	—	—	—	M/10	7,30–7,60	M/10	7,30–7,60	—	—

a. $^5J_{H_3-H_7}$ = 0,50 Hz.
b. $^4J_{H_{4a}-H_6}$ = 1,70 Hz.
c. $^5J_{CH_3-CH_3}$ = 1,00 Hz.
d. $^5J_{H_3-H_7}$ = 0,72 Hz.
e. E = $CO_2C_2H_5$, Ph = C_6H_5.
f. $^5J_{H_3-H_7}$ = 0,89 Hz.

groupe méthyle voisin permet de fixer la position du cycle à trois chaînons du côté opposé à l'atome de deutérium.

Dans le cas des deux thiophéno[*b*]monohomotropones **2***e* et **3***e*, l'analyse des couplages à longue distance permet de conclure. Ainsi pour l'isomère **2***e* on note un couplage ^5J en « zig-zag » entre le proton thiophénique H_3 et le proton éthylénique H_7. Ce couplage n'apparaît pas dans le cas de **3***e* pour lequel la disposition des liaisons est telle que le zig-zag est « cassé ». L'analyse comparative des spectres de **2***e* et **2′***e* d'une part et **3***e* et **3′***e* d'autre part confirme cette attribution structurale (voir tableau 3).

(2) *Thiophéno[b]bishomotropones*

L'ensemble des données de rmn des thiophéno[*b*]bishomotropones figure dans le tableau 4.

Si les spectres de rmn des thiophéno[*c*]bishomotropones (1) présentent une grande symétrie tant pour les composés *cis* que pour leurs isomères *trans*, il n'en est plus de même pour les thiophéno[*b*]bishomotropones par suite de la dissymétrie intrinsèque à la série [*b*].

Le dérivé *trans* **4***f* présente deux systèmes AMX entre 1,0 et 3,0 ppm. Dans le même domaine de fréquence l'isomère *cis* **5***f* montre deux systèmes plus fortement couplés de type ABX. Cependant l'examen comparatif de ces données est insuffisant pour préciser la nature *cis* ou *trans* de ces thiophéno[*b*]bishomotropones. Aussi, nous avons analysé les spectres rmn des alcools dérivés. Leur examen comparatif (voir fig. 3) montre que deux alcools isomères sont isolés au départ de **4***f* alors qu'un seul alcool apparaît lors de la réduction de **5***f*.

(3) *Cycloocta et cyclonona[b]thiophénones*

L'examen comparatif des données de rmn des composés **10**, **11** et **12** et celles de leurs analogues deutériés **10′**, **11′** et **12′** a permis de préciser la structure de ces dérivés.

Dans le cas de la cyclonona[*b*]thiophénone **12** l'existence de

et des dihydro-4,4a 3b*H*-cyclopropa [3,4]cyclohepta[2,1-*b*]thiophénones-5, **3**

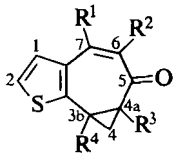

3

Troponiques				Cyclopropaniques								Constantes de couplage						
H_6		H_7		H_{3b}		H_{4a}		H_{4endo}		H_{4exo}								J_{1-2} ou
m/i	δ	m/i	δ	m/i	δ	m/i	δ	m/i	δ	m/i	δ	J_{3b-4a}	$J_{3b-4endo}$	$J_{3b-4exo}$	$J_{4a-4endo}$	$J_{4a-4exo}$	$J_{4endo-4exo}$	J_{2-3}
2d/1[b]	5,94	2d/1[a]	6,91	3d/1	2,60	4d/1[b]	2,54	3d/1	1,47	3d/1	1,93	8,41	6,98	9,02	6,28	9,19	4,60	4,98
—	—	M/1[f]	6,69	2d/1	2,57	—	—	2d/1	1,75	2d/1	1,63	—	6,69	8,96	—	—	4,57	5,13
—	—	—	—	2d/1	2,56	—	—	2d/1	1,75	2d/1	1,63	—	6,70	9,00	—	—	4,60	5,13
—	—	—	—	2d/1	2,53	—	—	2d/1	1,99	2d/1	1,54	—	7,00	8,92	—	—	4,57	5,13
—	—	d/1[d]	7,69	t/1	3,22	—	—	d/2	2,11	d/2	2,11	—	8,54	8,54	—	—	0,00	5,13
—	—	—	—	t/1	3,22	—	—	d/2	2,11	d/2	2,11	—	8,54	8,54	—	—	0,00	5,13
—	—	d/1	7,03	2d/1	3,02	—	—	2d/1	2,56	2d/1	2,18	—	7,17	9,17	—	—	5,14	5,10
—	—	—	—	2d/1	3,02	—	—	2d/1	2,55	2d/1	2,18	—	7,13	9,17	—	—	5,12	5,11
—	—	d/1	7,03	—	—	—	—	d/1	2,55	d/1	2,17	—	—	—	—	—	5,09	5,10
—	—	q/1	6,68	2d/1	2,57	—	—	2d/1	1,88	2d/1	1,67	—	6,84	9,03	—	—	4,58	4,95
—	—	q/1	6,66	—	—	—	—	d/1	1,88	d/1	1,68	—	—	—	—	—	4,60	5,00
—	—	—	—	2d/1	2,53	—	—	2d/1	2,19	2d/1	1,55	—	6,81	8,85	—	—	4,89	0,00
—	—	s/1	7,69	2d/1	3,28	—	—	2d/1	2,20	2d/1	2,13	—	7,51	10,92	—	—	4,70	5,25
—	—	s/1	7,69	—	—	—	—	d/1	2,20	d/1	2,12	—	—	—	—	—	4,80	5,25
—	—	s/1[a]	7,72	3d/1	2,91	3d/1[b]	2,75	3d/1	1,93	3d/1	1,97	8,99	6,63	8,50	6,92	8,62	5,38	5,35
—	—	s/1	7,02	2d/1	3,04	—	—	2d/1	2,70	2d/1	2,22	—	7,07	9,21	—	—	5,22	5,20
—	—	—	—	2d/1	3,04	—	—	2d/1	2,70	2d/1	2,22	—	7,10	9,20	—	—	5,23	5,20
—	—	s/1	7,00	—	—	—	—	d/1	2,69	d/1	2,22	—	—	—	—	—	5,10	5,20

deux motifs —CH_2—CH_2—CHPh— inéquivalents et indépendants rend l'analyse spectrale délicate.

Le recours à un spectre COSY[4] est nécessaire pour préciser les connexions des dix protons inéquivalents. Nous avons fait figurer de part et d'autre de la diagonale les connexions relatives à chacun des deux systèmes de cinq protons (voir fig. 4).

Le spectre calculé[5] avec les valeurs mesurées sur le spectre à une dimension coïncide parfaitement avec ce dernier (voir fig. 5). Nous avons également fait figurer le spectre de **12'**, analogue deutérié de **12**. On constate ainsi :

(*i*) que les signaux des protons H_{4endo} et H_{4exo} sont tous deux concernés par la présence d'un atome de deutérium en position 4,

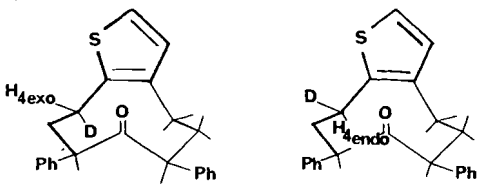

(*ii*) qu'il est possible d'assigner les deux motifs —CH_2—CH_2—CHPh— sur la base de la comparaison des deux spectres.

L'examen attentif des valeurs des constantes de couplage (voir partie expérimentale) permet de préciser la conformation

4. Le spectre COSY a été obtenu à l'aide du micro-programme BRÜKER COSY .AU. Paramètres introduits : 512 expériences; 32 signaux collectés; 4 signaux ignorés; deuxième dimension 2K; première dimension 1K; multiplication sinusoïdale déphasée de $\pi/10$ dans les deux dimensions; délai de recyclage 2 s; délai initial entre les deux impulsions : 3 μs; angles d'impulsion 90° et 90° (8 μs).

5. Programme de simulation PANIC (Bibliothèque BRÜKER). Largeur des raies : 0,5 Hz. Ce program est limité à 9 spins inéquivalents. On peut cependant dans notre cas scinder le calcul en traitant successivement deux systèmes *indépendants* de 5 spins non équivalents et en additionnant les deux sous-spectres ainsi obtenus.

TABLEAU 4. Caractéristiques rmn des tétrahydro-4,4a,6,6a

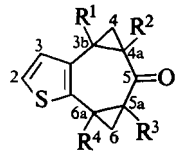

4, 5

Composé	Configuration	R^1	R^2	R^3	R^4	Thiophéniques H_2 m/i	H_2 δ	H_3 m/i	H_3 δ	Exocycliques de R^2 m/i	de R^2 δ	de R^3 m/i	de R^3 δ
4*a*	*trans*	H	H	H	H	d/1	7,01	2d/1	6,83	—	—	—	—
4*e*	*trans*	H	E[a]	E	H	d/1	7,05	d/1	6,85	qd/1	4,32	qd/1	4,31
										qd/1	4,24	qd/1	4,23
										t/6	1,32	t/6	1,32
4′*e*	*trans*	H	E	E	D	d/1	7,05	d/1	6,85	qd/1	4,32	qd/1	4,31
										qd/1	4,24	qd/1	4,23
										t/6	1,32	t/6	1,32
4*f*	*trans*	H	Ph[a]	Ph	H	d/1	7,08	d/1	6,92	M/10	~7,30	M/10	~7,30
4′*f*	*trans*	H	Ph	Ph	D	d/1	7,08	d/1	6,91	M/10	~7,30	M/10	~7,30
4″*f*	*trans*	D	Ph	Ph	H	d/1	7,08	d/1	6,91	M/10	~7,30	M/10	~7,30
5*f*	*cis*	H	Ph	Ph	H	d/1	7,15	2d/1[b]	6,94	M/10	~7,00	M/10	~7,00

Constantes de couplage

Composé	J_{3b-} J_{3b-4a}	J_{3b-} $_{4endo}$	J_{3b-} $_{4exo}$	J_{4a-} $_{4endo}$	J_{4a-} $_{4exo}$	J_{4endo} $_{4exo}$	J_{5a-6a}	J_{6a-} $_{6endo}$	J_{6a-} $_{6exo}$	J_{5a-} $_{6endo}$	J_{5a-} $_{6exo}$	J_{6endo} $_{6exo}$	J_{2-3}
4*a*	9,24	5,63	8,31	6,44	8,40	5,18	9,42	6,26	8,62	6,18	8,48	5,13	5,05
4*e*	—	7,23	9,21	—	—	5,00	—	7,07	9,35	—	—	5,07	5,18
4′*e*	—	7,25	9,32	—	—	5,07	—	—	—	—	—	4,95	5,18
4*f*	—	6,64	9,08	—	—	4,57	—	6,20	8,89	—	—	4,49	5,13
4′*f*	—	6,64	9,11	—	—	5,22	—	—	—	—	—	5,09	5,19
4″*f*	—	—	—	—	—	5,40	—	6,29	8,91	—	—	5,08	5,19
5*f*	—	5,70	8,76	—	—	4,27	—	5,49	8,44	—	—	4,36	5,29

a. E = $CO_2C_2H_5$, Ph = C_6H_5.
b. $^4J_{H_3-H_{6a}}$ = 1,21 Hz.

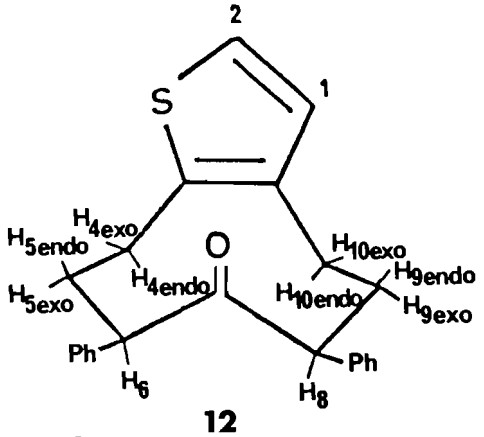

12

$^3J_{H_{4endo}-H_{5endo}}$ = 7,29 Hz
$^3J_{H_{5endo}-H_6}$ = 12,38 Hz
$^3J_{H_{10endo}-H_{9endo}}$ = 7,47 Hz
$^3J_{H_{9endo}-H_8}$ = 12,34 Hz

privilégiée qu'adopte cette molécule. Pour l'un des motifs —CH_2—CH_2—CHPh—, un seul des cinq protons échange trois couplages importants et un couplage plus faible. Il s'agit nécessairement du proton H_{5endo}. En effet, outre la constante géminée (13,81 Hz) échangée entre ce proton et H_{5exo}, H_{5endo} présente deux couplages vicinaux importants (12,38 et 7,29 Hz) correspondant à des interactions diaxiales respectivement avec H_6 et H_{4endo}. Enfin la valeur peu élevée de la constante H_{5endo}–H_{4exo} (3,73 Hz) est attribuable à une interaction de type axial–équatorial. Un raisonnement identique peut être tenu à propos du proton H_{9endo} et la conformation privilégiée qu'adopte cette molécule peut alors être proposée et représentée selon le schéma ci-dessous.

Conclusion

La réactivité des thiophéno[*b*]tropones vis-à-vis du méthylure de diméthylsulfoxonium ne diffère pas fondamentalement de celle de leurs isomères [*c*]. La structure des thiophéno[*b*]monohomotropones obtenues découle de l'examen comparatif des spectres de rmn à champ moyen des composés et de leurs analogues deutériés. L'analyse spectrale à haut champ des produits de réduction a contribué à élucider les problèmes structuraux liés à l'isomérie *cis*/*trans* des systèmes bishomo-

3b*H*,5a*H*-dicyclopropa[3,4:6,7]cyclohepta[1,2-*b*]thiophénones-5, **4** et **5**

Protons															
						Cyclopropaniques									
H_{3b}		H_{4a}		H_{4endo}		H_{4exo}		H_{6a}		H_{5a}		H_{6endo}		H_{6exo}	
m/i	δ	m/i	δ	m/i	δ	m/i	δ	m/i	δ	m/i	δ	m/i	δ	m/i	δ
3d/1	$2,27_2$	3d/1	2,18	3d/1	1,80	3d/1	1,37	3d/1	$2,27_3$	3d/1	2,14	3d/1	1,45	3d/1	1,34
2d/1	2,95	—	—	2d/1	1,98	2d/1	1,76	2d/1	2,97	—	—	2d/1	1,90	2d/1	1,76
2d/1	2,96	—	—	2d/1	1,98	2d/1	1,76	—	—	—	—	d/1	1,91	d/1	1,77
2d/1	2,73	—	—	2d/1	2,22	2d/1	1,49	2d/1	2,86	—	—	2d/1	2,06	2d/1	1,44
2d/1	2,74	—	—	2d/1	2,20	2d/1	1,48	—	—	—	—	d/1	2,07	d/1	1,44
—	—	—	—	d/1	2,22	d/1	1,53	2d/1	2,86	—	—	2d/1	2,05	2d/1	1,44
2d/1	2,78	—	—	2d/1	1,58	2d/1	1,27	3d/1[b]	2,90	—	—	2d/1	1,44	2d/1	1,14

troponiques. L'action de l'amalgame de zinc conduit à des cycloocta et cyclonona[*b*]thiophénones dont la structure est déterminée par analyse des spectres de rmn à haut champ.

Partie expérimentale

Les analyses élémentaires ont été effectuées par le Service Central d'Analyse du C.N.R.S. Les spectres de rmn ^1H ont été enregistrés à 100 MHz sur un appareil JEOL FX 100 et à 400 MHz sur un appareil Brüker WM 400. Un échantillon de 5 mg est, sauf indication contraire, dissous dans 0,2 cm^3 de $CDCl_3$. Les déplacements chimiques sont donnés en ppm par rapport à $SiMe_4$ et les constantes de couplage en Hz (résolution digitale : 0,01 Hz). Les multiplicités sont indiquées comme suit : s (singulet), d (doublet), t (triplet), q (quadruplet), m (multiplet).

A. Matières premières

1. *Thiophéno[*b*]tropones*

Les thiophéno[*b*]tropones mises en oeuvre ont été préparées par les méthodes décrites dans la littérature (6) : cyclohepta[*b*]thiophénone-6, **1***a*, *F* = 94°C; diméthyl-5,7 cyclohepta[*b*]thiophénone-6, **1***b*, *F* = 83°C; triméthyl-5,7,8 cyclohepta[*b*]thiophénone-6, **1***c*, *F* = 73°C; triméthyl-4,5,7 cyclohepta[*b*]thiophénone-6, **1***d*, *F* = 80°C; oxo-6 cyclohepta[*b*]thiophéne dicarboxylate-5,7 de diéthyle, **1***e*, *F* = 103°C; diphényl-5,7 cyclohepta[*b*]thiophénone-6, **1***f*, *F* = 140°C (rmn ^{13}C, 100 MHz, δ ppm/TMS : 187,2 (CO), 132,5 (C4), 131,6 (C3), 130,6 (C8), 128,5 (C2).

2. *Thiophéno[*b*]tropones deutériées*

*Diméthyl-5,7 cyclohepta[*b*]thiophénone-6 (D-8), 1'*b

La préparation est identique à celle de son analogue non deutérié **1***b*. Au départ de diformyl-2,3 thiophène (CDO-3) (14 g, 100 mmol) et de 13 g (150 mmol) de pentanone-3 on isole 16,5 g (Rdt = 87%) de **1'***b*; *F* = 80°C. *Anal.* calc. pour $C_{11}H_9DOS$: C 69,08, H 4,74, D 1,05, O 8,37, S 16,77; trouvé : C 69,3, H 4,8, D 1,0, O 8,6, S 16,5.

*Oxo-6 cyclohepta[*b*]thiophène dicarboxylate-5,7 de diéthyle (D-8), 1'*e

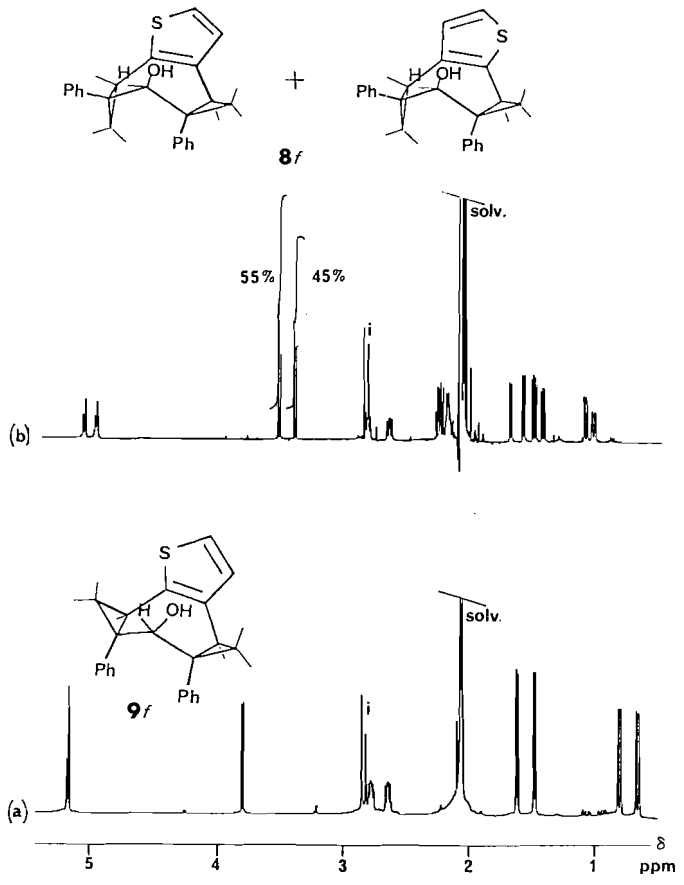

FIG. 3. Spectres rmn ^1H (400 MHz, $(CD_3)_2CO$) des thiophéno[*b*]-bishomotroponols; (a) **9***f*, (b) **8**. i : impureté du solvant deutérié.

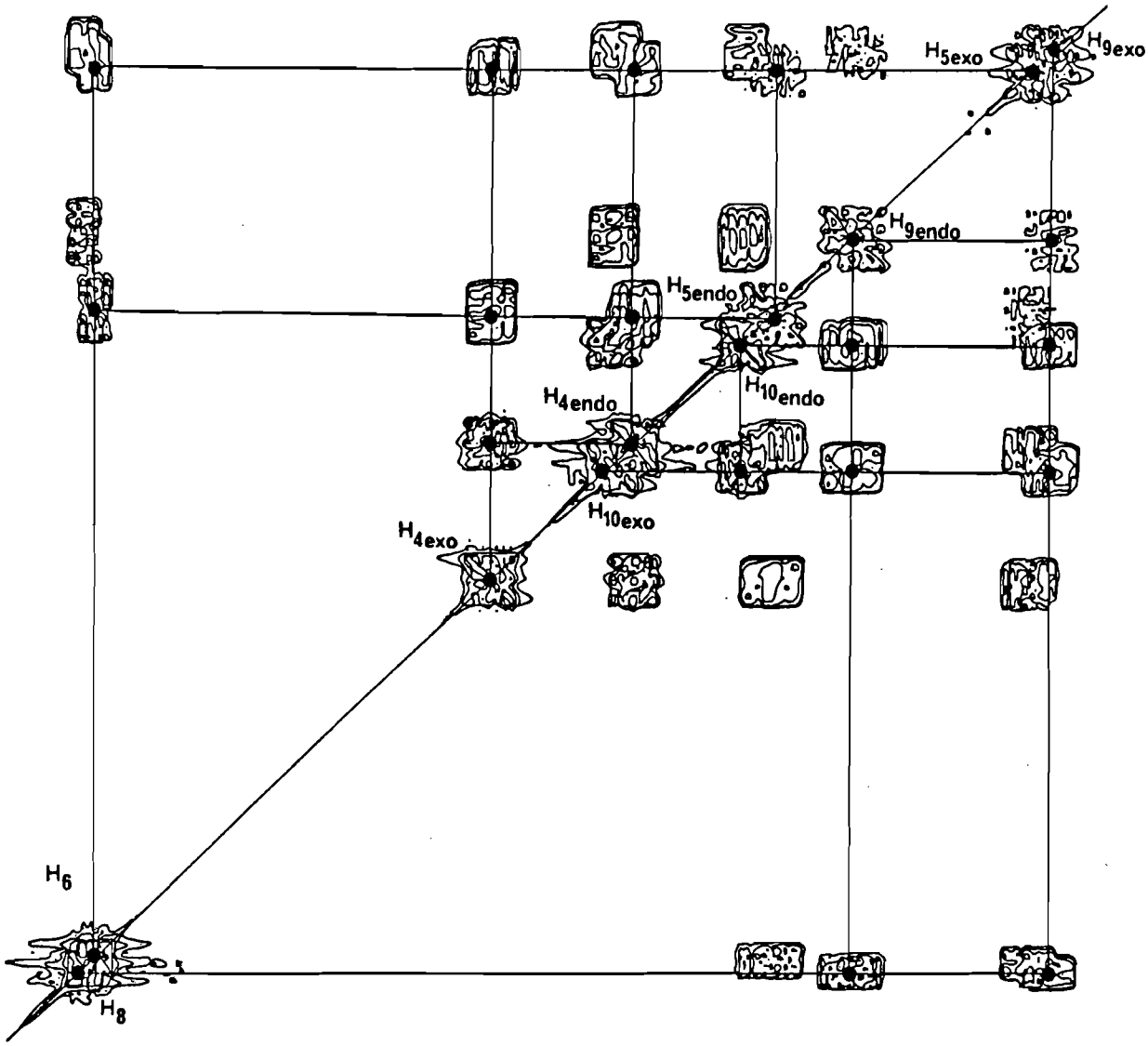

FIG. 4. Spectre COSY (400 MHz, $CDCl_3$) du composé **12** montrant les connexions des deux motifs —CH_2—CH_2—CHPh indépendants.

Dans les mêmes conditions que **1***e*, au départ de diformyl-2,3 thiophène (CDO-2), **1′***e* est obtenu avec un rendement de 78%; F = 103°C. *Anal.* calc. pour $C_{15}H_{13}DO_5S$: C 58,62, H 4,26, D 0,65, O 26,03, S 10,43; trouvé : C 58,6, H 4,2, D 0,6, O 26,2, S 10,5.

*Diphényl-5,7 cyclohepta[*b*]thiophénone-6 (D-8), 1′*f *et diphényl-5,7 cyclohepta[*b*]thiophénone-6 (D-4), 1″*f

On procède comme pour **1***f* respectivement au départ de diformyl-2,3 thiophène (CDO-2) ou (CDO-3) (Rdts = 79 et 68%); F = 138 et 138°C. *Anal.* calc. pour $C_{21}H_{13}DOS$: C 79,97, O 5,07, S 10,16; trouvé pour **1′***f* : C 80,5, O 5,1, S 10,0; trouvé pour **1″***f* : C 80,1, O 5,0, S 10,1.

*B. Cyclopropa et dicyclopropa cyclohepta[*b*]thiophénones-5*

Les thiophéno[*b*]homotropones ont été préparées dans des conditions voisines (voir tableau 5) qui ne seront détaillées que dans l'exemple suivant.

*Triméthyl-4a,6,7 dihydro-4,4a 3b*H*-cyclopropa[3,4]cyclohepta-[2,1-*b*]thiophénone-5,* **3***d*

À une suspension de 1,92 g (40 mmol) d'hydrure de sodium (50% dans l'huile minérale), préalablement lavée par trois fois 50 cm^3 d'éther de pétrole on ajoute 8,80 g (40 mmol) d'iodure de triméthylsulfoxonium (7) et 50 cm^3 de *N,N*-diméthylformamide (DMF). Après 1 h de contact l'ylure obtenu est filtré et additionné à une solution de 2,04 g (10 mmol) de **1***d* dans 50 cm^3 de DMF. Le milieu se colore progressivement en brun. L'agitation est poursuivie 12 h, puis le mélange est versé sur 200 cm^3 d'eau acidifiée (pH ~2). La phase aqueuse est extraite à l'éther et les phases organiques réunies sont lavées à l'eau jusqu'à neutralité, séchées sur sulfate de magnésium et les solvants sont évaporés. Le solide brut obtenu est chromatographié sur acide silicique (éluant : éther–hexane 1:2), puis recristallisé dans 40 cm^3 de ce même mélange de solvants. On obtient 1,57 g (Rdt = 72%) du composé **3***d*; F = 119°C.

Trois autres thiophéno[*b*]homotropones ont été obtenues par décarboalkoxylation des homotropones correspondantes selon les protocoles suivants :

*Dihydro-4,4a 3b*H*-cyclopropa[3,4]cyclohepta[1,2-*b*]thiophénone-5,* **2***a*

Au départ de 0,96 g (3 mmol) de **2***e* et 0,25 g de chlorure de lithium dans 60 cm^3 de DMSO à reflux on isole 0,25 g (Rdt = 47%) de **2***a*; F = 57°C; rmn δ (400 MHz) : 7,35 (d, H_2, J = 4,98 Hz), 7,13 (2d, H_3, J = 4,98 et 0,70 Hz), 6,91 (2d, H_7, J = 12,57 et 0,70 Hz), 5,94 (2d, H_6, J = 12,57 et 1,70 Hz), 2,60 (3d, H_{3b}, J = 8,41, 9,02 et 6,98 Hz), 2,54 (4d, H_{4a}, J = 8,41, 9,19, 6,28 et 1,70 Hz), 1,93 (3d, H_{4exo}, J = 9,02, 9,19 et 4,60 Hz), 1,47 (3d, H_{4endo}, J = 6,98, 6,28 et 4,60 Hz). *Anal.* calc. pour $C_{10}H_8OS$: C 68,15, H 4,58, O 9,08, S 18,20; trouvé : C 68,3, H 4,6, O 9,2, S 18,1.

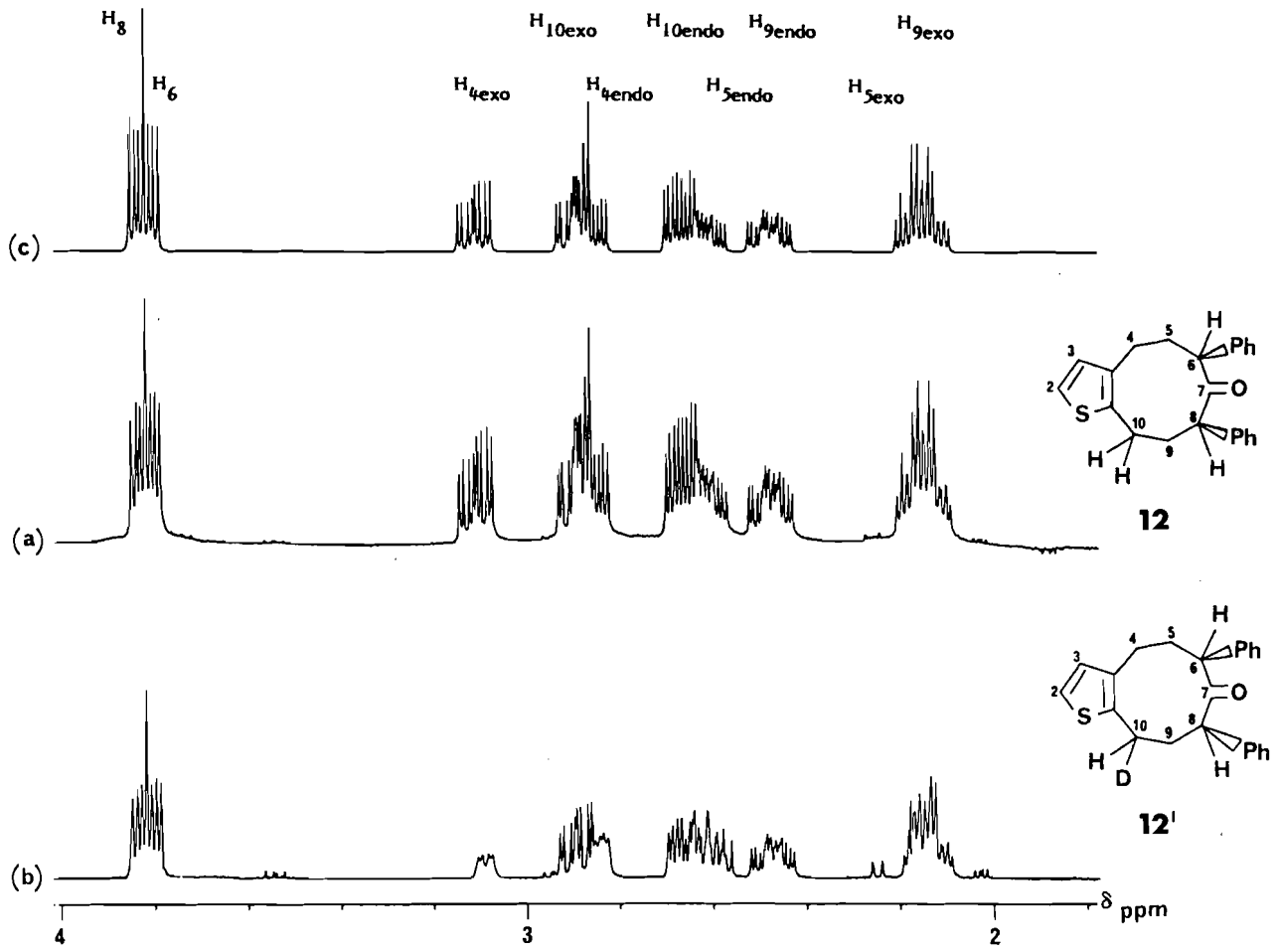

FIG. 5. Spectres rmn ^1H (400 MHz, $CDCl_3$) : (a) du composé **12**; (b) de **12'**, analogue deutérié de **12**; (c) spectre calculé de **12**.

*Oxo-5 dihydro-4,4a 3b*H-*cyclopropa[3,4]cyclohepta[2,1-*b*]thiophènecarboxylate-6 d'éthyle, 3*g

Au départ de 0,18 g de **3***e*, 0,05 g de chlorure de lithium et en opérant comme précédemment on isole 0,09 g (Rdt = 43%) de **3***g*. Ce composé a été uniquement caractérisé par son spectre de rmn protonique; rmn δ (400 MHz) : 7,72 (s, H_7), 7,07 (d, H_2, J = 5,35 Hz), 7,00 (d, H_1, J = 5,35 Hz), 4,29 (q, —OCH_2—, J = 7,08 Hz), 2,91 (3d, H_{3b}, J = 8,99, 8,51 et 6,63 Hz), 2,75 (3d, H_{4a}, J = 8,99, 8,62 et 6,92 Hz), 1,97 (3d, H_{4exo}, J = 8,51, 8,62 et 5,38 Hz), 1,93 (3d, H_{4endo}, J = 6,63, 6,92 et 5,38 Hz).

trans *Tétrahydro-4,4a,6,6a 3b*H,*5a*H-*dicyclopropa[3,4:6,7]cyclohepta[1,2-*b*]thiophénone-5, 4*a

Le composé **4***a*, 1,83 g (6 mmol) et 0,51 g (12 mmol) de chlorure de lithium conduisent après 2 h de chauffage à reflux dans 120 cm^3 de DMSO à 0,70 g (Rdt = 61%) de **4***a*; F = 88°C. *Anal.* calc. pour $C_{11}H_{10}OS$: C 69,44, H 5,30, O 8,41, S 16,85; trouvé : C 69,8, H 5,3, O 8,4, S 16,3. Les caractéristiques rmn de ce composé apparaissent dans le tableau 3.

*C. Dérivés de reduction des cyclopropa et dicyclopropa cyclohepta[*b*]-thiophénones-5*

*1. Cyclopropa et dicyclopropa[*b*]thiophène-ols-5*

*Diphényl-4a,6 dihydro-4,4a 3b*H-*cyclopropa[3,4]cyclohepta[1,2-*b*]thiophène-ol-5, 6*f *et diphényl-4a,6 dihydro-4,4a 3b*H-*cyclopropa[3,4]cyclohepta[2,1-*b*]thiophène-ol-5, 7*f

À une suspension de 0,76 g (20 mmol) de $LiAlH_4$ dans 40 cm^3 d'éther anhydre on ajoute goutte à goutte à 0°C une solution de 1,64 g (5 mmol) du mélange **2***f* + **3***f*. Après 2 h de contact l'excès d'hydrure est détruit par 2 cm^3 d'eau. Le précipité formé est filtré et lavé par trois fois 10 cm^3 d'éther. Les phases éthérées sont lavées, séchées et le solvant est évaporé. On obtient 1,3 g (Rdt = 80%) du mélange **6***f* + **7***f*; rmn δ (400 MHz, $(CD_3)_2CO$) : 7,20–7,50 (M, 24H arom.), 4,92 (d, C*H*OH (**6***f*), J = 5,08 Hz), 4,88 (d, C*H*OH (**7***f*), J = 5,13 Hz), 3,93 (d, CHO*H* (**7***f*), J = 5,13 Hz), 3,92 (d, CHO*H* (**6***f*), J = 5,08 Hz), 2,93 (2d, H_{3b} (**7***f*), J = 5,93 et 9,81 Hz), 2,26 (2d, H_{3b} (**6***f*), J = 6,09 et 10,07 Hz), 1,75 (2d, H_{4endo} (**7***f*), J = 4,00 et 5,93 Hz), 1,71 (2d, H_{4endo} (**6***f*), J = 4,09 et 6,09 Hz), 1,06 (2d, H_{4exo} (**7***f*), J = 4,00 et 9,81 Hz), 1,01 (2d, H_{4exo} (**6***f*), J = 4,09 et 10,07 Hz).

trans-*Diphényl-4a,5a tétrahydro-4,4a,6,6a 3b*H,*5a*H-*dicyclopropa[3,4:6,7]cyclohepta[1,2-*b*]thiophène-ol-5, 8*f

Au départ de 2,00 g de **4***f* (5,85 mmol) et de 1,14 g de $LiAlH_4$ (30 mmol) on isole 1,52 g (Rdt = 76%) de **12***f*; F = 110°C; rmn δ (400 MHz, $(CD_3)_2CO$) : 7,1–7,6 (M, 24H arom.), 5.05 (d, CHO*H*, J = 7,08 Hz), 4,96 (d, CHO*H*, J = 7,32 Hz), 3,52 (d, C*H*OH, J = 7,08 Hz), 3,39 (d, C*H*OH, J = 7,32 Hz), 1,0–3,0 (M, 12H aliph.). *Anal.* calc. pour $C_{23}H_{20}OS$: C 80,19, H 5,85, O 4,65, S 9,31; trouvé : C 80,2, H 5,9, O 4,6, S 9,2.

cis-*Diphényl-4a,5a tétrahydro-4,4a,6,6a 3b*H,*5a*H-*dicyclopropa-[3,4:6,7]cyclohepta[1,2-*b*]thiophène-ol-5, 9*f

La réduction de 0,02 g de **5***f* (~0,06 mmol) conduit à 0,005 g de **9***f* (Rdt ~ 25%); F = 172°C. Ce composé a uniquement été caractérisé par son spectre de rmn : rmn δ (400 MHz, $(CD_3)_2CO$) : 6,8–7,3 (M, 12H arom.), 5,16 (d, CHO*H*, J = 6,30 Hz), 3,79 (d, C*H*OH, J = 6,30 Hz), 2,77 (2d, H_{6a}, J = 5,38 et 9,16 Hz), 2,64 (2d, H_{3b}, J = 5,58 et 9,50 Hz), 1,61 (2d, H_{6endo}, J = 5,38 et 3,25 Hz), 1,47 (2d, H_{4endo}, J = 3,19 et 5,58 Hz), 0,79 (2d, H_{6exo}, J = 3,25 et 9,16 Hz), 0,65 (2d, H_{4exo}, J = 3,19 et 9,50 Hz).

TABLEAU 5. Caractéristiques des réactions et des dihydro-4,4a 3b*H*-cyclopropa[3,4]cyclohepta[1,2-*b*]thiophénones-5, **2**, dihydro-4,4a 3b*H*-**4** et **5**

Substrat de départ	R^1	R^2	R^3	R^4	Rapport ylure/tropone	Solvant réactionnel	Eluant de séparation[b]	Produit(s) obtenus(s)	Rendement(s) (%)	Solvant(s) de recristallisation[b]
1*b*	H	CH_3	CH_3	H	5:1	DMF	A–F (1:3)	**2***b*	25	B
								3*b*	8	—
1′*b**	H	CH_3	CH_3	D	5:1	DMF	A–F (1:3)	**2′***b*	10	B
								3′*b*	3	—
1*c*	H	CH_3	CH_3	CH_3	8:1	DMF	—	**2***c*	46	B
1*d*	CH_3	CH_3	CH_3	H	4:1	DMF	A–B (1:2)	**3***d*	72	A–B (1:2)
1*f*	H	Ph[a]	Ph	H	1:1	DMF	B–C (1:1)	**2***f*	46,5[c]	B–C (2:1)
								3*f*	28,5[c]	
1*f*	H	Ph	Ph	H	4:1	DMSO	B–C (1:1)	**2***f* + **3***f*	4	B–C (2:1)
								4*f*	71	B–C (2:1)
								5*f*	2	B–C (2:1)
1′*f*	H	Ph	Ph	D	2,5:1	DMF	B–C (1:1)	**2′***f* + **3′***f*	15	B–C (2:1)
								5′*f*	42	B–C (2:1)
1″*f*	D	Ph	Ph	H	5:1	DMSO	B–C (1:1)	**2″***f* + **3″***f*	3	B–C (2:1)
								5″*f*	59	B–C (2:1)
1*e*	H	E[a]	E	H	1,5:1	DMF	A–F (2:1)	**2***e*	10	A–B (1:1)
								3*e*	10	A–F (1:2)
1*e*	H	E	E	H	3:1	DMF	—	**4***e*	33	B–C (10:1)
1′*e**	H	E	E	D	1,5:1	DMF	A–F (2:1)	**2′***e*	6	A–B (1:1)
								3′*e*	1	A–F (1:2)
1′*e*	H	E	E	D	3:1	DMF	—	**4′***e*	30	B–C (10:1)

a. E = $CO_2C_2H_5$, Ph = C_6H_5.

b. A : éther anhydre; B : hexane; C : chlorure de méthylène; D : éther de pétrole; F : pentane.

c. Proportions relatives calculées par intégration des signaux rmn des protons cyclopropaniques.

*Les rendements en composés deutériés sont souvent plus faibles que ceux signalés pour leur analogues protonés car ces réactions ont été conduites sur de faibles quantités de réactifs.

2. *Cyclopropacycloocta et cyclopropacyclonona thiophénones-5*

*Diphényl-4a,6 hexahydro-4,4a,5,6,7,8 3b*H*-cyclopropa[3,4]cyclo-octa[1,2-*b*]thiophénone-5, **10**, diphényl-4a,6 hexahydro-4,4a,5,6,7,8 3b*H*-cyclopropa[3,4]cycloocta[2,1-*b*]thiophénone-5, **11***

Au départ de 4,06 g (14 mmol) de chlorure mercurique, de 13,08 g de zinc et de 1,71 g (5 mmol) de **4***f* portés à reflux pendant 12 h dans 100 cm^3 d'éthanol et 10 cm^3 d'acide chlorhydrique (d = 1,19) on isole 1,06 g (Rdt = 70%) du mélange **10** + **11**; rmn δ (400 MHz) (caractéristiques des ponts méthyléniques) : 2,28 (2d, H_{4endo} (**11**), J = 3,80 et 6,19 Hz), 2,15 (2d, H_{4endo} (**10**), J = 4,13 et 6,66 Hz), 1,32 (2d, H_{4exo} (**11**), J = 3,80 et 8,72 Hz), 1,21 (2d, H_{4exo} (**10**), J = 4,13 et 9,17 Hz). *Anal.* calc. pour $C_{23}H_{20}OS$: C 80,19, H 5,85, O 4,64, S 9,31; trouvé : C 80,3, H 5,8, O 4,8, S 9,1.

*Composés **10**, **11** et diphényl-6,8 hexahydro-5,6,7,8,9,10 4*H*-cyclonona[1,2-*b*]thiophénone-7, **12***

En procédant avec une quantité relative plus importante d'amalgame de zinc (préparé au départ de 2,70 g (10 mmol) de chlorure mercurique et de 13,08 g de zinc), 0,68 g (2 mmol) du composé **4***f* conduisent à 0,17 g (Rdt = 22%) du mélange **10** + **11** précédemment décrit et à 0,15 g (Rdt = 22%) de **12**; F = 155°C; rmn δ (400 MHz) : 6,80–7,10 (M, 12H arom.), 3,83 (2d, H_8, J = 12,34 et 4,58 Hz), 3,81 (2d, H_6, J = 12,38 et 4,27 Hz), 3,11 (3d, H_{4exo}, J = 15,40, 3,73 et 9,28 Hz), 2,89 (3d, H_{10exo}, J = 14,57, 3,35 et 9,48 Hz), 2,86 (3d, H_{4endo}, J = 15,40, 7,29 et 3,96 Hz), 2,67 (3d, H_{10endo}, J = 14,57, 7,47 et 3,42 Hz), 2,62 (4d, H_{5endo}, J = 12,38, 3,73, 7,29 et 13,81 Hz), 2,47 (4d, H_{9endo}, J = 12,34. 3,35, 7,47 et 13,90 Hz), 2,16 (4d, H_{5exo}, J = 4,27, 9,28, 3,96 et 13,81 Hz), 2,13 (4d, H_{9exo}, J = 4,58, 9,48, 3,42 et 13,90 Hz). *Anal.* calc. pour $C_{23}H_{22}OS$: C 79,73, H 6,40, O 4,62, S 9,26; trouvé : C 79,3, H 6,3, O 4,6, S 9,2.

*Diphényl-4a,6 hexahydro-4,4a,5,6,7,8 3b*H*-cyclopropa[3,4]cyclo-octa[1,2-*b*]thiophénone-5 (D-8), **10′**, diphényl-4a,6 hexahydro-4,4a,5,6,7,8 3b*H*-cyclopropa[3,4]cycloocta[2,1-*b*]thiophéne-5 (D-3b), **11′** et diphényl-6,8 hexahydro-5,6,7,8,9,10 4*H*-cyclonona[1,2-*b*]thiophénone-7 (D-10), **12′***

Dans les mêmes conditions que celles que nous venons de décrire, 0,50 g (1,45 mmol) du composé **4′***f*, 2,03 g (7,5 mmol) de chlorure mercurique et 6,54 g de zinc conduisent à 0,07 g (Rdt = 14%) du mélange **10′** + **11′** et à 0,09 g (Rdt = 18%) de **12′**; F = 149°C. Composés **10′** + **11′** : rmn δ (400 MHz) : (caractéristiques des ponts méthyléniques) 2,27 (d, H_{4endo} (**11′**), J = 3,91 Hz), 2,14 (2d, H_{4endo} (**10′**), J = 4,00 et 6,59 Hz), 1,31 (d, H_{4exo} (**11′**), J = 3,91 Hz), 1,21 (2d, H_{4exo} (**10′**), J = 4,00 et 9,04 Hz). *Anal.* calc. pour $C_{23}H_{19}DOS$: C 79,96, O 4,63, S 9,28; trouvé : C 79,6, O 5,0, S 9,0. Composé **12′** : *Anal.* calc. pour $C_{23}H_{21}DOS$: C 79,49, O 4,60, S 9,23; trouvé : C 79,6, O 4,4, S 9,2.

1. B. HANQUET, R. GUILARD et P. FOURNARI. Bull. Soc. Chim. Fr. 571 (1977).
2. B. HANQUET, R. GUILARD et Y. DUSAUSOY. J. Chem. Soc. Perkin Trans. 1, 983 (1985).
3. B. HANQUET, M. FARNIER, R. GUILARD, C. LECOMTE et Y. DUSAUSOY. Can. J. Chem. **63**, 2089 (1985).
4. E. VEDEJS. Organic reactions. Vol. 22. Wiley, New York. 1975. Chap. 3.
5. Y. DUSAUSOY, B. HANQUET et R. GUILARD. Acta Crystallogr. Sect. B, **37**, 1367 (1981).
6. R. GUILARD et P. FOURNARI. Bull. Soc. Chim. Fr. 1437 (1971).
7. E. J. COREY et M. CHAYKOVSKY. J. Am. Chem. Soc. **87**, 1353 (1965).

cyclopropa[3,4]cyclohepta[2,1-*b*]thiophénones-5, **3** et des tétrahydro-4,4a,6,6a 3b*H*,5a*H*-dicyclopropa[3,4:6,7]cyclohepta[1,2-*b*]thiophénones-5,

		Analyse centésimale							
		C		H		O		S	
F ou Eb (°C)	Formule(s) moléculaire(s)	Calc.	Tr.	Calc.	Tr.	Calc.	Tr.	Calc.	Tr.
48	$C_{12}H_{12}OS$	70,55	70,6	5,92	5,9	7,83	7,7	15,69	15,7
180/14	$C_{12}H_{12}OS$	70,55	70,6	5,92	6,1	7,83	7,7	15,69	15,5
48	$C_{12}H_{11}DOS$	70,20	69,3	—	—	7,79	7,8	15,62	15,0
180/14	$C_{12}H_{11}DOS$	70,20	70,1	—	—	7,79	7,8	15,62	15,3
103	$C_{13}H_{14}OS$	71,52	71,3	6,46	6,5	7,33	7,4	14,69	14,5
119	$C_{13}H_{14}OS$	71,52	71,4	6,46	—	7,33	7,2	14,69	14,8
—	$C_{22}H_{16}OS$	80,47	79,9	4,91	4,8	4,87	5,3	9,74	9,8
—	$C_{22}H_{16}OS$								
150	$C_{23}H_{18}OS$	80,67	79,6	5,26	5,3	4,67	4,9	9,36	9,5
190	$C_{23}H_{18}OS$	80,67	80,6	5,26	5,3	4,67	4,7	9,36	9,1
—	$C_{22}H_{15}DOS$	80,22	80,2	—	—	4,86	5,3	9,71	9,7
186	$C_{23}H_{17}DOS$	80,43	80,5	—	—	4,66	4,7	9,34	9,3
—	$C_{22}H_{15}DOS$	80,22	80,3	—	—	4,86	5,2	9,71	9,5
189	$C_{23}H_{17}DOS$	80,43	80,5	—	—	4,66	4,7	9,34	9,3
100	$C_{16}H_{16}O_5S$	59,98	60,2	5,03	5,2	24,97	24,8	10,01	9,9
66	$C_{16}H_{16}O_5S$	59,98	60,1	5,03	5,0	24,97	24,9	10,01	10,1
95	$C_{17}H_{18}O_5S$	61,06	61,1	5,43	5,5	23,92	23,9	9,59	9,9
100	$C_{16}H_{15}DO_5S$	59,79	60,0	—	—	24,89	24,7	9,97	9,9
66	$C_{16}H_{15}DO_5S$	59,79	59,6	—	—	24,89	24,8	9,97	9,7
90	$C_{17}H_{17}DO_5S$	60,87	60,7	—	—	23,85	23,5	9,56	9,4

The internal rotational potential in benzyl chloride

TED SCHAEFER, RUDY SEBASTIAN, AND GLENN H. PENNER
Department of Chemistry, University of Manitoba, Winnipeg, Man., Canada R3T 2N2
Received December 2, 1985

TED SCHAEFER, RUDY SEBASTIAN, and GLENN H. PENNER. Can. J. Chem. **64**, 1372 (1986).

The ^{1}H nmr spectra of benzyl chloride in dilute CS_2 and acetone-d_6 solutions are analyzed. The long-range coupling constants are consistent only with a low-energy conformation in which the C—Cl bond lies in a plane perpendicular to the benzene plane. Geometry optimized computations at the STO 3G level of molecular orbital theory agree with this conclusion and yield a nearly pure twofold barrier to internal rotation of 8.6 kJ/mol. In CS_2 solution the long-range couplings yield 8.8 kJ/mol, rising to 11.2 kJ/mol in acetone solution. This increase in the internal barrier in a polar solvent is similar to that found for benzyl fluoride, but in the latter the barrier itself is very much smaller than in benzyl chloride.

TED SCHAEFER, RUDY SEBASTIAN et GLENN H. PENNER. Can. J. Chem. **64**, 1372 (1986).

On a analysé les spectres rmn du ^{1}H du chlorure de benzyle qui ont été déterminés dans des solutions diluées de CS_2 et d'acétone-d_6. Les constantes de couplage à longue distance ne sont en accord qu'avec une conformation de basse énergie dans laquelle la liaison C—Cl serait dans une plan perpendiculaire au plan du benzène. Des calculs optimisés de la géométrie, effectués au niveau STO 3G de la théorie des orbitales moléculaires, sont en accord avec cette conclusion et conduisent à une barrière binaire pratiquement pure, de 8,6 kJ/mol, pour la rotation interne. Cette augmentation de la barrière interne dans un solvant polaire est semblable à celle qui a été observée dans le cas du fluorure de benzyle; toutefois, dans ce dernier cas, la barrière elle-même est beaucoup plus faible que dans le cas du chlorure de benzyle.

[Traduit par la revue]

Introduction

Early Raman (1) and Kerr constant (2) data implied that **1** is the low-energy conformer of benzyl chloride in solution, while an infrared and Raman spectral study apparently detected all three conformers (3). For the 3,5-dichloro derivative in benzene-d_6 solution the long-range proton–proton coupling constants were interpreted to mean that **2** is of lowest energy and that the internal barrier to rotation, assumed twofold, was 8.8 ± 1.7 kJ/mol (4).

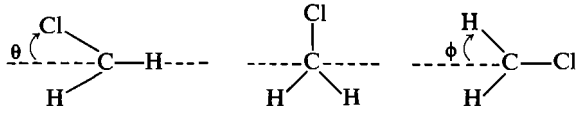

1 **2** **3**

The electron diffraction pattern of benzyl chloride in the gas phase was consistent with essentially **1** as the average structure or with **2** and a concomitant twofold internal barrier to rotation of 6.3 kJ/mol (5). Reconsideration of the data suggested that V_2 is nearer 8.8 kJ/mol (6). Recent ^{1}H nmr spectra of benzyl chloride dissolved in two nematic phases are consistent only with conformer **1**, apparently to the exclusion of **2** and **3** (7). It was stated, however, that independent information about the shape of the potential function for internal motion was required for a more rigorous discussion.

In this paper we report extensive geometry optimized STO 3G MO calculations for the internal potential of benzyl chloride. The ^{1}H nmr spectra in CS_2 and acetone-d_6 are analyzed in order to investigate solvent perturbations of the internal barrier.

Experimental

A 2.5 mol% solution of benzyl chloride in CS_2, containing 10 mol% of C_6D_{12} and 0.5 mol% of TMS, was transferred to a 5-mm od nmr tube. The solution was degassed by several cycles of the freeze–pump–thaw technique and the nmr tube was flame-sealed. The same treatment was given to a 2.2 mol% solution of benzyl chloride in acetone-d_6, which also contained 0.5 mol% TMS.

The ^{1}H nmr spectra were accumulated at a probe temperature of 300 K and at 300 MHz on a Bruker AM300 spectrometer. Wide sweepwidths referenced the spectra with respect to TMS. Each spectral region was examined in detail, the sweepwidth and data region being adjusted to give acquisition times of about 40 s. The digital resolution was about 0.025 Hz. Four to sixteen scans were acquired. Zero filling to twice the original data region was done before transforming the FIDs using a small amount of gaussian multiplication. The linewidths at half height were approximately 0.04 Hz. STO 3G MO (9) computations employed the computer program MONSTERGAUSS (10) and utilized an Amdahl 470/V8 system. INDO and CNDO/2 computations (11, 12) were also done on this system.

Results and discussion

Spectral analyses

These were done with a locally modified version of the computer program NUMAR1T (13). The spectral parameters are collected in Table 1, where they are compared with those obtained (14) from a self-assigning analysis of an ^{1}H nmr spectrum at 100 MHz for a 20 mol% solution in acetone. Considering that the linewidth at half height of the peaks in the latter spectrum was 0.148(2) Hz, compared to the ca. 0.04 Hz at 300 MHz, the agreement between the parameters is very good. However, the small long-range couplings are expected to be more accurately given by the present analyses because of the larger number of resolved splittings observable in the spectra at 300 MHz.

Figure 1 displays the observed and calculated spectra of the methylene protons in CS_2 solution.

STO 3G MO calculations

When all bond angles and lengths were allowed to vary, with the proviso that the carbon framework of the benzene moiety remained a regular hexagon, the relative energies of the conformers could be fit by eq. [1]. The angle θ is 90° for **2** above

$$[1]\quad V(\theta)/\text{kJ mol}^{-1} = 8.58 \pm 0.01 \sin^2(\theta + 90°) - 0.24 \pm 0.01 \sin^2 2\theta$$

TABLE 1. The ^{1}H nmr spectral parameters for benzyl chloride in CS_2 and acetone solutions

Parameter	Value		
	CS_2[a]	Acetone-d_6	
$\nu_{(CH_2)}$	1338.428(1)[d]	1409.659(1)[b,d]	—
ν_2	2179.386(1)[d]	2234.024(1)[d]	739.722(2)[c,e]
ν_3	2173.560(1)[d]	2213.506(1)[d]	733.191(2)[e]
ν_4	2161.172(1)[d]	2200.325(1)[d]	728.937(4)[e]
$^3J_{23}$	7.723(1)[f]	7.740(1)	7.752(5)
$^3J_{34}$	7.475(2)	7.495(1)	7.497(5)
$^4J_{26}$	1.978(2)	1.974(1)	1.978(6)
$^4J_{24}$	1.251(2)	1.247(1)	1.242(4)
$^4J_{35}$	1.409(2)	1.408(1)	1.406(6)
$^5J_{25}$	0.589(1)	0.607(1)	0.605(3)
$^4J(H,CH_2)$	−0.518(1)	−0.483(1)	−0.491(3)[g]
$^5J(H,CH_2)$	0.287(2)	0.280(1)	0.295(4)[g]
$^6J(H,CH_2)$	−0.358(1)	−0.337(1)	−0.331(6)[g]
Calculated transitions	370	351	—
Assigned transitions	319	302	—
Peaks observed	175	192	—
Largest deviation	0.028	0.016	—
Root mean square deviation	0.009	0.005	—

[a]For a 2.5 mol% solution in CS_2 containing 10 mol% C_6D_{12} and 0.5 mol% TMS, probe temperature being 300 K.
[b]For a 2.0 mol% solution in acetone-d_6 containing 0.5 mol% TMS at 300 K.
[c]For a 20 mol% solution in acetone-d_6.
[d]To high frequency of internal TMS at 300.135 MHz.
[e]To high frequency of internal TMS at 100 MHz (14).
[f]Numbers in parentheses represent standard deviations in the last significant figure.
[g]Because the linewidth in this spectrum was 0.15 Hz, these long-range couplings are probably considerably less reliable than those in the other columns, extracted from spectra with linewidths of about 0.04 Hz.

and seven values were used in the fit, the errors being given at the 95% confidence level. The completely optimized structure of the low-energy conformer **2** is shown in Fig. 2.

According to these computations the barrier is predominantly twofold, with a very small fourfold component. In the discussion below of the long-range couplings, the internal barrier will be taken as twofold.

Long-range couplings and the internal potential

(i) CS_2/C_6D_{12} solution

It has been demonstrated that $^6J(H,CH_2) \equiv {}^6J$ is directly proportional to $\sin^2\phi$, where ϕ is the angle by which the C—H bond of the sidechain twists out of the benzene plane (15–17). If the value of ^6J is known at $\phi = 90°$, then the observed ^6J yields the expectation value, $\langle\sin^2\phi\rangle$. The latter can be related to the twofold barrier by a hindered rotor model (17). A recent precise analysis of the ^{1}H nmr spectrum of toluene yields ^6J as −1.204(4) Hz at $\phi = 90°$ (8).

However, the magnitude of this number decreases in the presence of electronegative α-substituents. Recent detailed studies of benzyl fluoride (18) and benzyl methyl ether and some derivatives (19) show that ^6J is −1.02 Hz for a CH_2OR group at 90° and is −0.95 Hz for CH_2F. The assumption of a linear dependence of ^6J on the electronegativity of the α-substituent yields ^6J as −1.06 Hz for CH_2Cl if the chlorine substituent has an electronegativity of 3.0 on the scale for which fluorine is placed at 3.92, OR at 3.31, and H at 1.78 (20–22).

Because ^6J is −0.358(1) Hz in CS_2 solution, $\langle\sin^2\phi\rangle$ follows

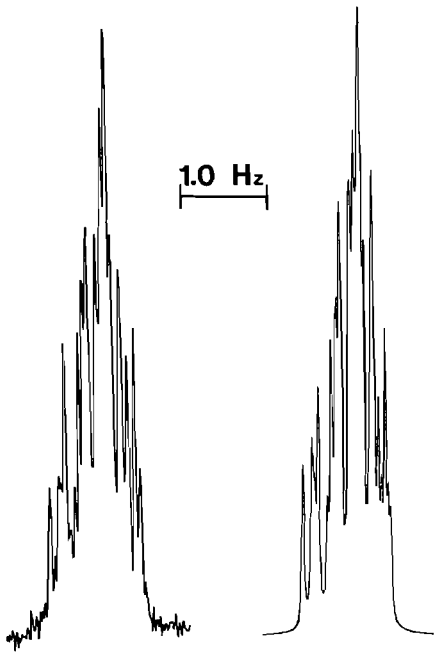

FIG. 1. The observed and computed ^{1}H nmr spectra of the methylene protons of benzyl chloride, for a 2.5 mol% CS_2 solution containing 10 mol% of C_6D_{12} and 0.5 mol% of TMS. The probe temperature is 300 K and the spectrometer frequency is 300.135 MHz. The linewidth at half height is between 0.03 and 0.04 Hz. The computed spectrum is based on the parameter values in Table 1.

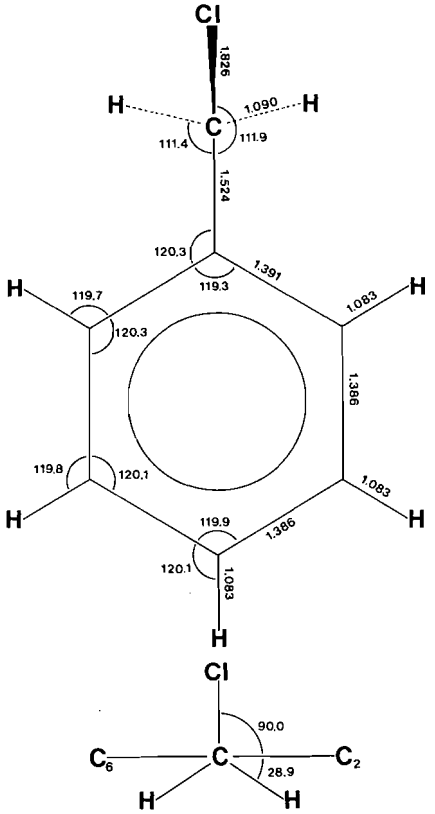

FIG. 2. The fully optimized structure of the stable conformer of benzyl chloride at the STO 3G level of molecular orbital theory. Its energy is −720.475480 au. The C(1)—C(α) bond makes an angle of 0.2° with the C(1)—C(4) axis. When the C—Cl bond lies in the benzene plane, the C(1)CCl angle increases to 114.75° and the C(2)C(1)C(α) angle is computed to increase also, to 123.2°. Therefore steric strain is indicated as at least one contribution to the internal barrier of rotation about the sp^2–sp^3 bond.

as 0.358/1.06 or 0.338. This value corresponds to a V_2 of 8.8 ± 0.4 kJ/mol in a table relating $\langle \sin^2 \theta \rangle$ to V_2, the temperature, and to the reduced moment of inertia of benzyl chloride (23), *if* it is assumed that the conformation of lowest energy is **2**. The quoted error assumes an error of 0.01 Hz in ^6J at $\phi = 90°$. This barrier in CS_2 solution agrees rather well with the 8.6 kJ/mol calculated by STO 3G MO methods above. Furthermore, it coincides with the 8.8 kJ/mol deduced by Scharfenberg from the electron diffraction data for the vapor (6). The average torsional angle associated with this barrier corresponds, not to 60° as in **1**, but to 67.5° (6). Such an average is also compatible with a hindered rotor model (24).

The dipole moment of benzyl chloride is 1.74 D in decalin (25) and is reported as 1.75–1.89 D in benzene solution (26). INDO MO computations for the STO 3G MO geometries give 2.21 D for **2** and 2.18 D for **3**, whereas the STO 3G MO values are 2.66 and 2.42 D, respectively. Both sets of data suggest an increase in the dipole moment as the C—Cl bond twists out of the ring plane but are clearly overestimates of the dipole moment magnitudes. Assuming a dipole moment of 1.7 D for **3** and 1.9 D for **2**, the dielectric continuum model (27), and allowing for the polarizability of the solute predicts an increase of at most 0.3 kJ/mol in the stability of **2** relative to **3** when benzyl chloride is dissolved in CS_2. The same model predicts a stabilization of **2** in acetone by about 0.5 kJ/mol, rather less than found below.

(ii) Acetone-d_6 solution

In this solution, ^6J is −0.337 (1) Hz and V_2 becomes 11.2 ± 0.4 kJ/mol, an increase of 2.4 ± 0.8 kJ/mol relative to the CS_2 solution. It happens that the J method (17) for internal barriers is most sensitive in this region of barrier magnitudes. The increase of 2.4 kJ/mol is reliable because its value is insensitive to the value taken for ^6J at $\phi = 90°$. Furthermore, a detailed study of long-range $^{13}C,^{19}F$, $^1H,^{19}F$, and $^1H,^1H$ couplings of benzyl fluoride in a range of solvents established that the conformer analogous to **2** became 2 kJ/mol more stable than that analogous to **3** when passing from CS_2 to acetone solution (18). It may also be noted that the dipole moment of benzyl fluoride (28) is equal to that of benzyl chloride within experimental error.

The notable difference between the two compounds is that the internal barrier in benzyl fluoride must be very small, probably less than 1 kJ/mol in CS_2 solution (18). Therefore the change in internal barrier caused by the polar acetone solvent is apparently independent of the intrinsic barrier, implying that for benzyl chloride the low-energy conformer **2** is being stabilized by the polar solvent and probably leaving the high-energy form **3** (steric barrier?) unchanged (see Fig. 2).

*(iii) **1** cannot be of lowest energy*

The discussion above assumes **2** as the stable conformer. However, suppose **1** were stable, as deduced from a classical approach to the ^1H nmr spectra in nematic solvents (7). For this conformer $\langle \sin^2 \phi \rangle$ is $(\sin^2 60° + \sin^2 0°)/2$ or 0.375, assuming that the barrier is not so high that averaging of the two ^6J values is prevented. Then ^6J becomes -1.06×0.375 or −0.398 Hz. Any internal motion in conformer **1** will cause this number to change towards −0.53 Hz because, in the limit of free internal rotation, $\langle \sin^2 \phi \rangle$ equals 0.5. Because the observed ^6J values are well below 0.398 Hz in magnitude, **1** cannot be the preferred conformer for benzyl chloride in CS_2 or acetone solutions. Only if ^6J at $\phi = 90°$ were less than 0.90 Hz in magnitude in CS_2 solution, would **1** be stable, and then only if the barrier in **1** were very large indeed.

(iv) Concerning $^5J(H,CH_2)$ and $^4J(H,CH_2)$

The orthobenzylic coupling in toluene has been written as (29)

$$[2] \quad {}^4J(H,CH_2)/Hz = -1.08 \sin^2 \phi - 0.32 \cos^2 \phi$$

For toluene the expectation values of $\sin^2 \phi$ and $\cos^2 \phi$ are both 0.5, so that ^4J should be −0.70 Hz, precisely as found in a recent analysis (8). It was also shown (29) that ^4J decreases in magnitude as the electronegativity of the α-substituent increases, at least for acenaphthene derivatives in which the substituent has a fixed orientation with respect to the π plane of the aromatic system.

If the multiplier of $\sin^2 \phi$ represents the σ–π or hyperconjugative term in the coupling mechanism, then it may be reasonable to assume a reduction in its magnitude in the same proportion suffered by ^6J, a sole σ–π coupling. If this assumption is correct, then it follows from the −0.518 Hz for ^4J in the CS_2 solution of benzyl chloride that the term in $\cos^2 \phi$ must also be reduced, by a factor of 0.92. For the acetone solution the calculated ^4J becomes −0.494 Hz, somewhat different from the observed −0.483 Hz.

Whatever the merit of the assumptions in this discussion, qualitatively it is clear that ^4J should be smaller in magnitude in acetone than in CS_2 solution, simply because ^4J is dominated by the $\sin^2 \phi$ term in eq. [2] and its expectation value is smaller in the acetone solution because **2** is stabilized. In other words, the

observed changes in ^4J and ^6J are both consistent with an increased V_2 in acetone solution if **2** is the stable conformer.

Turning to ^5J, it has been postulated (8) to obey eq. [3] for toluene.

[3] $^5J(H,CH_2) = 0.336\langle\sin^2\phi\rangle + 0.322\langle\sin^2(\phi/2)\rangle$

The first term represents the $\sigma-\pi$ term and in benzyl chloride should also be reduced, presumably by a factor of 1.06/1.20. It is not known whether the σ electron term, in $\sin^2(\phi/2)$, increases or decreases in the presence of an electronegative α-substituent.

An electronegative *ortho* substituent increases the σ electron component of ^5J, for example in 2,6-difluorotoluene (30). If the ^5J of 0.287 Hz for benzyl chloride in CS_2 solution is to be reproduced by an equation like [3], then the α-chlorine substituent must increase the σ electron term. One might write $^5J = 0.287 = 0.336(1.06/1.20)(0.338) + 0.322(0.5)R$ because for a twofold barrier $\langle\sin^2(\phi/2)\rangle$ is 0.5. The factor R becomes 1.16. Application of this factor to the acetone solution yields 0.281 Hz as compared to the observed 0.280(1) Hz.

In other words, the observed decrease of ^5J in going from the CS_2 to the acetone solution is interpreted to arise from the decreased $\sigma-\pi$ component in the latter, the σ electron term being a constant whatever the value of R. Qualitatively, this interpretation is consistent with the behaviour of ^4J and ^6J in the two solvents.

(v) Concerning the barrier in 3,5-dichlorobenzyl chloride

In benzene-d_6 solution, $^6J(H,CH_2)$ is $-0.40(1)$ Hz (4). It was assumed (4), on the basis of arguments now known to be incorrect, that ^6J at $\phi = 90°$ was -1.14 ± 0.02 Hz, from which it followed that 8.8 ± 1.7 kJ/mol represented the internal barrier to rotation. The value of $-1.06(1)$ Hz for the extremum of ^6J yields an internal twofold barrier of 5.7 ± 0.9 kJ/mol.

In CS_2 solution, V_2 is 8.8 ± 0.4 kJ/mol for benzyl chloride. The difference of 3.1 ± 1.3 kcal/mol is most likely real because, for benzyl fluoride, a variety of coupling data show that the conformer analogous to **3** is stabilized by 2 kJ/mol by chlorine substituents at the two *meta* positions. In other words, because **2** is the most stable conformer of benzyl chloride, the two *meta* chlorine substituents *lower* the internal barrier. The stabilization of the conformer with the halogen substituent in-plane may well be very similar for benzyl chloride and benzyl fluoride if intramolecular dipole interactions are responsible; the dipole moments of the two compounds are so very similar. Yet, it is interesting that the in-plane conformer of benzenethiol is also stabilized by *meta* chlorine substituents (31). The barrier in benzenethiol is presumably dominated by conjugative interactions.

Conclusions

In CS_2 solution the only reasonable interpretation of the long-range proton coupling constants in benzyl chloride is that the conformation of lowest energy is the one in which the C—Cl lies in a plane perpendicular to the benzene ring. The derived twofold internal barrier is in agreement with that computed by STO 3G MO methods and with the latest treatment of electron diffraction patterns. In acetone-d_6 solution the barrier increases by about 2 kJ/mol, according to the long-range couplings.

A recent discussion of the vibrational spectra of liquid benzyl chloride (32) concludes that the internal barrier is sixfold with an upper magnitude of 16.0 kJ/mol.

Acknowledgements

We are grateful to the Natural Sciences and Engineering Research Council of Canada for financial assistance.

1. L. Verdonck and G. P. Van Der Kelen. Spectrochim. Acta, Part A, **28**, 51 (1972); **28**, 55 (1972).
2. K. E. Calderbank, R. J. W. Le Fevre, and R. K. Pierens. J. Chem. Soc. B, 1463 (1970).
3. W. A. Seth-Paul and H. Shino. Spectrochim. Acta, Part A, **31**, 1605 (1975).
4. T. Schaefer, L. J. Kruczynski, and W. J. E. Parr. Can. J. Chem. **54**, 3210 (1976).
5. N. I. Sadova, L. V. Vilkov, I. Hargittai, and J. Brunvoll. J. Mol. Struct. **31**, 131 (1976).
6. P. Scharfenberg. J. Chem. Phys. **77**, 4791 (1982).
7. M. Longeri, G. Chidichimo, and K. Bucci. Org. Magn. Reson. **22**, 408 (1984).
8. T. Schaefer, R. Sebastian, and G. H. Penner. Can. J. Chem. **63**, 2597 (1985).
9. W. J. Hehre, R. Ditchfield, R. F. Stewarts, and J. A. Pople. J. Chem. Phys. **52**, 2769 (1970).
10. M. R. Petersen and R. A. Poirier. MONSTERGAUSS. Department of Chemistry, University of Toronto, Toronto, Ontario, 1981.
11. J. A. Pople, J. W. McIver, and N. S. Ostlund. J. Chem. Phys. **49**, 2965 (1968).
12. P. Dobosh and N. S. Ostlund. QCPE, **11**, 281 (1975).
13. A. R. Quirt and J. S. Martin. J. Magn. Reson. **5**, 318 (1971); J. S. Martin, A. R. Quirt, and K. E. Worvill. The nmr program library. Daresbury Laboratory, Daresbury, U.K.
14. D. S. Stephenson and G. Binsch. J. Magn. Reson. **37**, 409 (1980).
15. R. Wasylishen and T. Schaefer. Can. J. Chem. **50**, 1852 (1972).
16. C. J. Macdonald and W. F. Reynolds. Can. J. Chem. **48**, 1002 (1970).
17. W. J. E. Parr and T. Schaefer. Acc. Chem. Res. **13**, 400 (1980).
18. T. Schaefer, J. Peeling, and R. Sebastian. Can. J. Chem. **63**, 3219 (1985).
19. R. Laatikainen. Magn. Reson. Chem. In press.
20. B. P. Dailey and J. N. Shoolery. J. Am. Chem. Soc. **77**, 3977 (1956).
21. J. R. Cavanaugh and B. P. Dailey. J. Chem. Phys. **34**, 1099 (1961).
22. M. L. Huggins. J. Am. Chem. Soc. **75**, 4123 (1953).
23. W. Danchura. Ph.D. Thesis, University of Manitoba, Winnipeg, Canada (1983).
24. T. A. Wildman. Chem. Phys. Lett. **75**, 383 (1980); **80**, 210 (1981).
25. F. Fairbrother. Proc. R. Soc. London, Part A, **142**, 173 (1933).
26. A. L. McClellan. Tables of experimental dipole moments. W. H. Freeman and Co., San Francisco. 1963.
27. R. J. Abraham and E. Bretschneider. *In* Internal rotation in molecules. *Edited by* W. J. Orville-Thomas. J. Wiley and Sons, New York. 1974. Chapt. 13.
28. M. T. Rogers. J. Am. Chem. Soc. **69**, 457 (1947).
29. M. Barfield, C. J. Fallick, K. Hata, S. Sternhell, and P. W. Westerman. J. Am. Chem. Soc. **105**, 2178 (1983).
30. T. Schaefer and R. Laatikainen. Can. J. Chem. **61**, 2785 (1983).
31. T. Schaefer, J. D. Baleja, and G. H. Penner. Can. J. Chem. **63**, 2471 (1985).
32. R. J. A. Ribeiro-Claro, A. M. D'A. Rocha Gonsalves, and J. J. C. Teixeira-Dias. Specterochim. Acta, Part A, **41**, 1055 (1985).

Motion about the C_{sp^2}—S bond in thioanisole and some derivatives by the *J* method

TED SCHAEFER AND JAMES D. BALEJA[1]

Department of Chemistry, University of Manitoba, Winnipeg, Man., Canada R3T 2N2

Received January 21, 1986

TED SCHAEFER and JAMES D. BALEJA. Can. J. Chem. **64**, 1376 (1986).

Conformations about the C_{sp2}—S bond in thioanisole and eight of its derivatives in solution are investigated by means of long-range spin–spin coupling constants over six bonds between the sidechain ^{13}C nucleus and the *para* ring proton or ^{19}F nucleus. According to geometry optimized STO 3G MO calculations the internal barrier to rotation is predominantly twofold in the gas phase in thioanisole and is 6.2 kJ/mol. In benzene solution the coupling constant yields 5.5(4) kJ/mol. *Para* fluorine and methyl substituents reduce the magnitude of the internal barrier, but *meta* methyl or chlorine substituents cause significant increases. In the presence of two *ortho* fluorine substituents the conformation of lowest energy has the C—S bond in a plane perpendicular to the aromatic plane, but the barrier may now contain a fourfold component. Addition of further fluorine substituents in the *meta* or *para* positions causes characteristic changes in conformational preferences of the thiomethyl group.

TED SCHAEFER et JAMES D. BALEJA. Can. J. Chem. **64**, 1376 (1986).

En se basant sue les constantes de couplage à longue distance à travers six liaisons entre les noyaux ^{13}C de la chaîne latérale et le proton ou un noyau ^{19}F en position *para* du cycle, on a étudié les conformations autour de la liaison C_{sp2}—S du thioanisole et de huit de ses dérivés en solution. Dans le cas du thioanisole en phase gazeuse et d'après des calculs d'OM au niveau STO 3G effectués sur des géométries optimisées, la barrière interne à la rotation est principalement binaire et s'élève à 6,2 kJ/mol. En solution dans le benzène, l'évaluation faite sur la base de la constante de couplage est égale à 5,5(4) kJ/mol. La présence de substituants fluor ou méthyle en position *para* réduit l'amplitude de la barrière interne; toutefois, la présence de substituants chlore ou méthyle en position *méta* provoque une augmentation importante de cette valeur. En présence de deux substituants fluor en position *ortho*, la conformation de plus basse énergie comporte une liaison C—S dans un plan qui est perpendiculaire au plan aromatique; toutefois, dans ce cas, la barrière peut maintenant contenir une composante quaternaire. L'addition d'autres substituants fluor en position *méta* provoque des changements des changements caractéristiques dans les préférences conformationnelles du groupement thiométhyle.

[Traduit par la revue]

Introduction

Although most experimental and theoretical methods (1–10) agree that the low energy conformation of thioanisole has all heavy atoms coplanar, the estimates of the barrier to rotation about the C_{sp2}—S bond vary from 1 kJ/mol (10) to 26 kJ/mol (2). Furthermore, no firm agreement exists as to the form of the potential function governing the motion about this bond, *local* minima having been suggested for various values of θ between 0 and 90° in **1** (3, 10). A pure twofold barrier, for example, has a

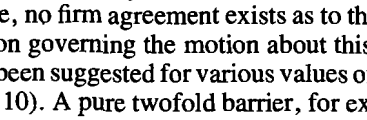

1

maximum at 90°, as would a barrier consisting of twofold and fourfold terms if the latter is relatively small. If it is substantial, then a local minimum can occur at 90°.

In thiophenol, in which the internal barrier is determined by $3p...\pi$ conjugation across the C—S bond, the potential hindering rotation is adequately described as twofold (11–13). In thioanisole, modification of such a simple form may be caused by interactions of the methyl group with, say, the *ortho* C—H bonds.

In view of the present uncertainties concerning the shape and magnitude of the barrier governing motion about the C_{sp2}—S bond in thioanisole, it seems reasonable to apply an independent method to this problem.

It is known that certain long-range spin–spin coupling constants between sidechain and ring nuclei have a simple conformational dependence (14). For example, ^6J(H,H) in toluene is proportional to $\sin^2\theta$, where θ is the angle by which the C—H bond twists out of the benzene plane (15). In a benzyl compound, then, the expectation value of $\sin^2\theta$ can be calculated in terms of the hindering potential and the temperature via a hindered rotor model, or classically, if preferred. If the value of ^6J(H,H) is known at $\theta = 90°$, then the measured value of ^6J(H,H) for the compound yields the expectation value of $\sin^2\theta$ and hence the magnitude of the potential barrier, whose form is assumed in the model (14).

In thioanisole the coupling constant of choice is $^6J(^1H,^{13}C)$. It is calculated to obey a $\sin^2\theta$ law. In 4-fluorothioanisole, the useful parameter would be $^6J(^{13}C,^{19}F)$, again involving the ^{13}C nucleus of the methyl group. Some success has been had with the corresponding couplings in anisole derivatives as indicators of conformational preferences (16).

Accordingly, this paper reports on the use of $^6J(^1H,^{13}C)$ and $^6J(^{13}C,^{19}F)$ in the measurement of internal barriers in thioanisole and a number of its derivatives. STO-3G MO computations, using fairly full geometry optimization procedures, are employed to provide hints about the form of the internal potentials.

Experimental

Compounds

^{13}C enriched thioanisole and its 2,6-dichloro, 3,5-dichloro, 3,5-dimethyl, and sym-tetrafluoro derivatives were prepared by adding (17) iodomethane-^{13}C (99 at.%, MSD Isotopes) to a mixture of the appropriate commercial thiophenol and anhydrous K_2CO_3 in dry acetone. The products were identified by nmr and mass spectroscopies.

Pentafluoro- and 4-methylthiophenol were methylated by addition of dimethyl sulfate to the aqueous sodium thiolate.

The 2,6-dibromo, 2,6-difluoro, 2,4,6-trifluoro, 2,6-dibromo-4-fluoro, and 2,6-dibromo-4-methyl derivatives of thioanisole were prepared from the corresponding anilines by treatment of the aqueous diazonium hydrosulfate salt with cuprous methylmercaptide, as devel-

[1]Present address: Department of Biochemistry, University of Alberta, Edmonton, Alberta.

TABLE 1. The ^{1}H nmr spectral parameters for thioanisole and thioanisole-α-^{13}C at 300 K

Parameter	Value		Parameter	Value	
ν_{CH_3}[a]	590.665(0)[b]	—[c]	$^5J_{25}$	0.548(0)[b]	0.550(0)[c]
$\nu_2 = \nu_6$	2131.905(1)[d]	2133.389(0)	^4J(H,^{13}C)	—	0.00
$\nu_3 = \nu_5$	2104.034(1)	2104.120(0)	^5JCH,^{13}C	—	0.078(1)
ν_4	2070.157(1)	2070.173(1)	^6J(H,^{13}C)	—	−0.147(1)
^5J(H,CH$_3$)	−0.140(0)	−0.137(0)	^1J(H,^{13}C)[e]	—	139.8
^6J(H,CH$_3$)	0.075(1)	0.079(0)	Peaks	178	202
^7J(H,CH$_3$)	−0.053(1)	−0.055(1)	Assigned peaks	167	194
$^3J_{23}$	7.938(1)	7.936(0)	Transitions calcd.	512	800
$^3J_{34}$	7.435(1)	7.436(1)	Transitions assigned	426	612
$^4J_{26}$	2.108(1)	2.104(1)	Largest deviation	0.014	0.017
$^4J_{24}$	1.155(1)	1.154(1)	Root mean square deviation	0.005	0.006
$^4J_{35}$	1.551(1)	1.551(1)	Line widths	0.045	0.045

[a]In Hz at 300.135 MHz to high frequency of internal tetramethylsilane.
[b]2 mol% of thioanisole in benzene-d_6.
[c]1.7 mol% of thioanisole-α-^{13}C in benzene-d_6.
[d]Numbers in parentheses are the standard deviations in the last significant figure.
[e]Not iterated on.

oped in this laboratory (18). Product identity was confirmed by ^{1}H,^{13}C,^{19}F nmr spectroscopies and by the mass spectra.

Sample preparation

Sampes for ^{1}H and ^{19}F nmr measurements were prepared by weight to consist of ca.2 mol% solutions in acetone-d_6 or benzene-d_6. Each solution was filtered through a pipette, containing cotton wool cleaned with CCl_4, into a 5-mm od nmr tube fitted with a ground-glass joint. Sample tubes were then degassed by at least five freeze–pump–thaw cycles and were flame-sealed.

Samples for ^{13}C nmr studies were prepared by volume or by weight as solutions in acetone-d_6 and were treated as above, except that 10-mm od sample tubes were employed.

Nuclear magnetic resonance measurements

^{1}H,^{13}C, and ^{19}F free induction decays were recorded on a Bruker WH90-DS spectrometer at a probe temperature of 305 K and at transmitter frequencies of 90.02, 84.70, and 22.63 MHz, respectively. The B_2 fields for multiple resonance experiments were calibrated with off-resonance techniques and could be regulated in 1-db steps (19). Some ^{1}H and ^{13}C nmr spectra were accumulated on a Bruker AM300 spectrometer when it became available in the later stages of the work.

In order to measure long-range couplings from protons to the ^{13}C nucleus of the methyl group, the INEPT pulse sequence was used (20). Other measurements used methods adequately described previously (16, 21). For the determination of very small splittings, resolution enhancement was obtained by multiplication with an increasing exponential function combined with a negative line broadening parameter, or by sine multiplication.

Computations

Ab initio molecular orbital calculations, using geometry optimization procedures, were performed at the STO-3G level (22) with the program MONSTERGAUSS (23). INDO MO FPT (24, 25) computations of spin–spin coupling constants employed the STO 3G optimized geometries. All computations were done with an Amdahl 470/V8 system.

Results and discussion

These were carried out with the programs LAME (26, 27) and NUMARIT (28) in iterative and non-iterative modes. Table 1 gives the ^{1}H nmr spectral parameters for thioanisole-α-^{13}C in benzene-d_6 solution. The ^{1}H nmr spectrum of unenriched thioanisole had previously been analyzed (21) and the comparison in Table 1 gives an indication of the precision obtainable. Figure 1 displays part of the nmr spectrum of the *meta* protons of the enriched compound.

Figures 2 and 3 illustrate how the signs of $^5J(^1H,^{13}C)$ and $^6J(^1H,^{13}C)$ were determined for 2,6-dichlorothioanisole. They are positive and negative, respectively, relatives to $^1J(^1H,^{13}C)$ in the methyl group. The latter is positive (29).

Figure 4 displays one of the four multiplets of the INEPT spectrum of the methyl ^{13}C nucleus in 2,6-dibromothioanisole. The large spacing arises from coupling to the *para* proton.

Table 2 gives the coupling parameters relevant to the discussion below.

The extrema in $^6J(^1H,^{13}C)$ and $^6J(^{13}C,^{19}F)$

In the equation $^6J = {}^6J_{90}\langle\sin^2\theta\rangle$, in which $^6J_{90}$ is the value of ^6J at $\theta = 90°$ and $\langle\sin^2\theta\rangle$ is the expectation value of $\sin^2\theta$ for a particular barrier, it is assumed that ^6J vanishes at $\theta = 0$. This assumption is valid for $^6J(^1H,^1H)$ couplings (14).

The assumption that $^6J(^1H,^{13}C)$ and $^6J(^{13}C,^{19}F)$ are proportional to $\sin^2\theta$ can be tested with INDO MO FPT calculations, which usually yield a reliable functional form of such long-range couplings even when the magnitudes of the couplings are not reproduced. For thioanisole, the calculations give $^6J(^1H,^{13}C)/Hz = -0.05 - 0.49\sin^2\theta$. As usual (15, 30, 31), the angle-independent term is taken as an artifact of the computation.

For 2,6-dichlorothioanisole, $^6J(^1H,^{13}C)$ is measured as −0.51(1) Hz and the barrier to internal rotation is calculated as 31.3 kJ/mol by STO 3G MO. Such a barrier, if twofold, corresponds to a $\langle\sin^2\theta\rangle$ of 0.96, suggesting a $^6J_{90}$ of −0.53 Hz. In 2,6-dibromothioanisole, $^6J(^1H,^{13}C)$ is −0.541(5) Hz. In this compound, the barrier to internal rotation must be larger than in the chloro derivative, so that −0.54 Hz appears as a reasonable approximation to $^6J_{90}$.

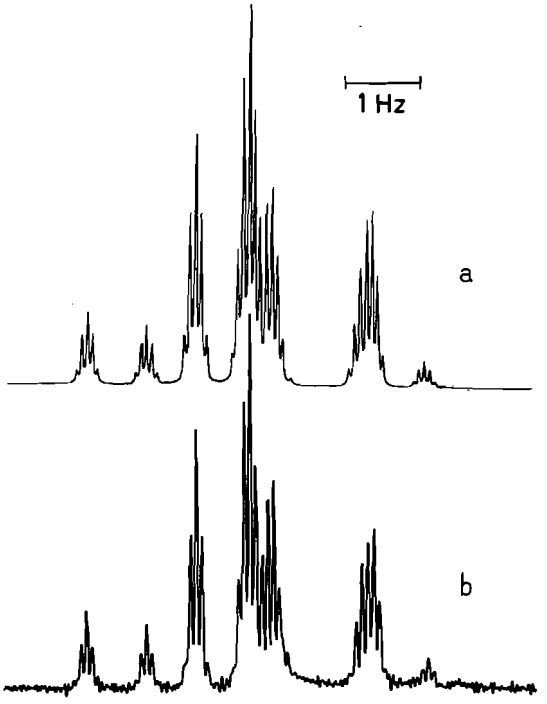

FIG. 1. Part of the *meta* ^{1}H nmr spectrum at 300 MHz and 300 K for a 1.7 mol% solution of thioanisole-α-^{13}C in benzene-d_6 solution. The smallest splittings in the observed spectrum in b are near 0.08 Hz and, according to the full analysis, are due to coupling over five bonds to the ^{13}C nucleus with a magnitude of 0.078(1) Hz. The quintet structure of some of the multiplets arises because the coupling over six bonds to the methyl protons also has a value near 0.08 Hz (see Table 1).

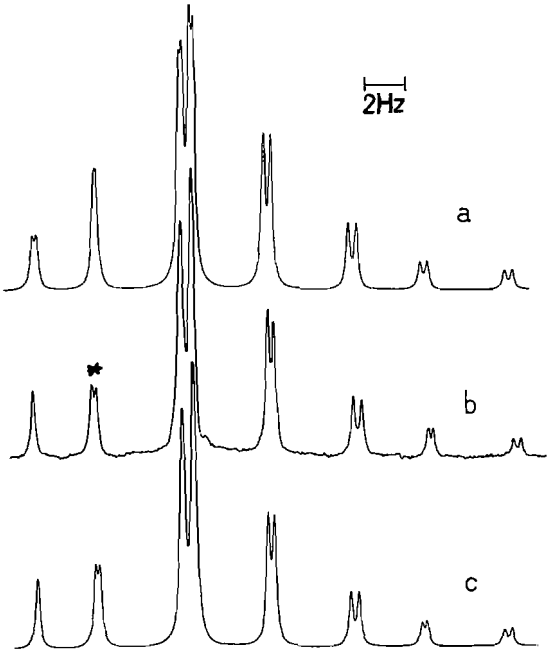

FIG. 2. The ^{1}H nmr spectrum of the ring protons of a 4 mol% solution of 2,6-dichlorothioanisole-α-^{13}C in acetone-d_6 at 300 K and 90 MHz is shown in b. In a the simulated spectrum has $^5J(^1H,^{13}C)/^6J(^1H,^{13}C)$ positive whereas in c this ratio is negative. Clearly, the couplings are of opposite sign. The band marked by an asterisk is shown with higher resolution in Fig. 3.

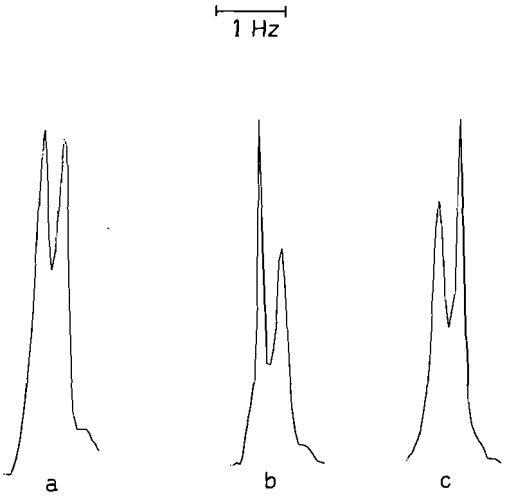

FIG. 3. In a is shown the band marked with an asterisk in Fig. 2, arising from the *meta* protons in 2,6-dichlorothioanisole-α-^{13}C. The peaks are broadened by coupling to the methyl protons. In b the methyl protons (those at high frequency) are being decoupled for one spin state of the ^{13}C nucleus, whereas in c the low frequency methyl proton band is being irradiated. The experiments show that $^1J(^1H,^{13}C)/^5J(^1H,^{13}C) > 0$.

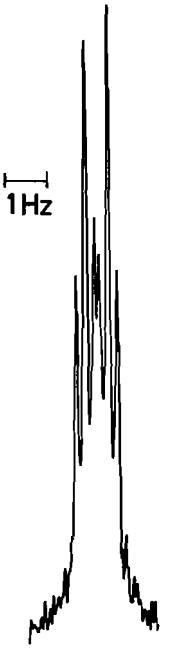

FIG. 4. One multiplet of the INEPT spectrum of the methyl ^{13}C nucleus of a 2 mol% solution of 2,6-dibromoanisole in acetone-d_6 at 300 K and 75.486 MHz. The large splitting arises from coupling to the *para* proton and is 0.541(5) Hz in magnitude. The triplets arise from a coupling of 0.217(5) Hz to the *meta* protons.

However, in a 2,6-dibromo-4-methylthioanisole, $^7J(^1H,^{13}C)$ becomes 0.606(5) Hz. If $^6J(^1H,^{13}C)$ is a pure σ–π coupling, then one expects that $^7J = -^6J$. Three possible reasons for the absence of this equality suggest themselves. First, it is known that a *para* methyl group decreases the $3p\ldots\pi$ conjugation in thiophenol and thereby decreases the twofold barrier by 1 kJ/mol (11). In the present thioanisole derivative the 4-methyl substituent would therefore further stabilize the $\theta = 90°$ conformation, leading to an increase in the magnitude of the hypothetical ^6J and therefore in ^7J. The observed increase of

TABLE 2. Internal rotational barriers for thioanisole and some derivatives

Substituent	$^6J(^1H,^{13}C)$ or $^6J(^{13}C,^{19}F)$	$<\sin^2\theta>^h$	V_2/kj[i]	V_2^l (STO 3G)
H[a]	−0.147(3)[f]	0.26(1)	5.4(4)	6.2
4-F[b]	0.474(4)	0.32(2)	3.8(4)	4.6
4-CH_3[b]	0.190(4)[g]	0.34(1)	3.3(3)	4.9
3,5-diCH_3[c]	−0.132(4)	0.24(1)	6.3(4)	6.6
3,5-diCl[c]	−0.087(5)	0.155(13)	9.9(9)	7.5
2,6-diF[c]	−0.420(3)	0.75(2)	5.9(8)[k]	
2,4,6-triF[d]	1.20(1)	0.78(2)	6.9(8)[k]	
2,3,5,6-tetraF[c]	−0.370(5)	0.66(2)	3.3(7)[k]	
pentaF[e]	1.19(2)	0.77(2)	6.5(8)[k]	

[a]For a 1.7 mol% solution in benzene-d_6.
[b]50 v/v% in acetone-d_6.
[c]2 mol% in acetone-d_6.
[d]4 mol% in acetone-d_6.
[e]27 mol% in acetone-d_6.
[f]In Hz, standard deviations being given in parentheses.
[g]This is $^7J(^1H,^{13}C)$.
[h]Based on $^6J(^1H,^{13}C) = -0.56 \pm 0.02$ Hz at $\theta = 90°$ and $^6J(^{13}C,^{19}F) = 1.54 \pm 0.04$ Hz at $\theta = 90°$.
[i]These twofold barriers follow from tables of $<\sin^2\theta>$ as a function of the barrier, the temperature, and reduced moment of inertia (42).
[k]These barriers are based on the assumption of a twofold barrier. See text.
[l]Based on geometry optimized structures.

10% is really rather too large, however. Second, it is conceivable that ^6J contains a *positive* non σ–π component and, because ^7J measures only the σ–π component, its magnitude is then larger than that of ^6J. Thirdly,it is possible that for the present couplings the equality in magnitudes is not to be expected, it having been postulated and observed (32–34) originally for $^1H,^1H$ couplings. Yet, to within experimental error (16) the equality holds for the corresponding anisole derivatives.

In view of these uncertainties about the value of $^6J_{90}$ and because a value of −0.54 Hz holds only if the barrier in the bromo derivative is infinite, it shall be assumed that $^6J_{90}$ has a value of -0.56 ± 0.02 Hz in the derivation of barriers below, and can be compared to the -0.63 ± 0.01 Hz deduced for anisole (16). The magnitude of the latter would be expected to be larger because hyperconjugation would be more efficient in anisole, the shorter bond lengths leading to larger overlap integrals.

Turning to $^6J(^{13}C,^{19}F)$, its value in 2,6-dibromo-4-fluorothioanisole is 1.48(1) Hz, actually equal to that observed in the corresponding anisole derivative (16). The INDO MO FPT calculations again support a $\sin^2\theta$ dependence of this coupling, but underestimate its magnitude, as they do for $^6J(^{13}C,^{19}F)$ in 4-fluoroanisole (16) and for $^6J(^1H,^{19}F)$ in 4-fluorotoluene (15). In the absence of more definite information, $^6J_{90}$ will be taken as 1.54(4) Hz to allow for the finite barrier in the compound above. Furthermore, any possible ^6J at $\theta = 0$ will be ignored. The same assumption for anisole derivatives led to reasonable conformational deduction (16).

The form of the hindering potential

When bond lengths and angles are allowed to vary, with the constraint that the carbon network of the benzene ring remain a planar hexagon, the STO 3G MO energies can be fit by $V_2/\text{kJ} = (6.23 \pm 0.24)\ \sin^2\theta$ at the 95% confidence level. The geometries are optimized at 15° intervals in θ, giving seven values in all. If a fourfold potential is assumed to be present, one has $V/\text{kJ} = (5.95 \pm 0.18)\ \sin^2\theta + (0.43 \pm 0.17)\ \sin^2 2\theta$. Perhaps a small fourfold component, amounting to about 7% of the twofold, is present. However, such a magnitude of V_4 will alter $<\sin^2\theta>$ by very little, less than the uncertainty introduced by that in $^6J_{90}$.

For 3,5-difluorothioanisole, the STO 3G MO energies are reproduced by $V_2/\text{kJ mol}^{-1} = 8.84 \pm 0.26\ \sin^2\theta$. The increase in the calculated barrier relative to thioanisole is expected on the basis of the perturbational approach to molecular orbital theory (35) and parallels that observed (12) for V_2 in the corresponding thiophenols.

It will be assumed below that, in the absence of *ortho* substituents, the rotational barrier is adequately described as twofold.

For 2,6-difluoroanisole the computed energies are fit by $V/\text{kJ} = (9.7 \pm 0.6)\ \sin^2\phi - (2.7 \pm 0.6)\ \sin^2 2\phi$ where φ is zero when the methyl group lies perpendicular to the benzene plane. The expectation value of $<\sin^2\theta>$ is 0.788 for this potential and is 0.844 if a twofold barrier with a magnitude of 9.7 kJ/mol is assumed. Therefore, for some of the compounds below, a barrier derived on the basis of a twofold potential will contain an error to be discussed further below.

The derived barriers and conformations

Table 2 contains the magnitudes of the internal barriers to rotation about the C_{sp2}—S bond for thioanisole and eight of its derivatives.

(*i*) *Thioanisole*

The present STO 3G MO results indicate a predominantly twofold barrier in the gas phase, only a little higher than the 5.4(4) kJ/mol deduced for the benzene solution. The latter number implies that the barrier lies towards the low end of the range of some 25 kJ/mol in the values found in the literature. In some of these experiments, an angle θ is computed. Thus, from dipole moment and induced birefringence data in CCl_4 solution, θ is deduced as 23 ± 5° (1), in agreement with deductions based on X-ray fluorescence spectra (8) at liquid nitrogen temperature.

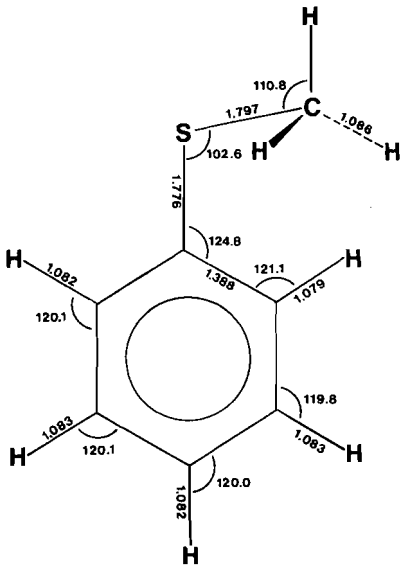

FIG. 5. The STO 3G MO geometry of the planar ground state of the thioanisole molecule with the carbon framework of the phenyl group as a regular haxagon. Note the deformation from 120° of the C2C1S angle, which becomes 120° of course for the perpendicular conformer. In the latter the C—S—C angle becomes 97.9° and the aromatic C—H bonds become 1.083 Å; the C_{sp2}—S bond increases to 1.787 Å and the C_{sp3}—S bond length becomes 1.803 Å. The electron diffraction structure (36) has a C—C bond length of 1.391(2) Å, a C_{sp2}—S bond length of 1.749(4) Å, and a C_{sp3}—S length of 1.803(4) Å. The C—S—C angle is 105.6(7)°, the S—C—H angle is 110.2(1.7)°, and the methyl group is apparently twisted out-of-plane by 45.3(2.8)°.

Electron diffraction patterns in the gas phase apparently fit a θ of 45 ± 10° (36). For a V_2 of 5.4(4) kJ/mol, the classical expectation value of θ is 27.6 ± 1.0° at 300 K, not very different from the value calculated (37) quantum mechanically from a hindered rotor model. A value of 45° is obtained for a zero barrier, of course. That out-of-plane populations are significant is also confirmed by nmr spectroscopy on thioanisole dissolved in liquid crystals (9).

Figure 5 gives the STO 3G MO structure for thioanisole in its lowest energy conformation. The figure caption compares the structure with that deduced from electron diffraction data and with the structure of the computed high energy form.

(ii) 4-Fluoro- and 4-methylthioanisole

Because the methylthio group is a π electron donor, the fluorine and methyl substituents act to decrease the $3p...\pi$ conjugation. If much of the barrier arises from this conjugation, as expected because the low-energy form is clearly planar, then the barriers to internal rotation in these two compounds should be lower than in thioanisole.

This decrease in V_2 is observed via the coupling constants and is also calculated by STO 3G MO methods (Table 2). A reduction of V_2 of thiophenol, caused by *para* fluorine or methyl substituents, has been noted (11).

The microwave barrier for 4-fluorothioanisole is 3.0 ± 1.0 kJ/mol and is based on the relative intensities of two band series in the low resolution spectrum in the gas phase at ambient temperatures (38). This value agrees with the 3.8(4) kJ/mol found in acetone solution in the present work.

(iii) 3,5-Dichloro- and 3,5-dimethylthioanisole

The increases in the internal barrier to rotation of the sulfhydryl group in the analogous thiophenols (relative to thiophenol) are the same as those found for the thioanisole in Table 2 (12). The change in the barrier caused by *meta* substituents has been discussed for the thiophenol derivatives in terms of perturbation molecular orbital theory and will not be repeated here. Qualitatively, the STO 3G MO barriers in Table 2 agree with the observed increases in barrier in solution for the two molecules.

(iv) 2,6-Difluorothioanisole

The two *ortho* fluorine substituents destabilize the planar (θ ± 0) conformation. In fact, $\langle\sin^2\theta\rangle$ becomes 0.75(2) in Table 2. If the barrier is purely twofold, then this number implies that the perpendicular (θ = 90°) conformation is of low energy and that the internal barrier is 5.9(8) kJ/mol. According to the STO 3G MO numbers, however, the magnitude of the fourfold component is about 30% of that of the twofold component. If a fourfold component exists, then a set of calculations of the classical expectation values of $\langle\sin^2\theta\rangle$ shows that the experimental value of 0.75 can be accommodated by a variety of combinations of twofold and fourfold potentials (note that the value of $\langle\sin^2\theta\rangle$ is not in question). If the restriction that $|V_4/V_2| \sim 0.3$ is applied, then 1.6/4.8 and −2.4/8.0 can be accommodated for V_4/V_2, for example.

In any event, it is clear that a significant barrier to internal rotation exists and that a given SCH_3 group spends much of its time nearer θ = 90° than θ = 0 at 300 K in acetone solution.

(v) Tri-, tetra-, and pentafluoro thioanisoles

When a *para* fluorine substituent is added to 2,6-difluorothioanisole, it is expected that the perpendicular conformer is further stabilized and that $\langle\sin^2\theta\rangle$ will increase, the *para* substituent causing a decrease in $3p...\pi$ conjugation. Although the errors in $\langle\sin^2\theta\rangle$ are rather large in Table 2, there is the consistency that V_2 drops by about 1 kJ/mol in moving from thioanisole to 4-fluorothioanisole, as it should because the planar conformer is stable for both compounds, whereas in moving from 2,6-difluoro- to 2,4,6-trifluorothioanisole an apparent increase occurs in $\langle\sin^2\theta\rangle$.

If two *meta* fluorine substituents are added to 2,6-difluorothioanisole, then by analogy to 3,5-dichlorothioanisole lower values of θ are expected to be more heavily populated. Indeed, the value of $\langle\sin^2\theta\rangle$ drops to 0.66(2), corresponding to an *apparent* V_2 of 3.3(7) kJ/mol.

Then, addition of one more fluorine substituent to tetrafluorothioanisole must again raise the magnitude of $\langle\sin^2\theta\rangle$. This occurs, to a value of 0.77(2), and it appears that a *para* fluorine substituent dominates the two *meta* substituents. Exactly the same phenomenon is observed for thiophenol derivatives in the sense that, although two *meta* chlorine substituents cause a remarkable increase in V_2, the addition of a *para* hydroxy substituent to 3,5-dichlorothiophenol brings V_2 back to a value similar to that in 4-methoxythiophenol (12). In terms of perturbation molecular orbital theory, it may be that the *para* substituent causes a first-order perturbation and, when it is present, the *meta* substituents are second-order perturbers. However, we have no more detailed interpretation of such a possibility.

Because of the rather large errors in the $\langle\sin^2\theta\rangle$ values for these fluorine derivatives, it is useful to have another set of parameters that substantiate the tentative conclusions about the conformational properties of these fluorine derivatives of thioanisole given in this section. Such a set is provided by $^5J(CH_3{}^{19}F)$, the long-range couplings between the methyl protons and the ^{19}F nuclei in the *ortho* C—F bonds.

The long-range $^5J(CH_3,{}^{19}F) \equiv {}^5J$

There is very little doubt that this coupling in anisole (16) and acetophenone (39) derivatives is a "through-space" (40) or proximate coupling. As such, its magnitude depends critically on the distance between the coupled nuclei. For ^5J in 2-fluoroacetophenone, for example, a semiempirical approach relates the magnitude of ^5J to $\cos^4\theta$, defined between $\theta = 0$ (methyl group *cis* to the C—F bond) and $\theta = 90°$ (39). In other words, ^5J decreases rapidly as the methyl group moves out of the benzene plane.

It appears eminently reasonable that ^5J in thioanisole derivatives is also a proximate coupling. If so, then it is arguable that, relative to its value in 2,6-difluorothioanisole, 0.746(5) Hz, its magnitude should decrease in 2,4,6-trifluorothioanisole because larger values of θ are now preferred. Indeed, ^5J is 0.588(1) Hz in the latter. Again, in 2,3,5,6-tetrafluorothioanisole the two *meta* substituents induce lower values relative to the 2,6-difluro derivative and ^5J increases to 0.907(2) Hz. The addition of a *para* fluorine substituent to yield the pentafluoro compound should now cause ^5J to drop. It does, to 0.722 Hz.

Quantitatively, the ^5J values support the arguments in the previous section concerning the degree of nonplanarity of the thiomethyl group. Indeed, if the V_2 values in Table 2 are used to calculate classical expectation values of θ, one finds a correlation coefficient of 0.903 (significant at the 90% confidence level) between ^5J and $\cos^4\theta$. The relationship implies a ^5J of 4.5 Hz at $\theta = 0$, a reasonable value. Of course, this correlation does not constitute a proof of the correctness of the barriers tabulated in Table 2, nor indeed that they are twofold. Parenthetically, the expectation value of 65° for θ in pentafluorothioanisole based on V_2 happens to agree with the conformational angle of 64 ± 5° deduced from Kerr constants (41) and X-ray fluorescence measurements (8).

Acknowledgments

We are grateful to Dr. James Peeling for the measurements on 4-fluorothioanisole and to the Natural Sciences and Engineering Research Council of Canada for financial support.

1. M. J. Aroney, R. J. W. LeFevre, R. K. Pierens, and M. G. N. The. J. Chem. Soc. London, B, 1132 (1971).
2. P. Palmieri, F. Tullini, B. Velino, and C. Zauli. Gazz. Chim. Ital. **105**, 919 (1975).
3. A. Schweig and N. Thon. Chem. Phys. Lett. **38**, 482 (1976).
4. E. Honegger and E. Heilbronner. Chem. Phys. Lett. **81**, 615 (1981).
5. P. S. Dewar, E. Ernstbrunner, J. R. Gilmore, M. Godfrey, and J. M. Mellor. Tetrahedron, **30**, 2455 (1974).
6. A. Modelli, D. Jones, F. P. Colonna, and G. Distefano. Chem. Phys. **77**, 153 (1983).
7. M. Mohraz, W. Jian-qi, E. Heilbronner, A. Soladie-Cavallo, and F. Matloubi-Maghadam. Helv. Chim. Acta, **64**, 97 (1981).
8. G. N. Dolenko, A. A. Voityuk, T. N. Delenko, and L. N. Mazalov. Zh. Strukt. Khim. **23**, 34 (1982).
9. J. W. Emsley, M. Longeri, C. A. Veracini, D. Catalano, and G. F. Pedulli. J. Chem. Soc. Perkin Trans. 2, 1289 (1982).
10. T. Matsushita, Y. Osamura, N. Misawa, K. Nishimoto, and Y. Tsuno. Bull. Chem. Soc. Jpn. **52**, 2521 (1979).
11. T. Schaefer and T. A. Wildman. Chem. Phys. Lett. **80**, 280 (1981).
12. T. Schaefer, J. D. Baleja, and G. H. Penner. Can. J. Chem. **63**, 2471 (1985).
13. N. W. Larsen and F. M. Nicolaisen. J. Mol. Struct. **22**, 29 (1974).
14. W. J. E. Parr and T. Schaefer. Acc. Chem. Res. **13**, 400 (1980).
15. R. Wasylishen and T. Schaefer. Can. J. Chem. **50**, 1852 (1972).
16. T. Schaefer, R. Laatikainen, T. A. Wildman, J. Peeling, G. H. Penner, J. Baleja, and K. Marat. Can. J. Chem. **62**, 1592 (1984).
17. L. F. Fieser and M. Fieser. Reagents in organic chemistry. J. Wiley and Sons,New York. 1967. p. 682.
18. J. D. Baleja. Synth. Commun. **14**, 215 (1984).
19. T. Schaefer and K. Marat. Org. Magn. Reson. **15**, 294 (1981).
20. G. A. Morris and R. Freeman. J. Am. Chem. Soc. **101**, 760 (1979).
21. T. Schaefer and J. D. Baleja. J. Magn. Reson. **60**, 131 (1984).
22. W. J. Hehre, R. F. Stewart, and J. A. Pople. J. Chem. Phys. **51**, 2657 (1969).
23. M. R. Petersen and R. A. Poirier. MONSTERGAUSS. Department of Chemistry, University of Toronto, Toronto, Ontario. 1981.
24. J. A. Pople, J. W. McIver, Jr., and N. S. Ostlund. J. Chem. Phys. **49**, 2960 2965 (1968).
25. P. Dobosh and N. S. Ostlund. QCPE, **11**, 281 (1975).
26. S. M. Castellano and A. A. Bothner-By. J. Chem. Phys. **41**, 3863 (1964).
27. C. W. Haigh. Annu. Rep. NMR Spectrosc. **4**, 311 (1971).
28. A. R. Quirt and J. S. Martin. J. Magn. Reson. **5**, 318 (1971); J. S. Martin, A. R. Quirt, and K. E. Worvill. The nmr program library. Daresbury Laboratory, Daresbury, U.K.
29. R. Freeman. J. Chem. Phys. **43**, 3087 (1965).
30. T. Schaefer, J. Peeling, and G. H. Penner. Can. J. Chem. **61**, 2773 (1983).
31. T. Schaefer, J. Peeling, G. H. Penner, A. Lemire, and R. Sebastian. Can. J. Chem. **63**, 24 (1985).
32. R. A. Hoffman. Mol. Phys. **1**, 326 (1958).
33. C. J. Macdonald and W. F. Reynolds. Can. J. Chem. **48**, 1002 (1970).
34. J. B. Rowbotham and T. Schaefer. Can. J. Chem. **52**, 489 (1974).
35. A. Pross and L. Radom. Prog. Phys. Org. Chem. **13**, 1 (1981).
36. N. M. Zaripov. Zh. Strukt. Khim. **17**, 741 (1976).
37. T. A. Wildman. Chem. Phys. Lett. **75**, 383 (1980); **80**, 210 (1981).
38. D. G. Lister, P. Palmieri, and C. Zauli. J. Mol. Struct. **35**, 299 (1976).
39. T. Schaefer, G. H. Penner, T. A. Wildman, and J. Peeling. Can. J. Chem. **63**, 2256 (1985).
40. J. Hilton and L. H. Sutcliffe. Prog. Nucl. Magn. Reson. Spectrosc. **10**, 27 (1975).
41. M. J. Aroney, L. Cleaver, R. K. Pierens, and R. J. W. LeFevre. J. Chem. Soc. Perkin Trans. 2, 1854 (1976).
42. W. Danchura. Ph.D. Thesis, University of Manitoba, Winnipeg, Manitoba. 1983.

A study of chromium-exchanged zeolites as potential catalysts for thermolysis of water

K. M. MIEDZINSKA AND B. R. HOLLEBONE
Department of Chemistry, Carleton University, Ottawa, Ont., Canada K1S 5B6
Received July 5, 1985[1]

K. M. MIEDZINSKA and B. R. HOLLEBONE. Can. J. Chem. **64**, 1382 (1986).

Evidence was found that the Cr(III)/Cr(II) redox cycle previously described to occur upon dehydration and rehydration of exchanged zeolite 13X, does not occur reversibly. Data suggest dimerization of the metal ion at high levels of exchange. The bridging provided by the oxygen atoms of the lattice probably stabilize these dimers and lead to initial but irreversible reduction at very low temperatures. Evidence also indicates irreversible formation of new lattices at very high dehydration temperatures.

K. M. MIEDZINSKA et B. R. HOLLEBONE. Can. J. Chem. **64**, 1382 (1986).

D'après des rapports antérieurs, les réactions de déshydratation et de réhydratation de réolites 13X échangées sont accompagnées d'un cycle rédox Cr(III)/Cr(II); on a trouvé que ce cycle ne se produit pas d'une façon réversible. Les données suggèrent que, à des niveaux élevés d'échange, il se produit une dimérisation de l'ion métallique. Le pontage qui est fourni par les atomes d'oxygène du réseau stabilise probablement ces dimères et, à des températures très basses, il conduit à une réduction initiale qui est irréversible. Les données indiquent aussi que, à des températures de déshydratation élevées, il se produit aussi une formation irréversible de nouveaux réseaux.

[Traduit par la revue]

Introduction

Amongst the many chemical systems which have been identified as potential systems for energy storage, metal ion doped zeolites which catalyse the thermolysis of water have been extensively studied (1–9). Both natural and synthetic zeolites absorb up to 30% by weight of water. The sites occupied by sodium ions and water bound within these lattices of various stoichiometries (10) have been characterized by crystallographic studies (1, 2, 4, 8) and infrared spectroscopy (3, 7, 11), epr (7) and nmr (12) as points of high symmetry in both the sodalite and supercages of the structure. These sites may be occupied by either aquated sodium ions or water but range in thermodynamic stability from the greatest in the sodalite cage to the least in the supercage as an approximate function of the availability of lattice oxygen binding sites at each position (13–15) (Fig. 1).

A large proportion of both the lattice sodium ions and water molecules can be displaced by exchange with a wide variety of transition metal or rare earth ions (7, 16). The degree of exchange depends on the critical dimension of the exchanging ion (17) and for the larger ions may involve the loss of some water ligands during insertion into the lattice (18). This can result in the stabilization of unusual coordination numbers (1, 7, 9, 19) or oxidation states (1, 7, 20, 21) which are of potential interest as catalytic sites. In particular, chromium(III) has been examined as a potential catalyst for thermolysis of water because of its facile reduction to the divalent form (22–24). In particular, studies of water thermolysis on Cr doped zeolites showed oxygen production under moderate temperature conditions (25, 26). However, the detailed behaviour of the chromium ion was not clarified and the overall reversibility of the system was not established.

In this work zeolites 13X and Y52 have been doped at many levels up to saturation with trivalent chromium. The structures both before and after thermal treatment have been examined by a variety of probes to determine the role played by the chromium ion. Using the same probes the systems have been recycled to examine reversibility and to discover whether they offer any potential as working catalysts for thermolytic energy conversion.

[1]Revision received January 31, 1986.

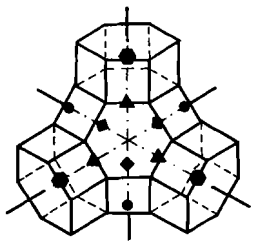

FIG. 1. Zeolite lattice and substitution sites: ●, Site I; ▲, Site I′; ●, Site II; ◆, Site II′.

Experimental

Sample preparation

Synthetic zeolites of the X lattice 13X (lot 139450 30049) and of the Y lattice LZ-Y52 (lot 020580) (previously known as SK-40) were obtained from Union Carbide Corporation Linde Division. Both powder samples were washed free of sodium silicates before use. All water was doubly distilled and deionized, all chemicals were reagent grade. Both zeolites were exchanged by overnight stirring in with trivalent chromium nitrate ($Cr(NO_3)_3.9H_2O$) solutions at concentrations of either 0.06 or 0.03 *M* in 300 mL of H_2O depending on the degree of exchange desired. The pH was maintained at 5 to 6 with 6 *N* NH_4OH and samples were mixed with Teflon stirrers while protected from light. With a minimum molar ratio of Cr/NH_4OH of 20:1 there was no evidence of the formation of $Cr(OH)^{2+}$. After exchange, samples were filtered and air dried to constant weight. Details may be found in Table 1.

Sample analysis

All samples were digested in a mixture of HF, NHO_3, and H_2SO_4 in Teflon vessels to dryness, then redissolved in 10% HF solution. Sodium was analysed gravimetrically as the magnesium uranyl acetate (27). Aluminum and chromium were determined by atomic absorption on a Perkin-Elmer, Model 5000, with HGA 500 graphite furnace atomic absorption spectrophotometer. Sample notation and data are given in Table 2.

Structural methods

Magnetic susceptibilities were measured by the Gouy method on a custom built magnetic balance incorporating a Cahn electrobalance, evacuated sample chamber with thermal control from 4 to 278 K and an electromagnet of variable field up to 9.2 kG. The instrument was calibrated with Mohr's salt.

Infrared spectra were obtained at low resolution on a Perkin Elmer Model 257 and at high resolution on a Perkin Elmer Model 257 spectrophotometer as Nujol mulls.

TABLE 1. Preparation chromium exchanged zeolites 13X and Y52

Sample	Amount zeolite ±0.01 g	Amount[a] exchanged $Cr(NO_3)_3 \cdot 9H_2O$	Footnotes
1-Cr^{3+}(13X)^{1}AD	25.00	8.00103	*b, e, h, j, l, o, q, s*
2-Cr^{3+}(13X)^{1}AD	25.03	8.00196	*b, e, h, j, l, o, q, s*
1-Cr^{3+}(13X)^{4}AD	25.00	7.9536	*c, f, h, k, l, o, q*
		7.9638	*c, f, h, k, m, o, q*
		3.4800	*c, f, h, k, m, o, q*
		3.5209	*c, g, h, k, m, o, q, s, t*
2-Cr^{3+}(13X)^{4}AD	25.0099	7.9974	*c, g, h, k, m, o, q*
		8.0009	*c, g, h, k, m, o, q*
		3.5009	*c, g, h, k, m, o, q*
		3.5382	*c, g, h, k, m, o, q, s, u*
3-Cr^{3+}(13X)^{4}AD	25.0271	8.0000	*c, g, h, k, m, o, q*
		7.9993	*c, g, h, k, m, o, q*
		3.5047	*c, g, h, k, m, o, q*
		3.5000	*c, g, h, k, m, o, q, s*
4-Cr^{3+}(13X)^{4}AD	25.0077	8.0008	*c, g, h, k, m, o, q*
		8.0000	*c, g, h, k, m, o, q*
		3.4991	*c, g, h, k, m, o, q*
		3.4995	*c, g, h, k, m, o, q*
1-Cr^{3+}(Y52)^{1}AD	10.0000	8.00453	*d, f, i, j, n, p, r, s*
2-Cr^{3+}(Y52)^{1}AD	10.0000	4.00443	*d, f, i, j, n, p, r, s*

[a]In g ± 0.0001 or 0.00001 as appropriate.
[b]pH of solution is 5.0.
[c]pH of solution is 5.5.
[d]pH of solution is 4.0.
[e]Solution stirred for 4 h.
[f]Solution stirred for 3 h.
[g]Solution stirred for 2 h.
[h]Time allowed for settling = 4 h.
[i]Time allowed for settling = 3 h.
[j]Filtered with Whatman #42.
[k]Filtered with Whatman #41.
[l]Filtrate clear and colourless.
[m]Filtrate clear green.
[n]Filtrate blue.
[o]Zeolite gray/green.
[p]Zeolite blue.
[q]pH of filtrate is 5.5.
[r]pH of filtrate is 4.5.
[s]Air dried for 2 days.
[t]Yield 29.133 ± 0.002 g.
[u]Yield 28.737 ± 0.002 g.

TABLE 2. Molecular formulas, molecular weights and percentages exchanged

Sample[a]	Molecular formula[b]	Al/Si ratio	Molecular weight[c]	Percentage exchanged[d]
13X theoretical	$Na_{86}(AlO_2)_{86}(SiO_2)_{106}$ 264 H_2O	1.23	18 176	
Y52 theoretical	$Na_{56}(AlO_2)_{56}(SiO_2)_{136}$ 250 H_2O	2.43	17 258	
13X	$Na_{87.8}(AlO_2)_{84.2}(SiO_2)_{114.2}$ 264.5 H_2O	1.36	18 225	
Y52	$Na_{52.9}(AlO_2)_{59.1}(SiO_2)_{132.9}$ 248.6 H_2O	2.25	17 164	
Cr^{3+}(13X)^{1}AD	$Cr_{6.9}$ $Na_{69.1}(AlO_2)_{84.2}(SiO_2)_{107.8}$ 265.8 H_2O	1.28	18 178	24.0
Cr^{3+}(13X)^{4}AD	$Cr_{10.4}Na_{50.8}(AlO_2)_{84.3}(SiO_2)_{107.8}$ 268.7 H_2O	1.28	17 991	36.3
Cr^{2+}(13X)^{1}C	$Cr_{6.5}$ $Na_{60.3}(AlO_2)_{84.2}(SiO_2)_{107.8}$ 263.8 H_2O	1.28	17 918	22.6
Cr^{3+}(Y52)^{1}AD	$Cr_{8.1}$ $Na_{29.6}(AlO_2)_{59.1}(SiO_2)_{132.8}$ 254.1 H_2O	2.25	17 163	18.6

[a]Samples are labelled in the following manner $N - M^{n+}(Z)^E$ *T*D, where *N* = number of sample; M = metal ion exchanged onto zeolite; *n* = oxidation state of M; Z = zeolite; *E* = number of times exchanged; *T* = temperature at which dehydration occurred, if any; D = drying technique used where VD = vacuum dried, OD = oven dried, AD = air dried, C = centrifuged.
[b]Cr ± 0.4, Na ± 0.2, AlO_2 ± 0.2, SiO_2 ± 0.4, H_2O ± 0.4.
[c]±1.0.
[d]% Exchange = 100 $aM_2/(86/eM_1)$ where *a* = actual weight of ion per gram of zeolite, M_1 = molecular weight of the exchanged cation, M_2 = molecular weight of the exchanged zeolite, *e* = oxidation state of the exchanging cation. Error ± 0.2.

Thermogravimetric analysis were performed on a Dupont Model 950 Thermogravemetric Analyser. Samples in platinum boats were heated at 10°C/min with a gravimetric time constant of 1 s. The instrument was standardized with calcium oxide under nitrogen using chrome alumel thermocouples.

Differential thermal analysis were performed on the Dupont Model 900 Differential Thermal Analyser. In HEAT mode, samples were heated at 20°/min with a baseline slope of zero. The instrument was standardized daily against glass, KNO_3 (127.7°), $KClO_4$ (299.5°C), and Ag_2SO_4 (412°).

Dehydration of exchanged zeolites

Samples in the area of 1 g were dehydrated to temperatures of 110, 150, 200, and 250°C. All samples were dehydrated on a vacuum line

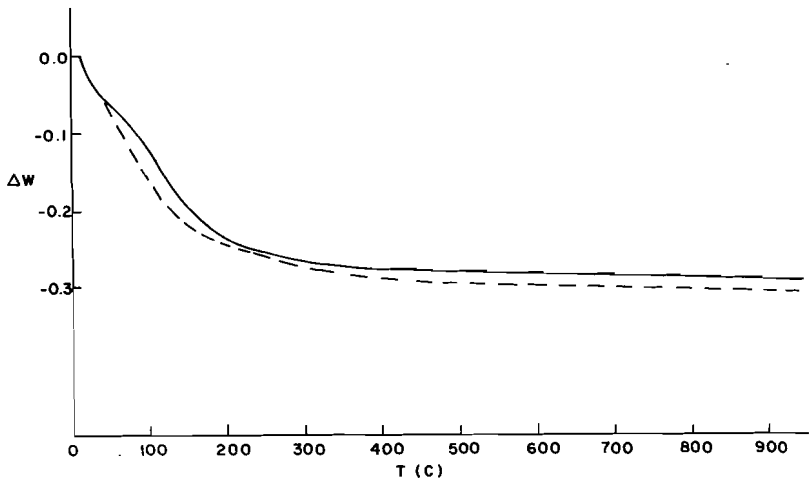

FIG. 2. Thermogravimetric analysis of Cr zeolite 13X (- - -) and zeolite 13X (——).

with a fore-pump and mercury diffusion pump system capable of pumping down to 10^{-3} mbar. Samples were evacuated in an electrically heated sand bath monitored by a thermometer in the sand at a depth equivalent to that of the sample. Samples were protected from the light and evacuated with heating up to as long as 60 h with continual evacuation. Samples were then cooled to room temperature (24°C) over a 24 h period under vacuum but with no further pumping. They were then transferred under nitrogen into sealed tubes.

Rehydration of exchanged zeolites

Samples were weighed out under nitrogen and immersed in 20 mL water for 48 h, being warmed to ~50°C. They were then filtered with tarred Whatman #42 paper and air dried under cover.

Results

Exchange and structures

In every case, all of the chromium of the first exchange was placed onto the lattice (as is evidenced by a colourless filtrate). Although the second filtrate remained green, and indicated that not all of the chromium made available to the lattice was exchanged, it was possible to place more chromium onto the frame in further exchanges. This was proven by analysis of the filrates, which showed high levels of sodium and significantly decreased levels of chromium.

The results in Table 1 show exchange levels from 18 to 36%. The framework structure of the samples was monitored by X-ray powder diffraction. It is known that in powder samples many X-ray intensities of zeolites are lost in the background or are confused by overlapping diffraction lines (11). The results indicated that all the samples remaind intact after exchange. Previous studies have shown exchange levels of only 6 Cr per zeolitic unit (28), yet this study has successfully exchanged 8.1 Cr^{3+} on Y52, 10.4 on 13X.

Thermogravimetric analysis

Water loss was calculated from the percentage weight loss of the samples. Samples were run both entirely hydrated and partially dehydrated (i.e. at 120°C). It was found that the total percentage weight losses of the partially dehydrated samples were equivalent to the percentage weight loss as extrapolated to the appropriate temperature of dehydration of fully hydrated sample.

Shown in Fig. 2 is an example of a TGA spectrum, specifically of unexchanged 13X and a chromium exchanged 13X.

The exchanged zeolites lose water more rapidly and continue to lose water at higher temperatures. The endothermic shift of water loss at moderate temperatures also seen in DTA spectra, indicates that the water is more loosely bound in exchanged systems (Table 3).

TABLE 3. Results of TGA analysis

	TGA analysis	
Sample	H_2O loss (mg)[a]	Sample size (mg)[b]
13X	2.85	10.90
Y52	2.69	10.31
$Cr^{3+}(13X)^1AD$	2.92	11.10
$Cr^{3+}(13X)^4AD$	2.65	9.85
$Cr^{2+}(13X)^1C$	2.37	9.09
$Cr^{3+}(Y52)^1AD$	2.52	9.42
13X(120)R	2.66	9.34
$13X(120R)^2$	2.46	10.46
Y52(120R)	2.10	10.32
$Y52(120R)^2$	2.83	10.15

[a] ±0.04.
[b] ±0.02.

Differential thermal analysis

Spectra were obtained on all samples of exchanged, unexchanged, dehydrated, and rehydrated zeolites. All samples were run against a glass reference and against the corresponding unexchanged zeolite where applicable. Characteristics are shown in Table 4.

Shown in Fig. 3 is an example of a DTA spectrum of unexchanged 13X and of chromium exchanged 13X with the 13X background removed by the differential operation of the instrument. Both the X and Y zeolite samples displayed plateaus in the 750°C range, indicating a phase transition and probable structural collapse. However, none of the samples showed any evidence of the intense exothermic peak expected. It is reasonable to assume that the framework is unstable upon dehydration and that the exothermic process of lattice destruction occurs between 100 and 350°C and is thus masked by the endothermic process of dehydration (6). This assumption was substantiated by X-ray crystallography of the sample at 500°C.

The 13X sample reveals three major areas of slow endother-

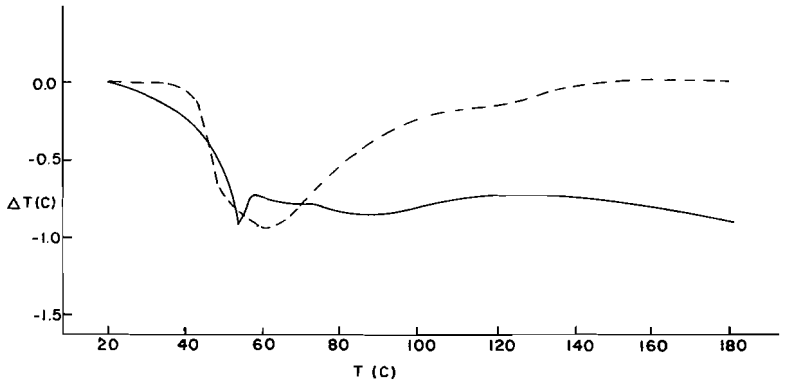

FIG. 3. Differential thermal analysis of Cr zeolite 13X (- - -) and zeolite 13X (——).

TABLE 4. Differential thermal analysis characteristics

Sample	Reference	Peaks *endo* (°C)	Peaks *exo* (°C)
13X	Glass	50 – 150	
		150 – 175	
		175 – 300	
13X(120)	Glass	225 – 350	
13X(150)	Glass	10 – 50	
13X(200)	Glass	20 – 60	60 – 90
		90	90 – 100
		90 – 125	100 – 150
Y52	Glass	15 – 80	80 – 85
		85 – 125	
Y52(150)	Glass	15 – 55	55 – 90
		70 – 80	
		80 – 110	
Y52(200)	Glass	70 – 80	75 – 100
		80 – 125	
		125 – 250	
1-Cr^{3+}(13X)^{4}AD	13X	100 – 350	
		110 – 240	
2-Cr^{3+}(13X)^{4}AD	13X	100 – 375	
		115 – 240	
1-Cr^{3+}(13X)^{4}120	13X	40 – 75	
		90 – 100	
		110 – 120	
1-Cr^{3+}(13X)^{4}120	Glass	90 – 250	
1-Cr^{3+}(13X)^{4}150	13X	15 – 60	
		75 – 150	
1-Cr^{3+}(13X)^{4}150	Glass	150 – 225	
1-Cr^{3+}(13X)^{4}120R	13X	25 – 65	
		85 – 225	
		240 – 290	
1-Cr^{3+}(13X)^{4}120R	Glass	85 – 100	85
		100 – 120	
		140 – 250	
1-Cr^{3+}(13X)^{4}200R	13X	10 – 65	
		85 – 180	
1-Cr^{3+}(13X)^{4}200R	Glass	85 – 150	80
1-Cr^{3+}(13X)^{4}250R	13X	80 – 250	
1-Cr^{3+}(13X)^{4}250R	Glass	110 – 325	110
1-Cr^{3+}(13X)^{4}120	(13X)120	200 – 310	75 – 100
		200 – 230	
1-Cr^{3+}(13X)^{4}150	(13X)150	275 – 350	80 – 110
1-Cr^{3+}(Y52)^{1}AD	Y52	75 – 125	
		125 – 200	
1-Cr^{3+}(Y52)^{1}200	(Y52)200	80 – 125	80
		240 – 300	
		350 –	

mic dehydration between 50 and 300°C (29). Upon dehydration to 120°C only the last region is seen and is shifted up to 225 to 300°C, suggesting that the remaining water molecules are very strongly bonded. The samples dehydrated at 150 to 200°C show endothermic peaks at the low temperature scale.

The Y52 on the other hand shows an exothermic peak in the midst of the endothermic area. As the sample is dehydrated the endothermic area remains relatively stable but the exothermic shifts up in temperature and becomes split.

When the chromium is exchanged onto 13X only one large endothermic area covering the same range as the 13X is observed within which there is a smaller area of faster loss. Upon dehydration to 120°C there is a shift to lower temperature as for 13X. Upon removal of the 13X background, the effect of the chromium is resolved into three endothermic peaks within the range shown by the entire sample. Upon elimination of the background of a similarly treated (13X)120, a sharp exothermic peak at 75–100°C and a large endothermic peak at 200–310°C, with the major portion at 200 to 230°C are observed. This would again suggest that there has been an internal phase transition (or perhaps another migration) and that the remaining water is very strongly bonded.

The DTA spectra of rehydrated samples show a strong exothermic peak immediately previous to three areas of *endo* activity, which lie within the endothermic area of the original sample. After removal of the zeolitic sample background one sees two endothermic areas appear, each preceded by a strong exothermic peak, again indicating internal migration. There is also a further endothermic area at a higher temperature than expected. There are clearly differences between the original exchanged samples and the de- and re-hydrated samples (30). The same pattern appears with the 150 and 200°C samples and also holds for the Y zeolites.

Magnetic susceptibilities

The instrument was calibrated with Mohr's salt (ferrous ammonium sulphate, $Fe(NH_4)_2(SO_4)_26H_2O$ MW 392.15, $\chi'_m = 32.04 \times 10^{-6}$ cgs at 22°C). Samples of Cr exchanged zeolites were run at three temperatures (room, helium and nitrogen) to determine if the magnetic susceptibilities were temperature independent. Thereafter all samples were run at room temperature. Samples were run at four field strengths, 0.65, 0.75, 0.84, and 0.92 Tesla. The gram and molar susceptibilities derived after applying instrument calibration factors and molecular weights respectively are given in Table 5. Errors are assessed from the initial weight, the standard deviation and the errors in molecular weights in Table 1.

The standard spin-only value for $\mu_{eff}(Cr^{3+})$ is 3.87 BM. All

TABLE 5. Magnetic susceptibilities and effective moments of exchanged zeolites

Sample	$\chi'_m \times 10^{-6}$ cgs ±0.0001%	μ_{eff} M^{n+}(Z) (BM) ±0.001%	μ_{eff} M^{n+} (BM)[a] ±0.01%
$Cr^{3+}(13X)^1AD$	169 698	20.02	2.90
$Cr^{3+}(13X)^1120$	84 428	14.12	2.05
$Cr^{3+}(13X)^1150$	85 282	14.19	2.06
$Cr^{3+}(13X)^1200$	84 861	14.16	2.05
$Cr^{3+}(13X)^1150R$	95 309	15.00	2.17
$Cr^{3+}(13X)^4AD$	166 698	19.84	1.91
$Cr^{3+}(13X)^4120$	147 178	18.65	1.79
$Cr^{3+}(13X)^4150$	92 550	14.79	1.42
$Cr^{3+}(13X)^4200$	132 331	17.68	1.70
$Cr^{3+}(13X)^4120R$	187 717	21.06	2.02
$Cr^{3+}(Y52)^1AD$	3 409	2.84	0.35
$Cr^{3+}(Y52)^1200$	82 430	13.95	1.72

[a] μ_{eff} of the metal ion alone is obtained by dividing the μ_{eff} of the total metal ion per mole of exchanged zeolite by the number of metal ions per unit cell as obtained from Table 1.

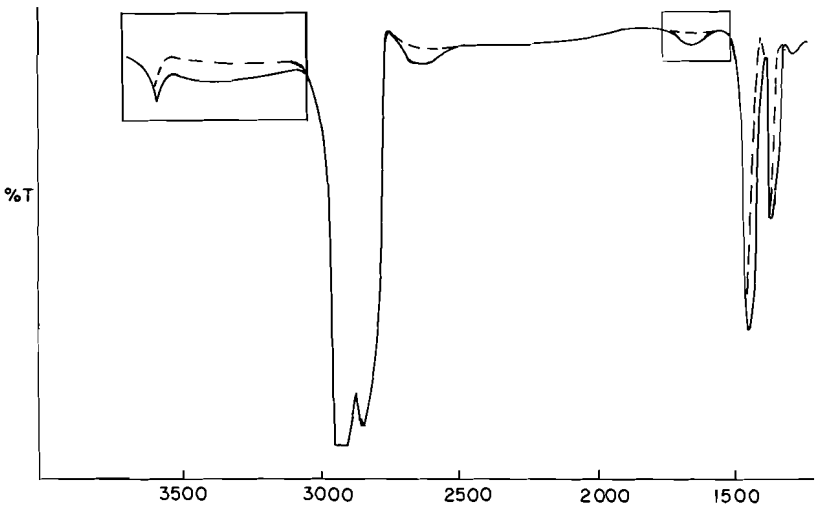

FIG. 4. Infrared spectra of Cr zeolite to 1500 cm^{-1}.

the results in Table 4 lie well below this value, decreasing with increasing dehydration temperature in most cases. The sharpest decrease is observed for dehydration at 120°C for the singly exchanged 13X is coincident with the first large endothermic peak in differential thermal analysis (Table 3). It also accompanies a distinct colour change from green to light grey. In the Y52 samples susceptibilities were also well below those expected in isolated Cr^{3+} but show an increase in samples dehydrated at 200°C.

Infrared spectra

Infrared spectra were obtained on all samples before and after dehydration or exchange. Typical low resolution spectra of 13X and Cr^{3+} 13X are shown in Figs. 4 and 5. High resolution spectra, reported in Table 6, were obtained in the ranges indicated on the low resolution spectra to observe the features which changed with treatments more closely.

Hydroxyl stretching bands occur in the range from 3000 to 3800 cm^{-1} for O—H bonds in various environments. The weak sharp band at 3750 cm^{-1} is exhibited by all zeolites and has been assigned to a terminal hydroxyl stretch (31). It disappears on dehydration and does not return during rehydration under the conditions of these experiments.

Bands appearing in the 3650 to 3680 cm^{-1} have been assigned to bridging hydroxyl stretching modes (31) in both zeolite 13X and Y52. Like the terminal stretch mode, they disappear on dehydration and do not return with rehydration. These bands are also altered by the extent of Cr^{3+} exchange. At 24% exchange, the 2680 cm^{-1} band in Y52 is lost but the 3650 band in both lattices is retained. Since initial exchange involves substitution in the sodalite cage at site I the 3680 cm^{-1} band is assigned to labile water in the sodalite cage bridging between Na^+ ions and the lattice. At 36% exchange in both lattices, the 3650 cm^{-1} disappears from 13X and is shifted to 3630 cm^{-1} in Y52. At this level of exchange sites in the supercages are occupied suggesting that the 3650 cm^{-1} band represents bridging hydroxyl groups in the supercage. The supercage of 13X is smaller than that of Y52 and having a lower Si/Al ratio as well, appears to lose all bridging water at this level of exchange while in Y52 some labile water is retained but the bridges are weaker.

A third band type near 3575 cm^{-1} is observed in all lattices and is persistent through all heat treatments. They are assigned as local Cr—OH hydroxyl stretch modes (31) of the exchanged ion or possibly those of occluded silica residues in the zeolite lattice.

A set of bands in the 1600 to 1700 cm^{-1} range is assigned to

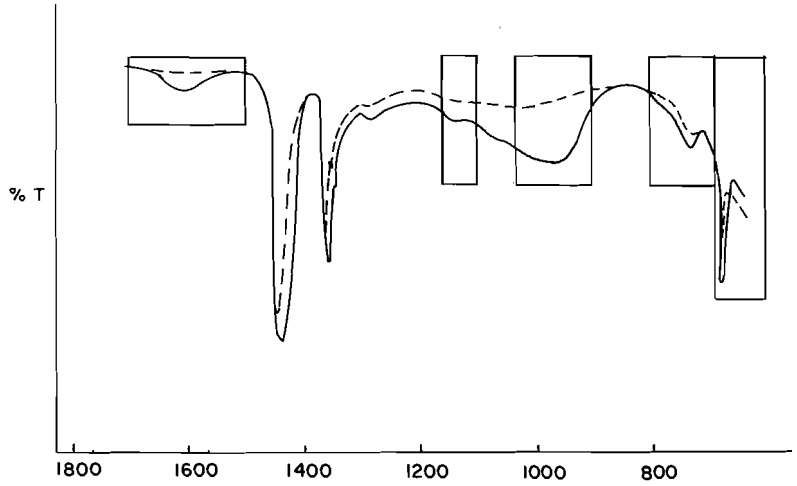

FIG. 5. Infrared spectra of Cr zeolite 13X (- - -) and zeolite 13X (——), 1800 to 700 cm^{-1}.

TABLE 6. Infrared spectral characteristics

Sample	Bands (cm^{-1})
13X	3750–3740, 3650, 3575, 2950, 2850, 2750–2550, 1700–1550, 1675, 1455, 1375, 1300, 1140(sh), 1050–950, 780–700, 775, 725, 660, 630
Y52	3750–3740, 3680, 3650, 3525, 3500–3100, 2500–2200, 2100–1900, 1660–1575, 1525, 1375, 1200–900, 1140, 1050–950, 1020, 780–680, 775, 725, 640
1-Cr^{3+}(13X)^{1}AD	3750–3740, 3650, 3570, 2950, 2850, 2750–2400, 1700–1600, 1450, 1375, 1150(sh), 1050–950, 780–680, 775, 725, 660, 630
1-Cr^{3+}(13X)^{4}AD	3750–3740, 3580, 2950, 2850, 2750–2500, 1750–1600, 1460, 135)75, 1360, 1150(sh), 1050–975, 780–680, 775, 725, 660, 630
1-Cr^{3+}(Y52)^{1}AD	3750–3740, 3630, 3575, 2950(sh), 2925, 2860(sh), 2850, 2850–2500, 1700–1575, 1460, 1350, 1325(sh), 1150(sh), 1050–950, 780–680, 775, 725, 660, 630
(13X)120	3750–3740, 3570, 2940(sh), 2920, 2840, 2750–2550, 1700–1600, 1460, 1375, 1360(sh), 1150, 1090–950, 780–700, 780, 720, 660, 630
(13X)120R	3750–3740, 3570, 2940(sh), 2920, 2840, 2750–2550, 1675–1600, 1460, 1375, 1360(sh), 1150, 1050–975, 780–700, 720, 660, 630
(13X)(120R)^2	3750–3740, 3570, 2940(sh), 2920, 2840, 2750–2550, 1700–1600, 1460, 1375, 1365(sh), 1150, 1050–950, 765–700, 765, 720, 660, 630
(13X) TGA	3750–3740, 3570, 2950, 2920, 2850, 2730, 2650, 1700–1600, 1460, 1470(sh), 1380, 1365(sh), 1150(sh), 1050–975, 760, 760–700, 720, 660, 630

water bending modes (31–33). Like the stretching modes they are lost on dehydration and do not reappear on rehydration. Their dependence on exchange is difficult to interpret. Similar results and difficulties are encountered with the low energy bands between 700 and 1100 cm^{-1}. The absence of any characteristic NH_4^+ bands is evidence of the purity of the zeolite with respect to the NH_4OH buffer.

Discussion

The structure of Na13X is well established by single crystal Na13X X-ray diffraction (8). The sites occupied by Na^+ ions are I and I′ with the water in I′ and II′ (8, 34). The sites occupied by replacement ions are also well documented on zeolite A (Cu^{2+}, Cu^+) (1) and zeolite A (Zn^{2+}) (2) by crystallography and many ions by infrared and epr spectroscopy (7, 13, 22, 23). The arrangements fall naturally into a progressive pattern of substitution which represent occupation of successively less stable sites (13). This corresponds directly with the decreasing availability of lattice oxygen ligands in sites I, I′, II′, and finally II (Fig. 1).

This theoretical sequence appears to be confirmed by the current experiments. The infrared spectra show the progressive

loss of lattice hydroxyl with increasing exchange levels in both X and Y lattices. At the same time, the spectra of the Y lattice suggest the free volume occupied by bridging hydroxyls of the supercage decreases. The thermal data show that there is an increase in the lattice water content on substitution but a decrease in its stability, since the endothermic peaks all shift to lower temperature.

All of these facts are consistent with the initial occupation of Site I by the dehydrated exchange ion (18). This site was formerly occupied by a four coordinate, tetrahedral $[Na^+(H_2O)_4]^+$ complex ion and the waters of coordination were hydrogen bound to the lattice oxygen of the sodalite cage. From the spectroscopic evidence, the infrared bands attributed to this hydrated ion have disappeared and the complexed sodium ion appears to have been expelled by the much larger deaquated chromium exchange ion, binding directly to the lattice oxygen. When the hydrogen bonds between the lattice and the water bound to the sodium ion are broken and the sodalite cage contains no coordinated water, molecules in the supercage from both the exchanged ion and the displaced sodium ions are more weakly bound. This is shown by the endothermic shifts in exchanged zeolite thermal data and the long wavelength shifts in the infrared of bridging hydroxyl.

While this exchange is occurring, it has been demonstrated that some hydroxyl oxygen may exchange with the lattice (35), probably because the lattice silicon remains a strong Lewis acid permitting splitting of the six rings (14). The processes of dehydration and exchange lead to symmetry reductions at the aluminum (12) when this exchange occurs.

For the exchange ion, the next most stable site is I′ or II′ (13) both of which provide three lattice oxygen and three waters of coordination in the supercage (36). Site II′ is probably occupied first if Site I is occupied because of Coulomb repulsion. Up to this level of exchange one would expect dilute magnetic behaviour. Immediately Sites I and I′ (37) are occupied, because II′ is also occupied, exchange ions become adjacent in the lattice, sharing lattice oxygen bridges on alternate faces of the 6-ring. This provides the opportunity for shared oxidation states (mixed valence states in partly reduced species) and the formation of metal–metal bonded dimers. Such dimers do not form between pairs of Cr^{3+} ions, but can form in mixed valence pairs or pairs of tetragonal d^4 Cr^{2+} ions (38). This is in sharp contrast to most doped zeolites in which the electronic configurations of the transition metal ions are not conducive to dimerization. As observed in iron doped lattices, bridging then occurs through lattice oxygen atoms (39).

The bridging provided by the lattice can stabilize these dimers and lead to reduction at very low temperatures. Evidence of this is seen in the progressively greying colour of the doped materials and the falling magnetic susceptibility, to be expected in the formation of deep red diamagnetic Cr^{2+} dimers.

At the highest levels of exchange, Site II must also be occupied (13). This can displace the ion in Site II′ towards that in Site I providing a further opportunity for dimerization. Such metal–metal bond formation could readily distort the supercage, as is observed at the highest exchange achieved in these experiments by powder crystallography.

There are distinct differences seen in the DTA spectra of the original exchanged zeolites and the rehydrated zeolites for both X and Y. The infrared spectra do not show the expected regrowth of water bending bonds, again indicating a breakdown of the bridging hydroxyls. This is further indication of lattices which have been irreversibly altered.

In conclusion, it appears that the reduction suggested by the earlier thermolysis research (25) proceeds very easily once the characteristic dimer formation of the d^4 system becomes possible at the higher levels of exchange. It appears to be completely irreversible. This is because the lattice under the stress of the dimer bonding collapes to a new form and is incapable of breaking the Cr^{2+}—Cr^{2+} bond when reoxydation is attempted.

Acknowledgements

The authors wish to thank Dr. Peter Bird and Dr. Ronald Westbury of Concordia University for the use of X-ray and thermogravimetric instruments, respectively, and generous assistance in interpretation of the data. We also wish to acknowledge the Department of Energy, Mines and Resources for use of the variable temperature magnetobalance. Support was provided by an NRC contract.

1. H. S. Lee and K. Seff. J. Phys. Chem. **85**, 397 (1981).
2. L. B. McCusker and K. Seff. J. Phys. Chem. **85**, 405 (1981).
3. M. Iwamoto, S. Morita, and S. Kagowa. J. Phys. Chem. **85**, 3955 (1981).
4. T. M. El-Akkad, A. M. Khalil, G. Attia, and S. Nashed. Thermochim. Acta, **52**, 19 (1982).
5. S. J. Kulkani and S. B. Kulkani. Thermochim. Acta, **52**, 93 (1982).
6. V. Dondeur and D. Vucelci. Thermochim. Acta, **68**, 91 (1983); **68**, 101 (1983); **68**, 113 (1983).
7. M. Iwamoto, M. Nakamura, H. Nagano, and S. Kagawa. J. Phys. Chem. **86**, 153 (1982).
8. J. J. Pluth and U. V. Smith. J. Am. Chem. Soc. **105**, 1192 (1983).
9. T. Ichikawa and L. Kevan. J. Am. Chem. Soc. **103**, 5355 (1983).
10. R. M. Barrer. Zeolites and clay minerals as sorbents and molecular sieves. Academic Press, New York. 1978.
11. P. A. Jacobs and R. von Ballmoos. J. Phys. Chem. **86**, 3050 (1982).
12. A. P. M. Kantgens, K. F. M. G. J. Scholle, and W. S. Veeman. J. Phys. Chem. **87**, 357 (1983).
13. Kyoung, Tai No, Hakze Chon, Talkye Ree, and Mu Shik Jhon. J. Phys. Chem. **85**, 2065 (1981).
14. S. Beran. J. Phys. Chem. **85**, 1956 (1981).
15. T. Ichikawa and L. Kevan. J. Am. Chem. Soc. **105**, 402 (1983).
16. M. W. Roberts and J. M. Thomas. Surfaces and defect properties of solids. Specialist Periodic Reports Chem. Soc. **4**, 1 (1976).
17. D. Fraenkel. Chemtech. 60 (1981).
18. J. M. Stencel, V. U. S. Rao, J. R. Dichl, K. H. Rhee, A. G. Dhere, and R. J. DeAngelis. J. Catal. **84**, 109 (1983).
19. R. Gopal, B. R. Hollebone, E. Jones, C. H. Langford, and R. Shigeishi. J. Chem. Soc. Chem. Commun. 291 (1980).
20. S. Djemel, M.-F. Guilleux, J. Jeanjean, J. F. Tempere, and D. Delafosse. J. Chem. Soc. Faraday Trans. I, **78**, 835 (1982).
21. M. Kermaree, D. Oliver, M. Richard, M. Che, and F. Bozon-Verduraz. J. Phys. Chem. **56**, 2818 (1982).
22. B. Wichterlova, Z. Tavaruzkova, and J. Novakova. J. Chem. Soc. Faraday Trans. I, **79**, 1573 (1983).
23. S. Beran, P. Jiru, and B. Wichterlova. J. Chem. Soc. Faraday Trans. I, **79**, 1591 (1983).
24. Z. Tvaruzkova and B. Wichterlova. J. Chem. Soc. Faraday Trans. I, **79**, 1591 (1983).
25. P. H. Kasai and R. J. Bishop. J. Phys. Chem. **81**, 1527 (1977).
26. K. Groenvald, P. P. M. M. Wittgen, C. E. Nuijten, and G. C. A. Schuit. J. Catal. **59**, 53 (1979).
27. A. I. Vogel. A textbook of quantitative inorganic analysis. Ed. 4. Longmans and Green and Co., London. 1978. p. 481.

28. C. L. ANGELL and P. C. SCHAFFER. J. Phys. Chem. **69**, 3463 (1965).
29. S. J. KULKARNI and S. B. KULKARNI. Thermochim. Acta, **54**, 251 (1982).
30. M. H. SIMONAT-GRANGE and F. B. HANNOUNI. Thermochim. Acta, **77**, 311 (1984).
31. L. M. KUSTOV, V. Y. BONOVKOV, and V. B. KAZANSKY. J. Catal. **72**, 149 (1981).
32. P. GALLEZOT, Y. BEN. TAARIT, and B. IMCLIK. J. Catal. **26**, 295 (1972).
33. N. P. EVONERIDES, B. BEAGLEY, and J. DERAYER. Inorg. Chim. Acta **20**, 243 (1976).
34. B. COUGHLAN and W. M. CARROLL. J. Chem. Soc. Faraday Trans. I, **72**, 2016 (1976).
35. R. VON BALLMOOS and W. M. MEIER. J. Phys. Chem. **86**, 2698 (1982).
36. F. V. HUNTER and J. SCHERZER. J. Catal. **20**, 246 (1971).
37. P. GALLEZOT and B. IMELIK. J. Phys. Chem. **77**, 652 (1973).
38. F. A. COTTON and G. WILKINSON. Advanced inorganic chemistry. 3rd ed. John Wiley and Sons, New York. p. 834.
39. W. N. DELGASS, R. L. GARTEN, and M. BOUDART. J. Phys. Chem. **73**, 2970 (1969).

Pseudoxandrine, pseudoxandrinine, oxandrine et oxandrinine, premières α ou α′ céto-bisbenzyltétrahydroisoquinoléines à pont biphénylique[1]

DIEGO CORTES, REYNALD HOCQUEMILLER ET ANDRÉ CAVÉ[2]
Laboratoire de pharmacognosie, Unité associée 496 Centre national de la recherche scientifique, Faculté de pharmacie, 92290 Châtenay-Malabry, France
JAIRO SAEZ
Universidad de Antioquia, Departamento de Química, AA1226 Medellin, Colombia
ET
ADRIEN CAVÉ
Centre de pharmacologie et endocrinologie, Institut national de la santé et de la recherche médicale – Centre national de la recherche scientifique, 34033 Montpellier, France

Reçu le 25 novembre 1985

DIEGO CORTES, REYNALD HOCQUEMILLER, ANDRÉ CAVÉ, JAIRO SAEZ et ADRIEN CAVÉ. Can. J. Chem. **64**, 1390 (1986).

Les alcaloïdes pseudoxandrine, pseudoxandrinine, oxandrine et oxandrinine ont été isolés d'une Annonacée colombienne, *Pseudoxandra* aff. *lucida*. Ces alcaloïdes appartiennent au petit groupe des bisbenzylisoquinoléines à pont biphénylique, C(11)—C(11′) et ils sont les premiers α ou α′ mono-céto-bisbenzyltétrahydroisoquinoléines. Ces structures ont été élucidées par sm, par des expériences de double résonance et nOe en rmn de ^{1}H, et par ^{13}C rmn.

DIEGO CORTES, REYNALD HOCQUEMILLER, ANDRÉ CAVÉ, JAIRO SAEZ, and ADRIEN CAVÉ. Can. J. Chem. **64**, 1390 (1986).

The alkaloids pseudoxandrine, pseudoxandrinine, oxandrine, and oxandrinine have been isolated from a Colombian Annonaceous, *Pseudoxandra* aff. *lucida*. These bases belong to the small group of bisbenzyisoquinolines with a C(11)—C(11′) biphenyl bond, and are the first α or α′ mono-keto-bisbenzyltetrahydroisoquinolines. These structures were elucidated by ms, ^{1}H nmr (including double resonance and nOe experiments), and ^{13}C nmr.

Introduction

Parmi les alcaloïdes isolés des écorces de l'espèce colombienne *Pseudoxandra* aff. *lucida* (1), il faut remarquer la présence de plusieurs bisbenzyltétrahydroisoquinoléines à pont biphénylique, dont l'antioquine, **1** (alcaloïde majeur (2)), qui a montré une intéressante activité spasmolytique;[3] la sécantioquine, première *seco*-bisbenzyltétrahydroisoquinoléine à pont biphénylique (3); et la medelline, première bisbenzyltétrahydroisoquinoléine à pont méthylènedioxy intramoléculaire (4). Quatre autre bisbenzyltétrahydroisoquinoléines mineures ont été isolées; elles sont caractérisées par la présence d'une cétone conjuguée en position α ou α′ : il s'agit de la pseudoxandrine, **2**, la pseudoxandrinine, **8**, l'oxandrine, **9**, et l'oxandrinine, **13**.

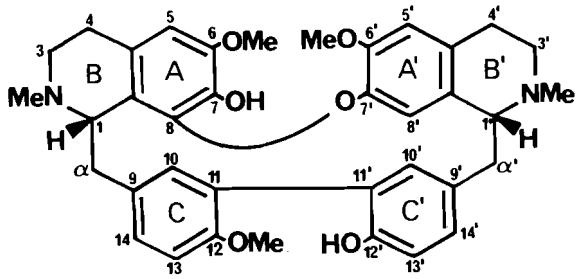

1 : antioquine

TABLEAU 1. Résonance magnétique nucléaire de ^{13}C de la pseudoxandrine, **2**, et de l'oxandrine, **9** ($CDCl_3$, 25,2 MHz)

	δ			δ	
Carbone	**2**	**9**	Carbone	**2**	**9**
C-1	84,4	63,8	C-1′	63,0	84,0
C-3	52,0	45,5	C-3′	45,2	53,0
C-4	35,2	22,6	C-4′	22,6	35,0
C-4a	121,9	124,4	C-4′a	127,6	131,2[e]
C-5	106,1	107,3	C-5′	114,1	113,2
C-6	145,8	146,4	C-6′	151,2	150,9
C-7	134,3	133,6	C-7′	143,3	139,8
C-8	141,5	137,0	C-8′	120,8	117,8[c]
C-8a	124,0	126,8[f]	C-8′a	126,7	126,9[f]
C-α	205,1	38,1	C-α′	39,5	205,5
C-9	136,4	131,2[e]	C-9	135,8	143,2
C-10	131,4[d]	134,8	C-10′	133,6	131,5[d]
C-11	131,6[c]	133,3[e]	C-11′	130,4[c]	131,9[e]
C-12	153,1	154,0	C-12′	153,9	153,1
C-13	110,9	117,7[c]	C-13′	117,5	111,2
C-14	129,5[d]	131,4[d]	C-14′	130,9[d]	129,6[d]
NMe-2	42,6[a]	41,7[a]	NMe-2′	43,1[a]	42,8[a]
OMe-6	56,2[b]	55,9	OMe-6′	55,9[b]	55,8[b]
OMe-12	—	56,4[b]	OMe-12′	56,2[b]	—

a,b,c,d,e,f. Valeurs interchangeables pour un même produit.

Résultats et discussion

La pseudoxandrine, **2**, est obtenue sous forme de poudre amorphe, $[\alpha]_D$ +23° (*c* 1,13, $CHCl_3$). Le spectre ir, montre la présence d'un groupement carbonylé de type arylcétone (ν(C=O) : 1680 cm^{-1}); ceci est confirmé par le spectre de ^{13}C rmn : 1 singulet à 205,1 ppm (voir Tableau 1). Son spectre de masse en impact électronique ($M^{+\cdot}$ 622, 100%) confirme sa nature dimérique. Les fragmentations principales conduisent

[1]Partie 62 dans la série « Alcaloïdes des Annonacées »; Partie 61 : voir réf. 4.

[2]Auteur à qui adresser toute correspondance.

[3]D'après une étude pharmacologique préliminaire, l'antioquine a montré sur duodénum isolé de Rat, à la concentration de 0,1 mg/mL, une inhibition de près de 50% des spasmes induits par l'acétylcholine et le chlorure de baryum.

Printed in Canada / Imprimé au Canada

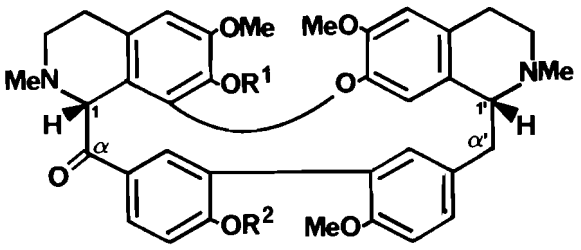

2 : $R^1 = R^2 = H$: pseudoxandrine

3 : $R^1 = R^2 = Ac$

4 : $R^1 = R^2 = Me$

par rupture de deux liaisons benzyliques (1–α et 1′–α′) à un ensemble bisisoquinoléique se traduisant sur le spectre par des pics à *m/z* 382, 192 et 191 correspondant respectivement aux ions monochargé et doublement chargé (5). Cette fragmentation est en faveur (*i*) d'une bisbenzyltétrahydroisoquinoléine à deux ponts, l'un diaryl-éther entre les unités isoquinoléines, l'autre biphénylique (6); (*ii*) d'une partie bisisoquinoléique diméthoxylée; (*iii*) de la présence de deux groupements phénoliques, l'un sur la partie bisisoquinoléique, l'autre sur la partie biphénylique.

Le spectre de ^1H rmn de la pseudoxandrine, **2**, montre que la molécule possède deux N-méthyles et trois méthoxyles. Les signaux correspondant aux protons en 1 et 1′ apparaissent l'un sous forme d'un doublet à 4,05 ppm, et l'autre sous forme d'un singulet à 4,25 ppm, laissant ainsi supposer que le groupement carbonyle de **2** est porté soit par le carbone α, soit par le carbone α′. Des expériences de découplage sélectif ont montré la présence de deux systèmes AMX appartenant aux noyaux C et C′.

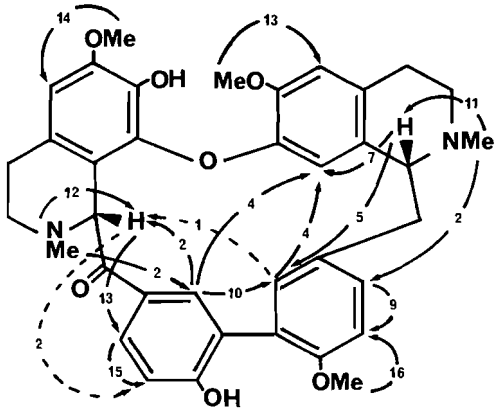

2 : pseudoxandrine, nOe

——→ nOe +

- - - - → nOe −

Par ailleurs, l'étude des dérivés diacétylé, **3**, et diméthylé, **4**, de la pseudoxandrine, a permis de confirmer l'existence, dans **2**, de deux OH phénoliques et de fixer leur position en 7 et en 12 (ou 12′).

L'analyse structurale de la pseudoxandrine, **2**, est complétée par la mesure des effets Overhauser nucléaires (7, 8), enregistrés à 360 MHz sous forme de spectres de différences (2). L'irradiation successive des singulets N—Me à 2,27 et 2,39 ppm fait apparaitre un effet de 11% sur le doublet H-1′ à 4,05 ppm et un effet de 12% sur le singulet H-1 à 4,25 ppm. Un effet plus faible de l'ordre de 2% indique la proximité de ce dernier groupe N—Me avec le proton aromatique H-10. L'irradiation des protons H-1 et H-1′ permet d'identifier les protons proches, 10 et 14 pour le premier et 8′ et 10′ pour le second. La proximité des protons 10 et 10′ découle de l'irradiation du signal de H-10 qui donne un effet de 10% sur H-10′, permettant ainsi de relier les deux unités benzylisoquinoléïques. Le positionnement du méthoxyle en 12′ découle d'un effet de 16% avec le proton aromatique 13′ déjà identifié lors des expériences de double irradiation. L'identification du H-5 et du méthoxyle 6 résulte de l'observation d'un effet de 14% sur le singulet à 6,42 ppm lors de l'irradiation sélective du méthoxyle à 3,85 ppm. L'irradiation du signal du méthoxyle 6′ à 3,63 ppm permet de localiser le proton 5′ à 6,66 ppm. Les deux OH phénoliques sont placés par déduction en 12 et en 7.

Un effet Overhauser négatif est observé sur H-13 lors de l'irradiation de H-1. Il met en évidence une disposition « en ligne » (9) des protons 1, 14 et 13. Un effet comparable est observé sur H-1 lors de l'irradiation de H-10′. On peut noter les proximités de NMe-2 avec H-10 et de H-1 avec H-14 qui traduisent un arrangement structural bien défini dans cette partie de la molécule. Ces expériences permettent donc de placer le carbonyle en position α.

La présence du groupe carbonyle a été confirmée soit par réduction au $NaBH_4$, soit par réduction de Clemmensen. En effet, la réduction de la diméthylpseudoxandrine **3**, par $NaBH_4$, conduit à la dihydrodiméthylpseudoxandrine, **5**. Quant à la réduction de la pseudoxandrine **2** par la méthode de Clemmensen (Zn/HCl), elle conduit, avec un faible rendement, à deux produits, **6** et **7**. L'examen des spectres de ^1H rmn et de masse (sm), montre qu'il s'agit de stéréoisomères. Le sm de ces deux

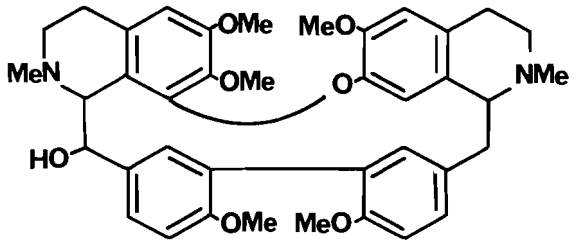

5

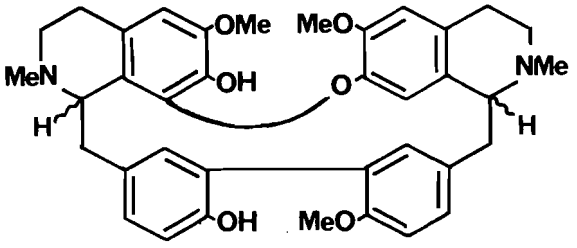

6 : 1*S*, 1′*R* : tiliageine

7 : 1*R*, 1′*R*

produits présente les mêmes fragmentations que celles de l'antioquine, **1** (2), et de la tiliageine, **6** (6). L'examen des courbes de dc (dichroïsme circulaire) de **2** et de **6** et **7** permet de proposer les stéréochimies. La courbe de dc de la pseudoxandrine, **2**, est identique à celle de l'antioquine, **1**, dont la configuration a été établie comme étant 1*S*, 1′*R* (1, 2). De plus, la courbe de dc de l'un des dérivés, **6**, obtenu par réduction de

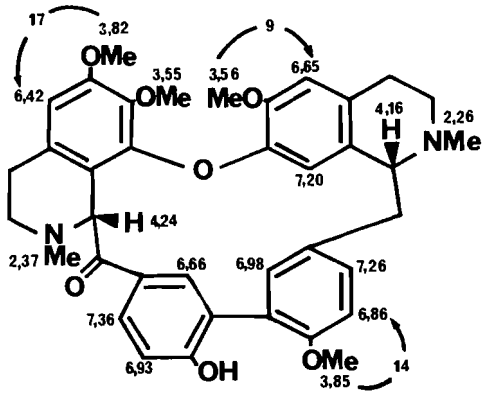

FIG. 1. Composé **8**: pseudoxandrinine, ^{1}H rmn et nOe; $J_{10-14} = J_{10'-14'} = 2$ Hz; $J_{14-13} = J_{14'-13'} = 8{,}5$ Hz.

Clemmensen de la pseudoxandrine, **2**, est identique à celle de l'antioquine, **1**, permettant de conclure que ce produit correspond à la tiliageine, **6**, dont la stéréochimie a été établie par biosynthèse (6). Le signe et la valeur du pouvoir rotatoire du dérivé **6** sont en accord avec cette hypothèse. La courbe de dc du deuxième produit, **7**, obtenu lors de la réduction de Clemmensen est inverse de celle de l'antioquine, **1**; ceci permet de supposer que par réduction au Zn/HCl de **2** on obtient les deux isomères, l'un **6** étant 1*S*, 1′*R*, l'autre **7** étant de configuration 1*R*, 1′*R*. Au vu des résultats de cette réduction, on peut envisager que celle-ci se fait par l'intermédiaire d'un énol, expliquant ainsi la non conservation de la stéréochimie en position 1.

La pseudoxandrinine **8** a une structure très proche de celle de la pseudoxandrine, **2**, comme le montre l'analyse de ses différents spectres. Le sm de **8** révèle un pic moléculaire ($M^{+\cdot}$ 636, $C_{38}H_{40}N_2O_7$), et des fragmentations qui montrent que la pseudoxandrinine, **8**, est une *O*-méthyl-7 pseudoxandrine. En effet, le spectre de ^{1}H rmn vient à l'appui de cette hypothèse (voir **8**, fig. 1). Une corrélation avec le dérivé diméthylé, **4**, de la pseudoxandrine, **2**, confirme la position des différents substituants. La configuration absolue de **8** est déduite de sa courbe de dc; celle-ci, identique à celles de la pseudoxandrine, **2**, et de l'antioquine, **1**, permet d'attribuer à **8** la configuration 1*S*, 1′*R*.

La troisième cétoamine isolée de *P.* aff. *lucida*, l'oxandrine, **9**, présente un $[\alpha]_D$ négatif en $CHCl_3$ (−11°) et positif en MeOH (+9°). Ses spectres uv, ir (C=O, 1680 cm^{-1}), ^{13}C rmn (s, 205,5 ppm; voir Tableau 1) et masse ($M^{+\cdot}$ 622 et *m/z* 381, 192, 191), présentent une grande similitude avec ceux de la pseudoxandrine, **2**. L'examen du spectre de ^{1}H rmn de **9** (fig. 2), et de celui de ses dérivés diacétylé, **10**, et diméthylé, **11**, confirme la parenté entre la pseudoxandrine, **2** et l'oxandrine, **9**. La structure de **9**, a été confirmée par mesure des effets Overhauser en ^{1}H rmn (voir **9** nOe). Lorsque le singulet à 4,21 (H-1 ou H-1′, voisin du carbonyle en α ou α′) est irradié, on note un nOe sur un des NMe (δ 2,32), sur un dd à δ 7,25 (H-14 ou H-14′) et sur le singulet à δ 7,12 correspondant au H-8′. Par contre l'irradiation du doublet à δ 3,80 (H-1 ou H-1′, voisin du CH_2 en α ou α′), provoque des effets Overhauser sur l'autre NMe (δ 2,33) et sur les protons du méthylène benzylique (H-α). Ces expériences montrent que le carbonyle de l'oxandrine appartient au monomère benzylisoquinoléine porteur du proton libre en position 8′. Il est à noter que les effets Overhauser observés par irradiation du H-1′ sont nettement moins intenses sur le H-8′ et plus prononcés sur le H-14′ pour l'oxandrine, **9**, que pour l'antioquine, **1** (2), et

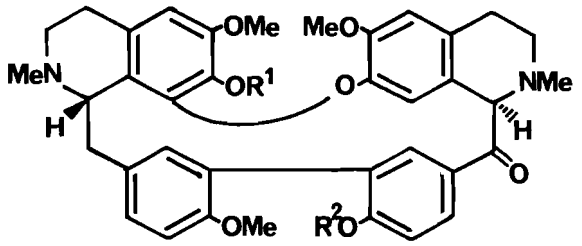

9: $R^1 = R^2 = H$: oxandrine

10: $R^1 = R^2 = Ac$

11: $R^1 = R^2 = Me$

13: $R^1 = H$; $R^2 = Me$: oxandrinine

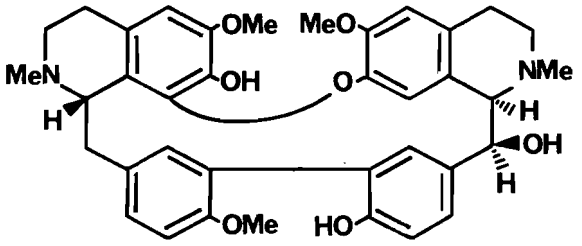

12: dihydrooxandrine

la pseudoxandrine, **2** (voir fig. 3). Comme le montre l'étude sur le modèle Dreiding, ces différences peuvent s'expliquer si la configuration en 1′ est inverse chez l'oxandrine, c'est-à-dire 1′*S*. Si cet argument est insuffisant à lui seul pour affirmer que l'oxandrine, **9**, a la configuration 1*S*, 1′*S* (les effets nOe en 1 sont identiques pour l'antioquine, **1** (2), et pour l'oxandrine, **9**), il est conforté par l'aspect de la courbe de dc de **9**, qui présente des effets Cotton opposés à ceux de l'antioquine, **1**.

De plus, si la réduction de **9**, par $NaBH_4$, conduisant à l'alcool majoritaire, **12**, ne confirme que l'existence du carbonyle en α′,[4] la réduction de **9** par Zn/HCl permet d'obtenir

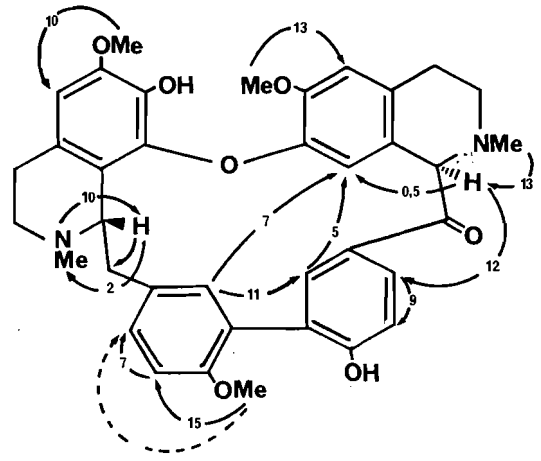

9: oxandrine, nOe

——→ nOe +

- - - - → nOe −

[4]La disposition en *cis* des H-1′ et H-α′ est démontrée d'une part par ^{1}H rmn ($J = 4$ Hz), d'autre part par déshydratation ($POCl_3$) et formation de l'énamine correspondante.

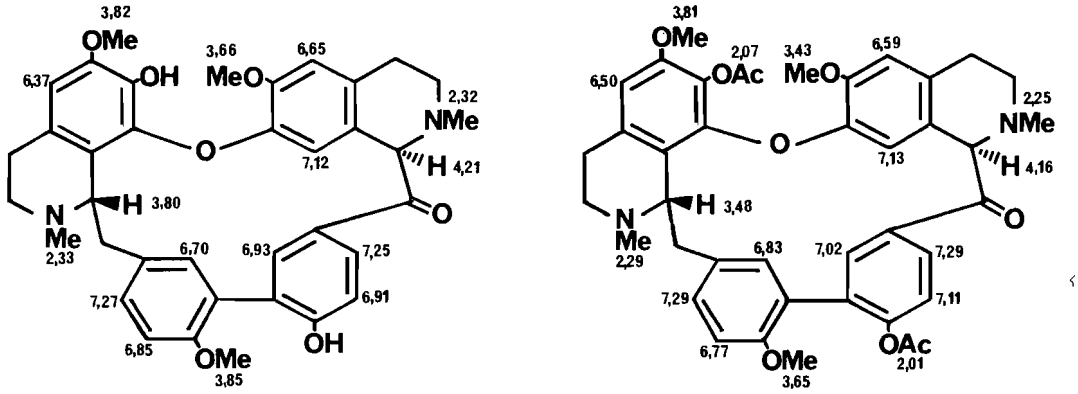

FIG. 2. Composé **9** : oxandrine, ^{1}H rmn; $J_{14-13} = J_{14'-13'} = 8{,}5$ Hz; $J_{10-14} = J_{10'-14'} = 2$ Hz. Composé **10**, ^{1}H rmn; $J_{14-13} = J_{14'-13'} = 8{,}5$ Hz; $J_{10-14} = J_{10'-14'} = 2$ Hz.

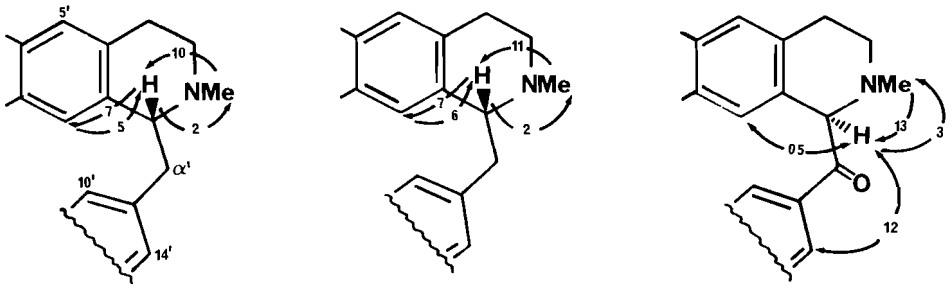

antioquine, **1** pseudoxandrine, **2** oxandrine, **9**

FIG. 3

deux produits isomères, dont l'un est identique à la (*S,R*)-antioquine, **1** (ccm, ir, dc, ^{1}H rmn, sm). Or, il a été montré pour la pseudoxandrine, **2**, que la réduction de Clemmensen menait à la formation de deux épimères. Il est donc logique que l'un des deux produits obtenus ait acquis la configuration 1′*R* et ait la même configuration que l'antioquine (1*S*, 1′*R*).

La configuration inverse en 1′ de l'oxandrine, **9**, par rapport à l'antioquine, **1**, pourrait être expliquée par l'existence d'un intermédiaire ènamine lors du processus oxydatif.

L'oxandrinine, **13**, a été obtenue en très faible quantité (0,1% des A.T. (alcaloïdes totaux)). L'ensemble de ses données spectrales (uv, ir, ^{1}H rmn, masse), montrent qu'il s'agit de la *O*-méthyl-12′ oxandrine. Ceci a été confirmé par la préparation de la méthyloxandrinine identique à la diméthyloxandrine, **11**. La courbe de dc de **13** est superposable à celle de l'oxandrine, **9**, et permet donc de lui proposer la configuration 1*S*,1′*S*.

La pseudoxandrine, **2**, et l'oxandrine, **9**, constituent les premiers exemples d'alcaloïdes α ou α′ céto-bisbenzyltétrahydroisoquinoléiques rencontrés jusqu'ici (10, 11). Elles peuvent être considérées comme des intermédiaires biogénétiques d'oxydation des bisbenzyltétrahydroisoquinoléines à pont biphénylique, dont la position α ou α′ est rendue favorable à des oxydations par la présence d'un hydroxyle phénolique en position *para*. Ce stade intermédiaire d'oxydation n'a jamais été décrit. En effet les structures des céto-bisbenzyltétrahydroisoquinoléines, décrites auparavant, ont été récemment révisées; il s'agit en réalité de *N*-formyl-bisbenzyltétrahydroisoquinoléines.[5] Cependant, des produits d'oxydation plus poussée ont été signalés, tels que les cétoimines (13) et les *seco*-bisbenzyltétrahydroisoquinoléines (14, 3).

Partie expérimentale

Pouvoirs rotatoires mesurés sur polarimètre Schmidt–Haensch, type Polartronic I. Spectres enregistrés sur les appareils suivants: uv, Unicam SP 1800; ir, Perkin Elmer 257; dc, auto-dichograph Mark V; sm, VG Micromass 70 et Nermag R10-10C; ^{1}H rmn, Cameca (250 MHz) et Brüker (360 et 500 MHz); ^{13}C rmn, Varian CFT 20 (25,2 MHz).

Extraction des alcaloïdes

Les écorces de *Pseudoxandra* aff. *lucida* (Annonaceae) ont été récoltées à San Luis, Antioquia (Colombie). L'extraction menée de façon habituelle fournit 1,5% d'alcaloïdes totaux non quaternaires. Les alcaloïdes totaux ont été chromatographiés sur colonne de Kieselgel 60. L'élution a été réalisée par des mélanges de polarité croissante de dichlorométhane et méthanol. (1, 2).

Pseudoxandrine, 2

Elle a été isolée amorphe (1% des A.T. (1, 2)); $C_{37}H_{38}N_2O_7$; $[\alpha]_D$ +23° (*c* 1,13, $CHCl_3$); $[\alpha]_D$ +60° (*c*, 0,1, MeOH); uv, λ_{max}, EtOH, nm (log ε) : 208 (4,78), 282 (3,94); EtOH + NaOH : 222 (4,96), 300 (4,24); ir, ν_{max}, film : 3340, 1680, 1605, 1510, 1460, 1305, 1270, 1240, 1120 cm^{-1}; dc, MeOH (c 3,56 × 10^{-4}), Δε (nm) : 0 (295), +5 ép. (277), +35,6 (242), 0 (228), −47 (218); ^{1}H rmn, $CDCl_3$, 360 MHz, δ : 2,27 (s, 3H, NMe-2′), 2,39 (s, 3H, NMe-2), 3,63 (s, 3H, OMe-6′), 3,85 (s, 3H, OMe-6), 3,86 (s, 3H, OMe-12′), 4,05 (d, 1H, H-1′), 4,25 (s, 1H, H-1), 6,42 (s, 1H, H-5), 6,66 (s, 1H, H-5′), 6,73 (d, 1H, H-10), 6,85 (d, 1H, H-13′), 6,95 (d, 1H, H-13), 6,96 (d, 1H, H-10′), 7,14 (s, 1H, H-8′), 7,20 (dd, 1H, H-14′), 7,36 (dd, 1H, H-14); $J_{14-13} = J_{14'-13'} = 8{,}5$ Hz; $J_{10-14} = J_{10'-14'} = 2$ Hz; ^{13}C rmn, voir Tableau 1; sm, IC (NH_3), *m/z* : 623 [$M^{+\bullet}$ + 1]; sm, IE, *m/z* (%) : 622 (100, [$M^{+\bullet}$]), 621 (80), 607 (18), 593 (14), 382 (3), 381 (8), 367

[5]Les structures des dicéto-bibenzyltétrahydroisoquinoléines, Thalrugosinone (12*a*) et Thalpindione (12*b*), ont été révisées (voir réf. 12*c*).

(4), 311 (11 [$M^{+\bullet}$/2]), 192 (8), 191,5 (8), 191 (30), 190 (9), 175 (4), 174 (3).

O,O-*diacétylpseudoxandrine, 3*

Préparée à partir de **2** (Ac_2O/Pyr); $[\alpha]_D$ +47° (*c*, 0,53, $CHCl_3$); uv, λ_{max}, EtOH, nm (log ϵ) : 212 (4,75), 281 (3,92); ir, ν_{max}, film : 1760, 1685, 1610, 1500 cm^{-1}; ^1H rmn, $CDCl_3$, 250 MHz, δ : 1,75 (s, 3H, OAc-7), 2,12 (s, 3H, OAc-12), 2,28 (s, 3H, NMe-2′), 2,72 (s, 3H, NMe-2), 3,62 (s, 3H, OMe-6′), 3,68 et 3,83 (2s, 6H, OMe-12′ et OMe-6), 4,29 (s, 1H, H-1), 6,50 (s, 1H, H-5), 6,71 (s, 1H, H-5′), 6,59–7,30 (7H, Ar–H); sm, IC (NH_3), *m/z* : 707[$M^{+\bullet}$+ 1]; sm, IE, *m/z* (%) : 706 (100 [$M^{+\bullet}$]), 705 (55), 691 (13), 664 (28), 663 (34), 622 (3), 621 (8), 423 (2), 381 (4), 368 (2), 206 (3), 204 (2), 191 (34), 175 (4).

O,O-*diméthylpseudoxandrine, 4*

Préparée à partir de **2** (CH_2N_2/Et_2O); $[\alpha]_D$ +6° (*c* 0,66, $CHCl_3$); uv, λ_{max}, EtOH, nm (log ϵ) : 210 (4,70), 286 (3,95); ir, ν_{max}, film : 1680, 1605 cm^{-1}; ^1H rmn, $CDCl_3$, 250 MHz, δ : (signaux doublés, déplacements chimiques moyens) 2,29 (3H, NMe-2′), 2,39 (3H, NMe-2), 3,52 (3H, OMe-7); 3,56 (3H, OMe-6′), 3,73, 3,79 et 3,84 (9H, OMe-6, OMe-12 et OMe-12′), 4,25 (1H, H-1), 6,02–7,26 (9H, Ar–H); sm, IC (NH_3) *m/z* : 651 [$M^{+\bullet}$ + 1]; sm, IE, *m/z* (%) : 650 (100, [$M^{+\bullet}$]), 649 (89), 635 (61), 621 (21), 607 (10), 395 (10), 382 (12), 381 (17), 368 (5), 354 (7), 325 (26), 311 (15), 206 (98), 198,5 (17), 198 (67), 192 (14), 191 (15), 190 (27), 175 (27), 174 (21).

Dihydrodiméthylpseudoxandrine, 5

Préparée à partir de **4** ($NaBH_4$/MeOH) selon la méthode décrite pour **12**; ir, ν_{max}, film : 1605, 1585, 1500 cm^{-1}; sm, IC, *m/z* : 653 [M^+ + 1], 652 [M^+], 639, 621, 395, 369, 206.

Réduction de la pseudoxandrine, 2, par Zn/HCl : produits 6 et 7

À 40 mg de **2** en solution dans 4 mL d'acide acétique sont additionnés 6 g de Zn pulvérisé et 12 mL de HCl 10 *N*; le mélange est porté à reflux pendant 68 h. Après extraction et purification du milieu réactionnel par ccm préparative, on obtient 3 mg du dérivé **6** et 2 mg du dérivé, **7**. Dérivé **6** : Tiliageine; [α] +192° (*c*, 0,12, $CHCl_3$) (litt. (6) [α] +132, Pyr); ir, ν_{max} film : 1610, 1580, 1500 cm^{-1}; dc, MeOH (*c*, $3,7 \times 10^{-4}$), $\Delta\epsilon$ (nm) : 0 (320), +1,9 (291), +3,8 (249), 0 (231), −3,9 (217); sm, IC, *m/z* : 609 [M^+ + 1], 608 [$M^{+\bullet}$], 381, 367, 191. Dérivé **7** : dc, MeOH (*c* $3,5 \times 10^{-4}$), $\Delta\epsilon$ (nm) : 0 (297), −4 (246), 0 (240), +25 (223), 0 (214); sm, IC, *m/z* : 609 [$M^{+\bullet}$ + 1], 608 [$M^{+\bullet}$], 381, 367, 191.

Pseudoxandrinine, 8

Amorphe (0,1% des A.T. (1, 2)); $C_{38}H_{40}N_2O_7$; $[\alpha]_D$ +7° (*c* 0,7, $CHCl_3$); uv, λ_{max}, EtOH, nm (log ϵ) : 208 (4,44), 224 ép. (4,34) 280 (3,80); EtOH + NaOH : 220 (4,90), 2,96 (4,33); ir, λ_{max}, film : 3340, 1675, 1600, 1500, 1270, 1230, 1120, 1070, 1020 cm^{-1}; dc, MeOH (*c* $5,1 \times 10^{-4}$), $\Delta\epsilon$ (nm) : 0 (362), −2,9 (341), 0 (313), +2,9 (296), +19 (249), 0 (232), −21,7 (219); ^1H rmn, 360 MHz, $CDCl_3$: voir fig. 1; sm, IE, *m/z* (%) : 636 (100, [$M^{+\bullet}$], 635 (85), 621 (28), 607 (12), 593 (6), 411 (2), 396 (1), 395 (2), 381 (5), 367 (1), 365 (9), 198,5 (5), 198 (19), 191 (3), 175 (6), 174 (6).

O-*méthylpseudoxandrinine*

Préparée à partir de **8** (CH_2N_2/Et_2O). Le produit méthylé obtenu est identique à la diméthylpseudoxandrine, **4**.

Oxandrine, 9

Amorphe (1% des A.T. (1, 2)); $C_{37}H_{38}N_2O_7$; $[\alpha]_D$ −11° (*c* 0,9, $CHCl_3$); $[\alpha]_D$ +9° (*c* 0,96, MeOH); uv, λ_{max} EtOH, nm (log ϵ) : 209 (4,73), 282 (4,02); EtOH + NaOH : 224 (4,92), 296 (4,30); ir, ν_{max}, film : 3320, 1670, 1605 cm^{-1}; dc, MeOH (*c* $2,57 \times 10^{-4}$), $\Delta\epsilon$ (nm) : 0 (310), −4,6 ép. (293), −25 (250), 0 (233), +80 (221), 0 (211); ^1H rmn, $CDCl_3$, 360 MHz : voir fig. 2 et **9**, nOe; ^{13}C rmn, voir Tableau 1; sm, IC (NH_3), *m/z* : 623 ($M^{+\bullet}$ + 1); sm, IE, *m/z* (%) : 622 (16 [$M^{+\bullet}$]), 381 (3), 367 (1), 192 (100), 191 (30), 175 (5).

O,O-*diacétyloxandrine, 10*

Préparée à partir de **9** (Ac_2O/Pyr); $[\alpha]_D$ +88° (*c* 0,9, $CHCl_3$); uv λ_{max}, EtOH, nm (log ϵ) : 224 (4,62), 282 (3,69); ir, ν_{max}, film : 1765, 1680, 1605 cm^{-1}; ^1H rmn, $CDCl_3$, 360 MHz : voir fig. 2; sm IC (isobutane), *m/z* : 707 [$M^{+\bullet}$ + 1]; sm, IE, *m/z* (%) : 706 (100, [$M^{+\bullet}$]), 664 (50), 663 (58), 649 (19), 437 (5), 381 (5), 368 (4), 353 (9), 191 (30).

O,O-*diméthyloxandrine, 11*

Préparée à partir de **9** (CH_2N_2/Et_2O); sm, IE, *m/z* (%) : 650 (100, [$M^{+\bullet}$]), 396 (1), 381 (12), 198 (60), 175 (39); ^1H rmn, 500 MHz, $CDCl_3$, δ : 2,26 (s, 3H, NMe-2′), 2,27 (s, 3H, NMe-2), 3,41 (s, 3H, OMe-7), 3,69 (s, 3H, OMe-6′), 3,74 et 3,76 (2s, 6H, OMe-12 et OMe-12′), 3,83 (s, 3H, OMe-6), 3,45 (m, 1H, H-1), 4,13 (s, 1H, H-1′), 6,44 (s, 1H, H-5), 6,58 (s, 1H, H-5′), 6,77 (d, 1H, H-10), 6,81 et 6,85 (2d, 2H, H-13 et H-13′), 7,02 (d, 1H, H-10′), 7,12 (s, 1H, H-8′), 7,26 (dd, 1H, H-14′), 7,28 (dd, 1H, H-14); $J_{14-13} = J_{14'-13'}$ = 8,5 Hz; $J_{10-14} = J_{10'-14'}$ = 2 Hz.

Dihydrooxandrine, 12

Du $NaBH_4$ (100 mg) est additionné en petites portions à une solution d'oxandrine, **9** (100 mg) dans le méthanol (10 mL) sous agitation, à température ambiante, pendant 30 min. Après évaporation, le résidu est redissous par HCl dilué, alcalinisé par l'ammoniaque et extrait par CH_2Cl_2. L'extrait est purifié par ccm (chromatographie sur couche mince) préparative sur silice (CH_2Cl_2/MeOH/NH_4OH 100 : 10:1). On obtient 30 mg de l'alcool majoritaire, **12**; $[\alpha]_D$ +140° (*c* 0,38, $CHCl_3$); uv, λ_{max}, EtOH, nm (log ϵ) : 210 (4,99), 285 (4,02); EtOH + NaOH : 220 (5,00), 292 (4,09); ir, ν_{max}, film : 3350, 1610 cm^{-1}; ^1H rmn, $CDCl_3$, 360 MHz, δ : 2,08 (s, 3H, NMe-2′), 2,35 (s, 3H, NMe-2), 3,42 (s, 3H, OMe-6′), 3,70 (s, 3H, OMe-6), 3,82 (s, 3H, OMe-12); système AB : 3,67 (d, 1H, H-1′), 5,30 (d, 1H, H-α′), $J_{1'-\alpha'}$ = 4 Hz, 6,32 (s, 1H, H-5), 6,57 (s, 1H, H-5′), 6,88 (d, 1H, H-13), 6,90–7,41 (6H, Ar-H); sm, IE, *m/z* (%) : 624 (100 [$M^{+\bullet}$]), 623 (60), 609 (34), 381 (3), 206 (14), 191 (27).

Réduction de l'oxandrine, 9, par Zn/HCl

La réduction de **9** selon la méthode précédemment décrite pour la pseudoxandrine, **2**, mène à deux produits, dont l'antioquine, **1** (ccm, ir, dc).

Oxandrinine, 13

Amorphe (0,1% des A.T. (1, 2)) : $C_{38}H_{40}N_2O_7$; $[\alpha]_D$ +60° (*c* 0,5, $CHCl_3$); uv, λ_{max}, EtOH, nm (log ϵ) : 208 (4,50), 282 (3,64); EtOH + NaOH : 216 (4,78), 290 (4,00); ir, ν_{max}, film : 3340, 1675, 1600, 1500; dc, MeOH (*c* $4,32 \times 10^{-4}$), $\Delta\epsilon$ (nm) : 0 (355), +1 (330), 0 (281), −2,5 (252), 0 (236), +8,5 (223), 0 (210); ^1H rmn, $CDCl_3$, 360 MHz, δ : 2,27 (s, 6H, NMe-2 et NMe-2′), 3,74 (s, 3H, OMe-6′), 3,80 (s, 3H, OMe-6), 3,84 (s, 6H, OMe-12 et OMe-12′), 4,18 (s, 1H, H-1′), 6,43 (s, 1H, H-5), 6,65 (s, 1H, H-5′), 6,81–7,32 (m, 7H, Ar-H); sm, IC, (NH_3), *m/z* : 637 [$M^{+\bullet}$ + 1]; sm, IE, *m/z* (%) : 636 ($M^{+\bullet}$), 635, 621, 607, 417, 411, 381, 368, 191, 190, 175, 174.

O-*méthyloxandrinine*

Préparée à partir de **13** (CH_2N_2/Et_2O). Le produit méthylé obtenu est identique à la diméthyloxandrine, **11**.

Remerciements

Les auteurs expriment leur gratitude au Dr. C. Merienne, de l'Institut d'Electronique Fondamentale d'Orsay, pour l'enregistrement des spectres de ^1H rmn à 250 MHz.

1. J. Saez. Thèse de Doctorat de l'Université Paris-Sud, 1985.
2. D. Cortes, J. Saez, R. Hocquemiller, A. Cavé et Ad. Cavé. J. Nat. Prod. **48**, 76 (1985).
3. D. Cortes, J. Saez, R. Hocquemiller et A. Cavé. C.R. Acad. Sci. Paris, **298**, Série II, 591 (1984).
4. D. Cortes, J. Saez, R. Hocquemiller, A. Cavé et Ad. Cavé. Heterocycles, **24**, 607 (1986).
5. M. Tomita, T. Kikuchi, K. Fujitani, A. Kato, H. Furukawa, Y. Aoyagi, M. Kitano et T. Ibuka. Tetrahedron Lett. 857 (1966); J. Baldas, I. R. C. Bick, T. Ibuka, R. S. Kapil et Q. N. Porter. J. Chem. Soc: Perkin Trans. 1, 592 (1972).

6. M. SHAMMA et J. L. MONIOT. Heterocycles, **4**, 1817 (1976); K. P. GUHA, B. MUKHERJEE et R. MUKHERJEE. J. Nat. Prod. **42**, 1 (1979); P. L. SHIFF, JR. J. Nat. Prod. **46**, 1 (1983).
7. L. D. HALL et J. K. M. SANDERS. J. Am. Chem. Soc. **102**, 5703 (1980).
8. D. NEUHAUS, R. N. SHEPPARD et I. R. C. BICK. J. Am. Chem. Soc. **105**, 5996 (1983).
9. J. H. NOGGLE et R. E. SCHIRMER. The nuclear Overhauser effect. Chemical applications. Academic Press, New York. 1971.
10. A. CAVÉ. Annonaceae alkaloids. *Dans* The chemistry and biology of isoquinoline alkaloids. *Editeurs*: J. D. Phillipson, M. H. Roberts et M. H. Zenk. Springer Verlag, Berlin. 1985. p. 79.
11. J. SAEZ, D. CORTES, R. HOCQUEMILLER et A. CAVÉ. Oxandrine and Pseudoxandrine, first α or α′ ketobisbenzylisoquinolines of natural origin. International Symposium: The chemistry and biology of isoquinoline alkaloids. Londres, 1984.
12. (*a*) W. N. WU, J. L. BEAL et R. W. DOSKOTCH. J. Nat. Prod. **43**, 143 (1980); (*b*) J. Nat. Prod. **43**, 372 (1980); (*c*) S. F. HUSSAIN, H. GUINAUDEAU, A. J. FREYER et M. SHAMMA. J. Nat. Prod. **48**, 962 (1985).
13. M. P. CAVA, K. T. BUCK et K. L. STUART. The bisbenzylisoquinoline alkaloids. Occurrence, structure and pharmacology. Vol. XVI. *Dans* The alkaloids. *Editeur*: R. H. F. Manske. Academic Press, New York. 1977. p. 279; J. WU, J. L. BEAL et R. W. DOSKOTCH. J. Org. Chem. **45**, 213 (1980); S. F. HUSSAIN, L. KHAN, H. GUINAUDEAU, J. E. LEET, A. J. FREYER et M. SHAMMA. Tetrahedron, **40**, 2513 (1984).
14. M. SHAMMA, J. E. FOY et G. A. MIANA. J. Am. Chem. Soc. **96**, 7809 (1974).

The crystal structure of *N*,*N*′-bismethoxycarbonyl-L-valyl-L-valine, a product of the rearrangement of the symmetrical anhydride of *N*-methoxycarbonyl-L-valine[1,2]

FARID R. AHMED
Division of Biological Sciences, National Research Council of Canada, Ottawa, Ont., Canada K1A 0R6
AND
FRANCIS M. F. CHEN AND N. LEO BENOITON
Department of Biochemistry, University of Ottawa, Ottawa, Ont., Canada K1H 8M5
Received September 5, 1985

FARID R. AHMED, FRANCIS M. F. CHEN, and N. LEO BENOITON. Can. J. Chem. **64**, 1396 (1986).

A side product accompanying the reaction of *N*-methoxycarbonyl-L-valine anhydride with an amino acid anion in aqueous dimethylformamide has been characterized by an X-ray analysis as *N*,*N*′-bismethoxycarbonyl-L-valyl-L-valine, $C_{14}H_{24}N_2O_7$. The crystals are orthorhombic, space group $P2_12_12_1$, $a = 14.581(2)$, $b = 17.110(2)$, $c = 6.970(1)$ Å, $Z = 4$. The structure was determined by the direct method, and refined by block-diagonal least squares to $R = 0.046$, $R_w = 0.053$ for 1759 reflections with $I \geq 3\sigma(I)$. The carboxy-terminal part of the dimer is in the *gauche* conformation while the other part is *trans*. Each molecule at (x, y, z) makes two hydrogen bonds O...H—O and N—H...O to the molecule at $(1 - x, y - 1/2, 1/2 - z)$ and similarly to that at $(1 - x, 1/2 + y, 1/2 - z)$ to form infinite ribbons along y.

FARID R. AHMED, FRANCIS M. F. CHEN et N. LEO BENOITON. Can. J. Chem. **64**, 1396 (1986).

Faisant appel à la diffraction des rayons-X, on a déterminé que le produit secondaire, qui accompagne la réaction de l'anhydride de la *N*-méthoxycarbonyl L-valine avec un anion d'acide aminé dans du diméthylformamide aqueux, est de la *N*,*N*′-bisméthoxycarbonyl L-valyl-L-valine, $C_{14}H_{24}N_2O_7$. Les cristaux sont orthorhombiques, groupe d'espace $P2_12_12_1$, avec $a = 14{,}581(2)$, $b = 17{,}110(2)$ et $c = 6{,}970(1)$ Å et $Z = 4$. On a déterminé la structure par la méthode directe et on l'a affinée par la méthode des moindres carrés (blocs diagonaux) jusqu'à des valeurs de $R = 0{,}046$ et $R_w = 0{,}053$ pour 1759 réflexions avec $I \geq 3\sigma(I)$. La portion carboxy terminale du dimère est dans une conformation *gauche* alors que l'autre partie est *trans*. Chacune des molécules dans l'environnement x, y, z forme deux liaisons hydrogènes O...H—O et N—H...O avec la molécule qui se trouve dans l'environnement $(1 - x, y - 1/2, 1/2 - z)$ et, de la même manière, avec celle en $(1 - x, 1/2 + y, 1/2 - z)$ pour former des rubans infinis le long de l'axe y.

[Traduit par la revue]

Introduction

The reaction of an *N*-alkoxycarbonylamino acid anhydride **1** with the amino acid anion **2** in aqueous dimethylformamide gives, after acidification, the expected *N*-protected dipeptide acid **3** and the *N*-alkoxycarbonylamino acid **4** (1). However, it also gives a third product which is strongly retained by a reversed phase high performance liquid chromatography column. Further investigation of the reaction using *N*-methoxycarbonyl-L-valine anhydride (**1***a*) revealed that the same product was generated in aqueous dimethylformamide containing sodium hydrogen carbonate in the absence of nucleophile **2**. Successive fractionation of an organic solvent extract of the acidified mixture led to the isolation of crystalline material, mp 149–150°C. It is this third product which is the subject of the present study.

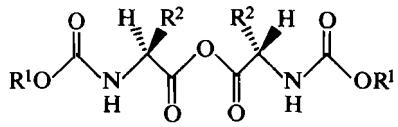

1

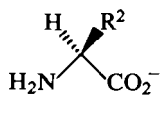

2

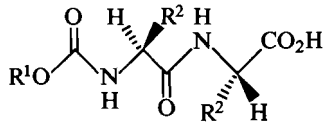

3

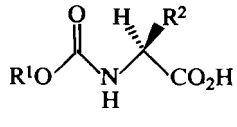

4

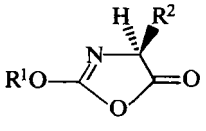

5

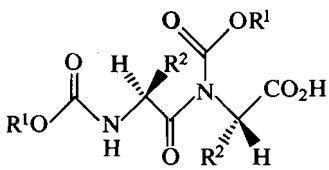

6

a $R^1 = CH_3$, $R^2 = CH(CH_3)_2$

[1]NRCC No. 25574.
[2]L-Valine = (2*S*)-2-amino-3-methyl-butanoic acid.

Experimental

Preparation of N,N′*-bismethoxycarbonyl-L-valyl-L-valine (6a)*

Crystalline *N*-methoxycarbonyl-L-valine anhydride (**1***a*) (1 mmol), obtained from the parent acid **4***a* using a soluble carbodiimide followed by aqueous washes (2, 3), was dissolved in dimethylformamide–water (3:1, 4 mL) containing $NaHCO_3$ (1.1 mmol). After 2 h at room temperature, the mixture was acidified with 1 *N* HCl, and extracted with dichloromethane (20 mL × 2). The extract was dried ($MgSO_4$), the solvent was removed with a rotary evaporator, and the final traces of dimethylformamide were removed with a vacuum pump. The residue was fractionated by crystallization from dichloromethane – light petroleum. **6***a* had mp 149–150°C; $[\alpha]_D^{22}$ −26.4° (*c*, 1 in $CHCl_3$); ir (KBr pellet): 3360, 3320, 2970, 1750 (urethane), 1730 (urethane), 1710 (acid), 1680 (amide) cm^{-1}; ^{1}H-nmr ($CDCl_3$) δ ppm vs. Me_4Si: 0.80, 0.81, 1.18, 1.26 (12H, 4 × d, $J = 7$ Hz, CH_3CH), 2.30 (2H, m, $(CH_3)_2CH$, 3.68 (3H, s, OC(1)H_3), 3.83 (3H, s, OC(16)H_3), 4.88 (1H, d, $J = 9$ Hz, αC(17)*H*), 5.48 (2H, b, α*CH*, N*H*; after D_2O exchange, 1H, d, $J = 4$ Hz, αC(6)*H*), 7.35 (1H, b, CO_2H); ms: *m*/*e* 332 (M* absent), 314 (M* − H_2O).

X-ray structure analysis of (6a)

Suitable crystals were obtained after four crystallization attempts from dichloromethane – light petroleum. The crystal selected for the

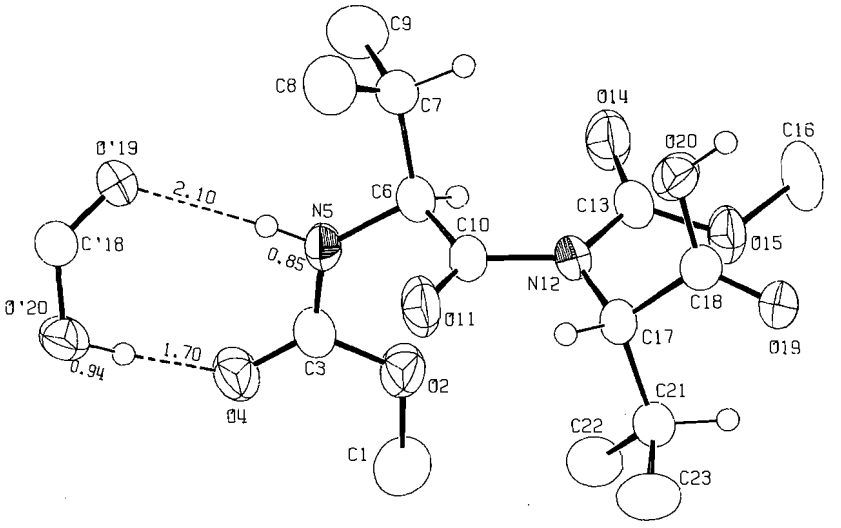

FIG. 1. ORTEP diagram of (**6***a*) showing the molecular structure with thermal ellipsoids drawn at 50% probability. The hydrogen bonds (dotted lines) have O(4)···O′(20) = 2.642(3) Å, O(4)···H—O′(20) = 174(5)°, N(5)···O′(19) = 2.929(3) Å, and N(5)—H···O′(19) = 164(3)°.

TABLE 1. Positional ($\times 10^4$) and thermal ($\times 10^4$) parameters

Atom	*x*	*y*	*z*	U_{eq}* (Å^2)
C(1)	2267(2)	655(2)	5669(7)	676
O(2)	3242(1)	795(1)	5512(4)	563
C(3)	3784(2)	164(2)	5416(5)	437
O(4)	3487(1)	−503(1)	5525(4)	553
N(5)	4662(2)	349(1)	5189(4)	464
C(6)	5014(2)	1142(1)	4990(5)	448
C(7)	6068(2)	1147(2)	5169(6)	575
C(8)	6546(3)	643(2)	3648(9)	864
C(9)	6342(3)	908(3)	7192(9)	957
C(10)	4715(2)	1472(1)	3047(5)	432
O(11)	4579(2)	1049(1)	1696(4)	595
N(12)	4584(2)	2285(1)	2848(4)	377
C(13)	4727(2)	2828(1)	4314(5)	432
O(14)	5122(2)	2710(1)	5795(4)	670
O(15)	4366(2)	3508(1)	3816(3)	491
C(16)	4591(3)	4172(2)	5003(6)	685
C(17)	4239(2)	2559(1)	968(4)	383
C(18)	4760(2)	3280(2)	308(4)	386
O(19)	4401(1)	3838(1)	−421(3)	453
O(20)	5654(1)	3214(1)	579(4)	518
C(21)	3186(2)	2691(2)	858(5)	474
C(22)	2654(2)	2170(2)	2234(7)	649
C(23)	2883(3)	2563(3)	−1227(7)	743

*$U_{eq} = (1/3)\sum_i\sum_j U_{ij}\, a_i^* a_j^* a_i a_j$.

X-ray analysis was in the shape of a triangular prism of dimensions 0.13 × 0.27 × 0.33 mm. The X-ray data were measured on an Enraf-Nonius CAD-4F diffractometer using Ni-filtered Cu radiation, λ(Kα$_1$) = 1.54056 Å. Crystal data at 22°C are:

$C_{14}H_{24}N_2O_7$ fw = 332.36

Orthorhombic, $P2_12_12_1$, a = 14.581(2), b = 17.110(2), c = 6.970(1) Å, V = 1738.9 Å^3, Z = 4, D_c = 1.269 g cm^{-3}, F(000) = 712, μ(Cu Kα) = 8.2 cm^{-1}.

The unit-cell parameters were derived by a least-squares fit of the 2θ values for 22 reflections with 25° < θ < 51°. Intensities were measured for the 2070 non-equivalent reflections within 2θ = 150°, in the ω–2θ scan mode with Δω = (0.7 + 0.14 tan θ)° plus 25% at each end for the background. Three standard reflections measured every hour showed minor variations of ±2% in their intensities. Corrections were applied for the scale variations and for Lorentz and polarization effects, but not for absorption. Of the measured reflections, 1759 with $I \geq 3\sigma(I)$ were considered observed and were employed in the analysis.

The structure was determined by the direct method with the aid of MULTAN (4), but the atom types were identified from the bond lengths after partial refinement. All the H atoms were located from a difference map and included in the refinement with isotropic temperature factors. Refinement was by block-diagonal least squares minimizing $\Sigma w(|F_o| - |F_c|)^2$ with $w = [1 + (|F_o|/20)^2]^{-1}$ for the observed reflections, but excluding the (200) reflection which showed extinction effect. Convergence was reached at $R = \Sigma||F_o| - |F_c||/\Sigma|F_o| = 0.046$ for the observed reflections, $R_w = [\Sigma w(|F_o| - |F_c|)^2/\Sigma w|F_o|^2]^{1/2} = 0.053$, $S = [\Sigma w(|F_o| - |F_c|)^2/(m - n)]^{1/2} = 0.53$, mean shift = 0.03σ and maximum shift = 0.54σ. The final difference map showed small fluctuations within −0.24 and 0.16 e Å^{-3}. Scattering factor curves were from refs. 5 and 6, and the computations were performed with the NRC system of crystallographic programs (7) and ORTEP (8).

Final atomic parameters are presented in Tables 1, 4, and 5.[3]

Results and discussion

The ^{1}H-nmr spectrum showed two methoxy singlets of equal intensity at δ 3.68 and 3.83 ppm, two non-equivalent isopropyl groups (four C*H*$_3$CH-doublets) and one D$_2$O-exchangeable acidic proton, thus indicating the compound to be a dimer of **4***a* with no D$_2$O-exchangeable N—H proton. On the other hand, the molecular ion at *m/e* 314 in the mass spectrum corresponded to that of a dimer of 2-methoxy-5(4*H*)-oxazolone **5***a* or **4***a* which had lost a molecule of water. The ir spectrum (KBr pellet) showed four sharp peaks in the 1680–1750 cm^{-1} carbonyl region. Our inability to arrive at a structure based on this information prompted an analysis by single crystal X-ray diffraction which characterized the compound as *N,N′*-bis-methoxycarbonyl-L-valyl-L-valine (**6***a*). It transpires that the mass spectrum of **6***a* does not indicate the molecular ion but M* − 18, and that the N—H proton is only slowly exchangeable by deuterium, requiring 24 hours for complete exchange. The compound is sensitive to alkali, being completely destroyed in 20 min in aqueous sodium hydrogen carbonate.

[3]The structure factor table, Table 4 (anisotropic thermal parameters for non-hydrogen atoms), and Table 5 (parameters for the H atoms) may be purchased from the Depository of Unpublished Data, CISTI, National Research Council of Canada, Ottawa, Ont., Canada K1A 0S2.

TABLE 2. Bond lengths (Å) and valence angles (deg)*

Atom 1	Atom 2	Distance	Atom 1	Atom 2	Distance
C(1)	O(2)	1.446(3)	N(12)	C(13)	1.397(4)
O(2)	C(3)	1.340(4)	N(12)	C(17)	1.480(4)
C(3)	O(4)	1.223(4)	C(13)	O(14)	1.199(4)
C(3)	N(5)	1.328(4)	C(13)	O(15)	1.323(3)
N(5)	C(6)	1.457(3)	O(15)	C(16)	1.443(4)
C(6)	C(7)	1.542(4)	C(17)	C(18)	1.520(4)
C(6)	C(10)	1.531(5)	C(17)	C(21)	1.554(4)
C(7)	C(8)	1.534(6)	C(18)	O(19)	1.202(4)
C(7)	C(9)	1.522(7)	C(18)	O(20)	1.322(3)
C(10)	O(11)	1.204(4)	C(21)	C(22)	1.522(5)
C(10)	N(12)	1.411(3)	C(21)	C(23)	1.535(6)

Atom 1	Atom 2	Atom 3	Angle	Atom 1	Atom 2	Atom 3	Angle
C(1)	O(2)	C(3)	116.8(3)	C(10)	N(12)	C(17)	116.5(2)
O(2)	C(3)	O(4)	122.7(3)	C(13)	N(12)	C(17)	119.2(2)
O(2)	C(3)	N(5)	112.5(3)	N(12)	C(13)	O(14)	126.1(3)
O(4)	C(3)	N(5)	124.8(3)	N(12)	C(13)	O(15)	109.5(2)
C(3)	N(5)	C(6)	124.9(3)	O(14)	C(13)	O(15)	124.4(3)
N(5)	C(6)	C(7)	110.4(2)	C(13)	O(15)	C(16)	116.8(3)
N(5)	C(6)	C(10)	109.1(2)	N(12)	C(17)	C(18)	110.8(2)
C(7)	C(6)	C(10)	110.7(2)	N(12)	C(17)	C(21)	115.2(2)
C(6)	C(7)	C(8)	113.2(3)	C(18)	C(17)	C(21)	111.2(2)
C(6)	C(7)	C(9)	109.6(3)	C(17)	C(18)	O(19)	123.7(3)
C(8)	C(7)	C(9)	111.7(3)	C(17)	C(18)	O(20)	112.4(2)
C(6)	C(10)	O(11)	121.1(3)	O(19)	C(18)	O(20)	123.9(3)
C(6)	C(10)	N(12)	119.3(2)	C(17)	C(21)	C(22)	112.8(3)
O(11)	C(10)	N(12)	119.6(3)	C(17)	C(21)	C(23)	108.1(3)
C(10)	N(12)	C(13)	124.3(2)	C(22)	C(21)	C(23)	111.5(3)

*Numbers in parentheses are estimated standard deviations.

The molecular structure depicted in Fig. 1 is shown to correspond to formula **6***a*. The corresponding bond lengths and valence angles are listed in Table 2. The bond lengths occur in the narrow ranges 1.520(4)–1.554(4) Å for C—C, 1.199(4)–1.223(4) Å for C=O, 1.322(3)–1.340(4) for C—O near a carbonyl group, otherwise 1.443(4)–1.446(3) Å. However, the C—N show wider variations, where the shortest is C(3)—N(5) = 1.328(4) Å and the longest is N(12)—C(17) = 1.480(4) Å.

In this dimer molecule, the conformation at C(6)—C(7) is *gauche* with H(6)—C(6)—C(7)—H(7) = −61(3)°, while that at C(17)—C(21) is close to *trans* with H(17)—C(17)—C(21)—H(21) = −147(3)°. Similarly, two different conformations were reported (9) for the two independent molecules in the unit cell of L-valine. Other torsion angles describing the molecular conformation are presented in Table 3.

Each molecule at (x, y, z) forms two intermolecular hydrogen bonds O(4)...H′(20)—O′(20) and N(5)—H(5)...O′(19) to the molecule at $(1 - x, y - 1/2, 1/2 - z)$, and two similar bonds to the molecule at $(1 - x, 1/2 + y, 1/2 - z)$ thus connecting the molecules into ribbons along y. The ribbons are held together in the structure by van der Waals interactions. The geometry of the hydrogen bonds is given in Fig. 1 and its legend. It should be noted that the observed intermolecular distances O(4)...O′(20) = 2.642(3) Å and N(5)...O′(19) = 2.929(3) Å of the hydrogen bonds are shorter than the sums of the corresponding van der Waals radii which were derived in a recent publication (10) as r(O) = 1.54 Å and r(N) = 1.60 Å.

The nmr data indicate that the conformations at C(6)—C(7) and C(17)—C(21), which are *gauche* and *trans* respectively in the crystal, are similar in the molecule in solution in deuterochloroform. A *trans* relationship with the isopropyl proton is indicated by the 9 Hz coupling constant for the proton on the α-carbon which is not linked to N—H, i.e. H(17). A *cis* relationship with the isopropyl proton is indicated by the coupling constant of 4 Hz, which becomes apparent after deuterium exchange, for the proton on the α-carbon which is linked to N—H, i.e. H(6).

TABLE 3. Some torsion angles (deg) describing the molecular conformation*

Bonds	Angle
C(1)—O(2)—C(3)—O(4)	−2.7(4)
O(2)—C(3)—N(5)—C(6)	−2.2(4)
C(3)—N(5)—C(6)—C(10)	−69.7(4)
N(5)—C(6)—C(10)—O(11)	−28.2(4)
C(7)—C(6)—C(10)—N(12)	−87.5(3)
C(6)—C(10)—N(12)—C(13)	1.4(4)
O(11)—C(10)—N(12)—C(17)	2.8(4)
C(10)—N(12)—C(17)—C(21)	96.6(3)
C(13)—N(12)—C(17)—C(18)	46.1(3)
O(19)—C(18)—C(17)—C(21)	−8.5(4)
O(15)—C(13)—N(12)—C(17)	10.7(4)
O(14)—C(13)—O(15)—C(16)	10.1(4)

*Numbers in parentheses are esitmated standard deviations.

Urethane acylation producing **6** has been encountered as a side-reaction in mixed anhydride couplings of *N*-protected glycine derivatives (11–14). The present work is the first characterization of a diacylimide **6** with $R^2 \neq H$, and the first

demonstration that urethane acylation occurs in aqueous solvents. It also confirms, as suggested (11, 14–16), that anhydride **1** is an immediate precursor of **6**. A subsequent publication will address in detail the chemistry implicated in the formation and decomposition of compound **6**.

Acknowledgements

This work was financially supported by the Medical Research Council of Canada, of which N.L.B. is a Career Investigator. We thank Mrs. M. E. Pippy for assistance with the computations.

1. N. L. BENOITON, F. M. F. CHEN, R. STEINAUER, and M. CHOUINARD. Int. J. Pep. Protein Res. **27**, 28 (1986).
2. F. M. F. CHEN, K. KURODA, and N. L. BENOITON. Synthesis, 928 (1978); 232 (1979).
3. A. PAQUET, F. M. F. CHEN, and N. L. BENOITON. Can. J. Chem. **62**, 1335 (1984).
4. P. MAIN, S. E. HULL, L. LESSINGER, G. GERMAIN, J. P. DECLERCQ, and M. M. WOOLFSON. MULTAN 78. Universities of York, England and Louvain-La-Neuve, Belgium. 1978.
5. International Tables for X-ray Crystallography. Vol. IV. Kynoch Press, Birmingham, England. 1974.
6. R. F. STEWART, E. R. DAVIDSON, and W. T. SIMPSON. J. Chem. Phys. **42**, 3175 (1965).
7. F. R. AHMED, S. R. HALL, M. E. PIPPY, and C. P. HUBER. J. Appl. Crystallogr. **6**, 309 (1973).
8. C. K. JOHNSON. ORTEP II. Report ORNL-3794, 2nd Rev. Oak Ridge National Laboratory, TN. 1971.
9. K. TORII and Y. IITAKA. Acta Crystallogr. B**26**, 1317 (1970).
10. S. C. NYBURG and C. H. FAERMAN. Acta Crystallogr. B**41**, 274 (1985).
11. T. WIELAND and B. HEINKE. Ann. Chem. **599**, 70 (1956).
12. K. D. KOPPLE and R. J. RENICK. J. Org. Chem. **23**, 1565 (1958).
13. P. SCHELLENBERG and J. ULLRICH. Chem. Ber. **92**, 1276 (1959).
14. R. B. MERRIFIELD, A. R. MITCHELL, and J. E. CLARKE. J. Org. Chem. **39**, 660 (1974).
15. H. KOTAKE and T. SAITO. Bull. Chem. Soc. Jpn. **39**, 853 (1966).
16. D. F. DETAR, R. SILVERSTEIN, and F. F. ROGERS. J. Am. Chem. Soc. **88**, 1024 (1966).

Fluorination of protected mannose derivatives using diethylaminosulfur trifluoride

IAN P. STREET AND STEPHEN G. WITHERS
Department of Chemistry, University of British Columbia, Vancouver, B.C., Canada V6T 1Y6
Received November 29, 1985

IAN P. STREET and STEPHEN G. WITHERS. Can. J. Chem. **64**, 1400 (1986).

3,4,6-Tri-*O*-benzyl-D-mannose and methyl 3,4,6-tri-*O*-benzyl-α-D-mannopyranoside were subjected to fluorination by diethylaminosulfur trifluoride and each produced two products. The former suffered fluorination at the anomeric centre to give the α-fluoride and, to a lesser extent, additionally at C-2 to give the 2-fluoro-2-deoxy-β-D-glucopyranosyl fluoride. The methyl mannoside underwent a methyl ether migration reaction to produce a 1:1 mixture of the α- and β-2-*O*-methyl glucosyl fluorides. A mechanism for this rearrangement is proposed and ^1H and ^{19}F nmr data are presented for all products.

IAN P. STREET et STEPHEN G. WITHERS. Can. J. Chem. **64**, 1400 (1986).

On a soumis le tri-*O*-benzyl-3,4,6 D-mannose et le tri-*O*-benzyl-3,4,6 α-D-mannopyrannoside de méthyle à une fluoration par le diéthylamino trifluorure de soufre; chacune des réactions conduit à deux produits. L'ose est fluoré au centre anomérique pour conduire au fluorure-α et à un degré moindre au fluorure de fluoro-2 déoxy-2 β-D-glucopyrannosyle, un produit qui a subi une fluoration supplémentaire au niveau du carbone-2. Le mannoside de méthyle subit une réaction de migration de l'éther méthylique qui conduit à un mélange 1:1 des fluorures des α- et β-*O*-méthyl-2 glucosyles. On propose un mécanisme pour cette transposition et on présente des données de rmn du ^1H et du ^{19}F pour tous les produits.

[Traduit par la revue]

Introduction

Considerable effort has been expended recently in the synthesis of fluorinated sugars, particularly of 2-fluoro-2-deoxy-D-glucose and 2-fluoro-2-deoxy-D-mannose (1–3). One reason for this has been the widespread use of [^{18}F]-labelled carbohydrates as probes for studying energy metabolism in the brain by means of positron emission tomography (4). In addition, fluorinated carbohydrates have been suggested to possess antitumour activity (5) and have also been used as probes of the active sites of proteins and enzymes that bind sugars (6).

Several different approaches to the synthesis of 2-deoxy-2-fluoro carbohydrates have been adopted, which fall into the two general categories of addition reactions to glucals and of nucleophilic displacement reactions (or epoxide ring openings) using fluoride (7). A particularly promising approach has been the use of diethylaminosulfur trifluoride (DAST) to convert a hydroxyl group to a fluorine with inversion of stereochemistry (8). In connection with our project on the use of fluorodeoxy sugars to probe the active sites of enzymes, we embarked upon a study of the use of DAST to effect fluorinations of 3,4,6-tri-*O*-benzyl-D-mannopyranose (**1**) and methyl 3,4,6-tri-*O*-benzyl-α-D-mannopyranoside (**2**) with a view to achieving a convenient and rapid synthesis of 2-fluoro-2-deoxy-D-glucose. Previous studies (9, 10) have suggested that displacement reactions at C-2 of mannosides proceed more efficiently with the β- than the α-mannosides. However, since the latter are more readily synthesized, possible routes through such intermediates would be considerably more convenient. This paper describes the results of these investigations.

Results and discussion

Since characterization of these compounds relies to a considerable extent upon ^{19}F nmr data on the fluorinated products, it is pertinent to review some relevant information (1) on this topic prior to discussion of results. In general, a fluorine attached to the anomeric centre will resonate well downfield (Φ = 136–151 ppm) of fluorine attached elsewhere on the sugar rings. In addition, α-D-pyranosyl fluorides tend to resonate at lower field strengths than the corresponding β-anomer. Geminal couplings to fluorine tend to be large (≈50 Hz) and vicinal ^1H–^{19}F couplings range from 0 Hz up to ≈30 Hz in a *trans*-diaxial relationship.

Reaction of DAST with 3,4,6-tri-O-benzyl-D-mannose (1)

Treatment of 3,4,6-tri-*O*-benzyl-D-mannose (**1**) (11) with three equivalents of DAST for 24 h at room temperature resulted in the formation of two major products, which were separated by column chromatography. The chromatographically more mobile fraction was identified as 2-deoxy-2-fluoro-3,4,6-tri-*O*-benzyl-β-D-glucopyranosyl fluoride (**3**) (30% isolated yield) while the slower product (18% isolated yield) was shown to be 3,4,6-tri-*O*-benzyl-α-D-mannopyranosyl fluoride (**4**).

Proof of structure for the former compound (**3**) was obtained from mass spectral data (m/z = 454) and from both ^1H and ^{19}F nmr spectroscopic data since, for example, two fluorine resonances were observed (Φ = 141.05 and 197.78) consistent with a 2-fluoro-2-deoxy-β-D-hexopyranosyl fluoride. Further, the fluorine resonance at C-2 showed only relatively small ^1H–^{19}F and ^{19}F–^{19}F couplings, other than the geminal coupling. All nmr data were very similar to those published for 3,4,6-tri-*O*-acetyl-2-deoxy-2-fluoro-β-D-glucopyranosyl fluoride (12). Additional proof of structure was provided by removal of the blockings groups via catalytic hydrogenolysis with Pd catalyst to yield the free sugar, since this compound was shown to be identical to an authentic sample of 2-deoxy-2-fluoro-β-D-glucosyl fluoride prepared by an alternative route (12), as demonstrated by tlc analysis and nmr spectroscopic data. No difluorinated product possessing the α-anomeric configuration was observed.

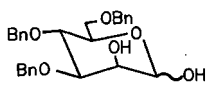

1

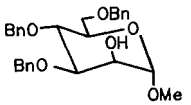

2

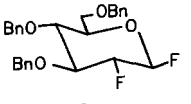

3

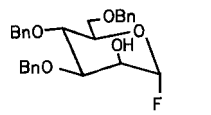

4

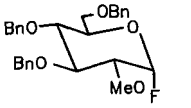

5

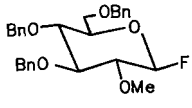

6

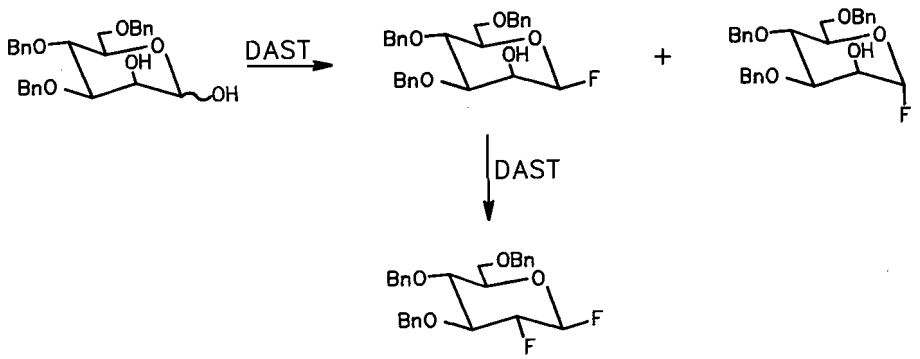

SCHEME 1

Only one resonance was observed (Φ = 140.98) in the ^{19}F nmr spectrum of the second compound, showing it to be a glycosyl fluoride, probably α-linked. The ^{1}H nmr data suggest it to be a mannosyl fluoride, since no large coupling was observed between H-2 and F-1 and between H-2 and H-3 as required for the glucosyl fluoride. Further, the ^{19}F nmr chemical shift measured is very close to that observed previously (13) for the compound 2,3,4,6-tetra-*O*-acetyl-α-D-mannopyranosyl fluoride (Φ = 138.8) and for α-D-mannopyranosyl fluoride itself (Φ = 138.8). Thus the compound was identified as 3,4,6-tri-*O*-benzyl-α-D-mannopyranosyl fluoride (**4**).

This mixture of products suggests that the initial reaction involves the formation of an anomeric mixture of mannopyranosyl fluorides of which only the β-anomer can then undergo a second, much slower, displacement reaction with DAST at C-2 to produce a difluorinated product (Scheme 1). Indeed, recent studies (14, 15) have shown that DAST is a very efficient reagent for the synthesis of appropriately protected glycosyl fluorides. It has also been noted by several authors (10, 11) that displacement reactions at C-2 of mannopyranosyl derivatives, with a charged nucleophile such as azide or fluoride, occur much more readily on sugars possessing the β-anomeric configuration than those of α-configuration. This is exemplified by the reaction of DAST with benzyl 3,4,6-tri-*O*-benzyl-β-D-mannopyranoside (16), which gave the desired displacement product in 80% yield, with a reaction time of only 5 min. Similar success has been achieved in effecting displacement of trifluoromethanesulfonate from C-2 of β-D-mannopyranosides using cesium fluoride (17), tetrabutylammonium fluoride (18), and tris(dimethylamino)sulfonium difluorotrimethyl silicate (19). In contrast, an attempt to displace trifluroromethanesulfonate from C-2 of methyl α-D-mannopyranoside using azide gave only a 30% yield of the desired 2-deoxy-2-azido-α-D-glucosyl derivative (20). In this case the major product was the result of a competing elimination reaction.

The reluctance of α-mannosides to undergo displacements at C-2 has been attributed to a variety of closely related factors. These include the high concentration of electron density in the required path of the incoming nucleophile due to the lone pair present on the α-anomeric substituent and, secondly, the unfavorable dipolar interactions that occur in the transition state between an axial anomeric substituent and the approaching nucleophile. Given the highly polar nature of the carbon–fluorine bond, it would be expected that the presence of an axial fluorine substituent at the anomeric centre would increase the magnitude of this latter effect. However, since the electron density associated with the fluorine would be held very close to the nucleus relative to the case for oxygen, it might be expected on this basis that such displacements would occur relatively more readily for a glycosyl fluoride than for an α-linked *O*-glycoside. Since all attempts to effect a displacement at C-2 of the α-mannopyranosyl fluoride (**4**) by DAST were unsuccessful, as were attempts to force the reaction of **1** with DAST towards a greater yield of the difluorinated sugar (**3**) by extending the reaction time or by heating, it must be concluded that the dipolar argument is probably the more reasonable in this case.

*Reaction of DAST with methyl 3,4,6-tri-*O*-benzyl-α-D-mannoside (2)*

In an effort to see if DAST could effect a displacement from C-2 of an α-mannopyranoside, methyl 3,4,6-tri-*O*-benzyl-α-D-mannopyranoside (**2**) was prepared as described (11) and treated with 3 equivalents of DAST in dichloromethane at reflux for 90 min. Instead of the expected displacement products, a 46% yield of a 1:1 anomeric mixture of 2-*O*-methyl-3,4,6-tri-*O*-benzyl-D-glucopyranosyl fluorides **5** and **6** was obtained. These were identified by a number of techniques as follows. The data are consistent with fluorine substitution at C-1 rather than C-2 since the ^{19}F nmr resonances appear well downfield in a region characteristic of glycosyl fluorides. A *gluco* rather than a *manno* configuration was assigned, since in the case of the α-fluoride (**5**) a large (25.61 Hz) coupling constant is observed between H-2 and F-1, a magnitude which is only observed for *trans*-diaxially related substituents, particularly at C-2. Similarly, for the β-anomer a large H-1 – H-2 coupling of 6.7 Hz is observed, which is again consistent only with a *trans*-diaxial arrangement of the two protons. Additionally, a long-range coupling between fluorine and the protons of the 2-*O*-methyl substituent (J = 1.05 Hz) is observed in the β-anomer (**6**). A similar fluorine–proton coupling over 5 bonds is observed in the two 2-*O*-methyl-3,4,6-tri-*O*-acetyl-D-glycosyl fluorides (13).

Mass spectral data are also consistent with these structures since the parent ion mass (m/z = 466) is identical for the two compounds isolated and in agreement with the proposed structure. Moreover a major peak (parent − 20) due to the loss of hydrogen fluoride is observed, consistent with the expected ready loss of fluoride from the anomeric centre. Further, acid catalysed hydrolysis of the product produces a single compound that contains no fluorine, as evidenced by the lack of ^{19}F–^{1}H couplings in the ^{1}H nmr. Such behaviour would be expected for a glycosyl fluoride but not for a 2-fluoro-2-deoxy sugar.

Thus, rather than effecting a displacement reaction at C-2, a methyl ether migration has occurred with the concomitant, or subsequent, attack of fluoride at the anomeric centre. A likely

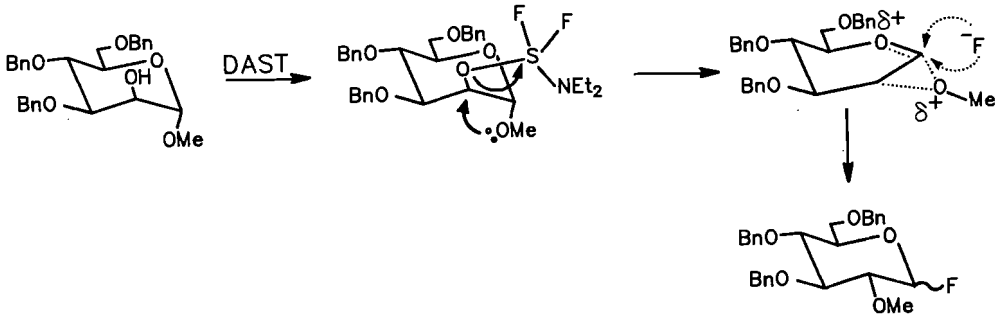

SCHEME 2

mechanism for this would involve the initial formation of the sulfoxo derivative at the axial hydroxyl group (see Scheme 2). Rather than suffer displacement by free fluoride ion, this highly reactive leaving group is instead displaced by intramolecular attack of the glycosidic oxygen atom to produce a 2-*O*-methyl glycosyl oxocarbonium ion intermediate, which undergoes attack by fluoride at the anomeric centre, apparently with equal ease from either face, to produce the (1:1) mixture of glycosyl fluorides. It is not, therefore, a thermodynamically controlled reaction. A concerted mechanism in which the sulfoxy derivative at C-2 provides a concerted intramolecular delivery of fluoride to the anomeric centre would not appear to be likely in this case since this would result in exclusive formation of the β-fluoride.

A migration of this type, to our knowledge, has not been reported before in fluorination attempts using DAST, although eliminations are common competing side reactions (1, 20). Indeed, in the case mentioned previously involving azide displacement of the highly reactive triflate from C-2 of a protected methyl-α-D-mannopyranoside, no evidence was obtained for a migration product, simply a product of an elimination reaction. However, migration has been observed in attempts to perform displacements of the highly reactive triflate leaving group (21), where a methyl ether migration from the anomeric centre to C-5 of a pentopyranosyl 5-triflate occurred.

Experimental

Thin-layer chromatography (tlc) was performed on Merck Silica Gel 60 F_{254} aluminum backed plates. Chromatograms were visualized by charring with 10% sulfuric acid in methanol. Flash chromatography was carried out on Merck Silica gel (230–400 mesh). The ^{1}H nmr spectra were recorded on a Brüker WH-400 spectrometer using $CDCl_3$ solutions and tetramethylsilane as an internal standard. Chemical shifts are expressed in δ and coupling constants (*J*) are given in hertz (s = singlet, d = doublet, t = triplet, m = multiplet). The ^{19}F nmr spectra were recorded on a Brüker HXS-270 operating at 254 MHz using a $CDCl_3$ solution and trifluoroacetic acid as an external standard. Chemical shifts are expressed in Φ, i.e. ppm upfield from $CFCl_3$, and coupling constants in hertz. Diethylaminosulfur trifluoride was obtained from Aldrich Chemical Co.

3,4,6-Tri-O-*benzyl-2-deoxy-2-fluoro*-β-D-*glucopyranosyl fluoride (3) and 3,4,6-tri*-O-*benzyl*-α-D-*mannopyranosyl fluoride (4)*

The compound 3,4,6-tri-*O*-benzyl-D-mannopyranose, 500 mg (1.1 mmol), was dissolved in dry dichloromethane (10 mL) and cooled to −20°C. Anhydrous conditions were maintained while DAST, 0.4 mL (3.3 mmol), was added and the reaction mixture allowed to slowly warm to room temperature. After a period of 24 h the reaction mixture was cooled to 0°C and, after cautious addition of 5 mL of methanol, stirred at room temperature for a further 2 h. The solvents were removed *in vacuo* and the resulting oil purified by flash chromatography using 95% methylene chloride/5% ethyl acetate. The chromatographically more mobile fraction was further purified on a second flash column using 90% *n*-pentane/10% ethyl acetate to yield 183 mg (0.4 mmol 36%) of the 2-deoxy-2-fluoro-β-D-glucopyranosyl fluoride (**3**); ^{19}F nmr data, Φ: 141.05 (dt, *J* = 52.71, 13.81 Hz, F-1), 197.78 (m, *J* = 50.6, 15.06, 3.47 Hz, F-2); ^{1}H nmr data δ: 5.33 (ddd, *J* = 52.74, 6.52, 3.89 Hz, 1H, H-1), 4.89, 4.83, 4.72, 4.59, 4.54, 4.51 (6 benzylic protons), 4.49 (m, *J* = 51 Hz, 8.0, 13.0 Hz, 1H, H-2), 3.79 (dt, *J* = 8.2, 10.3 Hz, 1H, H-3), 3.78–3.70 (m, 3H, H-4, H-6, H-6′), 3.61 (m, 1H, H-5), 7.34–7.14 (m, 15 aromatic protons). Mass spectrum, *m/z*: 454.

The second fraction (from the first column) yielded 92 mg (0.2 mmol, 18%) of the α-D-mannopyranosyl fluoride (**4**). ^{19}F nmr data, Φ: 140.98 (d, *J* = 49.47 Hz); ^{1}H nmr data, δ: 7.35–7.17 (m, 15H, aromatic protons), 5.66 (dd, *J* = 1.7, 49.56, 1H, H-1), 4.82–4.52 (m, 6H, 6 benzylic protons), 4.08 (m, 1H, H-2), 3.92 (t, *J* = 8.5 Hz, 1H, H-4), 3.90 (m, 1H, H-5), 3.86 (dd, *J* = 8.1, 1.9 Hz, 1H, H-3), 3.77 (dd, *J* = 3.9, 11.0 Hz, 1H, H-6), 3.70 (dd, *J* = 1.8, 11.0 Hz, 1H, H-6′), 2.82 (br s, removed on addition of D_2O, C-2—O*H*). Mass spectrum, *m/z*: 452.

3,4,6-Tri-O-*benzyl-2*-O-*methyl*-α- *and* β-D-*glucopyranosyl fluorides (5 and 6)*

Methyl 3,4,6-tri-*O*-benzyl-α-D-mannopyranoside, 222 mg (0.48 mmol), was dissolved in 10 mL of anhydrous methylene chloride and cooled to −20°C under anhydrous conditions. DAST, 0.180 mL (1.24 mmol) was added and the reaction temperature maintained at −20°C for 30 min. After allowing the reaction mixture to warm to room temperature it was heated gently to reflux for 90 min. The mixture was then cooled to 0°C and, after cautious addition of 5 mL of methanol, stirred for 1 h at room temperature. After removal of the solvents the product mixture was separated by flash chromatography using 10% ethyl acetate/90% *n*-pentane. The first compound eluted was found to be 3,4,6-tri-*O*-benzyl-2-*O*-methyl-β-D-glucopyranosyl fluoride (**6**) (48 mg, 0.11 mmol, 23%); ^{19}F nmr data, Φ: 138.61 (dd, *J* = 53.29, 12.21 Hz); ^{1}H nmr data, δ: 7.35–7.13 (m, 15H, aromatic), 5.15 (dd, *J* = 6.7, 52.0 Hz, 1H, H-1), 4.88–4.54 (6H, 6 benzylic protons), 3.72, 3.67, 3.57 (5H, H-3, H-4, H-5, H-6, H-6′), 3.58 (d, *J* = 1.05 Hz, 3H, C-2—OCH_3), 3.25 (m, *J* = 6.5, 8.1, 12.1 Hz, 1H, H-2). Mass spectrum, *m/z*: 466.

Further elution with the same solvent system gave the chromatographically less mobile compound 3,4,6-tri-*O*-benzyl-2-*O*-methyl-α-D-glucopyranosyl fluoride (54 mg, 0.12 mmol, 24%); ^{19}F nmr data, Φ: 149.87 (*J* = 53.45, 25.65 Hz); ^{1}H nmr data, δ: 7.36–7.13 (m, 15H, 15 aromatic protons), 5.73 (dd, *J* = 2.7, 54.0, 1H, H-2), 4.91–4.50 (6H, 6 benzylic protons), 3.95–3.66 (m, 5H, H-3, H-4, H-5, H-6, H-6′), 3.55 (s, 3H, C-2—OCH_3), 3.55 (m, *J* = 2.67, 9.46, 25.61 Hz, 1H, H-2). Mass spectrum, *m/z*: 466.

Acknowledgements

This research was supported by the Natural Sciences and Engineering Research Council of Canada, the Research Corporation, and the British Columbia Health Care Research Foundation; we also thank the B.C. Science Council for a G.R.E.A.T. scholarship to I.P.S.

1. A. A. E. PENGLIS. Adv. Carbohydr. Chem. Biochem. **38**, 195 (1981).
2. A. B. FOSTER and J. H. WESTWOOD. Pure Appl. Chem. **35**, 147 (1973).
3. P. W. KENT. Ciba Found. Symp. Carbon Fluorine Compd., Elsevier, New York. 1972. pp. 169–238.
4. A. P. WOLF. Semin. Nucl. Med. **11**, 2 (1981).
5. J. B. SHATTON, H. P. MORRIS, and S. WEINHOUSE. Cancer Res. **29**, 11 (1969).
6. Y. ITTAH and C. P. J. GLAUDEMANS. Carbohydr. Res. **95**, 189 (1981).
7. E. M. BESSEL, A. B. FOSTER, and J. H. WESTWOOD. Biochem. J. **128**, 199 (1972).
8. M. SHARMA and W. KORYTNYK. Tetrahedron Lett. **6**, 573 (1977); C. W. SOMAWARDHANA and E. G. BRUNNGRABER. Carbohydr. Res. **121**, 51 (1983); W. J. MIDDLETON. J. Org. Chem. **40**, 574 (1975); T. J. TEWSON and M. J. WELCH. J. Org. Chem. **43**, 1090 (1978); P. J. CARD. J. Org. Chem. **48**, 393 (1983).
9. A. C. RICHARDSON. Carbohydr. Res. **10**, 395 (1969).
10. M. MILJKOVIC, M. GLIGORIJEVIC, and D. GLISIN. J. Org. Chem. **39**, 3223 (1974).
11. N. E. FRANKS and R. MONTGOMERY. Carbohydr. Res. **6**, 286 (1968).
12. L. D. HALL, R. N. JOHNSON, J. ADAMSON, and A. B. FOSTER. Can. J. Chem. **49**, 118 (1971).
13. L. D. HALL, J. F. MANVILLE, and M. S. BHACCA. Can. J. Chem. **47**, 1 (1969).
14. WM. ROSENBROOK, D. A. RILEY, and P. A. LARTEY. Tetrahedron Lett. **26**, 3 (1985).
15. G. H. POSNER and S. R. HAINES. Tetrahedron Lett. **26**, 5 (1985).
16. A. DESSINGES, A. OLESKER, G. LUKACS, and T. T. THANG. Carbohydr. Res. **126**, C6 (1984).
17. S. LEVY, E. LIVNI, D. ELMALEH, and W. CURATOLO. J. Chem. Soc. Chem. Commun. 972 (1982).
18. T. HARADAHIRA, M. MAEDA, Y. KAI, and M. KOJIMA. J. Chem. Soc. Chem. Commun. 364 (1985).
19. W. A. SZAREK, G. W. HAY, and B. DOBOSZEWSKI. J. Chem. Soc. Chem. Commun. 663 (1985).
20. J. N. VOS, J. H. VAN BOOM, C. A. A. VAN BOECKEL, and T. BEETZ. J. Carbohydr. Chem. **3**, 117 (1984).
21. V. K. IYER and J. P. HORWITZ. J. Org. Chem. **47**, 644 (1982).

Use of camphor in pseudoguaianolide synthesis

JOHN H. HUTCHINSON, THOMAS MONEY,[1] AND SUSAN E. PIPER
Department of Chemistry, University of British Columbia, Vancouver, B.C., Canada V6T 1Y6

Received December 18, 1985

JOHN H. HUTCHINSON, THOMAS MONEY, and SUSAN E. PIPER. Can. J. Chem. **64**, 1404 (1986).

Stereoselective alkylation of a bicyclic lactone (**9**) derived from (+)-camphor (**5**) is the basis of a synthetic route to bicyclic enone (**3**) which could be used as a key intermediate in helenanolide synthesis.

JOHN H. HUTCHINSON, THOMAS MONEY et SUSAN E. PIPER. Can. J. Chem. **64**, 1404 (1986).

On utilise l'alcoylation stéréosélective de la lactone bicyclique **9**, provenant du (+)-camphre (**5**), pour préparer l'énone bicyclique **3** qui peut être utilisée comme intermédiaire clé dans la synthèse de l'hélènanolide.

[Traduit par la revue]

Pseudoguaianolides are sesquiterpenoid lactones which are classified as helenanolides (cf. helenalin (**1**)) or ambrosanolides (cf. ambrosin (**2**)) on the basis of their configuration at the C(10) position. The cytotoxic activity (1) and structural complexity of the helenanolides and ambrosanolides has stimulated considerable interest in their total synthesis and several imaginative routes to specific sesquiterpenoids of each class have been reported (2–13). A recent report (13) by Lansbury and co-workers describing the synthesis of a pseudoguaianolide intermediate by ring cleavage of 9-iodocamphor oxime prompts us to record our synthetic studies in this area.

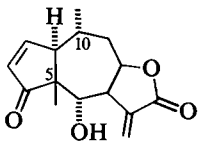

1

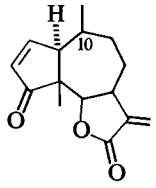

2

As part of our general investigations on the use of camphor as a chiral starting material in natural product synthesis (**9**) (14, 15) we have recently been involved in the development of simple synthetic routes from (+)-camphor (5) to epimeric dienones, **3** and **4**, which have considerable potential as intermediates in the

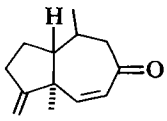

3

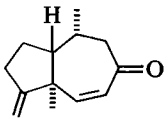

4

synthesis of *ent*-helananolides and *ent*-ambrosanolides, respectively.[2] The synthetic route to dienone (**3**) involves an intermediate bicyclic lactone (14, 15) which is readily synthesized from 9,10-dibromocamphor (**7**) (14*a*)[3] by the previously reported procedure (15) (cf. Scheme 1). Subsequent alkylation of **9** with methyl iodide provided the expected 4 β-methyl derivative **10** as the only isolable product in ~55% yield. The stereochemistry of the methyl group in this compound was supported by nmr evidence, i.e. the 4α-hydrogen signal, on irradiation with the C(4)-methyl resonance frequency, collapsed to a doublet with a coupling constant (J = 12 Hz) consistent with its *anti* relationship with the 5 β-hydrogen atom.[4] Methanolysis of lactone (**10**) followed by protection of the alcohol group and reduction of the ester provided monocyclic alcohol (**11**) in ~65% overall yield from **9**. Conversion of **11** to the corresponding iodide (**12**) followed by treatment with the carbanion derived from 2-methyl-1,3-dithiane (19) yielded an intermediate which was hydrolyzed ($CH_3I/CH_3CH{:}H_2O/CaCO_3$) (20*a*, 20*b*,[5] 20*c*) to provide silyloxyketone (**13**) in 45% overall yield. Removal of the silyl protective group followed by oxidation (PDC/CH_2Cl_2) (21) and intramolecular aldol condensation [(*i*) (KOH/MeOH; (*ii*) $MsCl/Et_3N$/DMAP/24 h)] of the intermediate keto-aldehyde (**14**) provided dienone **3** in ~70% yield.[6]

Dienone (**3**)[7] is structurally similar to racemic intermediates (**15***a*, *b*) used by other research groups in published synthetic routes to helenanolides and it is expected that this synthetic intermediate will be convertible to optically pure helenanolides by adaptation of previously published procedures (2, 5).

Experimental

Unless otherwise stated, the following are implied. Melting points (mp) were determined on a Kofler micro heating stage and are uncorrected. For gas–liquid chromatography a Hewlett-Packard gas chromatograph (Model 5830A) was used with 6 ft × ⅛ in. column (3% OV-17). Capillary glc analysis was carried out on a Hewlett-Packard 5880A gas chromatograph employing a flame ionization detector and using a W.C.O.T. narrow bore (0.21 mm × 12 m) Carbowax 20 M column. Helium was used as the carrier gas. The ^1H nmr spectra were recorded on Bruker WH-400, Nicolet Oxford H-270 or Bruker WP-80 instruments. Signal positions are given in delta (δ) with tetramethylsilane (TMS) as an internal reference. Signal multiplicity and integrated areas are indicated in parentheses. The solvent used was deuteriochloroform. Infrared spectra were recorded on a Perkin-Elmer 137 spectrophotometer and optical rotations were measured using a Perkin-Elmer 141 polarimeter. Low resolution mass spectra were obtained using a Varian/MAT Kodel CH4B mass spectrometer and high resolution mass spectra using a Kratos MS50 instrument. Microanalysis were

[1]To whom all correspondence should be addressed.

[2]Dienones (**3**) and (**4**) are synthons for the *ent*-helenanolides and *ent*-ambrosanolides, respectively. To synthesize enantiomers of (**3**) and (**4**) would involve C(3)-bromination (Br_2/HOAc) of commercially availible (−)-camphor as the first step in the sequence. (−)-Camphor is relatively expensive and although this extra expense can be avoided to some extent by oxidizing commercially available (−)-borneol with hypochlorite (16–18), the convenience of starting with (+)-3-bromocamphor (**6**) prompted us to conduct our initial investigations in the *ent*- series.

[3]Our published (14*a*) yield (~60%) for the conversion of 3,9,10-tribromocamphor to 9,10-dibromocamphor (**7**) has been increased to ~90% by conducting the selective debromination (Zn/HOAc/ether) in an ice-bath for 30 min.

[4]Structure (**10**) has recently been confirmed by X-ray chrystallographic analysis; S. J. Rettig and J. Trotter, unpublished results.

[5]In the absence of $CaCO_3$ the double bond was isomerized to the endocyclic position and the silyl protective group was removed.

[6]The synthesis of dienone (**3**) was previously described at the C.I.C. Conference, Montreal, June 3–6, 1984.

[7]The conversion of (+)-9,10-dibromocamphor (**7**) to epimeric dienone (**4**), a potential intermediate in ambrosanolide synthesis, is currently being investigated in our laboratory.

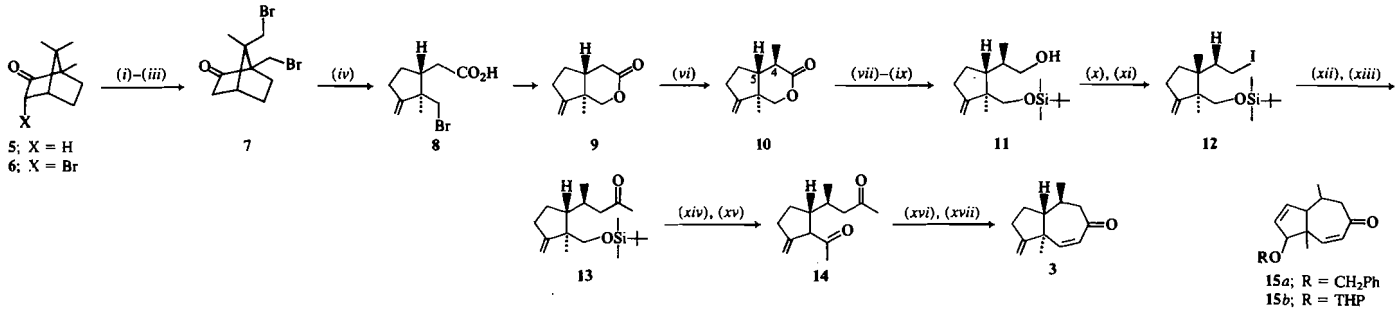

(*i*) $Br_2/ClSO_3H$/4 h, (*ii*) $Br_2/ClSO_3H$/5 days; (*iii*) Zn/HOAc/5°C/0.5 h; (*iv*) KOH/H_2O/THF; (*v*) KOH/DMSO:H_2O (99:1)/Ag_2O/65°C/12 h; (*vi*) LDA/THF/ −78°C; CH_3I; (*vii*) MeOH/H^+; (*viii*) Bu^tMe_2SiCl/DMAP/CH_2Cl_2; (*ix*) $LiAlH_4$/THF; (*x*) MsCl/Et_3N; (*xi*) NaI/HMPA; (*xii*) 2-methyldithiane/BuLi/THF; (*xiii*) CH_3I/CH_3CN:$H_2O/CaCO_3/\Delta$; (*xiv*) Bu_4NF/THF/20°C; (*xv*) PDC/CH_2Cl_2; (*xvi*) KOH/MeOH; (*xvii*) MsCl/Et_3N/DMAP/24 h; DBU.

SCHEME 1

performed by Mr. P. Borda, Microanalytical Laboratory, University of British Columbia.

Methyl lactone (10)

LDA was generated at 0°C under argon by adding *n*-butyllithium (1.6 *M* in hexane; 2.5 mL; 4.0 mmol) dropwise to a stirred solution of diisopropylamine (0.56 mL) in dry THF (30 mL) and stirring for 30 min. The mixture was cooled to −78°C and a solution of lactone (**9**) (15) (0.65 g, 3.92 mmol) in THF (26 mL) was added dropwise by means of a cannula. After 30 min at −78°C, methyl iodide (0.75 mL; 12 mmol) was added and the mixure warmed to room temperature and stirred for 1.5 h. Addition of saturated aqueous ammonium chloride followed by extraction with ether, drying ($MgSO_4$) and removal of solvent gave a yellow solid (0.70 g) which was shown by capillary glc to consist of one major (~60%) component. Column chromatography (silica gel; petroleum-ether:ether, 4:1) of the crude product afforded methyl lactone (**10**) as white needles (0.39 g; 55% yield). ν_{max} (CCl_4) 1730, 1645, 890 cm^{-1}; δ ($CDCl_3$, 400 MHz) 1.08 (d, 3H, $J \sim 1$ Hz), 1.31 (d, 3H, $J = 7$ Hz), 4.22 (d, 1H, $J = 10$ Hz), 4.34 (d, 1H, $J = 10$ Hz), 4.61 (t, 1H, $J = 2.5$ Hz), 4.82 (1H, t, $J = 2$ Hz). M.W. calcd. For $C_{11}H_{16}O_2$: 180.1150; found (high resolution mass spectrometry): 180.1149. *Anal.* calcd. for $C_{11}H_{16}O_2$: C 73.29, H 8.95; found: 73.22, H 9.01.

Silyl ether alcohol (11)

A solution of methyl lactone (**10**) (0.521 g, 2.89 mmol) in anhydrous methanol (15 mL) containing 1 drop of concentrated H_2SO_4 was stirred at room temperature for 1.5 h. The mixture was quenched with saturated aqueous sodium hydrogen carbonate, poured into saturated brine, extracted several times with ethyl acetate, and the organic layers dried ($MgSO_4$) and evaporated to give the corresonding hydroxy-ester as a colorless oil (0.61 g, 99% yield). δ ($CDCl_3$, 80 MHz) 0.875 (s, 3H), 1.2 (d, 3H, $J = 6$ Hz), 3.2 (D) and 3.55 (D) (AB quartet, $J = 12$ Hz), 3.7 (s, 3H), 4.85 (t, 1H, $J = 2$ Hz), 4.97 (t, 1H, $J = 2$ Hz).

Freshly sublimed *t*-butyldimethylsilyl chloride (2.89 g; 19.15 mmol) was added to a mixture of the above hydroxy-ester (1.35 g; 6.38 mmol) and dimethylaminopyridine (DMAP) (2.34 g; 19.14 mmol) in dry CH_2Cl_2 (50 mL) at room temperature. After 48 h the mixture was poured into ice-cold dilute hydrochloric acid (0.5 *M*) and extracted several times with CH_2Cl_2. Washing (water) and drying ($MgSO_4$) of the organic layers afforded, after solvent removal, a pale yellow oil. Column chromatography (silica gel; petroleum ether:ether 24:1) provided the TBDMS etherester as a colorless mobile oil (1.93 g, 93% yield). δ ($CDCl_3$, 80 MHz): 0.025 (s, 6H), 0.875 (s, 9H), 0.9 (s, 3H), 1.15 (d, 3H, $J = 6$ Hz), 3.25 (d) and 3.40 (d) (AB quartet, $J = 10$ Hz), 3.7 (s, 3H), 3.78 (t, 1H, $J = 2$ Hz), 3.88 (t, 1H, $J = 2$ Hz).

Lithium aluminum hydride (0.156 g; 4.1 mmol) was added portionwise to a stirred solution of the above ester (1.35 g; 4.13 mmol) in dry THF (30 mL) at 0°C. After 1 h at 0°C the mixture was poured into ice-cold brine, acidified with dilute hydrochloric acid (0.5 *M*), and extracted several times with ethyl acetate. Drying ($MgSO_4$) and removal of the solvent afforded a pale yellow oil (1.2 g; 98% yield). Column chromatography (silica gel; petroleum ether:ether 9:1) provided pure alcohol (11). $[\alpha]_D$ −45.0 (c, 0.22, CH_2Cl_2); *M/e* (relative intensity): 241 (16) ($M^+ - C_4H_9$), 149 (76), 107 (94), 89 (62), 75 (100); δ ($CDCl_3$, 400 MHz): 0.03 (s, 3H), 0.05 (s, 3H), 1.08 (s, 9H), 1.1 (s, 3H), 1.16 (d, 3H, $J = 7$ Hz), 1.74 (s, 1H, disappears on addition of D_2O), 3.64 (1H, dd, $J = 10$ Hz), 3.68 (d) and 3.77 (d) (2H, AB quartet, $J = 10$ Hz), 3.85 (1H, dd, $J = 10$ Hz and 5 Hz), 4.92 (br, s, 1H), 5.07 (br s, 1H). *Anal.* calcd. for $C_{17}H_{34}OSi$: C 68.39, H 11.48; found: C 68.60, H 11.50.

Silyl ether iodide (12)

Mesyl chloride (0.35 mL; 4.5 mmol) was added dropwise to a stirred mixture of alcohol (**11**) (1.22 g; 4.09 mmol), triethylamine (0.63 mL; 4.5 mmol), and DMAP (0.244 g; 2 mmol) in dry CH_2Cl_2 (30 mL) at 0°C. Stirring for 1.5 h followed by pouring into ice-cold dilute HCl (0.5 *M*), extraction with CH_2Cl_2, drying ($MgSO_4$), filtration and evaporation afforded the corresponding mesylate as a pale yellow oil (1.5 g, 97% yield), which was used without further purification. *M/e* (relative intensity): 361 ($M^+ - CH_3$), 319 (1.2), 281 (0.5), 244 (0.8), 153 (49.3), 149 (100); δ ($CDCl_3$, 80 MHz): 0.05 (s, 6H), 0.92 (s, 9H), 0.98 (s, 3H), 0.98 (d, 3H, $J = 7$ Hz), 3.00 (s, 3H), 3.32 (d) and 3.45 (d) (2H, AB quartet, $J = 10$ Hz), 3.85–4.38 (m, 2H), 4.75 (t, 1H, 2 Hz), 4.80 (t, 1H, 2 Hz).

Sodium iodide (5.31 g; 35.4 mmol) was added portionwise to a stirred solution of the above mesylate (2.22 g; 5.9 mmol) in HMPA (dry; 60 mL) at 0°C under argon. The mixture was allowed to warm to room temperature and stirred in the dark for 25–48 h while being monitored at regular intervals by tlc (petroleum ether:ether, 4:1, silica). The reaction was worked up by pouring into saturated brine, extracting several times with ether and washing the organic layer with aqueous sodium hydrogen sulphite and water. Removal of the solvent provided a pale-yellow oil which, after column chromatography (silica; petroleum ether:ether, 9:1) afforded pure iodide (**12**) as a colorless oil (1.96 g; 82% yield). *M/e* (relative intensity): 393 (0.3, $M^+ - CH_3$), 351 (43.8), 309 (1.25), 281 (0.6), 263 (5.07), 223 (9.03), 185 (18.28), 149 (87.56), 107 (100); δ ($CDCl_3$, 400 MHz): 0.02 (s, 3H), 0.04 (s, 3H), 0.9 (s, 9H), 0.94 (s, 3H), 0.98 (d, 3H, $J = 7$ Hz), 1.37 (m, 1H), 1.8 (m, 2H), 2.05 (m, 1H), 2.31 (m, 2H), 3.13 (dd, 1H, $J = 10$ Hz and $J = 8$ Hz), 3.36 (dd, 1H, $J = 10$ Hz and 4 Hz), 3.34 (1H, d, $J = 10$ Hz), 3.43 (1H, d, $J = 10$ Hz), 4.75 (t, 1H, $J = 2$ Hz), 4.88 (t, 1H, $J = 2$ Hz). *Anal.* calcd. for $C_{17}H_{33}OSiI$: C 49.99, H 8.14; found: C 50.46, H 8.33.

Silyl ether ketone (**13**)

n-Butyllithium (1.6 *M* in hexane, 2.36 mL, 3.77 mmol) was added, dropwise over 10 min, to a stirred solution of 2-methyl-1,3-dithiane (0.5 g; 3.77 mmol) in dry THF (10 mL) at −20°C under argon. After 3 h a solution of iodide (**12**) (0.52 g; 1.274 mmol) in THF (10 mL) was added and the mixture stirred at −20°C for 1 h and 20°C for 15 h. Acidification with aqueous ammonium chloride followed by extraction with ether and workup in the usual way afforded a yellow oil which was purified by column chromatography (silica; petroleum ether:ether,

100:1) to provide the dithiane silyl ether as a colorless oil (0.42 g; 80% yield); δ (400 MHz) 0.01 (s, 3H), 0.015 (s, 3H), 0.88 (s, 9H), 0.90 (d, 3H, $J = 7$ Hz), 1.04 (s, 3H), 1.46 (s, 3H), 2.36 (m, 2H), 2.84 (m, 4H), 3.16 (1H, d, $J = 10$ Hz), 3.33 (1H, d, $J = 10$ Hz), 4.75 (br s, 1H), 4.84 (br s, 1H).

The above dithiane derivative (0.2 g; 0.48 mmol) and anhydrous calcium carbonate (145 mg, 1.45 mmol) was heated in a solution (13 mL) of acetonitrile, water, and methyl iodide (v/v, 10:2:1) at ~80°C for 1.5 h. Excess acetonitrile and methyl iodide were removed *in vacuo*, water added, and the mixture extracted several times with ethyl acetate. Removal of solvent afforded a colorless oil (0.13 g; 82% yield) which, after column chromatography (silica, petroleum ether:ether, 24:1), afforded pure methyl ketone (**13**) (0.11 g, 71% yield); ν_{max} (cm^{-1}, film): 1720, 1650, 840. $[\alpha]_D = -35.00$, (c 0.4, CH_2Cl_2); *M/e* (relative intensity): 225 (16.7), 210 (29.5), 175 (15.7), 159 (18.5); δ (400 MHz): 0.01 (s, 3H), 0.015 (s, 3H), 0.83 (d, 3H, $J =$ 6 Hz), 0.88 (s, 9H), 0.97 (s, 3H), 1.59 (m, 1H), 1.74 (m, 1H), 1.87 (m, 1H), 2.12 (s, 3H), 2.26 (m, 3H), 2.56 (dd, 1H, $J = 15$ Hz and 5 Hz), 3.28 (d, 1H, $J = 10$ Hz), 3.39 (d, 1H, $J = 10$ Hz), 4.74 (br s, 1H), 4.86 (br s, 1H). *Anal.* calcd. for $C_{19}H_{36}O_2Si$: C 70.31, H 11.18; found: C 70.38, H 11.20.

Keto aldehyde (14)

Tetrabutylammonium fluoride (TBAF) (1.0 *M* in THF; 3.21 mL, 3.21 mmol) was added to a flask containing ketone (**13**) (0.52 g, 1.6 mmol) under argon at room temperature and the mixture stirred for 3 h. The reaction mixture was extracted with ethyl acetate, and worked up in the usual way to provide crude keto alcohol (400 mg) as a yellow oil. ν_{max} (cm^{-1}, film): 3600–3150, 1710, 1650. δ ($CDCl_3$, 80 MHz) 0.9 (d, 3H, $J = 7$ Hz), 0.95 (s, 3H), 2.15 (s, 3H), 3.5 (d, 2H, $J =$ 7 Hz), 4.8 (t, 1H, $J = 2$ Hz), 4.95 (t, 1H, $J = 2$ Hz).

To a stirred solution of the crude keto alcohol (0.335 g; 1.6 mmol) in dry CH_2Cl_2 (15 mL) was added pyridine dichromate (PDC) (2.0 g, 5.32 mmol). The mixture was stirred at room temperature for 20 h before filtering through a pad of celite/silica gel/$MgSO_4$. Evaporation of the organic solution afforded a yellow oil which, after column chromatography (silica; petroleum ether:ether, 4:1) provided keto-aldehyde (**14**) (0.246 g, 74% yield over two steps) as a colorless oil. ν_{max} (cm^{-1}, film): 1710, 1700, 1640, 890. δ ($CDCl_3$, 80 MHz): 0.95 (d, 3H, $J = 7$ Hz), 1.1 (s, 3H), 2.1 (s, 3H), 4.68 (t, 1H, $J = 2$ Hz), 5.08 (t, 1H, $J = 2$ Hz), 9.28 (s, 1H). *M/e* (relative intensity): 208 (1.2 M^+), 194 (1.8), 136 (13.7), 121 (20.6), 43 (40.9).

Bicyclic enone (3)

A potassium hydroxide solution (10%, 3.0 mL) was added to a stirred solution of keto-aldehyde (**14**) (0.327 g; 1.572 mmol) in methanol (20 mL) at room temperature and the mixture stirred for 3 h. After this time acidification of the reaction mixture followed by extraction with ethyl acetate and workup in the usual way gave crude aldol (0.327 g) as a white crysalline solid.

Mesyl chloride (0.27 g, 0.183 mL; 2.36 mmol) was added dropwise to a stirred mixture of crude aldol (0.327 g, 1.572 mmol), triethylamine (0.328 mL; 2.36 mmol) and DMAP (0.192 g, 1.572 mmol) in dry CH_2Cl_2 (10 mL) at 0°C. Stirring was continued at 0°C for 3.5 h, after which time DBU (0.469 mL, 3.14 mmol) was added. The mixture was allowed to warm to room temperature and stirred for 20 h before removal of solvent *in vacuo*. Column chromatography (silica; petroleum ether:ether, 19:1) of the resultant brown oil provided enone (**3**) (0.223 g, 75% yield) as a colorless oil. ν_{max} (cm^{-1}, film): 1670, 1640, $[\alpha]_D = -102.42$ (c 0.33, CH_2Cl_2). δ ($CDCl_3$, 400 MHz): 1.11 (d, 3H, $J = 7$ Hz), 1.18 (s, 3H), 1.43 (m, 1H), 1.72 (6 line multiplet, 1H), 1.98 (m, 2H), 2.28–2.4 (m, 2H), 2.49–2.58 (m, 1H), 3.06 (dd, 1H, $J =$ 12 Hz and 8 Hz), 4.92 (t, 1H, 2 Hz), 4.95 (t, 1H, 2.5 Hz), 5.96 (dd, 1H, $J = 12$ Hz and 1 Hz), 6.8 (d, 1H, $J = 12$ Hz). *M/e* (relative intensity): 190.1358 (41.9), 175.1123 (35.24), 161.0977 (17.32), 120.0939 (54.07), 105.0704 (79.71), 91.0550 (100). *Anal.* calcd. for $C_{13}H_{18}O$: C 82.06, H 9.53; found: C 82.15, H 9.50.

Acknowledgement

We thank Natural Sciences and Engineering Research Council of Canada, Ottawa, Canada for a research grant.

1. (*a*) P. A. Grieco, K. Hiroi, J. A. Noguez, Y. Masaki, M. Nishizawa, A. Rosewosky, S. Oppenheim, and H. Lazarus. J. Med. Chem. **20**, 71 (1977) and references therein; (*b*) K.-H. Lee, H. Furukawa, and E.-S. Huang. J. Med. Chem. **15**, 609 (1972).
2. (*a*) M. R. Roberts, and R. H. Schlessinger. J. Am. Chem. Soc. **101**, 7626 (1979); (*b*) G. J. Quallich and R. H. Schlessinger. **100**, 7627 (1979).
3. (*a*) P. T. Lansbury, D. G. Hangauer, Jr., and J. P. Vacca. J. Am. Chem. Soc. **102**, 3964 (1980) and references therein; (*b*) P. T. Lansbury, A. K. Serelis, J. E. Hengeveld, and D. G. Hangauer, Jr. Tetrahedron, **36**, 2701 (1980); (*c*) P. T. Lansbury and J. P. Vacca. Tetrahedron Lett. 2623 (1982); (*d*) P. T. Lansbury and T. E. Nickson. Tetrahedron Lett. 2627 (1982).
4. (*a*) F. E. Ziegler and J.-M. Fang. J. Org. Chem. **46**, 825 (1981); (*b*) F. E. Ziegler, J.-M. Fang, and C. C. Tam. J. Am. Chem. Soc. **104**, 7174 (1982) and references therein.
5. (*a*) P. A. Grieco, G. F. Majetich, and Y. Ohfune. J. Am. Chem. Soc. **104**, 4226 (1982) and references therein; (*b*) P. A. Grieco, Y. Ohfune, G. F. Majetich, and C.-L. J. Wang. J. Am. Chem. Soc. **104**, 4233 (1982); (*c*) P. A. Grieco, Y. Ohfune, and G. F. Majetich. J. Org. Chem. **48**, 360 (1983) and references therein.
6. (*a*) C. H. Heathcock, C. M. Tice, and T. C. Germroth. J. Am. Chem. Soc. **104**, 6081 (1982) and references therein; (*b*) C. H. Heathcock, S. L. Graham, M. C. Pirrung, F. Plavac, and C. T. White. *In* The total synthesis of natural products. Vol. 5. *Edited by* J. W. ApSimon. Wiley, New York. 1982.
7. (*a*) P. Kok, P. De Clercq, and M. E. Vandewalle. J. Org. Chem. **44**, 4553 (1979); (*b*) M. Demuynck, P. De Clercq, and M. Vandewalle. J. Org. Chem. **44**, 4863 (1979).
8. J. A. Marshall and R. H. Ellison. J. Am. Chem. Soc. **98**, 4312 (1976).
9. M. F. Semmelhack, A. Yamashita, J. C. Tomesch, and J. Hirotsu. J. Am. Chem. Soc. **100**, 5545 (1978).
10. P. A. Wender, M. A. Eissenstrat, and M. P. Filosa. J. Am. Chem. Soc. **101**, 2196 (1979).
11. R. Kretchmer and W. J. Thompson. J. Am. Chem. Soc. **98**, 3379 (1976).
12. K. Nagao, M. Chiba, I. Yoshimura, and S.-W. Kim. Chem. Pharm. Bull. **29**, 2733 (1981).
13. P. T. Lansbury, D. J. Mazur, and J. P. Springer. J. Org. Chem. **50**, 1632 (1985).
14. (*a*) W. M. Dadson, M. Lam, T. Money, and S. E. Piper. Can. J. Chem. **61**, 343 (1983); (*b*) J. Hutchinson, T. Money, and S. E. Piper. J. Chem. Soc. Chem. Commun. 455 (1984); (*c*) J. H. Hutchinson and T. Money. Tetrahedron Lett. **26**, 1819 (1985); (*d*) T. Money. Natural Product Rep. **2**, 253 (1985); (*e*) J. H. Hutchinson and T. Money. J. Chem. Soc. Chem. Commun. 288 (1986).
15. J. H. Hutchinson, T. Money, and S. E. Piper. Can. J. Chem. **64**, 854 (1986).
16. R. V. Stevens, K. T. Chapman, and H. N. Weller. J. Org. Chem. **45**, 2030 (1980).
17. S. O. Nwaukwa and P. M. Keehn. Tetrahedron Lett. **23**, 35 (1982).
18. R. V. Stevens, K. T. Chapman, C. A. Stubbs, W. W. Tam, and K. F. Albizati. Tetrahedron Lett. **23**, 4647 (1982).
19. (*a*) D. Seebach and E. J. Corey. J. Org. Chem. **40**, 231 (1975); (*b*) B.-T. Grobel and D. Seebach. Synthesis, 357 (1977).
20. (*a*) M. Fetizon and M. Jurion. J. Chem. Soc. Chem. Commun. 382 (1972); (*b*) R. L. Markezich, W. E. Willy, B. E. McCarry, and W. S. Johnson. J. Am. Chem. Soc. **93**, 4414 (1973); (*c*) B. M. Trost, M. Preckel, and L. M. Leichter. J. Am. Chem. Soc. **97**, 2224 (1975).
21. E. J. Corey and G. Schmidt. Tetrahedron Lett. 399 (1979).

Improved syntheses of hydroxy acid precursors of macrolide pheromones of cucujid grain beetles[1,2]

A. C. OEHLSCHLAGER,[3] E. CZYZEWSKA, R. AKSELA, AND H. D. PIERCE, JR.
Department of Chemistry, Simon Fraser University, Burnaby, B.C., Canada V5A 1S6

Received May 27, 1985[4]

A. C. OEHLSCHLAGER, E. CZYZEWSKA, R. AKSELA, and H. D. PIERCE, JR. Can. J. Chem. **64**, 1407 (1986).

Syntheses of 11- and 12-hydroxy-(*Z*)-3-dodecenic, 11- and 12-hydroxy-(*Z*,*Z*)-3,6-dodecadienic, and 13-hydroxy-(*Z*,*Z*)-5,8-tetradecadienic acids are reported. These unsaturated hydroxy acids are precursors of male-produced macrolide aggregation pheromones of grain beetles of the genera *Cryptolestes* and *Oryzaephilus*. The sequence of reactions for synthesis of the hydroxy-(*Z*)-3 acids was carboxylation of the dilithium salt of 10- or 11-hydroxy undecyne, deconjugation of the resulting carboxylic acids with $NaNH_2$ in THF/liquid ammonia to a mixture of 2,3-allenic and 3-alkynoic acids, and hydrogenation of the mixture with P-2 nickel catalyst. This latter reaction gave only the desired hydroxy-(*Z*)-3-alkenoic acids. The convergent point in the syntheses of the diunsaturated hydroxy-(*Z*,*Z*) acids was the coupling of the dimagnesium salt of 3-butyn-1-ol or 5-hexyn-1-ol to the appropriate functionalized propargylic bromide. The resulting 1,4-diacetylenic alcohols were oxidized with Jones reagent to the corresponding carboxylic acids, which were hydrogenated over P-2 nickel catalyst and deprotected.

A. C. OEHLSCHLAGER, E. CZYZEWSKA, R. AKSELA et H. D. PIERCE, JR. Can. J. Chem. **64**, 1407 (1986).

On rapporte des synthèses des acides hydroxy-11 (et 12) dodécène-3(*Z*) oïques, hydroxy-11 (et 12) dodécadiène-3(*Z*),6(*Z*) oïques et hydroxy-13 tétradécadiène-5(*Z*),8(*Z*) oïque. Ces acides hydroxylés et insaturés sont des précurseurs de phérémones d'aggrégation, produites par les mâles de coléoptères des classes génériques *Cryptolestes* et *Oryzaephilus*. La synthèse des acides hydroxylés portant une double liaison en position 3(*Z*) implique la carboxylation du sel de dilithium de l'hydroxy-10 (ou 11) undécyne, puis une déconjugaison des acides carboxyliques qui en résultent, à l'aide de $NaNH_2$ dans du THF/ammoniac liquide, qui conduit à un mélange d'acides allèniques-2,3 et alcyne-3 oïques et finalement une hydrogénation du mélange sur un catalyseur P-2 de nickel. Cette dernière réaction ne conduit qu'aux hydroxy-acides alcène-3(*Z*) oïques désirés. Le point de convergence des synthèses des hydroxy-acides di'insaturés-(*Z*,*Z*) est le couplage du sel de dimagnésium du butyne-3 ol ou de l'hexyne-5 ol avec le bromure propargylique fonctionnalisé d'une façon appropriée. On a oxydé les alcools di-acétyléniques-1,4 qui en résultent avec le réactif de Jones; on a hydrogéné les acides carboxyliques correspondants sur un catalyseur P-2 de nickel et on les a ensuite déprotégé.

[Traduit par la revue]

Introduction

During the past several years, we have reported (1–6) the discovery of seven macrolide aggregation pheromones for five species of grain beetles (Table 1). These well-known cucujids are economically-important pests during grain storage, food processing and distribution, and in households. The beetles infest a wide variety of stored-product commodities such as grain, cereal-based foods, nuts, chocolate, oil seeds and cake, raisins and other dried fruits, and spices.

Our initial syntheses (7–9) of these macrolides were long and, in cases, inefficient, but furnished sufficient amounts of the pheromones for laboratory bioassays. In order to supply selected macrolides for laboratory trap tests and limited field trials, we have devised more efficient syntheses of the ω and ω − 1 hydroxy acid precursors of macrolides **1**–**4** and **6**. As in previous approaches, we have utilized functionalized alkynes for carbon–carbon bond formation by coupling with appropriate electrophiles and for conversion into the required *Z*-olefinic bonds. In this paper, we report new syntheses for the hydroxy acid precursors of macrolides **1** and **6** and improved routes to those of macrolides **2**–**4**.

Results and discussion

*Hydroxy (Z)-3-alkenoic acids **8** and **14***

Alkylation of the lithium salt of 1-octyne with methyloxirane gave alkynol **9**, which was isomerized to terminal alkyne **10** with sodium 3-aminopropylamide in 1,3-diaminopropane (11). While carboxylation of the dilithium salt of **10** gave a good yield of hydroxy acid **11**, deconjugation of **11** with sodium amide in liquid ammonia – THF (10, 11) always gave a mixture containing desired **12** and conjugated allenic acid **13** with the former predominating (Scheme 1). Fortunately, this mixture was stereospecifically reduced to (*Z*)-3-alkenoic acid **8** with P-2 nickel (7–9).

The efficiency and ease of execution of the combined sequence of carboxylation, deconjugation, and reduction suggested its use for the synthesis of **14**, the precursor of macrolide **6**. Commercially available 10-undecen-1-ol, **15**, was converted by published methods (12) to 10-undecyn-1-ol, **16**, which was carboxylated to give **17** (Scheme 1). Deconjugation of **17** also gave a mixture of β,γ-alkynoic and allenic acids (**18** and **19**) but the mixture was reduced cleanly with P-2 nickel to the (*Z*)-3-acid **14**.

Reduction with P-2 nickel of conjugated allenes **13** and **19** to (*Z*)-3 acids **8** and **14** depends upon the presence of the carboxyl group since reduction under similar conditions of disubstituted allenes bearing a carbomethoxy, hydroxymethylene, or acetoxymethylene gave mixtures of regioisomers and stereoisomers of the possible alkenes (E. Czyzewska, unpublished results). Apparently, the polar carboxyl group or carboxylate anion (generated from ethylene diamine in the catalytic system) complexes with the nickel surface so that only the least hindered side of the allene bond is reduced.

Our new five-step routes to acids **8** and **14** proceed in overall yields of 40–50%, a 2- to 3-fold improvement upon our previously reported syntheses (7, 8), and avoid protection and

[1]Coleoptera: Cucujidae.

[2]Research supported by the Natural Sciences and Engineering Research Council of Canada through Operating Grant A0851 and Strategic Grant G0958.

[3]Author to whom correspondence may be addressed.

[4]Revision received February 11, 1986.

TABLE 1. Distribution of macrolide lactones in *Cryptolestes* and *Oryzaephilus* spp.[a]

	1	2	5	6	7	3	4
C. ferrugineus	P	+	P	–	+	–	+
C. pusillus	–	–	–	P	P	+	–
C. turcicus	–	–	–	–	P	–	P
O. mercator	P	P	–	–	+	+	+
O. surinamensis	–	P	–	–	+	P	P

[a]P, pheromone; +, produced by males in minor or trace amounts; –, absent in sp.

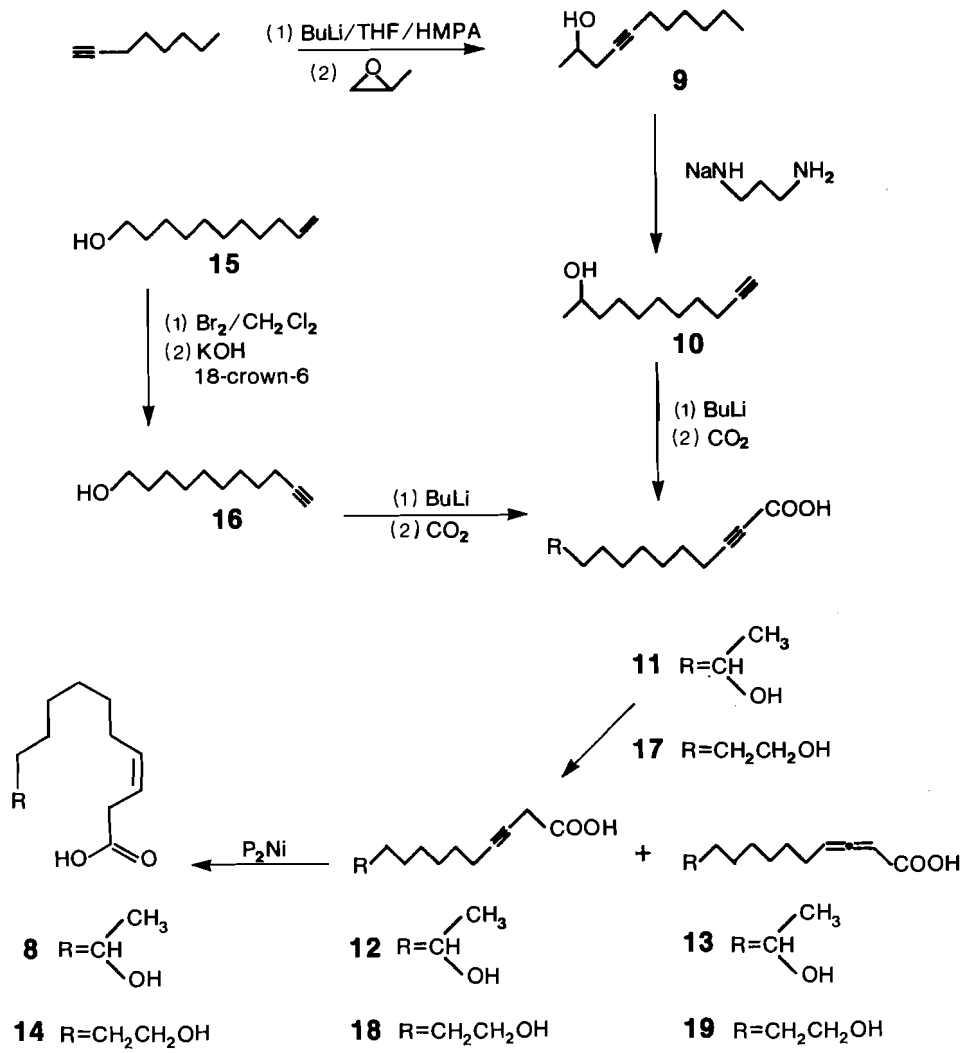

SCHEME 1

deprotection of hydroxyl groups, and chromic acid oxidation for generation of 3-alkynoic acids from homopropargylic alcohols. Use of (*R*)- or (*S*)-methyloxirane would permit synthesis of chiral isomers of **8**.

*Hydroxy (Z,Z)-dienic acids **26**, **35**, and **41***

The convergent point of our previous syntheses of **26** and **35** (Schemes 2 and 3) was the coupling of **20** with the appropriately substituted alkyne. This procedure, while efficient, required for **26** the selective removal of a *tert*-butyldimethylsilyl group in the presence of a MEM-protected hydroxyl. This process gave only moderate yields, and we desired a route to avoid these steps. Recently, Nicolaou *et al.* reported that the dimagnesium salt of 3-butyn-1-ol coupled efficiently to propargylic bromides in the presence of CuCl (14). Thus we redirected our effects to the syntheses of substituted propargylic bromides.

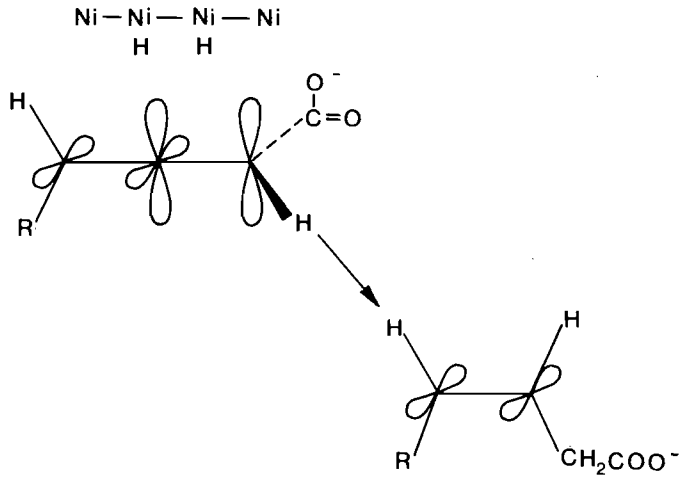

For the synthesis of **26** (Scheme 2), commercially available 3-heptyn-1-ol was isomerized to 6-heptyn-1-ol, which was protected to give the known (13) MEM derivative, **21**. Chain extension of **21** with formaldehyde (10) gave propargylic alcohol **22**, which was converted to bromide **24** via tosylate **23**. Bromide **24** coupled with the Grignard dianion of 3-butyn-1-ol in HMPA/THF using cuprous chloride catalysis to give the previously prepared (9) diyne **25** in excellent yield. It is noteworthy that the reaction failed to yield any coupled product if HMPA was omitted. Diyne **25** was oxidized to the carboxylic acid, which was deprotected and reduced to **26**. The present route to **26** through intermediate **25** requires nine steps and proceeds in 14% overall yield, a 60% improvement over our previous synthesis (9).

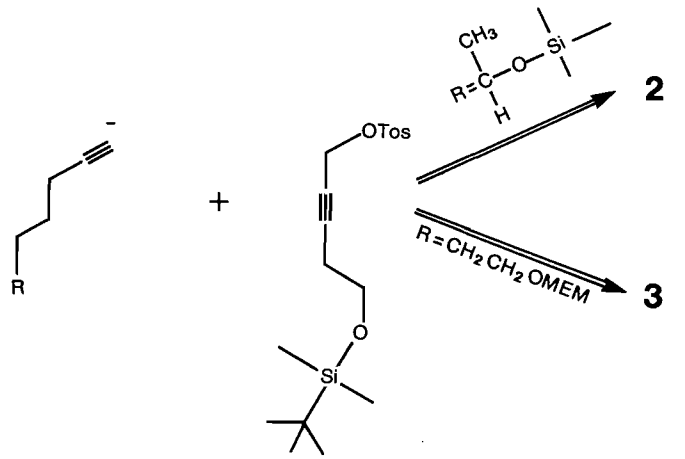

20

For the synthesis of **35**, bromide **32** was prepared in 35% overall yield from chloroalcohol **27** and was coupled with the dianion of 3-butyn-1-ol to give diynic alcohol **33** in 80% yield (Scheme 3). However, conversion of **33** to **35** by several different routes gave low yields. For example, deprotection of **33** and subsequent oxidation of **34** with chromic acid to the intermediate keto acid, which was sequentially reduced with $NaBH_4$ and P-2 nickel, gave **35** in 14% overall yield. We have been able to increase the yield of **35** to 24% by careful monitoring of the P-2 nickel reduction of **34**. Chromic acid oxidation of **33** prior to deprotection of the C-11 hydroxyl led to a mixture of products in which no component exceeded 30%. Diyne to diene reduction of **34** with P-2 nickel proceeded well (67–74%) but subsequent Jones oxidation (inverse addition) (16) of the resulting dienic, 1,11-diol to the corresponding dienic keto acid proceeded in only 30% yield.

The synthesis of acid **41** commenced with conversion of **36** (17) to bromide **37**, which was coupled with the Grignard dianion of 5-hexyn-1-ol (Scheme 4). Oxidation of **38** with Jones reagent gave keto acid **39**, which was sequentially reduced with $NaBH_4$ and P-2 nickel to hydroxy (*Z*,*Z*)-dienic acid, **41**. Our new synthesis of **41** proceeds with an overall yield of 46%, which is considerably better than the 27% obtained by our previous route.

Experimental

Hewlett–Packard 5880A and 5890A gas chromatographs fitted with capillary inlet systems, flame-ionization detectors, and WCOT columns (15 or 30 m × 0.25 mm id) of glass or fused silica were employed for analyses by gas–liquid chromatography (gc). Columns were coated with OV-101, SP-2100, or DB-1 liquid phases. Injection port and detector temperatures were 260 and 275°C, respectively. Helium was the carrier gas.

Column chromatography was performed by the flash chromatography method on silica gel (Kieselgel 60, 40–63 μm, E. Merck, Darmstadt). Solvents were distilled before use.

Low-resolution mass spectra were obtained on a Hewlett–Packard 5985B coupled gas chromatograph – mass spectrometer using electron-impact ionization at 70 eV or chemical ionization (CI) with isobutane as the ionizing gas. High resolution mass spectra were obtained on a Kratos MS80 RFA mass spectrometer interfaced with a Carla Erba gas chromatograph equipped with a 15 m × 0.25 mm id, DB-1 fused silica column. The ir spectra of neat samples between NaCl plates were determined on a Perkin–Elmer 599B spectrophotometer. The ^1H nmr spectra were recorded in $CDCl_3$ on Varian EM 360 or Brüker 400 WM spectrometers.

All reactions requiring anhydrous and (or) oxygen-free conditions were run in flame-dried glassware under a positive pressure of nitrogen or argon. Tetrahydrofuran (THF) was freshly distilled from lithium aluminum hydride. Dimethylformamide (DMF) and hexamethylphosphoramide (HMPA) were distilled from calcium hydride under reduced pressure. 1,3-Diaminopropane (1,3-DAP) was distilled from barium oxide. Rotary evaporation at water aspirator pressure was employed to concentrate or remove solvent from solutions obtained by extractive work-up of reactions. Due to instability of the 1,4-diyne intermediates, all subsequent reactions on these intermediates were carried out without purification.

Preparation of 4-undecyn-2-ol (9)

To a solution of 1-octyne (15 g, 0.136 mol) in 120 mL of dry THF under argon at −40°C was added dropwise 78 mL of 2.1 *M* *n*-BuLi in hexane (0.164 mol). After completion of addition, the mixture was warmed to 0°C over 30 min, and then cooled to −20°C. Dry HMPA (45 mL) was added, followed by dropwise addition over 45 min of racemic methyloxirane (9.5 g, 0.164 mol) in HMPA (45 mL). The reaction was stirred at −20°C for 30 min, warmed to 20°C over 4 h, and stirred an additional 12 h. The mixture was poured into ice-water (100 mL) and extracted with ether (4 × 50 mL). The combined organic extracts were washed with brine, dried ($MgSO_4$), and concentrated with no heating. Distillation of the residue gave **9** (18) (21.5 g, 94%); bp 65–72°C (0.2 Torr; 1 Torr = 133.3 Pa). Mass calcd. for $C_{11}H_{20}$: 168 (M^+); found: 169 ($M^+ + 1$, CI, isobutane).

Preparation of 10-undecyn-2-ol (10)

To a suspension of $NaNH_2$ (41.2 g, 1.1 mol, 6 equiv.) in 500 mL of liquid ammonia (10) was added 250 mL of 1,3-DAP (dried over KOH). Most of the ammonia was then evaporated at 50°C (water bath), and the last traces were removed at water pump pressure while maintaining the contents of the flask at 40°C for 15 min. 4-Undecyn-2-ol, **9** (29.6 g, 0.176 mol), was added and the reaction heated at 80°C for 2 h. The reaction mixture was then poured into 400 mL of ice-water and extracted with ether (4 × 50 mL). The ether extracts were dried ($MgSO_4$) and concentrated to yield **10** (21.5 g, 72.5%, 98% pure by gc), which was used in the subsequent reaction without further

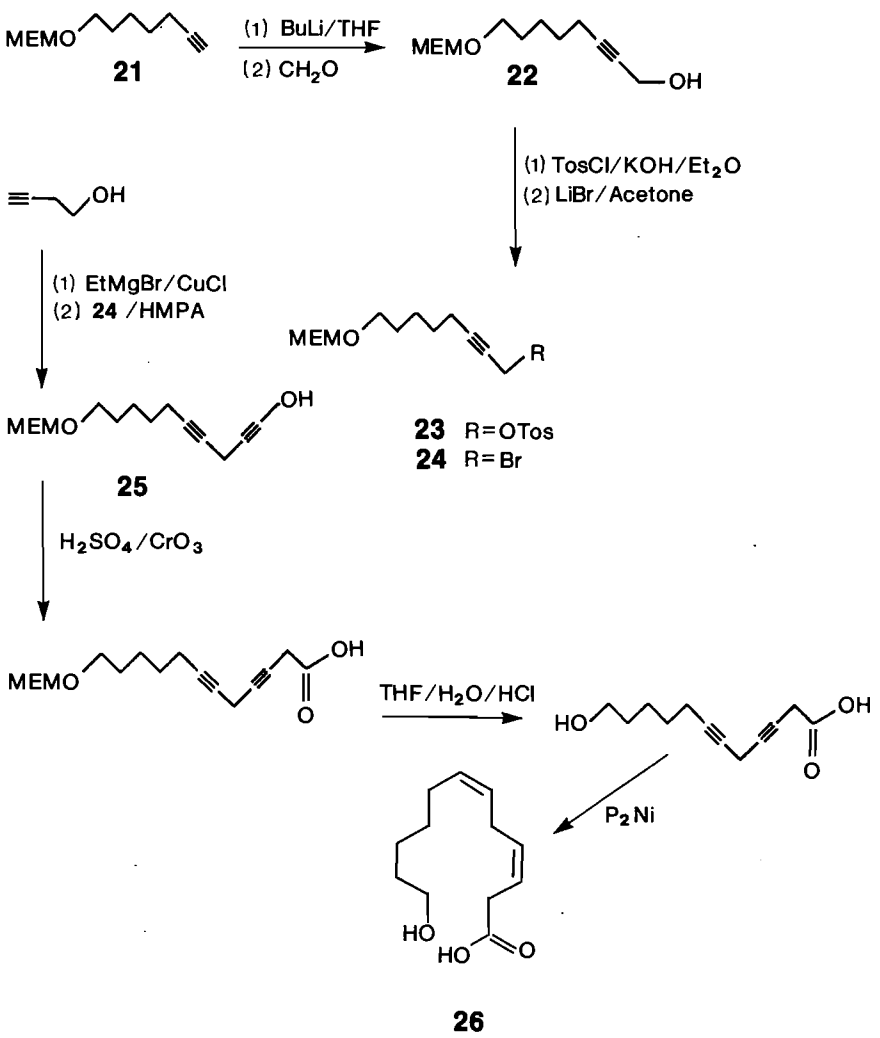

SCHEME 2

purification; ir (film): 2135 (s, C≡C) cm^{-1}. *Exact Mass* calcd. for ($C_{11}H_{20}O - CH_3$): 153.1279; found: 153.1297.

Preparation of 11-hydroxy-2-dodecynoic acid (11)

To 400 mL of dry THF under argon at −10°C was added 141 mL of 2.1 *M n*-butyllithium (0.296 mol) in hexane. To this was added 19.8 g (0.118 mol) of **10** in 50 mL THF. The temperature was raised to 0°C, and CO_2 from a cylinder was bubbled in for 30 min. The reaction was warmed to room temperature and quenched by the sequential addition of 50 mL saturated aqueous NH_4Cl solution and 200 mL 5 *N* HCl. The resulting solution was extracted with ether (4 × 200 mL). The combined extracts were dried ($MgSO_4$) and concentrated to give a 95% yield of **11**. An analytical sample (>90% pure by gc) of the methyl ester of **11** was prepared by treatment of a small portion of the product with diazomethane. Ester: ^1H nmr ($CDCl_3$) δ: 1.18 (d, 3H, J = 6 Hz, C(12) H), 1.20–1.66 (m, 13H, CH_2, OH), 2.32 (t, 2H, J = 7 Hz, C(4) H), 3.76 (s, 3H, OCH_3), 3.80 (m, 1H, C(11) H). Carboxylic acid: ir (film): 3350 (br, COOH), 2240 (s, C≡C), 1720 (s, C=O) cm^{-1}.

Preparation of 12 and 13 from 11

To the suspension of $NaNH_2$ (8.4 mmol) in 50 mL liquid ammonia was added **11** (0.3 g, 1.4 mmol) in 5 mL THF. After 30 min, 4 g of powdered ammonium chloride was added, and the ammonia was removed by heating at 50°C. The reaction was cooled to room temperature, and ether (100 mL), crushed ice (20 g), and sufficient 5 *N* HCl to lower the pH to 1 were added. The solution was saturated with NH_4Cl and extracted with ether (3 × 50 mL). The ether extracts were combined, dried ($MgSO_4$), and concentrated to yield nearly quantitative amounts of **12** and **13**. A small sample (0.1 g) of the product mixture was esterified with diazomethane. Gas chromatographic analysis of the esterified mixture revealed two principle (>90%) peaks in a ratio of 6:1–2:1 (depending on the run): ^1H nmr ($CDCl_3$) δ: 1.19 (d, J = 6 Hz, C(12) H), 1.2–1.6 (m, 10H, CH_2, OH), 3.26 (t, 1.5 H, C(2) H), 3.57 (s, 3H, OCH_3), 3.80 (m, 1H, C(11) H), 5.58 (d, 0.25H, J = 15 Hz, C(2) H), 5.62 (q, ≈0.25H, J = 9.5, 15 Hz, C(4) H). Mass calcd. for $C_{13}H_{22}O_3$ (both compounds): 226 (M^+); found: 227 (M^+ + 1, CI, isobutane, both compounds).

Reduction of 12 and 13 to 8

A mixture of **12** and **13** (2.8 g, 13 mmol) was reduced with P-2 nickel by the procedure previously reported (7). The product (2.5 g, 89%) was identical to 11-hydroxy-(*Z*)-3-dodecenoic acid, **8**, prepared earlier (8).

Preparation of 10-undecyn-1-ol, 16

To a solution of 26 g (0.153 mol) of 10-undecen-1-ol, **15**, in 100 mL of CH_2Cl_2 at 4°C was added slowly 24.5 g (0.153 mol) of bromine in 100 mL of CH_2Cl_2 (12). Removal of solvent gave 46.7 g (92%) of 10,11-dibromoundecan-1-ol as a liquid that was a single component by gc. To a solution of crude product in 800 mL of heptane was added powdered KOH (19.9 g, 0.301 mol, 2.12 equiv.) and 18-crown-6 (0.375 g, 1.42 mmol). The reaction was carried out and worked up according to the published procedure (12) to give 18.8 g (80%) of alkynol **16**; ir (film): 3360 (br, OH), 3320 (s, C≡CH), 2130 (s, C≡C) cm^{-1}.

Preparation of 12-hydroxy-2-dodecynoic acid, 17

Alkynol **16** (2.3 g, 13.7 mmol) was carboxylated in nearly quantitative yield by the procedure described above for **10**. The methyl

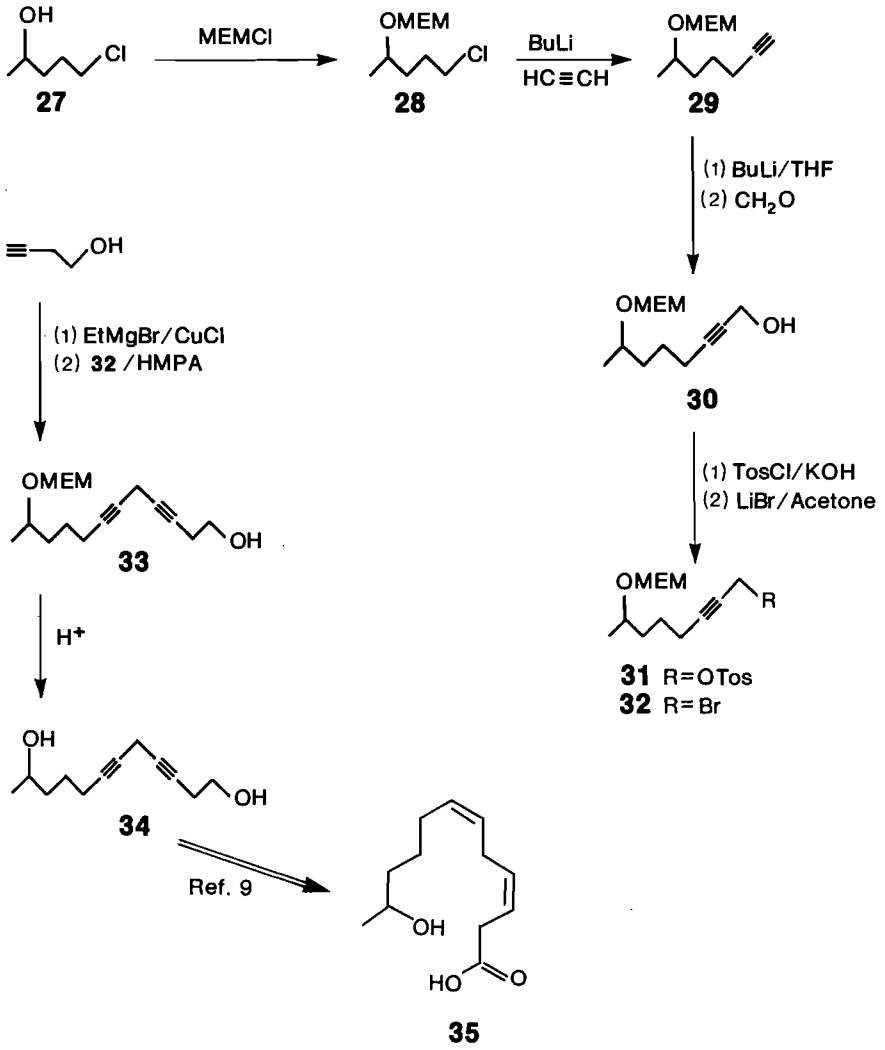

SCHEME 3

ester (CH_2N_2) of **17** (96% pure by gc) gave acceptable nmr and ir spectra. *Exact Mass* calcd. for ($C_{12}H_{20}O_3$ − CH_3O): 195.1385; found: 195.1370.

Preparation of 18 and 19 from 17

The deconjugation of **17** (6.1 g, 19 mmol) was conducted (Na, 8 equiv., 50 mL liquid NH_3, 80 mL THF) according to the procedure described for **11** to yield 5.6 g (92%) of a mixture (3:2–4:1, by gc of methyl esters) of **18** and **19**. The mixture of methyl esters (CH_2N_2) of **18** and **19** gave acceptable nmr and ir spectra.

Reduction of 18 and 19 to 14

Reduction of the mixture of **18** and **19** from the above preparation (5.6 g) with P-2 nickel yielded 5.5 g of **14**, which was identical by gc–ms (as the methyl ester) and nmr with that prepared previously (7).

Preparation of [(2-methoxyethoxy)methoxy]-6-heptyne, 22

3-Heptyn-1-ol was isomerized to the terminal alkyne in 90% yield as described for **9**, which was then protected as the (2-methoxyethoxy)methyl ether in 81% yield (15). Compound **21** gave ^1H nmr and mass spectra identical to that prepared previously (9). To a solution of **21** (32 g, 0.16 mol) in THF (500 mL) under argon, while maintaining the temperature below 0°C, was added dropwise *n*-BuLi in hexane (96 mL, 2.5 *M*, 0.24 mol). The resulting solution was stirred at 0°C for 30 min. Dry paraformaldehyde (7.7 g, 0.26 mol) was added in one portion. The mixture was warmed to 20°C over several hours and stirred at 20°C for 12 h. The reaction was worked up by pouring into ice-water (100 mL) and extracting with ether (4 × 50 mL). The ether extract was dried ($MgSO_4$) and concentrated to give 25.7 g (70%) of **22** (75% pure by gc). *Exact Mass* calcd. for ($C_{12}H_{22}O_4$ − CH_3O): 199.1334; found: 199.1333.

Preparation of 8-[(2-methoxyethoxy)methoxy]-2-heptyn-1-yl p-toluenesulfonate, 23

The crude product (38.6 g,0.17 mol) from the previous reaction was stirred with *p*-toluenesulfonyl chloride (35.2 g, 0.185 mol) and powdered KOH (47.1 g, 0.84 mol) in 500 mL dry ether at 0°C. After 30 min the reaction was poured into ice-water (300 mL) and the organic layer removed. The aqueous layer was extracted with ether (2 × 150 mL). The combined organic extracts were washed with brine, dried ($MgSO_4$), and concentrated without heating. Final traces of solvent were removed under vacuum (0.1 Torr) for 4 h, yielding the tosylate **23** as an oil (60.28 g, 93%). Tosylate **23** gave one spot on tlc (hexane:EtOAc, 3:1) and was used without further purification.

Preparation of 8-[(2-methoxyethoxy)methoxy]-2-heptyn-1-yl bromide, 24

Tosylate **23** (40 g, 0.104 mol) and LiBr (18 g, 0.21 mol) in 600 mL dry acetone were stirred at room temperature for 1 h. The solution was concentrated at room temperature, diluted with 500 mL of water, and extracted with ether (2 × 200 mL). The combined ether extracts were dried ($MgSO_4$) and concentrated to yield 31 g (100%) of crude product, which was purified by flash chromatography on silica gel (200 g;

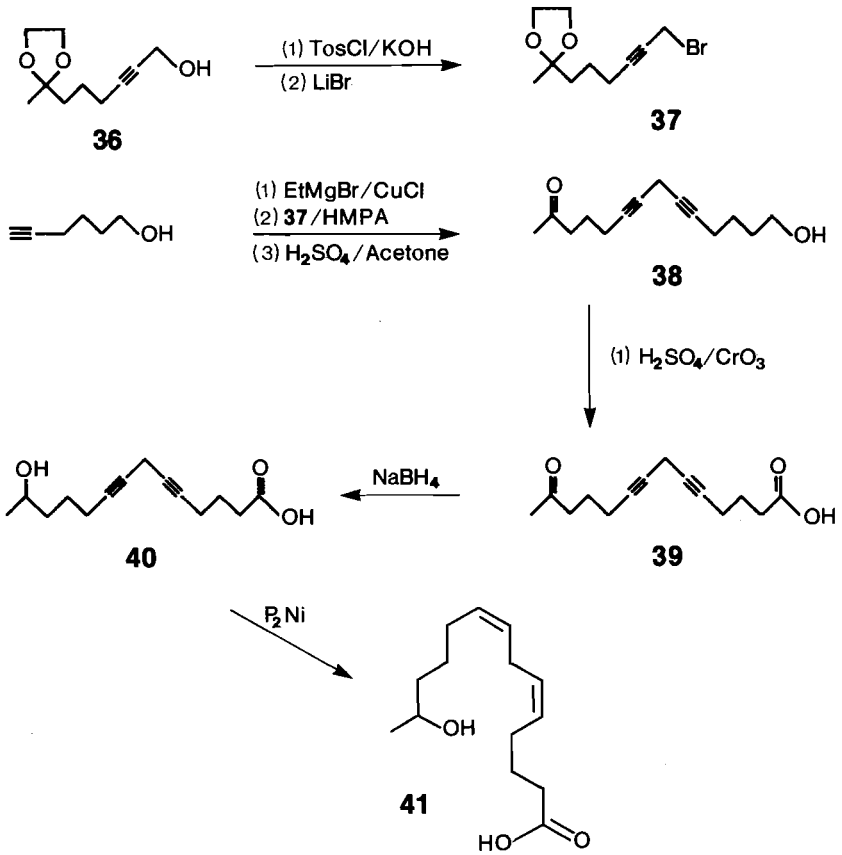

SCHEME 4

hexane:EtOAc, 4:1) to yield 15 g (50%) of **24** (80% pure by gc). *Exact Mass* calcd. for ($C_{12}H_{21}O_3Br$ − Br): 213.1490; found: 213.1468.

Preparation of 12-[(2-methoxyethoxy)methoxy]-3,6-dodecadiyn-1-ol, 25

A 2.25 *M* solution of EtMgBr (7.1 mL, 15.95 mmol) in THF was added dropwise to 3-butyn-1-ol (0.58 g, 8.24 mmol) in 40 mL dry THF. The resulting suspension was refluxed for 2 h. Cuprous chloride (0.85 g, 8.64 mmol) was added to the cooled (room temperature) mixture, which was stirred a further 0.5 h. Bromide **24** (1.06 g, 3.75 mmol) in 10 mL dry HMPA was added at ice-bath temperature. The ice bath was removed. The reaction mixture was stirred for 2.5 h, poured into 50 mL cold saturated NH_4Cl solution, and extracted with ether (3 × 50 mL). The combined ether extracts were washed with saturated NH_4Cl solution (50 mL) and brine. The ether extract was dried ($MgSO_4$) and concentrated to yield 1.1 g (92%) of the crude **25** (89% pure by gc). The ^1H nmr, ms, and ir data of **25** were equivalent to those previously obtained (9).

Preparation of 5-chloro-2-pentanol, 27

To a stirred solution of $NaBH_4$ (10.0 g, 0.264 mol) in 200 mL of 95% EtOH at 0°C was added dropwise over 2 h a solution of 5-chloro-2-pentanone (30 g, 0.249 mol) in 50 mL of 95% EtOH. After 1 h, acetone (50 mL) was added and most of the solvent was evaporated. Water (250 mL) was added to the residue, and the solution was extracted with ether (3 × 100 mL). The ether extracts were combined, dried ($MgSO_4$), and evaporated. The residue was distilled to give 27.5 g (90%) of **27** (98% pure by gc); bp 89–90°C (25 Torr).

Preparation of 5-chloro-2-[(methoxyethoxy)methoxy] pentane, 28

Reaction of chloro alcohol **27** with MEM chloride by the literature procedure (13) gave **28** in 89% yield (93% pure by gc); bp 60–70°C (0.1 Torr); ^1H nmr ($CDCl_3$) δ: 1.16 (d, 3H, J = 6.6 Hz, CH_3), 1.55–1.65 (m, 2H, C(3)), 1.80–1.91 (m, 2H, C(4)), 3.36 (s, 3H, OCH_3), 3.50–3.58 (m, 4H, OCH_2CH_2O), 3.66–3.76 (m, 3H, C(2), C(5)), 4.68–4.76 (dd, 2H, OCH_2); ms, *m/e* (%, rel. int.): 105 (55%), 89 (100%), 73 (18%), 59 (78%).

Preparation of 6-[(2-methoxyethoxy)methoxy]-1-heptyne, 29

A stream of dry acetylene was used to saturated 180 mL of dry THF at ice-bath temperature. To this solution, 2.1 *M* *n*-BuLi in hexane (65 mL, 0.136 mol) was added dropwise while maintaining the temperature at 5–10°C. After stirring the mixture for 0.5 h at 10°C, 5-chloro-2-[(2-methoxyethoxy)methoxy]-pentane, **28** (20.4 g, 0.097 mol), in 50 mL of dry HMPA was added dropwise. The reaction mixture was warmed to room temperature and stirred under an acetylene atmosphere for 24 h. The reaction was quenched by pouring into ice-water (150 mL) and extracting with ether (5 × 50 mL). The combined ether extracts were washed with water (75 mL) and brine (2 × 75 mL), dried ($MgSO_4$), and concentrated. Distillation of the residue gave 19.5 g (94%) of **29** (93% pure by gc); bp 65–70°C (0.2 Torr); ir (film): 3295, 2118 cm^{-1}; ^1H nmr ($CDCl_3$) δ: 1.13 (d, 3H, J = 6.6 Hz, CH_3), 1.50–1.67 (m, 4H, C(4), C(5)), 1.95 (t, 1H, J = 2.5 Hz, C(1)), 2.18 (tt, 2H, J = 7, 2.5 Hz, C(3)), 3.40 (s, 3H, OCH_3), 3.56 (m, 2H, OCH_2CH_2O), 3.70 (m, 2H, OCH_2CH_2), 3.75 (m, 1H, C(6)), 4.70–4.78 (dd, 2H, OCH_2O). *Exact Mass* calcd. for ($C_{11}H_{20}O_3$ − CH_3O): 169.1229; found: 169.1248.

Preparation of 7-[(2-methoxyethoxy)methoxy]-2-octyn-1-ol, 30

6-[(2-Methoxyethoxy)methoxy]-1-heptene, **29**, was chain-extended to **30** in 62% yield by the procedure described above for **22**: bp 120–130°C (0.3 Torr); ir (film): 3360, 2220 cm^{-1} (90% pure by gc); ^1H nmr ($CDCl_3$) δ: 1.14 (d, 3H, J = 6.6 Hz, C(8)), 1.50–1.66 (m, 4H, C(5), C(6)), 2.18 (tt, 2H, J = 7, 2.5 Hz, C(4)), 2.32 (br s, 1H, OH), 3.40 (s, 3H, OCH_3), 3.56 (m, 2H, OCH_2CH_2O), 3.70 (m, 2H, OCH_2CH_2O), 3.75 (m, 1H, C(7)), 4.18 (br s, 2H, C(1)), 4.70–4.78 (dd, 2H, OCH_2O). *Exact Mass* calcd. for ($C_{12}H_{22}O_4$ − CH_3O): 199.1334; found: 199.1376.

Preparation of 1-bromo-7-[(2-methoxyethoxy)methoxy)-2-octyne, 32

Bromide **32** was prepared from **30** in 69% yield by the procedure described for **24** and was purified by distillation; bp 120–130°C (0.1 Torr); ir (film): 2200 cm^{-1}; ^1H nmr ($CDCl_3$) δ: 1.14 (d, 3H, J = 6.6 Hz, C(8)), 1.50–1.66 (m, 4H, C(5), C(6)), 2.18 (tt, 2H, J = 7, 2.5 Hz, C(4)), 3.40 (s, 3H, OCH_3), 3.56 (m, 2H, OCH_2CH_2O), 3.70

(m, 2H, OCH_2CH_2O), 3.75 (m, 1H, C(7)), 3.92 (t, 2H, J = 2.6 Hz, C(1)), 4.70–4.78 (dd, 2H, OCH_2O); ms, m/e (%, rel. int.): 173 (12%), 171 (12%), 159 (7%), 157 (7%), 144 (23%), 146 (23%), 107 (35%), 79 (50%), 65 (45%), 55 (40%), 45 (100%). *Exact Mass* calcd. for ($C_{12}H_{21}O_3Br$ − Br): 213.1491; found: 213.1504.

Preparation of 11-[(2-methoxyethoxy)methoxy]-3,6-dodecadiyn-1-ol, 33

Bromide **32** was coupled to 3-butyn-1-ol as described above for **25** to give **33** (83% pure by gc) in 98% crude yield; ^{1}H nmr ($CDCl_3$) δ: 1.13 (d, 3H, J = 6.6 Hz, C(12)), 1.50–1.66 (m, 4H, C(9), C(10)), 1.95 (t, 1H, J = 5, 3 Hz, OH), 2.17 (m, 2H, C(8)), 2.43 (m, 2H, C(2)), 3.13 (quint., 2H, J = 2.2 Hz, C(5)), 3.40 (s, 3H, OCH_3), 3.56 (m, 2H, OCH_2CH_2O), 3.69–3.78 (m, 5H, OCH_2CH_2O, C(1), C(11)), 4.70–4.78 (dd, 2H, OCH_2O).

Preparation of 3,6-dodecadiyn-1,11-diol, 34

The crude diyne **33** prepared above (5.44 g, 0.019 mol) was stirred for 18 h at 20°C in 195 mL of THF:H_2O:conc. HCl (8:2:1 by volume). The reaction was quenched by pouring into 200 mL of ice-water and extracted with ether (2 × 100 mL). The ether extract was washed with brine (2 × 100 mL), dried ($MgSO_4$), and concentrated to yield 3.7 g (100%) of **34**, which gave ^{1}H nmr and mass spectra identical to those obtained previously (9).

Preparation of 2-methyl-2-(6-bromo-4-hexynyl)-1,3-dioxolane, 37

Bromide **37** was prepared in 89% yield from **36** by the procedure used to prepare **24**. The crude product (82% pure by gc) was employed for the following reaction; ir (film): 2220 cm^{-1}; ^{1}H nmr (60 MHz, $CDCl_3$) δ: 1.53–1.82 (m, 4H, $2CH_2$), 2.12–2.40 (m, 2H, $CH_2C{\equiv}C$), 3.90 (br s, 4H, OCH_2CH_2O), 3.95 (br s, 2H, CH_2Br). *Exact Mass* calcd. for ($C_{10}H_{15}O_2Br$ − Br): 167.1072; found: 167.1070.

Preparation of 13-oxo-5,8-tetradecadiyn-1-ol, 38

To 5-hexyn-1-ol (0.64 g, 6.5 mmol) in 40 mL of THF was added 5.6 mL of 2.25 *M* EtMgBr (12.6 mmol) in THF. The mixture was refluxed for 2 h and cooled to ice-bath temperature, whereupon CuCl (0.64 g, 6.5 mmol) was added. After 0.5 h of stirring, **37** (0.94 g, 3.8 mmol) in 10 mL of dry HMPA was added. The reaction was stirred overnight and then poured into 50 mL of saturated NH_4Cl solution. The product was isolated by extraction with ether (3 × 25 mL). The combined ether extracts were worked up with saturated NH_4Cl solution (2 × 25 mL) and brine (2 × 40 mL), dried ($MgSO_4$), and concentrated to give 1.1 g of the crude hydroxy ketal, which was 95% pure by gc. To this ketal in 40 mL of acetone was added 3 drops of 3.5 *M* H_2SO_4. After 5 h of stirring at 25°C, K_2CO_3 (1 g) was added. The solution was then filtered and concentrated to give 0.85 g of **38**, which was 85% pure by gc analysis; ir (film): 2238 cm^{-1}; ^{1}H nmr ($CDCl_3$) δ: 1.53–1.68 (m, 4H, C(2), C(3)), 1.75 (quint., 2H, J = 7.3 Hz, C(11)), 2.15 (s, 3H, C(14)), 2.16–2.23 (m, 4H, C(4), C(10)), 2.55 (t, 2H, J = 7.3 Hz, C(12)), 3.08 (quint., 2H, J = 2.1 Hz, C(7)), 3.65 (t, 2H, J = 7 Hz, C(1)). *Exact Mass* calcd. for $C_{14}H_{20}O_2$: 220.1463; found: 220.1455.

Preparation of 13-oxo-5,8-tetradecadiynoic acid, 39

Crude keto-alcohol **38** (0.8 g, ≈3.8 mmol) in reagent acetone (40 mL) was added dropwise over 1 h at ice-bath temperature to CrO_3 (1.64 g, 16.4 mmol) dissolved in 3.5 *M* H_2SO_4 (16.5 mL). The ice bath was removed, the reaction stirred at 20°C for 4 h, poured into ice-water (300 mL), and extracted with ether (4 × 50 mL). The ether extract was washed with brine (2 × 50 mL), dried ($MgSO_4$), and concentrated to give 0.87 g of **39** (78% overall from **37**), which was 80% pure by gc (as the methyl ester, CH_2N_2); ^{1}H nmr ($CDCl_3$) δ: 1.75 (quint., 2H, J = 7 Hz, C(3)), 1.83 (quint., 2H, J = 7 Hz, C(11)), 2.16 (s, 3H, C(14)), 2.17–2.29 (m, 4H, C(4), C(10)), 2.52 (t, 2H, J = 7 Hz, C(2)), 2.56 (t, 2H, J = 7 Hz, C(12)), 3.08 (quint., 2H, J = 2.1 Hz, C(7)). *Exact Mass* calcd. for ($C_{15}H_{20}O_3$ − CH_3): 233.1177; found: 233.1209.

Preparation of 13-hydroxy-5,8-tetradecadiynoic acid, 40

Keto-acid **39** (0.69 g, 2.9 mmol) was dissolved in 95% ethanol (10 mL) and cooled to −20°C, whereupon $NaBH_4$ (0.16 g, 4.1 mmol) was added in one portion. The reaction was slowly warmed to 0°C, cooled to −20°C, and acidified with 3.5 *N* HCl. Brine (40 mL) was added and the solution extracted with ether (4 × 40 mL). The ether extract was washed with brine (2 × 40 mL), dried ($MgSO_4$), and concentrated to give 0.76 g (87%) of **40**, which was 80% pure by gc when analyzed as the methyl ester (CH_2N_2); ir (film): 3600–2500, 2240, and 1710 cm^{-1}. *Exact Mass* calcd. for ($C_{15}H_{22}O_3$ − CH_3): 235.1334; found: 235.1325.

Preparation of 13-hydroxy-(Z,Z)-5,8-tetradecadienoic acid, 41

Reduction of hydroxy acid **40** (0.66 g, 1.8 mmol) with P-2 nickel (7) gave, after work-up, 0.69 g (73%) of crude **41** whose nmr and mass spectra matched those previously reported (9).

1. J. H. Borden, M. C. Dolinski, L. Chong, V. Verigin, H. D. Pierce, Jr., and A. C. Oehlschlager. Can. Entomol. **111**, 581 (1979).
2. A. M. Pierce, J. H. Borden, and A. C. Oehlschlager. Can. J. Zool. **59**, 1980 (1981).
3. J. W. Wong, V. Verigin, A. C. Oehlschlager, J. H. Borden, H. D. Pierce, Jr., A. M. Pierce, and L. Chong. J. Chem. Ecol. **9**, 451 (1983).
4. A. M. Pierce, H. D. Pierce, Jr., J. H. Borden, and A. C. Oehlschlager. J. Agric. Biol. Chem. **33**, 848 (1985); J. G. Millar, H. D. Pierce, Jr., A. M. Pierce, A. C. Oehlschlager, and J. H. Borden. J. Chem. Ecol. **11**, 1071 (1985); J. G. Millar, H. D. Pierce, Jr., A. M. Pierce, A. C. Oehlschlager, J. H. Borden, and A. C. Barak. J. Chem. Ecol. **11**, 1053 (1985).
5. H. D. Pierce, Jr., A. M. Pierce, J. G. Millar, J. W. Wong, V. G. Verigin, A. C. Oehlschlager, and J. H. Borden. Proc. 3rd International Working Conference on Stored-Product Entomology. Manhattan, Kansas, 1984. p. 121.
6. A. M. Pierce, H. D. Pierce, Jr., J. G. Millar, J. H. Borden, and A. C. Oehlschlager. Proc. 3rd International Working Conference on Stored-Product Entomology. Manhattan, Kansas, 1984. p. 107.
7. J. G. Millar, A. C. Oehlschlager, and J. W. Wong. J. Org. Chem. **48**, 4404 (1983).
8. A. C. Oehlschlager, J. W. Wong, V. G. Verigin, and H. D. Pierce, Jr. J. Org. Chem. **48**, 5009 (1983)
9. J. G. Millar and A. C. Oehlschlager. J. Org. Chem. **49**, 2332 (1984).
10. L. Brandsma. Preparative acetylenic chemistry. Elsevier Publishing Company, Amsterdam, London, New York. 1971.
11. H. Hommes and L. Brandsma. Recl. Trav. Chim. Pays-Bas, **96**, 160 (1977); S. R. Abrams. Can. J. Chem. **62**, 1333 (1984); M. M. Midland, R. L. Halterman, C. A. Brown, and A. Yamaichi. Tetrahedron Lett. 4171 (1981).
12. C. E. Bishop and G. W. Marow. J. Org. Chem. **48**, 657 (1983); E. V. Dehmlow and M. Lissel. Tetrahedron, **37**, 1653 (1981).
13. E. J. Corey, J.-L. Gras, and P. Ulrich. Tetrahedron Lett. 809 (1976).
14. K. C. Nicolaou, N. A. Petasis, W. S. Li, T. Ladduwahetty, J. L. Randall, S. E. Webber, and P. E. Hernandez. J. Org. Chem. **48**, 5400 (1983).
15. J. Hooz and S. S. H. Gilani. Can. J. Chem. **46**, 86 (1968).
16. B. C. Holland and N. W. Gilman. Synth. Commun. **4**, 203 (1974).
17. B. D. Johnston and A. C. Oehlschlager. J. Org. Chem. **47**, 5384 (1982).
18. K. Utimoto, C. Lambert, Y. Fukuda, H. Shiragami, and H. Nozaki. Tetrahedron Lett. **25**, 5423 (1984).

A CIDEP study of the photooxidation of benzoquinone in trifluoroacetic acid

MARJORY T. CRAW, M. CATHERINE DEPEW, AND JEFFREY K. S. WAN[1]
Department of Chemistry, Queen's University, Kingston, Ont., Canada K7L 3N6

Received October 1, 1985

MARJORY T. CRAW, M. CATHERINE DEPEW, and JEFFREY K. S. WAN. Can. J. Chem. **64**, 1414 (1986).

The combined techniques of electron spin resonance and CIDEP have been used to probe the reactions of 1,4-*p*-benzoquinone in trifluoroacetic acid. The results led to the establishment of two distinct mechanisms, a thermal and a photochemical pathway, for the formation of the one-electron oxidized species in this solvent. In addition it has also been found that by using time-resolved CIDEP the neutral 1,4-*p*-benzohydroquinone radical may be readily observed under various conditions.

MARJORY T. CRAW, M. CATHERINE DEPEW et JEFFREY K. S. WAN. Can. J. Chem. **64**, 1414 (1986).

On a fait appel à une combinaison de techniques de résonance paramagnétique électronique et CIDEP pour étudier les réactions de la benzoquinone-1,4 dans l'acide trifluoroacétique. Les résultats tendent à suggérer l'existence de deux mécanismes distincts, une voie thermique et une autre photochimique, pour la formation des espèces oxydées par un électron que l'on retrouve dans ce solvant. De plus, l'utilisation de la technique CIDEP résolue en fonction du temps permet d'observer facilement le radical benzohydroquinone-1,4 dans ces conditions.

[Traduit par la revue]

Introduction

Thermal and photoredox reactions involving benzoquinones have long been the subject of considerable general interest (1, 2). The intermediates in many of these reactions are commonly referred to as "semiquinones," which include the neutral and charged forms. Of the charged semiquinone radicals, the radical anion is readily observed by both optical and esr (electron spin resonance) spectroscopy; the corresponding one-electron oxidized species have, however, been more difficult to observe and are thought to be stable only in strongly acidic media (3, 4). Thus, trifluoroacetic acid, TFA, generally acknowledged for its ability to solvate and stabilize organic cations due to its acidity and low nucleophilicity (5, 6), has been used in this laboratory for the time-resolved CIDEP[2] studies of organic radical cations (7–9). Both a theoretical investigation (10) and an experimental study (7, 11) have concluded that the major stabilization effect arises from an interaction of the trifluoromethyl group and the organic cation.

The photochemical formation of polarized benzoquinone radical cations in TFA has been used as a model system for the charge transfer process involving heterocyclic sulfur-containing compounds (8). It was confirmed that secondary polarization observed in the radical cations of heterocyclic sulfur compounds resulted directly from the rapid charge transfer process:

$$BQ^{\ddagger} * + S \rightarrow BW + S^{\ddagger} *$$

An alternate, direct primary photochemical process such as

$$^3BQ^* + S \rightarrow \dot{S}^+ * + BQ^{\dot{-}} *$$

is unlikely, as the resultant $BQ^{\dot{-}} *$ radical anion was never observed in these systems. It was also clear that the primary polarized benzoquinone radical species is the radical cation, since neither a neutral nor an anion radical could lead to a charge transfer process resulting in the formation of the sulfur radical cation.

While the polarized benzoquinone radical cation in TFA provided a model system for CIDEP study of charge transfer reactions, the mechanism for the thermal and photochemical production of the radical cation in TFA remained unresolved. Because of the great deal of general interest in the radical cation studies in TFA, we have systematically investigated the photooxidation of benzoquinone in TFA and related solvents by the combination of esr and time-resolved CIDEP methods.

The results provide some insight into the complex mechanism for the formation of the benzoquinone radical cation in trifluoroacetic acid. It was further unambiguously established that the trifluoroacetyl moiety served only to enhance the stabilization of the radical cation and was not involved in the formation steps. These conclusions will be of great interest to organic reactions in TFA in general.

Experimental

Benzoquinone was supplied by Aldrich and repeatedly recrystallized from ethanol and sublimed before use. Trifluoroacetic acid was obtained from Alfa Chemicals. All other chemicals were reagent grade and used without further purification. All samples were purged with oxygen-free nitrogen before experimentation.

For the variable temperature studies, oxygen was evacuated from the samples by the freeze-thawing technique. The esr spectra were recorded on a Varian E3 spectrometer with a variable temperature control accessory. The samples were irradiated inside the cavity using a 200-W super pressure mercury arc lamp. CIDEP experiments were also conducted on the Varian E3 spectrometer using a 1-MW Molectron N_2 laser; the CIDEP transients were directly detected without modulation using a Hewlett Packard wide-band preamplifier and a Princeton Applied Research model 162 boxcar integrator. The polarization spectra were then displayed and stored on a Nicolet microcomputer-controlled oscilloscope connected to a Hewlett Packard 7475A digital plotter. In some cases the microwave signal was increased to a significant extent by using a "homemade" amplifier that essentially magnified the microwave signal prior to modulation and utilized a Narda solid-state GaAs preamplifier narrowly tuned to the cavity frequency.

Kinetic measurements were carried out using the Nicolet computer oscilloscope, the intensity of the esr signal being monitored before, during, and after irradiation. The decay rates of the radicals were calculated assuming pseudo-first-order kinetics.

Results and discussion

When a solution of benzoquinone (BQ) in TFA was placed in the cavity of the esr spectrometer at room temperature, a fairly weak signal consisting of 5 lines was observed. Photolysis of this solution resulted in an increase in the signal intensity; the *g* factor and hyperfine splitting constant were the same as those observed thermally. The splitting pattern is indicative of a

[1]Author to whom correspondence may be addressed.

[2]CIDEP: chemically induced dynamic electron polarization.

1:4:6:4:1 quintet, consistent with the formation of a radical with 4 equivalent protons. The proposed structure of this species is that shown (**1**), with the unpaired electron being delocalized over the whole π system.

1

The g factor (2.0040) and splitting constant (a_H = 2.22 G) measured for this species are very similar to those reported previously (12) for the radical anion, i.e. g = 2.0046 and a_H = 2.36 G, suggesting that, as with the anion (13), the cation has a quininoid structure with planar geometry. The assignment of **1** was further supported by an INDO calculation using the structural parameters given by Shinagawa and Shinagawa (13). In addition, benzoquinone-d_4 was synthesized and the radical cation spectrum showed a major single peak with unresolved hyperfines due to the d-atoms.

It is not immediately obvious why the benzoquinone radical cation and the radical anion have such similar proton hyperfine splittings, granted that they are produced in very different media. This point deserves some further examination. We have thus listed in Table 1 all our experimental observations and the standard INDO molecular orbital calculations of all three charged forms of possible paramagnetic intermediates of p-benzoquinone. It is apparent that in all three cases the ring protons have similar hyperfine splittings, which do not seem to be sensitive to the charges they carry. Another example of the insensitivity of splittings of atoms in the ring to the charges is that of phenoxazine (T. S. Liu and J. Retsky, private communication). Since in the case of benzoquinone radicals all the ring protons lie in the nodal plane of the unpaired π-electron, we thought that a more reliable test for differentiating the changes in hyperfine splitting with charge would be the symmetrical 2,5-dimethyl-p-benzoquinone. The experimental observations of both the 2,5-dimethyl-p-benzoquinone radical cation in TFA and the corresponding radical anion in IPA are given in Table 1. Although both have the same hyperfine pattern (septet of triplets), it is clear that the major septet splitting due to the six equivalent methyl protons is substantially different. As well, we should also mention that many of the substituted p-benzoquinones we tested do not form radical cations, although the corresponding radical anions are usually observable in basic medium. These include duroquinone and tetrachloro-p-benzoquinone.

Returning to the esr parameters of p-benzoquinone radicals, it is further worthwhile to point out that the radical cation and the radical anion have rather different relaxation times. In both cw (continuous wave) and time-resolved polarized esr spectra, the line width of the radical cation is several times greater than the corresponding radical anion. This phenomenon is also exhibited by comparing the line width of the phenoxazine radical cation and its neutral counterpart, as well as for the 2,5-dimethyl-p-benzoquinone radical cation and anion systems.

The significant line-broadening effect in the radical cation spectrum observed in TFA is probably caused by the strong interaction of the radical cation with the trifluoromethyl moiety. The phenomenon thus lends further support to the importance of the unique stabilization effect of TFA towards radical cations.

The cw optical spectra of p-benzoquinone in three different solvents, IPA, ethanol with NaOH, and TFA, have also been recorded. In separate esr measurements, the NaOH solution showed a strong signal of the radical anion while the TFA solution exhibited the weaker signal of the radical cation. Although some different appearances in the near uv band around 300 nm are evident in all three different spectra, little conclusion can be drawn in these experiments as the solvent effect in such systems can be dominating.

TABLE 1. Calculated and experimental proton hyperfine splittings (gauss) of p-benzoquinone radical ions

	INDO results	Experimental observations
	a_H = 2.56	a_H = 2.33 (in alcohol)
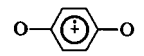	a_H = 2.14	a_H = 2.22 (in TFA)
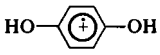	a_H = 1.67 a_{OH} = 5.08	a_H = 2.24 a_{OH} = 5.08 (in H_2SO_4)
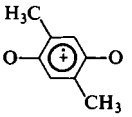	—	a_{CH3} = 3.30 a_H = 0.90 (in TFA)
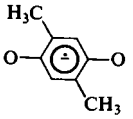 [a]	—	a_{CH3} = 2.30 a_H = 1.70 (in water)

[a]Taken from ref. 19.

The presence of the benzoquinone radical cation was further established by chemical evidence given below. When photolysis ceased, the photochemically generated signal decayed to an intensity similar to that detected before irradiation. The rate constant for this decay was calculated as 3.83×10^3 s^{-1}, assuming pseudo-first-order kinetics. However, when the temperature was raised in stages from 23 to 60°C the thermal signal intensity increased more than sevenfold, reflecting the increasing radical steady-state concentration.

When the solvent was changed from TFA to acetic acid, no signal was observed before photolysis. Irradiation of this sample resulted in the observation of only the neutral semiquinone radical (**2**) (14), with splitting constants as shown.

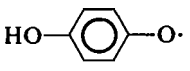

$a_H ortho$ = 5.11 G
$a_H meta$ = 0.28 G
a_{OH} = 1.79 G

2

Although the radical cation may possibly form, it may not persist long enough for cw observation due to a lack of solvent stabilization. On the other hand, if the radical species observed in TFA was to be assigned to the unlikely radical anion, there would have been no reason at all why the same radical anion could not be observed in acetic acid. The photochemical production of the neutral semiquinone radical can be accounted for by the triplet abstraction from the methyl group of acetic acid.

In time-resolved CIDEP experiments with benzoquinone in TFA, the broadened polarized radical cation spectrum observed is given in Fig. 1. The strong, totally emissive polarization is characteristic of the photochemical triplet mechanism but a minor contribution of E/A polarization from the radical pair mechanism is clearly evident. Thus, the low-field lines are

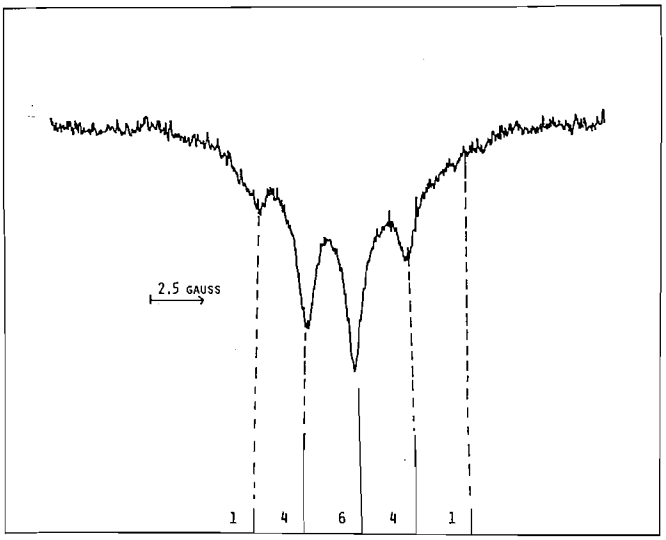

FIG. 1. The polarization spectrum of the 1,4-*p*-benzoquinone radical cation ($B\dot{Q}^+$) in TFA recorded 1.0 μs after the laser flash.

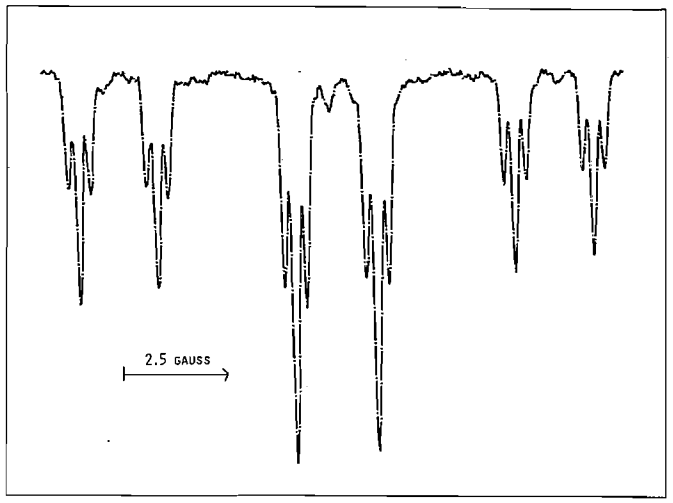

FIG. 2. The polarization spectrum of the neutral radical of 1,4-*p*-benzoquinone ($B\dot{Q}H$) in CH_3COOH/IPA recorded 1.0 μs after the laser flash.

relatively stronger in emission than the high field lines. The "thermalized" radicals produced simultaneously during the CIDEP experiments are not detected in the time-resolved observations. A simple mechanism, which can account for both the thermal and photochemical observations involving oxidation of benzoquinone in TFA, can be represented by the following:

[1] $BQ + CF_3COOH \rightleftharpoons BQH^+ + CF_3COO^-$

[2] $BQ + BQH^+ \xrightarrow{\Delta} B\dot{Q}^+ + B\dot{Q}H$

[3] $BQ + h\nu \rightsquigarrow {}^3BQ^*$ (*denotes spin polarization)

[4] ${}^3BQ^* + BQH^+ \longrightarrow B\dot{Q}^{+}* + B\dot{Q}H^*$

[5] $B\dot{Q}H^* + H^+ \longrightarrow B\dot{Q}H_2^+$

Benzoquinone, having two reactive carbonyl groups, is likely to undergo some degree of protonation at thermal equilibrium:

$$\rangle C{=}O + H^+ \rightleftharpoons \rangle \overset{+}{C}{-}OH$$

As well, protonation can also occur at the quininoid ring. Thus, Davies and co-workers (16) have proposed the intermediacy of a carbenium ion in the photolysis of cyclopentadiene derivatives in TFA. Once formed, this species is thought to rapidly lose a hydrogen atom to form the cyclopentadienyl radical cation.

In the thermal oxidation of benzoquinone in TFA, reaction [2] may involve either a hydrogen atom transfer from BQH^+ to BQ or a direct charge transfer between the two. Since the product radicals are the same and the thermal radicals do not exhibit CIDEP, we are not able to distinguish the detailed step involved. It is obvious that reaction [2] is endothermic but the activation energy barrier may not have to be substantial, since the reactants and the products are almost structurally degenerate. Nevertheless, the thermal reaction [2] is indeed temperature dependent, as evidenced by the experimental results. While the $B\dot{Q}^+$ would be stabilized by the trifluoromethyl moiety, the companion neutral semiquinone radical $B\dot{Q}H$ decayed rapidly in acidic medium (17).

In the photochemical oxidation, reaction [3] involved the intersystem crossing to the triplet sublevels of benzoquinone, ${}^3BQ^*$, causing the spin polarization to be in the emissive mode (15). Subsequent reaction of the polarized triplet in reaction [4] will conserve the spin polarization in the primary radicals, provided the reaction is faster or comparable to the triplet spin lattice relaxation, which is normally in the nanosecond region in liquid medium. Again, *we are not able to distinguish whether reaction [4] is a charge transfer or a H atom abstraction process*. The counter radical, $B\dot{Q}H^*$, was not evident in the "integrated" time-resolved CIDEP spectrum (Fig. 1), although in the benzoquinone-d_4 experiments a minor triplet component due to the dihydroxysemiquinone radical cation, **3**, became observable. The formation of **3**,

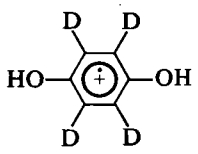

3

can be accounted for in reaction [5].

In order to confirm the necessary protonation step in reaction [1] and the role of the trifluoroacetyl group, experiments were conducted with BQ in trifluoroacetic anhydride [$(CF_3CO)_2$] instead of TFA. In this case we could not detect any esr signal at all before or after irradiation, but by adding one drop of water to the sample the esr spectrum corresponding to the benzoquinone radical cation was immediately observed. This clearly shows that this reaction requires hydrogen ions in solution and not merely the presence of the trifluoroacetyl moiety. On the other hand, when formic acid was used as solvent, *no thermal signal was detected*. During photolysis a relatively weaker cw and polarized radical cation spectrum was observed. The rate of decay of the $B\dot{Q}^+$ in formic acid was measured as $1.03 \times 10^4\ s^{-1}$, some three times faster than that observed in TFA. Thus, formic acid is capable of protonating the quinone; however, the difference in the decay rate of the radical cation in this solvent and in TFA suggests that the cation radical is considerably more stable in the presence of CF_3COO^-. This agrees well with results we obtained previously where it was found that as one descends the series CF_3COOH, CF_2COOH, and CFH_2COOH stabilization of radical cations decreases (7).

The photochemical observation of $B\dot{Q}^+$ in both TFA and formic acid and not in acetic acid may be accounted for by the

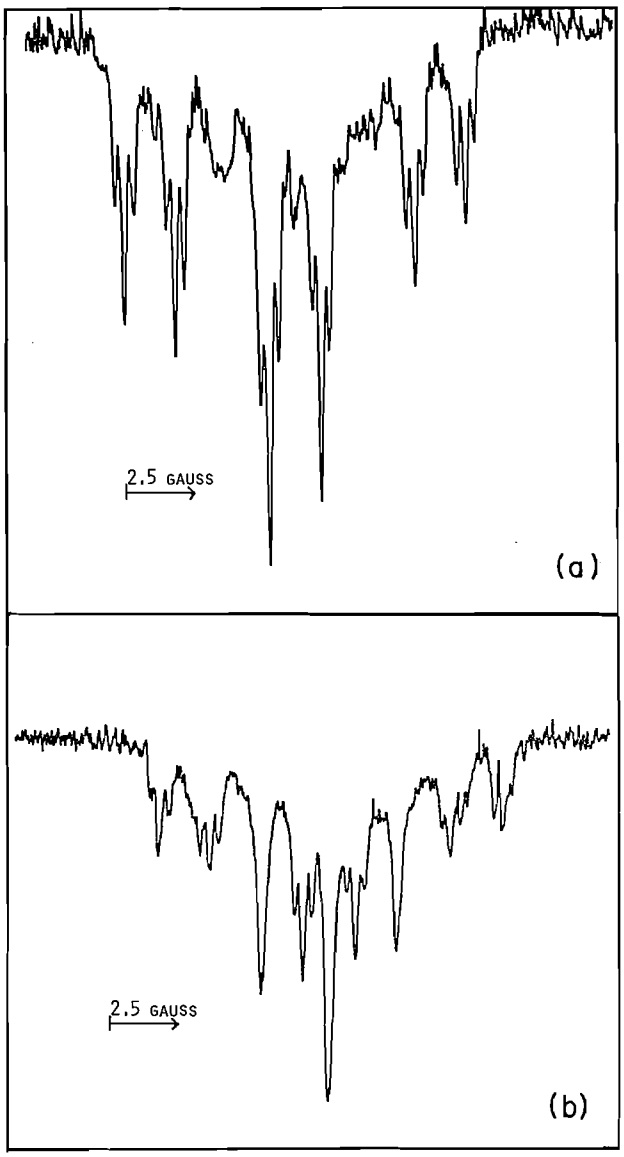

FIG. 3. The polarization spectrum of 1,4-*p*-benzoquinone in ethanol recorded (a) 0.5 μs and (b) 1.5 μs after the laser flash; see text.

somewhat lower p*K*a values of the former two acids and the lack of stabilization of $B\dot{Q}^+$ in acetic acid. The inability to observe polarization from $B\dot{Q}H$ in acetic acid may result from a decrease in the rate of $\dot{H}$ abstraction in this solvent compared with, for example, isopropyl alcohol. Indeed, if the solvent used consists of a 1:1 mixture of acetic acid/isopropyl alcohol intense emissive polarization (Fig. 2) corresponding to the neutral hydroquinone radical is observed. The slower rate of H abstraction in acetic acid relative to alcohol solvents may be explained in terms of a switching of the lowest lying excited states to the π,π^* character (1, 18). The observation of such an intense polarization signal for the neutral hydroquinone radical was rather surprising since this species is not very stable and was difficult to observe in the conventional esr experiment.

We have conducted further CIDEP experiments with BQ in ethanol solvent. The polarization spectra obtained for this system 0.5 μs and 1.5 μs after the laser pulse are shown in Figs. 3. As may be seen, only the neutral semiquinone radical is observed after 0.5 μs, whereas increasing the delay time led to a spectrum that becomes the superposition of two species, the neutral semiquinone and $BQ^{\dot{-}}$, suggesting that in this case the neutral radical is the precursor to the anion radical.

It is rather satisfying that in the laboratory one can indeed control the experimental conditions to yield CIDEP spectra of all the three forms of the benzoquinone radicals: the neutral semiquinone radical, the benzoquinone radical anion, and the benzoquinone radical cation. The present study of the oxidation of 1,4-*p*-benzoquinone provides a model system for which further investigations of structurally similar molecules, particularly those of biological significance such as vitamin K and vitamin E, will be developed.

Acknowledgements

This research was supported by the Natural Sciences and Engineering Research Council of Canada.

1. D. R. KEMP and G. PORTER. Proc. R. Soc. London, A, **326**, 117 (1971).
2. R. A. MORTON (*Editor*). Biochemistry of quinones. Academic Press, New York, NY. 1965.
3. J. R. BOLTON and A. CARRINGTON. Proc. Chem. Soc. 385 (1962).
4. J. R. BOLTON, A. CARRINGTON, and J. DOS SANTOS-VEIGA. Mol. Phys. **5**, 465 (1962).
5. J. E. NORLANDER and W. E. KELLY. J. Am. Chem. Soc. **91**, 996 (1969).
6. T. W. BENTLY, F. L. SCHADT, and P. SCHLEYER. J. Am. Chem. Soc. **94**, 992 (1974).
7. M. C. DEPEW, L. ZHONGLI, and J. K. S. WAN. Spectrosc. Lett. **16**, 451 (1983).
8. M. C. DEPEW, L. ZHONGLI, and J. K. S. WAN. J. Am. Chem. Soc. **105**, 2480 (1983).
9. M. T. CRAW, M. C. DEPEW, and J. K. S. WAN. Phosphorus Sulfur. 1985. In press.
10. J. J. DANNENBERG. Agnew. Chem. Int. Ed. Engl. **14**, 641 (1975).
11. U. SVANHOLM and V. D. PARKER. Tetrahedron Lett. 471 (1972).
12. K. SCHEFFLER and H. B. STEGMAN. Ber. Bunsenges. Physik. Chem. **67**, 864 (1963).
13. Y. SHINAGAWA and Y. SHINAGAWA. J. Am. Chem. Soc. **100**, 67 (1978).
14. T. E. GOUGH. Trans. Far. Soc. **1**, 2321 (1966).
15. M. C. DEPEW and J. K. S. WAN. Magn. Reson. Rev. **8**, 85 (1983).
16. J. L. COURTNEIDGE, A. G. DAVIES, and S. N. YAZDI. J. Chem. Soc. Chem. Commun. 570 (1984).
17. E. J. LAND and G. PORTER. Proc. Chem. Soc. 84 (1960).
18. D. HOLTON and D. MURPHY. J. Chem. Soc. Faraday Trans. 1, **78**, 1223 (1982).
19. J. A. PEDERSEN. J. Chem. Soc. Perkin Trans. 2, 424 (1973).

Electrochemical nucleation in the electroreduction of silver(I) from molten calcium nitrate tetrahydrate

SURENDER K. JAIN[1] AND KEITH E. JOHNSON[2]

Department of Chemistry, University of Regina, Regina, Sask., Canada S4S 0A2

Received February 26, 1985[3]

SURENDER K. JAIN and KEITH E. JOHNSON. Can. J. Chem. **64**, 1418 (1986).

The electroreduction of silver(I) on a platinum electrode from its solution in molten calcium nitrate tetrahydrate has been studied using voltammetric, chronopotentiometric, and chronoamperomeric techniques. The early stages of metal deposition appear to be controlled by a nucleation step as indicated by potential overshoots in chronopotentiometric and maxima in chronoamperometric transients. From the rising portion of the current–time transients, the number-density of the surface nuclei has been estimated. Diffusion coefficients calculated from the data obtained from different techniques are in good agreement.

SURENDER K. JAIN et KEITH E. JOHNSON. Can. J. Chem. **64**, 1418 (1986).

Utilisant des techniques voltamétriques, chronopotentiométriques et chronoampérométriques, on a étudié l'électro-réduction de l'argent(I) sur une électrode de platine à partir de sa solution dans du nitrate de calcium tétrahydraté, à l'état fondu. Il semble que les premières étapes de la déposition du métal sont controlées par une étape de nucléation qui est indiquée par des excès de potentiel dans la chronopotentiométrie et par des maxima dans les espèces transitoires de la chronoampérométrie. En se basant sur la portion qui augmente des espèces transitoires de la courbe du courant en fonction du temps, on a pu évaluer la densité numérique des noyaux de surface. Les coefficients de diffusion qui ont été calculés à partir des données obtenues à l'aide de ces diverses techniques sont en bon accord.

[Traduit par la revue]

Introduction

Physico-chemical studies of hydrated melts have been reported over recent years by various workers (1–11). Braunstein *et al.* (12) reported the polarographic diffusion coefficients of Cd^{2+} in aqueous nitrate melts. Moynihan and Angell (13) measured the diffusion coefficients of Ag^+, Tl^+, and Cd^{2+} in molten calcium nitrate tetrahydrate by chronopotentiometry using a mercury pool electrode for Tl^+ and Cd^{2+} and a platinum foil electrode for Ag^+. Lovering (14, 15) for the first time studied systematically the electro-reduction of a large number of inorganic cations in a variety of molten hydrates and reported their polarographic half-wave potentials and diffusion coefficients.

Recently, Bansal and Plambeck (16, 17), have investigated the electrochemical reduction of various cations in molten calcium nitrate tetrahydrate using chronopotentiometric and cyclic voltammetric techniques. These authors have also studied the reduction of Ag^+, Tl^+, and Cd^{2+} by ac chronopotentiometry (18). It is noticeable that while the authors presented ac and dc chronopotentiograms for Tl^+ and Cd^{2+}, only the ac chronopotentiogram was included for the reduction of Ag^+. Moynihan and Angell (13) did not report any abnormality in the potential–time transients for the reduction of Ag^+ on a platinum electrode. These observations prompted us to investigate in detail the electroreduction of Ag^+ from its solutions in molten calcium nitrate tetrahydrate. Our results concerning electroreduction of Ag^+ on a platinum electrode using voltammetric, chronopotentiometric, and chronoamperometric techniques, presented in this paper, show that the electrodeposition of silver from molten calcium nitrate tetrahydrate involves the formation and growth of nuclei in the early stages of the reaction, i.e. before a uniform deposit has been formed over the electrode surface.

Experimental

Calcium nitrate tetrahydrate (BDH, AnalaR) and silver nitrate (Shawinigan Reagent) were used without further purification. The gravimetric analysis of calcium nitrate hydrate gave the water-to-salt mole ratio as 4.00 ± 0.005. Densities of the melt corresponding to this composition were obtained from the works of Ewing and Mikovsky (19). About 140 g of the melt were used for each experiment. As the solubility of oxygen in this melt is negligible (13, 16), no precaution was taken to exclude air from the system, save for tightly capping the cell to avoid loss of water.

The cell containing the melt was kept immersed in an oil bath thermostated to ± 0.1°C. The bath stirrer was turned off to avoid mechanical vibrations only during the measurements. The working electrode consisted of a 0.5 mm diameter bright platinum wire sealed into a 6 mm diameter soda–lead glass tubing so that about 9 mm length of wire protruded from the seal. The exact length and diameter were measured by optical micrometry. The auxiliary electrode was a platinum flag of large area and the reference electrode was a 0.8 mm diameter silver wire loosely coiled at one end and immersed in a silver nitrate (0.05 mol kg^{-1}) solution in molten calcium nitrate tetrahydrate held in a fritted glass tube. All electrochemical work was done using a PAR Electrochemical system (model 170) and x-y recorder (Houston Instruments-Type 2000).

After each scan, the electrode was held at an anodic potential for a few minutes to strip off the deposited metal and the solution stirred well before recording the next scan. Each scan was repeated at least twice.

Results

Linear sweep and cyclic voltammetry

The theoretical treatment of linear sweep voltammetry for the electrode processes involving the reversible deposition of a soluble or insoluble product is available (20). Berzins and Delahay (21) treated the case where reversible charge transfer resulted in the deposition of an insoluble product. From their treatment it can be shown that the peak current (i_p) for the reversible deposition of an insoluble metal at any temperature is given by the equation

$$[1] \quad i_p = 6346\, n^{3/2} A C D^{1/2} v^{1/2} T^{-1/2}$$

where i_p is the peak current in amperes, n is the number of electrons involved in the charge transfer process, A is the area of the electrode in cm^2, C is the concentration (mol L^{-1}), D is the diffusion coefficient ($cm^2\ s^{-1}$), and v is the voltage scan rate ($V\ s^{-1}$).

[1]On leave from Hindu College, University of Delhi, Delhi-110007, India.

[2]To whom all correspondence should be addressed.

[3]Revision received February 10, 1986.

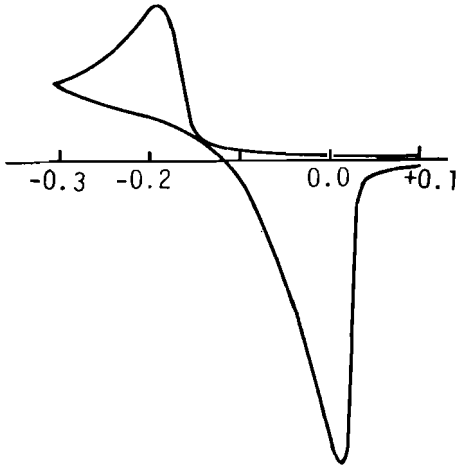

FIG. 1. A typical cyclic voltammogram for Ag^+ in molten calcium nitrate tetrahydrate at 30.7°C. Scan rate: 100 mV s^{-1}; $C_{Ag+} = 15.72 \times 10^{-3}$ mol/L. X axis values are in volts against Ag/Ag^+ (0.05 mol kg^{-1}) reference electrode.

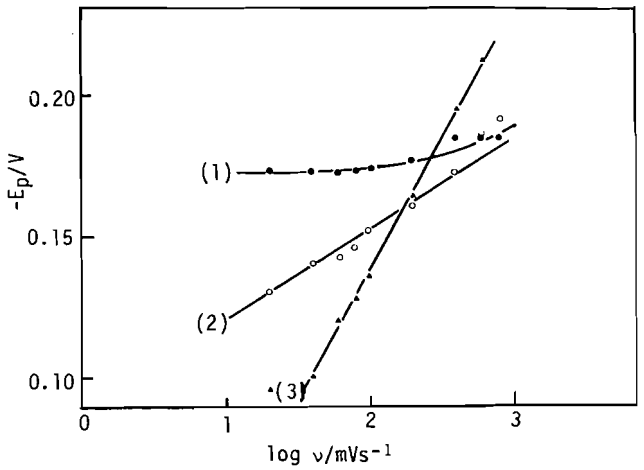

FIG. 2. Plots of E_p vs. log v for the voltammetric reduction of Ag^+ at 55°C. C_{Ag+}: (*1*) 2.62×10^{-3}; (*2*) 15.72×10^{-3}; (*3*) 58.17×10^{-3} mol L^{-1}.

Assuming that the activity of the deposited metal remains constant and equal to unity, the peak (20, 21) and half-peak (22) potentials are given by:

$$[2] \quad E_p = E^0 + \frac{RT}{nF} \ln fC - \frac{0.854RT}{nF}$$

$$[3] \quad R_{p/2} = E^0 + \frac{RT}{nF} \ln fC - \frac{0.0815RT}{nF}$$

where f is the activity coefficient of the solute and all other terms have their usual significance.

Combining eqs. [2] and [3], one can write,

$$[4] \quad \Delta E = E_p - E_{p/2} = -\frac{0.7725RT}{nF}$$

Thus, the peak and half-peak potentials depend upon the concentration of the electroactive species, and would shift to more positive (anodic) values with an increase in solute concentration. The difference, $E_p - E_{p/2}$ ($= \Delta E$) on the other hand is independent of the concentration. For a reversible process, E_p, $E_{p/2}$, and ΔE are independent of the scan rate.

A typical cyclic voltammogram for the reduction of Ag^+ from its solution in molten calcium nitrate tetrahydrate at 55°C is presented in Fig. 1. It illustrates two important features, namely the unusually steep rise in current as the cathodic peak potential is approached and the equally sharp fall in current after the anodic peak. This latter characteristic is consistent with the stripping of an insoluble deposit from the electrode surface. The anodic peak current exceeds that for the cathodic process, being simply a function of the reversal potential, but within measurable limits the quantities of charge involved in cathodic and anodic half-cycles are always the same. However, the rising part of the cathodic peak is too steep and the peak potential is at too cathodic a value relative to the reversible potential for a simple diffusion-controlled process. In the multicyclic runs, the peak potentials for the reduction process in the subsequent cycles shift to more anodic values.

The peak and half-peak potentials were estimated from the recorded voltammograms and presented in Table 1. The peak and half-peak potentials for the reduction process showed a cathodic shift with an increase in the scan rate while the anodic peak potential remained practically unaltered. However, at low

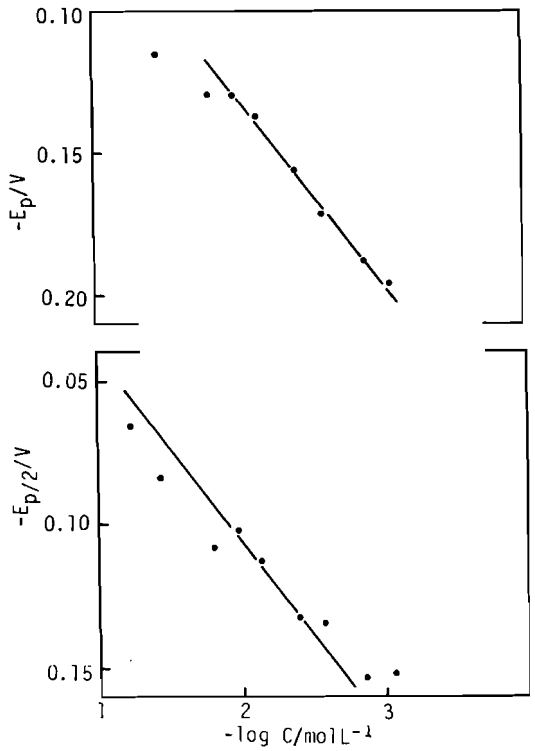

FIG. 3. $E_{p/2}$ and E_p shown as a function of log C for voltammetric reduction of Ag^+ at 55°C. Sweep rate 20 mV s^{-1}.

concentration E_p and $E_{p/2}$ remained virtually constant over the scan rate 20–200 mV s^{-1}. The differences $E_p - E_{p/2}$ showed a considerable scatter but were in the vicinity of 40 ± 20 mV as compared to the theoretical value of 21.8 mV calculated from eq. [4] for a one-electron process at 55°C. The variation of E_p with scan rate does not obey any simple relationship. However, the linear dependence of E_p on log v predicted for an irreversible process is evident at higher concentrations (Fig. 2). Although the peak and half-peak potentials shifted to more anodic values with an increase in the concentration of Ag^+ at any given scan rate, the plots of $E_{p/2}$ and E_p vs. log C resulted in straight lines with the theoretical slopes predicted by eqs. [2] and [3] only at low scan rates. Typical plots for the reduction of silver at a scan rate of 20 mV s^{-1} are shown in Fig. 3. At higher scan rates, the straight line plots exhibited lesser slopes. The

TABLE 1. E_p, $E_{p/2}$, and ΔE as a function of sweep rate for the reduction of Ag^+ in molten calcium nitrate tetrahydrate at 328.1 K

Scan rate/mV s^{-1}	E_p/V	$E_{p/2}$/V	ΔE/V	E_p/V	$E_{p/2}$/V	ΔE/V
		0.86 m*M*			1.30 m*M*	
20	−0.196	−0.152	−0.044	−0.188	−0.152	−0.036
40	−0.204	−0.156	−0.048	−0.192	−0.152	−0.040
60	−0.208	−0.152	−0.056	−0.196	−0.152	−0.044
80	−0.208	−0.152	−0.056	−0.196	−0.152	−0.044
100	−0.212	−0.156	−0.056	−0.200	−0.152	−0.048
200	−0.220	−0.162	−0.058	−0.200	−0.152	−0.048
300	−0.220	−0.172	−0.048	−0.212	−0.158	−0.054
400	—	—	—	−0.212	−0.160	−0.052
		2.62 m*M*			3.86 m*M*	
20	−0.172	−0.134	−0.038	−0.156	−0.132	−0.024
40	−0.172	−0.134	−0.038	−0.160	−0.133	−0.027
60	−0.172	−0.134	−0.038	−0.168	−0.136	−0.032
80	−0.172	−0.134	−0.038	−0.170	−0.136	−0.034
100	−0.174	−0.134	−0.040	−0.180	−0.138	−0.042
200	−0.176	−0.134	−0.042	−0.180	−0.138	−0.042
300	−0.180	−0.136	−0.044	−0.185	−0.139	−0.046
400	−0.184	−0.136	−0.048	−0.188	−0.138	−0.050
500	−0.184	−0.136	−0.048	−0.188	−0.142	−0.046
600	−0.184	−0.137	−0.047	−0.192	−0.156	−0.036
800	−0.184	−0.146	−0.038	−0.192	—	—
		7.19 m*M*			10.46 m*M*	
20	−0.138	−0.112	−0.026	−0.130	−0.102	−0.028
40	−0.140	−0.112	−0.028	−0.134	−0.108	−0.026
60	−0.144	−0.116	−0.028	−0.138	−0.108	−0.030
80	−0.154	−0.122	−0.032	−0.144	−0.118	−0.026
100	−0.156	−0.124	−0.032	−0.156	−0.123	−0.033
200	−0.164	−0.126	−0.038	−0.162	−0.125	−0.037
300	−0.172	−0.128	−0.044	−0.168	−0.124	−0.044
400	−0.180	−0.132	−0.048	−0.176	−0.128	−0.048
500	−0.188	−0.134	−0.054	−0.176	−0.128	−0.048
600	−0.188	−0.133	−0.055	−0.178	−0.128	−0.050
800	−0.188	−0.134	−0.054	−0.184	−0.136	−0.048
1000	−0.188	—	—	—	—	—
		15.72 m*M*			36.03 m*M*	
20	−0.130	−0.108	−0.022	−0.116	−0.084	−0.032
40	−0.140	−0.112	−0.028	−0.128	−0.090	−0.038
60	−0.142	−0.112	−0.030	−0.132	−0.094	−0.038
80	−0.146	−0.112	−0.034	−0.138	−0.096	−0.042
100	−0.152	−0.095	−0.057	−0.140	−0.100	−0.040
200	−0.160	−0.114	−0.046	−0.160	−0.103	−0.057
300	−0.168	−0.118	−0.050	−0.176	−0.120	−0.056
400	−0.172	−0.118	−0.054	−0.184	−0.128	−0.056
500	−0.180	−0.121	−0.059	−0.192	−0.140	−0.052
600	−0.185	−0.126	−0.059	−0.220	−0.152	−0.068
800	−0.190	−0.121	−0.069	−0.212	−0.160	−0.074
1000	—	—	—	−0.234	−0.160	−0.074
		58.17 m*M*				
20	−0.096	−0.066	−0.030			
40	−0.111	−0.072	−0.039			
60	−0.120	−0.076	−0.044			
80	−0.128	−0.080	−0.048			
100	−0.136	−0.084	−0.052			
200	−0.164	−0.096	−0.068			
300	−0.180	−0.106	−0.074			
400	−0.194	−0.112	−0.082			
500	−0.206	−0.128	−0.078			
600	−0.212	−0.142	−0.070			
800	−0.256	−0.168	−0.088			
1000	−0.268	−0.178	−0.090			

*Concentrations are expressed on the molar scale. Pt-wire electrode area = 0.1379 cm^2.

TABLE 2. Diffusion coefficients of Ag^+ in molten calcium nitrate tetrahydrate as a function of concentration (at 328.1 K), obtained from different methods

	Voltammetric	Chronopotentiometric	Chronoamperometric
$10^3\ C$/mol L^{-1}	$10^7\ D_{Ag+}$ /cm^2 s^{-1}	$10^7\ D_{Ag+}$ /cm^2 s^{-1}	$10^7\ D_{Ag+}$ /cm^2 s^{-1}
0.86	2.4	—	—
1.30	3.4	—	—
2.62	3.5	—	—
3.86	5.0	—	—
7.19	4.9	—	—
9.15	—	3.2	—
10.46	4.7	—	—
15.72	5.0	—	—
17.08	—	4.6	—
26.45	—	4.5	2.8
36.03	5.5	—	—
42.08	—	4.5	3.1
58.17	6.0	—	—

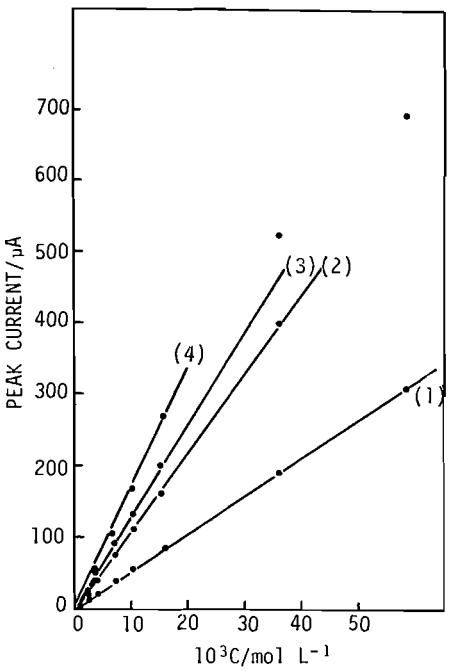

FIG. 4. Voltammetric peak current (i_p) shown as a function of concentration at various sweep rates: (*1*) 20; (*2*) 100; (*3*) 200; (*4*) 400 mV s^{-1}.

peak current (i_p) versus $v^{1/2}$ plots (not shown) for different Ag^+ concentrations were linear only up to a scan rate of about 200 mV s^{-1}, as is to be expected for a simple diffusion-controlled process. At all concentrations above this scan rate negative deviations were observed.

The i_p vs. concentration plots were linear (Fig. 4) in the low concentration region and up to a sweep rate of about 400 mV s^{-1}. The diffusion coefficients of Ag^+ were evaluated from the linear part of the i_p vs. $v^{1/2}$ plots. The calculated values are recorded in Table 2.

It was shown by Mamantov *et al.* (22) that for a reversible deposition of an insoluble substance at the electrode surface, the plot of log $(i_p - i)$ vs. E approaches linearity in the approximate range $(0.5–0.9)i_p$ with a slope equal to $2.2nF/RT$. The present results show that while such a correlation is found to hold good at low sweep rates, the range of linearity of such plots is very narrow at higher sweep rates. A typical set of data is presented in Fig. 5 to illustrate this point.

TABLE 3. Diffusion coefficients of Ag^+ at various temperatures in molten calcium nitrate tetrahydrate obtained from voltammetric data; concentrations of $Ag^+ = 15.72 \times 10^{-3}$ mol L^{-1}

T (K)	$10^7\ D_{Ag+}$
303.9	1.2
313.7	1.9
328.1	4.9
343.1	9.6

E_D (Arrhenius equation) = 47.7 kJ mol^{-1}

In view of the experimental evidence presented here, it can be concluded that some other factor, kinetic or otherwise, is involved in the reduction of Ag^+ on the platinum electrode.

In Table 3 are presented the voltammetric diffusion coefficients at different temperatures. The Arrhenius equation described adequately the temperature dependence of the diffusion coefficients over the temperature range 304–343 K: the activation energy for the diffusion process was found to be 47.7 kJ mol^{-1}.

Chronopotentiometry

The reduction of Ag^+ on a platinum electrode from its solutions in molten calcium nitrate tetrahydrate was also investigated by chronopotentiometry. A typical chronopotentiometric transient is shown in Fig. 6. Apart from a small maximum at the beginning of the transition time, the transient has a characteristic shape. Another feature frequently observed during the recording of chronopotentiometric transients was the appearance of a small, second transition at more cathodic potentials during the deposition of silver from its solutions in calcium nitrate tetrahydrate melt.

The theoretical potential of the working electrode during constant current electrolysis is given by (20),

$$[5] \quad E = E^0 + \frac{RT}{nF} \ln \left[c - \frac{2it^{1/2}}{nF\pi^{1/2}D^{1/2}} \right]$$

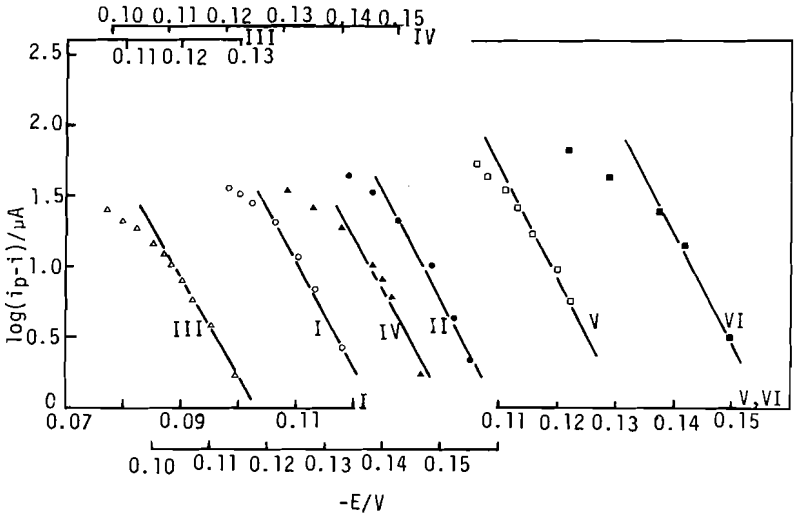

FIG. 5. Plots of log $(i_p - i)$ vs. E constructed from voltammograms at different concentration and sweep rates at 55°C. Sweep rates: I, III, and V: 20 mV s^{-1}; II, IV, and VI: 200 mV s^{-1}. Concentration: III and IV, 7.19 × 10^{-3}; I and II, 10.46 × 10^{-3}; V and VI, 15.72 × 10^{-3} mol L^{-1}.

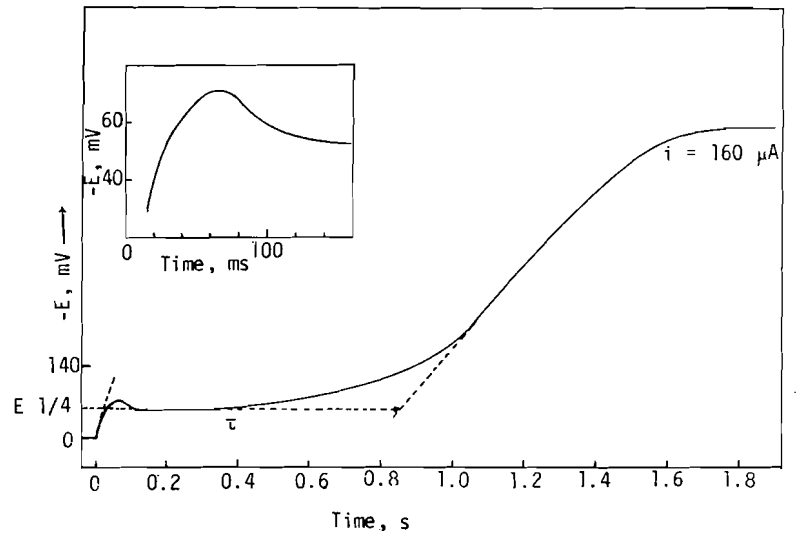

FIG. 6. Chronopotentiogram for the reduction of Ag^+ from its solution in molten calcium nitrate tetrahydrate at 55°C. The concentration of $AgNO_3$ = 17.108 × 10^{-6} mol cm^{-3}.

where E^0 is the standard electrode potential of the metal–metal ion couple, n is the number of electrons involved in the electron-transfer step, i is the current density (A cm^{-2}), D is the diffusion coefficient (cm^2 s^{-1}), c is the bulk concentration (mol cm^{-3}) of the reducible species, and R, T, F have their usual significance. From eq. [5], it can be seen that the potential of the microelectrode would approach infinity at the time τ (called the transition time) which is defined as

$$[6] \qquad \tau^{1/2} = \frac{n\pi^{1/2}FcD^{1/2}}{2i}$$

In actual practice, the potential of the microelectrode rapidly increases to such a value that some other electrode process, such as deposition of another ion or the electrolysis of the solvent itself, takes over. Thus, from eq. [6], the square root of the transition time, at any concentration, should vary linearly with i^{-1}.

In the present work, the square root of the transition time, evaluated using the method of Delahay and Berzins (23), for concentrations over the range 17.08 × 10^{-6} – 42.08 × 10^{-6} mol cm^{-3} varied linearly with the inverse of the current and the plots passed through the origin (Fig. 7). However, the deviations from linearity at the lowest concentration, 9.15 × 10^{-6} mol cm^{-3}, are apparent. The ratio of transition times for the reduction and oxidation processes was 1:1, which is a typical value for the deposition of an insoluble product. This is confirmed by the logarithmic plots in Fig. 8 in which, however, the marked deviations from linearity at the beginning of the transient are a reflection of the overshoot in the beginning of the potential–time transients. The τ values and the related parameters for the reduction of Ag^+ from its solutions in molten calcium nitrate tetrahydrate at various concentrations and current densities at 55°C are included in Table 4. The average values of diffusion coefficients for Ag^+ compare reasonably well with those obtained from the voltammetric data (Table 2). These observations indicate that the conditions for semi-infinite linear diffusion were operative during the measurements.

The present chronopotentiometric results have been analyzed to determine whether an adsorption process is responsible for

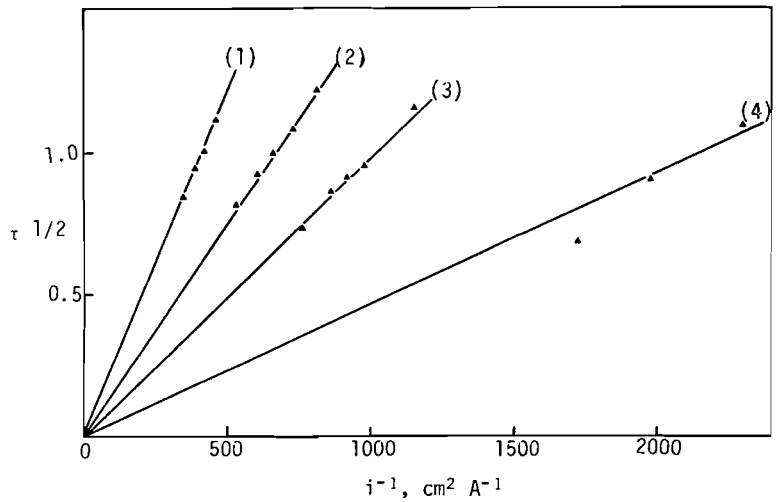

FIG. 7. Plots of $\tau^{1/2}$ vs. i^{-1} for the chronopotentiometric reduction of Ag^+ from calcium nitrate tetrahydrate melts (at 55°C) at different concentrations. The c_{Ag+} are: (*1*) 42.08×10^{-6}; (*2*) 26.45×10^{-6}; (*3*) 17.08×10^{-6}; (*4*) 9.15×10^{-6} mol cm^{-3}. Pt-wire electrode area 0.1379 cm^2.

TABLE 4. Chronopotentiometric data for the reduction of Ag^+ in molten calcium nitrate tetrahydrate at 328.1 K; Pt microelectrode area = 0.1379 cm^2, reference electrode: Ag/Ag^+ (0.05 mol kg^{-1})

$10^6 c_{Ag+}$	$10^4 i_0$	τ	$10^4 i_0\tau^{1/2}$	$i_0\tau^{1/2}/c_{Ag+}$	$10^7 D_{Ag+}$
mol cm^3	A cm^{-2}	s	A cm^{-2} s$^{1/2}$	A cm s$^{1/2}$ mol^{-1}	cm^2 s^{-1}
9.15	4.35	1.2	4.563	52.08	3.7
	5.08	0.81	4.563	49.87	3.4
	5.80	0.46	3.951	43.18	2.5
17.08	8.70	1.3	10.058	58.89	4.7
	10.15	0.88	9.524	55.76	4.2
	10.88	0.82	10.157	59.47	4.8
	11.60	0.73	9.900	57.96	4.6
	13.05	0.56	9.768	57.19	4.5
26.45	12.23	1.5	15.038	56.85	4.4
	13.78	1.2	14.890	56.29	4.3
	15.23	0.98	15.106	57.11	4.4
	16.68	0.85	15.359	58.06	4.6
	18.85	0.66	15.317	57.91	4.6
42.08	21.75	1.2	24.068	57.19	4.5
	23.93	1.2	24.121	57.32	4.5
	26.11	0.89	24.600	58.46	4.7
	29.01	0.70	24.338	57.84	4.6

the observations recorded in the present study. The plots of $i\tau$ vs. i^{-1} and vs. $\tau^{1/2}$ according to the AR, SR, and SAR models of adsorption (24) were constructed. These plots for different concentrations as shown in Fig. 9, are linear and pass through the origin, thereby indicating that an adsorption phenomenon is not operative in the present case. The slopes of $i\tau$ vs. i^{-1} and $\tau^{1/2}$ plots yielded diffusion coefficients of Ag^+ identical to those obtained from Sand's equation (Table 5).

Chronoamperometry

The electroreduction of Ag^+ was also studied by the potential step technique. In the present work, the magnitude of the applied potential step (η) was varied systematically by -5 to -10 mV from the equilibrium potential (against 0.05 mol kg^{-1} Ag^+). The resultant current–time transients for a typical concentration are shown in Fig. 10. For a simple diffusion-controlled process, the current response to a potentiostatic pulse should decay with time for all values of η. In the present study, the I–t curves show maxima at potentials close to the potential of Ag^+ reduction, but are of normal shape both at potentials less cathodic than the reduction and in the region of diffusion control. The position and the height of the maxima are very sensitive to both the applied potential and the concentration of Ag^+.

The current–time relationship for semi-infinite cylindrical diffusion is given by (20)

$$[7] \quad I(t) = \frac{zFADc}{r_0}\left(\frac{1}{\sqrt{\pi\phi}} + \frac{1}{2} - \frac{1}{4}\left(\frac{\phi}{\pi}\right)^{1/2} + \frac{\phi}{8}\cdots\right)$$

where r_0 is the radius and A the area of cylindrical wire electrode, and $\phi = Dt/r_0^2$. For ordinary times, all but the first

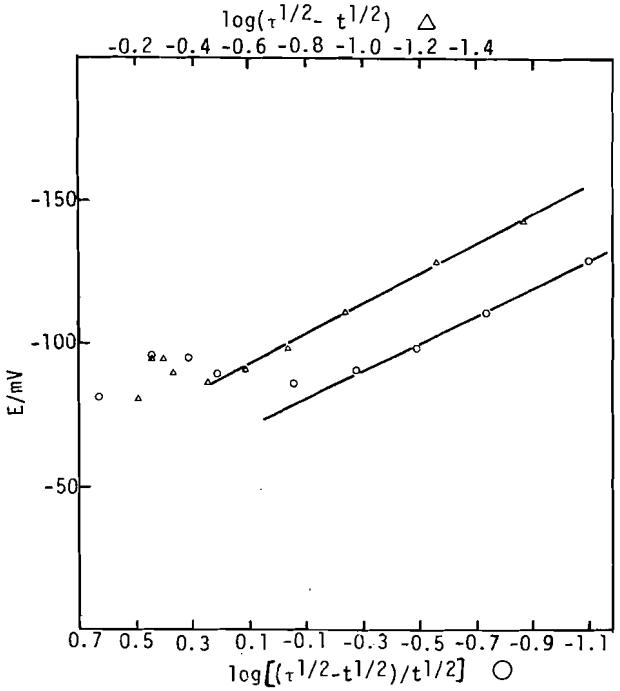

FIG. 8. Plots of E vs. $\log\{(\tau^{1/2} - t^{1/2})/t^{1/2}\}$ and $\log(\tau^{1/2} - t^{1/2})$ for the reduction of Ag^+ from calcium nitrate tetrahydrate at 55°C. $c_{Ag+} = 17.08 \times 10^{-6}$ mol cm^{-3}; $i = 13.05 \times 10^{-4}$ A cm^{-2}; $\tau = 0.56$ s.

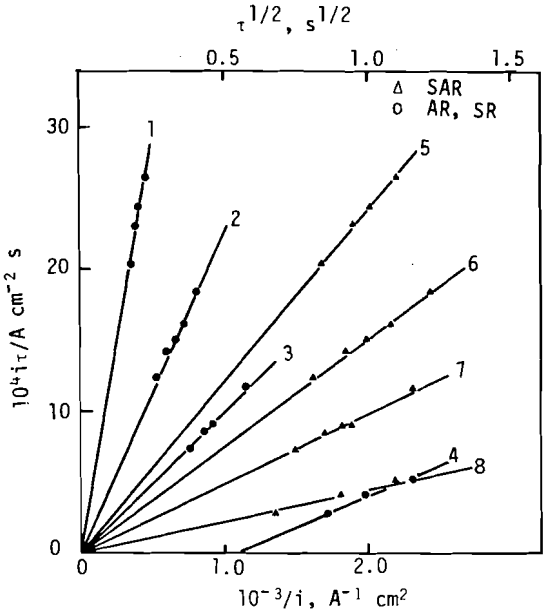

FIG. 9. Plots of $i_0\tau$ vs. i^{-1} and $\tau^{1/2}$ constructed from chronopotentiometric data for the reduction of Ag^+ from molten calcium nitrate tetrahydrate. $c_{Ag+} = (1, 5)\,42.08 \times 10^{-6}$; $(2, 6)\,26.45 \times 10^{-6}$; $(3, 7)\,17.08 \times 10^{-6}$; $(4, 8)\,9.15 \times 10^{-6}$ mol cm^{-3}.

two terms in the parentheses can be neglected, and the current is still a linear function of $t^{-1/2}$ as in the case of linear diffusion. Figure 11 shows a typical current–time$^{-1/2}$ correlation in which, for $6 \geq t \geq 0.4$, a linear relationship is observed. The diffusion coefficient calculated from the linear portion of the plot was estimated to be 3.14×10^{-7} cm^2 s^{-1}. Using this value for the diffusion coefficient, the value of the intercept ($= FADc/2r_0$) was calculated and is compared with that

TABLE 5. Chronopotentiometric diffusion coefficient of Ag^+ in molten calcium nitrate tetrahydrate as calculated using different models; temperature = 328.1 K

	$10^7 D_{Ag+}$ /cm^2 s^{-1}		
$10^6 c$ mol cm^{-3}	AR, SR	SAR	Sand's
9.15	—	3.1	3.2
17.08	4.7	4.5	4.6
26.45	4.4	4.4	4.5
42.08	4.5	4.5	4.5

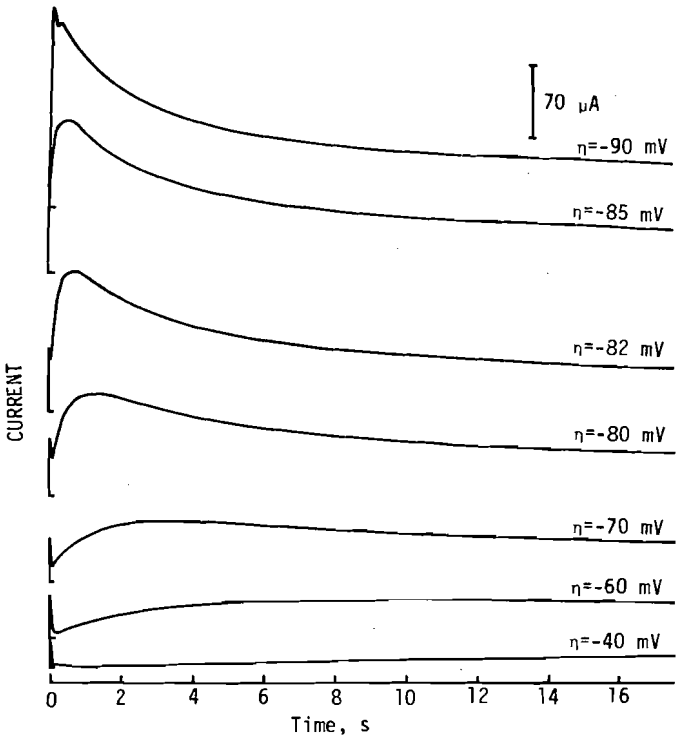

FIG. 10. Current response to a potentiostatic inpulse shown as a function of time and the applied potential step (η). $c_{Ag+} = 42.08 \times 10^{-6}$ mol cm^{-3}.

obtained by extrapolating the linear portion. The two values were, respectively, 3.7 μA and 7 μA. In view of the uncertainty involved in the extrapolation, the disagreement cannot be considered significant. The diffusion coefficient obtained by this method is also given in Table 2. The average values for the diffusion coefficient of Ag^+ obtained in the present study at 55°C appear to be in reasonably good agreement with the value of 2.15×10^{-7} cm^2 s^{-1} (at 50°C) reported by Lovering (14). The slightly lower value of Lovering could be due to the combined effects of a slightly lower temperature of measurement and the possible loss of water during his measurements (25). The rising portion of the current–time transients followed the I–$t^{1/2}$ relationship. All I–$t^{1/2}$ plots (not shown) in the present study passed through the origin and had slopes which were strongly dependent on the applied potential step. Our studies, however, did not show the existence of any "induction period" necessary before the nucleation and growth processes could proceed, as observed by Hills *et al.* (26) in their studies. As apparent from the work of these authors, the induction period decreased rapidly as the potential step became more cathodic.

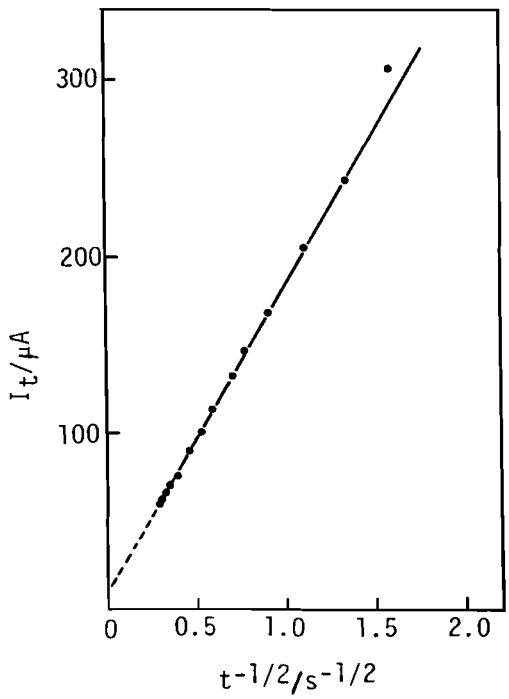

FIG. 11. I_t vs. $t^{1/2}$ plot constructed from the chronoamperometric curve at an applied potential of −160 mV at 55°C. $c_{Ag+} = 42.08 \times 10^{-6}$ mol cm^{-3}.

We feel that the potential steps applied in the present study are probably such that the induction period becomes too short to be observed.

Discussion

The unusual behavior of Ag^+ upon reduction in molten calcium nitrate tetrahydrate as observed in the present study indicates that the electrode process is not a simple reversible one. One possible explanation could be the existence of adsorption phenomena, which are well known in aqueous electrodeposition as well as in molten salts (27–31). The $i\tau$ vs. i^{-1} and $\tau^{1/2}$ plots for different concentrations, constructed from the chronopotentiometric data obtained in the present study (Fig. 9) pass through the origin, thereby speaking against the adsorption process influencing the mechanism of Ag^+ reduction under the conditions of the present investigations. As the usual effect of nucleation is the appearance of a maximum in the chronoamperometric and chronopotentiometric curves, another convincing and probably physically more relevant explanation is the existence of a nucleation step at the beginning of the electrodeposition of the metal. Hills *et al.* (26) have observed almost identical phenomena during the reduction of Ag^+ from molten nitrates and also during the electrodeposition of silver on platinum and graphite and of mercury on graphite from aqueous solutions (26). Mamantov and co-workers have also observed a nucleation step in the electrodeposition of aluminum (31), zirconium (31), and iron (33) on solid microelectrodes in chloroaluminate melts.

The formation and growth of an electro-deposited phase is a complex process. Fleischmann and Thirsk (34) have reviewed the different possible types of growth mechanisms when the electrodeposited metal is the same as that of the substrate. According to Hills *et al.* (26) for a hemispherical diffusion, the potentiostatic time transient for *instantaneous* nucleation can be described through the equation,

TABLE 6. The number-density of silver nuclei (N_0/cm^2) evaluated through eq. [10]

$\eta_{applied}$/mV	$10^6 \frac{dI}{dt^{1/2}} \Big/$ A s$^{-1/2}$	$10^{-5} N_0$/cm^2
−40	2.0	1.32
−60	16.5	8.70
−70	44.6	23.53
−80	121.2	63.94
−90	256.0	135.07

Electrode area = 0.1379 cm^2
Concentration of $AgNO_3 = 42.08 \times 10^{-6}$ mol cm^{-3}
Density of silver = 10.47 g cm^{-3}
D_{Ag+} (chronoamperometric) $= 3.14 \times 10^{-7}$ cm^2 s^{-1}

$$[8] \quad I(t) = nFN_0 \frac{\pi(2Dc)^{3/2}M^{1/2}t^{1/2}}{\rho^{1/2}}$$

and that for *progressive* nucleation through the expression,

$$[9] \quad I(t) = \frac{4nFk_nN_0\pi(Dc)^{3/2}M^{1/2}t^{3/2}}{3\rho^{1/2}}$$

in which N_0 is the number of nuclei formed, M and ρ are the molar mass and density of the electro-deposited metal, D and c are the diffusion coefficient and concentration of the electroactive species, t is the time, and k_n is the rate constant for the formation of nuclei. All other terms have their usual significance.

In a subsequent publication, Gunawardena, Hills, and Montenegro (35) showed that a more appropriate equation representing the middle rising portion of the current-time transient is

$$[10] \quad I(t) = \frac{1.04nF\pi(2Dc)^{3/2}M^{1/2}N_0t^{1/2}}{\rho^{1/2}}$$

As predicted by eq. [10], the I vs. $t^{1/2}$ linear plots pass through the origin in the present case, thereby indicating that the deposition of silver under these conditions is a process involving instantaneous three-dimensional nucleation followed by growth controlled by the hemispherical diffusion of Ag^+ from the melt. The potential dependence of the growth current at any given concentration implies that the total number of available nucleation sites is potential dependent, i.e., there is a distribution of nucleation sites of different energies which nucleate at different overpotentials.

The number-density of the nuclei at the electrode surface, as calculated from the slopes of I–$t^{1/2}$ plots, are presented in Table 6.

In view of the observations resulting from the analysis of the current–time transients, it is possible to explain the abnormal chronopotentiometric and voltammetric behaviour relating to the electrodeposition of silver from molten calcium nitrate tetrahydrate. The small overshoot observed at the beginning of each chronopotentiogram can be seen as the nucleation overpotential, which must be attained before bulk deposition can proceed. Once nucleation has taken place, the charge-transfer process, being rapid, no longer requires this overpotential and as a result the potential of the working electrode falls to normal before the transient of the expected shape is completed. The *frequent* appearance of a small second overpotential at more cathodic potentials during the deposition of silver from this hydrate melt may be due to a secondary nucleation process.

Examining for such a possibility during the electrodeposition of silver on platinum from molten nitrates by scanning electron micrographs, Hills *et al.* (26) could actually see that, at lower overpotentials, the deposit grows only in patches over the electrode surface and that the remainder of the surface is not nucleated until higher overpotentials are reached.

Although at the moment we are unable to correlate the cathodic shift of cathodic peak-potentials at higher sweep rates with the chronopotentiometric and chronoamperometric results, the near constancy of the anodic peak potentials appears to be consistent with the existence of a nucleation step, for during anodic stripping no overpotential would be required. The anodic shift of the reduction peak potentials in subsequent cycles of multicyclic runs, which has been suggested as one of the criteria for nucleation (32), further supports the occurrence of a nucleation step during initial stages of Ag^+ reduction.

Acknowledgements

The authors wish to thank the Natural Sciences and Engineering Research Council for financial support. One of us (S.K.J.) acknowledges with pleasure the cooperation and help extended by Drs. F. W. Yerhoff, Luc Verdet, and P. O. Ikekwere during his stay (1982–1983) at the University of Regina.

1. C. A. ANGELL. J. Electrochem. Soc. **112**, 1224 (1965).
2. C. A. ANGELL. J. Phys. Chem. **69**, 2137 (1965).
3. C. A. ANGELL. J. Phys. Chem. **70**, 3988 (1966).
4. J. BRAUNSTEIN, L. ORR, and W. MACDONALD. J. Chem. Eng. Data, **12**, 415 (1967).
5. J. BRAUNSTEIN, A. R. ALVAREZ-FUNES, and H. BRAUNSTEIN. J. Phys. Chem. **70**, 1734 (1966).
6. C. T. MOYNIHAN. J. Phys. Chem. **70**, 3399 (1966).
7. C. T. MOYNIHAN and A. FRATIELLO. J. Am. Chem. Soc. **89**, 5546 (1967).
8. S. K. JAIN. J. Chem. Eng. Data, **18**, 397 (1973).
9. S. K. JAIN. J. Phys. Chem. **82**, 1272 (1978).
10. S. K. JAIN and R. TAMAMUSHI. Sci. Papers IPCR (Japan), **74**, 73 (1980).
11. S. K. JAIN and R. TAMAMUSHI. Can. J. Chem. **58**, 1697 (1980).
12. J. BRAUNSTEIN, L. ORR, A. R. ALVAREZ-FUNES, and H. BRAUNSTEIN. J. Electroanal. Chem. **15**, 337 (1967).
13. C. T. MOYNIHAN and C. A. ANGELL. J. Phys. Chem. **74**, 736 (1970).
14. D. G. LOVERING. Coll. Czech. Chem. Commun. **37**, 3697 (1972).
15. D. G. LOVERING. J. Electroanal. Chem. **50**, 91 (1974).
16. N. P. BANSAL and J. A. PLAMBECK. J. Electrochem. Soc. **124**, 1036 (1977).
17. N. P. BANSAL and J. A. PLAMBECK. Electrochim. Acta, **23**, 1053 (1978).
18. N. P. BANSAL and J. A. PLAMBECK. Electrochim. Acta, **23**, 697 (1978).
19. W. W. EWING and R. J. MIKOVSKY. J. Am. Chem. Soc. **72**, 1390 (1950).
20. P. DELAHAY. New instrumental methods in electrochemistry. Interscience, New York. 1954.
21. T. BERZINS and P. DELAHAY. J. Am. Chem. Soc. **75**, 555 (1953).
22. G. MAMANTOV, D. L. MANNING, and J. M. DALE. J. Electroanal. Chem. **9**, 253 (1965).
23. P. DELAHAY and T. BERZINS. J. Am. Chem. Soc. **75**, 2486 (1953).
24. R. W. MURRAY and D. J. GROSS. Anal. Chem. **38**, 392 (1966).
25. D. G. LOVERING. J. Electrochem. Soc. **126**, 985 (1979).
26. G. J. HILLS, D. J. SCHIFFRIN, and J. THOMPSON. Electrochim. Acta, **19**, 657 (1974).
27. M. F. BELL and J. A. HARRISON. J. Electroanal. Chem. **41**, 15 (1973).
28. H. A. LAITINEN and R. A. OSTERYOUNG. *In* Fused salts. *Edited by* B. R. Sundheim. McGraw Hill, New York. 1964.
29. R. NARAYAN, D. G. LOVERING, and D. INMAN. Chem. Commun. 386 (1966).
30. D. INMAN, R. S. SETHI, and R. SPENCER. J. Electroanal. Chem. **29**, 137 (1971).
31. R. NARAYAN and D. INMAN. J. Polarogr. Soc. **11**, 27 (1965).
32. P. ROLLAND and G. MAMANTOV. J. Electrochem. Soc. **123**, 1299 (1976).
33. B. GILBERT, G. MAMANTOV, and K. W. FUND. Inorg. Chem. **14**, 1802 (1975).
34. M. FLEISCHMANN and H. R. THIRSK. Advances in electrochemistry and electrochemical engineering. Vol. 3. *Edited by* P. Delahay and C. W. Tobias, Interscience, New York. 1963.
35. G. A. GUNAWARDENA, G. J. HILLS, and I. MONTENEGRO. Electrochim. Acta, **23**, 693 (1978).

Detection of deuterium labelling by two-dimensional $^{1}H,^{13}C$ nuclear magnetic resonance shift correlation with ^{2}H decoupling

PAUL B. REESE, LAIRD A. TRIMBLE, AND JOHN C. VEDERAS[1]
Department of Chemistry, University of Alberta, Edmonton, Alta., Canada T6G 2G2

Received December 13, 1985

PAUL B. REESE, LAIRD A. TRIMBLE, and JOHN C. VEDERAS. Can. J. Chem. **64**, 1427 (1986).

Methylene groups that are stereospecifically labelled with deuterium can be easily observed using deuterium-decoupled 2-dimensional proton/carbon nmr shift correlation spectroscopy in either normal or CH-selective mode. Application of the technique to [3-^{2}H]camphors **2**, **3**, and **4** shows that overlap of other ^{13}C resonances does not interfere with the ^{2}H detection. Such experiments with [3-^{2}H]-*N*-benzoylphenylalanine methyl esters **6** and **7** demonstrate that identification of labelled diastereotopic hydrogens can be done if they are separated by 0.1 ppm in the ^{1}H nmr spectrum. Fully deuterated carbons (e.g., CD_3 methyl, CD_2 methylene, CD methine) cannot be observed by this approach, as seen by the study of pregnenolone acetate (**9**) randomly deuterated at C-17 and C-21. The technique is ideal for cases with extensive overlap of other proton and carbon resonances because high chemical shift dispersion in two dimensions separates the signals of interest. This nmr method was used to show that hydrogenation of cholesteryl acetate (**10**) with deuterium gas and palladium catalyst exchanges the C-7 α-hydrogen to give **12**. The detection limit is estimated at 10% deuterium per site unless ^{13}C-labelled compounds are used.

PAUL B. REESE, LAIRD A. TRIMBLE et JOHN C. VEDERAS. Can. J. Chem. **64**, 1427 (1986).

Utilisant la spectroscopie de corrélation des déplacements rmn proton/carbone bidimensionnelle, découplée pour le deutérium et opérée soit en mode normal ou en mode sélectif pour le CH, on peut facilement observer les groupements méthylènes qui sont marqués d'une façon stéréospécifique avec du deutérium. L'application de cette technique aux camphres-[^{2}H-3] **2**, **3** et **4** permet de montrer que le recouvrement des autres résonances ^{13}C n'interfère pas avec la détection du ^{2}H. De telles expériences avec les esters méthyliques de la *N*-benzoylphénylalanine-[^{2}H-3] **6** and **7** permet de démontrer que l'identification des hydrogènes diastéréotopes marqués peut être faite s'ils sont séparés par 0,1 ppm dans le spectre rmn du ^{1}H. En se basant sur une étude réalisée sur de l'acétate de pregnénolone (**9**) deutéré au hasard dans les positions C-17 et C-21, on peut conclure que les carbones complètement deutérés (par exemple, méthyles CD_3, méthylènes CD_2 et méthine CD) ne peuvent pas être observés par cette approche. Dû au fait que les déplacements chimiques subissent une grande dispersion lorsqu'on opère en deux dimensions et que cette propriété permet de séparer les signaux qui présentent de l'intérêt, la technique est toutefois idéale pour les cas où il existe beaucoup de recouvrement avec les résonances d'autres protons ou carbones. On a utilisé cette méthode rmn pour démontrer que l'hydrogènation de l'acétate de cholestéryle (**10**) avec du deutérium gazeux en présence d'un catalyseur de palladium échange l'hydrogène-α en C-7 pour conduire au composé **12**. On a évalué que la limite de détection est égale à 10% de deutérium par site, à moins que l'on utilise des composés marqués au ^{13}C.

[Traduit par la revue]

Introduction

Labelling studies employing nmr detection of hydrogen isotopes are increasingly popular because they provide considerable insight into biological and chemical mechanisms (1, 2). The most widely used isotope, deuterium, is routinely observed by changes induced in ^{1}H nmr spectra and by direct ^{2}H nmr measurements (3). Alternatively, it may be detected by differences in the ^{13}C nmr spectra of carbons that are directly attached to deuterium (e.g., α-isotope shifts) (2, 4, 5) or two bonds away (β-isotope shifts) (4, 6, 7). However, determining which of two diastereotopic hydrogens on a methylene group is deuterium labelled is often difficult by any of these techniques even if the ^{1}H nmr assignment is known. At low levels of isotopic enrichment ^{1}H nmr differences are normally obscured by intense signals due to unlabelled material, whereas ^{2}H nmr spectra frequently suffer from extensive overlap of resonances because chemical shift similarities are exacerbated by quadrupole broadening. Although addition of lanthanide shift reagents can sometimes overcome the latter problem (8), the procedure does involve contamination of a potentially valuable sample. Use of normal ^{1}H-decoupled ^{13}C nmr spectroscopy for stereochemical analysis is even more limited since ^{2}H-induced isotope shifts (4) are often of similar magnitude for each of the diastereotopic methylene hydrogens. In principle, tritium labelling in combination with ^{3}H nmr can circumvent these difficulties because of the excellent spectral characteristics of this isotope; however, the accompanying high levels of radioactivity have restricted its use so far (9, 10).

Modern nmr pulse methods[2] possess considerable promise for defining the position and extent of deuterium labelling. Among such techniques that have been applied to deuterated systems (12), two-dimensional chemical shift correlation of deuterium with carbon-13 (13) or correlation of deuterium with protons (14) could potentially provide information on the stereochemistry of labelling at a methylene group. Recently we reported in preliminary form (15) the use of two-dimensional proton/carbon-13 nmr shift correlation with deuterium decoupling to examine stereospecifically deuterated systems. This approach has already proved valuable in analyzing the stereochemistry of an enzymatic reaction (16). In the present work, full experimental details of this method, its limitations, and additional applications to more complex systems are described.

Results and discussion

In order to test the utility as well as the shortcomings of the deuterium-decoupled $^{1}H,^{13}C$ nmr shift correlation method, four systems were examined. These are (*1*) [3-^{2}H]camphor, in which the ^{1}H resonances of interest are well separated in the ^{1}H nmr spectrum, but another interfering carbon signal (C-4) appears within 0.1 ppm of C-3 in the ^{13}C nmr spectrum; (*2*) *N*-benzoyl-[3-^{2}H]phenylalanine methyl ester, in which the

[1]Author to whom correspondence should be addressed.

[2]For reviews, see ref. 11*a*; for partial INADEQUATE spectrum of camphor, see ref. 11*b*.

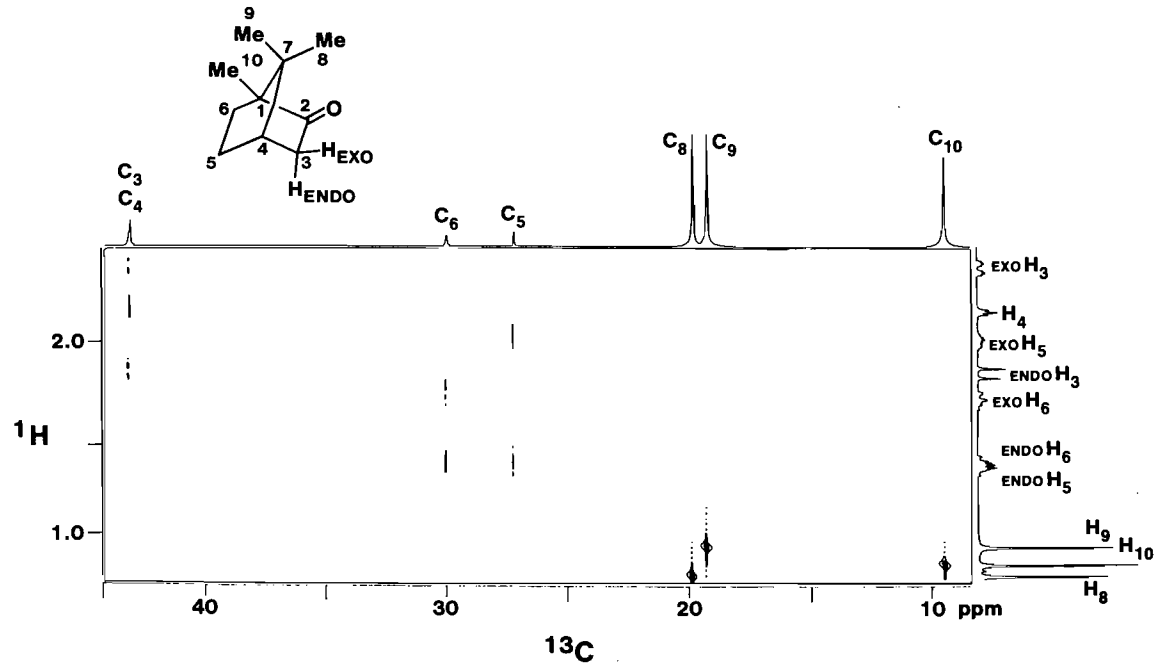

FIG. 1. Normal $^1H,^{13}C$ shift correlation spectrum of unlabelled camphor (**1**). Corresponding sections of the ^1H nmr (400 MHz) and ^{13}C nmr (100.6 MHz) are shown on the vertical and horizontal axes, respectively.

^1H nmr chemical shifts of the C-3 methylene hydrogens are within 0.1 ppm, but the attached carbon signal is well separated; (*3*) [17,21-^2H]pregnenolone acetate, in which methine and methyl groups are partially deuterated; and (*4*) [5,6,7-^2H]cholestanyl acetate, in which the hydrogen resonances of interest are buried in the ^1H nmr "steroidal envelope" and the corresponding carbon signals are flanked by numerous other peaks. Use of a selective $^1H,^{13}C$ correlation pulse sequence (17) that gives signals only for carbons bearing a single hydrogen (CH plots) is also described.

Camphor

Since a number of ^{13}C nmr assignments of camphor (**1**) in various solvents have been reported (18–20), spin echo Fourier transform (SEFT) (21) and 2D INADEQUATE (11, 22) techniques were employed to confirm an earlier assignment (19).[3] A previous ^1H nmr assignment (20) was verified by normal heteronuclear proton–carbon shift correlation (11, 23) (Fig. 1), homonuclear proton–proton decoupling experiments, and examination of $Eu(fod)_3$-induced shifts[3] in proton and carbon spectra. The resulting values given in Table 1 are in complete agreement with a very recent nmr study (24) of camphor (**1**).[4] The exchangeable C-3 methylene hydrogens of camphor (**1**) are well resolved in the ^1H nmr spectrum (*endo* at 1.84 ppm, *exo* at 2.36 ppm). However, the C-3 and C-4 carbon resonances appear within 0.1 ppm of each other in ^{13}C nmr spectra, and slight temperature or concentration changes can shift their positions sufficiently to cause complete overlap.

Endo-, *exo-*, and bis-deuterated camphors **2**, **3**, and **4**, respectively, were prepared by literature procedures (26). Each of these compounds was separately mixed with unlabelled camphor (**1**) in a 2:1 ratio (labelled:unlabelled). Normal two-dimensional $^1H,^{13}C$ chemical shift correlations (23) with broad-band deuterium decoupling were done on each of these samples. The portions of the spectra containing the C-3 methylene and C-4 methine groups are shown as the CH_n plots in the top row of Fig. 2. Application of the selective heteronuclear correlation pulse sequence (17) with deuterium decoupling and the variable pulse angle θ set to 90° produced the simpler CH plots in the bottom row of Fig. 2. These display only those carbons bearing a single proton. In each case A and B are signals due to correlation of the C-3 methylene carbon of unlabelled camphor (**1**) with the attached *exo* and *endo* hydrogens, respectively. Resonance X results from the C-4 methine group of **1**. Comparison of the complete and the CH-only correlation plots of pure **1** to the corresponding plots of mixtures of **1** with **2** or **3** shows the appearance of two additional signals: Y and either C or E. Signal Y results from the C-4 methine being shifted upfield on the horizontal ^{13}C chemical shift axis due to the presence of single deuteriums at C-3 (β-isotope shift) (4, 6).

TABLE 1. Chemical shifts of camphor (**1**)[a]

Position	δ ^1H	δ ^{13}C
1	—	57.6 (s)
2	—	217.9 (s)
3	2.36 (*exo*) 1.84 (*endo*)	43.4 (t)
4	2.10	43.5 (d)
5	1.96 (*exo*) 1.41 (*endo*)	27.4 (t)
6	1.68 (*exo*) 1.34 (*endo*)	30.2 (t)
7	—	46.8 (s)
8	0.83	19.8 (q)
9	0.95	19.3 (q)
10	0.91	9.3 (q)

[a]For conditions see Experimental.

[3]See supplementary material for 2D INADEQUATE spectra and $Eu(fod)_3$ studies of camphor (**1**). This material may be purchased from the Depository of Unpublished Data, CISTI, National Research Council of Canada, Ottawa, Ont., Canada K1A 0S2.

[4]Our results and those in ref. 24 show that a different ^1H nmr assignment (25) is incorrect.

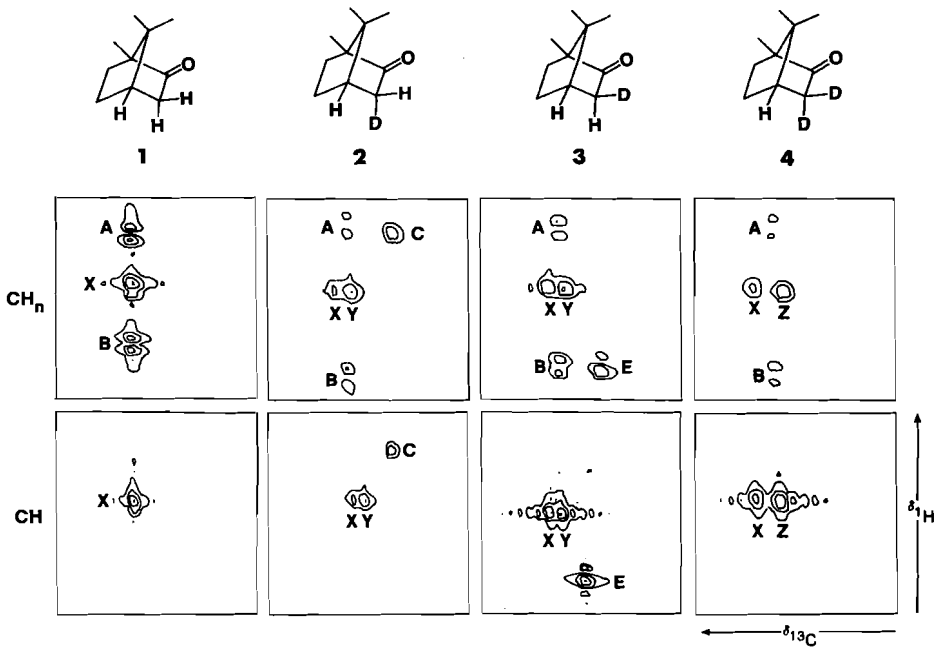

FIG. 2. Deuterium-decoupled normal (CH_n) and selective (CH) proton/carbon shift correlation plots of the C-3 methylene and C-4 methine region of camphor. In each plot the chemical shift increases from 1.76 to 2.43 ppm for ^1H on the vertical axis and from 42.76 to 43.93 ppm for ^{13}C on the horizontal axis (right to left).

The signals labelled C and E arise from C-3 carbons bearing a single proton in the *exo* or *endo* positions, respectively. The large upfield α-isotope shift caused by deuterium on directly-bonded carbon (2, 4) effects the substantial separation of undeuterated (A, B) and deuterated (C, E) methylene signals. In the bis-deuterated camphor (**4**), *Z* is the C-4 methine resonance that is shifted upfield by the two deuteriums on C-3.

The spectra depicted in Fig. 2 clearly demonstrate that stereospecific deuterium labelling can be easily determined by either the normal or selective correlation method even if other interfering carbon resonances are present. The main advantage of the selective correlation is simplification of the plots for easier visualization. However, it is generally necessary to run complete correlation spectra with unlabelled material present as internal standard to be certain of correct assignment of new signals arising from the deuterated compound. With either full or selective correlation techniques, complete broad-band deuterium decoupling is essential, and normally requires a ^{19}F lock (C_6F_6). It is also extremely important to use a relaxation delay (ca. 3 s) between pulse sequences to guarantee optimal observation of correlation signals.

In order to estimate the lower limit of detection of singly deuterated methylene groups by this method, the ratio of unlabelled camphor (**1**) to labelled compounds **2** or **3** was varied. Correlation experiments done using the same conditions as before (see Experimental) on samples containing 20% monodeuterated camphor and 80% unlabelled **1** still gave clean correlation plots similar to those in Fig. 2. These results in combination with normal one-dimensional broad-band $^1H,^2H$-decoupled ^{13}C nmr spectroscopy suggest that the lower detection limit may be in the range of 10% deuterium on natural abundance carbon-13 (1.1%) if the number of scans and experiment time are considerably increased.

N-*Benzoylphenylalanine methyl ester*

Frequently the resonance of a methylene carbon is well resolved in the ^{13}C nmr spectrum, but the chemical shifts of attached diastereotopic hydrogens are very similar. To test the deuterium-decoupled correlation method in such circumstances, a racemic mixture of (2*S*,3*S*)- and (2*R*,3*R*)-*N*-benzoyl[2,3-$^2H_2$]phenylalanine methyl esters (**6**) was prepared by literature procedures (27) and mixed with the corresponding unlabelled compound **5** (28) in a 2:1 ratio. A mixture of all possible stereoisomers of the C-3 monodeuterated derivative **7** was generated by enolization of **6** and quenching with unlabelled acetic acid. This was mixed with unlabelled material **5**, in the same fashion, before nmr analysis.

In the normal ^1H nmr spectrum ($CDCl_3$) the diastereotopic hydrogens of *N*-benzoylphenylalanine methyl ester (**5**) appear at 3.20 and 3.29 ppm as the A and B parts of an ABX system. The corresponding methylene carbon displays a well-separated resonance at 38.0 ppm. Two-dimensional proton/carbon shift correlation experiments with deuterium decoupling on **5** and its mixtures with **6** and **7** produced the plots shown in Fig. 3. These expansions of the C-3 methylene region of the full (CH_n) and selective (CH) correlations clearly display additional signals for **6** and **7** due to the presence of CHD groups. The correlation of the upfield hydrogen of **6** with an isotope-shifted carbon resonance shows that the downfield methylene hydrogen has been replaced by deuterium. Since **7** is nonstereospecifically labelled, the CHD group exists in both possible relative configurations. As a result, two isotope-shifted correlation signals are observed.

The observed deuterium-induced α-isotope shift on the horizontal carbon axis is the essential feature that allows detection of deuterated methylenes. However, a small upfield shift in the position of the deuterated species can also be seen on the vertical proton chemical shift axis. Deuterium isotope shifts on ^1H nmr resonance positions have been reported previously (4, 29), but are usually too small to be readily noticed. They seem to be a general phenomenon, which is easily observed in the deuterium-decoupled $^1H,^{13}C$ shift correlation spectra.

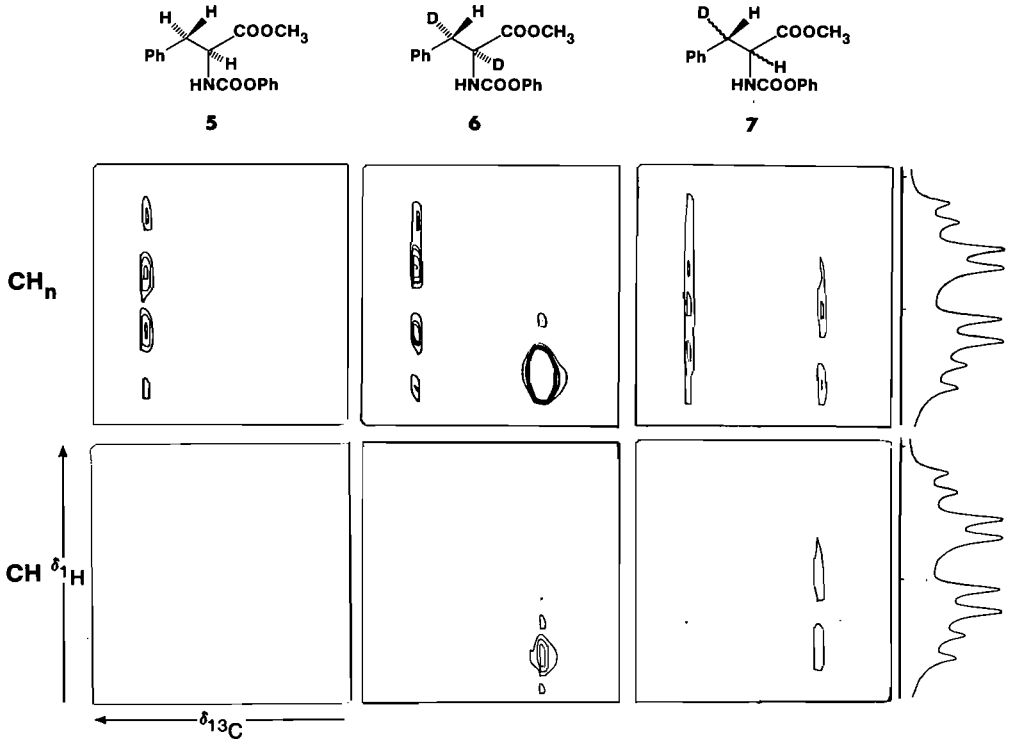

FIG. 3. Normal (CH_n) and selective (CH) proton/carbon correlations (deuterium decoupled) of the C-3 region of *N*-benzoylphenylalanine methyl esters. Compound **6** is racemic and **7** is a mixture of all stereoisomers. The corresponding ^1H nmr of **5** is shown on each vertical axis (3.12–3.36 ppm).

Pregnenolone acetate

In order to examine use of this method with other types of deuterated systems, the hydrogens at C-17 and C-21 of pregnenolone (**8**) (Scheme 1) were partially exchanged in basic media containing 50% labile deuterium. Acetylation afforded **9** as a statistical mixture of d_0, d_1, d_2, d_3, and d_4 species. Although deuterium substitution at C-17 produces the expected changes in the ^1H nmr and fully decoupled (^1H,^2H) ^{13}C nmr spectra of **9**, the ^1H,^{13}C shift correlation methods are ineffective at detecting the methine label because only species bearing hydrogen at C-17 give signals. Similarly, molecules having three deuteriums at the C-21 methyl cannot be seen in the correlation spectra of that region (Fig. 4). However, the CHD_2, CH_2D, and CH_3 species are all readily visible in the full deuterium-decoupled proton/carbon correlation spectrum (CH_n) because of the additive nature of the α-isotope effect of deuterium on carbon (4). Unfortunately, the presence of deuterium unfavorably alters Overhauser enhancement and relaxation of directly attached carbons (2, 30) such that not all the peak areas are a direct measure of the extent of ^2H labelling. This is also true in the regular fully decoupled (^1H,^2H) ^{13}C nmr spectrum. The β-isotope shift method developed by Staunton and co-workers (6) may be the most widely applicable approach to examine deuterium content at methines and methyl groups (7). The deuterium/carbon-13 shift correlation technique recently reported by Wesener and Günther (13) could be advantageous in cases of extensive ^{13}C resonance overlap, and should give signals for all deuterated methine and methyl species.

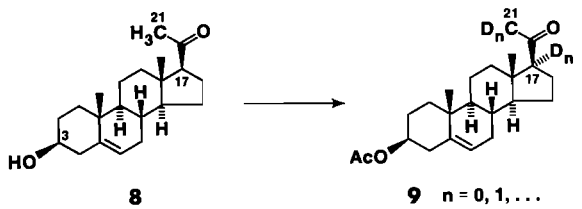

SCHEME 1

Cholestanyl acetate

One of the most common problems in measuring deuterium content at labelled methylene groups is overlap of other proton resonances. This overlap can make definitive identification of labelled sites impossible by routine one-dimensional nmr methods. To rigorously test the present technique in such a situation, cholesteryl acetate (**10**) was reduced to unlabelled and deuterated cholestanyl acetates **11** and **12**, respectively (Scheme 2). The reaction of **10** with deuterium gas and palladium on charcoal (5%) in ethyl acetate containing acetic acid-d_4 labelled C-5, C-6, and C-7 of **12**, in analogy to the previously reported (31) reduction with platinum catalyst. Carbons bearing deuterium could be identified from α- and β-isotope shifts in the normal fully decoupled (^1H,^2H) ^{13}C nmr spectra of a 1:2 mixture of **11** and **12**. Thus C-4, C-8, and C-10 exhibited smaller β-isotope shifts (4), whereas C-5, C-6, and C-7 each showed a larger α-isotope shift as well as the small β-shifts (Table 2). The ^{13}C nmr spectral assignments are in accord with those previously reported by two other groups (32, 33). The known configuration at C-5, the preference for *syn* addition of hydrogen, and the well-precedented interaction of the steroid α-face with palladium (34) suggested that the deuteriums at C-6 and C-7 were on the α-side. However, this cannot be directly determined by routine ^1H nmr, ^2H nmr, or ^{13}C nmr analysis because the resonances of interest are buried in the "steroid envelope".

The deuterium-decoupled proton/carbon correlation spec-

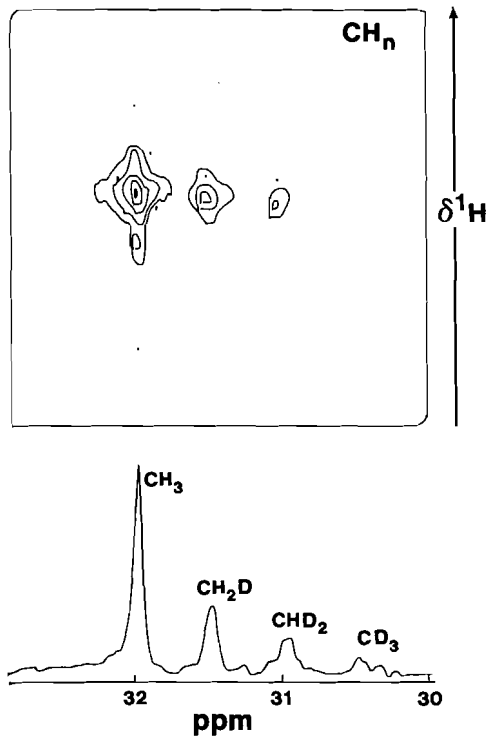

FIG. 4. Deuterium-decoupled proton/carbon correlation of the C-21 methyl region of **9** showing various labelled species. The fully decoupled (^1H,^2H) ^{13}C nmr spectrum is displayed underneath for comparison. The chemical shift increases from 1.40 to 2.73 ppm for ^1H on the vertical axis.

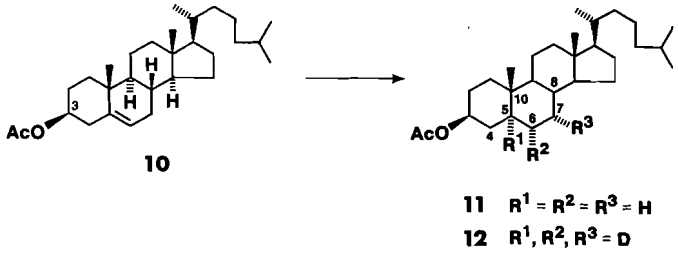

SCHEME 2

TABLE 2. ^2H-induced isotope shifts in ^{13}C nmr of [5,6,7-^2H]-3β-acetoxycholestane (**12**)[a]

Position	Shift type[b]	Magnitude (ppm)[c]
4	β	0.12
5	α	0.57
	β	0.10
6	α	0.50
	β[d]	0.10
7	α	0.48
	β	0.13
8	β	0.12
10	β	0.12

[a]For measurement conditions see Experimental.
[b]α refers to directly attached ^2H, β refers to ^2H two bonds away.
[c]All shifts upfield.
[d]Shifts due to ^2H at C-7 and to ^2H at C-5 are same size.

trum of the 1:2 mixture of **11** and **12** clearly shows that the upfield axial (α-face) hydrogen at C-7 is deuterium labelled (Fig. 5). In the expansion of section A from the large plot (Fig. 6), signals F and G are due to correlation of the C-7 carbon to the directly attached equatorial (downfield) and axial (upfield) hydrogens (35) of unlabelled cholestanyl acetate (**11**). Signals H and J result from the same correlation in molecules of the deuterated derivative **12**, which have no deuterium at C-7 but do bear a deuterium two bonds away at C-6 that causes an upfield β-isotope shift on the carbon axis. Signal K arises from molecules of **12** having axial deuterium at C-7 (large α-isotope shift), but no deuterium at C-6. The intense peak L is due to molecules of **12** having axial deuterium at C-7 (large α-isotope shift) and a single deuterium at C-6 (smaller β-isotope shift). Lack of any correlation between the axial hydrogen at C-7 and any carbon signal having an α-isotope shift demonstrates that deuterium labelling is completely stereospecific at that site (i.e., all C-7 ^2H is axial).

Unfortunately the axial and equatorial hydrogens at C-6 of cholestanyl acetate (**11**) could not be resolved in the ^1H nmr spectrum. These diastereotopic protons give rise to a single resonance in the proton/carbon shift correlation spectrum of unlabelled **11** in either chloroform-*d* (Fig. 5) or benzene-d_6. Examination of the spectra of cholestan-3-one gave a similar result. A recent report on correlation experiments with a different steroid system also showed that the C-6 hydrogen resonances have essentially identical chemical shifts (36). The region of the deuterium-decoupled proton/carbon correlation spectrum containing the C-6 methylene is expanded in section B of Fig. 6. Resonance M comes from unlabelled material **11**, whereas the other additional signals (N, P, Q) are due to carbons of **12** having deuterium directly attached (P, Q) and (or) two bonds away (N, Q). Although no stereochemical information about the deuterium at C-6 is available from this two-dimensional spectrum, it does remove interference from the overlapping carbon resonances of C-16 and C-25. In contrast, the stereospecific labelling at C-7 can be clearly seen.

Conclusions

The deuterium-decoupled proton/carbon nmr shift correlation technique is ideal for observation of stereospecifically ^2H-labelled methylene groups in complex systems (e.g., **12**). This method takes advantage of the high chemical shift dispersion available in ^{13}C nmr to separate signals of interest, and avoids obscuring the methylene proton AB system through resonance broadening common in ^2H nmr. The large upfield deuterium-induced α-isotope shift on ^{13}C resonance positions cleanly separates the correlation peaks of partially deuterated carbons from corresponding signals of unlabelled material. Key resonances due to monodeuterated methylenes can be isolated further through application of a selective pulse sequence (17), which generates correlation plots containing only CH groups. The technique is also excellent for detecting small ^2H-induced isotope shifts on ^1H nmr resonances. Some resolution of the methylene AB signals in ^1H nmr is essential for stereochemical identification, but this separation of resonances can be much smaller (≤0.1 ppm) than with ^2H nmr or correlation of deuterium with other nuclei (13, 14). Of course, as with other nmr methods, determination of the absolute stereochemistry must be done by independent means.

The major current limitation of this technique is instrumental; it is necessary to lock on ^{19}F while decoupling ^2H and pulsing

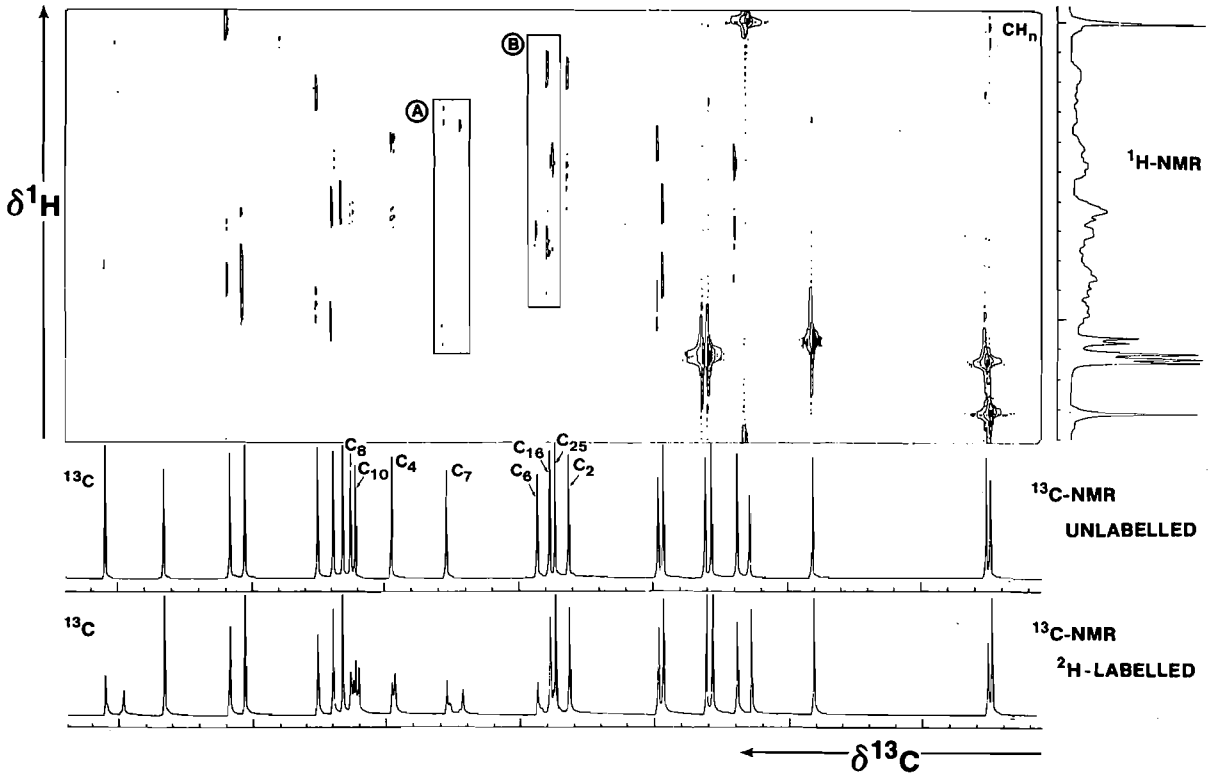

FIG. 5. Deuterium-decoupled proton/carbon correlation of deuterated 3β-acetoxycholestane (**12**). The corresponding 400-MHz ^{1}H nmr spectrum (0.59–2.05 ppm) is shown on the vertical axis and the 100.6-MHz ^{13}C nmr spectra (10.6–47.0 ppm) of unlabelled and ^{2}H-labelled material are displayed on the horizontal axis. See Fig. 6 for expansions of the regions labelled A and B.

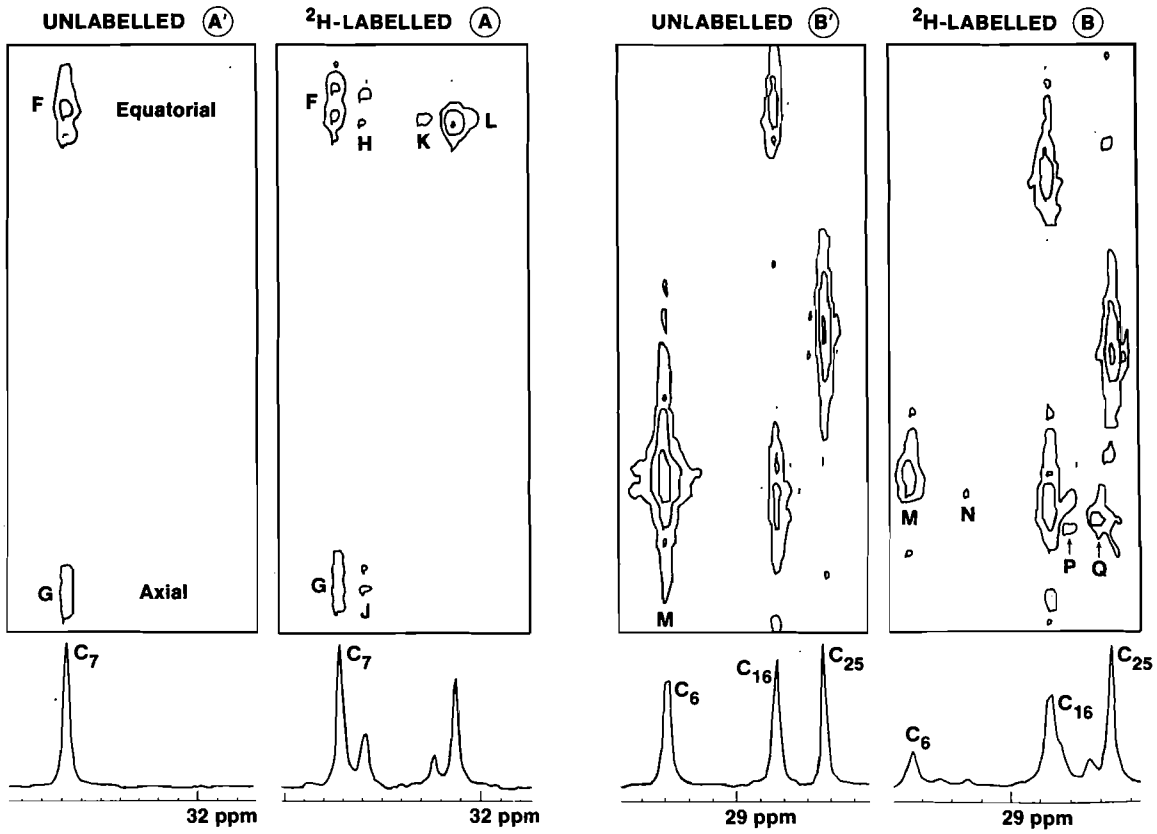

FIG. 6. Deuterium-decoupled proton/carbon correlations of the regions containing C-7 (A′ and A) and C-6 (B′ and B) of unlabelled 3β-acetoxycholestane and the ^{2}H-labelled analog **12**. The sections A and B are also shown in Fig. 5 for comparison.

^1H and ^{13}C frequencies. Wider distribution of commercially-available triple resonance probes in the future will overcome this difficulty. This method is not applicable to fully deuterated carbons that bear no hydrogen (e.g., CD_3), and is generally not ideal for quantitative determination of deuterium content. As with other 2D nmr spectra, another limitation is the amount of material available for study. A correlation experiment on a sample whose concentration is 0.8 *M* in a 5-mm tube takes about 1 h (400 MHz for ^1H). It is clear that 64 t_1 points are sufficient to obtain the required information. The appearance of the spectra could certainly be improved by use of more t_1 values, but only at the expense of valuable spectrometer time. At least 10% ^2H per site is necessary for detection at natural abundance levels of ^{13}C (1.1%). However, shorter instrument time and much greater sensitivity can be achieved if the compound is enriched with ^{13}C at the deuterated carbons. Such double labelling of precursors is now routine in biochemical investigations. One application of this nmr method has already been described (16), and work on its use in biosynthetic studies will be reported shortly.

Experimental

Melting points were recorded on a Thomas Hoover apparatus and are uncorrected. Infrared (ir) spectra were measured on chloroform solutions using a Nicolet 7199 FT spectrometer. Mass spectra were obtained on a KRATOS A.E.I. MS50 spectrometer using electron impact (70 eV) and chemical ionization (NH_3) modes. Commercial chemicals were of reagent grade and were purified as necessary according to standard procedures (37).

Nuclear magnetic resonance spectra

A Brüker WH400 spectrometer (400 MHz ^1H, 100.6 MHz ^{13}C) was used to obtain spectra on samples in $CDCl_3$ (unless otherwise noted) using 5-mm tubes at 25°C. All chemical shifts are reported in parts per million (δ scale) from tetramethylsilane as internal standard. All ^2H-decoupled nmr spectra were done using a ^{19}F lock on C_6F_6 (5–20% v/v added to sample). Heteronuclear proton/carbon shift correlations with broad-band deuterium decoupling employed previously described pulse sequences to obtain the complete (23) and selective (17) two-dimensional plots. For the latter, the variable pulse angle θ was set to 90°. All correlation experiments used: a relaxation delay = 3 s between scans; 1 K FID's for 64 values of t_1; zero filling to 512 points in f_1 (^1H) and 2 K in f_2 (^{13}C). In each case a Gaussian window function was applied to both f_1 and f_2 with the line broadening set equal to the number of Hz/pt after zero filling, and the Gaussian broadening was set to zero. For camphor (2.36 *M* solution): f_1 (^1H) = 1060 Hz; f_2 (^{13}C) = 5000 Hz; acquisition time 0.10 s; 4 scans/t_1 increment. For *N*-benzoylphenylalanine methyl esters (1.29 *M*): f_1 (^1H) = 800 Hz; f_2 (^{13}C) = 1800 Hz; acquisition time = 0.28 s; 8 scans/t_1 increment. For pregnenolone acetates (3β-acetoxypregn-5-en-20-one) (0.89 *M*): f_1 (^1H) = 1400 Hz; f_2 (^{13}C) = 1700 Hz; acquisition time = 0.31 s; 12 scans/t_1 increment. For cholestanyl acetates (3β-acetoxycholestane) (0.81 *M*): f_1 (^1H) = 585 Hz; f_2 (^{13}C) = 3600 Hz; acquisition time = 0.14 s; 16 scans/t_1 increment.

Deuterated camphors 2, 3, and 4

The monodeuterated compounds **2** and **3** were prepared by the procedures of Joshi and Warnhoff and the bis-deuterated camphor **4** was made according to Thomas and Wilholm (26). All three were sublimed before use to give chromatographically pure materials with the expected physical and spectral properties.

For [3-*endo*-^2H]camphor (**2**): ^1H nmr signal at δ 1.78 reduced by 80%. *Exact Mass* calcd. for $C_{10}H_{15}{}^2HO$: 153.1265; found: 153.1274.

For [3-*exo*-^2H]camphor (**3**): ^1H nmr signal at δ 2.29 (3 *exo* H) reduced by 75%, at 1.78 (3 *endo* H) relative intensity unchanged. *Exact Mass* calcd. for $C_{10}H_{15}{}^2HO$: 153.1265; found: 153.1273.

For [3,3-$^2H_2$]camphor (**4**): ^1H nmr signals at δ 1.78 and 2.29 completely absent. *Exact Mass* calcd. for $C_{10}H_{14}{}^2H_2O$: 154.1317; found: 154.1327.

N-Benzoylphenylalanine methyl esters 5, 6, and 7

The unlabelled compound **5** was prepared by literature procedures (28). The racemic mixture of (2*S*,3*S*)- and (2*R*,3*R*)-*N*-benzoyl[2,3-$^2H_2$]phenylalanine methyl esters (**6**) was synthesized by the method of Battersby and co-workers except that the intermediate azlactone was cleaved by methanol according to Buckles *et al.* (27). For the preparation of **7** a solution of **6** (2.0 g, 7.0 mmol) in tetrahydrofuran (THF) (15 mL) was added to a cold (−78°C) solution of THF (20 mL) and lithium diisopropylamide (1.5 *M* *n*-BuLi (14 mL, 20 mmol), diisopropylamine (3.0 mL, 21 mmol)) under Ar atmosphere. Stirring was continued for 30 min, acetic acid (5.0 mL, 80 mmol) was added, and the mixture was allowed to warm to 20°C. The solution was diluted with ether and washed with concentrated aqueous NaCl and sodium bicarbonate. The organic phase was dried, concentrated *in vacuo*, filtered through a short column of silica gel (70–230 mesh), and recrystallized from ethyl acetate–ether to give 1.95 g (97%) of *N*-benzoyl[3-^2H]phenylalanine methyl ester (**7**) as a mixture of all possible stereoisomers. This material showed the expected physical and spectral properties. For **7**: mp 84–86°C; ^1H nmr signals at δ 3.20 and 3.29 (1H total, d, J = 6 Hz, H at C-3), 5.06 (1H, br t, J = 6 Hz, H at C-2). *Exact Mass* calcd. for $C_{17}H_{16}{}^2HNO_3$: 284.1272; found: 284.1272.

[17,21-^2H]-3β-Acetoxypregn-5-en-20-one (9)

Commercially available (Sigma) pregnenolone (**8**) (2.0 g, 6.3 mmol) in THF (20 mL) was mixed with a solution of NaOH (50 mg), H_2O (1 mL), D_2O (1 mL), methanol (2 mL), and methanol-d_1 (2 mL). This was heated to reflux for 48 h, the solvent was removed *in vacuo*, and the steroid was extracted with ethyl acetate. This extract was washed with water, dried, and concentrated *in vacuo* to give 2.0 g of pregnenolone deuterated randomly in the 17 and 21 positions. A portion of this (1.5 g, 4.2 mmol) was dissolved in pyridine (8 mL) and treated with acetic anhydride (2 mL, 20 mmol) at 20°C overnight. The mixture was poured into excess cold (4°C) aqueous hydrochloric acid, and the steroid was extracted with ethyl acetate. The extract was washed with water and sodium bicarbonate solution, dried, and concentrated *in vacuo*. Recrystallization from ethyl acetate gave 1.5 g (ca. 88%) of pregnenolone acetate **9** randomly deuterated at C-17 and C-21. Comparison to authentic unlabelled material (38) showed the expected physical and spectroscopic properties: mp 147–149.5°C (lit. (38) mp 149–150°C); ^1H nmr signals at δ 2.1 (H-21) and 2.55 (H-17) reduced. The mass spectrum (ms) exhibits ions (M^+ − HOAc) at 302.2538, 301.2486, 300.2427, 299.2366, and 298.2301 for tetra-, tri-, di-, mono-, and non-deuterated compounds, respectively. Pure unlabelled compound gave *Exact Mass* calcd. for ($C_{23}H_{34}O_3$ − CH_3COOH): 298.2298; found: 298.2301.

3β-Acetoxy-5α-cholestanes 11 and 12

Palladium (5% on carbon) (200 mg) was stirred in dry ethyl acetate (2.5 mL) under deuterium gas (1 atm.) for 10 min. A solution of 3β-acetoxycholest-5-ene (**10**) (1.00 g, 2.33 mmol) in warm ethyl acetate (5 mL) was added, followed by acetic acid-d_1 (5 mL). The mixture was stirred under deuterium for 48 h, filtered, and concentrated *in vacuo*. The ^1H nmr showed that the reaction was 95% complete but purification was difficult. The mixture was therefore dissolved in dichloromethane (15 mL), cooled to 4°C, treated with *m*-chloroperoxybenzoic acid (800 mg), and allowed to stir at 20°C for 10 h. The solution was washed with aqueous sodium sulfite and sodium bicarbonate, dried, concentrated *in vacuo*, and redissolved in acetone. A solution of periodic acid dihydrate (500 mg) in water (5 mL) was added and the mixture was heated to reflux 1 h. Sodium bicarbonate (185 mg) was added to the cooled solution; the mixture was then concentrated *in vacuo* and partitioned between concentrated aqueous NaCl and ethyl acetate. The organic phase was dried, concentrated *in vacuo*, and chromatographed on silica gel (70–230 mesh) with 10% ethyl acetate – light petroleum ether. The resulting 600 mg (60%) of pure [5α,6α,7α-$^2H_3$]-3β-acetoxycholestane (**12**) was recrystallized from ethyl acetate. The undeuterated compound **11** was prepared analogously, and showed physical and spectral properties in accordance with literature reports (32, 33, 39, 40). For deuterated compound **12**: mp 99–102°C;

^{1}H nmr almost indistinguishable from that of unlabelled analog **11** (40); ms *m/e* (*relative intensity*): 433.3985 (*61*), 432.3925 (*55*), 431.3858 (*21*), 430.3795 (*6*).

Acknowledgements

We are grateful to Dr. Richard N. Moore, Glen Bigam, and Dr. Thomas T. Nakashima for valuable discussions and technical assistance. We greatly appreciate financial support from the National Institutes of Health (GM 29826), the Natural Sciences and Engineering Research Council of Canada, and the Alberta Heritage Foundation for Medical Research.

1. T. J. Simpson. *In* Biosynthesis. Vol. 7. Royal Society of Chemistry, London. 1984. pp. 1–44.
2. M. J. Garson and J. Staunton. Chem. Soc. Rev. 539 (1979).
3. H. C. Jarrell and I. C. P. Smith. *In* The multinuclear approach to NMR spectroscopy. *Edited by* J. B. Lambert and F. G. Riddell. D. Reidel, Boston. 1983. pp. 133–149.
4. P. E. Hansen. Annu. Rep. NMR Spectrosc. **15**, 105 (1983).
5. A. K. Demetriadou, E. D. Laue, and J. Staunton. J. Chem. Soc. Chem. Commun. 1125 (1985); U. Sankawa, Y. Ebizuka, H. Noguchi, Y. Isikawa, S. Kitaghawa, Y. Yamamoto, T. Kobayashi, and Y. Iitak. Tetrahedron, **39**, 3583 (1983); C. R. Hutchinson, L. Shu-Wen, A. G. McInnes, and J. A. Walter. Tetrahedron, **39**, 3507 (1983).
6. J. Staunton and C. Abell. J. Chem. Soc. Chem. Commun. 856 (1981).
7. Y. Tomita, M. Arata, and Y. Ikeshiro. J. Chem. Soc. Chem. Commun. 1087 (1985); R. N. Moore, G. Bigam, J. K. Chan, A. M. Hogg, T. T. Nakashima, and J. C. Vederas. J. Am. Chem. Soc. **107**, 3694 (1985); F. E. Scott, T. J. Simpson, L. A. Trimble, and J. C. Vederas. J. Chem. Soc. Chem. Commun. 756 (1984).
8. F. Nicotra, F. Ronchetti, G. Russo, L. Toma, P. Gariboldi, and B. M. Ranzi. J. Chem. Soc. Perkin Trans. 1, 521 (1985); J. M. Schwab and J. B. Klassen. J. Am. Chem. Soc. **106**, 7217 (1984); P. M. Harrison and P. Quinn. J. Chem. Soc. Chem. Commun. 879 (1983).
9. E. A. Evans, D. C. Warrell, J. A. Elvidge, and J. R. Jones. Handbook of tritium NMR spectroscopy and applications. J. Wiley and Sons, Chichester, U.K. 1985.
10. J. N. S. Evans, P. E. Fagerness, N. E. Mackenzie, and A. I. Scott. J. Am. Chem. Soc. **106**, 5738 (1984); D. H. G. Crout, M. Lutstorf, and P. J. Morgan. Tetrahedron, **39**, 3457 (1983).
11. (*a*) R. Benn and H. Günther. Angew. Chem. Int. Ed. Engl. **22**, 350 (1983); J. N. Shoolery. J. Nat. Prod. **47**, 226 (1984); (*b*) H. Günther and P. Schmitt. Naturwissenschaften, **71**, 342 (1984).
12. P. L. Rinaldi and N. J. Baldwin. J. Am. Chem. Soc. **105**, 7523 (1983); J. R. Wesener, P. Schmitt, and H. Günther. J. Am. Chem. Soc. **106**, 10 (1984); C. Abell, D. M. Doddrell, M. J. Garson, E. D. Laue, and J. Staunton. J. Chem. Soc. Chem. Commun. 694 (1983); T. T. Nakashima, R. E. D. McClung, and B. K. John. J. Magn. Reson. **58**, 27 (1984).
13. J. R. Wesener and H. Günther. J. Am. Chem. Soc. **107**, 1537 (1985).
14. H. Bleich, S. Gould, P. Pitner, and J. Wilde. J. Magn. Reson. **56**, 515 (1984); S. J. Gould, V. A. Palaniswamy, H. Bleich, and J. Wilde. J. Chem. Soc. Chem. Commun. 1075 (1984).
15. L. A. Trimble, P. B. Reese, and J. C. Vederas. J. Am. Chem. Soc. **107**, 2175 (1985).
16. J. G. Kelland, M. M. Palcic, M. A. Pickard, and J. C. Vederas. Biochemistry, **24**, 3263 (1985).
17. T. T. Nakashima, B. K. John, and R. E. D. McClung. J. Magn. Reson. **59**, 124 (1984), and references therein.
18. J. B. Grutzner, M. Jautelat, J. B. Dence, R. A. Smith, and J. D. Roberts. J. Am. Chem. Soc. **92**, 7107 (1970); E. Lipmaa, T. Pehk, J. Paasivirta, N. Belikova, and A. Plate. Org. Magn. Reson. **2**, 581 (1970); F. Bohlmann, R. Zeisberg, and E. Klein. Org. Magn. Reson. **7**, 426 (1975); T. Terao, H. Miura, and A. Saika. J. Am. Chem. Soc. **104**, 5228 (1982).
19. J. B. Stothers, C. T. Tan, and K. C. Teo. Can. J. Chem. **51**, 2893 (1973).
20. P. V. Demarco, D. Doddrell, and E. Wenkert. J. Chem. Soc. Chem. Commun. 1418 (1969), and references therein.
21. D. L. Rabenstein and T. T. Nakashima. Anal. Chem. **51**, 1465A (1979).
22. A. Bax, R. Freeman, and T. A. Frenkiel. J. Am. Chem. Soc. **103**, 2102 (1981).
23. G. A. Morris and L. D. Hall. J. Am. Chem. Soc. **103**, 4703 (1981).
24. C. Yu and G. C. Levy. J. Am. Chem. Soc. **106**, 6533 (1984).
25. D. M. Grant, J. Curtis, W. R. Croasmun, D. K. Dalling, F. W. Wehrli, and S. Wehrli. J. Am. Chem. Soc. **104**, 4492 (1982).
26. G. C. Joshi and E. W. Warnhoff. J. Org. Chem. **37**, 2383 (1972); A. F. Thomas and B. Wilholm. Tetrahedron Lett. 1309 (1965).
27. R. H. Wightman, J. Staunton, A. R. Battersby, and K. R. Hanson. J. Chem. Soc. Perkin Trans. 1, 2355 (1972); R. E. Buckles, R. Filler, and L. Hilfman. J. Org. Chem. **17**, 233 (1952).
28. J. Schnyder and M. Rottenburg. Helv. Chim. Acta, **58**, 521 (1975).
29. R. A. Bernheim and H. Batiz-Hernandez. J. Chem. Phys. **45**, 2261 (1966).
30. J. B. Stothers. *In* Topics in carbon-13 NMR spectroscopy. Vol. 1. *Edited by* G. C. Levy. John Wiley, New York. 1974. pp. 236–237.
31. D. K. Fukushima and T. F. Gallagher. J. Am. Chem. Soc. **77**, 139 (1955).
32. J. W. Blunt and J. B. Stothers. Org. Magn. Reson. **9**, 439 (1977).
33. H. J. Reich, M. Jautelat, M. T. Messe, F. J. Weigert, and J. D. Roberts. J. Am. Chem. Soc. **91**, 7445 (1969).
34. S. Nishimura, M. Murai, and M. Shiota. Chem. Lett. 1239 (1980); S. Nishimura, I. Takahashi, M. Shiota, and M. Ishige. Chem. Lett. 877 (1981).
35. W. A. Thomas. Annu. Rep. NMR Spectrosc. **3**, 91 (1970).
36. T. Kikuchi, S. Kadota, S. Matsuda, and H. Suehara. Tetrahedron Lett. **25**, 2565 (1984).
37. D. D. Perrin, W. L. F. Armdrego, and D. R. Perrin. Purification of laboratory chemicals. 2nd ed. Pergamon Press, New York. 1982.
38. A. Wettstein. Helv. Chim. Acta, **23**, 1373 (1940).
39. E. B. Hershberg, E. P. Oliveto, C. Gerald, and L. Johnson. J. Am. Chem. Soc. **73**, 1144 (1951).
40. T. A. Wittstruck, J. K. Sliwowski, and E. Caspi. J. Chem. Soc. Perkin Trans. 1, 1403 (1977).

Further analysis of surface bond lengths measured for chemisorption on metal surfaces

K. A. R. MITCHELL, S. A. SCHLATTER, AND R. N. S. SODHI

Department of Chemistry, University of British Columbia, 2036 Main Mall, Vancouver, B.C., Canada V6T 1Y6

Received November 15, 1985

K. A. R. MITCHELL, S. A. SCHLATTER, and R. N. S. SODHI. Can. J. Chem. **64**, 1435 (1986).

This paper compares bond lengths deduced from the methods of surface crystallography with predictions from the Pauling–Schomaker–Stevenson approach and from a new alternative approach suggested by recent work of Brown and Altermatt. Examples considered are specifically for X—M surface bond lengths where atoms X from groups 16 or 17 are adsorbed on well-defined surfaces of a metal M. The alternative approach introduced here is parametrised with reference to structural data from solid compounds of formula MX. The two predictive approaches considered, when used together, appear to be quite adequate for guiding choices of trial model structures to be included in surface crystallographic analyses with low-energy electron diffraction (LEED); also they seem reasonable for checking the general reliability (or otherwise) of surface bond length data. Two further features introduced by this work are (*i*) evidence that the Cl—Ag distance reported by LEED for Cl adsorbed on the Ag(100) surface is broadly consistent with the structure of solid AgCl; (*ii*) evidence for S adsorbed on the Fe(110) surface that these analyses can guide investigations of lateral relaxations of surface metal atoms. As more reliable structural data become available, extensions of these analyses should help to identify the finer details in X—M bond lengths which result from the special coordination arrangements occurring at surfaces.

K. A. R. MITCHELL, S. A. SCHLATTER et R. N. S. SODHI. Can. J. Chem. **64**, 1435 (1986).

Dans ce travail, on compare les longueurs des liaisons déduites à l'aide de méthodes de cristallographie de surface avec les prédictions qui peuvent être faites à l'aide de l'approche de Pauling–Schomaker–Stevenson ainsi qu'à partir d'une nouvelle approche qui a été suggérée par un travail de Brown et Altermatt. Les exemples qui sont considérés sont reliés spécifiquement aux longueurs des liaisons X—M de surface, dans lesquelles les atomes X provenant des groupes 16 et 17 sont adsorbés sur des surfaces bien définies d'un métal M. Dans l'approche alternative introduite dans ce travail, on attribue les paramètres par référence avec des données de structure de composés solides de formule MX. Lorsqu'on utilise ensemble les deux méthodes de prédiction, elles semblent assez adéquates pour guider dans le choix de structures modèles qui peuvent être introduites dans des analyses de surfaces cristallographiques établies à l'aide de la diffraction électronique à basse énergie (LEED); elles semblent aussi raisonables pour vérifier la fiabilité générale (ou autre) des données relatives aux longueurs de liaison de surface. Dans ce travail, on a aussi introduit les deux caractéristiques suivantes: (*i*) les données relatives au fait que la distance Cl—Ag déterminée par LEED pour du Cl adsorbé sur la surface (100) de l'argent est généralement en accord avec la structure du AgCl solide; (*ii*) le fait que les analyses des données relatives au S adsorbé sur la surface (110) du fer peuvent servir de guide dans des études de relaxations latérales d'atomes métalliques de surface. Au fur et à mesure que des données de structure deviendront disponibles, des extensions de ces analyses devraient aider à identifier les détails plus fins des longueurs des liaisons X—M qui résultent d'arrangements spéciaux de coordinations se produisant sur les surfaces.

[Traduit par la revue]

Introduction

Structural information now becoming available for chemisorption on well-defined metal surfaces is opening a new dimension for structural chemistry. A recent review (1) discussed some approaches for assessing the general reasonableness, or otherwise, of structural data being produced by the methods of surface crystallography. This discussion emphasised the near-neighbour X—M interatomic distances observed when main-group atoms (X) are chemisorbed on crystallographically well-defined surfaces of metals (M). The approach of utilising bond order – bond length relations of the type used by Pauling, in combination with the Schomaker–Stevenson scheme for determining single-bond distances (2), often worked quite well for estimating surface X—M bond lengths, although a few instances remained of more substantial discrepancies between predicted and experimental values. The discrepancy for O adsorbed on the (111) surface of aluminum was identified as a problem for the Pauling–Schomaker–Stevenson (PSS) approach, although the situation was somewhat ambiguous in other cases, including that for Cl adsorbed on the (100) surface of silver. For the latter, the structural determination with low-energy electron diffraction (LEED) (3) appears basically reliable, but in terms of Pauling-type atomic radii the reported Cl—Ag distance seems long compared with the corresponding Cl—Cu distance for Cl adsorbed on Cu(100) (4, 5).

Another approach for predicting surface bond distances is to use bond valence – bond length relations deduced from computer analyses of solid state structures (6). A recent application to O—M interatomic distances at surfaces with specific expressions so given by Brown and Altermatt (7) showed improvements compared with the PSS approach, especially for predicting nearest-neighbour and next-nearest-neighbour bond lengths for O adsorbed on long-bridge sites of (110) surfaces of face-centered cubic metals (8). Models for the common adsorption sites observed in surface crystallography are detailed in ref. 9.

Potentially the Brown–Altermatt approach seems likely to provide a powerful scheme for interpreting surface structures, although the range of combinations of X and M for which bond valence – bond length expressions have been reliably established is still restricted. The expressions used in ref. 8 were for examples where the oxidation states of M were comparatively low (e.g. 1 or 2), however many of the other expressions provided by Brown and Altermatt are for M with oxidation states which seem too high for applications to chemisorption structures. Nevertheless, for future reference, it is noted that Brown and Altermatt also proposed an algorithm for estimating these expressions for wider ranges of atom combinations and oxidation states (7).

The present paper explores a new procedure which contains the gist of the Brown–Altermatt approach, while enabling estimates to be made for X—M surface bond lengths for a wide

TABLE 1. X—M interatomic distances from surface crystallographic techniques for adsorption of X atoms belonging to either group 16 or 17, and compared with values predicted by the PSS approach and by eq. [1]; n identifies the numbers of near-neighbours for atom X on the surface, and the values of r_0 for use in eq. [1] have been estimated for compounds of formula MX

				X—M distances (Å)		
X	Surface	r_0 (Å)	n	PSS	Eq. [1]	Surface crystallography
O	Ag(110)	1.84*	2	2.07	2.05	2.06(12)
			2	2.27	2.15	2.17(12)
Cl	Ag(100)	2.11	4	2.48	2.62	2.64(3)
I	Ag(111)	2.36	3	2.79	2.77	2.80(13), 2.87(14), 2.83(15)
O	Al(111)	1.65*	3	1.97	1.80	1.79(16), 1.81(17), 1.76(18)
O	Co(100)	1.71	4	2.00	1.97	1.94(19)
Cl	Cu(100)	1.84	4	2.34	2.35	2.37(4), 2.38(5)
I	Cu(100)	2.11	4	2.73	2.62	2.69(20)
I	Cu(111)		3	2.63	2.52	2.66(20)
O	Cu(100)	1.69	4	2.01	1.95	1.97(21), 1.94(22)
O	Cu(110)		2	1.88	1.84	1.84(23)
			2	2.21	2.09	2.00(23)
S	Cu(100)	1.99*	4	2.27	2.25	2.28(24)
Te	Cu(100)	2.32*	4	2.64	2.58	2.62(25)
Te	Cu(111)		6	2.78	2.73	2.69(25)
O	Fe(100)	1.75	4	2.10	2.11	2.08(26)
			1	1.98	2.01	2.02(26)
S	Fe(100)	2.04	4	2.31	2.34	2.30(27)
			1	2.54	2.60	2.52(27)
S	Fe(110)		2	2.18	2.21	2.17(28)
			2	2.37	2.40	2.36(28)
O	Ir(110)	1.87*	2	1.85	1.87	1.93(29)
O	Ir(111)		3	1.99	2.02	2.04(30)
S	Ir(111)	2.18*	3	2.25	2.33	2.28(31)
O	Ni(100)	1.67	4	1.99	1.93	1.98(32–34), 1.96(35)
O	Ni(110)		2	1.86	1.81	1.78(36)
			2	2.22	2.09	1.95(36)
O	Ni(111)		3	1.89	1.82	1.88(37)
S	Ni(100)	1.97*	4	2.25	2.23	2.19(32, 33, 38), 2.23(39)
S	Ni(110)		4	2.37	2.35	2.32(40), 2.35(41)
			1	2.24	2.18	2.18(40), 2.17(41)
S	Ni(111)		3	2.15	2.12	2.02(41)
Se	Ni(110)	2.09	4	2.39	2.35	2.28(32), 2.35(33, 42)
Se	Ni(110)		4	2.48	2.44	2.42(43)
			1	2.48	2.39	2.35(43)
Se	Ni(111)		3	2.29	2.24	2.31(43)
Te	Ni(100)	2.23	4	2.62	2.49	2.59(32), 2.52(33)
S	Pd(100)	2.07*	4	2.36	2.33	2.35(44)
S	Pd(111)		3	2.26	2.22	2.22(53)
S	Pt(111)	2.07*	3	2.28	2.22	2.28(45)
O	Rh(111)	1.82*	3	1.99	1.97	1.98(46)
S	Rh(100)	2.13*	4	2.33	2.39	2.30(47)
S	Rh(110)		4	2.49	2.52	2.45(48)
			1	2.22	2.31	2.12(48)
S	Rh(111)		3	2.23	2.28	2.18(49)
O	Ta(100)	1.80	4	2.16	2.06	2.00(ave)(50)
O	W(110)	1.89*	3	2.02	2.04	2.08(51)
O	Zr(0001)	1.90	6	2.39	2.31	2.31(52)

*Values estimated with Brown and Altermatt's algorithm (7); see text.

range of chemisorption systems and coordination arrangements. Several reasons can be identified for needing to predict surface bond lengths. One is to indicate reasonable structural models for testing with multiple-scattering calculations during LEED crystallographic analyses. A second reason involves assessing the general reliability of a determined surface structure. Finally, a third, but prospective, reason involves probing the finer details of determined bond distances to identify aspects of the surface chemical bonding. The latter is required as a step toward understanding energetics and important molecular processes on surfaces, including catalysis.

Calculations and results

The Brown–Altermatt (BA) method (7) depends on the expression

[1] $r = r_0 - 0.85 \log s$

for a particular interatomic distance of bond valence s, where r_0 is the corresponding distance for a bond of unit valence. Given r_0, X—M bond lengths can be calculated with eq. [1] on the assumption that the sum of bond valencies at each X equals the atomic valence v, which in the following is taken as the normal group value (e.g. 1 for F, Cl, ...; 2 for O, S, ...). For the case that X adsorbs on a metallic surface with n equivalent neighbouring M atoms, all the bond valencies equal v/n.

The present work explores ways for deducing plausible values of r_0 in situations which have not yet been assessed in detail by the type of procedures discussed by Brown and Altermatt. Specifically an attempt is made to deduce r_0 from the known coordination numbers of X and the corresponding sets of X—M neighbouring interatomic distances in a reference solid of formula MX. This particular choice is made in part because there is an appreciable amount of reference data available for this formula type, and therefore many systems can be readily compared on an equal footing. Other factors encouraging this choice are (*i*) the metal's oxidation state is necessarily fairly low (e.g. +1 or +2 when X is a halogen or chalcogen respectively), which seems appropriate for surface metal atoms, and (*ii*) this approach is broadly consistent with that which recently used detailed BA expressions for investigating structural data for oxygen chemisorption (8).

When information is available for more than one structure for a particular reference compound, such as AgI (10), a value of r_0 is determined for each and an average taken. Also, when structural information is unavailable (or uncertain) for a compound MX, the required value of r_0 is estimated with Brown and Altermatt's algorithm (7), except for metal sulphides where each BA estimate is systematically reduced by 0.08 Å (since otherwise the M—S surface bond lengths predicted by the algorithm appear to be too long when compared with experimental data or with predictions with the PSS approach). X—M bond lengths from surface crystallography are compared in Table 1 with predicted values for examples where X is either a group 16 or group 17 atom. The predicted values are from the PSS approach, as discussed in ref. 1, and from the use of eq. [1] as outlined above. For the latter, entries in Table 1 identify the value of r_0 used in each case for parametrising the analysis. Wherever possible values of r_0 were estimated with structural data compiled by Wyckoff (11), but where such data are unavailable the r_0 values were estimated from Brown and Altermatt's algorithm as described above (such values are identified with an asterisk in Table 1).

Discussion

For O adsorbed on the surfaces of Ag(110), Cu(110), Fe(100), and Ni(110), for S adsorbed on Fe(100), Ni(110), and Rh(110), and for Se adsorbed on Ni(110), two sets of X—M bond lengths are given in Table 1; these are to M atoms in the top metal layer and to those in the second metal layer. The latter are often predicted less well than for bonds to top layer M atoms, and in part this is because the calculations always assume that the topmost interlayer spacing in the metal equals the bulk value. Some distortions from bulk vertical spacings are now being recognised experimentally in this context, and this forms a topic of increasing interest; nevertheless, it probably remains premature to include such effects in an analysis (extensions from the treatment here would need to consider X—M and M—M bonding simultaneously). Even with the less reliable predictions for X—M bond distances to second metal layers, the average discrepancy between predicted surface bond distances and experimental values is about 0.05 Å with this use of eq. [1]; the average discrepancy for the PSS model as applied in ref. 1 is about 30% larger.

Overall the level of correspondence found with eq. [1] is more than sufficient for guiding choices of trial structures for LEED crystallography. Further, predictions from the two methods together appear to provide a helpful framework for assessing the general reliability of a surface structural determination. For example the problem associated with the PSS approach for O on Al(111) is avoided by using eq. [1]; additionally the comparison in Table 1 for this equation apparently supports the essential reliability of the LEED structural analysis for Cl on Ag(100). Thus the surface bond lengths for Cl adsorbed on the (100) surfaces of silver and copper are shown here to be generally consistent with the bulk structural data for AgCl and CuCl. Excluding bond distances to second layer metal atoms, there is just one example (S adsorbed on Ni(111)) where both approaches give predictions which disagree with the experimental value by 0.10 Å or more. For the use of eq. [1] alone, larger discrepancies occur for I on Cu(111) and for the adsorption of S on surfaces of rhodium. Incidentally, for the latter, if the solid $Rh_{17}S_{15}$ (54) is used to parametrise eq. [1], a value of r_0 equal to 2.01 Å is suggested. Then the predicted S—Rh bond distances on the (100), (110) (two), and (111) surfaces are 2.27, 2.45, 2.11, and 2.16 Å respectively, and the average discrepancy from the experimental values is reduced markedly compared with the values given for the use of eq. [1] in Table 1. For the latter, the estimated value of r_0 has already been reduced by 0.08 Å from that given by the BA algorithm. This reduction is empirical, and the evidence for S—Rh bonds may indicate that some further refinement could be advantageous; in any event the fundamental reasons for the need for this correction factor are not clear at present.

The LEED crystallographic analysis for S adsorbed on Fe(110) shows that the surface metal atoms relax laterally (28), and accordingly our analysis allows the top layer metal atoms to relax so that the two pairs of neighbouring S—Fe distances become more similar. The calculations made here for this system considered metal distortion from the unrelaxed (bulk) structure through to the fully "jammed" structure for the topmost layer, which is the structure observed by LEED (28). The average calculated S—Fe bond distances are found to decrease monotonically from the unrelaxed to the jammed structure according to both the PSS model and the use of eq. [1]. The distortion induced by S in the Fe(110) surface layer is appreciable. For the unreconstructed model, eq. [1] predicts pairs of bond lengths equal to 2.14 and 2.58 Å. The latter are significantly different from the values 2.21 and 2.40 Å which minimise the average S—Fe bond distance (and therefore are assumed to approximate the circumstances for maximum adsorption energy).

The values of r_0 used in this work for O—M bonds are generally close to those taken from Brown and Altermatt's tables and used in the recent analysis by two of the authors (8) (where common systems are treated the predicted O—M bond lengths in Table 1 equal those in ref. 8 to within 0.01 Å on average). To elaborate for O—Ni bonds, a value of r_0 equal to 1.67 Å (suggested by the structure of solid NiO) is used here, whereas 1.654 Å was used previously. One addition to the information in Table 1 for O adsorbed on Ni(100) should be noted, and this concerns the LEED analysis by Demuth *et al.* (55) which suggests that O atoms may be displaced from the 4-fold centre sites toward the bridge-bonding positions. No

confirmation has yet been provided for this structure, which has two pairs of O—Ni interatomic distances at 1.75 Å and 2.14 Å for each O atom. However, the structure proposed by Demuth *et al.* corresponds to a total bond valence of 2.17 at O when eq. [1] is used with r_0 equal to 1.67 Å. Indeed r_0 would just need to be reduced to 1.64 Å to give exact consistency with the conventional group valence of 2; therefore this structure is broadly consistent with the requirements of the BA relations.

Concluding remarks

This study, along with that published previously (1), should be seen as a preliminary investigation to interpret the structural data which are now emerging from the methods of surface crystallography. A very close overall correspondence between experiment and prediction cannot be expected at this stage, in part because of uncertainties which necessarily occur in the surface structural determinations. These are difficult to estimate in general, but the most recent and carefully made structural analyses yield X—M bond lengths which are likely to be accurate to within 0.03 Å. The choice made here of the reference compounds for parametrising eq. [1] is arbitrary, although the note made above for S adsorbed on rhodium suggests that refinements may be appropriate as more reliable structural data become available. However, for now, there is consistency in using a constant formula type, and, in any event, the bonding arrangement for X adsorbed on a well-defined crystallographic plane of a solid metal M is normally different from that occurring in any actual solid formed by X and M. Nevertheless, with carefully-made surface structural analyses, there remains the hope that extensions to the basic approach reported here should help to identify the finer details in X—M bond lengths which result from the special coordination arrangements required at surfaces.

Acknowledgement

We gratefully acknowledge the support of this research provided by the Natural Sciences and Engineering Research Council of Canada.

1. K. A. R. MITCHELL. Surface Sci. **149**, 93 (1985).
2. L. PAULING. The nature of the chemical bond. Cornell University Press, Ithaca, NY. 1960.
3. E. ZANAZZI, F. JONA, D. W. JEPSEN, and P. M. MARCUS. Phys. Rev. B**14**, 432 (1976); E. ZANAZZI and F. JONA. Surface Sci. **62**, 61 (1977).
4. P. H. CITRIN, D. R. HAMANN, L. F. MATTHEIS, and J. E. ROWE. Phys. Rev. Lett. **49**, 1712 (1982).
5. D. WESTPHAL, A. GOLDMANN, F. JONA, and P. M. MARCUS. Solid State Commun. **44**, 685 (1982).
6. I. D. BROWN. *In* Structure and bonding in crystals. Vol. 2. *Edited by* M. O'Keefe and A. Navrotsky. Academic Press, New York. 1981. p. 1.
7. I. D. BROWN and D. ALTERMATT. Acta Crystallogr. B**41**, 244 (1985).
8. K. A. R. MITCHELL and S. A. SCHLATTER. Can. J. Chem. **63**, 3631 (1985).
9. G. A. SOMORJAI. Chemistry in two dimensions: surfaces. Cornell University Press, Ithaca, NY. 1981.
10. M. J. MOORE and J. S. KASPER. J. Chem. Phys. **48**, 2446 (1968).
11. R. W. G. WYCKOFF. Crystal structures. Vol. 1. Interscience, New York. 1960.
12. A. PUSCHMANN and J. HAASE. Surface Sci. **144**, 559 (1984).
13. F. FORSTMANN, W. BERNDT, and P. BÜTTNER. Phys. Rev. Lett. **30**, 17 (1973).
14. P. H. CITRIN, P. EISENBERGER, and R. C. HEWITT. Phys. Rev. Lett. **41**, 309 (1978).
15. M. MAGLIETTA, E. ZANAZZI, U. BARDI, D. SONDERICKER, F. JONA, and P. M. MARCUS. Surface Sci. **123**, 141 (1982).
16. J. STÖHR, L. I. JOHANSSON, S. BRENNAN, M. HECHT, and J. N. MILLER. Phys. Rev. B**22**, 4052 (1980).
17. F. SORIA, V. MARTÍNEZ, M. C. MUÑOZ, and J. L. SACEDÓN. Phys. Rev. B**24**, 6926 (1981).
18. D. NORMAN, S. BRENNAN, R. JAEGER, and J. STÖHR. Surface Sci. **105**, L297 (1981).
19. M. MAGLIETTA, E. ZANAZZI, U. BARDI, F. JONA, D. W. JEPSEN, and P. M. MARCUS. Surface Sci. **77**, 101 (1978).
20. P. H. CITRIN, P. EISENBERGER, and R. C. HEWITT. Phys. Rev. Lett. **45**, 1948 (1980).
21. J. G. TOBIN, L. E. KLEBANOFF, D. H. ROSENBLATT, R. F. DAVIS, E. UMBACH, A. G. BACA, D. A. SHIRLEY, Y. HUANG, W. M. KANG, and S. Y. TONG. Phys. Rev. B**26**, 7076 (1982).
22. U. DÖBLER, K. BABERSCHKE, J. STÖHR, and D. A. OUTKA. Phys. Rev. B**31**, 2532 (1985).
23. U. DÖBLER, K. BABERSCHKE, J. HAASE, and A. PUSCHMANN. Phys. Rev. Lett. **52**, 1437 (1984).
24. J. J. BARTON, C. C. BAHR, Z. HUSSAIN, S. W. ROBEY, J. G. TOBIN, L. E. KLEBANOFF, and D. A. SHIRLEY. Phys. Rev. Lett. **51**, 272 (1983).
25. F. COMIN, P. H. CITRIN, P. EISENBERGER, and J. E. ROWE. Phys. Rev. B**26**, 7060 (1982).
26. K. O. LEGG, F. JONA, D. W. JEPSEN, and P. M. MARCUS. Phys. Rev. B**16**, 5271 (1977).
27. K. O. LEGG, F. JONA, D. W. JEPSEN, and P. M. MARCUS. Surface Sci. **66**, 25 (1977).
28. H. D. SHIH, F. JONA, D. W. JEPSEN, and P. M. MARCUS. Phys. Rev. Lett. **46**, 731 (1981).
29. C.-M. CHAN, K. L. LUKE, M. A. VAN HOVE, W. H. WEINBERG, and S. P. WITHROW. Surface Sci. **78**, 386 (1978).
30. C.-M. CHAN and W. H. WEINBERG. J. Chem. Phys. **71**, 2788 (1979).
31. C.-M. CHAN and W. H. WEINBERG. J. Chem. Phys. **71**, 3988 (1979).
32. J. E. DEMUTH, D. W. JEPSEN, and P. M. MARCUS. Phys. Rev. Lett. **31**, 540 (1973).
33. M. VAN HOVE and S. Y. TONG. J. Vacuum Sci. Technol. **12**, 230 (1975).
34. G. HANKE, E. LANG, K. HEINZ, and K. MÜLLER. Surface Sci. **91**, 551 (1980).
35. J. STÖHR, R. JAEGER, and T. KENDELEWICZ. Phys. Rev. Lett. **49**, 142 (1982); S. Y. TONG, W. M. KANG, D. H. ROSENBLATT, J. G. TOBIN, and D. A. SHIRLEY. Phys. Rev. B**27**, 4632 (1983).
36. H. NIEHUS and G. COMSA. Surface Sci. **151**, L171 (1985).
37. P. M. MARCUS, J. E. DEMUTH, and D. W. JEPSEN. Surface Sci. **53**, 501 (1975).
38. D. H. ROSENBLATT, J. G. TOBIN, M. G. MASON, R. F. DAVIS, S. D. KEVAN, D. A. SHIRLEY, C. H. LI, and S. Y. TONG. Phys. Rev. B**23**, 3828 (1981).
39. S. BRENNAN, J. STÖHR, and R. JAEGER. Phys. Rev. B**24**, 4871 (1981).
40. J. F. VAN DER VEEN, R. M. TROMP, R. G. SMEENK, and F. W. SARIS. Surface Sci. **82**, 468 (1979).
41. J. E. DEMUTH, D. W. JEPSEN, and P. M. MARCUS. Phys. Rev. Lett. **32**, 1182 (1974).
42. D. H. ROSENBLATT, S. D. KEVAN, J. G. TOBIN, R. F. DAVIS, M. G. MASON, D. A. SHIRLEY, J. C. TANG, and S. Y. TONG. Phys. Rev. B**26**, 3181 (1982).
43. D. H. ROSENBLATT, S. D. KEVAN, J. G. TOBIN, R. F. DAVIS, M. G. MASON, D. R. DENLEY, D. A. SHIRLEY, Y. HUANG, and S. Y. TONG. Phys. Rev. B**26**, 1812 (1982).
44. W. BERNDT, R. HORA, and M. SCHEFFLER. Surface Sci. **117**, 188 (1982).
45. K. HAYEK, H. GLASSL, A. GUTMANN, H. LEONHARD, M. PRUTTON, S. P. TEAR, and M. R. WELTON-COOK. Surface Sci. **152/3**, 419 (1985).
46. P. C. WONG, K. C. HUI, M. Y. ZHOU, and K. A. R. MITCHELL. Surface Sci. **165**, L21 (1986).

47. S. HENGRASMEE, P. R. WATSON, D. C. FROST, and K. A. R. MITCHELL. Surface Sci. **87**, L249 (1979).
48. S. HENGRASMEE, P. R. WATSON, D. C. FROST, and K. A. R. MITCHELL. Surface Sci. **92**, 71 (1980).
49. P. C. WONG, M. Y. ZHOU, K. C. HUI, and K. A. R. MITCHELL. Surface Sci. **163**, 172 (1985).
50. A. V. TITOV and H. JAGODZINSKI. Surface Sci. **152/3**, 409 (1985).
51. M. A. VAN HOVE and S. Y. TONG. Phys. Rev. Lett. **35**, 1092 (1975).
52. K. C. HUI, R. H. MILNE, K. A. R. MITCHELL, W. T. MOORE, and M. Y. ZHOU. Solid State Commun. **56**, 83 (1985).
53. F. MÁCA, M. SCHEFFLER, and W. BERNDT. Surface Sci. **160**, 467 (1985).
54. S. GELLER. Acta Crystallogr. **15**, 1198 (1962).
55. J. E. DEMUTH, N. J. DINARDO, and G. S. CARGILL III. Phys. Rev. Lett. **50**, 1373 (1983).

^{13}C magnetic resonance studies. 124.[1] Preparative ring expansions of bicyclic ketones by homoketonization of cyclopropoxide analogs

VIJAY PATEL,[2] ARTHUR J. RAGAUSKAS,[3] AND J. B. STOTHERS
Department of Chemistry, University of Western Ontario, London, Ont., Canada N6A 5B7

Received January 14, 1986

VIJAY PATEL, ARTHUR J. RAGAUSKAS, and J. B. STOTHERS. Can. J. Chem. **64**, 1440 (1986).

Homoketonization of some readily prepared cyclopropoxides provides a new synthetic method for ring expansion of the [2.2.1] and [2.2.2] ring systems. Cyclopropanation of the trimethylsilyl enol ethers derived from a variety of polycyclic ketones affords the required cyclopropyl silyl ethers, which may be ketonized directly or hydrolyzed to the corresponding cyclopropanols before ketonization. The results for fourteen examples serve to define the scope of the ring expansion process, and the silyl enol ethers, cyclopropyl silyl ethers, and most of the corresponding cyclopropanols have been characterized by ^{13}Cmr. The stereochemistry of the ketonization leading to ring expansion has been established by deuterium labelling experiments.

VIJAY PATEL, ARTHUR J. RAGAUSKAS et J. B. STOTHERS. Can. J. Chem. **64**, 1440 (1986).

L'homocétonisation de quelques éthers cyclopropaniques facilement accessibles fournit une nouvelle méthode de synthèse pour l'extension de cycle des systèmes [2.2.1] et [2.2.2]. La cyclopropanation des éthers énoliques triméthylsilylés, obtenus à partir de diverses cétones bicycliques, conduit aux éthers cyclopropyl/silyles requis qui peuvent soit être transformés en cétones directement soit être hydrolysés en cyclopropanols correspondants avant de les soumettre à la réaction de cétonisation. Les résultats obtenus avec quatorze exemples permettent de définir la généralité de ce processus d'extension de cycle; de plus, on a caractérisé les éthers énoliques silylés, les éthers cyclopropyle/silyles et la plupart des cyclopropanols correspondants en faisant appel à la rmn du ^{13}C. En se basant sur les résultats d'expériences réalisées à l'aide de produits marqués au deutérium, on a pu établir la stéréochimie de la réaction de cétonisation qui conduit à l'extension de cycle.

[Traduit par la revue]

Introduction

Efficient regiospecific homologation of unsymmetrical ketones has been the objective of many synthetic procedures and although the treatment of ketones with diazoalkanes (1), diazoacetic esters (2), and the Tiffeneau–Demjanov reaction (3) often proceeds in good yield these processes generally lead to mixtures of two regioisomers. Recently, in the course of an examination of the homoketonization of some highly substituted polycyclic cyclopropoxides (4), we found that the analogous derivatives of less highly substituted bicyclic [2.2.1] and [2.2.2] systems undergo ring expansion preferentially upon homoketonization (5), thereby affording an attractive new method of regiospecific homologation since the direction of ring expansion is predetermined by the structure of the cyclopropoxide species as outlined in Scheme 1. This sequence, developed by Girard and Conia (6) for a series of acyclic and monocyclic ketones, was utilized to generate several polycyclic

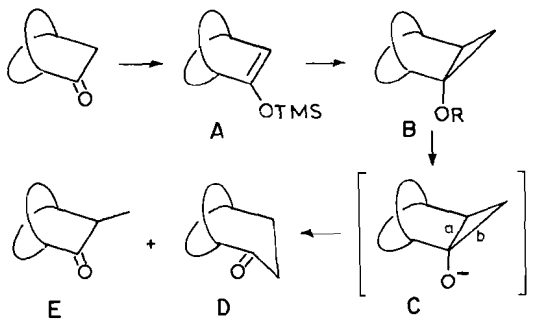

SCHEME 1

cyclopropanol derivatives to examine their behavior upon cleavage via homoketonization. Treatment of a given ketone with lithium diisopropylamide (LDA) followed by reaction with trimethylsilyl chloride (TMSCl) and triethylamine afforded the trimethylsilyl enol ether **A**; this procedure is a modification of that described by House *et al.* (7). Cyclopropanation with methylene iodide and a zinc–silver couple gave **B** (R = Me_3Si) which may be converted to the corresponding cyclopropanol **B** (R = H) with dilute HCl in tetrahydrofuran. In each case, a single cyclopropyl ether was formed in the cyclopropanation reaction and the orientation of the three-membered ring was deduced from the ^{13}C shielding data. Homoketonization via **C** can be accomplished directly from the ether **B** (R = Me_3Si) by base-catalyzed cleavage or by deprotonation of the cyclopropanol **B** (R = H) with dilute base. In either case, **C** is rapidly ketonized to a mixture of ketones with the ring-expanded isomer **D** as the major component for systems having one- or two-carbon bridges in the bicyclic skeleton. The minor product **E** is the α-methyl derivative of the initial ketone. For systems having one 3-carbon bridge the α-methyl ketone is the major product. The ^{13}Cmr spectra served to identify the ketonic products in each case. Protonation of the carbanion leading to **D**, generated upon ketonization of **C**, can occur with either retention or inversion of configuration and the stereochemistry of the process has been established by ^{13}C studies of the product from the requisite deuterium labelling experiments in four systems. We wish to describe the results of this study in this paper.

Results and discussion

Originally our interest in an examination of homoketonization of cyclopropoxide units in polycyclic systems arose from our ongoing investigation of homoenolization in polycyclic ketones. As an initial step, the sequence outlined in Scheme 1 was carried out with norcamphor (**1***a*) as a model compound for the development of the required preparative procedures for related ketones. The conversion of **1***a* to its trimethylsilyl enol ether followed by cyclopropanation and treatment with dilute

[1]For Part 123, see ref. 27; for Part 122, see ref. 28; for Part 121, see ref. 29.

[2]Present address: Research and Development Department, 3M Canada Inc., London, Ont., Canada.

[3]Present address: Department of Chemistry, University of Alberta, Edmonton, Alta., Canada.

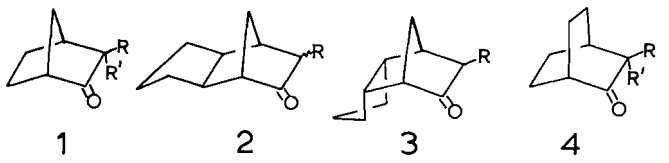

1 2 3 4

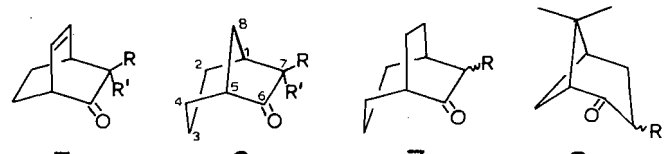

5 6 7 8

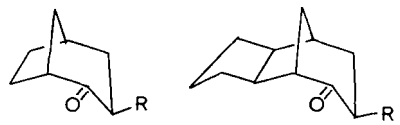

9 10

a R = R' = H
b R = Me; R' = H
c R = R' = Me

acid gave tricyclo[3.2.1.$0^{2,4}$]octan-2-ol in 60% overall yield, which, upon treatment with base at room temperature, afforded an essentially quantitative yield of bicyclo[3.2.1]octan-2-one. Clearly, we had observed a simple *regiospecific* ring expansion under mild conditions. To explore the potential of this process, ketones **2***a*–**10***a* were selected for further examination, since these provide a systematic series through the [2.2.1], [2.2.2], [3.2.1], [3.2.2], and [3.1.1] ring systems. The ketonization of **C** (Scheme 1) involves cleavage of either bond *a* or *b*, leading to either ring expansion to **D** (via *a* cleavage) or the α-methyl derivative **E** of the starting ketone (via *b* cleavage). The results for the series **1***a*–**10***a* should shed light on the balance between these two modes of cleavage.

Ketones **1***a*–**10***a* were converted to their trimethylsilyl enol ethers by reaction with LDA and TMSCl in 75–98% yields upon isolation by short-path distillation under reduced pressure. These enol ethers were characterized by their ^{13}Cmr spectra and the data are collected in Table 1, which includes precise mass measurements for most of the products. Cyclopropanation with CH_2I_2 and a Zn–Ag couple afforded the expected Simmons–Smith product, in each case as a single isomer as revealed by glc analysis and ^{13}Cmr; the ^{13}C data are listed in Table 2. Mild acid-catalyzed ether cleavage of these substituted cyclopropyl ethers furnished the corresponding cyclopropanols in high yield. For several examples, the cyclopropanol was isolated and examined by ^{13}Cmr; these shielding data are included in Table 2, from which it is evident that the trimethylsilyl group on oxygen in the ether has very minor effects on the skeletal carbon shieldings.

The orientation of the methylene group introduced by the Simmons–Smith cyclopropanation reaction was evident for **11***a*, derived from norcamphor (**1***a*), by the ^{13}C shielding data since the cyclopropyl methylene has marked effects on the methano bridge carbon in polycyclic systems as shown by the data for **15**–**17**. The *exo*- and *endo*-cyclopropyl rings produce major shielding and deshielding effects, respectively, at the methano bridge carbon. Exactly analogous trends have been observed for the saturated analogs of **15**–**17** (8), the tricyclo[3.1.1.$0^{2,4}$]- and tetracyclo[4.1.0.$0^{2,4}0^{3,5}$]heptane (9), and the tricyclo[3.3.1.$0^{2,4}$]- and tetracyclo[3.3.1.$0^{2,4}0^{6,8}$]nonane (10) systems. The observed methylene signals for **11***a* at δ_C 9.8, 24.7, 29.1, and 31.2, therefore, clearly show that this product arises by *exo*-cyclopropanation. In the event of *endo* cyclopropanation, the methano carbon would appear in the range of 45–50 ppm; the absence of such absorption in the spectra of **11***a*–*f*, **13***a*,*b* and *e*,*f* established the *exo* orientation of the cyclopropyl ring in each case. For **12***c*,*d* and *g*,*h* derived from the bicyclooctenones **5***a* and **5***b*, the *endo* disposition of the cyclopropyl ring is based on the observed olefinic shieldings in the range δ_C 129.6–132.8, which are upfield from those in bicyclooctene, δ_C 134.1 (11), and the upfield shift exhibited by C-8 in **12***c*,*d*, ascribable to a γ-*gauche* interaction with the neighboring oxygen nucleus; the data for several bicyclooctene derivatives (11) support this assignment. Cyclopropanation of **18**, derived from nopinone (**8***a*), was expected to favor formation of **14***a* since addition to the other side of the double bond would be hindered by the *syn* methyl group; strong support for the assigned structure is provided by the data for a series of 6,6-dimethyltricyclo[4.1.1.$0^{2,4}$]octanes (12). Specifically, the shieldings for the 2,6,6-trimethyl derivative are remarkably similar to those for **14***b*, as expected, since the shielding effects of hydroxyl and methyl substituents are known to be very similar, apart from the α-effects. The orientation of the cyclopropyl ring in **13***c*,*d*, **14***c*, *d*, and *e* is more difficult to assign with certainty although an examination of molecular models led us to the indicated assignments. It may be noted that epimerization of *exo*-3-methylbicyclo[2.2.1]octan-2-one (**9***b*) fails to produce detectable amounts of the *endo*-3-methyl isomer (13), which clearly suggests that isomers **14***c*, *d*, and

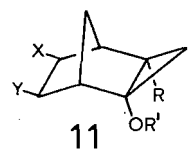

11

	R'	R	X	Y
a	TMS	H	H	H
b	H	H	H	H
c	TMS	H	exo-$(CH_2)_3$	
d	TMS	H	endo-$(CH_2)_3$	
e	TMS	Me	H	H
f	H	Me	H	H

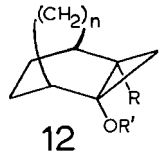

12

	n	R'	R
a	2	TMS	H
b	2	H	H
c	2(Δ^6)	TMS	H
d	2(Δ^6)	H	H
e	2	TMS	Me
f	2	H	Me
g	2(Δ^6)	TMS	Me
h	2(Δ^6)	H	Me

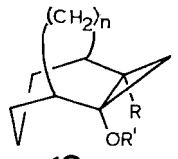

13

	n	R'	R
a	1	TMS	H
b	1	H	H
c	2	TMS	H
d	2	H	H
e	1	TMS	Me
f	1	H	Me

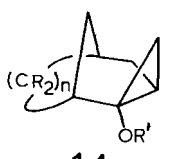

14

	n	R'	R_2
a	1	TMS	Me_2
b	1	H	Me_2
c	2	TMS	H_2
d	2	H	H_2
e	2	TMS	exo-$(CH_2)_3$

TABLE 1. ^{13}C shieldings,[a] yields, and precise masses of the trimethylsilyl enol ethers derived from ketones **1–10**

Ketone	Yield[b] (%, enol ether)	δ_C C-1	C-2	C-3	C-4	C-5	C-6	C-7	C-8	C-9	C-10	C-11	Me_3Si	Me	*Exact Mass*[c]
1*a*	76	45.9	161.5	104.9	41.4	28.2	24.9	47.3					0.0		
2*a*	98	45.2	46.2	(31.1)	(31.1)	31.5	49.8	50.6	164.4	106.7	40.7		0.1		222.1440 (calcd.)
															222.1445 (obsd.)
3*a*	90	47.5	44.5	(29.2)	(29.0)	(31.0)	47.8	50.4	161.6	103.2	52.4		0.0		222.1440 (calcd.)
															222.1444 (obsd.)
4*a*	80	36.1	156.9	105.1	30.4	27.4	26.4	26.4	27.4				0.3		196.1283 (calcd.)
															196.1279 (obsd.)
5*a*	95	42.9	160.1	104.9	36.4	(136.4)	(133.1)	25.2	26.4				0.2		194.1127 (calcd.)
															194.1121 (obsd.)
6*a*	84	37.9	26.9	19.3	24.6	42.4	157.2	101.8	44.0				0.1		196.1283 (calcd.)
															196.1269 (obsd.)
7*a*	80	31.5	32.0	23.5	29.6	38.9	158.5	106.1	27.1	26.6			0.4		210.1440 (calcd.)
															210.1444 (obsd.)
8*a*	90	48.4	159.4	95.5	31.5	41.2	38.7	28.2					0.4	21.2	210.1440 (calcd.)
														26.2	210.1441 (obsd.)
9*a*	75	41.8	157.3	97.4	(35.7)	33.5	(34.9)	30.7	34.4				0.5		
10*a*	89	40.5	46.7	33.1	28.6	33.7	50.1	54.2	158.0	97.3	30.3	35.0	0.6		236.1596 (calcd.)
															236.1594 (obsd.)
1*b*	73	46.1	153.2	116.3	45.9	(26.5)	(26.7)	45.6					0.5	10.0	
4*b*	67	36.5	148.4	115.2	36.2	27.4	26.6	26.6	27.4				0.6	13.7	210.1440 (calcd.)
															210.1447 (obsd.)
5*b*	67	43.0	151.4	115.5	42.4	(135.7)	(133.7)	25.4	26.3				0.6	18.7	208.1283 (calcd.)
															208.1273 (obsd.)

[a]In ppm from internal TMS for C_6D_6 solutions, calibrated from the central line of the solvent signal (δ_C 128.0); values in parentheses may be interchanged.
[b]Isolated by Kugelrohr distillation and the purity assessed by glc (see Experimental).
[c]For analytical samples obtained by glc.

TABLE 2. ^{13}C shieldings,[a] yields, and precise masses of several polycyclic cyclopropyl trimethylsilyl ethers and corresponding cyclopropanols

Compound	Yield[b] (%)	δ_C C-1	C-2	C-3	C-4	C-5	C-6	C-7	C-8	C-9	C-10	C-11	Me_3Si	Me	*Exact Mass*[d]
11*a*	78	42.5	61.0	9.8	22.2	36.6	29.1	24.7	31.2				1.1		196.1289 (calcd.)
															196.1278 (obsd.)
11*b*		41.9	59.8	9.7	22.5	36.7	28.8	24.7	31.1						124.0888 (calcd.)
															124.0884 (obsd.)
11*c*	94	41.1	48.4	(31.3)	28.2	(31.0)	43.7	46.9	62.8	13.8	23.9	24.8	1.2		236.1596 (calcd.)
															236.1596 (obsd.)
11*d*	87	41.2	48.1	(29.4)	26.5	(28.9)	47.1	45.5	60.3	10.4	17.5	34.9	0.0		236.1596 (calcd.)
															236.1601 (obsd.)
11*e*	58	43.1	63.4	15.1	21.7	41.1	25.2	23.5	31.8				1.0	12.7	210.1440 (calcd.)
															210.1434 (obsd.)
11*f*		42.7	62.4	15.2	22.7	41.6	25.2	23.7	31.8					12.7	
12*a*	70	32.2	58.1	11.5	23.0	25.3	26.0	25.1	22.6	23.4			1.3		210.1440 (calcd.)
															210.1447 (obsd.)
12*b*		31.7	56.6	11.7	23.3	25.4	26.0	25.4	22.7	23.4					
12*c*	90	38.6	57.5	10.7	18.1	31.6	132.4	129.9	21.2	25.4			1.2		208.1283 (calcd.)
															208.1281 (obsd.)
12*d*		38.4	55.9	11.1	18.7	31.8	132.8	129.6	21.4	25.4					136.0888 (calcd.)
															136.0891 (obsd.)
12*e*	75	32.7	62.1	17.0	22.8	31.2	25.1	24.9	22.5	23.2			1.1	16.0	224.1596 (calcd.)
															224.1604 (obsd.)
12*f*		32.3	60.5	17.3	23.5	31.5	25.4	24.9	22.6	23.3				15.7	
12*g*	55	39.2	60.8	16.5	17.0	37.4	(131.8)	(132.3)	20.6	22.0			1.2	14.9	222.1440 (calcd.)
															222.1435 (obsd.)
12*h*		38.7	59.3	16.7	18.3	37.7	(131.9)	(132.1)	20.8	22.1				14.6	
13*a*	70	39.1	62.5	13.6	25.2	34.8	32.2	19.5	28.9	34.3			1.5		210.1440 (calcd.)
															210.1447 (obsd.)
13*b*		38.5	61.5	13.7	25.6	35.0	31.9	19.4	28.4	34.2					138.1045 (calcd.)
															138.1039 (obsd.)
13*c*	51	37.1	59.6	16.3	26.1	31.7	34.8	22.0	30.2	22.0	24.5		1.5		224.1596 (calcd.)
															224.1600 (obsd.)
13*d*		36.9	57.9	16.6	26.8	31.8	34.8	22.1	30.3	21.9	24.5				
13*e*	[c]	40.4	65.4	19.8	25.1	38.2	29.5	19.1	28.7	34.3			1.1	13.1	224.1596 (calcd.)
															224.1590 (obsd.)
13*f*		39.3	64.3	19.8	26.0	38.5	29.3	19.1	28.1	34.1				12.9	
14*a*	66	47.2	61.0	20.0	16.6	28.6	42.1	41.0	26.8				1.5	21.4	224.1596 (calcd.)
														26.7	224.1591 (obsd.)
14*b*		46.7	60.2	19.8	17.2	28.6	41.7	40.8	26.5					21.0	152.1196 (calcd.)
														26.3	152.1201 (obsd.)
14*c*	67	40.1	60.9	20.2	15.3	(35.3)	32.9	29.8	27.3	(34.1)			1.5		210.1440 (calcd.)
															210.1447 (obsd.)
14*d*		39.7	59.1	20.5	15.9	(35.2)	32.9	29.8	27.3	(34.1)					
14*e*	76	39.5	44.8	34.7	28.1	33.0	45.2	48.8	61.6	15.2	20.2	28.5	1.4		250.1753 (calcd.)
												33.2(C-12)			250.1759 (obsd.)

[a]In ppm from internal TMS for C_6D_6 solutions, calibrated from the central solvent peak (δ_C 128.0); similar values in parentheses may be interchanged.
[b]For the cyclopropyl ethers, acid hydrolysis to the corresponding cyclopropanols proceeded in 90–95% yields.
[c]See text.
[d]For analytical samples obtained by glc.

TABLE 3. Homoketonizations of cyclopropyl derivatives of ketones **1***a*–**10***a*

Initial ketone	Cyclopropyl derivative	Temperature (°C)	Products[a] Ring-expansion Compound	%	α-Methylation Compound	% (*exo*:*endo*)
1*a*	**11***a*	25	**9***a*	>98	**1***b*	Trace
		83		96		4 (1:1)
	11*b*	25		>98		Trace
		83		93		7 (1:1)
2*a*	**11***c*	0	**10***a*	>99	**2***b*	—
		25		>98		Trace
		83		94		6 (1:1)
3*a*	**11***d*	0	**19**	68	**3***b*	32 (*exo*)
4*a*	**12***a*	25	**20***a*	70	**4***b*	30
		83		50		50
	12*b*	25		73		27
		83		47		53
5*a*	**12***c*	25	**Δ⁶-20***a*	95	**5***b*	5
	12*d*	0		95		5
		25		92		8 (0.5)
		83		87		13
6*a*	**13***a*	0	**21**	60	**6***b*	40
		25		52		48 (1:1)
		83		32		68
7*a*	**13***d*	25	**22**	~5[b]	**7***b*	~95 (1:1)
8*a*	**14***a*	25		—	**8***b*	>99 (5:1)
	14*b*	25		—		>99
9*a*	**14***c*	25	**23**	23	**9***b*	77 (*exo*)
	14*d*	25		20		80
10*a*	**14***e*	25	[c]	—	**10***b*	>95 (*exo*)

[a]Proportions of products determined by glc (±3%); *exo*:*endo* ratios estimated by ^{13}Cmr (±5%).
[b]Estimated by ^{13}Cmr since insufficient resolution obtained by glc.
[c]Minor component presumably a condensation product (^{13}Cmr).

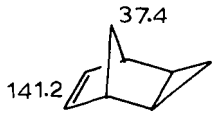

15

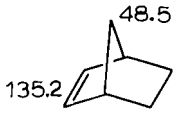

16

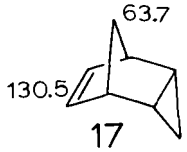

17

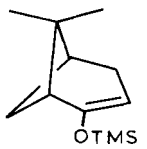

18

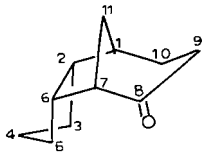
19

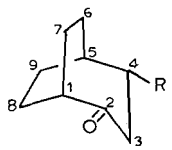
20 *a* R = H *b* R = Me

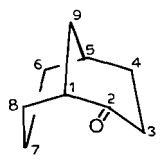
21

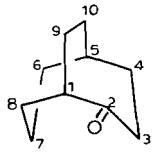
22

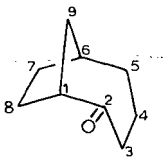
23


24

e are significantly more stable than their *endo* counterparts, thereby precluding formation of the latter. The lack of appropriate model data renders the assignments for **13***c*,*d* more tenuous and these indeed may have *endo*-cyclopropyl rings but, in any event, the cyclopropanation reaction gave a single isolable addition product.

In the early stages of this project, the cyclopropanols were obtained from the trimethylsilyl ethers to permit direct generation of the corresponding cyclopropoxide for examination of the homoketonization process. While the acid-catalyzed ether cleavage proceeds in essentially quantitative yield, the cyclopropanols are much less stable than their corresponding trimethylsilyl ethers and, consequently, do not store well. Furthermore, these cyclopropanols tend to decompose on attempted analysis by glc, yielding the α-methyl derivative of the initial ketone. As examples, it was found that a single α-methyl ketone was found in >80% yield for **11***b* → **1***b*, **12***d* → **5***b*, **13***b* → **6***b*, and **14***b* → *exo*-**8***b*. Since the α-methyl ketones are not epimerized on the glc columns, this shows that their stereochemistry is predetermined by the structure of the cyclopropanol. Thus these transformations confirm the stereochemical assignments for these cyclopropanols. Treatment of the cyclopropyl ethers with base, however, accomplishes cleavage and homoketonization of the resulting cyclopropoxide in one step and was shown to give the same mixture of products. For preparative purposes this is clearly the method of choice for cleavage of the cyclopropyl ring.

The results for homoketonization of the cyclopropanated

TABLE 4. ^{13}C shieldings[a] and precise masses of ring-expanded ketones from **1***a*, **4***a*,*b*, **5***a*,*b*, **7***a*, and **9***a*

Compound	δ_C C-1	C-2	C-3	C-4	C-5	C-6	C-7	C-8	C-9	C-10	Me	*Exact Mass*[d] calcd.	obsd.
20*a*	45.4	217.4	38.7	29.2	28.0	24.8	22.3	22.3	24.8			138.1045	138.1039
Δ^6-**20***a*	49.3	209.7	39.4	30.7	31.2	136.7	127.9	24.1	25.0			136.0888	136.0883
22*b*	47.0	216.2	44.3	34.2	35.5	35.2	21.6	28.5	24.4	25.2			
23	52.0	217.3	42.6	20.9	(35.9)	38.9	30.6	29.4	(36.1)			138.1045	138.1041
4-Me-**9***a*[c]	50.3	213.8	43.4	37.2	40.4	22.4	28.1	38.6			19.4	138.1045	138.1043
20*b*	44.8	217.2	47.2	35.3	34.5	26.9	22.3	23.0	18.8		22.0	152.1201	152.1195
Δ^6-**20***b*	48.4	209.8	48.5	(37.78)	(37.85)	138.3	126.5	23.9	17.9		21.9	150.1045	150.1041

[a]In ppm from internal TMS in $CDCl_3$ solutions; values in parentheses may be interchanged.
[b]Data obtained from a mixture with **7***b*.
[c]Data previously reported (4) but not assigned.
[d]For analytical samples obtained by glc.

derivatives of the ten ketones **1***a*–**10***a* are summarized in Table 3; for five of these cases the trimethylsilyl cyclopropyl ethers and their corresponding cyclopropanols were examined to establish that both routes give the same product mixture within experimental error. In each case, the α-methyl ketones were readily identified by their ^{13}C spectra, all of which had been reported previously: **1***b* (15), **2***b*, **3***b*, and **10***b* (11), **4***b* and **5***b* (17), **6***b*–**9***b* (13). The ring-expanded ketones were shown to be isomeric by ms and their ^{13}C spectra lacked methyl absorption; the ^{13}C shieldings are listed in Table 4 except for **19** (16) and **21** (18) for which these data have been published.

From the product mixtures for the derivatives of **1***a* and **2***a* it is readily apparent that ring expansion is the highly favored mode for ketonization in these [2.2.1] systems. In fact, the efficacy of this new process for ring expansion in **1***a* led to the examination of **2***a* as a model system for a proposed synthesis of hirsutene, which required an analogous ring expansion of the Δ^3-derivative of **2***a* as a key step and was subsequently found to work well (14). For **3***a*, the third member of the [2.2.1] family, ring expansion is clearly favored although to a lesser extent than the others. For both of the [2.2.2] systems, **4***a* and **5***a*, ring expansion is favored, more highly so in the unsaturated case. With the isomeric bicyclo[3.2.1]octanones, **6***a* and **9***a*, however, the proportion of ring-expanded product decreases significantly, especially for the latter in which the initial carbonyl group is in the 3-carbon bridge. For the remaining examples **7***a*, **8***a*, and **10***a*, their α-methyl derivatives were obtained in >95% yields. In the case of **7***a*, the ring-expanded product was clearly identified, although it was not obtained in a pure state because all separation attempts with glc failed to resolve the product mixture, and the proportions of **22** and **7***b* were estimated from the ^{13}C spectrum of the mixture. For **8***a*, the only product was **8***b*, as a 5:1 mixture of *exo* and *endo* isomers. The minor component (<5%) formed from **10***a* appeared to be a condensation product from its ^{13}C spectrum, but this material was not fully characterized.

The results in Table 3 show clearly that there is a delicate balance between the two modes of ring opening for these cyclopropoxides with the ratio of bond cleavage *a*:*b* (see **C**, Scheme 1) varying from ~100:1 to ~1:100. It is also apparent that cleavage leading to ring expansion is increasingly favored with decreasing reaction temperature for **11***a*–*c*, **12***a*–*d*, and **13***a*. Two major opposing factors governing the regioselectivity in a given system can be envisaged. Cleavage of bonds *a* and *b* will lead to incipient secondary and primary carbanions, respectively, and the latter may be inherently favored because of the greater stability of the 1° species and the fact that it should be less hindered for protonation. On the other hand, cleavage of bond *a* can be expected to relieve ring strain in some systems thereby rendering it the favored mode of reaction, i.e. a dependence on product stability. Presumably the importance of this factor will diminish as the size of the bridges in the ring system increase, and the proportion of ring-expanded product will reflect this trend. It is apparent that ring expansion is decreasingly favored in the saturated series in the order: [2.2.1], [2.2.2], [3.2.1], [3.2.2], and the unsaturated [2.2.2] skeleton gives a higher proportion of ring expansion than its saturated counterpart; these trends agree with expectations. It may be noted that ring expansion is less favored in the **3***a* system than in the isomeric **2***a* system. This also fits nicely with expectations, since **10***a* formed in the latter case will be more stable than the isomeric **19** arising from **3***a* because the favored conformation of the six-membered ring in each will be different. The chair form, readily adopted in **10***a*, would be destabilized by nonbonded interactions with the *endo*-3- and -5-methylenes in **19** rendering a boat-like conformation more favorable, thereby destabilizing **19** relative to **10***a*. In any event, the homoketonization results show that the sequence in Scheme 1 is useful for preparative ring expansions in the [2.2.1], [2.2.2], and related systems. As examples we have utilized this sequence for the corresponding homologations of the tricyclo[3.2.1.$0^{2,4}$]octan-6-ones (10) and of tricyclo[5.2.1.$0^{1,5}$]decan-8-one (**24**) (19).

The opening of cyclopropoxide **C** to the ring-expanded ketone **D** (Scheme 1) can proceed with retention or inversion of configuration at the carbanionic site and the stereochemistry of the process can be determined by cleavage in a deuterated medium as illustrated by *a* and *b*, respectively, in Scheme 2 for cyclopropoxide **25** formed from **11***a* and **11***b*. In general, ketonizations of cyclopropoxides in polycyclic systems are found to undergo inversion of configuration, but some strained systems exhibit retention (20) and it was, therefore, of interest to determine the stereoselectivities in the **1***a*, **2***a*, **5***a*, and **6***a* systems. To distinguish between paths *a* and *b*, **11***a* was cleaved in KOD/*t*-BuOD at 25°C and the product treated with KOH/MeOH to back-exchange the α-deuterium incorporated after the cleavage. The ^{13}Cmr spectrum of a 1:1 mixture of **9***a* with the **9***a*-d_1 obtained in this manner was recorded to observe the effects of the 4-deuterium on its neighboring carbon absorptions to determine its stereochemistry. The orientation of the deuterium is revealed by the magnitude of the vicinal

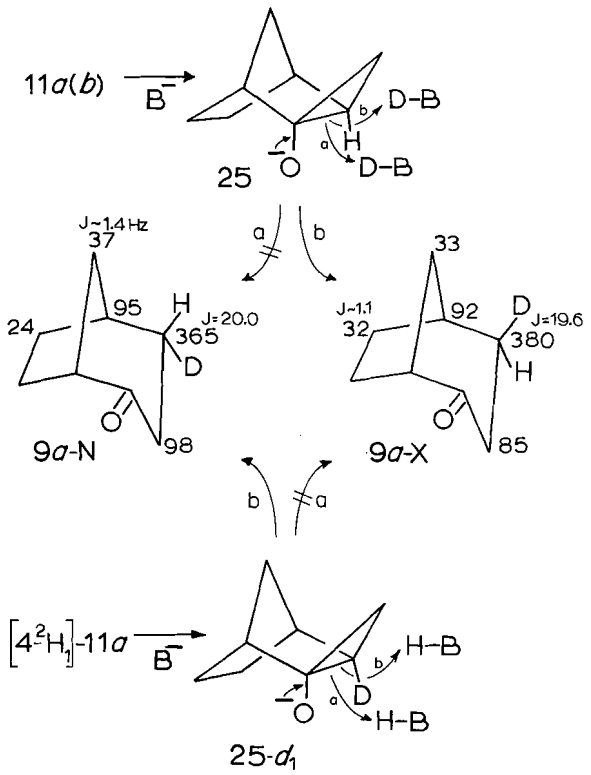

SCHEME 2

^2H–^{13}C coupling interactions and the ^2H-induced isotope shifts (21). From this spectrum *exo*-deuterium incorporation was revealed; the observed isotope effects on the ^{13}C shieldings in ppb and the resolved vicinal couplings are shown in **9***a*-**X**. A key feature is the observation of vicinal ^{13}C–^2H coupling for C-6 with $J = 1.1$ Hz, while C-8 is only slightly broadened; this is indicative of deuterium antiperiplanar to C-6 and, therefore, in the *exo* orientation. To confirm this conclusion, a sample of [3,3-$^2H_1$]-**1***a* was converted to [4-$^2H_1$]-**11***a*, which was subsequently opened with NaOH/MeOH to form **9***a*-d_1. The ^{13}C spectrum of a 1:1 mixture of this material and **9***a* exhibited the ^2H effects shown for **9***a*-**N** (Scheme 2). In this case, the C-8 pattern revealed a vicinal coupling of 1.4 Hz while the C-6 signal was slightly broadened by the deuterium, indicating that C-8 and ^2H-4 are antiperiplanar, i.e. *endo*-^2H-4. These data establish that the cleavage of **25** proceeds with inversion. It may be noted that the patterns for C-3 and C-5 exhibited resolved geminal couplings of 0.6 Hz with ^2H-4; thus an upper limit of ca. 0.3 Hz may be suggested for the C-6, ^2H-4 vicinal interaction. The analogous experiments with **11***c* and [10-$^2H_1$]-**11***c* gave the isomeric monodeuterated ketones **10***a*-**X** and **10***a*-**N**, respectively, exhibiting the ^2H–^{13}C couplings and ^2H-induced shifts noted in the structural formulas. These constitute good evidence of the presence of *exo*- and *endo*-deuterium, respectively, at C-10 and, hence, for inversion of configuration upon homoketonization of the cyclopropoxide generated from **11***c*.

Treatment of **13***a* with KOD/*t*-BuOD, followed by back-exchange with KOH/MeOH, furnished a sample of **21**-d_1, tentatively identified as **21**-**X**, having the ^2H effects in the ^{13}C spectrum indicated. A sample of [4-$^2H_1$]-**13***a*, prepared from [7,7-$^2H_2$]-**6***a*, was opened with NaOH/MeOH to form **21**-d_1, which displayed the ^2H effects shown in **21**-**N** in its ^{13}C spectrum. These assignments required reversal of the shieldings

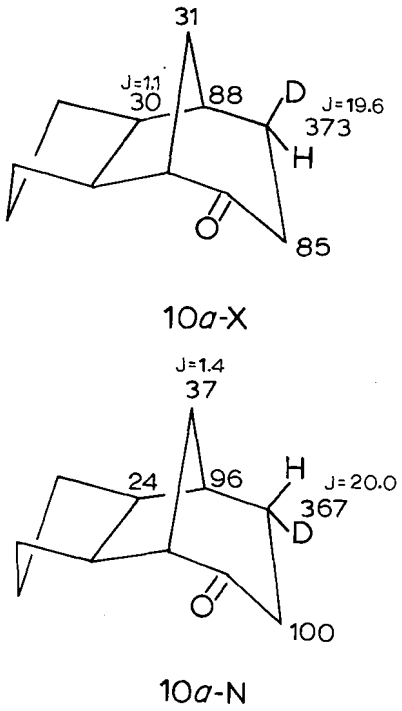

originally ascribed (18) to C-6 and C-9, but followed from the fact that the methylene absorption at δ_C 32.5 (C-6) exhibits vicinal ^{13}C-^2H coupling in both monodeuterated samples while that at δ_C 32.0 (C-9) has resolvable coupling in only one. For each of these samples, geminal couplings of 0.5 Hz were readily resolved for C-3 and C-5. The six-membered ring containing the carbonyl group in **21** will be a mixture of chair and skew-boat forms, thereby rendering the ^2H effects different from those found for the isomeric pairs of [4-$^2H_1$]-**9***a* and [10-$^2H_1$]-**10***a* described above. In either conformation, an *endo*-4-deuterium atom (**21**-**N**) will be antiperiplanar to C-9 and resolvable vicinal coupling would be expected. For the *exo*-4-^2H isomer, however, the dihedral angles relating the deuterium atom and C-9 will be ca. 60° and ca. 90° for the chair and skew-boat forms for which the vicinal coupling is expected to be small. On this basis, we conclude that ketonization of **13***a* also proceeds with inversion.

The stereochemistry of cyclopropoxide cleavage was also examined in the unsaturated [2.2.2] system. Treatment of **12***c* with KOD/*t*-BuOD, followed by back-exchange with KOH/MeOH, gave a sample of the monodeuterated ring-expanded ketone **26**-**N**. Its ^{13}C spectrum exhibited distinctive ^2H effects in four of the signals while the olefinic absorption at δ_C 136.7 was slightly broadened. In contrast, the spectrum of a sample of this ketone obtained by cleavage of [4-$^2H_2$]-**12***c* with NaOH/MeOH revealed vicinal ^{13}C–^2H coupling of 1.1 Hz for this olefinic signal whereas the C-6 signal was only broadened, but shifted by 32 ppb; this is consistent with structure **26**-**X**. Thus, homoketonization of **23***c* proceeds with inversion of configuration.

The ^2Hmr spectra of each of the monodeuterated ketones obtained in these homoketonization experiments were recorded to determine the stereoselectivity of the cleavages. In each case, a single ^2H signal was observed, indicating that the stereoselectivities are >98% favoring inversion of configuration for each system. The positions of these signals in $CHCl_3$ solutions were (δ): 1.70 (**9***a*-**X**), 1.79 (**9***a*-**N**), 1.67 (**10***a*-**X**), 1.83 (**10***a*-**N**), 2.06 (**21**-**X**), 1.79 (**21**-**N**), 1.91 (**26**-**N**), and 1.79

TABLE 5. Base-catalyzed homoketonizations of **11***e*,*f*, **12***f*,*h*, and **13***f*

Initial ketone	Cyclopropyl derivative	Temperature (°C)	Products: Ring-expansion Compound	Ring-expansion %	α,α-Dimethyl derivatives Compound	α,α-Dimethyl derivatives %
1*b*	**11***e*	25	4-Me-**9***a*[a]	37	**1***c*	63
		83		20		80
	11*f*	25		35		65
4*b*	**12***f*	25	**20***b*	Trace	**4***c*	>99
5*b*	**12***h*	25	Δ[6]-**20***b*	22	**5***c*	78
		83		19		81
6*b*	**13***f*	25	[b]	<10	**6***c*	>90

[a]Reference 4.
[b]The proportion of ring-expanded product (?) was estimated by glc but the material was not identified.

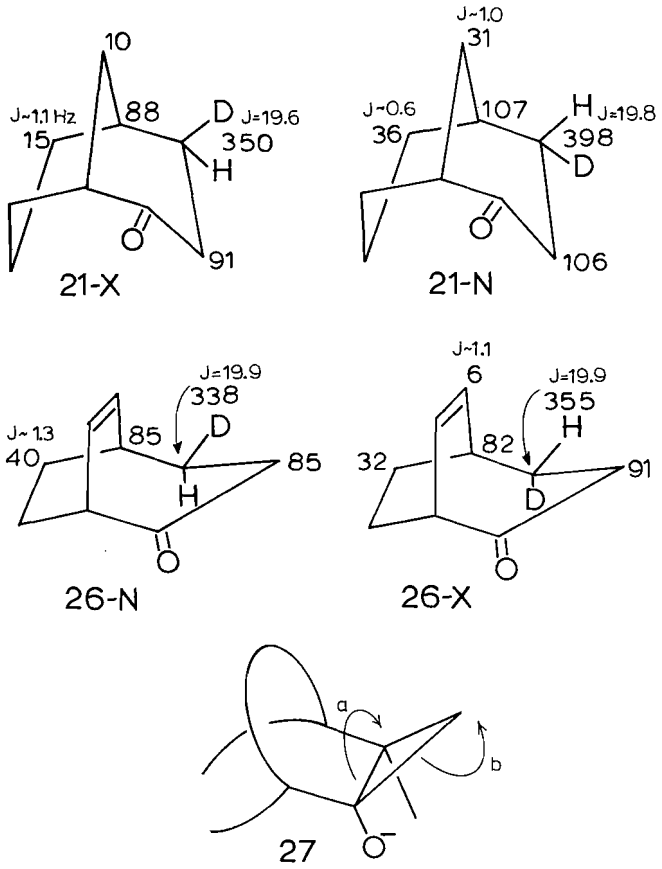

(**26-X**). Thus, in each case, the presence of product arising by opening with retention would give rise to a separately resolved ^2H signal; the absence of such signals establishes the high stereoselectivity noted.

After the discovery of homoenolization (22) in camphenilone (**1***c*), Nickon, Lambert, and Oliver showed that β-proton abstraction also occurred at the α-methyl carbons (23) and a homoenolate anion such as **27** was suggested as a possible intermediate for α-methyl exchange. Subsequently, many examples of this exchange process under homoenolization conditions have been found for mono-, bi-, and tricyclic ketones, having *gem*-dimethyl substitution at the α-methylene positions (20). Although **27** can open in two ways, with ring expansion (path *a*) or to regenerate the initial α,α-dimethyl ketone (path *b*), ring-expanded products have not been detected for any of the cyclic systems examined; path *a*, however, has been found to be important in acyclic systems. Our original examination of **1***a* was intended to develop the preparative procedures for an investigation of **1***b* and related ketones to test for the possible intermediacy of species such as **27** in the α-methyl exchange process. In fact, four systems were examined and the results are listed in Table 5, while the ^{13}C shieldings for the trimethylsilyl enol ethers and their cyclopropanated derivatives are included in Tables 1 and 2. In each case the α,α-dimethylated ketones were readily identified by ^{13}Cmr (**1***c* (15), **4***c*, **5***c* (17), and **6***c* (13)), which also served to characterize the new ring-expanded ketones 4-Me-**9***a*, **20***b*, and Δ[6]-**20***b* (Table 4); it can be noted that the generation of the trimethylsilyl enol ether from **6***b* proved difficult and a pure product was not isolated. However, the cyclopropanation reaction led to a mixture of components of which the major one could be isolated by preparative glc and was characterized as **13***e* (Table 2). From the results in Table 5 it is apparent that cleavage leading to the α,α-dimethyl ketones is strongly favored, indicating that **27** opens preferentially via a primary carbanion (path *b*) rather than a tertiary species (path *a*), which is consistent with the greater stability of the former. This mode is increasingly favored with increasing temperature, suggesting that **27** is a reasonable intermediate for α-methyl exchange under typical homoenolization temperatures of 185°C or higher. Since α-methyl exchange is known (20) to be very slow ($k \sim 10^{-7}\ s^{-1}$), small amounts of ring-expanded products, formed by the less-favored opening of **27**, may have escaped detection; presumably these could readily undergo aldol condensation under homoenolization conditions.

In summary, the sequence outlined in Scheme 1 provides an efficient method for regioselective ring expansion in [2.2.1], [2.2.2], and related systems and can be carried out under mild conditions. Furthermore, the homoketonization of the cyclopropoxides proceeds with high stereoselectivity, thereby providing a means of generating selectively deuterated ring-expanded products that may be useful for other studies.

Experimental

Boiling points are uncorrected. Gas–liquid chromatography was carried out on Varian 920 and 3700 instruments using columns of 6% FFAP or 10% SE-30 on Chromosorb W, as indicated. Tetrahydrofuran (THF) and ether were dried over sodium and freshly distilled before

use. Diisopropylamine, triethylamine, and pyridine were distilled from CaH_2 and stored over 4A molecular sieves. Norcamphor (**1***a*) and bicyclo[5.2.1.$0^{2,6}$]decan-8-one (**2***a*) are commercially available (Aldrich). All other starting ketones were prepared in earlier studies and additional material was generated using the same procedures: **1***b* (15), **3***a*, **10***a* (16), **4***a*,*b*, **5***a*,*b* (17), **6***a*,*b*, **7***a*, **8***a*, **9***a* (13).

Infrared spectra were recorded with a Beckman 4250 instrument and mass spectra were obtained on a Varian MAT-311A system at 70 eV (direct inlet). Routine ^{1}Hmr spectra were obtained with either Varian T-60 or EM-360 instruments while data for pure samples were collected with a Varian XL-200 instrument. The latter spectrometer and a Varian XL-300 were employed to record the ^{2}H and ^{13}Cmr spectra and comparison of the fully decoupled ^{13}C spectra with those obtained with either the APT (24) or DEPT (25) sequences identified the methyl, methylene, methine, and fully-substituted carbon signals.

General procedure for the preparation of the trimethylsilyl enol ethers

Freshly distilled THF (20 mL) and diisopropylamine (30 mmol) were added to a flame-dried flask under nitrogen and cooled to −78°C. Upon the addition of *n*-butyllithium (25 mmol) in *n*-hexane via syringe, the mixture was stirred for 30–45 min before dropwise addition of a solution of the ketone (20 mmol) in THF (5 mL). While the stirring continued, a quenching solution of chlorotrimethylsilane (30 mmol), triethylamine (10 mmol), and THF (7 mL) was prepared in a flame-dried, nitrogen-purged centrifuge tube. The precipitate was removed by centrifugation and the clear solution added to the enolate solution. The reaction mixture was stirred at −78°C briefly and then allowed to warm to room temperature while stirring was continued for 0.5–3 h before cooling to 0°C. A cold, saturated aqueous Na_2CO_3 solution (30 mL) was added with vigorous stirring; the product was isolated by pentane extraction and purified by Kugelrohr distillation. With the exception of the enol ether from **6***b*, which could not be obtained in a pure form, the trimethylsilyl enol ethers were characterized by ^{13}Cmr and precise mass measurements, which are listed in Table 1 together with the isolated yields for each enol ether; the purity of each product was assessed by glc analysis (FFAP) and found to be ≧95% in each case. The product from **1***a*, bp 85–90°C/10 Torr (1 Torr = 133.3 Pa); ir (film): 1605 cm^{-1}; from **1***b*, bp 75–80°C/6 Torr; ir (film): 1670 cm^{-1}; from **2***a*, bp 92–94°C/0.4 Torr; ir (film): 1610 cm^{-1}; from **3***a*, bp 89–94°C/0.2 Torr; ir (film): 1614 cm^{-1}; from **4***a*, bp 62–66°C/17 Torr; ir (film): 1642 cm^{-1}; from **4***b*, bp 85–90°C/14 Torr; ir (film): 1640 cm^{-1}; from **5***a*, bp 60–64°C/17 Torr; ir (film): 1657 cm^{-1}; from **5***b*, bp 45–50°C/1 Torr; ir (film): 1685 cm^{-1}; from **6***a*, bp 100–115°C/15 Torr; ir (film): 1622 cm^{-1}; from **7***a*, bp 110–115°C/4 Torr; ir (film): 1665 cm^{-1}; from **8***a*, bp 95–100°C/10 Torr; ir (film): 1646 cm^{-1}; from **9***a*, bp 90–95°C/4 Torr; ir (film): 1660 cm^{-1}; from **10***a*, bp 85–90°C/0.2 Torr; ir (film): 1660 cm^{-1}.

Cyclopropanation of the trimethylsilyl enol ethers

A modification of the procedure described by Girard and Conia (6) was employed. To a flask fitted with a reflux condenser, nitrogen purge, and magnetic stirrer was added a zinc–silver couple (55 mmol). The apparatus was flame-dried and then cooled to room temperature before the addition of CH_2I_2 (30 mmol) in anhydrous Et_2O (10 mL). The mixture was warmed until refluxing occurred without external heating. Upon cessation of reflux a solution of enol ether (16 mmol) in Et_2O (35 mL) was added and this mixture was heated under reflux for several hours before cooling to 0°C. Pyridine–ether (1:1) solution was added until no further precipitation occurred and the precipitate was removed by filtration and washed with Et_2O. After evaporation of the solvent, the residue was taken up in *n*-pentane and the last traces of precipitate were removed before drying over $MgSO_4$. After the solvent was evaporated, the product was isolated by Kugelrohr distillation and its purity assessed by glc (FFAP or SE-30). Analytical samples were obtained by glc and characterized by ^{13}Cmr and precise mass measurements, listed in Table 2 with the isolated yields. For each ether, the reflux time, purity, bp, and principal ir absorption were:

11*a*: 25.5 h; >96%; bp 110–115°C/15 Torr; ir (film): 3085, 2980, 1340, 1245, 835 cm^{-1}; **11***c*: 25.5 h; >95%; bp 56–58°C/0.3 Torr; ir (film): 3060, 2940, 1250, 833 cm^{-1}; **11***d*: 14 h; >90%; isolated without distillation; ir (film): 3060, 2950, 1250, 870 cm^{-1}; **11***e*: 20 h; >95%; bp 64–68°C/2 Torr; ir (film): 3060, 2975, 1250, 845 cm^{-1}; **12***a*: 6 h; >94%; bp 75–80°C/15 Torr; ir (film): 3078, 2945, 1250, 1195, 840 cm^{-1}; **12***c*: Zn–Ag (40 mmol), CH_2I_2 (20 mmol), 24 h; >93%; bp 75–80°C/5 Torr; ir (film): 3050, 3008, 2950, 1255, 1198, 840 cm^{-1}; **12***e*: 50 h; >90%; bp 80–85°C/1 Torr; ir (film): 3025, 2950, 1245, 1190, 835 cm^{-1}; **12***g*: Zn–Ag (30 mmol), CH_2I_2 (16 mmol), 20 h; >90%; bp 80–85°C/2 Torr; ir (film): 3050, 3000, 2950, 1250, 1188, 840 cm^{-1}; **13***a*: 18 h; >93%; bp 130–135°C/15 Torr; ir (film): 3020, 2955, 1254, 879, 840 cm^{-1}; **13***c*: 20 h; >90%; bp 125–130°C/4 Torr; ir (film): 3075, 2950, 1250, 830 cm^{-1}; **13***e*: 25 h; >85%; bp 135–140°C/8 Torr; ir (film): 3065, 2950, 1250, 835 cm^{-1}; **14***a*: 2 cycles of 23 h each; >98%; bp 75–80°C/2 Torr; ir (film): 3078, 2920, 1240, 1185, 840 cm^{-1}; **14***c*: 25 h; >90%; bp 100–105°C/2 Torr; ir (film): 3080, 2950, 1250, 840 cm^{-1}; **14***e*: 18 h; >90%; isolated by preparative glc without distillation; ir (film): 3000, 2950, 1190, 850 cm^{-1}.

Preparation of cyclopropanols

To a solution composed of 10% 0.1 *M* aqueous HCl and 90% THF was added the pure cyclopropyl silyl ether, obtained by preparative glc, and the reaction mixture stirred at room temperature for 0.5–3 h. After removal of THF under reduced pressure, the residue was taken up in pentane and dried over $MgSO_4$. Evaporation of the pentane yielded the corresponding cyclopropanol in essentially quantitative yield, which was characterized by ^{13}Cmr and, in several cases, precise mass measurement. These data are collected in Table 2. **14***b* crystallized on standing: mp 92–95°C (from pentane–methanol); ir (CCl_4): 3160, 3079, 2918, 1185 cm^{-1}.

Homoketonization experiments

(a) Cyclopropanols

The cyclopropanol (20 mmol) was added to a solution of KOH/*t*-BuOH (1.26 *M*, 10 mL) at the desired temperature and the solution was stirred for 0.5 h (83°C), 2 h (25°C), 24 h (0°C). After the addition of H_2O (15 mL), the ketonic products were isolated by pentane extraction (3 × 20 mL) and the combined extracts dried over $MgSO_4$. The oily residue (>85% yield in each case) remaining after removal of solvent was analyzed by glc (FFAP) to determine the composition of the product mixture. In each case, the α-methylated ketones were known from earlier studies in these laboratories and were readily identified by coinjection. Preparative glc provided samples of each component for examination by ^{13}Cmr to confirm their identities. The ^{13}C data for the ketones that had not been previously encountered in our earlier work are listed in Table 4 together with precise mass measurements. For each cyclopropanol, triplicate runs were done at a given temperature and the average compositions of these product mixtures are collected in Tables 3 and 5; the results were reproducible within limits of ±2%.

(b) Trimethylsilyl cyclopropyl ethers

To methanolic NaOH solution (3 *M*, 5 mL), maintained at the desired temperature, was added the silyl cyclopropyl ether (15 mmol, glc collected) and the mixture was stirred for 20–25 h (0°C, 25°C) or 2 h (83°C) before the addition of aqueous NaCl solution (10 mL). The ketonic products were isolated in >85% yields and assessed as described above for the corresponding cyclopropanols. The compositions of the product mixtures (averaged from triplicate runs) are listed in Tables 3 and 5 while the ^{13}C data for new ketones are collected in Table 4.

*Homoketonizations of the monodeuterated cyclopropyl ethers (**11**a–d_1, **11**c–d_1, **12**c–d_1, **13**a–d_1)*

*(i) Preparation of **1**a–d_2, **2**a–d_2, **5**a–d_2, and **6**a–d_2*

A modification of the procedure described by Hunter *et al.* (26) was employed. To a solution of anhydrous potassium carbonate (2.7 g) in D_2O (22.7 mL, 99.8% D, minimum isotopic purity, Merck, Sharp & Dohme) was added ketone **1***a* (5.0 g) under nitrogen and the mixture refluxed for 18 h. The ketone was recovered by pentane extraction (3 × 15 mL) and the extracts dried over $MgSO_4$ before evaporation of the solvent. After an additional cycle (18 h), [3,3-$^2H_2$]-**1***a* (4.3 g,

84%) was recovered and its ^{13}C spectrum indicated nearly complete exchange at the α-methylene site.

An analogous sample of [9,9-$^2H_2$]-**2***a* (2.2 g, 55% yield) was obtained upon treatment of **2***a* (4.0 g) with K_2CO_3 (1.2 g) in D_2O (12 mL) after four cycles with reflux times of 11, 40, 158, and 83 h.

Essentially complete exchange of the α-methylene hydrogens in **5***a* (0.5 g) was realized by refluxing with K_2CO_3 (0.2 g) in D_2O (2.0 mL) for 17 h under nitrogen. Pentane extraction furnished a solid product that upon sublimation gave [3,3-$^2H_2$]-**5***a* (0.46 g, 90% yield).

The same treatment of **6***a* (2.0 g) with K_2CO_3 (2.5 g) in D_2O (25 mL) at reflux for 12 h yielded **6***a*-d_x (2.0 g) for which the ^{13}C spectrum indicated ca. 50% exchange of the α-methylene hydrogens. Hence, a solution of **6***a*-d_x (2.0 g) in anhydrous dioxane (4 mL) was added to a 1 *M* NaOD/D_2O solution (25 mL) and refluxed under nitrogen for 16 h. Pentane extraction furnished [7,7-$^2H_2$]-**6***a* (1.5 g, 75% yield) for which the ^{13}C spectrum indicated essentially complete exchange of the α-methylene hydrogens.

(*ii*) The trimethylsilyl enol ethers of the dideuterated ketones just described were generated following the same procedures used for the parent ketones using 1.5 molar equivalents of LDA and TMSCl. Treatment of these enol ethers with the Simmons–Smith reagent (Zn–Ag, CH_2I) gave the corresponding cyclopropyl silyl ethers in the same yields as those obtained for their unlabelled counterparts.

(*iii*) Cyclopropyl ether **11***a*-d_1 (45 mg, 2.3 mmol) was added to methanolic NaOH solution (3 *M*, 7 mL) and the mixture was stirred overnight at room temperature. After the addition of H_2O (7 mL)), the product was extracted with pentane (3 × 15 mL) and the combined extracts were washed with H_2O (2 × 15 mL) before drying over $MgSO_4$. Removal of the solvent by evaporation gave an oil (28 mg, 98% yield), which by glc (FFAP) was >99% pure **9***a*-d_1; ms: 3.4% d_0, 97.6% d_1 (0.976 D/molecule); which was shown to be [*endo*-4-$^2H_1$]-**9***a*-**N**) by ^{13}Cmr (see text); ^2Hmr ($CHCl_3$) δ: 1.79.

The same treatment of **11***c*-d_1 (48 mg) gave [*endo*-10-$^2H_1$]-**10***a* (32 mg, 95% yield, >99% pure); ms: 6.8% d_0, 93.2% d_1 (0.932 D/molecule); ^2Hmr ($CHCl_3$) δ: 1.83; shown to be **10***a*-**N** by ^{13}Cmr (see text).

For **12***c*-d_1 and **13***a*-d_1, the product mixture isolated by pentane extraction was separated by preparative glc (FFAP) to obtain the requisite samples of the deuterated ketones: [*exo*-4-$^2H_1$]-Δ^6-**20***a* (88% yield, >98% pure); ms: 8.8% d_0, 91.2% d_1, (0.912 D/molecule); ^2Hmr ($CHCl_3$) δ: 1.79 and shown to be **26-X** by ^{13}Cmr (see text); [*endo*-4-$^2H_1$]-**21** (51% yield); ms: 3.3% d_0, 96.7% d_1 (0.967 D/molecule); ^2Hmr ($CHCl_3$) δ: 1.79; and found to be **21**-**N** by ^{13}Cmr (see text).

Homoketonizations of **11**a, **11**c, **12**c *and* **13**a *in deuterated base*

To a solution of KOD/*t*-BuOD (95% deuterated, 1 *M*, 6 mL) was added **11***a* (0.32 g) and the mixture stirred at room temperature under nitrogen overnight. After the addition of H_2O (4 mL), the product was extracted with pentane (4 × 10 mL) and the combined extracts washed with 10% NaCl solution (2 × 10 mL) and H_2O (10 mL) before drying over $MgSO_4$. Removal of the solvent gave an oil (0.20 g), which was treated with methanolic NaOH (3 *M*, 6 mL) and stirred at room temperature overnight. Pentane extraction, as in the first step, gave [*exo*-4-$^2H_1$]-**9***a* (140 mg, 70%); ms: 50.5% d_0, 49.5% d_1 (0.495 D/molecule); ^2Hmr ($CHCl_3$) δ: 1.70; identified as **9***a*-**X** by ^{13}Cmr (see text).

The same sequence with **11***c* (100 mg) using KOD/*t*-BuOD (95% deuterated, 1 *M*, 1.6 mL) followed by methanolic NaOH solution (1 *M*, 1.6 mL) gave [*exo*-10-$^2H_1$]-**10***a* (67 mg, 96%); ms: 28.5% d_0, 68.7% d_1, 2.8% d_2 (0.743 D/molecule); ^2Hmr ($CHCl_3$) δ: 1.67; shown to be **10***a*-**X** by ^{13}Cmr (see text).

Cyclopropyl ether **12***c* (55 mg) was stirred with NaOD/CD_3OD solution (99.8% deuterated, 1 *M*, 5 mL) at room temperature under nitrogen overnight. The product isolated by pentane extraction as described above was treated similarly with methanolic NaOH solution (3 *M*, 5 mL) and reisolated by pentane extraction to afford [*exo*-4-$^2H_1$]-Δ^6-**20***a* (33 mg, 91%); ms: 4.2% d_0, 95.1% d_1, 0.7% d_2 (0.965 D/molecule); ^2Hmr ($CHCl_3$) δ: 1.91; identified as **26**-**N** by ^{13}Cmr (see text).

Exactly analogous treatment of **13***a* gave [*exo*-4-$^2H_1$]-**21** in 70% yield; ms: 3.2% d_0, 92.2% d_1, 4.6% d_2 (1.014 D/molecule); ^2Hmr ($CHCl_3$) δ: 2.06; identified as **21-X** by ^{13}Cmr (see text).

Acknowledgements

We are grateful for the financial support provided by the Natural Sciences and Engineering Research Council of Canada.

1. C. D. GUTSCHE and D. REDMORE. Carbocyclic ring expansion reactions. Academic Press, New York. 1968. Chapt. 4.
2. W. L. MOCK and M. E. HARTMAN. J. Org. Chem. **42**, 459 (1977).
3. P. A. SMITH and D. R. BAER. Org. React. **11**, 157 (1960).
4. V. PATEL and J. B. STOTHERS. Can. J. Chem. **58**, 2728 (1980).
5. Y. HOYANO, V. PATEL, and J. B. STOTHERS. Can. J. Chem. **58**, 2730 (1980).
6. C. GIRARD and J.-M. CONIA. J. Chem. Res. (M), 2346 (1978).
7. H. O. HOUSE, L. J. CZUBA, M. GALL, and H. D. OLMSTEAD. J. Org. Chem. **34**, 2324 (1969).
8. A. K. CHENG and J. B. STOTHERS. Org. Magn. Reson. **6**, 355 (1977).
9. M. CHRISTL and R. HERBERT. Org. Magn. Reson. **12**, 150 (1979).
10. A. J. RAGAUSKAS and J. B. STOTHERS. Can. J. Chem. **63**, 1250 (1985).
11. J. B. STOTHERS and C. T. TAN. Can. J. Chem. **54**, 917 (1976).
12. P. BRUN, J. CASANOVA, J. HATEUR, J. P. ZAHRA, and B. WAEGELL. Org. Magn. Reson. **12**, 537 (1979).
13. S. H. GROVER, D. H. MARR, J. B. STOTHERS, and C. T. TAN. Can. J. Chem. **53**, 1351 (1975).
14. B. A. DAWSON, A. K. GHOSH, J. L. JURLINA, A. J. RAGAUSKAS, and J. B. STOTHERS. Can. J. Chem. **62**, 2521 (1984).
15. J. B. STOTHERS, C. T. TAN, and K. C. TEO. Can. J. Chem. **51**, 2893 (1973).
16. B. A. DAWSON and J. B. STOTHERS. Org. Magn. Reson. **21**, 217 (1983).
17. K. R. STEPHENS, J. B. STOTHERS, and C. T. TAN. *In* Mass spectrometry and nmr in pesticide chemistry. *Edited by* R. Haque and J. F. Biros. Plenum Press, New York, NY. 1974. pp. 179–196.
18. K. YAMADA, S. MANABE, Y. KYOTANI, M. SUZUKE, and Y. HIRATA. Bull. Chem. Soc. Jpn. **52**, 186 (1979).
19. J. L. JURLINA, H. A. PATEL, and J. B. STOTHERS. Can. J. Chem. **62**, 1159 (1984).
20. N. H. WERSTIUK. Tetrahedron, **39**, 205 (1983).
21. R. AYDIN, J. R. WESENER, H. GUNTHER, R. L. SANTILLAN, M. E. GARIBAY, and P. JOSEPH-NATHAN. J. Org. Chem. **49**, 3845 (1984).
22. A. NICKON and J. L. LAMBERT. J. Am. Chem. Soc. **84**, 4604 (1962).
23. A. NICKON, J. L. LAMBERT, and J. E. OLIVER. J. Am. Chem. Soc. **88**, 2787 (1966).
24. S. PATT and J. N. SHOOLERY. J. Magn. Reson. **46**, 535 (1982).
25. D. M. DODDRELL, D. T. PEGG, and M. R. BENDALL. J. Magn. Reson. **48**, 323 (1982).
26. D. H. HUNTER, Y. LIN, A. L. MCINTYRE, D. J. SHEARING, and M. ZVAGULIS. J. Am. Chem. Soc. **95**, 8327 (1973).
27. R. D. STIPANOVIC, A. STOESSL, J. B. STOTHERS, D. W. ALTMAN, A. A. BELL, and P. HEINSTEIN. J. Chem. Soc. Chem. Commun. 100 (1986).
28. J. P. WIEBE, C. DELINE, K. D. BUCKINGHAM, V. DAVE, and J. B. STOTHERS. Steroids, **45**, 39 (1985).
29. A. STOESSL and J. B. STOTHERS. Can. J. Chem. **64**, 1 (1986).

Structural studies of 1,3-dioxa-2-silacycloalkanes[1,2]

A. W. HANSON, A. W. MCCULLOCH, AND A. G. MCINNES

Atlantic Research Laboratory, National Research Council of Canada, 1411 Oxford St., Halifax, N.S., Canada B3H 3Z1

Received October 24, 1985

A. W. HANSON, A. W. MCCULLOCH, and A. G. MCINNES. Can. J. Chem. **64**, 1450 (1986).

Crystal structure analyses of 1,3-dioxa-2,2-diphenyl-2-sila-5,6-benzocycloheptane (**1**), 2,9-disila-1,3,8,10-tetraoxa-2,2,9,9-tetraphenyl-5,6,12,13-dibenzocyclotetradecane (**2**), 2,10-disila-2,2,10,10-tetramethyl-1,3,9,11-tetraoxa-5,7,13,15-dibenzocyclohexadecane (**3**), 2,7-disila-2,2,7,7-tetramethyl-1,3,6,8-tetraoxa-4,5,9,10-dibenzocyclodecane (**4**), and 2,4-disila-2,2,4,4-tetraphenyl-1,3,5-trioxa-6,7-benzocycloheptane (**11**) are reported. Facile acid-catalyzed reaction of 2,7-disila-1,3,6,8-tetraoxa-2,2,7,7-tetraphenyl-4,5,9,10-dibenzocyclodecane (**8**) with water gives 1,3-di(2-hydroxyphenoxy)-1,3-disila-2-oxa-1,1,3,3-tetraphenylpropane (**12**). The latter in turn decomposes in a base-catalyzed reaction to give a mixture of **11** and catechol.

A. W. HANSON, A. W. MCCULLOCH et A. G. MCINNES. Can. J. Chem. **64**, 1450 (1986).

On rapporte des analyses des structures cristallines des dioxa-1,3 diphényl-2,2 sila-2 benzo-5,6 cycloheptane (**1**), disila-2,9 tétraoxa-1,3,8,10 tétraphényl-2,2,9,9 dibenzo-5,6,12,13 tétradécane (**2**), disila-2,10 tétraméthyl-2,2,10,10 tétraoxa-1,3,9,11 dibenzo-5,7,13,15 cyclohexadécane (**3**), disila-2,7 tétraméthyl-2,2,7,7 tétraoxa-1,3,6,8 dibenzo-4,5,9,10 cyclodécane (**4**) et disila-2,4 tétraphényl-2,2,4,4 trioxa-1,3,5 benzo-6,7 cycloheptane (**11**). Le disila-2,7 tétraoxa-1,3,6,8 tétraphényl-2,2,7,7 dibenzo-4,5,9,10 cyclodécane (**8**) réagit facilement avec l'eau, sous l'influence des acides, pour donner le di(hydroxy-2 phénoxy)-1,3 disila-1,3 oxa-2 tétraphényl-1,1,3,3 propane (**12**). Ce dernier composé, par réaction catalysée par les bases, se décompose pour donner un mélange de **11** et de catéchol.

[Traduit par la revue]

Introduction

The rather diverse literature on the intriguing chemistry of 1,3-dioxa-2-silaheterocycles has been summarised in a recent review by Cragg and Lane (1). These workers have undertaken a comprehensive investigation of the preparation and spectroscopic properties of such compounds. As part of an ongoing study in this laboratory of the biological role of silicon, we have over the past few years conducted a study of model interactions of dihydroxy compounds with dichlorosilanes which in many respects closely parallels that of Cragg and Lane.

1,3-Dioxa-2-silacycloalkanes are usually prepared by reaction of diols with difunctional silanes. Monomeric, dimeric, and polymeric products are obtained, with the stability of the product being dependent on ring size and substitution. Physical studies, such as nmr and X-ray diffraction, of such products have been extremely limited. In this article we therefore wish to describe the X-ray structure analyses of five compounds: the 7-membered monomer **1**, 14-membered dimer **2**, 16-membered dimer **3**, and 10-membered dimer **4**, as well as the trioxa derivative **11** (see Figs. 1–5). We have also studied in detail the chemistry of the dimeric compound **8**, obtained by reaction of catechol with dichlorodiphenylsilane.

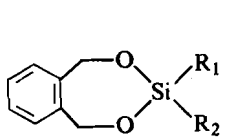

1 $R_1 = R_2 = \phi$
5 R_1 = Me; $R_2 = \phi$
6 $R_1 = R_2$ = Me

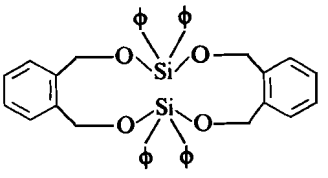

2

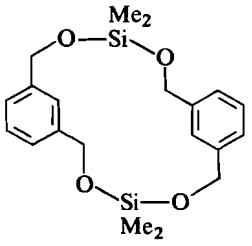

3

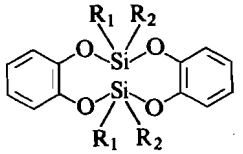

4 $R_1 = R_2$ = Me
7 R_1 = Me; $R_2 = \phi$
8 $R_1 = R_2 = \phi$

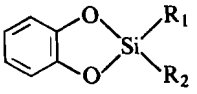

9 $R_1 = R_2$ = Me
10 $R_1 = R_2 = \phi$

Results and discussion

Preparation of 1,3-dioxa-2-silacycloalkanes

Birkofer and Stuhl have reported (2) that reaction of 1,2-benzenedimethanol with dichlorodiphenylsilane yields the benzodioxasilacycloheptane **1**. Since the submission of this manuscript Cragg and Lane have reported details of the isolation of **1** and its dimer **2** from a similar reaction (15). In our hands the predominant reaction product was the monomer **1**, mp 128–130°C, with **2**, mp 251–253°C, being obtained as a minor product.

The reactions of 1,3-benzenedimethanol with dichlorosilanes have not previously been investigated. Steric constraints in this case preclude monomer formation. We have isolated in good yield the crystalline dimer **3**, mp 162–164°C, from reaction of 1,3-benzenedimethanol with dichlorodimethylsilane.

The reactions of catechol with dichlorosilanes have received considerable attention (1), and it has been shown that the monomeric 1,2-phenylenedioxysilanes (e.g. **9**) undergo reversible dimerisation (e.g. to **4**): dissociation to monomer is favoured at elevated temperatures (3). X-ray diffraction studies have been carried out on a number of *o*-phenylenedioxy siliconates in which the silicon atom is either pentacoordinated (4–7) or hexacoordinated (8). Myer and Nagorsen have also presented X-ray diffraction data for the tetracoordinated bis(*o*-phenylenedioxy)silane (9), although the planar structure they propose has been subsequently questioned by Dunitz (10). No X-ray study has been carried out on compounds of type **4** or **9**. Hence we have also prepared and analysed **4**, mp 87–90°C, from reaction of catechol with dichlorodimethylsilane.

[1]NRCC No. 25582.

[2]Presented in part at the 6th International Symposium on Organosilicon Chemistry, Budapest, August 1981.

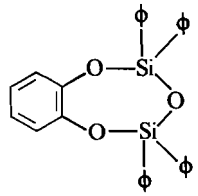

11

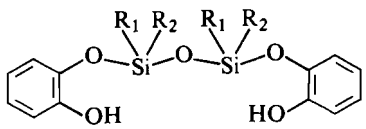

12 $R_1 = R_2 = \phi$
13 $R_1 = R_2 = Me$

Carbon-13 and silicon-29 nmr data for **1** and **3** are presented in Table 1. Compound **2** was not sufficiently soluble to permit high-resolution nmr investigation. Carbon-13 nmr also confirmed that the analogous reactions of 1,2-benzenedimethanol with dichloromethylphenylsilane and dichlorodimethylsilane afforded chiefly the monomeric products **5** and **6**. The chemical shifts of the methylene carbon and the aryl carbon geminal to oxygen are very similar to those of the corresponding carbons of **1** (Table 1).

Through comparison with the ^{13}C spectrum of **4** we have likewise identified the dimeric compounds **7** and **8** as major products of reaction of catechol with dichloromethylphenylsilane and dichlorodiphenylsilane (Table 2). When a solution of **4** was allowed to stand at room temperature new low-intensity ^{13}C signals were observed for the monomer **9**. In particular, the chemical shifts of the aryl carbons bonded to or geminal to oxygen resemble those of 1,3-benzodioxole, while in the more flexible **4** the shifts of these carbons correspond more closely to those of catechol itself. Creation of the five-membered ring results in a downfield shift of ~3 ppm in the oxygen-bonded carbon and an upfield shift of ~8 ppm in the carbon geminal to oxygen. Analogous small signals presumably due to **10** were observed at 113.90 and 148.85 ppm in freshly-prepared $CDCl_3$ solutions of **8**.

Chemistry of dimer 8

Cragg and Lane have reported that reaction of catechol with dichlorodiphenylsilane affords dimer **8**, for which they report a melting point of 126–130°C (11). They were unable to explain why the mp was significantly lower than those (157–171°C) previously reported by other workers (11).

In our hands the reaction yielded two major solid products. The first, with low solubility in acetone and mp 167–172°C, has all the ^1H, ^{13}C, and ^{29}Si nmr features reported by Cragg and Lane for **8** (11). Using X-ray analysis we have established the structure of the second product, which crystallized from petroleum ether/ethyl acetate with mp 136–138°C, as **11**, a compound postulated by Cragg and Lane as a product of distillation of **8** (11). The ^{29}Si shift of −32.71 ppm is very close to that (−32.58 ppm) quoted by them for their distillate.

These discrepancies led us to closely examine the chemistry of dimer **8**. As a consequence, we have further observed that **8** reacts readily with moisture to give the dihydroxy derivative **12**, mp 128–130°C. The closeness of this mp to that reported for **8** by Cragg and Lane suggests that during the crystallization process they inadvertently caused conversion to **12**.

These authors did produce ^{13}C spectra showing the initial stages of decomposition of **8** (11). When a $CDCl_3$ solution of

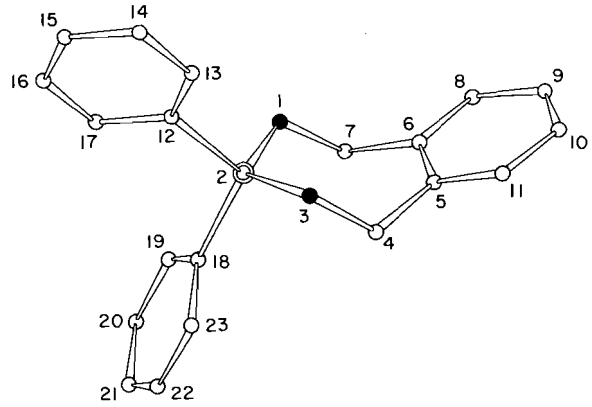

FIG. 1. 1,3-Dioxa-2,2-diphenyl-2-sila-5,6-benzocycloheptane, **1**. In this and other figures carbon, oxygen, and silicon atoms are represented by open, solid, and open double circles, respectively.

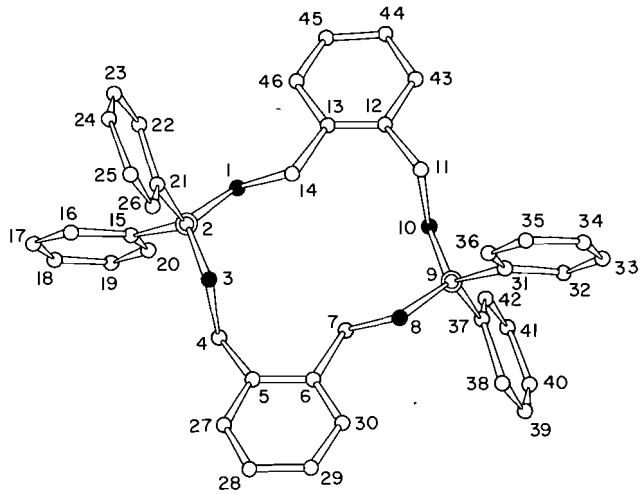

FIG. 2. 2,9-Disila-1,3,8,10-tetraoxa-2,2,9,9-tetraphenyl-5,6,12,13-dibenzocyclotetradecane, **2**.

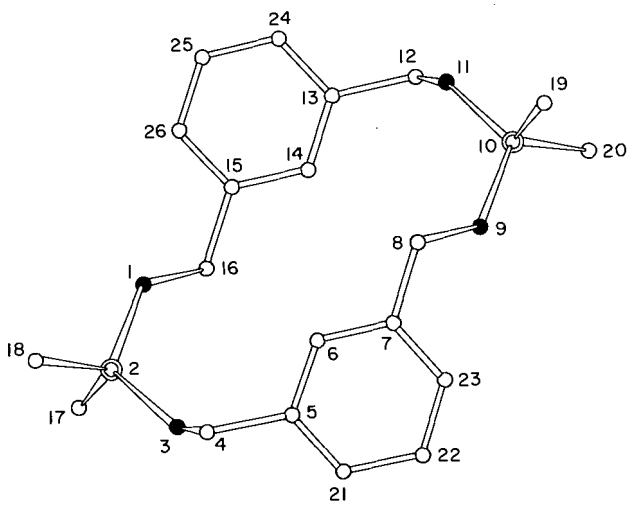

FIG. 3. 2,10-Disila-2,2,10,10-tetramethyl-1,3,9,11-tetraoxa-5,7,13,15-dibenzocyclohexadecane, **3**.

our **8** was allowed to stand at room temperature and monitored by ^{13}C nmr, we observed the same type of initial change. However, after 15 days the spectrum showed only signals for **12**. A similar conversion was obtained when an acetone or benzene suspension of **8** was refluxed for 2–3 h. Atmospheric

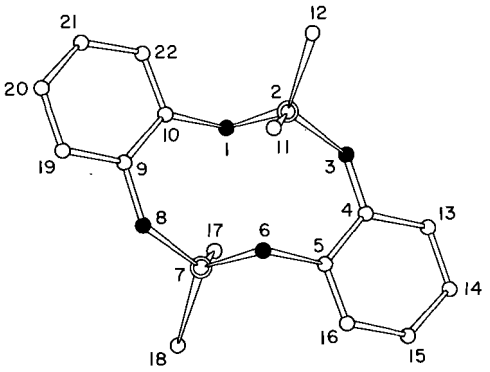

FIG. 4. 2,7-Disila-2,2,7,7-tetramethyl-1,3,6,8-tetraoxa-4,5,9,10-dibenzocyclodecane, **4**.

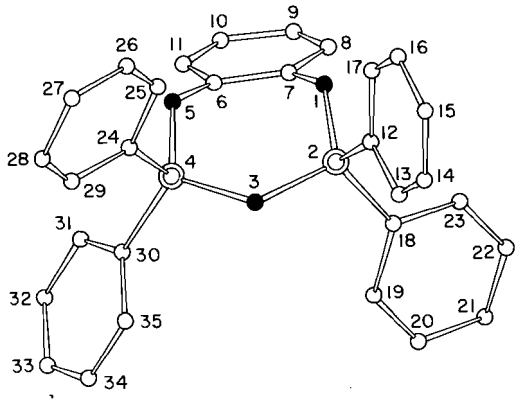

FIG. 5. 2,4-Disila-2,2,4,4-tetraphenyl-1,3,5-trioxa-6,7-benzocycloheptane, **11**.

moisture is responsible for the slow conversion of **8** to **12** in organic solvents. The time required for complete conversion in chloroform at room temperature can be reduced to 6 h by addition of a few drops of water.

The generality of the process was demonstrated by the analogous conversion of **4** to **13** (21 days in $CHCl_3$ at room temperature), the ^{13}C nmr of which is given in Table 2.

The structure of **12** follows from consideration of its ^1H, ^{13}C, and ^{29}Si nmr spectra and from its facile breakdown to **11** and catechol, in the presence of a small amount of pyridine. The same products were obtained from the pyridine-promoted breakdown of **8**. ^1H, ^{13}C, and ^{29}Si nmr spectra have been obtained for **8**, **11**, and **12**. The ^1H nmr data (Table 3) reveal the ratio of catechol ring hydrogens to Si-phenyl hydrogens, as well as the presence of OH groups in **12**. The ^{13}C spectra (Table 2) establish the symmetrically substituted catechol rings of **8** and **11** and the equivalence of both such rings in **8**, as well as the asymmetrically substituted catechol rings of **12**, and their equivalence. As expected, the ring methine carbon geminal to the hydroxyl group in **12** was three-bond coupled to both the hydroxyl proton and the hydrogen at the *meta* ring carbon, thus appearing as a doublet of triplets. The remaining three methine carbons on the catechol ring each appeared as a doublet of doublets, showing three-bond coupling to only a single *meta* hydrogen. Finally, the ^{29}Si nmr spectra confirmed that all three compounds possessed only tetra-coordinated Si atoms.

The conversion of **8** to **12** (and of **4** to **13**) presumably involves protonation and formation of a transient silanol the oxygen of which attacks the second silicon atom (Fig. 6). It seems likely that hydrogen-bonding (involving the phenolic proton, silanol group, and the oxygen under attack as in Fig. 6) determines the direction of the final rupture of the Si—O bond to give the second phenolic group of **12**, since no **11** was detected in the reaction products. Base-catalyzed reaction of **12** leads directly to **11** and catechol as shown in Fig. 6.

The isolation of **11** as a major product of reaction of catechol with dichlorodiphenylsilane can be explained on the basis of the facile base-catalyzed conversion of **8**. Not unexpectedly, we have found that the ratio of these two products is very sensitive to the reaction conditions, since this would be controlled by factors such as the concentration of moisture and free pyridine available to catalyze conversion of **8** to **11**.

Crystallography

All procedures were executed at a nominal temperature of 24°C, using Ni-filtered CuKα radiation ($\lambda\alpha_1$ = 1.54056 Å). The space groups were deduced from single-crystal photographs. The unit-cell constants were derived by least-squares analysis of the diffractometer (Picker four-circle) angles of a sufficient number of automatically centred reflections in the range $100° < 2\theta < 130°$. The intensities of all independent reflections with $2\theta < 130°$ were measured with θ–2θ scans, and individual reflection profiles were analysed as described by Grant and Gabe (12). There was no evidence of decay during these measurements for any of the specimens. Absorption corrections (Gaussian integration) were applied for **1**, **3**, **4**, and **11**. Crystals of **2** were invariably found to be twinned on $(\bar{1}\,0\,1)$. For the specimen studied the volume ratio of twin elements was estimated to be 0.63:0.37. The intensities corresponding to the larger element were recorded and used in the analysis. Because of the twinning, absorption correction was not considered feasible for this specimen. The problem of overlapping reflections was treated pragmatically. For the $(\bar{h}\,0\,h)$ reflections the overlap of (equivalent) reflections was total, and the observed intensities could be appropriately scaled. Two instances of incomplete overlap (of non-equivalent reflections) were revealed by anomalous profiles, and the reflections affected were excluded from the analysis. Complete, or nearly-complete overlaps could not be detected in this way, however, and the intensities of some reflections were undoubtedly overestimated. At a late stage in the refinement, therefore, all reflections with $F_c \gg F_o$ (an additional 33, or 2% of the data set) were also excluded. The structure determined for this compound is undoubtedly correct, but the possibility of unusual systematic errors in the final atomic parameters should not be disregarded. All structures were solved uneventfully by direct methods (MULTAN (13)). Refinement was by block-diagonal least-squares, minimizing $\Sigma w\Delta F^2$, where $1/w = \sigma^2(F_o) + kF_o^2$. The hydrogen atoms were either assigned reasonable positions (C—H = 1.08 Å) or located in ΔF syntheses. The thermal motion was assumed to be isotropic for the hydrogen atoms, and anisotropic for the others. Refinement was terminated when all indicated parameter shifts were acceptably small ($<0.1\sigma$). The final ΔF syntheses indicated no detail inconsistent with the proposed structures (Figs. 1–5). The atomic coordinates are given in Tables 4 to 8, and selected bond lengths, bond angles, and torsion angles in Tables 9 to 13. The computer programs and the source of atomic scattering factors are identified in ref. 14. Cragg and Lane have suggested (1) that large SiOC bond angles may be a characteristic of all 1,3,2-dioxasilacycloalkanes. This is certainly true for **4** (126.0° and 137.0°) but for **1**, **2**, and **3** these angles range from 118.6° to 125.1° (mean 121.6°). In the *trioxa* derivative **11**, the corresponding values are 126.1° and 131.1°, while the SiOSi angle is 134.9°.

TABLE 1. ^{13}C and ^{29}Si nmr data ($CDCl_3$) for **1**, **3**, **5**, and **6**

Compound	δ_{Si}	*C*—O	*C*—C—O	aryl *C*	Si—R			
					CH_3	*C*-1′	*C*-2′	*C*-3′	*C*-4′
1	−23.69	66.36	139.19	128.24, 129.23		132.23	134.76	127.96	130.57
5		66.08	139.32	128.21, 129.16	−2.87	134.07	134.07	128.06	130.23
6		65.53	139.17	128.06, 128.88	−2.75				
3	−1.55	64.81	140.82	125.90, 128.47	−2.87				

TABLE 2. ^{13}C and ^{29}Si nmr data for catechol-based compounds ($CDCl_3$)

Compound	δ_{Si}	Catechol ring			δ_C CH_3	Si—R			
		C—O	*C*—C—O	*C*—C—C—O		C-1′	C-2′	C-3′	C-4′
Catechol		144.8	115.8	120.1					
1,3-Benzodioxole		147.5	108.7	121.6					
4	−5.14	145.14	121.60	122.76	−2.05				
9		148.54	113.48	121.12	−0.85				
7	−19.76	145.01	121.56	122.90	−3.70	134.09	134.02	128.01	130.54
8	−37.02	144.80	121.49	122.71		131.59	135.02	127.75	130.57
11	−32.71	144.72	122.37	123.25		131.95	134.56	127.84	130.73
12*	−37.98	141.14	115.47	120.01		131.73	134.49	128.18	131.05
		146.79	118.60	122.94					
13		141.34	115.41	120.06	−0.69				
		146.94	118.50	122.67					

*The high-resolution spectrum showed 115.47 (dt, 159.9, 7.5), 118.60 (dd, 159.27, 7.5), 120.01 (dd, ^1J not measurable, 8.0), 122.94 (dd, 160.2, 8.4).

TABLE 3. ^1H nmr data ($CDCl_3$)

Compound	δ_H (ppm)		
	Catechol ring	Si-phenyl	OH
8	6.70 (s, 4H)	7.2–7.45 (m, 6H)	
		7.45–7.75 (m, 4H)	
11	6.70–7.04	7.19–7.38 (m, 12H)	
	(sym. m, 4H)	7.60–7.76 (m, 8H)	
12	6.43–6.96 (m, 8H)	7.15–7.65 (m, 20H)	5.45 (s, 2H)

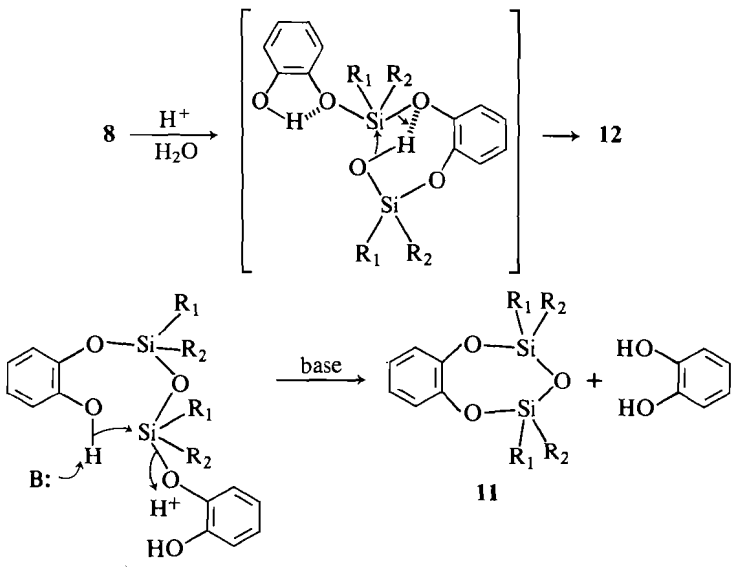

FIG. 6. Conversions of **8** to **12** and of **12** to **11**.

TABLE 4. Atomic coordinates (esd's) and equivalent isotropic B value (B_{eq}, Å^2)* for **1** (H-atoms omitted)

Atom	x	y	z	B_{eq}
O(1)	0.40330(8)	0.24864(19)	0.24284(15)	3.6
Si(2)	0.41183(3)	0.35395(8)	0.11336(6)	3.3
O(3)	0.49324(8)	0.40266(20)	0.12946(15)	3.7
C(4)	0.52924(13)	0.4855(3)	0.2451(3)	4.3
C(5)	0.55317(12)	0.3783(3)	0.3618(2)	3.7
C(6)	0.50598(13)	0.2970(3)	0.4219(2)	3.7
C(7)	0.42866(13)	0.3134(3)	0.3737(2)	4.1
C(8)	0.53139(16)	0.2020(3)	0.5317(3)	4.9
C(9)	0.60267(17)	0.1910(4)	0.5823(3)	5.8
C(10)	0.64792(15)	0.2717(4)	0.5240(3)	5.7
C(11)	0.62342(13)	0.3623(4)	0.4137(3)	4.9
C(12)	0.38850(12)	0.2340(3)	−0.0400(2)	3.5
C(13)	0.43713(14)	0.1395(3)	−0.0829(3)	4.4
C(14)	0.42003(17)	0.0536(4)	−0.1992(3)	6.2
C(15)	0.35453(20)	0.0621(4)	−0.2748(3)	6.8
C(16)	0.30643(18)	0.1540(4)	−0.2365(3)	6.4
C(17)	0.32247(14)	0.2407(4)	−0.1203(3)	4.7
C(18)	0.35620(11)	0.5336(3)	0.1029(2)	3.3
C(19)	0.29524(12)	0.5336(3)	0.1507(2)	3.8
C(20)	0.25256(12)	0.6645(3)	0.1389(3)	4.5
C(21)	0.26991(15)	0.7976(3)	0.0794(3)	4.9
C(22)	0.32960(15)	0.8028(3)	0.0309(3)	5.0
C(23)	0.32741(13)	0.6714(3)	0.0427(3)	4.3

*In this and following tables, $B_{eq} = 8\pi^2(U_{11} + U_{22} + U_{33})/3$.

Crystal and other numerical data[3]

(1) $C_{20}H_{18}O_2Si$ fw = 318.4
Monoclinic, a = 19.735(1), b = 8.4424(6), c = 10.3032(4) Å, β = 102.08(1)° (25 reflections), V = 1678.6 Å^3, space group $P2_1/n$ (alt. $P2_1/c$, No. 14), Z = 4, ρ_c = 1.259 g cm^{-3}. Nominal crystal dimensions 0.5 × 0.2 × 0.07 mm, μ = 12.6 cm^{-1}, absorption corrections 1.08 to 1.32. A total of 2858 reflections were scanned ($\pm h$, $+k$, $+l$), giving 1950 with $I > 2\sigma(I)$. Final R = 0.035 (0.064 including the unobserved), R_w = 0.048, k in weighting scheme, 0.0005. H atom parameters were refined.

(2) $C_{40}H_{36}O_4Si_2$ fw = 636.9
Triclinic, a = 9.334(3), b = 12.179(3), c = 7.724(3) Å, α = 91.22(2), β = 103.54(2), γ = 99.24(2)° (23 reflections), V = 841.0 Å^3, space group $P\bar{1}$ (No. 2), Z = 1, ρ_c = 1.257 g cm^{-3}, molecular symmetry, centre. Nominal crystal dimensions 0.4 × 0.13 × 0.07 mm, μ = 12.7 cm^{-1}, no absorption corrections. A total of 2853 reflections were scanned ($\pm h$, $+k$, $\pm l$) giving 1595 with $I > 2\sigma(I)$, but 35 were omitted from the refinement procedure. Final R = 0.055 (0.133 for all reflections), R_w = 0.075, k in weighting scheme, 0.001. H-atom parameters were not refined (U_{iso} = 0.10 Å^2).

(3) $C_{20}H_{28}O_4Si_2$ fw = 388.6
Monoclinic, a = 10.914(1), b = 11.646(3), c = 8.094(2) Å, β = 95.28(2)° (36 reflections), V = 1024.4 Å^3, space group $P2_1/c$ (No. 14), Z = 2, ρ_c = 1.259 g cm^{-3}, molecular symmetry, centre. Nominal crystal dimensions 0.4 × 0.27 × 0.27 mm, μ = 17.0 cm^{-1}, absorption corrections 1.42 to 1.66. A total of 1749 reflections were scanned ($\pm h$, $+k$, $+l$), giving 1581 with $I > 2\sigma(I)$. Final R = 0.032 (0.036 including the unobserved), R_w = 0.052, k in weighting scheme, 0.0002. H atom parameters were refined.

[3]Complete set of supplementary data may be purchased from the Depository of Unpublished Data, CISTI, National Research Council of Canada, Ottawa, Ont., Canada K1A 0S2.

TABLE 5. Atomic coordinates (esd's) and B_{eq} (Å^2) for **2** (H-atoms omitted); other atoms omitted can be derived from their centrosymmetrically related equivalents by the operation $(1-x, 2-y, 1-z)$ (see Fig. 2)

Atom	x	y	z	B_{eq}
O(1)	0.2559(3)	0.9041(2)	0.3225(4)	4.3
Si(2)	0.25541(14)	0.78673(10)	0.42211(17)	3.4
O(3)	0.3971(3)	0.7957(3)	0.5954(4)	4.0
C(4)	0.3978(5)	0.8470(4)	0.7651(6)	4.0
C(5)	0.5521(5)	0.8679(4)	0.8835(6)	3.5
C(13)	0.3427(5)	1.0382(3)	0.1278(6)	3.3
C(14)	0.3839(6)	0.9562(5)	0.2655(7)	5.2
C(15)	0.0759(5)	0.7619(4)	0.4904(6)	3.5
C(16)	−0.0067(6)	0.6553(4)	0.4854(8)	5.6
C(17)	−0.1344(6)	0.6376(5)	0.5523(9)	7.2
C(18)	−0.1832(6)	0.7264(5)	0.6211(9)	6.6
C(19)	−0.1051(6)	0.8309(5)	0.6245(8)	5.9
C(20)	0.0228(5)	0.8485(4)	0.5603(7)	4.4
C(21)	0.2764(5)	0.6750(4)	0.2703(6)	3.8
C(22)	0.1775(6)	0.6519(5)	0.1032(7)	5.3
C(23)	0.1895(7)	0.5677(5)	−0.0148(8)	6.7
C(24)	0.2989(8)	0.5036(5)	0.0351(9)	7.6
C(25)	0.3965(7)	0.5238(5)	0.1962(9)	7.1
C(26)	0.3881(6)	0.6080(4)	0.3150(7)	5.2
C(27)	0.5927(6)	0.7940(4)	1.0119(7)	4.5
C(28)	0.7323(6)	0.8091(4)	1.1279(7)	5.0
C(45)	0.1663(6)	1.0972(4)	−0.1162(7)	4.6
C(46)	0.2036(5)	1.0216(4)	0.0106(6)	3.7

TABLE 6. Atomic coordinates (esd's) and B_{eq} (Å^2) for **3** (H-atoms omitted); other atoms omitted can be derived from their centrosymmetrically related equivalents by the operation $(1-x, 1-y, -z)$ (see Fig. 3)

Atom	x	y	z	B_{eq}
O(1)	0.22098(11)	0.49042(10)	0.02001(14)	3.5
Si(2)	0.16814(4)	0.40774(4)	0.16139(5)	2.9
O(3)	0.27989(10)	0.33833(10)	0.26720(14)	3.2
C(4)	0.36325(16)	0.38724(17)	0.39595(21)	3.4
C(5)	0.49401(15)	0.38062(14)	0.35157(19)	3.0
C(6)	0.53934(15)	0.46314(13)	0.24786(19)	3.0
C(15)	0.34093(15)	0.54002(14)	−0.20614(20)	2.9
C(16)	0.29319(17)	0.44507(14)	−0.10296(22)	3.8
C(17)	0.06891(17)	0.29330(17)	0.06510(24)	4.1
C(18)	0.08800(19)	0.50580(18)	0.29386(25)	4.6
C(21)	0.57149(17)	0.29357(15)	0.41176(22)	3.6
C(22)	0.69097(17)	0.28808(16)	0.36920(24)	4.1
C(23)	0.73429(15)	0.37088(16)	0.26623(22)	3.6

(4) $C_{16}H_{20}O_4Si_2$ fw = 332.5
Monoclinic, a = 8.944(1), b = 7.820(1), c = 13.159(2), β = 113.45(1)° (22 reflections), V = 844.4 Å^3, space group $P2_1/c$ (No. 14), Z = 2, ρ_c = 1.307 g cm^{-3}, molecular symmetry, centre. Specimen geometry: isosceles-triangular plate, thickness = 0.17 mm, base = height = 0.5 mm, μ = 19.8 cm^{-1}, absorption corrections 1.37 to 2.00. A total of 1440 reflections were scanned ($\pm h$, $+k$, $+l$), giving 1297 with $I > 2\sigma(I)$. Final R = 0.032 (0.037 including the unobserved), R_w = 0.045. k in weighting scheme, 0.00005. H-atom parameters were refined.

(11) $C_{30}H_{24}O_3Si_2$ fw = 488.7
Monoclinic, a = 16.587(1), b = 11.416(1), c = 14.112(1) Å, β = 106.35(1)° (30 reflections), V = 2564.1 Å^3, space group $P2_1/n$ (alt. $P2_1/c$, No. 14), Z = 4, ρ_c = 1.266 g cm^{-3}.

TABLE 7. Atomic coordinates (esd's) and B_{eq} (Å^2) for **4** (H-atoms omitted); other atoms omitted can be derived from their centrosymmetrically related equivalents by the operation $(1-x, -y, -z)$ (see Fig. 4)

Atom	x	y	z	B_{eq}
O(1)	0.59338(15)	0.05135(16)	0.11102(10)	3.2
Si(2)	0.40814(6)	0.11174(6)	0.09606(4)	3.1
O(3)	0.29351(16)	−0.06003(18)	0.05813(10)	3.8
C(9)	0.7776(2)	0.1551(2)	0.0357(1)	3.0
C(10)	0.7198(2)	0.1579(2)	0.1197(1)	2.9
C(11)	0.3350(3)	0.2898(3)	−0.0022(2)	4.6
C(12)	0.4081(3)	0.1597(3)	0.2331(2)	4.6
C(19)	0.9094(2)	0.2565(3)	0.0453(2)	4.0
C(20)	0.9827(3)	0.3614(3)	0.1363(2)	4.5
C(21)	0.9248(3)	0.3647(3)	0.2183(2)	4.4
C(22)	0.7948(2)	0.2633(3)	0.2103(2)	3.8

TABLE 8. Atomic coordinates (esd's) and B_{eq} (Å^2) for **11** (H-atoms omitted)

Atom	x	y	z	B_{eq}
O(1)	0.46257(11)	0.12138(14)	0.12352(12)	4.4
Si(2)	0.45607(4)	0.24153(6)	0.05731(5)	4.0
O(3)	0.44410(11)	0.35229(14)	0.12495(12)	4.4
Si(4)	0.42223(4)	0.36683(6)	0.22979(5)	4.2
O(5)	0.44259(11)	0.24277(15)	0.29044(13)	4.8
C(6)	0.5065(2)	0.1626(2)	0.2987(2)	4.4
C(7)	0.5166(2)	0.1028(2)	0.2172(2)	4.2
C(8)	0.5791(2)	0.0187(2)	0.2291(2)	5.0
C(9)	0.6301(2)	−0.0063(3)	0.3229(2)	5.7
C(10)	0.6193(2)	0.0504(3)	0.4035(2)	6.1
C(11)	0.5574(2)	0.1353(3)	0.3920(2)	5.5
C(12)	0.3631(2)	0.2197(2)	−0.0495(2)	4.3
C(13)	0.3486(2)	0.2950(3)	−0.1293(2)	5.8
C(14)	0.2773(2)	0.2821(4)	−0.2094(2)	7.9
C(15)	0.2218(2)	0.1945(4)	−0.2112(3)	8.3
C(16)	0.2353(2)	0.1184(4)	−0.1343(3)	8.4
C(17)	0.3059(2)	0.1291(3)	−0.0530(2)	6.1
C(18)	0.5532(2)	0.2685(2)	0.0212(2)	4.1
C(19)	0.5921(2)	0.3784(2)	0.0347(2)	4.7
C(20)	0.6639(2)	0.3985(3)	0.0051(2)	6.0
C(21)	0.6987(2)	0.3113(3)	−0.0370(3)	6.9
C(22)	0.6617(2)	0.2026(3)	−0.0510(3)	7.4
C(23)	0.5893(2)	0.1806(2)	−0.0221(2)	5.8
C(24)	0.3080(2)	0.3874(2)	0.2102(2)	4.4
C(25)	0.2523(2)	0.2980(2)	0.1677(2)	5.4
C(26)	0.1667(2)	0.3081(3)	0.1533(2)	6.0
C(27)	0.1339(2)	0.4098(3)	0.1790(3)	6.5
C(28)	0.1873(2)	0.4996(3)	0.2196(3)	8.2
C(29)	0.2734(2)	0.4891(3)	0.2355(3)	6.5
C(30)	0.4868(1)	0.4889(2)	0.2986(2)	4.7
C(31)	0.5349(2)	0.4769(3)	0.3956(2)	6.9
C(32)	0.5813(2)	0.5731(4)	0.4448(3)	8.7
C(33)	0.5795(2)	0.6783(3)	0.3985(3)	8.1
C(34)	0.5327(2)	0.6915(3)	0.3028(3)	7.2
C(35)	0.4874(2)	0.5964(3)	0.2538(2)	5.9

Nominal crystal dimensions 0.21 × 0.31 × 0.37 mm, μ = 14.84 cm^{-1}, absorption corrections 1.25 to 1.47. A total of 4381 reflections were scanned ($\pm h, +k, +l$), giving 3081 with $I > 3\sigma(I)$. Final $R = 0.040$ (0.062 including the unobserved), $R_w = 0.057$, k in weighting scheme, 0.0005. H atom parameters were not refined.

TABLE 9. Selected bond lengths (Å), torsion angles (deg), and bond angles (deg) for **1**; in this and subsequent tables the torsion angles are defined by the atoms comprising the inner, silicon-containing ring

Bond	Length	Torsion angle
Si(2)—O(1)	1.641(2)	54.3
Si(2)—O(3)	1.633(2)	−55.7
Si(2)—C(12)	1.852(2)	
Si(2)—C(18)	1.862(2)	
O(1)—C(7)	1.444(3)	−79.7
O(3)—C(4)	1.435(3)	80.4
C(4)—C(5)	1.500(4)	−64.7
C(6)—C(7)	1.509(4)	66.7
C(5)—C(6)	1.401(3)	−0.5

Bonds	Angle	Bonds	Angle
O(1)—Si(2)—O(3)	108.7(1)	Si(2)—O(1)—C(7)	118.6(2)
O(1)—Si(2)—C(12)	110.4(1)	Si(2)—O(3)—C(4)	120.8(2)
O(1)—Si(2)—C(18)	109.2(1)	O(3)—C(4)—C(5)	112.9(2)
O(3)—Si(2)—C(12)	106.7(1)	O(1)—C(7)—C(6)	113.7(2)
O(3)—Si(2)—C(18)	110.9(1)	C(4)—C(5)—C(6)	121.5(2)
C(12)—Si(2)—C(18)	111.0(1)	C(5)—C(6)—C(7)	122.0(2)

TABLE 10. Selected bond lengths (Å), torsion angles (deg) and bond angles (deg) for **2**

Bond	Length	Torsion angle
Si(2)—O(1)	1.638(3)	54.0
Si(2)—O(3)	1.635(3)	80.2
Si(2)—C(15)	1.854(5)	
Si(2)—C(21)	1.841(5)	
O(1)—C(14)	1.427(6)	161.0
O(3)—C(4)	1.438(6)	−166.3
C(4)—C(5)	1.494(6)	82.5
C(13)—C(14)	1.501(7)	149.5
C(5)—C(6)	1.401(6)	−1.2

Bonds	Angle	Bonds	Angle
O(1)—Si(2)—O(3)	111.3(2)	Si(2)—O(1)—C(14)	121.3(3)
O(1)—Si(2)—C(15)	105.0(2)	Si(2)—O(3)—C(4)	122.7(3)
O(1)—Si(2)—C(21)	110.1(2)	O(3)—C(4)—C(5)	110.7(4)
O(3)—Si(2)—C(15)	110.9(2)	O(1)—C(14)—C(13)	111.1(4)
O(3)—Si(2)—C(21)	106.0(2)	C(4)—C(5)—C(6)	122.3(4)
C(15)—Si(2)—C(21)	113.6(2)	C(12)—C(13)—C(14)	119.5(4)

Experimental

The ^{13}C (20 MHz) nmr spectra were recorded in $CDCl_3$ on a Varian FT-80A spectrometer with internal ^{2}H lock to the solvent and at a temperature of 35°C. The spectra were acquired with SW 4132, AT 0.99, FA 23°, ^{1}H irradiation at 80 Hz, $\gamma H_2/2H\pi \sim 4000$ Hz, modulation bandwidth 2000 Hz (broadband decoupling). ^{29}Si nmr spectra with broadband ^{1}H-decoupling were obtained at 71.73 MHz using a Nicolet Magnetics 360 spectrometer. Samples ($CDCl_3$; 10 mm tubes) were treated with $Cr(acac)_3$ (5 mg/mL) to decrease spin–lattice relaxation time T_1 and suppress the nuclear Overhauser enhancement which has the potential to cause nulling of ^{29}Si signals. Other conditions were as follows: temperature 21°C, spectral width ±10 kHz, quadrature phase detection, acquisition time 0.41 s, 90° pulses (40 µs), delay between acquisitions 1 s to 10 s.

1,3-Dioxa-2,2-diphenyl-2-sila-5,6-benzocycloheptane, 1, and 2,9-disila-1,3,8,10-tetraoxa-2,2,9,9-tetraphenyl-5,6,12,13-dibenzocyclotetradecane 2

A solution of dichlorodiphenylsilane (25.28 g, 0.10 mol) in toluene

TABLE 11. Selected bond lengths (Å) torsion angles (deg) and bond angles (deg) for **3**

Bond	Length	Torsion angle
Si(2)—O(1)	1.640(1)	56.5
Si(2)—O(3)	1.638(1)	76.8
Si(2)—C(17)	1.844(2)	
Si(2)—C(18)	1.842(2)	
O(1)—C(16)	1.427(2)	−174.1
O(3)—C(4)	1.437(2)	−119.1
C(4)—C(5)	1.505(2)	82.3
C(15)—C(16)	1.507(2)	137.7
C(5)—C(6)	1.396(2)	179.4
C(6)—C(7)	1.380(2)	−176.0

Bonds	Angle	Bonds	Angle
O(1)—Si(2)—O(3)	111.2(1)	Si(2)—O(3)—C(4)	125.1(1)
O(1)—Si(2)—C(17)	111.1(1)	O(3)—C(4)—C(5)	111.0(1)
O(1)—Si(2)—C(18)	105.0(1)	O(1)—C(16)—C(15)	110.9(1)
O(3)—Si(2)—C(17)	104.2(1)	C(4)—C(5)—C(6)	120.3(2)
O(3)—Si(2)—C(18)	111.9(1)	C(14)—C(15)—C(16)	120.0(2)
C(17)—Si(2)—C(18)	113.7(1)	C(5)—C(6)—C(7)	121.6(2)
Si(2)—O(1)—C(16)	121.4(1)		

TABLE 12. Selected bond lengths (Å), torsion angles (deg), and bond angles (deg) for **4**

Bond	Length	Torsion angle
Si(2)—O(1)	1.657(1)	165.8
Si(2)—O(3)	1.642(1)	−75.3
Si(2)—C(11)	1.835(2)	
Si(2)—C(12)	1.842(2)	
O(1)—C(10)	1.372(2)	−114.8
O(3)—C(4)	1.363(2)	23.8
C(4)—C(5)	1.395(3)	−4.7

Bonds	Angle	Bonds	Angle
O(1)—Si(2)—O(3)	106.1(1)	C(11)—Si(2)—C(12)	113.4(1)
O(1)—Si(2)—C(11)	111.0(1)	Si(2)—O(1)—C(10)	126.0(1)
O(1)—Si(2)—C(12)	109.4(1)	Si(2)—O(3)—C(4)	137.0(1)
O(3)—Si(2)—C(11)	113.7(1)	O(3)—C(4)—C(5)	122.7(2)
O(3)—Si(2)—C(12)	102.8(1)	C(4)—C(5)—O(6)	118.6(2)

(50 mL) was added to a stirred, hot (~100°C) mixture of 1,2-benzenedimethanol (13.82 g, 0.10 mol) and pyridine (16 mL, 0.198 mol) in toluene (200 mL). After refluxing for 3 h the precipitated solid was filtered and the toluene evaporated. Trituration of the residue with ether gave colorless solid (29.68 g). Treatment of the latter with refluxing ethyl acetate gave **2** as insoluble solid (2.67 g, 8.4%). The pure compound was obtained as colorless prisms, mp 251–253°C (toluene) (lit. 245–250°C (1)).

Successive concentrations of the ethyl acetate-soluble fraction gave **1** as a colorless solid (20.57 g, 64.7%): the pure compound was obtained as colorless prisms, mp 128–130°C (ethyl acetate) (lit. 129–131°C (1)).

Analogous reactions of 1,2-benzenedimethanol with dichloromethylphenylsilane and dichlorodimethylsilane afforded viscous oils. Compounds **5** and **6** were identified as the major components by ^{13}C nmr (Table 1).

2,10-Disila-2,2,10,10-tetramethyl-1,3,9,11-tetraoxa-5,7,13,15-dibenzocyclohexadecane, ***3***

Dichlorodimethylsilane (13.3 g, 0.103 mol) in toluene (50 mL) was added to a stirred, hot (100°C) solution of 1,3-benzenedimethanol (13.82 g, 0.10 mol) and pyridine (16 mL, 0.198 mol) in toluene (200 mL). Work-up after 3 h as above gave a viscous oil which crystallized on cooling. Trituration with ether gave **3** as an insoluble solid (11.77 g, 60.7%): the pure compound was obtained as colorless prisms, mp 162–164°C (ethyl acetate).

TABLE 13. Selected bond lengths (Å), torsion angles (deg), and bond angles (deg) for **11**

Bond	Length	Torsion angle
Si(2)—O(1)	1.646(2)	−52.1
Si(2)—O(3)	1.630(2)	−12.4
Si(2)—C(12)	1.845(3)	
Si(2)—C(18)	1.848(3)	
Si(4)—O(3)	1.628(2)	19.5
Si(4)—O(5)	1.640(2)	37.8
Si(4)—C(24)	1.851(3)	
Si(4)—C(30)	1.856(3)	
O(1)—C(7)	1.389(3)	68.9
O(5)—C(6)	1.380(3)	−62.3
C(6)—C(7)	1.387(4)	0.1

Bonds	Angle	Bonds	Angle
O(1)—Si(2)—O(3)	108.3(1)	O(5)—Si(4)—C(24)	103.8(1)
O(1)—Si(2)—C(12)	104.9(1)	O(5)—Si(4)—C(30)	111.8(1)
O(1)—Si(2)—C(18)	119.1(1)	C(24)—Si(4)—C(30)	113.4(1)
O(3)—Si(2)—C(12)	111.8(1)	Si(2)—O(1)—C(7)	126.1(2)
O(3)—Si(2)—C(18)	107.0(1)	Si(2)—O(3)—Si(4)	134.9(1)
C(12)—Si(2)—C(18)	113.0(1)	Si(4)—O(5)—C(6)	131.1(2)
O(3)—Si(4)—O(5)	108.7(1)	O(5)—C(6)—C(7)	121.7(2)
O(3)—Si(4)—C(24)	111.0(1)	O(1)—C(7)—C(6)	121.2(2)
O(3)—Si(4)—C(30)	108.0(1)		

2,7-Disila-2,2,7,7-tetramethyl-1,3,6,8-tetraoxa-4,5,9,10-dibenzocyclodecane, ***4***

A solution of dichlorodimethylsilane (26.6 g, 0.206 mol) in toluene (50 mL) was added to a hot (~80°C), stirred mixture of catechol (22.0 g, 0.20 mol) and pyridine (32 mL, 0.396 mol) in toluene (200 mL). After refluxing for 3 h and standing overnight at room temperature the precipitate was filtered off. Toluene was distilled from the filtrate to give a semi-crystalline mass (29.08 g): compound **4** was obtained as colorless prisms (16.42 g, 49.5%), mp 87–90°C (petroleum ether) (lit. 84–88°C (11)).

Crystalline **7**, mp 117–121°C (lit. 109–115°C (11)), was isolated from an analogous reaction of catechol with dichloromethylphenylsilane.

2,7-Disila-1,3,6,8-tetraoxa-2,2,7,7-tetraphenyl-4,5,9,10-dibenzocyclodecane, ***8****, and 2,4-disila-2,2,4,4-tetraphenyl-1,3,5-trioxa-6,7-benzocycloheptane,* ***11***

Analogous reaction of dichlorodiphenylsilane (25.28 g) and catechol (11.01 g) in the presence of pyridine (15.65 g) and toluene (250 mL) was carried out at 100°C for 3 h. The precipitated pyridine hydrochloride was filtered off and the filtrate concentrated by evaporation under reduced pressure. A colorless precipitate (11.39 g) was collected. This was washed with warm acetone to leave dimer **8** as a colorless solid (11.045 g, 38%), mp 167–172°C.

Distillation of toluene from the filtrate gave a viscous oily residue which gradually crystallized. The trioxa derivative **11** was obtained as colorless prisms (7.06 g, 29%), mp 136–138°C (petroleum ether/ethyl acetate).

1,3-Di(2-hydroxyphenoxy)-1,3-disila-2-oxa-1,1,3,3-tetraphenylpropane, ***12***

A solution of dimer **8** (2.00 g) in chloroform (20 mL) was allowed to stand at room temperature for 15 days. Evaporation of the solvent and

crystallization gave **12** as colorless prisms (1.602 g, 78%), mp 128–130°C (petroleum ether/ether acetate).

Complete conversion to **12** was obtained after **8** (500 mg) was stirred for 6 h at room temperature in chloroform (10 mL) to which water (4 drops) had been added. Complete conversion was also obtained when suspensions of **8** (1 g) in 30 mL of acetone or benzene were refluxed for 2 or 4 h, respectively: the solid slowly dissolved as the reaction progressed.

*Pyridine-catalyzed decomposition of **12***

A solution of **12** (1.00 g) in chloroform (20 mL) containing pyridine (1 drop) was stirred at room temperature for 30 min. The petroleum ether insoluble portion of the product afforded catechol as a colorless solid (88 mg, 48%) identified by mp (100–106°C), mixed mp (100–105°C) and nmr. Crystallization of the petroleum ether soluble component gave **11** (371 mg, 46%), mp 134–137°C (petroleum ether/ethyl acetate). When the reaction time was increased to 1 h the isolated yields of catechol and **11** were 86% and 74%, respectively.

The same breakdown products (**11** and catechol) were isolated after a solution of **8** (1 g) in chloroform (20 mL) was treated with 1 drop of pyridine and allowed to stand at room temperature for 24 h.

*1,3-Di(2-hydroxyphenoxy)-1,3-disila-2-oxa-1,1,3,3-tetramethylpropane, **13***

When a solution of **4** in $CDCl_3$ was allowed to stand at room temperature for 21 days, essentially quantitative conversion to **13** was observed.

Acknowledgements

We wish to thank Mrs. M. G. Flack and Mrs. M. Wile for excellent technical assistance. We also thank Dr. J. A. Walter for the ^{29}Si nmr spectra, some of which were obtained at the Atlantic Regional Magnetic Resonance Centre at Dalhousie University, Halifax.

1. R. H. Cragg and R. D. Lane. J. Organomet. Chem. **267**, 1 (1984); R. D. Lane. Ph.D. Thesis, University of Kent at Canterbury. 1983.
2. L. Birkofer and O. Stuhl. J. Organomet. Chem. **164**, C1 (1979).
3. H. Meyer, G. Nagorsen, and A. Weiss. Z. Naturforschung. **30**b, 488 (1975).
4. F. P. Boer, J. J. Flynn, and J. W. Turley. J. Am. Chem. Soc. **90**, 6973 (1968).
5. J. J. Harland, R. O. Day, J. F. Vollano, A. C. Sau, and R. R. Holmes. J. Am. Chem. Soc. **103**, 5269 (1981).
6. R. R. Holmes, R. O. Day, V. Chandrasekhar, and J. M. Holmes. Inorg. Chem. **24**, 2009 (1985).
7. R. R. Holmes, R. O. Day, V. Chandrasekhar, J. J. Harland, and J. M. Holmes. Inorg. Chem. **24**, 2016 (1985).
8. J. J. Flynn and F. P. Boer. J. Am. Chem. Soc. **91**, 5756 (1969).
9. H. Meyer and G. Nagorsen. Angew. Chem. Int. Ed. Engl. **18**, 551 (1979); E.-U. Wurthwein and P. V. Schleyer. Angew. Chem. Int. Ed. Engl. **18**, 553 (1979).
10. J. D. Dunitz. Angew. Chem. Int. Ed. Engl. **19**, 1034 (1980); G. Nagorsen and H. Meyer. Angew. Chem. Int. Ed. Engl. **19**, 1034 (1980).
11. R. H. Cragg and R. D. Lane. J. Organomet. Chem. **270**, 25 (1984).
12. D. F. Grant and E. J. Gabe. J. Appl. Crystallogr. **11**, 114 (1978).
13. G. Germain, P. Main, and M. M. Woolfson. Acta Crystallogr. A**27**, 368 (1971).
14. (*a*) A. C. Larson and E. J. Gabe. Computing in crystallography. Delft University Press, Delft, Holland. 1978. p. 81; (*b*) International Tables for X-Ray Crystallography, Vol. IV. Kynoch Press, Birmingham, England. 1974.
15. R. H. Cragg and R. D. Lane. J. Organomet. Chem. **289**, 23 (1985).

The reactions of $O(^3P)$ with 2-propanone, 2-butanone, and 3-pentanone

JOHN M. ROSCOE
Department of Chemistry, Acadia University, Wolfville, N.S., Canada B0P 1X0

Received July 30, 1985[1]

JOHN M. ROSCOE. Can. J. Chem. **64**, 1458 (1986).

The reactions of $O(^3P)$ with 2-propanone, 2-butanone, and 3-pentanone have been studied kinetically as a function of temperature and substrate concentration. The absolute rate constants for these reactions in the gas phase, in the units $M^{-1}\,s^{-1}$, obey the following relations.

$$O + \text{2-propanone: } \ln k = 20.28\pm0.18 - (2.1\pm0.2) \times 10^3/T$$

$$O + \text{2-butanone: } \ln k = 20.02\pm0.19 - (1.3\pm0.3) \times 10^3/T$$

$$O + \text{3-pentanone: } \ln k = 19.48\pm0.32 - (1.0\pm0.5) \times 10^3/T$$

The activation energies for these reactions are comparable to those for the reactions of $O(^3P)$ with alcohols, but the preexponential factors for the reactions of $O(^3P)$ with these ketones are significantly smaller than those for the analogous reactions with alcohols. The available data indicate that the reactivity of $O(^3P)$ toward ketones shows a variation with polar effects of substituents which is similar to that found for the reactions of OH with ketones.

JOHN M. ROSCOE. Can. J. Chem. **64**, 1458 (1986).

On a étudié la variation de la cinétique des réactions du $O(^3P)$ avec la propanone-2, la butanone-2 et la pentanone-3 en fonction de la température et de la concentration des substrats. Les constantes absolues de ces vitesses de réaction en phase gazeuse, exprimées en $M^{-1}\,s^{-1}$, obéissent aux relations suivantes:

$$O + \text{2-propanone: } \ln k = 20{,}28\pm0{,}18 - (2{,}1\pm0{,}2) \times 10^3/T$$

$$O + \text{2-butanone: } \ln k = 20{,}02\pm0{,}19 - (1{,}3\pm0{,}3) \times 10^3/T$$

$$O + \text{3-pentanone: } \ln k = 19{,}48\pm0{,}32 - (1{,}0\pm0{,}5) \times 10^3/T$$

Les énergies d'activation de ces réactions sont comparables à celles des réactions du $O(^3P)$ avec les alcools; toutefois, les facteurs préexponentiels pour les réactions du $O(^3P)$ avec ces cétones sont beaucoup plus faibles que ceux observés pour les réactions analogues avec les alcools. Les données disponibles indiquent que la réactivité du $O(^3P)$ avec les cétones varie avec les effets polaires des substituants d'une façon semblable à celle qui a été observée pour les réactions de OH avec les cétones.
[Traduit par la revue]

Introduction

We recently reported an analysis of kinetic data for the reactions of $O(^3P)$ with C_1 to C_4 alcohols (1). The results indicated that the inductive effect of the OH group was significant at CH bonds which were not α to OH. The Arrhenius preexponential factors for these reactions were consistently smaller than those for reactions of $O(^3P)$ with alkanes and were insensitive to the structure of the alcohol except for a statistical dependence on the number of α-CH bonds. The activation energies for the reactions of $O(^3P)$ with alcohols were some 2 to 4 times smaller than those for the analogous alkane reactions as a result of the strong inductive effect of the OH group. A Taft linear free energy analysis showed that the reactions of $O(^3P)$ with alcohols had a sensitivity to polar effects midway between the analogous reactions with alkanes and aldehydes and that the reactions of $O(^3P)$ consistently showed somewhat stronger polar effects than the corresponding reactions of OH.

The reactions of $O(^3P)$ with ketones described here were investigated for several reasons. Kinetic data for these reactions are very scarce. The only previous study of such reactions of which we are aware (2) reported that, for the reaction of $O(^3P)$ with 2-propanone, the activation energy was comparable to, or somewhat larger than, that for the reaction of $O(^3P)$ with methanol. The Arrhenius preexponential factor, however, was found to be some 5 to 10 times smaller than the recently reported values for the reaction of $O(^3P)$ with methanol (3–5). It seemed useful to test the generality of this result. Ketones also provide the opportunity to investigate the effects of substitution on both sides of a very polar functional group. It was of interest to estimate the extent to which polar effects due to substitution on one side of the carbonyl would be felt on the other side of the carbonyl. Finally, the comparatively wide range of substitution possible in ketones provides an excellent opportunity to seek correlations between Arrhenius parameters and to further explore the sensitivity of reactions of $O(^3P)$ to polar effects.

Experimental

The reactions were studied in a conventional discharge-flow system similar to those used in earlier work in this laboratory (6, 7). The cylindrical reaction vessel was coated with boric acid to inhibit heterogeneous recombination of $O(^3P)$. The substrate entered the reactor through a moveable inlet and the concentration of $O(^3P)$ was monitored at a fixed point at the downstream end of the reaction vessel. The pressures used in the experiments ranged from 0.9 to 1.2 Torr (1 Torr = 133.3 Pa) and linear flow velocities in the reaction vessel ranged from 600 to 1300 cm s^{-1}.

Oxygen atoms were formed by titrating $N(^4S)$ atoms with NO in order to avoid interference from O_2 (6, 8). $N(^4S)$ was produced by dissociating purified N_2 with a microwave-driven discharge. The concentration of $O(^3P)$ produced in this way was kept small by passing only a small part of the total nitrogen flow through the discharge, the remainder of the nitrogen mixing with the products of the discharge upstream from the NO inlet. This arrangement made it possible to achieve more than a 1000-fold excess of ketone. This was essential to avoid secondary reactions of $O(^3P)$, particularly with OH, while permitting a reasonably wide variation in ketone concentration as required in the kinetic analysis. The concentration of $O(^3P)$ was determined by measuring the intensity of the emission from electronically excited NO_2 produced by adding a small amount of NO in excess of that required to completely consume the $N(^4S)$. The rate constants

[1]Revision received February 26, 1986.

obtained in this way were independent of the amount of excess NO used.

The ketones (Fisher, Certified) were purified by repeated fractional distillation until no impurities could be detected by gas chromatography. Their purity was estimated on this basis to be better than 99.995%. Gas chromatographic analysis of both starting materials and reaction products was done on an 8-ft column packed with Porapak Q using a thermal conductivity detector because of the need to measure water. The purity of the starting materials was also confirmed on an 8-ft 1% Carbowax column using a flame ionization detector. Reaction products were trapped with liquid nitrogen, warmed to room temperature, and then removed from the flow system for injection into the gas chromatograph. Because of the large concentration of ketone used in these experiments, the ketone could be used as an internal standard for determination of the reaction products.

Experiments in which a constant amount of NO in slight excess of $N(^4S)$ was added through the moveable inlet at various distances along the reactor in the absence of ketone indicated that heterogeneous recombination of $O(^3P)$ was negligible over the range of reaction times used in the kinetic experiments. However, as in our recent work on the reactions of $O(^3P)$ with the butanols (1), adsorption of the substrate and (or) reaction products on the walls of the reaction vessel produced a substantial extraneous first-order heterogeneous loss route for $O(^3P)$. In an effort to keep this effect constant during a given set of kinetic experiments, the moveable inlet was always moved upstream during a run and was moved slowly enough to allow the system to stabilize between successive measurements of the concentration of $O(^3P)$. After a kinetic experiment, the substrate flow was turned off, the moveable reactant inlet was returned to the downstream end of the reaction vessel, and a new kinetic experiment was not started until the $O(^3P)$ concentration had returned to its previous value in the absence of reactant. The pseudo-first-order plots obtained in this way were reproducible, had linear correlation coefficients better than 0.98, and gave slopes with standard deviations less than 2%. As indicated in Fig. 1, the pseudo-first-order rate constants could be adequately represented by

[1] $$k_{obs} = k_0 + k_R[RC{:}OR']$$

in which k_R is the rate constant for the reaction of $O(^3P)$ with ketone in the gas phase and k_0 refers to the complicating first-order wall loss for $O(^3P)$. Values of k_R were obtained from plots such as those in Fig. 1 covering a factor of up to 8 in ketone concentration. Values of k_R obtained in this way were reproducible to within 20% or better. Both the pseudo-first-order rate constants and the Arrhenius parameters obtained from them were calculated by weighted least squares with weights $y^2/\sigma^2(y)$ where $y = k_R$ in the Arrhenius expression and $y = O(^3P)$ signal in the pseudo-first-order analysis of $O(^3P)$ decay. The data in the pseudo-first-order analysis were within two standard deviations of the regression line while the data used in the Arrhenius expressions were at the 95% confidence level or better.

Results and discussion

The earlier work on the reaction of $O(^3P)$ with 2-propanone (2) demonstrated clearly that the initial step in the reaction is

[2] $$CH_3C{:}OCH_3 + O \rightarrow CH_2C{:}OCH_3 + OH$$

Subsequent reactions that must be considered are

[3] $$O + OH \rightarrow O_2 + H$$

[4] $$OH + CH_3C{:}OCH_3 \rightarrow CH_2C{:}OCH_3 + H_2O$$

[5] $$2\ CH_2C{:}OCH_3 \rightarrow \text{products}$$

[6] $$O + CH_2C{:}OCH_3 \rightarrow \text{products}$$

Reaction [3] may be suppressed relative to reaction [4] by using a sufficient excess of 2-propanone (or of the appropriate ketone in the other reactions studied, assuming they occur by the same kind of mechanism). The concentration ratio of ketone to $O(^3P)$ required to accomplish this will be indicated by $[H_2O]/\Delta[O] = 1$ where $\Delta[O]$ is the reduction in [O] due to reaction. For $[CH_3C{:}OCH_3]/[O]_0 > 150$ the measured yield of H_2O was equal to the consumption of $O(^3P)$ while ratios less than 100 gave yields of H_2O that were clearly less than the consumption of $O(^3P)$. Similar results were obtained for the other ketones although the ketone/$O(^3P)$ ratio required for quantitative elimination of reaction [3] varied somewhat from one ketone to another. The ratio of ketone to $O(^3P)$ was always kept greater than that required to ensure that reaction [3] was negligible.

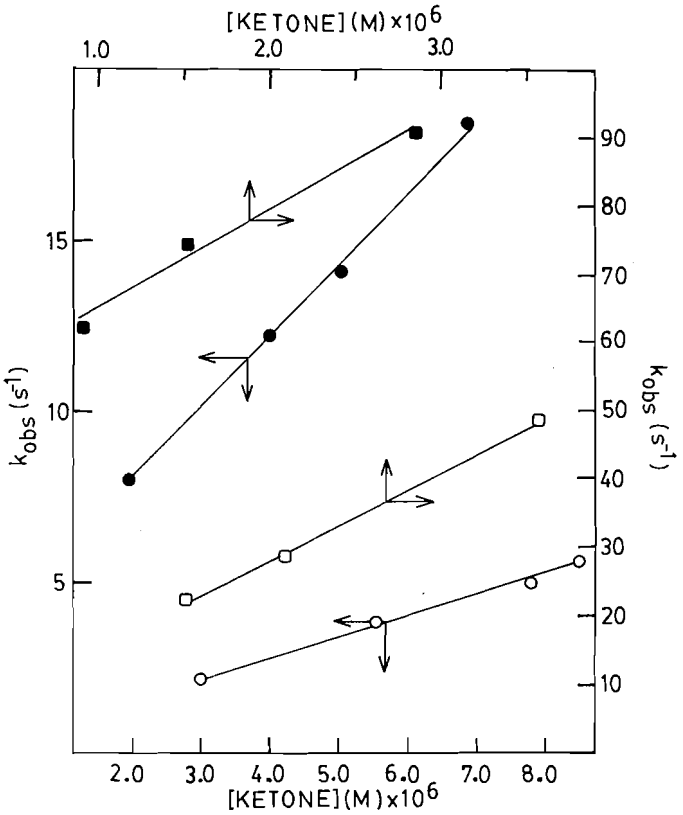

FIG. 1. Concentration dependence of pseudo-first-order rate constants (k_{obs}). ○, O + 2-propanone, 301 K; ●, O + 2-propanone, 371 K; □, O + 2-butanone, 318 K; ■, O + 3-pentanone, 344 K.

The effect on $O(^3P)$ decay kinetics of intervention by reaction [6] is less clear-cut than was the case for reaction [3]. If reaction [6] occurs by addition, it simply represents an extra loss route for $O(^3P)$ that does not lead to H_2O. The observation that, with a sufficiently large excess of ketone, the yield of H_2O could be made equal to the consumption of $O(^3P)$ indicates that addition of $O(^3P)$ to the organic radical formed in the initial step of the reaction is not important under the conditions used to determine the rate constants. It is, of course, possible for reaction [6] to proceed by hydrogen abstraction producing OH, which would then yield H_2O via reaction [4], setting up a chain for removal of $O(^3P)$. Such a mechanistic complication would not be detected by measuring the yield of H_2O. There are, however, both theoretical and experimental reasons to conclude that this version of reaction [6] was also unimportant. The extent of intervention of reaction [6] will depend on the concentration of the organic radical ($CH_2C{:}OCH_3$ in the case of 2-propanone) and this, in turn, will depend on the initial concentration of $O(^3P)$. The initial concentration of $O(^3P)$ was varied by approximately a factor of 5 for each reaction studied with no detectable effect on the value of the rate constant. This

TABLE 1. Summary of kinetic data

Temperature (K)	Pressure (Torr)	$[O]_0 \times 10^8$ (M)	[Ketone] $\times 10^6$ (M)	k_{obs} (s^{-1})	$k_R \times 10^{-6}$ ($M^{-1}\ s^{-1}$)
O + 2-propanone:					
301	0.891	1.22	2.98	2.11	0.61
	0.891	1.15	5.52	3.80	$k_0 = 0.3\ s^{-1}$ [a]
	0.978	1.21	7.77	4.96	
	1.14	1.42	8.50	5.59	
301	1.58	12.5	6.11	6.73	1.29
	1.64	23.2	5.09	6.93	$k_0 = -0.4\ s^{-1}$ [b]
	1.68	21.2	13.8	17.6	
	1.51	20.4	7.59	9.36	
301	1.40	25.8	3.44	12.5	2.47
	1.59	27.2	9.37	24.7	$k_0 = 4.1\ s^{-1}$ [b]
	1.36	25.4	2.12	8.75	
	1.55	27.1	7.93	26.8	
313	0.728	1.70	3.80	4.60	0.76
	0.736	1.64	5.33	4.87	$k_0 = 1\ s^{-1}$
	0.760	1.57	7.77	7.52	
316	0.891	0.544	3.04	4.04	0.77
	0.987	0.604	3.24	3.53	$k_0 = 1.4\ s^{-1}$
	1.00	0.550	8.32	7.77	
343	0.925	1.81	3.00	4.75	1.84
	1.01	1.96	3.73	6.61	$k_0 = -0.5\ s^{-1}$
	1.04	1.90	6.42	11.2	
371	0.925	2.48	1.94	7.94	2.14
	0.816	1.96	3.98	12.2	$k_0 = 3.8\ s^{-1}$
	0.807	1.87	5.04	14.1	
	0.960	2.27	6.85	18.4	
437	0.816	0.648	0.808	15.3	6.41
	0.816	0.624	1.87	19.8	$k_0 = 10\ s^{-1}$
	0.824	0.631	1.88	25.0	
	0.816	0.570	4.30	37.8	
474	0.899	0.576	1.30	32.6	6.76
	0.874	0.540	2.25	32.2	$k_0 = 22\ s^{-1}$
	0.882	0.521	3.52	53.1	
	0.899	0.498	5.24	55.5	
494	0.824	0.825	0.991	40.1	10.4
	0.832	1.16	3.30	61.3	$k_0 = 29\ s^{-1}$
	0.832	1.10	4.59	78.9	
515	0.969	0.649	1.54	46.5	8.39
	1.00	0.664	1.99	45.5	$k0 = 32\ s^{-1}$
	0.969	0.610	3.26	59.6	
542	0.891	0.384	1.09	31.5	18.8
	0.908	0.381	1.85	46.4	$k_0 = 12\ s^{-1}$
	0.891	0.365	2.41	61.5	
	0.899	0.359	3.07	67.2	
565	0.934	0.445	0.939	42.1	14.4
	0.951	0.442	1.64	53.7	$k_0 = 29\ s^{-1}$
	0.987	0.447	2.37	62.2	
	0.969	0.429	2.89	70.8	
O + 2-butanone:					
308	0.775	0.509	2.00	28.6	6.65
	0.775	0.486	3.71	42.3	$k_0 = 16\ s^{-1}$
	0.775	0.477	4.38	43.5	
315	0.951	0.781	1.83	42.2	11.2
	0.969	0.777	2.98	68.4	$k_0 = 25\ s^{-1}$
	0.978	0.771	3.75	61.9	
318	0.978	0.452	1.51	22.2	10.6
	0.978	0.446	2.09	28.6	$k_0 = 2\ s^{-1}$
	0.987	0.437	3.56	48.8	
373	0.943	0.284	1.54	91.6	15.6
	0.943	0.279	2.18	120.	$k_0 = 74\ s^{-1}$
	0.943	0.273	3.04	117.	

TABLE 1. (*concluded*)

Temperature (K)	Pressure (Torr)	$[O]_0 \times 10^8$ (M)	[Ketone] $\times 10^6$ (M)	k_{obs} (s^{-1})	$k_R \times 10^{-6}$ ($M^{-1}\ s^{-1}$)
437	0.916	0.737	0.516	44.2	30.4
	0.925	0.735	0.904	64.0	$k_0 = 32\ s^{-1}$
	0.916	0.709	1.76	83.8	
457	0.960	0.421	0.892	59.5	39.0
	0.960	0.416	1.24	83.5	$k_0 = 29\ s^{-1}$
	0.951	0.399	2.29	117.	
484	0.925	0.297	1.25	98.8	30.0
	0.934	0.289	2.32	165.	$k_0 = 73\ s^{-1}$
	0.951	0.284	3.41	164.	
O + 3-pentanone:					
308	0.951	0.444	2.12	55.3	6.38
	0.951	0.439	2.17	56.1	$k_0 = 41\ s^{-1}$
	0.960	0.437	3.38	63.9	
	0.951	0.430	3.70	64.0	
316	0.951	0.311	2.06	42.0	7.98
	0.951	0.308	2.54	46.0	$k_0 = 26\ s^{-1}$
	0.951	0.300	3.74	55.4	
320	0.908	0.264	0.956	13.5	18.7
	0.916	0.264	1.47	38.2	$k_0 = 1\ s^{-1}$
	0.908	0.256	2.42	43.6	
324	0.969	0.125	0.810	8.26	16.2
	0.960	0.124	1.13	22.0	$k_0 = -1\ s^{-1}$
	0.978	0.123	2.16	32.8	
330	1.01	0.360	0.852	48.6	10.6
	1.00	0.350	1.84	51.2	$k_0 = 37\ s^{-1}$
	1.01	0.348	2.56	67.5	
344	0.934	0.350	0.911	62.0	14.3
	0.925	0.342	1.51	74.3	$k_0 = 50\ s^{-1}$
	0.925	0.330	2.86	90.8	
346	0.960	0.282	1.41	63.4	15.0
	0.960	0.281	1.64	71.2	$k_0 = 44\ s^{-1}$
	0.960	0.272	2.90	87.2	
372	0.943	0.206	1.36	77.0	21.5
	0.943	0.203	1.95	78.3	$k_0 = 43\ s^{-1}$
	0.951	0.198	3.26	115.	
439	0.969	0.690	0.805	99.0	36.3
	0.960	0.670	1.51	133.	$k_0 = 72\ s^{-1}$
	0.960	0.663	1.82	133.	
443	0.891	0.832	1.03	99.6	37.2
	0.891	0.803	2.12	154.	$k_0 = 65\ s^{-1}$
	0.891	0.792	2.53	158.	
	0.899	0.794	2.78	163.	
500	0.951	0.322	1.00	119.	22.9
	0.951	0.317	1.49	145.	$k_0 = 100\ s^{-1}$
	0.951	0.312	1.92	140.	
545	0.960	0.991	0.735	123.	39.5
	0.960	0.969	1.35	158.	$k_0 = 100\ s^{-1}$
	0.978	0.974	1.73	183.	
	0.969	0.956	1.97	162.	

[a]Values of the heterogeneous component of k_{obs} have been listed to indicate the approximate magnitude of the extraneous loss of $O(^3P)$.

[b]These data are included to indicate the effect of an inadequate excess of 2-propanone. The values of k_R at these temperatures require a significant stoichiometric correction.

suggests that reaction [6] was unimportant as a loss route for $O(^3P)$. In order for reaction [6] to be important, the ratio $k_1[CH_3C{:}OCH_3]/k_6[CH_2C{:}OCH_3]$ would need to be less than about 10. This is unlikely for two reasons. The concentration of the organic radical is likely to be substantially smaller than that of $O(^3P)$ during at least the first half-life. Since the ketone/$O(^3P)$ ratio ranges from about 100 to over 1000 this would require k_1/k_6 to be less than 0.01. For comparable preexponential factors, this would require reaction [6] to have an activation energy more than 2.5 kJ/mol less than that for reaction [1]. Alternatively, for comparable activation energies reaction [6] would require a preexponential factor more than 10 times larger than that for reaction [1]. Such large variations in preexponential factor or activation energy between reactions [1]

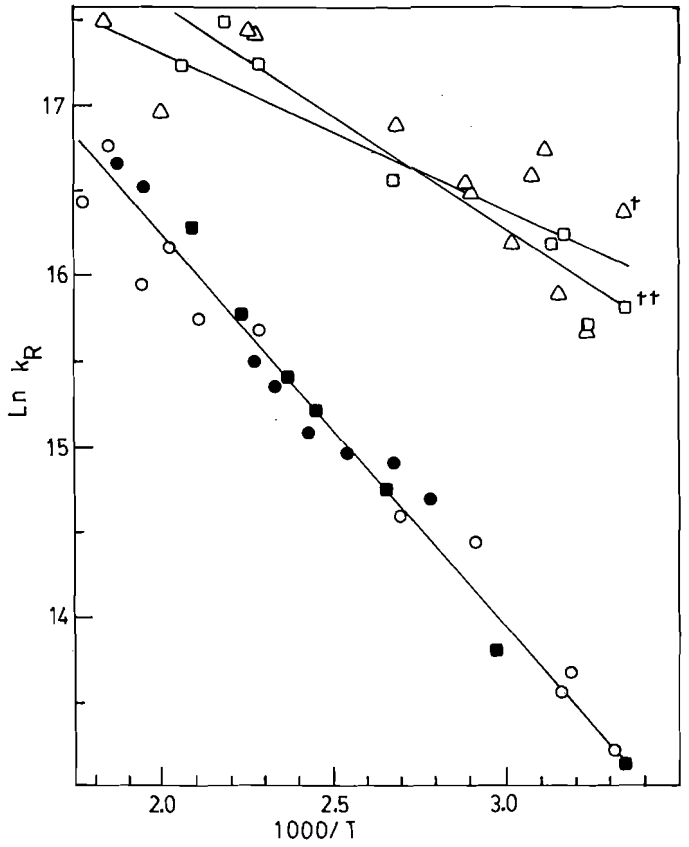

FIG. 2. Arrhenius plots for the reactions of $O(^3P)$ with ketones. O + 2-propanone: ○, this work; ●, ref. 2, mass spectrometric results; ■, ref. 2, esr results, experimental rate constants divided by the suggested stoichiometric coefficient of 3; O + 2-butanone: □, this work; □††, calculated from the linear free energy correlation of ref. 10 using the experimental rate constant for OH + 2-butanone reported in ref. 11; O + 3-pentanone: △, this work; △†, calculated from the linear free energy correlation of ref. 10 using the experimental rate constant for OH + 3-pentanone reported in ref. 12.

and [6] seem unreasonable in view of the similarities in the organic reactant in these reactions. Finally, intervention by reaction [6] as a hydrogen abstraction reaction would increase the rate constants measured experimentally above the correct value for the absolute rate constant by a factor equal to the chain length. This effect would show up as a larger than expected value for the preexponential factors of the reactions. In fact, the preexponential factors are significantly smaller than those for the reactions of $O(^3P)$ with either alcohols or alkanes.

The effect of an inadequate excess of 2-propanone is indicated in the data for the first three temperatures in Table 1. The first data set spans $[CH_3C{:}OCH_3]/[O]_0$ ratios of about 8–35, the second, ratios of about 22–65, and the third, ratios of about 245–641. In all cases, good first-order atom decays were observed and within each range of $[CH_3C{:}OCH_3]/[O]_0$ ratios the pseudo-first-order rate constant was linearly related to the concentration of 2-propanone. It is clear, however, that the slopes of such relations, representing the homogeneous bimolecular rate constant, decrease systematically with decreasing initial concentration of $O(^3P)$ but with 2-propanone concentrations falling in the same range for each data set. As noted earlier, the effect of decreasing the initial concentration of $O(^3P)$ will be to decrease the concentration of the $CH_2C{:}OCH_3$ radical relative to 2-propanone, thereby decreasing the importance of secondary reactions of $O(^3P)$ with $CH_2C{:}OCH_3$. This

TABLE 2. Summary of Arrhenius parameters

Ketone	$A \times 10^{-8}$ ($M^{-1}s^{-1}$)	E_a (kJ mol^{-1})	Reference
2-Propanone	9. ± 3	18. ± 3.	2[a]
2-Propanone	6.4 ± 4	17. ± 2.	This work
2-Butanone	5.0 ± 0.9	10. ± 2.	This work
3-Pentanone	2.9 ± 0.9	8.6 ± 3.7	This work

[a]Recalculated from the mass spectrometric data of ref. 2 by the *y*-weighted least-squares method used for the data obtained in this work.

behaviour may be compared with that observed by Lee and Timmons (2). They found that rate constants for the reaction of $O(^3P)$ with 2-propanone, measured by following the pseudo-first-order loss of $O(^3P)$ by esr spectroscopy, were about a factor of three larger than those obtained by using mass spectrometry to follow the loss of 2-propanone in the presence of a large excess of $O(^3P)$. While they do not quote an absolute concentration of $O(^3P)$, comparison with earlier work from their laboratory (9) suggests that their esr experiments were made with $[O(^3P)] \sim 10^{-7}\,M$ (~4% dissociation of O_2). Their $[CH_3C{:}OCH_3]/[O]_0$ ratios would then fall about in the range 30–100 where we also found significant stoichiometric corrections. Our initial concentrations of $O(^3P)$ are in the range $2 \times 10^{-8}\,M - 3 \times 10^{-9}\,M$ in the experiments with 2-propanone while our absolute concentrations of 2-propanone fall in the same range as those used by Lee and Timmons. A gradual variation in the stoichiometric correction with $[CH_3C{:}OCH_3]/[O]_0$ ratio would not be noticed over a modest range of values of this ratio because of the experimental scatter inherent in such measurements, and reasonably linear dependence of the pseudo-first-order rate constant on the concentration of 2-propanone might be expected. Good linear first-order atom decays would also be observed provided the stoichiometric factor is constant and the consumption of 2-propanone is negligible over the range of reaction times examined. The effects of variable stoichiometric corrections only become evident when the ratio of reactant concentration to atom concentration is varied by several orders of magnitude as in our work and in the comparison of the mass spectrometric and esr results reported by Lee and Timmons.

In view of the above comments, it seems unlikely that extraneous loss routes for $O(^3P)$ had a significant effect on the values calculated for the rate constants of the reactions studied here. At least in the reaction of $O(^3P)$ with 2-propanone, perhaps the most convincing evidence of this is the excellent agreement between our results and those in the literature (2) as shown in Fig. 2. The data falling on that Arrhenius plot cover an overall range of $[CH_3C{:}OCH_3]/[O]_0$ of from 0.015 to 1500, suggesting that both this work and the earlier measurements have adequately eliminated the effects of secondary reactions. There are no data in the literature for the temperature dependence of the reactions of $O(^3P)$ with 2-butanone and 3-pentanone. However, the linear free energy correlation of Gaffney and Levine (10) may be combined with measurements of the rate constants for the reactions of OH with these ketones (11, 12) to estimate the rate constants for their reactions with $O(^3P)$ at 298 K. The values calculated in this way are indicated in Fig. 2 and are in good agreement with our experimental values.

The Arrhenius parameters for the reactions studied are summarized in Table 2. The activation energies are comparable to those found for the reactions of $O(^3P)$ with alcohols (1)

TABLE 3. Summary of data for Taft correlations[a]

Reaction	k_{298} (M^{-1} s^{-1})	σ*	E_s	Reference
O + 2-propanone	4.04×10^5	0.49	1.24	2
O + 2-propanone	5.33×10^5	0.49	1.24	This work
O + 2-butanone[b]	7.70×10^6	0.00, 0.49	0.00, 1.24	This work
O + 3-pentanone	9.37×10^6	0.00	0.00	This work
OH + 2-butanone[b]	5.66×10^8	0.00, 0.49	0.00, 1.24	11
OH + 2-pentanone	2.85×10^9	−0.10	−0.07	12
OH + 2-hexanone	5.52×10^9	−0.115	−0.36	12
OH + 4-methyl-2-pentanone	8.73×10^9	−0.19	−0.47	12
OH + 3-pentanone	1.11×10^9	0.00	0.00	12
OH + 3-hexanone	4.19×10^9	−0.10	−0.07	12

[a]In all cases the reference compound is the one for which σ* = E_s = 0.00 by definition.

[b]For the series of ketones CH_3C:OR, the reference compound is by convention the one for which R = C_2H_5 since both sides of the carbonyl must be bound to carbon to yield a ketone. Similarly, for the series of ketones C_2H_5C:OR, the reference compound is the one for which R = C_2H_5. Thus, 2-butanone is both the reference compound for the series CH_3C:OR and the compound for which R = H in the series C_2H_5C:OR.

and show the expected trend to smaller values with increasing accumulation of secondary α-CH bonds. The preexponential factors show a systematic variation approximately in proportion to the number of α-CH bonds. This is similar to the behaviour observed in the reactions of O(^3P) with alcohols in which the first step is hydrogen abstraction, mainly from the α-CH, and is consistent with a similar initial step in the reactions of O(^3P) with ketones.

The preexponential factors for the reactions of O(^3P) with ketones measured here are some 5–10 times smaller than those for the reactions of O(^3P) with alcohols. They are also an order of magnitude or more smaller than the preexponential factors for the reactions of O(^3P) with alkanes. This kind of behaviour has been observed consistently in the reactions of O(^3P) with organic compounds containing oxygen (e.g. refs. 1–7). It has been postulated that because of the electrophilic nature of the oxygen atom, attack tends to occur preferentially at electron-rich centers such as the OH group in alcohols and the double bonds in ketones and olefins (2). The resulting complex in reactions of O(^3P) with olefins can yield stabilized products such as epoxides. However, such stabilized products are not possible in the reactions of O(^3P) with alcohols and ketones and, at the pressures encountered in experiments in a discharge flow system, these addition complexes simply dissociate again to starting material. Such an explanation would predict that the preexponential factors become smaller with increasing availability of electron density in functional groups such as —OH and >C=O at which O(^3P) is unable to react. This is consistent with the observed decrease in preexponential factor from reactions of O(^3P) with alcohols to the reactions of O(^3P) with ketones.

The transmission of polar effects from the alkyl group on one side of the carbonyl to the one on the other side may be estimated by comparing the rate constants at 300 K for the reactions of O(^3P) with the three ketones studied here. In the reaction of O(^3P) with 2-butanone there are two kinds of α-CH bonds and one kind of β-CH bond so that the composite rate constant for abstraction is

$$[7] \quad k_{C_4H_8O} = k_{CH_3} + k_{C_2H_5}$$

Here k_{CH_3} is the rate constant for abstraction of hydrogen from the CH_3 group bound to the carbonyl and $k_{C_2H_5}$ is the composite rate constant for abstraction from the C_2H_5 group on the other side of the carbonyl. Similarly, the rate constant for reaction of O(^3P) with 3-pentanone can be written

$$[8] \quad k_{C_5H_{10}O} = 2k_{C_2H_5}$$

On the assumption that $k_{C_2H_5}$ is approximately the same for 2-butanone and 3-pentanone, the value of k_{CH_3} at 300 K in 2-butanone is $3 \times 10^6 M^{-1}$ s^{-1}. This is significantly larger than the value of k_{CH_3} ($2.7 \times 10^5 M^{-1}$ s^{-1}) calculated from the rate constant for the reaction of O(^3P) with 2-propanone at 300 K. In fact, operation of polar effects would tend to make the value of $k_{C_2H_5}$ estimated from the reaction of O(^3P) with 3-pentanone larger than the value appropriate to 2-butanone. This suggests that the estimate of $3 \times 10^6 M^{-1}$ s^{-1} for k_{CH_3} in 2-butanone might best be regarded as a lower limit. The estimate of k_{CH_3} in 2-butanone is subject to a probable uncertainty of as much as 70% since it is calculated as the difference between two rate constants of comparable magnitude. The qualitative indication is, however, that extension of the alkyl group in 2-propanone from CH_3 to C_2H_5 increases the reactivity of the remaining CH_3 group.

It is instructive to use the Taft relation (13) to compare the sensitivity to polar effects of the reactions of O(^3P) with ketones. The relevant data are summarized in Table 3. The correlations are less satisfactory than those in the recent analysis of the reactions of O(^3P) with alcohols (1) for two reasons. First, there are too few data for the reactions of O(^3P) with ketones to provide a good correlation. However, comparison of the limited data available provides an estimate of −2 for the value of ρ* for the reactions of O(^3P) with CH_3C:OR and −0.2 for the value of ρ* for the reactions of O(^3P) with C_2H_5C:OR. While there are more data for the reactions of OH with ketones, the Taft correlation suffers from the lack of accurate kinetic data for the reaction of OH with 2-propanone, restricting the analysis to a rather narrow range of values of the substituent parameter. The kinetic data for the reactions of OH with ketones of the type C_2H_5C:OR are also badly scattered, preventing estimation of an accurate value of the reaction parameter, ρ*, for this series of ketones. Nevertheless, a value of −4 may be estimated for ρ* for the reactions of OH with the series of ketones CH_3C:OR and a value of about −0.5 may be estimated for the reactions of OH with the series of ketones C_2H_5C:OR. This indicates a close

parallel between the sensitivities toward polar effects exhibited by the reactions of ketones with OH and with $O(^3P)$. A similar, although less dramatic, dependence of ρ^* on general reactivity was observed in the Taft analysis of reactions of $O(^3P)$ and OH with a wide range of substrates (1). The effect is also consistent with the observation that ρ^* should become less negative as reactivity increases (14).

Acknowledgement

Financial support for this work was provided by the Natural Sciences and Engineering Research Council of Canada.

1. JOHN M. ROSCOE. Can. J. Chem. **61**, 2716 (1983).
2. J. H. LEE and RICHARD B. TIMMONS. Int. J. Chem. Kinet. **9**, 133 (1977).
3. R. L. FAILES, D. L. SINGLETON, G. PARASKEVOPOULOS, and R. S. IRWIN. Int. J. Chem. Kinet. **14**, 371 (1982).
4. H. H. GROTHEER and TH. JUST. Chem. Phys. Lett. **78**, 71 (1981).
5. D. G. KEIL, T. TANZAWA, E. G. SKOLNIK, R. B. KLEMM, and J. V. MICHAEL. J. Chem. Phys. **75**, 2693 (1981).
6. C. M. OWENS and J. M. ROSCOE. Can. J. Chem. **54**, 984 (1976).
7. A. L. AYUB and J. M. ROSCOE. Can. J. Chem. **57**, 1269 (1979).
8. N. WASHIDA. J. Chem. Phys. **75**, 2715 (1981).
9. H. F. LEFEVRE, J. F. MEAGHER, and R. B. TIMMONS. Int. J. Chem. Kinet. **4**, 103 (1972).
10. J. S. GAFFNEY and S. Z. LEVINE. Int. J. Chem. Kinet. **11**, 1197 (1979).
11. R. A. COX, K. F. PATRICK, and S. A. CHANT. Environ. Sci. Technol. **15**, 587 (1981).
12. R. ATKINSON, S. M. ASCHMANN, W. P. L. CARTER, and J. N. PITTS, JR. Int. J. Chem. Kinet. **14**, 839 (1982).
13. N. B. CHAPMAN and J. SHORTER. Advances in linear free energy relationships. Plenum, London. 1972.
14. J. E. LEFFLER and E. GRUNWALD. Rates and equilibria of organic reactions. Wiley, New York. 1963.

COMMUNICATION

High-field ^{2}Hmr spectrometry of deuteriated 1,3,3-trimethylbicyclo[2.2.1]heptan-2-ones. Determination of geminal deuterium isotope effects on deuterium chemical shift

NICK HENRY WERSTIUK, GEORGE TIMMINS, AND BRIAN SAYER
Department of Chemistry, McMaster University, Hamilton, Ont., Canada L8S 4M1

Received January 24, 1986

NICK HENRY WERSTIUK, GEORGE TIMMINS, and BRIAN SAYER. Can. J. Chem. **64**, 1465 (1986).

By a high-field ^{2}Hmr study of deuteriated 1,3,3-trimethylbicyclo[2.2.1]heptan-2-ones (fenchones), we have established that the geminal deuterium isotope effects on the *exo*-6-, *endo*-6-, and methyl deuterons are 1.46 ± 0.06 Hz (0.019 ppm), 1.61 ± 0.06 Hz (0.021 ppm), and 1.46 ± 0.06 Hz (0.019 ppm), respectively. From this study it is clear that high-field ^{2}Hmr has the potential of providing directly all the information on the degree of deuterium substitution at carbon previously obtained indirectly by ^{13}Cmr, while retaining the ability to identify chemically nonequivalent deuterons.

NICK HENRY WERSTIUK, GEORGE TIMMINS et BRIAN SAYER. Can. J. Chem. **64**, 1465 (1986).

En appliquant la technique de la rmn du ^{2}H à haut champ à des triméthyl-1,3,3 bicyclo[2.2.1]heptanones-2 (fenchones), on a établi que les effets isotopiques geminaux du deutérium des deutérons *exo*-6, *endo*-6 ainsi que ceux des groupements méthyles sont respectivement 1,46 ± 0,06 Hz (0,019 ppm), 1,61 ± 0,06 Hz (0,021 ppm) et 1,46 ± 0,06 Hz (0,019 ppm). Sur la base de cette étude, il est clair que la rmn du ^{2}H à haut champ possède le potentiel de fournir directement toutes les informations relatives au degré de substitution par des deutérium (jusqu'à maintenant on ne pouvait obtenir cette information qu'indirectement en se basant sur la rmn du ^{13}C) tout en gardant la possibilité d'identifier les deutérons qui ne sont pas équivalents du point de vue chimique.

[Traduit par la revue]

Although many cases of deuterium isotope effects on ^{1}H and ^{13}C chemical shifts have been documented (1), there is a paucity of examples of deuterium isotope effects on deuterium chemical shift, basically because the dispersion of the signals is narrow. By using a high-field spectrometer and resolution enhancement, this problem has been obviated. In this communication, we report on a ^{2}Hmr study at 76.78 MHz of deuteriated 1,3,3-trimethylbicyclo[2.2.1]heptan-2-ones (fenchones (**1**)). We document the first examples of geminal deuterium isotope effects on deuterium chemical shift and establish, because the effects are additive, that this direct method has potential of providing all the information on the degree of substitution at carbon previously obtained indirectly by ^{13}Cmr (1–3) while retaining the ability to identify chemically nonequivalent deuterons. This method should prove to be useful not only for monitoring ^{1}H–^{2}H (H–D) exchange but for determining isotopic enrichment in biosynthetic studies as well.

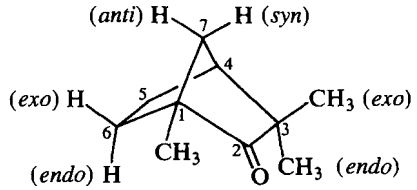

1

The fenchones used in this study were obtained by homoenolization of the ketone in deuteriated medium (Table 1). The ^{2}Hmr spectra[1] of the fenchones, obtained at identical concentrations (0.040 g/mL in CCl_4) at 30°C, are given in Fig. 1. Spectra A, B, D, and E were obtained by using resolution enhancement. Spectrum C is the original spectrum obtained under standard conditions corresponding to D.

TABLE 1. Preparation of deuteriated fenchones

Entry	Conditions	Deuterium incorporation
1	$(CH_3)_3COD/(CH_3)_3COK^a$ 187°C/40 h	1.00
2	$(CH_3)_3COD/(CH_3)_3COK^a$ 197°C/50 h	1.30
3	$(CH_3)_3COD/(CH_3)_3COK^b$ 220°C/304 h	1.52
4	$(CD_3)_3COD/(CD_3)_3COK^c$ 220°C/304 h	3.75

[a]Fenchone (0.100 g) was reacted in a base solution prepared by dissolving potassium (0.100 g) in $(CH_3)_3COD$ (2.0 mL).
[b]Fenchone (0.255 g) was reacted in a base solution prepared by dissolving potassium (0.255 g) in $(CH_3)_3COD$ (5.0 mL).
[c]Fenchone (0.176 g) was reacted in a base solution prepared by dissolving potassium (0.207 g) in $(CD_3)_3COD$ (4.0 mL).

Signals at δ 1.491 and 1.359 of A, the spectrum of fenchone-$d_{1.00}$ (entry 1), show that, as expected (2), *exo*-6-H undergoes exchange faster than *endo*-6-H. The signals at lower frequency flanking these signals are due to fenchone with two deuterons at C-6 and the isotope shifts for *exo*-3 and *endo*-D are +0.019 ppm (1.46 ± 0.06 Hz) and +0.021 ppm (1.61 ± 0.06 Hz), respectively.

Spectrum B is the resolution-enhanced spectrum of fenchone-$d_{1.30}$ (entry 2). In this case, there is 43% of species with two deuterons at C-6, 7% of species that have a single deuteron (δ 0.997) in the *exo*-3 methyl, and ~1% of species labelled at the bridgehead methyl (δ 1.092). That the weak signal at δ 0.978 is due to species with two deuterons in the *exo* methyl rather than the *endo*-3 methyl deuteriated species is established by the fact that the chemical shift difference is ~0.019 ppm. This conclusion is supported by the fact that the difference in

[1]Deuterium magnetic resonance spectra were obtained at 76.78 MHz on a Brüker AM 500 spectrometer operating at 11.75 *T* with broadband proton decoupling. Four hundred transients were acquired in each case using a 45° pulse with an acquisition time of 4.1 s. Initially, memory size was 16K; this was zero-filled to 64K giving a digital resolution of 0.06 Hz/point. Resolution enhancement was achieved with the "Gaussian multiplication" feature available with Brücker software.

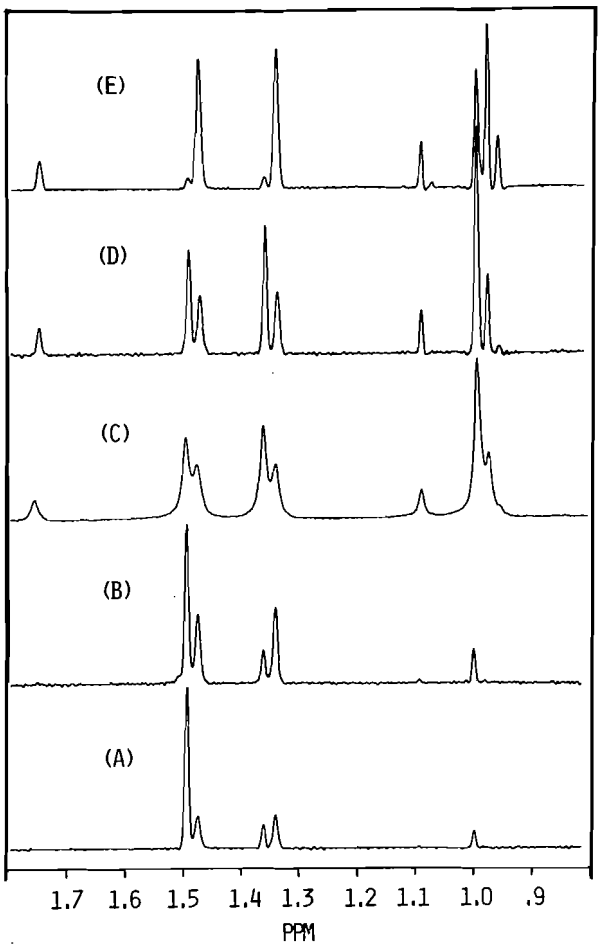

FIG. 1. (A) Resolution-enhanced ^{2}Hmr spectrum (76.78 MHz, CCl_4) of fenchone-$d_{1.00}$. (B) Resolution-enhanced ^{2}Hmr spectrum of fenchone-$d_{1.30}$. (C) ^{2}Hmr spectrum of fenchone-$d_{1.52}$. (D) Resolution-enhanced ^{2}Hmr spectrum of fenchone-$d_{1.52}$. (E) Resolution-enhanced spectrum of fenchone-$d_{3.75}$.

chemical shift between the *exo* and *endo* methyls is only 0.005 ppm as established from the 500-MHz ^{1}Hmr spectrum. In this case, the *exo*-D and *endo*-D shifts also are +0.019 ppm (1.46 ± 0.05 Hz) and +0.021 ppm (1.61 ± 0.06 Hz), respectively.

Spectrum D of fenchone-$d_{1.52}$ (entry 3) shows, as established previously, that the 6-position is equilibrated with the deuterium pool, which is gradually diluted as $(CH_3)_3COD$ is converted to isobutene (4). That is, the intensities of the peaks due to *exo*-6-D, *endo*-6-D, and the 6-d_2 species are roughly equal. The intensity of the peak due to *exo*-6-D is slightly lower than the intensity of the peak due to *endo*-6-D and slightly lower than the sum of the peaks due to the 6-d_2 species. This is so because exchange at the *exo*-6 position is faster than exchange at the *endo*-6 position and thereby more rapidly reflects the dilution of the deuterium pool. The *exo*-D and *endo*-D shifts are the same as the shifts in the previous two cases. The signals of δ 0.997, 0.978, and 0.959, with identical separations of 0.019 ppm, of relative intensity 100, 35, and 4 are due to the *exo*-3 methyl containing one, two and three deuterons, respectively. Close examination of the peak at δ 0.997 indicates that there is a perceptible shoulder on its low frequency side (Δδ 0.01), more pronounced in E, that must be due to deuterium in the *endo* methyl. The signal at δ 1.748 is due to deuterium at the *syn*-7 position (4, 5). By comparison, spectrum C, corresponding to D, obtained under standard conditions clearly shows doubly and triply labelled species as shoulders. It is important to note that in each resolution-enhanced spectrum, the intensities of the signals due to the *exo*- and *endo*-deuterons of the C-6 dideuteriated species are roughly within 90% of each other. This indicates that resolution enhancement does not seriously distort the intensities as the natural line widths of the deuterium resonances are similar. Caution should be exercised when applying this method to resonances of very different line widths.[2]

Spectrum E of fenchone-$d_{3.75}$ (entry 4) shows conclusively that the ketone is essentially fully deuteriated at C-6. The *exo*-D and *endo*-D shifts are identical to the shifts determined in the first three cases. The weak signal on the low frequency side of the peak at δ 1.092 indicates that a small amount of the fenchone is doubly labelled at the bridgehead methyl. The signals at δ 0.997, 0.978, and 0.959 indicate that the *exo*-3 methyl is 36% singly labelled, 48% doubly labelled, and 16% triply labelled. The shoulder on the peak at δ 0.997 due to deuteriated *endo*-3 methyl is more pronounced than it is in D (*vide supra*). The isotope shift of a deuteron of a methyl group by a deuteron is 0.019 ppm and for two deuterons it is 0.038 ppm (2.92 ± 0.06 Hz). On the other hand, from four determinations of the isotope shifts at C-6, it appears that the shift of *exo*-D (1.46 ± 0.06 Hz) is slightly less than the shift (1.62 ± 0.06 Hz) of *endo*-D.

Acknowledgements

We thank the Natural Sciences and Engineering Research Council of Canada and McMaster University for financial support of the high-field NMR facility.

1. H. H. MANTSCH, H. SAITO, and I. C. P. SMITH. Prog. NMR Spectrosc. **11**, 211 (1977).
2. A. L. JOHNSON, J. B. STOTHERS, and C. T. TAN. Can. J. Chem. **53**, 212 (1975).
3. J. R. WESNER, P. SCHMITT, and H. GÜNTHER. J. Am. Chem. Soc. **106**, 10 (1984).
4. N. H. WERSTIUK and G. TIMMINS. Can. J. Chem. **63**, 526 (1985).
5. N. H. WERSTIUK, S. YEROUSHALMI, and G. TIMMINS. Can. J. Chem. **61**, 1945 (1983).

[2]Studies of larger molecules are planned. In cases where line widths are vastly different, computerized curve-fitting may yield useful data.

Structure électronique et réactivité des pyridyl-isothiocyanates. Étude quantique et photoélectronique[1]

C. GUIMON ET G. PFISTER-GUILLOUZO
Laboratoire de physico-chimie moléculaire, Unité associée 474, Institut universitaire de recherche scientifique, Avenue de l'Université, 64000 Pau, France
D. ILAVSKY
Department of Organic Chemistry, Slovak Technical University, 880 37 Bratislava, Czechoslovakia
ET
M. MARCHALIN ET A. MARTVON
Research Institute for Drugs, 801 00 Bratislava, Czechoslovakia
Reçu le 4 décembre 1985

C. GUIMON, G. PFISTER-GUILLOUZO, D. ILAVSKY, M. MARCHALIN et A. MARTVON. Can. J. Chem. **64**, 1467 (1986).

À l'aide de calculs quantiques associés aux données de la spectroscopie photoélectronique ultraviolette (spu), nous montrons que la régiosélectivité des cycloadditions du pyridyl-2 isothiocyanate et de divers dipoles 1–3 est gouvernée par les orbitales frontières. Les différentes cycloadditions (4 + 2, 2 + 3, 2 + 2) dépendent en effet du recouvrement de ces orbitales, ce qui met en relief l'importance des interactions secondaires, c'est-à-dire de la localisation des orbitales sur les atomes adjacents aux liaisons qui se forment au cours de l'addition.

C. GUIMON, G. PFISTER-GUILLOUZO, D. ILAVSKY, M. MARCHALIN, and A. MARTVON. Can. J. Chem. **64**, 1467 (1986).

On the basis of molecular orbital calculations made in association with ultraviolet photoelectron spectroscopy (ups), it is demonstrated that the regioselectivity of the cycloadditions of pyridyl-2-isothiocyanate with 1,3-dipoles is directed by frontier orbitals. The different cycloadditions (4 + 2, 2 + 3, 2 + 2) vary with the overlap of these orbitals and this shows the importance of secondary interactions, namely the localization of the orbitals on the atoms adjacent to the bonds that are formed during the addition.

[Traduit par la revue]

La réactivité du groupement isothiocyanate vis-à-vis de dipoles 1–3 ou de systèmes éthyléniques a été largement étudiée. Cependant, si les réactions de cycloaddition concernant des alkyl ou des aryl isothiocyanates sont relativement bien connues, celles de ce groupement lié à des hétérocycles n'ont fait l'objet que de peu de travaux.

Nous présentons ici, dans le but d'interpréter les nombreuses réactions de cycloadditions présentées par ce composé, une analyse de la structure électronique du pyridyl isothiocyanate. Cette analyse prend comme support une technique expérimentale, la spectroscopie photoélectronique à rayonnement ultraviolet (spu) (He I, He II) associée aux méthodes quantiques, MNDO (avec minimisation de l'énergie par rapport aux paramètres géométriques) et EHT (Extended Hückel Theory).

Nous nous sommes placés dans l'hypothèse de réactions concertées et gouvernées par les orbitales frontières (HOMO : orbitale occupée la plus haute, LUMO : orbitale vacante la plus basse).

Partie expérimentale et théorique

Les spectres photoélectroniques (He I, He II) ont été enregistrés sur un appareil PS 18 Perkin Elmer et sur un spectromètre modèle 0078 des PhotoElectron Spectrometer Laboratories Ltd. La résolution des bandes est en moyenne de 25 meV pour les spectres enregistrés avec la radiation He I (21,21 eV). L'étalonnage a été effectué dans tous les cas par rapport aux pics $^2P_{1/2}$ et $^2P_{3/2}$ du xénon (12,13 et 13,43 eV) et de l'argon (15,76 et 15,94 eV).

Les potentiels d'ionisation ont été calculés dans le cadre de l'approximation de Koopmans (1) à l'aide de la méthode MNDO (2) après une minimisation complète de l'énergie totale par rapport aux paramètres géométriques, ceci pour l'isothiocyanate, le pyridyl-2 isothiocyanate et tous les réactifs envisagés. Dans le cas des pyridyl-3 et -4 isothiocyanates nous avons utilisé les géométries minimisées du fragment isothiocyanate et du cycle pyridinique (3).

I. Structure électronique des pyridyl-isothiocyanates

La structure électronique des divers pyridyl-isothiocyanates peut être facilement déduite de la structure électronique déjà bien connue de la pyridine et de l'isothiocyanate lui-même. Les orbitales moléculaires occupées les plus hautes sont en effet des combinaisons linéaires des orbitales localisées sur les deux fragments, combinaisons pondérées par le recouvrement et l'écart énergétique de ces orbitales. Nous avons schématisé les interactions entre les orbitales localisées sur les fragments dans la figure 1, en se référant aux valeurs expérimentales des potentiels d'ionisation déterminées par spectroscopie photoélectronique (tableau 1).

Les deux orbitales occupées les plus hautes de l'isothiocyanate sont de symétrie π mais orthogonales entre elles (4, 5), l'une (π) se conjuguant avec le système π du cycle, l'autre (π') étant dans le plan σ.

Dans le cas du méthylisothiocyanate, ces deux orbitales sont quasiment dégénérées. En effet, la bande correspondant à l'éjection d'un électron issu de l'orbitale π' apparaît comme un épaulement de la bande associée à l'orbitale π (fig. 2). Du fait de son faible recouvrement avec les orbitales σ du cycle, cette orbitale reste pratiquement pure dans les différents pyridyl-isothiocyanates (9,8, 9,6 et 9,8 eV). La localisation prononcée de cette orbitale sur l'atome de soufre est traduite par une baisse d'intensité de la bande correspondante dans les spectres enregistrés avec la radiation He II (figures 3 et 4). Ceci est en accord avec toutes les observations antérieures et les calculs de section efficace de photoionisation qui prévoient dans les spectres He II, une intensité relative plus faible pour les bandes

1. Part XX de « Application of photoelectron spectroscopy to molecular properties ». Part XIX : réf. 30.

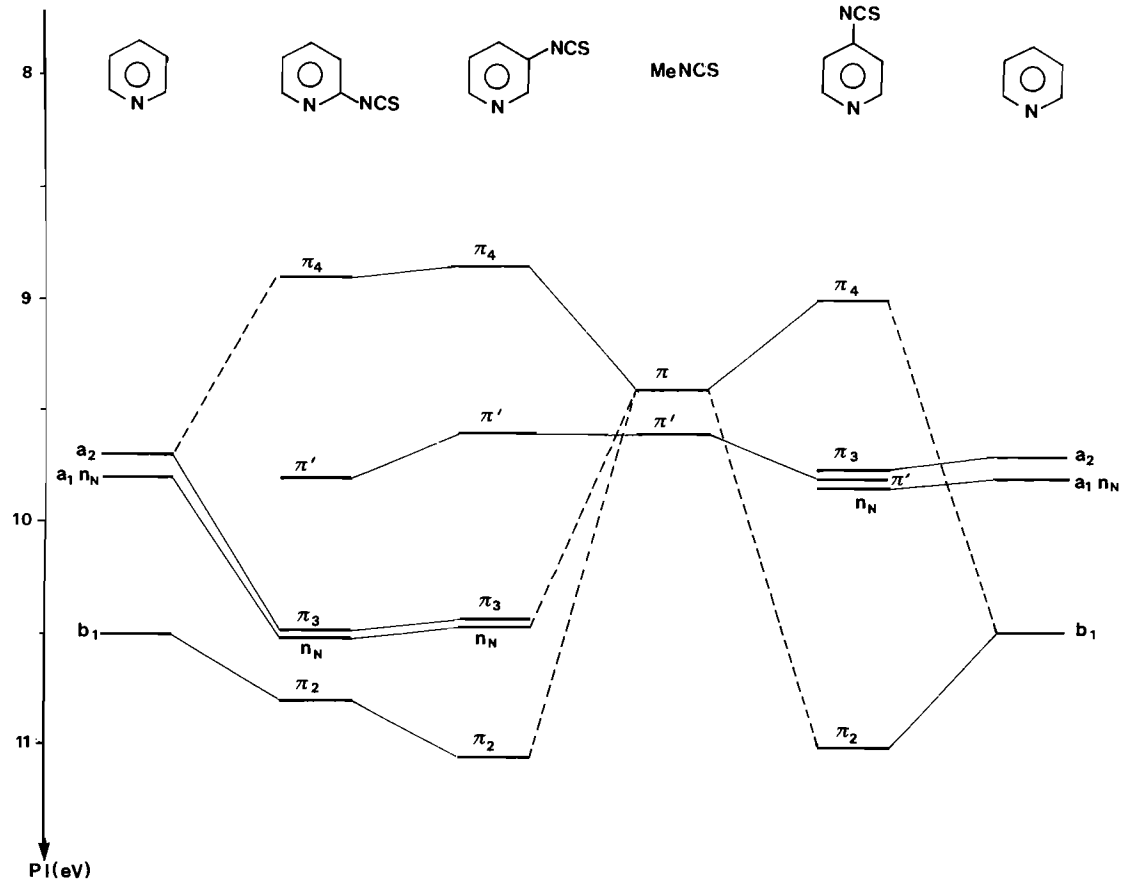

FIG. 1. Diagramme d'interaction entre les orbitales occupées les plus hautes de la pyridine et du groupement isothiocyanate.

associées aux orbitales localisées sur les atomes de la 3ème période (S) par rapport à celles résultant de l'éjection d'un électron plus localisé sur des atomes de la 2ème période (C, N, O) (6–10).

L'orbitale π localisée en grande partie également sur l'atome de soufre mais aussi sur l'atome d'azote (fig. 6) présente un recouvrement important avec les deux orbitales π_{b_1} et π_{a_2} de la pyridine (11, 12). Lorsque le groupement isothiocyanate est placé en position *ortho* ou *méta*, l'interaction de ces orbitales donne trois combinaisons π_2, π_3 et π_4 (fig. 1). Du fait de leur position énergétique, les orbitales π_{b_1}, π_{a_2} et π interviendront de façon majoritaire respectivement dans les combinaisons π_2, π_3 et π_4. Cette dernière est d'ailleurs associée à une bande diminuant d'intensité dans les spectres He II (figures 3, 4 et 5). La stabilisation plus prononcée de l'orbitale π_2 dans le pyridyl-3 isothiocyanate vient d'une localisation supérieure de l'orbitale π_{b_1} de la pyridine sur le sommet 3 (*méta*) par rapport au sommet 2 (*ortho*). Nous remarquons pour ces deux composés, une stabilisation conséquente (0,6 eV) de l'orbitale non liante n_N de la pyridine due selon toute vraisemblance à un effet inductif du groupement isothiocyanate.

Dans le cas du pyridyl-4 isothiocyanate, l'orbitale π interagit seulement avec l'orbitale π_{b_1} (l'orbitale π_{a_1} présentant un noeud sur le sommet *para*) pour donner les combinaisons π_2 et π_4. Les trois autres orbitales (π', n_N et π_{a_2}) restent donc pratiquement pures et se trouvent accidentellement dégénérées (figures 1 et 5).

Les calculs MNDO effectués dans le cadre de l'approximation de Koopmans (PI $\sim -\epsilon_i$) reflètent assez bien cette analyse qualitative et expérimentale, du moins au niveau des orbitales

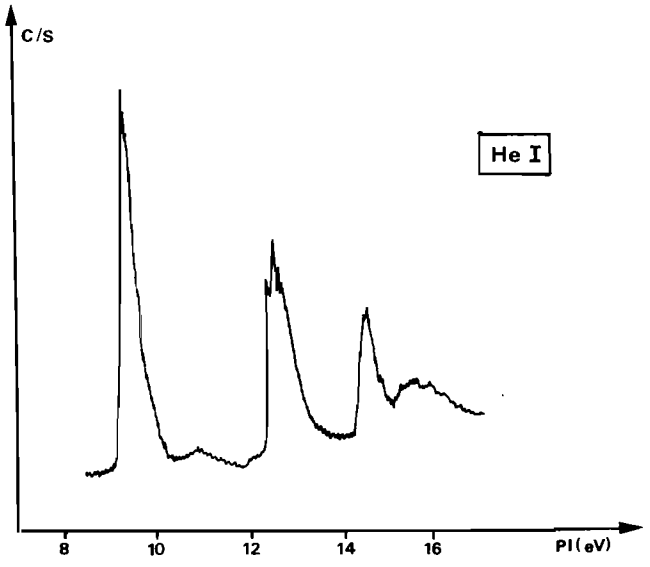

FIG. 2. Spectre photoélectronique (He I) du méthylisothiocyanate.

de type π. En effet la séquence de ces orbitales est bien respectée et les valeurs des potentiels d'ionisation sont reproduites avec un décalage maximum de 0,8 eV, ce qui est un résultat satisfaisant pour une méthode semi-empirique qui ne prend en compte ni les effets de corrélation, ni la réorganisation des ions. Comme pour toutes les autres méthodes cependant, elle a tendance à surestimer d'environ 1 eV les potentiels d'ionisation associés à la paire libre de l'azote pyridinique. Ceci

TABLEAU 1. Potentiels d'ionisation (eV) expérimentaux (verticaux) et calculés (MNDO dans le cadre de l'approximation de Koopmans) de divers isothiocyanates; (↓) bandes diminuant d'intensité en He II

Isothiocyanate		Potentiels d'ionisation (eV)				
Méthylisothiocyanate	exp.	9,4 (↓)	9,6 (↓)	12,62	14,6	
	calc.	10,03(π)	10,47(π')			
Pyridyl-2 isothiocyanate	exp.	8,9 (↓)	9,8 (↓)	10,5	10,5	10,8
	calc.	9,38(π)	10,45(π')	10,77(π)	11,58(n)	11,05(π)
Pyridyl-3 isothiocyanate	exp.	8,85(↓)	9,6 (↓)	10,45	10,45	11,05
	calc.	9,45(π)	10,35(π')	10,68(π)	11,65(n)	11,37
Pyridyl-4 isothiocyanate	exp.	9,0 (↓)	9,8	9,8	9,8	11,0 (↓)
	calc.	9,76(π)	10,24(π)	10,46(π')	11,45(n)	11,53(π)

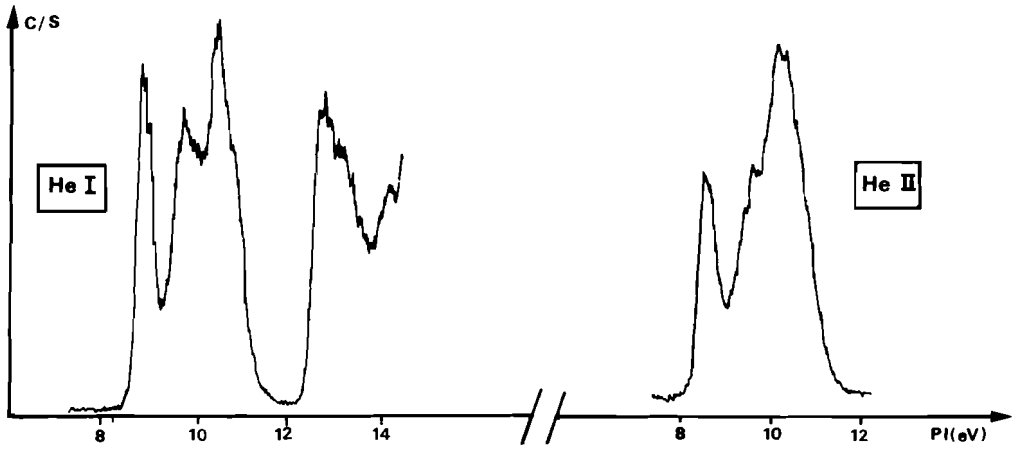

FIG. 3. Spectre photoélectronique (He I, He II) du pyridyl-2 isothiocyanate.

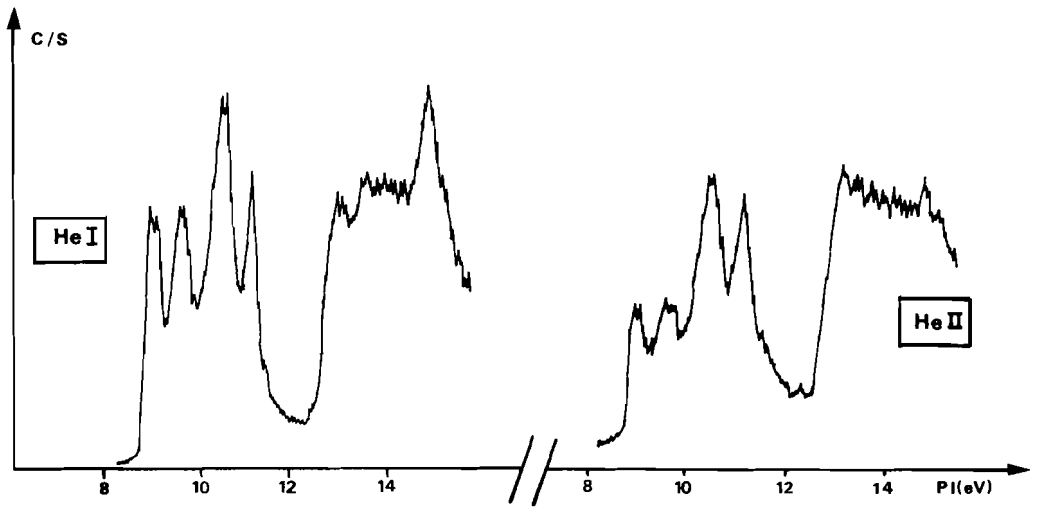

FIG. 4. Spectre photoélectronique (He I, He II) du pyridyl-3 isothiocyanate.

est dû aux effets de polarisation plus importants dans le cas de l'éjection d'un électron très localisé et qui ne sont pas pris en compte dans l'approximation de Koopmans.

II. Réactivité du pyridyl-2 isothiocyanate

Comme nous le soulignons dans l'introduction, le pyridyl-2 isothiocyanate présente une réactivité très intéressante, que ce soit avec les composés dipolaires 1–3, tel que l'acide hydrazoïque ou le diazométhane ou avec différentes molécules comportant une liaison C=N (imines, isocyanates, isothiocyanates, carbodiimides, hydrazones). Toutes ces réactions conduisent à l'obtention d'hétérocycles à 4, 5 ou 6 chaînons selon le type de cycloaddition (2 + 2, 2 + 3 ou 4 + 2).

De nombreux travaux ont mis en évidence le rôle prépondérant des interactions entre les orbitales frontières HOMO (orbitales occupées les plus hautes) et LUMO (orbitales vacantes les plus basses) des différents réactifs dans la plupart des cycloadditions (13–17). En effet, lors de l'approche des

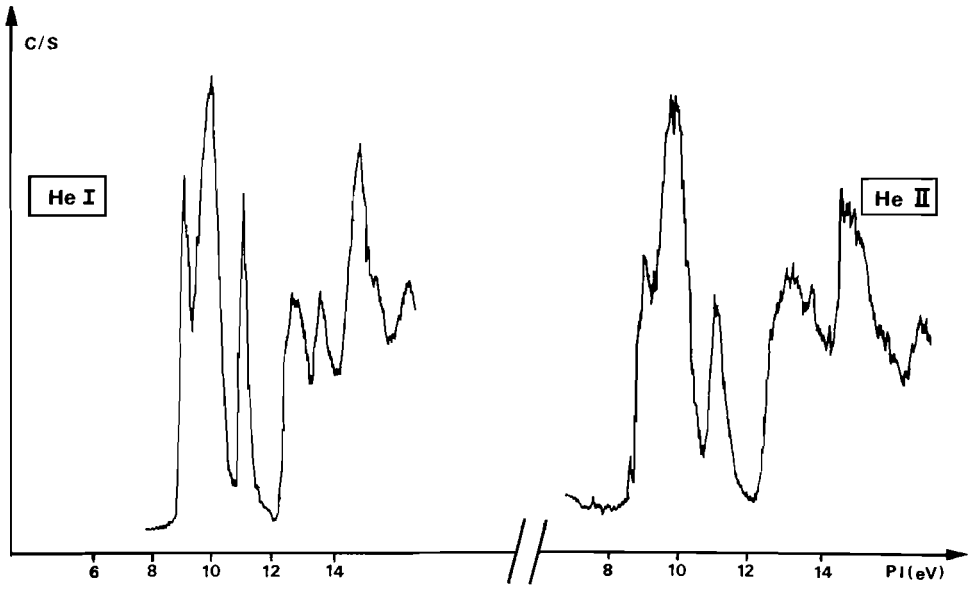

FIG. 5. Spectre photoélectronique (He I, He II) du pyridyl-4 isothiocyanate.

deux réactifs, les orbitales virtuelles les plus basses de chacun d'eux interagissent avec les orbitales occupées les plus hautes de l'autre réactif ce qui conduit à une stabilisation de l'énergie du supersystème. Cette stabilisation est proportionnelle au recouvrement de ces orbitales et inversement proportionnelle à leur écart énergétique. Si l'on admet que les interactions coulombiennes peuvent être négligées (ce qui est généralement le cas pour des réactions concertées), la théorie des perturbations du second ordre permet d'estimer cette énergie de stabilisation.

Dans la plupart des cas, la presque totalité de cette énergie vient de l'interaction de la plus haute orbitale occupée de type π de chaque réactif avec la plus basse vacante π de l'autre réactif, car les autres orbitales de même type sont, ou beaucoup plus stables (pour les occupées) ou beaucoup moins stables (pour les virtuelles), ce qui augmente la valeur du dénominateur et rend donc négligeable le terme correspondant. La régiosélectivité des cycloadditions suit souvent l'ordre donné par l'interaction principale qui correspond à la seule prise en considération des atomes (1 et 2 de la molécule A et 1′ et 2′ de la molécule B) entre lesquels se forment les liaisons (1–1′ et 2–2′).

Ainsi, l'énergie d'interaction principale $\Delta E'$ dans l'état de transition est donnée par la somme des interactions HOMO (A) – LUMO (B) et HOMO (B) – LUMO (A) (18–21) :

$$\Delta E' = \frac{[(C_{\text{HOMO}\,1}\,C_{\text{LUMO}\,1'} + C_{\text{HOMO}\,2}\,C_{\text{LUMO}\,2'})\beta]^2}{E_{\text{HOMO A}} - E_{\text{LUMO B}} - Q} + \frac{[(C_{\text{HOMO}\,1'}\,C_{\text{LUMO}\,1} + C_{\text{HOMO}\,2'}\,C_{\text{LUMO}\,2})\beta]^2}{E_{\text{HOMO B}} - E_{\text{LUMO A}} - Q}$$

$C_{\text{HOMO}\,1}$ et $C_{\text{LUMO}\,1}$ (ou $C_{\text{HOMO}\,2}$ et $C_{\text{LUMO}\,2}$ ou $C_{\text{HOMO}\,1'}$ et $C_{\text{LUMO}\,1'}$ ou $C_{\text{HOMO}\,2'}$ et $C_{\text{LUMO}\,2'}$) représentent les coefficients des orbitales atomïques P_π sur l'atome 1 (ou 2, ou 1′, ou 2′) dans les orbitales moléculaires frontières occupée (HOMO) et virtuelle (LUMO) respectivement d'énergie $E_{\text{HOMO A}}$ et $E_{\text{LUMO A}}$ (ou $E_{\text{HOMO B}}$ et $E_{\text{LUMO B}}$)·β qui est l'intégrale d'échange entre les orbitales atomiques 1 et 1′ ou 2 et 2′ est proportionnelle à l'intégrale de recouvrement de ces orbitales. Comme nous l'avons fait remarquer précédemment, $\Delta E'$ est donc fonction de la structure de l'état de transition à la fois par

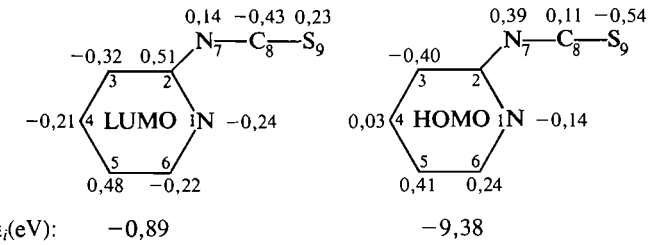

FIG. 6. Valeurs propres et vecteurs propres associés aux orbitales frontières π du pyridyl-2 isothiocyanate calculés par la méthode MNDO (2) avec optimisation de l'énergie totale par rapport à la géométrie moléculaire.

l'intermédiaire de l'intégrale β et par celui du paramètre Q dont la valeur croît lorsque les deux réactifs se rapprochent (21).

Si la prise en compte de cette seule interaction principale suffit à expliquer la régiosélectivité de la cycloaddition de molécules simples, elle est souvent insuffisante pour rendre compte de la réactivité de composés conjugués. Dans ce cas, il faut considérer l'interaction des orbitales frontières dans leur globalité et donc estimer un terme analogue à $\Delta E'$, $\Delta E''$, correspondant à des interactions secondaires et qui tient compte des coefficients des orbitales atomiques sur les autres sommets. Ces interactions secondaires, qui jouent un rôle non négligeable dans le cas d'un recouvrement important de ces orbitales atomiques, sont naturellement fonction de la position respective des réactifs dans l'état de transition. Le terme $\Delta E''$ viendra alors s'ajouter ou se retrancher à $\Delta E'$ selon que le recouvrement sera positif (lobes en phase) ou négatif (lobes en opposition de phase).

Les composés réagissant avec le groupement isothiocyanate sont de deux types, d'une part les imines, d'autre part, les dipoles 1–3. Nous présentons dans les figures 6 et 7 l'énergie et la localisation des orbitales frontières (HOMO et LUMO) de tous les réactifs étudiés, calculées par la méthode MNDO après minimisation de l'énergie totale par rapport à tous les paramètres géométriques. On peut immédiatement remarquer qu'au niveau des sommets entre lesquels s'établissent les liaisons, la forme générale des orbitales frontières est pratiquement iden-

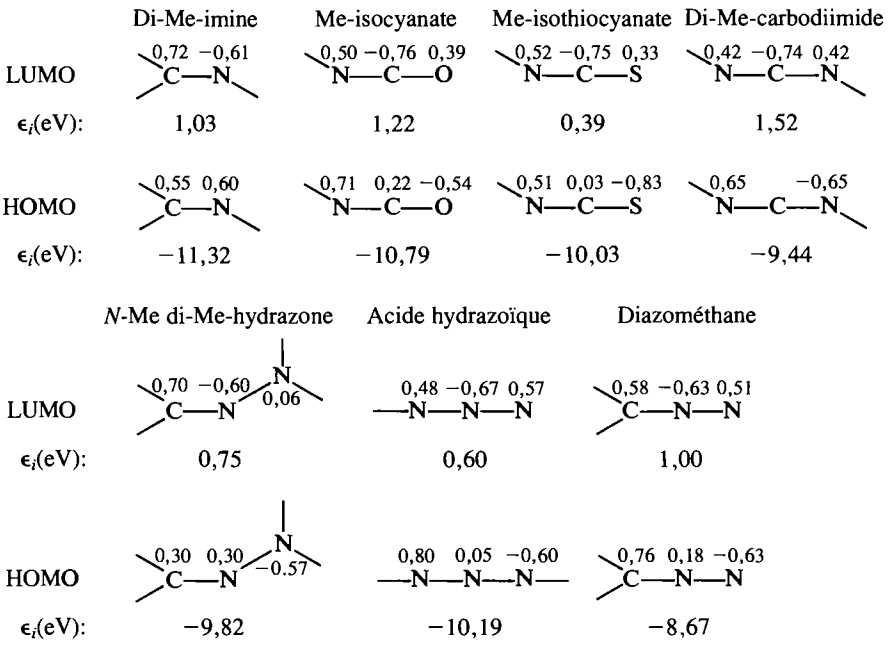

FIG. 7. Valeurs propres et vecteurs propres associés aux orbitales frontières π de différents réactifs impliqués dans la cycloaddition du pyridyl-2 isothiocyanate. Ces valeurs ont été calculées par la méthode MNDO (22) avec optimisation de l'énergie totale par rapport à tous les paramètres géométriques.

tique pour tous ces composés. Les différences de régiosélectivité relevées dans la littérature ne peuvent donc provenir seulement des interactions principales, mais doivent être liées à l'existence de certaines interactions secondaires. Dans la discussion ci-dessous, nous allons tenter d'analyser l'importance relative de ces deux types d'interactions dans les diverses cycloadditions. Celles-ci peuvent être de trois types, 4 + 2, 2 + 3 et 2 + 2, suivant que les sommets réagissant sont, pour le pyridyl-isothiocyanate, l'atome d'azote intracyclique et l'atome de carbone extracyclique (4 + 2) ou deux atomes contigus du groupement NCS (2 + 3 et 2 + 2) et pour les autres réactifs deux atomes voisins (4 + 2 et 2 + 2) ou deux atomes en position 1–3 (2 + 3).

N-*Éthylydene-methylamine*

R^1 et R^2 étant des groupements alkyls, la régiosélectivité de cette réaction doit suivre les interactions principales, les interactions secondaires étant pratiquement inexistantes. La cycloaddition 2 + 2 doit être défavorisée de part le faible

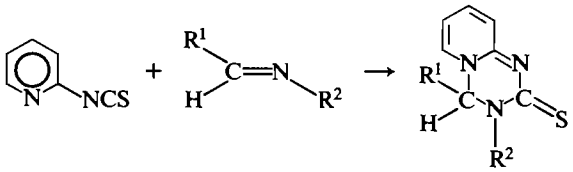

recouvrement entre la LUMO du pyridyl-isothiocyanate et l'HOMO de l'imine, la première présentant des lobes en opposition de phase sur les sommets contigus de NCS, la seconde étant en phase sur C—N. Seule est donc envisageable une addition 4 + 2 (les sommets attaqués par l'imine étant le carbone C_8 et l'azote N_1) qui fait intervenir des sommets présentant des lobes en phase entre les LUMO et les HOMO. La régiosélectivité dépend du recouvrement des orbitales frontières dans l'état de transition. Celui-ci sera d'autant plus important que les liaisons se formeront entre les sommets ayant la localisation de ces orbitales la plus élevée, c'est-à-dire, entre l'atome de carbone de l'imine et l'atome d'azote de la pyridine d'une part et l'atome d'azote de l'imine et l'atome de carbone du groupement NCS d'autre part. C'est bien ce qui a été observé expérimentalement (22).

Isocyanates et isothiocyanates

Comme dans le cas précédent, quel que soit l'hétéroatome X (oxygène ou soufre), le type de la cycloaddition observé est 4 + 2 (22). C'est également vrai lorsque R est un noyau pyridinique, c'est-à-dire, lorsque la cycloaddition correspond à une dimérisation (23, 24). Cette dernière s'effectue très facilement pour donner un dimère très stable thermodynamiquement.

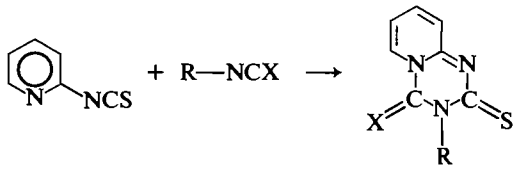

Si l'on ne tient compte que des interactions principales (fig. 6), deux types de cycloadditions sont possibles, à savoir 4 + 2 et 2 + 2. Dans ce dernier cas, les atomes de carbone et de soufre du groupement fonctionnel s'accrochent respectivement aux atomes de soufre et de carbone de l'autre groupement. Seuls en effet ces atomes présentent au niveau des orbitales frontières des lobes en phase ce qui augmente le recouvrement entre les LUMO et les HOMO et favorise les interactions stabilisantes. Il apparaît toutefois que la cycloaddition 4 + 2 est favorisée par les interactions secondaires stabilisantes, celles-ci n'existant pas lors de l'approche du type 2 + 2.

Nous avons visualisé ces interactions dans la figure 8. Elles sont particulièrement importantes entre l'HOMO du pyridyl-2 isothiocyanate et la LUMO de R—NSX au niveau des deux atomes d'azote extracycliques et surtout au niveau de l'atome de soufre (dans l'HOMO) et du carbone C_3 du cycle pyridinique (dans la LUMO) du fait de la localisation importante sur ces atomes des orbitales correspondantes (fig. 6).

De façon à apprécier l'importance de ces interactions, nous avons effectué un calcul EHT (25) sur la supermolécule dans

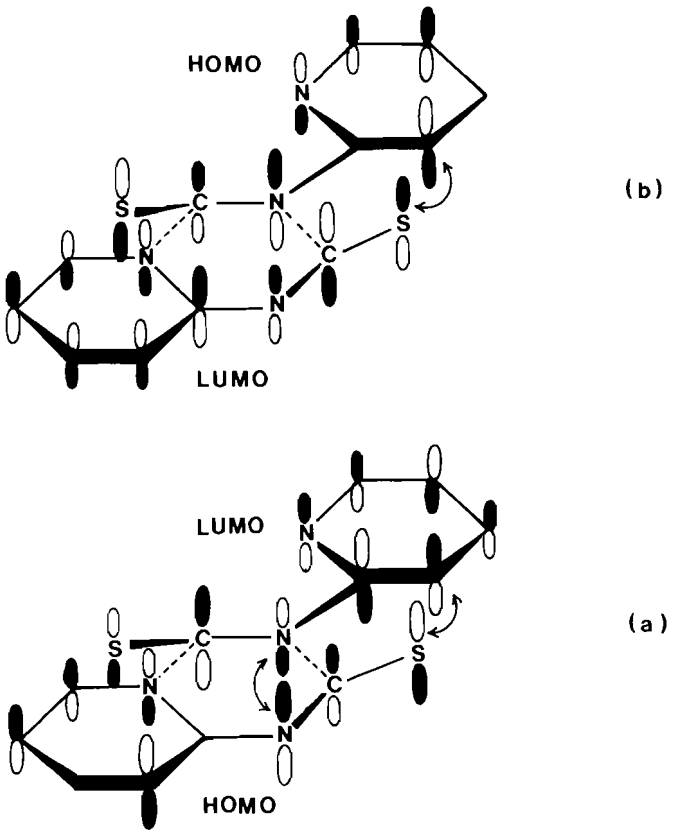

FIG. 8. Interactions primaires (...) et secondaires (↔) stabilisantes lors de la dimérisation du pyridyl-2 isothiocyanate.

son état de transition supposé, c'est-à-dire les deux molécules étant dans des plans parallèles distants de 2,25 Å l'un de l'autre (fig. 8). D'après diverses études théoriques (26), on peut en effet considérer que cette structure représente approximativement l'état de transition de l'addition dans l'hypothèse d'une réaction concertée. Il semble probable que pour un système donné, la distance entre les plans moléculaires est pratiquement constante lors les différentes approches. Il s'en suit que le terme Q de l'équation donnant $\Delta E'$ peut également être considéré comme constant, ce qui rend possible des corrélations entre la régiosélectivité des réactions étudiées et la valeur des recouvrements entre les orbitales des deux réactifs. Ces recouvrements sont tirés d'un calcul FMO (Fragment Molecular Orbitals) (27).[2]

Ainsi, le recouvrement entre l'HOMO d'une pyridyl-2 isothiocyanate et la LUMO de l'autre dans l'approche présentée dans la figure 8 (a) est de 0,1086, tandis que le recouvrement LUMO–HOMO (fig. 8 (b)) est seulement de 0,0104. Cette approche telle qu'elle est schématisée dans la figure 8 semble préférentielle puisque un calcul similaire sur ce système où l'on a fait tourner la molécule supérieure de 180° autour de l'axe C—N exocyclique donne comme recouvrements 0,0898 et 0,0074. Ces recouvrements plus faibles s'expliquent par le décalage des deux cycles, ce qui minimise les interactions secondaires. De plus, l'interaction destabilisante HOMO–HOMO est dans ce cas légèrement supérieure (0,0160 contre 0,0046).

Carbodiimide

Ce composé de symétrie D_{2h} peut en principe, comme les précédents, donner lieu à une cycloaddition 2 + 2 ou 4 + 2. Dans le cas où les groupements substituants R sont des groupements alkyls, les interactions secondaires sont négligeables et seules sont à considérer les interactions principales. Au vu des coefficients reportés dans les figures 6 et 7, il semble que doit être privilégiée l'addition 2 + 2 où les atomes d'azote et de carbone de la diimine se lient respectivement aux atomes de carbone et de soufre du groupement NCS, à cause en particulier de la forte localisation de l'HOMO du pyridyl isothiocyanate sur l'atome de soufre, ce qui renforce l'interaction stabilisante HOMO (NCS) – LUMO (NCN). Cette conclusion est confirmée par diverses études expérimentales (22, 28) :

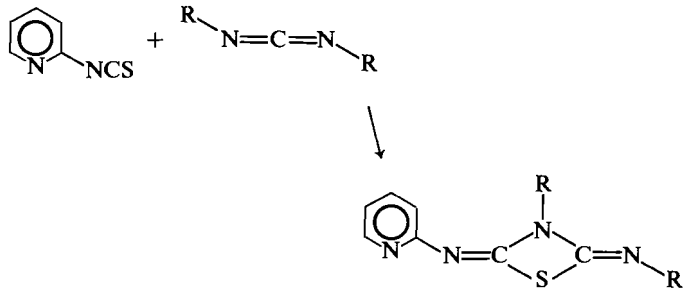

Lorsque R est un groupement conjugué, il faut prendre en compte les interactions secondaires de la même manière que pour l'étude de la dimérisation. Comme dans ce cas donc, l'addition 4 + 2 doit être favorisée grâce en particulier à la proximité de l'atome de soufre et de l'atome de carbone en position *ortho* du groupement aryl (fig. 8). Ce résultat est en accord avec les données expérimentales dont nous disposons (22) :

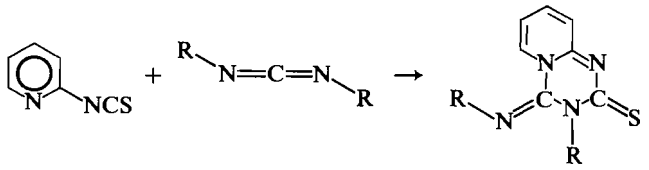

Hydrazone

Ce composé a la possibilité de s'additionner selon le schéma 4 + 2 mais également selon le schéma 2 + 3 où l'atome d'azote amino se lie à l'atome de carbone de NCS pour donner une triazole-thione après migration de l'atome d'hydrogène de l'azote amino sur l'azote imino :

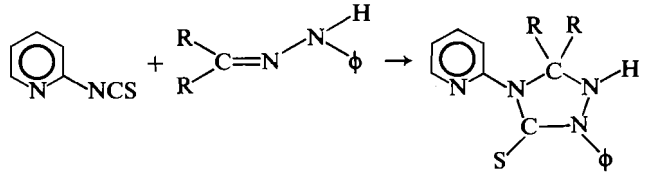

Si l'on considère la localisation des orbitales frontières au niveau des sommets en compétition (N_1, N_7, C_8 de la pyridine et C, N, N de l'hydrazone) des deux réactifs, il semble que les interactions principales soient plus stabilisantes pour la cycloaddition 2 + 3 que pour la 4 + 2, en particulier au niveau du recouvrement HOMO (NCS) – LUMO (CNN).

Ceci est bien traduit par le calcul EHT – FMO puisque le

2. Afin d'estimer quantitativement les interactions entre les orbitales ϕ_k localisées sur les différents fragments qui composent une molécule (ou super molécule) donnée, on effectue un calcul EHT sur la molécule complète, ce qui donne les orbitales moléculaires ψ_i sur la base des orbitales atomiques χ_j ($\psi_i = \Sigma_j a_{ij} \chi_j$), puis un calcul identique pour chaque fragment ($\phi_k = \Sigma_j b_{kj} \psi_j$). Un simple produit matriciel donne alors les orbitales moléculaires ψ_i sur la base des orbitales semi-localisées ϕ_k ($\psi_i = \Sigma_k c_{ik} \phi_k$). Il en est de même de la matrice des recouvrements entre les orbitales localisées ϕ_k.

recouvrement de ces deux orbitales est de 0,0094 pour l'addition 2 + 3 et de 0,0021 pour l'addition 4 + 2.[3] De même les recouvrements entre la LUMO (NCS) et l'HOMO (CNN) sont respectivement égaux à 0,0065 (addition 2 + 3) et à 0,0001 (addition 4 + 2). Les résultats concernant la phényl hydrazone (24) font bien état d'une addition 2 + 3 avec le pyridyl-2 isothiocyanate.

Acide hydrazoïque; diazométhane

L'addition de ces deux dipoles 1–3 sur le groupement isothiocyanate donne un thiatriazole ou un thiadiazole après une migration d'un atome d'hydrogène du dipole sur l'azote du groupement NCS (24, 29). À priori deux types d'additions sont

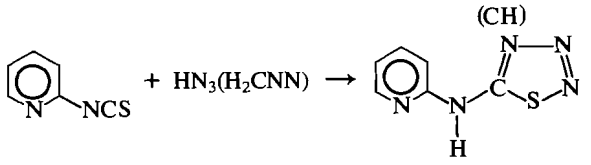

possibles si l'on regarde la forme des orbitales frontières des deux réactifs (figures 6 et 7). D'une part les atomes de carbone et d'azote des extrémités du diazométhane (ou les deux atomes 1 et 3 de l'acide hydrazoïque peuvent se lier respectivement aux atomes de carbone et de soufre du groupement isothiocyanate (résultat expérimental) ou aux atomes de carbone et d'azote de ce groupement. (Cette dernière régiosélectivité semble favorisée par rapport à celle où les deux atomes cités du diazométhane s'accrochent respectivement aux atomes d'azote et de carbone de NCS, ceci grâce à un recouvrement LUMO (NCS) – HOMO (CNN) bien supérieur.)

Ici encore la régiosélectivité de la cycloaddition est bien traduite par les interactions entre les orbitales frontières des deux composés. En effet un calcul EHT–FMO montre que la cycloaddition observée expérimentalement correspond à un recouvrement LUMO (NCS) – HOMO (CNN) dans l'état de transition nettement plus important que pour l'autre approche (0,1164 contre 0,0760).

Conclusion

L'analyse de la structure électronique du pyridyl-2 isothiocyanate nous a permis de rendre compte de manière satisfaisante de la réactivité vis-à-vis de divers dipoles 1–3 et de composés possédant une liaison C=N. La régiosélectivité des cycloadditions semble être gouvernée par les orbitales frontières et plus particulièrement par le recouvrement de celles-ci. Il a toutefois été nécessaire d'inclure dans nos raisonnements qualitatifs à la fois les interactions principales et secondaires, c'est-à-dire de considérer les orbitales dans leur globalité et non, comme il a été souvent proposé, de s'en tenir aux seules interactions principales (correspondant aux sommets entre lesquels se forment les liaisons). On a ainsi pu mettre en évidence l'importance de ces interactions secondaires qui sont souvent à l'origine du type de cycloaddition observé (4 + 2, 2 + 3 ou 2 + 2).

3. Ces recouvrements ont des valeurs plus faibles que ceux calculés pour la dimérisation car nous avons éloigné légèrement les plans moléculaires à cause de la gêne stérique provoquée par les groupements méthyles R de l'hydrazone.

1. T. Koopmans. Physica, **1**, 104 (1934).
2. M. J. S. Dewar et W. Thiel. J. Am. Chem. Soc. **99**, 4899; **99**, 4907 (1977).
3. S. Khayar. Thèse de 3ème cycle, Pau (1982).
4. S. Cradock, E. A. V. Ebsworth et J. D. Murdoch. J. Chem. Soc. 86 (1972).
5. B. J. M. Neijzen et C. A. De Lange. J. Electron Spectrosc. Relat. Phenom. **18**, 179 (1980).
6. A. Katrib, T. P. Debies, R. J. Colton, T. H. Lee et J. W. Rabalais. Chem. Phys. Lett. **22**, 196 (1973).
7. A. Schweig et W. Thiel. J. Electron Spectrosc. Relat. Phenom. **3**, 27 (1974), et réf. citées.
8. C. Guimon, D. Gombeau, G. Pfister-Guillouzo, L. Asbrink et J. Sandstrom. J. Electron Spectrosc. Relat. Phenom. **4**, 49 (1974).
9. T. H. Gan, J. B. Pell et G. D. Willet. Chem. Phys. Lett. **48**, 483 (1977).
10. H. Daamen et A. Oskam. Inorg. Chem. Acta, **27**, 209 (1978).
11. R. Gleiter, E. Heilbronner et V. Hornung. Helv. Chim. Acta, **55**, 255 (1972).
12. E. Heilbronner, J. P. Maier et E. Haselbach. *Dans* Physical methods in heterocyclic chemistry. Vol. VI. *Editeur*: A. R. Katritzky. Academic Press, New York. 1974. p. 22.
13. K. Fukui. Molecular orbitals in chemistry, physics and biology. *Editeurs*: P. O. Lowdin et B. Pullman. Academic Press, New-York. 1964; Bull. Chem. Soc. Jpn. **39**, 498 (1966).
14. R. Hoffmann et R. B. Woodward. J. Am. Chem. Soc. **87**, 4388 (1965).
15. L. Salem. J. Am. Chem. Soc. **90**, 543 (1968); **90**, 553 (1968).
16. K. N. Houk. J. Am. Chem. Soc. **95**, 4092 (1973).
17. K. N. Houk, J. Sims, C. R. Watts et L. J. Luskus. J. Am. Chem. Soc. **95**, 7301 (1973).
18. M. J. S. Dewar. The molecular orbital theory of organic chemistry, McGraw–Hill, New York. 1969.
19. R. Sustmann. Tetrahedron Lett. 2717 (1971).
20. R. Sustmann et H. Trill. Angew Chem. Int. Ed. Engl. **11**, 838 (1972).
21. N. G. Rondan, K. N. Houk et R. A. Moss. J. Am. Chem. Soc. **102**, 1770 (1980).
22. M. Marchalin, J. Svetlik et A. Martvon. Collect. Czech. Chem. Commun. **46**, 2557 (1981).
23. K. E. Fahrenholtz, W. Benz, J. F. Blount et T. H. Williams. J. Org. Chem. **45**, 4219 (1980).
24. M. Marchalin, J. Svetlik et A. Martvon. Collect. Czech. Chem. Commun. **46**, 2428 (1981).
25. R. Hoffmann. J. Chem. Phys. **39**, 1397 (1963).
26. G. Leroy, M. T. Nguyen et M. Sana. Tetrahedron, **34**, 2459 (1978).
27. R. Hoffmann, H. Fujimoto, J. R. Swenson et C. C. Wan. J. Am. Chem. Soc. **95**, 7644 (1973).
28. G. L'Abbe, L. Van Meervelt et G. S. D. King. Bull. Soc. Chim. Belges, **90**, 1185 (1981).
29. M. Marchalin et A. Martvon. Collect. Czech. Chem. Commun. **45**, 2329 (1980).
30. C. Guimon, G. Pfister-Guillouzo, B. Chaudret et R. Poilblanc. J. Chem. Soc. Dalton Trans. 43 (1985).

Complexes of hybrid ligands. Comparative studies on two cationic Pt^{2+} complexes of a fluorinated alkoxy-thioether ligand: solid-state structures and evidence for coupled ring-thioether inversion in solution[1]

RENÉ T. BOERÉ, NICHOLAS C. PAYNE, AND CHRISTOPHER J. WILLIS[2]
Department of Chemistry, The University of Western Ontario, London, Ont., Canada N6A 5B7
Received September 4, 1985[3]

RENÉ T. BOERÉ, NICHOLAS C. PAYNE, and CHRISTOPHER J. WILLIS. Can. J. Chem. **64**, 1474 (1986).

Complete structural determinations are reported for two cationic platinum(II) complexes of the chelating, hybrid, alkoxythioether ligand $CH_3SCH_2O(CF_3)_2O^-$ with phosphine coligands and BF_4^- counterions. Complex **1**, $[Pt(PPh_3)_2\{CH_3SCH_2C(CF_3)_2O\}]BF_4$, $C_{42}H_{37}BCl_2F_{10}OP_2PtS$ (CH_2Cl_2 solvate) is monoclinic, space group $P2_1/c$, with $a = 12.2534(9)$, $b = 18.584(2)$, $c = 19.612(3)$ Å, $\beta = 97.36(1)°$, $V = 4466(1)$ Å^3, $Z = 4$. Complex **2**, $[Pt(PPh_2Me)_2\{CH_3SCH_2C(CF_3)_2O\}]BF_4$, $C_{31}H_{31}BF_{10}OP_2PtS$, is orthorhombic, space group $Pna2_1$, with $a = 23.093(4)$, $b = 11.362(3)$, $c = 12.880(2)$ Å, $V = 3379(2)$ Å^3, $Z = 4$. The structures show the five-membered chelate ring to have similar conformations in the two complexes, the CH_3S and axial CF_3 groups being in an *anti* conformation.

The structural results are discussed in relation to previous nmr studies on these and related complexes. It is concluded that an anisotropic shielding effect on the CH_3S and CF_3 resonances is present in both complexes, but that it is significantly greater in **1**, where PPh_3 is the coligand, and anomalies in the ^{19}F nmr spectra are explained on this basis. A careful consideration of the nmr data, in light of the crystal structures, demonstrates the persistence of preferred chelate ring conformations in solution. Thioether inversion induces ring inversion in these complexes.

RENÉ T. BOERÉ, NICHOLAS C. PAYNE et CHRISTOPHER J. WILLIS. Can. J. Chem. **64**, 1474 (1986).

On rapporte les déterminations complètes des structures de deux complexes cationiques du Pt(II) avec du $CH_3SCH_2C(CF_3)_2O^-$ (l'alcoolate d'un thioéther qui est un ligand hydrure, chélatant), des coligands phosphines et des contre-ions BF_4^-. Le complexe **1**, $[Pt(PPh_3)_2\{CH_3SCH_2C(CF_3)_2O\}]BF_4$, $C_{42}H_{37}BCl_2F_{10}OP_2PtS$ (CH_2Cl_2 solvaté), est monoclinique, groupe d'espace $P2_1/c$ avec $a = 12,2534(9)$, $b = 18,584(2)$ et $c = 19,612(3)$ Å, $\beta = 97,36(1)°$, $V = 4466(1)$ Å^3 et $Z = 4$. Le complexe **2**, $[Pt(PPh_2Me)_2\{CH_3SCH_2C(CF_3)_2O\}]BF_4$, $C_{31}H_{31}BF_{10}OP_2PtS$, est orthorhombique, groupe d'espace $Pna2_1$, avec $a = 23,093(4)$, $b = 11,362(3)$, $c = 12,880(2)$ Å, $V = 3379(2)$ Å^3 et $Z = 4$. Les structures comprennent un cycle à cinq chaïnons qui est chélaté de manière a assumer des conformations semblables dans les deux complexes; les groupements CH_2S et CF_3 axial sont dans des conformations *anti*.

On discute des résutats structuraux en relation avec des études rmn qui ont été faites antérieurement sur ces complexes et sur d'atures qui leur sont reliés. On en conclut que l'effet de blindage anisotrope sur les résonances des groupements CH_3S et CF_3 est présent dans les deux complexes: toutefois, il est de beaucoup plus important dans le complexe **1**, dans lequel le PPh_3 est le coligand; on peut expliquer les anomalies du spectres rmn ^{19}F sur cette base. Un examen attentif des données de la rmn, à la lumière des structures cristallines, démontre que les conformations privilégiées du cycle chélate persistent même en solution. Dans ces complexes, l'inversion du thioéther induit une inversion du cycle.

[Traduit par la revue]

Introduction

We have recently reported (1) the preparation and structural characterization by nmr of some cationic Pt^{2+} complexes of the bidentate, anionic, fluoro-alkoxy thioether ligands R—S—CH_2—$C(CF_3)_2$—O^- (R = Me or Ph).[4] The energetics of thioether inversion in complexes **1–7** were investigated by the dynamic nmr method:

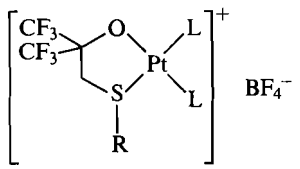

R = Me, L = PPh_3 (**1**); L = PPh_2Me (**2**); L = $PPhMe_2$ (**3**); L = PMe_3 (**4**); R = Ph, L = PPh_3 (**5**); L = PPh_2Me (**6**); L = $PPhMe_2$ (7)

In the course of this work, we noted unusual *upfield* coordination chemical shifts for the SCH_3 groups in **1–3**, an effect which has been postulated as due to the aromatic ring anisotropy of a neighbouring phosphine ligand (3, 4). We also noted anomalous effects in the ^{19}F nmr, where the CF_3 groups in compound **1** appeared equivalent at temperatures where all of the other complexes showed the doublet-of-quartets pattern associated with inequivalence.

In order to probe the origin of these two effects, we have determined the solid-state structures of **1** and **2** by single-crystal X-ray crystallography.

The results, reported here, show that both complexes have very similar geometry, and that phenyl rings from the neighbouring phosphines are indeed oriented in such a way as to induce the observed shifts in the ^1H nmr. Consideration of data for the two systematic series of compounds **1–4** and **5–7** shows that the anomalies in the ^{19}F nmr are due to the same effect.

Structure determination

General

The synthesis of the complexes has been described previously (1). Colourless crystals of each compound were grown by slow evaporation from ethanol/dichloromethane solutions; compound **1** crystallized as a dichloromethane solvate.

Compound 2, X-ray data collection and reduction

Preliminary Weissenberg and precession photography showed Laué symmetry and systematic absences consistent with the orthorhombic

[1]Presented in part at the 67th Annual CIC Conference, Montreal, June 1984.

[2]To whom all correspondence should be addressed.

[3]Revision received March 5, 1986.

[4]We abbreviate the ligands as Me—S—O^- and Ph—S—O^-.

TABLE 1. Summary of crystal and data collection parameters

	Compound **2**	Compound **1**
Molecular formula	$C_{31}H_{31}BF_{10}OP_2PtS$	$C_{42}H_{37}BCl_2F_{10}OP_2PtS$
Formula weight	909.5	1118.6
Crystal class	Orthorhombic	Monoclinic
Laué symmetry	*mm*2	2/*m*
a	23.093(4) Å	12.2534(9) Å
b	11.362(3) Å	18.5835(22) Å
c	12.880(2) Å	19.6115(25) Å
β	—	97.356(8)°
V	3379(2) Å^3	4466(1) Å^3
Z	4	4
d(obs)[a]	1.79(1) g cm^{-3}	1.72(1) g cm^{-3}
d(calcd)	1.788	1.664
Systematic absences	*0kl: k + l = 2n + 1*	*h0l: h = 2n + 1*
	hk0; h = 2n + 1	*0k0: k = 2n + 1*
Space group	*Pna*2$_1$, # 33	*P*2$_1$/*c*, # 14
Diffractometer	Enraf/Nonius CAD 4	
Radiation	Mo Kα_1, graphite monochromatized, λ = 0.70930 Å	
Aperture	4 mm × (1.3–5.9) mm	
Data collected	$h \leq 0, -1 \leq k, l \leq 0$	$h \geq 0, k \geq 0, \pm l$
θ range	$0 \leq 2\theta \leq 60°$	$0 \leq 2\theta \leq 50°$
Scan type	ω/2θ	ω/2θ
Scan speed	1.3–4.0 deg min^{-1}	1.5–5.0 deg min^{-1}
Backgrounds	25% above and below calculated scan width	
Standard reflections	$\bar{2}2,0,0$ / 0,10,0 / 0,0,12	$0,\bar{1}0,0$ / 5,0,0 / 0,0,2
Loss in intensity	0.10 % per hour	−0.04 % per hour
Crystal dimensions	0.50 × 0.45 × 0.45 mm^3	0.31 × 0.28 × 0.20 mm^3
Crystal volume	0.0631 mm^3	0.0140 mm^3
μ	41.52 cm^{-1}	35.10 cm^{-1}
Absorption correction	Gaussian, ABSCOR	Analytical, AGNOST
Range transmission coefficient	0.185–0.302	0.446–0.539
Crystal faces	{110}, {100}, {01$\bar{1}$} (001)	{100}, {010}, {001} {011}, {111}, {$\bar{1}$11}, (10$\bar{2}$)
Reflections collected	5589	8166
No. averaged/% agreement	773, —	345, 0.6%
No. unique data in final cycle	3939	5660
σ; *p* value	$F_o > 3\sigma(F_o)$; 0.04	$F_o > 3\sigma(F_o)$; 0.04
Variables, final cycle	220	289
Final R_1[b]	0.0364	0.0405
Final weighted R_2[c]	0.0448	0.0382

[a]By neutral buoyancy in $C_2H_4Br_2/CCl_4$.
[b]$R_1 = \Sigma||F_o| - |F_c||/\Sigma|F_o|$.
[c]$R_2 = \{\Sigma w(|F_o| - |F_c|)^2/\Sigma wF_o^2\}^{1/2}$.

space groups *Pnma* (# 62) and *Pna*2$_1$ (# 33) (5). Cell constants suggested four formula units per unit cell, which in *Pnma* requires cations at special positions with either mirror or inversion symmetry, both of which are inconsistent with the assumed cation structure in an ordered crystal. Since there were no signs of disorder, space group *Pna*2$_1$ was chosen. A suitably sized crystal of **2** was cleaved perpendicular to [001] from an elongated prism. Details of crystal parameters, intensity data measurements (6) and data processing (7) are summarized in Table 1. No appreciable crystal decomposition occurred during data collection. Crystal dimensions were measured on an optical microscope, face indices assigned by optical goniometry, and an absorption correction was applied (8). For both structures neutral atom scattering factors were taken from Cromer and Waber (9), with those for hydrogen from Stewart, Davidson, and Simpson (10). Anomalous dispersion contributions were included for Pt, Cl, S, and P atoms (11). The function minimized was $\Sigma w(|F_o| - |F_c|)^2$, where the weight w is defined as $4|F_o|/\sigma^2(F_c^2)$, and p values were 0.04 for each structure (12).

Preliminary structure solution and refinement were carried out on a PDP 11/23+ computer (7). The position of the Pt atom and inner coordination sphere were determined by heavy-atom methods. Further solution was hampered by a persistent pseudo mirror-symmetry perpendicular to c, but all the non-hydrogen atoms were eventually located in a series of difference-Fourier syntheses without refinement. Although the CH_2Cl_2 solvent molecule was not disordered, and the carbon and chlorine atoms could be assigned anisotropic thermal parameters, there was significant disorder of the tetrafluoroborate anion, which was finally described by using three rigid groups of varying multiplicities.[5]

In the final stages of the refinement phenyl rings were included as idealized 6-atom rigid groups (C—C = 1.392 Å) with individual isotropic thermal parameters (13). Since *Pna*2$_1$ is an acentric space-group, a preliminary test was performed to determine the hand of the crystal. Inverting the model led to a slight increase in the R factors, and refinement was therefore continued on the original choice of hand.

[5]Computer programs used included local modifications of the following for the CDC Cyber 835 at the University of Western Ontario: WOCLS, full-matrix least-square refinement, from J. A. Ibers' NUCLS; Patterson and Fourier Syntheses, FORDAP, by A. Zalkin: ORFFE, Functions and Errors, by W. R. Busing, K. O. Martin, and H. A. Levy, and ORTEPII, crystal structure illustrations, by C. K. Johnson.

Hydrogen atoms were located in a difference-Fourier synthesis with electron densities ranging from 0.8(3) to 0.3(3) e $Å^{-3}$, and included in subsequent refinements at idealized locations with C—H = 0.95 Å and isotropic temperature factors 110% of that of the attached atom. A further two cycles of refinement with all non-group atoms assigned anisotropic thermal parameters gave $R_1 = 0.034$, $R_2 = 0.044$. The best model for the anion consisted of three tetrahedra of F atoms, with multiplicities of 50, 25, and 25% and the group origins tied to the position of a boron atom assigned an anisotropic thermal parameter. A full description of the different disorder models tried has been deposited.[6] On varying the group orientation angles and individual atom isotropic temperature factors, agreement factors of $R_1 = 0.036$ and $R_2 = 0.045$, with electron density residuals of 0.9(2), 0.9(2), and 0.8(2) e $Å^{-3}$ (top three peaks) were obtained. A final check on the handedness of the crystal was performed at this stage, again showing the inverted model to be inferior. A statistical analysis suggested the presence of secondary extinction, so a correction was applied (14). Two further cycles of least-squares refinement, with appropriate adjustment of the H-atom positions, led to convergence with agreement factors of $R_1 = 0.036$ and $R_2 = 0.045$. The largest parameter shift was 0.215 of its esd, associated with the x-coordinate of the origin of the Ph(4) group. The error in an observation of unit weight was 4.2 electrons. The secondary extinction coefficient refined to $5.9(2) \times 10^{-6}$. A final difference-Fourier map showed a peak of 1.1(2) e $Å^{-3}$ associated with the carbon atoms of one phenyl ring. The largest residual in the vicinity of the anion was only 0.9(2) e $Å^{-3}$. A statistical analysis of R_2 in terms of $|F_o|$, diffractometer setting angles, and $\lambda^{-1} \sin\theta$ showed no unusual trends.

Compound 1, X-ray data collection and reduction

Preliminary Weissenberg and precession photographs showed the space group to be $P2_1/c$. General conditions of data recording (6) and processing (7) were as described for compound **2** and are recorded in Table 1. An analytical absorption correction using the program AGNOST was applied.[7] Preliminary structure solution and refinement were carried out on a PDP 11/23+ computer. The position of the Pt atom was determined from an origin-removed Patterson synthesis, and subsequent difference-Fourier syntheses located all 60 non-hydrogen atoms (7). Two cycles of full-matrix least-squares refinement with the four heaviest atoms assigned anisotropic thermal parameters, and the phenyl rings as idealized groups (13), gave agreement factors $R_1 = 0.60$, $R_2 = 0.065$. Use of absorption-corrected data and the variation of individual temperature factors for the group atoms during two further cycles of refinement gave $R_1 = 0.048$, $R_2 = 0.051$. At this point a Fourier synthesis over the anion region of the unit cell showed only mild disorder, with the electron-density plot dominated by five major peaks consistent with a BF_4^- anion. The anion was therefore refined as individual atoms assigned anisotropic thermal parameters and two further cycles led to $R_1 = 0.044$ and $R_2 = 0.045$. The hydrogen atom positions were located on a total-difference Fourier map, at peak heights ranging from 0.8(3) to 0.3(3) e $Å^{-3}$, and were included in idealized positions as in the refinement of the structure of compound **2**. In the final cycles of refinement, employing 5660 unique data with $F_o \geq 3\sigma(F_o)$, 289 parameters were varied to convergence with $R_1 = 0.041$ and $R_2 = 0.038$. The largest parameter shift was 0.6 of its esd, that of the y-coordinate of $F(10)$. A final difference-Fourier map showed peaks of 1.2(1) e $Å^{-3}$ near the anion, 1.0(1) e $Å^{-3}$ near C(24), and 0.9(1) e $Å^{-3}$ near Cl(2). This suggests that any disorder in the BF_4^- ion is adequately accounted for in the anisotropic model, although the geometry of the model is not that of an ideal tetrahedron.

Final atomic positions and U_{equiv} of non-hydrogen atoms for compounds **1** and **2** are given in Tables 2 and 3, respectively,

TABLE 2. Atomic positional ($\times 10^4$) and thermal ($\times 10^3$) parameters for **1**

Atom	x	y	z	U_{equiv}
Pt	2086.9(2)	431.2(2)	2288.0(2)	31.4(1)
Cl1	801(3)	−3310(2)	754(2)	141(3)
Cl2	−593(3)	−2687(2)	1659(2)	151(3)
S	404(2)	663(1)	1610(1)	46(1)
P1	3913(1)	346(1)	2726(1)	36(1)
P2	1424(2)	−273(1)	3074(1)	35(1)
F1	2572(5)	2602(3)	1489(3)	99(5)
F2	1140(5)	2168(3)	1825(3)	89(4)
F3	1082(5)	2533(3)	801(3)	106(5)
F4	3031(5)	846(3)	308(3)	101(5)
F5	3605(5)	1864(3)	621(3)	100(5)
F6	2137(5)	1758(4)	−76(3)	115(5)
F7	2948(8)	−1526(5)	154(7)	234(11)
F8	1234(7)	−1659(6)	−83(6)	219(10)
F9	1982(13)	−1277(9)	802(5)	304(16)
F10	1980(8)	−679(6)	−49(8)	300(14)
O	2704(4)	1118(3)	1622(3)	46(3)
C1	−252(8)	−130(5)	1240(4)	77(7)
C2	1010(6)	981(4)	858(4)	48(5)
C3	2036(6)	1431(4)	1092(4)	42(5)
C4	1719(8)	2192(5)	1300(5)	60(6)
C5	2709(8)	1476(5)	483(5)	61(6)
C6	−10(10)	−2595(7)	922(7)	122(11)
B	2011(12)	−1271(9)	194(7)	79(9)
C21	4460(4)	1159(2)	3174(3)	40(2)
C22	5475(4)	1151(3)	3584(3)	59(2)
C23	5893(4)	1781(3)	3901(3)	67(3)
C24	5296(5)	2419(3)	3807(3)	75(3)
C25	4282(5)	2426(2)	3397(3)	81(3)
C26	3863(3)	1796(3)	3080(3)	61(3)
C31	4657(4)	264(3)	1988(2)	37(2)
C32	4389(3)	−292(2)	1521(3)	47(2)
C33	4975(4)	−379(3)	963(2)	60(2)
C34	5830(4)	91(3)	873(2)	62(3)
C35	6098(4)	647(3)	1340(3)	61(3)
C36	5511(4)	734(2)	1897(2)	50(2)
C11	4384(4)	−394(2)	3299(2)	40(2)
C12	4328(4)	−316(2)	3999(3)	49(2)
C13	4609(5)	−889(3)	4444(2)	68(3)
C14	4945(5)	−1540(3)	4189(3)	77(3)
C15	5000(5)	−1618(2)	3488(3)	65(3)
C16	4719(4)	−1045(3)	3043(2)	49(2)
C41	−69(3)	−359(3)	2953(3)	40(2)
C42	−590(5)	−1012(2)	2782(3)	56(2)
C43	−1733(5)	−1045(3)	2660(3)	80(3)
C44	−2356(3)	−424(4)	2710(3)	84(3)
C45	−1835(4)	229(3)	2881(3)	59(3)
C46	−691(4)	261(2)	3002(3)	51(2)
C51	1637(5)	108(3)	3940(2)	41(2)
C52	2159(5)	773(3)	4033(3)	52(2)
C53	2356(5)	1075(2)	4687(3)	70(3)
C54	2032(5)	711(4)	5248(2)	83(3)
C55	1511(5)	46(4)	5156(3)	94(4)
C56	1313(5)	−255(2)	4502(3)	83(3)
C61	1915(4)	−1196(2)	3046(3)	43(2)
C62	2069(5)	−1457(3)	2400(2)	56(2)
C63	2316(5)	−2180(3)	2317(3)	77(3)
C64	2408(5)	−2643(2)	2880(4)	90(3)
C65	2254(5)	−2382(3)	3526(3)	102(4)
C66	2007(5)	−1658(4)	3069(2)	78(3)

anisotropic temperature factors are given in supplementary Tables S-I and S-II, group parameters in Table S-III, hydrogen atom positions and temperature factors in Tables S-IV and S-V, and values of $10|F_o|$ and $10|F_c|$ in Tables S-VII and S-VIII.

[6]A description of the models explored in an attempt to describe the anion disorder, anisotropic thermal parameters, hydrogen atom parameters, rigid group parameters, weighted least-square planes, and structure amplitudes may be purchased from the Depository of Unpublished Data, CISTI, National Research Council of Canada, Ottawa, Ont., Canada K1A 0S2.

[7]AGNOST, adsorption program by Cahen and Ibers (15*a*), using the analytical method of de Meulenaer and Tompa (15*b*).

TABLE 3. Atomic positional ($\times 10^4$) and thermal ($\times 10^3$) parameters for **2**

Atom	x	y	z	U_{equiv}
Pt	2049.1(2)	1020.1(3)	2500	29.3(2)
S	2377(1)	2847(3)	1895(3)	40(2)
P1	1951(1)	−896(3)	2983(2)	31(1)
P2	1108(1)	1539(2)	2501(6)	34(1)
F1	3218(4)	−405(8)	672(7)	76(7)
F2	2711(4)	1067(9)	320(6)	80(7)
F3	3618(4)	1131(9)	109(7)	95(8)
F4	4283(3)	1611(9)	1726(8)	87(7)
F5	4036(3)	−155(8)	2152(7)	79(7)
F6	3941(4)	1259(11)	3228(8)	79(8)
O	2914(3)	581(6)	2506(15)	38(4)
C1	2319(6)	3889(11)	2940(12)	59(9)
C2	3158(5)	2515(13)	1891(11)	49(8)
C3	3274(5)	1203(11)	1853(11)	41(7)
C4	3212(6)	731(14)	713(12)	52(9)
C5	3879(7)	983(16)	2280(12)	50(11)
C6	2544(5)	−1308(12)	3870(11)	49(8)
C7	616(5)	547(11)	1860(11)	45(8)
B	3848(11)	5574(22)	3250(19)	112(19)
C11	2009(4)	−1830(8)	1864(6)	36(3)
C12	1721(4)	−1506(7)	958(7)	48(3)
C13	1741(4)	−2235(9)	90(6)	55(4)
C14	2048(4)	−3288(8)	128(7)	58(4)
C15	2336(4)	−3612(7)	1033(9)	88(6)
C16	2317(4)	−2883(9)	1901(7)	74(5)
C21	1303(3)	−1347(7)	3657(6)	37(3)
C22	910(4)	−2150(7)	3245(5)	44(3)
C23	409(3)	−2431(7)	3791(7)	57(4)
C24	301(3)	−1911(8)	4750(7)	63(4)
C25	694(4)	−1108(8)	5162(5)	54(4)
C26	1195(3)	−826(7)	4616(6)	46(3)
C31	815(4)	1799(8)	3805(5)	41(3)
C32	1188(3)	2130(8)	4601(7)	47(3)
C33	974(4)	2319(8)	5597(6)	56(4)
C34	386(4)	2177(9)	5797(6)	67(5)
C35	12(3)	1846(9)	5001(8)	75(5)
C36	227(3)	1657(8)	4005(7)	56(4)
C41	971(4)	2889(6)	1781(6)	41(3)
C42	720(4)	3871(8)	2244(5)	50(4)
C43	600(4)	4867(7)	1652(8)	67(5)
C44	732(4)	4881(7)	598(7)	79(5)
C45	983(4)	3898(9)	134(5)	58(4)
C46	1103(4)	2902(7)	726(7)	49(3)
F7	3782	5043	4241	134
F8	3762	6807	3336	116
F9	3435	5094	2552	145
F10	4415	5350	2870	131
F7*	3926	4706	2468	132
F8*	3247	5766	3410	86
F9*	4114	6641	2931	92
F10*	4105	5181	4189	85
F7**	4285	6452	3202	98
F8**	4110	4452	3377	110
F9**	3522	5587	2315	73
F10**	3476	5804	4104	113

Structure descriptions

A comparison of selected interatomic distances and bond angles for the two cations is shown in Table 4, while weighted least-square planes are presented in Table S-VI.

Perspective ORTEP stereoviews of the cations in compounds **1** and **2**, with atoms drawn as 50% probability thermal ellipsoids, are shown as Figs. 1 and 2, respectively.

TABLE 4. Selected bond lengths and angles[a]

Bonds	Length (Å) Compound **2**	Compound **1**	Average[b]
Pt—S	2.343(3)	2.347(2)	2.345(3)
Pt—P(1)	2.275(3)	2.297(2)	—
Pt—P(2)	2.251(3)	2.251(3)	2.251(3)
Pt—O	2.058(6)	2.041(5)	2.050(6)
S—C(1)	1.797(14)	1.789(9)	1.79(1)
S—C(2)	1.841(13)	1.832(8)	1.84(1)
C(2)—C(3)	1.516(18)	1.531(10)	1.52(1)
O—C(3)	1.377(17)	1.366(8)	1.37(1)
C(3)—C(4)	1.570(19)	1.535(11)	1.55(2)
C(3)—C(5)	1.522(20)	1.538(11)	1.53(2)

Bonds	Angle (deg) Compound **2**	Compound **1**	Average
S—Pt—O	84.4(2)	83.8(1)	84.1(2)
S—Pt—P(2)	94.6(1)	97.28(7)	—
P(1)—Pt—P(2)	98.8(1)	97.14(7)	—
P(1)—Pt—O	82.2(2)	81.9(1)	82.1(2)
Pt—S—C(1)	108.1(4)	113.3(3)	—
Pt—S—C(2)	97.9(5)	95.6(3)	—
Pt—O—C(3)	117.3(8)	121.2(4)	—
C(1)—S—C(2)	102.2(6)	98.4(4)	—
S—C(2)—C(3)	111.9(9)	109.7(5)	110.8(7)
O—C(3)—C(2)	112.2(11)	112.6(6)	112.4(9)
O—C(3)—C(4)	110.0(11)	109.7(7)	109.9(9)
C(2)—C(3)—C(4)	110.5(12)	110.9(7)	111(1)
C(2)—C(3)—C(5)	108.2(12)	107.3(7)	108(1)
C(4)—C(3)—C(5)	115.5(12)	109.6(7)	—

[a]Bond lengths in Å, angles in deg. Estimated standard deviations are given in parentheses and refer to the least significant digit(s).

[b]Observed differences applied to a normal distribution using accepted criteria before averaging (2), estimated standard deviations are the root-mean-square values.

The common atom numbering scheme for the hybrid ligand in both complexes is shown in the line diagram:

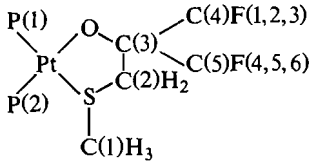

In the PPh_3 complex **1**, C(11), C(21), and C(31) are bonded to P(1), and C(41), C(51), and C(61) to P(2). In the PPh_2Me complex **2**, C(6)(Me), C(11)(Ph) and C(21)(Ph) are bonded to P(1), and C(7)(Me), C(31)(Ph), and C(41)(Ph) to P(2). In both cases, F(7), F(8), F(9), and F(10) are bonded to boron in the anion.

Both of the structures are composed of discrete cations and anions. In **1**, the shortest intermolecular contact is 2.33 Å between one of the hydrogen atoms on C(2) and a fluorine atom in the anion. In **2**, one intermolecular H—H contact (2.24 Å) is less than the sum of the covalent radii, and there are also several short contacts between phenyl-ring hydrogens and BF_4^- anions.

The basic geometry of both cations is similar. Coordination around the platinum atom is distorted square-planar in each, with adjacent angles greater than 90° [P(1)—Pt—P(2), S—Pt—P(2)] or less than 90° [P(1)—Pt—O, S—Pt—O]. The large inter-phosphorus angles (97–99°) are consistent with general observations on complexes containing *cis*-coordinated

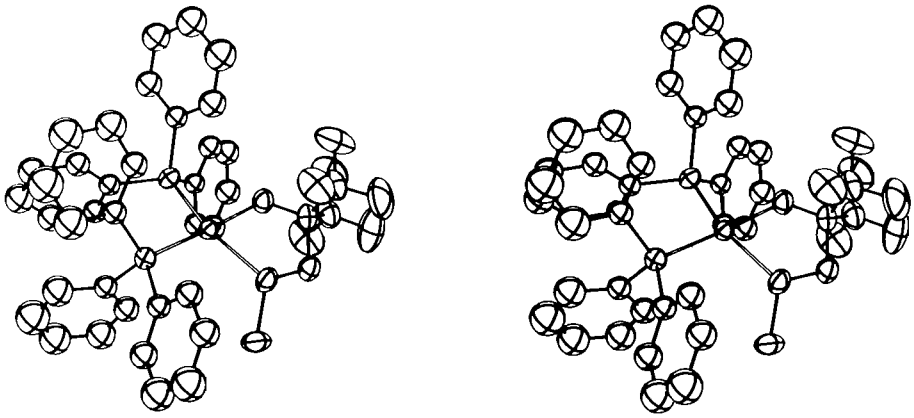

FIG. 1. ORTEP stereoviews of the cation in compound **1**.

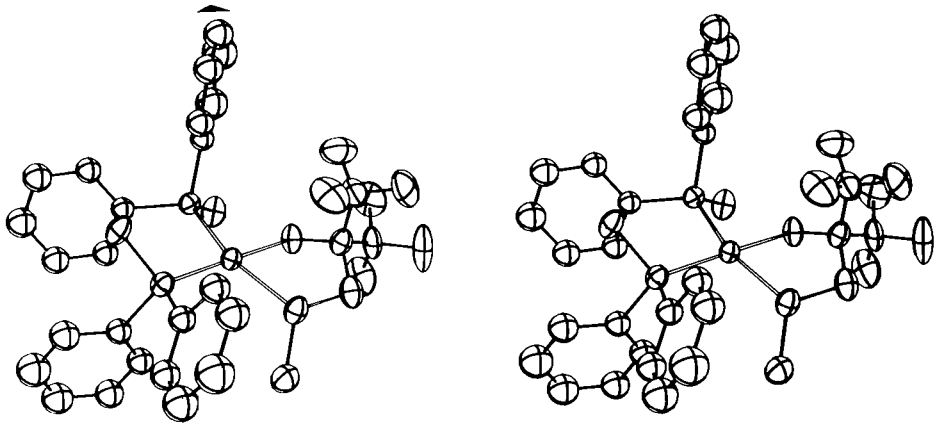

FIG. 2. ORTEP stereoviews of the cation in compound **2**.

phenyl phosphines. The similar values for the angles between coordinated phosphorus and sulfur (95–97°) suggest that the thioether methyl substituent also has considerable steric bulk, which in turn is likely to influence the chelate ring conformations. The "bite" angle of the chelating ligand does not differ significantly between the two complexes, and the average of 84.1(2)° is similar to other known examples in which Pt^{2+} or Pd^{2+} is incorporated into a five-membered ring with one first-row and one second-row donor atom (16).

The average Pt—S bond length in the two complexes is 2.345(3) Å. This is significantly longer than the range 2.21(1)–2.292(6) Å reported for Pt—S bonds *trans* to halides, amines, or thioethers (17). A longer bond [2.33(1) Å] is found in the complex **8** (18) which is, to our knowledge, the only other structure reported in which a thioether is *trans* to a phosphine on platinum(II):

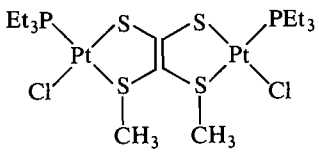

8

The average Pt—O bond length of 2.050(6) Å in **1** and **2** is within the normal range. A survey[8] of ten crystal structures published in 1980–1983 shows a range of 1.98–2.06 Å, with a mean of 2.02(3) Å. Previously reported values for Pt—O bonds in fluorinated alkoxy derivatives of platinum include 1.992(5) Å in (COD)Pt[—$OC(CF_3)_2$—O—$C(CF_3)_2^-$] (19) and 2.024(21) and 2.032(9) Å in *cis*-$(R_3P)_2$Pt[—O—$C(CF_3)_2$—O—$C(CF_3)_2$—O—], where R_3P = $MePPh_2$ and PPh_3, respectively (20).

For each of the complexes **1** and **2**, the bond from Pt to the phosphine *trans* to the thioether, Pt—P(1), is longer than that to the phosphine *trans* to the alkoxy group, Pt—P(2). The Pt—P(2) distance, at 2.251(3) Å, is identical in **1** and **2** and is marginally longer than the values of 2.223(9) and 2.244(4) Å found previously for R_3P—Pt *trans* to a fluorinated alkoxy group (19). However, there is a significant difference between the Pt—P(1) bond length of 2.292(3) Å found in complex **1** and that of 2.275(3) Å in **2**. This may be attributed to the greater degree of steric crowding, and the associated departure from strict square-planar geometry, that is found with the bulkier triphenylphosphine in **1**.

The average C—O bond length of 1.37(1) Å is significantly shorter than the normal sp^3-carbon to oxygen bond length of 1.43(1) Å. We have found very similar values in several other fluorinated alkoxides (21, 22).

The geometry of the chelate ring is similar in the structures of **1** and **2**. In both, the sulfur methyl substituent is located *anti* to the more axial of the two CF_3 groups, presumably to minimize intramolecular $CH_3 \leftrightarrow CF_3$ repulsion. In other complexes of CF_3-substituted thioether complexes, the least sterically hindered arrangement is found in the solid state (23). For example,

[8]Using the program CRYSTOR for searching the Cambridge crystallographic data base, through the courtesy of the Canadian Institute for Scientific and Technical Information, Ottawa.

TABLE 5. Anisotropic shielding of CH_3S and CF_3 groups (ppm)[a]

Complex	Phosphine	$\delta(CH_3S)$	$\Delta\delta(CH_3S)$[b]	$\delta(CH_3)(A)$	$\delta(CH_3)(B)$	$\delta\Delta(CF_3)$[c]
			Complexes of Me—S—O$^-$:			
1[d]	PPh_3	1.96	−0.83	−76.2	−76.2	0
2[d]	PPh_2Me	2.13	−0.66	−76.1	−76.8	+0.7
3[e]	$PPhMe_2$	2.74	−0.05	−76.5	−78.1	+1.6
4[d]	PMe_3	2.79	—	−76.0	−77.9	+1.9
			Complexes of Ph—S—O$^-$:			
5[e]	PPh_3			−76.4	−76.8	+0.4
6[e]	PPh_2Me			−76.4	−77.0	+0.6
7[e]	$PPhMe_2$			−76.3	−77.5	+1.2

[a]^{1}H nmr at 100 MHz; ^{19}F nmr at 94.1 MHz; experimental details are given in ref. 1.
[b]Referred to PMe_3 complex.
[c]$\delta\Delta = \delta(CF_3)(A) - \delta(CF_3)(B)$.
[d]Solvent CD_2Cl_2.
[e]Solvent $CDCl_3$; allow ~0.5 ppm shift difference between solvents.

in **9**, the CF_3 group and the CH_3 substituent β to it on the chelate backbone are mutually *anti* (24). Similarly in complex **10**, each of the S—CH_3 groups is *anti* to the adjacent CF_3 group (25).

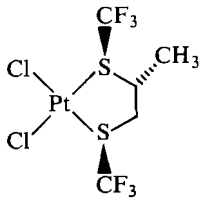

9

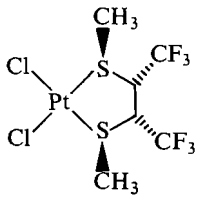

10

As can been seen in the stereoviews, the conformations of **1** and **2**, though similar, do differ significantly. In both structures, four out of the five atoms making up the ring are close to coplanarity. However, in **2** it is the carbon atom carrying the CF_3 groups, C(3), which is 0.51 Å *above* the plane, while in **1** it is the methylene carbon atom, (C)2), which is 0.63 Å *below* the plane. We have observed very similar situations in complexes of the closely-related ligand $Ph_2PCH_2C(CF_3)_2O^-$ (26), and it seems to be a general trend for Pt and Pd complexes of these ligands to adopt a conformation with four coplanar atoms in a five-membered chelate ring. It is unclear whether these differing conformations are due to differing steric requirements of the phosphine ligands, or merely to crystal packing forces, but either points to a low-energy distortion coordinate between them.

Discussion

Anisotropic shielding of the SCH_3 group

We have attributed a large shielding of the methyl resonance in the complex $PtCl(Me—S—O)(PPh_3)$ to the ring-current effect of an *adjacent* PPh_3 group (1). Similar shielding effects are observed in the cationic complexes **1–4**, and our postulate that there is an interaction between the sulfur methyl groups of Me—S—O$^-$ and the phosphine phenyl rings is now substantiated by the structural results on complexes **1** and **2**. As Figs. 1 and 2 show, an aromatic ring makes an almost exactly perpendicular approach to the CH_3—S substituent. In solution, the phosphines would be expected to undergo rapid reorientation about the Pt—P bond, and the methyl groups would therefore experience an average shielding influence from the rotating phenyl rings. The size of the influence will depend upon the number of aromatic substituents on the phosphine and upon their relative freedom to re-orient about their P—C axes. In Table 5, the dependence of $\delta(CH_3S)$ on the coligand is presented.

The shift in $[Pt(Me—S—O)(PMe_3)_2]^+$ was taken as the zero-point, from which we calculate an anisotropic shielding effect, Δδ, which increases with the number of aromatic rings on the adjacent phosphine. The palladium analogue of **1** has $\delta(CH_3—S) = 1.77$ ppm, implying a large Δδ for this complex as well. Ring anisotropy effects have been postulated before to explain upfield shifts; for example, in a series of dimethylcarboxamido platinum complexes (3) and in a ruthenium(II) complex (4), but have not previously been substantiated by a full structural determination.

The perpendicular approach of the phosphine rings to the CF_3 groups is also evident on the stereoviews. For the nmr data (Table 5), we define Δδ as the *difference* in chemical shift between the two CF_3 groups. In the absence of ring anisotropy effects, at temperatures low enough to slow inversion at sulfur, the CF_3 groups in complexes of these ligands give doublet-of-quartet patterns, with $J(F_A, F_B)$ of about 10 Hz. The chemical shift separation, Δδ, varies considerably in different types of R—S—O$^-$ complexes (1, 27), making it essential to consider a systematic range of compounds in order to draw significant conclusions about specific influences on Δδ. We report here two such series, namely **1–4** and **5–7**. In each, there is a systematic variation in $\Delta\delta(CF_3)$ with change in phosphine, such that, in each series, Δδ decreases in the sequence $PMe_3 > PPhMe_2 > PPh_2Me > PPh_3$. This variation closely matches the anisotropic shielding of the methyl groups, and we therefore suggest that the CF_3 groups are also affected by ring currents on adjacent phosphine ligands. Supporting evidence comes from the complex $PtCl(Me—S—O)(PPh_3)$, in which chloro is adjacent to the CF_3 groups and $\Delta\delta(CF_3)$ is 1.6 ppm (1).

In the PPh_3 complex **1**, Δδ = 0, whereas the similar complex of the ligand Ph—S—O$^-$, **5**, has a small, but non-zero, separation. This suggests that the observation of a single resonance for the CF_3 groups on **1** is the result of a *fortuitous* negation of inherently different chemical shifts by the ring current effects. The crystal structures of **1** and **2** substantiate this conclusion, since differences between the two structures are not sufficient to explain the chemical shifts on any other basis.

Preferred conformation in solution

A direct consequence of the observation of ring anisotropy effects on the CF_3 groups is that the chelate rings of complexes **1–7** maintain a preferred conformation in solution; that is, for a

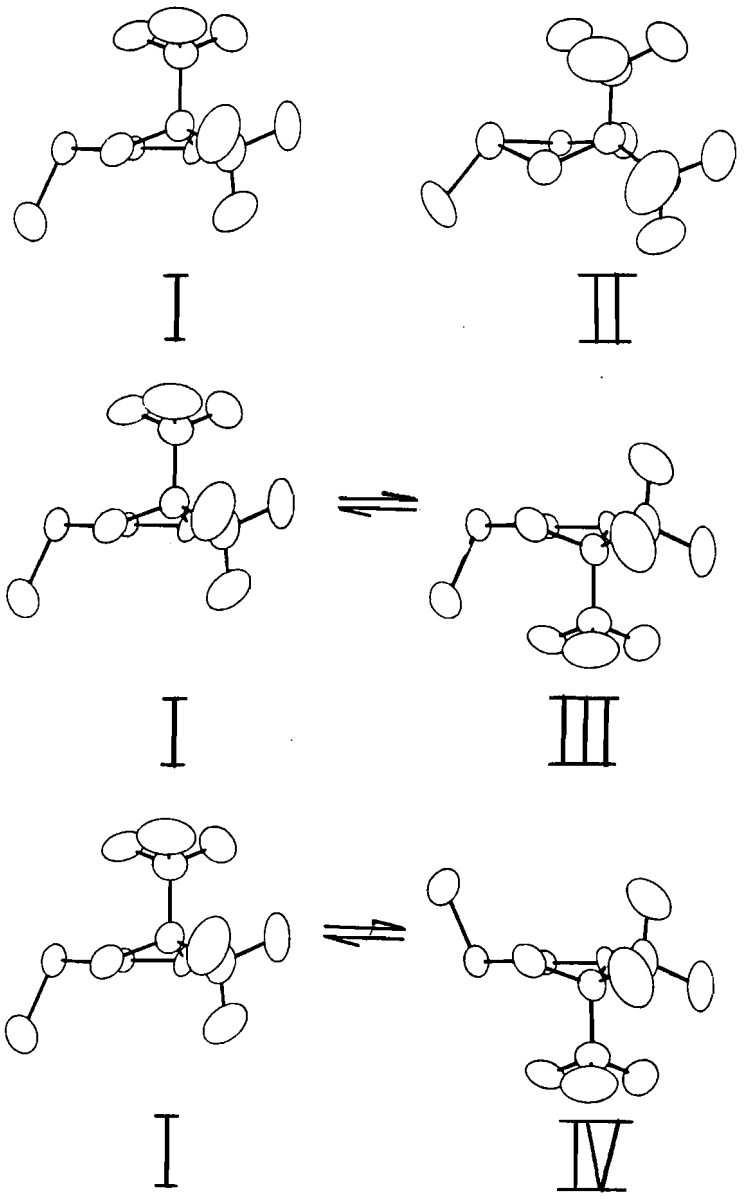

FIG. 3. Possible chelate ring conformations.

given enantiomer, the axial and equatorial CF_3 groups do *not* exchange in the manner shown by **I** ↔ **III** in Fig. 3, or at least that the lifetime of **I** is long with respect to that of **III**.

Since the two conformations are of different energy, this is perhaps not surprising, but the difference is subtle and not immediately obvious. Configurations **I**, **II**, and **III** are, of course, *representations* of the three static structures; we do not mean to imply that the differences between the solid-state conformations are maintained in solution. All that is required to explain the observed nmr behaviour is that complete ring inversion does not occur at low temperatures, since rapid **I** ↔ **III** exchange would average the CF_3 environments with respect to the adjacent phenyl rings, resulting in no net effect on their chemical shifts. The lower-energy species is probably I, with the CH_3—S group *anti* to the more axial CF_3 group, minimizing CH_3 ↔ CF_3 interactions. This aspect of the solid-state structures *is* maintained in solution, and only when thioether inversion becomes rapid does the complete ring inversion occur (shown as **I** ↔ **IV** in Fig. 3).

Ring conformational changes in five-membered metal–sulfur ring systems are usually very low energy processes, and are thus rapid at temperatures well below those required for thioether inversion (28). For this reason, and because most work has employed symmetrically substituted dithioethers, preferred conformations are rarely seen in such complexes. We have previously reported the nmr parameters of the platinum(II) perfluoropinacolato complex of 2,5-dithiahexane, Pt(PFP)(DTH), **11** (29).

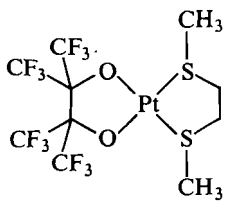

11

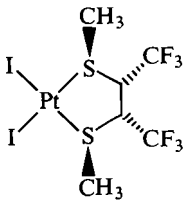

12

The *anti*-isomer of **11** has inequivalent CF_3 groups, which indicates a preferred conformation of the PFP ring, presumably

that which minimizes interaction with the CH_3—S groups of DTH.

Preferred conformations have also been reported in complexes of $CF_3SCH_2CH(CH_3)SCH_3$ (24), $CH_3SCH(CF_3)SCH_3$ (30), and $CH_3SCH_2CH(CF_3)SCH_3$ (23, 30). The presence of two chiral centres in the PtX_2 complexes of these ligands means that preferred conformations can be detected through the abundance of specific diastereomers, and **12** exists in solution entirely as the *syn* diastereomer, where $CH_3 \leftrightarrow CF_3$ interactions are at a minimum. There is an excellent correlation between known solid-state structures and the most abundant stereoisomer in solution for these complexes (23–25).

The absence of a second chiral centre in **1** and **2** makes it difficult to follow the chelate ring dynamics in our complexes, as has been done for **12**. The excellent agreement between the activation energies for thioether inversion measured independently from the ^1H and ^{19}F nmr suggests that the CH_3 and CF_3 groups are rendered equivalent by the same process, which we believe to be the coupled ring-thioether inversion represented by **I** ↔ **IV** in Fig. 3.

Conclusions

The crystal structures of **1** and **2** clearly show the origin of the anomalous chemical shifts observed for the SCH_3 and CF_3 groups. In complexes of the thioether ligands Me—S—O^- and Ph—S—O^-, with bulky CF_3 substituents, subtle steric interactions control the conformations of the chelate rings in the solid state and in solution; the power of the combined use of ^1H and ^{19}F nmr to monitor the latter has been demonstrated. As a consequence of the large substituents and the low symmetry, preferred conformations, correlating with solid-state structures, exist in solution.

Acknowledgements

We are grateful for financial support of this work provided by the Natural Sciences and Engineering Research Council of Canada through operating grants to N.C.P. and C.J.W. and a postgraduate scholarship to R.T.B.

1. R. T. Boeré and C. J. Willis. Can. J. Chem. **64**, 492 (1986).
2. G. H. Stout and L. H. Jensen. X-ray structure determination. MacMillan, New York. 1968.
3. C. R. Green and R. J. Angelici. Inorg. Chem. **11**, 2095 (1972).
4. D. M. Roundhill, S. G. Roundhill, W. B. Beaulieu, and U. Bagchi. Inorg. Chem. **19**, 3365 (1980).
5. International tables for X-ray crystallography. D. Reidel Publishing Co. Vol. A. 1963.
6. Enraf-Nonius CAD4F Users' Manual, Enraf-Nonius, Delft, 1984.
7. Enraf-Nonius Structure Determination Package, SDS-Plus Version 1.0, 1982.
8. P. Coppens, L. Leiserowitz, and D. Rabinowich. Acta Crystallogr. **18**, 1035 (1965).
9. D. T. Cromer and J. T. Waber. Acta Crystallogr. **18**, 104 (1965).
10. R. F. Stewart, E. R. Davidson, and W. T. Simpson. J. Chem. Phys. **42**, 3175 (1965).
11. D. T. Cromer and J. Liberman. J. Chem. Phys. **53**, 1891 (1970).
12. W. R. Busing and H. A. Levy. J. Chem. Phys. **16**, 563 (1957).
13. R. Eisenberg and J. A. Ibers. Inorg. Chem. **4**, 773 (1965).
14. W. H. Zachariasen. Acta Crystallogr. A**2**, 212 (1968).
15. (*a*) D. Cahen and J. A. Ibers. J. Appl. Crystallogr. **5**, 298 (1965); (*b*) J. de Meulenaer and H. Tompa. Acta Crystallogr. **19**, 1014 (1965).
16. L. P. Battaglia, B. A. Corradi, G. C. Palmieri, M. Nardelli, and T. M. E. Vidoni. Acta Crystallogr. B**29**, 762 (1973).
17. S. G. Murray and F. R. Hartley. Chem. Rev. **81**, 365 (1981).
18. B. Cetinkaya, P. B. Hitchcock, M. F. Lappert, P. L. Pye, and D. B. Shaw. J. Chem. Soc. Dalton Trans. 434 (1979).
19. M. Green and J. A. K. Howard. J. Chem. Soc. Dalton Trans. 2065 (1977).
20. A. Modinos and P. J. Woodward. J. Chem. Soc. Dalton Trans. 2134 (1975).
21. E. Konefal, S. J. Loeb, D. W. Stephan, and C. J. Willis. Inorg. Chem. **23**, 538 (1984).
22. R. T. Boeré, W. M. Brown, D. W. Stephan, and C. J. Willis. Inog. Chem. **24**, 593 (1985) and references therein.
23. W. N. Hunter, K. W. Muir, and D. W. A. Sharp. J. Fluorine Chem. **21**, 19 (1982).
24. (*a*) R. J. Cross *et al.* J. Chem. Soc. Chem. Commun. 291 (1976); (*b*) L. Manijlovic-Muir, K. W. Muir, and T. Solomun. Inorg. Chim. Acta, **22**, 69 (1977).
25. W. N. Hunter, K. W. Muir, and D. W. A. Sharp. Acta Crystallogr. C**40**, 37 (1984).
26. C. D. Montgomery, N. C. Payne, and C. J. Willis. Inorg. Chim. Acta. In press.
27. R. T. Boeré and C. J. Willis. Can. J. Chem. **63**, 3530 (1985).
28. E. W. Abel, K. G. Orrell, and S. K. Bhargava. Progr. Inorg. Chem. **32**, 1 (1984) and references therein.
29. R. T. Boeré and C. J. Willis. Inorg. Chem. **24**, 1059 (1985).
30. R. J. Cross, D. S. Rycroft, D. W. A. Sharp, and H. Torrens. J. Chem. Soc. Dalton Trans. 2434 (1980).

Further syntheses with nitroxide α,β-unsaturated aldehydes and allylic bromides

KÁLMÁN HIDEG,[1] JÓZSEF CSEKÖ, AND H. OLGA HANKOVSZKY
Central Laboratory Chemistry, University of Pécs, H-7643 Pécs, P.O. Box 99, Hungary
AND
PÁL SOHÁR
EGIS Pharmaceuticals, Spectroscopic Department, H-1475 Budapest, P.O. Box 100, Hungary
Received February 15, 1985[2]

KÁLMÁN HIDEG, JÓZSEF CSEKÖ, H. O. HANKOVSZKY, and PÁL SOHÁR. Can. J. Chem. **64**, 1482 (1986).

The enhanced reactivity of nitroxide allylic bromides is used for preparation of spin-labelled analogues of biologically active compounds (morphine, Nalorphine, barbituric acid, choline and acetyl choline). Nitroxide α,β-unsaturated aldehydes are reacted with phosphoranes to give nitroxide polyenes. The nitroxides are reduced to diamagnetic *N*-hydroxy hydrochloride salts, which can be converted in the presence of base to *N*-acetoxy derivatives.

KÁLMÁN HIDEG, JÓZSEF CSEKÖ, H. O. HANKOVSZKY et PÁL SOHÁR. Can. J. Chem. **64**, 1482 (1986).

On fait appel à la grande réactivité des nitroxydes des bromures allyliques pour préparer des analogues de composés biologiquement actifs (morphine, Nalorphine, acide barbiturique, choline et acétyl choline) portant des marqueurs de spin. On a fait réagir des nitroxydes d'aldéhydes α,β-non saturés avec des phosphoranes pour obtenir des nitroxydes de polyènes. On a réduit les nitroxydes pour obtenir les chlorhydrates diamagnétiques de dérivés *N*-hydroxylés qui peuvent être transformés, en présence de base, en dérivés *N*-acétoxylés.

[Traduit par la revue]

Introduction

It is essential in spin labelling of various biomolecules (drugs, hormones, and amino acids) to achieve minimal perturbation of their function (1–3). Besides this there are other important factors requiring optimization, such as the use of a spin label reagent with high but selective reactivity, and to achieve a stable labelled molecule in which its nitroxide moiety shows relatively high resistance toward reduction reactions.

In earlier work spin-labelled analogues of drug molecules such as morphine, barbiturate, and acetylcholine have been reported, e.g. morphine was alkylated on its phenolic hydroxyl group with 1-oxyl-2,2,5,5-tetramethyl-3-iodoacetamidopyrrolidine and used for spin-label immunoassay (4). The preparation of diacylated morphines (5), the 6-amino[2,2,6,6-tetramethyl-4-piperidyl-1-oxyl]morphine, and -codeine with marginal biological activity (6) are also known. Commercially available 5-(2-aminoethyl)-5-isopentylbarbituric acid was acylated with ethyl 1-oxyl-2,2,5,5-tetramethylpyrrolidine-3-carbonyl carbonate (7). The spin-labelled acetylcholines having the 2,2,6,6-tetramethylpiperidine-1-oxyl moiety are also known (7–9) and have been used in various membrane studies (10).

Preparation of a spin-labelled diene, 1-oxyl-4-vinyl-2,2,6,6-tetramethyl-1,2,5,6-tetrahydropyridine in a multistep synthesis started from triacetonamine, and its Diels–Alder reaction with maleic anhydride has been described (11).

Allylic halides offer enhanced reactivity (for reviews, see ref. 12), and therefore we have used nitroxide allylic halides for alkylating biomolecules. For preparation of dienes by the Wittig reaction we used α,β-unsaturated aldehydes, which can conveniently be obtained by oxidation (e.g. by MnO_2) of the corresponding allylic alcohol (13).

Results and discussion

The first objective of the present paper is to give further examples of the advantages of unsaturated aldehydes and allylic halides in preparation of spin-labelled analogues of the aforementioned molecules. In our laboratory the preparation of spin-labelled α,β-unsaturated aldehydes (**1**), (14), (**3**) (15) and allylic halides (**2**) (16), (**4**) (15) have been developed.

1 (R = CHO)
2 (R = CH_2Br)

3 (R = CHO)
4 (R = CH_2Br)

It is an advantage of allylic compounds that they are more reactive in nucleophilic displacement than their saturated analogues, and thus substitution reactions can be carried out more easily under milder conditions. However, it is important to know whether the nucleophilic displacement has taken place with or without allylic rearrangement (12) (Scheme 1). If the compounds are diamagnetic, the structure of the products can be proved by nmr investigation. In the case of paramagnetic compounds it is necessary to convert them to diamagnetic derivatives, most conveniently by reduction. When compounds are not sensitive to hydrogenation the reduction to *N*-hydroxy derivatives could be carried out by catalytic hydrogenation (17). in the case of olefinic nitroxides this method cannot be applied.

Another known convenient method for the reduction of

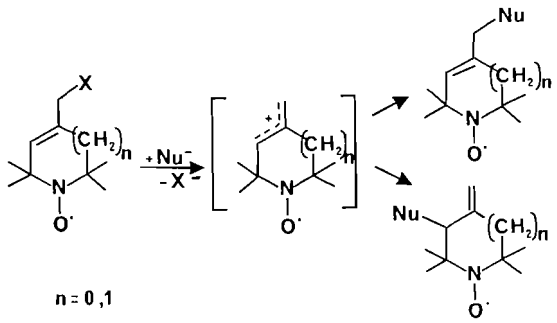

SCHEME 1

[1]Author to whom correspondence may be addressed.
[2]Revision received February 21, 1986.

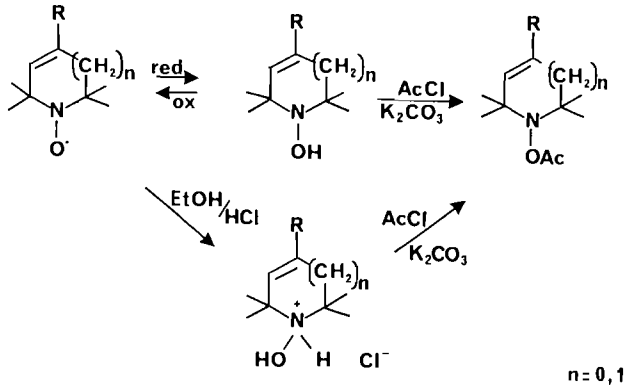

SCHEME 2

nitroxides is the reduction by aqueous ascorbic acid (18). Really, all the types of paramagnetic molecules in this paper can be reduced to the corresponding *N*-hydroxy derivatives by an excess of ascorbic acid. However, during isolation of the *N*-hydroxy compounds some of them are oxidized back spontaneously to nitroxide so quickly that this method could not be used. Since the nitroxides can be converted in alcohol with strong acid to *N*-hydroxy salts (19) we prepared, in most of the cases, the *N*-hydroxy hydrochloride salts, then directly acetylated them to stable *N*-acetoxy derivatives in the presence of base (triethylamine or potassium carbonate).

In this type of substitution reaction the position of the allylic double bond did not change. The ^1H and ^{13}C nmr spectra of compounds obtained from each reaction type showed that reactions with **2** and **4** had taken place without allylic rearrangement (see Table 1 and Experimental). The allyl halides (**2**, **4**) used for alkylation of morphines have not only the advantage of higher reactivity observed in alkylation of morphine, with **2**, on the phenolic hydroxyl to **5** (16), or with **4** to **6**, but in alkylating the normorphine molecule with **2** or **4** the *N*-allyl labelled derivatives (**7**, **8**) can be obtained. When normorphine was reacted with excess of reagents **2** and **4**, the biradicals (**9** and **10**) were obtained.

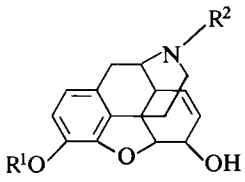

5 (R^1 = X, R^2 = Me)
6 (R^1 = Y, R^2 = Me)
7 (R^1 = H, R^2 = X)

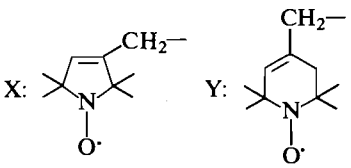

8 (R^1 = H, R^2 = Y)
9 (R^1 = R^2 = X)
10 (R^1 = R^2 = Y)

It turned out that while the *N*-allyl morphine (Nalorphine) is an antagonist of morphine according to Snyder's bioassay method (20), **7** and **8** are moderate agonists. The inhibition of electrically induced contraction of guinea pig intestine (ID_{50}), morphine: 7×10^{-6} mol, normorphine: 7×10^{-6} mol (20); **7**: 3×10^{-6}; **8**: 1×10^{-6} mol. The sodium ion index (Nalorphine 3, morphine 38) (20) of **7** is 7, and of **8** is 20.[3] The 3-*O*-labelled derivatives (**5**, **6**) proved less active than the *N*-allyl derivatives (**7**, **8**). The ^1H and ^{13}C nmr spectra of the dihydrochloride salt of **7** (11) were not informative enough to investigate the question of allylic rearrangement; therefore it was acetylated to **12**, whose nmr spectra proved the structure (Table 1, Experimental).

[3]A. Borsodi, unpublished data.

The *N*-hydroxy derivative of **6** was converted into the *N*,*O*-diacetoxy derivative, whose nmr spectra correspond to non-rearranged product (**13**).

Spin-labelled malonic esters (**14**, **15**) were prepared from the corresponding malonates with **2** or **4** in a phase-transfer (PHT) reaction, using tetrabutylammonium hydrogen sulfate (TBAH) as PHT catalyst. The nmr spectra of *N*-hydroxy hydrochloride salts (**16** and **17**) obtained from **14** and **15** showed that no allylic rearrangement had taken place during the alkylation, because the position of the signal of the olefinic proton (or carbon) and the methylene protons (or carbon) remain as they are in the hydrochloride salts of the allylic alcohols: 1-hydroxy-3-

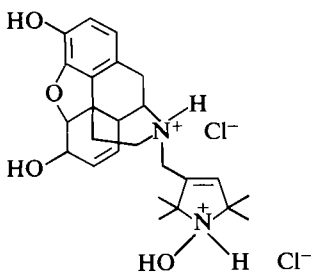

11

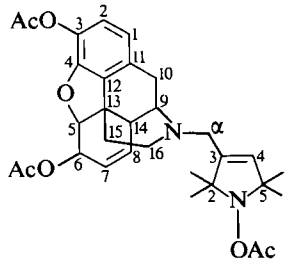

12

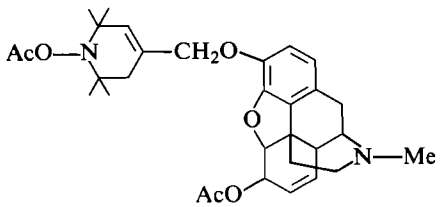

13

hydroxymethyl-2,2,5,5-tetramethyl-3-pyrroline hydrochloride (**18**) and 1-hydroxy-4-hydroxymethyl-2,2,6,6-tetramethyl-1,2,5,6-tetrahydropyridine hydrochloride (**19**). (The nitroxide allylic alcohols (13, 16) were starting compounds in the synthesis of α,β-unsaturated aldehydes **1** and **3** and allylic bromides **2** and **4**.)

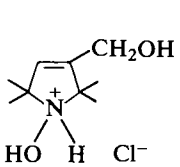

18

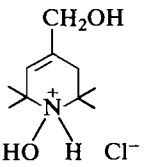

19

The ring closure reactions of malonates **14** and **15** with urea in the presence of sodium ethoxide in dry ethanol gave spin-labelled barbituric acids **20** and **21**.

The experience of preparation of spin-labelled maleimides from spin-labelled amines with maleic anhydride showed that the ring closure was always accompanied by the formation of undesired iso-maleimide (**22**) as by-product (21, 22). We wished to utilize the high reactivity of **2** and **4** for preparation of maleimides **23** and **24** from allyl halides (**2**, **4**) with silver maleimide or maleimide (in a PHT reaction). Compounds **23** and **24** could be obtained but the yields were very low; **23** was identical with a sample prepared earlier by the alternative route from amine and maleic anhydride (23).

The advantageous reactivity of allylic halides was also utilized for preparation of spin-labelled choline and acetylcholine with minimal perturbance to either choline or acetylcholine. By quaternization of *N*,*N*-dimethylamino ethanol or its *O*-acetyl

TABLE 1. The ^1H and ^{13}C nmr chemical shifts ($\delta_{TMS} = 0$ ppm) of the spin-labelled part (of pyrroline or dehydropiperidine rings) of compounds **12**, **13**, **16–19**, **32**, **38***a,b*, **39***a,b*, and **43** in DMSO-d_6 or $CDCl_3$ solution (**12**, **13**, **32**, **39***a,b*, **43**) at 250 (^1H) and 20 (^{13}C) MHz

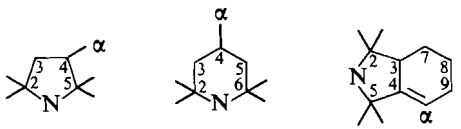

Compound	CH_3 (2,5/2,6)[a] 4 × s (4 × 3H)	H-3 s (1H)	H-5[b] (2H)	H(α)	C-2,5/2,6[a]	C-3	C-4	C-5[b]	(α)	CH_3 (2,5/2,6)[a]
12	1.24 (9H), 1.27 (3H)	5.48	—	~3.15[c]	68.3[d]	131.8[e]	129.6[f]	—	53.0	~20,[g] ~25[g]
13	1.14, 1.15, 1.21, 1.22	5.55	2.0–2.5[h]	~4.5[c]	57.4, 59.3	128.4[e]	127.39[f]	38.9	71.7	20.5, 21.9, 28.1, 29.5
16	~1.2,[g] ~1.4,[g] ~1.55[g]	5.06	—	3.08[j]	76.4, 80.0	129.4[e]	139.5	—	32.7	~23.8,[g] ~25.0[g]
17	1.25, 1.35, 1.40, 1.50	5.45	2.00,[c] 2.75[c]	2.58[j]	66.1, 67.8	129.3	131.4	39.0	?[k]	~25[g]
18	1.37, 1.42, 1.56[d]	5.71	—	4.01[j]	76.8, 78.8	127.6	145.5	—	58.4	~24.5,[g] ~25.5[g]
19	1.28, 1.38, 1.50, 1.55	5.55	2.15,[c] 2.75[c]	3.82[j]	66.7, 68.3	125.0	134.6	38.1	64.8	~25[g]
32	1.25,[d] 1.32[d]	5.59	—	6.14[l]	68.3, 71.1	130.2[e]	142.7	—	130.7[e]	~25[g]
38*a*	1.33, 1.47,[d] 1.72[g]	3.75[m]	—	5.95	73.9, 74.2	47.5	146.3	—	121.2	22.4, 25.9, 26.8, ?
38*b*	1.16, 1.39, 1.59, 1.64	2.85[m,n]	—	6.05	73.9, 75.2	43.2	143.5	—	120.6	24.2, 25.2, 25.7, 28.7
39*a*	1.10, 1.28, 1.34, ~1.55[g]	3.35[m]	—	5.64	64.7, 65.1	47.3	149.5	—	115.8	24.3,[d] 25.6, 25.9
39*b*	1.11, 1.24, 1.25, 1.37	~2.65[m,o]	—	5.70	65.1, 66.8	43.3	147.9	—	115.1	24.1, 24.5, 25.1, 26.7
41	1.35, 1.42 (9H)	5.83	—	5.95[v]	78.2, 80.7	129.4	142.8	—	139.0[e]	~24.9,[g] ~25.9[g]
44	1.17, 1.19, 1.20, 1.28	5.46	2.17,[p] 2.42[p]	6.33[r]	58.1, 60.4	134.3	129.8	38.0	138.1	21.4, 22.8, 29.1, 30.4

[a]2,6 for compounds **13**, **17**, **19** and **43**; 2,5 for all others.
[b]In case of compounds **13**, **17**, **19** and **43**.
[c]AB-like multiplet (2H) with broadened lines.
[d]Two coincident signals.
[e,f,i]Reversed assignments may be possible.
[g]Broadened, diffuse signals.
[h]Hidden by the multiplets of the morphine skeleton.
[j]Singlet (2H).
[k]Overlapped by the solvent signal.
[l]dd (11.3, 17.8 Hz).
[m]Probable assignment only. Due to line broadening and overlap of multiplets it is not possible to assign the H-3, -7, -8, -9 signals unanimously.
[n]Overlapping signals.
[o]Partly overlapped by the solvent signal.
[p]AB-multiplet, $J = 16.4$ Hz.
[r]dd (10.8 and 17.5 Hz).
[s]Overlapping lines, proved by DEPT experiment.
[t]May be one of the lines assigned to CH_3 (2,5).
[u]Overlapping bands of the maleimide ring and the acetyl group.
[v]d ($J(trans) = 15.8$ Hz).

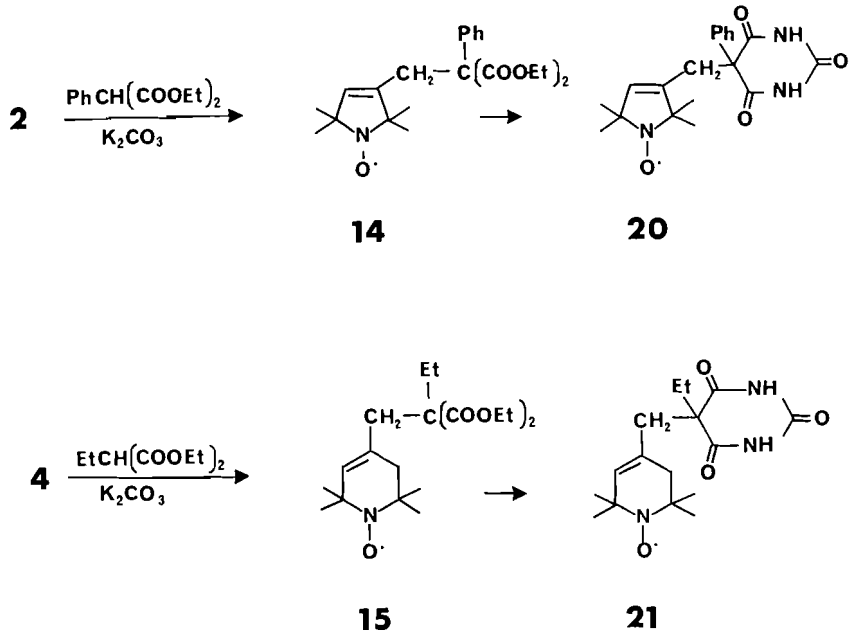

SCHEME 3

derivative with **2** and **4**, spin-labelled cholines **25**, **26** or acetylcholines **27**, **28** were conveniently prepared. These compounds, showing close resemblance to the Me_3N^+ moiety of the non-labelled compounds, may be useful for biological studies and investigation of the structure – biological activity relationship.

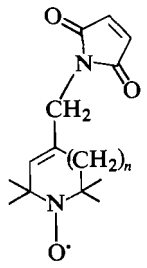

23 (n = 0)
24 (n = 1)

In another set of experiments the unsaturated aldehydes (**1**, **3**) were utilized as convenient synthons for preparation of polyenes. For an ongoing collaboration with polymer chemists we wished to use a spin-labelled diene for investigation of polystyrene polymerization. Utilizing a phase-transfer Wittig reaction (24) of **1** with methylidene phosphorane, formed *in situ* 2,2,5,5-tetramethyl-3-vinyl-3-pyrroline-1-oxyl (**29**) was obtained.

However, the application of paramagnetic dienes in a free radical polymerization procedure might not be possible because of the involvement of the nitroxide moiety in the polymerization as an inhibitor (25).

Therefore the diene (**29**) first was reduced either with ascorbic acid to *N*-hydroxy diene (**30**), then *O*-acetylated to **32**, or else **29** was dissolved in ethanol saturated with HCl, then incubated for several hours at room temperature and precipitated with ether. The $CHCl_3$ solution of *N*-hydroxy hydrochloride **31** in the presence of K_2CO_3 was acylated with excess acetyl chloride to **32**. The *O*-acetyl protecting group as an active ester group can be easily hydrolyzed with aqueous alkali and oxidized again spontaneously, by air or with PbO_2, to nitroxide (**29**). This

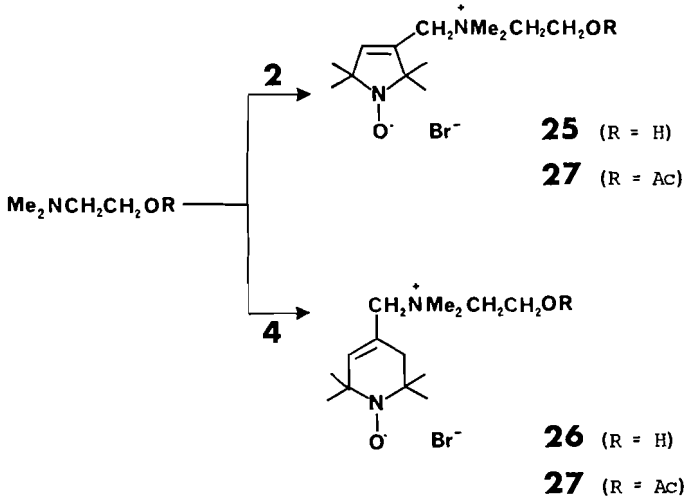

SCHEME 4

method of protection was successfully applied in a polystyrene copolymerization study (26).

Compound **29** was reacted with maleic anhydride to a new spin-labelled anhydride reagent (**33**), with the known spin-labelled maleimide **24** to a biradical (**34**). However, it was also necessary to prepare further adducts to determine the configuration of these adducts, because the anhydride **33** is sensitive toward the above-mentioned reduction methods, and the biradical **34** has signals that partly overlap the signals of ring junction protons (or carbons). Therefore **29** was reacted with *N*-methyl maleimide to give **35**, and with *N*-ethyl maleimide to give **36**,

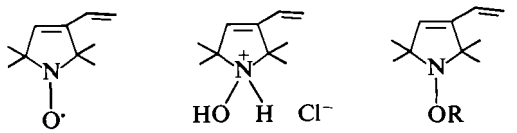

29 **31** **30** (R = H) **32** (R = Ac)

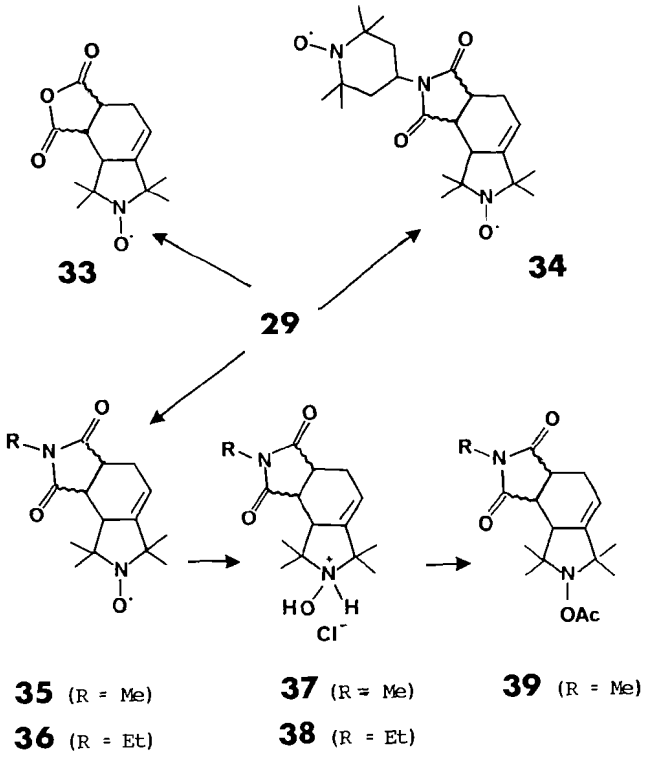

SCHEME 5

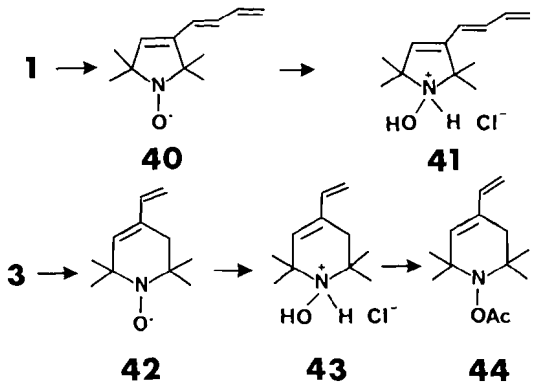

SCHEME 6

which are mixtures of two isomers (*a* and *b*), differing in the configuration of C-3, -7, -8. Diamagnetic *N*-hydroxy salts of **36***a,b* were separated (**38***a,b*) as well as the *O*-acetyl derivatives **39***a,b* obtained via *N*-hydroxy salts (**37***a,b*). Carbon chemical shifts showed that the major isomers formed in the cyclization are the stereochemically more stable ones, while the minor compounds are the more crowded molecules. Determination of the stereostructure of these diastereomers is in progress and will be published elsewhere.

Compound **1**, with allyl triphenylphosphorane, gave a nitroxide triene **40**. The nmr spectra of reduced derivatives **41** showed that the trienes have *E* configuration.

The Wittig reaction of **3** with methylidene phosphorane formed *in situ* gave **42**, which was converted into **43**, then **44**.

Experimental

The compounds were purified by flash column chromatography on Kieselgel 60 (0.040–0.063 mm, Merck). The esr (electron spin resonance) spectra were obtained from 10^{-3} *M* solution on a Zeiss ER9 spectrometer. All of the monoradicals exhibited three equidistant lines a_N = 14.3–15.3 G. The mass spectra were measured on a Varian MAT-SM-1 mass spectrometer. Melting points were measured using a Boetius micro instrument and are not corrected. The ir spectra of radicals were measured with a Zeiss Specord 75 type of instrument; ir spectra of diamagnetic compounds were run in KBr discs on a Brüker IFS-113v FT spectrometer equipped with an Aspect 2000 computer.

The nmr spectra were recorded in 5- or 10-mm tubes at room temperature on a Brüker WM-250 (^{1}H) or WP-80SY FT spectrometer (^{13}C) controlled by an Aspect 2000 computer at 250.13 (^{1}H) or 20.14 MHz (^{13}C) in $CDCl_3$ or DMSO-d_6 solution using the deuterium signal of the solvent as the lock and TMS as internal reference. The most important measuring parameters were as follows: sweep width: 5 kHz; pulse width: 1 (^{1}H) or 3.5 (^{13}C) μs (ca. 20° or 30° flip angle); acquisition time 1.64 s; number of scans: 16 or 2^{10}–2^{16}; computer memory: 16K; Lorentzian exponential multiplication for signal-to-noise enhancement (LB 0.7 or 1.0 Hz) and complete proton noise decoupling (ca. 1.5 W) for ^{13}C measurements were applied.

DEPT[4] experiments (27) were performed (in the case of compounds **13** and **32**) in a standard way (28) using only the θ = 135° pulse to separate CH/CH_3 and CH_2 lines phased "up" and "down", respectively. Typical acquisition data were: number of scans: 128–12 K; relaxation delay for protons: 3 s; 90° pulse width: 10.8 and 22.8 μs for ^{13}C and ^{1}H, respectively. The estimated value for *J*(C,H) resulted in a 3.7-ms delay for polarization.

Spectral data of the common (spin-labelled) part of the compounds investigated were tabulated (Table 1); further parameters of the very different structures are listed separately (the footnotes in Table 1 are also referred to throughout the Experimental). It is to be noted that many of the nmr signals are broadened (lines of multiplets have coalesced) due probably to residual free radical contaminations. Consequently, and because of poor solubilities or coincidences with the solvent peaks, it was not possible to determine proton–proton coupling constants for compounds **38***a,b* and **39***a,b* nor to identify some carbon lines in the case of **38***a,b*. The assignments of carbons of the morphine skeleton are based on literature data (29).

General method for the preparation of hydroxylamine hydrochloride salts (Method A)

The nitroxide compound was dissolved in EtOH saturated with HCl (5 mL) and allowed to stand overnight. Then ether was added and the crystalline product was filtered.

General method for the preparation of N*-acetoxy compounds (Method B)*

To a stirred mixture of hydroxylamine hydrochloride salt (1 mmol) and potassium carbonate (2 mmol) in dry chloroform, acetylchloride (2 mmol) was added. After 20 min water was added, the organic phase washed with a solution of $NaHCO_3$, water, dried, and evaporated.

*Preparation of 3-spin-labelled morphine derivatives (**5**, **6**). General procedure*

The allylic bromo compound (**2** or **4**) (0.50 mmol) was added to a suspension of morphine base (143 mg, 0.50 mmol) and K_2CO_3 (100 mg) in DMF, and the mixture was heated (70°C) for 2 h, diluted with a solution of NH_4Cl, extracted with $CHCl_3$ (3 × 10 mL), dried, and evaporated. The pure product (**5** or **6**) was obtained by preparative thin-layer chromatography (Merck, Kieselgel 60; chloroform:ether: ethanol, 4:4:1). Compound **5** was identical in all respects with the compound prepared from the corresponding mesylate (16). Yield: 110 mg (48%) (**6**); mp 156–157°C; ir (Nujol): 3400–3200 (OH), 1520 (C=C) cm^{-1}; ms, *m/e*: M^+ 451 (9), 437(13), 436(6), 421(13). *Anal.* calcd. for $C_{27}H_{35}N_2O_4$ (451.59): C 71.81, H 7.81, N 6.20; found: C 72.05, H 7.51, N 5.98.

Preparation of N*-spin-labelled normorphine derivatives (**7**, **8**). General procedure*

The nitroxide allylic bromo compound (**2** or **4**) (0.50 mmol) was added to a suspension of normorphine (135 mg, 0.50 mmol) and K_2CO_3 (100 mg) in DMF and the mixture was heated (70°C) for 2 h,

[4]DEPT: Distortionless Enhancement by Polarization Transfer.

diluted with a solution of NH_4Cl, extracted with $CHCl_3$ (3 × 10 mL), and the organic phase was dried and evaporated. The pure product (**7** or **8**) was obtained by preparative thin-layer chromatography (Merck, Kieselgel 60; chloroform:ether:ethanol, 4:4:1). Yield: 125 mg (59%) (**7**); mp > 250°C; ir (Nujol): 3500–3100 (OH) cm^{-1}. *Anal.* calcd. for $C_{25}H_{31}N_2O_4$ (423.54): C 70.94, H 7.38, N 6.61; found: C 70.72, H 7.49, N 7.05. Yield: 100 mg (45%) (**8**); mp > 200°C; ir (Nujol): 3500–3100 (OH) cm^{-1}; ms, *m/e*: M^+ 437(49), 429(100), 407(22), 284(24). *Anal.* calcd. for $C_{26}H_{33}N_2O_4$ (437.56): C 71.37, H 7.60, N 6.40; found: C 71.28, H 7.72, N 6.29.

*Preparation of bis spin-labelled normorphine derivatives (**9**, **10**). General procedure*

The allylic bromo compound (**2** or **4**) (1 mmol) was added to a suspension of normorphine base (135 mg, 0.50 mmol) and K_2CO_3 (100 mg) in DMF, and the mixture was heated (70°C) for 2 h, diluted with a solution of NH_4Cl, extracted with $CHCl_3$ (3 × 10 mL), dried, and evaporated. The pure product (**9** or **10**) was obtained by preparative thin-layer chromatography (Merck, Kieselgel 60; $CHCl_3$:ether:ethanol, 4:4:1). Yield: 140 mg (49%) (**9**); mp 92–93°C; ir (Nujol): 3500–3100 (OH) cm^{-1}. *Anal.* calcd. for $C_{34}H_{45}N_3O_5$ (575.75): C 70.93, H 7.88, N 7.30; found: C 70.96, H 8.05, N 7.33. Yield: 94 mg (31%) (**10**); mp 191–192°C; ir (Nujol): 3500–3100 (OH) cm^{-1}; ms, *m/e*: M^+ 603 (0.2), 152 (100). *Anal.* calcd. for $C_{36}H_{49}N_3O_5$(603.84): C 71.61, H 8.18, N 6.96; found: C 71.93, H 8.34, N 7.02.

*Preparation of hydrochloride salt of **7** (**11**)*

From **7** (450 mg, 1.1 mmol) according to *Method A*. Yield: 500 mg (94%) mp > 250°C; ir ($CHCl_3$): 3400–3200 (OH) cm^{-1}. *Anal.* calcd. for $C_{25}H_{32}N_2O_4 \cdot 2HCl$ (497.47): C 60.36, H 6.89, N 5.63, Cl 14.15; found: C 59.99, H 6.93, N 5.64, Cl 14.59.

Preparation of N*-acetoxy derivative of **7** (**12**)*

From **11** (450 mg, 0.90 mmol) according to *Method B*. Yield: 300 mg (61%); mp 129–130°C; ir (KBr): 1774 (C═O, phenolic ester), 1738 (C═O, allylic ester), 1247, 1207, 1038 (C—O) cm^{-1}; ^1H nmr: CH_3(Ac): 2.14, 2.16, 2.27, 3 × s (3 × 3H); H-9: 3.45, m (1H); H-5: 5.10, dd (5.5, 0.7 Hz); H-6: ~5.15, m (1H); H-8: 5.40, ~d (~10 Hz); H-7: 5.62, ~d (~10 Hz); H-1: 6.58, d (8.2 Hz); H-2: 6.76, d (8.2 Hz); ^{13}C nmr: CH_3(Ac): 19.1, 20.5, 22.1; CH_2(10): 20.5; CH_2(15): 35.4; CH(14): 40.8; CH_2(16): 43.6; C-13: 44.5; CH(9): 57.5; CH(6): 71.3; CH(5): 89.0; CH(1): 119.2; CH(2): 122.0; CH(8): 128.6;[f] C-12: 131.2;[e] CH(7): 132.1;[i] C-11: 132.2;[i] C-3: 141.1; C-4: 149.7; C═O: 168, 170.3, 171.3. *Anal.* calcd. for $C_{31}H_{38}N_2O_7$ (550.68): C 67.62, H 6.96, N 5.09; found: C 67.41, H 6.88, N 4.98.

Preparation of N*-acetoxy derivative of **6** (**13**)*

From **6** (1.5 g, 3.3 mmol) by *Method A*, then *Method B* (without isolation of hydrochloride salt). The pure product (**13**) was obtained by flash chromatography ($CHCl_3$:MeOH, 20:1). Yield: 250 mg (14%); mp 63–64°C; ir ($CHCl_3$): 1750, 1735 (C═O) cm^{-1}; ^1H nmr: CH_3(Ac): 2.10, 2.14, 2 × s (2 × 3H); CH_3N: 2.43, s (3H); H-9: 3.35, m (1H); H-5: 5.10, d (~6 Hz); H-6: 5.16, m (1H); H-8: 5.44, ~d (~10 Hz); H-7: 5.63, ~d (~10 Hz); H-2: 6.50, d (~9 Hz); H-1: 6.64, d (~9 Hz); ^{13}C nmr: CH_3(Ac): 17.4, 19.6;[s] CH_2(10): 19.6;[s] CH_2(15): 34.4; CH(14): 39.5; C-13: 41.5; NCH_3: 41.9; CH_2(16): 45.6; CH(9): 58.1; CH(6): 67.1; CH(5): 86.8; CH(2): 116.5; CH(1): 118.1; C-11: 126.7; CH (8): 127.35;[f] C-12: 129.9; CH(7): 130.5;[e] C-3: 139.5; C-4: 146.3; C═O: 169.0, 169.6. *Anal.* calcd. for $C_{31}H_{40}N_2O_6$ (536.67): C 69.38, H 7.51, N 5.22; found: C 69.48, H 7.80, N 5.52.

*Preparation of spin-labelled diethyl phenylmalonate (**14**)*

A solution of NaOH (2 *N*, 3.6 mL) was added to a CH_2Cl_2 solution (9 mL) of diethyl phenylmalonate (710 mg, 3 mmol), TBAH (1.222 g, 3.6 mmol), and **2** (839 mg, 3.6 mmol) and stirred at room temperature for 16 h. The organic layer was separated, dried, evaporated, and chromatographed on a silica gel column with CCl_4/ether, to give **14**. Yield: 700 mg (60%); mp 100–101°C; ir (Nujol): 1725 (C═O) cm^{-1}. *Anal.* calcd. for $C_{22}H_{30}NO_5$ (388.49): C 68.02, H 7.78, N 3.61; found: C 68.00, H 7.49, N 3.56.

*Preparation of spin-labelled diethyl ethylmalonate (**15**)*

A solution of NaOH (2 *N*, 3.6 mL) was added to a solution of diethyl ethylmalonate (565 mg, 3 mmol), TBAH (1.222 g, 3.6 mmol), and **4** (89 mg, 3.6 mmol) in CH_2Cl_2 (9 mL) and stirred at room temperature for 16 h. The organic layer was separated, dried, evaporated, and chromatographed on a silica gel column with CCl_4/ether, to give **15**. Yield: 400 mg (37%), red oil; ir ($CHCl_3$): 1720 (C═O) cm^{-1}. *Anal.* calcd. for $C_{19}H_{32}NO_5$ (354.48): C 64.38, H 9.10, N 3.95; found: C 64.46, H 8.91, N 3.84.

*Preparation of hydrochloride salt of **14** (**16**)*

From **14** (194 mg, 0.50 mmol) according to *Method A*. Yield: 200 mg (94%); mp 130–132°C; ir (KBr): 3100–2400 (OH + N^+H), 1753, 1725 (C═O), 1240, 1200, 1028 (C—O) cm^{-1}; ^1H nmr: CH_3(OEt): 1.16, t (7.0 Hz), 6H; CH_2(OEt): 4.20, qa (4H); ArH: 7.3–7.5, m (5H); OH + NH: ~11.6, ~12.0, 2 × br s (2 × 1H); ^{13}C nmr: CH_3(OEt): 15.3; C_{quat}: 62.5; CH_2(OEt): 63.4; C_{Ar}-2′, -6′: 129.7,[e] 129.8;[e] C_{Ar}-1′: 137.1; C═O: 170.8. *Anal.* calcd. for $C_{22}H_{31}NO_5 \cdot HCl$ (425.96): C 62.03, H 7.57, N 3.29, Cl 8.32; found: C 61.79, H 7.70, N 3.01, Cl 8.62.

*Preparation of hydrochloride salt of **15** (**17**)*

From **15** (177 mg, 0.50 mmol) according to *Method A*. Yield: 170 mg (91%); mp 130–131°C; ir (KBr): 3100–2400 (OH + N^+H), 1749, 1726 (C═O), 1225, 1182, 1036 (C—O) cm^{-1}; ^1H nmr: CH_3(C-Et): 0.78, t (7.4 Hz, 3H); CH_3(OEt): 1.19, t (7.1 Hz, 6H); CH_2(C-Et): 1.85, qa (2H); CH_2(OEt): 4.13, qa (4H); OH + NH: ~11.5, ~12.4, 2 × br s (2 × 1H); ^{13}C nmr: CH_3(C-Et): 9.9; CH_3(OEt): 15.4; CH_2(C-Et): 26.5; C_{quat}: 59.1; CH_2(OEt): 62.6; C═O: 172.1. *Anal.* calcd. for $C_{19}H_{33}NO_5 \cdot HCl$ (391.94): C 58.23, H 8.74, N 3.57, Cl 9.04; found: 58.57, H 8.60, N 3.47, Cl 9.02.

*Preparation of 1-hydroxy-3-hydroxymethyl-2,2,5,5-tetramethyl-3-pyrroline hydrochloride (**18**)*

From 1-oxyl-3-hydroxymethyl-2,2,5,5-tetramethyl-3-pyrroline (170 mg, 1 mmol) according to *Method A*. Yield: 184 mg (88%) mp 157–159°C; ir (KBr): 3450, 3325, 3200–2500 (OH + N^+H), 1107 (C—O) cm^{-1}; ^1H nmr: OH + NH: ~11.6, ~12.2, 2 × br s (2 × 1H). *Anal.* calcd. for $C_9H_{17}NO_2 \cdot HCl$ (207.70): C 52.05, H 8.73, N 6.75, Cl 17.07; found: C 52.26, H 8.91, N 6.93, Cl 17.19.

*Preparation of 1-hydroxy-4-hydroxymethyl-2,2,6,6-tetramethyl-1,2,5,6-tetrahydropyridine hydrochloride (**19**)*

From 1-oxyl-4-hydroxymethyl-2,2,6,6-tetramethyl-1,2,5,6-tetrahydropyridine (184 mg, 1 mmol) according to *Method A*. Yield: 165 mg (90%) mp 176–177°C; ir (KBr): 3425, 3200, 2675 (OH, HN^+ − OH, N^+H) cm^{-1}; ^1H nmr: OH + NH: ~11.4, ~12.5, 2 × br s (2 × 1H). *Anal.* calcd. for $C_{10}H_{19}NO_5 \cdot HCl$ (221.73): C 54.17, H 9.03, N 6.32, Cl 15.99; found: C 53.94, H 9.23, N 6.59, Cl 16.08.

*Preparation of 5-phenyl-5-[(1-oxyl-2,2,5,5-tetramethyl-3-pyrroline-3-yl)methyl]barbituric acid (**20**)*

A solution of **14** (388 mg, 1 mmol) in dry EtOH was added to a solution of urea (300 mg, 5 mmol) in sodium ethoxide (1 *M*, 3 mL, 3 mmol) and refluxed for 15 h. The reaction mixture was acidified with 1 *N* HCl and extracted with $CHCl_3$. The organic phase was washed with water, dried, evaporated, and chromatographed on a silica gel column with chloroform/ether, to give **20**. Yield: 150 mg (43%); mp 138–140°C; ir ($CHCl_3$): 3300–2700 (NH), 1750, 1690 (C═O), 1600 (C═C) cm^{-1}; ms, *m/e*: M^+ 355(5), 288(8), 258(11), 232(50). *Anal.* calcd. for $C_{19}H_{22}N_3O_4$ (356.41): C 64.03, H 6.22, N 11.79; found: C 63.89, H 6.54, N 12.07.

*Preparation of 5-ethyl-5-[(1-oxyl-2,2,6,6-tetramethyl-1,2,5,6-tetrahydropyrid-4-yl)methyl]barbituric acid (**21**)*

To a solution of urea (300 mg, 5 mmol) in sodium ethoxide (1 *M*, 3 mL, 3 mmol), a solution of **15** (354 mg, 1 mmol) in dry EtOH was added dropwise. The reaction mixture was refluxed for 15 h, acidified with 1 *N* HCl, and extracted with $CHCl_3$. The organic phase was washed with water, dried, evaporated, and chromatographed on a silica gel column with $CHCl_3$/ether, to give **21**. Yield: 140 mg (43%); mp 156–157°C; ir ($CHCl_3$): 3300–2700 (NH), 1750, 1710 (C═O) cm^{-1};

ms, *m/e*: M^+ 322(33), 308(15), 136(34), 135(17). *Anal.* calcd. for $C_{16}H_{24}N_3O_4$ (322.40): C 59.61, H 7.50, N 13.03; found: C 59.82, H 7.57, N 13.02.

Preparation of spin-labelled maleimides (23, 24) Method I

In a three-necked flask equipped with a nitrogen inlet was placed maleimide (97 mg, 1 mmol), powdered anhydrous K_2CO_3 (83 mg, 0.6 mmol), powdered KOH (73 mg, 1.1 mmol), and 18-crown-6 (26 mg, 0.1 mmol) in toluene (8 mL). The mixture was stirred under nitrogen at room temperature for 24 h, then **2** or **4** (1,1 mmol) in toluene (1 mL) was added. The mixture was stirred for 18 h at reflux. The reaction mixture was cooled to room temperature, and the inorganic salts were filtered off and washed with saturated KCl solution (3 × 20 mL), dried, and evaporated. The product **23** or **24** was obtained with preparative thin-layer chromatography (Merck, Kieselgel 60; CCl_4:ether 4:1). Yield 20 mg (8.0%) (**23**). Compound **23** was identical in all respects with the compound that has been described in the literature (23). Yield: 20 mg (7.6%) (**24**); mp 110–112°C; ir ($CHCl_3$): 1730, 1710 (C=O) cm^{-1}. *Anal.* calcd. for $C_{14}H_{19}N_2O_3$ (263.31): C 63.86, H 7.27, N 10.64; found: C 64.01, H 7.13, N 10.36.

Method II

The silver maleimide was prepared by the method of Schwartz and Lerner (30). A mixture of allylic bromo compound (**2** or **4**) (1 mmol) and silver maleimide (1.1 mmol) in dry benzene (5 mL) was refluxed for 16 h. The silver salts were removed by filtration. After evaporation of the solvent the residue was chromatographed on silica gel to give the spin-labelled maleimide compound. Yield: 23 mg (9.2%) (**23**); 25 mg (9.6%) (**24**).

Preparation of spin-labelled choline derivatives (25, 26). General procedure

Compound **2** or **4** (0.50 mmol) was added to 2-dimethylaminoethanol (45 mg, 0.50 mmol). After a few minutes the crystalline product was filtered, then washed with ether. Yield: 56 mg (35%) (**25**); mp 184–186°C; ir (Nujol): 3500–3100 (OH) cm^{-1}. *Anal.* calcd. for $C_{13}H_{26}BrN_2O_2$ (322.27): C 48.45, H 8.13, Br 24.80, N 8.69; found: C 48.40, H 8.07, Br 24.63, N 8.48. Yield: 72 mg (41%) (**26**); mp 160–162°C; ir (Nujol): 3500–3100 (OH) cm^{-1}. *Anal.* calcd. for $C_{14}H_{28}BrN_2O_2$ (336.29): C 50.00, H 8.39, Br 23.76, N 8.33; found: C 49.90, H 8.56, Br 23.42, N 8.43.

Preparation of spin-labelled acetylcholine derivatives (27, 28). General procedure

Compound **2** or **4** (0.50 mmol) was added to 2-(dimethylamino) ethyl acetate (66 mg, 0.50 mmol). After a few minutes the crystals of product were filtered, then washed with ether. Yield: 82 mg (45%) (**27**); mp 121–123°C; ir (Nujol): 1740 (C=O) cm^{-1}. *Anal.* calcd. for $C_{15}H_{28}BrN_2O_3$ (364.31): C 49.46, H 7.75, Br 21.93, N 7.69; found: C 49.66, H 7.58, Br 21.90, N 7.51. Yield: 81 mg (43%) (**28**); mp 142–144°C; ir (Nujol): 1735 (C=O) cm^{-1}. *Anal.* calcd. for $C_{16}H_{30}BrN_2O_3$ (378.35): C 50.80, H 7.99, Br 21.12, N 7.40; found: C 50.81, H 7.98, Br 21.05, N 7.37.

Preparation of 1-oxyl-3-vinyl-2,2,5,5-tetramethyl-3-pyrroline (29) From 1

Anhydrous K_2CO_3 (3.5 g) and the aldehyde (**1**) (3.36 g, 0.02 mol) were added to a solution of triphenylmethylphosphonium iodide (8.4 g, 0.02 mol) in dioxane, refluxed for 24 h, filtered off, evaporated, and the residue purified by chromatography on a silica gel column with chloroform/ether, to give **29** as a dark red oil. Yield: 1.8 g (54%); ir ($CHCl_3$): 1630, 1590 (C=C—C=C) cm^{-1}; ms, *m/e*: M^+ 166(20), 152(26), 151(30), 136(32). *Anal.* calcd. for $C_{10}H_{16}NO$ (166.25): C 72.25, H 9.70, N 8.43; found: C 71.92, H 9.59, N 8.27.

From 32

To a solution of *N*-acetoxy diene (**32**) (104 mg, 0.50 mmol) in MeOH (2 mL) was added 1 *N* aqueous NaOH (2 mL) and the solution allowed to stand for 30 min. It was then extracted with chloroform, the organic phase dried ($MgSO_4$), stirred with PbO_2 (1 g) for 10 min, filtered, and evaporated. The product is identical with compound **29** obtained by *Method I*. Yield: 50 mg (60%).

Preparation of hydrochloride salt of 29 (31)

From **29** (166 mg, 1 mmol) according to *Method A*. Yield: 186 mg (91%); mp 140–141°C. *Anal.* calcd. for $C_{10}H_{17}NO{\cdot}HCl$ (203.72): C 58.96, H 8.91, N 6.88, Cl 17.40; found: C 59.20, H 9.13, N 6.91, Cl 16.96.

N-*Acetoxy-3-vinyl-2,2,5,5-tetramethyl-3-pyrroline (32) From 29*

A solution of ascorbic acid (3.52 g, 0.02 mol) in water (10 mL) was added to a solution of **29** (1.66 g, 0.01 mol) in methanol (5 mL). After decolorization the solution (10 min) was extracted with chloroform, dried ($MgSO_4$), evaporated, and added to a stirred mixture of acetylchloride (1.17 g, 0.015 mol) and potassium carbonate (2.76 g, 0.02 mol) in dry chloroform. After 20 min water was added, the organic layer washed with a solution of $NaHCO_3$, water, dried, and evaporated to give **32** as a colorless oil. Yield: 1.15 g (55%); ir (KBr): 1774 (C=O), 1202 (C—O), 999 (=CH) cm^{-1}; ^1H nmr: $=CH_2$: 5.14, *d* (*J*(*cis*) = 11.3 Hz), 5.42, *d* (*J*(*trans*) = 17.8 Hz); ^{13}C nmr: CH_3(Ac): 19.1; $=CH_2$: 115.9; C=O: 171.3; ms, *m/e*: M^+ 209(2,2), 194(13), 167(10), 152(100). *Anal.* calcd. for $C_{12}H_{19}NO_2$ (209.29): C 68.87, H 9.15, N 6.69; found: C 68.70, H 8.85, N 7.09.

From 31

From **31** (186 mg, 0.92 mmol) according to *Method B*: the pure product was obtained by flash chromatography (*n*-hexane:ethyl acetate, 4:1), and it was identical with compound **32** obtained with *Method I*. Yield: 189 mg (99%).

1,1,3,3-Tetramethyl-2-oxyl-1,3,4,5,6,9-hexahydroindol-3,4-dicarboxylic anhydride (33)

Maleic anhydride (60 mg, 0.7 mmol) and toluene-4-sulfonic acid (5 mg) were added to a solution of **29** (166 mg, 1 mmol) in dry benzene, then refluxed for 4 h. After this the reaction mixture was evaporated and purified with preparative thin-layer chromatography (Merck, Kieselgel 60; $CHCl_3$:ether, 1:1) to give **33**. Yield: 70 mg (27%); mp 136–137°C; ir ($CHCl_3$): 1870, 1795 ($(CO)_2O$) cm^{-1}; ms, *m/e*: M^+ 264(100), 225(10), 166(18), 151(16). *Anal.* calcd. for $C_{14}H_{18}NO_4$ (264.32): C 63.62, H 6.86, N 5.30; found: C 63.68, H 6.97, N 5.14.

Preparation of adduct of 29 and N-*(1-oxyl-2,2,6,6-tetramethyl-4-piperidyl)maleimide (34)*

N-(1-oxyl-2,2,6,6-tetramethyl-4-piperidyl)maleimide (22) (251 mg, 1 mmol) and toluene-4-sulfonic acid (5 mg) were added to a solution of **29** (166 mg, 1 mmol) in dry benzene, refluxed for 12 h, evaporated, and purified by preparative thin-layer chromatography (Merck, Kieselgel 60; CCl_4:ether, 1:1), to give **34**. Yield: 110 mg (26%); mp 108–110°C; ir ($CHCl_3$): 1860, 1790 (C=O) cm^{-1}; esr: five lines of biradical with $a_{N/2}$ = 8.71G. *Anal.* calcd. for $C_{23}H_{35}N_3O_4$ (417.55): C 66.16, H 8.45, N 10.06; found: C 66.07, H 8.91, N 10.21.

Preparation of adducts of 29 with N-*methylmaleimide (35a, 35b)*

N-Methylmaleimide (1.55 g, 0.014 mol) was added to a solution of **29** (2.25 g, 0.014 mol) in dry toluene and the reaction mixture was refluxed for 12 h, evaporated, and purified with flash chromatograhy (*n*-hexane:ethyl acetate, 2:1) to give two main products. The first product eluting from the column was **35***a*. Yield: 0.2 g (5%); mp 161–162°C; ir ($CHCl_3$): 1775, 1705 (C=O, imide) cm^{-1}. *Anal.* calcd. for $C_{15}H_{21}N_2O_3$ (277.36): C 64.96, H 7.63, N 10.10; found: C 65.08, H 8.00, N 10.30. The second product was **35***b*. Yield: 1.4 g (37%); mp 130–131°C; ir ($CDCl_3$): 1775, 1695 (C=O, imide) cm^{-1}. *Anal.* calcd. for $C_{15}H_{21}N_2O_3$ (277.36): C 64.96, H 7.63, N 10.10; found: C 64.62, H 7.43, N 9.79.

Preparation of adducts of 29 with N-*ethylmaleimide (36a, 36b)*

N-Ethylmaleimide (250 mg, 2 mmol) was added to a solution of **29** (332 mg, 2 mmol) in dry toluene, refluxed for 12 h, evaporated, and purified by flash chromatograhy (*n*-hexane:ethyl acetate, 2:1) to obtain two stereoisomer products. The first product eluting from the column was **36***a*. Yield: 56 mg (9%), mp 164–166°C; ir ($CHCl_3$): 1775, 1690 (C=O, imide) cm^{-1}. *Anal.* calcd. for $C_{16}H_{23}N_2O_3$ (291.37): C 65.96, H 7.96, N 9.61; found: C 66.12, H 8.04, N 9.63. The second product was **36***b*. Yield: 184 mg (31%); mp 131–132°C; ir (in $CHCl_3$): 1770,

1690 (C=O, imide) cm^{-1}. *Anal.* calcd. for $C_{16}H_{23}N_2O_3$ (291.37): C 65.96, H 7.96, N 9.61; found: C 66.04, H 8.17, N 9.90.

Preparation of hydrochloride salts of **35**a *and* **35**b (**37**a, **37***b*)

From **35***a* (200 mg, 0.7 mmol) according to *Method A* to give **37***a*. Yield: 155 mg (70%); mp 209–210°C; ir ($CHCl_3$): 1775, 1705 (C=O, imide) cm^{-1}. *Anal.* calcd. for $C_{15}H_{22}N_2O_3 \cdot HCl$ (314.83): C 57.23, H 7.36, N 8.90, Cl 11.26; found: 57.63, H 7.72, N 8.90, Cl 11.38.

From **35***b* (300 mg, 1 mmol) according to *Method A* to give **37***b*. Yield: 270 mg (86%); mp 163–164°C; ir ($CHCl_3$): 1770, 1695 (C=O, imide) cm^{-1}. *Anal.* calcd. for $C_{15}H_{22}N_2O_3 \cdot HCl$ (314.83): C 57.23, H 7.36, N 8.90, Cl 11.26; found: 57.26, H 7.63, N 8.79, Cl 11.49.

Preparation of hydrochloride salts of **36**a *and* **36**b (**38**a, **38***b*)

From **36***a* (50 mg, 0.17 mmol) according to *Method A* to give **38***a*. Yield: 49 mg (87%); mp 142–144°C; ir (KBr): 3100–2200 (OH + HN^+), 1772, 1690 (C=O, imide) cm^{-1}; ^1H nmr: CH_3(NEt): 1.00, t (7.1 Hz); H-9: ~2.35,[c,m] ~3.5;[c,m] H-8: 3.00,[m] ~s (1H); H-7: 3.25,[m] ~t (broad lines, ^1H); CH_2(NEt): 3.36, qa (2H); ^{13}C nmr: CH_3(Et): 14.2; NCH_2: 34.9; C-7, -8; ?;[k] C-9:[t] NC=O: 180.0.[n] *Anal.* calcd. for $C_{16}H_{24}N_2O_3 \cdot HCl$ (328.84): C 58.44, H 7.66, N 8.52, Cl 10.78; found: C 58.62, H 7.39, N 8.26, Cl 11.02.

From **36***b* (50 mg, 0.17 mmol), according to *Method A* to give **38***b*. Yield: 50 mg (89%); mp 161–163°C; ir (KBr): 3100–2300 (OH + N^+H), 1776, 1699 (C=O, imide) cm^{-1}; ^1H nmr: CH_3(NEt): 1.07, t (7.2 Hz); H-9: 1.90,[m] ~tt (1H), 2.85, m;[m,n] H-8: 2.6, m;[o] H-7: 3.25, dd (~10, ~5 Hz); ^{13}C nmr: CH_3(Et): 14.2; NCH_2: 34.6; C-7, -8: ?;[k] C-9:[t] NC=O: 179.5, 179.9. *Anal.* calcd. for $C_{16}H_{24}N_2O_3 \cdot HCl$ (328.84): C 58.44, H 7.66, N 8.52, Cl 10.78; found: C 58.13, H 7.36, N 8.45, Cl 10.88.

Preparation of N-*acetoxy derivatives of* **35**a *and* **35**b (**39**a, **39***b*)

From **37***a* (150 mg, 0.5 mmol) according to *Method B*. The pure product was obtained by flash chromatography (*n*-hexane:ethyl acetate, 2:1). Yield: 100 mg (62%); (**39***a*); mp 125–126°C; ir (KBr): 1772, 1699 (C=O, imide), 1745 (Ac), 1231 (C—O) cm^{-1}; ^1H nmr: H-9: ~2.2,[s] ~2.85;[s] CH_3(Ac): 2.30, br s (3H); H-8: ~2.5[s] (1H); NCH_3: 2.91, s (3H); H-7: 3.10, t (~8 Hz); ^{13}C nmr: CH_2(9): 18.8; CH_3(Ac): 21.4; NCH_3: 28.1; C-7, -8: 40.3, 41.4; C=O(Ac): 173.3; NC=O: 176.4, 178.4. *Anal.* calcd. for $C_{17}H_{24}N_2O_4$ (320.41): C 63.73, H 7.55, N 8.74; found: C 63.45, H 7.99, N 8.44.

From **37***b* (250 mg, 0.8 mmol) by *Method B*. The pure product was obtained by flash chromatography (*n*-hexane:ethyl acetate, 2:1). Yield: 175 mg (68%) (**39***b*); mp 128–129°C; ir (KBr): 1772, 1701[u] (C=O), 1200 (C—O) cm^{-1}; ^1H nmr: H-9: 1.90,[n] 2.85,[m,n] (2 × *m* (2 × 1H); CH_3(Ac): 2.15, s (3H); H-7: ~2.75, m;[m] H-8: ~2.85, m;[m,n] NCH_3: 3.00, s (3H); ^{13}C nmr: CH_3(Ac): 18.9; NCH_3: 30.4; C-7, -8: 38.7, 39.7; C=O(Ac): 170.7; NC=O: 178.6, 178.9. *Anal.* calcd. for $C_{17}H_{24}N_2O_4$ (320.41): C 63.73, H 7.55, N 8.74; found: C 63.48, H 7.62, N 8.94.

*Preparation of 1-oxyl-3-(1,3-butadienyl)-2,2,5,5-tetramethyl-3-pyrroline (**40**)*

The anhydrous K_2CO_3 (1.75 g) and the aldehyde (**1**) (1.68 g, 0.01 mol) were added to a solution of allyltriphenylphosphonium chloride (3.38 g, 0.01 mol) in dioxane, then refluxed for 24 h, filtered off, evaporated, and the residue purified by flash chromatography (*n*-hexane: ethyl acetate, 9:1) to give **40** as a red oil. Yield: 670 mg (35%); ir ($CHCl_3$): 1620, 1595, 1580 (C=C) cm^{-1}; ms, *m/e*: M^+ 192(53.5), 177(47), 162(53.5), 119(100). *Anal.* calcd. for $C_{12}H_{18}NO$ (192.29): C 74.96, H 9.44, N 7.28; found: C 74.85, H 9.46, N 6.99.

*Preparation of hydrochloride salt of **40** (**41**)*

From **40** (384 mg, 2 mmol) according to *Method A*. Yield: 300 mg (65%); mp 149–151°C; ir (KBr): 3250–2250 (OH + N^+H) cm^{-1}; ^1H nmr: $=CH_2$: 5.12, *d* (*J*(*cis*) = 9.9 Hz); 5.24, d (*J*(*trans*) = 16.6 Hz); =CH(β): 6.54 dd ($J_{\alpha,\beta}$(*trans*) = 15.8 Hz, $J_{\beta,\gamma}$(*vic*) = 10.6 Hz); =CH(γ): 6.30 ~dt ($J_{\gamma,\delta}$(*trans*) = 16.6 Hz, $J_{\gamma,\delta}$(*cis*) ≅ $J_{\beta,\gamma}$(*vic*) = 10.3 Hz); ^{13}C nmr: $=CH_2$: 122.8; =CH(β): 125.1;[e] =CH(γ): 136.8.[e] *Anal.* calcd. for $C_{12}H_{19}NO \cdot HCl$ (229.76): C 62.74, H 8.77, N 6.10, Cl 15.43; found: C 62.82, H 8.61, N 6.02, Cl 15.91.

*Preparation of 1-oxyl-4-vinyl-2,2,6,6-tetramethyl-1,2,5,6-tetrahydropyridine (**42**)*

Anhydrous K_2CO_3 (1.75 g) and the aldehyde (**3**) (1.82 g, 0.01 mol) were added to a solution of triphenylmethylphosphonium iodide (4.2 g, 0.01 mol) in dioxane, then refluxed for 24 h, filtered off, evaporated, and the residue purified by flash chromatography (*n*-hexane:ethyl acetate, 9:1) to give **42** as a red oil. Yield: 750 mg (42%). Compound **42** was identical in all respects with the compound that has been described in the literature (11).

*Preparation of hydrochloride salt of **42** (**43**)*

From **42** (180 mg, 1 mmol) according to *Method A*. Yield: 150 mg (69%); mp 157–158°C; ir (KBr): 1650, 1610 (C=C—C=C) cm^{-1}. *Anal.* calcd. for $C_{11}H_{19}NO \cdot HCl$ (217.75): C 60.68, H 9.26, N 6.43, Cl 16.28; found: C 60.52, H 9.57, N 6.27, Cl 16.21.

Preparation of N-*acetoxy derivative of **42** (**44**)*

From **43** (108 mg, 0.5 mmol) according to *Method B*. The pure product (**44**) was obtained by flash chromatography (*n*-hexane:ethyl acetate, 9:1) as a colorless oil. Yield: 138 mg (62%); ir (KBr): 1768 (C=O), 1196 (C—O), 989 (=CH, olefin) cm^{-1}; ^1H nmr: CH_3(Ac): 2.12 s (3H); $=CH_2$: 4.99, *d* (*J* (*cis*) = 10.8 Hz), 5.08, *d* (*J* (*trans*) = 17.5 Hz); ^{13}C nmr: CH_3(Ac): 18.6; $=CH_2$: 111.5. *Anal.* calcd. for $C_{13}H_{21}NO_2$ (223.33): C 69.92, H 9.48, N 6.27; found: C 70.17, H 9.61, N 6.13.

Acknowledgements

This work was supported in part by the Hungarian Academy of Sciences, Grant No 301/A/82. The authors are indebted to Dr. J. Belágyi for the esr spectra and for the mass spectra to Dr. J. Jerkovich, Institute for Drug Research, Budapest, to Dr. J. B. Csákvári and Mr. A. Fürjes for technical assistance, and to Mrs. M. Ott for the microanalyses.

1. L. J. Berliner (*Editor*). Spin labeling, theory and applications. Vols. I and II. Academic Press, New York. 1976 and 1979.
2. G. I. Likhtenshtein. Method spinovykh metok v molekularnoi biologii. Nauka, Moscow. 1973 (in Russian); translation: G. I. Likhtenshtein. Spin labeling, methods in molecular biology. Wiley–Interscience, New York. 1976.
3. J. F. W. Keana. Synthesis and chemistry of nitroxide spin labels. *In* Spin labeling in pharmacology. *Edited by* J. L. Holtzman. Academic Press, London. 1984.
4. R. K. Leute, E. F. Ullman, A. Goldstein, and L. A. Herzenberg. Nature (New Biol.), **236**, 93 (1972).
5. W. Y. Wu, L. G. Abood, M. Gates, and R. W. Kreilick. Mol. Pharmacol. **13**, 766 (1977).
6. J. A. Cella and J. A. Kelley. J. Pharm. Sci. **66**, 1054 (1977).
7. C. F. Chignell, D. K. Starkweather, and R. H. Erlich. J. Med. Chem. **15**, 876 (1972).
8. G. M. Rosen and M. B. Abou-Donia. Synth. Commun. **5**, 415 (1975).
9. E. J. Rauckman, G. M. Rosen, and M. B. Abou-Donia. Org. Prep. Proced. Int. **8**, 159 (1976).
10. R. D. Kornberg and H. M. McConnell. Biochemistry, **10**, 1111 (1971).
11. A. B. Shapiro, L. N. Skripnichenko, V. V. Pavlikov, and E. G. Rozantsev. Izv. Akad. Nauk SSSR, Ser. Khim. 151 (1979).
12. R. H. De Wolfe and W. G. Young. Chem. Rev. **56**, 753 (1956); Allylic reactions. *In* The chemistry of functional groups. The chemistry of alkenes. *Edited by* S. Patai. J. Wiley and Sons, London. 1972. p. 681.
13. A. Fatiadi. Synthesis, **65**, 133 (1976).
14. K. Hideg, H. O. Hankovszky, L. Lex, and Gy. Kulcsár. Synthesis, 911 (1980).
15. J. Csekő, H. O. Hankovszky, and K. Hideg. Can. J. Chem. **63**, 940 (1985).

16. H. O. HANKOVSZKY, K. HIDEG, and L. LEX. Synthesis, 914 (1980).
17. T. D. LEE and J. F. W. KEANA. J. Org. Chem. **43**, 4226 (1978).
18. C. M. PALEOS and P. DAIS. J. Chem. Soc. Chem. Commun. 345 (1977).
19. E. G. ROZANTSEV. Free nitroxyl radicals. Plenum Press, New York. 1970. p. 207.
20. S. H. SNYDER. Sci. Am. **236**, 44 (1977).
21. M. D. BARRAT, A. P. DAVIES, and M. T. A. EVANS. Eur. J. Biochem. **24**, 280 (1971); B. J. GAFFNEY. The chemistry of spin labels. *In* spin labeling, theory and applications. Vol. I. *Edited by* L. J. Berliner. Academic Press, New York. 1976. pp. 193 and 214.
22. A. YU. MISHARIN and O. L. POLYANOVSKY. Izv. Akad. Nauk SSSR, Ser. Khim. 2526 (1974).
23. J. L. DRYER, H. BEINERT, J. F. W. KEANA, H. O. HANKOVSZKY, K. HIDEG, S. S. EATON, and G. R. EATON. Biochim. Biophys. Acta, **745**, 229 (1983).
24. Y. LE BIGOT, M. DELMAS, and A. GASET. Synth. Commun. **12**, 107 (1982).
25. W. G. MILLER. Spin-labeled synthetic polymers. *In* Spin labeling, theory and applications. Vol. II. *Edited by* L. J. Berliner. Academic Press, New York. 1979. p. 173.
26. P. SIMON, L. SÜMEGI, A. ROCKENBAUER, F. TÜDÓS, J. CSEKÓ, and K. HIDEG. Micromolecules, **18**, 1137 (1985).
27. D. P. BURUM and R. R. ERNST. J. Magn. Reson. **39**, 163 (1980).
28. D. M. DODDRELL and D. T. PEGG. J. Am. Chem. Soc. **102**, 6388 (1980).
29. F. I. CARROL, G. G. MORELAND, G. A. BRINE, and J. A. Kepler. J. Org. Chem. **41**, 996 (1976).
30. A. L. SCHWARTZ and L. M. LERNER. J. Org. Chem. **39**, 21 (1974).

$n-\pi$ Electron donor–acceptor complexes. III. Aliphatic amines with dicyanobenzenes. Electric and steric effects of the *N*-substituents on complex formation

JORGE D. ANUNZIATA, NORMA S. GALAVERNA, JOAQUÍN O. SINGH, AND JUANA J. SILBER[1]

Departamento de Química y Física, Universidad Nacional de Río Cuarto, Estafeta 9, Rio Cuarto, 5800. Córdoba, Argentina

Received November 11, 1985

JORGE D. ANUNZIATA, NORMA S. GALAVERNA, JOAQUÍN O. SINGH, and JUANA J. SILBER. Can. J. Chem. **64**, 1491 (1986).

The interaction of several aliphatic amines as *n*-donors with 1,2-, 1,3-, and 1,4-dicyanobenzenes as π acceptors in *n*-hexane has been studied. The spectroscopic behaviour of the mixtures leads us to propose that Electron Donor – Acceptor (EDA) complexes are formed. Correlations of the experimental data with the amine structure were performed for the amine–1,4-dicyanobenzene complexes. By means of free energy related substituents and regression analysis, the electronic and steric effects of three N-substituents were quantitatively separated. Thus, with *K* representing the stability constants of the complexes, the values of log *K* are correlated with Taft's polar substituent constants, σ^*, and Hancock's corrected steric substituent constants, E_s^C. The results allowed the proposal of a probable structure of the complex, at least with respect to the donor orientation.

JORGE D. ANUNZIATA, NORMA S. GALAVERNA, JOAQUÍN O. SINGH et JUANA J. SILBER. Can. J. Chem. **64**, 1491 (1986).

On a étudié l'interaction, dans le *n*-hexane, entre plusieurs amines aliphatiques agissant comme donneurs et les dicyano-1,2 (et -1,3 et -1,4) agissant comme accepteurs π. Le comportement spectroscopique des mélanges nous a conduit à proposer qu'il y a formation de complexes donneur–accepteur d'électrons (DAE). Pour les complexes des amines avec le dicyano-1,4 benzène, on a établi des corrélations entre les valeurs expérimentales et la structure de l'amine. Au moyen de relations d'énergie libre des substituants et d'analyse de régréssion, les effets électroniques et stériques des trois substituants du N ont pu être séparés quantitativement. De cette façon, les valeurs de log *K*, en prenant *K* comme la constante de stabilité des complexes, sont en corrélation avec la constante polaire de Taft du substituant, σ^*, et la constante stérique corrigée de Hancock du substituant, E_s^C. Les résultats permettent de proposer une structure probable du complexe, au moins par rapport à l'orientation du donneur.

[Traduit par la revue]

Introduction

Continuing our work involving the interactions between *n*-electron donors with π-electron acceptors (1, 2), in the presence investigation we wish to report the study of EDA (Electron Donor–Acceptor) complexation between aliphatic amines and 1,2-, 1,3-, and 1,4-dicyanobenzenes (DCB) in *n*-hexane as solvent.

We have previously determined the weak character of the EDA complexes formed between benzonitrile and aliphatic amines in the same solvent (1). The presence of another cyano group in the aromatic ring would be expected to increase its electron acceptor character since its electron affinity is also increased (3).

The π-acceptor properties of dicyano and the polycyanobenzenes in particular have been thoroughly studied in relation to π donors (4–7) with which fairly strong complexes have been encountered. However, in studies of the photochemical reactions of the dicyanobenzenes with some aliphatic amines in polar solvents, it has been proposed that the EDA complex formation in the ground state is either absent or very weak (8, 9) since these systems do not exhibit any charge-transfer absorption band.

In this work we were able to measure the stability constants (*K*) of aliphatic amines with dicyanobenzenes and correlate these values with the amine structure. It is known that the steric properties of the substituents attached to the electron donor can influence the magnitude of the complex association constant, which is smaller than that expected simply from the electronic effects when there is a close approach of the donor and the acceptor (10–12).

The reactivity of the aliphatic amines towards lone-pair acceptors is generally governed by the polar and steric factors of the three N-substituents (13–16). We have analyzed the effect of these types of substituents from a number of aliphatic amines upon complex formation with 1,4-DCB. The analyses were carried out by means of free energy substituent parameters (17), which allowed quantitative determination of the magnitude of the steric effects with respect to the polar effect. The correlations obtained are compared with other types of amine–EDA complexes and as $n-\sigma$ (14, 17) and $n-\upsilon$ (17, 18).

Experimental

n-Hexane (Carlo Erba R.P.) was purified as previously described (1); diethyl, triethyl, *n*-butyl, di-*n*-butyl, tri-*n*-butyl, *n*-propyl, di-*n*-propyl, tri-*n*-propyl, isopropyl, isobutyl, di-isobutyl, *tert*-butyl, and *sec*-butyl amines (Aldrich Chem. Co.) were dried with KOH pellets and distilled in a dry nitrogen atmosphere over metallic sodium.

All the reagents were degassed and distilled in a high vacuum line just before use to ensure anhydrous conditions. To obtain reproducible results special care should be taken to assure the purity of the amine. The latter was controlled by the ultraviolet (uv) cutoff point and gas–liquid chromatography (glc) (Porapak Q., Apiezon L.). 1,2-DCB (Aldrich Chem. Co.), 1,3-DCB (Fluka), and 1,4-DCB (Fluka) were recrystallized several times from triply distilled water and then sublimed under vacuum.

Spectra were obtained in thermostatted cells in a Cary 17 spectrophotometer. The working temperatures were 15, 27, and 40±0.1°C.

Solutions were prepared by weighing. The ranges of concentration used were $0.5 \times 10^{-4} - 6 \times 10^{-4}$ *M* for the DCBs and 0.2–3 *M* for the amines. All solutions were freshly prepared prior to use.

Data processing was performed on a Digital PDP 11/34 computer.

Results

Characterization of the EDA complexes and measurement of stability constants

The spectral characteristics of the mixtures of amines with DCBs show the same general features previously observed for the amine–benzonitrile (1) and amine–dinitrobenzene (2) systems. Thus, although no new band is observed, there is an appreciable deviation from additivity of the optical density with

[1]Author to whom correspondence may be addressed.

TABLE 1. Experimental results for the K values and ε_{AD} for diethylamine–DCB complexes in n-hexane and 27°C and λ = 294 nm

Acceptor	K ($dm^3\ mol^{-1}$)[a]	ε_{AD} ($dm^3\ mol^{-1}\ cm^{-1}$)[b]	Correlation coefficient	$E_{1/2}$ (eV)
1,2-DCB	0.060 ± 0.006	2360	0.9980	−2.12
1,3-DCB	0.180 ± 0.010	460	0.9990	−2.17
1,4-DCB	0.088 ± 0.009	3870	0.9988	−1.97

[a]The error in K was calculated as in ref. 1.
[b]$\varepsilon_{AD} = \varepsilon_A + \varepsilon_D + \varepsilon_C$.
[c]$E_{1/2}$ = half-wave potential (ref. 31).

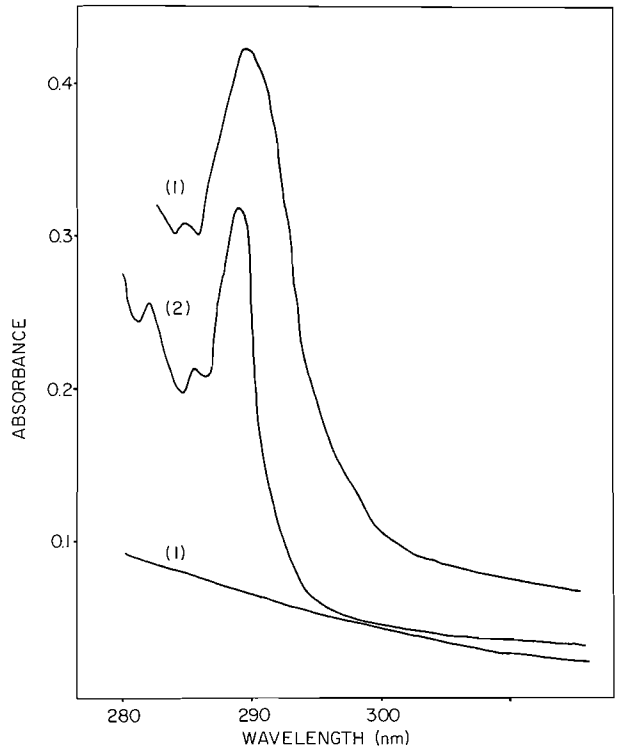

FIG. 1. Typical spectral results: (1) n-BA 3.04 M; (2) 1,4-DCB 1.75×10^{-4} M; (3) mixture of n-BA 3.04 M and 1,4-DCB 1.75×10^{-4} M. Solvent: n-hexane; temperature: 27 ± 0.1°C.

respect to that of either component alone. This effect was best observed in a range of wavelengths from 290 to 320 nm. Typical spectral results are shown in Fig. 1.

The enhanced absorbance for the amine–DCB systems was interpreted as due to a specific interaction of the type of EDA complexation.

Thus if a 1:1 complex is assumed, the observed absorbance, A_T, of a system can then be interpreted as the sum of three components (eq. [1]).

$$[1] \quad A_T = A_A + A_D + A_D$$

where A_A, A_D, and A_{AD} stand for the absorbance of the acceptor (DCB), the donor (amine), and the complex at equilibrium.

A value of absorbance, A_C, can now be defined as a function of the experimental value, A_T, and the corresponding values for the initial concentration of the acceptor, A_{A_0}, and the donor, A_{D_0} (eq. [2]).

$$[2] \quad A_C = A_T - (A_{A_0} + A_{D_0})$$

Hence, A_C is a measure of the deviation from additivity of the mixtures, and in every system was calculated for several ratios of amine–DCB where the amine concentration, D_0, was always at least 500-fold in excess with respect to the DCB concentrations, A_0. The most accurate measurements could be performed at 294 nm, which was therefore the wavelength chosen to calculate K. K can be determined graphically by utilizing a known equation derived (19) for the case in which the absorption of the complex overlaps with that of the donor and the acceptor, such as eq. [3].

$$[3] \quad \frac{A_0 D_0}{A_C(A_0 + D_0)} = \frac{1}{K\varepsilon_C}\frac{1}{(A_0 + D_0)} + \frac{1}{\varepsilon_C}$$

where A_0 and D_0 are the initial concentrations of the acceptor and the donor and $\varepsilon_C = \varepsilon_{AD} - (\varepsilon_D + \varepsilon_A)$, where ε_{AD}, ε_D, and ε_A are the molar extinction coefficients of the complex, the donor, and acceptor, respectively, at the chosen wavelength. The values of K and ε_C, thus calculated, are used to initiate an iterative procedure previously described (1, 2), which provides more reliable values under our experimental conditions. The results obtained for the amine complexes with the three acceptors are depicted in Table 1. On the other hand, Table 2 shows the results for the complexes of 1,4-DCB with the thirteen amines studied, to analyze the effect of the structure of the donor on the stability of the complexes.

The behaviour of K with temperature for every system gives values of $-\Delta H$ of the order of 12 ± 1.0 kJ mol^{-1}, which are consistent with the values expected for the formation of weak EDA complexes (20).

Correlations of K *with the structure of the amines*

Earlier works correlated the reactivity of amines with the total polar effects of the three N-substituents by using the summation of the Taft σ* values ($\Sigma\sigma^*$) (13). The deviation of the data for the "hindered" amines from the apparent correlation for the "unhindered" compounds was only qualitatively attributed to the steric effect of bulky N-substituents (17). Since the steric effect of the three N-substituents is not additive (21), we attempted to separate the polar and steric effects of these N-substituents, namely R^1, R^2, and R^3, by means of the known (14) multiparameter eq. [4].

$$[4] \quad \log K = \rho^*\Sigma\sigma^* + a_1E_S^C(R^1) + a_2E_S^C(R^2) + a_3E_S^C(R^3) + C$$

where $E_S^C(R^1)$, $E_S^C(R^2)$, and $E_S^C(R^3)$ are respectively the Hancock (22) corrected steric constants of N-substituents. R^1, R^2, and R^3 where $E_S^C(R^1) \geq E_S^C(R^2) \geq E_S^C(R^3)$; ρ^*, a_1, a_2, a_3 are the susceptibility constants, and C is the intercept.

The value of E_S^C is a steric constant E_S, corrected by the hyperconjugation effect of α-hydrogen atoms, which is related to the Hancock constant by eq. [5].

TABLE 2. Values of log K and ε_{AD} for amines–1,4-DCB complexes in n-hexane at 27°C and λ = 294 nm

Amines	$-\log K$ ($dm^3\ mol^{-1}$)[a]	ε_{AD} ($dm^3\ mol^{-1}\ cm^{-1}$)[b]	Correlation coefficient	I_p (eV)[c]	$-\log K_{calc.}$ ($dm^3\ mol^{-1}$)[d]
Diethyl	1.06	3870	0.9960	8.01	0.94
Triethyl	1.19	3370	0.9889	7.50	1.13
n-Propyl	0.79	1630	0.9984	8.78	0.96
Isopropyl	1.19	2850	0.9981	8.72	1.03
Di-*n*-propyl	1.47	6420	0.9989	7.84	1.46
Tri-*n*-propyl	2.25	8070	0.9852	7.23	2.10
n-Butyl	1.00	2090	0.9967	8.71	0.95
Isobutyl	1.19	3370	0.9888	8.70	1.22
sec-Butyl	1.28	2940	0.9991	8.70	1.32
tert-Butyl	1.48	3880	0.9976	8.64	1.52
Di-*n*-butyl	1.09	4450	0.9958	7.69	1.47
Di-isobutyl	2.70	11600	0.9879	—	2.55
Tri-*n*-butyl	2.00	8310	0.9876	7.00	2.14

[a]The error in K was calculated, as in ref. 1, to be less than 15% in every case.
[b]$\varepsilon_{AD} = \varepsilon_C + \varepsilon_A + \varepsilon_D$.
[c]Data from ref. 32.
[d]Values calculated from eq. [4] (see text).

TABLE 3. Correlations for reactivity data of aliphatic amines[a] in EDA complexes

$$\log K = \rho^*\Sigma\sigma^* + a_1E_s^C(R^1) + a_2E_s^C(R^2) + a_3E_s^C(R^3) + C$$

Systems	log K	a_1	a_2	a_3	c	n^b	s^c	r^d	F^e
Amines – 1,4-DCB[f]	−1.63 ($dm^3\ mol^{-1}$)	1.65	1.50	0.48	−0.23	13	0.285	0.960	23.5
Amines–BMe_3[g]	−4.878 (atm^{-1})	14.585	4.879	1.461	0.001	17	0.569	0.876	9.9
Amines–iodine[h]	−2.265 ($dm^3\ mol^{-1}$)	1.878	0.908	0.469	4.283	24	0.266	0.956	50.3

[a]σ^* and E_s^C values are taken from ref. 17.
[b]The number of data used in the correlation.
[c]Standard deviation.
[d]Multiple correlation coefficient.
[e]F value of the correlation.
[f]This work.
[g]Association in gas phase, data from ref. 17.
[h]EDA complex, data from ref. 17.

[5] $E_S^C = E_S - 0.306(3 - n_H)$

where n_H is the number of α-hydrogen atoms.

In eq. [4], the overall effects of the N-substituents of the aliphatic amines on lone-pair acceptors are quantitatively factored into electronic and steric effects.

The correlation according to eq. [4] and the multiple regression analysis for the equilibrium constants of Table 2 are gathered in Table 3.

Employing the correlation obtained by means of eq. [4], we now compared the values calculated for log K (reported in Table 2) to the experimental data. From this comparison and by considering the high confidence level obtained in the correlation (F-values in Table 3), we were able to presume that this equation takes into account both polar and steric effects in these types of complexes and it therefore has good predictive value.

Discussion

The fact that we were able to determine a finite value of K and a constant value of ε_{AD} for the DCB – aliphatic amine systems is interpreted as though we were actually detecting a complex at equilibrium. However, if these are indeed EDA complexes, they are undoubtedly weak. Furthermore, we expect that these complexes have a 1:1 stoichiometry, as in the n–π systems previously studied (1, 2). Problems of solubility prevented experiments in the presence of an excess of DCB, as were carried out for the benzonitrile systems. Nevertheless, we feel that our conclusions are justified by the fact that the data fit equations derived for 1:1 complexes, even when the concentration of DCBs was varied more than tenfold within the entire range of the donor. Moreover, other types of interaction, such as electrostatic or dipolar forces that may contribute to gain stabilization (23, 24), cannot be altogether disregarded. Previous work performed in our laboratory on the solvatochromism of the uv spectra of π-acceptors such as benzonitrile (25), and more recently with nitrobenzene and DCBs (26), demonstrated that the solvent effects of the aliphatic amines cannot be accounted for only by the dipolar interactions and that EDA complex formation should be postulated.

In agreement with the latter statement we could consider that the charge transfer band of these complexes is not observed due to the overlap of these bands with those of the donor and the acceptor. Therefore, its maximum should appear in a uv region that is not experimentally accessible under the conditions required to detect these weak complexes.

The theory for EDA complexes (20) predicts a correlation of

the position of the maximum of the charge-transfer transition (λ_{max}) with the ionization potential (I_P) of the donor and electron affinity (E_A) of the acceptor.

We could attempt to establish these correlations for the amine–1,4-DCB systems, by considering that $\varepsilon_{AD\,max}$ is not drastically different for the various amines (1, 2) and that it can be assumed the calculated ε_{AD} at 294 nm represents the extinction coefficient of the tail of the charge-transfer band. Consequently, an increase in ε_{AD} reflects the shift in λ_{max}. Then, by inspection of Table 2, it can be observed that ε_{AD} increases as I_P decreases. Moreover, the tendency observed is very similar to the corresponding I_2 – aliphatic amine (14) and 1,3,5-trinitrobenzene – aliphatic amine complexes (27, 28). These correlations lead us to conclude that the interactions of 1,4-DCB–aliphatic amines are the result of intermolecular EDA complexes.

On the other hand, and following the same reasoning for a given donor, a greater value of ε_{AD} would be obtained for an acceptor with a greater E_A. If we compare the half-wave potential, $E_{1/2}$, taken as a measure of E_A (29) with the values of ε_{AD} for the amine complexes with the three DCBs (Table 1), the predicted trend is actually observed.

Then, all the evidence agrees with the assumption of an EDA complex formation. It should be noted that the K values for the amine–DCB complexes are higher than those obtained for the corresponding amines with benzonitrile (1). This is also expected, since the presence of a second electron-withdrawing cyano group increases the acceptor strength of the aromatic ring.

The analysis of the applications of eq. [4] to correlate the K values in the amine–1,4-DCB systems with the structure of the amines yields some interesting results. As shown in Table 3, a negative ρ^* value is obtained; then, the greater the electron-donating ability of the N-substituents, the greater also the association reactivity of the amines. On the other hand, the positive a_1, a_2, and a_3 values show that bulkier substituents give rise to smaller K values. These susceptibility constants of the steric terms decrease in the order of $a_1 > a_2 > a_3$. This means that K values are more sensitive to the steric effect of R^1 (the smallest group) and least sensitive to that of R^3.

If our data are compared with the same type of correlation obtained for other EDA complexes (see Table 3), such as the amine–iodine (14, 17) in *n*-hexane and amine–trimethylboron (17, 18), it is observed that the ratio of $a_1:a_2:a_3$ is nearly 4:3:1 for our systems, while it is 4:2:1 for the iodine systems and 10:3:1 for the trimethylboron complexes. This comparison, in principle, suggests the idea that the relative significance of the steric effects of the component substituents seems to be similar in the 1,4-DCB–amine and iodine–amine complexes but very different from that of the trimethylboron complexes.

A high value of negative ρ^* as observed for the latter complexes indicates strong complexation, which is derived from a closer approach of the donor and acceptor.

However, a much lower value of negative ρ^* for the 1,4-DCB–amine system implies looser complexes, and consequently the susceptibility to steric factors is also lower.

Apparently the steric effects of R^1 and R^2 in the 1,4-DCB–amine complexes are similar but much greater than R^3. This would mean that the bulkier N-substituent, R^3, tends to be at a greater distance from the acceptor moiety than R^1 and R^2. In this manner, if we assume that the approach of the lone-pair electrons of the donor is perpendicular to the benzene ring, the geometry of these complexes would be as in structure **I**.

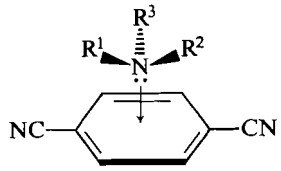

I

In the case of 1,4-DCB, the more symmetric of the acceptors under study, the geometry of **I** seems to be quite reasonable. In support of this idea, it can be cited that theoretical calculations for the $n-\pi$ complexes between aliphatic amine and *p*-benzoquinones (30) showed that the *n*-donor always approaches in a manner perpendicular to the plane of the ring.

With respect to 1,2- and 1,3-DCB, more data are needed to support certain conclusions. However, the fact that 1,3-DCB gives the greater value of K (Table 1) can be explained only if orientational complexes are proposed (2). In this case, there will be a preferential approach of the donor to the region of the smallest electronic density in the benzene ring. This region would be between both cyano groups where the sum of the inductive and resonance effects is the greatest, that is to say an approach toward position 2 in 1,3-DCB. No preferential region of this type can be postulated for 1,2- and 1,4-DCB by this undoubtedly very simplified analysis. The preferential site of attack has been proposed for other $n-\pi$ complexes (30).

Work is now in progress to gather more data for the 1,2- and 1,3-DCB–amine complexes, together with theoretical calculations to establish the probable geometry of these complexes.

Acknowledgements

This work has been partially supported by the Consejo Nacional de Investigaciones Científicas y Técnicas (CONICET) and the Consejo de Investigaciones Científicas y Técnicas de la Provincia de Córdoba (CONICOR), Argentina.

1. J. ANUNZIATA, J. O. SINGH, and J. J. SILBER. Can. J. Chem. **59**, 1291 (1981).
2. J. O. SINGH, J. D. ANUNZIATA, and J. J. SILBER. Can. J. Chem. **63**, 903 (1985).
3. G. BRIEGLEB. Angew. Chem. Int. Engl. **3**, 617 (1964).
4. G. M. BENNET and R. L. WAIN. J. Chem. Soc. 1108 (1936).
5. M. E. PEOVER. Trans. Faraday Soc. **58**, 2370 (1962).
6. A. S. BAILEY, B. R. HEEN, and J. M. LANGDON. Tetrahedron, **19**, 161 (1963).
7. R. FOSTER and T. J. THOMSON. Trans. Faraday Soc. **59**, 2287 (1963).
8. M. OHASHI and K. MIYAKE. Chem. Lett. 615 (1977).
9. M. OHASHI, K. MIYAKE, and K. TSUJIMOTO. Bull. Chem. Soc. Jpn. **53**, 1683 (1980).
10. J. M. PEARSON, S. R. TURNER, and A. LEDWITH. Molecular association. Vol. 2. *Edited by* R. Foster. Academic Press, New York. 1979. Chapt. 2.
11. M. CHARTON. J. Org. Chem. **31**, 2991 (1966).
12. D. NICHOLS and H. J. WEINTRAUB. Int. J. Quantum Chem. Quantum Biol. Symp. **9**, 205 (1982).
13. R. W. TAFT, JR. Steric effects in organic chemistry. *Edited by* M. S. Newman. Wiley, New York, NY. 1956. p. 556.
14. H. YADA, J. TANAKA, and S. NAGAKURA. Bull. Chem. Soc. Jpn. **33**, 1660 (1960).
15. K. F. WONG and S. NG. J. Chem. Soc. Faraday Trans. 2, **71**, 622 (1975).
16. (*a*) H. C. BROWN and G. G. PAI. J. Org. Chem. **46**, 4713 (1981); (*b*) H. C. BROWN, J. CHANDRASEKHARAN, and K. K. WANG. J. Org. Chem. **48**, 3689 (1983).

17. CH. TAKAYAMA, T. FUJITA, and M. TAKAJIMA. J. Org. Chem. **44**, 2871 (1979).
18. H. C. BROWN, D. H. MCDANIEL, and O. HÄFLIGER. Determination of organic structures by physical methods. Vol. 1. *Edited by* E. A. Braude and F. C. Nachod. Academic Press, New York, NY. 1955. p. 634.
19. S. D. ROSS and M. M. LABES. J. Am. Chem. Soc. **79**, 76 (1957).
20. R. S. MULLIKEN and W. B. PERSON. Molecular complexes. Wiley, New York. 1962.
21. J. SHORTER. Correlation analysis in organic chemistry. Oxford Chem. Series, Clarendon Press. 1973.
22. C. K. HANCOCK, E. A. MEYERS, and B. J. YAGER. J. Am. Chem. Soc. **83**, 4211 (1961).
23. (*a*) E. G. MCRAE. J. Phys. Chem. **61**, 562 (1957); (*b*) W. LIPTAY. Angew. Chem. Int. Ed. Engl. **8**, 177 (1969).
24. K. M. C. DAVIS. Molecular association. Vol. 1. *Edited by* R. Foster. Academic Press, New York. 1975. p. 151.
25. J. ANUNZIATA, J. O. SINGH, and J. CHESSA DE SILBER. An. Asoc. Quím. Argentina, **71**, 401 (1983).
26. (*a*) L. ZINGARETTI, J. ANUNZIATA, J. SINGH, N. TOSELLI, and J. J. SILBER. Proceedings of the Third Physical Chemistry Congress, Argentina. 1983; (*b*) N. TOSELLI, J. ANUNZIATA, J. SINGH, and J. J. SILBER. IVth Physical Chemistry Congress, Argentina. 1985.
27. R. FOSTER and R. K. MACKIE. Tetrahedron, **16**, 119 (1961).
28. R. FOSTER and R. K. MACKIE. J. Chem. Soc. 3843 (1962).
29. R. FOSTER. Organic charge transfer complexes. Academic Press, New York. 1969.
30. M. J. M. CAMPBELL, B. DEMETRIOU, and R. JONES. J. Chem. Soc. Perkin Trans. **2**, 917 (1983).
31. P. H. RIEGER, I. BERNAL, W. H. REINMUTH, and C. K. FRAENKEL. J. Am. Chem. Soc. **85**, 683 (1963).
32. R. C. WEAST (*Editor*). Handbook of chemistry and physics. 65th ed. The Chemical Rubber Co., Cleveland, Ohio. 1984. E.70.

Atomic properties and the reactivity of carbenes

PRESTON J. MACDOUGALL[1] AND RICHARD F. W. BADER
Department of Chemistry, McMaster University, Hamilton, Ont., Canada L8S 4M1

Received November 26, 1985

PRESTON J. MACDOUGALL and RICHARD F. W. BADER. Can. J. Chem. **64**, 1496 (1986).

The properties of the atoms in a number of substituted carbenes and silylene provide an understanding of the relative stabilities of their lowest lying singlet and triplet states and of their differing chemical reactivities. The theory of atoms in molecules defines all of an atom's properties, including its energy. In this research one finds that the methylenic carbon or silicon atom is energetically most stable in the triplet state of each system, while the ligands are most stable in the corresponding singlet state. It is also found that the average electron populations of the carbon and silicon atoms are largest in the triplet states. In systems where the carbon or silicon atom bears a net positive charge, as found in $CHNH_2$, CF_2, and SiH_2, the excess in the transfer of charge to the more electronegative ligands in the singlet states stabilizes the ligands more than it destabilizes the central atom. These systems have singlet ground states. The relative susceptibility of singlet and triplet carbenes to electrophilic and nucleophilic attack is determined by the properties of the Laplacian of the charge distribution. This quantity assimilates the model of localized electrons in terms of local concentrations of electronic charge. It also determines regions from which electronic charge is locally depleted. These regions are found to coincide with those where the lowest-lying vacant orbital is concentrated.

PRESTON J. MACDOUGALL et RICHARD F. W. BADER. Can. J. Chem. **64**, 1496 (1986).

Les propriétés des atomes dans un certain nombre de carbènes et de silylènes substitués fournissent une base pour la compréhension des stabilités relatives de leurs états singulet et triplet de plus basses énergies ainsi que de leurs diverses réactivités chimiques. La théorie l'atome dans les molécules définit toutes les propriétés des atomes, y compris leur énergie. Dans cette recherche, on trouve que les atomes de carbone ou de silicium méthyléniques sont, d'un point de vue énergétique, plus stable dans l'état triplet de chaque système alors que les ligands sont plus stables dans l'état singulet correspondant. On a aussi trouvé que les populations électroniques moyennes des atomes de carbone et de silicium sont plus élevées dans les états triplets. Dans les systèmes les atomes de carbone ou de silicium portent une charge positive nette, comme dans où $CHNH_2$, CF_2 et SiH_2, l'excès dans le transfert de charge vers les ligands plus électronégatifs des états singulets a comme effet de plus stabiliser les ligands que de déstabiliser l'atome central. Les états fondamentaux de ces systèmes sont singulets. En se basant sur les propriétés de la distribution de charge de Laplace, on a déterminé les susceptibilités relatives des carbènes singulet et triplet aux réactions d'attaque électrophile et nucléophile. Cette fonction assimile le modèle des électrons localisés en fonction de concentrations locales de la charge électronique. On détermine aussi les régions à partir desquelles la charge électronique est localement épuisée. On a trouvé que ces régions coïncident avec celles dont l'orbitale basse vacante est concentrée.

[Traduit par la revue]

Introduction

This paper relates the chemistry of carbenes and related compounds to the properties of their constituent atoms and the bonds which link them. The atoms and bonds are in turn defined in terms of salient properties of the charge distribution, properties that are determined by the forces acting within the system. Thus the concepts of atoms and bonds serve to both summarize the physics of a system and provide for its translation into the language of chemistry.

The chemistry of a carbene is dependent upon its spin multiplicity (1). On the basis of *chemical* evidence methylene has been shown to have a triplet ground state (2*a*). This was in accord with Herzberg's earlier spectroscopic findings (2*b*). Difluoromethylene and silylene, SiH_2, on the other hand, possess singlet ground states (3). This paper relates the relative stabilities of the singlet and triplet states to the properties of the central carbon or silicon atom and to the behaviour of the nonbonded charge concentrations in the valence shells of these atoms. These charge concentrations, two in a triplet and one in a singlet, are described not within an orbital model but rather in terms of a property of the total charge density, its Laplacian. The total charge density exhibits local maxima only at the positions of nuclei and its topology, while providing the basis for the definition of atoms and molecular structure (4), gives no indication of concentrations of charge as anticipated in terms of the Lewis electron pair model or localized orbital models of electronic structure. On the other hand, the Laplacian of a scalar function such as ρ, the quantity $\nabla^2\rho$, magnifies any local variations in the function. Just as energy changes of chemical interest are found to be only small fractions of the total energy of a molecular system, so chemically important properties are found to correspond to relatively small local variations in the charge density. These local variations in the otherwise smooth topology of ρ are translated by its Laplacian into the familiar model of localized bonded and nonbonded "electron pairs", i.e. local concentrations of electronic charge (5).

When the Laplacian of ρ is negative at a given point in space ($\nabla^2\rho < 0$), it means that the value of ρ at that point is greater than the average of its values at all neighbouring points. A local maximum in $-\nabla^2\rho$ thus means that electronic charge is concentrated or compressed in the region of the maximum. Correspondingly, a local minimum in $-\nabla^2\rho$ means that charge is locally depleted, or that the charge density is expanded in the region of the minimum. It must be borne in mind that stationary points in the Laplacian of ρ do not determine maxima or minima in ρ itself but rather the points where electronic charge is locally compressed ($\nabla^2\rho < 0$) or expanded ($\nabla^2\rho > 0$).

Singlet carbenes are known to exhibit ambiphilic characteristics. It has been shown that the local charge concentrations and depletions, the lumps and holes in a charge distribution as defined by the Laplacian of ρ, determine the sites of electrophilic and nucleophilic attack, respectively (5). The sizes and shapes of these lumps and holes in the charge distributions of a variety of carbenes, silylenes, and vinylidenes are used to rationalize the predominance of either electrophilic or nucleophilic behaviour in these molecules.

[1]To whom all correspondence should be addressed.

TABLE 1. Geometries and energies

System	Geometrical parameters (deg, Å)	E(HF) (hartrees)
CLi_2(T)	C—Li = 1.924, θ = 111.93	−52.60030
CH_2(T)	C—H = 1.072, θ = 131.14	−38.92549
CH_2(S)	C—H = 1.099, θ = 102.82	−38.87631
CF_2(T)	C—F = 1.304, θ = 118.70	−236.60895
CF_2(S)	C—F = 1.283, θ = 104.48	−236.66074
SiH_2(T)	Si—H = 1.472, θ = 118.15	−289.98958
SiH_2(S)	Si—H = 1.510, θ = 93.45	−289.99605
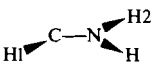 (T)	C—H1 = 1.078, C—N = 1.384, N—H2 = 0.999, ∡(H1CN) = 125.43, ∡(CNH2) = 144.38, ∡(H1CNH2) = 128.61	−93.96268
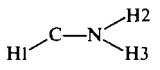 (S)	C—H1 = 1.098, C—N = 1.308, N—H2 = 0.997, N—H3 = 1.000, ∡(H1CN) = 106.38, ∡(H1CNH2(3)) = 119.35(125.80)	−93.98368
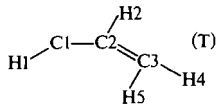 (T)	C1—H1 = 1.073, C1—C2 = 1.385, C2—C3 = 1.390, ∡(H1C1C2) = 132.98, ∡(C1C2C3) = 124.81, C2—H2 = 1.079, C3—H4 = 1.074, C3—H5 = 1.076, ∡(C1C2H2) = 117.15, ∡(C2C3H4(5)) = 121.01(121.36)	−115.83818
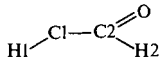 (T)	C1—H1 = 1.072, C1—C2 = 1.524, C2—O = 1.233, C2—H2 = 1.090, ∡(H1C1C2) = 131.96, ∡(C1C2H2) = 117.43, ∡(C1C2O) = 122.88	−151.66398
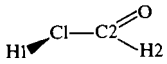 (S)	C1—H1 = 1.091, C1—C2 = 1.443, C2—O = 1.192, C2—H2 = 1.108, ∡(H1C1C2) = 110.96, ∡(C1C2O) = 129.03, ∡(C1C2H2) = 108.21, ∡(H1C1C2O) = −95.2, ∡(H1C1C2H2) = 88.9	−151.61163
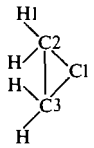 (S)	C1—C2 = 1.495, C2—C3 = 1.478, C2—H1 = 1.078, ∡(C1C2C3) = 59.26, ∡(C1C2H1) = 116.05, ∡(C3C1C2H1) = 111.1	−115.77445
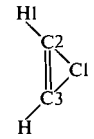 (S)	C1—C2 = 1.408, C2—C3 = 1.310, C2—H1 = 1.070, ∡(C2C1C3) = 55.43, ∡(C1C2H1) = 148.15	−114.62434
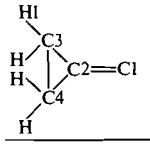 (S)	C1—C2 = 1.275, C2—C3 = 1.491, C3—C4 = 1.483, C3—H1 = 1.076, ∡(C3C2C4) = 59.66, ∡(C2C3H1) = 116.18, ∡(C1C2C3H1) = 70.49	−153.63403

Calculations

The results for the singlet states were obtained from single determinantal calculations using the 6-31G** basis set. Calculation of the triplet state functions used the same basis but employed the unrestricted SCF procedure (the 6-21G** basis was used for singlet and triplet SiH_2). All geometries were optimized at either of these two levels of theory and the results are given in Table 1. The bonds in CLi_2 are ionic with little directional character and the bending force constant for this molecule is very small. The predicted geometries of such triatomic molecules are very dependent upon the adequacy of the basis set used to describe the negatively charged central atom.[2] With the addition of an extra set of diffuse s, p, and d functions on the C atom the CLi_2 molecule in its triplet state is predicted to be bent with a bond angle of 111.9°. The molecule is still a floppy one and the energy difference between the linear and equilibrium geometries is only 1.4 kcal/mol. Convergence difficulties were encountered in the calculation of the singlet state of this molecule, but it has been previously shown that the ground state of CLi_2 is a triplet (7). The singlet state of formylmethylene is calculated to have a nonplanar geometry at the 6-31G** basis set as previously reported by Bouma *et al.* (8). We find a slightly lower energy for this state than that found by Bouma *et al.*, who state that with correlation, formylmethylene isomerizes to ketene.

In the linear geometry of a carbene the $2p_z$ and $2p_x$ orbitals on carbon (the $3a_1$ and $1b_1$ orbitals, respectively, of the bent molecule) are degenerate and of π symmetry. With an increasing departure from linearity the $3a_1$ orbital becomes increasingly more stable than the $1b_1$ orbital. Thus for linear or near linear geometries Hund's rule applies to yield a $^3\Sigma_g$ or $^3B_1$ ground state from the configurations $\ldots\pi^2$ or $\ldots 3a_1 1b_1$. For a strongly bent geometry the ground state will be a singlet, $\ldots 3a^2$,

[2]Grev and Schaefer (6) have found that two sets of d orbitals are necessary to properly describe the ground state of CSi_2, which is bent. We have since calculated that the net charge on C in this molecule is −2.69 e. We employed their expanded basis set for C in our geometry optimization of triplet CLi_2.

$^1A_1$. Thus there is a close connection between the geometry and spin multiplicity of a carbene and one notes in Table 1 that the calculated bond angles of the triplet states are always larger than those of the singlets.

A $^1A_1$ state is also obtained by double occupation of the $1b_1$ orbital and the ground state of a singlet carbene is better described in terms of a linear combination of these two lowest $^1A_1$ determinantal state functions. A two-state CI calculation (at the single-state geometries) was carried out for CH_2, CF_2, and SiH_2 to determine its effect on the properties of the electronic charge distribution. The contribution of the upper state to the total charge distribution was only a few percent in each case. While the effect on the singlet–triplet energy separation was significant, the quantitative changes in ρ amounted to only a few percent and qualitatively the charge distributions were left unaltered. These results are summarized in the Appendix. Our two configuration CI calculations impose the frozen orbital approximation. Two configuration SCF calculations which do not invoke this approximation give smaller singlet–triplet splitting energies, 22.0 and 12.8 kcal/mol for methylene (9, 10). The latter was obtained using a basis of quality similar to ours.

A recent review emphasizes the sensitivity of the singlet–triplet splitting to the level of theory used (11).

Atomic properties and ground state multiplicities

As has been demonstrated (12) and recently reviewed for the chemical reader (13), the atomic boundaries and the network of bonds are determined by the gradient vector field of the charge density (see Fig. 1). The atomic boundaries exhibit a zero flux in the gradient vectors of ρ and they thus satisfy the quantum condition for the definition of a subsystem with well-defined properties. Five atomic properties will be used in the present investigation:

(*a*) atomic charge of atom Ω, $q(\Omega)$ is obtained by integration of ρ over the basin of atom Ω to obtain its average electron population $N(\Omega)$ followed by the subtraction of this average electron population from the nuclear charge, Z_Ω,

$$[1] \quad q(\Omega) = Z_\Omega - \int_\Omega \rho d\tau = Z_\Omega - N(\Omega)$$

(*b*) Atomic dipole $\boldsymbol{\mu}(\Omega)$ is obtained by weighting the integration of ρ with the position vector $\boldsymbol{r}$ with origin at the nucleus of Ω,

$$[2] \quad \boldsymbol{\mu}(\Omega) = \int_\Omega \boldsymbol{r}\rho d\tau$$

(*c*) Spin population $S(\Omega)$, is obtained by integrating the spin density $\sigma(\boldsymbol{r}) = \rho^\alpha(\boldsymbol{r}) - \rho^\beta(\boldsymbol{r})$, the difference between the α- and β-spin densities, over the basin of Ω to give the average number of excess α electrons (if $S(\Omega) > 0$) on atom Ω (14)

$$[3] \quad S(\Omega) = \int_\Omega \sigma(\boldsymbol{r}) d\tau$$

(*d*) The degree of localization of the electrons on atom Ω and denoted by $l(\Omega)$ is obtained by integrating the Fermi hole over the basin of the atom, $F(\Omega,\Omega)$, and comparing it with the average number of electrons in the atom (15*a*)

$$[4] \quad F(\Omega,\Omega) = -\Sigma_{i,j}[\int_\Omega \phi_i \phi_j d\tau]^2$$

Conceptually this is equivalent to averaging, over all reference coordinates within atom Ω, the extent to which the "exchange charge density" (15*b*) is contained within that atom. The limiting value of the integrated Fermi hole, $F(\Omega,\Omega)$, is $-N(\Omega)$. At this limit the $N(\Omega)$ electrons are completely localized on atom Ω, there is no exchange of these electrons with other electrons in the system and the fluctuation in the average population $N(\Omega)$ is zero. Thus the ratio $|F(\Omega,\Omega)/N(\Omega)|$ determines the fraction of the maximum possible localization and when multiplied by 100 determines the percent localization of the electrons on atom Ω, $l(\Omega)$.

(*e*) The energy of atom Ω, $E(\Omega)$, is most simply obtained by integrating the kinetic energy density over the atom to obtain its average kinetic energy, $T(\Omega)$. Since the atom is a quantum subsystem, the virial theorem applies and $E(\Omega) = -T(\Omega)$.[3] For equilibrium geometries, as is true here, the sum of the atomic energies equals the total energy of the molecule,

$$E = \Sigma_\Omega E(\Omega)$$

We begin with a discussion of the atomic properties of the systems listed in Table 2. The ground states of CH_2 and the systems listed above it are triplets, while those of the remaining systems are singlets. The charge distributions of CH_2 and SiH_2 shown in Fig. 1 serve to illustrate the definition of atomic boundaries and how the resulting atomic properties reflect the principal features of a charge distribution. There is an almost equal sharing of bonding density between C and H in saturated hydrocarbons, $q(H) = -0.06$ e in CH_4. This remains true for the two states of methylene where the charges on H are of even smaller magnitude. In SiH_2 there is a substantial transfer of charge from Si to H as is evident in the display of ρ; the distribution on H is expanded and more diffuse compared to that for CH_2, and ρ is separately localized in each atomic basin to a greater extent in SiH_2 than it is in CH_2. This difference in the degree of localization of charge is quantified by the values of $l(\Omega)$ (Table 2) which show that the electrons on the H atoms in SiH_2 are 76% localized compared to a value of only 48% in CH_2.

The properties of ρ at the bond saddle point serve to characterize the nature of the bond (Table 3). The value of ρ at the bond saddle point, the quantity ρ_b, tends to smaller values as the bonding tends towards the ionic limit. Thus ρ_b is greater for CH_2 than it is for SiH_2 which in turn possesses a value greater than that for CLi_2, for which the bonding is ionic. One notes that the remaining core density on each Li atom is highly localized (Table 2). Negative values of $\nabla^2\rho_b$, the value of the Laplacian of ρ at the bond saddle point, indicate that the negative curvatures of ρ (those perpendicular to the bond) dominate the interaction. This behaviour is typical of a shared interaction such as is found in CH_2 — charge is accumulated along the bond path as a result of the perpendicular contractions of ρ (5, 16). In SiH_2, $\nabla^2\rho_b > 0$ indicating that the Si—H interactions are dominated by the contractions of ρ away from the interatomic surface towards each of the nuclei. This behaviour is typical of bonds with substantial charge transfer and localized atomic distributions. The reader is again referred to Fig. 1 to appreciate the differing behaviours associated with a large ρ_b and negative $\nabla^2\rho_b$ value and a low ρ_b and positive $\nabla^2\rho_b$ value.

There is considerable charge transfer from carbon to fluorine and nitrogen (Table 2) and the $\nabla^2\rho_b$ values for the C—F and

[3] Because the approximate state functions used here do not satisfy the Hellmann–Feynman theorem, there are small net forces calculated for the nuclei at the equilibrium geometry. Thus the ratio $|E/T|$ differs slightly from unity. The values of $T(\Omega)$ were multiplied by the $|E/T|$ ratio in order that the sum of the atomic energies would equal E. These are small corrections, the ratios for the triplet and singlet states, respectively, are 1.0001 and 0.9991 for CH_2, 1.0002 and 1.0004 for SiH_2.

TABLE 2. Atomic properties of carbenes

YXY′	q(X)	q(Y)	q(Y′)	S(X)	S(Y)	S(Y′)	E(T)−E(S)†	ΔE(X)	ΔE(Y)	ΔE(Y′)	μ(X)*	l(Y)
LiCLi (T)	−1.824	+0.912	+0.912	+1.984	+0.008	+0.008					−1.98	98% (Li)
HC(C′H=CH_2) (T)	−0.094	+0.019	+0.075 (C′H, +0.074) (CH_2, +0.002)	+1.675	+0.023	(C′H, −0.442) (CH_2, +0.746)					0.33	
(T)	−0.064	+0.046	+0.018 (C′H, +1.109) (O, −1.091)	+1.754	+0.014	(C′, −0.314) (O, +0.511)					0.26	
HC(C′H=O)						(H, +0.035)	−33	−49	+3	+13‡		
(S)	+0.009	+0.035	−0.044 (C′H, +1.287) (O, −1.332)								0.90	44% (H)
(T)	−0.055	+0.028	+0.028	+1.973	+0.014	+0.014					0.30	
HCH							−31	−75	+22	+22		
(S)	+0.088	−0.044	−0.044								1.03	48% (H)
(T)	+0.510	+0.010	−0.520 (N, −1.330) (H, +0.405)	+1.710	+0.064	+0.226					1.02	
$HC(NH_2)$							+13	−130	+29	+114		
(S)	+0.696	−0.098	−0.598 (N, −1.448) (H, +0.425)								1.67	49% (H)
(T)	+1.440	−0.720	−0.720	+1.632	+0.184	+0.184					1.90	
FCF							+32	−116	+74	+74		
(S)	+1.552	−0.776	−0.776								3.13	95% (F)
(T)	+1.476	−0.738	−0.738	+1.648	+0.176	+0.176					2.48	
HSiH							+4	−20	+12	+12		
(S)	+1.508	−0.754	−0.754								2.56	76% (H)

*Atomic dipoles in atomic units. 1 au = 2.542 D. A positive value for μ means the negative end of dipole is directed away from ligands.
†All energy differences are in kcal mol^{-1} and all refer to E(triplet state) − E(singlet state).
‡The individual atomic contributions to ΔE from the formyl group are: ΔE(C′) = −59, ΔE(O) = +74, and ΔE(H) = −2 all in kcal mol^{-1}.

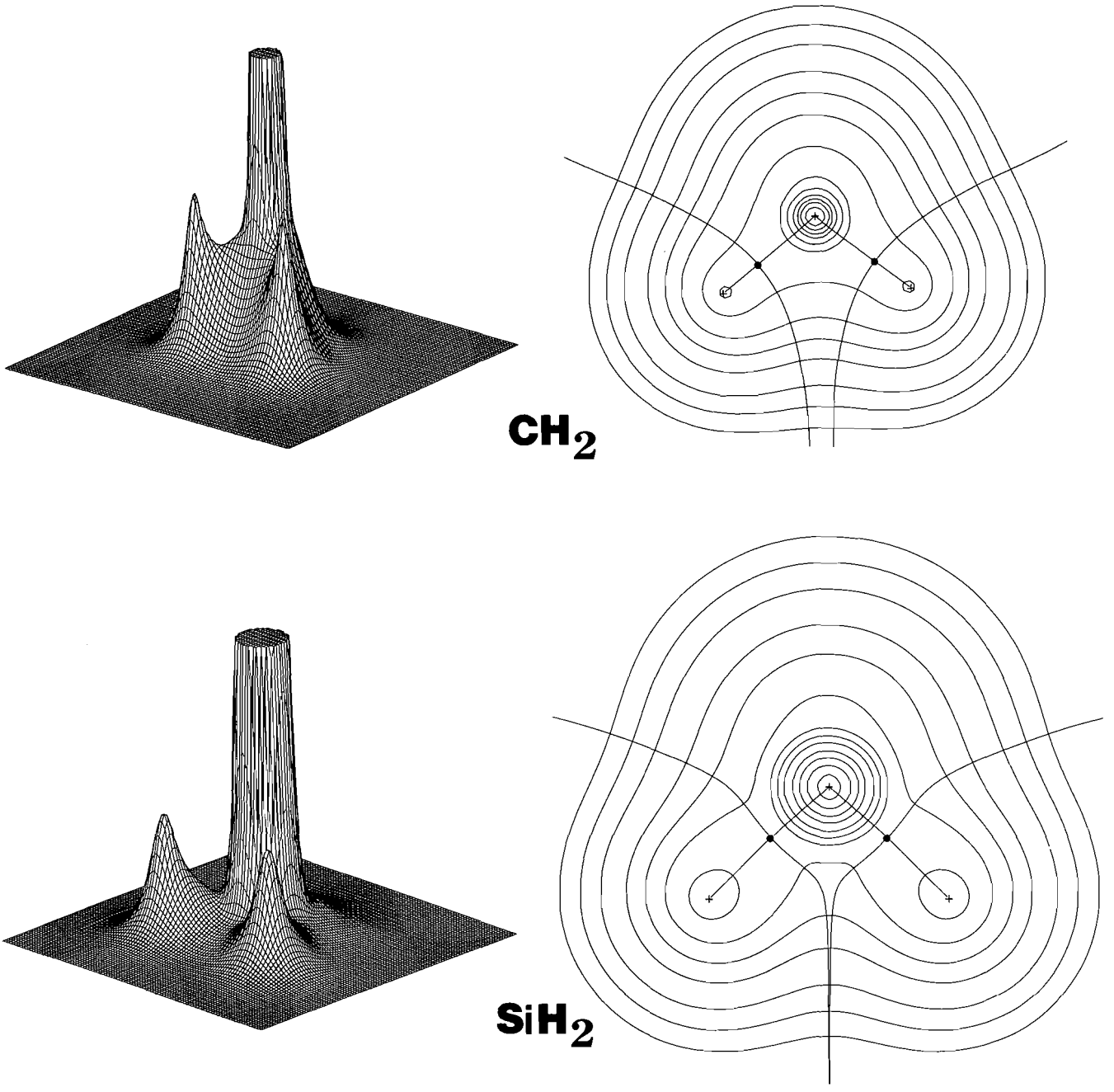

FIG. 1. Contour maps and corresponding relief maps of the singlet charge distributions in the plane of the nuclei for CH_2 and SiH_2. The same vertical scaling is used in the relief maps. The maxima in ρ at the positions of the C and Si nuclei are not shown. The black dots on the contour map denote the positions of the bond saddle points. Also shown are the bond paths and the atomic boundaries defined by the interatomic surfaces. As illustrated in the relief maps, the value of ρ at a bond saddle point ρ_b, is the minimum value attained by ρ along the bond path and the maximum value attained in the interatomic surface. A bond path and its associated surface are defined respectively by the gradient vectors of ρ which originate and terminate at the bond saddle point. The contour values in au are 0.002, 0.004, and 0.008 increasing by powers of 10 to a maximum value of 20 au.

C—N bonds indicate that these interactions are dominated by a contraction of charge towards each of the nuclei. These interactions are, however, not ionic but very polar shared interactions as indicated by the relatively large values of ρ_b.

Essentially all of the unpaired spin density is localized on the carbon atom in the triplet states of CLi_2 and CH_2. There is a small excess in the transfer of β-spin density compared to α-spin density to the carbon atom in these systems with the result that the ligands have small net α spin populations. In $CHNH_2$, CF_2, and SiH_2 there is a significant delocalization of the spin density onto the ligands as a result of the transfer of charge to the ligands from the carbon and silicon atoms in these molecules. There is also a significant delocalization of the spin density in formylmethylene and vinylmethylene into the CH=O and CH=CH_2 fragments. Since there is no net transfer of charge from the methylenic carbon in these two molecules, the spin delocalization is accomplished through a spin polarization rather than by a transfer of charge. From the data given in Table 2 it is seen that the spin populations of the methylenic carbons are reduced from the value of two. Negative spin populations, approximately

TABLE 3. Bond properties and reactivity sites

System	Bond	ρ_b au	$\nabla^2\rho_b$ au	ϵ†	Nonbonded maxima $\nabla^2\rho$ au	Hole in VSCC Width* au	Hole in VSCC $\nabla^2\rho$ au
CLi_2 (T)	C—Li	0.035	+0.224	0.08 ⊥	−0.50	No hole	—
$HCC'H{=}C''H_2$ (T)	C—H	0.292	−1.117	0.02 ⊥	−0.50	No hole	—
	C—C′	0.321	−0.975	0.21 ⊥			
	C′—C″	0.318	−0.956	0.26 ⊥			
HCC′H=O (T)	C—H	0.294	−1.153	0.01 ⊥	−0.51	No hole	—
	C—C′	0.314	−0.975	0.18 ⊥			
	C′=O	0.387	+0.495	0.11 ⊥			
	C′—H	0.296	−1.157	0.03 ⊥			
(S)	C—H	0.292	−1.142	0.18 ⊥	−1.44	1.3	+0.4
	C—C′	0.315	−1.019	0.19 ⊥			
	C′=O	0.428	+0.500	0.06 ⊥†			
	C′—H	0.283	−1.073	0.01			
CH_2 (T)	C—H	0.291	−1.113	0.04 ⊥	−0.46	No hole	—
(S)	C—H	0.290	−1.112	0.18	−1.55	1.4	+0.3
$HCNH_2$ (T)	H—C	0.288	−1.086	0.07 ⊥	−0.57	1.2	+0.08
	C—N	0.304	−0.624	0.10 ⊥			
	N—H	0.359	−1.966	0.05			
$HCNH_2$ (S)	H—C	0.288	−1.094	0.11	−1.55	1.3	+0.21
	C—N	0.335	−0.022	0.48			
(*cis*)	N—H	0.362	−2.065	0.04 ⊥			
(*trans*)	N—H	0.366	−2.016	0.04 ⊥			
CF_2 (T)	C—F	0.273	+0.894	0.93 ⊥	−1.04	1.6	+0.4
(S)	C—F	0.289	+0.719	0.42	−1.91	1.8	+0.3
SiH_2 (T)	Si—H	0.117	+0.345	0.13 ⊥	−0.08	4.1	+0.08
(S)	Si—H	0.112	+0.297	0.16	−0.14	3.2	+0.04

†⊥ indicates major axis is perpendicular to the plane of the Y—X—Y′ nuclei. In singlet formylmethylene the major axis of the C′=O bond is perpendicular to the plane of the formyl group. All other bonds have their major axis in the Y—X—Y′ plane.

*There are two such holes in the singlet states of all systems, while only one in the triplet states.

equal to the reduction in S(C), are present on the adjacent carbon atoms. The terminal oxygen and carbon atoms again have positive spin populations. The presence of alternating net spin populations on neighbouring atoms as a mechanism for spin delocalization has been previously noted (14). This mechanism is different from that operative in the amino- and difluoro-molecules where there is a simple transfer of charge and all the atoms exhibit spin populations of the same sign.

The final property listed in Table 3 is the bond ellipticity ϵ defined as $\epsilon = (\lambda_1/\lambda_2 - 1)$ where λ_1 and λ_2 are the magnitudes of the two negative curvatures of ρ at the bond saddle point with $\lambda_1 > \lambda_2$ (17). When these two curvatures are not equal, the charge density in the interatomic surface falls off from its maximum value at the saddle point more slowly in the plane containing the smallest of the two curvatures, indicating that charge density is preferentially accumulated in this particular plane. The C=C bond in ethylene, for example, has $\epsilon > 0$ and the axis of the smaller curvature lies in the plane perpendicular to the plane of the nuclei — charge density is preferentially accumulated in the plane of the "π" orbital. The data in Table 3 indicate that the charge of the methylenic bonds is preferentially accumulated in the plane of the nuclei in the singlet molecules and in the plane perpendicular to this for all of the triplet molecules.

A carbon–carbon bond order n can be defined in terms of the value of ρ_b (17), giving $n = 1, 2, 3$, respectively for ethane, ethylene, and acetylene. In terms of the bond order and bond ellipticity parameters, one can show that in addition to the spin polarization present in the formyl- and vinylmethylenes, there is an essentially complete delocalization of the π density in these systems. The two C—C bonds in vinylmethylene have equal bond orders of 1.6 and similar ellipticities with their major axes in the π plane. The C—C bond order in the triplet state of formylmethylene is 1.5 again indicating a delocalization of the π density. The spin populations, bond orders, and bond ellipticities indicate that vinylmethylene is best described as a vinyl radical with an extra unpaired and localized σ electron resulting from the loss of a terminal hydrogen atom. Hutton *et al.* (18) have arrived at the same description of this molecule on the basis of its esr spectrum.

The perturbation of the nonbonded charge density on carbon is minimal in the methylene systems because of the essentially equal sharing of the bonding charge density between the C and H atoms. This is reflected in the near zero atomic charges on carbon in these systems and in their small atomic dipoles. Hence the triplet state is of lower energy than the singlet state for methylene because of Hund's rule, as it is for the carbon atom itself. Indeed the singlet–triplet energy gaps are of the same order of magnitude for the two systems. The relative singlet–triplet stabilities in the remaining systems will be discussed by comparing the properties of their charge distributions with those for the two corresponding states of CH_2.

The single most distinguishing feature of the examples listed in Table 2 relative to methylene is the extent and direction of charge transfer. A transfer of charge from the ligands to the carbon as in CLi_2 leaves the triplet as the ground state. When charge is transferred to the ligands as in $CHNH_2$, CF_2, and SiH_2, the singlet state is more stable than the triplet. In the two

remaining systems where the methylenic carbon is bonded to another carbon atom, the net charges on C are similar to those found in CH_2 itself and the triplet states are again the ground states. One notes as well that the central carbon and silicon atoms of the triplet states are more electronegative than they are in the corresponding singlets; q(C) is more negative for the triplet than for the singlet state in every system listed in Table 2.

The energies listed in Table 2, $\Delta E(\Omega)$, are the differences in the atomic energies between the triplet and singlet states for each molecular system. We first discuss the systems with a charge transfer from carbon or silicon to the ligands. In each of these systems the central atom is most stable in the triplet state and its energy change is the largest of the atoms in the molecule. The ligands, on the other hand, are most stable in the singlet states. These relative atomic stabilities parallel the differences in the average atomic populations between the triplet and singlet states. The populations for C and Si are largest in the triplet states while those for H, N, and F are largest in the singlet states. In the $CHNH_2$, CF_2, and SiH_2 systems the excess in the transfer of charge to the more electronegative ligands in the singlet states stabilizes the ligands more than it destabilizes the less electronegative central atom and the singlet states are most stable. Given the differing populations in these systems, the favoured state is the singlet as the largest amount of negative charge is placed on the most electronegative atoms in this state.

The singlet–triplet atomic charge and energy differences for formylmethylene follow the same patterns as those already discussed if the formyl group is considered as a single entity. Within this group there is a significant charge transfer from the carbon to the oxygen atom. The oxygen atom has its largest electron population and lowest energy in the singlet state and behaves as do the ligands discussed above. The formyl carbon, however, possesses a larger population and its lowest energy in the triplet state, both differences being greater than for the methylenic carbon. As discussed above there is a polarization of the spin density and a delocalization of the π density in this molecule and in the related vinylmethylene. This delocalization of the charge density and the accompanying alternation of the spin population leads to a greater stabilization of the two neighbouring carbon atoms in the triplet states of these unsaturated carbenes than it does to the terminal carbon and oxygen atoms in the corresponding singlet states, and the ground states are triplets.

The methylenic carbon always possesses a larger electron population and lower energy in the triplet than in the singlet state of a carbene. From the examples studied here it is found that the triplet is the ground state when carbon bears a net negative charge. Thus this extra stabilization of the methylenic carbon in the triplet state dominates the total singlet–triplet energy difference when the net charge on carbon is negative. When there is a substantial transfer of charge to the ligands and carbon bears a net positive charge, the ground state is a singlet.

Previous workers have attributed a triplet ground state in vinylmethylene to a delocalization of π density and a singlet ground state in systems with ligands possessing unshared pairs of electrons as in CF_2 to a back-donation of the π density (19–21). This latter argument does not account for the existence of a singlet ground state in SiH_2. Harrison *et al.* (22) have proposed that electronegative substituents differentially stabilize singlet carbenes, while electropositive substituents stabilize triplet carbenes. It has also been argued that π donors stabilize the singlet more than the triplet, while π acceptors have the opposite effect (23).

The orbital model of π back-donation wherein an electronegative atom such as fluorine or nitrogen donates electronic charge to a less electronegative atom such as carbon is not apparent as such in the properties of a total charge distribution. For example, π back-donation is predicted to occur in the singlet states of CF_2 and $CHNH_2$ and yet the methylenic carbon has a larger electron population in the triplet than in the singlet states of these two systems. Also, as noted in Table 3, the ellipticities of the C—F and C—N bonds in the singlet molecules have their major axes in the plane of the nuclei, opposite to what is found for bonds with partial π character. It is a general observation that in a bond X—Y with significant charge transfer from X to Y there is a polarization of both atomic charge distributions in the direction counter to the direction of the charge transfer (24). What one observes is that the magnitude of the atomic *back-polarization* on Y parallels the anticipated consequences of the π *back-donation* model. Thus, the magnitude of μ(Y) is largest when there is an orbital vacancy on X; in CH_3F, μ(F) = 0.32 au while in singlet CF_2, μ(F) = 0.52 au. Also, within the carbene series, μ(F) and μ(N) are larger in the singlet states than in the triplets (Table 4). The π-donation model is invoked to account for unusually short X—Y bond lengths and the data in Table 4 show that the state, singlet or triplet, with the shortest X—Y bond also has the largest value for μ(Y). In CF_2 or $CHNH_2$ this is the anticipated singlet state while in SiH_2, where the ligand has no unshared electrons, it is the triplet. However, the polarization of H is of the same magnitude as the others despite this difference.

The triplet ground states of formyl and vinylmethylene have been accounted for in terms of the π-acceptor model (23). As already noted, the present theory provides a quantitative assessment of both spin and charge delocalization through the assignment of corresponding atomic populations, bond orders, and bond ellipticities. As demonstrated below, the properties of the Laplacian of ρ provide the mechanism underlying the atomic back-polarizations and charge delocalizations.

Valence charge concentrations and ground state multiplicities

The Laplacian of ρ for a free atom reflects the quantum shell structure by exhibiting a corresponding number of alternating pairs of regions of charge concentration ($\nabla^2\rho < 0$), and charge depletion ($\nabla^2\rho > 0$) beginning with a spike-like concentration at the nucleus. Upon bonding, local maxima and minima are formed in the valence shell of charge concentration (VSCC) and the number of resulting bonded and nonbonded maxima thus formed are in general agreement with localized models of electronic structure.

The local concentrations of charge in the valence shell of an atom as determined by the Laplacian of ρ mimic not only the model of localized bonded and nonbonded pairs, they also reflect the presence of local concentrations of unpaired electrons. In Fig. 2 the Laplacian distribution for triplet CF_2 exhibits two distinct maxima on the carbon atom in the symmetry plane perpendicular to the plane of the nuclei. The singlet state of the same molecule exhibits a single nonbonded maximum on carbon. The magnitude of this single maximum (corresponding to the model of a localized electron pair) is larger than the two identical maxima present in the triplet state, each of which models a single unpaired electron. The values of the nonbonded maxima in the Laplacian of ρ are given in Table 3. Similar observations apply to the other pairs of molecules listed in Table 3 (Fig. 3) with the exceptions of CHCH=O and $CHCH{=}CH_2$. In these molecules the triplet states exhibit a single nonbonded

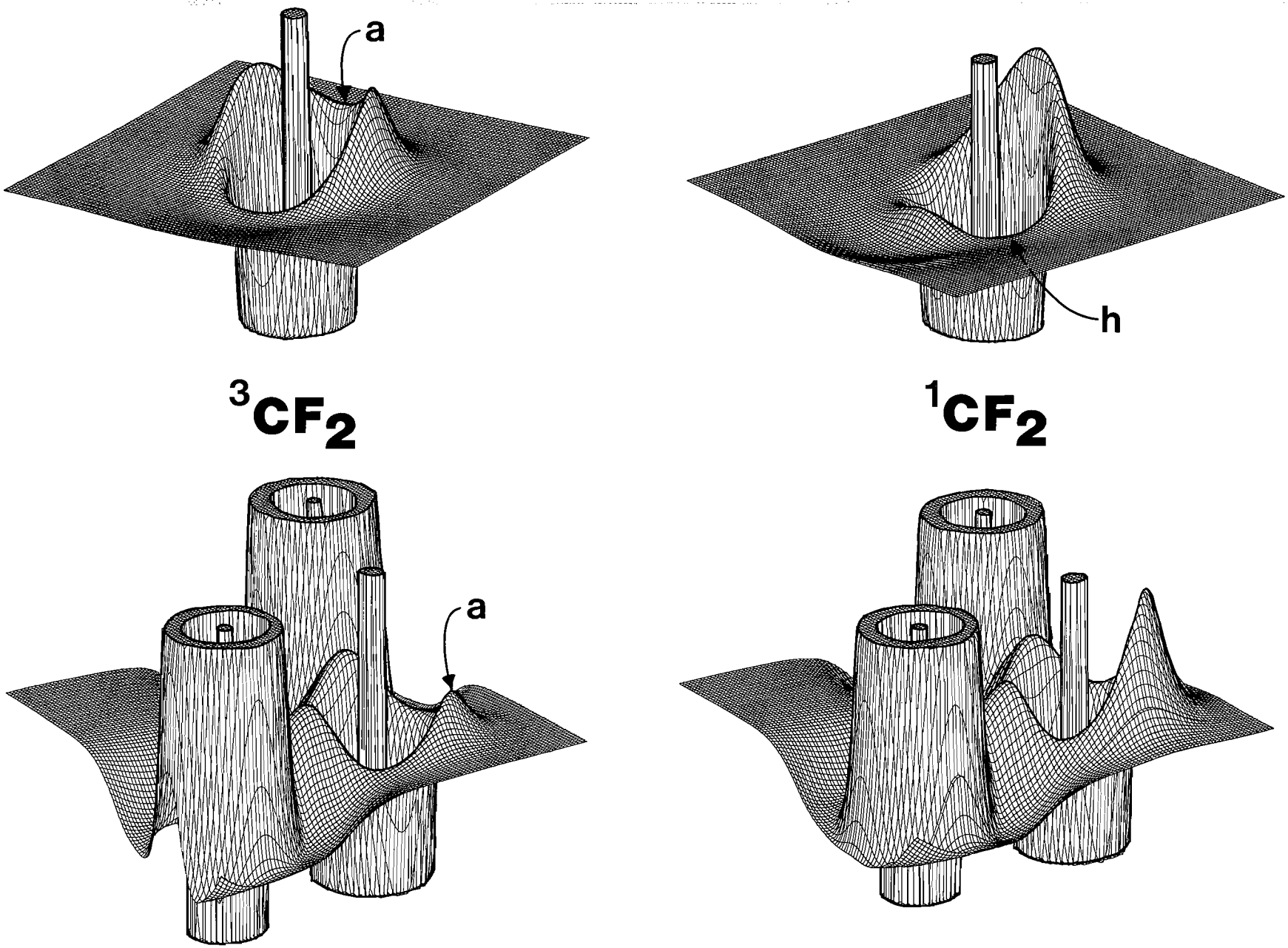

FIG. 2. Displays of the Laplacians of the charge distributions for the triplet and singlet states of CF_2. The lower diagrams are for the plane of the nuclei, the upper ones for the perpendicular symmetry plane containing the C nucleus. The function plotted is $-\nabla^2\rho$, a maximum in this function denoting a maximum in the concentration of charge. The core or first quantum shell of each atom exhibits a spike-like charge concentration at the nucleus surrounded by a deep region of charge depletion. This is followed by the valence shell of charge concentration (VSCC) and the outer or valence region of charge depletion. The VSCC of carbon in the triplet state shows two bonded maxima and two nonbonded maxima in the perpendicular plane. The point labelled **a** in the lower diagram is not a maximum. It is *another* view of the saddle point **a** between the nonbonded maxima. The VSCC of carbon in the singlet state also shows two bonded maxima but only a single, larger, nonbonded maximum. The point labelled **h** and its mirror point are positions where the VSCC on carbon has been broken. There is no radial maximum or lip defining a shell at these points. The maxima present in the VSCC's of the F atoms are not shown as they are larger by a factor of ten than those on the carbons.

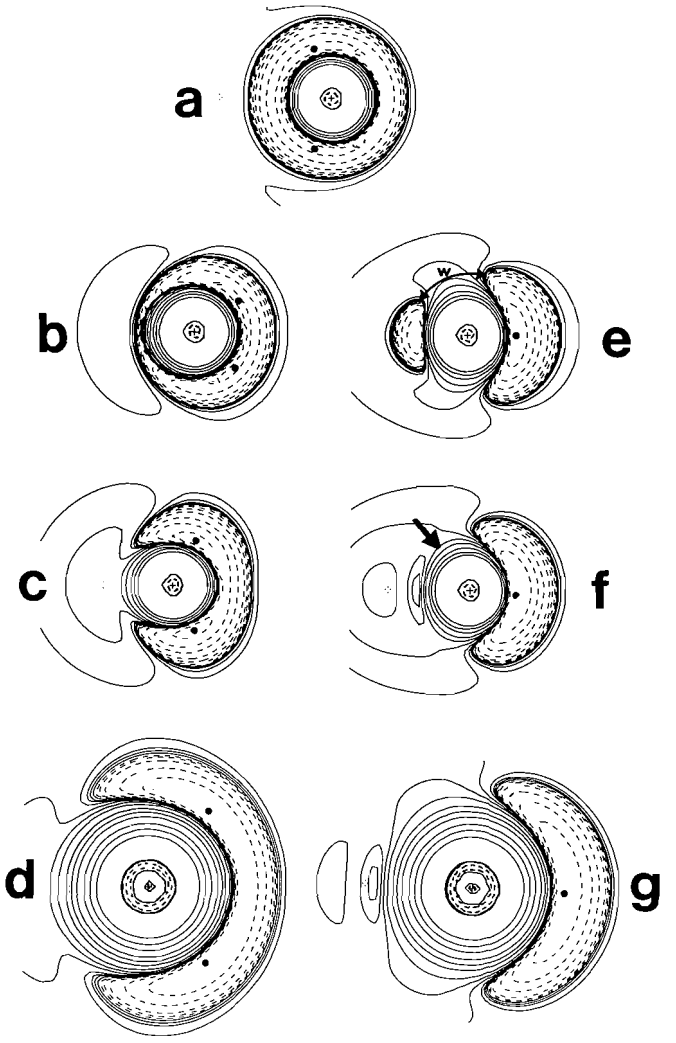

FIG. 3. Contour plots of $\nabla^2\rho$ in symmetry planes perpendicular to the plane of the nuclei containing the C or Si nucleus. For the triplets (*a*) CLi_2, (*b*) CH_2, (*c*) CF_2, and (*d*) SiH_2 and for the singlets (*e*) CH_2, (*f*) CF_2, and (*g*) SiH_2. The right-hand side of each figure corresponds to the nonbonded side of the C or Si atom. Dashed lines denote negative values — regions where charge is concentrated. Solid lines denote positive values — regions of charge depletion. Each dot denotes a maximum in $-\nabla^2\rho$, a maximum in charge concentration. Each triplet state exhibits two and each singlet one such maxima in this plane. Figures (*c*) and (*f*) are the contour maps corresponding to the top two relief diagrams of Fig. 2. Contour values in au are ±0.002, ±0.004, ±0.008 increasing in powers of 10 up to ±8.0.

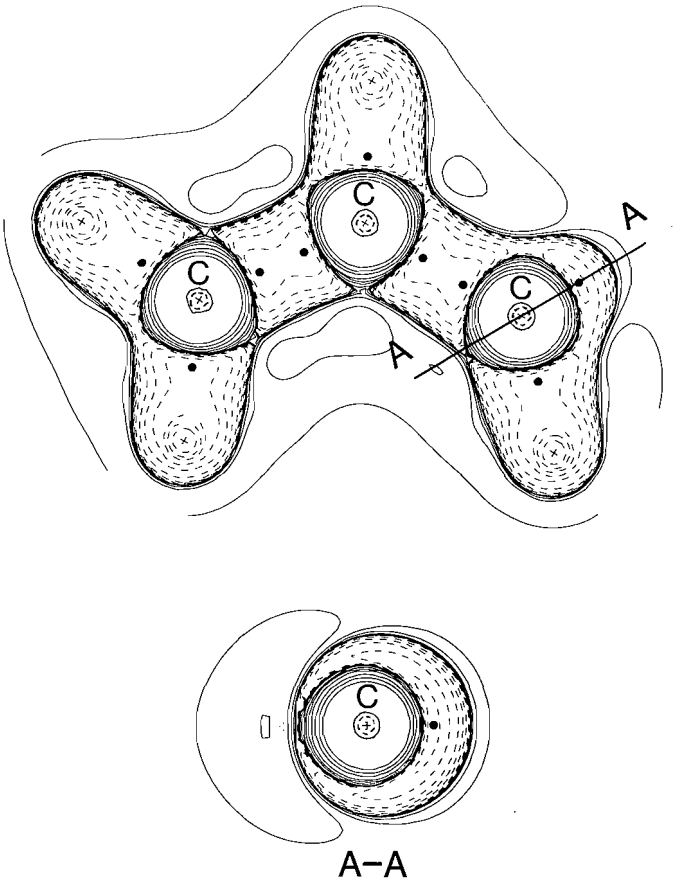

FIG. 4. Contour plot of the Laplacian of ρ for the triplet state of vinylmethylene; in the plane of the nuclei (upper diagram) and the cross-section, A—A, through the divalent carbon. The dots denote the bonded and the single nonbonded maximum in charge concentration.

maximum (Fig. 4) as a result of the delocalization of the π density into the CH=CH_2 and CH=O fragments.

We begin with some general observations. The nonbonded maxima in the singlet states are considerably larger than those in the triplet states. In those molecules which have a triplet ground state there are no regions of charge depletion (or holes as we shall refer to them) in the VSCC and the nonbonded maxima are not pronounced.[4] This behaviour is typified by the methylenic carbon in vinylmethylene as illustrated in Fig. 4. The delocalization of the valence charge concentration is most pronounced in the triplet state of CLi_2 where the C atom bears a large net negative charge (Fig. 3*a*). The VSCC is also polarized towards the ligands in this molecule to the extent that what correspond to nonbonded maxima in the other examples are now maxima on the *bonded* side of the molecule. The nonbonded charge in the singlet states of these molecules on the other hand is very localized (Fig. 3*e*) with the result that regions of charge depletion or holes are also present in the VSCC of the methylenic carbon in the singlet state, in accord with their ambiphilic nature. For the molecules which have singlet ground states, the nonbonded maxima are large and very pronounced in both the singlet and triplet states of each system as illustrated for CF_2 in Fig. 2. In these systems the ligands bear substantial negative charges and the methylenic carbon atom is strongly polarized into its nonbonded region, more so in the singlet than in the triplet states (see μ(C) values in Table 2). Correspondingly the single nonbonded maximum in the singlet is approximately twice the magnitude of either maximum in the triplet. Thus as a consequence of the charge transfer to the ligands, the nonbonded charge concentrations on carbon are localized and holes are present in the VSCC's in both the singlet *and* triplet states of these molecules.

In summary, in carbenes where the methylenic carbon is neutral or negatively charged, there is a delocalization of the nonbonded charge concentration in the triplet state while the nonbonded charge concentration is localized in the singlet state. In these systems the ground state is the delocalized triplet. In carbenes where there is a substantial charge transfer to the

[4]The magnitude of $\nabla^2\rho$ at the intervening saddle points is only a few percent less than its value at the maxima, and the extrema are not pronounced.

ligands the VSCC of the methylenic carbon is very localized into bonded and nonbonded charge concentrations in both the triplet and singlet states. The localization is greatest in the singlet states and these are the ground states in such systems.

Substituent effects on chemical reactivity

The extent of atomic back-polarization of Y in an X—Y bond can be rationalized in terms of the properties of the Laplacian of ρ. Of interest is the case where Y has unshared pairs of electrons, such as fluorine. In an axially symmetric system such as H—F, fluorine exhibits a uniform nonbonded torus of charge concentration subtending an angle at the nucleus of 101.2°. The manner and extent to which this torus of nonbonded charge is polarized in a system without axial symmetry is determined by the properties of the VSCC of the bonded neighbour, X. If X does not possess an orbital vacancy then its VSCC does not exhibit any pronounced regions of charge depletion. In this case the polarization of the nonbonded torus of charge concentration of F is very slight and the small maxima induced in the torus are staggered with respect to the bonded maxima on X.[5] In ClF_5 for example, the axial F exhibits four nonbonded maxima which are staggered with respect to the four bonded maxima on the Cl atom. In CH_3F, fluorine has three nonbonded maxima which are staggered with respect to the three bonded maxima on carbon. The maxima induced in the nonbonded torus by these polarizations exceed in value the resulting minima in $\nabla^2\rho$ by less than 1.0% and correspondingly, the atomic back-polarization of F is relatively small.

In the case where X possesses an orbital vacancy the polarization of the nonbonded torus on F and the resulting back-polarization of its density are very pronounced. In the singlet state of CF_2, the VSCC on carbon exhibits two pronounced holes so positioned as to mimic a vacant $p\pi$ orbital, Fig. 3*c*. The VSCC of carbon in a carbocation exhibits the same pattern of charge depletion. In singlet CF_2 the density on F, including the nonbonded torus of charge concentration, undergoes significant polarization towards the regions of charge depletion on carbon. The result is the formation of two minima and two maxima in the nonbonded torus. Since the minima result from the polarization of the nonbonded charge towards the holes on carbon, the nonbonded maxima on fluorine now eclipse the maxima on carbon. These are large effects; the resulting nonbonded maxima on fluorine exceed the minima in the nonbonded torus of charge concentration by 25% and the atomic dipole is large (Table 4). This situation parallels the model of π back-donation, but as previously noted there is only a polarization of the atomic charge on Y, not a transfer back to the vacancy on X.

The VSCC of carbon in triplet CF_2 has regions of charge depletion in the plane of the nuclei (Figs. 2 and 3*c*). The nonbonded torus on F undergoes a polarization similar to that in the singlet state, but to a lesser extent. The resulting nonbonded charge maxima exceed the minima by 8% and they again eclipse the nonbonded maxima on carbon which are above and below the plane of the nuclei in this case. The atomic polarization on F is also less than in the singlet state. In the orbital model of a triplet carbon every orbital on carbon is at least singly occupied and hence no π back-donation is expected. The Laplacian of ρ, by indicating the presence of regions of charge depletion on carbon, does correctly anticipate atomic back-polarization in the triplet case. Since the holes on carbon are less pronounced in the triplet than in the singlet state, the extent of polarization is less.

These same mechanisms are operative in the $CHNH_2$ system. In the singlet state of this molecule the —NH_2 group is planar so as to align the nonbonded charge concentration on nitrogen with

[5]Cremer and Kraka (25) have proposed that the staggered conformation results from maximum avoidance of vicinal bonded charge concentrations.

TABLE 4. Bond distances and atomic dipoles

YXY′	R(X—Y′) Å	μ(Y′) au
CF_2 (S)	1.283	0.524
CF_2 (T)	1.304	0.414
$HCNH_2$ (S)	1.308	0.518
$HCNH_2$ (T)	1.384	0.230
SiH_2 (S)	1.510	0.418
SiH_2 (T)	1.472	0.452

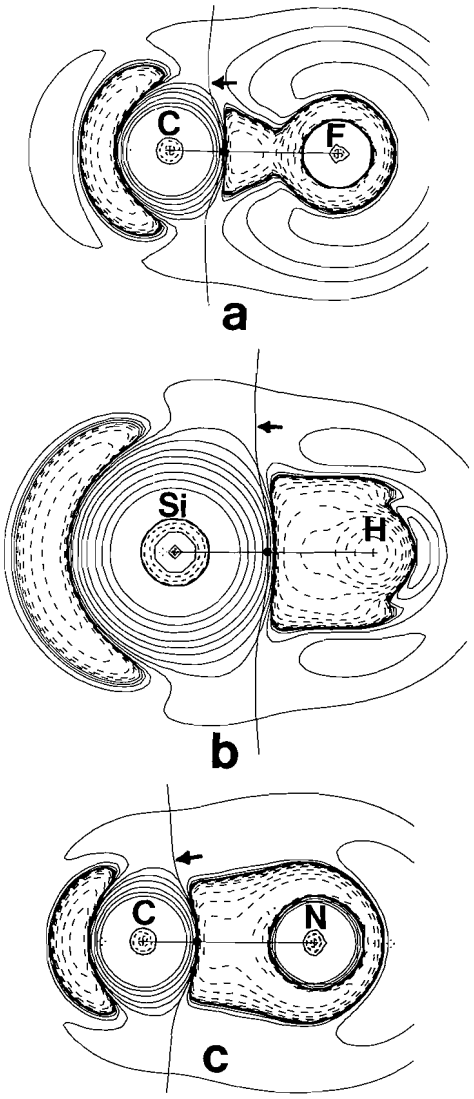

FIG. 5. Contour diagrams of $\nabla^2\rho$ with bond paths and interatomic surfaces overlayed. These are planes perpendicular to the planes of the nuclei, containing one of the bond axes. For (*a*) singlet CF_2, (*b*) singlet SiH_2, and (*c*) singlet $CHNH_2$. The arrows indicate the effect of back-polarization on the interatomic surfaces. In the absence of strong back-polarization, as in CH_3F or CH_3NH_2, the surfaces are not pushed in the direction indicated by the arrows.

TABLE 5. Structural and atomic properties of cyclic carbenes

System	Bond	$\nabla^2\rho_b$ au	ϵ†	n	$q(\Omega)$	μ(C1) *au	Nonbonded maximum $\nabla^2\rho$ au	Hole in VSCC Width au	Hole in VSCC $\nabla^2\rho$ au
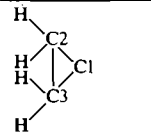	C1—C2	−0.608	0.600	1.09	C1 −0.015	+1.08	−1.35	1.3	+0.4
	C2—C3	−0.547	0.556	1.04	C2 +0.052				
	C2—H	−1.072	0.032		H −0.022				
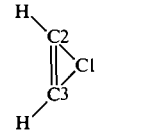	C1—C2	−0.738	0.621	1.33	C1 +0.221	+1.38	−1.30	1.2	+0.18
	C2—C3	−0.921	0.067	1.83	C2 −0.181				
	C2—H	−1.218	0.044		H +0.070				
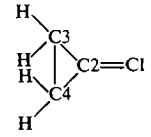	C1—C2	−1.461	0.482 ⊥	2.60	C1 +0.123	+1.10	−1.45	1.0	+0.3
	C2—C3	−0.467	0.645	0.93	C2 −0.487				
	C3—C4	−0.596	0.382	1.06	C3 +0.188				
	C3—H	−1.156	0.023		H −0.003				

*1 au = 2.542 D, a positive μ value means that the negative end of the dipole is directed away from the ligands.
†⊥ indicates that the major axis is perpendicular to the plane of the ring. All other bonds have their major axis in the plane of the ring.

the π-like region of charge depletion on carbon. The nitrogen is polarized towards carbon to such an extent that it no longer possesses a nonbonded charge concentration and its atomic dipole is large, Table 4. In triplet $CHNH_2$ the nitrogen atom is pyramidal and possesses a nonbonded charge concentration as does N in NH_3 (5). The VSCC of carbon in the triplet state has a region of charge depletion in the plane of the H—C—N nuclei and the nonbonded charge concentration on N is aligned with it. As with CF_2, the polarization of the ligand is less pronounced in the triplet than in the singlet.

The shape of the interatomic surface illustrates the effect that such back-polarization has on an X—Y bond (Fig. 5). It is observed that the bulging in these interatomic surfaces is not axially symmetric, but that in the singlet states it is more pronounced above and below the plane of the nuclei. It is also observed that the extent of bulging increases as μ(Y) increases.

In ref. 5 it was proposed that nonbonded maxima in $-\nabla^2\rho(r)$ are sites of electrophilic attack and points of maximum charge depletion in the VSCC are sites of nucleophilic attack. It is generally found that VSCC's of atoms with incomplete valence shells, such as C in carbenes, do not completely envelope the nucleus. In Fig. 2 any radial line from the C nucleus in triplet CF_2 passes through a maximum as it crosses the VSCC, but in the case of the C atom in singlet CF_2 there exist radial paths which do not pass over such a "lip". As a result a critical point corresponding to a point of maximum charge depletion in the VSCC does not exist. To characterize the susceptibility of such atoms to nucleophilic attack we report (Tables 3 and 5) the width of the hole in the VSCC. This measurement is illustrated in Fig. 3*e*. We also report the value of $\nabla^2\rho$ at the hole center. To characterize the susceptibility of the divalent atoms to electrophilic attack, the values of $\nabla^2\rho$ at the nonbonded maxima are reported in Tables 3 and 4.

The triplet states of CH_2 and CLi_2 do not exhibit regions of charge depletion in the VSCC's of the methylenic carbon atoms. Hence the triplet states of these molecules are not susceptible to attack by nucleophiles. They are, however, very susceptible to attack by electrophiles. The delocalized nature of the nonbonded charge concentration in these molecules indicates that it is easily polarized, thereby accounting for their reactive nature towards electrophiles. As pointed out earlier, singlet carbenes have both lumps and holes in their VSCC's, making them susceptible to both electrophilic and nucleophilic attack (Fig. 3). The singlet states of carbenes in which charge is transferred to the ligands are found to be less susceptible to nucleophilic attack than singlet CH_2 (26). The arrow in Fig. 3*f* indicates that the direction of approach of a nucleophile to the VSCC of the C atom in singlet CF_2 is at an acute angle to the C—F bond axes. The resulting electron–electron repulsion between the approaching nucleophile and the negatively charged F atoms creates a barrier to nucleophilic attack. This same argument applies to singlet SiH_2 and singlet $CHNH_2$. Sosa and Schlegel have calculated that indeed the singlet states of CF_2 and SiH_2 have high insertion barriers relative to that of singlet CH_2, and that the angle of approach is as described above for both CF_2 and SiH_2 (27). The small hole width and completion of the VSCC of the C atom in singlet $CHNH_2$ indicate it is less susceptible to nucleophilic attack than singlet CH_2, even before ligand–nucleophile repulsions are considered.

The delocalization of spin and charge density in α,β-unsaturated methylenes was previously discussed. As mentioned, these systems are best described as biradicals with one of the unshared electrons delocalized into the π system. Thus, the reactivity of these systems will be free radical-like. As a result of the presence of a single nonbonded charge concentration (Fig. 4), they are predicted to be less reactive than alkylmethylenes which have two such maxima. Singlet formylmethylene has been predicted to rearrange easily to ketene via an intramolecular αC—H insertion (8). This rearrangement is foreshadowed by the alignment of the αC—H bond with the hole in the VSCC of the divalent C atom and the unusually small angle this bond makes with the C—C bond axis, 108.2° compared to 117.4° in the triplet state. This is an example of a singlet carbene with a ligand which possesses no unshared electrons. In the absence of an unshared pair the density of the C—H bond is polarized towards the hole in the VSCC of the methylenic carbon, as indicated by its low ρ_b value (Table 5). This behaviour is analogous to hyperconjugation in carbocations (17).

The reactivity of the singlet states of two cyclic carbenes and a vinylidene (Table 5) are considered next. Others have shown

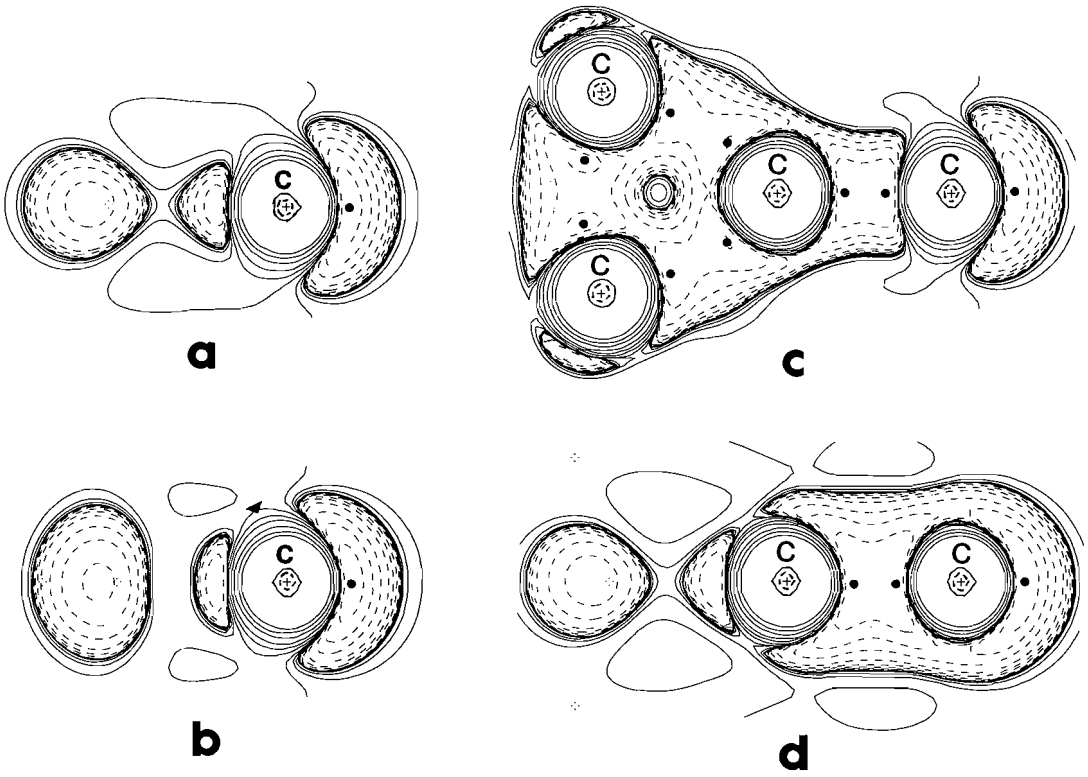

FIG. 6. Contour plots of $\nabla^2\rho$. Local maxima in $-\nabla^2\rho$ are denoted by solid circles. (*a*) The symmetry plane bisecting the ring in cyclopropylidene. Note the delocalization of charge into the center of the ring. (*b*) A similar plane in cyclopropenylidene. The triangle indicates a critical point in the VSCC of the methylenic carbon atom corresponding to a site of nucleophilic attack. There is a mirror site as well. (*c*) The plane containing the ring nuclei in cyclopropylidenecarbene. The sites of nucleophilic attack on the methylenic carbon are also in this plane. (*d*) The plane containing the π bond in cyclopropylidenecarbene.

that they possess singlet ground states (20, 28). Considering the small bond angle in three-membered ring carbenes (59.3° in cyclopropylidene and 55.4° in cyclopropenylidene), one can account for the singlet ground states of these systems by recalling that the $3a_1$ orbital becomes increasingly more stable relative to the $1b_1$ orbital as θ(RCR) decreases. Note that in the latter two examples in Table 5 there is significant charge transfer from the methylenic C atom to its neighbouring atom(s). Hence the singlet ground states of these systems agree with the charge transfer argument as well.

In cyclopropylidene the two types of C—C bonds differ only slightly from the C—C bond in cyclopropane for which n = 0.99 and ϵ = 0.49. On the basis of the data in Tables 3 and 5, the reactivity of the methylenic carbon in cyclopropylidene is predicted to be similar to that of singlet CH_2; susceptible to both nucleophilic and electrophilic attack. A comparison of Figs. 3*e* and 6*a* illustrates this similarity.

Cyclopropenylidene has been predicted to be unreactive towards nucleophiles (29). The bond orders given in Table 5 indicate that there is some delocalization of charge in this system. The effect of this on the VSCC of the methylenic C atom is illustrated in Fig. 6*b*. In this case there is a point of maximum charge depletion in the VSCC of the methylenic C atom, that is, a critical point in $\nabla^2\rho$. Because of this delocalization, charge is much less depleted at this point than in other carbenes. Thus one would predict cyclopropenylidene to be even less susceptible to nucleophilic attack than singlet $CHNH_2$, for example. Even though the data in Table 5 predict the nonbonded charge concentration on cyclopropylidene to be similar in reactivity to that of cyclopropenylidene, nucleophilic behaviour will be dominant in the latter because of its greater selectivity as an electrophile (26).

The final example is cyclopropylidenecarbene. This vinylidene has an unusually short C2=C1: bond (1.275 Å) and a correspondingly high bond order (n = 2.60). The partial triple-bond character of the C1—C2 bond arises from conjugation with the three-membered ring (17). This is suggested by the reduction in the bond order of the adjacent C—C bonds, n(C2—C3) = 0.932. The extent of charge concentration in the π plane (Fig. 6*d*) illustrates the highly nucleophilic nature of this C=C: fragment (30). Figure 6*c* shows the plane containing the hole in the VSCC of the methylenic carbon atom, $\nabla^2\rho$ at the hole center $\approx +0.4$, roughly that for singlet CH_2. However, the hole width is extremely small resulting from the extent that the bonded and nonbonded charge concentrations cover the VSCC, reducing the size of the region a nucleophile can attack.

Conclusions

1. We find the energy of the central atom to be lower in the triplet state while the energy of the ligand is lower in the singlet state. It is also found that the average electron population of the central atom is largest in the triplet state. As a result, transfer of charge to the ligands preferentially stabilizes the singlet state while transfer of charge to the central atom stabilizes the triplet state. We expect these observations to remain valid at higher levels of theory. The trend is supported by performing a two-state CI calculation on singlet methylene, for which ΔE(C) = −68 kcal/mol and ΔE(H) = +21 kcal/mol (cf. Table 2). These observations allow one to rationalize, non-empirically, the

ground state multiplicities of simple carbenes in terms of well-defined atomic properties.

2. The orbital model of π back-donation is found to be inconsistent with the observed properties of the charge density. Instead, back-polarization of negatively charged ligands is found to be the operative mechanism that accounts for the trends in X—Y bond lengths (Table 4).

3. In unsaturated carbenes it is found that spin polarization, and not charge transfer, stabilizes the triplet states.

4. Finally, the properties of the Laplacian distribution allow one to discuss carbene reactivity in terms of an observable property directly related to the energetics of the system.

A previous model based on electronegativity (22) was deemed "unnecessary in understanding substituent effects on ST (singlet–triplet) gaps" in the publication of a more recent model. The latter model was based on empirical π-acceptor and π-donor indices derived from Mulliken population analyses (23). On the basis of conclusions 1, 2, and 3 above, the latter model is unnecessary also.

Acknowledgements

Acknowledgement is made to the donors of The Petroleum Research Fund, administered by the American Chemical Society, for partial support of this research. One of us (P.J.M.) wishes to thank the Xerox Research Centre of Canada for the award of a Graduate Research Fellowship.

1. P. S. Skell and R. C. Woodsworth. J. Am. Chem. Soc. **78**, 4496 (1956); **78**, 6427 (1956); **81**, 3383 (1959).
2. (*a*) F. A. L. Anet, R. F. W. Bader, and A.-M. Van der Auwera. J. Am. Chem. Soc. **82**, 3217 (1960); R. F. W. Bader and J. I. Generosa. Can. J. Chem. **43**, 1631 (1965); (*b*) G. Herzberg. Proc. R. Soc. London, Ser. A, **262**, 291 (1961).
3. C. W. Bauschlicher, H. F. Schaefer, III, and P. S. Bagus. J. Am. Chem. Soc. **99**, 7106 (1977); M. E. Colvin, R. S. Grev, H. F. Schaefer, III, and J. Bicerano. Chem. Phys. Lett. **99**, 399 (1983).
4. R. F. W. Bader, S. G. Anderson, and A. J. Duke. J. Am. Chem. Soc. **101**, 1389 (1979); R. F. W. Bader, T. T. Nguyen-Dang, and Y. Tal. J. Chem. Phys. **70**, 4316 (1979).
5. R. F. W. Bader, P. J. MacDougall, and C. D. H. Lau. J. Am. Chem. Soc. **106**, 1594 (1984).
6. R. S. Grev and H. F. Schaefer, III. J. Chem. Phys. **82**, 4126 (1985).
7. A. Mavridis and J. F. Harrison. J. Am. Chem. Soc. **104**, 3827 (1982).
8. W. J. Bouma, R. H. Nobes, L. Radom, and C. E. Woodward. J. Org. Chem. **47**, 1869 (1982).
9. J. H. Meadows and H. F. Schaefer, III. J. Am. Chem. Soc. **98**, 4383 (1976).
10. C. W. Bauschlicher and I Shavitt. J. Am. Chem. Soc. **100**, 739 (1978).
11. I. Shavitt. Tetrahedron, **41**, 1531 (1985).
12. R. F. W. Bader, T. T. Nguyen-Dang, and Y. Tal. Rep. Prog. Phys. **44**, 893 (1981); R. F. W. Bader and T. T. Nguyen-Dang. Adv. Quantum Chem. **14**, 63 (1981).
13. R. F. W. Bader. Acc. Chem. Res. **18**, 9 (1985).
14. R. F. W. Bader and R. A. Gangi. J. Am. Chem. Soc. **93**, 1831 (1971); R. F. W. Bader, M. E. Stephens, and R. A. Gangi. Can. J. Chem. **55**, 2755 (1977).
15. (*a*) R. F. W. Bader and M. E. Stephens. J. Am. Chem. Soc. **97**, 7391 (1975); (*b*) J. C. Slater. Quantum theory of atomic structure. Vol. II. McGraw-Hill, New York. 1960.
16. R. F. W. Bader and H. Essén. J. Chem. Phys. **80**, 1943 (1984).
17. R. F. W. Bader, T. S. Slee, D. Cremer, and E. Kraka. J. Am. Chem. Soc. **105**, 5061 (1983).
18. R. S. Hutton, M. L. Manion, H. D. Roth, and E. J. Wasserman. J. Am. Chem. Soc. **96**, 4681 (1974).
19. R. Gleiter and R. Hoffmann. J. Am. Chem. Soc. **90**, 5457 (1974).
20. N. C. Baird and K. F. Taylor. J. Am. Chem. Soc. **100**, 1333 (1978).
21. L. Pauling. J. Chem. Soc. Chem. Commun. 688 (1980).
22. J. F. Harrison, R. C. Liedtke, and J. F. Liebman. J. Am. Chem. Soc. **101**, 7162 (1979).
23. P. H. Mueller, N. G. Rondan, K. N. Houk, J. F. Harrison, D. Hooper, B. H. Willen, and J. F. Liebman. J. Am. Chem. Soc. **103**, 5049 (1981).
24. R. F. W. Bader and W. H. Henneker. J. Am. Chem. Soc. **87**, 3063 (1965); R. F. W. Bader, P. M. Beddall, and P. E. Cade. J. Am. Chem. Soc. **93**, 3095 (1971).
25. D. Cremer and E. Kraka. J. Am. Chem. Soc. **107**, 3811 (1985).
26. R. A. Moss. Acc. Chem. Res. **13**, 58 (1980).
27. C. Sosa and H. B. Schlegel. J. Am. Chem. Soc. **106**, 5847 (1984).
28. J. W. Kenney, III, J. Simons, G. D. Purvis, and R. J. Bartlett. J. Am. Chem. Soc. **100**, 6930 (1978).
29. T. J. Lee, A. Bunge, and H. F. Schaefer, III. J. Am. Chem. Soc. **107**, 137 (1985).
30. P. J. Stang. Chem. Rev. **78**, 383 (1978).

Appendix

Effect of two state CI on properties of singlet CH_2

Property	Value	
	One configuration	Two configurations
$E(^1T) - E(^0S)$	−30.86 kcal/mol*	−26.72 kcal/mol
$E(^0S)$	−38.8763 au	−38.8829 au
q(H)	−0.0473 e	−0.0438 e
C—H bond		
ρ_b	0.2905 au	0.2899 au
$\nabla^2\rho_b$	−1.1225 au	−1.1182 au
ϵ	0.1746	0.1628
Nonbonded charge concentration		
$\nabla^2\rho(r)$	−1.5537 au	−1.4696 au

*This value reduces to −27.7 kcal/mol when $E(^1T)$ is obtained from a restricted open-shell calculation rather than from UHF. This value compares favourably with the value −26.2 kcal/mol obtained in ref. 10 which used a basis set of similar size, but with different exponents for the *d* functions in the singlet and triplet states.

Convenient synthesis, X-ray crystal structure, and Raman spectrum of the heptasulphide dianion, S_7^{2-}, in $[PPN]_2S_7 \cdot 2EtOH$

TRISTRAM CHIVERS,[1] FRANK EDELMANN, JOHN F. RICHARDSON, AND KENNETH J. SCHMIDT
Department of Chemistry, The University of Calgary, Calgary, Alta., Canada T2N 1N4

Received January 13, 1986

TRISTRAM CHIVERS, FRANK EDELMANN, JOHN F. RICHARDSON, and KENNETH J. SCHMIDT. Can. J. Chem. **64**, 1509 (1986).

The S_7^{2-} ion is readily prepared in high yield by the reaction of [PPN]SH with *cyclo*-S_8 in ethanol. The crystal and molecular structures of $[PPN]_2S_7 \cdot 2EtOH$ have been determined by X-ray crystallography. The crystals are monoclinic and belong to the space group $P2_1$, a = 13.199(2), b = 19.414(2), c = 14.046(2) Å, β = 94.027(6)°, V = 3590.3(7) Å^3, Z = 2. The final R and R_w values were 0.064 and 0.060, respectively. The S_7^{2-} ion is an unbranched chain of sulphur atoms in the *cis,trans,cis*-configuration with torsion angles of 89.99(18), 71.84(16), 76.54(16), and 94.19(18)°. The S—S distances (in Å) become progressively smaller in the sequence d(S—S central) [2.072(3) and 2.070(3)] > d(S—S internal) [2.050(2) and 2.037(3)] > d(S—S) terminal [2.044(3) and 2.026(4)]. The Raman spectrum of the S_7^{2-} ion in $[PPN]_2S_7 \cdot 2EtOH$ exhibits characteristic S—S stretching vibrations at 503, 453, 419, and 395 cm^{-1}.

TRISTRAM CHIVERS, FRANK EDELMANN, JOHN F. RICHARDSON et KENNETH J. SCHMIDT. Can. J. Chem. **64**, 1509 (1986).

La réaction du [PPN]SH avec le *cyclo*-S_8 dans l'éthanol permet de préparer facilement et avec un très bon rendement l'ion S_7^{2-}. Faisant appel à la diffraction des rayons-X, on a déterminé les structures cristalline et moléculaire du $[PPN]_2S_7 \cdot 2EtOH$. Les cristaux sont monocliniques, groupe d'espace $P2_1$ avec a = 13,199(2), b = 19,414(2) et c = 14,046(2) Å, β = 94,027(6)°, V = 3590,3(7) Å^3 et Z = 2. Les valeurs finales de R et R_w sont respectivement 0,064 et 0,060. L'ion S_7^{2-} est une chaîne linéaire d'atomes de soufre dans la configuration *cis,trans,cis* avec des angles de torsion de 89,99(18), 71,84(16), 76,54(16) et 94,19(18)°. Les distances S—S (en Å) deviennent de plus en plus courtes dans la séquence d(S—S central) [2,072(3) et 2,070(3)] > d(S—S interne) [2,050(2) and 2,037(3)] > d(S—S terminal) [2,044(3) et 2,026(4)]. Le spectre Raman de l'ion S_7^{2-}, tel qu'il existe dans le $[PPN]_2S_7 \cdot 2EtOH$, présente les vibrations d'élongation caractéristiques aux S—S, soit des bandes à 503, 453, 419 et 395 cm^{-1}.

[Traduit par la revue]

Introduction

Recent developments in the chemistry of transition metal polysulphides have stimulated interest in the characterization of long-chain polysulphide anions, S_x^{2-} ($x > 6$) (1). Several investigations have provided evidence for the formation and instability of such anions in solution (2–4). Solubility and uv–visible spectroscopic measurements indicate that solutions of lithium polysulphides in DMSO or THF contain chains with an *average* of 9–10 sulphur atoms (2). Earlier studies of the electrochemical reduction of *cyclo*-S_8 have established that the S_8^{2-} ion is unstable with respect to disproportionation to S_6^{2-} and sulphur in dilute DMF (3) or DMSO (4) solutions (10^{-3} – 10^{-4} *M*) in the presence of R_4N^+ salts. Long chain polysulphide anions can, however, be stabilized in the solid state by the presence of larger counter-ions.

In 1983 Coucouvanis *et al.* reported the unexpected formation of $[Ph_4P]_2S_7$ in moderate yield from the reaction of MoS_9^{2-} with an excess of sodium diethyldithiocarbamate in the presence of $[Ph_4P]Cl$ (5). The S_7^{2-} ion was shown to be an unbranched chain in the *trans,trans,trans*-configuration by X-ray crystallography (5). Subsequently, more direct routes for the preparation of salts of S_x^{2-} anions ($x > 6$) have been described. The compounds $[Ph_4As]_2S_7$ (6) and $[Ph_4P]_2S_8$ (7) were obtained in 80% yields by addition of $[Ph_4As]Cl$ or $[Ph_4P]Cl$, respectively, to an ethanol solution of Na_2S_4. The S_{12}^{2-} ion was isolated as its PPN^+ salt ($PPN^+ = (Ph_3P)_2N^+$) from the reaction of [PPN]Cl with *cyclo*-S_8 in the presence of potassium carbonate (8).

In an attempt to stabilize the initial product of the nucleophilic cleavage of an S_8 ring we have investigated the reaction of [PPN]SH with *cyclo*-S_8 in ethanol and found that it produces a high yield of $[PPN]_2S_7 \cdot 2EtOH$ rather than $[PPN][HS_9]$. The crystal and molecular structures of $[PPN]_2S_7 \cdot EtOH$ have been determined by X-ray crystallography and the Raman spectrum of this salt is compared with that of $[PPN]_2S_{12}$.

[1]To whom all correspondence should be addressed.

Experimental

Reagents and general procedures

[PPN]Cl (9), NaSH (10), and $[PPN]_2S_{12}$ (8) were prepared by the literature procedures. All solvents were dried and distilled before use: C_2H_5OH (Na/diethylphthalate), CH_3CN (CaH_2, P_2O_5, CaH_2). The preparation of $[PPN]_2S_7$ was carried out under an atmosphere of dry nitrogen, but the manipulation of crystalline samples of this salt was performed in air.

Infrared spectra were recorded as Nujol mulls (CsI windows) on a Perkin-Elmer 467 grating spectrophotometer (4000–250 cm^{-1}). Raman spectra were obtained on a Jarrell-Ash Model 25-100 double monochromator calibrated with carbon tetrachloride. A Coherent Radiation CR4 Argon ion laser fitted with an Innova plasma tube was used to obtain exciting radiation at 514 nm. Samples were mounted in a 6 cm diameter stainless steel ring on a bed of dry KBr, which was rotated at about 1000 rpm to prevent thermal decomposition.

Preparation of $[PPN]_2S_7$

(*a*) A solution of [PPN]SH was prepared by stirring a mixture of NaSH (0.30 g, 5.4 mmol) and [PPN]Cl (3.1 g, 5.4 mmol) in ethanol (30 mL) at 23°C (11) for 2 h. The precipitate of sodium chloride was removed by filtration and ethanol (80 mL) and *cyclo*-S_8 (0.60 g, 2.3 mmol) were added to the clear filtrate with vigorous stirring. The solution turned orange rapidly and a strong smell of H_2S was detected. After 5 min, a small amount of unreacted sulphur (ca. 0.10 g) was removed by filtration and the bright orange filtrate was allowed to stand at 23°C for 1 day whereupon large, ruby red crystals formed. After 2 days these crystals were separated by filtration, washed with ethanol (2 × 30 mL), and dried in air to give $[PPN]_2S_7 \cdot 2C_2H_5OH$ (2.5 g, 1.9 mmol). *Anal.* calcd. for $C_{76}H_{72}N_2O_2P_4S_7$: C 65.49, H 5.21, N 2.01, S 16.10; found: C 64.82, H 5.20, N 2.05, S 16.58. One of these crystals was used in the X-ray structural determination.

(*b*) In order to optimize the yield of $[PPN]_2S_7$ a slightly different procedure was used. A solution of [PPN]SH was prepared as described

above using the same quantities of reagents except that the total volume of ethanol was only 40 mL. Addition of *cyclo*-S_8 (0.50 g, 2.0 mmol) to this solution produced an orange–red precipitate within 1 min. After 15 min some unreacted sulphur was still present, so the mixture was stirred at 23°C for 18 h by which time sulphur was no longer evident in the orange precipitate. The product was isolated by filtration, washed with ethanol (2 × 10 mL), and dried in air to give $[PPN]_2S_7 \cdot 2EtOH$ (2.65 g, 2.0 mmol), which had a Raman spectrum identical to that of the crystalline sample prepared in (*a*). Powdered samples obtained by this procedure sometimes contain small amounts of *cyclo*-S_8 as indicated by Raman bands at 471, 218, and 152 cm^{-1} (12). *Cyclo*-S_8 can be removed from these samples by Soxhlet extraction with *n*-pentane for 24–48 h.

X-ray crystallography

Crystal data:

$C_{76}H_{72}N_2O_2P_4S_7$ fw = 1393.78

Space group $P2_1$, a = 13.199(2), b = 19.414(2), c = 14.046(2) Å, β = 94.027(6)°, V = 3590.3(7) Å^3, Z = 2, ρ_c = 1.29 g cm^{-3} (21(1)°C, MoKα, λ = 0.71069 Å, graphite monochromator), μ(MoKα) = 3.51. $F(000)$ = 1458 and crystal description: red, multi-faceted blocks, approx. 0.30 × 0.30 × 0.33 mm.

An examination of the crystalline sample using both binocular and polarising microscopes showed the bulk of the sample to be composed of twinned crystals. Six crystals were mounted and photographed on an Enraf-Nonius CAD4F diffractometer before one was found having ω scans of suitable quality for data collection. Intensity data were collected using the ω–2θ scan technique with a scan range of 1.5(0.80 + 0.142 tan θ) and scan speeds varying from 0.6 to 3.3° min^{-1}. Three standard reflections measured every 2400 s of X-ray exposure time showed a variation of less than 1% during the data acquisition period. The intensity of the reflection data dropped off rapidly with increasing θ and collection was terminated at a maximum θ of 25°. A total of 6486 unique reflections were measured for the octants $+h, -k, \pm l$, of which 4362 were considered observed ($F_o > 3\sigma(F_o)$, where σ was derived from counting statistics). The data were corrected for background, Lorentz and polarization effects but an absorption correction was not carried out. Details concerning data collection and reduction can be found in ref. 13. The choice of space group as $P2_1$ is ambiguous. The choice of the acentric space group was supported by the distribution of E values (K curve). Although the independent cations almost lie about a centre of symmetry, this is not exact and, more importantly, the anion and solvate molecules do not satisfy the conditions necessary for $P2_1/m$. Examination of the intensity data collected and cell reduction (performed using a modification of TRACER II by S. L. Lawson, see ref. 14) failed to show the presence of a higher symmetry cell.

The coordinates of the S and P atoms were determined by direct methods (MULTAN 78) (15). Structure factor and difference Fourier calculations revealed the positions of the remaining non-hydrogen atoms. The structure was refined by block-diagonal least-squares techniques (4 blocks) based on F, minimizing the function $\Sigma w(|F_o| - |F_c|)^2$, where $w = [\sigma(F_o)^2 + 0.0001F^2]^{-1}$. All computations were performed using the XRAY 76 system of programs (16). Scattering factors were taken from refs. 17 (non-H) and 18 (H) and anomalous dispersion corrections were included for non-hydrogen atoms (19). Phenyl H atoms were included in calculated positions with isotropic thermal parameters set to 1.1 times B_{eq} of the atom to which they are bonded. H atoms associated with the solvent molecule could not be located. The model did not converge easily, with the average Δ/σ being 0.6 in the final cycle. We attribute this oscillation in parameters to the near-centric distribution of the PPN^+ cations in the cell. In the final cycle there were 5594 observations (observed reflections plus those for which $I_c > 3\sigma(I_o)$) and 458 variables with the agreement factors $R = \Sigma(||F_o| - |F_c||)/\Sigma(|F_o| = 0.064$ and $R_w = [\Sigma w(|F_o| - |F_c|)^2/\Sigma w|F_o|]^{1/2} = 0.060$. The final GOF value was 1.15 and the largest peak of residual electron density was 0.6 e Å^{-3} (in the region of C(3)—C(4)).

The positional and isotropic thermal parameters for the non-hydrogen atoms of $[PPN]_2S_7 \cdot 2EtOH$ are given in Table 1. Tables giving the anisotropic thermal parameters (SI), positional and thermal parameters for H atoms (SII), bond lengths and angles (SIII), and the structure factors (SIV) have been placed in the Depository of Unpublished Data.[2]

The estimated standard deviations quoted in the tables are those derived from counting statistics and least-squares refinement. In view of the relative weakness of the intensity data, these calculated esds are probably underestimated, particularly for bond lengths and angles. It is difficult to evaluate the exact standard deviation, but it should be noted that differences between chemically equivalent bonds may not be significant.

Results and discussion

Synthesis of $[PPN]_2S_7$

The reaction of [PPN]SH with *cyclo*-S_8 in ethanol in a 1:1 molar ratio proceeded rapidly at room temperature to give $[PPN]_2S_7$ and a considerable amount of unreacted sulphur. Presumably the initially formed HS_9^- ion decomposes with loss of H_2S to give S_7^{2-} and sulphur. In subsequent reactions, the stoichiometry was adjusted in order to optimize the yield of $[PPN]_2S_7$ according to the following overall reaction.

$$2[PPN]SH + 6/8S_8 \rightarrow [PPN]_2S_7 + H_2S$$

The product can be recovered from ethanol solution either as large, ruby red crystals or, from more concentrated solutions, as an orange powder in ca. 80% yield. In aprotic donor solvents such as acetonitrile or DMF, $[PPN]_2S_7$ disproportionates to give polysulphur radical ions, e.g. $S_3^{\cdot-}$, cf. $[Ph_4P]_2S_7$ (5). Crystalline samples of this salt can be stored at room temperature for several days without decomposition. After several weeks the deposition of elemental sulphur is noticeable and can readily be detected by Raman spectroscopy (*vide infra*). Samples should be stored under an inert atmosphere at low temperatures in order to minimize the decomposition.

Crystal and molecular structures of $[PPN]_2S_7 \cdot 2EtOH$

An ORTEP drawing of the S_7^{2-} ion in $[PPP]_2S_7 \cdot 2EtOH$ is shown in Fig. 1 and the packing of the ions in the crystal is depicted in Fig. 2. Polysulphide chains, S_x^{2-} ($x \geq 5$), present interesting possibilities of isomerism because the dihedral angles $S_1S_2S_3/S_4S_5S_6$ etc. are normally close to 90° (20). For example, the S_6^{2-} ion can have three isomers, (*cis*,*cis*), (*cis*,*trans*), or (*trans*,*trans*) and there are six possible conformations of the S_7^{2-} ion.[3] Previous X-ray structural investigations have revealed only *all cis*- or, more frequently, *all trans*-conformations for S_x^{2-} (x = 5–7) (22). The former configuration is present in *cyclo*-S_8 while the latter is the configuration of the helices of fibrous sulphur and of the S_7^{2-} ion in $(Ph_4P)_2S_7$ (5). By contrast, the S_7^{2-} ion in the PPN^+ salt adopts a *cis*,*trans*,*cis* arrangement of sulphur atoms and thus provides the first example of a polysulphide chain that is not in either an *all cis*- or an *all trans*-conformation. This conformation is similar to the regular alternating *cis*,*trans* structure of *cyclo*-S_{12} (23).

The bond lengths, bond angles, and torsion angles of the S_7^{2-} ions in $[Ph_4P]_2S_7$ and $[PPN]_2S_7 \cdot 2EtOH$ are compared in Table 2. A trend towards progressively smaller S—S bond distances in the sequence d(S—S central) > d(S—S internal) > d(S—S

[2]Tables SI–SIV may be purchased from the Depository of Unpublished Data, CISTI, National Research Council of Canada, Ottawa, Ont., Canada K1A 0S2.

[3]These numbers do not include the possible existence of pairs of enantiomers for each isomer. A succinct discussion of the stereochemistry of polysulphide chains is given in ref. 21.

TABLE 1. Positional ($\times 10^4$) and isotropic thermal ($\times 10$) parameters for the non-H atoms of $(PPN)_2S_7 2EtOH$

Atom	x	y	z	B_{eq}/B_{iso}*
S(1)†	5745(2)	5451(0)	−3338(2)	60(1)
S(2)	6233(2)	4490(1)	−2927(2)	50(1)
S(3)	7235(2)	4541(1)	−1746(2)	53(1)
S(4)	8685(2)	4636(1)	−2209(2)	47(1)
S(5)	9205(2)	5627(1)	−1937(2)	50(1)
S(6)	10214(2)	5601(1)	−772(2)	55(1)
S(7)	9487(2)	5671(1)	449(2)	67(1)
P(1)	2972(1)	7779(1)	5284(1)	28(1)
P(2)	1923(2)	8934(1)	6159(1)	29(1)
N(1)	2637(5)	8553(3)	5480(4)	35(3)
C(1)	4312(5)	7776(4)	5182(5)	34(1)
C(2)	4840(7)	7170(5)	5142(6)	52(2)
C(3)	5894(8)	7194(6)	5038(7)	67(3)
C(4)	6343(8)	7809(6)	4983(7)	68(2)
C(5)	5869(8)	8401(6)	5020(7)	67(3)
C(6)	4830(6)	8396(5)	5124(6)	47(2)
C(11)	2367(5)	7484(4)	4176(5)	32(1)
C(12)	1948(6)	7939(4)	3509(5)	38(2)
C(13)	1500(6)	7715(5)	2640(6)	45(2)
C(14)	1480(7)	7032(5)	2433(6)	48(2)
C(15)	1920(7)	6563(5)	3073(6)	50(2)
C(16)	2387(6)	6793(5)	3934(6)	45(2)
C(21)	2708(6)	7167(4)	6202(5)	31(1)
C(22)	1777(7)	6846(4)	6175(6)	44(2)
C(23)	1535(7)	6429(5)	6962(7)	55(2)
C(24)	2225(8)	6358(5)	7689(7)	60(2)
C(25)	3137(9)	6654(6)	7730(8)	75(3)
C(26)	3418(7)	7077(5)	6965(7)	52(2)
C(31)	1508(5)	9731(4)	5598(5)	29(1)
C(32)	2071(6)	10016(4)	4880(5)	38(2)
C(33)	1762(6)	10632(5)	4476(6)	49(2)
C(34)	929(7)	10972(5)	4772(6)	51(2)
C(35)	388(6)	10705(5)	5468(6)	45(2)
C(36)	676(6)	10074(4)	5910(6)	42(2)
C(41)	2589(6)	9147(4)	7284(5)	35(2)
C(42)	3539(7)	8903(5)	7495(6)	55(2)
C(43)	4075(9)	9075(6)	8337(8)	81(3)
C(44)	3639(7)	9501(5)	8967(6)	55(2)
C(45)	2710(6)	9758(4)	8784(6)	44(2)
C(46)	2188(6)	9589(4)	7932(5)	40(2)
C(51)	803(5)	8470(4)	6378(5)	30(1)
C(52)	608(6)	8205(5)	7268(6)	46(2)
C(53)	−254(7)	7788(5)	7361(7)	59(2)
C(54)	−897(7)	7668(5)	6594(7)	58(2)
C(55)	−717(7)	7919(5)	5723(6)	53(2)
C(56)	133(7)	8330(4)	5605(6)	45(2)
P(3)	8084(1)	8009(1)	402(1)	29(1)
P(4)	6909(2)	9086(1)	1293(1)	28(1)
N(2)	7697(4)	8759(3)	642(4)	34(3)
C(61)	7429(5)	7680(4)	−662(5)	30(1)
C(62)	7537(6)	7005(4)	−939(6)	39(2)
C(63)	7019(7)	6760(5)	−1767(7)	52(2)
C(64)	6427(7)	7178(5)	−2315(6)	53(2)
C(65)	6306(7)	7861(5)	−2094(6)	56(2)
C(66)	6832(6)	8122(4)	−1232(6)	46(2)
C(71)	9402(5)	8060(4)	186(5)	29(1)
C(72)	9859(6)	8705(4)	121(5)	38(2)
C(73)	10883(6)	8755(4)	−67(6)	44(2)
C(74)	11422(6)	8173(4)	−189(5)	44(2)
C(75)	10995(6)	7533(4)	−120(6)	44(2)
C(76)	9965(6)	7471(4)	82(5)	39(2)
C(81)	7934(6)	7392(4)	1329(5)	33(1)
C(82)	7114(6)	6958(4)	1323(6)	42(2)
C(83)	7005(7)	6502(5)	2098(6)	52(2)
C(84)	7692(7)	6526(5)	2829(7)	55(2)
C(85)	8505(8)	6936(6)	2866(7)	71(3)
C(86)	8644(7)	7390(5)	2100(6)	50(2)
C(91)	5860(5)	8543(3)	1520(5)	30(1)
C(92)	5140(6)	8411(4)	774(6)	44(2)
C(93)	4320(7)	7958(5)	933(6)	55(2)
C(94)	4280(7)	7671(5)	1800(6)	52(2)
C(95)	4986(6)	7761(5)	2518(6)	50(2)
C(96)	5776(6)	8218(4)	2396(5)	42(2)
C(101)	7499(6)	9356(4)	2415(5)	33(1)
C(102)	8525(6)	9287(4)	2607(6)	40(2)
C(103)	8989(6)	9472(5)	3483(6)	50(2)
C(104)	8416(7)	9729(5)	4157(6)	54(2)
C(105)	7386(6)	9844(4)	3992(6)	45(2)
C(106)	6935(6)	9654(4)	3094(5)	39(2)
C(111)	6394(5)	9847(4)	711(5)	30(1)
C(112)	5497(6)	10144(4)	980(5)	37(2)
C(113)	5124(6)	10735(5)	533(6)	52(2)
C(114)	5619(7)	11025(5)	−179(7)	57(2)
C(115)	6513(7)	10766(5)	−437(6)	59(2)
C(116)	6924(6)	10154(4)	3(5)	40(2)
C(7)	2062(9)	4410(6)	3074(9)	91(8)
C(8)	1506(11)	4518(6)	2156(9)	88(8)
O(1)	915(10)	5038(6)	2151(7)	155(9)
C(9)	5372(11)	574(10)	6965(10)	128(10)
C(10)	4855(11)	338(7)	6137(8)	103(9)
O(2)	5498(6)	385(5)	5386(6)	104(6)

*All S, P, N atoms and the two molecules of EtOH solvate were refined anisotropically and are thus listed with B_{eq} thermal parameters.

†The y coordinate for S(1) was set to define the origin.

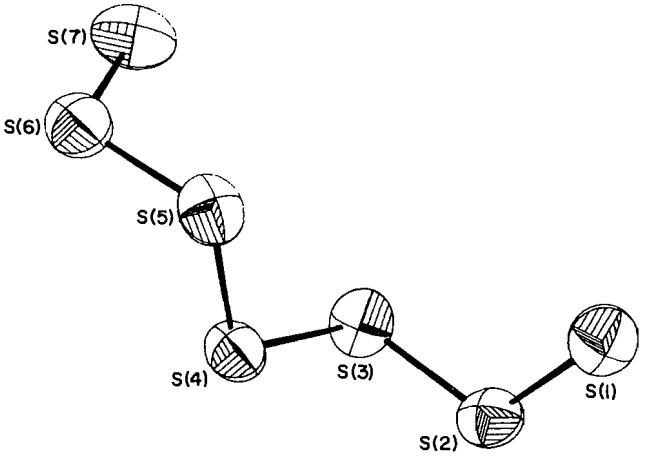

FIG. 1. ORTEP plot (50% probability ellipsoids) of the S_7^{2-} ion in $[PPN]_2S_7 \cdot 2EtOH$ showing the atomic numbering scheme.

terminal) is observed for both salts, but the attenuation is less pronounced in $[PPN]_2S_7 \cdot 2EtOH$. In contrast, it should be noted that the values of the S—S distances in the *all-trans* S_6^{2-} ion of ethylenediammonium hexasulphide alternate, the shortest being the internal S—S bond (22), whereas no significant difference between internal and terminal S—S bond lengths was found for $[Bu_4N]_2S_6$ (24). The average S—S bond length in $[PPN]_2S_7 \cdot 2EtOH$ is 2.050(3) Å [cf. 2.030(2) Å in $[Ph_4P]_2S_7$ (5)]. The average S—S—S angle of 109.4(2)° in $[PPN]_2S_7 \cdot 2EtOH$ is very similar to the value of 109.3(1)° found for $[Ph_4P]_2S_7$ (5). There are substantial differences, however, in the torsion angles

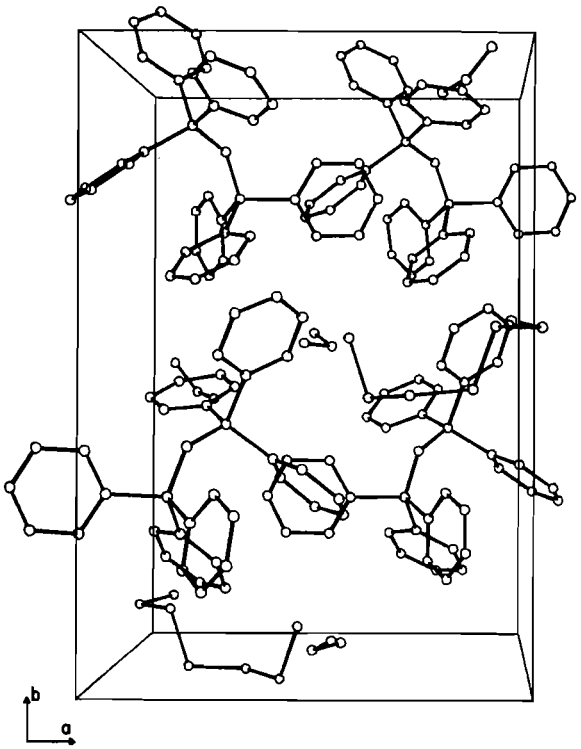

FIG. 2. Unit cell of $[PPN]_2S_7 \cdot 2EtOH$.

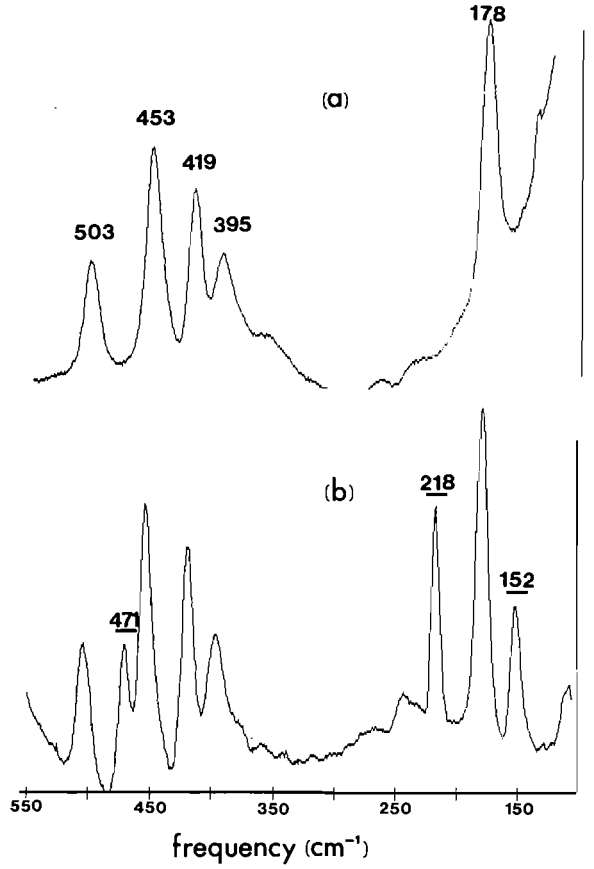

FIG. 3. Raman spectra of (*a*) $[PPN]_2S_7 \cdot 2EtOH$ and (*b*) $[PPN]_2S_7 \cdot 2EtOH$ containing cyclo-S_8.

TABLE 2. Bond distances (Å), angles (deg), and dihedral angles (deg) in the S_7^{2-} ion

	Length	
Bond	$[PPN]_2S_7$*	$[Ph_4P]_2S_7$†
S(1)—S(2)	2.044(3)	1.995(2)
S(2)—S(3)	2.050(3)	2.036(2)
S(3)—S(4)	2.072(3)	2.062(2)
S(4)—S(5)	2.070(3)	2.062(2)
S(5)—S(6)	2.037(3)	2.037(2)
S(6)—S(7)	2.026(4)	1.990(2)
	Angle	
Atoms	$[PPN]_2S_7$	$[Ph_4P]_2S_7$
S(1)—S(2)—S(3)	110.9(2)	111.30(10)
S(2)—S(3)—S(4)	107.9(1)	108.59(9)
S(3)—S(4)—S(5)	109.1(1)	106.75(10)
S(4)—S(5)—S(6)	108.3(1)	108.77(10)
S(5)—S(6)—S(7)	110.9(2)	111.09(10)
	Dihedral angle	
Planes	$[PPN]_2S_7$	$[Ph_4P]_2S_7$
S(1)S(2)S(3)/S(2)S(3)S(4)	89.99(18)	73.29(10)
S(2)S(3)S(4)/S(3)S(4)S(5)	71.84(16)	74.41(10)
S(3)S(4)S(5)/S(4)S(5)S(6)	76.54(16)	65.22(10)
S(4)S(5)S(6)/S(5)S(6)S(7)	94.19(18)	79.86(10)

*The esd's may be underestimated (see Experimental section).
†Data taken from ref. 5.

observed for the S_7^{2-} ion in these two salts. These differences are largest for the outermost torsion angles and can probably be attributed to the different chain conformations (*cis,trans,cis* for the PPN^+ salt vs. *trans,trans,trans* for the Ph_4P^+ salt). Previous structural studies of polysulphide anions have revealed torsion angles of ca. 90° for *all trans*-conformations and torsion angles of ca. 72° for *all cis*-conformations (22). Unlike cyclic sulphur allotropes (25), there appears to be no obvious correlation between S—S bond lengths and torsion angles in anionic polysulphide chains.

Raman spectra of $[PPN]_2S_7 \cdot 2EtOH$ and $[PPN]_2S_{12}$

Raman spectroscopy is the technique of choice for the characterization of cyclic (12) and linear (26) homonuclear sulphur species. A typical Raman spectrum of the S_7^{2-} ion in $[PPN]_2S_7 \cdot 2EtOH$ is shown in Fig. 3*a*. Characteristic S—S stretching vibrations are observed at 503, 453, 419, and 395 cm^{-1} and a strong SS deformation mode occurs at 178 cm^{-1}. The presence of *cyclo*-S_8, which sometimes arises in freshly prepared powders or in the crystalline product upon prolonged standing at room temperature, can be detected readily by the observation of characteristic Raman bands at ca. 470, 216, and 150 cm^{-1} (Fig. 3*b*) (27). Thus the Raman spectrum provides an excellent criterion of purity for samples of $[PPN]_2S_7$. The S_8^{2-} ion in $[Ph_4P]_2S_8$ is reported to exhibit S—S stretching bands at 500, 459, 431, and 390 cm^{-1} and a deformation band at 282 cm^{-1} in the ir spectrum (7).

We also obtained the Raman spectrum of the recently described PPN^+ salt of the dodecasulphide anion, S_{12}^{2-} (8), for

comparison with that of $[PPN]_2S_7$. The characteristic S—S stretching vibrations for $[PPN]_2S_{12}$ appeared at 515, 460 sh, 434, and 350 sh cm^{-1}.

Summary and conclusions

The reaction of [PPN]SH with *cyclo*-S_8 in ethanol provides a rapid, high yield synthesis of either powdered or crystalline samples of $[PPN]_2S_7 \cdot 2EtOH$ of high purity. An X-ray structural investigation of this product showed it to contain the first example of an anionic polysulphide chain which is not in either an *all cis*- or an *all trans*-conformation. This salt could prove to be a convenient reagent for the synthesis of derivatives of *cyclo*-octasulphur in which one sulphur atom is replaced by a transition metal, e.g. $(Me_3P)MS_7$ (M = Ru, Os) (28), or a main group element, e.g. S_7TeX_2 (X = Cl, Br) (29, 30). It is apparent that large cations are not only capable of stabilizing long polysulphide anions, S_x^{2-} ($x > 6$), in the solid state but that, under different reaction conditions, the same cation may stabilize different polysulphide chains e.g. $[PPN]_2S_7$ and $[PPN]_2S_{12}$ or $[Ph_4P]_2S_7$ and $[Ph_4P]_4S_8$.

Acknowledgements

We thank the Natural Sciences and Engineering Research Council of Canada for financial support (operating and infrastructure grants), Dr. R. A. Kydd for advice on the use of the Raman spectrometer, and Dr. K. A. Kerr for the use of the diffractometer.

1. M. Draganjac and T. B. Rauchfuss. Angew. Chem. Int. Ed. Engl. **24**, 742 (1985) and references therein.
2. R. D. Rauh, F. S. Shuker, J. M. Marston, and S. B. Brummer. J. Inorg. Nucl. Chem. **39**, 1761 (1977).
3. R. Martin, W. Doub, J. Roberts, and D. Sawyer. Inorg. Chem. **12**, 1921 (1973).
4. J. Badoz-Lambling, R. Bonnaterre, G. Cauquis, M. Delamar, and G. Demange. Electrochim. Acta, **21**, 119 (1976).
5. M. G. Kanatzidis, N. C. Baenziger, and D. Coucouvanis. Inorg. Chem. **22**, 290 (1983).
6. C. Schumacher, E. Herdtweck, and K. Dehnicke. Z. Anorg. Allg. Chem. In press.
7. B. Czeska and K. Dehnicke. Z. Naturforsch. **40b**, 120 (1985).
8. F. Seel and M. Wagner. Z. Naturforsch. **40b**, 762 (1985).
9. J. K. Ruff and W. J. Schlientz. Inorg. Synth. **15**, 84 (1974).
10. R. E. Eibeck. Inorg. Synth. **7**, 128 (1963).
11. R. G. W. Gingerich and R. J. Angelici. J. Am. Chem. Soc. **101**, 5604 (1979).
12. R. Steudel. Top. Current Chem. **102**, 149 (1982).
13. T. Chivers, R. T. Oakley, R. Pieters, and J. F. Richardson. Can. J. Chem. **63**, 1063 (1985).
14. S. L. Lawson and R. A. Jacobsen. Ames Laboratory Report IS-1141; USAEC: Iowa State University, Ames, IA. April 1965.
15. P. Main, S. E. Hull, L. Lessinger, G. Germain, J.-P. Declercq, and M. M. Woolfson. MULTAN 78, A system of computer programs for the automatic solution of crystal structures from X-ray diffraction data. University of York, York, England. 1978.
16. J. M. Stewart (*Editor*). Technical Report TR-446. Computer Science Centre, University of Maryland.
17. D. T. Cromer and J. B. Mann. Acta Crystallogr. A**24**, 321 (1968).
18. R. F. Stewart, E. Davidson, and W. Simpson. J. Chem. Phys. **42**, 3175 (1965).
19. International tables for X-ray crystallography. Kynoch Press, Birmingham, England. 1974.
20. A. F. Wells. Structural inorganic chemistry. 5th ed. Clarendon Press, Oxford. 1984. p. 727.
21. R. Rahman, S. Safe, and A. Taylor. Q. Rev. Chem. Soc. **24**, 208 (1970).
22. P. Böttcher, H. Buchkremer-Hermanns, and J. Baron. Z. Naturforsch. **39b**, 416 (1984) and references therein.
23. J. Steidel, R. Steudel, and A. Kutoglu. Z. Anorg. Allg. Chem. **476**, 171 (1981).
24. R. G. Teller, L. J. Krause, and R. C. Haushalter. Inorg. Chem. **22**, 1809 (1983).
25. R. Steudel. Z. Naturforsch. **38b**, 543 (1983).
26. T. Chivers and C. Lau. Inorg. Chem. **21**, 453 (1982).
27. G. Gautier and M. Debeau. Spectrochim. Acta, A**32**, 1007 (1976).
28. J. Gotzig, A. L. Rheingold, and H. Werner. Angew. Chem. Int. Ed. Engl. **23**, 814 (1984).
29. J. Weiss and M. Pupp. Angew Chem. Int. Ed. Engl. **9**, 463 (1970).
30. J. Weiss and M. Pupp. Acta Crystallogr. B**28**, 3653 (1972).

Preparation of *exo*-6-benzyl-*exo*-2-(*m*-hydroxyphenyl)-1-dimethylaminomethylbicyclo[2.2.2.]octane. A non-peptide mimic of enkephalins

PATRICE C. BÉLANGER AND CLAUDE DUFRESNE

Medicinal Chemistry Department, Merck Frosst Canada Inc., P.O. Box 1005, Pointe Claire/Dorval, P.Q., Canada H9R 4P8

Received December 4, 1985

PATRICE C. BÉLANGER and CLAUDE DUFRESNE. Can. J. Chem. **64**, 1514 (1986).

A model for the active conformation of methionine enkephalin was derived from computer modeling. From this model, a target was designed and synthesized using bicyclo[2.2.2]octane as a structural template. Thus, a key intermediate, *exo*-6-benzoyl-1-carboethoxybicyclo[2.2.2]-2-octene was prepared via a Diels–Alder reaction using ethyl dihydrobenzoate and phenylvinylketone. It was subsequently modified to *exo*-6-benzyl-1-dimethylaminobicyclo[2.2.2]-2-octene. This intermediate was hydroborated and oxidized to the ketone on which the second aromatic group was introduced using a Grignard reaction, eventually giving rise to the desired target, *exo*-6-benzyl-*exo*-2-(*m*-hydroxyphenyl)-1-dimethylaminobicyclo[2.2.2]octane. Biological testing demonstrated weak activity with this compound.

PATRICE C. BÉLANGER et CLAUDE DUFRESNE. Can. J. Chem. **64**, 1514 (1986).

Utilisant un ordinateur, on a déssiné un modèle pour la conformation active de la méthionine encéphaline. À partir de ce modèle, on a choisi une cible que l'on a synthétisée en utilisant le bicyclo[2.2.2]octane comme support de la structure. On a donc préparé un intermédiaire clé, le benzoyl-6-*exo* carboéthoxy-1 bicyclo[2.2.2]octène-2, par le biais d'une réaction de Diels–Alder entre le dihydrobenzoate d'éthyle et la phénylvinylcétone. On l'a subséquemment transformée en benzyl-6-*exo* diméthylamino-1 bicyclo[2.2.2]octène-2. On a procédé à une réaction d'hydroboration de cet intermédiaire et on l'a oxydé en une cétone. En procédant à une réaction de Grignard sur la benzyl-6-*exo* diméthylamino-1 bicyclo[2.2.2]octanone-2, on a éventuellement obtenu le produit désiré, le benzyl-6-*exo* (*m*-hydroxyphényl)-2-*exo* diméthylamino-1 bicyclo[2.2.2]octane. Les tests biologiques exécutés avec ce composé n'ont mis en évidence qu'une faible activité.

[Traduit par la revue]

Introduction

The discovery of the enkephalins (1, 2) has renewed the hope that the development of analgesics without the side effects associated with the narcotic analgesics might be possible. With the help of the Merck Molecular Modeling System (MMMS) (3), a model for the bioactive conformation of the enkephalins was developed. The process involved a combination of the structure–activity relationships known for the opiates (4) and for the enkephalins (5), of the distance between the two aromatic systems (6) (estimated to be approximately 10 Å from fluorescence studies of enkephalin analogs), and of modeling and comparing with known opiates. Another feature of this model is the presence of a β turn, which adds rigidity to the flexible enkephalin backbone and also acts as a template for positioning the key groups (tyrosine and phenylalanine phenyl groups) in space as is found in the very active opiates such as etorphin (7). The bicyclo[2.2.2]octane derivative **2** is such a structure that gave a good fit with the model and also possesses the two aromatic groups found in the enkephalins. The methionine part is absent from the proposed target and justification for this is found in the high degree of analgesic activity in some of the tetrapeptide analogs of the enkephalins (8). Using such a model, it was hoped to obtain activity of the μ-type with compounds having mixed agonist and antagonist activity on oral administration.

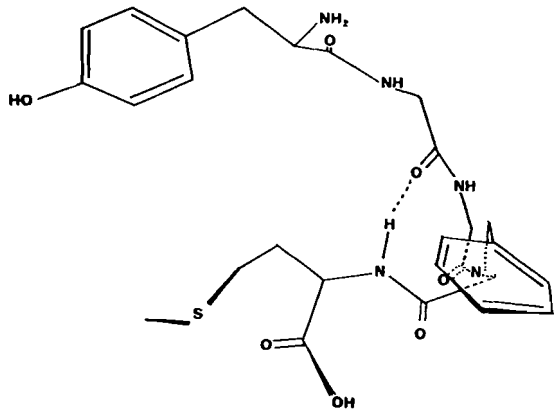

1

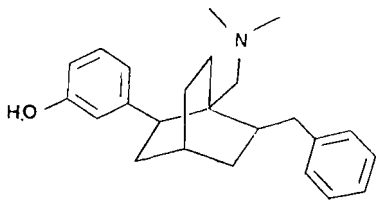

2

Results and discussion

A retrosynthetic analysis of the bicyclo[2.2.2] structure **2** suggested as a key intermediate the keto ester **3**, the product expected to result from the Diels–Alder reaction of ethyl dihydrobenzoate **4** with vinyl phenyl ketone **5**, followed by functionalizations to the desired target **2**. Four possible geometrical isomers are possible, and a stereospecific approach can reduce the number of possible isomers to give the desired 2,6 *exo* relationship suggested by the modeling experiments.

The key intermediate **3** was synthesized via a Diels–Alder reaction. Thus, ethyl dihydrobenzoate **4**, prepared according to the indications of Hünig and Kahanek (9), reacted readily with vinylphenylketone **5** affording **3** in 46% yield as the major compound. Among the other products of this Diels–Alder reaction, the *exo* isomer was also found to be present in 13%, giving rise to a mixture of 4.4:1. Obviously this mixture has not

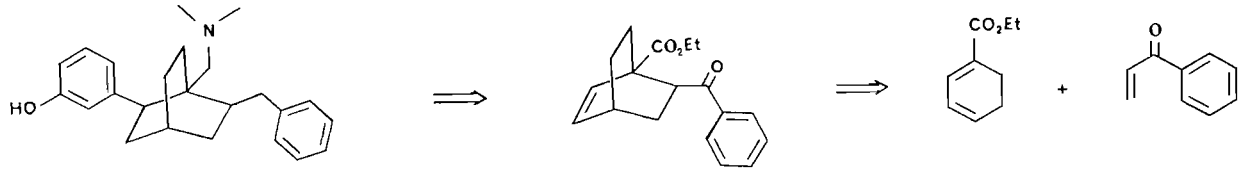

2 3 4 5

SCHEME 1

reached equilibrium, as the ratio of the *endo*:*exo* mixture was found to be 3.2:1 when pure *endo* or pure *exo* isomers alone were equilibrated by stirring in ethanol containing sodium ethoxide for 3 days at room temperature.

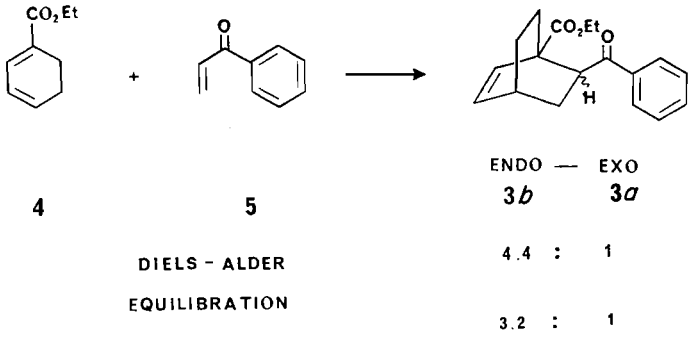

Nuclear magnetic resonance (nmr) spectra can clearly distinguish the *endo* and *exo* relationship, as can be seen by the chemical shift of the olefinic protons that appear to be influenced by the ketone in position 6. In the *exo* isomer, the two protons H-2 and H-3 absorb at 6.20 and 6.45 ppm as a triplet ($J_{3,2}$ = 6 Hz, $J_{3,4}$ = 8 Hz) and as a doublet (J = 4 Hz), whereas in the *endo* isomer, H-2 and H-3 appeared as a doublet (J = 8 Hz) and a triplet ($J_{3,2}$ = 6 Hz, $J_{3,4}$ = 8 Hz), at 6.20 and at 6.85 ppm, the downfield shift of 0.40 ppm being attributed to the influence of the benzoyl carbonyl.

Ortho orientation was easily demonstrated chemically by reducing **3** with sodium borohydride followed by treating the resulting alcohols **6** with phosphorous tribromide. γ-Lactones **7**, readily characterized by their infrared band at 1790 cm^{-1}, were obtained (10).

Base hydrolysis of **3** led to the keto acid **8**, which was submitted to the conditions of the Wolff–Kishner reaction, affording the carboxylic acid **9** in low yield.

Such a result forced us to change the strategy at this stage and, accordingly, the approach outlined in Scheme 3 was used as an alternative route to **2**.

Consequently, the treatment of the *endo* ketoacid **8** with thionyl chloride in chloroform gave the β,γ-unsaturated lactone **10**. This lactone **10** was then ammonolysed by reacting it at room temperature with anhydrous ammonia dissolved in tetrahydrofuran (THF). Analysis of the reaction mixture revealed the formation of the desired *exo* ketoamide **11** as the major product and of the *endo* ketoamide **12** as a minor product. The ratio of *exo* to *endo* was determined to be 2:1. This result is not too surprising as protonation of the intermediate enolate is expected to take place from the least hindered face, which is the face opposite to the ethano bridge. The nmr spectra of the *exo* isomer **11** show the olefinic protons absorbing as a multiplet between 6.35 and 6.55 ppm whereas the *endo* isomer **12** has its corresponding multiplet as a broad and less defined absorption located between 5.7 and 6.7 ppm.

The benzoyl group is now placed with the desired stereochemistry and the reduction of the carbonyl group remains to be carried out to ascertain the proper positioning of the phenylalanine equivalent.

Since the lithium aluminium hydride (LAH) reduction of **11** afforded a mixture of *exo* amino alcohols **13** in variable yields, due most likely to the formation of insoluble salts, it was found that the best approach to achieve this conversion was to carry it out on the nitrile **14**, readily prepared by the treatment of ketoamide **11** with trifluoroacetic anhydride in a mixture of pyridine and dioxane. LAH reduction of the resulting nitrile **14** provided a more reliable higher yielding and efficient preparation of **13**. There were no attempts to separate the diastereoisomers at this stage as, in the next step, the removal of the hydroxyl group eliminated this source of potential problems.

Reduction of **13** by lithium in liquid ammonia according to the indications of Hall *et al.* (11) gave **15**, where the benzyl group is now in place as a phenylalanine equivalent. The Eschweiler–Clark reaction (12) was performed on **15** in a boiling mixture of 37% aqueous formaldehyde solution and formic acid, leading to **16**, a derivative bearing the dimethylamino group that affords the basic nitrogen deemed necessary for analgesic activity.

The remaining problem to tackle was the introduction of the tyrosine equivalent, the *m*-hydroxyphenyl group. This was best achieved by hydroborating the double bond of intermediate **16**. This reaction gave rise to the isomeric alcohols **17***a* and **17***b* after decomposing the amine–borane complex by a base hydrolysis. A mixture of four isomers are possible and were indeed present in the mixture. However, the pair of the two regioisomers were readily separated by preparative hplc (high performance liquid chromatography) from the other pair as the difference of polarity was such that a pair required the incorporation of methanol in the eluent. This behavior is probably due to hydrogen bonding, possible in the case of **17***a* because of the proximity of the hydroxyl group and the dimethylamino group but not possible in the case of **17***b*. Each pair of regioisomers was oxidized to the corresponding ketone by Jones oxidation (13).

The structural assignment of the pair of regioisomers **17***a* and **17***b*, which was based on polarity considerations, was confirmed by the analysis of the nmr spectra of their corresponding ketones **18***a* and **18***b*. Thus, isomer **18***a* has a CH_2 group α to the carbonyl with a bridgehead proton next to it and its nmr shows that H-3a at 2.88 ppm is a doublet of doublets with coupling constants of 3.7 Hz and 14.0 Hz for the coupling of protons H-3a,H-4 and H-3a,H-3b, respectively. On the other hand, isomer **18***b*, having an isolated CH_2 group *ortho* to the carbonyl, shows the absorption of these protons H-2a and H-2b as an AB pair of doublets centered at 2.50 ppm with a coupling constant of 17 Hz.

The Grignard addition of *m*-methoxyphenylmagnesium bromide on ketone **18***a* allowed the introduction of the tyrosine equivalent. The mixture of tertiary alcohols **20** was dehydrated by treating it with *p*-toluenesulfonic acid in refluxing benzene,

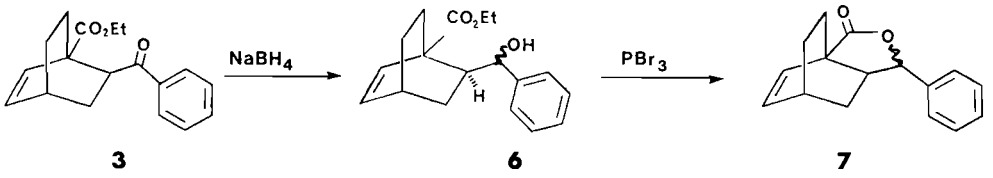

3 6 7

SCHEME 2

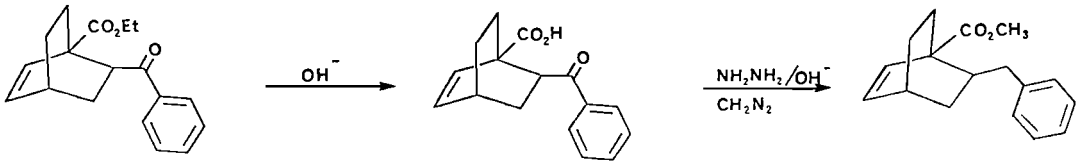

3 8 9

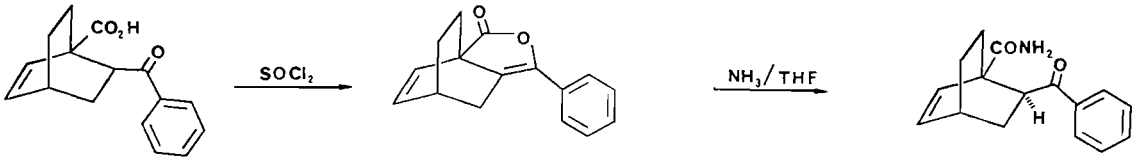

8 10 11

+

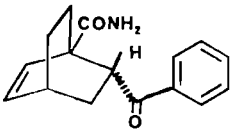

12

SCHEME 3

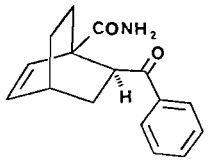

11

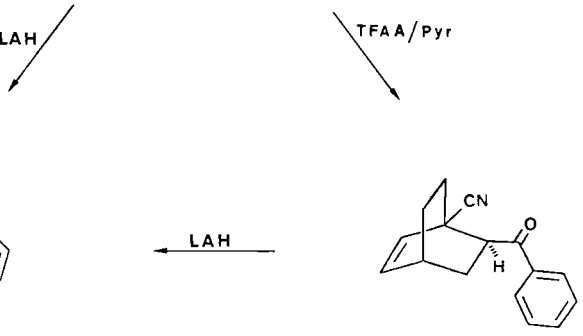

13 14

SCHEME 4

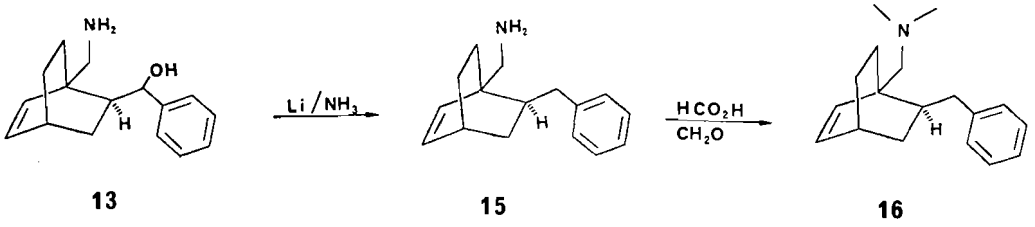

13 15 16

SCHEME 5

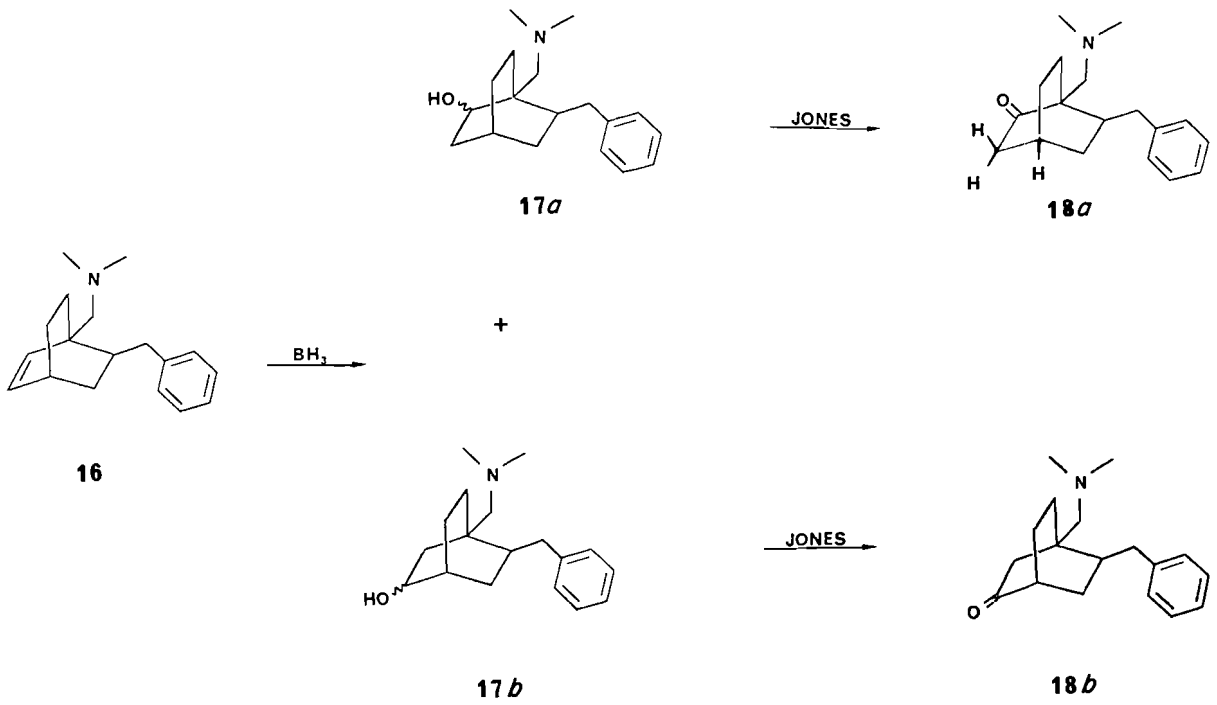

SCHEME 6

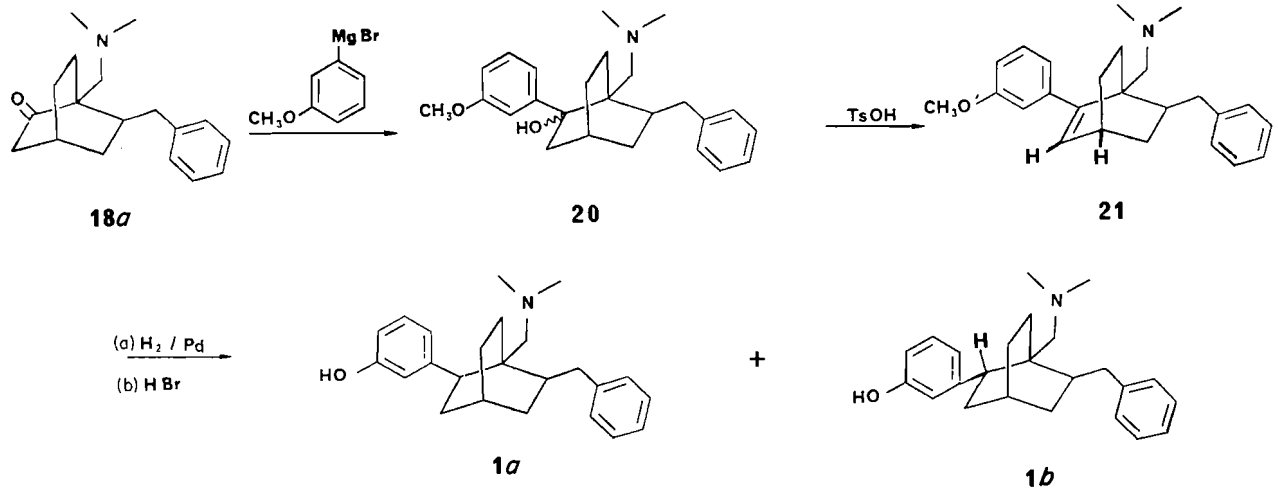

SCHEME 7

thus affording the olefinic product **21**. The olefinic proton absorbs at 5.95 ppm as a doublet having a coupling constant of 6.0 Hz, again in agreement with the proofs of structure of the alcohols **17** and ketones **18**. Hydrogenation of the olefin **21** gave a mixture of two products. Two isomers can be expected from this catalytic hydrogenation but preferential absorption was expected to occur from the least hindered face. Indeed, the reduction gave a major isomer, assigned as the desired isomer, based on the preferential attack of the double bond. The other isomer was assigned as having the *m*-methoxyphenyl group *endo* and was isolated in small amounts.

Deblocking the phenolic function in **22** was carried out by

refluxing **22** in a mixture of concentrated hydrogen bromide in acetic acid, leading to the isolation of the desired target **1**.

Compound **1** and its *endo* isomer were tested in the ^{3}H-Naloxone binding assay (14) and they were found to have only weak binding activity with a IC_{50} (mean inhibitory concentration) of 225 n*M* and 1025 n*M* respectively. Under the same conditions, morphine and methionine enkephalin had a IC_{50} of 4.5 n*M* and 9.0 n*M* respectively. When tested on rats in the hot plate assay (15), both isomers were found to be analgesic at 64 mg/kg when administered orally. Under these conditions, methionine enkephalin was inactive because of poor absorption and morphine was active at 2 mg/kg. Two reasons can be invoked to explain this disappointing biological activity. First of all, there may be a need for the missing methionine portion. Also, the glycine amides are considered as spacers that positioned the key aromatic groups in the correct spatial relationship. The use of the bicyclo[2.2.2]octane system to act as a spacer could be too great a change, as it was shown that slight modifications of the Gly-2 and Gly-3 amide carbonyls result in a marked decrease of the in vitro biological activities (16).

Experimental

Melting points were taken on a Thomas Hoover apparatus in open capillary tubes and are uncorrected. Infrared spectra were recorded on a Perkin–Elmer 267 grating spectrophotometer and were recorded as KBr disks unless otherwise noted. A Varian EM-360 spectrometer was used to record nmr spectra in deuterochloroform unless otherwise indicated. Proton chemical shifts are relative to tetramethylsilane (TMS) as internal standard. Elemental analyses were performed by Galbraith and Associates, Knoxville, TN.

All reactions as well as column chromatographic separations were monitored routinely with the aid of thin-layer chromatography (tlc) using precoated 0.25-mm silica gel GF plates, Analtech, visualized by charring with sulfuric acid.

Preparative hplc separations were performed on a Waters PrepLC/System 500 preparative liquid chromatograph using PrepPAK-500/Silica cartridges (5.7 × 30 cm). The peaks were detected with a differential refractive index detector and the flow rate was 200 mL/min, unless otherwise indicated.

endo-*6-Benzoyl-1-carboethoxybicyclo[2.2.2]-2-octene (3)*

Ethyl dihydrobenzoate **4** (335.3 g, 2.21 mol), 1-phenyl-3-propen-1-one **5** (347 g, 2.63 mol), and hydroquinone (32 g, 0.29 mol) were heated under nitrogen at 150°C for 24 h. The mixture was purified by preparative hplc eluting with 10% ether in hexane to yield *endo*-6-benzoyl-1-carboethoxybicyclo[2.2.2]-2-octene **3***a* (286 g, 46%) and *exo*-6-benzoyl-1-carboethoxybicyclo[2.2.2]-2-octene **3***b* (65 g, 13%); *endo*, mp 52–60°C; *exo*: oil.

3*a*: ir: 1725 (CO_2Et), 1680 (C=O) cm^{-1}; ^{1}H nmr (ppm): 0.9–3 (m, 10H, aliphatic protons), 4.15 (m, 3H, OCH_2 + 1 proton), 6.2 (t, 1H, H-3), 6.85 (d, J = 8 Hz, 1H, H-2), 7.45 (m, 3H, *para* and *meta* aromatic protons), 7.95 (m, 2H, *ortho* protons). *Anal.* calcd. for $C_{18}H_{20}O_3$: C 76.08, H 7.09; found: C 76.18, H 7.16.

3*b*: ir: 1725 (CO_2Et), 1680 (C=O) cm^{-1}; ^{1}H nmr (ppm): 0.9–3 (m, 10H, aliphatic protons), 4.15 (m, 3H, OCH_2 + 1 proton), 6.2 (t, 1H, H-3), 6.45 (d, J = 4 Hz, 1H, H-2), 7.45 (m, 3H, *para* and *meta* aromatic protons), 7.95 (m, 2H, *ortho* protons). *Anal.* calcd. for $C_{18}H_{20}O_3$: C 76.08, H 7.09; found: C 76.22, H 7.18.

Equilibrium of endo-*6-benzoyl-1-carboethoxybicyclo[2.2.2]-2-octene (3*a*)*

The *endo* isomer **3***a* (0.1 g, 0.35 mmol) was dissolved in ethanol (3 mL) of a sodium ethoxide solution prepared by reacting sodium (0.2 g) with ethanol (10 mL). The solution was left at room temperature for 3 days. Analysis by hplc, using a μ-Porasil column (Waters Scientific), eluting with hexane – ethyl acetate in a ratio of 8:2 (v/v), gave a ratio of 73:27 in favor of the more polar *endo* isomer **3***a*.

Equilibration of exo-*6-benzoyl-1-carboethoxybicyclo[2.2.2]-2-octene (3*b*)*

The *exo* isomer **3***b* (0.1 g, 0.35 mmol) was dissolved in ethanol (3 mL) of a sodium ethoxide solution prepared by reacting sodium (0.2 g) with ethanol (10 mL). The solution was left at room temperature for 3 days. Analysis by hplc, using the conditions described above, gave a ratio of 76:24 in favor of the more polar *endo* isomer **3***a*.

endo-*6-Benzoylbicyclo[2.2.2]-2-octene-1-carboxylic acid (8)*

endo-6-Benzoyl-1-carboethoxybicyclo[2.2.2]-2-octene (75 g, 0.26 mol) in ethanol (65 mL) was added to a solution of potassium hydroxide (52.8 g, 0.94 mol) in ethanol (200 mL). The mixture was refluxed for 4 h. The solvent was removed under vacuum, and the residue was taken up in water and extracted with ether. The aqueous layer was then acidified, the solid was filtered, and then air-dried to yield *endo*-6-benzoylbicyclo[2.2.2]-2-octene-1-carboxylic acid (**8**) (58.6 g, 87%), mp 249–253°C; ir: 1700 (CO_2H), 1675 (C=O) cm^{-1}; ^{1}H nmr (ppm): 0.9–2.4 (m, 7H, aliphatic protons), 3.95 (mq, J = 6 Hz, H-4, 6.15 (t, J = 8 Hz, 1H, H-3), 6.65 (d, J = 8 Hz, 1H, H-2), 7.50 (m, 3H, *para* and *meta* aromatic protons), 7.85 (m, 2H, *ortho* protons). *Anal.* calcd. for $C_{16}H_{16}O_3$: C 74.98, H 6.29; found: C 74.98, H 6.47.

Enol lactone (10)

endo-6-Benzoylbicyclo[2.2.2]-2-octene-1-carboxylic acid (**8**) (7 g, 27 mmol) was suspended in chloroform (100 mL) and thionyl chloride (14 mL, 0.19 mol) was added. After a reflux period of 3 h, the solution was evaporated to dryness to yield crude enol lactone **10** (6.5 g, 100%). An analytical sample obtained by preparative tlc had mp 100–105°C; ir: 1800 (CO), 1680 (C=C) cm^{-1}; ^{1}H nmr (ppm): 1.75 (m, 4H, aliphatic protons), 2.55 (m, 2H, CH_2), 3.10 (m, 1H, aliphatic proton), 6.40 (m, 2H, olefinic protons), 7.45 (m, 5H, aromatic protons). *Anal.* calcd. for $C_{16}H_{14}O_2$: C 80.65, H 5.92; found: C 80.67, H 5.95.

exo-*6-Benzoylbicyclo[2.2.2]-2-octene-1-carboxamide (11)*

Enol lactone (**10**) (46 g, 0.19 mol) dissolved in tetrahydrofuran (50 mL) was added slowly to a saturated solution of gaseous ammonia in THF (100 mL). After stirring the mixture at room temperature for 6 days, it was evaporated to dryness. Trituration of the mixture of *endo* and *exo* isomers in ether yielded pure *exo* **11**, sparingly soluble in ether (30 g, 61%), mp 165–168°C. The mother liquors contained 16 g of a mixture of the isomers enriched in the *endo* isomer; ir: 3490, 3170 (NH), 1678 (CO), 1670 ($CONH_2$) cm^{-1}; ^{1}H nmr (ppm): 1.55 (m, 5H, aliphatic protons), 2.65 (m, 2H, CH_2), 3.70 (q, 1H), 5.85 (broad peak, 2H, NH_2), 6.45 (d, 2H, olefinic protons), 7.45 (m, 3H, *para* and *meta* aromatic protons), 7.85 (m, 2H, *ortho* protons). *Anal.* calcd. for $C_{16}H_{17}O_2N$: C 75.28, H 6.71, N 5.48; found: C 75.29, H 6.92, N 5.34.

exo-*6-benzoyl-1-cyanobicyclo[2.2.2]-2-octene (14)*

To *exo*-6-benzoylbicyclo[2.2.2]-2-octene-1-carboxamide **11** (2.6 g, 10 mmol) dissolved in anhydrous dioxane (250 mL) and pyridine (23 mL) and maintained at 0°C, was added carefully trifluoroacetic anhydride (2.2 mL). The reaction mixture was heated at 50°C for 3 h and was poured into ice and water. It was then extracted with ether, the organic phases were washed with 5% sodium bicarbonate, with brine, dried (Na_2SO_4), and concentrated *in vacuo* to yield, after crystallization from cold ether, *exo*-6-benzoyl-1-cyanobicyclo[2.2.2]-2-octene **14** (2.2 g, 93%), mp 80–81°C; ir: 2240 (CN), 1680 (C=O) cm^{-1}; ^{1}H nmr (ppm): 1.60 (m, 5H, aliphatic protons), 2.70 (m, 2H, CH_2), 3.55 (q, 1H, J = 8 Hz, H-4), 6.35 (m, 2H, J = 2 Hz, olefinic protons), 7.50 (m, 3H, *meta* and *para* aromatic protons), 7.85 (m, 2H, *ortho* aromatic protons). *Anal.* calcd. for $C_{16}H_{15}ON$: C 80.98, H 6.37, N 5.90; found: C 80.80, H 6.32, N 5.84.

exo-*6-(α-hydroxybenzyl)-1-aminomethylbicyclo[2.2.2]-2-octene (13)*

Preparation from keto amide 11

To *exo*-6-benzoylbicyclo[2.2.2]-2-octene-1-carboxamide **11** (1.2 g, 4.7 mmol) dissolved in THF (20 mL) was added slowly a solution of LAH (0.5 g, 13.5 mmol) in THF (10 mL) and the mixture was refluxed for 24 h. The reaction mixture was poured into ice and water. It was then extracted with ether, the organic phases were washed with 5% sodium bicarbonate, with brine, dried (Na_2SO_4), and concentrated *in*

vacuo to yield a residue that was purified by chromatography on alumina to give *exo*-6-(α-hydroxybenzyl)-1-aminomethylbicyclo[2.2.2]-2-octene **13** (0.38 g, 33%), mp 118–120°C; ir: 3365, 3320, 3290 (NH_2, OH) cm^{-1}; ^1H nmr (ppm): 0.9–2.5 (m, 8H, aliphatic protons), 3.05 (m, 2H, CH_2), 3.65 (s, 3H, NH_2, OH), 4.45 (d, J = 10 Hz, 1H, CHO), 6.10 (m, 2H, J = 2 Hz, olefinic protons), 7.20 (s, 5H, aromatic protons). *Anal.* calcd. for $C_{16}H_{21}ON$: C 78.97, H 8.69, N 5.75; found: C 78.70, H 8.90, N 5.55.

Preparation from nitrile ***14***

Similarly, the reduction of nitrile **14** (2.2 g, 9.2 mmol) by LAH (1 g, 26.3 mmol) in THF (40 mL) proceeded well to give 60% yield of **13** whose properties were identical to those of the product obtained from the reduction of the amide **11**.

exo-*6-Benzyl-1-aminomethylbicyclo[2.2.2]-2-octene (**15**)*

exo-6-(α-Hydroxybenzyl)-1-aminomethylbicyclo[2.2.2]-2-octene **13** (11 g, 45 mmol) in THF (75 mL) was added dropwise to a solution of lithium (6 g, 0.86 mol) in liquid ammonia (500 mL). Stirring was maintained for 2 h and then solid ammonium chloride (30 g) was added to the reaction mixture, followed by the careful addition of water. The aqueous mixture was extracted with methylene chloride, the organic phases were washed with brine, dried (Na_2SO_4), and concentrated *in vacuo* to yield a residue that was purified by preparative hplc, eluting with 4% methanol in chloroform containing 0.4% NH_4OH to give *exo*-6-benzyl-1-aminomethylbicyclo[2.2.2]-2-octene (**15**) (8.6 g, 84%), mp 102–104°C. The hydrochloride had mp 243–245°C; ir: 3300 (NH_2) cm^{-1}; ^1H nmr (ppm): 1.0–3.0 (m, 14H, aliphatic protons), 6.20 (m, 2H, J = 4 Hz, olefinic protons), 7.15 (s, 5H, aromatic protons). *Anal.* calcd. for $C_{16}H_{21}NCl$: C 72.84, H 8.40, N 5.31, Cl 13.43; found: C 72.70, H 8.37, N 5.21, Cl 13.23.

exo-*6-Benzyl-1-dimethylaminomethylbicyclo[2.2.2]-2-octene (**16**)*

exo-6-Benzyl-1-aminomethylbicyclo[2.2.2]-2-octene **15** (5 g, 22 mmol), formic acid (100 mL), and 35% aqueous formaldehyde (5 mL) were refluxed under nitrogen for 5 h. The volatiles were removed under vacuum and the residue was taken up in water (100 mL). The resulting solution was neutralized with 5% sodium bicarbonate, extracted with methylene chloride, dried (Na_2SO_4), and evaporated to yield **16** (5 g, 89%). Its hydrochloride had mp 237–240°C; ^1H nmr (ppm): 1.0–3.0 (m, 18H, aliphatic protons), 6.25 (m, 2H, J = 4 Hz, olefinic protons), 7.10 (s, 5H, aromatic protons). *Anal.* calcd. for $C_{18}H_{26}NCl$: C 74.02, H 8.98, N 4.80, Cl 12.15; found: C 73.90, H 9.01, N 4.80, Cl 12.34.

exo-*6-Benzyl-2-hydroxy-1-dimethylaminomethylbicyclo[2.2.2]-2-octane (**17**a, **17**b)*

exo-6-Benzyl-1-dimethylaminomethylbicyclo[2.2.2]-2-octene (**16**) (9 g, 35 mmol) dissolved in THF (20 mL) was treated with diborane (50 mL, 1 *M* solution in THF, 50 mmol) at 0°C under nitrogen for a period of 2 h. Sodium hydroxide (50 mL, 3 *N*) and 30% hydrogen peroxide (50 mL) were slowly and successively added to the mixture, which was then refluxed for 1 h to hydrolyse the amine–borane complex. The two phases were separated and the aqueous phase was extracted with ether. The organic phases were combined and washed with brine, dried (Na_2SO_4), and concentrated *in vacuo* to yield a residue that was purified by preparative hplc, eluting with 10% methanol in chloroform containing 0.1% NH_4OH to yield 6-benzyl-2-hydroxy-1-dimethylaminomethylbicyclo[2.2.2]-2-octane (**17***a*) as the less polar isomer (6.2 g, 65%) and 6-benzyl-3-hydroxy-1-dimethylaminomethylbicyclo[2.2.2]-2-octane (**17***b*) as the more polar isomer (1.7 g, 18%).

Isomer ***17***a: ir: 3390 (OH) cm^{-1}: ^1H nmr (ppm): 1.0–2.0 (m, 7H, aliphatic protons), 2.0–3.0 (m, 13H, aliphatic protons), 3.95 (m, 1H, CH), 7.20 (s, 5H, aromatic protons), 7.85 (br s, 1H, OH). *Anal.* calcd. for $C_{18}H_{27}NO$: C 79.12, H 9.89, N 5.12; found: C 79.64, N 9.97, N 4.98.

Isomer ***17***b: ir: 3390 (OH) cm^{-1}; ^1H nmr (ppm): 1.0–2.9 (m, 21H, aliphatic protons), 2.90 (m, 1H, CH), 7.20 (s, 5H, aromatic protons). *Anal.* calcd. for $C_{18}H_{27}NO$: C 79.12, H 9.89, N 5.12; found: C 79.40, H 9.71, N 4.85.

exo-*6-Benzyl-2-keto-1-dimethylaminomethylbicyclo[2.2.2]-2-octane (**18**a)*

exo-6-Benzyl-2-hydroxy-1-dimethylaminomethylbicyclo[2.2.2]-2-octane (**17***a*) (5 g, 18 mmol) dissolved in acetone (100 mL) was cooled at 0°C and 1.1 *M* Jones reagent (18 mL, 19.8 mmol) was added dropwise to the solution. The mixture was stirred for 4 h at 0°C and was poured into water (50 mL). It was extracted with methylene chloride. The organic phase was washed with brine, dried (Na_2SO_4), and concentrated *in vacuo* to yield *exo*-6-benzyl-2-keto-1-dimethylaminomethylbicyclo[2.2.2]-2-octane (**18***a*) (4.8 g, 91%) as an oil; ir: 1715 (CO) cm^{-1}; ^1H nmr (ppm): 1.0–2.3 (m, 2H, aliphatic protons), 2.5 (s, 2H, CH_2N), 2.70 (d of d, J = 11.2 Hz, 14 Hz, H-3b), 2.90 (d of d, J = 3.7 Hz, 14.0 Hz, H-3a), 3.03 (s, 3H, CH_3), 3.07 (s, 3H, CH_3), 3.35 (2H, q, J_{ab} = 14 Hz, CH_2), 7.25 (m, 5H, aromatic protons). *Anal.* calcd. for $C_{18}H_{25}NO$: C 79.65, H 9.28, N 5.16; found: C 79.74, H 9.40, N 5.00.

exo-*6-Benzyl-3-keto-1-dimethylaminomethylbicyclo[2.2.2]-2-octane (**18**b)*

exo-6-Benzyl-3-hydroxy-1-dimethylaminomethylbicyclo[2.2.2]-2-octane (**17***a*) (2.5 g, 9 mmol) dissolved in acetone (100 mL) was cooled at 0°C and 1.1 *M* Jones reagent (9 mL, 9.9 mmol) was added dropwise to the solution. The mixture was stirred for 4 h at 0°C and was poured into water (50 mL). It was extracted with methylene chloride. The organic phase was washed with brine, dried (Na_2SO_4), and concentrated *in vacuo* to yield *exo*-6-benzyl-3-keto-1-dimethylaminomethylbicyclo[2.2.2]-2-octane (**18***b*) (2.0 g, 90%) as an oil; ir: 1730 (CO) cm^{-1}; ^1H nmr (ppm): 1.0–2.3 (m, 10H, aliphatic protons), 2.40 (d, J = 14 Hz, H-3b), 2.90 (d, J = 14.0 Hz, H-3a), 2.82 (s, 3H, CH_3), 2.88 (s, 3H, CH_3), 3.16 (2H, q, J_{ab} = 14 Hz, CH_2), 7.25 (m, 5H, aromatic protons). *Anal.* calcd. for $C_{18}H_{25}NO$: C 79.65, H 9.28, N 5.16; found: C 79.70, H 9.22, N 5.04.

endo- *and* exo-*6-benzyl-2-(*m*-methoxyphenyl)-2-hydroxy-1-dimethylaminomethylbicyclo[2.2.2]-2-octane (**20**)*

To *m*-methoxyphenylmagnesium bromide prepared by the reaction of magnesium (0.97 g, 40 mmol) with *m*-bromoanisole (7.5 g, 40 mmol) in THF (50 mL) was added dropwise a solution of *exo*-6-benzyl-2-keto-1-dimethylaminomethylbicyclo[2.2.2]-2-octane (**18***a*) (4 g, 14.7 mmol) at room temperature. After stirring for 30 min, the reaction mixture was quenched by adding water (14 mL). The aqueous mixture was extracted with chloroform. The organic phase was washed with brine, dried (Na_2SO_4), and concentrated *in vacuo* to yield a residue that was purified by preparative hplc, eluting with 1% methanol in chloroform containing 1% NH_4OH to give a mixture of *endo*- and *exo*-6-benzyl-2-(*m*-methoxyphenyl)-2-hydroxy-1-dimethylaminomethylbicyclo[2.2.2]-2-octane (**20**) (3.3 g, 59%), mp 85–89°C; ir: 3200 (OH) cm^{-1}; ^1H nmr (ppm): 1.0–3.0 (m, 20H, aliphatic protons), 3.75 (s, 3H, CH_3), 6.40 (s, 1H, OH), 7.15 (m, 9H, aromatic protons). *Anal.* calcd. for $C_{25}H_{33}NO_2$: C 79.11, H 8.76, N 3.69; found: C 79.38, H 8.40, N 3.99.

exo-*6-Benzyl-2-*m*-methoxyphenyl-1-dimethylaminomethylbicyclo[2.2.2]-2-octane (**21**)*

The mixture of *endo*- and *exo*-6-benzyl-2-(*m*-methoxyphenyl)-2-hydroxy-1-dimethylaminomethylbicyclo[2.2.2]-2-octane (**20**) (0.59 g, 1.55 mmol) was refluxed for 2 h in benzene containing traces of *p*-toluenesulfonic acid. The reaction mixture was washed with brine, dried (Na_2SO_4), and concentrated *in vacuo* to yield *exo*-6-benzyl-2-*m*-methoxyphenyl-1-dimethylaminomethylbicyclo[2.2.2]-2-octene (**21**) (0.58 g, 100%), mp 88–100°C. Its hydrochloride had mp 162–164°C; ^1H nmr (ppm): 1.85–2.55 (m, 17H, aliphatic protons), 3.70 (s, 3H, CH_3), 3.75 (d, 1H, CH), 6.00 (d, J = 6 Hz, 1H, H-3), 6.85 (m, 4H, aromatic protons), 7.15 (m, 5H, aromatic protons). *Anal.* calcd. for $C_{25}H_{31}NO$: C 72.84, H 8.15, N 3.39; found: C 73.12, H 8.36, N 3.26.

exo-*6-Benzyl*-exo-*2-*m*-methoxyphenyl-1-dimethylaminomethylbicyclo[2.2.2]-2-octane (**22**a)*

exo-6-Benzyl-*exo*-2-*m*-methoxyphenyl-1-dimethylaminoethylbicyclo[2.2.2]-2-octene (2.9 g, 8 mmol) in ethanol (150 mL) was hydro-

genated at 50 psi (1 psi = 6.9 kPa) over 5% palladium on charcoal (0.35 g) for a period of 1 h. After filtering through Celite, the filtrate was concentrated *in vacuo* to yield 2.9 g of a mixture of epimers. The crude mixture was chromatographed on silica gel, eluting with chloroform treated with 0.1% NH_4OH, giving *exo*-6-benzyl-*exo*-2-*m*-methoxyphenyl-1-dimethylaminomethylbicyclo[2.2.2]-2-octane (**22***a*) (1.8 g, 62%) as the major isomer and *endo*-6-benzyl-*exo*-2-*m*-methoxyphenyl-1-dimethylaminomethylbicyclo[2.2.2]-2-octane (**5***b*) as the minor isomer (150 mg).

The hydrochloride of the major isomer had mp 238–240°C.

Isomer **22**a: ^{1}H nmr (ppm): 1.60–2.10 (m, 21H, aliphatic protons), 3.05 (m, 2H, H-4, H-5), 3.70 (s, 3H, CH_3), 6.85 (m, 4H, aromatic protons), 7.10 (m, 5H, aromatic protons). *Anal.* calcd. for $C_{25}H_{35}NO$: C 75.10, H 8.51, N 3.50; found: C 74.97, H 8.46, N 3.41.

Isomer **22**b: ^{1}H nmr (ppm): 1.60–2.10 (m, 21H, aliphatic protons), 3.05 (m, 2H, H-4, H-5), 3.70 (s, 3H, CH_3), 6.85 (m, 4H, aromatic protons), 7.10 (m, 5H, aromatic protons). *Anal.* calcd. for $C_{25}H_{35}NO$: C 75.10, H 8.51, N 3.50; found: C 75.21, H 8.36, N 3.51.

exo-*6-Benzyl*-exo-*2*-m-*hydroxyphenyl-1-dimethylaminomethylbicyclo[2.2.2]-2-octane (1*a)

exo-6-Benzyl-*exo*-2-*m*-methoxyphenyl-1-dimethylaminomethylbicyclo[2.2.2]-2-octane (**22***a*) (0.46 g, 1.27 mmol) in acetic acid (5 mL) and 48% hydrobromic acid (5 mL) was refluxed under nitrogen for a period of 24 h. The mixture was neutralized with concentrated ammonia, extracted with methylene chloride, the organic phase was washed with brine, dried (Na_2SO_4), and concentrated *in vacuo* to yield *exo*-6-benzyl-*exo*-2-*m*-hydroxyphenyl-1-dimethylaminomethylbicyclo[2.2.2]-2-octane (**1***a*) (0.43 g, 97%). After purification by tlc, it had mp 155–157°C. Its hydrochloride had mp 264–265°C; ^{1}H nmr (ppm): 1.60–2.10 (m, 19H, aliphatic protons), 3.05 (m, 2H, H-4, H-5), 5.48 (s, 1H, OH), 6.85 (m, 4H, aromatic protons), 7.10 (m, 5H, aromatic protons). *Anal.* calcd. for $C_{24}H_{32}NOCl \cdot 0.5H_2O$: C 73.01, H 8.36, N 3.54; found: C 73.34, H 8.42, N 3.44.

endo-*6-Benzyl*-exo-*2*-m-*hydroxyphenyl-1-dimethylaminomethylbicyclo[2.2.2]-2-octane (1*b)

endo-6-benzyl-*exo*-2-*m*-methoxyphenyl-1-dimethylaminomethylbicyclo[2.2.2]-2-octane (**22***b*) (0.10 g, 0.27 mmol) in acetic acid (3 mL) and 48% hydrobromic acid (3 mL) was refluxed under nitrogen for a period of 24 h. The mixture was neutralized with concentrated ammonia, extracted with methylene chloride, the organic phase was washed with brine, dried (Na_2SO_4), and concentrated *in vacuo* to yield *exo*-6-benzyl-*exo*-2-*m*-hydroxyphenyl-1-dimethylaminomethylbicyclo[2.2.2]-2-octane (**1***b*) (0.08 g, 80%), isolated as an oil. Its hydrochloride had mp 150–153°C; ^{1}H nmr (ppm): 1.60–2.10 (m, 19H, aliphatic protons), 3.05 (m, 2H, H-4, H-5), 6.85 (m, 5H, aromatic protons, OH), 7.10 (m, 5H, aromatic protons). *Anal.* calcd. for $C_{24}H_{32}NOCl$: C 74.71, H 8.30, N 3.63; found: C 74.41, H 8.58, N 3.41.

Preparation of 1-carboethoxy-6-(α-hydroxybenzyl)bicyclo[2.2.2]-2-octene (6)

To a solution of 1-carboethoxy-6-benzoylbicyclo[2.2.2]-2-octene (280 mg, 1 mmol) in methanol (10 mL) was added sodium borohydride (40 mg) and the reaction mixture was stirred at room temperature for 15 min. The mixture was poured into water and extracted with ether, washed with brine, dried (Na_2SO_4), and concentrated *in vacuo*. The residue was chromatographed on silica gel, eluting with benzene to yield 254 mg of 1-carboethoxy-6-(α-hydroxybenzyl)bicyclo[2.2.2]-2-octene; ir: 3480 (OH), 1720 (CO) cm^{-1}; ^{1}H nmr (ppm): 1.60–2.10 (m, 13H, aliphatic protons), 4.00 (m, 3H, CH_2, CHO), 6.35 (m, 2H, olefinic protons), 7.23 (m, 5H, aromatic protons). *Anal.* calcd. for $C_{18}H_{22}O_3$: C 75.49, H 7.74; found: C 75.22, H 7.71.

Preparation of lactone (7)

To a solution of 1-carboethoxy-6-(α-hydroxybenzyl)bicyclo[2.2.2]-2-octene (154 mg, 0.53 mmol) in ether (5 mL) was added phosphorous oxychloride (100 mg) and the reaction mixture was stirred at room temperature for 30 min. The mixture was poured into water and extracted with ether, washed with brine, dried (Na_2SO_4), and concentrated *in vacuo*. The residue was chromatographed on silica gel, eluting with benzene to yield 129 mg of lactone (**7**); ir: 1780 (CO) cm^{-1}; ^{1}H nmr (ppm): 1.30–2.70 (m, 8H, aliphatic protons), 4.73 (d, J = 10 Hz, 1H, CHO), 6.10 (d, J = 8 Hz, 1H, H-2), 6.50 (t, J = 6 Hz, 1H, H-3), 7.27 (m, 5H, aromatic protons). *Anal.* calcd. for $C_{16}H_{15}O_2$: C 79.97, H 6.71; found: C 79.78, H 6.90.

Preparation of 1-carboethoxy-6-benzylbicyclo[2.2.2]-2-octene

A solution of 1-carboethoxy-6-benzoylbicyclo[2.2.2]-2-octene (280 mg, 1 mmol) and potassium hydroxide (300 mg) in ethylene glycol (10 mL) was heated at 100°C for a period of 45 min. At this point, all ester was found to be hydrolysed to its corresponding acid. Hydrazine (0.5 mL) was then added and the temperature was brought up to 200°C and maintained at that temperature for 2 h. The reaction mixture was then poured onto water and extracted with ether, washed with brine, dried (Na_2SO_4), and concentrated *in vacuo*. The residue was taken up in ether and treated with an excess of diazomethane. Evaporation of the ether gave a residue (207 mg) that was purified by chromatography on silica gel, eluting with 10% ether in hexane to yield 17 mg of 1-carbomethoxy-6-benzylbicyclo[2.2.2]-2-octene as an oil; ir: 1730 (CO) cm^{-1}; ^{1}H nmr (ppm): 1.50–2.70 (m, 10H, aliphatic protons), 3.83 (s, 3H, CH_3), 6.30 (m, 2H, H-2 and H-3), 7.27 (m, 5H, aromatic protons); mass spectrum: M^+ 256.

Acknowledgements

The authors wish to thank Dr. P. Gund and G. M. Smith (Merck Sharp and Dohme Research Laboratories, Rahway, New Jersey) for their help and discussions regarding the Merck Molecular Modeling System, Dr. R. N. Young and Dr. J. Rokach (Merck Frosst Canada Inc.) for useful and frequent discussions on the synthetic work, and Dr. P. S. Anderson and Dr. F. M. Robinson (Merck Sharp and Dohme Research Laboratories, West Point, Pennsylvania) for numerous discussions on analgesics. The authors wish also to acknowledge the support of Dr. R. L. Hudgin, Ms. S. Charleson, and Ms. A. Rackham (Merck Frosst Canada Inc.) for the determination of biological activities of the compounds.

1. (*a*) J. Hughes. Brain Res. **88**, 295 (1975); (*b*) J. Hughes, T. W. Smith, H. W. Kosterlitz, L. A. Fothergill, B. A. Morgan, and H. R. Morris. Nature (London), **258**, 577 (1975).
2. H. W. Kosterlitz (*Editor*). Opiates and endogeneous opioid peptides. Elsevier/North Holland Biomedical Press, Amsterdam, The Netherlands. 1976.
3. P. Gund, J. D. Andose, J. B. Rhodes, and G. M. Smith. Science, **208**, 1425 (1980).
4. G. De Stevens. Analgetics. Academic Press, New York. 1965.
5. J. S. Morley. Annu. Rev. Pharmacol. Toxicol. 82 (1980).
6. P. W. Schiller, C. F. Yam, and M. Lis. Biochemistry, **16**, 1831 (1977).
7. A. F. Bradbury et al. Nature (London), **260**, 793 (1976).
8. R. C. A. Frederickson, R. Nickander, E. L. Smithwick, R. Shuman, and F. H. Norris. Opiates and endogeneous opioid peptides. Elsevier/North Holland Biomedical Press, Amsterdam, The Netherlands. 1976. p. 239.
9. S. Hünig and H. Kahanek. Chem. Ber. **90**, 238 (1957).
10. L. J. Bellamy. The infrared spectra of complex molecules. Chapman and Hall, London. 1975. p. 212.
11. S. S. Hall, S. D. Lipsky, F. J. McEnroe, and A. P. Bartels. J. Org. Chem. **36**, 2588 (1971).
12. H. T. Clark, H. B. Gillespie, and S. Z. Weisshaus. J. Am. Chem. Soc. **55**, 4571 (1933).
13. K. Bowden, I. M. Heilbron, E. R. H. Jones, and B. C. L. Weedon. J. Chem. Soc. 39 (1946).
14. C. B. Pert, S. H. Snyder, and E. L. May. J. Pharmacol. Exp. Ther. **196**, 316 (1976).
15. N. B. Eddy and D. Leimbach. J. Pharmacol. Exp. Ther. **107**, 385 (1953).
16. M. Szelke. International Narcotic Research Conference, North Falmouth, Mass. June 11–15, 1978.

Solute–solvent effects in the dissociation of thymolsulfonephthalein (an uncharged acid) in aqueous mixtures of acetonitrile (ACN), urea, and dimethyl sulfoxide (DMSO)

A. L. De and A. K. Atta

Department of Chemistry, Presidency College, Calcutta-700 073, India

Received August 12, 1985[1]

A. L. De and A. K. Atta. Can. J. Chem. **64**, 1521 (1986).

The thermodynamic first dissociation constants, $({}_sK)_{H_2A}$ of thymolsulfonephthalein (H_2A), an uncharged acid, have been determined at 25°C in aqueous mixtures of 10, 30, 50, 70, and 80 wt% acetonitrile (ACN), 11.52, 20.31, 29.64, and 36.83 wt% urea, 20, 40, 60, and 80 wt% dimethyl sulfoxide (DMSO) by spectrophotometric measurements. The solvent effect represented by $\partial(\Delta G^0) = 2.303RT[p({}_sK)^N - p({}_wK)^N]$ is found to increase in ACN + H_2O system as mol% ACN increases in the solvent. In contrast, the corresponding values in urea + H_2O as well as DMSO + H_2O solvent systems decrease with increase in proportion of organic component in the solvent, the decrease being sharp in urea + H_2O. The results have been discussed in terms of the standard Gibbs energies of transfer of H^+ from water to the mixed solvent, $\Delta G_t^0(H^+)$ and the relative values of the standard Gibbs energies of transfer of HA^-, $\Delta G_t^0(HA^-)$ and of $\Delta G_t^0(H_2A)$ in all the solvent systems. The overall dissociation behaviour of the acid (H_2A) is found to be dictated by the specific solute-solvent interactions of the species participating in the dissociation equilibria.

A. L. De et A. K. Atta. Can. J. Chem. **64**, 1521 (1986).

Faisant appel à des mesures spectrophotométriques et opérant à 25°C, dans des mélanges aqueux à 10, 30, 50, 70 et 80% (poids) d'acétonitrile (ACN), à 11,52, 20,31, 29,64 et 36,83% (poids) d'urée et 20, 40, 60 et 80% (poids) de diméthylsulfoxyde (DMSO), on a déterminé les premières constantes de dissociation thermodynamiques, $({}_sK)_{H_2A}$, de la thymolsulfonephtaléine (H_2A), un acide qui n'est pas changé. On a trouvé que, dans le système ACN/H_2O, l'effet de solvant représenté par l'équation $\partial(\Delta G^0) = 2{,}303RT[p({}_sK)^N - p({}_wK)^N]$ augmente avec une augmentation de la concentration de ACN dans le solvant. Par ailleurs, les valeurs correspondantes dans les systèmes de solvant urée/H_2O et DMSO/H_2O diminuent avec une augmentation de la proportion du composé organique dans le solvant; la diminution est rapide dans le système urée/H_2O. On discute des résultats en fonction des énergies standard de Gibbs pour le transfert des ions H^+ de l'eau vers le solvant mixte, $\Delta G_t^0(H^+)$ et des valeurs relatives des énergies standard de Gibbs pour le transfert des ions HA^-, $\Delta G_t^0(HA^-)$, et de l'acide H_2A, $\Delta G_t^0(H_2A)$, dans tous les systèmes de solvants. On a trouvé que le comportement global de la dissociation de l'acide (H_2A) est dicté par les interactions spécifiques soluté/solvant des espèces qui participent dans l'équilibre de la dissociation.

[Traduit par la revue]

Introduction

Despite extensive (1–9) studies the solvent effect on the dissociation of weak Brønsted acids can hardly be considered completely understood. Previously solvent effect was believed to be chiefly guided by the change of dielectric constant of the solvents. But recent observation that the extent of proton transfer processes differs in different isodielectric solvent systems (8, 9) leads to recognize that the dielectric constant can not be the sole factor but the chemical nature of the cosolvents also plays an important role in dictating the overall solvent effects.

In this paper attempts have been made to examine the solvent effects on proton transfer equilibria of the neutral acid, thymolsulfonephthalein in a series of aqueous binary mixtures of several cosolvents having different physicochemical properties such as urea, dimethyl sulfoxide (DMSO) and acetonitrile (ACN), in light of the solvation behaviour of the species involved in the dissociation equilibria. Unlike DMSO + H_2O (10) and ACN + H_2O (11) mixtures, the dielectric constant (ϵ_s) value of urea + H_2O (12) increases with the increase in organic component of the solvent in the mixture (ϵ_s values are shown in Table 4). Such an analysis is expected to reveal important information on the solvation behaviour of the species involved in the dissociation equilibria, as would be guided by the influence of varying acidity, basicity, dispersion, structural and electronic characteristics of the cosolvents and their aqueous mixtures besides the varying Born-type electrostatic interactions on the ionic species involved. Dissociation constants of monopositively charged acids in urea + H_2O (7*c*, *d*), ACN + H_2O (7*e*), and DMSO + H_2O (13, 14) were reported earlier and the study is now extended to uncharged acid.

The structures of thymolsulfonephthalein may be represented by **I** to **III**.

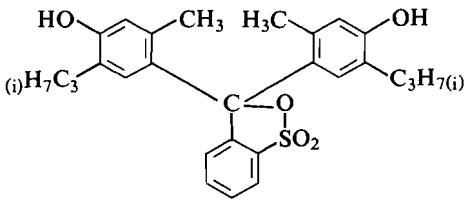

I

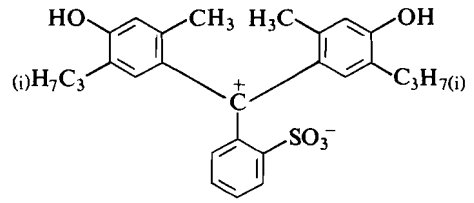

II

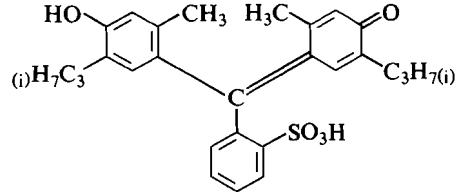

III

[1]Revision received February 28, 1986.

TABLE 1. Data for spectrophotometric determination of $p({}_sK)_{H_2A}$ of thymolsulfonephthalein in ACN + H_2O mixtures at 25°C

m_{HCl}	A	$p({}_sK)'_{H_2A}$	m_{HCl}	A	$p({}_sK)'_{H_2A}$
10 wt% ACN; [indicator] = 1.64×10^{-5} M			70 wt% ACN; [indicator] = 1.65×10^{-5} M		
Completely basic	0.013	—	Completely basic	0.013	—
0.005101	0.093	1.634	0.001925	0.167	2.405
0.01023	0.151	1.641	0.002883	0.209	2.404
0.01534	0.193	1.655	0.003853	0.241	2.403
0.02037	0.220	1.647	0.005769	0.287	2.405
0.02556	0.247	1.657	0.007701	0.320	2.410
0.03061	0.270	1.671	0.009642	0.342	2.407
0.03578	0.284	1.663	0.01149	0.361	2.414
0.04089	0.302	1.678	0.01353	0.377	2.419
0.04588	0.318	1.694	0.01546	0.387	2.415
Completely acidic	0.548	—	Completely acidic	0.553	—
30 wt% ACN; [indicator] = 1.57×10^{-5} M			80 wt% ACN; [indicator] = 1.43×10^{-5} M		
Completely basic	0.009	—	Completely basic	0.004	—
0.003910	0.092	1.768	0.000569	0.131	2.849
0.007822	0.145	1.771	0.001139	0.199	2.849
0.01165	0.187	1.790	0.001706	0.244	2.855
0.01566	0.218	1.795	0.002271	0.276	2.861
0.02349	0.260	1.798	0.003425	0.317	2.860
0.02740	0.281	1.817	0.004523	0.345	2.874
0.03127	0.299	1.835	0.005669	0.359	2.858
0.03514	0.308	1.828	0.007347	0.378	2.860
0.04305	0.331	1.846	0.008016	0.386	2.873
Completely acidic	0.530	—	Completely acidic	0.488	—
50 wt% ACN; [indicator] = 1.21×10^{-5} M					
Completely basic	0.009	—			
0.003330	0.088	1.970			
0.006654	0.133	1.972			
0.009992	0.166	1.984			
0.01336	0.192	2.001			
0.01657	0.203	1.979			
0.01998	0.222	2.001			
0.02331	0.230	1.988			
0.02663	0.243	2.007			
0.03005	0.255	2.027			
Completely acidic	0.403	—			

The probable structure of thymolsulfonephthalein in solution in red colour acid form is **II** or **III**. Kolthoff *et al.* (15) considered acid form of a thymolsulfonephthalein as a hybrid, $A^{\pm}$ (acid–base type $A^{\pm}B^{\pm -}$). While studying the salt effect and medium effect on the dissociation of *m*-cresolsulfonephthalein in methanol–water, Bates *et al.* (16) has indicated that the behaviour of activity coefficient function does not lend support to one of the three possible structures A^0B^-, $A^{\pm}B^-$, or $A^{\pm}B^{\pm -}$.

The neutral thymolsulfonephthalein can be written (17) as H_2A since it has two ionizable hydrogen atoms, one of which undergoes ionization in the acid range (step *i*) and the other in the alkaline range (step *ii*). The two steps may be represented in reaction [1].

$$[1]\quad \underset{\text{(red)}}{H_2A} \underset{\text{step } i}{\overset{-H^+}{\rightleftharpoons}} \underset{\text{(yellow)}}{HA^-} \underset{\text{step } ii}{\overset{-H^+}{\rightleftharpoons}} \underset{\text{(blue)}}{A^{2-}}$$

The first stages of ionization of neutral H_2A in the mixed solvent SH is represented by reaction [2]

$$[2]\quad H_2A + SH \rightleftharpoons HA^- + SH_2^+$$

Experimental

Purification of ACN (18) (BDH), DMSO (19) (Merck), and water (18) have been described. DMSO + H_2O and urea + H_2O mixtures were prepared by weight and dry HCl gas was passed into respective solvents to produce HCl solution. Molal concentration of HCl was obtained by titrating weighed amounts of solution dissolved in water against standard aqueous alkali using phenolphthalein as the indicator. Stock HCl solution in ACN + H_2O mixture was, however, obtained by mixing weighed amounts of standard aqueous HCl solution and pure ACN in suitable proportion to give the desired solvent composition. This procedure in ACN + H_2O was necessary for stable absorbance readings and reproducibility of result. Thymolsulfonephthalein (pro-analysis, E. Merck) was used as such. Dissociation constants were determined spectrophotometrically using the method described for some acids earlier (5*a*, 20, 21). As H_2A is a relatively strong acid, it is possible to achieve considerable variation in the degree of dissociation by varying the concentration of added strong acid, HCl permitting determination of $p({}_sK)_{H_2A}$ without recourse to buffer solution. A series of solutions were prepared in 10 cm^3 amounts by adding weighed amounts of HCl solution, indicator solution, and the appropriate solvent. Simple calculation gave the molalities of HCl. The spectral

TABLE 2. Data for spectrophotometric determination of $p({}_sK)_{H_2A}$ of thymolsulfonephthalein in urea + H_2O mixtures at 25°C

m_{HCl}	A	$p({}_sK)'_{H_2O}$	m_{HCl}	A	$p({}_sK)'_{H_2A}$
11.52 wt% urea; [indicator] = 1.53×10^{-5} M			29.64 wt% urea; [indicator] = 1.62×10^{-5} M		
Completely basic	0.012	—	Completely basic	0.013	—
0.01874	0.077	1.029	0.01891	0.039	0.573
0.03751	0.121	1.051	0.03784	0.062	0.608
0.05615	0.150	1.052	0.05682	0.080	0.619
0.07514	0.180	1.083	0.07557	0.100	0.657
0.09364	0.198	1.085	0.09463	0.113	0.660
0.1121	0.217	1.104	0.1140	0.131	0.694
0.1312	0.233	1.118	0.1327	0.145	0.714
0.1493	0.247	1.133	0.1513	0.157	0.729
Completely acidic	0.513	—	Completely acidic	0.536	—
20.31 wt% urea; [indicator] = 1.46×10^{-5} M			36.83 wt% urea; [indicator] = 1.55×10^{-5} M		
Completely basic	0.012	—	Completely basic	0.013	—
0.01796	0.050	0.799	0.01957	0.032	0.412
0.03583	0.078	0.817	0.03906	0.049	0.452
0.05396	0.101	0.831	0.05868	0.062	0.457
0.07194	0.123	0.859	0.07836	0.078	0.502
0.08942	0.144	0.891	0.09793	0.090	0.516
0.1073	0.156	0.890	0.1185	0.105	0.552
0.1249	0.175	0.927	0.1366	0.113	0.555
0.1447	0.186	0.930	0.1577	0.130	0.602
Completely acidic	0.491	—	Completely acidic	0.519	—

absorbances were determined at 25 ± 0.2°C using a PMQ II CARL ZEISS spectrophotometer with 1 cm cells at 548 nm where the absorbance shows a maximum for the acid form in water. The limiting absorbances of the acid form (H_2A) were determined in concentrated solution of HCl (4–6 M), (in ACN + H_2O, the values of m_{HCl} used were much less and for the limiting absorption of the completely acid form, a very much smaller amount of concentrated HCl was required when compared to other solvent systems) but that for the base form (HA^-) was determined in the respective solvents without any addition of alkali (16, 22). The absorbance readings were corrected, where necessary, for the identical total concentration of the indicator. The indicator solution in pure solvent contained virtually exclusively the species HA^- and there was no trace of A^{2-} because measurement at 598 nm (the maximum absorption wavelength of blue form, A^{2-}) showed no absorption at all (21).

Results

For determination of thermodynamic dissociation constant, $({}_sK)_{H_2A}$ (subscript s refers to mixed solvent) an extrapolation function $p({}_sK)'_{H_2A}$ defined by reaction [3] was constructed (20) by combining mass law expression for reaction [2] with the Debye–Hückel expression for activity coefficient.

$$[3]\quad p({}_sK)'_{H_2A} = -\log m_{SH^+_2} - \log (m_{HA^-}/m_{H_2A}) + 2S_f\sqrt{\mu}(1 + Ba_0\sqrt{\mu})^{-2} = p({}_sK)_{H_2A} + f(\mu)$$

where $m_{SH^+_2}$ is the relative molality of H^+ in the solution, $S_f = 1.824 \times 10^6(\epsilon_s T)^{-3/2}$ and $B = 50.29(\epsilon_s T)^{-1/2}$ are the Debye–Hückel constants, a_0 is the ion-size parameter, μ is the ionic strength being equal to $\mu = m_{HCl} \cdot d_s$ where d_s is the density of the solvent. Densities were available from literature (10–12). The concentration of the ionic species obtained from dissociation of H_2A being extremely small compared to that of m_{HCl}, their contribution to the ionic strength can be neglected. As indicator concentration is very small, the value of $m_{SH^+_2}$ is practically the same as that of m_{HCl}. Dielectric constant values (ϵ_s) required for calculation of Debye–Hückel constants were available from literature (10–12). The value of concentration ratio, $m_{HA^-}/m_{H_2A} = (A - A_a)/(A_b - A)$ were obtained (5*a*, 20) from absorbances A_a, A_b, and A of the completely acid form (H_2A), completely base form (HA^-), and the mixture of the two forms measured at an identical total concentration of the indicator in the same cell. In eq. [3], $({}_sK)'_{H_2A}$ is the apparent dissociation constant which becomes equal to thermodynamic dissociation constant, $({}_sK)_{H_2A}$ at an ionic strength of zero. $p({}_sK)'_{H_2A}$ values were calculated by considering $a_0 = 0$, because, this numerical value resulted in linear $p({}_sK)'_{H_2A}$ plots. Other value of a_0 (= 1, 2 etc.) also produces straight lines with different slopes but have no effect on $p({}_sK)_{H_2A}$ values.

The values of m_{HCl}, spectral absorbances (A), and $p({}_sK)'_{H_2A}$ are listed in Tables 1–3. $p({}_sK)_{H_2A}$ values in the molal scale in the three solvent systems are given in Table 4. The uncertainty in the pK values is about ±0.01 unit. pK value of H_2A in water, i.e., $p({}_wK)_{H_2A}$ reported recently (17) agreed completely with the literature value (23).

Discussion

To make a valid comparison (5*b*, 7, 8, 24) of the results in different solvents, it is necessary to use dissociation constants in the mole fraction scale, $p({}_sK)^N_{H_2A}$ which is related to molal scale value by the equation (2, 7) $p({}_sK)^N_{H_2A} = p({}_sK)_{H_2A} + \log 1000/M_{SH}$ where M_{SH} is the average molecular weight of the mixed solvent. Solvent effect on the dissociation can be represented by (8*b*)

$$[4]\quad \text{Solvent effect} = \partial(\Delta G^0) = {}_s\Delta G^0 - {}_w\Delta G^0 = 2.303RT[p({}_sK)^N_{H_2A} - p({}_wK)^N_{H_2A}] = 2.303RT[p({}_sK)_{H_2A} - p({}_wK)_{H_2A} - \log M_{SH}/M_w]$$

TABLE 3. Data for spectrophotometric determination of $p({}_sK)_{H_2A}$ of thymolsulfonephthalein in DMSO + H_2O mixtures at 25°C

m_{HCl}	A	$p({}_sK)'_{H_2A}$	m_{HCl}	A	$p({}_sK)'_{H_2A}$
20 wt% DMSO; [indicator] = 1.85×10^{-5} M			60 wt% DMSO; [indicator] = 1.57×10^{-5} M		
Completely basic	0.014	—	Completely basic	0.012	—
0.08091	0.122	1.521	0.01503	0.086	1.196
0.01628	0.186	1.517	0.03009	0.132	1.212
0.02835	0.254	1.536	0.04497	0.163	1.219
0.03642	0.281	1.532	0.06014	0.189	1.233
0.05401	0.329	1.540	0.07513	0.211	1.251
0.07319	0.359	1.535	0.09026	0.224	1.248
0.09254	0.388	1.555	0.1046	0.240	1.266
0.1193	0.412	1.561	0.1195	0.254	1.283
Completely acidic	0.622	—	Completely acidic	0.523	—
40 wt% DMSO; [indicator] = 1.63×10^{-5} M			80 wt% DMSO; [indicator] = 1.41×10^{-5} M		
Completely basic	0.012	—	Completely basic	0.011	—
0.01465	0.111	1.319	0.01499	0.058	1.057
0.02451	0.153	1.332	0.03001	0.089	1.085
0.03920	0.199	1.350	0.04495	0.109	1.085
0.05784	0.242	1.373	0.05986	0.127	1.105
0.07300	0.263	1.373	0.07474	0.141	1.115
0.08841	0.286	1.393	0.08998	0.156	0.141
0.1024	0.298	1.394	0.1049	0.164	1.143
0.1186	0.319	1.424	0.1197	0.178	1.176
Completely acidic	0.550	—	Completely acidic	0.468	—

TABLE 4. Values of $p({}_sK)_{H_2A}$ (molal scale), $\partial(\Delta G^0)$, $\Delta G_t^0(H^+)$, and $\Delta G_t^0(HA^-) - \Delta G_t^0(H_2A)$ for thymolsulfonephthalein in aqueous mixtures of ACN, urea, and DMSO at 25°C (ΔG^0 values are in kJ mol^{-1} (mole fraction scale))

Wt% co-solvent	Mol% co-solvent	ϵ_s[a]	$p({}_sK)_{H_2A}$	$\partial(\Delta G^0)$	$\Delta G_t^0(H^+)$[b]	$\Delta G_t^0(HA^-) - \Delta G_t^0(H_2A)$
				ACN + water mixtures		
0	0	78.4	1.60[c]	0	0	0
10	4.65	74.5	1.62	0.03	−1.8	1.8
30	15.84	65.0	1.76	0.46	−3.8	4.3
50	30.52	55.1	1.96	1.24	−4.3	5.5
70	50.61	47.0	2.40	3.33	−3.3	6.6
80	63.73	42.9	2.85	5.66	−2.6	8.3
				Urea + water mixtures		
11.52	3.78	83.90	1.01	−3.57	−1.5	−2.1
20.31	7.10	87.95	0.78	−5.06	−2.9	−2.2
29.64	11.21	91.76	0.55	−6.56	−4.5	−2.1
36.83	14.88	94.43	0.39	−7.64	−5.9	−1.7
				DMSO + water mixtures		
20	5.45	77.9	1.52	−0.87	−3.3	2.4
40	13.33	76.4	1.31	−2.57	−8.4	5.8
60	25.7	73.3	1.19	−3.87	−16.7	12.8
80	48.0	64.7	1.04	−5.56	—	—

[a]Dielectric constant values of ACN + H_2O (11), urea + H_2O (12), and DMSO + H_2O (10) mixtures were taken from literature. Some of the values in ACN + H_2O were obtained by interpolation.

[b]$\Delta G_t^0(H^+)$ values in ACN + water have been obtained from ref. 18 by interpolation and the values in DMSO + water and urea + water have been taken from refs. 28 and 29, respectively. Uncertainty in $\Delta G_t^0(H^+)$ values are ±0.2 kJ mol^{-1}.

[c]Reference 17.

where $({}_wK)_{H_2A}$ and M_w are the dissociation constant in pure water and molecular weight of water, respectively. Values of $\partial(\Delta G^0)$ in mole fraction scale are summarised in Table 4.

Figure 1 depicts the variation of $\partial(\Delta G^0)$ with mol% non-aqueous component. $\partial(\Delta G^0)$ increases gradually with increase in mol% ACN. In contrast, the corresponding value in urea + H_2O and DMSO + H_2O decreases with increase in proportion of organic co-solvent in the mixed solvent, the decrease being sharp in urea + H_2O. Solvent effect on the dissociation of positively charged acids has also been found to be unusually large (7*c*, *d*) in urea + H_2O solvent systems.

Solvent effect is determined by the interactions of H^+, H_2A,

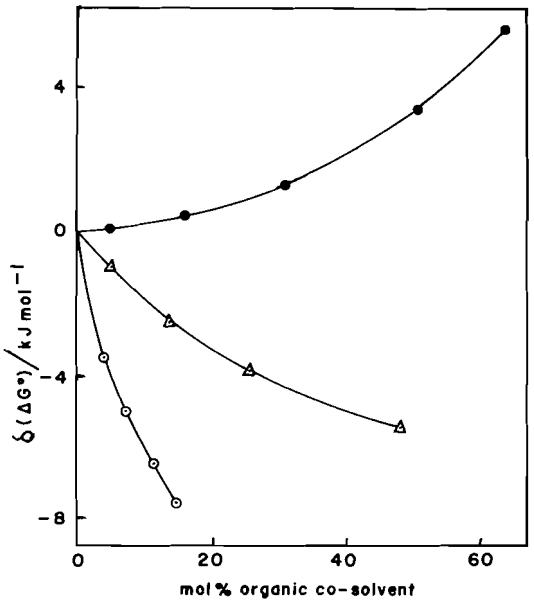

FIG. 1. Variation of $\partial(\Delta G^0)$ of thymolsulfonephthalein in aqueous mixtures of DMSO (△), ACN (●), and urea (○) at 298.15 K.

and HA^- with the solvent molecules and is better understood in terms of $\Delta G_t^0(i)$ values in eq. [5] of all the three species involved in the dissociation equilibrium (3, 20)

$$[5] \quad \partial(\Delta G^0) = \Delta G_t^0(H^+) + \Delta G_t^0(HA^-) - \Delta G_t^0(H_2A)$$

where $\Delta G_t^0(i)$ is the Gibbs energy change accompanying the transfer of one mole of species i from the standard state in water to the standard state in the solvent concerned, both on the mole fraction scale.

$\Delta G_t^0(H^+)$ values for all the solvent systems based on widely used (25–27) extrathermodynamic method using the reference electrolyte [RE = Ph_4AsBPh_4 (Ph = phenyl)] assumption, $\Delta G_t^0(Ph_4As^+) = \Delta G_t^0(Ph_4B^-) = \frac{1}{2}\Delta G_t^0(Ph_4AsBPh_4)$ are available in literature (18, 28, 29). $\Delta G_t^0(H^+)$ values are found to be increasingly negative in DMSO + H_2O and urea + H_2O indicating increased stabilization of H^+ and the increased solvation of H^+ is dictated by the co-solvent-induced basicity of the solvents (28, 29). $\Delta G_t^0(H^+)$ for ACN + H_2O passes through a minimum. $\Delta G_t^0(H^+)$ for pure ACN is positive (18) (not shown

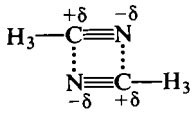

A

in Fig. 2). In spite of fairly large negative charge on nitrile N atom of ACN molecule, the protophobic character of ACN may arise from the possible formation of dimers (**A**) which are shown from ir studies to exist in pure ACN. Negative charge centres of nitrile N atom is not available for H^+ solvation and ACN behaves as protophobic solvent. Thus, the initial increased solvation of H^+ can be attributed to the increased basicity of aqueous ACN resulting from the breakdown (30) of three-dimensional ice-like water (31) structure releasing more basic monomeric water molecules. The "non-aqueous" water, containing increased number of monomeric water molecules, is effectively a more basic solvent (3). Moreover, these water monomers and ACN molecules may lead to the formation of intercomponent hydrogen-bonded complexes (32) (**B**) and (**C**)

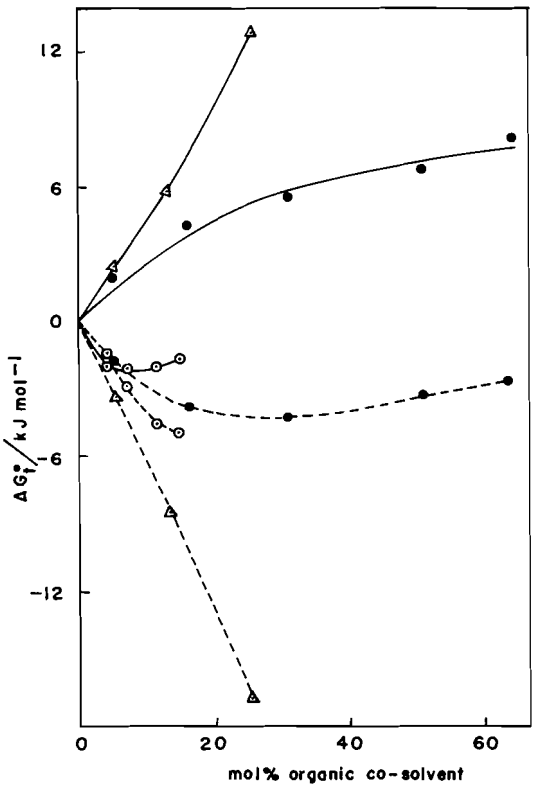

FIG. 2. Variation of $\Delta G_t^0(HA^-) - \Delta G_t^0(H_2A)$ of thymolsulfonephthalein [solid line] and $\Delta G_t^0(H^+)$ [dotted line] in aqueous mixtures of DMSO (△), ACN (●), and urea (○) at 298.15 K.

resulting in an increased basicity of the hydroxyl oxygen itself due to the presence of N lone pair.

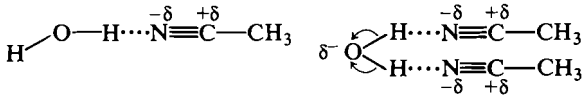

B C

Increasing trend in $\Delta G_t^0(H^+)$ at higher ACN mol% may be partly attributed to the Born-type electrostatic interaction and partly to the protophobic character of ACN. Values of $\Delta G_t^0(H^+)$ facilitates the evaluation of the combined term $\Delta G_t^0(HA^-) - \Delta G_t^0(H_2A)$ from eq. [5]. Variations of $\Delta G_t^0(H^+)$ and $\Delta G_t^0(HA^-) - \Delta G_t^0(H_2A)$ (Table 4) with mol% organic co-solvent shown in Fig. 2. Value of $\Delta G_t^0(HA^-) - \Delta G_t^0(H_2A)$ in urea + H_2O decreases and passes through a minimum. On the other hand, the corresponding value in ACN + H_2O and DMSO + H_2O increases with mol% organic component, the value passing through more positive magnitudes in DMSO + H_2O.

The dispersion interaction contribution to the combined term is expected to be cancelled to a large extent. The solvents, however, differ in their dielectric constant (ϵ_s) values and solvating capabilities. ϵ_s value increases as urea is added to water, but the value decreases on addition of ACN or DMSO. Contribution to Gibbs energy of transfer of HA^- due to Born-type electrostatic interaction (3) is positive in aqueous mixtures of ACN or DMSO and negative in urea + H_2O. Again, ϵ_s value of DMSO + H_2O being greater than that of ACN + H_2O of similar mol% non-aqueous component, electrostatic interaction should impart less positive contribution to $\Delta G_t^0(HA^-)$ in DMSO + H_2O than in ACN + H_2O. Contrary behaviour as reflected in relative positions of $\Delta G_t^0(HA^-) - \Delta G_t^0(H_2A)$ curves in DMSO + H_2O and ACN + H_2O (Fig. 2) may be

attributed to stronger anion desolvating capability of DMSO compared to ACN. Destabilization of anion in DMSO + H_2O and ACN + H_2O is likely to stem from the weak H-bond donating capability and the location (33) of positive end of the solvent dipole at a sterically unapproachable position of the molecule. From this point of view, the non-linearity of and increased number of $—CH_3$ groups in DMSO make positive end of the dipole less available to anion than in ACN and this is probably responsible for the observed relative behaviour of $\Delta G_t^0(HA^-) - \Delta G_t^0(H_2A)$ in DMSO + H_2O and ACN + H_2O.

In case of urea + H_2O, besides the negative contribution to $\Delta G_t^0(HA^-)$ due to Born electrostatic effect, further stabilization of HA^- is expected from "acid–base type" interaction of the negative charge centre of HA^- with the Zwitterionic form $\overset{+}{N}H_2{=}C(NH_2)O^-$, the actual contributor to the resonating structure of urea. The Zwitterionic structure of urea molecule probably makes it more acidic compared to water molecule. For this reason, hydrogen bond formed by HA^- are expected to be stronger with urea than with water, causing greater stabilization of HA^- and more negative ΔG_t^0 values with increasing proportion of urea in the solvent. The upward trend of $\Delta G_t^0(HA^-) - \Delta G_t^0(H_2A)$ after passing through a minimum is consistent with those observed (28, 29) for some anions like benzoate, Cl^-, OH^-. The upward trend after passing through a minimum is explained by the interaction of the solute species at that structurally critical region of the mixed solvents.

Interaction of H^+ is reflected in $\Delta G_t^0(H^+)$ values which may be considered as a measure of basicities of the solvents relative to water (3). In conclusion it may be said that very large negative magnitude of $\Delta G_t^0(H^+)$ in DMSO + H_2O compared to that in ACN + H_2O is primarily responsible for contrasting dissociation behaviour of H_2A in these two solvent systems and maximum acidic strength of H_2A in urea + H_2O is due primarily to combined effect of stability of both H^+ and HA^- ions in the mixed solvent relative to that in water.

1. R. P. Bell. The proton in chemistry. Cornell University Press, Ithaca, New York. 1959.
2. E. J. King. Acid–base equilibria. Pergamon, London. 1965.
3. R. G. Bates. *In* Hydrogen-bonded solvent systems. *Edited by* A. K. Covington and P. Jones. Taylor and Francis, London. 1968. p. 49.
4. C. H. Rochester and B. Rossall. Trans. Faraday Soc. **65**, 992 (1969); **65**, 1004 (1969); (*b*) G. H. Parsons, C. H. Rochester, and C. E. C. Wood. J. Chem. Soc. B, 533 (1971); (*c*) G. H. Parsons and C. H. Rochester. J. Chem. Soc. Faraday Trans. 1, **71**, 1058 (1975); **71**, 1069 (1975); (*d*) C. H. Rochester and S. A. Sclosa. J. Chem. Soc. Faraday Trans. 1, **75**, 2781 (1979); **77**, 579 (1981).
5. E. E. Sager, R. A. Robinson, and R. G. Bates. J. Res. Nat. Bur. Stand. **68**A, 305 (1964); (*b*) R. G. Bates, J. S. Falcone, Jr., and A. Y. W. Ho. Anal. Chem. **46**, 2004 (1974); (*c*) M. Paabo, R. G. Bates, and R. A. Robinson. J. Phys. Chem. **70**, 247 (1966); (*d*) P. Schindler, R. A. Robinson, and R. G. Bates. J. Phys. Chem. **72**, 141 (1968); (*e*) E. S. Etz, R. A. Robinson, and R. G. Bates. J. Solution Chem. **6**, 503 (1972); (*f*) Z. Pawlak and R. G. Bates. J. Solution Chem. **4**, 817 (1975); **5**, 213 (1976); (*g*) R. A. Batler, C. A. Vega, and R. G. Bates. J. Solution Chem. **9**, 293 (1980).
6. B. Nowak and Z. Pawlak. J. Chem. Soc. Faraday Trans. 1, **78**, 2693 (1982).
7. K. K. Kundu, A. L. De, and M. N. Das. J. Chem. Soc. Perkin Trans. 2, 2963 (1972); (*b*) A. L. De. Electrochim. Acta, **28**, 1643 (1983); (*c*) A. L. De. Electrochim. Acta, **29**, 683 (1984); (*d*) A. L. De. Ind. J. Chem. **23**A, 820 (1984); (*e*) A. L. De and T. K. De. Can. J. Chem. **62**, 1776 (1984); (*f*) A. L. De and T. K. De. Can. J. Chem. **62**, 2245 (1984); (*g*) A. L. De. Ind. J. Chem. **23**A, 352 (1984).
8. K. K. Kundu, A. L. De, and M. N. Das. J. Chem. Soc. Dalton Trans. 386 (1972); (*b*) K. Bose and K. K. Kundu. J. Chem. Soc. Perkin Trans. 2, 1208 (1979).
9. A. L. De. Electrochim. Acta, **29**, 471 (1984).
10. (*a*) K. H. Khoo. J. Chem. Soc. A, 2932 (1971); (*b*) A. K. Das. Ph.D. Thesis. Jadavpur University, Calcutta. 1980.
11. C. Moreau and G. Douheret. (*a*) Thermochem. Acta, **8**, 385 (1975); (*b*) J. Chem. Thermodyn. **8**, 403 (1976).
12. K. K. Kundu and K. Mazumdar. J. Chem. Soc. Faraday I, **69**, 806 (1973).
13. R. K. Wolford. J. Phys. Chem. **68**, 3392 (1964).
14. S. Janardhanan and C. Kalidas. Ind. J. Chem. **22**A, 17 (1983).
15. I. M. Kolthoff and L. S. Guss. J. Am. Chem. Soc. **60**, 2516 (1938).
16. D. Rosenthal, H. B. Hetzer, and R. G. Bates. J. Am. Chem. Soc. **86**, 549 (1964).
17. A. L. De and A. K. Atta. J. Chem. Soc. Perkin II. In press.
18. K. Das, A. K. Das, and K. K. Kundu. Electrochim. Acta, **26**, 471 (1981).
19. B. G. Cox. J. Chem. Soc. Perkin II, 607 (1973).
20. A. L. De and A. K. Atta. Can. J. Chem. **63**, 3129 (1985).
21. A. L. De. Ind. J. Chem. **22**A, 932 (1983).
22. E. E. Sager, H. J. Keegan, and S. F. Acru. J. Res. Nat. Bur. Stand. **31**, 323 (1943).
23. R. G. Bates. Determination of pH. John Wiley and Sons, New York. 1964. p. 193.
24. R. A. Robinson and R. H. Stokes. Electrolyte solutions. 2nd ed. Butterworths, London. 1965. p. 353.
25. O. Popovych, A. Gibolsky, and D. H. Berne. Anal. Chem. **44**, 81 (1972).
26. O. Popovych. Anal. Chem. **46**, 2009 (1974).
27. B. G. Cox, G. R. Hedwig, A. J. Parkar, and D. W. Watts. Aust. J. Chem. **27**, 477 (1974).
28. (*a*) K. K. Kundu and A. K. Das. J. Solution Chem. **9**, 226 (1979); (*b*) K. Das, K. Bose, and K. K. Kundu. Electrochim. Acta, **26**, 479 (1981).
29. A. K. Das and K. K. Kundu. Ind. J. Chem. **15**A, 771 (1977).
30. (*a*) K. W. Morcom and R. W. Smith. J. Chem. Thermodyn. **1**, 503 (1969); (*b*) R. E. Robertson and S. E. Sugamari. Can. J. Chem. **50**, 1353 (1972); (*c*) S. Schiavo and B. Scrosati. Z. Phys. Chem. **9**, 102 (1976).
31. F. Franks and D. J. G. Ives. Q. Rev. Chem. Soc. **20**, 1 (1966).
32. A. Le Narvor, E. Gentric, and P. Saumagne. Can. J. Chem. **49**, 1933 (1971).
33. W. R. Davidson and P. Kebarb. J. Am. Chem. Soc. **98**, 6125 (1976).

Diaulusterols A and B from the skin extracts of the dorid nudibranch *Diaulula sandiegensis*

DAVID E. WILLIAMS, STEPHEN W. AYER, AND RAYMOND J. ANDERSEN[1]

Departments of Oceanography and Chemistry, University of British Columbia, Vancouver, B.C., Canada V6T 1W5

Received January 14, 1986

DAVID E. WILLIAMS, STEPHEN W. AYER, and RAYMOND J. ANDERSEN. Can. J. Chem. **64**, 1527 (1986).

Two new steroids, diaulusterol A (**2**) and diaulusterol B (**3**), have been isolated from skin extracts of the dorid nudibranch *Diaulula sandiegensis*. The proposed structures of **2** and **3** are based on spectral arguments.

DAVID E. WILLIAMS, STEPHEN W. AYER et RAYMOND J. ANDERSEN. Can. J. Chem. **64**, 1527 (1986).

On a isolé deux nouveaux stéroïdes, le diaulustérol A (**2**) et la diaulustérol B (**3**), des écorces de la *Diaulula sandiegensis*. On propose les structures **2** et **3** en se basant sur des données spectrales.

[Traduit par la revue]

Introduction

The intertidal and subtidal regions of the Pacific Coast of North America are inhabited by sizable populations of a large number of species of dorid nudibranchs (1). Many of the species have distributional ranges that extend along the entire coastline from Alaska to Mexico. A series of examinations of the dorid *Cadlina luteomarginata*, collected at several California (2) and British Columbia (3) sites, showed that its skin chemistry differed from one collecting site to another. It was simultaneously shown that the majority of metabolites present in the skin extracts of *C. luteomarginata* were obtained from sponges in the nudibranch's diet, and that the observed variation in skin chemistry was a consequence of changing diet with changing collection site.

Diaulula sandiegensis is another dorid which has a documented distribution range that extends from Alaska to Cape San Lucas, Mexico (1). Walker and Faulkner isolated a series of nine chlorinated acetylenes related to **1** from specimens of *D. sandiegensis* collected at Point Loma, California (4). We have examined specimens of *D. sandiegensis* collected in Barkley Sound, British Columbia, and found them to contain the two new steroids, diaulusterol A (**2**) and diaulusterol B (**3**).

D. sandiegensis was collected by hand using SCUBA (−1 to −15 m) on exposed rocky reefs in Barkley Sound. Freshly collected animals were immediately immersed in methanol and allowed to extract at 2°C for two days. The extraction solvent was decanted from the nudibranchs, evaporated *in vacuo*, and the residue was partitioned between brine and ethyl acetate. Fractionation of the ethyl acetate soluble material by flash, LH20, and reverse-phase chromatography produced pure samples of diaulusterol A (**2**) and diaulusterol B (**3**).

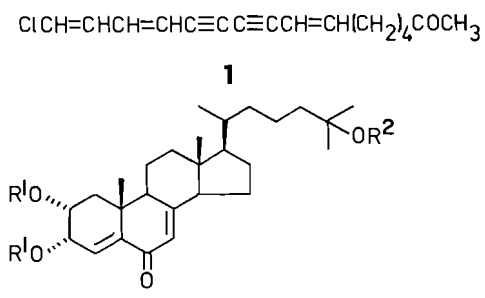

1

2 R^1=H R^2= ‡-$COCH_2CHOHCH_3$

3 $R^1 = R^2$ = H

4 R^1 = Ac R^2= ‡-$COCH_2CHOAcCH_3$

5 R^1 = Ac R^2 = H

Diaulusterol A (**2**) was isolated as a uv (ultraviolet) absorbing clear oil that showed ir (infrared) bands at 3380, 1722, 1660, and 1620 cm^{-1} appropriate for hydroxyl, saturated carbonyl, unsaturated carbonyl, and alkene functionalities. The electron impact mass spectrum of **2** provided little information since no parent ion was observed. Diaulusterol A (**2**) showed resonances for 31 carbon atoms in its ^{13}C nmr spectrum and its ^1H nmr spectrum showed a series of methyl resonances at 0.65 (s, 3H), 0.96 (d, J = 7 Hz, 3H), 1.17 (s, 3H), and 1.46 (s, 6H) ppm that indicated a steroidal structure. Other notable features in the ^1H nmr spectrum of **2** were an additional methyl resonance at 1.21 (d, J = 7 Hz, 3H), three carbinol methine proton resonances at 3.90 (dt, J = 11, 5 Hz, 1H), 4.15 (m, 1H), and 4.28 (t, J = 5 Hz, 1H), and two olefinic proton resonances at 5.87 (t, J = 1 Hz, 1H) and 6.54 (d, J = 5 Hz, 1H) ppm.

We found that **2** steadily decomposed to give a complex mixture of very polar materials when it was exposed to nmr solvents or other manipulations. Acetylation of **2** with acetic anhydride and pyridine generated the triacetate **4**, which proved to be a very stable substance. Triacetate **4** was shown by mass spectrometry to have a molecular formula of $C_{37}H_{54}O_9$, which represents the addition of six carbon atoms to the 31 that were observed in the ^{13}C nmr spectrum of **2**. Three new methyl resonances at 2.06, 2.08, and 2.12 in addition to the observed downfield shifts of the carbinol methine resonances to 5.14, 5.23, and 5.64 ppm in the ^1H nmr spectrum of **4** confirmed the formation of a triacetate.

Subtraction of the atoms present in the three acetyl residues from the molecular formula of **4** resulted in a molecular formula of $C_{31}H_{48}O_6$ for diaulusterol A (**2**). Three of the oxygen atoms in this formula could be accounted for by the three secondary alcohols (^{13}C nmr 64.4 (d), 65.2 (d), and 66.7 (d)) that underwent acetylation. The ir (1722 and 1660 cm^{-1}) and ^{13}C nmr spectra (172.4 (s) and 188.7 (s) ppm) of **2** revealed that the remaining oxygen atoms were present as ester and cross-conjugated ketone functionalities.

A decoupling experiment further elaborated the ester containing fragment. Thus, irradiation of the carbinol methine resonance at 4.15 in the ^1H nmr spectrum of **2** collapsed the methyl doublet at 1.21 to a singlet, and simplified two resonances at 2.34 (dd, J = 9, 16 Hz, 1H) and 2.42 (dd, J = 4, 16 Hz, 1H) ppm to an AB quartet (J = 16 Hz). This isolated six-proton spin system was assigned to a 3-hydroxybutanoate moiety.

[1]Author to whom correspondence may be addressed.

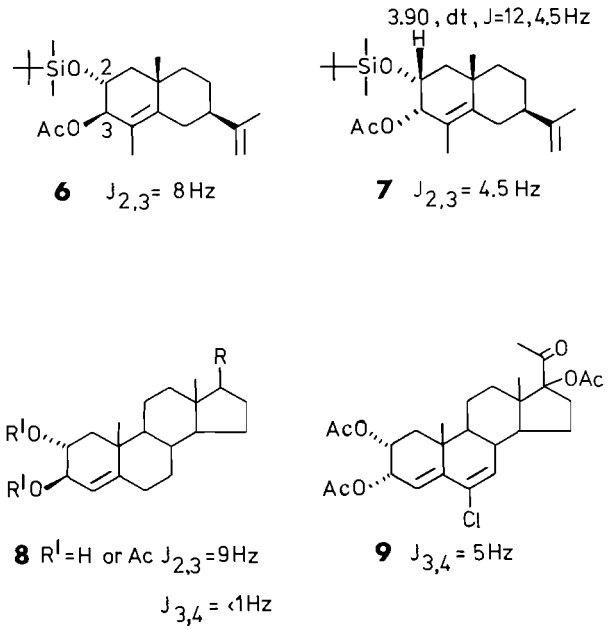

FIG. 1. Models for the ^{1}H spin system in ring A of Diaulusterol A.

Subtraction of the four carbons of this fragment from the molecular formula of **2** leaves the 27 carbons of a basic steroid skeleton, supporting our hypothesis of a steroidal structure for **2**. A ^{1}H nmr resonance at 1.46 (s, 6H) and a ^{13}C nmr resonance at 83.6 (s) ppm indicated that the butanoate fragment was attached to C25 of the steroid sidechain.

A second series of ^{1}H nmr decoupling experiments allowed the placement of much of the remaining functionality on the steroid nucleus. Irradiation of the methine proton at 3.90 in the spectrum of **2** collapsed the methine resonance at 4.28 to a doublet (J = 5 Hz) and simplified a pair of resonances at 1.75–1.85 ppm to an apparent AB quartet. Irradiation of the methine resonance at 4.28 simplified the multiplet at 3.90 to a doublet of doublets (J = 5, 11 Hz) and collapsed the doublet at 6.54 to a singlet, while irradiation at 6.54 simplified the methine resonance at 4.28 to a doublet (J = 5 Hz). The only way to situate this five-proton spin system on a steroid nucleus was to assign the resonances at 1.75–1.85 to a pair of geminal protons at C1, the resonances at 3.90 and 4.28 to carbinol methine protons at C2 and C3, respectively, and the resonance at 6.54 to an olefinic proton at C4. The demonstration of a nOe (nuclear Overhauser enhancement) between the methyl protons at 1.26 (C19) and a methine proton at 5.14 (H2) in the triacetate **4** required that H2 be β. An additional nOe between the methine proton at 5.14 (H2) and its vicinal neighbor, which appears at 5.64 (H3) ppm in the ^{1}H nmr spectrum of **4**, showed that H3 was also β. Comparison of the observed coupling constants for this spin system in **2** and **4** to the corresponding coupling constants in the model compounds **6–9** (5–7) confirmed our assignment (see Fig. 1).

The remaining functionality indicated by the spectral data and required by the molecular formula of **2** was a cross-conjugated ketone and a trisubstituted olefin. Having established the nature of the A ring in **2**, there was no choice but to place the ketone functionality at C6 and the olefin at C7—C8. The resulting proton and ^{13}C nmr assignments for diaulusterol A (**2**), which are given in Table 1, are in good agreement with the proposed structure. Also consistent with the structural assignment is the splitting of the C7 olefinic proton resonance (5.87 ppm) into a

TABLE 1. Partial nmr assignments for diaulusterol A (**2**). Chemical shifts are in ppm from TMS

Carbon	^{1}H	^{13}C
2	3.90, dt, J = 11, 5 Hz	66.7* (CH)[a]
3	4.28, t, J = 5 Hz	64.4 (CH)
4	6.54, d, J = 5 Hz	128.1 (CH)
5	—	146.2 (C)
6	—	188.7 (C)
7	5.87, t, J = 1 Hz	123.6 (CH)
8	—	166.9 (C)
18	0.65	12.5 (CH_3)
19	1.17	21.1& (CH_3)
21	0.96, d, J = 7 Hz	18.7 (CH_3)
25	—	83.6 (C)
26	1.46	26.1 (CH_3)
27	1.46	26.2 (CH_3)
28	—	172.4 (C)
29	2.34, dd, J = 9, 16 Hz; 2.42, dd, J = 4, 16 Hz	42.1 (CH_2)
30	4.15, m	65.2* (CH)
31	1.21, d, J = 7 Hz	22.3& (CH_3)

* and & mean the assignments may be interchanged.
[a]Hydrogen attachments were determined using ADEPT.

triplet (J = 1 Hz) via allylic coupling to the C14 and C9 protons, and the observation of intense fragment ions at m/z 582 (M^+ − HOAc), 522 (M^+ − (2 × HOAc)), 496 (M^+ − (3-acetoxybutanoic acid) via McLafferty), and 265 (M^+ − (sidechain + (2 × HOAc)) daltons in the mass spectrum of **4**.

The observed chemical shifts for the C18 (^{1}H: 0.65; ^{13}C: 12.75 ppm) and C21 (^{1}H: 0.96; ^{13}C: 18.75 ppm) methyl groups in **2** were virtually identical to those reported for cholesterol (C18: 0.67, 12.0; C21: 0.90, 18.8 ppm), suggesting that the relative configurations at C13, C14, C17, and C20 were identical in the two molecules. This information, coupled with the above arguments for ring A, allowed us to assign the relative stereochemistry of diaulusterol A (**2**) as shown. Irradiation of the C18 methyl protons in **4** failed to induce an observable nOe into the C14 proton and irradiation of the C19 methyl protons likewise failed to induce an nOe into the C9 proton. This negative evidence, while not proving the stereochemical assignment, is at least consistent with it.

Diaulusterol B (**3**) was also isolated as a clear oil that was shown by mass spectrometry to have a molecular formula of $C_{27}H_{42}O_4$ (M^+; calcd.: 430.3083; found: 430.3055). The ^{1}H nmr spectrum of **3** was identical to that of **2** in all respects except for the absence of the resonances due to the 3-hydroxybutanoate residue. Diaulusterol B was therefore assigned structure **3**. Treatment of the triol **3** with acetic anhydride and pyridine at room temperature generates the diacetate **5** as expected. We found diaulusterol B (**3**) in rapidly processed extracts of *D. sandiegensis*, thereby eliminating the possibility that it is an artifact formed by hydrolysis of diaulusterol A (**2**).

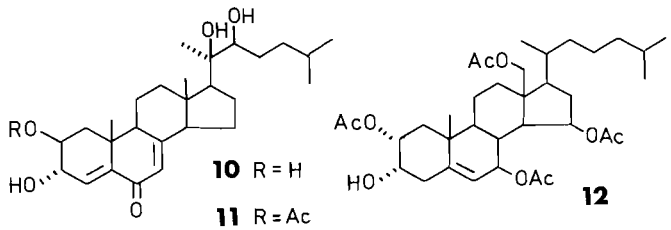

Diaulusterols A (**2**) and B (**3**) are related to pinnasterol (**10**) and acetylpinnasterol (**11**) (8), which were isolated from the red alga *Laurencia pinnata*. All four steroids share structural features with the ecdysones, and compounds **10** and **11** showed biological activity as insect moulting hormones. The 25-(3-hydroxybutanoate) residue and the 2-α,3-α diol array of the diaulusterols are not commonly encountered in naturally occurring steroids. One of the small number of steroids containing a 2-α,3-α diol is compound **12**, which was recently isolated from the marine hydroid *Eudendrium glomeratum* (9).

Our results, in combination with previous findings of Walker and Faulkner (4), have shown that *Dialula sandiegensis* represents another example of a dorid nudibranch that has different skin chemistry at different collecting sites. It seems reasonable to assume that the steroids found in the British Columbia specimens and the chlorinated acetylenes found in the California specimens are being produced by the different dietary organisms found at the two locations; however, an actual dietary source of the metabolites has not been identified at either collecting site.

Experimental

The ^{1}H nmr spectra were recorded on Varian XL-300 and Brüker WH-400 spectrometers. The ^{13}C nmr spectra were recorded on a Varian XL-300 spectrometer. TMS (tetramethylsilane) was used as an internal standard. Low resolution mass spectra were recorded on an AEI MS902 spectrometer and high resolution mass spectra on an AEI MS50 instrument. The ir spectra were recorded on a BOMEM Fourier Transform spectrometer. The uv–visible spectra were recorded on a Bausch and Lomb Spectronic-2000 spectrometer.

Merck silica gel 230–400 mesh was used for flash and preparative thin-layer chromatography (tlc) and a Whatman Magnum-9 ODS-3 column was used for preparative hplc. Sephadex LH-20 resin was used for molecular exclusion chromatography. R_f's are listed for all compounds in an analytical tlc system using ethyl acetate as an eluent.

Specimens of *Diaulula sandiegensis* (152 animals) were collected on several exposed rocky reefs (−1 to −15 m) in Barkley Sound, British Columbia. Freshly collected animals were immediately immersed in methanol and allowed to extract at 2°C for two days, after which the methanol was decanted off and replaced with fresh solvent. The first and second methanol extracts were combined and evaporated *in vacuo*. The resulting residue was partitioned between brine (200 mL) and ethyl acetate (5 × 125 mL). Evaporation of the combined ethyl acetate extracts gave a brown oil (1.4 g).

Flash chromatography of the brown oil (1:1 acetone – methylene chloride) gave a fraction (90 mg) that contained diaulusterols A (**2**), B (**3**), and fats. LH20 chromatography (1:4 methanol – chloroform) removed most of the fats. The resulting enriched mixture of compounds **2** and **3** (47 mg) was purified via reverse phase hplc (7:3 methanol – water) to yield pure steroids as clear oils (**2**: 24 mg; **3**: 3.2 mg).

Diaulusterol A (2): R_f 0.18; ir (film): 3380, 2940, 2870, 1722, 1660, 1620, 1455, 1375, 875, and 750 cm^{-1}; ^{1}H nmr ($CDCl_3$): 0.65 (s, 3H), 0.96 (d, J = 7 Hz, 3H), 1.17 (s, 3H), 1.21 (d, J = 7 Hz, 3H), 1.46 (s, 6H), 2.34 (dd, J = 9, 16 Hz, 1H), 2.42 (dd, J = 4, 16 Hz, 1H), 3.90 (dt, J = 5, 11 Hz, 1H), 4.15 (m, 1H), 4.28 (t, J = 5 Hz, 1H), 5.87 (t, J = 1 Hz, 1H), and 6.54 (d, J = 5 Hz, 1H); ^{13}C nmr ($CDCl_3$): 12.5, 18.7, 20.4, 21.1, 21.8, 22.3, 22.6, 26.1, 26.2, 27.6, 35.8, 35.9, 38.5, 38.6, 40.6, 41.1, 43.7, 44.5, 47.8, 56.0, 56.2, 64.4, 65.2, 66.7, 83.6, 123.6, 128.1, 146.2, 166.9, 172.4, and 188.7 ppm.

Diaulusterol A triacetate (4): Diaulusterol A (**2**) (24 mg) was stirred overnight at room temperature in a solution of pyridine – acetic anhydride (3:1; 8 mL). Evaporation of the reagents under high vacuum generated a residue that was purified via preparative tlc to give pure acetate **4** (27 mg): clear oil; R_f 0.56; uv (MeOH) λ_{max}: 264 nm (12 800); ^{1}H nmr ($CDCl_3$): 0.68 (s, 3H), 0.99 (d, J = 7 Hz, 3H), 1.26 (s, 3H), 1.32 (d, J = 8 Hz, 3H), 1.46 (s, 6H), 2.06 (s, 3H), 2.08 (s, 3H), 2.12 (s, 3H), 2.46 (dd, J = 6, 18 Hz, 1H), 2.60 (dd, J = 8, 18 Hz, 1H), 5.14 (dt, J = 14, 5 Hz, 1H), 5.27 (m, 1H), 5.64 (m, 1H), 5.92 (bs, 1H), and 6.47 (d, J = 7 Hz); ms: 642 (M^+), 582, 522, 496, 494, 376, 361, 265, 249, 171, 147, 129, 119. *Exact Mass* calcd.: 642.3768; found: 642.3779.

Diaulusterol B (3): clear oil; R_f 0.15; ^{1}H nmr ($CDCl_3$): 0.65 (s, 3H), 0.97 (d, J = 7 Hz, 3H), 1.17 (s, 3H), 1.23 (s, 6H), 3.88 (m, 1H), 4.27 (m, 1H), 5.87 (bs, 1H), 6.54 (d, J = 5 Hz, 1H); ms: 430 (M^+), 412, 397, 394. *Exact Mass* calcd.: 430.3083; found: 430.3055.

Diaulusterol B diacetate (5): Prepared as described above for **4**. Compound **5**: clear oil; R_f 0.55; uv (MeOH) λ_{max}: 264 nm; ^{1}H nmr ($CDCl_3$): 0.67 (s, 3H), 0.98 (d, J = 7 Hz, 3H), 1.24 (s, 9H), 2.04 (s, 3H), 2.08 (s, 3H), 5.12 (m, 1H), 5.61 (m, 1H), 5.89 (bs, 1H), 6.43 (d, J = 7 Hz, 1H).

Acknowledgements

The authors would like to thank Mike LeBlanc and the staff of the Bamfield Marine Station for assistance collecting *D. sandiegensis*. Financial support was provided by the Natural Sciences and Engineering Research Council of Canada and by a UBC–UGF to D.W.

1. D. W. Behrens. *In* Pacific Coast Nudibranchs. Sea Challengers, Los Osos, California. 1980.
2. J. E. Thompson, R. P. Walker, S. J. Wratten, and D. J. Faulkner. Tetrahedron, **38**, 1865 (1982).
3. (*a*) J. Hellou, R. J. Andersen, and J. Thompson. Tetrahedron, **38**, 1875 (1982); (*b*) K. Gustafson, R. J. Andersen, H. Cun-Heng, and J. Clardy. Tetrahedron Lett. **26**, 2521 (1985).
4. R. P. Walker and D. J. Faulkner. J. Org. Chem. **46**, 1475 (1981).
5. A. Murai, M. Ono, A. Akibo, and T. Masamune. Chem. Soc. Jpn. Bull. **55**, 1195 (1982).
6. (*a*) K. Shimada, T. Nambara, I. Uchida, and M. Kupchan. Heterocycles, **12**, 1445 (1979); (*b*) M. Mihailovic, J. Forsek, L. Lorenc, Z. Maksimovic, H. Fuher, and J. Kalvoda. Helv. Chim. Acta, **52**, 459 (1969).
7. S. Honma, S. Iwamura, K. Iizuka, A. Kambegawa, and K. Shida. Chem. Pharm. Bull. **25**, 2019 (1977).
8. A. Fukuzawa, Y. Kumagai, T. Masamune, A. Furusaki, C. Katayama, and T. Matsumoto. Tetrahedron Lett. **22**, 4085 (1981).
9. E. Fattorusso, V. Lanzotti, S. Magno, and E. Novellino. J. Org. Chem. **50**, 2868 (1985).

Phosphazène : une étude théorique du spectre d'ionisation[1]

DANIELLE GONBEAU, JEAN-LUC GARCIA ET GENEVIÈVE PFISTER-GUILLOUZO[2]

Institut universitaire de recherche scientifique, Laboratoire de physico-chimie moléculaire, Unité associée 474, Avenue de l'université, 64000 PAU, France

Reçu le 22 novembre 1985

DANIELLE GONBEAU, JEAN-LUC GARCIA et GENEVIÈVE PFISTER-GUILLOUZO. Can. J. Chem. **64**, 1530 (1986).

Une étude des sections efficaces de photoionisation du phosphazène HP=NH a été réalisée dans le cadre de la méthode MSXα. Les résultats obtenus, concernant les ionisations mettant en jeu les paires du phosphore et de l'azote, ont été confrontés à ceux déduits qualitativement d'un examen des localisations dans la fonction d'état initial. Parallèlement, les phénomènes de réorganisation électronique au niveau des ions générés par photoionisation ont été discutés.

DANIELLE GONBEAU, JEAN-LUC GARCIA, and GENEVIÈVE PFISTER-GUILLOUZO. Can. J. Chem. **64**, 1530 (1986).

A study of photoionization cross sections was undertaken in MSXα on the phosphazene HP=NH. For the ionizations involving the phosphorus and nitrogen lone pairs, the results were discussed and compared with those obtained from examination of localizations in the initial state. In parallel the electronic reorganization effects encountered in the ionic states were also analyzed.

En spectroscopie photoélectronique (ultraviolet) l'analyse des variations d'intensité des bandes observées expérimentalement notamment par passage du rayonnement HeI (21,22 eV) à HeII (40,81 eV) est un outil puissant d'attribution largement utilisé.

Sur la base de règles qualitatives, fondées sur les calculs de sections efficaces atomiques et l'examen des localisations dans les orbitales moléculaires mises en jeu lors des ionisations (1), l'interprétation des variations expérimentales d'intensité a été réalisée avec succès pour de nombreux systèmes moléculaires. Les limites d'une telle démarche apparaissent pour des molécules hétéroatomiques. Dans le cas des triazaphospholes par exemple (2), les variations d'intensité lors du passage HeI/HeII ne peuvent être toutes interprétées à partir des localisations des orbitales ionisées.

Ceci nous a conduit à examiner de façon plus rigoureuse les sections efficaces de photoionisation pour une molécule de petite taille présentant précisément deux hétéroatomes de période différente. Compte tenu des études expérimentales réalisées nous avons fait choix de l'entité modèle HP=NH.

Étant donné les limites mises en évidence d'une interprétation basée sur la considération du seul état initial, nous avons estimé par une approche multiconfigurationnelle l'importance des phénomènes de relocalisation dans les ions.

1. Conditions de calcul

Les calculs de sections efficaces de photoionisation ont été menés dans le cadre de la méthode MSXα particulièrement bien adaptée à ce type de problèmes.

En effet, l'extension de cette méthode à l'étude d'états du continu (3) permet l'évaluation dans un formalisme homogène des fonctions d'état initial et d'état final intervenant au niveau du moment de transition; elle se révèle par là même d'approximation moins grossière que les nombreux calculs effectués sur la base d'une représentation de l'état final par une onde plane.

Nous avons travaillé dans des conditions identiques à celles définies lors d'une étude antérieure (4): (*i*) au niveau des atomes les paramètres α optimisés par Schwarz (5) ont été utilisés avec une moyenne pondérée des α atomiques pour les régions intersphère et outersphère; (*ii*) les rayons des sphères atomiques ont été déterminés de façon non empirique (6) en réduisant de 12% les rayons obtenus à l'itération 0 pour des sphères englobant un nombre d'électrons égal au numéro atomique; (*iii*) l'évaluation des fonctions d'état initial et d'état final a été réalisée avec le même potentiel (prise en compte à chaque itération de calcul MSXα de la correction de Latter (7) pour le calcul des états initiaux); (*iv*) pour chaque atome et pour le calcul de toutes les fonctions d'état initial (i) une valeur $l_{max} = l + 1$ a été adoptée. Pour les fonctions d'état final (f) des valeurs $l_{max\,f} = l_{max\,i} + 1$ ont été choisies. Dans le cas de l'outersphère l_{max} a été déterminée par examen de la convergence des résultats.

Les potentiels d'ionisation ont été évalués selon le formalisme de l'état de transition (8).

Les effets de relocalisation dans l'état final ont été obtenus en Hartree Fock à l'aide d'une méthode de pseudo potentiel (9) (inclue dans le programme Hondo (10) avec des bases de valence d'un niveau double zeta (ζ) et une fonction de polarisation de type *d* sur le phosphore. Les interactions de configurations ont été réalisées dans le cadre de la méthode CIPSI (11) qui met en oeuvre conjointement la méthode des variations (pour les interactions les plus fortes) et une méthode perturbative (pour l'effet des déterminants moins importants).

Les conditions générales de calcul adoptées sont identiques à celles précisées lors d'un précédent travail (12).

2. Calculs MSXα sur H—P=N—H

Les calculs ont été effectués pour les deux conformères *trans* et *cis* de HP=NH.

Récemment le premier dialkyl imino phosphane *t*Bu—P=N—*t*Bu (conformation *trans*) a été détecté par Niecke et Flick (13). Il a été généré et caractérisé en spectroscopie photoélectronique par thermolyse du dimère (14).

La conformation *cis* du phosphazène correspond quant à elle à une disposition intervenant au niveau des hétérocycles à phosphore dicoordiné examinés par ailleurs (2).

2.1. Potentiels d'ionisation

Les résultats obtenus pour les deux isomères sont présentés dans le tableau 1.

Pour l'isomère *trans*, en accord avec des résultats antérieurs (15) les premier et troisième potentiels d'ionisation à 10,95 eV et 14,29 eV sont attribués respectivement à des ionisations

1. Part XXIX de «Application of photoelectron spectroscopy to molecular properties.» Part XXVIII : réf. 21.

2. Auteur à qui adresser toute correspondance.

TABLEAU 1. HP=NH (*trans* et *cis*). Niveaux d'énergie, distributions de charge et potentiels d'ionisation (PI) en MXSα

	Orbitale	Energie (eV)	Distribution de charge (%) P	N	$H^{(N)}$	$H^{(P)}$	Int.	Out	PI théoriques (eV)
HP=NH	5a′	−7,708	31	23	1	9	23	12	10,95
trans	1a″	−9,048	17	40			37	5	12,32
	4a′	−10,964	22	36	1	6	29	5	14,29
	3a′	−12,441	28	31	7	18	10	6	15,68
	2a′	−16,418	34	27	9	11	15	4	19,86
HP=NH	5a′	−7,909	33	13	2	16	17	19	11,25
cis	1a″	−9,164	17	41			32	10	12,46
	4a′	−9,255	20	49	1	1	13	17	12,49
	3a′	−13,256	27	25	5	20	16	7	16,78
	2a′	−16,044	33	32	10	7	11	7	19,53

PI expérimentaux (*t*Bu—P=N—*t*Bu, *trans*) (14) 8,11 eV; 9,70 eV; 10,10 eV. Paramètres géométriques de HP=NH *trans* et HP=NH *cis* définis lors d'un précédent travail (15).

mettant en jeu les orbitales 5a′ et 4a′, combinaisons liante (n^+) et antiliante (n^-) des paires libres des atomes de phosphore et d'azote. il faut remarquer une localisation plus grande sur le phosphore en ce qui concerne l'orbitale 5a′ et au contraire un poids plus important sur l'azote pour l'orbitale 4a′ (tableau 1).

Le potentiel d'ionisation à 12,32 eV correspond à l'ionisation faisant intervenir l'orbitale 1a″ caractéristique de la liaison $\pi_{P=N}$.

L'attribution des deux premiers potentiels d'ionisation est en accord avec celle proposée expérimentalement par Elbel *et al.* (14) pour le dérivé tertiobutylé : PI (n^+) (8,11 eV) < PI (π) (9,70–10,10 eV). En dépit de l'effet bien connu des groupements tertiobutylés (stabilisation de l'état ionique) les potentiels d'ionisation obtenus théoriquement sont trop profonds.

En ce qui concerne l'isomère *cis* (tableau 1), une séquence analogue σ, π, σ est observée pour les dernières orbitales occupées avec une interaction des paires en *trans* nettement plus importante qu'en *cis*, respectivement de 3,3 et 1,2 eV. Il faut noter également que les orbitales 5a′ et 4a′ correspondent respectivement aux combinaisons n^- et n^+ des paires des atomes de phosphore et d'azote. Elles présentent toutefois les mêmes localisations que dans l'isomère *trans*, à savoir poids important sur le phosphore pour l'orbitale 5a′, forte localisation sur l'azote pour 4a′.

Nous observons une position quasiment inchangée du potentiel d'ionisation associé à l'ionisation mettant en jeu l'orbitale $\pi_{P=N}$ (isomère *trans* : 12,32 eV, isomère *cis* : 12,46 eV).

2.2. *Sections efficaces et paramètres d'asymétrie*

Les résultats obtenus pour les sections efficaces différentielles de photoionisation (directement comparables aux intensités des bandes expérimentales) et les paramètres d'asymétrie ont été visualisés sous forme de courbes (figures 1 et 2) pour les trois premiers états initiaux de chaque isomère.

Un balayage en énergie cinétique par pas de 5 eV a été effectué dans un domaine compris entre 5 eV et 50 eV et les énergies de photons correspondant aux deux sources de rayonnement HeI (21,22 eV) et HeII (40,81 eV) ont été matérialisées par des traits verticaux.

Dans le cas de l'isomère *trans* une diminution est observée lorsqu'on passe d'un rayonnement HeI à HeII pour les trois états (fig. 1).

Toutefois, des différences apparaissent pour les états initiaux 5a′ et 4a′ mettant en jeu les paires libres des atomes de phosphore et d'azote. En effet, la diminution en passant de $h\nu$ = 21,22 eV à $h\nu$ = 40,81 eV est nettement plus grande pour l'état initial 5a′ correspondant à la combinaison n^+ que pour l'état initial 4a′ associé à la combinaison n^-.

En ce qui concerne les paramètres d'asymétrie leurs variations en fonction de l'énergie des photons, font apparaître également des allures bien différenciées pour les deux états initiaux 5a′ et 4a′.

Les résultats obtenus pour l'isomère *cis* (fig. 2) permettent de remarquer une diminution des sections efficaces en fonction de l'énergie des photons incidents pour les trois premiers états initiaux. Par contre, la plus forte diminution est observée dans ce cas pour l'état initial 4a′. Ce résultat est particulièrement intéressant compte tenu des localisations observées au niveau des orbitales 5a′ et 4a′.

En effet, comme nous l'avons vu, l'orbitale 5a′ présente le poids le plus important sur l'atome de phosphore alors que l'orbitale 4a′ est fortement localisée sur l'azote. Sur la base des règles habituelles, l'ionisation mettant en jeu l'orbitale 5a′ devrait ainsi être associée à une bande diminuant nettement d'intensité en passant d'un rayonnement HeI à HeII vis-à-vis de celle correspondant à l'ionisation faisant intervenir l'orbitale 4a′. Les calculs réalisés conduisent à des résultats inverses puisque la diminution la plus importante de section efficace est notée pour l'état initial 4a′.

Ces résultats mettent ainsi en évidence les limites des règles qualitatives dans ce cas. La seule analyse de la fonction d'état initial est insuffisante pour discuter des variations d'intensité en fonction de l'énergie des photons incidents.

Par ailleurs, l'examen des résultats obtenus pour les isomères *cis* et *trans* montre que la plus nette diminution de section efficace intervient dans les deux cas pour les états initiaux correspondant à la combinaison n^+ des paires du phosphore et de l'azote (5a′ pour l'isomère *trans*, 4a′ pour l'isomère *cis*).

Ainsi, les sections efficaces associées aux états initiaux caractéristiques des paires libres des atomes de phosphore et d'azote paraissent plus affectées par la «symétrie» des combinaisons des paires que par la localisation plus ou moins importante sur l'atome de phosphore dans la fonction d'état initial. Une remarque similaire peut être faite en ce qui concerne

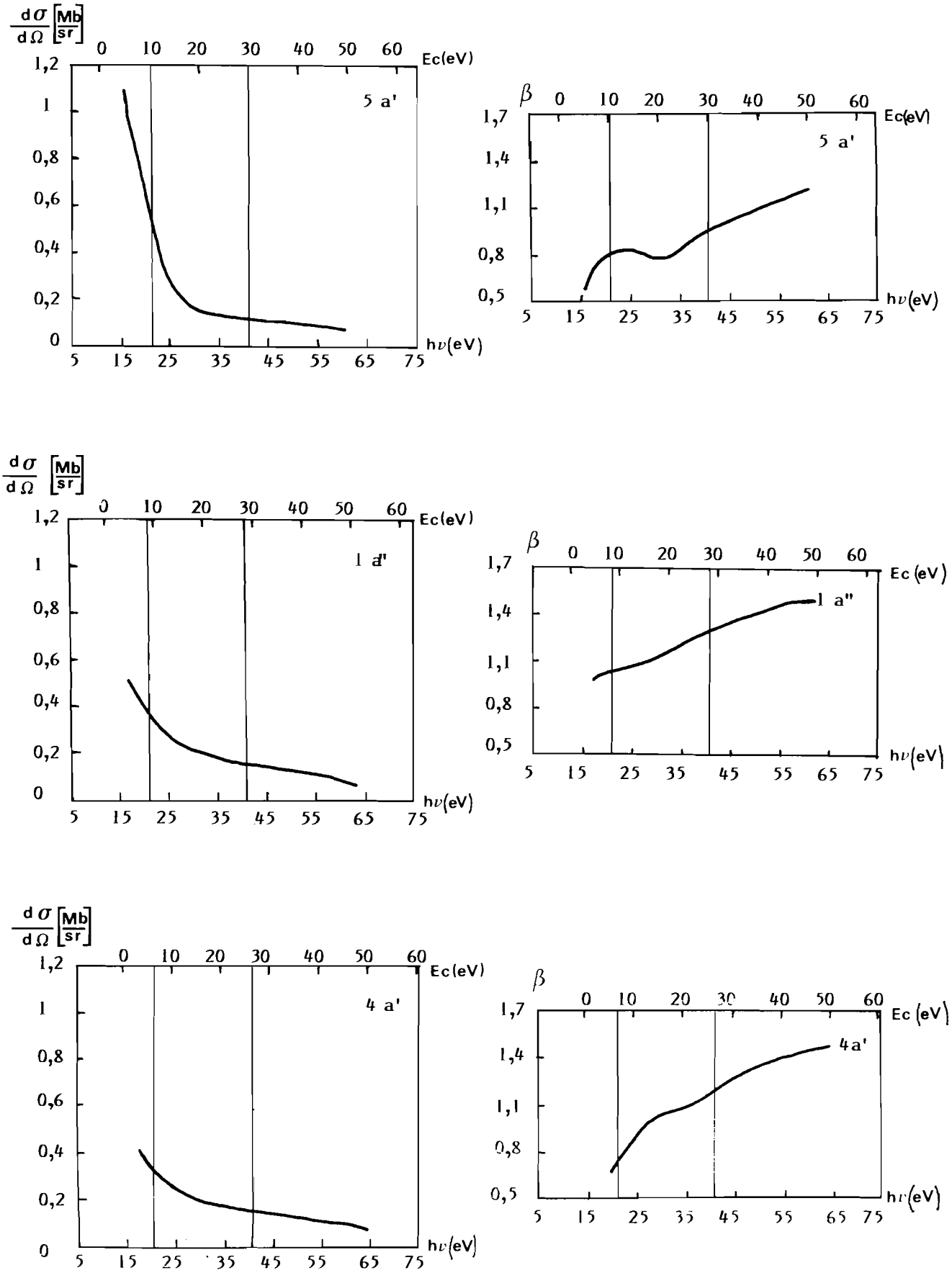

FIG. 1. HP=NH *trans* : orbitales $5a'$, $1a''$, $4a'$. Sections efficaces différentielles de photoionisation et paramètres d'asymétrie.

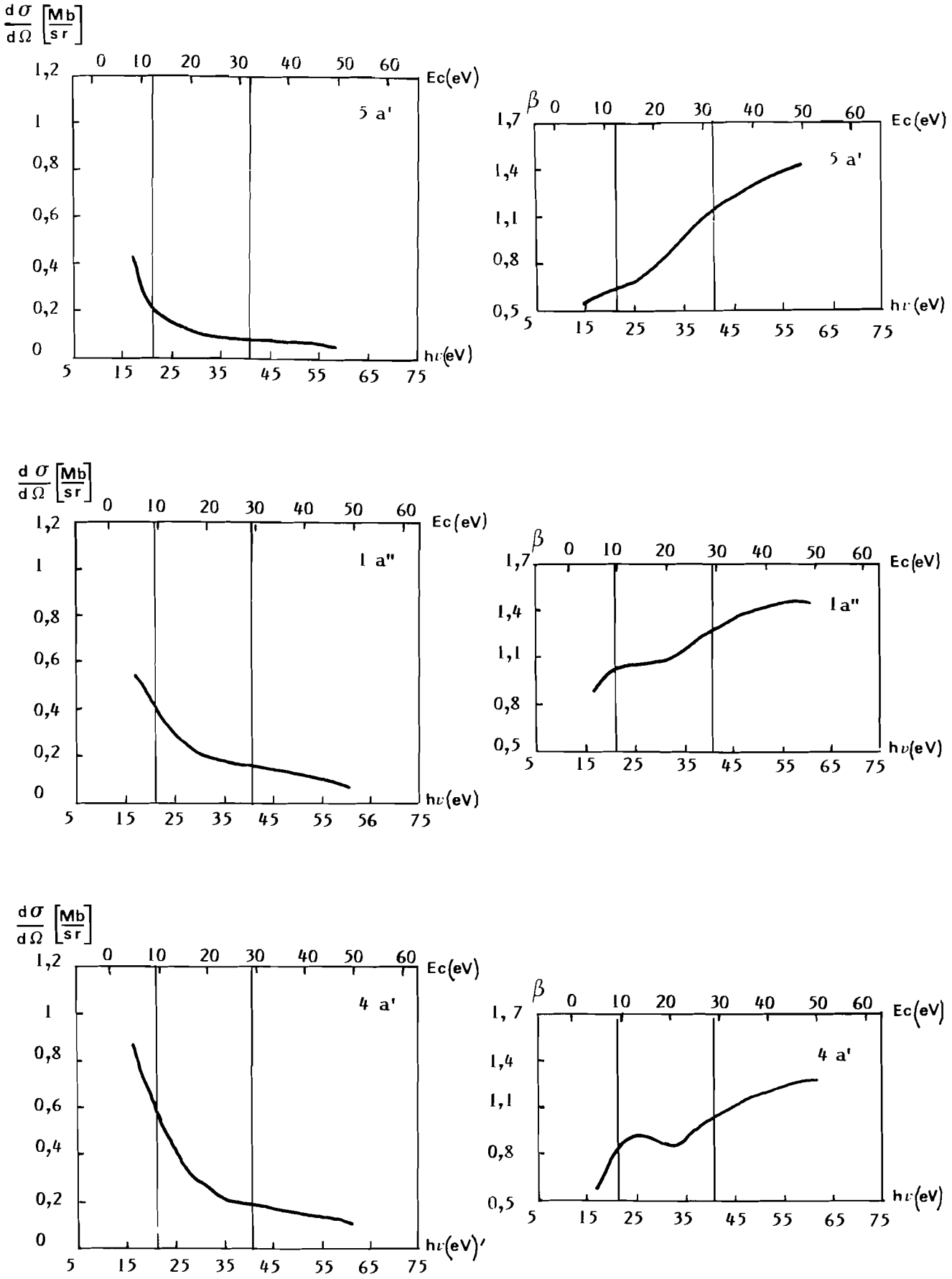

FIG. 2. HP=NH *cis* : orbitales $5a'$, $1a''$, $4a'$. Sections efficaces différentielles de photoionisation et paramètres d'asymétrie.

TABLEAU 2. HP=NH *trans*. Potentiels d'ionisation calculés (CIPSI)

États	PI Koopmans (eV)	Correction de polarisation	Correction de corrélation	PI corrigés (eV)	PI calculés par CIPSI	PI expérimentaux *t*Bu—P=N—*t*Bu
$^2A'$	10,61	−0,37	0,24	10,03	8,878	8,11
$^2A''$	11,75	−0,68	0,58	11,65	11,739	9,70
$^2A'$	14,58	−0,68	0,18	14,08	12,346	10,10
$^2A'$	16,08	−0,57	0,23	15,69		

TABLEAU 3. HP=NH *cis*. Potentiels d'ionisation calculés (CIPSI)

États	PI Koopmans (eV)	Correction de polarisation	Correction de corrélation	PI corrigés (eV)	PI calculés par CIPSI
$^2A'$	10,66	−0,26	0,26	10,66	9,34
$^2A''$	11,85	−0,71	0,57	11,71	11,72
$^2A'$	12,86	−0,96	0,21	12,11	11,13
$^2A'$	17,64	−0,49	0,19	17,34	

les paramètres d'asymétrie puisque des variations de β du même type sont observées pour les états $5a'$ (*cis*), $4a'$ (*trans*) d'une part et pour $4a'$ (*cis*), $5a'$ (*trans*) d'autre part.

Ces conclusions rejoignent celles de Price *et al.* (16) et les observations expérimentales sur CS_2, CO_2, COS où les bandes associées aux orbitales $\sigma_g(2p)$ présentent d'appréciables diminutions d'intensité par rapport aux bandes $\sigma_u(2p)$.

3. Phénomènes de relocalisation au niveau des ions générés par photoionisation de H—P=N—H

Les calculs MSXα ont été réalisés dans le cadre d'une approche monoélectronique et, en particulier, le caractère multiélectronique du processus de photoémission n'a pas été pris en compte dans la description de l'état final.

Or, pour interpréter les modifications d'intensité non explicables précisément à partir des localisations calculées dans l'état initial, on invoque parfois des possibilités de réorganisation de l'ion.

Nous avons donc entrepris d'examiner l'importance de ces phénomènes de relocalisation et procéder pour cela à des calculs Hartree Fock avec interaction de configurations.

Au niveau SCF (self-consistent field), nous obtenons pour les dernières orbitales occupées une séquence identique à celle précédemment déterminée en MSXα. Les potentiels d'ionisation dans le cadre de l'approximation de Koopmans sont assez voisins de ceux obtenus avec le formalisme de l'état de transition (tableaux 1–3). Pour l'isomère *trans*, les valeurs des potentiels d'ionisation obtenues sont trop élevées vis-à-vis des données expérimentales.

Il est cependant bien connu que dans cette approximation, on ne prend pas en compte les effets de polarisation et de corrélation qui peuvent affecter différemment les niveaux π et ceux caractéristiques des paires libres de ces systèmes.

Les effets de polarisation sont d'autant plus importants que les «trous» sont localisés et donc attendus les plus forts pour les paires libres; il contribuent généralement à diminuer les potentiels d'ionisation alors que les effets de corrélation les augmentent et ceci particulièrement pour les liaisons π (17).

À l'aide d'un processus déjà utilisé par ailleurs (12, 18) et qui présente l'avantage de ne nécessiter qu'un temps de calcul de l'ordre d'une itération SCF par potentiel d'ionisation nous avons estimé les corrections de polarisation et de corrélation.

Les résultats obtenus (tableaux 2 et 3) ne mettent en évidence que peu de changements sur les écarts respectifs des trois potentiels d'ionisation avec pour les deux premiers une compensation quasi totale des effets de polarisation et de corrélation.

Nous avons donc réalisé des calculs perturbationnels complets à l'aide du programme CIPSI.

Pour l'isomère *trans*, nous constatons (tableau 2), compte tenu de l'effet des groupements tertiobutyles (stabilisation de l'état ionique), un accord satisfaisant avec les données expérimentales, le premier potentiel d'ionisation étant toutefois un peu trop bas.

Dans le cas de l'isomère *cis* (tableau 3), nous observons une inversion des deuxième et troisième potentiels d'ionisation.

Il est important de remarquer que ces modifications notables ont leur principale origine dans l'effet de corrélation spécifique des ions; l'importance de ce terme a déjà été soulignée par Cederbaum (19) et Chong (20) et mise en évidence lors d'une étude réalisée sur le diméthyl diphosphène (12).

Dans les cas considérés ici, il est particulièrement important pour les ionisations mettant en jeu les orbitales combinaisons des paires libres de P et de N, de part la présence d'une orbitale virtuelle π* assez basse.

Après avoir examiné l'importance des effets de polarisation et de corrélation, nous avons analysé à l'aide des matrices densité après interaction de configuration les phénomènes de relocalisation au niveau des deux premiers ions σ.

Les résultats présentés sur la figure 3 pour le phosphazène *trans* font apparaître pour l'ion mettant en jeu l'orbitale $5a'$ un «trou» totalement délocalisé sur les deux atomes de phosphore et d'azote; au niveau de l'ion associé à l'orbitale $4a'$, le «trou» paraît un peu plus localisé sur l'atome de phosphore.

Dans le cas du phosphazène *cis*, des conclusions voisines peuvent être déduites de l'examen de la figure 3 avec toutefois un «trou» plus nettement localisé sur le phosphore en ce qui concerne l'ion correspondant à l'orbitale $4a'$.

Si la structure électronique globale de ces ions est assez différente de l'image que l'on pouvait en avoir à partir du seul examen des localisations des orbitales moléculaires mises en jeu

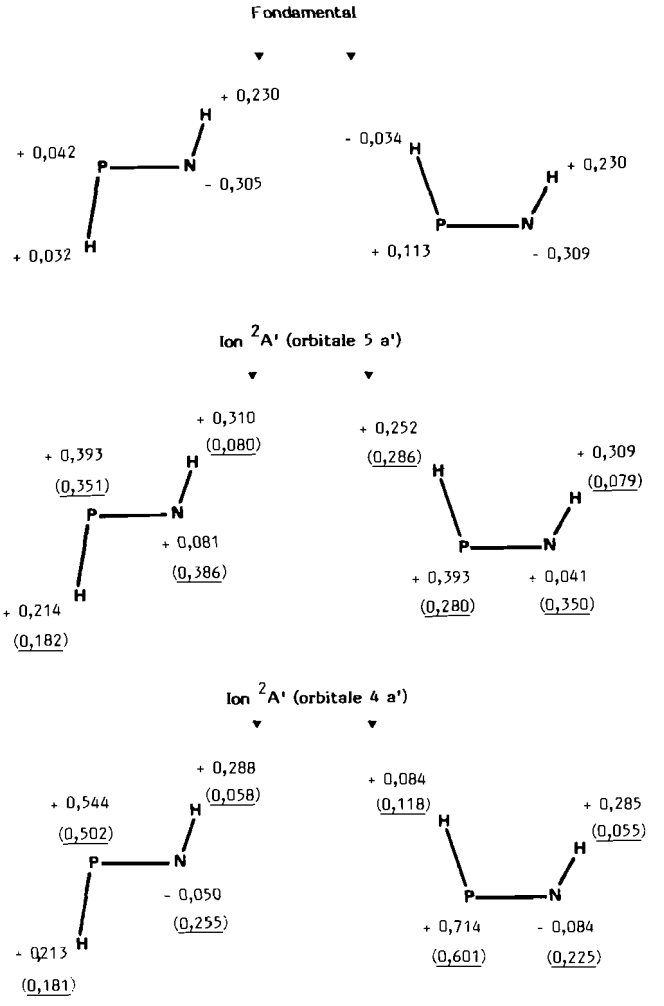

FIG. 3. HP=NH. Isomères *trans* et *cis*. Charges nettes après interaction de configurations. (Ecarts en charges nettes entre les ions et le fondamental.)

lors de l'ionisation, on constate toutefois que ces phénomènes de relocalisation ne sont pas très importants.

Toutefois, les calculs des sections efficaces pour les deux isomères mettent en évidence un comportement similaire pour les états associés respectivement à l'orbitale $5a'$ de l'isomère *trans* et à l'orbitale $4a'$ de l'isomère *cis*. Les résultats obtenus ici ne font apparaître aucune analogie de ce type puisqu'au contraire une localisation du «trou» sur le phosphore n'intervient que pour les ions correspondant aux orbitales $4a'$ des isomères *cis* et *trans*.

Les mêmes remarques avaient pu être déduites de l'analyse de travaux similaires (2) sur les isomères α et β des triazaphospholes. Quel que soit l'ion examiné, aucune corrélation n'avait pu être établie entre les variations d'intensité HeI/HeII observées expérimentalement et la plus ou moins grande localisation du «trou» sur l'atome de phosphore dans les différents ions formés.

4. Conclusion

L'étude réalisée sur le phosphazène HP=NH nous a permis de dégager un certain nombre de points importants concernant les sections efficaces de photoionisation des états ioniques provenant de l'éjection d'électrons des paires libres du phosphore et de l'azote.

Tout d'abord, il apparaît que la seule considération des localisations dans la fonction d'état initial est insuffisante pour interpréter correctement les variations d'intensité. Un des points essentiels mis en évidence apparaît être la phase entre les orbitales atomiques intervenant dans l'orbitale moléculaire ionisée liée à la pseudo symétrie du système.

De plus il semble, d'après l'analyse des phénomènes de réorganisation électronique au niveau des ions générés par photoionisation, que ce type de phénomène ne peut être en corrélation directe avec les variations des sections efficaces.

Remerciements

Les auteurs remercient le Docteur J. P. Flament (Unité Associée 465, École Polytechnique) pour leur avoir communiqué le programme de calcul permettant d'obtenir les matrices densité après interaction de configurations.

1. (*a*) P. DECHANT, A. SCHWEIG et W. THEIL. Angew. Chem. Int. Ed. Engl. **12**, 308 (1973); (*b*) A. SCHWEIG et W. THIEL. J. Chem. Phys. **60**, 951 (1974).
2. D. GONBEAU, G. PFISTER-GUILLOUZO, J. BARRANS et M. H. PALMER. Chem. Phys. **95**, 243 (1985).
3. D. DILL et J. L. DEHMER. J. Chem. Phys. **61**, 692 (1974).
4. J. L. GARCIA, D. GONBEAU, G. PFISTER-GUILLOUZO, M. ROCH et J. WEBER. Can. J. Chem. **63**, 1518 (1985).
5. K. SCHWARZ. Phys. Rev. B, **5**, 2466 (1972).
6. J. G. NORMAN, JR. J. Chem. Phys. **61**, 4630 (1974).
7. R. LATTER. Phys. Rev. **81**, 385 (1955).
8. J. C. SLATER. Quantum theory of molecules and solids. Vol. 4. McGraw–Hill, New York. 1974.
9. (*a*) P. DURAND et J. C. BARTHELAT. Theor. Chem. Acta, **38**, 283 (1975); (*b*) J. C. BARTHELAT et P. DURAND. Gazz. Chim. Ital. **108**, 225 (1978).
10. M. DUPUIS, J. RYS et H. F. KING. J. Chem. Phys. **65**, 111 (1976).
11. (*a*) B. HURON, J. P. MALRIEU et P. RANCUREL. J. Chem. Phys. **58**, 5745 (1973); (*b*) M. PELISSIER. Thèse Université Paul Sabatier, Toulouse, France (1980).
12. D. GONBEAU et G. PFISTER-GUILLOUZO. J. Electron Spectrosc. Relat. Phenom. **33**, 279 (1984).
13. E. NIECKE et W. FLICK. Angew. Chem. Int. Ed. Engl. **12**, 585 (1973).
14. S. ELBEL, A. ELLIS, E. NIECKE, H. EGSGAARD et L. CARLSEN. J. Chem. Soc. Dalton Trans. **5**, 879 (1985).
15. D. GONBEAU, G. PFISTER-GUILLOUZO et J. BARRANS. Can. J. Chem. **61**, 1371 (1983).
16. W. C. PRICE, A. W. POTTS et D. G. STREETS. *Dans* Electron spectroscopy. *Editeur*: D. A. Shirley. North Holland, Amsterdam. 1972.
17. J. P. MALRIEU. Journée sur la spectroscopie photoélectronique. Paris, Mars 1978.
18. G. TRINQUIER. J. Am. Chem. Soc. **104**, 6969 (1982).
19. S. CEDERBAUM. Chem. Phys. Lett. **25**, 562 (1975).
20. J. CHONG. J. Electron Spectrosc. Relat. Phenom. **7**, 429 (1975).
21. M. C. LASNE, J. L. RIPOLL, C. LAFON, D. GONBEAU et G. PFISTER-GUILLOUZO. Nouv. J. Chim. **10**, 69 (1986).

Vitamin D relatives. Part I. B-thiophene-des-A-cholestanes. Solvolytic reactions of some derivatives of 2,2-disubstituted cyclohexane-1,4-diol and 4-hydroxycyclohexan-1-one

JACEK W. MORZYCKI
Department of Chemistry, University of Warsaw, Pasteura 1, 02093 Warszawa, Poland

Received December 6, 1985

JACEK W. MORZYCKI. Can. J. Chem. **64**, 1536 (1986).

Some derivatives of des-A-cholestane with a thiophene ring B have been prepared from triketone **2**. The reactions of tosylates of C-10 alcohols (**7***b*, **9***b*, and **8***c*) leading to A-ring ethers (**10** and **11**) and olefin **5**, respectively, have been studied. The solvolysis of tosylate **4***c* and the Bamford–Stevens reactions of *p*-tosylhydrazones **3***c* and **13***b* are also discussed.

JACEK W. MORZYCKI. Can. J. Chem. **64**, 1536 (1986).

Utilisant la tricétone **2** comme produit de départ, on a préparé quelques dérivés du des-A-cholestane comportant un thiophène comme cycle B. On a étudié les réactions des tosylates des alcools en C-10 (**7***b*, **9***b* et **8***c*) qui conduisent respectivement aux éthers du cycle A (**10** et **11**) et à l'oléfine **5**. On discute aussi des réactions de solvolyse du tosylate **4***c* et des réactions de Bamford–Stevens des *p*-tosylhydrazones **3***c* and **13***b*.

[Traduit par la revue]

In the course of our studies on the synthesis of vitamin D relatives (1, 2) we have drawn attention to 6,9-epithio-tachysterol **A** as a possible intermediate. The allylic oxidation of this compound, followed by desulfurization, as well as photochemical and thermal isomerization (3) could afford an important, active metabolite of vitamin D_3, i.e. 1α-OH-D_3 (4). In an attempted synthesis of 6,9-epithio-tachysterol **A**, the starting ketone **1** (5) with the double bond C(9)—C(10) was subjected to ozonolysis. The resulting triketone **2** contained a 1,4-dicarbonyl system that reacted with phosphorus pentasulfide to give the thiophene derivative **3***b* (6) in good yield. In the next step the problem of the 19-methyl group migration from the 5β position to its former (in cholesterol) 10β position arose. It was expected that generation of a carbonium ion at C-10 should provide a driving force for the reaction. We assumed that the secondary carbonium ion adjacent to the quaternary carbon C-5 is likely to rearrange, to give a more stable tertiary carbonium ion by migration of a substituent (methyl, thienyl) or ring bond.

The carbon atom C-10 exists in compound **3***b* in the form of a carbonyl group and one of the best ways to the desired carbonium ion seemed to be the decomposition (7*a*) of 10-toluene-*p*-sulfonylhydrazone **3***d* under basic conditions (Bamford–Stevens reaction). The reaction afforded the unrearranged $\Delta^{1(10)}$ olefin **4***a* as the major product. The failure of this reaction prompted us to study the solvolytic reactions (7*b*) of *p*-toluenesulfonates of the C-10 alcohols. The $NaBH_4$ reduction of ketone **3***b* yielded a single epimer of alcohol **7***a*. As expected (attack of hydride from the less hindered side of the molecule), the compound obtained had the 10α-OH configuration. Proton nmr showed the equatorial orientation of both hydroxyl and acetoxyl groups (the broad signals of axial 10β ($w/2$ = 15 Hz) and 3α ($w/2$ = 20 Hz) protons at δ = 3.66 and 5.13, respectively) in the dominating conformation *B*. The alternative chair conformation *A* with the *anti*-coplanar arrangement of 10α-OH and 5β-CH_3 is less stable due to 1,3-diaxial interaction of 3β-acetoxyl and methyl groups. The reaction of 10α-tosylate **7***b* with KOH/diethylene glycol/diglyme (diglyme: diethylene glycol dimethyl ether) at 120°C afforded ether **10** in good yield. The product was apparently formed by an intramolecular attack of the 3β-alkoxyl ion from the back side on carbon C-10 in the boat conformation, which becomes more significant at higher temperature. This S_N2 type reaction unequivocally confirmed the *trans* relationship of 3β-acetate to the leaving group in the starting material **7***b*. Unfortunately the formation of the oxygen bridge precluded the development of a carbonium ion at C-10 and, at the same time, the retropinacolic rearrangement. To avoid this complication and to increase the contribution of the conformation with an axial hydroxyl (or tosyloxyl) group, we decided to study the solvolysis of compound **8***c* with the inverted configuration of acetate at C-3. Acetylation with inversion (8) of hydroxy-ketone **3***a* gave **6**. The $NaBH_4$ reduction of ketone **6** resulted in the formation of two products in the ratio 4:3. The less polar, major product appeared to be the 10α alcohol **8***a*. The ^1H nmr spectra confirmed the domination of the expected conformation *C*, with the axial substituent at C-10 and the equatorial 3α-acetate, either in the case of free alcohol **8***a* or its tosylate **8***c* (δ 5.08 (m, $w/2$ = 24 Hz, 3β-H) and 4.57 ($w/2$ = 6 Hz, 10β-H)).

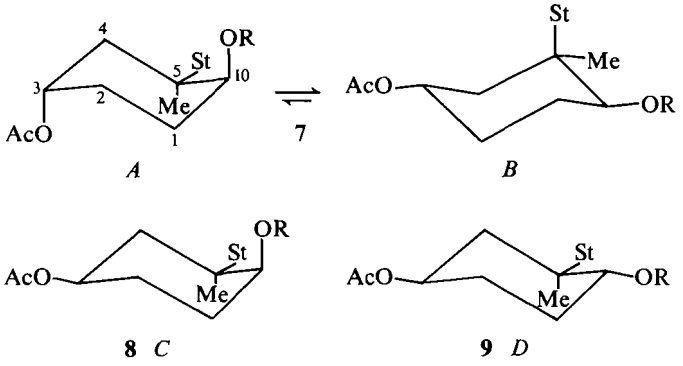

The second, more polar product was identified as the 10β alcohol **9***a*. The formation of significant amounts of epimeric alcohol **9***a* can be explained by taking into consideration its relative stability. In the preferred conformation *D*, either alcohol **9***a* or its tosylate **9***b* (δ 4.96 (m, $w/2$ = 22 Hz, 3β-H), 4.75 (m, $w/2$ = 18 Hz, 10α-H)) contained three equatorial substitutents, and only the small methyl group that occupied the axial position was involved in the 1,2-ae interaction with a 10β substituent.

The solvolysis of 10α-tosylate **8***c* was carried out under the same conditions as described in the case of compound **7***b*. Although the preferred conformation *C* seemed to be the most favourable for the methyl group migration, the reaction afforded $\Delta^{1(10)}$ olefin **5** and no rearranged products were detected. The

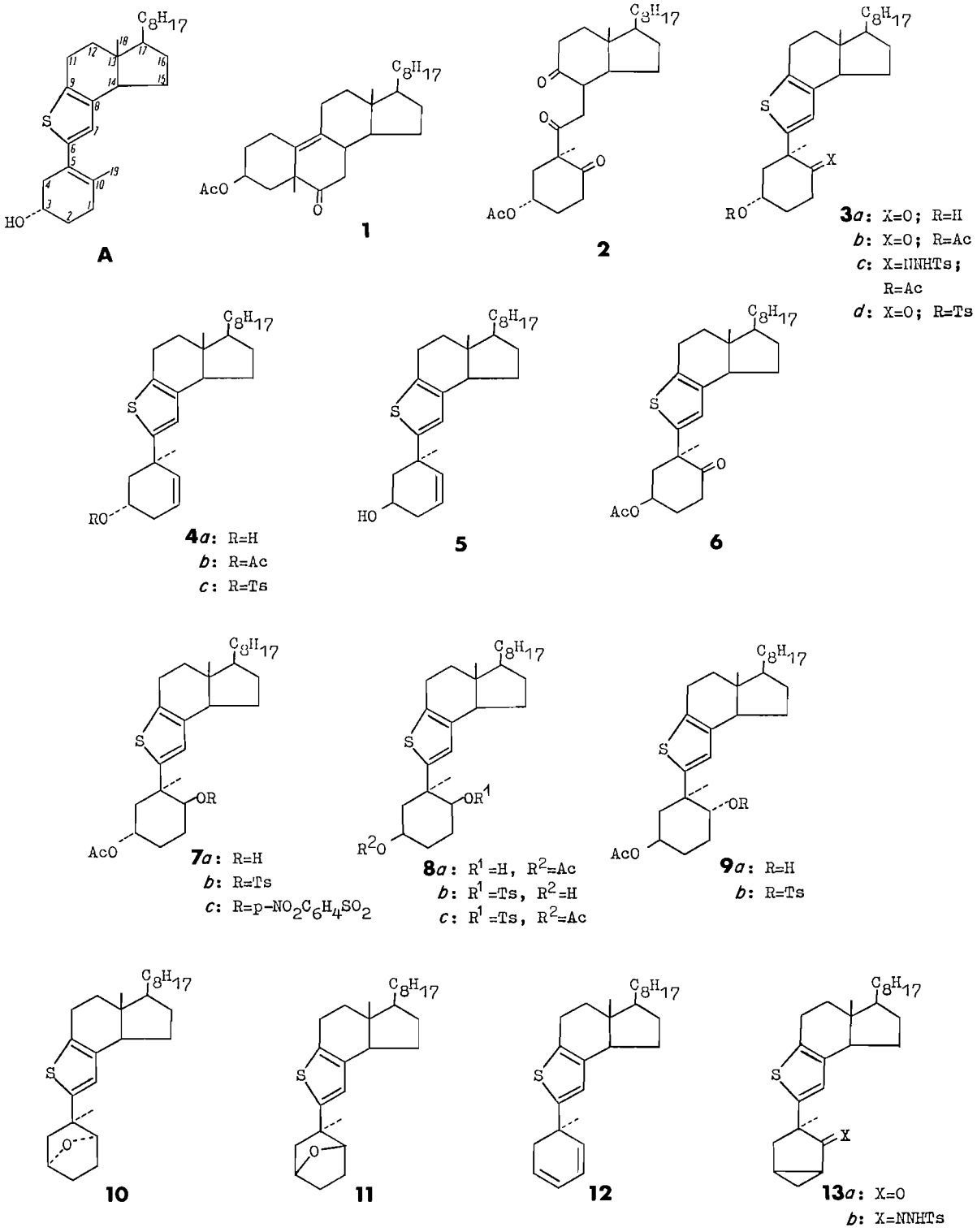

SCHEME 1

minor product of the reaction appeared to be hydroxy-tosylate **8***b* (the elimination of TsOH must be slower than the intramolecular substitution observed in the case of **7***b*). The similar reaction of the 10β-tosylate **9***b* resulted in the formation of α-ether **11** as the only isolable product. This intramolecular displacement proceeded in the same way as described above for compound **7***b*. In this case a nucleophilic attack took place from the opposite, α, side of the molecule as required by the structure of the starting material.

Since we failed to obtain the rearranged products by solvolytic methods from tosylates of the C-10 alcohols, we tried some other reactions that could afford at least partial positive charge at C-10. Such a reaction was the solvolysis of tosylate **4***c*, which should proceed with participation of π-electrons of the double bond. A nonclassical carbocation with a considerable charge at C-10 could be a suitable intermediate for rearrangement. The compound **4***c* was obtained by tosylation of homoallylic alcohol **4***a*, the product of the decomposition of *p*-tosylhydrazone **3***c*

already described. However, the reaction, carried out in the same manner as described previously, yielded only the product of a simple elimination of *p*-TsOH, diene **12**. Another attempt was the Bamford–Stevens reaction of *p*-tosylhydrazone **13***b*. The α-cyclopropyl ketone **13***a* was easily obtained from oxo-tosylate **3***d* by the reaction with sodium isopropoxide in almost quantitative yield. Unfortunately the decomposition of **13***b* under basic conditions led to a complex mixture of products, which were not analysed.

Eventually, we brought about the migration of the 19-methyl group by solvolysis of *p*-nitrobenzenesulfonate **7***c* in refluxing acetic acid in the presence of sodium acetate. Under these conditions, mainly the products of methyl migration were formed, in addition to a small amount of unrearranged olefin **4***b*. However, 6,9-epithio-tachysteryl acetate (λ_{max} 294 nm, δ 1.88 (br s, 19-H)), obtained in low yield, was accompanied by a number of other products (e.g. the $\Delta^{4(5)}$ isomer, nonpolar products of rearrangement with concomitant 3β-acetate elimination). The process requires further studies, which are under way.

Experimental

The melting points were determined on a Boetius micro melting point apparatus and are uncorrected. Optical rotations were measured on a Perkin–Elmer 241 polarimeter in chloroform solutions at $c = 1.0$ unless otherwise stated. The ir spectra were recorded on UR-20 and Unicam SP 1100 spectrophotometers. The ^{1}H nmr spectra were taken at 100 mHz (JEOL INM-4H-100 and Brüker instruments) in $CDCl_3$ solutions with TMS as an internal standard. Column chromatography was performed on silica gel (Kieselgel 60, 70–230 mesh, Merck). Thin-layer chromatograms were developed on aluminium tlc sheets precoated with silica gel F_{254} and visualized with 50% sulfuric acid after heating. All solvents were dried and freshly distilled prior to use. The starting ketone **1** was prepared according to the procedure described in ref. 5.

Triketone 2

A solution of β,γ-unsaturated ketone **1** (2.5 g) in hexane (100 mL) was cooled to −70°C in a Dry Ice – acetone bath and then treated with ozone. An excess of ozone was removed by passing a stream of oxygen, the reaction mixture was allowed to warm up to room temperature, and hexane was evaporated under reduced pressure. The residue was dissolved in acetic acid (30 mL) and stirred with zinc dust (2.5 g) for 45 min. The reaction mixture was diluted with ether (250 mL) and all inorganic material was filtered off. The filtrate was washed with water, sodium bicarbonate solution, again with water, and dried over anhydrous sodium sulfate. The solvent was removed and the crude product was purified on a silica gel column. Triketone **2** (1.9 g) was eluted with benzene–ether (9:1); $[\alpha]_D^{27}$ −68.2°; ν_{max} (neat): 1732, 1713, and 1698 cm^{-1}; δ: 5.42 (m, 1H, 3α-H), 2.08 (s, 3H, CH_3COO—), 1.38 (s, 5β-CH_3), 1.03 (s, 13β-CH_3). *Anal.* calcd. for $C_{29}H_{46}O_5$: C 73.4, H 9.8; found: C 73.5, H 9.7.

β-Oxo-thiophenes 3

To a stirred solution of triketone **2** (500 mg) in anhydrous THF (50 mL) were added phosphorus pentasulfide P_4S_{10} (1 g) and potassium hydrogen carbonate (1 g) and the reaction mixture was refluxed for 1 h. Most of the solvent was distilled off and the residue was dissolved in tetrachloromethane and water. The organic solution was washed with water, dried, and evaporated. Silica gel column chromatography of the crude product afforded compound **3***b* in a pure form (310 mg; 62%) eluted with benzene–ether (1%). At the end of elution some fractions containing **3***b* were contaminated by a slightly more polar furan analog (δ: 6.10 (s, 7-H)). Therefore it is recommended to leave the crude product for a few days in CCl_4 solution before chromatography to get rid of the unstable furan derivative. Compound **3***b*: $[\alpha]_D^{27}$ −72°; ν_{max} ($CHCl_3$): 1730, 1716, and 1261 cm^{-1}; λ_{max} (EtOH): 240 nm (ε 4950); δ: 6.53 (s, 1H, 7-H), 5.43 (m, 1H, 3α-H), 2.08 (s, 3H, CH_3COO—), 1.37 (s, 5β-CH_3), 0.61 (s, 13β-CH_3). *Anal.* calcd. for $C_{29}H_{44}O_3S$: C 73.7, H 9.4; found: C 73.6, H 9.4.

The hydrolysis of **3***b* was carried out in the following way. Compound **3***b* (140 mg) was dissolved in ethanol (20 mL) and a solution of potassium hydroxide (200 mg) in water (1 mL) was added dropwise. The reaction mixture was kept at 40°C for 1 h. The usual work-up afforded hydroxy-ketone **3***a* as an amorphous solid, $[\alpha]_D^{24}$ −76°; ν_{max} (KBr): 3430 and 1721 cm^{-1}; δ: 6.38 (s, 1H, 7-H), 4.30 (m, 1H, 3α-H), 3.41 (bs, 1H, —OH), 1.36 (s, 5β-CH_3), 0.60 (s, 13β-CH_3).

*3β-Hydroxy-olefin 4*a

Compound **3***b* (150 mg) and toluene-4-sulfonic acid hydrazide (250 mg) were dissolved in diglyme (2 mL) – diethylene glycol (5 mL) mixture, and acetic acid (0.5 mL) was added. The reaction mixture was stirred at 70°C for 4 h; tlc control showed the disappearance of all the starting material. A solution of *p*-tosylhydrazone **3***c* obtained in such a way was treated with KOH (2.5 g) and the temperature was increased to 140°C. The reaction was maintained at this temperature until evolution of N_2 stopped (about 30 min). After cooling, the reaction mixture was poured into 3% sulfuric acid and extracted with methylene chloride. The extract was dried over sodium sulfate and evaporated (the rest of the diglyme and glycol was removed under high vacuum) and the residue was chromatographed on a silica gel column. The product, olefin **4***a*, was eluted with benzene–ether (3%). Yield 76 mg; $[\alpha]_D^{24}$ +114°; ν_{max} ($CHCl_3$): 3610 and 1034 cm^{-1}; δ: 6.37 (s, 1H, 7-H), 5.69 (almost s, 2H, 1-H and 10-H), 3.90 (m, 1H, 3α-H), 1.41 (s, 5β-CH_3), 0.61 (s, 13β-CH_3). *Anal.* calcd. for $C_{27}H_{42}OS$: C 78.2, H 10.2; found: C 78.4, H 10.1.

*3β,10α-Diol 3-monoacetate 7*a

A stirred solution of compound **3***b* (200 mg) in benzene (15 mL) – methanol (15 mL) was treated with sodium borohydride (50 mg). After 30 min at room temperature the solvents were removed, chloroform and 5% sulfuric acid were added, and the chloroform layer was separated, washed with water, and dried over sodium sulfate. The evaporation of the solvent afforded essentially pure 10α-alcohol **7***a* in almost quantitative yield; mp 170–171°C (from hexane); $[\alpha]_D^{26}$ +32.5° (*c* 0.9); ν_{max} (KBr): 3474, 1718, and 1272 cm^{-1}; λ_{max} (EtOH): 241 nm (ε 6900); δ: 6.61 (s, 1H, 7-H), 5.13 (m, $w/2 = 20$ Hz, 1H, 3α-H), 3.66 (m, $w/2 = 15$ Hz, 1H, 10β-H), 2.05 (s, 3H, CH_3COO—), 1.83 (s, —OH), 1.42 (s, 5β-CH_3), 0.62 (s, 13β-CH_3). *Anal.* calcd. for $C_{29}H_{46}O_3S$: C 73.4, H 9.8; found: C 73.5, H 9.6.

Compound **7***a* (70 mg) and *p*-TsCl (170 mg) were dissolved in anhydrous pyridine (3 mL) and the solution was allowed to stand at room temperature for 24 h. The usual work-up gave tosylate **7***b*, which was used in the next experiment.

3β,10β-Ether 10

Tosylate **7***b* from the previous experiment was dissolved in diglyme (3 mL), potassium hydroxide (1.2 g) in diethylene glycol (3 mL) was added, and the vigorously stirred reaction mixture was heated at 120°C for 1 h. After cooling, the reaction mixture was poured into dilute hydrochloric acid and extracted with tetrachloromethane. The extract was washed with water, dried over sodium sulfate, and evaporated. The crude product **10** was filtered through a layer of silica gel in a benzene–ether (2%) solution. Yield 39 mg; $[\alpha]_D^{26}$ +18° (*c* 0.86); ν_{max} ($CHCl_3$): 1017 cm^{-1}; λ_{max} (EtOH): 241 nm (ε 7000); δ: 6.42 (s, 1H, 7-H), 4.64 and 4.23 (2 × m, 2 × 1H, —CH—O—CH—), 1.42 (s, 5β-CH_3), 0.62 (s, 13β-CH_3). *Anal.* calcd. for $C_{27}H_{42}OS$: C 78.2, H 10.2; found: C 78.5, H 10.2.

3α-Acetoxy-ketone 6

To a stirred solution of 3β-hydroxy-ketone **3***a* (300 mg) triphenylphosphine (250 mg), and acetic acid (100 mg) in anhydrous tetrahydrofuran (5 mL) was added diethyl azodicarboxylate (180 mg), and the reaction mixture was allowed to stand at room temperature for 24 h. The solvent was evaporated and the residue was chromatographed on a silica gel column. The steroidal product **6** was eluted with benzene–ether (5%). Yield 220 mg; $[\alpha]_D^{24}$ −6.0°; ν_{max} ($CHCl_3$): 1730 and 1705 cm^{-1}; δ: 6.37 (s, 1H, 7-H), 5.24 (m, 1H, 3β-H), 1.93 (s, 3H,

CH_3COO—), 1.49 (s, 5β-CH_3), 0.62 (s, 13β-CH_3). *Anal.* calcd. for $C_{29}H_{44}O_3S$: C 73.7, H 9.4; found: C 73.9, H 9.5.

3α,10α-Diol- and 3α,10β-diol-3-monoacetates ***8***a *and* ***9***a

A solution of compound **6** (200 mg) in benzene–methanol (1:1; 30 mL) was treated with $NaBH_4$ (50 mg) at room temperature for 1 h. The usual work-up of the reaction mixture, followed by the chromatographic separation of products on a silica gel column afforded 10α-alcohol ***8a*** (108 mg) and 10β-alcohol ***9a*** (82 mg); both products were eluted with benzene–ether (6%).

Compound ***8a***: $[\alpha]_D^{24}$ +65.0°; ν_{max} (neat): 3620, 1732, and 1248 cm^{-1}; δ: 6.53 (s, 1H, 7-H), 5.02 (m, 1H, 3β-H), 3.68 (m, 1H, 10β-H), 2.06 (s, 3H, CH_3COO—), 1.78 (s, —OH), 1.39 (s, 5β-CH_3), 0.61 (s, 13β-CH_3). *Anal.* calcd. for $C_{29}H_{46}O_3S$: C 73.4, H 9.8; found: C 73.7, H 9.8.

Compound ***9a***: $[\alpha]_D^{24}$ +63.8°; ν_{max} (neat): 3525, 1739, and 1248 cm^{-1}; δ: 6.56 (s, 1H, 7-H), 5.00 (m, 1H, 3β-H), 3.77 (m, 1H, 10α-H), 2.00 (s, 3H, CH_3COO—), 1.38 (s, 5β-CH_3), 0.62 (s, 13β-CH_3). *Anal.* calcd. for $C_{29}H_{46}O_3S$: C 73.4, H 9.8; found: C 73.6, H 9.7.

Both alcohols were converted into the corresponding tosylates ***8c*** or ***9b*** by dissolving the starting material (70 mg) in anhydrous pyridine (3 mL) together with *p*-tosyl chloride (300 mg). The reactions were allowed to stand at 30°C for 1 week. The standard work-up followed by chromatographic purification (tosylates were eluted with benzene–ether (2%) in both cases) afforded compounds ***8c*** or ***9b*** in almost quantitative yields.

8c: δ: 7.26 (AA′BB′, J = 8.4 Hz, 4H, arom. H), 6.38 (s, 1H, 7-H), 5.08 (m, $w/2$ = 24 Hz, 1H, 3β-H), 4.57 (m, $w/2$ = 6 Hz, 1H, 10β-H), 2.40 (s, 3H, Ar-CH_3), 2.03 (s, 3H, CH_3COO—), 1.35 (s, 5β-CH_3), 0.58 (s, 13β-CH_3).

9b: δ: 7.27 (AA′BB′, J = 8.2 Hz, 4H, arom. H), 6.37 (s, 1H, 7-H), 4.96 (m, $w/2$ = 22 Hz, 1H, 3β-H), 4.75 (m, $w/2$ = 18 Hz, 1H, 10α-H), 2.40 (s, 3H, Ar-CH_3), 1.97 (s, 3H, CH_3COO—), 1.38 (s, 5β-CH_3), 0.58 (s, 13β-CH_3).

3α,10α-Ether ***11***

To a solution of tosylate ***9b*** (67 mg) in diglyme (3 mL) was added potassium hydroxide (1.2 g) in diethylene glycol (3 mL). The reaction mixture was heated at 120°C and stirred for 1 h. The reaction was quenched in cold water, acidified with hydrochloric acid, and extracted with tetrachloromethane. The extract was washed with water, dried (anhydrous Na_2SO_4), and evaporated. The crude produce was purified on a silica gel column. 3α,10α-Ether **11** (37 mg) was eluted with benzene–ether (1%); $[\alpha]_D^{24}$ +33.5°; ν_{max} ($CHCl_3$): 995 cm^{-1}; λ_{max} (EtOH): 240 nm (ε 6200); δ: 6.49 (s, 1H, 7-H), 4.65 and 4.36 (2 × m, 2 × 1H, —CH—O—CH—), 1.42 (s, 5β-CH_3), 0.54 (s, 13β-CH_3). *Anal.* calcd. for $C_{27}H_{42}OS$: C 78.2, H 10.2; found: C 78.5, H 10.1.

3α-Hydroxy-olefin ***5***

The solvolysis of tosylate ***8c*** (70 mg) was carried out in exactly the same manner as in the previous experiment. The reaction products were separated on a silica gel column. The elution with benzene–ether (4%) afforded 3α-hydroxy-olefin **5** (36 mg). With benzene–ether (7%), hydroxy-tosylate ***8b*** (10 mg) was eluted.

Compound **5**: $[\alpha]_D^{24}$ + 61°; ν_{max} ($CHCl_3$): 3618 and 1038 cm^{-1}; δ: 6.47 (s, 1H, 7-H), 5.68 (m, 1H, 1-H), 4.08 (m, 1H, 3β-H), 1.45 (s, 5β-CH_3), 0.63 (s, 13β-CH_3). *Anal.* calcd. for $C_{27}H_{42}OS$: C 78.2, H 10.2; found: C 78.4, H 10.4.

Compound ***8b***: $[\alpha]_D^{24}$ +52°; ν_{max} ($CHCl_3$): 3606, 1178, and 901 cm^{-1}; δ: 7.27 (AA′BB′, J = 8.4 Hz, 4H, arom. H), 6.41 (s, 1H, 7-H), 4.54 (m, 1H, 10β-H), 3.98 (m, 1H, 3β-H), 2.41 (s, 3H, Ar-CH_3), 1.34 (s, 5β-CH_3), 0.59 (s, 13β-CH_3).

Diene ***12***

3β-Hydroxy-olefin ***4a*** (80 mg) and *p*-tosyl chloride (300 mg) were dissolved in anhydrous pyridine and allowed to stand for 16 h. Thin-layer chromatography showed complete conversion and the pyridine was then evaporated at room temperature. The residue was dissolved in diglyme (2 mL) and a solution of KOH (0.8 g) in diethylene glycol was added. The reaction mixture was vigorously stirred and heated at 110°C for 30 min. The reaction was quenched in cold water, acidified with HCl, and extracted with tetrachloromethane. The solvent was removed from the extract dried over sodium sulfate, and the crude product was purified by filtration through a layer of silica gel in a benzene – petroleum ether (1:4) solution. Yield of diene **12**, 56 mg; $[\alpha]_D^{25}$ +155°; ν_{max} ($CHCl_3$): 2965 and 1471 cm^{-1}; λ_{max} (EtOH): 244 (ε 12 000) and 256 (ε 11 600) nm; δ: 6.51 (s, 1H, 7-H), 5.86 (m, 4H, 1-H, 2-H, 3-H, and 10-H), 1.42 (s, 5β-CH_3), 0.64 (s, 13β-CH_3). *Anal.* calcd. for $C_{27}H_{40}S$: C 81.8, H 10.2; found: C 81.5, H 10.0.

α-Cyclopropylketone ***13***a

A solution of compound ***3a*** (140 mg) and *p*-tosyl chloride (500 mg) in anhydrous pyridine (5 mL) was allowed to stand at room temperature for 16 h. Pyridine was removed under high vacuum and a solution of sodium isopropoxide in isopropanol (prepared from 1 g of sodium and 80 mL of i-PrOH) was added. The suspension obtained was refluxed for 1 h. Then water was added and isopropanol was distilled off under reduced pressure. The steroidal product was extracted with benzene, and the extract was dried over sodium sulfate and evaporated. The crude product was purified on a silica gel column, and α-cyclopropylketone ***13a*** (105 mg) was eluted with benzene; mp 69–70°C; $[\alpha]_D^{25}$ +19.8°; ν_{max} ($CHCl_3$): 1699 cm^{-1}; δ: 6.48 (s, 1H, 7-H), 1.42 (s, 5β-CH_3), 0.61 (s, 13β-CH_3). *Anal.* calcd. for $C_{27}H_{40}OS$: C 78.6, H 9.8; found: C 78.5, H 9.8.

The *p*-tosylhydrazone of α-cyclopropylketone ***13b*** was obtained in a manner similar to that described earlier for compound ***3c*** (the reaction was somewhat slower and required more acetic acid). Its decomposition (Bamford–Stevens reaction), however, resulted in the formation of a complex mixture of products, which was not studied further.

Acknowledgements

Sincere thanks are extended to Professor W. J. Rodewald for useful discussions. This investigation was supported by the Polish Academy of Sciences.

1. (*a*) J. W. Morzycki, J. Jurek, and W. J. Rodewald. Can. J. Chem. **64**, 1540 (1986); (*b*) Tetrahedron Lett. **26**, 4243 (1985).
2. J. W. Morzycki, H. K. Schnoes, and H. F. DeLuca. J. Org. Chem. **49**, 2148 (1984).
3. P. J. Kocienski and B. Lythgoe. J. Chem. Soc. Perkin Trans. 1, 1400 (1980).
4. H. F. DeLuca, H. E. Paaren, and H. K. Schnoes. Top. Curr. Chem. **83**, 1 (1979).
5. W. J. Szczepek. Acta Chimica Hung. In press.
6. P. G. Sammes (*Editor*). Comprehensive organic chemistry. Vol. 4. Pergamon Press, Oxford. 1979. p. 829.
7. (*a*) D. N. Kirk and M. P. Hartshorn. Steroid reaction mechanisms. Elsevier, Amsterdam. 1968. p. 339; (*b*) pp. 41, 107, 228.
8. A. K. Bose, B. Lal, W. A. Hoffman, and M. S. Manhas. Tetrahedron Lett. 1619 (1973).

Synthesis of 8-methylene-des-AB-cholestan-9-one by cholesterol degradation[1]

JACEK W. MORZYCKI,[2] JAROSŁAW JUREK, AND WŁADYSŁAW J. RODEWALD
Department of Chemistry, University of Warsaw, Pasteura 1, 02093 Warszawa, Poland

Received December 6, 1985

JACEK W. MORZYCKI, JAROSŁAW JUREK, and WŁADYSŁAW J. RODEWALD. Can. J. Chem. **64**, 1540 (1986).

The short synthetic route from 3β-acetoxy-5β-methyl-19-norcholest-9(10)-en-6-one (**1**) to 8-methylene-des-AB-cholestan-9-one (**8**) is described. Compound **8** is a convenient intermediate for the synthesis of relatives of vitamin D_3 by the A → CD route.

JACEK W. MORZYCKI, JAROSŁAW JUREK et WŁADYSŁAW J. RODEWALD. Can. J. Chem. **64**, 1540 (1986).

On décrit une voie de synthèse courte pour transformer l'acétoxy-3β méthyl-5β nor-19 cholestène-9(10) one-6 (**1**) en méthylène-8 des-AB cholestanone-9 (**8**). Le composé **8** est un intermédiaire utile pour la synthèse, par le biais de la route A → CD, de composés apparentés à la vitamine D_3.

[Traduit par la revue]

Considerable interest surrounds des-AB- and des-A-B-seco-cholestane derivatives since they serve (2) as intermediates for the synthesis of relatives of vitamin D_3. These systems can be obtained either by total synthesis (3) or by degradation of cholesterol (4). The degradative approach avoids many of the stereochemical problems of a total synthesis and consists of successive cleavage of two bonds in ring B of the cholestane skeleton. Continuing studies (1) on des-A-B-seco steroids, our attention has been drawn to the synthesis of des-AB cholestanes containing one carbon atom substituent attached to C-8. The easily available ketone **1** (5) (from cholesterol in 4 steps)[3] seemed to be an excellent starting material for this purpose. The same compound was used by Lythgoe and co-workers in the synthesis of 8-hydroxymethyl-des-AB-cholest-8-ene (**12***a*) (6). Compound **12***a* was obtained in good yield and then successfully converted to 1α-hydroxy-vitamin D_3 (7). However, the multi-step Lythgoe synthesis of **12**, though efficient, was somewhat troublesome and therefore we considered alternative, more direct, methods of ketone **1** degradation (8). The most promising one seemed to be the oxime **2** fragmentation to an unsaturated nitrile, the reaction that was expected to predominate under Beckmann rearrangement conditions. We assumed that the ozonolysis of the C(9)—C(10) double bond in hypothetic nitrile **A**, followed by HCN elimination, should afford α-methylene ketone **8**.

Compound **2***a* reacted with $POCl_3$/Py to give a chromatographically inseparable mixture of nitriles in addition to a small amount of lactam **3**. However, spectral analysis of the mixture suggested a high content of nitrile **4**. The whole nitrile fraction was ozonized and the complex mixture of products was subjected to column chromatography. The major product appeared to be compound **5**, thus confirming structure **4** as the most significant compound of the nitriles mixture. Since we failed to obtain **8** in this way some changes in our synthetic strategy were necessary. We decided to inverse the order of transformations and to study the oxime **6***a* fragmentation reaction. We planned to obtain compound **6***a* by ozonolysis of the C(9)—C(10) double bond of the protected oxime, followed by hydrolysis of a protective group. It has been found (9) that γ-oxo-ketoximes undergo a heterolytic 5-centre fragmentation reaction to α,β-unsaturated ketones and nitriles. A similar fragmentation could also be expected in the case of **6***a*. The protection of oxime as acetate **2***b* appeared to be sufficient against ozone, and diketone **6***b* was obtained in 80% yield. The oxime acetyl group was selectively and almost quantitatively removed by hydrolysis with $NaHCO_3$/MeOH. Unfortunately, the compound obtained did not react either with TsCl/Py or with TsCl/MeOH/NaOH (9) (except for hydrolysis of 3β-OAc). However, on treatment with $POCl_3$/Py, it unexpectedly underwent fragmentation to α-methylene ketone **8** in about 50% yield. Under these conditions the normal Beckmann rearrangement of compound **6***a* was rather anticipated (10). The A-ring fragment is probably water soluble, as we could not find it in the benzene extract of the reaction products in spite of careful analysis. In some experiments a small amount of slightly more polar by-product **9** was obtained. The formation of oxazine **9** was also unexpected unless the structure **6***a* of the starting material was incorrect. These results prompted us to reexamine a structure of the product of oxime acetate **6***b* hydrolysis. We found that its hydroxyl group (ν_{max} ($CHCl_3$): 3582 cm^{-1}) is resistant to acetylation under mild conditions. This suggested that either the hydroxyl group is strongly engaged in an intramolecular hydrogen bond or, more likely, it is tertiary and the actual structure is **7**. Carbon-13 nmr distinguishes between these two possibilities. The comparison of the C-9 chemical shifts in ^{13}C nmr spectra of **6***b* (δ: 211.3 $\rangle C{=}O$) and the hydrolysis product (δ: 95.7 $\rangle C(OH)(OR)$) unequivocally confirmed the cyclic structure **7** of the latter compound and showed that it is a mixture of two epimers **7***a* and **7***b* in a ratio of approximately 7:3 (calculated from the integration of the anomeric carbon signals at δ 95.7 and 96.0) (11). The mixture is inseparable by chromatographic methods but it may be enriched in α-anomer **7***a* by crystallization from petroleum ether. In further experiments it was checked that oxazine **9** was not an intermediate in the reaction and that the presence of base (pyridine) is important for the fragmentation progress. The tentative mechanism of the reaction is shown in Scheme 1. However, it is also possible that during the reaction there is an equilibrium between **7***a*, **7***b*, and an open chain tautomer, i.e., **6***a*. The hydroxyl group of the free oxime **6***a* is easily accessible and therefore it reacts faster with $POCl_3$ than **7** (*a* or *b*) to give the corresponding ester. The fragmentation of this intermediate could be similar to that shown for the compound **7** derivative.

[1]Part V in our series on des-A- and des-A-B-seco steroids. For part IV, see ref. 1.

[2]Author to whom correspondence may be addressed.

[3]The improved synthesis of **1** from cholesterol was recently elaborated by Szczepek (5*b*).

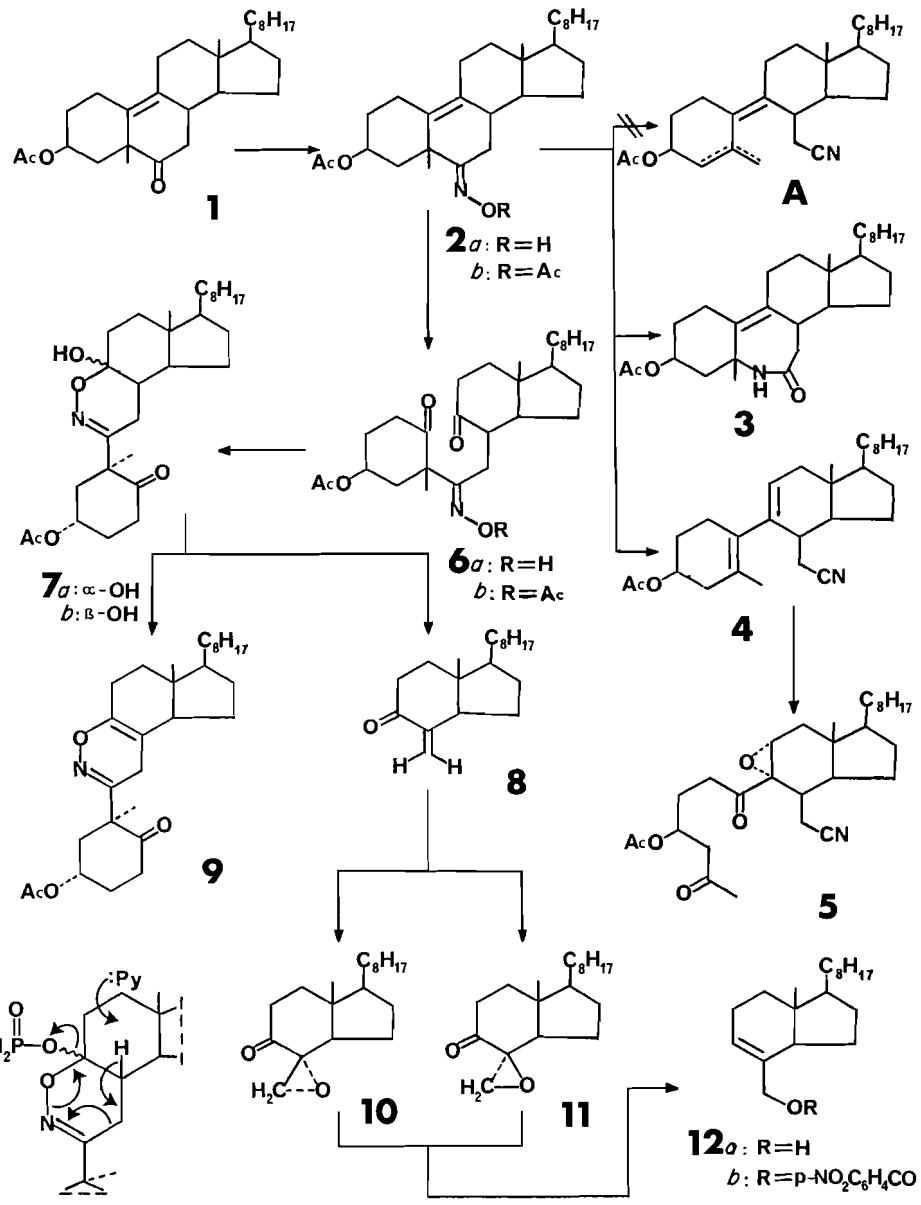

SCHEME 1

The virtual utility of the des-AB compound **8** for the synthesis of relatives of vitamin D_3 and some analogs of natural steroids seems to be clear (12). To confirm its structure by chemical means and to demonstrate its application in the vitamin D field, the α-methylene ketone **8** was converted to the known allylic alcohol **12***a* by Wharton's two-step procedure (13). In the first step compound **8** was oxidized with hydrogen peroxide/NaOH/MeOH to yield a mixture of epoxy ketones **10** and **11** in the ratio 2:3. Each of them (or a mixture of both epimers) was then reduced with hydrazine at room temperature to give the same product **12***a*. Physical constants and spectral properties of its *p*-nitrobenzoyl derivative **12***b* proved to be almost identical with the data given for this compound in the literature (6).

Experimental

The melting points were determined on a Boetius micro melting point apparatus and are uncorrected. Optical rotations were measured on a Perkin–Elmer 241 polarimeter in chloroform solutions at $c = 1.0$ unless otherwise stated. The ir spectra were recorded on UR-20 and Unicam SP 1100 spectrophotometers. The ^1H and ^{13}C nmr spectra were taken at 100 MHz (JEOL INM-4H-100 and Brüker) in $CDCl_3$ solutions with TMS as an internal standard. The mass spectra were recorded on a LKB 9000 spectrometer at 70 eV. Column chromatography was performed on silica gel (Kieselgel 60, 70–230 mesh, Merck). Thin-layer chromatograms were developed on aluminium sheets tlc precoated with silica gel F_{254} and visualized with 50% sulfuric acid after heating. All solvents were dried and freshly distilled prior to use. The starting ketone **1** was prepared according to the procedure described in ref. 5*b*.

*Oxime 2*a

A solution of ketone **1** (5.0 g) and hydroxylamine hydrochloride (8.0 g) in methanol (100 mL) and pyridine (25 mL) was refluxed for 20 min. After cooling, the reaction mixture was poured into ice-water (400 mL), acidified with dilute hydrochloric acid, and extracted with chloroform (3 × 150 mL). The combined organic extracts were washed with water and dried over anhydrous Na_2SO_4. The solvent was removed under reduced pressure and the residue was purified by silica gel column chromatography. The elution with benzene–ether (9:1) afforded oxime **2***a* (4.3 g), which was used in the next step without any further purification. An analytical sample of **2***a* was obtained by

preparative tlc of oxime **2***a* (100 mg) eluted from the column. The plates were developed four times in benzene. This procedure got rid of the more polar *Z* isomer,[4] which makes up about 5% of the crude product. The pure compound **2***a* crystallized from petroleum ether, mp 151–153°C; $[\alpha]_D^{26}$ +39°; ν_{max} ($CHCl_3$): 3589, 3300, 1732, 1667, and 1268 cm^{-1}; δ: 5.11 (m, 1H, 3α-H), 2.07 (s, 3H, CH_3COO—), 1.42 (s, 5β-CH_3), 0.78 (s, 13β-CH_3). *Anal.* calcd. for $C_{29}H_{47}NO_3$: C 76.1, H 10.3; found: C 75.9, H 10.2.

Beckmann rearrangement of oxime **2**a

To a solution of compound **2***a* (900 mg) in pyridine (20 mL) cooled to −10°C a well-chilled mixture of $POCl_3$ (1 mL) and pyridine (20 mL) was added. The temperature (−10°C) was maintained for 10 min, then the reaction mixture was poured into ice-water (400 mL), acidified with dilute HCl, and extracted with chloroform (3 × 70 mL). The chloroform extracts were washed with water and dried over anhydrous Na_2SO_4. The solvent was evaporated and the residue was subjected to column chromatography. The benzene elution afforded a mixture of nitriles (450 mg). The elution with a benzene–ether (3:1) mixture yielded lactam **3** (150 mg), mp (from methanol) 132–135°C; $[\alpha]_D^{26}$ +105°; ν_{max} (neat): 3220, 1740, 1668, 1642 (shoulder), and 1250 cm^{-1}; δ: 5.95 (s, 1H, —NH), 5.03 (m, 1H, 3α-H), 2.05 (s, 3H, CH_3COO—), 1.63 (s, 5β-CH_3), 0.79 (s, 13β-CH_3). *Anal.* calcd. for $C_{29}H_{47}NO_3$: C 76.1, H 10.3; found: C 75.8, H 10.3.

Ozonolysis of the nitriles mixture

The nitrile fraction from the preceding experiment (80 mg) was dissolved in hexane (100 mL), cooled in a Dry Ice – acetone bath, and ozonized until a blue colour appeared. Hexane was removed under reduced pressure and zinc dust (200 mg) in acetic acid (5 mL) was added. The above mixture was stirred for 2 h, diluted with ether (200 mL), and the zinc was filtered off. The filtrate was washed with water, then with sodium bicarbonate solution, again with water, and dried over sodium sulfate. The crude product was chromatographed on a silica gel column. The benzene–ether (4:1) mixture eluted epoxy-diketone **5** (24 mg), $[\alpha]_D^{27}$ +6.2°; ν_{max} (neat): 2259, 1740, 1724, 1712, and 1250 cm^{-1}; δ: 5.26 (m, 1H, 3α-H), 3.15 (m, 1H, 11β-H), 2.15 (s, 3H, CH_3CO—), 2.01 (s, 3H, CH_3COO—), 0.81 (s, 13β-CH_3); *m/e*: 487 (M^+, 0.5%), 427 (M^+ − HOAc, 13%), 314 (M^+ − HOAc − C_8H_{17}, 23%), 124 (100%). *Anal.* calcd. for $C_{29}H_{45}NO_5$: C 71.4, H 9.3; found: C 71.3, H 9.3.

Ozonolysis of oxime acetate **2**b

Oxime acetate **2***b* was obtained by acetylation of oxime **2***a* (4.0 g) under standard conditions (15 mL of Ac_2O, 50 mL of Py, room temperature, 4 h). The usual work-up afforded the crude product, homogenous in tlc (4.25 g); $[\alpha]_D^{26}$ +53°; ν_{max} (neat): 1770, 1739, 1681, and 1637 cm^{-1}; δ: 5.19 (m, 1H, 3α-H), 2.18 (s, 3H, CH_3COON=), 2.07 (s, 3H, CH_3COO—), 1.52 (s, 5β-CH_3), 0.75 (s, 13β-CH_3).

A solution of the above oxime acetate **2***b* (140 mg) in hexane (150 mL) was cooled to −20°C. A stream of ozone (about 10 L/h) was passed through the solution for 3 min. Hexane was removed under reduced pressure and zinc dust (200 mg) in acetic acid (5 mL) was added. The further work-up was identical to the previous experiment. The silica gel column chromatography of crude product afforded diketone **6***b* (119 mg) eluted with benzene–ether (9:1), $[\alpha]_D^{25}$ −30°; ν_{max} ($CHCl_3$): 1770, 1730, 1712, and 1633 cm^{-1}; δ: 5.43 (m, 1H, 3α-H), 2.21 (s, 3H, CH_3COON=), 2.03 (s, 3H, CH_3COO—), 1.34 (s, 5β-CH_3), 1.02 (s, 13β-CH_3); ^{13}C nmr, δ: 211.3 (C-9), 208.9 (C-10), 170.2 (C=O in 3β-acetate), 169.4 (C=O in oxime acetate), 167.6 (C-6), 68.2 (C-3). *Anal.* calcd. for $C_{31}H_{49}NO_6$: C 70.0, H 9.3; found: C 69.8, H 9.3

The selective hydrolysis of compound **6**b

To a solution of compound **6***b* (400 mg) in methanol (100 mL) was added sodium bicarbonate (0.5 g), and the reaction mixture was stirred at room temperature for 1.5 h. $NaHCO_3$ was filtered off, the filtrate was acidified with acetic acid (to pH 6), and methanol was removed under reduced pressure. The residue was redissolved in benzene (150 mL), the solution obtained was washed with water, dried over sodium sulfate, and the solvent was evaporated. The crude product, **7** (361 mg), homogenous in tlc, was crystallized several times from petroleum ether, mp 137–138°C; $[\alpha]_D^{25}$ −29°; ν_{max} ($CHCl_3$): 3582, 1729, 1713, and 1260 cm^{-1}; δ: 5.40 (m, 1H, 3α-H), 2.08 (s, 3H, CH_3COO—), 1.25 (s, 5β-CH_3); ^{13}C nmr, δ: 209.2 (C-10), 170.2 (C=O in acetate), 157.6 (C-6), 95.7 (C-9), 68.3 (C-3). *Anal.* calcd. for $C_{29}H_{47}NO_5$: C 71.1, H 9.7; found: C 70.9, H 9.7.

8-Methylene-des-AB-cholestan-9-one (8) and oxazine **9**

A solution of compound **7** (a crude material was used that is actually a mixture of anomers **7***a* and **7***b*; 104 mg) in pyridine (20 mL) was chilled to 0°C and treated with $POCl_3$ (1.5 mL) in cold pyridine (10 mL). The reaction mixture was allowed to stand in the refrigerator (5°C) for 1 h, then poured into ice-water, acidified with dilute HCl, and extracted with benzene. The extract was washed with water, dried over sodium sulfate, and the solvent was evaporated. The residue was subjected to column chromatography. The least polar compound, α-methylene-ketone **8**, was eluted with benzene (32 mg); $[\alpha]_D^{25}$ +45°; ν_{max} ($CHCl_3$): 3100 (w, CH_2=), 1693, and 1625 cm^{-1}; λ_{max}: 234 nm (ε 4100); δ: 6.15 and 5.20 (2 × m, 2 × 1H, H_2C=), 0.72 (s, 13β-CH_3); *m/e*: 276 (M^+, 10%), 163 (M^+ − C_8H_{17}, 100%). *Anal.* calcd. for $C_{19}H_{32}O$: C 82.5, H 11.7; found: C 82.5, H 11.6.

Further elution with benzene afforded oxazine **9** (7 mg); $[\alpha]_D^{25}$ −14°; ν_{max} ($CHCl_3$): 1730, 1715, 1678, 1620 (w), and 1260 cm^{-1}; δ: 5.21 (m, 1H, 3α-H), 2.09 (s, 3H, CH_3COO—), 1.26 (s, 5β-CH_3), 0.77 (s, 13β-CH_3); *m/e*: 471 (M^+, 10%), 43 (100%). The benzene–ether (9:1) mixture eluted unreacted starting material **7** (21 mg).

The oxidation of 8-methylene-des-AB-cholestan-9-one (8) with hydrogen peroxide

A flask with a solution of α-methylene-ketone **8** (72 mg) in methanol (10 mL) and 30% hydrogen peroxide (1.6 mL) was placed in an ice-water bath. To the vigorously stirred reaction mixture 20% aqueous sodium hydroxide (0.4 mL) was added dropwise during 10 min. After 4 h of continuous stirring the mixture was poured into water and extracted with ether. The usual work-up provided an oily product, which was chromatographed on a silica gel column. The benzene elution afforded α-epoxide **10** (23 mg); $[\alpha]_D^{25}$ +73° (*c* 1.0 in CCl_4); ν_{max} ($CHCl_3$): 1719 cm^{-1}; δ: 3.15 and 2.53 (2 × d, J = 6 Hz, 2 × 1H, H_2C—C—), 0.92 (s, 13β-CH_3); *m/e*: 292 (M^+, 22%), 43 (100%).

The benzene–ether (9:1) mixture eluted β-epoxide **11** (34 mg); $[\alpha]_D^{25}$ +38° (*c* 1.0 in CCl_4); ν_{max} ($CHCl_3$): 1720 cm^{-1}; δ: 3.04 and 2.74 (2 × d, J = 6 Hz, 2 × 1H, H_2C—C—), 0.98 (s, 13β-CH_3); *m/e*: 292 (M^+,

17%), 43 (100%).

Allylic alcohol **12**a *and its* p*-nitrobenzoate* **12**b

To a solution of epoxide (**10** and (or) **11**; 60 mg) in methanol (10 mL) cooled to 0°C in an ice-water bath was added portionwise a solution of anhydrous hydrazine (1 mL) in methanol (4 mL). The reaction mixture was allowed to stand for 1 h at 0°C and for another hour at room temperature, then poured into water and extracted with benzene. The solvent was removed from the dried (anhydrous Na_2SO_4) extract, and the oily product, allylic alcohol **12***a*, was directly subjected to *p*-nitrobenzoylation (60 mg of *p*-$NO_2C_6H_4COCl$, 6 mL of pyridine, room temperature, 4 h). The reaction mixture was diluted with benzene (80 mL), washed several times with an aqueous solution of cupric sulfate, with water, and dried over sodium sulfate. The solvent was evaporated and the crude product was purified by column chromatography. *p*-Nitrobenzoate **12***b* was eluted with hexane–benzene (3:1) and crystallized from ethanol; mp 103–104.5°C (lit. (6) mp 100–103°C); $[\alpha]_D^{25}$ +16.5°; ν_{max} (KBr): 1729, 1670, 1530, 1352, and 1290 cm^{-1}; δ: 8.20 (m, 4H, arom H), 5.70 (m, 1H, 9-H), 4.75 (almost s, 2H, —CH_2OCO—), 0.71 (s, 13β-CH_3); *m/e*: 427 (M^+, 2%), 260 (M^+ −

[4]The *E* configuration of the major oxime **2***a* was unequivocally proved by its further transformations, i.e. the formation of lactam **3** and particularly the cyclization of B-seco-oxime **6***a* to **7**.

p-$NO_2C_6H_4CO_2H$, 48%), 147 ($M^+ - p$-$NO_2C_6H_4CO_2H - C_8H_{17}$, 100%). *Anal.* calcd. for $C_{26}H_{37}NO_4$: C 73.0, H 8.7; found: C 72.8, H 8.8.

Acknowledgements

We thank Dr Z. Bończa-Tomaszewski and Dr R. Siciński for their helpful interest. Financial support of this research by the Polish Academy of Sciences is gratefully acknowledged.

1. W. J. Szczepek, J. W. Morzycki, Z. Bończa-Tomaszewski, M. Chodyński, and W. J. Rodewald. Can. J. Chem. **62**, 1081 (1984).
2. (*a*) M. L. Hammond, A. Mourino, and W. H. Okamura. J. Am. Chem. Soc. **100**, 4907 (1978); (*b*) R. G. Harrison, B. Lythgoe, and P. W. Wright. J. Chem. Soc. Perkin Trans. 1, 2654 (1974); (*c*) H. Nemoto, X. M. Wu, H. Kurobe, M. Imara, K. Fukumoto, and T. Kametani. Tetrahedron Lett. **25**, 3095 (1984).
3. (*a*) S. R. Wilson and M. S. Haque. Tetrahedron Lett. **25**, 3147 (1984); (*b*) P. S. Littlewood, B. Lythgoe, and A. K. Saksena. J. Chem. Soc. (C), 2955 (1971); (*c*) P. J. Kocienski, B. Lythgoe, and D. A. Roberts. J. Chem. Soc. Perkin Trans. 1, 834 (1978).
4. (*a*) A. Windaus and W. Grundmann. Ann. **524**, 295 (1936); (*b*) R. S. Davidson, W. H. H. Günter, S. M. Waddington-Feather, and D. A. Roberts. J. Chem. Soc. Perkin Trans. 1, 892 (1980).
5. (*a*) P. Kočovsky and V. Černy. Collect. Czech. Chem. Commun. **42**, 2415 (1977); (*b*) W. J. Szczepek. Acta Chim. Hung. In press.
6. P. J. Kocienski, B. Lythgoe, and D. A. Roberts. J. Chem. Soc. Perkin Trans. 1, 897 (1980).
7. P. J. Kocienski and B. Lythgoe. J. Chem. Soc. Perkin Trans. 1, 1400 (1980).
8. J. W. Morzycki, J. Jurek, and W. J. Rodewald. Tetrahedron Lett. **26**, 4243 (1985).
9. W. Eisele, C. A. Grob, E. Renk, and H. von Tschammer. Helv. Chim. Acta, **51**, 816 (1968).
10. E. S. Olson and J. H. Richards. J. Org. Chem. **33**, 434 (1968).
11. (*a*) A. Ejchart and L. Kozerski. Spektrometria Magnetycznego Rezonansu Jądrowego ^{13}C. PWN, Warszawa 1981. Chapt. Carbohydrates. p. 247 (in Polish); (*b*) L. Que, Jr. and G. R. Gray. Biochemistry, **13**, 146 (1974).
12. (*a*) R. A. Micheli, Z. G. Hajos, N. Cohen, D. R. Parrish, L. A. Portland, W. Sciemanna, M. A. Scott, and P. A. Wehrli. J. Org. Chem. **40**, 675 (1975); (*b*) N. Cohen, B. L. Banner, W. F. Eichel, D. R. Parish, and G. Saucy. J. Org. Chem. **40**, 681 (1975).
13. (*a*) P. S. Wharton and D. M. Bohlen. J. Org. Chem. **26**, 3615 (1961); (*b*) W. R. Benn and R. M. Dobson. J. Org. Chem. **29**, 1142 (1964).

Infrared spectroscopic studies of solvent effects on the conformation of *n*-alkanes[1]

H. L. CASAL, P. W. YANG, AND H. H. MANTSCH
Division of Chemistry, National Research Council of Canada, Ottawa, Ont., Canada K1A 0R6

Received January 27, 1986

H. L. CASAL, P. W. YANG, and H. H. MANTSCH. Can. J. Chem. **64**, 1544 (1986).

The infrared spectra of specifically deuterated *n*-tridecane-7,7-d_2 pure and mixed with several linear and branched hydrocarbons have been measured as a function of temperature. The average *gauche* fraction at the middle of the *n*-tridecane chain has been determined from the intensities of conformation-specific CD_2 rocking bands. The results indicate that the concentration of *gauche* rotamers in the centre of the *n*-C_{13} chains varies with the solvent. For example, when *n*-tridecane is dissolved in other *n*-hydrocarbons the *gauche* concentration decreases when the chain length of the solvent is shorter than *n*-C_{13} and increases when the solvent chains are longer than *n*-C_{13}. However, no simple, direct correlation is found between these solvent-induced changes in *gauche* concentration and measured thermodynamic quantities of mixing.

H. L. CASAL, P. W. YANG et H. H. MANTSCH. Can. J. Chem. **64**, 1544 (1986).

Opérant à diverses températures, on a mesuré les spectres infrarouges du *n*-tridécane-d_2-7,7 soit à l'état pur soit sous forme de mélange avec plusieurs hydrocarbures linéaires ou ramifiés. En se basant sur les intensités des bandes de vibration de rotation du CD_2 qui sont spécifiques aux conformations, on a déterminé la fraction moyenne de conformères *gauche* qui existe au centre de la chaîne du *n*-tridécane. Les résultats indiquent que la concentration de rotamères *gauche* dans le centre des chaînes *n*-C_{13} varie avec le solvant. Par exemple, lorsqu'on dissout du *n*-tridécane dans d'autres hydrocarbures linéaires, la concentration de conformères *gauche* diminue si la longueur de la chaîne du solvant est plus courte que celle du *n*-C_{13} alors qu'elle augmente lorsque les chaînes du solvant sont plus longues que celle du *n*-C_{13}. Toutefois, il n'existe aucune corrélation directe entre ces changements, induits par le solvant, dans les concentrations de conformères *gauche* et les quantités thermodynamiques de mélange qui ont été mesurées.

[Traduit par la revue]

Introduction

The conformation, flexibility, and constitution of liquid hydrocarbons in their pure state or in mixtures with each other play an important role in determining their macroscopic behaviour. There currently is considerable interest in understanding the molecular-level phenomena associated with the measured macroscopic thermodynamic properties of mixing hydrocarbons with each other (1). The measured thermodynamic functions such as excess enthalpy or volume are a manifestation of interactions at the molecular level. The ΔH of mixtures of alkanes might be expected to be particularly simple since methyl and methylene groups in normal or branched alkanes may be taken as similar. Thus, the components of the mixture will be of the same chemical nature. Furthermore, differences in free volume between the alkane components of a mixture produce only small negative contributions to ΔH. More significant contributions to ΔH can arise from order effects, which may be of two kinds, one *intramolecular* involving *gauche–trans* isomerism and the other *intermolecular* involving orientational order of the alkane molecules. However, the time-averaged thermodynamic measurements are unable to resolve the relative significance of intramolecular isomerism and intermolecular short-range order in the total contribution to the observed excess thermodynamic quantities. The changes in packing (orientational order) must have an effect on the ability of these chain molecules to adopt different conformations. Thus, the two effects (inter- and intramolecular) cannot be easily separated. Spectroscopic methods are appropriate to attempt measurements of one or the other of these effects (or both together). For example, light scattering experiments have been used to measure changes in short-range intermolecular order (1, 2); on the other hand, Raman spectra indicated that within experimental error the total *gauche* concentration of liquid *n*-$C_{16}H_{34}$ is the same in the pure state and in CCl_4 solutions (2). The spectra of pure liquid hydrocarbons and their mixtures with each other are practically identical and the determination of their individual *gauche* concentrations is therefore a challenging problem. Isotopic labelling can be used to address this problem.

The results reported here represent an attempt to determine the average *gauche* concentration of one hydrocarbon in solution with other hydrocarbons. The method used for these measurements is based on the unique sensitivity of the infrared-active CD_2 rocking vibrations of specifically labelled *n*-hydrocarbons. This method was first introduced by Snyder to study the conformation of solid polyethylene (3). It was later used to study solid-state hydrocarbons (4) and also to measure *gauche* defect concentration in solid fatty acids (5). The spectra of specifically labelled *n*-hydrocarbons in the liquid state have also been analysed in detail and the necessary background for quantitative studies of chain conformation in hydrocarbon mixtures is available (6).

Experimental

n-Tridecane-7,7-d_2 (*n*-C_{13}-7,7-d_2) was purchased from Merck, Sharp & Dohme (Montreal, Canada). Its chemical purity was determined to be 99.2% from gas–liquid chromatography. Its isotopic purity was 98% atom D. The solvents used, cyclohexane, 2,2,4-trimethyl-pentane, *n*-heptane, *n*-octane, *n*-hexadecane, 2-methylpentane, 2,2-dimethylpentane, 3-methylpentane, 2,2-dimethylbutane, 2,3-dimethylbutane, and 3,3-dimethylpentane were from Aldrich (gold label) and were used as received.

Series of infrared spectra were recorded between 10 and 50°C using a Digilab FTS-11 Fourier transform infrared spectrometer equipped with a wide-range (~450 cm^{-1} cut off) HgCdTe detector. The samples consisted of neat liquid *n*-C_{13}-7,7-d_2 and its mixtures (always 50% by volume) with the above-mentioned solvents. Spectra were measured from solutions contained in cells of 50 μm path length with KBr windows. The resolution was 2 cm^{-1} and 200 interferograms were accumulated for each spectrum. The temperature was measured by a copper–constantan thermocouple in contact with the cell windows. The integrated band intensities due to the different conformers were measured by calculating the area of the observed bands from

[1]NRCC No. 25423.

TABLE 1. Observed frequencies[a] for the CD_2 rocking vibrational mode of an isolated CD_2 group in the interior of a normal hydrocarbon chain

ν_{obs} (cm^{-1})	Conformer[b]
622	ttt
646	tgg
652	tgt
680	ggt

[a]From ref. 6.
[b]The underlined symbols refer to the bond pair being monitored; in the present case of *n*-C_{13}-7,7-d_2, this bond pair is C_6—C_7; identical to C_7—C_8.

band-fitted spectra. An iterative band-fitting program was used and spectra were processed after baseline correction due to the overlapping signals from the non-deuterated moieties of *n*-C_{13}-7,7-d_2 and solvents.

Results and discussion

The infrared bands due to the rocking vibrations of isolated CD_2 groups in a polymethylene chain occur between 600 and 680 cm^{-1}. For quantitative measurements of these bands, the solvents selected for study must not give rise to bands in this region which could interfere with the CD_2 rocking bands. The solvents used in this study were selected on that basis and the results presented here are from mixtures where the solvent bands do not overlap with the conformationally-sensitive CD_2 rocking signals from *n*-C_{13}-7,7-d_2.

The CD_2 rocking vibrations are almost completely decoupled from other vibrational modes of the unlabelled chain. The frequencies of the CD_2 rocking modes are uniquely sensitive to the conformation of the neighbouring C—C bonds as well as to the position of the CD_2 group in the chain. In Table 1 we summarize the observed frequencies for a CD_2 group in an otherwise non-labelled hydrocarbon chain. The values of the frequencies listed in Table 1 are for a CD_2 group in the interior of a chain and are from ref. 6.

In the spectra of long *n*-hydrocarbons ($n \geq 11$) the two bands at 646 and 652 cm^{-1}, due to tgg and tgt conformers respectively, overlap to such an extent that their separation is not possible. Therefore, we have meausred the combined area under the band at ~650 cm^{-1} (see Fig. 1) and refer to this quantity as I_{650}. Thus I_{650} represents the total intensity due to *tg* conformers (from tgg and tgt bond pairs). The area under the ttt band at ~622 cm^{-1} is termed I_{622} and represents the intensity due to the all-*trans* conformers. From these values, and following the derivations of ref. 6, the relative *gauche* concentration at the middle of the *n*-C_{13} chain is:

$$[1] \quad r_g(C_6—C_7) \equiv \frac{1}{2}[r_g(C_6) + r_g(C_7)] \cong \frac{n_{gt}}{n_{tt}} = \frac{1}{2}\frac{I_{650}}{I_{622}} \times A_r$$

where $r_g(C_6—C_7)$ is the ratio of the numbers of *trans–gauche* pairs to the numbers of *trans–trans* pairs and A_r is the relative absorptivity of the *tg* (~650 cm^{-1}) and *tt* (~622 cm^{-1}) bands. A_r has been determined to be 1.00 ± 0.07 for the rocking bands of CD_2 groups in the interior of chains (6); we shall use 1.0 as the value. From eq. [1], the average *gauche* fraction can be expressed as (6):

$$[2] \quad f_g(C_6—C_7) = \left[\frac{1}{r_g(C_6—C_7)} + 1\right]^{-1} \cong \frac{I_{650}}{I_{650} + 2I_{622}}$$

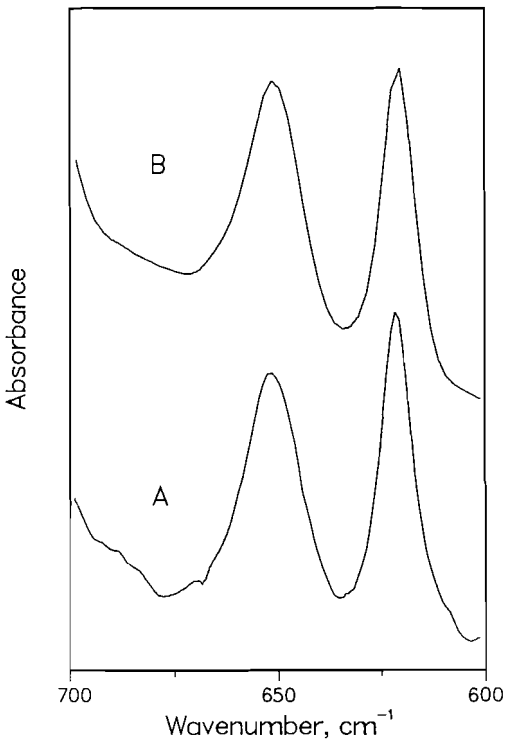

FIG. 1. Infrared spectrum (600–700 cm^{-1}) of *n*-C_{13}-7,7-d_2 pure (A) and as a 50% vol/vol solution in *n*-heptane (B).

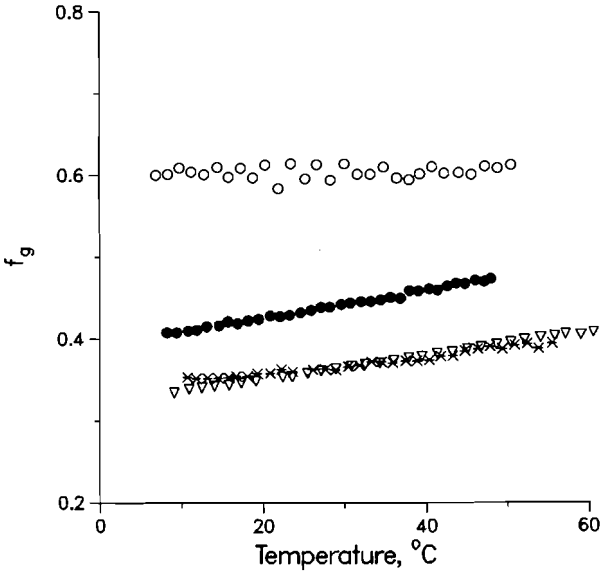

FIG. 2. Temperature dependence of the average *gauche* fraction (f_g) in *n*-C_{13}-7,7-d_2; neat liquid (●), and 50% vol/vol solutions of *n*-C_{13}-7,7-d_2 in: *n*-heptane (▽); *n*-octane (*); and *n*-hexadecane (○).

This is the quantity that we have calculated from the spectra of *n*-C_{13}-7,7-d_2.

Effect of solvent chain length on f_g

The temperature dependence of f_g for neat *n*-C_{13}-7,7-d_2 is compared in Fig. 2 with that for *n*-C_{13}-7,7-d_2 mixed with *n*-heptane, *n*-octane, and *n*-hexadecane. The values of f_g for *n*-C_{13} mixed with *n*-heptane and *n*-octane are practically identical. They are smaller than those for pure *n*-C_{13}. For example, at 25°C, $f_g = 0.43$ in pure *n*-C_{13} whereas $f_g = 0.36$ in *n*-C_{13} dissolved in either *n*-heptane or *n*-octane. Thus, when

n-C_{13} is mixed with these two solvents the concentration of *gauche* conformers at the middle of the n-C_{13} chain is less than in the pure state.

The case of n-C_{13}-7,7-d_2 mixed with n-hexadecane is the opposite, see Fig. 2. In this case the concentration of *gauche* conformers is much larger in solution than in the pure state f_g = 0.60 for the n-hexadecane solution compared to f_g = 0.43 for neat n-C_{13} at 25°C. The effect of n-C_{16} is to disorder (from the point of view of the *gauche* concentration) the n-C_{13} chains.

Taken together, the results of Fig. 2 can be summarized as indicating that when a normal hydrocarbon is mixed with another normal hydrocarbon of different chain length the concentration of *gauche* conformers in the middle of the longer hydrocarbon *decreases* (compare pure n-C_{13} with the solution of n-C_{13} in n-C_7 and n-C_8). On the other hand, the hydrocarbon with the shorter chain is disordered (i.e. the *gauche* concentration *increases*) when dissolved in a longer homologue. (Compare pure n-C_{13} with the solution in n-C_{16}.)

The observed heats of mixing of n-hydrocarbons with each other are invariably positive at ordinary temperatures (7) which is indicative at either inter- or intramolecular disorder being introduced upon mixing. An increase in f_g for an n-alkane could be accompanied by a positive enthalpy change. On mixing two n-alkanes of different chain length the longer alkane could contribute negatively and the shorter positively to the total ΔH. However, the total contribution of the intramolecular conformational part of the disorder to the observed heats of mixing cannot be derived from the present experiments since in each measurement the behaviour of only one of the components in the mixture is monitored.

Effect of branching of the solvent molecules

The effect of branching of the solvent hydrocarbon was studied by comparing the values of f_g (in n-C_{13}) when n-C_{13} was mixed with n-heptane and with two of its branched isomers, 2,2-dimethylpentane and 3,3-dimethylpentane; the corresponding results are shown in Fig. 3*A*. A comparison between n-octane and its branched isomer 2,2,4-trimethylpentane is shown in Fig. 3*B*.

The data of Fig. 3*A* show that the effect of n-heptane, 2,2-dimethylpentane, and 3,3-dimethylpentane on the values of f_g in n-C_{13} is similar. In all cases f_g is smaller in solution than in the pure state. Moreover, at 25°C the values of f_g are practically the same (~0.36) for all three mixtures.

In the presence of n-heptane and of its two branched isomers, the n-C_{13} chain contain less *gauche* conformers than in the pure state; thus, these three solvents create order in the n-C_{13} chains. However, the measured heats of mixing of n-hexadecane with n-heptane, 2,2-dimethylpentane, and 3,3-dimethylpentane are positive (102, 237, and 138 J/mol (8) respectively), indicating that order is destroyed on mixing a long n-alkane with these heptanes. The disorder introduced at the *intermolecular* (short range orientational) level must therefore compensate for the order created in n-C_{13} at the *intramolecular* level. In principle, intramolecular disorder could also be introduced in the solvent molecules while n-C_{13} is ordered. This is expected to be the case for n-heptane as solvent, following the data for different chain length presented above. However, in the case of 3,3-dimethylpentane the molecular shape does not allow for the introduction of *gauche* conformers due to steric crowding of the methyl groups and a similar situation occurs in 2,2-dimethylpentane. Therefore, since a large compensation of the intramolecular order created in n-C_{13} is not expected to come from 2,2-dimethylpentane and 3,3-dimethylpentane, intermolecular effects could be invoked. That is, when *order* is created at the intramolecular level in n-C_{13} the *disorder* introduced at the intermolecular level overcompensates to yield positive heats of mixing.

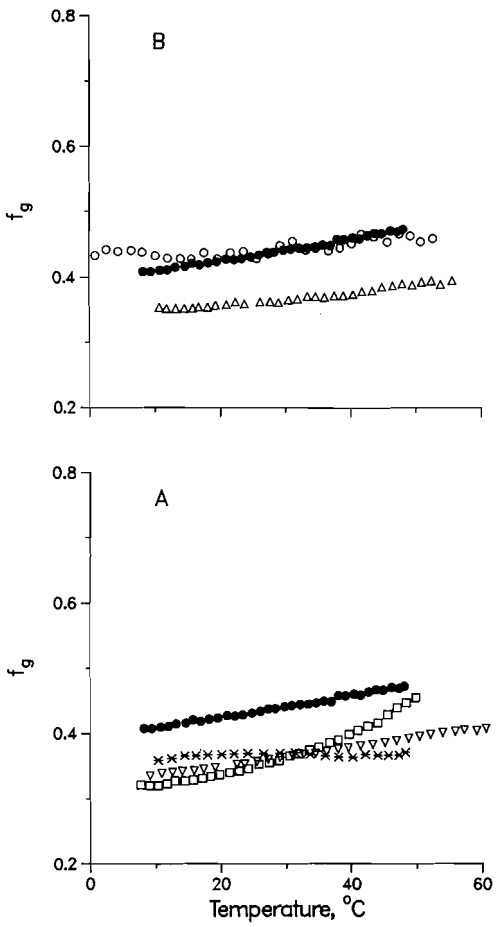

FIG. 3. *A*: Temperature dependence of f_g in n-C_{13}-7,7-d_2; pure liquid (●), and as 50% vol/vol solutions of n-C_{13}-7,7-d_2 in: n-heptane (▽), 2,2-dimethylpentane (*), and 3,3-dimethylpentane (□). *B*: Temperature dependence of f_g in n-C_{13}-7,7-d_2: pure liquid (●), and as 50% vol/vol solutions of n-C_{13}-7,7-d_2 in 2,2,4-trimethylpentane (○) and n-octane (△).

A comparison of the f_g values in n-C_{13} dissolved in n-octane and iso-octane is shown in Fig. 3*B*. In this case the branched isomer, iso-octane, produces no effect on the *gauche* bond concentration in the middle of the n-C_{13} chain. The same values of f_g are found for neat n-C_{13} and n-C_{13} mixed with iso-octane. This is in contrast to the situation with the linear hydrocarbon n-octane as solvent where the f_g value (i.e. the concentration of *gauche* conformers) is markedly smaller in solution than in neat n-C_{13}.

We have also measured the spectra of n-C_{13}-7,7-d_2 dissolved in cyclohexane and in four isomers of n-C_6: 2-methylpentane, 3-methylpentane, 2,2-dimethylbutane, and 2,3-dimethylbutane. The values of f_g derived from these spectra at 25°C are given in Table 2. The values of f_g for n-C_{13} mixed with the branched isomers of n-C_6 are smaller than f_g for neat n-C_{13} (see Table 2). Thus, these branched hydrocarbons induce a smaller concentration of *gauche* conformers at the centre of the n-C_{13} chain. As the value of f_g was not measured for n-C_{13} mixed with n-hexane the effect of these branched isomers of n-C_6 can not be

TABLE 2. Average *gauche* fraction (f_g) at the centre of the n-C_{13} chain measured from spectra of n-C_{13}-7,7-d_2 mixed with different solvents at 25°C

Solvent	f_g
None	0.43
Cyclohexane	0.46
2-Methylpentane	0.37
3-Methylpentane	0.38
2,2-Dimethylbutane	0.35
2,3-Dimethylbutane	0.38

compared directly with that of n-C_6. However, the close similarity of f_g in n-C_{13}-7,7-d_2 mixed with n-C_7 or n-C_8 (Fig. 2) allows us to speculate that f_g for n-C_{13} mixed with n-C_6 should be almost the same (i.e. ≈ 0.36). On that basis there are no large differences between f_g measured in the branched C_6 solvents and the linear C_6, a similar situation to that found for n-C_{13} mixed with n-C_7 and its branched isomers (Fig. 3*A*).

The value of f_g for n-C_{13} dissolved in cyclohexane is larger than that for pure n-C_{13} indicating (see Table 2) that the concentration of *gauche* conformers at the centre of the n-C_{13} chain is larger than in neat n-C_{13}. Cyclohexane is generally referred to as a globular solvent and from the intermolecular point of view it is an "order breaking" solvent when mixed with n-hydrocarbons (9). The effect of cyclohexane on the concentration of *gauche* conformers in the n-C_{13} chains is not very pronounced, i.e. there is only a slight increase in f_g between n-C_{13} in the pure state and that in cyclohexane solution. This would indicate that the large values of the enthalpy of mixing found for solutions of cyclohexane and hydrocarbons would probably be best explained by intermolecular contributions to the mixing phenomena.

Concluding remarks

The data presented herein demonstrate that the concentration of *gauche* conformers in n-hydrocarbons in mixtures is a function of the solvent. The *gauche* concentration in n-tridecane has been measured by utilizing the CD_2 rocking vibrations of a CD_2 group in position 7 of the n-tridecane chain. Thus, the present measurements only apply to the centre of the chain and no information is available regarding conformation at chain positions close to the terminal methyl groups. Positional dependence of the *gauche* concentration is known to occur in the case of solid n-hydrocarbons (4).

The magnitude of the changes observed in the values of f_g cannot be related directly to the differences in the energy difference between *gauche* and *trans* conformers (ΔE_{gt}). This is because our observable "I_{650}" is the combined intensity of bands due to tgt and tgg conformers. Thus, I_{650} contains contributions from conformers with one and two *gauche* bonds and their separation is not possible.

Although the present changes in the f_g values cannot be readily and easily correlated with thermodynamic measurements on the enthalpy of mixing they suggest that changes in the concentration of *gauche* conformers do not play the most important role in determining the macroscopic observables. For example, dissolving n-C_{13} in a branched alkane induces a decrease in the concentration of *gauche* conformers leading to a prediction of negative ΔH. However, the enthalpy of mixing of such a system is positive (9).

In the case of mixtures of n-hydrocarbons differing only in chain length a trend emerges in the dependence of the *gauche* concentration with chain length. In a given mixture, the concentration of *gauche* conformers *decreases* for the longer n-hydrocarbon and the opposite occur for the shorter n-hydrocarbon. In order to determine whether the two effects compensate each other, or whether more disorder is introduced in one component compared to the order created in the other component, it would be necessary to utilize two specifically-deuterated hydrocarbons that differ considerably in chain length.

Finally, while the present results are limited to a few solvents, it is demonstrated that this approach represents a direct method of determining the *gauche* concentration of n-hydrocarbons and should be useful to study other solvent systems.

Acknowledgements

We are grateful to Drs. D. Patterson and M. Costas for their valuable advice and suggestions. We also thank Dr. R. G. Snyder for providing us with a preprint of ref. 6.

1. A. HEINTZ and R. LICHTENTHALER. Angew. Chem. Int. Ed. Engl. **21**, 184 (1982); S. N. BHATTACHARYYA, M. COSTAS, D. PATTERSON, and H. V. TRA. Fluid Phase Equilibria, **20**, 27 (1985).
2. E. W. FISCHER, G. R. STOBL, M. DETTENMAIER, M. STAMM, and STEIDLE. Discuss. Faraday Soc. **68**, 26 (1979).
3. R. G. SNYDER and M. W. POORE. Macromolecules, **6**, 708 (1973).
4. R. G. SNYDER, M. MARONCELLI, H. L. STRAUSS, C. A. ELLIGER, D. G. CAMERON, H. L. CASAL, and H. H. MANTSCH. J. Am. Chem. Soc. **105**, 133 (1983); M. MARONCELLI, H. L. STRAUSS, and R. G. SNYDER. J. Chem. Phys. **82**, 2811 (1985).
5. G. ZERBI, G. MINONI, and A. P. TULLOCH. J. Chem. Phys. **78**, 5853 (1983).
6. M. MARONCELLI, H. L. STRAUSS, and R. G. SNYDER. J. Phys. Chem. **89**, 4390 (1985).
7. J. S. ROWLINSON and F. L. SWINTON. Liquids and liquid mixtures. 3rd ed. Butterworth, London. 1959.
8. M. BARBE and D. PATTERSON. J. Solution Chem. **9**, 753 (1980).
9. A. HEINTZ and R. N. LICHTENTHALER. Ber. Bunsenges. Phys. Chem. **83**, 567 (1979).

A pulse radiolysis study of solvated electrons in *tert*-butanol/water solutions

JOANNA CYGLER,[1] NORMAN V. KLASSEN, AND CARL K. ROSS
Division of Physics, National Research Council of Canada, Ottawa, Ont., Canada K1A 0R6

Received September 13, 1985

JOANNA CYGLER, NORMAN V. KLASSEN, and CARL K. ROSS. Can. J. Chem. **64**, 1548 (1986).

Many solutes, added to water in amounts of a few mol%, cause an increase in the yield of solvated electrons (e_s^-) measured by pulse radiolysis. A pulse radiolysis study of *tert*-butanol (*t*BuOH) in D_2O has been carried out to investigate this phenomenon. Detailed measurements of the yield, measured as $G\epsilon_{max}(e_s^-)$, and the decay of solvated electrons were made at 6, 25, and 46°C over the range 0–5 mol% *t*BuOH. The maximum $G\epsilon_{max}(e_s^-)$ occurs at about 1 mol% *t*BuOH, but the exact concentration depends on the temperature of the sample and the time after the pulse at which the measurement is made. Three factors are examined as contributing to the increased $G\epsilon_{max}(e_s^-)$ in the presence of *t*BuOH and certain other solutes. They are (*i*) the change in viscosity produced by the added solute, (*ii*) the scavenging of OH radicals by the solute, thereby reducing the reaction of OH with e_s^-, and (*iii*) the possibility that the addition of the solute leads to an increase in the thermalization distance of the secondary electrons. It is concluded that effects (*i*) and (*ii*) are sufficient to explain the existing experimental data.

JOANNA CYGLER, NORMAN V. KLASSEN et CARL K. ROSS. Can. J. Chem. **64**, 1548 (1986).

Lorsqu'on ajoute de faibles quantités (quelques mol%) de plusieurs solutés dans de l'eau, la radiolyse pulsée permet de mesurer une augmentation du rendement d'électrons solvatés (e_s^-). Dans le but d'évaluer ce phénomène, on a effectué une étude de la radiolyse pulsée du *tert*-butanol (*t*-BuOH) dans le D_2O. Opérant à 6, 25 et 46°C et à des concentrations de *t*-BuOH allant de 0 à 5 mol%, on a effectué des mesures détaillés des rendements, mesurés sous la forme de $G\epsilon_{max}(e_s^-)$, et des vitesses de déclin des électrons solvatés. La valeur maximale pour $G\epsilon_{max}(e_s^-)$ est observée autour de 1 mol% de *t*-BuOH; toutefois, la concentration exacte dépend de la température de l'échantillon et du temps qui s'est écoulé entre la pulsation et le moment où la mesure est faite. On a examiné trois facteurs qui pourraient contribuer à une augmentation de la valeur de $G\epsilon_{max}(e_s^-)$ en présence de *t*-BuOH et de certains autres solutés. Il s'agit (*i*) du changement de viscosité provoqué par l'addition du soluté, (*ii*) d'un piégeage des radicaux OH par le soluté qui réduit la réaction des OH avec les e_s^- et (*iii*) de la possibilité que l'addition du soluté conduise à une augmentation de la distance de thermalisation des électrons secondaires. On en conclut que les effets (*i*) et (*ii*) sont suffisants pour expliquer les données expérimentales existantes.

[Traduit par la revue]

Introduction

A recent series of papers by Leu, Jha, Freeman, and Cygler (1–3) on alcohol–water solutions describes in considerable detail the effect of solution composition on the yield of solvated electrons (e_s^-) at 1 μs and on properties of e_s^- such as the width of its absorption band at half height and the wavelength of maximum absorption. Pulse radiolysis studies of alcohol–water solutions revealed that the maximum $G\epsilon_{max}(e_s^-)$ occurs at a few mol% alcohol, where the spectrum of e_s^- is not noticeably different from that in water (2, 3). A similar effect was observed by Tran-Thi, Koulkes-Pujo, Sutton, and Anitoff (4) for the addition of less than 2 mol% of several amides and dimethyl sulfoxide to water. Leu, Jha, and Freeman (2) concluded that the increased $G\epsilon_{max}(e_s^-)$ results from an increase in the thermalization distance of the secondary electrons brought about by a stiffening of the solvent structure by the added alcohol. Tran-Thi *et al.* (4) explained the increase in $G\epsilon_{max}(e_s^-)$ by the more conventional argument that scavenging of OH radicals by the solute reduces the extent to which OH radicals react with e_s^-.

It seemed worthwhile to study another system in detail to test these models further. We chose *tert*-butanol–water solutions because *tert*-butanol (*t*BuOH) represents the extremes of two properties which are important for these models, namely the effect of the solute on the structure of the solution and the reaction of the solute with OH radicals. Compared to most monohydric, aliphatic alcohols, *t*BuOH reacts rather slowly with OH (5) but, at the same time, *t*BuOH has an unusually strong effect on the structure of the solution (refs. 6–15, and references therein).

We carried out pulse radiolysis measurements of $G\epsilon_{max}(e_s^-)$ and the decay kineties of e_s^- using *t*BuOH/D_2O solutions at 6, 25, and 46°C. Under most conditions, we observed a maximum $G\epsilon_{max}(e_s^-)$ at about 1 mol% *t*BuOH. We conclude that the increase in $G\epsilon_{max}(e_s^-)$ caused by the addition of small amounts of alcohol to water, as reported here and elsewhere, is most reasonably explained by the increase in viscosity, and the scavenging of OH, by the added alcohol.

Experimental

tert-Butanol (Fisher Certified) was purified by repeated recrystallization (16) and its absorption spectrum was found to be structureless at wavelengths down to 220 nm. Its water content, as measured by the Karl Fisher method, was 4.94 mg cm^{-3}. D_2O (99.8 atom% D) was used as received from Merck, Sharp and Dohme. Solutions of *t*BuOH in D_2O were prepared by weight. The densities of the solutions were measured at 25°C. The density variation over the temperature range 6–46°C was assumed to be the same for all solutions in the range 0–5 mol% *t*BuOH (17).

Samples were deaerated by bubbling with argon (Airco, Superpurified) for 60 min and were sealed off in Suprasil cells of 5 mm optical pathlength. The cells were supported in the open air for measurements at "room temperature", and in a quartz Dewar with Suprasil windows for measurements at 6, 25, and 46°C. The temperature in the Dewar was maintained with a flow of nitrogen gas, regulated to ±1°C, and was measured with an HP model 2802A digital thermometer with the platinum resistance probe in contact with the metal cell holder.

Irradiations were carried out using single 40 ns pulses of 35 MeV electrons from a linear accelerator. Aluminum plates of 6–10 mm thickness were used to attenuate and spread the electron beam. The dose to the sample was always close to 1.4 krad per pulse, except for the measurements shown in Fig. 1, where a dose of about 6 krad per pulse was used. Dosimetry was carried out using O_2-saturated 5×10^{-3} *M* KSCN, taking $G\epsilon_{475}(SCN)_2^- = 2.2 \times 10^4$ *M* cm^{-1} (100 eV)$^{-1}$ at mid-pulse. Account was taken of the electron densities of the various

[1]Present address: Department of Medical Physics, Cross Cancer Institute, 11560 University Avenue, Edmonton, Alta., Canada T6G 1Z2.

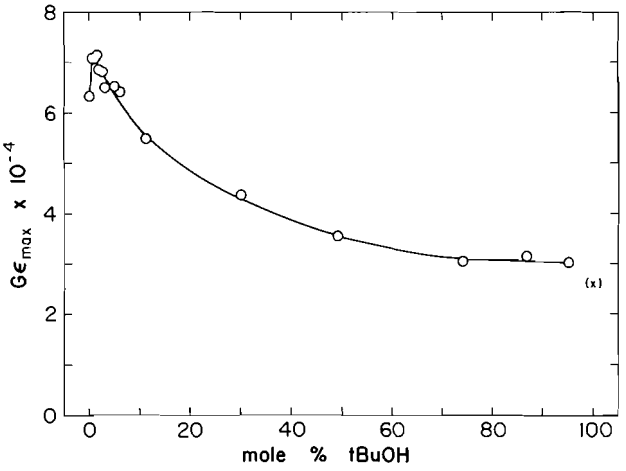

FIG. 1. $G\epsilon_{max}(e_s^-)$, for tBuOH/D_2O solutions at about 21°C, versus mol% tBuOH measured at 100 ns after the start of a 40 ns pulse. The data point (×) for pure tBuOH at 27°C, 100 ns, was calculated from the experimental data used in ref. 16.

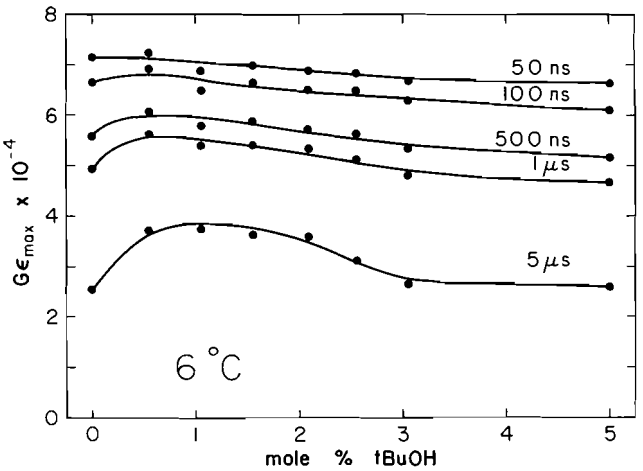

FIG. 2. $G\epsilon_{max}(e_s^-)$ versus mol% tBuOH for tBuOH/D_2O solutions at 6°C. The times after the start of the 40 ns pulse are indicated.

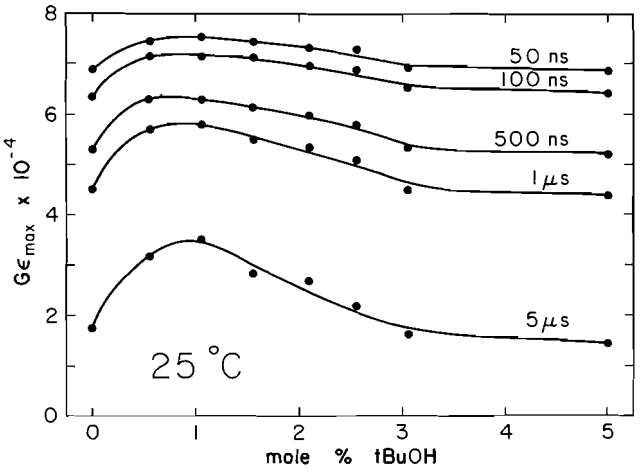

FIG. 3. $G\epsilon_{max}(e_s^-)$ versus mol% tBuOH for tBuOH/D_2O solutions at 25°C. The times after the start of the 40 ns pulse are indicated.

solutions at each temperature. Pulse-to-pulse variations in the dose were monitored with a secondary emission monitor (SEM).

The equipment and techniques used to measure optical absorption have been described previously (18–20). Measurements between 500 and 900 nm were made using an EG&G SHS-100 silicon photoiodide and a 50Ω load resistor, the system having a response time of 10 ns. Above 900 nm, a Barnes A-100 detector with a response time of 50 ns was used.

Apart from the data shown in Fig. 1, the present results were compiled from measurements made on one set of samples covering the range 0–5 mol% tBuOH/D_2O. These measurements are in good agreement with measurements made on another set of samples covering the same concentration and temperature range. Each value reported for $G\epsilon_{max}(e_s^-)$ at 100 ns is the average of six measurements. The measurements reported were made on solutions which had already received at least 10 krad. The present study required that the averaged values of $G\epsilon_{max}(e_s^-)$ for a given sample on a given day be reproducible to ±1%. This was achieved by careful attention to all details. Poorer reproducibility was found for solutions which had received an accumulated dose of less than 10 krad. A very important procedure was the careful "lining up" of the electron beam to avoid, as much as possible, instabilities in the beam during the day. If a dose variation greater than ±10% occurred, as evidenced by the SEM readings, a recalibration of the SEM against the dosimetry solution was carried out. The SEM signal was found not to be exactly proportional to the optical density of the dosimetry solution. Therefore, a calibration curve of optical density vs. SEM signal was prepared each day.

The day-to-day variation in $G\epsilon_{max}(e_s^-)$ was greater than the variation during a single day. $G\epsilon_{max}(e_s^-)$ measured using a given sample varied by ±2% from one day to another. The average $G\epsilon_{max}(e_s^-)$ for a given solution at a given temperature was determined relative to $G\epsilon_{max}(e_{aq}^-)$ in neat D_2O at the same temperature on the same day. This value of $G\epsilon_{max}(e_{aq}^-)$ was, in turn, normalized to $G\epsilon_{max}(e_{aq}^-)$ in neat D_2O determined at 6, 25, and 46°C on a day when the utmost care was taken to ensure reproducibility. In this way, we arrived at an internally consistent set of results.

Results

D_2O was used instead of H_2O because of a concurrent study (21) which required D_2O. The use of D_2O has not caused any serious problems for our effort to understand the variation of $G\epsilon_{max}(e_s^-)$ with tBuOH concentration in aqueous solutions.

$G\epsilon_{max}(e_s^-)$ was measured at room temperature (about 21°C) for tBuOH/D_2O solutions covering the range 0–95 mol% tBuOH. The values of $G\epsilon_{max}(e_s^-)$ at 100 ns after the start of the pulse are shown in Fig. 1. The measurements at each concentration included a determination of $\lambda_{max}(e_s^-)$ which agreed with the published values (1). From 0–10 mol% tBuOH, $\lambda_{max}(e_s^-)$ remained constant at 720 (±10) nm. At higher tBuOH concentrations, λ_{max} moved to longer wavelengths. In tBuOH/D_2O solutions, there is an increase in $G\epsilon_{max}(e_s^-)$ on going from 0 to about 1 mol% tBuOH, followed by a decrease on going to higher tBuOH concentrations. The overall appearance of Fig. 1 is similar to that found by Leu *et al.* (2) for several alcohol–water systems. Included in Fig. 1 is a data point for $G\epsilon_{max}(e_s^-)$ at 100 ns in pure tBuOH at 27°C estimated from the experimental data used in ref. 16.

Having ascertained that the variation of $G\epsilon_{max}(e_s^-)$ with tBuOH concentration in water-rich solutions is similar to that in other alcohol–water solutions, we made a more detailed study of $G\epsilon_{max}(e_s^-)$ for solutions covering the concentration range 0–5 mol% tBuOH at 6, 25, and 46°C. The results are shown in Figs. 2, 3, and 4 for 50, 100, 500, 1000, and 5000 ns after the start of the pulse. No significant changes were found in the shape or the λ_{max} of the e_s^- spectrum over the range 0–5 mol% tBuOH at a given temperature, in agreement with the results of Leu, Jha, and Freeman (1). We adopted values of 697, 720, and 747 nm for λ_{max} at 6, 25, and 46°C, respectively. This variation in λ_{max} with temperature was calculated from the temperature

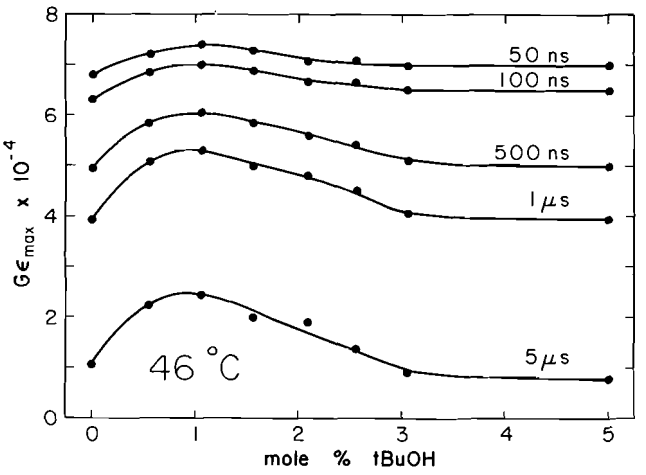

FIG. 4. $G\epsilon_{max}(e_s^-)$ versus mol% *t*BuOH for *t*BuOH/D_2O solutions at 46°C. The times after the start of the 40 ns pulse are indicated.

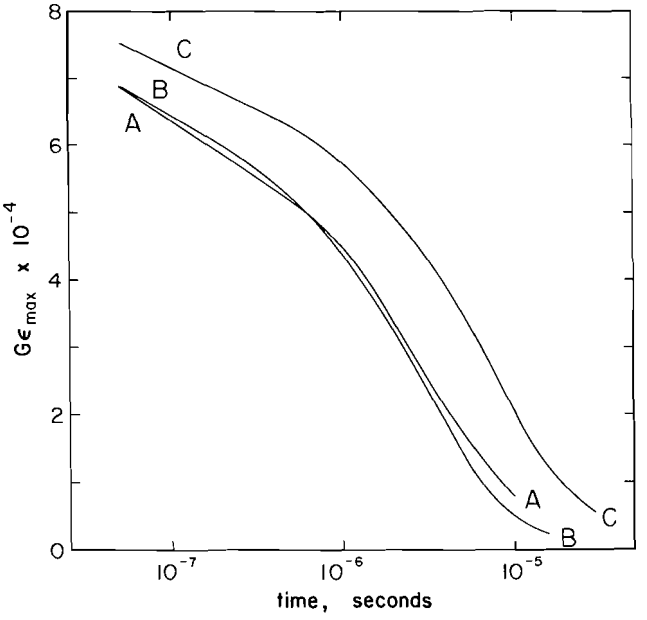

FIG. 5. $G\epsilon_{max}(e_s^-)$, for *t*BuOH solutions at 25°C, versus time. A, B, and C correspond to 0, 5.0, and 1.04 mol% *t*BuOH, respectively.

variation of e_{aq}^- in H_2O found by Michael, Hart, and Schmidt (22). Our less complete examination of λ_{max} agreed with these values. Any measurements made slightly off λ_{max} were corrected by use of the spectral shape of e_{aq}^- (23).

We measured $G\epsilon_{max}(e_{aq}^-)$ to be 6.32×10^4 at 720 nm in pure D_2O at 25°C, 100 ns. For e_{aq}^- in H_2O at 27°C, λ_{max} = 720 nm and $\epsilon_{max} = 1.9 \times 10^4$ (23). However, ϵ_{max} would have been 2.0×10^4 if the authors had used the same value of $G\epsilon_{475}(SCN)_2^-$ as we did for dosimetry. Assuming that the spectral shape of e_{aq}^- in ref. 23 also applies to e_{aq}^- in D_2O, and combining it with $\epsilon_{700}(e_{aq}^-)$ in $D_2O = 2.02 \times 10^4$ (24), we arrive at $\epsilon_{max}(e_{aq}^-) = 2.04 \times 10^4$ in D_2O at room temperature. Hence, our value $G\epsilon_{max}(e_{aq}^-) = 6.32 \times 10^4$ in D_2O at 25°C, 100 ns, leads to $G(e_{aq}^-) = 3.1$. In H_2O, Buxton determined $G(e_{aq}^-) = 2.8$ at 120 ns after a 5 ns pulse (25). Combined with an 11% higher yield of e_{aq}^- in D_2O than in H_2O (24), this predicts $G(e_{aq}^-) = 3.1$ in D_2O at 120 ns after a 5 ns pulse. Asmus and Fendler (26) reported $G(e_{aq}^-) = 3.06 \pm 0.05$ in D_2O, based on scavenging with millimolar SF_6.

The decay of e_s^- measured for D_2O, 1.04 mol% *t*BuOH and 5.0 mol% *t*BuOH at 25°C is shown in Fig. 5. The 24% decay of e_s^- between 50 and 500 ns for our 1.4 krad pulse in D_2O (curve A, Fig. 5) agrees with similar measurements in H_2O (27). The reactions from 1 μs onwards presumably follow homogeneous kinetics and can be modeled using MACKSIM, a computer program used to simulate water radiolysis (28, 29). The decay of e_{aq}^- in D_2O (curve A, Fig. 5) was successfully simulated using MACKSIM and a set of rate constants for D_2O (5, 24, 30, 31). A simulation assuming no D_2O_2 present before the pulse showed insufficient decay of e_{aq}^- from 10^{-6}–10^{-5} s indicating that accumulated D_2O_2 plays a role. Because of the decomposition of accumulated D_2O_2 by the room light and the analyzing light, its concentration preceding a pulse is unknown. Curve A (Fig. 5) was well simulated with an initial concentration of D_2O_2 of 3.5×10^{-6} *M*, i.e., twice the concentration produced by a single pulse, but not with initial D_2O_2 concentrations of 0 or 11×10^{-6} *M*.

Discussion

Spur and non-spur electrons and the free-ion yield

In the present study of *t*BuOH/D_2O solutions, in the study of Leu, Jha, and Freeman of other alcohols and water (2), and in the study of Tran-Thi, Koulkes-Pujo, Sutton, and Anitoff of amides etc. in water (4), it was found that the addition of solute, up to a few mol%, to water at room temperature caused an increase in $G\epsilon_{max}(e_s^-)$ over the time scale of the pulse radiolysis measurements. At yet higher solute concentrations, $G\epsilon_{max}(e_s^-)$ decreased. Leu *et al.* (2) attributed the increase in $G\epsilon_{max}(e_s^-)$ to an increase in the free-ion yield brought about by an increase in the thermalization distance of the secondary electrons, whereas Tran-Thi *et al.* (4) attributed it to OH scavenging by the solute.

Those solvated electrons which react with radiation-produced species in the spur, and whose decay obeys non-homogeneous kinetics, will be called spur electrons, $(e_s^-)_{sp}$. The remainder of the solvated electrons, those whose reactions obey homogeneous kinetics, will be called non-spur electrons, $(e_s^-)_{nsp}$. We assume that the free-ion yield, G_{fi}, as used by Leu *et al.*, corresponds to $G(e_s^-)_{nsp}$. The free-ion yield is the yield of electrons which escape eventual recombination with their geminate cations. Although G_{fi} is a very useful concept for the reactions of electrons in low dielectric media such as hydrocarbons, where most e_s^- reacts with cations, it is less useful in the case of water where much e_s^- reacts with a neutral species, the OH radical.[2] The G_{fi} concept is particularly inappropriate to apply to the changes caused by adding alcohol to water if the decay rate of e_s^- is affected significantly by the scavenging of OH. The addition of alcohol to water causes an increase in viscosity. This affects the spur reaction of e_s^- with OH through the reaction rate constant and the diffusion coefficients. By contrast, G_{fi} depends on the dielectric constant and might be affected quite differently. For these reasons we prefer to discuss e_s^- in alcohol–water solutions in terms of $G(e_s^-)_{sp}$ and $G(e_s^-)_{nsp}$. Johnson and Salmon (33) have addressed the inadequacy of G_{fi} to describe the reactions of e_s^- in methanol.

Scavenging experiments are often used to determine $G(e_s^-)_{nsp}$, using the fact that a reagent added at millimolar concentrations cannot compete effectively for e_s^- within the spur where

[2]W. G. Burns communicated to the authors that a computer simulation of reactions in water irradiated at low dose rates indicated that 57% of the decay of e_s^- at times earlier than 10 ns is due to reaction with the hydroxyl radical.

reactive species are present in high concentration, but can compete effectively outside the spur where the concentration of radiation-produced species is very low. In experiments in which only e_s^- is followed, $(e_s^-)_{nsp}$ can be separated from $(e_s^-)_{sp}$ by using the fact that spur decay is faster than non-spur decay. This method was used by Leu *et al.* (2) who applied eq. [1] of ref. 2 to $G(e_s^-)$, measured at times when spur decay was essentially complete, to calculate the maximum $G(e_s^-)_{nsp}$. We agree with their conclusion that the increased $G\epsilon_{max}(e_s^-)$ they observed on adding alcohol to water was caused by an increased $G(e_s^-)_{nsp}$ (which they call G_{fi}). It remains to be decided what caused the increased $G(e_s^-)_{nsp}$.

tBuOH–water

We find a maximum in $G\epsilon_{max}(e_s^-)$ versus *t*BuOH concentration at about 1 mol% *t*BuOH in D_2O at 25°C. For methanol, ethanol, and 1-propanol solutions in H_2O, the maxima are reported to occur at 2 mol% alcohol, but the few concentrations used in the 1–3 mol% range makes the maximum values of $G\epsilon_{max}(e_s^-)$ and the concentrations at which they occur somewhat uncertain. For 2-propanol/H_2O the maximum is reported to occur at 3 mol% alcohol (3). These maximum values of $G\epsilon_{max}(e_s^-)$ are greater than in the absence of alcohol by 12% for methanol, 15% for ethanol, 23% for 1-propanol, 16% for 2-propanol, and 11% for *t*BuOH/D_2O, the latter being the value at 50 ns, 25°C in Fig. 3. The general trend is for a greater maximum value the greater the value of the product k(OH + alcohol) × (concentration of alcohol at maximum $G\epsilon$). This trend implicates OH scavenging as a factor contributing to the change in $G\epsilon_{max}(e_s^-)$. Figures 2, 3, and 4 show that the ratio of the value of $G\epsilon_{max}(e_s^-)$ for 1 mol% *t*BuOH to the value for water increases with time. This is expected if OH is scavenged by *t*BuOH to produce a hydroxyalkyl radical which is less reactive towards e_s^- than is OH. We believe that this is a major reason for the increase in $G\epsilon_{max}(e_s^-)$ with added *t*BuOH (up to 1 mol% *t*BuOH).

At 6°C, 50 ns, unlike the situation at 25 and 46°C, 50 ns, the value of $G\epsilon_{max}(e_s^-)$ for 1 mol% *t*BuOH is about the same as the value in D_2O. If the greater $G(e_s^-)_{nsp}$ in 1 mol% *t*BuOH than in D_2O found at 50 ns at both 25 and 46°C were due to an increased thermalization distance in 1 mol% *t*BuOH, then the same effect should occur at 6°C but it does not. Several authors (15, 34–36) have concluded that the increased order brought about by adding small amounts of alcohol to water is a larger effect at lower temperatures. Therefore, if an increased thermalization distance were the cause of the maximum in $G\epsilon_{max}(e_s^-)$ versus *t*BuOH concentration we would expect this effect to be more pronounced at 6°C than at 25°C. This is not the case. Therefore, an increased thermalization distance is eliminated as the cause of the maxima observed. On the other hand, if the phenomenon is due to OH scavenging it should develop more rapidly at higher temperatures, just as we have observed. The fact that the rate constant k(OH + *t*BuOH) is much smaller than the diffusion controlled limit (5) makes it plausible that the activation energy for this reaction is sufficiently large to significantly slow down the OH scavenging at 6°C. The familiar maximum in $G\epsilon_{max}(e_s^-)$ versus mol% *t*BuOH, which appears only at longer times at 6°C, is attributed to an increase in the lifetime of $(e_s^-)_{nsp}$ caused by the eventual scavenging of OH by *t*BuOH.

$G(e_s^-)_{nsp}$ in alcohol–water solutions depends on the interplay of a number of factors. The dielectric constant is important in determining what fraction of electrons react with geminate ions. The fraction of electrons which react with OH in the spur will change with viscosity depending on how the diffusion coefficients change relative to the change in the reaction rate constant. Scavenging of OH radicals during and after the completion of spur reactions will change the decay rate of $(e_s^-)_{nsp}$. The concentration of alcohol at which the increase in $G\epsilon_{max}(e_s^-)$ changes to a decrease depends on these and other factors. The concentration of amides at which the maximum in $G\epsilon_{max}(e_s^-)$ occurs was suggested by Tran-Thi *et al.* (4) to depend also on the scavenging of presolvated electrons by the solute.

OH scavenging or increased thermalization distance?

The effect on $G\epsilon_{max}(e_s^-)$ of adding a few mol% *t*BuOH to D_2O is consistent with scavenging of OH by *t*BuOH to produce a hydroxyalkyl radical which is less reactive than OH towards e_s^-. The results are not consistent with the proposal of Leu, Jha, and Freeman (2) that such effects are mainly due to an increase in the thermalization distance of the electron. The strongest evidence in favour of the proposal by Leu *et al.* comes from their analysis of the measurements of Jonah, Matheson, Miller, and Hart (37) of e_s^- decay between 0.1 and 3.3 ns in water and 3 *M* EtOH. We now reexamine those results to see if an explanation other than that of Leu *et al.* is feasible.

Leu *et al.* dismissed OH scavenging as a factor for the 1.6-fold slower decay, between 0.1 and 3.3 ns, of e_s^- in 3 *M* ethanol (EtOH) than in water (37) because the factor 1.6 is so close to the 1.7-fold increase in viscosity on going from water to 3 *M* EtOH. The decay curve for e_s^- in 3 *M* EtOH superimposes the curve in water (37) if the times of the former are reduced 1.6-fold taking 0.1 ns as time zero. However, this treatment is rather insensitive to the shapes of the curves for 3 *M* EtOH and for water because both curves must coincide at the time taken as zero regardless of the reduction factor which is used to make them coincide at 3 ns. Given the rate constant of $1.3 \times 10^9\ M^{-1}\ s^{-1}$ for the reaction (OH + EtOH) in 3 *M* EtOH (the rate constant in water (5) corrected for the different viscosity of 3 *M* EtOH as indicated below), the OH radicals are half converted to the ethanol radical, ·EtOH,

$$OH + EtOH \rightarrow H_2 + \cdot EtOH$$

by about 0.18 ns, and entirely converted within a few ns. The analysis of Leu *et al.* implies that ·EtOH reacts as rapidly with e_s^- as does OH which seems unlikely because ·EtOH must have a smaller diffusion coefficient than OH. Another problem with the analysis of Leu *et al.* is that other studies indicate that the 1.7-fold increase in viscosity on going from water to 3 *M* EtOH leads to a reduction of (1.3–1.4)-fold in rate constants (38, 39). The complex dependence of e_s^- rate constants on viscosity when drastically changing the solution composition has been remarked upon (3).

We have analyzed the e_s^- decays from (0.1–3.3) ns, reported by Jonah *et al.* (37) in their Fig. 3, and conclude that they are satisfactorily explained by a combination of viscosity and scavenging effects. We assumed that $G(e_s^-)$ in both water and 3 *M* EtOH are the same at 1 ps. The decay of e_s^- in water between 1 ps and the earliest experimental point (Fig. 3, ref. 37) was determined from the solid curve in Fig. 20 of ref. 40 and the decay at longer times was taken from ref. 37. The decay of e_s^- in 3 *M* EtOH before the earliest experimental point was taken to be 1.4 times slower than in water (see preceding paragraph). The result is a higher value of $G(e_s^-)$ in 3 *M* EtOH than in water at the time of the earliest experimental point. The decay in water was superimposed on the decay in 3 *M* EtOH by multiplying the

time in water by a factor graduated from 1.4 at $\leq 10^{-10}$ s to 1.9 at 8×10^{-10} s to 2.0 at 1.2×10^{-9} s. Qualitatively, this sort of graduated factor is what one would expect if the OH radicals were being replaced by a less mobile ·EtOH radical over this time period. As described in the next paragraph, the factors seem reasonable. Hence, there appears to be no need to invoke an increased thermalization distance in 3 *M* EtOH to explain Fig. 3 of ref. 37.

The value of the rate constant of the reaction of e_s^- with ·EtOH has not been reported. A value of $8 \times 10^9\ M^{-1}\ s^{-1}$ has been reported for the reaction of e_s^- with the corresponding radical of methanol, $\cdot CH_2OH$, in methanol (32). The rate constant for the reaction of e_s^- with ·EtOH was estimated using the following assumptions; (*a*) the decay of e_s^- in 3 *M* EtOH is 2.0 times slower than in water at 1 ns, when all OH has been scavenged, (*b*) about 57% of the decay of e_s^- in the spur in water is due to reaction with OH (see footnote 2), and (*c*) all rate constants are 1.4 times smaller in 3 *M* EtOH than in water. On this basis we estimate that $k(e_s^- + \cdot EtOH) \simeq 1 \times 10^{10}\ M^{-1}\ s^{-1}$ in 3 *M* EtOH.

Acknowledgements

The authors wish to thank C. Jonah for replying to enquiries about ref. 37. They are very grateful to W. G. Burns for carrying out a computer simulation of the spur processes in irradiated water. The assistance of the Analytical Section of the Division of Chemistry, National Research Council of Canada, who did the Karl Fischer titrations on *t*BuOH, is gratefully acknowledged.

1. A.-D. Leu, N. K. Jha, and G. R. Freeman. Can. J. Chem. **60**, 2342 (1982).
2. A.-D. Leu, N. K. Jha, and G. R. Freeman. Can. J. Chem. **61**, 1115 (1983).
3. J. Cygler and G. R. Freeman. Can. J. Chem. **62**, 1265 (1984).
4. T. H. Tran-Thi, A. M. Koulkes-Pujo, J. Sutton, and O. Anitoff. Radiat. Phys. Chem. **23**, 77 (1984).
5. L. M. Dorfman and G. E. Adams (*Editors*). Reactivity of the hydroxyl radical in aqueous solutions. Natl. Stand. Ref. Data Ser. Natl. Bur. Stand. (U.S.), **46** (1973).
6. C. de Visser, G. Perron, and J. E. Desnoyers. Can. J. Chem. **55**, 856 (1977).
7. D. A. Armitage, M. J. Blandamer, K. W. Morcom, and N. C. Treloar. Nature, **219**, 718 (1968).
8. T. L. Broadwater and R. L. Kay. J. Phys. Chem. **74**, 3802 (1970).
9. Y. Y. Akhadov. Dielectric properties of binary solutions. Pergamon Press, New York. 1981.
10. H. Endo and O. Nomoto. Bull. Chem. Soc. Jpn. **46**, 3004 (1973).
11. K. Iwasaki and T. Fujiyama. J. Phys. Chem. **81**, 1908 (1977).
12. K. Ueberreiter. Makromol. Chem. Rapid Commun. **1**, 139 (1980).
13. J. A. Lanning, M. J. Pikal, and J. Q. Chambers. J. Phys. Chem. **78**, 70 (1974).
14. F. Franks and D. J. G. Ives. Q. Rev. **20**, 1 (1966).
15. F. Franks. *In* Hydrogen-bonded solvent systems. *Edited by* A. K. Covington and P. Jones. Taylor and Francis Ltd. London. 1968. pp. 31–47.
16. G. G. Teather and N. V. Klassen. Int. J. Radiat. Phys. Chem. **7**, 475 (1975).
17. R. T. Emmet and F. J. Millero. J. Chem. Engin. Data, **20**, 351 (1975).
18. G. G. Teather, N. V. Klassen, and H. A. Gillis. Int. J. Radiat. Phys. Chem. **8**, 477 (1976).
19. C. K. Ross, K. H. Lokan, and G. G. Teather. Comput. Chem. **3**, 89 (1979).
20. T. K. Cooper, D. C. Walker, H. A. Gillis, and N. V. Klassen. Can. J. Chem. **51**, 2195 (1973).
21. J. Cygler, N. V. Klassen, and G. G. Teather. Rad. Phys. Chem. **27**, 47 (1986).
22. B. D. Michael, E. J. Hart, and K. H. Schmidt. J. Phys. Chem. **75**, 2798 (1971).
23. G. L. Hug (*Editor*). Optical spectra of nonmetallic inorganic transient species in aqueous solution. Natl. Stand. Ref. Data Ser. Natl. Bur. Stand. (U.S.), **69**, 6 (1981).
24. E. M. Fielden and E. J. Hart. Rad. Res. **33**, 426 (1968).
25. G. V. Buxton. Proc. R. Soc. London A, **328**, 9 (1972).
26. K.-D. Asmus and J. H. Fendler. J. Phys. Chem. **73**, 1583 (1969).
27. C. N. Trumbore, W. Youngblade, and D. R. Short. J. Phys. Chem. **88**, 5057 (1984).
28. A. W. Boyd, M. B. Carver, and R. S. Dixon. Radiat. Phys. Chem. **15**, 177 (1980).
29. C. K. Ross, N. V. Klassen, and G. D. Smith. Med. Phys. **11**, 653 (1984).
30. E. J. Hart and E. M. Fielden. J. Phys. Chem. **72**, 577 (1968).
31. Z. D. Draganic, O. I. Micic, and M. T. Nedadovic. J. Phys. Chem. **72**, 511 (1968).
32. D. W. Johnson and G. A. Salmon. Radiat. Phys. Chem. **10**, 294 (1977).
33. D. W. Johnson and G. A. Salmon. Can. J. Chem. **55**, 2030 (1977).
34. E. M. Arnett and D. R. McKelvey. J. Am. Chem. Soc. **88**, 5021 (1966).
35. A. G. Mitchell and W. F. K. Wynne-Jones. Discuss. Faraday Soc. **15**, 161 (1953).
36. E. M. Arnett. *In* Physico-chemical processes in mixed aqueous solvents. *Edited by* F. Franks. Heinemann Educational Books Ltd., London. 1967. pp. 124, 125.
37. C. D. Jonah, M. S. Matheson, J. R. Miller, and E. J. Hart. J. Phys. Chem. **80**, 1267 (1976).
38. B. H. Milosavlevic and O. I. Micic. J. Phys. Chem. **82**, 1359 (1978).
39. B. Cercek. Int. J. Radiat. Phys. Chem. **7**, 223 (1975).
40. W. G. Burns, H. E. Sims, and J. A. B. Goodall. Radiat. Phys. Chem. **23**, 142 (1984).

Monoozonides of chloro-substituted conjugated dienes: preparation, stability, and some chemical reactions

KARL GRIESBAUM,[1] ASHIS R. BANDYOPADHYAY, AND MARTIN MEISTER
Engler-Bunte-Institut, Bereich Petrochemie, Universität Karlsruhe (TH), D-7500 Karlsruhe, Federal Republic of Germany

Received January 2, 1986

KARL GRIESBAUM, ASHIS R. BANDYOPADHYAY, and MARTIN MEISTER. Can. J. Chem. **64**, 1553 (1986).

The chlorodienes (*E*)-4-chloro-3-methyl-1,3-hexadiene (**5***a*), (*E*)- and (*Z*)-4-chloro-2,3-dimethyl-1,3-hexadiene (**5***b*/**6***b*), (*E*,*E*)-5-chloro-4-methyl-2,4-heptadiene (**5***c*), (4*E*)- and (4*Z*)-5-chloro-3,4-dimethyl-2,4-heptadiene (**5***d*/**6***d*), chloroprene (**11***a*), and 2-chloro-3-methyl-1,3-butadiene (**11***b*) are selectively ozonized at the non-chlorinated double bonds to give the corresponding monoozonides **7**, **8**, and **12**. Further ozonolyses of the monoozonides of **5***b* and of **11***b* in methanol as well as epoxidation of the monoozonide of **5***b* and subsequent reaction of the resulting chloroepoxide with $AgBF_4$ are described.

KARL GRIESBAUM, ASHIS R. BANDYOPADHYAY et MARTIN MEISTER. Can. J. Chem. **64**, 1553 (1986).

Les chlorodiènes chloro-4 méthyl-3 hexadiène-1,3(*E*) (**5***a*), chloro-4 diméthyl-2,3 hexadiène-1,3(*E*) et (*Z*) (**5***b*/**6***b*), chloro-5 méthyl-4 heptadiène-2(*E*),4(*E*) (**5***c*), chloro-5 diméthyl-3,4 heptadiène-2,4(*E*) et -4(*Z*) (**5***d*/**6***d*), chloroprène (**11***a*) et chloro-2 méthyl-3 butadiène-1,3 (**11***b*) subissent des réactions sélectives d'ozonolyse au niveau des doubles liaisons qui ne sont pas chlorées pour conduire aux monoozonides correspondants **7**, **8** et **12**. On décrit aussi des ozonolyses subséquentes des monoozonides de **5***b* et de **11***b* qui ont été effectuées dans le méthanol ainsi que la réaction d'époxydation du monoozonide de **5***b* suivie d'une réaction subséquente avec du $AgBF_4$.

[Traduit par la revue]

Introduction

In recent years we prepared the α,β-unsaturated ozonides **1***a* (1), **1***b*–**1***f* (2), and **1***g* (3) by monoozonolyses of the corresponding conjugated dienes. The stability of these ozonides varied considerably, depending on the nature of the substituents R^1 and R^2. In an attempt at assessing the influence of chlorine substituents upon the formation and stability of α,β-unsaturated ozonides, we have now ozonided substrates **5***a*–**5***d*, **6***b*, and **6***d*, bearing the chlorine substituent in a terminal position of the conjugated diene system, as well as substrates **11***a* and **11***b* having 2-chloro-substituted conjugated diene systems.

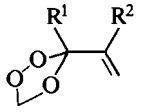

1

	a	*b*	*c*	*d*	*e*	*f*	*g*
R^1	CH_3	CH_3	H	C_6H_5	C_6H_5	CH_3	$(CH_3)_3C$
R^2	CH_3	H	CH_3	C_6H_5	CH_3	C_6H_5	$(CH_3)_3C$

Results and discussion

The hitherto unknown chlorodienes of structures **5** and **6** have been prepared by aldol condensations of 3-pentanone (**2**) with appropriately substituted components of structure **3**, followed by sequential reactions of the respective condensation products (**4**) with phosphorus pentachloride and potassium *tert*-butoxide. The configurations at the chlorinated double bonds of **5** and **6** have been assigned based on the experience (4) that the signal of the CH_3 group appears at lower field if the chlorine and the CH_3 substituents have a *cis* arrangement. The non-chlorinated double bond of **5***c* has been assigned an *E* configuration based on the large coupling constant (15.0 Hz) of the vinylic protons; the configurations of the non-chlorinated double bonds of **5***d* and **6***d* have not been determined. In a variation of a published procedure (5), diene **11***b* has been obtained from addition of HCl to 2-methyl-1-butene-3-yne.

Treatment of the dienes **5***a*–**5***d*, **6***b*, and **6***d* with ca. 0.8 molar equivalents of ozone in pentane at −78°C led to predominant attack at the non-chlorinated double bonds of the diene systems to yield mixtures of the corresponding monoozonide **7** or **8** and the corresponding carbonyl fragment **9** or **10**, respectively, whereas no ozonides derived from the chloro-substituted double bonds could be detected. Ozonides **7***a*, **7***b*, **7***c*, **7***d*, **8***b*, and **8***d* have been isolated in yields of 82, 30, 41, 40, 7, and 11%, respectively, based on the deficient amount of ozone applied. They are colorless liquids of considerable thermal stability, as evidenced by the fact that they gave rise to sharp peaks in gas chromatography (gc) and to molecular ions in gc–ms (mass spectral) analyses. Ozonides **7***c*, **7***d*, and **8***d* consisted of mixtures of the corresponding *cis*–*trans* isomers with respect to the positions of the substituents at the ozonide rings. In the case of **7***c*, the mixture has been separated and the isomers have been stereochemically assigned based on the assumption that the isomer having the longer gc retention time has *cis* configuration, as has been observed for other pairs of isomeric ozonides (6). Reductions with triphenyl phosphine gave **9***a* from **7***a* and **7***c*, **9***b* from **7***b* and **7***d*, and **10***b* from **8***b* and **8***d*.

Ozonolyses of dienes **11***a* and **11***b* under the aforementioned conditions resulted also in predominant attack at the non-chlorinated double bonds to give mixtures of the corresponding monoozonides (**12**) and carbonyl fragments (**13**); ozonides derived from the chloro-substituted double bonds again could not be detected. The liquid ozonides **12***a* and **12***b* have been isolated in 51 and 31%, respectively. It is known from other experiments[2] that the primary ozonide of **11***b* forms ca. 80% of **13***b*. Since ketone fragments usually do not undergo cycloadditions with carbonyl oxides to give ozonides (7), one would have expected a maximum yield of ca. 20% for ozonide **12***b*. The actual yield of 31% for **12***b* suggests, therefore, that at least part of the ozonide has been indeed formed by cycloaddition of **13***b* with the carbonyl oxide of formaldehyde. This leads to the conclusion that the α-chloro substituent activates the carbonyl group of **13***b*.

The α-chloro-substituted ozonides **12***a* and **12***b* are less stable than the β-chloro-substituted ozonides of structures **7**

[1]Author to whom correspondence may be addressed.

[2]K. Griesbaum and M. Meister, unpublished results.

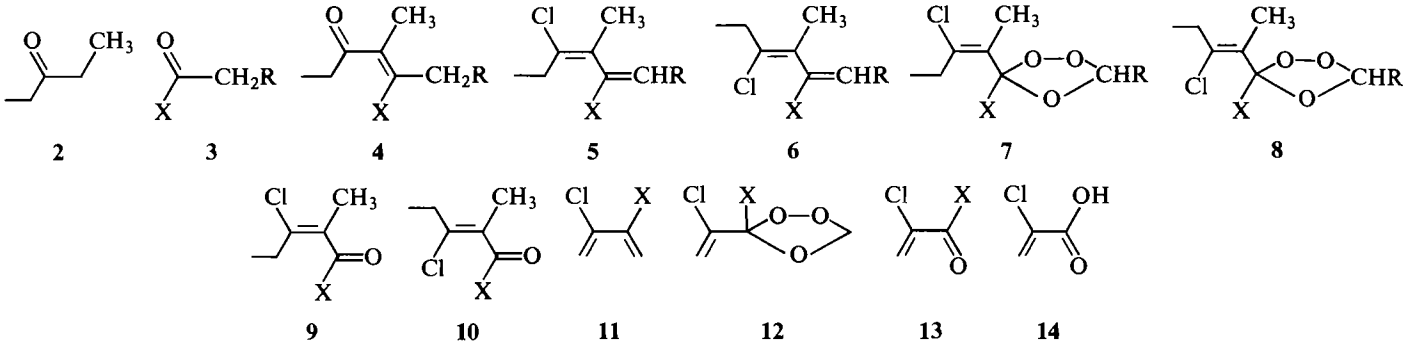

2 3 4 5 6 7 8

9 10 11 12 13 14

	a	*b*	*c*	*d*
X	H	CH_3	H	CH_3
R	H	H	CH_3	CH_3

and **8**, as evidenced by spontaneous decompositions during gc analyses and upon shock treatment. Treatment of the ozonides with dimethyl sulfide (DMS) gave a mixture of **13***a* and **14** starting from **12***a*, and **13***b* starting from **12***b*. The formation of **14** is rationalized by attack of the co-product DMSO (dimethylsulfoxide) at the allylic hydrogen of **12***a* and subsequent cleavage of the ozonide **12***a* in the same manner as had been experienced previously with other ozonides (2).

It appeared interesting to test the ozonolysis of representative examples of α- and β-chloro-substituted α,β-unsaturated ozonides, such as **7***b* and **12***b*, in methanol. For, based on previous experience with the direction of ozone cleavage of monochloro-substituted double bonds (8), such reactions should lead to **16** and **20**, respectively, as primary, and to **17** and **21**, respectively, as secondary products. To our knowledge, compounds of types **17** and **20** are unknown and though ozonides of type **21** are known, they have never been obtained via the corresponding acyl chloride precursors of type **20**.

Treatment of **7***b* with ozone in methanol/$CDCl_3$ at −78°C and subsequent warming of the mixture gave fragments **18** and **19** in a molar ratio of ca. 1:2, along with methyl formate and dimethoxymethane. Proton nmr analysis provided no evidence for the formation of **17** and showed, in fact, that the ozonide ring was no longer existent, as evidenced by the absence of the signals for the protons of the CH_2 group of the ozonide ring. It is concluded, therefore, that either **17** or its precursor **16** decomposes, possibly catalyzed by hydrogen chloride, to give two equivalents of **19** and products derived from the CH_2 moiety. Concurrently, **15** is solvolyzed by methanol to give **18**.

Ozonolysis of ozonide **12***b* in CH_3OD at −78°C afforded a mixture of **21** and **22** in nearly equimolar amounts, from which ozonide **21** has been isolated in 31% yield. Its structure was established by independent preparation via ozonolysis of methyl methacrylate (**23***a*) and by reduction with DMS to give **23***b*.

Recently, we had shown that α,β-unsaturated ozonides can be readily converted into the corresponding epoxides by treatment with peracid (1). It appeared, therefore, interesting to examine the epoxidation of representative examples of the chlorinated α,β-unsaturated ozonides obtained in the present study. Treatment of ozonide **7***b* with *m*-chloroperbenzoic acid yielded two stereoisomeric epoxyozonides of structure **24** and the α-chloro-β-ketoozonide **25**, the latter probably by post isomerization of **24**. The stereochemical identity of the epoxyozonides (**24**) has not been elucidated; they have been arbitrarily denoted as **24***A* and **24***B*. Reductions with triphenyl phosphine gave **26** from **24***A* and **24***B*, and **27** from **25**.

Epoxyozonide **24***A* gave a spontaneous reaction with $AgBF_4$ to yield the α,β-unsaturated ozonide **30** and two isomeric α-fluoro-β-ketoozonides, **31***A* and **31***B*, of unassigned stereochemistry. On the basis of previous results with substituted 2-chlorooxiranes (9), these products can be rationalized by dechlorination of **24** with silver ions, followed by ring opening of the ensuing carbenium ion **28** to give carbenium ion **29**. The latter, in turn, may undergo deprotonation to give **30** or reaction with the BF_4 anion to give **31**.

Treatment of ozonides **12***a* and **12***b* with *m*-chloroperbenzoic acid failed to yield the corresponding epoxyozonides and hence their reactions with $AgBF_4$ could not be examined.

The following conclusions are drawn from the foregoing results: (*1*) Both 1-chloro- and 2-chloro-substituted conjugated dienes can be converted into monoozonides by selective ozone attack at the respective non-chlorinated double bonds. However, monoozonides of 2-chloro-substituted dienes appear to be less stable than those of 1-chloro-substituted dienes. (*2*) Carbonyl oxides that are attached to an ozonide ring as in **16** could not be trapped with methanol to give stable α-hydroperoxyozonides of type **17**. Instead, the reaction led to abnormal products, resulting from cleavage of the carbon single bond that

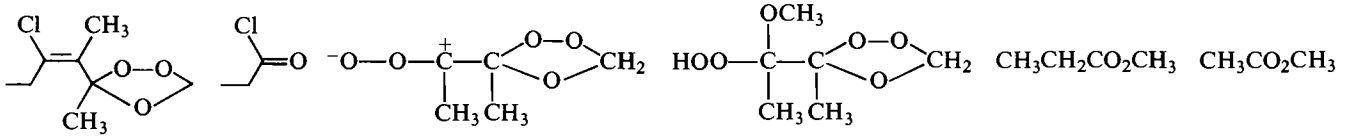

7*b* **15** **16** **17** **18** **19**

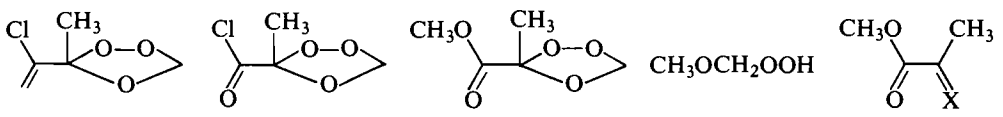

12*b* **20** **21** **22** **23**

a: X = CH_2; *b*: X = O

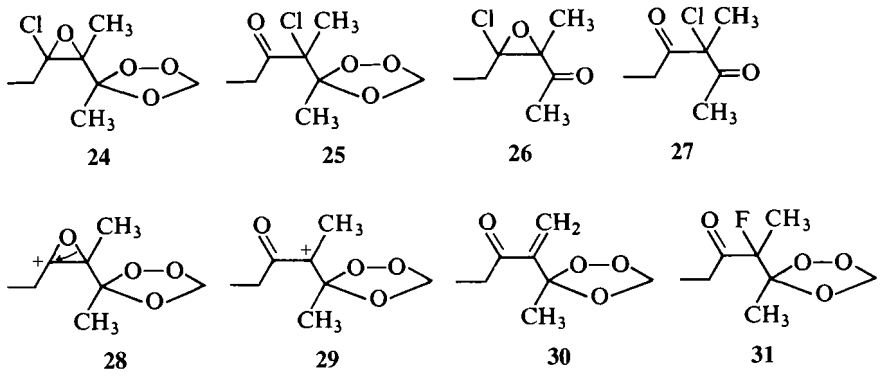

links the carbonyl oxide moiety with the ozonide moiety. This is reminiscent of the behavior of α-oxo-carbonyl oxides, which also preferentially evade trapping by methanol and lead to abnormal products via cleavage of the carbon single bond that links the oxo and the carbonyl oxide moiety (10). (*3*) α-Chlorooxo-ozonides like **20** can be trapped by methanol to give α-methyl carboxylated ozonides. This is noteworthy, for in view of the notorious instability of α-ketoozonides one would have expected that the electron-withdrawing effect of chlorine renders α-chlorooxo-ozonides even less stable. The fact that **20** could be trapped by methanol at low temperature does not exclude, however, that it is unstable at elevated temperatures. In fact, we suspect that it was the corresponding α-chlorooxo-ozonide that caused a violent explosion of the crude product from the diozonolysis of **11***a* in pentane after it had reached room temperature.

Materials and methods

Materials

Chemicals, solvents, and technical gases were of commercial grades.

Analytical methods

The ^{1}H nmr and ^{13}C nmr spectra were routinely recorded on Bruker instrument WP 60, and in special cases on Bruker instruments WH 250 and WM 300; ir spectra were recorded on a Beckman IR 4260 spectrometer and mass spectra on a Hewlett Packard instrument 5985 B. The gc analyses were carried out on a Shimadzu GC/6A and on a Varian 1400 instrument, using a temperature program of 60–160°C at 4°C/min and glass columns with the following sizes and packings: (A) 0.3 × 300 cm, 5% Carbowax 20 M on Chromosorb G; (B) 0.3 × 500 cm, 5% Carbowax 20 M on Chromosorb G; (C) 0.3 × 300 cm, 5% Nitrilesiliconoil XE 60 on Chromosorb G; (D) 0.3 × 50 cm, 5% Nitrilesiliconoil XE 60 on Chromosorb G. Temperature of injection port 200°C for conditions A, B, C and 70°C for condition D.

Preparation of **5**a

To a suspension of 639 g (3.07 mol) of phosphorus pentachloride and 3 L of ether, a solution of 229.2 g (2.05 mol) of 4-methyl-4-hexene-3-one (**4***a*) (11) in 1 L of ether was added dropwise at room temperature with vigorous stirring. Then the mixture was refluxed with stirring for 24 h, cooled to room temperature, and 1 L of an aqueous solution of 10% sodium carbonate was added dropwise. The organic phase was separated, the aqueous phase was extracted with ether, and the extracts were combined with the organic phase. The combined ether solutions were washed with aqueous sodium bicarbonate and dried over sodium sulfate. After removal of the ether in a rotary evaporator, there remained 284.5 g of a light brown liquid. A mixture of 76.0 g (0.68 mol) of potassium *tert*-butoxide in 200 mL of dry *tert*-butanol and 55.7 g of the above liquid was refluxed with stirring for 24 h. Then 200 mL of water was added at room temperature and the mixture was extracted twice with 500 mL, each time, of *n*-pentane. The combined extracts were washed twice with 500 mL of water and dried over sodium sulfate. After removal of *n*-pentane in a rotary evaporator there remained 19.0 g of a brown liquid. The latter was divided into two equal parts, which were separately processed by flash chromatography (12) (column 5 × 46 cm; 390 g of silica gel; *n*-pentane) to give a total of 7.4 g of **5***a* of approximately 86% purity. The latter product was again submitted to flash chromatography under the same conditions to give 3.2 g of **5***a* of 97% purity according to gc analysis (condition C).

*(E)-4-Chloro-3-methyl-1,3-hexadiene (***5**a*):* colorless liquid; ir (film): 1625 cm^{-1}; ^{1}H nmr (250 MHz, $CDCl_3$, TMS), δ: 1.14 (t, J = 7.5 Hz, 3H), 1.95 (t, J = 0.8 Hz, 3H), 2.57 (q, J = 7.5 Hz, 2H), ABX system with δ_A 5.12 (1H), δ_B 5.25 (1H), δ_X 6.68 (1H), J_{AB} = 1.4 Hz, J_{AX} = 11.0 Hz, J_{BX} = 17.0 Hz; ms, *m/e* (relative intensity): 132, 130 (25, 75) M^+, 117, 115 (12, 38) $(M - CH_3)^+$, 95 (100) $(M - Cl)^+$; gc t_R (condition C) 8.3 min. The neat substance discolored at room temperature, therefore no elemental analysis was attempted. The stereochemical assignment of **5***a* is based on the fact that mono-ozonolysis followed by reduction gave **9***a*.

Preparation of **5**c was by the same procedure as described for the preparation of **5***a*: Reaction of 320.0 g (1.54 mol) of phosphorus pentachloride in 1 L of ether and 129.1 g (1.0 mol) of 4-methyl-4-heptene-3-one (**4***c*) (11) in 1 L of ether yielded 173.0 g of a light brown liquid. Reaction of 25.2 g (0.225 mol) of potassium *tert*-butoxide in 200 mL of *tert*-butanol and 27.0 g of the above brown liquid gave 16.3 g of crude **5***c*. This was divided into two equal parts, which were separately processed by flash chromatography as described for **5***a* to give a total of 6.2 g of a colorless liquid. From the latter, pure **5***c* was isolated by flash chromatography under the same conditions as above.

*(E,E)-5-Chloro-4-methyl-2,4-heptadiene (***5**c*):* colorless liquid; ir (film): 1605 cm^{-1}; ^{1}H nmr ($CDCl_3$, TMS), δ: 1.10 (t, J = 7.3 Hz, 3H), 1.92 (s, 3H), 2.52 (q, J = 7.3 Hz, 2H), ABX_3 system with δ_A 6.32 (1H), δ_B 5.63 (1H), δ_X 1.75 (3H), J_{AB} = 15.0 Hz, J_{BX} = 1.2 Hz, J_{AX} = 6.3 Hz; ms, *m/e* (relative intensity): 146, 144 (30, 88) M^+, 131, 129 (18, 52) $(M - CH_3)^+$, 109 (100) $(M - Cl)^+$; gc t_R (condition C) 13.3 min.

Preparation of **5**b *and of* **6**b

A solution of 258.0 g (3 mol) of 3-pentanone, 388.8 g (3.6 mol) of chlorotrimethylsilane, and 727.2 g (7.2 mol) of triethyl amine in 1.2 L of dimethyl formamide was refluxed with stirring for 24 h, cooled to room temperature, and extracted three times with *n*-pentane. The combined extracts were sequentially washed with 1 *N* aqueous hydrochloric acid, with a 5% aqueous solution of sodium bicarbonate and water, and subsequently dried over sodium sulfate. The *n*-pentane was distilled off through a 30-cm packed column and the residue was distilled at vacuum through the same column to give 369.6 g (78%) of 3-trimethylsiloxy-2-pentene having a bp of 76–77°C at 85 Torr (1 Torr = 133.3 Pa).

To a solution of 789.2 g (4.19 mol) of titanium tetrachloride in 250 mL of dichloromethane, 241.3 g (4.16 mol) of acetone and subsequently 671.2 g (4.25 mol) of 3-trimethylsiloxy-2-pentene were added dropwise with stirring at ca. 0°C, and the mixture was kept stirring at room temperature for 16 h. Then 1 L of a 10% aqueous solution of sodium bicarbonate was added, the organic layer was separated, the aqueous layer was extracted with dichloromethane, the extracts were combined with the organic layer, and dichloromethane

was removed in a rotary evaporator at room temperature and 15 Torr. To the liquid residue, 5 g of *p*-toluenesulfonic acid and 1 L of benzene were added and the benzene was distilled off through a 30-cm packed column. The liquid residue was added to 1 L of ether, sequentially washed with a 5% aqueous solution of sodium bicarbonate and water, dried over sodium sulfate, and filtered. From the filtrate the ether was removed at room temperature and 15 Torr and the residue was distilled through a 30-cm packed column. The fraction distilling at 67–73°C (30–23 Torr) comprised 263 g and contained 78% of 4,5-dimethyl-4-hexene-3-one (**4***b*); ^{1}H nmr ($CDCl_3$, TMS), δ: 1.08 (t, J = 7.5 Hz, 3H), 1.75 (s, 3H), 1.81 (s, 6H), 2.53 (q, 2H).

To a suspension of 416.0 g (2.0 mol) of phosphorus pentachloride in 1.8 L of ether, a solution of 126.0 g (1.0 mol) of the above crude **4***b* in 1 L of ether was added dropwise at room temperature with vigorous stirring, and the reaction product was worked up in the manner described above for the preparation of **5***a*. After removal of pentane there remained 118.6 g of a brown liquid, which was distilled through a 30-cm packed column to afford 69.4 g of a distillate with a bp of 83–87°C (110 Torr). Distillation of the latter through a 1-m spinning band column afforded 19.7 g of a fraction with a bp of 89°C (110 Torr) containing 88% of **5***b* and 10% of **6***b* as shown by gc analysis. From this distillate samples of pure **5***b* and **6***b* have been isolated by pgc (preparative gas chromatography) (glass column, 0.7 × 300 cm, 5% Carbowax 20 M on Chromosorb G; 60–160°C at 3°C/min).

*(E)-4-Chloro-2,3-dimethyl-1,3-hexadiene (**5**b)*: colorless liquid; ir (film): 1640 cm^{-1}; ^{1}H nmr ($CDCl_3$, TMS), δ: 1.21 (t, J = 7.2 Hz, 3H), 1.83 (m) and 1.90 (s, partly overlapping signals of 6H altogether), 2.45 (q, J = 7.2 Hz, 2H), 4.78 (m, 1H), 4.97 (m, 1H); ms, *m/e* (relative intensity): 146, 144 (26, 100) M^+, 131, 129 (7, 16) $(M - CH_3)^+$, 109 (90) $(M - Cl)^+$; gc t_R (condition A) 5.7 min. *Anal.* calcd. for $C_8H_{13}Cl$ (144.7): C 66.43, H 9.06, Cl 24.51; found: C 66.53, H 8.91, Cl 24.33.

*(Z)-4-Chloro-2,3-dimethyl-1,3-hexadiene (**6**b)*: colorless liquid; ir (film): 1640 cm^{-1}; ^{1}H nmr ($CDCl_3$, TMS), δ: 1.12 (t, J = 7.3 Hz, 3H), 1.80 (s) and 1.83 (m, overlapping signals of 6H altogether), 2.41 (q, J = 7.3 Hz, 2H), 4.83 (m, 1H), 5.05 (m, 1H); ms, *m/e* (relative intensity): 146, 144 (33, 100) M^+, 131, 129 (8, 25) $(M - CH_3)^+$, 109 (38) $(M - Cl)^+$; gc t_R (condition A) 6.3 min. *Anal.* calcd. for $C_8H_{13}Cl$ (144.7): C 66.43, H 9.06, Cl 24.51; found: C 66.25, H 8.82, Cl 24.40.

Preparation of **5**d *and* **6**d was by the same procedure as described above for the preparation of **5***b* and **6***b*: Reaction of 361.3 g (1.91 mol) of titanium tetrachloride in 1.4 L of dichloromethane with 137.4 g (1.91 mol) of 2-butanone and 301.0 g (1.91 mol) of 3-trimethylsiloxy-2-pentene gave 102.0 g of a colorless distillate, bp 94–99°C (50 Torr). Reaction of 302.8 g (1.46 mol) of phosphorus pentachloride in 1.5 L of ether with 102.0 g of the above distillate and subsequent distillation of the crude product through a 30-cm packed column gave 47.0 g of a slightly brown liquid, bp 83–87°C (42 Torr). Reaction of 2.77 g (24.7 mmol) of potassium *tert*-butoxide in 30 mL of *tert*-butanol with 3.9 g of the above liquid gave 2.03 g of crude product, from which 0.66 g of **5***d* and 0.43 g of **6***d* were isolated by flash chromatography (column 5 × 45 cm, 166 g of silica gel; *n*-pentane).

*(4E)-5-Chloro-3,4-dimethyl-2,4-heptadiene (**5**d)*: colorless liquid; ir ($CDCl_3$): 1640 cm^{-1}; ^{1}H nmr (300 MHz, $CDCl_3$, TMS), δ: 1.07 (t, J = 7.3 Hz, 3H), 1.84 (t, J = 0.9 Hz, 3H), 2.36 (qq, J = 7.3 and 0.9 Hz, 2H), A_3B_3X system with δ_A 1.62 (3H), δ_B 1.68 (3H), δ_X 5.23 (1H), J_{AB} = 1.1 Hz, J_{AX} = 6.7 Hz, J_{BX} = 1.5 Hz; ^{13}C nmr ($CDCl_3$, TMS, broad band decoupled), δ: 13.37, 13.45, 15.30, 19.55, 29.41, 121.73, 132.17, 135.81, 136.44; ms, *m/e* (relative intensity): 160, 158 (9, 23) M^+, 123 (18) $(M - Cl)^+$; gc t_R (condition B) 15.2 min. *Anal.* calcd. for $C_9H_{15}Cl$ (158.7): C 68.12, H 9.53, Cl 22.34; found: C 68.18, H 9.37, Cl 22.24.

*(4Z)-5-Chloro-3,4-dimethyl-2,4-heptadiene (**6**d)*: colorless liquid; ir ($CDCl_3$): 1635 cm^{-1}; ^{1}H nmr (300 MHz, $CDCl_3$, TMS), δ: 1.11 (t, J = 7.3 Hz, 3H), 1.78 (t, J = 0.6 Hz, 3H), 2.38 (qq, J = 7.3 and 0.6 Hz, 2H), A_3B_3X system with δ_A 1.64 (3H), δ_B 1.70 (3H), δ_X 5.25 (1H), J_{AB} = 1.1 Hz, J_{AX} = 6.8 Hz, J_{BX} = 1.5 Hz; ^{13}C nmr ($CDCl_3$, TMS, broad band decoupled), δ: 12.51, 13.36, 14.71, 19.15, 28.94, 121.69, 129.20, 134.94, 137.46; ms, *m/e* (relative intensity): 160, 158 (9, 18) M^+, 123 (16) $(M - Cl)^+$; gc t_R (condition B) 16.2 min. *Anal.* calcd. for $C_9H_{19}Cl$ (158.7): C 68.12, H 9.53, Cl 22.34; found: C 68.01, H 9.32, Cl 22.43.

*Chloroprene (**11**a)* was available as a 50% solution in toluene. It was isolated by distillation through a 80-cm packed column at 200 Torr into a receiver cooled to −20°C and then stored at −20°C in the presence of added hydroquinone. Before each ozonolysis reaction, an adequate amount was redistilled through a 20-cm packed column under the above conditions; gc t_R (condition B) 5.3 min; 99% purity.

*Preparation of 2-chloro-3-methyl-1,3-butadiene (**11**b)*

A mixture of 30.0 g copper-I chloride, 12.0 g ammonium chloride, and 56.0 g (0.84 mol) 2-methyl-1-butene-3-yne (13) in 210 mL of concentrated hydrochloric acid was shaken for 4 h at room temperature in a 400-mL sealed glass ampoule. The dark product was submitted to steam distillation, the aqueous phase of the distillate was neutralized with potassium carbonate, extracted with dichloromethane, and the extracts combined with the organic phase of the distillate, dried over potassium carbonate, and distilled through a 30-cm packed column in the presence of hydroquinone. The fraction boiling at 47–49°C (158 Torr) was redistilled through a 1-m spinning band column at 158 Torr to give pure **11***b*. It was stored at −20°C in the presence of hydroquinone and redistilled at 158 Torr through a 20-cm packed column immediately before its use.

*2-Chloro-3-methyl-1,3-butadiene (**11**b)*: colorless liquid; ^{1}H nmr ($CDCl_3$, TMS), δ: 1.98 (m, 3H), 5.17 (m, 1H), 5.43 (s, 2H), 5.59 (m, 1H).

General procedure for the ozonolysis reactions

Solutions of the substrates in *n*-pentane were ozonized at −78°C. The product mixtures were warmed up to room temperature, the solvent was removed in a rotary evaporator at 15 Torr and room temperature, and the peroxidic liquid residues were separated by flash chromatography (pentane:ether 30:1, column 4 × 46 cm, 270 g of silica gel for the isolation of **7***b* and **8***b*; column 2 × 65 cm, 110 g of silica gel for the isolation of the remaining ozonides).

Ozonolysis of **5**a

A solution of 0.65 g (5 mmol) of **5***a* in 10 mL of pentane was treated with 3.8 mmol of ozone to give 0.86 g of liquid residue, from which 0.58 g (82%) of **7***a* and 0.01 g (2%) of **9***a* were isolated.

*3-[(E)-2-Chloro-1-methyl-1-butenyl]-1,2,4-trioxolane (**7**a)*: colorless liquid; ir (film): 1645 cm^{-1}; ^{1}H nmr ($CDCl_3$, TMS), δ: 1.16 (t, J = 7.3 Hz, 3H), 1.83 (s, 3H), 2.52 (q, J = 7.3 Hz, 2H), 5.12 (s, 1H), 5.35 (s, 1H), 5.84 (s, 1H); ^{13}C nmr (300 MHz, $CDCl_3$, TMS), δ: 13.36 (q, J = 128.8 Hz), 13.66 (q, J = 129.2 Hz), 28.85 (t, J = 127.3 Hz), 95.08 (dd, J = 173.8 and 166.4 Hz), 100.21 (d, J = 178.6 Hz), 123.70 (s), 143.32 (s); ms, *m/e* (relative intensity): 180, 178 (2, 7) M^+, 150, 148 (6, 19) $(M - CH_2O)^+$, 134, 132 (34, 100) $(M - CH_2O_2)^+$; gc t_R (condition D) 10.5 min. *Anal.* calcd. for $C_7H_{11}ClO_3$ (178.6): C 47.07, H 6.20, Cl 19.85; found: C 46.94, H 6.20, Cl 19.76.

*(E)-3-Chloro-2-methyl-2-pentenal (**9**a)*: colorless liquid; ^{1}H nmr ($CDCl_3$, TMS), δ: 1.29 (t, J = 7.2 Hz, 3H), 1.91 (s, 3H), 2.92 (q, J = 7.3 Hz, 2H), 10.03 (s, 1H); ms, *m/e* (relative intensity): 134, 132 (34, 100) M^+, 119, 117 (3, 13) $(M - CH_3)^+$, 97 (31) $(M - Cl)^+$; gc t_R (condition B) 15.4 min.

Ozonolysis of a mixture of **5**b *and* **6**b

A solution of 2.88 g (20 mmol) of **5***b* and **6***b* in a ratio of 9:1 in 30 mL of pentane was treated with 16 mmol of ozone to give 2.72 g of liquid residue, from which 930 mg (30%) of **7***b*, 210 mg (7%) of **8***b*, 265 mg (11%) of **9***b*, and 75 mg (3%) of **10***b* have been isolated.

*3-[(E)-2-Chloro-1-methyl-1-butenyl]-3-methyl-1,2,4-trioxolane (**7**b)*: colorless liquid; ir (film): 1645 cm^{-1}; ^{1}H nmr (300 MHz, $CDCl_3$, TMS) ABM_3X_3 system with δ_A 2.44 (1H), δ_B 2.73 (1H), δ_M 1.88 (3H), δ_X 1.15 (3H), J_{AB} = 13.0 Hz, J_{AM} = 0.8 Hz, J_{AX} = J_{BX} = 7.3 Hz, δ: 1.59 (s, 3H), 5.07 (s, 1H), 5.16 (s, 1H); ^{13}C nmr ($CDCl_3$, TMS), δ: 12.99 (q, J = 129.4 Hz), 17.04 (q, J = 126.7 Hz), 22.46 (q, J = 127.6 Hz), 30.4 (t, J = 125.3 Hz), 94.1 (dd, J = 149.1 and

167.0 Hz), 109.31 (s), 137.00 (s), 137.55 (s); ms, *m/e* (relative intensity): 194, 192 (15, 41) M^+, 148, 146 (68, 85) $(M - CH_2O_2)^+$, 133, 131 (30, 82) $(M - C_2H_5O_2)^+$, 67 (77) $(C_5H_7)^+$, 43 (100) $(CH_3CO)^+$; gc t_R (condition D) 9.2 min. *Anal.* calcd. for $C_8H_{13}ClO_3$ (192.6): C 49.88, H 6.80, Cl 18.41; found: C 49.92, H 6.79, Cl 18.54.

*3-[(Z)-2-Chloro-1-methyl-1-butenyl]-3-methyl-1,2,4-trioxolane (**8**b)*: colorless liquid; ir ($CDCl_3$): 1640 cm^{-1}; ^1H nmr (300 MHz, $CDCl_3$, TMS) $A_2M_3X_3$ system with δ_A 2.42 (2H), δ_M 1.80 (3H), δ_X 1.12 (3H), $J_{AM} = 0.6$ Hz, $J_{AX} = 7.4$ Hz, $J_{MX} = 0$ Hz, δ: 1.69 (s, 3H), 5.06 (s, 1H), 5.18 (s, 1H); ^{13}C nmr (300 MHz, $CDCl_3$, TMS), δ: 12.23 (q, $J = 129.6$ Hz), 15.34 (q, $J = 129.6$ Hz), 20.55 (q, $J = 129.6$ Hz), 30.78 (t, $J = 129.6$ Hz), 93.76 (dd, $J = 166.8$ and 171.6 Hz), 108.94 (s), 131.35 (s), 132.83 (s); ms, *m/e* (relative intensity): 194, 192 (10, 29) M^+, 148, 146 (48, 78) $(M - CH_2O_2)^+$, 133, 131 (29, 72) $(M - C_2H_5O_2)^+$, 67 (78) $(C_5H_7)^+$, 43 (100) $(CH_3CO)^+$; gc t_R (condition D) 10.8 min. *Anal.* calcd. for $C_8H_{13}ClO_3$ (192.6): C 49.88, H 6.80, Cl 18.41; found: C 50.05, H 6.83, Cl 18.31.

*(E)-4-Chloro-3-methyl-3-hexene-2-one (**9**b)*: colorless liquid; ir (film): 1690, 1600 cm^{-1}; ^1H nmr ($CDCl_3$, TMS), δ: 1.16 (t, $J = 6.9$ Hz, 3H), 2.03 (t, $J = 0.9$ Hz, 3H), 2.28 (s, 3H), 2.53 (q, $J = 6.9$ Hz, 2H); ^{13}C nmr (300 MHz, $CDCl_3$, TMS), δ: 12.99 (q, $J = 128.2$ Hz), 17.41 (q, $J = 129.2$ Hz), 29.76 (q, $J = 128.2$ Hz), 30.65 (t, $J = 128.2$ Hz), 132.85 (s), 145.09 (s), 201.27 (s); ms, *m/e* (relative intensity): 148, 146 (19, 61) M^+, 133, 131 (18, 49) $(M - CH_3)^+$, 67 (51) $(C_5H_7)^+$, 43 (100) $(CH_3CO)^+$; gc t_R (condition C) 15.6 min. *Anal.* calcd. for $C_7H_{11}ClO$ (146.6): C 57.34, H 7.56, Cl 24.18; found: C 57.43, H 7.57, Cl 24.12.

*(Z)-4-Chloro-3-methyl-3-hexene-2-one (**10**b)*: colorless liquid; ir (film): 1700 cm^{-1}; ^1H nmr ($CDCl_3$, TMS), δ: 1.16 (t, $J = 7.3$ Hz, 3H), 1.86 (s, 3H), 2.39 (s, 3H), 2.45 (q, $J = 7.3$ Hz, 2H); ^{13}C nmr (300 MHz, $CDCl_3$, TMS), δ: 11.84 (q, $J = 127.9$ Hz), 15.82 (q, $J = 128.9$ Hz), 29.19 (t, $J = 128.9$ Hz), 29.87 (q, $J = 127.9$ Hz), 133.34 (s), 134.22 (s), 204.11 (s); ms, *m/e* (relative intensity): 148, 146 (33, 100) M^+, 133, 131 (31, 95) $(M - CH_3)^+$, 67 (60) $(C_5H_7)^+$, 43 (46) $(CH_3CO)^+$; gc t_R (condition C) 18.5 min. *Anal.* calcd. for $C_7H_{11}ClO$ (146.6): C 57.34, H 7.56; found: C 57.47, H 7.70.

*Ozonolysis of **5**c*

A solution of 0.72 g (5 mmol) of **5***c* in 10 mL of pentane was treated with 4 mmol of ozone to give 0.95 g of liquid residue, from which 157 mg (20%) of *cis*-**7***c*, 163 mg (21%) of *trans*-**7***c*, and 68 mg (13%) of **9***a* have been isolated.

cis-*3-[(E)-2-Chloro-1-methyl-1-butenyl]-5-methyl-1,2,4-trioxolane (*cis-**7**c)*: colorless liquid; ir (film): 1650 cm^{-1}; ^1H nmr ($CDCl_3$, TMS), δ: 1.16 (t, $J = 7.3$ Hz, 3H), 1.47 (d, $J = 5.0$ Hz, 3H), 1.85 (s, 3H), 2.52 (q, $J = 7.3$ Hz, 2H), 5.46 (q, $J = 5.0$ Hz, 1H), 5.93 (s, 1H); ^{13}C nmr (300 MHz, $CDCl_3$, TMS), δ: 13.37 (q, $J = 127.0$ Hz), 13.71 (q, $J = 132.1$ Hz), 17.84 (q, $J = 128.0$ Hz), 28.82 (t, $J = 127.0$ Hz), 100.60 (d, $J = 178.9$ Hz), 101.99 (d, $J = 172.8$ Hz), 125.16 (s), 142.20 (s); ms, *m/e* (relative intensity): 194, 192 (7, 22) M^+, 150, 148 (8, 21) $(M - CH_3CHO)^+$, 134, 132 (23, 68) $(M - CH_3CHO_2)^+$, 125 (100) $(M - ClO_2)^+$, 67 (65) $(C_5H_7)^+$; gc t_R (condition D) 12.4 min. *Anal.* calcd. for $C_8H_{13}ClO_3$ (192.6): C 49.88, H 6.80, Cl 18.41; found: C 49.74, H 6.76, Cl 18.63.

trans-*3-[(E)-2-Chloro-1-methyl-1-butenyl]-5-methyl-1,2,4-trioxolane (*trans-**7**c)*: colorless liquid; ir (film): 1640 cm^{-1}; ^1H nmr ($CDCl_3$, TMS), δ: 1.16 (t, $J = 7.3$ Hz, 3H), 1.47 (d, $J = 4.9$ Hz, 3H), 1.84 (s, 3H), 2.48 (q, $J = 7.3$ Hz, 2H), 5.39 (q, $J = 4.9$ Hz, 1H), 5.90 (s, 1H); ^{13}C nmr (300 MHz, $CDCl_3$, TMS), δ: 13.38 (q, $J = 128.8$ Hz), 13.79 (q, $J = 128.8$ Hz), 16.07 (q, $J = 128.0$ Hz), 28.85 (t, $J = 128.8$ Hz), 100.85 (d, $J = 178.6$ Hz), 102.57 (d, $J = 170.5$ Hz), 123.82 (s), 143.28 (s); ms, *m/e* (relative intensity): 194, 192 (9, 27) M^+, 150, 148 (8, 24) $(M - CH_3CHO)^+$, 134, 132 (21, 62) $(M - CH_3CHO_2)^+$, 125 (100) $(M - ClO_2)^+$, 67 (50) $(C_5H_7)^+$; gc t_R (condition D) 11.3 min.

*Ozonolysis of **5**d*

A solution of 627 mg (4 mmol) of **5***d* in 10 mL of pentane was treated with 152 mg (3.2 mmol) of ozone to give 713 mg of liquid residue, from which 264 mg (40%) of **7***d* and 96 mg (21%) of **9***b* have been isolated.

*3-[(E)-2-Chloro-1-methyl-1-butenyl]-3-methyl-1,2,4-trioxolane (**7**d)*: colorless liquid consisting of two stereoisomers of **7***d* in a ratio of ca. 3:1, as evidenced by the intensities of the $CH_3(CH)$ signals that appeared in different chemical shift positions; ir (film): 1640 cm^{-1}; ^1H nmr ($CDCl_3$, TMS), major isomer, δ: 1.14 (t, $J = 7.3$ Hz), 1.42 (d, $J = 4.9$ Hz), 1.57 (s), 1.88 (s), 2.55 (q, $J = 7.3$ Hz), 5.31 (q, $J = 4.9$ Hz); minor isomer, δ: 1.14 (t, $J = 7.3$ Hz), 1.38 (d, $J = 4.9$ Hz), 1.55 (s), 1.88 (s), 2.55 (q, $J = 7.3$ Hz), 5.31 (q, $J = 4.9$ Hz); ms, *m/e* (relative intensity): 208, 206 (13, 39) M^+, 193, 191 (4, 13) $(M - CH_3)^+$, 148, 146 (16, 31) $(M - CH_3CHO_2)^+$, 139 (94) $(M - ClO_2)^+$, 127 (50) $(M - CH_3CHOCl)^+$, 111 (30) $(M - CH_3CHOOCl)^+$, 67 (69) $(C_5H_7)^+$, 43 (100) $(CH_3CO)^+$; gc t_R (condition D) 10.3 min. *Anal.* calcd. for $C_9H_{15}ClO_3$ (206.7): C 52.30, H 7.31, Cl 17.16; found: C 52.31, H 7.24, Cl 17.00.

*Ozonolysis of **6**d*

A solution of 427 mg (2.7 mmol) of **6***d* in 10 mL of pentane was treated with 100 mg (2.1 mmol) of ozone to give 408 mg of liquid residue, from which 48 mg (11%) of **8***d* and 190 mg (60%) of **10***b* have been isolated.

*3-[(Z)-2-Chloro-1-methyl-1-butenyl]-3-methyl-1,2,4-trioxolane (**8**d)*: colorless liquid consisting of two stereoisomers of **8***d* in a ratio of 5:1 based on the intensities of the $CH_3(CH)$ signals that appeared in different chemical shift positions; ir (film): 1640 cm^{-1}; ^1H nmr ($CDCl_3$, TMS), major isomer, δ: 1.11 (t, $J = 7.4$ Hz), 1.42 (d, $J = 4.9$ Hz), 1.68 (s), 1.80 (s), 2.38 (q, $J = 7.4$ Hz), 5.32 (q, $J = 4.9$ Hz); minor isomer, δ: 1.11 (t, $J = 7.4$ Hz), 1.36 (d, $J = 4.9$ Hz), 1.65 (s), 1.80 (s), 2.38 (q, $J = 7.4$ Hz), 5.32 (q, $J = 4.9$ Hz).

*Reductions of ozonides **7**a–**7**d and **8**d*

A solution of the respective ozonide in $CDCl_3$ was admixed with 40 mg of triphenylphosphine in an nmr tube and the tube was repeatedly shaken; ^1H nmr and gc analyses showed the formation of **9***a* from **7***a* and **7***c*, of **9***b* from **7***b* and **7***d*, and of **10***b* from **8***b* and **8***d*.

*Ozonolysis of **11**a*[3]

A solution of 2.445 g (27.6 mmol) of **11***a* in 33 mL of *n*-pentane was treated with 21.4 mmol of ozone at −78°C. Then 1 mL of methanol, 1 g of sodium bicarbonate, and 1 g of sodium sulfate were added, the mixture was kept stirring at −10°C until it became neutral, then was filtered and the solids washed with dichloromethane. The filtrate was distilled at room temperature and 0.2 Torr into a series of three traps kept at 0°C, −25°C, and −78°C. The fraction collected at −78°C (20 mL) contained pentane and dichloromethane, along with trace amounts of **13***a*. The fraction collected at −25°C (0.2 g) contained **12***a* and **13***a* in a ratio of 93:7. The fraction collected at 0°C consisted of 1.40 g (51%) of ozonide **12***a*, according to ^1H nmr analysis. For analytical purposes a sample of it was further purified by preparative thick layer chromatography (20 × 20 cm silica gel plate, trichloromethane:hexane 1:1) and subsequently distilled at room temperature and 0.1 Torr.

*3-(1-Chloroethenyl)-1,2,4-trioxolane (**12**a)*: colorless, shock sensitive liquid; ir (film): 1638 (C=C) cm^{-1}; ^1H nmr (300 MHz, $CDCl_3$, TMS), δ: 5.19 (s, 1H), 5.32 (s, 1H), 5.62 (m, 1H), 5.63 (d, $J = 1.9$ Hz, 1H), 5.79 (dd, $J = 1.9$ and 0.7 Hz, 1H); ^{13}C nmr ($CDCl_3$, TMS), δ: 94.64 (td, $J = 171$ and ca. 2 Hz), 100.45 (dm, $J = 176$ Hz), 118.49 (dd, $J = 164$ and 163 Hz), 134.58 (m); ms, *m/e* (relative intensity): 138, 136 (7, 22) M^+, 106, 104 (24, 47) $(M - O_2)^+$, 75 (44) $(M - C_2H_2Cl)^+$, 63, 61 (44, 100) $(C_2H_2Cl)^+$. *Anal.* calcd. for $C_4H_5ClO_3$ (136.5): C 35.19, H 3.69, Cl 25.97; found: C 35.27, H 3.62, Cl 25.88.

*2-Chloropropenal (**13**a)* has been identified by gc and ^1H nmr analysis with the help of an authentic sample, which was obtained by

[3] **Caution!** Application of more than one equivalent of ozone in pentane should be avoided, since treatment of chloroprene (**11***a*) with excess ozone in pentane at −78°C and subsequent warm-up of the mixture led to a violent explosion soon after the product had reached room temperature.

the following procedure: A mixture of 84.0 g (1.5 mol) of propenal and 200 mL of water was saturated with chlorine at ca. 0°C, a trace of *tert*-butyl-1,2-dihydroxybenzene was added, and the product was submitted to steam distillation. The organic phase of the distillate was dried over sodium sulfate, filtered, and distilled through a 20-cm packed column; bp 46°C (40 Torr); ^{1}H nmr ($CDCl_3$, TMS) AB-system with δ_A 6.44 (1H), δ_B 6.60 (1H), J_{AB} = 2.0 Hz, δ: 9.47 (s, 1H); ms, *m/e* (relative intensity): 92, 90 (36, 100) M^+, 63, 61 (12, 33) $(M - CHO)^+$; gc t_R (condition B) 14.1 min.

Treatment of ***12***a *with DMS*

To a mixture of 307.0 mg (4.9 mmol) of dimethyl sulfide and 1.5 mL of $CDCl_3$ a solution of 219.0 mg (1.6 mmol) of ***12a*** in 1.5 mL of $CDCl_3$ was added dropwise and kept stirring for 2 h at 0°C. Then 0.11 mL of methanol was added and stirring was continued for 21 h at room temperature; ^{1}H nmr analysis showed the presence of ***13a*** and of ***14*** (δ 6.03, d and 6.56, d, J = 1.5 Hz) in a ratio of 83:17, along with DMS (δ 2.12), DMSO (δ 2.62), and methoxymethanol (δ 3.44 and 4.74, s, each) (1).

Ozonolysis of ***11***b

A solution of 1.991 g (19.4 mmol) of ***11b*** in 30 mL of pentane was treated with 15 mmol of ozone at −78°C and worked up as described in the ozonolysis of ***11a***. The filtrate was concentrated by evaporation of solvent in a rotary evaporator at room temperature and reduced pressure. From the liquid concentrate (5 mL), 710 mg (31%) of ***12b*** and 100 mg (6%) of ***13b*** were isolated by flash chromatography (column 2.2 × 160 cm, 250 g silica gel, dichloromethane). Ozonide ***12b*** was subsequently distilled at room temperature and 10^{-2} Torr.

*3-(1-Chloroethyl)-3-methyl-1,2,4-trioxolane (****12****b)*: colorless, shock sensitive liquid; ir ($CDCl_3$): 1632 (C=C) cm^-; ^{1}H nmr ($CDCl_3$, TMS), δ: 1.71 (s, 3H), 5.11 (s, 1H), 5.34 (s, 1H), AB system with δ_A 5.45 (1H), δ_B 5.75 (1H), J_{AB} = 1.5 Hz; ^{13}C nmr ($CDCl_3$, TMS), δ: 20.14 (q, J = 130 Hz), 94.79 (dd, J = 174 and 167 Hz), 106.66 (s), 115.00 (t, J = 164 Hz), 139.37 (s); ms, *m/e* (relative intensity): 152, 150 (0.3, 0.8) M^+, 89 (16) $(M - C_2H_2Cl)^+$, 63, 61 (8, 23) $(C_2H_2Cl)^+$, 43 (100) $(CH_3CO)^+$. *Anal.* calcd. for $C_5H_7ClO_3$ (150.6): C 39.89, H 4.68, Cl 23.54; found: C 39.88, H 4.52, Cl. 23.35.

*2-Chloro-1-butene-3-one (****13****b)* has been identified by gc, ms, and ^{1}H nmr analysis with the help of an authentic sample that was obtained by the following procedure: A solution of 70.0 g (1.0 mol) of 1-butene-3-one in 150 mL of dichloromethane was saturated with chlorine at ca. 0°C, neutralized with sodium bicarbonate, dried over magnesium sulfate, filtered, and concentrated in a rotary evaporator at room temperature and 25 Torr. The liquid residue (153.0 g) was added dropwise to a stirred mixture of 130 mL (1.1 mol) of quinoline and a trace amount of *tert*-butyl-1,2-dihydroxybenzene at 115°C and 160 Torr, after which the resulting ***13b*** was distilled off through a 15-cm packed column. The distillate (35 g) was immediately redistilled through a 20-cm packed column in the presence of trace amounts of *tert*-butyl-1,2-dihydroxybenzene to give 10.5 g (10%) of ***13b*** as a colorless liquid; ^{1}H nmr ($CDCl_3$, TMS), δ: 2.46 (s, 3H), AB system with δ_A 6.08 (1H), δ_B 6.39 (1H), J_{AB} = 2.0 Hz; ms, *m/e* (relative intensity): 106, 104 (26, 76) M^+, 63, 61 (13, 39) $(M - CH_3CO)^+$, 43 (100) $(CH_3CO)^+$; gc t_R (condition B) 14.4 min. The material undergoes polymerization.

Reduction of ***12***b *with DMS*

To a mixture of 44.6 mg (0.72 mmol) of DMS in 0.4 mL of $CDCl_3$ was added a solution of 40.6 mg (0.27 mmol) of ***12b*** in 0.4 mL of $CDCl_3$ at room temperature; ^{1}H nmr analysis after 24 h showed the presence of ***13b*** and of DMSO (δ 2.63, s) in a ratio of 1:1.

Ozonolysis of ***7***b *in* $CH_3OH/CDCl_3$

A solution of 101 mg (0.522 mmol) of ***7b*** and 67 mg (2.1 mmol) of methanol in 2 mL of $CDCl_3$ was treated with ozone at −60°C until it turned blue, was then flushed with nitrogen, warmed up to room temperature, and admixed with 70 mg (0.417 mmol) of 1,1,2,2-tetrachloroethane as a standard; ^{1}H nmr analysis ($CDCl_3$, TMS) showed the presence of ***18*** (δ 1.15, t, J = 7.2 Hz, $CH_3(CH_2)$; 2.33, q, CH_2) and of ***19*** (δ 2.06, s, CH_3CO) in a molar ratio of 1:2, as well as methyl formate (δ 3.77, d, J = 0.8 Hz, CH_3O; 8.05, m, CH) and dimethoxymethane (δ 4.59, s, CH_2); gc analysis (condition B) with the help of authentic samples confirmed the presence of ***18*** (t_R = 6.6 min) and ***19*** (t_R = 5.1 min).

Ozonolysis of ***12***b *in* CH_3OD

A solution of 190 mg (1.3 mmol) of ***12b*** in 1.8 mL of CH_3OD was ozonized at −78°C until it turned blue, was flushed with nitrogen, admixed with 500 mg each of sodium bicarbonate and sodium sulfate, warmed up to 0°C, and diluted with 15 mL of dichloromethane. The salts were filtered off and the filtrate was concentrated at room temperature and 12 Torr; ^{1}H nmr analysis ($CDCl_3$, TMS) of the liquid residue (2 mL) showed the presence of ***21*** and ***22*** (δ 4.98, s, CH_2) (14) in a ratio of 1:0.9. By flash chromatography (column 2 × 30 cm, 50 g silica gel, dichloromethane), 60 mg (31%) of ***21*** was isolated.

Preparation of ***21*** *by ozonolysis of* ***23***a

A solution of 1.034 g (10.3 mmol) of ***23a*** in 14 mL of pentane was ozonied at −78°C until it turned blue, was then flushed with nitrogen, warmed up to room temperature, and kept until the original precipitate had dissolved. The mixture was concentrated in a rotary evaporator at room temperature and 20 Torr. From the liquid residue 1.05 g (72%) of ***21*** was isolated by flash chromatography and subsequently distilled at room temperature and at a pressure below 10^{-4} Torr.

*3-Carbomethoxy-3-methyl-1,2,4-trioxolane (****21****)*: colorless, shock sensitive liquid; ir (CCl_4): 1768 (C=O) cm^{-1}; ^{1}H nmr ($CDCl_3$, TMS), δ: 1.71 (s, 3H), 3.82 (s, 3H), 5.09 (s, 1H), 5.40 (s, 1H); ^{13}C nmr ($CDCl_3$, TMS), δ: 18.50 (q, J = 131 Hz), 53.04 (q, J = 148 Hz), 95.16 (d, d, J = 175 and 167 Hz), 103.95 (s), 168.83 (s); ms, *m/e* (relative intensity): 149 (100) $(M + 1)^+$ by chemical ionization; 89 (31) $(M - CO_2CH_3)^+$, 59 (24) $(CO_2CH_3)^+$, 43 (100) $(CH_3CO)^+$ by electron impact ionization. *Anal.* calcd. for $C_5H_8O_5$ (148.1): C 40.54, H 5.44; found: C 40.45, H 5.48.

Reduction of ***21*** *with DMS*

A solution of 40.0 mg (0.64 mmol) of DMS in 0.4 mL of $CDCl_3$ was admixed with 27.5 mg (0.18 mmol) of ***21*** in 0.4 mL of $CDCl_3$; ^{1}H nmr analysis with the help of authentic samples showed the presence of ***23b*** (δ 2.49, s and 3.88, s) and of DMSO (δ 2.62, s) in a ratio of 1:1.

Epoxidation of ***7***b

A solution of 1.38 g (7.2 mmol) of ***7b*** and 1.49 g (8.6 mmol) of *m*-chloroperbenzoic acid in 30 mL in dichloromethane was refluxed for 32 h and decanted from a colorless precipitate, which appeared during cooling to room temperature. The precipitate was washed with pentane, the decanted pentane was admixed with the main solution, and the mixture was concentrated in a rotary evaporator at room temperature and 15 Torr. The liquid residue (1.78 g) was separated by flash chromatography (column 4 × 46 cm, 280 g of silica gel, pentane:ether 20:1) to give 190 mg (13%) of ***24A***, 60 mg (4%) of ***24B***, and 60 mg (4%) of ***25***.

*3-Methyl-3-(*cis*-3-chloro-3-ethyl-2-methyl-2-oxiranyl)-1,2,4-trioxolanes (****24****)*

Isomer ***24***A: colorless liquid; ir (film): no absorption in the regions of the C=C and C=O stretching bands; ^{1}H nmr ($CDCl_3$, TMS), δ: 1.22 (t, J = 7.2 Hz, 3H), 1.57 (s, 3H), 1.64 (s, 3H), 2.26 (m, 2H), 5.04 (s, 1H), 5.16 (br s, 1H).

Isomer ***24***B: colorless liquid; ir (film): no absorption in the regions of the C=C and C=O stretching bands; ^{1}H nmr ($CDCl_3$, TMS), δ: 1.22 (t, J = 6.9 Hz, 3H), 1.54 (s, 3H), 1.68 (s, 3H), 2.20 (m, 2H), 4.99 (s, 1H), 5.21 (s, 1H).

*3-Methyl-3-(2-chloro-3-oxo-2-pentyl)-1,2,4-trioxolane (****25****)*: colorless liquid; ir (film): 1770 (C=O) cm^{-1}; ^{1}H nmr ($CDCl_3$, TMS), δ: 1.07 (t, J = 7.2 Hz, 3H), 1.57 (s, 3H), 1.76 (s, 3H), 2.84 (m, 2H), 5.18 (m, 2H).

Reduction of ***24***A *and of* ***24***B *with triphenylphosphine*

Solutions of ***24A*** and of ***24B*** in $CDCl_3$ were admixed with 40 mg of triphenylphosphine, each in nmr tubes at room temperature. The

^{1}H nmr analyses after 5 min showed in each case the presence of **26**. In addition, a precipitate appeared, probably polymeric formaldehyde.

trans-*2-Acetyl-3-chloro-3-ethyl-2-methyloxirane (26)* has been identified by comparison of ^{1}H nmr data with those of authentic **26**, which was obtained by the following procedure: A solution of 1.52 g (10.4 mmol) of **9***b* and 2.02 g (11.7 mmol) of *m*-chloroperbenzoic acid in 20 mL of dichloromethane was refluxed for 48 h, decanted from a colorless precipitate, and concentrated at room temperature and 15 Torr. The residual liquid (2.1 g) was separated by flash chromatography (same conditions as for **24** above) to give 65 mg (4%) of **26** as a colorless liquid; ^{1}H nmr ($CDCl_3$, TMS), δ: 1.13 (t, J = 7.0 Hz, 3H), 1.68 (s, 3H), 1.83 (center of m, overlapping with the singlet at 1.68), 2.22 (s, 3H).

Reduction of **25** was by the same procedure as that of **24**. The ^{1}H nmr analysis ($CDCl_3$, TMS) showed the presence of **27**; δ: 1.11 (t, J = 7.4 Hz, 3H), 1.75 (s, 3H), 2.32 (s, 3H), 2.72 (q, J = 7.4 Hz, 2H).

Reaction of **24**A *with* $AgBF_4$

To a solution of 630 mg (3.2 mmol) of $AgBF_4$ in 10 mL of ether, 560 mg (2.7 mmol) of **24***A* in 5 mL of ether was added dropwise with stirring at −10°C. The mixture was kept stirring at −10°C for 30 min and then separated by flash chromatography (column 5 × 40 cm, 318 g of silica gel, pentane:ether 10:1) to give 110 mg (24%) of **30**, 105 mg (20%) of **31***A*, and 30 mg (6%) of **31***B*.

3-Methyl-3-(oxo-1-pentene-2-yl)-1,2,4-trioxolane (30): colorless liquid; ir (film): 1685 (C=O), 1620 (C=C) cm^{-1}; ^{1}H nmr ($CDCl_3$, TMS), δ: 1.11 (t, J = 7.1 Hz, 3H), 1.75 (s, 3H), 2.67 (q, J = 7.1 Hz, 2H), 5.09 (s, 1H), 5.18 (s, 1H), 6.07 (s, 1H), 6.22 (s, 1H); ^{13}C nmr (300 MHz, $CDCl_3$, TMS), δ: 8.16 (q, J = 132.7 Hz), 22.48 (q, J = 132.7 Hz), 32.88 (t, J = 123.4 Hz), 94.31 (dd), 107.58 (s), 124.88 (dd), 147.58 (s), 201.13 (s).

3-Methyl-3-(2-fluoro-3-oxo-2-pentyl)-1,2,4-trioxolanes (31)

Isomer **31**A: colorless liquid; ^{1}H nmr ($CDCl_3$, TMS), δ: 1.05 (t, 7.1 Hz, 3H), 1.49 (d, J_{FH} = 1.8 Hz, 3H), 1.54 (d, J_{FH} = 22.5 Hz, 3H), 2.71 (m, 2H), 5.13 (s, 1H), 5.18 (s, 1H).

Isomer **31**B: colorless liquid; ^{1}H nmr ($CDCl_3$, TMS), δ: 1.05 (t, J = 7.2 Hz, 3H), 1.49 (d, J_{FH} = 22.0 Hz, 3H), 1.53 (d, J_{FH} = 2.4 Hz, 3H), 2.71 (m, 2H), 4.93 (d, J_{FH} = 1.1 Hz, 1H), 5.07 (s, 1H).

Acknowledgements

Support of this research by the Fonds der Chemischen Industrie and by Bayer AG, Leverkusen, is gratefully acknowledged.

1. K. Griesbaum, H. Keul, S. Agarwal, and G. Zwick. Chem. Ber. **116**, 409 (1983).
2. K. Griesbaum and G. Zwick. Chem. Ber. **118**, 3041 (1985).
3. K. Griesbaum, W. Volpp, and R. Greinert. J. Am. Chem. Soc. **107**, 5309 (1985).
4. Z. Arnold and J. Zemlicka. Collect. Czech. Chem. Commun. **24**, 2385 (1959).
5. H. W. Carothers and D. D. Coffman. J. Am. Chem. Soc. **54**, 4071 (1932).
6. R. W. Murray, R. D. Youssefyeh, and P. R. Story. J. Am. Chem. Soc. **89**, 2429 (1967).
7. P. S. Bailey. *In* Ozonation in organic chemistry. Vol. 1. Academic Press, New York. 1978. p. 25.
8. H. Keul and K. Griesbaum. Can. J. Chem. **58**, 2049 (1980).
9. H. Keul, B. Pfeffer, and K. Griesbaum. Chem. Ber. **117**, 2193 (1984).
10. K. Griesbaum and G. Zwick. Chem. Ber. **119**, 229 (1986).
11. R. Heilman, P. Arnold, and G. Scheuerbrandt. Bull. Soc. Chim. Fr. 1337 (1961).
12. W. C. Still, M. Kahn, and A. Mitra. J. Org. Chem. **43**, 2923 (1978).
13. C. D. Hurd and W. D. McPhee. J. Am. Chem. Soc. **71**, 398 (1949).
14. M. Meister, G. Zwick, and K. Griesbaum. Can. J. Chem. **61**, 2385 (1983).

Synthesis of 6-alkynylated uridines

HIROMICHI TANAKA, KAZUHIRO HARAGUCHI, YACHIYO KOIZUMI, MARIKO FUKUI, AND TADASHI MIYASAKA[1]

School of Pharmaceutical Sciences, Showa University, Hatanodai 1-5-8, Shinagawa-ku, Tokyo 142, Japan

Received November 22, 1985

This paper is dedicated to Professor Morio Ikehara on the occasion of his retirement from Osaka University in March 1986

HIROMICHI TANAKA, KAZUHIRO HARAGUCHI, YACHIYO KOIZUMI, MARIKO FUKUI, and TADASHI MIYASAKA. Can. J. Chem. **64**, 1560 (1986).

6-Alkynylated uridines, a hitherto unknown class of compounds, were synthesized by a coupling reaction of terminal alkynes with 6-iodo-2′,3′-*O*-isopropylidene-5′-*O*-methoxymethyluridine in the presence of bis(triphenylphosphine)palladium(II) chloride and copper(I) iodide. 6-Ethynyl-2′-deoxyuridine was also prepared by using 6-iodo-3′,5′-*O*-(tetraisopropyldisiloxan-1,3-diyl)-2′-deoxyuridine as a starting material.

HIROMICHI TANAKA, KAZUHIRO HARAGUCHI, YACHIYO KOIZUMI, MARIKO FUKUI et TADASHI MIYASAKA. Can. J. Chem. **64**, 1560 (1986).

Faisant appel à une réaction de couplage des alcynes terminaux avec l'iodo-6 *O*-isopropylidène-2′,3′ *O*-méthoxyméthyl-5′ uridine, en présence de chlorure de bis(triphénylphosphine) palladium(II) et d'iodure de cuivre(I), on a synthétisé des uridines portant des groupements alcynes en position 6, une classe de composés qui étaient jusqu'à maintenant inconnue. On a aussi préparé de l'éthynyl-6 déoxy-2′ uridine en utilisant l'iodo-6 (tétraisopropyldisiloxane-1,3 diyl)-3′,5′ déoxy-2′ uridine comme produit de départ.

[Traduit par la revue]

Because of their significant biological activities, 5-alkynylated pyrimidine nucleosides in general and 5-alkynylated uracil nucleosides in particular have attracted considerable attention in the field of nucleoside chemistry.

The earlier method for the preparation of these compounds is based on the classical condensation method wherein protected sugar derivatives and appropriate bases were used (1–3). Later, on the basis of a modified procedure for the coupling reaction of terminal alkynes with aryl halides reported by Sonogashira *et al.* (4), Robins and co-workers described an elegant application of this method for the preparation of 5-alkynyluracil nucleosides (5–7).

While an alternative method for the coupling reaction is also available (8), Robins' approach, palladium–copper catalyzed coupling of terminal alkynes with 5-iodouracil nucleosides, seems to be most widely applicable to the modification of nucleosides, as has been shown in the synthesis of 6-, 8-, and 2-alkynylated purine nucleosides (9, 10).

On the other hand, although 6-ethynyluracil has been prepared and found to suppress the proliferation of leukemia L1210, B-16 melanoma, and Lewis lung carcinoma cells (11), pyrimidine nucleosides having an alkynyl group in the C-6 position have not yet appeared in the literature. This might be related to the fact that the classical condensation method with 6-substituted pyrimidines has almost always resulted in the predominant formation of N^3-glycosylated products (12–15).

We have recently published a series of papers on the lithiation of nucleosides, which furnished general access to the modification of their base moieties (16–20). 6-Substituted uridines, which have thus far been difficult to synthesize, are now easily accessible by our method (16), the lithiation of 2′,3′-*O*-isopropylidene-5′-*O*-methoxymethyluridine (**1**) with LDA (lithium diisopropylamide) and subsequent reactions of the lithiated species with electrophiles. An apparent candidate for synthesizing 6-alkynyluridines might be a 6-iodouridine derivative that can be prepared by using iodine as an electrophile in the above reaction (21, 22).

Thus 6-iodo-2′,3′-*O*-isopropylidene-5′-*O*-methoxymethyluridine (**2**), prepared in 76% yield from **1** according to the published procedure (22), was deprotected by treatment with 50% aqueous trifluoroacetic acid (TFA) to produce **3** as crystals (mp 130–132°C) in quantitative yield. However, the use of **3** as a starting material resulted in the formation of an intractable mixture of products under Robins' conditions with DMF as a cosolvent. Accordingly, we then examined the coupling reaction of **2** with terminal alkynes.

Treatment of **2** with phenylacetylene in triethylamine at 60°C for 2 h under positive pressure of dry argon in the presence of bis(triphenylphosphine)palladium(II) chloride and copper(I) iodide gave a 71% yield of the 6-[2-(phenyl)ethynyl]uridine derivative (**4**) after column chromatography on silica gel. The presence of an alkynyl group in **4** was clear from the ir spectrum (ν 2180 cm^{-1}); ^{1}Hmr ($CDCl_3$: δ 6.02, H-1′; δ 6.40, H-5; δ 7.26–7.56, phenyl) and ms (M^+ m/z: 428) spectra were in good agreement with its structure. Other terminal alkynes also work equally well, as shown in Table 1. It should be mentioned that protection of the hydroxyl group in propargyl alcohol was not necessary to effect smooth coupling with **2**. The 6-ethynyluridine derivative (**8**) was obtained from its trimethylsilyl precursor (**7**) upon treatment with methanolic ammonia. Since the use of silica gel decreased the isolated yield of **8** to a considerable extent, magnesium silicate was used as an adsorbent in its column chromatography.

A similar coupling reaction of the 5-bromo-6-iodouridine derivative **10**, accessible from **9** by LDA lithiation followed by iodination, with phenylacetylene was also carried out. It was found, however, that most of **10** was deiodinated during the reaction, leading to the isolation of **9** in 50% yield.

Concurrent deprotection of 2′,3′-*O*-isopropylidene and the 5′-*O*-methoxymethyl groups in the above products (**4–6** and **8**) was accomplished with 50% TFA at room temperature to furnish the corresponding 6-alkynyluridines (**11–14**) in good yields. The results are summarized in Table 2.

Finally, the C-6 ethynylation of 2′-deoxyuridine was examined by using 6-iodo-3′,5′-*O*-(tetraisopropyldisiloxan-1,3-diyl)-2′-deoxyuridine (**15**) as a starting material (18).

Compound **15** was subjected to reaction with trimethylsilylacetylene under Robins' conditions for 1 h. As the resulting

[1]Author to whom correspondence may be addressed.

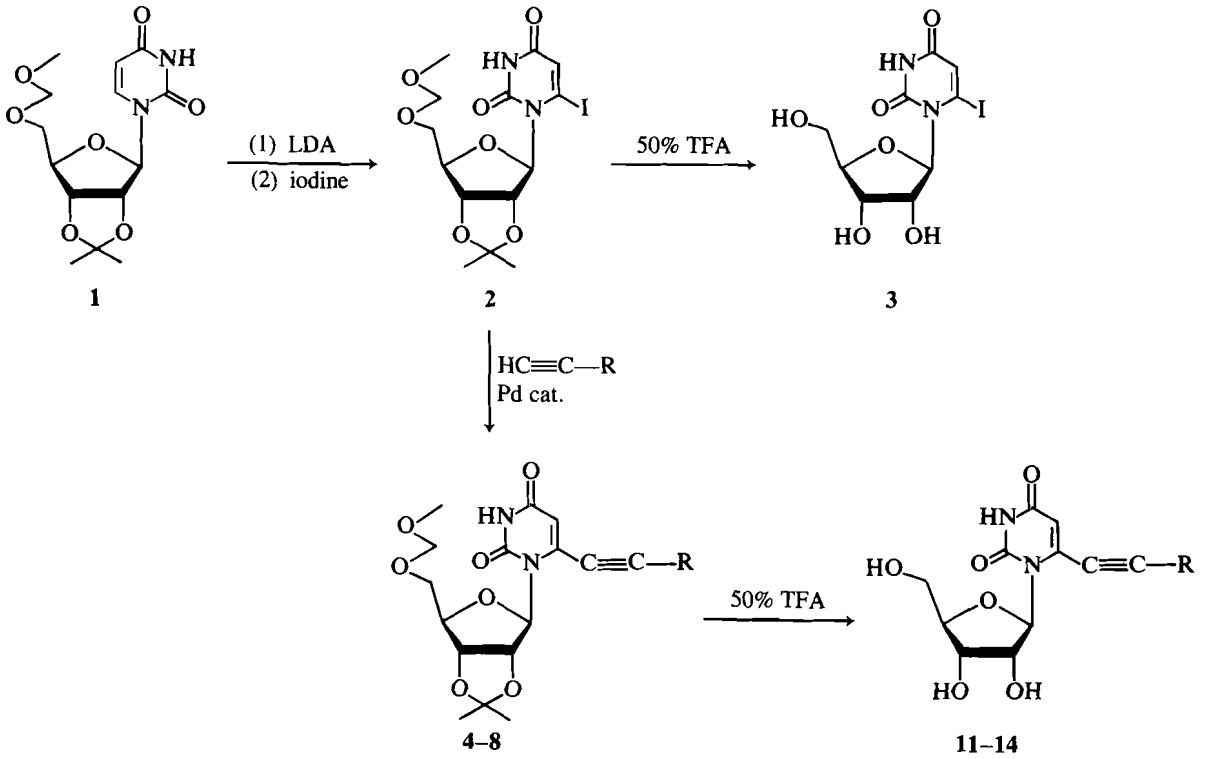

SCHEME 1

TABLE 1. Yields and ^{1}Hmr data of **4–8**

Product	R	Yield (%)	Proton magnetic resonance chemical shifts (δ: ppm) in $CDCl_3$								
			H-1′	H-2′	H-3′	H-4′	CH_2-5′	H-5	CH_2OCH_3	Isopr. Me	Others
4	Ph	71	6.02	5.21	4.82	4.33	3.75	6.41	4.66 3.36	1.57 1.37	7.26–7.56 phenyl
5	$(CH_2)_3Me$	74	6.33	5.19	4.87	4.25	3.76	5.86	4.66 3.35	1.56 1.35	0.96, 1.26–1.70, and 2.51 hexynyl
6	CH_2OH	73	6.25	5.19	4.86	4.23	3.76	5.96	4.66 3.37	1.57 1.36	2.68 and 4.54 CH_2OH
7	$SiMe_3$	68	6.33	5.17	4.82	4.29	3.74	5.90	4.63 3.33	1.52 1.33	0.26 $SiMe_3$
8	H	70*	6.29	5.19	4.86	4.28	3.76	6.01	4.66 3.36	1.56 1.36	3.78 C≡CH

*Yield from **7**.

product (**16**) could not be obtained in pure form even after column chromatography on magnesium silicate, the mixture containing **16** was treated with tetrabutylammonium fluoride (TBAF) in THF for 1 h. This and successive column chromatography of the reaction mixture gave 6-ethynyl-2′-deoxyuridine (**17**, mp 202–204°C) in 32% yield from **15**.

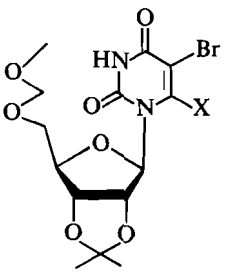

9 X = H
10 X = I

Biological evaluation of the compounds involved in this study is presently under investigation.

Experimental

Melting points were determined with a Yanagimoto micro melting point apparatus and are uncorrected. The ^{1}Hmr spectra were measured with an appropriate internal standard of tetramethylsilane (TMS) or sodium-2,2-dimethyl-2-silapentane 5-sulfonate (DSS), with a JEOL JNM-FX 100 spectrometer. The abbreviations used are as follows: s, singlet; d, doublet; dd, double doublet; t, triplet; q, quartet; m, multiplet; br, broad. Mass spectra were taken on a JEOL JMS-D 300 spectrometer. The uv and ir spectra were recorded on Shimadzu UV-240 and JASCO A-102 spectrophotometers, respectively. Unless otherwise noted, column chromatography was carried out on silica gel (Wakogel CC-200). Thin-layer chromatography (tlc) was performed on silica gel (precoated silica gel plate 60 F_{254}, Merck). Compounds **4**, **5**, **7**, and **8**, being noncrystalline, were not analyzed; however their crystalline deprotected products **11**, **12**, and **14** were analyzed.

TABLE 2. Yields and ^{1}Hmr data of **11–14**

Product	R	Yield (%)	Proton magnetic resonance chemical shifts (δ: ppm) in DMSO-d_6						
			H-1′	H-2′	H-3′	H-4′	CH_2-5′	H-5	Others
11	Ph	84	5.99	4.52 – 4.59		4.07	3.55	6.08	7.49–7.63 phenyl
12	$(CH_2)_3Me$	74	5.91	4.54	4.05	3.66	3.53	5.82	0.91, 1.50, and 2.50 hexynyl
13*	CH_2OH	83	6.14	4.82	4.38	3.97	3.83	6.13	4.53 C≡C—CH_2
14	H	62	5.87	4.58	3.69	3.56	3.27	6.00	5.28 C≡CH

*The ^{1}Hmr spectrum was measured in D_2O.

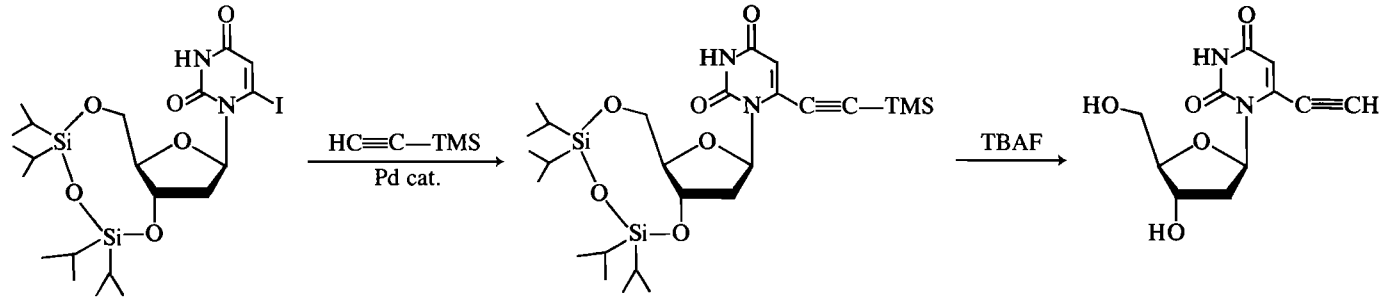

SCHEME 2

6-Iodo-2′,3′-O-isopropylidene-5′-O-methoxymethyluridine (2)

For the preparation and physical data of this compound see ref. 22.

6-Iodouridine (3)

A solution of **2** (500 mg) in 50% TFA (7 mL) was stirred for 6 h at room temperature. The mixture was evaporated to dryness and the whole residue was chromatographed on a silica gel column. Elution with 6% EtOH in $CHCl_3$ gave **3** (407 mg, 100%). Crystallization from EtOH furnished an analytically pure sample (327 mg, 80%, mp 130–132°C); $\lambda_{max}(H_2O)$: 269 nm (ε 9300), $\lambda_{min}(H_2O)$: 237 nm (ε 4200); ^{1}Hmr (DMSO-d_6, after adding D_2O), δ: 3.32 (2H, m, CH_2-5′), 3.78 (1H, m, H-4′), 4.08 (1H, t, H-3′), 4.54 (1H, dd, H-2′), 5.74 (1H, d, J = 3.4 Hz, H-1′), 6.35 (1H, s, H-5); ms m/z: 238 (B + 1). *Anal.* calcd. for $C_9H_{11}O_6N_2I$: C 29.37, H 3.12, N 7.85; found: C 29.20, H 3.00, N 7.57.

2′,3′-O-Isopropylidene-5′-O-methoxymethyl-6-[2-(phenyl)ethynyl]uridine (4)

Phenylacetylene (0.3 mL, 3.16 mmol) was added to a mixture of **2** (604 mg, 1.33 mmol), $Pd(Ph_3P)_2Cl_2$ (93 mg, 0.13 mmol), and CuI (25 mg, 0.13 mmol) in Et_3N (10 mL). The mixture was stirred at 60°C for 2 h under positive pressure of dry argon. The solvent was evaporated and the resulting residue was chromatographed on a silica gel column. Elution with 0.5% EtOH in $CHCl_3$ gave **4** (403 mg, 71%) as foam; ir (KBr) ν: 2180 cm^{-1}; λ_{max}(MeOH): 305 nm, λ_{min}(MeOH): 239 nm; ms m/z: 428 (M^+), 413 (M − Me), 212 (B + 1).

6-Hexynyl-2′,3′-O-isopropylidene-5′-O-methoxymethyluridine (5)

This compound was prepared from **2** (574 mg) and hexyne (207 mg) by the procedure for the preparation of **4**. Silica gel column chromatography (0.5% EtOH in $CHCl_3$) gave 395 mg (74%) of **5** as syrup; ir (KBr) ν: 2230 cm^{-1}; λ_{max}(MeOH): 284 nm, λ_{min}(MeOH): 246 nm; ms m/z: 408 (M^+), 393 (M − Me).

6-(3-Hydroxypropynyl)-2′,3′-O-isopropylidene-5′-O-methoxymethyluridine (6)

This compound was prepared from **2** (299 mg) and propargyl alcohol (74 mg) by the procedure for the preparation of **4**. Silica gel column chromatography (2% EtOH in $CHCl_3$) gave 182 mg (73%) of **6** as amorphous powder. Crystallization from EtOH furnished an analytically pure sample (71 mg, 28%, mp 146–148°C); ir (KBr) ν: 2220 cm^{-1}; λ_{max}(MeOH): 287 nm (ε 10 800), λ_{min}(MeOH): 251 nm (ε 3000); ms m/z: 382 (M^+), 367 (M − Me). *Anal.* calcd. for $C_{17}H_{22}N_2O_8$: C 53.88, H 7.05, N 5.98; found: C 53.50, H 7.32, N 5.80.

2′,3′-O-Isopropylidene-5′-O-methoxymethyl-6-[2-(trimethylsilyl)ethynyl]uridine (7)

This compound was prepared from **2** (1.24 g) and trimethylsilylacetylene (538 mg) by the procedure for the preparation of **4**. Silica gel column chromatography (1% EtOH in $CHCl_3$) gave 843 mg of **7** as a syrup; ir ($CHCl_3$) ν: 2100 cm^{-1}; λ_{max}(MeOH): 284 nm, λ_{min}(MeOH): 240 nm; ms m/z: 424 (M^+), 209 (B + 1).

6-Ethynyl-2′,3′-O-isopropylidene-5′-O-methoxymethyluridine (8)

A solution of **7** (166 mg) in NH_3/MeOH (10 mL) was kept standing at room temperature for 2 h. The mixture was evaporated to dryness and the resulting residue was chromatographed on a column of magnesium silicate (Florisil®). Elution with 10% EtOAc in benzene gave 104 mg (70%) of **8** as a foam; ir ($CHCl_3$) ν: 2100 cm^{-1}; λ_{max}(MeOH): 284 nm, λ_{min}(MeOH): 244 nm; ms m/z: 352 (M^+), 337 (M − Me).

5-Bromo-2′,3′-O-isopropylidene-5′-O-methoxymethyluridine (9)

5-Bromo-2′,3′-*O*-isopropylideneuridine (4.1 g) was added to a mixture of dry acetone (50 mL), dry dimethoxymethane (100 mL), and methanesulfonic acid (1.5 mL). The resulting solution was stirred at room temperature for 5 h. The reaction was quenched by adding aqueous $NaHCO_3$ and the organic solvents were removed by evaporation. Extraction with $CHCl_3$ followed by chromatographic purification on silica gel (1% EtOH in $CHCl_3$) gave 4.38 g (95%) of **9** as syrup. Crystallization from ether furnished an analytically pure sample (4.15 g, 90%, mp 134–135°C); λ_{max}(MeOH): 276 nm (ε 9400), λ_{min}(MeOH): 240 nm (ε 1700); ^{1}Hmr ($CDCl_3$) δ: 1.37 (3H, s, isopr. Me), 1.60 (3H, s, isopr. Me), 3.41 (3H, s, CH_2OCH_3), 3.80 (2H, m, CH_2-5′), 4.45 (1H, m, H-4′), 4.72 (2H, s, CH_2OCH_3), 4.77–4.89 (2H, m, H-2′ and H-3′), 5.99 (1H, d, J = 2.0 Hz, H-1′), 8.06 (1H, s, H-6), 8.64 (1H, br, NH); ms m/z: 407 and 405 (M^+), 392 and 390 (M − Me). *Anal.* calcd. for $C_{14}H_{19}N_2O_7Br$: C 41.34, H 4.75, N 7.16; found: C 41.29, H 4.70, N 6.88.

5-Bromo-6-iodo-2′,3′-O-isopropylidene-5′-O-methoxymethyluridine (10)

LDA (2.5 mmol) in THF (20 mL) was placed in a three-necked flask equipped with a nitrogen-inlet adapter, thermometer, and rubber

septum. To this, a solution of **9** (407 mg, 1.0 mmol) in THF (10 mL) was added, under positive pressure of dry argon, at a rate such that the temperature did not exceed −70°C. After the mixture was stirred for 1 h, iodine (569 mg, 2.2 mmol as I_2) in THF (15 mL) was added while maintaining the temperature below −70°C. The mixture was stirred for 1.5 h below −70°C, quenched with AcOH (0.14 mL), and allowed to warm to room temperature. The whole was evaporated to dryness and the residue was chromatographed on a silica gel column (0.5% EtOH in $CHCl_3$). This afforded 462 mg (87%) of **10**. Crystallization from acetone–hexane gave an analytically pure sample (329 mg, 62%, mp 198–199°C); λ_{max}(MeOH): 278 nm (ε 8200), λ_{min}(MeOH): 242 nm (ε 3400); ^{1}Hmr ($CDCl_3$) δ: 1.36 (3H, s, isopr. Me), 1.58 (3H, s, isopr. Me), 3.37 (3H, s, CH_2OCH_3), 3.74 (2H, m, CH_2-5′), 4.30 (1H, m, H-4′), 4.66 (2H, s, CH_2OCH_3), 4.85 (1H, dd, H-3′), 5.18 (1H, dd, H-2′), 6.35 (1H, d, J = 1.5 Hz, H-1′), 9.02 (1H, br, NH); ms m/z: 519 and 517 (M − Me), 318 and 316 (B + 1). *Anal.* calcd. for $C_{14}H_{18}N_2O_7BrI$: C 31.54, H 3.40, N 5.25; found: C 31.83, H 3.49, N 5.23.

*6-(2-Phenyl)ethynyluridine (**11**)*

A solution of **4** (143 mg) in 50% THA (2 mL) was stirred at room temperature overnight. The mixture was evaporated to dryness and the whole residue was chromatographed on a silica gel column. Elution with 4% EtOH in $CHCl_3$ gave **11** (100 mg, 84%) as amorphous powder; ir (KBr) ν: 2180 cm^{-1}; λ_{max}(MeOH): 308 nm (ε 19 100), λ_{min}(MeOH): 242 nm (ε 9400); ms m/z: 212 (B + 1). *Anal.* calcd. for $C_{17}H_{16}N_2O_6$: C 59.30, H 4.68, N 8.13; found: C 59.17, H 4.68, N 8.00.

*6-Hexynyluridine (**12**)*

This compound was prepared from **5** (363 mg) by the procedure for the preparation of **11**. Silica gel column chromatography (5% EtOH in $CHCl_3$) gave 212 mg (74%) of **12** as foam; ir ($CHCl_3$) ν: 2220 cm^{-1}; λ_{max}(H_2O): 287 nm (ε 12 000), λ_{min}(H_2O): 251 nm (ε 2000); ms m/z: 206 (B + 1). *Anal.* calcd. for $C_{15}H_{20}N_2O_6$: C 55.55, H 6.22, N 8.64; found: C 55.27, H 6.46, N 8.39.

*6-(3-Hydroxypropynyl)uridine (**13**)*

This compound was prepared from **6** (117 mg) by the procedure for the preparation of **11**. Silica gel column chromatography (5–10% EtOH in $CHCl_3$) gave 64 mg (83%) of **13**. Crystallization from EtOAc furnished an analytically pure sample (21 mg, 27%, mp 174–176°C); ir ($CHCl_3$) ν: 2220 cm^{-1}; λ_{max}(H_2O): 287 nm (ε 11 000), λ_{min}(H_2O): 250 nm (ε 2100); ms m/z: 166 (B + 1). *Anal.* calcd. for $C_{12}H_{14}N_2O_7$: C 48.32, H 4.73, N 9.39; found: C 48.14, H 4.73, N 9.28.

*6-Ethynyluridine (**14**)*

This compound was prepared from **8** (241 mg) by the procedure for the preparation of **11**. Column chromatography of Florisil gave 114 mg (62%) of **14**. Crystallization from MeOH furnished an analytically pure sample (59 mg, 32%, mp 217–219°C); ir (KBr) ν: 2100 cm^{-1}; λ_{max}(H_2O): 285 nm (ε 9900), λ_{min}(H_2O): 245 nm (ε 1100); ms m/z: 137 (B + 2). *Anal.* calcd. for $C_{11}H_{12}N_2O_6$: C 49.25, H 4.51, N 10.45; found: C 49.35, H 4.50, N 10.25.

*6-Ethynyl-2′-deoxyuridine (**17**)*

Ethynylation of **15** (500 mg) was carried out by the procedure for the preparation of **4** using trimethylsilylacetylene (165 mg) as a terminal alkyne. After column chromatography on Florisil, the mixture containing **16** was treated with TBAF·$3H_2O$ (1.25 g) in THF (10 mL) at room temperature for 1 h. Evaporation of the solvent followed by chromatographic purification on Florisil (5% EtOH in $CHCl_3$) gave **17** (68 mg, 32%) as crystalline powder, which was analytically pure (mp 202–204°C); ir (KBr) ν: 2280 cm^{-1}; λ_{max}(H_2O): 285.5 nm (ε 10 600), λ_{min}(H_2O): 243.5 nm (ε 1400); ^{1}Hmr (DMSO-d_6) δ: 1.92–2.13 (1H, m, H-2′), 2.64–2.92 (1H, m, H-2′), 3.41–3.70 (3H, m, H-4′ and CH_2-5′), 4.22 (1H, m, H-3′), 5.26 (1H, s, C≡CH), 5.97 (1H, d, H-5), 6.35 (1H, dd, H-1′), 11.52 (1H, br, NH); ms m/z: 136 (B + 1). *Anal.* calcd. for $C_{11}H_{12}N_2O_5$: C 52.38, H 4.80, N 11.11; found: C 52.46, H 4.92, N 10.83.

Acknowledgement

We would like to thank Miss Emiko Inoue for her skillful assistance.

1. J. Perman, R. A. Sharma, and M. Bobek. Tetrahedron Lett. 2427 (1976).
2. A. S. Jones, P. Serafinowski, and R. T. Walker. Tetrahedron Lett. 2459 (1977).
3. P. J. Barr, A. S. Jones, P. Serafinowski, and R. T. Walker. J. Chem. Soc. Perkin Trans. 1, 1263 (1978).
4. K. Sonogashira, Y. Tohda, and N. Hagihara. Tetrahedron Lett. 4467 (1975).
5. M. J. Robins and P. J. Barr. Tetrahedron Lett. **22**, 421 (1981).
6. M. J. Robins and P. J. Barr. J. Org. Chem. **48**, 1854 (1983).
7. E. De Clercq, J. Descamps, J. Balzarini, J. Giziewicz, P. J. Barr, and M. J. Robins. J. Med. Chem. **26**, 661 (1983).
8. P. Vincent, J.-P. Beaucourt, and L. Pichat. Tetrahedron Lett. **22**, 945 (1981).
9. S. Koyama, Z. Kumazawa, and N. Kashimura. Nucleic Acids Symposium Series, **11**, 41 (1982).
10. A. Matsuda, M. Shinozaki, T. Miyasaka, H. Machida, and T. Abiru. Chem. Pharm. Bull. **33**, 1766 (1985).
11. A. C. Schroeder, A. Bloch, J. L. Perman, and M. Bobek. J. Med. Chem. **25**, 1255 (1982).
12. W. V. Curran and R. B. Angier. J. Org. Chem. **31**, 201 (1966).
13. T. Ueda and U. Tanaka. Chem. Pharm. Bull. **18**, 1491 (1970).
14. U. Niedballa and H. Vorbrüggen. J. Org. Chem. **39**, 3660 (1974).
15. L. Pichat and G. Chatelain. Bull. Chim. Soc. Fr. 1833 (1970).
16. H. Tanaka, H. Hayakawa, and T. Miyasaka. Tetrahedron, **38**, 2635 (1982).
17. H. Tanaka, Y. Uchida, M. Shinozaki, H. Hayakawa, A. Matsuda, and T. Miyasaka. Chem. Pharm. Bull. **31**, 787 (1983).
18. H. Tanaka, H. Hayakawa, S. Iijima, K. Haraguchi, and T. Miyasaka. Tetrahedron, **41**, 861 (1985).
19. H. Hayakawa, H. Tanaka, and T. Miyasaka. Tetrahedron, **41**, 1675 (1985).
20. H. Tanaka, M. Hirayama, A. Mastuda, T. Miyasaka, and T. Ueda. Chem. Lett. 589 (1985).
21. H. Tanaka, A. Matsuda, S. Iijima, H. Hayakawa, and T. Miyasaka. Chem. Pharm. Bull. **31**, 2164 (1983).
22. H. Tanaka, H. Hayakawa, K. Haraguchi, and T. Miyasaka. Nucleosides nucleotides, **4**, 607 (1985).

H–D exchange of 1-methylcycloalkenes in dilute acid at elevated temperatures

NICK HENRY WERSTIUK AND GEORGE TIMMINS
Department of Chemistry, McMaster University, Hamilton, Ont., Canada L8S 4M1

Received January 13, 1986

NICK HENRY WERSTIUK and GEORGE TIMMINS. Can. J. Chem. **64**, 1564 (1986).

Specifically deuteriated cycloalkenes 1-trideuteriomethylcyclopentene-2,5,5-d_6 (**1***b*), 1-trideuteriomethylcyclohexene-2,6,6-d_6 (**2***b*), 1-trideuteriomethylcycloheptene-2,7,7-d_6 (**3***b*), and 1-trideuteriomethylcyclooctene-2,8,8-d_6 (**4***b*) have been prepared from the corresponding protiated substrates **1***a*, **2***a*, **3***a*, and **4***a* using a modified HTDA exchange method. The perlabelled analogues of **1***a* and **2***a*, **5** and **6**, have been synthesized by the same method.

NICK HENRY WERSTIUK et GEORGE TIMMINS. Can. J. Chem. **64**, 1564 (1986).

Faisant appel à une méthode d'échange au HTDA modifiée et utilisant les substrats protonés **1***a*, **2***a*, **3***a* et **4***a* comme produits de départ, on a préparé les cycloalcènes deutérés spécifiquement suivants: trideutérométhyl-1 cyclopentène-d_6-2,5,5 (**1***b*), trideutérométhyl-1 cyclohexène-d_6-2,6,6 (**2***b*), trideutéréméthyl-1 cycloheptène-d_6-2,7,7 (**3***b*) et trideutérométhylcyclooctène-d_6-2,8,8 (**4***b*). On a aussi synthétisé les analogues perdeutérés de **1***a* et **2***a*, **5** et **6**, en faisant appel à la même méthode.
[Traduit par la revue]

Introduction

Initial studies of the application of high temperature – dilute acid (HTDA) exchange have established that a wide range of aromatic compounds can be specifically labelled or perlabelled (1–6, 8). In continuing these studies, we examined a series of straight-chained alkenes and cycloalkenes in an attempt to prepare a group of labelled substrates that could be elaborated into labelled aliphatic compounds by standard transformations (7). To establish whether or not a methyl group can act as an anchor for the double bond and thereby promote specific H–D exchange of alkenes, we have studied the H–D exchange of 1-methylcyclopentene (**1***a*), 1-methylcyclohexene (**2***a*), 1-methylcycloheptene (**3***a*), and 1-methylcyclooctene (**4***a*). A modified HTDA method was used as described previously (7) to reduce the extent of substitution and to reduce the temperature and the reaction time. In the modified method, a cosolvent such as decalin is used and the reaction solutions are agitated by a rocking motion of the pressure vessel used to contain the reaction tubes. In this paper we report that specifically deuteriated cycloalkenes **1***b*, **2***b*, **3***b*, and **4***b* can easily be prepared using this method as well as the perdeuteriated analogues of **1***a* and **2***a*, **5** and **6**.

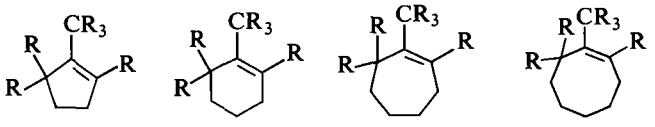

1 *a*, R = H; *b*, R = D

2 *a*, R = H; *b*, R = D

3 *a*, R = H; *b*, R = D

4 *a*, R = H; *b*, R = D

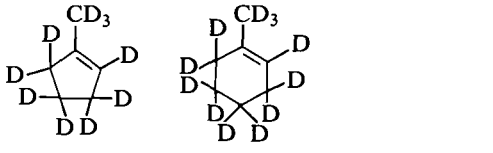

5 **6**

Results and discussion

*H–D exchange of 1-methylcyclopentene (1*a*)*

When **1***a* was treated under HTDA conditions using non-deuteriated medium (entry 1, Table 1), the major product was identified as **1***a* by its ^{1}Hmr spectrum. The ^{1}Hmr spectrum of the minor component indicated that it was a mixture of 3-methyl- and 4-methylcyclopentene (7). Under similar conditions in deuteriated medium (entry 2), **1***a* incorporates 6.03 D atoms per molecule (0.4% d_0, 0.5% d_1, 0.7% d_2, 1.2% d_3, 3.5% d_4, 15.2% d_5, 57.0% d_6, 11.5% d_7, 6.9% d_8, 2.7% d_9, and 0.5% d_{10} species). The ^{2}Hmr spectrum (Fig. 1a) showed three signals at δ 1.68 (CD_3), δ 2.17 (D-5), and δ 5.28 (D-2) and shoulders at δ 1.81 and δ 2.24 that correspond to small amounts of deuterium at C-4 and C-3, respectively. Confirmation of the deuterium distribution was obtained from the ^{1}Hmr spectrum that exhibited signals at δ 1.81 (bt, H-4), δ 2.24 (bt, H-3) and weak signals (<5%) due to residual protons at the other locations. This pattern of deuterium incorporation indicates that initial electrophilic attack by D_3O^+ occurs at C-2 to yield a tertiary cation and elimination of a proton from the methyl, C-2, or C-6 results in preferential H–D exchange at these three positions. The methyl group acts as an "anchor" for the double bond and thereby for the exchange. When a larger scale reaction was carried out (see Experimental), **1***b* was obtained in 79.6% yield by distillation from the decalin layer. It should be a simple matter to scale up the reaction even further. At 210°C (entry 3) full equilibration of the hydrogens with the deuterium pool was achieved and 9.43 D atoms per molecule (0.4% d_6, 2.2% d_7, 9.1% d_8, 30.4% d_9, 57.9% d_{10} species) are incorporated, but only 64.6% of perdeuteriated 1-methylcyclopentene (**5**) remained.

*H–D exchange of 1-methylcyclohexene 2*a

1-Methylcyclohexene, under the same conditions as **1***a*, reacts in a similar fashion (entry 4) and **2***a* is the major product as identified by its ^{1}Hmr spectrum. Although the minor products were not identified it is likely that they are identical to the products obtained from the exchange and rearrangement of cycloheptene (7) where the 1-methylcyclohexyl cation is an intermediate. When **2***a* was heated in deuteriated medium (entry 5), 5.82 D atoms (0.4% d_2, 0.6% d_3, 3.0% d_4, 17.5% d_5, 72.5% d_6, 3.3% d_7, 2.1% d_8, 0.5% d_9 species) were incorporated. The pattern of incorporation observed for **1***a* is seen in the ^{2}Hmr (δ 1.62, CD_3; δ 1.89, D-6; δ 5.40, D-2) (Fig. 1b) and ^{1}Hmr (δ 1.58, 4H, m, H-4 and H-5; δ 1.96, 2H, t, H-3) spectra. When a larger scale reaction was run (see Experimental), **2***b* (85%) was isolated as a mixture with lower-boiling isomers (15%) in 72% yield by distillation from the decalin layer. To obtain pure **2***b*, a preparative gc separation or a spinning band distillation would be required. At 210°C (entry

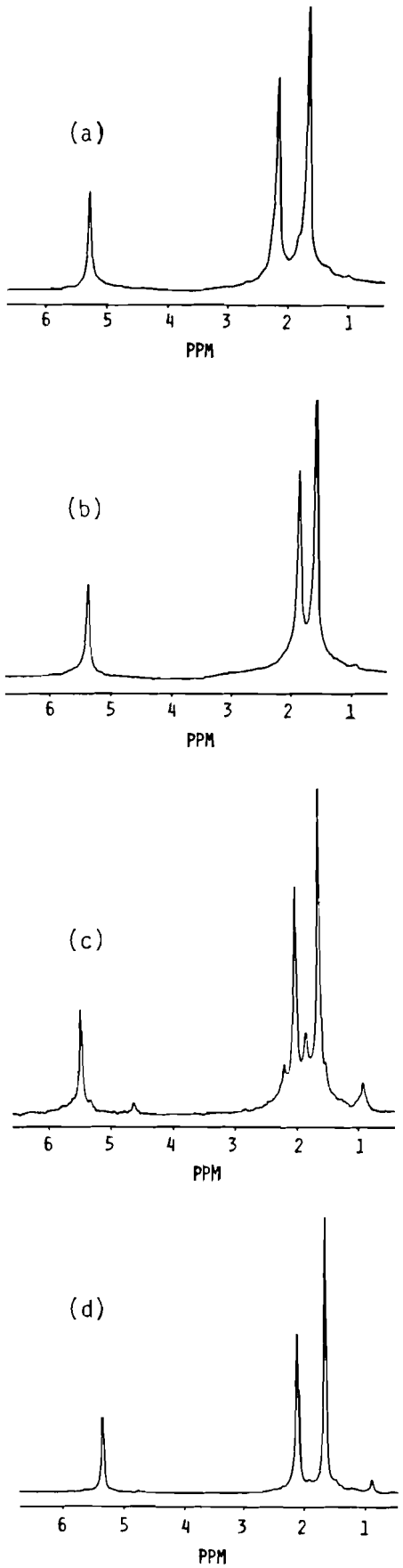

FIG. 1. The ^{2}Hmr (38.4 MHz, CCl_4) spectra of 1-methylcyclopentene-$d_{6.03}$ (a), 1-methylcyclohexene-$d_{5.82}$ (b), 1-methylcycloheptene-$d_{6.13}$ (c), and 1-methylcyclooctene-$d_{6.23}$ (d).

6), **2***a* is essentially equilibrated with the deuterium pool and 11.2 D atoms are incorporated per molecule (0.3% d_6, 0.9% d_7, 1.4% d_8, 4.1% d_9, 13.3% d_{10}, 34.1% d_{11}, and 45.9% d_{12} species) and by gc analysis it was established that **2***b* made up 62.4% of the product.

H–D exchange of 1-methylcycloheptane (3a)

Exchange of **3***a* at 162°C resulted in some rearrangement (entry 7), but the specifically deuteriated substrate was the major product. In this case, commercially supplied **3***a* used in the experiments was found to contain a major impurity (14%) of slightly longer retention time than **3***a* on the analytical gc. Because the boiling points were so similar, attempts to purify **3***a*, even by preparative gc, failed and the mixture was used in these exchange studies. Mass spectral analysis of the major product isolated from the reaction described in entry 7 established that 6.13 D atoms were incorporated per molecule. That the d_6 species (3.3% d_4, 14.6% d_5, 59.6% d_6, 5.1% d_7, 10.1% d_8, 2.0% d_9, 4.3% d_{10}) is the major component indicates that exchange of **3***a* is highly selective. The ^{2}Hmr spectrum (Fig. 1c) shows peaks at δ 5.52 (~1D, D-2), δ 2.05 (~2D, D-7), and δ 1.66 (~3D, CD_3) expected on the basis of the ^{1}Hmr if exchange occurs selectively at C-2, C-7, and the methyl group. The other peaks that make up 15–20% of the ^{2}Hmr signals are assumed to be due to the impurity in the starting material. Loss of the signals in the ^{1}Hmr of **3***b* at the shift positions listed confirms the presence of deuterium at these locations and corroborates our assignment.

H–D exchange of 1-methylcyclooctene (4a)

At 162°C (entry 8) **4***a* underwent some rearrangement, but the selectively deuteriated cycloalkene **4***b* was the major product. Mass spectral analysis of **4***b* (1.5% d_4, 11.6% d_5, 68.4% d_6, 7.7% d_7, 6.1% d_8, 2.0% d_9, 1.8% d_{10}, 0.8% d_{11}), isolated by preparative gc, showed that 6.23 D atoms were incorporated into **4***a*. The ^{1}Hmr showed the loss of signals at δ 5.28 (H-2), δ 2.07 (H-7), and δ 1.63 (CH_3). The ^{2}Hmr spectrum (Fig. 1d) confirms the location of the deuterium with the signals located at δ 5.47, δ 2.01, and δ 1.66.

Conclusions

This establishes that the modified HTDA method provides an easy route to specifically deuteriated 1-trideuteriomethylcycloalkenes **1***b*, **2***b*, **3***b*, and **4***b*, as well as the perdeuteriated analogues **5** and **6**. Since the methyl group is an effective "anchor" for the double bond in these systems, we expect that other groups (ethyl, phenyl, etc.) will exhibit this effect as well.

Experimental

Analyses were carried out on a Tracor model 560 chromatograph equipped with a Varian Areograph model 485 electronic integrator using 6 ft × 4 mm id 3% OV-1 on 100–120 mesh Supelcoport and 30 ft × 1/8 in. 23% SP-1700 on 80–100 mesh Chromosorb PAW columns. Preparative collections were performed on a Varian A-700 gas chromatograph equipped with a 5 ft × 1/4 in. 15% SE-30 on 80–100 mesh Chromosorb W column. Products were characterized by ^{1}Hmr spectroscopy. Deuterium analyses were carried out on a VG Micromass 7070F mass spectrometer at low ionizing voltage (12–15 eV).

H–D exchange of cycloalkenes

In a typical reaction, **1***a* (0.20 g), 0.26 *M* HCl/H_2O or 0.26 *M* DCl/D_2O (5 mL), and decalin (1 mL) were sealed under vacuum in a medium-walled Pyrex tube after the solution was degassed via three freeze–pump–thaw cycles. The tube was heated in a 600-mL Parr pressure vessel containing water to equalize the pressure. Mixing was

TABLE 1. H–D exchange of 1-methylcycloalkenes

Entry	Substrate	Conditions	Relative percent yields	Excess D atoms per molecule
1	**1***a*	H, 178°C, 14 h	Other(6.5), **1***a*(91.6), other(1.9)	
2	**1***a*	D, 172°C, 17 h	Other(1.9), **1***b*(87.0),	**1***b*, 6.03
3	**1***a*	D, 210°C, 15 h	Other(9.2), **1***c*(64.6), other(3 components, 26.3)	**5**, 9.43
4	**2***a*	H, 178°C, 14 h	Other(6.7), **2***a*(91.5), other(1.7)	
5	**2***a*	D, 172°C, 17 h	Other(11.1), **2***b*(88.0), other(0.9)	**2***b*, 5.82
6	**2***a*	D, 210°C, 15 h	Other(3 components, 30.6) **2***c*(62.4), other(6, 9)	**6**, 11.2
7	**3***a*	D, 154°C, 18 h	Other(2 components, 17.3) **3***b*(82.7)	**3***b*, 6.13
8	**4***a*	D, 162°C, 15 h	Other(3 components, 18.0) **4***b*(81.8)	**4***b*, 6.23

[a]H indicates 0.26 *M* HCl/H_2O and D indicates 0.26 *M* DCl/D_2O. The temperature was controlled to ±3°.

[b]The products are listed in order of increasing gc retention time.

accomplished by a rocking motion of the vessel. The tube was cooled, opened, the decalin layer was withdrawn, analyzed by analytical gc, and the products isolated by preparative gc. The results of studies on **1***a*, **2***a*, **3***a*, and **4***a* are given in Table 1.

Preparation of deuteriated 1-methylcyclopentene

Two tubes prepared in the usual manner, each containing **1***a* (0.32 g), decalin (1.6 mL), and 0.26 *M* DCl/D_2O (8 mL), were heated at 142°C for 18.5 h in the Parr vessel. The tubes were cooled, opened, and the deuteriated cyclopentenes (0.55 g, 79.6%) were isolated from the decalin using a short-path distillation apparatus. Analytical gc analysis showed that the product consisted of 92% **1***b*, and 8% of the 3-methyl and 4-methyl isomers. Mass spectral analysis established that the cycloalkenes consisted of 0.1% d_4, 17.0% d_5, 76.5% d_6, 4.6% d_7, 1.3% d_8, and 0.5% d_9 species over natural abundance corresponding to an incorporation of 5.91 D atoms per molecule; ^{2}Hmr δ 5.28, δ 2.18, δ 1.68.

Preparation of specifically deuteriated 1-methylcyclohexene

Three tubes each, containing **2***a* (0.32 g), decalin (1.6 mL), and 0.26 *M* DCl/D_2O (8 mL), were heated at 160°C for 19 h in the Parr vessel. The tubes were opened and the deuteriated cyclohexenes (0.73 g, 72%) were isolated from the combined decalin layers by distillation through a 10-cm Vigreux column at atmospheric pressure into a Dry Ice cooled receiver. Analytical gc analysis showed that the product consisted of 75.9% **2***b* and another component (24.1%) of shorter retention time; ms: 0.2% d_3, 1.0% d_4, 11.4% d_5, 55.8% d_6, 9.1% d_7, 7.7% d_8, 6.0% d_9, 5.0% d_{10}, 2.9% d_{11}, 0.9% d_{12} species (6.60 D atoms per molecule); ^{2}Hmr δ 5.37, δ 1.86, δ 1.59.

Acknowledgements

We thank the Natural Sciences and Engineering Research Council of Canada for financial support. We are indebted to Mr. B. Sayer for obtaining the ^{2}Hmr spectra.

1. N. H. WERSTIUK and T. KADAI. Can. J. Chem. **51**, 1485 (1973).
2. N. H. WERSTIUK and T. KADAI. Can. J. Chem. **52**, 2169 (1974).
3. N. H. WERSTIUK and T. KADAI. U.S. Patent No. 3, 989, 705 (1976).
4. N. H. WERSTIUK and T. KADAI. Canadian Patent No. 1048556 (1979).
5. N. H. WERSTIUK and G. TIMMINS. Can. J. Chem. **59**, 1022 (1981).
6. N. H. WERSTIUK and G. TIMMINS. Can. J. Chem. **59**, 3218 (1981).
7. N. H. WERSTIUK and G. TIMMINS. Can. J. Chem. **63**, 530 (1985).
8. N. H. WERSTIUK. *In* Isotopes in physical and biomedical sciences. *Edited by* J. R. Jones and E. Buncel. Elsevier, New York. In press.

Open chain nitrogen compounds. Part XI.[1] 3,7-Bis(arylazo)-1,3,5,7-tetraazabicyclo[3,3,1]nonanes: the reaction of diazonium ions with ammonia–formaldehyde mixtures

ROBERT D. SINGER AND KEITH VAUGHAN[2]
Department of Chemistry, Saint Mary's University, Halifax, N.S., Canada B3H 3C3

AND

DONALD L. HOOPER
Department of Chemistry, Dalhousie University, Halifax, N.S., Canada B3H 3J5

Received August 6, 1985[3]

ROBERT D. SINGER, KEITH VAUGHAN, and DONALD L. HOOPER. Can. J. Chem. **64**, 1567 (1986).

Reaction of a series of diazonium salts with either hexamine or an aqueous mixture of ammonia–formaldehyde affords 3,7-bis(arylazo)-1,3,5,7-tetraazabicyclo[3,3,1]nonanes; several new examples of this novel class of bicycloheterocycle have been prepared and characterized. Analysis of the low-temperature nmr spectra of one compound in this series shows that the bicyclic system prefers the chair–chair conformation. The bis(arylazo)tetraazabicyclononanes, which are surprisingly stable in aqueous buffer compared to analogous triazenes of open-chain structure, do undergo slow decomposition at slightly acidic pH in an acetone–buffer mixture. The apparent product of this decomposition is the arylamine, which is observed as the Mannich condensation product, $ArNH.CH_2CH_2COCH_3$.

ROBERT D. SINGER, KEITH VAUGHAN et DONALD L. HOOPER. Can. J. Chem. **64**, 1567 (1986).

La réaction d'une série de sels de diazonium, soit avec de l'hexamine ou avec une solution aqueuse d'ammoniac et de formaldéhyde, conduit aux bis (arylazo)-3,7 tétraaza-1,3,5,7 bicyclo[3.3.1]nonanes; on a ainsi préparé et caractérisé plusieurs nouveaux composés de cette nouvelle classe d'hétérocycles bicycliques. L'analyse du spectre rmn, déterminé à basse température, de l'un des composés de cette série permet de démontrer que le système bicyclique existe d'une façon préférentielle dans la conformation chaise–chaise. Par comparaison avec les triazènes analogues en chaînes ouvertes, la stabilité des bis(arylazo) tétraazabicyclononanes dans des solutions aqueuses de tampons est surprenante; dans des solutions légèrement acides, dans un tampon dans de l'acétone, ils subissent toutefois une décomposition lente. Le produit apparent de cette décomposition est l'arylamine qui est observée sous la forme de produit de condensation de Mannich, $ArNH.CH_2CH_2COCH_3$.
[Traduit par la revue]

Introduction

The reaction of diazonium salt solutions with ammonia–formaldehyde mixtures is of interest to us for several reasons. Firstly, the expected 1:1:1 coupling product would be the novel monomethyloltriazene, **1***a*, which would be a new type of triazene and is the analogue of the previously reported (1) *N*-methyl-*N*-hydroxymethyltriazenes **1***b*. Stable hydroxymethyltriazenes of type **1***b* have been reported as the products of diazonium coupling of methylamine–formaldehyde mixtures (2, 3), and have been shown to have significant anti-tumour activity against mouse tumour models in vivo (4). Consequently, the extension of these diazonium coupling reactions to ammonia–formaldehyde mixtures might be expected to afford triazenes of type **1***a*, which should themselves have interesting biological properties. A particular biological significance attached to structure **1***a* is the possibility that a triazene of this type might be a metabolite of the cytotoxic 1-aryl-3-methyltriazene, $ArN{=}N{-}NHCH_3$; it has been shown that such a triazene undergoes metabolism under in vitro microsomal incubation (5), but free formaldehyde could not be detected (6).

Furthermore, it has been reported (7, 8) that diazonium coupling with hexamethylenetetramine (the condensation product of ammonia and formaldehyde) affords the bisarylazotetraazabicyclononanes (**2**). These bicyclic heterocycles are close structural analogues of the bis(triazenylmethyl)methylamines (**3**) (3, 9), which can also be obtained from diazonium coupling with methylamine–formaldehyde mixtures under appropriate conditions. We were interested to prepare the

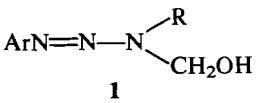

1
a R = H
b R = Me

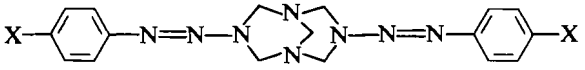

2
a X = Cl
b X = Br
c X = CN
d X = NO_2
e X = CO_2Et
f X = $CONH_2$
g X = $COCH_3$

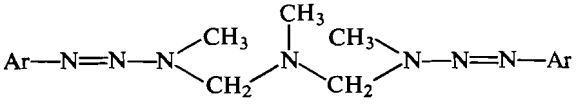

3 *a* Ar = *p*-Br.C_6H_4—

bicyclic heterocycles **2**, to compare their solution chemistry with that of the bis-triazenes **3** and also to determine if the diazonium coupling with ammonia–formaldehyde could be persuaded to follow a pathway to triazenes of type **1***a* rather than of type **2**.

Results and discussion

Reaction of *p*-cyanobenzenediazonium chloride with hexamethylenetetramine (HMT) afforded a high yield of the

[1]For part X see Can. J. Chem. **64**, 799 (1986).
[2]Author to whom correspondence may be addressed.
[3]Revision received February 26th, 1986.

TABLE 1*a*. Yields and physical and spectroscopic data of the 3,7-bis(arylazo)-1,3,5,7-tetraazabicyclo[3,3,1]nonanes[a]

Compound no.	X	Method	Yield (%)	Melting point (°C)	Solvent	Ultraviolet λ_{max} (nm) (ε)	Infrared (cm^{-1})
2*a*	Cl	A	38	166–168	Ethanol		1580(w)
2*b*	Br	A	38	187–190.5	Ethanol	287 (29 095)	1580(w)
2*c*	CN	A B	46 90	254–255	Ethanol/DMSO	302 (34 643)	2220 1600
2*d*	NO_2	A	60	281–283.5[b]	DMSO	348 (29 326)	1605 1595 1510 1340
2*e*	CO_2Et	A	73	185–186	Ethanol	304 (33 059)	1710 1615
2*f*	$CONH_2$	A	52	282–285	$DMSO/CHCl_3$		3460 3400 3170 1635 1600
2*g*	$COCH_3$	A	73	222.5–225.5	Ethanol	306 (24 270)	1675 1600

[a]See Table 1*b* for elemental analysis and Tables 2 and 3 for nmr data.
[b]Literature (7) mp 244°C.

TABLE 1*b*. Elemental analysis of 3,7-bis(arylazo)-1,3,5,7-tetraazabicyclo[3,3,1]nonanes (**2**)

Compound no.	X	Formula	Calculated (%)				Found (%)			
			C	H	N	X	C	H	N	X
2*a*	Cl	$C_{17}H_{18}N_8Cl_2$	50.4	4.4	27.7	17.5	50.5	4.5	27.6	16.9
2*b*	Br	$C_{17}H_{18}N_8Br_2$	41.3	3.6	22.7	32.4	41.3	3.7	22.4	31.9
2*c*	CN	$C_{19}H_{18}N_{10}$	59.1	4.7	36.3	—	59.2	4.7	36.0	—
2*d*	NO_2	$C_{17}H_{18}N_{10}O_4$	47.9	4.2	32.9	—	47.5	4.3	32.2	—
2*e*	$CO_2C_2H_5$	$C_{23}H_{28}N_8O_4$	57.5	5.8	23.3	—	57.2	5.8	23.2	—
2*g*	$COCH_3$	$C_{21}H_{24}N_8O_2$	60.0	5.7	26.7	—	60.1	5.8	26.7	—

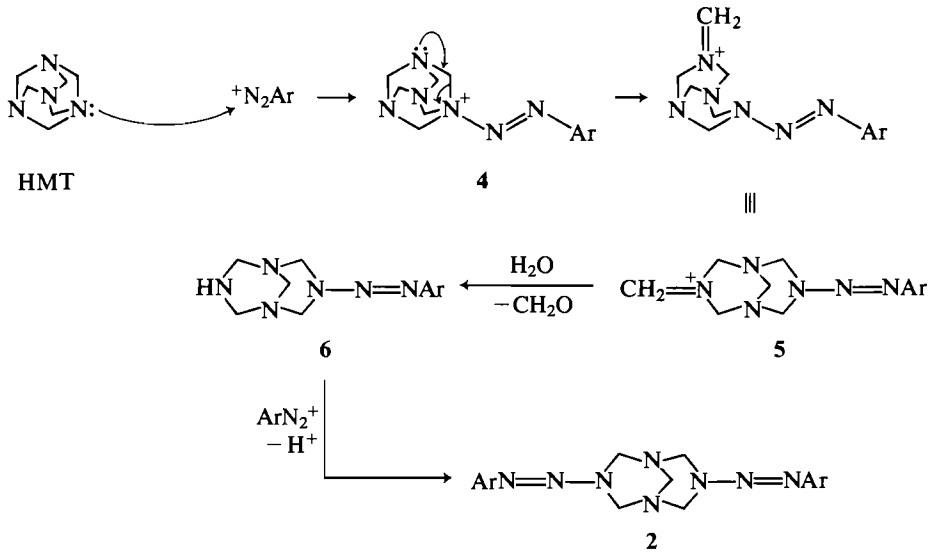

SCHEME 1

TABLE 2. The ^1H nmr spectra of the bis(arylazo)tetraazabicyclononanes (**2**) in $CDCl_3$

Compound no.	X	δ (ppm) X	N—CH_2—N (bridging)	N—CH_2—N (non-bridging)	Aromatic AA'BB'
2*a*	Cl[a]	—	4.40(2H, s)	4.6(1H, br) 4.8(3H, br) 5.4(4H, br)	7.05 (8H)
2*b*	Br[a]	—	4.38(2H, s)	4.8(4H, br) 5.4(4H, br)	7.0 (8H)
2*c*	CN[b]	—	4.45(2H, s)	4.50(2H, br) 5.10(2H, br) 5.18(2H, br) 6.02(2H, br)	7.17 7.19 7.37 7.39 } (8H)
2*e*	CO_2Et[b]	1.37(6H, t, J = 7.1 Hz) 4.31(4H, q, J = 7.1 Hz)	4.13(2H, s)	4.47(2H, br) 5.15(4H, br) 6.05(2H, br)	7.13 7.15 7.73 7.75 } (8H)
2*f*	$CONH_2$[a]	—	4.40(2H, s)	4.8(4H, br) 5.3(4H, br)	7.0–7.7 (8H)
2*g*	$COCH_3$[a]	2.5(6H, s)	4.40(2H, s)	5.0(8H, very broad)	7.1–7.6 (8H)

[a]60 MHz.
[b]360 MHz.

bis(arylazo)tetraazabicyclononane **2***c*, which was also obtained, in lesser yield, by reaction of the diazonium salt with varying composition mixtures of ammonia and formaldehyde. The optimum ratio of ArN_2^+:NH_3:CH_2O for maximum yield of **2***c* was observed to be 1:2:10 and these proportions were used to prepare the other bis(arylazo)tetraazabicyclononanes (**2***a*, *b*, *d*–*g*). Percentage yields are shown in Table 1*a*. These bicyclic heterocycles were characterized by ir, nmr, mass spectra, and elemental analysis.

The mass spectrum of the *p*-cyano derivative **2***c* shows a molecular ion at m/z 386, consistent with the bis(arylazo)tetraazabicyclononane structure. Principal fragments occur at m/z 130 (p-$NC.C_6H_4N_2^+$) and 256, arising from cleavage of the triazene moiety at the N2—N3 bond, and at m/z 358, due to loss of N_2 from the molecular ion. The ethyl ester analogue **2***e* was also characterized by mass spectroscopy, giving the expected molecular ion at m/z 480.

The formation of the bis(arylazo)heterocycles **2** from the ammonia–formaldehyde diazonium coupling suggests that the predominant species in the NH_3–CH_2O solution is HMT. A reasonable mechanism for the conversion HMT → **2** is shown in Scheme 1. Attachment of the electrophilic diazonium ion at one of the four equivalent nitrogen atoms of HMT affords the triazenium ion **4** and initiates ring cleavage, typical of an aminal (10), to give the iminium ion **5**. Hydrolysis of **5** and loss of formaldehyde leads to the mono(arylazo)tetraazabicyclononane **6**; further diazonium coupling to the secondary amino position of **6** gives the observed product (**2**). The apparent reluctance of **2** to undergo further diazo coupling at the bridgehead nitrogen atoms may simply be a consequence of the insolubility of **2** in the aqueous medium.

Formation of a triazene of type **1***a* requires diazonium coupling to the carbinolamine, NH_2CH_2OH, the 1:1 condensation product of ammonia and formaldehyde, which is recognized to be an intermediate in the formation of HMT from ammonia and formaldehyde (11). Accordingly, we investigated the reaction of *p*-cyanobenzenediazonium cation with NH_3:CH_2O mixtures ranging in composition from 2:1 to 1:10. The higher ratio of NH_3:CH_2O did result in lower yield of the HMT-derived product **2***c*, but we could find no spectroscopic evidence for formation of the monohydroxymethyltriazene **1***a* in any of the reaction mixtures. Furthermore, none of these reaction mixtures contained even trace amounts of the aniline (p-$NC.C_6H_4.NH_2$), which would be the most likely degradation product to arise from decomposition of **1***a*. If **1***a* is formed under these conditions, we must assume that it does not survive the reaction conditions or work-up, and undergoes further condensation with NH_3–CH_2O to give a product of type **2**.

Examination of the nmr spectra of the bis(arylazo)tetraazabicyclononanes **2** reveals the nature of the conformational structure of these fused saturated bicyclic heterocycles. The possible conformations for a tetraazabicyclo[3,3,1]nonane system are chair–chair, chair–boat, and boat–boat. Not surprisingly, the preferred conformation in a majority of cases is the chair–chair, but the introduction of bulky substituents at positions 3 and 7 results in preference for the chair–boat conformation (12).

The ^1H nmr spectra of the bis(arylazo)tetraazabicyclononanes **2** (Table 2) show considerable broadening of several signals. For example, in the spectrum of **2***c*, the higher-field portion of the aromatic AA'BB' system is slightly broadened, and all but one of the ring N-methylene signals are severely broadened. Similar broadening of N—CH_2 signals is observed in the ^1H nmr spectrum of the ethyl ester analogue **2***e*, although two of the broad signals overlap at δ 5.15 (compare **2***c*, which has broad signals resolved at δ 5.10 and 5.18). The equilibrium process responsible for this broadening also causes broadening of some signals in the ^{13}C nmr spectrum of **2***e* (Table 3); consistent with the ^1H nmr spectrum of **2***e*, one of the N—CH_2—N signals is sharp (δ 69.9), whereas those at δ 63.7 and 72.1 are broad.

The structure of **2***e* and the nature of the equilibrium process

TABLE 3. The ^{13}C nmr signals in the spectrum of 3,7-bis(*p*-ethoxycarbonylphenylazo)-1,3,5,7-tetraazabicyclo[3,3,1]nonane (**2***e*) in $CDCl_3$

δ (ppm)	Assignment
14.3	CH_3
60.6	$O—CH_2$
63.7 (br)	$N—CH_2—N$ (non-bridging)
69.9	$N—CH_2—N$ (bridging)
72.1 (br)	$N—CH_2—N$ (non-bridging)
120.2	aromatic *C*H
127.7	aromatic *C* (adj. to C=O)
130.1	aromatic *C*H
153.0	aromatic *C* (adj. to N=N)
166.2	*C*=O

responsible for nmr line-broadening is revealed by an analysis of the ^1H and ^{13}C nmr spectra at low temperatures (−58°C). The broad signals in the ^{13}C spectrum at δ 63.7 and 72.1 split into two sets of two singlets at δ 62.86/72.27 and 63.59/71.68, of unequal intensity. The aromatic signals at δ 127.7, 130.1, and 153.0 are also split, each into two signals of unequal intensity, in the low temperature spectrum. The unequal intensity of these sets suggests that the low temperature system is a mixture of two nonequivalent thermodynamically distinguishable isomers. The only consistent interpretation of these observations is that the components of the mixture are the *syn* and *anti* forms of the chair–chair conformation, **7***a* and **7***b* respectively, which are essentially the rotamers arising from restricted rotation around the N2′—N3′ bond of the triazene moiety (13).[4] The major rotamer, presumably **7***b*, is responsible for the more intense set of signals at δ 62.86 and 72.27; on the basis of the proximity of the ring carbons to the electron lone pairs on the central nitrogens of the triazene unit, we can assign the low-field signal at δ 62.86 to the more deshielded equivalent carbons 2 and 6, and the high-field signal at δ 72.27 to carbons 4 and 8 in structure **7***b*. Similarly the signal at δ 63.59 is assigned to the equivalent carbons 2 and 8 and at δ 71.68 to carbons 4 and 6 in the minor rotamer **7***a*. The signal at δ 69.9, assigned to the bridging methylene group (C-9), is not distinguishable in the two rotamers, presumably because it is sufficiently far removed from the site of rotamerism.

The low temperature ^1H nmr spectrum of **2***e* confirms this interpretation. The aromatic signals resolve into two closely spaced sets of AA′BB′ systems, and the $O—CH_2$ group resolves into two closely spaced quartets, but the resolution of the signals in the N-methylene region provides unequivocal evidence for the proposed structures **7***a* and **7***b*. The bridging methylene (C-9) protons resolve into two singlets, at δ 4.5 for the major rotamer (**7***b*) and at δ 4.48 in **7***a*. This observation is clearly inconsistent with a chair–boat conformation, in which the protons at C-9 would be nonequivalent and give rise to one or more AB patterns. The remaining methylene protons of **7***b* separate into two quite different AB patterns, one with a large chemical shift difference (δ 6.10, 6.06, 4.54, and 4.50), the

[4]A much less likely interpretation would be similar rotamers of the boat–boat molecular conformation. It has recently been shown for the analogous 3,7-diazabicyclo[3,3,1]nonane that substituents such as nitroso or ethoxycarbonyl attached to the 3- and 7-nitrogens confer sp^2 hybridization character on these nitrogens. The geometry at these nitrogens is planar and the preferred conformation adopted is the "twin-chair" (15).

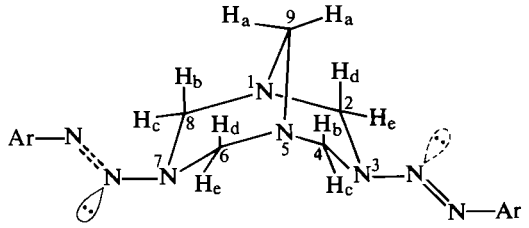

anti **7***b*

(Ar = *p*-$EtO_2C.C_6H_4$−)

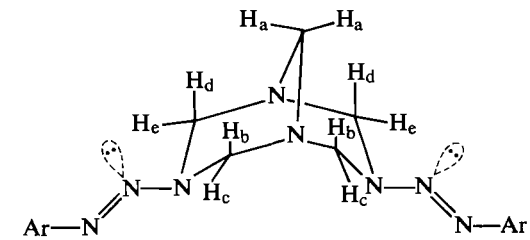

syn **7***a*

other with a small chemical shift difference (δ 5.19, 5.15, 5.13, and 5.09). The minor rotamer **7***a* also gives two distinguishable AB patterns from the N-methylene protons at carbons 2, 4, 6, and 8: δ 6.04, 6.00, 4.47, and 4.43, and δ 5.30, 5.26, 5.22, and 5.18. These observations are consistent with the equivalence of positions 4 with 8 and 2 with 6 in structure **7***b*, and of positions 2 with 8 and 4 with 6 in structure **7***a*, and thus confirms the conformational assignments.

These conclusions are consistent with the observations of Stefaniak *et al.* (8) with the analogous 3,7-bis(nitroso)- and 3,7-bis(acetyl)-1,3,5,7-tetraazabicyclo[3,3,1]nonanes, which exist as similar *syn* and *anti* isomers. However, the broadening of the signals from the ring methylene protons in 3,7-bis(arylazo) analogues was incorrectly presumed by them to arise from quadrapolar relaxation induced by the nitrogen nuclei in the 3,7 substituents (8).

In view of the close structural similarity of the tetraazabicyclononanes **2** to the previously reported (9) bis-triazenes **3**, it was of interest to us to compare the aqueous solution chemistry of these molecules. We have shown that bis-triazenes undergo facile hydrolysis in phosphate buffer (with 1.7% DMSO) at pH 7.5 to give the corresponding arylamine, via the intermediate 1-aryl-3-methyltriazene, ArN=N.NHMe; for example, the *p*-bromophenyl-bistriazene (**3***a*) decays with a half-life of 12.0 min at a pH 7.5 (13). This ease of decomposition has been attributed to the aminal character of the bis-triazene (14). The *p*-bromo- and *p*-ethoxycarbonylphenyl-tetraazabicyclononanes (**2***b* and **2***e*) were hydrolysed in pH 7.5 phosphate buffer under identical conditions to those used in the hydrolysis of **3***a*; surprisingly **2***b* and **2***e* were found to be stable under these conditions. No change in the uv spectrum of either substrate was seen over a 24-h period.

The ethyl ester **2***e* was also found to be stable in (*a*) a 4:1 (v/v) acetone–water mixture at 37°C, (*b*) acetone – pH 7.5 phosphate buffer at 37°C, and (*c*) refluxing ethanol. Slow decomposition of **2***e* was evident when dissolved in a mixture of acetone – phosphate buffer and the pH adjusted to 4.5. However, even after 20 h under these conditions some starting material remained. The reaction in acetone – pH 4.5 buffer was accelerated by refluxing for 5 h and afforded an identifiable product, the β-anilino-butanone (**8**).

Characterization of **8** is based on ir, nmr, and mass spectral

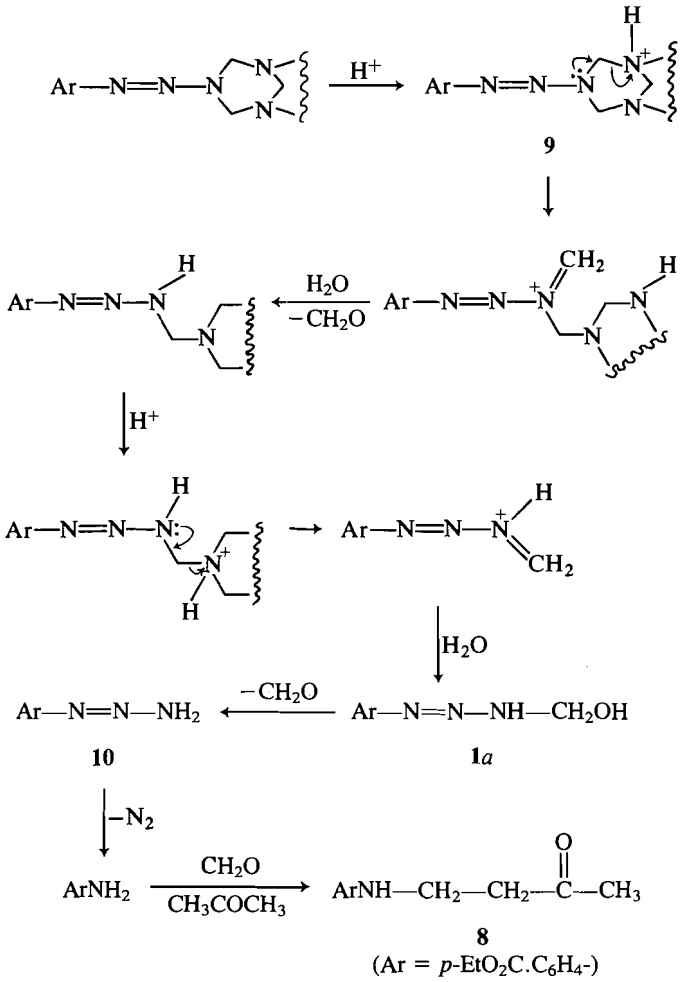

SCHEME 2

data, and on comparison with an authentic sample.[5] The formation of the ketone **8** from **2***e* must derive from hydrolysis of **2***e* to the aniline (ethyl *p*-aminobenzoate), which could then condense by a Mannich reaction with formaldehyde, released during hydrolysis, and acetone from the medium, eq. [1]:

$$[1]\quad ArNH_2 + CH_2O + CH_3{-}\overset{O}{\overset{\|}{C}}{-}CH_3 \xrightarrow{H^+} ArNHCH_2CH_2\overset{O}{\overset{\|}{C}}CH_3$$

The remaining question is the pathway of hydrolysis of **2***e* to the arylamine. A possible mechanism is shown in Scheme 2, in which the reaction is initiated by protonation at either N1 or N5 of **2** to give the cation **9**. Aminal type dissociation of **9** initiates a cascade of reactions resulting in formation of two moles of the elusive monohydroxymethyltriazene **1***a*. Loss of formaldehyde from **1***a* affords the unstable triazene **10**, which spontaneously loses nitrogen to afford the aniline.

The lower reactivity of **2** towards hydrolysis, compared to **1***a*, suggests weaker basic character of the N1 or N5 nitrogens in **2** compared to the analogous aminal nitrogen in the bis-triazene. The less basic character of these nitrogens could arise from the less exposed nature of the nitrogen lone pairs resulting from the constraints of the bicyclic system. The bonds around the analogous nitrogen in the bis-triazene **3** are much more mobile, giving more accessibility for protonation of the nitrogen lone pair.

Although we must conclude from this study that the 1-aryl-3-hydroxymethyltriazene **1***a* cannot be isolated from a 1:1:1 coupling reaction of the diazonium cation, ammonia, and formaldehyde, the possible intermediacy of **1***a* in the hydrolysis of **2** offers some encouragement that compounds of type **2** may be useful as "pro-drugs" for this hydroxymethyltriazene (**1***a*). Thus it is reasonable to assume that the bis(arylazo)tetraazabicyclononanes **2** may have useful biological properties; this is presently under investigation.

Experimental

Melting points were recorded with a Kofler hot-stage melting point apparatus and are uncorrected. Infrared spectra were recorded in Nujol mulls with Perkin Elmer 299 and 1300 spectrophotometers. The uv spectra were recorded with a Unicam SP8-400 uv–visible spectrophotometer, and nmr spectra were recorded with a Varian EM360 (60 MHz) or a Nicolet 360NB (360 MHz) spectrometer. Microanalyses were carried out by the Canadian Microanalytical Service, Vancouver, B.C.

3,7-Bis(arylazo)-1,3,5,7-tetraazabicyclo[3,3,1]nonanes (2)

General procedure

Method A. The arylamine (0.02 mol) was dissolved in 2 *M* hydrochloric acid (30 mL, 0.06 mol) and diazotized at 0°C with a solution of sodium nitrite (1.52 g, 0.022 mol) in water over a period of 1 h. The diazonium salt solution was filtered, if necessary, to remove turbidity and a mixture of concentrated ammonia (2.43 g, 0.04 mol) and 37% aqueous formaldehyde (16.17 g, 0.20 mol) was added slowly to the clear diazonium salt solution. After stirring for 0.25 h, the mixture was neutralized with saturated sodium bicarbonate, whereupon the product precipitated immediately. The precipitated triazene (**2**) was filtered, dried and recrystallized from an appropriate solvent. Yields and physical properties are given in Tables 1*a* and 1*b*.

Method B. In this slightly modified procedure, the diazonium salt (0.02 mol) was treated with a solution of hexamethylenetetramine (0.7 g) in water, the mixture neutralized with $NaHCO_3$ and worked up as described above.

4-(p-Ethoxycarbonylphenylamino)butan-2-one (8)

3,7-Bis(*p*-ethoxycarbonylphenylazo)-1,3,5,7-tetraazabicyclo[3,3,1]nonane (**2***e*) (70 mg) was dissolved in a mixture of acetone (25 mL) and phosphate buffer (5 mL, pH 7.5). The pH was adjusted to 4.5 by addition of 2 *M* hydrochloric acid (approximately 5 drops). The solution was refluxed for 5 h; the excess acetone was evaporated under vacuum, whereupon the product precipitated from the aqueous residue. Filtration, then washing with water and a little ethanol afforded the anilino-ketone **8** (30 mg, 87.5%), mp 95°C (from CH_2Cl_2); ir: 3370, 1710, and 1680 cm^{-1}; δ($CDCl_3$): 1.35(3H, t, *J* 7 Hz, CH_3), 2.16(3H, s, CH_3—CO), 2.75 (2H, t, *J* 6 Hz, CH_2—CO), 3.46(2H, t, *J* 6 Hz, N—CH_2), 4.30(3H, q + br s, O—CH_2 and NH), 6.48/6.59/7.80/7.91 (4H, m, AA′BB′, aromatic); M^+ 235, *m/z*: 192 ($EtO_2C.C_6H_4NHCH_2CH_2^+$), 190 ($M^+$ − OEt), 179 ($EtO_2C.C_6H_4NH{-}CH_3^+$), 178 ($EtO_2C.C_6H_4.NHCH_2^+$), 150 ($EtO_2C.C_6H_5^+$), 120 ($OC.C_6H_4.NH_2^+$).

Acknowledgements

The award of an NSERC Undergraduate Research Award (to R.D.S.) is gratefully acknowledged. Other financial assistance was provided by the Saint Mary's University Senate Research Committee. The authors are also grateful to the Atlantic Regional Magnetic Resonance centre, Dalhousie University, for the high-field nmr spectra. We also thank the Chemistry Department at Dalhousie University for the mass spectra.

[5]An authentic sample of **8** was prepared by a modified Mannich procedure. Ethyl *p*-aminobenzoate was refluxed with formaldehyde in acetone – pH 4.5 phosphate buffer for 24 h. Evaporation of the acetone and extraction with chloroform afforded, from the dry chloroform extract, a product identical with that obtained from reaction of **2***e* as described. The conventional Mannich procedure (Organic Syntheses, Coll. Vol. IV, p. 281) was too vigorous and afforded only a dark oil.

1. A. GESCHER, J. A. HICKMAN, R. J. SIMMONDS, M. F. G. STEVENS, and K. VAUGHAN. Tetrahedron Lett. 5041 (1978).
2. C. M. HEMENS, H. W. MANNING, K. VAUGHAN, R. J. LAFRANCE, and Y. TANG. Can. J. Chem. **62**, 741 (1984).
3. S. C. CHENG, M. L. DE S. FERNANDES, J. ILEY, and M. E. N. ROSA. J. Chem. Res. (S), 108 (1983).
4. K. VAUGHAN, Y. TANG, G. LLANOS, J. K. HORTON, R. J. SIMMONDS, J. A. HICKMAN, and M. F. G. STEVENS. J. Med. Chem. **27**, 357 (1984).
5. P. FARINA, A. GESCHER, J. A. HICKMAN, J. K. HORTON, M. D'INCALCI, D. ROSS, M. F. G. STEVENS, and L. TORTI. Biochem. Pharmacol. **31**, 1887 (1982).
6. J. R. P. GODIN, K. VAUGHAN, and K. W. RENTON. Can. J. Physiol. Pharmacol. **59**, 1234 (1981).
7. P. DUDEN and M. SCHARFF. Justus Liebigs Ann. Chem. **288**, 231 (1985).
8. L. STEFANIAK, T. URBANSKI, M. WITANOWSKI, A. R. FARMINER, and G. A. WEBB. Tetrahedron, **30**, 3775 (1974).
9. H. W. MANNING, C. M. HEMENS, R. J. LAFRANCE, Y. TANG, and K. VAUGHAN. Can. J. Chem. **62**, 749 (1984).
10. M. J. GIDLEY and J. K. M. SANDERS. J. Pharm. Pharmacol. **35**, 712 (1983).
11. H. H. RICHMOND, G. S. MYERS, and G. F. WRIGHT. J. Am. Chem. Soc. **70**, 3659 (1948).
12. S. K. BHATTACHARJEE and K. K. CHACKO. Tetrahedron, **35**, 1999 (1979).
13. M. H. AKHTAR, R. S. MCDANIEL, M. FESER, and A. C. OEHLSCHLAGER. Tetrahedron, **24**, 3899 (1968).
14. H. W. MANNING, L. M. CAMERON, R. J. LAFRANCE, K. VAUGHAN, and R. RAJARAMAN. Anti-Cancer Drug Design, **1**, 37 (1985).
15. P. H. MCCABE, N. J. MILNE, and G. A. SIM. J. Chem. Soc. Chem. Commun. 625 (1985).

Effect of geometry on the thermodynamic properties of micellar systems: trialkylamine oxides in water

GASTON CARON, NADIA GÉLINAS, AND JACQUES E. DESNOYERS[1]

Department of Chemistry, Université de Sherbrooke, Sherbrooke (Qué.), Canada J1K 2R1

Received January 3, 1986

GASTON CARON, NADIA GÉLINAS, and JACQUES E. DESNOYERS. Can. J. Chem. **64**, 1573 (1986).

The apparent molar volumes, heat capacities, relative enthalpies, and isentropic compressibilities of symmetrical trialkylamine oxides and cyclohexyldimethylamine oxide were measured in water at 25°C. The data were in most cases analyzed with a mass-action model which was previously developed (J. Phys. Chem. **87**, 1397 (1983)) for micellar systems. Trimethylamine oxide shows no sign of micellization while the three next members of this homologous series and cyclohexyldimethylamine oxide form aggregates with relatively low aggregation numbers. The thermodynamic data were compared with those of assymmetrical amine oxides to investigate the effect of geometry on the micellar properties. The thermodynamic properties of the solutes in the pre-micellar region show a very good group additivity which is independent of geometry. On the other hand, with symmetrical isomers, the CMCs are much larger, the aggregation numbers smaller and the thermodynamic functions of micellization larger. These geometrical factors can be taken advantage of for thermal energy storage.

GASTON CARON, NADIA GÉLINAS et JACQUES E. DESNOYERS. Can. J. Chem. **64**, 1573 (1986).

Les volumes, capacités calorifiques, enthalpies relatives et compressibilités isentropiques molaires apparents des oxydes de trialkylamines symétriques et du cyclohexyldiméthylamine ont été mesurés dans l'eau à 25°C. Les données ont été analysées, dans la plupart des cas, au moyen d'un modèle d'action de masse développé précédemment (J. Phys. Chem. **87**, 1397 (1983)) pour les systèmes micellaires. Il n'y a aucune évidence de micellisation dans le cas de l'oxyde de triméthylamine, alors que les trois prochains homologues ainsi que l'oxyde du cyclohexyldiméthylamine forment des aggrégats avec des nombres d'aggrégation relativement faibles. Les données thermodynamiques ont été comparées avec celles des oxydes d'amines symétriques pour étudier l'effet de la géométrie sur les propriétés micellaires. Les propriétés des solutés dans la région pré-micellaire démontrent en général une très bonne additivité de groupe, indépendante de la géométrie. Par contre, avec les isomères symétriques, les CMCs sont plus grandes, les nombres d'aggrégation plus petits et les fonctions thermodynamiques de micellisation plus grandes. Il est possible de prendre avantage de ces facteurs géométriques pour le stokage thermique de l'énergie.

Introduction

The solvation of hydrophobic solutes in water enhances the structure of water in the vicinity of the solute, and this is characterized by high apparent molar heat capacities (1). Even though the specific heat capacity of the pure additives is generally lower than that of pure water, these solute–solvent interactions may lead to an overall larger specific heat capacity of the solution relative to pure water. This phenomenon can in principle be exploited for thermal energy storage. Unfortunately, hydrophobic solutes often tend to micellize or undergo some microphase transitions in water, and these aggregation processes are accompanied by a large reduction in heat capacity. It would therefore be useful to investigate the conditions under which hydrophobic solutes can remain soluble in water up to relatively high concentrations and not undergo micellization.

It is well known that the geometry of hydrophobic solutes affects significantly their physical properties in water. For example, important differences are observed between *n*-butanol and *tert*-butanol (2). The differences are even more evident with tetraalkylammonium halides. Nonyltrimethylammonium bromide is a typical ionic surfactant with a critical micellar concentration (CMC) of 0.14 mol kg^{-1} (3). On the other hand, tetrapropylammonium bromide, which has the same formula weight, does not show any sign of association in water before 1.3 mol kg^{-1} (4).

For a better understanding of the geometrical factors, it is preferable to study nonionic systems where complications due to the charges are avoided. Alcohols are hydrophobic solute but their limited solubility in water prevents the study of the longer-chain homologs at high concentration where hydrophobic interactions and association are more pronounced. Amine oxides, on the other hand, are much more soluble in water, and recently the thermodynamic properties of alkyldimethylamine oxides were reported for alkyl chains up to decyl (5, 6). It was also shown that this homologous series was ideal for the testing of a mass-action model for micellization. The thermodynamic properties of the symmetrical trialkylamine oxides have not been investigated. This series could therefore be an appropriate one to investigate the influence of geometry of the solute on the thermodynamics of micellization. Cyclohexyldimethylamine oxide will also be investigated with some properties for the same purpose.

While our prime interest is in heat capacities, precise volume data are also required to convert the heat capacities per unit volume, obtained with a flow calorimeter, into specific heat capacities. Enthalpies are also useful to predict the equilibrium displacement contribution to heat capacities, and it is this contribution which causes the high heat capacities in the micellar region (6). Finally, it was felt that compressibilities could be informative on the influence of pressure on the system.

Experimental

The techniques used for the measurement of densities (7), heat capacities (8), enthalpies of dilution (9), and isentropic compressibilities (3) have all been described previously and are the same as the ones used for the long-chain amine oxides (5, 6) and alkylammonium bromides (3).

The symmetrical trialkylamine oxides (CX) and cyclohexyldimethylamine oxide (HC1) were prepared by the oxidation of the corresponding amine with hydrogen peroxide, as described previously for assymetrical amine oxides (6). The main difficulty encountered with the present amine oxides came from the difficulty, and often impossibility, of purification by recrystallization in view of the high hygroscopic nature of these substances.

[1]To whom correspondence should be sent at Institut National de la Recherche Scientifique, C.P. 7500, Ste-Foy (Qué.), Canada G1V 4C7.

TABLE 1. Volumes and heat capacities of trialkylamine oxides in water at 25°C

m (mol kg^{-1})	$10^3(d-d_0)$ (g cm^{-3})	$V_{2,\phi}$ (cm^3 mol^{-1})	$10^3(\sigma-\sigma_0)/\sigma_0$	$C_{P,2,\phi}$ (J K^{-1} mol^{-1})	m (mol kg^{-1})	$10^3(d-d_0)$ (g cm^{-3})	$V_{2,\phi}$ (cm^3 mol^{-1})	$10^3(\sigma-\sigma_0)/\sigma_0$	$C_{P,2,\phi}$ (J K^{-1} mol^{-1})
Cyclohexyldimethylamine oxyde					Triethylamine oxide				
0.0790	0.795	133.87	−1.404	466.67	0.0942	0.240	114.94	−1.115	428.97
0.1046	1.010	133.77	−1.921	463.66	0.1902	0.509	114.78	−2.080	431.61
0.3739	3.715	133.15	−6.688	460.45	0.2899	0.823	114.59	−3.283	428.58
0.6063	8.106	132.70	−10.691	457.53	0.3870	1.147	114.42	−4.542	425.58
1.0930	11.134	131.92	−18.421	453.48	0.4964	1.556	114.21	−5.509	426.89
1.5182	15.395	131.41	−25.329	448.49	0.6391	2.140	113.92	−7.004	425.59
2.1348	21.097	130.93	−36.866	438.15	0.7198	2.482	113.79	−7.916	424.42
2.7432	25.973	130.71	−51.256	424.01	0.8576	3.100	113.54	−9.279	423.54
3.6002	31.723	130.62	−77.148	398.96	0.9663	3.617	113.36	−10.416	422.40
4.1129	34.435	130.71	−94.209	384.32	1.1135	4.331	113.13	−12.053	420.50
4.7099	37.105	130.85	−114.689	368.21	1.3000	5.316	112.82	−14.090	418.20
5.2393	39.077	131.01	−132.894	355.07	1.7207	7.613	112.22	−19.351	411.61
6.0229	41.499	131.25	−157.470	339.77	2.0906	9.753	111.75	−24.653	406.13
6.9701	43.812	131.54	−192.514	326.33	2.4418	11.771	111.37	−29.708	399.45
7.8240	45.467	131.79	−205.713	315.40	2.8699	14.187	110.99	−37.135	391.22
					3.2767	16.372	110.69	−45.112	382.91
Trimethylamine oxide					3.5397	17.695	110.55	−50.476	377.79
0.2728	0.601	73.07	−8.07	178.53	4.0437	20.019	110.34	−61.341	368.19
0.5072	1.140	72.99	−14.84	177.27	4.8225	22.901	110.23	−79.665	353.69
0.7651	1.781	72.86	−22.13	176.00	5.4258	24.516	110.28	−95.639	341.92
1.0548	2.540	72.73	−30.10	174.64	6.0411	25.645	110.43	−111.608	331.58
1.3111	3.260	72.58	−36.99	173.40	6.9771	27.993	110.40		
1.5132	3.837	72.50	−42.36	172.32	7.8050	28.999	110.57		
1.8422	4.835	72.34	−50.95	170.49	9.0001	29.511	110.95		
2.2406	6.089	72.16	−61.09	168.37	10.6610	28.837	111.59		
2.2365	7.396	71.98	−70.25	167.49	12.1140	26.888	112.28		
3.0058	8.649	71.82	−79.38	165.13	14.8660	23.788	113.23		
3.5801	10.664	71.57	−92.84	162.18					
4.0970	12.521	71.36	−103.96	160.40	Tripropylamine oxide				
4.6067	14.357	71.17	−114.90	158.26	0.0908	−0.258	162.60	0.88	719.03
5.2120	16.551	70.96	−127.22	156.07	0.2010	−0.474	162.20	1.97	718.15
					0.3114	−0.592	161.75	3.11	717.86
Tributylamine oxide					0.3974	−0.637	161.46	3.98	717.28
0.1096	−0.852	209.95	3.89	1026.5	0.4985	−0.632	161.12	5.08	717.39
0.1441	−1.081	209.70	5.22	1029.8	0.6094	−0.589	160.81	6.19	716.65
0.1552	−1.150	209.64	5.63	1030.0	0.7845	−0.397	160.32	7.95	715.70
0.1956	−1.400	209.47	7.53	1035.8	0.9734	−0.094	159.85	9.81	714.73
0.2451	−1.684	209.21	9.34	1039.2	1.1420	0.235	159.50	10.90	711.75
0.2837	−1.873	208.99	11.26	1046.6	1.3972	0.781	159.05	11.91	706.29
0.3447	−2.175	208.75	13.75	1051.1	1.5852	1.196	158.79	11.49	699.57
0.3691	−2.276	208.63	14.99	1052.1	1.7973	1.653	158.55	10.50	692.05
0.5008	−2.822	208.21	21.85	1068.8	1.9832	1.934	158.45	8.58	684.00
0.5907	−3.161	207.99	26.62	1078.1	2.2626	2.359	158.32	4.46	670.87
0.6805	−3.520	207.89	31.15	1084.5	2.4808	2.569	158.29	−0.87	657.57
0.6940	−3.546	207.83	31.56	1083.4	2.5860	2.657	158.29	−3.33	651.99
0.7054	−3.604	207.84	32.24	1085.0	3.0292	2.581	158.47	−18.60	622.41
0.7741	−3.891	207.82	35.12	1086.0	3.5404	2.079	158.82	−38.32	591.20
0.8752	−4.331	207.83	38.69	1084.3	3.7711	1.568	159.07	−48.72	576.56
1.0212	−5.074	208.01	41.44	1072.2	5.1277	−2.327	160.57	−107.71	509.25
1.2119	−6.233	208.43	39.24	1037.9	5.9871	−5.504	161.56	−142.24	478.15
1.4884	−8.195	209.21	21.17	971.7	7.0579	−9.577	162.67	−181.60	447.21
1.7223	−10.040	209.93	11.50	912.7	9.8045	−19.446	164.95	−250.58	408.31
1.9016	−11.520	210.48	−2.49	869.4	11.8922	−25.648	166.19	−287.24	392.64
2.4617	−16.324	212.09	−46.51	763.7	15.1760	−34.011	167.72	−331.00	376.39
2.8874	−19.954	213.17	−79.15	703.4					
4.4905	−31.557	216.31	−179.22	573.2					
5.6728	−40.390	217.94	−232.09	526.4					

Cyclohexylamine was purchased from Eastman Kodak and cyclohexyldimethylamine was then synthesized by methylation of the primary amine as described by Clarke *et al.* (10).

Trimethylamine oxide (C1) was purchased as such from Princeton Laboratories and used after filtration on millipore. For the other three homologs (C2, C3, and C4) and HC1, the purified amines, from Aldrich, were heated to 65°C, and cold hydrogen peroxide (30% solution from Fisher) was then added at the rate of one drop per second in the proportion of 1.2 mol of peroxide to 1 mol of amine. After the addition had been completed, the mixture was warmed to 70°C until the upper phase, the amine, had disappeared. The reaction time was about 5 h for C2 and 72 h for C4. After completion of the reaction, manganese dioxide was added in catalytic quantity to eliminate all excess of H_2O_2. The complete elimination of the peroxide was checked with iodide

TABLE 2. Isentropic compressibilities of trialkylamine oxides in water at 25°C

m (mol kg^{-1})	$10^5\,\beta_s$ (bar^{-1})	$10^4\,K_{s,2,\phi}$ (cm^3 bar^{-1} mol^{-1})	m (mol kg^{-1})	$10^5\,\beta_s$ (bar^{-1})	$10^4\,K_{s,2,\phi}$ (cm^3 bar^{-1} mol^{-1})
Trimethylamine oxide			Tripropylamine oxide		
0.096	4.437	−9.88	0.348	4.160	−24.26
0.221	4.385	−9.93	0.553	4.160	−22.42
0.6575	4.211	−9.80	0.726	3.875	−20.90
0.9403	4.106	−9.73	0.927	3.745	−19.17
1.3719	3.953	−9.61	1.219	3.582	−16.47
1.6264	3.868	−9.54	1.422	3.488	−14.20
1.9187	3.775	−9.42	1.628	3.403	−12.12
2.1801	3.695	−9.32	1.866	3.318	−9.63
2.4848	3.606	−9.19	2.242	3.215	−5.51
2.6905	3.549	−9.00	2.867	3.108	1.35
3.2467	3.405	−8.81	3.766	3.051	10.58
3.5826	3.323	−8.27	4.376	3.050	16.02
3.9206	3.246	−8.04	5.294	3.076	22.90
4.2747	3.170	−7.61	6.303	3.125	29.08
4.8908	3.048	−7.01	7.708	3.209	35.92
6.8134	2.748	−6.05	9.230	3.303	41.61
7.2199	2.596	−6.39	12.187	3.474	49.55
			16.937	3.694	57.45
			21.961	3.861	62.08
Triethylamine oxide			Tributylamine oxide		
0.0918	4.410	−21.62	0.0493	4.418	−24.94
0.2293	4.314	−21.51	0.1199	4.338	−24.07
0.4062	4.197	−21.01	0.3768	4.088	−18.01
0.5759	4.090	−20.63	0.6617	3.875	−10.45
0.8128	3.752	−19.45	0.8163	3.789	−5.67
1.1739	3.536	−18.40	1.0429	3.696	−1.95
1.6216	3.390	−17.54	1.3143	3.630	11.17
2.2789	3.269	−16.66	1.5806	3.595	19.44
2.6636	3.138	−15.50	1.9930	3.573	29.90
3.0115	3.035	−14.36	2.3629	3.534	34.75
3.4381	2.925	−12.91	2.6449	3.530	39.26
3.7502	2.857	−11.75	2.9565	3.556	44.53
4.2872	2.757	−9.85	3.3475	3.576	49.43
8.0907	2.452	2.02	3.8620	3.612	55.23
8.8069	2.448	4.02	4.6316	3.668	61.83
9.9678	2.454	6.96	5.5352	3.730	67.92
12.114	2.486	11.41	6.6116	3.821	73.55
14.866	2.551	15.86	7.4238	3.882	77.09
			12.5	4.195	90.73

starch paper. The excess amine was removed by three extractions with petroleum ether. The C2 and C3 products were used as such, while C4 and HC1 were recrystallized in diethyl ether.

Stock solutions were prepared and their molality determined by conductimetric titration with hydrochloric acid. Solutions were then prepared by dilution, by mass, using distilled deionized water.

Results

The changes in density ($d - d_0$) and in relative changes in heat capacity per unit volume $(\sigma - \sigma_0)/\sigma_0$ from which apparent molar volumes, $V_{2,\phi}$ and heat capacities $C_{P,2,\phi}$ can be derived (7, 8) are given in Table 1. The density and heat capacity per unit volume of pure water at 25°C were taken as 0.997047 g cm^{-3} and 4.1793 J K^{-1} cm^{-3}. The isentropic compressibilities β_s were calculated from sound velocities (10) and are given in Table 2 along with the derived apparent molar isentropic compressibilities $K_{S,2,\phi}$. The value of $\beta_{S,0}$ at 25°C was taken as 44.77×10^{-6} bar^{-1}. The integral enthalpies of dilution, ΔH_{ID} for a dilution ratio f are reported in Table 3. These enthalpies of dilution were converted to relative apparent molar enthalpies by least-squares fitting of the data with an equation of the type

$$[1] \quad L_{2,\phi} = Am + Bm^2 + \ldots$$

from which

$$[2] \quad \Delta H_{ID} = \Delta L_{2,\phi} = A(fm - m) + B(f^2m^2 - m^2)$$

The parameters A and B are given in Table 4.

The concentration dependence of the apparent molar quantities of the symmetrical amine oxides are shown in Figs. 1 to 4, while $V_{2,\phi}$ and $C_{P,2,\phi}$ of HC1 are shown in Fig. 5. The corresponding partial molar compressibilities are also shown in Fig. 4. These trends are typical of the behaviour of surfactants in water, except that the CMC is observed at much higher concentrations than with single chain surfactants. The enthalpies of dilution could not be measured in the post-micellar region since incomplete mixing was observed at these high

TABLE 3. Enthalpies of dilution of trialkylamine oxides in water at 25°C

m (mol kg^{-1})	fm (mol kg^{-1})	ΔH_{ID} (J mol^{-1})	m (mol kg^{-1})	fm (mol kg^{-1})	ΔH_{ID} (J mol^{-1})
Trimethylamine oxide					
0.09700	0.04518	−24.5	1.4028	0.59743	−1319
0.19627	0.09106	−49.3	1.4028	0.59747	−1303
0.19627	0.09106	−52.8	1.4028	0.59755	−1302
0.29857	0.13796	−78.0	1.5590	0.67240	−1528
0.29857	0.13797	−77.4	1.5959	0.67234	−1515
0.29857	0.13796	−81.9	1.6876	0.72873	−1698
0.40546	0.18663	−111.2	1.6760	0.72883	−1683
0.40546	0.18660	−108.6	1.8547	0.72854	−1992
0.40546	0.18660	−112.1	1.8547	0.72925	−1987
0.50290	0.23238	−140.4	1.9804	0.77234	−2164
0.50290	0.23239	−141.1	1.9804	0.77236	−2167
0.50290	0.23239	−139.2	2.9370	1.1880	−3450
0.59961	0.27604	−167.5	2.9370	1.1881	−3460
0.59961	0.27606	−167.2	2.9370	1.1881	−3467
0.70276	0.32230	−199.5			
0.70276	0.32231	−200.4	Tripropylamine oxide		
0.70276	0.32231	−201.1	0.19697	0.09311	−4288
0.79600	0.36379	−229.0	0.19697	0.09310	−4313
0.79600	0.36380	−229.4	0.40258	0.18714	−8903
0.90535	0.41209	−267.3	0.65778	0.29963	−1561
0.90535	0.41215	−266.3	0.81073	0.36490	−1968
0.99998	0.45365	−302.5	1.1973	0.52181	−3157
0.99998	0.45359	−300.2	1.1973	0.52185	−3135
1.0968	0.49580	−336.9	1.3477	0.58076	−3620
1.0968	0.49573	−336.0	1.3884	0.59655	−3741
1.0063	0.54656	−374.8	1.5837	0.67071	−4470
1.2063	0.54652	−373.0	1.7869	0.74567	−5215
1.2978	0.58607	−411.5	2.0409	0.83654	−6217
1.2978	0.58599	−412.9	2.1536	0.89704	−6559
1.3923	0.62652	−448.3	3.9784	1.1897	−10715
1.3923	0.62655	−441.4	3.0784	1.1898	−10842
1.4891	0.66782	−487.2	3.3068	1.2594	−11643
1.4891	0.66786	−484.5	3.3068	1.2594	−11705
1.7936	0.79578	−614.1	4.0431	1.4707	−14639
1.7936	0.79575	−611.3	4.0431	1.4707	−14791
2.0200	0.86079	−732.2			
2.0200	0.86081	−733.7	Tributylamine oxide		
			0.15035	0.07331	−750.2
Triethylamine oxide			0.22036	0.10754	−1100
0.19482	0.09047	−142.5	0.35836	0.17112	−1892
0.40769	0.18690	−312.4	0.46320	0.22062	−2522
0.40769	0.18690	−313.1	0.59599	0.28024	−3383
0.70081	0.31574	−561.3	0.75622	0.34735	−4525
0.70081	0.31574	−563.8	0.83574	0.38413	−5112
0.70081	0.31574	−569.6	0.99027	0.44862	−6368
0.94730	0.42072	−808.2	1.0671	0.47723	−7007
0.94730	0.42072	−799.3	1.1317	0.50315	−7510
1.1950	0.51499	−1088	1.8414	0.76622	−12308
1.1959	0.51499	−1083	2.0074	0.82339	−10474
			2.0074	0.82338	−10087

TABLE 4. Parameters of eq. [2] for trialhylamine oxides in water at 25°C

Solute	A	B	m_{max}
Trimethylamine oxide	469 ± 1	56.3 ± 0.6	2.02
Triethylamine oxide	1270 ± 10	188 ± 6	1.98
Tripropylamine oxide	3960 ± 10	412 ± 6	2.15
Tributylamine oxide	9260 ± 50	1680 ± 40	1.13

concentrations, and the magnitude of the enthalpies was becoming too large for the microcalorimeter.

Thermodynamic data of micellar systems can be fitted by least-squares using a recently developed mass-action model (6). The parameters that are extracted from the data, or those need to be fixed, are the following: Y_2^0 = partial molar quantity of solute 2 at infinite dilution; A_Y = second virial coefficient for the interactions between monomers; Y_2^M = partial molar quantity of the surfactant in the micellar form; A_Y^M = interaction

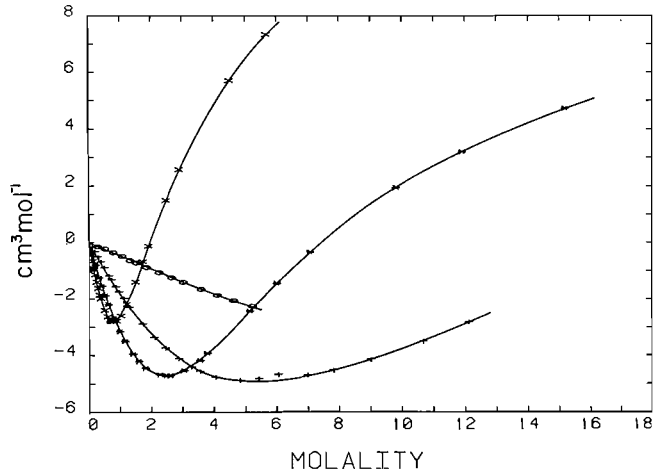

FIG. 1. Apparent molar volumes of trialkylamine oxides in water at 25°C.

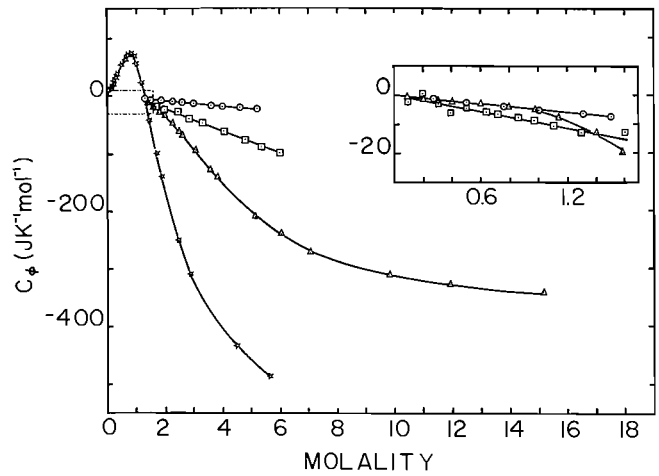

FIG. 2. Apparent molar heat capacities of trialkylamine oxides in water at 25°C.

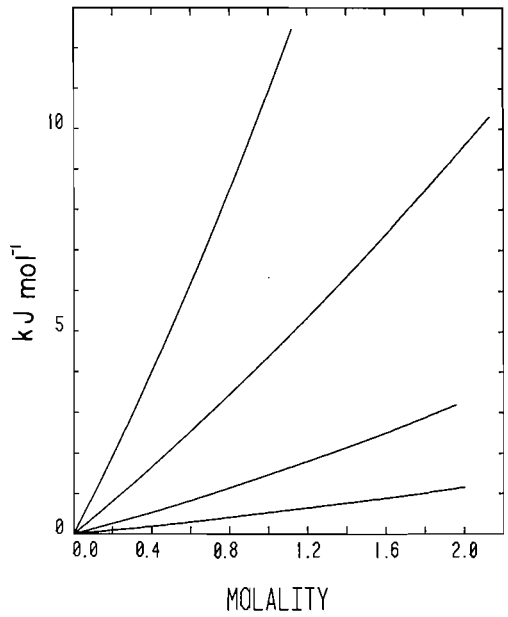

FIG. 3. Apparent molar relative enthalpies of trialkylamine oxides in water at 25°C.

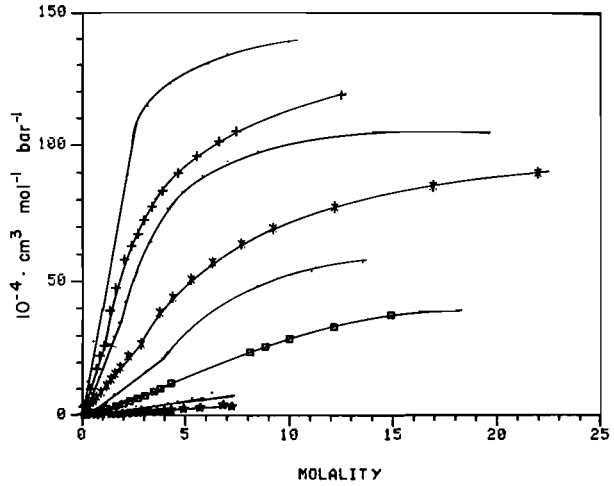

FIG. 4. Apparent and partial (full line) molar isentropic compressibilities of trialkylamine oxides in water at 25°C. The bottom curve is for C1 and the top curve for C4.

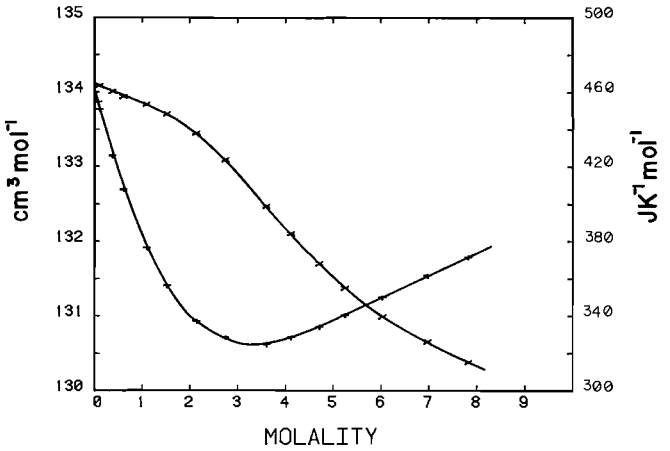

FIG. 5. Apparent molar volumes and heat capacities of cyclohexyldimethylamine oxide in water at 25°C.

parameter in the post-micellar region; m_I = critical micellar concentration on the molality scale and defined as the inflection point in the fraction of monomers; N = aggregation number; EQUIL = equilibrium displacement contribution to heat capacities, $(\Delta H_M/T)^2/R$, and to compressibilities, $(\Delta V_M)^2/RT$, where ΔH_M and ΔV_M are the enthalpies and volumes of micellization; and s is standard deviation.

With medium chain length surfactants, it is possible to extract all the above parameters from the least-squares fit. With alkyldimethylamine oxides, the model was quantitative, even without the parameter $A_Y{}^M$ (6). The aggregation numbers that were extracted were quite reasonable, independent of the property and to a first approximation independent of temperature. The model is not as successful with the symmetrical amine oxides, primarily due to the lack of data points at high concentration and in the inflection region. As a result, the convergence was difficult and some of the parameters extracted were not always realistic, especially $Y_2{}^M$ and EQUIL. Still, the aggregation numbers extracted were of the order of 3 for C2, 4 for C3, and 6 for C4. These aggregation numbers are of the correct magnitude for such surfactants. When convergence was not achieved or slow, some of the parameters were fixed at reasonable values. The parameters obtained from the least-

TABLE 5. Thermodynamic parameters of trimethylamine oxide in water at 25°C

Property	Y_2^0	A_Y
$V_\phi/(cm^3\ mol^{-1})$	73.15	−0.452
$C_\phi/(J\ K^{-1}\ mol^{-1})$	180.0	−4.8
$10^4\ K_{s,2,\phi}/(cm^3\ bar^{-1}\ mol^{-1})$	−9.9	0.68

squares are given in Tables 5 and 6. In the case of C1, no evidence of micellization is observed with most properties. Therefore, only Y_2^0 and A_Y are given.

The aggregation numbers, the CMC, and the thermodynamic changes during micellization of HC1 are comparable to those of the symmetrical amine oxides. Cyclisation of the chain therefore has no major effect on the micellization properties.

Discussion

The standard thermodynamic quantities Y_2^0 are functions of the intrinsic contribution and of the solute–solvent interactions. The parameters V_2^0 and $C_{P,2}^0$ of the symmetrical and assymmetrical (6) amine oxides are compared with the tetraalkylammonium bromides (3, 11) in Fig. 6. Symmetrical and assymmetircal amine oxides fall on the same lines and these slopes are, in a first approximation, identical to those of the ammonium salts. In the case of HC1 (not shown), both the volumes and heat capacities fall below the line of the other amine oxides as expected since there is one less H atom in this solute. The CH_2 contribution to these two functions is independent of the presence of a charge or of the symmetry. The CH_2 contribution of the amine oxides is 15.7 $cm^3\ mol^{-1}$ for V_2^0 and

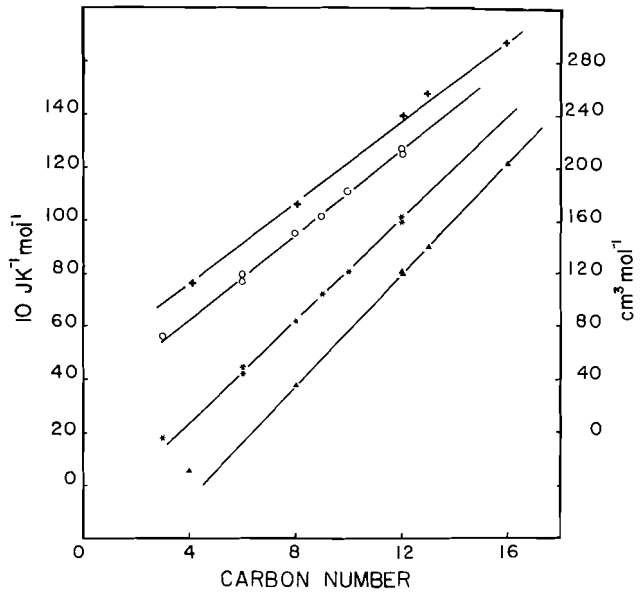

FIG. 6. Dependence of the standard thermodynamic functions on the total number of carbon atoms in the chains: + and ○, V_2^0 of R_4NBr and amine oxides, respectively; * and ▲, $C_{P,2}^0$ of amine oxides and R_4NBr, respectively.

95 $J\ K^{-1}\ mol^{-1}$ for $C_{P,2}^0$. These results are in good agreement with the values obtained by other authors (2, 12–14).

The situation is not as simple with compressibilities. The dependence of $K_{S,2}^0$ on the number of carbon atoms appears to be the same for all the systems (see Fig. 7) implying a constant CH_2 contribution of -1.5×10^{-4} $cm^3\ bar^{-1}\ mol^{-1}$, again in good agreement with other authors (15, 16). On the other hand,

TABLE 6. Parameters from the mass-action model*

Parameters	Value			
	HC1	C2	C3	C4
$V_2^0/(cm^3\ mol^{-1})$	134.03	115.13	162.81	210.52
$A_V/(cm^3\ mol^{-2}\ kg)$	−2.409	−1.891	−3.327	−5.614
$V_2^M/(cm^3\ mol^{-1})$	146.90	121.66	182.95	229.78
$A_V^M/(cm^3\ mol^{-2}\ kg)$	(0)	0.44	(0)	0.20
$m_I/(mol\ kg^{-1})$	2.491	3.879	2.855	1.160
N	3.027	3.496	3.763	3.915
$s/(cm^3\ mol^{-1})$	0.024	0.053	0.061	0.020
$C_{P,2}^0/(J\ K^{-1}\ mol^{-1})$	465.55	430.13	722.15	1017.0
$A_C/(J\ K^{-1}\ mol^{-2}\ kg)$	−11.22	−4.115	−10.98	96.51
$C_{P,2}^M/(J\ K^{-1}\ mol^{-1})$	145.54	147.95	258.76	(360)
$A_C^M/(J\ K^{-1}\ mol^{-2}\ kg)$	7.55	(0)	(0)	−17.30
$m_I/(mol\ kg^{-1})$	3.377	3.014	(2.8)	(1.16)
N	(6.00)	(3)	7.938	9.797
EQUIL/$(J\ K^{-}\ mol^{-1})$	32.76	67.80	5.42	73.63
$s/(J\ K^{-1}\ mol^{-1})$	0.97	3.4	3.33	5.88
$10^4\ K_{s,2}^0/(cm^3\ bar^{-1}\ mol^{-1})$		−21.56	−26.85	−25.51
$10^4\ A_k/(cm^3\ bar^{-1}\ mol^{-2}\ kg)$		1.694	7.644	13.87
$10^4\ K_{s,2}^M/(cm^3\ bar^{-1}\ mol^{-1})$		(28.2)	(78.5)	111.27
$10^4\ A_k^M/(cm^3\ bar^{-1}\ mol^{-2}\ kg)$		(0)	(0)	(0)
$m_I/(mol\ kg^{-1})$		8.744	3.413	(1.16)
N		(3)	3.760	3.609
10^4 EQUIL/$(cm^3\ bar^{-1}\ mol^{-1})$		32.99	0.75	2.33
$10^4\ s/(cm^3\ bar^{-1}\ mol^{-1})$		0.38	0.10	1.34

*Values in parentheses were fixed.

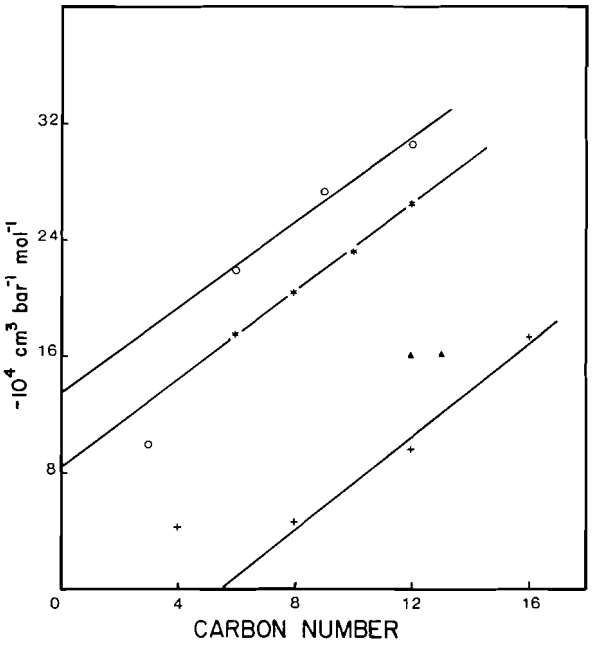

FIG. 7. Dependence of standard partial molar isentropic compressibilities on the total number of carbon atoms in the chains: ○, symmetrical amine oxides; *, assymmetrical amine oxides; +, symmetrical R_4NBr; ▲, assymmetrical R_4NBr.

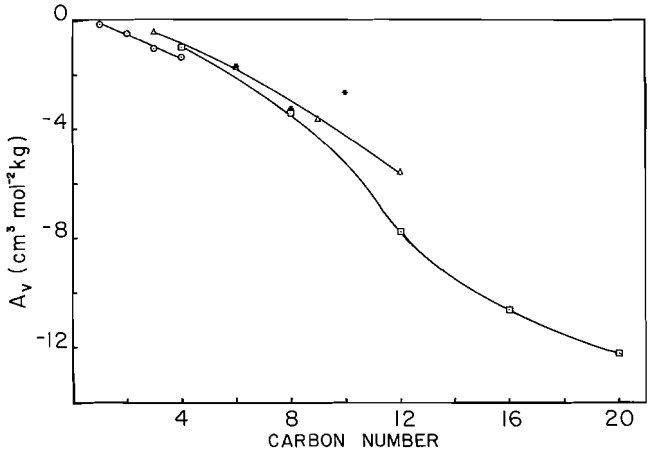

FIG. 8. Dependence of parameter A_V on the number of carbon atoms.

the symmetry of the solute affects the magnitude of $K_{S,2}^0$; the symmetrical amine oxides are more negative while the symmetrical ammonium salts (15) are more positive than the corresponding linear isomers (3). It is not easy to explain why the symmetry affects compressibilities but not heat capacities and volumes. It would be necessary to examine corresponding correlations in non-aqueous solvents and in the pure liquid state before venturing an explanation.

The second virial coefficients, as seen from Tables 5 and 6 change in a fairly regular way with chain length. The parameter A_V is plotted against the number of carbon atoms in the chains and compared with the assymmetrical amine oxides, tetraalkylammonium bromides and alcohols (17) in Fig. 8. All the solutes fall approximately on the same straight line. This is also approximately true for A_H. This linearity suggests that these virial coefficient are approximately additive as it was observed for free energies (18).

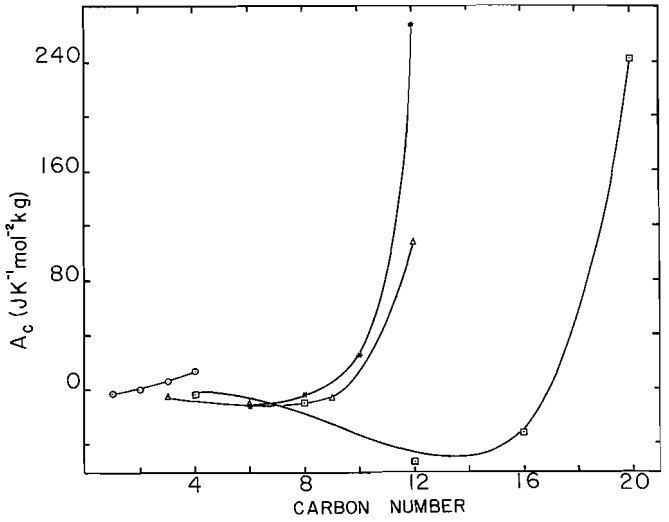

FIG. 9. Dependence of parameter A_C on the number of carbon atoms.

A similar plot is shown for A_C in Fig. 9. No simple correlation can be made in this case. The values of A_C of the amine oxides are approximately equal to zero up to 9 carbons and then increase sharply. The corresponding values for tetraalkylammonium bromides decrease up to 12 carbons and again increase. For the alcohols, A_C increases steadily. The interpretation of this parameter is not simple since it contains two main contributions. The interaction between two monomers as they approach each other lead to a partial dehydration of the hydrophobic chains and this causes a negative contribution to A_C. By analogy with equilibrium constants there is also a relaxational or equilibrium displacement contribution as the temperature is increased. This will cause a positive contribution to A_C since it is proportional to $(A_H)^2$. These two contributions cancel each other for the lower homologs, but the relaxational contribution rapidly takes over with the more hydrophobic solutes where A_H is large.

The equilibrium displacement contribution to heat capacities is again of similar magnitude for symmetrical and assymmetrical (6) amine oxides. This contribution is sufficiently large to produce a hump in $C_{P,2\phi}$ in the micellar region for octyldimethylamine oxide and C4. This, of course, implies that both these surfactants have comparable large enthalpies of micellization.

The main differences between the symmetrical and assymmetrical isomers are in the micellar parameters. With the symmetrical isomers, the CMCs are much larger, the aggregation numbers small and the change ΔY_2^M larger.

Conclusion

The present study indicates that the thermodynamic properties of monomeric hydrophobic solutes of different geometries can to a large extent be predicted by group additivity. On the other hand, the association or aggregation of such solutes in water depend significantly on the shape of the molecules; micellization is favored with long-chain amphiphilic solutes, while bulky solutes show much less tendency to aggregate. The thermodynamic functions of micellization are also strongly dependent on geometry.

The present study also shows that the heat capacity per unit volume of a solution of tributylamine oxide can be increased

by about 4% relative to pure water in the concentration region where the apparent molar heat capacity goes through a maximum. While this solute is not of much interest for energy storage in view of its thermal instability, these results suggest that bulky hydrophobic solutes might meet the requirements for improving the energy storage of aqueous solutions. The ideal solute would have to be hydrophobic, stable, highly soluble in water, with a large enthalpy of transition and a small heat capacity of transition. Such conditions can usually be met at low temperatures. Work is under way to investigate such possibilities.

Acknowledgements

The authors are grateful to the Natural Sciences and Engineering Council of Canada and to the Quebec Ministry of Education for financial support.

1. J. E. DESNOYERS and C. JOLICOEUR. *In* Treatise of electrochemistry. Vol. 5. *Edited by* J. O'M. Bockris, B. E. Conway, and E. Yeager. Plenum Press, New York. 1982. p. 1.
2. C. JOLICOEUR and G. LACROIX. Can. J. Chem. **54**, 624 (1976).
3. R. DELISI, C. OSTIGUY, G. PERRON, and J. E. DESNOYERS. J. Colloid Interf. Sci. **71**, 147 (1979).
4. W.-Y. WEN and K. NARA. J. Phys. Chem. **71**, 3907 (1967).
5. J. E. DESNOYERS, R. LELISI, D. ROBERTS, and G. PERRON. *In* Solution chemistry of surfactants. Vol. 1. *Edited by* K. L. Mittal. Plenum Press, New York. 1979. p. 221.
6. J. E. DESNOYERS, G. CARON, R. DELISI, D. ROBERTS, A. ROUX, and G. PERRON. J. Phys. Chem. **87**, 1397 (1983).
7. P. PICKER, E. TREMBLAY, and C. JOLICOEUR. J. Solution Chem. **3**, 377 (1974).
8. P. PICKER, P. A. LEDUC, P. PHILIP, and J. E. DESNOYERS. J. Chem. Thermodyn. **3**, 631 (1971).
9. J.-L. FORTIER, P. A. LEDUC, P. PICKER, and J. E. DESNOYERS. J. Solution Chem. **2**, 467 (1973).
10. H. T. CLARKE, H. B. GILLESPIE, and S. F. WEISSHAUS. J. Am. Chem. Soc. **55**, 4571 (1933).
11. G. PERRON, N. DESROSIERS, and J. E. DESNOYERS. Can. J. Chem. **54**, 2163 (1976).
12. G. PERRON and J. E. DESNOYERS. Fluid Phase Equil. **2**, 239 (1979).
13. S. CABANI, P. GIANI, V. MOLLICA, and L. LEPORI. J. Solution Chem. **10**, 563 (1981).
14. T. NAKAJIMA, T. KOMATSU, and T. NAKAGAWA. Bull. Chem. Soc. Jpn. **48**, 783 (1975).
15. J. G. MATHIESON and B. E. CONWAY. J. Chem. Soc. **70**, 752 (1974).
16. T. NAKAJIMA, T. KOMATSU, and T. NAKAGAWA. Bull. Chem. Soc. Jpn. **48**, 788 (1975).
17. G. PERRON and J. E. DESNOYERS. J. Chem. Thermodyn. **13**, 1105 (1981).
18. J. J. SAVAGE and R. H. WOOD. J. Solution Chem. **5**, 733 (1976).

Sulphur-33 nuclear magnetic resonance spectroscopy of sulphones[1]

JEFFREY HOYLE, J. STUART GROSSERT,[2] DONALD L. HOOPER, AND SUBRAMANIAN SOTHEESWARAN[3]
Department of Chemistry, Dalhousie University, Halifax, N.S., Canada B3H 4J3

Received September 5, 1985

JEFFREY HOYLE, J. STUART GROSSERT, DONALD L. HOOPER, and SUBRAMANIAN SOTHEESWARAN. Can. J. Chem. **64**, 1581 (1986).

The sulphur-33 nmr spectra of 28 sulphones were measured in deuterochloroform solutions at 27.716172 MHz. The spectra were referenced with respect to an external aqueous ammonium sulphate solution and the chemical shifts lay in the range 0 ± 20 ppm, with many lines having a half-height width of less than 200 Hz. Instrumental parameters that affect the spectra were studied. Some of the sulphur-33 resonances can be correlated well with carbon-13 or oxygen-17 resonances in appropriate analogous compounds, and with the Taft σ* parameter.

JEFFREY HOYLE, J. STUART GROSSERT, DONALD L. HOOPER et SUBRAMANIAN SOTHEESWARAN. Can. J. Chem. **64**, 1581 (1986).

Opérant à 27,716172 MHz et dans des solutions de deutérochloroforme, on a mesuré les spectres rmn du ^{33}S de 28 sulfones. Les déplacements chimiques, qui se situent dans l'intervalle de 0 ± 20 ppm, sont exprimés par rapport à une solution aqueuse de sulfate d'ammonium untilisée comme référence externe; les largueurs à mi-hauteur de plusieurs raies ne dépassent pas 200 Hz. On a étudié les paramètres reliés aux instruments qui peuvent affecter les spectres. On a pu établir une bonne corrélation entre les résonances en rmn du ^{33}S et soit le paramètre σ* de Taft ou les résonances en rmn du ^{13}C du ^{17}O de composés analogues appropriés.

[Traduit par la revue]

Introduction

Sulphur-33 was one of the first nuclei for which the nmr phenomenon was observed (1), yet for many years the nucleus received no further attention (2), undoubtedly due in a large measure to its low receptivity and to the quadrupole moment of the nucleus, which gives rise to significant line broadening in the spectra of many molecules. This line broadening is greatly decreased when the sulphur nucleus experiences a significant and reasonably symmetrical electric field gradient, such that the sulphur-33 resonance in SF_6 is actually a clearly defined septet (2, 3). Sulphones also give usefully narrow lines, although this fact was not reported until 1981 (4). This pioneering study suffers from rather large uncertainties in the values of the chemical shifts reported, presumably due to the use of a relatively low-field spectrometer. The increasingly wide availability of high-field, multinuclear nmr spectrometers has facilitated studies on the sulphur-33 nucleus, and a number of papers reporting useful nmr results on organosulphur compounds have recently appeared (5–9). These studies show that the sulphur-33 nucleus in sulphones resonates over a relatively narrow chemical shift range. The resonance frequencies are structure dependent and are generally quite different from the much broader lines found for other less oxidized sulphur-containing functional groups (6, 8). A range of sulphones has been studied, but as yet no systematic correlation of structures and chemical shifts has been reported. Furthermore, there is an unfortunate lack of standardization in the choice of reference compound, this ranging from carbon disulphide (5–7), which has a relatively broad resonance, to sulpholane (8), and ammonium sulphate (9, 10), which has a narrow resonance.

Results and discussion

As a result of other ongoing work (11, 12), we had in hand a series of sulphones with a wide range of substituents representing a systematic variation in the environment of the sulphone group. The results from measuring the sulphur-33 nmr resonances for these compounds are reported in Table 1.

The chemical shifts in this study are reported as δ values with respect to an external 5 *M* aqueous solution of ammonium sulphate. The sulphate ion gives a narrow line and its use as a reference line has been thoroughly investigated by Lutz *et al.* (10), who compared its suitability to that of carbon disulphide. Carbon disulphide has been used as a reference by a number of other workers (5, 7), but it exhibits a broad line ($W_{1/2}$ > 250 Hz), which means that accurate measurement of its resonance frequency is more difficult than a similar measurement for a narrow resonance.

A comparison of some chemical shifts reported in the literature and some from the present work is presented in Table 2. The results at times show sizeable differences between reported chemical shifts and line widths, such that some standardization of recording techniques is desirable.

The narrow chemical shift range required that a number of spectral variables were assessed. This was done using a sample of ethyl phenyl sulphone (Table 1, entry #13), which exhibits a resonance line of intermediate width (>100 Hz). The number of data points used to acquire a spectrum is important; for a spectral window of 1000 Hz, at least 8K data points were required to give reproducible values of line width and frequency. For any nucleus of low receptivity, detection requires the smallest possible delay time between switching off the transmitter and switching on the receiver. However, this exacts a penalty in the rolling baseline resulting from acoustic ringing, which was minimized by deleting ("left shifting") some points of the expanded FID (free induction decay) display. The number of points deleted is a function of the sample as well as the number of scans; for this particular sample at least 4 points had to be deleted to assure consistent measurements of line frequency and line width. In addition, it was found that very careful phasing of the resultant absorption signal was essential for accurate measurement of line frequencies. Variations of up to 1 ppm were observed for apparently trivial errors in phasing. Finally, it was also found necessary to use an FID exponential multiplicand more positive than −10 in order to obtain consistent line width values (136–140 Hz for this sample).

[1]Taken in part from the Ph.D. thesis of J.H., August 1984.
[2]Author to whom correspondence may be addressed.
[3]Visiting Professor from the University of Peradeniya, Sri Lanka.

TABLE 1. Sulphur-33 chemical shifts and line widths of certain sulphones, together with carbon-13 data for analogous carbon compounds

Entry	Sulphone	δ-*S*(ppm)*	$W_{1/2}$(Hz)	Carbon compound	δ-*C*(ref.)†
1	$MeSO_2Me$	−12.8	15	$MeCH_2Me$	16.1(14)
2	$EtSO_2Et$	4.9	50	$EtCH_2Et$	34.6(14)
3	$Pr^iSO_2Pr^i$	18.1	120	$Pr^iCH_2Pr^i$	49.1(15)
4	$MeSO_2CH_2Cl$	−7.2	90	$MeCH_2CH_2Cl$	26.3(16)
5	$MeSO_2CHCl_2$	−0.2	280	$MeCH_2CHCl_2$	37.3
6	$MeSO_2CCl_3$	4.5	300	$MeCH_2CCl_3$	48.3
7	$MeSO_2CH_2Br$	−10.3	95	$MeCH_2CH_2Br$	26.3(16)
8	$MeSO_2CH_2Ph$	−16.7	40	$MeCH_2CH_2Ph$	24.8(16)
9	$MeSO_2CHClMe$	0.9	40	$MeCH_2CHClMe$	33.8(17)
10	$PhCH_2SO_2CH_2Ph$	−3.3	20	$PhCH_2CH_2CH_2Ph$	32.9(15)
11	$PhCH_2SO_2CHClMe$	3.5	110	$PhCH_2CH_2CHClMe$	44.1
12	$PhCH_2SO_2CHClPh$	4.1	330	$PhCH_2CH_2CHClPh$	44.3
13	$PhSO_2CH_2CH_3$	−7.0	125	$PhCH_2CH_2CH_3$	38.3(16)
14	$PhSO_2CHClMe$	−6.6	50	$PhCH_2CHClMe$	47.9
15	$PhSO_2CH_2Ac$‡	−20.0	150	$PhCH_2CH_2Ac$	29.8(15)
16	$PhSO_2CH_2Bz$‡	−18.8	350	$PhCH_2CH_2Bz$	30.0(15)
17	$PhSO_2CH(SPh)Ac$	−17.0	350	$PhCH_2CH(SPh)Ac$	37.8
18	$MeSO_2CH(SMe)Bz$	4.0	325	$MeCH_2CH(SMe)Bz$	23.3
19	$MeSO_2CH(SEt)Bz$	5.9	120	$MeCH_2CH(SEt)Bz$	23.3
20	$MeSO_2CH(SPh)Bz$	4.0	400	$MeCH_2CH(SPh)Bz$	23.3
21	$MeSO_2CH_2Bz$	−12.1	215	$MeCH_2CH_2Bz$	17.7(18)
22	$MeSO_2CHMeBz$	−1.3	100	$MeCH_2CHMeBz$	26.1
23	$MeSO_2CHClBz$	−3.7	200	$MeCH_2CHClBz$	27.3
24	$MeSO_2CHBrBz$	−5.0	400	$MeCH_2CHBrBr$	27.3
25	$MeSO_2CH_2C(OCH_2)_2Ph$	−11.7	100	$MeCH_2CH_2C(OCH_2)_2Ph$	40.3
26	$EtSO_2CH_2SO_2Et$	−10.0	>500	$EtCH_2CH_2CH_2Et$	26.1(14)
27	$(CH_2)_5SO_2$	−9.8	45	$(CH_2)_5CH_2$	27.1(14)
28	$[(CH_2)_4CHCl]SO_2$	−9.6	100	$[(CH_2)_4CHCl]CH_2$	36.9(15)

*Chemical shifts are reported in $CDCl_3$ with respect to external 5 *M* ammonium sulphate in water.

†These carbon-13 chemical shifts were obtained from the reference listed in parentheses or were calculated using the Lindeman–Adams procedure (13).

‡Ac = CH_3CO—; Bz = PhCO—.

TABLE 2. Comparison of the sulphur-33 chemical shifts (ppm)* and line widths ($W_{1/2}$, Hz) between this work and literature values for selected compounds

Compound	This work	Ref. 5	Ref. 6	Ref. 7	Ref. 8
$MeSO_2Me$	−12.8(15)	−12(50)	−17(46)	−12(20)	−10(6.8)
$EtSO_2Et$	+4.9(50)	+2(70)	+3(92)	+2(100)	—
$PhCH_2SO_2CH_2Ph$	−3.3(20)	−2(120)	—	−1(100)	—
$PhSO_2Ph$	—	−20(120)	−24(161)	−22(70)	−21(48)
$(CH_2)_5SO_2$	−9.8(45)	−10(50)	−11(92)	—	—
$(CH_2)_4SO_2$	—	+38(50)	+36(69)	—	+39(10)

*For comparison purposes chemical shifts are all referenced to sulphate anions assuming that the carbon disulphide resonance is 332 ppm upfield from that of sulphate ions (3).

We have found that sulphone mixtures such as $MeSO_2CH_2Cl$ and $MeSO_2CHCl_2$ or $PhSO_2CH_2COMe$ and $MeSO_2CH_2COPh$ showed the same chemical shifts as were found for the individual compounds, viz. Table 1, entries 4, 5 and 15, 21, respectively. Entries 17–20 showed only a single sulphur-33 resonance and this arose from the more highly oxidized sulphur atom.

The correlation of chemical shifts with structure has long been studied and various empirical correlations such as that due to Lindeman and Adams (13) for carbon-13 chemical shifts in alkanes are widely used. Another correlation of possible relevance to sulphur-33 spectra is the report of a linear correlation of oxygen-17 chemical shifts in ethers with the carbon-13 chemical shift in the analogous alkanes. In the case of simple compounds, with only alkyl substituents to the oxygen, there is a linear correlation between these chemical shifts (δ-*O* vs. δ-*C*), with a resulting slope of 3.2, that has been suggested (19) can be related to the difference in size and electron density of the 2*p* orbitals of oxygen and carbon, although the actual agreement between the measured slope and the calculated difference is somewhat tenuous (3.2 vs. 2.3).

When we plotted the sulphur-33 chemical shifts of the simple dialkyl sulphones (entries 1–3, and literature values (5) for di-*n*-propyl sulphone, and di-*n*-butyl sulphone) versus the carbon-13 shifts of the analogous alkanes (13), a linear regression analysis gave a correlation of the form δ-*S* = 0.92 δ-*C*

TABLE 3. Sulphur-33, carbon-13, and σ* data for certain sulphones and analogous carbon compounds

Entry	Sulphone	δ-*S* (ppm)†	σ*	Carbon compound	δ-*C*
1	$MeSO_2Me$	−12.8	0.00	$MeCH_2Me$	16.1
2	$EtSO_2Et$	4.9	−0.10	$EtCH_2Et$	34.6
3	$Pr^iSO_2Pr^i$	18.1	−0.19	$Pr^iCH_2Pr^i$	49.1
4	$Pr^nSO_2Pr^n$	1‡	−0.115	$Pr^nCH_2Pr^n$	29.5
5	$Bu^nSO_2Bu^n$	4‡	−0.13	$Bu^nCH_2Bu^n$	30.0
6	$MeSO_2CH_2Cl$	−7.2	1.05	$MeCH_2CH_2Cl$	26.3
7	$MeSO_2CHCl_2$	−0.2	1.94	$MeCH_2CHCl_2$	37.3
8	$MeSO_2CCl_3$	4.5	2.65	$MeCH_2CCl_3$	48.3
9	$MeSO_2CH_2Br$	−10.3	0.99§	$MeCH_2CH_2Br$	26.3
10	$MeSO_2CH_2Ph$	−16.7	0.215	$MeCH_2CH_2Ph$	24.8

σ is the Taft polar substituent parameter, cf. ref. 23.
†Taken from Table 1.
‡These values taken from ref. 5.
§This value is estimated from σ_1, cf. ref. 21.

− 26.5; however, the correlation coefficient was only 0.992. This correlation might well be improved by higher field measurements and the use of a narrow reference line for the spectra of the compounds that were not available to us. The slope of the line is only about 30% of the corresponding line from δ-*O* vs. δ-*C*, and, while the slope of this line has been suggested to be related to a function of the oxygen bonding orbitals (19), it is much less certain which orbitals would be involved in the bonding of a sulphone (a complex functionality) as compared to an ether (a simple functionality). However, it does appear that the sulphone sulphur atom in dialkyl sulphones is affected by changes of carbon atoms in the alkyl chains in a similar manner as is a carbon atom in an alkane, and thus substituent parameters based on the Lindeman–Adams approach (13) could be used to estimate approximate sulphur-33 chemical shifts in dialkyl sulphones. More examples are required to confirm this and will be the subject of further work.

In contrast to the simple dialkyl sulphones, the introduction of polar substituents in the side chain led to resonances at different values. Entries 4–12 in Table 1 contain haloalkyl or arylalkyl side chains. Regression analysis of the data for a plot of δ-*S* vs. δ-*C* yielded a line of slope 0.762 and a correlation coefficient of 0.909. No similar correlations were obviously possible for the remaining entries in the table, but it should be noted that some of the δ-*C* values were calculated and there will be uncertainties in these in the case of more complex structures.

Since we have shown that a plot of δ-*S* vs. δ-*C* for sulphones and analogous carbon compounds produces a straight line for simple dialkyl compounds, and other workers have shown a similar correlation for ethers (19), it seemed reasonable to investigate a correlation of δ-*S* vs. δ-*O* for simple dialkyl sulphones and ethers. Using the data for the same five dialkyl sulphones detailed above together with the corresponding data for ethers (19), a linear correlation was obtained with slope of 0.29 and a correlation coefficient of 0.991.

In addition to the above correlations between chemical shifts, we have also compared the sulphur-33 chemical shifts with a standard parameter that correlates electronic effects of substituents. Such Hammett-type correlations have been reported on for carbon-13 nuclei, in general concentrating on the study of substituted aromatic compounds (20, 21). Relatively few studies on aliphatic compounds appear to have been made (22); these have focused on the Taft polar substituent constant, σ* (23). We have examined similar correlations for both the sulphur-33 and carbon-13 resonances with σ* for the compounds from the first eight entries in Table 1, together with some values taken from the literature; these are presented in Table 3. Linear regression analysis of entries 1–5 produced an equation of the form $\delta\text{-}S = -155\,\sigma^* - 13.3$ with a correlation coefficient (r) of 0.967. Similar treatment of entries 6–10 gave $\delta\text{-}S = 8.78\,\sigma^* - 18.0$ ($r = 0.991$). Analogous treatments of the carbon chemical shifts and σ* gave $\delta\text{-}C = -160\,\sigma^* + 14.7$ ($r = 0.930$) and $\delta\text{-}C = 10.2\,\sigma^* + 18.6$ ($r = 0.951$), respectively.

The correlations between δ-*S* and δ-*C* or δ-*O* are superior to the correlations between δ-*S* or δ-*C* and σ*, but this is perhaps to be expected since in the former case correlations are being made between similar parameters whereas in the latter the correlation is between a chemical shift and a parameter derived from acid equilibrium constants. As has been mentioned previously (21), it may be unwise to attempt correlations between chemical shifts and reactivity of molecules. However, there does seem to be a better correlation between δ-*S* and σ* compared to δ-*C* vs. σ*, which may be indicative of the more polar nature of the sulphonyl group. Further work is required to substantiate this, but the results presented in the present work do offer three alternative approaches of some practical value for the prediction of the chemical shift of the sulphur-33 nucleus in a substantial range of sulphones.

Experimental

Spectroscopy

The sulphur-33 nuclear magnetic resonance spectra reported were obtained using a Nicolet 360 NB nmr spectrometer, coupled to an Oxford Instruments superconducting magnet and a Nicolet 1280 data acquisition system. The spectrometer was operated at a frequency of 27.716172 MHz with quadrature detection, a total sweep width of 5000 Hz, and a pulse width of 35 μs (90° pulse) with a pulse delay of 1 s between pulses. A delay of approximately 200 μs was used between the pulse and acquisition to minimize the effects of acoustic ringing, and hence a rolling base line; the spectrum was collected over 819.2 ms (acquisition time) and stored using 16K data points. The probe temperature was 20 ± 1°C and typically 500–10 000 transients were collected; a Butterworth filter was used for all measurements. The deuterium resonance of the solvent was used both for locking and shimming the spectrometer.

An external standard of 5 *M* ammonium sulphate in water was used to measure chemical shift values, the absolute frequency of which was measured before and after each series of runs, and was found to be invariant. Samples were run in regular 10-mm diameter tubes, in

$CDCl_3$ solutions, and had a concentration of 100–500 mg of sample per 2 mL of solvent. Chemical shift values are reported with an uncertainty of ±1%. Proton spin decoupling was not used.

Preparation of the sulphones

The sulphones in Table 1, entries 1–3, 8, 10, 13, and 27, were either commercially available or were prepared by oxidation of the corresponding sulphide using H_2O_2 in methanol containing ammonium molybdate (24). Those from entries 4–7, 15, 21, 23, 24, and 28 were available from previous work (11, 12, 25). All other compounds were prepared by literature procedures and their purities were checked using both nmr spectroscopy and comparison of melting points with the reported values (26–29).

Acknowledgements

All sulphur-33 nmr spectra were obtained at the Atlantic Regional Magnetic Resonance Centre in Halifax, N.S. and we are grateful to Mr. Bruce MacDonald for collecting these. We are also grateful to NSERC (Canada) and to Dalhousie University for financial support, and one of us (J.H.) is most appreciative of the award of an I. W. Killam Memorial Scholarship.

1. S. S. Dharmatti and H. E. Weaver. Phys. Rev. **83**, 845 (1951).
2. C. Rodger, N. Sheppard, H. C. E. McFarlane and W. McFarlane. *In* Nmr and the periodic table. *Edited by* R. K. Harris and B. E. Mann. Academic Press, London. 1978; P. Granger. *In* Nmr of newly accessible nuclei. Vol. 2. *Edited by* P. Laszlo. Academic Press, New York. 1983. p. 388.
3. R. E. Wasylishen, C. Connor, and J. Friedrich. Can. J. Chem. **62**, 981 (1984).
4. R. Faure, E. J. Vincent, J. M. Ruiz, and L. Lena. Org. Magn. Reson. **15**, 401 (1981).
5. D. L. Harris and S. A. Evans, Jr. J. Org. Chem. **47**, 3355 (1982).
6. R. Annunziata and G. Barbarella. Org. Magn. Reson. **22**, 250 (1984).
7. L. Cassidei, V. Fiandanese, G. Marchese, and O. Sciacovelli. Org. Magn. Reson. **22**, 486 (1984).
8. T. C. Farrar, B. M. Trost, S. L. Tang, and S. E. Springer-Wilson. J. Am. Chem. Soc. **107**, 262 (1985).
9. J. F. Hinton and D. Buster. J. Magn. Reson. **57**, 494 (1984).
10. O. Lutz, A. Nolle, and A. Schwenk. Z. Naturforsch. Teil A, **28**, 1370 (1973).
11. J. S. Grossert, P. K. Dubey, G. H. Gill, T. S. Cameron, and P. A. Gardner. Can. J. Chem. **62**, 798 (1984).
12. J. S. Grossert, J. Hoyle, and D. L. Hooper. Tetrahedron, **40**, 1135 (1984).
13. L. P. Lindeman and J. Q. Adams. Anal. Chem. **43**, 1245 (1971).
14. E. Breitmaier, G. Haas, and W. Voelter. Atlas of carbon-13 NMR data. Plenum, New York. 1976.
15. Sadtler Research Laboratories Inc. Standard carbon-13 NMR spectra, 1976–present.
16. V. Formacek, L. Desnoyer, H. P. Kelterhals, T. Keller, and J. T. Clerc. ^{13}C data bank. Vol. 1 Brüker Physik. 1976.
17. B. Boyd (*Editor*). Selected carbon-13 NMR spectral data. Thermodynamics Research Centre, Texas A & M University, Texas. 1983.
18. L. F. Johnson and W. C. Jankowski. Carbon-13 NMR spectra. Wiley–Interscience, New York. 1972.
19. T. T.-T. Nguyen, C. Delseth, J.-P. Kintzinger, P.-A. Carrupt, and P. Vogel. Tetrahedron, **36**, 2793 (1980); J.-P. Kintzinger. *In* Oxygen-17 and silicon-29 (NMR, Basic Principles and Progress, Vol. 17), *Edited by* P. Diehl, E. Fluck, and R. Kosfeld. Springer-Verlag, Berlin. 1981; H. Iwamura, T. Sugawara, Y. Kawada, K. Tori, R. Muneynki, and R. Noyori. Tetrahedron Lett. 3449 (1979).
20. G. C. Levy, R. L. Lichter, and G. L. Nelson. Carbon-13 nuclear magnetic resonance spectroscopy. 2nd ed. Wiley, New York. 1980. Chapt. 4; D. A. R. Happer, S. M. McKerrow, and A. L. Wilkinson. Aust. J. Chem. **30**, 1715 (1977).
21. E. A. Hill and H. E. Guenther. Org. Magn. Reson. **16**, 177 (1981).
22. T. Pehk and E. Lippmaa. Org. Magn. Reson. **3**, 679 (1971); T. Pehk, E. Lippmaa, V. V. Sevostjanova, M. M. Krayuschkin, and A. J. Tarasova. Org. Magn. Reson. **3**, 783 (1971).
23. T. H. Lowry and K. S. Richardson. Mechanism and theory in organic chemistry. 2nd ed. Harper and Row, New York. 1981. p. 137.
24. H. S. Schultz, H. B. Freyermouth, and S. R. Buc. J. Org. Chem. **28**, 1140 (1963).
25. J. S. Grossert and R. F. Langler. Can. J. Chem. **55**, 407 (1977).
26. J. S. Grossert, J. Hoyle, S. Sotheeswaran, P. K. Dubey, and D. L. Hooper. Submitted.
27. J. S. Grossert and P. K. Dubey. J. Chem. Soc. Chem. Commun. 1183 (1982).
28. H. O. House and J. K. Larson. J. Org. Chem. **33**, 61 (1968).
29. C. M. Suter. The organic chemistry of sulfur. Wiley, New York. 1944. Chapt. VII.

Metabolites produced by the Scleroderris canker fungus, *Gremmeniella abietina*.[1] Part 1

WILLIAM A. AYER, YUMIKO HOYANO, M. SOLEDADE PEDRAS, AND IAN VAN ALTENA
Department of Chemistry, The University of Alberta, Edmonton, Alta., Canada T6G 2G2

Received February 7, 1986

WILLIAM A. AYER, YUMIKO HOYANO, M. SOLEDADE PEDRAS, and IAN VAN ALTENA. Can. J. Chem. **64**, 1585 (1986).

The metabolites produced in liquid culture by the Ascomycetous fungus *Gremmeniella abietina* (Lagerb.) Morelet, the causative agent of Scleroderris canker in pines, have been investigated. The major metabolite, which we have named sclerodin, is (−)-4,7-dihydroxy-2,3,3,9-tetramethyl-2,3-dihydronaphtho[1,2-*b*]furan-5,6-dicarboxylic anhydride (**1**), the enantiomer of the so-called "naphthalic anhydride from atrovenetin". Several highly colored compounds, including the enantiomer of atrovenetinone (**3**), the blue compound **6**, the red acenaphthenequinone derivative **8** (sclerodione), and the yellow 8-hydroxysclerodin (**12**) were also obtained. The blue compound **6**, named Scleroderris blue, has been prepared from **3**, and sclerodione (**8**) has been transformed into sclerodin (**1**).

WILLIAM A. AYER, YUMIKO HOYANO, M. SOLEDADE PEDRAS et IAN VAN ALTENA. Can. J. Chem. **64**, 1585 (1986).

On a étudié les métabolites qui sont produits dans un milieu du culture liquide par les champignons Ascomycetous *Gremmeniella abietina* (Lagerb.) Morelet, les agents qui causent la nécrose de Scleroderris dans les pins. Le métabolite principal, que l'on a appelé sclérodine, est l'anhydride de l'acide (−)-dihydroxy-4,7 tétraméthyl-2,3,3,9 dihydro-2,3 naphto[1,2-*b*]furanne dicarboxylique-5,6 (**1**), l'énantiomère du produit appelé «anhydride naphtalique de l'atrovénétine». On a aussi obtenu plusieurs composés fortement colorés, comme l'énantiomère de l'atrovénétinone (**3**), le composé bleu (**6**), le dérivé rouge de l'acénaphtènequinone (**8**, sclérodione) et l'hydroxy-8 sclérodine (**12**) qui est jaune. On a préparé le composé bleu (**6**), que l'on a dénommé bleu de Scléroderris, à partir du composé **3**; par ailleurs, on a transformé la sclérodione (**8**) en sclérodine (**1**).

[Traduit par la revue]

Introduction

The Ascomycetous fungus *Gremmeniella abietina* (Lagerb.) Morelet (= *Scleroderris lagerbergii*) is a virulent pathogen of pine trees in many parts of the world, causing defoliation, cankers, and mortality.[2] In North America the disease caused by this fungus, commonly known as *Scleroderris* canker, is regarded as one of the most serious tree nursery and reforestation diseases. The disease is also prevalent in Europe, where it is known as Brunchorstia dieback, and in Japan. We felt that an investigation of the metabolites produced when the fungus is grown in liquid culture might lead to identification of the compounds responsible for symptom expression and we now report the structures of the major metabolites.

Gremmeniella abietina was grown at 16–17°C on a medium of 10% V-8 juice containing 1% added glucose (3), either in still culture or in a stirred and aerated fermentation apparatus. Best yields of metabolites were obtained from the still cultures. Extraction (CH_2Cl_2) of the filtered culture broth yielded ca. 0.05 g/L of crude metabolites, while Soxhlet extraction (CH_2Cl_2) of the mycelium provided substantially more material (ca. 0.45 g from the mycelium of a 1-L growth).

The thin-layer chromatogram of the crude metabolites displayed a colorful array of compounds. These compounds were separated by silica gel chromatography to give, in order of elution, a blue compound, a colorless strongly fluorescent compound, a red compound, a dark burgundy compound, a yellow compound, and a mixture of brownish materials from which two compounds have been identified.

The colorless, strongly fluorescent compound, mp 256–257°C, $C_{18}H_{16}O_6$, shows carbonyl absorption in the ir at 1705 and 1665 cm^{-1} and readily forms a diacetyl derivative absorbing at 1778, 1760, and 1724 cm^{-1}. The ^1H nmr spectrum (Table 1) shows clearly defined signals for all sixteen protons: 2 methyl singlets, a secondary methyl doublet coupled to a methine hydrogen *geminal* to oxygen, an aromatic methyl, an aromatic hydrogen, and two H-bonded phenolic hydrogens.

The ^{13}C nmr spectrum shows five carbon singlets in the region δ 150–170 (three aromatic carbons bearing oxygen and two high-field carbonyls), six aromatic carbon singlets (δ 93–150), an aromatic carbon doublet (δ 117), and six aliphatic carbons (four methyl carbons, a secondary carbon bonded to oxygen (δ 92), and a quaternary carbon). A search of the literature revealed that this compound, for which we propose the name sclerodin, is the anhydride **1**, its diacetyl derivative being compound **1***a*. The enantiomer of sclerodin (**1**) was first obtained by oxidation of atrovenetin **2** (4) and later was isolated from cultures of *Penicillium herquei* (5) and subsequently from other fungi (6–8). Comparison of sclerodin (**1***a*) with an authentic sample of the enantiomer verified the identity in all respects other than optical rotation.[3]

Atrovenetin (**2**) has been shown to have the *R* configuration at C-2′ (9) and it provides the dextrorotatory form of **1** on oxidation (4). The absolution configuration of the (+) form of the anhydride has also been determined directly by X-ray crystallography (8). This is the first time the levorotatory form of the anhydride **1** has been isolated from natural sources. The (+) form has been obtained from *Penicillium herquei* (5), *Roesleria pallida* (6), *Roesleria hypogea*,[4] and *Aspergillus silvaticus* (8). The rotation of the anhydride isolated from *Fusicoccum putrefaciens* (7) was not reported.

The dark burgundy compound, which causes a green discoloration on contact with the skin and a blue-green discoloration of paper, was shown by high resolution electron impact mass spectrometry (eims) and chemical ionization mass spec-

[1]Preliminary accounts of parts of this work have already appeared (1, 2).

[2]For a good summary of all aspects of this disease see the book cited in ref. 2. This publication gives the proceedings of an international symposium on Scleroderris canker on conifers held in Syracuse, U.S.A., in 1983.

[3]We thank Professor L. C. Vining for kindly providing authentic samples of the enantiomer of **1** and of the ethanolate of atrovenetinone.

[4]H. Musso, personal communication.

TABLE 1. ^{1}H nuclear magnetic resonance data for metabolites and derivatives of *G. abietina*[a]

Compound	Signal (δ) (multiplicity, *J*(Hz))							
	H-4′(5′)	H-1′	H-5′(4′)	$ArCH_3$	H-2′	H-8	OH	Other
1	1.32	1.51 (d, 7)	1.55	2.84	4.72 (q, 7)	6.85	11.43 11.64	
1*b*[b]	1.29	1.34 (d, 6)	1.55	3.73	4.60 (q, 6)	6.95		
1*b*	1.29	1.48 (d, 7)	1.53	2.90	4.65 (q, 7)	7.05		4.10, 4.14 (OCH_3)
3[c]	1.26	1.46 (d, 7)	1.50	2.75	4.79 (q, 7)	6.89	13.15 14.09	
8	1.29	1.48 (d, 8)	1.54	2.75	4.67 (q, 8)	6.66	7.48 7.79	
8*a*	1.28	1.50	1.56	2.90	4.74	7.02		2.46, 2.52 ($OCOCH_3$)
9	1.25	1.48 (d, 7)	1.53	2.68	4.75 (q, 7)	6.77		
9*a*	1.22	1.45 (d, 7)	1.56	2.68	4.17 (q, 7)	6.74		4.17, 4.50 (OCH_3)
12*a*	1.32	1.50 (d, 6.5)	1.56	2.83	4.73 (q, 6.5)		6.47 11.94	4.10 (OCH_3)
12*a*[b]	1.34	1.45 (d, 6.5)	1.56	3.09	4.67 (q, 6.5)		4.95	4.12 (OCH_3)
12*b*	1.32	1.52 (d, 7)	1.56	2.88	4.67 (q, 7)			3.92, 4.13, 4.14 (OCH_3)

[a]In $CDCl_3$ unless otherwise noted.
[b]In pyridine-d_5.
[c]In DMSO-d_6.

trometry (cims) to possess the molecular formula $C_{19}H_{16}O_6$. The ^{1}H nmr spectrum (Table 1) was very similar to that of the anhydride **1**. The ^{13}C nmr spectrum, determined in DMSO-d_6, shows carbonyl peaks at δ 198 and 196 (those of the anhydride **1** appear at ~δ 166) and a signal at δ 88, which is not present in the spectrum of the anhydride. When the spectrum is determined in CD_2Cl_2, additional carbonyl signals appear near δ 176 and the intensity of the signal at δ 88 is diminished. These data suggested that the compound is the triketone **3**, present mainly in DMSO as the hydrate **4***a*. The enantiomer of this compound, atrovenetinone, has previously been prepared (5) by oxidation of atrovenetin (**2**) with benzoquinone. Atrovenetinone was characterized as its crystalline ethanolate. Crystallization of the dark burgundy compound from ethanol provided pale yellow needles of **4***b*, which showed the same spectral characteristics (^{1}H nmr, ir) and tlc behavior as an authentic sample of the enantiomer.[2] Aerial oxidation of **4***a* gave the levorotatory anhydride, **1**, confirming the absolute stereochemistry at C-2′. It was found that when a solution of compound **3** was painted on freshly peeled pine, the characteristic blue-green color of *Scleroderris* infected wood developed.

When the solvent system used for the chromatographic separation of **3** contained acetone, the acetone adduct **5***a* (as a mixture of epimers) was obtained instead of compound **3**. Compound **5***a*, which readily forms a diacetyl derivative **5***b*, is an artifact formed during separation since it is not present in the original extract. Treatment of **3** with acetone in the presence of a catalytic amount of acetic acid readily gives **5***a*.

The blue compound proved rather unstable and difficult to purify, but after repeated silica gel chromatography and crystallization from ethanol, a deep blue crystalline material was obtained. Efforts to determine the molecular formula of this compound, which we believe to be responsible, at least in part, for the bluish-green coloration of the wood of *Scleroderris* infected pine, were initially unsuccessful. The highest mass peak in the eims appeared at *m/z* 337 and corresponded to the ion $C_{19}H_{15}NO_5$. Another prominent peak occurred at *m/z* 326 ($C_{19}H_{18}O_5$). The cims did not afford a recognizable parent ion. However, field desorption mass spectrometry[5] suggested a molecular weight of 663 amu. Addition of the two high mass eims fragments then suggested that the molecular formula is $C_{38}H_{33}NO_{10}$ (mw 663). The ^{1}H nmr spectrum is similar to that of the anhydride **1** and the triketone hydrate **4***a* with most signals doubled. When a solution of the blue compound in $CHCl_3$ is allowed to stand in the presence of air, sclerodin (**1**) is obtained. The ultraviolet–visible spectrum ($CHCl_3$) of the blue compound shows λ_{max} 268, 368, 405 (sh), and 608 nm. Narasimhachari and Vining (5) have previously suggested that the characteristic green pigment of *Penicillium herquei* might be formed by a ninhydrin-like reaction between atrovenetinone (**3**) and amino acids, but they were unable to completely characterize the pigment. In our hands, treatment of a buffered solution of glycine with atrovenetinone (**3**) in aqueous dioxane (10) and purification of the product by flash chromatography gave blue crystalline material identical in all respects with the compound isolated from *G. abietina*. The pigment, for which we suggest the trivial name Scleroderris blue, thus possesses structure **6**. Scleroderris blue (**6**) changes color with changing pH: in basic solution it appears green whereas in acidic solution it is deep blue. Since the uv spectrum of **6** is almost identical with that reported (5) for the green pigment of *P. herquei*, we believe that this pigment also has structure **6**.

The red compound, mp 210–212°C, $C_{19}H_{16}O_5$, has one

[5]We thank Professor G. Wood, University of Windsor, for the field desorption spectrum.

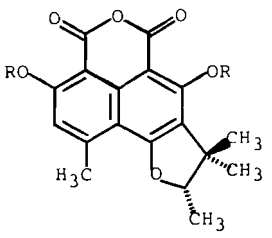

1 R = H
1*a* R = Ac
1*b* R = CH_3

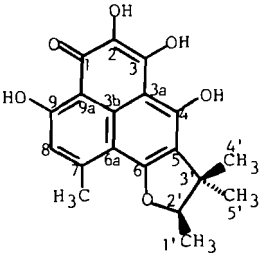

2

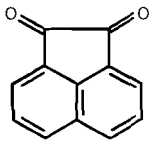

7

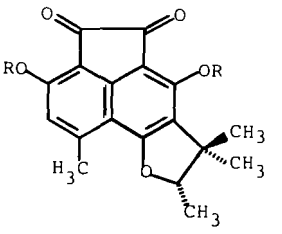

8*a* R = H
8*b* R = Ac

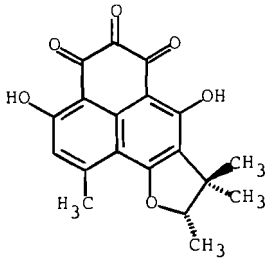

3

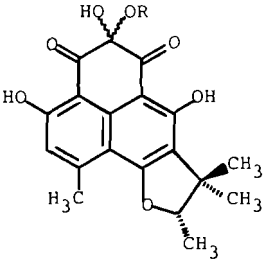

4*a* R = H
4*b* R = CH_2CH_3

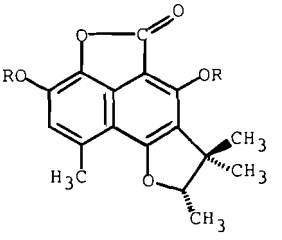

9 R = H
9*a* R = CH_3

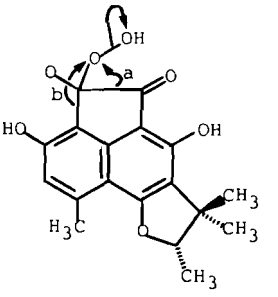

10

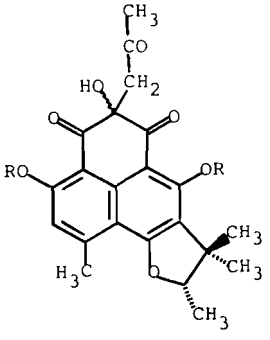

5*a* R = H
5*b* R = AC

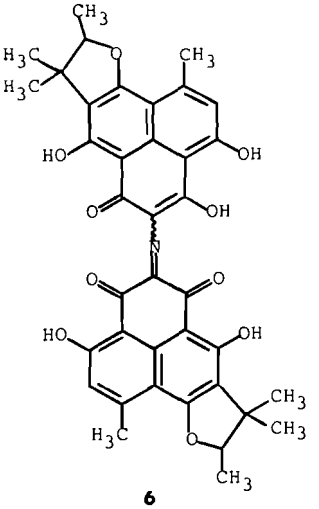

6

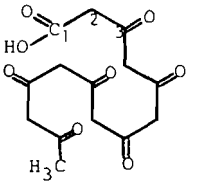

11

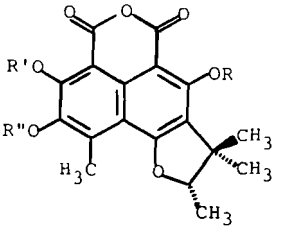

R = R' = R" = H
12*a* R = CH_3 R' = R" = H
12*b* R = R' = R" = CH_3

oxygen less than the anhydride **1**. The ^1H nmr spectrum (Table 1) is very similar to that of **1** but the ^{13}C nmr spectrum shows ketonic carbonyls at δ 189.8 and 186.3. The ir spectrum shows carbonyl absorption at 1714 and 1690 cm^{-1}. This compound readily forms a diacetyl derivative, the ir spectrum of which shows carbonyl absorption at 1780 and 1740 cm^{-1}. Acenaphthenequinone (**1**) absorbs at 1785 and 1724 cm^{-1} (11). This evidence suggested that the red compound, for which we propose the name sclerodione, has structure **8** (the diacetate is **8***a*). The structure was confirmed by alkaline peroxide oxidation of **8** to give, after acidification, the anhydride **1** (migration "a" in **10**), along with the lactone **9**, the product of Dakin oxidation (migration "b" in **10**) followed by peroxide cleavage of the resulting α-ketoacid. The orientation of the lactone ring in **9** was proven by methylation (CH_2N_2) to give **9***a*. The ether **9***a* shows two distinct methoxyl signals in the ^1H nmr, one at δ 4.17 and one at δ 4.50. The latter signal must be deshielded by the lactone carbonyl group. Irradiation of the methoxyl protons at δ 4.17 causes an 8.8% nOe (nuclear Overhauser effect) enhancement of the aromatic proton, whereas irradiation of the δ 4.50 methoxyl signal causes no detectable nOe enhancement. To the best of our knowledge, sclerodione (**8**) represents the first acenaphthenquinone isolated from natural sources. Biosynthetic studies (12) have shown that the naturally occurring phenalenones of the atrovenetrin (**2**) type are prenylated heptaketides formed from a heptaketide chain folded as in **11**. In a subsequent paper in this series[6] we will show that the *G. abietina* metabolites are formed by this pathway and that it is C-2 of **11** which is lost in the formation of both **1** and sclerodione (**8**).

The more polar components of the *G. abietina* extract (brownish streak on tlc) proved difficult to purify. However, after the crude material was treated with ethereal diazomethane, a bright yellow crystalline compound $C_{19}H_{18}O_7$ was isolated by ptlc. The compound is assigned structure **12***a* on the basis of the following observations. Its ^1H nmr spectrum (Table 1) is similar to that of the anhydride **1** except that it lacks the C-8 aromatic proton signal and it shows an aromatic methoxyl at δ 4.10. The ^{13}C nmr spectrum is similar to that of **1** except that the signal for C-8 in **1** (d, δ 117.4) is replaced by a singlet in the δ 150 ppm region and the aromatic methyl signal is shifted upfield to δ 15.1 (δ 23.6 in **1**) as is expected for a methyl *ortho* to a phenolic OH

[6]W. A. Ayer, M. S. Pedras, and D. E. Ward, manuscript in preparation.

(13). When the ^1H nmr spectrum is determined in pyridine-d_5, the aromatic methyl is shifted downfield by 0.26 ppm, indicating the hydroxyl at C-8 is not methylated (14). Since the methoxyl CH_3 did not experience a pyridine-induced shift, it is believed to be located at C-4 rather than C-9, although this is not rigorously established. Treatment of **12***a* with ethereal diazomethane furnished the trimethyl ether **12***b*. Trimethyl ether **12***b* was also isolated from the ptlc of the diazomethane treated polar compounds. It is presumed that compound **12** (8-hydroxysclerodin) is produced by the fungus and that **12***a* is formed during the diazomethane treatment. It is worthwhile noting that the anhydride carbonyls in the monomethyl ether **12***a* absorb at 1750 and 1685 cm^{-1}, while in the trimethyl ether they absorb at 1760 and 1725 cm^{-1}. In the anhydride **1**, where both carbonyls are H-bonded, the carbonyl absorption appears at 1705 and 1665 cm^{-1}.

Preliminary tests indicate that the crude metabolites of *G. abietina* cause symptoms (browning of needles) similar to those caused by the fungus in pine seedlings.[7] Biological testing of the individual compounds is being initiated. We feel that the greenish discoloration of the wood of pines suffering from Scleroderris canker may be due to the presence of the colored compounds described herein, particularly **6**, although we have not as yet attempted to isolate the compounds from diseased wood.

Experimental

All solvents except diethyl ether were distilled prior to use. ACS quality anhydrous diethyl ether was used without purification. Skellysolve B refers to Skelly Oil Company light petroleum, bp 62–70°C. Pyridine was distilled from CaH_2 and stored over molecular sieves, acetic anhydride was dried over P_2O_5 and distilled from sodium acetate.

Analytical thin-layer chromatography (tlc) was carried out on glass microscope slides (75 × 25 or 75 × 50 mm) coated (ca 0.3 mm) with silica gel G (E. Merck, Darmstadt, or Terochem, Edmonton) containing 1% electronic phosphor (General Electric, Cleveland). Preparative thin-layer chromatography (ptlc) was carried out on glass plates (20 × 20 cm) coated (0.6 mm) with the same adsorbent. Materials were detected by visualization under an ultraviolet (uv) lamp (254 or 350 nm) or by spraying with a solution of vanillin (1%) in concentrated sulphuric acid. Flash chromatography (15) was performed using Merck Silica Gel 60 (40–63 μm). Small scale column chromatography was performed with Silica Gel 60 (<0.08 mm, Macherey Nagel, Dueren) whereas larger scale chromatography was carried out with Silica Gel 60 (0.05–0.2 mm, Macherey Nagel, Dueren).

High resolution mass spectra (hrms) were recorded on an A.E.I. MS-50 mass spectrometer coupled to a DS 50 computer. Chemical ionization mass spectra (cims) were recorded on an A.E.I. MS-9 spectrometer. Data are reported as *m/z* (relative intensity). Unless diagnostically significant, peaks with intensities less than 20% of the base peak are omitted. Infrared (ir) spectra were recorded on a Nicolet 7199 interferometer. Ultraviolet (uv) spectra were recorded on a Unicam SP 1700 ultraviolet spectrophotometer. ^1H nuclear magnetic resonance (^1H nmr) spectra were measured with a Varian HA-100 spectrometer, a Varian HA-100 spectrometer interfaced to a Digilab FTS/NMR-3 data system, a Brüker WH-200 spectrometer, or a Brüker WH-400 spectrometer. Carbon-13 nuclear magnetic resonance (^{13}C nmr) spectra were measured on a Brüker HFX-90 spectrometer interfaced to a Nicolet 1085 computer, a Varian HA-100 spectrometer interfaced to a Digilab FTS/NMR-3 data system, or a Brüker WH-200 spectrometer. All nuclear magnetic resonance measurements employed tetramethylsilane (TMS) as an internal standard and are reported in ppm downfield from TMS (δ). Optical rotations were measured on a Perkin Elmer Model 141 polarimeter. Melting points were determined on a Fisher–Johns melting point apparatus and are uncorrected.

Growth of Gremmeniella abietina *and isolation of metabolites*

Slant cultures of *Gremmeniella abietina* (strain C-699 or strain C-708, Canadian Forestry Service) were maintained on potato dextrose agar at 4°C. Two 250-mL shake cultures (10% filtered V-8 juice and 1% glucose medium) in 500-mL Erlenmeyer flasks were inoculated with one slant tube culture and the inoculum was gently shaken for 4 weeks at 15–17°C. Ten 2.8-L Fernbach flasks each containing 1 L of the same liquid medium were inoculated with ca. 50 mL each of an aqueous suspension of mycelium and the flasks were kept at 15–17°C for 4 weeks. The mycelium was separated by filtration through cheesecloth and the wet mycelium was extracted in a Soxhlet extractor with CH_2Cl_2 for 2 days. The broth was filtered again through a pad of Celite and the filtrate was extracted three times with CH_2Cl_2. The mycelium extract gave ~0.5 g/L of the crude metabolites while the broth extract gave ~0.05 g/L. Separation of the crude metabolites (mycelium) by flash chromatography (15) gave, in order of elution (solvent system $CHCl_3$:Skellysolve B:acetic acid (10:10:1)), fractions rich in a blue compound, a colorless, strongly fluorescent compound, a red compound, a dark burgundy compound, a yellow compound, and a mixture of brownish materials. The fractions were further purified as indicated for the individual components.

*Sclerodin (**1**)*

Sclerodin (**1**) was obtained after silica gel column chromatography (R_f 0.9 ($CHCl_3$:CH_3OH:acetic acid, 97:5:1)) and crystallization from 95% ethanol or CH_2Cl_2 – Skellysolve B, mp 256–257°C; $[\alpha]_D^{24}$ −72.6°C (*c* 1.34, $CHCl_3$); ir ($CHCl_3$ cast): 3100 (br), 1705, 1665, 1610, 1460, 1335, 1043, 870, 820 cm^{-1}; ^1H nmr, see Table 1; ^{13}C nmr ($CDCl_3$) δ: 14.5, 20.7, 23.6, 25.6, 43.5, 92.1, 93.5, 97.3, 108.5, 117.2, 119.1, 135.4, 149.8, 164.9, 165.4, 166.0, 166.1; hrms, *m/z* calcd. for $C_{18}H_{16}O_6$ (M^+): 328.0948; found: 328.0944 (31), 313 (100). The ir and ^1H nmr spectra of sclerodin were identical with those of an authentic sample of the enantiomer.

*Diacetylsclerodin (**1**a)*

Sclerodin (**1**) was stirred in an excess of acetic anhydride and pyridine overnight at room temperature. The reaction mixture was evaporated to dryness. The pale yellow compound was recrystallized from chloroform – Skellysolve B, mp 178–180°C; $[\alpha]_D$ −32.5° (*c* 0.48, $CHCl_3$); ir ($CHCl_3$ cast): 1778, 1760, 1724, 1605, 1600 cm^{-1}; hrms, *m/z* calcd. for $C_{22}H_{20}O_8$: 412.1158; found: 412.1161 (10.5), 370 (26), 328 (64), 314 (26), 313 (100).

*Sclerodin dimethyl ether (**1**b)*

Sclerodin (**1**) (60 mg) in CH_2Cl_2 was treated with excess ethereal diazomethane for 12 h. After evaporation of the solvent, the residue was purified by chromatography (eluant benzene:acetone, 9:1) and crystallization (CH_2Cl_2 – Skellysolve B) to give the dimethyl ether **1***b*, mp 193–194°C; $[\alpha]_D$ −84.0° (*c* 0.42, $CHCl_3$); ir ($CHCl_3$): 1740, 1714, 1600, 1590, 1560 cm^{-1}; ^1H nmr, see Table 1; ^{13}C nmr ($CDCl_3$): δ 14.0, 21.5, 24.0, 25.8, 43.9, 56.3, 62.6, 90.9, 100.6, 101.2, 110.7, 113.1, 125.1, 137.4, 147.3, 157.6, 157.8, 163.9, 164.3, 165.6; hrms, *m/z* calcd. for $C_{20}H_{20}O_6$: 356.1260; found: 356.1262 (55), 341 (100), 297 (19).

*Triketone (**3**) and triketone ethanolate (**4**b)*

The crude dark burgundy fraction was further purified by flash chromatography using ether:CH_2Cl_2 (4:1) as the eluant. Crystallization from acetone–benzene provided dark purple crystals of **3**, mp 220–222°C; ir (CH_2Cl_2 cast): 3390, 1720, 1634, 1605 cm^{-1}; ^1H nmr, see Table 1; hrms, *m/z* calcd. for $C_{19}H_{16}O_6$: 340.0947; found: 340.0942 (28), 327 (18), 312 (25), 297 (100), 269 (42). Crystallization of **3** from 95% ethanol gave pale yellow crystals of the ethanolate **4***b*, mp 223–226°C, identical (ir, ^1H nmr) with an authentic sample of atrovenetinone ethanolate. Because of the strong absorption of **3** in the visible, and because of the low solubility of **4***b* in ethanol, it was not possible to obtain meaningful $[\alpha]_D$ values for these substances.

*Acetone adduct of **3** (**5**a)*

Compound **5***a*, shown to be an artifact produced during isolation

[7] Y. Hiratsuka, Northern Forest Research Centre, Edmonton, personal communication.

when acetone was employed as an eluant, was prepared by stirring compound **3** (20 mg) in acetone (2 mL) containing acetic acid (10 drops) at room temperature for 2 h. The reaction was monitored by tlc until no compound **3** remained and then the product was isolated and purified by ptlc ($CHCl_3$:CH_3OH:acetic acid, 189:10:1) to give **5***a* (13 mg) as an amorphous solid; ir ($CHCl_3$ cast): 3400, 1730, 1710, 1635, 1605; uv (CH_3OH): λ_{max} (ε): 221 (33 000), 230 (27 000 shoulder), 252 (30 000 shoulder), 260 (41 000), 341 (15 000), 364 (11 000 shoulder) nm; ^1H nmr ($CDCl_3$), δ: 13.32, 12.80 (phenolic OH's), 6.76 (q, J = 1 Hz, H-8), 4.64 (q, J = 6.5 Hz, H-2′), 3.70 (bs, OH), 3.30 (s, $COCH_2$), 2.78 (d, 1 Hz, $ArCH_3$), 2.23 (s, $COCH_3$), 1.52 (s, H-5′ (4′)), 1.46 (d, J = 6.5 Hz, H-1′), 1.30 (s, H-4′ (4′)); hrms, m/z calcd. for $C_{22}H_{22}O_7$: 398.1368; found: 398.1364 (45); 383 (4), 355 (28), 313 (100), 297 (28), 157 (14).

Scleroderris blue (6)

Scleroderris blue (**6**), the least polar of the colored compounds, was isolated from the early dark blue colored fractions of the flash chromatography by ptlc over silica gel (double elution, eluant Skellysolve B:acetone:acetic acid (15:4:1)). Crystallization from ethanol gave tiny deep blue crystals, mp >300°C; ir ($CHCl_3$ cast): 2930, 2858, 1730, 1608, 1550, 1485, 1440, 1384, 1335, 1308; uv ($CHCl_3$) λ_{max} (ε): 268 (30 000), 368 (23 000), 405 (sh), 608 (18 000); ^1H nmr ($CDCl_3$),[8] δ: 1.12 (6H, bd), 1.18 (6H, bs), 1.35 (6H, bs), 2.73 (6H, bs), 4.58 (2H, m), 6.80 (2H, bs), 13.5 (2H, bs), 14.5 (2H, bs); ^1H nmr (pyridine-d_5),[8] δ: 1.20 (6H, bs), 1.36 (6H, bd), 1.41 (6H, bs), 2.74 (6H, bs), 4.55 (2H, m), 6.92 (2H, bs); molecular weight: 663 amu (determined by field desorption mass spectrometry).

Preparation of Scleroderris blue (6) from triketone 3

Triketone **3** (8.7 mg) was dissolved in dioxane (2 mL). Glycine (15 mg) in phosphate buffer (pH 7, 1 mL) was added and the reaction mixture was heated at 60°C overnight. The reaction mixture was concentrated and then extracted with CH_2Cl_2. The residue was purified by ptlc ($CHCl_3$: acetic acid, 99:1) to give compound **6** (2 mg) identical in all respects (tlc, uv, ir, ms) with naturally occurring Scleroderris blue.

Aerial oxidation of Scleroderris blue

A small amount of compound **6** was dissolved in dioxane and a drop of 6 *N* HCl was added. After a few minutes of shaking, the blue color disappeared. The solution was diluted with water and extracted with methylene chloride. The organic layer was dried and evaporated to give a white solid, which proved to be identical with sclerodin **1** (ir, tlc). The anhydride **1** was also obtained when a chloroform solution of **6** was left at room temperature for several days.

Sclerodione (8)

Sclerodione has an R_f on tlc only slightly less than the triketone **3** and is often difficult to observe. It may be visualized on tlc by spraying with vanillin – sulfuric acid to give a distinct purple spot. It may be separated by ptlc (double elution) using $CHCl_3$:Skellysolve B:acetic acid (14:5:1) as the eluant. Crystallization from CH_2Cl_2 – Skellysolve B gives bright red crystals, mp 210–212°C; $[\alpha]_D$ −115.3° (*c* 0.17, $CHCl_3$); ir ($CHCl_3$ cast): 3480, 1714, 1690, 1625, 1610 cm^{-1}; ^1H nmr, see Table 1; ^{13}C nmr ($CDCl_3$), δ: 14.5, 21.0, 22.0, 25.8, 43.3, 92.0, 106.2, 107.2, 109.2, 117.4, 119.6, 146.4, 150.9, 154.3, 154.9, 164.3, 186.3, 189.8; hrms, m/z calcd. for $C_{18}H_{16}O_5$: 312.0998; found: 312.0997 (50), 297 (100), 284 (6), 269 (55).

Diacetylsclerodione (8a)

Sclerodione (5 mg) was treated with acetic anhydride and pyridine at room temperature overnight. Evaporation and chromatography of the residue on silica gel (eluant $CHCl_3$) gave diacetylsclerodione (**8***a*) as an oil; ir (film): 1780, 1740, 1710, 1610, 1590 cm^{-1}; ^1H nmr, see Table 1; hrms, m/z calcd. for $C_{22}H_{20}O_7$: 296.1202; found: 396.1214 (16), 354 (25), 312 (100), 297 (92), 269 (22).

Oxidation of sclerodione (8)

Sclerodione (**8**, 10 mg) was dissolved in dioxane (3 mL). Potassium hydroxide (50 mg) in methanol (2 mL) was added followed by 30% hydrogen peroxide (0.1 mL). The reaction mixture was heated at 50°C for 10 min, cooled and acidified with dilute H_2SO_4, then extracted with CH_2Cl_2. The residue (6 mg) was chromatographed on silica gel (5 g), eluting with Skellysolve B:$CHCl_3$ (1:1) containing 0.1% acetic acid. Sclerodin (**1**) (2 mg) was eluted first, then the lactone **9** (1.4 mg); ir ($CHCl_3$ cast): 1726, 1660, 1640, 1620 cm^{-1}; ^1H nmr, see Table 1; hrms, m/z calcd. for $C_{17}H_{16}O_5$: 300.0998; found: 300.0997 (60), 285 (100), 267 (10), 257 (9). The dimethyl ether **9***a* was prepared by treating compound **9** with ethereal diazomethane.

8-Hydroxysclerodin methyl ether (12a) and 8-hydroxysclerodin trimethyl ether (12b)

A portion (100 mg) of the brownish, polar fraction obtained from the extract by flash chromatography was dissolved in ether and treated with excess ethereal diazomethane for 1 h. The residue left after removal of the solvent was purified by ptlc (eluant, ether: Skellysolve B : acetic acid (75:25:1)) to give 8-hydroxysclerodin methyl ether (**12***a*, 10 mg) as yellow crystals (from ether – Skellysolve B), mp 213–214°C; $[\alpha]_D$ −16° (*c*, 0.11, $CHCl_3$); ir ($CHCl_3$ cast): 3400, 1750, 1685, 1600 cm^{-1}; uv (MeOH) λ_{max} (ε): 211 (28 400), 234 (17 300), 257 (26 900), 309 (3280), 356 (8360), 396 (10 700 sh), 409 (11 000) nm; ^1H nmr: see Table 1; hrms, m/z calcd. for $C_{19}H_{18}O_7$: 358.1052; found: 358.1064 (76), 343 (100).

The less polar trimethyl ether **12***b* (2 mg) was also isolated from the ptlc. It could be prepared from **12***a* by treatment with diazomethane. Compound **12***b* was obtained as a glassy solid: ir ($CHCl_3$ cast): 1760, 1725, 1575 cm^{-1}; ^1H nmr, see Table 1; hrms, m/z calcd. for $C_{21}H_{22}O_7$: 386.1366; found: 386.1366 (97), 371 (100), 353 (11), 343 (9), 327 (17).

[8]Most of the peaks are poorly resolved overlapping signals.

Acknowledgements

We gratefully acknowledge the financial support provided by the Natural Sciences and Engineering Research Council of Canada. We thank Dr. Y. Hiratsuka, Northern Forest Research Centre, Edmonton, for bringing this problem to our attention and for providing cultures of *G. abietina*, Dr. G. Wood, University of Windsor, for the field desorption mass spectrum of compound **6**, and Prof. L. Vining, Dalhousie University, for samples of the enantiomers of compounds **1** and **4***b*.

1. W. A. Ayer, Y. Hoyano, I. van Altena, and Y. Hiratsuka. Rev. Latinoamer. Quim. **13**, 84 (1982).
2. W. A. Ayer and Y. Hiratsuka. *In* Scleroderris canker of conifers. *Edited by* P. D. Manion. Martinus Nijhoff, Dr. W. Junk Publishers, The Hague. 1984. pp. 54–58.
3. C. E. Dorworth. Can. J. Bot. **50**, 751 (1972).
4. D. H. R. Barton, P. de Mayo, and G. A. Raistrick. Tetrahedron, **6**, 48 (1959); I. C. Paul and G. A. Simm. J. Chem. Soc. 1097 (1965).
5. N. Narasimhachari and L. C. Vining. Can. J. Chem. **41**, 641 (1963).
6. G. W. van Eijk. Phytochemistry, **10**, 3263 (1971).
7. C. Rossi and R. Ubaldi. Ann. Ist. Super. Sanita, **9**, 320 (1973).
8. K. Homma, K. Fukuyama, Y. Katsube, Y. Kimura, and T. Hamosaki. Agric. Biol. Chem. **44**, 1333 (1980).
9. J. S. Brooks and G. A. Morrison. J. Chem. Soc. Chem. Commun. 1359 (1971).
10. H. Wittman, A. K. Mueller, and E. Ziegler. Monatsh. Chem. **100**, 497 (1969).
11. J. G. Grasseli. Atlas of spectral data and physical constants for organic compounds. Chemical Rubber Co. Press, Cleveland. 1973. p. B92.
12. T. J. Simpson. J. Chem. Soc. Perkin Trans. 1, 1233 (1979).
13. J. B. Stothers. Carbon-13 NMR spectroscopy. Academic Press, New York. 1972. p. 202.
14. P. V. Demarco, E. Farkas, D. Doddrell, B. L. Mylari, and E. Wenkert. J. Am. Chem. Soc. **90**, 5480 (1968).
15. W. C. Still, M. Kahn, and A. Mitra. J. Org. Chem. **43**, 2923 (1978).

Alternariol: evidence for biosynthesis via norlichexanthone

E. E. STINSON,[1] W. B. WISE, R. A. MOREAU, A. J. JUREWICZ, AND P. E. PFEFFER

Eastern Regional Research Center,[1] United States Department of Agriculture, Agricultural Research Service, Philadelphia, PA 19118, U.S.A.

Received May 1, 1985[2]

E. E. STINSON, W. B. WISE, R. A. MOREAU, A. J. JUREWICZ, and P. E. PFEFFER. Can. J. Chem. **64**, 1590 (1986).

Alternaria molds produce numerous mycotoxins including many α-dibenzopyrones such as alternariol (AOH) and related polyketides. AOH, presumed to be the initial α-dibenzopyrone produced, has for 20 years been considered to be biosynthesized from a single polyketide chain in a single step reaction. The present study presents evidence that the reaction may proceed through an intermediate, norlichexanthone (NLX). Bond cleavage and rearrangement of NLX to form AOH may be similar to aflatoxin B_1 formation from sterigmatocystin. The 2-D INADEQUATE experiment was used to assign the ^{13}C spectrum of AOH and to distinguish between possible mechanisms by which AOH may be synthesized from 1-^{13}C and 2-^{13}C acetates via NLX.

E. E. STINSON, W. B. WISE, R. A. MOREAU, A. J. JUREWICZ et P. E. PFEFFER. Can. J. Chem. **64**, 1590 (1986).

Les moisissures *Alternaria* produisent diverses mycotoxines, y compris plusieurs α-dibenzopyrones, comme l'alternariol (AOH) et des polycétides apparentés. Il est supposé que le AOH est l'α-dibanzopyrone qui est produite initialement et, depuis plus de 20 ans, on a considéré que ce composé est produit par une biosynthèse impliquant une seule chaîne polycétide réagissant au cours d'une seule réaction. Dans le présent travail, on présente des données suggérant que le réaction procède peut-être par le biais d'un intermédiaire, la norlichexanthone (NLX). Il est possible que le bris de la liaison et la transposition de la NLX pour former le AOH se produisent d'une façon semblable à ce qui se produit lors de la formation de l'aflotoxine B_1 à partir de la stérigmatocystine. On a fait appel à des expériences de 2-D INADEQUATE pour attribuer le spectre rmn du ^{13}C du AOH et pour distinguer entre les mécanismes possibles pour la synthèse du AOH à partir d'acétates marqués au ^{13}C dans les positions 1 et 2 et par le biais de la NLX.

[Traduit par la revue]

The *Alternaria*, a group of molds frequently involved in food spoilage, produce a wide variety of metabolites including the mycotoxins alternariol (AOH) (**1**) and alternariol monomethyl ether (AME) (**2**). These have been identified in food products contaminated by *Alternaria* (1). We became interested in the biosynthesis of these substances during the course of an investigation into the structure of fungal polyketide synthetases. The soluble enzyme responsible for the production of AOH seemed a good candidate for this study because of what then appeared to be the direct nature of the reaction. The synthesis of AOH had been reported to involve assembling a heptaketide chain, aromatizing, and release of the AOH in a single step. The pattern given for assembly of AOH and AME from 1-^{14}C acetate is shown in **3** (2, 4). A procedure was given for partial purification of the enzyme. The resulting solution also possessed O-methyltransferase activity capable of forming AME from AOH by a transmethylation reaction involving S-adenosyl methionine (SAM) (2, 3).

We report results of the present study, which indicate that NLX is a precursor of AOH.

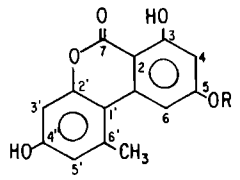

1-2

1, R = H
2, R = Me

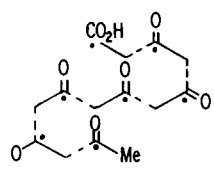

3

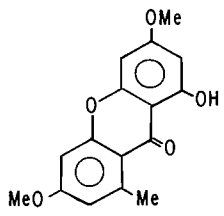

4

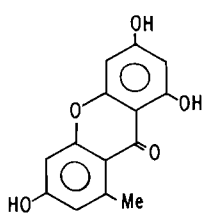

5

Results and discussion

During our investigation, repeated attempts to duplicate the purification procedure for AOH synthetase were unsuccessful (5, 6). Using a cell-free extract prepared from a high AOH-producing strain, NRRL 6434, of *A. tenuis*, the species employed in the earlier biosynthetic studies, no production of AOH could be confirmed upon addition of ^{14}C labeled Ac-CoA and Mal-CoA to the cell-free extract.

However, we observed incorporation of ^{14}C Ac-CoA and Mal-CoA into materials on numerous zones of the tlc (thin-layer chromatography) plate, with heavy ^{14}C incorporation into a zone immediately above AOH. The same cell-free extract also catalyzed the formation of large amounts of ^{14}C AME in the presence of AOH and ^{14}C SAM (as Gatenbeck had observed for his preparation), although whole cells of this strain of the fungus produce mainly AOH, not AME. Our inability to confirm the formation of AOH led us to consider the possibility that the previous group may actually have reported the formation of some other component that could not be separated from AOH by the methods then available.

Our detection method for AOH used the high resolution power of tlc and the automated linear analyzer for ^{14}C detection instead of the less selective paper chromatography used by the previous group (2).

Also, the previous group relied upon repeated recrystallization of product, which had been diluted with a large excess of exogenous AOH, to constant specific activity as confirmation that the counts were in the AOH rather than in some impurity. They used H_2O–EtOH mixtures as solvent, although it is known that recrystallization from solvent pairs often leads to impure material. In fact, it had been reported previously that recrys-

[1]Author to whom correspondence may be addressed.
[2]Revision received March 31, 1986.

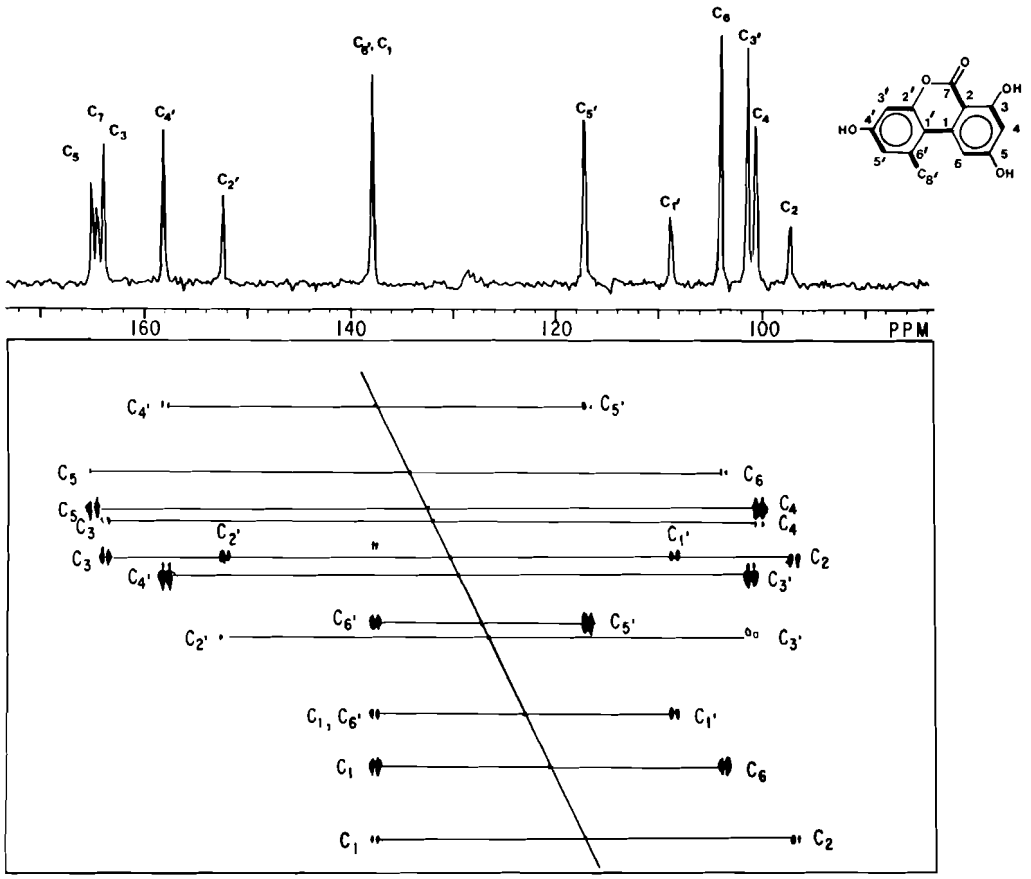

FIG. 1. 100-MHz ^{13}C 2-D INADEQUATE contour plot for a 0.95 *M* solution of alternariol (biosynthetically prepared from equal amounts of [1-^{13}C] and [2-^{13}C] acetates). Total acquisition time, 84 h. 1-D nmr shown above.

tallization from this solvent mixture (H_2O–EtOH) failed to remove a colored impurity from AOH (7). This was also our experience, as tlc examination disclosed that careful precipitation of AOH by the described method actually resulted in retention of a number of congeners.

An alternative mechanism for AOH biosynthesis has been suggested (1), which would proceed through the rearrangement of xanthone, in analogy to a well-documented step in aflatoxin biosynthesis (8). This notion is strongly supported by the recent isolation from *Penicillium notatum* of lichenxanthone (**4**) as a congener of AME (9). The same general mechanism, oxidative cleavage of an aromatic ring followed by rotation of the fragmented aryl structure, has also been reported in the formation of the α-pyrone structure of chartreusin in the *Streptomycetae* (10). These and other considerations led us to consider norlichexanthone, NLX (**5**), as a possible precursor.

Incorporation of norlichexanthone (NLX)

Particular care was taken with the purification procedure used to establish incorporation of norlichexanthone into AOH since it appears that the radioactivity measured in the earlier work (2, 3) may not have been associated with alternariol.

^{14}C-labeled norlichexanthone was added to a stationary culture of *Alternaria tenuis* shortly after vigorous growth had ceased (Day 10). Previous experiments in our laboratory had shown that this was the period for optimal incorporation of ^{14}C-labeled acetate into AOH. The mycelia were harvested after a suitable incubation period (Days 10–12), and extracted with ethyl acetate. AOH was isolated from this mycelial extract. Two different solvent systems were used in succession for flash chromatography, and a normal and a reverse phase system were used for final purification by preparative tlc. Purification of the metabolite to constant specific radioactivity by these procedures indicated 3.8% incorporation of NLX into AOH in vivo.

^{13}C spectral assignment of alternariol

As a prerequisite for investigation of the biosynthetic pathway to the production of AOH via NLX, it was necessary to establish an unambiguous assignment of the complete ^{13}C spectrum of this molecule. The ^{13}C shifts of alternariol have previously been only partly assigned (12), but we were able to make a full assignment by means of 2-D ^{13}C INADEQUATE nmr (13). To this end, we used alternariol produced by *Alternaria tenuis* grown on a medium supplemented with 1-^{13}C and 2-^{13}C acetate in equal amounts (Fig. 1). It was anticipated that ^{13}C–^{13}C coupling would be observed with greater probability (and thus the signal enhancement would be greater) between C1 and C2 of each pair of adjacent acetate residues, beginning at C6′–C5′. A similar phenomenon has been observed with 1-D ^{13}C nmr (14). The starting point in assigning the signals from the aromatic carbons was the signal of the ring carbon C6′ (138.3 ppm) directly bonded to the C8′ methyl group at 25.3 ppm. This signal was identified by the proton coupled ^{13}C spectra (not shown), which showed a quartet (5.8 Hz) at this location. In addition, long range 3-bond coupling was observed from the CH_3 group to the signal with split resonances (due to this geminal proton; 160 Hz) centered at 117.6 ppm, which was thus identified as C5′.

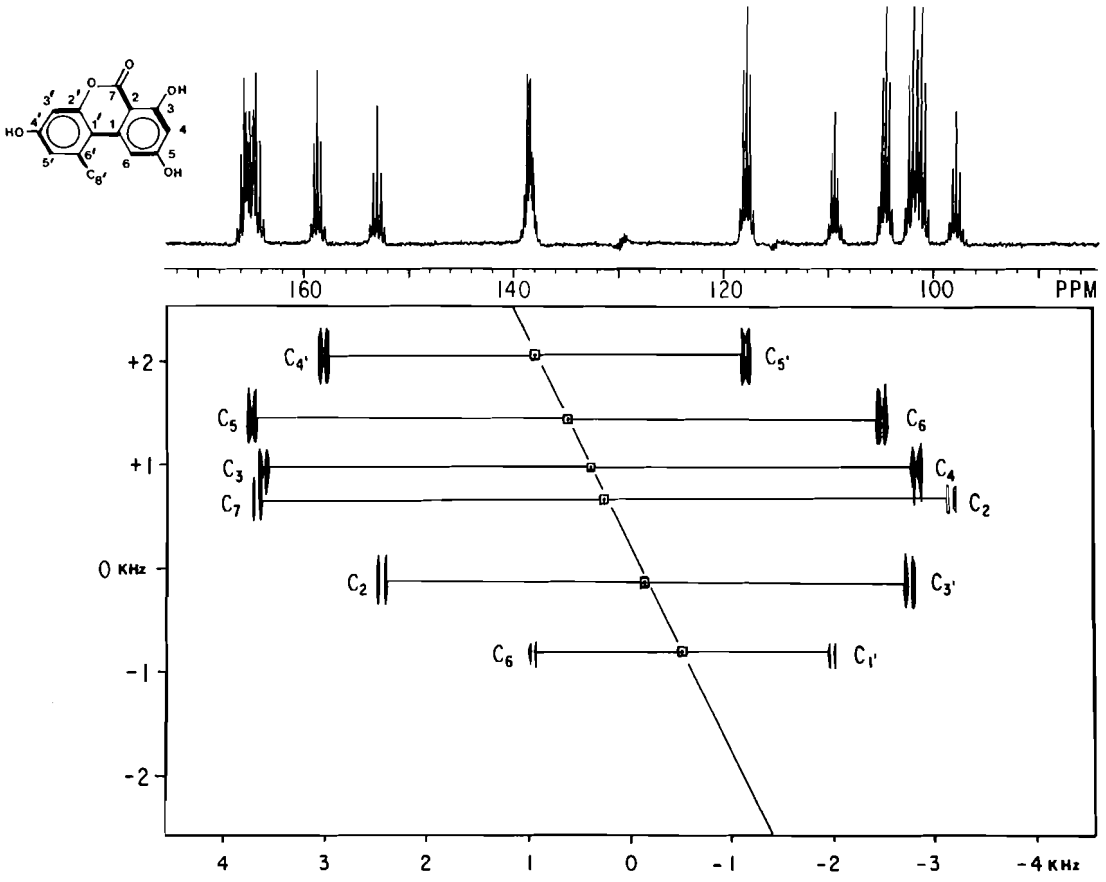

FIG. 2. 100-MHz ^{13}C 2-D INADEQUATE contour plot for a 0.47 *M* solution of alternariol (biosynthetically prepared from [1,2-^{13}C] acetate). Only the 5-kHz region in the vicinity of $F_1 = 0$ is shown. Total acquisition time from this spectrum was 38 h. 1-D nmr shown above.

The resulting 2-D contour plot (Fig. 1) of connectivities (one-dimensional spectrum displayed above) shows the expected lower intensity of response for connectivities between those carbon pairs originating from intact acetate units. The dynamic range difference between these and the enriched ^{13}C–^{13}C coupled carbons occurring at the junction between adjacent acetate units is not large enough to pose any observational difficulty and thus we were able to proceed with a full assignment of carbon signals from this single experiment. The longer spin-lattice relaxation times of the quaternary carbon pairs (C2′–C1′, C6′–C1′, C1–C2) contributed to the lower spectral responses for these resonances.

Possible mechanism for the biosynthesis of alternariol

Table 1 lists the full spectral assignment for alternariol.

Utilizing these assignments, an nmr experiment that examined AOH enriched using 2-^{13}C acetate established that the biosynthetic pathway for AOH starts at the C8′ and proceeds through the molecule with uniform enrichment of ^{13}C at alternate carbons located at 8′, 5′, 3′, 1′, 6, 4, and 2. This experiment agrees with the alternating pattern found with 1-^{14}C acetate (4) and presented in **3**.

To determine whether the biosynthesis of AOH involves cleavage of acetate units, we examined the nmr spectra of AOH synthesized by *Alternaria tenuis* when grown on medium containing 1,2-^{13}C acetates. The results of this experiment are clearly illustrated by the 2-D INADEQUATE contour plot shown in Fig. 2. As is evident, every carbon pair in this spectrum is coupled, which shows retention of intact acetate units throughout the molecule. This pattern of incorporation also agrees with **3**. This experiment gave no indication of a mixture of coupling patterns for AOH, indicating that no randomization had occurred.

No evidence that would indicate uncoupled carbon or a randomized pattern was observed in any of our ^{13}C nmr experiments. This would imply that the biosynthesis is under

TABLE 1. Nuclear magnetic resonance spectral assignment for AOH

Assignment	Shift σ[a]	Multiplicity[b]	σ[a] 2-D connectivities
C-8′	25.3	Quartet	—[c]
C-6′	138.3	Singlet	109.0, 117.6
C-5′	117.6	Doublet	138.3, 158.4
C-4′	158.4	Singlet	117.6, 101.6
C-3′	101.6	Doublet	158.4, 152.6
C-2′	152.6	Singlet	101.6, 109.0
C-1′	109.0	Singlet	138.3, 152.6, 138.1
C-1	138.1	Singlet	104.4, 97.4, 109.0
C-2	97.4	Singlet	138.1, 164.7
C-3	164.1	Singlet	97.4, 100.9
C-4	100.9	Doublet	164.1, 165.5
C-5	165.5	Singlet	100.9, 104.4
C-6	104.4	Doublet	165.5, 138.1
C-7	164.7	Singlet	97.4[d]

[a]Shift expressed in ppm relative to the solvent, DMSO, assigned a value of 39.5 ppm.
[b]Large one-bond C—H coupling only.
[c]Not in the spectral range.
[d]Assigned on basis of 1,2-^{13}C INADEQUATE experiment.

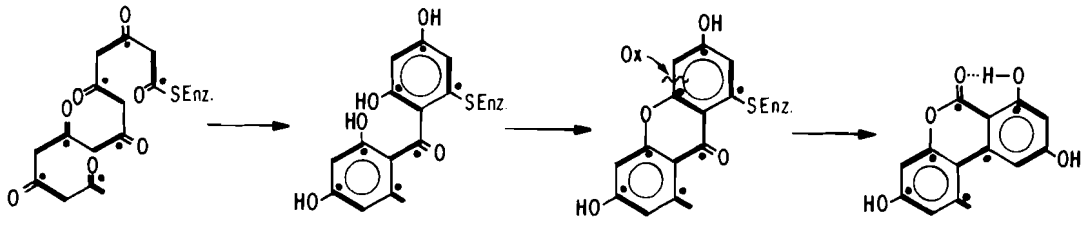

SCHEME 1

close steric control by the enzyme that prevents free rotation of aryl groups. The high rate of incorporation of NLX into AOH that is described in the Experimental probably indicates that NLX (or a very similar compound) is on the main biosynthetic route for AOH.

Scheme 1 presents a biosynthetic mechanism for biosynthesis of AOH that meets the above criteria. In this scheme, the point of attachment between the enzyme and the polyketide is shown as the active end of the polyketide chain, although the attachment could have migrated or could even involve several points of contact. The polyketide chain is assembled on the surface of the enzyme in a configuration that facilitated the formation of NLX. After rupture of the aromatic phloroglucinol ring, limited rotation of the aryl fragment and ring closure would produce the coupling pattern observed in AOH. This mechanism may require a second enzyme for oxidative cleavage of the aromatic ring. A reversible "retro-aldol" cleavage would result in destruction of an aromatic ring (which would be unlikely from free energy considerations), while oxidative fission of aromatic groups is widespread in the fungi (15, 16).

Other heptaketide assembly patterns and reactions can be suggested in addition to the mechanism shown in Scheme 1. For example, schemes can be devised in which (*1*) the phloroglucinol portion of the polyketide is assembled in a counterclockwise pattern, or (2) the polyketide chain could be assembled in the benzophenone configuration reported for griseofulvin biosynthesis (where NLX is also produced) (17). These mechanisms are more complex than that shown in Scheme 1 as they all require controlled rotation of aromatic groups to result in the observed AOH coupling pattern.

Experimental

Solvents were reagent "distilled in glass" quality. The yeast extract and potato dextrose agar were from Difco Laboratories (Detroit, Mich.). Analytical tlc was on scored, precoated plates fluorescent under 254 nm ("Uniplate", Silica Gel GF, 250 μm, Analtech, 75 Blue Hen Drive, Newark, DE 19711). Column chromatography was by the "flash chromatography" method (11) using the Ace Glass apparatus (Vineland, NJ) and 230–400 mesh silica gel (Merck, grade 60; Aldrich Chemical Co., Milwaukee, WI 53201). Sodium [1-^{13}C] and [1,2-^{13}C] acetate, 99% ^{13}C, and deuterated solvents were purchased from KOR (Cambridge, MA). Sodium [2-^{13}C] acetate, 99%, was purchased from Stohler Isotope Chemicals (Waltham, MA). Evaporations were done at room temperature or under a N_2 stream. Mass spectra were obtained using the direct injection probe (DIP) mode of the Hewlett–Packard 5885 mass spectrometer. The infrared spectra were obtained using a 237B Perkin–Elmer spectrophotometer and KBr discs. Authentic samples of norlichexanthone, both natural carbon and ^{14}C-labeled at the ketone carbon (30 000 cpm/mg), were kindly supplied by Dr. Constance M. Harris, Vanderbilt University, Nashville, TN.

Fungal cultures and production of labeled mycotoxin

The culture of *Alternaria tenuis* NRRL 6434, a strain with high production of AOH and a simple metabolic pattern that facilitated purification, was obtained from the Northern Regional Research Center, USDA/ARS, Poeria, IL. A single spore isolate from this strain was maintained on potato/dextrose agar. Fresh cultures of this isolate were started at frequent intervals, and portions of well sporulated 14–18 day old mycelia were used to innoculate 250-mL Erlenmeyer flasks each containing 60 mL of modified Czapex-Dox (MCD) medium. This medium contained 40 g glucose, 1.0 g yeast extract, 1.0 g $NaNO_3$, 1.0 g KH_2PO_4, 0.5 g $MgSO_4 \cdot 7H_2O$, 0.25 g NH_4Cl, 0.25 g KCl, 0.25 g NaCl, 0.01 g $FeSO_4 \cdot 7H_2O$, and 0.01 g $ZnSO_4 \cdot 7H_2O$, made up to 1 L with H_2O (18). These flasks were then incubated as stationary cultures in the dark at 25°C. Spiking with precursors was started on the 12th day and continued until the 16th day. The precursors were added by injecting the solutions into the MCD media beneath the mycelial cap. The flasks were then gently rotated without submerging any portion of the cap to mix the added precursor with the media. The acetates were added as 50 mg/0.2 mL aqueous solution per day and the NLX was added as 0.167 mg NLX/0.02 mL absolute EtOH per day. The mycelial cap was removed intact on the 17th day, and the cap was extracted three times by homogenizing with 30 mL MeOH for 1 min in a Waring Blendor and filtering. The extracts were combined and 50 mL H_2O was added. The solution was then extracted 3 times with 50 mL $CHCl_3$. The combined $CHCl_3$ solutions were concentrated by evaporation and the AOH was isolated and purified by flash chromatography. The column was developed first with 1 L of $CHCl_3$ to remove fast moving materials, and then developed with 1 L $CHCl_3$ solutions containing 2, 5, and 10% MeOH. The AOH emerged in the 2 and 5% MeOH eluates. The AOH was then repurified by flash chromatography using a hexane–EtOAc gradient. The AOH emerged at 25% EtOAc – hexane.

In a typical run, the yield of AOH obtained from 5 flasks was 307 mg. For unknown reasons, the yield of AOH and incorporation of precursors was highly variable. For most acetate runs under these conditions, incorporation into AOH was between 3 and 7% as determined by ms (mas spectra). The identity and purity of NLX and AOH were determined by ir, ms, and tlc with 5 solvent systems: toluene – glacial HOAc, 9:1; $CHCl_3$ – 1.6% EtOH; CH_2Cl_2–acetone, 95:5; toluene–EtOAc–HCO_2H, 6:3:1; and $(Et)_2O$–hexane–HOAc, 8:2:0.5. The yield of purified AOH from the flash column during the NLX incorporation experiment was 76.5 mg.

Thin-layer chromatography used 250-μm "Uniplates" (Analtech) using Silica Gel GF for normal phase and Silica Gel RPS for reversed phase tlc. The respective solvents were toluene – ethyl acetate – H_2O (6:3:1, v/v basis) and H_2O–methanol (65:35, v/v). ^{14}C activity on channeled tlc plates was detected by use of the tlc linear analyzer (Model LB 27 C, Berthold Analytical Instruments, 28 Charron Ave., Nashua, NH). Samples of the AOH obtained from the flash chromatographic columns were further purified by 3 preparative tlc purifications using each of these systems. Specific activity was determined by calculating ^{14}C activity (determined on a Beckman LS 8100 scintillation counter with "Aquasol" scintillation cocktail, New England Nuclear, Boston, MA) vs. peak height at 280 nm (Beckman Model 35 Spectrophotometer). The specific activity was constant after the first purification with each system.

Nuclear magnetic resonance parameters

Carbon-13 nmr spectra were measured in a 5-mm probe at 100.4 MHz using a JEOL GX-400 spectrometer system that included a 9.4 T Oxford narrow bore magnet and DEC LSI 11/23 data system. All data processing was with the JEOL Plexus software, version 2. Broadband ^{1}H decoupling was accomplished through the use of Waugh-type sequences (19, 20), and proton coupled ^{13}C spectra were measured

with grated decoupling in order to retain the nuclear Overhauser enhancements.

The two-dimensional studies were performed using the "INADEQUATE" pulse sequence proposed by Mareci and Freeman (21), where the final "read" pulse is allowed to have an arbitrary flip angle:

$$90°(X)-\tau-180°(Y)-\tau-90°(X)-t_1-\alpha(X)$$

τ was chosen to optimize conversion in double-quantum coherence in the usual manner, $\tau = (4J_{CC})^{-1}$, and the echo components emphasized by selecting $\alpha = 135°C$.

The 2-D INADEQUATE spectrum of alternariol (prepared utilizing [1-^{13}C] and [2-^{13}C] acetate) was obtained by processing an initial data matrix (t_1Xt_2) of 128 × 1024 points, representing spectra widths ($F_1 \times F_2$) of 5 kHz × 9 kHz. The $\pi/2$ pulse width was 11.4 μs, and τ was 4.386 ms corresponding to $J_{CC} = 57$ Hz. An overall recycle delay of 4.5 s was used to acquire 512 scans for each value of the incremented delay t_1. The 1-D spectrum reproduced above the 2-D contour plot was produced by transforming 1 K data acquired in a 9-kHz window using a 17.5 Hz broadening factor.

Finally, the 2-D data spectrum of alternariol (prepared utilizing [1,2-^{13}C] acetate) was obtained by processing an initial data matrix ($t_1 \times t_2$) of 512 × 1024 points representing spectral widths ($F_1 \times F_2$) of 100 kHz × 9 kHz. Other parameters were the same as in the previous experiment; however, only 64 scans were acquired at each t_1 value. The attached 1-D spectrum was prepared from a 32 K transform of data acquired in the same 9-kHz window, and a broadening factor of 2 Hz was used in data processing.

All 2-D data sets were double Fourier transformed utilizing trapezoidal window functions to approximate the sine-bell functions frequently used to improve the appearance of two-dimensional contour plots.

1. E. E. Stinson. J. Food Prot. **48**, 80 (1984).
2. S. Gatenbeck and S. Hermodsson. Acta Chem. Scand. **19**, 65 (1965).
3. S. Sjoland and S. Gatenbeck. Acta Chem. Scand. **20**, 1053 (1966).
4. R. Thomas. Biochem. J. 748 (1961).
5. E. E. Stinson and R. A. Moreau. 23rd Annual Meeting of the Phytochemical Society of North America, Tucson, Ariz. 1983. (Abstract).
6. E. E. Stinson and R. A. Moreau. 24th Annual Meeting of the Phytochemical Society of North America, Boston, Mass. 1984. (Abstract).
7. H. Raistrick, C. E. Stickings, and R. Thomas. Biochem. J. **55**, 421 (1953).
8. P. S. Steyn, R. Vleggaar, and P. L. Wessels. The biosynthesis of aflatoxin and its congeners. *In* The biosynthesis of mycotoxins. *Edited by* P. A. Steyn. Academic Press, New York and London. 1980. pp. 105–155.
9. J. E. Holker, E. O'Brien, and T. J. Simpson. J. Chem. Soc. Perkin Trans. 1, 1365 (1983).
10. P. L. Canham, L. C. Vining, A. G. McInnes, J. A. Walter, and J. L. C. Wright. Can. J. Chem. **55**, 2450 (1977).
11. W. C. Still, M. Kahn, and A. Mitra. J. Org. Chem. **43**, 2023 (1978).
12. R. J. Cole and R. H. Cox. Handbook of toxic fungal metabolites. Academic Press, New York and London. 1981. p. 616.
13. A. Bax, R. Freeman, T. A. Frankiel, and M. H. Levitt. J. Magn. Reson. **43**, 478 (1981).
14. H. Seto, T. Sato, and H. Yonehare. J. Am. Chem. Soc. **95**, 4861 (1973).
15. J. A. Buswell, K.-E. Eriksson, J. K. Gupta, S. G. Hamp, and I. Nordh. Arch. Microbiol. **131**, 366 (1982).
16. D. L. Crawford, M. J. Barder, A. L. Pometto III, and R. L. Crawford. Arch. Microbiol. **131**, 140 (1982).
17. C. M. Harris, J. S. Roberson, and T. M. Harris. J. Am. Chem. Soc. **98**, 5380 (1976).
18. M. R. Mass, M. A. Woody, and F. S. Chu. J. Food Saf. **3**, 39 (1981).
19. J. S. Waugh. J. Magn. Reson. **49**, 517 (1982).
20. J. S. Waugh. J. Magn. Reson. **50**, 30 (1982).
21. T. H. Mareci and R. Freeman. J. Magn. Reson. **48**, 158 (1982).

Excess volumes, viscosities, enthalpies, and Gibbs free energies for mixtures of methyl isobutyl ketone + *n*-pentanol and methyl isobutyl ketone + isoamyl alcohol at 298.15 K

ROQUE RIGGIO[1] AND HECTOR E. MARTINEZ
Facultad de Ciencias Naturales, Universidad Nacional de Salta, Buenos Aires 177, 4400 Salta, República Argentina

AND

HORACIO N. SOLIMO[2]
Facultad de Ciencias Exactas, Universidad Nacional de Salta, Buenos Aires 177, 4400 Salta, República Argentina

Received November 29, 1984[3]

ROQUE RIGGIO, HECTOR E. MARTINEZ, and HORACIO N. SOLIMO. Can. J. Chem. **64**, 1595 (1986).

Three excess functions (molar volumes, viscosities, and molar enthalpies) for the methyl isobutyl ketone + *n*-pentanol and methyl isobutyl ketone + isoamyl alcohol systems at 298.15 K were calculated from measured densities, viscosities, and enthalpies, respectively. The UNIFAC group contribution method was used in order to estimate the activity coefficients which were then employed to calculate the excess molar Gibbs free energy. An attempt to explain the experimental results in terms of molecular interactions was made.

ROQUE RIGGIO, HECTOR E. MARTINEZ et HORACIO N. SOLIMO. Can. J. Chem. **64**, 1595 (1986).

En faisant appel aux valeurs mesurées à 298,15 K pour les densités, les viscosités et les enthalpies, on a calculé les valeurs respectives des fonctions d'excès (volumes, viscosités et enthalpies molaires) des systèmes méthyl isobutyl cétone/*n*-pentanol et méthyl isobutyl cétone/alcool isoamylique. Dans le but de déterminer les coefficients d'activité, qui ont été utilisés pour calculer l'énergie libre molaire en excès de Gibbs, on a utilisé la méthode UNIFAC des contributions des groupes. On a essayé d'expliquer les résultats expérimentaux en fonction d'interactions moléculaires.

[Traduit par la revue]

Introduction

The excess thermodynamic properties of binary liquid solutions are fundamental for the design of industrial equipment and for the interpretation of liquid state, particularly when polar–polar liquids are the components of the mixtures. Continuing our study on these type of systems (1) we report here the excess molar volumes (V^E), viscosities (η^E), enthalpies (H^E), and Gibbs free energies (G^E) for the following mixtures: (*i*) methyl isobutyl ketone (MIK) + *n*-pentanol (P_1) and (*ii*) methyl isobutyl ketone (MIK) + isoamyl alcohol (IA).

Experimental

Materials

Methyl isobutyl ketone, *n*-pentanol, and isoamyl alcohol (all Merck Darmstadt p.a.) were dried over anhydrous K_2CO_3 and fractionally distilled under nitrogen atmosphere. In each case the middle fraction was collected and maintained over 3 Å molecular sieve for *n*-pentanol and isoamyl alcohol and 4 Å molecular sieve for methyl isobutyl ketone to prevent water absorption. The mixtures were prepared by mixing accurately weighed quantities of the pure liquids. Caution was taken to prevent evaporation.

Density (ρ) and refractive index (n_D)

Densities were determined with an Anton Paar DMA46 calculating density meter with a built-in thermostat. We have estimated that the reported densities were accurate to within ± 0.1 kg m^{-3}. The refractive indexes of the pure components (sodium D line) were measured with a Jena dipping refractometer with an accuracy of ± 0.00002.

Viscosity (η)

The measurements were carried out with a Cannon-Fenske viscometer calibrated with doubly distilled water and benzene (accuracy $\pm 0.5\%$). For refractive index and viscosity, a thermostatically controlled bath, constant to ± 0.01°C, was used.

Calorimetric measurements

The heats of mixing of the binary systems were measured with an accuracy of $\pm 1\%$ in a modified adiabatic calorimeter as described by Loiseleur (2, 3).

Results

The experimental physical properties of the pure liquids are reported in Table 1, along with the literature values for comparison.

The excess thermodynamic functions were calculated with the following equations:

$$[1] \quad \eta^E = \eta - \eta^{id} = \eta - \exp(x_1 \ln \eta_1 + x_2 \ln \eta_2)$$

$$[2] \quad V^E = V - (x_1V_1 + x_2V_2) = [(x_1M_1 + x_2M_2)/\rho] - (x_1V_1 + x_2V_2)$$

$$[3] \quad H^E = H_m$$

$$[4] \quad G^E = RT(x_1 \ln \gamma_1 + x_2 \ln \gamma_2)$$

where V, V_1, and V_2 = molar volumes of the mixture and the pure components, respectively; H_m = molar enthalpy of the mixture; η, η_1, and η_2 = viscosities of the mixture and the pure components, respectively; η^{id} = viscosity of ideal mixture; γ_1 and γ_2 = activity coefficients of components 1 and 2 in the solution phase, based on the pure solvent standard state; ρ = density of solution; and x_1 and x_2 = molar fraction of the first and second component, respectively.

The experimental molar fractions, densities, viscosities, and excess molar enthalpies for the MIK + P_1 and MIK + IA systems at 298.15 K are listed in Table 2.

The excess thermodynamic functions were fitted to the equation:

$$[5] \quad Y^E = x(1 - x) \sum_{j=0}^{n} a_j(2x - 1)^j$$

where Y^E is the excess function (V^E, H^E, G^E, or η^E). The a_j's coefficients which gave the best fit to eq. [5] are summarized in

[1]To whom correspondence should be addressed.

[2]Present address: Instituto de Física, Facultad de Ciencias Exactas y Tecnología, Universidad Nacional du Tucumán, Avda., Independencia 1800, 4000 San Miguel de Tucumán, República Argentina.

[3]Revision received April 10, 1986.

TABLE 1. Experimental physical properties of the pure liquids at 298.15 K*

	ρ		η		n_D	
Component	Exp.	Lit. (18)	Exp.	Lit. (18)	Exp.	Lit. (18)
MIK	796.3	796.1	0.543	0.542	1.39360	1.3933
IA	807.1	807.1	3.48	—	1.40523	1.4052
P_1	811.0	811.5	3.35	3.347	1.40783	1.4079

*Units: ρ, kg m^{-3}; η, mPa s.

TABLE 2. Experimental values of density, viscosity, and excess molar enthalpy for the MIK + P_1 and MIK + IA systems at 298.15 K*

MIK + P_1					MIK + IA				
x_{MIK}	ρ	η	x_{MIK}	H^E	x_{MIK}	ρ	η	x_{MIK}	H^E
0.0000	811.0	3.35	0.0000	0	0.0000	807.1	3.48	0.0000	0
0.1011	809.5	2.47	0.1023	568	0.1006	805.8	2.58	0.1015	513
0.1974	808.2	1.89	0.2049	1029	0.2027	804.5	1.89	0.2046	842
0.3040	806.6	1.46	0.3042	1157	0.3201	803.1	1.40	0.3177	986
0.4023	805.1	1.20	0.4055	1317	0.3948	802.2	1.20	0.4002	1023
0.5022	803.7	1.00	0.5194	1320	0.5073	801.0	0.965	0.5051	1071
0.6064	802.0	0.856	0.6166	1217	0.6072	799.9	0.839	0.6095	1035
0.7079	800.6	0.738	0.7024	1133	0.7013	799.0	0.728	0.7073	956
0.7955	799.3	0.668	0.7857	861	0.8032	798.1	0.648	0.8072	796
0.8962	797.8	0.592	0.9015	527	0.8927	797.2	0.595	0.9055	490
1.0000	796.3	0.543	1.0000	0	1.0000	796.3	0.543	1.0000	0

*Units: ρ, kg m^{-3}; η, mPa s; H^E, J mol^{-1}.

TABLE 3. Coefficients and standard errors for representations of the excess functions by eq. [5]*

	MIK(1) + P_1(2)				MIK(1) + IA(2)			
	$10^6 V^E$	η^E	H^E	G^E	$10^6 V^E$	η^E	H^E	G^H
a_0	−0.3342	−1.3727	5264.18	3245.41	0.1510	−1.6131	4250.90	1359.15
a_1	0.0411	1.7296	−421.53	−20.02	0.0257	1.7579	−10.05	−353.29
a_2	0.0504	−1.1278	1264.26	100.72	−0.0284	−0.7596	2257.11	98.47
σ_{Y^E}	0.008	0.007	40.0	0.06	0.03	0.08	70.0	0.64

*Units: V^E, m^3 mol^{-1}; η^E, mPa s; H^E and G^E, J mol^{-1}.

Table 3. The choice of the appropriate number of constants was based on the variation with n of the standard error of the estimated, as defined by:

$$[6] \quad \sigma_{Y^E} = [\Sigma(Y^E_{obs} - Y^E_{calcd})^2/(n_{obs} - n)]^{1/2}$$

where the sum is taken over the n_{obs} results.

The UNIFAC group contribution method (4) was used in order to estimate the activity coefficients γ_1 and γ_2, using the new parameters (5). They are listed in Table 4.

The following equation was used:

$$[7] \quad \ln \gamma_i = \ln \gamma_i^c + \ln \gamma_i^r$$

where γ_i^c = combinatorial term for the i component and γ_i^r = residual term for the i component.

The excess molar Gibbs free energy was calculated from eq. [4], using the γ_i's obtained by the UNIFAC method, and the excess molar entropy is defined by:

$$[8] \quad TS^E = H^E - G^E$$

TABLE 4. Activity coefficients for the MIK + P_1 and MIK + IA systems at 298.15 K calculated by UNIFAC method

	MIK(1) + P_1(2)		MIK(1) + IA(2)	
x_{MIK}	γ_1	γ_2	γ_1	γ_2
0.0	3.89	1.00	2.09	1.00
0.1	2.93	1.02	1.69	1.01
0.2	2.31	1.06	1.44	1.04
0.3	1.89	1.13	1.28	1.08
0.4	1.59	1.24	1.18	1.13
0.5	1.39	1.39	1.11	1.19
0.6	1.24	1.60	1.06	1.25
0.7	1.13	1.89	1.03	1.32
0.8	1.06	1.39	1.01	1.39
0.9	1.01	2.91	1.00	1.47
1.0	1.00	3.83	1.00	1.55

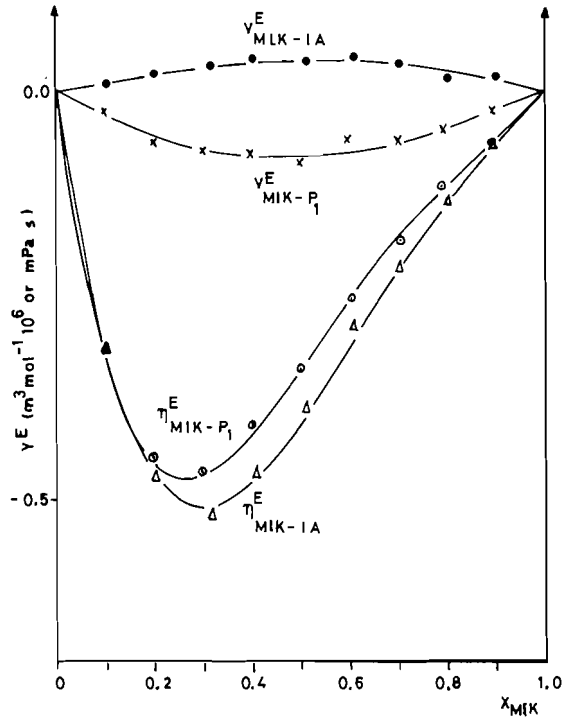

FIG. 1. Molar excess volumes and excess viscosities of methyl isobutyl ketone + *n*-pentanol and methyl isobutyl ketone + isoamyl alcohol mixtures as 298.15 K. Curves are least-square representations by eq. [5].

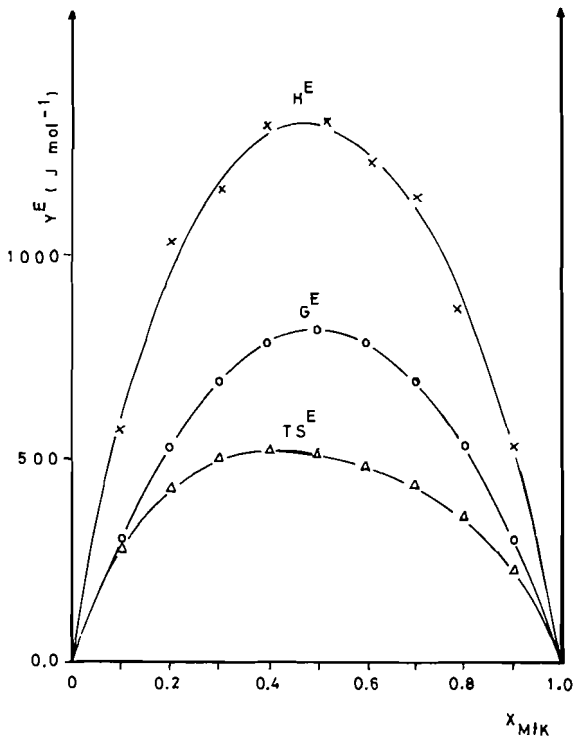

FIG. 2. Molar excess enthalpies, entropies and Gibbs free energies of methyl isobutyl ketone + *n*-pentanol mixtures at 298.15 K. Curves are least-square representations by eq. [5].

Discussion

Figure 1 shows the dependence of the excess molar volume with the composition for the MIK + P_1 and MIK + IA systems, where the first one is negative and the second one positive over the entire range of concentration, but in both cases the values are close to zero.

When alcohols, which exist in a highly associated form in the pure state (6, 7), are mixed with polar solvents (ketones) the monomerization occurs and new specific interactions appear in the solution (8). The disruption of the hydrogen-bonded alcohol structure gives rise to a positive contribution to V^E, which depends: (*i*) on the dielectric constant of the ketone (9) and (*ii*) on the chain length (10) and degree of branching (11) in the alcohol which decrease the self-asociation in the pure state. On the other hand, the interactions between unlike molecules in both systems are surely weaker than the sum of the interactions between like molecules. This also produces a positive contribution to V^E. If the factors that affect V^E were only these, the excess molar volume for the MIK + P_1 and MIK + IA systems should be strongly positive. Since these systems show negative and positive (but close to zero) values, respectively, it is evident that other factors are involved. Among the main ones we can mention the interstitial accommodation of the ketone within the hydrogen-bonded alcohol structure (12, 13) and the possibility of formation of new chemical species in the solution both producing contraction effect that counterbalance the expansive effects mentioned above. From the experimental results we deduce that the interstitial accommodation of the ketone within the hydrogen-bonded alcohol structure is more important than the formation of new chemical species, since both systems are endothermic (see Figs. 2 and 3) and the excess viscosity is negative (see Fig. 1).

The possibility of the geometrical fit of the ketone decreases when the branching of the alcohol increases, yielding positive V^E values as a consequence of the steric hindering. In agreement with this, the system MIK plus the highly branched *t*-amyl alcohol (14) shows a $V^E \cong 0.27$ at the maximum (near $x_{MIK} = 0.6$).

The dependence of V^E on the chain length can be appreciated by comparison with the values obtained for the systems MIK + *n*-butanol and MIK + isobutyl alcohol (1) where greater negative values were obtained.

It was found that for *n*-alkanols + *n*-heptane mixtures the positive contribution produced by breaking of the hydrogen bond between the alcohol molecules diminished with the size of the alcohol (10, 15) which is opposite to the results observed between MIK + P_1 – MIK + *n*-butanol and MIK + IA – MIK + isobutyl alcohol. This dissimilarity is probably *due* to the greater size difference (13) within the MIK–butanols as compared to the MIK–pentanols systems. It is not possible to invoke that the more negative values of V^E observed for the systems employing butanols are due to the formation of stronger hydrogen bonds, since their η^E values are more negative than those for the systems with pentanols.

We conclude that the breakdown of the alcohol structure is the primary contributor to the mixture effect for the systems reported here. This leads to negative values for the excess viscosity (see Fig. 1) which is interpreted by Fort and Moore (26) in terms of dominant dispersion forces.

The endothermic behavior for the MIK + P_1 and MIK + IA systems (see Figs. 2 and 3) is due to the consumption of energy necessary to produce the breakdown of the alcohol structure which is not compensated by the energy developed by the formation of new chemical species in the solution. Conse-

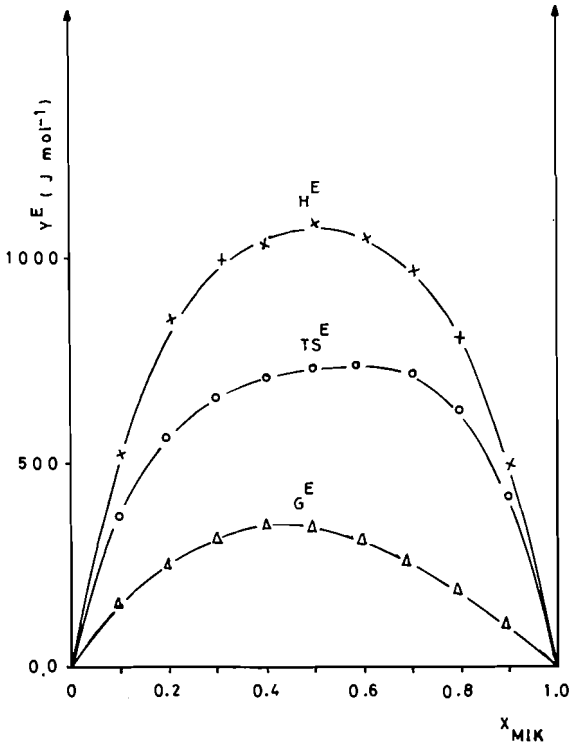

FIG. 3. Molar excess enthalpies, entropies and Gibbs free energies of methyl isobutyl ketone + isoamyl alcohol mixtures at 298.15 K. Curves are least-square representations by eq. [5].

quently, the global energy of the hydrogen bonds O—H···O in the *n*-pentanol and isoamyl alcohol must be greater than those of the same type of bonds in the intermolecular complexes (17). The greater positive values of H^E for the MIK + P_1 system with respect to the MIK + IA one could be interpreted in terms of the stronger self-association for the first system.

The positive values of S^E (see Figs. 2 and 3) are in agreement with the conclusions indicated above since this sign is indicative that the disruption of the alcohol structure is more important than the intermolecular association.

Acknowledgement

We wish to thank the INENCO-CONICET-UNSa, República Argentina, for financial support.

1. R. RIGGIO, J. F. RAMOS, M. HERNANDEZ UBEDA, and J. A. ESPÍNDOLA. Can. J. Chem. **59**, 3305 (1981).
2. H. N. SÓLIMO, R. RIGGIO, F. DAVOLIO, and M. KATZ. Can. J. Chem. **53**, 1258 (1975).
3. H. LOISELEUR, J. MERLIN, and R. A. PARIS. J. Chim. Phys. **62**, 1380 (1965).
4. A. FREDENSLUND, J. GMEHLING, and P. RASMUSSEN. Vapor–liquid equilibria using INIFAC. Elsevier Scientific Publishing Co., Amsterdam – Oxford – New York. 1977.
5. S. SKJOLD-JØRGENSEN, P. RASMUSSEN, and A. FREDENSLUND. Chem. Eng. Sci. **37**, 99 (1982).
6. H. C. VAN NESS, J. VAN WINKLE, H. H. RICHTOL, and H. E. HOLLINGER. J. Phys. Chem. **71**, 1483 (1967).
7. G. C. PIMENTEL and A. L. MCCLELLAN. The hydrogen bond. W. H. Freeman and Co., San Francisco. 1960.
8. J. E. HOUSE, JR. Trans. Ill. Acad. Sci. 123 (1966).
9. M. V. P. RAO and P. R. NAIDU. Indian J. Chem. **11**, 242 (1973).
10. A. J. TRESZCZANOWICZ and G. C. BENSON. J. Chem. Thermodyn. **10**, 967 (1978).
11. K. NAKANISHI and H. SHIRAI. Bull. Chem. Soc. Jpn. **43**, 1634 (1970).
12. D. E. G. JONES, I. A. WEEKS, S. C. ANAND, R. W. WETMORE, and G. C. BENSON. J. Chem. Eng. Data, **17**, 501 (1972).
13. G. C. BENSON and O. KIYOHARA. J. Chem. Eng. Data, **21**, 362 (1976).
14. H. N. SÓLIMO, R. RIGGIO, and H. E. MARTINEZ. J. Sol. Chem. **15**, 283 (1986).
15. A. J. TRESZCZANOWICZ and G. C. BENSON. J. Chem. Thermodyn. **9**, 1189 (1977).
16. R. J. FORT and W. R. MOORE. Trans. Faraday Soc. **62**, 1112 (1966).
17. K. N. MARSH. Pure Appl. Chem. **55**, 467 (1983).
18. J. A. RIDDIC and W. B. BUNGER. Organic solvents. Vol. II. 3rd ed. Wiley-Interscience, New York. 1970.

Enantiospecific synthesis of optically pure (*S*)-(+)-3-hydroxy-1-phenyl-1-butanone by bakers' yeast reduction

ROBERT CHÊNEVERT[1] AND SONIA THIBOUTOT

Département de chimie, Faculté des sciences et de génie, Université Laval, Québec (Qué.), Canada G1K 7P4

Received December 10, 1985

ROBERT CHÊNEVERT and SONIA THIBOUTOT. Can. J. Chem. **64**, 1599 (1986).

Bakers' yeast reduces 1-phenyl-1,3-butanedione with high chemo- and enantio-selectivity to give (*S*)-(+)-3-hydroxy-1-phenyl-1-butanone. The enantiomeric purity (>98%) was determined by nmr analysis using a chiral shift reagent and the absolute configuration was determined by correlation with ethyl (*S*)-(+)-3-hydroxybutyrate.

ROBERT CHÊNEVERT et SONIA THIBOUTOT. Can. J. Chem. **64**, 1599 (1986).

La levure de boulanger réduit la phényl-1 butanedione-1,3 d'une manière chimio et énantiosélective pour conduire à la (*S*)-(+)-hydroxy-3 phényl-1 butanone-1. La pureté énantiomérique (>98%) est mesurée par une analyse de rmn à l'aide d'un réactif de déblindage chiral. La configuration absolue est établie par corrélation avec le (*S*)-(+)-hydroxy-3 butyrate d'éthyle.

Introduction

Asymmetric synthesis has relied on the use, as starting materials, of optically active compounds that are members of the so-called "chiral carbon pool," i.e. easily available chiral substances produced by living organisms including amino acids, terpenes, carbohydrates, etc. (1–3). The composition of the chiral carbon pool is limited and there is an interest in its expansion. Biochemical transformation mediated by enzymes or microorganisms is an efficient tool for the preparation of chiral compounds. Reduction of unnatural ketone substrates by fermenting baker's yeast has received renewed attention for the preparation of chiral alcohols (4–8). We report here on the preparation of enantiomerically pure (*S*)-(+)-3-hydroxy-1-phenyl-1-butanone by bakers' yeast reduction of 1-phenyl-1,3-butanedione.

Results and discussion

The reduction was carried out by treating 1-phenyl-1,3-butanedione with a fermenting yeast – sugar–water suspension according to the basic procedure currently used (9). This reduction gave a single product in 33% yield (40% yield based on the unrecovered starting material), which was identified as pure (*S*)-(+)-3-hydroxy-1-phenyl-1-butanone (eq. [1]). The

[1] 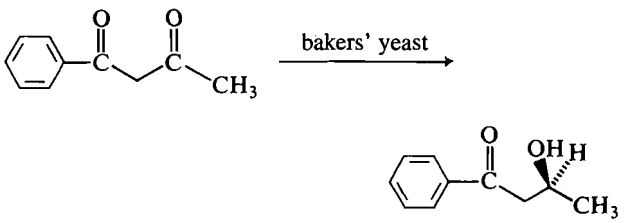

reaction is characterized by extraordinary selectivity: First, only the carbonyl group in position 3 is reduced. This chemoselectivity is unexpected because yeast reduces substituted acetophenones (4). Second, the reaction is enantioselective and only the (*S*)-(+) enantiomer is produced.

Enantiomeric composition of the product was determined by nuclear magnetic resonance analysis using tris[3-(heptafluoropropylhydroxymethylene)-*d*-camphorato]europium(III) as a chiral shift reagent (10). Polarimetry cannot be used because, to the best of our knowledge, none of the pure enantiomers has been reported so far. The nmr analysis requires the use of racemic 3-hydroxy-1-phenyl-1-butanone, which was prepared by condensation between acetaldehyde and benzoylacetic acid according to a known procedure (11). We also prepared this racemate by double reduction of 1-phenyl-1,3-butanedione with sodium borohydride followed by selective oxidation of the benzylic alcohol with pyridinium dichromate (eq. [2]). Figure 1A shows

[2] 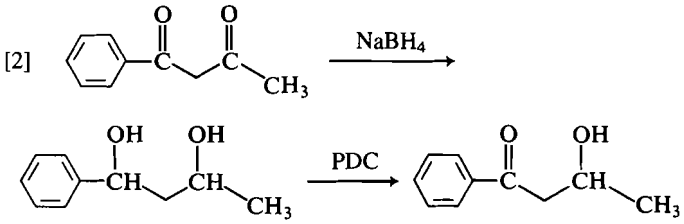

the well-resolved ^{1}H nmr signals for the methyl group of racemic 3-hydroxy-1-phenyl-1-butanone in the presence of 0.1 equivalent of Eu(hfc)$_3$. The partial spectrum (Fig. 1B) of the yeast reduction product shows only one doublet and there is no trace of a second doublet. The optical purity obtained is above 98%.

Attention was next turned to the determination of the absolute configuration of the title compound. The absolute configuration of the product obtained by microbial reduction of a carbonyl group containing a large group L and a small group S to the alcohol may be determined by application of Prelog's rule (12). According to this rule, which was initially postulated for the reduction of decalones by *Curvularia lunata*, the hydrogen transfer proceeds on the Re-face of the prochiral ketone to give the *S* alcohol, thus the reduction reported here should give the *S* enantiomer. In view of the fact that yeast has now been shown to have at least three carbonyl-reducing enzymes at its disposal,

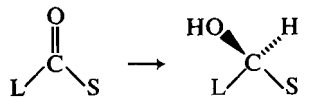

with different enantio-differentiating abilities (13), caution must be exercised, and the absolute configuration was confirmed by correlation with ethyl (*S*)-(+)-3-hydroxybutanoate obtained from yeast reduction of ethyl acetoacetate. The absolute configuration of this compound is firmly established (9). Reaction of phenylmagnesium bromide with ethyl (*S*)-(+)-3-hydroxybutanoate in the presence of triethylamine afforded (*S*)-(+)-3-hydroxy-1-phenyl-1-butanone (eq. [3]). In the presence of several equivalents of a tertiary aliphatic amine, the Grignard reaction with an ester gives a ketone as the major

[1]Author to whom correspondence may be addressed.

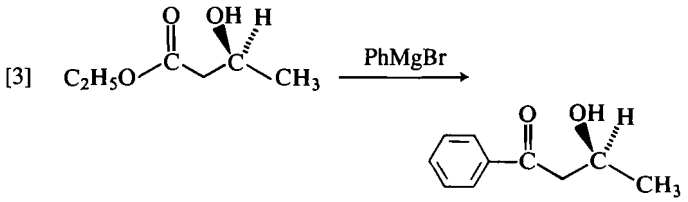

product (14). Therefore, the yeast reduction of 1-phenyl-1,3-butanedione gives the title compound with *S* configuration.

Experimental

The ^{1}H nmr spectra were recorded on a Varian XL-200 spectrometer. Eu(hfc)$_3$ and 1-phenyl-1,3-butanedione were purchased from Aldrich Chemical Co. bakers' yeast (*Saccharomyces cerevisiae*, type 1) was purchased from Sigma Chemical Co. Ethyl (*S*)-(+)-3-hydroxybutanoate was prepared according to known procedures (9, 15).

Bakers' yeast reduction of 1-phenyl-1,3-butanedione

A mixture of sucrose (30 g) and fresh bakers' yeast (20 g) in water (150 mL) gave, after 1 h at 30°C, a rapid evolution of carbon dioxide. 1-Phenyl-1,3-butanedione (1.62 g, 10 mmol) was added, and the fermenting suspension was stirred for another 24 h at room temperature. A warm (ca. 40°C) solution of 20 g sucrose in 50 mL of water was then added. Stirring was continued for 5 days at room temperature. The mixture was worked up by first adding 20 g of Celite and then filtering. The filtrate was saturated with sodium chloride and extracted with methylene chloride (continuous extraction). The organic phase was dried over magnesium sulfate, filtered, and concentrated with a rotary evaporator. The residue was purified by column chromatography (silica gel, methylene chloride – diethyl ether 96:4 as eluant) to give starting material (284 mg) and (*S*)-(+)-3-hydroxy-1-phenylbutanone (541 mg, 33% yield) as an oil; $[\alpha]^{25}$ +50.5° (*c* 0.12, $CHCl_3$); ir (neat): 3440, 3045, 2950, 1670, 1590, 1200, 1105, 1040 cm^{-1}; nmr ($CDCl_3$): 1.31 (3H, d, J = 6.5 Hz), 3.10 (2H, d, J = 6.0 Hz), 3.44 (1H, s), 4.40 (1H, m), 7.46 (3H, m), 7.93 (2H, dd, J_{ortho} = 8.0 Hz, J_{meta} = 2.0 Hz); ms *m/e* (relative intensity): 164 (M^+, 11), 146 (17), 105 (100), 77 (53).

3-Hydroxy-1-phenyl-1-butanone (racemic mixture)

1-Phenyl-1,3-butanedione (1.62 g, 10 mmol) reacts with sodium borohydride (0.38 g, 10 mmol) in ethanol (25 mL) to afford, after 90 min, 1-phenyl-1,3-butanediol (1.52 g) as a colorless liquid. Yield 92%; ir (neat): 3400, 3049, 2955, 1590, 1210, 1105 cm^{-1}; nmr ($CDCl_3$): 1.16 (3H, d, J = 6.5 Hz), 1.79 (2H, t, J = 7.0 Hz), 4.01 (1H, m), 4.92 (1H, m), 7.36 (5H, s); ms *m/e* (relative intensity): 166 (M^+, 10), 107 (85), 105 (70), 79 (100), 77 (87), 51 (26).

A solution of 1-phenyl-1,3-butanediol (5.6 mmol, 923 mg), and pyridinium dichromate (16) (2.1 g, 5.6 mmol) in methylene chloride (25 mL) was stirred at room temperature for 3 h. The reaction mixture was diluted with ether, filtered, and evaporated. The crude product was purified by column chromatography (silica gel, chloroform–ether, 50:50) to give racemic 3-hydroxy-1-phenyl-1-butanone. Yield 538 mg, 59%. Spectroscopic data are described above (see also ref. 11).

(S)-(+)-3-Hydroxy-1-phenyl-1-butanone from ethyl (S)-(+)-3-hydroxybutanoate

Ethyl (*S*)-(+)-3-hydroxybutanoate (528 mg, 4 mmol, ee (enantiomeric excess) = 85%) in anhydrous benzene (5 mL) was slowly added at 5–10°C to a freshly prepared solution of phenylmagnesium bromide (1.45 g, 8 mmol) and triethylamine (11) (2.42 g, 24 mmol) in anhydrous benzene – ether solution (6 mL – 4 mL). The reaction mixture was stirred at 5–10°C for 2 h and then treated with 4 *N* hydrochloric acid. The organic layer was washed first with water, then with 5% aqueous sodium hydrogen carbonate solution, and again with water, and evaporated. The crude product was purified by column chromatography (silica gel, chloroform–ether 60:40 as eluent) to give (*S*)-(+)-3-hydroxy-1-phenyl-1-butanone (360 mg, 55% yield); $[\alpha]^{25}$ +42.5° (*c* 0.70, $CHCl_3$); ir (neat): 3440, 3045, 2950, 1670, 1590, 1200, 1105, 1040 cm^{-1}; nmr ($CDCl_3$): 1.31 (3H, d, J = 6.5 Hz), 3.10 (2H, d, J = 6.0 Hz), 3.44 (1H, s), 4.40 (1H, m), 7.46 (3H, m), 7.93 (2H, dd, J_{ortho} = 8.0 Hz, J_{meta} = 2.0 Hz); ms *m/e* (relative intensity): 164 (M^+, 11), 146 (17), 105 (100), 77 (53).

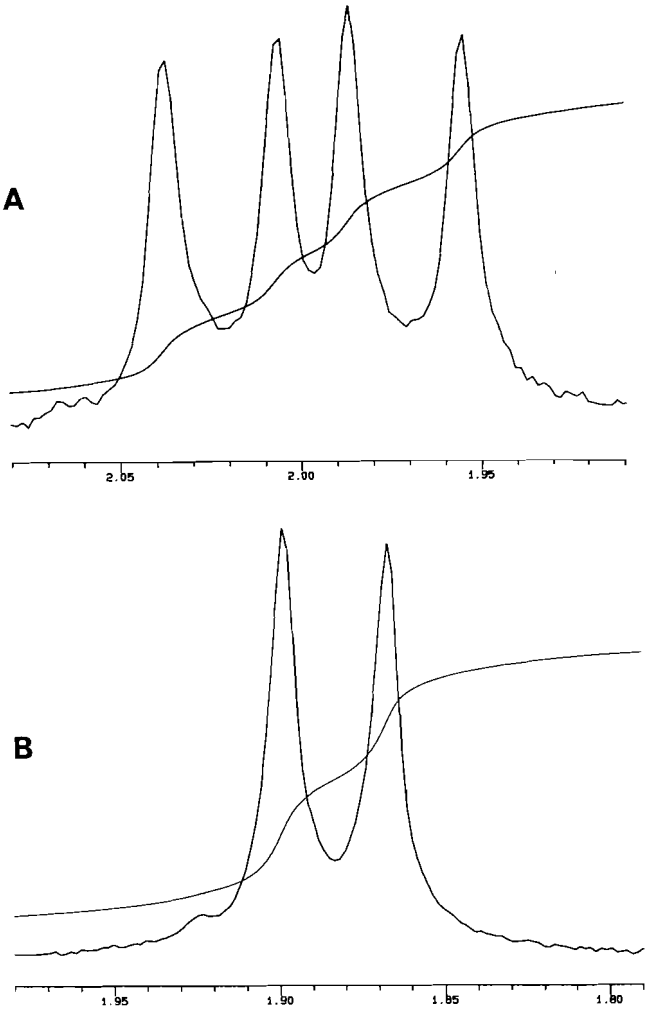

FIG. 1. 200-MHz ^{1}H nmr spectra of a solution prepared from (A) racemic 3-hydroxy-1-phenyl-1-butanone and (B) the product obtained by fermentation, in the presence of 0.1 equivalent of Eu(hfc)$_3$. The upper trace is slightly displaced to lower field due to the use of a slightly different concentration. The shoulder at δ 1.925 in (B), not being a doublet, cannot be due to the other enantiomer, and its signal area is less than 2% of the large doublet.

Acknowledgements

Support for this work by the Natural Sciences and Engineering Research Council of Canada and by the "Ministère de l'éducation", Québec, is gratefully acknowledged.

1. J. W. SCOTT. *In* Asymmetric synthesis. Vol. 4. *Edited by* J. D. Morrison and J. W. Scott. Academic Press, New York. 1984. Chapt. 1.
2. B. SEURIG and D. SEEBACH. Helv. Chim. Acta, **60**, 1175 (1977).
3. D. SEEBACH and H. O. KALINOWSKI. Nachr. Chem. Tech. **24**, 415 (1976).
4. C. J. SIH and C. S. CHEN. Angew. Chem. Int. Ed. Engl. **23**, 570 (1984).
5. K. MORI, H. MORI, and T. SUGAI. Tetrahedron, **41**, 919 (1985).
6. C. FUGANTI, P. GRASSELLI, and S. SERVI. J. Chem. Soc. Perkin Trans. 1, 241 (1983).
7. D. W. BROOK, P. G. GROTHANS, and W. L. IRWIN. J. Org. Chem. **47**, 2820 (1982).

8. T. KITAHARA and K. MORI. Tetrahedron Lett. **26**, 451 (1985).
9. D. SEEBACH, M. A. SUTTER, R. H. WEBER, and M. F. ZÜGER. Org. Synth. **63**, 1 (1984).
10. R. R. FRASER. *In* Asymmetric synthesis. Vol. 1. *Edited by* J. D. Morrison. Academic Press, New York. 1983. Chapt. 9.
11. W. RIED and W. KUNSTMANN. Chem. Ber. **100**, 605 (1967).
12. V. PRELOG. Pure Appl. Chem. **9**, 119 (1964).
13. W. R. SHIEH, A. S. GOPALAN, and C. J. SIH. J. Am. Chem. Soc. **107**, 2993 (1985).
14. I. KIKKAWA and T. YORIFUJI. Synthesis, 878 (1980).
15. D. D. RIDLEY and M. STRALOW. J. Chem. Soc. Chem. Commun. 400 (1975).
16. E. J. COREY and G. SCHMIDT. Tetrahedron Lett. 399 (1979).

The proximate spin–spin coupling, $^5J(F,CH_3)$, as a quantitative conformational indicator in alkylfluorobenzenes and related compounds

TED SCHAEFER, RUDY SEBASTIAN, GLENN H. PENNER, AND S. R. SALMAN[1]
Department of Chemistry, University of Manitoba, Winnipeg, Man., Canada R3T 2N2

Received January 27, 1986

TED SCHAEFER, RUDY SEBASTIAN, GLENN H. PENNER, and S. R. SALMAN. Can. J. Chem. **64**, 1602 (1986).

The through-space or proximate nuclear spin–spin coupling constant, $^5J(F,CH_3) \equiv {}^5J$, between methyl protons and ring fluorine nuclei in alkylfluorobenzenes is postulated as $^5J/\text{Hz} = A\langle\cos^4\theta\rangle + B\langle\sin^2(\theta/2)\rangle$, θ being the torsional angle for the C_{sp^2}—C_{sp^3} bond. *A* and *B* are obtained from the known internal rotational behaviour in 2,6-difluoroethylbenzene and the corresponding cumene derivative. The parameterization is tested on the observed ^5J in derivatives of 2,4,6-tri-*tert*-butyl- and 2,4,6-tri-isopropyl-fluorobenzene, in 2-chloro-6-fluoroisopropylbenzene, 2,6-difluoro-α-methylstyrene, and *N*-methyl-8-fluoroquinolinium halides. A prediction is made for ^5J in 2,6-difluoro-*tert*-butylbenzene. It appears that the present parameterization allows the derivation of approximate torsional potentials from proximate couplings, for example in α,α-dimethyl-2,6-difluorobenzyl alcohol.

TED SCHAEFER, RUDY SEBASTIAN, GLENN H. PENNER et S. R. SALMAN. Can. J. Chem. **64**, 1602 (1986).

On considère que les constantes de couplage spin–spin à travers l'espace (ou par proximité nucléaire), $^5J(F,CH_3) \equiv {}^5J$, entre les protons méthyles et les noyaux de fluor d'alkylfluorobenzènes peuvent être représentées par l'équation $^5J/\text{Hz} = A\langle\cos^4\theta\rangle + B\langle\sin^2(\theta/2)\rangle$ dans laquelle θ est l'angle de torsion par la liaison C_{sp^2}—C_{sp^3}. On a obtenu les valeurs de *A* et de *B* à partir du comportement connu pour la rotation interne dans le difluoro-2,6 éthylbenzène et le dérivé cumène correspondant. On a évalué les paramètres sur la valeur de ^5J observée dans des dérivés des tri-*tert*-butyl-2,4,6 et tri-isopropyl-2,4,6 fluorobenzène, dans le chloro-2 fluoro-6 isopropylbenzène, le difluoro-2,6 α-méthylstyrène et dans les halogénures du *N*-méthyl fluoro-8 quinolinium. On fait une prédiction relative à la valeur de ^5J dans le difluoro-2,6 *tert*-benzène. Il semble que les paramètres actuels permettent de dériver les potentiels approximatifs de torsion à partir de couplage approximatifs, comme dans l'alcool α,α-diméthyl difluoro-2,6 benzylique.

[Traduit par la revue]

Introduction

Proximate spin–spin coupling constants are those for which nuclear spin state information is transmitted via interactions between electron orbitals in proximate bonds or even between orbitals centered on the coupled nuclei (1–4). It follows that the magnitude of the coupling constants is very sensitive to the distance between the coupled nuclei and is often difficult to calculate reliably (4–10) or to relate quantitatively to common conformational parameters such as torsion angles. An early study of some alkyl derivatives of fluorobenzene (3) demonstrated a steep dependence of $^5J(F,CH_3) \equiv {}^5J$, the coupling over five formal bonds to methyl protons in the sidechain, on the distance between the fluorine nucleus and the carbon nucleus of the methyl group. The distance was estimated from models. Although ^5J gives a good indication of the preferred conformation of the sidechain, it is not obvious how ^5J can be related quantitatively to the potential governing the internal rotation about the C_{sp^2}—C_{sp^3} bond. For example, it is very likely that this potential in 2,6-difluoroethylbenzene, **1**, is predominantly twofold (11–14) and that, as in ethylbenzene itself (12, 14), the most stable conformation has θ as 90°. Again, the cumene derivative, **2**, has θ as 60° in the conformation of lowest energy (11). It is therefore expected and observed that ^5J in **1** is less than

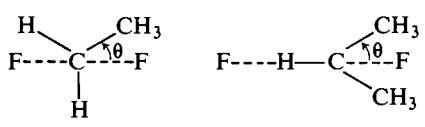

1 **2**

^5J in **2** (11). ^5J is relatively easily measured and can often be obtained by inspection of an nmr spectrum. Hence, if ^5J could be quantitatively related to θ, then it could be used to extract the hindering potential governing the motion of the sidechain.

Now, the proximate couplings $^5J(H,CH_3)$ in anisole and $^5J(F,CH_3)$ in 2-fluoroacetophenone apparently obey a $\cos^4\theta$ law (10, 15). For the former, INDO MO FPT computations (15) agree with such a θ dependence. However, such computations are unreliable for the proximate $^5J(F,CH_3)$ for reasons discussed previously (10). The assumption that $^5J \propto \cos^4\theta$ in 2-fluoroacetophenone, where θ is defined between 0 and 90° only, led to a reasonable interpretation of ^5J in this compound and its 6-fluoro derivative, and of its temperature dependence in the two compounds (10).

However, it is known[2] that the $2p_z$ orbital on the oxygen atom of the carbonyl group in acetophenone prevents efficient transmission of spin state information via the exocyclic bonds, so that the simple θ dependence for the proximate coupling mechanism may well have to be augmented by another contribution in alkylfluorobenzenes, particularly for $90° < \theta < 180°$.

In this paper, ^5J values in **1**, **2**, and **3** (α,α-dimethyl-2,6-

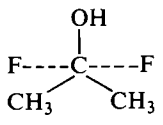

3

difluorobenzyl alcohol) are examined with a view to establishing ^5J as a quantitative measure of hindered rotation about the C_{sp^2}—C_{sp^3} bond. As applications, ^5J values in 2-chloro-6-fluoroisopropylbenzene, 3,5-dibromo-2-fluoroisopropylbenzene, and α-methyl-2,6-difluorostyrene are discussed, and a prediction is made for ^5J in 2,6-difluoro-*tert*-butylbenzene. Some literature values of ^5J are also examined.

The θ dependence of $^5J \equiv {}^5J(F, CH_3)$

The derivation of a relationship between ^5J and θ is facilitated by the following considerations. The values of $\cos^4\theta$ for rigid

[1]Permanent address: Department of Chemistry, University of Baghdad, Baghdad, Iraq.

[2]Unpublished work in this laboratory and private communication from Dr. R. Laatikainen.

conformers defined at 30, 60, and 90° are 0.5625, 0.0625, and zero, respectively. As the internal barrier decreases from infinity and approaches zero, $\langle\cos^4\theta\rangle$, the expectation value of $\cos^4\theta$, approaches 0.375 in each example. Hence, in **1** and **2** a vanishing barrier should yield identical values of ^5J. They are not identical, of course, and are ±0.301(3) and +0.956(3) Hz in **1** and **2**, respectively (11). In **1**, the most stable conformation has θ as 90°, whereas in **2** it is the one with θ = 60° (11). If ^5J were simply proportional to $\langle\cos^4\theta\rangle$ and if these two angles defined rigid conformations, then $^5J_0$, the value at θ = 0°, would follow as 31 Hz in **2** and infinity in **1**.[3] Neither value is reasonable, the latter for obvious reasons and the former because it also seems too large when compared, for example, to the $^5J_0$ of 8.15 Hz deduced for 2-fluoroacetophenone (10) or to the 8.8 Hz observed for the *N*-methyl-8-fluoroquinolinium iodide (8), in which θ approximates to zero. Because the C—C—C(H_3) bond angles in these latter two compounds are near 120° but are probably nearer 110° in **1** and **2**, a value of ^5J of about 10 Hz seems reasonable for the latter compounds.

Now, the barrier to rotation about the C_{sp^2}—C_{sp^3} bond in **1**, assumed twofold, is 25.5 ± 8.4 kJ/mol (11). At 300 K, such a barrier corresponds to a classical $\langle\cos^4\theta\rangle$ of 0.01 ± 0.01. Again, a dependence of ^5J only on $\cos^4\theta$ would imply a $^5J_0$ of 60 Hz or larger. It is apparent that another coupling mechanism contributes to ^5J.

Therefore, write eq. [1]

$$[1]\quad {}^5J/\mathrm{Hz} = ({}^5J_0/2)\langle\cos^4\theta\rangle + {}^5J_{180}\langle\sin^2(\theta/2)\rangle$$

in which the second term arises from a σ electron mechanism (16, 17) having its maximum in the all-*trans* arrangement of the intervening bonds. A σ–π electron contribution, varying as $\sin^2\theta$, is rejected because no coupling is observed between ^{19}F and methyl ^1H nuclei in 4-fluoroethylbenzene (18). For a twofold barrier, $\langle\sin^2(\theta/2)\rangle$ is 0.5 (16). Proceeding on this assumption and also taking ^5J in **1** as positive, one has $0.301(3) = ({}^5J_0/2)(0.01 \pm 0.01) + 0.5\,{}^5J_{180}$ for **1**. In **2** the enthalpy of activation for rotation about the C_{sp^2}—C_{sp^3} bond is 25.4(4) kJ/mol (11), yielding $+0.956(3) = ({}^5J_0/2)0.143(1) + 0.5\,{}^5J_{180}$. It follows that $^5J_0$ is 9.16 ± 0.65 Hz, an apparently reasonable magnitude in terms of the previous arguments, and that $^5J_{180}$ is 0.60 ± 0.10 Hz. In 2,6-difluoroalkylbenzenes, therefore, eq. [2] represents the θ dependence of ^5J. Note that

$$[2]\quad {}^5J(F_2CH_3)/\mathrm{Hz} = (9.16 \pm 0.65)/2(\langle\cos^4\theta\rangle) + (0.30 \pm 0.05)$$

twofold barriers are assumed and that $\langle\cos^4\theta\rangle$ is defined for $0 \le \theta \le 90°$ but that for $\langle\sin^2(\theta/2)\rangle$ this angle is defined between 0 and 180°. In a 2-fluoroalkylbenzene, for example, the coefficient of $\langle\cos^4\theta\rangle$ would become 9.16 ± 0.65 Hz and the second term would be $(0.60 \pm 0.10)\langle\sin^2(\theta/2)\rangle$ Hz.

Tests of the conformational eq. [2]

(i) 2,6-Difluoro-α,α-dimethylbenzyl alcohol, 3

In this molecule, ^5J is +2.031(1) Hz. Therefore $\langle\cos^4\theta\rangle$ is 0.38 ± 0.03 if the barrier is twofold. For a zero internal barrier $\langle\cos^4\theta\rangle$ is 0.375, so that an ambiguity is introduced by the error estimate. If **3** is the stable form, then V_2 ranges between 0 and 6 kJ/mol, because $0.3750 \le \langle\cos^4\theta\rangle \le 0.5625$. If the conformation analogous to **2** is the most stable, then $0.0625 \le \langle\cos^4\theta\rangle \le 0.375$ and an upper limit to V_2 becomes 1 kJ/mol. It is known[4] that the conformation analogous to **3** is favored by less than 25 kJ/mol in 2,6-difluorobenzyl alcohol. For the isopropyl derivative, **2**, the conformation with θ = 30°, analogous to **3**, lies 25 kJ/mol above **2**. Hence a simple additivity scheme for the interpretation of the barrier in **3** does not hold.

In order to ascertain the conformation of lowest energy for **3**, $^6J_p(^1H,^{13}C)$ was measured as (−)0.222(6) Hz in the derivative containing a $^{13}CH_3$ group (see Experimental). In 2,6-dichloroethylbenzene, this coupling is (−)0.618 ± 0.016 Hz (19) and is a close approximation to its value at θ = 90°. Furthermore, it seems clear that $^6J_p(^1H,^{13}C)$ varies as $\sin^2\theta$. Then, allowing for the electronegativity of the hydroxyl group in **3** and assuming that $^6J_{90}(^1H,^{13}C)$ is reduced in the same proportion (20*a*) as $^6J_{90}$(H,H), it follows that a *lower* limit to $\langle\sin^2\theta\rangle$ is 0.42. This value of $\langle\sin^2\theta\rangle$ corresponds to a V_2 of 3.3 kJ/mol *and* to a preferred conformation as shown in **3** (θ = 30°). For this choice of θ the proximate ^5J formulation suggests a V_2 of 3.0 ± 3.0 kJ/mol (from 0 to 6 kJ/mol). Equation [2] is successful to the extent of finding a very low barrier compared to those in **1** and **2**.

*(ii) Prediction for 2,6-difluoro-*tert*-butylbenzene, 4*

Because of the threefold symmetry of the *tert*-butyl group, $\langle\cos^4\theta\rangle$ will always average to 0.375, no matter what the most stable conformation or the barrier are. Consequently, eq. [2] predicts a ^5J of 2.0 ± 0.2 Hz because $\langle\sin^2(\theta/2)\rangle$ will be 0.5 under these conditions. **4** has not been made. However, ^5J is available for some 3-X-2,4,6-tri-*tert*-butylbenzenes (3) and is discussed next.

*(iii) $^5J(F,CH_3)$ in 3-X-2,4,6-tri-*tert*-butylbenzenes, 5*

As the size of X increases in **5**, the conformation in which one

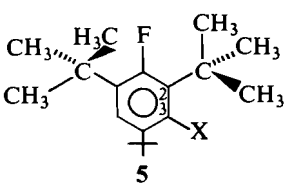

5

methyl group eclipses the C—F bond increases in stability. Accordingly, ^5J increases from 0.9 Hz for X = H to 4.2 Hz for X = Br. For compounds of this symmetry, eq. [2] must be written as eq. [3].

$$[3]\quad {}^5J(F,CH_3)/\mathrm{Hz} = (9.16 \pm 0.65)\langle\cos^4\theta\rangle + (0.60 \pm 0.10)\langle\sin^2(\theta/2)\rangle$$

For free rotation (zero barrier) ^5J becomes 3.74 ± 0.39 Hz, while for a rigid **5**, where one methyl group eclipses the C—F bond, the average ^5J is 3.35 ± 0.27 Hz (remember that $\langle\cos^4\theta\rangle$ is defined for $0 \le \theta \le 90°$). Again, for a rigid **5** in which two methyl groups are staggered about the C—F bond, the average ^5J is reduced to 0.58 ± 0.06 Hz. Accordingly, when neither rigid conformers nor completely free internal rotations exist, ^5J should lie between 0.52 and 4.03 Hz in magnitude. The ^5J of 4.2 Hz when X = Br must be interpreted in this model as caused by distortion of the sidechain geometry by the relatively large bromine substituent, such that the methyl group eclipsing the C—F bond moves about 0.1 Å closer to the fluorine substituent. A distortion of this magnitude can cause an increase of about 0.6 Hz in ^5J (3). That a substituent at C-3 in **5** can distort the molecule is also indicated by the change in ^5J observed for the *tert*-butyl group at C-6. Of course, the barriers to internal rotation in **5** are not known, but are needed to compute ^5J from

[3] Note that $^5J = ({}^5J_0/2)\langle\cos^4\theta\rangle$ because there are two *ortho* fluorine substituents and because, in line with the remarks in the introduction, $\langle\cos^4\theta\rangle$ is defined between 0° and 90° only.

[4] Unpublished work in this laboratory.

eq. [3]. That the barriers might well be substantial might be inferred from the following example.

(iv) 2-Chloro-6-fluoroisopropylbenzene, 6

Compound **6** obeys the equilibrium **6***a* ⇄ **6***b* with $K = 7.6$ at 300 K (20*b*).

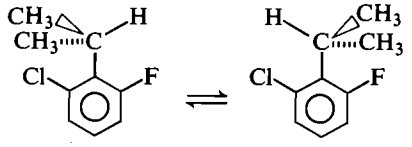

6*a* **6***b*

The enthalpy of activation for interconversion of **6***a* and **6***b* is 38.1(3) kJ/mol and $^5J(F,CH_3)$ is 1.61 Hz. Although the potential function for the rotation about the exocyclic C—C bond is not known from these data, the following approach allows an estimate of ^5J from eq. [3]. In **6***b* the potential hindering small amplitude torsions must be rather similar to V_2 in **2**, 25.5 kJ/mol. Therefore take $\langle\cos^4\theta\rangle$ to be 0.143(1) as discussed above for **2**, yielding ^5J as 1.46 ± 0.15 Hz in **6***b*. In **6***a*, only the term in $\langle\sin^2(\theta/2)\rangle$ contributes and will be 0.45 ± 0.08 Hz. Hence eq. [3] yields an estimate of 0.88 (1.46 ± 0.15) + 0.12 (0.45 ± 0.08) or 1.34 ± 0.14 Hz, where 0.88 is the fractional population of **6***b*. This estimate of ^5J lies 0.27 ± 0.14 Hz below the observed value of 1.61 Hz.

(v) 3,5-Dibromo-2-fluoroisopropylbenzene, 7

$^5J(F,CH_3)$ is 0.51(1) Hz in **7**. There is considerable freedom of motion about the C_{sp^2}—C_{sp^3} bond, as shown by the $^6J(H,CH)$ of −0.233(5) Hz. This coupling vanishes when the α C—H bond sits in the ring plane (11, 21–23). The simplest potential describing the motion of the isopropyl group contains onefold and twofold terms. An approximation to V_1 can be had from 2,6-diisopropylfluorobenzene, in which $^5J(F,CH_3)$ is 0.49(1) Hz in magnitude (same as in **7**) and $^5J_m(H,CH)$ is 0.420(7) Hz. The latter coupling is stereospecific (17, 24) and would be 0.63 Hz if this compound existed in a rigid conformation having the α C—H bond *cis* to the C—F bond.[5] Assuming a barrier sizeable compared to *kT* (see below), a free energy difference of 1.8 kJ/mol favoring the C—H *cis* over the C—H *trans* conformation can be deduced (24). The assumption that the entropy difference is negligible yields a value of 0.5 for the **7***a* ⇆ **7***b* equilibrium at 305 K.

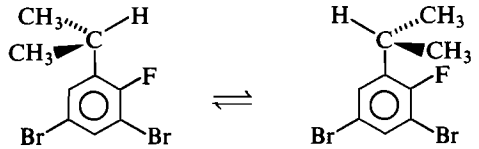

7*a* **7***b*

For rigid conformers ^5J follows as 0.55 ± 0.03 Hz, compared to the observed value of 0.51 ± 0.01 Hz. Of course, the twofold barrier to rotation in the absence of the fluorine substituent is 7.6 ± 0.8 kJ/mol (25) and is 25.5 ± 0.4 kJ/mol in **2**. At 305 K some considerable torsional amplitudes about the C_{sp^2}—C_{sp^3} bond therefore occur, particularly in **7***a*. Therefore write $V = V_1\sin^2(\psi/2) + V_2\sin^2\psi$, where ψ is zero in **7***a*, as the most simple potential function governing the torsion. V_1 is taken as 1.8 kJ/mol. Computation of the classical averages of $\cos^4\theta$ and $\sin^2(\theta/2)$, with the proviso that contributions to $\langle\cos^4\theta\rangle$ occur only when the methyl group lies in the quadrant containing the C—F bond, proceeds for a range of V_2 values. A reasonable fit to the observed ^5J of 0.51 Hz occurs for a V_2 of 22 ± 2 kJ/mol.

(vi) 2,6-Difluoro-α-methylstyrene, 8

In this compound, ^5J is 0.95(2) Hz. If eq. [2] applies, then $\langle\cos^4\theta\rangle$ is 0.142 ± 0.012. Because $\langle\cos^4\theta\rangle < 0.375$, the most stable conformation must have the methyl group in a plane perpendicular to the benzene plane. The assumption of a twofold barrier yields V_2 as 5.8 ± 0.5 kJ/mol. Of course, the C(1)—C—CH_3 bond angle is no doubt larger than in an sp^3 bonding situation, which would cause a decrease in $^5J_0$ in eq. [2]. If $^5J_0$ were as small as 8.0 Hz, somewhat smaller than in 2-fluoroacetophenone, then $\langle\cos^4\theta\rangle$ would be 0.162, corresponding to a V_2 of 5.1 kJ/mol. The classical expectation value of θ is 63(1)° for this range of V_2 values, where θ is measured from the ring plane.

In α-methylstyrene, θ has been deduced as 30° from ultraviolet spectroscopy (26) and as 29 ± 6°C from photoelectron spectral data (27). In 4-fluoro-α-methylstyrene, $^6J(^{13}C,^{19}F)$ indicates a V_2 of 5.9 kJ/mol, the preferred conformation having θ as 0° and a $\langle\theta\rangle$ of 27 ± 1°. In other words, the presence of the two *ortho* fluorine substituents alters the stable conformers from one in which θ is 0° to the one in which θ is 90°. The change in the magnitude of the barrier is apparently about 11 kJ/mol.

However, in styrene V_4 amounts to 26% of V_2 (28) and is of opposite sign to V_2. Although the observed $^5J(F,CH_3)$ in **8** unequivocally establishes the perpendicular conformer as the one of lowest energy, the assumption that V_4 and V_2 are of comparable magnitude is also compatible with a $\langle\cos^4\theta\rangle$ of 0.142. Thus, measuring the zero of energy from θ = 90° gives V_2 and V_4 as 5.0 and −4.5 kJ/mol, respectively, or as 11.5 and 9.8 kJ/mol. Now, STO 3G MO computations with geometry optimization (29*a*) agree that V_2 and V_4 differ in sign in styrene, although they overestimate V_2 by 27%. Identical (29*a*) computations on **8** yield V_2 and V_4 as 11.5(8) and 9.1(8) kJ/mol, respectively. It seems that $^5J(F,CH_3)$ is therefore compatible with a twofold barrier of 5.8 kJ/mol or with a barrier consisting of larger twofold and fourfold components of very similar magnitudes (it may be noted that STO 3G MO computations on **1** yield a small V_4 component for the internal rotation barrier, consistent with the assumptions made in previous sections).

(vii) N-methyl-8-fluoroquinolinium iodide and chloride, 9a and 9b

$^5J(F,CH_3)$ is +8.8 Hz in these molecules (8). In terms of eq. [3], the coupling should be 9.1 ± 0.6 Hz, assuming a planar rigid structure. Of course, the intervening bond angles are distorted from ideal 120° bond angles (8), yet the molecule is effectively planar. Considering that the bond lengths in the fragments used to derive eq. [3] are probably somewhat larger than in **9**, the coupling magnitude in the latter is probably consistent with the discussion in the previous sections.[6]

[5]Full analysis of ^1H nmr and ^{19}F nmr spectra of 2,6-diisopropylfluorobenzene is problematic because of the nature of its spin system. However, $^6J_p(H,CH)$ is −0.22(3) Hz, the same as in **7**, implying very similar motional characteristics of the isopropyl groups in the two compounds.

[6]A referee asks how the present treatment applies to $^5J(F,CH_2)$ in 5-fluoro-3,3-dimethyl-1,2,3,4-tetrahydrophenanthrene (29*b*). This coupling is indeed an interesting one from the viewpoint of proximate coupling mechanisms. However, the present paper relates to reorienting methyl groups (hence $^5J(F,CH_3)$ refers to an average over three methyl protons), which, in general, are part of a larger reorienting part of the molecule (angle θ).

TABLE 1. The ^{1}H nmr spectral parameters for 2,6-difluoro-α-methyl-α-methyl-^{13}C-benzyl alcohol[a]

Parameter	Value	Parameter	Value
$\nu(CH_3)$[b]	705.333(0)[c]	^4J(H,F)	6.099(4)
$\nu(^{13}CH_3)$	704.871(0)	^5J(H,F)	−1.438(5)
$\nu_3 = \nu_5$	2251.098(2)	^4J(F,F)	6.769(7)
ν_4	2351.963(3)	^3J(H,H)	8.315(3)
^1J(H,C)	127.447(1)	^4J(H,H)	1.289(5)
^3J(H,C)	4.315(1)	$^4J(CH_3,CH_3)$	0.501(0)
^5J(H,C)	0.000(5)	Calcd. transitions	80[d] 544[e]
^6J(H,C)	(−)0.222(6)	Assigned transitions	63 355
$^5J(F,CH_3)$	2.030(1)	Largest difference	0.042 0.018
$^5J(F,^{13}CH_3)$	2.032(1)	RMS deviation	0.014 0.006
^3J(H,F)	12.040(4)		

[a]For a 3.0 mol% solution in CS_2, containing 10.0 mol% C_6D_{12} and 0.5 mol% TMS at 300 K.
[b]In Hz at 300.135 MHz to high frequency of internal TMS.
[c]Numbers in parentheses are standard deviations in the last significant figure.
[d]From a separate analysis of the ring proton spectrum.
[e]From an analysis of the spectrum from the methyl protons.

Experimental

The preparation and analyses of the ^{1}H and ^{19}F nmr spectra of **1** have been described (11), as have the synthesis and analysis of the ^{1}H nmr spectrum of **2** (11, 30).

The analysis of the ^{1}H nmr spectrum of **3**, the compound being an intermediate in the synthesis of **2** (30), yielded $^5J(F,CH_3)$ as 2.032(1) Hz for a 3.1 mol% solution in CS_2 at 305 K. The ^{1}H nmr spectrum was calibrated on a HA100 spectrometer by procedures previously described in detail (31). $^5J(F,CH_3)$ was independent of concentration from 3 to 0.4 mol% in CS_2. Weak double irradiation experiments (32) showed that $^5J(F,CH_3)$ was of opposite sign to $^5J(F,OH)$ in **3**. The latter coupling is negative in 2-fluorobenzyl alcohol (33), implying $^5J(F,CH_3)$ as positive in **3**. The positive sign is expected, the coupling being positive in **2**, **7**, **8**, and **9**.

The synthesis of **3** containing a $^{13}CH_3$ group proceeded in a straightforward way by reaction of 2,6-difluoroacetophenone with the Grignard reagent prepared from ^{13}C-enriched methyl iodide. The ^{1}H nmr spectrum of a 3.0 mol% solution in CS_2, containing also 10 mol% C_6D_{12} and 0.5 mol% TMS, was obtained on an AM300 nmr spectrometer at a probe temperature of 300 K. This spectrum was analyzed with the computer program NUMARIT (34), as modified by R.S. The spectral parameters appear in Table 1. Figure 1 displays the ^{1}H nmr spectrum of the methyl group for this compound.

Compound **6** was prepared in the same manner as **2** (11, 30). Analysis of the ^{1}H nmr spectrum of **2** as a dilute solution in benzene-d_6 at 90 MHz yielded $^5J(F,CH_3)$ as 1.61(1) Hz.

Compound **7** was derived from 2-aminocumene via bromination and diazotization in the standard way. Its ^{1}H nmr and ^{19}F nmr spectra were accumulated on a WH90 nmr spectrometer from a dilute solution in acetone-d_6 by methods standard in this laboratory (31). Analyses of the spectra and double irradiation experiments yielded the germane result that $^5J(F,CH_3)$ was +0.51(1) Hz.

The 2,6-diisopropylfluorobenzene was synthesized via the diazonium salt of the corresponding aniline derivative. The ^{1}H nmr and ^{19}F nmr spectra of a 5 mol% solution in CCl_4, recorded on a WH90 spectrometer, arise from an ABB′XX′R spin system. The spectra were insensitive to $^4J_{46}$ and had other peculiarities that are of no interest here. However, an analysis gave $^5J(H,CH)$ as 0.420(7) Hz, $^5J(F,CH_3)$ as 0.492(5) Hz, and $^6J(H,CH)$ as −0.22(3) Hz, relevant to the discussion above. An analysis of the ^{19}F nmr spectrum, obtained while decoupling the methyl protons, utilized the self-assigning program DAVINS (35) in a manner described previously (11), and yielded $^4J(F,CH)$ as 0.40(1) Hz.

The styrene derivative, **8**, was also an intermediate in the synthesis of **2** (11, 30). For a dilute solution in CS_2, $^5J(F,CH_3)$ was 0.95(2) Hz.

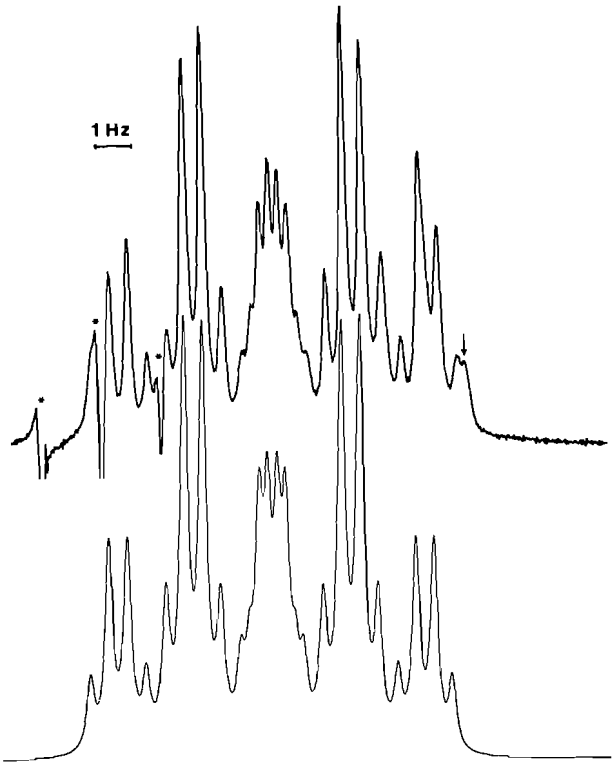

FIG. 1. The observed and calculated methyl ^{1}H nmr spectrum at 300 MHz and 300 K of a 3 mol% solution in CS_2 of 2,6-difluoro-α-methyl-α-methyl-^{13}C-benzyl alcohol. The line widths at half height are 0.2 Hz, probably arising from small unresolved long-range coupling to ring protons and the hydroxyl proton. The artifactual distortion of one side of the observed spectrum, indicated by asterisks, is not present in the ^{1}H nmr spectrum of the $^{13}CH_3$ group. An impurity peak, indicated by an arrow, is also present in the observed spectrum and impurities may also account for the anomalous intensity of a nearby peak.

Acknowledgements

We are grateful to the Natural Sciences and Engineering Research Council of Canada for financial assistance.

1. J. D. ROBERTS, D. R. DAVIES, and R. P. LUTZ. J. Am. Chem. Soc. **83**, 246 (1961).

2. J. HILTON and L. H. SUTCLIFFE. Prog. Nucl. Magn. Reson. Spectrosc. **10**, 27 (1975).
3. P. C. MYRE, J. W. EDMONDS, and J. D. KRUGER. J. Am. Chem. Soc. **88**, 2459 (1966).
4. R. E. WASYLISHEN and M. BARFIELD. J. Am. Chem. Soc. **97**, 4545 (1975).
5. T. SCHAEFER, S. R. SALMAN, and T. A. WILDMAN. Can. J. Chem. **58**, 2364 (1980).
6. T. SCHAEFER, K. MARAT, A. LEMIRE, and A. F. JANZEN. Org. Magn. Reson. **18**, 90 (1982).
7. T. SCHAEFER, R. SEBASTIAN, R. P. VEREGIN, and R. LAATIKAINEN. Can. J. Chem. **61**, 29 (1983).
8. M. BARFIELD, S. R. WALKER, K. A. CLARK, G. W. GRIBBLE, K. W. HADEN, W. J. KELLY, and C. S. LE HOULLIER. Org. Magn. Reson. **20**, 92 (1982).
9. T. A. WILDMAN. Ph.D. Thesis, University of Manitoba. 1982.
10. T. SCHAEFER, G. H. PENNER, T. A. WILDMAN, and J. PEELING. Can. J. Chem. **63**, 2256 (1985).
11. T. SCHAEFER, R. P. VEREGIN, R. LAATIKAINEN, R. SEBASTIAN, K. MARAT, and J. L. CHARLTON. Can. J. Chem. **60**, 2611 (1982).
12. T. SCHAEFER, L. KRUCZYNSKI, and W. NIEMCZURA. Chem. Phys. Lett. **38**, 498 (1976).
13. A. MILLER and D. W. SCOTT. J. Chem. Phys. **68**, 1317 (1978).
14. M. S. FARAG. Diss. Abstr. Int. B, **35**, 1594 (1974).
15. T. SCHAEFER and R. LAATIKAINEN. Can. J. Chem. **61**, 224 (1983).
16. T. SCHAEFER, T. A. WILDMAN, and R. SEBASTIAN. Can. J. Chem. **60**, 1924 (1982).
17. T. SCHAEFER and R. LAATIKAINEN. Can. J. Chem. **61**, 2785 (1983).
18. T. SCHAEFER, J. PEELING, G. H. PENNER, A. LEMIRE, and R. SEBASTIAN. Can. J. Chem. **63**, 24 (1985).
19. T. SCHAEFER, J. PEELING, and G. H. PENNER. Can. J. Chem. **61**, 2773 (1983).
20. (*a*) T. SCHAEFER, J. PEELING, and R. SEBASTIAN. Can. J. Chem. **63**, 3219 (1985); (*b*) R. LAATIKAINEN. J. Magn. Reson. **64**, 375 (1985).
21. R. WASYLISHEN and T. SCHAEFER. Can. J. Chem. **50**, 1852 (1972).
22. C. J. MACDONALD and W. F. REYNOLDS. Can. J. Chem. **48**, 1002 (1970).
23. W. J. E. PARR and T. SCHAEFER. Acc. Chem. Res. **13**, 400 (1980).
24. T. SCHAEFER, B. A. ADDISON, R. SEBASTIAN, and T. A. WILDMAN. Can. J. Chem. **59**, 1656 (1981).
25. T. SCHAEFER, W. J. E. PARR, and W. DANCHURA. J. Magn. Reson. **25**, 167 (1977).
26. G. K. HAMER, I. R. PEAT, and W. F. REYNOLDS. Can. J. Chem. **51**, 915 (1973).
27. T. KOBAYASHI, T. ARAI, H. SAKURAGI, K. TOKUMARU, and C. UTSONOMIYA. Bull. Chem. Soc. Jpn. **54**, 1658 (1981).
28. J. M. HOLLAS, H. MUSA, T. RIDLEY, P. H. TURNER, K. H. WEISENBERGER, and V. FAWCETT. J. Mol. Spectrosc. **94**, 437 (1982).
29. (*a*) T. SCHAEFER and G. H. PENNER. Chem. Phys. Lett. **114**, 526 (1985); (*b*) G. W. GRIBBLE and W. J. KELLY. Tetrahedron Lett. **26**, 3779 (1985).
30. R. P. VEREGIN. M.Sc. thesis, University of Manitoba. 1982.
31. T. SCHAEFER and R. SEBASTIAN. J. Magn. Reson. **41**, 395 (1980).
32. R. FREEMAN and W. A. ANDERSON. J. Chem. Phys. **37**, 2053 (1962).
33. T. SCHAEFER and W. J. E. PARR. J. Chem. Phys. **65**, 1197 (1976).
34. A. R. QUIRT and J. S. MARTIN. J. Magn. Reson. **5**, 318 (1971); J. S. MARTIN, A. R. QUIRT, and K. E. WORVILL. The NMR program library. Daresbury Laboratory, Daresbury, U.K.
35. D. S. STEPHENSON and G. BINSCH. J. Magn. Reson. **37**, 395 (1980); Quantum chemistry program exchange, **13**, 378 (1979).

Squaraine chemistry. On the anomalous mass spectra of bis(4-dimethylaminophenyl)squaraine and its derivatives

KOCK-YEE LAW,[1] F. COURT BAILEY, AND LYNN J. BLUETT
Xerox Corporation, 800 Phillips Road, 0114-39D, Webster, NY 14580, U.S.A.

Received May 13, 1985[2]

KOCK-YEE LAW, F. COURT BAILEY, and LYNN J. BLUETT. Can. J. Chem. **64**, 1607 (1986).

The electron impact (EI) mass specra of bis(4-dimethylaminophenyl)squaraine **1** and its derivatives **2–14** have been studied. Ions of mass number higher than the molecular ion, which are shown to be precursors of fragment ions of lower mass numbers, are observed. From the structure–property relationship, these ions are assigned to M + $CHR^{\dagger}$ and M + $H_2^{\dagger}$, where CH_2R is the alkyl group in the *N,N*-dialkylanilino moiety of squaraine. Evidence is provided that the formation of M + $CHR^{\dagger}$ and M + $H_2^{\dagger}$ is the result of alkyl transfer and H transfer reactions within a squaraine aggregate rather than intermolecular vapor phase reactions in the mass spectrometer. This molecular aggregate is later shown to be a trimer by analysis of metastable ion data and chemical ionization mass spectrometry. The fragmentation sequence of this trimeric species is elucidated with the assistance of metastable ions. Results show that the trimer may break down to monomeric and dimeric species upon electron impact; alternatively, the four-membered ring of the central squaraine in the trimer may cleave to generate two species of approximately equal mass number. These two species usually dominate the mass spectrum and further fragment into M + $CHR^{\dagger}$ and M + $H_2^{\dagger}$. Detailed fragmentation schemes for M + $CHR^{\dagger}$ and M + $H_2^{\dagger}$ are proposed and discussed.

KOCK-YEE LAW, F. COURT BAILEY et LYNN J. BLUETT. Can. J. Chem. **64**, 1607 (1986).

On a étudié les spectres de masse sous impact électronique de la bis(diméthylamino-4 phényl)squaraine (**1**) et de ses dérivés **2–14**. On a observé la présence d'ions de masses plus élevées que celle de l'ion moléculaire et on démontre que ce sont les précurseurs d'ions fragmentés de masses plus basses. En se basant sur des relations entre la structure et les propriétés, on a attribué ces ions aux entités M + $CHR^{\dagger}$ et M + $H_2^{\dagger}$ dans lesquelles CH_2R représente un groupement alkyle de la portion *N,N*-dialkylamino de la squaraine. On présente des données confirmant que la formation des entités M + $CHR^{\dagger}$ et M + $H_2^{\dagger}$ provient de réactions de transfert d'hydrogène ou de groupements alkyles à l'intérieur d'un agrégat de squaraine plutôt que de réactions intermoléculaires en phase vapeur à l'intérieur du spectromètre. En se basant sur une analyse des données relatives aux ions métastables et sur la spectrométrie de masse par ionisation chimique, on démontre de plus que cet agrégat moléculaire est un trimère. On a élucidé l'ordre de fragmentation de cette espèce trimère en se basant sur les ions métastables. Les résultats démontrent que, sous impact électronique, le trimère se brise en des espèces monomère et dimère; il est aussi possible que le cycle à quatre chaînons de la squaraine centrale du trimère se brise pour générer deux espèces de masses approximativement égales. Ces deux espèces dominent habituellement les spectres de masse et les fragmentations subséquentes en M + $CHR^{\dagger}$ et M + $H_2^{\dagger}$. On propose et discute des schémas détaillés des fragmentations en M + $CHR^{\dagger}$ et M + $H_2^{\dagger}$.

[Traduit par la revue]

Introduction

Squaraines are 1,3-disubstituted products obtained from squaric acid and *N,N*-dialkylanilines (1). The synthesis of squaraines is simple and has been reviewed several times in the literature (2). Owing to the strong exciton interactions, squaraines exhibit intense and panchromatic absorption from the visible to the near-infrared (400–1000 nm) in the solid state. These features have made them very attractive for various technological applications in industry, e.g., electrophotographic imaging (3), organic solar cells (4), ablative optical recording (5), etc.

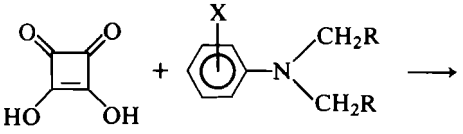

Squaric acid *N,N*-dialkylaniline

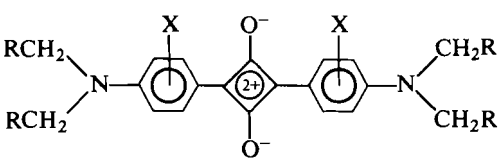

Squaraine

While the technological use of these compounds has been extensive and a large number of squaraine structures have been synthesized (6), very little attention has been devoted to the fundamental properties of squaraines. Squaraines have been typically characterized by elemental analysis, visible absorption, and ir (infrared) (1). Mass spectrometry, one of the basic analytic tools for structure determination of organic compounds, has rarely been used.

During the course of our investigation on the photoconductive properties of squaraines, we have used electron impact (EI) mass spectrometry as a routine tool for structural characterization and have found that squaraines exhibit very unusual mass spectrometric properties.[3] Ions of mass numbers higher than the molecular ion (M^+) were frequently observed. Here we report our investigation on the anomalous mass spectra of squaraines **1–14** (structures in Fig. 1). The mechanism of formation of these high molecular weight ions and their subsequent fragmentation processes are studied. Our results show that molecular aggregates of squaraines are precursors of the lower mass number fragments observed in the mass spectra. These molecular aggregates fragment upon electron impact to either molecular ions or high molecular weight intermediate ions.

[1]Author to whom correspondence may be addressed.
[2]Revision received February 11, 1986.

[3]A preliminary account of this work was presented at the 186th ACS National Meetings, Washington, D.C., August 28 – September 2, 1983.

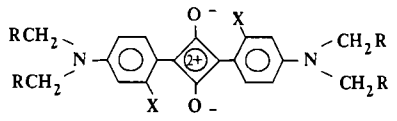

squaraine		
1	X=H	R=H
2	H	CH_3
3	H	C_2H_5
4	H	C_3H_7
5	CH_3	H
6	CH_3	CH_3
7	CH_3	C_3H_7
8	F	H
9	OCH_3	H
10	OCH_3	CH_3
11	C_2H_5	H

12

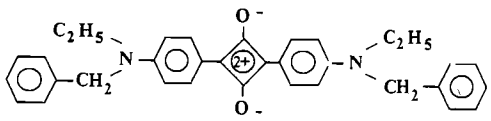

13

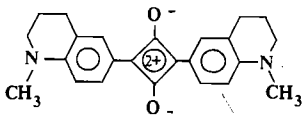

14

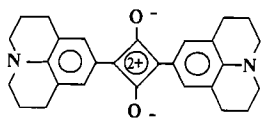

FIG. 1. Structures of squaraines **1–14**.

The latter species, which usually dominate the mass spectrum, further fragment into the characteristic mass spectrometric pattern of squaraine. The prospect of using mass spectrometry as an analytical tool for structure elucidation is discussed.

Experimental

Materials

Squaric acid, *N,N*-dimethylaniline, *N,N*-diethylaniline, *N,N*-dimethyl-*m*-toluidine, and *N,N*-di-*n*-butylaniline were purchased from Aldrich; *N,N*-diethyl-*m*-toluidine was obtained from Pfaltz & Bauer, *N*-ethyl-*N*-benzylaniline was a gift from Hardwicke Chemical Company. All these materials were used as received. *N,N*-Dimethyl-3-fluoroaniline, *N,N*-dimethyl-3-methoxyaniline, *N,N*-diethyl-3-methoxyaniline, *N,N*-dimethyl-3-ethylaniline, *N,N*-dipropylaniline, and *N,N*-dibutyl-3-methylaniline were prepared by alkylating an aniline derivative (Aldrich) with trialkyl phosphate (Aldrich) as described in the literature (7). All solvents were best commercial quality and were used without further purification.

General technique

Melting points were taken on a capillary melting point apparatus (Thomas Hoover) and are uncorrected. Elemental analyses were performed by Galbraith Laboratories. Spectra were recorded by means of the following instruments: infrared, Perkin–Elmer 283; ^{1}H nmr, Brüker WP-80; uv–vis, Cary 17.

Electron impact (EI) mass spectra were recorded on a Nuclide 12-90G magnetic sector mass spectrometer. Samples were introduced using the solid probe direct insertion inlet sytem and were usually heated slowly from ~25°C to a threshold temperature where strong ion current was obtained. The threshold temperature varied from 80°C to ~140°C and was at least 100°C below the melting point or the decomposition point of a specific compound. An ionization voltage of 70 eV regulated at 100 μA ionizing current was used.

Chemical ionization (CI) mass spectra of **1** were recorded on a triple quadrupole gc/ms spectrometer from Finnigan at Oneida Research Service. The vaporization temperature of **1** was ~150°C and the CI reagent gas (CH_4, NH_3, CH_2Cl_2, and N_2O) pressure was about 0.4 Torr (1 Torr = 133.3 Pa).

Squaraine synthesis

Squaraines were prepared by reacting one equivalent of squaric acid and two equivalents of *N,N*-dialkylanilines in a mixture of toluene (or benzene) and 1-butanol at reflux for ~8 h (8). Two work-up procedures were used and they are outlined as follows:

A. Pigment samples[4]

After cooling, the product was filtered, then washed with methanol and ether. All samples obtained are analytically pure.

B. Dye samples[4]

After cooling, solvent was removed under reduced pressure. Impurities were removed by extracting the mixture with ether. Squaraine product was then isolated from the residue by column chromatography on silica gel (Baker, 60–200 mesh) using chloroform as eluent. The physical properties and the spectroscopic data of these compounds are tabulated in Tables 1 and 2.

Results and discussion

Synthesis and characterization

Squaraines were prepared from squaric acid and *N,N*-dialkylanilines (8). Pigment samples were isolated from the product mixture by filtration and were usually analytically pure. As seen in Table 1, they all have high melting points (>200°C). As the length of the alkyl chain at the nitrogen increases, their solubility in organic solvents increases and this is accompanied by a decrease in melting point of the solid. The chemical yields of these soluble squaraines were low (<10%) and might be attributable to secondary reactions of squaraines with *N,N*-dialkylanilines in the product mixture.[5] Pure squaraines were isolated and purified by chromatographic techniques.

Squaraines exhibit intense absorption in the visible region in solution; their absorption maxima vary from 600 to 680 nm depending on the substituents at the nitrogen and in the phenyl ring. More detailed discussion on the electronic properties of squaraines will be addressed elsewhere.[6] In the ir spectra (Table 1) squaraines show no C=O stretching at ~1700 cm^{-1}. Instead, strong absorption bands at ~1600 cm^{-1} are observed and they are attributable to the C···C stretching in the four-membered ring and the phenyl ring. The absence of any C=O stretching is a strong indication of extensive bond delocalization in the four-membered ring of squaraine.

Owing to the high solubility of squaraine dyes prepared in this work, we were able to record ^{1}H nmr spectra on a routine nmr spectrometer. Results in Table 2 show that the chemical shifts of all the aliphatic protons are observed in the expected region. The chemical shifts of the aromatic protons are, however, quite characteristic and are worth further discussion.

Two sets of doublets at δ ~6.8 and ~ 8.3 ppm are observed for squaraines **2–4** and **12**, and they can be assigned to the β protons and the α protons in the phenyl ring, respectively. The

[4]Pigments denote colorants having very low solubility in various solvents and dyes generally refer to soluble colorants.

[5]Squaraines are known to react with amines to form adducts. In the case of tertiary aromatic amines, 1:1 squaraine–amine adducts have been isolated and characterized (9). In this work, we have found in controlled experiments that squaraines react with *N,N*-dialkylanilines to form colorless products. Although these colorless substances have not yet been characterized, we believe that the low chemical yield of squaraine dyes is at least in part the result of the consumption of squaraine in secondary reactions.

[6]K. Y. Law, manuscripts in preparation.

TABLE 1. Synthesis and properties of squaraines

Squaraine	Procedure	Yield (%)	Melting point (°C)	Infrared (cm^{-1})[a]	Analysis	C	H	N	F
1	A	60	296–297 (lit. 270)[b]	1584					
2	B	6	187–187.5	1584	calcd.	76.56	7.50	7.44	
					found	76.38	7.59	7.21	
3	B	9	186–186.5	1610 1580	calcd.	77.74	8.39	6.48	
					found	77.68	8.35	6.32	
4	B	7.4	186–186.5	1578	calcd.	78.65	9.08	5.73	
					found	78.84	9.19	5.60	
5[c]	A	30–50	251–251.5	1580					
6	B	7.6	198–199	1595	calcd.	77.19	7.97	6.92	
					found	76.91	8.03	6.72	
7	B	3	130–133	1600 1582	calcd.	79.02	9.36	5.42	
					found	79.21	9.46	5.38	
8	A	23	295–296	1595	calcd.	67.44	5.09	7.87	10.67
					found	67.37	5.21	7.85	10.68
9	A	9.5	230 (dec.)	1595	calcd.	69.46	6.36	7.36	
					found	69.29	6.47	7.22	
10	B	8.7	198–199	1610 1580	calcd.	71.53	7.39	6.42	
					found	71.10	7.39	6.29	
11	A	24	213–217	1586	calcd.	76.56	7.50	7.44	
					found	76.71	7.49	7.28	
12	B	2.5	196.5–197.5	1614 1580	calcd.	81.57	6.44	5.60	
					found	81.48	6.46	5.63	
13[c]	A	55	206–207.5	1588	calcd.	77.39	6.50	7.52	
					found	77.21	6.70	7.46	
14[c]	A	35	220–221	1590					

[a]In KBr.
[b]Reference 2*b*.
[c]The structures of these squaraines have been disclosed in patent literature, see ref. 6.

TABLE 2. ^1H nuclear magnetic resonance data of squaraine dyes synthesized in this work

Squaraine	Solvent	δ, ppm from TMS
2	CD_2Cl_2	1.25 (t, 12H, J = 7.5 Hz), 3.5 (q, 8H, J = 7.5 Hz), 6.8 (d, 4H, J = 9.8 Hz), and 8.32 (d, 4H, J = 9.8 Hz)
3	CD_2Cl_2	1.20 (t, 12H, J = 7.0 Hz), 1.3–2.0 (M, 8H), 3.42 (t, 8H, $J \sim$ 8.3 Hz), 6.76 (d, 4H, J = 9.5 Hz), and 8.28 (d, 4H, J = 9.5 Hz)
4	CD_2Cl_2	0.98 (t, 12H, J = 7.5 Hz), 1.1–1.92 (m, 16H), 3.46 (t, 8H, J = 7.5 Hz), 6.76 (d, 4H, J = 9.5 Hz), and 8.29 (d, 4H, J = 9.5 Hz)
6	CD_2Cl_2	1.29 (t, 12H, J = 7.4 Hz), 2.9 (s, 6H), 3.54 (q, 8H, J = 7.4 Hz), 6.5–6.7 (m, 4H), and 8.9 (d, 2H, J = 10.2 Hz)
7	CD_2Cl_2	1.0 (t, 12H, J = 7.5 Hz), 1.1–1.9 (m, 16H), 2.88 (s, 6H), 3.43 (t, 8H, J = 8.3 Hz), 6.4–6.7 (m, 4H), and ~8.9 (d, 2H, J = 10 Hz)
9	$CDCl_3$	3.24 (s, 12H), 4.09 (s, 6H), 6.1–6.7 (m, 4H), and 8.55 (d, 2H, J = 9.2 Hz)
10	$CDCl_3$	1.27 (t, 12H, J = 7.5 Hz), 3.52 (q, 8H, J = 7.5 Hz), 4.0 (s, 6H), 6.0–6.5 (m, 4H), and 8.82 (d, 2H, J = 9.5 Hz)
11	CD_2Cl_2	1.23 (t, 6H, J = 7.5 Hz), 3.19 (s, 12H), 3.43 (q, 4H, J = 7.5 Hz), 6.5–6.7 (m, 4H), and 9.04 (d, 2H, J = 10 Hz)
12	CD_2Cl_2	1.3 (t, 6H, J = 7.5 Hz), 3.68 (q, 4H, J = 7.5 Hz), 4.72 (s, 4H), 6.87 (d, 4H, J = 9.6 Hz), 7.1–7.5 (m, 10H), and ~8.3 (d, 4H, J = 9.6 Hz).
13	$CDCl_3$	1.98 (p, 4H, J = 6.5 Hz), 3.83 (t, 4H, J = 6.5 Hz), 3.17 (s, 6H), 3.50 (t, 4H, J = 6.5 Hz), 6.69 (d, 2H, J = 9.2 Hz), and 8.15–8.45 (m, 4H).

coupling constant of the α and the β protons is ~9–10 Hz, a typical coupling constant for aromatic protons in the adjacent position. This assignment is supported by ^{1}H nmr data of squaraines **6**, **7**, **9**, **10**, and **11**. In these squaraines, because of the α substitution, the integration of low-field to high-field

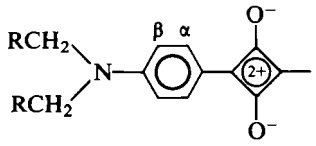

aromatic protons is 2:4. On the other hand, when the β-position is substituted, such as in squaraine **13**, the integration becomes 4:2. A similar assignment was also reported earlier by Kazmaier *et al.* in their ^{1}H nmr study of squaraine pigment.[7]

The chemical shift of the α protons varies from δ 8.3 to 9 and is about 1–1.5 ppm lower field than the aromatic protons in the corresponding *N*,*N*-dialkylanilines (δ ~ 7–7.3 ppm). The mechanism of the deshielding of the α protons has recently been studied and will be reported elsewhere.[6]

Electron impact mass spectra of squaraines

The electron impact (EI) mass spectra of squaraines **1**–**4** are presented in Figs. 2–5. All four squaraines give apparently clean mass spectra. The unusual feature of the results lies in the consistent occurrence of ions of mass numbers higher than the expected molecular ion. Ions at *m*/*z* 334, 404, 474, and 544, which correspond to the addition of a CH_2, a C_2H_4, a C_3H_6, and a C_4H_8 unit to the molecular ions of **1**, **2**, **3**, and **4**, respectively, are observed. These results suggest that these high molecular weight ions have a general formula of (M + CHR). In addition to M + CHR$^{+\cdot}$, ions at (*M* + 2), which are assigned to the addition of two hydrogen atoms to M^+, are also observed. Molecular ions are usually detectable, but their relative intensities are weak. The observation of M + CHR$^{+\cdot}$ and M + $H_2$$^{+\cdot}$ suggests that some kind of intermolecular alkyl transfer and H transfer reactions are occurring in the mass spectrometer.

Lower mass number fragment ions also appear to be very general and unique. The structures of these fragment ions are assigned on the basis of the structure–property relationship established from the mass spectra of squaraines **1**–**11**.[8] The relative intensities of these fragment ions are tabulated in Table 3. The formation of fragment ions **15** and **18** is very unusual because the carbon α to the phenyl ring in squaraine is bonded to neither an oxygen atom nor a hydrogen atom; the formation of **15** and **18** indicates the occurrence of molecular rearrangement processes in the mass spectrometer. A more detailed discussion of these rearrangement processes will be presented in later sections.

The changes in fragmentation patterns as a function of ionization voltage have been studied for some of these squaraines. A gradual dominance of M + CHR$^{+\cdot}$ and M + $H_2$$^{+\cdot}$ in the mass spectrum is observed when the ionization voltage is lowered. These results, along with the metastable ion data and structure–property relationships presented in this paper, suggest that M + CHR$^{+\cdot}$ and M + $H_2$$^{+\cdot}$ are precursors of the lower mass number fragment ions (10).

Very similar mass spectrometric results are obtained for squaraines **5**–**7** (Table 3). In addition to M + $H_2$$^{+\cdot}$, M + CHR$^{+\cdot}$ at *m*/*z* 362, 432, and 572 are observed for **5**, **6**, and **7**, respectively. The fragmentation pattern is found to be very similar to those of **1**–**4** as well. Analogous mass spectra are also obtained for **8**–**11** and results are tabulated in Table 3.

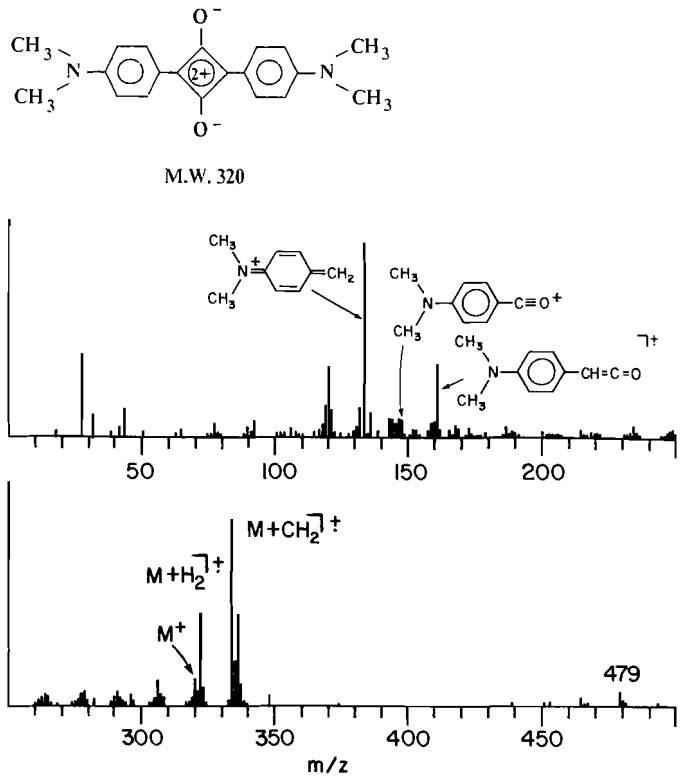

FIG. 2. EI mass spectrum of squaraine **1**.

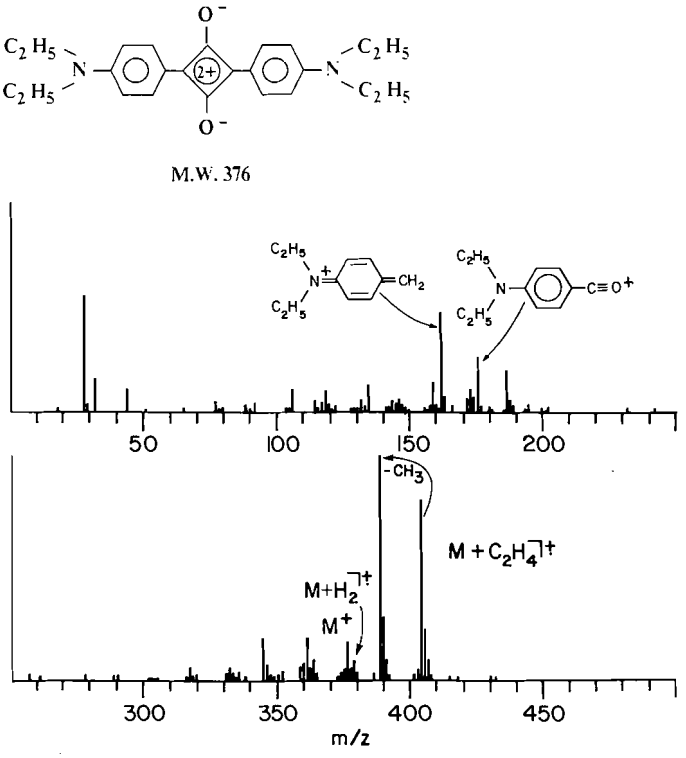

FIG. 3. EI mass spectrum of squaraine **2**.

[7]Reference 13.

[8]In the case of **1**, precise mass analyses were carried out for all fragment ions. Our results show that the observed values are in excellent agreement with the calculated values of all the proposed structures.

TABLE 3. Mass spectral data of squaraines

Squaraine	M^+	$M + CHR^{\urcorner\ddagger}$	Ion peak, m/z (rel. intensity)					
			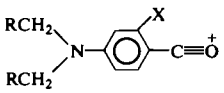 **15**	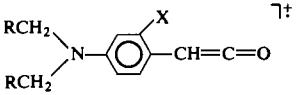 **16**	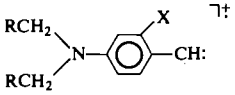 **17**	$M + H_2^{\urcorner\ddagger}$	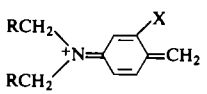 **18**	Base peak
1	320(13)	334(95)	148(13)	161(37)	—	322(48)	134(100)	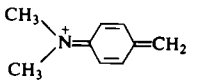
2	376(16)	404(80)	176(75)	—	—	378(9)	162(44)	$M + CH^{\urcorner\ddagger}$
3	432(5)	474(16)	204(36)	—	—	434(3)	190(100)	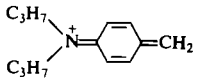
4	488(0)	544(83)	232(56)	—	—	490(6.7)	218(91)	$M + CH^{\urcorner\ddagger}$
5	348(24)	362(100)	162(6.5)	175(71)	147(45)	350(47)	148(28)	$M + CH_2^{\urcorner\ddagger}$
6	404(2)	432(16)	—	—	177(28)	406(100)	—	$M + H_2^{\urcorner\ddagger}$
7	516(4)	572(69)	—	—	233(82)	518(69)	—	$M + CH^{\urcorner\ddagger}$
8	356(10)	370(100)	166(5)	179(43)	151(26)	358(5)	152(20)	$M + CH_2^{\urcorner\ddagger}$
9	380(2)	394(100)	—	191(22)	163(20)	382(17)	164(9)	$M + CH_2^{\urcorner\ddagger}$
10	436(3)	464(4)	206(21)	219(11)	191(2)	438(67)	192(100)	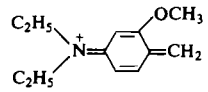
11	376(10)	390(100)	176(4.5)	189(25)	161(11)	378(32)	162(33)	$M + CH_2^{\urcorner\ddagger}$
12	500(16)	528(34) 590(9.6)	238(33)	—	—	502(11)	224(85)	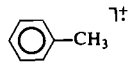
13	372(3)	386(3)	174(6)	187(6)	159(7)	374(32)	160(100)	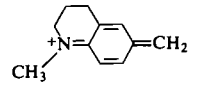
14	424(0)	—	—	—	—	426(10)	186(100)	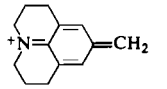

TABLE 4. Cross-over experiment

Ion	m/z	
	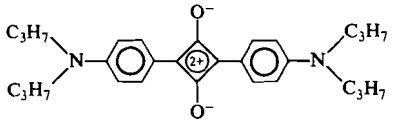 **3**	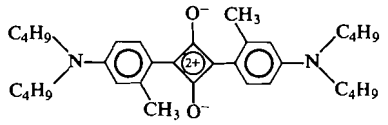 **7**
	Pr_2SQ	Bu_2SQ
M^+	432	516
(M + CHR) ion	474	572
Cross-over ion	488	558

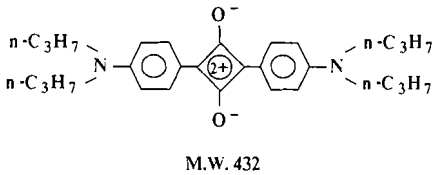

M.W. 432

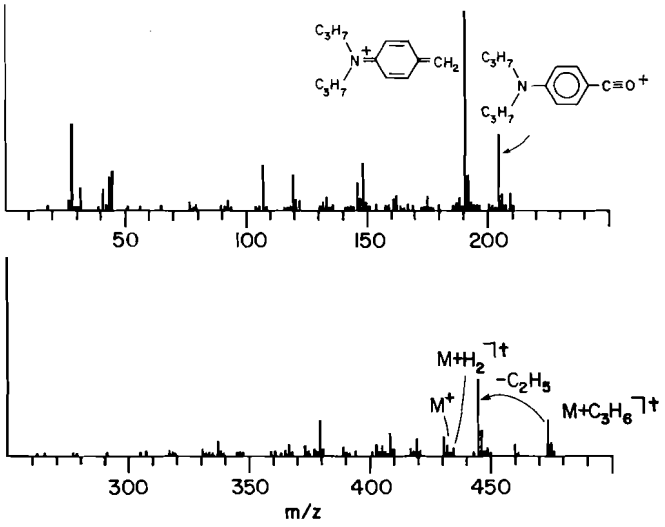

FIG. 4. EI mass spectrum of squaraine **3**.

The mass spectrum of **12** serves as another illustration of the interesting mass spectrometry of squaraine. There are two different alkyl groups at the nitrogen of **12** and two M + $CHR^{\dagger}$ are expected. Indeed, they are observed at m/z 528 and 590 and are assigned to M + $C_2H_4^{\dagger}$ and M + CH—$C_6H_5^{\dagger}$, respectively (Table 3). The mass spectrometric pattern of **12** is also found to be identical with those of **1–11** and the spectral data are included in Table 3.

Precursors of the fragment ions observed in the mass spectra of squaraines

The mass spectral data of **1–12** suggest that M + $CHR^{\dagger}$ and M + $H_2^{\dagger}$ are precursors of fragment ions of lower mass numbers. Their formation is presumably due to intermolecular alkyl transfer and H transfer reactions (see Scheme 1). Under the high vacuum conditions in the mass spectrometer, however, intermolecular reactions in the vapor phase are very unlikely. It is therefore very probable that these intermolecular reactions might just occur within a molecular aggregate of squaraine. In the following, we present methodology and results on the elucidation and identification of this aggregate.

(i) Cross-over experiment

Squaraines **3** and **7** were chosen for a cross-over experiment for the following reasons: (*1*) both **3** and **7** have a very similar vaporization temperature; (*2*) the mass spectra of **3** and **7** show no interference of the expected cross-over ions; (*3*) mixed aggregates of **3** and **7** can easily be prepared by solvent evaporation of a methylene chloride solution of **3** and **7**. The expected fragment ions in the cross-over experiments are summarized in Table 4.

The EI mass spectrum of the solid solution of **3** and **7** is shown in Fig. 6. In addition to the expected ions Pr_2SQ + $C_3H_6^{\dagger}$ at m/z 474 and Bu_2SQ + $C_4H_8^{\dagger}$ at m/z 572, two cross-over ions Pr_2SQ + $C_4H_8^{\dagger}$ at m/z 488 and Bu_2SQ + $C_3H_6^{\dagger}$ at m/z 558 are observed. While these spectral results clearly suggest that molecular aggregates of squaraines are precursors of the mass spectra of squaraines, a control experiment still must be performed so that the possibility of vapor phase reaction can be ruled out.

In the control experiment, **3** and **7** were placed in two fine capillary tubes. These two tubes were placed in the solid probe such that they were physically separated but were evaporated simultaneously. If vapor phase reactions were the cause of M + $CHR^{\dagger}$, cross-over M + $CHR^{\dagger}$ ions should be seen. The absence of cross-over M + $CHR^{\dagger}$ in Fig. 7 allows us to establish positively that molecular aggregates of squaraines are indeed precursors of the mass spectra.

The electronic properties of squaraines have been studied recently.[6] Squaraines are intramolecular charge-transfer complexes with the central four-membered ring being an electron acceptor (A) and the *N,N*-dialkylanilino moiety being an electron donor (D). In the solid state, intermolecular D–A interactions are shown to be very extensive and interplanar distances of squaraines are found to be ~3.5 Å[9] (*3b*, 11). It is thus not unreasonable to conclude that, due to the presence of strong D–A interactions in the solid state, squaraines vaporize as aggregates.

(ii) Metastable ion studies

Further questions that remain to be answered are the identity of the aggregate and the fragmentation processes of the aggregate. Numerous unsuccessful efforts have been made to search for the dimers and trimers of squaraines in the EI mass spectra. The absence of these species is presumably due to their low stability under the experimental conditions. The necessity of having an aggregate as a precursor for the mass spectrometry of squaraine has prompted us to study the metastable ions of

[9]K. Y. Law, unpublished X-ray data.

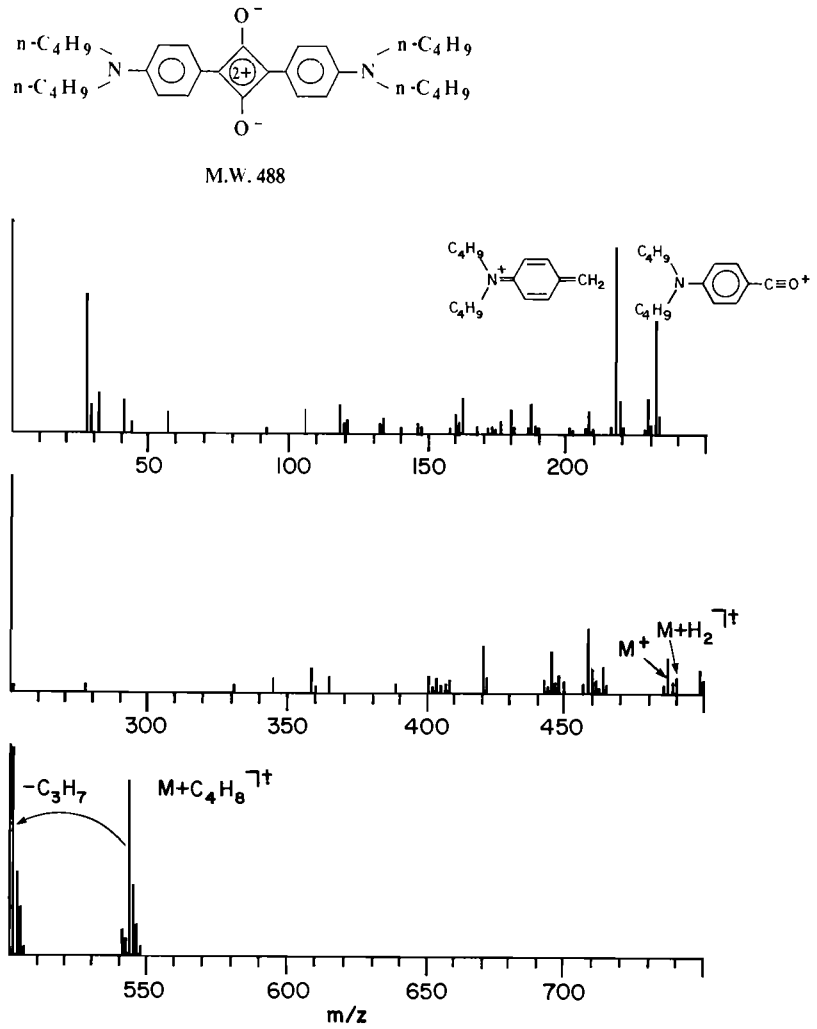

FIG. 5. EI mass spectrum of squaraine **4**.

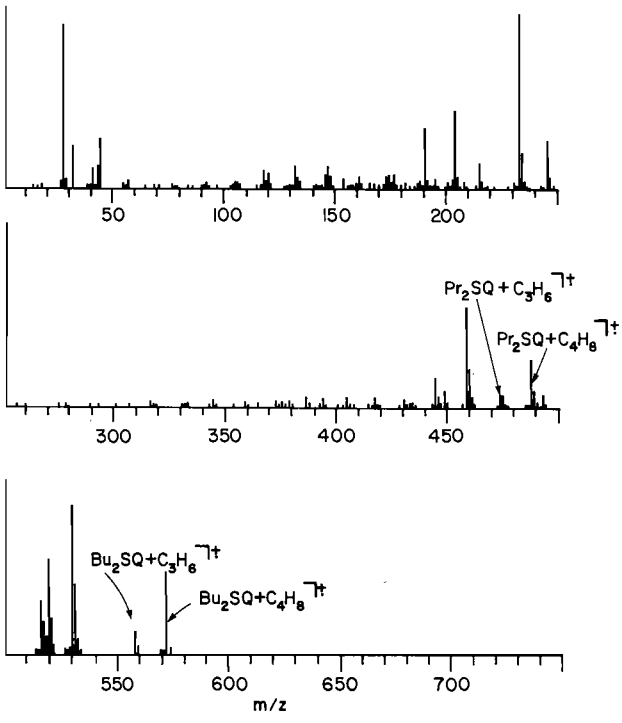

FIG. 6. EI mass spectrum of solid solution of **3** and **7**.

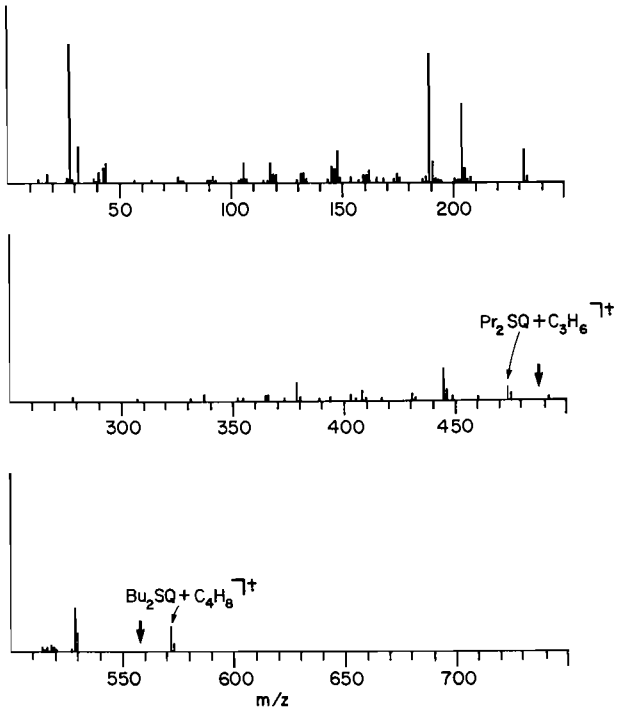

FIG. 7. EI mass spectrum of (**3** + **7**).

TABLE 5. Metastable ion data of **1**

m/z of metastable ion	Decay scheme	Fragmentation process	Remarks
280.6	334 → 306	$M + CH_2{}^{\cdot+} \rightarrow CO$	[a]
253.0	479 → 348	$1.5M - H^{\cdot+} \rightarrow M + CH_2 + CH_2{}^{\cdot+}$	[a]
238.5	960 → 479	$3M^+ \rightarrow 1.5M - H^{\cdot+}$	[a]
233	479 → 334	$1.5M - H^{\cdot+} \rightarrow M + CH_2{}^{\cdot+}$	[a]
110	161 → 133	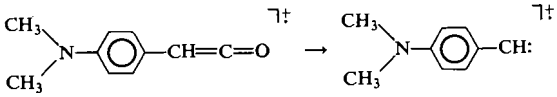	Scheme 3 path i
103.8	334 → 186	[a]	Scheme 3 path g
77.6	334 → 161	$M + CH_2{}^{\cdot+} \rightarrow$ 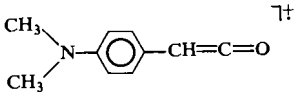	Scheme 3 path f

[a]See text for discussion.

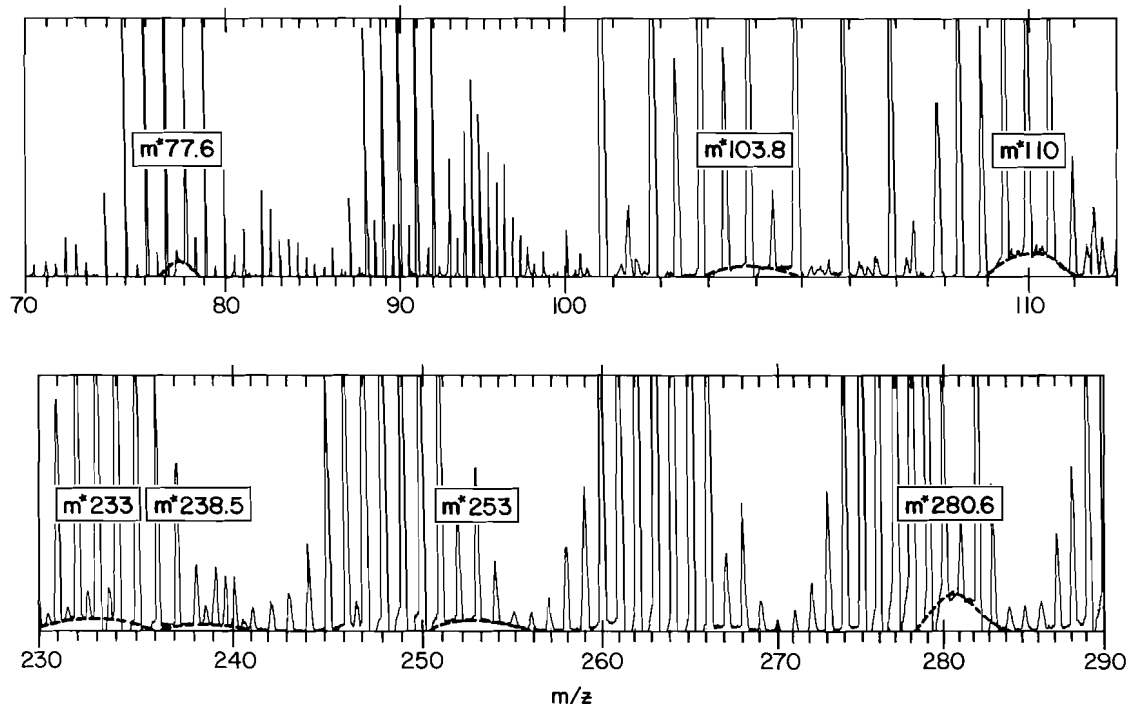

FIG. 8. Metastable ion peaks in the EI mass spectrum of **1**.

all our EI mass spectra. Our results show that metastable ions of squaraines bearing long alkyl chains are usually generated by dealkylation processes and they contribute very little to the understanding of the mass spectrometry of squaraine. On the other hand, metastable ions of squaraines having an *N,N*-dimethylamino moiety are very informative. Metastable ion peaks observed in the mass spectrum of **1** are presented in Fig. 8 and the data are tabulated in Table 5.

The impact of these metastable ions on the fragmentation processes will be discussed later. At present, we concentrate on the interpretation of evidence for the identity of the molecular aggregate. The metastable ion at *m/z* 238.5 is an exciting finding because it accounts for fragmentation of the trimer of **1** (*m/z* 960) to an ion at *m/z* 479. This 479 ion is actually observable in Fig. 2 and is assigned to $1.5M - H^{\cdot+}$ (see later for discussion). As seen in Table 5, one of the fragmentation processes of ion 479 is to fragment ion 334 ($M + CH_2{}^{\cdot+}$), which is the precursor of lower mass number ions; this result thus provides *the first evidence that the trimer is the precursor of the lower mass number fragment ions in the mass spectra of squaraines*.

Further evidence in support of the trimer comes from the metastable ions in squaraines **5** and **8**. Metastable ions at *m/z* 262.5 and 267.5 are observed in the EI mass spectra of **5** and **8**, respectively, and they may be explained in terms of fragmentation processes $3M^+ \rightarrow 1.5M - H^{\cdot+}$ and $3M^+ \rightarrow 1.5M^{\cdot+}$ for **5** and **8** respectively. These results not only suggest that the trimer precursor is very general, but also show that one of the fragmentation processes of the trimer is the cleavage of the four-membered ring of the central squaraine to form two species of approximately equal mass number.

(iii) Chemical ionization (CI) mass spectra of 1

The encouraging results in Table 5 prompted us to search for more direct evidence for the trimer. Using **1** as a model squaraine, we have performed a large number of CI experiments

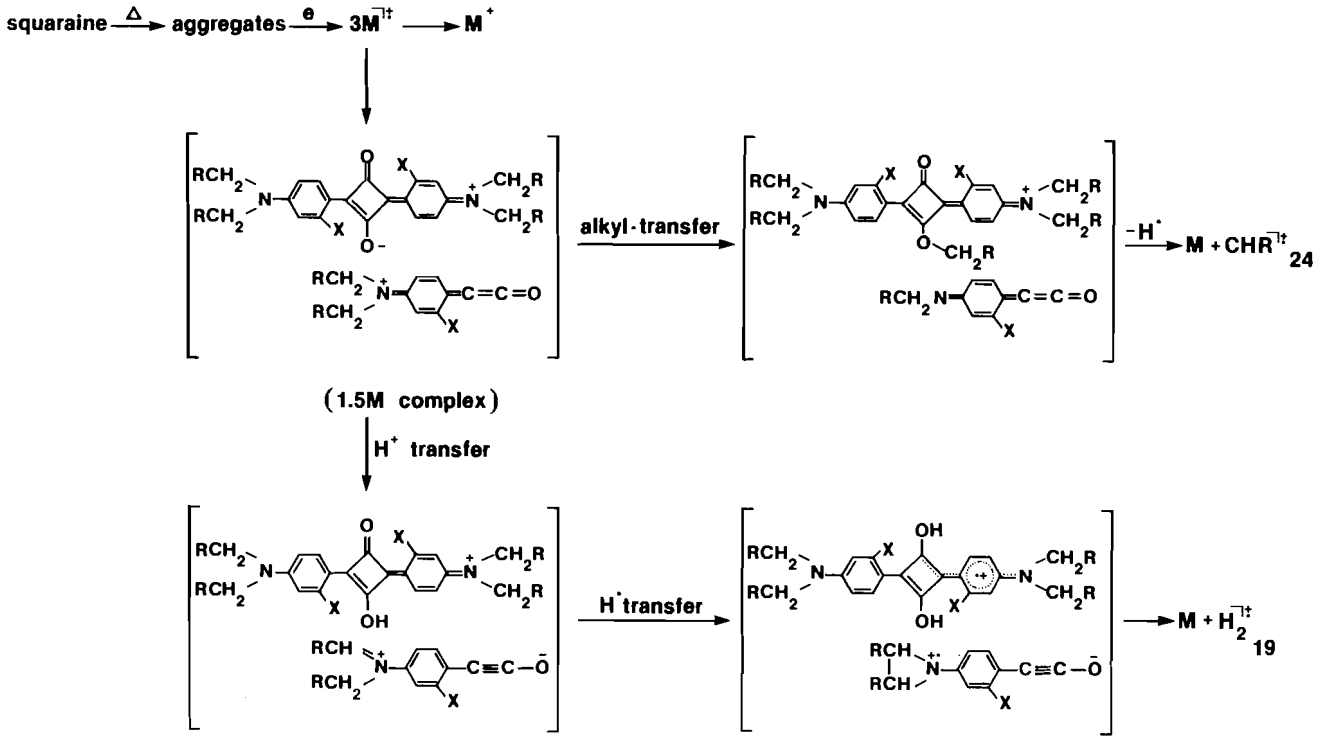

SCHEME 1. Proposed fragmentation processes of squaraine aggregates.

in the hope that the trimer of **1** would become discernible under milder ionization conditions.

Several ionization gases, including methane, isobutane, ammonia, and methylene chloride, were used and CI mass spectra very similar to the one shown in Fig. 2 were obtained. On the other hand, a very different mass spectrum was recorded when N_2O was used as ionization gas. As seen in Fig. 9, a base peak at m/z 321, which is assigned to M + $H^{\cdot+}$, is observed.[10] Dimeric and trimeric species at m/z 641 and 961 are also observed at higher spectral sensitivities.[10] The identity of the 961 peak was further confirmed by a ms/ms experiment where two peaks at m/z 320 (base peak) and 642, which are assigned to M^+ and 2M + $H_2^{\cdot+}$ of **1** respectively, are seen (Fig. 10). On the basis of these findings, we conclude that the trimers of squaraines are precursors of the lower mass number fragments in the mass spectra.

Fragmentation processes

(i) Mechanism of the formation of M + $CHR^{\cdot+}$ and M + $H_2^{\cdot+}$

Two simple, logical fragmentation processes can be envisioned for these trimers and both have been observed experimentally. The first process involves the fragmentation of the trimer to monomeric and dimeric species. The occurrence of this process is supported by the CI ms/ms spectrum of **1** (Fig. 9).

The second process involves the cleavage of the four-membered ring of the central squaraine in trimer. The occurrence of this process is supported by results in Table 5 and the metastable ion data of squaraines **5** and **8**. This ring cleavage reaction is not unexpected, but the surprising result is the formation of a species with mass number ~1.5M. Squaraines are strong intramolecular D–A complexes and extensive intermolecular D–A interactions are known to occur in the solid state. As noted earlier, due to the preservation of this intermolecular D–A interaction squaraines vaporize as aggregates rather than monomeric species in the vapor phase. This in turn generates the unique mass spectrometry. The formation of this ~1.5M species can thus be visualized as an extension of the D–A interaction between a squaraine molecule and an *N,N*-dialkylanilino moiety after the ring cleavage.[11]

While there is sufficient evidence to support our conclusion that the trimer of squaraine is the precursor of the mass spectrum, and this trimer undergoes fragmentation to give immediate ions M^+, $1.5M^+$, or 1.5M − $H^{\cdot+}$ upon electron impact, the evidence from these intermediate ions to M + $CHR^{\cdot+}$ and M + $H_2^{\cdot+}$, which are shown to be precursors of the lower mass number fragment ions, is less strong. Major evidence for the formation of M + $CHR^{\cdot+}$ and M + $H_2^{\cdot+}$ from 1.5M − $H^{\cdot+}$ is obtained from the EI mass spectrum of **1** (Fig. 2). In addition to M + $CH_2^{\cdot+}$ and M + $H_2^{\cdot+}$, weak fragment ions corresponding to the addition of two CH_2 units (m/z 348) and to the addition of one hydrogen atom and one methyl group (m/z 336) are observed in the EI mass spectrum of **1**.[8] These results suggest that there are two active sites for radical reactions in a squaraine. In **1**, these two sites may combine with two hydrogen atoms to give M + $H_2^{\cdot+}$ at m/z 322, or they may combine with one hydrogen

[10]The peaks at m/z 321, 641, and 961 are assigned to M + $H^{\cdot+}$, 2M + $H^{\cdot+}$, and 3M + $H^{\cdot+}$, respectively. The addition of a hydrogen atom to these species is due to the presence of moisture in the ionization gas (Drs. R. Isensee and J. Slayback, private communication).

[11]The formation of a complex between squaraine and an electron donor was also observed in another occasion in the mass spectrometer. In the CI experiment of **1**, when CH_2Cl_2 was used as ionization gas, ion peaks at m/z 355 and 675 were recorded in the negative ion mass spectrum. These two ions are assigned to the complexes between chloride ion with the monomer and the dimer of **1** respectively.

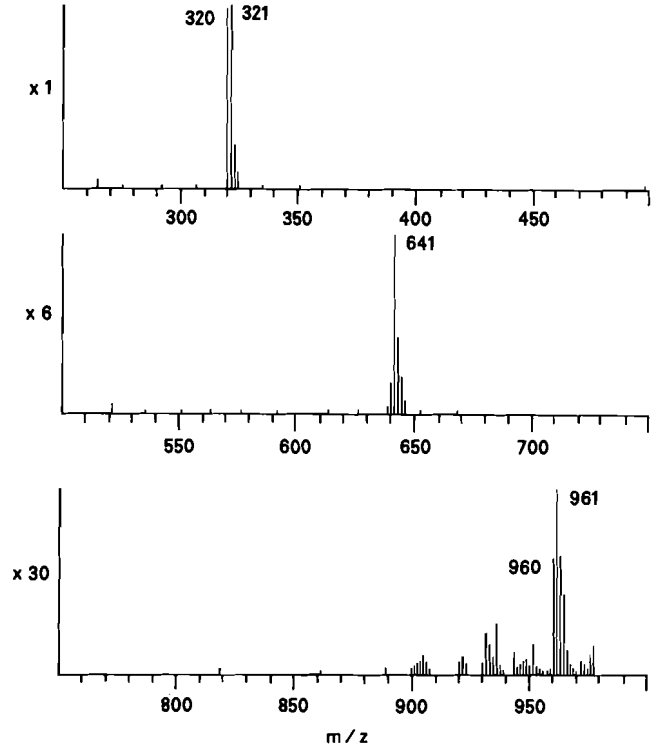

FIG. 9. CI (N_2O) mass spectrum of squaraine **1**.

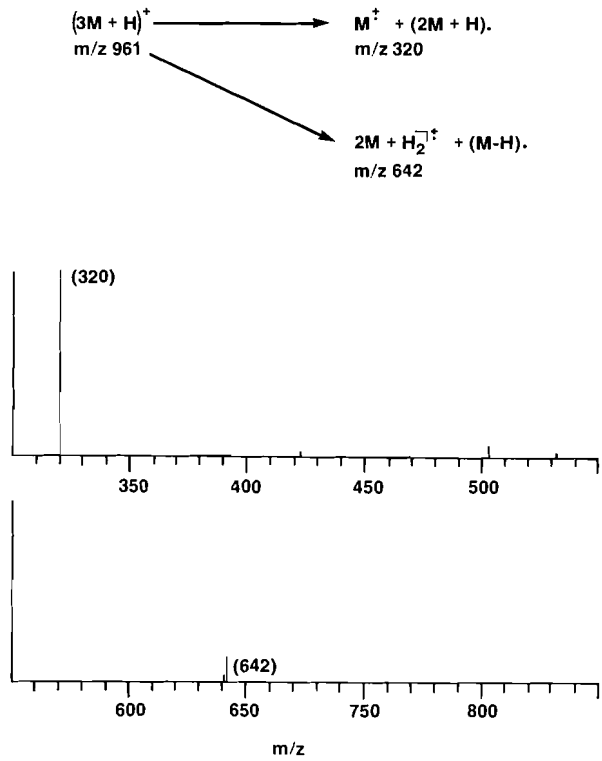

FIG. 10. CI ms/ms spectrum of ion 961.

atom and one methyl group to give M + H + $CH_3]^+$ at m/z 336. These two sites may combine with one or two methyl group(s) following radical disproportionation reactions to give M + $CH_2]^+$ at m/z 334 and M + CH_2 + $CH_2]^+$ at m/z 348. The only locations in **1** that are capable of accommodating these radical reactions are the C—O bonds. Using the metastable ion data in Table 5, we are able to show that at least two of these radical products, namely M + $CH_2]^+$ and M + CH_2 + $CH_2]^+$, are generated from 1.5M − $H]^+$. Because of the similar nature of the above radical reactions, we have assumed that M + $H_2]^+$ and M + H + $CH_3]^+$ are also generated in a similar way.

TABLE 6. Metastable ion data of **14**

m/z metastable ion	Decay scheme	Fragmentation process
346.5	426 → 384	M + $H_2]^+$ − C_3H_6
161	214 → 186	0.5M + $H_2]^+$ − CO
134.5	186 → 158	186 − C_2H_4
120.9	172[a] → 144	172 − C_2H_4

[a]The structure of m/z 172 is assigned to 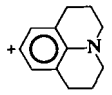

The distribution of these radical reactions is expected to vary as the structure of squaraine changes. Usually, M + $H_2]^+$ and M + $CHR]^+$ are major fragmentation products of 1.5M + $H]^+$ (or $1.5M^+$). It may be a coincidence that all four possibilities of radical reactions are observed in the EI mass spectrum of **1**.

The mass spectrometry of *N,N*-dialkylaniline was also studied briefly and results show that dealkylation and dehydrogenation reactions are major fragmentation processes. It is, therefore, possible that, due to dealkylation and dehydrogenation reactions of the *N,N*-dialkylanilino moiety in the 1.5M species, hydrogen atoms or alkyl radicals are generated and captured by the neighboring squaraine molecule to form M + $CHR]^+$ and M + $H_2]^+$. As demonstrated earlier in the cross-over experiment, intermolecular vapor phase exchange reactions are not occurring in the mass spectrometer. If M + $CHR]^+$ and M + $H_2]^+$ are indeed formed by radical processes, they must be formed via some kind of intermediate complexes. A proposed scheme for the formation of M + $CHR]^+$ and M + $H_2]^+$ from $1.5M]^+$ is depicted in Scheme 1. More sophisticated experimentation is needed to elucidate the exact mechanism of these processes.

(ii) Fragmentation of M + $H_2]^+$

To facilitate our understanding of the detailed fragmentation processes of M + $CHR]^+$ and M + $H_2]^+$, we studied the EI mass spectra of **13** and **14**, in which the alkyl transfer reactions in these squaraines are structurally restricted and prohibited, respectively. The mass spectral data of **13** and **14** are included in Table 3. The EI mass spectrum of **14**, from which M + $CHR]^+$ is expected to be absent, is presented in Fig. 11 for comparison purposes. The results in Table 3 show a gradual dominance of the mass spectrum by M + $H_2]^+$ and ion **18** from **1** → **13** → **14**. The base peaks for the mass spectra of **13** and **14** are at m/z 160 and 186 and are assigned to

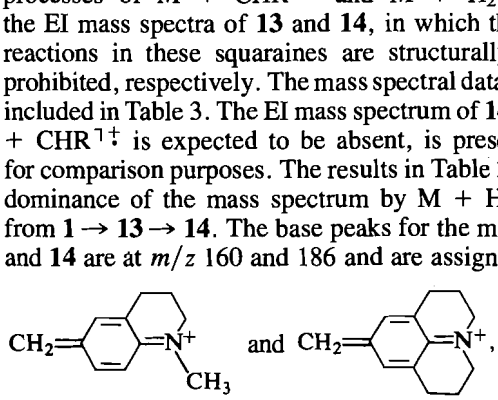

respectively. As expected, no M + $CHR]^+$ type species are detectable in the mass spectrum of **14** (Fig. 11).

Metastable ions of the mass spectrum of **14** have been studied. The data and the proposed fragmentation processes are shown in Table 6. Our results again reveal that dealkylation reactions are important fragmentation processes for the *N,N*-

TABLE 7. Additional metastable ion data for Schemes 2 and 3

Squaraine	*m/z* of metastable ion	Decay scheme	Fragmentation process	Remarks
2	374.6	404 → 389	$M + CHR^{\dagger\cdot} \xrightarrow{-R} M + CH^{\dagger\cdot}$	Scheme 3, path h
3	417.5	474 → 445	$M + CHR^{\dagger\cdot} \xrightarrow{-R} M + CH^{\dagger\cdot}$	Scheme 3, path h
	163.9	216 → 188	$0.5M^{\dagger\cdot} \xrightarrow{-CO}$ 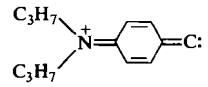	Scheme 2, path d
4	461.7	544 → 501	$M + CHR^{\dagger\cdot} \xrightarrow{-R} M + CH^{\dagger\cdot}$	Scheme 3, path h
6	402.6	432 → 417	$M + CHR^{\dagger\cdot} \xrightarrow{-R} M + CH^{\dagger\cdot}$	Scheme 3, path h
7	489.5	572 → 529	$M + CHR^{\dagger\cdot} \xrightarrow{-R} M + CH^{\dagger\cdot}$	Scheme 3, path h
8	127.0	179 → 151	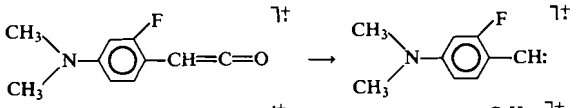	Scheme 3, path i
11	137.5	189 → 161	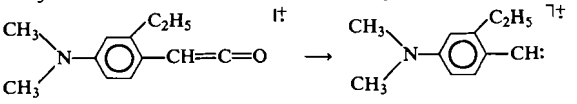	Scheme 3, path i
	67.4	378 → 160	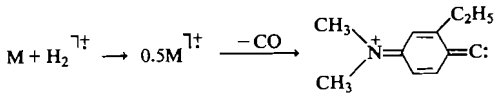	Scheme 2, paths b and d

dialkylanilino moiety. The most important metastable ion is at *m/z* 161 and is assigned to the decarbonylation reaction of 0.5M + $H_2^{\dagger\cdot}$ (*m/z* 214) to

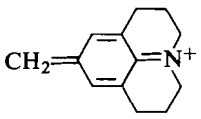

(*m/z* 186).

On the basis of the structure–property relationship for the mass spectra of **1**, **13**, and **14**, a general fragmentation scheme for M + $H_2^{\dagger\cdot}$ is shown in Scheme 2. The structure of M + $H_2^{\dagger\cdot}$, **19**, is drawn by analogy to the dihydrosquaraine species obtained from dimerization of ketene (12). Ring opening of the cyclobutenone structure in **19** will give **20**. After the cleavage of the weakest C—C bond in **20**, two species, **21** (*m/z* 0.5M) and **22** (*m/z* 0.5M + 2), are obtained. Decarbonylation of **21** and **22** (paths c and d) generates **23** and **18**, respectively. In **14**, the occurrence of path c is supported by metastable ion at *m/z* 161.

Additional evidence in support of Scheme 2[12] comes from metastable ions from the EI mass spectra of **3** and **11** (Table 7). Metstable ions at 163.9 and 67.4 are observed in the EI mass spectra of **3** and **11**, respectively, and they can be used to describe decarbonylation reactions as shown in path d of Scheme 2.

(iii) Fragmentation to M + CHR$^{\dagger\cdot}$

The mass spectral results of **1**, **13**, and **14** (Table 3) show that

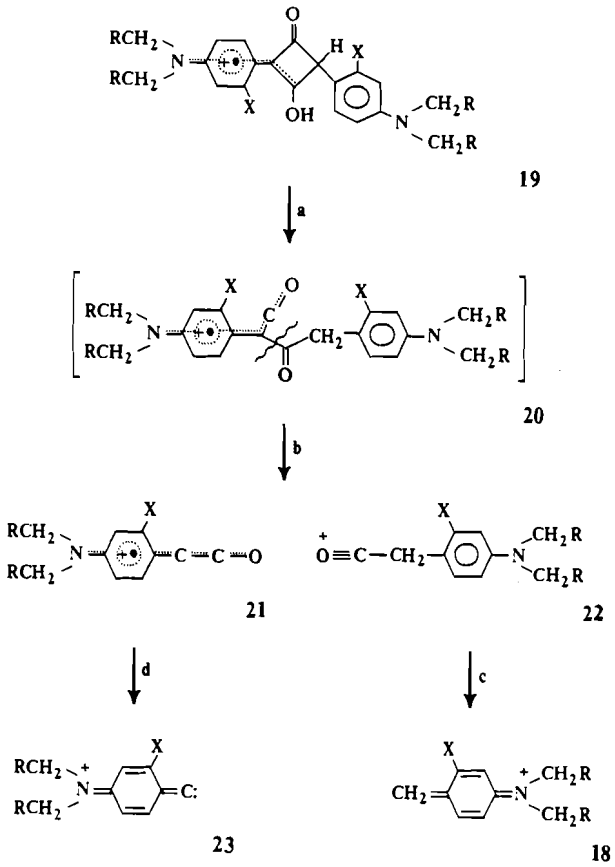

SCHEME 2. Fragmentation of M + $H_2^{\dagger\cdot}$.

[12]The EI mass spectrum of the dihydrosquaraine reported in ref. 12 has recently been studied. Fragmentation processes identical to those described in Scheme 2 are observed.

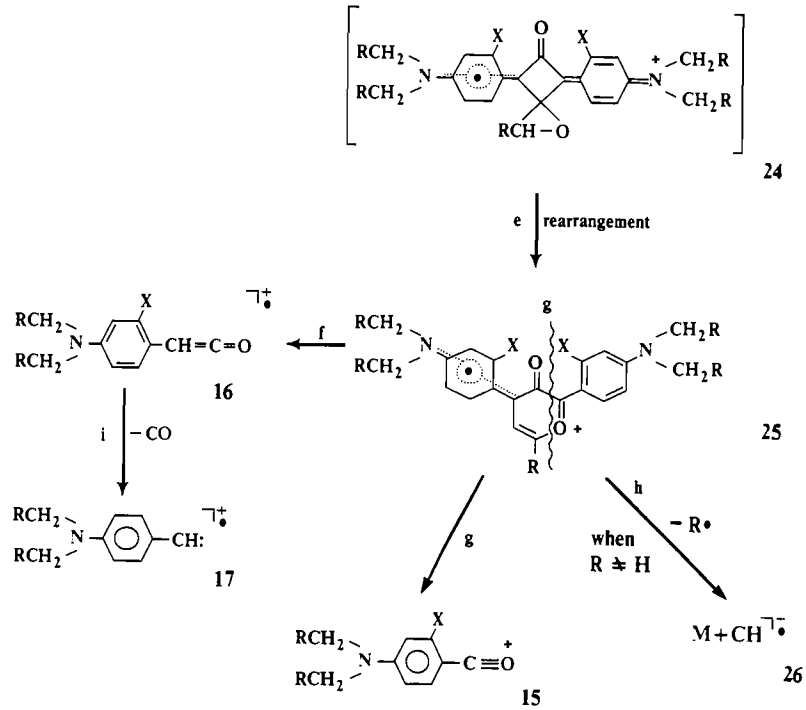

SCHEME 3. Fragmentation of M + CHR^{+}.

the intensity of fragment ion M + CHR^{+} decreases as the restriction of the alkyl transfer reaction increases. Assuming that there are two major fragmentation processes contributing to the EI mass spectrum of **1** (the fragmentation processes of M + CHR^{+} and M + H_2^{+}), the contribution of the fragmentation processes in Scheme 2 may be subtracted and results show that ions **15**, **16**, and **17** are associated with M + CHR^{+}. A general scheme for the formation of these three ions from M + CHR^{+} is presented in Scheme 3.

The proposed structure of M + CHR^{+} is **25**. Structure **25** fulfills all the requirements of M + CHR^{+} from the structure–property viewpoint. It has a very stable structure and is thus compatible with the observed high intensity of M + CHR^{+} in the mass spectra of squaraines. It can undergo sequential C—O and C—C bond cleavages (path g) to give a rearranged ion, **15**. Further evidence supporting structure **25** will be discussed later. In addition to the cleavage reaction in path g, **25** can also fragment into **16** (path f).[13] Ion **16** subsequently undergoes a decarbonylation reaction to give ion **17** (path i). The occurrence of paths f and i is supported by metastable ions of squaraine **1** (Table 5), and of squaraines **8** and **11** (Table 7). When R is not hydrogen, **25** will lose an R group to give ion **26** with general formula weight of (*M* + 13) (path h).[13] This dealkylation reaction is supported by a large number of metastable ion data (Table 7). The structure of **26**, however, cannot be deduced from the present data because there are five R groups in **25**.

As discussed earlier, M + CH_2^{+} of **1** is obtained from a radical addition–disproportion process, and the reaction site is the C—O group; thus the likely structure of M + CH_2^{+} would actually be an analog of **24**. The necessity of having a very stable M + CH_2^{+} that fragments into **15** leads us to propose that **24** is a primary product and that **24** undergoes a ring-expansion reaction (path e) to give a more stable ion **25**. In the case of squaraine **1**, the specific structure of M + CH_2^{+} is **27**.

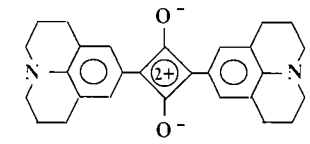

M.W. 424

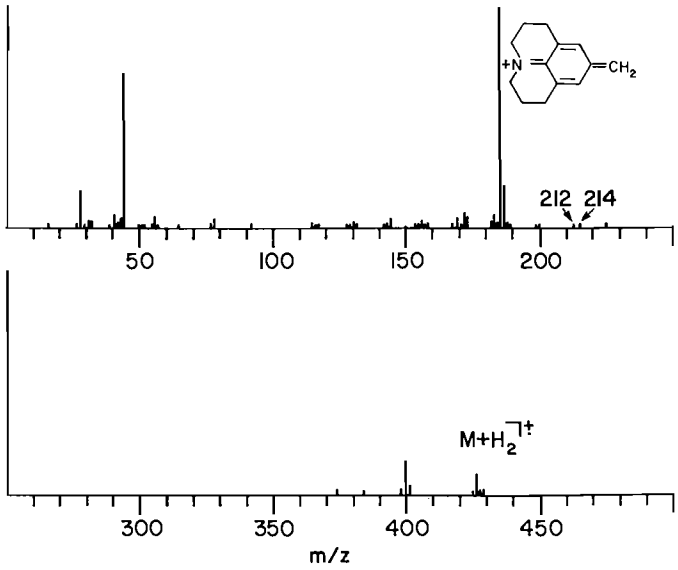

FIG. 11. EI mass spectrum of squaraine **14**.

The structural assignment of **27** is substantiated by metastable ion data. Results in Table 5 show that three metastable ions are

[13]There is also a possibility that both ions **16** and M + CH^{+} are derived directly from **24** instead of from **25**. The present data do not allow us to distinguish these two possibilities.

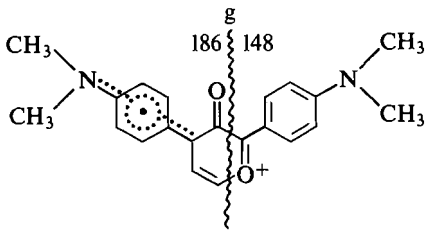

27 (*m/z* 334)

associated with **27**. The first metastable ion is at *m/z* 280.6 and is shown to derive from a decarbonylation reaction of **27**. The second metastable ion is at *m/z* 103.8 and is shown to derive from fragmentation process **27** (*m/z* 334) to an ion at *m/z* 186. The counter fragment of 186 is at *m/z* 148, which is assigned to

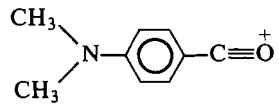

an analog of **15**. Therefore, metstable ion *m/z* 103.8 not only gives positive evidence of a parent–daughter relation between **27** and

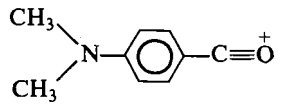

(also **25** and **15**), but also provides structural information about the location of bond cleavage in path g. The third metastable ion is at *m/z* 77.6 and is due to fragmentation of **27** to *p-N,N*-dimethylaminophenyl ketene ion. The structural information obtained from the above three metastable ions suggests that **27** should have a carbonyl group and a *p-N,N*-dimethylaminophenyl ketene skeleton; it is also made up of two fragments, of *m/z* of 186 and 148. **27** appears to satisfy all these criteria comfortably and we are confident in the correctness of the structural assignment of **27** (also of **25**).

Summary and remarks

In summary, the EI mass spectra of squaraines **1–14** have been studied. Our results show that without exception, due to the strong intermolecular D–A interactions of squaraine molecules in the solid state, squaraines vaporize thermally as molecular aggregates in the mass spectrometer. The participation of non-exchanging molecular aggregates was revealed by a cross-over experiment. Metastable ion data and chemical ionization mass spectrometry subsequently showed that this aggregate is a trimer. Ionization of this aggregate by electron impact results predominantly in an intermediate fragment ion of formula weight about 1.5 times the molecular weight of the squaraine. This ion fragments primarily to M + $CHR^{\neg\ddagger}$ and M + $H_2^{\neg\ddagger}$. Further fragmentation of M + $CHR^{\neg\ddagger}$ and M + $H_2^{\neg\ddagger}$ generates the general and unique mass spectrometric pattern of squaraine. Since information about the substituents at the nitrogen can be revealed by M + $CHR^{\neg\ddagger}$ and the molecular weight of a squaraine can be obtained from M + $H_2^{\neg\ddagger}$ and M^+ or independent chemical ionization experimentation, it appears that, given the understanding of the fragmentation processes in this work, mass spectrometry may become a useful tool for structure determination of squaraines.

Acknowledgements

We thank Drs. R. Isensee and J. Slayback (Oneida Research Services) for recording the CI mass spectra of **1**.

1. R. West. Oxocarbons. Academic Press, New York. 1980. Chapt. 10.
2. (*a*) A. H. Schmidt. Synthesis, 961 (1980); (*b*) H. E. Sprenger and W. Ziegenbein. Angew. Chem. Int. Ed. Engl. **7**, 430 (1968); (*c*) G. Maahs and P. Hegenberg. Angew. Chem. Int. Ed. Engl. **5**, 888 (1966).
3. (*a*) A. C. Tam and R. D. Balanson. IBM J. Res. Dev. **26**, 186 (1982); (*b*) R. E. Wingard. IEEE Trans. Appl. Ind. 1251 (1982); (*c*) A. C. Tam. Appl. Phys. Lett. **37**, 978 (1980); (*d*) R. J. Melz, R. B. Champ, L. S. Chang, C. Chiou, G. S. Keller, L. C. Liclican, R. B. Neiman, M. D. Shattuck, and W. J. Weiche. Photogr. Sci. Eng. **21**, 73 (1977).
4. (*a*) R. O. Loutfy, C. K. Hsiao, and P. M. Kazmaier. Photogr. Sci. Eng. **27**, 5 (1983); (*b*) D. L. Morel. Mol. Cryst. Liq. Cryst. **50**, 127 (1979); (*c*) V. Y. Merritt. IBM J. Res. Dev. **22**, 353 (1978); (*d*) D. L. Morel, A. K. Ghosh, T. Feng, E. L. Stogryn, P. E. Purwin, R. F. Shaw, and C. Fishman. Appl. Phys. Lett. **32**, 495 (1978); (*e*) V. Y. Merritt and H. J. Hovel. Appl. Phys. Lett. **29**, 414 (1976).
5. (*a*) D. J. Gravesteijn, C. Steenbergen, and J. van der Veen. Proc. SPIE Int. Soc. Opt. Eng. **420**, 327 (1983); (*b*) V. P. Jipson and C. R. Jones. J. Vac. Sci. Technol. **18**, 105 (1981); (*c*) V. P. Jipson and C. R. Jones. IBM Technical Disclosure Bulletin, **24**, 298 (1981).
6. U.S. Patents 3,617,270; 3,824,099; 4,175,956; 4,471,041 and 4,486,520.
7. A. I. Vogel. Textbook of practical organic chemistry. 4th ed. *Revised by* B. S. Furniss, A. J. Hannaford, V. Roger, P. W. G. Smith, and A. R. Tatchell. Longman, London and New York. 1978. Chapt. IV.
8. H. E. Sprenger and W. Ziegenbein. Angew. Chem. Internat. Ed. Engl. **5**, 894 (1966).
9. (*a*) A. Treibs and K. Jacob. Ann. Chem. **699**, 143 (1966); (*b*) A. Treibs, K. Jacob, and R. Tribollet. Ann. Chem. **741**, 101 (1970).
10. M. C. Hamming and N. G. Foster. Interpretation of mass spectra of organic compounds. Academic Press, New York and London. 1972. Chapt. 5.
11. M. Tristani-Kendra and C. J. Eckhardt. J. Chem. Phys. **81**, 1160 (1984).
12. D. G. Farnum, J. R. Johnson, R. E. Hess, T. B. Marshall, and B. J. Webster. Am. Chem. Soc. **87**, 5191 (1965).
13. P. M. Kazmaier, G. Hamer, and B. Burt. 11th Northeast Regional Meeting, Rochester, New York. October 18–21, 1981. p. 140.

Synthesis of cyclopentane analogs of (2′- and 3′-deoxy-*erythro*-pentofuranosyl and ribofuranosyl)-2-thiouracil nucleosides

LUCJAN J. J. HRONOWSKI AND WALTER A. SZAREK
Department of Chemistry, Queen's University, Kingston, Ont., Canada K7L 3N6

Received September 3, 1985[1]

LUCJAN J. J. HRONOWSKI and WALTER A. SZAREK. Can. J. Chem. **64**, 1620 (1986).

Three new carbocyclic analogs of nucleosides having the 2-thiouracil base have been synthesized. The cyclopentyl groups in these nucleosides are (±)-{(1β,3α,4β)-3-hydroxy-4-(hydroxymethyl)cyclopentyl} (see **31**), (±)-{(1β,2α,4β)-2-hydroxy-4-(hydroxymethyl)cyclopentyl} (see **32**), and (±)-{(1β,2α,3α,4β)-2,3-dihydroxy-4-(hydroxymethyl)cyclopentyl} (see **33**). The nucleosides were prepared by coupling the appropriate hydroxy derivatives of *cis*-3-aminocyclopentanemethanol with 3-ethoxypropenoyl isothiocyanate (**21**) followed by cyclization in 15 *N* aqueous ammonia to give the 2-thiouracil nucleosides. In addition a modified and shortened synthetic route is described for the synthesis of (±)-(1β,2α,3α,4β)-4-amino-2,3-dihydroxycyclopentanemethanol (**19**). The ^{1}H nmr spectra at 200 MHz of all of the synthetic intermediates, the 2-thiouracil nucleosides, and of the corresponding carbocyclic analogs of uracil nucleosides are discussed. It is shown that each nucleoside has a characteristically unique ^{1}H nmr spectrum and that in general the protons in the sulfur-containing compounds resonate at lower fields than those in the corresponding oxygen-containing compounds. The magnitude of this downfield shift is inversely related to the number of bonds separating a particular proton from the sulfur atom.

LUCJAN J. J. HRONOWSKI et WALTER A. SZAREK. Can. J. Chem. **64**, 1620 (1986).

On a synthétisé trois nouveaux analogues carbocycliques de nucléosides qui possèdent une base thio-2 uracile. Les groupements cyclopentyles de ces nucléosides sont les suivants: le (±)-(hydroxy-3α (hydroxyméthyl)-4β cyclopentyle-1β) (voir le composé **31**), le (±)-(hydroxy-2α (hydroxyméthyl)-4β cyclopentyle-1β) (voir le composé **32**) et le (±)-(dihydroxy-2α,3α (hydroxyméthyl)-4β cyclopentyle-1β) (voir le composé **33**). On a préparé les nucléosides en procédant à un couplage des dérivés hydroxylés appropriés de l'amino-3 cyclopentaneméthanol-*cis* avec l'isocyanate d'éthoxy-3 propènoyle (**21**) qui est suivi par une cyclisation dans de l'ammoniaque 15 *N* pour donner les nucléosides le thio-2 uracile. De plus, on décrit une voie de synthèse modifiée et racourcié pour la synthèse du (±)-amino-4β dihydroxy-2α,3α cyclopentaneméthanol-1β (**19**). On discute des spectres rmn du ^{1}H à 200 MHz de tous les intermédiaires de synthèse, de tous les nucléosides du thio-2 uracile et des analogues carbocycliques correspondants des nucléosides d'uracile. On démontre que chaque nucléoside possède une spectre rmn du ^{1}H qui est caractéristique et que, en général, les résonances des protons des composés contenant du soufre apparaissent à des champs plus bas que ceux des résonances des produits contenant de l'oxygène. L'amplitude de ce déplacement vers des champs plus faibles est reliée d'une façon inverse avec le nombre de liaisons qui sépare un proton particulier de l'atome de soufre.

[Traduit par la revue]

Introduction

A variety of carbocyclic analogs of pyrimidine nucleosides have been shown to possess anticancer and (or) antiviral activity (1–5). In some of these analogs, for example, carbodine (2), which is the carbocyclic analog of cytidine, and the carbocyclic analog of thymidine (3), the only chemical modification from the naturally occurring compounds is the replacement of the furanose-ring oxygen by a methylene group; the antineoplastic and antiviral activities in these compounds are a consequence of this single modification. However, the carbocyclic analog of uridine was shown to be inactive against KB cells in culture or L1210 leukemia in vivo (6), and the carbocyclic analogs containing 5-fluorouracil showed only modest activity against P388 leukemia in vivo (4).

In a previous report (7) we described the regiospecific synthesis of cyclopentane analogs of (2′- and 3′-deoxy-*threo*-pentofuranosyl)-2-thiouracil nucleosides; in a preliminary study (8) the 2′-deoxy nucleoside was shown to inhibit the growth of K562 cells in culture. The observations by several workers (9, 10) that 2-thiouracil and various derivatives of 2-thiouracil are selectively incorporated into murine melanomas suggest that nucleosides containing the 2-thiouracil base should be synthesized and tested against the melanomas. The present report describes the synthesis of three carbocyclic analogs of 2-thiouracil nucleosides, **31**–**33**. These analogs were prepared by an approach similar to that used by Shealy and O'Dell (6) for the synthesis of the carbocyclic analogs of uracil nucleosides (**28**–**30**). The approach involves the prior preparation of appropriately substituted cyclopentylamines (11–13) followed by the elaboration of the base moiety at the amino substituent using the procedures of Shaw and Warrener (14, 15); in the present work, the cyclopentylamine **19** was prepared by a modified and shorter route.

[1]Revision received April 8, 1986.

Results and discussion

The synthesis of all of the compounds shown in Scheme 1[2] has been described previously by Shealy and O'Dell (11, 12). Compound **1**, however, was prepared by oxidation of *exo*-5-norbornen-2-yl acetate with potassium permanganate using an adaptation of the method of Birch *et al.* (17) as described previously (7). Because of the important synthetic utility of the compounds, a detailed analysis of their high-resolution ^{1}Hmr spectra has been performed in the present work.

Characterization by 200-MHz ^{1}Hmr spectroscopy of the synthetic intermediates shown in Scheme 1

In Table 1 the ^{1}Hmr chemical shifts of **2** are compared to those of (±)-(1β,3β,4β)-4-acetoxy-1,3-cyclopentanedicarboxylic acid anhydride (**2***a*) (compound **3** in ref. 7), the isomer in which the acetoxy group is in the *cis* configuration. The spectra of these two compounds in $CDCl_3$ show some signifi-

[2]Structures **1**–**12**, **16**–**19**, and **22**–**33** depict only one enantiomer of racemic mixtures. The relative configurations of substituent groups on the cyclopentane ring are specified by the α,β system used for steroids (16). Substituents that are written below the plane of the cyclopentane ring are designated α and those above the plane of the ring as β.

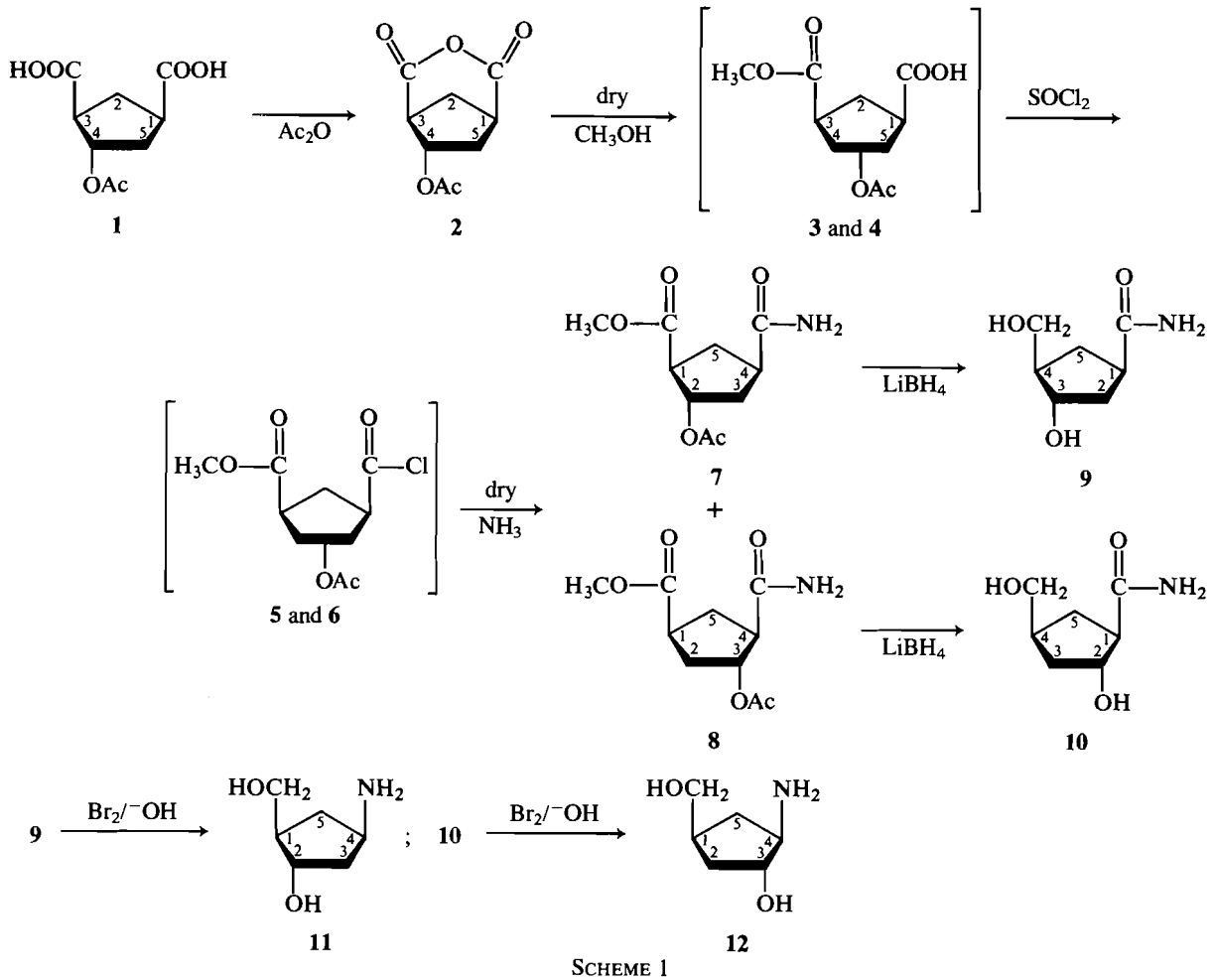

SCHEME 1

TABLE 1. ^{1}H magnetic resonance chemical shift data[a] in $CDCl_3$ for **2** and **2***a*[b]

Proton	Compound 2	2a
1	3.34–3.40	3.26
2	2.17 (J = 12.9, 3.9 Hz)	1.94 (J = 13.1, 4.0 Hz)
2′	2.33	2.36
3	3.34–4.0	3.66
4	5.31 (^3J = 7.2, 2.6 Hz)	5.44 (^3J = 9.8, 6.4, 3.7 Hz)
5[c]	2.05–2.18	2.65 (J = 15.3, 9.8, 7.0 Hz)
5′[c]	2.63 (J = 15.6, 7.2, 1.6 Hz)	2.00
OAc	2.09	2.07

[a]More complete Hmr data for **2** are found in the experimental section, and for **2***a* in ref. 7.

[b]Compound **2***a* is (±)-(1β,3β,4β)-4-acetoxy-1,3-cyclopentanedicarboxylic acid anhydride (compound **3** in ref. 7).

[c]Assignments have been made on the basis of the coupling to H-4.

cant differences. The signal of H-4 resonates at δ 5.44 in the case of the *cis* compound (**2***a*) and at δ 5.31 in the case of **2**, and, as expected, much larger vicinal coupling constants are observed for this proton in the case of the *cis* compound than in **2** (see Table 1). The chemical shifts of H-1 and H-3 are also quite different in the two isomers. In the spectrum of the *cis* compound the signals of these protons are separated by 0.40 ppm, whereas in the spectrum of compound **2** they have similar chemical shifts with the multiplets overlapping in the δ 3.34–3.40 region. The vicinal coupling constants for H-2 and H-2′ are similar for both isomers although the chemical shifts of the H-2 protons are quite different (see Table 1). The chemical shifts of the acetoxy-methyl protons are very similar for both compounds.

Table 2 shows the chemical shifts in Me_2SO-d_6 of **7** and **8** and of the corresponding *cis* isomers (±)-methyl (1β,2β,4β)-2-acetoxy-4-carbamoylcyclopentanecarboxylate (**7***a*) and (±)-methyl (1β,3β,4β)-3-acetoxy-4-carbamoylcyclopentanecarboxylate (**8***a*) (compounds **5** and **9**, respectively, in ref. 7). The ^{1}Hmr spectra of each of the four isomers are quite different although they do show some trends. The signals for the amide protons ($CONH_2$) in the spectra of all four isomers appear as two well-separated, broadened singlets. The proton bonded to the carbon bearing the acetoxy group resonates at slightly different fields in the different isomers; however, the gross appearance of these multiplets in the spectra of compounds **7** and **8** is that of an overlapping doublet of triplets, whereas in the spectra of the *cis* isomers these multiplets appear as triplets of doublets, as would be expected for two *trans* vicinal couplings and one *cis* vicinal coupling in the former pair, and two *cis* vicinal and one *trans* vicinal coupling in the latter pair of isomers. In the spectra of compounds **7** and **8** the multiplets owing to the four methylene protons are very similar, having very similar coupling constants, although small differences in the chemical shifts do occur, as shown in Table 2. In the case of the corresponding *cis* isomers these multiplets are more complex and greater differ-

TABLE 2. ^{1}H magnetic resonance chemical shift data[a] in Me_2SO-d_6 for **7**, **8**, **7***a*,[b] and **8***a*[b]

Proton	Compound			
	7	**8**	**7***a*	**8***a*
1	2.87	2.98	3.06	2.91
2	5.20	1.85	5.22	1.90–2.27
2′	—	2.11	—	1.90–2.27
3	1.82	5.11	1.81	5.24
3′	2.02	—	2.21	—
4	2.82	2.74	2.64	2.78
5	1.81	1.80	1.96–2.11	1.90–2.27
5′	2.21	2.23	1.96–2.11	1.90–2.27
OMe	3.62	3.63	3.58	3.61
OAc	1.99	2.00	1.90	1.90
$CONH_2$	6.87	6.94	6.84	6.84
$CONH_2$	7.38	7.39	7.30	7.22

[a]More complete ^{1}Hmr data for **7** and **8** are found in the experimental section, and for **7***a* and **8***a* in ref. 7.

[b]Compound **7***a* is (±)-methyl(1β,2β,4β)-2-acetoxy-4-carbamoylcyclopentanecarboxylate (**5** in ref. 7); compound **8***a* is (±)-methyl(1β,3β,4β)-3-acetoxy-4-carbamoylcyclopentanecarboxylate (**9** in ref. 7).

TABLE 3. ^{1}H magnetic resonance chemical shift data[a] in Me_2SO-d_6 for **9**, **10**, **9***a*,[b] and **10***a*[b]

Proton	Compound			
	9	**10**	**9***a*	**10***a*
1	2.75	2.41	2.65	2.44
2	1.58	4.08	1.65	4.18
2′	1.76	—	1.93	—
3	3.85	1.53	4.01	1.34
3′	—	1.53	—	1.75–1.89
4	1.75–2.0	2.14	1.82	2.04
5	1.29	1.28	1.31–1.51	1.60
5′	1.75–2.0	1.87	1.8 –2.0	1.75–1.89
CH_2OH	3.25	3.25	3.35	3.33
CH_2OH	3.39	3.25	3.59	3.33
CH_2OH	4.45–4.51	4.48	4.24	4.58
OH at C-2	—	4.72	—	4.84
OH at C-3	4.45–4.51	—	4.71	—
$CONH_2$	6.68	6.74	6.92	6.91
$CONH_2$	7.24	7.19	7.45	7.28

[a]More complete ^{1}Hmr data for **9** and **10** are found in the experimental section, and for **9***a* and **10***a* in ref. 7.

[b]Compound **9***a* is (±)-(1β,3β,4β)-3-hydroxy-4-(hydroxymethyl)cyclopentanecarboxamide (compound **6** in ref. 7); compound **10***a* is (±)-(1β,2β,4β)-2-hydroxy-4-(hydroxymethyl)cyclopentanecarboxamide (compound **10** in ref. 7).

ences in their appearance are observed at 200 MHz. The H-1 (and also the H-4) proton in each of the four isomers resonates at a characteristically different chemical shift, as shown in Table 2. Finally, the acetoxy-methyl protons in **7** and **8** resonate at δ 1.99 and 2.00, respectively, whereas in the *cis* isomers they resonate at δ 1.90.

The chemical shifts of the protons in compounds **9** and **10** and in their *cis* isomers are shown in Table 3. Each of the isomers has a characteristically different spectrum; however, in general, the signals for the *cis* isomers are found slightly further downfield relative to the corresponding ones for the *trans* compounds. In the spectrum of compound **9** the non-equivalence of the methylene protons of the hydroxymethyl substituent was clearly observed, as was also the case in the *cis* analog (±)-(1β,3β,4β)-3-hydroxy-4-(hydroxymethyl)cyclopentanecarboxamide (**9***a*) (ref. 7); however, in **10**, as was seen also for the *cis* analog (±)-(1β,2β,4β)-2-hydroxy-4-(hydroxymethyl)cyclopentanecarboxamide (**10***a*) (ref. 7), the chemical shifts of these protons were the same. Spin–spin decoupling experiments on compounds **9** and **10** allowed unambiguous and direct assignment of the multiplets and a confirmation of the structures assigned previously to these compounds by less direct methods using chemical and ^{1}Hmr evidence obtained on compounds that were derived from **9** and **10** (12).

TABLE 4. ^{1}H magnetic resonance chemical shift data[a] in Me_2SO-d_6 for **11**,**12**,**11***a*,[b] and **12***a*[b]

Proton	Compound			
	11	**12**	**11***a*	**12***a*
1	1.78	2.12	1.71–1.97	1.85–2.08
2	3.88	1.45	4.00	1.31
2′	—	1.63	—	1.71–1.89
3	1.44	3.53	1.39	3.73
3′	1.62	—	1.71–1.97	—
4	3.3	2.85	3.23	2.95
5	0.94	0.94	1.12	1.08
5′	1.98	1.91	1.71–1.97	1.71–1.89
CH_2OH	3.3–3.4	3.25	3.37	3.29
CH_2OH	3.3–3.4	3.25	3.59	3.29

[a]More complete ^{1}Hmr data for **11** and **12** are found in the experimental section, and for **11***a* and **12***a* in ref. 7.

[b]Compound **11***a* is (±)-(1β,2β,4β)-4-amino-2-hydroxycyclopentanemethanol (compound **22** in ref. 7); compound **12***a* is (±)-(1β,3β,4β)-4-amino-3-hydroxycyclopentanemethanol (compound **17** in ref. 7).

The chemical shift data for **11** and **12** and for their *cis* analogs, given in Table 4, illustrate several interesting trends including shielding effects by vicinal hydroxyls. An identical chemical shift and coupling pattern were observed for the H-5 proton in the spectra of **11** and **12**. The chemical shifts of the protons at C-3 in **11** are essentially identical to those of the protons at C-2 in **12**; however, the coupling constants obtained from the two pairs of multiplets are quite different (see experimental section). The chemical shifts of the H-5′ proton in **11** and **12** are slightly different; however, the largest difference in chemical shifts for corresponding protons was observed for the protons at C-1 and C-4. In the spectrum of compound **11** these protons resonate at δ 1.78 and 3.3, respectively, whereas in the spectrum of **12** they resonate at δ 2.12 and 2.85, respectively. Thus, the effect of the *cis* vicinal hydroxyl group in these carbocyclic compounds is to shield adjacent protons, causing them to resonate further upfield; this type of shielding by a *cis* vicinal hydroxyl has been observed previously for a variety of carbohydrate derivatives including nucleosides and nucleotides (18–21). The ^{1}Hmr spectra of the *cis* analogs (**11***a* and **12***a*) also show a shielding effect by the *trans* vicinal hydroxyls, although of a slightly smaller magnitude, as illustrated by the chemical shifts for H-4 in the spectra of **11***a* and **12***a* (see Table 4). Similar shielding effects by vicinal hydroxyls were observed for compounds **9**, **10**, **9***a*, and **10***a* (see Table 3).

*Synthesis of (±)-(1β,2α,3α,4β)-4-amino-2,3-dihydroxycyclopentanemethanol (**19**)*

Since the time of the first stereoselective synthesis of compound **19** by Shealy and Clayton (13, 22) several different approaches have been developed for the synthesis of this amine

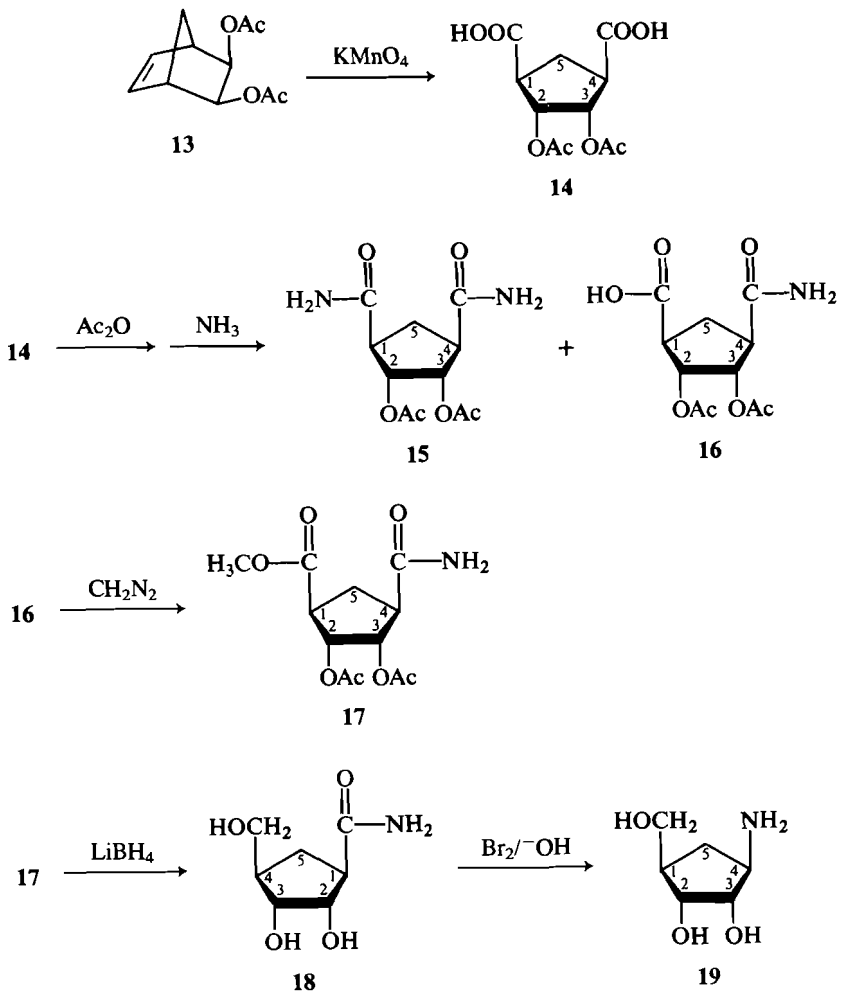

SCHEME 2

(23–25) and its protected derivatives (26, 27). The present approach (see Scheme 2) is a modification of the synthesis described by Shealy and Clayton (13, 22) and requires fewer synthetic steps. Compound **14** was prepared by oxidation of **13** with potassium permanganate, instead of sodium permanganate as was used by Shealy and Clayton (13, 22). Compound **16** was prepared as described previously (13); this procedure afforded also the diamide **15**. Esterification of **16** with diazomethane gave **17** in 79% yield; this compound was then reduced with lithium borohydride to give **18**, in high yield, from which compound **19** was prepared by a Hofmann reaction in aqueous medium.

^{1}H magnetic resonance spectra of compounds in Scheme 2

High-resolution ^{1}Hmr spectra at 200 MHz were obtained for the compounds shown in Scheme 2 (see Experimental). The assignment of the signals in the spectra of compounds **16** and **17** has been made with the aid of spin–spin decoupling experiments and by comparison of the chemical shifts of corresponding protons in the two compounds. All of the corresponding protons in compounds **16** and **17** have essentially identical chemical shifts and coupling constants except for the proton at C-1. In the case of compound **16** this proton resonates at δ 2.91, whereas in the case of the ester derivative **17** its signal is shifted downfield to δ 3.03. A similar downfield shift of the signal for the corresponding proton on esterification of the carboxyl group was observed previously in the spectra of the *cis* analogs (compounds **4** and **5** in ref. 7). Thus, once the identity of the H-1 signal had been established, it was possible to assign the remaining signals in the spectra of **16** and **17** by spin–spin decoupling. The assignment of the ^{1}Hmr signals in the spectra of compounds **18** and **19** also has been made with the aid of spin–spin decoupling experiments.

Synthesis of the nucleoside analogs

3-Ethoxypropenoyl isothiocyanate (**21**), which was synthesized as described by Shaw and Warrener (15), was coupled with the aminohydroxycyclopentanemethanols **11**, **12**, and **19** to give the corresponding thioureas **25**, **26**, and **27**, respectively (see Scheme 3). The thioureas were then cyclized using 15 *N* aqueous ammonia to give the 2-thiouracil nucleoside analogs **31**, **32**, and **33**, respectively. The analogous ureas, namely **22**, **23**, and **24**, and the uracil nucleoside analogs, namely **28**, **29**, and **30** (6), were also synthesized in the present study in order to determine their ^{1}Hmr spectra and to compare them to those of the thio analogs.

^{1}H magnetic resonance spectra of compounds in Scheme 3

The ^{1}Hmr spectra of the $C_2H_5OCH{=}CHCONHCONH{-}$ fragments in compounds **22–24** are very similar to each other with a variation in the chemical shifts of corresponding protons of less than 0.02 ppm. Similarly, the corresponding protons in the $C_2H_5OCH{=}CHCONHCSNH{-}$ fragments have essentially identical chemical shifts in the spectra of compounds **25–27**, with the largest variation, namely ±0.03 ppm, occurring for the CSNH protons. However, the chemical shifts of the

TABLE 5. ^{1}H magnetic resonance chemical shift data[a] in Me_2SO-d_6 for **22–27**

	Compound					
Proton	**22**	**23**	**24**	**25**	**26**	**27**
1′	4.16	3.69–3.85	3.87	4.65	4.28	4.38
2′	1.55	3.69–3.85	3.50–3.66	1.65	3.90–4.04	3.62–3.75
2″	1.73–1.90	—	—	1.94	—	—
3′	3.87	1.55	3.50–3.66	3.90	1.59	3.62–3.75
3″	—	1.55	—	—	1.59	—
4′	1.73–1.90	2.03–2.25	1.88	1.85	2.13–2.36	1.92
5′	1.10	1.12	1.04	1.18	1.17	1.04
5″	2.13	2.03–2.25	2.11	2.28	2.13–2.36	2.32

[a]More complete ^{1}Hmr data for each compound are found in the experimental section.

protons in the sulfur-containing fragments occur further downfield than those of the corresponding protons in compounds **22–24**. The magnitude of the downfield shift varies with the distance from the sulfur atom; for example, the CH_3 protons in compounds **25–27** resonate only 0.01 ppm further downfield, whereas the signals of the CSNH protons are shifted ~2.43 ppm downfield relative to the corresponding signals in the spectra of compounds **22–24**.

The chemical shift data for the cyclopentyl protons in compounds **22–27** are summarized in Table 5. In general, corresponding protons in compounds **25–27** resonate further downfield than those in compounds **22–24**. The magnitude of this downfield shift varies inversely with the number of bonds by which a particular proton is separated from the sulfur atom.

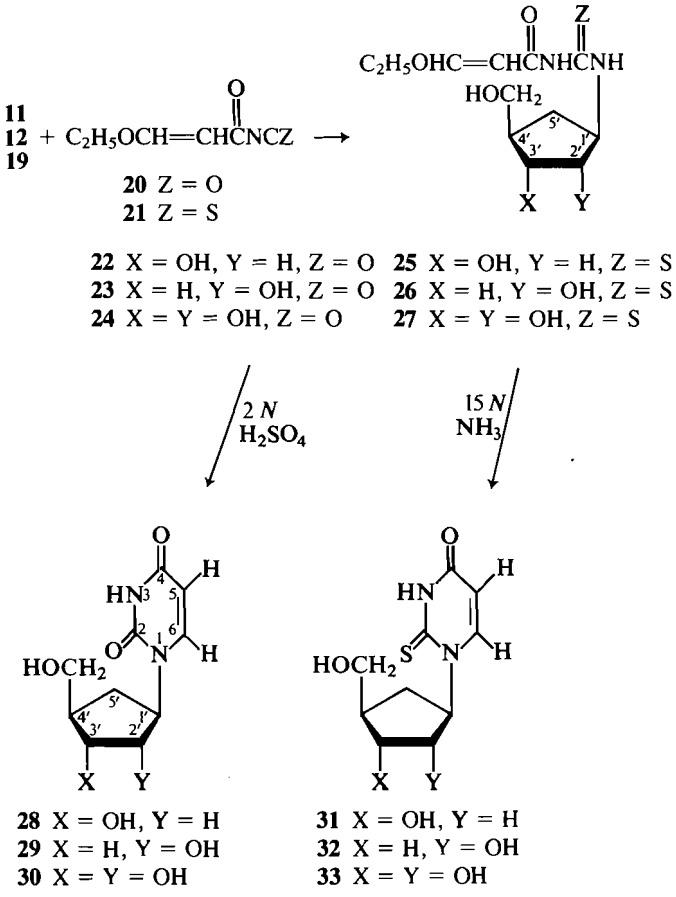

SCHEME 3

Thus, the signals for the protons at C-1′ in compounds **25–27** are shifted downfield by ~0.50 ppm relative to those of the corresponding protons in compounds **22–24**, whereas the signals for the protons at C-3′ or C-4′ are shifted downfield by only ~0.04 ppm. Table 5 also shows that, in the cases of compounds **22–27**, the *cis* vicinal hydroxyl has a shielding effect on H-1′ and H-4′ that is similar to that seen above for the cases of compounds **9–12** (see Tables 3 and 4).

Table 6 summarizes the chemical shift data of the nucleoside analogs **28–33**. The values for the corresponding protons on the uracil base are essentially identical in the cases of **28–30**, as are those for the corresponding protons on the 2-thiouracil base in the cases of **31–33**; however, the chemical shifts of the corresponding protons on the 2-thiouracil base are shifted downfield relative to those on the uracil base. In general, the chemical shifts of protons on the cyclopentane ring are shifted downfield in the spectra of the 2-thiouracil analogs relative to those of the uracil analogs. An exception to this pattern occurs for the H-5′ protons, which in the cases of the 2-thiouracil analogs resonate upfield relative to those in the cases of the uracil analogs (see Table 6). As shown by the chemical shift data for the H-1′ protons in Table 6, the *cis* vicinal hydroxyls have shielding effects in the nucleosides that are similar to those seen above for compounds **9–12** and **22–27**. The chemical shift data in Table 6 also show that each nucleoside has a unique and characteristic spectrum and one which is significantly different from the spectra of the nucleoside analogs that have the hydroxyls in the *cis* configuration (7).

Ultraviolet spectra of ***31–33***

The ultraviolet spectra of the 2-thiouracil nucleoside analogs **31–33** are very similar to each other and closely resemble those of 1-methyl-2-thiouracil (28) at the corresponding pH's.

Preliminary biological evaluation

Compounds **31–33** were tested for cell-growth inhibition using cultured L1210 cells as described previously (29). No cell-growth inhibition by these compounds was observed at concentrations as high as 10^{-3} *M*. Further biological studies are in progress.

Conclusions

Three new carbocyclic analogs of 2-thiouracil nucleosides have been synthesized. In addition, the carbocyclic analogs of uracil nucleosides first synthesized by Shealy and O'Dell (6) were synthesized and their ^{1}Hmr spectra were compared to those of the 2-thiouracil analogs. As shown previously for the carbocyclic analogs of uracil nucleosides, which contained the

TABLE 6. ^{1}H magnetic resonance chemical shift data[a] in Me_2SO-d_6 for **28–33**

Proton	Compound					
	28	**29**	**30**	**31**	**32**	**33**
3	11.21	11.21	11.20	12.53	12.58	12.6
5	5.58	5.59	5.59	5.99	6.00	6.01
6	7.69	7.68	7.69	7.85	7.85	7.87
1′	4.95	4.45	4.57–4.68	5.96	5.55	5.67
2′	1.71–2.00	4.14	3.97	1.80–1.99	4.22	4.05
2″	1.71–2.00	—	—	1.80–1.99	—	—
3′	3.97	1.56	3.71	4.01	1.59	3.73
3″	—	1.76	—	—	1.78	—
4′	1.71–2.00	2.16	1.85–2.08	1.80–1.99	2.04–2.26	1.95
5′	1.36	1.37	1.26	1.32	1.20	1.08
5″	2.08	1.96	1.85–2.08	2.20	2.04–2.26	2.18
CH_2OH	3.34–3.56	3.29–3.35	3.33–3.45	3.34–3.56	3.29–3.35	3.33–3.47
CH_2OH	4.63	4.60	4.70	4.65	4.64	4.73
OH at C-2	—	5.05	4.89	—	5.11	4.94
OH at C-3	4.75	—	4.60	4.79	—	4.67

[a]More complete ^{1}Hmr data for each compound are found in the experimental section.

hydroxyl in the *cis* configuration (7), the replacement of the oxygen by a sulfur atom at C-2 has a profound effect on the chemical shifts of not only the base protons but also of the protons on the cyclopentane ring. In general, the protons in the sulfur-containing compounds resonate at lower fields than the corresponding protons in the oxygen-containing compounds.

A modified route for the synthesis of (+)-(1β,2α,3α,4β)-4-amino-2,3-dihydroxycyclopentanemethanol (**19**) is described, which contains fewer steps than that described by Shealy and Clayton (13). The ^{1}Hmr spectra at 200 MHz of the synthetic intermediates leading to all of the nucleosides described in the present work have been determined also, and compared with the ^{1}Hmr spectra of the corresponding synthetic intermediates leading to the carbocyclic analogs of nucleosides having the hydroxyl group in the *cis* configuration (7).

Experimental

Melting points were determined on a Fisher–Johns apparatus and are uncorrected. The ^{1}Hmr spectra were determined on a Brüker CXP-200 spectrometer at 200 MHz. Chemical shifts (δ) are given relative to Me_4Si (δ = 0). The coupling constants quoted are observed, uncorrected values; the instrument-resolution error is ±0.3 hertz. Assignments of chemical shifts and coupling constants were made with the aid of spin-decoupling experiments. The following abbreviations are used in describing ^{1}Hmr signals: singlet (s), doublet (d), triplet (t), quartet (q), quintuplet (qu), sextuplet (se), multiplet (m), and broadened (br). Ultraviolet spectra were recorded on a Perkin–Elmer 552 spectrophotometer. Thin-layer chromatography (tlc) was performed using silica gel 60 F-254 plates (BDH Chemicals). The developed plates were dried and sprayed with a solution of ceric sulfate (1%) and molybdic acid (1.5%) in 10% aqueous sulfuric acid, and heated at ~150°C. Unless otherwise indicated, the same solvent was used for both tlc and column chromatography.

(±)-(1β,3β,4α)-4-Acetoxy-1,3-cyclopentanedicarboxylic acid anhydride (2)

(±)-*exo*-5-Norbornen-2-yl acetate (30) was oxidized with $KMnO_4$ to (±)-(1β,3β,4α)-4-acetoxy-1,3-cyclopentanedicarboxylic acid (7), which was then converted into compound **2** using acetic anhydride as described by O'Dell and Shealy (11); mp 118–120°C (lit. (11) mp 119–120°C); ^{1}Hmr (200 MHz, Me_2SO-d_6) δ: 1.94 (1H, d of t, J_{gem} = 12.8, ^3J = 4.1 Hz, H-2), 2.03 (3H, s, OAc), 2.06 (1H, d of d of d of d, J_{gem} = 15.5, $^3J_{5,1}$ = 7.4, $^3J_{5,4}$ = 2.9, J = 1.5 Hz, H-5), 2.49 (1H, m, H-2′), 2.54 (1H, m, H-5′), 3.25–3.36 (2H, m, H-1 and H-3), 5.23 (1H, br d of d, $^3J_{4,5'}$ = 7.4, $^3J_{4,5}$ = 2.9 Hz, H-4). Spin–spin decoupling was performed at H-4; ^{1}Hmr (200 MHz, $CDCl_3$) δ: 2.05–2.18 (1H, m, H-5), 2.09 (3H, s, OAc), 2.17 (1H, d of t, J_{gem} = 12.9, ^3J = 3.9 Hz, H-2), 2.33 (1H, m, J_{gem} = 12.9 Hz, H-2′), 2.63 (1H, d of d of d, J_{gem} = 15.6, $^3J_{5',4}$ = 7.2, J = 1.6 Hz, H-5′), 3.34–3.40 (2H, m, H-1 and H-3), 5.31 (1H, m, $^3J_{4,5'}$ = 7.2, J = 2.6 Hz, H-4).

(±)-Methyl (1β,2α,4β)-2-acetoxy-4-carbamoylcyclopentanecarboxylate (7) and (±)-methyl (1β,3α,4β)-3-acetoxy-4-carbamoylcyclopentanecarboxylate (8)

Compound **2** was converted into compounds **7** and **8** as described by O'Dell and Shealy (11). Compound **2** was stirred in dry methanol at room temperature to give a mixture of compounds **3** and **4**. The solvent was removed and treatment of the mixture with $SOCl_2$ in benzene gave compounds **5** and **6**, which were then converted into compounds **7** and **8** using anhydrous NH_3 in benzene. Compounds **7** and **8** were isolated by silica gel column chromatography using toluene–acetone (3:2 (v/v)) as solvent. Compound **7** had R_f 0.23 (15:1 (v/v) methylene chloride – 2-propanol). mp 105–106°C (lit. (12) mp 108–109°C); ^{1}Hmr (200 MHz, Me_2SO-d_6) δ: 1.81 (1H, d of t, J_{gem} = 12.7, ^3J = 10.0 Hz, H-5), 1.82 (1H, m, J_{gem} = 13.2, $^3J_{3,4}$ = 8.4, $^3J_{3,2}$ = 3.8 Hz, H-3), 1.99 (3H, s, OAc), 2.02 (1H, m, J_{gem} = 13.2, $^3J_{3',4}$ = 9.9, $^3J_{3',2}$ = 7.1 Hz, H-3′), 2.21 (1H, d of t, J_{gem} = 12.7, ^3J = 8.0 Hz, H-5′), 2.82 (1H, m, H-4), 2.87 (1H, t of d, $^3J_{1,2}$ = 4.2 Hz, H-1), 3.62 (3H, s, OMe), 5.20 (1H, m, $^3J_{2,3'}$ = 7.1 Hz, H-2), 6.87 (1H, br s, $CONH_2$), 7.38 (1H, br s, $CONH_2$). Spin–spin decoupling was performed at H-2. Compound **8** had R_f 0.38 (15:1 (v/v) methylene chloride – 2-propanol), mp 61–70°C (lit. (12) mp 73 and 80°C); ^{1}Hmr (200 MHz, Me_2SO-d_6) δ: 1.80 (1H, d of t, J_{gem} = 12.7, ^3J = 10.1 Hz, H-5), 1.85 (1H, d of d of d, J_{gem} = 14, $^3J_{2,1}$ = 7.9, $^3J_{2,3}$ = 3.9 Hz, H-2), 2.00 (3H, s, OAc), 2.11 (1H, d of d of d, J_{gem} = 14, $^3J_{2',1}$ = 9.7, $^3J_{2',3}$ = 7.0 Hz, H-2′), 2.23 (1H, d of t, J_{gem} = 12.7, ^3J = 8.1 Hz, H-5′), 2.74 (1H, t of d, ^3J = 8.9, $^3J_{4,3}$ = 4.8 Hz, H-4), 2.98 (1H, m, H-1), 3.63 (3H, s, OMe), 5.11 (1H, d of t, $^3J_{3,2'}$ = 7.0, ^3J = 4.1 Hz, H-3), 6.94 (1H, br s, $CONH_2$), 7.39 (1H, br s, $CONH_2$). Spin–spin decoupling was performed at H-3.

(±)-(1β,3α,4β)-3-Hydroxy-4-(hydroxymethyl)cyclopentanecarboxamide (9)

Compound **9** was prepared by reduction of **7** using lithium borohydride in tetrahydrofuran as described previously (11); mp 124–127°C (lit. (12) mp 127–128°C); ^{1}Hmr (200 MHz, Me_2SO-d_6) δ: 1.29 (1H, d of d of d, J_{gem} = 11.9, $^3J_{5,1}$ = 9.2, $^3J_{5,4}$ = 7.3 Hz, H-5),

1.58 (1H, m, J_{gem} = 13.0, $^3J_{2,1}$ = 8.1, $^3J_{2,3}$ = 3.4 Hz, H-2), 1.76 (1H, d of d of d, J_{gem} = 13.0, $^3J_{2',1}$ = 9.2, $^3J_{2',3}$ = 6.2 Hz, H-2'), 1.75–2.0 (2H, m, H-4 and H-5'), 2.75 (1H, m, H-1), 3.25 (1H, m, J_{gem} = 10.5, $^3J_{to\,H\text{-}4}$ = 6.4 Hz, CH_2OH), 3.39 (1H, m, J_{gem} = 10.5, $^3J_{to\,H\text{-}4}$ = 6.1 Hz, CH_2OH), 3.85 (1H, m, $^3J_{3,2'}$ = 6.2, $^3J_{3,4}$ = 3.8, $^3J_{3,2}$ = 3.4 Hz, H-3), 4.45–4.51 (2H, m, OH), 6.68 (1H, br s, $CONH_2$), 7.24 (1H, br s, $CONH_2$). The amide and hydroxyl protons were exchanged with D_2O in the ^{1}Hmr determination. Spin–spin decoupling was performed at H-5, H-2, H-1, H-3, and CH_2OH.

*(±)-(1β,2α,4β)-2-Hydroxy-4-(hydroxymethyl)cyclopentanecarboxamide (**10**)*

Compound **10** was prepared by reduction of **8** using lithium borohydride in tetrahydrofuran as described previously (11); mp 117–124°C (lit. (12) mp 123–124°C); ^{1}Hmr (200 MHz, Me_2SO-d_6) δ: 1.28 (1H, d of t, J_{gem} = 12.7, ^3J = 9.5 Hz, H-5), 1.53 (2H, d of d, $^3J_{to\,H\text{-}4}$ = 7.9, $^3J_{to\,H\text{-}2}$ = 6.1 Hz, H-3 and H-3'), 1.87 (1H, d of t, J_{gem} = 12.7, ^3J = 7.7 Hz, H-5'), 2.14 (1H, m, H-4), 2.41 (1H, d of d of d, $^3J_{1,5}$ = 10.1, $^3J_{1,5'}$ = 8.0, $^3J_{1,2}$ = 5.9 Hz, H-1), 3.25 (2H, m, $^3J_{to\,H\text{-}4}$ = 6.4 Hz, CH_2OH), 4.08 (1H, m, H-2), 4.48 (1H, br t, ^3J = 4.7 Hz, CH_2OH), 4.72 (1H, br d, $^3J_{to\,H\text{-}2}$ = 4.3 Hz, OH at 2), 6.74 (1H, br s, $CONH_2$), 7.19 (1H, br s, $CONH_2$). Spin–spin decoupling was performed at H-5, H-5', H-4, H-3, H-2, H-1, and CH_2OH.

*(±)-(1β,2α,4β)-4-Amino-2-hydroxycyclopentanemethanol (**11**)*

A Hofmann hypobromite reaction in water was performed on **9** as described previously (11) to give compound **11**; R_f 0.41 (4:1 (v/v) ethanol – 15 *N* aqueous ammonia); ^{1}Hmr (200 MHz, Me_2SO-d_6) δ: 0.94 (1H, d of t, J_{gem} = 12.6, ^3J = 7.4 Hz, H-5), 1.44 (1H, m, J_{gem} = 12.7, ^3J = 6.7 Hz, H-3), 1.62 (1H, m, J_{gem} = 12.7, $^3J_{3',4}$ = 6.8, $^3J_{3',2}$ = 4.6 Hz, H-3'), 1.78 (1H, m, H-1), 1.98 (1H, m, J_{gem} = 12.6, ^3J = 7.5 Hz, H-5'), 3.3 (1H, m, H-4), 3.3–3.4 (2H, m, CH_2OH), 3.88 (1H, d of t, $^3J_{2,3}$ = 6.7, $^3J_{2,3'}$ = $^3J_{2,1}$ = 4.6 Hz, H-2). Spin–spin decoupling was performed at H-2 and H-5.

*(±)-(1β,3α,4β)-4-Amino-2-hydroxycyclopentanemethanol (**12**)*

A Hofmann hypobromite reaction in water was performed on **10** as described previously (11) to give compound **12**; R_f 0.59 (4:1 (v/v) ethanol – 15 *N* aqueous ammonia); ^{1}Hmr (200 MHz, Me_2SO-d_6) δ: 0.94 (1H, d of t, J_{gem} = 12.8, ^3J = 7.1 Hz, H-5), 1.45 (1H, m, J_{gem} = 13.3, $^3J_{2,1}$ = 9.2, $^3J_{2,3}$ = 5.2 Hz, H-2), 1.63 (1H, m, J_{gem} = 13.3, ^3J = 6.6 Hz, H-2'), 1.91 (1H, d of d of d, J_{gem} = 12.8, $^3J_{5',1}$ = 8.7, $^3J_{5',4}$ = 6.6 Hz, H-5'), 2.12 (1H, m, H-1), 2.85 (1H, t of d, ^3J = 6.8, $^3J_{4,3}$ = 5.1 Hz, H-4), 3.25 (2H, d, $^3J_{to\,H\text{-}1}$ = 6.0 Hz, CH_2OH), 3.53 (1H, m, H-3). Spin–spin decoupling was performed at δ 3.25 and 3.53.

*(1β,2α,3α,4β)-2,3-Diacetoxy-1,4-cyclopentanedicarboxylic acid (**14**)*

Compound **13** (13) (65.2 g, 0.31 mol) was dissolved in isooctane (0.7 L) and layered on top of water (3.5 L), and the mixture was cooled to 5°C. To the stirred mixture potassium permanganate (188 g, 1.19 mol) in water (3 L) was added over a period of 3 h. During the addition of the potassium permanganate a steady stream of CO_2 was passed through the reaction mixture and the temperature was maintained at 5–10°C using an external ice bath. Immediately after the potassium permanganate had been added, SO_2 was passed through the reaction mixture until it became clear, during which process the temperature was maintained below 15°C. The volume of the reaction solution was reduced to 1.2 L. It was then cooled in an ice bath, acidified with concentrated hydrochloric acid (85 mL), and extracted with diethyl ether (7 × 400 mL) to give a solid (72.6 g, 85%). This material was recrystallized from ethyl acetate to give **14** (65.2 g, 76.7%) as a white crystalline solid, mp 163–168°C (lit (13) mp 169–171°C); ^{1}Hmr (200 MHz, Me_2SO-d_6) δ: 1.88 (1H, d of t, J_{gem} = 13.4, ^3J = 8.6 Hz, H-5), 2.01 (6H, s, OAc), 2.43 (1H, d of t, J_{gem} = 13.4, ^3J = 9.4 Hz, H-5'), 2.96 (2H, t of d, ^3J = 8.8, ^3J = 4.6 Hz, H-1 and H-4), 5.25 (2H, m, H-2 and H-3), 12.71 (2H, br s, CO_2H).

*(1β,2α,3α,4β)-2,3-Diacetoxy-1,4-cyclopentanedicarboxamide (**15**) and (±)-(1β,2α,3α,4β)-2,3-Diacetoxy-4-carbamoylcyclopentanecarboxylic acid (**16**)*

Compound **14** (32.0 g, 0.117 mol) was suspended in acetic anhydride (400 mL) and the mixture was heated on a steam bath for 1 h. Volatile components were evaporated to give a light brown oil (36 g). The oil was dissolved in dry tetrahydrofuran (500 mL) and the solution was cooled to 5°C. Anhydrous ammonia was blown over the stirred reaction solution (which was maintained at 5–10°C) for 25 min. The solvent was evaporated and the remaining white solid was dissolved in water (150 mL). Insoluble material was removed by filtration and washed with water (25 mL) that was combined with the filtrate. The filtrate was cooled to ice-bath temperature and an additional crop of a white solid was collected by filtration. The above two crops of solid (7.5 g) were shown to be (1β,2α,3α,4β)-2,3-diacetoxy-1,4-cyclopentanedicarboxamide (**15**), mp 230°C (dec.) (lit (13) mp 230°C (dec.)); ^{1}Hmr (200 MHz, Me_2SO-d_6) δ: 1.67 (1H, d of t, J_{gem} = 12.9, ^3J = 9.9 Hz, H-5), 1.98 (6H, s, OAc), 2.20 (1H, d of t, J_{gem} = 12.9, ^3J = 8.9 Hz, H-5'), 2.84 (2H, t of d, ^3J = 9.2, ^3J = 4.8 Hz, H-1 and H-4), 5.15 (2H, m, H-2 and H-3), 7.00 (2H, br s, $CONH_2$), 7.46 (2H, br s, $CONH_2$). The cold filtrate was acidified (pH ~2) with concentrated hydrochloric acid and left at 4°C overnight. The solution was then extracted with diethyl ether (5 × 200 mL). On evaporation of the diethyl ether an oil (10 g) was obtained, which was shown by ^{1}Hmr spectroscopy to be a mixture consisting predominantly of compound **15**. The aqueous layer was then extracted with ethyl acetate (7 × 200 mL). On evaporation of the ethyl acetate a crystalline solid separated, which was collected by suction and washed with a small amount of ethyl acetate to give **16** (12.7 g 40%), mp 164°C (lit. (13) mp 166°C and 182–183°C); ^{1}Hmr (200 MHz, Me_2SO-d_6) δ: 1.77 (1H, d of t, J_{gem} = 13.1, ^3J = 9.2 Hz, H-5), 1.99 (6H, s, OAc), 2.32 (1H, d of t, J_{gem} = 13.1, ^3J = 9.1 Hz, H-5'), 2.89 (1H, t of d, ^3J = 9.0, $^3J_{4,3}$ = 6.8 Hz, H-4), 2.91 (1H, t of d, ^3J = 9.6, $^3J_{1,2}$ = 5.4 Hz, H-1), 5.12 (1H, d of d, $^3J_{3,4}$ = 6.8, $^3J_{3,2}$ = 5.3 Hz, H-3), 5.28 (1H, m, H-2), 7.04 (1H, br s, $CONH_2$), 7.52 (1H, br s, $CONH_2$), 12.64 (1H, br s, CO_2H).

*(±)-Methyl (1β,2α,3α,4β)-2,3-diacetoxy-4-carbamoylcyclopentanecarboxylate (**17**)*

Compound **16** (12.7 g, 46 mmol) was dissolved in methanol (250 mL) and was methylated with diazomethane using procedures described previously (7, 31). The solution was left in the fume hood until the yellow color due to the slight excess of diazomethane faded. The solvent was evaporated and the residue was fractionated by column chromatography on silica gel to give a white solid (10.55 g, 79%), mp 85–90°C, R_f 0.35 (3:3:1 (v/v/v) toluene – ethyl acetate – 2-propanol); a second chromatographic separation on a silica gel column gave material having mp 89–91°C; ^{1}Hmr (200 MHz, Me_2SO-d_6) δ: 1.79 (1H, d of t, J_{gem} = 13.2, J = 9.3 Hz, H-5), 2.00 (6H, s, OAc), 2.34 (1H, d of t, J_{gem} = 13.2, ^3J = 9.2 Hz, H-5'), 2.90 (1H, t of d, ^3J = 8.8, $^3J_{4,3}$ = 6.5 Hz, H-4), 3.03 (1H, t of d, ^3J = 9.3, $^3J_{1,2}$ = 6.2 Hz, H-1), 3.64 (3H, s, OMe), 5.13 (1H, d of d, $^3J_{3,4}$ = 6.5, $^3J_{3,2}$ = 5.3 Hz, H-3), 5.28 (1H, m, H-2), 7.09 (1H, br s, $CONH_2$), 7.55 (1H, br s, $CONH_2$). Spin–spin decoupling was performed at H-2. *Anal.* calcd. for $C_{12}H_{17}O_7N$: C 50.17, H 5.97, N 4.88; found: 50.00, H 5.86, N 4.85.

*(±)-(1β,2α,3α,4β)-2,3-Dihydroxy-4-(hydroxymethyl)cyclopentanecarboxamide (**18**)*

A solution containing lithium borohydride (6.5 g, 298 mmol) in tetrahydrofuran (400 mL) was refluxed in 1 h and cooled to ~40°C. To this solution was added a solution of compound **17** (13.73 g, 47.8 mmol) in tetrahydrofuran (100 mL), and the reaction solution was heated at reflux temperature for 2 h. The solution was cooled to ice-bath temperature and diluted dropwise with water (200 mL); there was then a slow addition of Amberlite IR-120 (H^+) cation-exchange resin (150 g). The mixture was stirred overnight. The resin was removed by filtration and washed with water (300 mL). The combined filtrate and washings were stirred with Amberlite IR-45 ($^-$OH) anion-exchange resin (260 g) to adjust the pH to neutrality. The resin was removed by filtration and washed with water (3 L). The combined filtrate and washings were evaporated to a semisolid, which was then evaporated with methanol (5 × 60 mL) to remove the boric acid as the methyl ester; an orange viscous oil (9.8 g) was obtained. The oil was stirred with tetrahydrofuran (60 mL) for 3 days and a light-brown solid was collected and dried over P_2O_5 at 60°C for 2 h to give a crude sample of **18** (7.83 g, 93%), which was shown by ^{1}Hmr spectroscopy to be

contaminated by small amounts of impurities. (The crude material was used for the preparation of **19**, as described below, without further purification.) A small sample (0.1 g) was purified by column chromatography on silica gel to give a single component having R_f 0.37 (5:1 (v/v) acetonitrile–water). This material was crystallized, from the minimal amount of ethanol necessary to dissolve the residue after evaporation of the chromatographic solvents and a drop of hexanes, to give a white solid that was collected by filtration and washed with diethyl ether, mp 135–137°C; ^{1}Hmr (200 MHz, Me_2SO-d_6) δ: 1.25 (1H, m, H-5), 1.76–1.97 (2H, m, H-4 and H-5′), 2.48–2.61 (1H, m, H-1), 3.21–3.43 (2H, m, CH_2OH), 3.59 (1H, q, ^3J = 4.3 Hz, H-3), 3.80 (1H, m, $^3J_{2,1}$ = 7.1, $^3J_{2,3}$ = 5.2 Hz, H-2), 4.33 (1H, d, $^3J_{\text{to H-3}}$ = 4.7 Hz, OH at position 3), 4.47 (1H, d, $^3J_{\text{to H-2}}$ = 6.2 Hz, OH at position 2), 4.50 (1H, t, ^3J = 5.1 Hz, CH_2OH), 6.75 (1H, br s, $CONH_2$), 7.19 (1H, br s, $CONH_2$). Spin–spin decoupling was performed at H-2 and H-3. *Anal.* calcd. for $C_7H_{13}O_4N$: C 47.99, H 7.48, N 8.00; found: C 47.73, H 7.49, N 7.89.

*(±)-(1β,2α,3α,4β)-4-Amino-2,3-dihydroxycyclopentanemethanol (**19**)*

A freshly prepared solution of $Ba(OH)_2 \cdot 8H_2O$ (70.0 g, 222 mmol) in water (1.42 L) was filtered to remove any $BaCO_3$ present, and then cooled to 5°C. To this solution Br_2 (2.25 mL, 44 mmol) was added; immediately after the Br_2 had dissolved, compound **18** (7.73 g, 44 mmol) in water (100 mL) was added in one portion, and the reaction solution was left at room temperature for 1 h. It was then heated at 60–70°C for 1 h and left at 4°C overnight. The cold reaction mixture was acidified with 3 *M* H_2SO_4 (150 mL) and centrifuged to remove the $BaSO_4$. The reaction solution was passed through a column of Amberlite CG-120 (H^+) cation-exchange resin (200 g). The resin was washed with water (3.3 L), which was discarded. Elution of the resin with 2 *N* aqueous ammonia followed by evaporation of the solvent gave an orange-brown oil (3.12 g). The oil was dissolved in ethanol (30 mL), which caused a sticky brown material to precipitate. The ethanol solution was decanted and evaporated to give **19** (2.95 g, 46%) as an orange oil; ^{1}Hmr (200 MHz, Me_2SO-d_6) δ: 0.88 (1H, m, J_{gem} = 11.8, ^3J = 7.3 Hz, H-5), 1.74–2.00 (2H, m, H-1 and H-5′), 2.96 (1H, m, H-4), 3.25–3.49 (3H, m, H-3 and CH_2OH), 3.66 (1H, t, ^3J = 4.7 Hz, H-2). Spin–spin decoupling was performed at H-2, H-4, and H-5.

*(±)-3-Ethoxy-*N*-{N′-[(1β,3α,4β)-3-hydroxy-4-(hydroxymethyl)cyclopentyl]carbamoyl}propenamide (**22**)*

Compound **22** was prepared by the coupling of 3-ethoxypropenoyl isocyanate (**20**) (6, 7, 14) with compound **11** as described by Shealy and O'Dell (6). After the volatile components had been evaporated, the crude oil was fractionated by column chromatography on silica gel to give **22** as a white solid, R_f 0.32 (2:2:1 (v/v/v) toluene – ethyl acetate – 2-propanol), mp 148–151°C (lit. (6) mp 138–140°C); ^{1}Hmr (200 MHz, Me_2SO-d_6) δ: 1.10 (1H, d of t, J_{gem} = 12.8, ^3J = 8.3 Hz, H-5′), 1.25 (3H, t, ^3J = 7.0 Hz, CH_3), 1.55 (1H, d of d of d, J_{gem} = 12.8, $^3J_{2',1'}$ = 7.9, $^3J_{2',3'}$ = 6.4 Hz, H-2′), 1.73–1.90 (2H, m, H-2″ and H-4′), 2.13 (1H, d of t, J_{gem} = 12.8, ^3J = 7.9 Hz, H-5″), 3.25–3.46 (2H, m, CH_2OH), 3.87 (1H, m, H-3′), 3.94 (2H, q, ^3J = 7.0 Hz, CH_3CH_2O), 4.16 (1H, se, ^3J = 7.7 Hz, H-1′), 4.55 (1H, t, $^3J_{\text{to }CH_2OH}$ = 5.2 Hz, CH_2OH), 4.59 (1H, d, $^3J_{\text{to H-3′}}$ = 4.5 Hz, OH at 3′), 5.50 (1H, d, ^3J = 12.2 Hz, H-2), 7.54 (1H, d, ^3J = 12.2 Hz, H-3), 8.49 (1H, br d, $^3J_{\text{to H-1′}}$ = 7.7 Hz, CONHCON*H*), 10.00 (1H, br s, CON*H*CONH). Spin–spin decoupling was performed at H-1′, H-5″, and at H-3′.

*(±)-3-Ethoxy-*N*-{N′-[(1β,2α,4β)-2-hydroxy-4-(hydroxymethyl)cyclopentyl]carbamoyl}propenamide (**23**)*

Compound **23** was prepared by the coupling of 3-ethoxypropenoyl isocyanate (**20**) (6, 7, 14) with compound **12** as described by Shealy and O'Dell (6). After the reaction solvents had been evaporated, the residue was dissolved in a minimal amount of methanol and fractionated by column chromatography on silica gel to give **23** (49% yield) as a white solid, R_f 0.38 (2:2:1 (v/v/v) toluene–ethyl acetate–2-propanol), mp 128–130°C (lit. (6) 126–128°C); ^{1}Hmr (200 MHz, Me_2SO-d_6) δ: 1.12 (1H, m, H-5′), 1.25 (3H, t, ^3J = 7.1 Hz, CH_3), 1.55 (2H, m, H-3′ and H-3″), 2.03–2.25 (2H, m, H-4′ and H-5″), 3.25–3.40 (2H, m, CH_2OH), 3.69–3.85 (2H, m, H-1′ and H-2′), 3.94 (2H, q, ^3J = 7.1 Hz, CH_3CH_2O), 4.57 (1H, t, $^3J_{\text{to }CH_2OH}$ = 5.2 Hz, CH_2OH), 4.85 (1H, d, $^3J_{\text{to H-2′}}$ = 4.3 Hz, HO at position 2′), 5.50 (1H, d, ^3J = 12.5 Hz, H-2), 7.55 (1H, d, ^3J = 12.5 Hz, H-3), 8.52 (1H, br d, $^3J_{\text{to H-1′}}$ = 6.9 Hz, CONHCON*H*), 10.03 (1H, br s, CON*H*CONH). Spin–spin decoupling was performed at the H-5′ proton.

*(±)-3-Ethoxy-*N*-{N′-[(1β,2α,3α,4β)-2,3-dihydroxy-4-(hydroxymethyl)cyclopentyl]carbamoyl}propenamide (**24**)*

Compound **24** was prepared by the coupling of 3-ethoxypropenoyl isocyanate (**20**) (6, 7, 14) with compound **19** as described by Shealy and O'Dell (6). After the reaction solvents had been evaporated, the crude oil was fractionated by column chromatography on silica gel to give **24** as a single component on tlc, R_f 0.43 (1:1:1 (v/v/v) toluene – ethyl acetate – 2-propanol); ^{1}Hmr (200 MHz, Me_2SO-d_6) δ: 1.04 (1H, d of t, J_{gem} = 13.0, ^3J = 7.8 Hz, H-5′), 1.24 (3H, t, ^3J = 7.1 Hz, CH_3), 1.88 (1H, m, H-4′), 2.11 (1H, d of t, J_{gem} = 13.0, ^3J = 8.7 Hz, H-5″), 3.25–3.44 (2H, m, CH_2OH), 3.50–3.66 (2H, m, H-2′ and H-3′), 3.87 (1H, qu, ^3J = 7.4 Hz, H-1′), 3.94 (2H, q, ^3J = 7.1 Hz, CH_3CH_2O), 4.42 (1H, d, $^3J_{\text{to H-3′}}$ = 4.3 Hz, OH at position 3′), 4.59 (1H, t, $^3J_{\text{to }CH_2OH}$ = 5.1 Hz, CH_2OH), 4.66 (1H, d, $^3J_{\text{to H-2′}}$ = 5.5 Hz, OH at position 2′), 5.51 (1H, d, ^3J = 12.5 Hz, H-2), 7.55 (1H, d, ^3J = 12.5 Hz, H-3), 8.53 (1H, br d, $^3J_{\text{to H-1′}}$ = 7.3 Hz, CONHCON*H*), 10.02 (1H, br s, CON*H*CONH). Spin–spin decoupling was performed at δ 1.88, 4.42, and 8.53.

*3-Ethoxypropenoyl isothiocyanate (**21**)*

Compound **21** was prepared from 3-ethoxypropenoyl chloride and potassium thiocyanate by a procedure similar to that of Shaw and Warrener (7, 15). A mixture of 3-ethoxypropenoyl chloride (7.27 g, 54 mmol) and potassium thiocyanate (5.25 g, 54 mmol) in acetonitrile (35 mL) was shaken at room temperature for 3.5 h and filtered to remove the potassium chloride. The salt was washed with a small amount of acetonitrile and the wash was combined with the filtrate. This acetonitrile solution of compound **21** was used immediately for the preparation of compounds **25**, **26**, and **27** without further processing.

*(±)-3-Ethoxy-*N*-{N′-[(1β,3α,4β)-3-hydroxy-4-(hydroxymethyl)cyclopentyl]thiocarbamoyl}propenamide (**25**)*

Compound **11** (3.32 g, 25 mmol) was dissolved in *N*,*N*-dimethylformamide (32 mL), and the solution was dried over 4 Å molecular sieves and cooled to ice-bath temperature; the acetonitrile solution (24 mL) of **21** (25 mmol, theoretical), prepared above, was added dropwise over a period of 10 min. The reaction solution was left at room temperature overnight and at 4°C for a day. The reaction solvents were evaporated and the resulting orange oil was evaporated with ethanol (2 × 10 mL). The oil was then fractionated by column chromatography on silica gel to give **25** (4.4 g, 61%) as a light-yellow solid, R_f 0.41 (3:3:1 (v/v/v) toluene – ethyl acetate – 2-propanol). The ^{1}Hmr spectrum showed only traces of impurities to be present in this material; ^{1}Hmr (200 MHz, Me_2SO-d_6) δ: 1.18 (1H, m, J_{gem} = 12.8, ^3J = 8.0 Hz, H-5′), 1.26 (3H, t, ^3J = 7.1 Hz, CH_3), 1.65 (1H, m, J_{gem} = 13.2, ^3J = 7.3, ^3J = 6.3 Hz, H-2′), 1.85 (1H, m, H-4′), 1.94 (1H, m, J_{gem} = 13.2, ^3J = 7.7, ^3J = 4.6 Hz, H-2″), 2.28 (1H, d of t, J_{gem} = 12.8, ^3J = 8.0 Hz, H-5″), 3.2–3.5 (2H, m, CH_2OH), 3.90 (1H, m, H-3′), 3.98 (2H, q, ^3J = 7.1 Hz, CH_3CH_2O), 4.58 (1H, t, $^3J_{\text{to }CH_2OH}$ = 5.1 Hz, CH_2OH), 4.65 (1H, m, H-1′), 4.66 (1H, d, $^3J_{\text{to H-3′}}$ = 4.1 Hz, OH at position 3′), 5.70 (1H, d, ^3J = 12.0 Hz, H-2), 7.59 (1H, d, ^3J = 12.0 Hz, H-3), 10.85 (1H, br s, CON*H*CSNH), 10.91 (1H, br d, $^3J_{\text{to H-1′}}$ = 7.7 Hz, CONHCSN*H*). Spin–spin decoupling was performed at δ 2.28, 3.90, and 10.85.

*(±)-3-Ethoxy-*N*-{N′-[(1β,2α,4β)-2-hydroxy-4-(hydroxymethyl)cyclopentyl]thiocarbamoyl}propenamide (**26**)*

The procedure for the preparation of compound **26** was the same as that for **25**. To an ice-cold *N*,*N*-dimethylformamide solution (45 mL) of compound **12** (3.27 g, 25 mmol) was added 24 mL of the acetonitrile solution of **21** (25 mmol, theoretical) over a period of 10 min. This reaction solution was treated as described by the preparation of **25** and the resulting orange oil was fractionated by column chromatography on silica gel to give **26** (3.55 g, 49%) as a light-yellow gum, R_f 0.45 (3:3:1

(v/v/v) toluene – ethyl acetate – 2-propanol). The ^{1}Hmr spectrum showed only traces of impurities to be present in this preparation; ^{1}Hmr (200 MHz, Me_2SO-d_6) δ: 1.17 (1H, m, H-5′), 1.26 (3H, t, ^3J = 7.1 Hz, CH_3), 1.59 (2H, m, H-3′ and H-3″), 2.13–2.36 (2H, m, H-4′ and H-5″), 3.29 (2H, m, CH_2OH), 3.90–4.04 (1H, m, H-2′), 3.98 (2H, q, ^3J = 7.1 Hz, CH_3CH_2O), 4.28 (1H, m, H-1′), 4.59 (1H, t, $^3J_{\text{to CH}_2\text{OH}}$ = 5.0 Hz, CH_2OH), 4.96 (1H, d, $^3J_{\text{to H-2′}}$ = 4.3 Hz, OH at position 2′), 5.70 (1H, d, ^3J = 12.2 Hz, H-2), 7.60 (1H, d, ^3J = 12.2 Hz, H-3), 10.87 (1H, br s, CONHCSNH), 10.93 (1H, br d, $^3J_{\text{to H-1′}}$ = 7.3 Hz, CONHCSNH). Spin–spin decoupling was performed at δ 3.29 and 4.28.

*(±)-3-Ethoxy-*N*-{N′-[(1β,2α,3α,4β)-2,3-dihydroxy-4-(hydroxymethyl)cyclopentyl]thiocarbamoyl}propenamide (27)*

The procedure for the preparation of compound **27** was the same as that for **25**. To an ice-cold *N*,*N*-dimethylformamide solution (12 mL) of compound **19** (0.55 g, 3.7 mmol) was added 4 mL of the acetonitrile solution of **21** (4 mmol, theoretical) over a period of 5 min. The reaction solution was treated as described for the preparation of **25** and the resulting brown oil was fractionated by column chromatography on silica gel to give **27** (0.503 g, 45% crude) as a yellow oil, R_f 0.34 (3:3:1 (v/v/v) toluene – ethyl acetate – 2-propanol). This oil was used for the preparation of **33** without further purification, although its ^{1}Hmr spectrum showed minor peaks due to impurities; ^{1}Hmr (200 MHz, Me_2SO-d_6) δ: 1.04 (1H, d of t, J_{gem} = 13.0, ^3J = 7.5 Hz, H-5′), 1.26 (3H, t, ^3J = 7.1 Hz, CH_3), 1.92 (1H, m, H-4′), 2.32 (1H, d of t, J_{gem} = 13.0, ^3J = 8.5 Hz, H-5″), 3.26–3.46 (2H, m, CH_2OH), 3.62–3.75 (2H, m, H-2′ and H-3′), 3.98 (2H, q, ^3J = 7.1 Hz, CH_3CH_2O), 4.38 (1H, qu, ^3J = 7.5 Hz, H-1′), 4.54 (1H, d, ^3J = 4.3 Hz, OH), 4.63 (1H, t, $^3J_{\text{to CH}_2\text{OH}}$ = 5.0 Hz, CH_2OH), 4.78 (1H, d, ^3J = 6.0 Hz, OH), 5.71 (1H, d, ^3J = 12.2 Hz, H-2), 7.60 (1H, d, ^3J = 12.2 Hz, H-3), 10.88 (1H, br s, CONHCSNH), 10.97 (1H, br d, $^3J_{\text{to H-1′}}$ = 7.3 Hz, CONHCSNH). Spin–spin decoupling was performed at δ 3.69 and 4.38.

*(±)-1-{(1β,3α,4β)-3-Hydroxy-4-(hydroxymethyl)cyclopentyl}-2,4(1*H*,3*H*)-pyrimidinedione (28)*

A solution containing **22** (0.209 g, 0.77 mmol) in 2 *N* H_2SO_4 (15 mL) was heated at reflux temperature for 0.5 h, cooled in an ice bath, and neutralized with 2 *N* NaOH. The water was evaporated and the residue was extracted with warm ethanol (3 × 10 mL). After the ethanol had been evaporated, the residue was fractionated by column chromatography on silica gel to give **28** (0.166 g, 95%) as a white solid, mp 158–160°C (dec.) (lit. (6) mp 160–163°C (dec.)), R_f 0.43 (9:1 (v/v) acetonitrile–water); ^{1}Hmr (200 MHz, Me_2SO-d_6) δ: 1.36 (1H, m, H-5′), 1.71–2.00 (3H, m, H-2′, H-2″, and H-4′), 2.08 (1H, d of t, J_{gem} = 12.5, ^3J = 7.7 Hz, H-5″), 3.34–3.56 (2H, m, CH_2OH), 3.97 (1H, m, H-3′), 4.63 (1H, t, $^3J_{\text{to CH}_2\text{OH}}$ = 5.1 Hz, CH_2OH), 4.75 (1H, d, $^3J_{\text{to H-3′}}$ = 4.2 Hz, OH at position 3′), 4.95 (1H, m, H-1′), 5.58 (1H, d, $^3J_{5,6}$ = 8.2 Hz, H-5), 7.69 (1H, d, $^3J_{6,5}$ = 8.2 Hz, H-6), 11.21 (1H, br s, H-3). Spin–spin decoupling at δ 1.36 and 4.75.

*(±)-1-{(1β,2α,4β)-2-Hydroxy-4-(hydroxymethyl)cyclopentyl}-2,4(1*H*,3*H*)-pyrimidinedione (29)*

A solution of **23** (0.44 g, 1.61 mmol) in 2 *N* H_2SO_4 (20 mL) was treated as described above for the preparation of **28**. The residue from the ethanol extract was fractionated by column chromatography on silica gel to give **29** (0.275 g, 75%) as a white solid, mp 174–177°C (lit. (6) mp 174–176°C), R_f 0.46 (9:1 (v/v) acetonitrile–water); ^{1}Hmr (200 MHz, Me_2SO-d_6) δ: 1.37 (1H, m, J_{gem} = 11.9, ^3J = 9.0 Hz, H-5′), 1.56 (1H, m, J_{gem} = 13.0, ^3J = 9.1, ^3J = 7.7 Hz, H-3′), 1.76 (1H, m, J_{gem} = 13.0, ^3J = 7.9, ^3J = 5.3 Hz, H-3″), 1.96 (1H, d of t, J_{gem} = 11.9, ^3J = 7.5 Hz, H-5″), 2.16 (1H, m, H-4′), 3.29–3.35 (2H, m, CH_2OH), 4.14 (1H, m, H-2′), 4.45 (1H, d of t, ^3J = 11.4, ^3J = 8.1 Hz, H-1′), 4.60 (1H, t, $^3J_{\text{to CH}_2\text{OH}}$ = 5.1 Hz, CH_2OH), 5.05 (1H, d, $^3J_{\text{to H-2′}}$ = 5.3 Hz, OH at position 2′), 5.59 (1H, d, $^3J_{5,6}$ = 8.2 Hz, H-5), 7.68 (1H, d, $^3J_{6,5}$ = 8.2 Hz, H-6), 11.21 (1H, br s, H-3). Spin–spin decoupling was performed at δ 4.14.

*(±)-1-{(1β,2α,3α,4β)-2,3-Dihydroxy-4-(hydroxymethyl)cyclopentyl}-2,4(1*H*,3*H*)-pyrimidinedione (30)*

A solution of **24** (0.113 g, 0.39 mmol) in 2 *N* H_2SO_4 (10 mL) was treated as described above for the preparation of **28**. The residue from the ethanol extract was fractionated by column chromatography on silica gel to give **30** (0.079 g, 84%), mp 165–173°C (lit. (6) mp 176–179°C), R_f 0.35 (9:1 (v/v) acetonitrile–water); ^{1}Hmr (200 MHz, Me_2SO-d_6) δ: 1.26 (1H, m, H-5′), 1.85–2.08 (2H, m, H-4′ and H-5″), 3.33–3.45 (2H, m, CH_2OH), 3.71 (1H, m, H-3′), 3.97 (1H, m, H-2′), 4.57–4.68 (1H, m, H-1′), 4.60 (1H, d, $^3J_{\text{to H-3′}}$ = 4.1 Hz, OH at position 3′), 4.70 (1H, t, $^3J_{\text{to CH}_2\text{OH}}$ = 5.0 Hz, CH_2OH), 4.89 (1H, d, $^3J_{\text{to H-2′}}$ = 6.4 Hz, OH at position 2′), 5.59 (1H, d, $^3J_{5,6}$ = 7.7 Hz, H-5), 7.69 (1H, d, $^3J_{6,5}$ = 7.7 Hz, H-6), 11.20 (1H, br s, H-3). Spin–spin decoupling was performed at δ 1.26, 3.71, 3.97, and 4.89.

*(±)-2,3-Dihydro-1-{(1β,3α,4β)-3-hydroxy-4-(hydroxymethyl)cyclopentyl}-2-thioxo-4-(1*H*)-pyrimidinone (31)*

A solution of **25** (4.2 g, 14.6 mmol) in 15 *N* aqueous ammonia (125 mL) was heated in a 90°C oil bath for 25 min. The solution was cooled to room temperature and the reaction solvents were evaporated. The residue was evaporated with ethanol (50 mL) and triturated with warm ethanol (50 mL). The mixture was cooled in an ice bath, and the precipitated material was collected by filtration and washed with ethanol to give a light-yellow solid (2.148 g), mp 169–172°C. The volume of the combined filtrate and wash was reduced and an additional amount (0.562 g) of a light-yellow solid was obtained, mp 167–173°C, for a total yield of 2.71 g (77%). An analytical sample was prepared by recrystallization from ethanol to give a faintly yellow solid, mp 174–175°C, R_f 0.46 (1:1:1 (v/v/v) toluene – ethyl acetate – 2-propanol); uv λ_{max} (C_2H_5OH): 219 (ε 17 200), 273 (13 700) nm; λ_{max} (0.01 *N* HCl in C_2H_5OH): 219 (ε 17 200), 273 (13 600) nm; λ_{max} (0.01 *N* NaOH in C_2H_5OH): 240 (ε 19 600), 273 (16 300) nm; ^{1}Hmr (200 MHz, Me_2SO-d_6) δ: 1.32 (1H, d of t, J_{gem} = 12.7, ^3J = 9.5 Hz, H-5′), 1.80–1.99 (3H, m, H-2′, H-2″, and H-4′), 2.20 (1H, d of t, J_{gem} = 12.7, ^3J = 7.8 Hz, H-5″), 3.34–3.56 (2H, m, CH_2OH), 4.01 (1H, m, H-3′), 4.65 (1H, t, $^3J_{\text{to CH}_2\text{OH}}$ = 4.7 Hz, CH_2OH), 4.79 (1H, d, $^3J_{\text{to H-3′}}$ = 3.9 Hz, OH at position 3′), 5.96 (1H, qu, ^3J = 8.8 Hz, H-1′), 5.99 (1H, d, $^3J_{5,6}$ = 8.2 Hz, H-5), 7.85 (1H, d, $^3J_{6,5}$ = 8.2 Hz, H-6), 12.53 (1H, br s, H-3). Spin–spin decoupling was performed at δ 2.20, 4.01, and 4.65. *Anal.* calcd. for $C_{10}H_{14}O_3N_2S$: C 49.57, H 5.82, N 11.56; found: C 50.14, H 6.00, N 11.79.

*(±)-2,3-Dihydro-1-{(1β,2α,4β)-2-hydroxy-4-(hydroxymethyl)cyclopentyl}-2-thioxo-4-(1*H*)-pyrimidinone (32)*

A solution of **26** (3.515 g, 12.2 mmol) in 15 *N* aqueous ammonia (100 mL) was heated in an oil bath at 90°C for 20 min. It was then treated as described for the preparation of **31** to give (in two crops) **32** (2.081 g, 71%) as a white solid, mp 217–220°C, R_f 0.45 (1:1:1 (v/v/v) toluene – ethyl acetate – 2-propanol). An analytical sample was prepared by recrystallization from ethanol, mp 219–220°C; uv λ_{max} (C_2H_5OH): 220 (ε 17 000), 274 (13 400) nm; λ_{max} (0.01 *N* HCl in C_2H_5OH): 220 (ε 16 800), 274 (13 300) nm; λ_{max} (0.01 *N* NaOH in C_2H_5OH): 240 (ε 20 000), 274 (15 700) nm; ^{1}Hmr (200 MHz, Me_2SO-d_6) δ: 1.20 (1H, m, H-5′), 1.59 (1H, d of t, J_{gem} = 13.1, ^3J = 8.4 Hz, H-3′), 1.78 (1H, m, J_{gem} = 13.1, ^3J = 8.1, ^3J = 5.0 Hz, H-3″), 2.04–2.26 (2H, m, H-4′ and H-5″), 3.29–3.35 (2H, m, CH_2OH), 4.22 (1H, m, H-2′), 4.64 (1H, t, $^3J_{\text{to CH}_2\text{OH}}$ = 5.2 Hz, CH_2OH), 5.11 (1H, d, $^3J_{\text{to H-2′}}$ = 5.0 Hz, OH at position 2′), 5.55 (1H, d of t, ^3J = 10.9, ^3J = 7.9 Hz, H-1′), 6.00 (1H, d, $^3J_{5,6}$ = 8.0 Hz, H-5), 7.85 (1H, d, $^3J_{6,5}$ = 8.0 Hz, H-6), 12.58 (1H, br s, H-3). Spin–spin decoupling was performed at δ 1.20 and 4.22. *Anal.* calcd. for $C_{10}H_{14}O_3N_2S$: C 49.57, H 5.82, N 11.56, S 13.23; found: C 50.09, H 5.98, N 11.88, S 13.26.

*(±)-2,3-Dihydro-1-{(1β,2α,3α,4β)-2,3-dihydroxy-4-(hydroxymethyl)cyclopentyl}-2-thioxo-4-(1*H*)-pyrimidinone (33)*

A solution of **27** (0.487 g, 1.60 mmol) in 15 *N* aqueous ammonia (25 mL) was heated in an oil bath at 100°C for 20 min. The reaction solvents were evaporated and the residue was fractionated by column chromatography on silica gel to give a while solid (0.263 g, 64%), R_f 0.53 (9:1 (v/v) acetonitrile–water). An analytical sample was prepared by recrystallization from methanol–ethanol to give a crystalline solid, mp 196–198°C; uv λ_{max} (C_2H_5OH): 220 (ε 16 900), 274 (13 100) nm; λ_{max} (0.01 *N* HCl in C_2H_5OH): 220 (ε 17 100), 274 (13 000) nm; λ_{max} (0.01 *N* NaOH in C_2H_5OH): 240 (ε 19 900), 273 (15 500) nm; ^{1}Hmr (200 MHz, Me_2SO-d_6) δ: 1.08 (1H, m, J_{gem} = 12.2, $^3J_{5',4'}$ = 7.7 Hz,

H-5′), 1.95 (1H, m, H-4′), 2.18 (1H, d of t, J_{gem} = 12.2, ^3J = 8.5 Hz, H-5″), 3.33–3.47 (2H, m, CH_2OH), 3.73 (1H, m, H-3′), 4.05 (1H, m, $^3J_{2',1'}$ = 9.6, $^3J_{\text{to OH at 2'}}$ = 6.5, $^3J_{2',3'}$ = 5.8 Hz, H-2′), 4.67 (1H, d, $^3J_{\text{to H-3'}}$ = 3.5 Hz, OH at position 3′), 4.73 (1H, t, $^3J_{\text{to C}H_2\text{OH}}$ = 5.0 Hz, CH_2OH), 4.94 (1H, d, $^3J_{\text{to H-2'}}$ = 6.5 Hz, OH at position 2′), 5.67 (1H, q, ^3J = 9.6 Hz, H-1′), 6.01 (1H, d, $^3J_{5,6}$ = 8.0 Hz, H-5), 7.87 (1H, d, $^3J_{6,5}$ = 8.0 Hz, H-6), 12.6 (1H, br s, H-3). Spin–spin decoupling was performed at δ 1.08, 3.4, 3.73, and 4.05. *Anal.* calcd. for $C_{10}H_{14}O_4N_2S$: C 46.50, H 5.46, N 10.85, S 12.41; found: C 46.62, H 5.54, N 10.84, S 12.18.

Acknowledgement

The authors are grateful to the Natural Sciences and Engineering Research Council of Canada for its support of this work in the form of a grant (to W.A.S.).

1. Y. F. SHEALY and C. A. O'DELL. J. Pharm. Sci. **68**, 668 (1979).
2. Y. F. SHEALY and C. A. O'DELL. J. Heterocycl. Chem. **17**, 353 (1980).
3. Y. F. SHEALY, C. A. O'DELL, and M. C. THORPE. J. Heterocycl. Chem. **18**, 383 (1981).
4. Y. F. SHEALY, J. L. FRYE, N. F. DUBOIS, S. C. SHADDIX, and R. W. BROCKMAN. J. Med. Chem. **24**, 1083 (1981).
5. Y. F. SHEALY, C. A. O'DELL, W. M. SHANNON, and G. ARNETT. J. Med. Chem. **26**, 156 (1983), and references therein.
6. Y. F. SHEALY and C. A. O'DELL. J. Heterocycl. Chem. **13**, 1015 (1976).
7. L. J. J. HRONOWSKI and W. A. SZAREK. Can. J. Chem. **63**, 2787 (1985).
8. L. J. J. HRONOWSKI. Ph.D. Thesis, Queen's University, Kingston, Ont. 1984.
9. F. WATJEN, O. BUCHARDT, and E. LANGVAD. J. Med. Chem. **25**, 956 (1982), and references therein.
10. L. DENCKER, B. LARSSON, K. OLANDER, and S. ULLBERG. Br. J. Cancer, **45**, 95 (1982).
11. C. A. O'DELL and Y. F. SHEALY. *In* Nucleic acid chemistry. Part I. *Edited by* L. B. Townsend and R. S. Tipson. John Wiley and Sons, Inc., New York. 1978. pp. 161–167.
12. Y. F. SHEALY and C. A. O'DELL. Tetrahedron Lett. 2231 (1969).
13. Y. F. SHEALY and J. D. CLAYTON. J. Am. Chem. Soc. **91**, 3075 (1969).
14. G. SHAW and R. N. WARRENER. J. Chem. Soc. 157 (1958).
15. G. SHAW and R. N. WARRENER. J. Chem. Soc. 153 (1958).
16. IUPAC–IUB. Revised tentative rules for nomenclature of steroids. J. Org. Chem. **34**, 1517 (1969).
17. S. F. BIRCH, W. J. OLDHAM, and E. A. JOHNSON. J. Chem. Soc. 818 (1947).
18. R. U. LEMIEUX and D. R. LINEBACK. Ann. Rev. Biochem. **32**, 155 (1963).
19. H. P. M. FROMAGEOT, B. E. GRIFFIN, C. B. REESE, J. E. SULSTON, and D. R. TRENTHAM. Tetrahedron, **22**, 705 (1966).
20. K. N. FANG, N. S. KONDO, P. S. MILLER, and P. O. P. Ts'O. J. Am. Chem. Soc. **93**, 6647 (1971), and references therein.
21. D. J. WOOD, F. E. HRUSKA, and K. K. OGILVIE. Can. J. Chem. **52**, 3353 (1974).
22. Y. F. SHEALY and J. D. CLAYTON. J. Am. Chem. Soc. **88**, 3885 (1966).
23. R. VINCE and S. DALUGE. J. Org. Chem. **45**, 531 (1980).
24. R. C. CERMAK and R. VINCE. Tetrahedron Lett. **22**, 2331 (1981).
25. B. L. KAM and N. J. OPPENHEIMER. J. Org. Chem. **46**, 3268 (1981).
26. A. HOLY. Collect. Czech. Chem. Commun. **41**, 647 (1976).
27. A. K. SAKSENA. Tetrahedron Lett. **21**, 133 (1980).
28. M. SANO. Chem. Pharm. Bull. **10**, 320 (1962).
29. L. J. J. HRONOWSKI and W. A. SZAREK. J. Med. Chem. **25**, 522 (1982).
30. G. ZWEIFEL, K. NAGASE, and H. C. BROWN. J. Am. Chem. Soc. **84**, 183 (1962).
31. A. VOGEL. Vogel's textbook of practical organic chemistry. 4th ed. *Revised by* B. S. Furniss, A. J. Hannaford, V. Rogers, P. W. G. Smith, and A. R. Tatchell. Longman, London and New York. 1978. p. 291.

The influence of the changing of P=O to P=S and P—O—R to P—S—R on the reactivity of phosphinate esters under alkaline hydrolysis conditions

ROBERT D. COOK,[1] SELIM FARAH,[2] LABIB GHAWI,[2] ADNAN ITANI,[2] AND JUBRAIL RAHIL[2]

Department of Chemistry, American University of Beirut, Beirut, Lebanon, and Department of Chemistry, Erindale College, University of Toronto, Mississauga, Ont., Canada L5L 1C6

Received February 14, 1986

ROBERT D. COOK, SELIM FARAH, LABIB GHAWI, ADNAN ITANI, and JUBRAIL RAHIL. Can. J. Chem. **64**, 1630 (1986).

Alkyl dialkylphosphinates, thionates, thioates, and dithioates have been studied under alkaline hydrolysis conditions in 60% DME – H_2O and pure H_2O. Substitution of S for O in the phosphoryl group has only a small rate retarding effect, typically less than a factor of 10. The effect of the similar replacement in the leaving group, however, can lead to rate increases greater than a factor of 100. Activation parameters were determined and the ΔS^* values range from −19 to −49 eu for the bimolecular reactions. The more negative values are for the esters with higher sulfur content and/or sterically large substituents. The results are discussed in terms of a pathway involving a pentacoordinate intermediate.

ROBERT D. COOK, SELIM FARAH, LABIB GHAWI, ADNAN ITANI et JUBRAIL RAHIL. Can. J. Chem. **64**, 1630 (1986).

Opérant dans un mélange à 60% de DME/eau ainsi que dans de l'eau pure, on a étudié les dialkylphosphinates, les thionates, les thioates et les dithioates d'alkyles dans des conditions d'hydrolyse alcaline. La substitution du S par un O dans le groupement phosphoryle provoque un faible ralentissement de la vitesse de la réaction et le rapport des deux vitesses est plus petit que 10. Toutefois, si l'on effectue un remplacement semblable dans le groupement nucléofuge, la vitesse de la réaction est augmentée par un facteur de plus de 100. On a déterminé les paramètres d'activation et, pour les réactions bimoléculaires, les valeurs des ΔS^* varient de −19 à −49 ue. Les valeurs les plus négatives sont liées aux esters comportant le plus grand nombre d'atomes de soufre et/ou les substituants les plus encombrants d'un point de vue stérique. On discute des résultats en fonction d'une voie réactionnelle impliquant un intermédiaire pentacoordonné.

[Traduit par la revue]

Introduction

The alkaline hydrolysis reactions of phosphorus esters, especially those of phosphates (1), have been extensively investigated. The reactions of phosphonates (1) and phosphinates (1, 2) have also been the subject of several reports. There have been, however, only a few reports on the effect of the replacement of oxygen by sulfur on the reactivity of these esters. There is interest in the reactivity of phosphorothioates because of their use as phosphate analogues in stereochemical studies of phosphoryl transfer reactions (3).

Ketelaar, Gersmann, and Koopmans have reported that a series of *p*-nitrophenyl phosphorothioates (P=S) hydrolyze 30 to 160 times slower in base solution than the corresponding phosphates (4). Breslow and Katz have shown that in the aqueous hydrolysis of the mono *p*-nitrophenyl ester of the phosphate dianion, the P=O esters reacts 60 times slower than the P=S (5). However in the enzymatic hydrolysis catalyzed by alkaline phosphatase the opposite is true with a reactivity ratio (P=O/P=S) of approximately 100. The authors suggested that a P=O/P=S ratio greater than 1 is an indication of an associative mechanism, while values less than 1 suggest a dissociative pathway (5). Chlebowski and Coleman have also reported a large rate difference in favor of the P=O ester in the Zn(II) alkaline phosphatase catalyzed hydrolysis of a phosphate monoester (6). Benkovic and Schray have, however, suggested that the use of the P=O/P=S reactivity ratio as a basis for the choice of reaction pathway may be misleading (7).

Little has been published on the hydrolysis of phosphinothionates. In one report (8), the authors find that, for $(ClCH_2)_2P(X)OC_2H_5$, the P=O/P=S ratio is 4 while, for $(C_2H_5)_2P(X)OC_2H_5$, the ratio is 0.70 for the reaction in base.

In order to understand more the effect of sulfur on the reactivity of phosphorus esters a series of phosphinate esters **1**–**4** was synthesized and studied under alkaline hydrolysis conditions. In these esters not only is the effect of sulfur in the P=X group studied but also in the leaving group.

Phosphinates, in general, hydrolyze via an associative pathway (2) and there is strong evidence that the reaction precedes via a pentacoordinate intermediate (reaction [1]).

[1] $R_2P(O)OR' + {}^-OH \underset{k_{-1}}{\overset{k_1}{\rightleftharpoons}}$ 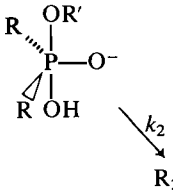 $\xrightarrow{k_2} R_2PO_2^- + R'OH$

Support for such an intermediate is plentiful in cyclic phosphorus esters (9) and there are also two reports supporting their existence in acyclic systems, one in a phosphonate (10) and one in a phosphinate (11). The results of this study will be analyzed in terms of a pathway involving an intermediate (reaction [1]).

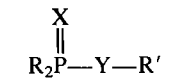

1 X = Y = O
2 X = S; Y = O
3 X = O; Y = S
4 X = Y = S

a, R = R′ = CH_3
b, R = C_2H_5; R′ = CH_3
c, R = *n*-C_3H_7; R′ = CH_3
d, R = *i*C_3H_7; R′ = CH_3
e, R = *i*C_4H_9; R′ = CH_3
f, R = *s*-C_4H_9; R′ = CH_3
g, R = R′ = C_2H_5
h, R = C_2H_5; R′ = *n*-C_3H_7
i, R = C_2H_5; R′ = *i*C_3H_7
j, R = C_2H_5; R′ = *i*C_4H_9
k, R = C_2H_5; R′ = *s*-C_4H_9

Results

The second-order rate constants for the alkaline hydrolysis of the alkyl dialkylphosphinates (**1**), phosphinothionates (**2**),

[1]Address for the academic years of 1984–1986 at the University of Toronto; present address: Bishop's University, Lennoxville, P.Q., Canada J1M 1Z7.

[2]Taken in part from the M.S. Theses of S.F., L.G., A.I., and J.R., American University of Beirut, Lebanon.

TABLE 1. Rate constants[a] for the alkaline hydrolysis of alkyl dialkylphosphinates in H_2O and 60% DME – H_2O

Compound	T (°C)	$k_2 \times 10^4\ M^{-1}\ s^{-1}$	
		H_2O[b]	60% DME – H_2O[b]
1*a*	30	—	340[c]
	40	115	—
	50	261	1108[c]
	60	511	—
1*b*	75	104	109[c]
1*c*	75	—	9.87
1*e*	75	4.16	—
1*f*	75	0.13	—
1*g*	75	11.8	14.7[c]
1*h*	75	7.94	8.82
1*i*	75	0.72	0.69[c]
1*j*	75	4.57	4.66
1*k*	75	0.30	—

[a]Average of two to three kinetic runs.
[b]Ionic strength kept at 0.1 *M* using $NaClO_4$.
[c]Reference 2*a*.

TABLE 2. Rate constants[a] for the alkaline hydrolysis of alkyl dialkylphosphinothionates in H_2O and 60% DME – H_2O

Compound	T (°C)	$k_2 \times 10^4\ M^{-1}\ s^{-1}$	
		H_2O[b]	60% DME – H_2O[b]
2*a*	30	487	331
	40	964	494
	50	1670	1010
2*b*	30	—	2.85
	50	—	12.4
	75	183	61.6
2*c*	30	—	1.17
	50	—	4.30
	62.5	—	9.88
	75	—	22.1
2*g*	75	32.5	—

[a]Average of two to three kinetic determinations.
[b]Ionic strength kept at 0.1 *M* using $NaClO_4$.

phosphinothioates (**3**), and phosphinodithioates (**4**) are given in Tables 1–4, respectively.

The activation parameters for selected esters are given in Table 5.

Discussion

General trends

(a) Influence of substituents on phosphorus

The alkyl substituents on phosphorus have a large effect on the reaction rate, especially in the esters with alkoxy leaving groups. Table 6 gives the relative rate data for the four ester systems, and for the sake of comparison, the results in a carboxylic ester series (12). Attempts to correlate the results in series 1 and 5 of Table 6 with the Taft polar equation (13) (eq. [2]), the Taft steric equation (eq. [3]), and the combined equation (eq. [4]) were not successful. Although phosphinates

$$[2] \quad \log k_R/k_{CH_3} = \sigma^*\rho^*$$

$$[3] \quad \log k_R/k_{CH_3} = \delta E_s$$

$$[4] \quad \log k_R/k_{CH_3} = \sigma^*\rho^* + \delta E_s$$

TABLE 3. Rate constants[a] for the alkaline hydrolysis of alkyl dialkylphosphinothioates in H_2O and 60% DME – H_2O

Compound	T (°C)	$k_2 \times 10^4\ M^{-1}\ s^{-1}$	
		H_2O[b]	60% DME – H_2O[b]
3*a*	0	10.6	—
	30	35.2	84.2
3*b*	30	16.7	29.5
	40	24.3	33.5
	50	39.3	57.4
3*c*	30	4.05	7.96
	50	6.94	11.4
3*d*	65	0.58	—
	85	2.65	—
	95	6.22	—
3*f*	65	0.39	—
	75	1.63	—
	85	2.08	—
3*g*	30	8.28	11.5
	40	11.1	27.8
	50	18.2	60.4
3*h*	30	5.0	11.9
	50	18.4	75.5
3*j*	50	6.22	12.2

[a]Average of two to three kinetic determinations.
[b]Ionic strength kept at 0.1 *M* using $NaClO_4$.

usually undergo hydrolysis by attack of ^-OH at phosphorus with subsequent P—O bond (2*a*) cleavage, Haake and Rahil (2*b*) have recently reported that the sterically hindered phosphinate, methyl diisopropylphosphinate, hydrolyzes with approximately 25% C—O bond cleavage. It is not surprising then that, with this mixed cleavage pattern for some esters, there is no correlation with the Taft equation when applied to the effect of substituents on phosphorus.

Alkyl substituents have a greater effect on phosphinate hydrolysis than on carboxylic ester hydrolysis in keeping with a tetrahedral phosphorus ground state going to a pentacoordinate intermediate rather than trigonal carbon going to a tetrahedral intermediate.

(b) Influence of the leaving groups

This topic can be discussed in two parts: (*i*) the influence of the atom Y (O or S) on the reaction rate and (*ii*) the influence of the alkyl group R′ on the reaction rate. Table 7 gives sample data for several compounds and indicates the general trend in which the SR′ esters are more reactive than the OR′ esters. This reactivity order is found in other phosphorus ester systems and reflects the lower basicity of the $^-SR'$ groups (14). It is, however, clear from the data that the difference in rate is larger in the less reactive more sterically hindered esters.

The effect of R′ on the reaction rate is shown in the relative rate data in Table 8. The nature of R′ has a much greater influence on the less reactive OR′ esters than on the SR′ esters. Also the structure of the leaving group appears to be much more important in phosphorus (OR′) ester hydrolysis (15) than in carboxylic ester hydrolysis (16) (Table 8). For series 1 and 3 there is an excellent correlation with Taft's σ* values (eq. [2]). For series 1 $\rho^* = 14.1$ ($r = 0.998$) and for series 3 $\rho^* = 3.0$ ($r = 0.994$). Haake and co-workers (2*a*) have previously obtained a $\rho^* = 8$ and $\delta = 1.5$ for three esters of the series $(C_2H_5)_2P(O)OR'$ and $\rho^* = 11$ and $\delta = 0.6$ for seven esters in the series $(C_6H_5)_2P(O)OR'$ using the Taft combined equation

TABLE 4. Rate constants[a] for the alkaline hydrolysis of alkyl dialkylphosphinodithioates at 60% DME – H_2O[b]

Compound	T °C	$k_2 \times 10^3\ M^{-1}\ s^{-1}$	Compound	T °C	$k_2 \times 10^3\ M^{-1}\ s^{-1}$
4*a*	0	13.7	**4***g*	30	0.66
	30	49.9		50	2.43
				62.5	8.56
4*b*	30	3.79	**4***h*	50	2.05
	40	6.22			
	50	11.1			
4*c*	30	2.55	**4***j*	50	1.89
	50	8.08		62.5	3.75
	75	26.6		75	7.62
4*d*	50	13.6	**4***k*	40	0.58
	62.5	24.0		50	1.11
	75	50.8		62.5	2.55

[a]Average of two to three kinetic determinations.
[b]Ionic strength kept at 0.1 M using $NaClO_4$.

TABLE 5. Activation parameters for the alkaline hydrolysis of selected phosphinate esters at 50°C

Compound	Solvent[a]	ΔG^* kcal/mol	ΔH^* kcal/mol	ΔS^* eu
1*a*	W	21.3	15.1	−19
	D[b]	20.3	11.5	−27
2*a*	W	20.1	11.0	−28
	D	20.4	11.6	−27
3*a*	W[c]	21.1	6.0	−49
4*a*	D[c]	20.9	6.7	−47
1*b*	D[b]	22.7	12.3	−32
2*b*	D	23.3	13.7	−30
3*b*	W	21.2	7.7	−41
	D	20.8	6.5	−44
4*b*	D	21.8	9.8	−37
2*c*	D	24.0	14.2	−30
4*c*	D	22.1	10.3	−38
1*g*	D[b]	24.3	14.3	−31
3*g*	W	21.5	7.0	−45
4*g*	D	22.8	11.3	−36
1*i*	D	26.1	12.5	−42
4*j*	D	23.0	11.6	−36
4*k*	D	23.3	13.1	−32

[a]D = 60% DME – H_2O, W = H_2O.
[b]T = 75°C; ref. 2*a*.
[c]T = 30°C.

(eq. [4]). The use of the Taft equation for alkyl substituents only has been recently criticized (17), however these excellent correlations for quite large rate differences especially in the case of series 1 would appear to be significant. It has previously been suggested that the large values of ρ* are due to the changing polarization of the oxygen from slightly positive in starting ester (**5**) to an oxygen which is negative in the transition state of the

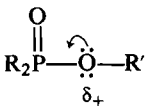

5

reaction (2*a*). A similar analysis of the results of Jones and Thomas (series 4 in Table 8) using the Taft equation (eq. [3]) gives a rather poor correlation with a ρ* value of 7.1 (r = 0.966). For carboxylic esters formation of the tetrahedral intermediate has been proposed as the rate-determining step in alkaline hydrolysis (18). The higher value of ρ* for alkyl diethylphosphinates supports a reaction in which there is a greater charge density on the oxygen of the leaving group in the rate-determining step than there is in the reaction of carboxylic esters.

The value of ρ* for the series with SR′ leaving groups is almost the same as that obtained by Kreevoy and co-workers (19) for the ionization of aliphatic thiols (ρ* = 3.5). The significance of this is discussed later.

(c) Influence of the atom doubly bonded to phosphorus

Table 9 gives a number of comparisons for the effect of the change in atom in P=X on the rate of hydrolysis of the phosphinates. Also given in Table 9 are selected literature values for other reactions of phosphorus and carboxylic esters. The general trend is that P=O compounds are more reactive than P=S compounds although there are some exceptions. This difference in reactivity has been attributed to differences in polarizability and solvation in the two systems (20).

In the case of the alkaline hydrolysis of a carboxylic ester and thionester, Campbell and Lapinskas (21) have suggested that a $k_{C=O}/k_{C=S} > 1$ supports rate-determining formation of a tetrahedral intermediate while a ratio less than 1, found for an aminolysis reaction, supports a rate-determining collapse of the intermediate. There are no similar trends in the hydrolysis reactions of phosphorus esters as reported in Table 9; it appears that the ratio is substituent, solvent, leaving group and nucleophile dependent. The only trend which is suggested by the results is that the effect of X in P=X appears to be greater when the nucleophile is neutral. The reactivity ratio P=O/P=S is also greater in the less reactive phosphate systems mentioned in the Introduction (4–6).

(d) Solvent effects

The hydrolysis reactions were carried out in two solvents only (60% DME – H_2O and H_2O). For P=O esters, regardless of the leaving group, the rates were slightly faster in the mixed solvent system (compound **1***i* is the only exception). If the transition state is considered as a large monoanion with its charge highly dispersed then the net change in solvation can be thought of as a highly solvated hydroxide going to a less solvated transition state, and it is, therefore, reasonable that the reaction rate would decrease in water. However, for the two P=S esters (**2***a* and **2***b*) studied in both solvents the opposite solvent effect is observed. Unfortunately the limited solubility of the P=S

TABLE 6. Relative rate data for the alkaline hydrolysis of phosphinates esters; influence of the alkyl substituents on phosphorus

Series	Ester	Relative rate data for R = CH_3	C_2H_5	n-C_3H_7	i-C_3H_7	i-C_4H_9	s-C_4H_9
1	$R_2P(O)OCH_3$[a]	10760	808	—	—	31.3	1
2	$R_2P(O)OCH_3$[b]	515	11	1	—	—	—
3	$R_2P(S)OCH_3$[c]	235	2.9	1	—	—	—
4	$R_2P(O)SCH_3$[d]	10.6	3.7	1	—	—	—
5	$R_2P(O)SCH_3$[e]	550	310	55	1.4	—	1
6	$R_2P(S)SCH_3$[f]	13	1.4	1	—	1.7	—
7	$RC(O)OC_2H_5$[g]	21	10	4	2.5	1	—

[a]This work; T = 75°C in H_2O.
[b]This work and ref. 2; T = 75°C in 60% DME – H_2O.
[c]This work; T = 50°C in 60% DME – H_2O.
[d]This work; T = 30°C in 60% DME – H_2O.
[e]This work; T = 50°C in H_2O.
[f]This work; T = 50°C in 60% DME – H_2O.
[g]Reference 12; T = 24.8°C in 70% acetone – H_2O.

TABLE 7. Relative rate data for the alkaline hydrolysis of phosphinate esters; influence of the heteroatom in the leaving group

Ester	Solvent[a]	T °C	k_S/k_O
$(CH_3)_2P(O)YCH_3$	D	30	1.03
$(C_2H_5)_2(O)YCH_3$	D	50	22[b]
$(C_2H_5)_2P(O)YC_2H_5$	W	75	77[c]
$(s$-$C_4H_9)_2P(O)YCH_3$	W	75	126
$(CH_3)_2P(S)YCH_3$	D	30	1.5
$(C_2H_5)_2P(S)YCH_3$	D	30	13.3
$(C_3H_7)_2P(S)YCH_3$	D	30	22

[a]D = 60% DME – H_2O; W = H_2O.
[b]Rate for $(C_2H_5)_2P(O)OCH_3$ from ref. 2*a*.
[c]Rate for $(C_2H_5)_2P(O)YC_2H_5$ extrapolated to 75°C.

esters in water prevented determining whether or not this is a general reversal of behavior. It is known that the P=S bond is considerably less solvated than the P=O bond (11, 14, 22) and this difference could account for the observed change but more esters should be studied as well as rates measured in a wider range of solvents.

(e) Activation parameters

The most obvious trends in the data of Table 5 are the lower ΔH^* for the P—S—R′ esters and the more negative ΔS^* for the esters with larger alkyl groups as well as for the esters with higher sulfur content. The lower ΔH^* can be attributed to the weak P—S bond (23) leading to an earlier transition state, while the change in ΔS^* can best be explained by the differences in solvation of the starting neutral S and O esters, which should be greater than the differences for the monocharged transition states. In the case of the esters with large alkyl groups, steric inhibition of solvation of the ester may be important. Such inhibition has been observed for these esters during the process of protonation (24).

Mechanistic considerations

There is clear evidence for pentacovalent intermediates in the alkaline hydrolysis of cyclic phosphorus esters (9, 25) as well as in the acid-catalyzed hydrolysis of an acyclic phosphinothionate (11). The strongest kinetic evidence for intermediate formation in the alkaline hydrolysis of acyclic phosphinates comes from linear free energy data on the hydrolysis of aryl phosphinates where, with one exception, the rate constants correlate with Hammett's σ values and not with the σ^- values of the substituents (26). These results suggest that there is no charge generation on the leaving group in the rate-determining step and therefore formation of the intermediate is suggested as the slow step. Formation of the intermediate should be rate-determining with any leaving group which is less basic than ^-OH (e.g., $^-SR'$ or ^-OAr) while breakdown of the intermediate will be rate-determining for $^-OR'$ leaving groups. The ρ* values obtained in this work for the OR′ and SR′ leaving groups are consistent with this hypothesis.

The closeness of the ρ* value for RSH ionization where some negative charge must exist on sulfur and the ρ* value of $R_2P(O)SR'$ esters appears to be an anomaly. It might be better to compare the latter value with that obtained for the hydrolysis of acetates (ρ* = 7.1) (16) where formation of the intermediate is also suggested as the rate-determining step (18). The ratio of the insulating effects of the S and O atoms has been calculated from ^{13}C—H coupling constants (Z_S/Z_O = 0.90) (27) and therefore the value of ρ* for the SR′ esters is even smaller than that which would be predicted from the hydrolysis of carboxylic esters.

The relative rate data of Table 6 also supports these conclusions in as much as the steric effects of the groups attached to phosphorus would be expected to be larger in the reaction where the intermediate is already fully formed before the transition state is reached (OR′ esters). These steric effect arguments can also account for the increasing $k_{POR'}/k_{PSR'}$ ratio with increasing size of the substituents on phosphorus (Table 7).

Conclusions

The general trend observed for phosphorus esters which hydrolyse via an associative pathway is that the P=O esters are more reactive than the P=S esters and, the more reactive the systems, the less the difference in reactivity. The greatest effect of this substitution should be observed in phosphate reactions with neutral nucleophiles and the least effect in phosphinate reactions with nucleophiles like ^-OH.

The results obtained for the effect of changing the leaving group are in line with most other observations on phosphorus esters where the basicity of the leaving group has a considerable influence on the reactivity of the ester.

Solvation appears to play an important role and more work in this area is certainly needed.

TABLE 8. Relative rate data for the alkaline hydrolysis of phosphinate esters; influence of the alkyl group in the leaving group

Series	Ester	Relative rate for R = CH_3	C_2H_5	n-C_3H_7	i-C_3H_7	i-C_4H_9	s-C_4H_9
1	$(C_2H_5)_2P(O)OR$[a]	342	39	26	2.4	15	1
2	$(C_2H_5)_2P(O)SR$[b]	9	3	3	—	1	—
3	$(C_2H_5)_2P(S)SR$[c]	10	2.2	1.9	—	1.7	1
4	$CH_3C(O)OR$[d]	33	14.3	8.3	2.2	5.5	1
5	$CH_3P(O)(OR)_2$[e]	600	40	—	1	—	—

[a]This work; T = 75°C in H_2O.
[b]This work; T = 50°C in H_2O.
[c]This work; T = 50°C in 60% DME – H_2O.
[d]Reference 16; T = 24.7°C in 70% acetone – H_2O.
[e]Reference 15; T = 80°C in H_2O.

TABLE 9. Influence on the atom doubly bonded to phosphorus on the rate of nucleophilic attack on phosphorus

Compound	Nucleophile	k[P=O]/k[P=S]
$(CH_3)_2P(X)OCH_3$	HO^-[a]	1.1
$(CH_3)_2P(X)SCH_3$	HO^-[b]	1.7
$(C_2H_5)_2P(X)OCH_3$	HO^-[c]	0.6
	HO^-[d]	1.8
$(C_2H_5)_2P(X)SCH_3$	HO^-[b]	8.3
$(C_2H_5)_2P(X)OC_2H_5$	HO^-[c]	0.4
$(C_6H_5)_2P(X)OC_6H_4CH_3$-$p$	HO^-[e]	33
$(ClCH_2)_2P(X)SC_2H_5$	HO^-[f]	25
$(ClCH_2)_2P(X)OC_2H_5$	HO^-[f]	4
$(C_6H_5)_2P(X)OC_6H_4NO_2$-$p$	$H_2NC_4H_9$[g]	25
$(C_2H_5O)_2P(X)OC_6H_4NO_2$-$p$	HO^-[h]	9.1
	H_2O[i]	56
$(C_2H_5O)_3P(X)$	HO^-[j]	6.6
$C_6H_5C(X)OC_6H_4NO_2$-p	HO^-[k]	8.3
	$H_2NC_2H_5$[k]	0.39

[a]This work; T = 50°C in 60% DME – H_2O.
[b]This work; T = 30°C in 60% DME – H_2O.
[c]This work; T = 75°C in H_2O.
[d]This work; T = 75°C in 60% DME – H_2O.
[e]Reference 39; T = 50°C in 50% EtOH – H_2O.
[f]References 8, 40; T = 25°C in H_2O.
[g]Reference 41; T = 30°C in CH_3CN.
[h]Reference 42; T = 25°C in H_2O.
[i]Reference 43; T = 37°C in pH = 7.4 in 0.067 M phosphate buffer.
[j]Reference 44; T = 25°C in H_2O.
[k]Reference 21; T = 25°C in 20% CH_3CH – H_2O.

All of the results are consistent with a reaction pathway involving an intermediate.

Experimental

Synthesis of the esters (for general synthesis, see ref. 28)

The esters were synthesized by known methods or variations of known methods as mentioned below:

Method 1: (for **1***a–c* and **1***g–k*)

[5] $3RMgX + P(S)Cl_3 \rightarrow R_2P(S)P(S)R_2$ (29)

Thiophosphoryl chloride in ether was added dropwise over a period of 4–5 h to an ether solution of the appropriate Grignard reagent at 0°C. The final mixture was poured carefully into an ice-cold 10% sulfuric acid solution. The product was extracted with ether.

[6] $R_2P(S)P(S)R_2 + 3SO_2Cl_2 \rightarrow R_2P(O)Cl + SOCl_2$ (30)

The sulfuryl chloride in benzene was added dropwise to a benzene solution of the biphosphine disulfide at room temperature. The solvent and $SOCl_2$ were distilled at atmospheric pressure and the acid chloride was distilled under diminished pressure.

[7] $R_2P(O)Cl + R'ONa \rightarrow R_2P(O)OR'$ (31)

A benzene solution of the acid chloride was added to a solution of alkoxide in its corresponding alcohol. The reaction mixture was initially filtered (-NaCl), then distilled at atmospheric pressure to remove solvents and finally the ester was vacuum distilled.

Method 2: (for **2***a–c* and **2***g–k*)

[8] $R_2P(S)P(S)R_2 + SO_2Cl_2 \rightarrow R_2P(S)Cl$ (32)

The procedure used was identical to reaction [6] except in this case with equimolar amounts of the reagents.

[9] $R_2P(S)Cl + R'ONa \rightarrow R_2P(S)OR'$ (31)

The procedure was identical to that of reaction [7].

Method 3: (for **2***a–c*, **3***g*, **3***h*, and **3***j*)

[10] $R_2P(S)Cl + 2NaOH \rightarrow R_2P(O)SNa$ (33)

An aqueous solution of sodium hydroxide was added to the acid chloride. The resulting mixture was evaporated to dryness giving a salt which is a mixture of the product and NaCl.

[11] $R_2P(O)SNa + R'X \rightarrow R_2P(O)SR'$ (34)

The above salt was refluxed with excess alkyl halide in acetonitrile. The solvent was partially evaporated and then the mixture was filtered. The resulting solution was fractionally distilled.

Method 4: (for **4***a–c*, **4***g*, **4***h*, and **4***j*)

[12] $R_2P(S)Cl + 2NaSH \rightarrow R_2P(S)SNa$ (35)

The acid chloride was added to a methanol solution of NaSH. The solution was evaporated to dryness giving the product and NaCl.

[13] $R_2P(S)SNa + R'X \rightarrow R_2P(S)SR'$ (34)

The procedure was identical to that of reaction [11].

Method 5: (for **1***d–f*, **2***d–f*, **3***d–f*, and **4***d–f*)

[14] $PCl_3 + 2RMgX \rightarrow R_2PCl$ (36)

An ether solution of the Grignard was added dropwise with vigorous stirring to an ether solution of PCl_3 at −40°C and under an inert atmosphere. The product was filtered and transferred to a distilling flask; the solution was then vacuum distilled.

[15] $R_2PCl + O_2 \rightarrow R_2P(O)Cl$

Oxygen was bubbled into a benzene solution of the phosphine. The reaction isotherm was moderated by a 10 volume excess of benzene. The acid chloride was vacuum distilled.

[16] $R_2PCl + S \rightarrow R_2P(S)Cl$

Table 10. Spectral data and physical constants for the phosphinate esters

Compound	Nuclear magnetic resonance spectral data (δ)[a]						ir (cm^{-1})[b]	B.P. °C/Torr		Reference
	HCP	*H*CCP	*H*CCCP	PYC*H*	PYCC*H*	PYCCC*H*	P=X	Observed	Literature	
1*a*	1.8(d) J = 13 Hz	—	—	3.70(d) J = 14 Hz	—	—	1210	78–79/12	66–67/10	47
1*b*	0.8–1.9(m)	0.8–1.9(m)	—	3.74(d) J = 14 Hz	—	—	1208	78/10	86–86.2/12	48
1*c*	0.8–1.8(m)	0.8–1.8(m)	0.8–1.8(m)	3.50(d) J = 14 Hz	—	—	1210	88–89/0.5	—	—
1*e*	1.0–1.8(m)	1.0–1.8(m)	1.0–1.1(d)	3.70(d) J = 14 Hz	—	—	1200	88–89/1.0	—	—
1*f*	1.0–1.8(m)	1.0–1.8(m)	1.0–1.8(m)	3.70(d) J = 14 Hz	—	—	1208	88–90/1.2	—	—
1*g*	0.8–2.0(m)	0.8–2.0(m)	—	4.03(m)	0.8–2.0(m)	—	1210	99–100/2.5	88–88.5/10	49
1*h*	0.8–2.0(m)	0.8–2.0(m)	—	3.80(m)	0.8–2.0(m)	0.8–2.0(m)	1205	82–84/0.5	103.4/13	48
1*i*	0.6–2.1(m)	0.6–2.1(m)	—	4.65(m)	0.6–2.1(m)	—	1205	106–108/2.5	95.5/14	48
1*j*	0.5–1.5(m)	0.5–1.5(m)	—	3.37(d×2)	0.5–1.5(m)	0.5–1.5(m)	1200	138–140/2.5	112/13	48
1*k*	0.7–1.8(m)	0.7–1.8(m)	—	4.25(m)	0.7–1.8(m)	0.7–1.8(m)	1205	92–94/2.5	—	
2*a*	1.85(d) J = 14 Hz	—	—	3.60(d) J = 14 Hz	—	—	755	79–80/2.5	65–66/10	47
2*b*	0.6–2.0(m)	0.6–2.0(m)	—	3.40(d) J = 14 Hz	—	—	750	114–115/2.5	75.6/7	50
2*c*	0.8–2.1(m)	0.8–2.1(m)	0.8–2.1(m)	3.40(d) J = 14 Hz	—	—	755	82/1.2	118–119/12	31
2*d*	1.0–1.6(m)	1.0–1.6(m)		3.82(d) J = 14 Hz	—	—	750	88–89/2.2	—	—
2*e*	1.3–1.7(m)	1.3–1.7(m)	1.1–1.2(d)	3.86(d) J = 14 Hz	—	—	750	94–96/2.1	—	—
2*f*	0.9–1.4(m)	0.9–1.4(m)	0.9–1.4(m)	3.65(d) J = 14 Hz			752	98–100/1.0	—	—
2*g*	0.8–2.2(m)	0.8–2.2(m)	—	4.00(m)	0.8–2.2(m)	—	752	48–50/0.2	—	—
2*h*	0.5–2.1(m)	0.5–2.1(m)	—	3.50(m)	0.5–2.1(m)	0.5–2.1(m)	750	88–89/2.4	65–68/0.2	51
2*i*	1.0–2.2(m)	1.0–2.2(m)	—	4.05(m)	—	—	750	88–90/1.0	96.5–97/11	31
2*j*	0.8–2.2(m)	0.8–2.2(m)	—	3.65(d×2)	0.8–2.2(m)	0.8–2.2(m)	750	96–97/0.75	—	—
2*k*	0.8–2.1(m)	0.8–2.1(m)	—	4.5(m)	0.8–2.1(m)	0.8–2.1(m)	755	122–124/2.0	—	—
3*a*	1.75(d) J = 13 Hz	—	—	2.27(d) J = 11 Hz	—	—	1176	102/4.6	106/12	52
3*b*	0.8–2.2(m)	0.8–2.2(m)	—	2.30(d) J = 11 Hz	—	—	1176	54/0.7	93/2	52
3*c*	1.2–2.2(m)	1.2–2.2(m)	1.0(t)	2.33(d) J = 11 Hz	—	—	1183	125/5.2	120–121/2.0	52
3*d*	1.9–2.1(m)	1.05(d×2)	—	2.17(d) J = 11 Hz	—	—	1180	113/4.6	88/1	52
3*e*	1.3–2.0(m)	1.3–2.0(m)	1.0–1.2(d)	2.25(d) J = 11 Hz	—	—	1185	66/0.005	—	—
3*f*	1.7–1.9(m)	0.6–1.4(m)	0.6–1.4(m)	2.08(d) J = 10 Hz	—	—	1180	130/4.0	—	—
3*g*	1.2–2.2(m)	1.2–2.2(m)	—	2.75(m)	1.2–2.2(m)	—	1183	108/3.2	102/4	52
3*h*	0.6–2.3(m)	0.6–2.3(m)	—	2.83(t×2)	0.6–2.3(m)	1.0–1.1(t)	1171	122/2.0	116–117/2	52
3*j*	1.2–2.4(m)	1.2–2.4(m)	—	2.67(d×2)	1.2–2.4(m)	0.9(d) J = 6 Hz	1175	127/5.0	—	—
4*a*	1.9(d) J = 13 Hz	—	—	2.27(d) J = 14 Hz	—	—	780	78–79/0.1	112–114/14	53
4*b*	0.7–2.0(m)	0.7–2.0(m)	—	2.20(d) J = 12 Hz	—	—	780	90–92/2.8	71.2/2.0	52
4*c*	0.7–2.1(m)	0.7–2.1(m)	—	2.10(d) J = 13 Hz	—	—	800	86–88/0.5	—	—
4*d*	2.0–2.2(m)	0.9–1.2(d×2)	—	2.20(d) J = 13 Hz	—	—	770	60–61/1.0	72/2.0	52
4*e*	1.2–1.7(m)	1.2–1.7(m)	1.0–1.2(d)	2.20(d) J = 9 Hz	—	—	830	98/1.3	—	—
4*g*	0.9–2.1(m)	0.9–2.1(m)	—	2.80(m)	0.9–2.1(m)	—	780	90/0.5	61–62/0.05	54
4*h*	0.7–2.0(m)	0.7–2.0(m)	—	2.90(m)	0.7–2.0(m)	0.7–2.0(m)	780	92/0.5	74–76/0.05	54
4*j*	0.7–2.1(m)	0.7–2.1(m)	—	2.70(m)	0.7–2.1(m)	0.7–2.1(m)	780	78/0.05	77–79/0.06	45
4*k*	0.7–2.0(m)	0.7–2.1(m)	—	3.20(m)	0.7–2.1(m)	0.7–2.1(m)	780	98/0.1	—	—

[a]Separation of the individual upfield resonances was not usually possible. All spectra integrated exactly for the downfield protons (PSC*H*) versus all the others.
[b]Reference 46.

Equimolar amounts of sulfur and the phosphine were gently warmed in benzene. Catalytic amounts of $AlCl_3$ were also occasionally used. The acid chloride was vacuum distilled.

The esters are now synthesized by reaction [7] for **1***d–f*, reaction [9] for **2***d–f*, reactions [10] and [11] for esters **3***d–f* and reactions [12] and [13] for esters **4***d–f*.

Method 6: (for **4***k*)

[17] $(C_2H_5)_2P(S)P(S)(C_2H_5)_2 + LiAlH_4 \rightarrow (C_2H_5)_2PH$ (29)

An ether suspension of the hydride was added to an ether solution of the biphosphine disulfide. The reaction was carried out in an inert atmosphere and was warmed for 1 h on a steam bath. After cooling, water was added carefully and the ether layer was separated and dried. The product was distilled in an inert atmosphere.

[18] $(C_2H_5)_2PH + (s\text{-}C_4H_9)_2S_2 \rightarrow (C_2H_5)_2P(S)SC_4H_9\text{-}s$ (37)

Equimolar amounts of the reagents in benzene were refluxed overnight under an inert atmosphere. The product was vacuum distilled.

Purification and identification of the esters

All esters were first distilled through a Vigreux column and then further purified by distillation on a Perkin-Elmer Model 151 teflon annular spinning band column. The uncorrected boiling points, nmr chemical shifts, and the P=X stretching frequencies are given in Table 10 as well as the literature values for the boiling points of the previously reported esters.

The identity and purity of the esters were checked by nmr; all of the esters have downfield bands due to $R_2P(Y)XCH$ which could be easily integrated versus all the upfield CH bands.

Kinetics

All rates were run in 50 mL volumetric flasks thermostatted in a constant temperature bath ($T \pm 0.2$°C). Weighed amounts of ester and $NaClO_4$ (to keep ionic strength constant at 0.1 *M*) were added to the flask followed by enough NaOH solution to make the ester and base concentrations equivalent. In the cases where a mixed solvent system was used, the DME was added to the ester and salt followed by the base and then the flask was topped up by the addition of 60% DME – H_2O solution. The DME was purified by the method of Wiberg (38). During the course of the reaction 4 mL aliquots were withdrawn and quenched in standard perchloric acid. The solution was back-titrated with standard base using a Radiometric Model ABU 11 autoburette and Radiometer Model 28 pH meter. Glass and standard calomel electrodes were used. The rate constants were calculated from eq. [19] where the slope is determined from a plot $1/(mL_{calcd} - mL_{titr})$ versus time in seconds; mL_{calcd} is the number of millilitres of titrating base necessary to neutralize the quenching acid and mL_{titr} is the number of millilitres of base necessary to titrate the aliquot of quenched reaction solution.

$$[19] \quad k_2(M^{-1}\,s^{-1}) = \frac{(\text{slope})(\text{No. of mL of aliquot})}{(\text{normality of back-titrating base})}$$

The reported rate constants were determined from a least-squares analysis of the data. The rate constants are averages of at least two kinetic runs; the correlation coefficients of the plots and the reproducibility of the data are excellent. The range of the rate constants reported in Tables 1–4 is better than ±5%. The ΔS^* values reported in Table 5 are not better than ±3 eu.

Rate studies could not be carried out on all the esters reported in Table 10 especially those of general structure $R_2P(S)OR'$. These esters when they contain more than 5 carbons are not soluble in H_2O and we were unable to measure their rates in 60% DME – H_2O because of problems of solvent decomposition over the period of time necessary for their reaction (2*b*).

Nuclear magnetic resonance monitoring in a reaction and analysis of products for $(C_2H_5)_2P(S)OCH_3$ indicates neither desulfurization, as was observed during the acid-catalyzed hydrolysis of $(CH_3)_2P(S)OCH_3$ (22*b*), nor alkyl group migration from O to S.

Acknowledgement

The authors thank the Arts and Sciences Research Committee of the American University of Beirut for financial support.

1. A. J. Kirby and S. G. Warren. The organic chemistry of phosphorus. Elsevier, Amsterdam. 1967. Chapt. 10; J. Emsley and C. D. Hall. The chemistry of phosphorus. John Wiley, New York. 1976. Chapt. 8.
2. (*a*) R. D. Cook, C. E. Diebert, W. Schwarz, P. C. Turley, and P. Haake. J. Am. Chem. Soc. **95**, 8088 (1973); (*b*) J. Rahil and P. Haake. J. Org. Chem. **46**, 3048 (1981).
3. F. Eckstein. Acc. Chem. Res. **12**, 204 (1979).
4. J. A. A. Ketelaar, H. R. Gersmann, and K. Koopmans. Rec. Tran. Chim. **71**, 1253 (1952); *cf.* D. F. Heath. J. Chem. Soc. 3796 (1956).
5. R. Breslow and I. Katz. J. Am. Chem. Soc. **90**, 7376 (1968).
6. J. F. Chlebowski and J. E. Coleman. J. Biol. Chem. **249**, 7192 (1974).
7. S. J. Benkovic and K. J. Schray. *In* The enzymes. Vol. 8. *Edited by* P. D. Boyer. Academic Press, New York. 1971. Part A, pp. 212, 213.
8. V. E. Bel'skii, N. N. Bezzubova, V. D. Akamsin, V. N. Eliseenkov, N. I. Rizpolozhenskii, and A. N. Puduvik. Dokl. Akad. Nauk SSSR, **197**, 85 (1971); Engl. Trans. p. 171.
9. F. H. Westheimer. Acc. Chem. Res. **1**, 70 (1968); K. Mislow. Acc. Chem. Res. **3**, 321 (1970); D. Marquarding, H. Klusacek, P. Gillespie, and F. Ramirez. Acc. Chem. Res. **4**, 288 (1971).
10. I. Sigal and F. H. Westheimer. J. Am. Chem. Soc. **101**, 752 (1979).
11. R. D. Cook and M. Metni. Can. J. Chem. **63**, 3155 (1985).
12. G. Davies and D. P. Evans. J. Chem. Soc. 339 (1940).
13. R. W. Taft, Jr. J. Am. Chem. Soc. **74**, 3120 (1952); R. W. Taft, Jr. *In* Steric effects in organic chemistry. *Edited by* M. S. Newman. J. Wiley, New York. 1956. Chapt. 13.
14. L. Almasi. *In* Sulfur in organic and inorganic chemistry. Vol. 1. *Edited by* A. Senning. M. Dekker, New York. 1971; V. E. Bel'skii, N. N. Naberezhnova, L. V. Nesterov, and A. Ya. Kessel'. Zh. Obshch. Khim. **46**, 1438 (1976); Engl. Trans. p. 1415.
15. R. F. Hudson and L. Keay. J. Chem. Soc. 2463 (1956).
16. R. W. A. Jones and J. D. R. Thomas. J. Chem. Soc. B, 661 (1966).
17. J. Shorter. Correlation analysis of organic reactivity. Research Studies Press, Chichester. 1982.
18. T. C. Bruice and M. F. Mayahi. J. Am. Chem. Soc. **82**, 3067 (1960); M. L. Bender and W. P. Jencks. J. Am. Chem. Soc. **83**, 4189 (1961).
19. M. M. Keevoy, E. T. Harper, R. E. Duvall, H. S. Wilgus, and L. T. Ditsch. J. Am. Chem. Soc. **82**, 4899 (1960); M. M. Keevoy, B. E. Eichinger, F. E. Stary, E. A. Katz, and J. H. Sellstedt. J. Org. Chem. **29**, 1641 (1964).
20. A. A. Neimysheva and I. L. Knunyants. Dokl. Akad. Nauk SSSR, **181**, 888 (1968); Engl. Trans. p. 697; A. A. Neimysheva, V. I. Savshuk, M. V. Ermolaeva, and I. L. Knunyants. Izv. Akad. Nauk SSSR Ser. Khim. 2222 (1968); Engl. Trans. p. 2104.
21. P. Campbell and B. A. Lapinskas. J. Am. Chem. Soc. **99**, 5378 (1977).
22. P. Haake, R. D. Cook, and G. Hurst. J. Am. Chem. Soc. **89**, 2650 (1967).
23. M. L. Huggins. J. Am. Chem. Soc. **75**, 4123 (1953).
24. K. A. Abbas and R. D. Cook. Can. J. Chem. **55**, 3540 (1977).
25. P. Haake, R. D. Cook, T. Koizumi, P. S. Ossip, W. Schwarz, and D. A. Tyssee. J. Am. Chem. Soc. **92**, 3828 (1970).
26. R. D. Cook and L. Rahhal-Arabi. Tetrahedron Lett. 3147 (1985).
27. I. F. Tupitsyn. Zh. Obshch. Khim. **52**, 986 (1982); Engl. Trans. p. 858.

28. K. SASSE. Methoden der organischen chemie. Houben-Weyl, Georg Thieme Verlag, Stuttgart. 1963. Vol. 12, Part 1; 1982. Vol. E-2; G. M. KOSOLAPOFF and L. MAIER (*Editors*). Organic phosphorus compounds. Vol. 6. Wiley-Interscience, New York. 1983.
29. K. ISSLIEB and A. TSCHACH. Chem. Ber. **92**, 704 (1959).
30. L. MAIER. Chem. Ber. **94**, 3056 (1961).
31. G. M. KOSOLAPOFF and R. M. WATSON. J. Am. Chem. Soc. **73**, 4101 (1951).
32. W. KUCHEN, H. BUCHWALD, K. STROLENBERG, and J. METTEN. Ann. **652**, 28 (1962).
33. C. BORECKI, J. MICHALSKI, and S. MUSSIEROWICZ. J. Chem. Soc. 4081 (1958).
34. T. A. MASTRYUKOVA, T. A. MELENT'EVA, and M. I. KABACHNIK. Zh. Obshch. Khim. **35**, 1197 (1965); Chem. Abstr. **63**, 11605 (1965).
35. T. A. MASTRYUKOVA, A. B. SHIPOV, and M. I. KABACHNIK. Zh. Obshch. Khim. **31**, 507 (1961); Chem. Abstr. **55**, 22101 (1961).
36. W. VOSKUIL and J. F. ARENS. Rec. Trav. Chim. **82**, 302 (1963).
37. M. GRAYSON and C. E. FARLEY. J. Org. Chem. **32**, 236 (1967).
38. K. B. WIBERG. Laboratory techniques in organic chemistry. McGraw-Hill, New York. NY. 1960. p. 246.
39. G. D. ELISEEVA, B. I. ISTOMIN, and A. V. KALABINA. Zh. Obshch. Khim. **48**, 1901 (1978); Engl. Trans. p. 1735; B. I. ISOTMIN, N. A. SUKHORUKOVA, A. V. KALABINA, and YU. I. SUKHORUKOV. Zh. Obshch. Khim. **52**, 2011 (1981); Engl. Trans. p. 1787.
40. V. E. BEL'SKII, M. V. EFREMOVA, and I. M. SHERMERGORN. Izv. Akad. Nauk. USSR, Ser. Khim. 923 (1967); Engl. Trans. p. 891.
41. R. D. COOK, W. A. DAOUK, A. N. HAJJ, A. KABBANI, A. KURKU, M. SAMAHA, F. SHAYBAN, and O. V. TANIELIAN. Can. J. Chem. **64**, 213 (1986).
42. D. F. HEATH. J. Chem. Soc. 3796 (1956).
43. D. F. HEATH. J. Chem. Soc. 3804 (1956).
44. K. A. ANIKIENKO, T. K. SKRIPACH, N. P. RODIONOVA, and M. K. BARANAEV. Kin. Katal. **6**, 196 (1965); Engl. Trans. p. 196.
45. V. D. AKAMSIN and N. I. RIZPOLOZHENSKII. Dokl. Akad. Nauk SSSR, **168**, 207 (1966); Chem. Abstr. **65**, 8953 (1966).
46. L. C. THOMAS. Interpretation of the infrared spectra of organophosphorus compounds. Heyden and Son Inc., London. 1974.
47. W. D. BURKHARDT, E. G. HOEHN, and J. GOUBEAU. Z. Anorg. Allg. Chem. **442**, 19 (1978).
48. A. I. RAZUMOV and O. A. MUKHACHEVA. Dokl. Akad. Nauk SSSR, **91**, 271 (1953); Chem. Abstr. **48**, 8725 (1954).
49. A. I. RAZUMOV and O. A. MUKHACHEVA. Zh. Obshch. Khim. **26**, 2463 (1956).
50. A. B. REMIZOV, I. YA. KURAMSHIN, A. V. AGANOV, and G. G. BUTENKO. Dokl. Akad. Nauk SSSR, **208**, 1118 (1973); Engl. Trans. p. 134.
51. T. A. MASTRYUKOVA, R. M. KALYANOVA, G. K. GENKINA, T. M. SHCHERBINA, V. A. SVOREN', and M. I. KABACHNIK. Zh. Obshch. Khim. **47**, 272 (1977); Engl. Trans. p. 2479.
52. I. YA. KURAMSHIN, A. A. MURATOVA, E. G. YARKOVA, A. A. MUSINA, F. KH. IZMAILOVA, and A. N. PUDOVIK. Zh. Obshch. Khim. **43**, 1456 (1973); Engl. Trans. p. 1446.
53. R. G. KOSTYANOVSKII, Y. I. ELNATANOV, and S. V. BONDARENKO. Izv. Akad. Nauk SSSR, Ser. Khim. 2835 (1975); Engl. Trans. p. 2726.
54. V. D. AKAMSIN and N. I. RIZPOLOZHENSKII. Izv. Akad. Nauk SSSR, Ser. Khim. 493 (1966); Chem. Abstr. **65**, 5480 (1966).

Kinetic solvent effects on acid-catalyzed hydrolysis of sucrose in aqueous mixtures of some protic, aprotic, and dipolar aprotic solvents

URMILA MANDAL, KAUSHIK DAS, AND KIRON KUMAR KUNDU[1]
Physical Chemistry Laboratories, Jadavpur University, Calcutta – 700 032, India

Received November 11, 1985[2]

URMILA MANDAL, KAUSHIK DAS, and KIRON KUMAR KUNDU. Can. J. Chem. **64**, 1638 (1986).

Rate constants of acid-catalyzed hydrolysis of sucrose (S) to D-glucose and L-fructose have been determined at 25°C by optical rotation measurements in aqueous mixtures of protophobic protic glycerol (GL), protophilic protic urea (UH), aprotic dioxane (D), and dipolar aprotic dimethyl sulphoxide (DMSO). Transfer free energies of the substrate sucrose, $\Delta G_t^0(S)$ have also been determined in the solvents from solubility measurements. These values as well as those of H^+, as obtained earlier by use of the widely used tetraphenylarsonium tetraphenylboron (TATB) reference electrolyte assumption, yielded transfer free energies of the transition state. The observed log (k_s/k_w) – composition profiles reveal that the rates increase monotonically in GL–water mixtures, that decrease more or less monotonically in UH– and DMSO–water mixtures, and decrease up to 10 mol% D in D–water mixtures, beyond which the values tend to increase. Examination of $\Delta G_t^0(i)$–composition profiles for the different species in each case indicates that the initial and transition state solvation get more or less compensated and the observed rates are dictated by the increased solvation of H^+ in aqueous UH, DMSO, and D co-solvent systems. But in GL–water mixtures the decreased solvation of the transition state compared with the initial state is overcome by the decreased solvation of H^+, thus resulting in the gradual enhancement of the rates of the reaction. The observed linearity of the correlative plots of $-\delta(\Delta G^{\neq})$ $[=RT \ln (k_s/k_w)]$ vs. $\Delta G_t^0(H^+)$ with distinctly different slopes in the two cases also substantiates the relative importance of H^+ solvation in dictating the rates of the reaction in these widely different aqueous co-solvents.

URMILA MANDAL, KAUSHIK DAS et KIRON KUMAR KUNDU. Can. J. Chem. **64**, 1638 (1986).

Opérant à 25°C, dans des mélanges aqueux de glycérol (GL) (protophobe et protique), d'urée (UH) (protophile et protique), de dioxanne (D) (aprotique) et diméthylsulfoxyde (DMSO) (depolaire et aprotique) et faisant appel à des mesures de rotation optique, on a mesuré les constantes de vitesse pour l'hydrolyse acido-catalysée du sucrose (S) en D-glucose et en L-fructose. En faisant appel à des mesures de solubilité, on a aussi déterminé les énergies libres de transfert $\Delta G_t^0(S)$ dans ces solvants. Ces valeurs ainsi que celles relatives au H^+ qui ont été obtenues antérieurement en utilisant l'hypothèse de l'électrolyte de référence tétraphénylborure de tétraphénylarsonium (TBTA) ont permis de déterminer les énergies libres de l'état de transition. Les courbes reliant la composition avec le log (k_s/k_w) révèlent que les vitesses augmentent d'une façon monotone dans le mélanges GL/eau, qu'elles diminuent d'une façon plus ou moins monotone dans les mélanges UH/eau et DMSO/eau alors que, dans des mélanges de D/eau, il se produit un ralentissement jusqu'à 10 mol% de D qui est suivi par une augmentation de la vitesse à des concentrations en D qui sont de plus en plus élevées. L'examen des courbes reliant la composition avec les $\Delta G_t^0(i)$ pour les différentes espèces, dans chaque cas, indique que la solvatation de l'état initial et de l'état de transition est plus ou moins compensée et que les vitesses observées sont dictées par une augmentation de la solvatation des ions H^+ dans les systèmes de co-solvants UH/eau, DMSO/eau et D/eau. Toutefois, dans les mélanges de GL/eau, la solvatation qui est plus faible dans l'état de transition que dans l'état initial est compensée par une solvatation réduite des ions H^+ et ceci conduit à une augmentation graduelle des vitesses de réaction. On a observé que les courbes établissant une corrélation entre le $-\delta(\Delta G^{\neq})$ $[= RT \ln (k_s/k_w)]$ et le $\Delta G_t^0(H^+)$ sont linéaires et qu'elles possèdent des pentes légèrement différentes; ces données confirment la relative importance de la solvatation des ions H^+ dans l'orientation de la réaction dans ces différentes co-solvants aqueux.

[Traduit par la revue]

Introduction

Until recent years kinetic solvent effects of reactions in different media were usually correlated with various empirical parameters of "solvent polarity" which sum up all the specific and non-specific interactions of the media with initial and transition states and are derived with the aid of the principle of linear free energy (LFE) relationships (1). Lately, however, increasing efforts (2–8) have been made to rationalize the kinetic solvent effects from thermodynamic points of view. One of these essentially involves splitting up the activation parameters into contributions of initial and transition states and hence to correlate and understand their behaviour in the light of the relevant physico-chemical properties of the solvents.

In a previous paper (9) such an attempt has been made for the alkaline hydrolysis of a triphenylmethyl dye viz crystal violet (CV^+), in aqueous mixtures of a number of protic, aprotic, and dipolar aprotic co-solvents with varied physico-chemical properties. The results revealed that the kinetic solvent effect of that reaction is not guided solely by OH^- or lyate S^-, as is widely believed, but also by the differences in relative stabilization of the initial and transition states of the substrates, which were found to vary with the nature of the co-solvents. Besides, while the stabilization of hydrophobic CV^+ is chiefly guided by dispersion and hydrophilic interactions of the co-solvents, that of the transition state, believed possibly to be outer-sphere complex, $[CV^+]S^-$, is augmented by the increased hydrogen-bonding propensity of the hydroxylic co-solvents in particular. Thus it transpires that, for complete understanding of the kinetic solvent effects on nucleophilic reactions, dissection of the activation parameters such as free energy of activation ($\Delta G^{\neq}$) into the contributions of the inidividual species involved should be highly rewarding.

In this paper we have extended our studies on kinetic solvent effects on the well known H_3O^+-catalyzed hydrolysis of D-sucrose to D-glucose and L-fructose, otherwise known as the inversion of cane sugar, in aqueous mixtures of protophobic protic glycerol (GL), protophilic protic urea (UH), aprotic dioxane (D), and dipolar aprotic dimethyl sulphoxide (DMSO) at 25°C. In fact, recently evaluated (10–12) transfer free energies of (ΔG_t^0) of different ions, including H^+ and OH^- or the lyate ion, S^-, (based on the widely used tetraphenylarsonium

[1]To whom all correspondence should be addressed.
[2]Revision received April 3, 1986.

TABLE 1. Kinetic and thermodynamic data for the hydrolysis of sucrose and the involved reacting species at 25°C in different aquo-organic solvents

Organic solvent	Wt.% co-solvent	mol% co-solvent	k (min^{-1})	$\delta(\Delta G^{\neq})$ (kJ mol^{-1})	Solubility (mol dm^{-3})	$\Delta G_t^0(S)$ (kJ mol^{-1})	$\Delta G_t^0(H^+)^{c-f}$ (kJ mol^{-1})	$\Delta G_t^0(X^{\neq})$ (kJ mol^{-1})
Glycerol[c]	0	0	1.88×10^{-3}[a]	0	2.64[b]	0	0	0
	23.1	5.53	2.53×10^{-3}	−0.74	1.98	0.78	1.38	1.42
	33.3	8.90	2.85×10^{-3}	−1.03	1.73	1.04	2.00	2.01
	50	16.35	3.53×10^{-3}	−1.56	1.19	1.97	3.28	3.69
	70	31.32	5.35×10^{-3}	−2.60	0.65	3.48	5.56	6.44
Urea[d]	10	3.22	7.19×10^{-4}	2.38	2.90	−0.23	−1.34	0.81
	20	6.97	5.27×10^{-4}	3.15	2.83	−0.17	−2.66	0.32
	30	11.38	1.98×10^{-4}	5.58	2.70	−0.06	−4.27	1.25
	40	16.65	1.15×10^{-4}	6.86	2.60	0.04	−5.75	1.08
DMSO[e]	10	2.49	1.00×10^{-3}	1.56	2.42	0.22	−1.34	0.44
	30	8.96	1.22×10^{-4}	6.79	2.03	0.66	−5.05	2.40
	50	18.73	4.03×10^{-5}	9.53	1.60	1.24	−10.87	−0.10
Dioxane[f]	10	2.22	8.33×10^{-4}	2.02	2.38	0.26	−1.41	0.87
	30	8.06	1.46×10^{-4}	6.33	1.87	0.86	−5.03	2.16
	50	16.98	2.02×10^{-4}	5.53	1.38	1.61	−3.15	3.99

[a]The value of k at 25°C as computed from the data on $k_{H_3O^+} = k/Ck_{H_3O^+}$ in ref. 17 is 2.1×10^{-3} min^{-1}.
[b]Reference 22.
[c]Reference 10.
[d]Reference 11.
[e]Reference 11.
[f]Reference 12.

tetraphenylboron (TATB) reference electrolyte assumption (13), $\Delta G_t^0(Ph_4As^+) = \Delta G_t^0(Ph_4B^-) = \frac{1}{2}\Delta G_t^0(Ph_4AsPh_4B)$ in different aquo-organic solvents including the above-noted co-solvents, have prompted us to take up the present study. The choice of these co-solvents rests on the fact that while $\Delta G_t^0(H^+)$ values are found to be increasingly positive in the case of less basic GL, and negative in the case of more basic protic UH and dipolar aprotic DMSO, that in aqueous D though increasingly negative at initial compositions, is less so beyond 10 mol% D. And these results led us to expect that if the relative catalytic activity of H^+ is largely dictated by the relative solvation of H^+, the rate of inversion of cane sugar will be enhanced in aqueous GL and increasingly inhibited in aqueous UH and DMSO and up to 10 mol% D and reversed beyond that composition, provided the relative solvation of the initial and transition states is not untowardly different from each other in each of these aquo-organic solvent systems. It was therefore considered particularly interesting to examine if the expected correspondence is more or less true or not. As the contributions of initial state solvation of the substrate are not known in these solvents, these have been determined by measuring the solubilities of sucrose in the solvents.

Experimental

The organic solvents were purified by the methods described earlier (9). The mixed solvents were prepared by mass dilution with triple distilled water. AnalaR (BDH) grade sucrose was used without further treatment. The rates of hydrolysis of sucrose were studied in aqueous mixtures of 0, 23, 33, 50, and 70 wt.% GL, 10, 30, and 50 wt.% D and DMSO and 10, 20, 30, and 40 wt.% UH, using 10% sucrose solution and an optimum concentration of 0.25 M HCl as the catalyst in the respective solvents. The rates of the reaction were followed after Guggenheim and Wiseman (14) by measuring the optical rotation of aliquots of the reaction mixtures with the help of a Hilger Standard Polarimeter, after duly freezing the rates of the reaction in the aliquots by adding minute excess of alkali beyond the point of neutralization. The latter was to eliminate "mutarotation lag" (14). As Guggenheim and Wiseman indicated, the hydrolysis of sucrose into D-glucose and L-fructose is followed by mutarotation of the products at rates greater by a factor of about 10^2 than that of the hydrolysis. Thus the optical rotation at any moment will differ by a small but not constant amount from the value it would have if mutarotation were instantaneous. This is often called the "mutarotation lag". The mutarotation lag if not estimated, could introduce an error in the rate constant of less than 1% but greater than 0.1%. Therefore, as suggested by Guggenheim and Wiseman, aliquot samples (10 mL) of the reaction mixtures were neutralized with a slight excess of alkali and diluted to 25 mL before measuring the optical rotation. Neutralization of the acid completely stops the hydrolysis of sucrose and further addition of minute excess of alkali completes mutarotation practically instantaneously.

Solubilities of sucrose in the solvents were determined at 25°C by measuring the optical rotation of the saturated solutions in the respective solvent mixtures. The saturated solutions were prepared (15) by adding sufficient amounts of sucrose to 30–40 mL of the respective solvents taken in tightly stoppered Jena bottles and shaken in a mechanical shaker for about 2–3 h. The solutions were then thermally equilibrated in a thermostat kept at 25°C for a few days with occasional shaking. Aliquots of these solutions were taken at 2–3 days intervals using specially designed pipettes fitted with G_3-Gooch discs at the delivery ends and after diluting appropriately with water the solutions were analyzed by noting the optical rotation. The procedure was repeated until successive readings agreed within ±1%. The solubilities in mol dm^{-3} so obtained for each of the mixtures in different solvent systems are given in Table 1. The transfer free energies of sucrose from water to the mixed solvents, $\Delta G_t^0(S)$ were obtained on molar scale by the usual relation (15, 16) and presented in Table 1.

Results and discussion

As the kinetic behaviour of the reaction in all the aquo-organic solvents is found to be exactly similar to that in water, the reaction can be assumed to be a case of specific hydrogen ion catalysis as in water (17). Thus we can for all these water-rich solvent mixtures postulate the equilibrium

$$S + H_3O^+ \underset{k_{-1}}{\overset{k_1}{\rightleftharpoons}} [S.H_3O]^+ \xrightarrow{k_2} \text{products}$$

where S is the substrate sucrose, H_3O^+ the solvated hydrogen ion and $k_2 \ll k_{-1}$. Now for a given concentration of HCl, $K(= k_1/k_{-1})$ will vary from solvent to solvent and the resulting changes in the concentration of the collision complex $[S.H_3O^+]$ will cause a change in the measured velocity constant k. Under these conditions

$$-\frac{dC_S}{dt} = k_2 C_{[S.H_3O]^+}$$

$$= k_2 K C_{H_3O^+} \frac{Y_{H_3O^+} Y_S}{Y_{[S.H_3O]^+}} C_S$$

We assume tentatively that the activity coefficient factor $(Y_{H_3O^+} Y_S / Y_{[S.H_3O]^+})$ being a ratio of the activity coefficients of the singly charged species multiplied by that of an uncharged species, is likely to be nearly unity at the low concentration of HCl used in each case. Thus, neglecting the effect of activity coefficient factor the rate can be expressed as follows

$$-\frac{dC_S}{dt} = k_2 K C_{H_3O^+} C_S = k C_S$$

where k, the observed pseudo-first-order rate constant, is $k_2 K C_{H_3O^+}$ at a particular concentration of H_3O^+ and $k_{H_3O^+}$, the second-order rate constant, is given by

$$k_{H_3O^+} = k/C_{H_3O^+} = k_2 K$$

So, at a particular concentration of HCl i.e. $C_{H_3O^+}$, the observed velocity constant k was obtained from the slope of the first order linear plot of $-\ln(\alpha_t - \alpha_\infty)$ vs. t where α_t and α_∞, were the optical reactions of the aliquots at time $t = t$ and $t = \infty$.[3]

In Table 1 are given the values of the velocity constant $k(\text{min}^{-1})$ (the number of moles of sucrose reacting per mole of sucrose per min) for the solvents at 25°C. Notably, the observed value of k in pure water compares fairly well with the value computed from Leininger and Kilpatrick's data (17) at different concentration of HCl.

The k values are referred to a particular catalyst concentration (viz. 0.25 *M* HCl) for all the co-solvent compositions and the effect of activity coefficient factor in the rate equation is likely to be negligibly small. Therefore these values, and in particular log (k_s/k_w) (where the subscript s refers to solvent and w to water), can be tentatively taken as a relative measure of the kinetic solvent effect on the reaction in the different solvents.

Thus from Fig. 1 where log (k_s/k_w) values are plotted against mol% co-solvents, it can be seen that the observed rate constant relative to that in water increases almost linearly with increasing composition of GL, while it decreases more or less monotonically with increasing composition of UH, DMSO, and up to 10 mol% D, beyond which the values take an upward trend. These results conform at least qualitatively with what is expected from the inverse behaviour of the transfer free energy of H^+, $\Delta G_t^0(H^+)$ with co-solvent compositions as indicated earlier. Thus, H^+ becomes a more active catalyst with increasing composition of GL as it becomes increasingly less stabilized due to the decreased basicity of the solvents (10). The reverse is true in the cases of more basic co-solvents like UH, DMSO, and to 10 mol% D beyond which it takes an opposite trend conforming to its decreased stabilization and hence increased catalytic activity. Thus it appears that the kinetics of the reaction

[3]A complete set of the experimental data obtianed at $C_{HCl} = 0.25$ *M*, may be purchased from the Depository of Unpublished Data CISTI, National Research Council of Canada, Ottawa, Ont., Canada K1A 0S2.

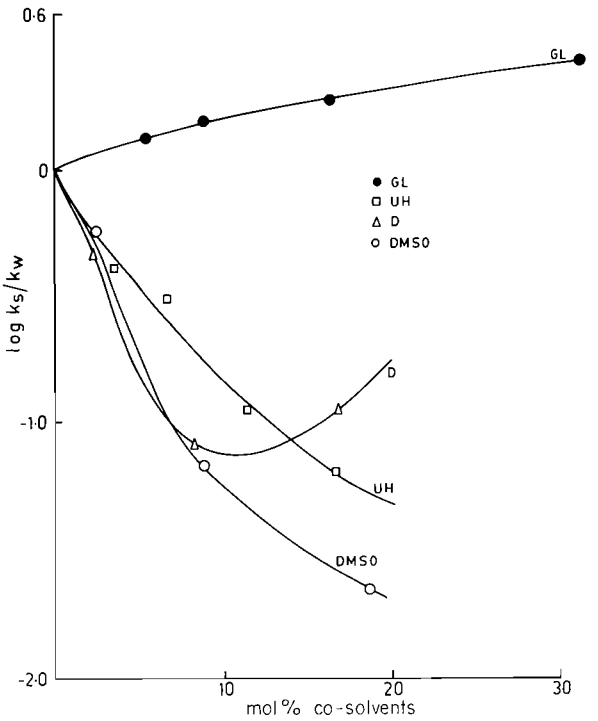

FIG. 1. Variation of log k_s/k_w with mol% co-solvent for the hydrolysis of sucrose (S) at 25°C in aqueous mixtures of glycerol (GL, ●); urea (UH, □); dioxane (D, △) and dimethyl sulphoxide (DMSO, ○).

are to a large extent dictated by the relative solvation of H^+; the more solvated the H^+, the less effective it is as a catalyst for the inversion of cane sugar.

To get a better indication of the relative contributions of different species guiding the rates of hydrolytic reactions a detailed analysis of the relative transfer free energies of activation $\delta(\Delta G^{\neq})$ would be useful. $\delta(\Delta G^{\neq})$ values were obtained after the Eyring equation

$$k = \frac{RT}{Nh} \exp^{-\Delta G^{\neq}/RT}$$

Moreover, as the concentration dependence of $\delta(\Delta G^{\neq})$ is expected to be fairly small (*vide* ref. 17), $\delta(\Delta G^{\neq})$ can be tentatively related to transfer free energies of the species involved in the reaction as follows (7)

$$\delta(\Delta G^{\neq}) = \Delta G_t^0(X^{\neq}) - \Delta G_t^0(S) - \Delta G_t^0(H^+)$$

The tentative values of the transfer free energies of the transition state, $\Delta G_t^0(X^{\neq})$ were then evaluated by use of the corresponding values of $\Delta G_t^0(S)$ and $\Delta G_t^0(H^+)$ (10–12) for the solvents. All these values are presented in the table.

Figure 2 illustrates $\Delta G_t^0(i)$–composition profiles of the different species involved, viz. H^+, S, and $X^{\neq}$ and also $\delta(\Delta G^{\neq})$ in the aqueous mixtures of the co-solvents GL and UH, and Fig. 3 those for DMSO and D. It is interesting to note that in GL–water mixtures ΔG_t^0 values of all the species are increasingly positive with the increase of GL and their relative order is $\Delta G_t^0(X^{\neq}) > \Delta G_t^0(H^+) \gg \Delta G_t^0(S)$. Evidently, while the observed increased destabilization of H^+ is the result of smaller basicity of glycerol (ROH) (10) compared to that of water, due to two electron-withdrawing —OH groups in the alkyl group R [$= CH_2(OH)CH(OH)CH_2$] that of sucrose is seemingly the result of steric effect imparted by GL molecules

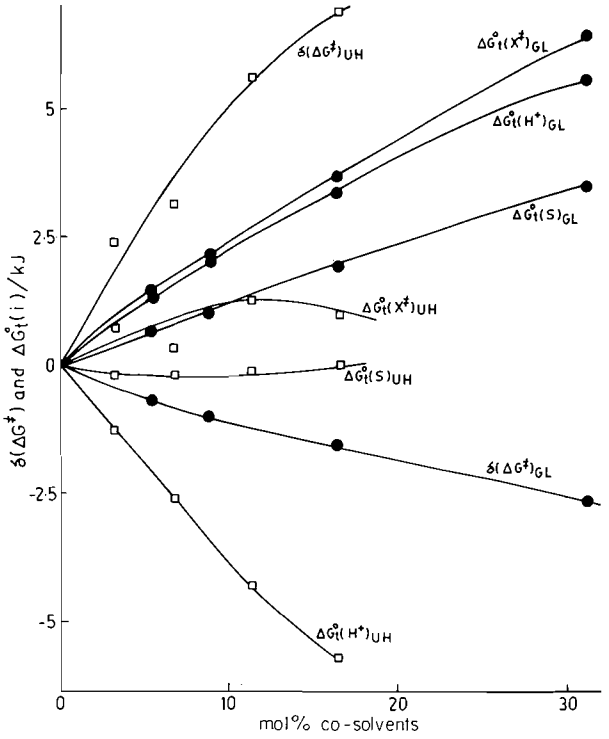

FIG. 2. Kinetic solvent effects $\delta(\Delta G^{\neq})$ for the hydrolysis of sucrose (S) and the involved transfer free energies (ΔG_t^0) of H^+, S and the transition state ($X^{\neq}$) on molar scale in aqueous mixtures of glycerol (GL, ●) and urea (UH, □) at 25°C.

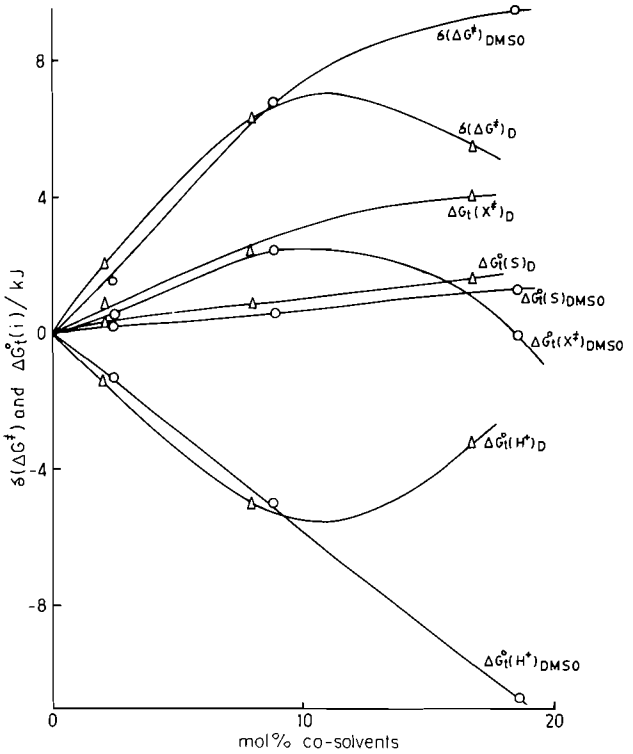

FIG. 3. Kinetic solvent effects $\delta(\Delta G^{\neq})$ for the hydrolysis of sucrose (S) and the involved transfer free energies (ΔG_t^0) of H^+, S and the transition state ($X^{\neq}$) on molar scale in aqueous mixtures of dioxane (D, △) and dimethyl sulphoxide (DMSO, ○) at 25°C.

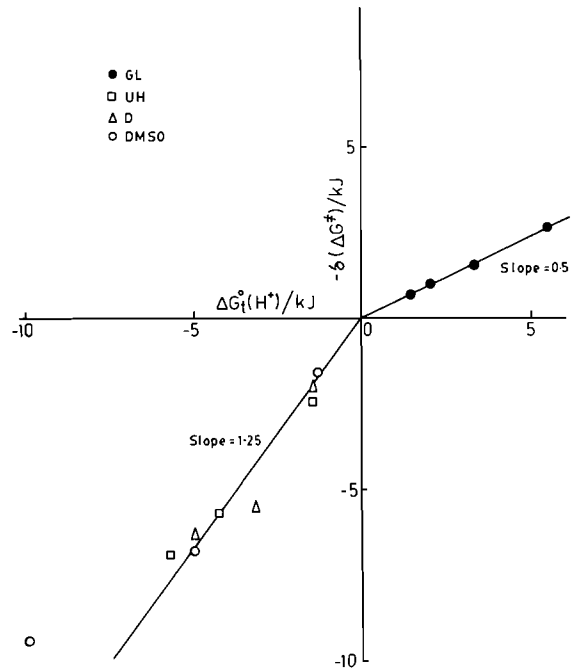

FIG. 4. Plots of $-\delta(\Delta G^{\neq})$ vs. $\Delta G_t^0(H^+)$ for the hydrolysis of sucrose in different aquo-organic solvents.

as compared to water. Evidently, the more pronounced destabilization observed of the transition state ($X^{\neq}$) which is effectively a protonated sucrose $[S.H_3O]^+$ (17), is attributable to the resultant effect of the steric hindrance of GL molecules and the decreased basicity of GL–water mixtures. Thus, it appears that although the transition state is increasingly destabilized relative to the initial state, the opposing resultant effects of increased destabilization of both H^+ and initial-state substrate (S) overcompensate the effect of the former and thus enhance the rate of the reaction with increased proportion of GL.

In the case of aqueous urea, however, the reverse is seemingly true. Thus, while $\Delta G_t^0(X^{\neq})$ values are slightly positive and have a tendency to pass through a maximum, $\Delta G_t^0(S)$ values remain almost invariant with UH composition, thus making $[\Delta G_t^0(X^{\neq}) - \Delta G_t^0(S)]$ values slightly positive. Evidently, increasingly large $-\Delta G_t^0(H^+)$ values result in the observed increasingly positive magnitudes of $\delta(\Delta G^{\neq})$ with increased proportion of use. Notably, while the increased pronounced stabilization of H^+ in UH–water mixtures is attributable to the resultant effects of increased basicity (11) and increased dielectric constant (18) of the solvents, the observed nearly invariant stabilization of sucrose with increased proportion of urea is possibly the effect of urea–water clusters (19) formed through 3 H-bond centres of zwitterionic forms of urea. The observed slight destabilization of the transition state $[S.H_3O]^+$ at initial composition of urea is also indicative of the larger interaction of water than that with possible urea–water clusters because of steric effect. And the observed trend of larger stabilization at higher composition is the result of the superimposed effects of increased basicity as well as the increased dielectric constant of the solvents. Thus the observed relatively small solvation of initial and transition states of sucrose is indicative of the small propensity of urea to form "specific complexes" with carbohydrates, as suggested by Moulik *et al.* (20) from the studies of alkaline degradation of D-fructose and D-glucose in the presence of urea.

In aqueous DMSO solutions while the composition profile of $\Delta G_t^0(S)$ (*vide* Fig. 3) remains almost invariant up to 20 mol% DMSO and that for X^+ takes a downward trend after exhibiting a small and broad maximum around 10 mol% DMSO, that for H^+ takes a sharp downward trend from the beginning. Seemingly, the stabilization of sucrose remains virtually unaltered because of opposing effects of hydrophobicity of 2 (—CH_3) groups and H-bonding propensity of the unhindered basic O-centre of the DMSO molecule. Also, the pronounced stabilization of the positively charged transition state $[S.H_3O]^+$ at higher compositions is the effect of increased basicity of DMSO–water mixtures resulting from the pronounced negative charge density on the O-centre of DMSO molecule due to the inductive effect of 2 (—CH_3) groups, and as reflected in the increased $-\Delta G_t^0$ values of H^+ and some alkali metal cations in these solvents (11). Evidently, at lower compositions enhanced solvation of H^+ dictates the decreased rate of reaction. But at higher concentrations enhanced solvation of the transition state over the initial state opposes the decreased catalytic activity of H^+ to some extent and thus results in the observed downward trend of $\delta(\Delta G^{\neq})$–composition profile (Fig. 3).

Exactly similar is the case in aqueous D at initial compositions but the reverse holds at higher compositions. In fact $\Delta G_t^0(H^+)$ has a downward trend at initial compositions because of the increased basicity of D + H_2O mixtures resulting from larger protophilicity of two basic O-centres of dioxane molecules (21). But, as explained earlier (12), because of the possible shifting of the equilibria between the aquo-complexes of "boat" and "chair" forms of dioxane molecules with increased proportion of D, the basicity decreases at higher compositions. Consequently, as $\Delta G_t^0(H^+)$ values have an upward trend at higher compositions, $\delta(\Delta G^{\neq})$ values take a downward trend, reflecting that the relative solvation of H^+ dictates the rate of the reaction. Moreover, as in DMSO–water mixtures, the observed invariance in solvation of sucrose with addition of D seemingly results partly from the opposing effects of hydrophobicity of 4 (—CH_2—) groups and the H-bonding propensity of the two basic O-centres of D molecules and partly from the possible aquo-dioxane complexes with little solvating capability because of steric factor. And the observed slight destabilization of the transition state $[S.H_3O]^+$ is possibly the resultant effects of steric hindrance of the solvating species like aquo–dioxane complexes, Born-type electrostatic interaction and the decreased basicity at higher compositions. Thus the effect of destabilization of transition state also partly contributes to the inhibition of the reaction, though to a small extent.

Thus if we sum up as in Fig. 4, where the correlative plots of $-\delta(\Delta G^{\neq})$ vs. $\Delta G_t^0(H^+)$ are depicted, it is found that while all the points in GL–water mixtures fall on a straight line in the first quadrant with a slope of about 0.5, those in aqueous D, DMSO, and UH fall on a single straight line in the third quadrant but with a slope of about 1.25. While the observed line in the first quadrant indicates that the rate of the reaction is largely enhanced due to the increased desolvation of H^+, that in the third quadrant indicates that the reaction is largely inhibited due to the increased solvation of H^+. The observed slope in the former case viz. 0.5 instead of 1.0, further suggests that initial and transition state solvation do not cancel each other but their resultant effect reduces the desolvation effect of H^+ by about 50%. In fact, as the ΔG_t^0–composition profiles of different reacting species viz. H^+, S, and X^+ in Fig. 2 suggest, the resultant effects of both H^+ and S overcome the opposing effect of the increased desolvation of the transition state and thus cause the observed enhancement of the reactions. On the other hand, in the cases of aqueous mixtures of UH, D, and DMSO, the observed slope of the linear plot in the third quadrant, viz. 1.25 instead of 1, suggests that the increased inhibition of the effect of H^+ due to increased solvation is further augmented by the resultant effects of initial and transition state solvation. As indicated earlier from the analysis of the relative $\Delta G_t^0(i)$–composition profiles of H^+, S, and X^+ in these solvent mixtures (Figs. 2 and 3), although the effect of initial state solvation is negligibly small, the increased desolvation of the transition state is responsible for further slowing down the reaction.

Thus it may be concluded that just as in the case of alkaline hydrolysis of crystal violet in different aquo-organic solvents, the present results also clearly demonstrate that the correlation of the relative solvation of the involved species of the reactions with relative physico-chemical properties of the solvents offer good insights into the kinetic solvent effects of reactions.

Acknowledgement

Authors wish to record their thanks to CSIR, Government of India, New Delhi, for financial assistance.

1. C. Reichardt. Angew. Chem. Int. Edn. Engl. **18**, 9 (1979).
2. M. H. Abraham. Prog. Phys. Org. Chem. 11, 1 (1974).
3. M. J. Blandamer and J. Burgess. Chem. Soc. Rev. **4**, 55 (1975).
4. A. J. Parker, D. Mayer, R. Schmid, and U. Gutman. J. Org. Chem. **43**, 1843 (1978).
5. E. Buncel and H. Wilson. Acc. Chem. Res. **12**, 42 (1979).
6. C. F. Wells. J. Chem. Soc. Dalton 1494 (1980).
7. J. B. F. N. Engberts. *In* Water: a comprehensive treatise. Vol. 6. *Edited by* F. Franks. Plenum Press, New York. 1976. p. 139 and references therein.
8. Y. Kondo, M. Ittoh, and S. Susabayashi. J. Chem. Soc. Faraday Trans. 1, **78**, 2793 (1982).
9. U. Mandal, S. Sen, K. Das, and K. K. Kundu. Can. J. Chem. In press.
10. I. N. Basumallick and K. K. Kundu. Can. J. Chem. **58**, 79 (1981).
11. A. K. Das and K. K. Kundu. J. Soln. Chem. **8**, 259 (1979).
12. A. Bhattacharya, J. Datta, K. Das, and K. K. Kundu. Ind. J. Chem. **21**A, 9 (1982).
13. B. G. Cox, G. R. Hedwig, A. J. Parker, and D. W. Watts. Aust. J. Chem. **27**, 477 (1974) and references therein.
14. E. A. Guggenheim and L. A. Wiseman. Proc. R. Soc. London, Sec. A, **17**, 203 (1950).
15. U. Mandal, S. Bhattacharya, S. Sen, and K. K. Kundu. J. Chem. Soc. Perkin Trans. II, 853 (1985) and references therein.
16. J. Datta and K. K. Kundu. Can. J. Chem. **61**, 625 (1983) and references therein.
17. P. M. Leininger and M. Kilpatrick. J. Am. Chem. Soc. **60**, 1268 (1938); **60**, 2891 (1938).
18. J. Wyman, Jr. J. Am. Chem. Soc. **55**, 4116 (1933).
19. A. K. Das and K. K. Kundu. J. Phys. Chem. **79**, 2604 (1975) and references therein.
20. S. P. Moulik, D. Basu, and P. K. Bhattacharya. Carbohydr. Res. **63**, 165 (1978).
21. J. Datta and K. K. Kundu. Can. J. Chem. **59**, 3149 (1981).
22. A. Siedell. Solubilities of organic compounds. Vol. II. 3rd ed. D. Van Nostrand Co. Inc., New York. 1941. p. 711.

The 2-mercapto-1-methylimidazolyl moiety as a bridging ligand in complexes of gallium, rhenium, and molybdenum

D. A. COOPER, S. J. RETTIG, A. STORR,[1] AND J. TROTTER[1]

Department of Chemistry, The University of British Columbia, Vancouver, B.C., Canada V6T 1Y6

Received October 2, 1985

D. A. COOPER, S. J. RETTIG, A. STORR, and J. TROTTER. Can. J. Chem. **64**, 1643 (1986).

The synthesis and characterization of complexes containing the 2-mercapto-1-methylimidazolyl ligand are described. $Me_2Ga(SCNCHCHNMe)$ occurs as a dimer, crystals of which are monoclinic, $C2/c$, a = 14.140(2), b = 7.4098(4), c = 18.024(2) Å, β = 106.38(1)°, Z = 4 dimers; the structure was determined by conventional heavy atom methods and refined by full-matrix least-squares techniques to a final R value of 0.039 for 1767 reflections. The crystal contains centrosymmetric dimeric molecules, with a central 8-membered ring, formed by mercaptoimidazolyl ligand bridging between dimethylgallium groups; gallium has tetrahedral geometry, with no tendency to five-coordination, Ga—S = 2.3697(8), Ga—N = 2.019(2) Å. Reaction of $Me_2Ga(pz)(SCNCHCHNMe)^-$, L^-, with $[Re(CO)_4Cl]_2$ results in the formation of $LRe(CO)_3$, whose physical properties indicate a *fac* arrangement of the organogallate ligand. Attempts to synthesize corresponding $LMo(\eta^3\text{-}C_4H_7)(CO)_2$ and $LMo(\eta^3\text{-}C_3H_5)(CO)_2$ complexes yielded the dimeric species $[Mo(\eta^3\text{-}C_4H_7)(CO)_2(SCNCHCHNMe)]_2$ and $[Mo(\eta^3\text{-}C_3H_5)(CO)_2(SCNCHCHNMe)]_2$. Crystals of the $[Mo(\eta^3\text{-}C_4H_7)(CO)_2(SCNCHCHNMe)]_2$ complex are monoclinic, $I2/a$, a = 15.057(2), b = 9.4853(9), c = 18.240(2) Å, β = 108.67(1)°, Z = 4 dimers, R = 0.028 for 2363 reflexions. The structure contains dimeric molecules with C_2 symmetry, and five fused rings, a central group of three 4-membered rings being formed by bonding of the S atoms of the ligands to both Mo atoms (in contrast to the gallium complex). The molecule has a U-shape, with Mo atoms having pseudo-octahedral environments, Mo—S = 2.6868(7), 2.5576(7), Mo—N = 2.253(2), Mo—CO = 1.950(2), Mo—C(allyl) = 2.259(3), 2.326(3) Å. Considerable strain in the chelate rings is indicated by angles as low as S—Mo—N = 63.9(1)°.

D. A. COOPER, S. J. RETTIG, A. STORR, and J. TROTTER. Can. J. Chem. **64**, 1643 (1986).

On décrit la synthèse et le caractérisation de complexes contenant le ligand mercapto-2 méthyl-1 imidazolyle. Le $Me_2Ga(SCNCHCHNMe)$ existe sous forme de dimère dont les cristaux sont monocliniques, groupe d'espace $C2/c$, avec a = 14,140(2), b = 7,4098(4), c = 18,024(2) Å, β = 106,38(1)° et Z = 4 dimères; on a déterminé la structure par les méthodes conventionnelles aux atomes lourds et on l'a affiné par la méthode des moindres carrés (matrice entière) jusqu'à une valeur finale de R de 0,039 pour 1767 réflexions. Les cristaux comportent des molécules dimères centrosymétriques, avec un noyau central à 8 chaînons, qui sont formés de ligands mercaptoimidazolyes servant de pont entre les groupements diméthylgallium; le gallium possède une géométrie tétraédrique, il n'a aucune tendance à donner une penta-coordination et Ga—S = 2,3697(8) alors que Ga—N = 2,019(2) Å. La réaction du composé $Me_2Ga(pz)(SCNCHCHNMe)^-$, L^-, avec le $[Re(CO)_4Cl]_2$ conduit à la formation du $LRe(CO)_3$ dont les propriétés physiques indiquent que le ligand arganogallate se trouve dans un arrangement *fac*. Des essais en vue de préparer les complexes correspondants $LMo(\eta^3\text{-}C_4H_7)(CO)_2$ et $LMo(\eta^3\text{-}C_3H_5)(CO)_2$ n'ont conduit qu'à la formation des espèces dimères $[Mo(\eta^3\text{-}C_4H_7)(CO)_2(SCNCHCHNMe)]_2$ et $[Mo(\eta^3\text{-}C_3H_5)(CO)_2(SCNCHCHNMe)]_2$. Les cristaux du complexe $[Mo(\eta^3\text{-}C_4H_7)(CO)_2(SCNCHCHNMe)]_2$ sont monocliniques, groupe d'espace $I2/a$, avec a = 15,057(2), b = 9,4853(9), c = 18,240(2) Å, β = 108,67(1)°, Z = 4 dimères et R = 0,028 pour 2363 réflexions. Chacune des structures contient des molécules dimères avec une symétrie C_2 et des cycles à cinq chaînons condensés, avec un groupement central de cycles à 4 chaînons qui sont formés par la liaison des atomes de S des ligands avec les deux atomes de Mo (et ceci est en opposition avec ce qui est observé avec le complexe de gallium). La molécule existe sous une forme en U et les atomes de Mo possèdent des environnements pseudo-octaédriques, Mo—S = 2,6868(7), 2,5576(7), Mo—N = 2,253(2), Mo—CO = 1,950(2), Mo—C(allyle) = 2,259(3), 2,326(3) Å. Une tension importante dans les cycles chélatés se réflète par des angles S—Mo—N qui sont aussi bas que 63,9(1)°.

[Traduit par la revue]

Introduction

In our continuing investigations on the reactivity of organogallium species with "active" hydrogen compounds, and the synthesis of anionic pyrazolylgallate ligands (ref. 1 and references therein), our attention has recently focussed on 2-mercapto-1-methyl-imidazole, **1**, as a molecule of potential interest.

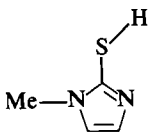

1

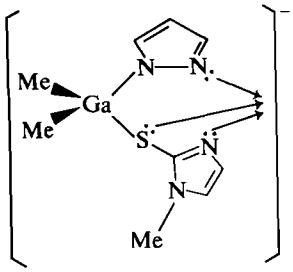

2

Thus, on the one hand, reaction of this molecule with Me_3Ga, with resulting elimination of methane, should afford a product for which numerous possible modes of oligomerization may be envisaged. On the other hand, reaction of the mercaptan with the $Me_3Ga(pz)^-$ anion should lead to the novel anionic ligand system, **2**. This has in fact been demonstrated by the synthesis of the octahedral $LRe(CO)_3$ complex in which the ligand **2** acts as a tridentate chelating ligand, thus extending the range of such complexes containing unsymmetrical pyrazolyl–gallate ligand systems (1). The present account also details X-ray analysis data on two novel structures, the dimers $[Me_2Ga(SCNCHCHNMe)]_2$ and $[Mo(\eta^3\text{-}C_4H_7)(CO)_2(SCNCHCHNMe)]_2$.

Experimental

Starting materials

Air-sensitive materials were handled in a nitrogen atmosphere. Tetrahydrofuran (THF), benzene, and CH_2Cl_2 were dried by refluxing over Na/benzophenone, potassium, and CaH_2, respectively, followed by distillation. $Mo(MeCN)_2(\eta^3\text{-}C_3H_5)(CO)_2Br$ and $Mo(MeCN)_2(\eta^3$-

[1]Authors to whom correspondence may be addressed.

TABLE 1. Micro-analyses and ir data for the complexes derived from the (SCNCHCHNMe) bridging ligand

Compound	Calcd. (%)			Found (%)			ν_{CO}(cm^{-1})*	
	C	H	N	C	H	N	In Nujol	Other
$[Me_2Ga(SCNCHCHNMe)]_2$	33.85	5.17	13.16	33.99	5.25	13.15		
$[Me_2Gapz(SCNCHCHNMe)]Re(CO)_3$	26.19	2.56	10.18	26.22	2.21	9.90	2010, 1900(br)	†2008, 1910(br)
$[Mo(\eta^3\text{-}C_3H_5)(CO)_2(SCNCHCHNMe)]_2$	35.18	3.26	9.12	35.54	3.39	8.43	1930(br), 1837(br)	‡1935(br), 1872, 1852
$[Mo(\eta^3\text{-}C_4H_7)(CO)_2(SCNCHCHNMe)]_2$	37.62	3.76	8.78	37.46	3.89	8.83	1955, 1935, 1865, 1840	‡1975, 1939, 1875, 1854

*br = broad.
†In dichloromethane.
‡In THF.

TABLE 2. ^{1}H nmr data for the complexes derived from the (SCNCHCHNMe) bridging ligand*

Compound	Ga-*Me*	N-*Me*	$H_\eta H_\rho$	"pyrazolyl"			"allyl"		
				H_β	H_γ	H_δ	H *anti*	H *syn*	Other
†$[Me_2Ga(SCNCHCHNMe)]_2$	10.22(s) 10.39(s)	6.44(s) 6.29(s)	2.72(d) 3.04(br)						
‡$[Me_2Gapz(SCNCHCHNMe)]Re(CO)_3$	10.12(s) 9.94(s)	7.49(s)	3.44(d) 4.34(d)	3.94(dd)	2.69(d)	2.12(d)			
†$[Mo(\eta^3\text{-}C_3H_5)(CO)_2(SCNCHCHNMe)]_2$		6.83(s)	3.28(d) 3.18(d)				8.60(d) 8.68(d) (J = 10 Hz)	6.58(d) 6.60(d) (J = 7 Hz)	6.18(br) H-unique
†$[Mo(\eta^3\text{-}C_4H_7)(CO)_2(SCNCHCHNMe)]_2$		6.80(s)	3.18(d) 3.23(d)				8.54(s) 8.90(s)	6.65(d) 7.05(d) J = 3 Hz)	8.28(s) allyl-Me

*s = single, d = doublet, t = triplet, br = broad, dd = doublet of doublets; $J_{HCCH} \approx 2$ for pz protons; see Fig. 2 for proton identification.
†Measured in d_6-acetone (τ acetone = 7.89 ppm).
‡Measured in C_6D_6 (τ benzene = 2.84 ppm).

$C_4H_7)(CO)_2Cl$ were prepared by literature methods (2). The allyl halides and acetonitrile were distilled before use, the latter being dried by refluxing over P_4O_{10}. $[Re(CO)_4Cl]_2$ was synthesized by a literature procedure (3) from rhenium carbonyl (Strem) and chlorine gas (Matheson). 2-Mercapto-1-methylimidazole (Aldrich) was used as supplied.

Preparation of $[Me_2Ga(SCNCHCHNMe)]_2$

$$2Me_3Ga + 2HSCNCHCHNMe \xrightarrow[\text{room temp./3 h}]{\text{THF}} [Me_2Ga(SCNCHCHNMe)]_2 + 2CH_4$$

2-Mercapto-1-methylimidazole (2.0 g; 18 mmol) and trimethylgallium (2.1 g; 18 mmol) were stirred in THF at room temperature for 3 h. After solvent removal *in vacuo* the residue was extracted with benzene. The filtrate, upon slow evaporation of the solvent, afforded colourless crystals of $[Me_2Ga(SCNCHCHNMe)]_2$ in approximately 90% yield. Analytical and spectroscopic data for the complex are given in Tables 1 and 2.

Preparation of $Na^+[Me_2Ga(pz)(SCNCHCHNMe)]^-$,

An equimolar amount of the mercaptoimidazole, **1**, in THF was added to a THF solution of $Na^+Me_3Ga(pz)^-$ (4) and the resultant mixture refluxed for ~40 h. An ir spectrum of the solution at this time indicated the complete absence of the ν_{SH} band (~2800 cm^{-1}) of the starting material. The cooled solution was then diluted to a known volume with THF and the standard solution stored under a nitrogen atmosphere.

Preparation of $[Me_2Ga(pz)(SCNCHCHNMe)]Re(CO)_3$

A two molar equivalent of the ligand was added to $[Re(CO)_4Cl]_2$ (0.292 g; 0.44 mmol) in THF. A 19-h reflux of the reactant solution effected the total disappearance of the carbonyl bands of the starting material in the ir spectrum of the reacting mixture. The solvent was then removed under vacuum and the residue extracted with benzene. The filtrate afforded small white crystals of the product, $[Me_2Ga(pz)(SCNCHCHNMe)]Re(CO)_3$, in approximately 50% yield. Analytical and spectroscopic data for the compound are presented in Tables 1 and 2.

Attempted preparation of $[Me_2Ga(pz)(SCNCHCHNMe)]Mo(\eta^3\text{-allyl})(CO)_2$, *and preparation of* $[Mo(\eta^3\text{-allyl})(CO)_2(SCNCHCHNMe)]_2$ *where* η^3-*allyl* = η^3-C_3H_5 *or* η^3-C_4H_7

$$2Mo(MeCN)_2(\eta^3\text{-}C_3H_5)(CO)_2Br + 2Na^-[Me_2Ga(pz)(SCNCHCHNMe)]^- \xrightarrow[\text{room temp./16 h}]{\text{THF}} [Mo(\eta^3\text{-}C_3H_5)(CO)_2(SCNCHCHNMe)]_2 + 2NaBr + 4MeCN + [Me_2Ga(pz)]_2$$

A similar equation holds for $Mo(MeCN)_2(\eta^3\text{-}C_4H_7)(CO)_2Cl$.

Addition of an equimolar amount of $Na^+[Me_2Ga(pz)(SCNCHCHNMe)]^-$ to a clear orange THF solution of $Mo(MeCN)_2(\eta^3\text{-allyl})(CO)_2X$ (~0.34 mmol) immediately resulted in precipitation of a fine white solid (presumably NaX), with concomitant shifts in the carbonyl stretching frequencies in the ir spectrum of the mixture. After stirring the reaction mixture at room temperature for 20 h, the solvent was removed *in vacuo* and the residues extracted with benzene. Subsequent evaporation of the solvent from the filtered solutions afforded orange crystals characterized as benzene solvate compounds. Heating at 70°C whilst under vacuum removed the residual benzene and gave analytically pure samples of $[Mo(\eta^3\text{-allyl})(CO)_2(SCNCHCHNMe)]_2$ in approximately 60% yields. Analytical and spectroscopic data for the two compounds are included in Tables 1 and 2. No $[Me_2Ga(pz)\cdot(SCNCHCHNMe)]Mo(\eta^3\text{-allyl})(CO)_2$ compounds were obtained.

X-ray crystallographic analyses

Bis(μ*-1-methylimidazole-2-thiolato-S,N2′)bis[dimethylgallium(III)]*

A crystal bounded by the six faces (followed by their distances in mm from a common origin: {0 0 1}, 0.24, {1 0 0}, 0.17, (1 2 0), 0.27, (0 −1 1), 0.28 was mounted in a general orientation. Unit-cell parameters were refined by least-squares on 2 sin θ/λ values for 25 reflections (2θ = 40–52°) measured on a diffractometer with Mo-$K\alpha$ radiation ($\lambda(K\alpha_1)$ = 0.70930, $\lambda(K\alpha_2)$ = 0.71359 Å). Crystal data at 22°C are:

$C_{12}H_{22}Ga_2N_4S_2$ fw = 425.9

Monoclinic, a = 14.140(2), b = 7.4098(4), c = 18.024(2) Å, β = 106.38(1)°, V = 1811.8(3) Å^3, Z = 4, ρ_c = 1.561 Mg m^{-3}, $F(000)$ =

TABLE 3. Final positional (fractional: Mo, Ga, S × 10^5; O, N, C × 10^4; H × 10^3) and isotropic thermal parameters (U × 10^3, Å^2) with estimated standard deviations in parentheses

Atom	x	y	z	U_{eq}^* or U_{iso}
		$[Me_2Ga(SCNCHCHNMe)]_2$		
Ga	57757(2)	41004(4)	41605(2)	46
S	40340(5)	42028(10)	38653(4)	49
N(1)	3874(2)	7081(3)	4787(1)	47
N(2)	3657(2)	7769(4)	3572(2)	53
C(1)	6047(3)	2219(6)	3476(2)	65
C(2)	6265(3)	6590(5)	4221(2)	61
C(3)	3854(2)	6425(4)	4093(2)	42
C(4)	3690(3)	8914(4)	4689(2)	61
C(5)	3558(3)	9347(5)	3955(3)	66
C(6)	3561(4)	7607(7)	2739(2)	79
H(1a)	662(3)	162(6)	365(2)	80(12)
H(1b)	604(3)	265(6)	295(3)	93(14)
H(1c)	558(3)	120(5)	342(2)	57(10)
H(2a)	682(4)	697(7)	399(3)	108(15)
H(2b)	612(4)	713(7)	458(3)	101(16)
H(2c)	593(3)	744(6)	370(2)	86(12)
H(4)	370(3)	958(5)	506(2)	64(11)
H(5)	352(4)	1033(7)	375(3)	96(14)
H(6a)	295(5)	715(9)	253(3)	122(21)
H(6b)	385(6)	878(10)	247(4)	175(28)
H(6c)	421(3)	717(7)	265(2)	87(13)
		$[Mo(\eta^3\text{-}C_4H_7)(CO)_2(SCNCHCHNMe)]_2$		
Mo	18404(2)	40871(2)	39108(1)	31
S	14919(5)	34997(8)	52338(4)	34
O(1)	2762(2)	4205(3)	2619(1)	68
O(2)	2594(2)	7154(3)	4036(2)	76
N(1)	1527(1)	1815(2)	4092(1)	32
N(2)	1311(2)	570(2)	5039(1)	34
C(1)	2407(2)	4126(3)	3085(2)	43
C(2)	2303(2)	6014(3)	3998(2)	47
C(3)	702(3)	3922(5)	2710(2)	60
C(4)	287(2)	4279(4)	3281(2)	54
C(5)	551(3)	5601(4)	3633(3)	61
C(6)	−377(3)	3302(6)	3493(3)	69
C(7)	1452(2)	1864(3)	4787(1)	30
C(8)	1424(2)	411(3)	3872(2)	38
C(9)	1298(2)	−349(3)	4449(2)	41
C(10)	1219(3)	226(4)	5788(2)	49
H(3a)	63(3)	300(4)	252(2)	75(13)
H(3b)	85(3)	461(5)	234(3)	89(14)
H(5a)	34(3)	582(5)	401(3)	91(16)
H(5b)	66(3)	635(4)	335(2)	68(12)
H(6a)	−34(3)	351(5)	400(3)	85(15)
H(6b)	−95(3)	343(4)	312(2)	65(11)
H(6c)	−26(3)	225(4)	339(2)	76(13)
H(8)	145(2)	20(3)	337(2)	48(9)
H(9)	129(3)	−133(4)	449(2)	64(11)
H(10a)	120(4)	104(5)	609(3)	114(20)
H(10b)	69(4)	0(6)	575(3)	118(20)
H(10c)	169(4)	−51(6)	609(3)	141(21)

*U_{eq} = (1/3) trace (diagonalized U), esd's not given.

TABLE 4. Bond lengths (Å) with estimated standard deviations in parentheses

Bond	Length (Å)	Bond	Length (Å)
	$[Me_2Ga(SCNCHCHNMe)]_2$		
Ga—S	2.3697(8)	N(1)—C(4)	1.385(4)
Ga—C(1)	1.970 (3)	N(2)—C(3)	1.344(4)
Ga—C(2)	1.962 (4)	N(2)—C(5)	1.385(5)
Ga—N(1)′	2.019 (2)	N(2)—C(6)	1.473(5)
S—C(3)	1.733 (3)	C(4)—C(5)	1.322(6)
N(1)—C(3)	1.335 (3)		
	$[Mo(\eta^3\text{-}C_4H_7)(CO)_2(SCNCHCHNMe)]_2$		
Mo—S	2.6868(7)	O(2)—C(2)	1.160(4)
Mo—N(1)	2.253 (2)	N(1)—C(7)	1.309(3)
Mo—C(1)	1.955 (3)	N(1)—C(8)	1.385(4)
Mo—C(2)	1.944 (3)	N(2)—C(7)	1.351(3)
Mo—C(3)	2.314 (3)	N(2)—C(9)	1.379(4)
Mo—C(4)	2.259 (3)	N(2)—C(10)	1.455(4)
Mo—C(5)	2.337 (4)	C(3)—C(4)	1.417(6)
Mo—S′	2.5576(7)	C(4)—C(5)	1.407(6)
S—C(7)	1.744 (3)	C(4)—C(6)	1.502(5)
O(1)—C(1)	1.142 (4)	C(8)—C(9)	1.339(4)

*Here and elsewhere primed atoms are related to unprimed atoms by the centre of symmetry $(1-x, 1-y, 1-z)$ for the Ga complex and by the twofold axis $(1/2-x, y, 1-z)$ for the Mo complex.

864, μ(Mo-$K\alpha$) = 30.9 cm^{-1}. Absent reflections: hkl, $h+k$ odd, and $h0l$, l odd, space group $C2/c$ (C_{2h}^6, No. 15) and molecular symmetry 1, from structure analysis.

Intensities were measured with graphite-monochromatized Mo-$K\alpha$ radiation on an Enraf-Nonius CAD4-F diffractometer. An ω–2θ scan at 2.87–10.06° min^{-1} over a range of (0.90 + 0.35 tan θ) deg in ω (extended by 25% on both sides for background measurement) was employed. Data were measured to $2\theta = 60°$ for $\pm h, +k, +l$. The intensities of three check reflections, measured every 3600 s throughout the data collection, remained constant to within 3.5%. After data reduction,[2] an absorption correction was applied using the analytical method (5, 6). Transmission factors ranged from 0.240 to 0.416. Of the 2621 independent reflections measured, 1767 (67.4%) had intensities greater than or equal to $3\sigma(I)$ above background where $\sigma^2(I) = S + 2B + (0.04(S-B))^2$ with S = scan count and B = normalized background count.

The systematic absences allow space groups Cc or $C2/c$, the latter being suggested by the E-statistics and by the Patterson function, from which the coordinates of the Ga and S atoms were determined. The remaining atoms, including hydrogen, were positioned from subsequent difference maps. In the final stages of refinement the non-hydrogen atoms were refined with anisotropic thermal parameters and the hydrogen atoms with isotropic thermal parameters. The scattering factors of ref. 7 were used for non-hydrogen atoms and those of ref. 8 for hydrogen atoms. Anomalous scattering factors from ref. 9 were used for the Ga and S atoms. The weighting scheme $w = 1/\sigma^2(F)$, where $\sigma^2(F)$ is derived from the previously defined $\sigma^2(I)$, gave uniform average values of $w(|F_o| - |F_c|)^2$ over ranges of both $|F_o|$ and sin θ/λ and was employed in the final stages of full-matrix refinement of 135 variables. Reflections with $I < 3\sigma(I)$ were not included in the refinement. Convergence was reached at $R = 0.039$ and $R_w = 0.045$ for 1767 reflections with $I \geq 3\sigma(I)$. For all 2621 reflections $R = 0.064$. The function minimized was $\Sigma w(|F_o| - |F_c|)^2$, $R = \Sigma||F_o| - |F_c||/\Sigma|F_o|$ and $R_w = (\Sigma w(|F_o| - |F_c|)^2/\Sigma w|F_o|^2)^{1/2}$.

On the final cycle of refinement the mean and maximum parameter shifts corresponded to 0.04 and 0.35σ, respectively. The mean error in an observation of unit weight was 1.716. A final difference map showed maximum fluctuations of −1.46 to +0.82 e Å^{-3} near gallium and was essentially featureless elsewhere. The final positional and thermal parameters appear in Tables 3 and 7,[3] respectively. Bond lengths, bond angles, and intra-annular torsion angles are given in Tables 4–6, respectively. Bond lengths and angles involving hydrogen and a complete list of torsion angles (Tables 8–10) have been deposited.[3] Measured and calculated structure factors have been placed in the Depository of Unpublished Data.[3]

Bis(μ-1-methylimidazole-2-thiolato-S,N²,S′)bis[(η³-2-methylallyl)dicarbonylmolybdenum]

Experimental details are as above except where noted. The six bounding faces of the crystal were: ±(1 1 0), 0.07, ±(−1 1 0), 0.08, {0 0 1}, 0.14 mm (from a common origin). Reflections used in the refinement of the unit-cell constants had $2\theta = 30$–40°. Crystal data are:

$C_{20}H_{24}Mo_2N_4O_4S_2$ fw = 640.4

Monoclinic, a = 15.057(2), b = 9.4853(9), c = 18.240(2) Å, β = 108.67(1)°, V = 2467.9(5) Å^3, Z = 4, ρ_c = 1.724 Mg m^{-3}, $F(000)$ = 1280, μ(Mo-$K\alpha$) = 11.9 cm^{-1}. Absent reflections: hkl, $h+k+l$ odd, and $h0l$, h odd, space group $I2/a$ [non-standard setting of $C2/c$ with equivalent positions: (0, 0, 0), (1/2, 1/2, 1/2) ± (x, y, z; 1/2 − x, y, $-z$)] and molecular symmetry 2, from structure analysis.

An ω–2θ scan at 1.06–10.06° min^{-1} over a range of (0.57 + 0.35 tan θ)° in ω was employed. Of 3586 independent reflections measured (to $2\theta = 60°$), 2363 had intensities greater than or equal to $3\sigma(I)$ above background. The intensities of the three standard reflections remained constant to within 2.5%. The data were corrected for absorption using the Gaussian integration method (5, 10), transmission factors ranging from 0.811 to 0.873 for 72 sampling points.

The choice of the centrosymmetric space group and the solution and refinement of the structure parallel that described above for $[Me_2Ga(SCNCHCHNMe)]_2$. Convergence was reached at $R = 0.028$ and $R_w = 0.030$ and 2363 reflections with $I \geq 3\sigma(I)$. For all 3586 reflections, $R = 0.066$. The mean and maximum parameter shifts of the final cycle of refinement were 0.028 and 0.29σ, respectively, and the mean error in an observation of unit weight was 1.217. The maximum fluctuations on the final difference map were −0.82 and +0.42 e Å^{-3}, both near Mo.

Spectra

Infrared spectra were recorded on a Perkin-Elmer 598 spectrometer. ^{1}H nmr spectra were recorded on Bruker WP-80 and Varian XL-300 instruments.

Results and discussion

The elimination of methane from the reaction of trimethylgallium and 2-mercapto-1-methylimidazole follows the pattern established for similar reactions involving gallium alkyls and compounds containing active hydrogen (1). The solid state structure of the product is shown in Fig. 1. The compound exists as dimeric units that display a novel eight-membered ring with the two gallium atoms in tetrahedral environments. In the structure the imidazolyl rings remain planar, allowing delocalization of the 6π electrons with concomitant gain in stabilization energy. There appears to be no tendency for the gallium centres to become 5-coordinate via an involvement with the second S atom (Ga···S = 3.711(1) Å), an arrangement that would lead to the existence of three fused 4-membered rings similar to those

[2]The computer programs used include locally written programs for data processing and locally modified versions of the following: ORFLS, full-matrix least-squares, and ORFFE, function and errors, by W. R. Busing, K. O. Martin, and H. A. Levy; FORDAP, Patterson and Fourier syntheses, by A. Zalkin; ORTEP II, illustrations, by C. K. Johnson.

[3]The structure factor table, Table 7 (anisotropic thermal parameters) and other material mentioned in the text are available, at a nominal charge, from the Depository of Unpublished Data, CISTI, National Research Council of Canada, Ottawa, Ont., Canada K1A 0S2.

TABLE 5. Bond angles (deg) with estimated standard deviations in parentheses

Bonds	Angle (deg)	Bonds	Angle (deg)
	$[Me_2Ga(SCNCHCHNMe)]_2$		
S—Ga—C(1)	104.79(12)	C(4)—N(1)—Ga′	122.2 (2)
S—Ga—C(2)	108.05(12)	C(3)—N(2)—C(5)	107.9 (3)
S—Ga—N(1)′	100.90(7)	C(3)—N(2)—C(6)	126.5 (3)
C(1)—Ga—C(2)	124.9 (2)	C(5)—N(2)—C(6)	125.7 (3)
C(1)—Ga—N(1)′	104.0 (2)	S—C(3)—N(1)	127.0 (2)
C(2)—Ga—N(1)′	111.46(14)	S—C(3)—N(2)	123.6 (2)
Ga—S—C(3)	100.97(9)	N(1)—C(3)—N(2)	109.4 (2)
C(3)—N(1)—C(4)	106.4 (3)	N(1)—C(4)—C(5)	109.6 (3)
C(3)—N(1)—Ga′	131.1 (2)	N(2)—C(5)—C(4)	106.7 (3)
	$[Mo(\eta^3\text{-}C_4H_7)(CO)_2(SCNCHCHNMe)]_2$		
S—Mo—N(1)	63.89(6)	C(4)—Mo—S′	169.18(9)
S—Mo—C(1)	162.73(10)	C(5)—Mo—S′	148.40(12)
S—Mo—C(2)	106.80(10)	Mo—S—C(7)	75.66(9)
S—Mo—C(3)	122.53(11)	Mo—S—Mo′	93.83(2)
S—Mo—C(4)	90.30(9)	C(7)—S—Mo′	111.06(9)
S—Mo—C(5)	86.26(11)	Mo—N(1)—C(7)	101.2 (2)
S—Mo—S′	80.96(2)	Mo—N(1)—C(8)	152.5 (2)
N(1)—Mo—C(1)	107.12(11)	C(7)—N(1)—C(8)	106.1 (2)
N(1)—Mo—C(2)	166.80(12)	C(7)—N(2)—C(9)	105.9 (2)
N(1)—Mo—C(3)	86.99(13)	C(7)—N(2)—C(10)	126.6 (3)
N(1)—Mo—C(4)	85.42(10)	C(9)—N(2)—C(10)	127.5 (3)
N(1)—Mo—C(5)	114.91(12)	Mo—C(1)—O(1)	176.7 (3)
N(1)—Mo—S′	85.02(6)	Mo—C(2)—O(2)	178.0 (3)
C(1)—Mo—C(2)	79.18(13)	Mo—C(3)—C(4)	69.8 (2)
C(1)—Mo—C(3)	69.23(14)	Mo—C(4)—C(3)	74.1 (2)
C(1)—Mo—C(4)	104.05(13)	Mo—C(4)—C(5)	75.2 (2)
C(1)—Mo—C(5)	111.00(14)	Mo—C(4)—C(6)	119.0 (2)
C(1)—Mo—S′	83.62(9)	C(3)—C(4)—C(5)	114.9 (4)
C(2)—Mo—C(3)	106.2 (2)	C(3)—C(4)—C(6)	121.9 (4)
C(2)—Mo—C(4)	104.57(14)	C(5)—C(4)—C(6)	123.1 (4)
C(2)—Mo—C(5)	72.01(14)	Mo—C(5)—C(4)	69.2 (2)
C(2)—Mo—S′	84.18(10)	S—C(7)—N(1)	118.9 (2)
C(3)—Mo—C(4)	36.07(14)	S—C(7)—N(2)	129.4 (2)
C(3)—Mo—C(5)	61.6 (2)	N(1)—C(7)—N(2)	111.6 (2)
C(3)—Mo—S′	147.95(12)	N(1)—C(8)—C(9)	108.8 (3)
C(4)—Mo—C(5)	35.59(14)	N(2)—C(9)—C(8)	107.6 (3)

TABLE 6. Intra-annular torsion angles (deg) standard deviations in parentheses

Atoms	Intra-annular torsion angle (deg)
$[Me_2Ga(SCNCHCHNMe)]_2$	
N(1)′—Ga—S—C(3)	99.96(12)
S—Ga—N(1)′—C(3)′	−76.0 (3)
Ga—S—C(3)—N(1)	−85.6 (2)
Ga′—N(1)—C(3)—S	6.0 (4)
$[Mo(\eta^3\text{-}C_4H_7)(CO)_2(SCNCHCHNMe)]_2$	
S′—Mo—S—Mo′	24.78(3)
S—Mo—S′—Mo′	−23.52(3)
N(1)—Mo—S—C(7)	2.88(10)
Mo—S—C(7)—N(1)	−5.1 (2)
Mo—N(1)—C(7)—S	6.0 (2)
S—Mo—N(1)—C(7)	−3.78(14)

observed in the structure of the molybdenum complex described below. The reason for this reluctance of the gallium centres to become five-coordinate is not clear, since this coordination number is common in "Ga—O" dimer species (11–14). The Ga—N distance of 2.019(2) Å in the present complex is comparable to, but slightly longer than the Ga—N distances of ~1.97 Å in other tetrahedral gallium species (15–17). Little information is available on Ga—S bond lengths; the length of 2.370(1) Å in the present structure lies between that of 2.321(2) Å in an aminomethylene–benzo[6]furanthionate complex (18), and those of 2.408–2.466(2) Å in a dithiocarbamate (19).

The reaction of the ligand **2** with $[Re(CO)_4Cl]_2$ resulted in a moderate yield of the tricarbonyl product $[Me_2Ga(pz)(SCNCHCHNMe)]Re(CO)_3$. The expected *facial* arrangement of the organogallate ligand in the product was confirmed by the ir and ^1H nmr data obtained for the complex. Thus, three strong ν_{CO} bands are expected for a *fac* arrangement, whereas a *mer* arrangement would lead to two weak ν_{CO} bands and one strong ν_{CO} band in the ir spectrum (20). The ir spectrum observed, although showing only two strong ν_{CO} bands, displays a broad lower frequency vibration that we attribute to two unresolved ν_{CO} bands. The ^1H nmr spectrum of the complex in C_6D_6 solvent (Fig. 2) is consistent with a *fac* arrangement for the organogallate ligand. Thus the "$GaMe_2$" grouping displays two distinct singlets at ~10τ, whereas for a *mer* arrangement a plane of symmetry in the molecule would render the two Ga—Me groups equivalent and hence lead to one signal in this region of

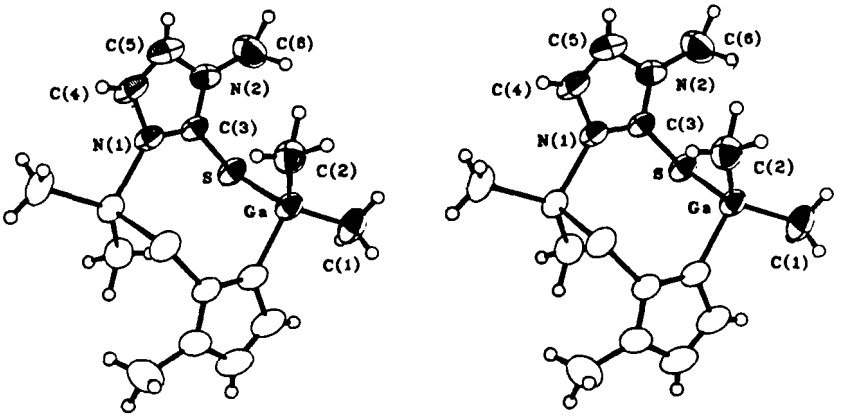

FIG. 1. Stereoscopic view of the $[Me_2GaS\overline{CNCHCHNMe}]_2$ molecule. 50% probability thermal ellipsoids are shown.

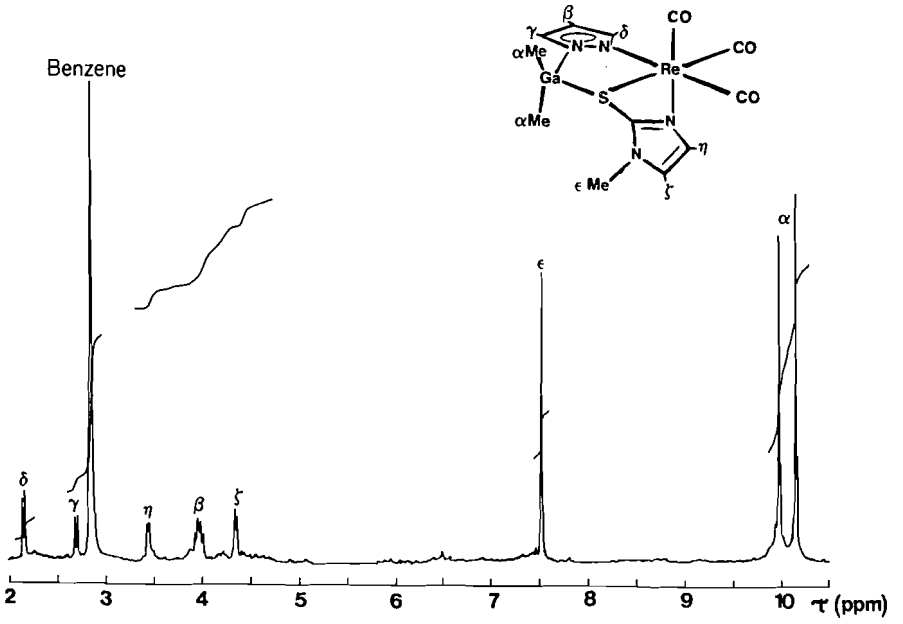

FIG. 2. 80 MHz ^1H nmr spectrum of $[Me_2Gapz(S\overline{CNCHCHNMe})]Re(CO)_3$ in C_6D_6.

the spectrum. It is worth noting that in the proposed structure the sulphur atom is three coordinate, unlike the sulphur atom in the $[Me_2Ga(S\overline{CNCHCHNMe})]_2$ dimer species, but analogous to the sulphur coordination in the $[Mo(\eta^3\text{-}C_4H_7)(CO)_2(S\overline{CNCHCHNMe})]_2$ dimer species described below.

In contrast to the successful coordination of the ligand **2** to the "$Re(CO)_3$" unit, attempts to synthesize analogous octahedral complexes incorporating the "$Mo(CO)_2(\eta^3\text{-allyl})$" moiety failed. However, the products obtained from these attempts were themselves of great interest. Thus, instead of the anticipated reaction sequence it became apparent that degradation of the ligand **2** had occurred and resulted in the formation of the dimeric species $[Mo(\eta^3\text{-allyl})(CO)_2(S\overline{CNCHCHNMe})]_2$. A second product in the reaction was identified as the $[Me_2Ga(pz)]_2$ dimer compound, which has been characterized previously (21).

The molybdenum-containing dimers have been characterized by ir, ^1H nmr, and mass spectral studies and, in addition, the X-ray structure determination of the $\eta^3\text{-}C_4H_7$-containing compound has been performed. The ir spectra of the complexes show four strong ν_{CO} bands, a pattern which would be predicted for the C_2 point group of these dimeric species (22). The ^1H nmr spectra of the complexes are also consistent with the dimeric structure found in the solid state (see below). The spectrum of the $[Mo(\eta^3\text{-}C_3H_5)(CO)_2(S\overline{CNCHCHNMe})]_2$ complex in d_6-acetone is shown in Fig. 3. Thus, the two *anti* protons of the allyl group are inequivalent, as are the two *syn* protons (these have very similar chemical shifts but are resolved at 300 MHz). The *N—Me* groups of the two imidazolyl ligands appear as a singlet in the spectrum, indicating equivalent environments in the molecule.

The mass spectra of the two complexes demonstrate their dimeric nature in the gas phase. For example, the mass spectrum of the $\eta^3\text{-}C_3H_5$ derivative displays a weak parent-ion signal at ~612, as well as other strong signals attributable to ions containing the dimeric unit $[Mo(S\overline{CNCHCHNMe})]_2$.

The results from the above-mentioned physical methods indicated the dimeric nature of the $[Mo(\eta^3\text{-}C_3H_5)(CO)_2(S\overline{CNCHCHNMe})]_2$ and $[Mo(\eta^3\text{-}C_4H_7)(CO)_2(S\overline{CNCHCHNMe})]_2$ complexes. Two possible structures that would account for our data are shown in Fig. 4*a* and *b*. In both of these proposals the molybdenum atoms attain an 18-electron configuration via a

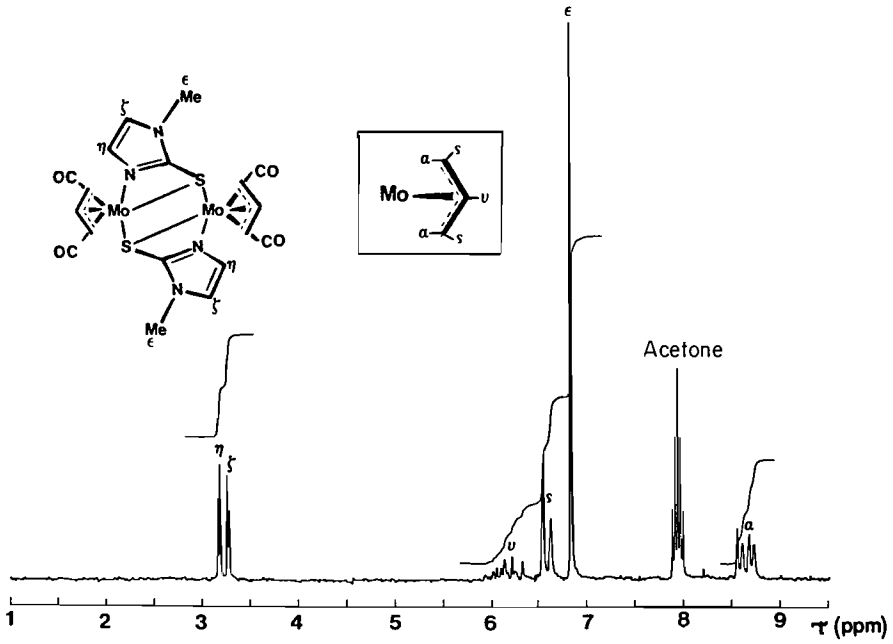

FIG. 3. 80 MHz ^{1}H nmr spectrum of $[Mo(\eta^3\text{-}C_3H_5)(CO)_2(\overline{SCNCHCHNMe})]_2$ in d_6-acetone.

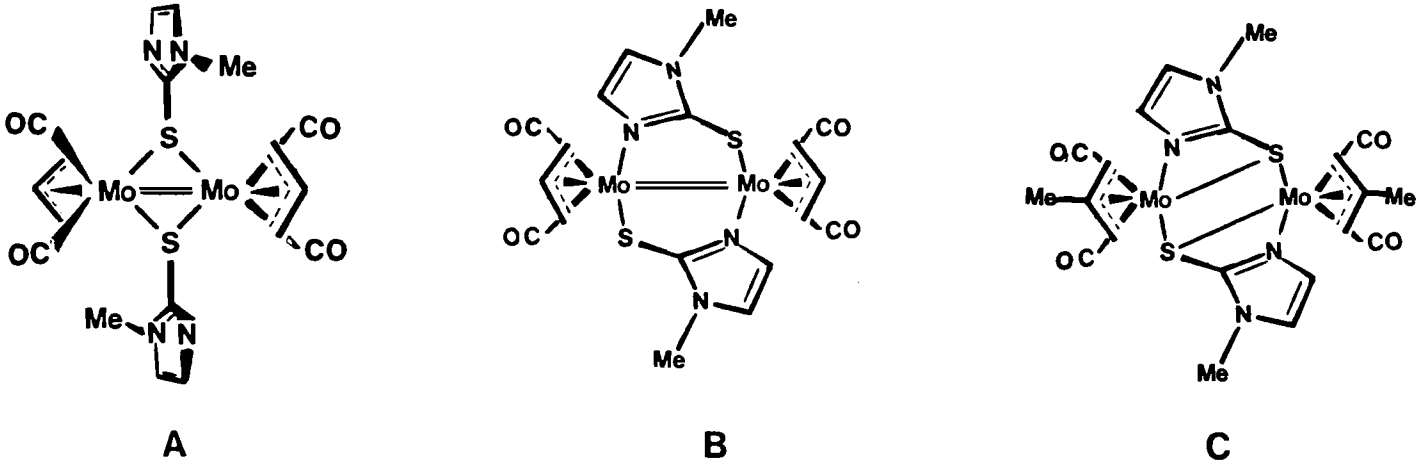

FIG. 4. Possible structures for the dimeric species, $[Mo(\eta^3\text{-allyl})(CO)_2(\overline{SCNCHCHNMe})]_2$.

Mo=Mo double bond. Although there are numerous examples of sulphur-bridged dimolybdenum species (23–26), the availability of the nitrogen lone pair on the unsubstituted nitrogen atom of the imidazolyl ligand prompted us to predict the arrangement shown in Fig. 4*b*. A single crystal X-ray structure determination of the $[Mo(\eta^3\text{-}C_4H_7)(CO)_2(\overline{SCNCHCHNMe})]_2$ complex was undertaken to examine this prediction. The resulting structure is shown in Fig. 5. The complex is indeed dimeric in the solid state but does not, in fact, display any Mo—Mo bonding interaction. The 18-electron count on each molybdenum centre is achieved by bridging S atoms. These 3-coordinate sulphur atoms adopt an arrangement similar to that predicted for the sulphur atom in the $[MeGa(pz)(\overline{SCNCHCHNMe})]$-$Re(CO)_3$ compound, but are evidently very different from the 2-coordinate sulphur atoms observed in the structure of the $[Me_2Ga(\overline{SCNCHCHNMe})]_2$ dimer species. The structure observed (Figs. 4*c* and 5) has crystallographically-imposed C_2 molecular symmetry, and exhibits a system of five fused rings arranged in an unusual U-shape. The ring sizes involved are, in order, five-, four-, four-, four- and five-membered. The central Mo_2S_2 ring is puckered (bond torsion angles of 24°, Table 6, Mo—S = 2.6868(7) Å in the MoSCN four-membered chelate ring, and Mo—S′ = 2.5576(7) Å; these distances are within the rather wide range found for Mo—S distances, the difference between the two values resulting probably from strain caused by the small bite of the mercaptoimidazole ligand (S···N = 2.640(2) Å) and from the influence of the different (carbonyl and allyl) *trans* ligands. The angles in the Mo_2S_2 ring are S—Mo—S′ = 80.96(2), Mo—S—Mo′ = 93.83(2)°, and the Mo···Mo cross-ring distance of 3.8313(4) Å precludes the possibility of significant metal–metal interaction. The Mo atoms are in a pseudo-octahedral environment, with the η^3-C_4H_7 ligand occupying one octahedral position, *cis* to one S and *trans* to the second S atom. Important bond distances are Mo—N = 2.253(2), mean Mo—CO = 1.950(2), Mo—C(allyl) = 2.259(3) (central C), mean = 2.326(3) Å (terminal carbons). Bond angles at Mo differ markedly from 90 and 180°C, as a result of the fused ring structure; in particular, S—Mo—N =

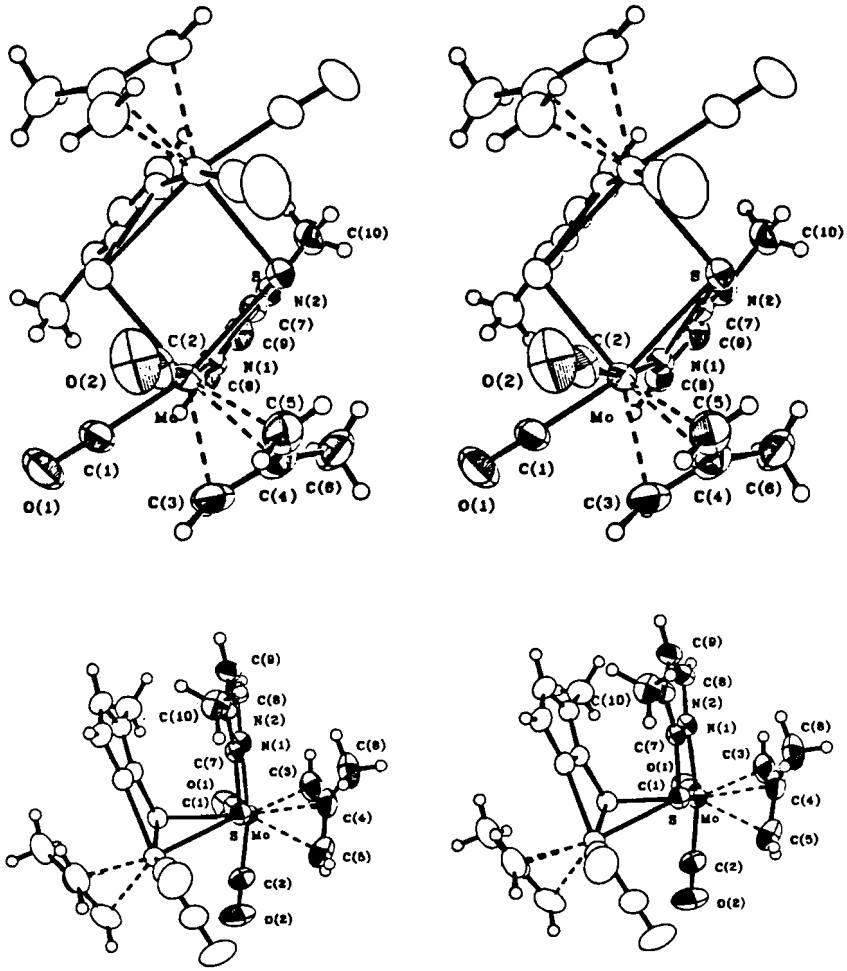

FIG. 5. Stereoscopic view of the $[Mo(\eta^3\text{-}C_4H_7)(CO)_2(S\overline{CNCHCHN}Me)]_2$ molecule. 50% probability thermal ellipsoids are shown.

63.9(1) and Mo—S—C = 75.7(1)° in the four-membered MoSCN ring. These latter angles suggest considerable strain in the MoSCN ring, although the ring is not far from planar (bond torsion angles 3–6(2)°, Table 6). The constraints introduced by the small bite of the mercaptoimidazole ligand probably also account for the non-occurrence of five-coordinate Ga in the dimethylgallium dimer (Fig. 1); here the S···N bite is 2.752(2) Å, and the formation of a Ga—S bond of about 2.40 Å would involve excessive strain in the four-membered chelate ring. The U-shape of the Mo complex (Fig. 5) results in the two imidazole rings being roughly parallel, with possible overlap of the two π-electron systems; the distances between the atoms of the rings are however too long (all >4 Å) to permit any significant interaction.

Acknowledgements

We thank the Natural Sciences and Engineering Research Council of Canada for financial support, and the University of British Columbia Computing Centre for assistance.

1. S. J. RETTIG, A. STORR, J. TROTTER, and K. UHRICH. Can. J. Chem. **62**, 2783 (1984).
2. R. G. HAYTER. J. Organomet. Chem. **13**, P1 (1968).
3. G. DOLCETTI and J. R. NORTON. Inorg. Synth. **16**, 35 (1976).
4. K. S. CHONG, S. J. RETTIG, A. STORR, and J. TROTTER. Can. J. Chem. **55**, 4166 (1977).
5. P. COPPENS, L. LEISEROWITZ, and D. RABINOVICH. Acta Crystallogr. **18**, 1035 (1965).
6. W. R. BUSING and H. A. LEVY. Acta Crystallogr. **22**, 457 (1967).
7. D. T. CROMER and J. B. MANN. Acta Crystallogr. Sect. A, **24**, 321 (1968).
8. R. F. STEWART, E. R. DAVIDSON, and W. T. SIMPSON. J. Chem. Phys. **42**, 3175 (1965).
9. D. T. CROMER and D. LIBERMAN. J. Chem. Phys. **53**, 1891 (1970).
10. J. DE MEULENAER and H. TOMPA. Acta Crystallogr. **19**, 1014 (1965).
11. S. J. RETTIG, A. STORR, and J. TROTTER. Can. J. Chem. **52**, 2206 (1974).
12. S. J. RETTIG, A. STORR, and J. TROTTER. Can. J. Chem. **53**, 58 (1975).
13. S. J. RETTIG, A. STORR, and J. TROTTER. Can. J. Chem. **54**, 1278 (1976).
14. S. J. RETTIG, A. STORR, and J. TROTTER. Can. J. Chem. **62**, 1705 (1984).
15. D. F. SHRIVER and C. E. NORDMAN. Inorg. Chem. **2**, 1298 (1963).
16. W. HARRISON, A. STORR, and J. TROTTER. J. Chem. Soc. Dalton Trans. 1554 (1972).
17. D. F. RENDLE, A. STORR, and J. TROTTER. J. Chem. Soc. Dalton Trans. 2252 (1973).
18. V. I. BREGADZE, N. G. FURMANOVA, L. M. GOLUBINSKAYA, O. Y. KOMPAN, Y. T. STRUCHKOV, V. A. BREN, ZH. V. BREN, A. E. LYUBARSKAYA, V. I. MINKIN, and L. M. SITKINA. J. Organomet. Chem. **192**, 1 (1980).

19. K. DYMOCK, G. J. PALENIK, J. SLEZAK, C. L. RASTON, and A. H. WHITE. J. Chem. Soc. Dalton Trans. 28 (1976).
20. D. M. ADAMS. Metal–ligand and related vibrations. Edward Arnold, London. 1967.
21. A. ARDUINI and A. STORR. J. Chem. Soc. Dalton Trans. 503 (1974).
22. F. A. COTTON. Chemical application of group theory. Wiley. 1963.
23. K. YAMANOUCHI, J. H. ENEMARK, J. W. MCDONALD, and W. E. NEWTON. J. Am. Chem. Soc. **99**, 3529 (1977).
24. J. T. HUNEKE, K. YAMANOUCHI, and J. H. ENEMARK. Inorg. Chem. **17**, 3695 (1978).
25. E. I. STEIFEL. Prog. Inorg. Chem. **22**, 1 (1977).
26. M. E. NOBLE, K. FOLTING, J. C. HUFFMAN, and R. A. D. WENTWORTH. Inorg. Chem. **22**, 3671 (1983).

Unimolecular fragmentation of some gaseous protonated amines

ERIC J. REINER, RAYMOND A. POIRIER,[1] MICHAEL R. PETERSON, IMRE G. CSIZMADIA, AND ALEX G. HARRISON[2]
Department of Chemistry, University of Toronto, Toronto, Ont., Canada M5S 1A1

Received February 14, 1986

ERIC J. REINER, RAYMOND A. POIRIER, MICHAEL R. PETERSON, IMRE G. CSIZMADIA, and ALEX G. HARRISON. Can. J. Chem. **64**, 1652 (1986).

The proton-transfer chemical ionization mass spectra of the C_3 to C_5 monoalkyl amines as well as a number of di- and tri-alkyl amines have been determined using H_3^+ and (in some cases) HCO^+ as protonating agent. The RNH_3^+ ions fragment to form alkyl ions R^+ and eliminate alkenes to form NH_4^+. In addition, abundant immonium ions are observed in the CI mass spectra corresponding to elimination of alkane from RNH_3^+ or to direct alkide ion abstraction from RNH_2; these ions serve to characterize the alkyl groups attached to the α-carbon atom of the amine. Although alkane elimination from RNH_3^+ is the thermochemically favoured reaction, only R^+ and NH_4^+ are formed in decomposition of metastable RNH_3^+ ions. The potential energy profile for fragmentation of i-$C_3H_7NH_3^+$ has been calculated by *ab initio* molecular orbital methods. These calculations show that CH_4 elimination has a large energy barrier additional to the reaction endothermicity while formation of NH_4^+ has only a small additional barrier and formation of $C_3H_7^+$ has no barrier additional to the endothermicity. It is concluded that the immonium ions probably arise primarily by direct alkide ion abstraction reactions.

ERIC J. REINER, RAYMOND A. POIRIER, MICHAEL R. PETERSON, IMRE G. CSIZMADIA et ALEX G. HARRISON. Can. J. Chem. **64**, 1652 (1986).

Utilisant le H_3^+ et (dans quelques cas) le HCO^+ comme agents protonants, on a déterminé les spectres de masse par ionisation chimique par transfert de proton des amines primaires en C_3 à C_5 ainsi que d'un certain nombre d'amines secondaires et tertiaires. Les ions RNH_3^+ se fragmentent pour former des ions alkyles R^+ ou pour éliminer des alcènes avec formation de NH_4^+. De plus, on observe la formation abondante d'ions immonium dans les spectres de masse par ionisation chimique et ceux-ci correspondent à une élmination d'alcane de l'ion RNH_3^+ ou à un enlèvement direct d'ion alkide à partir du RNH_2; ces ions servent à caractériser les groupements alkyles attachés à l'atome de carbone en α de l'amine. Même si l'élimination d'alcane à partir de l'ion RNH_3^+ est la réaction qui est thermodynamiquement favorisée, il ne se forme que les ions R^+ et NH_4^+ lors de la décomposition des ions métastables RNH_3^+. Utilisant des méthodes d'orbitales moléculaires *ab initio*, on a calculé les profiles d'énergie potentielle pour la fragmentation de l'ion i-$C_3H_7NH_3^+$. Ces calculs démontrent que l'élimination de CH_4 est soumise à une forte barrière énergétique qui s'additionne à l'endothermicité de la réaction alors que la formation de l'ion NH_4^+ n'est soumise qu'à une faible barrière additionnelle et que la formation de l'ion $C_3H_7^+$ n'est soumise à aucune barrière additionnelle par rapport à l'endothermicité de la réaction. On en conclut que les ions immonium proviennent probablement de réactions primaires d'abstractions directes de l'ion alkide.

[Traduit par la revue]

Introduction

The proton transfer chemical ionization mass spectra of aliphatic amines have seen little systematic study (1). By analogy with the behaviour of protonated aliphatic alcohols, which have been studied extensively (2–4), the major fragmentation reactions of the protonated amines, RNH_3^+, might be expected to be elimination of NH_3 forming the corresponding alkyl ion. In agreement with this prediction two early limited studies (5, 6) reported significant yields of R^+ ions, although, because of the high proton affinity of ammonia, fragmentation was not particularly facile (7). In contrast to these few results Colosimo and Brancaleoni (8) have reported that, in the H_2 chemical ionization mass spectra of the C_1 to C_4 alkyl amines, very low or negligible intensities are observed for the alkyl ions formed by loss of NH_3 from RNH_3^+. Rather, the base peak reported corresponds either to formation of NH_4^+ or to formation of immonium ions resulting, nominally, from elimination of an alkane molecule.

We report here the results of a detailed study of the proton transfer chemical ionization mass spectra of the C_3 to C_5 monoalkyl amines as well as selected dialkyl and trialkyl amines. In contrast to the results of Colosimo and Brancaleoni (8), we observe, for the monoalkyl amines, RNH_2, significant yields of R^+ alkyl ions although, in agreement with them, we also observe significant yields of NH_4^+ and immonium ions arising, nominally, by alkane elimination from RNH_3^+. Thermochemically, alkane elimination is the most favourable fragmentation reaction for protonated alkyl amines. However, this reaction is not observed for low energy RNH_3^+ ions fragmenting in the metastable ion time frame; rather formation of R^+ and NH_4^+ are the only metastable ion fragmentation reactions observed for the RNH_3^+ ions studied. Clearly the critical reaction energies are not the same as the reaction enthalpies. Metastable ion fragmentation reactions occur near the threshold for fragmentation of the decomposing species and it is well known (9, 10) that, near the threshold, the relative rates are determined primarily by the critical reaction energies. Thus the unimolecular chemistry of such ions is best understood in terms of the potential energy profile (11) for the ion. For species such as protonated amines it is extremely difficult to establish such a potential energy profile by experimental methods. Therefore, to reach a better understanding of the unimolecular chemistry of protonated alkyl amines we have calculated by *ab initio* molecular orbital methods the potential energy surface for a representative case, protonated isopropyl amine. The results of these calculations, as well as the detailed chemical ionization and metastable ion studies, are presented in the following.

Experimental

Proton transfer chemical ionization mass spectra were obtained using either a DuPont 21-290 single-focusing magnetic deflection mass spectrometer equipped with a chemical ionization source or with an

[1]Present address: Department of Chemistry, Memorial University, St. John's, Nfld., Canada A1B 3X7.

[2]Author to whom correspondence may be addressed.

AEI MS-902 double-focusing (BE) mass spectrometer also equipped with a chemical ionization source. Comparable spectra were obtained from each machine. In both cases the source temperature was ~150°C with samples being introduced from a heated inlet system at ~150°C. Reagent gas pressures were ~0.3 Torr and the ionizing electron energy was 70 eV. Reagent gases used were H_2 and 10% CO/90% H_2. The former produces H_3^+ as the proton transfer reagent ion while the latter produces HCO^+. The proton affinity of H_2 is ~422 kJ mol^{-1} (1) while that of CO is ~590 kJ mol^{-1} (1). Since the proton affinities of the amines are of the order of 920 kJ mol^{-1} (1) protonation of the amines by H_3^+ is ~500 kJ mol^{-1} exothermic and protonation by HCO^+ is ~330 kJ mol^{-1} exothermic, an exothermicity similar to protonation by the common proton transfer reagent CH_5^+; the use of HCO^+ has the advantage that the background is less extensive.

The unimolecular fragmentation reactions of the protonated amines, which occur in the metastable ion time-frame ($k = 10^4$–10^6 s^{-1}), were investigated by the MIKES technique (12) using a VG Analytical ZAB-2FQ mass spectrometer. The feature of the ZAB-2FQ instrument essential for the present work is that it is a reverse geometry (magnetic sector preceding the electric sector) double-focusing mass spectrometer. This configuration permits selection of the ion corresponding to the protonated amine by the magnetic sector, unimolecular fragmentation of this mass-selected ion in the drift region between the two sectors with identification of the ionic fragmentation products from their kinetic energies by scanning the electric sector (12). In studying the unimolecular metastable ion fragmentation reactions the protonated amines were preprared using H_2, CH_4, and i-C_4H_{10} as chemical ionization reagent gases. The CH_4 reagent gas produces CH_5^+ and $C_2H_5^+$ ($PA(CH_4)$ = 546 kJ mol^{-1} (1), $PA(C_2H_4)$ = 684 kJ mol^{-1} (1)) as reagent ions while i-C_4H_{10} produces $C_4H_9^+$ ($PA(i\text{-}C_4H_8)$ = 824 kJ mol^{-1} (1)) as the reagent ion. The variation of reagent gas thus permits a study of the effect of protonation exothermicity on the metastable ion characteristics.

All compounds used were commercially available and showed no detectable impurities in their mass spectra.

Results and discussion

Chemical ionization mass spectra

Table 1 records the H_2 and CO/H_2 chemical ionization mass spectra of n-propyl and i-propyl amine. Despite the high proton affinity of NH_3, which is a measure of the R^+—NH_3 bond strength (7),[3] the MH^+ ion signals are very low because of the large exothermicity of the protonation reaction. Two fragmentation reactions of the MH^+ ion are clearly established, reaction [1] involving elimination of NH_3 and reaction [2] involving formation of the ammonium ion.

[1] $C_3H_7NH_3^+ \rightarrow C_3H_7^+ + NH_3$

[2] $\rightarrow NH_4^+ + C_3H_6$

The $C_3H_5^+$ ion presumably arises by further fragmentation of the $C_3H_7^+$ ion. Two additional primary product ions are the $(M - H)^+$ ion at m/z 58 and the immonium ion (m/z 30 and m/z 44, respectively). This latter ion may arise either by direct alkide ion abstraction from RNH_2 by the reagent ion or by elimination of an alkane molecule from the MH^+ ion (reaction [3]).

[3] $R_1\text{—}CH(R_2)\text{—}NH_3^+ \rightarrow R_2CH{=}NH_2^+ + R_1H$

$\rightarrow R_1CH{=}NH_2^+ + R_2H$

The origin of this product will be discussed in detail later; the important point is that it serves to identify the alkyl group(s) attached to the α-carbon of the amine.

[3]Implicit in this statement is the assumption that alkyl cation affinities will parallel proton affinities.

TABLE 1. H_2 and CO/H_2 CI mass spectra of propyl amines

		Relative abundance			
		n-$C_3H_7NH_2$		i-$C_3H_7NH_2$	
m/z	Ion	H_2CI	CO/H_2CI	H_2CI	CO/H_2CI
60	MH^+	2	12	1	2
59	$M^{+\cdot}$	15	18	4	1
58	$(M - H)^+$	59	35	37	21
45	$MH^+ - CH_3$	1	—	4	—
44	$MH^+ - CH_4$	32	12	89	85
43	$C_3H_7^+$	100	100	100	77
42	$C_3H_6^+$	4	1	6	1
41	$C_3H_5^+$	46	22	22	12
30	$MH^+ - C_2H_6$	96	37	5	1
18	NH_4^+	90	79	80	100

The present H_2CI mass spectra are in quantitative disagreement with the spectra reported by Colosimo and Brancaleoni (8). Thus, they report the intensity ratios m/z 43:m/z 30:m/z 18 = 12:100:26 for n-propyl amine compared to 100:96:90 in our work. For i-propyl amine they do not report any ion signals at m/z 44 or m/z 43 which is in sharp contrast to our results. Although chemical ionization mass spectra are less reproducible than electron impact spectra these differences are greater than one would expect to observe. By comparison with earlier studies of the CI of amines (5, 6) and the known behaviour of alcohols under proton transfer CI conditions (2–4) the present results would appear to be a better representation of the behaviour expected of gaseous protonated amines.

Tables 2 and 3 record, respectively, the H_2 and CO/H_2 CI mass spectra of the four butyl amines as well as the spectra of diethyl amine and dimethyl ethyl amine. The butyl amines show the same fragmentation reactions as the propyl amines with NH_4^+ and $C_4H_9^+$ ($RNH_3^+ - NH_3$) being prominent as well as the immonium ions arising by nominal alkane elimination from MH^+. Thus, in the latter category, the two primary amines show intense $(M - C_3H_7)^+$ ion signals, t-butyl amine shows an intense $(M - CH_3)^+$ ion signal and s-butyl amine shows both $(M - CH_3)^+$ and $(M - C_2H_5)^+$ ion signals, the latter being more intense. These ion signals provide direct information on the alkyl group(s) attached to the α-carbon of the amine. The $C_3H_5^+$ ion presumably arises by further fragmentation of $C_4H_9^+$; the $C_2H_5^+$ ion also would be expected to arise by further fragmentation of $C_4H_9^+$ (13); however, formation of this ion is obscured by ion signals in the reagent ion spectrum (HCO^+ in CO/H_2 and a background N_2H^+/HCO^+ ion signal in H_2). Again our H_2CI mass spectra are in disagreement with the results of Colasimo and Brancaleoni (8) who do not report any ion signals for $C_4H_9^+$ (m/z 57).

The spectra of diethyl amine and dimethylethyl amine, also recorded in Tables 2 and 3, show more abundant MH^+ and $(M - H)^+$ ion signals than do the monoalkyl amines. This is in agreement with the CH_4CI mass spectra of triethyl amine and a number of polytertiary amines (14) which also show abundant MH^+ and $(M - H)^+$ ion signals. The di- and tri-alkyl amines of Tables 2 and 3 also show abundant ion signals arising, nominally, by CH_4 elimination from MH^+. In addition, a new reaction channel opens, involving ethylene elimination from MH^+, forming protonated ethyl amine and protonated dimethyl amine, respectively, at m/z 46.

Table 4 records the main ions observed in the H_2 CI mass

TABLE 2. H_2CI mass spectra of C_4 amines

		Relative abundance					
m/z	Ion	n-$C_4H_9NH_2$	i-$C_4H_9NH_2$	s-$C_4H_9NH_2$	t-$C_4H_9NH_2$	$(C_2H_5)_2NH$	$(CH_3)_2NC_2H_5$
74	MH^+	2	2	1	—	14	9
73	$M^{+\cdot}$	8	12	4	2	40	44
72	$(M - H)^+$	22	47	40	21	100	100
59	$MH^+ - CH_3$	—	—	—	—	5	2
58	$MH^+ - CH_4$	8	44	55	84	92	43
57	$C_4H_9^+$	23	47	59	100	7	2
56	$C_4H_8^+$	1	3	3	2	3	2
55	$C_4H_7^+$	4	12	12	9	—	—
46	$MH^+ - C_2H_4$	—	—	—	—	39	55
45	$MH^+ - C_2H_5$	1	—	2	—	1	1
44	$MH^+ - C_2H_6$	8	3	100	2	39	14
43	$C_3H_7^+$	5	7	9	1	2	1
42	$C_3H_6^+$	3	4	8	3	4	5
41	$C_3H_5^+$	38	67	72	31	2	1
30	$MH^+ - C_3H_8$	100	100	25	2	28	2
18	NH_4^+	44	52	99	24	99	1

TABLE 3. CO/H_2 CI mass spectra of C_4 amines

		Relative abundance					
m/z	Ion	n-$C_4H_9NH_2$	i-$C_4H_9NH_2$	s-$C_4H_9NH_2$	t-$C_4H_9NH_2$	$(C_2H_5)_2NH$	$(CH_3)_2NC_2H_5$
74	MH^+	15	9	3	1	100	61
73	$M^{+\cdot}$	18	15	2	1	71	100
72	$(M - H)^+$	27	28	19	4	79	92
59	$MH^+ - CH_3$	—	1	1	2	2	2
58	$MH^+ - CH_4$	11	23	26	75	99	69
57	$C_4H_9^+$	95	100	65	100	4	3
56	$C_4H_8^+$	1	3	—	1	4	2
55	$C_4H_7^+$	4	7	6	4	—	—
46	$MH^+ - C_2H_5$	(18)*	(10)*	(16)*	(3)*	25	12
45	$MH^+ - C_2H_5$	1	1	—	—	3	1
44	$MH^+ - C_2H_6$	5	—	100	—	22	11
43	$C_3H_7^+$	5	3	3	1	2	2
42	$C_3H_6^+$	2	1	4	—	2	7
41	$C_3H_5^+$	31	23	23	12	1	—
30	$MH^+ - C_3H_8$	100	52	2	—	14	2
18	NH_4^+	60	20	73	16	6	3

*This ion is not seen in H_2CI mass spectra and may arise by reaction of HCO^+ with amine, possibly

$$HCO^+ + RNH_2 \rightarrow HCONH_3^+ + (R - H)$$

spectra of eight isomeric pentyl amines. A major reaction channel involves elimination of NH_3 from MH^+ to form $C_5H_{11}^+$ (m/z 71), which shows extensive fragmentation to form $C_3H_7^+$ (m/z 43). For the purposes of identifying the amine the most important ions are those arising by nominal akane elimination from MH^+. Thus the primary amines of formula $C_4H_9CH_2NH_2$ show an abundant ion signal at m/z 30 corresponding to elimination of C_4H_{10}, amines with the structure $C_3H_7CH(NH_2)CH_3$ show an intense signal at m/z 44 corresponding to C_3H_8 elimination while $C_2H_5CH(NH_2)C_2H_5$ and $C_2H_5C(NH_2)(CH_3)_2$ both show an intense peak at m/z 58 corresponding to elimination of C_2H_6. The elimination of CH_4 is a much less structure-specific reaction and, thus, provides little structural information.

Figure 1 compares the H_2CI mass spectra of 2-amyl amine and t-amyl amine with the H_2CI of the corresponding alcohols. The H_3O^+ ion signal, analogous to the NH_4^+ ion signal, was not recorded for the alcohols because of interference from background water in the instrument. Two major differences are observed between the amines and the alcohols. First, the intensities of the alkane elimination products are much more intense for the amines, thereby providing much more definitive information concerning alkyl substitution on the α-carbon. Second, the $C_5H_{11}^+$ alkyl ions, formed by HX elimination from RXH^+, show much more extensive fragmentation for the amines. The origin of this latter difference has been discussed previously (15).

Table 5 records the H_2CI mass spectra of four C_5 di- and tri-alkyl amines. Abundant $(M - H)^+$ ion signals are observed as well as the immonium ions arising by nominal alkane elimination from MH^+; this latter reaction involves cleavage of the C—C bond α to the nitrogen function. In addition, as discussed previously for the C_4, di- and tri-alkyl amines, olefin elimination from MH^+ is quite prominent. Thus both the

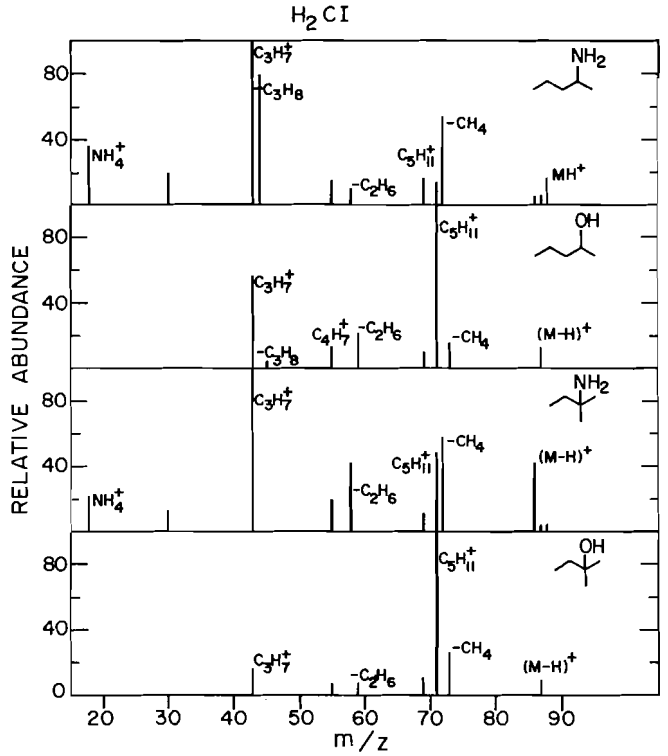

FIG. 1. Comparison of the H_2CI mass spectra of amyl amines and amyl alcohols.

protonated methyl butyl amines show elimination of C_4H_8 while *N*-ethyl propyl amine shows elimination of C_3H_6 and *N*-methyl diethyl amine shows elimination of C_2H_4. These olefin elimination reactions also help to characterize the amines.

Fragmentation of protonated amines as metastable ions

Two fragmentation channels are observed for RNH_3^+ ions in the metastable ion time frame, formation of NH_4^+ by elimination of alkene and formation of the alkyl ion, R^+, by loss of NH_3. Thus, *n*-$C_3H_7NH_3^+$ showed formation of $C_3H_7^+$ and NH_4^+ in the ratio 23:100 while *i*-$C_3H_7NH_3^+$ showed a ratio of 1:100 in metastable ion fragmentation reactions. The results obtained for the protonated butyl amines are presented in Table 6 for three different protonating reagents with different protonation exothermicity. The protonated primary amines, *n*-$C_4H_9NH_3^+$ and *i*-$C_4H_9NH_3^+$ show abundant formation of $C_4H_9^+$ on the metastable ion time scale, with the relative abundance of NH_4^+ increasing with increasing exothermicity of the initial protonation reaction. By contrast, the protonated secondary and tertiary amines show dominant formation of NH_4^+ in metastable ion fragmentation reactions with the relative product yields being insensitive to the exothermicity of the protonation reaction. The pentyl amines were studied only following protonation by *i*-C_4H_{10}. The results, presented in Table 7, are similar to the results for the protonated butyl amines in that the primary amines favour formation of the alkyl ion, $C_5H_{11}^+$, while the secondary and tertiary amines strongly favour formation of NH_4^+ in the metastable ion fragmentation reactions.

The metastable ion fragmentation reactions correspond to reactions with rate constants in the range 10^4 to 10^6 s^{-1} defined by the parameters of the instrument; normally the relative ion abundances depend strongly on the critical reaction energies. Changing the exothermicity of the protonation reaction does not change the range of rate constants but appears to change the

TABLE 4. H_2CI mass spectra of amyl amines

		Relative abundance									
		NH2		NH2		NH2		NH2		NH2	
m/z	Ion										
88	MH^+	14	15	7	18	17	15	58	7		
87	$M^{+\bullet}$	21	14	17	18	10	5	5	4		
86	$(M-H)^+$	43	29	31	53	58	43	49	41		
72	$MH^+ - CH_4$	8	9	47	19	26	50	17	57		
71	$C_5H_{11}^+$	7	10	19	14	12	18	14	49		
58	$MH^+ - C_2H_6$	4	6	—	13	8	—	73	42		
44	$MH^+ - C_3H_8$	—	—	—	—	100	59	14	—		
43	$C_3H_7^+$	90	91	100	100	97	100	100	100		
30	$MH^+ - C_4H_{10}$	100	100	47	81	18	10	31	7		
18	NH_4^+	26	22	21	24	27	18	34	17		

TABLE 5. H_2CI mass spectra of some C_5 di- and tri-alkyl amines

m/z	Ion	$CH_3NH(CH_2)_3CH_3$	$CH_3NHCH(CH_3)CH_2CH_3$	$C_2H_5NHCH_2CH_2CH_3$	$CH_3N(C_2H_5)_2$
88	MH^+	31	7	16	23
87	$M^{+\cdot}$	33	19	48	52
86	$(M - H)^+$	100	60	100	100
72	$MH^+ - CH_4$	13	36	37	41
60	$MH^+ - C_2H_4$	—	—	—	42
58	$MH^+ - C_2H_6$	10	100	90	—
57	$C_4H_9^+$	24	18	—	9
46	$MH^+ - C_3H_6$	—	—	43	—
45	$MH^+ - C_3H_7$	—	3	6	—
44	$MH^+ - C_3H_8$	84	7	22	10
43	$C_3H_5^+$	—	5	31	—
41	$C_3H_5^+$	9	9	8	—
32	$MH^+ - C_4H_8$	38	30	2	—
30	$MH^+ - C_4H_{10}$	4	14	29	—
18	NH_4^+	2	3	23	—

TABLE 6. Metastable ion fragmentation of protonated butyl amines

	% of total metastable ion signal					
	i-$C_4H_{10}CI$		CH_4CI		H_2CI	
Amine	$C_4H_9^+$	NH_4^+	$C_4H_9^+$	NH_4^+	$C_4H_9^+$	NH_4^+
n-$C_4H_9NH_3^+$	73	27	40	60	38	62
i-$C_4H_9NH_3^+$	86	14	67	33	64	36
s-$C_4H_9NH_3^+$	5	95	1	99	5	95
t-$C_4H_9NH_3^+$	4	96	2	98	5	95

TABLE 7. Metastable ion fragmentation of protonated pentyl amine

	% of metastable ion signal i-$C_4H_{10}CI$	
Amine	$C_5H_{11}^+$	NH_4^+
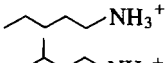	58	42
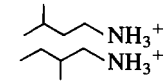	83	17
	72	28
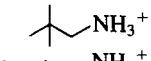	56	44
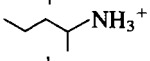	6	94
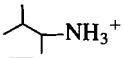	29	71
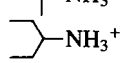	3	97
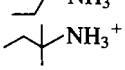	1	99

distribution of internal energies in the metastable ion energy window (16). By contrast, fragmentation reactions occurring in the ion source following protonation represent higher energy reactions ($k > 10^6$ s^{-1}) and the relative product yields may reflect both the effect of critical reaction energies and frequency factors on the rates of fragmentation. The relative metastable ion abundances observed for the butyl amines suggest that for the primary amines formation of $C_4H_9^+$ has a lower critical reaction energy than formation of NH_4^+ with the opposite prevailing for the secondary and tertiary amine. The absence of any metastable transition corresponding to elimination of alkane implies that this reaction has a considerably higher critical reaction energy.

It is of interest to compare this approximate ordering of critical reaction energies with calculated reaction endothermicities. This comparison is made in Table 8 for the propyl and butyl amines which shows the calculated ΔH_{react} and relative ion abundances for metastable ion fragmentation reactions and in the H_2 and CO/H_2 chemical ionization mass spectra. In the thermochemical calculations we have assumed that primary alkyl ions are not formed but that hydrogen shifts occur to form the appropriate secondary or tertiary alkyl ion. The thermochemical data used in the calculations are summarized in the Appendix.

Several interesting points arise from the comparison of the relative abundances with the reaction thermochemistry. First, for the secondary and tertiary protonated amines, alkane elimination has by far the lowest enthalpy of reaction yet this fragmentation reaction is not observed for metastable ion fragmentation reactions. This strongly suggests that the critical energy for alkane elimination is considerably greater than the reaction endothermicity. The high yields of the alkane elimination products in the CI mass spectra, which emphasize fragmentation reactions of ions with greater internal energies, are consistent either with a very favourable frequency factor for the reaction *or* with formation of these products by a direct alkide ion abstraction reaction. For the secondary and tertiary amines the favoured formation of NH_4^+ over R^+ in metastable ion fragmentation reactions is in agreement with the reaction thermochemistry; the increase in the relative yields of the alkyl ions in the CI mass spectra indicates that the reaction forming these products has a more favourable frequency factor. For the primary amines the relative metastable fragmentation yields of alkyl ions and NH_4^+ are not in agreement with the calculated enthalpies of reaction since large yields of alkyl ions are observed despite the fact that the reaction has a greater endothermicity. These results imply that, at least for the primary amines, formation of NH_4^+ has a critical reaction energy greater than the reaction endothermicity. The variation of relative metastable ion yields with protonation exothermicity (Table 6) also supports the conclusion that formation of $C_4H_9^+$ has the

TABLE 8. Thermochemistry and relative yields of fragmentation reactions

Amine	Fragmentation products	ΔH_{react}*	m*†	CO/H_2CI	H_2CI
n-$C_3H_7NH_3^+$	$CH_2NH_2^+ + C_2H_6$	114	0	37	96
	i-$C_3H_7^+ + NH_3$	206	23	100	100
	$NH_4^+ + C_3H_6$	102	100	79	90
i-$C_3H_7NH_3^+$	$CH_3CHNH_2^+ + CH_4$	52	0	85	89
	i-$C_3H_7^+ + NH_3$	223	1	77	100
	$NH_4^+ + C_3H_6$	119	100	100	80
n-$C_4H_9NH_3^+$	$CH_2NH_2^+ + C_3H_8$	120	0	100	100
	s-$C_4H_9^+ + NH_3$	200	67	95	23
	$NH_4^+ + C_4H_8$	95	100	60	44
i-$C_4H_9NH_3^+$	$CH_2NH_2^+ + C_3H_8$	130	0	52	100
	t-$C_4H_9^+ + NH_3$	143	100	100	47
	$NH_4^+ + C_4H_8$	105	49	20	52
s-$C_4H_9NH_3^+$	$CH_3CHNH_2^+ + C_2H_6$	71	0	100	100
	s-$C_4H_9^+ + NH_3$	217	1	65	59
	$NH_4^+ + C_4H_8$	113	100	73	99
t-$C_4H_9NH_3^+$	$(CH_3)_2CNH_2^+ + CH_4$	30	0	75	84
	t-$C_4H_9^+ + NH_3$	168	2	100	100
	$NH_4^+ + C_4H_8$	131	100	16	24

*kJ mol^{-1}.
†CH_4CI.

lower critical reaction energy for the primary amines. This result contrasts with the conclusions derived for the protonated secondary and tertiary amines.

These differences between the calculated reaction endothermicities and the apparent critical reaction energies prompted us to undertake the calculation of the potential energy surface for the fragmentation of a representative protonated amine by *ab initio* molecular orbital methods. We have chosen protonated *i*-propyl amine for study. The details of these calculations are presented in the following section. Further discussion of the fragmentation of protonated amines follows in light of these calculations.

Potential energy profile for fragmentation of i-$C_3H_7NH_3^+$

The potential energy profile for fragmentation of protonated isopropyl amine was determined by *ab initio* self-consistent field (SCF) molecular orbital calculations. Three fragmentation reaction were considered, viz.

[3] i-$C_3H_7NH_3^+ \rightarrow CH_3CHNH_2^+ + CH_4$

[4] $\rightarrow i$-$C_3H_7^+ + NH_3$

[5] $\rightarrow NH_4^+ + C_3H_6$

A 3-21G (17) split valence basis set was used to optimize the geometries of all the species by use of *ab initio* SCF calculations in the MONSTERGAUSS system (18).[4] Geometry optimization of all species, except the transition states, was achieved by simultaneous variation of bond lengths and bond angles using the analytic first derivatives of energy in conjunction with Davidon's optimally conditional (OC) algorithm (20). The norm of the gradient vector was less than 5×10^{-4} mdyn at convergence for all cases. Geometry optimization of the transition state structures (TS $-$ NH_4^+ and TS $-$ CH_4) was accomplished using the VA05AD (VA) sum of squares optimization technique (21). In this method the Hessian matrix was evaluated by gradient differences and diagonalized to determine the order of the critical point. Again the norm of the gradient vector was less than 5×10^{-4} mdyn for convergence. The structures of all stable species are listed in Table 9 while the structures of the two transition states and the one intermediate detected are shown in Fig. 2.

The single point energies of the 3-21G-optimized structures were calculated using a 6-31G* (22) basis set and are listed in Table 10. Because all the reactions are isodesmic reactions of closed shell species, the correlation and relativistic energies may be assumed to be relatively constant and neglect of these terms will introduce errors of no more than 4–17 kJ mol^{-1} in calculated energy differences (30). All calculations were performed on the Gould 32/9705 computer, Department of Chemistry, University of Toronto.

The calculated potential energy profile is shown in Fig. 3. Reaction [3], elimination of CH_4, entails a 1,3-hydrogen/proton shift from nitrogen to carbon in which the hydrogen/proton inserts itself between the central carbon (C_1) and the departing methyl group; the transition state structure is shown in Fig. 2. The calculated barrier for this reaction is 389 kJ mol^{-1}, much higher than the theoretically calculated endothermicity of 50 kJ mol^{-1}; this latter value is in good agreement with the endothermicity (52 kJ mol^{-1}) derived from the thermochemical data. Reaction [4], loss of NH_3, was found to proceed without a barrier additional to the endothermicity with the $C_3H_7^+$ and NH_3 products merely drifting apart with no maximum in the potential energy curve. The calculated reaction endothermicity is in good agreement with the experimental endothermicity.

Reaction [5], formation of NH_4^+, was found to proceed by a transition state with an energy 40 kJ mol^{-1} above the final products; the structure of this transition state is shown in Fig. 2. In essence, in this reaction the C—N bond lengthens and the NH_3 group moves towards one of the methyl groups with some lengthening of a C—H bond. Of particular interest is the observation of the minimum in the surface between the transition state and the final products. This minimum corres-

[4]MONSTERGAUSS includes GAUSSIAN 80 (19) and geometry optimization by analytic first derivative methods.

TABLE 9. Calculated equilibrium geometries

Molecule or ion	Geometrical parameters
NH_3	$r(NH) = 1.003$ $\angle(HNH) = 112.4$
CH_4	$r(CH) = 1.083$ $\angle(HCH) = 109.5$
NH_4^+	$r(NH) = 1.021$ $\angle(NHN) = 109.5$
$CH_2NH_2^+$ 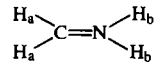	$r(CH) = 1.268$, $r(H_aC) = 1.072$, $r(H_bN) = 1.010$ $\angle(H_aCN) = 120.2$, $\angle(H_bNC) = 122.2$
C_3H_6 (C_s) 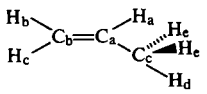	$r(C_aC_b) = 1.316$, $r(C_aC_c) = 1.510$, $r(H_aC_a) = 1.076$, $r(H_bC_b) = 1.075$, $r(H_cC_b) = 1.073$, $r(H_dC_c) = 1.083$, $r(H_eC_c) = 1.086$, $\angle(H_aC_aC_b) = 119.6$ $\angle(H_bC_bC_a) = 121.8$, $\angle(H_cC_bC_a) = 121.8$ $\angle(C_bC_aC_c) = 124.7$, $\angle(H_eC_cC_a) = 119.7$ $\angle(H_eC_cC_aC_b) = 120.5$
$C_3H_7^+$ (C_{2v}) 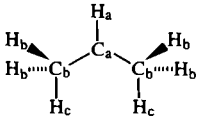	$r(H_aC_a) = 1.079$, $r(C_aC_b) = 1.455$ $r(H_bC_b) = 1.095$, $r(H_cC_b) = 1.077$ $\angle(H_aC_aC_b) = 117.3$, $\angle(H_cC_bC_a) = 114.1$ $\angle(H_bC_bC_a) = 108.7$, $\angle(H_aC_aC_bH_b) = 124.0$
$C_2H_6N^+$ (C_s) 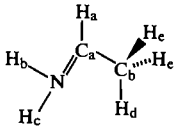	$r(C_aN) = 1.275$, $r(C_aC_b) = 1.485$ $r(H_bN) = 1.008$, $r(H_cN) = 1.009$ $r(H_dC_b) = 1.080$, $r(H_aC_a) = 1.075$ $r(H_eC_b) = 1.087$, $\angle(H_aC_aN) = 117.3$ $\angle(H_bNC_a) = 122.1$, $\angle(H_cNC_a) = 122.1$ $\angle(H_dC_bC_a) = 112.9$, $\angle(H_eC_bC_a) = 108.9$ $\angle(NC_aC_b) = 124.2$, $\angle(H_aC_aC_bH_e) = 121.9$
$C_3H_{10}N^+$ (C_s) 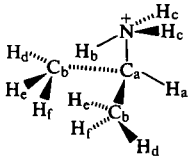	$r(NC_a) = 1.571$, $r(H_aC_a) = 1.079$ $r(H_bN) = 1.018$, $r(H_cN) = 1.017$ $r(C_bC_a) = 1.528$, $r(H_dC_b) = 1.084$ $r(H_fC_b) = 1.084$, $r(H_eC_b) = 1.083$ $\angle(H_aC_aN) = 104.3$, $\angle(H_bNC_a) = 109.8$ $\angle(H_cNC_a) = 110.7$, $\angle(C_bC_aN) = 107.6$ $\angle(H_dC_bC_a) = 111.1$, $\angle(H_eC_bC_a) = 112.0$ $\angle(H_fC_bC_a) = 108.6$, $\angle(C_bC_aNH_a) = 118.6$ $\angle(H_dC_bC_aN) = -63.4$, $\angle(H_dC_bC_aH_e) = 122.7$ $\angle(H_fC_bC_aH_d) = 118.5$, $\angle(H_cNC_aH_a) = 119.7$

ponds to a proton bound dimer of propene and ammonia and has the structure shown in Fig. 2. The binding energy of the dimer was found to be 42 kJ mol^{-1}.

The calculated potential energy profile adequately rationalizes the experimental data obtained for the fragmentation of protonated isopropyl amine. The high critical reaction energy for elimination of CH_4 precludes observation of this reaction channel in metastable ion fragmentation reactions despite the favourable thermochemistry. Instead formation of NH_4^+ has the lowest critical reaction energy and, in agreement, this is the dominant metastable ion fragmentation product. The high abundance of the CH_4 elimination product, particularly in the CO/H_2 CI mass spectrum, remains to be resolved. Protonation of isopropyl amine by ground state HCO^+ is only ~324 kJ mol^{-1} exothermic while the barrier for elimination of CH_4 is ~389 kJ mol^{-1}; thus elimination of CH_4 should not be

TABLE 10. Calculated energies of participating species with 3-21G geometries

Molecule or ion	Energy (hartrees) 6-31G	3-21G
NH_3	−56.18251	−55.87220
CH_4	−40.19517	−39.97688
NH_4^+	−56.53055	−56.23386
C_3H_6	−117.07140	−116.42401
$C_3H_7^+$	−117.38060	−116.72620
$CH_3CHNH_2^+$	−133.44277	−132.70564
$(CH_3)_2CHNH_3^+$	−173.65756	−172.71387
TS—NH_4^+	−173.58538	−172.62685
TS—CH_4	−173.50362	−172.55088
C_3H_6—H^+—NH_3	−173.61986	−172.59444

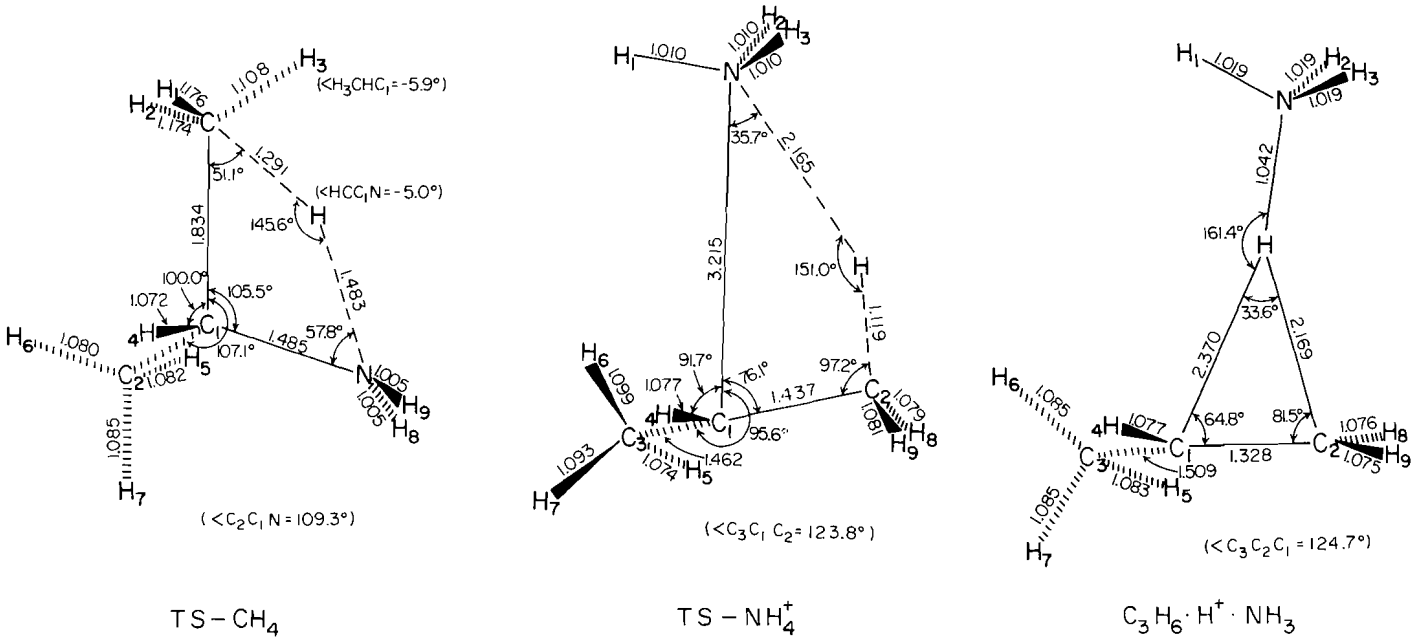

FIG. 2. Calculated structures of transition states and intermediates.

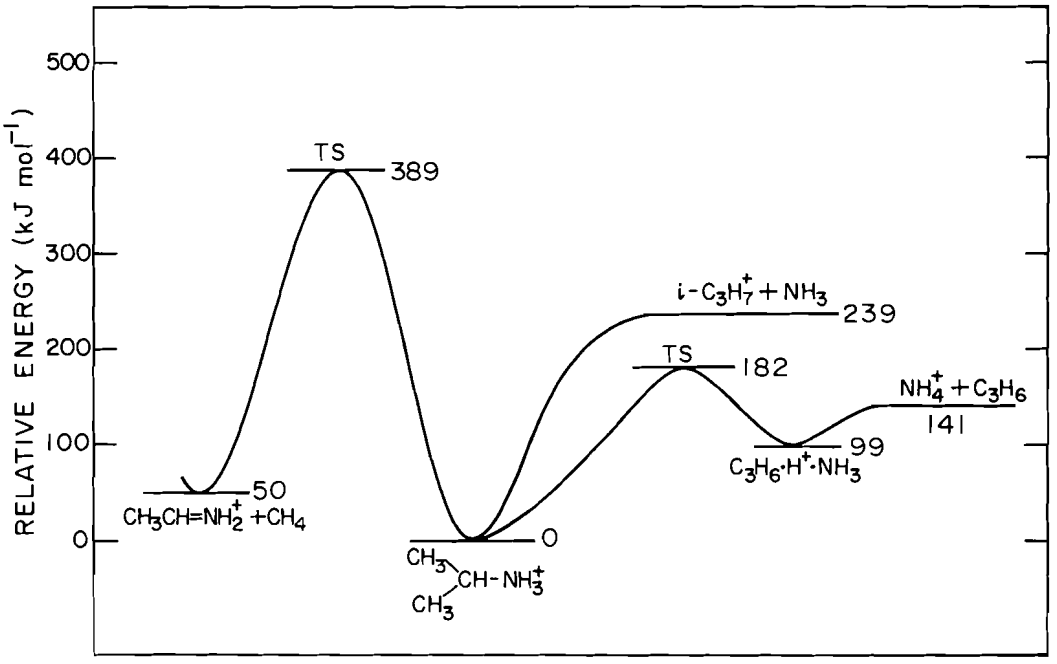

FIG. 3. Potential energy profile for i-$C_3H_7NH_3^+$.

observed. However, to qualify this statement it should be noted that it is unlikely that all of the HCO^+ ions are in their ground state under our experimental conditions. In view of the high energy barrier for alkane elimination it might be argued that alkane elimination does not occur from protonated amines but rather that the relevant signals in the CI mass spectra arise by a different mechanism such as direct alkide ion abstraction by the reagent ion. We have observed (unpublished results) that alkane elimination occurs from protonated alkyl amines activated by a high energy (8 keV) collision but that it is of only minor importance for protonated amines activated by a low energy (100 eV) collision. The results to date suggest that the average energy transformed from translational energy into internal energy is approximately the same for both high energy and low energy collisions (23, 24) but that in the high energy collisions there is a low probability tail extending to high internal energies (24). It appears that it is these high energy ions which fragment by alkane elimination. Such high energies probably are not achieved to a significant extent in chemical ionization systems and it is likely that the reaction occurring is largely an alkide ion abstraction reaction rather than alkane elimination from the protonated amine.

There remains the question of why the protonated primary butyl amines show abundant formation of $C_4H_9^+$ in metastable ion fragmentation reactions while the secondary and tertiary amines do not. The reasons are not clear. The thermochemistry favours formation of NH_4^+ and the calculated barrier for this reaction is not sufficient to reverse the thermochemical arguments. We must assume that, for reasons unknown, for protonated *n*-butyl and *i*-butyl amines, the barrier is even higher than that calculated for the *i*-propyl amine. We have not attempted to calculate this barrier since for the butyl amines there is a possible ambiguity concerning the mechanism of the reaction, i.e., an uncertainty as to the hydrogen lost with the NH_4^+.

Acknowledgements

The purchase of ZAB 2FQ for the Ontario Regional Ion Chemistry Laboratory (ORICL) at the University of Toronto was made possible by a grant from the Natural Sciences and Engineering Research Council of Canada, who also have supported the present research. E.J.R. gratefully acknowledges the award of University of Toronto Open Fellowships.

1. A. G. HARRISON. Chemical ionization mass spectrometry. CRC Press, Boca Raton, FL. 1983.
2. F. H. FIELD. J. Am. Chem. Soc. **92**, 2672 (1970).
3. H. ICHIKAWA and A. G. HARRISON. Org. Mass Spectrom. **13**, 389 (1978).
4. J. A. HERMAN and A. G. HARRISON. Can. J. Chem. **59**, 2125 (1984).
5. I. JARDINE and C. FENSELAU. J. Am. Chem. Soc. **98**, 5086 (1976).
6. H. E. AUDIER, A. MILLET, C. PERRET, J. C. TABET, and P. VARENNE. Org. Mass Spectrom. **13**, 315 (1978).
7. F. H. FIELD. *In* Mass spectrometry. Ser. 1, Vol. 5. MTP Rev. Sci. Phys. Chem. *Edited by* A. Maccoll. Butterworth, London. 1972.
8. M. COLOSIMO and E. BRANCALEONI. Org. Mass Spectrom. **17**, 286 (1982).
9. C. W. TSANG and A. G. HARRISON. *In* Biochemical applications of mass spectrometry. *Edited by* G. R. Waller. John Wiley, New York. 1972.
10. I. HOWE, D. H. WILLIAMS, and R. D. BOWEN. Mass spectrometry, principles and applications. McGraw-Hill, New York. 1981.
11. R. D. BOWEN and D. H. WILLIAMS. *In* Rearrangements in ground and excited states. Vol. 1. *Edited by* P. deMayo. Academic Press, New York, NY. 1980. Chapt. 2.
12. K. R. JENNINGS. *In* Ionic processes in the gas phase. *Edited by* M. A. Almoster Ferreira. Dordrecht. 1984.
13. R. D. BOWEN and D. H. WILLIAMS. J. Chem. Soc. Perkin Trans. II, 1479 (1976).
14. T. A. WHITNEY, L. P. KLEMANN, and F. H. FIELD. Anal. Chem. **43**, 1048 (1971).
15. E. J. REINER and A. G. HARRISON. Org. Mass Spectrom. **19**, 343 (1984).
16. A. G. HARRISON, T. GAUMANN, and D. STAHL. Org. Mass Spectrom. **18**, 517 (1983).
17. J. S. BINKLEY, J. A. POPLE, and W. J. HEHRE. J. Am. Chem. Soc. **102**, 939 (1980).
18. M. R. PETERSON and R. A. POIRIER. MONSTERGAUSS. Department of Chemistry, University of Toronto, Toronto, Canada.
19. J. S. BINKLEY, R. A. WHITESIDE, R. KRISHNAN, R. SEEGER, D. J. DEFREES, H. B. SCHLEGEL, and J. A. POPLE. Q.C.P.E. **13**, 406 (1981).
20. W. C. DAVIDON and L. NAZARETH. Technical Memos 303 and 306, Applied Physical Division, Argonne National Laboratories, Argonne, IL. 1977.
21. M. J. D. POWELL. Subroutine VAO5AD, AERE Subroutine Library, Harwell, Didcot, Berkshire, U.K.
22. W. J. HEHRE, R. DITCHFIELD, and J. A. POPLE. J. Chem. Phys. **56**, 2257 (1972); P. C. HARIHARAN and J. A. POPLE. Theoret. Chim. Acta (Berlin), **28**, 213 (1973).
23. S. NACSON and A. G. HARRISON. Int. J. Mass Spectrom. Ion Proc. **63**, 325 (1985).
24. H. I. KENTTAMAA and R. G. COOKS. Int. J. Mass Spectrom. Ion Proc. **64**, 79 (1985).
25. J. D. COX and G. PILCHER. Thermochemistry of organic and organometallic compounds. Academic Press, New York. 1970.
26. D. H. AUE and M. T. BOWERS. *In* Gas phase ion chemistry. Vol. 2. *Edited by* M. T. Bowers. Academic Press, New York. 1979.
27. H. M. ROSENSTOCK, K. DRAXL, B. W. STEINER, and J. T. HERRON. J. Phys. Chem. Ref. Data, **6**, Suppl. 1 (1977).
28. F. P. LOSSING and G. P. SEMELUK. Can. J. Chem. **48**, 955 (1970).
29. F. P. LOSSING, Y.-T. LAU, and A. MACCOLL. Can. J. Chem. **59**, 2228 (1981).
30. P. ČÁRSKY and M. URBAN. *Ab initio* calculations: methods and applications in chemistry. Lecture Notes in Chemistry 16, Springer Verlag, New York. 1980.

Appendix

The enthalpies of formation of the protonated amines were derived from the reported proton affinities through the relationship

[6] $$PA(RNH_2) = \Delta H_f^0(RNH_3^+) - \Delta H_f^0(RH^+) - \Delta H_f(RNH_2)$$

using $\Delta H_f^0(H^+) = 1531.4$ kJ mol^{-1} (27). The relevant data are summarized in Table 11. Other thermochemical data used were $\Delta H_f^0(i\text{-}C_3H_7^+) = 803$ kJ mol^{-1}, $\Delta H_f^0(s\text{-}C_4H_9^+) = 766$ kJ mol^{-1} and $\Delta H_f^0(t\text{-}C_4H_9^+) = 699$ kJ mol^{-1}, all taken from Lossing and Semeluk (28). $\Delta H_f^0(NH_3) = -46.0$ kJ mol^{-1}, $\Delta H_f^0(CH_4) = -75.3$ kJ mol^{-1}, $\Delta H_f^0(C_2H_6) = -83.7$ kJ mol^{-1} and $\Delta H_f^0(C_3H_6) = -20.9$ kJ mol^{-1} were from ref. 27 while the enthalpies of formation of the immonium ions are (29) $\Delta H_f^0(CH_2NH_2^+) = 745$ kJ mol^{-1}, $\Delta H_f^0(CH_3CHNH_2^+) = 657$ kJ mol^{-1}, $\Delta H_f^0(CH_3CH_2CHNH_2^+) = 636$ kJ mol^{-1}, and $\Delta H_f^0((CH_3)_2CNH_2^+) = 590$ kJ mol^{-1}.

TABLE 11. Thermochemical data for protonated amines

Amine	ΔH_f (kJ mol^{-1})*	PA (kJ mol^{-1})†	$\Delta H_f(RNH_3^+)$ (kJ mol^{-1})
n-$C_3H_7NH_2$	−70.2	914.2	546.8
i-$C_3H_7NH_2$	−83.8	918.0	529.7
n-$C_3H_9NH_2$	−95.0	916.3	520.1
i-$C_4H_9NH_2$	−103.6	918.4	509.6
s-$C_4H_9NH_2$	−106.3	922.6	502.5
t-$C_9H_9NH_2$	−120.9	925.9	484.5

*From ref. 25.
†From ref. 26.

Ternary charge-transfer complexes. III.[1] Complexes with Group V elements in the anion[2]

SYDNEY BROWNSTEIN,[3] ERIC GABE, FLORENCE LEE, AND ANDREJ PIOTROWSKI
Division of Chemistry, National Research Council of Canada, Ottawa, Ont., Canada K1A 0R9

Received October 8, 1985[4]

SYDNEY BROWNSTEIN, ERIC GABE, FLORENCE LEE, and ANDREJ PIOTROWSKI. Can. J. Chem. **64**, 1661 (1986).

$NOMX_6$·aromatic charge-transfer complexes are formed where M may be P, As, or Sb, X may be F or Cl, and aromatic may be benzene or a methyl-substituted benzene. Nuclear magnetic resonance and optical spectral parameters are given and three crystal structures reported. Appreciable conductivity is found for $NOSbCl_6$·polystyrene and $NOSbF_6$·hexamethylbenzene.

SYDNEY BROWNSTEIN, ERIC GABE, FLORENCE LEE et ANDREJ PIOTROWSKI. Can. J. Chem. **64**, 1661 (1986).

On a observé qu'il se forme des complexes de transfert de charge du type $NOMX_6$·aromatique, dans lesquels M = P, As ou Sb, X = F ou Cl et aromatique = du benzène ou un benzène substitué par un groupement méthyle. On rapporte les données relatives aux spectres rmn et optiques ainsi trois structures cristallines. On a trouvé que les composés $NOSbCl_6$·polystyrène et $NOSbF_6$·hexaméthylebenzène donnent lieu à une conductivité appréciable.

[Traduit par la revue]

Introduction

The preparation of stable charge transfer complexes of NOCl, MCl_n, and an aromatic hydrocarbon has been reported (1). The variation in properties and stabilities of such complexes as a function of the anion has been described when a Group III or IV element is the central atom in the anion (2). In this article the properties of such complexes will be presented where the central element of the counter ion is from Group V of the periodic table and the halogen is chlorine or fluorine.

Following is a brief history of the nitrosyl salts which were used in this study. $NOPF_6$ is well characterized (3). There is some evidence for a complex between NOCl and $AsCl_3$ but no complex has been isolated (4, 5). $NOAsF_6$ (3), $NOSbCl_6$ (6), and $NOSbF_6$ (3) have been well characterized.

Antimony pentachloride itself reacts with aromatic hydrocarbons to give charge-transfer complexes (7) and to substitute chlorine for hydrogen (8). Under some conditions $SbCl_5$ will react with hexamethylbenzene to give the stable radical cation 4-methylene-1,2,3,5,6-hexamethylcyclohexadiene-2,5 (9). Antimony pentachloride also reacts with $SOCl_2$ to give $SOCl_2 \cdot SbCl_5$ (10) and with $POCl_3$ to give $POCl_3 \cdot SbCl_5$ (11). Complex formation has been reported between antimony pentachloride and NO (12), NO_2Cl (13), ICl_3 (14), and SCl_4 (15).

Nitrosyl tetrachloroantimonate has been prepared by the decomposition of $SbCl_3 \cdot 2NOCl \cdot NOBCl_4$ (4). $POCl_3$ and $SbCl_3$ are also reported to form a complex (16). There has been some study of complexes between $SbCl_3$ and aromatic compounds and 1:1 complex formation is claimed (17).

Experimental

Chemicals

Nitrosyl chloride, nitrosyl fluoride, arsenic trichloride, arsenic pentafluoride, phosphorus trifluoride, phosphorus tri- and pentachloride, nitric oxide, anthracene, *p*-dichlorobenzene, hexamethylbenzene, anisole, 4-methyl-*N*,*N*-dimethylaniline, 9,10-dimethylanthracene, and antimony trifluoride were used as purchased. Phosphorus pentafluoride was stored over phosphorus pentoxide in order to inhibit formation of POF_3. Antimony pentachloride and pentafluoride were vacuum-distilled and antimony trichloride vacuum-sublimed before transfer under vacuum to storage containers. $POCl_3$, $SOCl_2$, and SCl_2 were also transferred to storage containers by vacuum distillation. Benzene, toluene, *p*-xylene, sulfur dioxide, methylene chloride, and neopentane were purified and stored as previously described (18). *N*,*N*-Dimethylaniline and *t*-butylbenzene were distilled under vacuum from sodium. Chlorobenzene was purified by low temperature crystallization and napthalene by vacuum sublimation. The salt $ICl_2^+SbCl_6^-$ was prepared from ICl, Cl_2, and $SbCl_5$ and purified by recrystallization.

$NOAsF_6 \cdot C_6(CH_3)_6$

AsF_5 (2.0 mmol) and NOF (2.0 mmol) were condensed into a reaction vessel closed with a "Teflon" stopcock along with 2 mL of sulfur dioxide. The mixture was thawed, shaken briefly to get a slurry of white solid, and all volatile materials removed under vacuum to give 1.82 mmol of $NOAsF_6$. An equivalent amount of hexamethylbenzene was added and the mixture dissolved in SO_2 to give a deep red solution. Methylene chloride was added and the solvent slowly removed to give a black crystalline solid which was stable in air.

$NOSbCl_6 \cdot (C_6H_5CH_3)_2$

To 0.3918 g of $NOSbCl_6$ dissolved in 3 mL of SO_2 was added 0.5 g of toluene by vacuum transfer. Some of the SO_2 was evaporated overnight and the remaining solution was held at −20°C for 20 h. The crystalline complex was separated by low temperature filtration: It is exceedingly sensitive to moisture. *Anal.* calcd. for $NOSbCl_6 \cdot C_{14}H_{16}$: H 2.94, C 30.64, N 2.55, Sb 26.66; found: H 3.06, C 30.16, N 2.69, Sb 23.39.

$NOSbCl_6 \cdot C_6(CH_3)_6$

Equivalent quantities of $NOSbCl_6$ and hexamethylbenzene were dissolved in SO_2 and the solvent slowly evaporated to give a nearly saturated solution at room temperature. Upon cooling crystals separated. The solution was decanted from the crystalline material, which is not sensitive to atmospheric moisture.

Magnetic resonance spectra were obtained on a Bruker AM 400 spectrometer at a magnetic field strength corresponding to 400 MHz for protons. Carbon and proton chemical shifts are reported with respect to tetramethylsilane, although neopentane was used as an internal reference since it is inert with respect to the compounds studied. A correction of 0.92 ppm was applied for protons and 31.4 ppm for ^{13}C. Fluorine resonance shifts are reported with respect to internal $CFCl_3$.

Visible spectra were obtained on a Carey 210 Spectrometer. Samples for conductivity measurements were prepared as pressed pellets in the same manner as, and using a die for, KBr infrared pellets. The resistance was measured between the parallel, adjustable plates of a General Radio type 1690 A dielectric sample holder with a General Radio type 1673 A automatic capacitance bridge operating at 1 kHz.

X-ray reflections were measured with Mo $K\alpha_1$ monochromatized radiation, (λ = 0.70932 Å) using a Picker diffractometer with the $\theta/2\theta$ scan technique and profile analysis (19). Reflections were considered significant with $I_{net} > 2.5\sigma(I_{net})$. The intensity data for $NOAsF_6$·hexamethylbenzene and $NOSbCl_6$·2toluene were collected at low temperature (115 K) in an attempt to minimize the effects of the

[1]The preceding article in this series is ref. 2.
[2]NRC No. 25724.
[3]To whom all correspondence should be addressed.
[4]Revision received April 9, 1986.

TABLE 1. Parameters from X-ray structural characterization

Compound	$NOAsF_x$·hexamethylbenzene $x \approx 6$	$NOSbCl_6$·hexamethylbenzene	$NOSbCl_6$·2toluene
Crystal type	Monoclinic	Orthorhombic	Orthorhombic
Space group	$C2/c$	$Pbcm$	$Pnma$
$2\theta_{max}$	50°	55°	60°
a, Å	12.858(3)	8.2357(5)	11.242(1)
b, Å	17.605(3)	19.466 (2)	15.961(2)
c, Å	13.297(3)	12.406 (1)	11.521(1)
β, deg	101.07 (2)	—	—
Z	8	4	4
D, calcd (Mg m^{-3})	1.71	1.76	1.76
Crystal dimensions (mm)	0.25 × 0.25 × 0.3	0.25 × 0.3 × 0.15	0.2 × 0.2 × 0.2
Unique reflections	2639	2382	3128
Significant reflections	1711	1488	1793
μ (mm^{-1})	2.35	2.21	2.13
R_f all data	0.128	0.092	0.167
R_f significant data	0.077	0.049	0.083
R_w all data	0.062	0.039	0.069
R_w significant data	0.062	0.039	0.069

NO and AsF_6 disorder. This was only partially successful and the accuracy of all these structures suffers because of disorder. Lorentz and polarization factors were applied but absorption corrections were not applied. X-ray structural data for $NOAsF_6$·hexamethylbenzene, $NOSbCl_6$·hexamethylbenzene and $NOSbCl_6$·2toluene are listed in Table 1. The structures of $NOAsF_6$·hexamethylbenzene and $NOSbCl_6$·hexamethylbenzene were solved by MULTAN (20) and refined by full-matrix least squares. The structure of $NOSbCl_6$·2toluene was solved by Patterson and heavy-atom techniques. Attempts to locate H-atoms from difference maps were not successful and positions for H-atoms on the ring were calculated. All calculations were performed with the NRC VAX system of programs (21). Scattering factors were taken from the International tables for X-ray crystallography (22). The final atomic positional parameters and mean temperature factors are given in Table 2 and the anisotropic temperature factors and structure factors are deposited as supplementary material.[5] The structure of $NOSbCl_6$·hexamethylbenzene has previously been reported in preliminary form (1). Bond lengths and angles are reported in Table 3.

The structure of $NOAsFx$·hexamethylbenzene consists of four entities $\frac{1}{2}(AsF_6)$, $\frac{1}{2}(AsF_x; x \approx 6)$, NO, and $C_6(CH_3)_6$. For AsF_6, the As atom is coordinated to six F atoms (three of them are equivalent atoms generated with a crystallographic two-fold rotation axis) to form an octahedron. The maximum deviation from an ideal octahedral angle is 0.9° and the As—F distances are 1.709(6) to 1.724(7) Å. For the disordered AsF_x, the As atom is coordinated to twelve partially occupied F atoms (six of them are equivalent atoms generated by a crystallographic center of symmetry) to form two distorted octahedra (one is As2 with F4, F5, F6, and their equivalents, the other is As2, F7, F8, F9, and their equivalents). The occupancy factors of the six F atoms are 0.59, 0.82, 0.51, 0.23, 0.41, and 0.33, with a sum of 2.89 × 2 = 5.78. The thermal parameters in this, and in the toluene adduct, have an unusual distribution. In particular the B_{iso} value of F5 is very high (9.7 Å^2) but this is probably an artifact of the refinement which has also given the highest occupancy to F5 (0.82). In our experience it is a mistake to attempt to explain such deviations when there is a high degree of disorder. The maximum deviation from an ideal octahedral angle is 6°. The As—F distances are 1.62(2) to 1.76(2) Å. The N—O distance is 1.13(2) Å. The aromatic C—C distances are 1.41(2) to 1.45(2) Å and the aromatic C—C methyl distances are 1.48(2) to 1.53(3) Å. The C—C—C angles are 119(1) to 122(1)°. The distances from the plane of the ring to the N atom and the O atom are 2.07(2) and 2.81(2) Å, respectively.

[5]Complete set of data may be purchased from the Depository of Unpublished Data, CISTI, National Research Council of Canada, Ottawa, Ont., Canada K1A 0S2.

The molecule $NOSbCl_6$·2toluene contains a mirror plane. The atoms Sb, N, O, Cl1, Cl2, Cl3, and Cl4 are situated on the plane with a toluene ring on either side of it. The shortest contact between the NO group and the aromatic ring is 2.41(3) Å.

For all three of these adducts, because of the structural disorder, it is not possible to unambiguously assign the nitrogen and oxygen atoms as shown. Reversing their relative positions causes an insignificant change in the agreement indices. The present assignment is preferred since it agrees with theoretical calculations (23).

Results and discussion

The typical deep red–brown colour associated with this family of charge transfer complexes is observed when $NOPF_6$ is brought into solution in sulfur dioxide by benzene and methyl-substituted benzenes. The fluorine resonance results of Table 4 show that complex formation has occurred. From the relative intensities of the signals from PF_6^- and the $CFCl_3$ reference it was found that complex formation was incomplete with $NOPF_6$ and benzene but essentially complete with the methyl-substituted benzenes. Proton and carbon resonance shifts and uv maxima are listed in Table 5. There is no reaction between PCl_5 and NOCl. PF_3 reacts with both NOF and NOCl to give POF_3.

The reddish-brown colour associated with this family of charge transfer complexes is observed in the ternary systems NOCl–$AsCl_3$ and mesitylene or hexamethylbenzene. Since the extent of association could not be readily established the systems were not studied further. $NOAsF_6$ and hexamethylbenzene form a stable charge-transfer complex. From the fluorine magnetic resonance results in SO_2 solution, listed in Table 4, there appears to be little effect of complexation upon AsF_6^-. Other spectral parameters for $NOAsF_6$ hexamethylbenzene are listed in Table 5. Pertinent structural features of the solid complex are listed in Tables 2 and 6. The unit cell contains two formula units of which one has the AsF_6^- in a disordered fashion. This is shown in Fig. 1, with the second NO and hexamethylbenzene units deleted for clarity. AsF_3 does not appear to complex with either NOCl nor NOF.

Spectral parameters for many complexes of $NOSbCl_6$ with aromatic compounds are listed in Table 5. The magnetic resonance and uv values are similar to those found for the corresponding compounds of the Group III and IV chlorides and fluorides (2). It was not possible to obtain the extinction

TABLE 2. Final atomic positional parameters and mean temperature factors

Atom	X^a	Y	Z	$B_{iso}{}^b$
		$NoSbCl_6$·hexamethylbenzene		
Sb	0.36638(9)	0.38528(4)	1/4	3.98(4)
Cl1	0.6448 (4)	0.35525(17)	1/4	7.42(21)
Cl2	0.0894 (4)	0.41512(15)	1/4	5.86(17)
Cl3	0.3183 (3)	0.30241(11)	0.11645(18)	7.27(13)
Cl4	0.4163 (3)	0.46735(10)	0.11605(16)	6.93(12)
C1	0.9676 (11)	0.5907 (4)	0.1953 (7)	6.6 (5)
C2	1.1029 (14)	0.6132 (5)	0.1398 (6)	6.8 (6)
C3	1.2450 (11)	0.6364 (3)	0.1928 (7)	6.2 (5)
C7	0.8196 (12)	0.5654 (6)	0.1344 (11)	14.0 (9)
C8	1.1093 (19)	0.6147 (6)	0.0145 (7)	15.6 (9)
C9	1.3962 (13)	0.6618 (5)	0.1301 (10)	13.0 (8)
N	0.0434 (17)	0.7137 (7)	1/4	13.3 (14)
O	0.0475 (20)	0.7605 (7)	0.1686 (15)	13.2 (12)
		$NOSbCl_6$·2toluene		
Sb	0.43378(9)	1/4	0.50111(16)	1.49(5)
Cl1	0.5775 (6)	1/4	0.3556 (5)	2.9 (3)
Cl2	0.2847 (6)	1/4	0.3492 (5)	2.7 (3)
Cl3	0.5865 (6)	1/4	0.6471 (5)	3.3 (3)
Cl4	0.2820 (6)	1/4	0.6370 (5)	2.7 (3)
Cl5	0.4349 (3)	0.10256(15)	0.5065 (5)	3.44(18)
C1	0.3511 (10)	0.4378 (7)	0.1042 (11)	2.1 (5)
C2	0.4755 (12)	0.4255 (8)	0.1163 (13)	3.0 (6)
C3	0.521 (3)	0.3872 (11)	0.0379 (19)	6.7 (12)
C4	0.5072 (22)	0.3649 (12)	−0.0679 (19)	8.1 (13)
C5	0.3698 (13)	0.3732 (7)	−0.0873 (12)	3.4 (6)
C6	0.3023 (9)	0.4105 (7)	0.0136 (14)	2.1 (5)
C7	0.2751 (12)	0.4764 (7)	0.2092 (15)	5.4 (8)
O	0.3595 (13)	1/4	0.1057	3.7 (7)
N	0.4635 (18)	1/4	0.1057	4.7 (11)
H2	0.517	0.451	0.188	3.5
H3	0.624	0.368	0.046	3.9
H4	0.546	0.352	−0.142	4.0
H5	0.328	0.349	−0.161	4.2
H6	0.212	0.415	−0.007	3.3
		$NOAsF_6$·hexamethylbenzene		
As1	0	0.68359(11)	1/4	1.76(11)
As2	0	1	0	2.37(11)
F1	−0.0447 (6)	0.6156 (4)	0.1603 (5)	2.9 (4)
F2	0.1206 (5)	0.6837 (5)	0.2119 (5)	3.4 (4)
F3	−0.0468 (7)	0.7524 (4)	0.1605 (5)	3.7 (4)
F4	−0.0297 (11)	1.0944 (7)	−0.0143 (9)	2.5 (5)
F5	0.0754 (12)	1.0117 (9)	−0.0838 (11)	9.7 (7)
F6	−0.1116 (19)	0.9795 (9)	−0.0854 (14)	4.3 (8)
F7	0.055 (4)	1.0814 (24)	−0.036 (3)	6.4 (16)
F8	−0.0467 (22)	0.9751 (11)	−0.1220 (17)	3.8 (8)
F9	−0.116 (3)	1.0551 (20)	−0.0150 (23)	6.6 (15)
C1	0.3330 (10)	0.8500 (7)	0.3235 (10)	1.9 (6)
C2	0.3404 (10)	0.9048 (8)	0.2434 (11)	2.3 (7)
C3	0.3643 (10)	0.8797 (8)	0.1479 (10)	2.4 (7)
C4	0.3723 (10)	0.8008 (7)	0.1284 (9)	1.7 (6)
C5	0.3580 (10)	0.7467 (7)	0.2072 (10)	1.7 (6)
C6	0.3405 (10)	0.7706 (7)	0.3037 (10)	2.0 (7)
C7	0.3101 (11)	0.8779 (7)	0.4263 (9)	3.0 (7)
C8	0.3242 (11)	0.9878 (7)	0.2643 (10)	3.3 (8)
C9	0.3775 (11)	0.9373 (8)	0.0658 (10)	3.2 (7)
C10	0.3928 (10)	0.7761 (7)	0.0273 (9)	2.3 (7)
C11	0.3598 (10)	0.6623 (6)	0.1831 (10)	2.5 (7)
C12	0.3274 (11)	0.7132 (7)	0.3880 (9)	2.8 (7)
O	0.1140 (7)	0.8766 (6)	0.2253 (8)	3.7 (6)
N	0.1821 (9)	0.8462 (6)	0.2006 (8)	2.4 (6)

[a]The estimated standard deviations refer to the last digit printed.
[b]B_{iso} is the mean of the principal axes of the thermal ellipsoid.

coefficient for the charge transfer band of the benzene complex since it appears as a shoulder on a more intense, shorter wavelength signal. It was also not possible to isolate a stable solid benzene adduct.

The stoichiometry of the toluene complex in solution is not established. With 2 equiv. of toluene for each $NOSbCl_6$ the proton chemical shifts are approximately intermediate between those for a 1:1 solution and for toluene itself. The extinction coefficient has been calculated on the basis of 1:1 and 2:1 complexes. In the solid, however, both elemental analysis and the crystal structure, which will be discussed in conjunction with those of the hexamethylbenzene adducts, indicate a 2:1 complex.

A solid adduct of 1:1 stoichiometry was isolated with *t*-bu-benzene. From the change in uv absorption with change in concentration an equilibrium constant of 1.2×10^4 was calculated for adduct formation. From the proton magnetic resonance spectrum as a function of concentration the solution stoichiometry was determined to be 1:1 for the *p*-xylene complex. The equilibrium constant for formation of this complex was calculated as 1.0×10^4 from the concentration dependence of the uv absorption.

The hexamethylbenzene adducts of $NOAsF_6$ and $NOSbCl_6$, and the toluene adduct of $NOSbCl_6$, whose crystal structures have been determined, have the parameters listed in Tables 2 and 6. It is immediately apparent that the N—O bond length for $NOSbCl_6$·hexamethylbenzene is much longer than for the other two complexes. It is also much longer than those found for $NOAlCl_4$ at 0.997 Å (25), NO at 1.15 Å (26), and NOCl at 1.14 Å (27). For $NOSbCl_6$·hexamethylbenzene the nitrogen is placed nearly symmetrically at an average separation of only 2.04 Å from the six ring carbons of hexamethylbenzene. The NO moiety is disordered with the oxygen appearing at either of two positions. Three of the $SbCl_6^-$ chlorines are 3.9 Å from an edge of the aromatic ring. There is no obvious regular stacking of units involving the aromatic rings but the closest description of long range order would be planes of aromatic rings alternating with planes of N—O groups with the $SbCl_6^-$ units in the same plane as the aromatic rings, but offset from the NO groups. At 45° to these planes are bands of $SbCl_6^-$ units alternating with bands containing the NO groups and the hexamethylbenzene moieties. The structure is illustrated in Fig. 2.

Packing in the toluene complex is not the same as for hexamethylbenzene because of the different stoichiometry. There are planes of toluene units alternating with planes of $SbCl_6^-$ units and bands of toluene and NO^+ species. The structure is shown in Fig. 3. There is considerable disorder in the orientation of the NO moiety which could not be fitted by reasonable models to improve the refinement of the structure. Therefore the NO bond length and the C—C bond lengths and angles are less precise than determined by the least-squares analysis. There do not appear to be simple planes of the various constituent units in the $NOAsF_6$·hexamathylbenzene complex.

The hexamethylbenzene adducts of $NOAsF_6$, $NOSbCl_6$, and $NOSbF_6$ are exceptional in that their reactivity towards moisture is sufficently slight that they may be manipulated in air without decomposition. The infrared spectrum of $NOSbCl_6$·hexamethylbenzene in a KBr pellet has a strong absorption at 1849 cm^{-1} assigned to the NO stretching mode and no signals at higher frequencies until those assigned to C—H stretching modes at 2920 and 2990 cm^{-1}. This NO absorption is at considerably lower energy than that found for $NOSbCl_6$ at 2189 cm^{-1} and for $NOAlCl_4$ at 2242 cm^{-1} (3), but in the region

TABLE 3. Bond lengths and angles

Bond	Length (Å)	Bonds[a]	Angle (deg)
Sb—Cl1	2.367(4)	Cl1—Sb—Cl2	180.00(8)
Sb—Cl2	2.354(3)	Cl1—Sb—Cl3	89.64(8) × 2
Sb—Cl3	2.346(2) × 2	Cl1—Sb—Cl4	89.90(8) × 2
Sb—Cl4	2.342(2) × 2	Cl2—Sb—Cl3	90.35(8) × 2
		Cl2—Sb—Cl4	90.11(8) × 2
		Cl3—Sb—Cl3′	89.85(9)
		Cl3—Sb—Cl4	89.86(8) × 2
		Cl3—Sb—Cl4′	174.47(9) × 2
		Cl4—Sb—Cl4′	90.42(8)
N—O	1.360(18) × 2	O—N—O′	95.95(13)
C1—C1′	1.357(17)	C2—C1—C1′	119.9 (8)
C1—C2	1.382(15)	C7—C1—C1′	119.9 (10)
C1—C7	1.517(13)	C2—C1—C7	120.2 (9)
C2—C3	1.416(15)	C1—C2—C3	122.5 (8)
C2—C8	1.556(12)	C1—C2—C8	122.1 (10)
		C3—C2—C8	115.5 (10)
C3—C3′	1.420(19)	C2—C3—C3′	117.7 (8)
C3—C9	1.549(12)	C2—C3—C9	122.2 (9)
		C9—C3—C3′	120.2 (9)
		$NOSbCl_6$·2toluene	
Sb—Cl1	2.328(7)	Cl1—Sb—Cl2	87.7 (2)
Sb—Cl2	2.423(6)	Cl1—Sb—Cl3	90.5 (2)
Sb—Cl3	2.404(6)	Cl1—Sb—Cl4	176.5 (2)
Sb—Cl4	2.316(6)	Cl1—Sb—Cl5	90.9 (1) × 2
Sb—Cl5	2.354(2) × 2	Cl2—Sb—Cl3	178.2 (2)
		Cl2—Sb—Cl4	88.8 (2)
		Cl2—Sb—Cl5	91.3 (1) × 2
		Cl3—Sb—Cl4	93.0 (2)
		Cl3—Sb—Cl5	88.7 (1) × 2
		Cl4—Sb—Cl5	89.2 (1) × 2
		Cl5—Sb—Cl5′[b]	176.9 (2)
N—O	1.17 (2)		
C1—C2	1.419(18)	C2—C1—C6	117.6 (12)
C1—C6	1.257(19)	C2—C1—C7	120.2 (12)
C1—C7	1.604(19)	C6—C1—C7	121.8 (11)
C2—C3	1.20 (3)	C1—C2—C3	114.3 (16)
C3—C4	1.28 (3)	C2—C3—C4	143.9 (22)
C4—C5	1.57 (3)	C3—C4—C5	103.2 (17)
C5—C6	1.510(2)	C4—C5—C6	114.8 (12)
		$NOAsF_6$·hexamethylbenzene	
As1—F1	1.709(6) × 2	F1—As1—F1′[c]	91.1 (3)
As1—F2	1.721(7) × 2	F1—As1—F2	89.8 (4) × 2
As1—F3	1.724(7) × 2	F1—As1—F2′	90.3 (4) × 2
		F1—As1—F3	89.1 (3) × 2
		F1—As1—F3′	179.1 (4) × 2
		F2—As1—F2′	179.8 (4)
		F2—As1—F3	90.6 (4) × 2
		F2—As1—Fe′	89.3 (4) × 2
		F3—As1—F3′	90.7 (3)
As2—F4	1.707(12) × 2		
As2—F5	1.625(15) × 2		
As2—F6	1.689(18) × 2		
As2—F7	1.71 (4) × 2		
As2—F8	1.676(20) × 2		
As2—F9	1.76 (3) × 2		
N—O	1.128(15)		
C1—C2	1.454(19)	C2—C1—C6	119.9 (12)
C1—C6	1.428(18)	C2—C1—C7	119.4 (11)
C1—C7	1.533(18)	C6—C1—C7	120.6 (11)
		C1—C2—C3	119.9 (12)
C2—C3	1.434(20)	C1—C2—C8	118.5 (12)
C2—C8	1.509(18)	C3—C2—C8	121.5 (12)
		C2—C3—C4	120.0 (12)

TABLE 3. (*concluded*)

Bond	Length (Å)	Bonds[a]	Angle (deg)
C3—C4	1.419(18)	C2—C3—C9	120.0 (12)
C3—C9	1.523(20)	C4—C3—C9	120.0 (12)
		C3—C4—C5	119.1 (12)
C4—C5	1.454(18)	C3—C4—C10	119.0 (11)
C4—C10	1.484(20)	C5—C4—C10	121.9 (11)
		C4—C5—C6	121.7 (11)
C5—C6	1.410(19)	C4—C5—C11	118.6 (11)
C5—C11	1.522(17)	C6—C5—C11	119.7 (11)
		C1—C6—C5	119.2 (12)
C6—C12	1.542(18)	C1—C6—C12	119.2 (12)
		C5—C6—C12	121.6 (11)

[a]Primed atoms are at $x, y, \frac{1}{2} - z$.
[b]Primed atoms are at $x, \frac{1}{2} - y, z$.
[c]Primed atoms are at $1 - x, y, \frac{1}{2} - z$.

TABLE 4. Fluorine resonance parameters for some group V fluorides and their complexes

Sample[a]	δ ^{19}F	J_{M-F}
PF_5[b]	−65.4	947
NR_4PF_6[b]	−71.0	711
$NOPF_6$·hexamethylbenzene	−66.9	713
AsF_5	−41.6	
NR_4AsF_6[b]	−63.6	937
$NOAsF_6$	−57.1	907
$NOAsF_6$·hexamethylbenzene	−58.9	920
AsF_3	−42.3	
SbF_5	−67 axial	
	−96 equatorial	
$NOSbF_6$·hexamethylbenzene	−115.9	1 950 ^{121}Sb
		1 050 ^{123}Sb

[a]In SO_2 solution.
[b]Reference 24.

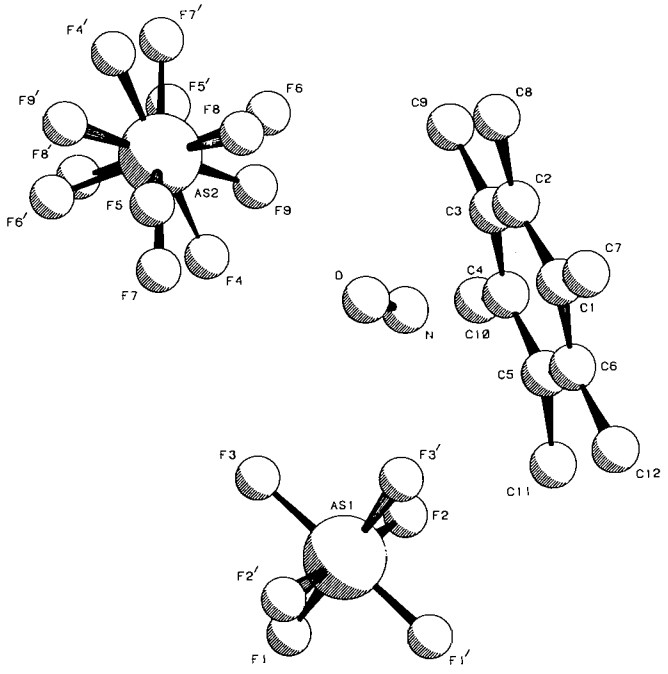

FIG. 1. The structure of $NOAsF_6$—hexamethylbenzene.

TABLE 5. Magnetic resonance and optical parameters for $NOMX_6$–aromatic complexes

Compound	δ^1H		$\delta^{13}C$		λ_{max} Å	ϵ
	CH_3	H	CH_3	C-aromatic		
$NOPF_6$-hexamethylbenzene	2.47		17.1	149.8	2750 shoulder	
$NOPF_6$-mesitylene	2.52	7.45	20.9	137.1		
				151.1		
$NOPF_6$-*p*-xylene	2.55	7.63	20.7	137.6		
				147.6		
$NOPF_6$-toluene	2.42	7.38	20.9	128.4 *p*		
		7.45		131.3 *o*		
				132.1 *m*		
				142.0		
$NOPF_6$-benzene		>7.34		>129.1		
$NOAsF_6$-hexamethylbenzene	2.39		17.1	149.1	3340	47 000
$NOSbCl_6$-hexamethylbenzene	2.47		18.2	150.2	3340	8 100
$NOSbCl_6$-*p*-xylene	2.58	7.67	20.8	137.8	3400	10 000
				148.0		
$NOSbCl_6$-*t*-butylbenzene	1.47	7.89	30.5	134.3	3390	5 000
		7.96	36.5	134.8		
		8.05		136.9		
				163.5		
$NOSbCl_6$-2toluene	2.47	7.46	20.8	129.8	3400	5 300
				132.6		
				133.2		
				144.3		
$NOSbCl_6$-toluene	2.78	8.05			3400	10 600
$NOSbCl_6$-benzene		7.81		136.7	3440	
$NOSbF_6$-hexamethylbenzene	2.48		17.1	150.1	2720	

TABLE 6. Bond lengths, stretching frequencies, and resistivities for some $NOMX_6$–aromatic complexes

Compound	ν_{NO}, cm^{-1}	Length, Å			Resistivity ohm cm
		N—O	Aromatic-N	Aromatic-O	
$NOAsF_6$-hexamethylbenzene	—	1.13	2.07	2.81	7.3×10^6
$NOSbCl_6$-hexamethylbenzene	1849	1.43	2.04	2.85	4.3×10^2
$NOSbCl_6$-2toluene	—	1.17	2.49	2.67	—
$NOSbF_6$-hexamethylbenzene	1850				3

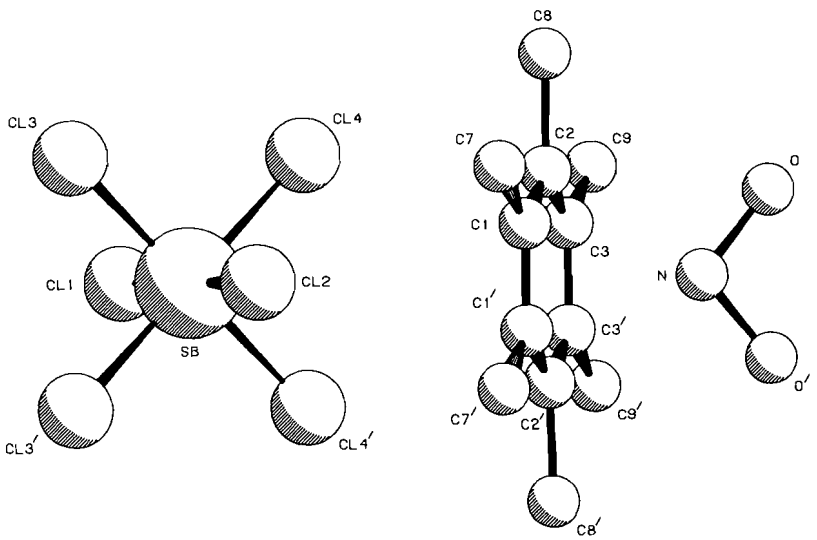

FIG. 2. The structure of $NOSbCl_6$—hexamethylbenzene.

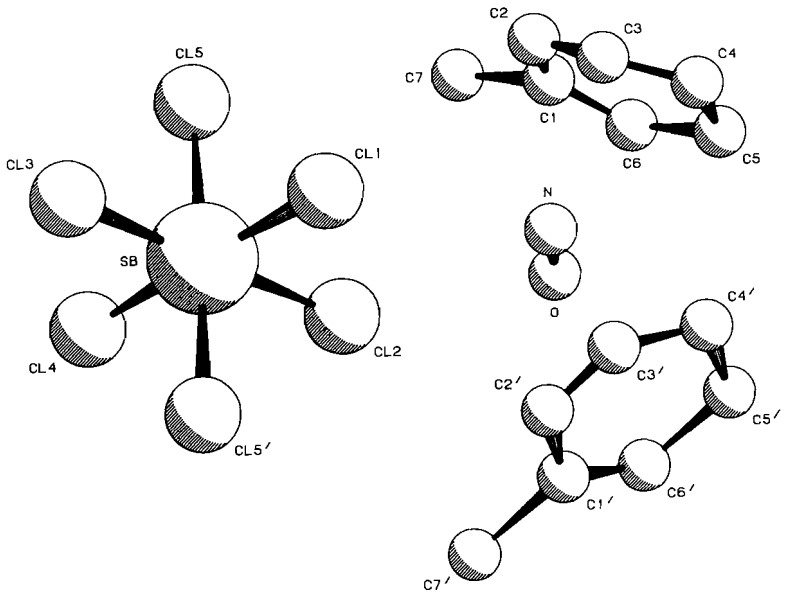

FIG. 3. The structure of $NOSbCl_6$—2toluene.

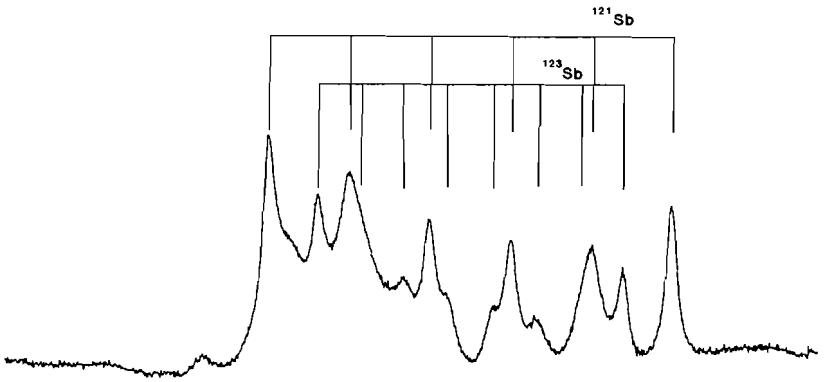

FIG. 4. The fluorine resonance spectrum of $NOSbF_6$—hexamethyl-benzene in SO_2 solution.

of co-ordinated nitrosyl groups. There was no strong ir signal from the NO group in $NOAsF_6$·hexamethylbenzene. The extreme moisture sensitivity of the toluene complex prevented measurement of its conductivity and infrared spectrum.

The conductivity of a crystalline sample of the $NOSbCl_6$·hexamethylbenzene adduct was found to be 4.2×10^{-4} ohm^{-1} cm^{-1} and it had a weak esr signal with $g = 2.008$ (1). A second, purer, sample had conductivity of 2.3×10^{-3} ohm^{-1} cm^{-1} and no esr signal. $NOSbCl_6$ and polystyrene also form a complex which is stable in air. Its conductivity as a pressed pellet was found to be 1.9×10^{-4} ohm^{-1} cm^{-1} and as a film cast from methylene chloride 1.6×10^{-2} ohm^{-1} cm^{-1}. Many other species reacted with $NOSbCl_6$ to initially yield colours similar to those of the already described charge transfer complexes followed rapidly by a further reaction, presumably chlorination. With anthracene as aromatic compound, 9,10-dichloroanthracene was isolated in 70% yield after hydrolysis of the reaction mixture. From *N,N*-dimethylaniline the *para* chloro product was identified by proton resonance spectroscopy.

The chemical shift of the ^{121}Sb resonance was not sensitive to complex formation but the line width decreased from extremely broad for $SbCl_5$ dissolved in SO_2 to 1 280 Hz for $NOSbCl_6$, to 610 Hz for the benzene complex and 370 Hz for the toluene complex.

Although $SOCl_2$ and $SbCl_5$ form a 1:1 complex (10) there is no evidence for a ternary charge-transfer complex with aromatic hydrocarbons. There is rapid chlorination of benzene by $SOCl_2 \cdot SbCl_5$ with gas evolution. A mass spectrum of the product is interpreted as mixture containing up to four chlorine atoms per molecule. The proton and carbon resonance spectra of a solution of $SOCl_2$, $SbCl_5$, and hexamethylbenzene in SO_2 are the same as those for $SbCl_5$ and hexamethylbenzene without $SOCl_2$. Presumably complex formation of $SbCl_5$ with hexamethylbezene is stronger than with $SOCl_2$. Chlorination was also observed with ICl_2SbCl_6.

The crystal structure of the 1:1 complex of $POCl_3$ and $SbCl_5$ has been determined (11). It was verified by ^{31}P resonance spectroscopy that complex formation also occurs in methylene chloride solution. Upon addition of 1 equiv. of hexamethylbenzene the ^{31}P signal of free $POCl_3$ appears as well as the proton and carbon resonance signals of the $SbCl_5$ hexamethylbenzene complex. It is therefore more likely that complex formation between $SbCl_5$ and hexamethylbenzene is higher than that between $SbCl_5$ and $POCl_3$ or a possible ternary complex, as was also observed with $SOCl_2$.

The reaction of NOCl and $SbCl_3$ yields $NOSbCl_6$. The only product isolated from the reaction of NO, $SbCl_3$, and hexamethylbenzene was $NOSbCl_6$—hexamethylbenzene. There was

no evidence from phosphorous resonance spectroscopy for complex formation between $POCl_3$ and $SbCl_3$ in CH_2Cl_2 solution, nor for formation of a ternary complex with hexamethylbenzene. Therefore among the systems studied with antimony chlorides, $NOSbCl_6$ is unique in the formation of charge-transfer complexes with aromatic compounds.

Fluorine resonance results for some antimony—fluorine species and for $NOSbF_6$·hexamethylbenzene are listed in Table 2. SbF_5 co-ordinates strongly with the SO_2 solvent to give axial and equatorial fluorine ligands (28). The chemical shifts and observable fluorine spin coupling in this system are strongly temperature- and concentration-dependant, the present results being for concentrated room temperature solutions. It was not previously possible to measure the antimony–fluorine spin coupling of SbF_6^- from the fluorine resonance spectrum of the ion due to rapid quadrupolar relaxation. An estimate of $J_{^{19}F-^{121}Sb}$ of 1 840 Hz for aqueous $KSbF_6$ was found from the ^{121}Sb spectrum (29). Figure 4 presents the fluorine resonance spectrum of $NOSbF_6$·hexamethylbenzene in SO_2 solution. Both the $^{19}F-^{121}Sb$ and $^{19}F-^{123}Sb$ spin couplings are clearly visible with a ratio of 1.86 which agrees with that of the gyromagnetic ratios (1.85). The spectral pattern is characteristic of coupling to a quadrupolar nucleus with the outer lines narrower and more intense (30). There is a broad impurity peak under the low field part of the pattern.

Ultraviolet and magnetic resonance parameters for the $NOSbF_6$·hexamethylbenzene complex are listed in Table 5, and the infrared and conductivity results are listed in Table 6. The high conductivity of this compound is noteworthy and might possibly lead to interesting applications (31). There appears to be a correlation of long N—O bond length, low N—O stretching frequency and high conductivity for the compounds listed in Table 6. It is possible that the conduction mechanism involves the unusually weakly bonded NO group and the π electrons of the nearby aromatic rings.

The characteristic colour of these charge transfer complexes is also found in the system SbF_5, NOCl, and hexamethylbenzene. The fluorine resonance spectrum shows the characteristic signal of the $NOSbF_6$·hexamethylbenzene species and other unassigned signals. Disproportionation amongst fluorine and chlorine containing antimony species probably occurs to give a mixture of products. The reaction of SbF_3, NOF, and hexamethylbenzene also gives $NOSbF_6$·hexamethylbenzene.

The fluorine-containing nitrosyl salts give stronger complexes than those containing chlorine as was also found for the Groups III and IV elements (2). Thus $NOPF_6$ gives complexes, but $NOPCl_6$ does not exist. $NOAsF_6$ gives a complex stable to dissociation while there is significant dissociation with the complex of $NOAsCl_4$. The conductivity of the $NOSbF_6$·hexamethylbenzene complex is much greater than that for the $NOSbCl_6$ complex suggesting stronger complex formation. The strength of complex formation appears to increase as one goes down the periodic table as with the Group IV elements (2). Thus there are no nitrosyl chloride complexes of phosphorus, partially dissociated ones with arsenic and strong ones with antimony.

1. S. Brownstein, E. Gabe, F. Lee, and L. Tan. J. Chem. Soc. Chem. Commun. 1566 (1984).
2. S. Brownstein, A. Morrisson, and L. Tan. Can. J. Chem. **64**, 265 (1986).
3. D. W. A. Sharp and J. Thorley. J. Chem. Soc. 3557 (1963).
4. T. C. Waddington and F. Klanberg. Z. anorg. allgem. Chem. **304**, 185 (1960).
5. J. Lewis and D. B. Sowerby. Rec. trav. chim. **75**, 615 (1956).
6. R. W. Asmussen. Z. anorg. allgem. Chem. **243**, 127 (1939).
7. P. R. Hammond and R. R. Lake. J. Chem. Soc. Chem. Commun. 987 (1968).
8. P. Kovacic and N. O. Brace. J. Am. Chem. Soc. **76**, 5491 (1954).
9. L. S. Singer and I. C. Lewis. J. Am. Chem. Soc. **87**, 4695 (1965).
10. D. E. Burge and T. H. Norris. J. Am. Chem. Soc. **81**, 2324 (1959).
11. C. I. Branden and I. Lindquist. Acta Chem. Scand. **17**, 353 (1963).
12. H. J. M. Bowen. J. Chem. Soc. 3637 (1954).
13. F. Seel, J. Nogradi, and R. Posse. Z. anorg. allgem. Chem. **269**, 197 (1952).
14. C. G. Vonk and E. H. Wiebenga. Acta Crystallogr. **12**, 859 (1959).
15. I. R. Beattie and H. Chudzynska. J. Chem. Soc. A, 984 (1967).
16. L. K. Ashrafullina, V. E. Belskii, and R. R. Shazidullin. Izv. Akad. Nauk SSSR, Ser. Khim. **7**, 1504 (1976).
17. H. H. Perkampus and E. Baumgarten. Z. Phys. Chem. **39**, 1 (1963).
18. L. K. Tan and S. Brownstein. J. Org. Chem. **48**, 302 (1983).
19. D. F. Grant and E. J. Gabe. J. Appl. Crystallogr. **11**, 114 (1978).
20. G. Germain, P. Main, and M. M. Woolfson. Acta Crystallogr. A**27**, 368 (1971).
21. E. J. Gabe, F. L. Lee, and Y. LePage. Crystallogr. Comput. **3**, 107 (1984).
22. International tables for X-ray crystallography. Vol IV. 1974. Kynoch Press, Birmingham, England. Table 2.2B, p. 99.
23. W. D. Reents, R. C. Haddon, and K. Raghavachari. Private communication.
24. S. Brownstein. Can. J. Chem. **47**, 605 (1969).
25. P. Barbier, G. Mairesse, J. P. Wignacourt, and F. Baert. Cryst. Struct. Commun. **5**, 633 (1976).
26. C. A. Burrus and W. Gordy. Phys. Rev. **92**, 1437 (1953).
27. J. A. A. Ketelaar and K. J. Palmer. J. Am. Chem. Soc. **59**, 2629 (1937).
28. J. Bacon, P. A. W. Dean, and R. J. Gillespie. Can. J. Chem. **47**, 1655 (1969).
29. E. L. Muetterties and W. D. Phillips. J. Am. Chem. Soc. **81**, 1084 (1959).
30. D. W. Aksnes, S. M. Hutchison, and K. J. Parker. Mol. Phys. **14**, 301 (1968).
31. S. Brownstein. Patent applications, Canadian: 458-579, U.S.; 752-082.

The structure and resonance Raman spectra – structure correlations for methyloxycarbonyl-L-phenylalanyl-L-alanine ethyl dithioester[1]

K. A. VARUGHESE, R. H. ANGUS, P. R. CAREY,[2] H. LEE, AND A. C. STORER
Division of Biological Sciences, National Research Council of Canada, Ottawa, Ont., Canada K1A 0R6

Received December 4, 1985

K. I. VARUGHESE, R. H. ANGUS, P. R. CAREY, H. LEE, and A. C. STORER. Can. J. Chem. **64**, 1668 (1986).

The structure of methyloxycarbonyl-L-phenylalanyl-L-alanine ethyl dithioester has been determined by X-ray crystallographic analysis. The N—C—C—S(thiol) and C—N—C—C(S) torsional angles are 141(1)° and −69(2)°, respectively. Consequently, the N and thiono (C=S) sulfur atoms are in close contact and the N···S(thiono) distance is 3.078(5) Å. The structure is a perturbed **A** conformer, which we designate **A′**, by analogy to a previously characterised **A** conformer (Huber *et al.*, Biochemistry, **21**, 3109 (1982)). The $\bar{\Phi}$, $\bar{\Psi}$ angles for the Phe residue are −87(2) and 151(2)°, respectively. A Raman spectroscopic study of a single crystal of the LL form and a resonance Raman (RR) spectroscopic study of powdered methyloxycarbonyl-L-phenylalanyl-DL-alanine ethyl dithioester establish the RR signature of the dithio moiety for the compound in the **A′** form. The RR spectrum of the dithioester in CCl_4 defines the RR signature for the $\mathbf{C_5}$ form in solution, while the RR spectrum from a solution in H_2O/CH_3CN provides information on the signatures of the **A** and **B** conformers. As for the case of *N*-benzoyl-DL-alanine dithioester, the **A** and $\mathbf{C_5}$ signatures of the title compound closely resemble those for glycine-based dithioesters but the key marker bands for the **B** conformer are shifted by ≈30 cm^{-1} to lower frequency compared to those for a glycine dithioester.

K. I. VARUGHESE, R. H. ANGUS, P. R. CAREY, H. LEE, and A. C. STORER. Can. J. Chem. **64**, 1668 (1986).

Faisant appel à la diffraction des rayons-X, on a déterminé la structure du dithioester éthylique de la méthyloxycarbonyl L-phénylalanyl L-alanine. Les angles de torsion N—C—C—S(thiol) et C—N—C—C(S) sont respectivement 141(1) et −69(2)°. En conséquence, les atomes d'azote et de soufre du thione (C=S) sont très près les uns des autres et la distance N···S(thiono) est égale à 3,078(5) Å. La structure est un conformère **A** déformé que l'on a appelé **A′** par analogie avec un conformère **A** caractérisé antérieurement (Huber et collaborateurs, Biochemistry, **21**, 3109 (1982)). Les angles $\bar{\Phi}$ et $\bar{\Psi}$ du groupement Phe sont respectivement −87(2)° et 151(2)°. Une étude par spectroscopie Raman d'un cristal unique de la forme LL et une étude par spectroscopie de résonance Raman (RR) du dithioester éthylique de la méthyloxycarbonyl L-phénylalanyl DL-alanine a permis de déterminer la signature RR de la portion dithio du composé dans sa forme **A′**. Le spectre RR du dithioester en solution dans le CCl_4 définit la signature RR de la form $\mathbf{C_5}$ en solution alors que le spectre RR du même composé en solution dans H_2O/CH_3CN fournit de l'information sur les signatures des conformères **A** et **B**. Comme ce fut le cas avec le dithioester de la *N*-benzoyl DL-alanine, les signatures **A** et $\mathbf{C_5}$ du composé mentionné dans le titre ressemblent beaucoup à celles des dithioesters des dérivés de la glycine; toutefois, par comparaison avec les bandes d'un dithioester de la glycine, les bandes principales du conformère **B** sont déplacés par environ 30 cm^{-1} vers les fréquences plus basses.

[Traduit par la revue]

Introduction

The reaction of amino acid or multipeptide thionoesters, $RC(=O)NHCHR'C(=S)OCH_3$, with a cysteine proteinase such as papain generates a transient dithioacyl-enzyme intermediate $RC(=O)NHCHR'C(=S)S$—papain, where the substrate is linked to the enzyme by the thiol sulfur of cysteine 25 (1, 2). The dithioester moiety has an intense electronic absorption band near 315 nm which provides the opportunity to obtain the resonance Raman (RR) spectrum of the dithioester group and the adjacent bonds (1, 2). By this means it is possible to monitor the vibrational spectrum of the group undergoing transformation in the active site and arrive at a detailed description of conformational events during enzymolysis.

Interpretation of the RR spectra of the enzyme-substrate intermediates has been greatly facilitated by joint Raman and X-ray crystallographic studies on model compounds of the type $RC(=O)NHCHR'C(=S)SC_2H_5$, which have led to a set of precise spectra–structure correlations. It has also been necessary to undertake an analysis of the conformational properties of these dithioesters in solution by Raman, RR, and FTIR spectroscopy (3, 4). Taking the crystallographic and spectroscopic results together, the findings are that in non-hydrogen bonding solvents such as CCl_4, glycine-based dithioesters exist in a major populational state known as $\mathbf{C_5}$ (1) in which the N—H forms a hydrogen bond to the thiono sulfur and the resultant five-membered ring is essentially planar (Fig. 1). There is a minor population of a state known as conformer **B** (1) in CCl_4 and this is the predominant form in H-bonding solvents such as H_2O. The **B**-form is also shown in Fig. 1 and has the N atom *cis* to the thiol sulfur as a consequence of a N···S(thiol) interaction. This form is essentially unique to dithio- and thiol-esters (5) and is of importance for the dithioacyl-enzymes with glycine in the P_1 position (which is the substrate amino acid linked to cysteine 25) since it is the sole conformational state in native $RC(=O)NHCH_2C(=S)S$—papains (6) and other plant cysteine proteinases (7). Returning to the model compounds, there is another conformational state found in hydrogen bonding solvents. This is the **A** form shown in Fig. 1; it is converted to the $\mathbf{C_5}$ conformer by a 90° rotation about the NH—CH_2 bond and the N—H group participates in H-bonding to solvent rather than bonding intramolecularly to the thiono sulfur. Conformers **A**, **B**, and $\mathbf{C_5}$ have separate and characteristic RR spectra which we refer to as RR signatures.

Initial studies on dithioacyl enzymes and their corresponding dithioester model compounds focused on species having glycine next to the dithio group. Since glycine is a rather atypical amino acid and since papain shows marked variations in reactivity with different amino acids in the P_1 position we have begun to extend our analysis to other amino acids. Firstly, we are investigating the conformational and RR spectral properties of dithioesters based on alanine. A recent study (8) demonstrated that

[1]NRC No. 25723.

[2]To whom all correspondence should be addressed.

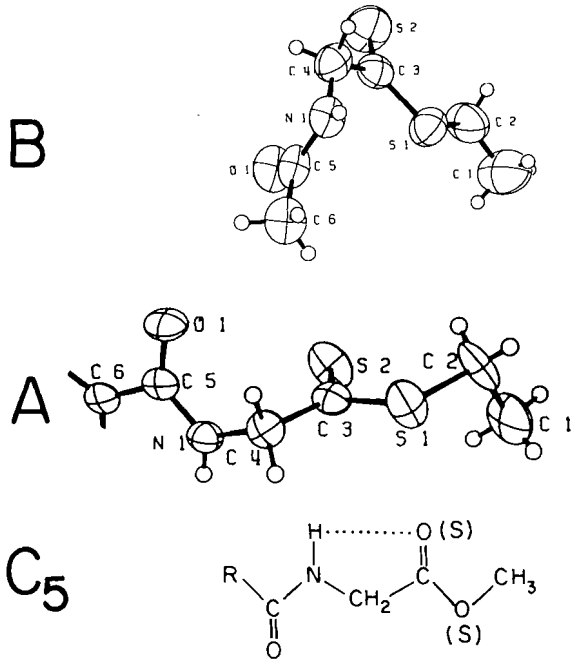

FIG. 1. Conformers **B**, **A**, and $\mathbf{C}_5$. The molecules shown are glycine derivatives; it is believed that alanine-based dithioesters have similar conformational preferences. Structures **A** and **B** are reproduced from ref. 16 with permission.

N-benzoylalanine ethyl dithioester crystallised as a **B**-like conformer and defined the RR signatures of the **B**, **A**, and $\mathbf{C}_5$ conformers for this molecule. The present work extends the analysis of alanine compounds to methyloxycarbonyl-L-phenylalanyl-L-alanine ethyl dithioester whose thionoester analog (—C(=S)OCH_3) is a particularly good substrate for papain (unpublished work, this laboratory). The LL form of the dithioester crystallised in a novel, perturbed **A**-like conformational state. It is the first reported structure of a dithioester based on a dipeptide and provides a useful addition to the catalogue of structure – RR spectra correlations.

Experimental

Materials

N-Methyloxycarbonylphenylalanyl-DL-alanine ethyl dithioester was prepared from its nitrile using a procedure previously described (9). The nitrile was produced by first, preparing the α-aminopropionitrile (0.01 equiv.) *in situ* (8), treating the α-aminopropionitrile mixture with *N*-methylmorpholine (0.01 equiv.) and then slowly adding it dropwise through a constant addition funnel into a cooled (−15°C, ice–salt) reaction mixture of methyloxycarbonylphenylalanine (0.01 equiv.), dissolved in CH_2Cl_2, previously treated with *N*-methylmorpholine and isobutyl chloroformate to produce the mixed anhydride of the *N*-protected amino acid (9). The reaction mixture was stirred for 1.5 h at −15°C and then at RT overnight. The water/organic mixture was separated and the water layer extracted twice with CH_2Cl_2. The organic extracts were combined, washed with 5% $NaHCO_3$, H_2O, 1 *N* HCl, H_2O, saturated NaCl solution and then dried over Na_2SO_4. The CH_2Cl_2 was removed and the oily residue was triturated with ether producing a white precipitate which was filtered, washed with ether, and air dried. The yield was 70%.

The purity of the *N*-methyloxycarbonylphenylalanyl-DL-alanine ethyl dithioester was checked by nmr and elemental analysis.

Crystal data

$C_{16}H_{22}N_2O_3S_2$ fw = 354.49

Tetragonal, $I4_1$, a = 15.198(3), c = 16.503(4) Å, ρ_c = 1.2354 g cm^{-3}, λ(CuKα) = 1.54178 Å, μ(CuKα) = 25.7 cm^{-1}. Crystal dimensions 0.1 × 0.2 × 0.5 mm.

Yellow crystals of *N*-methyloxycarbonyl-L-phenylalanyl-L-alanine ethyl dithioester were obtained by diffusing *n*-hexane into a solution of the DL compound in ether. The unit cell constants were measured using 23 reflections in the 2θ range 36 to 45°.

The intensity data were measured using Ni-filtered CuKα radiation (λ_1 = 1.5405 Å, λ_2 = 1.5443 Å) with a CAD4 diffractometer to a 2θ limit of 150°, by scanning ω/2θ; Δω = 0.70 + 0.35 tan θ (deg); aperture 4.0 + 0.4 tan θ (mm) and take off angle of 2.5°. The intensities of the reflections were monitored using three standard reflections and there were no systematic changes in the intensities. An empirical φ absorption correction (10) was applied. The intensity data reduction and the application of absorption correction were carried out by a program written by K. I. Varughese and G. Kartha (unpublished work). The ratio of the maximum to minimun transmissions was 1.28. Of the 2031 unique reflections measured 1746 had $F_o \geqq 2\sigma(F)$ and were used in the least-squares refinements. The structure was solved using the computer program MULTAN 80 (11) and refined by the block-diagonal least-squares program. Hydrogens were located with the help of difference electron density maps and stereochemical criteria. None of the hydrogens bonded to C(1) were located, but all the remaining 19 hydrogens were included in the structure factor calculations and refinement. In the refinement, thermal vibrations of hydrogens were treated isotropically while nonhydrogens were treated anisotropically. The *z*-coordinate of the S(1) was held fixed during the refinement. The refinement converged at an R ($\Sigma|\Delta F|/\Sigma|F_o|$) of 0.066. In the refinement weights were assigned from the counting statistics. The final weighted R was 0.075. The atomic scattering factors were taken from the International tables for X-ray crystallography (12). All crystallographic calculations otherwise noted were done with the NRC set of crystallographic programs (13). The final ΔF map was essentially featureless. The maximum peak and minimum trough in it were 0.5 and −0.4 e Å^{-3}, respectively.

Spectral data

The 647.1 nm excited Raman spectrum of methyloxycarbonyl-L-phenylalanyl-L-alanine ethyl dithioester was obtained using a Jarrell-Ash 25-400 spectrometer-based system (14); approximately 50 mW of laser power and a spectral slit width of 8 cm^{-1} were used. The 324 nm excited RR spectra of methyloxycarbonyl-L-phenylalanyl-DL-alanine ethyl dithioester in a powdered form were obtained using a system equipped with a multichannel detector (15). The solid material was used to coat the inside of a spinning quartz nmr tube and examined in the backscattering geometry. RR spectra from the dithioester in solution were obtained from 1–2 mL of solution, stirred by a small magnetic "pip", and contained in a quartz cuvette. The solution samples were examined in the 90° excitation–observation geometry. For the RR spectra, approximately 70 mW of 324 nm Kr^+ laser power was used and the spectral slit width of the spectrograph was set at 12 cm^{-1}.

Results and discussion

The crystal structure of methyloxycarbonyl-L-phenylalanyl-L-alanine ethyl dithioester

Crystals were grown from a solution containing both the LD and LL forms but the crystals selected for X-ray crystallographic analysis were solely in the LL form. The positional and thermal parameters of non-hydrogen atoms in methyloxycarbonyl-L-phenylalanyl-L-alanine ethyl dithioester are given in Table 1. For the hydrogen atoms these parameters are available as supplementary material.[3] The structure is depicted in Fig. 2.

[3]Tables of observed and calculated structure factors, positional and thermal parameters of hydrogen atoms and anisotropic temperature factors of non-hydrogen atoms may be purchased from the Depository of Unpublished Data, CISTI, National Research Council of Canada, Ottawa, Ont., Canada K1A 0S2.

TABLE 1. Positional and thermal parameters of nonhydrogen atoms*

Atom	x	y	z	B_{eq}
S(1)	90287(12)	21005(14)	46156	7.6
S(2)	96062(14)	39054(13)	49452(20)	8.7
O(1)	11362(2)	2483(3)	3901(2)	4.7
O(2)	13806(2)	2165(2)	4612(2)	4.7
O(3)	14158(2)	2239(2)	3289(2)	4.7
N(1)	11337(3)	2891(3)	5203(2)	4.3
N(2)	13097(3)	3091(3)	3762(2)	3.6
C(1)	7293(5)	2190(6)	4396(7)	8.9
C(2)	8046(5)	2740(7)	4349(6)	9.3
C(3)	9737(3)	2860(4)	4965(4)	4.9
C(4)	10530(4)	2426(4)	5384(3)	4.8
C(5)	10370(5)	2419(6)	6290(4)	8.0
C(6)	11702(3)	2890(3)	4464(3)	3.6
C(7)	12518(3)	3443(3)	4376(3)	3.4
C(8)	13688(3)	2479(3)	3941(3)	3.5
C(9)	14842(5)	1622(5)	3415(5)	6.8
C(10)	12281(4)	4399(4)	4163(3)	4.5
C(11)	13039(4)	5010(3)	4232(4)	4.5
C(12)	13457(5)	5342(4)	3572(4)	6.2
C(13)	14203(6)	5871(5)	3655(5)	7.3
C(14)	14497(5)	6069(4)	4405(5)	7.4
C(15)	14097(5)	5763(5)	5073(5)	6.8
C(16)	13358(4)	5248(4)	4992(4)	5.5

*B_{eq} is calculated as $(8\pi^2/3)(U_{11} + U_{22} + U_{33})$. The coordinates are multiplied by 10^5 for sulfur atoms and by 10^4 for the rest.

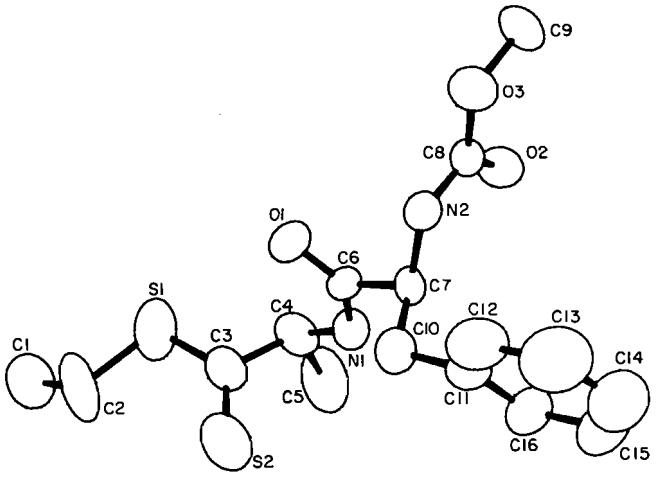

FIG. 2. The thermal elipsoid plot of methyloxycarbonyl-L-phenylalanyl-L-alanine ethyl dithioester.

Some relevant torsional angles are given in Table 2 and bond distances and bond angles are given in Fig. 3.

Since the RR spectrum is a sensitive probe of conformation in the —C(=O)NHCH(CH_3)C(=S)SC_2H_5 fragment, emphasis is given to the conformational properties of this part of the molecule. For the nine glycine- and alanine-based dithioesters analysed thus far eight structures have been found to occur as the so-called conformer **B**, in which the C(=O)NHCHRC(=S)SC_2H_5 nitrogen and thiol sulfur atoms are essentially *cis*, i.e. the NHCHR—CS torsional angle is small, between +10 and −20° (Fig. 1). Only one structure, *N*-(*p*-nitrobenzoyl)glycine ethyl dithioester, has been found where the N and thiol S atoms are *trans*, with the $NHCH_2$—CS(thiol) torsional angle equal to −172° (16); this structure we call conformer **A** (Fig. 1). Therefore, the present structure (Fig. 2) makes a valuable addition to our knowledge of *non*-**B** conformers. The key N(1)C(4)—C(3)S(1) torsional angle (designated $\overline{\Psi}'$) is 141.1(14)° (standard deviations refer to the least significant digit) with the C(6)N(1)—C(4)C(3) angle (Φ') being −69.2(22)°. These compare with the corresponding values for the conformer **A** of *N*-(*p*-nitrobenzoyl)glycine of −171.7° ($\overline{\Psi}$) and −86.2° (Φ) and contrast to typical conformer **B** values of ±15° ($\overline{\Psi}'$) and −80° ($\overline{\Phi}'$). Obviously the $\overline{\Phi}'$, $\overline{\Psi}'$, values are more **A**-like than conformer **B**-like and we describe the present compound as an **A**′ conformer.

One interesting observation is that the N···S(thiono) distance is 3.078(5) Å for the present compound compared to 3.043 Å in the crystalline form of *N*-(*p*-nitrobenzoyl)glycine ethyl dithioester. As the absolute values of the $\overline{\Psi}'$ angles differ by 32° a larger difference in N···S distances might be expected. However, in the present PheAla dithioester compared to the *p*-nitrobenzoylglycine structure the N(1)—C(4)—C(3) and C(4)—C(3)—S(2) angles are contracted by 3.6 and 2.3°, respectively. The N···S(thiono) distances are shorter than the sum of the van der Waals radii for N and S (3.35 Å) in both compounds, suggesting that an attractive N···S interaction exists and the contraction of the N(1)—C(4)—C(3) and C(4)—C(3)—S(2) angles in the present PheAla analog gives some support to this idea. Since there is a paucity of data concerning sulfur to nitrogen interactions for C=S groups, compared to sulfur nitrogen interactions involving sulfur in a X—S—Y bonding scheme (17, 18), further structures with C=S···N contacts are needed to develop stereochemical criteria for the interaction and to confirm that it does indeed exist.

For the phenylalanine residue the Ramachandran ($\overline{\Phi}$, $\overline{\Psi}$) values are −87.0(20) and 150.9(16)°, respectively. The χ_1 (N(2)—C(7)—C(10)—C(11)) and χ_2 (C(7)—C(10)—C(11)—C(12)) torsional angles are −68.6(19) and 106.1(21)°, respectively. At the dithioester end of the molecule, the —SC_2H_5 group takes up a fairly extended configuration with C(1)—C(2)—S(1)—C(3) equal to −153.9(18)°, a wide range of values have been determined for this parameter (8) and the values are probably determined by crystal packing forces. The bonds meeting at C(3) and C(6) are planar and there is no evidence for pyramidalisation at either atom. There are two intermolecular hydrogen bonds in the crystal; the parameters for these are given in Table 3.

Resonance Raman signatures of the different conformations of methyloxycarbonyl-L-phenylalanyl-DL-alanine ethyl dithioester

The 647.1 nm excited Raman spectrum of a single crystal of methyloxycarbonyl-L-phenylalanyl-L-alanine ethyl dithioester is given in Fig. 4. It is not possible to obtain 324 nm excited resonance Raman spectra from a single crystal due to problems associated with photodecomposition. Therefore, RR spectra of the solid form were obtained from powdered material coating the inside of a quartz spinning nmr cell and examined in the back-scattering geometry. Powdered samples from various origins were examined, e.g. from crushed crystals of the LL stereoisomer, or precipitated from a LL, LD mixture in a number of solvents. The RR spectrum shown in Fig. 5 is from a powder containing a 50:50 mixture of the LD and LL forms and the major features are indistinguishable from the RR spectrum of a powder sample of crushed crystals of the LL stereoisomer. There were insufficient quantities of the LL crystals to obtain high quality RR data from the LL form alone. Most of the features in the RR

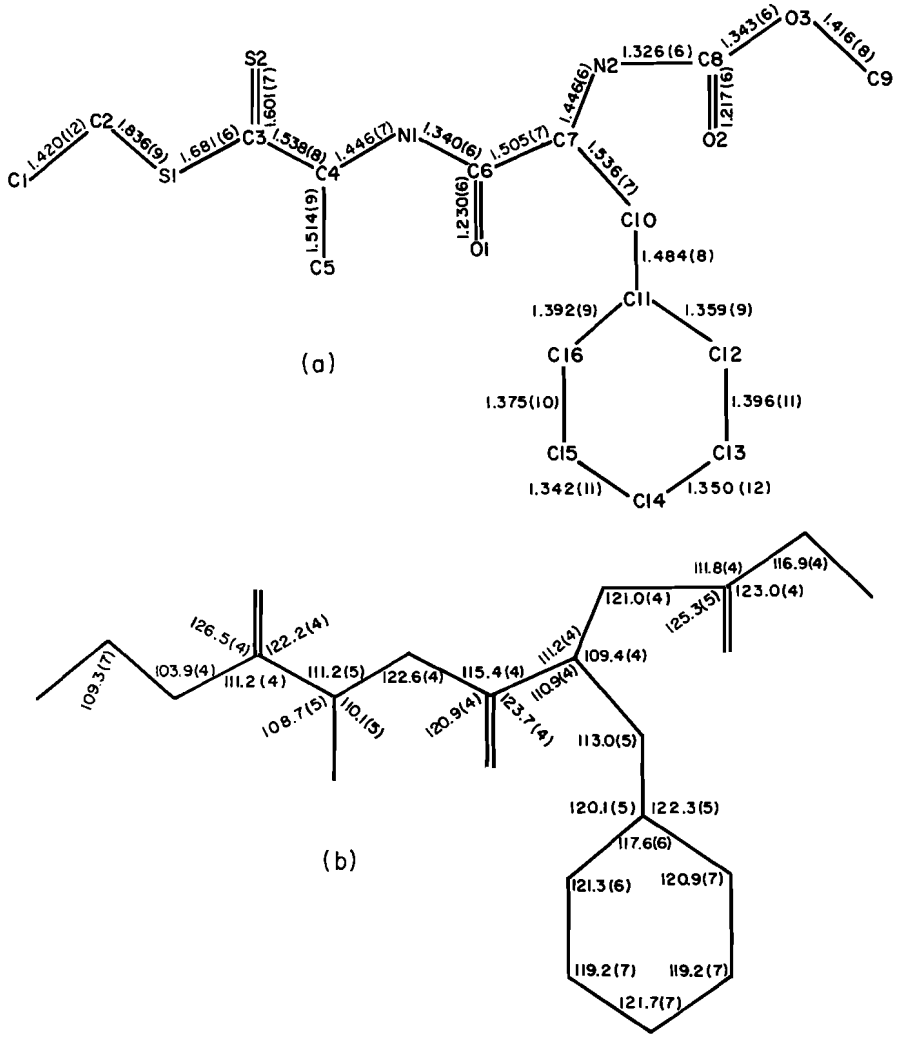

FIG. 3. (*a*) Bond lengths and (*b*) angles for methyloxycarbonyl-L-phenylalanyl-L-alanine ethyl dithioester.

TABLE 2. Selected torsional angles*

Atoms				Angle (deg)
C1	C2	S1	C3	−153.9(18)
C2	S1	C3	S2	−7.4(19)
C2	S1	C3	C4	168.1(14)
C3	C4	N1	C6	−69.2(22)
S1	C3	C4	N1	141.1(14)
S2	C3	C4	N1	−43.1(23)
C8	N2	C7	C6	−87.0(20)
N1	C6	C7	N2	150.9(16)
C4	N1	C6	C7	177.3(16)
C7	N2	C8	O3	179.9(15)
N2	C7	C10	C11	−68.6(19)
N2	C7	C6	O1	−31.5(24)
C7	C10	C11	C12	106.2(21)
C7	C10	C11	C16	−72.6(23)
C9	O3	C8	N2	176.8(16)

*Standard deviations refer to the least significant digit, (18) means 1.8°.

TABLE 3. Hydrogen bond parameters*

Bonds	Length (Å) D—H	H···A	D···A	Angle (deg) D—H···A
N(1)—H—O(1)	0.75(8)	2.18(7)	2.870(6)	154(7)
N(2)—H—O(3)	0.93(5)	2.04(6)	2.959(5)	169(6)

*D = donor, A = acceptor.

spectrum can be associated with peaks in the normal Raman spectrum of the single crystal. It appears that the normal Raman features at 1186 and 1162 cm^{-1} (Fig. 4) are both RR-active and that they are unresolved in the RR spectrum to form the broad band seen at 1174 cm^{-1} (Fig. 5). The intense RR peak at 1099 cm^{-1} probably corresponds to the shoulder seen at 1096 cm^{-1} in the normal Raman spectrum (Fig. 4). The weak to medium RR peaks at 1033, 1008, and 902 cm^{-1} can also be seen in the Raman spectrum at or near these frequencies the (1008 cm^{-1} band appears as a shoulder on the intense 1003 cm^{-1} feature). The broad RR feature centered at 667 cm^{-1} cannot be identified in the Raman spectrum due to interference, in the latter, from a laser plasma line. This line could not be removed completely under the experimental conditions employed. The RR peaks near 578 and 561 cm^{-1} probably correspond to the features seen at 577 and 555 cm^{-1} in the Raman spectrum of the single crystal. The intense RR peaks at 1174, 1099, and 667 cm^{-1} were observed in the same position in the poorer quality RR spectrum of the LL form (data not

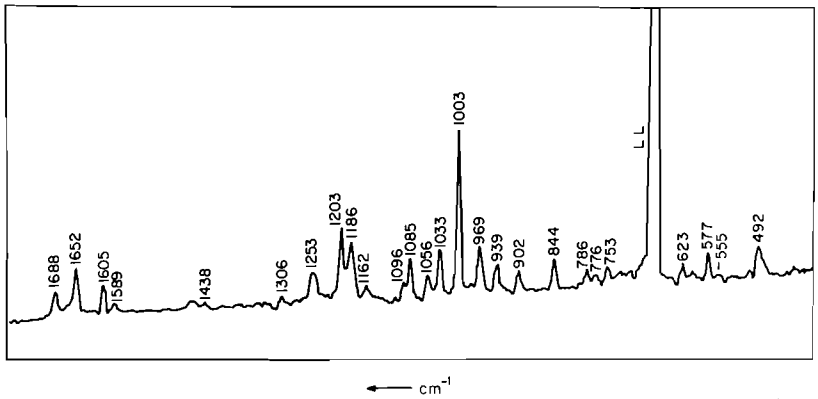

FIG. 4. The 647.1 nm excited Raman spectrum of a single crystal of methyloxycarbonyl-L-phenylalanyl-L-alanine ethyl dithioester; LL = laser plasma line.

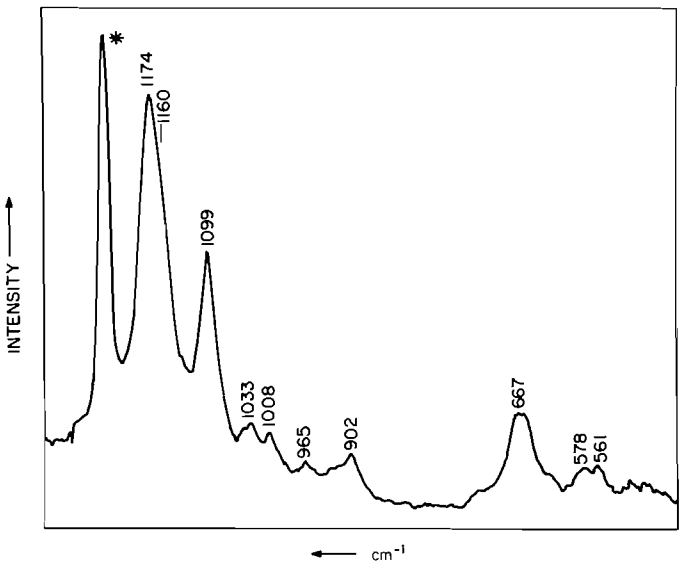

FIG. 5. The 324 nm excited resonance Raman spectrum of powdered methyloxycarbonyl-L-phenylalanyl-DL-alanine ethyl dithioester. The peak marked with an asterisk is due to a laser plasma line.

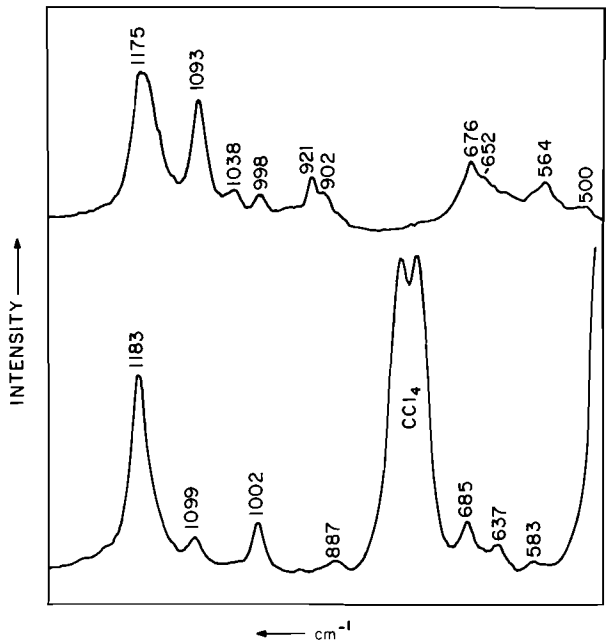

FIG. 6. Resonance Raman spectra (324 nm excitation) of methyloxycarbonyl-L-phenylalanyl-DL-alanine ethyl dithioester, $\sim 5 \times 10^{-4}$ *M* in H_2O/CH_3CN (19:1) (top) and $\sim 10^{-3}$ *M* in CCl_4 (bottom). In the top spectrum the peak at 921 cm^{-1} is due to CH_3CN; in the bottom spectrum the doublet near 750 cm^{-1} is due to CCl_4.

shown), thus these data establish a partial RR signature of an alanine-based dithioester in an **A′** type conformation which, in turn, constitutes a useful addition to our catalogue of spectra–structure correlations.

Our knowledge of the conformational properties of *N*-acyl glycine dithioesters (3, 4) and *N*-benzoylalanine ethyl dithioester (8) in solution allows us to delineate the structure – RR spectra correlations, for the major RR peaks, for methyloxycarbonyl-L-phenylalanyl-DL-alanine ethyl dithioester in solution. Figure 6 compares the RR spectra of the PheAla dithioester in H_2O/CH_3CN (19:1 v/v) and CCl_4. The spectra in Fig. 6 are very similar to the RR spectra of *N*-benzoylalanine ethyl dithioester in H_2O/CH_3CN and CCl_4 (Figs. 7 and 8 in ref. 8); thus, the conformational preferences in the $—C(=O)NHCH(CH_3)C(=S)SC_2H_5$ fragment of this molecule and the present PheAla dithioester must be very similar. In H_2O/CH_3CN both molecules assume a mixed population of **A** and **B** type conformers about the dithioester moiety. In the spectrum in H_2O/CH_3CN the **A** conformer makes the major contribution to intensity in the 1175 and 652–676 cm^{-1} regions and, on the basis that it increases in intensity in CCl_4 solution, probably to the peak near 1000 cm^{-1}. Further evidence that the 1000 cm^{-1} band is found for only **A** or $\mathbf{C_5}$ conformers is that it is absent in the RR spectrum of solid *N*-benzoylalanine ethyl dithioester, which is in a **B** conformer, but is present when this compound is dissolved in H_2O or CCl_4 where the **A** and $\mathbf{C_5}$ conformers, respectively, are expected. The RR spectrum of the solid (Fig. 5) also indicates that the **A** conformer contributes part of the intensity of the 1093 cm^{-1} feature seen in Fig. 6 (top). The position of the peaks near 1175 and 660 cm^{-1} are very similar to those found for the **A** conformers of *N*-acylglycine ethyl dithioesters. The main **B** conformer markers occur in the spectrum from H_2O/CH_3CN solution (Fig. 6) at 1093 and 564 cm^{-1}. Unlike the **A** conformer case, the alanine **B** conformer peaks at 1093 and 564 cm^{-1} are shifted to lower frequency by some 30 cm^{-1} compared to the corresponding **B** features in *N*-acyl glycine dithioester.

A further difference between *N*-acylglycine and *N*-acylalanine dithioesters concerns the overlap of **A** and **B** conformer markers in the 1090–1190 cm^{-1} region. For the **A**-like conformers, *N*-acylglycine dithioesters have just a single intense

feature near 1170 cm^{-1} (16), in addition to this feature *N*-acylalanine dithioesters have a medium intensity peak near 1100 cm^{-1} (Fig. 5). For the **B**-like conformers, *N*-acylglycine dithioesters have an intense band near 1135 cm^{-1} and a weak to medium intensity peak near 1165 cm^{-1} (17) whereas in the most thoroughly studied *N*-acylalanine dithioester case, *N*-benzoylalanine ethyl dithioester, the intense 1100 cm^{-1} **B**-marker is accompanied by two medium intensity bands near 1140 and 1169 cm^{-1} (8). Thus, it appears that in the 1090–1190 cm^{-1} region greater care has to be taken to disentangle **A** and **B** markers in the case of the alanine-based dithioesters than in the case of glycine-based dithioesters.

In CCl_4, the predominant conformation of the glycine- and alanine-based dithioesters examined thus far is $\mathbf{C}_5$. From the marked similarity between the RR spectra of these molecules (4, 8) and the present example it is very likely that the alanine—dithioester portion in the majority of molecules of methyloxycarbonyl-L-phenylalanyl-DL-alanine ethyl dithioester in CCl_4 takes up a $\mathbf{C}_5$ conformation. The 1183, 685, and 637 cm^{-1} are characteristic $\mathbf{C}_5$ markers. The peak seen in Fig. 6 at 1002 cm^{-1} is also observed at this position for *N*-benzoylalanine ethyl dithioester in CCl_4 (8), but not for any *N*-acylglycine derivatives (4). Therefore it is likely that this feature is alanine specific. It may be associated with the C_α—CH_3 moiety (8) and appears to increase in relative intensity in the $\mathbf{C}_5$ conformer (Fig. 6). A further point of note is the 1099 cm^{-1} feature in CCl_4, which may contain contributions from the $\mathbf{C}_5$ conformer and from the small amount of the **B**-form present, is much less intense than the corresponding band in the spectrum of the solid. Thus, the 1099 cm^{-1} peak is less intense in the $\mathbf{C}_5$ compared to the corresponding band in the **A** conformer.

1. P. R. CAREY and A. C. STORER. Pure Appl. Chem. **57**, 225 (1985).
2. P. R. CAREY and A. C. STORER. Ann. Rev. Biophys. Bioeng. **13**, 25 (1984).
3. A. C. STORER, Y. OZAKI, and P. R. CAREY. Can. J. Chem. **60**, 199 (1982).
4. H. LEE, A. C. STORER, and P. R. CAREY. Biochemistry, **22**, 4781 (1983).
5. C. P. HUBER, P. R. CAREY, S.-C. HSI, H. LEE, and A. C. STORER. J. Am. Chem. Soc. **106**, 8263 (1984).
6. A. C. STORER, H. LEE, and P. R. CAREY. Biochemistry, **22**, 4789 (1983).
7. P. R. CAREY and Y. OZAKI. Biochem. Biophys. Res. Commun. **117**, 725 (1983).
8. R. H. ANGUS, P. R. CAREY, H. LEE, A. C. STORER, and K. I. VARUGHESE. Can. J. Chem. **63**, 2169 (1985).
9. P. R. CAREY, R. H. ANGUS, H. LEE, and A. C. STORER. J. Biol. Chem. **259**, 14357 (1984).
10. A. C. T. NORTH, D. C. PHILIPS, and F. C. MATHEWS. Acta Crystallogr. A**24**, 351 (1968).
11. P. MAIN, S. J. FISKE, S. E. HULL, L. LESSINGER, G. GERMAIN, J-P. DECLERCQ, and M. M. WOOLFSON. MULTAN 80. A system of computer programs for automatic solution of crystal structures from X-ray diffraction data. University of York, England and University of Louvain, Louvain, Belgium. 1980.
12. International tables for X-ray crystallography. Vol. III. Kynoch Press: Birmingham. 1968. p.202.
13. F. R. AHMED, S. R. HALL, M. E. PIPPY, and C. P. HUBER. J. Appl. Crystallogr. C, 309 (1973) (NRC Crystallographic Programs for IBM/360 system, accession No. 133-147).
14. K. KUMAR and P. R. CAREY. J. Chem. Phys. **63**, 3697 (1975).
15. P. R. CAREY and L. R. SANS CARTIER. J. Raman Spectrosc. **14**, 271 (1983).
16. C. P. HUBER, Y. OZAKI, D. H. PLIURA, A. C. STORER, and P. R. CAREY. Biochemistry, **21**, 3109 (1982).
17. K. I. VARUGHESE, A. C. STORER, and P. R. CAREY. J. Am. Chem. Soc. **106**, 8252 (1984).
18. R. E. ROSENFIELD, R. PARTHASARATHY, and J. D. DUNITZ. J. Am. Chem. Soc. **99**, 4860 (1977).

COMMUNICATIONS

Concerning the Si—Li bonding in phenylsilyllithiums as studied by variable temperature ^{7}Li nuclear magnetic resonance[1]

ERWIN BUNCEL[2] AND T. KRISHNAN VENKATACHALAM
Department of Chemistry, Queen's University, Kingston, Ont., Canada K7L 3N6

AND

ULF EDLUND
Department of Chemistry, Umeå University, S-90187 Umeå, Sweden

Received February 4, 1986

ERWIN BUNCEL, T. KRISHNAN VENKATACHALAM, and ULF EDLUND. Can. J. Chem. **64**, 1674 (1986).

A variable temperature ^{7}Li nmr study of equimolar mixtures of two structurally related phenylsilyllithiums supports a bimolecular exchange mechanism between monomeric structures as being responsible for the collapse of the ^{7}Li signals of the two species. The different exchange rates indicated in MTHF and THF parallel the observations from a Si—Li coupling study. The experimental data provide support for a mainly ionic Si—Li bond, although some orbital interaction is indicated.

ERWIN BUNCEL, T. KRISHNAN VENKATACHALAM et ULF EDLUND. Can. J. Chem. **64**, 1674 (1986).

Les résultats d'une étude des spectres rmn du ^{7}Li, effectuée à des températures variables sur des mélanges équimoléculaires de deux phényl silyl lithium reliées par leur structure, sont en accord avec la suggestion qu'un mécanisme d'échange bimoléculaire entre les structures monomères est responsable de la coalescence des signaux ^{7}Li des deux espèces. Les diverses vitesses d'échange dans le MTHF et le THF sont parallèles à celles obtenues lors d'une étude du couplage Si—Li. Les données expérimentales fournissent un support à l'hypothèse d'une liaison Si—Li qui serait principalement ionique, même s'il semble exister quelques interactions entre orbitales.

[Traduit par la revue]

Introduction

The precise nature of bonding in organolithium compounds has been a topic of considerable controversy (1). On the basis of recent *ab initio* calculations it has been argued that the carbon–lithium bond is predominantly ionic, i.e. ca 80% ionic character, and in fact more ionic than the Li—F bond (2). ^{13}C nmr studies of organolithium compounds have been most informative of the carbon–lithium bonding character in solution where the existence of ^{13}C—^{6}Li coupling has been taken as strong evidence of covalent character of the carbon–lithium bond (3).

Less attention has been paid to the bonding situation in organosilyllithium compounds. However, based on the very similar ^{7}Li chemical shifts, it was claimed that the ionicity of the Si—Li bond should be similar to that of the C—Li bond (4). Additionally, in the nmr study of diisopropylphenylsilyllithium, the diastereotopic isopropyl groups remain nonequivalent up to 185°C, indicating a slow inversion on the ^{1}H nmr time-scale (4). The ionic character of the Si—Li bond has recently received support from *ab initio* study, which showed that the Si—Li bond is to some extent stronger than the C—Li bond, and also that the ionic bonding in the $SiH_3^-Li^+$ ion pair is more extensive than in $CH_3^-Li^+$, due to the greater electron affinity of SiH_3 compared to CH_3 (5).

We have found by means of a ^{13}C nmr study of phenylsilyllithium and other phenyl-substituted germyl, stannyl, and plumbyl anions, a strong similarity in the charge distribution of the phenyl rings, indicating that most of the negative charge resides on the metal atom, contrasting with the situation in the corresponding phenylmethyl carbanion systems (6). Moreover, a lithium-nmr study of the phenylsilyllithium species suggested that the Si—Li interaction was equal to or stronger than the association found for Ph_3CLi, in ethereal solvents (7).

Additional support for this suggestion was recently provided by a study (8) of these phenylsilyllithiums using ^{29}Si nmr. The existence of ^{29}Si—$^{6(7)}$Li couplings provided evidence of sufficient Si–Li orbital overlap to allow a mechanism for some charge transfer with spin-polarization necessary for scalar coupling. Moreover, a slight concentration dependence of the coupling in $PhMe_2Si^7Li$ in THF solvent at −80°C, suggested that a bimolecular exchange process could be responsible for the collapse of the coupling (8). However, an alternative explanation would be that ion-pair dissociative processes are responsible for the collapse of the coupling as a result of temperature and medium changes.

We have sought further evidence to distinguish between these possibilities using a methodology which has been established in various organometallic exchange processes (9). If the ^{7}Li resonances for two structurally related species rapidly equilibrating at ambient temperature are significantly different, then one should, by lowering the temperature, be able to see separate ^{7}Li signals. The following experiments have been performed using a Bruker AM-400 multinuclear nmr instrument with LiCl (1 *M*) in D_2O as external standard (Table 1).

(*1*) The two species Ph_3SiLi and $Ph_2MeSiLi$, obtained by lithium metal cleavage of Ph_3Si—$SiMePh_2$ in THF, gave a single resonance of ca. 1 Hz linewidth at room temperature. Successive lowering of the temperature to −90°C resulted in a line broadening up to 18 Hz but no distortion in the Lorentzian line shape could be detected. This observation parallels that in the ^{29}Si nmr study (8) of the two separate compounds in the

[1]Carbanion mechanisms. Part 15. For Part 14, see ref. 7.
[2]To whom all correspondence should be addressed.

TABLE 1. ^{7}Li nmr data for 1:1 mixtures of silyllithiums as a function of temperature

Species	Solvent	T (°C)	δ (ppm)	$\nu_{1/2}$ (Hz)
Ph_3SiLi + $Ph_2MeSiLi$	THF	22	2.27	3.0
		−60	2.26	12.0
		−90	2.26	18.0
Ph_3SiLi + $PhMe_2SiLi$	THF	22	2.22	4.0
		−40	2.25	10.0
		−60	2.25	19.0
		−80	2.30	47.0
		−85	2.33, 2.13	56.0
		−90	2.33, 2.10	54.0
Ph_3SiLi + $Ph_2MeSiLi$	MTHF	22	2.20	13.0
		−40	2.20	28.0
		−60	2.22	37.0
		−70	2.19	37.0
		−75	2.26, 2.17	41.0
		−80	2.28, 2.17	45.0
		−85	2.30, 2.17	48.0
		−90	2.30, 2.17	51.0

same solvent in which no coupling was revealed even at −100°C.

(*2*) Similar experiments using the pair of silyllithiums Ph_3SiLi and $PhMe_2SiLi$ showed a different kind of behaviour. At ca. −80°C a distorted signal was observed which on further lowering of the temperature to −90°C showed two overlapping peaks with a separation $\Delta\delta = 0.23$. This shift difference is approximately the same as the difference calculated from ^{7}Li nmr data of the separate species ($\Delta\delta = 0.13$) (7). This observation compares with the well resolved multiplet of the ^{29}Si signal observed in THF at −100°C of $PhMe_2SiLi$ found previously (8).

(*3*) The final experiment refers to the pair of species Ph_3SiLi and $Ph_2MeSiLi$ but changing the solvent to 2-methyltetrahydrofuran (MTHF). In this case the non-Lorentzian behaviour is already noted at −70°C and on lowering the temperature to −90°C, two partially resolved peaks of equal intensity are observed (Fig. 1). Again, the chemical shift difference of $\Delta\delta = 0.13$ could be measured, which within experimental accuracy is the same as the value derived for the separate species ($\Delta\delta = 0.10$). In the scalar coupling study (8), both these compounds gave rise to multiplets at −100°C in MTHF solvent.

It is noteworthy that the coupling constant ($^1J[^{29}Si, ^7Li] = 51$ Hz) (7) and the ^{7}Li peak separation (20 Hz) are of reasonably similar magnitude in these cases. This suggests that the coalescence point in the two experiments should be found in a comparable temperature range, provided that the collapse is caused by the same mechanism. This is in agreement with the observations.

One would have expected that a dissociative process would lead to some change in π-polarization of the ^{13}C signals of the phenyl carbons, the ^{29}Si chemical shifts and, most significantly, of the ^{7}Li nmr signals. Such changes were not observed in our earlier studies (6–8) or in the present study. Especially noteworthy is the approximate temperature independence found for the ^{7}Li chemical shifts of all these silyllithium species (Table 1). If a change in ion-pair equilibrium is occurring one would expect a significant upfield shift of several ppm on going to solvent separated species (7, 10). The fact that in the present study the splitting was observed in a narrow temperature

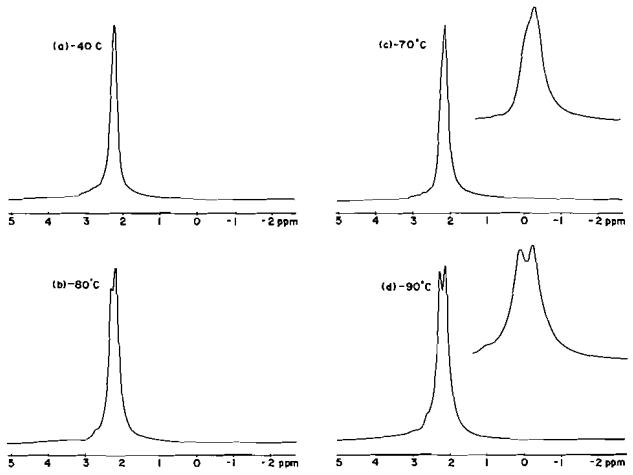

FIG. 1. Variable temperature ^{7}Li nmr spectra of an equimolar mixture of Ph_3SiLi and $Ph_3MeSiLi$ in 2-methyltetrahydrofuran (MTHF).

interval, added to the earlier observations that there is a slight concentration dependence of the ^{29}Si–^{7}Li coupling at a given temperature, provides strong support for a bimolecular exchange process between the monomeric species.

No attempt has been made to evaluate rate constants for exchange due to the possibility of trace amounts of radical anions which could be formed during the lithium metal reduction and which could cause efficient line broadening. This is suggested by the exchange experiments where the line-width reproducibility at ambient temperature is unsatisfactory for a line-shape analysis to be performed. Moreover, anion – radical anion exchange could be a dynamic process on the nmr time scale (11). A further consideration is that line-broadening of the ^{7}Li signal at low temperature could arise from a more efficient quadrupolar relaxation (3*a*, 12), as well as slow exchange. This complication could, however, be avoided if the less quadrupolar ^{6}Li isotope were used (3).

The data presented in this study are thus consistent with a significant, although minor, Si—Li bonding character (orbital interaction) in the organosilyllithium compounds under investigation. Further support for an ionic description is given by the very similar lithium chemical shifts of the phenylsilyllithiums. Thus the lithium chemical shifts do not respond to the significant ^{29}Si chemical shift changes observed along the series Ph_3SiLi ($\delta_{THF}^{^{29}Si} = -9.0$) → $Ph_2MeSiLi$ ($\delta_{THF}^{^{29}Si} = -20.6$) → $PhMe_2SiLi$ ($\delta_{THF}^{^{29}Si} = -27.8$) (13).

The observation of a well-resolved ^{29}Si–^{7}Li coupling at low temperature also supports a mainly ionic description. The ^{29}Si–^{7}Li coupling is expected to be quenched by quadrupolar-induced relaxation if the bond covalency is significantly large, in parallel with the behaviour of propyllithium (14). The silicon–lithium bonding character therefore seems to be closer to that found for lithium acetylides (15). In this context, it is noted that through-space mechanisms have been suggested, for instance to account for the observation of ^{19}F, ^{19}F coupling in certain sterically congested bicyclic structures (16).

To conclude, the present study of the structures of phenylsilyllithiums supports an orbital interaction between the silicon and lithium atoms, although the bonding is believed to be mainly ionic. Moreover, the results are consistent with the observation of Si–Li scalar coupling at low temperature and with conclusions from *ab initio* calculations (5).

Acknowledgements

Support of this research by grants from the Swedish Natural Science Research Council (U.E.) and the Natural Sciences and Engineering Research Council of Canada (E.B.) is gratefully acknowledged. Helpful correspondence and the provision of unpublished information by Professor Paul Schleyer is also acknowledged.

1. (*a*) A. STREITWIESER, JR., J. E. WILLIAMS, JR., S. ALEXANDRATOS, and J. M. MCKELVEY. J. Am. Chem. Soc. **98**, 4778 (1976); (*b*) J. D. DILL, P. V. R. SCHLEYER, J. S. BINKLEY, and J. A. POPLE. J. Am. Chem. Soc. **99**, 6159 (1977); (*c*) G. D. GRAHAM, D. S. MARYNICK, and W. N. LIPSCOMB. J. Am. Chem. Soc. **102**, 4572 (1980); (*d*) T. CLARK, C. ROHDE, and P. V. R. SCHLEYER. Organometallics, **2**, 1344 (1983); (*e*) S. M. BACHRACH and A. STREITWIESER, JR. J. Am. Chem. Soc. **106**, 2283 (1984); (*f*) E. BUNCEL. Carbanions. Mechanistic and isotopic aspects. Elsevier, Amsterdam. 1975; (*g*) D. H. O'BRIEN. *In* Comprehensive carbanion chemistry. Vol. 1. *Edited by* E. Buncel and T. Durst. Elsevier, Amsterdam. 1980; (*h*) E. BUNCEL and B. C. MENON. J. Org. Chem. **44**, 317 (1979); (*i*) B. C. MENON, H. F. SHURVELL, J. P. COLPA, and E. BUNCEL. J. Mol. Struct. **78**, 29 (1982).
2. A. E. REED, R. B. WEINSTOCK, and F. WEINHOLD. J. Chem. Phys. **83**, 735 (1985).
3. (*a*) G. FRAENKEL, M. HENRICHS, J. M. HEWITT, B. M. SU, and M. J. GECKLE. J. Am. Chem. Soc. **102**, 3345 (1980); (*b*) D. SEEBACH, R. HÄSSIG, and J. GABRIEL. Helv. Chim. Acta, **66**, 308 (1983).
4. J. B. LAMBERT and M. URDANETA-PEREZ. J. Am. Chem. Soc. **100**, 157 (1978).
5. B. T. LUKE, J. A. POPLE, M.-B. KROGH-JESPERSEN, Y. APELOIG, J. CHANDRASEKHAR, and P. V. R. SCHLEYER. J. Am. Chem. Soc. In press.
6. E. BUNCEL, T. K. VENKATACHALAM, U. EDLUND, and B. ELIASSON. J. Chem. Soc. Chem. Commun. 1476 (1984).
7. E. BUNCEL, T. K. VENKATACHALAM, B. ELIASSON, and U. EDLUND. J. Am. Chem. Soc. **107**, 303 (1985).
8. U. EDLUND, T. LEJON, T. K. VENKATACHALAM, and E. BUNCEL. J. Am. Chem. Soc. **107**, 6408 (1985).
9. T. L. BROWN. Acc. Chem. Res. **1**, 23 (1968).
10. R. H. COX and H. W. TERRY, JR. J. Magn. Reson. **104**, 317 (1974).
11. (*a*) B. ELIASSON, T. LEJON, and U. EDLUND. J. Chem. Soc. Chem. Commun. 591 (1984); (*b*) K. MÜLLEN. Chem. Rev. **84**, 607 (1984).
12. J. F. MCGARRITY and C. A. OGLE. J. Am. Chem. Soc. **107**, 1805 (1985).
13. U. EDLUND, T. LEJON, T. K. VENKATACHALAM, and E. BUNCEL. To be published.
14. G. FRAENKEL, A. M. KRAENKEL, M. J. GECKLE, and F. SCHLOSS. J. Am. Chem. Soc. **101**, 4745 (1979).
15. (*a*) G. FRAENKEL and P. PRAMANIK. J. Chem. Soc. Chem. Commun. 1527 (1983); (*b*) R. HÄSSIG and D. SEEBACH. Helv. Chim. Acta, **66**, 2269 (1983).
16. J. HILTON and L. H. SUTCLIFFE. Prog. Nucl. Magn. Resn. Spectrosc. **10**, 27 (1975).

Synthesis and structural characterization of an unusual silylzirconium hydride complex

CLARE AITKEN AND JOHN F. HARROD
Chemistry Department, McGill University, Montreal, Que., Canada H3A 2K6

AND

EDMOND SAMUEL
Ecole Nationale Supérieure de Chimie de Paris, UA 403, CNRS, Paris, France

Received February 25, 1986

CLAIRE AITKEN, JOHN F. HARROD, and EDMOND SAMUEL. Can. J. Chem. **64**, 1677 (1986).

Dimethylzirconocene and dihydridozirconocene both catalyze the dehydrogenative coupling of primary and secondary organosilanes. Primary silanes give linear polysilanes and secondary silanes give tetraorganodisilanes. The reaction of dimethylzirconocene with a small excess of phenylsilane gives the unusual unsymmetrically substituted zirconocenesilylhydride dimer: $Cp_2Zr(SiMePhH)(\mu\text{-}H)_2(PhH_2Si)ZrCp_2$. The structure of this product is deduced from a combination of nmr and crystallographic results. Although the nmr data suggest that dihydridozirconocene reacts with phenylsilane to give the corresponding symmetrical dimer (Me replaced by H) in solution, attempts to isolate this compound have not been successful.

CLAIRE AITKEN, JOHN F. HARROD et EDMOND SAMUEL. Can. J. Chem. **64**, 1677 (1986).

Le diméthylzirconocène et le dihydridozirconocène catalysent tous les deux le couplage déshydrogénant des organosilanes primaires et secondaires. Les silanes primaires conduisent à des polysilanes linéaires; les silanes secondaires donnent des tétraorganodisilanes. La réaction du diméthylzirconocène avec un léger excès de phénylsilane conduit à un produit inhabituel, le dimère substitué d'une façon non symétrique de l'hydrure de zirconocènesilyle, $Cp_2Zr(SiMePhH)(\mu\text{-}H)_2(PhH_2Si)ZrCp_2$. On a déduit la structure de ce produit en se basant sur une combinaison de données rmn et cristallographiques. Même si les données de la rmn suggèrent que, en solution, le dihydrozirconocène réagit avec le phénylsilane pour conduire au dimère symétrique correspondant (le Me est remplacé par un H), on n'a pas réussi à isoler ce composé.

[Traduit par la revue]

We recently reported that dimethyltitanocene and its analogues are effective catalysts for the dehydrogenative coupling of primary organosilanes to organopolysilanes according to reaction [1] (1, 2)

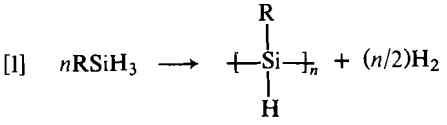

[1] $n\text{RSiH}_3 \longrightarrow \text{-[-Si(R)(H)-]}_n\text{-} + (n/2)\text{H}_2$

We now report that dimethylzirconocene, **1**, is also an effective catalyst for the same reaction. Unlike the analogous titanium compound, **1** also catalyses the coupling of secondary organosilanes to tetraorganodisilanes. The zirconium system has also provided a novel organometallic product which, whilst showing little catalytic activity, probably throws light on the mechanism of the polymerization reaction.

Shortly after the addition of a small amount of **1** (ca. 1 mol%) to phenylsilane, **2**, either neat or in solution in a hydrocarbon solvent, the initially colourless solution turns yellow and then deep orange. Accompanying these color changes there is a vigorous evolution of hydrogen and rapid formation of poly(phenylsilylene) (for details of polymer characterization, see refs. 1, 2). At room temperature a similar reaction with diphenylsilane was extremely sluggish, but at 65°C a smooth coupling to 1,1,2,2-tetraphenyldisilane occurred. Dimethyltitanocene does not effectively catalyze this dimerization reaction, but gives an oligomeric polysilane mixture in small yield.

Reaction of **1** in toluene with a severalfold excess of **2** gave a dark orange solution from which precipitated a yellow crystalline solid, **3**. (*Anal.* calcd. for $C_{33}H_{38}Si_2Zr_2$: C 58.87, H 5.69, Si 8.34; found, C 58.41, H 5.86, Si 8.73). After washing with ether to remove traces of polymer, this solid gave the ^{1}H-nmr spectrum shown in Fig. 1. The spectrum of the product arising from a reaction with an excess of $PhSiD_3$ is also shown in Fig. 1. From these spectra we can draw the following conclusions: the molecule contains (*1*) two slightly inequivalent bridging hydrides coupled to each other (AB quartet at δ −5.09 and −4.96, J_{H-H} = 11 Hz), (*2*) a methyl group of the kind $(CH_3)SiH$ (doublet at δ 0.58, J_{H-H} = 4 Hz, becomes a singlet in the deutero-compound), and a multiplet at δ 4.87 (coupled to the δ 0.58 resonance and absent in the deutero-compound), (*3*) a sharp singlet at δ 4.78, absent in deutero-compound, assigned to $PhSiH_2$, (*4*) four inequivalent η^5-cyclopentadienyl groups (δ 5.28, 5.37, 5.43, and 5.50), (*5*) two phenyl groups (peaks at δ 7.55–7.65 due to *ortho*-protons and complex multiplet at δ 7.20–7.35 due to *meta*- and *para*-protons). A natural abundance ^{29}Si spectrum, obtained using a DEPT (distortionless enhancement by polarization transfer) pulse sequence (3) is shown in Fig. 2. Two Si resonances are observed: a doublet of unresolved multiplets (δ 15.81, J_{Si-H} = 168 Hz) and a triplet of doublets (δ −7.86, J_{Si-H} = 147 and 15 Hz). These results lead to the conclusion that the compound **3** has the following structure:

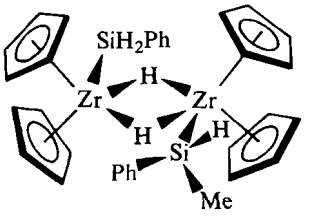

3

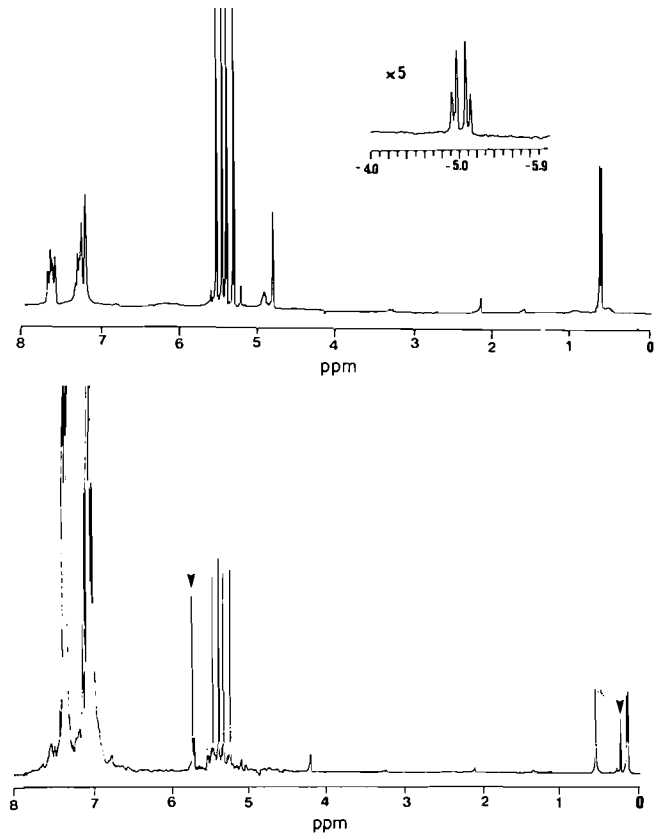

FIG. 1. Upper spectrum: ^{1}H-nmr spectrum of **3** in benzene-d_6. Lower spectrum: the product of an in situ reaction of Cp_2ZrMe_2 with an excess of $PhSiD_3$ in benzene-d_6. The resonance at ca. 0.1 ppm is due to CH_3D liberated in the reaction. Arrows indicate peaks due to an impurity.

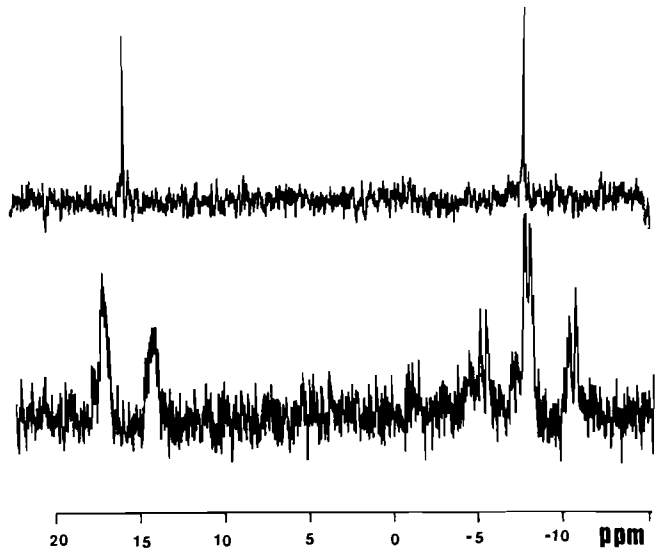

FIG. 2. Natural abundance ^{29}Si-nmr spectrum of **3**. Upper spectrum proton decoupled.

The observation of the high field hydride protons as an AB quartet and of the four inequivalent Cp resonances allows definitive exclusion of the possibility that **3** is a mixture of two different symmetrical silyl complexes. The chemical shifts of the hydride and Cp resonances are in the same region as has been observed for the structurally similar $[Cp_2ZrH_2]_2$ (4, 5), where Cp is either η^5-cyclopentadienyl or η^5-methylcyclopentadienyl. The ^{29}Si resonances are at unusually high field, compared to shifts reported for other transition metal silyls (6). The orange solution resulting from dissolution of $[Cp_2ZrH_2]_2$ in a toluene solution of **2** gives a sharp, single Cp resonance at δ 5.4 and a singlet due to hydride at δ −4.9. We have not been able to isolate this product as a crystalline solid, but it is almost certainly the symmetrical —SiH_2Ph compound.

Complicated disorder problems have so far hindered the refinement of the crystal structure of **3** to a statisfactory confidence level. However, the gross features of the molecule, as concluded from the nmr study, are supported by the X-ray results.[1]

The compound **3** is formally a dimer of (*a*) the product of oxidative addition of $PhSiH_3$ to zirconocene and (*b*) the product of the insertion of a phenylsilylene moiety into the Zr—C bond of a zirconocenemethylhydride species. The sequence of reactions which eventually lead to the formation of this species is clearly very complicated. Even though it is produced almost quantitatively in near-stoichiometric reactions and is the only zirconocene species observable by nmr in catalytic reactions, its low activity as a catalyst for the phenylsilane polymerization reaction indicates that it is possibly aborted from the catalytic cycle. One possible interpretation is that the trapping of a silylene by insertion into a Zr—CH_3 bond, rather than a Zr—Si bond somehow blocks the reaction. It is also possible that the actual catalytic species are not observable by nmr, either due to rapid dynamic rearrangements, or to paramagnetism. Although paramagnetic Zr compounds are relatively rare (7, 8), weak esr signals are observed in the reaction products of **1** with **2**. The strength of these signals is enormously increased by irradiation with uv light. The intense signals consist of a doublet (g = 1.990, $A(^1H)$ = 5.6 G), reminiscent of the paramagnetic hydrides produced by irradiation of zirconocenedihydride dimers (8), and a doublet of triplets (g = 2.0047, $A(^1H_1)$ = 11.2 G, $A(^1H_2)$ = 5.6 G) reminiscent of the mixed valence hydride of titanocene produced by reaction of dimethyltitanocene with silicon hydrides (9).

Acknowledgements

Thanks are due to the Natural Sciences and Engineering Research Council of Canada, the Fonds FCAC du Quebec, and the Dow Corning Corporation for financial support of this work.

1. C. AITKEN, J. F. HARROD, and E. SAMUEL. J. Organomet. Chem. **279**, C11 (1985).
2. C. AITKEN, J. F. HARROD, and E. SAMUEL. J. Am. Chem. Soc. **108**, 4059 (1986).

[1]The crystallographic study is being carried out by the Laboratoire de Diffraction des Rayons-X, Université de Montréal. The crystals studied were monoclinic, a = 8.86, b = 16.34, c = 10.25 Å, β = 90.82°. Space group $P2_1/c$ was deduced from systematic absences ($h0l$, $l \neq 2n$; $0k0$, $k \neq 2n$). The structure solved in this space group consists of pairs of centrosymmetrically related $(\eta^5\text{-}C_5H_5)_2Zr$ units with relative orientation and Zr—Zr separation observed for $[\eta^5\text{-}(C_5H_5)_2ZrH_2]_2$ (4). This suggests that the two units of the dimer are held by a similar pair of bridging hydrides. In the present structure the non-bridging hydrides are replaced by silyl groups. One of the C_5H_5 groups is severely disordered and the electron density for the Si—CH_3 group is more consistent with half occupancy at the two sites of the dimer. However, there is no disordering of the Si atoms corresponding to reflection through the plane perpendicular to the Si—Zr—Zr—Si plane, indicating that the crystal contains a single diastereomer. The present level of refinement (R = 12) does not allow an interpretation of the disorder in terms of superimposed ordered chemical units. Attempts to resolve this difficulty are continuing.

3. D. M. DODRELL, D. T. PEGG, and M. R. BENDALL. J. Magn. Reson. **48**, 323 (1982).
4. S. B. JONES and J. L. PETERSEN. Inorg. Chem. **20**, 2889 (1985).
5. D. G. BICKLEY, H. NGUYEN, P. BOUGEARD, B. SAYER, R. C. BURNS, and M. J. MCGLINCHEY. J. Organomet. Chem. **246**, 257 (1983).
6. B. COLEMAN. *In* NMR of newly accessible nuclei. Vol. 2. *Edited by* P. Laszlo. Academic Press, Inc. 1983. p. 214.
7. M. F. LAPPERT, C. J. PICKERT, P. I. RILEY, and P. I. H. YARROW. J. Chem. Soc. Dalton Trans. 805 (1981); M. F. LAPPERT, P. I. RILEY, and P. I. H. YARROW. J. Chem. Soc. Chem. Commun. 305 (1979); G. M. WILLIAMS and J. SCHWARTZ. J. Am. Chem. Soc. **104**, 1122 (1982); K. I. GELL, T. V. HARRIS, and J. SCHWARTZ. Inorg. Chem. **20**, 481 (1981); E. SAMUEL. Inorg. Chem. **22**, 2967 (1983).
8. C. S. BAIGUR, S. B. JONES, and J. L. PETERSEN. Organometallics, **4**, 1929 (1985).
9. E. SAMUEL and J. F. HARROD. J. Am. Chem. Soc. **106**, 1859 (1984).

Reactions of alicyclic ketones in carbon tetrachloride. I. The kinetics of the chlorination of cyclopentanone and cyclohexanone catalyzed by hydrogen chloride

EIZE J. STAMHUIS,[1] HENK MAATMAN,[2] HENK STINISSEN,[3] AND GEERT E. H. JOOSTEN[4]

Department of Chemical Engineering, The State University of Groningen, Nijenborgh 16, 9747 AG Groningen, The Netherlands

Received July 10, 1985[5]

EIZE J. STAMHUIS, HENK MAATMAN, HENK STINISSEN, and GEERT E. H. JOOSTEN. Can. J. Chem. **64**, 1681 (1986).

The kinetics of the direct chlorination of cyclopentanone (cp) and cyclohexanone (ch) in carbon tetrachloride, catalyzed by hydrogen chloride, was studied. The rate of chlorination, measured by flow and stopped-flow techniques, is zero order in chlorine; the order in cp and ch increases from 1 at [cp] and [ch] of 0.01 *M* concentration to 2 at concentrations of 1 *M*. This is explained by self-association of the ketones in carbon tetrachloride solutions. The order in hydrogen chloride is 1. Since this compound is one of the products, the reaction is *autocatalytic*. Deuterium isotope effects and the kinetic data strongly point to a mechanism in which the oxygen-protonated *monomeric* ketone is α-carbon deprotonated in a rate-determining step. This step, which is catalyzed by the bases cp or ch, respectively, leads to the corresponding enol as intermediate. The enol is then chlorinated very rapidly. In addition to the chloro ketone, very reactive chloride anions are formed. A small fraction of these anions deprotonate α- or α′-carbon atoms of the oxygen-conjugate acid of the monochloro ketone. The remainder are captured by HCl to form energetically more favored Cl--$(HCl)_n$ complexes with $n = 1, 2$, or 3. This explains why, even at low conversions of the ketones, substantial amounts of the various dichloro isomers are formed in addition to monochloro products. A rate expression is derived, which excellently describes the experimentally obtained rates of chlorination of cp and ch over a range of reaction rates of more than three decades.

EIZE J. STAMHUIS, HENK MAATMAN, HENK STINISSEN et GEERT E. H. JOOSTEN. Can. J. Chem. **64**, 1681 (1986).

Opérant dans le tétrachlorure de carbone, on a étudié la cinétique de la chloration directe, catalysée par le chlorure d'hydrogène, de la cyclopentanone (cp) et de la cyclohexanone (ch). Les vitesses de chloration, mesurées par des techniques de flux et de flux stoppés, sont d'ordre zéro en chlore alors que l'ordre en cp et en ch augmente de 1 (lorsque les concentrations de ces cétones sont égales à 0,01 *M*) à 2 (lorsque ces concentrations sont égales à 1 *M*). On explique cette observation par une auto-association des cétones dans des solutions dans le tétrachlorure de carbone. L'ordre en chlorure d'hydrogène est égal à 1. Puisque le chlorure d'hydrogène est un des produits, on doit classer la réaction comme *autocatalysique*. Les effets isotopiques du deutérium ainsi que les données cinétiques suggèrent fortement un mécanisme impliquant, dans l'étape qui détermine la vitesse, la déprotonation du carbone-α d'une cétone *monomère* protonée par l'oxygène. Cette étape, qui est catalysée respectivement par les bases cp et ch, conduit aux énols correspondants, comme intermédiaires. L'énol est alors chloré très rapidement. Une petite fraction de ces anions déprotone les atomes de carbones-α et -α′ de l'acide conjugé de l'oxygène de la cétone monochlorée. Le reste est capturé par le HCl pour former des complexes Cl--$(HCl)_n$ ($n = 1$, 2 et 3) qui sont plus favorisés du point de vue énergétique. Ceci explique pourquoi, même à des taux de conversions en cétones très faibles, il se forme des quantités substantielles de diverses cétones dichlorées aux côtés des produits monochlorés. On a dérivé une expression pour les vitesses qui décrit d'une façon excellente les vitesses expérimentales de chloration des cétones cp et ch, à des taux de réaction s'étalant sur trois ordres de grandeur.

[Traduit par la revue]

In polar media the acid-catalyzed halogenation of ketones usually proceeds by a rate-determining base-catalyzed α-carbon deprotonation of the oxygen-conjugate acid (1*a*). A reactive enol is produced that rapidly is halogenated in a subsequent step, according to Scheme 1. As far as aqueous and other polar

[1] $$—COCH_2— + HA \leftrightarrows —\overset{+}{C}OHCH_2— + A^-$$

[2] $$—\overset{+}{C}OHCH_2— + B \rightarrow —C(OH)=CH— + HB^+ \text{ (slow)}$$

[3] $$—C(OH)=CH— + Hal_2 \rightarrow —COCHHal + HHal \text{ (fast)}$$

HA : general acid
B : general base
Hal_2 : halogen

SCHEME 1

protic solvents are concerned, the mechanism of the reaction of Scheme 1, as well as the identity of the catalytic species HA and B, are quite well known (1*b*, 2, 3*a*). However, the direct halogenation of ketones under acidic conditions in inert solvents of low dielectric constant appears to be significantly more complicated (3*b*, 4, 5). Although acid–base catalysis is clearly demonstrated (4), the experimental results obtained so far do not permit a general description of the mechanism involved in the reaction (3*b*). Assuming a prototropic isomerization in non-polar aprotic solvents analogous to that in aqueous solutions, it has been suggested that the second proton transfer involves another ketone molecule acting as the basic species. This would result in a higher kinetic order than the first in the substrate (1*c*). Actually such a catalytic action is proposed by Boyer and de Aguirre (6). They studied the indirect bromination of cyclohexanone in benzene by *N*-bromosuccinimide, catalyzed by chloro acetic acids. However, the contribution of the reaction catalyzed by the ketone relative to those of other basic species was small and the mechanism could not be established.

The interpretation of the kinetic results of the direct halogenation of ketones is further complicated by a rather low selectivity of the monohalogenated product, even at deficient amounts of the halogen (7), and further by the partial self-association of the ketone molecules in solvents of low dielectric constant (8) and the *autocatalytic* nature of the reaction by the production of hydrogen halide as acid catalyst. To obtain more insight into the factors that determine the course of this type of reaction, a study is made of the hydrogen chloride catalyzed direct chlorination of cyclopentanone (cp) and cyclohexanone (ch) in carbon

[1]Author to whom correspondence may be addressed.
[2]Present address: Enka, Arnhem, The Netherlands.
[3]Present address: Methanol Chemie, Delfzijl, The Netherlands.
[4]Present address: N.V. Nederlandse Gasunie, Groningen, The Netherlands.
[5]Revision received April 18, 1986.

tetrachloride under homogeneous conditions. In this paper we present the results of the kinetic measurements. In order to explain the kinetic data, the selectivity of the chlorination to the various products is also investigated. A kinetic rate equation is derived that quantitatively describes the experimental results, taking into account the partial self-association of the ketone molecules. Combining the kinetic data with the values of the primary kinetic deuterium isotope effects, obtained from the rates of chlorination of ch and of 2,2,6,6-tetradeuteriocyclohexanone (2,2,6,6-ch-d_4) using in each case HCl and DCl as catalysts, makes it possible to determine a mechanism for the reactions involved that is consistent with the experimental results.

Experimental

Materials

Chlorine and hydrogen chloride were obtained from Matheson, purity >99.5 and 99.0%, respectively. Carbon tetrachloride: Merck, Pro Analyse, purity >99.8%. The ch and cp (Merck, Zur Synthese, purity 99%) were distilled at reduced pressure (3.4 and 2.7 kPa, respectively). Fractions between 357 and 358 K for ch and 303 and 304 K for cp were collected for use. It is necessary to maintain a reduced pressure during the distillation of the ketones to prevent thermal dimerization and subsequent formation of the corresponding hydroxyketones. These compounds would interfere in the experiments since they are much more reactive towards chlorine than the starting ketones themselves. Distillation at atmospheric pressure is not recommended because it leads very easily to the formation of hydroxyketones, in concentrations of more than 500 ppm, during the time that the condensed liquid film cools down.

2,2,6,6-ch-d_4 was synthesized from ch and D_2O with DCl and D_3PO_4 as catalysts (9); bp 338 K at 4.1 kPa. The ir spectrum was identical with that given by the Aldrich ir catalog (10). The degree of deuteration was 96% as determined by mass spectroscopy. DCl was generated by the action of D_2O on benzoyl chloride at 373 K (11) and dissolved in carbon tetrachloride. Entrainment of benzoyl chloride did not occur, as was shown by ^{1}H nmr and glc. 2-Chlorocyclohexanone (2-mcch) and 2-chlorocyclopentanone (2-mccp) were obtained from Aldrich (purity >98%) and distilled at 1.3 kPa and 1.6 kPa, respectively. Fractions between 355 and 357 K and 346 and 348 K, respectively, were collected for use.

Analytical techniques

Gas–liquid chromatographic (glc) analyses were performed on a Perkin–Elmer 900 gas–liquid chromatograph, provided with a TCD and an FID detector. For hplc analysis a DuPont model 820 was used, equipped with a Kipp automatic injection system and a Tracor 970 A adjustable wavelength scanning uv detector. The glc and hplc instruments were connected with a Spectra Physics Autolab IV system for peak integration. The uv spectra were recorded on a Zeiss PMQII spectrophotometer and ir spectra were measured on a Perkin–Elmer 457. Mass and ^{1}H nmr spectra were recorded on an AEI-MS9 and a JEOL-C-60 AL, respectively (Department of Organic Chemistry). The chlorinated products, present in the reaction mixtures, were separated by hplc. Detection was performed by uv at 310 nm and 290 nm for the chlorinated cyclopentanones and cyclohexanones, respectively. Identification of the dichloro compounds was carried out by ir, mass spectrometry, and ^{1}H nmr after separation by glc and trapping of the pure compounds. The spectra were in accordance with published data (12, 13).

Titration of chlorine and hydrogen chloride

Samples of carbon tetrachloride, containing Cl_2 and HCl, were analysed for Cl_2 by adding them to an aqueous solution of 0.1 *N* KI. The heterogeneous mixture was stirred vigorously and titrated with 0.1 or 0.01 *N* aqueous thiosulphate. Starch was used as end point indicator. The mixture was then analysed for HCl by titration with 0.1 or 0.01 *N* aqueous sodium hydroxide, using Methyl Red as indicator. The latter titration did not interfere with that for Cl_2, as was thoroughly checked.

Kinetics and instrumentation

The kinetics of the chlorination of ch and cp was measured by a continuous flow technique and by a stopped-flow method (apparatus from Aminco Morrow). In both cases a dilute solution of the ketone in carbon tetrachloride and a dilute solution of chlorine and hydrogen chloride in carbon tetrachloride were rapidly mixed. The flow rate used in the continuous flow technique was always sufficiently high to ensure turbulent flow. The residence time distribution in the reactor was calculated to be negligible (14). The reactor volume, measured from the mixing chamber (a T-joint) to the middle of the transmission cell, was varied between 0.3×10^{-6} and 0.4×10^{-6} m^3. The internal diameter of the reaction tube was 1.5×10^{-3} m. Flow rates used were 3.2×10^{-6} to 1.2×10^{-5} m^3 s^{-1}. Therefore plug flow was assumed. Resulting reaction times ranged from 100 to 500 ms. The conversion of chlorine was determined by measuring the extinction of chlorine at $\lambda = 345$ nm (ε_{Cl_2}: 8200 m^3 kmol^{-1} m^{-1}). A crucial point in both techniques is to realize a very small ratio between the mixing time (t_m) of the two solutions and the reaction or residence time (τ). In our experiments t_m/τ was always smaller than 0.01. The mixing time is thus negligible. Reaction samples were taken and analysed for chlorinated ketones as described in the materials section. The conversion of the ketones was always less than 10%, in most cases even less than 5% to prevent autocatalytic effects. The reaction rates measured by the continuous flow technique and those by the stopped-flow method agreed within the experimental reproducibility. The self- or auto-association of ch and cp in carbon tetrachloride was determined by freezing point depression measurements (15). The apparent molecular mass, $\bar{M}_w$, can be related to the value of the fraction, α, of the ketone existing as monomer by

$$[4] \qquad \bar{M}_w = 2M_w/(1 + \alpha)$$

From α the association constant, K_A, was calculated by

$$[5] \qquad K_A = \frac{[\text{dimer ketone}]}{[\text{monomer ketone}]^2} = \frac{(1 - \alpha)}{2\alpha^2[X]_0}$$

$[X]_0$ being the total ketone concentration. It is assumed that the ratio of the concentrations of trimer ketone and dimers is negligible. (In Appendix I an equation is derived for the calculation of α).

Results and discussion

Reaction products

The direct acid-catalyzed chlorination of ketones does not usually proceed with high selectivity to the monochloro compounds (2). It may be expected that the formation of mono- and di-chlorinated compounds takes place consecutively and that the amount of higher chlorinated products only becomes substantial at appreciable fractional conversions of the ketone. However, as has been proven in the chlorination of 4-*tert*-butylcyclohexanone in carbon tetrachloride at 274–278 K, the monochloro ketone is not necessarily the precursor of the *cis*,*trans*-2,6-dichloro-4-*tert*-butylcyclohexanone (7). If a comparable reaction takes place, e.g. the chlorination of unsubstituted alicyclic ketones, the presence of dichlorinated products may be expected, even at low fractional conversions of the ketones. As a consequence, a correct interpretation of the kinetic results is only possible in connection with a known product distribution. Therefore, the selectivity to the distinct chlorinated ketones was studied at various concentrations of chlorine, hydrogen chloride, and ketone.

The selectivity $S(Y)$ of the chlorinated ketone, Y, is defined as

$$[6] \qquad S(Y) = \frac{[Y]}{[\text{mccp}] + [g\text{-2,2-dccp}] + [c\text{-2,5-dccp}] + [t\text{-2,5-dccp}]}$$

where Y: relevant chlorinated ketone; mccp: 2-chlorocyclopen-

TABLE 1. The selectivity, $S(Y)$, of the chlorinated products (Y), in the chlorination of cyclopentanone (cp). $[cp]_0 = 0.19\ M$, $T = 297$ K. $S(Y)$ and η_{cp} in percentages; $[Cl_2]_0$ and [HCl] in M

$[Cl_2]_0$	[HCl]	η_{cp}	S(2-mccp)	S(*g*-2,2-dccp)	S(*c*-2,5-dccp)	S(*t*-2,5-dccp)	S(2,2,5-tccp)
0.007	0.066	2.8	86	*	7.1	6.9	
0.014	0.072	6.2	84	0.5	6.4	9.1	
0.026	0.078	13	84	0.6	6.9	8.5	
0.042	0.083	18	82	0.9	7.7	9.4	
0.046	0.075	18	82	0.9	7.7	8.1	1.3

*Concentration below the detection limit.

TABLE 2. The influence of [HCl] on the selectivity, $S(Y)$, of the chlorinated products (Y), in the chlorination of cyclopentanone (cp). $[cp]_0 = 0.19\ M$, $[Cl_2]_0 = 0.014\ M$, $T = 297$ K. $S(Y)$ and conversion, η_{cp}, in percentages; [HCl] in M

[HCl]	η_{cp}	S(2-mccp)	S(*g*-2,2-dccp)	S(*c*-2,5-dccp)	S(*t*-2,5-dccp)
0.043	6.8	84	0.6	7.2	8.2
0.072	6.2	85	0.6	7.2	7.2
0.096	6.5	87	0.9	6.5	5.6
0.130	7.0	86	0.4	7.9	5.0

TABLE 3. The influence of [cp] on the selectivity, $S(Y)$, of the chlorinated products (Y), in the chlorination of cyclopentanone (cp). $[Cl_2]_0 = 0.023\ M$, $[HCl] = 0.05\ M$, $T = 297$ K. $S(Y)$ and conversion, η_{cp}, in percentages; $[cp]_0$ in M

$[cp]_0$	η_{cp}	S(2-mcch)	S(*g*-2,2-dccp)	S(*c*-2,5-dccp)	S(*t*-2,5-dccp)
0.11	18	84	0.6	7.7	7.7
0.19	13	84	0.6	7.2	8.2
0.48	3.9	86	0.4	6.1	6.5
0.96	1.8	83	0.7	8.0	8.3
1.50	1.4	83	0.5	8.7	7.8

tanone; *g*-2,2-dccp: *gem*-2,2-dichlorocyclopentanone; *c*-2,5-dccp: *cis*-2,5-dichlorocyclopentanone; and *t*-2,5-dccp: *trans*-2,5-dichlorocyclopentanone.

A similar expression holds for the selectivity of the chlorinated cyclohexanones. The selectivities of the different chlorinated products, obtained at conversions (η_x) of the ketone (X) up to 18%, are summarized in Tables 1–3.

Even at fractional conversions of cp that are lower than 3%, S(2-mccp) was found to be at most 86%. At higher ketone conversions S(2-mccp) decreases. Although the dichlorination does lead mainly to approximately equal amounts of *cis*- and *trans*-2,5-dichlorocyclopentanone, slight but not negligible amounts of the *gem*-2,2-dccp isomer are formed (Table 1). The product distribution obtained in the chlorination of ch in a conversion range of 1.8–19% is summarized in Tables 4 and 5.

The data of these tables show a maximum selectivity of 2-chlorocyclohexanone (2-mcch) of 81%. Although *gem*-2,2-dichlorocyclohexanone and *cis*-2,6-dcch could be detected, the concentrations were in most cases too low for a quantitative analysis. As might be expected, the product distribution did not vary when a time lag (up to a few days) was introduced between moment of reaction and analysis (5).

Kinetics

During the chlorination of ch and cp a linear decrease of the concentration of chlorine with increasing reaction time was observed up to conversions of chlorine of more than 90%, indicating a zero-order dependence on chlorine. The influence of the concentration of hydrogen chloride on the rate of chlorination of ketones was measured at several hydrogen chloride concentrations ranging from 10^{-2} to $10^{-1}\ M$. To prevent autocatalysis by hydrogen chloride, care was taken to avoid a substantial increase in its concentration during an experiment. In most cases the ratio of the concentrations of ketone and chlorine had a value of at least 20. Nevertheless, in the evaluation of the reaction order of hydrogen chloride a logarithmic mean value of initial and final concentration of this compound was used.

TABLE 4. The influence of [HCl] on the selectivity, $S(Y)$, of the chlorinated products (Y), in the chlorination of cyclohexanone (ch). $[Cl_2]_0 = 0.045\ M$, $[ch]_0 = 0.20\ M$, $T = 294$ K. $S(Y)$ and conversion, η_{ch}, in percentages; [HCl] in M

[HCl]	η_{ch}	S(2-mcch)	S(*c*-2,6-dcch)	S(*t*-2,6-dcch)
0.032	17	81	*	19
0.064	18	80	*	20
0.150	19	80	2	18

*Detected, but concentration too low for quantitative analysis.

The chlorination of cp is found to be virtually first order in hydrogen chloride over the complete range of concentrations of cp (Fig. 1). The chlorination of ch demonstrates an order of 1.2

TABLE 5. The influence of [ch] on the selectivity, $S(Y)$, of the chlorinated products (Y), in the chlorination of cyclohexanone (ch). $[Cl_2]_0 = 0.018$–$0.022\ M$, $[HCl] = 0.065\ M$, $T = 294$ K. $S(Y)$ and conversion, η_{ch}, in percentages; $[ch]_0$ in M

$[ch]_0$	η_{ch}	S(2-mcch)	S(*t*-2,6-dcch)
0.21	7.2	83	17
0.25	7.3	81	19
0.46	3.1	81	19
0.80	1.8	80	20

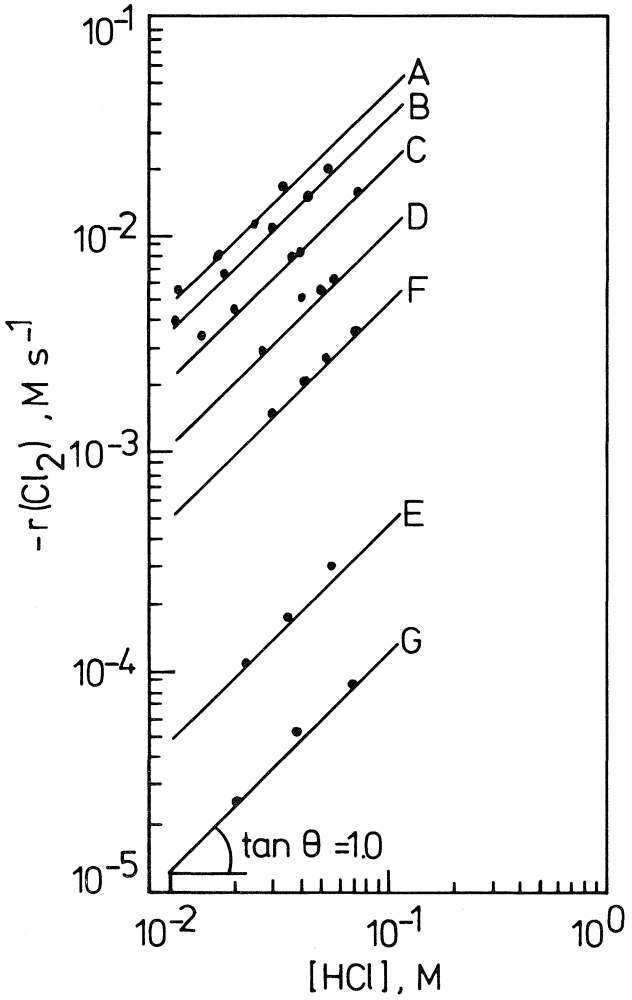

FIG. 1. The influence of the concentration of hydrogen chloride on the rate of chlorination of cp at 298 K. Ketone concentrations (in M): A: 2.00; B: 1.50; C: 1.00; D: 0.50; E: 0.25; F: 0.064; G: 0.032.

in hydrogen chloride (Fig. 2). From the experimental data for the determination of the order in hydrogen chloride at various ketone concentration levels, the dependence of the rate of reaction on the ketone concentration was calculated. This dependence is shown in Figs. 3 and 4. At low concentrations the reaction order is nearly 2 and at high concentrations it approximates 1.

So far, the zero order in chlorine points to a mechanism that is in part analogous to that of the chlorination in aqueous solutions. This is supported by the observation that the zero order in chlorine changes to first order at very low ($<2 \times 10^{-4}\ M$) concentrations of chlorine. It is therefore reasonable to assume that the chlorination step (at concentrations $>2 \times 10^{-4}\ M$) is a relatively very rapid process, but that another reaction earlier in the sequence is rate determining. However, the kinetic data presented so far are not sufficient to establish which reaction is rate determining.

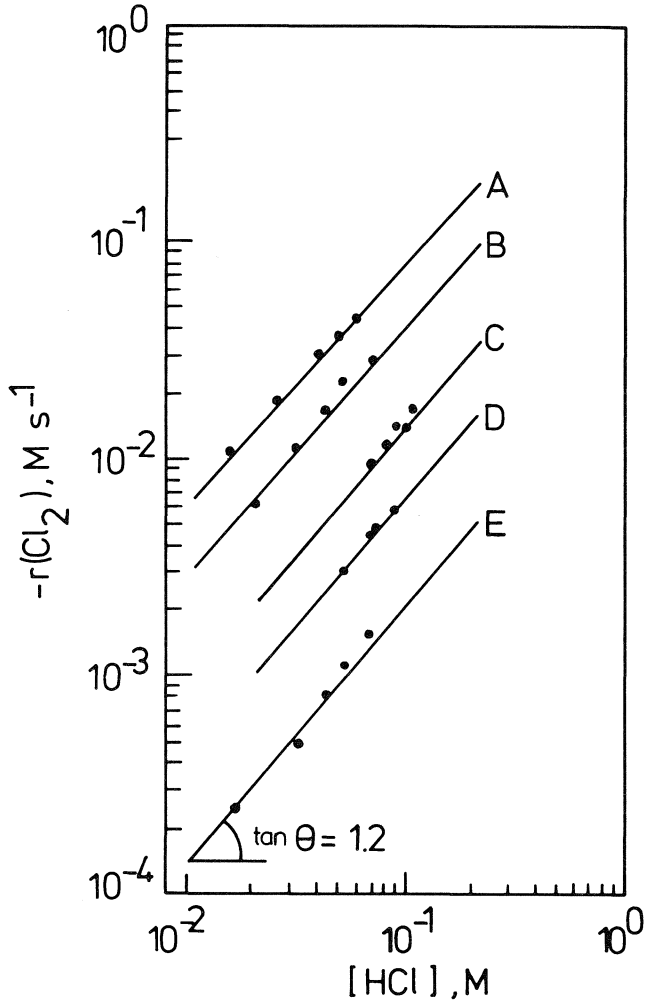

FIG. 2. The influence of the concentration of hydrogen chloride on the rate of chlorination of ch at 294 K. Ketone concentrations (in M): A: 1.00; B: 0.50; C: 0.24; D: 0.100; E: 0.050.

The self-association of cp and ch

The dependence of the reaction order of the ketone on the ketone concentration may be explained by self-association of the ketone molecules in carbon tetrachloride. Evidence for this self-association was obtained from measurements of the freezing point depression of ketone solutions in CCl_4. The apparent molecular weight of the ketones thus determined was always much larger than that of the monomers. More accurate values of the association constants $K_{A,cp}$ and $K_{A,ch}$ than those determined from freezing point measurements are obtained by fitting a derived expression for the reaction rates, given below, with the experimental reaction rates, since for both compounds a large number of reaction rates, determined over a wide range of ketone and hydrogen chloride concentrations, are available. This results in $K_{A,cp} = 3\ M^{-1}$ at 298 K and $K_{A,ch} = 4\ M^{-1}$ at 294 K. The self-association of cp and ch in carbon tetrachloride may be ascribed to a dipole–dipole interaction of the carbonyl group.

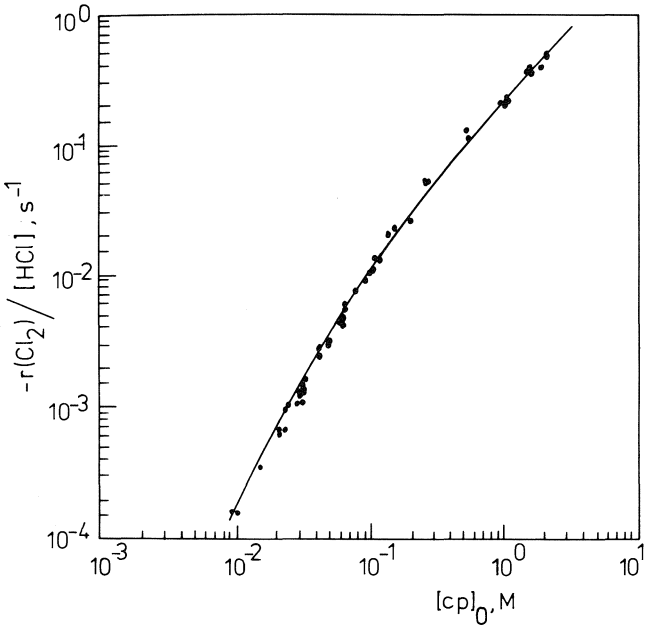

FIG. 3. The influence of $[cp]_0$ on the rate of chlorination at 298 K. Experimental values (●); the smooth curve is calculated with eq. [18] and the constants from Table 8.

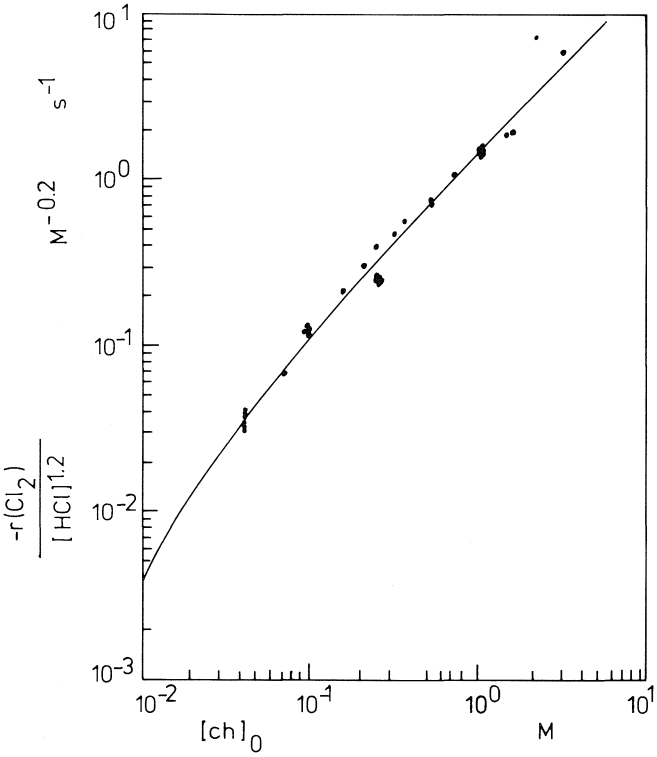

FIG. 4. The influence of [ch] on the rate of chlorination at 294 K. Experimental (●); the smooth curve is calculated with eq. [18] and the constants from Table 8.

Kinetic isotope effects of the chlorination of cyclohexanone in carbon tetrachloride

The kinetic results, given so far, are not sufficient to obtain a reliable mechanism for the hydrogen chloride catalyzed chlorination of cp and ch in carbon tetrachloride. Therefore the primary deuterium isotope effects were determined. Rates of chlorination of ch and of 2,2,6,6-ch-d_4 (cd) were measured,

TABLE 6. Rate constants of the chlorination of cyclohexanone (ch) and 2,2,6,6-cyclohexanone-d_4 (cd), catalyzed by HCl and DCl. [HCl] = 0.05–0.08 M, [DCl] = 0.05–0.07 M, $[Cl_2]_0 <$ 0.010 M, T = 294 K; [ch] and [cd] in M. For [ch] and [cd] = 0.1, k in $M^{-1.9}$ s^{-1}; for [ch] and [cd] = 0.5, k = $M^{-1.2}$ s^{-1}

[ch] or [cd]	$k_{ch, HCl}$	$k_{ch, DCl}$	$k_{cd, HCl}$	$k_{cd, DCl}$
0.1	5.9	14	1.1	2.0
0.5	1.9	3.7	0.52	0.78

using in both cases HCl as well as DCl as catalyst. Scheme 2 shows the combinations and the corresponding reaction rate constants.

[7] $\text{ch} + Cl_2 \xrightarrow[k_{ch, HCl}]{HCl} \text{products}$

[8] $\text{ch} + Cl_2 \xrightarrow[k_{ch, DCl}]{DCl} \text{products}$

[9] $\text{cd} + Cl_2 \xrightarrow[k_{cd, HCl}]{HCl} \text{products}$

[10] $\text{cd} + Cl_2 \xrightarrow[k_{cd, DCl}]{DCl} \text{products}$

SCHEME 2

On account of the varying order in ch, the experiments were carried out at two ketone concentrations, one in the region of reaction order approaching two and one in the first-order region. The reaction rate constants $k_{x,z}$ (x = ch, cd; z = HCl, DCl) were calculated from the kinetic expression:

[11] $$-r(Cl_2) = k_{x,z}[x]^n[z]^p$$

where $-r(Cl_2)$: rate of production of chlorine, M s^{-1}, with the following ketone or deuterated ketone concentrations and reaction orders

$$[x] = 0.1\ M \quad n = 1.7 \quad p = 1.2$$

$$[x] = 0.5\ M \quad n = 1.0 \quad p = 1.2$$

The values of the rate constants are summarized in Table 6. The primary (catalyst) kinetic isotope effects, $k_{ch, HCl}/k_{ch, DCl}$ and $k_{cd, HCl}/k_{cd, DCl}$, derived from Table 6, are approximately 0.5 and 0.6, respectively.

The primary (substrate) kinetic isotope effects $k_{ch, HCl}/k_{cd, HCl}$ and $k_{ch, DCl}/k_{cd, DCl}$ range between 3.7 and 7.0. Combination of the two sets of primary isotope effects strongly points to a base-catalyzed rate-determining proton abstraction from the α-carbon atom of the carbonyl-oxygen protonated ketone molecule, leading to the corresponding enol. The enol is subsequently chlorinated rapidly as long as enough chlorine is present, thus explaining the observed zero order in chlorine. The values of the primary kinetic isotope effects derived from Table 6 for the proton abstraction from the α-carbon atom at low and at high ketone concentrations are, though not equal, of the same order of magnitude. This leads to the conclusion that at both concentrations the rate-determining step is the same. All the experimental data presented so far strongly point to a mechanism that is in part analogous to that of the acid-catalyzed chlorination of ketones in aqueous solution. However, the mechanism is more complicated, as indicated by the varying order in ketone. This varying order in ketone may be explained

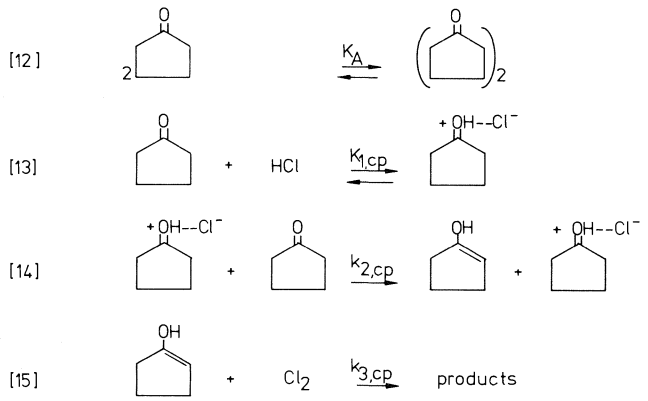

SCHEME 3

by assuming self-association of the ketones in the apolar solvent carbon tetrachloride.

The first step in the chlorination is the protonation of the carbonyl group by hydrogen chloride. In principle the monomer as well as the dimer can be protonated, but as the base strength of the carbonyl groups of the dimer may be expected to be lower by the dipole–dipole interaction, it is reasonable to assume that the monomer will be protonated preferentially and therefore be the reactive species in the chlorination.

The acid-catalyzed halogenation and enolization of ketones does not only show acid catalysis, but proceeds by a combined acid–base catalyzed step. In aqueous solution the base can be water or the basic component of the buffer system. In apolar aprotic media it is not immediately clear which species, present in the solution, acts as base. In the next section, evidence will be given that the ketone molecule itself acts as basic catalyst.

Proposed reaction scheme

A proposed reaction mechanism for the hydrogen chloride catalyzed chlorination of cp in carbon tetrachloride is presented in Scheme 3. An analogous scheme applies to the chlorination of ch. In step [14] the monomeric ketone acts as base.

From Scheme 3 a kinetic expression for the rate of reaction of chlorine can be derived.

$$[16] \quad -r(\mathrm{Cl_2}) = \frac{[2 - S(\mathrm{Y})]}{S(\mathrm{Y})} K_1 k_2 [\mathrm{cp}]^2 [\mathrm{HCl}]$$

In eq. [16] [cp] is unknown due to the dimerization. An expression for [cp] in terms of the total ketone concentration $[\mathrm{cp}]_0$ and the equilibrium constant K_A of the self-association can be derived, see Appendix I. This leads to

$$[17] \quad [\mathrm{cp}] = \frac{-1 + \sqrt{(1 + 8K_A[\mathrm{cp}]_0)}}{4K_A}$$

Substitution of eq. [17] in eq. [16] results in:

$$[18] \quad -r(\mathrm{Cl_2}) = \frac{[2 - S(\mathrm{Y})]}{S(\mathrm{Y})} K_1 k_2 \frac{\{-1 + \sqrt{(1 + 8K_A[\mathrm{cp}]_0)}\}^2}{16K_A^2} [\mathrm{HCl}]$$

It is clear that this rate expression shows the desired varying order in ketone. When

$$[19] \quad K_A[\mathrm{cp}]_0 \ll 1, \quad -r(\mathrm{Cl_2}) \sim [\mathrm{cp}]_0^2[\mathrm{HCl}]$$

$$[20] \quad K_A[\mathrm{cp}]_0 \gg 1, \quad -r(\mathrm{Cl_2}) \sim [\mathrm{cp}]_0[\mathrm{HCl}]$$

Intermediate values of $K_A[\mathrm{cp}]_0$ give reaction orders in ketone between 1 and 2. Fitting the derived expression to the experimental reaction rates yields the equilibrium constant of the association K_A and the concentration independent factor K_1k_2 in eq. [18]. The value of K_1k_2 can be interpreted as the overall reaction rate under conditions of $\alpha \rightarrow 1$ (see Appendix I).

TABLE 7. Equilibrium constants of the self-association of cp and ch, and the overall reaction rate constants at low ketone concentrations, derived from the chlorination experiments

Ketone	Temperature (K)	K_A (M^{-1})	K_1k_2 $M^{-(p+1)}\,s^{-1}$
cp*	298	3	1.6
ch*	294	4	15.5

*Order in hydrogen chloride is p. For cp, p = 1.04; for ch, p = 1.2.

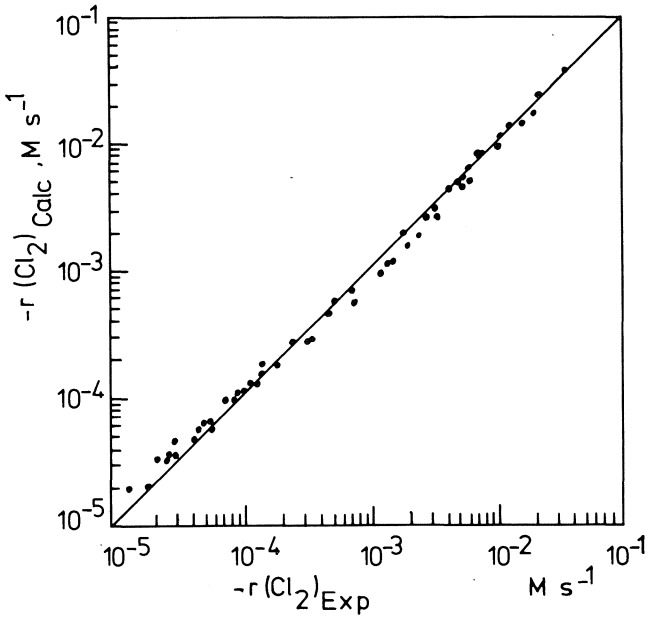

FIG. 5. Comparison between calculated (eq. [18], S (2-mccp) = 86%, constants from Table 8) and experimental rates of chlorination of cp. T = 298 K.

Analogous equations as derived for cp also apply to ch. Table 7 summarizes the values of K_A and K_1k_2 for cp and ch.

In Figs. 5 and 6 a comparison between the experimental reaction rates and those calculated on the basis of Scheme 3 and eq. [18] is presented. The experimental and calculated data agree excellently for both ketones over a range of reaction rates of more than *three* decades. This lends credit to the concept of a partial association of the polar ketone molecules in carbon tetrachloride and also strongly indicates that the proposed mechanism as shown by the reactions of Scheme 3 is correct.

The deprotonation of the α-carbon is rate determining and is catalyzed by the ketone molecule, acting as base. The proposed mechanism explains also that the experimental order in the ketone is 2 in the concentration range of the ketone where the self-association plays a minor role, i.e. for [cp] and [ch] < 0.1 M. More evidence on this point will be given in a following paper on the chlorination of the 2-chlorocycloketones.

As far as the rate-determining base-catalyzed deprotonation is concerned, as represented by eq. [14], the only other basic species present as potential catalyst, besides the ketone mole-

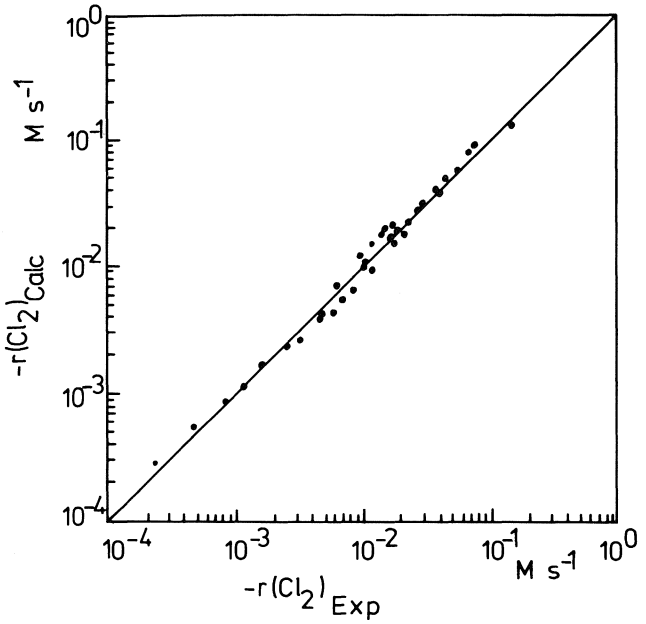

FIG. 6. Comparison between calculated (eq. [18], S (2-mcch) = 81%, constants from Table 8) and experimental rates of chlorination of ch. T = 294 K.

cule, would be the chloride anion. However, it is very unlikely that its concentration will be of any significance in this apolar medium. The maximal concentration would be in the order of that of the protonated ketone, which is very small. Besides, free Cl^- ions will be captured by HCl. Quantum mechanical calculations show a gain in energy of 129.3 kJ mol^{-1} by the formation of a homoconjugated complex $Cl^-...HCl$, a further gain of 79 kJ mol^{-1} for complexation with a second HCl molecule (linear configuration), and another 67.5 kJ mol^{-1} when a third HCl molecule enters the complex (equilateral configuration with Cl^- in the center).[6]

Though in these calculations no allowance was made for entropy and solvent effects, a rapid complexation of the free chloride anions by HCl molecules in this inert medium seems very likely. It may be expected that the basic properties of the $Cl^-...(HCl)_n$ complexes will be less than that of the free chloride anion. A significant contribution of chloride anion catalysis to the rate-determining step of eq. [14] may therefore be rejected. As mentioned above, the selectivity, S(Y), of the 2-chloro ketones never exceeds 86% and even at very low fractional conversions of the ketone a mixture of the three isomeric dichloro ketones is formed. The rate of chlorination of the 2-chloro ketones is much smaller than that of the unsubstituted compounds (16). Therefore a normal consecutive chlorination of the monochloro ketone can be excluded. A possible explanation may be that some of the incipient chloride anions formed in the chlorination of the enolic double bond will, before being captured by an HCl molecule to form a $Cl^-...(HCl)_n$ complex, attack an α- or α′-carbon hydrogen, leading to an enol as precursor of a dichloro compound. This process will in principle not stop after the introduction of two chlorine atoms and indeed 2,2,5-trichlorocyclopentanone is detected (Table 1). The observation that, besides *cis*- and *trans*-2,5-dccp, *gem*-2,2-dccp is also formed and that the presence of small amounts of *gem*-2,2-dcch could be detected cannot be explained by the mechanism proposed by Teo and Warnhoff (7). They studied the direct chlorination of 4-*tert*-butylcyclohexanone. Besides the *cis*- and *trans*-2-chloro ketones, *cis,trans*-2,6-dichloro-4-*tert*-butylcyclohexanone was also formed. The authors concluded that the latter compound was the result of a concerted dichlorination of the starting ketone. Such a mechanism excludes the formation of a *gem*-2,2-dichloro ketone. However, from Tables 1 and 2 it is clear that *gem*-2,2-dccp is actually formed and at a rate much larger than experimentally obtained in the chlorination of 2-mccp, even when the latter reaction is catalyzed (eq. [14]) by the stronger base cp instead of 2-mccp, as will be shown in the following paper in this series. We therefore believe that in the chlorination of cp and ch a rapid consecutive reaction catalyzed by the chloride anion, rather than a concerted mechanism, is responsible for the formation of substantial amounts of one or more of the dichloro isomers. This is shown in Scheme 4 for cp. The species that is formed as intermediate and is converted into the dichlorinated product may be regarded as an intimate ion pair.

The relative reactivities of cyclopentanone and cyclohexanone

From Table 7 it can be concluded that the ratio of the overall rate constants for ch and cp is about 10. Since the values of K_1 and k_2 are not known separately, it is hard to tell whether the high value of this ratio should be ascribed to the difference in basicity of the ketones (eq. [13]) or to the difference in acidity of the α-hydrogen atoms (eq. [14]). Campbell and Edward (17) have measured the basicities of ch and cp in concentrated sulphuric acid and obtained pK values of −6.8 and −7.5, respectively. The higher basicity of ch not only means a higher concentation of the oxygen-protonated species relative to that of cp but also a relative increase in reactivity of the deprotonation of the α-carbon atoms by the action of the ketone base.

The ratio of the cis- *and* trans-*dichloro compounds formed*

As mentioned before, the chlorination of cp gives nearly equal amounts of *cis*- and *trans*-2,5-dccp, whereas *trans*-2,6-dcch is formed almost exclusively in the chlorination of ch. This can be understood by considering the conformation of the reactive chloro enols of both ketones. A model of 5-chloro-1-cyclopenten-1-ol shows that this enol is nearly flat and that the chlorine atom lies almost in the plane of the ring. Therefore the steric hindrance for the attack of molecular chlorine on the double bond from above or below the ring may be expected to be approximately the same, the *trans* attack being slightly favoured. In the 6-chloro-1-cyclohexen-1-ol molecule the Cl atom takes a much more pronounced axial position (13), leading to a much larger steric hindrance for an approach of a chlorine molecule from the *cis* position. Therefore virtually only *trans*-2,6-dcch is formed. Dang Quoc-Quan (13) reports that the *cis* isomer is thermodynamically the more stable isomer. However, equilibration of the isomerization only occurs at an appreciable rate above 360 K in acidic media. In our experiments virtually no *trans–cis* conversion was observed, as shown by analysis of samples of reaction mixtures even after several days of storage.

The influence of the temperature

In the reaction rate expression (eq. [18]) the overall reaction rate constant is compounded from several contributions. The

[6]Quantum mechanical calculations with an extended basis set on the $Cl^-...(HCl)_n$ complex, with n = 1, 2, and 3, were carried out by Prof. Dr. W. C. Nieuwpoort and Mrs. A. van den Bergh–van Dop, Dept. of Chemical Physics, The State University of Groningen, The Netherlands. For n = 1, 2, the complexes were assumed to be linear, for n = 3, the HCl molecules were assumed to be arranged around the central chloride ion in one plane at angles of 120°.

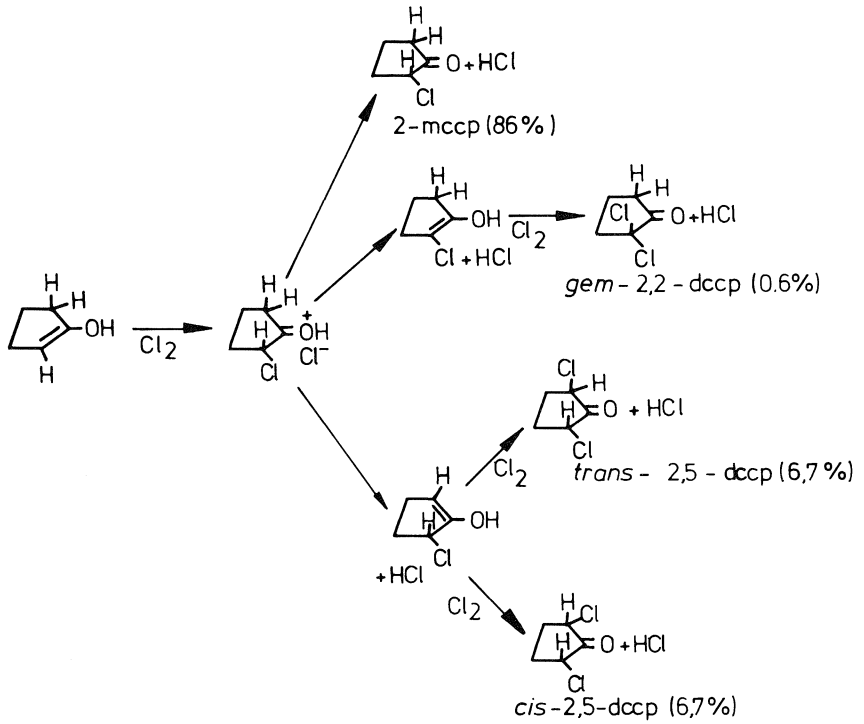

SCHEME 4

relative importance of these contributions varies with the concentration of the ketone. Each contribution probably has a different dependence on the temperature. Therefore we may expect that the measured activation energy of the overall reaction will vary with the ketone concentration. The apparent activation energy was therefore measured at two ketone concentrations [X]:

(*i*) At low ketone concentration, where the order of ketone is nearly 2. In this region eq. [18] degenerates to

$$[21] \quad -r(Cl_2) = \frac{[2 - S(Y)]}{S(Y)} K_1 k_2 [X]_0^2 [HCl] = \frac{[2 - S(Y)]}{S(Y)} k_{exp} [X]_0^2 [HCl]$$

(*ii*) At ketone concentrations of 0.5 *M* and more, where the order in ketone is 1, eq. [18] becomes

$$[22] \quad -r(Cl_2) = \frac{[2 - S(Y)]}{S(Y)} \frac{K_1 k_2}{2K_A} [X]_0 [HCl] = \frac{[2 - S(Y)]}{S(Y)} k_{exp} [X]_0 [HCl]$$

The experimentally determined activation energy, calculated from the rates of chlorination at 6 temperatures in the range of 279–314 K, was 15 kJ mol^{-1} at low and 25 kJ mol^{-1} at higher ($\geq$0.5 *M*) ketone concentrations for both cp and ch. The experimental rate constants, k_{exp}, are presented in Fig. 7.

The difference between the enthalpy values at low and high ketone concentrations may be ascribed to the influence of the temperature on the equilibrium constant of the self-association of the ketone molecules, K_A, the $-\Delta H_A^0$ for the self-association being 10 kJ mol^{-1}. This value is rather close to that of 12 kJ mol^{-1} determined for both the enthalpy of association of acetone in hexadecane (18) and the enthalpy of association of nitrobenzene in carbon tetrachloride (19). Arrhenius plots of the compounded reaction rate constants $K_1 k_2$ calculated from eq. [18] and corrected for the temperature dependence of K_A show

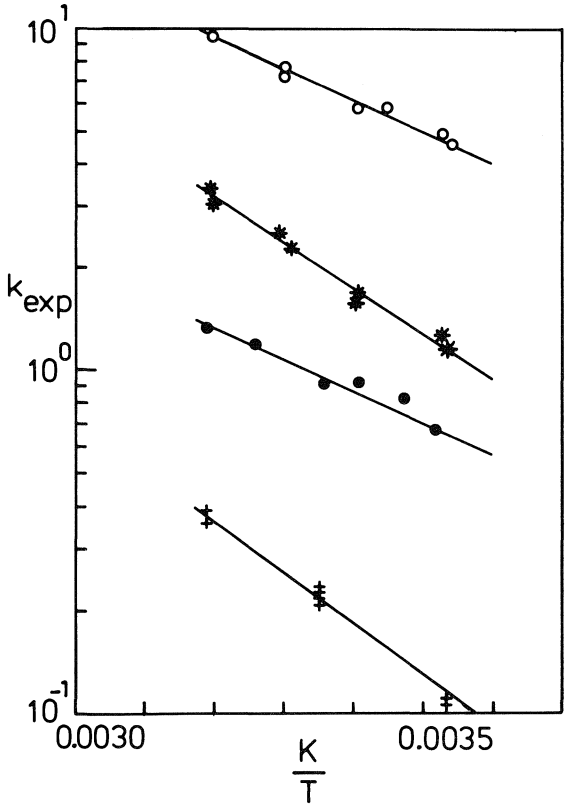

FIG. 7. The Arrhenius plots of the chlorination of cyclopentanone and cyclohexanone in carbon tetrachloride solutions at different ketone concentrations; ●, [cp] = 0.053 *M* (eq. [21]); +, [cp] = 0.50 *M* (eq. [22]); ○, [ch] = 0.10 *M* (eq. [21]); *, [ch] = 0.47 *M* (eq. [22]).

$K_1 k_2$ for cp as well as ch to be indeed independent of the ketone concentration, Fig. 8.

Values of activation energy, Arrhenius frequency factors, and enthalpy of the self-association are summarized in Table 8. The resemblance of the values of the enthalpy for the self-

TABLE 8. Influence of the temperature on the rate of chlorination of cp and ch, according to the mechanism given in Scheme 3. For cp, $p = 1.04$; for ch, $p = 1.2$; $S(Y)$ in percentages

Ketone	$S(Y)$	Temperature range (K)	K_1k_2 $(M^{-(p+1)}\,s^{-1})$	K_A (M^{-1})
cp	86	279–313	$6.8\ 10^2 \exp(-1.5\ 10^4/RT)$	$5.3\ 10^{-2} \exp(10^4/RT)$
ch	81	279–314	$7.2\ 10^3 \exp(-1.5\ 10^4/RT)$	$6.7\ 10^{-2} \exp(10^4/RT)$

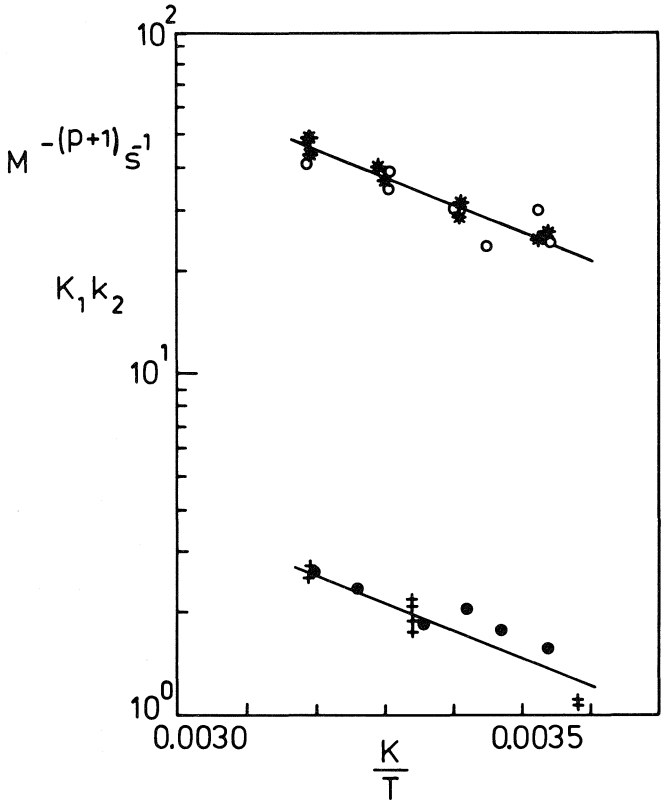

FIG. 8. Arrhenius plots of the chlorination of cyclopentanone and cyclohexanone in carbon tetrachloride solutions. The compounded reaction rate constant K_1k_2 from the proposed reaction model as a function of the reciprocal temperature at the ketone concentrations as indicated in Fig. 7; $p = 1.0$ for cyclopentanone, $p = 1.2$ for cyclohexanone.

association of cp and ch to those of acetone and nitrobenzene and the fact that the compounded reaction rate constants are independent of the ketone concentration lend credibility to the proposed reaction mechanism as presented in Scheme 3.

In the following paper the kinetics and mechanism of the hydrogen chloride catalyzed chlorination of 2-mcch and 2-mccp in carbon tetrachloride will be described.

Acknowledgements

We thank Prof. Dr. W. C. Nieuwpoort and Mrs. A. van den Bergh – van Dop for the quantum mechanical calculations on the Cl...$(HCl)_n$ systems and Prof. Dr. J. B. F. N. Engberts, Department of Organic Chemistry, State University of Groningen, for fruitful discussions.

1. R. P. BELL. The proton in chemistry. 2nd ed. Chapman and Hall, London. 1973. (*a*) pp. 141–146; (*b*) pp. 171–181; (*c*) p. 148.
2. H. O. HOUSE. Modern synthetic reactions. 2nd ed. W. A. Benjamin, Inc., Menlo Park. 1972. pp. 459–478.
3. A. J. WARING. Ketones. *In* Comprehensive organic chemistry. Vol. 1. *Edited by* J. F. Stoddart. Pergamon Press, Oxford. 1979. (*a*) pp. 1024–1027; (*b*) pp. 1037–1039.
4. E. C. GILBERT, R. E. JONES, D. C. MCLEAN, and E. SHERMAN. Ind. Eng. Chem. Prod. Res. Dev. **14**, 2 (1975).
5. Y. JASOR, M. GAUDRY, A. MARQUET, and M. BETTAHAR. Bull. Soc. Chim. Fr. 2732 (1973).
6. G. BOYER and I. DE AGUIRRE. Bull. Soc. Chim. Fr. 4016 (1972).
7. K. E. TEO and E. W. WARNHOFF. J. Am. Chem. Soc. **95**, 2728 (1973).
8. R. L. LYNCH, S. D. CHRISTIAN, and H. E. AFFSPRUNG. J. Phys. Chem. **73**, 3273 (1969).
9. J. SEIBL and T. GAUMANN. Helv. Chim. Acta, **46**, 2857 (1963).
10. C. J. POUCHERT. The Aldrich library of infrared spectra. 2nd ed. Aldrich Chem. Company. 1975. p. 1034.
11. H. C. BROWN and C. GROOT. J. Am. Chem. Soc. **64**, 2223 (1942).
12. Q.-Q. DANG. C.R. Acad. Sci. Paris, Ser. C, **262**, 924 (1966).
13. Q.-Q. DANG. Thèse de Doctorat en Sciences, Paris, 1966.
14. O. LEVENSPIEL. Chemical reaction engineering. 2nd ed. John Wiley and Sons, Inc., New York. 1972. pp. 282–290.
15. A. W. DAVIDSON. Laboratory manual of physical chemistry. 4th ed. J. Wiley and Sons, Inc., New York. 1956. p. 251.
16. E. J. STAMHUIS, H. MAATMAN, and G. E. H. JOOSTEN. Can. J. Chem. **64**, 1690 (1986).
17. H. J. CAMPBELL and J. T. EDWARD. Can. J. Chem. **38**, 2109 (1960).
18. T. F. LIN, S. D. CHRISTIAN, and H. E. AFFSPRUNG. J. Phys. Chem. **71**, 968 (1967).
19. R. W. TAFT, G. B. KLINGENSMITH, and S. EHRENSON. J. Am. Chem. Soc. **87**, 3620 (1965).

Appendix I

The concentration of cp in solutions of carbon tetrachloride

The dimerization of cyclopentanone in carbon tetrachloride is represented by

[A-1] $2\,cp \overset{K_A}{\leftrightarrows} (cp)_2$

K_A is defined by eq. [5]. From this equation the fraction of the total ketone present in the monomeric form, $\alpha = [cp]/[cp]_0$, is obtained in terms of K_A and the total ketone concentration, $[cp]_0$:

$$[A\text{-}2] \quad \alpha = \frac{-1 + \sqrt{(1 + 8K_A[cp]_0)}}{4K_A[cp]_0}$$

Only the positive root has physical significance, resulting in the following expression for the concentration of the monomeric species:

$$[A\text{-}3] \quad [cp] = \frac{-1 + \sqrt{(1 + 8K_A[cp]_0)}}{4K_A}$$

A similar expression can be derived for the concentration of monomeric cyclohexanone in carbon tetrachloride.

Reactions of alicyclic ketones in carbon tetrachloride. II. Kinetics of the chlorination of 2-chlorocyclopentanone and 2-chlorocyclohexanone, catalyzed by hydrogen chloride

EIZE J. STAMHUIS,[1] HENK MAATMAN,[2] AND GEERT E. H. JOOSTEN[3]

Department of Chemical Engineering, the State University of Groningen, Nijenborgh 16, 9747 AG Groningen, The Netherlands

Received July 10, 1985[4]

EIZE J. STAMHUIS, HENK MAATMAN, and GEERT E. H. JOOSTEN. Can. J. Chem. **64**, 1690 (1986).

The kinetics of the direct chlorination of 2-chlorocyclopentanone (2-mccp) and 2-chlorocyclohexanone (2-mcch) in carbon tetrachloride, catalyzed by hydrogen chloride, were studied. Reaction products are all the possible 2,2-, 2,5-, and 2,6-dichloro compounds. The ratios depend on the concentrations of the monochloro compound and hydrogen chloride. Surprisingly, even at conversions of the monochloro compound as low as 2%, 2,2,5-trichlorocyclopentanone and 2,2,6-trichlorocyclohexanone, respectively, are also formed. The chlorination reaction of both monochloro ketones shows zero order in chlorine. The order in hydrogen chloride is 1.3. The order in 2-mccp and 2-mcch varies somewhat with the concentration of the ketone and was found to be roughly 1.7. The variation in reaction order is explained by a partial self-association of the ketones. The ketones act as substrates as well as basic catalysts in the rate-determining α- or α′-carbon deprotonation. General base catalysis is clearly demonstrated by a strong increase in the rate of chlorination of 2-mccp upon addition of cyclopentanone (cp) to the reaction mixture, which agrees with the mechanism as presented in a previous paper. Kinetic equations derived from the reaction models for the "separate" and "mixed" ketone chlorinations accurately describe the observed rates of the chlorination of 2-mccp and 2-mcch in the concentration range of 0.04–1.0 M.

EIZE J. STAMHUIS, HENK MAATMAN et GEERT E. H. JOOSTEN. Can. J. Chem. **64**, 1690 (1986).

Opérant dans le tétrachlorure de carbone, on a étudié la cinétique de la chloration directe, catalysée par le chlorure d'hydrogène, des chloro-2 cyclopentanone (2-mccp) et cyclohexanone (2-mcch). Les produits de la réaction correspondent à tous les produits possibles pour les disubstitutions en -2,2, -2,5 et -2,6. Les rapports varient avec les concentrations initiales de composé monochloré et de chlorure d'hydrogène. Il est surprenant de noter, à des taux de transformation du dérivé monochloré aussi bas que 2%, qu'il y a aussi formation, selon le cas, de trichloro-2,2,5 cyclopentanone ainsi que de trichloro-2,2,6 cyclohexanone. Par rapport au chlore, l'ordre de la réaction de chloration des deux cétones monochlorées est égal à zéro. Par rapport au chlorure d'hydrogène, il est égal à 1,3. Par rapport aux cétones 2-mccp et 2-mcch, l'ordre varie en fonction de la concentration des cétones; il s'établit approximativement à 1,7. On explique cette variation de l'ordre par rapport aux cétones en fonction d'une auto-association partielle des cétones. Les cétones agissent comme substrats ainsi que comme catalyseurs basiques dans la déprotonation des carbones α et α′ qui détermine la vitesse de la réaction. On a facilement mis en évidence une catalyse générale des bases en notant la grande augmentation de la vitesse de chloration de la 2-mccp par addition de cyclopentanone (cp) au milieu réactionnel; cette observation est en accord avec le mécanisme proposé dans notre travail antérieur. À des concentrations allant de 0,04 à 1,0 *M*, les équations cinétiques que l'on peut dériver des modèles réactionnels proposés pour des réactions de chlorations "séparées" et "mélangées" des cétones décrivent adéquatement les vitesses observées pour la chloration des cétones 2-mccp et 2-mcch.

[Traduit par la revue]

Introduction

In a previous paper the kinetics of the chlorination of cyclopentanone (cp) and cyclohexanone (ch) in carbon tetrachloride, catalyzed by hydrogen chloride, are described (1). A kinetic model is developed that is consistent with the experimental results over a broad range of concentrations of both ketones. A mechanism is proposed, which explains the kinetic results.

As to the product distribution, it was found experimentally that even at very low fractional conversions of the ketone, besides the 2-monochloro products, considerable amounts of the three isomeric dichloro ketones are also formed. This could not be explained by a normal consecutive chlorination of the monochloro ketones. To obtain more insight into the reactions involved, the kinetics of the chlorination of 2-chlorocyclopentanone (2-mccp) and 2-chlorocyclohexanone (2-mcch) in carbon tetrachloride, catalyzed by hydrogen chloride, were studied.

Experimental

Materials

Cyclopentanone and cyclohexanone were purified as reported in the previous paper (1). 2-Chlorocyclopentanone (Merck), purity >98%, was distilled and the fraction 346–348 K (1.6 kPa) was collected and used for the experiments. 2-Chlorocyclohexanone (Aldrich), purity >98%, was distilled and the fraction 355–357 K (1.3 kPa) was collected. Suppliers and specifications of chlorine, hydrogen chloride, and carbon tetrachloride are the same as reported in the previous paper (1).

Kinetic methods

The chlorination reactions were carried out in a thermostated ultraviolet transmission cell of 10×10^{-6} m^3 with a light path length of 2×10^{-2} m, equipped with a magnetic stirrer and placed in a Zeiss PMQ II spectrophotometer. Kinetic runs were carried out by rapidly mixing a solution of hydrogen chloride and chlorine in CCl_4, with a solution of 2-chloro ketone and hydrogen chloride in CCl_4. The concentration of chlorine was subsequently followed as a function of time by measuring the extinction of an optimal wavelength of 336 nm ($\varepsilon_{Cl_2} = 4200\ M^{-1}\ m^{-1}$).

Initial chlorine concentrations were determined by titration before mixing and from the extinction of the reaction mixture at time $t = 0$. Afterwards the mass balance on the chlorination products was calculated. The balance always agreed with 4%. All products were

[1]Author to whom correspondence may be addressed.

[2]Present address: Enka, Arnhem, The Netherlands.

[3]Present address: N.V. Nederlandse Gasunie, Groningen, The Netherlands.

[4]Revision received April 18, 1986.

TABLE 1. The selectivity $S(Z)$ of the chlorinated products (Z) in the chlorination of 2-chlorocyclopentanone (2-mccp). T = 294 K, [HCl] and [2-mccp] in M

[HCl]	[2-mccp]	mccp conversion (%)	S(*g*-2,2-dccp)	S(*c*-2,5-dccp)	S(*t*-2,5-dccp)	S(2,2,5-tccp)
0.033	1.10	13	0.16	0.31	0.47	0.02
0.055	0.10	13	0.14	0.35	0.49	0.03
0.033	0.90	2	0.05	0.40	0.53	0.02
0.060	0.90	2	0.02	0.47	0.45	0.05
0.081	0.90	2	0.00	0.46	0.49	0.05

analyzed by hplc. In some cases a stopped-flow technique was used as described in the preceding paper (1).

Results and discussion

Product distribution

After each kinetic run of the chlorination of 2-mccp the reaction mixture was analyzed quantitatively. In all experiments, including those at fractional conversions of 2-mccp down to 2%, some 2,2,5-trichlorocyclopentanone (2,2,5-tccp) was formed. In the chlorination of 2-mcch similar results were obtained. From the analytical results the selectivities, $S(Z)$, to the individual di- and trichlorinated ketones, (Z), were calculated according to

$$S(Z) = \frac{[Z]}{[gem\text{-}2,2\text{-dccp}] + [cis\text{-}2,5\text{-dccp}] + [trans\text{-}2,5\text{-dccp}] + [2,5,5\text{-tccp}]}$$

with *gem*-2,2-dccp: *gem*-2,2-dichlorocyclopentanone; *cis*-2,5-dccp: *cis*-2,5-dichlorocyclopentanone; *trans*-2,5-dccp: *trans*-2,5-dichlorocyclopentanone; and 2,5,5-tccp: 2,5,5-trichlorocyclopentanone.

The experimental isomer distributions obtained in the chlorination of 2-mccp at two conversions, η, of the starting ketone, and at several initial concentrations of the reactants, are summarized in Table 1. The content of *gem*-2,2-dccp decreases with increasing 2-mccp concentrations. The same applies to the ratio of *cis*-2,5-dccp to *trans*-2,5-dccp, although to a much lesser extent.

The observed selectivities will be discussed further on in this paper.

Kinetics

The experiments carried out in the temperature range of 284–314 K show a zero reaction order in chlorine. Figures 1 and 2 give the rate of disappearance of chlorine vs. the concentration of hydrogen chloride at several concentrations of 2-mccp and 2-mcch, respectively.

In view of the *autocatalytic* nature of the reaction, the chlorination was always carried out up to only a few percent conversion of the ketone to avoid a substantial increase in the concentration of hydrogen chloride. If necessary, corrections were made for the hydrogen chloride formed. From Figs. 1 and 2 an order in hydrogen chloride of 1.3 for both ketones can be calculated. From the rates at various ketone concentrations the order in monochloro ketone was determined to be roughly 1.7. Just as in the chlorination of the unsubstituted ketones, this value is not constant over the entire concentration range.

Figures 3 and 4 show the experimental results (points) and the calculated rates (drawn lines) based upon the kinetic model, which is given below.

Kinetic model

The observed variation of the reaction order of the monochloro ketones with the ketone concentrations as shown in Figs. 3 and 4 is reasonable in the light of the proposed mechanism for the chlorination of cyclopentanone and cyclohexanone as presented in the previous paper (1). This variation in order is brought about by a partial self-association of the monochloro ketones. Analogous to the reaction model of the chlorination of the parent ketones the rate expression is:

$$[1] \quad -r(Cl_2) = \frac{(2 - S_d)}{S_d} K_1 k_2 \times \left[\frac{-1 + \sqrt{1 + 8K_A[Y]_0}}{4K_A}\right]^2 [HCl]^{1.3}$$

Y: 2-mccp, 2-mcch; K_1: equilibrium constant of the ketone-oxygen protonation given by eq. [3] in Scheme 2; k_2: rate constant of the rate determining α- or α′-carbon deprotonation of the oxygen-protonated ketone (substrate) by the same ketone acting as base; K_A: equilibrium constant of the self-association of Y; and S_d: selectivity of the chlorination to the combined dichloro compounds. The values of the parameters as determined from the experimental results by a least-squares method are summarized in Table 2.

The calculated rates of chlorination obtained by substituting the parameters of Table 2 in eq. [1] agree well with the experimental rates of reaction (drawn curves in Figs. 3 and 4).

The values of the association constants K_A of the monochloro compounds in carbon tetrachloride are considerably lower than those of the parent ketones. This is the reason for the smaller variation in the reaction order in the monochloro ketones over the experimental range of concentrations compared to those of the parent ketones.

The influence of the temperature on the rate of chlorination of 2-mccp, measured at ketone concentrations of 0.10 and 0.23 M, is in fact composed of a contribution of the compounded chlorination reaction rate constant K_1k_2 and of the self-association of the monochloro ketone as represented by the term $(-1 + \sqrt{1 + 8\,K_A[Y]_0})^2/16\,K_A^2$ in eq. [1]. Correcting for the

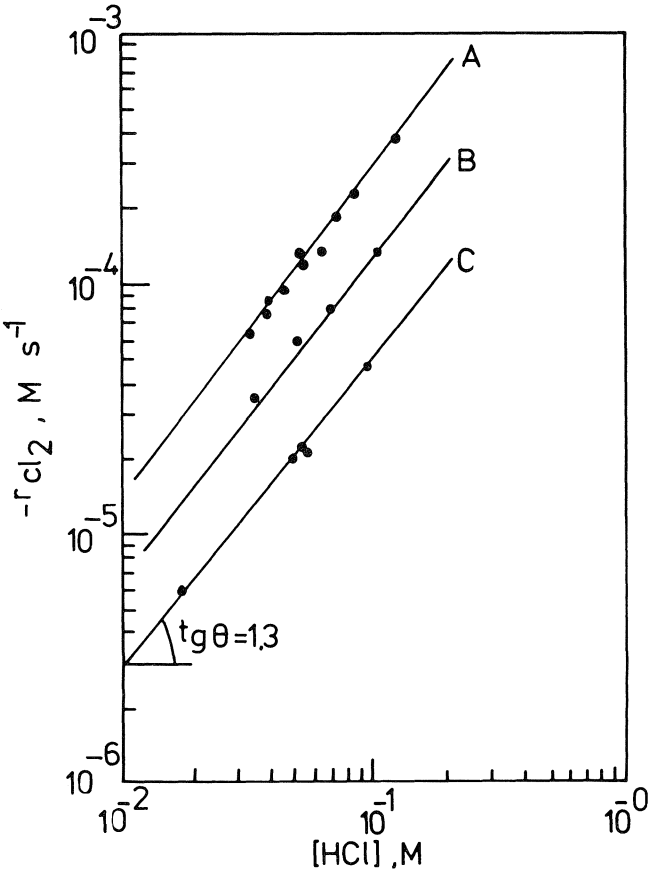

FIG. 1. The influence of the concentration of hydrogen chloride on the rate of chlorination of 2-mccp at 294 K. Ketone concentrations (in *M*): A: 0.30; B: 0.20; C: 0.10.

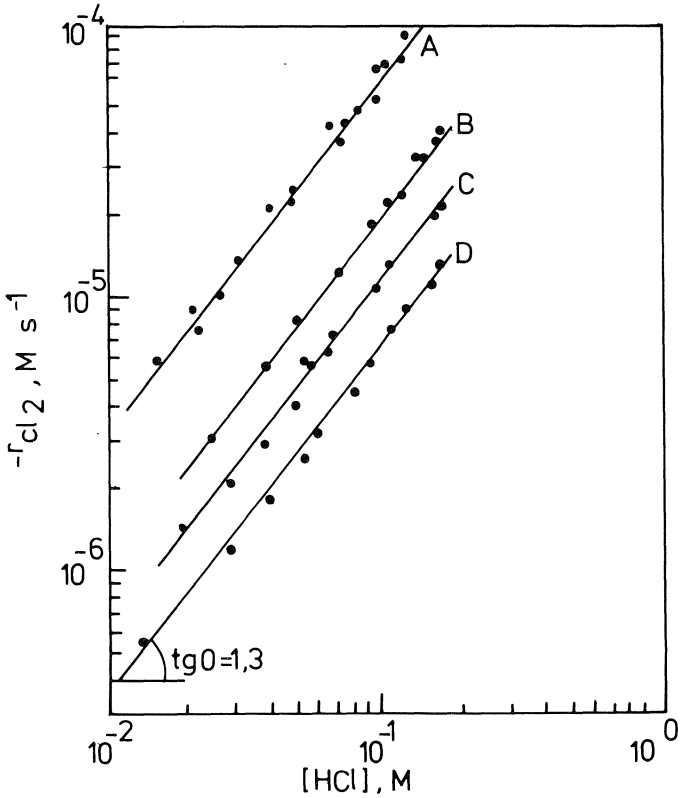

FIG. 2. The influence of the concentration of hydrogen chloride on the rate of chlorination of 2-mcch at 294 K. Ketone concentrations (in *M*): A: 0.44, B: 0.34; C: 0.16; D: 0.12.

latter contribution, assuming an enthalpy of self-association ($-\Delta H_A^0$) of 10 kJ mol^{-1} as found for cp and ch (1), the compounded rate constant K_1k_2 at various temperatures could be calculated and its temperature dependence expressed in an Arrhenius equation. The value of the activation energy, E_a(2-mccp), of the chlorination reaction is found to be 22 kJ mol^{-1} and the pre-exponential factor 900 $M^{-2.3}$ s^{-1}.

As might be concluded from the presence of trichloro compounds in the reaction mixture, part of the monochloro ketones is rapidly chlorinated to products containing two more chlorine atoms than the original reactant. For the parent ketones a similar behaviour was observed (1). However, the extent of this rapid consecutive reaction is smaller for the monochloro compounds, leading to about 5% of the trichloro ketones. Analogous to the explanation given in the previous paper for the formation of dichloro ketones directly from cp and ch, part of the oxygen-protonated dichloro compound formed by the chlorination of the monochloro ketone forms an intimate ion pair with a very reactive chlorine anion. This ion pair will subsequently lead to dichloro enol molecules as precursors of the trichloro ketone, according to Scheme 1.

This process must compete with an oxygen deprotonation of the dichloro compound by probably the same chloro anion. The lower reactivity and the smaller number of the remaining α-hydrogen atoms in the dichloro ketones with respect to the 2-chloro compounds are most probably responsible for the fact that in the chlorination of 2-mccp and 2-mcch only 5% trichloro ketones are formed, whereas in the chlorination of cp and ch approximately 17% of the dichloro derivatives are produced.

TABLE 2. Equilibrium constants of the self-association, K_A, of 2-mccp and 2-mcch, and the compounded reaction rate constant of the chlorination at 294 K

Ketone	K_A (M^{-1})	K_1k_2 ($M^{-2.3}$ s^{-1})
2-mccp	0.5	0.10
2-mcch	0.5	0.011

Both the unsubstituted ketones and the monochloro derivatives show similar behaviour regarding the chloride base-catalyzed rapid consecutive chlorination. It may therefore be expected that this reaction is not limited to this class of ketones, but will occur quite generally in the acid-catalyzed direct chlorination of ketones in apolar solvents. It may well be the main reason for the generally observed low selectivities of desired products in the direct halogenation of aldehydes and ketones.

The chlorination of 2-chlorocyclopentanone, catalyzed by cyclopentanone

The kinetic results for the chlorination of cp, 2-mccp, ch, and 2-mcch, obtained so far, permit the calculation of the selectivities to the mono-, di-, and trichlorinated products over a large range of fractional ketone conversions. At high conversions of the unsubsituted ketones the calculated values of the selectivities to the monochlorinated products were found to be much higher than those obtained experimentally, indicating more complicated kinetics than expected. The kinetic measure-

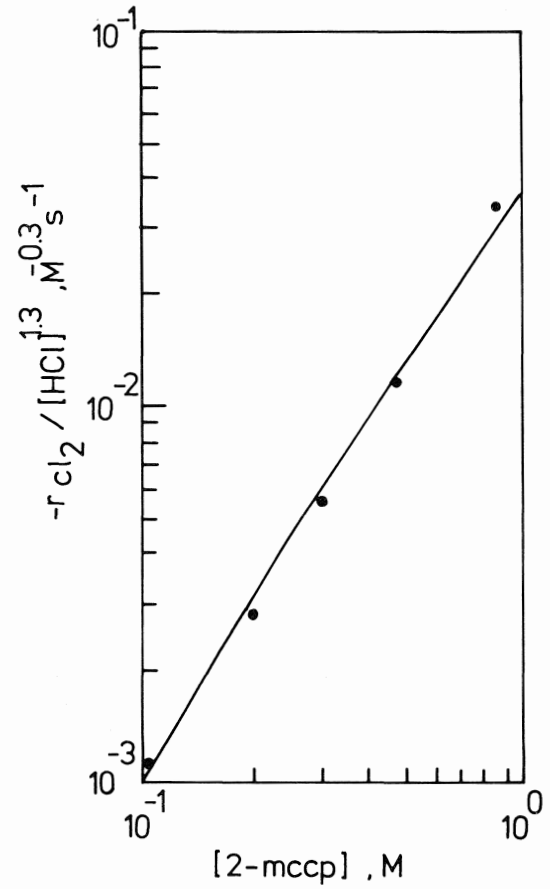

FIG. 3. The influence of the concentration of 2-mccp on the rate of chlorination at 294 K. Experimental (●); the smooth curve is calculated with eq. [1] and the constants from Table 2.

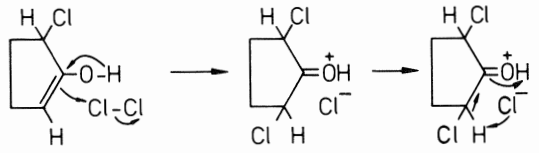

SCHEME 1

ments described thus far could be explained by a mechanism in which the ketone molecule is not only the substrate but also a base catalyst. This was confirmed by the results of two sets of primary kinetic isotope effects for ch (1). This raises the question whether addition of unsubstituted ketone to reaction mixtures containing 2-monochloro ketone would demonstrate base catalysis by the unsubstituted ketone in the proton removal from an α- or α′-carbon atom of the 2-chloro ketone on the one hand, and base catalysis by the 2-monochloro compound in the chlorination of the unsubstituted ketone on the other hand, thus explaining the deviations between experimental and calculated selectivities. Closer inspection shows that base catalysis by the 2-monochloro compound probably is negligible relative to that by the unsubstituted ketone: the pK_A values of the monochloro ketones, and thus their basicities, are significantly lower than those of the unsubstituted ketones, the difference being 2–3 pK_A units (2–4). The base catalysis by the parent ketone in the chlorination of the monochloro compound may be significant, however. This would lead to a considerable decrease in selectivity to the monochloro product in the chlorination of cp or

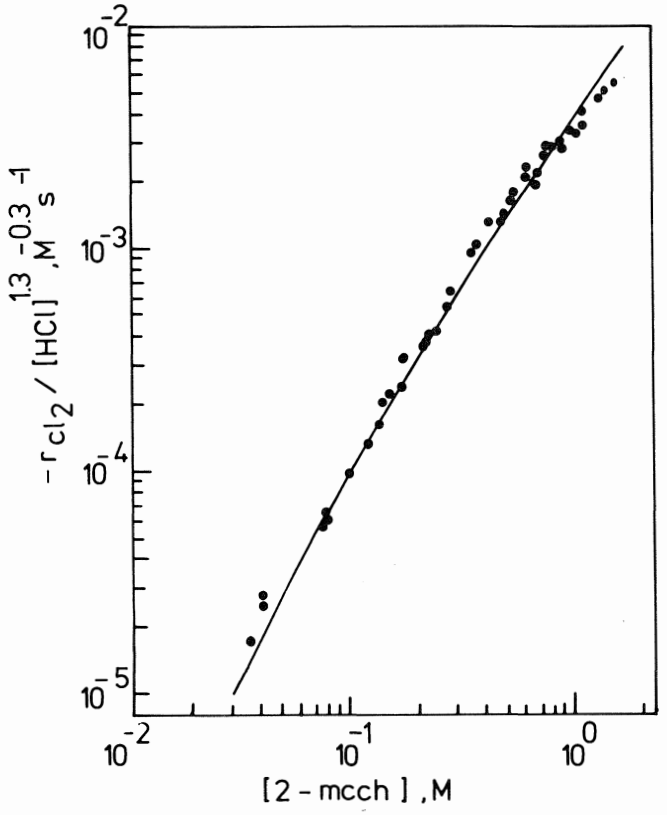

FIG. 4. The influence of the concentration of 2-mcch on the rate of chlorination at 294 K. Experimental (●); the smooth curve is calculated with eq. [1] and the constants from Table 2.

ch at higher conversions. The following reaction scheme gives the chlorination of 2-mccp catalyzed by cp (Scheme 2).

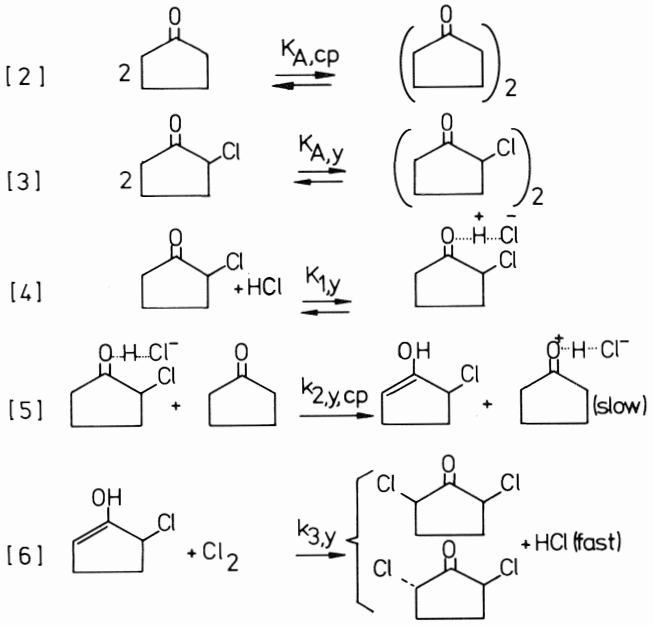

Y: 2-mccp

SCHEME 2

An analogous scheme applies to the chlorination of 2-mcch catalyzed by ch.

The various equilibrium and rate constants are, from now on, provided with an index to distinguish between values for the unsubstituted ketone X and the monochloro ketone Y.

TABLE 3. The contribution of the cp catalyzed chlorination of 2-mccp. $K_{A,cp} = 3\ M^{-1}$, $K_{A,2\text{-mccp}} = 0.5\ M^{-1}$; $T = 294$ K; X = cp, Y = 2-mccp; $S_z = 0.95$; $-r(Cl_2,Y,X)$ is the rate of disappearance of chlorine in the chlorination of substrate ketone Y, catalyzed by ketone X

[HCl] (M)	$[X]_0$ (M)	$[Y]_0$ (M)	$-10^4\ r(Cl_2)_{exp}$ ($M\ s^{-1}$)	$-10^4\ r(Cl_2,X,X)_{calc.}$ ($M\ s^{-1}$)	$-10^4\ r(Cl_2,Y,Y)_{calc.}$ ($M\ s^{-1}$)	$-10^4\ r(Cl_2,Y,X)_{exp}$ ($M\ s^{-1}$)	$-10^4\ r(Cl_2,Y,X)_{calc.}$ ($M\ s^{-1}$)	$K_{1,Y}k_{2,Y,X}$* ($M^{-2}\ s^{-1}$)
0.057	0.086	0.68	22.4	5.51	5.90	11.0	7.10	0.60
0.054	0.037	0.29	3.84	1.09	1.28	1.47	1.70	0.34
0.051	0.046	0.29	4.69	1.55	1.19	1.95	1.94	0.39
0.046	0.052	0.30	5.47	1.77	1.09	2.61	1.99	0.51
0.039	0.069	0.29	4.98	2.47	0.85	1.66	2.07	0.31
0.091	0.026	0.20	2.20	0.45	1.36	0.39	1.53	0.099
0.110	0.081	0.14	13.3	9.14	0.87	3.29	3.52	0.36
0.110	0.069	0.09	10.6	6.79	0.44	3.37	2.07	0.64
0.12	0.044	0.11	6.14	3.38	0.70	2.06	1.87	0.43
0.11	0.033	0.14	3.96	1.74	0.86	1.36	1.67	0.32
0.089	0.022	0.14	2.44	0.63	0.70	1.11	0.94	0.46
0.12	0.050	0.09	6.72	4.14	0.50	2.08	1.73	0.47
0.13	0.034	0.046	2.75	2.32	0.18	0.25	0.72	0.078

*The mean value of $K_{1,Y}k_{2,Y,X}$ is 0.39 ± 0.17 (standard deviation).

Based on Scheme 2, the rate of disappearance of chlorine in the chlorination of the monochloro ketone in a ketone – monochloro ketone mixture is given by

$$[7]\quad -r(Cl_2) = \frac{(2 - S_z)}{S_z} \times K_{1,Y}k_{2,Y,X}\left[\frac{-1 + \sqrt{1 + 8K_{A,Y}[Y]_0}}{4K_{A,Y}}\right] \times \left[\frac{-1 + \sqrt{1 + 8K_{A,X}[X]_0}}{4K_{A,X}}\right][HCl]$$

S_z: selectivity to the dichloro ketones; X: cp or ch; Y: 2-mccp or 2-mcch; $[X]_0$: total concentration of the unsubstituted ketone X; $[Y]_0$: total concentration of the monochloro ketone Y; $K_{1,Y}k_{2,Y,X}$: compounded reaction rate constant, based on Scheme 2, with X the unsubstitued ketone, here as base catalyst, and Y the monochloro ketone, here as substrate; in $M^{-2}\ s^{-1}$.

In an actual reaction mixture the rate of chlorine consumption will be larger as, parallel with the reactions given in Scheme 2, the chlorination of cp catalyzed by cp and of 2-mccp catalyzed by 2-mccp will also take place.

To determine the value of $K_{1,mccp}k_{2,mccp,cp}$, a number of experiments were carried out in which 2-mccp was chlorinated in the presence of cp. The results are presented in Table 3. The rates of chlorination of cp catalyzed by cp, and of 2-mccp catalyzed by 2-mccp, were subtracted from the observed rates. From the resulting difference, the compounded rate constant, $K_{1,mccp}k_{2,mccp,cp}$, was calculated, using eq. [7]. Thus a value of $0.39 \pm 0.17\ M^{-2}\ s^{-1}$ was obtained at a temperature of 294 K.

As well as self-association of the ketones, one may expect association of cp and 2-mccp molecules. By using a geometric mean value of $K_{A,X,Y}$ for this "cross-association," the greatest difference in the calculated[5] selectivity to 2-mccp with and without this kind of association was only 2%, even at a total ketone concentration of $2.5\ M$. The impact of the cross-association on the results of the mixed ketone experiments was therefore neglected.

Table 4 gives the values of the compounded reaction rate constant for the various combinations of substrate and base catalyst. The estimated values in Table 4 were obtained as follows. The difference in the values of the compounded rate constant for cases III and IV can be ascribed to the different catalytic activities of the bases acting in both cases. The relative activity of the bases is therefore $0.39/0.1 = 3.9$. If it be assumed that the ratio of the catalytic activities of the bases in cases I and II is the same, a value of $1.6/3.9 \approx 0.4$ is obtained for the rate constant in case II.[6]

A similar reasoning was applied in estimating the constant in case VI. The ratio of the catalytic activities of the unsubstituted and monosubstituted ketones as base is 3.9 for cp and approximately 150 for ch (comparison between cases III and IV, VII and VIII).

[5]As calculated from a computer simulation of a number of chlorination experiments, carried out in a trickle-bed reactor at 293 K.

[6]The rate-determining step in the chlorination of the ketones studied is expressed by eq. [5]. To a first approximation, this rate depends on the concentrations of substrate and catalyst, the acidity of the α-carbon hydrogen, which is removed, the basicity (nucleophilicity) of the catalyst-base, and other effects like steric hindrance in the activated complex. To estimate the value of the compounded rate constant for case II, these effects were taken into account qualitatively. As to the steric hindrance, a proportional increase in the series I–IV of Table 4 was assumed.

TABLE 4. The measured and estimated reaction rate constants based on the mechanism presented in Scheme 2. $K_{A,cp} = 3\ M^{-1}$, $K_{A,ch} = 4\ M^{-1}$, $K_{A,2\text{-mccp}} = K_{a,2\text{-mcch}} = 0.5\ M^{-1}$

Case	Substrate	Base catalyst	Compounded rate constant	Value compounded rate constant ($M^{-2}\ s^{-1}$)
I	cp	cp	$K_{1,cp}k_{2,cp,cp}$	1.6
II	cp	2-mccp	$K_{1,cp}k_{2,cp,mccp}$	0.4*
III	2-mccp	cp	$K_{1,mccp}k_{2,mccp,cp}$	0.39
IV	2-mccp	2-mccp	$K_{1,mccp}k_{2,mccp,mccp}$	0.1
V	ch	ch	$K_{1,ch}k_{2,ch,ch}$	15.5
VI	ch	2-mcch	$K_{1,ch}k_{2,ch,mcch}$	0.1*
VII	2-mcch	ch	$K_{1,mcch}k_{2,mcch,ch}$	1.5†
VIII	2-mcch	2-mcch	$K_{1,mcch}k_{2,mcch,mcch}$	0.01

*Estimated value.
†Estimated from computer simulations of chlorination experiments in a trickle-bed reactor.

In aqueous media a decrease of 2–3 pK_A units was found for the first chlorine atom introduced (2). It may be expected that such a decrease in basicity would result in ratios of these overall rate constants much larger than those experimentally obtained. However, as is well known, large differences in basicities as found in aqueous media diminish in an apolar solvent like carbon tetrachloride. This is brought about by strong ion-pair formation (5).

It is striking that the ratio of the overall rate constants of chlorination of the unsubstituted and monosubstituted ketones is 4 for cp (cases I and III) and 10 for ch (cases V and VII), in those cases that the unsubstituted ketone acts as basic catalyst. That these ratios are considerably larger than 1 is probably due to the lower basicities of the monochloro derivatives and to the smaller number of α-carbon and α′-carbon hydrogens available in the latter compounds with respect to the unsubstituted ketones. The extra decrease in reactivity of 2-mcch relative to 2-mccp with a factor of 2.5 might be ascribed to the exceptional position of the chlorine atom in 2-mcch. When dissolved in hexane, carbon tetrachloride, or iso-octane, this position is preferentially axial as a consequence of the electrostatic repulsion between the dipoles of the carbonyl group and the carbon chlorine in the equatorial position (6, 7), despite an increase in steric hindrance by the interaction of this α-carbon chlorine with the α′-axial hydrogen. Energetically, the hydrogen most favorable for enolization is this α′-carbon hydrogen, leading to 6-chloro-1-cyclohexen-1-ol. Just as in 2-mcch, the chlorine atom in this intermediate also takes a very pronounced axial position (6), leading to a much larger steric hindrance for an approach of a chlorine molecule from the *cis* position in the subsequent step. Therefore, virtually only *trans*-2,6-dichlorocyclohexanone is formed, as is indeed observed. One may expect that this route is only slightly influenced by the type of basic catalyst used. The selectivities to the dichlorocyclohexanones in the chlorination of ch catalyzed by the chloride anions in the intimate ion-pair mechanism can then also be understood, and indeed *trans*-2,6-dcch is formed almost exclusively (ref. 1, Tables 4 and 5).

Very likely the preferential axial position of the α-chlorine in 2-mcch in apolar media results in a lower basicity of the carbonyl group for this ketone with respect to 2-mccp. This explains the large difference in the ratios of the compounded rate constants for cases III and IV, and VII and VIII, respectively.

The selectivities S(*Z*)

In contrast to the 6-chloro-1-cyclohexen-1-ol molecule, a model of 5-chloro-1-cyclopenten-1-ol shows that this enol is nearly flat. The position of the chlorine atom is almost in the plane of the ring, *trans* attack of the chlorine molecule being slightly favored. Therefore a ratio of *S*(*trans*-2,5-dccp) and *S*(*cis*-2,5-dccp) of slightly larger than one may be expected in the chlorination of 2-mccp. Table 1 shows this to be actually the case. As was observed earlier (8), *S*(*gem*-2,2-dccp) appears to be dependent on the concentrations of the reagents. Table 1 shows that *S*(*gem*-2,2-dccp) decreases almost linearly with increasing concentrations of both 2-mccp and hydrogen chloride. Although the data are not sufficient to draw pertinent conclusions, this selectivity may well be related to the dielectric constant of the reaction mixture. At increasing concentrations of 2-mccp and (or) hydrogen chloride the dielectric constant will increase. It may be expected that the repulsion of the carbonyl and α-C—Cl dipoles will decrease with increasing dielectric constant of the medium. If acid–base catalyzed enolization is favoured by a planar configuration of the carbonyl group and the α-carbon–hydrogen bond, an increase in *S*(*gem*-2,2-dccp) at decreasing dielectric constant may indeed be expected. For at low dielectric constant the α-carbon chlorine is forced into the axial position and the α-carbon hydrogen then turns into the plane of the C=O group.

It should be mentioned that virtually no *cis–trans* conversion takes place after the reaction, as was proven by analysis of samples of the reaction mixtures, even after several days of storage at reaction temperatures. This is in agreement with observations by others (see ref. 6, p. 12, and ref. 8).

Conclusions

It is clear that the direct chlorination of the cyclic ketones in carbon tetrachloride, catalyzed by hydrogen chloride, is much more complicated than expected on the basis of literature data on chlorination reactions in polar media. This is mainly due to the fact that the substrate and products themselves also act as basic catalysts in the reaction. It may be pointed out that, actually, more reactions occur than described in this contribution. Although not kinetically investigated, batch experiments with ch always show the formation of small amounts of 2,2,6,6-tetrachlorocyclohexanone, as long as ch is present. This indicates a ch catalyzed enolization of the dichloro- and, to

a small extent, of the trichlorocyclohexanone. Besides, very small amounts of the tetrasubstituted compound may also be formed in the rapid consecutive chloride-anion catalyzed enolization of the oxygen-protonated dichloro ketones. Similar results were obtained in the chlorination of cp.

It should be mentioned that chlorination of ch and cp with excess of chlorine leads to a mixture of α,α'-chlorinated products, containing on the average not more than 2.3–2.5 chlorine atoms per ketone molecule. High conversions to 2,2,6,6-tetrachlorocyclohexanone are possible, using an organic base like collidine as catalyst (9).

1. E. J. STAMHUIS, H. MAATMAN, H. STINISSEN, and G. E. H. JOOSTEN. Chem. **64**, 1681 (1986).
2. G. C. LEVY. Chem. Commun. 1257 (1966); J. Am. Chem. Soc. **92**, 6238 (1970).
3. P. METZGER, A. CASADEVALL, and E. CASADEVALL. Tetrahedron, **31**, 733 (1975); **31**, 744 (1975).
4. H. J. CAMPBELL and J. T. EDWARD. Can. J. Chem. **38**, 2109 (1960).
5. R. P. BELL. The proton in chemistry. 2nd ed. Chapman and Hall, London. 1973. Chapt. 4.
6. Q.-Q. DANG. Thesis, Paris, 1962. p. 32.
7. N. L. ALLINGER, J. ALLINGER, L. A. FREIBERG, R. F. CZAJA, and N. A. LEBEL. J. Am. Chem. Soc. **82**, 5876 (1960).
8. Y. JASOR, M. GAUDRY, A. MARQUET, and M. BETTAHAR. Bull. Soc. Chim. Fr. 2732 (1973).
9. E. C. GILBERT, R. E. JONES, D. C. MCLEAN, and E. SHERMAN. Ind. Eng. Chem. Prod. Res. Dev. **14**, 2 (1975).

The crystal structure and vibrational spectrum of $(C_8H_{20}N_2)[InBr_5(H_2O)]\cdot H_2O$, a salt of the 1,1,4,4-tetramethylpiperazonium dication containing the aquopentabromoindate complex anion

GEORGE R. CLARK, CLIFTON E. F. RICKARD, AND MICHAEL J. TAYLOR[1]

Department of Chemistry, University of Auckland, Auckland 1, New Zealand

Received January 10, 1986

GEORGE R. CLARK, CLIFTON E. F. RICKARD, and MICHAEL J. TAYLOR. Can. J. Chem. **64**, 1697 (1986).

The preparation, crystal structure, and vibrational spectra of the title compound are reported. The compound crystallizes in the triclinic space group $P\bar{1}$, with $a = 7.386(2)$, $b = 8.637(1)$, $c = 16.546(2)$ Å, $\alpha = 97.40(1)°$, $\beta = 95.51(2)°$, $\gamma = 112.91(2)°$, $V = 951.6$ Å^3, $\rho_{obs} = 2.43$ g cm^{-3}, $Z = 2$, $\rho_{calcd} = 2.424$ g cm^{-3} (MoK_α, $\lambda = 0.71069$ Å). The structure was solved by direct methods and electron density maps, and refined by full-matrix least squares to the final $R = 0.038$ for 3343 observed reflections. The structure consists of *N,N,N′,N′*-tetramethylpiperazonium cations containing a six-membered C_4N_2 heterocycle, $InBr_5(OH_2)^{2-}$ anions, and additional H_2O solvent molecules. Infrared and Raman spectral bands of the $InBr_5(OH_2)^{2-}$ complex are assigned on the basis of C_{4v} skeletal symmetry, and the H_2O molecule of crystallization is also detected spectroscopically.

GEORGE R. CLARK, CLIFTON E. F. RICKARD et MICHAEL J. TAYLOR. Can. J. Chem. **64**, 1697 (1986).

On rapporte la préparation, la structure cristalline et les spectres vibrationnels du composé mentionné dans le titre. Le composé cristallise dans le groupe d'espace triclinique, $P\bar{1}$, avec $a = 7,386(2)$, $b = 8,637(1)$ et $c = 16,546(2)$ Å, $\alpha = 97,40(1)$, $\beta = 95,51(2)$ et $\gamma = 112,91(2)°$, $V = 951,6$ Å^3, $\rho_{obs} = 2,43$ g cm^{-3}, $Z = 2$, $\rho_{calcd} = 2,424$ g cm^{-3} (MoK_α, $\lambda = 0,71069$ Å). On a résolu la structure par des méthodes directes et des cartes de densités électroniques et on l'a raffinée par la méthode des moindres carrés (matrice entière) jusqu'à une valeur de $R = 0,038$ pour 3343 réflexions observées. La structure comporte des cations *N,N,N′,N′*-tétraméthylpipérazonium contenant un hétérocycle à six chaînons C_4N_2, des anions $InBr_5(OH_2)^{2-}$ et des molécules additionnelles d'eau de solvation. On a attribué les bandes observées dans les spectres ir et Raman du complexe $InBr_5(OH_2)^{2-}$ sur la base d'une symétrie du squelette C_{4v}; la spectroscopie permet aussi de détecter la molécule d'eau de cristallisation.

[Traduit par la revue]

Introduction

Heterocyclic dipositive cations, which are easily prepared by reaction of *N,N,N′,N′*-tetramethyl-1,2-ethanediamine (tmen) with methylene dihalides or 1,2-dihalogenoalkanes, may be used as counterions for the isolation of complex anions, especially those possessing a double negative charge (1). Here we report structural investigations of the compound 1,1,4,4-tetramethylpiperazonium aquopentabromoindate monohydrate, $(C_8H_{20}N_2)[InBr_5(H_2O)].H_2O$, **1**, obtained as crystals from an aqueous solution in which a mixture of indium bromide complexes is believed to exist (2).

The anion in **1** is $InBr_5(OH_2)^{2-}$ and its characterisation completes the series of six-coordinate indium halide complex anions $InX_n(OH_2)_{6-n}^{3-n}$ (X = Cl or Br; $n = 4$–6) for which crystallographic and spectroscopic data are available (3). Also revealed are the dimensions of the *N,N,N′,N′*-tetramethylpiperazonium dication, containing a six-membered C_4N_2 heterocycle, which may be compared with those of the analogous five-membered ring imidazolidinium dication (from tmen and CH_2Cl_2), the structure of which was determined recently (4).

Experimental

Preparative, analytical, and spectroscopic aspects

Aqueous solutions of indium bromide were prepared by dissolving the metal in concentrated HBr, by dissolving $InBr_3$ in water, or by the addition of KBr to $In(NO_3)_3$ solution (3:1 KBr to $In(NO_3)_3$). 1,1,4,4-Tetramethylpiperazonium dibromide, prepared from tmen and 1,2-dibromoethane (1), was added in aqueous solution so as to afford a slight excess based on the quantity of In^{3+}. Crystalline products formed on mixing the solutions. Larger, well-shaped crystals for the present study were obtained by evaporation of a solution from which an initial crop had already been obtained. These were collected and dried by contact with filter paper. *Anal.* calcd. for $(C_8H_{20}N_2)InBr_5.2H_2O$: C 13.83, H 3.48, N 4.03; found: C 14.14, H 3.50, N 4.32.

[1]To whom all correspondence should be addressed.

Raman spectra were recorded with a Jasco R300 spectrometer, using Ar^+ laser excitation (488 or 514 nm) from a Coherent Radiation CR4 source operating at 200 mW. Infrared spectra were measured using a Perkin-Elmer 597 spectrometer for the range 4000–200 cm^{-1}, and in the far-infrared (400–40 cm^{-1}) using a Grubb-Parsons Cube MkII interferometer linked to an IBM PC microcomputer. The low-frequency spectra indicated the presence of an indium bromide complex anion (5). In some samples two intense ν(In—Br) Raman peaks were seen near 170 cm^{-1}, separated by ca. 5 cm^{-1}, and small shifts (less than 10 cm^{-1}) between one sample and another were noticed in the position of several bands due to the cation, particularly the rocking modes. These effects are probably associated with minor conformational changes in the ions concerned. In an attempt to eliminate this factor, care was taken to select the material for X-ray and spectroscopic analysis from the same batch of crystals.

X-ray studies

Crystals of the title compound are colourless prisms. A crystal with approximate dimensions 0.23 × 0.18 × 0.13 mm was affixed to the end of a glass fibre and positioned on a Enraf-Nonius CAD-4 diffractometer. Accurate unit cell parameters were derived from a least-squares fit to the setting angles of 25 high-θ reflections widely dispersed through reciprocal space. The diffraction pattern contained no systematic absences in a triclinic distribution, and the space group was deduced to be $P\bar{1}$ rather than $P1$ on the basis of intensity statistics. The data were corrected for Lorentz and polarization effects, and scaled to allow for isotropic decay of intensity standards (maximum decay 10%). Absorption corrections were from empirical curves derived from azimuthal scans, with maximum and minimum correction factors being 0.9992 and 0.6749, respectively (6). The crystal density was measured by flotation in CH_2Br_2/*c*-hexane mixtures.

The positions of the indium and bromine atoms were obtained by direct methods using the SHELX program (7), and the lighter atoms were found in a subsequent electron density map. No attempt was made to locate hydrogen atoms. The structure was refined anisotropically by full-matrix least squares to convergence at $R = 0.038$ and $R_w = 0.043$ for 3343 unique observed reflections. The function minimised during least-squares calculations was $\Sigma w(|F_o| - |F_c|)^2$, with $w = 1/[\sigma^2(F)$

TABLE 1. Summary of crystal data, intensity collection, and structural refinement for $(C_8H_{20}N_2)[InBr_5(OH_2)].H_2O$

Cell constants	$a = 7.386(2)$ Å, $b = 8.637(1)$ Å, $c = 16.546(2)$ Å, $\alpha = 97.40(1)°$, $\beta = 95.51(2)°$, $\gamma = 112.91(2)°$
Cell volume	951.6 Å^3
Space group	$P\bar{1}$ (No. 2)
Z	2
M_r	694.6
ρ_{calcd}	2.424 g cm^{-3}
ρ_{obs}	2.43 g cm^{-3}
$F(000)$	652
Absorption coefficient	123.3 cm^{-1}
Radiation	Mo K_α, $\lambda = 0.71069$ Å
θ range	1–30°
Scan type	$\omega/2\theta$
Background time/scan time	0.5
Total reflections measured	5750
Unique data, $I > 3\sigma(I)$	3343
No. of refined parameters	163

$+ gF^2]$ and final g of 2.606×10^{-3}. $S = [\Sigma w(|F_o| - |F_c|)^2/(m - n)]^{1/2} = 0.748$. The maximum residual electron density in a final difference map (0.93 e Å^{-3}) was a spurious peak close to the indium atom position. Structure determination and refinement were performed on the University of Auckland IBM 4341 computer.

Details of the crystal, intensity data collection, and structure refinement are summarized in Table 1. Atomic positions and equivalent isotropic temperature factors are given in Table 2. Anisotropic thermal parameters, and tables of observed and calculated structure factor amplitudes, are available as Supplementary Data.[2]

Figure 1 shows the packing within the centrosymmetric unit cell. Figure 2 gives the cation with the atomic numbering scheme for C and N atoms, and Fig. 3 shows the $InBr_5(OH_2)^{2-}$ anion.

Results and discussion

Preparative aspects

Aqueous solutions of indium chloride or bromide are known to contain mixtures of complex anions, including species with water molecules coordinated to the metal (2, 8, 9). A variety of solids can be crystallised from these solutions by use of metal or alkylammonium cations, and include examples in which additional halide as well as a complex anion is present, e.g. $(MeNH_3)_4InBr_7$ contains Br^- and $InBr_6^{3-}$ ions (5, 10). Our objective was to see whether the use of a bulky dication would facilitate the isolation of a dianion from the mixture present in a indium bromide solution. $(Me_4N)_2InBr_5$, prepared by Tuck *et al.* (5), appears from spectroscopic evidence, to contain $InBr_4^-$ and Br^- ions. With the Me_4N^+ cation, the chloride system can furnish either $(Me_4N)_2[InCl_5]$ or $(Me_4N)_2[InCl_5(H_2O)]$ depending on the reaction medium (5). We find that indium bromide solutions to which the $Me_2N(C_2H_4)_2NMe_2^{2+}$ cation is added yield a crystalline product, and the position of ν(In—Br) bands in Raman and ir spectra indicates that a five- or six-coordinate indium complex is present. A crystal of this compound was selected for X-ray examination and the same product was investigated spectroscopically.

Structural studies

The crystal structure of **1** consists of discrete dipositive cations, $InBr_5(OH_2)^{2-}$ complex anions, and an additional H_2O solvent molecule which is linked to the coordinated water molecule of the anion by hydrogen bonding (Fig. 1). The separation between the oxygen atoms of the H_2O molecules is 2.79 Å, which suggests a hydrogen bond length of ca. 1.8 Å, a usual value. A "difference" Fourier map shows electron density along the O---O vector connecting the two water molecules, but fails to locate the proton precisely. All other interatomic distances involving the second water molecule and O or Br atoms are in excess of 3.3 Å, so that further bond formation is ruled out. The crystals of **1** are stable in the atmosphere at room temperature but become cloudy on the surface when in contact with acetone or alcohol, probably through loss of the solvent molecule from the lattice.

Figure 2 shows the structure of one of the two crystallographically distinct dications, the six-membered rings of which adopt a regular chair conformation. Bond distances and angles are given in Table 3. Note that the atomic numbering for the second dication is N(2) and C(5)—C(8). The C—N bond

TABLE 2. Atomic positions and equivalent isotropic temperature factors

Atom	x	y	z	B_{eq} (Å^2)*
In	0.41207(7)	0.29144(5)	0.74691(3)	1.91
Br(1)	0.30432(11)	0.19322(9)	0.58433(4)	2.65
Br(2)	0.15667(12)	−0.01502(8)	0.75969(5)	2.99
Br(3)	0.54826(11)	0.35141(9)	0.90738(5)	2.79
Br(4)	0.69748(11)	0.57327(9)	0.72567(5)	2.96
Br(5)	0.16052(11)	0.43997(9)	0.76283(5)	2.79
O(1)	0.6464 (8)	0.1738 (7)	0.7303 (3)	3.11
O(2)	0.5554 (11)	−0.1161 (8)	0.8028 (5)	5.15
N(1)	0.0266 (8)	−0.1645 (6)	−0.0123 (3)	1.90
N(2)	0.8202 (8)	0.3360 (7)	0.4771 (3)	2.10
C(1)	0.1993 (9)	0.0077 (8)	0.0043 (5)	2.34
C(2)	−0.1515 (10)	−0.1450 (8)	−0.0545 (5)	2.39
C(3)	0.0794 (11)	−0.2857 (9)	−0.0719 (5)	2.53
C(4)	−0.0154 (12)	−0.2387 (9)	0.0645 (5)	2.80
C(5)	0.9982 (11)	0.3722 (9)	0.4347 (5)	2.73
C(6)	0.8106 (10)	0.5052 (9)	0.5081 (5)	2.52
C(7)	0.8213 (12)	0.2350 (9)	0.5441 (5)	2.91
C(8)	0.6325 (12)	0.2334 (10)	0.4144 (5)	3.29

*Temperature factors of anisotropically refined atoms are given in the form of the isotropic equivalent thermal parameter defined as $B_{eq} = (8/3)\pi^2\Sigma_i\Sigma_j U_{ij} a_i^* a_j^* a_i \cdot a_j$.

[2]Complete set of data may be purchased from the Depository of Unpublished Data, CISTI, National Research Council of Canada, Ottawa, Ont., Canada K1A 0S2.

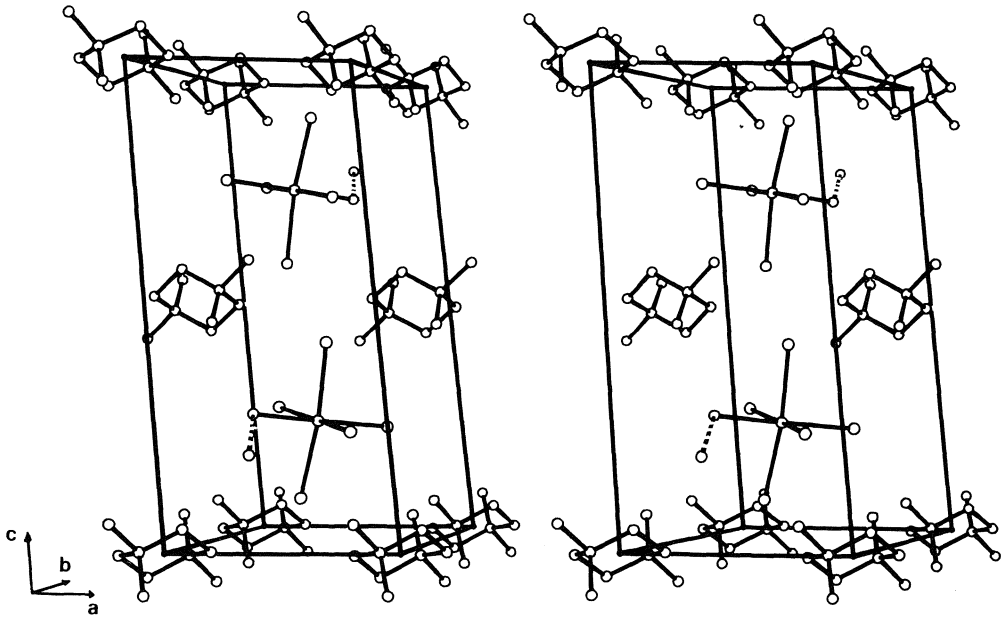

FIG. 1. Stereoscopic view of the unit cell packing of $(C_8H_{20}N_2)[InBr_5(OH_2)].H_2O$.

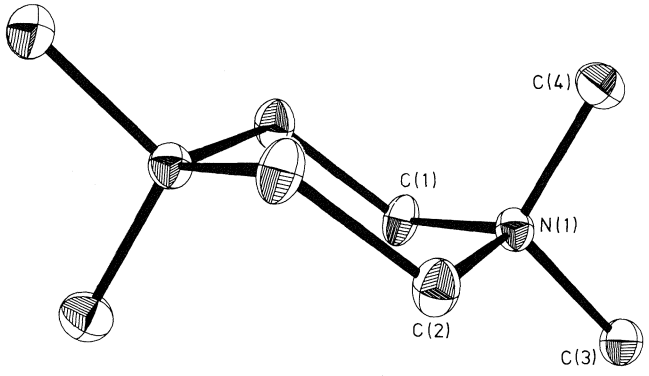

FIG. 2. The molecular framework of the 1,1,4,4-tetramethylpiperazonium cation, $Me_2N(C_2H_4)_2NMe_2^{2+}$.

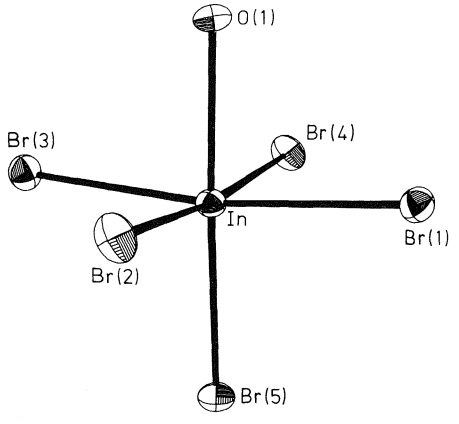

FIG. 3. The molecular structure of the aquopentabromoindate anion, $InBr_5(OH_2)^{2-}$.

lengths, in the range 1.50–1.53 Å, are normal values for quaternary nitrogen and are similar to those of the 1,1,3,3-tetramethylimidazolidinium dication (4). This latter species, the five-membered ring cyclic cation derived from tmen and a methylene dihalide, has a short C—C distance of 1.48 Å. In the present six-membered ring the C—C distance is larger, 1.533 Å, and is slightly greater than the corresponding bond length in piperazine (1.527 Å) or 1,4-dimethylpiperazine (1.521 Å) (11). These two molecules have C—N bonds of 1.45–1.47 Å: those of the present heterocycle are significantly longer, with C—N(ring) distances which average 1.507 Å, and are similar to those found in the tetraamidopiperazonium dication, which has C—N(ring) distances of 1.510 and 1.513 Å and a C—C distance of 1.521 Å (12).

The structure of the $InBr_5(OH_2)^{2-}$ anion is shown in Fig. 3, with bond lengths and angles in Table 4. The average In—Br distance, 2.644 Å, comes between those of $InBr_4(OH_2)_2^-$ and $InBr_6^{3-}$, which are 2.613 Å (13) and 2.670 Å (14), respec-

TABLE 3. Bond distances (Å) and angles (deg) in the 1,1,4,4-tetramethylpiperazonium dication*

Cation 1		Cation 2	
Bond	Distance	Bond	Distance
C(1)—N(1)	1.505(8)	C(5)—N(2)	1.495(8)
C(2)—N(1)	1.508(9)	C(6)—N(2)	1.516(8)
C(3)—N(1)	1.531(8)	C(7)—N(2)	1.499(9)
C(4)—N(1)	1.501(9)	C(8)—N(2)	1.521(9)
C(1)—C(2)′	1.533(8)	C(5)—C(6)′	1.527(9)
Cation 1		**Cation 2**	
Bonds	Angle	Bonds	Angle
C(1)—N(1)—C(2)	107.8(5)	C(5)—N(2)—C(6)	107.8(5)
C(1)—N(1)—C(3)	107.7(5)	C(5)—N(2)—C(7)	112.5(6)
C(1)—N(1)—C(4)	112.7(5)	C(5)—N(2)—C(8)	109.2(5)
C(2)—N(1)—C(3)	108.5(5)	C(6)—N(2)—C(7)	112.8(5)
C(2)—N(1)—C(4)	111.8(5)	C(6)—N(2)—C(8)	106.4(6)
C(3)—N(1)—C(4)	108.3(5)	C(7)—N(2)—C(8)	107.8(6)
C(2)′—C(1)—N(1)	112.0(5)	C(6)′—C(5)—N(2)	111.5(6)

*Primed atoms are related to unprimed atoms by inversion through the centres of symmetry.

TABLE 4. Bond distances (Å) and angles (deg) in the $[InBr_5(OH_2)]^{2-}$ complex anion

Bond	Distance
In—Br(1)	2.658(1)
In—Br(2)	2.635(1)
In—Br(3)	2.656(1)
In—Br(4)	2.619(1)
In—Br(5)	2.651(1)
In—O	2.344(5)

Bonds	Angle	Bonds	Angle
Br(1)—In—Br(2)	86.97(4)	Br(1)—In—O	85.2(1)
Br(2)—In—Br(3)	89.50(5)	Br(2)—In—O	87.7(1)
Br(3)—In—Br(4)	92.00(5)	Br(3)—In—O	85.5(1)
Br(1)—In—Br(4)	90.20(4)	Br(4)—In—O	84.2(1)
Br(1)—In—Br(5)	94.24(4)		
Br(2)—In—Br(5)	95.49(5)		
Br(3)—In—Br(5)	95.22(5)		
Br(4)—In—Br(5)	92.63(5)		

tively. Six-coordinate aquochloro complexes of indium also show an increase in bond length with increased charge on the anion (15).

For $InBr_5(OH_2)^{2-}$, the In—O distance of 2.344 Å makes this the longest indium–oxygen bond so far measured, exceeding the values of 2.224 Å in the chloride analogue $InCl_5(OH_2)^{2-}$ (16), 2.261 Å in $InBr_4(OH_2)_2^-$ (13), and 2.15 Å in $In(OH_2)_6^{3+}$ (17). A value of 2.287 Å has been estimated for the In—O distance in $(NH_4)_2[InBr_5(H_2O)]$ from an analysis of the single crystal ^{115}In nqr spectrum (18). The greater In—O distance of the present structure may be due in part to the effect of hydrogen bonding to the additional water molecule. Inspection of the bond angles of the present complex reveals a significant displacement of atoms Br(1)—Br(4) towards oxygen, the average of the set of Br—In—O angles being 85.6°. At the same time In—Br(2) and In—Br(4) bonds are noticeably shorter than the other three In—Br bonds, and close in length to those of $InBr_4(OH_2)_2^-$, but we can see no obvious explanation for this.

Vibrational spectroscopy

In the vibrational spectra of crystalline samples, bands due to the $Me_2N(C_2H_4)_2NMe_2^{2+}$ cation are readily identified by comparison with our measurements of the tetramethylpiperazonium halide salts in the solid state or in solution. These are reported and the assignment of the spectrum of this species is considered elsewhere (1). Remaining features are attributable to the $InBr_5(OH_2)^{2-}$ complex anion, and to the second water molecule which accompanies it in the crystal. Table 5 shows that the present spectrum closely resembles that of $Cs_2InBr_5(OH_2)$, reported by Adams and Lock (19) in a survey of some aquohalogeno complexes. Vibrational modes of the $InBr_5O$ unit, according to the idealised point group symmetry of C_{4v}, form the representation $4A_1 + 2B_1 + B_2 + 4E$ in which all species are Raman-active and A_1 and E species are also infrared-active, so that 8 of the 11 fundamentals should appear in both spectra. All these modes are anticipated to occur in the region below 400 cm^{-1}, with symmetric In—Br stretching expected to be close to the value of 172 cm^{-1} in $(MeNH_3)_4InBr_7$ which contains the octahedral $InBr_6^{3-}$ anion (5). The previous reports of $InBr_5(OH_2)^{2-}$ (9, 19, 20) did not give a detailed assignment. Our assignment in Table 5 is supported by comparison with the closely similar vibrational spectrum of $SbBr_5(OEt_2)$ which has a coordination sphere isoelectronic with $InBr_5O$ (21), and also takes advantage of single crystal Raman spectroscopy of the chloro complex $InCl_5(OH_2)^{2-}$ in the Cs^+ (22) and K^+ (16) salts. The infrared and Raman spectra of $InBr_5(OH_2)^{2-}$ are in reasonable agreement with predictions for C_{4v} symmetry. In particular we note that, although the pattern of In—Br bond lengths indicates that the structure is closer to

TABLE 5. Vibrational spectra of the $InBr_5(OH_2)^{2-}$ anion (cm^{-1})

$Me_2N(C_2H_4)_2NMe_2[InBr_5(H_2O)].H_2O$*		$Cs_2[InBr_5(H_2O)]$†		
Infrared	Raman	Infrared	Raman	Assignment‡
3500m,sh	3500w,sh	3500sh		$\nu(O—H)_{asym}$
3430s,br	3435wm	3425s		$\nu(O—H)_{sym}$
3280m,vbr	3280vw,br			$\nu(O—H)_{uncoord}$
1625w	1630vw			$\delta(HOH)_{uncoord}$
1593m, 1575w	1595vw	1576w		$\delta(HOH)$
540m,br		520m		$\rho_r(H_2O)$
		380ms		$\rho_w(H_2O)$
(265w)§	(265w)§	260ms	263wm	$\nu(In—OH_2)$, A_1
192vs	190w	190vs	193wm	$\nu(In—Br)$, E
177vs		175vs		$\nu(In—Br)$ out-of-phase, A_1
	170vs		172vs	$\nu(In—Br)$ in-phase, A_1
	165w,sh			$\nu(In—Br)$, B_1
145m	143m, 118w	148s, 121m	140ms, 115w,sh	$\delta(OInBr)$, $B_1 + E$
102s, 80w,sh	98s, 75m, 63w	100s, 79w, 64ms	102s, 76w, 63w	$\delta(BrInBr)$, $A_1 + B_2 + 2E$

*Bands due to cation are omitted.
†Reference 19.
‡Symmetry species are assigned on the basis of C_{4v} for $InBr_5O$.
§Overlapped by a cation band at 275 cm^{-1}.

C_{2v} than C_{4v} symmetry, the spectrum does not approach the number of bands (21 Raman, 19 ir) required by the lower symmetry. In contrast to the case of $K_2InCl_5(OH_2)$ (16), we observe no factor group splitting attributable to coupling within the centrosymmetric cell. This is not surprising since the bulky tetramethylpiperazonium cations will serve to isolate the anions from one another.

Six modes of $InBr_5(OH_2)^{2-}$ should involve the water molecule coordinated to indium. ν(In—O), which was tentatively located between 260 and 320 cm^{-1} in previous work (19, 20), is probably masked by a cation band at 275 cm^{-1}. A lower value, compared with 300–350 cm^{-1} in $InCl_5(OH_2)^{2-}$ salts (16, 19, 22), is matched by a significant increase in the In—O bond length from 2.224(9) Å in $InCl_5(OH_2)^{2-}$ (16) to 2.344(5) Å in $InBr_5(OH_2)^{2-}$. Other vibrations, namely the stretching, bending, rocking, and wagging modes of the coordinated water molecule, give rise to broad bands which are generally strong in ir and very weak in Raman spectra. All of these excepting the wagging mode are observed and readily assigned as in Table 5. The δ(HOH) bend has been noted as a useful indication of the purity of specimens of aquohalogen complexes since it is very sharp and has a characteristic frequency, e.g., 1576 cm^{-1} for salts containing $InBr_5(OH_2)^{2-}$ (19). With this criterion, and by comparison with the ir spectrum of $Cs_2[InBr_5(H_2O)]$ (19), the ν(O—H) and δ(HOH) frequencies belonging to the complex anion can be distinguished from those of the uncoordinated water molecule within the crystal, which are also assigned in Table 5. For this solvent molecule, ν(O—H) stretching is observed as a broad band, centred at the relatively low frequency of 3280 cm^{-1}, in accordance with the presence of hydrogen bonding which is also deduced from the crystallographic findings.

Acknowledgement

Support in the form of equipment grants from the New Zealand Universities' Grants Committee is gratefully acknowledged.

1. J. A. Creighton and M. J. Taylor. Can. J. Chem. To be submitted.
2. M. P. Hanson and R. A. Plane. Inorg. Chem. **8**, 746 (1969).
3. D. G. Tuck. Comprehensive coordination chemistry. Pergamon, Oxford. In press.
4. M. A. Khan, C. Peppe, and D. G. Tuck. Can. J. Chem. **62**, 1662 (1984).
5. J. Gislason, M. H. Lloyd, and D. G. Tuck. Inorg. Chem. **10**, 1907 (1971).
6. A. C. T. North, D. C. Phillips, and F. S. Mathews. Acta Crystallogr. A**24**, 351 (1968).
7. G. M. Sheldrick. SHELX-76 Program for Crystal Structure Determination, University Chemical Laboratory, Cambridge, U.K. 1976.
8. T. Jarv, J. T. Bulmer, and D. E. Irish. J. Phys. Chem. **81**, 649 (1977).
9. J. P. Wignacourt, G. Mairesse, P. Barbier, A. Lorriaux-Rubbens, and F. Wallart. Can. J. Chem. **60**, 1947 (1982).
10. M. A. Khan and D. G. Tuck. Acta Crystallogr. B**37**, 683 (1981).
11. M. Davis and D. Hassel. Acta Chem. Scand. **17**, 1181 (1963).
12. J. Lex and K.-H. Linke. Chem. Ber. **109**, 2684 (1976).
13. J. P. Wignacourt, G. Mairesse, and P. Barbier. Acta Crystallogr. B**36**, 669 (1980).
14. M. A. Khan and D. G. Tuck. Acta Crystallogr. B**37**, 683 (1981).
15. J. G. Contreras, F. W. B. Einstein, M. Gilbert, and D. G. Tuck. Acta Crystallogr. B**33**, 1648 (1977).
16. J. P. Wignacourt, A. Lorriaux-Rubbens, G. Mairesse, P. Barbier, and F. Wallart. Spectrochim. Acta, **36**A, 403 (1980).
17. M. Maeda and H. Ohtaki. Bull. Chem. Soc. Jpn. **50**, 1893 (1977).
18. K. Yamada, N. Weiden, and A. Weiss. J. Mol. Struct. **111**, 217 (1983).
19. D. M. Adams and P. J. Lock. J. Chem. Soc. A, 2801 (1971).
20. S. A. Cotton and J. F. Gibson. J. Chem. Soc. A, 1696 (1971).
21. C. J. Adams and A. J. Downs. J. Inorg. Nucl. Chem. **34**, 1829 (1972).
22. D. M. Adams and D. C. Newton. J. Chem. Soc. Dalton Trans. 681 (1972).

Phosphoryl to carbonyl migration of amino groups in mixed anhydrides

JILL SYMES AND TOMASZ A. MODRO[1]

Department of Organic Chemistry, University of Cape Town, Rondebosch 7700, South Africa

Received January 23, 1986

JILL SYMES and TOMASZ A. MODRO. Can. J. Chem. **64**, 1702 (1986).

Mixed anhydrides derived from carboxylic and amidophosphoric acids, $(RO)(R'_2N)P(O)OC(O)R''$ (**1**), undergo unimolecular fragmentation yielding carboxyamides, $R''C(O)NR'_2$, and metaphosphate esters, $ROPO_2$. The mechanism of the amino group transfer was studied for substrate **1***a* (**1**, R = R′ = Me; R″ = Ph); solvent as well as substituent effects indicate little (if any) charge development in the transition state. The effects of solvents and Lewis acids on the reaction rate and the activation parameters determined for **1***a* can be explained best in terms of stabilizing interactions with either carboxyamide or metaphosphate being formed in the course of reaction. The transfer of a functional group from one acyl center to another was investigated for other anhydride systems and the relative contributions of the fragmentation vs. disproportionation of substrates are discussed.

JILL SYMES et TOMASZ A. MODRO. Can. J. Chem. **64**, 1702 (1986).

Les anhydrides mixtes, $(RO)(R'_2N)P(O)OC(O)R''$ (**1**), obtenus à partir d'acides carboxyliques et d'acides amidophosphoriques subissent des fragmentations unimoléculaires conduisant aux carboxyamides, $R''C(O)NR'_2$, et aux esters métaphosphates, $ROPO_2$. On a étudié le mécanisme de transfert du groupement aminé dans le substrat **1***a* (**1**, R = R′ = Me; R″ = Ph); les effets de solvant ainsi que les effets de substituant indiquent qu'il n'y a que peu (s'il en existe) de développement de charge dans l'état de transition. Dans le cas du composé **1***a*, on a déterminé les effets des solvants et des acides de Lewis sur les vitesses de réaction et sur les paramètres d'activation; les meilleures explications pour ces résultats sont basées sur les interactions stabilisantes qui se forment au cours de la réaction soit avec le carboxyamide ou le métaphosphate. On a étudié le transfert d'un groupement fonctionnel d'un centre acyle à un autre dans d'autres systèmes d'anhydrides et on discute des contributions relatives à la fragmentation des substrats par rapport à leur disproportionation.

[Traduit par la revue]

The ability of a functional group, such as alkyl ester OR, to migrate from one phosphoryl centre to another in a phosphoric anhydride was noticed as early as 1914 (1), when the formation of trialkyl phosphates was found to occur on thermal decomposition of tetraalkyl pyrophosphates. Reorganisation between structural units in an anhydride system was confirmed in later studies (2) on the polyphosphate esters with insecticidal properties. In the case of mixed anhydrides of dialkylphosphoric and carboxylic acids the major reaction is the disproportionation to a pair of symmetrical anhydrides; the reaction has been used (3) as a synthetic route to tetraalkyl pyrophosphates. It was reported, however (3), that when the mixed anhydrides contained a dialkylamide group, a considerable quantity of *N,N*-dialkylcarboxyamide was also formed, e.g.:

$$(Me_2N)_2P(O)OC(O)Me \xrightarrow{\Delta} Me{-}C(O)NMe_2$$

SCHEME 1

In consequence, acyl phosphates can undergo fragmentation according to two independent pathways; (*i*) the (necessarily) bimolecular disproportionation to symmetrical anhydrides; (*ii*) the fragmentation (possibly unimolecular) occurring within the anhydride framework and involving the transfer of a functional group from the phosphoryl to the adjacent acyl centre. The stoichiometry of this fragmentation (Scheme 2) requires reduction of the coordination number of phosphorus and the formation of (besides the carboxyderivative **2**) the metaphosphate-type product **3**.

While the phosphoramidate function shows high migratory reactivity in mixed anhydrides (see Scheme 1), N-substituted pyrophosphoramides of the Schradan type appear to be thermally stable (4). Thermal disproportionation leading to symmetrical anhydrides is characteristic of dialkylacyl phosphates (2), but mixed carboxylic–dihalophosphoric anhydrides, $RC(O)OP(O)X_2$

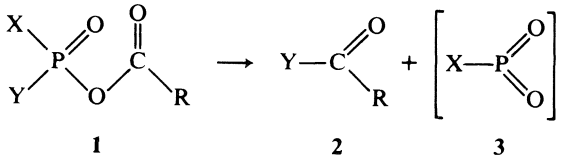

1 **2** **3**

SCHEME 2

(X = F, Cl) yield upon distillation acyl halides RC(O)X (5). It seems, therefore, that the migratory aptitude of a group bonded to phosphorus in an anhydride system is a complex function of the nature of both the migrating group and the acceptor acyl centre. Although the chemistry of acyl phosphates has been extensively investigated with respect to their reactivity towards nucleophiles (6), no systematic studies have been carried out on the fragmentations of these diacyl systems under non-nucleophilic conditions. In this paper we report our results on the rearrangement of phosphoric–carboxylic anhydrides containing a phosphoramidate group (**1**, Y = NRR′).

Results and discussion

We have reported recently (7) that the reaction between tetramethylammonium salts of N-substituted methylphosphoramidic acids **4***a,b*, with benzoyl chloride (**5***a*) results in a facile and quantitative conversion to the corresponding N-substituted benzamide derivatives, **6***a,b* (Scheme 3). In the present work we extended this reaction to substrates containing secondary phosphoramidate functions (**4***c,d,e*) and found that they react smoothly with acetyl chloride yielding the corresponding acetamides (**6***c,d,e*). The obvious implication of Scheme 3 is that the initial reaction between **4** and **5** results in the formation of the mixed phosphoric–carboxylic anhydrides (**1**, R = Ph, Me; X = OMe; Y = NR′R″), which subsequently rearrange according to Scheme 2, yielding the carboxyamides **2** (Y = NR′R″). We therefore concentrated our further investigation on a selected pair of substrates (**4***a*, **5***a*) to demonstrate the

[1]Author to whom correspondence should be addressed.

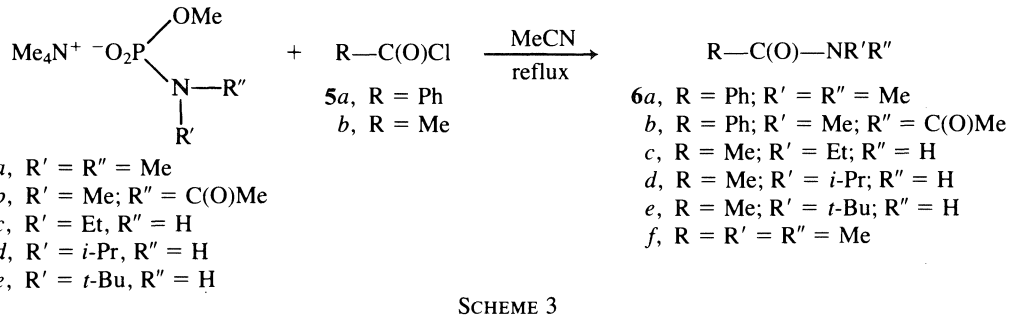

SCHEME 3

intermediate formation of the anhydride **1***a* (**1**, R = Ph; X = OMe; Y = NMe_2) and to study the mechanism of its fragmentation.

When **4***a* and **5***a* are allowed to react at room temperature, the only product obtained (after filtration of $Me_4N^+Cl^-$) is the expected mixed anhydride **1***a*. Although this compound can be stored in a refrigerator for several weeks, it decomposes slowly at room temperature, yielding *N*,*N*-dimethylbenzamide (**6***a*) and the polymeric, phosphorus-containing material, probably a product of self-condensation of methyl metaphosphate (**3***a*, X = OMe). The fragmentation can easily be followed by ^{1}H nmr spectroscopy due to the disappearance of the *N*-methyl signal of the P(O)NMe_2 group in **1***a* (δ 2.80, d, J_{HP} 11 Hz), and the appearance of the *N*-methyl signal of **6***a* (δ 3.0, br s). Under no circumstances were we able to detect any formation of methyl benzoate, i.e. a product expected from the migration of the OMe group in **1***a* rather than the NMe_2 group to the benzoyl carbon atom (Scheme 4).

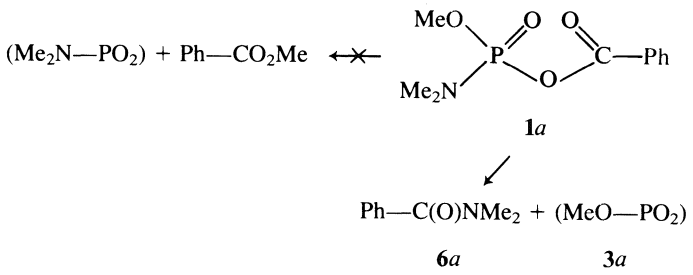

SCHEME 4

If the fragmentation of **1***a* presented in Scheme 4 is a unimolecular process, it yields initially **3***a* in its monomeric form. In order to obtain evidence for the formation of "free" **3***a*, we carried out the trapping experiment described by Clapp and Westheimer (8), involving phosphorylation of *N*-methylaniline by the metaphosphate species (Scheme 5). When **1***a* was heated at 50°C in CD_3CN in the presence of 2.5 mol-equivalents of *N*-methylaniline for 60 h, the ^{1}H nmr of the solution revealed complete disappearance of the substrate and the formation (in addition to **6***a*) of the salt **4***f* whose spectroscopic features were identical to those reported in the literature (8).

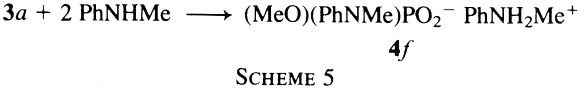

SCHEME 5

Rate measurements

The changes in the ^{1}H nmr spectra of solutions of **1***a* that accompany its conversion to **6***a* (Scheme 3) could also be employed in determination of the rates of fragmentation. As can be seen from Table 1, which shows the effect of substrate concentration on the rate of fragmentation, the reaction follows first-order kinetics.

TABLE 1. Rates of formation of **2***a* from **1***a* at 68.0°C

[Substrate] (*M*)	Solvent	$10^6 k_1$[a] (s^{-1})	*r*	$10^6 k_2$[a] ($M^{-1}s^{-1}$)	*r*
0.182	Acetone-d_6	1.95	0.994	2.43	0.993
0.364	Acetone-d_6	1.85	0.992	1.18	0.990
		Average: 1.90 ± 0.07		Average: 1.805 ± 0.88	
0.187	$CDCl_3$	1.49	0.994	1.86	0.988
0.373	$CDCl_3$	1.65	0.988	1.04	0.986
		Average: 1.57 ± 0.11		Average: 1.45	± 0.58

[a]Calculated according to the first- and second-order rate law, respectively.

The unimolecular collapse of anhydrides **1** may proceed according to a variety of mechanistic patterns, from a fully concerted pathway to the stepwise mechanism, involving a charge-separated intermediate. These two extreme cases are presented for **1***a* in Scheme 6. To provide experimental evidence for the "concerted" or "charge-separated" type of mechanism of fragmentation, we measured the rates of P → C dimethylamine group transfer in **1***a* as a function of reaction medium, temperature, catalyst, and substituents introduced to the benzene ring.

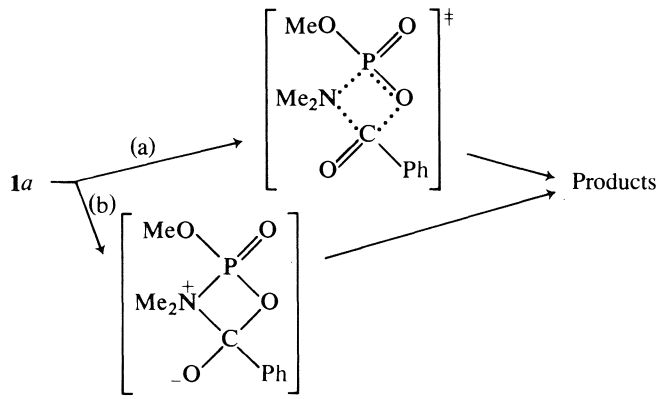

SCHEME 6

Table 2 lists rate constants obtained for fragmentation of **1***a* (Scheme 4) in four solvents and at different temperatures. Because of the rapid solvolysis of the anhydride linkage in **1**, the choice of reaction media was obviously limited to non-hydroxylic solvents, and because of the kinetic method, only deuterated solvents were used. The accuracy of the kinetic measurements is not very high. There are at least two reasons for the relatively poor reproducibility of the individual k_1 values. Firstly, since the formation of **6***a* is slow (typical value for $t_{\frac{1}{2}}$ is at least 1 week), it is difficult to exclude participation of any competing reactions for **1***a*, such as nucleophilic cleavage of the anhydride system, or the disproportionation process. Secondly,

TABLE 2. Rates of formation of **2***a* from **1***a*; [substrate] = 0.18 *M*

Temperature (°C)	$10^6 \times k_1$ (s^{-1})[a]			
	CCl_4	$CDCl_3$	$(CD_3)_2CO$	CD_3CN
45	0.34	0.18	0.48	0.83
50				2.07
58		0.72		
62	0.45	1.51	1.17	4.22
68			1.90	
71		4.56		
72	0.89		2.94	11.4

[a]Average of two runs; ± ≤10%.

TABLE 3. Substituent effects on the rate of fragmentation of mixed anhydrides (**1**, X = MeO, Y = NMe_2; R = *p*-Z-C_6H_4); $CDCl_3$, 70°C

Substrate	Z	$10^6 k_1$ (s^{-1})
1*a*	H	5.1
1*b*	MeO	4.1
1*c*	Cl	2.2
1*d*	NO_2	2.4

fragmentation of **1***a* is subject to the catalytic effect of a variety of species (*vide infra*), so traces of impurities present in the substrate or in the reaction medium can affect the reaction rate. The general trend for the medium effects on reaction rate can, nevertheless, be obtained; the rate of fragmentation decreases in the following order of solvents employed: $CD_3CN > (CD_3)_2CO \approx CDCl_3 > CCl_4$. The variations in the k_1 values are, however, small (the maximum value of k_{rel}, $k_{CD_3CN}/k_{CCl_4} \approx 13$) and the observed order of reactivities follows only approximately the usual (9) solvent polarity scales. The small effect of solvents on the rate of fragmentation of **1***a* would support the mechanism involving the isopolar transition state (Scheme 6, path a). For comparison, a concerted fragmentation of 3-methyl-2,5-dihydrothiophen-1,1-dioxide shows almost negligible dependance on solvent change ($k_{sulfolane}/k_{n\text{-decane}} = 1.8$) (10), while the thermolysis of α-chlorobenzyl methyl ether, involving formation of the chloride–oxocarbonium ion pair, is subject to a dramatic solvent effect ($k_{CH_3CN}/k_{CCl_4} = 166\,000$) (11). Additional support for the mechanism involving little (if any) charge development in the transition state for the fragmentation was obtained from the substituent effects on the reaction rate (Table 3). Not only does substitution involving a change of 1.05 σ units (substrates **1***d* and **1***b*) result in merely a 1.7-fold variation in the rate, but the observed order of reactivities does not reflect the electron-donating or -withdrawing properties of substituents Z.[2] In the absence of any correlation of k_1 values with substituent constants σ_z, we attribute small variations in reaction rate listed in Table 3 to solvation effects of substituents Z, which can possibly influence the conformational flexibility of the anhydride system **1**, necessary for the amino group transfer to occur.

During the initial experiments on the fragmentation reaction it had been noted that the rate of benzamide formation depended on the presence of other species, e.g. the unreacted acyl chloride used for the preparation of **1**. We have determined the effect of added benzoyl chloride on the rate of fragmentation of pure **1***a*, and have supported the data by demonstrating the catalytic effect of another Lewis acid, iodine, on the reaction rate. The results are given in Table 4.

TABLE 4. Rates of formation of **2***a* from **1***a* at 45°C; initial concentration of **1***a* = 0.28 *M*

Solvent	Catalyst (*M*)	$10^6 k_1$ (s^{-1})	k_{rel}
$CDCl_3$	—	0.144	1
	5*a* (0.065)	1.40	9.7
	5*a* (0.26)	1.67	11.6
CCl_4	—	0.35	1
	I_2 (0.033)	1.64	4.7
	I_2 (0.118)	2.49	7.1

TABLE 5. Activation parameters for first-order fragmentation of **1***a*

Solvent	r^a	$\Delta H^{\ddagger}$/kcal mol^{-1}	$\Delta S^{\ddagger}$/cal K^{-1} mol^{-1}
$CDCl_3$	0.995	27.3 ± 2.0	−4.0 ± 5.6
CD_3CN	0.999	20.7 ± 0.7	−21.4 ± 4.8
$(CD_3)_2CO$	0.985	13.5 ± 2.0	−42.6 ± 5.0

[a]Correlation coefficient for the slope of the ln k_1 *vs.* 10^3 $1/T$ plot.

In our opinion, the most plausible explanation for the catalytic effects presented in Table 4 is the stabilizing interaction between the added Lewis acid and the incipient benzamide molecule being formed via the transition state depicted in Scheme 6 (path a). The equilibrium constants for complexation of a variety of covalent halide compounds and carboxylic amides are of the order of $K = 10^2$–10^3 (13), and the formation of the adduct of **6***a* with iodine in CCl_4 at 25°C was found to be accompanied by a free energy change of −0.8 kcal/mol (14).

Rate data included in Table 2 enabled us to calculate activation parameters for the fragmentation of **1***a* in three solvents ($CDCl_3$, acetone-d_6, CD_3CN) (Table 5); the accuracy of the kinetic measurements in CCl_4 was too low to prepare a reliable Arrhenius plot.

It can be seen from Table 5 that the decrease in the enthalpy of activation on moving from chloroform to acetone is largely compensated by the unfavourable change in activation entropy, resulting in small and ill-defined solvent effects on the reaction rate. The observed variations in the $\Delta S^{\ddagger}$ values indicate that in the chloroform–acetonitrile–acetone series a higher degree of solvent organisation is achieved in the transition state (relative to the initial state). We attribute these entropy changes to increasing nucleophilic solvation of the incipient methyl metaphosphate, effectively "freezing out" solvent molecules. Metaphosphate species are highly electrophilic by virtue of their readily accessible σ* and π* unoccupied orbitals (15), and their donor–acceptor interactions with solvents such as acetonitrile, as well as electrophile–nucleophile reactivity with respect to ketones, are well documented (16). Since ketones are stronger bases than nitriles, both in terms of HBA (17) and Brønsted (18) basicity, they also may be expected to interact more strongly than nitriles with such a powerful Lewis acid as $MeOPO_2$. As a result, activation entropy for NMe_2 group transfer is not far from zero for the poorly solvated transition state in $CDCl_3$ (and similar in magnitude to that obtained for thermal α,β-elimination of alkyl acetates (19)), but is highly negative in

[2]It may be noted at this point that the addition of semicarbazide (N-nucleophile) to aromatic aldehydes follows the Hammett equation with ρ = 0.9 (12).

acetone, where solvent molecules become involved in nucleophilic solvation of the metaphosphate formed. Solvent effects on the magnitude of the free enthalpy of activation are, however, large; $\Delta H^{\neq}$ is reduced by half when chloroform is replaced by acetone, and the intermediate value was obtained in acetonitrile. This result indicates that some polarity in the transition state (or intermediate) may be responsible for the observed dependence of $\Delta H^{\neq}$ on solvent polarity.[3] The order of the decrease in the $\Delta H^{\neq}$ values (Table 5) does not follow, however, the polarity of solvents involved, which increases in the order: chloroform < acetone < acetonitrile (9). This suggests that specific rather than general solvent effects operate in the transition state, with acetone being most effective in stabilizing the incipient metaphosphate product. It seems therefore that solvent effects on the activation parameters of the fragmentation are based on Lewis acid–base rather than dipole–dipole interactions.

In summary, we believe that the reaction represented in Scheme 4 probably does not involve significant charge development in the transition state (in the sense of distinct addition–elimination steps as shown in pathway b, Scheme 6), but is subject to both Lewis acid catalysis and nucleophilic solvation effects as a consequence of the nature of the reaction products.

Mixed anhydrides **1**, used as precursors for carboxyamides **6** (Scheme 3) were prepared by condensation of phosphate salts with carboxylic acid chlorides. The same anhydrides and, consequently, the same fragmentation products could be obtained by treating carboxylic salts with the corresponding phosphorochloridates. We have prepared **1***a* by the latter route, and decomposed it *in situ* to the expected product **6***a*. In this case, however, the reaction mixture contained small quantities of a new product that was absent in previous experiments, and which was subsequently identified as methyl *N,N,N',N'*-tetramethylphosphorodiamidate (**9**). The formation of this product can only be explained by partial disproportionation of **1***a* to benzoic anhydride and the pyrophosphoric diester diamide **8**, which then undergoes fragmentation with NMe_2 group transfer from one phosphoryl centre to another, yielding diamidoester **9** (Scheme 7).

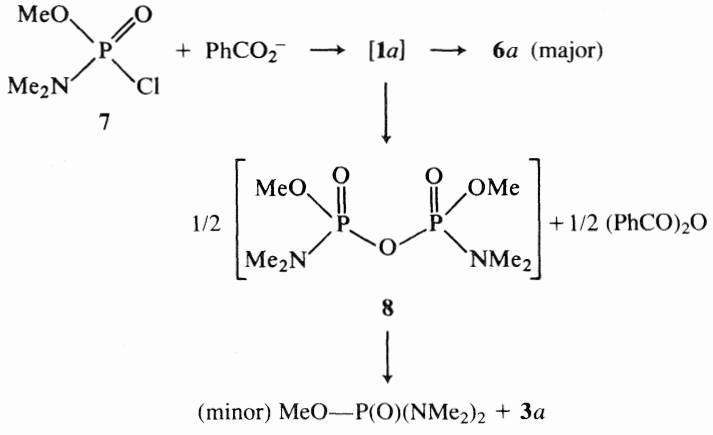

SCHEME 7

This result indicates that the selectivity in the non-nucleophilic cleavage (fragmentation vs. disproportionation) of the mixed anhydrides of the type **1** can be a sensitive function of reaction conditions and (or) the composition of the reaction mixture.

Related systems

Fragmentation represented in Scheme 2 has also been confirmed for anhydrides derived from diamidophosphoric acid. Mixed anhydride **1***e* (**1**, R = Ph; X = Y = NMe_2) has been prepared from benzoyl chloride and the tetramethylammonium salt of tetramethyldiamidophosphoric acid (**10**) and was found to yield, upon heating, benzamide (**6***a*), in a manner analogous to that of **1***a* (Scheme 8).

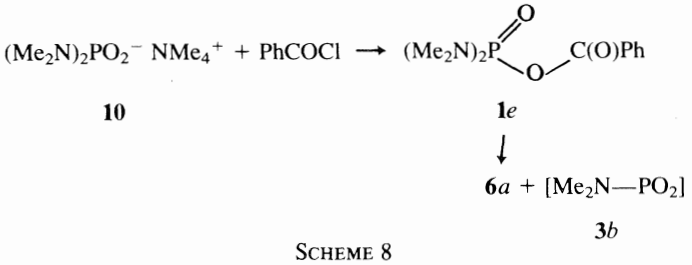

SCHEME 8

Reactivity of **1***e* relative to that of **1***a* is given in Table 6. The observed rate enhancement can be attributed to the greater stability (21) of the nitrogen-substituted metaphosphate systems, as compared with the PO_3-type species; such a difference should also be reflected in the transition states leading to products **3***a* and **3***b*, respectively.

In mixed anhydrides derived from dialkylphosphates (**1**, X = Y = OR), no migration of an alkoxy group OR from phosphoryl to carbonyl functions was observed. Dimethylbenzoyl phosphate **1***f* (**1**, R = Ph; X = Y = OMe), prepared either by condensation of dimethyl phosphorochloridate with benzoate anion (22) or from benzoyl chloride and dimethyl phosphate salt, disproportionated thermally to benzoic anhydride and tetramethyl pyrophosphate, but no methyl benzoate could be detected within the accuracy of ^1H nmr spectroscopy and tlc (thin-layer chromatography). Similarly, dimethylacetyl phosphate **1***g* (**1**, R = Me; X = Y = OMe), prepared from trimethyl phosphate and acetyl chloride (23), could be distilled, but upon storing at room temperature for a period of 6 months yielded significant quantities of acetyl anhydride and tetramethyl pyrophosphate with no evidence for any methyl acetate formed.

It seems, therefore, that the migratory (phosphoryl to carbonyl) aptitude of an amino group in a mixed anhydride system is much higher than that of an alkoxy substituent. Simple calculations, based on the magnitudes of the energies of the bonds being broken or formed during the fragmentation, show that the bond-energy changes that accompany amino group migration are ca. 18 kcal mol^{-1} more favourable than those expected for the OR group transfer. This difference could be responsible for shifting the reactivity of mixed anhydrides of the

TABLE 6. Rates of formation of **2***a* from **1***e* at 45.0°C

Solvent	$10^6 k_1$ (s^{-1})	r	k_{rel}[a]
CCl_4	3.50	0.983	5
$CDCl_3$	4.31	0.994	12
$(CD_3)_2CO$	5.97	0.985	6
CD_3CN	6.86	0.991	4

[a]Relative to **1***a*, after correcting to a single NMe_2 group.

[3]MO calculations on the fragmentation represented in Scheme 2 (**1**, X, Y = NH_2, OH; R = H) are currently being carried out (20). Although the results confirm in principle the concerted mechanism with no distinct intermediate occurring along the reaction coordinate, dipole moments calculated for the substrate, transition states, and products indicate some charge separation in the course of the reaction.

1*a*–**1***e* type towards the intramolecular amino group transfer rather than the bimolecular disproportionation reaction.

Experimental

Melting points (uncorrected) were determined on a Fisher–Johns apparatus. The ^{1}H nmr spectra were recorded on 60-MHz Varian EM 360 and 100-MHz Varian XL 100 spectrometers with TMS or DDS as internal standards. Aluminium-backed silica gel plates (Merck, Kieselgel 60 F_{254}) were used for tlc. Gas chromatography (gc) was performed on a gas chromatography Q Carlo Erba 4200 instrument using a 2-m column packed with 3% silicone SE-30 (G.C. Grade), and He as a carrier gas; FID, injection and detection temperature 250°C; ethyl benzoate as internal standard. Analyses for C, H, and N were carried out at the University of Cape Town. All solvents and commercial reagents were dried and purified by conventional means before use.

Materials

Dimethylphosphorochloridate was prepared from PCl_3, MeOH, and SO_2Cl_2 (24); 63%, bp 45°C (2 Torr) (lit. (24) bp 55–57°C (2–3 Torr) (1 Torr = 133.3 Pa)); ^{1}H nmr ($CDCl_3$) δ: 3.98 (d, J_{HP} 14 Hz). Methyl-*N*,*N*-dimethylphosphoroamidochloridate (**7**) was prepared from methylphosphorodichloridate and two equivalents of dimethylamine in ether with cooling in Dry Ice. Oil (69%); ^{1}H nmr ($CDCl_3$) δ: 2.72 (6H, d, J_{HP} 13 Hz, NMe_2), 3.85 (3H, d, J_{HP} 15 Hz, OMe). Tetramethylphosphorodiamidochloridate was prepared from $POCl_3$ and four equivalents of dimethylamine (25); 88%, bp 70–72°C (0.6 Torr) (lit. (25) bp 79–82°C (0.6 Torr)); ^{1}H nmr ($CDCl_3$) δ: 2.70 (d, J_{HP} 13 Hz). Dimethyl-*N*,*N*-dimethylphosphoramidate was prepared from dimethylphosphorochloridate and two equivalents of dimethylamine (26); 71%, bp 33°C (0.2 Torr) (lit. (26) bp 72°C (11 Torr)); ^{1}H nmr ($CDCl_3$) δ: 2.75 (6H, d, J_{HP} 10 Hz, NMe_2), 3.72 (6H, d, J_{HP} 11 Hz, OMe). Methyl-*N*,*N*,*N*′,*N*′-tetramethylphosphorodiamidate was prepared from the diamidochloridate and sodium methoxide in methanol; 44%, bp 46–48°C (0.5 Torr); ^{1}H nmr ($CDCl_3$) δ: 2.65 (12H, d, J_{HP} 10 Hz, NMe_2), 3.60 (3H, d, J_{HP} 11 Hz, OMe). Dimethyl-*N*-alkylphosphoramidates, $(MeO)_2P(O)NHR$, were prepared from dimethylphosphorochloridate and two equivalents of the corresponding amine in ether. After filtration, ethereal solutions were washed with water and dried, the solvent removed, and the products were used in further steps without purification; ^{1}H nmr ($CDCl_3$), R = Et, δ: 1.12 (3H, t, J_{HH} 7 Hz, β-Me), 2.97 (3H, m, CH_2 and N-H), 3.66 (6H, d, J_{HP} 11 Hz, OMe); R = i-Pr, δ: 1.18 (6H, d, J_{HH} 7 Hz, β-Me), 3.30 (1H, m, CH), 3.69 (6H, d, J_{HP} 12 Hz, OMe); R = *t*-Bu, δ: 1.28 (9H, s, β-Me), 3.70 (6H, d, J_{HP} 11 Hz, OMe).

Tetramethylammonium phosphates **4***a*,*c*,*d*,*e*, and $(MeO)_2PO_2^-$ NMe_4^+ were prepared according to the following procedure: 0.013 mol of a substrate was dissolved in 8 mL of dry acetonitrile and 14.5 mL of 5.4 *M* solution of trimethylamine in dry acetonitrile (ca. 6 mol-equivalents) were added. The solution was sealed in a glass tube and heated at 80°C overnight. After cooling, the precipitate was filtered off, washed quickly with cold, dry acetonitrile, and stored in a desiccator over P_4O_{10}. **4***a*: 76% (very hygroscopic); ^{1}H nmr (D_2O) δ: 2.60 (6H, d, J_{HP} 8 Hz, NMe_2), 3.21 (12H, s, NMe_4^+), 3.51 (3H, d, J_{HP} 10 Hz, OMe). *Anal.* calcd. for $C_7H_{21}N_2O_3P$: C 39.6, H 9.9, N 13.2%; found: C 39.1, H 9.9, N 14.3%. **4***c*, ^{1}H nmr (D_2O) δ: 1.09 (3H, t, J_{HH} 7 Hz, β-Me), 2.82 (2H, m, CH_2), 3.18 (12H, s, NMe_4^+), 3.45 (3H, d, J_{HP} 10 Hz, OMe). **4***d*, ^{1}H nmr (D_2O) δ: 1.09 (6H, d, J_{HH} 3 Hz, β-Me), 2.88 (1H, m, CH), 3.15 (12H, s, NMe_4^+), 3.75 (3H, d, J_{HP} 11 Hz, OMe). **4***e*, ^{1}H nmr (D_2O) δ: 1.25 (9H, s, β-Me), 3.20 (12H, s, NMe_4^+), 3.70 (3H, d, J_{HP} 11 Hz, OMe). $(MeO)_2PO_2^-$ NMe_4^+: 64% (as a monohydrate); ^{1}H nmr (D_2O) δ: 3.18 (12H, s, NMe_4^+), 3.55 (6H, d, J_{HP} 11 Hz, OMe).

Salt **10** could not be prepared in the same way since the starting methyl-*N*,*N*,*N*′,*N*′-tetramethylphosphorodiamidate proved unreactive towards demethylation by trimethylamine. **10** was prepared in the following way: $(Me_2N)_2P(O)Cl$ (0.022 mol) was added slowly with cooling and stirring to the aqueous solution of two mol-equivalents of tetramethylammonium hydroxide. Stirring was continued for 3 h, water was removed under reduced pressure, and the residue was dried by adding three times 20 mL of benzene and distilling to dryness. The final product consisted of equimolar quantities of **10** and NMe_4^+ Cl^-; 99.5%; ^{1}H nmr (D_2O) δ: 2.50 (12H, d, J_{HP} 10 Hz, PNMe), 3.10 (24H, s, NMe_4^+). *Anal.* calcd. for $C_{12}N_{36}N_4O_2PCl$: C 43.0, H 10.8, N 16.7%; found: C 42.5, H 11.1, N 15.7%. This product was used for the synthesis of **1***e* without further purification.

6*a* was prepared by adding benzoyl chloride to the solution of the equimolar quantity of dimethylammonium chloride in water containing three equivalents of NaOH, extracting with benzene, and removing benzene under reduced pressure; 85%; mp 40–42°C; ^{1}H nmr ($CDCl_3$) δ: 3.00 (6H, br s, NMe_2), 7.35 (5H, s, Ph). *Anal.* calcd. for $C_9H_{11}NO$: C 72.5, H 7.4, N 9.4%; found: C 72.6, H 7.4, N 9.4%. **6***f* was prepared by adding acetyl chloride to the solution of ca. 2.5 mol-equivalents of dimethylamine in ether, leaving the solution overnight, filtering, removing ether, and distilling the crude product; 20%; bp 34°C (0.2 Torr); ^{1}H nmr ($CDCl_3$) δ: 2.09 (3H, s, MeCO), 2.98 (6H, d, NMe_2). *Anal.* calcd. for C_4H_9ON: C 55.2, H 10.3, N 16.1%; found: C 54.6, H 10.3, N 15.8%.

Formation of amides **6** from salts **4** and acid chlorides **5** (Scheme 3): 1 mmol of **5** was added to a suspension of 1 mmol of **4** in 12 mL of dry acetonitrile and the mixture was stirred and heated under reflux for 4 h. After cooling, the white precipitate ($NMe_4^+Cl^-$) and glassy material (presumably polymeric methyl metaphosphate) were removed by filtration, washed with acetonitrile, and the solvent removed under reduced pressure. Examination of the residue by ^{1}H nmr ($CDCl_3$), tlc, or gc indicated that amides **6** were the only products present. Individual products were identified by comparison with authentic samples or by comparing their ^{1}H nmr spectra with those reported in the literature (27).

Synthesis of mixed anhydrides **1**

1*a*: **4***a* (3.5 mmol) was suspended in dry acetonitrile (20 mL) and a solution of **5***a* (2.6 mmol) in acetonitrile (20 mL) was added dropwise with stirring at room temperature. Stirring was continued for 3 h, dry CCl_4 (10 mL) was added, the mixture was filtered, and the solvent was removed under reduced pressure. CCl_4 (10 mL) was added, the mixture filtered again, and solvent removed. The resultant product was stored in the refrigerator; 93% (based on **5***a*); oil; ^{1}H nmr ($CDCl_3$) δ: 2.80 (6H, d, J_{HP} 11 Hz, NMe_2), 3.90 (3H, d, J_{HP} 12 Hz, OMe), 7.45 (3H, m, *m*+*p* arom.), 8.10 (2H, m, *o*-arom.). *Anal.* calcd. for $C_{10}H_{14}NO_4P$: C 49.4, H 5.8, N 5.8%; found: C 49.2, H 5.9, N 5.8%. Anhydrides **1***b*–**1***f* were prepared in the analogous way. **1***b*: oil; ^{1}H nmr ($CDCl_3$) δ: 2.75 (6H, d, J_{HP} 11 Hz, NMe_2), 3.85 (3H, s, C-OMe), 3.88 (3H, d, J_{HP} 11 Hz, P-OMe), 6.95 (2H, d, J_{HH} 10 Hz, 3,5-H_2), 8.05 (2H, d, J_{HH} 10 Hz, 2,6-H_2). *Anal.* calcd. for $C_{11}H_{16}NO_5P$: C 48.4, H 5.9, N 5.1%; found: C 47.8, H 6.2, N 5.1%. **1***c*: solid; ^{1}H nmr ($CDCl_3$) δ: 2.78 (6H, d, J_{HP} 11 Hz, NMe_2), 3.85 (3H, d, J_{HP} 12 Hz, OMe), 7.35 and 8.00 (2 × 2H, d, J_{HH} 10 Hz, 3,5-H_2 and 2,6-H_2). *Anal.* calcd. for $C_{10}H_{13}NO_4ClP$: C 43.2, H 4.7, N 5.0%; found: C 43.2, H 4.8, N 5.2%. **1***d*: solid; ^{1}H nmr ($CDCl_3$) δ: 2.80 (6H, d, J_{HP} 11 Hz, NMe_2), 3.92 (3H, d, J_{HP} 12 Hz, OMe), 8.33 (4H, m, arom.-H). *Anal.* calcd. for $C_{10}H_{13}N_2O_6P$: C 41.7, H 4.5, N 9.7%; found: C 41.8, H 4.8, N 9.8%. **1***e*: oil; ^{1}H nmr ($CDCl_3$) δ: 2.85 (12H, d, J_{HP} 11 Hz, NMe_2), 7.60 (3H, m, *m*+*p* arom.), 8.20 (2H, m, *o*-arom.). Since **1***e* always contained small quantities of $NMe_4^+Cl^-$, no satisfactory analysis was obtained for this product. **1***f*: oil; ^{1}H nmr ($CDCl_3$) δ: 3.95 (6H, d, J_{HP} 12 Hz, OMe), 7.45 (3H, m, *m*+*p* arom.), 8.10 (2H, m, *o*-arom.). *Anal.* calcd. for $C_{10}H_{11}O_5P$: C 47.0, H 4.8%; found: C 45.8, H 4.8%.

Reaction of **3**a *with* N-*methylaniline* (Scheme 5)

1*a* (20 μL) and *N*-methylaniline (22 μL) were dissolved in CD_3CN (0.4 mL) in the nmr tube; the tube was sealed and heated in a water bath at 50°C for 59 h. The final spectrum showed complete disappearance of **1***a* and the presence of signals expected for **6***a* and the salt **4***f*. Products **6***a* and **4***f* were identified by comparing the ^{1}H nmr spectrum of the reaction solution with the ^{1}H nmr characteristics of **6***a* obtained for the authentic sample of this compound, and of **4***f*, as reported in the literature (8). **6***a*, δ: 3.05 (6H, br s), 7.40 (5H, s). **4***f*, δ: 2.90 (3H, s,

NMe^+), 3.20 (3H, d, J_{HP} 9 Hz, P-NMe), 3.70 (3H, d, J_{HP} 11 Hz, OMe), 7.20 (10H, m, 2 × Ph) (lit. (8) δ: 2.9 (3H, s), 3.2 (3H, d, J_{HP} 8 Hz), 3.7 (3H, d, J_{HP} 12 Hz), 7.3 (10H, m)).

Reaction of ***7*** *with benzoic acid* (Scheme 7)

A solution of **7** (13 mmol) in acetonitrile (30 mL) and ether (10 mL) was added dropwise with stirring and cooling to a solution of benzoic acid (10 mmol), triethylamine (6 mmol), and DMF (10 mmol) in acetonitrile (30 mL). The mixture was then heated under reflux for 1 h, ether (50 mL) was added, the mixture was filtered, and solvents were removed under reduced pressure. The oily product was dissolved in chloroform (35 mL), washed with water (3 × 20 mL), dried, and evaporated under reduced pressure. The ^{1}H nmr of the product indicated the presence of ***6a*** (δ 3.05, 6H, br s; 7.4–8.1, 5H, m) and another, phosphorus-containing product (δ 2.68, 12H, d, *J* 10 Hz; 3.68, 3H, d, *J* 11 Hz). The product was separated by gc yielding **9** (9%, t_R 4.6 min) and ***6a*** (58%, t_R 9.7 min), which were identified by comparison with authentic samples.

Reaction of ***10*** *with* ***5****a* (Scheme 8)

10 (9.8 mmol) was suspended in dry acetonitrile (10 mL) and a solution of ***5a*** (6.6 mmol) in acetonitrile (15 mL) was added dropwise with stirring. The mixture was then heated under reflux for 4 h, cooled, filtered, and the solvent removed under reduced pressure. The resultant solid product was recrystallized from petroleum ether (bp 30–40°C) and identified as ***6a***; mp 39–41°C. When the reaction was carried out at room temperature and aliquots (4 mL) were withdrawn at intervals and worked up as before, the intermediate formation of ***1e*** was demonstrated by ^{1}H nmr spectroscopy (δ 2.80, 12H, d, J_{HP} 11 Hz, NMe_2).

Reaction of $(MeO)_2PO_2^-$ *with* ***5****a*

Tetramethylammonium dimethylphosphate (1.5 mmol) was suspended in dry acetonitrile (15 mL) and ***5a*** (1.55 mmol) in acetonitrile (15 mL) was added with stirring at room temperature. Stirring was then continued at room temperature for 3.5 h with removal of aliquots (4 mL) at various times; all aliquots were filtered, evaporated under reduced pressure, and the residue examined by ^{1}H nmr spectroscopy ($CDCl_3$). After carrying out the reaction for 3.5 h at room temperature, the mixture was heated under reflux for 4 h, again with removal of aliquots, which were worked up as before. Spectra obtained before heating showed the appearance of a new product (δ 3.99, d, J_{HP} 10 Hz), identified as dimethylbenzoyl phosphate. After 1 h of heating under reflux, however, this product had disappeared almost entirely and a new product had appeared (δ 3.72, d, J_{HP} 10 Hz), and remained unchanged over the period of further heating. This product was identified as tetramethyl pyrophosphate. No methyl benzoate or trimethyl phosphate were found in the reaction mixture, as demonstrated by the addition of authentic samples. The mixture of dimethylbenzoyl phosphate and tetramethyl phosphate was also obtained when dimethyl phosphorochloridate was allowed to react with benzoic acid in acetonitrile in the presence of triethylamine and DMF and the product distilled under reduced pressure (bp 120–125°C (0.5 Torr)).

Reaction of trimethyl phosphate with ***5****b*

Trimethyl phosphate (0.113 mol), ***5b*** (0.073 mol), and triethylamine (2 drops) were heated at 56–58°C for 12 h (23). Distillation of the product yielded dimethylacetyl phosphate; bp 68–71°C (0.2 Torr); ^{1}H nmr ($CDCl_3$) δ: 2.20 (3H, s, C-Me), 3.90 (6H, d, J_{HP} 11.5 Hz, OMe). The ^{1}H nmr of this product, recorded after 6 months of standing at room temperature, showed that marked changes had taken place: new signals appeared at δ 2.08 (s) and δ 3.78 (d, J_{HP} 10 Hz). These signals were assigned to acetic anhydride and tetramethyl pyrophosphate, as confirmed by addition of authentic samples. Again, no methyl acetate or trimethyl phosphate could be detected in the reaction mixture.

Rate measurements

In a typical run, mixed anhydride (20 μL) was dissolved in deuterated solvent (0.4 mL) in an nmr tube, and the tube was sealed and incubated in a thermostatted water bath of the required temperature. Progress of reaction was monitored periodically by ^{1}H nmr: the amount of carboxyamide product present at various times was calculated as a percentage by determining the ratio

$$X(\%) = \frac{100A}{A + B}$$

where A = increment (per proton) for the carboxyamide measured from integration of the $C(O)NMe_2$ signal at δ ca. 3.0 (in mm/H); and B = increment (per proton) for the anhydride substrate measured from integration of the $P(O)NMe_2$ signal at δ ca. 2.75 (mm/H). The value of $X(\%)$ was then substituted into the first-order rate law term:

$$k_1 t = \ln\left(\frac{100}{100 - X}\right)$$

Reactions were followed to ca. 70% completion. All runs gave linear plots with r values of 0.990–0.995.

Since the rates of fragmentation are sensitive to the presence of various substances (see Discussion), great care was taken to make certain that the rate constants used for determination of relative reactivity, solvent or catalytic effects, and temperature effects were obtained, as far as possible, under identical conditions. For example, the Arrhenius plots (Table 2) were obtained for each solvent by carrying out all kinetic measurements simultaneously and using the same sample of ***1a*** and the same bottle of solvent. Similarly, the effect of catalyst (Table 4) was measured using the same sample of ***1a*** for all runs, and the effect of substituents (Table 3) was determined using the same $CDCl_3$ as a solvent.

Acknowledgement

Financial assistance of the University of Cape Town and the Council for Scientific and Industrial Research is gratefully acknowledged.

1. D. Balarev. Z. Anorg. Allg. Chem. **88**, 145 (1914); **99**, 191 (1917).
2. S. A. Hall and M. Jacobson. Ind. Eng. Chem. **40**, 694 (1948); E. Schwarzmann and J. R. Van Wazer. J. Am. Chem. Soc. **83**, 365 (1961).
3. K. A. Petrov and A. A. Neimysheva. J. Gen. Chem. USSR (Engl. Transl.), **29**, 1793 (1959).
4. A. D. F. Toy and E. N. Walsh. Inorg. Synth. **7**, 73 (1963).
5. F. Effenberg and G. König. Chem. Ber. **114**, 916 (1981).
6. G. Di Sabato and W. P. Jencks. J. Am. Chem. Soc. **83**, 4393 (1961); **83**, 4400 (1961).
7. T. F. Hendrickse, V. Mizrahi, and T. A. Modro. Phosphorus Sulfur, **20**, 93 (1984).
8. C. H. Clapp and F. H. Westheimer. J. Am. Chem. Soc. **96**, 6710 (1974).
9. C. Reichardt. Solvent effects in organic chemistry. Verlag Chemie, New York. 1979.
10. N. S. Isaacs and A. A. R. Laila. J. Chem. Soc. Perkin Trans. 2, 1470 (1976).
11. H. Kwart and P. A. Silver. J. Org. Chem. **40**, 3019 (1975).
12. B. M. Anderson and W. P. Jencks. J. Am. Chem. Soc. **82**, 1773 (1960).
13. D. P. N. Satchel and R. S. Satchel. Chem. Rev. **69**, 251 (1969).
14. R. L. Carlson and R. S. Drago. J. Am. Chem. Soc. **84**, 2320 (1962).
15. L. M. Loew and W. R. MacArthur. J. Am. Chem. Soc. **99**, 1019 (1977).
16. F. H. Westheimer. Chem. Rev. **81**, 313 (1981).
17. M. J. Kamlet and R. W. Taft. J. Am. Chem. Soc. **98**, 2886 (1976).
18. V. G. Sheverina, G. S. Karetnikov, P. S. Pyryalova, N. P. Egorov, S. K. Titova, and Y. P. Kortikov. Zh. Fiz. Khim. **54**, 1865 (1980).
19. B. K. Carpenter. Determination of organic reaction mechanisms. Wiley–Interscience, New York. 1984. Chapt. 7.2.

20. H. S. RZEPA, J. SYMES, and T. A. MODRO. In preparation.
21. E. NIECKE and W. FLICK. Angew. Chem. Internat. Ed. Engl. **13**, 134 (1974).
22. F. CRAMER and M. WINTER. Chem. Ber. **94**, 989 (1961).
23. K. SASSE. Organische Phosphorverbindungen. G. Thieme Verlag, Stuttgart. 1964. p. 564.
24. B. FISCHER and J. MICHALSKI. Rocz. Chem. **26**, 688 (1952).
25. B. C. SAUNDERS, H. G. COOK, J. D. ILETT, G. J. STACEY, H. G. WATSON, I. G. E. WILDING, and S. J. WOODCOCK. J. Chem. Soc. 2921 (1949).
26. G. KAMAI and F. M. KHARRASOVA. Zh. Obshch. Khim. **27**, 3064 (1957).
27. L. A. LA PLANCHE and M. T. ROGERS. J. Am. Chem. Soc. **86**, 337 (1964).

Contraction de cycle dans la substitution d'un triflate osidique

ANNIE GROUILLER

Service de chimie biologique de l'Institut national des sciences appliquées de Lyon, Bâtiment 406, 20 Avenue A. Einstein, 69621 Villeurbanne CEDEX, France

Reçu le 4 novembre 1985

ANNIE GROUILLER. Can. J. Chem. **64**, 1709 (1986).

La substitution nucléophile par le benzoate de sodium du trifluorométhanesulfonate en 2 de l'azido-3 (ou du *O*-benzoyl-3) désoxy-4 α-DL-*thréo*-pentopyrannoside de méthyle (**1** ou **4**) procède avec une contraction du cycle pyrannose en cycle furannose, en C-2. Cette contraction n'est nullement observée lors d'une substitution avec l'azoture de lithium.

ANNIE GROUILLER. Can. J. Chem. **64**, 1709 (1986).

Benzoate displacement of the 2-triflyl derivative of methyl 3-azido or 3-*O*-benzoyl-4-deoxy-α-DL-*threo*-pentopyranoside (**1** or **4**) occurs with a pyranose to furanose contraction reaction at C-2. This contraction is not observed with an azido displacement.

Différentes contractions du cycle pyrannosique en cycle furannosique ont été récemment observées lors de la substitution nucléophile de sulfonates (1) ou au cours de leur désulfonyloxylation réductive (2). Nous-mêmes, dans le cadre d'un programme de synthèse d'azido-nucléosides à squelette désoxy-pentopyrannosyle (3), nous avions observé (4) que le traitement par le benzoate de sodium de l'anomère α de l'azido-3 didésoxy-3,4 *O*-trifluorométhanesulfonyle-2-DL-*thréo*-pentopyrannoside de méthyle (**1**) conduisait à un mélange de deux composés : le dérivé benzoylé attendu **2** de substitution et en quantité prépondérante le produit **3** de contraction du cycle pyrannose en cycle furannose.[1]

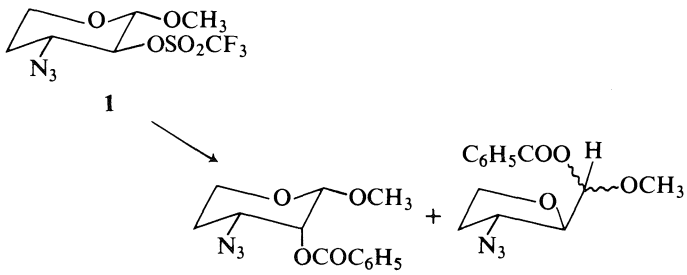

1 **2** **3**

Ce résultat avait été interprété comme provenant d'une part de l'encombrement stérique dû aux conformations équatoriales des groupements méthoxyle et azido, d'autre part de la relation antipériplanaire qui existait entre la liaison C-1/oxygène hétérocyclique et celle C-2/sulfonate. Par la suite, nous avons constaté (5) que le triflate **4**, traité dans les mêmes conditions par de l'azoture de lithium ne donnait naissance qu'à la formation du produit de substitution **5**. Or la configuration et la conformation des deux triflates **1** et **4** étaient la même. Seules changeaient la nature du groupement porté par le sucre en position 3 et celle du nucléophile utilisé.

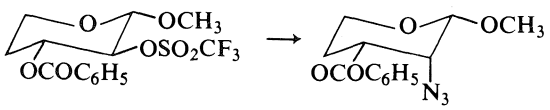

4 **5**

Pour discerner quel était le facteur déterminant, nous avons alors traité, toujours dans les mêmes conditions, d'une part l'azido-sucre **1** par l'azoture de lithium, d'autre part le benzoate **4** par le benzoate de sodium: dans le premier cas nous n'observons pas de contraction de cycle, mais que la formation du dérivé diazido de substitution **6**; dans le second cas, à côté du dibenzoate **7**, le produit de contraction de cycle **8** est formé dans un rapport de 3:2,5. Ces différents composés ont été purifiés et séparés par chromatographie sur colonne de gel de silice. Ils ont été identifiés d'après leur spectre de masse et leurs spectres de rmn du proton et du carbone 13.

Nous pouvons alors conclure que contrairement à l'hypothèse émise précédemment par nous (4) et par d'autres auteurs (6) pour expliquer cette contraction de cycle, l'attaque intramoléculaire du nucléophile par l'arrière du cycle sur le carbone 2 n'est pas dûe à la conformation de la molécule, mais à la nature du nucléophile utilisé : elle a lieu aussi bien avec le radical azido qu'avec le groupement benzoyle en position 3 équatoriale, à condition que le nucléophile utilisé soit le benzoate de sodium et non l'azoture de lithium. Généralement, la substitution S_N2 de

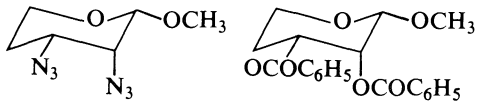

6 **7**

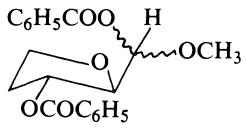

8

sulfonates en 2 de pyrannosides par des nucléophiles chargés est difficile et bien souvent impossible à cause d'un alignement défavorable des dipôles formés dans l'état de transition (7), sauf si le sulfonate est un triflate, excellent nucléofuge (8). Cependant, dans le cas de l'ion benzoate qui présente une concentration plus élevée en charge négative que l'ion azoture, l'attaque d'un triflate selon un mécanisme S_N2 est peut-être plus difficile qu'avec N_3^- : un déplacement interne (ou une contraction de cycle) peut alors entrer en compétition ou même devenir l'évènement principal.

Ces produits de contraction de cycle nous ouvrent une voie intéressante à la synthèse de C-nucléosides.

Partie expérimentale

Appareils et méthodes

La purification des composés a été réalisée par chromatographie sur gel de silice (Kieselgel 60 F_{254}, Merck 10757). Les spectres de rmn ont été enregistrés par le Service de rmn de la Faculté de Pharmacie de

[1]Tous nos composés sont racémiques; les formules représentent un seul énantiomère.

Marseille à 200 MHz pour ^1H et 50,3 MHz pour ^{13}C. Les déplacements chimiques sont exprimés en ppm, le tétraméthylsilane étant pris comme référence zéro. Les spectres de masse ont été obtenus en ionisation chimique (NH_3) par le Service Central d'Analyse du CNRS à Solaize.

Protocole général

Une solution de triflate (1,66 mmol) dans de l'hexaméthylphosphoramide (40 mL) est chauffée 5 h à 90°C avec 1,5 équiv. d'azoture de lithium (130 mg) ou de benzoate de sodium (360 mg). Le mélange réactionnel est versé sur de l'eau (50 mL) et extrait par de l'éther (200 mL). La phase organique est séchée sur sulfate de magnésium et évaporée sous pression réduite. Le résidue obtenu est purifié par chromatographie sur colonne sèche de gel de silice.

*Diazido-2,3 tridésoxy-2,3,4 α-DL-*érythro *pentopyrannoside de méthyle (**6**)*

Huile à partir de **1** (4) et d'azoture de lithium; rendement, 71%; R_f 0,68 (acétate d'éthyle – hexane, 1:1); ^1H rmn ($CDCl_3$) δ : 4,43 (d, $J_{1,2}$ = 2,0 Hz, H-1), 4,15–4,0 (sext, $J_{3,4a}$ = 3,6, $J_{3,4b}$ = 11 Hz, H-3), 3,73 (q, $J_{2,3}$ = 3,6 Hz, H-2), 3,67–3,38 (m, H-5a,b), 2,10–1,72 (m, H-4a,b); ^{13}C rmn ($CDCl_3$) δ : 100,8 (C-1), 61,1 (C-2), 60,3 (C-5), 58,3 (OCH_3), 58,0 (C-3), 26,3 (C-4); sm *m/e* : 216 (MNH_4^+).

*Désoxy-4 di-*O*-benzoyl-2,3 α-DL-*érythro *pentopyrannoside de méthyle (**7**) et benzoyl-méthyl acétal de l'anhydro-2,5 désoxy-4* O*-benzoyl-3 DL ribose (**8**)*

Huiles à partir de **4** (5) et de benzoate de sodium; rendement global, 57% (dont 26% de **7** et 31% de **8**, séparés par chromatographie sur colonne sèche de gel de silice avec comme éluant le mélange acétate d'éthyle – hexane 1:2).

7 : R_f 0,57 (acétate d'éthyle – hexane, 1:2); ^1H rmn ($CDCl_3$) δ : 8,08–7,97 et 7,60–7,33 (m, 5H, Ph), 5,57–5,46 (m, $J_{2,3}$ = 2 Hz, H-2 et H-3), 4,80 (d, $J_{1,2}$ = 2 Hz, H-1), 4,29–4,14 (m, $J_{5a,5b}$ = 8 Hz, H-5a), 3,71–3,55 (m, H-5b), 3,51 (s, OCH_3), 2,20–2,05 (m, H-4); ^{13}C rmn ($CDCl_3$) δ : 166 (CO), 135–126 (C_6H_5), 98,7 (C-1), 68,6 (C-2), 68,2 (C-3), 58,8 (C-5), 56,4 (OCH_3), 28,2 (C-4); sm *m/e* : 374 (MNH_4^+), 325 ($M - OCH_3$).

8 : R_f 0,48 (acétate d'éthyle – hexane, 1:2); ^1H rmn ($CDCl_3$) δ : 8,14–7,98 et 7,63–7,40 (m, 5H, Ph), 6,20 (d, $J_{1,2}$ = 4 Hz, H-1), 5,70 (sext, $J_{3,4a}$ = 2, $J_{3,4b}$ = 3,6 Hz, H-3), 4,37 (q, $J_{2,3}$ = 2 Hz, H-2), 4,2–3,90 (m, H-5a,b), 3,57 (s, OCH_3), 2,48–2,26 et 2,20–2,05 (m, H-4a et H-4b); ^{13}C rmn ($CDCl_3$) δ : 166 (CO), 135–126 (C_6H_5), 97,8 (C-1), 84 (C-2), 76 (C-3), 68,5 (C-5), 58 (OCH_3), 34 (C-4); sm *m/e* : 374 (MNH_4^+), 325 ($M - OCH_3$), 220 ($M - OCH_3 - COC_6H_5$), 191 (M-chaîne latérale).

Remerciements

Nous tenons à remercier le CNRS (UA 495) et l'INSERM (U 205) de leur aide financière.

1. G. Berti, G. Catelani, F. Colonna, M. Ferretti et L. Monti. Gazz. Chim. Ital. **115**, 85 (1985).
2. H. H. Baer, D. J. Astles, H. C. Chin et L. Siemsen. Can. J. Chem. **63**, 432 (1985).
3. G. Carret, A. Grouiller et H. Pacheco. Carbohydr. Res. **111**, 59 (1982).
4. A. Grouiller, H. Bazin et C. Gagnieu. Tetrahedron Lett. 2559 (1982).
5. G. Carret. Thèse d'Universtité n° 90, Université Claude Bernard, Lyon I. 1984.
6. J. Jarý, P. Novak et Z. Samek. Liebigs Ann. Chim. **740**, 98 (1970); V. Pozsgay et A. Neszmélyi. Tetrahedron Lett. 211 (1980).
7. A. C. Richardson. Carbohydr. Res. **10**, 395 (1969).
8. H. H. Baer et B. Radatus. Carbohydr. Res. **144**, 77 (1985).

An MNDO study of dipyridopyrazinium and relation cations: instability of certain fused heteroaromatic dications with two bridgehead nitrogens

JEFFREY G. EAVES, DAVID PARKER,[1] AND NIGEL RUDGEWICK-BROWN
Department of Chemistry, University of Durham, South Road, Durham DH1 3LE, U.K.

Received February 3, 1986

JEFFREY G. EAVES, DAVID PARKER, and NIGEL RUDGEWICK-BROWN. Can. J. Chem. **64**, 1711 (1986).

MNDO calculations are reported for the series of closed shell aromatic and heteroaromatic molecules and cations **1** to **7**. The 14π dipyrido-dications **1***a* and **2***a* are considerably less stable than their dihydro-analogues **1***b* and **2***b* and perhaps should not be considered to be "aromatic" cations.

JEFFREY G. EAVES, DAVID PARKER et NIGEL RUDGEWICK-BROWN. Can. J. Chem. **64**, 1711 (1986).

On rapporte des calculs MNDO effectués sur la série des molécules et des cations aromatiques et hétéroaromatiques **1** à **7** à couches fermées. Les dipyridodications **1***a* et **2***a* à 14 électrons π sont beaucoup moins stables que leurs analogues dihydro **1***b* et **2***b*; on ne devrait peut-être pas les considérer comme des cations "aromatiques".

[Traduit par la revue]

Introduction

The series of condensed heteroaromatic systems which incorporates pyridinium cations has been studied in detail, mainly as a result of the herbicidal activity of certain derivatives (1). More recently, dipyridinium cations have been shown to be components of a novel class of organic metals (2). However, the dipyrido[1,2-*a*:1′,2′-*d*]pyrazinium ring system, **1**, and the related pyrimidinium cation **2** have been relatively poorly studied (3, 4). We have recently been studying the structure and reactivity of some dipyridopyrazinium cations (4). During the course of this work it became apparent that the putative aromatic cations **1***a* and **2***a* had not been defined. These dications are of particular interest as they may be expected to accept an electron readily, forming stable radical cations, as required for efficient herbicidal action. There was a need therefore to assess the relative stability of these dications compared to their dihydro-analogues, **1***b* and **2***b*, relating this to a series of mono- and dications of comparable structure, **3** to **7**. This series was chosen in order to compare the effect of varying overall charge, π-electron number and the location of the nitrogen atoms (i.e. at bridgehead positions or otherwise).[2] The cations selected include the commercial herbicide "diquat" **6***b* (5), and its dehydro-analogue **6***a* both of which are well-defined dications. The 12π anthracene dication, **5***a*, is also included. It has been characterised electrochemically recently (6) and was shown to be highly unstable with a life-time of the order of seconds at −50°C in liquid sulphur dioxide.

Discussion and results

A series of geometry optimised MNDO molecular orbital calculations has been undertaken in order to compare the relative stability of **1***a* and **2***a* and their dihydro analogues, **1***b* and **2***b*, to the related aromatic and heteroaromatic systems **3** to **7**. The calculations were carried out using Dewar's MNDO program (9) with the aid of a CDC 7600 or an IBM 370/168 computer. The geometric parameters were optimised and the appropriate point-group symmetry of **1** to **7** was utilised where necessary. It was therefore assumed that the aromatic species **1***a* to **7***a* were flat.

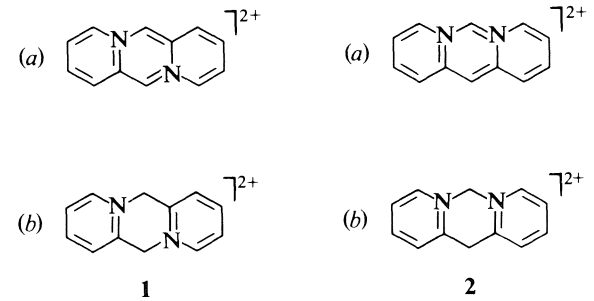

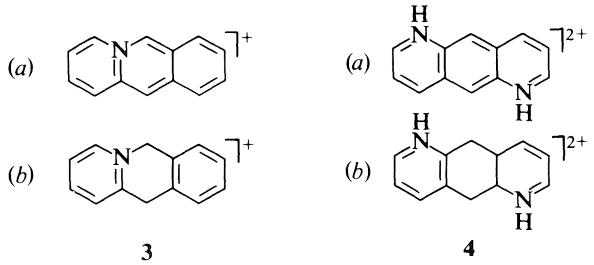

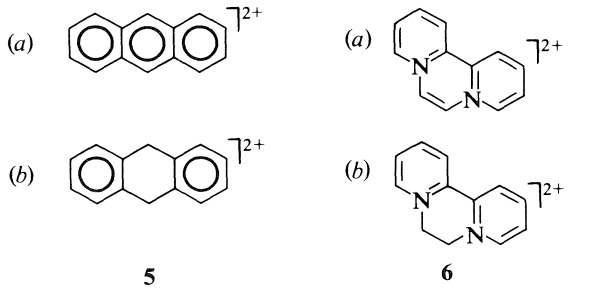

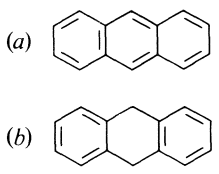

[1]To whom all correspondence should be addressed.

[2]Some of these systems have been examined previously using a semi-empirical PPP-SCFMO method (7, 8).

TABLE 1. MNDO calculated gas-phase enthalpies of formation[a] (kcal mol^{-1})

	ΔH_f^θ (**1***a*–**7***a*)	ΔH_f^θ/dihydro analogue (**1***b*–**7***b*)	$\delta(\Delta H_f^\theta)_{calcd}$ **n**(*a*) − (*b*)
1	495.8	457.5	+38.3
2	496.8	458.2	+38.6
3	225.3	204.6	+20.7
4	451.6	429.9	+21.7
5	504.8	544.4	−39.6
6	483.5	463.3	+20.2
7[b]	58.9 (55.2)	37.8 (38.2)	+21.1 (17.0)

[a]The mean absolute error in values has been calculated to be 7.2 kcal mol^{-1} for cationic systems and 6.3 kcal mol^{-1} for neutrals (9).
[b]Experimental value is given in parentheses (10).

(i) Heats of formation

In Table 1 the calculated gas-phase enthalpies of formation for the "aromatic" systems **1***a* to **7***a* are compared with the values for the corresponding dihydro systems, **1***b* to **7***b*. A striking feature of this comparison is the high *difference* in heats of formation ($(\delta\Delta H_{f\,calcd}^\theta)$, column 3) for **1** and **2** (38.5 kcal mol^{-1}) compared to **3**, **4**, **6**, and **7** where the difference averages 20.9 kcal mol^{-1}. The heats of formation for the pyrazinium and pyrimidinium dications **1***a* and **2***a* and the anthracene dication **5***a* are quite similar, despite the fact that the former are formally 14π aromatic dications and the latter is an anti-aromatic 12π system. This suggests that **1***a* and **2***a* are uniquely unstable within the series considered. The calculated difference in enthalpy of formation for **6***a* and **6***b* is 20.2 kcal mol^{-1}, in line with **3**, **4**, **6**, and **7** but in contrast to **1** and **2**. It would seem that the instability of **1***a* and **2***a* is not simply associated with the occurrence of two bridgehead nitrogens, as occurs also in **6***a* and **6***b*.

In the case of anthracene, experimental and calculated heats of formation may be compared (10). Both sets of values fall within the mean error of the calculation, as expected for such simple molecules (9). Finally it is worth noting that the conjugated 12π dication **5***a*, is notably more stable than its (5+5)π dihydro analogue, **5***b*. In the latter case the dication may be considered as two independent 5π aryl cations in which the positive charge is localised within each of the outer rings.

(ii) Molecular geometries and frontier orbital energies

For the series **1***a* to **7***a* it was expedient to assume that the cations and molecules were flat with the appropriate point-group

TABLE 2. Selected frontier molecular orbitals[a]

Compound	HOMO (energy/eV)	NHOMO (energy/eV)	LUMO (energy/eV)
1*a*	−16·5 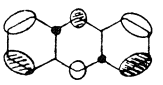	−18·4 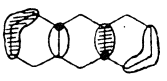	−10·3 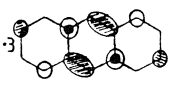
2*a*	−16·6 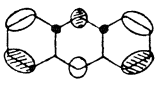	−18·1 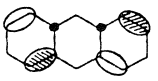	−10·1 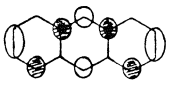
3*a*	−12·4 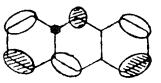	−13·6 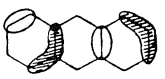	−5·5 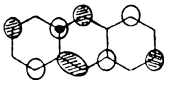
4*a*	−16·7 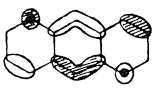	−17·5 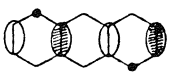	−9·5 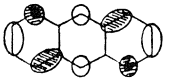
5*a*	−17·2 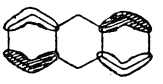	−17·5 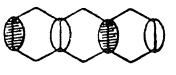	−11·3 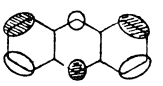
6*a*	−17·6 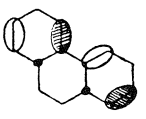	−17·7 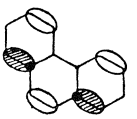	−9·7 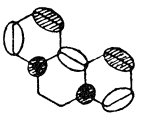
6*b*	−17·5 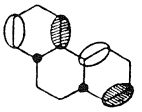	−18·7 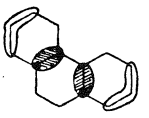	−9·6 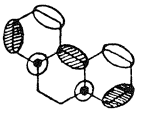
7*a*	−8·0 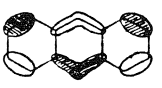	−9·0 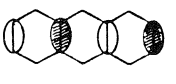	−0·8 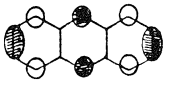

[a]As deduced from examination of the elements of the eigenvector matrix, examining the atomic orbital coefficients for each molecular orbital.

symmetries.[3] For the dihydro-systems **1***b*, **2***b*, **3***b*, **4***b*, **6***b*, and **7***b* the central ring is calculated to be non-planar with dihedral angles between the planes of the two aromatic rings of 148, 149, 141, 153, 10, and 141°, respectively. The experimental values from the reported X-ray structures of **1***b* (4), **6***b* (11), and **7***b* (12) are 141, 20, and 145° showing reasonable agreement bearing in mind the perturbing influence on cation molecular geometry of nearest anions (4, 11) and crystal packing effects. Generally, the calculated and experimental bond lengths show good agreement.

The C(1)—C(9) bond length for the central ring of the "diquat" derivative **6***a* is calculated to be 1.36 Å in close agreement with both the experimental value of 1.35 Å and the commonly accepted bond length for an isolated alkene bond of 1.34 Å. This correlation suggests that the bond is perhaps best regarded as olefinic rather than aromatic in character. This is similar to the behaviour of the C(9)—C(10) double bond in phenanthrenes, although this point was overlooked by workers dicussing the crystal structure of **6***b* (5).

(iii) Charge distribution and frontier molecular orbitals.

Within the heteroaromatic rings of the dihydro systems **1***b*, **2***b*, **3***b*, **4***b*, and **6***b*, a pronounced $+/-$ alternation of net atomic charge density is consistently found. This may be associated with effective *delocalisation* of charge around the pyridinium ring. Such charge alternation is also found for the two outer rings in **6***a*: indeed the calculated values accord closely with those of **6***b*. This suggests that in **6***a* the positive charge is not effectively delocalised into the central ring and that **6***a* effectively behaves like **6***b* with a linking, but only weakly conjugating double bond. In the 14π systems **3***a* and **4***a*, such charge alternation is also observed in each heterocyclic ring.

Effective charge delocalization, as evidenced by this $+/-$ charge alternation, *does not* occur to such an extent with **1***a*, **2***a*, and **5***a*. In these three systems, there is a localization of charge on the ring atoms, which presumably must destabilise the system, raising its overall energy (as evidenced by their high heats of formation with respect to the dihydro analogues, Table 1). Again it is worth noting that the anthracene dication is behaving in a similar manner to the putative aromatic systems **1***a* and **2***a*. Further insight into the relative stability of these systems comes from an examination of their frontier molecular orbitals, Table 2. Examination of the calculated eigenvector matrix gives the atomic orbital coefficients for each molecular orbital from which the pictorial MO's shown in Table 2 have been simply derived. Inspection of Table 2 reveals that in the two highest-occupied MO's of **1***a*, **2***a*, and **5***a*, no π orbital overlap through the central ring occurs. This presumably may be related to the lack of charge delocalisation discussed above. In contrast, effective π-orbital overlap through the central ring is consistently observed in the HOMO or NHOMO for **3***a*, **4***a*, and **7***a*.

Given the similarity of **1***a* and **2***a* to the 12π anthracene dication **5***a*, it is tempting to speculate that they may not reasonably be termed "aromatic", despite the fact that they formally contain 14π-electrons in a conjugated, cyclic array. Their inherent instability, as manifested by the high differential heat of formation with respect to their dihydro-analogues, the lack of effective charge delocalisation around the ring and by the fact that they have eluded preparation, clearly sets them apart from the related systems considered in this study.

[3]Tables of frontier orbital energies, molecular bond lengths, and atomic charge densities are available from the authors, on request.

Acknowledgements

We thank SERC for a studentship (J.G.E.) and Dr. H. S. Rzepa and Professor D. T. Clark for some helpful comments.

1. W. R. Boon. Outlook Agr. **4**, 163 (1964); Chem. Ind. (London), 782 (1965).
2. G. J. Ashwell. Nature (London), **290**, 686 (1981).
3. E. E. Glover and G. H. Morris. J. Chem. Soc. 3366 (1965); 3885 (1965); G. A. Abbott, D. Leaver, and K. C. Mathur. J. Chem. Res. M, 2846 (1978); A. L. Black and L. A. Summers. Chem. Commun. 582 (1970).
4. M. R. Bryce, J. G. Eaves, J. A. K. Howard, O. Johnson, and D. Parker. J. Chem. Soc. Perkin Trans. II, 433 (1985).
5. P. D. Sullivan and M. L. Williams. J. Am. Chem. Soc. **98**, 1711 (1976).
6. M. Dietrich, J. Mortensen, and J. Heinze. Ang. Chem. Int. Ed. Engl. **24**, 508 (1985).
7. V. Galasso. Theoret. Chim. Acta, **11**, 417 (1968).
8. V. Galasso and G. De Alti. Gass. Chim. Ital. **100**, 421 (1970).
9. M. J. S. Dewar and W. Thiel. J. Am. Chem. Soc. **99**, 4899, 4907 (1977).
10. J. D. Cox and G. Pilcher. Thermochemistry of organic and organometallic compounds. Academic Press, New York. 1970.
11. R. Mason. Acta Crystallogr. **17**, 547 (1964).
12. W. G. Ferrier and R. Iball. Chem. Ind. (London), 1296 (1954); T. Brennan, E. F. Putkey, and M. Sundaralingham. Chem. Commun. 1490 (1971); F. Leroy, C. Courseille, M. Daney, and F. Bouas-Laurent. Acta Crystallogr. **32**B, 2792 (1976).

Kinetic and equilibrium studies of the σ-adduct forming reactions of 1,3,5-trinitrobenzene and picryl chloride with some carbon bases

MICHAEL R. CRAMPTON, TERENCE P. KEE, AND JENNIFER R. WILCOCK
Department of Chemistry, Durham University, Durham, DH1 3LE, England

Received February 19, 1986

MICHAEL R. CRAMPTON, TERENCE P. KEE, and JENNIFER R. WILCOCK. Can. J. Chem. **64**, 1714 (1986).

Reaction of 1,3,5-trinitrobenzene (TNB) with the malononitrile anion in methanol yields a carbon-bonded σ-adduct, (**3**). Ionisation of the remaining exocyclic hydrogen is favourable and yields the dianion (**4**). The initial reaction of 1-chloro-2,4,6-trinitrobenzene similarly occurs at an unsubstituted ring position, but is followed by slower nucleophilic attack at the 1-position yielding the substituted product. A major difference in the reaction of the ethyl malononitrile anion with TNB is that the adduct formed (**11**) has no readily dissociable proton. Hence, here, conversion to the carbon-bonded adduct is less favourable. Kinetic and equilibrium data are reported for these reactions and are compared with data for adduct formation involving methoxide ions.

MICHAEL R. CRAMPTON, TERENCE P. KEE et JENNIFER R. WILCOCK. Can. J. Chem. **64**, 1714 (1986).

La réaction du trinitro-1,3,5 benzène (TNB) avec l'anion malononitrile, dans le méthanol, conduit à un produit conduisant à la formation d'un adduit-σ lié à un carbone (**3**). L'ionisation de l'hydrogène exocyclique résiduel est favorable et conduit au dianion **4**. La réaction initiale du chloro-1 trinitro-2,4,6 benzène se produit de la même manière à la position non-substituée du cycle; toutefois, elle est suivie d'une attaque nucléophile plus lente au niveau de la position 1 qui conduit au produit substitué. Une différence importante dans la réaction de l'anion éthylmalononitrile avec le TNB est que l'adduit qui se forme, **11**, ne porte pas de proton dissociable. Alors, sa conversion en un adduit lié par le carbone est moins favorable. On rapporte les données cinétiques et d'équilibre de ces réactions et on les compare avec les données obtenues pour la formation d'adduits impliquant les ions méthylates.

[Traduit par la revue]

Many carbon-bonded σ-adducts have been characterised from the reactions of activated aromatic molecules with carbon bases (1, 2). However, relatively few kinetic studies of these systems have been reported, due in part to the difficulty of generating the nucleophiles under conditions suitable for such studies. A notable exception here is the work of Kaválek, Štěrba, and co-workers which showed that carbanions generated from malonic acid derivatives were suitable nucleophiles (3–5).

In this paper we report kinetic and equilibrium data for the reactions of malononitrile anion with 1,3,5-trinitrobenzene and with picryl chloride (1-chloro-2,4,6-trinitrobenzene) in methanol, and equilibrium data for reaction of the ethyl malononitrile anion with 1,3,5-trinitrobenzene. The results are important in that the equilibrium constants give a measure of the carbon basicities of the nucleophiles (thermodynamic affinity for carbon) while the rate constants measure their nucleophilicity and nucleofugality. There is current interest in the comparison of these quantities for different types of nucleophile, and in different types of reaction (6, 7).

Results and discussion

Acidities of malononitrile and ethyl malononitrile in methanol

The pK_a of malononitrile in water is reported (7–10) as 11.2. Carbanions were generated in methanol, as shown in reaction [1], by reaction of (**1**, R = H, Et) with methoxide ions. Values of K_{CH} determined spectrophotometrically are in Tables 1 and 2. These values are related by eq. [2] to K_a, the acid dissociation constants of the carbon acids and K_M, the autoprotolysis constant of methanol. Since the value (11) for pK_M is 16.92 we obtain values for pK_a in methanol for (**1**, R = H) of 14.14 and for (**1**, R = Et) of 15.60. The acid weakening effect of the ethyl group may be attributed partially to its polar effect and partially to steric inhibition of solvation of the anion (11).

$$[1]\quad \underset{\mathbf{1}}{RCH(CN)_2} + MeO^- \overset{K_{CH}}{\rightleftharpoons} \underset{\mathbf{2}}{RC(CN)_2^-}$$

$$[2]\quad K_{CH} = K_a/K_M$$

TABLE 1. Equilibrium data for reaction of malonotrile[a] with sodium methoxide in methanol at 25°C

10^3 [NaOMe]/M	Absorbance (226 nm)[b]	K_{CH}[c]/L mol^{-1}
0	0.01	
0.95	0.55	620
1.90	0.80	620
4.75	1.10	600
6.65	1.18	570
9.5	1.26	580
19	1.37	600

[a]Concentration is 1×10^{-4} M.
[b]Absorption is due to carbanion. These are initial values determined by stopped flow spectrophotometry. Values correspond to cell of 1 cm path length.
[c]Calculated as $(A - 0.01)/(1.49 - A)[NaOMe]_{eq}$ where A represents absorbance.

Reaction of malononitrile anion with 1,3,5-trinitrobenzene (TNB)

Our results are best interpreted by Scheme 1 which allows for the reaction of TNB with methoxide ions to produce **5**. This reaction, which is known to be very rapid on the stopped-flow timescale (12) and for which K_{OMe} has (13) the value 17 L mol^{-1}, was minimized by working with [MeO$^-$] ≤ 0.01 M. In all cases the fraction of substrate present in the form of **5** *at equilibrium* was negligibly small. The visible spectrum of the TNB-malononitrile adduct present at equilibrium had λ_{max} at ca. 450 nm with a shoulder at longer wavelength and was typical of 1:1 adducts of TNB with carbon bases (2). However, small variations of spectral shape were observed depending on the residual concentration of methoxide ions and provide evidence

TABLE 2. Equilibrium data for reaction of ethylmalononitrile with potassium methoxide in methanol at 25°C

(**1**, R = Et)/M	[KOMe]/M	Absorbance (238 nm)[a]	K_{CH}[b]/L mol^{-1}
0.0005	0.0020	0.24	21
0.0005	0.0035	0.41	21
0.0005	0.0050	0.56	21
0.0005	0.0100	1.0	20
0.0002	0.0200	0.75	23
0.0002	0.0400	1.20	25
0.0001	0.10	0.90	—
0.0001	0.20	1.00	—
0.0001	0.50	1.07	—
0.0025	0.00075	0.42	20
0.0050	0.00075	0.87	21
0.0050	0.00050	0.55	20

[a]Determined by conventional spectrophotometry using 1 cm cell. Values extrapolated to zero time.
[b]Calculated as [**2**]/[**1**][MeO$^-$] using extinction coefficients of 1.2×10^4 L mol^{-1} cm^{-1} for (**2**, R = Et) and zero for (**1**, R = Et).

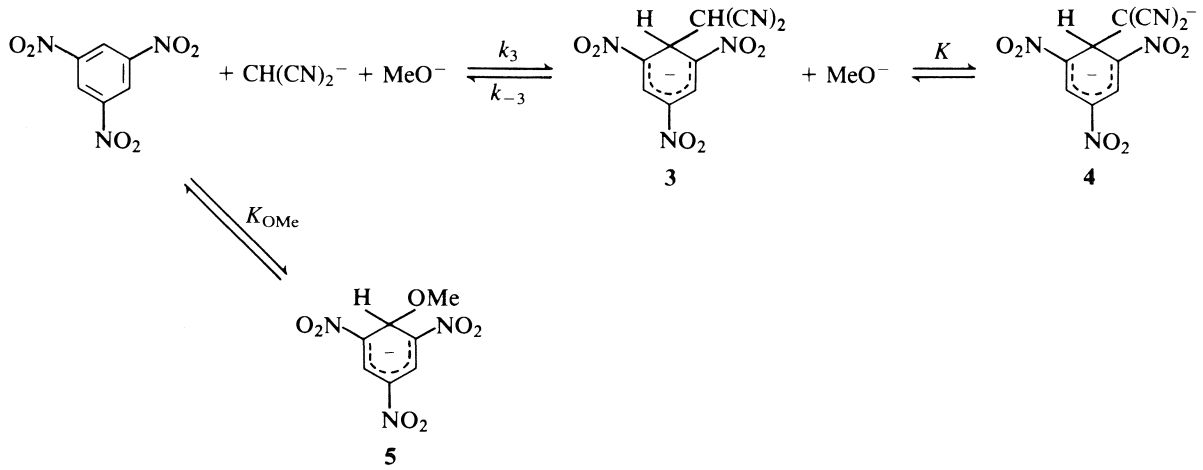

SCHEME 1

for the ionisation **3** ⇌ **4**. With [MeO$^-$] > 10^{-3} M, the spectrum had λ_{max} 460 nm, 520 (sh) and is attributed to the dianion **4**, while with [MeO$^-$] < 10^{-4} M (in buffer solutions) the spectrum showed λ_{max} 440 nm, 525 sh indicating the predominance of **3**. It is to be expected that the adduct **3** should be a stronger acid than malononitrile since it is known that the $C_6H_2(NO_2)_3^-$ group, although negatively charged, is electron withdrawing relative to hydrogen (14, 15).

Kinetic measurements were made by stopped-flow spectrophotometry, one syringe containing a mixture of TNB and malononitrile in methanol and the other a solution of sodium methoxide in methanol. We worked with concentrations [NaOMe] ≫ [malononitrile] ≫ [TNB] and a single first order process was observed in the visible region. Rate constants are in Table 3. The proton transfers involving the formation of the malononitrile anion, and the equilibration of **3** and **4** are expected to be fast on the stopped-flow time-scale (16). On that basis, and allowing for the rapid equilibrium formation of **5** we obtain eq. [3]

$$[3] \quad k_{obs} = \frac{k_3[CH(CN)_2^-]}{1 + K_{OMe}[MeO^-]} + \frac{k_{-3}}{1 + K[MeO^-]}$$

where K is the equilibrium constant for reaction of **3** with methoxide ions to give **4**. Plots, in Fig. 1, at constant methoxide concentration of k_{obs} versus $[CH(CN)_2^-]/(1 + K_{OMe}[MeO^-])$ were linear. The slopes gave a value for k_3 of $(3 \pm 0.5) \times 10^5$ L mol^{-1} s^{-1}. The values of the intercepts are inversely proportional to the sodium methoxide concentration, indicating that the condition $K[MeO^-] \gg 1$ applies, and giving a value for k_{-3}/K of 0.26 ± 0.02 mol L^{-1} s^{-1}. Hence we obtain a value for $K_3K(= k_3K/k_{-3})$ of $(1.1 \pm 0.3) \times 10^6$ L^2 mol^{-2}.

In order to separate the values of K_3 and K it was necessary to work in solutions containing very low concentrations of methoxide ions. This was achieved by using buffer solutions prepared from 4-bromophenol, whose pK_a value in methanol is known (11) to be 13.61. Equilibrium absorbances obtained using conventional spectrophotometry were measured at λ_{max} and also at 550 nm and are reported in Table 4. Because of the fairly fast decomposition reaction these are the values extrapolated to zero time. We define the equilibrium constant, K_{obs}, by eq. [4] where A is the measured absorbance and A_∞ is the value corresponding to complete conversion of TNB to adduct. If the reasonable assumption is made that the extinction coefficients of **3** and **4** at λ_{max} are the same then it is readily shown that K_{obs} is related to K_3 and K by eq. [5].

$$[4] \quad K_{obs} = \frac{A}{(A_\infty - A)} \cdot \frac{1}{[CH(CN)_2^-]}$$

TABLE 3. Kinetic data for reaction of 1,3,5-trinitrobenzene[a] with (**2**, R = H) in methanol at 25°C

$10^4[CH_2(CN)_2]_{stoich}/M$	$10^4[NaOMe]_{stoich}$[b]$/M$	$10^4[CH(CN)_2^-]$[c]$/M$	k_{obs}[d]$/s^{-1}$
1.0	30	0.64	99
2.0	30	1.27	115
3.0	30	1.88	120
3.5	30	2.19	132
5.0	30	3.09	155
1.5	50	1.12	74
3.0	50	2.22	103
5.0	50	3.68	160
1.0	60	0.78	60
1.5	60	1.17	68
2.0	60	1.56	80
3.0	60	2.33	103
4.0	60	3.10	120
1.0	100	0.86	50
2.0	100	1.71	78
3.0	100	2.56	98
4.0	100	3.41	120

[a]Concentration is 5×10^{-6} *M*.
[b]Ionic strength, 0.01 *M* with sodium chloride.
[c]Calculated from the stoichiometric concentrations of malononitrile and sodium methoxide, using a value for K_{CH} of 600 L mol^{-1}.
[d]Measured by stopped-flow spectrophotometry of 460 nm.

TABLE 4. Equilibrium data for reaction of 1,3,5-trinitrobenzene[a] with malononitrile in buffer solutions at 25°C

			Absorbances[d]		
$[CH_2(CN)_2]_{stoich}/M$	$10^4[MeO^-]$[b]$/M$	$10^4[CH(CN)_2^-]$[c]$/M$	λ_{max}	550 (nm)	K_{obs}/L mol^{-1}
0.01	0.48	2.8	0.10	0.05	73
0.02	0.47	5.5	0.195	0.10	74
0.01	0.95	5.4	0.28	0.14	110
0.01	0.95	5.4	0.26	0.13	102
0.02	0.90	10.2	0.46	0.23	99
0.01	1.44	8.0	0.50	0.25	139
0.01	1.80	9.8	0.72	0.35	172
0.005	1.90	5.2	0.43	0.20	183
0.01	2.30	12.2	1.00	0.47	205
0.005	2.60	6.8	0.65	0.30	220

[a]Concentration is 2×10^{-4} *M*.
[b]Residual methoxide concentration in 4-bromophenol/4-bromophenoxide buffers. Since the concentrations of buffer components (ca. 0.1 *M*) were not in a very large excess of the malononitrile concentration, a correction has been applied for depletion of base by formation of malononitrile anion. Ionic strength was maintained at 0.01 *M*.
[c]Calculated from eq. [1] using a value for K_{CH} of 600 L mol^{-1}.
[d]The extinction coefficients were determined to be 2.5×10^4 L mol^{-1} cm^{-1} at λ_{max}, and 1.15×10^4 L mol^{-1} cm^{-1} at 550 nm. These measurements were made using large excesses of [malononitrile] and [methoxide] over [TNB].

[5] $K_{obs} = K_3(1 + K[MeO^-]$

A plot, Fig. 2, of K_{obs} versus methoxide concentration gave values for K_3 of 37 L mol^{-1} (intercept) and for K of 2.1×10^4 L mol^{-1} (slope/intercept). Similar treatment of the data at 550 nm yielded values for K_3 of 42 L mol^{-1} and for K of 1.9×10^4 L mol^{-1}. The slopes of these plots give a value for the product K_3K of 8×10^5 L^2 mol^{-2}, in reasonable accord with that obtained from the kinetic measurements.

We now have two ways of calculating the value for k_{-3}. From the knowledge that the value of k_{-3}/K is 0.26 mol L^{-1} s^{-1} and the known value for K we obtain a value of 5500 ± 1000 s^{-1}. The second value, obtained from k_3/K_3, is 7500 ± 2000 s^{-1}. Our preferred value is 6500 ± 2000 s^{-1}.

Reaction of malononitrile anion with picryl chloride

Mixing solutions in methanol of picryl chloride (1-chloro-2,4,6-trinitrobenzene) and malononitrile in the presence of base produced a transient red colour, which we take to signify σ-adduct formation, followed by a strong permanent yellow colour λ_{max} 442 nm, ϵ 2.5×10^4 L mol^{-1} cm^{-1} which may be attributed to the substitution product. There is very strong evidence (1, 2, 17, 18) that nucleophilic attack at unsubstituted positions of picryl chloride is a considerably faster process than is attack at the chloro-substituted position. Hence we interpret the reactions by Scheme 2. Here the initially observed σ-adduct is **6** which in the presence of methoxide will be present largely in the ionised form **7**. The rate-determining step in the substitution reaction is expected (1, 2) to be formation of the intermediate **8**

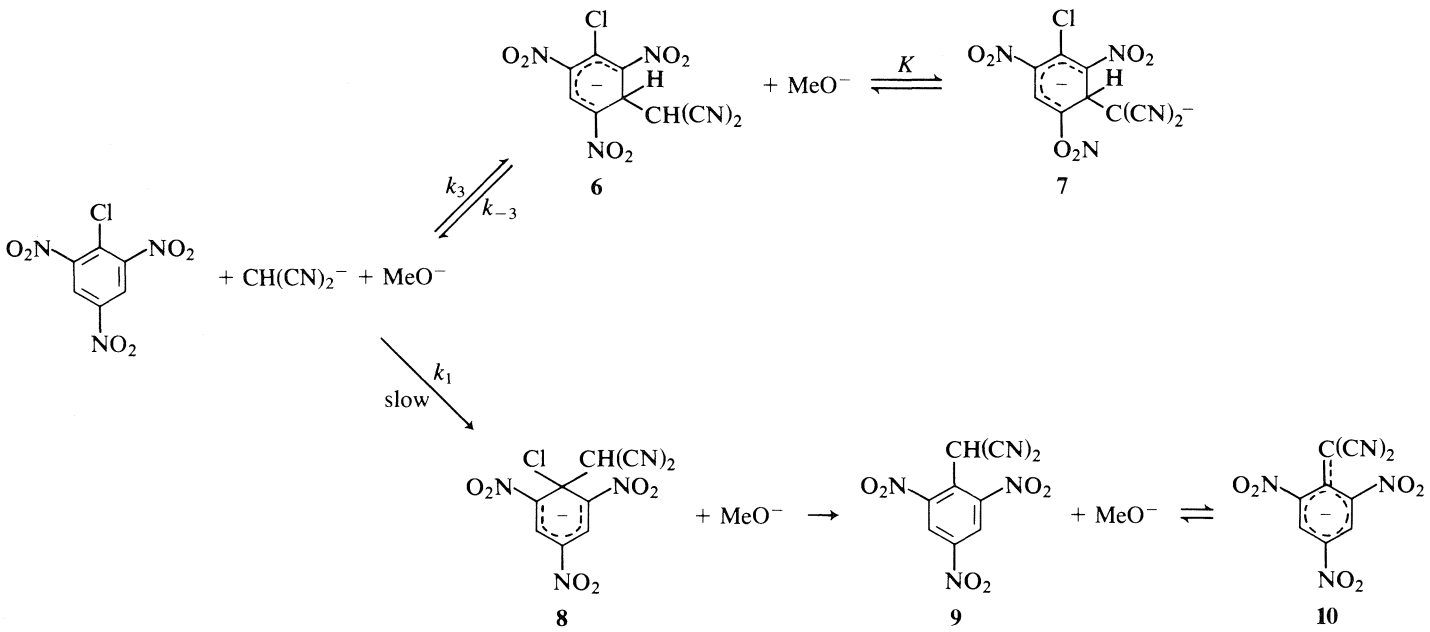

SCHEME 2

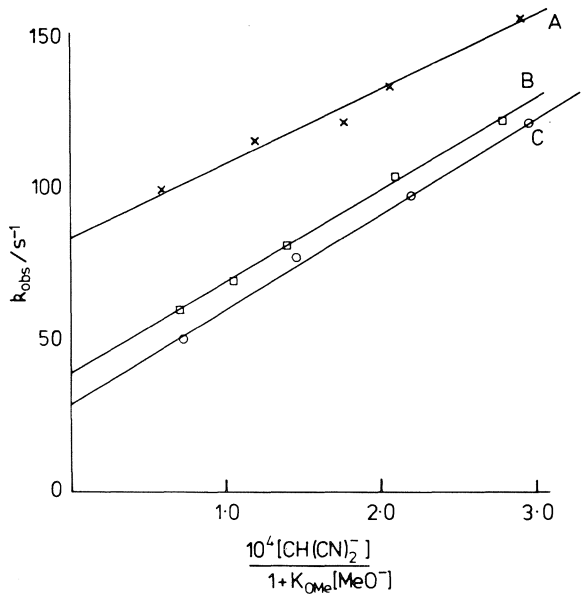

FIG. 1. Plots of k_{obs} versus $10^4[CH(CN)_2^-]/(1 + K_{OMe}[MeO^-])$ for solutions containing the following concentrations of sodium methoxide in methanol: *A*, 0.003 mol L^{-1}; *B*, 0.006 mol L^{-1}; *C*, 0.010 mol L^{-1}.

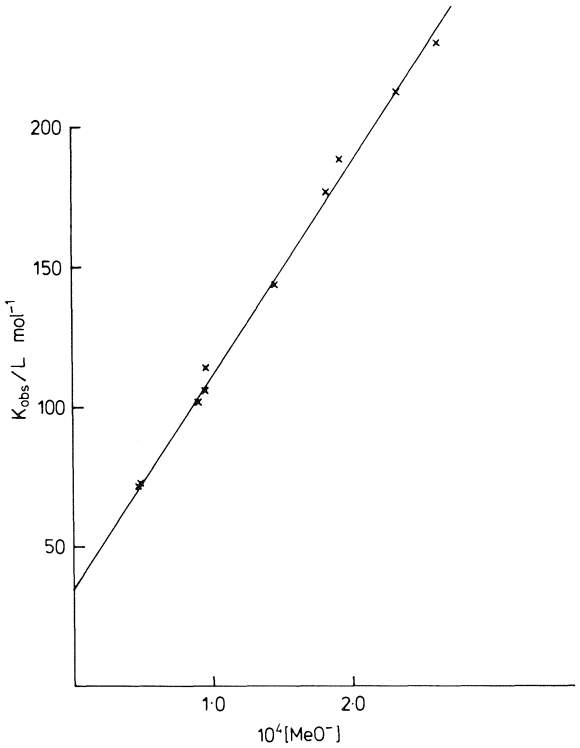

FIG. 2. Plot according to eq. [5] for the reaction of TNB with malononitrile in buffer solutions. Data at λ_{max}.

which will then rapidly expel chloride ion to yield **9**. In the presence of base **9** is expected (19, 20) to be largely ionised to **10**.

Kinetic measurements, made by stopped-flow spectrophotometry under first-order conditions, showed the presence of two well-separated processes. The rate expression for the fast process which is colour forming at 526 nm and may be identified with formation of **7** is similar to eq. [3] for reaction of TNB. However, since here methoxide attack at the 3-position may be neglected (the equilibrium constant is known (21) to have the low value of 2.6 L mol^{-1}) we obtain eq. [6]. It is readily shown

$$[6] \quad k_{fast} = k_3[CH(CN)_2^-] + \frac{k_{-3}}{1 + K[MeO^-]}$$

$$[7] \quad k_{slow} = \frac{k_1[CH(CN)_2^-]}{1 + K_3[CH(CN)_2^-] + KK_3[CH(CN)_2^-][MeO^-]}$$

that the rate expression appropriate for the slow process, colour fading at 526 nm, is eq. [7].

Data are presented in Table 5. A plot of k_{fast} versus $[CH(CN)_2^-]$ was linear with slope, k_3, 3×10^4 L mol^{-1} s^{-1} and intercept $k_{-3}/(1 + K[MeO^-])$ of 22 ± 2 s^{-1}. We expect the value of K for ionisation of **6** to be rather similar to the value for ionisation of the TNB adduct (3), since the negative charge

TABLE 5. Rate data for the reaction of picryl chloride[a] with (**2**, R = H) in methanol at 25°C

$10^4[CH_2(CN)_2]_{stoich}/M$	$[NaOMe]_{stoich}/M$	$10^4[CH(CN)_2^-]^b/M$	$k_{fast}{}^c/s^{-1}$	$k_{slow}{}^d/s^{-1}$	$k_{calcd}{}^e$
5	0.01	4.3	35		
10	0.01	8.5	45	0.74	0.71
20	0.01	16.7	73	0.96	0.99

[a]Concentration is 1×10^{-5} *M*.
[b]Calculated from the stoichiometric concentrations of malononitrile and sodium methoxide, using a value for K_{CH} of 600 L mol^{-1}.
[c]Colour forming reaction at 526 nm.
[d]Fading reaction at 526 rm.
[e]Calculated from eq. [7] with k_1 1.75×10^3 L mol^{-1} s^{-1}, and KK_3, 1.4×10^5 L^2 mol^{-1}. Account was taken of the depletion of methoxide concentration in the formation of the malononitrile anion.

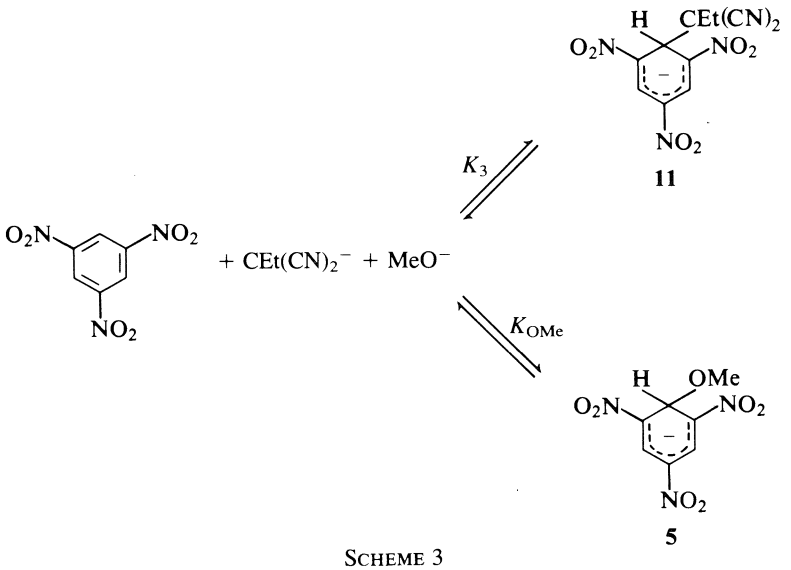

SCHEME 3

produced can not be directly delocalised into the ring. Assuming a value for *K* of 2×10^4 L mol^{-1}, as found for the TNB–adduct, we obtain a value for k_{-3} of 4400 s^{-1}. From the rate of the slower reaction we obtain a value for k_1 of 1.75×10^3 L mol^{-1} s^{-1}.

In a study of the reaction of picryl chloride with diethyl malonate Leffek and Matinopoulos-Scordou (20) observed a σ-adduct which they thought was the intermediate on the substitution pathway. It is worth noting that, in the present case, the assumption that the observed adduct has structure **8** leads to the conclusion that expulsion of chloride is slower by at least three orders of magnitude than is expulsion of the malononitrile anion. We think this is unlikely.

It is of interest to compare, Table 6, the data for picryl chloride with that for TNB. The pattern is very similar to that previously observed with oxygen bases. Thus the value of K_3 for picryl chloride is ca. six times smaller than the value for TNB (the corresponding ratios for reaction with methoxide ions (21) and with hydroxide ions (18, 22) are 6.5 and 5, respectively) and this change is due largely to a decrease in the value of k_3 while values of k_{-3} are similar. The value of k_1 for attack at the 1-position of picryl chloride is ca. 20 times lower than that for attack at the unsubstituted 3-position and ca. 200 times lower than that for attack at ring-positions of TNB. The origins of these effects have been discussed recently (22).

Reaction of ethylmalononitrile anion with TNB

Visible spectra indicate the rapid formation of a mixture of the carbon-bonded adduct (**11**) with λ_{max} 430 nm (ε, 2.5×10^4 L mol^{-1} cm^{-1}), 520 nm and the methoxide adduct (**5**),

TABLE 6. Comparison of rate and equilibrium constants for reaction of (**2**, R = H) with TNB and with picryl chloride

	Value	
Parameter	TNB	Picryl chloride
k_3/L mol^{-1} s^{-1}	3×10^5	3×10^4
k_{-3}/s^{-1}	6500	4400
K_3/L mol^{-1}	40	7
k_1/L mol^{-1} s^{-1}	—	1.75×10^3

λ_{max} 420, 490 nm (Scheme 3). A very much slower reaction gives a species probably a di-adduct (2, 3), with a single absorption in the visible region (490 nm).

A major difference from the reaction with (**2**, R = H) is that here the adduct formed, **11**, has no readily dissociable proton. Hence the favourable ionisation equilibrium, **3** ⇌ **4**, observed with the corresponding malononitrile adduct is absent. As a result conversion of TNB to the carbon-bonded adduct is considerably reduced and formation, at equilibrium, of the methoxide adduct **5** can more readily compete. To minimize this latter pathway we kept the concentration of ethyl malononitrile in large excess of the methoxide concentration. Equilibrium optical densities were measured at 430 nm and at 550 nm and are in Table 7. After correction of the values at 430 nm for the contribution due to **5** we obtain a value for K_{CH} of 33 ±

TABLE 7. Equilibrium data for the reaction of 1,3,5-trinitrobenzene[a] with (**2**, R = Et) in methanol at 25°C

				Absorbances			
$[EtCH(CN)_2]_{stoich}/M$	$[KOMe]_{stoich}/M$	$[EtC(CN)_2^-]^b/M$	$[MeO^-]^c/M$	A (430 nm)	A^d (430 nm)	A (550 nm)	K_3^e/L mol^{-1}
0.25	0.010	0.0084	0.0016	0.23	0.21	0.096	32
0.25	0.020	0.0166	0.0034	0.40	0.36	0.19	36
0.25	0.040	0.0329	0.0071	0.56	0.51	0.24	35
0.25	0.060	0.0485	0.0115	0.64	0.56	0.27	32
0.075	0.010	0.0060	0.0040	0.21	0.16	0.08	34
0.10	0.010	0.0066	0.0034	0.22	0.18	0.09	35
0.20	0.010	0.0081	0.0019	0.20	0.18	0.08	28
0.30	0.020	0.0172	0.0028	0.35	0.32	0.15	29

[a]Concentration is 4×10^{-5} M.
[b]Calculated from the stoichiometric concentrations of ethylmalononitrile and methoxide with a value for K_{CH} of 21 L mol^{-1}.
[c]Residual methoxide concentration.
[d]After subtraction of absorbance calculated for the methoxide adduct, (**5**). K_{OMe} = 17 L mol^{-1}.
[e]Calculated as $A^d(430)/(1.00 - A(430))[EtC(CN)_2^-]$. AT 430 nm both **11** and **5** have ϵ, 2.5×10^4 L mol^{-1} cm^{-1}.

TABLE 8. Comparison of equilibrium and rate data for reaction of nucleophiles with 1,3,5-trinitrobenzene in methanol

	Value for nucleophile					
Parameter	$CH(CN)_2^-$	$CEt(CN)_2^-$	CN^-	MeO^-	EtS^-	PhS^-
$(pK_a^{Nuc})^a$	14.1	15.6	13.3[c]	16.9	15	10.9
K_3^b/L mol^{-1}	40	33	200[d]	17	3500[f]	2[f]
k_3/L mol^{-1} s^{-1}	$(3 \pm 0.5) \times 10^5$	—	16[d]	7050[e]	—	—
k_{-3}/s^{-1}	6500 ± 2000	—	0.08[d]	305[e]	—	—

[a]Refers to the conjugate acid of the nucleophile, e.g. $CH_2(CN)_2$.
[b]Equilibrium constant for adduct formation at an unsubstituted position of TNB.
[c]From ref. 6.
[d]From ref. 23. Measurements refer to 80/20 v/v methanol/water.
[e]From ref. 12.
[f]From ref. 24.

5 L mol^{-1}. The data at 550 nm, where **5** shows very small absorption, lead to an identical value for K_{CH}.

Comparison of equilibrium and kinetic data

Values obtained in the present work are collected in Table 8 and are compared with some values from the literature. Values of K_3 give a measure of the carbon basicities (24, 25) of the nucleophiles, as judged by the σ-adduct forming reaction with TNB, while values of k_3 measure nucleophilicities, and k_{-3} nucleofugalities. The results show that the effect of the ethyl group in enhancing the proton basicity of the ethylmalononitrile anion relative to the malononitrile anion is not carried through in the σ-adduct forming reaction. This may reasonably be attributed to the destabilising effect of steric crowding in the adduct **11**, which is formed by reaction of the trisubstituted carbanion at a somewhat hindered site (26).

The K_3 values show that the carbon basicity towards TNB of $CH(CN)_2^-$ is greater than that of methoxide by a factor of ca. 2. However, after taking account of the pK_a difference between the two bases we obtain a ratio of ca. 10^3. This is consistent with other observations which show that carbon bases have considerably higher carbon basicities than oxygen bases of similar proton basicity (7, 25). The data in Table 8 also indicate the enhanced carbon basicities, relative to methoxide, of cyanide ion and of sulphur bases.

The value of k_3 for $CH(CN)_2^-$ is ca. 40 times larger than the corresponding value for MeO^- while the ratio for k_{-3} values is ca. 20. This is in accord with results of Bernasconi *et al.* (7) which show that relatively low intrinsic barriers may be expected for reactions involving delocalised cyano-substituted carbanions. The relatively high nucleofugality of the malononitrile anion observed here is paralleled in carbonyl-forming elimination reactions (7), but contrasts with the low nucleofugality expected in olefin-forming reaction (6, 7). In the latter class of reactions the cyanide ion is found (6) to be an extremely poor leaving group with a nucleofugality at least six orders of magnitude lower than that of methoxide ion. Our results show that expulsion of cyanide from the TNB adduct is slower than the corresponding expulsion of methoxide by a factor of ca. 4000. This, while confirming the poor leaving group ability of the cyanide ion, suggests that the range of nucleofugalities to be expected in σ-adduct decompositions may be lower than observed in olefin-forming eliminations.

Experimental

1,3,5-Trinitrobenzene, 1-chloro-2,4,6-trinitrobenzene, malononitrile, and 4-bromophenol were purified commercial specimens. Ethyl malononitrile was prepared from ethyl malonic acid in three stages. In the first stage di-esterification was accomplished by refluxing in ethanol-containing sulphuric acid. Reaction of the di-ester with aqueous ammonia yielded the di-amide which was dehydrated by refluxing from phosphorus pentoxide. The product was purified immediately before use by prep-scale gas chromatography. The ^{1}H nmr spectrum showed bands at δ 4.70 (t, 7 Hz), 2.0 (pentet, 7 Hz),

1.10 (t, 7 Hz). Mr. J. Banks is thanked for this preparation. Solutions of alkali-metal methoxides were prepared by dissolving clean sodium or potassium in AnalaR methanol under nitrogen. Cloudiness in the resulting solutions was removed on centrifugation. Concentrations were determined by titration with standardised acid. The AnalaR methanol used as solvent was de-gassed before use.

Ultraviolet/visible spectra were measured using a Pye-Unicam SP8-100 recording spectrometer of a Hi-Tech SF3L stopped-flow instrument. The latter instrument was used for kinetic studies which were made under first order conditions. Quoted rate coefficients are the mean of at least five determinations and are precise to ±5%.

1. E. Buncel, M. R. Crampton, M. J. Strauss, and F. Terrier. Electron deficient aromatic– and heteroaromatic–base interactions. Elsevier, 1984.
2. M. R. Crampton. Adv. Phys. Org. Chem. **7**, 211 (1969); M. J. Strauss. Chem. Rev. **70**, 667 (1970); G. A. Artamkina, M. P. Egorov, and I. P. Beletskaya. Chem. Rev. **82**, 427 (1982).
3. I. Kolb, V. Macháček, and V. Štěrba. Collect. Czech. Chem. Commun. **41**, 1914 (1976).
4. J. Kaválek, A. Ashtaq, and V. Štěrba. Collect. Czech. Chem. Commun. **44**, 1453 (1979).
5. J. Kaválek, V. Macháček, and V. Štěrba. Collect. Czech. Chem. Commun. **42**, 2928 (1977).
6. C. J. M. Stirling. Acc. Chem. Res. **12**, 198 (1979); C. J. M. Stirling and M. Varma. J. Chem. Soc. Chem. Commun. 553 (1981).
7. C. F. Bernasconi, K. A. Howard, and A. Kanavarioti. J. Am. Chem. Soc. **106**, 6827 (1984); C. F. Bernasconi, J. L. Zitomer, J. P. Fox, and K. A. Howard. J. Org. Chem. **49**, 482 (1984).
8. J. R. Jones. The ionisation of carbon acids. Academic Press. 1973.
9. R. H. Boyd and C. Wang. J. Am. Chem. Soc. **87**, 430 (1965).
10. K. Bowden and R. Stewart. Tetrahedron, **21**, 261 (1965).
11. C. H. Rochester and B. Rossall. J. Chem. Soc. Perkin Trans. II, 743 (1967).
12. C. F. Bernasconi. J. Am. Chem. Soc. **92**, 4682 (1970).
13. M. R. Crampton and H. A. Khan. J. Chem. Soc. Perkin Trans. II, 710 (1973).
14. M. R. Crampton. J. Chem. Soc. B, 2112 (1971).
15. E. Buncel and J. G. K. Webb. Can. J. Chem. **52**, 630 (1974).
16. F. Hibbert, F. A. Long, and E. A. Walters. J. Am. Chem. Soc. **93**, 2829 (1971); F. Hibbert. Comprehensive chemical kinetics. **8**, 97 (1977).
17. M. R. Crampton, M. A. El Ghariani, and H. A. Khan. Tetrahedron, **28**, 3299 (1972).
18. B. Gibson and M. R. Crampton. J. Chem. Soc. Perkin Trans. II, 648 (1979).
19. J. Kaválek, M. Pastonek, and V. Štěrba. Collect. Czech. Chem. Commun. **43**, 1401 (1978).
20. K. J. Leffek and A. E. Matinopoulos-Scordou. Can. J. Chem. **55**, 2656 (1977); **55**, 2664 (1977).
21. L. H. Gan and A. R. Norris. Can. J. Chem. **52**, 18 (1974).
22. M. R. Crampton and C. Greenhalgh. J. Chem. Soc. Perkin Trans. II. 187 (1986).
23. D. N. Brooke. Ph.D. Thesis, University of Durham. 1981.
24. M. R. Crampton. J. Chem. Soc. B, 1208 (1968).
25. J. Hine and R. D. Weimar. J. Am. Chem. Soc. **87**, 3387 (1965).
26. A. D. A. Al Aruri and M. R. Crampton. J. Chem Soc. Perkin Trans. II, 807 (1981).

Enthalpies of solution of urea in water–alkanol mixtures and the enthalpic pair interaction coefficients of urea and several nonelectrolytes in water

HENRYK PIEKARSKI
Institute of Physical Chemistry, University of Lódź, ul. Nowotki 18, Lódź, 91-416 Poland

AND

GUS SOMSEN
Department of Chemistry, Vrije Universiteit, De Boelelaan 1083, 1081 HV Amsterdam, The Netherlands

Received January 30, 1986

HENRYK PIEKARSKI and GUS SOMSEN. Can. J. Chem. **64**, 1721 (1986).

Enthalpies of solution of urea in binary mixtures of isopropanol, *s*-butanol, and ethoxyethanol with water have been measured at high water content. Those in the binaries isopropanol + water and ethoxyethanol + water show endothermic maxima at 8 and 4 mol% alkanol, respectively. Enthalpic pair interaction coefficients are calculated for the interactions between urea and the alkanols and discussed in connection with these coefficients for interactions between urea and other nonelectrolytes and between *N,N*-dimethylformamide and several nonelectrolytes. The enthalpic pair interaction coefficients correlate linearly with the heat capacity change on hydration of the nonelectrolytes and with the enthalpy of hydrophobic hydration of the alkanols.

HENRYK PIEKARSKI et GUS SOMSEN. Can. J. Chem. **64**, 1721 (1986).

Opérant dans des mélanges contenant une forte proportion d'eau, on a déterminé les enthalpies de solution de l'urée dans des mélanges binaires d'isopropanol, de *s*-butanol et d'éthoxyéthanol avec de l'eau. Les solutions dans des mélanges binaires d'isopropanol + eau et éthoxyéthanol + eau présentent respectivement des maxima endothermiques à 8 et à 4 mol% d'alcanol. On a calculé les coefficients d'interaction des paires enthalpiques pour les interactions entre l'urée et les alcanols et on en discute en relation avec les mêmes coefficients pour les interactions entre l'urée et d'autres non-électrolytes et entre le *N,N*-diméthylformamide et plusieurs non-électrolytes. Il existe une corrélation linéaire entre les coefficients d'interaction des paires enthalpiques et les changements de capacité calorifique lors de l'hydratation des non-électrolytes ainsi qu'avec l'enthalpie de l'hydratation hydrophobe des alcanols.

[Traduit par la revue]

Introduction

Much attention has recently been devoted to the so called "enthalpic pair interaction coefficients" h_{xy} of solutes in dilute solutions. These coefficients are regarded as a measure of the heat effect (i.e. the enthalpy of interaction) when two solute particles approach each other. Enthalpic interaction coefficients can be obtained from enthalpies of dilution (interactions between similar solutes) and enthalpies of mixing or of dissolution leading to three-component systems (interactions between dissimilar solutes) (1–3). The theoretical calculation of pair interaction coefficients by statistical mechanical methods has been performed by several authors (1, 4, 5), but has to face the problem that the results are sensitive to subtle details in the adopted potentials of mean force of the solute particles. In another line of approach the attention has been focussed on the interpretation of qualitative and quantitative variations of the interaction coefficients within groups of more or less related compounds (2, 3, 6–15). The group additivity concept developed by Savage and Wood (6) to correlate enthalpic pair interaction coefficients of a wide range of nonelectrolytes (mainly alcohols, polyhydroxy compounds, and amides) in water has been found to be very useful in predicting unknown values. A similar group additivity concept was employed by Heuvelsland, De Visser, and Somsen (16) to the analysis of interactions in systems containing ionic solutes (tetraalkylammonium bromides) in water as well as in the nonaqueous solvent *N,N*-dimethylformamide (DMF). Also the enthalpic interaction coefficients for NaI–alcohol pairs in aqueous solution appeared to be a sum of group contributions (17).

In a previous paper of one of the present authors (H.P., ref 17) the enthalpic pair interaction coefficients were analyzed in terms of correlations between h_{xy} and other properties of the solutes. In this way it seemed possible to find which interaction in the investigated aqueous systems gives the leading contribution to h_{xy}. All systems contained one electrolyte (NaI) with different nonelectrolytes. Simple correlations were found between h_{xy} (NaI–nonelectrolyte) in water and the molecular polarizability (α) of the nonelectrolyte as well as its Kosower acidity parameter (Z). However, the correlations are not general and hold only for groups of related compounds. The aim of this study is to explore the possibilities for a more general correlation of pair interaction coefficients with solute properties, using solutes with different molecular structure. The systems DMF–nonelectrolyte and urea–nonelectrolyte both in aqueous solution were selected for this purpose since there are many data in the literature concerning the pair interaction coefficients in these systems (2, 6, 9, 13, 14, 18). In order to enlarge the number of data for our analysis, we have determined experimentally some additional h_{xy} values for urea–nonelectrolyte interactions by measuring the enthalpies of solution of urea (U) in aqueous solutions of isopropanol (*i*-PrOH), *s*-butanol (*s*-BuOH), and ethoxyethanol (EEtOH).

Experimental

Urea, purissimum (POCh, Gliwice, Poland) was recrystallized from doubly distilled water and dried under vacuum for several days at 330 K. Isopropanol, analytically pure (POCh Gliwice, Poland), *s*-butanol, A.R. (Reanal, Hungary), and ethoxyethanol, analytically pure (Loba Chemie), were purified and dried by standard methods (19). Solutions of the alcohols in water were prepared by weight.

Enthalpies of solution of urea in the different solvent mixtures were measured in an isoperibol type calorimeter. The spherical glass calorimetric vessel with a capacity of 100 cm^3 was equipped with a calibration heater, stainless steel stirrer, and two thermistors as temperature sensors. Small glass ampoules containing the substance to

TABLE 1. Enthalpies of solution of urea in aqueous solutions of isopropanol (*i*-PrOH), sec-butanol (*s*-BuOH) and ethoxyethanol (EEtOH) at 298.15 K

Mass % of nonelectrolyte	ΔH_{sol} (kJ mol^{-1})		
	i-PrOH	*s*-BuOH	EEtOH
0	15.29 ± 0.03	15.29 ± 0.03	15.29 ± 0.03
2.5	15.68 ± 0.03	15.69 ± 0.03	15.45 ± 0.02
5.0	16.11 ± 0.03	16.16 ± 0.02	15.61 ± 0.02
7.5	—	16.56 ± 0.04	15.72 ± 0.04
10.0	16.84 ± 0.04	16.95 ± 0.04	15.82 ± 0.03
12.5	—	17.28 ± 0.03	—
15.0	17.51 ± 0.02	17.65 ± 0.05	15.94 ± 0.02
20.0	17.91 ± 0.03		15.73 ± 0.04
25.0	17.78 ± 0.04		15.33 ± 0.03
30.0	17.32 ± 0.05		14.94 ± 0.04

be dissolved can be attached to the stirrer. The dissolution process was initiated by crushing the ampoule against the bottom of the calorimetric vessel. The thermistors were connected to a multivibrator system which generates a rectangular wave. Its frequency changes correspond to changes of the temperature of the calorimeter. The frequency was measured by means of a digital frequencymeter type PFL-21 (Kabid, Poland). Its sensitivity of ±1 Hz corresponds to a temperature change of about 2×10^{-5} K. The calorimeter resides in a hermetically closed brass jacket with a capacity of about 1 dm^3 within a water thermostat. The temperature stability of the thermostat was better than 1×10^{-3} K.

Results

The final concentration of the urea solutions ranged from 0.006 to 0.015 mol dm^{-3}. No concentration dependence (outside the error limits) of the enthalpies of solution was observed and consequently the measured enthalpies were regarded as those at infinite dilution ΔH^{∞}_{sol}.

The values of ΔH^{∞}_{sol} for urea in aqueous solutions of *i*-PrOH, *s*-BuOH, and EEtOH at 298.15 K are listed in Table 1. The dissolution enthalpy of urea in water obtained by us (15.29 ± 0.03 kJ mol^{-1}) is in very good agreement with literature data: 15.28 kJ mol^{-1} (20), 15.29 kJ mol^{-1} (21), 15.30 kJ mol^{-1} (2), 15.31 kJ mol^{-1} (22).

Discussion

Enthalpies of solution

The enthalpies of solution of urea in the mixtures of water with isopropanol, *s*-butanol, and ethoxyethanol are plotted in Fig. 1 as a function of the mole percentage of the organic component. The curves representing the enthalpies of solution for urea in water + *i*-PrOH and water + EEtOH exhibit maxima at low alcohol contents. A similar extremum in ΔH^{∞}_{sol} has been observed in the urea – water – tertiary butanol system studied by Desnoyers *et al.* (2), as well as in all electrolyte–water–alkanol systems studied thus far. When it is assumed that these maxima are related to structure-making or -stabilizing effects of the alkanols when they are added to water (23–26), it appears that such effect is larger for the more globular solute *i*-PrOH than for the longer and non-branched molecule EEtOH.

Enthalpic pair interaction coefficients

From the enthalpy of solution data we have calculated the enthalpic pair interaction coefficients h_{xy} for the interaction urea–nonelectrolyte in water. The method of calculation has

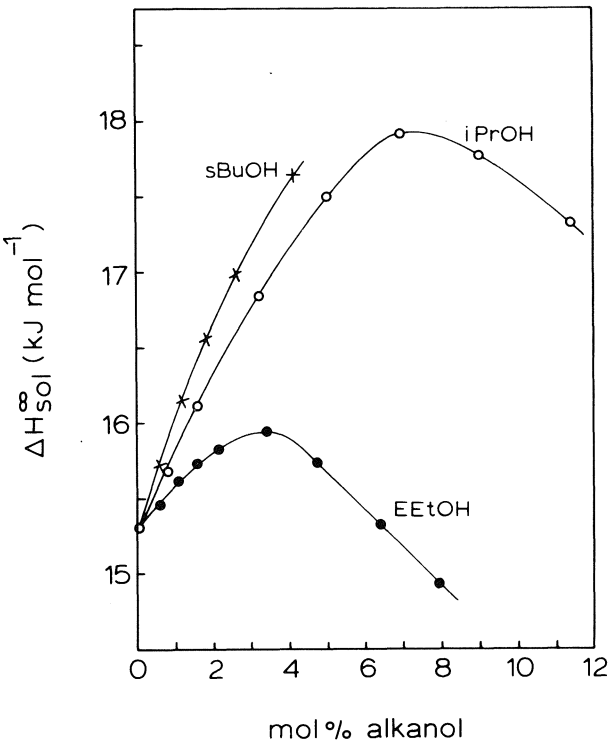

FIG. 1. Enthalpies of solution of urea in mixtures of water with isopropanol (*i*-PrOH), *s*-butanol (*s*-BuOH), and ethoxyethanol (EEtOH) vs. mol% of the nonaqueous component.

been described previously (17) and the results are given in Table 2. In Table 2 are collected also a number of values obtained in other investigations on urea–nonelectrolyte and DMF–nonelectrolyte interactions. There are a few general trends in the h_{xy} values. In all cases where interaction coefficients with DMF and with urea are known, the coefficients involving an interaction with DMF are more positive than those corresponding to an interaction with urea. Also, the interaction coefficients with DMF as well as with urea become more positive when the co-solute carries more or larger alkyl groups.

The interaction between molecules in aqueous solution leads to modification of the hydration structures (co-spheres) around the molecules. Due to an overlap of co-spheres some of the hydration water molecules may change their spatial arrangement from the co-sphere structure to a structure typical for bulk water (1, 28, 29). For correlation with enthalpic coefficients it may therefore be appropriate to pay attention to functions that are known to be sensitive to structural changes in solution. The entropy of hydration ΔS_h, probably the best function for this purpose, is only known in a few cases for the systems investigated here. Another function exhibiting comparable behaviour with respect to structural changes in solution as the entropy is the heat capacity (30). In order to reflect the contribution of the solvent to the total partial molar heat capacity of the solute, we have used values relative to the molar heat capacity in the gaseous state, i.e. heat capacities of transfer defined by

$$\delta C_p = \bar{C}^{\infty}_{p,2} - C^{g}_{p,m}$$

in which $\bar{C}^{\infty}_{p,2}$ is the partial molar heat capacity of a solute at infinite dilution in water and $C^{g}_{p,m}$ is the molar heat capacity of the same solute in the vapour phase. Values of δC_p are

TABLE 2. Enthalpic pair interaction coefficients h_{xy} of solutes X (DMF and urea) and co-solutes Y in water at 298.15 K

	h_{xy} (J kg mol^{-2})			h_{xy} (J kg mol^{-2})	
Co-solute Y	DMF	Urea	Co-solute Y	DMF	Urea
1, MeOH	531[a]		**12**, glucose		−378[e]
2, EtOH	762[a]	319[b]	**13**, mannitol	852[f]	
3, *n*-PrOH	1024[a]	424[b]	**14**, *n*-hexylamine	1632[a]	
4, *i*-PrOH	1020[a]	499 ± 13[c]	**15**, urea	−156[a]	−350[e,g]
5, *n*-BuOH	1300[a]	475[b]	**16**, formamide	136[a]	
6, *i*-BuOH	1236[a]		**17**, *N*-methylformamide	419[a]	−109[e]
7, *s*-BuOH	1296[a]	623 ± 18[c]	**18**, dimethylformamide	617[a]	−156[a]
8, *t*-BuOH	1281[a]	715[d]	**19**, *N*-methylacetamide		0[e]
9, *n*-PenOH	1506[a]		**20**, *N*-butylacetamide	1263[a]	
10, *t*-PenOH	1583[a]		**21**, acetone		50[h]
11, EEtOH		314 ± 7[c]	**22**, tetrahydrofuran		295[h]

[a]Reference 14, the uncertainty of the h_{xy} values in this reference has been estimated at 15%.
[b]Reference 27.
[c]This paper.
[d]Reference 2.
[e]Reference 6.
[f]Reference 13.
[g]Reference 3.

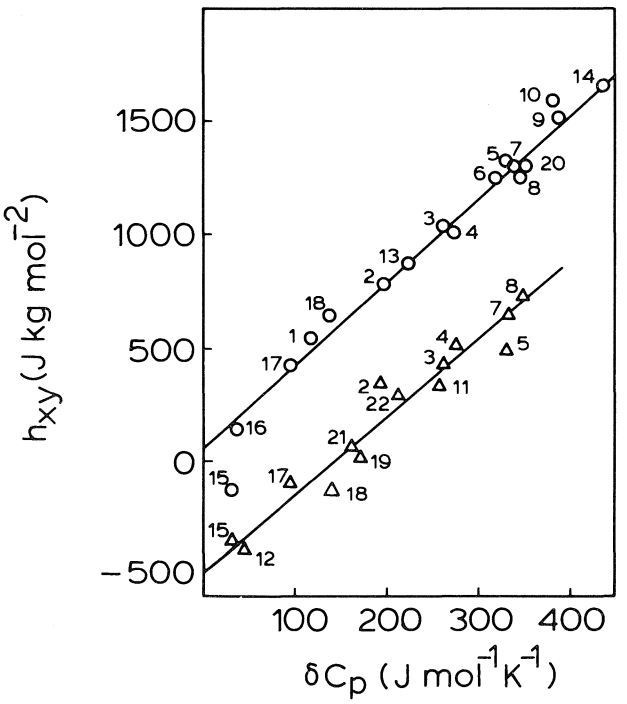

FIG. 2. The dependence of the enthalpic pair interaction coefficients h_{xy} for DMF–nonelectrolyte (circles) and urea–nonelectrolyte (triangles) interactions on the heat capacity of transfer ($\bar{C}_{p,2} - C_{p,m}$) of the nonelectrolyte from vapour phase to high dilution in water. The numbers correspond to those given in Table 2.

given in a compilation of Cabani *et al.* (31). The relation of the pair interaction coefficients h_{xy} for pairs: DMF–nonelectrolyte Y, and for pairs urea–nonelectrolyte Y with δC_p is presented in Fig. 2. As can be seen in this figure, there is a good linear correlation for interactions with DMF as well as for interactions with urea. The slope of the line correlating δC_p with h_{xy} values for pairs DMF–nonelectrolyte is 3.63 ± 0.12 kg mol^{-1} K^{-1}; that for pairs urea–nonelectrolyte amounts to 3.25 ± 0.22 kg mol^{-1} K^{-1}.

Values of h_{xy} will depend primarily on three effects: (*a*) the hydration of a separate molecule X; (*b*) the hydration of a separate molecule Y; and (*c*) the interaction between molecules X and Y when they approach each other. For a given particle X effect *a* will be constant. The linear dependences of h_{xy} for a given X with a hydration property of the varying co-solute Y, as found in Fig. 2, strongly suggests that effect *b* is more important than effect *c*. The two separate lines obtained in Fig. 2 demonstrate that h_{xy} is also determined by the difference in hydration between DMF and urea molecules (effect *a*). Since the slopes of the lines are approximately equal, it may be concluded that the cosphere overlap of the different co-solutes with DMF changes in the same way as that with urea. Again specific effects (*c*) seem to be of minor importance. However, they may be present in some cases. For instance, the deviations of the h_{xy} value for the DMF–urea interaction from both linear relations in Fig. 2 may well be due to this, since they are both far beyond the experimental uncertainty.

In water, part of the co-solutes given in Fig. 2 are hydrophobically hydrated. As a measure for their hydrophobicity the enthalpy of hydrophobic hydration Hb(W) of the nonelectrolyte may be adopted which is defined by De Visser and Somsen (32) and evaluated for the alcohols by Rouw (14). In the h_{xy} values would depend mainly on the hydrophobic hydration effect, a simple correlation between h_{xy} and Hb(W) should be expected. Figure 3 shows a plot of h_{xy} for DMF–alkanol interactions and for urea–alkanol interactions vs. Hb(W) of the alkanol. The good linear correlation for these systems confirms the conclusion about the influence of the hydration of the co-solute drawn above.

Values of h_{xy} for urea–nonelectrolyte interactions may also be compared with those for NaI–nonelectrolyte interaction published recently (17). Figure 4 shows that there is a good correlation between the two series of values. The slope of the line correlating these data is close to unity (0.99 ± 0.07). Hence,

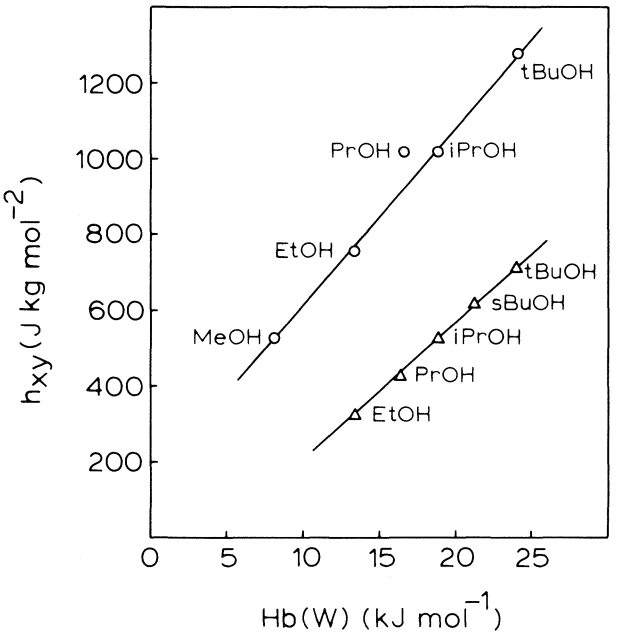

FIG. 3. The correlation between the hydrophobic hydration enthalpy Hb(W) of alkanols and the enthalpic pair interaction coefficients h_{xy} for DMF–alkanol and urea–alkanol pairs.

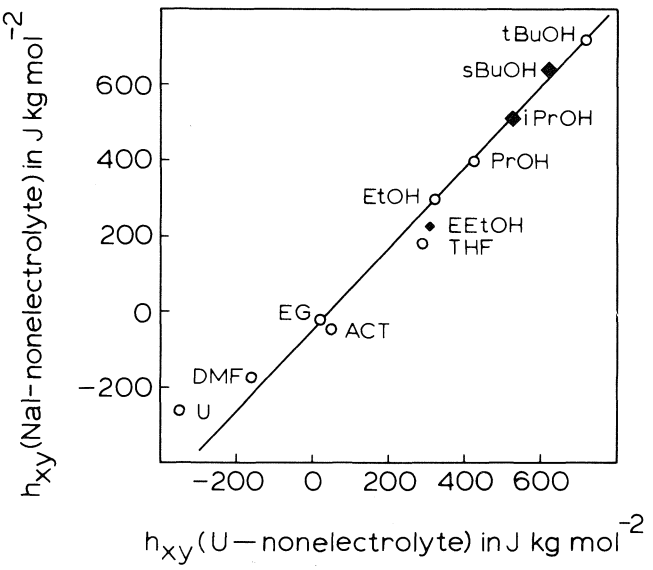

FIG. 4. The correlation between the enthalpic pair interaction coefficients h_{xy} for urea–nonelectrolyte pairs and for the NaI–nonelectrolyte pairs. EG = ethylene glycol; ACT = acetonitrile; THF = tetrahydrofuran; ◆: our data (the dimensions refer to the error limits); ○: literature data.

from the point of view of enthalpic pair interaction coefficients, the differences between urea–nonelectrolyte and electrolyte–-nonelectrolyte are predominantly quantitative. Probably there is some similarity in the hydration of urea and ionic solutes. The urea molecule has proton-donor and proton-acceptor as well as electron-donor and electron-acceptor properties. For this reason it might interact in a way comparable to that for cations and anions.

1. H. L. FRIEDMAN and C. V. KRISHNAN. J. Solution Chem. **2**, 119 (1973).
2. J. E. DESNOYERS, G. PERRON, L. AVEDIKIAN, and J.-P. MOREL. J. Solution Chem. **5**, 631 (1976).
3. F. FRANKS, M. D. PEDLEY, and D. S. REID. J. Chem. Soc. Faraday Trans. I, **72**, 359 (1976).
4. A. H. CLARK, F. FRANKS, M. D. PEDLEY, and D. S. REID. J. Chem. Soc. Faraday Trans. I, **73**, 290 (1977).
5. L. R. PRATT and D. CHANDLER. J. Solution Chem. **9**, 1 (1980).
6. J. J. SAVAGE and R. H. WOOD. J. Solution Chem. **5**, 733 (1976).
7. B. Y. OKAMOTO, R. H. WOOD, and P. T. THOMPSON. J. Chem. Soc. Faraday Trans. I, **74**, 1990 (1978).
8. G. PERRON, D. JOLY, J. E. DESNOYERS, L. AVEDIKIAN, and J.-P. MOREL. Can. J. Chem. **56**, 552 (1978).
9. F. FRANKS and M. D. PEDLEY. J. Chem. Soc. Faraday Trans. I, **77**, 1341 (1981).
10. G. BARONE, E. CASTRONUOVO, and V. ELIA. J. Solution Chem. **9**, 607 (1980).
11. G. M. BLACKBURN, T. H. LILLEY, and E. WALMSLEY. J. Chem. Soc. Faraday Trans. I, **76**, 915 (1980).
12. G. PERRON and J. E. DESNOYERS. J. Chem. Thermodyn. **13**, 1105 (1981).
13. I. R. TASKER and R. H. WOOD. J. Solution Chem. **11**, 295 (1982).
14. A. ROUW. Thesis, Free University, Amsterdam. 1982.
15. M. BLOEMENDAL and G. SOMSEN. J. Solution Chem. **12**, 83 (1983).
16. W. J. M. HEUVELSLAND, C. DE VISSER, and G. SOMSEN. J. Chem. Soc. Faraday Trans. I, **77**, 1191 (1981).
17. H. PIEKARSKI. Can. J. Chem. **61**, 2203 (1983).
18. V. ABATE, G. BARONE, G. CASTRONUOVO, V. ELIA, and V. SAVINO. J. Chem. Soc. Faraday Trans. I, **80**, 759 (1984).
19. A. WEISSBERGER, E. S. PROSKAUER, J. A. RIDDICK, and E. E. TOOPS, JR. Organic solvents. Interscience Publishers, New York. 1955.
20. C. DE VISSER, H. J. M. GRÜNBAUER, and G. SOMSEN. Z. Physik Chem. N.F. **97**, 69 (1975).
21. M. Y. SCHRIER, P. J. TURNER, and E. E. SCHRIER. J. Phys. Chem. **79**, 1391 (1975).
22. E. P. EGAN and B. B. LUFF. J. Chem. Eng. Data, **11**, 192 (1966).
23. G. NEMETHY and H. A. SCHERAGA. J. Phys. Chem. **66**, 1773 (1964).
24. O. YA. SAMOILOV. Zhur. Strukt. Khim. **7**, 15 (1964); **7**, 175 (1964).
25. G. NEMETHY. Ann. Ist. Super. Sanita, **6**, 487 (1970).
26. K. P. MISHCHENKO and G. M. POLTORATSKII. Problems of thermodynamics and structure of aqueous and nonaqueous electrolyte solutions. Plenum, New York. 1972.
27. G. BARONE, P. CACACE, G. CASTRONUOVO, M. COZZOLINO, and V. ELIA. Proc. 2nd Czechoslovak Conf. Calorimetry, Prague and Liblice, Sept. 1982. p. 111.
28. J. E. DESNOYERS, M. AREL, G. PERRON, and C. JOLICOEUR. J. Phys. Chem. **73**, 3346 (1969).
29. F. FRANKS. Water, a comprehensive treatise. Vol. 2. Plenum, New York. 1972. Chapt. 5.
30. H. S. FRANK and W. Y. WEN. Discuss. Faraday Soc. **24**, 133 (1957).
31. S. CABANI, P. GIANNI, V. MOLICA, and L. LEPORI. J. Solution Chem. **10**, 563 (1981).
32. C. DE VISSER and G. SOMSEN. J. Phys. Chem. **78**, 1719 (1974).

Composés du phosphore dicoordonné : action des amines sur les triazaphospholes-1,2,4,3 substitués en 2,5. Étude thermodynamique de l'équilibre de formation des triazaphospholines et caractérisation de leurs dérivés tétracoordonnés

MARIE-THÉRÈSE BOISDON, LUCIEN LOPEZ, CHRISTIAN MALAVAUD ET JEAN BARRANS[1]
Centre national de la recherche scientifique, Unité associée 454, Université Paul Sabatier, 118 Route de Narbonne, 31062 Toulouse CEDEX, France

ABDELAZIZ CHABANE
École nationale d'ingénieurs de Gabès, Tunisie

ET

RAYMONDE MATHIS
Laboratoire des hétérocycles du phosphore et de l'azote, 118 Route de Narbonne, 31062 Toulouse CEDEX, France

Reçu le 8 novembre 1985

MARIE-THÉRÈSE BOISDON, LUCIEN LOPEZ, CHRISTIAN MALAVAUD, JEAN BARRANS, ABDELAZIZ CHABANE et RAYMONDE MATHIS. Can. J. Chem. **64**, 1725 (1986).

Les amines réagissent sur les triazaphospholes-1,2,4,3 substitués en 2,5 pour conduire à des composés d'addition en 1,2 selon une réaction équilibrée. Cet équilibre est mis en évidence d'une part par abaissement de la température, d'autre part par voie chimique : l'addition de soufre, de sélénium ou d'azoture (X) déplace entièrement l'équilibre vers le composé d'addition 1,2 :

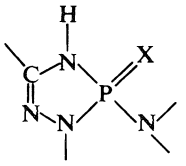

Les grandeurs thermodynamiques associées à cet équilibre ont été déterminées dans quelques cas.

MARIE-THÉRÈSE BOISDON, LUCIEN LOPEZ, CHRISTIAN MALAVAUD, JEAN BARRANS, ABDELAZIZ CHABANE, and RAYMONDE MATHIS. Can. J. Chem. **64**, 1725 (1986).

The oxidation of 2,5-disubstituted 1,2,4,3-triazaphospholes with amines gives 1,2 addition products by an equilibrium reaction. This equilibrium has been proved by temperature lowering and also by chemical reaction: addition of sulfur, selenium, or azide (X) shifts the equilibrium to the 1,2 addition products:

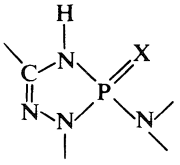

The thermodynamical parameters associated with this equilibrium have been determinated in some cases.

Introduction

Nous avons observé au laboratoire (1) que les triazaphospholes-1,2,4,3 substitués en 2,5 par des groupements alkyles ou phényles **1** réagissent avec les amines primaires et secondaires pour conduire à des amino-3 triazaphospholines **2** suivant une réaction réversible. Deux types de réaction étaient envisagés : *voie a* : la simple addition 1,2; et *voie b*: une addition 1,1 suivie d'un réarrangement.

La rmn (résonance magnétique nucléaire) à température variable n'a pas permis de mettre en évidence la présence d'un groupement P—H; néanmoins nous ne pouvons pas exclure la voie b.

En effet des travaux récents d'addition d'amine sur des phosphazènes acycliques (2) ont conduit à l'observation des

[1]

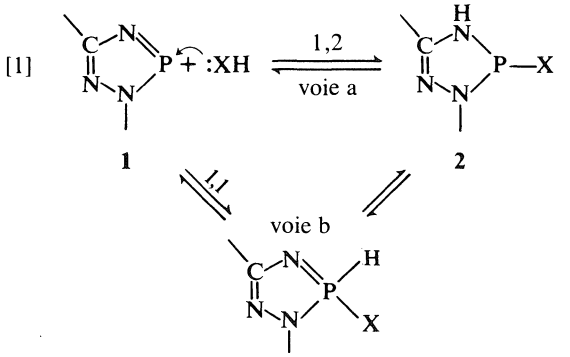

1. Auteur à qui adresser toute correspondance.

deux types d'addition suivant la nature du reste R :

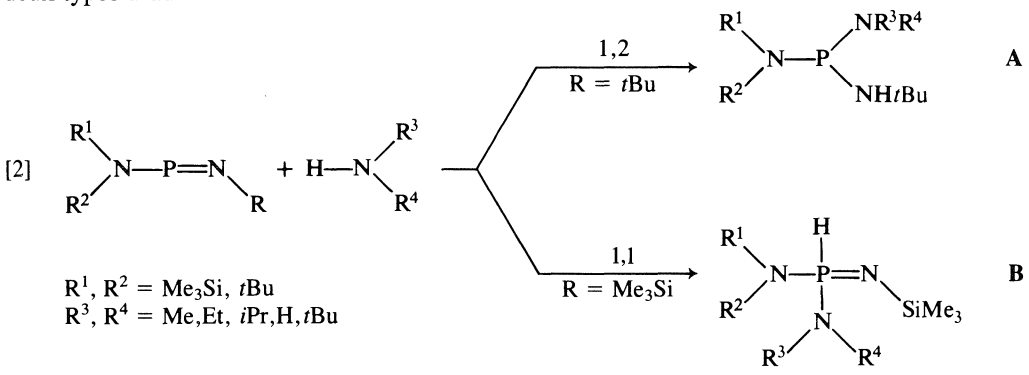

Les auteurs considérent que la formation de **A** ou de **B** est liée à des effets stériques et électroniques. Dans le cas particulier de l'aniline, et lorsque R = $SiMe_3$, il y a *équilibre* entre les formes **A** et **B**. Lorsque l'encombrement est trop grand autour de l'atome de phosphore, la réaction n'a pas lieu; par exemple, la diisopropylamine ne réagit pas lorsque R = *t*Bu.

Nous avons repris l'étude de l'addition oxydante d'amine sur les dérivés **1** en diversifiant les amines et les restes portés par le composé phosphoré (tableau 1).

Ce travail comportera deux parties : 1. Mise en évidence de l'équilibre [1] par abaissement de la température avec détermination des paramètres thermodynamiques et étude des facteurs de l'équilibre. 2. Déplacement de l'équilibre par voie chimique et étude des dérivés formés **3**, **4** et **5**.

I. Étude thermodynamique de l'équilibre

Influence de la nature de l'amine

Nous avons tenté de détecter la présence éventuelle du composé d'addition 1,1 en utilisant des amines silylées et en opérant, dans certains cas, à basse température (addition des réactifs vers −50°C). Dans tous les cas, le seul produit observé a été l'amino-3 triazaphospholine-1,2,4,3 **2**.

L'abaissement de la température du mélange réactionnel a permis d'observer la formation d'adduits avec l'aniline, la tertiobutylamine ou l'ammoniac, qui nous avaient semblé initialement inactives sur les Me-2 triazaphospholes-1,2,4,3 (1).

Une étude thermodynamique de l'équilibre suivant :

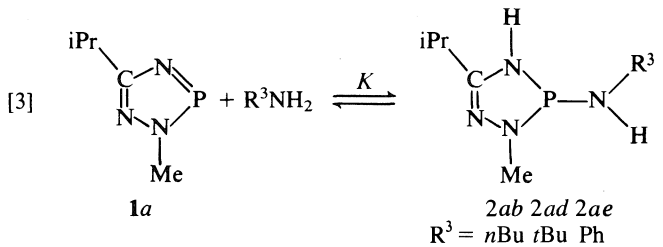

a été faite par rmn de ^{31}P sur des mélanges stoechiométriques en solution dans le toluène. L'établissement de l'équilibre est rapide; il est atteint en moins de 2 min à température ordinaire, de 10 min à −50°C.

Les résultats des mesures sont rassemblés sur la figure 1 et dans le tableau 2.

La constante de l'équilibre dépend notamment de la force de la nouvelle liaison P—N formée. C'est ainsi qu'avec l'aniline moins basique (pK_b = 9,37) que la *n*-butylamine (pK_b = 3,23),

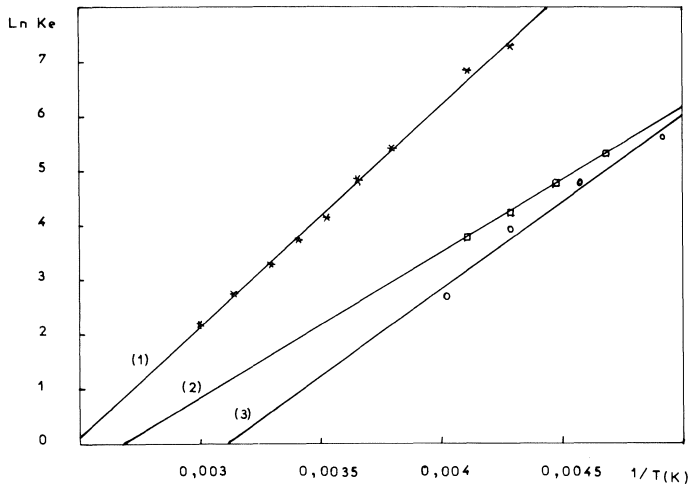

FIG. 1. Variation de la constante de l'équilibre [3] en fonction de la température (solvant : toluène). * **1***a* + $nBuNH_2$; □ **1***a* + $tBuNH_2$; ○ **1***a* + $PhNH_2$.

(3), le doublet de l'azote déjà engagé dans la conjugaison avec le phényle n'est pas disponible pour renforcer la liaison P—N par retrocoordination. On a bien : $K(n\text{Bu}) > K(\text{Ph})$. Par ailleurs avec la tertiobutylamine (pK_b = 3,17), de basicité comparable à celle de la *n*-butylamine, le produit formé est destabilisé par une gêne stérique entre le groupement *t*Bu et le groupement méthyle porté par l'azote N2 du cycle ($K(n\text{Bu}) > K(t\text{Bu})$).

Influence du solvant

Les solvants basiques (DMSO, pyridine) favorisent la formation des dérivés **2**. Dans l'équilibre : **1***c* + $nBuNH_2 \rightleftharpoons$ **2***cb*, la constante K_{308} est environ dix fois plus élevée dans le DMSO que dans le toluène et six fois plus dans la pyridine que dans le toluène (K_{308} (tol.) = 3,8; K_{308} (DMSO) = 75; K_{308} (pyr.) = 22). Le solvant basique doit stabiliser le composé P^{III} formé, par solvatation de l'hydrogène très acide (4) lié à l'azote N4 du cycle.

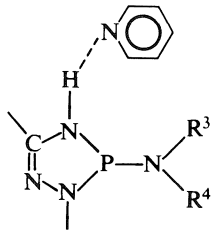

TABLEAU 1. Réactifs et composés formés

Triazaphospholes (a–e)

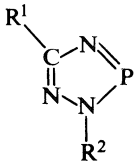

		a	*b*	*c*	*d*	*e*
1 (*a–e*)	R^1	*i*Pr	CH_2Ph	Ph	Ph	Ph
	R^2	Me	Me	Me	Ph	$SiMe_3$

Amines **7** (*a–r*)

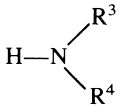

	a	*b*	*c*	*d*	*e*	*f*	*g*	*h*	*i*
R^3	H	nBu	CH_2Ph	*t*Bu	Ph	*CHMePh	CH_2*t*Bu	Me	Et
R^4	H	H	H	H	H	H	H	Me	Et

	j	*k*	*l*	*m*	*n*	*o*	*p*	*q*	*r*
R^3	C_2H_4Cl	iPr	Ph			Pr	CH_2Ph	*t*Bu	$SiMe_3$
R^4	C_2H_4Cl	iPr	Ph			$SiMe_3$	$SiMe_3$	$SiMe_3$	$SiMe_3$

Composés formés

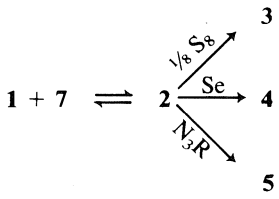

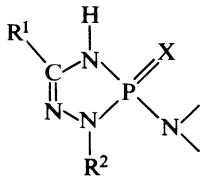

X :	S	Se	NR
	2	**3**	**4**	**5**

Appellation des composés formés : **N***xy*

N : caractérise la famille des composés (**2–5**)
x : caractérise le triazaphosphole de départ (*a–e*)
y : caractérise le reste amino (*a–r*)

ex.: 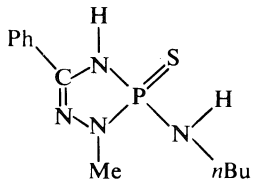 **3***cb*

Cette stabilisation a été observée dans l'étude de l'équilibre (5) :

[4] 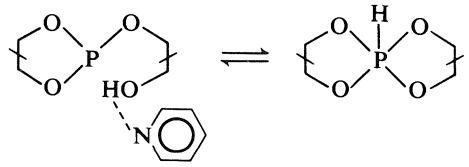

Influence du substituant R^2 du triazaphosphole

On observe un déplacement de l'équilibre vers la formation de l'amino-3 triazaphospholine lorsque R^2 = Ph (**1***d*) par rapport aux cas où R^2 = Me (**1***a*, **1***b*, **1***c*) (Tableau 3).

La présence d'un groupement phényle en position 2 doit favoriser la conjugaison avec le cycle triazaphospholine et renforcer l'interaction $p\pi$–$d\pi$ entre l'azote exocyclique et le phosphore. Ces effets stabilisent l'aminotriazaphospholine.

Lorsque R^2 = $SiMe_3$, l'effet (−*I*) du silicium se traduit sur le triazaphosphole **1***e* par un déblindage du signal de rmn de ^{31}P ($\Delta\delta$ ^{31}P = +24 ppm). L'accroissement de l'électrophilie du phosphore doit favoriser l'addition d'amines. En fait, on obtient le même pourcentage de P^{III} qu'avec **1***c* (R^2 = Me) par suite de l'encombrement stérique du groupement $SiMe_3$.

Étude par rmn de ^{31}P des triazaphospholines **2**

Déplacements chimiques

Les déplacements chimiques observés en rmn de ^{31}P sont faibles (50–80 ppm) par rapport à ceux donnés généralement dans la littérature pour les tris(amino)phosphines et les amino-3 diazaphospholidines-1,3,2 (80–120 ppm) (2*a*, 6, 7). Toutefois les amino-3 tetrazaphospholines-1,2,4,5,3 (8) ont des déplacements chimiques encore plus faibles (~35 ppm).

Isomérie de rotation

De nombreuses études ont été faites sur la conformation stéréodynamique de mono, bis ou tris(amino)phosphines et d'aminodiazaphospholidines-1,3,2 s'appuyant sur des expériences de rmn de ^1H et ^{13}C à température variable (9–11) et sur

TABLEAU 2. Grandeurs thermodynamiques de l'équilibre [3] (solvant : toluène)

	R^3	Conc. (mol/L)	K_{298K} (1/mol)	ΔH^0 (kJ/mol)	ΔS^0 (J/mol K)	ΔG_{298K} (kJ/mol)	Coeff. de régression
2*ab*	*n*Bu	0,855	35,0	−33,8	−84,0	−8,8	0,997
2*ae*	Ph	0,827	1,9	−26,7	−83,2	−1,9	0,988
2*ad*	*t*Bu	1,815	5,7	−22,1	−59,4	−4,4	0,9997

TABLEAU 3. Caractéristiques de l'équilibre [3] (R^1 = Ph, R^4 = H)

	R^3							
	CH_2Ph		*n*Bu		*t*Bu		Ph	
R^2	% P^{III}	*K*	% P^{III}	*K*	% P^{III}	*K*	% P^{III}	*K*
Me	51	1,6	76,5	3,8	0	0	0	0
Ph	100		100		70	4,2	100*	

Mesures effectuées par rmn de ^{31}P à 308 K. Solvant : toluène. *K* (L/mol).
*Plusieurs composés.

des déterminations de structures par diffraction des rayons X (11*b* et 12). Dans tous les composés cycliques étudiés, l'atome d'azote exocyclique est hybridé en sp^2, et lorsque la rotation autour de la liaison P—N(*exo*) est bloquée, on observe en rmn des valeurs très différentes des constantes de couplage du phosphore avec les carbones ou les protons des substituants portés par cet azote exocyclique (tableau 4).

Dans les amino-3 triazaphospholines-1,2,4,3 **2**, on observe à la température ordinaire un seul signal en rmn de ^{31}P, même pour $R^3 \neq R^4$; de plus les protons méthyléniques du composé **2***cc* ($R^3 = CH_2C_6H_5$) restent équivalents même à −70°C, ce qui implique une rotation rapide autour de la liaison P—N(*exo*).

Remarquons que lorsque l'azote exocyclique porte des groupements encombrants (R^3 = *t*Bu ou $SiMe_3$), on observe à basse température un dédoublement du signal de rmn de ^{31}P. Pour **2***ad* (tol., T.O. (température ordinaire)) : δ ^{31}P = 63,7; à −70°C δ ^{31}P = 66,0 (75%) et 56,2 (25%). En supposant les populations des deux sites égales, on a calculé la barrière à la rotation autour de P—N(*exo*) : $\Delta G^{\ddagger}$ = 41,8 kJ mol^{-1}. Cette valeur est voisine de celle obtenue dans le cas de la diisopropylamino-2 diméthyl-3 diazaphospholidine-1,3,2 (tableau 4).

L'étude des spectres de rmn de ^{15}N de ces différents composés donne une valeur de $J_{PN(exo)}$ particulièrement élevée (80–100 Hz) (tableau 4), correspondant à un fort caractère *s* de la liaison P—N.

L'ensemble de ces résultats : (*i*) faible valeur de δ ^{31}P, (*ii*) rotation restreinte autour de la liaison P—N, et (*iii*) valeur élevée du couplage, $^1J_{PN(exo)}$, s'explique par une rétrocoordination $p\pi$–$d\pi$ entre N(*exo*) et P dans le plan du cycle et nous permet d'envisager pour les amino-3 triazaphospholines une structure autour de l'atome de phosphore comparable à celle des amino-3 tétrazaphospholènes-1,2,4,5,3 (8*a*).

II. Mise en évidence par voie chimique de l'équilibre [3]

La formation de triazaphospholine dans un mélange stoechiométrique de triazaphosphole et d'amine à température ambiante a été également prouvée par des réactions secondaires sur le composé du phosphore tricoordonné, qui déplacent totalement l'équilibre précédent. C'est ainsi que le soufre, le sélénium, les azotures réagissent facilement sur les mélanges pour donner des composés du phosphore tétracoordonné pentavalent (tableau 1).

1. Dérivés soufrés (thioaminotriazaphospholines) 3

On peut envisager deux voies d'accès aux composés du phosphore tétracoordonné pentavalent :

[5]

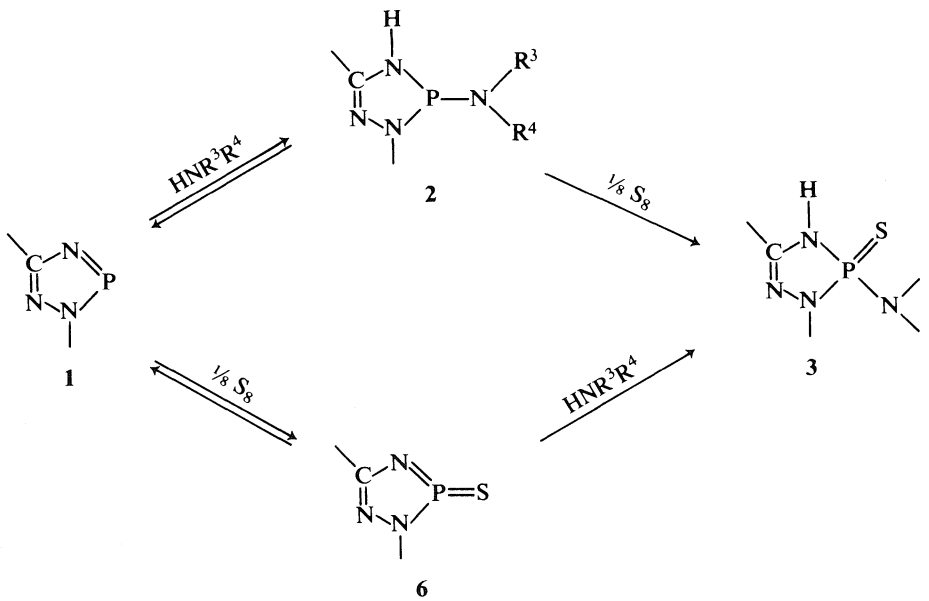

TABLEAU 4. Caractéristiques rmn de ^{13}C et ^{15}N d'aminophospholines et phospholidines

Composé	δ ^{13}CH ($^2J_{PC}$, Hz)	Barrière de rot. P—N (kJ/mol)	δ ^{15}N* ($^1J_{PN}$, Hz)	Réf.
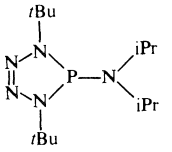	44,4 (±8,2) 47,4 (±28,7)			8*a*
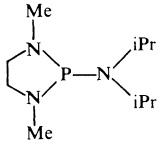	46,8 (−8,2) 42,5 (26,0)	42,2	N(*endo*) −353,8(51) N(*exo*) −286,0(96)	9*a*
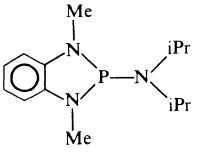	42,9 (+26,9) 44,9 (−8,6)	55,2	N(*endo*) −316,8(55,6) N(*exo*) −267,9(98,9)	9*b*
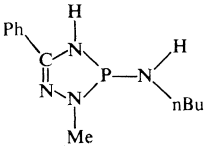	δ $N^{13}CH_2$ 35,85 (21,8) 38,92 (8,7)		N1 −109,15 N2 −257,45(65,5) N4 −282,13(53,1) N(*exo*) −295,91(83,9)($^1J_{NH}$ = 78)	
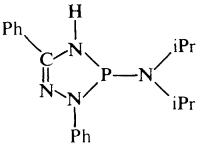	46,21 (9,7)		N1 −111,78 N2 −215,80(66,0) N4 −272,50(53,85) N(*exo*) −254,88(95,9)	

*Référence NO_2Me.

En effet le soufre réagit à température ambiante sur les dérivés de l'aminophosphazène —N—P=N— (13), et bien que l'atome de phosphore des triazaphospholes soit beaucoup moins nucléophile que celui des aminophosphazènes, on ne peut éliminer le second chemin de réaction.

De plus nous avons observé récemment que le soufre réagissait sur les triazaphospholes dans la pyridine après plusieurs heures de chauffage à 105°C (par exemple δ ^{31}P (**6***d*) = 39,8); compte tenu de cette faible réactivité, on peut penser que les vitesses de réaction par ces deux voies sont très différentes et que la première doît être beaucoup plus grande.

La réaction est totale, souvent exothermique; elle conduit à des composés solides, peu solubles dans les solvants organiques hydrocarbonés mais très solubles dans l'acétone et la pyridine.

L'ammoniac conduit à une nouvelle famille de thiophosphoramides, particulièrement stables vis-à-vis de l'eau lorsque R^2 = Ph (il faut plus de 24 h à 35°C pour hydrolyser complètement le composé **3***da*).

Caractéristiques de résonance magnétique nucléaire

Les déplacements chimiques en rmn de ^{31}P sont peu différents de ceux des triazaphospholines correspondantes. Ils se situent autour de 65 ppm pour R^2, R^3, R^4 aliphatiques, et autour de 55 ppm pour R^2 ou R^3 = Ph. Ces grandeurs sont comparables à celles de la littérature pour un environnement comparable de l'atome de phosphore (6).

En rmn de ^1H, les signaux correspondant aux groupements NH endo- et exocycliques sont nettement distincts : δ NH(*endo*) = 10,5–11,8 ppm dans la pyridine et δ N(*exo*) = 6,5–7 ppm. Un léger abaissement de température est souvent nécessaire pour observer les couplages proton–phosphore, dont les grandeurs sont également très différentes : $^2J_{PNH(endo)}$ = 17–21 Hz et $^2J_{PNH(exo)}$ = 5–7,2 Hz sauf pour $R^3 = CH_2Ph$ ($^2J_{PNH(exo)}$ = 21,2 Hz pour **3***cc* et 20 Hz pour **3***dc*) et pour R^3 = *t*Bu et Ph ($^2J_{PNH(exo)}$ = 18 Hz pour **3***cd*, **3***ce*, **3***dd* et **3***de*).

Caractéristiques infrarouges

Nous avons observé essentiellement les vibrateurs NH de ces composés, à l'état solide et en solution dans CCl_4. Les valeurs observées, en accord avec les donnés de la littérature (4, 7, 14, 15), confirment le caractère particulièrement acide du proton porté par l'azote endocyclique N4, et la forte délocalisation électronique dans l'enchaînement :

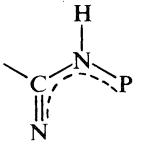

2. Dérivés séléniés

Le sélénium a été également utilisé pour mettre en évidence l'équilibre étudié. Sa plus grande réactivité sur les composés du phosphore tricoordonné a permis d'obtenir plus rapidement

certains dérivés, notamment avec la tertiobutylamine. Toutefois avec la diphénylamine, la réaction reste incomplète.

Les produits formés cristallisent très rapidement dans le toluène et sont ensuite très peu solubles et oxydables. On peut noter l'échange sélénium–oxygène dans le DMSO. Ainsi **4***cb* en solution dans le DMSO conduit à l'oxyde de triazaphospholine correspondant de même déplacement chimique (δ ^{31}P = 20,45 ppm) que le produit d'oxydation directe par l'ozone de **3***cc*. Un tel échange n'a pas lieu avec les dérivés soufrés (R^2 = Me).

Les déplacements chimiques de rmn de ^{31}P des dérivés séléniés sont inférieurs d'une dizaine de ppm à ceux des dérivés soufrés homologues. Dans certains composés, on a pu noter le couplage $^1J_{PSe}$(~850 Hz) grâce aux bandes satellites dues à ^{77}Se (16).

3. Addition d'azotures

Alors que les azotures sont inactifs sur les triazaphospholes à température ordinaire, ils réagissent très facilement sur les amino-3 triazaphospholines avec départ d'azote pour conduire aux amino-3 imino-3 triazaphospholines-1,2,4,3. Ils permettent donc, comme le soufre et le sélénium, de déplacer entièrement l'équilibre. Par précipitation par l'éther, on isole des poudres blanches dont la stabilité dépend du reste amino. Il peut y avoir dimérisation par ouverture de la liaison P=NR, comme cela a été observé au laboratoire sur les iminophospholanes à cycle dioxa, oxaza ou diaza (17).

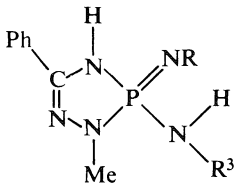

R^3	R	δ ^{31}P
CH_2Ph	Ph	53,4 et − 50,4 ($CDCl_3$
Ph	CH_2Ph	40,25 (CH_2Cl_2)
		39,95 (pyr.)

5

Conclusion

Malgré la variété des substituants portés par le triazaphosphole et l'amine, nous n'avons jamais détecté la présence de composés d'addition 1,1, même en opérant à basse température et en utilisant des substituants silylés donnant des environnements voisins de ceux de E. Niecke (8*a*) et V. D. Romanenko (2*a*). On peut donc conclure que l'addition d'amine sur les triazaphospholes par la voie **B** est peu probable ou en tout cas nettement défavorisée.

La rmn de ^{31}P à température variable nous a permis de voir que cette addition est générale et équilibrée, de mesurer les constantes d'équilibre pour divers réactifs et de déterminer la valeur de la barrière à la rotation P—N(*exo*) pour R = *t*Bu. Cette liaison a un caractère double partiel que confirme la valeur élevée du couplage $^1J_{P^{15}N}$.

La réaction qui présente une enthalpie libre standard négative est défavorisée par les amines peu basiques ou encombrées. Inversement, on favorise la formation de l'aminotriazaphospholine en substituant l'azote N2 du cycle par un groupement phényle.

Dans certains cas où l'addition de l'amine ou de l'ammoniac est très défavorisée, l'introduction de soufre, de sélénium ou d'azoture permet l'addition totale avec formation du composé du phosphore tétracoordonné. L'action de l'ammoniac sur les triazaphospholes en présence de soufre est une méthode simple d'obtention des thiodihydroamino-3 phospholines, permettant de caractériser la présence de σ^2-λ^3-phosphazènes.

Dans les thiotriazaphospholines, le proton porté par l'azote N4 du cycle est particulièrement acide et peut donner lieu à des réactions de substitution.

Partie expérimentale

Les spectres de rmn ont été enregistrés : d'une part sur spectrographe Perkin–Elmer R32 (onde continue (υ_0 = 90 MHz) (sans lock) pour ^1H; FT (calculateur Nicolet TT7) (sans lock) pour ^{31}P) et d'autre part sur spectrographe Brüker WM 250 (pour ^{13}C (υ_0 = 62,83 MHz) réf. int. TMS; pour ^{15}N (υ_0 = 25,34 MHz) réf. ext. NO_2Me en présence de triacétylacétonate de chrome (0,08 mol L^{-1}) (NS = 57 000)).

L'étude spectrométrique infrarouge a été réalisée à l'aide d'un spectrographe PERKIN–ELMER, modèle 125, à double faisceau, sur les échantillons à l'état pur dispersés dans une pastille de bromure de potassium (~1,5 mg dans 150 mg de KBr), ou en solution dans des cuves de 10 cm pour CCl_4.

Les spectres de masse on été obtenus par impact électronique sous 75 eV sur spectromètre quadripolaire RIBER modèle QML-SI.

Triazaphospholines 2

La plupart des amino-3 H-4 triazaphospholines-1,2,4,3 substituées en 2,5 **2**, ont été observées par rmn de ^{31}P dans le mélange réactionnel (toluène) à l'équilibre soit à température ordinaire (T.O.) (33°C), soit à basse température. **2***aa* (−30°C) : 65,8; **2***ab* (T.O.) : 66,5; **2***ac* (T.O.) : 67; **2***ad* (−30°C) : 63,7 et (−70°C) : 66,0 et 56,2 (3:1) coalescence à −50°C; **2***ae* (−20°C) : 57,1 et (−30°C) : 66,1 et 54,3 (1:15); **2***ag* (T.O.) : 77,9; **2***ba* (−30°C) : 69,1; **2***bf* (T.O.) : 65,0; **2***bg* (T.O.) : 70,2; **2***ca* : (−30°C) : 66,1; **2***cb* (T.O.) : 69,8; **2***cc* 69,2; **2***cd* (−30°C) : 66,4; **2***ce* (−30°C) : 55,4; **2***ch* (T.O.) : 82,6; **2***cj* (T.O.) : 78,8; **2***ch* (T.O.) : 79,5; **2***cp* (T.O.) : 77 et (−30°C) 81,9 et 76,8 (1:3); **2***cq* (−30°C) : 65 et (−70°C) 67,3 et 57,3 (2:1) coalescence à −45°C; **2***cm* (−30°C); 87; **2***db* (T.O.) : 65,5 ($^2J_{PH}$ = 31,5); **2***dc* (T.O.) : 65,0 ($^2J_{PH}$ = 34); **2***dd* (T.O.) : 61,5 ($^2J_{PH}$ = 16 et 33); **2***de* (T.O.) : 59,7; **2***dm* (T.O.) : 65,5; **2***dk* (T.O.) : 70,4 ($^2J_{PH}$ = 38); **2***dr* (−25°C) : 75; **2***ea* (T.O.) : 71,3; **2***eb* (T.O.) : 68,9.

2*cn* Méthode A (7) : On mélange 10 mmol de morpholine dissoute dans 10 mL de benzène anhydre et 10 mmol de triazaphosphole en solution dans 20 mL de benzène. La réaction est exothermique. On concentre la solution obtenue sous le vide de la trompe à eau. Le produit formé cristallise plus ou moins vite. Il est recristallisé dans le benzène sous atmosphère inerte car il est hygroscopique et oxydable à l'air; *F* (benzène) 63°C; ν_{NH} (KBr) : 3300, 3200 cm^{-1}; ν_{NH} (sol.) (4); δ ^{31}P (tol. + pyr.) : 78,5; δ H(C_6D_6) : 8,1 et 7,32 (2H et 3H, m, Ph), 3,25 (3H, d, $^3J_{HP}$ = 8,0, NMe), 2,65 et 3,4 (4H, m, $(CH_2)_4$). *Anal.* calc. pour $C_{12}H_{17}N_4PO$: C 54,59; H 6,49; N 21,22; P 11,76; tr. : C 53,67; H 6,44; N 20,67; P 11,48.

2*dn* Méthode A : *F* (benzène) 128°C; ν_{NH} (sol.) (4); δ ^{31}P (pyr.) : 77; δ H(C_6H_6) : 8,1, 7,75 et 7,3 (2H, 2H, 6H, m, 2Ph), 3,3 et 2,8 (8H, m, $(CH_2)_4$). *Anal.* calc. pour $C_{17}H_{19}N_4PO$: C 62,63; H 5,87; N 17,19; P 9,52; tr. : C 61,79; H 5,97; N 16,70; P 9,39.

Thiotriazaphospholines (3)

3*aa* Méthode B : 20 mmol de triazaphosphole **1***a*, dissoutes dans 5 mL de toluène sec, sont ajoutées à la quantité stoechiométrique de soufre élementaire. On fait barboter un courant d'ammoniac sec jusqu'à disparition du soufre. Il se produit un net échauffement et au bout d'une ou deux minutes, le produit formé cristallise sous forme d'une poudre blanche qui est filtrée, lavée plusieurs fois à l'hexane et séchée sur P_2O_5 sous pression réduite; *F* (hexane) 151–152°C; ν_{NH} (KBr) : 3392, 3250, 3205–3310; (CCl_4) : 3496 et 3388; (NH_2) : 3452 dissym. NH(*endo*); (diox.) : 3370–3380, 3283 cm^{-1}; δ ^{31}P (pyr.) : 66,9; δ H (C_5D_5N + $CDCl_3$, −10°C) : 10,35 (1H, d, $^2J_{PH}$ = 19,3 coalescence à 30–32°C, NH(*endo*)), 6,25 (2H, d, $^2J_{PH}$ = 5,7, coalescence vers 46°C, NH_2(*exo*)), 3,28 (3H, d, $^3J_{PH}$ = 9,8, NCH_3), 2,62 (1H, m, $^3J_{HH}$ = 7, *H*C), 1,16 (6H, d, $^3J_{HH}$ = 7, $C(CH_3)_2$. *m/z* : 192 (M^+ (100)), 177 (M − A) (17), 159 (M − SH) (91), 144 (**1***a* + 1) (15) (A = amine). *Anal.* calc. pour $C_5H_{13}N_4PS$: C 31,25; H 6,77; N 29,17; P 16,14; tr. : C 31,01; H 6,75; N 27,05; P 16,93.

Méthode C : Un mélange équimoléculaire de 5 mmol de triazaphosphole, amine et soufre en solution dans 0,5 mL de toluène conduit à

T.O. au dérivé soufré, observé *in situ* par rmn de ^{31}P ou en solution pyridinique quand il cristallise dans le toluène. **3***ab* δ P (tol.) : 64,3; **3***ad* δ P (tol.) : 57,8; **3***ae* δ P (pyr.) : 55,6; **3***ag* δ P (tol.) : 65,15; **3***al* δ P (tol.) : 57,5; δ P (pyr.) : 59,5; δ H (pyr., T.O.) : 10,36 (1H, d, $^2J_{PH}$ = 21, NH(*endo*)), 3,52 (3H, d, $^3J_{PH}$ = 9,0, NC*H*$_3$), 2,66 (1H, m, $^3J_{HH}$ = 7, C*H*), 1,10 (6H, d, $^3J_{HH}$ = 7, C(CH$_3$)$_2$).

3*ba* Méthode B : *F* (hexane) 135–137°C; ν_{NH} (KBr) : 3360–3362, 3255, 3130, 3060; (CCl_4) : 3497 et 3388 (NH_2), 3446 et 3428–3430 (NH(*endo*)); (diox.) : 3380, 3275, 3250–3260 cm^{-1}; δ P (pyr.) : 66,9; δ H (pyr., −20°C) : 10,9 (1H, d, $^2J_{PH}$ = 19,5, NH(*endo*)), 7,55 et 7,4 (2H et 3H, m, Ph), 6,9 (2H, d, $^2J_{PH}$ = 6,0, NH_2), 3,45 (3H, d, $^3J_{PH}$ = 10, NCH_3), 3,85 (2H, s large, CH_2Ph); *m/z* : 240 (M^+ (23)), 207 (M − A) (32), 191 ± 1 (**1***b*) (25), 91 $PhCH_2$ (100). *Anal.* calc. pour $C_9H_{13}N_4PS$: C 45,00; H 5,41; N 23,33; P 12,92; tr. : C 45,05; H 5,62; N 23,18; P 12,89.

3*bc* Méthode D : On laisse environ 1 heure à température ambiante en atmosphère inerte, un mélange équimoléculaire de 20 mmol de triazaphosphole, d'amine et de soufre dans 3 mL de toluène. On contrôle l'achèvement de la réaction par rmn de ^{31}P. La solution est concentrée, le produit formé est précipité par addition d'hexane, filtré, lavé plusieurs fois à l'hexane, parfois recristallisé dans le benzène (7); *F* (benzène) 155°C; ir (4); δ P (tol.) : 66; δ H (tol. + pyr., −20°C) : 10,1 (1H, d, $^2J_{PH}$ = 20,5, N*H*(*endo*)), 7,25 (10H, Ph), 6,23 (1H, dt, $^2J_{PH}$ = 22 et $^3J_{HH}$ = 7,2, NH(*exo*)), 4,2 (2H, dd, $^3J_{HH}$ = 7,2 et $^3J_{HP}$ = 15,2, NCH_2Ph), 3,75 (2H, $^2J_{HH}$ = 16, $^4J_{HP}$ = 1, CCH_2Ph), 3,25 (3H, d, $^3J_{PH}$ = 9,1, NCH_3). *Anal.* calc. pour $C_{16}H_{19}N_4PS$: C 58,23; H 5,80; N 16,98; P 9,40; tr. : C 58,51; H 5,97; N 16,51; P 9,40.

3*bf* Méthode C : δ P (tol.) : 60,9 et 60,3; **3***bg* δ P (tol.) : 70,2.

3*ca* Méthode B : *F* (hexane) 155–157°C; ν_{NH} (KBr) : 3405, 3290, 3265–3270, 3220–3230; (CCl_4) : 3495 et 3387 (NH_2), 3457 et 3450 (NH(*endo*)); (diox.) : 3380, 3275–3280 cm^{-1}; δ P (pyr.) : 66,7; δ H (pyr., −20°C) : 11,0 (1H, d, $^2J_{PH}$ = 18,7, NH), 8,05 et 7,4 (2H et 3H, m, Ph), 6,77 (2H, d, $^2J_{PH}$ = 5,0, coalescence à 30°C, NH_2), 3,3 (3H, d, $^3J_{PH}$ = 10,0, NCH_3); *m/z* : 226 (M^+ (60)), 193 (M − SH) (42), **1***c* (44), 104 (PhCNH) (100). *Anal.* calc. pour $C_8H_{11}N_4PS$: C 42,48; H 4,88; N 24,78; P 13,72; tr. : C 43,16; H 4,93; N 23,63; P 13,58.

3*cb* Méthode D : *F* (hexane) 99–100°C; ν_{NH} (KBr) : 3350, 3200; (CCl_4) : 3458, 3450, 3425, 3420; (diox.) : 3300–3305, 3255–3260 cm^{-1}; δ P (tol.) : 63,8; δ H (pyr., −10°C) : 11,05 (1H, d, $^2J_{PH}$ = 18,5, NH(*endo*)), 8,23 et 7,43 (2H et 3H, m, Ph), 6,85 (1H, dt, $^2J_{PH}$ = 21, $^3J_{HH}$ = 6,5, NH(*exo*)), 3,38 (3H, d, $^3J_{PH}$ = 9, NCH_3), 2,93 (2H, m, $^3J_{HNCH}$ = 6,5, $^3J_{HCCH}$ = 6, $^3J_{PH}$ ~ 13, NCH_2—), 1,35 et 1,16 (4H, m, C—CH_2—CH_2), 0,68 (3H, t, $^3J_{HH}$ = 7, CCH_3); δ ^{13}C (J_{PC}) ($CDCl_3$, T.O.) : 146,12 (5,6) C1, 138, 131,5–126,0 (Ph), 42,23 (8,9) NCH_3, 35,85 (21,8) N—CH_2—, 21,91 et 20,72 (CH_2—CH_2), 14,46 (2,2) CH_3; *m/z* : 282 (M^+ (9)), 254 (M − SH) (0,7), 231 (3,8), 210 (A) (3,5), 127–128 (**1***c*) (100).

3*cc* Méthode D (7) : *F* (benzène) 163°C; ir (4); δ P (tol.) : 63,8; δ H (pyr., −20°C) : 11,2 (1H, d, $^2J_{PH}$ = 19,1, NH(*endo*)), 7,85 et 7,2 (2H et 8H, m, 2Ph), 7,86 (1H, d, $^2J_{PH}$ = 21,2 et $^3J_{HH}$ = 7,0, NH(*exo*)), 4,3 (2H, dd, $^3J_{HCNH}$ = 6,5, $^3J_{HCNP}$ = 15, NCH_2Ph), 3,35 (3H, d, $^3J_{PH}$ = 9,1, NCH_3). *Anal.* calc. pour $C_{15}H_{17}N_4PS$: C 57,01; H 5,42; N 17,73; P 9,82; tr. : C 56,80; H 5,57; N 17,50; P 9,80.

3*cd* Méthode D : *F* (hexane) 100–103°C; ν_{NH} (KBr) : 3490, 3350, 3225, 3110–3115; (CCl_4) : 3460–3465, 3445–3450, 3395; (diox.) : 3260–3270 cm^{-1}; δ P (tol.) : 58,9 et δ P (pyr.) : 60,1; δ H ($CDCl_3$, −35°C) : 8,8 (1H, d, $^2J_{PH}$ = 21, NH(*endo*)), 7,8 et 7,5 (2H et 3H, m, Ph), 3,8 (1H, d, $^2J_{PH}$ = 18, NH(*exo*)), 3,35 (3H, d, $^3J_{PH}$ = 8,5, NC*H*$_3$), 1,3 (9H, s, $C(CH_3)_3$; *m/z* : 282 (M^+ (14)), 231 (8), 226 (M − *t*Bu + 1) (14), 211 (M − A) (7), 193 (226 − SH) (18), 177 (**1***c*) (100). *Anal.* calc. pour $C_{17}H_{21}N_4PS$: C 59,30; H 6,10; N 16,28; P 9,01; tr. : C 61,60; H 6,37; N 16,15; P 6,87.

3*ce* Méthode D : *F* (benzène) 193°C; ν_{NH} (KBr) : 3363, 3140, 3100; (CCl_4) : 3455, 3445, 3400; (diox.) : 3245 dissym. cm^{-1}; δ P (pyr.) : 55,5; δ H (pyr., −20°C) : 11,7 (1H, d, $^2J_{PH}$ = 17, NH(*endo*)), 10,14 (1H, d, $^2J_{PH}$ = 18, NH(*exo*)), 8,15, 7,45 et 7,22 (10H, m, 2Ph); 3,42 (3H, d, $^3J_{PH}$ = 8,4, NC*H*$_3$); *m/z* : 302 (M^+ − 1) (16), 231 (17), 210 (M − SH) (4), 117 (**1***c*) (43). *Anal.* calc. pour $C_{14}H_{15}N_4PS$: C 55,63; H 4,97; N 18,54; P 10,26; tr. : C 55,40; H 4,91; N 18,30; P 10,35.

3*ch* Méthode D : δ P (tol.) : 69,4; δ H (pyr., T.O.) : 10 (1H, large, NH), 3,2 (3H, d, $^3J_{PH}$ = 8, NCH_3(*endo*)), 2,8 (6H, d, $^3J_{PH}$ = 11, $N(CH_3)_2$ *exo*).

3*cj* Méthode C : δ (tol.) : 68,4.

3*ck* Méthode C : δ (tol.) : 63,4.

3*cl* Méthode D : *F* (hexane) 208–216°C; ν_{NH} (KBr) : 3320, 3295; (CCl_4) : 3450–3455, 3435, (diox.) : 3240–3250 dissym. cm^{-1}; δ P (tol.) : 59,1; δ H (pyr., T.O.) : 11,1 (1H, d, $^2J_{PH}$ = 20, NH), 7,7 et 7,1 (2H et 13H, m, 3 Ph), 3,43 (3H, d, $^3J_{PH}$ = 8,4, NCH); *m/z* : 378 (M^+ (0,04)), 231 (7), 177 (**1***c*) (22), 169 (Ph_2NH) (100), 168 (Ph_2NH − 1) (50). *Anal.* calc. pour $C_{20}H_{19}N_4PS$: C 63,49; H 5,03; N 14,81; P 8,20; S 8,47; tr. : C 62,00; H 4,87; N 14,95; P 8,58; S 8,28.

3*cm* Méthode D : *F* (hexane) 136°C (déc.); ν_{max} (KBr) : 3220, 3160 cm^{-1}; δ P (tol.) : 64,2; δ H (tol., −65°C) : 11,2 (1H, m, NH), 8,3 et 7,5 (5H, m, Ph), 3,47 (3H, d, $^3J_{PH}$ = 8, NCH_3); *m/z* : 252 (210 (M − A) (5), 117 (**1***c*) (100)). *Anal.* calc. pour $C_{10}H_{13}N_4PS$: C 47,62; H 5,6; N 22,22; P 12,30; S 12,70; tr. : C 47,30; H 5,56; N 19,12; P 8,59; S 14,86.

3*cn* Méthode D (7) : *F* (benzène) 141°C; ir (4); δ P (pyr.) : 67,5; δ H (pyr., −20°C) : 9,13 (1H, d, $^2J_{PH}$ = 20, NH), 7,95 et 7,3 (2H et 3H, m, Ph), 3,5 (8H, m, $(CH_2)_4$), 3,25 (3H, d, $^3J_{PH}$ = 9, NCH_3). *Anal.* calc. pour $C_{12}H_{17}N_4OPS$: C 48,69; H 5,79; N 18,93; P 10,48; tr. : C 48,43; H 5,70; N 18,67; P 10,55.

3*cp* Méthode C : δ P (tol.) : 72,1 instable.

3*cq* Méthode D : *F* (hexane) 120–125°C; δ P (tol.) : 67,1; δ H (pyr., T.O.) : 8,2 et 7,2 (m, Ph), 5,0 (1H, d, $^2J_{PH}$ = 16,4, NH), 3,2 (3H, d, $^3J_{PH}$ = 9,3, NCH_3), 1,4 (9H, s, $C(CH_3)_3$), 0,4 (9H, s, $NSi(CH_3)_3$); *m/z* : 354 (M^+ (82)), 298 (M − *t*Bu + 1) (17), 282 (M − $SiMe_3$ + 1) (19), 265 (M − *t*Bu − S) (11), 250 (M − $SiMe_3$ − S) (11), 209 (M − A) (45), 177–176 (**1***c*) (100). *Anal.* calc. pour $C_{15}H_{27}N_4PSSi$: N 15,82; P 8,76; tr. : N 16,83; P 8,58.

3*da* Méthode B : *F* (hexane) 210–220°C; ν_{NH} (KBr) : 3450, 3270–3275, 3220–3225; (CCl_4) : 3493 et 3385 (NH_2), 3450 et 3437 (NH(*endo*)); (diox.) : 3340, 3260 cm^{-1}; δ P (pyr.) : 59,0; δ H (pyr., −50°C) : 12,1 (1H, d, $^2J_{PH}$ = 20, NH(*endo*)), 8,56 (2H, d, $^2J_{PH}$ = 8, NH_2), 8,15–8,30 et 7–7,7 (10H, m, 2Ph); *m/z* : 288 (M^+ (34)), 273 (M − A) (30), 239 (**1***d*) (100). *Anal.* calc. pour $C_{13}H_{13}N_4PS$: C 54,17; H 4,51; N 19,44; P 10,76; tr. : C 53,85; H 4,67; N 19,31; P 10,45.

3*db* Méthode C : δ P (tol.) : 55,4

3*dc* Méthode D : *F* (tol.) 123–125°C; ν_{NH} (KBr) : 3215, 3170–3180; (CCl_4) : 3455–3435; (diox.) : 3240, 3190–3200 cm^{-1}; δ P (tol.) : 54,8; δ H (pyr., −40°C) : 11,95 (1H, d, $^2J_{PH}$ = 18, NH *endo*), 8,85 (d, *J* = 20, NH *exo*), 8,5, 8,25, 7,6 et 7,3 (m, 3 Ph), 4,5 (2H, dd, $^3J_{PH}$ = 14, $^3J_{HH}$ = 6, NCH_2Ph); *m/z* : 378 (272 (M − A) traces), 247 (M − A − NH) (13), 231 (100). *Anal.* calc. pour $C_{20}H_{19}N_4PS$: C 63,49; H 5,03; N 14,81; P 8,20; S 8,47; tr. : C 63,43; H 4,84; N 14,83; P 8,23; S 8,26.

3*dd* Méthode D : *F* (hexane) 100–103°C; ν_{NH} (KBr) : 3290; (CCl_4) : 3454, 3436, 3392 cm^{-1}; δ P (tol.) : 52,1; δ H (pyr. + $CDCl_3$, −50°C) : 11,2 (1H, d, $^2J_{PH}$ ~ 20, NH(*endo*)), 8,25 et 7,7–7,3 (2H et 8H, m, 2Ph), 6,77 (1H, d, $^2J_{PH}$ = 18, NH(*exo*)); *m/z* : 44 (M^+ (10,4)), 288 (M − *t*Bu + 1) (9,6), 272 (M − A) (2), 239 (**1***d*) (100)). *Anal.* calc. pour $C_{17}H_{21}N_4PS$: C 59,30; H 6,10; N 16,28; P 9,01; tr. : C 61,60; H 6,37; N 16,15; P 6,87.

3*de* Méthode D : *F* (hexane) 82–87°C; ν_{NH} (KBr) : 3360, 3200; (CCl_4) : 3455, 3437, 3397; (diox.) : 3240–3250, 3220 cm^{-1}; δ P (tol.) 47,15; δ H ($CDCl_3$ + pyr., −30°C) : 11,75 (1H, d, $^2J_{PH}$ = 21, NH(*endo*)), 9,64 (1H, d, $^2J_{PH}$ = 18, NH(*exo*)), 8,2–8,0 et 7,6–6,8 (10H, m, 2Ph); *m/z* : 364 (M^+ (6)), 273 (M − A) (1,5), 239 (**1***d*) (100).

3*dj* Méthode C : δ P (CH_2Cl_2 + tol.) : 60,5.

3*dk* Méthode D : poudre jaune instable, *F* (hexane) 159°C; ν_{max} (KBr) : 3230, 3160; (CCl_4) : 3445 cm^{-1}; δ P (tol.) : 53,6, δ H (pyr., −15°C) : 11,8 (d, $^2J_{PH}$ = 22 NH(*endo*)), 8,25, 7,55 et 7,3 (10H, m, 2 Ph), 3,7 (2H, m, CH), 1,20 et 11,6 (12H, 2d, $^3J_{HH}$ = 6, $(C(CH_3)_2)_2$); *m/z* : 372 (M^+ (12)), 272 (M − A) (2), 239 (**1***d*) (100), 231 (90)).

3*dm* Méthode D : *F* (hexane) 126°C (déc.); δ P (pyr.) : 57,8. *Anal.* calc. pour $C_{15}H_{15}N_4PS$: C 57,33; H 4,78; N 17,83; P 9,87; tr. : C 58,42; H 5,90; N 15,73; P 8,07.

3*dn* Méthode B (7) : *F* (benzène) 206°C; ir (4); δ P (pyr.) : 61; δ H (tol. + pyr., −30°C) : 11,8 (1H, d, $^2J_{PH}$ = 21, NH), 8,0 et 7,4 (2H

et 3H, m, Ph), 3,4 (8H, m, $(CH_2)_4$). *Anal.* calc. pour $C_{17}H_{19}N_4OPS$: C 57,03; H 5,35; N 15,65; P 8,67; tr. : C 57,15; H 5,39; N 15,82; P 8,78.

3*do* Méthode C : δ P (tol.) : 61,9; **3***dp* δ P (tol.) : 61,4; **3***dr* δ P (tol.) : 60,9.

3*ea* Méthode C : δ P (tol.) : 67,8 (30%) et 67,0 (70%); **3***eb* δ P (tol. + $CDCl_3$) : 67,8 ($^2J_{PH}$ = 17,8; $^3J_{PH}$ = 11,6); **3***ed* δ P (tol.) : 62,8 ($^2J_{PNH}$ = 15,3 et 20,0).

Ces trois derniers composés sont instables et perdent facilement $SiMe_3$.

Selenotriazaphospholines ***4***

4*cb* δ P (DMSO) : 54,2 ($^1J_{PSe}$ = 853 ± 10 Hz); δ H (pyr., −15°C) : 11,45 (1H, d, $^2J_{PH}$ = 20, NH(*exo*)), 6,15 (1H, d, ^2J = 22, NH(*endo*)), 3,35 (3H, d, $^3J_{PH}$ = 9).

4*cc F* 96–98°C; δ P (CH_2Cl_2) : 54,1 ($^1J_{PSe}$ = 832 ± 10 Hz).

4*cd F* 152°C; δ P (tol.) : 47,1 ($^1J_{PSe}$ = 843 ± 5); δ H (pyr., −15°C) : 11,45 (1H, d, $^2J_{PH}$ = 21, NH(*endo*)), 8,23 et 7,45 (2H et 3H, m, Ph), 6,15 (1H, d, $^2J_{PH}$ = 21 NH(*exo*)), 3,33 (3H, d, $^3J_{PH}$ = 9, NCH_3), 1,10 (9H, s, $C(CH_3)_3$); *m/z* : 329 (M^+ (traces)), 193 (M^+ − Se − *t*Bu) (15), 232 (M^+ − SeH − CH_3 − 2) (7), 177 (**1***c*) (100).

Amino-3 iminotriazaphospholines ***5***

5*cc F* (hexane) 228°C; ν_{max} (KBr) : 3220–3140 (NH); (CCl_4) : 3460f, 3410 et 3220–3160; (diox.) : 3360f, 3250 cm^{-1}; δ ^{31}P (CH_2Cl_2) : 40,25; δ H (pyr.) : 9,55 (1H, large NH(*endo*)), 8,68 (2H) et 7,33 (14H) très larges (3Ph et NH), 4,28 (2H, d, $^3J_{PH}$ = 12,2 NCH_2), 3,28 (3H, d, $^3J_{PH}$ = 6,2, NCH_3); *m/z* : 375 (300 (1,5) (M − Ph + 2)), 106 (100) ($PhCH_2NH$). *Anal.* calc. pour $C_{21}H_{22}N_5P$: C 67,20; H 5,87; N 18,67; P 8,27; tr. : C 65,86; H 6,06; N 18,19; P 7,99.

Remerciements

Les auteurs remercient M. Gerard Commenges pour l'enregistrement du spectre rmn de ^{15}N, Mme. C. Vidal pour le traitement des données rmn permettant d'accéder aux grandeurs thermodynamiques et Mme. A. Colomer pour l'enregistrement des spectres infrarouges.

1. Y. Charbonnel et J. Barrans. Tetrahedron, **32**, 2039 (1976).
2. (*a*) L. N. Markovskii, V. D. Romanenko et A. V. Ruban. Phopshorus Sulfur, **9**, 221 (1980); (*b*) V. D. Romanenko, A. V. Ruban, N. N. Kalibabchuck, S. V. Iksanova et L. N. Markovski. Zh. Obshch. Khim. **51**, 1726 (1981).
3. C. R. C. Handbook of chemistry and physics. 63ème éd. CRC Press, Boca Raton, FL. 1982–1983.
4. R. Mathis, A. Chabane, Y. Charbonnel et J. Barrans. C.R. Acad. Sci. Ser. B, **282**, B-67 (1976).
5. A. Munoz, M. Sanchez, M. Koenig et R. Wolf. Bull. Soc. Chim. 2193 (1974).
6. (*a*) F. Ramirez, A. V. Patwardhan, H. J. Hugler et C. P. Smith. Tetrahedron Lett. **26**, 3053 (1966); (*b*) D. Bernard. Thèse de Doctorat, Université Paris VI. 1974. N°. 9610; (*c*) Y. Charbonnel. Thèse de Doctorat, Université Toulouse III. 1975. N°. 656; (*d*) C. Malavaud. Thèse de Doctorat, Université Toulouse. 1980. N°. 944; (*e*) L. Lopez, J. P. Majoral, A. Meriem, Th, N'Gando M'Pondo, J. Navech et J. Barrans. J. Chem. Soc. Chem. Commun. 184 (1984).
7. A. Chabane. Thèse de Doctorat, Université Toulouse III. 974. N°. 1616.
8. (*a*) E. Niecke et H. G. Schafer. Chem. Ber. **115**, 185 (1982); (*b*) S. Pohl, E. Niecke et H. G. Schäfer. Angew. Chem. Int. Ed. Engl. **17**, 136 (1978).
9. J. H. Hargis, W. B. Jennings, S. D. Worley et M. S. Tolley. J. Am. Chem. Soc. **102**, 13 (1980); (*b*) W. B. Jennings, D. Randall, S. D. Worley et J. H. Hargis. J. Chem. Soc. Perkin Trans. 2, 1411 (1981).
10. (*a*) A. H. Cowley, M. J. S. Dewar, W. R. Jackson et W. B. Jennings. J. Am. Chem. Soc. **92**, 5206 (1970); (*b*) J. P. Albrand, A. Cogne, D. Gagnaire et J. B. Robert. Tetrahedron, **28**, 819 (1972); (*c*) M. P. Simmonin et R. M. Lequan. J. Chem. Soc. Chem. Commun. 1204 (1972).
11. S. D. Worley, J. H. Hargis, L. Chang et G. A. Mattson. J. Electron. Spectrosc. Relat. Phenom. **25**, 135 (1982); (*b*) W. B. Jennings et M. S. Tolley. J. Chem. Soc. Perkin Trans. 2, 1207 (1984); (*c*) W. B. Jennings et M. Rutherford. Tetrahedron Lett. **25**, 3131 (1984).
12. (*a*) D. E. Schiff, J. W. Richardson, R. A. Jacobson, A. H. Cowley et J. Lasch. Inorg. Chem. **23**, 3373 (1984); (*b*) K. Paxton et Th. A. Hamor. J. Chem. Soc. Dalton Trans. 647 (1978); (*c*) E. Niecke, M. Engelmann, H. Zorn, B. Krebs and G. Henkel. Angew. Chem. Int. Ed. Engl. **19**, 710 (1980).
13. O. J. Sherer et N. Kuhn. J. Organomet. Chem. **82**, C_3 (1974).
14. J. Khemdoudi. Thèse de spécialité, Université Toulouse III. 1975.
15. R. A. Nyquist. Spectrochim. Acta, **19**, 713 (1963).
16. D. E. Schiff, J. W. Richardson, R. A. Jacobson, A. H. Cowley, J. Lasch and J. G. Verkade. Inorg. Chem. **23**, 3373 (1984).
17. M. R. Marre, M. Sanchez, J. F. Brazier, R. Wolf et J. Bellan. Can. J. Chem. **60**, 456 (1982).

Sulphur cation chemistry in a fuel-rich, CH_4–O_2 flame with OCS additive

NICHOLAS S. KARELLAS AND JOHN M. GOODINGS

Department of Chemistry and Centre for Research in Experimental Space Science, York University, 4700 Keele Street, Downsview, Ont., Canada M3J 1P3

Received February 17, 1986

NICHOLAS S. KARELLAS and JOHN M. GOODINGS. Can. J. Chem. **64**, 1733 (1986).

A fuel-rich, methane–oxygen, premixed flame at atmospheric pressure was doped with 0.2 mol% of OCS. More than 40 different sulphurous cations were observed in the mass range < 100 u by sampling the flame into a flame-ion mass spectrometer. Ion concentration profiles along the flame axis are presented, together with mass spectra at fixed points in the flame. In the reaction zone, primary sulphur ions CH_xS^+ (x = 1, 3, 5) undergo extensive ion–molecule reactions (association and condensation) with CH_4/CH_3, C_2H_2, and OCS to form a considerable variety of secondary sulphurous cations. Just downstream of the reaction zone, the ion chemistry is somewhat different; it appears to be dominated by reactions of primary sulphur ions including H_xS^+ (x = 0–3) with C_2H_2 present as an intermediate. A few ions (H_xS^+, OS^+, S_2^+) persist throughout the burnt gas region in equilibrium with the natural flame ions CHO^+ and H_3O^+. These sulphurous cation signals show the evolution of the sulphur chemistry, both ionic and neutral, through the flame reaction zone into the burnt gas downstream where H_2S, not SO_2, is the major product in fuel-rich combustion.

NICHOLAS S. KARELLAS and JOHN M. GOODINGS. Can. J. Chem. **64**, 1733 (1986).

Une flamme pré-mélangée de méthane/oxygène, riche en combustible, a été dopée avec 0,2 mol% de OCS. En procédant à un échantillonage de la flamme dans un spectromètre de masse, on a détecté plus de 40 de cations différents, de masse inférieure à 100 unités, qui contiennent du soufre. On présente les courbes des concentrations ioniques en fonction de l'axe de la flamme ainsi que les spectres de masse à des points définis de la flamme. Dans la zone de la réaction, les ions sulfurés primaires, CH_xS^+ dans lesquels x = 1, 3 et 5, subissent des réactions ion/molécules importantes (association et condensation) avec la paire CH_4/CH_3, le C_2H_2 et le OCS; il y a ainsi formation d'une variété importante de cations sulfurés secondaires. Juste après la zone réactionnelle, la chimie des ions est un peu différente; elle semble être dominée par des réactions des ions sulfurés primaires, y compris H_xS^+ (x = 0–3), avec le C_2H_2 qui est présent comme intermédiaire. Quelques ions (H_xS^+, OS^+ et S_2^+) sont présents partout dans le région des gaz ayant subi la combustion et ils sont en équilibre avec les ions normaux de la flamme, comme le CHO^+ et le H_3O^+. Ces signaux dus à des cations sulfurés démontrent l'évolution de la chimie du soufre, tant ionique que neutre, de la zone réactionnelle de la flamme à celle des gaz formés après la combustion; dans toutes ces zones, c'est le H_2S et non pas le SO_2 qui est le produit majeur de la combustion dans des mélanges riches en combustible.

[Traduit par la revue]

Introduction

Gaseous sulphur compounds are poured into the atmosphere mainly by stationary plants for electrical power generation, space heating, smelting, paper making and sulphuric acid manufacture. The effects of both short-range and long-range transport of sulphur pollutants are increasingly recognized in connection with respiratory diseases, acid rain, and general environmental damage, both urban and rural. At the same time, detection methods for pollutants of many types have improved dramatically in the past 20 years, particularly with regard to specificity (1). A great deal of the sulphur pollution arises from combustion processes; coal is the fuel most likely to have a high sulphur content.

Any hydrocarbon flame contains a wide variety of natural ions, both positive and negative. If sulphur is present in the flame in whatever form, it will be chemically ionized to give sulphurous anions and cations. These can serve as a probe of the sulphur chemistry if the ion chemistry is reasonably well understood. The ions present in a flame at atmospheric pressure can be sampled through a nozzle into a flame-ion mass spectrometer. The method is advantageous because all types of sulphur ions can be detected with equal facility, ion identification is highly specific in the chemically complex flame environment, and all regions of the flame can be probed including the reaction zone where the sulphur chemistry originates upstream. Two such studies of sulphurous negative ions have already been completed in which a fuel-rich, CH_4–O_2 flame was doped with 0.2 mol% first of OCS (2), and then with H_2S and SO_2 for comparison with OCS (3). The types of sulphurous anions detected were relatively few (S^-, HS^-, OS^-, O_2S^-, O_3S^-, HO_3S^-, $CH_3O^-.O_2S$, O_4S^-, HO_4S^-) and were essentially confined to the flame reaction zone.

The present study involves observations of sulphurous positive ions in the same fuel-rich, CH_4–O_2 flame, again doped with 0.2 mol% of OCS. Typical ion concentration profiles measured along the flame axis are presented. Obviously, the chemical ionization (CI) processes for positive ions are different, and more than five times as many cations as anions were detected at mass numbers below 100 u. This considerable variety of cations was measured for presentation by taking mass spectra at three different points in the flame. The sulphurous cation chemistry can be understood in terms of addition and condensation reactions of primary sulphur ions with the CH_4 fuel (or CH_3 radicals derived from it), with C_2H_2 present as a major intermediate, and with S atoms supplied directly by the OCS additive. It is significant that a number of the sulphur cations, unlike most of the anions, can be detected everywhere in the flame; in the reaction zone, downstream of it, and also throughout the burnt gas region.

Experimental

All of the ion concentration measurements were performed on the same CH_4–O_2 flame of fuel-rich composition (equivalence ratio ϕ = 2.15) whose ion chemistry we have studied extensively in the past (4, 5). It was of the laminar premixed type with a conical luminous reaction zone (height ≃ 5 mm, base diameter ≃ 3 mm, thickness ≃ 0.3 mm) to facilitate ionic sampling along the flame axis into the mass spectrometer. The flame has a burnt gas velocity of approximately 1 m s^{-1} and an adiabatic flame temperature of 2460 K, although the measured temperature of the equilibrium burnt gas was close to 2200 K. The flame was stabilized at atmospheric pressure on a simple,

tubular, quartz burner (2.3 mm id) surrounded by a flowing argon shield to minimize the entrainment of atmospheric air. Provision was made to add 0.2 mol% of OCS to the premixed gas in exactly the same way as was done previously for the sulphurous anion studies (2). The additive could be introduced or removed without altering the flame. All gases were used straight from the cylinders without further purification (CH_4 > 99.0%, O_2 > 99.6%, Ar > 99.9%, OCS > 97.5%). The burner was mounted on a motor-driven carriage with accurate alignment of the flame axis with the sampling orifice of the mass spectrometer. The calibrated burner drive provided spatial resolution of ±0.02 mm along the flame axis (designated z) for measurements of ion concentration profiles.

The flame-ion mass spectrometer has been described previously in detail (4). The flame burned against a 60°, conical, chromium, sampling nozzle of orifice diameter ca. 0.1 mm mounted in a water-cooled flange of the type described by Hayhurst and Telford (6). The sampled ions pass through two stages of differential pumping into a quadrupole mass filter. The mass-analyzed ions are detected with a parallel-plate Faraday collector connected to a vibrating reed electrometer having a grid-leak resistance of 10^{10} ohms. The ion signal magnitudes in the figures are quoted in volts based on the detected ion current passing through 10^{10} ohms. The mass spectra shown below have been corrected for mass discrimination in the filter against ions of high m/e measured at high resolving power. The dynamic range of sensitivity of the apparatus is five orders of magnitude.

A method has been described (4) involving a relatively sharp minimum in the pressure profile of the sampled gas for locating a reproducible origin ($z = 0$) in the *flame* (not referred to the burner). It corresponds to the downstream edge of the luminous reaction zone on the flame axis. In this way, a family of ion profiles at different mass numbers m/e can be accurately overlaid on the distance scale z. It is also an important consideration, when comparing mass spectra at a fixed point on the flame axis with and without OCS additive, to be able to return to the same point on the flame axis.

Neutral sulphur chemistry

Approximate concentration profiles for the important neutral species appropriate to our flame are given in Fig. 1 adapted from Hastie's studies of a similar fuel-rich flame (7). The profiles reflect our use of an argon shield to suppress the secondary downstream combustion region which is evident in Hastie's work. Figure 1 shows the expected fall of CH_4 and O_2 through the reaction zone, and the rapid rise of the major neutral products H_2, CO, and H_2O as well as H atoms; the HO concentration actually overshoots its equilibrium value in this region. Because of the relatively weak C—S bond, OCS is an efficient donor of S atoms in reaction with a variety of flame species. Thus, when OCS is added to the premixed gas, the following series of reactions might be expected to be balanced, or nearly so, in the flame reaction zone; relevant data are given in Table 1 drawn from Westley's compilation of recommended rate constants for combustion reactions (8)

[1] $OCS + H \rightleftharpoons HS + CO$

[2] $HS + H_2 \rightleftharpoons H_2S + H$

[3] $H_2S + HO \rightleftharpoons HS + H_2O$

[4] $HS + H \rightleftharpoons S + H_2$

[5] $S + HO \rightleftharpoons OS + H$

[6] $OS + HO \rightleftharpoons O_2S + H$

Combined with a balanced reaction not involving sulphur species

[7] $H_2O + H \rightleftharpoons HO + H_2$

the overall net reaction of [1] to [7] is

[8] $OCS + 2HO \rightleftharpoons O_2S + CO + H_2$

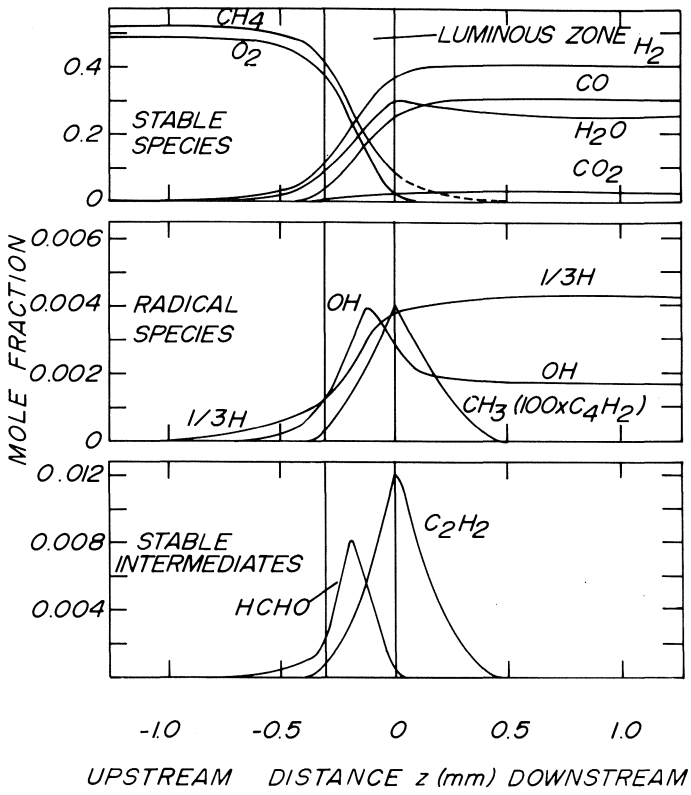

FIG. 1. Approximate concentration profiles for important neutral species adapted from Hastie's studies of a similar fuel-rich flame.

Because of the HO radical overshoot, O_2S and OS will be enhanced in the flame reaction zone, particularly when reactions involving molecular oxygen are considered

[9] $S + O_2 \rightleftharpoons OS + O$

[10] $OS + O_2 \rightleftharpoons O_2S + O$

before the oxidant is consumed. This will not be the case downstream, however, since the concentrations of CO and H_2 continue to rise, whilst that of HO falls to its equilibrium value. In addition, minor reactions can lead to diatomic sulphur

[11] $S + OCS\ (HS, OS) \rightleftharpoons S_2 + CO\ (H, O)$

In any event, a variety of sulphurous neutrals (e.g. S, HS, H_2S, OS, O_2S, S_2) will be present in the reaction zone of this fuel-rich flame.

Well downstream in the equilibrium burnt gas, the identity of the original sulphur additive is, of course, lost and only the quantity of sulphur present is important. For this flame, exactly 0.2 mol% of OCS in the premixed unburnt gas translates into 0.1285 mol% of sulphur species in the burnt gas; that is, each mole of unburnt reagents combusts to give 1.556 mol of products. Equilibrium concentrations of various sulphur species in the burnt gas can be found from calculated equilibrium constants for reactions [1] to [6] and also [11] to [13]

[12] $CS + HO \rightleftharpoons HS + CO$

[13] $CS + OCS \rightleftharpoons CS_2 + CO$

All the necessary standard free energies of formation at 2200 K are listed in JANAF Tables (11). For a few minor species (e.g. HO_2S), thermodynamic data are not available. The equilibrium concentrations of nine sulphur species, and also those of the important non-sulphurous neutrals, are given in Table 2. The figures show the preponderance of H_2S over O_2S in this

TABLE 1. Reactions involving sulphurous neutral species

No.	Reaction	Rate constant[a]	Uncertainty factors[b]	T (K)[c]	Reference
[1]	$OCS + H \rightarrow HS + CO$	2.2×10^{-14}	0.8/1.3	298	9
[2]	$H_2S + H \rightarrow HS + H_2$	2.1×10^{-12}	0.5/1.5	470	9
[3]	$H_2S + HO \rightarrow HS + H_2O$	8.4×10^{-12}	0.5/1.5	900	9
[4]	$HS + H \rightarrow S + H_2$	2.5×10^{-11}	0.5/1.5	298	9
	[d]$S + H_2 \rightarrow HS + H$	2.0×10^{-13}	0.5/1.5	2000	9
[5]	$S + HO \rightarrow OS + H$	4.7×10^{-11}		2000	10
	$\rightarrow HS + O$	1.7×10^{-13}		2000	10
	[d]$OS + H \rightarrow S + HO$	1.1×10^{-12}		2000	10
	$\rightarrow HS + O$	2.2×10^{-15}		2000	10
[9]	$S + O_2 \rightarrow OS + O$	2.3×10^{-12}	0.5/1.5	450	9
	[d]$OS + O \rightarrow S + O_2$	3.7×10^{-12}		2000	10
[10]	$OS + O_2 \rightarrow O_2S + O$	1.5×10^{-13}	0.3/1.7	2000	9
	[d]$O + O_2S \rightarrow OS + O_2$	3.3×10^{-14}	0.3/1.7	2000	9
[11*a*]	$S + OCS \rightarrow S_2 + CO$	1.0×10^{-12}	0.3/3.0	2000	9
[11*b*]	$S + HS \rightarrow S_2 + H$	4.7×10^{-11}		2000	10
[11*c*]	$S + OS \rightarrow S_2 + O$	1.5×10^{-13}		2000	10

[a]Rate constants are given in units of cm^3 molecule^{-1} s^{-1}.
[b]The uncertainty factors f/F indicate that the value of the rate constant k lies in the range $fk_0 < k < Fk_0$ around its central value k_0 (8).
[c]Each rate constant has been calculated at a temperature as close to 2000 K as the available data permit.
[d]This is the backward direction of the reaction appearing immediately above in the table.

TABLE 2. Calculated equilibrium burnt gas composition at 2200 K of the fuel-rich flame doped with 0.2 mol% of OCS

Usual species	Mole fraction	Sulphur species	Mole fraction	% Sulphur[a]
H_2	0.4120	H_2S	6.483×10^{-4}	50.45
CO	0.2978	HS	2.944×10^{-4}	22.91
H_2O	0.2514	OS	1.396×10^{-4}	10.86
CO_2	0.0349	O_2S	1.248×10^{-4}	9.72
H	3.63×10^{-3}	S	0.436×10^{-4}	3.39
HO	3.05×10^{-4}	OCS	0.172×10^{-4}	1.34
O	1.91×10^{-6}	S_2	0.171×10^{-4}	1.33
Σ	1.0000	CS	4.05×10^{-8}	0.00315
		CS_2	2.03×10^{-9}	0.000158
		Σ	0.001285	100.00

[a]These percentages of the total sulphur present in the burnt gas are calculated on a molar basis.

fuel-rich flame, and also the relatively high concentrations of HS and OS. Species involving C—S bonds are very minor.

Results

Sulphur cation profiles

The effect on the total positive ion profile of adding 0.2 mol% of OCS is shown in Fig. 2. The ion signal was enhanced in the reaction zone, located upstream of $z = 0$ (negative z in Fig. 2) and, to a lesser extent, downstream in the burnt gas but the peak value remained unchanged within experimental error. Profiles of individual ionic species which showed a change with the addition of OCS were measured in the mass range 32–100 u. Broadly speaking, these profiles were of four types. A number of them, particularly those at high mass numbers, showed a relatively sharp peak in the reaction zone; Fig. 3 gives an example at 77 u. Others exhibited a fairly broad maximum just downstream of the reaction zone before tailing out into the burnt gas; Fig. 4 at 47 u is a typical example.

A third group of ions, of which Fig. 5 at 59 u is typical, showed both effects; namely, a fairly sharp peak in the reaction zone and a broader one downstream. A fourth group is comprised of a few distinctive profiles like that given in Fig. 6 at 48 u which showed an even broader maximum further downstream with the signal persisting throughout the burnt gas; in the case of Fig. 6, a sulphur peak was also noted in the flame reaction zone. In all, sulphurous cation signals, many of them large, were observed at 47 mass numbers below 100 u. This behaviour is in marked contrast to the sulphurous anion signals studied previously with OCS additive in the same flame (2) which were attributable to just nine negative ion species.

Mass spectra

In order to organize this large quantity of data for presentation, mass spectra were recorded at three distinct positions on the flame axis. These three positions could be accurately reproduced with and without OCS additive with the aid of the profiles shown in Fig. 7. The first position is defined in the flame reaction zone at the peak of the profile at 43 u corresponding to $z = -0.15$ mm. This profile, due to protonated ketene, CH_2COH^+, is the largest ion signal present in the reaction zone and is a very useful marker because its peak position does not change when OCS is added to the flame. Mass spectra recorded at this position are shown in Figs. 8 and 9. The solid lines were measured with OCS present and the dashed lines with OCS

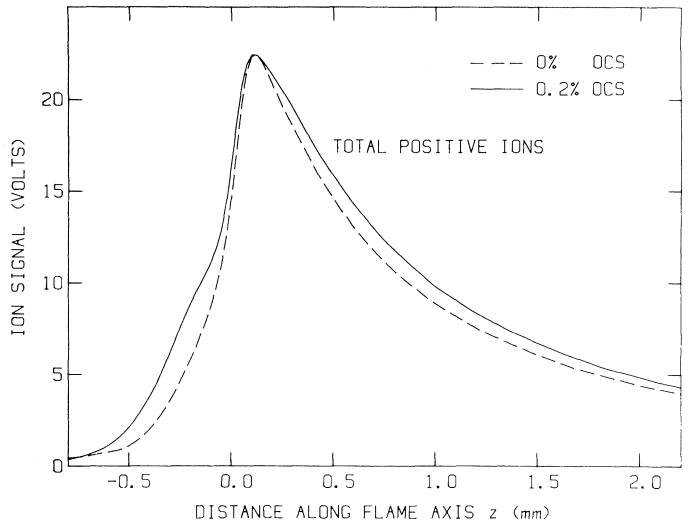

FIG. 2. Total positive ion profiles with, and without, 0.2 mol% of OCS additive. The flame reaction zone is located upstream of $z = 0$.

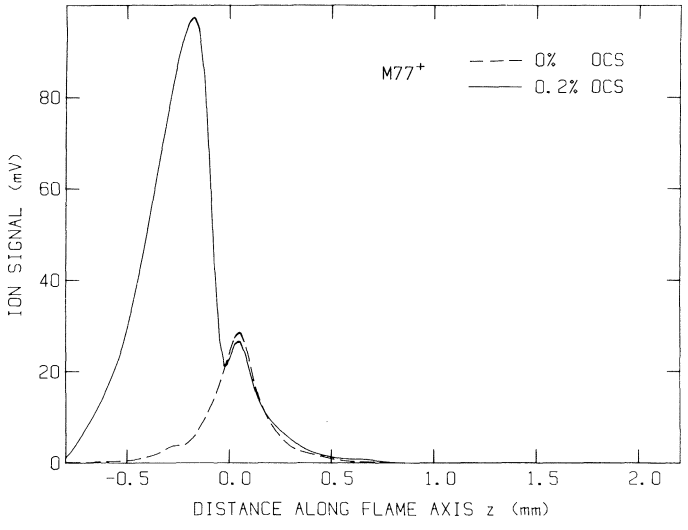

FIG. 3. Typical sulphurous cation profile with 0.2 mol% of OCS additive showing a concentration peak in the flame reaction zone; this example at 77 u is due to CHS_2^+. The dashed profile was measured with OCS absent.

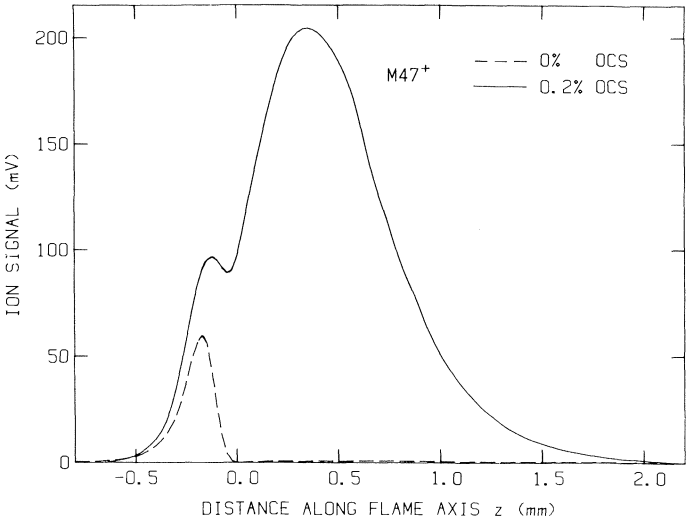

FIG. 4. Typical sulphurous cation profile with 0.2 mol% of OCS additive showing a fairly broad maximum just downstream of the flame reaction zone; this example at 47 u is due to CH_3S^+. The dashed profile was measured with OCS absent.

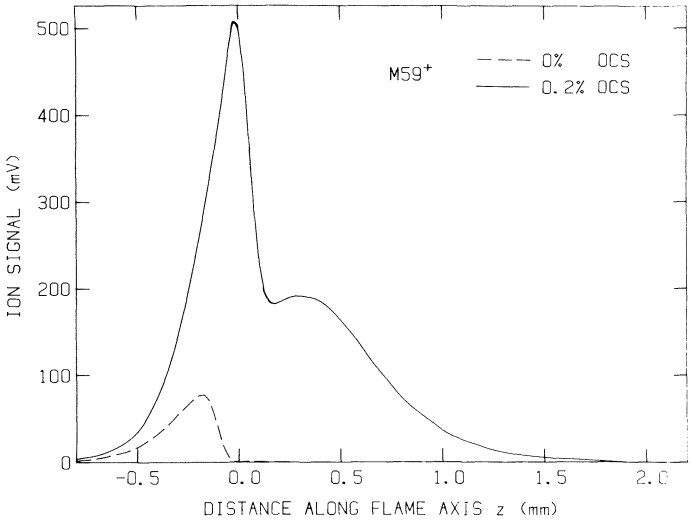

FIG. 5. Typical sulphurous cation profile with 0.2 mol% of OCS additive showing maxima both in the flame reaction zone and just downstream of it; this example at 59 u is due to $C_2H_3S^+$. The dashed profile was measured with OCS absent.

absent. For clarity, the spectra are divided up between Fig. 8 where sulphurous cations are involved, and Fig. 9 where the ion signals decrease or show little change with OCS addition.

The second position is defined at $z = 0.2$ mm on the flame axis in the vicinity of the broad profile maxima. It is designated 0.15 mm downstream of the very large $C_3H_3^+$ profile peak at 39 u which occurs at $z = 0.05$ mm as shown in Fig. 7. Although the $C_3H_3^+$ peak decreased somewhat in magnitude with the addition of OCS, it is a useful marker because the peak position does not shift. Mass spectra recorded at this position are given in Figs. 10 and 11. The data are presented in exactly the same way as those for Figs. 8 and 9.

Further downstream in Fig. 7, the very broad maximum of the persistent H_3O^+ profile at 19 u decreased and shifted considerably with OCS addition, and is not a useful marker. Thus, a third position is defined at $z = 0.5$ mm downstream, still with reference to the $C_3H_3^+$ profile peak as a marker. Figure 12 gives the mass spectra of sulphurous cations recorded at this position whose profiles persist far downstream throughout the burnt gas like H_3O^+ in Fig. 7 or OS^+ at 48 u in Fig. 6.

Discussion

Sulphurous cations may form in a number of ways. From Fig. 2, the total ion signal is appreciably higher in the flame reaction zone when OCS is present. One possible explanation is the existence of a new chemi-ionization source reaction involving sulphur such as

[14] $CH + S \rightarrow CHS^+ + e^- \qquad \Delta H^0 = 38$

(Standard heats of reaction ΔH^0 are given in kcal mol^{-1} at 298 K.) This is analogous to the established fundamental ionization reaction in hydrocarbon flames (12)

[15] $CH + O \rightarrow CHO^+ + e^- \qquad \Delta H^0 = -5$

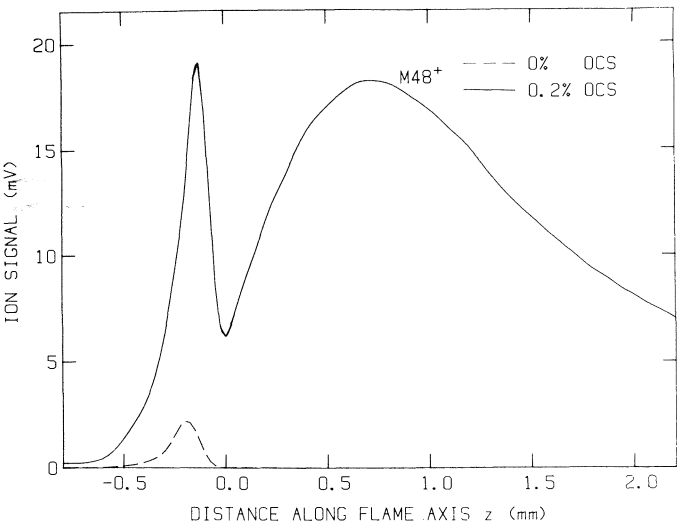

FIG. 6. Typical sulphurous cation profile with 0.2 mol% of OCS additive showing a broad maximum downstream in the flame which persists throughout the burnt gas region. This example at 48 u is due to OS^+; the additional peak in the reaction zone probably represents CH_4S^+. The dashed profile was measured with OCS absent.

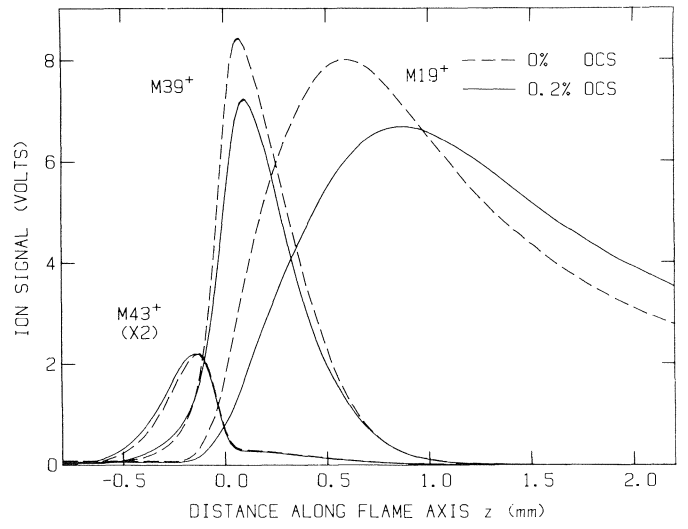

FIG. 7. Major non-sulphurous positive ion profiles with, and without, 0.2 mol% of OCS additive used to locate position markers on the flame axis. The ions represent $C_2H_3O^+$ at 43 u in the reaction zone, $C_3H_3^+$ at 39 u just downstream of it, and H_3O^+ at 19 u which persists throughout the burnt gas region.

However, reaction [14] is an unlikely process because it is considerably endothermic, and also because the CHS^+ profile (not shown) did not commence as far upstream as many profiles of other ionic species. An alternative explanation might be a decreased rate of ion recombination when the flame is doped with OCS. At the present time, we do not have a satisfactory explanation of the enhanced total ion signal in the flame reaction zone, but further work is in progress to clarify the situation.

If chemi-ionization involving sulphur is not a major mechanism, the first sulphur ions to appear in the flame, which we shall designate here as primary sulphur ions, must result from ion–molecule reactions of natural flame ions with sulphurous neutrals. The most obvious example is the formation of $CHOS^+$ at 61 u by exothermic proton transfer from CHO^+ to the OCS additive

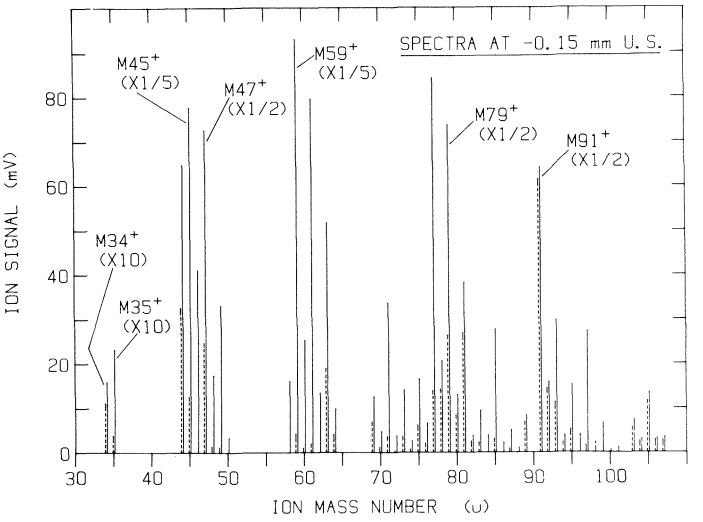

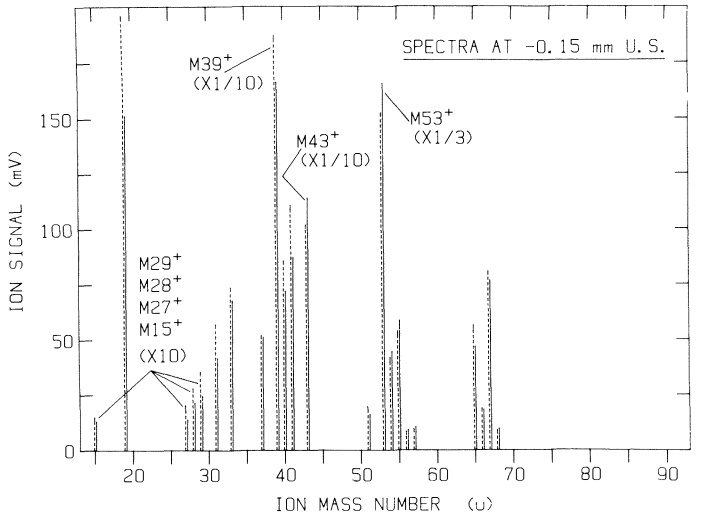

FIG. 8. Mass spectra measured in the reaction zone both with (solid lines) and without (dashed lines) OCS additive emphasizing sulphurous cations.

FIG. 9. Mass spectra measured in the reaction zone both with (solid lines) and without (dashed lines) OCS additive emphasizing non-sulphurous cations.

[16] $CHO^+ + OCS \rightarrow CHOS^+ + CO \qquad \Delta H^0 = -9$

Data for a number of relevant ion–molecule reactions involving sulphurous species like reaction [16] are given in Table 3 which is based mainly on Albritton's compilation (13). Not surprisingly, the $CHOS^+$ profile (not shown) was observed to commence very far upstream in the flame reaction zone. In addition, secondary sulphurous cations can form with comparatively large rates of production if primary sulphur ions react with major flame neutrals.

It will become apparent that the downstream sulphur ion chemistry at $z = 0.2$ mm exemplified by Fig. 10 is a simpler case of the ion chemistry in the reaction zone. For this reason, the downstream spectra will be discussed first before proceeding to Fig. 8.

Downstream sulphurous ion chemistry

Figure 13 is a simplified version of the mass spectra shown in Fig. 10 giving just the differences in signal magnitudes due to

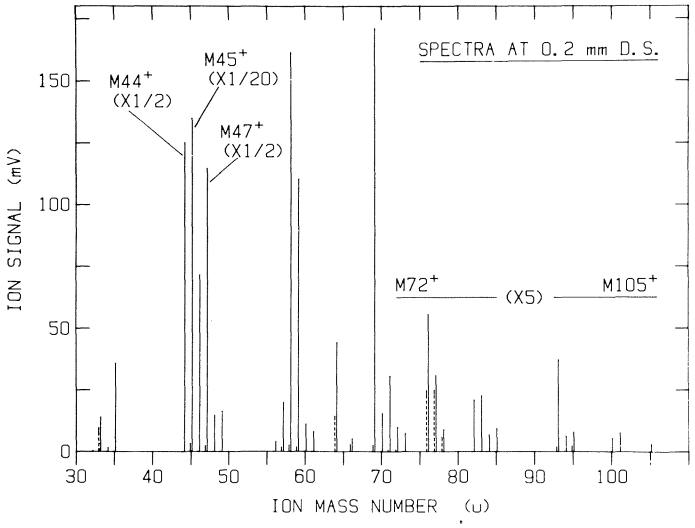

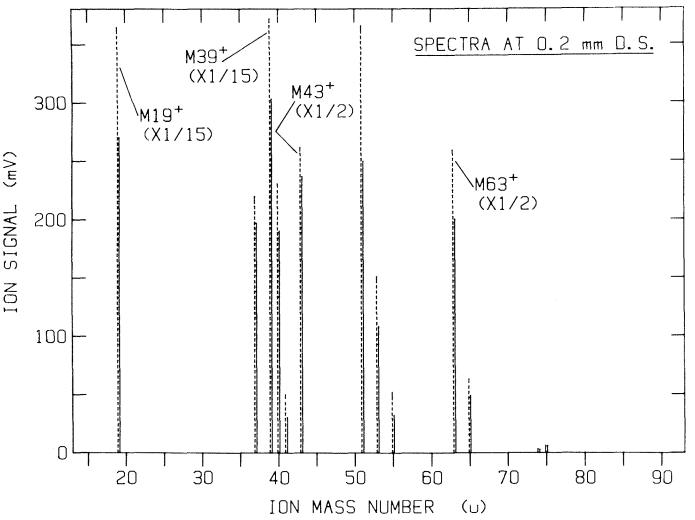

FIG. 10. Mass spectra measured just downstream of the reaction zone both with (solid lines) and without (dashed lines) OCS additive emphasizing sulphurous cations.

FIG. 11. Mass spectra measured just downstream of the reaction zone both with (solid lines) and without (dashed lines) OCS additive emphasizing non-sulphurous cations.

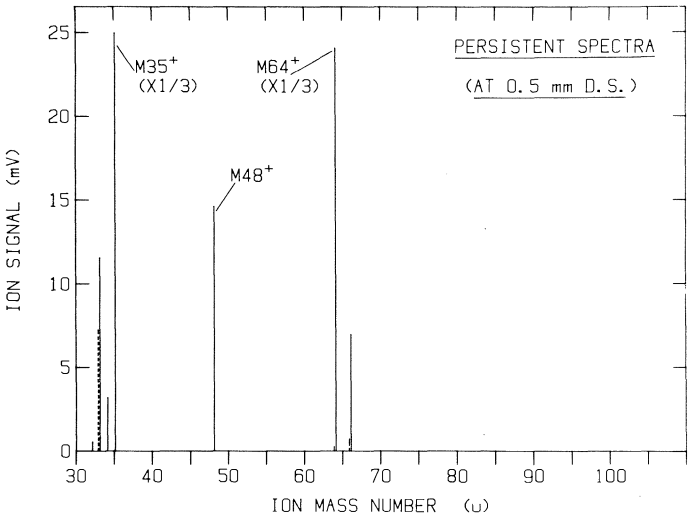

FIG. 12. Mass spectra measured at $z = 0.5$ mm both with (solid lines) and without (dashed lines) OCS additive of those sulphurous cations whose profiles persist throughout the burnt gas region.

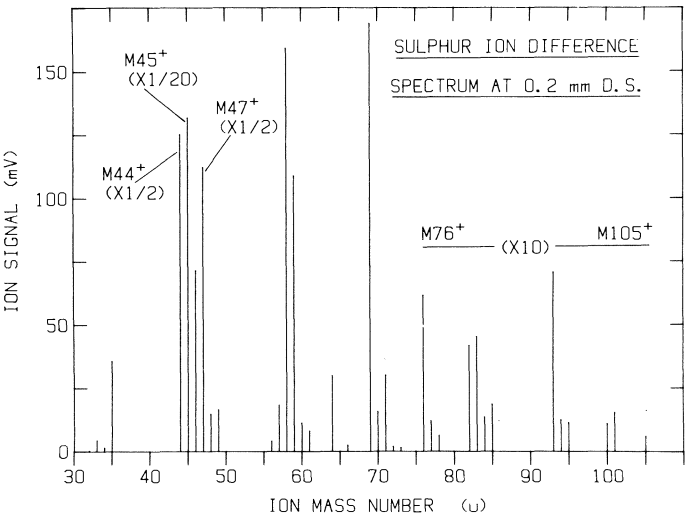

FIG. 13. Difference mass spectrum of just the sulphurous cation signals measured just downstream of the flame reaction zone.

sulphur cations at $z = 0.2$ mm downstream. The ions at 33–35 u can arise from protonated S, HS, and H_2S whose proton affinities (PA's) are fairly high. Table 4 lists the PA's of a number of sulphur species and also those of their oxygen analogues for comparison purposes; the values are taken from the recent compilation of Lias *et al.* (19). For a given pair, it is significant that the sulphur value is higher than the oxygen one in every case. The tiny S^+ ion signal at 32 u can arise by H atom stripping of HS^+

[17] $HS^+ + H\ (HO) \rightarrow S^+ + H_2\ (H_2O) \qquad \Delta H^0 = -20\ (-35)$

since the concentrations of H and HO will be near their equilibrium values 0.2 mm downstream. Similar H atom stripping reactions are exothermic for the $H_2S^+ \rightarrow HS^+$ and $H_3S^+ \rightarrow H_2S^+$ conversions as well.

The next group of ions in the mass range 44–49 u is comprised of CH_xS^+ ($x = 0$–3) and probably OS^+ and HOS^+. The large signals observed at 45 and 47 u may derive in part from proton transfer to CS and HCHS (thioformaldehyde) whose PA's given in Table 4 are high. Otherwise, a number of possible reactions leading to CHS^+ and CH_3S^+ have been measured at room temperature, and are listed in Table 3. For example, there is a series of reactions of CH_x^+ ($x = 0$–3) ions with H_2S

[18] $C^+ + H_2S \rightarrow CHS^+ + H \qquad \Delta H^0 = -127$
$\rightarrow H_2S^+ + C \qquad \Delta H^0 = -19$

[19] $CH^+ + H_2S \rightarrow CHS^+ + H_2 \qquad \Delta H^0 = -137$
$\rightarrow H_3S^+ + C \qquad \Delta H^0 = -23$

[20] $CH_2^+ + H_2S \rightarrow CHS^+ + H + H_2 \qquad \Delta H^0 = -29$
$\rightarrow CH_3S^+ + H \qquad \Delta H^0 = -75$
$\rightarrow H_3S^+ + CH \qquad \Delta H^0 = 4$

[21] $CH_3^+ + H_2S \rightarrow CH_3S^+ + H_2 \qquad \Delta H^0 = -54$

and a similar series involving CH_x^+ with OCS. At 48 and 49 u, OS^+ and HOS^+ are favoured over CH_4S^+ and CH_5S^+.

TABLE 3. Ion–molecule reactions involving sulphurous species

No.	Reaction	Product ratio (%)	Rate constant[a]	Error (%)	T (K)	Reference
[16]	$CHO^+ + OCS \rightarrow CHOS^+ + CO$		1.1×10^{-9}	±20	300	14
[18]	$C^+ + H_2S \rightarrow CHS^+ + H$	75	1.7×10^{-9}	±20	300	15
	$\rightarrow H_2S^+ + C$	25				
[19]	$CH^+ + H_2S \rightarrow CHS^+ + H_2$	70	2.1×10^{-9}	±20	300	15
	$\rightarrow H_3S^+ + C$	30				
[20]	$CH_2^+ + H_2S \rightarrow CHS^+ + H + H_2$	10	2.3×10^{-9}	±20	300	15
	$\rightarrow CH_3S^+ + H$	80				
	$\rightarrow H_3S^+ + CH$	10				
[21]	$CH_3^+ + H_2S \rightarrow CH_3S^+ + H_2$		1.2×10^{-9}	±20	300	15
	$CH^+ + OCS \rightarrow CHS^+ + CO$	55	1.9×10^{-9}	±20	300	15
	$\rightarrow CHOS^+ + C$	45				
	$CH_2^+ + OCS \rightarrow CHS^+ + CHO$	60	1.8×10^{-9}	±20	300	15
	$\rightarrow CH_2S^+ + CO$	40				
	$CH_3^+ + OCS \rightarrow CH_3S^+ + CO$		1.2×10^{-9}	±20	300	15
[27]	$H_3O^+ + H_2S \rightarrow H_3S^+ + H_2O$		1.9×10^{-9}	±20	296	16
[27]	$H_3S^+ + H_2O \rightarrow H_3O^+ + H_2S$		3.3×10^{-12}	±40	296	16
[28]	$H_2S^+ + H_2O \rightarrow H_3O^+ + HS$		8.1×10^{-10}	±25	295	17
[29]	$HS^+ + H_2O \rightarrow H_3O^+ + S$		6.3×10^{-10}	±25	295	17
[33]	$OS^+ + H_2S \rightarrow S_2^+ + H_2O$		9.4×10^{-10}	±30	300	18
	$CHO^+ H_2S \rightarrow H_3S^+ + CO$		1.4×10^{-9}	±30	300	18
	$S^+ + H_2S \rightarrow H_2S^+ + S$	>80	7.3×10^{-10}	±50	300	18
	$\rightarrow S_2^+ + H_2$	<20				
	$S^+ + H_2S \rightarrow S_2^+ + H_2$	72	8.8×10^{-10}	±20	295	17
	$\rightarrow HS_2^+ + H$	23				
	$\rightarrow H_2S^+ + S$	5				
	$HS^+ + H_2S \rightarrow H_3S^+ + S$	47	1.0×10^{-9}	±20	295	17
	$\rightarrow HS_2^+ + H_2$	28				
	$\rightarrow H_2S^+ + HS$	25				
	$H_2S^+ + H_2S \rightarrow H_3S^+ + HS$		1.0×10^{-9}	±20	295	17
[35]	$H_3S^+ + HCHO \rightarrow CH_3O^+ + H_2S$		2.2×10^{-9}	±25	296	16
	$CH_3O^+ + H_2S \rightarrow H_3S^+ + HCHO$		2.2×10^{-10}	±55	296	16
	$H_3S^+ + CH_4 \rightarrow$		$<5 \times 10^{-13}$	±20	295	17
	$H_2S^+ + CH_4 \rightarrow$		$<5 \times 10^{-13}$	±20	295	17
	$HS^+ + CH_4 \rightarrow CH_3S^+ + H_2$	90	5.4×10^{-10}	±20	295	17
	$\rightarrow CH_3^+ + H_2S$	10				
	$S^+ + CH_4 \rightarrow CH_3S^+ + H$	95	4.0×10^{-10}	±25	295	17
	$\rightarrow CHS^+ + H_2 + H$	5				

[a]Rate constants are given in units of cm^3 $molecule^{-1}$ s^{-1}.

TABLE 4. Proton affinities (PA's) of sulphur species with their oxygen counterparts

Oxygen species			Sulphur species		
Ion mass AH^+ (u)	Neutral A	PA (kcal mol^{-1})	Ion mass AH^+ (u)	Neutral A	PA (kcal mol^{-1})
17	O	116.3	33	S	158.3
18	HO	143.6	34	HS	165
19	H_2O	166.5	35	H_2S	170.2
29	CO	141.9	45	CS	175
31	HCHO	171.7	47	HCHS	184.7
33	CH_3OH	181.9	49	CH_3SH	187.4
43	CH_2CO	198.0	59	CH_2CS	201.2
45	CH_3CHO	186.6	61	CH_3CHS	194.6
	CO_2	130.9		OCS	151
47	C_2H_5OH	188.3	63	C_2H_5SH	190.8
	$(CH_3)_2O$	192.1		$(CH_3)_2S$	200.6
			77	CS_2	164.4
			79	$(CH_3)_2SO$	211.3

Although the PA of CH_3SH given in Table 4 is high, and presumably that of the CH_3S radical also, these species are more likely to be found in the reaction zone and not downstream. On the other hand, the downstream concentration of OS even at z = 0.2 mm will be relatively high tending towards the calculated value given in Table 2. Although PA(OS) is not known, proton transfer to form HOS^+ followed by H atom stripping to give OS^+ is the most logical mechanism. Further support for this hypothesis comes from Fig. 12 where a sulphur profile at 48 u, undoubtedly OS^+, was observed to persist far downstream throughout the burnt gas.

The signal at 64 u is due to S_2^+, not O_2S^+, since the peak height at 66 u is 8.5% of that at 64 u in keeping with the natural abundance of the ^{34}S isotope of 4.22%. The group of ions observed at 76–78 u appears to represent $CH_xS_2^+$ (x = 0–2) disulphide ions. The ion with x = 1 at 77 u amounts to protonated carbon disulphide for which the H atom stripping reactions

[22] $CHS_2^+ + H(HO) \rightarrow CS_2^+ + H_2(H_2O) \qquad \Delta H^0 = -18\,(-33)$

are exothermic (20). Similarly, the signal at 78 u probably results from H atom stripping of $CH_3S_2^+$ at 79 u. Better evidence for CHS_2^+ and $CH_3S_2^+$ at 77 and 79 u comes from Figs. 3 and 8 in the flame reaction zone where the measured signals are much larger. The profiles of both ions were observed to commence very far upstream like that of $HCOS^+$.

The next step in the explanation comes from Hastie's neutral profiles (7) shown in Fig. 1. He observed the formation of acetylene as an intermediate having a peak concentration > 1% near the downstream edge of the reaction zone. Flame-ion evidence for acetylene comes from the very large $C_3H_3^+$ peak shown in Fig. 7 at the same position in our flame; C_2H_2 is the neutral reagent for the formation of $C_3H_3^+$ (4, 21). Acetylene is the key ingredient. All the other high-mass ions in Fig. 13 are explicable in terms of ion–molecule reactions of C_2H_2 with the ion groups at 32–35, 44–49, and 76–78 u. Acetylene is known to participate in ion-molecule association/condensation reactions (4, 22–24) of the types

[23] $$X^+ + C_2H_2 \xrightarrow{M} \begin{cases} C_2H_2X^+ \\ \rightarrow C_2HX^+ + H \\ \rightarrow C_2X^+ + H_2 \end{cases}$$

where M is a third body. Downstream in the flame where the H and HO concentrations are high, the C_2X^+ product is favoured because $C_2H_2X^+$ and C_2HX^+ are subject to H atom stripping. In general, the expected mechanism for secondary sulphurous ion formation is the addition of 24–26 mass units to ions of lower mass. Thus, acetylene addition to the H_xS^+ (x = 0–3) ions at 32–35 u produces the ion groups at 57–61 and 82–85 u. In particular, the large ion signals 35 → 59 → 83 differ by 24 u except that the peak at 58 u is greater than that at 59 u. (Note that the reverse is true in the reaction zone, Fig. 8.) However, H atom stripping of protonated thioketene at 59 u should be exothermic such that the larger signal at 58 u is not surprising

[24] $C_2H_3S^+ + H(HO) \rightarrow C_2H_2S^+ + H_2(H_2O)$

That reaction [24] would be exothermic stems from the fact that the oxygen analogue of the reaction involving protonated ketene is thermoneutral

[25] $C_2H_3O^+ + H \rightarrow C_2H_2O^+ + H_2 \qquad \Delta H^0 = 0.4$

Although PA(CH_2CS) is slightly greater than PA(CH_2CO) in Table 4, the ionization energy IE(CH_2CS) should be at least 1 eV less than IE(CH_2CO) = 9.614 eV (20), and the exothermicity of reaction [24] follows.

In the same way, acetylene addition to the $CH_xS^+/OS^+/HOS^+$ group of ions at 44–49 u produces the ion groups at 69–73 u and 93–95 u. In particular, the large ion signals in each group, 45 → 69 → 93, differ by 24 u. Also, the addition of acetylene to the $CH_xS_2^+$ ions grouped at 76–78 u accounts for the signals observed at 100, 101, and even 105 (i.e. $CH_3S_2^+$ + 26 u). In summary, three groups of protonated primary ions modified by H atom stripping plus acetylene addition/condensation reactions account for essentially all of the sulphurous cations observed in Fig. 13. An exception is S_2^+ which will be discussed further in the next section.

Persistent downstream ion profiles

Figure 12 is a mass spectrum of sulphurous cations whose profiles persist far downstream throughout the burnt gas like those shown for OS^+ and H_3O^+ in Figs. 6 and 7, respectively. The CHO^+ profile (not shown) is similar in this fuel-rich flame, and is indicative of a proton transfer equilibrium with H_3O^+

[26] $CHO^+ + H_2O \rightleftharpoons H_3O^+ + CO \qquad \Delta H^0 = -24.6$

(ΔH^0 values are quoted for the forward direction.) In the same way, all of the sulphurous ions represented in Fig. 12 (S^+, HS^+, H_2S^+, H_3S^+, OS^+, S_2^+) must come into equilibrium with H_3O^+ and CHO^+ downstream. The four H_xS^+ (x = 0–3) ions can be formed by proton transfer reactions involving H_3O^+

[27] $H_3O^+ + H_2S \rightleftharpoons H_3S^+ + H_2O \qquad \Delta H^0 = -3.7$

[28] $H_3O^+ + HS \rightleftharpoons H_2S^+ + H_2O \qquad \Delta H^0 = 2$

[29] $H_3O^+ + S \rightleftharpoons HS^+ + H_2O \qquad \Delta H^0 = 8.2$

in combination with the H atom stripping reactions

[30] $H_3S^+ + H(HO) \rightleftharpoons H_2S^+ + H_2(H_2O) \qquad \Delta H^0 = -6\,(-21)$

[31] $H_2S^+ + H(HO) \rightleftharpoons HS^+ + H_2(H_2O) \qquad \Delta H^0 = -14\,(-29)$

[17] $HS^+ + H(HO) \rightleftharpoons S^+ + H_2(H_2O) \qquad \Delta H^0 = -20\,(-35)$

which are exothermic in every case. For the latter three reactions, the rates of the endothermic back reactions are aided by the high equilibrium concentrations of H_2 and H_2O quoted in Table 2. But H_2S^+, HS^+, and S^+ are, of course, ionized H_2S, HS, and S which have ionization energies (IE's) of 10.47, 10.41, and 10.36 eV, respectively (20, 25). These IE's are all slightly higher than those of OS (10.31 eV) and S_2 (9.37 eV) such that OS^+ and S_2^+ could be formed by exothermic charge transfer processes; for example

[32] $H_2S^+ + OS \rightleftharpoons OS^+ + H_2S \qquad \Delta H^0 = -3$

Table 3 lists rate constants for a number of fast reactions which link these ions together and increase the rate of attainment of equilibrium; for example

[33] $OS^+ + H_2S \rightleftharpoons S_2^+ + H_2O \qquad \Delta H^0 = -47$

Thus, persistent ion signals are found in the burnt gas involving reasonably abundant sulphur neutrals (see Table 2) whose PA's are relatively high, and/or whose IE's are relatively low.

In principle, some of the ion–molecule reactions involving sulphurous species might be used to determine equilibrium constants K in the burnt gas. For example, reaction [27] yields

[34] $$K_{27} = \frac{[H_2O]}{[H_2S]} \times \frac{[H_3S^+]}{[H_3O^+]}$$

in terms of calculated neutral concentrations given in Table 2 and the measured ion signal ratio. Hence, $\Delta G^0 = -RT \ln K$ for

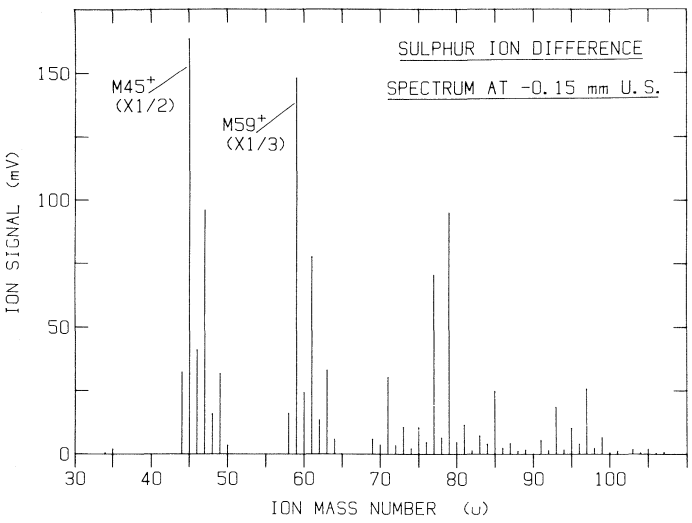

FIG. 14. Difference mass spectrum of just the sulphurous cation signals measured in the flame reaction zone.

such a reaction can be determined at the flame temperature provided that equilibrium is attained. We intend to consider some of these quantitative aspects in a future publication.

Sulphur ions in the reaction zone

Figure 14 is a simplified version of the mass spectra shown in Fig. 8 giving just the differences in signal magnitudes due to sulphur cations at $z = -0.15$ mm upstream in the reaction zone. Clearly the sulphur ion chemistry is more complicated than that shown in Fig. 13 for the downstream region. Here, the aim will be to high-light the main features without attempting to explain every peak. Thus, the explanation will concentrate on the larger ion signals having odd mass numbers recognizing that the ions of even mass can generally be produced by H atom stripping reactions.

In what respects is the reaction zone chemically different from the downstream region? Hastie's neutral profiles in Fig. 1 show the rise of formaldehyde as an intermediate whose concentration reaches a peak value of approximately 0.8 mol%. In addition, the acetylene concentration rises steadily through the reaction zone, and also that of methyl radicals from the decay of the methane fuel. Finally, the OCS additive retains its identity and serves as a donor of S atoms in reactions with other ions, giving CO as a neutral product.

In the first place, Fig. 14 shows that the H_xS^+ ($x = 0$–3) ion signals are much smaller than those measured downstream. This is partly due to the fact that the concentrations of S, HS, and H_2S have not yet reached their downstream equilibrium values. In addition, the PA's of all three neutrals given in Table 4 are less than that of formaldehyde; Table 3 indicates that the proton transfer reaction

$$[35] \quad H_3S^+ + HCHO \rightarrow CH_3O^+ + H_2S \qquad \Delta H^0 = -1.5$$

has a very high rate constant at room temperature (16). Although H_3S^+ does not react with CH_4 (17) it might well do so with CH_3 radicals

$$[36] \quad H_3S^+ + CH_3 \rightarrow CH_5S^+ + H \qquad \Delta H^0 = 0$$

at the flame temperature.

For the next ion group, let us focus attention primarily on the ion signals at 45, 47, and 49 u. Sources of the first two ions, CHS^+ and CH_3S^+, are given in Table 3 involving reactions of the CH_x^+ ($x = 0$–3) ions with OCS rather than with H_2S given

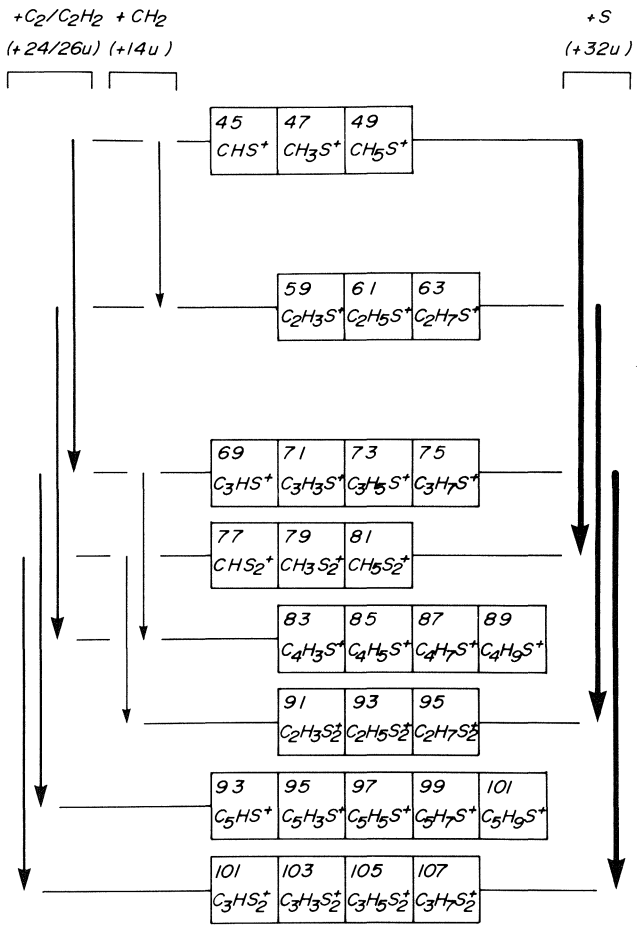

FIG. 15. Reaction flow diagram of the sulphurous ion chemistry in the flame reaction zone showing reactions of primary sulphur ions with C_2H_2, CH_4/CH_3, and with the OCS additive.

previously for the downstream region (reactions [18] to [21]). The ion at 49 u is likely to be CH_5S^+ rather than HOS^+ in the reaction zone. It might arise via reaction [36] or, if the mercaptan CH_3SH is present, by proton transfer since PA(CH_3SH) is high (see Table 4).

We are suggesting that these three CH_xS^+ ($x = 1, 3, 5$) ions in reactions with CH_4/CH_3, C_2H_2, and OCS are the primary reagents for essentially all the major sulphurous cations observed at higher mass numbers in Fig. 14. Thus, reactions with CH_4/CH_3 will result in the addition of a methylene group to the parent ion increasing its mass by 14 u

$$[37] \quad C_nH_mS^+ + CH_4\ (CH_3) \rightarrow C_{n+1}H_{m+2}S^+ + H_2\ (H)$$

Acetylene will add in much the same way as discussed previously for the downstream region

$$[38] \quad C_nH_mS^+ + C_2H_2 \xrightarrow{M} C_{n+2}H_{m+2}S^+ \rightarrow C_{n+2}H_mS^+ + H_2$$

except that the lower temperature of the reaction zone might be expected to favour the first channel; i.e., acetylene reactions will increase the parent mass by 26 or 24 u. Finally, reactions with OCS will add sulphur giving a mass increase of 32 u

$$[39] \quad CH_xS^+ + OCS \rightarrow CH_xS_2^+ + CO \qquad (x = 1, 3, 5)$$

The anomalously large signal at 79 u might involve $(CH_3)_2SOH^+$ as well as $CH_3S_2^+$ since PA(dimethylsulphoxide) = 211.3 kcal mol^{-1} is so high. Figure 15 presents a reaction scheme which closely follows the observations of the sulphurous cations given in

Fig. 14. In particular, the preservation of the relative signal magnitudes for the CH_xS^+ ($x = 1, 3, 5,$) ion triad at higher mass numbers should be noted. In general, H atom stripping is not observed to occur to the same extent as was the case downstream; the concentration of H atoms has not yet reached its equilibrium value upstream in the flame reaction zone.

Conclusions

When a fuel-rich, CH_4–O_2 flame is doped with 0.2 mol% of OCS, a number of conclusions can be drawn about the involvement of the sulphur additive in the flame chemistry as inferred from observations of flame cations.

(*1*) A great variety of different sulphurous cations has been detected at roughly half the mass numbers below 100 u.

(*2*) Concentration profiles of sulphurous ions measured along the flame axis show three characteristic shapes or combinations of them; fairly sharp peaks in the reaction zone, broader maxima just downstream of it, or even broader maxima still further downstream with ion signals which persist throughout the burnt gas.

(*3*) Upstream in the reaction zone, the CH_xS^+ ($x = 1, 3, 5$) ions are the major sulphurous ions to be formed first. Essentially all the rest of the sulphurous cations are secondary ions formed by addition (i.e. association) or condensation reactions of CH_xS^+ with (*a*) CH_4/CH_3, (*b*) C_2H_2, or (*c*) S from the OCS additive.

(*4*) Just downstream of the reaction zone, the primary sulphurous cations are H_xS^+ ($x = 0$–3) in addition to CH_xS^+ and possibly OS^+/HOS^+ as well. Essentially all the rest of the sulphur ions in this flame region can be explained by reactions of the primary cations with just C_2H_2, although ions of even mass number can be produced by H atom stripping reactions with H and HO.

(*5*) The few sulphur ions which persist throughout the burnt gas (H_xS^+ ($x = 0$–3), OS^+ and S_2^+) must be equilibrated with the natural flame ions CHO^+ and H_3O^+. These signals may be useful analytically for downstream sulphur determinations of H_2S, HS, OS, and S_2, but a cation link with O_2S is not immediately apparent.

(*6*) In the burnt gas region of this fuel-rich flame, equilibrium calculations show that H_2S accounts for about half, and HS nearly one quarter, of the total sulphur present; OS and O_2S amount to about 10% each. For fuel-rich combustion in general, it is of interest to know just where, and if, H_2S is subsequently oxidized to O_2S.

(*7*) The OCS additive is a very effective donor of S atoms in reaction with either ions or neutral species present in the flame.

(*8*) From observations of mass spectra, it is apparent that the sulphur cation chemistry closely mimics the oxygen cation chemistry with a separation of 16 mass units. Comparatively large sulphur ion signals are obtained from a small concentration of additive because the proton affinities of the sulphur species are larger, and ionization energies are smaller, than those of their oxygen analogues.

(*9*) When compared with previous studies of sulphurous negative ions (2, 3), it is clear that a much greater variety of sulphurous positive ions was observed. This bears out the general contention that electron-deficient cations are better candidates for molecular growth by condensation reactions than are electron-rich anions.

Acknowledgement

Support of this work by the Natural Sciences and Engineering Research Council of Canada under Grant No. A-1604 is gratefully acknowledged.

1. R. M. Harrison. CRC Critical Rev. Anal. Chem. **15**, 1 (1984).
2. J. M. Goodings, K. Elguindi, and D. K. Bohme. Can. J. Chem. **61**, 1703 (1983).
3. J. M. Goodings, K. Elguindi, D. K. Bohme, and A. Fox. Can. J. Chem. **64**, 689 (1986).
4. J. M. Goodings, D. K. Bohme, and C.-W. Ng. Combust. Flame, **36**, 27 (1979).
5. J. M. Goodings, D. K. Bohme, and C.-W. Ng. Combust. Flame, **36**, 45 (1979).
6. A. N. Hayhurst and N. R. Telford. Combust. Flame, **28**, 67 (1977).
7. J. W. Hastie. Combust. Flame, **21**, 187 (1973).
8. F. Westley. Table of recommended rate constants for chemical reactions occurring in combustion. NSRDS-NBS 67, U.S. Government Printing Office, Washington, DC. 1980.
9. D. L. Baulch, D. D. Drysdale, J. Duxbury, and S. J. Grant. Evaluated kinetic data for high temperature reactions. Vol. 3. Homogeneous gas phase reactions of the O_2–O_3 system, the CO–O_2–H_2 system, and of sulphur containing species. Butterworths, London. 1976.
10. S. W. Benson, D. M. Golden, R. W. Lawrence, R. Shaw, and R. W. Woolfolk. Estimating the kinetics of combustion including reactions involving oxides of nitrogen and sulphur. U.S. Environmental Protection Agency Report No. EPA-600/2-2-75-019. August, 1975.
11. (*a*) D. R. Stull and H. Prophet (*Editors*). JANAF Thermochemical Tables, 2nd ed. NSRDS-NBS 37, U.S. Government Printing Office, Washington, DC. 1971; (*b*) M. W. Chase, J. L. Curnutt, A. T. Hu, H. Prophet, A. N. Syverud, and L. C. Walker. JANAF Thermochemical Tables, 1974 Suppl. J. Phys. Chem. Ref. Data, **3**, 311 (1974); (*c*) M. W. Chase, J. L. Curnutt, H. Prophet, R. A. McDonald, and A. N. Syverud. JANAF Thermochemical Tables, 1975 Suppl. J. Phys. Chem. Ref. Data, **4**, 1 (1975); (*d*) M. W. Chase, J. L. Curnutt, R. A. McDonald, and A. N. Syverud. JANAF Thermochemical Tables, 1978 Suppl. J. Phys. Chem. Ref. Data, **7**, 793 (1978); (*e*) M. W. Chase, J. L. Curnutt, J. R. Downey, R. A. McDonald, A. N. Syverud, and E. A. Valenzuela. JANAF Thermochemical Tables, 1982 Suppl. J. Phys. Chem. Ref. Data, **11**, 695 (1982).
12. H. F. Calcote. Eighth Symposium (International) on Combustion. Williams & Wilkins, Baltimore, MD. 1962. p. 184.
13. D. L. Albritton. Ion–neutral reaction rate constants measured in flow reactors through 1977. Atomic Data and Nuclear Data Tables, **22**, No. 1. July, 1978.
14. N. G. Adams, D. Smith, and D. Grief. Int. J. Mass Spectrom. Ion Phys. **26**, 405 (1978).
15. N. G. Adams and D. Smith. Chem. Phys. Lett. **54**, 530 (1978).
16. K. Tanaka, G. I. Mackay, and D. K. Bohme. Can. J. Chem. **56**, 193 (1978).
17. D. Smith, N. G. Adams, and W. Lindinger. J. Chem. Phys. **77**, 3365 (1981).
18. J. P. Liddy, C. H. Freeman, and M. J. McEwan. Astrophys. Lett. **16**, 155 (1975).
19. S. G. Lias, J. F. Liebman, and R. D. Levin. Evaluated gas phase basicities and proton affinities of molecules; heats of formation of protonated molecules. J. Phys. Chem. Ref. Data, **13**, 695 (1984).
20. R. D. Levin and S. G. Lias. Ionization potential and appearance potential measurements, 1971–1981. NSRDS-NBS 71, U.S. Government Printing Office, Washington, DC. 1982.
21. J. M. Goodings, K. K. Bohme, and T. M. Sugden. Sixteenth Symposium (International) on Combustion, The Combustion Institute, Pittsburgh, PA. 1977. p. 891.
22. C. Vinckier, M. P. Gardner, and K. D. Bayes. Sixteenth Symposium (International) on Combustion, The Combustion Institute, Pittsburgh, PA. 1977. p. 881.
23. F. W. Brill and J. R. Eyler. J. Phys. Chem. **85**, 1091 (1981).
24. N. M. Simo and W. S. Koski. J. Phys. Chem. **88**, 5320 (1984).
25. H. M. Rosenstock, K. Draxl, B. W. Steiner, and J. T. Herron. J. Phys. Chem. Ref. Data, **6**, Suppl. No. 1. 1977.

Synthèse et caractérisation du α-hydroxy, ω-(4-*N*,*N*-diméthylaminophényl) polystyrène

GÉRARD BEINERT

Institut Charles Sadron, Centre national de la recherche scientifique, 6, rue Boussingault, 67083 Strasbourg, France

ET

MITCHELL A. WINNIK

Lash Miller Chemical Laboratories, Department of Chemistry and Erindale College, University of Toronto, Toronto, Ont., Canada M5S 1A1

Reçu le 13 août 1985[1]

GÉRARD BEINERT et MITCHELL A. WINNIK. Can. J. Chem. **64**, 1743 (1986).

Dans le but d'étudier la formation d'exciplexes intramoléculaires, nous avons préparé comme intermédiaires de synthèse des polystyrènes qui portent quantitativement à l'une des extrémités de la chaîne une fonction alcool, et à l'autre le groupe *N*,*N*-diméthylaminophényle. Ce groupe chromophore a été introduit dans le polymère par amorçage de la polymérisation anionique du styrène au moyen d'une solution contenant du potassio-1 (*N*,*N*-diméthylamino-4)phényl-1 éthane. En desactivant ensuite le polymère «vivant» par de l'oxiranne, on obtient la fonction alcool. Une méthode simple de préparation de cet amorceur consiste à faire réagir un excès de potassium sur une solution d'éthoxy-1 (*N*,*N*-diméthylamino-4)phényl-1 éthane dans le THF. Malgré son instabilité relative, cette solution se présente comme un amorceur efficace de la polymérisation du styrène.

GÉRARD BEINERT and MITCHELL A. WINNIK. Can. J. Chem. **64**, 1743 (1986).

To prepare polymers carrying a donor chromophore at one end and an acceptor chromophore at the other, anionic initiators carrying the 4-*N*,*N*-dimethylaminophenyl group were synthesized by two different methods. These polymers were needed for the purpose of studying intramolecular cyclization via observation of exciplex formation. It was established that metal cleavage of appropriately substituted ethers was the most advantageous way to synthesize these functionalized initiators. These compounds proved very reactive toward styrene, yielding quantitatively polymers bearing 4-(*N*,*N*-dimethylaminophenyl) groups at one end of the chain. At the other end of the chain, induced deactivation of the "living" sites by means of oxirane created a hydroxy function that could be used in a later step to attach various other groups. Attachment of pyrene to this end would lead to a system in which intramolecular exciplex formation could occur.

Introduction

La dynamique de cyclisation de chaînes macromoléculaires par formation intramoléculaire de complexes de type excimère ou exciplexe suscite depuis quelques années un vif intérêt (1). Pour réaliser de telles études, il est nécessaire de disposer de polymères linéaires—et si possible bien définis—portant des fonctions aux extrémités de leur chaîne. Dans le cas des exciplexes qui nous occupe ici, les deux fonctions doivent être de nature différente, l'une ayant un caractère donneur, l'autre accepteur d'électrons. Nous avons choisi la fonction *N*,*N*-diméthylamino-4 phényle (DAP) comme groupe donneur. Le présent article a pour objet de décrire la préparation de polystyrènes portant cette fonction à une extrémité de leur chaîne, l'autre étant dotée d'une fonction alcool susceptible de servir ultérieurement de point d'ancrage pour différents groupes chromophores de type accepteur.

L'objectif que nous nous sommes fixé implique l'utilisation d'un amorceur anionique comportant la fonction DAP afin de pouvoir utiliser l'oxiranne pour la formation de la fonction hydroxy à l'autre extrémité de la chaîne.

Nous avons donc conçu deux méthodes permettant de préparer des composés organo-métalliques fonctionnalisés par le groupe en question et nous avons étudié le comportement de ces composés en tant qu'amorceurs de la polymérisation anionique du styrène.

On sait en effet que la polymérisation anionique sans transfert, ni terminaison, constitue une méthode de choix pour la préparation de polymères de masse molaire déterminée et de faible polymolécularité, et pour la fonctionnalisation des extrémités de chaîne par désactivation sélective à l'aide d'un réactif approprié. L'objectif visé pourrait donc être atteint s'il s'avère possible d'amorcer la polymérisation du styrène par un composé organo-métallique portant la fonction DAP, et si la désactivation par l'oxiranne conduit effectivement à une fonction OH à l'autre extrémité de la chaîne (schéma 1) : l'action du chlorure de (pyrényl-1)-4 butyryle sur cette dernière devrait en effet permettre d'accéder à des chaînes polymères portant des fonctions différentes à leurs extrémités, et susceptibles de conduire à la formation d'exciplexes intramoléculaires.

Résultats et discussions

Il semble établi que le groupe *N*,*N*-diméthylamino n'entraîne pas de réactions parasites en polymérisation anionique. Par exemple Worsfold (2) a obtenu des polystyrènes marqués quantitativement à l'une des extrémités de leur chaîne en amorçant la polymérisation du styrène par le lithio-1 (*N*,*N*-diméthyl)amino-3 propane.

Le problème consiste donc à préparer un amorceur organo-métallique portant la fonction DAP. Deux voies s'offrent à nous : (*i*) la réaction d'addition d'un composé organo-métallique R^-M^+ sur le (*N*,*N*-diméthylamino-4)isopropényl benzène (DAB) dans des conditions choisies de façon à éviter la polymérisation intempestive de ce monomère; et (*ii*) la réaction de clivage par le potassium d'un éther comportant un groupe DAP.

Méthode procédant par addition

Le (*N*,*N*-diméthylamino-4)isopropényl benzène a été préparé selon la méthode de Seymour et Wolfstirn (3). La réaction d'addition d'un composé organo-métallique sur un dérivé de l'α-méthylstyrène ne peut se produire de façon satisfaisante que si le caractère nucléophile de l'organo-métallique est très accusé. C'est pourquoi nous avons choisi les trois composés suivants : le *sec*-butyllithium (*s*BuLi), le potassio-2 phényl-2 propane (PIK) et le potassio-1 phényl-1 éthane (PEK), dont

1. Révision reçue le 2 avril 1986.

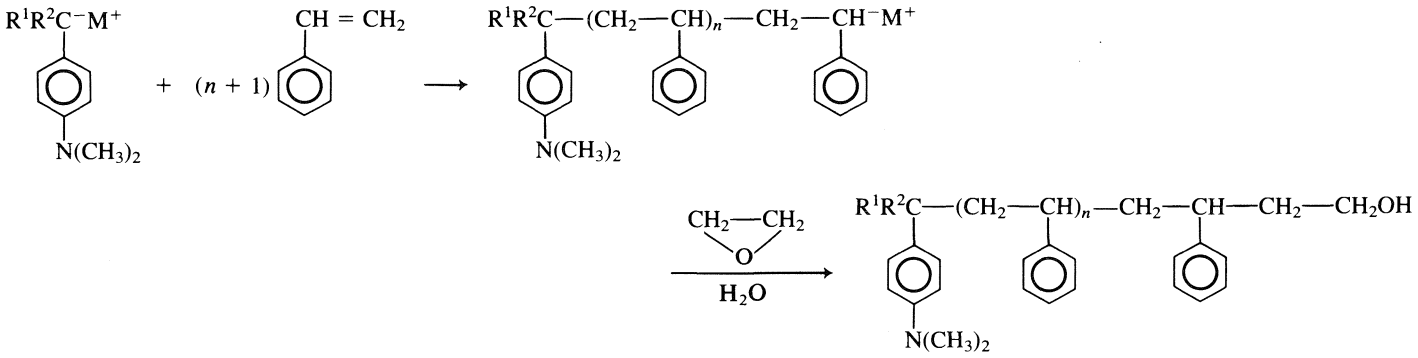

SCHÉMA 1

l'efficacité en tant qu'amorceurs n'est plus à démontrer. Le dernier mentionné a été utilisé en particulier pour la synthèse de polystyrènes de structure «idéale» ne comportant aucun groupe étranger au polymère (4) ainsi que pour la synthèse de copolymères séquencés polystyrène–polyoxyéthylène.

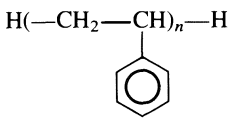

Le potassio-1 phényl-1 éthane peut être obtenu selon le procédé de Benkeser *et al.* (6) qui consiste à métaller l'éthylbenzène par un alkyl-potassium. Une méthode plus facile consiste à traiter une solution de bis(phényl-1 éthyl)éther dans le THF par du potassium. Cette réaction, étudiée par Gillman et McNinch (7) dans le cas du lithium, est transposable au potassium et conduit à une solution d'amorceur efficace pour la polymérisation du styrène (8). Il faut noter que, dans le cas qui nous occupe, la présence de phényl-1 éthanolate de potassium, qui se forme simultanément, n'est pas gênante.

La réaction d'addition a été conduite à 50°C dans le benzène, dans le cas du *s*BuLi, et à 25°C dans le THF pour les deux autres composés organo-métalliques. La solution est agitée pendant 2 h. On ajoute ensuite le styrène goutte à goutte, puis l'oxiranne destiné à la formation de fonctions hydroxyle. Il faut noter à cet égard que lorsque le potassium est le contre-ion, il est impératif d'opérer à une température suffisamment basse pour qu'un seul motif —CH_2—CH_2—O— se fixe en bout de chaîne, et que la polymérisation de l'oxiranne ne puisse avoir lieu.

Les résultats de nos essais sont rassemblés au tableau 1, et appellent quelques commentaires :

Pour vérifier le taux de fixation du groupe DAP en bout de chaîne, nous avons comparé entre elles les valeurs de la masse molaire moyenne en nombre $\bar{M}_n$ obtenue par chromatographie liquide d'exclusion (SEC) et de la masse molaire calculée à partir de l'absorption du chromophore, en faisant l'hypothèse que chaque chaîne porte *une* telle fonction, $\bar{M}_{uv}$. Nous avons supposé que le coefficient d'absorption molaire ε du groupe DAP est égal à celui d'un composé modèle : le *N*,*N*-diméthyl-amino-4 *tert*-butyl benzène que nous avons préparé au laboratoire (9) par alkylation de l'amino-4 *tert*-butyl benzène. La valeur de ε que nous avons trouvée à 300 nm est de 2 530 L mol^{-1} cm^{-1}, cette mesure étant effectuée sur un mélange d'isomères *para* (96,7%) et *ortho* (3,2%) caractérisé par chromatographie en phase gazeuse. Le point d'ébullition du composé modèle est de 121°C sous 1 600 Pa.

Il apparait dans le tableau 1 que les valeurs du rapport $\bar{M}_n/\bar{M}_{uv}$ sont dans tous les cas inférieures à l'unité. Cela peut s'expliquer par la lenteur de la réaction d'addition de R^-M^+ sur le DAB. Il faut noter que les conditions de concentration et de température n'étaient pas propices à la polymérisation du DAB. Par conséquent, la fonctionnalisation incomplète ne peut résulter que de la présence d'amorceur résiduel non fonctionnel (*s*BuLi, PIK, PEK) qui a participé à l'amorçage de la polymérisation du styrène.

Méthode procédant par clivage

La réaction déjà mentionnée de clivage du bis(phényl-1 éthyl)éther par le potassium nous a incité à avoir recours à une méthode semblable pour la synthèse du potassio-1 (*N*,*N*-diméthylamino-4)phényl-1 éthane. La synthèse de l'éther correspondant, le bis[(*N*,*N*-diméthylamino-4)phényl-1 éthyl]éther, et de l'éther dissymétrique, le (*N*,*N*-diméthylamino-4)phényl-1 éthyl éthyl éther, sont originales, le rendement étant bien meilleur dans le second cas.

La réaction de clivage s'effectue en milieu THF à −20°C, avec un excès de potassium. Le milieu réactionnel devient rouge foncé et contient alors un amorceur de polymérisation efficace, qui doit être consommé (schéma 2) dans les heures qui suivent, car sa stabilité n'est par très élevée. Même conservée à −20°C la solution évolue, sa viscosité s'accroît et son utilisation devient hasardeuse. Par contre, conservée à −75°C, elle est utilisable pendant une semaine.

Nous avons constaté que le dosage classique des sites actifs par l'acétanilide conduit dans ce cas à des résultats erronés. Il suffit en effet de 0,5 molécule d'acétanilide pour titrer un site organo-métallique. Ce résultat peut surprendre, mais il est reproductible, et peut être lié au caractère fortement nucléophile d'un carbanion benzylique substitué en *para* par un groupe donneur.

Les résultats des expériences de polymérisation effectuées à l'aide des solutions d'amorceur fonctionnel obtenues par clivage d'éther figurent au tableau 2. Comme précédemment, le taux de fonctionnalisation réalisé par amorçage a été déterminé par le rapport $\bar{M}_n/\bar{M}_{uv}$. Le composé modèle que nous avons utilisé pour la détermination du coefficient d'absorption molaire ε est ici le *N*,*N*-diméthylamino-4 isopropyl benzène préparé par

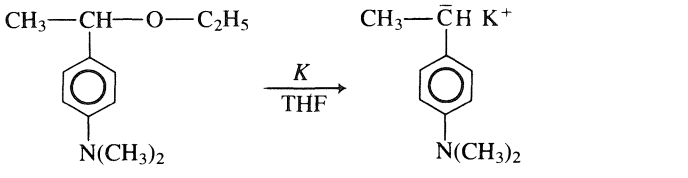

SCHÉMA 2

TABLEAU 1. Conditions expérimentales et résultats de la polymérisation amorcée par DAB

Amorceur	Solvant	T_{am} (°C)	Durée (h)	$T_{pol.}$ (°C)	$\bar{M}_n$ (g mol^{-1})	$\bar{M}_{uv}$ (g mol^{-1})	$\bar{M}_n/\bar{M}_{uv}$
DAB + *s*BuLi	Benzène	50	2	50	21 000	65 000	0,32
DAB + PIK	THF	25	2	−65	18 000	70 500	0,25
DAB + PEK	THF	25	4	−65	25 000	52 600	0,48

T_{am} : température à laquelle on prépare la solution d'amorceur; durée : temps durant lequel on laisse réagir le DAB sur l'organoalcalin R^-M^+; $T_{pol.}$: température à laquelle s'effectue la polymérisation du styrène; $\bar{M}_n$: masse molaire moyenne en nombre déterminée par chromatographie liquide d'exclusion; $\bar{M}_{uv}$: masse molaire moyenne déterminé par spectrométrie uv.

TABLEAU 2. Masse molaire des polymères préparés par la méthode procédant par clivage

$\bar{M}_n$ (g mol^{-1})	$\bar{M}_w$ (g mol^{-1})	$\bar{M}_{uv}$ (g mol^{-1})	$\bar{M}_w/\bar{M}_n$	$\bar{M}_n/\bar{M}_{uv}$
3 250	3 600	3 270	1,11	0,99
4 770	5 300	4 370	1,11	1,09
7 700	9 200	7 440	1,19	1,03
11 400	12 300	11 800	1,09	0,97
18 600	19 900	14 850	1,07	1,25
22 800	23 900	18 200	1,05	1,25
28 300	32 100	24 100	1,13	1,17
61 000	67 000	45 000	1,10	1,36
124 000	138 000	97 000	1,11	1,28

$\bar{M}_n$, $\bar{M}_w$: masse molaire moyenne en nombre et en poids déterminée par chromatographie liquide d'exclusion; $\bar{M}_{uv}$: masse molaire moyenne déterminée par spectrométrie uv.

réaction de deux molécules d'iodure de méthylmagnésium sur la *N,N*-diméthylamino-4 bénzaldehyde selon la méthode de Sachs (10, 11). Le produit brut est purifié par distillation, puis par chromatographie liquide sur silice, l'éluant étant le benzène, et enfin par redistillation. Son point d'ébullition se situe à 64°C sous 30 Pa. Le coefficient d'absorption molaire mesuré en solution dans le THF est de $\varepsilon = 2\,050$ L mol^{-1} cm^{-1} à 304 nm.

D'autre part, l'étude des chromatogrammes d'exclusion (SEC) permet d'évaluer la polymolécularité des échantillons, liée elle aussi à l'efficacité de l'amorceur.

En vue de s'assurer que des adsorptions imputables aux groupes fonctionnels ne conduisent pas à des valeurs erronées des masses molaires déterminées par SEC, nous avons comparé sur quelques échantillons les masses molaires moyennes en poids $\bar{M}_w$ et $\bar{M}_{ddl}$ déterminées par SEC et par diffusion de la lumière. Nous avons aussi vérifié que l'incrément d'indice de réfraction dn/dc du polystyrène fonctionnalisé est le même que celui du polystyrène classique soit 0,186 mL g^{-1} à 632 nm dans le THF. Ces valeurs figurent au tableau 3. Les écarts relevables ne sont pas supérieurs aux erreurs de mesures habituelles.

Bien que nos essais couvrent un large domaine de masses molaires, on peut considérer que la méthode proposée donne entière satisfaction. En effet, les valeurs de $\bar{M}_n/\bar{M}_{uv}$ voisines de l'unité attestent une fonctionnalisation quantitative. Les valeurs plus élevées sont probablement dues à des espèces chromophores résiduelles retenues par le polymère.

Dans le tableau 4 figure l'évolution de $\bar{M}_{uv}$ en fonction du nombre des précipitations d'un polymère; les variations observées étayent notre hypothèse.

Le tableau 5 rassemble les caractéristiques des produits isolés lors d'un essai spécial qui avait pour objectif la préparation d'un polymère fonctionnel de très faible masse molaire. Ce test supplémentaire d'efficacité de l'amorceur fonctionnel a pleinement confirmé les conclusions antérieures.

Partie expérimentale

Toutes les opérations mettant en oeuvre un carbanion ont été effectuées sous une légère surpression d'argon dans un appareillage étanche désormais classique.

Le THF est séché sur KOH, puis distillé sur fil de sodium; il est redistillé sur complexe benzophénone–sodium dans une ampoule étanche, puis conservé sous argon. Le styrène est séché sur $CaCl_2$, puis distillé sur fil de sodium. L'oxiranne est dégazé, puis distillé sur fil de sodium. Les mesures de SEC ont été réalisées sur un appareil équipé de 3 colonnes Shodex A 801, A 802 et A 803, la détection étant assurée par un réfractomètre différentiel Waters.

Les déterminations spectrophotométriques uv ont été effectuées sur un appareil Beckman Acta V.

(N,N-Diméthylamino-4)phényl-1 éthyl éthyl éther

Dans un ballon muni d'un décanteur de type Dean et Stark, on porte à ébullition durant 24 h 700 mL de benzène, 300 mL d'éthanol, 100 g (0,61 mole) de (*N,N*-diméthylamino-4)phényl-1 éthanol (10, 11) et 0,50 g d'acide *p*-toluène sulfonique. Après refroidissement, on ajoute 10 mL d'une solution de méthanolate de sodium (0,4 mol L^{-1}) dans du méthanol. On évapore les solvants, on redissout le produit dans 500 mL d'éther, puis on lave et on sèche sur sulfate de sodium. Enfin on évapore l'éther et on distille le résidu (115 g). On recueille 80 g. Eb. : 80–85°C (200 Pa). On conserve le produit sous argon.

Amorceur

On place 10 g (0,25 mol) de potassium dans 100 mL de THF, puis on abaisse la température à −20°C. On ajoute ensuite 10 mL (0,10 mol) de (*N,N*-diméthylamino-4)phényl-1 éthyl éthyl éther (éthoxy-1 (*N,N*-diméthylamino-4)phényl-1 éthane). La solution devient rapidement rouge. On maintient l'agitation la nuit. Dosée par l'acétanilide, la concentration en sites carbanioniques de cette solution est 0,34 mol L^{-1}.

Polymérisation du styrène

Exemple 1

À 250 mL de THF maintenu à −70°C on ajoute goutte à goutte 9 mL d'une solution de l'amorceur à une concentration de 0,34 mol L^{-1}. On ajoute ensuite goutte à goutte 25 g de styrène. La température croît rapidement à −40°C. Quand elle revient à −70°C, on ajoute 2 mL d'oxiranne, puis on enlève le bain réfrigérant. La décoloration du milieu réactionnel n'est pas immédiate. Quand elle se produit, vers −50°C, on ajoute successivement un peu de méthanol, 1 mL d'acide chlorhydrique, puis 2 mL d'ammoniaque. On filtre la solution pour éliminer le KCl, puis on précipite le polymère par 2 L de méthanol. On dissout et reprécipite le polymère avec les mêmes volumes de THF et de méthanol. Rendement quantitatif : $\bar{M}_n = 7\,700$ g mol^{-1}; $\bar{M}_w = 9\,200$ g mol^{-1}, $\bar{M}_{uv} = 7\,440$ g mol^{-1}.

Exemple 2

À 250 mL de THF maintenu à −70°C on ajoute 70 mL d'une solution d'amorceur de concentration 0,48 mL L^{-1}. On ajoute ensuite goutte à goutte 25 g de styrène. La température croît jusqu'à −50°C. On ajoute alors 5 mL d'oxiranne puis on enlève le bain réfrigérant. Après

TABLEAU 3. Comparaison des masses molaires moyennes déterminées par SEC et par diffusion de la lumière

$\bar{M}_n$ (g mol^{-1})	$\bar{M}_w$ (g mol^{-1})	$\bar{M}_{ddl}$ (g mol^{-1})	$\bar{M}_{uv}$ (g mol^{-1})	$\bar{M}_{ddl}/\bar{M}_n$	$\bar{M}_{ddl}/\bar{M}_w$	$\bar{M}_n/\bar{M}_{uv}$
34 900	36 800	38 000	32 700	1,05	1,03	1,07
37 300	41 100	42 000	35 000	1,10	1,02	1,06
66 100	73 600	79 000	58 200	1,11	1,07	1,13
92 400	102 300	108 000	77 300	1,10	1,06	1,19
114 000	130 000	144 000	99 000	1,14	1,11	1,15

$\bar{M}_n$, $\bar{M}_w$: masse molaire moyenne en nombre et en poids déterminée par chromatographie liquide d'exclusion; $\bar{M}_{ddl}$: masse molaire moyenne en poids déterminée par diffusion de la lumière; $\bar{M}_{uv}$: masse molaire moyenne déterminée par spectrométrie uv.

TABLEAU 4. Évolution de la masse molaire moyenne en fonction du nombre des precipitations

Nombre des précipitations	$\bar{M}_{uv}$ (g mol^{-1})
1	69 000
2	99 000
3	102 300
4	103 300
5	105 200

$\bar{M}_{uv}$: mass molaire moyenne déterminé par spectrométrie uv.

TABLEAU 5. Caractéristiques du polymère de faible mass molaire

	M_n (g mol^{-1})	M_w (g mol^{-1})	M_{uv} (g mol^{-1})	$\bar{M}_w/\bar{M}_n$	$\bar{M}_n/\bar{M}_{uv}$	O % (*c*)	O % (*t*)
F 1	3 220	3 820	3 260	1,19	0,99	0,49	0,60
F 2	1 990	2 200	1 600	1,11	1,24	0,80	1,11

$\bar{M}_n$, $\bar{M}_w$: masse molaire moyenne en nombre et en poids déterminée par chromatographie liquide d'exclusion; $\bar{M}_{uv}$: masse molaire moyenne déterminée par spectrometrie uv; O % (*c*) : taux en oxygène calculé, soit le rapport $16/\bar{M}_n$; O % (*t*) : taux en oxygène déterminé par analyse chimique élémentaire.

décoloration du milieu réactionnel, à −30°C, on introduit 7 mL d'acide chlorhydrique puis 9 mL d'ammoniaque. On filtre la solution pour éliminer le KCl, puis on précipite le polymère par 4 L de méthanol. On filtre 11,5 g de polymère. Ce produit est dissous dans 50 mL de THF puis reprécipité par 1 L de méthanol contenant 2 mL d'ammoniaque. Enfin on filtre 10,5 g (F 1) de polymère.

Les filtrats sont alors rassemblés. On évapore les solvants, redissout le résidue dans 150 mL de benzène, agite la solution avec un peu de gel de silice, filtre, puis précipite le polymère par un mélange de 2 L de méthanol, 200 mL d'eau et 2 mL d'ammoniaque. Ce polymère est d'aspect collant. On le redissout dans 10 mL de benzène. Après lyophilisation, on obtient 6,9 g (F 2) de polymère sous forme poudreuse.

Conclusion

L'action du potassium sur une solution de (*N*,*N*-diméthylamino-4)phényl-1 éthyl éthyl éther conduit à un composé organo-métallique qui est un amorceur anionique efficace agissant par addition. Lorsqu'on provoque la polymérisation du styrène par cette solution d'amorceur, et lorsqu'on fait réagir ensuite de l'oxiranne sur les sites carbanioniques, on obtient un polymère portant à l'une des extrémités de sa chaîne le groupe *N*,*N*-diméthylamino-4 phényle et à l'autre extrémité la fonction alcoolate.

Remerciements

Les auteurs expriment leurs vifs remerciements à M. F. Isel pour l'aide efficace qu'il leur a apportée dans la réalisation de ce travail.

1. M. A. WINNIK, A. M. SINCLAIR et G. BEINERT. Can. J. Chem. **63**, 1300 (1985).
2. D. J. WORSFOLD. J. Polym. Sci. Polym. Chem. Ed. **21**, 2237 (1983).
3. D. SEYMOUR et K. B. WOLFSTIRN. J. Am. Chem. Soc. **70**, 1177 (1948).
4. S. S. YEN. Makromol. Chem. **81**, 152 (1965).
5. H. XIE et P. ZHOU. Polym. Mat. Sci. Eng. **51**, 664 (1984).
6. R. A. BENKESER, A. E. TREVILLYAN et J. HOOZ. J. Am. Chem. Soc. **84**, 4971 (1962).
7. H. GILMAN et H. A. MCNINCH. J. Org. Chem. **26**, 3723 (1961).
8. A. LAPP, G. BEINERT et G. PICOT. Makromol. Chem. **185**, 453 (1984).
9. D. CRAIG. J. Am. Chem. Soc. **57**, 195 (1935).
10. F. SACHS et L. SACHS. Ber. **38**, 517 (1905).
11. F. SACHS et L. SACHS. Ber. **38**, 511 (1905).

Utilisation de l'*ortho*-tolidine pour l'étude des réactions des halogénates et halogénites[1]

GUY SCHMITZ ET HENRI ROOZE

Université libre de Bruxelles, Faculté des sciences appliquées, 50 avenue F. Roosevelt, 1050 Bruxelles, Belgique

Reçu le 29 janvier 1986

GUY SCHMITZ et HENRI ROOZE. Can. J. Chem. **64**, 1747 (1986).

Nous avons montré précédemment, que l'*ortho*-tolidine simplifie fortement l'étude cinétique des réactions redox du chlorite en réagissant avec des produits intermédiaires et en supprimant des réactions secondaires. Cette étude établit la validité de la méthode dans le cas de réactions du bromate. Pour la réaction bromate–bromure elle donne la loi classique d'ordre quatre avec $k = 1{,}54\ M^{-3}\ s^{-1}$ en milieu perchlorique de force ionique 1 *M* à 25°C, et une constante d'acidité de l'acide bromique valant 2,9. Cette méthode est ensuite utilisée pour étudier la réaction entre le bromate et le chlorite, réaction complexe en absence d'*ortho*-tolidine. On obtient la loi cinétique

$$-\frac{d[BrO_3^-]}{dt} = k[BrO_3^-][HClO_2][H^+]$$

avec $k = 0{,}83 + 0{,}76\ [H^+]$ dans les mêmes conditions. Si $[H^+] = 0{,}1\ M$ l'énergie d'activation apparente vaut 47,4 kJ/mol.

GUY SCHMITZ and HENRI ROOZE. Can. J. Chem. **64**, 1747 (1986).

We have shown previously that *ortho*-tolidine greatly simplifies the kinetic study of redox reactions of chlorite by reacting with intermediate products and eliminating side reactions. The present study shows the validity of the method in the case of bromate reactions. For the bromate–bromide reaction it gives the classical fourth-order rate law with $k = 1.54\ M^{-3}\ s^{-1}$ in perchloric acid solutions at 25°C and 1 *M* ionic strength, and an acidity constant of bromic acid of 2.9. This method is then used to study the reaction between bromate and chlorite, a complex reaction in the absence of *ortho*-tolidine. The rate law is

$$-\frac{d[BrO_3^-]}{dt} = k[BrO_3^-][HClO_2][H^+]$$

with $k = 0.83 + 0.76\ [H^+]$ in the same conditions. If $[H^+] = 0.1\ M$ the apparent activation energy is 47.4 kJ/mol.

Introduction

L'*ortho*-tolidine (biphényl-4,4′ diamino-3,3′ diméthyl) permet d'obtenir simplement et avec précision les caractéristiques cinétiques de nombreuses réactions redox des halogénates et halogénites. Nous avons discuté antérieurement ses propriétés et les avons mises à profit pour étudier la cinétique de la dismutation du chlorite catalysée par les ions Cl^- (1) et par le fer (2).

En résumé, ni le chlorate ni le chlorite n'oxydent l'*ortho*-tolidine avec une vitesse mesurable. Par contre le chlore, l'acide hypochloreux et le dioxyde de chlore l'oxydent extrêmement rapidement. Le produit de son oxydation présente, si le pH est inférieur à 2,5, une bande d'absorption intense ayant son maximum à 440 nm. Les absorbances mesurées sont reproductibles et, si la concentration en *ortho*-tolidine n'est pas trop élevée, suffisamment stables pour permettre des mesures très précises. Nous avons généralement utilisé des concentrations inférieures à $5 \times 10^{-4}\ M$.

L'élimination de produits intermédiaires des réactions étudiées simplifie leurs mécanismes et le coefficient d'absorption molaire élevé de l'*ortho*-tolidine oxydée, 59 700 $M^{-1}\ cm^{-1}$, permet une mesure aisée de leurs vitesses initiales. Nous montrons dans cet article que cette méthode est également utile pour étudier des réactions du bromate, en particulier la réaction bromate–chlorite.

Technique expérimentale

Les solutions de chlorite de sodium sont préparées à partir de chlorite commercial purifié par trois recristallisations successives. Elles sont conservées dans le noir en milieu légèrement basique et standardisées par iodométrie. Elles restent stables pendant plusieurs jours et donnent des résultats reproductibles. Le bromate de la qualité «pour analyses» est recristallisé, les traces de bromure qu'il contient pouvant influencer certains résultats. L'acidité est fixée avec de l'acide perchlorique et la force ionique avec du perchlorate de sodium «pour analyses», utilisés sans purification supplémentaire.

Les réactifs, conservés dans un thermostat, sont mélangés rapidement et transférés dans la cuvette thermostatisée d'un spectrophotomètre Beckman DBGT. Sauf précision contraire, la température est maintenue à 25 ± 0,1°C. Les conditions expérimentales sont toujours telles que l'on mesure des vitesses initiales. En enregistrant, en fonction du temps, l'absorbance à 440 nm due à l'oxydation de l'*ortho*-tolidine, on obtient des droites dont les pentes donnent ces vitesses. La linéarité des enregistrements est importante car elle assure qu'au cours d'une mesure on peut négliger la dégradation de l'*ortho*-tolidine oxydée. Nous abrégerons la formule de l'*ortho*-tolidine en NH_2RNH_2 et celle de sa forme oxydée en NHRNH.

$$\frac{d[NHRNH]}{dt} = \frac{1}{59700}\frac{dA}{dt} \qquad (M/s)$$

Réaction de l'*ortho*-tolidine avec le brome

L'*ortho*-tolidine est oxydée extrêmement rapidement par le brome suivant [1]. Nous avons obtenu le même maximum d'absorbance à 440 nm avec le même coefficient d'absorption molaire que dans le cas du chlore (cf. fig. 1). Comme dans ce cas le pH doit être inférieur à 2,5 et il est préférable de limiter la concentration en *ortho*-tolidine à $5 \times 10^{-4}\ M$. Avec un excès de Br_2 on obtient $[NHRNH] = [NH_2RNH_2]_0$ ce qui montre que l'*ortho*-tolidine n'est pas bromée.

[1] $\quad NH_2RNH_2 + Br_2 \rightarrow NHRNH + 2Br^- + 2H^+$

En milieux très acides (1 *M* en $HClO_4$) ou avec des concentrations en Br^- supérieures à $10^{-2}\ M$ nous avons obtenu des rapports $[NHRNH]/[Br_2]_0$ inférieurs à 1. Ceci ne résulte pas de la réversibilité de la réaction [1] (nous avons vérifié que Br^- ne réduit pas NHRNH) mais probablement de traces

1. Article n°4 de la série «Mécanisme des réactions du chlorite et du dioxyde de chlore.»

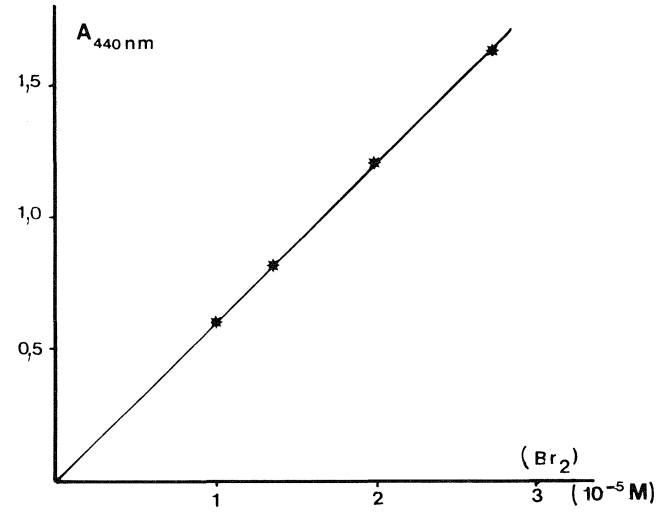

FIG. 1. Réaction de l'*ortho*-tolidine avec le brome. $[NH_2RNH_2] = 5 \times 10^{-5}\ M$; $[HClO_4] = 0{,}02\ M$.

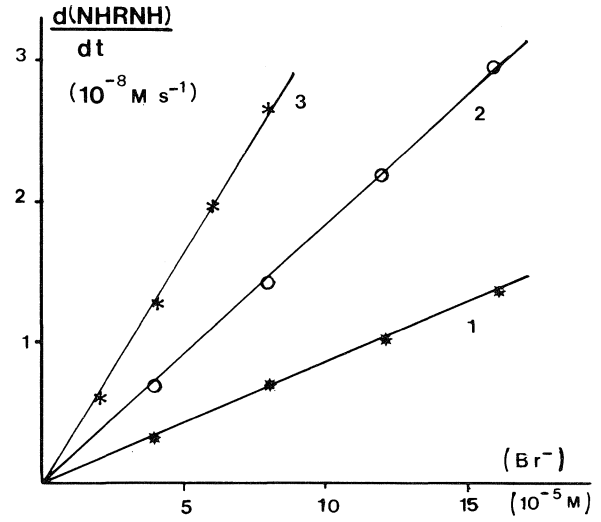

FIG. 2. Réaction bromate–bromure. $[NH_2RNH_2] = 10^{-4}\ M$. $[HClO_4] = 0{,}203$, $[NaBrO_3] = 5 \times 10^{-4}\ M$ (1); $[HClO_4] = 0{,}203$, $[NaBrO_3] = 10^{-3}\ M$ (2); $[HClO_4] = 0{,}406$, $[NaBrO_3] = 5 \times 10^{-4}\ M$ (3).

d'impuretés oxydables dans les réactifs. Par exemple, l'addition préalable d'un peu d'iodure réduit la quantité de NHRNH formée : une fraction du brome oxyde l'iodure en iode et celui-ci n'oxyde pas l'*ortho*-tolidine. Un tel effet peut fausser le dosage du brome par l'*ortho*-tolidine mais pas nos mesures cinétiques : après oxydation de ces impuretés la vitesse de formation de NHRNH devient bien proportionnelle à la vitesse de réaction. Quoi qu'il en soit, ce qui constitue la garantie finale de la validité de nos mesures est la linéarité des enregistrements de l'absorbance en fonction du temps. Les vitesses sont déduites des pentes de ces droites et indépendantes du temps zéro.

Cinétique de la réaction bromate–bromure en présence d'*ortho*-tolidine

L'*ortho*-tolidine n'est pas oxydée directement par le bromate avec une vitesse mesurable. La très faible vitesse d'oxydation que l'on peut parfois observer dépend de la pureté des réactifs. Il faut en particulier éliminer les traces d'halogénures dans le bromate.

Dans une solution acide de bromate et de bromure on obtient la réaction classique [2].

$$[2] \quad BrO_3^- + 5Br^- + 6H^+ \rightarrow 3Br_2 + 3H_2O$$

En présence d'*ortho*-tolidine le brome ainsi formé réagit rapidement suivant [1] et l'on obtient globalement [3].

$$[3] \quad BrO_3^- + 3NH_2RNH_2 \rightarrow Br^- + 3NHRNH + 3H_2O$$

L'étude de cette réaction nous a permis d'une part de confirmer la validité de la méthode à l'*ortho*-tolidine dans le cas des réactions du bromate, d'autre part de préciser l'effet du pH sur la réaction [2] en milieux très acides.

La réaction [2] obéit à la loi cinétique [4] (3–8).

$$[4] \quad -\frac{d[BrO_3^-]}{dt} = k_4[BrO_3^-][Br^-][H^+]^2$$

En présence d'*ortho*-tolidine l'étape déterminante reste la même et on déduit de [3] :

$$\frac{d[NHRNH]}{dt} = 3\,k_4[BrO_3^-][Br^-][H^+]^2$$

Nos mesures de vitesses initiales de formation de l'*ortho*-tolidine oxydée sont en parfait accord avec cette loi. Quelques résultats montrant l'ordre 1 par rapport au bromure sont repris sur la figure 2. Nous avons également vérifié l'ordre 1 par rapport au bromate (10^{-4}–$10^{-3}\ M$). Les vitesses sont indépendantes de la concentration de l'*ortho*-tolidine (10^{-4} ou $4 \times 10^{-4}\ M$). Elles diminuent si la force ionique I augmente, comme observé dans les travaux antérieurs. Avec $[HClO_4] = 0{,}1\ M$ et $[NaClO_4]$ variable, nous avons obtenu des vitesses dans les rapports 1,52:1,03:1,00 respectivement pour $I = 0{,}1$, 0,5 et 1,0 M.

TABLEAU 1. Réaction bromate–bromure

$[HClO_4]$ (M)	k_{exp} ($M^{-3}\ s^{-1}$)	k_4 ($M^{-3}\ s^{-1}$)
0,102	1,55 ± 0,04(7)	1,60
0,203	1,38 ± 0,03(9)	1,48
0,203	1,46 ± 0,04(8)	1,56
0,406	1,30 ± 0,07(8)	1,48
0,813	1,23 ± 0,03(11)	1,57

$T = 25°C$, $I = 1\ M$. Les nombres de mesures sont indiqués entre parenthèses, les erreurs correspondent aux écarts-types.

Les valeurs des constantes cinétiques obtenues pour différentes acidités, avec une force ionique fixée à 1 M, sont indiquées dans le tableau 1. La colonne k_{exp} donne les valeurs de k_4 calculées en prenant pour $[BrO_3^-]$ la concentration totale en bromate. On constate que k_{exp} diminue lorsque l'acidité augmente. Ceci s'explique par l'équilibre [5].

$$[5] \quad BrO_3^- + H^+ = BrO_3H$$

Soient $[NaBrO_3]$ la concentration totale en bromate et K_a la constante d'acidité de l'acide bromique.

$$[BrO_3^-] = \frac{K_a}{K_a + [H^+]}[NaBrO_3]$$

$$k_4 = \left[1 + \frac{[H^+]}{K_a}\right] k_{exp}$$

En prenant $K_a = 2{,}9\ M^{-1}$ on obtient des valeurs de k_4 indépendantes de l'acidité. Elles sont indiquées dans le tableau 1 et donnent en moyenne :

$$k_4 = 1{,}54\ M^{-3}\ s^{-1} \qquad (T = 25°C,\ I = 1\ M)$$

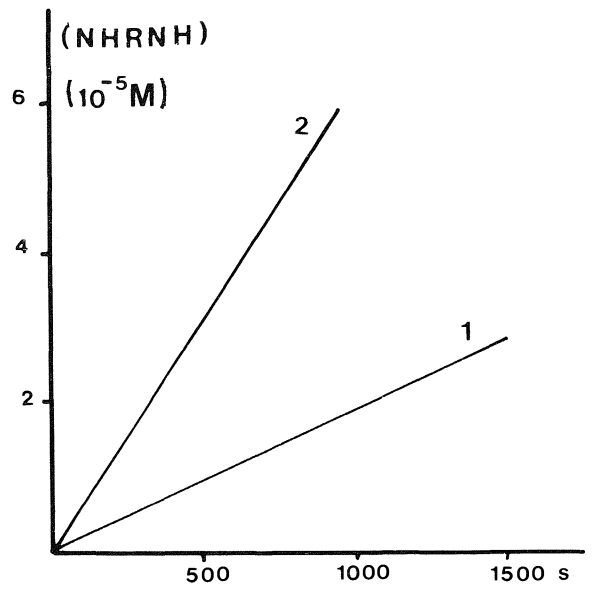

FIG. 3. Réaction bromate–chlorite. $[NH_2RNH_2] = 10^{-4}\,M$. $[HClO_4] = 0{,}102$, $[NaClO_2] = 1{,}24 \times 10^{-5}$, $[NaBrO_3] = 5 \times 10^{-3}\,M$ (1); $[HClO_4] = 0{,}404$, $[NaClO_2] = 1{,}00 \times 10^{-5}$, $[NaBrO_3] = 5 \times 10^{-3}\,M$ (2).

L'effet de l'équilibre [5] n'était pas apparu dans les travaux antérieurs car l'acidité, soit était trop faible pour qu'il apparaisse, soit avait varié parallèlement à la force ionique et l'effet de celle-ci était dominant. La valeur adoptée de K_a est tout à fait raisonnable et se compare favorablement à une estimation antérieure : $pK_a = 0{,}7$ (9). Les valeurs antérieures de k_4 permettant une comparaison avec la nôtre sont 2,32 et 1,18 pour $I = 1\,M$ (4, 6) et 1,86 pour $I = 0{,}8\,M$ (8).

Cinétique de la réaction bromate–chlorite en présence d'*ortho*-tolidine

Cette réaction présente un intéret particulier d'une part dans le cadre du mécanisme de réactions périodiques (10), d'autre part parce que sa première étape correspond à l'échange d'un seul électron au contraire des réactions classiques halogénates–halogénures.

Lorsqu'on mélange des solutions de bromate et de chlorite on obtient un système dont l'évolution aussi bien stoechiométrique que cinétique est très complexe. La première étape est [6].

[6] $BrO_3^- + HClO_2 + H^+ \rightarrow BrO_2 + ClO_2 + H_2O$

Le BrO_2 et le ClO_2 peuvent ensuite réagir de diverses manières. Thompson (11) a étudié cette réaction en présence d'alcool allylique qui, en captant le produit intermédiaire HOBr, élimine certaines complications. Cependant, même ainsi la stoechiométrie dépend des conditions expérimentales. Par contre, en présence d'*ortho*-tolidine on obtient simplement la stoechiométrie [7].

[7] $BrO_3^- + 3NH_2RNH_2 \rightarrow Br^- + 3NHRNH + 3H_2O$

Les expériences de la figure 3 montrent que le chlorite n'est pas consommé : la vitesse est inchangée alors que l'on a oxydé une quantité d'*ortho*-tolidine nettement supérieure à la quantité de chlorite introduite. L'expérience (2) a été faite en présence de 5×10^{-5} ion g/L d'Ag^+ pour éliminer l'effet des ions Br^- produits par [7] qui sinon apparaîtrait aux conversions élevées. Par contre, lors de toutes les expériences ci-après, les conversions sont restées suffisamment faibles (quelques pourcents) pour que cet effet soit négligeable. Rappelons que nos conditions expérimentales sont toujours telles que les enregistrements d'absorbances en fonction du temps soient linéaires et que l'on mesure des vitesses initiales.

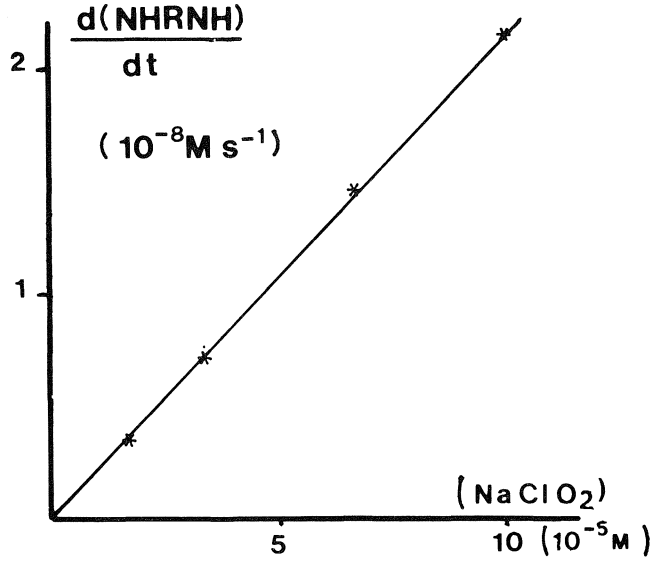

FIG. 4. Réaction bromate–chlorite. $[HClO_4] = 0{,}102$, $[NaBrO_3] = 10^{-3}$, $[NH_2RNH_2] = 10^{-4}\,M$, $I = 1\,M$, $T = 25°C$.

La simplification du mécanisme se comprend aisément. La première étape reste [6] car l'*ortho*-tolidine ne réagit ni avec le bromate ni avec le chlorite. Ensuite nous savons qu'elle est oxydée très rapidement par le ClO_2 suivant [8].

[8] $2ClO_2 + NH_2RNH_2 \rightarrow 2HClO_2 + NHRNH$

Le BrO_2 formé par [6] pourrait de même être réduit par l'*ortho*-tolidine en $HBrO_2$. Cependant celui-ci ne peut pas s'accumuler dans le système et, quel que soit le mécanisme de la réduction, on obtient la réaction globale [9].

[9] $2BrO_2 + 5NH_2RNH_2 \rightarrow 2Br^- + 2H^+ + 5NHRNH + 4H_2O$

En combinant [6], [8] et [9] on obtient [7], et

$$\frac{d[NHRNH]}{dt} = 3r_6$$

1. Résultats à 25°C et I = *0,1–1* M

Les figures 4 et 5 donnent quelques exemples de nos mesures établissant l'ordre 1 par rapport au bromate et au chlorite. L'ensemble des résultats obtenus est résumé dans le tableau 2. Les constantes k_{exp} sont définies par

$$\frac{d[NHRNH]}{dt} = k_{exp}[NaBrO_3][NaClO_2][H^+] + r_{Fe}$$

où $[NaBrO_3]$ et $[NaClO_2]$ désignent les concentrations totales et r_{Fe} la vitesse de la catalyse par le fer de l'oxydation de l'*ortho*-tolidine par le chlorite (2). Après purification des réactifs cette correction reste assez faible, généralement moins de 5%, pour permettre une détermination précise de k_{exp}. Soient K_{a1} et K_{a2} les constantes d'acidité de $HBrO_3$ et de $HClO_2$. Posons

$$r_6 = k_6[BrO_3^-][HClO_2][H^+]$$

On obtient

$$k_{exp} = 3\frac{K_{a1}}{K_{a1} + [H^+]}\frac{[H^+]}{K_{a2} + [H^+]}k_6$$

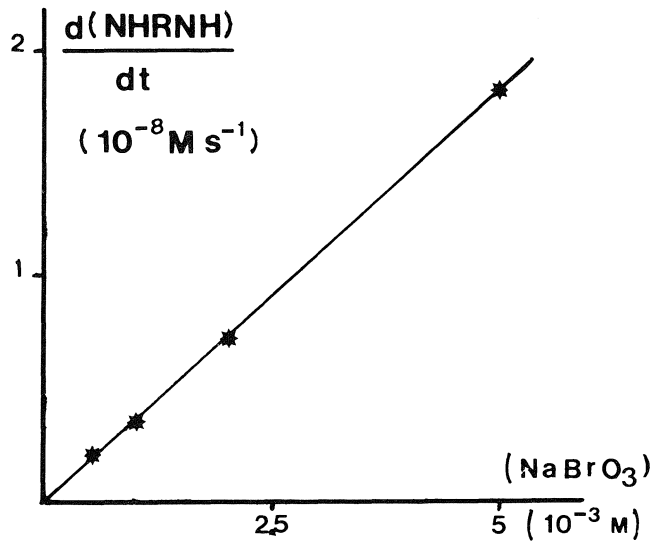

FIG. 5. Réaction bromate–chlorite. $[HClO_4] = 0{,}102$, $[NaClO_2] = 1{,}69 \times 10^{-5}$, $[NH_2RNH_2] = 10^{-4}\ M$, $I = 1\ M$, $T = 25°C$.

TABLEAU 2. Réaction bromate–chlorite

$[HClO_4]$ (M)	$[NaBrO_3]$ (M) $\times 10^3$	$[NaClO_2]$ (M) $\times 10^4$	k_{exp} ($M^{-2}\ s^{-1}$)	k_6 ($M^{-2}\ s^{-1}$)
0,10[a,b]	1	0,24	2,98 ± 0,05(8)	1,22
0,10[a]	1	0,12–1,2	2,95 ± 0,06(8)	1,21
0,10[a]	0,5–5	0,24	3,00 ± 0,09(8)	1,23
0,10	1	0,17–1,0	2,08 ± 0,04(8)	0,89
0,10	0,5–5	0,17	2,12 ± 0,06(8)	0,91
0,20	1	0,17	2,44(2)	0,97
0,30	1	0,17	2,65(2)	1,05
0,40	1	0,17	2,90(2)	1,17
0,10	1	0,40–1,6	2,14 ± 0,07(6)	0,92
0,10	0,5–5	0,40	2,15 ± 0,11(15)	0,92
0,20	1	0,40	2,47(2)	0,99
0,30	1	0,40	2,56(2)	1,02
0,40	1	0,40	2,80(2)	1,13

$T = 25°C$; $I = 1\ M$.
[a] $I = 0{,}1\ M$.
[b] Vérification de l'invariance de la vitesse pour $[NH_2RNH_2] = 5 \times 10^{-5} - 5 \times 10^{-4}\ M$. Les nombres de mesures sont indiqués entre parenthèses, les erreurs correspondent aux écarts-type.

Les valeurs de K_{a2} ont été mesurées par Hong et Rapson (12) en fonction de la force ionique. Ils ont obtenu $K_{a2} = 1{,}74 \times 10^{-2}$ pour $I = 0{,}1\ M$ et $2{,}4 \times 10^{-2}$ pour $I = 1\ M$. La valeur de K_{a1} pour $I = 1\ M$ a été déduite de notre étude de la réaction bromate–bromure. Si elle varie en fonction de la force ionique comme K_{a2} on obtient $K_{a1} = 2{,}1$ pour $I = 0{,}1\ M$. Le choix de cette constante n'influence quasi pas le calcul de k_6.

Quelques mesures faites à des forces ioniques comprises entre 0,1 et 1 M avec $[HClO_4] = 0{,}1\ M$ indiquent que k_{exp} varie à peu près comme l'inverse de K_{a2}, c'est-à-dire comme γ_{HClO_2}.

L'examen du tableau 2 montre que k_6 augmente avec l'acidité. Thompson (11) avait obtenu :

$$r_6 = k_6[BrO_3^-][HClO_2][H^+]^{1,2}$$

Nous verrons que, tenant compte de K_{a1} et K_{a2}, ses résultats comme les nôtres se laissent mieux représenter par :

$$r_6 = (k_6' + k_6''[H^+])[BrO_3^-][HClO_2][H^+]$$

TABLEAU 3. Réaction bromate–chlorite. Effet de la température

T (°C)	k_{exp} ($M^{-2}\ s^{-1}$)
33,3	5,04 ± 0,35(7)
25,0	2,98 (Tableau 2)
17,5	1,81 ± 0,10(6)
3,4	0,67 ± 0,04(11)

$[HClO_4] = 0{,}1$; $[NaClO_2] = 2{,}2 \times 10^{-5}\ M$; $[NaBrO_3] = 5 \times 10^{-4} - 0{,}01\ M$; $I = 0{,}1\ M$.

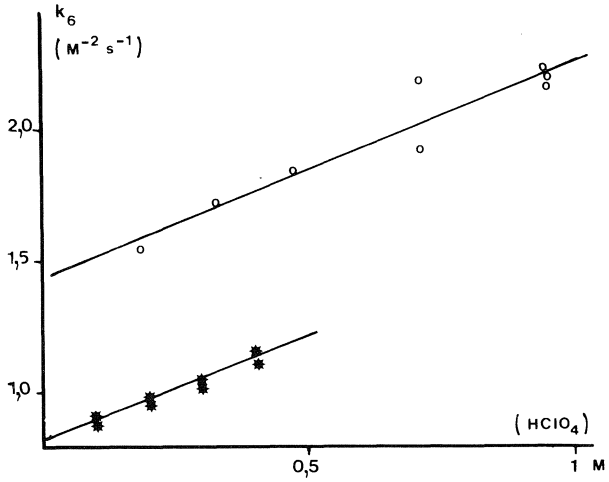

FIG. 6. Constantes cinétiques de la réaction bromate–chlorite à 25°C. Comparaison de nos valeurs (*) pour $I = 1\ M$ avec celles de Thompson (o) pour $I = 1{,}93\ M$.

2. Effet de la température, I = *0,1* M

Nos mesures de k_{exp} à différentes températures sont résumées dans le tableau 3. On en déduit une énergie d'activation de 47,4 kJ/mol. Comme k_{exp} dépend de l'acidité cette valeur n'est en toute rigueur valable que pour l'acidité à laquelle elle a été déterminée, soit $[HClO_4] = 0{,}1\ M$. Remarquons cependant que Thompson a obtenu une valeur pratiquement identique, 47,7 kJ/mol, pour $[HClO_4] = 1{,}92\ M$.

Conclusion et discussion

Pour discuter le mécanisme de réactions complexes, telles que les réactions périodiques, il est souhaitable de connaître les constantes cinétiques de leurs composantes. La méthode à l'*ortho*-tolidine permet de mesurer simplement et avec précision certaines de ces constantes.

Nous avons confirmé la validité de cette méthode dans le cas de réactions du bromate et déterminé la constante d'acidité de l'acide bromique. Nous l'avons ensuite utilisée pour mesurer la vitesse de l'étape déterminante de la réaction bromate–chlorite.

Pour interpréter l'effet de $[H^+]$ sur la vitesse de cette réaction il faut tenir compte des constantes d'acidité de l'acide chloreux et de l'acide bromique. La figure 6 montre que la variation de k_6 en fonction de $[H^+]$ est linéaire : $k_6 = 0{,}83 + 0{,}76[H^+]$. Cette figure reprend également les valeurs de k_6 déduites des mesures de Thompson (11), en remarquant que ses constantes k_a correspondent, avec nos notations, à $k_{exp}[H^+]/3$. Elles sont compatibles avec les nôtres, compte tenu de la différence de force ionique et des incertitudes affectant les mesures en absence d'*ortho*-tolidine. Cette variation de k_6 peut, par exemple, être interprétée par [5], [10], [11] et [12].

[10] $HBrO_3 + H^+ = BrO_2^+, H_2O$

[11] $BrO_2^+, H_2O + ClO_2^- \rightarrow BrO_2 + ClO_2 + H_2O$

[12] $BrO_2^+, H_2O + HClO_2 \rightarrow BrO_2 + ClO_2 + H_2O + H^+$

On obtient ainsi $k_6 = k_{11}K_{10}K_{a2}/K_{a1} + k_{12}K_{10}[H^+]/K_{a1}$.

1. G. SCHMITZ et H. ROOZE. Can. J. Chem. **59**, 1177 (1981).
2. G. SCHMITZ et H. ROOZE. Can. J. Chem. **62**, 2231 (1984).
3. A. SKRABAL et S. R. WEBERITSCH. Monatsh. **36**, 211 (1915).
4. H. A. YOUNG et W. C. BRAY. J. Am. Chem. Soc. **54**, 4284 (1932).
5. A. SKRABAL et H. SCHREINER. Monatsh. **65**, 213 (1935).
6. W. C. BRAY et H. A. LIEBHAFSKY. J. Am. Chem. Soc. **57**, 51 (1935).
7. M. SCLAR et L. RIESCH. J. Am. Chem. Soc. **58**, 667 (1936).
8. M. WRONSKA et M. WAWRZENCZYK. Z. phys. Chem. (Leipzig), **256**, 183 (1975).
9. PAUL PASCAL (*Éditeur*). Nouveau traité de chimie minérale. Tome XVI. Masson, Paris. 1960. p. 435.
10. M. ORBAN et I. R. EPSTEIN. J. Phys. Chem. **87**, 3212 (1983).
11. R. C. THOMPSON. Inorg. Chem. **12**, 1905 (1973).
12. C. C. HONG et W. H. RAPSON. Can. J. Chem. **46**, 2053 (1968).

Structure électronique des dianions $B_{12}H_{12}^{2-}$ et $B_9C_2H_{11}^{2-}$

ANNICK GOURSOT ET EDOUARD PÉNIGAULT[1]

Laboratoire de photochimie générale, Unité associée au Centre national de la recherche scientifique, n° 431, École Nationale Supérieure de Chimie, 3 rue A. Werner, F-68093 Mulhouse CEDEX, France

HENRY CHERMETTE

Institut de physique nucléaire (et IN2P3), Université de Lyon I, 43 boulevard du 11 novembre 1918, F-69622 Villeurbanne CEDEX, France

ET

JOSEPH G. FRIPIAT

Laboratoire de chimie théorique appliquée, Facultés Universitaires, 61 rue de Bruxelles, B-5000 Namur, Belgique

Reçu le 17 octobre 1985

ANNICK GOURSOT, EDOUARD PÉNIGAULT, HENRY CHERMETTE et JOSEPH G. FRIPIAT. Can. J. Chem. **64**, 1752 (1986).

Des calculs MS-Xα d'orbitales moléculaires ont été réalisés pour les dianions $B_{12}H_{12}^{2-}$ et $B_9C_2H_{11}^{2-}$. Leurs structures électroniques sont discutées en relation avec les distributions de charge de groupe. Cette étude conduit à une hiérarchie des sites d'attaque électrophile dans l'ion dicarbollyle, le bore opposé à la liaison C—C dans la face pentagonale étant le site le plus favorable.

ANNICK GOURSOT, EDOUARD PÉNIGAULT, HENRY CHERMETTE, and JOSEPH G. FRIPIAT. Can. J. Chem. **64**, 1752 (1986).

MS-Xα molecular orbital calculations have been performed on the dianions $B_{12}H_{12}^{2-}$ and $B_9C_2H_{11}^{2-}$. Their electronic structures are discussed in terms of group charge distributions. For the dicarbollide ion, this study indicates a most probable electrophilic attack on the boron site opposite to the C—C bond, on the pentagonal face.

La nature originale des liaisons chimiques que le bore est susceptible d'établir, tant avec lui-même qu'avec des hétéroéléments, favorise la formation d'unités structurales polyédriques, qui peuvent être complètes ou fragmentaires (1*a*). Une unité complète, ou structure *closo*, est décrite par un polyèdre dont toute face est trigonale et tout sommet occupé par un bore ou un hétéroélément. Toute structure fragmentaire dite *nido*, dérive formellement d'une structure *closo*, par élimination de l'un des sommets du polyèdre de référence.

Le dianion du dodécaborane ($B_{12}H_{12}^{2-}$) est l'archétype d'une structure *closo* régulière. Les B occupent les sommets d'un icosaèdre (fig. 1a) dont les 20 faces sont des triangles équilatéraux égaux (groupe de symétries I_h). Les métallocarboranes $(B_9C_2H_{11})_2M$, ou complexes bis-dicarbollyle du métal M de transition, ont une structure comptant deux unités icosaédriques irrégulières, qui sont opposées par un sommet commun occupé par M. Le ligand intervenant dans ces complexes est l'ion dicarbollyle $B_9C_2H_{11}^{2-}$, qui a une structure *nido* dérivant de l'icosaèdre. En dehors de ses faces trigonales, le polyèdre résultant comporte une face qui s'appuie sur 5 sommets sensiblement coplanaires (2), deux d'entre eux étant occupés par un carbone (fig. 1b). La nature des interactions métal–ligand dans les complexes $(B_9C_2H_{11})_2M$ en fait des complexes sandwich présentant une analogie marquée avec les métallocènes (3).

Il a été montré, antérieurement, que la méthode d'orbitales moléculaires SCF-MS-Xα conduit à une description satisfaisante de la structure électronique de divers composés sandwich, qu'il s'agisse de métallocènes (4) ou de complexes bis-aryle du chrome (5). Dans la perspective d'étudier divers métallocarboranes sandwich, nous avons effectué, dans un premier temps, l'étude Xα des structures électroniques de l'ion (3)-1,2-dicarbollyle et de son précurseur formel, $B_{12}H_{12}^{2-}$. En fait, la référence à $B_{12}H_{12}^{2-}$ vaut pour de nombreux autres composés à déficience électronique (boranes, hétéroboranes et dérivés), c'est-à-dire des composés dont le nombre total d'électrons de valence est inférieur à celui des orbitales atomiques (OA) de valence. À notre connaissance, la littérature ne rapporte pas d'étude d'orbitales moléculaires (OM) concernant l'ion dicarbollyle. Il en va différemment de $B_{12}H_{12}^{2-}$ et son étude Xα élargit le champ des comparaisons entre modèles issus de méthodes différentes. Jusqu'à maintenant, la méthode Xα a été rarement sollicitée pour étudier des édifices polyatomiques déficients en électrons (6). De nouvelles exploitations du modèle Xα offrent donc, aussi, l'intérêt de pouvoir contribuer à mieux faire apprécier l'étendue de sa fiabilité.

Géometrie et paramètres de calcul

La géométrie de $B_{12}H_{12}^{2-}$ (groupe I_h) est issue de la structure radiocristallographique de son sel dipotassique (7), le premier à avoir été isolé (8). Toute distance entre 2 B voisins de la cage icosaédrique régulière est de 1,775 Å, tandis que la longueur de toute liaison B—H est 1,07 Å.

La géométrie de l'ion (3)-1,2-dicarbollyle est tirée d'un étude radiocristallographique du complexe sandwich neutre $(B_9C_2H_{11})_2Ni$ (9). Pour rendre le modèle compatible avec l'existence d'un miroir, de légères corrections sont apportées aux positions atomiques. Ce miroir est le seul élément de symétrie du modèle (group C_s) et se confond avec le plan médiateur de la liaison C—C. Hormis B4 et B7, voisins des C sur la face pentagonale (fig. 1b), les éléments B occupent certains sommets d'un icosaèdre régulier. La distance séparant 2 éléments B voisins et occupant de tels sites, ainsi que les distances entre B8 et ses autres plus proches voisins (B4 et B7), s'identifient à la moyenne (1,785 Å) des distances expérimentales homologues, dans les 2 cages du complexe sandwich de référence. Tout élément H est positionné à l'extérieur de la cage, sur la demi-droite issue du centre de l'icosaèdre régulier cité et passant par l'élément, B ou C, auquel il est lié. Toute distance B—H ou C—H est confondue, dans le modèle, avec la moyenne (respectivement 1,08 ou 0,94 Å) des distances expérimentales de même nature. Le plan contenant les 5 voisins B de

1. Auteur à qui adresser toute correspondance.

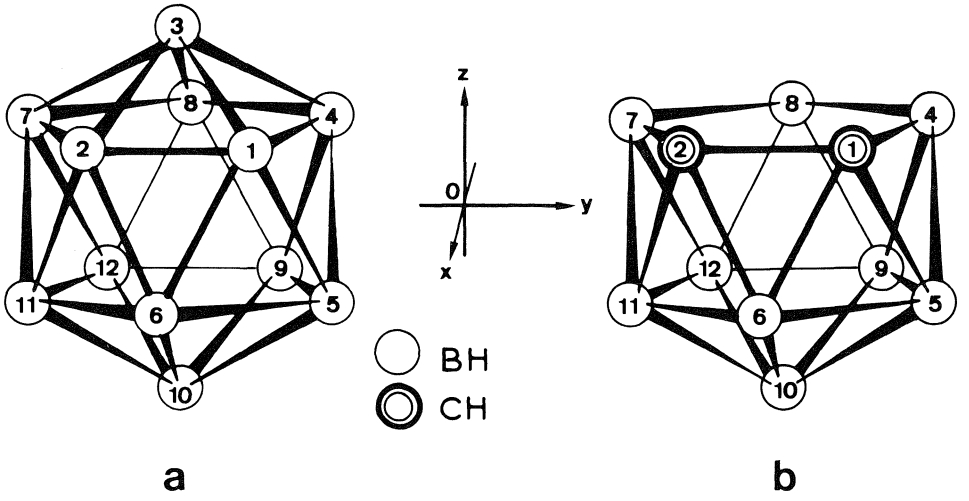

FIG. 1. Structures schématiques (a) de $B_{12}H_{12}^{2-}$ et (b) de l'ion (3)-1,2-dicarbollyle avec numérotation conventionnelle (22, 3) des groupes BH et CH.

B10 (fig. 1b) fait, avec la face pentagonale de l'ion dicarbollyle, un angle dièdre de 1,5°. Les éléments de la face pentagonale, les plus proches du plan des 5 B, sont C1 et C2, l'arête C1—C2 étant parallèle à ce plan. Les valeurs des autres distances interatomiques du modèle sont mentionnées dans un schéma topologique (fig. 2).

La version standard de la méthode SCF-MS-Xα (10) est utilisée sans orientation des spins. Le procédé de l'état de transition de Slater (11) sert à la détermination des énergies d'excitation de $B_{12}H_{12}^{2-}$. Pour les 2 dianions, le critère d'auto-cohérence du potentiel final est meilleur que 10^{-3}.

Les paramètres MS-Xα sont rassemblés dans le tableau 1. Le procédé non empirique de Norman (12) a été utilisé pour définir les sphères atomiques, de sorte que les sphères de 2 éléments directement liés soient sécantes. Dans le modèle de $B_{12}H_{12}^{2-}$, tout rayon atomique est pris égal à 88% du rayon de la sphère qui renfermerait le même nombre d'électrons que l'atome neutre, dans la superposition des densités atomiques. Pour l'ion dicarbollyle, les rayons atomiques r_C et $r_{H(C)}$ sont calculés selon le mode précédent et les rayons r_B et $r_{H(B)}$ sont identifiés à ceux retenus pour $B_{12}H_{12}^{2-}$. Les valeurs des paramètres d'échange de B (0,76531) et C (0,75928) sont celles optimalisées par Schwarz (13). Le paramètre d'échange de H (0,77725) est celui proposé par Slater (14). La moyenne des valeurs atomiques, pondérée par le nombre d'atomes, est adoptée pour les régions interatomique (Int.) et extramoléculaire (Ext.). La sphère circonscrite aux sphères atomiques constitue, par sa surface, la limite commune à ces 2 régions. Elle sert aussi de sphère de Watson (15) dont la charge (+2,5 pour chaque dianion) simule l'environnement et assure le signe négatif aux premiers niveaux énergétiques virtuels.

Dans tous les calculs rapportés, les ondes multiples de la région extramoléculaire sont développés sur une base d'ondes correspondant à $l \leqslant 4$ pour $B_{12}H_{12}^{2-}$ et $l \leqslant 3$ pour $B_9C_2H_{11}^{2-}$. Dans les sphères atomiques des deux dianions, les valeurs limites de l sont zéro pour H et 1 pour B et C.

Résultats et discussion

Le tableau 2 rassemble le type de symétrie, la population, la répartition de la charge et l'énergie en rydbergs (1 Ry = 0,5 ua = 13,6 eV), pour toute OM occupée et les 4 OM virtuelles les plus basses, dans l'état fondamental de $B_{12}H_{12}^{2-}$. Les énergies

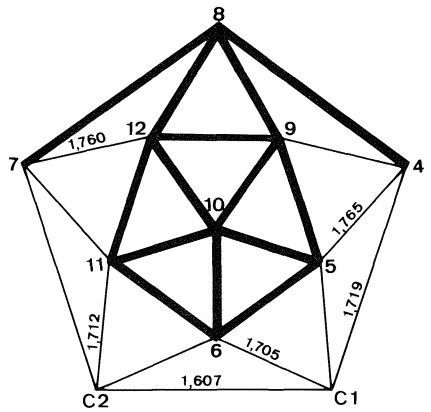

FIG. 2. Distances interatomiques (en Å) dans la cage de l'ion (3)-1,2-dicarbollyle, tout trait renforcé désignant une distance B—B de 1,785 Å.

TABLEAU 1. Paramètres MS-Xα (rayons atomiques en ua) des dianions $B_{12}H_{12}^{2-}$ et $B_9C_2H_{11}^{2-}$

Paramètre	$B_{12}H_{12}^{2-}$	$B_9C_2H_{11}^{2-}$
$r_{H(B)}$	1,3428	1,3428
$r_{H(C)}$		1,1599
r_B	1,8087	1,8087
r_C		1,7176
r_{ext}	6,5550	6,6000
$\alpha_{int} = \alpha_{ext}$	0,77128	0,77073

des OM de valence occupées, calculées par 2 méthodes semi-empiriques à champ auto-cohérent (ou SCF), sont rappelées dans un but de comparaison. Il s'agit des méthodes PRDDO et MNDO, respectivement utilisées par Lipscomb (1*b*) et par Dewar et McKee (16).

L'OM occupée la plus haute (ou HOMO) est $1g_u$. Elle est dégénérée d'ordre 4 et saturée par 8 électrons, conformément au diamagnétisme de $B_{12}H_{12}^{2-}$ (17). Pour des raisons de symétrie, les OA participant à l'HOMO sont exclusivement des orbitales p des éléments B, de sorte que $1g_u$ est non liante vis-à-vis de B—H. En revanche, $1g_u$ décrit des interactions B—B liantes qui contribuent à la cohésion de la cage.

TABLEAU 2. Niveaux d'énergie et distribution de charge de $B_{12}H_{12}^{2-}$ à l'état fondamental; (*a*) réf. 1*b*, (*b*) réf. 16, (*c*) nos résultats

					Distribution de charge (en %)				
		E (Ry)			B		H		
OM	Occ.	(*a*)	(*b*)	(*c*)	*s*	*p*	*s*	Int.	Ext.
$1g_g$	0			−0,041		42		43	15
$3h_g$	0			−0,059	3		1	9	87
$3t_{1u}$	0			−0,096	3	2	2	10	83
$3a_g$	0			−0,117	2	3	1	10	84
$1g_u$	8	−0,134	−0,190	−0,637		69		30	1
$2h_g$	10	−0,202	−0,252	−0,712	1	66	18	15	
$2t_{1u}$	6	−0,380	−0,426	−0,895	2	61	33	2	2
$1t_{2u}$	6	−0,436	−0,542	−0,975	23	22	52		3
$1h_g$	10	−0,670	−0,854	−1,085	33	22	36	7	2
$2a_g$	2	−0,564	−0,712	−1,090	1	52	40	5	2
$1t_{1u}$	6	−1,070	−1,415	−1,293	57	11	17	14	1
$1a_g$	2	−1,365	−2,199	−1,512	69	9	5	17	
$1s$B	24	−14,4		−13,18	100				

L'OM virtuelle la plus basse (ou LUMO) est $3a_g$. Elle est très diffuse, ainsi que les 2 OM virtuelles ($3t_{1u}$ et $3h_g$) qui la suivent dans l'échelle des énergies croissantes. Ces 3 premières OM virtuelles sont non liantes. Elles sont presque exclusivement localisées dans les régions extramoléculaire (pour la plus grande part) et interatomique. Les OA engagées dans l'OM virtuelle suivante ($1g_g$) sont, pour des raisons de symétrie, exclusivement des orbitales *p* des éléments B. L'OM $1g_g$ est antiliante et elle est localisée, essentiellement et pour parts sensiblement égales, dans les sphères atomiques B et dans la région interatomique.

La hiérarchie énergétique qualitative des OM de valence occupées est, à l'exception de l'inversion des niveaux $1h_g$ et $2a_g$, la même que celle établie par les auteurs cités précédemment. En fait, cette inversion n'a pas vraiment de signification, les 2 niveaux Xα concernés étant si proches (0,005 Ry) qu'ils sont assimilables à des niveaux fortuitement dégénérés. D'une méthode de calcul à l'autre, la seule comparaison énergétique qui soit significative, concerne les écarts entre niveaux. L'ensemble des distances énergétiques successives séparant les 5 niveaux occupés les plus hauts, définis par les calculs PRDDO et MNDO, est en assez bond accord avec le calcul Xα, le meilleur accord concernant les résultats PRDDO (1*b*). Par ailleurs, la méthode PRDDO et, plus encore, la méthode MNDO, conduisent à une beaucoup plus grande stabilisation relative des bas niveaux de valence ($1h_g$, $1t_{1u}$, $1a_g$), que ne le fait la méthode Xα. Il s'ensuit que les écarts successifs Xα, entre ces niveaux, sont systématiquement et très nettement inférieurs à ceux calculés par les 2 autres méthodes.

L'écart énergétique entre LUMO et HOMO est remarquable par son importance (0,52 Ry = 7,07 eV). Il est compatible avec diverses observations expérimentales (17), en particulier avec la très grande stabilité polarographique de $B_{12}H_{12}^{2-}$, tant vis-à-vis de l'oxydation que de la réduction. Par ailleurs, le spectre d'absorption uv–visible ne présente qu'une queue de bande, située à la limite (200 nm) du domaine exploré. Un calcul Xα concernant les transitions permises par symétrie, situe un maximum d'absorption à 165 nm pour la transition de moindre énergie HOMO → LUMO et à 150 nm pour la transition $1g_u \rightarrow 1g_g$.

Lipscomb (18) utilise des liaisons covalentes multicentriques pour rendre compte de la cohésion de la cage icosaédrique de $B_{12}H_{12}^{2-}$. Deux types de liaison sont distingués dans ce modèle : toute liaison B—H est classiquement covalente tandis que toute liaison B—B est électroniquement déficiente, vis-à-vis du schéma covalent traditionnel. L'extension de ce modèle à l'ensemble des boranes de structure *closo* ou *nido* et à leurs dérivés isoélectroniques (en particulier les carboranes) a permis de dégager des règles empiriques, qui relient le type structural de la cage polyédrique à son nombre de paires électroniques liantes. Ces règles ont reçu récemment une démonstration rigoureuse (19) et s'énoncent comme suit. Les liaisons dans le squelette polyédrique d'un borane *closo* $B_nH_n^{2-}$ ($n > 4$) sont assurées par $n + 1$ paires électroniques liantes, tandis que $n + 2$ paires sont nécessaires s'il s'agit d'un borane *nido* $B_nH_n^{4-}$ (ou, en particulier, d'un carborane isoélectronique). Compte tenu des électrons engagés dans les *n* liaisons covalentes B—H (et C—H dans un carborane), c'est au total $2n + 1$ et $2n + 2$ paires électroniques liantes, qui interviennent respectivement dans les structures *closo* et *nido*. Toutes les OM de valence occupées de $B_{12}H_{12}^{2-}$ étant liantes, leur population électronique totale (soit 50e) est donc conforme à la règle spécifique aux structures *closo*.

L'examen du tableau 2 montre que les OM de valence peuplées, à l'exception de $1g_u$ et $1t_{2u}$, décrivent à la fois des interactions B–B et des interactions B–H. Pour des raisons de symétrie, l'HOMO $1g_u$ est exclusivement concernée par les premières et l'OM $1t_{2u}$ par les secondes.

Les orbitales *p* des B participent à toute OM de valence peuplée et contribuent (sauf dans $1t_{2u}$) de manière prépondérante à l'ensemble des interactions B–B, qui font de $B_{12}H_{12}^{2-}$ un véritable cluster moléculaire. La plus grande part des interactions B–B est décrite par les 2 OM de plus basse énergie ($1a_g$ et $1t_{1u}$ où les orbitales des B sont à caractère *s* largement dominant) et par les 3 OM de plus haute énergie ($2t_{1u}$, $2h_g$, $1g_u$ à caractère *p* pratiquement exclusif). Toutefois, l'OM $2t_{1u}$ rend compte aussi d'interactions B–H qui sont sensiblement de même importance que les interactions B–B. Les niveaux se situant entre les 2 domaines à forte interactions B–B, correspondent à une prédominance marquée (voire exclusive pour $1t_{2u}$) des interactions B–H.

Il est possible d'obtenir une image de la configuration

électronique des éléments B et H, dans $B_{12}H_{12}^{2-}$, en attribuant la charge de la région interatomique, à la fois aux sphères atomiques B et H, et la charge de la région extramoléculaire, exclusivement aux sphères atomiques H. Ces répartitions sont faites, pour toute OM, proportionnellement aux charges des sphères atomiques et conduisent aux configurations électroniques suivantes : $2s^{0,91}\ 2p^{2,09}$ pour B et $1s^{1,17}$ pour H. Il en résulte une charge nette nulle sur B, la charge formelle (−0,17) de tout groupe BH étant portée par H. Un autre mode de répartition de la charge de la région extramoléculaire consisterait à l'attribuer, comme celle de la région interatomique, à la fois aux sphères B et H. Eu égard à la faible population électronique (0,71e) de la région extramoléculaire, les configurations électroniques précédentes n'en seraient pas affectées de manière sensible. En effet, d'un mode de calcul à l'autre, la plus grande différence concernant les populations d'un même sous-couche atomique est inférieure au seuil de signification (0,05).

Le tableau 3 regroupe le type de symétrie, l'énergie et la répartition de la charge de quelques OM de l'ion (3)-1,2-dicarbollyle, dans son état fondamental. Il s'agit, d'une part, d'OM peuplées (les 4 les plus basses en énergie et les 9 les plus hautes) et, d'autre part, d'OM virtuelles (les 2 les plus basses en énergie et l'OM $14a''$). Toutes les OM peuplées sont saturées par 2e et sont liantes, conformément à la règle de dénombrement des paires électroniques liantes dans une structure *nido*.

La filiation structurale formelle de $B_{12}H_{12}^{2-}$ à l'ion dicarbollyle, ne s'accompagne que d'une diminution de 2 électrons de valence. Cette situation est favorable à la recherche de corrélations entre les niveaux d'énergie des 2 dianions. A cet effet, il faut considérer l'abaissement de symétrie $I_h \rightarrow C_s$ et les applications suivantes concernant les représentations irréductibles de I_h, sous-tendues par les OM de $B_{12}H_{12}^{2-}$:

$$A_g \rightarrow A' \qquad T_{1u}\ (\text{ou } T_{2u}) \rightarrow 2A' + A''$$

$$H_g \rightarrow 3A' + 2A'' \qquad G_g\ (\text{ou } G_u) \rightarrow 2A' + 2A''$$

Le premier niveau de valence occupé de $B_{12}H_{12}^{2-}$ ($1a_g$) correspond à celui ($1a'$) de l'ion dicarbollyle. Au-delà de ces niveaux et dans le sens des énergies croissantes, il est possible de faire correspondre à tout niveau dégénéré d'ordre n de $B_{12}H_{12}^{2-}$, une séquence de n niveaux consécutifs de l'ion dicarbollyle, sans qu'il y ait recouvrement des domaines énergétiques de 2 séquences adjacentes. Dans cette démarche, la dégénérescence fortuite des niveaux $2a_g$ et $1h_g$ de $B_{12}H_{12}^{2-}$ conduit à les confondre en un niveau unique qui serait dégénéré d'ordre 6. En ce qui concerne l'HOMO $1g_u$ de $B_{12}H_{12}^{2-}$, il lui correspond dans l'ion dicarbollyle, une séquence comportant les 3 niveaux occupés les plus hauts en énergie ($8a''$, $9a''$, $15a'$) ainsi que la LUMO $16a'$.

Dans l'échelle des énergies croissantes, toutes les OM virtuelles de l'ion dicarbollyle jusqu'au niveau $14a''$ exclu, sont diffuses, essentiellement dans la région extramoléculaire. L'OM $14a''$ rend compte, exclusivement, d'interactions antiliantes entre des OA p des éléments de la cage polyédrique, à l'exception de B10. La contribution au niveau $14a''$ des éléments appartenant à la face pentagonale est d'environ 2 fois celle des autres éléments de la cage et la participation la plus grande concerne les OA p_z des C. C'est par l'intermédiaire de l'OM virtuelle $14a''$ que se ferait, dans un complexe métallique, un éventuel don électronique en retour du métal au ligand.

Le niveau énergétique de l'HOMO est plus élevé dans l'ion dicarbollyle (−0,484 Ry) que dans $B_{12}H_{12}^{2-}$ (−0,637 Ry). L'écart énergétique LUMO–HOMO est important dans le

TABLEAU 3. Energie et répartition de la charge de quelques OM de $B_9C_2H_{11}^{2-}$, à l'état fondamental (le niveau occupé le plus haut en énergie est $15a'$, saturé par 2 électrons)

		Distribution de charge (en %)																																			
		C1, 2		B4, 7		B5, 11		B6		B8		B9, 12		B10		H1, 2		H4, 7		H5, 11		H6		H8		H9, 12		H10			
OM	E(Ry)	s	p	s	p	s	p	s	p	s	p	s	p	s	p	s	p	s	p	s	p	s	p	s	p	s	p	s	p	Int.	Ext.
$14a''$	−0,025		16		5		5		2		2		6																	17	47
$17a'$	−0,117		1			1	1	1	1																					18	77
$16a'$	−0,195	2	1	1	1		1				1		1																	41	51
$15a'$	−0,484	1	9	1	13		1		3	1	21		7		2			1					1	1					36	2
$9a''$	−0,488	1	15	1	26		10				4		3		3			1		1									34	1
$8a''$	−0,621		7		19		7		4		15		14		3			1		1									28	1
$14a'$	−0,646		6		12		12				1		36		2			2		2									26	1
$13a'$	−0,673		2		6		9		11	1	8		14		16	1						3	6		2				21	
$7a''$	−0,687		9	1	9		23		8				4		14	1	6			5					1				19	
$6a''$	−0,722	1	13		9		18		7		2	1	17		2	4	3								9				14	
$12a'$	−0,724		25		5		6		7		6		9		7							1	2		1		6		24	1
$11a'$	−0,788		33		12		11		1		2		7		3			7		4			2		4		1		12	1
$3a'$	−1,232	1	6	8		4	3	15	1	9		8	2	5	2	3	3	3		1		6	3		3		2		14	1
$2a'$	−1,386	8	8	4	2	8	2	1	1	4	1	21	1	11	1	10				1					3		2		11	
$1a''$	−1,418	39	11	6	1	9	1		2				1			25	1			2									2	
$1a'$	−1,635	50	1	3	1	7	2	8	2	1		2		2		11													10	

TABLEAU 4. Configuration électronique des éléments et charges nettes (en e) dans les dianions $B_{12}H_{12}^{2-}$ et $B_9C_2H_{11}^{2-}$

Dianion	Nature et n° de groupe	Configuration électronique			Charge nette		
		B ou C		H			
		$2s$	$2p$	$1s$	B ou C	H	Groupe
$B_{12}H_{12}^{2-}$	BH qlcq.	0,91	2,09	1,17	0	−0,17	−0,17
$B_9C_2H_{11}^{2-}$	CH 1, 2	1,21	2,86	1,09	−0,07	−0,09	−0,16
	BH 4, 7	0,87	2,16	1,17	−0,03	−0,17	−0,20
	BH 5, 11	0,88	2,06	1,18	+0,06	−0,18	−0,12
	BH 6	0,90	2,02	1,19	+0,08	−0,19	−0,11
	BH 8	0,89	2,26	1,19	−0,15	−0,19	−0,34
	BH 9, 12	0,88	2,15	1,17	−0,03	−0,17	−0,20
	BH 10	0,89	2,12	1,19	−0,01	−0,19	−0,20

premier dianion (0,29 Ry = 3,94 eV) mais il est nettement inférieur à l'écart homologue dans le second (0,52 Ry = 7,07 eV). Par ailleurs, la distance énergétique séparant la LUMO du plus bas niveau de valence peuplé est sensiblement la même dans les 2 dianions (19,6 eV pour l'ion dicarbollyle et 19 eV pour $B_{12}H_{12}^{2-}$).

Le tableau 3 révèle une quasi-dégénérescence des 2 niveaux occupés de plus haute énergie ($9a''$ et $15a'$), séparés de seulement 0,004 Ry = 0,05 eV. Dans ces conditions, il n'est pas étonnant que l'ordre énergétique relatif de ces 2 niveaux soit susceptible de s'inverser, selon la méthode d'orbitales moléculaires retenue. Ainsi, une étude MNDO de divers carboranes (20) signale, sans autre détail, que la symétrie de l'HOMO de l'ion dicarbollyle est de type a''. La même étude est beaucoup plus explicite en ce qui concerne $B_9C_2H_{13}$, isoélectronique de l'ion dicarbollyle. Dans ce carborane neutre, les 2 niveaux peuplés les plus hauts en énergie sont distants de 0,62 eV et sont, par ordre d'énergie croissante, $15a'$ et $9a''$ (HOMO).

Les contributions moyennes des sphères atomiques, à la charge des 3 niveaux occupés de plus haute énergie ($8a''$, $9a''$ et $15a'$) de l'ion dicarbollyle, sont les plus importantes pour les éléments définissant la face pentagonale. Par atome, les contributions sont croissantes dans l'ordre : C1, C2 < B4, B7 < B8. La nature des composantes relatives à ces atomes, dans les 3 OM considérées, privilégie la présence des électrons dans des régions sensiblement axées sur les 5 arêtes fictives issues du sommet vacant n°3 de la structure *nido* (fig. 1). Les 4 niveaux occupés, énergétiquement les plus proches des précédents (c'est-à-dire $6a''$, $7a''$, $13a'$ et $14a'$), s'en distinguent très nettement par leur distribution de charge. Ce sont les contributions des éléments hors de la face pentagonale de la cage, qui y sont largement majoritaires. Il en résulte que les OM jouant le rôle primordial dans l'établissement d'une liaison π de coordination, entre un métal de transition et l'ion dicarbollyle (donneur de 3 doublets électroniques), sont les 3 occupées les plus hautes en énergie.

Les interactions B–H interviennent dans tous les niveaux de valence de l'ion dicarbollyle, à l'exception du premier ($1a'$). Toutefois, la somme des contributions aux interactions B–H, des 2 niveaux suivant $1a'$ (c'est-à-dire $1a''$ et $2a'$) et des 4 niveaux les plus hauts en énergie (c'est-à-dire $14a'$, $8a''$, $9a''$, $15a'$) n'atteint pas 5%. Les interactions B–H prédominent dans la suite des 9 niveaux (dont 3 de type de symétrie a'') comprise entre $5a'$ (−1,094 Ry) et $10a'$ (−0,840 Ry). Les interactions B–H sont quasi exclusives dans les 3 niveaux médians ($7a'$, $4a''$, $8a'$) de cette suite.

Les interactions C–H sont assurées dans une proportion voisine de 4/5 par les 6 OM de valence les plus basses en énergie, les 2 premières ($1a'$, $1a''$) décrivant à elles seules presque la moitié de ces interactions.

Les interactions entre éléments du squelette polyédrique sont présentes dans tous les niveaux sauf les 3 remarqués précédemment ($7a'$, $4a''$, $8a'$). En s'écartant de ces niveaux et quel que soit le sens de variation de l'énergie, les interactions croissent rapidement dans la cage polyédrique, pour devenir majoritaires dans deux ensembles de niveaux. Il s'agit des 4 niveaux de plus basse énergie, où les électrons engagés ont un caractère s dominant, et des 9 niveaux les plus élevés à caractère p quasi exclusif.

Le tableau 4 rapporte les configurations électroniques des éléments de l'ion dicarbollyle et les charges nettes qui en résultent. À titre de référence, les grandeurs homologues de $B_{12}H_{12}^{2-}$ sont aussi rappelées. Le mode de calcul utilisé pour l'ion dicarbollyle est le même que celui développé pour $B_{12}H_{12}^{2-}$. La remarque concernant l'influence du mode de calcul sur la configuration électronique des éléments de $B_{12}H_{12}^{2-}$, demeure valable pour l'ion dicarbollyle. La faible population électronique (0,60e) de la région extramoléculaire de l'ion dicarbollyle, conduit aux mêmes conclusions. Quant aux charges nettes de groupe, d'un mode de calcul à l'autre, elles se reproduisent à 0,01 près, c'est-à-dire très largement en-deçà du seuil de signification.

Lipscomb et coll. (21) on fait une étude PRDDO de l'ion $C_2B_9H_{12}^-$, isoélectronique de l'ion dicarbollyle. En adoptant les hypothèses qui sous-tendent cette étude, il est possible de dégager quelques tendances concernant la réactivité de l'ion dicarbollyle. D'après ces auteurs, les processus réactionnels ioniques seraient contrôlés par les charges nettes de groupe, plutôt que par la distribution de charge dans les niveaux occupés de plus haute énergie. Cette distribution, en revanche, régirait les processus réactionnels covalents. Compte tenu du seuil de signification, la population électronique de l'OA $2s$ de B se conserve pratiquement d'un groupe BH à l'autre. Il en est de même de la population électronique de l'OA $1s$ de H. La valeur moyenne pondérée de la première (0,88) et celle de la seconde (1,18), sont pratiquement confondues avec les grandeurs homologues de $B_{12}H_{12}^{2-}$ (respectivement 0,91 et 1,17). C'est donc, exclusivement, la population de l'OA $2p$ de B qui, en créant des différences de charge nette d'un groupe à l'autre, est susceptible d'induire une réactivité sélective. Ainsi, une attaque électrophile devrait se faire préférentiellement sur le site B8 (chargé −0,15 et le plus éloigné des C sur la face pentagonale).

Quant à une attaque nucléophile, si elle est possible, elle interviendrait en priorité sur les sites B6 ou B5, 11 (chargés +0,08 ou +0,06 et les plus proches des C en dehors de la face pentagonale). La reconnaissance expérimentale de ces sites privilégiés d'attaque, prouverait que les états réactifs de transition de l'ion dicarbollyle, dépendent principalement de la distribution statistique de charge, à l'état fondamental.

Il convient de souligner que les contributions de C et H à la charge nette de groupe sont très peu différentes, de sorte que les liaisons C—H sont pratiquement apolaires. Il en est de même de la liaison B—H du groupe 8. En revanche, les liaisons B—H des groupes 5, 11 et 6 ont une polarité accrue par rapport à toute liaison B—H de $B_{12}H_{12}^{2-}$. Il devrait en résulter une accentuation du caractère hydrure, pour les groupes concernés. Quant aux autres liaisons B—H de l'ion dicarbollyle, elles ont sensiblement la même polarité que dans $B_{12}H_{12}^{2-}$.

En conclusion, les analyses comparées des fonctions d'onde Xα de $B_{12}H_{12}^{2-}$ et $B_9C_2H_{11}^{2-}$ et des distributions de charge qui en résultent ont permis d'apprécier l'important effet de polarisation induit par les C. Cet effet est vraisemblablement le facteur essentiel de la stabilité de la structure *nido* de l'ion dicarbollyle. L'absence d'effet analogue dans un ion $B_{11}H_{11}^{4-}$, qui serait de même structure et isoélectronique du précédent, peut faire douter de son existence tandis que sa mise en évidence expérimentale reste à établir.

Remerciements

Les calculs ont été effectués au Centre de Calcul du CNRS de Strasbourg–Cronenbourg.

1. (*a*) E. L. MUETTERTIES (*Editeur*). Boron hydride chemistry. Academic Press, New York. 1975. Chapt. 1; (*b*) W. L. LIPSCOMB. *Dans* Boron hydride chemistry. *Editeur* : E. L. Muetterties. Academic Press, New York. 1975. Chapt. 2.
2. R. N. GRIMES. Carboranes. Academic Press, New York. 1970.
3. M. F. HAWTHORNE, D. C. YOUNG, T. D. ANDREWS, D. V. HOWE, R. L. PILLING, A. D. PITTS, M. REINTJES, L. F. WARREN,JR. et P. A. WEGNER. J. Am. Chem. Soc. **90**, 879 (1968).
4. (*a*) A. GOURSOT, E. PÉNIGAULT et J. WEBER. Nouv. J. Chim. **3**, 675 (1979); (*b*) J. WEBER, A. GOURSOT et E. PÉNIGAULT. J. Mol. Struct. **60**, 397 (1980); (*c*) J. WEBER, A. GOURSOT, E. PÉNIGAULT, J. H. AMMETER et J. BACHMANN. J. Am. Chem. Soc. **104**, 1491 (1982).
5. (*a*) J. WEBER, M. GEOFFROY, A. GOURSOT et E. PÉNIGAULT. J. Am. Chem. Soc. **100**, 3995 (1978); (*b*) J. WEBER, E. P. KUNDIG, A. GOURSOT et E. PÉNIGAULT. Can. J. Chem. **63**, 1734 (1985).
6. (*a*) H. J. T. PRESTON, J. J. KAUFMAN et W. S. KOSKI. Int. J. Quantum Chem. Symp. **9**, 137 (1975); (*b*) G. BAMBAKIDIS et R. P. WAGNER. J. Phys. Chem. Solids, **42**, 1023 (1981).
7. J. A. WUNDERLICH et W. N. LIPSCOMB. J. Am. Chem. Soc. **82**, 4427 (1960).
8. A. R. PITOCHELLI et M. F. HAWTHORNE. J. Am. Chem. Soc. **82**, 3228 (1960).
9. D. ST CLAIR, A. ZALKIN et D. H. TEMPLETON. J. Am. Chem. Soc. **92**, 1173 (1970).
10. K. H. JOHNSON. Adv. Quantum Chem. **7**, 143 (1973).
11. J. C. SLATER. Adv. Quantum Chem. **6**, 1 (1972).
12. J. G. NORMAN, JR. J. Chem. Phys. **61**, 4630 (1974).
13. K. SCHWARZ. Phys. Rev. B : Solid State, **5**, 2466 (1972).
14. J. C. SLATER. Int. J. Quantum Chem. Symp. **7**, 533 (1973).
15. R. E. WATSON. Phys. Rev. **111**, 1108 (1958).
16. M. J. S. DEWAR et M. L. MCKEE. Inorg. Chem. **17**, 1569 (1978).
17. E. L. MUTTERTIES et W. H. KNOTH. Polyhedral boranes. Marcel Dekker, Inc., New York. 1968.
18. W. N. LIPSCOMB. Boron hydrides. W. A. Benjamin, Inc., New York. 1963.
19. (*a*) A. J. STONE. Inorg. Chem. **20**, 563 (1981); (*b*) A. J. STONE et M. J. ALDERTON. Inorg. Chem. **21**, 2297 (1982).
20. M. J. S. DEWAR et M. L. MCKEE. Inorg. Chem. **19**, 2662 (1980).
21. J. H. HALL, JR., D. A. DIXON, D. A. KLEIR, T. A. HALGREN, L. D. BROWN et W. N. LIPSCOMB. J. Am. Chem. Soc. **97**, 4202 (1975).
22. R. ADAMS. Inorg. Chem. **2**, 1087 (1963).

Thioether complexes of tungsten hexacarbonyl

C. Robert Lucas

Department of Chemistry, Memorial University of Newfoundland, St. John's, Nfld., Canada A1B 3X7

Received October 9, 1985[1]

C. Robert Lucas. Can. J. Chem. **64**, 1758 (1986).

The preparation of a series of organic and organometallic thioethers R_3MSR' (M = C, Si, Ge, or Sn) is reported. From these, several new compounds of type **1** are synthesized, some of which contain *para*-substituted aryl functions for R and R′. In hexane solution in the carbonyl stretching region of the ir and in the uv there is evidence for a degree of multiple bonding, at least in the M—S—W—CO portion of these molecules. Multiple bonding extending into aromatic R or R′ is small or non-existent and cannot be assessed precisely because of spontaneous decomposition of the complexes. All the complexes undergo a thermally initiated decomposition, the ease of which depends on the nature of R, R′, and M. The unusual W(I) thiolate *cis*-$[(CO)_4W\text{-}\mu\text{-}SR']_2$ is the thermal decomposition product.

C. Robert Lucas. Can. J. Chem. **64**, 1758 (1986).

On rapporte la préparation d'une série de thioéthers R_3MSR' (M = C, Si, Ge ou Sn) organiques et organométalliques. En partant de ceux-ci, on a synthétisé plusieurs nouveaux composés du type **1**; dans certains de ces composés, R et R′ représentent quelquefois des fonctions aryles substituées en position *para*. La région carbonyle des spectres ir, mesurés solution dans l'hexane, ainsi que les spectres uv suggèrent qu'il existe un certain degré de liaisons multiples, au moins dans la portion M—S—W—CO de ces molécules. Par ailleurs, il n'y a que peu ou pas d'extension de cette liaison multiple dans les portions aromatiques R et R′; de plus, on ne peut pas en déterminer d'une façon précise l'étendue à cause de la décomposition spontanée des complexes. Tous les complexes subissent une décomposition initiée thermiquement et la facilité de cette réaction dépend de la nature de R, R′ et de M. The thiolate inhabituel du W(1), $[(CO)_4W\text{-}\mu\text{-}SR']_2$-*cis*, est le produit de la décomposition thermique.

[Traduit par la revue]

Introduction

It has been shown (1) that in complexes of type **1** the presence of a degree of multiple bonding between M and S, S and W, and W and CO can be detected by ir spectroscopy when M = Si, Ge, or Sn. It is of interest to know whether this can be detected by other physical methods, whether it extends into R and R′ if they are aromatic, and whether the multiple bonding has any

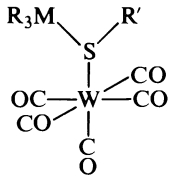

1

significant impact on the structure or chemical properties of the molecule.

Experimental

Spectroscopic data were obtained using the following instruments: ir, Perkin Elmer Model 283; nmr, Varian EM 360 or Bruker WP80 FT; mass spectra, VG Micromass 7070HS, uv, Cary Model 17. Analyses were performed by Canadian Microanalytical Service Ltd.

Ligands

All thiols and halides were obtained commercially except for *para*-$CF_3—C_6H_4—SH$, (*para*-Cl—$C_6H_4)_3GeCl$, (*para*-MeO—$C_6H_4)_3GeCl$, and (*para*-$CF_3—C_6H_4)_3GeCl$.

para-$CF_3—C_6H_4$-*SH*

To a mixture of concentrated HCl (10 mL) and ice (10 g) was added dropwise $CH_3—C_6H_4—NH_2$ (8.0 g, 6.3 mL, 50 mmol) at −4°C. To this was added dropwise a solution of $NaNO_2$ (3.7 g, 55 mmol) in H_2O (9 mL) also at −4°C. The cold diazonium salt solution was added dropwise to a solution of $KS_2COC_2H_5$ (9.4 g, 60 mmol) in H_2O (12 mL) at 45°C and stirred for 4 h. The solution was poured over chopped ice and the layers separated. The aqueous layer was extracted with ether (3 × 40 mL) and the extracts added to the organic layer which was then washed with 10% Na_2CO_3 and H_2O before being dried over $CaCl_2$. Volatiles were removed in vacuum, 95% ethanol (35 mL) was added to the residue and the mixture refluxed under an atmosphere of dry nitrogen while K_2CO_3 (12.2 g, 88 mmol) was added in small portions at a rate to maintain boiling. The mixture was refluxed overnight under an inert atmosphere. Water (75 mL) was added and the mixture extracted with ether (3 × 40 mL). The extracts were washed with 10% Na_2CO_3 (3 × 50 mL) and the washings were added to the aqueous phase previously separated which was then acidified to pH 3 with concentrated HCl and extracted with ether (3 × 40 mL). The extracts were dried over $CaCl_2$ and distilled. The product was an evil smelling oil boiling at 57°C at 8 mm Hg. Yield 1.4 g (16%).

(para-*Cl—*$C_6H_4)_3GeCl$, (para-*MeO—*$C_6H_4)_3GeCl$, *and* (para-*$CF_3—C_6H_4)_3GeCl$*

These compounds which are required for the preparation described below were obtained from the appropriate aryl bromide and $GeCl_4$ via a Grignard reaction in tetrahydrofuran and were used subsequently without isolation.

$Pb(SR)_2$

Lead mercaptides were obtained by stirring overnight stoichiometric mixtures of lead(II) acetate trihydrate and the appropriate thiols in 50% ethanol/water. The yellow precipitates were removed, washed several times with water and then alcohol, and dried in vacuum. Yields are typically >95%.

Me_3SiSPh, Me_3GeSPh, Ph_3CSPh, Ph_3GeSPh, (para-*Cl—*$C_6H_4)_3GeSPh$ (para-*MeO—*$C_6H_4)_3GeSPh$, (para-*$CF_3—C_6H_4)_3GeSPh$,* para-*Cl—*$C_6H_4—S—SiMe_3$, para-*MeO—*$C_6H_4—S—SiMe_3$, para-*$CF_3—C_6H_4—S—SiMe_3$*

These compounds were prepared by suspending $Pb(SR)_2$ (10 mmol) and the appropriate halide (20 mmol) in tetrahydrofuran (100 mL) and refluxing the mixture with stirring under an inert atmosphere until the suspended solids had turned white. Solids and solvent were removed to obtain crude products. Those that were mobile oils were distilled at reduced pressures under an inert atmosphere while those that were solids were recrystallized from benzene/hexane or were chromatographed in benzene/hexane on Florisil before being recrystallized.

Me_3SnSPh and Ph_3SnSPh

These compounds were prepared in tetrahydrofuran from stoichio-

[1]Revision received April 15, 1986.

metric mixtures of the appropriate organometal halide and thiophenol in presence of pyridine as a base. The solvent was removed under reduced pressure and the white crystalline products purified by recrystallization from benzene/hexane.

Ph_3SiSPh[2]

Diazabicyclo[2.2.2]octane (DABCO) (2.2 g, 20 mmol) was dissolved in dry toluene (15 mL) and thiophenol (2.2 g, 2.1 mL, 20 mmol) was added dropwise. The suspension was stirred for 2 h under a $CaCl_2$ drying tube and then filtered. The residue was dried under vacuum. Yield 3.1 g (70%) of DABCO.HSPh. Mp 95–97°C.

DABCO.HSPh (3.1 g, 14 mmol) and Ph_3SiCl (4.1 g, 14 mmol) were suspended in dry benzene (50 mL) and stirred under a $CaCl_2$ drying tube for 5 days. The suspension was filtered and the filtrate was concentrated under reduced pressure until a nearly colourless oil remained which crystallized on standing and from hexane.

(para-Cl—C_6H_4)$_3$CSPh and (para-MeO—C_6H_4)$_3$CSPh

Both compounds were obtained from the appropriate aryl bromide via its Grignard reagent which was first used with CO_2 to form the carboxylic acid and its methyl ester and then the tertiary carbinol by addition of the Grignard reagent to the methyl ester.

Thus, *para*-MeO—C_6H_4COOMe (6.6 g, 41.5 mmol) in dry tetrahydrofuran (25 mL) was added dropwise with stirring to MeO—C_6H_4—MgBr (125 mmol) in tetrahydrofuran (150 mL) and the mixture refluxed overnight. To this was added dropwise a saturated solution of NH_4Cl (20 mL) and water (40 mL). The mixture was stirred until two layers developed at which time they were separated and the aqueous layer washed with ether (3 × 50 mL). The washings were added to the organic layer which was then treated with 5% HCl, 10% $NaHCO_3$ and H_2O, and finally dried over $CaCl_2$. The solvent was removed to leave (MeO—C_6H_4)$_3$COH as an orange oil. Yield 6.0 g (41%).

The carbinol (3.5 g, 10 mmol) was suspended in dry ether (50 mL) containing PhSH (2.2 g, 2.0 mL, 20 mmol) and concentrated H_2SO_4 (0.3 mL) was added. The mixture was stirred for 24 h under a drying tube. Sodium hydroxide (1.0 mol/L, 35 mL) was added and the mixture stirred vigorously. The aqueous layer was separated and washed with CH_2Cl_2 (2 × 50 mL). All organic phases were combined, filtered through celite, and dried over $CaCl_2$. The solvent was removed to give a sticky yellow solid which was dissolved in benzene and chromatographed on Florisil to produce an off-white solid. Yield 2.2 g (50%).

(*para*-Cl—C_6H_4)$_3$CSPh was obtained similarly.

Complexes

A general method for the preparation of the type **1** complexes has been reported (1) with typical yields of 30%.

Mass spectra of the freshly prepared complexes did not show molecular ion peaks except for (Me_3GeSPh)$W(CO)_5$ and [(Cl—C_6H_4)$_3$GeSPh]$W(CO)_5$. Spectra of the other complexes consisted of peaks corresponding to $[ligand]^+$, $[R_3M]^+$, $[R'S]^+$, $[W(CO)_n]^+$ (n = 1–4), and ligand fragments.

cis-*[(OC)$_4$W-μ-SPh]$_2$*

Tungsten hexacarbonyl (5.3 g, 15 mmol) was dissolved in dry tetrahydrofuran (200 mL) in a Pyrex flask fitted with a double surface condenser, a magnetic stirrer, and a gas dispersion inlet tube. The top of the condenser was connected to an oil bubbler and the solution was irradiated for 4 h with a 100 W uv lamp while stirring and passing a stream of nitrogen bubbles through the solution. The lamp was switched off and Ph_3SiSPh (5.5 g, 15 mmol) dissolved in dry, degassed tetrahydrofuran (50 mL) was added under an inert atmosphere. The solution was refluxed for 24 h. Solvent was removed in vacuum and the residue extracted with hexane until the extracts were nearly colourless. The extracts were concentrated and chromatographed on Florisil using hexane as eluant. The first material to be removed is a green, non-terminal carbonyl substance which is followed by $W(CO)_6$, *cis*-[$(OC)_4W$-μ-SPh]$_2$, (Ph_3SiSPh)$W(CO)_5$, and $Ph_3SiSiPh_3$. The green *cis*-[$(OC)_4W$-μ-SPh]$_2$ was separated from its solvent, placed in a sublimer, and some $W(CO)_6$ removed by sublimation at 40°C and 0.1 mm Hg. The residue was recrystallized from hexane. Yield 1.3 g (22%). Mp 93°C (decomp). Mass spectrum: parent ion m/e = 810 not seen. Fragments with high abundance have m/e = 405, 268, 240, and 109 corresponding to $[(OC)_4WSPh]^+$, $[W(CO)_n]^+$ (n = 2–4) and $[PhS]^+$. *Anal.* calcd. for $C_{20}H_{10}O_8S_2W_2$: C 29.65, H 1.24, W 45.39; found C 29.72, H 1.96, W 45.50.

[2]A previously reported preparation of this compound, in our hands, gave no Ph_3SiSPh. However, the physical properties of Ph_3SiSPh prepared as described above agree with those previously reported (2).

Results and discussion

Many of the ligands employed in this study were obtained by the lead mercaptide process originally reported by Abel (3) as a method for (alkylthio)trimethylsilanes.

The lead mercaptides were prepared by precipitation from alcoholic solutions containing thiol and lead acetate trihydrate.

The thiols are available commercially or can be prepared easily from a diazonium salt and potassium ethyl xanthate.

The preferred route to R_3MSR' (M = C, R = substituted phenyl), however, starts from *para*-substituted aryl bromides and involves conversion of their Grignard reagents into methyl esters to which more Grignard is added forming tertiary carbinols. The carbinols are converted to thioethers by treatment with PhSH in the presence of mineral acid.

In two cases, neither of the routes already discussed is appropriate. Tertiary butyl chloride does not react with $Pb(SPh)_2$ even after 3 days in refluxing tetrahydrofuran and treatment of it with PhSH in the presence of a base leads only to isobutene. To prepare Me_3CSPh, addition of PhSH to isobutene in the presence of H_2SO_4 is the preferred route (4).

The lead mercaptide method also fails to yield Ph_3SiSPh. That compound can be obtained, however, from mixtures of PhSH and Ph_3SiCl in presence of the special base diazabicyclo[2.2.2]octane.

Some properties of the thioethers are listed in Table 1. All act as monodentate ligands to transition metals and we have already described some of their complexes (1).

In that earlier study, we examined several compounds of type **1** in hydrocarbon solution by vibrational spectroscopy in the carbonyl stretching region. Data from that and from the present studies (Table 2) were treated according to Cotton and Kraihanzel (5) to obtain approximate carbonyl stretching force constants and then by Graham's method (6) to obtain $\Delta\sigma$ and $\Delta\pi$ factors. Results are in Table 2 and are displayed graphically in Fig. 1 which also shows that all R_3MSR' ligands lie between triphenylphosphine and pyridine and near acetonitrile in terms of their σ-donor/π-acceptor abilities.

As will be discussed below, many of the complexes undergo a spontaneous decomposition to a *cis*-disubstituted carbonyl system which has ir and Raman absorptions in the same region as the B_1 mode of the type **1** complexes. Consequently, the type **1** complexes reported here which were not reported in our earlier study cannot be isolated in an analytically pure state. Furthermore, the frequency of their B_1 modes cannot be determined with precision due to the presence of overlapping bands from the decomposition product. Nonetheless, the other three bands expected for a molecule with C_{4v} local symmetry are well resolved and are sufficient to calculate all constants and the frequency of the partially obscured B_1 mode (Table 2) (7).

Reproducibility of the spectra is such that the probable error in the measured frequencies is <1 cm^{-1}. The effect of such an error is to introduce uncertainties of less than ± 0.07 for $\Delta\pi$ and ± 0.09 for $\Delta\sigma$ (Fig. 1).

The spectra appear as predicted by theory (7). The signifi-

TABLE 1.

Compound	Mp/bp (°C)	Yield	Nuclear magnetic resonance data[a]
Me_3CSPh	50 at 1.1 mm Hg	58%	1.28(s)(9); 7.4(m)(5)
Me_3SiSPh	38 at 0.1 mm Hg	66%	0.23(s)(9); 7.2(m)(5)
Me_3GeSPh	51 at 0.1 mm Hg	81%	0.44(s)(9); 7.2(m)(5)
Me_3SnSPh	98 at 0.1 mm Hg	75%	0.38(s)(9); 7.2(m)(5)[b]
Ph_3CSPh	107–108	85%	7.2(m)
Ph_3SiSPh	97–98	79%	7.2(m)
Ph_3GeSPh	95–96	68%	7.3(m)
Ph_3SnSPh	102–103	74%	7.3(m)
$(Cl—C_6H_4)_3CSPh$	146–150	81%	7.04(m); 7.27(s); 7.43(s)[c]
$(Cl—C_6H_4)_3GeSPh$	101–103	66%	7.1(m); 7.23(d, J_{AB} = 2.3 Hz); 7.31(d, J_{AB} = 2.3 Hz)[c]
$(MeO—C_6H_4)_3CSPh$	150–152	50%	3.77(s)(9); 6.70(d, J_{AB} = 9.3 Hz)(6); 7.01(m)(5); 7.24(d, J_{AB} = 9.3 Hz)(6)[c]
$(MeO—C_6H_4)_3GeSPh$	viscous oil	71%	3.80(s)(9); 6.89(m, J_{AB} = 8.5 Hz)(6); 7.2(m)(5); 7.49(m, J_{AB} = 8.5 Hz)(6)[c]
$(CF_3—C_6H_4)_3GeSPh$	viscous oil	38%	7.05(m, J_{AB} = 8.6 Hz); 7.3(m); 7.44(m, J_{AB} = 8.6 Hz)[d]
$Me_3SiS—C_6H_4—Cl$	59–61 at 0.1 mm Hg	73%	0.17(s)(9); 6.88(d, J_{AB} = 7.0 Hz)(2); 7.09(d, J_{AB} = 7.0 Hz)(2)[c]
$Me_3SiS—C_6H_4—OMe$	67–71 at 0.1 mm Hg	70%	0.00(s)(9); 3.51(s)(3); 6.50(d, J_{AB} = 8.9 Hz)(2); 7.03(d, J_{AB} = 8.9 Hz)(2)[c]
$Me_3SiS—C_6H_4—CF_3$	30–35 at 0.1 mm Hg	16%	0.31(s)(9); 7.18(d, J_{AB} = 8.7 Hz)(2); 7.39(d, J_{AB} = 8.7 Hz)(2)[c]

[a]In ppm from internal TMS. Data presented as δ (multiplicity)(relative intensity). Solvent $CDCl_3$ unless otherwise noted.
[b]d^6-acetone, $^2J^{117}Sn—^1H$ = 53.8 Hz, $^2J^{119}Sn—^1H$ = 56.3 Hz.
[c]CCl_4.
[d]^1H spectrum in CCl_4, ^{19}F spectrum 63.8(s) in $CDCl_3$ vs. $CFCl_3$.

TABLE 2. Infrared data from hexane solutions of $W(CO)_5L$

L in $W(CO)_5L$	ν_{CO} in cm^{-1}					Force constants (mdyn/Å)			Graham parameters (mdyn/Å)	
	A_1^1	B_1	E		A_1^2	k_1	k_2	k_i	Δσ	Δπ
Me_3CSPh[a]	2077.7	1988.0	1948.6	1945.5	1933.1	15.26	15.96	0.33	0	0
Me_3SiSPh[a]	2078.2	1987.8	1949.6	1945.3	1934.0	15.30	15.96	0.32	−0.04	+0.04
$Me_3SiS—C_6H_4—Cl$	2076.4	1987.6[b]	1951.2	1944.2	1932.1	15.26	15.95	0.32	−0.02	+0.01
$Me_3SiS—C_6H_4—OMe$	2077.7	1987.4[b]	1948.7	1944.9	1934.0	15.30	15.95	0.32	−0.06	+0.05
Me_3GeSPh[a]	2075.8	1987.9	1946.5	1942.0	1927.6	15.06	15.96	0.35	+0.20	−0.20
Me_3SnSPh[a]	2074.3	1986.0	1943.9	1938.2	1923.7	14.97	15.93	0.36	+0.23	−0.26
Ph_3CSPh[a]	2077.4	1988.1	1949.8	1944.5	1932.3	15.24	15.96	0.32	−0.02	+0.02
$(MeO—C_6H_4)_3CSPh$	2076.3	1987.5[b]	1950.1	1944.9	1932.1	15.26	15.95	0.32	−0.02	+0.01
Ph_3SiSPh	2075.5	1985.2[b]	1947.4	1942.0	1932.0	15.27	15.92	0.32	−0.09	+0.05
Ph_3GeSPh[a]	2075.0	1986.6	1947.8	1943.2	1923.6	15.09	15.94	0.33	+0.13	−0.15
$(Cl—C_6H_4)_3GeSPh$	2077.8	1986.2[b]	1947.3	1942.0	1920.1	15.07	15.93	0.33	+0.13	−0.16
$(MeO—C_6H_4)_3GeSPh$	2078.0	1986.8[b]	1948.0	1943.0	1924.4	15.14	15.94	0.33	+0.08	−0.10
$(CF_3—C_6H_4)_3GeSPh$	2079.0	1987.2[b]	1950.0	1941.1	1920.5	15.08	15.95	0.33	+0.16	−0.17
Ph_3SnSPh[a]	2074.8	1987.4	1945.2		1923.0	15.03	15.95	0.34	+0.21	−0.22
Ph_3P[c]	2074	1981	1943		1943	15.58	15.85	0.30	−0.54	+0.43
MeCN[c]	2083	—	1948		1931	15.22	16.00	0.31	+0.12	−0.08
PY[d]	2076	1980	1933		1895	14.59	15.83	0.37	—	—
$C_6H_{11}NH_2$[d]	2071	1974	1929		1894	14.65	15.74	0.35	+0.17	−0.39

[a]Data from ref. 1.
[b]Calculated value of ν.
[c]Data from ref. 24.
[d]Data from ref. 23.

cance of the force constants and Graham parameters has been discussed previously (1) and while the absolute values of the force constants may be disputed, differences between them for a series of closely related compounds are generally accepted as meaningful (8). As previously demonstrated (1), there is a relationship between the relative σ- and π-bonding abilities of the ligands and the nature of R and M in them. This relationship can be detected by vibrational spectroscopy and rationalized in terms of the electron density on sulfur which is affected both by the electronegativity of groups bound to sulfur and by the extent of $p\pi \rightarrow d\pi$ S → M bonding.

To determine whether vibrational spectroscopy can also detect changes in the carbonyls caused by *para*-substituents in aromatic R or R′, the substituents —CF_3, —Cl, —H, and —OMe, covering a range of electron-donating and -withdrawing abilities, indicated by their Hammett σ-values, were introduced. There is, however, no change within experimental error (Fig. 1), in the σ- and π-bonding ability of the ligands as their *para*-substituents are altered. This is not surprising when M = C in R_3MSR' since the absence of *d* orbitals on M prevents transmission of electronic effects except through the σ bonds. Thus, the influence of the *para*-substituents should diminish

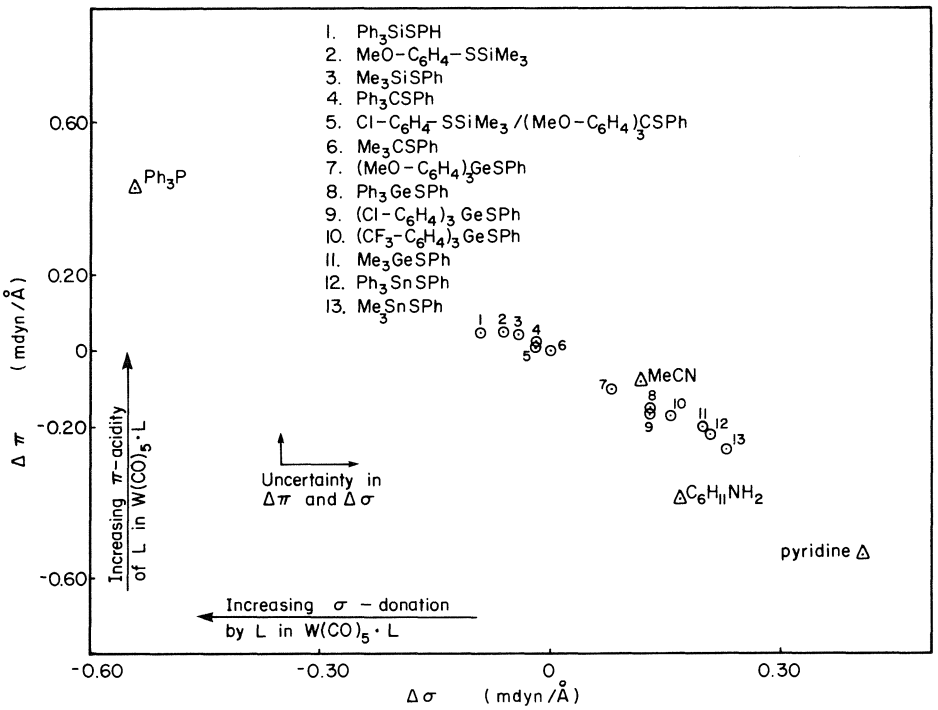

FIG. 1. Graham parameters for $W(CO)_5 \cdot L$ as a function of L: ⊙, data from this work; △, data from cotton (refs. 23 and 24) for comparison.

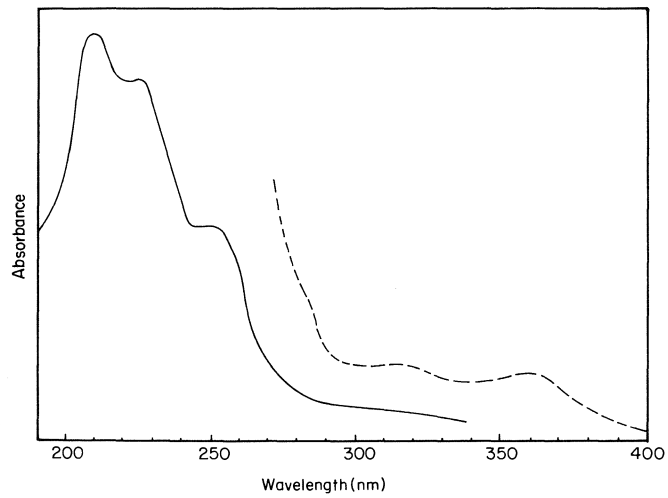

FIG. 2. Electronic spectrum of $W(CO)_5(Ph_3GeSPh)$: — $\sim 10^{-5}$ mol/L; --- $\sim 10^{-4}$ mol/L in hexane at room temperature.

rapidly with distance from the ring, becoming undetectably small over the four bonds to the carbonyls. This explanation probably reasonably describes the situation for the germanium–thioether complexes too because the extent of Ge—S π-bonding is small as has been shown in X-ray (9) and spectroscopic (1) studies.

When the *para*-substituent is on R′, however, it lies one bond closer to the carbonyls and to the sulfur atom and a greater effect might therefore be expected. That no significant change was detected is probably due to the fact that the uncertainty in Δσ and Δπ (discussed above) is larger than the changes caused by varying the *para*-substituent. This is consistent with the relatively small changes in Δσ and Δπ observed when R is changed from methyl to phenyl in these systems.

In an attempt to develop a more sensitive assessment of electronic effects, the uv spectra of some of the complexes

TABLE 3. Tungsten-to-thioether charge transfer wavelength

L in $W(CO)_5L$	λ (nm)
Me_3CSPh	231
Ph_3CSPh	235
Me_3GeSPh	220
Ph_3GeSPh	224
Me_3SnSPh	212
Ph_3SnSPh	215

were examined. A typical spectrum (Fig. 2) consists of a series of moderately intense metal-to-ligand charge transfer bands between 200 and 260 nm and two much weaker *d*–*d* transitions between 300 and 400 nm. One of the charge transfer bands is particularly sensitive to the nature of the ligand and moves as the ligand is changed (Table 3). By analogy with other $W(CO)_5L$ species, this band is assigned to a tungsten-to-thioether transition involving essentially *d* orbitals on both tungsten and sulfur (10).

If the sulfur *d*-orbital energies are affected by both the electro-negativity and by the extent of π-bonding to adjacent atoms or groups as discussed above, the energy of this charge transfer band should be affected also, assuming a reasonably constant energy for the tungsten orbitals. That such is indeed the case is illustrated in Fig. 3. As the groups attached to sulfur are changed in such a manner as to lower the electron density on sulfur (1), the π acidity of the ligand increases as the tungsten and sulfur *d* orbitals become closer in energy.

As noted earlier several of the type **1** complexes spontaneously decompose and their electronic spectra are uninterpretable due to overlapping bands. The decompositions, which can be represented in general by reaction [1], are thermally but not photochemically induced, their ease being sensitive to the nature of R and R′, with some occurring even in the solid state.

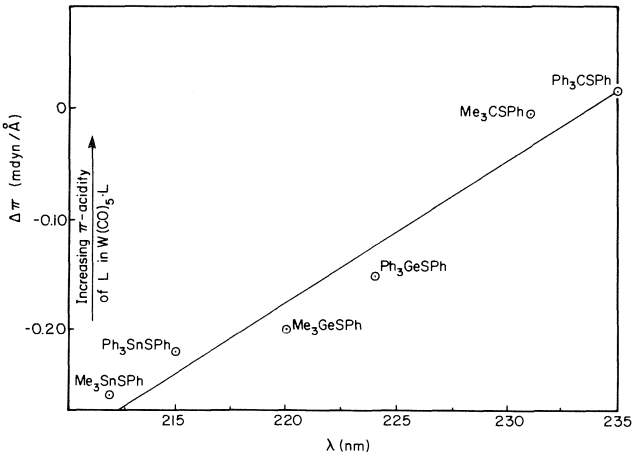

FIG. 3. π-acidity of L in $W(CO)_5 \cdot L$ vs. tungsten-to-thioether charge transfer wavelength.

[1] $2W(CO)_5(R_3MSR') \xrightarrow{\Delta} [W(CO)_4(SR')]_2 + (R_3M)_2$

For example, when R_3MSR' = $(Cl—C_6H_4)_3CSPh$ or $Me_3SiS—C_6H_4—CF_3$, the decomposition is so rapid that the type **1** complexes cannot be detected even in freshly prepared hexane extracts of the crude reaction products. By contrast, when R_3MSR' = Ph_3GeSPh, significant decomposition can only be accomplished by refluxing overnight. Irradiation of the same solution at room temperature for a similar period gives only small amounts of the desired products. Exactly which features of the ligand control the ease with which the decompositions proceed is not clear although when M = Si or when R or R′ are substituted phenyl, the decompositions seem to occur more readily.

Hexane solutions of the unusual W(I) thiolates which are products of these decompositions have ir spectra in the carbonyl stretching region consisting of four bands. For $W_2(CO)_8(SPh)_2$, these occur at 2038(s), 1979(m), 1973(m), and 1964(vs) cm^{-1}. Such spectra are consistent with a *cis*-disubstituted structure with C_{2v} local symmetry. Based on intensity arguments (11), the highest energy band can be assigned to the A_1 mode involving *trans* carbonyls and the lowest energy band to the B_1 mode. Since the *trans* force constant, k_1, must be less than the *cis* force constant, k_2 (5), there is only one satisfactory assignment of the two bands of intermediate frequency. Thus, the A_1 mode involving the *cis* carbonyls occurs at 1979 cm^{-1} and the B_2 mode occurs at 1973 cm^{-1}. Force constants obtained using these assignments are k_1 = 15.93, k_2 = 16.01, and k_i = 0.22 mdyn/Å.

Preliminary structural studies by X-ray methods (12) have confirmed the *cis*-disubstituted nature of the compound when R′ = Ph and that it is dimeric as indicated in reaction [1]. These studies also show that the W—W distance of 297.2(1) pm is substantially less than the 344 pm predicted from previously reported covalent radii (13).[3] Furthermore, the angles at S are acute while those at tungsten are obtuse. These observations suggest the presence of a W—W bond which is consistent with the appearance of a narrow phenyl multiplet 7.3 ppm from TMS in the ^1H nmr spectrum. In the absence of a W—W bond, some broadening or shift of the signal due to paramagnetism of a formally W(I) species might be expected. Analogous compounds of Group VI metals are rare, but $[Mo_2(SBu^t)_2(CO)_8]$ (14) is structurally similar and is also diamagnetic.

No study of the decomposition mechanism has been undertaken, but certain observations point to processes for which precedent exists. Thus, one could envisage the following stages occurring within the mechanism.

[2] $W(CO)_5(R_3MSR') \rightarrow W(CO)_5SR' + (1/2)(R_3M)_2$

[3] $W(CO)_5SR' \rightarrow W(CO)_4SR' + CO$

[4] $2W(CO)_4SR' \rightarrow (OC)_4W(SR')_2W(CO)_4$

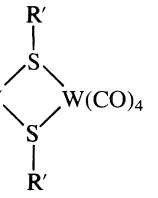

Reaction [2] involves cleavage of an M—S bond which has been demonstrated, at least in the case of M = Si, to be a facile process for the free ligand even under mild conditions (3, 15). Furthermore, there is evidence to suggest that when the ligand is coordinated, the central metal can assist in an M—S cleavage (16). The next stage (reaction [3]) requires loss of a *cis* carbonyl which could occur as a result of a *cis* labilizing process such as has been observed in related systems (17) and finally, reaction [4] involves dimerization similar to that observed for related complexes of Ru and W (18–21).

A structural study of Ge—S and Sn—S bonds in organometallic thioethers (9) found no shortening in the M—S bonds compared to the calculated lengths (22) and concluded that M—S multiple bonding was not structurally significant in these compounds. From our evidence, it would appear (Fig. 1) that the significance of M—S multiple bonding is greatest when M = Si and diminishes considerably when M = Ge or Sn. An X-ray study of Ph_3SiSPh was therefore undertaken (12) and the Si—S bond was found to have a length of 215.6(2) pm. This represents a shortening of >4 pm compared to the calculated length (22).

In conclusion, the effects of M—S multiple bonding in organometallic thioethers can be detected by both ir and uv spectroscopy. Such bonding diminishes in magnitude from Si through Ge to Sn, having structural significance only when M = Si and even then the M—S bond is cleaved with ease in the complexes. Whether multiple bonding extends into aromatic R and R′ cannot be determined with certainty although if such bonding exists it must be small.

Acknowledgements

This work was supported in part by the Natural Sciences Engineering and Research Council of Canada and by the Department of Chemistry, Memorial University of Newfoundland. The assistance of Mr. A. Clase and Mr. R. Whalen (some preparations and spectroscopy) and of Dr. B. Gregory and Miss M. Baggs (mass spectra) is gratefully acknowledged.

1. C. R. LUCAS. Can. J. Chem. **61**, 1096 (1983).
2. D. BRANDES. J. Organomet. Chem. **136**, 25 (1977).
3. E. W. ABEL. J. Chem. Soc. 4406 (1960).
4. V. N. IPATIEFF, H. PINES, and B. S. FRIEDMAN. J. Am. Chem. Soc. **60**, 2731 (1938).
5. F. A. COTTON and C. S. KRAIHANZEL. J. Am. Chem. Soc. **84**, 4432 (1962).
6. W. A. G. GRAHAM. Inorg. Chem. **7**, 315 (1968).
7. P. S. BRATERMAN. Metal carbonyl spectra. Academic Press, New York. 1975. pp. 68–72.

[3]Throughout this work, esd's are in parentheses and refer to the last digit printed.

8. F. A. COTTON and G. WILKINSON. Advanced inorganic chemistry. 4th ed. John Wiley and Sons, Toronto. 1980. pp. 1077–1079.
9. J. PICKARDT, H. SCHUMANN, C. F. CAMPANA, and L. F. DAHL. J. Organomet. Chem. **216**, 245 (1981).
10. A. B. P. LEVER. Inorganic electronic spectroscopy. 2nd ed. Elsevier, Oxford. 1984. pp. 275–285.
11. L. E. ORGEL. Inorg. Chem. **1**, 25 (1962).
12. C. R. LUCAS, E. GABE, and M. J. NEWLANDS. Unpublished results.
13. R. BAU, S. A. GRAHAM, and R. D. WILSON. J. Organomet. Chem. **91**, C49 (1975).
14. M. KAMATA, T. YOSHIDA, S. OTSUKA, K. HIROTSU, and T. HIGUCHI. J. Am. Chem. Soc. **103**, 3572 (1981).
15. H. VAHRENKAMP and R. KURY. Studies in inorganic chemistry. Vol. 5. *Edited by* A. Muller and B. Krebs. Elsevier, Oxford. 1984. p. 125.
16. P. J. DOSSOR, C. EABORN, and D. R. M. WALTON. J. Organomet. Chem. **71**, 207 (1974).
17. D. J. DARENSBOURG. Adv. Organomet. Chem. **21**, 113 (1982).
18. C. G. KUEHN and H. TAUBE. J. Am. Chem. Soc. **98**, 689 (1976).
19. M. HERBERHOLD and G. SUS. Angew. Chem. Int. Ed. **15**, 366 (1976).
20. M. HERBERHOLD and G. SUSS. J. Chem. Res. S246 (1977); M2720 (1977).
21. R. KURY and H. VAHRENKAMP. J. Chem. Res. S30 (1982); M0401 (1982).
22. J. E. HUHEEY. Inorganic chemistry. 3rd ed. Harper and Row, New York. 1983. p. 258.
23. C. S. KRAIHANZEL and F. A. COTTON. Inorg. Chem. **2**, 533 (1963).
24. F. A. COTTON. Inorg. Chem. **3**, 703 (1964).

ipso Nitration. XXVIII.[1] Nitration of 4-substituted toluenes: 1,2 adducts[2]

ALFRED FISCHER,[3] DEBORAH L. FYLES, GEORGE N. HENDERSON, AND SUMIT RAY MAHASAY
Department of Chemistry, University of Victoria, Victoria, B.C., Canada V8W 2Y2

Received February 10, 1986

ALFRED FISCHER, DEBORAH L. FYLES, GEORGE N. HENDERSON, and SUMIT RAY MAHASAY. Can. J. Chem. **64**, 1764 (1986).

Nitration of 4-acetamido-, 4-chloro-, and 4-methoxy-toluene in acetic anhydride gives in each case a *cis* 1,2 nitronium acetate adduct in addition to the nitro substitution product(s). Nitration of 4-fluorotoluene gives a pair of diastereomeric 1,4 nitronium acetate adducts and the *cis* 1,2 adduct.

ALFRED FISCHER, DEBORAH L. FYLES, GEORGE N. HENDERSON et SUMIT RAY MAHASAY. Can. J. Chem. **64**, 1764 (1986).

En plus de conduire à la formation de produits substitués par un groupement nitro, la nitration des acétamido-4, chloro-4 et méthoxy-4 toluènes effectuée dans l'anhydride acétique conduit aussi, dans chaque cas, à la formation d'un adduit nitronium acétate-1,2-*cis*. Lors de la nitration du fluoro-4 toluène, il y a formation de l'adduit 1,2-*cis* ainsi que d'une paire d'adduits nitronium acétates-1,4 diastéréoisomères.

[Traduit par la revue]

Nitration in acetic anhydride of aromatic compounds in which a substituted position is activated often leads to the formation of nitronium acetate adducts in which the nitro group is attached to the activated substituted site (3, 4). There are many examples in the polymethylbenzenes and *p*-alkyltoluenes (5–11). In these reactions the nitration of *p-tert*-butyltoluene appears anomalous in that it gives both 1,2 and 1,4 adducts (12), whereas only a pair of diastereomeric 1,4 adducts is formed in all of the other cases. In this paper we describe the nitration of 4-X-toluenes (X = F, Cl, OMe, NHCOMe) leading, in each case, to the formation of a 1,2 adduct and, in the case of 4-fluorotoluene, to a pair of diastereomeric 1,4 adducts. In a previous paper we described the structure and stereochemistry of the adduct formed on the nitration of 4-bromotoluene (1). Nitration of 4-bromo- and 4-methoxytoluene has been investigated previously by Clemens *et al.* (13). They obtained 4-methyl-4-nitrocyclohexadienone from both substrates and did not detect the formation of dienes.[4]

Results and discussion

Nitrations were carried out under conditions that led to optimum yields of the adducts and which were determined by carrying out preliminary reactions on a 0.5-mmol scale and following the reactions by nuclear magnetic resonance spectroscopy (^{1}H nmr). For preparative nitrations the reaction temperature was −40°C and trifluoroacetic anhydride was added to increase the activity of the nitrating mixture (4) in the cases of the less reactive substrates (X = F, Cl, I, NHAc). Reaction mixtures were neutralized by the addition of aqueous ammonia at low temperature or by addition to cold aqueous sodium bicarbonate followed by stirring for 1.5 h. Generally the composition of the reaction product isolated after work-up was the same as that present in the reaction mixture prior to work-up. The adduct from 4-chlorotoluene, like that from 4-bromotoluene (1), was crystallized directly from the reaction product. In the cases of the other substituted toluenes the product mixtures were separated by chromatography. The adduct from 4-acetamidotoluene was particularly labile, undergoing aromatization even at −20°C. However, it was obtained pure following two successive chromatographic separations at −78°C. The adducts from 4-fluorotoluene were also reactive, being subject to autocatalytic acid-catalysed loss of the elements of acetyl fluoride to form first 4-methyl-4-nitrocyclohexa-2,5-dienone, which in turn rearranged to 4-methyl-2-nitrophenol (15).

As in the case of 4-bromotoluene, 4-chlorotoluene gave an adduct and two substitution products, whereas the methoxy and acetamidotoluenes gave only the adduct and the 3-nitro derivative (Table 1). Nitration of 4-fluorotoluene was strikingly different from that of 4-bromo- and 4-chlorotoluene in that the major product was the 1,4 adduct (81%) obtained as a pair of

TABLE 1. Product distributions from the nitration of 4-X-toluenes in acetic anhydride: amount of product/mol% with the nitro group at the indicated position.

	Observed				Calculated[a]			
X	1[b]	2	3	4	1	2	3	4
F[c]	100	0	0	0	96	0	4	0
Cl[d]	70	17	13	0	73	9	14	3
Br[e]	64	28	8	0	69	13	18	0
I[e]	*f*	*f*	*f*	*f*	62	18	18	<2
OMe[g]	30	0	70	0	47	0	53	0
NHAc[h]	35	0	65	0	40	0	60	0

[a]Calculated product distributions are based on isomer distributions for nitration of toluene (16) and the relevant monosubstituted benzenes (see text) using data from the references indicated.
[b]For 4-fluorotoluene the product was a mixture of 1,2 adduct (8%), 1,4 adduct (81%), and dienone (11%). For the other substrates only the 1,2 adduct was present.
[c]Reference 17.
[d]See text.
[e]Reference 18.
[f]Adduct <10%; substitution product(s) present; 4-nitrotoluene major product (>50%).
[g]Reference 19*a*.
[h]Reference 20.

[1]For part XXVII, see ref. 1.
[2]For a preliminary communication, see ref. 2.
[3]Author to whom correspondence may be addressed.
[4]The ^{1}H nmr spectrum of 4-methyl-4-nitrocyclohexa-2,5-dienone that they reported (δ: 1.95, 5.66, 6.53 ppm) differs significantly from that reported by Myhre and co-workers (14) (1.96, 6.35, 7.15 ppm). When we repeated the nitration of 4-bromotoluene under the conditions described (13), we observed diene but not dienone in the reaction mixture and only 40% of the 4-bromotoluene reacted. Pure samples of the dienone have been characterized unambiguously by various workers and its formation at higher temperatures from 4-methylanisole is now well established.

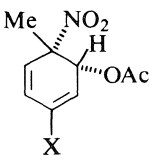
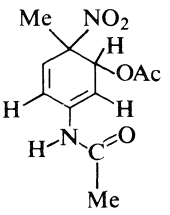
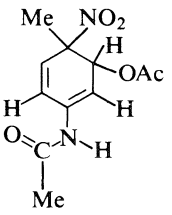


1 X = Br
2 X = Cl
3 X = F
4 X = OMe
5 X = NHAc
6 X = *t*-Bu

5*i* **5***ii* **7**

diastereomers. Only a small amount (8%) of 1,2 adduct was formed and no nitro substitution product was observed. Some 4-methyl-4-nitrocyclohexadienone was also obtained (11%) but, since this is a product of further reaction of the dienes (*vide supra*), it is likely that it was not formed as a primary reaction product. Nitration of 4-iodotoluene gave a very small amount of adduct (<10%), which was not isolated. The predominant product was 4-nitrotoluene, accompanied by the liberation of iodine. Substitution product(s) was also formed. Nitration of 4-(*N*,*N*-dimethylamino)toluene gave nitroaromatic product and no adduct was observed. Attempted nitration of 4-(*N*-methylamino)toluene resulted in the formation of the anilide. Nitration of 4-(*N*-methylacetamido)toluene gave an adduct that did not survive the work-up procedure.Nitration of 4-acetoxytoluene (4-methylphenyl acetate) gave the dienone, as previously observed (14), but no diene, even at −60°C.

Structure and spectra of the adducts

The structures of the dienes **1**, **2**, **3**, **4**, and **5** were initially assigned on the basis of spectral information. Elemental analyses are consistent with the addition of acetyl nitrate to the substrate aromatic. Such addition is confirmed by the infrared spectra, which exhibit strong absorptions around 1750 (for $OCOCH_3$) and 1550 cm^{-1} (for NO_2). The ultraviolet spectra (λ_{max} = 257–271 nm, $\varepsilon = 350\ m^2\ mol^{-1}$) show that the dienes are conjugated, since isolated double bonds absorb below 253 nm (21). There are three arrangements of conjugated double bonds that can be derived from addition to a 4-substituted toluene. Using the enumeration of toluene,[5] these may be described a 1,3-diene, a 1,5-diene, and a 2,4-diene. In the 1,3-diene both sp^3 carbon atoms have an attached hydrogen atom. However, the ^{13}C nmr spectra (Table 2) indicate that there is one sp^3 carbon atom with an attached hydrogen atom (δ_C = 70 ppm, doublet splitting in the gated spectrum J = 150 Hz), and one sp^3 carbon atom with no attached hydrogen (δ_C = 87 ppm, singlet in the gated spectrum). Moreover, this structure cannot account for the 10-Hz splitting in the ^1H nmr spectra (Table 3), which points to the presence of adjacent vinylic protons. In the 1,5-diene structure the variable substituent (4-X) is attached to an sp^3 carbon that has no attached hydrogen (either the nitro or the acetate group must also be attached to this carbon). However, in the ^{13}C nmr spectra the position of the fully substituted sp^3 carbon absorption is relatively invariant (δ_C = 87 ppm), which points to a constant substitution pattern. Correspondingly, the sp^2 carbon that has no attached hydrogen has widely ranging absorption (δ_C = 122.6–159.4 ppm) consistent with the 4-X substituent being located at this carbon. Only the 2,4-diene structure is consistent with the position of the absorptions of these two carbon atoms.

[5]The toluene enumeration is used in Table 1. The other tables use the appropriate enumeration for the cyclohexadienyl acetates.

The nitro group must be located at position 1 because the chemical shift of the fully substituted carbon (δ_C = 87 ppm) is the same as that of the sp^3 carbon of 4-methyl-4-nitrocyclohexa-2,5-dieone to which are attached the nitro and methyl groups. The acetate group is thus at position 6. In the case of diene **1** an X-ray crystal structure determination confirmed the structure assigned on the basis of the spectral data and gave the stereochemistry, the nitro and acetate groups being *cis* to each other (1). It seems reasonable to conclude that the 1,2 addition of acetyl nitrate, which is stereoselective in all of the substrates investigated and which is also stereoselective in the case of 4-*tert*-butyltoluene (12), is in all cases a *syn* addition. Shift reagent studies applied to the two members of a pair of diastereomeric adducts have been used to determine the stereochemistry of 1,4-adducts in which the acetate group is secondary (22), but the method could not be applied to the 1,2-dienes obtained in this work since a pure sample of the second diastereomer was not generally available.

Other features of the nmr spectra of the 1,2 adducts are as follows (enumeration now follows that exemplified in 3-chloro-6-methyl-6-nitrocyclohexa-2,4-dienyl acetate). In the ^1H nmr the methyl group protons resonate at 1.8 ppm and the acetate methyl protons resonate at 2.0 ppm. The protons of the methoxy group of diene **4** are at 3.60 ppm and those of the acetamido methyl group in diene **5** at 2.10 ppm. The absorptions of the 1 and 2 protons were distinguished from those of the 4 and 5 protons by the 6-Hz coupling of the former as compared with the 10-Hz coupling of the latter. The individual assignments of the absorptions of the 1 and 2 protons were made on the basis that the 1-proton absorption should be essentially invariant in position, and is therefore the absorption at 5.5 ppm, whereas the 2-proton absorption should be affected by the variation of the 3-substituent, which is vinylic to it, and thus this absorption ranges from 5.0 to 6.5 ppm. These assignments were confirmed in the cases of dienes **1** and **2** by selective proton decoupling of the 1-H from the C-1 in the ^{13}C spectra. The assignments of the 4 and 5 protons were made on the basis of long range coupling constants. Thus, in **2** the 1-H is coupled to one of 4-H and 5-H (J = 1.6 Hz) and 2-H is coupled to the other (J = 2.0 Hz). The four-bond 1,5 and 2,4 couplings should be larger than the five-bond 1,4 and 2,5 couplings and the 4-H and 5-H were assigned to reflect this. In the dienes **1** and **2** there is in addition a small 2,5 coupling (J = 0.6 Hz). Decoupling experiments were carried out on dienes **1** and **2**. In **1** the 1-H absorption appeared as a doublet of doublets (J = 6.2 Hz and 1.8 Hz). The 2-H absorption appeared as a doublet of a doublet of a doublet (J = 6.2 Hz, 1.8 Hz, 0.6 Hz). Irradiation of 1-H (5.45 ppm) caused the large coupling in 2-H to disappear, and the smallest coupling disappeared when the 5-H was irradiated (6.45 ppm). The 5-H absorption itself appeared as a doublet of a doublet of a doublet (J = 10.2 Hz, 1.8 Hz, 0.6 Hz), which collapsed to a doublet of a doublet (J = 10.2 Hz and 0.6 Hz) when the 1-H was irradiated. The 4-H absorption appeared as a doublet of a doublet (J = 10.2 Hz and 1.8 Hz). Similar observations were made on **2**. In diene **3** the signal due to 2-H is shifted upfield and it overlaps with the peak of the 1-H (5.6 ppm). Addition of the shift reagent tris-(1,1,1,2,2,3,3-heptafluoro-7,7-[$^2H_6$]dimethyl-4,6-[$^2H_3$]octanedionato)europium(III) (Eu([$^2H_9$]fod)$_3$) separated the 1-H peak from that of 2-H and allowed the coupling constants to be determined. The 2-H signal is shifted even further upfield in **4** (to 4.97 ppm). The five-bond coupling between 2-H and 5-H is absent in **3** and **4**.

The ^1H nmr spectrum of **5** is temperature dependent, the

TABLE 2. The ^{13}C nmr spectra of 3-X-6-methyl-6-nitrocyclohexa-2,4-dienyl acetates

Compound	X	Chemical shifts, ppm								
		6-CH_3	OAc	C-1	C-2	C-3	C-4	C-5	C-6	CO
1[a]	Br	23.1	20.6	70.4	122.0	122.6	127.8	128.5	86.8	169.0
2	Cl	23.2	20.6	70.2	118.1	133.6	126.1	129.4	87.2	169.5
3	F	23.4	20.9	73.1	98.2	159.4	120.1	131.5	87.9	169.4
4	OMe[b]	22.6	19.6	70.8	87.8	155.2	122.7	128.4	87.3	168.6
5	NHAc[c]	23.3	20.7	70.3	102.6	134.3	122.7	129.1	87.7	169.2[d]
6[e]	*t*-Bu	23.5	20.8	70.5	113.0	147.5	125.0	126.9	87.7	169.7

[a]From ref. 1.
[b]OCH_3 53.8 pm.
[c]$NHCOCH_3$ 170.0 or 169.2 and 24.5 pm.
[d]Or 170.0 pm.
[e]From ref. 12.

TABLE 3. The ^1H mr spectra of 3-X-6-methyl-6-nitrocyclohexa-2,4-dienyl acetates

Compound	X	Chemical shifts, ppm						Coupling constants, Hz				
		6-CH_3	OAc	1-H	2-H	4-H	5-H	1,2	1,5	2,4	2,5	4,5
1[a]	Br	1.77	1.98	5.45	6.37	6.13	6.45	6.15	1.76	1.80	0.55	10.23
2	Cl	1.78	1.99	5.53	6.12	6.03	6.55	6.13	1.65	1.97	0.61	10.20
3	F	1.82	1.98	5.57	5.57	6.03	6.64	6	1	2	0	10.5
4	OMe[b]	1.77	1.95	5.62	4.97	5.93	6.56	6.57	1.52	1.75	0	10.20
5	NHAc[c]	1.78	1.95	5.62	6.49	6.09	6.59	6.55	1.53	1.70	0	10.30
6[d]	*t*-Bu	1.67	1.95	5.53	5.74	6.24	6.38	5.6	1.2	1.6	0.8	10.3

[a]From ref. 1.
[b]OCH_3 3.60 pm.
[c]For NHAc shifts see Table 4.
[d]From ref. 12.

TABLE 4. Temperature dependence of ^1H chemical shifts of **5**

T, K	Chemical shifts, ppm							
	6-CH_3	OAc	NHAc	NH	1-H	2-H	4-H	5-H
229	1.77	1.95	2.10	8.32	5.61	6.53	6.08	6.59
241	1.78	1.95	2.10	8.22	5.62	6.49	6.09	6.59
249	1.78	1.95	2.10	8.00	5.62	6.46	6.10	6.59
273	1.78	1.94	2.09	7.50	5.62	6.43	6.11	6.58
298	1.78	1.96	2.11	[a]	5.62	6.33	6.13	6.58

[a]Very broad.

greatest variation being exhibited by the N-H followed by the 2-H and 4-H (Table 4). The C—N bond of an amide has partial double bond character, as a consequence of the amide group resonance, and hence rotation about the carbonyl nitrogen bond is hindered. In monosubstituted amides the rotamers differ in energy and therefore participate unequally in the thermal equilibrium. For N-alkyl compounds the predominant planar rotamer is the one with the alkyl groups (attached to the N and C=O) *anti* to each other (23). In the case of diene **5** such geometry gives rise to two limiting structures, **5***i* and **5***ii*, differing by rotation about the diene-N bond. In *i* the 2-H and in *ii* the 4-H lies in the deshielding zone of the carbonyl group. The chemical shifts of these protons thus vary with the relative orientation of the carbonyl group and their values at a particular temperature will be determined by the weighted average of the populations of rotamers *i* and *ii* in the equilibrium. From Table 4 it can be seen that the signal of 2-H shifts upfield and that of 4-H shifts downfield with increase in temperature. This suggests that structure *ii* is favored with increase in temperature, and that structure *i* is thermodynamically favored over *ii*.

The ^{13}C spectra of dienes **1** and **2** had two peaks due to methyl carbons, of which the lower field signal (δ_C = 23 ppm) was twice the intensity of the other (δ_C = 20 ppm). In the single frequency decoupled ^{13}C spectrum, obtained by irradiating the protons on the acetyl methyl group (δ = 1.95 ppm), the lower field signal (23 ppm) appeared as a quartet whereas the higher field signal became a singlet. This allowed the assignment of the lower field signal with the higher intensity to the ring methyl and the higher field signal as the acetyl methyl. The methyl signals are relatively invariant throughout the series and this assignment also applies to **3**, **4**, and **5**. The signal at C-2 was assigned on the basis of the effect of the substituent attached to the adjacent C-3; in all compounds this was expected to move the C-2 peak to higher fields and thus the highest field signal of the peaks attributable to C-2, C-4, and C-5 was assigned to C-2. The trends in the shifts of the C-2 and C-3 atoms in dienes **1**–**6** parallel those reported for the β and α carbons, respectively, of the monosubstituted ethylenes (24, 25), confirming the assignments (Table 5). The assignments of C-4 and C-5 were made on the basis of single frequency decoupling of the splitting by the protons attached to each carbon in the case of diene **4** and by the C-5 proton in other cases. As would be expected, the C-4 signal is more affected by the adjacent substituent than is the signal of the more remote C-5 (Tables 2 and 5). Furthermore, the relative shifts for the C-4 atoms parallel those for the C-2 atoms with the magnitudes of the relative shifts attenuated, reflecting the lower bond order for the 3–4 bond compared with the 2–3 bond. The

relative shifts for C-5 do not parallel those for C-2 and C-4. In the case of diene **3** the fluorine–carbon coupling, largest at C-3 and decreasing with increase of the separation of the carbon and the fluorine, supports the assignments made.

The structures of the 1,4 dienes **7***a* and **7***b* were also established by spectral studies. The presence of nitro and ester groups is evident from the ir. The symmetry apparent in both the ^1H and ^{13}C spectra clearly demonstrates that these must be 1,4 adducts and this is confirmed by the absence of strong uv absorption above 250 nm (the weak absorption, $<30\ m^2\ mol^{-1}$, is probably from an impurity). The 1,2 adduct from *p-tert*-butyltoluene has the C-1 absorption (toluene enumeration) at lower field (88 ppm) than does the 1,4 adduct (85 ppm). Correspondingly, in **3** the absorption is at lower field (87.9 ppm) than in **7***b* (83.2 ppm). In **7***b* the absorptions of 2-H and 3-H, and C-2 and C-3, and in **7***a* of 2-H and 3-H, were assigned in accordance with the expectation that the fluorine–proton 3-bond coupling should be larger than the 4-bond coupling and the fluorine–carbon 2-bond coupling should be larger than the 3-bond coupling. Addition of Eu([$^2H_9$]fod)$_3$ moved the CH_3 protons of **7***b* downfield to a greater extent (relative slope 0.17) than the corresponding protons of **7***a* (0.125). This indicates that **7***a* is the *E* isomer (from *syn* addition) and **7***b* the *Z* (*anti* addition).

Reactivities and positional selectivities of 4-substituted toluenes

The conditions required for nitration reflect the relative reactivities of the aromatic compounds. A longer reaction time, a higher mole-proportion of nitrating agent, a higher temperature, and the presence of trifluoroacetic anhydride (4) are required for deactivated substrates. Based on these features, the substrates belonging to the 4-X-toluene series can be arranged in order of decreasing reactivity as: OMe > (*t*-Bu, F) > Cl > Br > NHAc. The lower reactivity of the acetamido compound is unexpected as it is known to be a stronger activating group than alkyl and halogen substituents. The apparent anomaly could be a consequence of the lower solubility of the substrate in the reaction mixture. Since solid acetanilide was added to the nitrating agent, the reaction medium was heterogeneous at the early stages of the reaction and the effective concentration of the aromatic in solution would have been less than calculated.

The reactivities of the different ring positions of the *p*-disubstituted benzenes can be calculated from the partial rate factors for nitration of the appropriate monosubstituted benzenes in acetic anhydride, using the assumption of additivity of the logarithms of these factors.[6] Partial rate factors for nitration of toluene in acetic anhydride are known for all positions including the *ipso* position (16). Partial rate factors for other monosubstituted benzenes are known for the *ortho*, *meta*, and *para* positions but not for the *ipso* position. An estimate of the relative partial rate factor at the *ipso* position of chlorobenzene can be derived from data for the nitration of chloromesitylene (26). The ratio of adduct (with nitro *ipso* to chloro) to 2-chloro-4-nitro-1,3,5-trimethylbenzene is 21:73 and this gives the partial rate factor ratio of 21:36.5, i.e. the position *ipso* to chlorine is 60% as reactive as the *meta* position. Thus, using the known $o_f:m_f:p_f$ (18), the relative partial rate factors for chlorobenzene are $i_f:o_f:m_f:p_f$ = 0.6:33:1.0:154, from which

[6]Absolute values of the partial rate factors are not required. The relative yields of the nitration products obtained from a monosubstituted benzene (the isomer distribution), with each yield being divided by the number of positions in the substrate giving rise to that product on nitration, gives the relative partial rate factors.

TABLE 5. Relative ^{13}C chemical shifts for 3-X-6-methyl-6-nitrocyclohexa-2,4-dienyl acetates and for X-ethylenes[a]

	Chemical shifts, ppm					
X	C-2	C-3	C-4	C-5	C-α	C-β
Br	3.9	−11.0	1.7	−0.9	−10.5	4.7
F	−19.9	25.8	−6.0	2.1	21.6	−28.9
OMe	−30.3	21.6	−3.4	−1.0	27.0	−31.9
NHAc	−15.5	0.7	−3.4	−0.3	3.9	−23.1
t-Bu	−5.1	13.9	−1.1	−2.5	23.6	−7.6

[a]The reference compound is the chloro derivative. Data for X-ethylenes from refs. 24 and 25.

the calculated product distribution on nitration of 4-chlorotoluene is as shown in Table 1. The yield of *m*-nitrochlorobenzene obtained on nitration of chlorobenzene is quite small and thus the partial rate factor for *meta* (and thus *ipso*) nitration is subject to significant error and the results should be interpreted semiquantitatively at best. Nevertheless the calculation correctly predicts that the adduct with nitro *ipso* to methyl should be the major product, that there should be very little adduct with nitro *ipso* to chlorine (none was found), and that both nitro-4-chlorotoluenes should be obtained (although less 2-nitro than 3-nitro is predicted, whereas the opposite was found). Analogous data are not available to estimate the factors for nitration *ipso* to the other substituents. However, it seems reasonable to assume that such *ipso* partial rate factors, like that for chloro, are small since adducts with nitro *ipso* to these substituents were not observed. Calculated and observed product distributions are shown in Table 1. 4-Fluorotoluene is predicted to give, almost completely, *ipso* adduct, as was observed. 4-Bromotoluene, like 4-chlorotoluene, is predicted and found to give the adduct as the major product as well as observable amounts of both nitrobromotoluenes. 4-Iodotoluene is also predicted to give mainly adduct (with nitro *ipso* to methyl) and lesser but significant amounts of both nitro substitution products. Less than 0.2% of nitrodeiodination occurs on the nitration of iodobenzene (27), from which it may be calculated that not more than 2% of nitrodeiodination should occur in 4-nitrotoluene (Table 1). Here observation is in conflict with prediction since the extent of nitration *ipso* to methyl is small and that *ipso* to iodine, as measured by the formation of 4-nitrotoluene, is large. Nitrosodeiodination may account for the formation of 4-nitrotoluene as the major nitration product. This is known to be the process by which apparent nitrodeiodination occurs in the nitration of very reactive iodoaromatics, although such cases involve substrates rather more reactive than 4-iodotoluene (19*b*). 4-Methoxytoluene and 4-acetamidotoluene, for which the methoxy and acetamido groups are known to be particularly strongly *ortho* directing (and very weakly *meta* directing) in acetic anhydride (19*c*), give, as predicted, only the 3-nitro substitution product in addition to the *ipso* product, the latter predicted and found to be the smaller component. Nitration of 4-methoxytoluene in 46–80% sulphuric acid gives 4-methyl-2-nitrophenol (38%) and 4-methoxy-3-nitrotoluene (62%) (28). *ipso* Nitration and capture of the *ipso* cation by water, followed by loss of methanol, gives the dienone, which rearranges to the nitrocresol. The constant yield of the nitrocresol over the wide range of acidity implies that all of the *ipso* cation is captured in up to 80% sulphuric acid. The extent of capture is similar to that directly observed

in acetic anhydride (30%). The nitration of 4-bromo- and 4-chlorotoluene has been investigated in 63–85% sulphuric acid (29). In both cases there is competition between capture of the *ipso*-nitrocyclohexadienyl cation by water and its rearrangement to (ultimately) the 4-halo-2-nitrotoluene. The data imply that there is a significant amount of attack *ipso* to methyl in the two halotoluenes, but they do not provide a quantitative measure of the extent of this reaction as is obtained from our studies.

Regioselectivity in nucleophilic trapping

A striking feature of the nitration of 4-substituted toluenes is the change in the preference for 1,2 versus 1,4 adduct formation with change in the 4-substituent. It is known that formation of the adduct is subject to kinetic control (30) and thus it is the energetics of the transition states for trapping of the *ipso* cation that determine the preferred adduct. It is plausible that the greater formation of 1,2 adduct in the case of *p-tert*-butyltoluene is the consequence of a steric effect since in the series of 4-alkyltoluenes (alkyl = Me, Et, i-Pr, *t*-Bu) it is only in the last case that 1,2 adduct is obtained and the alkyl groups should have very similar electronic effects, but markedly different steric effects. However, the same explanation cannot be invoked to account for the formation of 1,2 adduct in the cases of the other substituents since none of these should have a large steric effect and most should be more similar to methyl than to *tert*-butyl. On the other hand, it is not apparent that an explanation can be found in terms of the electronic effects of the 4-substituents since, in terms of inductive effects as measured by σ_I (31), the order of electron-donating ability is Me > OMe > Br > Cl > F and, in terms of resonance effects (σ^+_R (31)) OMe > F > Cl > Br > Me. Neither order, nor the order of the sums, groups fluoro with methyl and accounts for the fact that these substituents promote 1,4 adduct formation.

Ab initio molecular orbital calculations carried out by Birch *et al.* indicate that the 4-substituted 1,2-dihydrobenzene is of lower energy than the 4-substituted 1,4-dihydrobenzene over a range of substituents (32). This supports the conclusion that adduct formation is subject to kinetic control since under equilibrium conditions the 1,2 adduct should be favoured for all substituents. The 1,4 adducts from those 4-substituted toluenes in which the substituent is a nucleofuge should undergo a facile elimination of this group as an acetyl derivative to form the dienone directly. However, dienone formation was not observed except in the case of 4-fluorotoluene. Thus the absence of the 1,4 adduct in the products from other 4-substituted toluenes cannot be attributed to its conversion to the dienone.

Experimental

Melting points are uncorrected and were determined on a Büchi SMP-20 melting point apparatus. Infrared spectra, calibrated with polystyrene, were recorded on a Perkin Elmer 283 spectrometer. Observations were made on potassium bromide discs for solids and on thin films between sodium chloride plates for liquids. Proton nuclear magnetic resonance spectra were recorded on Perkin Elmer R-12B (60 MHz), Perkin Elmer R-32 (90 MHz), or Brüker WM 250 (250 MHz) spectrometers. The nmr spectra of nitration reaction mixtures were recorded with the acetic anhydride peak at 2.15 ppm as the lock signal. For all other solutions either tetramethylsilane (90 MHz) or the solvent deuterium signal (250 MHz) was used as the lock signal. The ^{13}C nmr spectra were obtained with a Nicolet TT-14 spectrometer (15.1 MHz) or the Brüker WM 250 spectrometer (62.9 MHz), using solutions in $CDCl_3$ with TMS as the internal standard. Ultraviolet spectra were recorded on a Beckman DU-8 spectrophotometer using methanol or methylene chloride as solvent. For high performance liquid chromatography (hplc) a Varian 5000 liquid chromatograph (analytical) and a Waters Prep LC system (preparative) were used. Elemental analysis was performed by Canadian Microanalytical Service Ltd., Vancouver, British Columbia.

4-Chlorotoluene and *p*-methylanisole were from Eastman. 4-Fluorotoluene was from Aldrich. 4-Iodotoluene was from ICN Pharmaceuticals. *p*-Acetotoluidide (4-acetamidotoluene) was prepared from *p*-toluidine (J. T. Baker), and *N*-methyl-*p*-acetotoluidide (4-(*N*-methylacetamido)toluene) from *N*-methyl-*p*-toluidine (Eastman), following Vogel's procedure for acetanilide (33).

Acetic anhydride was certified ACS from Fisher. Trifluoroacetic anhydride was Aldrich gold label (99 + %). Fuming nitric acid (Fisher, 300 cm^3) was purified by distilling from urea (10 g) and sulphuric acid (500 cm^3) at below 40°C and stored at −25°C.

Solvents for chromatography including pentane (reagent, Fisher), ether (Fisher), and petroleum ether (reagent, Fisher) were dried over sodium and distilled before use. Silica gel (60–200 mesh, Davison Commercial grade H), neutral alumina (Brockman Activity I), and alumina (80–200 mesh, Fisher) deactivated with 3% (v/v) distilled water were used for chromatography. Anhydrous magnesium sulphate was used to dry solutions in organic solvents.

Nitration of 4-chlorotoluene

A nitrating mixture was prepared by the careful addition of acetic anhydride (75 g, 0.75 mmol), with stirring, to freshly distilled nitric acid (18.9 g, 0.3 mmol) at −78°C. The mixture was then warmed to 0°C, stirred for 15 min at 0°C, and cooled to −40°C. Trifluoroacetic anhydride (20.8 g, 0.15 mmol) was then slowly added to the mixture at −40°C. A solution of 4-chlorotoluene (18.99 g, 0.15 mol) in acetic anhydride (15 g, 0.15 mol) was added dropwise over 30 min to the stirred nitrating mixture at −40°C. Stirring was continued for 1 h at −40°C and the mixture was then cooled to −78°C and poured into ether (80 cm^3) at −78°C. Ammonium hydroxide (450 cm^3, 28%) was added in small portions to the stirred mixture and stirring was continued for an additional 1 h while the mixture warmed to ambient temperature. The ether layer was separated and the residue was washed with ether (400 cm^3). The combined ether solution was washed with cold water (4 × 300 cm^3) and dried. Removal of ether on the rotovapor at 15°C yielded a brown oil (31 g). The ^1H nmr spectrum of the crude mixture indicated the presence of (*Z*)-3-chloro-6-methyl-6-nitrocyclohexa-2,4-dienyl acetate (**2**) (70%), 4-chloro-3-nitrotoluene (13%), and 4-chloro-2-nitrotoluene (17%). Crystallization from ether–pentane (500 cm^3, 1:4) at −20°C afforded crude **2** (12 g), which on recrystallization gave colorless crystals, mp 49–50°C; ir (KBr): 1740 and 1230 ($OCOCH_3$), 1555 and 1375 (NO_2) cm^{-1}; uv (CH_3OH): 263 nm (390 m^2 mol^{-1}); ^1H nmr (250 MHz, $CDCl_3$): Table 3; ^{13}C nmr ($CDCl_3$, 62.9 MHz): Table 2. *Anal.* calcd. for $C_9H_{10}NO_4Cl$: C 46.61, H 4.29, N 5.92; found: C 46.67, H 4.35, N 6.05.

Nitration of 4-fluorotoluene

4-Fluorotoluene (12.4 g, 0.13 mol) was nitrated in a mixture of acetic anhydride (0.55 mol), trifluoroacetic anhydride (0.05 mol), and nitric acid (0.20 mol) following the general procedure described for 4-chlorotoluene. The ^1H nmr spectrum of the reaction mixture showed it to be a mixture of 1,4 diene (81%), 1,2 diene (8%), and 4-methyl-4-nitrocyclohexadienone (11%). On work-up a red-yellow oil was obtained, which contained 1,4 diene (73%), 1,2 diene (8%), and dienone (19%); hplc of the oil with 70% ether-pentane eluent gave a mixture of dienes (17.9 g) in the first fraction and the dienone (2.66 g) in the second. The ratio of 1,4 to 1,2 diene was 9:1. Further chromatography of the diene mixture using 50% ether–pentane as solvent gave a mixture of 1,2 and 1,4 dienes in the first fraction and (*Z*)-1-fluoro-4-methyl-4-nitrocyclohexa-2,5-dienyl acetate (**7***b*) (8.9 g, 32% yield) in the second. Diene **7***b* was isolated as a red oil and had uv (CH_2Cl_2): 269 nm (28 m^2 mol^{-1}); ir (film) 1765 and 1220 ($OCOCH_3$), 1550 and 1365 (NO_2) cm^{-1}; ^1H nmr (270 MHz, $CDCl_3$) δ: 1.81 (s, 3, 4-C*H*$_3$), 2.08 (s, 3, OCOC*H*$_3$), 6.34 (dd, 2, 2-*H* and 6-*H*), 6.49 (dd, 2, 3-*H* and 5-*H*) ppm, J_{23} = 10.5, $J_{2,1\text{-F}}$ = 5.0, $J_{3,1\text{-F}}$ = 0.7 Hz; ^{13}C nmr (15.1 MHz, $CDCl_3$, 0°C) δ_C: 21.7 (OCO*C*H$_3$), 25.4 (J_{CF} = 3.7 Hz, 4-*C*H$_3$), 83.2 (J_{CF} = 3.7 Hz, *C*-4), 102.6 (J_{CF} =

206.4 Hz, *C*-1), 126.1 (J_{CF} = 27.4 Hz, *C*-2, *C*-6), 132.2 (J_{CF} = 9.8 Hz, *C*-3, *C*-5), 167 (J_{CF} = 1.8 Hz, O*C*OCH$_3$) ppm.

The mixture of dienes was triturated with a solution of 25% ether–pentane and gave crystals of (*E*)-1-fluoro-4-methyl-4-nitrocyclohexa-2,5-dienyl acetate (**7***a*) (1.1 g, 4% yield). On recrystallization from ether–pentane **7***a* had mp 45–47°C; uv (CH_2Cl_2): 280 nm (8 m^2 mol^{-1}); ir (KBr): 1750 and 1210 (OCOCH$_3$), 1555 and 1350 (NO_2) cm^{-1}; ^{1}H nmr ($CDCl_3$, 0°C) δ: 1.81 (s, 3, 4-C*H*$_3$), 2.09 (s, 3, OCOC*H*$_3$), 6.49 (d, 4, 2-*H*, 3-*H*, 5-*H*, 6-*H*) ppm, J_{23} = 10 Hz, $J_{2\text{-H,F}}$ = 4 Hz, the coupling constants were determined after addition of the shift reagent Eu(fod)$_3$ to separate the chemical shifts of the overlapping peaks. Diene **7***a* readily decomposed to 4-methyl-4-nitrocyclohexadienone.

The solution from the trituration contained a mixture of equal amounts of 1,2 diene and 1,4 diene. The mixture was chromatographed using 25% ether–pentane as solvent. The first fraction contained the 1,2 diene and 4-methyl-2-nitrophenol (a decomposition product via the dienone). 3-Fluoro-6-methyl-6-nitrocyclohexa-2,4-dienyl acetate (**3**) was crystallized from the mixture. Recrystallization from ether–pentane gave colourless crystals, mp 45.5–47°C, uv (CH_2Cl_2): 256.5 nm (394 m^2 mol^{-1}); ir (KBr): 1745 and 1230 (OCOCH$_3$), 1555 and 1375 (NO_2) cm^{-1}; ^{1}H nmr (270 MHz, $CDCl_3$) δ: 1.82 (s, 3, 6-C*H*$_3$), 1.98 (s, 3, OCOC*H*$_3$), 5.57 (m, 2, 1-*H* and 2-*H*), 6.03 (ddd, 1, 4-*H*), 6.64 (ddd, 1, 5-*H*) ppm, J_{12} = 6, J_{15} = 1, $J_{1,3\text{-F}}$ = 5, J_{24} = 2, $J_{2,3\text{-F}}$ = 6, J_{45} = 10.5, $J_{4,3\text{-F}}$ = 6, $J_{5,3\text{-F}}$ = 5 Hz, addition of the shift reagent separated the overlapping peaks at 5.57 ppm and allowed the determination of the coupling constants between the 1-H, 2-H and 3-F; ^{13}C nmr (15.1 MHz, $CDCl_3$, 0°C) δ$_C$: 20.9 (OCO*C*H$_3$), 23.4 (6-*C*H$_3$), 73.1 (J_{CF} = 12.6 Hz, *C*-1), 87.9 (*C*-6), 98.2 (J_{CF} = 19.5 Hz, *C*-2), 120.1 (J_{CF} = 37.1 Hz, *C*-4), 131.5 (J_{CF} = 9.9 Hz, *C*-5), 159.4 (J_{CF} = 259.7 Hz, C-3), 169.4 (O*C*OCH$_3$) ppm. *Anal.* calcd. for $C_9H_{10}NO_4F$: C 50.24, H 4.68, N 6.51; found: C 50.58, H 4.69, N 6.45.

Nitration of 4-methylanisole

A solution of 4-methylanisole (54.6 g, 0.445 mol) in acetic anhydride (45.4 g, 0.445 mol) was added dropwise with stirring at −40°C over 30 min to a nitrating mixture prepared from nitric acid (56 g, 0.89 mol) and acetic anhydride (182 g, 1.78 mol). After complete addition, the mixture was stirred for 30 min at −40°C, then transferred into a three-necked 3-dm^3 round-bottom flask fitted with a mechanical stirrer, a low temperature thermometer, and an ammonia condenser, and containing 1.5 dm^3 ether at −78°C. Ammonia was condensed into the mixture until the temperature, which had risen to −60°C, fell again to −78°C. The mixture was then alkaline to litmus. Excess ammonia was removed on the aspirator while the temperature rose to 0°C over a period of 60 min. The mixture was then neutral to litmus. The ether layer was decanted into a separating funnel and the residue was washed with more ether (750 cm^3). The combined ether solution was washed with cold water (4 × 500 cm^3) and dried. Removal of the ether at 15°C yielded a reddish brown oil (80 g). The ^{1}H nmr spectrum of this mixture showed the composition as (*Z*)-3-methoxy-6-methyl-6-nitrocyclohexa-2,4-dienyl acetate (**4**) (30%) and 4-methyl-2-nitroanisole (70%). Crystallization from ether–pentane mixture at −20°C afforded, in three successive crops, crude diene **4** (26 g). On recrystallization, colorless crystals of **4** were obtained, mp 101.5–103.5°C; ir (KBr): 1735 and 1235 (OCOCH$_3$), 1545 and 1370 (NO_2), 1450 (OCH$_3$) cm^{-1}; uv (CH_2Cl_2): 271.3 nm (290 m^2 mol^{-1}); ^{1}H nmr ($CDCl_3$, 250 MHz): Table 3; ^{13}C nmr ($CDCl_3$, 62.9 MHz): Table 2. *Anal.* calcd. for $C_{10}H_{13}NO_5$: C 52.86, H 5.77, N 6.16; found: C 53.00, H 5.94, N 6.14.

Nitration of 4-acetamidotoluene

Finely powdered 4-acetamidotoluene (1.49 g, 10 mmol) was added to a nitrating mixture prepared from nitric acid (3.15 g, 50 mmol), acetic anhydride (15 g, 150 mmol), and trifluoroacetic anhydride (2.1 g, 10 mmol) at −40°C. The mixture was stirred at −40°C for 2 h, cooled to −78°C, and added to ether (500 cm^3) at −78°C. Ammonium hydroxide (100 cm^3, 28%) was added slowly, with stirring, and stirring was continued for an additional 2 h at −78°C. The ether layer was decanted and stored at −78°C. The residue was dissolved in cold water (250 cm^3), transferred to a separating funnel containing ether previously cooled to −20°C, and extracted. The combined ether solution was quickly washed with cold brine (4 × 250 cm^3), dried at −78°C, and filtered, through a jacketed filtering funnel maintained at −78°C, into a 1-dm^3 round-bottom flask cooled to −78°C. The ether was removed on a rotovapor connected to a high vacuum pump via a Dry Ice condenser followed by three liquid nitrogen traps. The evaporation flask was maintained at −40°C. The ^{1}H nmr spectrum of the yellow residue (2 g), taken at −40°C, indicated the presence of (*Z*)-3-acetamido-6-methyl-6-nitrocyclohexa-2,4-dienyl acetate (**5**) (35%) and 4-methyl-2-nitroacetanilide (65%). The mixture was chromatographed on activated silica gel (mesh size 60–200, 75 g) contained in a jacketed filtering funnel cooled to −78°C. Solvent used as eluent was cooled under nitrogen, in a jacketed dropping funnel, to −78°C. All fractions were collected in flasks cooled to −78°C, and evaporated below −40°C. Elution, first with 60% ether – petroleum ether and then with 80% ether – petroleum ether, gave 4-methyl-2-nitroacetanilide, mp 95–96°C (lit. (34) mp 96°C); ^{1}H nmr (250 MHz, $CDCl_3$) δ: 2.22 (s, 3, C*H*$_3$), 2.32 (s, 3, NHCOC*H*$_3$), 7.38 (dd, 1, 5-*H*), 7.92 (d, 1, 3-*H*), 8.54 (d, 1, 6-*H*), 10.12 (s, 1, N*H*) ppm, J_{35} = 1.85, J_{56} = 8.70 Hz; ^{13}C nmr (62.9 MHz, $CDCl_3$) δ$_C$: 20.5 (*C*H$_3$), 25.5 (NHCO*C*H$_3$), 122.2 (*C*-6), 125.5 (*C*-3), 132.5 (*C*-4), 133.5 (*C*-1), 136.4 (*C*-2), 136.8 (*C*-5), 168.9 (NH*C*OCH$_3$). The 90% ether – petroleum ether fraction contained 30% of the nitrotoluidide and 70% of **5**. The mixture (500 mg) was rechromatographed on silica gel (75 g) under the same conditions. Pure diene **5** was eluted in the 100% ether fraction and was characterized by nmr, Tables 2 and 3.

Nitration of other substrates

4-Iodotoluene was nitrated under conditions similar to those used for 4-chlorotoluene. The substrate was insoluble in acetic anhydride at −40°C. At 0°C 4-nitrotoluene was the major product but other substitution products were also apparent in the nmr. Iodine was present in the solution. When the reaction was carried out using methylene chloride to dissolve the iodotoluene, some small peaks were present in the diene region of the spectrum in addition to the peaks of the aromatic nitro products.

4-(*N*-methylacetamido)toluene was nitrated with nitric acid in acetic anhydride and trifluoroacetic anhydride at −40°C. Up to 30% of diene was observed by nmr, in addition to substitution product. The diene disappeared when the temperature was raised to 0°C. The diene also did not survive when the reaction mixture at −40°C was worked up.

4-(*N*,*N*-dimethylamino)toluene was nitrated at −40°C in acetic anhydride containing 1 mol proportion of nitric acid. Only substitution product was formed.

4-Methylphenyl acetate was nitrated with nitric acid in acetic anhydride at −40°C and also at −60°C but only 4-methyl-4-nitrocyclohexa-2,5-dienone was observed.

N-methyl-*p*-toluidine was reacted with nitric acid in acetic anhydride at −40°C but only acetylation occurred.

Acknowledgements

We thank Dr. Orson Chan for the 270-MHz nmr spectrum, the Natural Sciences and Engineering Research Council of Canada for financial support, and the University of Victoria for the award of a Fellowship (to S.R.M.).

1. G. W. Bushnell, A. Fischer, G. N. Henderson, and S. Ray Mahasay. Can. J. Chem. Accepted for publication.
2. A. Fischer, D. L. Fyles, and G. N. Henderson. J. Chem. Soc. Chem. Commun. 513 (1980).
3. D. J. Blackstock, A. Fischer, K. E. Richards, J. Vaughan, and G. J. Wright. Chem. Commun. 641 (1970).
4. A. Fischer, G. N. Henderson, and L. M. Iyer. Can. J. Chem. **63**, 2390 (1985).
5. D. J. Blackstock, J. R. Cretney, A. Fischer, M. P. Hartshorn, K. E. Richards, J. Vaughan, and G. J. Wright. Tetrahedron Lett. 2793 (1970).
6. A. Fischer and J. N. Ramsay. J. Am. Chem. Soc. **96**, 1614 (1974).

7. A. FISCHER and R. RÖDERER. Can. J. Chem. **54**, 423 (1976).
8. A. FISCHER and D. R. A. LEONARD. Can. J. Chem. **54**, 1795 (1976).
9. A. FISCHER and K. C. TEO. Can. J. Chem. **56**, 258 (1978).
10. A. FISCHER, G. N. HENDERSON, and R. J. THOMPSON. Aust. J. Chem. **31**, 1241 (1978).
11. A. FISCHER and K. C. TEO. Can. J. Chem. **56**, 1758 (1978).
12. A. FISCHER and R. RÖDERER. Can. J. Chem. **54**, 3978 (1976).
13. A. H. CLEMENS, M. P. HARTSHORN, K. E. RICHARDS, and G. J. WRIGHT. Aust. J. Chem. **30**, 103,(1977).
14. C. E. BARNES, K. S. FELDMAN, M. W. JOHNSON, H. W. H. LEE, and P. C. MYHRE. J. Org. Chem. **44**, 3925 (1979).
15. C. E. BARNES and P. C. MYHRE. J. Am. Chem. Soc. **100**, 973 (1978).
16. A. FISCHER and G. J. WRIGHT. Aust. J. Chem. **27**, 217 (1974).
17. J. R. KNOWLES, R. O. C. NORMAN, and G. K. RADDA. J. Chem. Soc. 4885 (1960).
18. J. D. ROBERTS, J. K. SANFORD, F. L. J. SIXMA, H. CERFONTAIN, and R. ZAGT. J. Am. Chem. Soc. **76**, 4525 (1954).
19. K. SCHOFIELD. Aromatic nitration. Cambridge University Press, Cambridge. 1980. (*a*) p. 243; (*b*) p. 209; (*c*) pp. 241–248.
20. S. R. HARTSHORN, R. B. MOODIE, and K. SCHOFIELD. J. Chem. Soc. B, 2454 (1971).
21. A. I. SCOTT. Interpretation of the ultraviolet spectra of natural products. Pergamon Press, Oxford. 1964. Chapt. 2.
22. A. FISCHER and J. N. RAMSAY. J. Chem. Soc. Perkin Trans. 2, 237 (1973).
23. H. KESSLER. Angew. Chem. Int. Ed. Engl. **9**, 219 (1970).
24. D. W. BROWN. J. Chem. Educ. **62**, 209 (1985).
25. R. J. ABRAHAM and P. LOFTUS. Proton and carbon-13 nmr spectroscopy. Heyden, London. 1978. p. 28.
26. A. FISCHER and S. S. SEYAN. Can. J. Chem. **56**, 1348 (1978).
27. R. G. COOMBES, D. H. G. CROUT, J. G. HOGGETT, R. B. MOODIE, and K. SCHOFIELD. J. Chem. Soc. B, 347 (1970).
28. J. W. BARNETT, R. B. MOODIE, K. SCHOFIELD, and J. B. WESTON. J. Chem. Soc. Perkin Trans. 2, 248 (1977).
29. R. B. MOODIE, K. SCHOFIELD, and J. B. WESTON. J. Chem. Soc. Perkin Trans 2, 1089 (1980).
30. A. FISCHER and G. N. HENDERSON. Can. J. Chem. **59**, 2314 (1981).
31. S. EHRENSON, R. T. C. BROWNLEE, and R. W. TAFT. *In* Progress in physical organic chemistry. Vol. 10. *Edited by* A. Streitweiser, Jr. and R. W. Taft. Interscience, New York, NY. 1973. p. 1.
32. A. J. BIRCH, A. L. HINDE, and L. RADOM. J. Am. Chem. Soc. **103**, 284 (1981).
33. A. I. VOGEL. Practical organic chemistry. 4th ed. Longmans, London. 1978. p. 684.
34. P. BOUCHET, G. JONCHERAY, R. JACQUIER, and J. ELGUERO. J. Heterocycl. Chem. **15**, 625 (1978).

Substrates for the differentiation of the *N*-acetylglucosaminyltransferases. Synthesis of βDGlcNAc(1→2)αDMan(1→6)βDMan and βDGlcNAc(1→2)αDMan(1→6)[αDMan(1→3)]βDMan glycosides

S. Hasan Tahir and Ole Hindsgaul[1]

Department of Chemistry, University of Alberta, Edmonton, Alta., Canada T6G 2G2

Received February 14, 1986

S. Hasan Tahir and Ole Hindsgaul. Can. J. Chem. **64**, 1771 (1986).

The trisaccharide βDGlcNAc(1→2)αDMan(1→6)βDMan (**2**) and the tetrasaccharide βDGlcNAc(1→2)αDMan(1→6)[αDMan(1→3)]βDMan (**3**) have been chemically synthesized as their 8-methoxycarbonyloctyl glycosides. Compounds **2** and **3**, both partial structures of naturally occurring asparagine linked oligosaccharides, are designed to function as selective substrates in *N*-acetylglucosaminyltransferase assays.

S. Hasan Tahir and Ole Hindsgaul. Can. J. Chem. **64**, 1771 (1986).

Faisant appel à des méthodes chimiques, on a synthétisé le trisaccharide β-DGlcNAc(1→2)αDMan(1→6)βDMan **2** ainsi que le tétrasaccharide β-DGlcNAc(1→2)αDMan(1→6)[αDMan(1→3)]βDMan **3**, tous les deux sous la forme de leur glycosides méthoxycarbonyl-8 octyles. Les composés **2** et **3**, qui sont des fractions d'asparagine qui l'on retrouve naturellement liée à des oligosaccharides, ont été préparés pour servir de substrats sélectifs dans des études sur la *N*-acétylglucosaminyltransférase.

[Traduit par la revue]

Introduction

About ten years ago, evidence began to accumulate that the carbohydrate structures of cell-surface glycoproteins and glycolipids became dramatically altered during both normal and abnormal cellular development (1–4). Consistent changes in cell-surface carbohydrate structures have now been shown to accompany the development of human melanoma, neuroblastoma, and colorectal, gastric, and pancreatic carcinoma (5). The occurrence of large fucosylated highly-branched glycopeptides is in fact one of the most reproducible correlates with the malignant transformation of cells (6). The functional significance, if any, of these cell-surface structural changes is not at all clear but these aberrant carbohydrate structures are attracting a great deal of clinical interest as potential tumor markers. The structures of many of these "tumor-associated" carbohydrates have been elucidated in recent years and major research efforts have gone into the production of the corresponding tumor-specific monoclonal antibodies (4, 7).

In 1984 Yamashita *et al.* (6) compared the carbohydrate structures of the membrane N-linked glycoproteins of baby hamster kidney (BHK) cells and their polyoma transformant (Py-BHK). They found that while the transformed cells synthesized the same (approximately 20) structures as did the normal cells, they produced more of the larger, more highly branched oligosaccharides. They proposed that the changes in the relative proportions of the cell-surface oligosaccharides observed on transformation could be explained by the elevation in the activity of a single enzyme, a glycosyltransferase, termed *N*-acetyl-β-D-glucosaminyltransferase V (GlcNAc-transferase V, GnT V), and subsequently showed (8) that the GnT V activity in Py-BHK cells was in fact elevated two-fold when compared with untransformed cells. This work (6, 8) therefore suggests that the activity of a single glycosyltransferase can, in itself, serve as a tumor marker. The detection of a change in a single specific enzymatic activity may be far simpler than the characterization and quantification of a highly heterogeneous mixture of cell-surface carbohydrate structures produced *as a result* of this single enzymatic change.

At least 7 different GlcNAc-transferases are known to be involved in the biosynthesis of the asparagine-linked oligosaccharides (6, 8–10). All of these enzymes use UDP-GlcNAc as the glycosyl donor and the difference between them lies in their specificity for different acceptor structures. To simplify the assay procedures for measuring these individual glycosyltransferase activities we have embarked on a synthetic program to provide carbohydrate structures that we expect will be substrates for only single preselected enzymes. Such substrates might include oligosaccharides where cross-reacting sugar residues are completely absent or where the interfering hydroxyl groups that might be acted on by other GlcNAc transferases are masked by either *O*-methylation or deoxygenation. This latter approach has recently (11, 12) been successfully applied in the differentiation of two competing α-L-fucosyltransferases in serum. To be truly useful, such substrates and their glycosylated products should also be amenable to simple rapid isolation from the incubation mixtures of cell extracts or fluids that contain the glycosyltransferase activities being assayed.

To test the practicability of this approach we chose to attempt the preparation of substrates selective for GnT V, since this glycosyltransferase is already attracting interest as a potential tumor marker. The heptasaccharide **1** (Fig. 1) is known to be a substrate for GnT V (as well as for other glycosyltransferases) and has been used to assay this enzyme. Recent work (13–17), from the laboratory of Lemieux, on the molecular basis for the binding of oligosaccharides by monoclonal antibodies and lectins strongly suggested that proteins were not likely to require carbohydrate surfaces much larger than that of a trisaccharide for faithful recognition. We expected that this situation might also hold true for the enzymatic specificity of glycosyltransferases and therefore envisioned the trisaccharide βDGlcNAc(1→2)αDMan(1→6)βDManOR (**2**) as a likely acceptor for GnT V. Our rationale for the choice of **2** can be seen in Fig. 1 where the structure of the natural heptasaccharide acceptor **1** is also shown. We set forth, therefore, to synthesize **2**, which contains the reactive target hydroxyl group acted on by the enzyme and one sugar residue on either side of the α-D-mannose residue bearing this hydroxyl group. Since we did not know whether this structure incorporated sufficient features for recognition by GnT V, the synthesis was planned in a way that also allowed the preparation of the tetrasaccharide **3**, which is closer in structure

[1]Author to whom correspondence may be addressed.

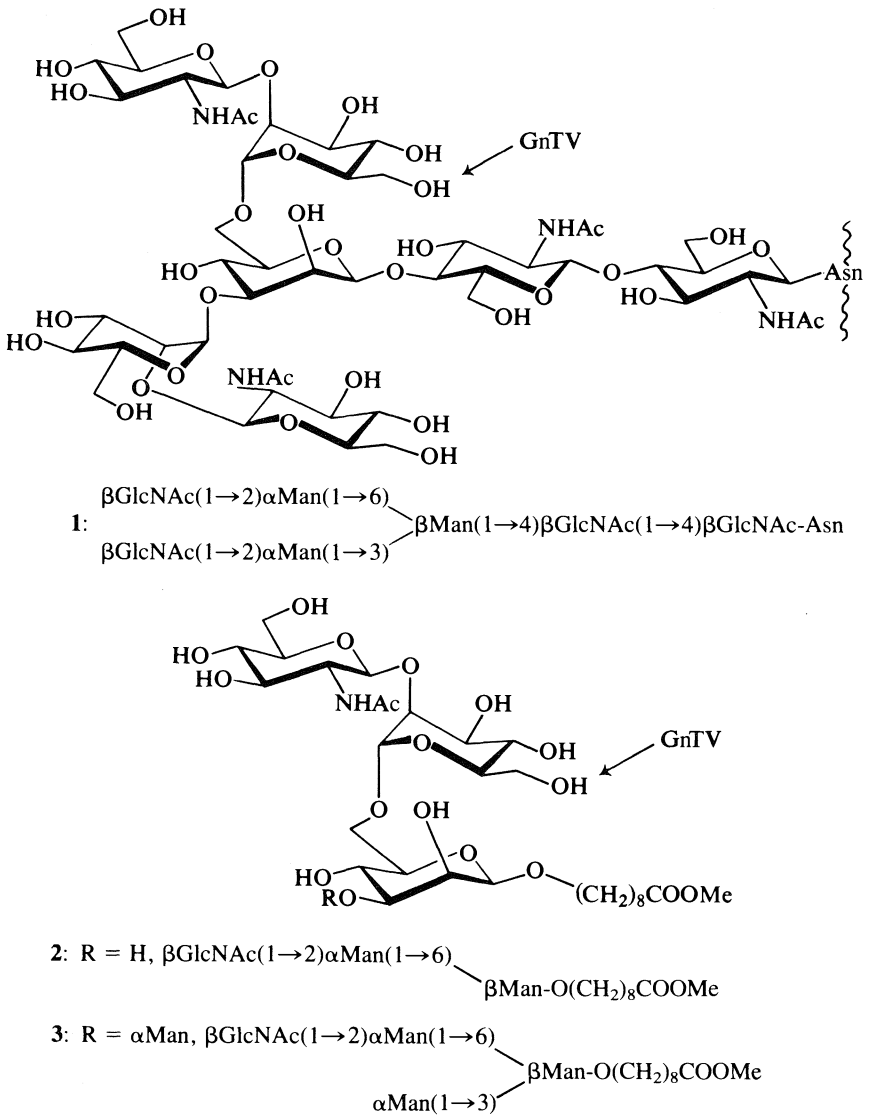

FIG. 1. A heptasaccharide acceptor (**1**) for GlcNAc-transferase V (GnT V) compared with the structures of the proposed synthetic acceptors **2** and **3**. The bold arrows show the primary hydroxyl group to which GnT V transfers an *N*-acetyl-β-D-glucosaminyl residue.

to the natural acceptor **1**. To facilitate the isolation of our glycosylated substrates from their enzymatic incubation mixtures, we elected to prepare **2** and **3** as their 8-methoxycarbonyloctyl glycosides (18), since inclusion of this hydrophobic group should facilitate adsorption on reverse phase (C-18) chromatography supports. This "linking arm" might also be used for the preparation of synthetic glycoconjugates.

Results and discussion

A retrosynthetic analysis of the target structures **2** and **3** suggested, as the key intermediate, the trisaccharide precursor **4**, which was protected in a manner to allow the selective liberation of the hydroxyl group at C-3 of the β-D-mannopyranosyl residue for subsequent glycosylation by **5**. A straightforward route to **4** from the glycosyl bromides **6**, **7**, and **8** was then apparent. Compounds **5** (19), **6** (20), and **7** (21) have already been described. A synthetic route to **8** was therefore required.

Methyl 4,6-*O*-benzylidene-α-D-mannopyranoside (**9**) was selectively allylated (22), via its 2,3-*O*-dibutylstannylidene derivative, to provide the 3-*O*-allyl derivative **10** in 82% yield. Benzylation of **10** then furnished the 2-*O*-benzyl derivative **11** in 90% yield. Reductive cleavage of the benzylidene group in **11** using $LiAlH_4$–$AlCl_3$, according to Liptak *et al.* (23), gave the 4-*O*-benzyl (**12**) and 6-*O*-benzyl (**13**) derivatives, in the ratio of 7:1, in a combined yield of 86%. Reaction of **12** with acetic anhydride in pyridine provided the 6-*O*-acetyl derivative **14**, which was acetolyzed (24) using acetic anhydride in the presence of a catalytic amount of sulfuric acid to afford 1,6-di-*O*-acetyl-3-*O*-allyl-2,4-di-*O*-benzyl-α-D-mannopyranose (**15**) in 77% yield.

Reaction of the diacetate **15** in dichloromethane, at 0°C, with hydrogen bromide that was dried by passage through a calcium sulfate column led to the formation of the glycosyl bromide **8** in essentially quantitative yield. When **15** was allowed to react with HBr gas introduced directly from the cylinder without passage through calcium sulfate, the thin-layer chromatogram (tlc) of the reaction mixture showed the presence of two products, the minor being the desired bromide **8**. The major product **16** had a slightly lower mobility in tlc. The ^1H nmr spectrum of the mixture of **8** and **16** indicated **16** to be the

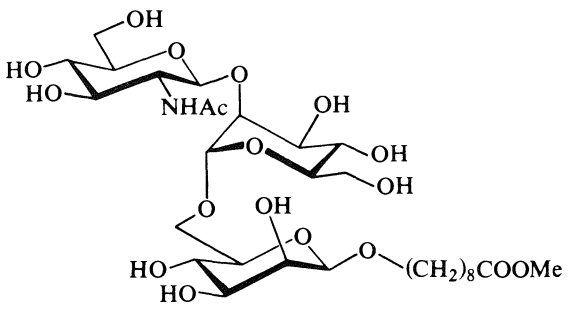

2

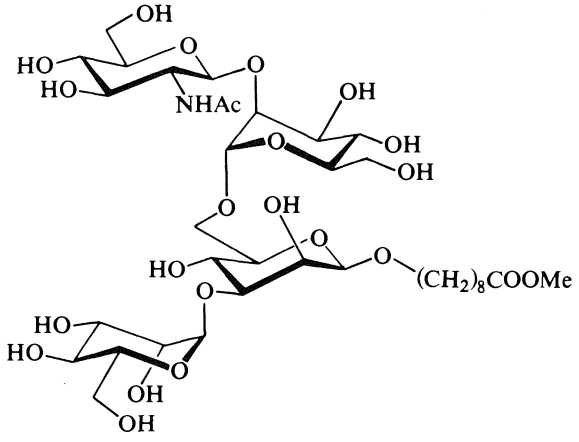

3

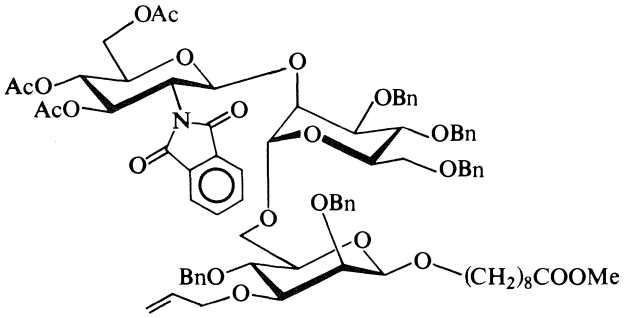

4

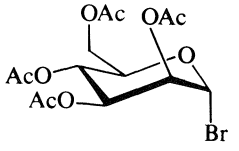

5

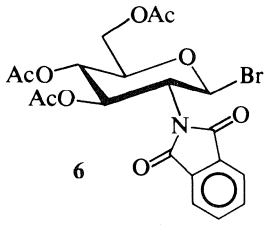

6

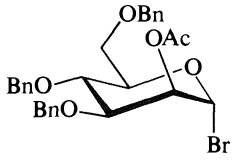

7

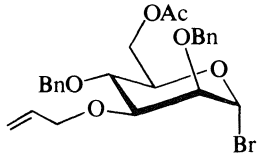

8

hydrobromination product of **8**, namely, 6-*O*-acetyl-2,4-di-*O*-benzyl-3-*O*-(3-bromopropyl)-α-D-mannopyranosyl bromide. This structural assignment was made to account for the observation of a triplet for two protons at δ 3.688 ($BrCH_2CH_2CH_2O$), a multiplet for two protons at δ 3.510 for $BrCH_2CH_2CH_2O$, and a two-proton multiplet at δ 2.119 for $BrCH_2CH_2CH_2O$. The ratio of **16** to **8** was determined to be 4:1 from this ^1H nmr spectrum.

Reaction of the glycosyl bromide **8** and 8-methoxycarbonyl-octanol according to Paulsen and Lockhoff (25), in the presence of an insoluble catalyst prepared by precipitation of silver silicate on aluminum oxide, provided a mixture of the β and α mannosides **17** (50–60%), which could not be separated chromatographically. That **17** was a mixture of the α and β glycosides was evident from the ^1H nmr spectrum, which showed a signal at δ 4.365 for H-1 of the β anomer and a doublet ($J_{1,2}$ = 2.0 Hz) at δ 4.824 for H-1 of the corresponding α anomer. The β:α ratio of this mixture, determined by integration of these signals in the ^1H nmr spectrum of **17**, was found to vary with the temperature of the reaction. At −78°C, the β and α anomers were produced in a 6:1 ratio, while at the higher temperatures of −20 and 0°C the ratios of β to α anomers were 4.3:1 and 3.5:1 respectively.

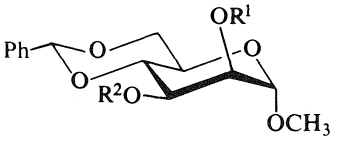

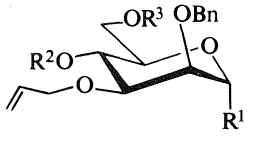

9 R^1 = H, R^2 = H
10 R^1 = H, R^2 = CH_2CHCH_2
11 R^1 = Bn, R^2 = CH_2CHCH_2
12 R^1 = OCH_3, R^2 = Bn, R^3 = H
13 R^1 = OCH_3, R^2 = H, R^3 = Bn
14 R^1 = OCH_3, R^2 = Bn, R^3 = Ac
15 R^1 = OAc, R^2 = Bn, R^3 = Ac
8 R^1 = Br, R^2 = Bn, R^3 = Ac

Treatment of the α/β mixture **17** with sodium methoxide in methanol effected the removal of the acetyl groups to provide **18**(β) and **19**(α), which could now be separated by column chromatography on silver nitrate impregnated silica gel. The ^{13}C nmr spectrum of the β glycoside **18** showed the signal for C-1 at 101.69 ppm ($J_{C\text{-}1,H\text{-}1}$ = 153.6 Hz) while the corresponding α anomer **19** showed C-1 at 98.25 ppm ($J_{C\text{-}1,H\text{-}1}$ = 168.2 Hz), in accord with the empirical rules formulated by

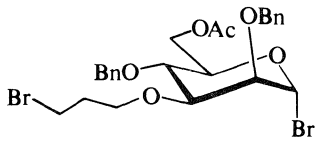

16

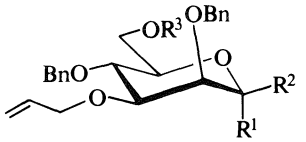

17(β) R^1 = H, R^2 = $O(CH_2)_8COOCH_3$, R^3 = Ac
17(α) R^1 = $O(CH_2)_8COOCH_3$, R^2 = H, R^3 = Ac
18(β) R^1 = H, R^2 = $O(CH_2)_8COOCH_3$, R^3 = H
19(α) R^1 = $O(CH_2)_8COOCH_3$, R^2 = H, R^3 = H

Bock and Pedersen (26) for the dependence of the one-bond C—H coupling on the anomeric configuration of pyranosides.

Condensation of the alcohol **18** and 2-*O*-acetyl-3,4,6-tri-*O*-benzyl-α-D-mannopyranosyl bromide (21) (**7**) using mercuric bromide and mercuric cyanide as promoters and acetonitrile as solvent furnished the α-linked disaccharide **20** in 77% yield. The resonances for both anomeric protons were observed in the ^{1}H nmr spectrum, at δ 4.911 ($J_{1',2'}$ = 2.0 Hz) and 4.334 ($J_{1,2} \approx 1$ Hz), while the ^{1}H-coupled ^{13}C nmr spectrum showed a doublet each for C-1 and C-1′ at δ 104.64 ($J_{C\text{-}1,H\text{-}1}$ = 154.7 Hz) and 97.77 ($J_{C\text{-}1',H\text{-}1'}$ = 170.4 Hz) respectively. One-bond C—H coupling constants of these magnitudes require the presence of the β and α glycosidic linkages as assigned (26).

Reaction of **20** with sodium methoxide in dry methanol provided the alcohol **21**, which was glycosylated with 3,4,6-tri-*O*-acetyl-2-deoxy-2-phthalimido-β-D-glucopyranosyl bromide (20) (**6**) according to Paulsen *et al.* (27), providing the trisaccharide **4** in 76% yield after chromatographic purification. The anomeric configuration of the newly introduced glycosyl residue was evident from the ^{1}H nmr spectrum of **4**, which showed a doublet at δ 5.573 ($J_{1'',2''}$ = 8.5 Hz) for H-1″. Isomerization of the allyl ether in **4** using tristriphenylphosphinerhodium(I) chloride (28), followed by hydrolysis of the resulting prop-1-enyl ether in the presence of mercuric chloride and mercuric oxide, then afforded the trisaccharide alcohol **22** in 85% yield.

Deacetylation of **22** using sodium methoxide in methanol led to the quantitative formation of **23**. Removal of the phthalimido group from **23**, and subsequent *N*-acetylation of the free amine as described by Bundle and Josephson (29), provided the acetyl derivative **24** in an overall yield of 60%. No evidence of attack at the 8-methoxycarbonyloctyl ester was obtained.

Finally, hydrogenolytic cleavage of the benzyl protecting groups of **24** using 5% palladium-on-charcoal as the catalyst, in 98% ethanol, furnished the target trisaccharide **2**, which was purified by size-exclusion chromatography on Bio-Gel P-2. Compound **2** was obtained as a white lyophilized powder in 85% yield.

Preparation of the tetrasaccharide **3** required the addition of an α-D-mannopyranosyl unit to the free 3-hydroxyl group of **22**, followed by deprotection. Reaction of **22** with 2,3,4,6-tetra-*O*-acetyl-α-D-mannopyranosyl bromide (19) (**5**) promoted by mercuric bromide and mercuric cyanide in dichloromethane, in the presence of 4 Å molecular sieves, gave the tetrasaccharide **25** in 65% yield. The anomeric configuration of the newly introduced mannopyranosyl unit of **34** was evident from its nmr spectra, where the signal for an additional anomeric proton

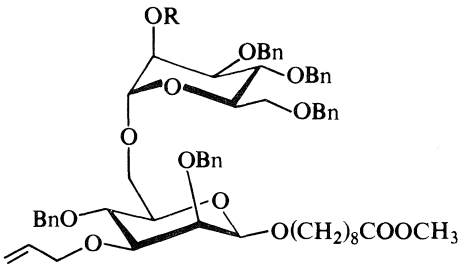

20 R = Ac
21 R = H

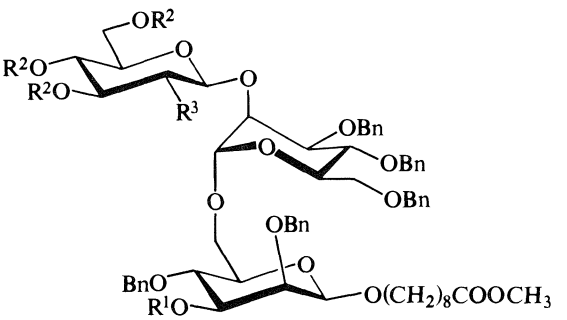

4 R^1 = CH_2CHCH_2, R^2 = Ac, R^3 = NPhth
22 R^1 = H, R^2 = Ac, R^3 = NPhth
23 R^1 = H, R^2 = H, R^3 = NPhth
24 R^1 = H, R^2 = H, R^3 = NHAc

appeared at δ 5.018 ($J_{1',2'} \approx 2$ Hz). The ^{13}C nmr spectrum showed the presence of four anomeric carbons: δ 101.95, $J_{C\text{-}1,H\text{-}1}$ = 152 ± 2 Hz; 97.64, $J_{C\text{-}1'',H\text{-}1''}$ = 170 ± 2 Hz; 96.60, $J_{C\text{-}1''',H\text{-}1'''}$ = 165 ± 2 Hz; and the new signal for the peracetylated α-linked mannose at δ 99.83, $J_{C\text{-}1',H\text{-}1'}$ = 169 ± 2 Hz.

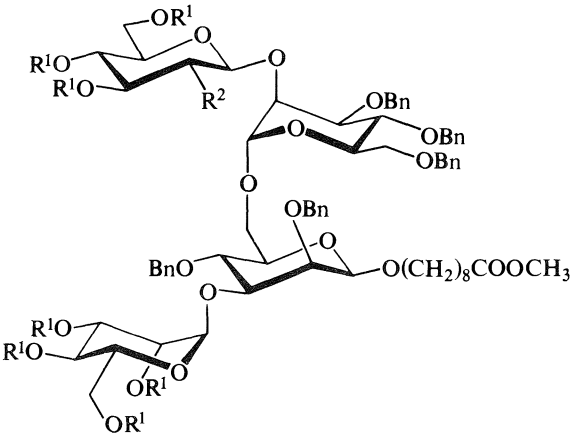

25 R^1 = Ac, R^2 = NPhth
26 R^1 = Ac, R^2 = NHAc

Conversion of **25** to **26** was effected in three steps without characterization of the intermediates involved. Deacetylation of **25** with sodium methoxide in methanol gave a white foam, which was refluxed with hydrazine in methanol to generate the free amine that, on treatment with acetic anhydride in pyridine, gave the peracetylated product **26** in 63% yield. Attempted *N*-acetylation of the intermediate free amine, obtained in the second step of the above sequence using acetic anhydride in methanol–water (1:1), gave a very polar hydroxylated derivative that proved difficult to purify by silica gel chromatography. Removal of the *O*-acetyl and *O*-benzyl protecting groups of **26** was accomplished by treatment with sodium methoxide in

methanol followed by hydrogenolysis over 5% palladium-on-charcoal. Filtration of the crude product through a column of Bio-Gel P-2 afforded the target tetrasaccharide **3** as a white lyophilized powder in a total yield of 85%.

The trisaccharide **2** is indeed an acceptor specific for GlcNAc-transferase V and detects the expected increase in activity of this enzyme on Rous sarcoma transformation of BHK cells. The tetrasaccharide **3** is a substrate for GlcNAc-transferase V and at least one other BHK GlcNAc-transferase. These results will be reported in detail elsewhere.[2]

Experimental

All solvents and reagents used were reagent grade and, in cases where further purification was required, standard procedures (30) were followed. Mercuric bromide was not purified before use. All solid reactants for glycosylation were dried overnight over phosphorus pentaoxide in a high vacuum prior to use. Solution transfers where anhydrous conditions were required were done under nitrogen using standard syringe techniques (31). Molecular sieves were purchased from BDH Chemicals, and the ratio of alcohol to molecular sieves in glycosylation was between 1:5 and 1:10 by weight.

Thin-layer chromatograms (tlc) were performed on precoated silica gel 60-F254 plates (E. Merck, Darmstadt) and visualized by quenching of fluorescence and (or) by charring after spraying with 5% sulfuric acid in ethanol. For flash chromatography (32) 40–63 μm (400–230 mesh) silica gel 60 (E. Merck No. 9385) and distilled solvents were used, and the ratio of silica gel to compound was in the range 50:1–100:1. Solvents were removed on a rotary evaporator under the vacuum of a water aspirator with bath temperatures of 40°C or lower. For gel filtration, Bio-Gel P-2 (200–400 mesh) (Bio-Rad Laboratories, Richmond, California, USA) was used.

Proton nuclear magnetic resonance (^{1}H nmr) spectra were recorded at either 400 MHz (Bruker WH-400) or 360 MHz (Bruker WM-360) with either tetramethylsilane (δ 0 in $CDCl_3$) or acetone (δ 2.225 in D_2O) as internal standard at ambient temperature. Carbon-13 nuclear magnetic resonance (^{13}C nmr) spectra were recorded at either 100.62 MHz (Bruker WH-400) or 90.56 MHz (Bruker WM-360) with either external tetramethylsilane (δ 0 in $CDCl_3$) or external 1,4-dioxane (δ 67.4 in D_2O) as reference standard. ^{1}H chemical shifts and coupling constants are reported as if they were first order. Assignments of ^{13}C resonances are tentative. Optical rotations were determined on a Perkin–Elmer 241 polarimeter in a 1-dm cell at ambient temperature (23 ± 1°C).

Protons of the allyl group present in the compounds described in this work were designated as H_a, H_b, H_c, H_d, and H_e as defined below. These protons generally showed the same coupling constants and thus the same multiplicity pattern in all the compounds examined and only the chemical shifts varied. The observed coupling constants were:

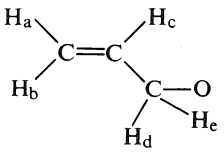

H_a, dddd, $J_{a,c}$ = 10.5 Hz, $J_{a,d}$ = 1.5 ± 0.5 Hz, $J_{a,e}$ = 1.5 ± 0.5 Hz, $J_{a,b}$ = 1.5 ± 0.5 Hz; H_b, dddd, $J_{b,c}$ = 17.0 Hz, $J_{b,d}$ = 1.5 ± 0.5 Hz, $J_{b,e}$ = 1.5 ± 0.5 Hz, $J_{a,b}$ = 1.5 ± 0.5 Hz; H_c, dddd, $J_{b,c}$ = 17.0 Hz, $J_{a,c}$ = 10.5 Hz, $J_{c,d}$ = 5.5 Hz, $J_{c,e}$ = 5.5 Hz; H_d, dddd, $J_{d,e}$ = 13.5 Hz, $J_{c,d}$ = 5.5 Hz, $J_{b,d}$ = 1.5 ± 0.5 Hz, $J_{a,d}$ = 1.5 ± 0.5 Hz; H_e, dddd, $J_{d,e}$ = 13.5 Hz, $J_{c,e}$ = 5.5 Hz, $J_{a,e}$ = 1.5 ± 0.5 Hz, $J_{b,e}$ = 1.5 ± 0.5 Hz.

*Methyl 3-*O*-allyl-2-*O*-benzyl-4,6-*O*-benzylidene-α-*D*-mannopyranoside (**11**)*

To a solution of methyl 3-*O*-allyl-4,6-*O*-benzylidene-α-D-mannopyranoside (22) (**10**) (13.60 g; 42.24 mmol) in dry benzene (500 mL) were added sodium hydride (about 80% dispersion in oil; 2.02 g) and benzyl bromide (7.55 mL; 63.35 mmol). The mixture was refluxed under nitrogen atmosphere for 16 h. After the mixture had cooled to room temperature, the excess of sodium hydride was decomposed by the addition of methanol (250 mL); then water (500 mL) was added. The organic layer was separated, washed with water, dried ($MgSO_4$), filtered, and concentrated. Purification of the major product could be achieved by gradient flash chromatography employing a mixture of hexane and ethyl acetate (the ratio of hexane – ethyl acetate was changed from 50:1 to 2:1 during elution). Finally **11** was obtained as a yellow oil (15.73 g; 90%); $[\alpha]_D$ +33.0° (*c* 1.4, chloroform); R_f 0.35 (hexane – ethyl acetate, 10:1); ^{1}H nmr ($CDCl_3$) δ: 7.505–7.259 (10H, arom.), 5.901 (1H, H_c allyl), 5.609 (s, 1H, $C_6H_5CHO_2$), 5.294 (1H, H_b allyl), 5.146 (1H, H_a allyl), 4.843 (d, 1H, J_{gem} = 12.0 Hz, C_6H_5CHHO), 4.725 (d, 1H, J_{gem} = 12.0 Hz, C_6H_5CHHO), 4.681 (d, 1H, $J_{1,2}$ = 2.0 Hz, H-1), 4.294–4.208 (2H, H_d allyl (δ 4.268) and H-6e (δ 4.244, dd, $J_{6a,6e}$ = 10.5 Hz, $J_{5,6a}$ = 4.5 Hz)), 4.185 (dd, 1H, $J_{6a,6e}$ = 10.0 Hz, $J_{5,6a}$ = 10.0 Hz, H-6a), 4.104 (1H, H_e allyl), 3.885–3.834 (2H, H-3 and H-4), 3.818 (dd, 1H, $J_{2,3}$ = 3.2 Hz, $J_{1,2}$ = 2.0 Hz, H-2), 3.761 (dd, 1H, $J_{4,5}$ = 10.0 Hz, $J_{5,6a}$ = 10.0 Hz, $J_{5,6e}$ = 4.5 Hz, H-5), 3.310 (s, 3H, CH_3O); ^{13}C nmr δ: 138.18, 137.72 (quat. arom.), 135.0 (CH_2=$CHCH_2O$), 128.64, 128.00, 127.87, 127.59, 125.00 (tert. arom.), 116.32 (CH_2=$CHCH_2O$), 101.43, 100.52 (C-1 and $C_6H_5CHO_2$), 79.09 (C-4), 76.47, 76.03 (C-2 and C-3), 73.56 ($C_6H_5CH_2O$), 68.79 (CH_2=$CHCH_2O$), 64.03 (C-6), 54.67 (C-5), 29.57 (CH_3O). *Anal.* calcd. for $C_{24}H_{28}O_6$: C 69.89, H 6.84; found: C 69.67, H 6.94.

*Methyl 3-*O*-allyl-2,4-di-*O*-benzyl-α-*D*-mannopyranoside (**12**) and methyl 3-*O*-allyl-2,6-di-*O*-benzyl-α-*D*-mannopyranoside (**13**)*

To a stirred solution of **11** (14.27 g; 34.59 mmol) in 1:1 diethyl ether – dichloromethane (300 mL) was added, portionwise, $LiAlH_4$ (3.95 g; 103.9 mmol) and the mixture was slowly heated to the boiling point. To the refluxing solution was added $AlCl_3$ (13.85 g; 103.9 mmol) in diethyl ether (150 mL) over a period of 70 min, when tlc indicated the absence of starting material. The mixture was cooled and the excess of $LiAlH_4$ was decomposed with ethyl acetate (75 mL), and $Al(OH)_3$ was precipitated by the addition of water (75 mL). After dilution with ether (400 mL), the organic layer was separated from the aqueous layer, which was back-extracted with ether (150 mL). The combined ether extracts were washed with water (3 × 150 mL), dried ($MgSO_4$), and concentrated to an oily residue, which tlc indicated to be a mixture of two compounds. The separation of these two products was achieved by flash chromatography using hexane – ethyl acetate (3:1) as eluent. Evaporation of the early fractions provided the minor product **13** (1.69 g) as an oil; $[\alpha]_D$ −6.25° (*c* 1.04, chloroform); R_f 0.47 (hexane – ethyl acetate, 2:1); ^{1}H nmr ($CDCl_3$) δ: 7.39–7.25 (10H, arom.), 5.906 (1H, H_c allyl), 5.283 (1H, H_b allyl), 5.185 (1H, H_a allyl), 4.778 (d, 1H, $J_{1,2}$ = 2.0 Hz, H-1), 4.730–4.665 (AB, 2H, J_{gem} = 12.0 Hz, $C_6H_5CH_2O$), 4.655–4.583 (AB, 2H, J_{gem} = 12.0 Hz, $C_6H_5CH_2O$), 4.070–3.938 (3H, H_d and H_e allyl overlapping with H-4 (δ 4.004, ddd, $J_{3,4}$ = 9.0 Hz, $J_{4,5}$ = 9.0 Hz, $J_{4,OH}$ = 2.0 Hz, simplified to dd with J_{OH} being absent on D_2O exchange)), 3.830–3.704 (4H, H-2, H-5, H-6a, and H-6b), 3.596 (dd, 1H, $J_{3,4}$ = 9.5 Hz, $J_{2,3}$ = 3.0 Hz, H-3), 3.354 (s, 3H, CH_3O), 2.578 (d, 1H, $J_{4,OH}$ = 2.0 Hz, D_2O exchangeable, 4-OH); ^{13}C nmr ($CDCl_3$) δ: 138.40, 138.37 (quat. arom.), 134.76 (CH_2=$CHCH_2O$), 128.37, 127.88, 127.66, 127.56 (tert. arom.), 117.22 (CH_2=$CHCH_2O$), 99.40 (C-1), 79.41 (C-3), 73.79 (C-2), 73.65, 72.78 ($C_6H_5CH_2O$), 71.58 (C-5), 70.73 (CH_2=$CHCH_2O$), 70.66 (C-6), 67.96 (C-4), 54.99 (CH_3O). *Anal.* calcd. for $C_{24}H_{30}O_6$: C 69.55, H 7.30; found: C 69.67, H 7.35.

Evaporation of the later fractions gave the major product **12** (10.78 g) as an oil; $[\alpha]_D$ +48.25° (*c* 0.97, chloroform); R_f 0.35 (hexane – ethyl acetate, 2:1); ^{1}H nmr ($CDCl_3$) δ: 7.42–7.24 (10H, arom.), 5.950 (1H, H_c allyl), 5.326 (1H, H_b allyl), 5.180 (1H, H_a allyl), 4.936 (d, 1H, J_{gem} = 11.0 Hz, C_6H_5CHHO), 4.813 (d, 1H, J_{gem} = 12.5 Hz, C_6H_5CHHO), 4.709–4.688 (2H, C_6H_5CHHO (δ 4.709, d, J_{gem} = 12.5 Hz) overlapping with H-1 (δ 4.690, d, $J_{1,2}$ = 2 Hz)), 4.638 (d, 1H, J_{gem} = 11.0 Hz, C_6H_5CHHO), 4.146–4.064 (2H, H_d and H_e allyl), 3.913 (dd, 1H, $J_{3,4}$ = 9.5 Hz, $J_{4,5}$ = 9.5 Hz,

[2]M. Pierce, J. Arango, S. H. Tahir, and O. Hindsgaul. Manuscript in preparation.

H-4), 3.840 (ddd, 1H, $J_{6a,6b}$ = 12.0 Hz, $J_{6,OH}$ = 5.5 Hz, $J_{5,6a}$ = 3.0 Hz, D_2O addition resulted in its collapse to dd with $J_{6,OH}$ having disappeared, H-6a), 3.81–3.72 (3H, H-2, H-3, and H-6b), 3.601 (ddd, 1H, $J_{4,5}$ = 9.5 Hz, $J_{5,6a}$ = 3.0 Hz, $J_{5,6b}$ = 5.0 Hz, H-5), 3.298 (s, 3H, CH_3O), 2.046 (dd, 1H, $J_{6a,OH}$ = 5.5 Hz, $J_{6b,OH}$ = 7.0 Hz, D_2O exchangeable, 6-OH); ^{13}C nmr ($CDCl_3$) δ: 138.56, 138.37 (quat. arom.), 134.96 (CH_2=$CHCH_2O$), 128.36, 128.02, 127.81, 127.67 (tert. arom.), 116.60 (CH_2=$CHCH_2O$), 99.47 (C-1), 79.92 (C-3), 75.13 ($C_6H_5CH_2O$), 74.88 (C-2 and C-4), 72.99 ($C_6H_5CH_2O$), 72.10 (C-5), 71.10 (CH_2=$CHCH_2O$), 62.42 (C-6), 54.72 (CH_3O). *Anal.* calcd. for $C_{24}H_{30}O_6$: C 69.55, H 7.30; found: C 69.42, H 7.37.

*Methyl 6-O-acetyl-3-O-allyl-2,4-di-O-benzyl-α-D-mannopyranoside (**14**)*

To a solution of **12** (10.30 g; 24.85 mmol) in dry pyridine (100 mL) was added acetic anhydride (7.5 mL; 79.54 mmol). The mixture was stirred under nitrogen atmosphere at room temperature overnight. The excess of acetic anhydride was decomposed by dropwise addition of ethanol (5 mL) to the ice-cold reaction mixture, and dichloromethane (300 mL) and water (250 mL) were then added. The aqueous layer was separated and back-extracted with dichloromethane (100 mL). The combined dichloromethane extracts were washed with 1 *N* aqueous HCl and saturated aqueous sodium bicarbonate. The organic phase was dried ($MgSO_4$), filtered, and evaporated under reduced pressure to give **14** (11.06 g; 98%) as a chromatographically pure oil; $[\alpha]_D$ +42.91° (*c* 1.03, chloroform); R_f 0.45 (hexane – ethyl acetate, 3:1); ^1H nmr ($CDCl_3$) δ: 7.41–7.25 (10H, arom.), 5.920 (1H, H_c allyl), 5.309 (1H, H_b allyl), 5.169 (1H, H_a allyl), 4.910 (d, 1H, J_{gem} = 11.0 Hz, C_6H_5CHHO), 4.778–4.691 (3H, $C_6H_5CH_2O$ (δ 4.778–4.691, AB, J_{gem} = 11.0 Hz) overlapping with H-1 (δ 4.718, d, $J_{1,2}$ = 2.0 Hz)), 4.561 (d, 1H, J_{gem} = 11.0 Hz, C_6H_5CHHO), 4.348–4.268 (2 × dd, 2H, $J_{6a,6b}$ = 12.0 Hz, $J_{5,6a}$ = 3.0 Hz, $J_{5,6b}$ = 5.0 Hz, H-6a and H-6b), 4.119–4.025 (2H, H_d and H_e allyl), 3.844 (dd, 1H, $J_{3,4}$ = 9.0 Hz, $J_{4,5}$ = 9.5 Hz, H-4), 3.781–3.706 (3H, H-3 (δ 3.766, $J_{2,3}$ = 3.5 Hz, $J_{3,4}$ = 9.5 Hz), H-2 (δ 3.743, $J_{1,2}$ = 2.0 Hz, $J_{2,3}$ = 3.5 Hz), and H-5), 3.31 (s, 3H, CH_3O), 2.05 (s, 3H, $OCOCH_3$); ^{13}C nmr ($CDCl_3$) δ: 170.80 ($OCOCH_3$), 138.34 (quat. arom.), 134.85 (CH_2=$CHCH_2O$), 128.36, 128.29, 128.08, 127.70, 127.60 (tert. arom.), 116.70 (CH_2=$CHCH_2O$), 99.10 (C-1), 79.89 (C-3), 75.07 ($C_6H_5CH_2O$), 74.50, 74.58 (C-2 and C-4), 72.66 ($C_6H_5CH_2O$), 70.98 (CH_2=$CHCH_2O$), 69.98 (C-5), 63.63 (C-6), 54.73 (CH_3O), 20.81 ($OCOCH_3$). *Anal.* calcd. for $C_{26}H_{32}O_7$: C 68.40, H 7.07; found: C 68.39, H 7.09.

*1,6-Di-O-acetyl-3-O-allyl-2,4-di-O-benzyl-α-D-mannopyranose (**15**)*

A solution of concentrated sulfuric acid (0.22 mL) in acetic anhydride (7.68 mL) was added dropwise to a solution of **14** (8.77 g; 19.65 mmol) in acetic anhydride (40 mL) at 0°C over 10 min. The mixture was stirred at 0°C for 25 min and at room temperature for 20 min. Then the reaction mixture was poured into dichloromethane (1 L) and ice-cold water (1 L) containing sodium bicarbonate, and the resulting mixture was stirred at room temperature for 30 min. The organic and aqueous layers were separated, and the aqueous layer was extracted with dichloromethane (500 mL). The dichloromethane solutions were combined and then washed with saturated aqueous sodium carbonate and water. Finally the organic phase was dried (Na_2SO_4), filtered, and concentrated. The residual syrup was purified by flash chromatography using hexane – ethyl acetate as eluent, the ratio of hexane to ethyl acetate being varied from 6:1 to 3:1 during elution. Removal of solvent from the early fractions provided the title compound as an oil (7.35 g; 77% yield); $[\alpha]_D$ +37.85 (*c* 0.93, chloroform); R_f 0.56 (hexane – ethyl acetate, 3:1); ^1H nmr ($CDCl_3$) δ: 7.431–7.273 (10H, arom.), 6.195 (d, 1H, $J_{1,2}$ = 2.0 Hz, H-1), 5.923 (1H, H_c allyl), 5.315 (1H, H_b allyl), 5.200 (1H, H_a allyl), 4.935 (d, 1H, J_{gem} = 10.5 Hz, C_6H_5CHHO), 4.840–4.766 (AB, 2H, J_{gem} = 12.0 Hz, $C_6H_5CH_2O$), 4.621 (d, 1H, J_{gem} = 10.5 Hz, C_6H_5CHHO), 4.384–4.310 (2 × dd, 2H, H-6a and H-6b), 4.095 (ddd, 2H, CH_2=$CHCH_2O$), 3.973 (dd, 1H, $J_{3,4}$ = 10.0 Hz, $J_{4,5}$ = 10.0 Hz, H-4), 3.893 (ddd, 1H, $J_{4,5}$ = 10.0 Hz, $J_{5,6a}$ = 4.0 Hz, $J_{5,6b}$ = 3.0 Hz, H-5), 3.814, 3.785 (2 dd, 2H, $J_{3,4}$ = 10.0 Hz, $J_{2,3}$ = 3.0 Hz, $J_{1,2}$ = 2.0 Hz, H-3 and H-2 respectively), 2.055 (s, 6H, $OCOCH_3$ × 2); ^{13}C nmr ($CDCl_3$) δ: 170.82, 168.82 ($OCOCH_3$), 138.08, 137.87 (quat. arom.), 134.68 (H_2C=$CHCH_2O$), 128.50, 128.40, 128.24, 127.93, 127.88, 127.83 (tert. arom), 117.04 (H_2C=$CHCH_2O$), 91.79 (C-1), 79.17 (C-3), 75.36 ($C_6H_5CH_2O$), 73.89, 73.39 (C-2 and C-4), 72.53 ($C_6H_5CH_2O$), 72.41 (C-5), 71.09 (H_2C=$CHCH_2O$), 63.24 (C-6), 20.98, 20.85 ($OCOCH_3$). *Anal.* calcd. for $C_{27}H_{32}O_8$: C 66.93, H 6.66; found: C 66.78, H 6.74.

*6-O-Acetyl-3-O-allyl-2,4-di-O-benzyl-α-D-mannopyranosyl bromide (**8**)*

Hydrogen bromide gas was passed for 30 min through a tube of calcium sulfate into a solution of **15** (5.80 g; 11.97 mmol) in dry dichloromethane (300 mL) at 0°C. The solution was then taken to dryness and the by-product acetic acid removed by evaporation of toluene (100 mL) from the residue (twice). Finally **8** was obtained as an oil, a portion of which was purified for elemental and nmr spectral analysis by flash chromatography using hexane – ethyl acetate (3:1) as eluent; $[\alpha]_D$ +133.08° (*c* 0.91, chloroform); R_f 0.60 (hexane – ethyl acetate, 3:1); ^1H nmr ($CDCl_3$) δ: 7.42–7.30 (10H, arom.), 6.444 (d, 1H, $J_{1,2}$ = 1.5 Hz, H-1), 5.936 (1H, H_c allyl), 5.350 (1H, H_b allyl), 5.233 (1H, H_a allyl), 5.955 (d, 1H, J_{gem} = 10.5 Hz, C_6H_5CHHO), 4.788–4.718 (AB, 2H, J_{gem} = 12.5 Hz, $C_6H_5CH_2O$), 4.613 (d, 1H, J_{gem} = 10.5 Hz, C_6H_5CHHO), 4.388–4.058 (2H, H-6a and H-6b), 4.243 (dd, 1H, $J_{3,4}$ = 9.0 Hz, $J_{2,3}$ = 3.0 Hz, H-3), 4.116 (d, 2H, *J* = 5 Hz, CH_2=$CHCH_2O$), 4.016–3.935 (3H, H-2 (δ 4.011, dd, $J_{2,3}$ = 3.0 Hz, $J_{1,2}$ = 1.5 Hz), H-4 and H-5), 2.065 (s, 3H, $OCOCH_3$); ^{13}C nmr ($CDCl_3$) δ: 170.57 ($OCOCH_3$), 137.90, 137.55 (quat. arom.), 134.37 (CH_2=$CHCH_2O$), 128.63, 128.44, 128.14, 127.97, 127.87, 127.73 (tert. arom.), 117.38 (CH_2=$CHCH_2O$), 87.41 (C-1), 78.41 (C-3), 78.31, 74.31, 73.57 (C-2, C-4, and C-5), 75.30, 72.89 ($C_6H_5CH_2O$), 71.21 (CH_2=$CHCH_2O$), 62.39 (C-6), 20.72 ($OCOCH_3$). *Anal.* calcd. for $C_{25}H_{29}O_6Br$: C 59.41, H 5.78, Br 15.81; found: C 59.48, H 5.82, Br 16.17.

*8-Methoxycarbonyloctyl 6-O-acetyl-3-O-allyl-2,4-di-O-benzyl-β-D-mannopyranoside (**17β**) and 8-methoxycarbonyloctyl 6-O-acetyl-3-O-allyl-2,4-di-O-benzyl-α-D-mannopyranoside (**17α**)*

8-Methoxycarbonyoctanol (18) (7.50 g; 39.89 mmol) and silver silicate/alumina (16.50 g) in dry dichloromethane (100 mL) were stirred at room temperature for 1 h. To the above mixture, which was cooled to −78°C, was added dropwise, with stirring, a solution of **8** (7.44 g; 14.72 mmol) in dry dichloromethane (75 mL) and stirring was continued for 2.5 h at −78°C, and for 10 h at room temperature. The mixture was diluted with dichloromethane (100 mL) and filtered through Celite. The filtrate was washed with water, dried (Na_2SO_4), and concentrated to a syrup that was purified by flash chromatography, using hexane – ethyl acetate (4.5:1) as eluent. A chromatographically inseparable 6:1 mixture of the β and α mannosides **17** was obtained as an oil (5.14 g; total yield 57%); ^1H nmr ($CDCl_3$) δ: 4.824 (d, $J_{1,2}$ = 1.5 Hz, H-1α), 4.365 (d, $J_{1,2} \approx 0.5$ Hz, H-1β), 2.059 (s, $OCOCH_3\alpha$), 2.050 (s, $OCOCH_3\beta$).

*8-Methoxycarbonyloctyl 3-O-allyl-2,4-di-O-benzyl-β-D-mannopyranoside (**18**) and 8-methoxycarbonyloctyl 3-O-allyl-2,4-di-O-benzyl-α-D-mannopyranoside (**19**)*

The mixture of α and β anomers **17** described above (4.39 g; 7.17 mmol) was dissolved in dry methanol (200 mL) containing a trace of sodium methoxide, and the resulting solution was stirred at room temperature overnight. Neutralization with Amberlite IR-120(H) resin followed by the removal of the resin and evaporation provided an oily residue (4.10 g) whose tlc on silica gel impregnated with silver nitrate showed it to be a mixture of two compounds. Purification of these two products was accomplished by flash chromatography on silver nitrate-impregnated silica gel (prepared by mixing silica gel (40–63 μm) with 17% by weight of finely powdered silver nitrate) using hexane – ethyl acetate as eluent, the ratio of hexane to ethyl acetate being decreased from 7:1 to 2:1 during elution. Evaporation of early fractions furnished the α anomer **19** (0.19 g) as an oil; $[\alpha]_D$ +30.8° (*c* 0.75, chloroform); ^1H nmr ($CDCl_3$) δ: 7.42–7.27 (10H, arom.), 5.965 (1H, H_c allyl),

5.345 (1H, H_b allyl), 5.194 (1H, H_a allyl), 4.945 (d, 1H, J_{gem} = 11.0 Hz, C_6H_5CHHO), 4.843–4.788 (2H, C_6H_5CHHO (δ 4.828, d, J_{gem} = 12.0 Hz) and H-1 (δ 4.790, d, $J_{1,2}$ = 2.0 Hz), 4.724 (d, 1H, J_{gem} = 12.0 Hz, C_6H_5CHHO), 4.655 (d, 1H, J_{gem} = 11.0 Hz, C_6H_5CHHO), 4.138 (br d, 2H, H_d and H_e allyl), 3.923 (dd, 1H, $J_{4,5}$ = 9.5 Hz, $J_{3,4}$ = 9.5 Hz, H-4), 3.870–3.579 (9H, H-2, H-3, H-5, H-6a, H-6b, $OCHHCH_2$, and OCH_3 (δ 3.665, s)), 3.329 (dt, 1H, J_{gem} = 9.0 Hz, J_{vic} = 6.5 Hz, $OCHHCH_2$), 2.303 (t, 2H, CH_2COOCH_3, J = 7.5 Hz), 2.098 (br s, 1H, D_2O exchangeable, OH), 1.620 (m, 2H, aliphatic), 1.510 (m, 2H, aliphatic), 1.29 (br s, 8H, remaining aliphatic); ^{13}C nmr ($CDCl_3$) δ: 174.15 ($COOCH_3$), 138.48, 138.43 (quat. arom.), 134.95 (CH_2=$CHCH_2O$), 128.35, 128.29, 128.07, 127.72, 127.67, 127.58 (tert. arom.), 116.47 (CH_2=$CHCH_2O$), 98.25 (C-1), 79.98 (C-3), 75.18 ($C_6H_5CH_2O$), 75.04, 75.01 (C-3 and C-4), 72.88 ($C_6H_5CH_2O$), 72.08 (C-5), 71.07 (CH_2=$CHCH_2O$), 67.61 (OCH_2CH_2), 62.46 (C-6), 51.33 ($COOCH_3$), 34.01 (CH_2COOCH_3), 29.32, 29.11, 29.06, 29.01, 25.99, 24.85 (aliphatic). *Anal.* calcd. for $C_{33}H_{46}O_8$: C 69.45, H 8.12; found: C 69.27, H 8.26.

Further elution provided a mixture of α and β anomers (0.9 g) which were in the ratio of 1:3 (α:β) by ^{1}H nmr.

Evaporation of the later fractions afforded the β anomer **18** (2.89 g) as an oil; $[\alpha]_D$ −51.33 (*c* 0.9, chloroform); ^{1}H nmr ($CDCl_3$) δ: 7.49–7.29 (10H, arom.), 5.893 (1H, H_c allyl), 5.288 (1H, H_b allyl), 5.17 (1H, H_a allyl), 4.969–4.858 (3H, $C_6H_5CH_2O$ (δ 4.969–4.800, AB, J_{gem} = 12.5 Hz) and C_6H_5CHHO (4.935, d, J_{gem} = 10.5 Hz)), 4.624 (d, 1H, J_{gem} = 10.5 Hz, C_6H_5CHHO), 4.408 (d, 1H, J = 1 Hz, H-1), 4.024–3.828 (6H, H-2, H-4, H-6a, $OCHHCH_2$, and CH_2=$CHCH_2O$), 3.763 (ddd, 1H, $J_{6a,6b}$ = 12.0 Hz, $J_{5,6b}$ = 6.0 Hz, $J_{6b,OH}$ = 6.0 Hz, simplified to dd with $J_{6b,OH}$ being absent on D_2O exchange, H-6b), 3.688 (s, 3H, OCH_3), 3.444–3.386 (2H, H-3 and $OCHHCH_2$), 3.316 (dt, 1H, $J_{4,5}$ = 9.5 Hz, $J_{5,6b}$ = 6.0 Hz, $J_{5,6a}$ = 3.0 Hz, H-5), 2.330 (t, 2H, CH_2COOCH_3, J = 7.5 Hz), 2.140 (t, 1H, $J_{6a,OH}$ = 6.0 Hz, $J_{6b,OH}$ = 6.0 Hz, D_2O exchangeable, OH), 1.670–1.628 (4H, aliphatic), 1.345 (8H, remaining aliphatic); ^{13}C nmr ($CDCl_3$) δ: 174.50 ($COOCH_3$), 138.66, 138.36 (quat. arom.), 134.70 (CH_2=$CHCH_2O$), 128.37, 128.28, 128.11, 128.03, 127.73, 127.37 (tert. arom.), 116.75 (CH_2=$CHCH_2O$), 101.69 (C-1, $J_{C\text{-}1,H\text{-}1}$ = 153.6 Hz), 82.33 (C-3), 75.77, 74.88, 73.90 (C-2, C-4, and C-5), 75.18, 73.86 ($C_6H_5CH_2O$), 70.58, 70.12 (CH_2=$CHCH_2O$ and OCH_2CH_2), 62.63 (C-6), 51.36 ($COOCH_3$), 34.04 (CH_2COOCH_3), 29.63, 29.16, 29.04, 26.01, 24.89 (aliphatic). *Anal.* calcd. for $C_{33}H_{46}O_8$: C 69.45, H 8.12; found: C 69.41, H 8.13.

*8-Methoxycarbonyloctyl 6-O-(2-O-acetyl-3,4,6-tri-O-benzyl-α-D-mannopyranosyl)-3-O-allyl-2,4-di-O-benzyl-β-D-mannopyranoside (**20**)*

To a solution of **18** (2.89 g; 5.06 mmol) in dry acetonitrile (60 mL) containing 4 Å molecular sieves were added, sequentially, mercuric bromide (2.19 g; 6.07 mmol), mercuric cyanide (1.53 g; 6.07 mmol), and a solution of 2-*O*-acetyl-3,4,6-tri-*O*-benzyl-α-D-mannopyranosyl bromide (21) (**7**) in dry acetonitrile (25 mL), which had been freshly prepared from 3,4,6-tri-*O*-benzyl-1,2-*O*-(methoxyethylidene)-β-D-mannopyranose (3.07 g; 6.07 mmol). The reaction mixture was stirred at room temperature for 1 h, and the mixture was then filtered through Celite. Evaporation of the solvent gave an oily residue, which was extracted 3 times with dichloromethane. The extracts were combined and washed successively with saturated aqueous potassium chloride, saturated aqueous sodium bicarbonate, water, and brine. The organic layer was dried (Na_2SO_4), filtered, and evaporated to dryness. The resulting oil was purified by flash chromatography using hexane–ethyl acetate (4:1) as eluent to provide the title compound as a syrup (4.07 g; 77%); $[\alpha]_D$ −6.07° (*c* 1.22, chloroform); R_f 0.3 (hexane–ethyl acetate, 3:1); ^{1}H nmr ($CDCl_3$) δ: 7.47–7.10 (25H, arom.), 5.86 (1H, H_c allyl), 5.459 (dd, 1H, $J_{2',3'}$ = 3.0 Hz, $J_{1',2'}$ = 2.0 Hz, H-2'), 5.270 (1H, H_b allyl), 5.159 (1H, H_a allyl), 4.980–4.825 (5H, H-1' (δ 4.911) and 4 × C_6H_5CHHO (d, J_{gem} = 11.0–12.5 Hz)), 4.680–4.650 (2d overlapping, 2H, J_{gem} = 10.5 and 12.0 Hz, $C_6H_5CH_2O$), 4.513–4.408 (4 × d, 4H, J_{gem} = 11.0–12.0 Hz, $C_6H_5CH_2O$), 4.334 (s, 1H, H-1), 3.930–3.590 (15H, $COOCH_3$ (δ 3.66), H-2, H-4, H-6a, H-6b, H-3', H-4', H-5', H-6a', H-6b', CH_2=$CHCH_2O$ and $OCHHCH_2$), 3.410–3.315 (3H, H-3, H-5, and $OCHHCH_2$), 2.283 (t, 2H, J = 7.5 Hz, CH_2COOCH_3), 2.133 (s, 3H, $OCOCH_3$), 1.620–1.513 (4H, aliphatic), 1.335–1.240 (8H, remaining aliphatic); ^{13}C nmr ($CDCl_3$) δ: 174.08 ($COOCH_3$), 170.12 ($OCOCH_3$), 139.00, 138.80, 138.53, 138.46, 138.05 (quat. arom.), 134.79 (CH_2=$CHCH_2O$), 128.27, 128.19, 128.13, 128.10, 127.97, 127.77, 127.70, 127.59, 127.54, 127.50, 127.38, 127.29, 127.23 (tert. arom.), 116.67 (CH_2=$CHCH_2O$), 101.64 (C-1, $J_{C\text{-}1,H\text{-}1}$ = 154.7 Hz), 97.77 (C-1', $J_{C\text{-}1',H\text{-}1'}$ = 170.4 Hz), 82.56 (C-3), 77.94 (C-3'), 74.80, 74.37, 73.91 (C-2, C-4, C-5, and C-4'), 71.36 (C-5'), 68.67 (C-2'), 74.91, 73.71, 73.30, 71.51 ($C_6H_5CH_2O$ × 5), 70.43, 69.79 (CH_2=$CHCH_2O$ and OCH_2CH_2), 68.98 (C-6'), 67.06 (C-6), 51.26 ($COOCH_3$), 34.05 (CH_2COOCH_3), 29.65, 29.23, 29.16, 29.07, 26.09, 24.92 (aliphatic), 20.99 ($OCOCH_3$). *Anal.* calcd. for $C_{62}H_{76}O_{14}$: C 71.24, H 7.33; found: 71.09, H 7.46.

*8-Methoxycarbonyloctyl 3-O-allyl-2,4-di-O-benzyl-6-O-(3,4,6-tri-O-benzyl-α-D-mannopyranosyl)-β-D-mannopyranoside (**21**)*

The disaccharide **20** (2.88 g; 2.76 mmol) was de-*O*-acetylated as described for the preparation of **18**. After removal of the resin by filtration the solvent was evaporated to afford **21** as chromatographically pure oil (2.73 g; 99%); $[\alpha]_D$ +3.13° (*c* 1.34, chloroform); R_f 0.32 (hexane–acetone, 3:1); ^{1}H nmr ($CDCl_3$) δ: 7.48–7.14 (25H, arom.), 5.883 (1H, H_c allyl), 5.288 (1H, H_b allyl), 5.170 (1H, H_a allyl), 5.258 (br s, 1H, $J_{1',2'} \leq 2$ Hz, H-1'), 4.968–4.795 (4 × d, 4H, J_{gem} = 11.0 and 12.5 Hz, $C_6H_5CH_2O$), 4.644–4.438 (6 × d, 6H, J_{gem} = 11.0–12.0 Hz, $C_6H_5CH_2O$), 4.335 (s, 1H, $J_{1,2} \leq 1$ Hz, H-1), 4.128 (br s, 1H, H-2'), 4.038–3.593 (15H, OCH_3 (δ 3.655, s), H-2, H-4, H-6a, H-6b, H-3', H-4', H-5', H-6a', H-6b', $OCHHCH_2$, and CH_2=$CHCH_2O$), 3.423–3.320 (3H, H-3, H-5, and $OCHHCH_2$), 2.355 (br s, 1H, D_2O exchangeable, OH), 2.284 (t, 2H, J = 7.5 Hz, CH_2COOCH_3), 1.59 (4H, aliphatic), 1.28 (8H, remaining aliphatic); ^{13}C nmr ($CDCl_3$) δ: 173.86 ($COOCH_3$), 139.04, 138.73, 138.59, 138.44, 138.03 (quat. arom.), 134.86 (CH_2=$CHCH_2O$), 128.49, 128.36, 128.29, 128.24, 128.07, 127.99, 127.89, 127.78, 127.62, 127.48, 127.40 (tert. arom.), 116.84 (CH_2=$CHCH_2O$), 101.73 (C-1), 99.77 (C-1'), 82.47 (C-3), 79.69 (C-3'), 75.24, 74.61, 74.36, 74.06 (C-3, C-4, C-5, and C-4'), 75.07, 74.94, 73.88, 73.41, 71.48 ($C_6H_5CH_2O$), 71.07 (C-5'), 70.54, 69.88 (CH_2=$CHCH_2O$ and OCH_2CH_2), 69.03 (C-6'), 68.01 (C-2'), 66.65 (C-6), 51.43 ($COOCH_3$), 34.12 (CH_2COOCH_3), 29.72, 29.29, 29.25, 29.14, 26.15, 24.99 (aliphatic). *Anal.* calcd. for $C_{60}H_{74}O_{13}$: C 71.83, H 7.44; found: C 71.59; H 7.31.

*8-Methoxycarbonyloctyl 6-O-[2-O-(3,4,6-tri-O-acetyl-2-deoxy-2-phthalimido-β-D-glucopyranosyl)-3,4,6-tri-O-benzyl-α-D-mannopyranosyl]-3-O-allyl-2,4-di-O-benzyl-β-D-mannopyranoside (**4**)*

To a solution of **21** (2.73 g; 2.73 mmol) in dry dichloromethane (75 mL) were added silver triflate (7.0 g; 27.25 mmol), *sym*-collidine (3.6 mL, 27.25 mmol), and 4 Å molecular sieves. To the resulting mixture, cooled to −50°C, was added dropwise a solution of 3,4,6-tri-*O*-acetyl-2-deoxy-2-phthalimido-β-D-glucopyranosyl bromide (20) (**6**) (2.30 g; 2.60 mmol) in dry dichloromethane (25 mL). The above mixture was stirred at −50°C for 15 min and then allowed to warm to room temperature over a period of 1 h. The tlc of the mixture revealed the presence of unreacted alcohol **21** (~30%). The reaction mixture was again cooled to −50°C and a solution of the bromide **6** (2.30 g; 2.60 mmol) in dry dichloromethane (25 mL) was added dropwise. After stirring at −50°C for 15 min, the mixture was allowed to attain room temperature, while stirring, over 1 h, by which time tlc showed the complete disappearance of **21**. The mixture was diluted with dichloromethane, and then filtered through Celite. The filtrate was washed sequentially with ice water, ice-cold 1 *N* HCl, and saturated aqueous sodium bicarbonate. The organic phase was dried (Na_2SO_4), filtered, and evaporated. The residual oil was purified by flash chromatography using hexane–acetone (3:1) as eluent to provide the title compound as a syrup (2.92 g; 76%); $[\alpha_D$ −23.04° (*c* 1.02, chloroform); R_f 0.17 (hexane–acetone, 3:1); ^{1}H nmr ($CDCl_3$) δ: 7.86–7.04 (29H, arom.), 5.901–5.790 (2H, H_c allyl and H-3" (δ 5.815, $J_{3'',4''}$

= 9.0 Hz, $J_{2'',3''}$ = 11.0 Hz)), 5.573 (d, 1H, $J_{1'',2''}$ = 8.5 Hz, H-1''), 5.303–5.143 (3H, H-4'' (δ 5.215, dd, $J_{4'',5''}$ = 10.0 Hz, $J_{3'',4''}$ = 9.0 Hz) and H_a and H_b allyl), 4.993 (d, 1H, J_{gem} = 13.0 Hz, C_6H_5CHHO), 4.890–4.735 (4 × d, 4H, J_{gem} = 11.0–12.5 Hz, $C_6H_5CH_2O$), 4.676 (d, 1H, $J_{1',2'}$ = 1.5 Hz, H-1'), 4.538–4.459 (2H, H-2'' (δ 4.513, dd, $J_{2'',3''}$ = 11.0 Hz, $J_{1'',2''}$ = 8.5 Hz) and C_6H_5CHHO (δ 4.475, d, J_{gem} = 12.0 Hz)), 4.400 (dd, 1H, $J_{2',3'}$ = 2.5 Hz, $J_{1',2'}$ = 2.5 Hz, H-2'), 4.373–4.303 (4H, H-1 (δ 4.344), H-6a'', and $C_6H_5CH_2O$), 4.233 (dd, 1H, $J_{6a'',6b''}$ = 12.5 Hz, $J_{5'',6b''}$ = 2.0 Hz, H-6b''), 4.063–3.245 (20H, $OCHHCH_2$ (δ 4.035, td, J_{gem} = 9.0 Hz, J_{vic} = 6.0 Hz), OCH_3 (δ 3.668, s), CH_2=$CHCH_2O$, $C_6H_5CH_2O$, H-2, H-3, H-4, H-5, H-6a, H-6b, H-3', H-4', H-5', H-6a', H-5'', $OCHHCH_2$), 2.989 (dd, 1H, $J_{6a',6b'}$ = 11.0 Hz, $J_{5',6b'}$ = 5.5 Hz, H-6b'), 2.31 (t, 2H, CH_2COOCH_3, J = 7.5 Hz), 2.055 (s, 3H, $OCOCH_3$), 2.024 (s, 3H, $OCOCH_3$), 1.863 (s, 3H, $OCOCH_3$), 1.70–1.59 (4H, aliphatic), 1.44–1.26 (8H, remaining aliphatic); ^{13}C nmr ($CDCl_3$) δ: 173.96 ($COOCH_3$), 170.42, 169.89, 169.21 ($OCOCH_3$ and phthalimido carbonyl), 138.69, 138.52, 138.36, 137.80 (benzyl quat. arom.), 134.55 (CH_2=$CHCH_2O$), 133.74 (phthalimido tert. arom.), 131.52 (phthalimido quat. arom.), 128.31, 128.19, 128.00, 127.92, 127.86, 127.63, 127.47, 127.43, 127.25, 127.19, 126.99 (benzyl tert. arom.), 123.16 (phthalimido tert. arom.), 116.52 (CH_2=$CHCH_2O$), 101.79 (C-1, $J_{C-1,H-1}$ = 152.8 Hz), 97.44 (C-1', $J_{C-1',H-1'}$ = 169.2 Hz), 96.48 (C-1'', $J_{C-1'',H-1''}$ = 165.1 Hz), 82.64 (C-3), 76.81, 74.54, 74.09, 73.75, 73.49, 72.88, 71.89, 71.45, 70.62, 69.01 (C-2, C-4, C-5, C-2', C-3', C-4', C-5', C-3'', C-4'', C-5''), 74.64, 73.63, 72.41, 70.33 ($C_6H_5CH_2O$), 70.11 (CH_2=$CHCH_2O$ and OCH_2CH_2), 69.40 (C-6'), 66.53 (C-6), 62.17 (C-6''), 54.25 (C-2''), 51.17 ($COOCH_3$), 33.86 (CH_2COOCH_3), 29.47, 29.10, 29.04, 28.90, 25.91, 24.74 (aliphatic), 20.56, 20.43, 20.24 ($OCOCH_3$). *Anal.* calcd. for $C_{80}H_{93}N_1O_{22}$: C 67.64, H 6.60, N 0.99; found: C 67.54, H 6.58, N 0.97.

*8-Methoxycarbonyloctyl 6-O-[2-O-(3,4,6-tri-O-acetyl-2-deoxy-2-phthalimido-β-D-glucopyranosyl)-3,4,6-tri-O-benzyl-α-D-mannopyranosyl]-2,4-di-O-benzyl-β-D-mannopyranoside (**22**)*

A solution of **4** (2.79 g; 1.97 mmol), tristriphenylphosphinerhodium(I) chloride (129 mg; 0.14 mmol), 1,8-diazabicyclo[2.2.2]octane (58 mg; 0.51 mmol) in ethanol–benzene–water (7:3:1; 100 mL) was refluxed for 24 h. The solvent was removed and the residue dissolved in acetone (100 mL) containing a trace amount of mercuric oxide (10–20 mg). To this solution was added a solution of mercuric chloride (3.0 g) in acetone–water (9:1; 50 mL), and the mixture was stirred at room temperature for 45 min. Following evaporation of the solvent, the residue was taken up in dichloromethane (250 mL). The dichloromethane solution was washed with 30% aqueous potassium bromide and water. The organic layer was dried (Na_2SO_4) and evaporated to give an oily residue that was purified by flash chromatography using toluene – ethyl acetate (3.5:1) as eluent. The title compound was obtained as a white foam (2.31 g; 85%); $[\alpha]_D$ −19.07 (*c* 0.97, chloroform); R_f 0.37 (toluene – ethyl acetate, 3:1); ^{1}H nmr ($CDCl_3$) δ: 7.88–7.07 (29H, arom.), 5.84 (dd, 1H, $J_{3'',4''}$ = 9.0 Hz, $J_{2'',3''}$ = 11.0 Hz, H-3''), 5.61 (d, 1H, $J_{1'',2''}$ = 8.5 Hz, H-1''), 5.221 (dd, 1H, $J_{4'',5''}$ = 9.0 Hz, $J_{3'',4''}$ = 9.0 Hz, H-4''), 5.063 (d, 1H, J_{gem} = 12.0 Hz, C_6H_5CHHO), 4.853 (d, 1H, J_{gem} = 11.0 Hz, C_6H_5CHHO), 4.778–4.733 (2 × d, 2H, J_{gem} = 11.0 and 12.0 Hz, $C_6H_5CH_2O$), 4.673 (d, 1H, $J_{1',2'}$ = 2.0 Hz, H-1'), 4.633 (d, 1H, J_{gem} = 12.0 Hz, C_6H_5CHHO), 4.543–4.476 (2H, H-2'' (δ 4.518, dd, $J_{2'',3''}$ = 11.0 Hz, $J_{1'',2''}$ = 8.5 Hz), C_6H_5CHHO (δ 4.491, d, J_{gem} = 12.0 Hz)), 4.433 (1H, $J_{1,2} \leq$ 1 Hz, H-1), 4.385–4.240 (5H, H-2', H-6a'', H-6b'' and $C_6H_5CH_2O$), 4.035–3.935 (4H, $OCHHCH_2$, H-5'', and $C_6H_5CH_2O$), 3.828–3.245 (14H, H-2, H-3, H-4, H-5, H-6a, H-6b, H-3', H-4', H-5', H-6a', $OCHHCH_2$ and OCH_3 (δ 3.651, s)), 2.998 (dd, 1H, $J_{6a',6b'}$ = 11.0 Hz, $J_{5',6b'}$ = 5.5 Hz, H-6b'), 2.380 (d, 1H, D_2O exchangeable, $J_{OH,H-3}$ = 10.0 Hz, OH), 2.290 (t, 2H, CH_2COOCH_3, J = 7.5 Hz), 2.056, 2.050 (2 × s, 6H, $OCOCH_3$), 1.860 (s, 3H, $OCOCH_3$), 1.68–1.58 (4H, aliphatic), 1.40–1.26 (8H, remaining aliphatic); ^{13}C nmr ($CDCl_3$) δ: 174.17 ($COOCH_3$), 170.63, 170.12, 169.40 ($OCOCH_3$ and phthalimido carbonyl), 138.77, 138.50, 138.37, 138.30, 138.10 (benzyl quat. arom.), 133.95 (phthalimido tert. arom.), 131.82 (phthalimido quat. arom.), 128.56, 128.36, 128.23, 128.13, 128.08, 127.72, 127.62, 127.59, 127.39, 127.21 (benzyl tert. arom.), 123.37 (phthalimido tert. arom.), 101.96 (C-1), 97.25 (C-1'), 96.61 (C-1''), 77.90, 77.22, 76.27, 74.39, 74.34, 74.07, 73.22, 72.12, 71.61, 70.80, 69.14 (C-2, C-3, C-4, C-5, C-2', C-3', C-4', C-5', C-3'', C-4'', and C-5''), 75.06, 74.83, 74.44, 72.63, 70.49 ($C_6H_5CH_2O$), 70.34 (OCH_2CH_2), 69.50 (C-6'), 66.58 (C-6), 62.33 (C-6''), 54.44 (C-2''), 51.38 ($COOCH_3$), 34.05 (CH_2COOCH_3), 29.61, 29.24, 29.19, 29.08, 26.06, 24.92 (aliphatic), 20.74, 20.62, 20.44 ($OCOCH_3$). *Anal.* calcd. for $C_{77}H_{89}N_1O_{22}$: C 66.99, H 6.50, N 1.01; found: C 66.74, H 6.43, N 0.84.

*8-Methoxycarbonyloctyl 6-O-[2-O-(2-deoxy-2-phthalimido-β-D-glucopyranosyl)-3,4,6-tri-O-benzyl-α-D-mannopyranosyl]-2,4-di-O-benzyl-β-D-mannopyranoside (**23**)*

Deacetylation of **22** (0.82 g; 0.59 mmol) was accomplished as described for the preparation of **18** to afford **23** as a white foam in quantitative yield; $[\alpha]_D$ −31.54°C (*c* 1.3, chloroform); R_f 0.2 (dichloromethane–methanol, 19:1); ^{1}H nmr ($CDCl_3$) δ: 7.66–7.06 (29H, arom.), 5.399 (d, 1H, $J_{1'',2''}$ = 8.0 Hz, H-1''), 5.035 (d, 1H, J_{gem} = 12.0 Hz, C_6H_5CHHO), 4.824–4.534 (6H, H-1' (δ 4.643) and $C_6H_5CH_2O$) (5 × d, J_{gem} = 12.5–11.0 Hz)), 4.408–4.241 (6H, H-1 (δ 4.408), H-2' (δ 4.248, dd, $J_{2',3'}$ = 2 Hz, $J_{1',2'}$ = 2 Hz), H-2'', H-3'', and $C_6H_5CH_2O$ (J_{gem} = 11.0 Hz)), 4.020–3.208 (21H, H-2, H-3, H-4, H-5, H-6a, H-6b, H-3', H-4', H-5', H-6a', H-4'', H-5'', H-6a'', H-6b'', OCH_2CH_2, $C_6H_5CH_2O$, and OCH_3 (δ 3.620, s)), 3.063–2.900 (2H, H-6b' (δ 2.918, dd, $J_{6a',6b'}$ = 10.5 Hz, $J_{5',6b'}$ = 5.5 Hz) and OH (br s, D_2O exchangeable)), 2.396 (d, 1H, $J_{3,OH}$ = 10.0 Hz, D_2O exchangeable, OH), 2.269 (t, 2H, J = 8.0 Hz, CH_2COOCH_3), 1.65–1.55 (4H, aliphatic), 1.39–1.26 (8H, remaining aliphatic); ^{13}C nmr ($CDCl_3$) δ: 174.43 ($COOCH_3$), 168.51 (phthalimido carbonyl), 138.68, 138.52, 138.35, 138.32, 138.05 (benzyl quat. arom.), 133.79 (phthalimido tert. arom.), 131.84 (phthalimido quat. arom.), 128.58, 128.38, 128.34, 128.26, 128.12, 128.03, 127.80, 127.70, 127.49, 127.44, 127.22 (benzyl. tert. arom.), 123.23 (phthalimido tert. arom.), 101.90 (C-1), 97.49 (C-1'), 96.84 (C-1''), 77.69, 77.26, 76.31, 75.65, 74.28, 74.13, 73.38, 72.07, 71.73 (C-2, C-3, C-4, C-5, Ç-2', C-3', C-4', C-5', C-3'', C-4'', and C-5''), 74.87, 74.77, 74.48, 72.63, 70.86 ($C_6H_5CH_2O$), 70.30 (OCH_2CH_2), 69.70 (C-6'), 66.65 (C-6), 62.21 (C-6''), 56.54 (C-2''), 51.45 ($COOCH_3$), 34.07 (CH_2COOCH_3), 29.61, 29.17, 29.04, 26.04, 24.88 (aliphatic). *Anal.* calcd. for $C_{71}H_{83}N_1O_{19}$: C 67.98, H 6.67, N 1.12; found: C 67.43, H 6.60, N 1.10.

*8-Methoxycarbonyloctyl 6-O-[2-O-(2-acetamido-2-deoxy-β-D-glucopyranosyl)-3,4,6-tri-O-benzyl-α-D-mannopyranosyl]-2,4-di-O-benzyl-β-D-mannopyranoside (**24**)*

Compound **23** (0.43 g; 0.34 mmol) in methanol (25 mL) containing hydrazine hydrate (0.14 mL of an 85% solution; 2.6 mmol) was refluxed for 12 h. The tlc showed the presence of the starting material in the reaction mixture. Therefore more hydrazine hydrate (0.07 mL of an 85% solution, 1.3 mmol) was added, the mixture was refluxed for another 4 h, and the solution was then taken to dryness. The residue was dissolved in methanol–water (1:1, 15 mL) and acetic anhydride (1 mL) was added. The resulting solution was stirred at room temperature for 2 h. Removal of solvent gave a white solid, which was purified by flash chromatography using dichloromethane–methanol (12:1) as eluent. Pure **24** was obtained as a white foam (0.24 g; 60%) $[\alpha]_D$ −20.46° (*c* 0.88, chloroform); R_f 0.61 (dichloromethane–methanol, 10:1); ^{1}H nmr ($CDCl_3$) δ: 7.42–7.16 (25H, arom.), 5.90–5.65 (br s, 1H, NH, D_2O exchangeable), 5.053 (d, 1H, J_{gem} = 12.0 Hz, C_6H_5CHHO), 4.913–4.825 (3H, $C_6H_5CH_2O$ (2 × d, J_{gem} = 11.0 Hz) and H-1' (δ 4.910, d, $J_{1',2'}$ = 2.0 Hz)), 4.743 (d, 1H, J_{gem} = 12.0 Hz, C_6H_5CHHO), 4.688–4.574 (3H, H-1'' and $C_6H_5CH_2O$) (2 × d, J_{gem} = 12.0 Hz)), 4.488–4.325 (5H, H-1 (δ 4.435) and $C_6H_5CH_2O$ (4 × d, J_{gem} = 12.0 and 11.0 Hz)), 4.253 (t, 1H, H-2'), 3.995–3.293 (23H, H-2, H-3, H-4, H-5, H-6a, H-6b, H-3', H-4', H-5', H-6a', H-6b', H-2'', H-3'', H-4'', H-5'', H-6a'', H-6b'', OH, OCH_2CH_2, and OCH_3 (δ 3.643, s)), 3.00–2.65 (br s, 2H, D_2O exchangeable, OH), 2.501 (d, 1H, $J_{3,OH}$ = 9.0 Hz, D_2O exchangeable, 3-OH), 2.276 (t, 2H, J = 7.0 Hz, CH_2COOCH_3), 1.840 (s, 3H, $NHCOCH_3$), 1.64–1.52 (4H,

aliphatic), 1.36–1.22 (8H, remaining aliphatic); ^{13}C nmr ($CDCl_3$) δ: 174.10 ($COOCH_3$), 172.37 ($NHCOCH_3$), 138.60, 138.39, 138.30, 137.93 (quat. arom.), 128.50, 128.34, 128.27, 128.17, 127.93, 127.73, 127.65, 127.58, 127.44 (tert. arom.), 101.90 (C-1), 99.23 (C-1′), 97.66 (C-1″), 77.62, 76.25, 75.83, 74.58, 74.39, 74.13, 73.71, 73.46, 71.64 (C-2, C-3, C-4, C-5, C-2′, C-3′, C-4′, C-5′, C-3″, C-4″, and C-5″), 74.75, 74.45, 73.20, 71.50, 70.30 ($C_6H_5CH_2O$), 68.85 (C-6′), 66.86 (C-6), 62.66 (C-6″), 59.07 (C-2″), 51.26 ($COOCH_3$), 33.99 (CH_2COOCH_3), 29.57, 29.11, 28.99, 25.99, 24.84 (aliphatic), 23.30 ($NHCOCH_3$). *Anal.* calcd. for $C_{65}H_{83}N_1O_{18}$: C 66.94, H 7.17, N 1.20; found: C 66.81, H 7.09, N 1.13.

8-Methoxycarbonyloctyl 6-O-[2-O-(2-acetamido-2-deoxy-β-D-glucopyranosyl)-α-D-mannopyranosyl]-β-D-mannopyranoside (2)

Compound **24** (45 mg; 0.039 mmol) was dissolved in 98% ethanol (9 mL), and 5% palladium-on-charcoal (45 mg) was added. The mixture was stirred under one atmosphere of hydrogen gas for 52 h. The catalyst was removed by filtration and, after solvent evaporation, the residue was passed through a column of Bio-Gel P2 (2.5 cm × 47 cm) using 10% aqueous ethanol as eluent. The carbohydrate-containing fractions were pooled, concentrated, and lyophilized to provide **2** as a white powder (23.5 mg; 85%); $[\alpha]_D$ −19.34° (*c* 0.91, water); R_f 0.57 (dichloromethane–methanol–water, 10:6:1); ^{1}H nmr (D_2O) δ: 4.920 (1H, $J_{1',2'}$ = 1.8 Hz, H-1′), 4.664 (1H, $J_{1,2} \leq 0.7$ Hz, H-1), 4.579 (1H, $J_{1'',2''}$ = 8.0 Hz, H-1″), 4.129 (dd, 1H, $J_{1',2'}$ = 1.4 Hz, $J_{2',3'}$ = 3.4 Hz, H-2′), 3.988–3.401 (22H, H-2 (δ 3.981, $J_{2,3}$ = 3.0 Hz), H-3′ (δ 3.844, $J_{3',4'}$ = 9.5 Hz, $J_{2',3'}$ = 3.5 Hz), H-2″ (δ 3.706, $J_{1'',2''}$ = 8.0 Hz), H-3, H-4, H-5, H-6a, H-6b, H-4′, H-5′, H-6a′, H-6b′, H-3″, H-4″, H-5″, H-6a″, H-6b″, OCH_2CH_2, and OCH_3 (δ 3.690)), 2.388 (t, 2H, *J* = 7.5 Hz, CH_2COOCH_3), 2.056 (s, 3H, $NHCOCH_3$), 1.68–1.50 (4H, aliphatic), 1.38–1.22 (8H, remaining aliphatic). The above ^{1}H nmr assignments were confirmed by homonuclear decoupling; ^{13}C nmr (D_2O) δ: 178.59 ($COOCH_3$), 175.59 ($NHCOCH_3$), 100.82 (C-1, $J_{C\text{-}1,H\text{-}1}$ = 159.4 Hz), 100.47 (C-1″, $J_{C\text{-}1'',H\text{-}1''}$ = 162.3 Hz), 97.72 (C-1′, $J_{C\text{-}1',H\text{-}1'}$ = 169.5 Hz), 77.35, 76.75, 75.35, 74.27, 74.10, 73.73, 71.43, 70.92, 70.84, 70.54, 68.20, 67.63 (C-2, C-3, C-4, C-5, C-2′, C-3′, C-4′, C-5′, C-3″, C-4″, C-5″, and OCH_2CH_2), 66.99 (C-6), 62.43 (C-6″), 61.55 (C-6′), 56.31 (C-2″), 52.91 ($COOCH_3$), 34.55 (CH_2COOCH_3), 29.46, 29.05, 28.97, 28.93, 25.82, 25.11 (aliphatic), 23.21 ($NHCOCH_3$). *Anal.* calcd. for $C_{30}H_{53}N_1O_{18}$: C 50.34, H 7.46, N 1.96; found: C 49.27, H 7.26, N 1.73.

8-Methoxycarbonyloctyl 6-O-[2-O-(3,4,6-tri-O-acetyl-2-deoxy-2-phthalimido-β-D-glucopyranosyl)-3,4,6-tri-O-benzyl-α-D-mannopyranosyl]-3-O-(2,3,4,6-tetra-O-acetyl-α-D-mannopyranosyl)-2,4-di-O-benzyl-β-D-mannopyranoside (25)

To a solution of the alcohol **22** (504 mg; 0.371 mmol) in dry acetonitrile (10 mL) containing 4 Å molecular sieves were added sequentially mercuric bromide (1.416 g; 3.93 mmol) and mercuric cyanide (988 mg; 3.95 mmol). To the resulting mixture was added a solution of 2,3,4,6-tetra-*O*-acetyl-α-D-mannopyranosyl bromide (19) (**5**) (0.915 g; 2.23 mmol) in dry acetonitrile (5 mL) in five portions with an interval of 30 min between additions, and the reaction mixture was strired for 2 h. Evaporation of the solvent gave an oily residue, which was extracted three times with dichloromethane. The organic extracts were combined and washed with saturated aqueous potassium chloride, saturated aqueous sodium bicarbonate, water, and brine. The dried organic layer (Na_2SO_4) was evaporated to give a foamy residue, which was purified by flash chromatography using toluene – ethyl acetate (3:1) as eluent. The title compound was obtained as a white foam (0.405 g; 65%); $[\alpha]_D$ +4.41° (*c* 0.98, chloroform); R_f 0.25 (toluene – ethyl acetate, 3:1); ^{1}H nmr ($CDCl_3$) δ: 7.88–7.02 (29H, arom.), 5.811 (dd, 1H, $J_{3''',4'''}$ = 10.0 Hz, $J_{2''',3'''}$ = 9.0 Hz, H-3‴), 5.574 (d, 1H, $J_{1''',2'''}$ = 8.5 Hz, H-1‴), 5.391–5.349 (2H, $J_{2',3'}$ = 3.0 Hz, H-2′ and H-3′), 5.240–5.094 (4H, H-4′, H-4‴, C_6H_5CHHO, and H-1 (δ 5.094) $J_{3',4'} = J_{4',5'}$ = 9.5 Hz, $J_{3''',4'''} = J_{4''',5'''}$ = 9.5 Hz), 4.893–4.750 (3H, J_{gem} = 11.5 Hz, and 13.0 Hz, 3 × C_6H_5CHHO), 4.696 (d, 1H, $J_{1'',2''}$ = 1.5 Hz, H-1″), 4.539–4.448 (2H, H-2‴ (δ 4.515, dd, $J_{1''',2'''}$ = 8.5 Hz, $J_{2''',3'''}$ = 10.5 Hz) and C_6H_5CHHO (J_{gem} = 11.5 Hz)), 4.440–4.284 (6H, H-1 (δ 4.440), H-2″ (δ 4.375, dd, $J_{1'',2''}$ = 2.0 Hz, $J_{2'',3''}$ = 2.0 Hz), H-6a‴, and 3 × C_6H_5CHHO (J_{gem} = 11.0 and 11.5 Hz)), 4.121 (dd, 1H, $J_{6a''',6b'''}$ = 12.0 Hz, $J_{5''',6b'''}$ = 1.5 Hz, H-6b‴), 4.098–3.235 (21H, H-2, H-3, H-4, H-5, H-6a, H-6b, H-5′, H-6a′, H-6b′, H-3″, H-4″, H-5″, H-6a″, H-5‴, OCH_2CH_2, $C_6H_5CH_2O$, OCH_3 (δ 3.674)), 2.953 (dd, 1H, $J_{6a'',6b''}$ = 10.5 Hz, $J_{5'',6''}$ = 6.0 Hz, H-6b″), 2.313 (t, 2H, *J* = 7.5 Hz, CH_2COOCH_3), 2.059–2.000 (6s, 18H, $OCOCH_3$ × 6), 1.868 (s, 3H, $OCOCH_3$), 1.74–1.54 (4H, aliphatic), 1.46–1.20 (8H, remaining aliphatic); ^{13}C nmr ($CDCl_3$) δ: 174.11 ($COOCH_3$), 170.58, 170.21, 170.06, 169.65, 169.47, 169.44, 169.35 ($OCOCH_3$ and phthalimido carbonyl), 138.75, 138.46, 137.73, 137.61 (phthalimido quat. arom.), 133.90 (phthalimido tert. arom.), 128.82, 128.46, 128.36, 128.15, 128.08, 128.03, 127.87, 127.54, 127.47, 127.36, 127.28, 127.18 (benzyl tert. arom.), 123.31 (phthalimido tert. arom.), 101.95 (C-1, $J_{C\text{-}1,H\text{-}1}$ = 152 ± 2 Hz), 99.83 (C-1′, $J_{C\text{-}1',H\text{-}1'}$ = 169 ± 2 Hz), 97.62 (C-1″, $J_{C\text{-}1'',H\text{-}1''}$ = 170 ± 2 Hz), 96.60 (C-1‴, $J_{C\text{-}1''',H\text{-}1'''}$ = 165 ± 2 Hz), 81.25, 76.29, 74.78, 74.48, 74.17, 72.90, 72.03, 71.80, 70.73, 69.33, 69.15, 68.98, 68.93, 65.94 (C-2, C-3, C-4, C-5, C-2′, C-3′, C-4′, C-5′, C-2″, C-3″, C-4″, C-5″, C-3‴, C-4‴, and C-5‴), 74.68, 74.58, 73.71, 72.52, 70.43 ($C_6H_5CH_2O$), 70.11 (OCH_2CH_2), 69.62 (C-6″), 66.29 (C-6), 62.44, 62.32 (C-6′ and C-6‴), 54.37 (C-2‴), 51.34 ($COOCH_3$), 34.02 (CH_2COOCH_3), 29.66, 29.27, 29.19, 29.07, 26.10, 24.89 (aliphatic), 20.69, 20.56, 20.40 ($OCOCH_3$). *Anal.* calcd. for $C_{91}H_{107}N_1O_{31}$: C 63.89, H 6.30, N 0.82; found: C 63.45, H 6.31, N 0.82.

8-Methoxycarbonyloctyl 6-O-[2-O-(3,4,6-tri-O-acetyl-2-acetamido-2-deoxy-β-D-glucopyranosyl)-3,4,6-tri-O-benzyl-α-D-mannopyranosyl]-3-O-[2,3,4,6-tetra-O-acetyl-α-D-mannopyranosyl]-2,4-di-O-benzyl-β-D-mannopyranoside (26)

Compound **25** (260 mg; 0.15 mmol) was de-*O*-acetylated as described for the preparation of **18** to provide a foamy solid that was dissolved in methanol (10 mL). To this solution was added hydrazine hydrate (0.4 mL of an 85% solution, 7.43 mmol) and the mixture was refluxed for 1 h. Removal of solvent gave a white residue from which traces of hydrazine were removed by evaporation of methanol (twice). The product was then dissolved in pyridine (3.5 mL) and acetic anhydride (3.5 mL), and stirred overnight at room temperature. Excess acetic anhydride was decomposed by dropwise addition of ethanol to the reaction mixture at 0°C, to which was then added dichloromethane and water. The aqueous layer was separated and back-extracted with more dichloromethane and the combined dichloromethane layers were washed with 1 *N* aqueous HCl and saturated aqueous sodium bicarbonate. The organic phase was dried (Na_2SO_4), filtered, and evaporated to give a foamy solid, which was purified by flash chromatography using hexane – ethyl acetate – ethanol (20:20:1) as eluent. Pure **26** was obtained as a white foam (154 mg; 62%) $[\alpha]_D$ +11.23 (*c* 1.18, chloroform); R_f 0.3 (hexane – ethyl acetate – ethanol, 20:20:1); ^{1}H nmr ($CDCl_3$) δ: 7.70–7.12 (25H, arom.), 5.613–5.523 (2H, H-3′‴ (δ 5.588) and NH (δ 5.533, d, *J* = 7.5 Hz)), 5.405–5.340 (2H, H-2′ (δ 5.399, dd, $J_{2',3'}$ = 3.5 Hz, $J_{1',2'}$ = 1.5 Hz) and H-3′ (δ 5.358, dd, $J_{3',4'}$ = 10.0 Hz, $J_{2',3'}$ = 3.5 Hz)), 5.213–4.990 (5H, H-4′ (δ 5.188, dd, $J_{4',5'}$ = 10.0 Hz, $J_{3',4'}$ = 10.0 Hz), C_6H_5CHHO (δ 5.133, d, J_{gem} = 13.0 Hz), H-1′ (δ 5.100), H-1‴ (δ 5.074, d, $J_{1''',2'''}$ = 8.5 Hz), and H-4‴ (δ 5.015, dd, $J_{4''',5'''}$ = 10.0 Hz, $J_{3''',4'''}$ = 10.0 Hz)), 4.905–4.765 (4H, H-1″ (δ 4.850, d, $J_{1'',2''}$ = 2.5 Hz) and 3 × C_6H_5CHHO (J_{gem} = 11.5–13.0 Hz)), 4.575–4.530 (2H, J_{gem} = 11.5 Hz and 12.0 Hz, $C_6H_5CH_2O$), 4.466–4.228 (6H, H-1 (δ 4.466), 3 × C_6H_5CHHO (J_{gem} = 12.0 Hz), H-2″ (δ 4.288, br s), H-6a‴ (δ 4.250, dd, $J_{6a''',6b'''}$ = 12.5 Hz, $J_{5''',6a'''}$ = 5.0 Hz)), 4.119–3.300 (13H, H-6b‴ (δ 4.100, dd, $J_{6a''',6b'''}$ = 12.0 Hz, $J_{5''',6b'''}$ = 2.0 Hz), H-2, H-3, H-4, H-5, H-6a, H-6b, H-5′, H-6a′, H-6b′, H-3″, H-4″, H-5″, H-6a″, H-6b″, H-2‴, H-5‴, OCH_2CH_2, and OCH_3 (δ 3.665)), 2.305 (t, 2H, CH_2COOCH_3, *J* = 7.5 Hz), 2.048–1.993 (21H, 7 × $OCOCH_3$), 1.779 (s, 3H, $NHCOCH_3$), 1.67–1.52 (4H, aliphatic), 1.40–1.14 (8H, remaining aliphatic); ^{13}C nmr ($CDCl_3$) δ: 174.22 ($COOCH_3$), 171.03, 170.70, 170.33, 170.15, 169.84, 169.59, 165.54 ($OCOCH_3$ and acetamido carbonyl), 138.71, 138.46, 137.91, 137.73 (quat.

arom.), 128.55, 128.50, 128.45, 128.37, 128.27, 128.22, 127.94, 127.87, 127.72, 127.61, 127.51, 127.41, 127.34 (tert. arom.), 101.90 (C-1), 99.83 (C-1′), 98.35 (C-1″), 98.09 (C-1‴), 81.09, 76.97, 76.52, 74.93, 74.48, 74.37, 73.57, 72.02, 71.61, 69.33, 69.20, 69.11, 68.90, 65.88 (C-2, C-3, C-4, C-5, C-2′, C-3′, C-4′, C-5′, C-2″, C-3″, C-4″, C-5″, C-3‴, C-4‴, and C-5‴), 74.93, 74.66, 73.74, 73.03, 70.77 ($C_6H_5CH_2O$), 70.59 (OCH_2CH_2), 69.27 (C-6″), 66.37 (C-6), 62.42 (C-6′ and C-6‴), 55.90 (C-2‴), 51.45 ($COOCH_3$), 34.07 (CH_2COOCH_3), 29.66, 29.33, 29.25, 29.14, 26.08, 24.94 (aliphatic), 23.27 ($NHCOCH_3$), 20.76, 20.68 ($OCOCH_3$). *Anal.* calcd. for $C_{85}H_{107}N_1O_{30}$: C 62.91, H 6.65, N 0.86; found: C 63.05, H 6.67, N 0.83.

8-Methoxycarbonyloctyl 6-O-[2-O-(2-acetamido-2-deoxy-β-D-glucopyranosyl)-α-D-mannopyranosyl]-3-O-(α-D-mannopyranosyl)-β-D-mannopyranoside (3)

Compound **35** (111 mg; 0.07 mmol) was de-*O*-acetylated as described for the preparation of **18** to provide a foamy solid (89 mg), which was dissolved in 98% ethanol (17 mL) and hydrogenolyzed over 5% palladium-on-charcoal (180 mg) at atmospheric pressure for 5 days. Processing, as described for **2**, gave **3** as a white amorphous solid (51 mg; 85%) following lyophilization; $[\alpha]_D$ +6.48° (*c* 0.91, water); R_f 0.28 (dichloromethane–methanol–water, 10:6:1); ^{1}H nmr (D_2O) δ: 5.104 (1H, $J_{1',2'}$ = 2.0 Hz, H-1′), 4.918 (1H, $J_{1'',2''}$ = 1.8 Hz, H-1″), 4.671 (1H, $J_{1,2} \leq$ 0.8 Hz, H-1), 4.579 (d, 1H, $J_{1''',2'''}$ = 8.0 Hz, H-1‴), 4.139 (2H, H-2 and H-2″), 4.065 (dd, 1H, $J_{2',3'}$ = 3.0 Hz, $J_{1'',2''}$ = 1.5 Hz, H-2′), 4.018–3.445 (26H, H-3′ (δ 3.891, $J_{3',4'}$ = 10.0 Hz, $J_{2',3'}$ = 3.0 Hz), H-3″ (δ 3.843, $J_{3'',4''}$ = 9.5 Hz, $J_{2'',3''}$ = 3.0 Hz), H-3 (δ 3.728, $J_{3,4}$ = 9.5 Hz), H-2‴ (δ 3.705), OCH_3 (δ 3.688, s), H-4, H-5, H-6a, H-6b, H-4′, H-5′, H-6a′, H-6b′, H-4″, H-5″, H-6a″, H-6b″, H-3‴, H-4‴, H-5‴, H-6a‴, H-6b‴, and OCH_2CH_2), 2.388 (t, 2H, CH_2COOCH_3, *J* = 7.5 Hz), 2.055 (s, 3H, $NHCOCH_3$), 1.66–1.50 (4H, aliphatic), 1.40–1.20 (8H, remaining aliphatic). The above ^{1}H nmr assignments were confirmed by homonuclear decoupling; ^{13}C nmr (D_2O) δ: 178.76 ($COOCH_3$), 175.66 ($NHCOCH_3$), 103.22 (C-1′, $J_{C\text{-}1',H\text{-}1'}$ = 172.0 Hz), 100.69 (C-1, $J_{C\text{-}1,H\text{-}1}$ = 159.1 Hz), 100.40 (C-1‴, $J_{C\text{-}1''',H\text{-}1'''}$ = 159.1 Hz), 97.61 (C-1″, $J_{C\text{-}1'',H\text{-}1''}$ = 169.3 Hz), 81.65, 77.14, 76.70, 75.12, 74.24, 74.18, 73.70, 71.24, 71.16, 70.94, 70.80, 70.49, 68.17, 67.67, 66.63 (C-2, C-3, C-4, C-5, C-2′, C-3′, C-4′, C-5′, C-2″, C-3″, C-4″, C-5″, C-3‴, C-4‴, and C-5‴), 70.99 (OCH_2CH_2), 66.63 (C-6), 62.49, 61.86, 61.51 (C-6′, C-6″, and C-6‴), 56.25 (C-2‴), 52.95 ($COOCH_3$), 34.59 (CH_2COOCH_3), 29.50, 29.11, 29.07, 28.99, 25.86, 25.15 (aliphatic), 23.22 ($NHCOCH_3$).

Acknowledgements

This research was supported by the Natural Sciences and Engineering Research Council of Canada and the Alberta Heritage Foundation for Medical Research. The microanalyses and the ^{1}H and ^{13}C nmr spectra were provided by the Analytical and Spectral Services Laboratory of this department. We are grateful to Chembiomed Ltd. (Edmonton) for a generous gift of 8-methoxycarbonyloctanol.

1. L. A. Smets and W. P. Van Beek. Biochim. Biophys. Acta, **738**, 237 (1984).
2. S.-I. Hakomori. Ann. Rev. Biochem. **50**, 733 (1981).
3. S.-I. Hakomori. Trends Biochem. Sci. **9**, 453 (1984).
4. T. Feizi and R. A. Childs. Trends Biochem. Sci. **10**, 24 (1985).
5. D. A. Cheresh, R. A. Reisfeld, and A. P. Varki. Science, **225**, 844 (1984).
6. K. Yamashita, T. Ohkura, Y. Tachibana, S. Takasaki, and A. Kobata. J. Biol. Chem. **259**, 10834 (1984).
7. J. L. Magnani. Biochem. Soc. Trans. **12**, 543 (1984).
8. K. Yamashita, Y. Tachibana, T. Ohkura, and A. Kobata. J. Biol. Chem. **260**, 3963 (1985).
9. H. Schachter. Clin. Biochem. **17**, 3 (1984).
10. H. Schachter, S. Narasimhan, P. Gleeson, and G. Vella. Can. J. Biochem. Cell Biol. **61**, 1049 (1983).
11. D. P. Khare, O. Hindsgaul, and R. U. Lemieux. Carbohydr. Res. **136**, 285 (1985).
12. J. Le Pendu, J. P. Cartron, R. U. Lemieux, and R. Oriol. Am. J. Hum. Genet. **37**, 749 (1985).
13. R. U. Lemieux, T. C. Wong, J. Liao, and E. A. Kabat. Mol. Immunol. **21**, 751 (1984).
14. U. Spohr, O. Hindsgaul, and R. U. Lemieux. Can. J. Chem. **63**, 2644 (1985).
15. O. Hindsgaul, D. P. Khare, M. Bach, and R. U. Lemieux. Can. J. Chem. **63**, 2653 (1985).
16. U. Spohr, N. Morishmia, O. Hindsgaul, and R. U. Lemieux. Can. J. Chem. **63**, 2659 (1985).
17. R. U. Lemieux, A. P. Venot, U. Spohr, P. Bird, G. Mandal, N. Morishima, O. Hindsgaul, and D. R. Bundle. Can. J. Chem. **63**, 2664 (1985).
18. R. U. Lemieux, D. R. Bundle, and D. A. Baker. J. Am. Chem. Soc. **97**, 4076 (1975).
19. W. A. Boommer. J. Am. Chem. Soc. **80**, 3372 (1958).
20. R. U. Lemieux, T. Takeda, and B. Y. Chung. A.C.S. Symposium Series, No. 39, 1979. pp. 90–115.
21. P. J. Garegg and L. Maron. Acta Chem. Scand. Ser. B, **33**, 39 (1979).
22. M. A. Nashed. Carbohydr. Res. **60**, 200 (1978).
23. A. Liptak, I. Jodal, and P. Nasasi. Carbohydr. Res. **44**, 1 (1975).
24. S. J. Sondheimer, R. Eby, and C. Schuerch. Carbohydr. Res. **60**, 187 (1978).
25. H. Paulsen and O. Lockhoff. Chem. Ber. **114**, 3102 (1981).
26. K. Bock and C. Pedersen. J. Chem. Soc. Perkin Trans. 2, 293 (1974).
27. H. Paulsen, W. Raulwald, and R. Lebuhn. Carbohydr. Res. **138**, 29 (1985).
28. E. J. Corey and J. W. Sugg. J. Org. Chem. **38**, 3224 (1973).
29. D. R. Bundle and S. Josephson. Can. J. Chem. **57**, 662 (1979).
30. D. D. Perrin, W. L. Armarego, and D. R. Perrin. Purification of laboratory compounds. 2nd ed. Pergamon Press, London. 1980.
31. G. W. Kramer, A. B. Levy, and M. M. Midland. *In* Organic Synthesis via Boranes. McGraw–Hill, New York. 1972. Chapt. 9.
32. W. C. Still, M. Kahn, and A. Mitra. J. Org. Chem. **43**, 2923 (1978).

The addition of electrophiles on ester enolates containing an oxygen in the β-position. A stereoelectronically controlled reaction

MAURICE CARON,[1] TAKESHI KAWAMATA, LUC RUEST, PIERRE SOUCY, AND PIERRE DESLONGCHAMPS[2]

Laboratoire de synthèse organique, Département de Chimie, Faculté des Sciences, Université de Sherbrooke, Sherbrooke (Qué.), Canada J1K 2R1

Received February 6, 1986

MAURICE CARON, TAKESHI KAWAMATA, LUC RUEST, PIERRE SOUCY, and PIERRE DESLONGCHAMPS. Can. J. Chem. **64**, 1781 (1986).

The enolate anion derived from spiro ketal methyl esters (**1**, **3**, and **4**) reacts with various electrophiles (PhSeBr, Ch_3I, O_2, I_2, $(CH_3S)_2$, and $(PhS)_2$) to yield as the major product, the isomer resulting from an equatorial approach of the electrophilic reagent. This stereochemically controlled reaction is discussed in terms of stereoelectronic effects that increase the electron density of the α face of the enolate anion.

MAURICE CARON, TAKESHI KAWAMATA, LUC RUEST, PIERRE SOUCY et PIERRE DESLONGCHAMPS. Can. J. Chem. **64**, 1781 (1986).

L'anion énolate d'esters méthyliques de spirocétal (**1**, **3** et **4**) réagit avec divers électrophiles (PhSeBr, CH_3I, O_2, I_2, $(CH_3S)_2$ et $(PhS)_2$) et donne, comme produit principal, l'isomère résultant d'une approche équatoriale de l'agent électrophilique. La stéréochimie de la réaction est discutée en tenant compte d'effets stéréoélectroniques qui augmentent la densité électronique de la face α de l'anion énolate.

In the course of our recent work on the formal total synthesis of erythromycin A (1), it was observed that the lithium ester enolate derived from spiroketal ester **1** (mixture of equatorial and axial isomers) (Scheme 1) gave, on reaction with phenylselenenyl bromide (2), a mixture of the isomeric phenylselenide esters **2***a* and **2***b* in a 12:88 ratio. The major formation of **2***b* was rationalized by invoking a stereoelectronic effect (3) that would favor an equatorial approach of phenylselenenyl bromide on the ester enolate intermediate.

To verify the generality of this process, we have studied the reactivity of the ester enolates derived from **3** and **4** with a variety of electrophilic reagents (C_6H_5SeBr, O_2, I_2, CH_3I, $(CH_3S)_2$, and $(C_6H_5S)_2$). We wish to report this work.

The synthesis of spiroketals **3**[3] and **4**[3] is depicted in Scheme 2. The lactone **8**,[4] a common intermediate for the preparation of **3** and **4**, was obtained from the Michael addition of dimethyl malonate on methyl methacrylate (→ **7**) followed by an aldol condensation with paraformaldehyde. The tetrahydropyranyl ether **9** of 3-butynol was prepared. The tetrahydropyranyl ether **11** of 5-hexyn-3-ol (**10**) was also obtained as shown. The lithium acetylides of **9** and that of **11** were then prepared and reacted with lactone **8** to give the hemiketals **12** and **13** respectively (4). Catalytic hydrogenation of **12** and **13** gave the corresponding saturated hemiketals **14** and **15**, which were cyclized under acidic conditions to give respectively spiroketal diesters **16** and **17** (5).

Decarbomethoxylation of spiroketal diester **16** with lithium chloride in wet dimethyl sulfoxide (6) gave a 83:17 mixture of axial and equatorial spiroketal monoester **3**, which could be separated by chromatography. Similarly, decarbomethoxylation of spiroketal diester **17** gave a 80:20 mixture of axial and equatorial monoester **4**. The epimers of **4** can also be obtained pure by chromatography. The enolates of **3** and **4** were generated (LDA in THF) starting from their respective axial and equatorial epimeric mixtures. The results obtained from the reaction of these two enolates with the various electrophiles are described in the experimental part and are summarized in Table 1.

In each case, the various equatorial and axial isomers obtained (**5***a*–*b* and **6***a*–*b*) were separated and obtained pure by chromatography. The assignment of configuration for the isomeric phenyl selenides **5***a* and **5***b* (E = PhSe) and for the methylated products **5***a* and **5***b* (E = Me) was rigorously established by finding the relative proportion of the equatorial and the axial isomer under equilibrating conditions. These two sets of isomers can be equilibrated under acidic conditions via the formation of tetrasubstituted dihydropyran intermediate. Indeed, under these conditions, isomer **5***a* can be converted via spiroketal opening into the mirror image of **5***b*. Equilibration of the phenyl selenides **5***a* and **5***b* (E = PhSe) gave a 25:75 ratio, and the major isomer was assigned as the equatorial isomer **5***b* because a PhSe is a larger group than a carbomethoxy. Similarly, equilibration of the methylated products **5***a* and **5***b* (E = CH_3) gave a 36:64 ratio, where the slightly major isomer was assigned as the equatorial isomer **5***b* on the basis that a methyl is slightly larger than a carbomethoxy group (7). This assignment was also confirmed by ^{13}C nmr analyses, which showed that for product **5***a* (E = CH_3) the carbon at position 4 appears as expected at higher field (33.9 ppm) than for compound **5***b* (E = CH_3) (36.6 ppm) due to a 1,3 diaxial interaction with axial methyl at position 2 (5).

In both isomeric series, ^1H nmr studies also showed (5) that the methoxy group of an axial ester always appears at a lower field that that of the equatorial one, and that the axial proton at position 4 is strongly deshielded by the axial substituent E (see Table 2). The configurational assignment for the isomeric compounds **2***a* and **2***b* and **6***a* and **6***b* (E = PhSe, OH, I, CH_3, CH_3S, and Phs) was established by spectral analysis by comparison with compounds **5***a* and **5***b* (E = PhSe and CH_3).

The results described in Table 1 show a very large preference for the formation of the equatorial isomer and it is unlikely that such a stereochemical control would be due only to steric effect.

[1]NSERCC and FCAR predoctoral fellowships: 1979–1982.

[2]Author to whom correspondence may be addressed.

[3]As these 1,7-dioxaspiro[5.5]undecane compounds are, in fact, the ketal derivatives of 1,9-dihydroxy-5-nonanone, we used the aliphatic chain numbering as indicated in structure **1**.

[4]Lactone **8** served also as a key intermediate in our formal total synthesis of erythromycin A (1).

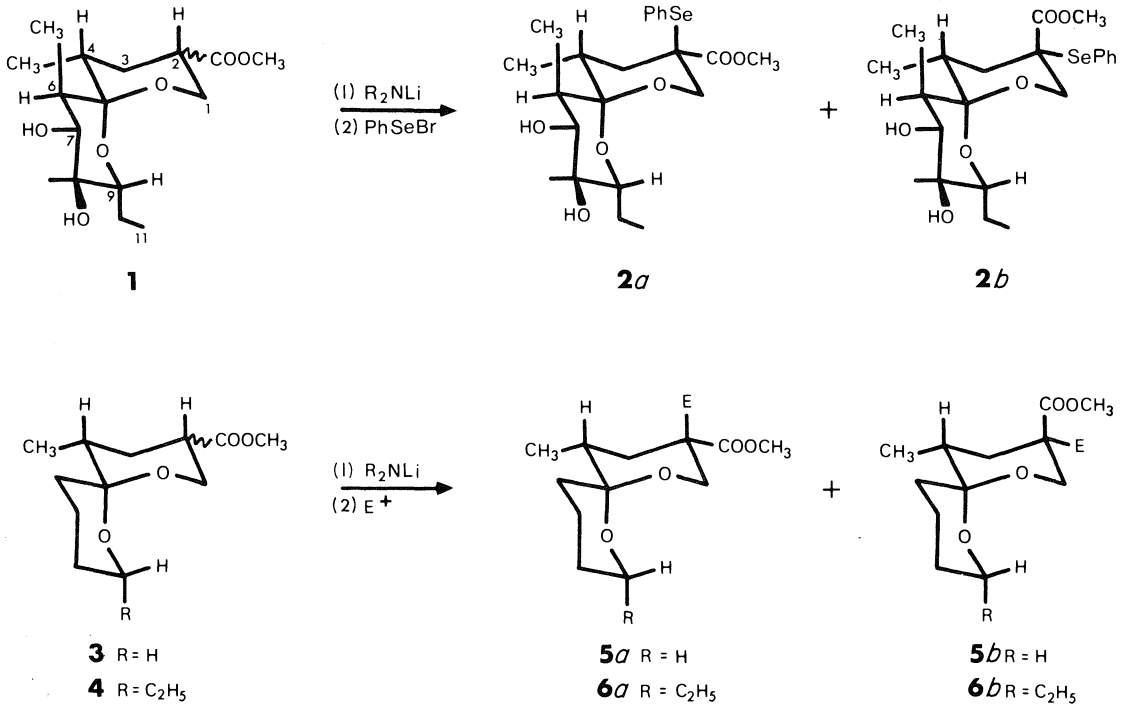

1 **2a** **2b**

3 R = H
4 R = C_2H_5

5a R = H
6a R = C_2H_5

5b R = H
6b R = C_2H_5

SCHEME 1

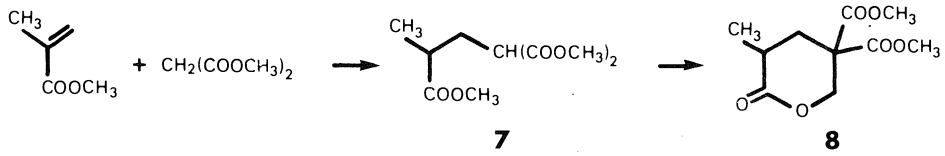

7 **8**

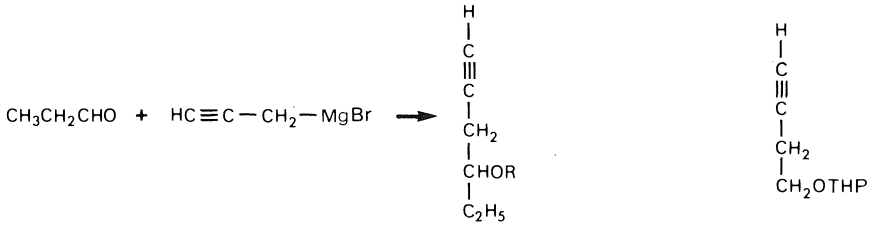

10 R = H
11 R = OTHP

9

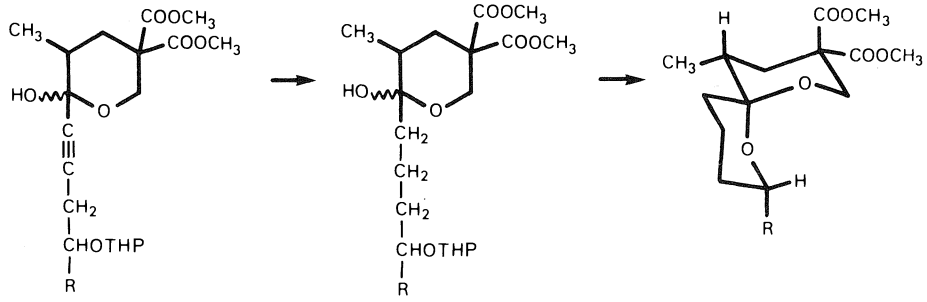

12 R = H
13 R = C_2H_5

14 R = H
15 R = C_2H_5

16 R = H
17 R = C_2H_5

SCHEME 2

TABLE 1. Addition of electrophilic reagents on ester enolates having an oxygen atom in the β-position

Substrate	Electrophilic reagent	Yield (%)	Isomers **2***a–b*, **5***a–b*, or **6***a–b* Axial	Equatorial
3	PhSeBr	69	10	90
	CH_3I	90	14	86
4	PhSeBr	77	12	88
	O_2	85	15	85
	I_2	95	13	87
	CH_3I	99	11	89
	$(CH_3S)_2$	99	<1	>99
	$(PhS)_2$	95	<1	>99
1	PhSeBr	92	12	88

TABLE 2. Chemical shifts of significative protons

Compounds	E	CO_2CH_3 Equatorial	CO_2CH_3 Axial	H_{C-4} Equatorial	H_{C-4} Axial
2*a, b*	PhSe	3.51	3.59	2.51	1.70
5*a, b*	PhSe	3.51	3.55	2.14	1.55
	CH_3	3.68	3.71	1.73	1.60
	H (**3**)	3.60	3.73	1.55	1.74
6*a, b*	PhSe	3.51	3.57	2.16	1.55
	OH	3.78	3.81	2.00	1.91
	I	3.802	3.803	2.02	1.80
	CH_3	3.67	3.71	1.85	1.82
	CH_3S	3.74	3.80	2.05	1.80
	PhS	3.60	3.61	2.18	1.80
	H (**4**)	3.66	3.72	1.54	1.75

We have suggested[5] that the observed selectivity might be a consequence of a stereoelectronic effect that renders the electron density on the α face of the enolate ester greater than that of the β face because the enolate anion **18** (Scheme 3) would be closer to the sp_3-hybridized equatorial anion **19** (a hybrid of **18** and **19**) than to the axial anion **20**. This would be due to the fact that the equatorial anion **19** is more stable, thus more important as a limiting structure, than the axial anion **20**. In the equatorial anion **19**, the carbon electron pair is antiperiplanar to the polar C—O bond; an additional stabilization due to the electronic delocalization resulting from the overlap of this electron pair with the antibonding orbital of that C—O bond is thus possible (n_C–σ^*_{O-C} overlap). This stereoelectronic effect is equivalent to the anomeric effect, except for the fact that the electron pair is on a carbon rather than an oxygen atom.

Krapcho and Dundulis (8) have reported the alkylation with methyl iodide of the enolate ester anion of methyl-4-*tert*-butylcyclohexane carboxylate. They have also studied the alkylation of methyl 2-methyl- and 3-methyl-cyclohexane carboxylate. In all cases, the major alkylated product was the "equatorial" isomer (84, 80, and 90% respectively) resulting from an equatorial approach of the alkylating agent.

Very similar results are thus obtained with the spiroketal and the cyclohexane methyl esters. Thus, the introduction of an oxygen in the cyclohexane ring does not influence much the axial:equatorial product ratio and one may simply conclude that steric rather than stereoelectronic factors govern the course of these reactions.

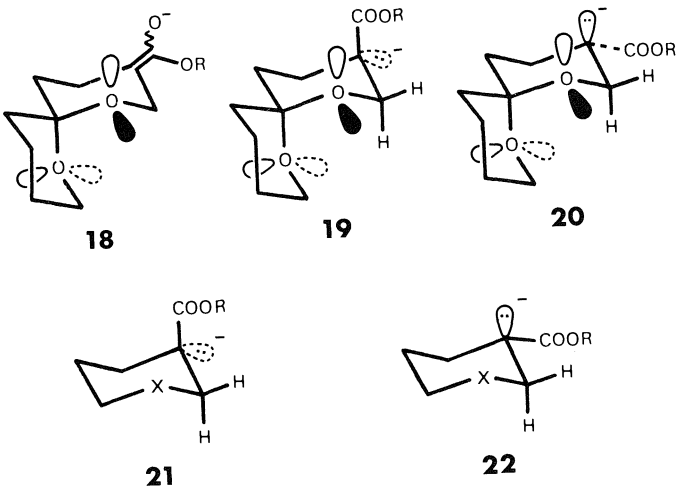

SCHEME 3

It is, however, also possible that the anion **21** (X = CH_2) is better stabilized than the anion **22** (X = CH_2) because a n_C–σ^*_{C-C} overlap in the former would be better than a n_C–σ^*_{H-C} overlap in the latter, and that the alkylation of cyclohexane ester would also be governed by stereoelectronic factors (9). When X = O, the electronic delocalization in anion **21** must, however, be more important than when Y = CH_2 and, on that basis, the former should produce more of the equatorial alkylated product than the latter. On the other hand, replacing a CH_2 group by an oxygen atom decreases the steric repulsion for the axial approach and more axial alkylated product should be formed. Thus, when X = O, the stereoelectronic and steric effects are favoring competing processes and must cancel each other. Consequently, the result observed with spiro ketal ester is similar to that found in cyclohexane ester.

In conclusion, the results that we are reporting cannot be considered as a clear demonstration that stereoelectronic effects play an important role in the alkylation of enolate ester having an oxygen atom in the β position because they can be rationalized either by a combination of steric and stereoelectronic effects or by steric effects only. Subsequent to this study, it was discovered that the influence of stereoelectronic effects can be observed very clearly by studying the relative rate of deprotonation of isomeric esters. This work is reported in the following article (10).

Experimental

The ir spectra were taken on a Perkin–Elmer 257 spectrophotometer. Proton nmr spectra were recorded on a Bruker WP-60 or Bruker WM-250 instrument. The following abbreviations have been used: s, singlet; d, doublet; dd, doublet of doublet; t, triplet; m, multiplet; and br, broad. Chemical shifts are reported in δ values relative to tetramethylsilane or chloroform as internal standard. Carbon nuclear magnetic resonance spectra were recorded on a Bruker HX-90 instrument. Mass spectra were obtained on Hitachi–Perkin–Elmer RMU-6A and Micromass ZAB-2F machines. Melting points were determined on a Buchi M-50 apparatus and are uncorrected. Ether, tetrahydrofuran, and 1,2-dimethoxyethane were dried by distilling over sodium benzophenone whereas benzene, dimethyl sulfoxide, and amines were distilled over calcium hydride. Anhydrous sodium sulfate was used as the drying agent in working up reactions. For flash

[5]See pages 283–284 in ref. 3*a*.

chromatography, Merck Kiesel gel 60 (230–400 mesh A.S.T.M.) was used. Thin-layer chromatography was performed using silica gel 60 F-250.

Triester 7

Dimethylmalonate (343 g, 2.6 mol) was added with stirring to a solution of sodium (12 g, 0.5 mol) in anhydrous methanol (800 mL) under nitrogen. A solution of methyl methacrylate (200 g, 2.0 mol) in methanol (150 mL) was then added and the mixture was refluxed for 9 h. The mixture was then concentrated by removal of methanol. The residue was dissolved in ether (600 mL), washed with hydrochloric acid (0.1 *N*, 3 × 20 mL), water (3 × 20 mL), and brine. The organic layer was dried over sodium sulfate, filtered, and the solvent was evaporated. The crude product was distilled under reduced pressure to give triester **7** (356 g, 76%); bp 100–102°C, 0.7 Torr (1 Torr = 133.3 Pa); ir ($CHCl_3$): 1735 and 1440 cm^{-1}; nmr ($CDCl_3$) δ: 3.73, 3.72, and 3.67 (three s, 3 × —OCH_3), 3.41 (1H, t, J = 6.0 Hz, —$HC(CO_2CH_3)_2$), 2.17 (3H, m, CH_2 and CH—CH_3), 1.18 (3H, d, J = 6.5 Hz, CH_3); *Mol. Wt.* (ms) calcd. for $C_{10}H_{16}O_6 - OCH_3$: m/e 201.0762; found: m/e 201.0751.

Lactone diester 8

Triester **7** (168 g, 0.72 mol) in dry benzene (500 mL) was added dropwise under nitrogen to a stirred suspension of sodium hydride (4.69 g, 0.19 mol) in dry benzene (200 mL). After the sodium hydride had disappeared, paraformaldehyde (54 g, 1.8 mol) was added and the mixture stirred for 3.5 h. The reaction mixture was then filtered, and washed with dilute hydrochloric acid (0.1 *N*, 3 × 200 mL) and water (2 × 200 mL). The extract was dried, filtered, and the solvent evaporated. The residue was purified either by distillation (bp 142–144°C, 0.4 Torr) or by hplc techniques (elution with toluene – ethyl acetate 9:1) to give lactone diester **8** (103 g, 62%); ir ($CHCl_3$): 1750, 1440, and 1260 cm^{-1}; nmr ($CDCl_3$) δ: 4.77 and 4.50 (2H, AB system, J_{AB} = 12 Hz, OCH_2), 3.78 (6H, s, 2 × OCH_3), 2.50 (3H, m, CH_2 and $CHCH_3$), 1.27 (3H, d, J = 6.1 Hz, CH_3); ms m/e: 230. *Mol. wt.* (ms) calcd. for $C_{10}H_{14}O_6$: m/e 230.0789; found: m/e 230.0789.

Hemiketal 12

To a stirred solution of acetylene **9** (10.2 g, 66 mmol) in tetrahydrofuran (75 mL) was added *n*-butyllithium (41.5 mL of 1.6 *M* solution in hexane, 66 mmol) at −78°C under nitrogen. After 30 min, a solution of lactone diester **8** (15.1 g, 66 mmol) was added and the mixture was stirred at −78°C for 45 min. A saturated solution of ammonium chloride was added and the mixture was extracted with ether (4 × 100 mL). The combined organic layers were dried and the solvents were evaporated to leave a crude product (21 g, 83%), which was not purified; ir ($CHCl_3$): 3580, 3400, 2180, 1740, 1260; nmr ($CDCl_3$) δ: 4.63 (1H, br t, O_2CH), 4.48 (1H, dd, J_{AB} = 12 Hz, J_w = 2 Hz) and 4.15 (1H, d, J_{AB} = 12 Hz) [$OCH_2C(CO_2CH_3)_2$], 3.7 (10H, m, 2 × CH_2O and 2 × OCH_3), 2.60 (3H, $CHCH_3$ and $CH_2C{\equiv}C$), 1.9–1.1 (8H, m, 4 × CH_2), 1.07 (3H, d, J = 6 Hz, CH_3); ms m/e: 366 ($M^+ - H_2O$).

Saturated hemiketal 14

A solution of acetylenic hemiketal **12** (828 mg, 2.16 mmol) in methanol (15 mL) was stirred under hydrogen with palladium-on-charcoal catalyst (5%, 43 mg) for 2 h. The solution was then filtered and methanol was evaporated to give crude saturated hemiketal **14** (807 mg, 96%), which was used without any further purification; ir ($CHCl_3$): 3600, 3440, 1740, 1260 cm^{-1}; nmr ($CDCl_3$) δ: 4.54 (1H, br t, O_2CH), 4.16 (2H, s, $OCH_2C(CO_2CH_3)_2$), 3.75 and 3.67 (6H, 2 s, 2 × OCH_3), 3.8–3.1 (4H, m, 2 × OCH_2), 2.32–1.57 (15H, m), 0.94 (3H, d, J = 6.0 Hz, CH_3); ms m/e: 370 ($M^+ - H_2O$).

Spiroketal diester 16

A solution of saturated hemiketal **14** (4.47 g, 12.27 mmol) in tetrahydrofuran (60 mL) was stirred with hydrochloric acid (1 *N*, 20 mL) for 2 h at 45°C. The mixture was then concentrated under vacuum and extracted with ether (3 × 30 mL). The organic layers were combined, dried, filtered, and the solvent was evaporated. The crude product was then refluxed in benzene (100 mL, Dean–Stark) with *p*-toluenesulfonic acid (200 mg) for 12 h. It was then purified by column chromatography on silica gel with hexane – ethyl acetate (3:2) as the solvent to give spiroketal diester **16** (see footnote 3) (2.49 g, 71%); mp 75–76°C; ir ($CHCl_3$): 1725, 1260 cm^{-1}; nmr ($CDCl_3$) δ: 4.21 (1H, dd, J_{AB} = 12 Hz, J_w = 1.9 Hz, H_{eq}-C1), 3.87 (1H, d, J_{AB} = 12 Hz, H_{ax}-C1), 3.78 (3H, s, OCH_3), 3.69 (3H, s, OCH_3), 3.7–3.5 (2H, m, H_2-C9), 2.3–1.1 (9H, m), 0.92 (3H, d, J = 6.1 Hz, CH_3). *Mol. Wt.* (ms) calcd. for $C_{14}H_{22}O_6$: m/e 286.1416; found: m/e 286.1426.

5-Hexyn-3-ol (10) (11)

To a mechanically stirred suspension of magnesium (48 g, 1.97 g-at.) and mercuric chloride (0.5 g, 1.8 mmol) in anhydrous ether (500 mL) was added under nitrogen a small quantity of propargyl bromide (8 g, 6 mL, 67.2 mmol). When the exothermic reaction started, the reaction mixture was cooled at −20°C (inner temperature). Then a solution of propargyl bromide (134 g, 1.13 mol, 100 mL) and propanal (53 g, 0.91 mol, 65.8 mL) in ether (500 mL) was added dropwise over a period of 3 h. The grey mixture was stirred at room temperature for 5 h, then cooled at 0°C, hydrolyzed with a saturated ammonium chloride solution (500 mL), and extracted with ether (4 × 500 mL). The combined organic layers were dried, filtered, and evaporated to an oil that was distilled under reduced pressure to yield pure 5-hexyn-3-ol (**10**) (67.5 g, 76%); bp 64°C, 25 Torr (lit. (11) bp 44°C, 10 Torr); ir ($CHCl_3$): 3580, 3460, 3310, 2100; nmr ($CDCl_3$) δ: 3.65 (1H, sextuplet, J = 6 Hz, H-C3), 2.40 (3H, m, H_2-C4 and OH), 2.05 (1H, t, H-C6), 1.58 (2H, m, H_2-C2), 0.96 (3H, t, J = 6.3 Hz, CH_3).

Tetrahydropyranyl ether 11

To a mixture of 5-hexyn-3-ol (**10**) (66.17 g, 0.67 mol) and freshly distilled dihydropyran (57.16 g, 0.67 mol) was added, with stirring, undistilled phosphorous trichloride (8 drops). After 4 h at 25°C, the mixture was diluted with ether (600 mL), washed with dilute sodium hydroxide solution (0.1 *N*, 2 × 250 mL), and the organic layer was dried, filtered, and evaporated. The crude product was distilled to give compound **11** (112.7 g, 92%); bp 79°C, 4.4 Torr; ir ($CHCl_3$): 3310, 2100, 1200–1040; nmr ($CDCl_3$) δ: 4.78 and 4.66 (1H, two br t, O_2CH), 3.66 (3H, m, H-C3 and OCH_2), 2.40 (2H, m, H_2-C4), 1.96 (1H, m, H-C6), 1.66 (8H, m, 4 × CH_2), 0.91 (3H, m, CH_3). *Mol. Wt.* (ms) calcd. for $C_{11}H_{17}O_2$: m/e 181.1228 ($M^+ - H$); found: m/e 181.1233.

Hemiketal 13

The preparation of this hemiketal was done as for hemiketal **12** (*vide supra*) with the following quantities: acetylene **11** (25.6 g, 141 mmol) in tetrahydrofuran (200 mL), *n*-butyllithium (88 mL, 1.6 *M*, 141 mmol), and lactone diester **8** (32.4 g, 141 mmol) in tetrahydrofuran (200 mL). The crude product (54.7 g, 94%) was not purified; ir ($CHCl_3$): 3600, 2210, 1740, 1260 cm^{-1}; nmr ($CDCl_3$) δ: 4.77 and 4.65 (1H, two br t, O_2CH), 4.51 (1H, dd, J_{AB} = 2 Hz) and 4.15 (1H, d, J_{AB} = 12 Hz) [$OCH_2C(CO_2CH_3)_2$], 3.75 (9H, m, CH_2O, H-COTHP, 2 × OCH_3), 2.51 (2H, m, H_2C—C═), 1.8–1.0 (10H, m), 0.98 (6H, m, 2 × CH_3); ms m/e: 395 ($M^+ - OH$).

Saturated hemiketal 15

A solution of acetylenic hemiketal **13** (25 g, 60.7 mmol) in methanol (250 mL) was hydrogenated over 10% Pd/C catalyst (1.5 g) for 2 h. After filtration of the mixture, the solvent was evaporated to leave a crude product **15** (24.6 g, 97%) that was not purified; ir ($CHCl_3$): 3600, 1740, 1240 cm^{-1}; nmr ($CDCl_3$) δ: 4.62 (1H, br t, O_2CH), 4.17 (2H, s, $OCH_2C(CO_2CH_3)_2$), 3.76–3.2 (9H, m, CH_2O, HCOTHP, 2 × OCH_3), 2.5–1.2 (17H), 0.92 (6H, m, 2 × CH_3).

Spiroketal diester 17

A solution of saturated hemiketal **15** (1.51 g, 3.65 mmol) in tetrahydrofuran (40 mL) was stirred with hydrochloric acid (1 *N*, 15 mL) for 4 h at 25°C. Water (10 mL) was then added and the mixture was extracted with ether (3 × 25 mL). The organic layer was dried, filtered, and the solvents were evaporated. The crude product was then refluxed in benzene (30 mL) with *p*-toluenesulfonic acid (85 mg, 7% w/w) for 12 h. The solvent was then evaporated and the residue

was purified by chromatography on silica gel (hexane – ethyl acetate, 9:1) to give spiroketal **17** (see footnote 3) (568 mg, 50%); ir ($CHCl_3$): 1735, 1260 cm^{-1}; nmr ($CDCl_3$) δ: 4.16 (1H, dd, J_{AB} = 11 Hz, J_w = 1.9 Hz, H_{eq}-C1), 3.87 (1H, d, J_{AB} = 11 Hz, H_{ax}-C1), 3.78 (3H, s, OCH_3), 3.70 (3H, s, OCH_3), 3.35 (1H, m, H-C9), 2.2–1.0 (11H, m), 0.90 (3H, t, J = 7 Hz, H_3-C11), 0.87 (3H, d, J = 6.5 Hz, H_3C-C4); ms m/e: 314 (M^+).

Spiroketal ***1***

Synthesis of this spiroketal has been reported elsewhere (1).

Decarboalkoxylation

(a) Spiroketal monoesters ***3*** *axial and equatorial*

A solution of diester **16** (2.34 g, 8.18 mmol), lithium chloride (694 mg, 16.9 mmol), and water (147 μL, 8.1 mmol) in dimethylsulfoxide (12 mL) was heated under nitrogen at 160°C for 1 h 40 min. The solvent was then evaporated under reduced pressure and the crude product was chromatographed on silica gel (hexane–ether 75:25) to give a mixture (1.64 g, 88%) of monoesters **3** (axial CO_2Me:equatorial CO_2Me 83:17, nmr integration of H-C2); ms m/e: 228 (M^+). A small quantity of the mixture was separated by preparative thin-layer chromatography.

Equatorial monoester **3** (less polar): ir ($CHCl_3$): 1735, 1250, 1150, 1070 cm^{-1}; nmr ($CDCl_3$) δ: 3.78 (1H, ddd, J_{AB} = 11 Hz, $J_{e,e}$ = 4.7 Hz, J_w = 1.6 Hz, H_{eq}-Cl), 3.66 (3H, s, OCH_3), 3.66 (1H, dd, J_{AB} = $J_{a,a}$ = 11 Hz, H_{ax}-C1), 3.63 (2H, m, H_2-C9), 2.75–2.60 (1H, m, H_{ax}-C2), 1.88–1.2 (8H, m), 1.54 (1H, m, H-C4), 0.94 (3H, d, J = 6.6 Hz, CH_3).

Axial monoester **3** (more polar): ir ($CHCl_3$): 1735, 1260, 1150, 1050 cm^{-1}; nmr ($CDCl_3$) δ: 4.07 (1H, dd, J_{AB} = 12 Hz, $J_{e,e}$ = 3 Hz, J_w = 2 Hz, H_{eq}-C1), 3.78 (1H, dd, J_{AB} = 12 Hz, $J_{a,e}$ = 3.4 Hz, H_{ax}-C1), 3.73 (3H, s, OCH_3), 3.62 (2H, m, H_2-C9), 2.55–2.42 (1H, narrow m, H_{eq}-C2), 2.0–1.1 (9H, m), 0.94 (3H, d, J = 6 Hz, CH_3).

(b) Spiroketal monoester ***4*** *axial and equatorial*

This reaction was done as for compound **3** with the following quantities: diester **17** (7.6 g, 24.2 mmol), dimethylsulfoxide (35 mL), lithium chloride (2.05 g, 48.4 mmol), and water (435 μL, 24.2 mmol). The purified monoesters (4.9 g, 79%, axial ester:equatorial ester 80:20, nmr integration of H-C2) were characterized on small scale, after separation by preparative thin-layer chromatography (hexane:ether, 85:15); ms m/e: 256 (M^+).

Equatorial monoester **4** (less polar): ir ($CHCl_3$): 1730, 1250, 1030 cm^{-1}; nmr ($CDCl_3$) δ: 3.74 (1H, ddd, J_{AB} = 11.1 Hz, $J_{e,a}$ = 4.9 Hz, J_w = 1.5 Hz, H_{eq}-C1), 3.63 (1H, dd, J_{AB} = $J_{a,a}$ = 11.1 Hz, H_{ax}-C1), 3.66 (3H, s, OCH_3), 3.44 (1H, m, H-C9), 2.66 (1H, heptet, H_{ax}-C2), 1.9–1.0 (11H, m), 0.93 (3H, t, J = 7.4 Hz, H_3-C11), 0.92 (3H, d, J = 6.6 Hz, H_3C-C4).

Axial monoester **4** (more polar): ir ($CHCl_3$): 1725, 1250, 1070 cm^{-1}; nmr ($CDCl_3$) δ: 4.00 (1H, ddd, J_{AB} = 11.3 Hz, $J_{e,e}$ = J_w = 1.7 Hz, H_{eq}-C1), 3.78 (1H, dd, J_{AB} = 11.3 Hz, $J_{a,e}$ = 3.4 Hz, H_{ax}-C1), 3.72 (3H, s, OCH_3), 3.43 (1H, m, H-C9), 2.47 (1H, narrow m, H_{eq}-C2), 1.95–1.0 (11H, m), 0.94 (3H, t, J = 7.4 Hz, H_3-C11), 0.89 (3H, d, J = 6.3 Hz, H_3C-C4).

Phenylselenide formation

(i) From spiroketal monoester ***3***

To a stirred solution of dry diisopropylamine (985 mg, 1.36 mL, 9.73 mmol) in dry tetrahydrofuran (15 mL) was added, under argon at −20°C, a solution of *n*-butyllithium (6.08 mL, 1.6 *M* in hexane, 9.73 mmol). After 10 min, to the cooled mixture (−78°C) was added dropwise a solution of monoester **3** (760 mg, 3.33 mmol) in tetrahydrofuran (15 mL). After 10 min at −78°C, the mixture was warmed at −50°C for 10 min and then cooled again at −78°C; then was added, via a cannula, a solution of phenylselenenyl bromide (9.73 mmol) freshly prepared at 0°C by the addition of bromine (249 μL, 4.86 mmol) to a solution of diphenyldiselenide (1.52 g, 4.86 mmol) in tetrahydrofuran (20 mL). The mixture was stirred 45 min at −78°C then hydrolyzed by the addition of saturated ammonium chloride solution (5 mL), and extracted with methylene chloride (3 × 120 mL). The combined organic layers were dried, filtered, and the solvents evaporated. Filtration of the extract on silica gel (hexane–ether, 3:1) afforded a purified mixture (880 mg, 69%) of selenides ***5a*** and *b* (10:90, E = PhSe—), which were separated by flash chromatography with hexane–ether (9:1) as a solvent.

Axial selenide ***5a*** (E = PhSe—) (less polar): ir ($CHCl_3$): 1720, 1440, 1260, 1070, 1030; nmr ($CDCl_3$) δ: 7.60 (2H), and 7.34 (3H) (two m, Ar-H), 3.80 (1H, d, J_{AB} = 12.7 Hz, H_{ax}-C1), 3.73 (1H, dd, J_{AB} = 12.7 Hz, J_w = 1.7 Hz, H_{eq}-C1), 3.58 (2H, m, H_2-C9), 3.51 (3H, s, OCH_3), 2.14 (2H, m, H_{eq}-C3 and H-C4), 1.92–1.1 (8H, m), 0.94 (3H, d, J = 6.8 Hz, CH_3). *Mol. Wt.* (ms) calcd. for $C_{18}H_{24}O_4Se$: m/e 384.0839; found: m/e 384.0835.

Equatorial selenide ***5b*** (E = PhSe) (more polar): mp 60–61°C; ir ($CHCl_3$): 1725, 1440, 1320, 1240, 1120, 1080, 1050; nmr ($CHCl_3$) δ: 7.57 (2H) and 7.33 (3H) (two m, Ar-H), 4.02 (1H, dd, J_{AB} = 11 Hz, J_w = 2.7 Hz, H_{eq}-C1), 3.85 (1H, d, J_{AB} = 11 Hz, H_{ax}-C1), 3.63 (2H, m, H_2-C9), 3.55 (3H, s, OCH_3), 2.13 (1H, ddd, J_{AB} = 12.7 Hz, $J_{e,a}$ = 4.0 Hz, J_w = 2.7 Hz, H_{eq}-C3), 1.82 (1H, dd, J_{AB} = $J_{a,a}$ = 12 Hz, H_{ax}-C3), 1.8–1.2 (7H, m), 0.89 (3H, d, J = 6.7 Hz); ms m/e: 384 (M^+).

Acid treatment of equatorial selenide ***5*** b (E = PhSe)

To a solution of equatorial selenide (34 mg, 0.088 mmol) in benzene (10 mL) was added *p*-toluenesulfonic acid (10 mg) and the mixture was refluxed (Dean–Stark) for 6 h under argon. The solvent was then evaporated and the residue filtered on silica gel to give a mixture (34 mg) of selenides ***5a*** and *b* (E = PhSe) (respectively 25:75, nmr integration).

(ii) From spiroketal monoester ***4***

Selenides ***6a*** and *b* (E = PhSe) were prepared exactly as selenides ***5a*** and *b* (*vide supra*) from the following quantity of monoester **4**: 170 mg, 0.66 mmol. Separation of the purified mixture (211 mg, 77%) led to axial (25 mg, 12%, less polar) and equatorial (186 mg, 88%, more polar) selenides ***6a*** and *b* (E = PhSe).

Axial selenide ***6a***: ir ($CHCl_3$): 1720, 1440, 1260, 1055, 1025; nmr ($CDCl_3$) δ: 7.59 (2H) and 7.32 (3H) (two m, Ar-H), 3.76 (1H, d, J_{AB} = 12 Hz, H_{ax}-C1), 3.70 (1H, dd, J_{AB} = 12 Hz, J_w = 1.7 Hz, H_{eq}-C1), 3.51 (3H, s, OCH_3), 3.43 (2H, m, H_2-C9), 2.16 (1H, m, H_{ax}-C4), 1.90 (1H, dd, J_{AB} = 14.3 Hz, $J_{a,a}$ = 11.7 Hz, H_{ax}-C3), 1.78 (1H, ddd, J_{AB} = 14.3 Hz, $J_{e,a}$ = 4.7 Hz, J_w = 1.7 Hz, H_{eq}-C3), 2.0–1.0 (8H, m), 0.93 (3H, d, J = 6.8 Hz, H_3C-C4), 0.87 (3H, t, J = 7.4 Hz, H_3-C11). *Mol. Wt.* (ms) calcd. for $C_{20}H_{28}O_4Se$: 412.1151; found: 412.1165.

Equatorial selenide ***6b***: ir ($CHCl_3$): 1720, 1440, 1240, 1160, 1110, 1070, 1005; nmr ($CDCl_3$) δ: 7.56 (2H) and 7.35 (3H) (two m, Ar-H), 4.00 (1H, dd, J_{AB} = 11 Hz, J_w = 2.7 Hz, H_{eq}-C1), 3.81 (1H, d, J_{AB} = 11 Hz, H_{ax}-C1), 3.57 (3H, s, OCH_3) 3.41 (1H, m, H-C9), 2.13 (1H, ddd, J_{AB} = 12.6 Hz, $J_{e,a}$ = 3.8 Hz, J_w = 2.7 Hz, H_{eq}-C3), 1.85 (1H, dd, J_{AB} = $J_{a,a}$ = 12.6 Hz, H_{ax}-C3), 1.85–1.0 (8H, m), 0.94 (3H, t, J = 7.3 Hz, H_3-C11), 0.87 (1H, d, J = 6.6 Hz, H_3C-C4); ms m/e: 412 (M^+).

(iii) From spiroketal monoester ***1*** [6]

To a stirred solution of dry cyclohexyl isopropylamine (2.88 mL, 15.8 mmol) in dry dimethoxyethane (DME) (10 mL) at −20°C was added under argon *n*-butyllithium (7.48 mL, 1.85 *M* in hexane, 13.8 mmol). After 10 min, to the mixture cooled at −78°C was added, via a cannula, a solution of monoester **1** (625 mg, 1.978 mmol) in DME (20 mL). The mixture was stirred 30 min at −78°C and 10 min at −50°C; then at −78°C was added a solution of phenylselenenyl bromide freshly prepared at 0°C by the addition of bromine (404 μL, 7.87 mmol) to a solution of diphenyldiselenide (2.451 g, 7.86 mmol) in DME (20 mL). After the addition, the mixture was stirred 1 h at −78°C, then hydrolyzed by the addition of saturated ammonium chloride solution (5 mL) and extracted with methylene chloride (3 × 120 mL). The combined organic layers were dried, filtered, and the solvents evaporated. Filtration of the extract on silica gel (hexane–ether, 3:1) afforded a purified mixture (854 mg, 92%) of selenides ***2a***

[6]The synthesis of compound **1** has been reported elsewhere (1).

and *b* (E = PhSe) (12:88), which were separated by flash chromatography with hexane–ether (9:1) as a solvent.

Axial selenide **2***a*: ir ($CHCl_3$): 3600, 3450, 1720, 1440, 1255, 1065, 1030, 1010 cm^{-1}; nmr ($CDCl_3$) δ: 7.59 (2H) and 7.35 (3H), (two m, Ar-H), 3.68 (1H, d, J_{AB} = 12.7 Hz, H_{ax}-C1), 3.62 (1H, d, J = 10.8 Hz, H_{ax}-C7), 3.59 (1H, dd, J_{AB} = 12.7 Hz, J_w = 1.7 Hz, H_{eq}-C1), 3.55 (3H, s, OCH_3), 3.24 (1H, dd, J = 10.4 Hz and J = 2.2 Hz, H-C9), 2.51 (1H, m, H-C4), 1.95–1.78 (3H, m, H_2-C3 and H-C6), 1.78–1.3 (2H, m, H_2-C10), 1.19 (3H, d, J = 6.6 Hz, H_3C-C6), 1.09 (3H, s, H_3C-C8), 0.94 (3H, t, J = 7.4 Hz, H_3C-11), 0.92 (3H, d, J = 6.8 Hz, H_3C-C4). *Mol. Wt.* (ms) calcd. for $C_{22}H_{32}O_6Se$: 472.1363; found: 472.1379.

Equatorial selenide **2***b*: ir ($CHCl_3$): 3600, 3450, 1725, 1440, 1240, 1030, 1010 cm^{-1}; nmr ($CDCl_3$) δ: 7.57 (2H) and 7.36 (3H) (two m, Ar-H), 3.94 (1H, dd, J_{AB} = 10.9 Hz, J_w = 2.6 Hz, H_{eq}-C1), 3.79 (1H, d, J_{AB} = 10.9 Hz, H_{ax}-C1), 3.59 (3H, s, OCH_3), 3.49 (1H, d, J = 10.4 Hz, H-C7), 3.23 (1H, dd, J = 10.5 Hz and J = 2.1 Hz, H-C9), 2.16 (1H, ddd, J_{AB} = 11.5 Hz, $J_{e,a}$ = ~3.5 Hz, J_w = 2.6 Hz, H_{eq}-C3), 1.82 (dd, J_{AB} = $J_{a,a}$ = 11.5 Hz, H_{ax}-C3), 2.1–1.1 (3H, m), 1.07 (3H, s, H_3-C8), 1.03 (3H, t, J = 7.4 Hz, H_3-C11), 0.88 (3H, d, J = 6.5 Hz, H_3C-C6), 0.86 (3H, d, J = 5.9 Hz, H_3C-C4). *Mol. Wt.* (ms) calcd. for $C_{22}H_{32}O_6Se$: 472.1363; found: 472.1365.

Hydroxylation of spiroketal monoester **4**

Anion derivative of spiroketal monoester **4** was prepared as previously described (*vide supra*, starting from 180 mg, 0.70 mmol of ester). Then, at −78°C, dry oxygen was slowly bubbled through the solution for a period of 1 h after which time dimethylsulfide (1 mL) was added. The mixture was warmed to room temperature, shaken with a slightly (pH 5) acidic potassium iodide solution (becomes brown), and extracted with methylene chloride (4 × 20 mL). The extract was washed with aqueous sodium thiosulfate solution, dried, filtered, and the solvent were evaporated. The crude extract was purified by flash chromatography (hexane–ether, 75:25) to give starting material **4** (22 mg, 12%), equatorial hydroxy-ester **6***b* (E = OH) (less polar, 122 mg, 64%), and axial hydroxy-ester **6***a* (E = OH) (more polar, 22 mg, 11.5%).

Equatorial hydroxy-ester **6***b*: ir ($CHCl_3$): 3580, 3520, 1720, 1440, 1240, 1055, 1045, 1020, 1010 cm^{-1}; nmr ($CDCl_3$) δ: 3.81 (3H, s, OCH_3), 3.70 (1H, dd, J_{AB} = 11 Hz, J_w = 2.1 Hz, H_{eq}-C1), 3.52 (1H, d, J_{AB} = 11 Hz, H_{ax}-C1), 3.42 (1H, m, H-C9), 2.79 (1H, s, OH), 1.91 (1H, m, H-C4), 1.88 (1H, ddd, J_{AB} = 12.7 Hz, $J_{e,a}$ = 3.9 Hz, J_w = 2.1 Hz, H_{eq}-C3), 1.79 (1H, dd, J_{AB} = $J_{a,a}$ = 12.7 Hz, H_{ax}-C3), 1.75–1.05 (8H, m), 0.94 (3H, t, J = 7.4 Hz, H_{ax}-C11), 0.92 (3H, d, J = 6.2 Hz, H_3C-C4). *Mol. Wt.* (ms) calcd. for $C_{14}H_{24}O_5$: *m/e* 272.1623; found *m/e*: 272.1628.

Axial hydroxy-ester **6***a*: ir ($CHCl_3$): 3540, 1730, 1440, 1240, 1090, 1080, 1055, 1015 cm^{-1}; nmr ($CDCl_3$) δ: 3.93 (1H, d, J_{AB} = 11.4 Hz, H_{ax}-C1), 3.78 (3H, s, OCH_3), 3.45 (1H, m, H-C9), 3.41 (1H, dd, J_{AB} = 11.4 Hz, J_w = 2.8 Hz, H_{eq}-C1), 3.05 (1H, s, OH), 2.13 (1H, dd, J_{AB} = $J_{a,a}$ = 12.6 Hz, H_{ax}-C3), 2.05–1.05 (10H, m), 0.95 (3H, t, J = 7.4 Hz, H_3-C11), 0.92 (3H, d, J = 6.6 Hz, H_3C-C4); ms *m/e*: 272 (M^+).

Iodine treatment of spiroketal monoester **4**

To a solution of anion derivative prepared as previously described from spiroketal monoester **4** (161 mg, 0.63 mmol) (*vide supra*) was added dropwise via a cannula, at −78°C, a solution of iodine (400 mg, 1.55 mmol) in tetrahydrofuran (3 mL). The mixture was stirred 10 min at −78°C, 10 min at −50°C, then hydrolyzed with ammonium chloride solution and extracted with methylene chloride (4 × 20 mL). The crude product was flash chromatographed (hexane:ether, 92:8) to give axial iodoester **6***a* (E = I) (30 mg, 12.5%, less polar) and equatorial iodoester **6***b* (E = I) (198 mg, 82.5%, more polar).

Axial iodoester **6***a*: ir ($CHCl_3$): 1730, 1440, 1290, 1260, 1055, 1020 cm^{-1}; nmr ($CDCl_3$) δ: 3.86 (1H, dd, J_{AB} = 13.1 Hz, J_w = 2.6 Hz, H_{eq}-C1), 3.80 (3H, s, OCH_3), 3.44 (1H, m, H-C9), 3.36 (1H, d, J_{AB} = 13.1 Hz, H_{ax}-C1), 2.03 (1H, ddd, J_{AB} = 15.4 Hz, $J_{e,a}$ = 3.7 Hz, J_w = 2.7 Hz, H_{eq}-C3), 2.02 (1H, m, H-C4), 1.52 (1H, dd, J_{AB} = 15.4 Hz, $J_{a,a}$ = 12.4 Hz, H_{ax}-C3), 1.95–1.02 (8H, m), 0.99 (3H, d, J = 6.6 Hz, H_3C-C4), 0.88 (3H, t, J = 7.5 Hz, H_3-C11). *Mol. Wt.* (ms) calcd. for $C_{14}H_{23}O_4I$: 383.0719; found: 383.0717.

Equatorial iodoester **6***b*: ir ($CHCl_3$): 1730, 1440, 1320, 1245, 1160, 1070, 1010 cm^{-1}; nmr ($CDCl_3$) δ: 4.23 (1H, dd, J_{AB} = 11.0 Hz, J_w = 2.7 Hz, H_{eq}-C1), 3.98 (1H, d, J_{AB} = 11.0 Hz, H_{ax}-C1), 3.80 (3H, s, OCH_3), 3.43 (1H, m, H-C9), 2.61 (1H, ddd, J_{AB} = 12.8 Hz, $J_{e,a}$ = 4.0 Hz, J_w = 2.7 Hz, H_{eq}-C3), 2.39 (1H, dd, J_{AB} = $J_{a,a}$ = 12.8 Hz, H_{ax}-C3), 1.85–1.04 (9H, m), 0.98 (3H, t, J = 7.4 Hz, H_3-C11), 0.90 (3H, d, J = 6.7 Hz, H_3C-C4): ms *m/e*: 383 (M^+).

Methyl derivative formation

From spiroketal monoester **3**

To a solution of anion derivative at −78°C prepared as described (*vide supra*) from spiroketal monoester **3** (75 mg, 0.33 mmol) was added methyl iodide (125 μL, 2.0 mmol) in tetrahydrofuran (1 mL). The mixture was stirred 30 min at −78°C, hydrolyzed with ammonium chloride solution, and extracted with methylene chloride (4 × 20 mL). The crude product was filtered on silica gel to give a mixture (71 mg, 90%) of **5***a* (E = CH_3) and **5***b* (E = CH_3) in a ratio of 14:86 (nmr integration of methoxy groups). Each compound was characterized after separation by thin-layer chromatography (hexane:ether, 9:1).

Axial methyl derivative **5***a* (less polar): ir ($CHCl_3$): 1725, 1165 cm^{-1}; nmr ($CDCl_3$) δ: 3.83 (1H, dd, J_{AB} = 11 Hz, J_w = 0.4 Hz vs. H_3C-C2, H_{ax}-C1), 3.68 (3H, s, OCH_3), 3.63 (1H, m, H_2-C9), 3.43 (1H, dd, J_{AB} = 11 Hz, J_w = 2.4 Hz, H_{eq}-Cl), 1.9–1.2 (9H, m), 1.34 (3H, s, H_3C-C2), 0.93 (3H, d, J = 6.5 Hz, H_3C-C4); nmr ^{13}C: 176.78 (CO_2), 96.99 (C5), 64.01 (C1), 60.5 (C9), 51.68 (OCH_3), 41.86 (C2), 35.60 (C6), 33.90 (C4), 31.40 (CH_3-C2), 25.15 (C8), 19.96 (C3), 18.60 (C7), 16.30 (CH_3-C4); ms *m/e*: 242.

Equatorial methyl derivative **5***b* (more polar): ir ($CHCl_3$): 1725, 1165 cm^{-1}; nmr ($CDCl_3$) δ: 3.95 (1H, dd, J_{AB} = 11.2, J_w = 2.8 Hz, H_{eq}-C1), 3.71 (3H, s, OCH_3), 3.59 (2H, m, H_2-C9), 3.36 (1H, d, J_{AB} = 11.2 Hz, H_{ax}-C1), 2.02–1.2 (9H, m), 1.03 (3H, s, H_3C-C2), 0.89 (3H, d, J = 6.7 Hz, CH_3-C4); nmr ^{13}C: 176.78 (CO_2), 97.10 (C5), 65.50 (C1), 60.60 (C9), 51.97 (OCH_3), 43.44 (C2), 36.60 (C4), 36.10 (C6), 31.21 (CH_3-C2), 25.20 (C8), 22.89 (C3), 18.50 (C7), 16.40 (CH_3-C4); ms *m/e*: 242.

From spiroketal monoester **4**

To a solution of anion derivative at −78°C prepared as described previously from spiroketal monoester **4** (170 mg, 0.664 mmol) (*vide supra*) was added dropwise a solution of methyl iodide (250 μL, 4.01 mmol) in tetrahydrofuran (2 mL). The mixture was stirred 30 min at −78°C, then hydrolyzed with ammonium chloride solution and extracted with methylene chloride (4 × 20 mL). The crude product was purified by flash chromatography (hexane:ether, 9:1) to give axial derivative **6***a* (E = CH_3) (19 mg, 11%, less polar) and equatorial derivative **6***b* (E = CH_3) (160 mg, 89%, more polar).

Axial methyl derivative **6***a*: ir ($CHCl_3$): 1725, 1295, 1250, 1130, 1068, 1050 cm^{-1}; nmr ($CDCl_3$) δ: 3.81 (1H, dd, J_{AB} = 11.1 Hz, J_w = 0.4 Hz vs. H_3C-C2, H_{ax}-C1), 3.67 (3H, s, OCH_3), 3.45 (1H, m, H-C9), 3.37 (1H, dd, J_{AB} = 11.1 Hz, J_w = 2.5 Hz, H_{eq}-C1), 1.91 (1H, dd, J_{AB} = $J_{a,a}$ = 12.6 Hz, H_{ax}-C3), 1.72 (1H, m, H_{eq}-C3), 1.9–1.1 (9H, m), 1.34 (3H, s, H_3C-C2), 0.93 (3H, t, J = 7.4 Hz, H_3-C11), 0.90 (3H, d, J = 6.6 Hz, H_3C-C4). *Mol. Wt.* (ms) calcd. for $C_{15}H_{26}O_4$: 270.1831; found: 270.1835.

Equatorial methyl derivative **6***b*: ir ($CHCl_3$): 1725, 1250, 1170, 1115, 1060, 1052 cm^{-1}; nmr ($CDCl_3$) δ: 3.93 (1H, dd, J_{AB} = 11.1 Hz, J_w = 2.7 Hz, H_{eq}-C1), 3.71 (3H, s, OCH_3), 3.41 (1H, m, H-C9), 3.34 (1H, d, J_{AB} = 11.1 Hz, H_{ax}-C1), 1.94 (1H, ddd, J_{AB} = 12.6 Hz, $J_{e,a}$ = 3.3 Hz, J_w = 2.7 Hz, H_{eq}-C3), 1.90–1.05 (9H, m), 1.45 (1H, dd, J_{AB} = $J_{a,a}$ = 12.6 Hz, H_{ax}-C3), 1.03 (3H, s, H_3C-C2), 0.94 (3H, t, J = 7.4 Hz, H_3-C11), 0.89 (3H, d, J = 6.6 Hz, H_3C-C4); ms *m/e*: 270 (M^+).

Acid treatment of equatorial methyl derivative **5**b (E = CH_3)

To a solution of equatorial methyl derivative **5***b* (15 mg, 0.062 mmol) in benzene (10 mL) was added *p*-toluenesulfonic acid (5 mg) and the mixture was refluxed (Dean–Stark) for 6 h under argon. Benzene was evaporated and the residue was filtered on silica gel to give a mixture

(14 mg) of methyl derivatives **5***a* and **5***b* (E = CH_3) in the proportion 36:64 respectively (nmr integration, OCH_3).

Methyl sulfide derivatives **6**a *and* **6**b (E = SCH_3)

To a solution of anion derivative, at −78°C, prepared as described previously from spiroketal monoester **4** (169 mg, 0.66 mmol) (*vide supra*), was added dropwise a solution of dimethyldisulfide (171 μL, 1.9 mmol) in tetrahydrofuran (2 mL). The mixture was stirred 30 min at −78°C, then hydrolyzed with ammonium chloride and extracted with methylene chloride (4 × 25 mL). The crude product was purified by flash chromatography (hexane:ether, 9:1) to give axial thiomethyl ester **6***a* (E = SCH_3) (1.5 mg, 0.7%, less polar) and equatorial thiomethyl ester **6***b* (E = SCH_3) (195 mg, 98%, more polar).

Axial sulfide derivative **6***a*: ir ($CHCl_3$): 1720, 1440, 1260, 1110, 1005 cm^{-1}; nmr ($CDCl_3$) δ: 3.80 (1H, d, J_{AB} = 12.4 Hz, H_{ax}-C1), 3.74 (3H, s, OCH_3), 3.69 (1H, dd, J_{AB} = 12.4 Hz, J_w = 2.4 Hz, H_{eq}-C1), 3.45 (1H, m, H-C9), 2.05 (1H, m, H-C4), 2.05 (3H, s, SCH_3), 2.01 (1H, m, H_{eq}-C3), 1.97 (1H, dd, J_{AB} = $J_{a,a}$ = 12.1 Hz, H_{ax}-C3), 1.90–1.0 (9H, m), 0.93 (3H, d, J = 6.3 Hz, H_3C-C4), 0.90 (3H, t, J = 7.4 Hz, H_3-C11). *Mol. Wt.* (ms) calcd. for $C_{15}H_{26}O_4S$: 302.1550; found: 302.1550.

Equatorial sulfide derivative **6***b*: ir ($CHCl_3$): 1725, 1460, 1440, 1320, 1240, 1075, 1015 cm^{-1}; nmr ($CDCl_3$) δ: 4.09 (1H, dd, J_{AB} = 10.9 Hz, J_w = 2.8 Hz, H_{eq}-C1), 3.80 (3H, s, OCH_3), 3.61 (1H, d, J_{AB} = 10.9 Hz, H_{ax}-C1), 3.45 (1H, m, H-C9), 2.13 (1H, ddd, J_{AB} = 12.4 Hz, $J_{e,a}$ = 3.4 Hz, J_w = 2.8 Hz, H_{eq}-C3), 2.07 (3H, s, SCH_3), 1.80 (1H, m, H-C4), 1.74 (1H, dd, J_{AB} = $J_{a,a}$ = 12.4 Hz, H_{ax}-C3), 1.86–1.02 (8H, m), 0.95 (3H, t, J = 7.3 Hz, H_3-C11), 0.92 (3H, d, J = 6.5 Hz, H_3C-C4); ms *m/e*: 302 (M^+).

Phenyl sulfide derivatives **6**a *and* **6**b (E = PhS)

To a solution of anion derivative, at −78°C, prepared as described from spiroketal monoester **4** (162 mg, 0.633 mmol) (*vide supra*) was added dropwise a solution of diphenyldisulfide (413 mg, 1.89 mmol) in tetrahydrofuran (2 mL). The mixture was stirred for 30 min at −78°C, then hydrolyzed with ammonium chloride solution and extracted with methylene chloride (4 × 25 mL). The crude product was purified by flash chromatography (hexane:ether, 92:8) to give axial thiophenyl ester **6***a* (E = PhS) (1.5 mg, 0.6%, less polar) and equatorial thiophenyl ester **6***b* (E = PhS) (216 mg, 94%, more polar).

Axial sulfide derivative **6***a*: ir ($CHCl_3$): 1725, 1440, 1260, 1055, 1010 cm^{-1}; nmr ($CDCl_3$) δ: 7.48 (2H) and 7.34 (3H) (two m, Ar-H), 3.76 (1H, d, J_{AB} = 12.4 Hz, H_{ax}-C1), 3.64 (1H, dd, J_{AB} = 12.4 Hz, J_w = 2.5 Hz, H_{eq}-C1), 3.61 (3H, s, OCH_3), 3.43 (1H, m, H-C9), 2.18 (1H, m, H-C4), 1.95 (1H, dd, J_{AB} = 14.2 Hz, $J_{a,a}$ = 12.3 Hz, H_{ax}-C3), 1.73 (1H, ddd, J_{AB} = 14.2 Hz, $J_{e,a}$ = 4.1 Hz, J_w = 2.5 Hz, H_{eq}-C3), 2.0–1.0 (9H, m), 0.92 (3H, d, J = 6.8 Hz, H_3C-C4), 0.87 (3H, t, J = 7.5 Hz, H_3-C11). *Mol. Wt.* (ms) calcd. for $C_{20}H_{28}O_4S$: 364.1706; found 364.1698.

Equatorial sulfide derivative **6***b*: ir ($CHCl_3$): 1730, 1440, 1320, 1240, 1045, 1010 cm^{-1}; nmr ($CDCl_3$) δ: 7.45 (2H) and 7.34 (3H) (two m, Ar-H), 3.98 (1H, dd, J_{AB} = 10.9 Hz, J_w = 2.8 Hz, H_{eq}-C1), 3.70 (1H, d, J_{AB} = 10.9 Hz, H_{ax}-C1), 3.61 (3H, s, OCH_3), 3.42 (1H, m, H-C9), 2.07 (1H, ddd, J_{AB} = 12.6 Hz, $J_{e,a}$ = 3.8 Hz, J_w = 2.8 Hz, H_{eq}-C3), 1.79 (1H, dd, J_{AB} = $J_{a,a}$ = 12.6 Hz, H_{ax}-C3), 1.80 (1H, m, H-C4), 1.85–1.02 (8H, m), 0.96 (3H, t, J = 7.3 Hz, H_3-C11), 0.89 (3H, d, J = 6.6 Hz, H_3C-C4); ms *m/e*: 364 (M^+).

Acknowledgements

Support for this work by the Natural Sciences and Engineering Research Council of Canada (NSERCC) and by the "Ministère de l'Éducation (FCAR)", Quebec, is gratefully acknowledged.

1. B. Bernet, P. M. Bishop, M. Caron, T. Kawamata, B. L. Roy, L. Ruest, G. Sauvé, P. Soucy, and P. Deslongchamps. Can. J. Chem. **63**, 2810 (1985); **63**, 2814 (1985); **63**, 2818 (1985).
2. (*a*) H. J. Reich, I. L. Reich, and J. M. Renga. J. Am. Chem. Soc. **95**, 5813 (1973); (*b*) K. B. Sharpless, R. F. Lauer, and A. Y. Teranishi. J. Am. Chem. Soc. **95**, 6137 (1973).
3. P. Deslongchamps. *In* Stereoelectronic effects in organic chemistry. Vol. 1. Organic Chemistry Series. *Edited by* J. E. Baldwin. Pergamon Press, Oxford, England. 1983.
4. (*a*) M. S. Kharash and O. Reinmuth. *In* Grignard reactions of non-metallic structures. Prentice–Hall, Englewood Cliffs, NJ. 1954. p. 574, and references quoted therein; (*b*) E. W. Colvin, R. A. Raphael, and J. S. Roberts. Chem. Commun. 858 (1971); (*c*) H. Ogura, H. Takahashi, and T. Itoh. J. Org. Chem. **37**, 72 (1972).
5. P. Deslongchamps, D. D. Rowawn, N. Pothier, G. Sauvé, and J. K. Saunders. Can. J. Chem. **59**, 1105 (1981); **59**, 1122 (1981); **59**, 1132 (1981).
6. (*a*) A. P. Krapcho and J. F. Weimaster. J. Org. Chem. **45**, 4105 (1980), and references quoted therein; (*b*) H. D. Banks. J. Org. Chem. **46**, 1743 (1981).
7. A. J. Hirsch. Top. Stereochem. **1**, 199 (1967).
8. A. P. Krapcho and E. A. Dundulis. J. Org. Chem. **45**, 3236 (1980).
9. A. S. Cieplak. J. Am. Chem. Soc. **103**, 4540 (1981).
10. A. Ndibwami and P. Deslongchamps. Can. J. Chem. **64**, 000 (1986).
11. A. Viola, J. H. MacMillan, R. J. Proverb, and B. L. Yates. J. Am. Chem. Soc. **93**, 6967 (1971).

Study on the enolization of alkylation of *cis* and *trans* 2-*tert*-5-X-1,3-dioxanes (X = CO_2CH_3, CHO, COPh, NO_2, and CN). Evidence for stereoelectronic control

ALEXIS NDIBWAMI[1] AND PIERRE DESLONGCHAMPS

Laboratoire de synthèse organique, Département de Chimie, Faculté des Sciences, Université de Sherbrooke, Sherbrooke (Qué.), Canada J1K 2R1

Received February 6, 1986

ALEXIS NDIBWAMI and PIERRE DESLONGCHAMPS. Can. J. Chem. **64**, 1788 (1986).

Alkylation of 2-*tert*-butyl-5-X-1,3-dioxanes (X = CO_2CH_3, COPh, and NO_2) was studied. Products resulting from an equatorial approach of the alkylating agent are preferentially formed when X = CO_2CH_3 and NO_2. Also, the *cis* isomers that have an equatorial hydrogen at C-5 were found to deprotonate at a faster rate than the *trans* isomers when X = CO_2CH_3, COPh, CHO, and CN. These results are compared with those obtained with methyl 2-*tert*-butyl cyclohexane carboxylate and are interpreted by taking into account stereoelectronic principles.

ALEXIS NDIBWAMI et PIERRE DESLONGCHAMPS. Can. J. Chem. **64**, 1788 (1986).

On a étudié l'alkylation des *tert*-butyl-2 X-5 dioxannes-1,3 (X = CO_2CH_3, COPh et NO_2). Les produits résultant d'une approche équatoriale d'un agent alkylant sont préférentiellement formés quand X = CO_2CH_3 et NO_2. Également, les isomères *cis* ayant un hydrogène équatorial en position 5 se déprotonent plus rapidement que les isomères *trans* quand X = CO_2CH_3, COPh, CHO et CN. Ces résultats sont comparés avec ceux obtenus avec le *tert*-butyl-4 carbométhoxy-1 cyclohexane et sont interprétés en tenant compte des principes du contrôle stéréoélectronique.

In the course of our investigation on the formal total synthesis of erythromycin A (1), it was found that the reaction of various electrophiles with the lithium enolate of spiroketal esters such as **1** (Scheme 1) gave the product **3**, having the E group in the equatorial position, as the major isomer (2, 3). We have suggested (2, 3) that this high selectivity might be due to the fact that, for stereoelectronic reasons caused by the presence of the ring oxygen, the electron density of the α face of the ester enolate **2** might be greater than that of the β face. This would be due to the fact that the enolate structure would correspond to a hybrid of enolates **4** and **5**, and that the other possible limiting structure **6** would not be important because it is energetically less favorable than **5**, in which the carbon electron pair is properly aligned to be delocalized in the antibonding orbital of the polar C—O bond (n_C–$\sigma^*_{O—C}$ overlap). As a result, the product resulting from an equatorial approach of the electrophile would be preferentially observed.

This stereoelectronic effect should also exist and likely be more important when two oxygens are present in the same ring, as in 1,3-dioxanes that have an enolizable functional group at C-5. Banks has recently obtained evidence in this respect by reporting (4) the decarboethoxylation of 1,3-dioxane diester **7**, which proceeds with high stereochemical control yielding a mixture of *cis* and *trans* monoesters **8** and **9** in an 87:13 ratio. Thus protonation of the enol ester intermediate that is produced in the decarboethoxylation of 1,3-dioxane diester **7** takes place preferably from the equatorial face, yielding the *cis* isomer **8**. In contrast, he observed that the decarboethoxylation of the corresponding cyclohexane diester **10** was not selective, yielding a ~1:1 ratio of *cis* and *trans* ethyl esters **11** and **12**.

Banks has explained the stereoselectivity in the decarboethoxylation of 1,3-dioxanes on the basis of the work of Klein (5): "attack on the intermediate carbanion **13** (Scheme 1) should be preferentially from the equatorial direction. The HOMO of this carbanion has antibonding interactions on its upper face of the axial non-bonding electron pair on the ring oxygens, producing an accumulation of electron density below the plane of the intermediate." This is an interesting theoretical explanation but our explanation based on the above stereoelectronic effect is also quite attractive.

To further study this problem, we have prepared and studied the alkylation and the relative rate of deprotonation of the *cis* and *trans* isomers of 2-*tert*-butyl-5-X-1,3-dioxane (X = CO_2CH_3, CHO, COPh, CN, and NO_2). We wish to report this work, which is discussed by taking into account stereoelectronic principles.

Results and discussion

Synthesis of starting materials

Formaldehyde was condensed with dimethyl malonate according to the method of Gault and Roesch (6) to give dimethyl bishydroxymethylmalonate (**14**) in 78% yield (Scheme 2). Acetalization (7) of **14** with pivalaldehyde gave the diester **15** (99% yield). Using the method of Krapcho and Weimasster (8), decarbomethoxylation of **15** gave a result similar to that previously observed by Banks (4) with diethyl ester, i.e. 80% yield of a mixture in a 89:11 ratio of *cis* and *trans* methyl esters **17** and **18**. Epimerization of this mixture with sodium methoxide in methanol gave 16.5 and 83.5% of esters **17** and **18** respectively. These two isomers can be separated by chromatography. The more stable isomer **18** was assigned the *trans* configuration and this was confirmed by ^{1}H nmr spectroscopy. In the *cis* isomer **17**, the hydrogen at C-5 shows a septet ($J_{ee} = J_{ea} = 1.3$ Hz) at 2.28 ppm, whereas in the *trans* isomer **18** the same hydrogen appears as a triplet of triplets at 2.94 ppm, with a large coupling constant ($J_{aa} = 11.2$ Hz). The axial orientation of the C-5 hydrogen in ester **18** is characterized by the large coupling constant and also by a low field chemical shift (2.94 ppm), which must be caused by the deshielding of the two axial electron pairs on the oxygen atoms of the dioxane ring.

Reduction of the mixture of esters **17** and **18** with lithium aluminium hydride (9) gave the corresponding mixture of epimeric alcohols, which was oxidized with pyridinium chlorochromate (10) to a nonseparable mixture of aldehydes **19** and **20**. Starting with pure ester **17** gave a mixture of aldehydes **19** and **20** in a 94:6 ratio, whereas pure ester **18** yielded the same products in a 25:75 ratio. Grignard reaction on a mixture of

[1]CIDA (Canadian International Development Agency) predoctoral fellowship (1982–1987).

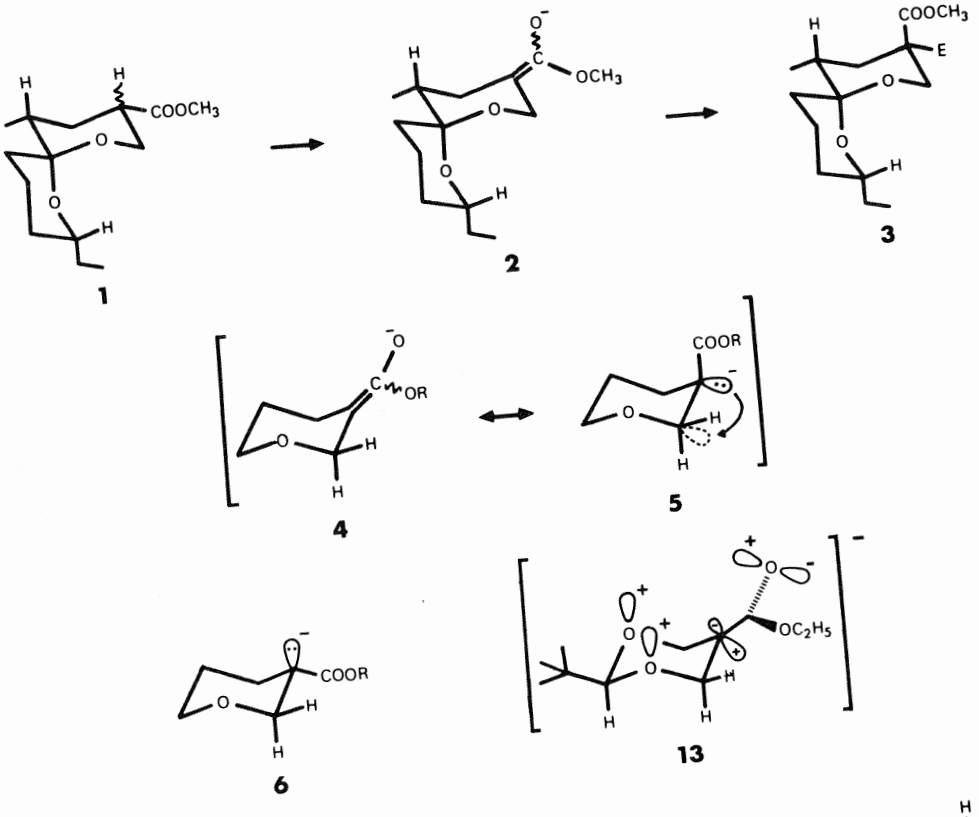

SCHEME 1

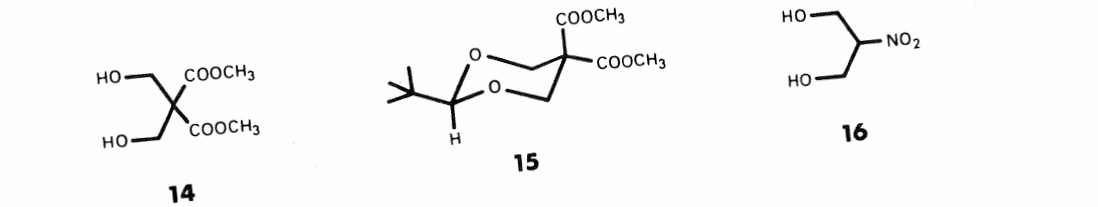

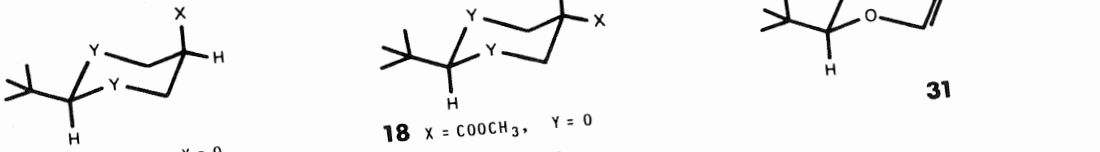

SCHEME 2

TABLE 1. Alkylation of 2-*tert*-butyl-5-X-1,3-dioxanes

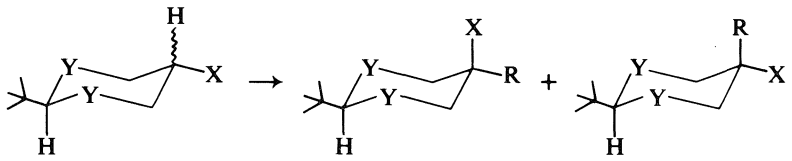

29 ("equatorial") **30** ("axial")

Starting material					
X	Y	Conditions	R—Y	Product ratio equat./axial	Yield
$COOCH_3$	O	LDA, THF, −78°C	CH_3—I	98:2	70
		LDA, DME, −78°C	CH_2=CH—CH_2Br	>95:5	66
COPh	O	LDA, THF, −78°C	CH_3—I	50:50	65
		LDA, THF, −78°C	CH_2=CH—CH_2Br	60:40	61
$COOCH_3$	CH_2	LDA, THF, −75°C	CH_3I	84:16	94.5[a]
NO_2	O	NaH, THF–DMF, 25°C	$pNO_2C_6H_4CH_2Br$	80:20	62
		NaH, THF–DMF, 25°C	D^+, H_2O	100:0	74

[a]Reference 15.

aldehydes **19** and **20** with phenyl magnesium bromide (11) followed by oxidation with pyridinium chlorochromate gave a mixture (ratio 85:15) of phenyl ketones **21** and **22** that can be separated by chromatography.

The *cis* and *trans* nitriles **23** and **24**, which can be obtained pure by chromatography, were prepared by treating a mixture of isomeric esters **17** and **18** with dimethylaluminium amide (12).

Treatment of nitromethane with paraformaldehyde in tetrahydrofuran–hexamethylphosphoramide (5:1) yielded the bishydroxymethylnitromethane (**16**) in 25% yield. Condensation of **16** with pivalaldehyde gave a mixture (ratio 93:7) of *cis* and *trans* nitro 1,3-dioxanes **25** and **26**, which can be obtained pure by chromatography. Finally, catalytic hydrogenation of 4-*tert*-butyl benzoic acid with platinum oxide gave the corresponding cyclohexane carboxylic acids (13), which on esterification with diazomethane yielded a mixture (74:26) of *cis* and *trans* methyl 4-*tert*-butylcyclohexane carboxylates **27** and **28**. Pure samples of each isomer were obtained by a careful chromatography.

Equilibration

The relative stability of the *cis* and the *trans* isomers of 2-*tert*-butyl-1,3-dioxanes having a functional group X at C-5 was determined by equilibration under basic conditions (CH_3ONa, CH_3OH). The isomeric nitro dioxanes **25** and **26** failed to undergo epimerization under the basic conditions used, the equilibration was carried out under acidic conditions (*p*-TSOH, benzene, reflux) presumably via acetal opening and reclosure. The results are the following: the *cis*:*trans* ratio is 16:84 for X = $COOCH_3$, 18:82 for X = COPh, ~50:50 for X = CHO, 75:25 for X = CN, and 63:37 for X = NO_2. Thus, the *trans* isomer (having an equatorial X group) is more stable when the X group is large (X = COOMe, COPh). No discrimination was observed for the smaller CHO group. The *cis* isomer is more stable when X = CN and NO_2, and the preferred axial orientation for these groups has been previously explained (14) on the basis of solvation, orbital interaction, and charge attraction (for NO_2).

Alkylation

Alkylation was carried out for 2-*tert*-butyl-5-X-1,3-dioxane (X = $COOCH_3$, COPh, and NO_2). The results are summarized in Table 1, which contains also the alkylation of methyl 4-*tert*-butylcyclohexane carboxylate recently reported by Krapcho and Dundulis (15).

The enolates of the methyl esters and phenyl ketones were generated with lithium diisopropyl amide (LDA) at −78°C in tetrahydrofuran or dimethoxyethane and alkylated with methyl iodide and allyl bromide. The enolate of the 5-nitro-1,3-dioxanes was produced with sodium hydride.

The rather high stereochemical control in the alkylation of the enolate ester of 1,3-dioxane (more than 95% of isomer **29** (X = $COOCH_3$, R = CH_3 or allyl)) is the result of an equatorial approach of the alkylating agent and it strongly supports the hypothesis of stereoelectronic control. On the other hand, the very poor selectivity observed with the phenyl ketone (even less than the cyclohexane methyl esters) indicates no stereoelectronic control. In this case, the enolate ion is more stable and thus much less reactive, since it is conjugated with an aromatic ring. This important additional stabilization may render the stereoelectronic effects caused by the ring oxygen comparatively less important at the transition state level because the activation energy of this alkylation process must be higher by comparison with that of the ester enolate. This explanation is also in agreement with the fact that in a reaction having a lower energy of activation, i.e. the deprotonation of the phenyl ketone (or the reverse process), the influence of stereoelectronic effects is then clearly observed (*vide infra*).

Attempts to alkylate the anion of nitro 1,3-dioxanes with methyl iodide or allyl bromide led to starting material and nonidentified products. Alkylation with *p*-nitrobenzyl bromide gave an 80:20 ratio of the "equatorial" and "axial" products **29** and **30** in 62% yield. A secondary product, the enol ether **31** (8% yield), which comes from the elimination of HNO_2 from the alkylated product, was also isolated from this reaction (16). The formation of C-alkylated products is, however, the result of an O-alkylation followed by an intramolecular rearrangement that might be a radical process (17). It is therefore difficult to appreciate the contribution of stereoelectronic effects in this case. However, it was found that quenching the nitro enolate with deuterium oxide led exclusively to the *cis* product **29** (X = NO_2, R = D) having a deuterium atom in the equatorial position.

In conclusion, this limited study indicates that stereoelec-

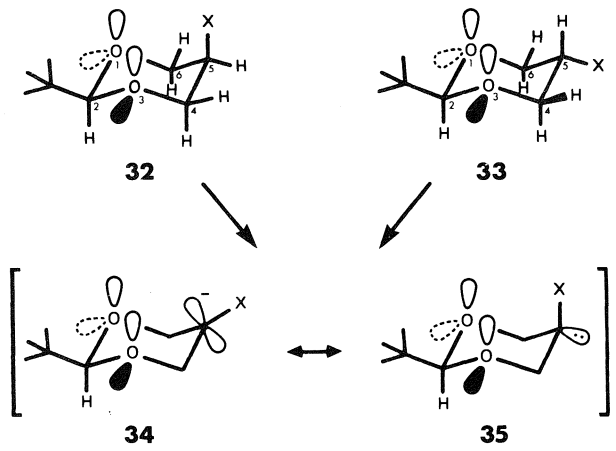

SCHEME 3

tronic factors may play a determining role only in the alkylation of the 1,3-dioxane ester. The specific equatorial protonation of the nitro enolate suggested, however, that the protonation of enolate or the reverse process, i.e. deprotonation, might be more appropriate processes to show the importance of stereoelectronic effects in the reactivity of enolates with electrophiles.

Deprotonation

If stereoelectronic effects are important at the transition state level for deprotonation, the *cis* isomer with an equatorial hydrogen at C-5 (Scheme 3) ought to be more readily deprotonated than the *trans* isomer, which has an axial hydrogen at C-5. In the *cis* isomers **32**, the equatorial C5—H bond to be broken is antiperiplanar to the polar C4—O3 and C6—O1 bonds, whereas in **33** the axial C5—H bond is antiperiplanar to the nonpolar axial C4—H and C6—H bonds. So, in **32**, the electron pair orbital of the equatorial C5—H bond can be delocalized by an interaction with the antibonding orbital (σ^*) of two polar C—O bonds. This electronic delocalization should therefore increase the acidity of the equatorial C-5 hydrogen, and deprotonation of the *cis* isomer **32** (to give the corresponding enolate anion, which should be a hybrid of **34** and **35**) should proceed at a faster rate than that of the *trans* isomer **33**.

The relative rate of deprotonation of the *cis* and *trans* isomers of 5-*tert*-butyl-1,3-dioxanes (X = $COOCH_3$, COPh, CHO, and CN) is shown in Table 2. Deprotonation of *cis* and *trans* methyl 2-*tert*-butyl cyclohexane carboxylate (**27** and **28**) was also measured. The analysis was made by comparing the time required to achieve 50% of deprotonation in each isomer. This was done by treating each isomer with sodium methoxide in methanol-O-*d* and the reaction was followed by ^1H nmr (250 MHz) spectroscopy. Aliquots were taken until the signal for the proton at C-5 had disappeared. A curve of the percentage of starting material versus time was drawn, from which the time that corresponds to 50% of deprotonation was determined ($t_{\frac{1}{2}}$). The 250-MHz ^1H nmr analysis showed clearly that in the dioxane series (X = $COOCH_3$, COPh, CHO, and CN), starting either with the *cis* or the *trans* isomers, only the *cis* monodeuterated isomers **36** were produced first, and the *trans* monodeuterated isomers **37** appeared slowly and became important only after a long period of time, indicating a large preference for an equatorial protonation of the anion.

The results show that the *cis* isomers are much more acidic than the *trans* isomers, when X = $COOCH_3$, COPh, and CHO, and on that basis, clearly, stereoelectronic effects must play a determining role in the relative acidity of these compounds. The

TABLE 2. Rate of deprotonation and deuterium incorporation

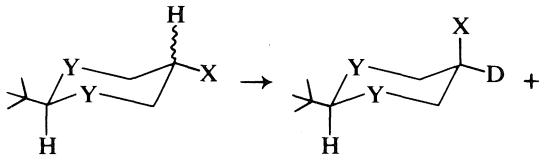

36 (*cis*)

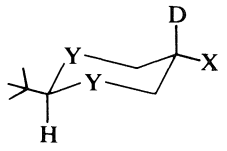

37 (*trans*)

Starting material					
Compounds	Geometry	Y	X	T (°C)	$t_{\frac{1}{2}}$
17	*cis*	O	$COOCH_3$	25°C	4 min
18	*trans*	O	$COOCH_3$	25°C	120 min
21	*cis*	O	COPh	−20°C	1 min
22	*trans*	O	COPh	−20°C	73 min
19	*cis*	O	CHO	−20°C	1 min
20	*trans*	O	CHO	−20°C	30 min
23	*cis*	O	CN	25°C	138 min
24	*trans*	O	CN	25°C	291 min
27	*cis*	CH_2	$COOCH_3$	25°C	101 h
28	*trans*	CH_2	$COOCH_3$	25°C	>8 days

cis nitrile is deprotonated at a slightly faster rate than the *trans* isomer and both are less acidic than the corresponding esters. Thus the type of stereoelectronic effects discussed above does not play a dominant role with nitriles. The *cis* methyl *tert*-butyl cyclohexane carboxylate **27** is also deprotonated at a slightly faster rate than the *trans* isomer **28**, but this can be due to steric effect only or to a combination of steric and less important stereoelectronic effects (due to overlap of the carbon electron pair with the C—C and C—H σ^* antibonding orbital (3)).

The isomeric cyclohexane esters are, however, much less acidic than the corresponding 1,3-dioxane esters, and this striking result indicates that the replacement of two methylene groups by two oxygen atoms in the cyclohexane ring has an enormous influence. This must be due to the inductive effect of the oxygen atoms, which increase the acidity of both the equatorial and axial hydrogen at C-5. The *cis* isomer would, however, be more acidic because in this isomer the equatorial C5—H bond is appropriately aligned in space (antiperiplanar to the C—O bonds) for an additional electronic delocalization.

We have already described that the enolate of the 5-nitro 1,3-dioxanes is protonated exclusively from the equatorial side. It can therefore be concluded that the protonation and deprotonation of 1,3-dioxanes having a functional group at C-5 take place with a very high degree of stereochemical control, and that these results can be taken as evidence that stereoelectronic effects play a key role in these processes.

Experimental

The infrared (ir) spectra were taken on a Perkin–Elmer 681 spectrophotometer. Proton nuclear magnetic resonance (^1H nmr) spectra were recorded on a Bruker WP-60, a Bruker WP-80, or a Bruker WM-250 instrument. Chemical shifts are reported in δ values (ppm) relative to tetramethylsilane or chloroform as internal standard.

Carbon nuclear magnetic resonance (^{13}C nmr) spectra were recorded on a Bruker WM-250 instrument. Melting points were determined on a Rinco M-50 apparatus, and are not corrected. Gas–liquid chromatography (glc) analysis was done on a Varian Aerograph 2868 or a Gas Chromatograph 5710A. The mass spectra (ms) were recorded on a VG Micromass ZAB-1F mass spectrometer.

Reactions were carried out under nitrogen or argon. Anhydrous magnesium sulfate was used as the drying agent in work-up of reactions.

*Dimethyl bishydroxymethylmalonate (**14**)*

To a mixture of potassium carbonate (1.25 g, 9 mmol) in water (4 mL) and 37% formalin (125 mL, 1.66 mol) was added methylmalonate (87.5 mL, 0.76 mol) in portions of 10 mL with agitation in a cold water bath. The solution was stirred at room temperature for 1 h, then a saturated aqueous solution of ammonium sulfate was added and the mixture extracted with ether. The aqueous layer was saturated with solid ammonium sulfate, and extracted again with ether followed by ethyl acetate. Drying and evaporation of the combined organic layers gave the diol **14** (115.6 g, 78%) after crystallization in ethyl acetate; mp 77–78°C; ir ($CHCl_3$): 3570, 3020, 2960, 1730, and 1040 cm^{-1}; ^1H nmr ($CDCl_3$) δ: 4.11 (4H, s, —CH_2OH), 3.79 (6H, s, —OCH_3), 2.85 (2H, br, —OH).

*2-tert-Butyl-1,3-dioxane-5,5-dicarboxylic acid dimethyl diester (**15**)*

Pivalaldehyde (12 mL, 0.11 mol), diol **14** (19.2 g, 0.1 mol), *p*-toluenesulfonic acid (0.8 g), and benzene (70 mL) were placed in a flask equipped with a Dean–Stark trap. The reaction mixture was kept at reflux temperature for 4 h, after which approximately 1.6 mL of water was removed. After cooling at room temperature, anhydrous sodium acetate (0.7 g) was added and the mixture stirred for 20 min. After filtration, the solution was diluted with ether and washed three times with water. Drying and evaporation of the organic phase gave pure diester **15** (25.8 g, 99%), which crystallized in hexane – ethyl acetate (2:8); mp 79°C; ir ($CHCl_3$): 3020, 2960, and 1735 cm^{-1}; ^1H nmr ($CDCl_3$) δ: 4.7 (2H, d of t, J = 11.46 Hz, 1.45 Hz, —OCH_2—, equatorial protons), 4.10 (1H, s, C2-H), 3.88 (2H, d of t, J = 11.46 Hz, 1.45 Hz, —OCH_2—, axial protons), 3.83 (3H, s, —OCH_3, axial ester), 3.71 (3H, s, —OCH_3, equatorial ester), 0.87 (9H, s, *tert*-butyl).

Cis *and* trans *2-tert-butyl-1,3-dioxane-5-carboxylic acid methyl esters (**17** and **18**)*

Lithium chloride (0.848 g, 20 mmol), water (0.54 g, 30 mmol), and diester **15** (2.6 g, 10 mmol) in 25 mL of dimethyl sulfoxide were mixed in a flask that was heated on an oil bath at 140–145°C for 4 h. The cooled solution was then poured into ice water, saturated with sodium chloride, extracted with hexane (5 × 30 mL), and the combined organic layers dried. An aliquot was analyzed by glc (column 5 ft × $\frac{1}{4}$ in. 5% FFAP on Chromosorb W; 60–80 mesh, 180°C), and showed 89% of *cis* isomer **17** and 11% of *trans* isomer **18**. Separation on silica gel with 5% ethyl acetate – hexane gave isomers **17** (1.44 g) and **18** (180 mg) in 80% combined yield. Cis *isomer **17**:* mp 35°C; ir ($CHCl_3$): 3000–2860 and 1735 cm^{-1}; ^1H nmr ($CDCl_3$) δ: 4.59 (2H, d of q, J = 11.8 Hz, 2.7 Hz, 1.4 Hz, —OCH_2—, equatorial protons), 4.12 (1H, s, C2-H), 3.84 (2H, d of q, J = 11.8 Hz, 3.1 Hz, 1.4 Hz, —OCH_2—, axial protons), 3.79 (3H, s, —OCH_3), 2.28 (1H, sept, J = 1.4 Hz, C5-H), 0.88 (9H, s, *tert*-butyl). Trans *isomer **18**:* mp 50–51°C; ir ($CHCl_3$): 3020–2880 and 1735 cm^{-1}; ^1H nmr ($CDCl_3$) δ: 4.37 (2H, apparent d of d of d, J = 11.7 Hz, 4.8 Hz, 1.4 Hz, —OCH_2—, equatorial protons), 4.03 (1H, s, C2-H), 3.75 (2H, apaprent d of d of d, J = 12.4 Hz, 10.5 Hz, 1.5 Hz, —OCH_2—, axial protons), 3.68 (3H, s, —OCH_3), 2.94 (1H, t of t, J = 12.3 Hz, 11.2 Hz, 4.7 Hz, C5-H), 0.91 (9H, s, *tert*-butyl).

Cis *and* trans *2-tert-butyl-5-formyl-1,3-dioxanes (**19** and **20**)*

Esters **17** and **18** (89:11 mixture) (2.63 g, 13 mmol) in ether (20 mL) were added during 1 h with stirring to a suspension of lithium aluminium hydride (2 g, 54 mmol) in ether (80 mL) at 0°C. The reaction mixture was stirred for an additional half-hour at room temperature. Saturated aqueous sodium sulfate solution (20 mL) was added at −40°C, and the mixture was poured into a saturated aqueous ammonium chloride solution (100 mL) and extracted with ether. The aqueous layer was filtered and the solution extracted with methylene chloride. The combined organic layers were dried and the solvents evaporated to afford, after flash chromatography with 40% ethyl acetate – hexane, 1.8 g (80%) of alcohol. Pyridinium chlorochromate (3.12 g, 14.5 mmol) and powdered molecular sieves 3 Å (3.35 g) were suspended in methylene chloride (50 mL). The above alcohol (1.68 g, 9.64 mmol) in methylene chloride (10 mL) was added and the reaction mixture stirred at room temperature for 1 h, then diluted with ether and filtered on Florisil. This afforded after evaporation a mixture of aldehydes **19** and **20** (1.39 g, 84%). A pure analytical sample of isomer **19** was obtained by fractional crystallization. *Isomer **19**:* mp 44–45°C; ir ($CHCl_3$): 2960, 2920, 2860, 1725, and 1150 cm^{-1}. ^1H nmr ($CDCl_3$) δ: 9.96 (1H, d, J = 0.7 Hz, —CHO), 4.55 (2H, d of t, J = 10.6 Hz, 1.4 Hz, —OCH_2—, equatorial protons), 4.15 (1H, s, C2-H), 3.95 (2H, d of m, J = 11 Hz, —OCH_2—, axial protons), 2.04 (1H, sept, J = 1.3 Hz, C5-H), 0.86 (9H, s, *tert*-butyl). *Isomer **20**:* ^1H nmr ($CDCl_3$) δ: 9.60 (1H, d, J = 1 Hz, —CHO), 4.34 (2H, d of d of d, J = 11.8 Hz, 4.7 Hz, 1.5 Hz, —OCH_2—, equatorial protons), 4.00 (1H, s, C2-H), 3.71 (2H, apparent t of d, J = 13 Hz, 10.5 Hz, 1.5 Hz, —OCH_2—, axial protons), 3.03 (1H, t of t of d, J = 13 Hz, 11 Hz, 4.7 Hz, 1.2 Hz, C5-H), 0.89 (9H, s, *tert*-butyl).

Cis *and* trans *2-tert-butyl-5-phenylketone-1,3-dioxanes (**21** and **22**)*

To a stirred solution of phenylmagnesium bromide (2.96 mL, 2.9 *M* in ether, 8.58 mmol) in ether (40 mL) at 0°C was added dropwise a solution of a mixture of aldehydes **19** and **20** (738 mg, 4.29 mmol) in anhydrous ether (5 mL). The reaction mixture was stirred for an additional 2 h at 0°C. Water (10 mL) was added, and the reaction mixture was allowed to warm to room temperature and then extracted with ether. The organic layer was dried and the ether evaporated to give, after flash chromatography with 20% ethyl acetate – hexane, 1.04 g (97%) of alcohol. Pyridinium chlorochromate (1.734 g, 8 mmol) and powdered molecular sieves 3 Å (2 g) were suspended in methylene chloride (150 mL). The above benzyl alcohol (1 g, 4 mmol) in methylene chloride (10 mL) was added and the mixture stirred at room temperature for 8 h. The solution was diluted with ether and filtered on Florisil. Separation on silica gel (1% acetone–chloroform) gave isomer **21** (85%) and isomer **22** (15%) (862 mg, 86.5% yield). *Isomer **21**:* mp 158–159°C; ir ($CHCl_3$): 3010, 2960, 2860, 1690, 1600, and 1150 cm^{-1}; ^1H nmr ($CDCl_3$): δ: 7.80–7.48 (5H, m, —C_6H_5), 4.58 (2H, d of q, J = 10.5 Hz, 1.3 Hz, —OCH_2—, equatorial protons), 4.14 (1H, s, C2-H), 4.05 (2H, d of d of t, J = 11.1 Hz, 3.7 Hz, 1.5 Hz, —OCH_2—, axial protons), 3.1 (1H, m, C5-H), 0.87 (9H, s, *tert*-butyl). *Isomer **22**:* mp 101–102°C; ^1H nmr ($CDCl_3$) δ: 7.97–7.50 (5H, m, —C_6H_5), 4.31 (2H, d of d of d, J = 11 Hz, 4.3 Hz, 1.8 Hz, —OCH_2—, equatorial protons), 4.13 (1H, s, C2-H), 3.93 (m, C5-H and —OCH_2—, axial protons), 0.94 (9H, s, *tert*-butyl).

Cis *and* trans *2-tert-butyl-5-cyano-1,3-dioxanes (**23** and **24**)*

Preparation of a solution of dimethylaluminium amide

To a solution of trimethylaluminium (15 mL, 2 *M* in toluene) in dry methylene chloride (5 mL) was added excess of ammonia (~10 mL) distilled from sodium. When the addition of ammonia was complete, the solution was stirred at room temperature until no more gas evolution. This makes an approximately 1.5 *M* solution of dimethylaluminium amide. A solution of a mixture of esters **17** and **18** (101 mg, 0.5 mmol) in dry xylene (20 mL) was treated with dimethylaluminium amide (700 μL, 1.05 mmol). The mixture was refluxed for 20 h, then cooled and treated with water (10 mL). The aqueous layer was extracted with ethyl acetate. The combined organic layers were dried and the solvents were evaporated under reduced pressure to give *cis* nitrile **23** (41.4%) and *trans* nitrile **24** (13%), after separation on silica gel with 5% ethyl acetate – benzene. *Isomer **33**:* mp 100–101°C; ir ($CHCl_3$): 2980, 2860, and 2245 cm^{-1}; ^1H nmr ($CDCl_3$) δ: 4.30 (2H, d of q, J = 11.9 Hz, 1.4 Hz, —OCH_2—, equatorial protons), 4.12 (1H, s, C2-H), 3.86 (2H, d of q, J = 11.6 Hz, 2.7 Hz, 1.3 Hz, —OCH_2—, axial protons), 2.57 (1H, sept, J = 1.3 Hz, C5-H), 0.94

(9H, singlet, *tert*-butyl). *Isomer **24**:* mp 118–119°C; ^{1}H nmr ($CDCl_3$) δ: 4.36 (2H, d of d, J = 11.5 Hz, 4.7 Hz, 1.5 Hz, —OCH_2—, equatorial protons), 4.10 (s, C2-H), 3.79 (2H, d of d of d, J = 12 Hz, 11.4 Hz, 1.5 Hz, —OCH_2—, axial protons), 3.03 (1H, t of t, J = 11.2 Hz, 4.7 Hz, C5-H), 0.88 (9H, s, *tert*-butyl).

*Bishydroxymethylnitromethane **16***

n-Butyllithium (19 mL, 1.56 *M* in hexane, 28.9 mmol) was added to a solution of nitromethane (780 μL, 14.43 mmol) in tetrahydrofuran–hexamethylphosphoramide (5:1). The mixture was stirred for 1 h at −78°C, then paraformaldehyde (1 g) was added in one portion and the reaction mixture was heated to room temperature and refluxed for 2 h. After cooling, saturated aqueous ammonium sulfate solution was added and the mixture extracted with ethyl acetate. The aqueous layer was saturated with solid ammonium sulfate and extracted again with ethyl acetate. The combined organic layers were dried and the solvents evaporated to give diol **16** (446 mg, 25.5%); ^{1}H nmr (acetone-d_6) δ: 4.86 (1H, quint, J = 5.9 Hz, CH), 4.56 (2H, br s, OH), 4.00 (4H, d, J = 5.9 Hz, CH_2).

Cis *and* trans 2-tert-*butyl-5-nitro-1,3-dioxanes (**25** and **26**)*

Pivaldehyde (380 μL, 3.5 mmol), trimethyl orthoformate (328 μL, 3 mmol), diol **16** (332 mg, 2.74 mmol), and *p*-toluenesulfonic acid (24 mg) in benzene (100 mL) were refluxed in a flask equipped with a condenser and a Dean–Stark trap. After 5 h the mixture was cooled and sodium acetate was added. After filtration, the solution was diluted with ether and washed with water. The organic layer was dried and the solvents evaporated. Flash chromatography with 40% ethyl acetate – hexane gave *cis* isomer **25** (308 mg, 59.5%) and *trans* isomer **26** (23.5 mg, 4.5%). *Isomer **25**:* mp 112–113°C; ir ($CHCl_3$): 2960, 1555, and 1150 cm^{-1}; ^{1}H nmr ($CDCl_3$) δ: 4.88 (2H, d of q, J = 11.8 Hz, 1.3 Hz, —OCH_2—, equatorial protons), 4.18 (1H, s, C2-H), 4.13 (1H, sept, J = 1.3 Hz, C5-H), 4.03 (2H, d of q, J = 11.8 Hz, 1.3 Hz, —OCH_2—, axial protons), 0.87 (9H, s, *tert*-butyl); ^{13}C nmr ($CDCl_3$) δ: 107.95 (C2), 77.45 (C5), 66.25 (C4, C6), 35 (C^{IV} of *tert*-butyl), 24.27 (CH_3 of *tert*-butyl); ms *m/e* (CI methane): 190 (MH^+), 143 (M − NO_2), 132 (M − $C(CH_3)_3$). *Isomer **26**:* ^{1}H nmr ($CDCl_3$) δ: 4.68 (1H, sept, J = 5 Hz, C5-H), 4.55 (2H, d of d of d, J = 11 Hz, 5.1 Hz, 1.5 Hz, —OCH_2—, equatorial protons), 4.07 (1H, s, C2-H), 3.98 (2H, d of d of d, J = 10.7 Hz, 1.4 Hz, —OCH_2—, axial protons), 0.90 (9H, s, *tert*-butyl).

Cis *and* trans *methyl 4*-tert-*butyl cyclohexane carboxylates (**27** and **28**)*

4-*tert*-Butyl benzoic acid (1 g, 5.6 mmol) and platinum oxide (112 mg) were suspended in glacial acetic acid (5 mL) in a hydrogenation apparatus. The mixture, mechanically stirred, was allowed to hydrogenate under hydrogen atmosphere (50 psi (1 psi = 6.9 kPa)) for 3 h at room temperature. The catalyst was removed by filtration and acetic acid evaporated. The resulting crude acid was dissolved in ether and diazomethane added dropwise at 0°C until the yellow coloration persisted. Ether was evaporated to give a mixture (74:26 as shown by glc) of *cis* and *trans* isomers **27** and **28** in a 95% overall yield. Analytically pure samples of each isomer were obtained by flash chromatography with 4% ethyl acetate – benzene. *Isomer **27**:* ir ($CHCl_3$): 2960, 2870, and 1740 cm^{-1}: ^{1}H nmr ($CDCl_3$) δ: 3.68 (3H, s, —OCH_3), 2.62 (1H, m, C1-H), 2.20–1.42 (4H, m, —CH_2—, equatorial protons), 1.60–1.10 (5H, m, C4-H and —CH_2—, axial protons), 0.82 (9H, s, *tert*-butyl); ^{13}C nmr ($CDCl_3$) δ: 175.59, 51.22, 47.96, 38.91, 32.40, 27.96, 27.36, and 23.79. *Isomer **28**:* ^{1}H nmr ($CDCl_3$) δ: 3.65 (3H, s, —OCH_3), 2.20 (1H, t of t, J = 12.6 Hz, 11.2 Hz, 3.7 Hz, C1-H), 2.14 (4H, m, —CH_2—, equatorial protons), 1.85–0.99 (5H, m, C4-H and —CH_2—, axial protons), 0.84 (9H, s, *tert*-butyl); ^{13}C nmr ($CDCl_3$) δ: 176.6, 51.3, 47.38, 43.43, 32.33, 29.52, 27.41, and 26.55.

2-tert-*Butyl-5-carbomethoxy-5-methyl-1,3-dioxanes (**29** and **30**)*

n-Butyllithium (900 μL, 1.7 *M* in hexane, 1.5 mmol) was added to a solution of diisopropylamine (210 μL, 1.5 mmol) in anhydrous tetrahydrofuran (10 mL) at 0°C and the mixture stirred for 30 min. The temperature was lowered to −78°C and ester **17** (89:11 mixture with isomer **18**) (101 mg, 0.5 mmol) in anhydrous tetrahydrofuran (1 mL) was added via a cannula. The reaction mixture was stirred for 1 h and methyl iodide (130 μL, 2 mmol) was added. The stirring was continued at −78°C for 30 min (reaction monitored by thin-layer chromatography). Saturated aqueous ammonium chloride solution (5 mL) was added and the mixture stirred at room temperature. The solution was extracted with ether, the organic layer washed with saturated aqueous sodium thiosulfate solution, dried, and the ether was evaporated. Gas–liquid chromatographic analysis showed methyl equatorial isomer **29** (98%) and methyl axial isomer **30** (2%) in 70% yield. The isomers were separated by flash chromatography with 20% ethyl acetate – hexane. *Isomer **29**:* mp 93–94°C; ir ($CHCl_3$): 2990–2860, 1738, and 1130–1100 cm^{-1}; ^{1}H nmr ($CDCl_3$) δ: 4.47 (2H, d, J = 11.2 Hz, —OCH_2—, equatorial protons), 4.06 (1H, s, C2-H), 3.76 (3H, s, —OCH_3), 3.37 (2H, d, J = 11.3 Hz, —OCH_2—, axial protons), 0.94 (3H, s, —CH_3), 0.87 (9H, s, *tert*-butyl); ^{13}C nmr ($CDCl_3$) δ: 174.86 (C=O), 107.67 (C2), 73.27 (C4, C6), 52.06 (—OCH_3), 42.4 (C5), 34.74 (C^{IV} of *tert*-butyl), 24.48 (CH_3 of *tert*-butyl), 17.57 (CH_3). *Isomer **30**:* mp 56–57°C; ir ($CHCl_3$): 3020–2880, 1730, and 1100 cm^{-1}; ^{1}H nmr ($CDCl_3$) δ: 4.01 (1H, s, C2-H), 3.91 (2H) and 3.83 (2H) (two doublets, J_{AB} = 11.1 Hz, —OCH_2—), 3.67 (3H, s, —OCH_3), 1.45 (3H, s, —CH_3), 0.92 (9H, s, *tert*-butyl); ^{13}C nmr ($CDCl_3$) δ: 174.01 (C=O), 107.8 (C2), 72.15 (C4, C6), 51.74 (—OCH_3), 41.01 (C5), 34.75 (C^{IV} of *tert*-butyl), 24.53 (CH_3 of *tert*-butyl), 18.97 (CH_3).

2-tert-*Butyl-5-allyl-5-carbomethoxy-1,3-dioxanes (**29** and **30**)*

n-Butyllithium (900 μL, 1.5 mmol) was added to a solution of diisopropylamine (210 μL, 1.5 mmol) in anhydrous dimethoxyethane at 0°C and the mixture stirred for 45 min. Ester **17** (89:11 mixture with isomer **18**) (101 mg, 0.5 mmol) was added at −78°C via a cannula. The solution was stirred for 1.5 h and allyl bromide (170 μL, 2 mmol) was added. The stirring was continued at −78°C for an additional 1.5 h, after which the mixture was warmed to room temperature. Saturated aqueous ammonium chloride solution (5 mL) was added and the solution extracted with ether. The organic layer was dried and the ether evaporated to give (after purification on silica gel with 20% ethyl acetate – hexane) a mixture (80 mg, 66%) of allyl equatorial isomer **29** (95%) and allyl axial isomer **30** (5%) as determined by glc. Pure analytical samples of each isomer were obtained by preparative gas–liquid chromatography at 130°C. *Isomer **29**:* ir ($CHCl_3$): 3080, 2960, 1730, 1640, and 1125 cm^{-1}; ^{1}H nmr ($CDCl_3$) δ: 5.60 (1H, m, olefinic proton), 5.03 (2H, m, olefinic protons), 4.45 (2H, d, J = 11.3 Hz, —OCH_2—, equatorial protons), 4.01 (1H, s, C2-H), 3.71 (3H, s, —OCH_3), 3.40 (2H, d, J = 11.3 Hz, —OCH_2—, axial protons), 2.02 (2H, d, J = 7.1 Hz, —CH_2—CH=CH_2), 0.83 (9H, s, *tert*-butyl); ^{13}C nmr ($CDCl_3$) δ: 173.58 (C=O), 131.14 (—CH=), 118.76 (=CH_2), 107.83 (C2), 72.20 (C4, C6), 51.88 (—OCH_3), 45.93 (C5), 37.1 (—CH_2—), 34.75 (C^{IV} of *tert*-butyl), 24.46 (CH_3 of *tert*-butyl). *Isomer **30**:* ^{1}H nmr ($CDCl_3$) δ: 6.00–4.90 (3H, m, olefinic protons), 4.17 (1H, s, C2-H), 4.01 (3.84 (4H, apparent doublet, J = 10 Hz, —OCH_2—), 3.66 (3H, s, —OCH_3), 2.68 (2H, d, J = 7 Hz, —CH_2—CH=), 0.92 (9H, s, *tert*-butyl); ^{13}C nmr ($CDCl_3$) δ: 172.68 (C=O), 133.13 (—CH=), 118.72 (=CH_2), 107.78 (C2), 70.13 (C4, C6), 51.54 (—OCH_3), 44.7 (C5), 35.97 (—CH_2—), 34.73 (C^{IV} of *tert*-butyl), 24.44 (—CH_3 of *tert*-butyl).

2-tert-*Butyl-5-methyl-5-phenylketone-1,3-dioxanes (**29** and **30**)*

n-Butyllithium (228 μL, 1.55 *M* in hexane) was added to a solution of diisopropylamine (51 μL, 0.35 mmol) in anhydrous tetrahydrofuran (5 mL) at 0°C and the mixture stirred for 1 h, after which the temperature was lowered to −78°C. Phenylketone **21** (35 mg, 0.14 mmol) in anhydrous tetrahydrofuran (3 mL) was added via a cannula and the reaction mixture stirred for 2 h. Methyl iodide (46 μL) was added at −78°C and the reaction stirred at this temperature for 2 h and at room temperature for 14 h. Saturated aqueous ammonium chloride solution (1 mL) was added and the solution extracted with ether. The organic layer was washed with saturated aqueous sodium thiosulfate solution, dried, and the solvents were evaporated. This gave, after flash chromatography with 20% ethyl acetate – hexane, methyl equatorial isomer **29** (50%) and methyl axial isomer **30** (50%) in 65% yield.

Isomer ***29****:* mp 148–149°C; ^{1}H nmr ($CDCl_3$) δ: 7.51 (5H, m, —C_6H_5), 4.71 (2H, d, J = 11 Hz, —OCH_2—, equatorial protons), 4.14 (1H, s, C2-H), 3.47 (2H, d, J = 11 Hz, —OCH_2—, axial protons), 1.07 (3H, s, —CH_3), 0.87 (9H, s, *tert*-butyl); ms *m/e*: 261 (M − H), 247 (M − CH_3), 205 (M − $C(CH_3)_3$). *Isomer* ***30****:* ^{1}H nmr ($CDCl_3$) δ: 7.66–7.49 (5H, m, —C_6H_5), 4.23 (2H, d, J = 11.1 Hz, —OCH_2—, equatorial protons), 4.02 (1H, s, C2-H), 3.86 (2H, d, J = 11 Hz, —OCH_2—, axial protons), 1.68 (3H, s, —CH_3), 0.94 (9H, s, *tert*-butyl); ms *m/e*: 261 (M − H), 247 (M − CH_3), 205 (M − $C(CH_3)_3$).

*2-*tert*-Butyl-5-allyl-5-phenylketone-1,3-dioxanes (****29*** *and* ***30****)*

n-Butyllithium (2.2 mL, 1.55 *M* in hexane) was added to a solution of diisopropylamine (486 μL, 3.4 mmol) in anhydrous tetrahydrofuran (5 mL) at 0°C and the mixture stirred for 1 h, then cooled to −78°C. Phenylketone **21** (280 mg, 1.125 mmol) in anhydrous tetrahydrofuran (5 mL) was added and stirring continued for 2.5 h. Allyl bromide (382.5 μL, 4.5 mmol) was added and the mixture allowed to stir at room temperature for 24 h. After habitual work-up and purification on silica gel with 1% acetone–chloroform, a mixture (202 mg, 61%) of allyl equatorial isomer **29** (60%) and allyl axial isomer **30** (40%) (determined by glc) was isolated. Analytically pure samples were obtained by careful fractional crystallization in hexane. *Isomer* ***29****:* ^{1}H nmr ($CDCl_3$) δ: 7.5 (5H, m, —C_6H_5), 6.5 (3H, m, olefinic protons), 4.71 (2H, apparent doublet, J = 11.6 Hz, —OCH_2—, equatorial protons), 4.13 (1H, s, C2-H), 3.54 (2H, apparent doublet, J = 11.7 Hz, —OCH_2—, axial protons), 2.22 (2H, d, J = 6.5 Hz, —CH_2—CH=), 0.86 (9H, s, *tert*-butyl); ms *m/e*: 288 (M), 231 (M − $C(CH_3)_3$). *Isomer* ***30****:* ^{1}H nmr ($CDCl_3$) δ: 7.50 (5H, m, —C_6H_5), 6.50 (3H, m, olefinic protons), 4.37 (2H, apparent doublet, J = 11.8 Hz, —OCH_2—, equatorial protons), 4.03 (1H, s, C2-H), 3.82 (2H, apparent doublet, —OCH_2—, axial protons), 3.00 (2H, d, J = 7 Hz, —CH_2—CH=), 0.94 (9H, s, *tert*-butyl).

*2-*tert*-Butyl-5-nitro-5-*p*-nitrobenzyl-1,3-dioxanes (****29*** *and* ***30****)*

To sodium hydride (washed from oil with hexane) (16 mg) suspended in anhydrous tetrahydrofuran – dimethylformamide (2:1) (3 mL) was added, at 0°C, nitrodioxane **25** (47.3 mg, 0.25 mmol) in tetrahydrofuran (0.5 mL). The mixture was stirred at room temperature for 1 h, and *p*-nitrobenzyl bromide (108 mg, 0.5 mmol) in tetrahydrofuran (1 mL) was added. The reaction was stirred at room temperature for an additional 2 h. Saturated aqueous ammonium chloride solution was added and the mixture was extracted with ether, the organic layer dried, and the ether evaporated. Separation on silica gel with 4% ethyl acetate – hexane afforded equatorial isomer **29** (49%) and axial isomer **30** (13%). Compound **31** (8%) resulting from elimination of HNO_2 was also isolated. *Isomer* ***29****:* ir ($CHCl_3$) δ: 8.18, 7.30 (4H, m, —C_6H_4—), 4.21 (2H, d of t, J = 10.1 Hz, 1.5 Hz, —OCH_2—, equatorial protons), 4.12 (1H, s, C2-H), 3.93 (2H, d of t, J = 11.6 Hz, 1.5 Hz, —OCH_2—, axial protons), 3.61 (2H, s, —CH_2—$C_6H_4NO_2$), 1.00 (9H, s, *tert*-butyl); ms *m/e*: 323 (M − H), 267 (M − $C(CH_3)_3$). *Isomer* ***30****:* ir ($CHCl_3$): 3020, 2960, 1660, 1520, 1350, and 1130 cm^{-1}; ^{1}H nmr ($CDCl_3$) δ: 8.21 (2H, d, J = 8.8 Hz, —$C_6H_4NO_2$), 7.47 (2H, d, J = 8.8 Hz, —$C_6H_4NO_2$), 5.15 (2H, s, —CH_2—$C_6H_4NO_2$), 5.15 and 4.46 (2 × 1H, d of t, J = 15.6 Hz, 14.2 Hz, 1.1 Hz, —OCH_2—, equatorial protons), 4.26 (2H, apparent triplet of triplet, J = 14.8 Hz, 14 Hz, 1.1 Hz, —OCH_2—, axial protons), 4.23 (1H, s, C2-H), 0.92 (9H, s, *tert*-butyl). *Compound* ***31****:* ir ($CHCl_3$): 3010, 2960, 2920, 1600, 1520, and 1100 cm^{-1}; ^{1}H nmr ($CDCl_3$) δ: 8.20 (2H, d, J = 6.8 Hz, —$C_6H_4NO_2$), 7.27 (2H, d, J = 7.1 Hz, —$C_6H_4NO_2$), 6.45 (1H, s, —OCH=), 4.85 (2H, d, J = 13.4 Hz, —OCH_2—), 4.48 (2H, s, —CH_2—$C_6H_4NO_2$), 4.30 (1H, s, C2-H), 0.92 (9H, s, *tert*-butyl); ms *m/e*: 276 (M − H), 220 (M − $C(CH_3)_3$).

Deuterium incorporation, typical example

Sodium metal (6 mg, 0.25 mmol) was dissolved in methanol-O-*d* (2 mL), and ester **17** (50.5 mg, 0.25 mmol) in methanol-O-*d* (2 mL) was added in one portion. Aliquots (250 μL each) were taken at 1, 5, 15, 30, 45 min, and more, quenched by saturated aqueous ammonium chloride solution, and extracted with ether. The organic layer was dried and the ether evaporated. The residue was dissolved in $CDCl_3$ and analyzed (250 MHz ^{1}H nmr).

Acknowledgements

Support for this work by the Natural Sciences and Engineering Research Council of Canada (NSERCC) and by the "Ministère de l'Éducation" (FCAR), Quebec, is gratefully acknowledged.

1. B. Bernet, P. M. Bishop, M. Caron, T. Kawamata, B. L. Roy, L. Ruest, S. Sauvé, and P. Deslongchamps. Can. J. Chem. **63**, 2810 (1985); **63**, 2814 (1985); **63**, 2818 (1985).
2. P. Deslongchamps. *In* Stereoelectronic effects in organic chemistry. Organic Chemistry Series. Vol. 1. *Edited by* J. E. Baldwin. Pergamon Press, Oxford, England. 1983. pp. 283–284.
3. M. Caron, T. Kawamata, L. Ruest, P. Soucy, and P. Deslongchamps. Can. J. Chem. **64**, 0000 (1985).
4. H. D. Banks. J. Org. Chem. **46**, 1743 (1981).
5. (*a*) J. Klein. Tetrahedron Lett. **44**, 4307 (1973); (*b*) J. Klein. Tetrahedron, **30**, 3349 (1974).
6. H. Gault and A. Roesch. Bull. Soc. Chim. 1411 (1937).
7. C. S. Rondestvedt, Jr. J. Org. Chem. **26**, 2247 (1961).
8. A. P. Krapcho and J. F. Weimasster. J. Org. Chem. **45**, 4105 (1980).
9. R. F. Nystrom and W. G. Brown. J. Am. Chem. Soc. **69**, 1197 (1947).
10. E. J. Corey and J. W. Suggs. Tetrahedron Lett. **31**, 2647 (1975).
11. M. P. Dreyfuss. J. Org. Chem. **28**, 3269 (1963).
12. J. L. Wood, N. A. Khatri, and S. M. Weinreb. Tetrahedron Lett. **51**, 4907 (1979).
13. H. A. Lau and H. Hart. J. Am. Chem. Soc. **81**, 4897 (1959).
14. (*a*) R. J. Abraham, H. D. Banks, E. L. Eliel, O. Hofer, and M. K. Kaloustian. J. Am. Chem. Soc. **94**, 1913 (1972); (*b*) M. K. Kaloustian, N. Dennis, S. Mager, S. A. Evans, I. Alcudia and E. L. Eliel. J. Am. Chem. Soc. **98**, 956 (1976).
15. A. P. Krapcho and E. A. Dundulis. J. Org. Chem. **45**, 3236 (1980).
16. (*a*) R. Beugelmans, A. Lechevallier, and H. Rousseau. Tetrahedron Lett. **24**, 1787 (1983); (*b*) M. P. Crozet and P. Vanelle. Tetrahedron Lett. **26**, 323 (1985).
17. V. I. Erashko, S. A. Shevelev, and A. A. Fainzil'berg. Russ. Chem. Rev. **35**, 719 (1966).

Study of photocatalytic reaction of methanol with water over Rh-, and Pd-loaded TiO_2 catalysts. The role of added alkali metal cations

SHUICHI NAITO

Research Centre for Spectrochemistry, Faculty of Science, The University of Tokyo, Hongo, Bunkyo-Ku, Tokyo, 113, Japan

Received January 31, 1986

SHUICHI NAITO. Can. J. Chem. **64**, 1795 (1986).

The product selectivity of the photocatalytic reaction of methanol with water is changed drastically by the addition of alkali metal cations to Rh- and Pd-loaded TiO_2 catalysts. Over alkali metal cation free catalysts, the main products are 1:1 ratio of H_2 and dimethoxymethane, which is replaced with H_2, methyl formate, and CO_2 over alkali metal cation added catalysts. The role of added alkali metal cations is the stabilization of the reaction intermediate as adsorbed formate instead of adsorbed formaldehyde, which causes the selectivity change from dimethoxymethane to methyl formate.

SHUICHI NAITO. Can. J. Chem. **64**, 1795 (1986).

Lors de la réaction photocatalytique du methanol et de l'eau, la sélectivité des produits change d'une façon drastique par l'addition de cations de métaux alcalins aux catalyseurs de TiO_2 saturés de Rh ou de Pd. Avec des catalyseurs ne contenant pas de cations de métaux alcalins, les produits principaux sont le H_2 et le diméthoxyméthane dans un rapport de 1:1; lorsque des cations de métaux alcalins sont ajoutés aux catalyseurs, les produits il y a formation de H_2, de formate de méthyle et de CO_2. Les cation des métaux alcalins qui sont ajoutés stabilisent l'intermédiaire réactionnel sous la forme d'une formate plutôt que de formaldéhyde adsorbé et ceci provoque le changement de sélectivieé du diméthoxyméthane vers le formate de méthyle.

[Traduit par la revue]

Extensive studies have been carried out to discover effective photocatalysts which convert solar energy into useful chemical compounds. Although many catalytic systems have been reported so far, they are mainly concerned with the efficiency of the photon energy conversion, and the control of the selectivity of the photoreaction has not attracted much attention. For instance, platinized titanium dioxide catalyzes many photoreactions including the decomposition of water (1–4), but the role of platinum tends to be recognized as an electron collector to receive electrons from the conduction band of TiO_2 and reduce the reactants. From the viewpoint of heterogeneous catalysis, it is interesting to modify these electron transfer sites and control the reaction selectivity.

Recently, we have reported that addition of alkali metal cations to Rh-, Pd-, and Pt-loaded TiO_2 catalysts can change the products selectivity of the photoreaction of methanol with water (5). The effect of alkali metal cation was remarkable and the main products changed drastically from H_2 and dimethoxymethane over Rh/TiO_2 to H_2, methyl formate, and CO_2 over $Rh–Na/TiO_2$. In this report, the role of the added alkali metal cations was studied in detail, by comparing the kinetic behaviour of alkali metal cation added catalysts with that of the catalysts free of alkali metal cations.

Experimental

The catalysts were prepared by a conventional impregnation method of precursor salts (5 wt%) onto TiO_2 powder (Aerosil P-25). For catalysts free of alkali metal cations, $RhCl_3$ and $(NH_4)_2PdCl_4$ were used as precursors. To add alkali metal cations, M_3RhCl_6 and M_2PdCl_4 (M = Li, Na, and Rb) type salts were employed.

The pretreatment of the catalysts was carried out as follows: 1 g of the catalyst was spread on the flat bottom of a quartz reaction cell (the area of the exposed catalyst was ca. 30 cm^2 and its depth was 1–2 mm), which was connected to a closed gas circulation system (total volume = ca. 305 cm^3). After evacuation at room temperature, the catalyst was reduced under 40 kPa of H_2 at 773 K for 20 h. Formed water was gathered in the liquid nitrogen cold trap of the circulation system. The dispersion of the reduced catalyst was determined by H_2 adsorption at room temperature (Rh/TiO_2 and $Rh–Na/TiO_2$ catalysts, 30–40% dispersion; and Pd/TiO_2 and $Pd–Na/TiO_2$ catalysts, 5–10% dispersion). The reduced catalyst exhibited photocatalytic activity for the reaction of methanol with water, but the rate was slow and not reproducible. To obtain constant activities, the catalyst was then oxidized under 40 kPa of O_2 at 573 K for 2 h prior to the photoreaction.

The reaction was carried out in the closed gas circulation system mentioned above. A mixture of methanol and water vapour was introduced in the system and the catalyst was irradiated by a 500 W Xe lamp (Ushio UXL500D) through the flat bottom of the reaction cell. In the reaction at room temperature, the reaction cell was air-cooled from the side and kept at 308 K in a stationary state under irradiation. For experiments on the determination of activation energy, the temperature was controlled by putting a bottom-opened furnace around the reaction cell. The products were analyzed by gas chromatography at certain intervals. For H_2 analysis, molecular sieve 13X column was used with Ar carrier at room temperature and for other products, Porapak Q column was used with He carrier at elevated temperatures. The identification of the products was performed by means of mass spectroscopy (UTI 100) as well as infrared spectroscopy (JASCO IRA-2) after the separation of each component by gas chromatography.

Results

Photoreaction over Rh/TiO_2 and Pd/TiO_2 catalysts

When a mixture of methanol and water vapour was introduced onto Rh/TiO_2 or Pd/TiO_2 catalyst under irradiation, a 1:1 ratio of H_2 and dimethoxymethane was formed as shown in Fig. 1. After 6 h, the irradiation was stopped and the reaction mixture was circulated in the closed system overnight without irradiation. No increase of H_2 and dimethoxymethane was observed during the dark reaction. When the catalyst was irradiated again, formation of H_2 and dimethoxymethane was restarted with similar rates as before. To study the dependence of the reaction rate upon the light intensity over Rh/TiO_2, the intensity of the Xe lamp was reduced to 40% using neutral density filter. The initial rates of H_2 and dimethoxymethane formation were changed from 0.074 and 0.082 mmol h^{-1} to 0.030 and 0.032 mmol h^{-1}, respectively. These results indicate that the reaction rates are proportional to the light intensity. The temperature dependence of the reaction was also examined over Rh/TiO_2 and Pd/TiO_2 catalysts. The results in Fig. 2 demonstrate that the rates of H_2 and dimethoxymethane formation were independent of the reaction temperature up to 368 K. Accordingly, it is strongly suggested that the photo-

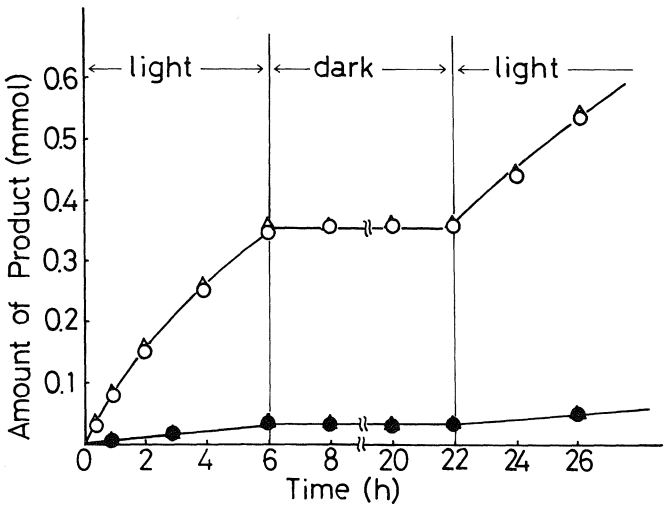

FIG. 1. Photocatalytic reaction of methanol with water over Rh/TiO_2 and Pd/TiO_2 at 308 K. (P_{H_2O} = 0.7 kPa, P_{CH_3OH} = 8.9 kPa): ○, H_2 (Rh); △, dimethoxymethane (Rh); ●, H_2 (Pd); ▲, dimethoxymethane (Pd).

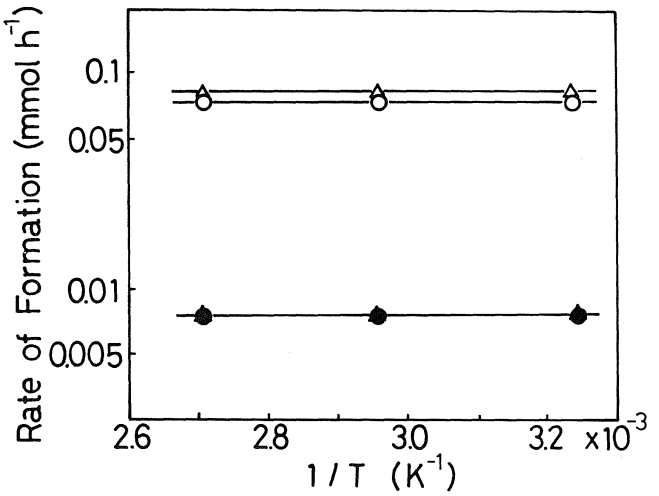

FIG. 2. Temperature dependence of the initial rate of the photocatalytic reaction of methanol with water over Rh/TiO_2 and Pd/TiO_2. (P_{H_2O} = 0.7 kPa, P_{CH_3OH} = 9.0 kPa): ○, H_2 (Rh); △, dimethoxymethane (Rh); ●, H_2 (Pd); ▲, dimethoxymethane (Pd).

excitation of the catalyst is involved in the rate-determining step of this reaction.

The pressure dependence of the reaction rate was examined over Rh/TiO_2 catalyst as shown in Fig. 3. Almost 1:1 ratio of H_2 and dimethoxymethane was formed at any pressure, but the dependency upon the partial pressures of water and methanol was different. In the case of water vapour lower than 1.5 kPa, the rate was proportional to the water pressure and reached a plateau abruptly at higher pressures. No such plateau was observed in the case of methanol, and the rate was of 0.5 order with respect to the partial pressure of methanol up to 15 kPa.

In order to study the role of water, the reaction with pure methanol vapour was attempted on Rh/TiO_2. It was recognized that the rate of H_2 evolution was very slow in the absence of water. This result was supported by the extrapolation to zero pressure of the water pressure dependence in Fig. 3, which shows almost zero rates for H_2 and dimethoxymethane formation.

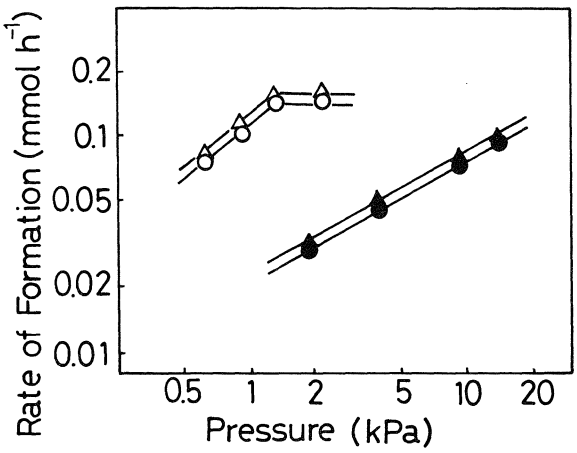

FIG. 3. Pressure dependence of the initial rate of the photocatalytic reaction of methanol with water over Rh/TiO_2 at 308 K. Open symbols: dependence of P_{H_2O} (P_{CH_3OH} = 9.0 kPa): ○, H_2; △, dimethoxymethane. Closed symbols: dependence on P_{CH_3OH} (P_{H_2O} = 0.7 kPa): ●, H_2; ▲, dimethoxymethane.

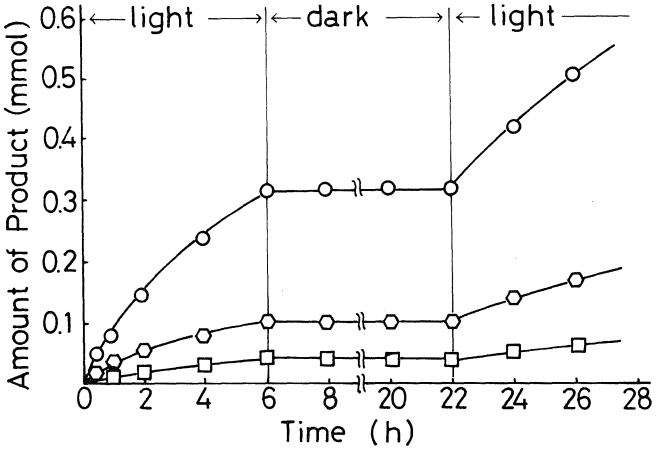

FIG. 4. Photocatalytic reaction of methanol with water over Rh–Na/TiO_2 at 308 K (P_{H_2O} = 0.7 kPa, P_{CH_3OH} = 9.0 kPa): ○, H_2; ○, methyl formate; □, CO_2.

Photoreaction over Rh–Na/TiO_2 and Pd–Na/TiO_2 catalysts

When a mixture of methanol and water vapour was introduced onto Rh–Na/TiO_2 catalyst under irradiation, H_2, methyl formate, and CO_2 were formed instead of dimethoxymethane as shown in Fig. 4. The ratio of formed products was almost constant during the reaction (in the case of Fig. 4, the ratio was H_2:$HCOOCH_3$:CO_2 = 9:3:1). Similar results were obtained over Pd–Na/TiO_2 catalyst. The dependency of the reaction rate upon the light intensity was studied over Rh–Na/TiO_2 by reducing the intensity of the Xe lamp with neutral filter. When the intensity was reduced to 40%, the initial rate of H_2 formation was changed from 0.082 mmol h^{-1} to 0.030 mmol h^{-1}, indicating almost proportional dependency. The initial rates of methyl formate and CO_2 formation were also changed from 0.016 and 0.008 mmol h^{-1} to 0.006 and 0.003 mmol h^{-1}, respectively.

The temperature dependence of the reaction was examined over Rh–Na/TiO_2 catalyst as shown in Fig. 5. The rate of H_2 formation was slightly dependent on the reaction temperature, and the apparent activation energy was measured as 4 kcal mol^{-1}. The rate of methyl formate formation decreased considerably

TABLE 1. Methanol–water and related reactions over various photocatalysts

Catalysts	Reactions	Conditions	Rates of H_2 formation (mmol h^{-1} g^{-1})	Selectivities[c] $CH_2(OCH_3)_2$ / H_2	Selectivities[c] $HCOOCH_3$ / CO_2	Selectivities[c] $2HCOOCH_3 + 3CO_2$ / H_2
Rh/TiO_2	$CH_3OH + H_2O$	Light	0.08	1.1	—	—
	CH_3OH + HCHO	Dark	>0.2[a]	—	—	—
$Rh–Na/TiO_2$	$CH_3OH + H_2O$	Light	0.08	—	2.0	0.91
	CH_3OH + HCHO	Dark	>0.2[a]	—	—	—
	CH_3OH + HCOOH	Dark	>0.15[b]	—	—	—
$Rh–Rb/TiO_2$	$CH_3OH + H_2O$	Light	0.07	—	3.0	0.82
$Rh–Li/TiO_2$	$CH_3OH + H_2O$	Light	0.05	—	0.45	0.85
Pd/TiO_2	$CH_3OH + H_2O$	Light	0.007	0.93	—	—
$Pd–Na/TiO_2$	$CH_3OH + H_2O$	Light	0.011	—	3.0	0.88

[a]The rate of dimethoxymethane formation.
[b]The rate of methyl formate formation.
[c]The detection limit of gas chromatography: ca. 1×10^{-6} mol for H_2 and ca. 5×10^{-6} mol for other products.

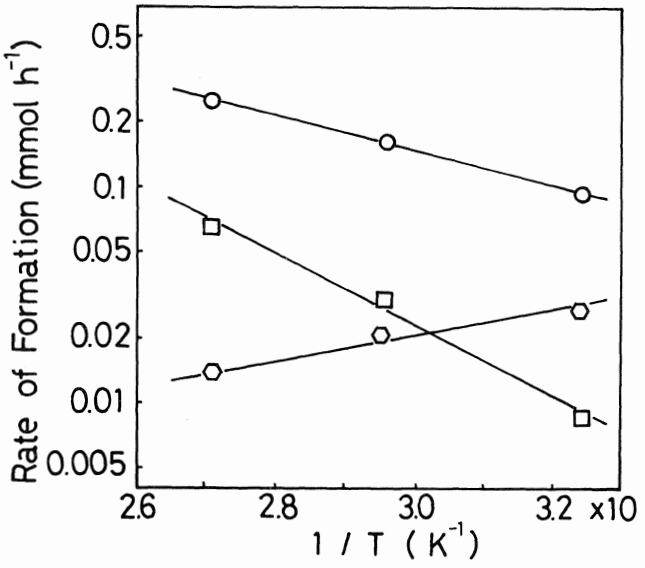

FIG. 5. Temperature dependence of the initial rate of the photocatalytic reaction of methanol with water over $Rh–Na/TiO_2$. (P_{H_2O} = 0.7 kPa, P_{CH_3OH} = 9.0 kPa): ○, H_2; ○, methyl formate; □, CO_2.

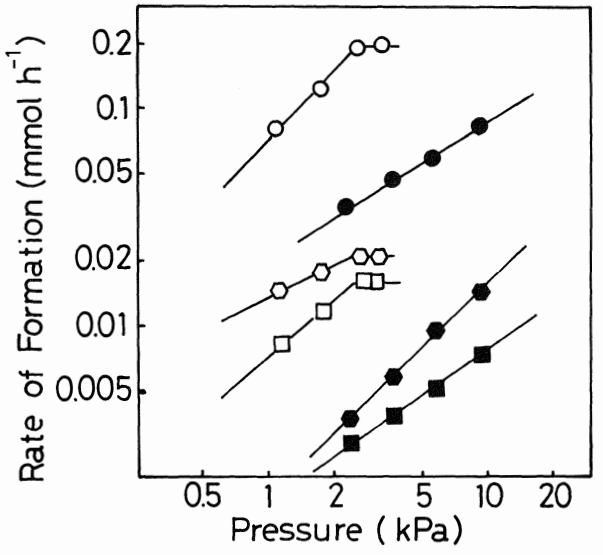

FIG. 6. Pressure dependence of the initial rate of the photocatalytic reaction of methanol with water over $Rh–Na/TiO_2$ at 308 K: (P_{H_2O} = 0.7 kPa, P_{CH_3OH} = 9.0 kPa). Open symbols: dependence of P_{H_2O} (P_{CH_3OH} = 9.0 kPa): ○, H_2; ○, methyl formate; □, CO_2. Closed symbols: dependence P_{CH_3OH} (P_{H_2O} = 0.7 kPa): ●, H_2; ●, methyl formate; ■, CO_2.

at higher temperatures. At the same time, the rate of CO_2 formation increased significantly with temperature, indicating the successive formation of these two products. The rates of CO_2 and methyl formate formation also depend on the alkali metal cations employed. As summarized in Table 1, over sodium- and rubidium-added catalysts, methyl formate was formed in higher amounts than CO_2, but over lithium-added catalyst, CO_2 was the main product even at room temperature.

The pressure dependence of the reaction was examined over $Rh–Na/TiO_2$ catalyst. As for the partial pressure of water, a dependency similar to the one observed in the case of Rh/TiO_2 was obtained. As shown in Fig. 6, the rate of H_2 formation was proportional to the partial pressure of water below 2 kPa, and reached a plateau at higher pressures. The variation of the CO_2 formation rate was similar to the one of H_2 (reaction order = 0.9), but for methyl formate a lower order than in the case of other products (reaction order = 0.6) was observed. The dependence was quite opposite in the case of methanol partial pressure. The reaction order was unity for methyl formate formation, but 0.6 for H_2 and CO_2 formations. The reaction scarcely proceeded when only methanol vapour was introduced on $Rh–Na/TiO_2$ or $Pd–Na/TiO_2$, which is consistent with the result of pressure dependence in Fig. 6.

Discussion

As shown in Figs. 1 and 4, the reaction of CH_3OH with H_2O did not proceed at all without irradiation over Rh-loaded TiO_2 catalyst. No reaction was observed either under dark or irradiation over Rh-loaded SiO_2 catalyst. These results indicate that photoexcitation of TiO_2 is indispensable to initiate the reaction.

[1] $TiO_2 + h\nu \rightarrow e^- + h^+$

Separated electrons and holes diffuse to the different active sites, where they react with H^+ and reducing agents to form

H_2 and oxidized products. In the present reaction, both water and methanol can be reducing agents. But the direct reaction between methanol and holes seems to be negligible on Rh and Pd catalysts, because the photoreaction did not proceed when pure methanol vapour was introduced over these catalysts as mentioned already. Moreover, Figs. 3 and 6 indicate the first order dependence of the reaction rates upon the partial pressure of water on both alkali metal cation added and free catalysts. Accordingly it is reasonable to suppose the photodissociation of weakly physisorbed water molecules to form OH radical as the first step of the reaction:

[2] $H_2O(a) + h^+ \rightarrow H^+(a) + \cdot OH(a)$

[3] $H^+(a) + e^- \rightarrow (1/2)H_2$ (on Rh or Pd)

The existence of such hydroxyl radical on TiO_2 under irradiation has been identified by Jaegar and Bard (6). The rate of H_2 formation was proportional to the light intensity and very little dependent on the reaction temperature. These facts suggest that the rate determining step of this reaction exists in reactions [1] to [3].

Over alkali metal cation free catalysts of Rh and Pd, the main products were H_2 and dimethoxymethane, and their molar ratio was 1:1 under the reaction conditions investigated. This result strongly suggests that the following reactions proceed over these catalysts:

[4] $CH_3OH + \cdot OH(a) \rightarrow HCHO(a) + H_2O + (1/2)H_2$

[5] $HCHO(a) + 2CH_3OH(a) \rightarrow CH_2(OCH_3)_2 + H_2O$

Reaction [4] is the oxidation of adsorbed methanol with OH radical to form adsorbed formaldehyde. Because formaldehyde was not detected at all in the gas phase during the reaction, reaction [5] to form dimethoxymethane should be fast. Actually, when a mixture of formaldehyde and methanol vapour was introduced on these catalysts, rapid formation of dimethoxymethane was observed even under the dark condition as summarized in Table 1.

When alkali metal cations were added to these catalysts, the product selectivity changed drastically and the formation of dimethoxymethane was not observed any more. But when a mixture of formaldehyde and methanol vapour was introduced over alkali metal cation added catalysts under the dark condition, dimethoxymethane was formed rapidly (Table 1). These results suggest that adsorbed formate may be formed directly from methanol under irradiation, without going via formaldehyde.

Similar effect of alkali metal cation addition has been reported on the selective formation of methanol from $CO–H_2$ reaction over similar catalysts. By adding sodium cation to Pd/SiO_2, the rate of methanol formation was accelerated more than 30 times compared to sodium-free catalyst (7). When formaldehyde, methanol, or $CO–H_2$ mixture was introduced over sodium added $Pd–Na/SiO_2$ catalyst, formation of adsorbed formate was observed by infrared spectroscopy, but no such infrared band was observed in the case of sodium cation free Pd/SiO_2 catalyst (8). From the tracer experiments using ^{13}CO and $C^{18}O$, it was demonstrated that active sites for methanol formation contain some surface oxygen O(s) which can stabilize reaction intermediate as formate, and alkali metal cations are effective for the preservation of such surface oxygen (9).

If we can postulate the existence of such surface structure for the alkali metal added catalysts in the present study, following reaction schemes can be proposed:

[6] $CH_3OH + \cdot OH(a) + O(s) \rightarrow HCOO(a) + H_2O + H_2$

[7] $HCOO(a) + \cdot OH(a) \rightarrow HCOOH(a) + O(s)$

[8] $HCOOH(a) + CH_3OH \rightarrow HCOOCH_3 + H_2O$

[9] $HCOOH(a) + \cdot OH(a) \rightarrow H_2O + CO_2 + (1/2)H_2$

Reaction [6] is the oxidation of adsorbed methanol with OH radical, which is similar to reaction [4]. But by the aid of surface oxygen O(s), formate is formed instead of formaldehyde. Stabilized formate may have a chance to be oxidized with another OH radical as shown in reaction [7]. Because no formic acid was detected in the gas phase during the reaction, reaction [8] should be fast, which could be confirmed by the introduction of methanol and formic acid vapour onto these catalysts (Table 1). From the results of Fig. 6, reaction [8] seems to show the first order dependence on the partial pressure of methanol suggesting the participation of weakly adsorbed methanol in this process. At room temperature, this step is much faster than step [9], but at higher temperatures, reaction [9] becomes a main step as indicated in Fig. 5.

By summing up reactions [1] to [9] formally, the following equations can be obtained for each product:

[10] $3CH_3OH \rightarrow H_2 + CH_2(OCH_3)_2 + H_2O$

[11] $2CH_3OH \rightarrow 2H_2 + HCOOCH_3$

[12] $CH_3OH + H_2O \rightarrow 3H_2 + CO_2$

From these equations it is easy to estimate the stoichiometry of the reaction. Equation [10] indicates the formation of H_2 and dimethoxymethane with a 1:1 ratio, which is the case on alkali metal cation free catalysts. Equations [11] and [12] suggest the formation of two hydrogen molecules per methyl formate, and three hydrogen molecules per CO_2 molecule over alkali metal cation added catalysts. Accordingly, if the reactions proposed above are correct, the following relation should be valid between the amounts of formed H_2, methyl formate, and CO_2:

[13] $[H_2] = 2[HCOOCH_3] + 3[CO_2]$

Calculated results according to eq. [13] were summarized in Table 1, which indicates that the proposed reaction schemes are consistent with the experimental results.

In the case of $Pd–Na/SiO_2$ catalyst, it was recognized that active sites for methanol formation may exist only in the vicinity of the palladium metal particle on the support, and their number is rather small (a few percent of the palladium atoms on the surface) (9). This situation seems to be also true in the present study. From the preparation method, it is supposed that formed surface structures are not uniform in both alkali metal cation added and free catalysts. Nevertheless, the effect of alkali metal cation addition was clear and caused a drastic change of the product selectivity over Rh and Pd catalysts, which strongly suggests the specificty of the active sites. As reported already (5), the photocatalytic behaviour of Pt/TiO_2 was considerably different from that of Rh or Pd catalysts in the photoreaction of methanol with water. The effect of alkali metal cation addition was not so clear over Pt/TiO_2, where methyl formate was formed even on the catalyst free of alkali metal cations. It has been also reported that in the case of $Pt–K/TiO_2$ catalyst (2 wt%, prepared by the photodecomposition of K_2PtCl_6), H_2 evolution was observed when only methanol vapour was introduced under irradiation (10, 11). This result suggests the existence of the direct reaction between holes and methanol, which was not the case on Rh and Pd catalysts. The explanation of the different catalytic behaviour with different metals or preparation methods is not clear at present, but they also suggest

the possibility of the selectivity control of the photocatalytic reactions by modifying the structures and chemical properties of the active sites.

1. G. M. SCHRAUZER and T. D. GUTH. J. Am. Chem. Soc. **99**, 7189 (1977).
2. T. KAWAI and T. SAKATA. J. Chem. Soc. Chem. Commun. 694 (1980).
3. H. MIYAMA, N. FUJII, and Y. NAGASE. Chem. Phys. Lett. **74**, 523 (1980).
4. H. REICHE and A. J. BARD. J. Am. Chem. Soc. **101**, 3127 (1979).
5. S. NAITO. J. Chem. Soc. Chem. Commun. 1211 (1985).
6. C. D. JAEGER and A. J. BARD. J. Phys. Chem. **83**, 3146 (1979).
7. Y. KIKUZONO, S. KAGAMI, S. NAITO, T. ONISHI, and K. TAMARU. Chem. Lett. 1249 (1981).
8. Y. KIKUZONO, S. KAGAMI, S. NAITO, T. ONISHI, and K. TAMARU. Faraday Discuss. Chem. Soc. 135 (1982).
9. S. NAITO, H. YOSHIOKA, H. ORITA, and K. TAMARU. Proc. 8th. Int. Congr. Catal. Berlin. III-207. 1984.
10. M. KAWAI, S. NAITO, K. TAMARU, and T. KAWAI. Chem. Phys. Lett. **98**, 377 (1983).
11. M. KAWAI, T. KAWAI, S. NAITO, and K. TAMARU. Chem. Phys. Lett. **110**, 58 (1984).

Chiral building blocks for amphotericin B[1,2]

DAVID LIANG,[3] HENRY W. PAULS, AND BERT FRASER-REID[4]
Paul M. Gross Chemical Laboratory, Duke University, Durham, NC 27706, U.S.A.

MICHAEL GEORGES
The Guelph–Waterloo Centre for Graduate Work in Chemistry, University of Waterloo, Waterloo, Ont., Canada N2L 3GL

AND

AZEEZ M. MUBARAK AND SŁAWOMIR JAROSZ
Department of Chemistry, University of Maryland, College Park, MD 20742, U.S.A.

Received November 4, 1985

DAVID LIANG, HENRY W. PAULS, BERT FRASER-REID, MICHAEL GEORGES, AZEEZ M. MUBARAK, and SŁAWOMIR JAROSZ. Can. J. Chem. **64**, 1800 (1986).

A general plan is outlined for disconnection of the polyene macrolides, which is aimed at achieving their syntheses, as well as facilitating the determination of their absolute configurations. The plan is exemplified by amphotericin B, **I**, the only family member of known absolute configuration. The major chiral component is a 20-carbon chain, **III**, which upon further retrosynthetic disconnection leads to three subunits, two of which correspond to the dideoxy hexoses **IV** and **V**. Although these are formally mirror images, they are best represented as the 3,4-dideoxyhexopyranoside, **1**, and the 3,5-dideoxyfuranose, **2**. Syntheses of **1** and **2** from readily available starting materials are described.

DAVID LIANG, HENRY W. PAULS, BERT FRASER-REID, MICHAEL GEORGES, AZEEZ M. MUBARAK et SŁAWOMIR JAROSZ. Can. J. Chem. **64**, 1800 (1986).

On présente un plan général de démembrement des macrolides polyéniques qui a pour but d'en réaliser la synthèse ainsi que de faciliter la détermination de leurs configurations absolues. Utilisant comme exemple l'amphotéricine B, le seul membre de la famille dont la configuration soit connue, on démontre comment le plan peut être opérationalisé. Le composant chiral principal est une chaîne à 20 atomes de carbone, **III**, qui conduit à trois sous-unités par un démembrement rétrosynthétique; deux de ces sous-unités correspondent aux didéoxy hexoses **IV** and **V**. Même si ces sous-unités sont formellement des images mirroirs, leurs meilleures représentations sont le didéoxy-3,4 hexopyrannoside **1** et le diéoxy-3,5 furannose **2**. On décrit les synthèses des composés **1** et **2** à partir de produits de départ facilement accessibles.

[Traduit par la revue]

Introduction

The polyene macrolides comprise a group of approximately 100 members (1), some of which have been in widespread clinical use for over 30 years, mainly for the treatment of yeast and candida infections (2–4), but also as antitumor agents (5) and in prostate therapy (6). Their skeleta are characteristically divided into a conjugated polyene chain (7) (from which the family name is derived), and an array that contains secondary hydroxyl groups in (almost) regular 1,3 relationships. The latter stereochemical feature currently attracts considerable attention (8).

In spite of the remarkable profile based on their clinical importance and unique structural features, the absolute stereochemistry is known for only one member, amphotericin B (**I**), which has yielded a crystalline derivative (9). However, in general, these antibiotics are amorphous, and their sensitivity to a wide variety of chemical reagents, as well as to light, renders chemical proof of structure very difficult. Synthetic activity has been remarkably light in comparison with other types of macrolides; however, the studies spearheaded by Masamune and co-workers (10), Nicolaou and Uenishi (11), Brooks *et al.* (12), and Floyd *et al.* (13) deserve particular note.

Our laboratory has been developing a general program on the polyene macrolides, which should facilitate proof of their structures and stereochemistry, relative and absolute, by a combination of degradative and synthetic studies. Our plans are necessarily based on the only member whose structure is known with certainty, that of amphotericin B, **I**, but there are several structural features that **I** shares with other polyene macrolides, which suggest that a general plan for degradation and (or) synthesis should be possible.

Retrosynthetic analysis

Logical points of disconnection of **I** are termini of the polyene chain (bonds **a** and **b**), and the lactone (bond **c**). The subunits thereby obtained are hexose **II**, and the uronic acid **III**. The regions of the latter designated **d** and **e** do not contain any contiguous chiral centers, and hence are logical sites for further retrosynthetic disconnections, resulting in segments **X**, **Y**, and **Z**.

Segment X

A plausible synthon for segment **X** is the 2,4-dideoxyhexose **IV**, which is conveniently represented as the methyl α-D-pyranoside, **1**.

Segment Y

Interestingly, a synthon for this segment is **V**, which, being the mirror image of **IV**, leads to the pyranoside **V***a*. However, pursuit of this analysis would require the use of an L-sugar, which would be uneconomical for a major synthetic undertaking. A more acceptable chiron (14) is the 3,5-dideoxyfura-

[1]Taken in part from Ph.D. theses: D.L., Duke University, 1985; H.P., Duke University, 1984; M.G., University of Waterloo, 1983.

[2]For preliminary communications dealing with this work, see refs. 27 and 31.

[3]Present addresses: D.L., Chemistry Department, University of South Carolina. H.P., Syntex, Inc., Mississauga, Ont., Canada. M.G., Xerox Research Centre, Mississauga, Ont., Canada. A.M., Ceylon Institute of Scientific and Polish Academy of Sciences, Warsaw, Poland.

[4]Author to whom correspondence may be addressed.

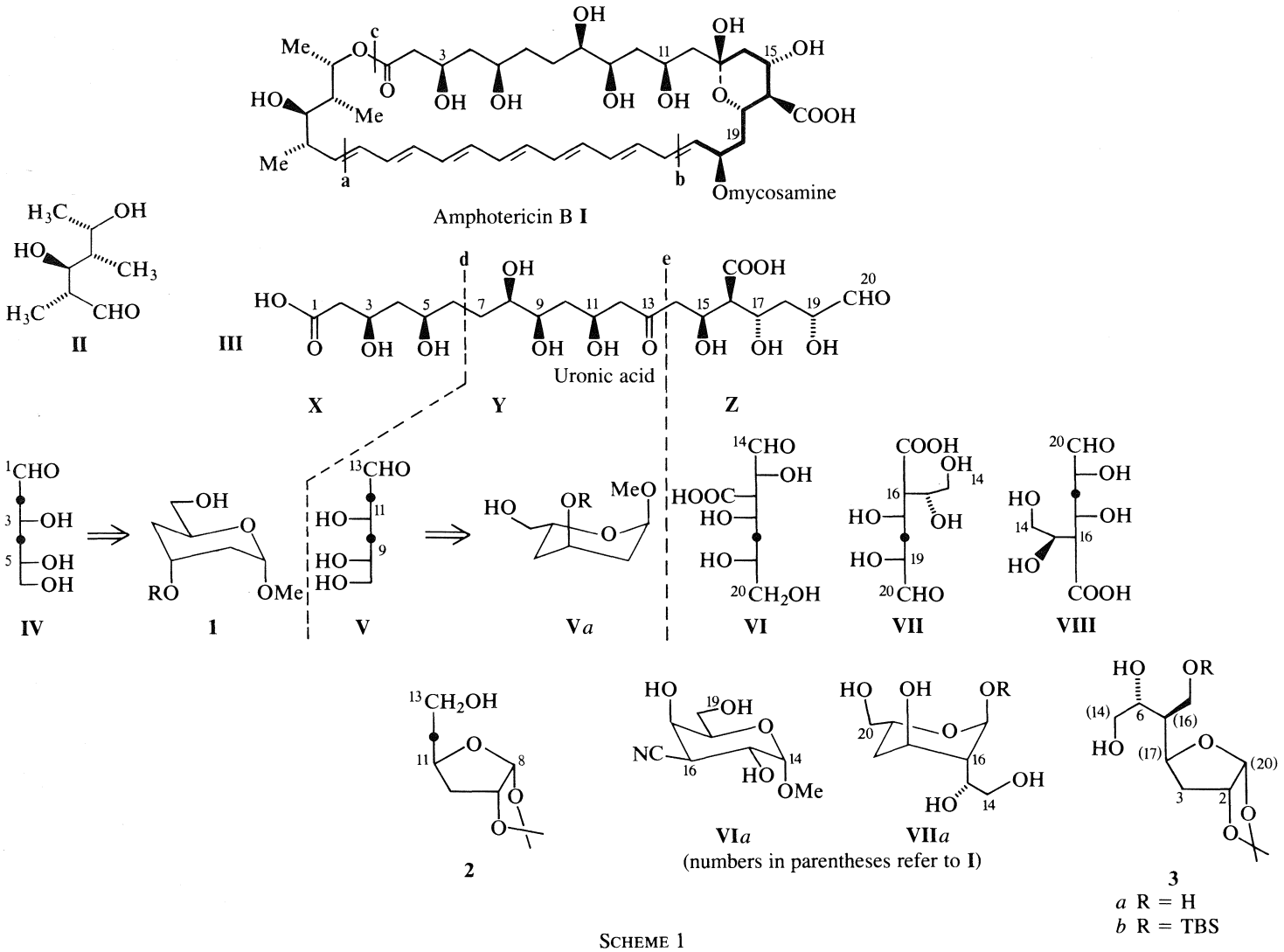

SCHEME 1

nose **2**, whose relationship to 1,2:5,6-di-*O*-isopropylidene-α-D-glucofuranose, **6***a*, is readily appreciated.

Segment Z

The C14—C15 portion is by far the most challenging, and its importance stems from the fact that the hemiketal feature that it represents (shown in heavy lines in **I**) is also found in most polyene macrolides (7). Thus this synthon could find general use in the synthesis of members of this family of macrolides.

The Fisher projections **VI**, **VII**, and **VIII** suggest three possible synthons for this segment. Structure **VI** initially seemed attractive since one approach would be via a 3-*C*-cyano sugar, such as **VI***a*, and although such compounds have been prepared by Guthrie and co-workers (15, 16) and ourselves (17), our preliminary explorations of this avenue did not prove promising.

In the case of **VII** and **VIII**, the C-15 stereocenter is "off template" and hence its stereocontrolled formation and verification present special challenges, as noted by us elsewhere (18). Synthon **III** correlates with the L-sugar **VII***a* and was therefore rejected for the reasons discussed above in connection with segment **Y**. Attention was therefore focused on VIII, which correlates with the furanose **3**.

Strategies for connecting the segments, such as olefination procedures and nucleophilic displacements, have been widely utilized in syntheses of macrolides from sugar precursors (14).

Synthetic studies

Chiron 1

This subunit was prepared routinely from the readily obtained 2-deoxy pyranoside **4** (19), by use of a variation of the procedure of Prugh and Deanna (20*b*). In our hands, unfortunately, acidic hydrolysis of the 4,6-*O*-benzylidene ring could not be accomplished without concomitant anomerisation, leading to

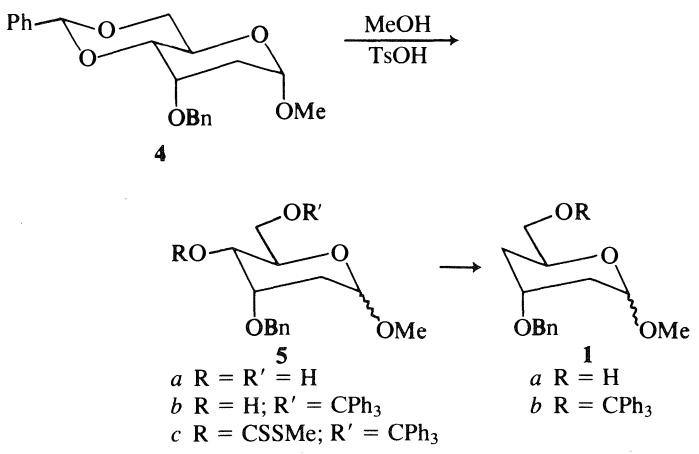

SCHEME 2

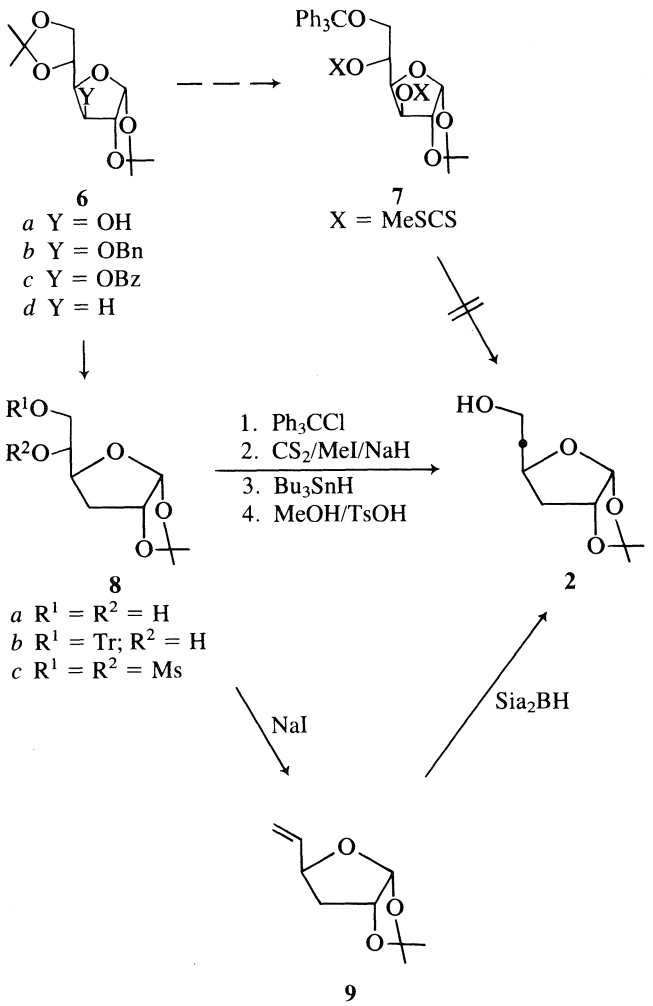

SCHEME 3

the α,β mixture **5***a*. Deoxygenation of the alcohol **5***b* was effected by the classical Barton–McCombie (21) procedure.

Chiron 2

The chiron **V** is a 3,5-dideoxy hexose and it seemed most expedient to remove the C-3 and C-5 oxygens simultaneously. However, we were unable to effect double deoxygenation of several doubly activated derivatives **7** (e.g. X = SO_2R, SCimidazoyl, SCSMe) by a variety of procedures. The product in each case was a complex mixture.

The deoxygenations therefore had to be done separately, and the logical starting point was the well-known 3-deoxy derivative **6***d* (21, 22), prepared most conveniently from **6***a* by the Barton procedure (21). Selective hydrolysis of **6***d* afforded the diol **8***a* (21, 22) and the tritylated derivative there of **8***b* was then subjected to the Barton deoxygenation followed by hydrolysis. However, the overall yield of **2** from **8***a* obtained by this route was 60% and so an alternative route was examined.

A more satisfactory yield (~80%) was achieved by hydroboration (23) of the alkene **9**. Of various procedures (24) tested for the preparation of this olefin, the reductive elimination of vicinal disulfonates, originated by Jones and Thomson (24*a*), proved to be the most convenient.

Chiron 3

In our first approach to the synthesis, we had hoped to make use of the alcohol **8***b*. Thus oxidation to **10** and a Horner–Emmons reaction afforded a 4:1 mixture (^{1}H nmr estimate) of the geometric isomers **11***a*. Reduction with DIBAL (diisobutylaluminum hydride) gave the allylic alcohols **11***b*, and hydroboration then led to **12** in excellent overall yield. However, the latter was obtained as a mixture of diastereomers of undetermined composition, as indeed as to be expected in view of the fact that the olefinic precursor, **11***b*, was a mixture of geometric isomers.

The uncertainty about the C-5 and C-6 configurations of **12** was a major problem for us. Our preliminary studies had suggested that, with C-5 alkenes such as **11***b*, the presence of a bulky substituent at C-3 could be used to control the facial selectivity of electrophilic additions. According to this observation, the desired C-5 and C-6 configurations of **3** could *both* be achieved, by ensuring that addition to the C-5 alkene occurred from the *re–re* face of a (*Z*) olefin such as **15**. The corresponding (*E*) olefin, **16**, would give the correct C-5, but incorrect C-6, configuration.

Stereoselective formation of a (*Z*) olefin therefore became the first requirement. The known diol **13***a* (25) was converted into ketone **14** by routine transformations. It was found that reaction with trimethylphosphonoacetate gave an inseparable 6:1 mixture of **15***a* and **16**. However, the corresponding Wittig reagent, carbomethoxymethylenetriphenylphosphorane, afforded **15***a* exclusively. Assignment of structure to these geometric isomers followed from the fact that treatment of each isomer with fluoride ion gave the hydroxyester **15***b* and the butenolide **17**, respectively, based upon their ir (infrared) and ^{1}H nmr spectral characteristics. Compound **15***b*, therefore, had the desired (*Z*) configuration, and hydrogenation over palladium gave two products that were assigned as the hydroxyester **18** and lactone **19***a* since, upon treatment of the mixture with *p*-toluenesulfonic acid for 6 h at room temperature, the more polar component was gradually transformed quantitatively into the less polar product, i.e. **18** → **19***a*.

A timely publication by Redlich and Neumann (26) also reported stereocontrolling effects on the hydrogenation of C-5 alkenes and, on the basis of these observations, the C-5 configuration of the lactone was tentatively assigned as shown in **19***a*. This assignment was subsequently established by X-ray analysis of a transformation product (27), and it was therefore apparent that hydrogenation of the double bond of **15** was favored from the *re–re* face. We then hoped to extend this selectivity to hydroboration.

The allylic alcohol **20***a* was obtained by DIBAL reduction of **15***a*, and upon hydroboration a 5:3 mixture of compounds **21** and **22***a* was formed. The structures of these compounds were established as follows. Firstly **21** was treated with thiocarbonyldiimidazole to give the thionocarbonate **23**, which was then reduced with tri-*n*-butyltin hydride according to the Barton–Subramanian procedure (28) to give **22***a*. The latter was hydrogenated over palladium in the presence of formic acid, and the resulting triol **22***b* was acetylated directly to give triacetate **22***c*.

Secondly, compound **19***a* was correlated with **22***c* by hydrogenolysis to give the hydroxylactone **19***b*, which upon reduction and acetylation gave the triacetate **22***c*.

These correlations indicated that the C-5 configurations in **19** and **21** were the same. Given (a) the *Z* configuration of **20** and (b) the mechanism of hydroboration (29), the C-6 hydroxyl configuration must therefore be as shown in **21**.

However, the high proportion of the by-product, **22***a*, was intolerable. This abnormal course of hydroboration responsible for its formation has been observed previously, and the mechanism that has been proposed is shown below (30). It is

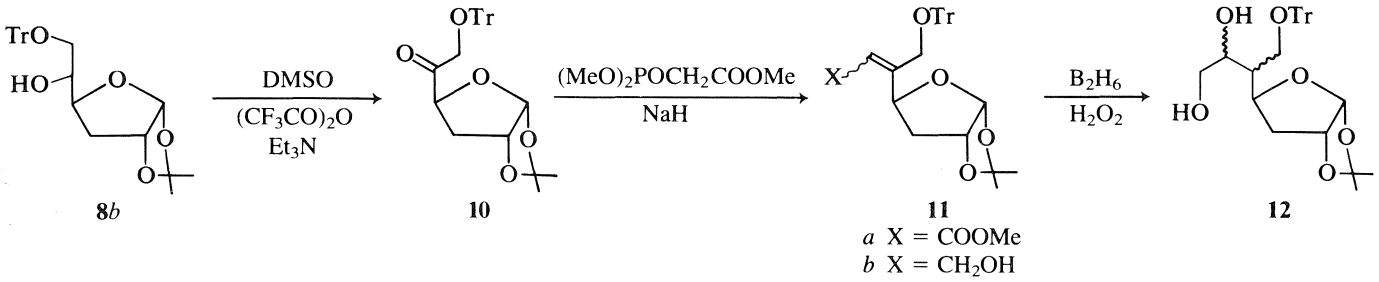

SCHEME 4

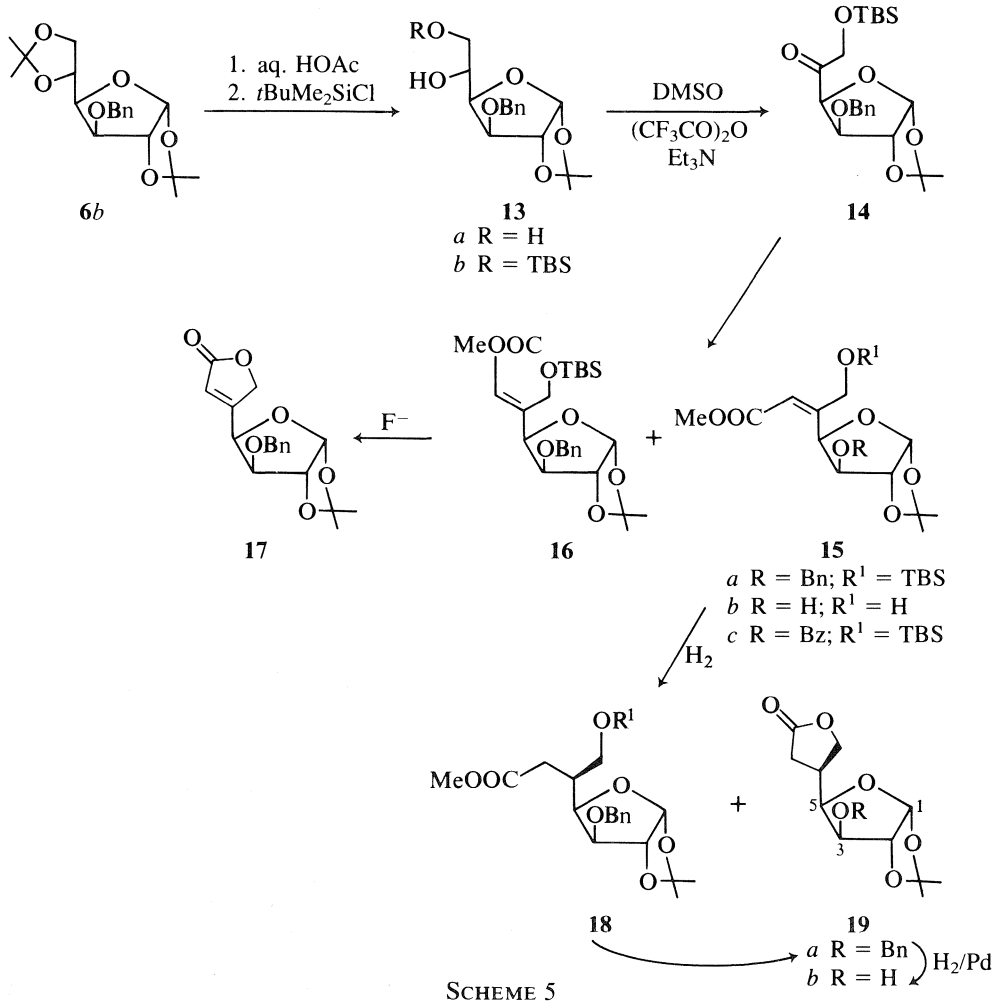

SCHEME 5

also known that this abnormal reaction can be suppressed by the use of dialkyl boranes, and in the light of this information, the protocol outlined in Scheme 7 was developed.

The germ of the idea (31) was that the reaction of a hindered borane with diol **20**b *would give the bis-boronate ester* **24**. *The bulky C-3 substituent of the latter should insure stereocontrolled approach from the* re–re *face of the double bond, and the bulky C-7 ester should suppress the formation of the abnormal product (such as* **22**). The starting material was the previously described benzoate **15***c* (27) from which **20***b* was readily obtained. Addition of disiamylborane did cause the rapid formation of a less polar product (tlc) presumed to be **24**; however, subsequent reaction was slow and upon work-up the starting material **20***b* was substantially recovered.

It emerged that the preferred reaction course was to allow **20***b* to stand with five equivalents of disiamylborane for 2 h at −78°C, whereupon complete formation of **24** was evident (tlc). Excess diborane was then added and the mixture was allowed to stand at room temperature, further additions of diborane being made if it was deemed necessary (tlc evidence). After the standard oxidative work-up, the triol **25** was isolated in 80% yield.

To prepare C-3 for deoxygenation selectively, triol **25** was treated with phosgene, which afforded the carbonate **26***a* in near quantitative yield. The Robbins variation (32) of the Barton–McCombie (21) reaction was then applied, affording **26***b* and **26***c* in 82 and 90% yields respectively.

Saponification of the carbonate group then afforded the diol **3***b*. From the numbering sequence shown (see Scheme 1), it is clear that **3***b* is a promising chiron for the hemiketal moiety of

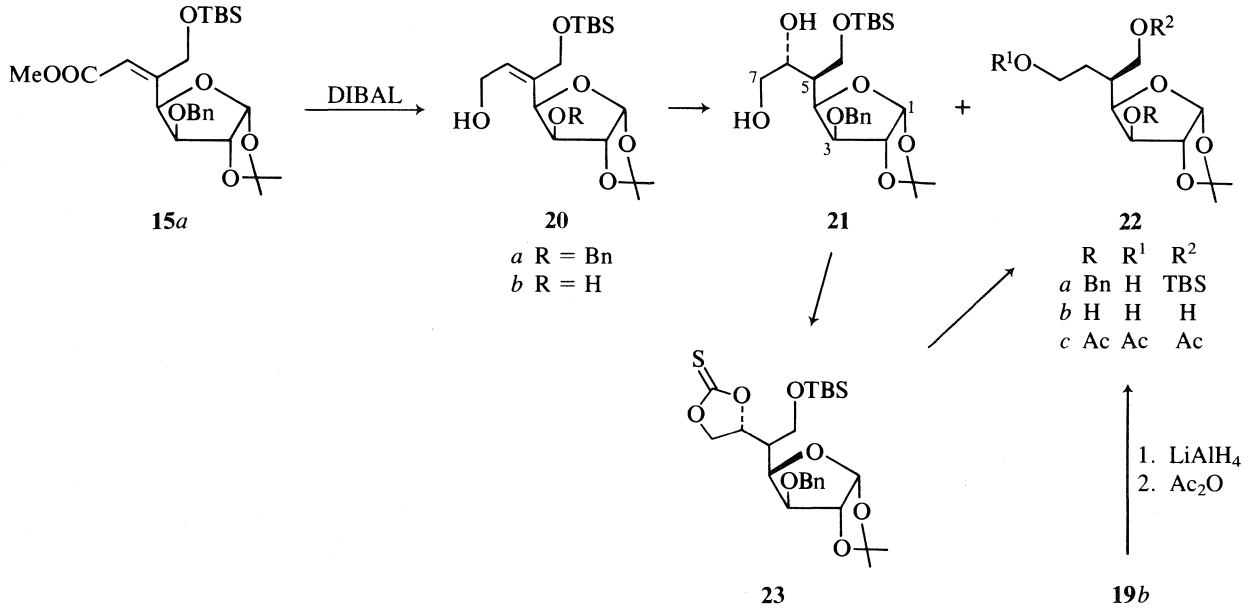

SCHEME 6

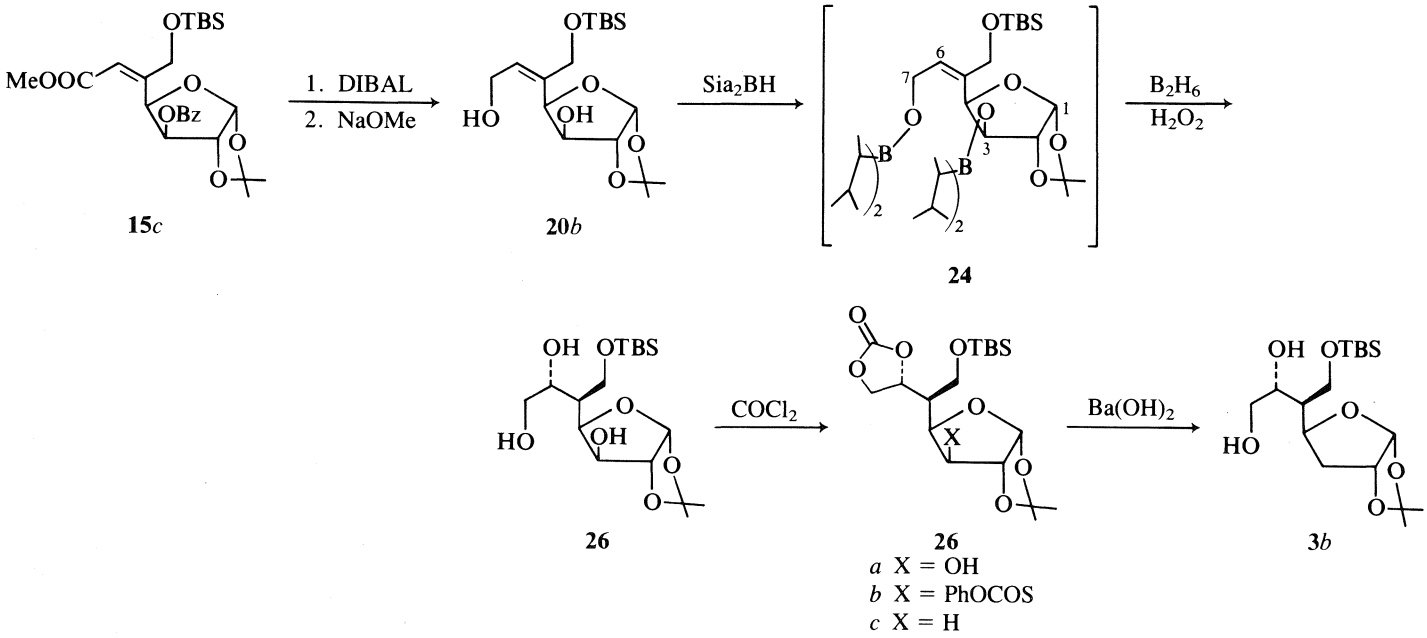

SCHEME 7

the polyene macrolides. The compound has been obtained with complete stereoselectivity, and the various functional groups are distinctively differentiated in order to facilitate docking with the other subunits. Studies in this direction are underway and will be reported in due course.

Experimental

General

Melting points were determined in capillary tubes using a Buchi Model 510 melting point apparatus and are uncorrected. Elemental analyses were performed by M-H-W Laboratories, Phoenix, Arizona. The ir spectra were recorded on Perkin–Elmer models 297 and 298 using sodium chloride cells and chloroform as solvent for solids, or sodium chloride plates for thin films of liquids or syrups. Optical rotations were determined at the sodium D line using a Perkin–Elmer 241 polarimeter. ^{1}H nmr spectra were determined on the following spectrometers: Varian EM-360A, Bruker NR-80, Varian XL-100, Varian XL 200, Bruker WM-250, or Bruker-WH-400. Unless otherwise stated the solvent was $CDCl_3$ with internal tetramethylsilane as the standard. The coupling constants were verified by homonuclear decoupling experiments. For the purpose of ^{1}H nmr interpretation, compound structures have been numbered in the schemes. Low resolution mass spectra were obtained using a Hitachi/Perkin–Elmer RMH-2 instrument, and high resolution mass spectra (hrms) were performed at the Research Triangle Park, North Carolina, with a VG7070F instrument. The progress of all reactions was monitored by thin-layer chromatography (tlc), which was performed on aluminum plates precoated with silica gel HF-254 (0.2-mm layers) containing a fluorescent indicator (Merck, 5539), with detection by uv (254 nm), charring with sulfuric acid spray, or charring with a solution of ammonium molybdate(VI) tetrahydrate (12.5 g) and cerium(IV) sulfate tetrahydrate (5.0 g) in 10% aqueous sulfuric acid (500 mL). Flash chromatography was performed using Kiesselgel 60 (230–400 mesh, E. Merck).

*Methyl 3-O-benzyl-2-deoxy-6-O-triphenylmethyl-α,β-D-*ribo*-hexopyranoside (5b)*

A solution of methyl 3-*O*-benzyl-4,6-*O*-benzylidene-α-D-*ribo*-hexopyranoside, **4** (19) (140 g, 0.39 mol), in $CHCl_3$ (700 mL) and

MeOH (700 mL) containing *p*-toluenesulfonic acid (5 g) was refluxed for 3 h. After cooling, the solution was neutralized with triethylamine (5 mL), concentrated *in vacuo*, and the oily residue was chromatographed on silica gel (400 g). Elution with cyclohexane – ethyl acetate (2:1) and EtOAc gave diol **5***a* (84.9 g, 80.5%) as an oil. The material was dissolved in methylene chloride (500 mL) containing triethylamine (70 mL) and triphenylmethyl chloride (87.3 g, 0.31 mmol) and *N,N*-dimethylaminopyridine (2 g) were added. After 15 h stirring at room temperature, the reaction mixture was evaporated *in vacuo*, diluted with ethyl acetate, washed with aqueous saturated NH_4Cl, NaCl, and $NaHCO_3$ solutions, then chromatographed on a silica gel column (1.5 kg). Elution with EtOAc–C_6H_{12} (1:4) gave 140 g (87%) of **5***b* as a syrupy, inseparable mixture of anomers. $[\alpha]_D^{20}$ + 37.3° (*c* 1.1, chloroform); ν_{max} (film): 3510 (OH) cm^{-1}; ^1H nmr (60 MHz) δ: 1.50–2.60 (m, 3H, H-2a, H-2e, OH), 3.42 (s, 3H, OCH_3), 3.20–4.20 (m, 5H, H-3, H-4, H-5, H-6a, H-6b), 4.55 (q, 2H, OCH_2Ph), 4.6 (m, 1H, H-1), 7.00–7.75 (m, 20H, OCH_2Ph, CPh_3). *Anal.* calcd. for $C_{33}H_{34}O_5$: C 77.62, H 6.71; found: C 77.38, H 6.56.

*Methyl 3-*O*-benzyl-2-deoxy-4-*O*-[(methylthio)thiocarbonyl]-6-*O*-triphenylmethyl-α,β-*D*-*ribo*-hexopyranoside (**5**c)*

To a suspension of NaH (12 g, oil free) in tetrahydrofuran (500 mL) was added a solution of compound **5***a* (128 g, 0.25 mol) in tetrahydrofuran (800 mL), and imidazole (1.2 g). The mixture was refluxed for 3 h under argon, and then carbon disulfide (75 mL) was added gradually. After 30 min under reflux methyl iodide (75 mL) was added gradually and, after an additional 2 h, the reaction mixture was cooled and quenched with acetic acid (40 mL), diluted with ethyl acetate, and washed with 3% dilute HCl, $NaHCO_3$, and NaCl solutions, then dried over anhydrous sodium sulfate, filtered, and evaporated *in vacuo*. The residue was purified by flash silica gel chromatography to give 140 g (95%) of the thiocarbonate **5***c* as a yellow syrup; R_f 0.54 (15% ethyl acetate – petroleum ether) for the β isomer, 0.44 for the α isomer; ^1H nmr (60 MHz, $CDCl_3$) for the α isomer, δ: 1.66–2.20 (m, 2H, H-2a, H-2e), 2.30 (s, 3H, SCH_3), 2.96–3.34 (m, 2H, H-6, H-6), 3.38 (s, 3H, OMe), 3.96–4.32 (m, 2H, H-3, H-5), 4.50 (s, 2H, $PhCH_2O$), 4.74 (br s, 1H, H-1), 5.86 (dd, 1H, $J_{4,5}$ = 9.6 Hz, $J_{3,4}$ = 4.0 Hz, H-4), 6.93–7.90 (m, 20H, $PhCH_2O$, Ph_3C); for the β isomer, δ: 1.50–2.20 (m, 2H, H-2a, H-2e), 2.34 (s, 3H, SMe), 2.90–3.22 (m, 2H, H-6, H-6), 3.42 (s, 3H, OMe), 4.06–4.35 (m, 2H, H-3, H-5), 4.46 (s, 2H, $PhCH_2O$), 4.78 (dd, 1H, $J_{1,2a}$ = 8.0 Hz, $J_{1,2e}$ = 3.0 Hz, H-1), 5.90 (dd, 1H, $J_{4,5}$ = 9.0 Hz, $J_{3,4}$ = 4.0 Hz, H-4), 6.90–7.70 (m, 20H, $PhCH_2O$, Ph_3C). *Anal.* calcd. for $C_{35}H_{36}O_5S_2$: C 69.97, H 6.04; found: C 69.42, H 6.12.

*Methyl 3-*O*-benzyl-2,4-dideoxy-α,β-*D*-*erythro*-hexopyranoside (**1**a)*

The crude oily xanthate **5***a* (140 g) was dissolved in toluene (1 L) containing 2,2-azobis(2-methylpropionitrile) (250 mg). The solution was added to tributyltin hydride (100 mL) in toluene (0.5 L). The mixture was boiled under argon for 24 h. Additional tributyltin hydride (50 mL) was added, and reflux was continued for 24 h. Concentration *in vacuo* gave a crude mixture, which was diluted with *n*-hexane (150 mL) and extracted with acetonitrile (100 mL × 2). The acetonitrile layer was concentrated *in vacuo*, and chromatographed on a silica gel column. Elution with cyclohexane – ethyl acetate (4:1) gave 120 g of material, which was assumed to be the tritylated derivative **1***b*. To the crude substance was added, directly, methanol (2.5 L) containing *p*-toluenesulfonic acid (5 g), and the mixture was stirred at room temperature for 6 h. The solution was then neutralized with triethylamine (10 mL), concentrated *in vacuo*, and chromatographed on a silica gel column. Elution with cyclohexane – ethyl acetate (4:1, then 1:1) gave 44 g (68%) of the anomeric mixture **1***a*; R_f 0.16 (30% ethyl acetate – petroleum ether); ^1H nmr (60 MHz) δ: 1.20–2.38 (m, 4H, H-2, H-4), 2.80 (br s, 1H, OH), 3.53 (s, 3H, OMe), 3.34–4.25 (m, 4H, H-3, H-5, H-6, H-6′), 4.55 (s, 2H, $PhCH_2$), 4.78 (dd, 1H, $J_{1,2e}$ = 2.0 Hz, $J_{1,2a}$ = 10 Hz, H-1), 7.35 (s, 5H, Ph). *Anal.* calcd. for $C_{14}H_{20}O_4$: C 66.64, H 7.99; found: C 65.80, H 7.89.

*3-Deoxy-1,2-*O*-isopropylidene-6-*O*-triphenylmethyl-α-*D*-hexofuranose (**8**b)*

A mixture of 3-deoxy-1,2-*O*-isopropylidene-α-D-*ribo*-hexofuranose, **8***a* (21, 22) (10.2 g, 50 mmol), triphenylmethyl chloride (14.6 g, 52.5 mmol), and *N,N*-dimethylaminopyridine (500 mg) was dissolved dimethylformamide (120 mL) and stirred at room temperature for 20 h. The reaction mixture was poured into ice water (100 mL) and then extracted with dichloromethane (3 × 200 mL). The combined organic extracts were washed with saturated ammonium chloride solution, water, and brine, dried (Na_2SO_4), and concentrated *in vacuo*. Flash chromatography of the residue afforded 19.6 g (88%) of **8***b*; R_f 0.50 (30% ethyl acetate – petroleum ether); $[\alpha]_D^{23}$ −15.8° (*c* 1.0, $CHCl_3$); ^1H nmr (80 MHz, $CDCl_3$) δ: 1.32, 1.52 (s, s, 6H, $C(CH_3)_2$), 1.67–2.55 (m, 3H, H-3, H-3′, OH, D_2O exchange), 3.22 (m, 1H, H-5), 3.74–4.50 (m, 3H, H-4, H-6, H-6′), 4.70 (t, 1H, *J* = 3.7 Hz, H-2), 5.78 (d, 1H, $J_{1,2}$ = 3.7 Hz, H-1). *Anal.* calcd. for $C_{28}H_{30}O_5$: C 75.31, H 6.77; found: C 75.44, H 6.67.

*3,5,6-Trideoxy-1,2-*O*-isopropylidene-α-D-*erythro*-hex-5-enofuranose (**9**)*

To a solution of the diol **8***a* (78 g, 0.382 mol) in tetrahydrofuran (400 mL) and pyridine (180 mL) was added methylsulfonyl chloride (131 g, 1.146 mol). The mixture was refluxed for 1.5 h and, after cooling, was concentrated *in vacuo*, diluted with ethyl acetate, washed with dilute solutions of HCl, $NaHCO_3$, and NaCl, then dried ($MgSO_4$). Evaporation gave a crude oil that was chromatographed on silica gel to yield compound **8***c* as a crystalline solid (46 g, 33.4%). The material was dissolved directly in butanone (1 L), sodium iodide (60 g, 0.4 mol) was added, and the solution was boiled under reflux overnight. The reaction mixture was diluted with diethyl ether, and washed with solutions of sodium thiosulfate, $NaHCO_3$, and NaCl. After drying over $MgSO_4$, the solution was concentrated *in vacuo* and the residue distilled at 45°C (1 Torr (1 Torr = 133.3 Pa)) to give **9** (15 g, 88%) as an oil; R_f 0.83 (50% ethyl acetate – petroleum ether); $[\alpha]_D^{23}$ −38.7° (*c* 1.0, $CHCl_3$); ^1H nmr (80 MHz) δ: 1.38, 1.58 (s, s, 6H, $C(CH_3)_2$), 1.60–1.86 (m, 1H, H-3), 2.22 (dd, 1H, *J* = 4.6 Hz, H-3β), 4.66 (m, 1H, H-4), 4.78 (t, 1H, *J* = 3.7 Hz, H-2), 5.14, 5.26, and 5.46 (m, 2H, H-6, H-6′), 5.88 (d, 1H, $J_{1,2}$ = 3.7 Hz, H-1), 5.92 (m, 1H, H-5). *Anal.* calcd. for $C_9H_{14}O_3$: C 63.51, H 8.29; found: C 63.47, H 8.26.

*3,5-Dideoxy-1,2-*O*-isopropylidene-α-D-*erythro*-hexofuranose (**2**)*

(a) Deoxygenation and detritylation of compound **8***b* (646 mg, 13.4 mmol) was carried out as described above for **5***b* → **5***c* → **1***a*. The product **2** (337 mg), obtained in 70% overall yield from **8***b*, was isolated as a colorless oil by chromatography.

(b) To a solution of disiamylborane (4.8 mmol) in tetrahydrofuran was added, dropwise, a solution of **9** (540 mg, 3.18 mmol) in tetrahydrofuran (5 mL) at 0°C under argon. After stirring at room temperature for 3 h, water (1 mL) was added dropwise at 0°C to destroy the excess of the reagent. The reaction mixture was oxidized by addition of 3 *N* sodium hydroxide (2 mL) in one portion and then 30% hydrogen peroxide (2 mL) dropwise, while maintaining the temperature at 20–25°C. After stirring for another 3 h at room temperature, the aqueous phase was saturated with sodium chloride. The tetrahydrofuran phase was separated and the aqueous layer was extracted with ether. The combined organic layers were dried ($MgSO_4$) and concentrated *in vacuo* and the excess water was removed azeotropically with toluene. Flash chromatography afforded compound **2** (537 mg, 90%) as a colorless syrup; R_f 0.20 (50% ethyl acetate – hexane); $[\alpha]_D^{23}$ −8.0° (*c* 1.05, chloroform); ^1H nmr (80 MHz) δ: 1.28, 1.48 (s, s, 6H, $C(CH_3)_2$), 1.60–2.35 (m, 5H, H-3, H-3′, H-5, H-5′, OH, D_2O exchange), 3.75 (m, 2H, H-6, H-6′), 4.33 (m, 1H, H-4), 4.68 (t, 1H, *J* = 3.7 Hz, H-2), 5.78 (d, 1H, $J_{1,2}$ = 3.7 Hz, H-1). *Anal.* calcd. for $C_9H_{16}O_4$: C 57.43, H 8.57; found: C 57.21, H 8.61.

*3-Deoxy-1,2-*O*-isopropylidene-6-*O*-triphenylmethyl-α-*D*-erythro-hexofuran-5-ulose (**10**)*

To a solution of dry dimethylsulfoxide (3.9 mL) in dichloromethane (50 mL), trifluoroacetic anhydride (5.8 mL) was added dropwise at −78°C under an argon atmosphere. After 15 min a solution of **8***b* (6.1 g, 13.7 mmol) in dichloromethane (60 mL) was added dropwise over a period of 45 min, and after another hour triethylamine (12 mL) was added dropwise, and the resulting solution was warmed up to

room temperature. The reaction solution was diluted with 200 mL of dichloromethane and then washed with saturated sodium bicarbonate, water, and brine, dried (Na_2SO_4), then concentrated *in vacuo*. Flash chromatography gave 5.8 g (96%) of ketone **10** as a syrup; R_f 0.42 (15% ethyl acetate – petroleum ether); $[\alpha]_D^{23}$ −1.33° (*c* 1.0, chloroform); ν_{max} ($CHCl_3$): 3000, 1730 cm^{-1}; ^1H nmr (60 MHz) δ: 1.15, 1.35 (s, s, 6H, $C(CH_3)_2$), 1.60 (dd, 1H, J = 4.0 Hz, J = 13.0 Hz, H-3α), 2.20 (dd, 1H, J = 4.0 Hz, H-3β), 3.90 (s, 2H, H-6, H-6′), 4.50 (t, 1H, J = 4.0 Hz, H-2), 4.62 (dd, 1H, J = 5.0 Hz, H-5), 5.62 (d, 1H, J = 4.0 Hz, H-1), 7.20 (m, 15H, Ph_3C). *Anal.* calcd. for $C_{28}H_{28}O_5$: C 75.65, H 6.35; found: C 75.59, H 6.31.

*Methyl 3,5,6-trideoxy-5-*C*-triphenylmethyloxy-1,2-*O*-isopropylidene-α-*D*-*erythro*-hept-5-(*E*,*Z*)-enofuranosyluronate (**11**a)*

To a suspension of 1.0 g (20.8 mmol) of 50% sodium hydride dispersion (prewashed with hexane) in dry benzene (60 mL) was added trimethylphosphonoacetate (2.6 g, 14.3 mmol) at room temperature under an argon atmosphere. After stirring at 35°C for 1 h, a solution of **10** (5.8 g, 13.06 mmol) in dry benzene (60 mL) was added to the reaction flask dropwise at room temperature. After stirring for 2 days the solution was diluted with ether and processed in the usual way. Flash chromatography gave 5.6 g (86%) of **11***a* as an inseparable 4:1 mixture of geometric isomers (based upon the integration of the methoxy peaks); R_f 0.58 (30% ethyl acetate – petroleum ether); $[\alpha]_D^{23}$ −33° (*c* 1.0, chloroform); ν_{max} ($CHCl_3$): 3000, 1710 (C=O), 1450 cm^{-1}; ^1H nmr (80 MHz) δ: 1.30, 1.58 (s, s, 6H, $C(CH_3)_2$), 1.50 (m, 1H, H-3), 2.53 (dd, 1H, J = 5.0 Hz, J = 13.0 Hz, H-3β), 3.80 (s, 3H, OCH_3), 4.00 (AB, 2H, J = 11.0 Hz, Δδ = 0.13 ppm, H-5, H-5′), 4.64 (t, 1H, J = 3.7 Hz, H-2), 5.63 (d, 1H, J = 3.7 Hz, H-1), 5.84 (dd, 1H, J = 4.4 Hz, J = 5.0 Hz, H-4), 6.45 (m, 1H, H-6), 7.32 (m, 15H, Ph_3C). *Anal.* calcd. for $C_{31}H_{32}O_6$: C 74.38, H 6.44; found: C 74.34, H 6.20.

*3,5,6-Trideoxy-5-*C*-triphenylmethyloxy-1,2-*O*-isopropylidene-α-*D*-*erythro*-hept-5-(*E*,*Z*)-enofuranose (**11**b)*

To a solution of **11***a* (3.5 g, 7 mmol) in diethyl ether, disobutylaluminum hydride (21 mL, 1.0 *M* in toluene) was added dropwise at 0°C under an argon atmosphere. After 4 h, 1 mL of water was added slowly at 0°C, followed by 1 mL of 15% aqueous sodium hydroxide and 3 mL of water. The inorganic salts were removed by filtration and the residue was rinsed with diethyl ether. The combined filtrates were dried ($MgSO_4$) and then concentrated *in vacuo*. Flash chromatography afforded 2.64 g (80%) of the allylic alcohol **11***b* as a white amorphous solid, mp 104–106°C (from ether – petroleum ether); R_f 0.29 (30% ethyl acetate – petroleum ether); $[\alpha]_D^{23}$ −18.4° (*c* 1.0, chloroform); ^1H nmr (80 MHz) δ: 1.18, 1.38 (s, s, 6H, $C(CH_3)_2$), 1.66–2.20 (m, 3H, H-3, H-3′, OH, D_2O exchange), 3.52 (br s, 2H, H-5, H-5′), 4.16 (d, 2H, J = 7.0 Hz, H-7, H-7′), 4.52 (t, 1H, J = 3.7 Hz, H-2), 4.84 (dd, 1H, J = 4.4 Hz, J = 5.0 Hz, H-4), 5.58 (d, 1H, J = 3.7 Hz, H-1), 5.94 (t, 1H, J = 7.0 Hz, H-6), 7.35 (m, 15H, Ph_3C). *Anal.* calcd. for $C_{30}H_{32}O_5$: C 76.25, H 6.82; found: C 76.06, H 6.61.

*Hydroboration of compound **11**b*

To a solution of diborane (16 mL, 1.0 *M* in tetrahydrofuran), which had been cooled to 0°C, was added a solution of **11***b* (2.5 g, 5.3 mmol) in tetrahydrofuran (20 mL) dropwise over a period of 1 h under an argon atmosphere. After 6 h, 1 mL of water was added slowly, followed by addition of 6 mL of 3 *N* aqueous sodium hydroxide and 6 mL of 30% hydrogen peroxide, maintaining the temperature at 20–25°C. After stirring for another 3 h at room temperature, the aqueous phase was saturated with sodium chloride. The tetrahydrofuran phase was separated and the aqueous layer was extracted with diethyl ether. The combined organic layers were dried over anhydrous magnesium sulfate and concentrated *in vacuo*. The excess of water was removed azeotropically with toluene, after which flash chromatography afforded **12** (2.3 g, 90%) as an amorphous solid; R_f 0.26 (50% ethyl acetate – petroleum ether); ^1H nmr (60 MHz) δ: 1.30, 1.50 (s, s, 6H, $C(CH_3)_2$), 1.70–2.24 (m, 3H, H-3′, H-5), 2.50–3.80 (m, 8H, H-4, H-6, H-7, H-7′, H-5, H-5′, 2 × OH), 4.68 (m, 1H, H-2), 5.75 (br d, 1H, H-1), 7.40 (m, 15H, Ph_3C). *Anal.* calcd. for $C_{30}H_{34}O_6$: C 73.45, H 6.98; found: C 73.38, H 6.93.

*3-*O*-Benzyl-6-*O*-tert-butyldimethylsilyl-1,2-*O*-isopropylidene-α-*D*-glucofuranose (**13**b)*

To a solution of 3-*O*-benzyl-1,2-*O*-isopropylidene-α-D-glucofuranose (**13***a*) (25) (17.4 g, 56.13 mmol), *N*,*N*-dimethylaminopyridine (1.0 g), and trimethylamine (23 mL) in dichloromethane (250 mL) was added *tert*-butyl-dimethylsilyl chloride (8.46 g, 56.13 mmol) at room temperature under an argon atmosphere. After 20 h the reaction mixture was poured into 100 mL of ice water, extracted with dichloromethane, and processed in the usual way to give **13***b* (23.1 g, 97%) as a colorless syrup; R_f 0.41 (15% ethyl acetate – petroleum ether); $[\alpha]_D^{23}$ −24.2° (*c* 1.0, chloroform); ^1H nmr (80 MHz) δ: 0.03 (s, 6H, $SiMe_2$), 0.89 (s, 9H, *t*BuSi), 1.30, 1.46 (s, s, 6H, $C(CH_3)_2$), 2.62 (d, 1H, J = 5.5 Hz, OH), 3.68–4.20 (m, 5H, H-3, H-4, H-5, H-6, H-6′), 4.57 (d, 1H, J = 3.7 Hz, H-2), 4.66 (s, 2H, $PhCH_2$), 5.89 (d, 1H, J = 3.7 Hz, H-1), 7.33 (s, 5H, Ph). *Anal.* calcd. for $C_{22}H_{36}O_6Si$: C 62.23, H 8.55; found: C 62.31, H 8.64.

*3-*O*-Benzyl-6-*O*-tert-butyldimethylsilyl-1,2-*O*-isopropylidene-α-*D*-xylo-hexofuran-5-ulose (**14**)*

Compound **13***b* (23.1 g, 54.48 mmol) was oxidized as described above for **8***b* → **10**. The product **14** (20.7 g, 90%) was a colorless syrup; R_f 0.41 (15% ethyl acetate – petroleum ether); $[\alpha]_D^{23}$ −91.98° (*c* 1.87, chloroform); ν_{max} ($CHCl_3$): 2950, 1740 (C=O), 1460 cm^{-1}; ^1H nmr (80 MHz) δ: 0.04 (s, 6H, $SiMe_2$), 0.90 (s, 9H, *t*BuSi), 1.30, 1.48 (s, s, 6H, $C(CH_3)_2$), 4.37 (d, 1H, $J_{3,4}$ = 3.5 Hz, H-3), 4.48 (s, 2H, H-6, H-6′), 4.52 (d, 2H, J = 3.5 Hz, $PhCH_2$), 4.58 (d, 1H, $J_{3,4}$ = 3.5 Hz, H-4), 4.88 (d, 1H, J = 3.7 Hz, H-2), 6.02 (d, 1H, $J_{1,2}$ = 3.7 Hz, H-1), 7.25 (s, 5H, Ph). *Anal.* calcd. for $C_{22}H_{34}O_6Si$: C 62.53, H 8.11; found: C 62.62, H 8.15.

*Methyl 3-*O*-benzyl-5-*C*-(tert-butyldimethylsilyloxymethyl)-5,6-dideoxy-1,2-*O*-isopropylidene-α-*D*-xylo-hept-5-(*Z*)-enofuranosyluranote (**15**a)*

A solution of **14** (16 g, 37.9 mmol) and carbomethoxymethylenetriphenylphosphorane (16 g, 50 mmol), in dry acetonitrile (50 mL) under argon, was refluxed for 2 h. Work-up in the usual way afforded **15***a* (15.2 g, 84%) after chromatography; R_f 0.63 (20% ethyl ether – petroleum ether); ν_{max} ($CHCl_3$): 2950, 1740 (C=O, unsaturated ester), 1660 cm^{-1}; ^1H nmr (80 MHz) δ: 0.05 (s, 6H, $SiMe_2$), 0.92 (s, 9H, *t*BuSi), 1.31, 1.50 (s, s, 6H, $C(CH_3)_2$), 3.62 (s, 3H, OCH_3), 4.35–4.73 (m, 6H, H-2, H-3, H-5, H-5′, $PhCH_2$), 5.86 (m, 1H, H-6), 5.95 (d, 1H, $J_{1,2}$ = 3.7 Hz, H-1), 6.17 (m, 1H, H-4), 7.30 (s, 5H, Ph). *Anal.* calcd. for $C_{25}H_{38}O_7Si$: C 62.73, H 8.00; found: C 62.70, H 7.96.

*5-*C*-Hydroxymethyl-5,6-dideoxy-1,2-*O*-isopropylidene-α-*D*-gluco-heptofuranuronic 1′,7-lactone (**19**b)*

To a solution of **15***a* (5.0 g, 10 mmol) in methanol (50 mL) was added ammonium fluoride (0.75 g, 20 mmol) in water (4 mL). The reaction mixture was refluxed for 3 h, cooled, and the methanol removed *in vacuo*. A solution of the residue (**15***b*) in benzene (100 mL) was hydrogenated over 5% platinum on carbon at a starting pressure of 500 psi (1 psi = 6.9 kPa). After 45 min the catalyst was removed by filtration and the filtrate was concentrated *in vacuo* to yield an oil that showed two components (tlc) assigned as **18** and **19***a*. To a solution of the oil in diethyl ether (100 mL) was added *p*-toluenesulfonic acid (120 mg, 0.6 mmol), and after 6 h at 23°C the reaction mixture was quenched with triethylamine, washed with brine, dried (Na_2SO_4), and concentrated *in vacuo* to afford 3.4 g (96%) of **19***a*. Debenzylation by hydrogenolysis (10% Pd/C) in ethanol was carried out in the usual way, to give **19***b* (1.9 g, 79%) as a crystalline material, mp 138–139°C; R_f 0.44 (5% methanol – methylene chloride); $[\alpha]_D^{20}$ −47.9° (*c* 0.4, chloroform); ν_{max} ($CHCl_3$): 3400 (hydrogen bonded OH), 2910, 1775 (lactone) cm^{-1}; ^1H nmr (400 MHz) δ: 1.31 (s, 3H, CCH_3), 1.49 (s, 3H, CCH_3), 1.57 (s, 1H, OH), 2.70 (ddd, 2H, H-7, H-7′), 3.00 (q, J = 8.0 Hz, 1H, H-5), 4.09–4.17 (m, 3H, H-3, H-6, H-6′), 4.46 (dd, J = 8.0 Hz, 1H, H-4), 4.50 (d, J = 3.7 Hz, 1H, H-2), 5.91 (d, J = 3.7 Hz, 1H, H-1). *Anal.* calcd. for $C_{11}H_{16}O_6$: C 54.09, H 6.60; found: C 54.14, H 6.76.

*3-O-Benzyl-5-C-(*tert*-butyldimethylsiloxymethyl)-5,6-dideoxy-1,2-O-isopropylidene-α-D-*xylo*-hept-5-(Z)-enofuranose (**20**a)*

Reduction of **15***a* (15.0 g, 31.4 mmol) with diisobutylaluminum hydride was carried out as described above for **11***a* → **11***b*. The product **20***a* (11.6 g, 82%) was a syrup; R_f 0.54 (50% ether – petroleum ether); ^{1}H nmr (80 MHz) δ: 0.05 (s, 6H, $SiMe_2$), 0.90 (s, 9H, *t*BuSi), 1.32, 1.48 (s, s, 6H, $C(CH_3)_2$), 1.75 (t, 1H, J = 5.4 Hz, OH), 3.92 (d, 1H, $J_{3,4}$ = 3.3 Hz, H-3), 4.00–4.28 (m, 4H, two H-7, two H-5′), 4.54 (d, 2H, J = 2.7 Hz, $PhCH_2$), 4.58 (d, 1H, J = 3.7 Hz, H-2), 4.92 (br d, 1H, J = 3.3 Hz, H-4), 5.94 (d and m, 2H, $J_{1,2}$ = 3.7 Hz, H-1, H-6; overlapping), 7.29 (s, 5H, Ph). *Anal.* calcd. for $C_{24}H_{38}O_6Si$: C 63.97, H 8.50; found: C 63.86, H 8.57.

*Hydroboration of compound **20**a (formation of compounds **15** and **16**a)*

Hydroboration of **20***a* (1.72 g, 3.78 mmol) was carried out as described for **11***b* → **12**. Flash chromatography of the product gave **21** (500 mg) and **22***a* (283 mg). For **21**: R_f 0.41 (50% ethyl acetate – petroleum ether); $[\alpha]_D^{23}$ −42.8° (*c* 0.90, chloroform); ^{1}H nmr (250 MHz) δ: 0.03 (d, 6H, J = 10.4 Hz, $SiMe_2$), 0.80 (s, 9H, *t*BuSi), 1.28, 1.44 (s, s, 6H, $C(CH_3)_2$), 2.20 (m, 1H, H-5), 2.70 (br s, 2H, two OH, D_2O exchange), 3.47 (dd, 1H, $J_{6,7a}$ = 4.3 Hz, J_{gem} = 11.3 Hz, H-7a), 3.70 (d, 2H, J = 5.0 Hz, two H-5′), 3.75 (dd, 1H, $J_{6,7b}$ = 3.0 Hz, J_{gem} = 11.3 Hz, H-7b), 3.84 (d, 1H, $J_{3,4}$ = 2.5 Hz, H-3), 3.98 (m, 1H, H-6), 4.32 (dd, 1H, $J_{3,4}$ = 2.5 Hz, J = 11.3 Hz, H-4), 4.54 (ABq, 2H, J = 11.3 Hz, PhCH_2), 4.60 (d, 1H, $J_{1,2}$ = 4.2 Hz, H-2), 5.90 (d, 1H, $J_{1,2}$ = 4.2 Hz, H-1), 7.30 (m, 5H, Ph). *Anal.* calcd. for $C_{24}H_{40}O_7Si$: C 61.51, H 8.60; found: C 61.36, H 8.83.

For **22***a*: R_f 0.67 (50% ethyl acetate – petroleum ether); ^{1}H nmr (250 MHz) δ: 0.03 (d, 6H, $SiMe_2$), 0.82 (s, 9H, *t*BuSi), 1.30, 1.45 (s, s, 6H, $C(CH_3)_2$), 1.82 (m, 2H, two H-6), 2.16 (m, 1H, H-5), 3.40 (dd, 1H, $J_{5,5'a}$ = 5.0 Hz, J_{gem} = 10.0 Hz, H-5′a), 3.56 (dd, 1H, $J_{5,5'b}$ = 2.5 Hz, J_{gem} = 10.0 Hz, H-5′b), 3.69 (t, 2H, J = 5.5 Hz, two H-7), 3.82 (d, 1H, $J_{3,4}$ = 2.5 Hz, H-3), 4.12 (dd and s, 2H, $J_{3,4}$ = 2.5 Hz, $J_{4,5}$ = 10.0 Hz, H-4, OH, D_2O exchange), 4.55 (ABq, 2H, J = 10.0 Hz, PhCH_2), 4.60 (d, 1H, $J_{1,2}$ = 4.2 Hz, H-2), 5.88 (d, 1H, $J_{1,2}$ = 4.2 Hz, H-1), 7.28 (m, 5H, Ph). *Anal.* calcd. for $C_{24}H_{40}O_6Si$: C 63.68, H 8.91; found: C 63.56, H 8.83.

*5-C-Acetoxymethyl-3,7-di-O-acetyl-5,6-dideoxy-1,2-O-isopropylidene-α-D-*gluco*-heptofuranose (**22**c)*

(a) Lactone **19***b* (0.123 g, 0.543 mmol) was dissolved in dry ether (25 mL), cooled in an ice water bath, and treated with lithium aluminum hydride (0.067 g, 1.76 mmol). The reaction mixture was warmed to room temperature and stirred, with the exclusion of moisture, for 1 h. Excess lithium aluminum hydride was destroyed with water and the solvent was removed. The residue (**22***b*) was dissolved in dry pyridine (30 mL) and treated with excess acetic anhydride (5 mL) for 1.5 h at room temperature. Work-up in the usual way afforded **22***c* (0.156 g, 76%); R_f 0.40 (50% ethyl acetate – petroleum ether); $[\alpha]_D^{23}$ −13.6° (*c* 1.1, $CHCl_3$); ^{1}H nmr (250 MHz) δ: 1.28, 1.48 (two s, 2 × 3H, $O_2C(CH_3)_2$), 1.74, 1.97–2.06 (two m, 2H, H-6a, H-6b), 2.01, 2.03, 2.09 (three s, 3 × 3H, 3 × $OCOCH_3$), 2.15 (m, 1H, H-5), 3.91–4.26 (m, 5H, H-4, H-7a, H-7b, H-1′a, H-1′b), 4.46 (d, 1H, H-2, $J_{1,2}$ = 3.7 Hz), 5.14 (d, 1H, H-3, $J_{3,4}$ = 3.2 Hz), 5.84 (d, 1H, H-1). *Anal.* calcd. for $C_{17}H_{26}O_9$: C 54.54, H 7.00; found: C 54.36, H 6.86.

(b) A mixture of compound **21** (530 mg, 1.08 mmol) and 1,1′-thiocarbonyldiimidazole (228 mg, 1.3 mmol) in 20 mL of dry tetrahydrofuran was refluxed under an argon atmosphere for 1 h. The reaction solution was partitioned between diethyl ether (50 mL) and cold 2 *N* hydrochloric acid (10 mL). The organic layer was separated, washed with water and brine, dried over anhydrous sodium sulfate, filtered, and evaporated *in vacuo* to give 518 mg (90%) of crude thionocarbonate **23**. A portion of the crude thionocarbonate (388 mg, 0.72 mmol), in tri-*n*-butyltin hydride (424 g, 1.44 mmol), and a catalytic amount of 1,1′-azobis(isobutyronitrile) in 20 mL of dry toluene was added to refluxing toluene over 10 min. After refluxing 3 h the mixture was treated with 5 mL of 10% aqueous sodium hydroxide at 40°C for 12 h. Work-up with the standard processing and flash chromatography provided pure compound **22***a*. A portion of the material (162 mg, 0.36 mmol), a catalytic amount of 10% palladium on activated carbon, and a few drops of 88% aqueous formic acid in 10 mL of methanol were stirred at room temperature under a hydrogen atmosphere. After 6 h the reaction mixture was filtered and evaporated *in vacuo*. The crude residue (**22***b*) was acetylated using the standard procedure, then treated with acetic anhydride and pyridine, to yield compound **22***c* (121 mg, 90%) whose physical properties were identical with those of the material described in part (a).

*5-C-(*tert*-Butyldimethylsiloxymethyl)-5,6-dideoxy-1,2-O-isopropylidene-α-D-*xylo*-hept-5-(Z)-enofuranose (**20**b)*

To a solution of 4.1 g (8.1 mmol) of the ester **15***c* (27) in 100 mL of dry toluene was added 24 mL of 1 *M* diisobutylaluminum hydride in toluene at 0°C, dropwise, over a period of 20 min under an argon atmosphere. After 3 h, tlc indicated that most of the starting material had been consumed. The reaction was quenched by addition of water at 0°C followed by 15% aqueous sodium hydroxide (1 mL) and water (3 mL). After vigorous stirring at room temperature for a few minutes, the white inorganic salts were removed by filtration, the residue was rinsed several times with ethyl acetate, and the combined filtrates were dried over anhydrous magnesium sulfate. The residue from evaporation was dissolved in dry methanol (100 mL) and then treated with a catalytic amount of sodium methoxide at room temperature. The saponification was monitored by tlc and, upon completion, the reaction mixture was poured into ice water and extracted with dichloromethane. The combined extracts were washed with cold dilute hydrochloric acid, saturated sodium bicarbonate, water, and brine, dried over anhydrous sodium sulfate, filtered, and concentrated *in vacuo*. The residue was purified by flash chromatography to give 2.1 g (72%) of pure diol **20***b* as a colorless syrup; R_f 0.45 (50% ethyl acetate – petroleum ether); $[\alpha]_D^{23}$ −38.4° (*c* 1.0, chloroform); ^{1}H nmr (80 MHz) δ: 0.08 (s, 6H, $SiMe_2$), 0.88 (s, 9H, *t*BuSi), 1.28, 1.45 (s, s, 6H, $C(CH_3)_2$), 2.48 (br s, 1H, OH), 3.80–4.46 (m, 6H, H-3, H-7, H-7′, H-5, H-5′, OH), 4.52 (d, 1H, J = 3.7 Hz, H-2), 5.03 (br s, 1H, H-4), 5.88 (m, 2H, $J_{1,2}$ = 3.7 Hz, H-1, H-6). *Anal.* calcd. for $C_{17}H_{32}O_6Si$: C 56.64, H 8.95; found: C 56.73, H 8.93.

*5-C-(*tert*-Butyldimethylsiloxymethyl)-5-deoxy-1,2-O-isopropylidene-L-*glycero*-α-D-*gluco*-heptofuranose (**25**)*

To a solution of disiamylborane (38 mmol) in dry tetrahydrofuran was added a solution of diol **20***b* (2.65 g, 7.36 mmol) in dry tetrahydrofuran (45 mL) at −78°C under an argon atmosphere, dropwise, over a period of 45 min. After stirring at −78°C for 2 h, the temperature was raised to −20°C, on the assumption (tlc evidence) that the formation of **24** was optional. A solution of 1 *M* borane in tetrahydrofuran (46 mL) was then added dropwise over a period of 45 min and the reaction mixture was stirred at room temperature for 16 h. Further portions of borane solution were added if necessary (tlc evidence). The reaction was quenched by addition of water (2 mL) to destroy the excess of borane, followed by 3 *N* sodium hydroxide and 30% hydrogen peroxide (30 mL of each) at 0°C. After vigorous stirring at room temperature for 6 h, the mixture was saturated with sodium chloride. The tetrahydrofuran phase was separated and the aqueous phase was extracted with ethyl acetate. The combined organic extracts were dried over anhydrous magnesium sulfate, filtered, and concentrated *in vacuo*. Excess water was removed azeotropically with toluene several times. The resulting residue was purified by flash chromatography to afford 2.22 g (80%) of pure triol **25** as a colorless syrup; R_f 0.21 (50% ethyl acetate – petroleum ether); $[\alpha]_D^{23}$ +7.8° (*c* 0.97, chloroform); ^{1}H nmr (250 MHz) δ: 0.06 (s, 6H, $SiMe_2$), 0.88 (s, 9H, *t*BuSi), 1.28, 1.47 (s, s, 6H, $C(CH_3)_2$), 2.14 (m, 2H, H-5, OH, D_2O exchange), 2.92 (br s, 1H, OH, D_2O exchange), 3.35 (br s, 1H, OH, D_2O exchange), 3.57–3.83 (m, 4H, H-3, H-6, H-5, H-5′), 3.86 (dd, 1H, $J_{3,4}$ = 2.5 Hz, J = 11.3 Hz, H-4), 4.13 (m, 2H, H-7, H-7′), 4.52 (d, 1H, J = 4.2 Hz, H-2), 5.88 (d, 1H, $J_{1,2}$ = 4.2 Hz, H-1). *Anal.* calcd. for $C_{17}H_{34}O_7Si$: C 53.94, H 9.12; found: C 53.76, H 9.05.

*5-C-(*tert*-Butyldimethylsiloxymethyl)-5-deoxy-1,2-O-isopropylidene-L-*glycero*-α-D-*gluco*-heptofuranose-6,7-carbonate (**26**a)*

To a stirred solution of triol **25** (1.14 g, 3.0 mmol) in dry dichloromethane (70 mL) and dry pyridine (35 mL) was added dropwise

14.4 mL of 12.5% phosgene in toluene at 0°C under an argon atmosphere over a period of 20 min. After 1 h the reaction was poured into 50 mL of ice water and then extracted with dichloromethane (2 × 50 mL). The combined organic extracts were washed with cold dilute hydrochloric acid, water, and brine, and dried (Na_2SO_4), filtered, and concentrated *in vacuo*. The residue was purified by flash chromatography to give **26***a* (1.1 g, 90%) as a colorless syrup; R_f 0.64 (50% ethyl acetate – petroleum ether); $[\alpha]_D^{23}$ +10.7° (*c* 1.47, chloroform); ν_{max} ($CHCl_3$): 3450 (OH), 2950, 2900, 1880 (C=O, cyclic carbonate) cm^{-1}; ^1H nmr (250 MHz) δ: 0.05 (s, 6H, $SiMe_2$), 0.85 (s, 9H, *t*BuSi), 1.27, 1.45 (s, s, 6H, $C(CH_3)_2$), 2.32 (m, 1H, H-5), 3.17 (br s, 1H, OH, D_2O exchange), 3.68 (dd, 1H, $J_{5,5'a}$ = 7.5 Hz, J_{gem} = 10.0 Hz, H-5′a), 3.90 (dd, 1H, $J_{5,5'b}$ = 2.5 Hz, J_{gem} = 10.0 Hz, H-5′b), 4.04 (dd, 1H, $J_{3,4}$ = 2.5 Hz, $J_{4,5}$ = 10.0 Hz, H-4), 4.18 (d, 1H, *J* = 2.5 Hz, H-3), 4.35 (t, 1H, *J* = 8.8 Hz, H-7a), 4.50 (d, 1H, *J* = 4.2 Hz, H-2), 4.61 (dd, 1H, *J* = 7.5 Hz, *J* = 10.0 Hz, H-7b), 4.76 (q, 1H, $J_{5,6}$ = $J_{6,7a}$ = 8.8 Hz, H-6), 5.82 (d, 1H, $J_{1,2}$ = 4.2 Hz, H-1). *Anal.* calcd. for $C_{18}H_{32}O_8Si$: C 53.44, H 7.97; found: C 53.43, H 8.00.

5-C-(tert-*Butyldimethylsiloxymethyl)-5-deoxy-1,2*-O-*isopropylidene-3*-O-*phenoxythiocarbonyl-L*-glycero-α-*D*-gluco-*heptofuranose-6,7-carbonate (**26**b)*

To a solution of the alcohol **26***a* (1.1 g, 2.7 mmol) and a catalytic amount of *N,N*-dimethylaminopyridine (~10 mg) in dry dichloromethane (50 mL) and dry pyridine (2 mL) was added phenyl chlorothionocarbonate (0.62 mL, 4.5 mmol) at room temperature under an argon atmosphere. After 3 h another more phenyl chlorothionocarbonate (0.2 mL) was added and the reaction was monitored by tlc. The reaction mixture was poured into 10 mL of ice water and extracted with 3 × 20 mL of dichloromethane. The combined organic extracts were washed with cold dilute hydrochloric acid, water, and brine, and dried over anhydrous sodium sulfate, filtered, and concentrated *in vacuo*. Flash chromatography gave **26***b* (1.2 g, 82%) as a yellow syrup; R_f 0.50 (50% ethyl acetate – hexane); $[\alpha]_D^{23}$ +9.4° (*c* 0.98, chloroform); ν_{max} ($CHCl_3$): 2950, 2900, 1800 (C=O), 1580, 1480 cm^{-1}; ^1H nmr (250 MHz) δ: 0.06 (d, 6H, $SiMe_2$), 0.88 (s, 9H, *t*BuSi), 1.31, 1.50 (s, s, 6H, $C(CH_3)_2$), 2.30 (ttt, 1H, *J* = 2.9 Hz, *J* = 9.8 Hz, H-5), 3.63 (dd, 1H, *J* = 3.3 Hz, J_{gem} = 10.8 Hz, H-5′a), 3.96 (dd, 1H, *J* = 3.3 Hz, J_{gem} = 10.8 Hz, H-5′b), 4.38 (t, 1H, *J* = 8.8 Hz, H-7a), 4.49 (dd, 1H, $J_{3,4}$ = 2.9 Hz, $J_{4,5}$ = 9.8 Hz, H-4), 4.62 (dd, 1H, *J* = 7.8 Hz, *J* = 8.8 Hz, H-7b), 4.72 (d, 1H, *J* = 4.2 Hz, H-2), 4.96 (q, 1H, *J* = 7.8 Hz, H-6), 5.64 (d, 1H, $J_{3,4}$ = 2.9 Hz, H-3), 5.92 (d, 1H, $J_{1,2}$ = 4.2 Hz, H-1), 7.05–7.50 (m, 5H, Ph). *Anal.* calcd. for $C_{25}H_{36}O_9SSi$: C 55.53, H 6.71, S 5.93; found: C 55.61, H 6.50, S 6.15.

5-C-(tert-*Butyldimethylsiloxymethyl)-3,5-dideoxy-1,2*-O-*isopropylidene-β-L*-talo-*heptofuranose-6,7-carbonate (**26**c)*

A mixture of compound **26***b* (1.2 g, 2.22 mmol), tri-*n*-butyltin hydride (0.9 mL, 3.33 mmol) and 2,2′-azobis(2-methylpropionitrile) (30 mg) in toluene (40 mL) was heated to reflux under an argon atmosphere. After 3 h the reaction mixture was cooled to room temperature and then concentrated *in vacuo*. Flash chromatography afforded compound **26***c* (775 mg, 90%) as a colorless syrup; R_f 0.15 (30% ethyl acetate – hexane); $[\alpha]_D^{23}$ +1.9° (*c* 1.35, chloroform); ν_{max} ($CHCl_3$): 3000, 1800 (C=O, cyclic carbonate), 1500 cm^{-1}; ^1H nmr (250 MHz) δ: 0.04 (s, 6H, $SiMe_2$), 0.88 (s, 9H, *t*BuSi), 1.29, 1.46 (s, s, 6H, $C(CH_3)_2$), 1.55 (m, 1H, H-3α), 1.80 (m, 1H, H-5), 2.25 (dd, 1H, $J_{2,3\beta}$ = $J_{3\beta,4}$ = 4.2 Hz, J_{gem} = 13.0 Hz, H-3α), 3.67 (dd, 1H, *J* = 3.1 Hz, J_{gem} = 10.2 Hz, H-5′a), 3.91 (dd, 1H, *J* = 3.1 Hz, J_{gem} = 10.2 Hz, H-5′b), 4.25 (ddd, 1H, $J_{3\beta,4}$ = 4.2 Hz, $J_{4,5}$ = 10.2 Hz, H-4), 4.38 (t, 1H, *J* = 9.3 Hz, H-7a), 4.62 (t, 1H, *J* = 8.3 Hz, H-7b), 4.70 (t, 1H, $J_{1,2}$ = $J_{2,3\beta}$ = 4.2 Hz, H-2), 4.90 (q, 1H, *J* = 8.3 Hz, H-6), 5.74 (d, 1H, $J_{1,2}$ = 4.2 Hz, H-1). *Anal.* calcd. for $C_{18}H_{32}O_7Si$: C 55.64, H 8.30; found: C 55.81, H 8.36.

5-C-(tert-*Butyldimethylsiloxymethyl)-3,5-deoxy-1,2*-O-*isopropylidene-β-L*-talo-*heptofuranose (**3**b)*

To a stirred solution of the carbonate **26***c* (215 mg, 0.56 mmol) in 215 mL of a water–methanol–tetrahydrofuran (1:1:1) mixture was added barium hydroxide octahydrate (100 mg). After stirring at room temperature for 30 min, the reaction mixture was neutralized with a stream of carbon dioxide gas, and then extracted with 3 × 20 mL of ethyl acetate. The combined organic extracts were dried over anhydrous magnesium sulfate, filtered, and concentrated *in vacuo*. Flash chromatography gave diol **3***b* (197 mg, 98%) as a colorless syrup; R_f 0.13 (30% ethyl acetate – petroleum ether); $[\alpha]_D^{23}$ −9.8° (*c* 1.25, chloroform); ^1H nmr (250 MHz) δ: 0.06 (s, 6H, $SiMe_2$), 0.88 (s, 9H, *t*BuSi), 1.28, 1.48 (s, s, 6H, $C(CH_3)_2$), 1.57 (m, 1H, H-3β), 1.82 (m, 1H, H-5), 2.15 (dd, 1H, $J_{2,3\beta}$ = $J_{3\beta,4}$ = 4.2 Hz, J_{gem} = 13.0 Hz, H-3β), 2.70 (dd, 1H, *J* = 6.3 Hz, *J* = 8.3 Hz, OH, D_2O exchange), 3.21 (d, 1H, *J* = 6.3 Hz, OH, D_2O exchange), 3.65–3.83 (m, 4H, two H-5′, H-7, H-7′), 3.93 (m, 1H, H-6), 4.32 (m, 1H, H-4), 4.71 (t, 1H, $J_{1,2}$ = $J_{2,3\beta}$ = 4.2 Hz, H-2), 5.78 (d, 1H, $J_{1,2}$ = 4.2 Hz, H-1). *Anal.* calcd. for $C_{17}H_{34}O_6Si$: C 56.32, H 9.45; found: C 56.32, H 9.31.

Acknowledgements

We are grateful to the Burroughs Wellcome Trust, Duke University, the University of Maryland, the Natural Sciences and Engineering Research Council of Canada, and the National Science Foundation (CHE 8304283) for support of this work. The help of Drs. Naoki Mitsuo and Masao Shiozaki is acknowledged.

1. J. D. Dutcher, M. B. Young, J. H. Sherman, W. Hibbits, and D. R. Walters. Antibiotic Annu. 886 (1956); J. D. Dutcher, D. R. Walters, and D. Wintersteiner. J. Org. Chem. **28**, 995 (1963); M. Von Saltza, J. D. Dutcher, J. Reid, and O. Wintersteiner. J. Org. Chem. **28**, 999 (1963); A. C. Cope, V. Axen, E. P. Burrows, and J. Weinlich. J. Am. Chem. Soc. **88**, 4228 (1966); E. Borowski, J. Zielinski, T. Ziminski, L. Falowski, P. Kolodziejczyk, J. Golik, and E. Jereczek. Tetrahedron Lett. 3909 (1970).
2. S. Waksman, and H. Lechevalier. *In* The actinomycetes. Vol. 3. Williams and Wilkins, Baltimore. 1962.
3. G. Hildick-Smith, H. Blank, and I. Sarkany. *In* Fungus diseases and their treatment. Little, Brown and Co., Boston. 1964.
4. S. C. Kinsky. *In* Antibiotics. Vol. 1. *Edited by* D. Gottlieb and P. D. Shaw. Springer Verlag, New York. 1967. p. 122, and references cited therein; R. W. Holz. *In* Antibiotics. Vol. 2. *Edited by* F. E. Hahn. Springer Verlag, New York. 1979. p. 313, and references cited therein.
5. I. K. Aronson, C. H. L. Rieger, K. Soltani, V. Tkalcevic, W. C. Chan, A. L. Lorincz, and G. Matz. Cancer, **43**, 101 (1979); B. A. Adelman, A. Bentman, P. Rosenthal, B. R. Smith, K. R. Bridges, and W. Holmes. Ann. Intern. Med. **91**, 323 (1979); E. Z. Ezdinli, D. D. O'Sullivan, L. P. Wasser, U. Kim, and L. Stutzman. J. Am. Med. Assoc. **262**, 258 (1979).
6. I. M. Tereshin. *In* Polyene antibiotics—present and future. University of Tokyo Press, Japan. 1976.
7. W. Oroshnik and A. D. Mebane. Prog. Chem. Org. Nat. Prod. **37**, 166 (1973); A. W. Norman, A. M. Spielvogel, and R. W. Wong. Adv. Lipid Res. **14**, 127 (1976).
8. T. Nakata, S. Takao, M. Fukui, T. Tanaka, and T. Oishi. Tetrahedron Lett. **24**, 3873 (1983); K. Narasaka and F. C. Pai. Tetrahedron, **40**, 2233 (1984); S. Kiyooka, H. Sasaoka, R. Fujiyama, and C. H. Heathcock. Tetrahedron Lett. **25**, 5331 (1984); P. A. Bartlett and K. K. Jernstedt. J. Am. Chem. Soc. **99**, 4829 (1977); M. Hirama and M. Uei. Tetrahedron Lett. **23**, 5307 (1982); B. H. Lipshutz and J. A. Kozlowski. J. Org. Chem. **49**, 1149 (1984).
9. W. Mechlinski, C. P. Schaffner, P. Ganis, and G. Avitabile. Tetrahedron Lett. 3873 (1970); P. Ganis, G. Avitabile, W. Mechlinski, and C. P. Schaffner. J. Am. Chem. Soc. **93**, 4560 (1970).
10. D. Boschelli, J. W. Ellingboe, and S. Masamune. Tetrahedron Lett. **25**, 3395 (1984); S. Masamune, T. Kaiho, and

D. S. GARVEY. J. Am. Chem. Soc. **104**, 5521 (1982); S. MASAMUNE, P. MA, H. OKUMOTO, J. W. ELLINGBOE, and Y. ITO. J. Org. Chem. **49**, 2837 (1984); P. MA, V. S. MARTIN, S. MASAMUNE, K. B. SHARPLESS, and S. M. VITI. J. Org. Chem. **47**, 1378 (1982).

11. K. C. NICOLAOU and J. UENISHI. J. Chem. Soc. Chem. Commun. 1292 (1982).
12. D. W. BROOKS and R. P. KELLOGG. Tetrahedron Lett. **23**, 4991 (1982); D. W. BROOKS and J. T. PALMER. Tetrahedron Lett. **24**, 3059 (1983).
13. D. M. FLOYD and A. W. FRITZ. Tetrahedron Lett. **22**, 2847 (1981); D. M. FLOYD and C. M. CIMARUSTI. Tetrahedron Lett. **20**, 4129 (1979).
14. S. HANESSIAN. *In* Total synthesis of natural products: the 'chiron' approach. Pergamon Press, New York. 1982.
15. B. E. DAVIDSON and R. D. GUTHRIE. J. Chem. Soc. Perkin Trans. 1, 658 (1972).
16. B. E. DAVIDSON, R. D. GUTHRIE, and A. T. MCPHAIL. J. Chem. Soc. Chem. Commun. 1273 (1968).
17. A. MUBARAK and B. FRASER-REID. J. Org. Chem. **47**, 4265 (1982).
18. B. FRASER-REID, L. MAGDZINSKI, and B. MOLINO. *In* Current trends in organic synthesis. *Edited by* H. Nozaki. Pergamon, New York. 1983; B. FRASER-REID, L. MAGDZINSKI, and B. MOLINO. J. Am. Chem. Soc. **106**, 731 (1984).
19. D. A. PRINS. J. Am. Chem. Soc. **70**, 3955 (1948).
20. (*a*) P. T. HO and S. CHUNG. Carbohydr. Res. **110**, 217 (1982); (*b*) J. D. PRUGH and A. A. DEANA. Tetrahedron Lett. **23**, 281 (1982); (*c*) Y. L. YANG and J. R. FALCK. Tetrahedron Lett. **23**, 4305 (1982).
21. D. H. R. BARTON and S. W. MCCOMBIE. J. Chem. Soc. Perkin Trans. 1, 1574 (1975).
22. E. J. HEDGELEY, W. G. OVEREND, and R. A. C. RENNIE. J. Chem. Soc. 4701 (1963).
23. K. C. NICOLAOU, M. R. PAVIA, and S. P. SEITZ. J. Am. Chem. Soc. **104**, 2027 (1982).
24. (*a*) J. K. N. JONES and J. L. THOMPSON. Can. J. Chem. **35**, 955 (1957); (*b*) D. HORTON, J. K. THOMSON, and C. G. TINDALL, JR. Methods Carbohydr. Chem. **6**, 297 (1972).
25. R. L. WHISTLER and W. C. LAKE. Methods Carbohydr. Chem. **6**, 286 (1972).
26. H. REDLICH and H. J. NEUMANN. Chem. Ber. **114**, 2020 (1981).
27. M. GEORGES, T. F. TAM, and B. FRASER-REID. J. Org. Chem. **50**, 5747 (1985); B. FRASER-REID, Z. BENKO, R. GUILIANO, K. M. SUN, and N. TAYLOR. J. Chem. Soc. Chem. Commun. 1029 (1984).
28. D. H. R. BARTON and R. SUBRAMANIAN. J. Chem. Soc. Perkin Trans. 1, 1718 (1977).
29. H. C. BROWN. *In* Boranes in organic chemistry. Cornell University Press, Ithaca, NY. 1972. p. 266.
30. H. C. BROWN and M. K. UNNI. J. Am. Chem. Soc. **90**, 2902 (1968); H. C. BROWN and R. M. GALLIVAN, JR. J. Am. Chem. Soc. **90**, 2906 (1968); H. C. BROWN and R. L. SHARP. J. Am. Chem. Soc. **90**, 2915 (1968), and references therein; K. H. SCHULTE-ELTE and G. OHLOFF. Helv. Chim. Acta, **50**, 153 (1967); D. J. PASTO and J. HICKMAN. J. Am. Chem. Soc. **90**, 4445 (1968).
31. D. LIANG, H. W. PAULS, and B. FRASER-REID. J. Chem. Soc. Chem. Commun. 1122 (1984).
32. M. J. ROBBINS and J. S. WILSON. J. Am. Chem. Soc. **103**, 932 (1981).

Electron transport in dense gases: limitations on the Ioffe-Regel and Mott criteria[1]

NORMAN GEE AND GORDON R. FREEMAN
Chemistry Department, University of Alberta, Edmonton, Alta., Canada T6G 2G2

Received January 2, 1986

NORMAN GEE and GORDON R. FREEMAN. Can. J. Chem. **64**, 1810 (1986).

In the gas phase, the Ioffe–Regel criterion that electron transport becomes modified when the mean free path equals the electron wavelength ($L = \lambda$) applies clearly only to helium and hydrogen, which have a net repulsive interaction with electrons. The Mott criterion, that when $L = \lambda/2\pi$ the electron is in a localized state, also applies to these two gases. The two criteria are less effective for molecules that have net attractive interactions with the electrons, because the interactions are not simply additive. They are not useful for xenon gas. The criteria are also assessed for: (*a*) several highly polarizable, spherical and nonspherical molecules; (*b*) polar molecules; (*c*) nitrogen and carbon dioxide, which form transient anions.

NORMAN GEE et GORDON R. FREEMAN. Can. J. Chem. **64**, 1810 (1986).

En phase gazeuse, le critère de Ioffe–Regel, selon lequel le transport d'électrons est modifié lorsque le parcours libre moyen est égal à la longueur d'onde de l'électron ($L = \lambda$), ne s'applique clairement que dans les cas de l'hélium et de l'hydrogène qui possèdent une interaction répulsive nette vis-à-vis les électrons. Le critère de Mott, selon lequel l'électron est dans un état localisé lorsque $L = \lambda/2\pi$, s'applique aussi à ces deux gaz. Dans les cas des molécules qui possèdent des interactions attractives pour les électrons, ces deux critères sont moins efficaces parce que les interactions ne sont alors pas additives. Ils ne sont pas utiles pour le xénone à l'état gazeux. On a aussi évalué ces critères pour : (*a*) plusieurs molécules hautement polarisables, sphériques et non-sphériques; (*b*) des molécules polaires et (*c*) pour l'azote et le dioxyde de carbone qui forment des anions transitoires.

[Traduit par la revue]

Introduction

In a gas at low densities the mobility μ of electrons is inversely proportional to the number density n of the gas, so:

[1] $$n\mu = \text{constant}$$

At sufficiently high densities $n\mu$ may either decrease (1–6) or increase (4–7) with increasing n, depending on the properties of the molecules and on n and the temperature T (4–6). There is no universal agreement about the causes of the changes in $n\mu$.

The effects of gas density on $n\mu$ are interpreted in terms of multibody scattering. What has come to be known as the Ioffe–Regel criterion for multibody scattering is often employed. Unfortunately there is confusion in the literature about the Ioffe–Regel criterion. The present work attempts to clarify the terminology, and to assess the applicability of the Ioffe–Regel criterion in a wide variety of gases.

2. Ioffe–Regel criteria

In 1960 Ioffe and Regel, in an article about amorphous and liquid semiconductors (8), discussed the limits of applicability of common theories of electronic conduction. The theories included assumptions about the mean velocity $\langle v \rangle$ and mean free path L of the electrons. Ioffe and Regel compared the magnitude of L with the average wavelength λ_T of the (nearly) free electrons and the average interatomic or intermolecular distance a of the medium.

The value of L can be obtained from the mobility of thermal, nearly free electrons by (from eqs. [13] and [17] in ref. 6*b*):

[2] $$L = \frac{1}{n\sigma_{ave}} = \frac{3}{e}\left(\frac{\pi m k_B T}{8}\right)^{1/2}\mu$$
$$= 4.17 \times 10^{-8}\, T^{1/2}\mu$$

where $\sigma_{ave} = \langle v \rangle / \langle v/\sigma_m \rangle$ is the momentum transfer cross section averaged over the Maxwellian velocity distribution, e and m are the electronic charge and mass, respectively, and k_B is Boltzmann's constant. The unit for L is m and for μ is (m^2/V s). At 300 K eq. [2] gives

[3] $$L = 7.2 \times 10^{-7}\,\mu$$

which agrees with Ioffe and Regel's room temperature value $L \approx 10^{-6}\,\mu(m^*/m_0)^{1/2}$, where the effective mass ratio m^*/m_0 is unity in the gas at low and moderate densities.

In many gases at $n \approx 1 \times 10^{26}$ molecules/m^3 electron mobilities at 300 K are of the order of 0.1 m^2/V s, so $L \approx 10^{-7}$ m. The value of a at this density is $\sim 10^{-9}$ m. The average de Broglie wavelength of the electron at this temperature is $\sim 10^{-8}$ m. Thus $L > \lambda_T > a$. By increasing n one decreases L as n^{-1}, and decreases a as $n^{-1/3}$; λ_T is varied for nearly free electrons by changing T.

Free forward motion with a mean velocity $\langle v \rangle$ only occurs over the mean distance L. Therefore Ioffe and Regel suggested that when L becomes smaller than λ_T "the concept of velocity of the charge carriers loses its meaning" (8). This means a modification of μ, but does not imply localization. However, when L calculated from eq. [3] has a value less than a "the mechanism of mobility itself must be altogether different, and the concept of mean free path has no meaning" (8). The value of L cannot in reality be less than a, so when eq. [3] indicates $L < a$ the electron must be in a localized state, and it migrates by hopping from site to site in a probabilistic manner. Equation [3] then does not apply.

The conditions, (*a*) $L \approx \lambda_T$ and (*b*) $L \approx a$, have been taken to depict multibody scattering and electron localization, respectively. The latter seems clear enough. The former is obscured by the wide variety of treatments of the average electron wavelength (8–18). The different treatments cause differences up to *eleven-fold* in the predicted densities where multibody scattering should become important (see Appendix 1). This large factor of eleven is made up of a factor of $6.3 = 2\pi$, caused by confusing wavelength λ with $\lambda/2\pi = \lambda\!\!\!^{-}$, and a factor of 1.8 caused by different methods of averaging over the Maxwellian velocity distribution. For the largest portion, 6.3-fold, it is convenient to distinguish by name λ, which is the distance over which the phase of the wave changes by one cycle, and $\lambda\!\!\!^{-}$, which is the distance over which the phase of the wave changes by one radian. Hence, λ is the *wavelength* and $\lambda\!\!\!^{-}$ is the *radianlength* (19). The names are useful in the visualization (20) of the processes.

For averaging λ over the Maxwellian velocity distribution we

[1]Assisted financially by the Natural Sciences and Engineering Research Council of Canada.

favor the 3-dimensional model and the inverse velocity, since $\lambda = h/mv$. Hence, the average wavelength and radianlength of electrons at temperature T are taken as

[4] wavelength $\lambda_T = h\langle v_{3d}^{-1}\rangle/m$
$$= h\left(\frac{2}{\pi m k_B T}\right)^{1/2}$$
$$= 1.49 \times 10^{-7}\, T^{-1/2}$$

[5] radianlength $\lambda\!\!\!^{-}_T = \hbar\langle v_{3d}^{-1}\rangle/m$
$$= 2.37 \times 10^{-8}\, T^{-1/2}$$

The one dimensional $\langle v_{1d}^{-1}\rangle$ equals infinity and cannot be used.

Mott changed the Ioffe–Regel criterion, although he did not change the name. Mott's criterion was that when L equals the "wavelength", $h/[2\pi(mk_BT)^{1/2}]$, the electron cannot be in a nearly free state, so it is in a localized state (11). As noted in Appendix 1, $h/[2\pi(mk_BT)^{1/2}]$ is a radianlength rather than a wavelength, so Mott's criterion is $L \approx \lambda\!\!\!^{-}_T$. Mott's is sort of a combination of the Ioffe–Regel criteria (*a*) and (*b*) and we call it the Mott criterion of localization.

3. Application of Ioffe–Regel $L \approx \lambda_T$, Mott $L \approx \lambda_T$, and $L \approx 2\lambda_T$

Iakubov (21) set out to quantify the Ioffe–Regel criterion (*a*), but actually used that of Mott. For the wavelength he used a formula for radianlength equivalent to (see Appendix 1)

[6] $\lambda\!\!\!^{-}_T = \hbar/m\alpha_{3d}$

where $\alpha_{3d} = (2k_BT/m)^{1/2}$ is the most probable speed. Iakubov suggested that for short range (repulsive) electron–atom interactions the "quantum interference" at high gas densities increased the effective collision frequency ν_{ef} of the electrons:

[7] $$\nu_{ef} = \nu\left(1 + \frac{\lambda\!\!\!^{-}_T}{L}\right)$$
$$= \nu(1 + \lambda\!\!\!^{-}_T n\sigma_{ave})$$

The mobility is inversely proportional to ν_{ef}:

[8] $$\mu \approx e/(m\nu_{ef})$$
$$\approx e/[m\nu(1 + \lambda\!\!\!^{-}_T n\sigma_{ave})]$$
$$= \mu_0/(1 + \lambda\!\!\!^{-}_T n\sigma_{ave})$$

When the deviation of μ_0 is small, $\lambda\!\!\!^{-}_T n\sigma_{ave} \ll 1$, eq. [8] is approximately

[9] $\mu/\mu_0 \approx (1 - \lambda\!\!\!^{-}_T n\sigma_{ave})$

Equation [9] empirically fits the density dependence of μ/μ_0 down to 0.4 in helium and hydrogen gases (13, 22). As it is also similar to Mott's localization criterion, its use is appealing. However, its derivation by way of eq. [8] is restricted to $\lambda\!\!\!^{-}_T n\sigma_{ave} \ll 1$. The choice of radianlength rather than wavelength as the parameter is related to the final localized state. The radianlength is a Bohr-type radius of a localized electron state, and the inverse radianlength is the exponential decay parameter of a Schrödinger-type ground state ($e^{-r/\lambda\!\!\!^{-}}$). For example, the hydrogen atom Bohr radius a_0 is a radianlength.

Atrazhev and Iakubov (15) apparently decided that a localized electron requires a space $2\lambda\!\!\!^{-}_T$ in dimension, which is a Bohr-type diameter. They modified eq. [9] to

[10] $\mu/\mu_0 = (1 - 2\lambda\!\!\!^{-}_T n\sigma_{ave})$

However, there is no general agreement about whether the factor in front of $\lambda\!\!\!^{-}_T$ should be exactly 2 (13, 22). This, in combination with the variety of methods of averaging the speed to obtain $\lambda\!\!\!^{-}_T$ (see Appendix 1) leaves flexibility in the equation.

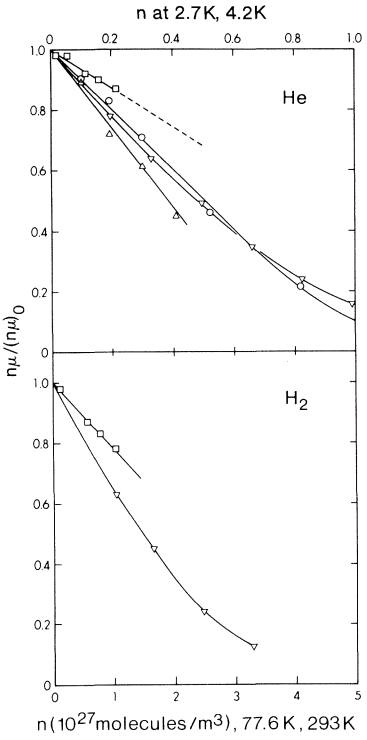

FIG. 1. Reduction of density normalized mobility $n\mu$ with increasing gas density n at several constant temperatures. He: △, 2.70 K, ref. 13; ○, 4.2 K, ref. 13; ▽, 77.6 K, ref. 24; □, ~293 K, data in ref. 2 extrapolated to zero field and normalized to the n = 10 and 28 (10^{25} molecules/m^3) results (see text). H_2: ▽, 77.6 K, ref. 24; □, ~293 K, ref. 2. The points were calculated from experimental data in the cited references.

Equation [10], like eq. [9], is related to the Mott criterion, not to that of Ioffe and Regel.

The Ioffe–Regel criterion means that when $L \approx \lambda$, $n\mu$ should be somewhat different than when $L \gg \lambda$ (8). When the electron–molecule interaction is repulsive (as when the molecule is nonpolar and has a very small polarizability) $n\mu$ decreases (negative effect) (15). When the electron–molecule interaction is attractive (as when the molecule is nonpolar and has a large polarizability) $n\mu$ increases (positive effect) (15). When the molecules are strongly polar the electron–molecule interaction is attractive and one might expect a positive effect, but a negative effect is observed (14, 17). These behaviors are quantitatively examined in the following sections.

(a) Molecules with low polarizability

Helium and hydrogen have small polarizabilities (23) and serve to illustrate the negative Ioffe–Regel effect (24). The condition

[11] $L = \lambda_T$

corresponds to

[12] $$\frac{1}{n\sigma_{ave}} = \frac{h}{m}\langle v_{3d}^{-1}\rangle$$

From eqs. [2] and [4], eq. [11] is satisfied at the Ioffe–Regel density:

[13] $n_{IR} = 0.28\,T(n\mu)_0$

where $(n\mu)_0$ is the low density value of $n\mu$ at temperature T. Thus the value of n_{IR} is extrapolated from low density behavior.

In helium over a hundred-fold range of temperatures, from 2.7 to 293 K, the value of $(n\mu)_{IR}/(n\mu)_0$ is 0.72 ± 0.02 (Fig. 1

TABLE 1. Density effects on electron transport in nonpolar fluids

Gas	$\frac{\bar{\alpha}^a}{4\pi\epsilon_0}$ (10^{-30} m^3)	$\mathcal{D}^a$ (10^{-30} C m)	T (K)	$\frac{T^b}{T_c}$	$(n\mu)_0{}^c$ (10^{24} molecules/m V s)	$n_{IR}{}^d$ (10^{25} molecules/m^3)	$\frac{n_{IR}{}^b}{n_c}$	$\frac{(n\mu)_{IR}{}^e}{(n\mu)_0}$	$\frac{(n\mu)_{2\chi}{}^e}{(n\mu)_0}$	$\frac{(n\mu)_{\chi}{}^e}{(n\mu)_0}$
He	0.2	0	2.70	0.52	300 (13)	23	0.022	0.70	—	—
			4.2	0.81	237 (13)	28	0.027	0.72	0.17	0.00013
			77.6	15	54 (24)	120	0.11	0.74	0.28	0.035
			293	56	25 (2)	205	0.20	0.74	—	—
H_2	0.8	0	77.6	2.3	35 (24)	76	0.082	0.72	0.25	0.025
			293	8.8	15.4 (2)	126	0.14	0.73	—	—
Ar	1.6	0	149	0.99	80 (29)	334	0.41	1.6	16	9[f]
			297	2.0	130 (29)	1080	1.34	>12 (30)	—	—
N_2	1.8	0	127	1.01	75 (37)	270	0.40	0.27	0.003[g]	7×10^{-5}[g]
			295	2.3	37 (37)	310	0.46	≤0.4	—	—
CO_2	2.6	0	295	0.97	1.9 (39)	16	0.025	0.9	0.06	0.003
			373	1.23	1.9 (39)	20	0.31	1.0	0.61	—
CH_4	2.6	0	194	1.02	28 (35)	152	0.25	1.0	1.4	29
			196	1.03	21 (34)	115	0.19	1.0	1.0	8
			293	1.54	34 (35)	280	0.46	2.0[h]	>15	<27
			295	1.55	36 (34)	300	0.49	1.9	>27	—
Xe	4.0	0	245	0.85	3.0 (4)	21	0.041	1.0	0.7[i]	—
			297	1.02	3.0 (4)	25	0.054	1.0	0.8[i]	~0.9[i]
			400	1.38	~3.0 (4)	~34	~0.07	1.0	≥1.0	≥2
C_2H_6	4.5	0	306	1.00	41 (40)	350	0.86	0.6[i]	>0.001[j]	—
			309	1.01	34 (41)	290	0.71	0.7[i]	<0.1[j]	—
			348	1.14	37 (41)	360	0.89	1.2	—	—
C_3H_8	6.3	0.28	370	1.00	19 (6*a*)	200	0.67	0.6[i]	~0.2[j,k]	—
			423	1.14	17 (5)	200	0.67	1.0	~0.3[j]	—
n-C_4H_{10}	8.1	≤0.17	426	1.00	13 (6*a*)	150	0.64	0.6[i]	~0.1[j]	—

[a]Mean polarizability $\bar{\alpha}$ and dipole moment $\mathcal{D}$, ref. 23. $\bar{\alpha}$ has SI units C m^2/V. To retain the familiar units m^3, we list $\bar{\alpha}/4\pi\epsilon_0$.
[b]T_c and n_c are the temperature and density of the critical fluid.
[c]Values from the references in parentheses indicated.
[d]Equation [13].
[e]Obtained from plots such as those in Fig. 1, constructed from data in refs. for $(n\mu)$, unless otherwise indicated. $n_{2\chi} = \pi n_{IR}$ and $n_{\chi} = 2\pi n_{IR}$.
[f]From $n\mu = 103 \times 10^{25}$ molecules/m V s at 87 K and $n = 21 \times 10^{27}$ molecules/m^3 (ref. 29), multiplied by the ratio of $(\chi_T/T^{3/2})^{-1}$ values at 149 and 87 K (ref. 31). At this density the isothermal compressibility $\chi_T = 1.4 \times 10^{-4}$ atm^{-1} at 149 K, and 2.2×10^{-4} atm^{-1} at 87 K (ref. 32). Thus $(n\mu)_{\chi} = 72 \times 10^{25}$ molecules/m V s at 149 K.
[g]From data in ref. 37*c*.
[h]±10%, extrapolated from data in ref. 7.
[i]Values slightly less than unity are caused by quasilocalization of electrons by density fluctuations in the gas.
[j]Values much less than unity are caused by the formation of localized states in the liquid.
[k]Using high density data from ref. 42.

and Table 1). The constancy of $(n\mu)_{IR}/(n\mu)_0$ over a hundredfold range of temperature confirms the validity of the Ioffe–Regel concept in helium.

In Fig. 1, the electrons in helium at 293 K were still slightly epithermal at the lowest field strength used (9×10^{-24} V m^2/molecule); the plots of drift velocity against field strength did not reach a slope of unity (2), in agreement with recent measurements in the same field range (25). Furthermore, Grünberg (2) evidently normalized his results at $n = 10$ and 28 (10^{25} molecules/m^3) to the $(n\mu)_0$ values of Crompton and co-workers (26), whereas in the denser gases used by Grünberg $n\mu$ should have been 1% and 3% lower, respectively. The points at 293 K were obtained by extrapolating Grünberg's data to zero field, assigning the average of the expected values $n\mu/(n\mu)_0 = 0.98$ to the equal sets at $n = 10$ and 28 (10^{25} molecules/m^3), and measuring the ratios at higher densities relative to that.

In hydrogen at 77.6 and 293 K the value of $(n\mu)_{IR}/(n\mu)_0$ is 0.72 ± 0.01 (Fig. 1 and Table 1). The behavior is the same as that in helium. The transient electron capture mechanism suggested by Frommhold (27) involving resonance with a rotational state of the molecule is therefore not the cause of the decrease of $n\mu$ in hydrogen. The decrease is caused by the constructive interference of the repulsive interactions of the electron with more than one molecule at a time, in accord with the Ioffe–Regel concept that electron transport is modified when $L \approx \lambda\!\!\!^{-}_T$.

Equation [10] predicts localization at

$$[14] \quad L = 2\lambda\!\!\!^{-}_T$$

where $\lambda\!\!\!^{-}_T$ is given by eq. [5]. If all the electrons had the same energy and if the scatterers were regularly spaced, a mean free path equal to $2\lambda\!\!\!^{-}$ should imply that a relatively completely localized state of the electrons had been formed. In a Maxwellian system ~30% of the electrons have $\lambda\!\!\!^{-} < \lambda\!\!\!^{-}_T$. Furthermore the scatterers are randomly distributed in space. At the density $n_{2\lambda}$ that satisfies eq. [14] the ratio $(n\mu)_{2\lambda}/(n\mu)_0$ is 0.17 in helium at 4.2 K and 0.27 ± 0.02 in helium and hydrogen at 77.6 K (Table 1). This is consistent with the $L = 2\lambda\!\!\!^{-}$ criterion of localization.

Mott's statement (11) that L cannot be smaller than $\lambda\!\!\!^{-}$ is commonly represented by saying that when

$$[15] \quad L = \lambda\!\!\!^{-}_T$$

the electron is in a localized state. In helium at a density that fulfills eq. [15], the experimental value of $(n\mu)_{\lambda}/(n\mu)_0$ is 1.34×10^{-4} at 4.2 K and 0.035 at 77.6 K (Table 1). In hydrogen at 77.6 K the ratio is 0.025. The electrons are localised. However, since $\lambda\!\!\!^{-}_T$ is the average of a wide distribution of values, the condition (15) is well past the threshold of localization and probably has less theoretical significance than condition [14].

Furthermore, the Ioffe–Regel condition (*b*), $L \approx a$, is well past the localization threshold.

(b) Molecules with larger polarizability

The preceding discussion applies to molecules that have a net repulsive interaction with the electrons. Molecules that have a large enough polarizability, such as argon and methane, have a net attractive interaction with thermal ($\lesssim$0.1 eV) electrons. In such gases the simultaneous interactions of an electron with more than one molecule at a time interfere destructively, so $n\mu$ increases in the multibody scattering regime (7, 15, 28).

In low density argon at 297 K the density normalized mobility is $(n\mu)_0 = 1.3 \times 10^{26}$ molecules/m V s (29). The value of n_{IR} is therefore 10.8×10^{27} molecules/m^3, which is 11% below the density where the mobility maximum occurs (30). Although 297 K is well above the highest temperature (158 K) used at this density, the results (30) indicate that in the supercritical gas at 297 K one would have $(n\mu)_{IR} > 1.6 \times 10^{27}$ molecules/m V s. Thus $(n\mu)_{IR}/(n\mu)_0 > 12$ (Table 1). Values of the ratio much greater than unity indicate that the electrons are in a conduction band.

TABLE 2. Electron scattering cross sections, dilute gas

Gas	T (K)	σ_{ave} (10^{-20} m^2) Obsd	Pol[a]	Obsd/Pol
Xe	145	63 (4)	249	0.25
	297	44 (4)	174	0.25
CH_4	150	7.8 (35)	200	0.04
	297	4.0 (35)	140	0.03
Ar	149	2.5 (29)	157	0.02
	297	1.1 (29)	111	0.01

[a]Equation [18].

At lower temperatures the values of $(n\mu)_0$ and n_{IR} are smaller, and the mobility ratio is smaller: at 149 K, $(n\mu)_{IR}/(n\mu)_0 = 1.6$ (Table 1). However, at the highest density $n_{2\lambda}$ the ratio is $(n\mu)_{2\lambda}/(n\mu)_0 = 16$ (Table 1). The still higher density $n_{\lambda} = 21 \times 10^{27}$ molecules/m^3 at 149 K is the density of liquid argon at its normal boiling point, 87 K. We used the model of Cohen and Lekner (31) and the isothermal compressibilities of the liquid at 87 and 149 K (32) to calculate the value of $(n\mu)_{\lambda}$ at 149 K from the value of $n\mu$ at the same density at 87 K (29). The resulting $(n\mu)_{\lambda}/(n\mu)_0 = 9$ is smaller than the lower density value $(n\mu)_{2\lambda}/(n\mu)_0 = 16$, because of the density dependence of the scattering length (33).

In methane (34, 35) the effects at n_{IR} and $n_{2\lambda}$ are smaller than in argon, and in xenon (4) they are smaller still (Table 1). This result is contrary to the initial expectation that the positive effect would be more pronounced at larger polarizabilities. It is the polarizability that determines whether the Ioffe–Regel effect is negative or positive (15).

The contribution of the polarization interaction to electron scattering by Xe, CH_4, and Ar can be assessed by comparison of σ_{ave} with that expected from the polarization potential. The scattering cross section expected from the polarization potential is (36)

$$[16] \quad \sigma_{pol} = \left(\frac{2.21\pi e}{4\pi\epsilon_0}\right)\left(\frac{\bar{\alpha}}{mv^2}\right)^{1/2}$$

Thus

$$[17] \quad \sigma_{pol,ave} = \langle v\rangle/\langle v/\sigma_{pol}\rangle = \left(\frac{2.21\pi e}{4\pi\epsilon_0}\right)\left(\frac{\bar{\alpha}}{m}\right)^{1/2}\frac{\langle v\rangle}{\langle v^2\rangle}$$

For a Maxwellian distribution of electrons at temperature T,

$$[18] \quad \sigma_{pol,ave} = 0.0150(\bar{\alpha}/4\pi\epsilon_0 T)^{1/2}$$

where σ is in m^2 and $\bar{\alpha}/4\pi\epsilon_0$ is in m^3 (the SI units of α are C m^2/V). The observed σ_{ave} of Xe is only 25% of $\sigma_{pol,ave}$, while those of CH_4 and Ar are only 4% and 2%, respectively (Table 2). Most of the electron–molecule attractive polarization interaction is cancelled by the short range Pauli repulsion

TABLE 3. Density effects on electron transport in polar gases

Gas	$\frac{\bar{\alpha}}{4\pi\epsilon_0}$ [a] (10^{-30} m^3)	$\mathscr{D}$ [a] (10^{-30} C m)	T (K)	$\frac{T}{T_c}$ [b]	$(n\mu)_0$ [c] (10^{22} molecules/m V s)	n_{IR} [d] (10^{25} molecules/m^3)	$\frac{n_{IR}}{n_c}$ [b]	$\frac{(n\mu)_{IR}}{(n\mu)_0}$ [e]	$\frac{(n\mu)_{2\lambda}}{(n\mu)_0}$ [e]	$\frac{(n\mu)_\lambda}{(n\mu)_0}$ [e]
CH_3OCH_3	5.2	4.3	407	1.02	82 (43)	9.3	0.028	0.9	0.8	0.5
CH_3NH_2	4.0	4.4	300	0.70	69 (44)	5.8	0.14	0.9	~0.3	—
NH_3	2.3	4.9	300	0.74	40 (44)	3.4	0.0041	0.9	0.4	0.2
			300	0.74	45 (17)	3.8	0.0045	0.9	0.7	0.3
			300	0.74	49 (10)	4.1	0.0049	0.9	0.7	0.2
			400	0.99	62 (10)	6.9	0.0083	0.9	0.7	0.4
			460	1.13	71 (10)	9.1	0.011	0.9	0.7	0.5
			600	1.48	78 (17)	13.3	0.016	0.9	0.7	—
CH_3OH	3.2	5.6	365	0.71	45 (6*b*)	4.6	0.009	0.9	—	—
			500	0.97	55 (6*b*)	7.7	0.015	>0.8	—	—
H_2O	1.5	6.1	463	0.72	31 (9)	3.9	0.0036	0.9	0.5	—
			523	0.81	34 (9)	5.0	0.0046	0.9	0.7	0.2

[a]Mean polarizability $\bar{\alpha}$ and dipole moment $\mathscr{D}$, ref. 23. $\bar{\alpha}$ has SI units C m^2/V. To retain the familiar units m^3, we list $\bar{\alpha}/4\pi\epsilon_0$.
[b]T_c and n_c are the temperature and density of the critical fluid.
[c]Values from the references in parentheses indicated.
[d]Equation [13].
[e]Obtained from plots such as those in Fig. 1, constructed from data in the refs. for $(n\mu)_0$, unless otherwise indicated. $n_{2\lambda} = \pi n_{IR}$ and $n_\lambda = 2\pi n_{IR}$.

between the electron and the filled valence electron shells of these molecules.

However, electron scattering is strong enough in low density xenon gas that n_{IR} corresponds to only ~10 atm pressure at 297 K; there is no enhancement of $n\mu$. Scarcely any enhancement of $n\mu$ occurs even at the 6.3 times higher density n_λ in xenon (Table 1). At much higher densities, $\sim 10 n_\lambda \approx 1$–2 ($10^{28}$ molecules/m^3), the value of $n\mu/(n\mu)_0$ is enormous, ~1000 (4). There is a large density effect, but it is not related to the Ioffe–Regel criterion.

If the positive Ioffe–Regel effect in argon and methane is indeed due to the density dependence of an attractive electron–molecule interaction (15), it should be at least as prominent in xenon. The absence of the effect in xenon suggests that the theoretical interpretation of the effects in argon and methane be reopened.

Recent attempts by Polischuk to explain the behavior in xenon and other gases are discussed in Appendix 2.

(c) Electron attachment

Nitrogen is a nonpolar molecule with an average polarizability similar to that of argon. The values of $(n\mu)_0$ at low temperatures are also similar in the two gases (Table 1) (29, 37). One might therefore expect similar values of $(n\mu)_{IR}/(n\mu)_0$ in nitrogen and argon at low temperatures. In fact the ratios are very different. In argon the ratio is greater than unity. In nitrogen it is smaller than unity, and even smaller than those in helium and hydrogen, which repel the electrons (Table 1). The deviation of $(n\mu)_{IR}/(n\mu)_0$ from unity is twice as great in nitrogen as in helium and hydrogen, and the deviation of $(n\mu)_{2\lambda}/(n\mu)_0$ is 100 times as great (Table 1). The behavior in nitrogen is explained by transient attachment of electrons to nitrogen molecules in the dense gas (37*a*).

Similarly, carbon dioxide can be compared to methane. They are nonpolar and have the same mean polarizability. The Ioffe–Regel ratio $(n\mu)_{IR}/(n\mu)_0$ is unity or slightly smaller in carbon dioxide, while in methane it is unity or greater. At higher densities the ratio $n\mu/(n\mu)_0$ becomes much smaller than unity in carbon dioxide and much larger than unity in methane (Table 1). Transient attachment of electrons occurs in dense carbon dioxide gas (3, 38, 39).

The Ioffe–Regel and Mott criteria should not be applied when electron attachment occurs.

(d) Nonspherical alkanes

There might be a small enhancement of $n\mu$ due to the Ioffe–Regel effect in ethane (40, 41), propane (5, 6, 42), and *n*-butane (6), but it is obscured by the decrease of $n\mu$ caused by quasilocalization (6, 40) under the conditions of experiment (Table 1). Heating the gas decreases the magnitude of the density fluctuations and therefore decreases the extent of quasilocalization; the value of $(n\mu)_{IR}/(n\mu)_0$ in ethane and propane increased to ≥ 1.0 (Table 1).

The $L = 2\lambda$ criterion applies to formation of localized states in the dense fluids; $(n\mu)_{2\lambda}/(n\mu)_0 \approx 0.1$ (Table 1).

There is an extensive literature about localized states of electrons in liquid, nonspherical hydrocarbons. The subject does not require discussion here. Example references are 5, 6, 40–42, and works cited therein.

(e) Polar compounds

The scattering cross sections of highly polar molecules for low energy ($\lesssim 0.1$ eV) electrons are large. The values of $(n\mu)_0$ are correspondingly low (compare values in Table 3 with those

in Table 1). The electron–dipole interaction is attractive and one might expect the Ioffe–Regel effect to be positive. However, it is slightly negative; $(n\mu)_{IR}/(n\mu)_0 = 0.9$ in dimethyl ether (43), methylamine (44), ammonia (10, 17, 44), methanol (6*b*), and water (9). The ratio in ammonia remains 0.9 over a two-fold range of temperature, 300–600 K (Table 3).

At the three-fold higher density $n_{2\lambda}$ the value of $(n\mu)_{2\lambda}/(n\mu)_0$ has only been reduced to 0.7, similar to $(n\mu)_{IR}/(n\mu)_0$ in the repulsive-interaction gases helium and hydrogen. At the still higher density n_λ a large degree of electron localization has still not been achieved (Table 3).

Polischuk's recent treatment of the behavior in water vapour (45*b*) is discussed in Appendix 2.

The scattering interaction does not change in a simple manner with density. Simple criteria such as those of Ioffe and Regel (8) and of Mott (11) are only of qualitative use in these gases. The criteria were devised for electron behavior in condensed phase semiconductors, where the internal electronic structure can change a lot from one material to another, but the density does not change much.

5. Conclusions

(*a*) The Ioffe–Regel criterion that $n\mu$ changes when $L \leq \lambda$ and the Mott criterion that $L \approx \lambda$ corresponds to a localized state of the electron, apply to gas density effects in helium and hydrogen, which have a net repulsive interaction with electrons.

(*b*) The Ioffe–Regel and Mott criteria are not useful when transient attachment of electrons occurs, nor when the molecules are highly polar.

(*c*) The positive Ioffe–Regel effect is not present in xenon, which brings into question the explanation of the effects in argon and methane.

1. J. L. Levine and T. M. Sanders, Jr. Phys. Rev. **154**, 138 (1967).
2. R. Grünberg. Z. Naturforsch. **23**a, 1994 (1968); **24**a, 1838 (1969).
3. H. Lehning. Phys. Lett. **28**A, 103 (1968).
4. S. S.-S. Huang and G. R. Freeman. J. Chem. Phys. **68**, 1355 (1978).
5. M. Nishikawa and R. A. Holroyd. J. Chem. Phys. **77**, 4678 (1982).
6. N. Gee and G. R. Freeman. (*a*) J. Chem. Phys. **78**, 1951 (1983); (*b*) Can. J. Chem. **61**, 1664 (1983).
7. H. Lehning. Phys. Lett. **29**A, 719 (1969).
8. A. F. Ioffe and A. R. Regel. Prog. Semiconductors, **4**, 237 (1960).
9. V. Giraud and P. Krebs. Chem. Phys. Lett. **86**, 85 (1982).
10. P. Krebs, K. Bukowski, V. Giraud, and M. Heintze. Ber. Bunsenges. Phys. Chem. **86**, 879 (1982).
11. N. F. Mott. Adv. Phys. **16**, 49 (1967).
12. L. M. Grossman. Thermodynamics and statistical mechanics. McGraw-Hill, New York. 1969. p. 313.
13. K. W. Schwartz. Phys. Rev. B, **21**, 5125 (1980).
14. P. Krebs. Ber. Bunsenges. Phys. Chem. **88**, 275 (1984).
15. V. M. Atrazhev and I. T. Iakubov. J. Phys. D: Appl. Phys. **10**, 2155 (1977).
16. K. W. Schwartz. Phys. Rev. Lett. **41**, 239 (1978).
17. L. G. Christophorou, J. G. Carter, and D. V. Maxey. J. Chem. Phys. **76**, 2653 (1982).
18. G. L. Braglia and V. Dallacasa. Phys. Rev. A. **26**, 902 (1982).
19. P. Lorrain and D. R. Corson. Electromagnetic fields and waves. 2nd ed. Freeman, San Francisco. 1970. p. 672.
20. N. J. Zabusky. Phys. Today, **37**, no. 7, 36 (1984).
21. I. T. Iakubov. High Temp. **10**, 158 (1972).
22. V. M. Atrazhev and I. T. Iakubov. Teplofiz. Vysek. Temp. USSR, **18**, 1292 (1980).
23. H. Stuart. *In* Landolt-Börnstein, Zahlenwerte und Funktionen. I. bd, 3 teil. *Edited by* A. Eucken and K. H. Hellwege. Springer-Verlag, Berlin. 1951. Sections 14206, 14207.
24. A. Bartels. Appl. Phys. **8**, 59 (1975).
25. G. Ramanan. Private communication.
26. R. W. Crompton, M. T. Elford, and R. L. Jory. Aust. J. Phys. **20**, 369 (1967).
27. L. Frommhold. Phys. Rev. **172**, 118 (1968).
28. A. Bartels. Phys. Lett. **44**A, 403 (1973).
29. S. S.-S. Huang and G. R. Freeman. Phys. Rev. A, **24**, 714 (1981).
30. J. A. Jahnke, L. Meyer, and S. A. Rice. Phys. Rev. A, **3**, 734 (1971).
31. M. H. Cohen and J. Lekner. Phys. Rev. **158**, 305 (1967).
32. A. L. Gosman, R. D. McCarty, and J. G. Hurst. Thermodynamic properties of argon. NSRDS-NBS 27. U.S. GPO, Washington, D.S., 1969.
33. J. Lekner. Phys. Lett. **27**, 341 (1968); Phys. Rev. **158**, 130 (1967).
34. N. E. Cipollini, R. A. Holroyd, and M. Nishikawa. J. Chem. Phys. **67**, 4636 (1977).
35. N. Gee and G. R. Freeman. Phys. Rev. A, **20**, 1152 (1979).
36. E. W. McDaniel. Collision phenomena in ionized gases. Wiley, New York. 1964. p. 445.
37. T. Wada and G. R. Freeman. (*a*) J. Chem. Phys. **72**, 6726 (1980); (*b*) Phys. Rev. A, **24**, 1066 (1981); (*c*) 1980 Annual Report Conf. Elect. Insul. Diel. Phen., National Academy Press, Washington, D.C., p. 386.
38. J. M. Warman, U. Sowada, and D. A. Armstrong. Chem. Phys. Lett. **82**, 458 (1981).
39. F. M. Jacobsen and G. R. Freeman. J. Chem. Phys. **84**, 3396 (1986).
40. N. Gee and G. R. Freeman. Phys. Rev. A, **22**, 301 (1980).
41. M. Nishikawa, R. A. Holroyd, and U. Sowada. J. Chem. Phys. **72**, 3081 (1980).
42. N. Gee and G. R. Freeman. Radiat. Phys. Chem. **15**, 267 (1980).
43. N. Gee and G. R. Freeman. Can. J. Chem. **60**, 1034 (1982).
44. J. C. Thompson, U. Even, and D. K. Blanks. J. Phys. Chem. **88**, 3709 (1984).
45. A. Ya. Polischuk. J. Phys. B: At. Mol. Phys. (*a*) **17**, 4789 (1984); (*b*) **18**, 829 (1985).
46. S. Altshuler. Phys. Rev. **107**, 114 (1957).

Appendix 1. Wavelength and radianlength

Each of the following eight formulas have been used to calculate the *wavelength* of electrons at temperature T; h is Planck's constant.

[*i*] $h(\pi/8mk_BT)^{1/2}$

This corresponds to the 7×10^{-9} m at room temperature given in ref. 8, and to $\langle k \rangle^{-1} = \langle \lambda^{-1} \rangle^{-1}$ in refs. 9 and 10.

[*ii*] $h(3/2mk_BT)^{1/2}$

This was incorrectly attributed to Ioffe and Regel (8) by Mott (11).

[*iii*] $h/[2\pi(mk_BT)^{1/2}]$

This corresponds to the 3×10^{-9} m at 100 K given in ref. 11.

[*iv*] $h/(mk_BT)^{1/2}$ (ref. 12)

[*v*] $h/(2\pi mk_BT)^{1/2}$ (refs. 12–14)

[*vi*] $h/[2\pi(2mk_BT)^{1/2}]$ (refs. 15–17)

The temperature in ref. 15 was used as an energy, so it

included k_B.

[*vii*] $h/(2mk_BT)^{1/2}$ (ref. 18)

[*viii*] $h/(8\pi mk_BT)^{1/2}$

This form is obtained when the empirical factor $\alpha = 1/2$, obtained by fitting a model to electron behavior in helium gas (13), is included where it seems to belong, in the wavelength factor.

The wavelengths estimated at a given T by these formulas can differ up to 11-fold, [*ii*]/[*vi*]. The differences are caused by different definitions of wavelength and different averaging procedures for the velocity.

Although all of the above formulas were called wavelength or average de Broglie wavelength by the authors cited, formulas [*iii*], [*vi*], and [*viii*] are actually for $\lambda\!\!\!^{-} = \lambda/2\pi$, which is 6.3-fold smaller than a wavelength. $\lambda\!\!\!^{-}$ is a *radianlength* (19). The radianlength is the counterpart of the *angular velocity* ω (radian/s). Angular velocity has been burdened with a number of imprecise names such as angular frequency, circular frequency, frequency, and radian frequency. The *frequency* ν (cycle/s) of a wave or oscillation is $\omega/2\pi$. In attempts to visualize wavelike properties of particles it is important to distinguish between wavelength and radianlength, and between frequency and angular velocity. The visualization of processes and concepts is of great utility, and will be more widely used in the future (20).

There are also differences between formulas [*i*] to [*viii*] due to the use of one dimensional ($1d$) or 3-dimensional ($3d$) speeds, and different types of averages over the Maxwellian distribution. The relevant $1d$ averages are

[*ix*] $\langle v_{1d}\rangle = (2k_BT/\pi m)^{1/2}$

[*x*] $\langle v_{1d}^2\rangle^{1/2} = (k_BT/m)^{1/2}$

while the $3d$ averages include

[*xi*] $\langle v_{3d}\rangle = (8k_BT/\pi m)^{1/2} = 2\langle v_{1d}\rangle$

[*xii*] $\langle v_{3d}^{-1}\rangle^{-1} = (\pi kT/2m)^{1/2}$

[*xiii*] $\langle v_{3d}^{-2}\rangle^{-1/2} = (k_BT/m)^{1/2} = \langle v_{1d}^2\rangle^{1/2}$

and the most probable speed

[*xiv*] $\alpha_{3d} = (2k_BT/m)^{1/2}$

The formulas therefore represent the following:

[i] wavelength$_{3d}$ $\lambda_{T,3d} = h/m\langle v_{3d}\rangle$
or half wavelength$_{1d}$ $\lambda_{T,1d}/2 = h/2m\langle v_{1d}\rangle$

[ii] approximate wavelength$_{1d} \approx h/m\langle v_{1d}\rangle$
or 2× wavelength$_{3d} \approx 2h/m\langle v_{3d}\rangle$

[iii] radianlength $\lambda\!\!\!^{-}_T = \hbar\langle v_{3d}^{-2}\rangle^{1/2}/m = \hbar/m\langle v_{1d}^2\rangle^{1/2}$

[iv] wavelength $= h\langle v_{3d}^{-2}\rangle^{1/2}/m = h/m\langle v_{1d}^2\rangle^{1/2}$

[v] $2\times$ radianlength$_{1d} = 2\hbar/m\langle v_{1d}\rangle$
or $4\times$ radianlength$_{3d} = 4\hbar/m\langle v_{3d}\rangle$

[vi] radianlength $= \hbar/m\alpha_{3d}$

[vii] wavelength $= h/m\alpha_{3d}$

[viii] radianlength$_{1d} = \hbar/m\langle v_{1d}\rangle$
or $2\times$ radianlength$_{3d} = 2\hbar/m\langle v_{3d}\rangle$

Equations [4] and [5] are preferred to the above eight in the dense gas context.

Appendix 2. Recent attempts

Polischuk, who was a co-worker of Iakubov, has recently made interesting attempts to explain the density dependence of $n\mu$ in xenon (45*a*) and in polar gases (45*b*). Although he made progress beyond earlier attempts, his work is obscured by the same language problems discussed in Appendix 1. There are other difficulties that deserve comment.

The density effect in nitrogen was classed with those in helium and hydrogen (45*a*, *b*), whereas the effect in nitrogen is due to electron capture (Table 1).

Models that use $\hbar = 1$, $h = 1$, $c = 1$ or $k_B = 1$ eliminate visualization of the physical processes. The ideas being advanced are then trapped behind jargon barriers and are not easily available to a broad audience. Polischuk used $\hbar = 1$ and $k_B = 1$, but in eq. [15] of ref. 45*b* he inserted $\hbar$ "which demonstrates the quantum nature of the density effect". His equation is quite complicated, but it is equivalent to the above eq. [7] multiplied by 0.5; $\Gamma = 0.5\nu$. However, he did not explain why the attractive electron–dipole potential should produce a negative rather than a positive effect of density on $n\mu$. Equation [3] of ref. 45*b* is simply the Altshuler cross section (46).

For nonpolar scatterers, Polischuk argued that the r_0 which occurs in terms such as $\alpha e^2/2(r_0^2 + r^2)^2$ is not simply a fitting parameter (45*a*), although it is simply that (33). He suggested that "r_0 can be estimated by the sizes of the outer electronic shell of the atom and by the effective radius of hard spheres". But he used values of r_0 for argon and xenon that were only 37% of the hard sphere radii estimated from the solid phase (29). A calculated curve for μ/μ_0 against xenon density is shown in Fig. 2 of ref. 45*a*, but values of the equation parameters are lacking. In particular, the values of the chemical potential and mobility threshold energy are needed at each density. Furthermore, electron quasilocalization and the drastic effect of temperature on it (4) were ignored.

The demicellization temperature of potassium *n*-octanoate in deuterium oxide as estimated from ^{1}H and ^{13}C nuclear magnetic resonance spectra

M. A. DESANDO AND L. W. REEVES

Department of Chemistry, University of Waterloo, Waterloo, Ont., Canada N2L 3G1

Received December 28, 1984[1]

M. A. DESANDO and L. W. REEVES. Can. J. Chem. **64**, 1817 (1986).

Measurements of the proton nmr peak positions and carbon-13 nmr chemical shifts as a function of concentration and of temperature estimate the demicellization temperature to be in the range ca. 115–227°C for potassium *n*-octanoate in deuterium oxide at concentrations around the critical micelle concentration.

M. A. DESANDO et L. W. REEVES. Can. J. Chem. **64**, 1817 (1986).

Opérant dans de l'oxyde de deutérium, à diverses températures et à diverses concentrations, on a mesuré les positions des bandes dans les spectres rmn du ^{1}H et du ^{13}C de l'octanoate de potassium; sur la base de ces résultats, on a évalué que la température de démicellisation, à des concentrations proches de la concentration micellaire critique, se situe entre 115 et 227°C.

[Traduit par la revue]

Introduction

Potassium *n*-octanoate in deuterium oxide ($^{2}H_2O$), as with aqueous solutions of other fatty acid salts, can form normal micelles (1–3) above the Krafft point (3) of the surfactant. Whereas considerable information is available on the properties of surfactant solutions around room temperature, very little is known on the behaviour of micelle-forming systems at high temperatures, especially above the boiling point of the solvent.

A study was therefore undertaken to obtain data on the nature of a simple two-component surfactant system, namely, potassium *n*-octanoate in $^{2}H_2O$, over a wide temperature range (29–154°C). The nmr method is a suitable one for the characterization of the species present in solution, and has the advantage over many other techniques of providing information on the environments and interactions of different parts of the molecule. It is possible to correlate spectral parameters such as resonance peak position to changes in the properties of the surfactant aggregates with variations in temperature.

There is substantial evidence from a number of experimental techniques that surfactants with a short alkyl chain ($\leq$8 carbon atoms) form small aggregates in water around room temperature (4). Sodium *n*-octanoate, for instance, self-associates into micelles with a mean aggregation number in the range 4–15 at temperatures around 25°C (5–7). Small micelles would be expected to be less stable than large ones, which would have stronger interactions among the larger more hydrophobic alkyl chains of the surfactant. Short-chain surfactants therefore tend to micellize via multiple equilibria (8, 9), whereas the self-association of long-chain surfactants may be described by a cooperative process where the monomer $\rightleftharpoons$ micelle equilibrium is dominant (1, 10). The micellization process of potassium *n*-octanoate in $^{2}H_2O$ is in contrast to that for long-chain surfactants that can form large micelles, e.g., 50–100 monomers per micelle (4).

The chemical nature of the surfactant, whether nonionic or ionic, bears on the variation of the critical micelle concentration (c.m.c), and hence the micelle stability, with temperature. Inherent in the c.m.c. value is a reflection of the ease of formation of the micelles, i.e., it has a dependence on the free energy of micellization (1, 4, 8, 10). A system that approaches thermal demicellization should, therefore, display an increase in the c.m.c. value at high temperatures. Indeed, the few experimental studies at elevated temperatures do show a monotonic increase of the c.m.c. with temperature. Consider, for instance, the works of Evans and Wightman (11) on cetyltrimethylammonium bromide, and Kunieda and Shinoda (12) on dioctadecyldimethylammonium chloride in water. These researchers were able to measure c.m.c. values at 166 and 200°C, respectively, which suggest that micelles exist at high temperatures. A theoretical treatment by Poland and Scheraga (13, 14) relates micelle stability to the hydrophobic character of the surfactant, e.g., alkyl chain length, and the c.m.c. They have calculated the temperature variation of the micelle size and, for a nonionic surfactant, demonstrate how micelles may not exist above a certain temperature.

From the literature data (1, 4, 11–18), a few basic features appear on the effects of temperature on micelle formation: (*i*) the c.m.c. possesses a parabolic-type variation with temperature, with the minimum usually around 25°C for ionic surfactants; and (*ii*) the size of ionic micelles appears to decrease with increasing temperature. Much information, however, is lacking on how temperature affects the self-association of surfactant amphiphiles.

One of the prime objectives of this study is, therefore, to observe the effects of high temperature on micellization, and subsequently to determine at which temperatures demicellization occurs, that is, the temperature above which micelle formation is not favoured.

Research on a simple micelle system will provide valuable information on temperature effects, which may be applied to lyotropic mesophases (19, 20), industrial processes involving surfactants (21), and to chemical evolution (22). Potassium *n*-octanoate was chosen for this work for the following reasons: (*i*) alkali metal salts of fatty acids do not decompose appreciably at higher temperatures; (*ii*) it has a high critical micelle concentration (c.m.c. ~0.30–0.40 *m* at ca. 25–35°C) (23), which allows for easier determination of the range of concentrations where most of the surfactant is in the micellar state; and (*iii*) it appears to form rather small micelles that are likely to disintegrate more completely at a lower temperature, and thus facilitate the detection of the demicellization temperature.

Experimental

Potassium *n*-octanoate was synthesized from the equimolar reaction of *n*-octanoic acid (Aldrich 99.5+%) with potassium hydroxide (Baker A.R.) in absolute ethanol, followed by several recrystallizations from absolute ethanol and rigorous drying *in vacuo*.

[1]Revision received April 11, 1986.

TABLE 1. Carbon-13 nmr chemical shifts (relative to external hexamethyldisiloxane) for the carbon atoms (numbered as position away from the CO_2^-) of potassium *n*-octanoate in the monomeric (δ_m) and micellar (δ_M) states in ^2H_2O

Temperature (°C)	δ_m (ppm)							δ_M (ppm)						
	C_2	C_3	C_4	C_5	C_6	C_7	C_8	C_2	C_3	C_4	C_5	C_6	C_7	C_8
37	36.660	24.920	27.240	27.740	30.050	20.980	12.447	37.074	25.450	28.162	28.748	30.953	21.654	12.882
55	37.000	25.198	27.450	28.040	30.318	21.206	12.586	37.305	25.671	28.233	28.882	31.002	21.702	12.931
75	37.254	25.409	27.640	28.230	30.480	21.300	12.727	37.514	25.783	28.354	29.041	31.129	21.779	12.951
86	37.400	25.530	27.800	28.410	30.620	21.510	12.800	37.657	25.893	28.431	29.090	31.206	21.822	12.971

Potassium *n*-octanoate (from laboratory stock) was washed several times with ethyl acetate and then dried *in vacuo* over $CaCl_2$ for a few days. Ethylene glycol (Baker A.R.) was refluxed over anhydrous sodium sulfate, distilled several times in dry nitrogen, and was then immediately sealed in an nmr tube.

Surfactant solutions of molal and, in a few cases, of molar concentrations (at 29°C) in ^2H_2O (99.8 atom %; Merck, Sharp and Dohme) were placed in the outer tubes of 5 or 10 mm od Wilmad precision coaxial nmr cells, with tetramethylsilane (TMS) (MSD Isotopes) in CCl_4 (~1% v/v) as the external reference for proton nmr spectra and neat hexamethyldisiloxane (Aldrich) for carbon-13 nmr spectra. Solutions for proton nmr spectra above 72°C were sealed in 5 mm od thick-wall nmr tubes. All resonance peak positions (in ppm) are relative to the external reference set to 0 ppm in the 1.88-T magnetic field of a Bruker WP-80 nmr spectrometer.

Variable temperature, natural abundance carbon-13 nmr spectra, with heteronuclear broad-band decoupling, were recorded at 20.12 MHz on the WP-80 spectrometer, and at 30°C and 62.95 MHz, with power gated decoupling, on a Bruker AM-250 nmr spectrometer.

Samples were allowed to attain thermal equilibrium, as confirmed from spectra taken over a period of time until constant values of resonance peak positions were observed (ca. 15–20 min at 29°C). In the case of high temperature measurements, the samples were preheated in a constant temperature bath to the desired temperature. In most cases, two or three proton nmr spectra were recorded for each sample. A typical uncertainty in the proton resonance peak position is ±0.003 ppm and the mean variation of the carbon-13 chemical shift for several measurements at 20.12 MHz is ±0.012 ppm. At 80 MHz the coupled spectra are second order, and so the term, peak position, has been applied to the proton nmr signals.

The temperature inside the 5-mm ^1H nmr probehead was determined from the equation of the line of best fit (from linear regression analysis) to the plot of frequency difference between the resonance peaks of neat ethylene glycol against observed temperature. The observed temperature was determined from measurements of the melting points of eight organic solids in a manner similar to that of Yamamoto and Yanagisawa (24). Melting points measured on a Meltemp block-heater type of apparatus were correlated to those determined from plots of spectral intensity versus the temperature set on a calibrated B-ST 100/700 temperature controller. At temperatures around and above the boiling point of ^2H_2O (101.4°C) it was necessary to use either degassed ^2H_2O – chlorosulfonic acid or ^2H_2O – sulfuric acid mixtures as the deuterium lock agents in the outer tubes of the coaxial nmr cells that contained the ethylene glycol.

Measurements of the relative intensities and areas of the proton resonance peaks as a function of concentration and temperature revealed that any evaporation of the solvent above 127°C resulted in a small change in concentration of the surfactant of the order of 10%. Corrections were not applied for bulk magnetic susceptibility in the coaxial samples as this was determined to be a small effect (25–27).

Results

The observed nmr peak is a weight average signal whose position (δ_{obs}) is dependent on the species present in solution; thus $\delta_{obs} = \Sigma(iC_i\delta_i)/C_T$, where the peak position (δ_i) and concentration (C_i) are for the species composed of i monomers, and C_T is the total surfactant concentration. Extrapolation of the δ_{obs} versus C_T curve to $C_T = 0$, i.e., infinite dilution, yields the δ_i value for the unassociated monomer (δ_m). Also, extrapolation of the δ_{obs} versus C_T^{-1} curve to infinite concentration ($C_T^{-1} \rightarrow O$) provides the value for the micellar state (δ_M) (26). The difference, $\Delta\delta = \delta_M - \delta_m$, is therefore a measure of the change in environment of a proton or set of magnetically equivalent protons upon entering the micellar state. In the case of ^{13}C nuclei, other factors may contribute to the chemical shift, notably, hybridization, and inductive and steric effects (28). Representative plots of δ_{obs} versus C_T^{-1} (Figs. 1 and 2) are given. Table 1 lists the carbon-13 nmr δ_m and δ_M values at different temperatures.

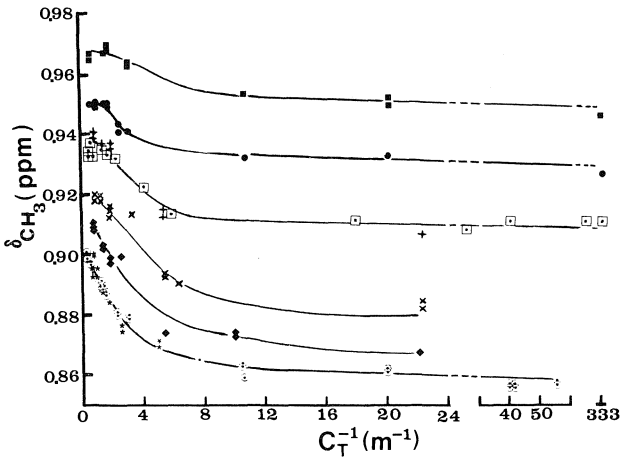

FIG. 1. Proton resonance peak position for the methyl group versus reciprocal total molal concentration of potassium *n*-octanoate in ^2H_2O; ⊙, 31°C; *, 32°C; ◆, 37°C, ×, 44°C; ⊡, 52°C; +, 54°C; ●, 61°C; ■, 72°C.

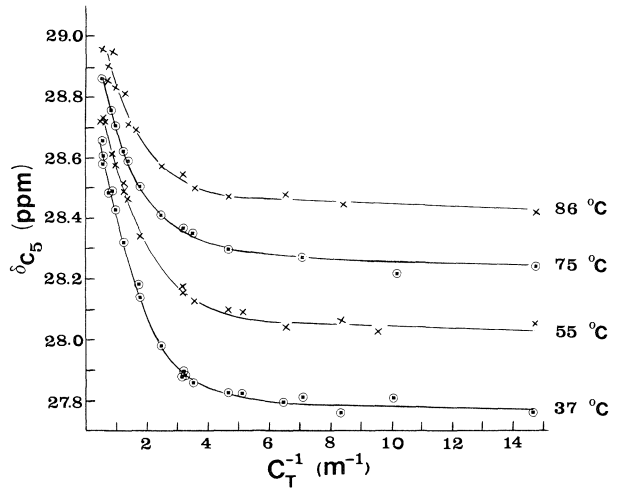

FIG. 2. Carbon-13 nmr chemical shift for the C_5 carbon atom versus reciprocal total molal concentration of potassium *n*-octanoate in ^2H_2O at different temperatures.

When TMS was not employed as an external reference, the difference in peak position, $\Delta\nu = \nu(\alpha\text{-}CH_2) - \nu(CH_3)$ was taken. The position of the centre peak of the resonance multiplet was used as $\nu(\alpha\text{-}CH_2)$. Plots of $\Delta\nu$ versus C_T yield the values ($\Delta\nu_m$) for the monomers at $C_T \rightarrow 0$ and the minima values in the plots of $\Delta\nu$ versus log C_T^{-1} (Fig. 3) were taken for the micellar state ($\Delta\nu_M$).

Critical micelle concentrations were determined from the intersection point, calculated from the equations of the lines (from linear regression analyses) of limiting slope in the plots of carbon-13 nmr chemical shift versus C_T^{-1}.

Discussion

The variations of the proton nmr peak positions as a function of the total potassium *n*-octanoate concentration in ^2H_2O are consistent with the model of normal micelle formation. For example, the difference in peak position ($\Delta\delta$) between the micellar and monomeric states is least for the α-CH_2 protons and increases with distance from the CO_2^- K^+ moiety (see Fig. 4). Over the temperature range 29–72°C the $\Delta\delta(CH_3)$ value is ca. 1.5–3.1 times larger than the $\Delta\delta(\alpha\text{-}CH_2)$ value and is in line with the fact that the methyl groups constitute the core of the

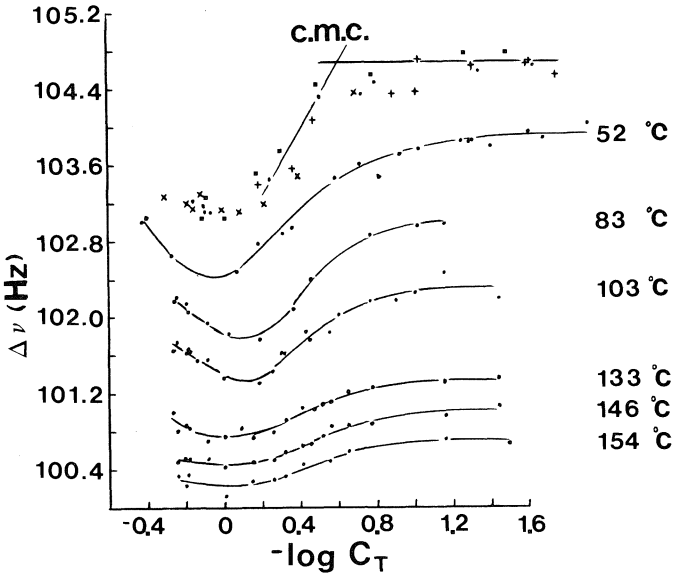

FIG. 3. Difference in peak positions ($\Delta\nu$) between the α-CH_2 and CH_3 resonances versus total molal concentration of potassium *n*-octanoate in ^2H_2O at different temperatures; ■, 29°C; +, 31°C; ×, 32°C; ●, 35°C.

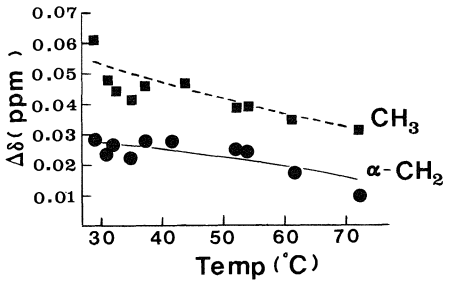

FIG. 4. Difference in proton resonance peak position ($\Delta\delta$) between the micellar and monomeric states for potassium *n*-octanoate in ^2H_2O at different temperatures (--- calculated from a computer generated least-squares fit (WATFIV LEAST).

micelle, whereas the methylene groups adjacent to the polar head groups of the amphiphile are near the surface of the micelle and, therefore, are subject to a substantial degree of hydration (29, 30). In fact, Halle and Carlström (29) have reported that fewer than two CH_2 groups of an amphiphile molecule are hydrated in the micelles of potassium *n*-octanoate in ^2H_2O at 28°C. At high temperatures the micelles are expected to be less stable and more hydrated. Enhanced dissociation of the micelles would lead the monomers to reside in a hydrated environment for longer periods of time, as is reflected in the decrease of $\Delta\delta$ with temperature over the range 29–72°C (Fig. 4).

Above ca. 70°C the volatility of the TMS in CCl_4 solution made it necessary to internally reference the peaks, e.g., the difference in peak position ($\Delta\nu$) between the α-CH_2 and CH_3 proton nmr signals was measured. Just as the characteristic peak positions, δ_m and δ_M, for the monomer and micelle, respectively, yield $\Delta\delta$, so the differences, $\delta_m(\alpha\text{-}CH_2) - \delta_m(CH_3) = \Delta\nu_m$ and $\delta_M(\alpha\text{-}CH_2) - \delta_M(CH_3) = \Delta\nu_m$, provide $\nu_M - \nu_m = \Delta(\Delta\nu)$. Micellization is also indicated from the discontinuity in the concentration dependence of $\Delta\nu$ at the c.m.c. (Fig. 3). The c.m.c. value from the $\Delta\nu$ versus log C_T^{-1} plot is similar to that from the proton nmr peak positions and the carbon-13 nmr chemical shifts (e.g., c.m.c. $\approx$ 0.30 *m* at 29°C (lit. (23) c.m.c. $\approx$ 0.30–0.40 *m* at ca. 25–35°C)). The latter are accepted

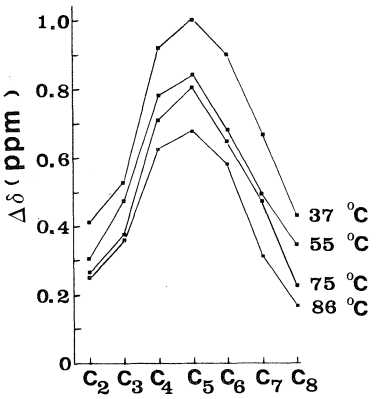

FIG. 5. Carbon-13 nmr chemical shift difference, $\Delta\delta$, between the micellar and monomeric states, for the carbon atoms of potassium *n*-octanoate in ^2H_2O at different temperatures.

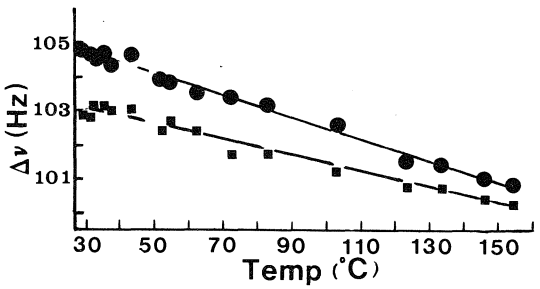

FIG. 6. Difference in peak positions between the α-CH_2 and CH_3 resonances for the monomeric, ●, and micellar, ■, states of potassium *n*-octanoate in ^2H_2O as a function of temperature.

TABLE 2. The demicellization temperature (in °C) of potassium *n*-octanoate in ^2H_2O as estimated from linear extrapolation of the carbon-13 nmr chemical shift difference, $\Delta\delta$, versus temperature plot to different values of $\Delta\delta$

	Carbon atom*						
	C_2	C_3	C_4	C_5	C_6	C_7	C_8
$\Delta\delta = 0$	161	182	199	204	182	140	117
$\Delta\delta = 0.012$†	157	179	197	202	180	138	115

*Subscript numeral corresponds to the position away from the CO_2^- carbon atom (C_1).

†Value at which the data extrapolate to the demicellization temperature, within the experimental error in $\Delta\delta$.

experimental parameters for the determination of c.m.c. values (26, 31). It is also worth noting that the shape of the $\Delta\nu$ versus log C_T^{-1} plot differs from that of δ versus C_T^{-1}, and this may be attributed to the different rates at which $\delta(\alpha\text{-}CH_2)$ and $\delta(CH_3)$ vary with the total surfactant concentration. The minimum position in the $\Delta\nu$ versus log C_T^{-1} plots is in all cases above the c.m.c., and has been chosen as an experimental $\Delta\nu_M$ value for the micelles. Intrinsically, the $\Delta\nu$ parameter behaves in an analogous manner to its parent parameter, δ, as reflected in the decrease in amplitude of both the δ and $\Delta\nu$ versus C_T^{-1} plots with temperature (Fig. 1 and 3).

A third parameter that affords information on demicellization phenomena is the ^{13}C nmr chemical shift. Because the ^{13}C nmr spectra are first order, it is possible to map the $\Delta\delta$ values as a function of position in the alkyl chain (Fig. 5). In contrast to the results from proton nmr spectra, the $\Delta\delta$ values from the ^{13}C spectra are higher for carbon atoms in the middle of the alkyl chain (see Fig. 5). One may explain the foregoing effect on the basis that carbon-13 chemical shifts are sensitive to conformational changes, e.g., *trans* ⇌ *gauche* rotational isomerism, with the *trans* rotamer being favoured in the micellar state (15, 16, 29). Elevation of the temperature will enhance rotations around the C—C bonds, and consequently alter the relative populations of the amphiphiles in the different rotameric states. Furthermore, conformational changes coupled with increased translational motion will weaken the hydrophobic bonding and thereby reduce the micelle stability. Increased temperature should thus induce a change in the ^{13}C nmr chemical shift, as observed from the plot of $\Delta\delta$ as a function of position along the alkyl chain (Fig. 5).

Collectively, the results from the variable temperature ^1H and ^{13}C nmr spectra suggest that potassium *n*-octanoate self-associates over a wide temperature range, 29°C to at least 103°C, and perhaps as high as 154°C. Also, the experimental results comply with a process that involves the dominance of complex processes, e.g., multiple equilibria, as exemplified by the enhanced curvature of the δ versus C_T^{-1} plot (Fig. 1) at the high temperatures. If a simple monomer ⇌ micelle equilibrium reaction exists, then the nmr peak position, or chemical shifts, as a function of C_T^{-1} will generate two straight lines ($\delta = \delta_M + (C_m/C_T)(\delta_m - \delta_M)$), which intersect at the critical micelle concentration (26). Deviations from ideal behaviour result in curved δ versus C_T^{-1} plots with larger radii of curvature for cases where the aggregates are small in size and the dominant mode of self-association is via multiple equilibria. From Figs. 1 and 3 it is obvious that the amplitude of the plots decreases and the curves tend toward the monomer line ($\delta = \delta_m$ and $\Delta\nu = \Delta\nu_m$) as the temperature increases.

Upon demicellization, surfactant monomers would be the predominant species in solution, and so the observed chemical shift would be that for the nonassociated amphiphiles, e.g., δ_m and $\Delta\nu_m$. This feature allows an estimate to be made of the demicellization temperature (DMT), for as the system tends toward the DMT, the micellar δ_M and $\Delta\nu_M$ values would, in effect, become more similar to the monomer δ_m and $\Delta\nu_m$ values (see Figs. 1–3 and 6). Two methods have been used to estimate the DMT from the ^1H nmr data, one by solving equations of the lines of δ and $\Delta\nu$ versus temperature (e.g. Fig. 6) of the monomers and micelles, for their intersection point, and the other from the temperature at which $\Delta\delta = 0$ and $\Delta(\Delta\nu) = 0$. The δ and $\Delta\delta$ data gave a DMT of ca. 127–157°C and the $\Delta\delta$ and $\Delta(\Delta\nu)$ data yielded a DMT of ca. 227°C.

The demicellization of potassium *n*-octanoate in deuterium oxide is well illustrated from the decrease in amplitude of the carbon-13 nmr $\Delta\delta$ as a function of position in the alkyl chain with increasing temperature (Fig. 5). Estimates of the DMT (115–199°C; see Table 2), from linear extrapolation of the ^{13}C nmr data to $\Delta\delta = 0$, are similar to the values (127–227°C) from the proton nmr experiments.

Although the DMT values must be considered as rough estimates, they do show some interesting and important features. In all cases the DMT (115–227°C) is above the boiling point of the solvent and in most cases is near or above the iceberg point of water (160°C) (32). Iceberg formation in water results from restructuring of the water molecules around hydrophobic entities (11, 32). This results in a change in entropy and has been attributed as a factor that affects the micellization process (1, 11). It is also significant that self-association of the surfactant into small aggregates exists above

TABLE 3. Critical micelle concentrations (in mol kg^{-1}) from plots of carbon-13 nmr chemical shifts, for different carbon atoms,* versus the reciprocal of the total potassium *n*-octanoate concentration in deuterium oxide at different temperatures

Temperature (°C)	Carbon atom							
	C_2	C_3	C_4	C_5	C_6	C_7	C_8	c.m.c.‡
30†	0.28	0.33	0.33	0.31	0.32	0.32	0.27	0.31
37	0.25	0.30	0.31	0.33	0.32	0.30	0.31	0.30
55	0.34	0.41	0.32	0.38	0.36	0.33	0.29	0.35
75	0.44	0.43	0.39	0.42	0.42	0.36	0.24§	0.39 (0.41)‖
86	0.42	0.40	0.41	0.43	0.41	0.45	0.17§	0.38 (0.42)‖

*Carbon atoms are numbered as position away from the CO_2^-.
†At 62.95 MHz on a Bruker AM-250 nmr spectrometer.
‡Mean c.m.c. value.
§These values may be appreciably in error owing to the enhanced curvature of the plots.
‖Mean c.m.c. without value from C_8.

the boiling point of ^2H_2O, where substantial changes in the bulk structure of the solvent occur.

It is not unreasonable that the demicellization temperature is above ca. 115°C. Consider the following: it is well established that alkali metal monoalkyl carboxylates with six to eight carbon atoms form small aggregates (16) in water above the c.m.c. Whereas potassium *n*-octanoate self-associates with up to ~10 monomers per micelle (29), it is questionable whether the hexanoate salt, with less than five monomers per aggregate, forms proper micelles, although it does display a c.m.c. at ca. 1.6 mol dm^{-3} at 25°C (23). Sodium pentanoate forms even smaller aggregates, dimers and trimers, and does not show a marked discontinuity in the physical parameter – concentration plot (33), although a c.m.c. has been assigned at 2.4 mol dm^{-3} at 20°C (23). A very short-chain amphiphile, such as sodium butyrate, exhibits little or no aggregation, as revealed from proton spin-lattice relaxation studies (33).

Some measure of the size of the micelles may be gained from a plot of log C_m versus log $(C_T - C_m)$, which is based on the single-step equilibrium model, where C_m is the concentration of unassociated monomers (34). The proton nmr data yield mean aggregation numbers ($\bar{n}$) in the range 3–6 monomers per micelle at 31°C and $\bar{n} \sim 2$ at 72°C, whereas the carbon-13 data give $\bar{n} \sim 9$ at 37°C and $\bar{n} \sim 4$ at 55°C. The $\bar{n}$ values should be considered as approximate, owing to the possibility of multiple equilibria and a polydispersity of aggregate sizes. Persson *et al.* (5) have determined similar $\bar{n}$ values of ~4–5 and 10–11 for sodium *n*-octanoate in ^2H_2O at 25°C.

The experimental results are in line with evidence that suggests small micelles form via multiple equilibria (18, 35), and with the quasielastic light scattering data of Mazer *et al.* (35), which reveal a decrease in the size of micelles with an increase in temperature over the range 10–85°C, for sodium dodecyl sulfate with sodium chloride in water. The aggregates formed by the alkali metal alkanoate surfactants should be very small at the high temperatures where the c.m.c. increases rapidly.

Both experimental and theoretical studies favour a parabolic or quadratic variation of the c.m.c. with temperature, the minimum value for ionic surfactants being around 25°C. From this work the c.m.c. (see Table 3) is observed to increase from ca. 0.30 *m* at 30°C to ca. 0.40 *m* at 86°C. These values are similar to those from the conductivity studies, by White and Benson, on potassium *n*-octanoate in water (36, 37). Even though the present work uses deuterium oxide as the solvent, it has been shown that ^2H_2O depresses the c.m.c. by only a small amount relative to the value in water (38).

One other point to be explored in the relation of the c.m.c. to micellization is the rate at which it changes with temperature. Literature data on the long-chain surfactants, tetradecyltrimethylammonium bromide (11) and dioctadecyldimethylammonium chloride (12) in water, reveal that the c.m.c. rises rapidly above 100°C. These results support the view that micellization becomes difficult above the boiling point of the solvent.

Finally, consider the fact that the binding energy of small micelles is less than that for large ones, and they would, therefore, be expected to demicellize at a lower temperature. The DMT for potassium *n*-octanoate corresponds to *RT* values of 3.2–4.2 kJ mol^{-1}, which are similar to the heat of dimerization of *n*-octanoic acid in water (ΔH_D = 4 kJ mol^{-1}) (39). It is consequently not unreasonable that the demicellization temperature of potassium *n*-octanoate in ^2H_2O at concentrations around the c.m.c. is in the range ca. 115–227°C, where surfactant dimers and monomers would be the predominant species in solution.

Conclusion

The experimental results from proton and carbon-13 nmr spectra provide the following information: (*i*) potassium *n*-octanoate forms aggregates over a wide temperature range, 29–154°C, and above the boiling point of deuterium oxide; (*ii*) complex or multiple equilibria appear to dominate the self-association process of the surfactant at high temperatures; and (*iii*) estimates of the demicellization temperature are in the range ~115 ≤ DMT ≤ 227°C where micelle formation is not favoured.

Acknowledgements

We wish to thank Pilar Orozco de Breña for her assistance and the Natural Sciences and Engineering Research Council of Canada for financing this project. Our gratitude is also expressed to Professor Kōzō Shinoda, of Yokohama National University, for valuable discussions.

1. C. TANFORD. The hydrophobic effect. Wiley, New York. 1973.
2. J. M. BROWN. Colloid science. Vol. 3. The Chemical Society Spec. Period. Rep., London. 1979. p. 253.
3. K. TSU, N. SAITO, and T. TAKEUCHI. J. Phys. Chem. **84**, 2287 (1980).

4. M. J. ROSEN. Surfactants and Interfacial Phenomena. John Wiley and Sons, New York. 1978.
5. B. PERSSON, T. DRAKENBERG, and B. LINDMAN. J. Phys. Chem. **83**, 3011 (1979).
6. B. LINDMAN, N. KAMENKA, M. PUYAL, B. BRUN, and B. JÖNSSON. J. Phys. Chem. **88**, 53 (1984).
7. T. ZEMB, M. DRIFFORD, M. HAYOUN, and A. JEHANNO. J. Phys. Chem. **87**, 4524 (1983).
8. P. MUKERJEE. Ber. Bunsenges. Phys. Chem. **82**, 931 (1978).
9. E. RUKENSTEIN and R. NAGARAJAN. J. Phys. Chem. **85**, 3010 (1981).
10. P. MUKERJEE. *In* Micellization, solubilization, and microemulsions. Vol. 1. *Edited by* K. L. Mittal. Plenum Press, New York. 1977. p. 186.
11. D. F. EVANS and P. J. WIGHTMAN. J. Colloid Interface Sci. **86**, 515 (1982).
12. H. KUNIEDA and K. SHINODA. J. Phys. Chem. **82**, 1710 (1978).
13. D. C. POLAND and H. A. SCHERAGA. J. Phys. Chem. **69**, 2431 (1965).
14. D. C. POLAND and H. A. SCHERAGA. J. Colloid Interface Sci. **21**, 273 (1966).
15. H. WENNERSTRÖM and B. LINDMAN. Phys. Rep. **52**, 1 (1979).
16. B. LINDMAN and H. WENNERSTRÖM. Topics Curr. Chem. **87**, 1 (1980).
17. D. ATTWOOD and A. T. FLORENCE. Surfactant systems. Chapman and Hall, London. 1983.
18. B. LINDMAN. *In* Surfactants. *Edited by* Th. F. Tadros. Academic Press, London. 1984. p. 83.
19. B. J. FORREST and L. W. REEVES. Chem. Rev. **81**, 1 (1981).
20. F. Y. FUJIWARA and L. W. REEVES. J. Phys. Chem. **84**, 653 (1980).
21. G. D. SMITH. *In* Solution chemistry of surfactants. Vol. 1. *Edited by* K. L. Mittal. Plenum Press, New York. 1979. p. 195.
22. R. M. LEMMON. Chem. Rev. **70**, 95 (1970).
23. P. MUKERJEE and K. J. MYSELS. Critical micelle concentrations of aqueous surfactant systems. Natl. Stand. Ref. Data Sevr. Nat. Bur. Stand., U.S. **36**, U.S. Dept. of Commerce, Washington D.C. (1971).
24. O. YAMAMOTO and M. YANAGISAWA. Anal. Chem. **42**, 1463 (1970).
25. B. J. BLACKBURN, F. E. HRASKA, and I. C. P. SMITH. Can. J. Chem. **47**, 4491 (1969).
26. N. MULLER and R. H. BIRKHAHN. J. Phys. Chem. **71**, 957 (1967).
27. H. GUSTAVSSON and B. LINDMAN. J. Am. Chem. Soc. **97**, 3923 (1975).
28. G. C. LEVY, R. L. LICHTER, and G. L. NELSON. Carbon-13 nuclear magnetic resonance spectroscopy. John Wiley & Sons, New York. 1980.
29. B. HALLE and G. CARLSTRÖM. J. Phys. Chem. **85**, 2142 (1981).
30. B. LINDMAN and B. BRUN. J. Colloid Interface Sci. **42**, 388 (1973).
31. K. J. MYSELS and P. MUKERJEE. Pure Appl. Chem. **51**, 1083 (1979).
32. K. SHINODA. J. Phys. Chem. **81**, 1300 (1977).
33. B. SVENS and I. DANIELSSON. J. Colloid Interface Sci. **41**, 298 (1972).
34. N. MULLER and F. E. PLATKO. J. Phys. Chem. **75**, 547 (1971).
35. N. A. MAZER, M. C. CAREY, and G. B. BENEDEK. *In* Micellization, solubilization and microemulsions. Vol. 1. *Edited by* K. L. Mittal. Plenum Press, New York. 1977.
36. P. WHITE and G. C. BENSON. Trans. Faraday Soc. **55**, 1025 (1959).
37. P. WHITE and G. C. BENSON. J. Phys. Chem. **64**, 599 (1960).
38. P. MUKERJEE, P. KAPAUAN, and G. MEYER. J. Phys. Chem. **70**, 783 (1966).
39. P. MUKERJEE. J. Phys. Chem. **69**, 2821 (1965).

The effects of high temperatures (29–123°C) on critical micelle concentrations in solutions of potassium *n*-octanoate in deuterium oxide: A nuclear magnetic resonance study

M. A. DESANDO AND L. W. REEVES

Department of Chemistry, University of Waterloo, Waterloo, Ont., Canada N2L 3G1

Received September 9, 1985[1]

M. A. DESANDO and L. W. REEVES. Can. J. Chem. **64**, 1823 (1986).

Critical micelle concentrations have been determined for potassium *n*-octanoate in deuterium oxide over a wide temperature range, 29–123°C, from the concentration dependence of proton nmr spectral parameters (peak positions, and vicinal splitting values of the α-CH_2 multiplet) and carbon-13 nmr chemical shifts. The c.m.c. varies from ca. 0.30 *m* at ca. 30°C to ca. 0.50 *m* at ca. 120°C and is at a minimum (0.30–0.35 *m*) in the temperature range ca. 30–50°C. $^{23}Na^+$ spin-lattice relaxation times reveal that a co-counterion (Na^+) different from that of the surfactant counterion (K^+) reflects the micellization process. A second critical micelle concentration has been observed around 1.0 *m* at ca. 30°C.

M. A. DESANDO et L. W. REEVES. Can. J. Chem. **64**, 1823 (1986).

Opérant dans l'oxyde de deutérium et à des températures aliant de 29 à 123°C et en se basant sur la variation des paramètres spectraux de la rmn du ^1H (déplacements chimiques et constantes de couplages vicinaux du multiplet du α-CH_2) et du ^{13}C (déplacements chimiques) avec la concentration, on a déterminé les concentrations micellaires critiques de l'octanoate de potassium. Ces c.m.c. varient d'environ 0,30 *m* à 30°C à environ 0,50 *m* à 120°C; elles passent par un minimum (0,30–0,35 *m*) dans l'intervalle de température de 30 à 50°C. Les temps de relaxation spin-réseau du $^{23}Na^+$ révèlent que la présence d'un contre-ion (Na^+) différent de celui présent dans les surfactants (K^+) se réflète dans le processus de micellisation. À 30°C, on a aussi observé une deuxième concentration micellaire critique autour de 1,0 *m*.

[Traduit par la revue]

Introduction

Amphiphiles of fatty acid salts are known to form normal micelles in water (1–5) around room temperature. Whereas considerable study has been done on the properties of surfactant solutions around the critical micelle concentration (c.m.c.), relatively little research has been performed on micelles at high temperatures and at high surfactant concentrations. There is uncertainty as to the nature of the changes that occur in the micelles as surfactant is added to the solution above the c.m.c, and at temperatures near and above the boiling point of water.

The critical micelle concentration is a fundamental parameter in the characterization of surfactant solutions, for it indicates the usually narrow range of concentrations separating the limits below which most of the surfactant is in the monomeric state and above which virtually all additional surfactant enters the micellar state (6). This definition has been subject to controversy as has been the concept of a c.m.c. A number of theories have been advanced to explain the occurrence of a critical micelle concentration (1, 6–9). The usefulness of c.m.c. values in the study of micelle formation, however, cannot be argued. For example, the variation of the c.m.c. with temperature can provide thermodynamic data and information on the nature of the surfactant self-association process.

In light of the importance of the c.m.c parameter, it is surprising that few studies have been carried out on its variation over a wide temperature range, which extends above the boiling point of water (10, 11). Research on surfactant systems is relevant to the industrial processes, e.g., the temperature for optimum detergency, and to biological phenomena such as temperature effects on membranes and the origin of life on the primitive earth.

It has been suggested that a second critical micelle concentration (c.m.c.$^{\#2}$) exists at concentrations higher than the critical micelle concentration (12–17). Some researchers believe that the c.m.c.$^{\#2}$ arises from a sphere-to-rod transition of the micelle geometry (16). Others attribute the c.m.c.$^{\#2}$ to a distortion of the micelles owing to increased binding of the counterions (ion condensation) and hence enhanced hydration of the micelles (13). Another explanation for the second critical concentration is that it occurs where the aggregates gain positional order because of increased electrical repulsions among the micelles (14). It has even been advanced that the changes in micelle structure at the c.m.c.$^{\#2}$ are so subtle that a very sensitive technique such as position annihilation is required to detect it (13).

The prime objective of the present work is therefore to study a simple ionic surfactant system, viz., potassium *n*-octanoate in ^2H_2O, by multinuclear nmr spectroscopy with a view to obtaining information on the temperature dependence of critical micelle concentrations.

Experimental

Potassium *n*-octanoate was prepared by neutralizing *n*-octanoic acid (Aldrich 99.5 + %) with an equimolar quantity of potassium hydroxide (Baker A.R.) in absolute ethanol. The product was recrystallized several times from absolute alcohol and rigorously dried *in vacuo*. Potassium *n*-octanoate (from laboratory stock) was washed several times with ethyl acetate to remove any residual acid, and was then dried *in vacuo* over anhydrous $CaCl_2$ for several days. Sodium chloride (Baker A.R.) was used without further purification. Ethylene glycol (Baker A.R.) was dried over anhydrous sodium sulfate during reflux in dry nitrogen gas prior to several distillations. Deuterium oxide (99.8 at.%) was purchased from Merck, Sharp & Dohme. The absence of recrystallizing solvents in potassium *n*-octanoate and water in ethylene glycol was checked from carbon-13 and proton nmr spectra.

Solutions of potassium *n*-octanoate in ^2H_2O were of molal concentration, except for those at 29°C, which were of molar concentration, and were contained in the outer tubes of thin-wall 5 mm od coaxial nmr cells (Wilmad WGS-5B1). Tetramethylsilane (TMS) in CCl_4 (~1 v/v) was used as the external reference in the inner tube of the nmr cell for proton spectra. Above 72°C the samples for proton spectra were contained in sealed thick-wall 5 mm od nmr tubes, without a reference material.

Proton nmr peak positions were measured relative to external TMS set to zero ppm on an 80-MHz (1.88-T field) Bruker WP-80 nmr spectrometer equipped with a PTS 160 frequency synthesizer and a B-ST 100/700 variable temperature controller. A typical uncertainty in

[1]Revision received April 11, 1986.

the proton nmr peak position is ±0.003 ppm. Corrections were not applied for bulk diamagnetic susceptibility in the coaxial samples, as no appreciable difference in peak position was noticed when the inner cell was present. The undecoupled proton nmr spectra are second order, and so the term, peak position, has been applied to the data.

$^{23}Na^+$ spin-lattice relaxation times were measured by the application of a $(\pi-\tau-\pi/2)_n$ pulse sequence via the inversion–recovery method at a frequency of 20.13 MHz at 29°C.

The temperature inside the ^1H probehead was measured from the linear equation for the difference in peak position of the ethylene glycol resonances as a function of observed temperature. The method employed to determine the observed temperature was similar to that of Yamamoto and Yamagisawa (18), and involved measurements of the melting points of eight organic solids, first on a Meltemp melting point apparatus and then on the nmr spectrometer. Ethylene glycol was sealed in the inner tube of a coaxial cell and the ^2H-lock agents (^2H_2O; ($^2H_2O/HSO_3Cl$ or $^2H_2O/H_2SO_4$ at ≥101°C)) in the outer tube.

Natural abundance, broad-band decoupled carbon-13 nmr spectra were recorded at 20.12 MHz on the Bruker WP-80 spectrometer, and power gated, broad-band decoupled carbon-13 nmr spectra, at 62.95 MHz and 30°C, on an AM-250 Bruker nmr spectrometer with a superconducting magnet. The ^{13}C nmr chemical shifts are relative to external hexamethyldisiloxane (98+%, Ald), and have a mean variation of ±0.012 ppm for several measurements.

Results

In accord with a single-step equilibrium model of micellization (monomer ⇌ micelle) the resonance peak position or chemical shift (δ) as a function of total surfactant concentration (C_T) can be expressed as:

$$[1] \quad \delta = \delta_M + [c.m.c.(\delta_m - \delta_M)]/C_T$$

where the subscripts m and M refer to the monomer and micelle, respectively (19). Inherent in the above equation is the condition that a plot of δ versus C_T^{-1} will consist of two straight lines that intersect at the critical micelle concentration (c.m.c). Factors such as multiple equilibria, polydispersity of micelle size, small aggregates, and structural transformations of the micelles may induce a degree of curvature in the δ versus C_T^{-1} plot, which increases as the system deviates from the simple equilibrium model. Modifications of eq. [1] have been formulated to consider ion-pair dissociation, but these have little effect on the shape of the curve (19).

Almost any physical property that varies with the degree of association of a solute will display a change in magnitude as the solute concentration is altered. Whether an abrupt change or discontinuity occurs at a certain concentration, e.g., the c.m.c., depends on the rate of change of the property (P) being observed. At the c.m.c., for example, d^3P/dC_T^3 is zero (20).

The c.m.c. values were determined, using linear regression analysis, from the intersection point of the lines of limiting slope of the spectral parameter (δ, $^3J_{HH}$, and T_1) versus the reciprocal of the total surfactant concentration C_T^{-1}) (Figs. 1–4). A low limit for the monomer line was set from the extrapolated value of the parameter–concentration curve to infinite dilution. The uncertainty in the c.m.c. value may be as high as ±0.05 m.

Although nmr chemical shifts (19) and spin-lattice relaxation times (21) have been used to determine c.m.c. values, the indirect nuclear spin–spin splitting value ($^3J_{HH}$) has not received much attention. The average vicinal proton ($H_1C_1C_2H_2$) splitting ($^3J_{H_1H_2}$) has been related empirically to the dihedral angle between the protons, by the Karplus equations for the ethanic molecules (22). Determinations of the $^3J_{HH}$ values, which are weight averaged ($^3J_{HH} = \Sigma x_i {}^3J_{HH_i}$; $^3J_{HH_i}$ is the splitting value for the species of mole fraction, X_i), for the monomeric and

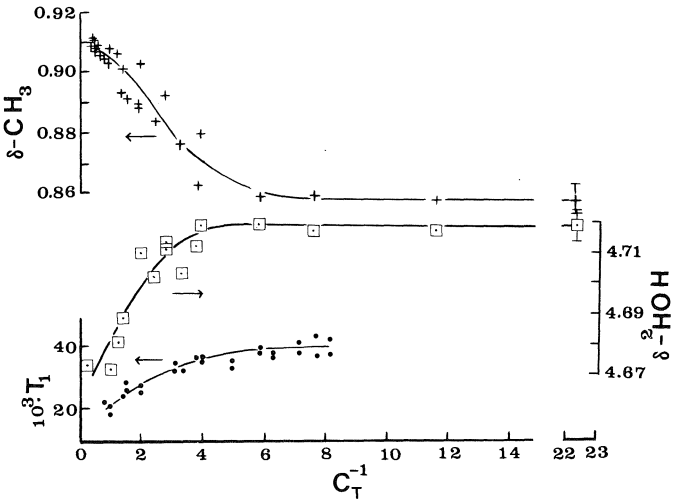

FIG. 1. ●, $^{23}Na^+$ spin-lattice relaxation time (T_1 in s); and nmr peak position (δ in ppm) for the residual proton signal in 99.8 at.% deuterium oxide (⊡, ^2HOH) and the methyl protons (+) as a function of the total surfactant concentration (C_T in mol kg^{-1}) for potassium n-octanoate:NaCl (3:1 mole:mole) in ^2H_2O at 31°C.

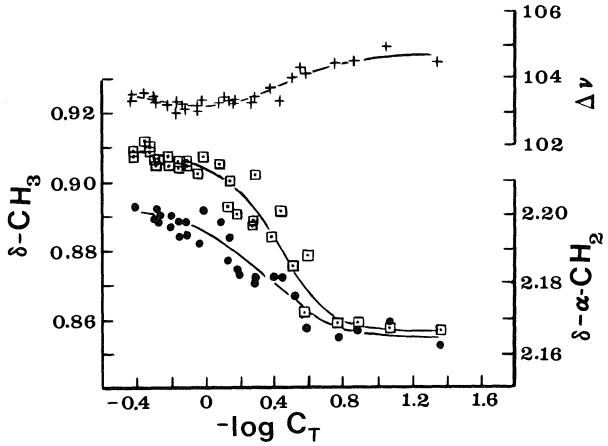

FIG. 2. Proton nmr peak position (δ in ppm) for the α-methylene (●) and methyl (⊡) protons, and the difference in peak position (+, $\Delta\nu = \nu(\alpha\text{-}CH_2) - \nu(CH_3)$ in Hz) as a function of the total surfactant concentration (C_T in mol kg^{-1}) for potassium n-octanoate:NaCl (3:1 mole:mole) in ^2H_2O at 31°C.

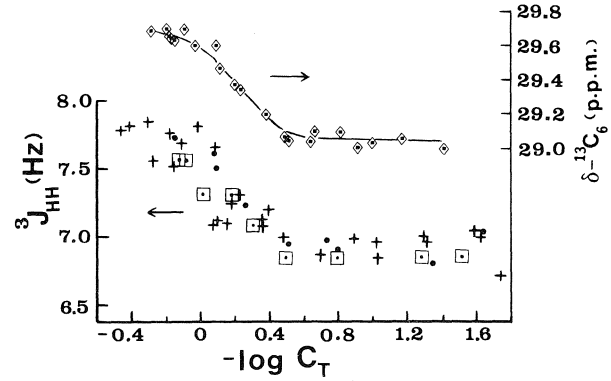

FIG. 3. Vicinal splitting value ($^3J_{HH}$) for the α-CH_2 protons and carbon-13 nmr chemical shift for carbon atom number six at 30°C (at 62.95 MHz) as a function of the total potassium n-octanoate concentration (C_T in mol kg^{-1}) in ^2H_2O: ⊡, 29°C; +, 31°C, ●, 35°C.

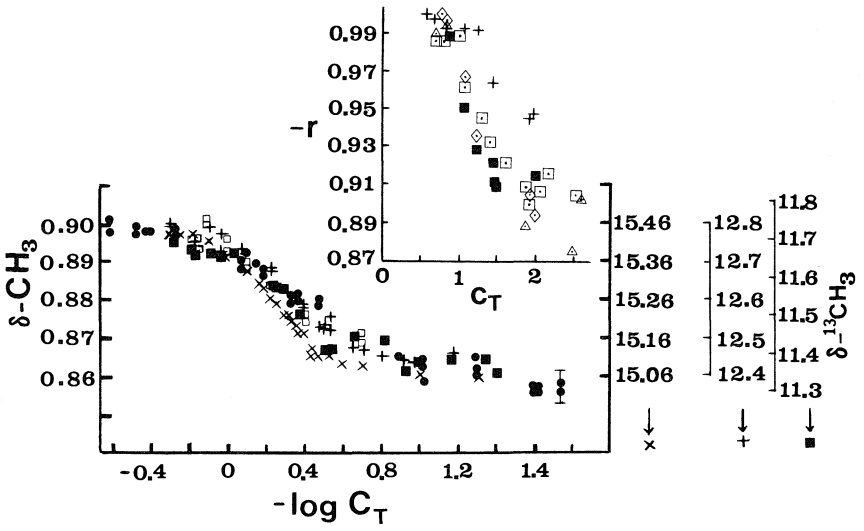

FIG. 4. The nmr peak positions (δ in ppm) of the methyl protons as a function of the total molal potassium *n*-octanoate concentration (C_T) expressed as $-\log C_T$, in ^2H_2O: □, 31°C; ●, 32°C; ^{13}C nmr chemical shifts of the CH_3 group (*vide infra*) (×, sodium *n*-octanoate in ^2H_2O (ref. 48)). Concentration (C_T in mol kg^{-1}) dependence of the correlation coefficient (r), from linear regression analysis, as each data point above the second critical micelle concentration is added to the line of best fit for the data below the second critical micelle concentration (ca. 1.0 *m*): (δ-CH_3; □, 31°C; △, 41°C); (^{13}C nmr (δ-CH_3) ■, 30°C (at 62.95 MHz); +, 37°C, ◇ 55°C, ×, lit. (ref. 48)).

TABLE 1. Critical micelle concentration (c.m.c.) values from nmr spectral parameters (proton nmr peak position (δ(^{1}H)), vicinal splitting value ($^3J_{HH}$) of the α-CH_2 proton resonance, and carbon-13 nmr chemical shifts (δ(^{13}C)) for potassium *n*-octanoate in deuterium oxide at different temperatures

	c.m.c. (mol kg^{-1})		
Temperature (°C)	δ(^{1}H)*	$^3J_{HH}$	δ(^{13}C)†
29	0.30	0.34	
30			0.31§
31	0.32	0.31	
35	0.29	0.31	
37	0.27	0.33	0.30
40	0.30	0.34	
49	0.29	0.32	
55			0.35
61	0.34	0.32	
75			0.41
83		0.46	
86			0.42
103		0.49	
123		0.52	
31‡	0.21	0.18	

*Average value from CH_3, α-CH_2, and $(CH_2)_4$ nmr data.
†Average value from alkyl carbon atoms nmr data.
‡Potassium *n*-octanoate:NaCl (3:1 mole:mole) in deuterium oxide; c.m.c. ~ 0.25 *m* from $^{23}Na^+$ spin-lattice relaxation time measurements at 29°C.
§At 62.95 MHz.

micellar states, give an indication of conformational changes in the surfactant ion pair, and possibly counterion binding upon micellization.

Spin-lattice relaxation times (T_1) were determined from the variation of the magnetization (M_z) along the z laboratory axis and thus the spectral intensity, as a function of the relaxation delay time between the π and $\pi/2$ pulses (23).

$$[2] \quad \ln (M_0 - M_z) = \ln (2M_0) - (t/T_1)$$

M_0 is the equilibrium magnetization before decay, $M_0 = -M_z$ at time $t = 0$.

Measurement of the c.m.c. value at different temperatures, from the various parameters (Table 1), allows for the calculation of thermodynamic quantities, such as the free energy (ΔG_{mic}), enthalpy (ΔH_{mic}), and entropy ΔS_{mic} of micellization, from a van't Hoff type of relation (10, 20, 24, 25):

$$[3] \quad \Delta G_{mic} = \Delta H_{mic} - T\Delta S_{mic} = \bar{n}(2 - \beta)RT \ln X_{c.m.c.}$$

In eq. [3] $\bar{n}$ is the mean aggregation number, $0 \leq \beta \leq 1$ ($\beta = 0$ for an electrically neutral micelle) is the degree of ionization of the micelle, and $X_{c.m.c.}$ is the c.m.c. in mole fraction units.

Discussion

It is observed from the plots of the proton resonance peak positions and carbon-13 nmr chemical shifts against the reciprocal of the total surfactant concentration that each of the different sets of magnetically equivalent nuclei reflects the micellization process, even the solvent (Fig. 1). Micellization is therefore a bulk phenomenon and is experienced by every part of the system. Although the water resonance signal has received some attention (26, 27), few studies have focussed on the alkyl group protons for the determination of the c.m.c. value. There are differences in the literature as to the extent of change in chemical shifts that the CH_3 and CH_2 protons experience as a function of the total surfactant concentration. Some researchers state that the alkyl proton resonances display little or no variation in chemical shift upon micelle formation (26–28). Odberg *et al.*, on the other hand, were able to determine c.m.c. values for the short-chain alkanoates from the alkyl proton nmr chemical shifts and differences in chemical shifts (29). Also, Fendler *et al.* observed appreciable changes in the chemical shifts of the CH_3 and CH_2 proton resonance signals of hexylammonium propionate in ^2H_2O (30).

One significant outcome of this study is that micellization is reflected in the abrupt change of the vicinal splitting value ($^3J_{HH}$) of the α-CH_2 protons around the c.m.c. (cf. c.m.c. from

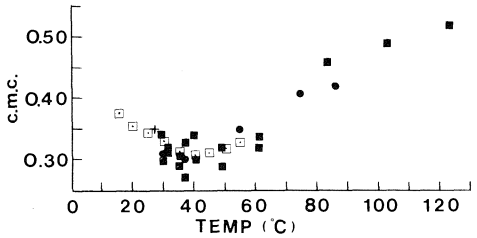

FIG. 5. Critical micelle concentration values (c.m.c. in mol kg^{-1}) at different temperatures for potassium *n*-octanoate in ^2H_2O: ■, from proton, and ●, from carbon-13 nmr spectral parameters (Table 1); ⊡, refs. 6, 24, and 51.

TABLE 2. Vicinal splitting values for the α-CH_2 protons of potassium *n*-octanoate in the monomeric ($^3J_{HH}$(m)) and micellar ($^3J_{HH}$(M)) states in ^2H_2O

Temperature (°C)	$^3J_{HH}$(m)(Hz)	$^3J_{HH}$(M)(Hz)
29	6.8	7.6
31	6.8	7.7
32	6.7	7.8
35	6.6	7.9
37	7.0	8.0
41	7.0	7.9
44	6.9	8.3
49	7.0	8.0
52	6.9	8.0
54	6.7	8.0
61	6.8	8.2
72	7.0	8.0
83	6.9	7.6
103	6.9	7.6
123	7.3	8.0
133	7.3	7.7
146	7.2	7.8
154	7.3	7.9
31*	7.5	7.9

*Potassium *n*-octanoate:NaCl (3:1 mole:mole) in ^2H_2O.

^{13}C nmr chemical shifts; see Fig. 3 and Table 1). Notice how the splitting values, at many temperatures, increase from ca. 7 Hz in the monomeric state to ca. 8 Hz in the micellar condition (Table 2). The variation of the $^3J_{HH}$ values may be accounted for by conformational changes around the headgroup and (or) increased binding of the cations to the micelles.

In the cases where NaCl is added in a 1:3 molar ratio to potassium *n*-octanoate in deuterium oxide the c.m.c. is obtained from the $^{23}Na^+$ spin-lattice relaxation time (Fig. 1), and agrees with that from the other parameters (see Table 1). Lindman *et al.* demonstrated, for binary solutions, the application of $^{23}Na^+$ spin-lattice relaxation times to the measurement of the c.m.c. (15, 31, 32). Clearly, the third component (electrolyte) experiences the formation of micelles. Exchange reactions of the type: $K^+Oc^- + Na^+ \rightleftharpoons Na^+Oc^- + K^+$ (Oc^- is *n*-octanoate) lead, in effect, to a mixed micelle. An indication of the interaction of the sodium cations with the micelles is forwarded by the $^{23}Na^+$ spin-lattice relaxation times (T_1) of the ternary solutions. At infinite dilution, the fact that T_1 ($\sim 4.6 \times 10^{-2}$ s) is ca. 40 times greater than the value $T_1 \sim 1.1 \times 10^{-3}$ s, in the micellar state, suggests enhanced interactions of the Na^+ with the *n*-octanoate ion. The former value compares to $T_1 \sim 4.1 \times 10^{-2}$ s for a solution of 0.25 molar NaCl in ^2H_2O and a literature value (33) of 5.0×10^{-2} s for a dilute solution of NaCl in water at 25°C.

A further indication of the effect of added electrolyte may be gained from the difference in peak position ($\Delta\delta$) between the micellar and monomeric states. When sodium chloride is present, $\Delta\delta$ increases by ca. 16% for the CH_3 protons as compared to ca. 77% for the α-CH_2 protons. These results suggest that although there are additional interactions among the hydrocarbon tails owing to the large size of the aggregates, there are also appreciable changes at the micelle surface. The decrease in the c.m.c. at 31°C from ca. 0.30 *m* to ca. 0.20 *m*, upon the addition of NaCl, testifies to the formation of large micelles.

Simple electrolytes, as well as high surfactant concentrations, are known to induce changes in the size and shape of micelles (2, 16, 34–49). However, the concentrations associated with the above phenomena, and the exact nature of the changes in the micellar solution, are not well understood. Above the c.m.c. a second critical micelle concentration may exist where the micelles undergo processes such as: (*i*) sphere (or globule)-to-rod transitions; (*ii*) increased hydration and binding of the counterions (ion condensation) (31); and (*iii*) greater positional order (14).

A second critical micelle concentration (c.m.c.$^{\#2}$) does in fact appear at ca. 1.0 *m* potassium *n*-octanoate in deuterium oxide (see Figs. 2 and 4). Statistically, the data may be correlated to two lines, one below and one above ca. 1.0 *m* potassium *n*-octanoate, as reflected in the correlation coefficient (Fig. 4). When the ^{13}C nmr data of Persson *et al.* (48), for sodium *n*-octanoate in ^2H_2O, are plotted along with the ^{13}C and ^1H nmr results from this work, the discontinuity around 1.0 *m* surfactant is quite obvious. Furthermore, when NaCl is added to the surfactant solutions, the second critical micelle concentration is again observed around 1.0 *m* potassium *n*-octanoate (Fig. 2).

Other cases in which researchers have utilized proton chemical shifts to detect a second critical micelle concentration are for potassium and sodium *n*-hexanoate at a 2 molar concentration in water (29). Gustavsson and Lindman reported a second break, at ca. 1.2 *m*, in the plot of $^{23}Na^+$ spin-lattice relaxation time versus total sodium *n*-octanoate concentration in ^2H_2O, along with an increase in the ratio of counterion to surfactant in the micelles (32). Aqueous solutions of cetylpyridinium chloride (16) and potassium oleate (17) display a second critical micelle concentration at around 10% by weight of surfactant, as compared to ca. 18% by weight for potassium *n*-octanoate in ^2H_2O from this study.

The variations of the spectral parameters with surfactant concentration suggest a progressive buildup of the micelles, via multiple equilibria reactions. If a monomer $\rightleftharpoons$ micelle equilibrium process is dominant, then a sharp transition point would be observed and the plot of δ versus concentration would generate two intersecting lines according to eq. [1]. Explicit in eq. [1] is the assumption that C_m = c.m.c., i.e., a constant monomer concentration above the c.m.c. If the number of free monomers changes with the total surfactant concentration there will be deviations from linearity in the plot of δ versus C_T^{-1}. There is experimental evidence that the unassociated monomer concentration decreases above the critical micelle concentration (50). Should there be a transition from spherical micelles (SM) to say globular, disk, cylindrical, or rod-shaped micelles (CM), then, for an equilibrium of the kind sphere $\rightleftharpoons$ rod, the nmr peak

position as a function of total surfactant concentration may take the form:

$$[4] \quad \delta = \delta_{CM} + \frac{\text{c.m.c.}^{\#2}}{C_T}(\delta_{SM} - \delta_{CM}); \quad \text{c.m.c.}^{\#2} = C_{SM}$$

assuming that all of the solute is in the two forms of micelles, i.e., no unassociated monomer. The presence of monomers would result in an expression of the form

$$[5] \quad \delta = (C_m\delta_m + \bar{n}C_{SM}\delta_{SM} + \bar{n}'C_{CM}\delta_{CM})/C_T$$

If $C_m \sim$ c.m.c. and $C_{SM} \sim$ c.m.c.$^{\#2}$, then

$$[6] \quad \delta = (\text{c.m.c.}\,\delta_m + \bar{n}\,\text{c.m.c.}^{\#2}\delta_{SM} + \bar{n}'C_{CM}\delta_{CM})/C_T$$

The total surfactant concentration can be expressed as

$$[7] \quad C_T = C_m + \bar{n}C_{SM} + \bar{n}'C_{CM} = \text{c.m.c.} + \bar{n}\,\text{c.m.c.}^{\#2} + n'C_{CM}$$

therefore,

$$[8] \quad C_{CM} = (C_T - \text{c.m.c.} - \bar{n}\,\text{c.m.c.}^{\#2})/\bar{n}'$$

Substitution of eq. [8] into eq. [6] and rearrangement yields

$$[9] \quad \delta = \delta_{CM} + \{[\text{c.m.c.}(\delta_m - \delta_{CM}) + \bar{n}\,\text{c.m.c.}^{\#2}(\delta_{SM} - \delta_{CM})]/C_T\}$$

When $\delta_{SM} = \delta_{CM}$ the above equation reduces to eq. [1] and two intersecting lines are observed in the plot of δ versus C_T^{-1}.

From the plots of δ against C_T^{-1} it is observed that the slope above the second transition point is less than that above the c.m.c.; thus from eqs. [1] and [9] one may infer:

$$[10] \quad \text{c.m.c.}(\delta_m - \delta_{SM}) > \text{c.m.c.}(\delta_m - \delta_{CM}) + \bar{n}\,\text{c.m.c.}^{\#2}(\delta_{SM} - \delta_{CM})$$

Other factors that may induce a change in the slope of the δ versus C_T^{-1} plot, above the c.m.c., are the concentration of the monomer and the size of the micelles. Notice in eqs. [6] and [9] that if C_m ($C_m \sim$ c.m.c.), $\bar{n}$, and $\bar{n}'$ vary with the total surfactant concentration then the slope will change. There is experimental evidence that the monomer concentration is at a maximum at the c.m.c. and that a polydispersity of aggregate sizes exists (50). If the $\bar{n}$ and $\bar{n}'$ values vary at different concentrations then slightly different δ_{SM} and δ_{CM} values would also be expected.

An expression ($\log C_m + \log nK = n \log (C_T - C_m)$; n is the mean aggregation number and K is the equilibrium constant) based on a single-step equilibrium model affords a rough estimate of the size of the micelles (46, 47). The average slope of the $\log C_m$ versus $\log (C_T - C_m)$ plot yields $\bar{n}$ in the range 3–6 monomers per micelle at 31°C from ^{1}H nmr spectra, and $n \sim 9$ at 37°C from ^{13}C nmr experiments. Literature values for sodium n-octanoate are $\bar{n} = 4$ to $\bar{n} = 15$ (48, 50). Some papers quote two $\bar{n}$ values for sodium n-octanoate, depending on the concentration interval studied (48). It is therefore very important that one understands the type of micelle present in a certain concentration interval and, therefore, the critical micelle concentrations, to interpret data on micelle systems.

Measurements of the c.m.c. values at temperatures in the range 29–123°C give additional information on the nature of micelle formation, in particular, the thermodynamics. Some ionic surfactants exhibit a minimum in the c.m.c. around room temperature, whereas for some nonionic and betaine surfactants the c.m.c. decreases with an increase in temperature (5). Critical micelle concentrations for bivalent metal alkyl sulfates appear to be independent of the temperature.

In the case of potassium n-octanoate in ^2H_2O, the c.m.c. shows little change, ca. 0.30–0.35 m, in the temperature range ca. 30–50°C and is at a minimum around 30–50°C, and then increases to ca. 0.52 m at 123°C. White and Benson observed a minimum in the c.m.c. of potassium n-octanoate plus a slight excess of KOH in water at 35°C, from conductivity measurements (24).

Analysis of the temperature variation of the c.m.c. allows for the determination of the enthalpy and entropy of micellization (eq. [3]). Mean aggregation numbers of 5–10 monomers per micelle and a degree of micelle ionization of $\beta = 0.7$–0.8 (from ref. 24) were applied in the calculations. The plot of ln c.m.c. (in mole fraction units) versus the reciprocal of the temperature yields $-101 \lesssim \Delta H_{mic} \lesssim -47$ kJ mol^{-1} and $117 \lesssim \Delta S_{mic} \lesssim 234$ J K^{-1} mol^{-1} above ~55°C. A decrease in the size of the micelles to dimers and trimers yields $-30 \lesssim \Delta H_{mic} \lesssim -19$ kJ mol^{-1}. The observed ΔH values compare with $\Delta H \sim -4$ to -12 kJ mol^{-1} at 45–55°C, from the conductivity data of White and Benson for potassium n-octanoate + KOH in water (24). Use of the van't Hoff relation for the derivation of enthalpies of micellization from c.m.c. values has been criticized on the basis that it assumes a temperature invariant micelle size, and the only reliable values are from conductivity experiments (24, 25). The ΔH_{mic} values do, however, indicate an exothermic process above ~55°C.

A factor that must be considered in the interpretation of the thermal dependence of the c.m.c. is the presence of the second critical micelle concentration. Boussaha and Ache demonstrated, using the positron annihilation technique, that the second critical micelle concentration for sodium n-octanoate/n-pentanol/H_2O decreases with increasing temperature (13). Mazer *et al.* determined, calorimetrically, the enthalpy for the process at the second critical concentration to be -1.74 ± 0.15 kJ mol^{-1}, for sodium dodecyl sulfate plus 0.6 molar sodium chloride in water (34). The aforementioned results imply subtle changes in the micelles at the second critical micelle concentration, yet appreciable changes in the nmr spectral parameters are noticed (Figs. 2 and 4).

Caution is advised in the study of micellization over wide temperature and surfactant concentration ranges, where both a critical micelle concentration and a second critical concentration occur and may vary at different rates with a change in temperature. Care should be taken to correlate the concentration dependence of a physical property on the total surfactant concentration to the proper critical micelle concentration, and to analyze the parameter–concentration plot over the appropriate range of concentrations associated with each phenomenon.

Conclusion

The study of micellization in potassium n-octanoate in deuterium oxide, over wide concentration and temperature intervals, reveals the following features:

(*i*) Proton nmr spectral parameters (peak position, and the vicinal splitting value of the α-CH_2 protons) yield the c.m.c. and the second critical micelle concentration, and the results are found to agree with those from carbon-13 nmr chemical shifts.

(*ii*) The c.m.c. shows little variation (ca. 0.30–0.35 m) with temperature in the range ca. 30–60°C, is at a minimum around 30–50°C, and increases up to ca. 0.52 m at 123°C (see Fig. 5).

(*iii*) A second critical micelle concentration exists around 1.0 *m* potassium *n*-octanoate in deuterium oxide at ca. 30–40°C.

1. C. TANFORD. The hydrophobic effect. 2nd ed. Wiley, New York. 1980.
2. B. LINDMAN and H. WENNERSTRÖM. Top. Curr. Chem. **87**, 1 (1980).
3. A. BEN-NAIM. Hydrophobic interactions. Plenum Press, New York. 1980.
4. P. MUKERJEE. Ber. Bunsenges Phys. Chem. **82**, 931 (1978).
5. M. J. ROSEN. Surfactants and interfacial phenomena. John Wiley and Sons, New York. 1978.
6. P. MUKERJEE and K. J. MYSELS. Critical micelle concentrations of aqueous surfactant systems. Data Sevr. Natl. Bur. Stand. U.S., **36**, U.S. Dept. of Commerce, Washington, D.C. (1971).
7. E. RUKENSTEIN and R. NAGARAJAN. J. Phys. Chem. **85**, 3010 (1981).
8. K. J. MYSELS and P. MUKERJEE. Pure Appl. Chem. **51**, 1083 (1979).
9. F. Y. LO, B. M. ESCOTT, E. J. FENDLER, E. T. ADAMS, JR., R. D. LARSEN, and P. W. SMITH. J. Phys. Chem. **79**, 2609 (1975).
10. D. F. EVANS and P. J. WIGHTMAN. J. Colloid Interface Sci. **86**, 515 (1982).
11. H. KUNIEDA and K. SHINODA. J. Phys. Chem. **82**, 1710 (1978).
12. T. KLASON. NMR studies of solubilization, hydrocarbon chain motion and the state of water in amphiphile–water systems. The Royal Institute of Technology, Stockholm. 1983.
13. A. BOUSSAHA and H. J. ACHE. J. Phys. Chem. **85**, 2444 (1981).
14. K. M. KALE, E. L. CUSSLER, and D. F. EVANS. J. Phys. Chem. **84**, 593 (1980).
15. B. LINDMAN and B. BRUN. J. Colloid Interface Sci. **42**, 388 (1973).
16. G. PORTE, Y. POGGI, J. APPELL, and G. MARET. J. Phys. Chem. **88**, 5713 (1984).
17. R. T. ROBERTS and G. P. JONES. Mol. Cryst. Liq. Cryst. **17**, 281 (1972).
18. O. YAMAMOTO and M. YANAGISAWA. Anal. Chem. **42**, 1463 (1970).
19. N. MULLER and R. H. BIRKHAHN. J. Phys. Chem. **72**, 583 (1968).
20. J. N. PHILLIPS. Trans. Faraday Soc. **51**, 561 (1955).
21. H. GUSTAVSSON and B. LINDMAN. J. Chem. Soc. Chem. Commun. 93 (1973).
22. J. M. EMSLEY, F. FEENEY, and L. H. SUTCLIFFE. High resolution nuclear magnetic resonance spectroscopy. Vol. 2. Pergamon Press, London. 1966.
23. T. C. FARRAR and E. D. BECKER. Pulse and Fourier transform NMR. Academic Press, New York. 1971.
24. P. WHITE and G. C. BENSON. Trans. Faraday Soc. **55**, 1025 (1959).
25. A. HOLTZER and M. F. HOLTZER. J. Phys. Chem. **78**, 1442 (1974).
26. J. CLIFFORD and B. A. PETHICA. Trans. Faraday Soc. **60**, 1483 (1964).
27. J. M. CORKILL, J. F. GOODMAN, and J. WYER. Trans. Faraday Soc. **65**, 9 (1969).
28. H. INOUE and T. NAKAGAWA. J. Phys. Chem. **70**, 1108 (1966).
29. L. ODBERG, B. SVENS, and I. DANIELSSON. J. Colloid Interface Sci. **41**, 298 (1972).
30. E. J. FENDLER, V. G. CONSTEIN, and J. H. FENDLER. J. Phys. Chem. **79**, 917 (1975).
31. B. LINDMAN *In* NMR of newly accessible nuclei. Vol. 1. *Edited by* P. Laszlo. Academic Press, New York. 1983.
32. H. GUSTAVSSON and B. LINDMAN. J. Am. Chem. Soc. **97**, 3923 (1975).
33. M. EISENSTADT and H. L. FRIEDMAN. J. Chem. Phys. **44**, 1407 (1966).
34. N. A. MAZER, M. C. CAREY, and G. B. BENEDEK. *In* Micellization, solubilization and microemulsions. Vol. 1. *Edited by* K. L. Mittal. Plenum Press, New York. 1977. p. 359.
35. N. A. MAZER and G. OLOFSSON. J. Phys. Chem. **86**, 4584 (1982).
36. P. MUKERJEE. *In* Micellization, solubilization and microemulsions. Vol. 1. *Edited by* K. L. Mittal. Plenum Press, New York. 1977. p. 171.
37. S. IKEDA. J. Phys. Chem. **88**, 2144 (1984).
38. G. PORTE, J. APPELL, and Y. POGGI. J. Phys. Chem. **84**, 3105 (1980).
39. A. FLAMBERG and R. PECORA. J. Phys. Chem. **88**, 3026 (1984).
40. E. LESSNER and J. FRAHM. J. Phys. Chem. **86**, 3032 (1982).
41. B. FORREST and L. W. REEVES. Chem. Rev. **81**, 1 (1981).
42. L. W. REEVES. Isr. J. Chem. **23**, 363 (1983).
43. J. ULMIUS and H. WENNERSTRÖM. J. Magn. Reson. **28**, 309 (1977).
44. U. HENDRIKSSON, L. ÖDBERG, J. C. ERIKSSON, and L. WESTMAN. J. Phys. Chem. **81**, 76 (1977).
45. G. LINDBLOM, B. LINDMAN, and L. MANDELL. J. Colloid Interface Sci. **42**, 400 (1973).
46. N. MÜLLER and F. E. PLATKO. J. Phys. Chem. **75**, 547 (1971).
47. B. PERSSON, T. DRAKENBERG, and B. LINDMAN. J. Phys. Chem. **80**, 2124 (1976).
48. B. PERSSON, T. DRAKENBERG, and B. LINDMAN. J. Phys. Chem. **83**, 3011 (1979).
49. T. ZEMB, M. DRIFFORD, M. HAYOUN, and A. JEHANNO. J. Phys. Chem. **87**, 4524 (1983).
50. B. LINDMAN, N. KAMENKA, M. PUYAL, B. BRUN, and B. JÖNSSON. J. Phys. Chem. **88**, 53 (1984).
51. B. HALLE and G. CARLSTRÖM. J. Phys. Chem. **85**, 2142 (1981).

Structure and conformation of the *N*-β-propionic acids of cyclohexan[*b*]indole and cyclooctan[*b*]indole

CARMEN ESTEBAN-CALDERON, MARTÍN MARTINEZ-RIPOLL, AND SEVERINO GARCÍA-BLANCO
Departamento de Cristalografía, Instituto Rocasolano, Consejo Superior de Investigaciones Científicas, Serrano, 119, Madrid-6, Spain

AND

FERNANDO TEMPRANO AND JOSÉ GONZALO RODRIGUEZ[1]
Departamento de Química Orgánica, Universidad Autonoma de Madrid, Canto Blanco, 28049-Madrid, Spain

Received July 16, 1984[2]

CARMEN ESTEBAN-CALDERON, MARTÍN MARTINEZ-RIPOLL, SEVERINO GARCÍA-BLANCO, FERNANDO TEMPRANO, and JOSÉ GONZALO RODRIGUEZ. Can. J. Chem. **64**, 1829 (1986).

The structures of cyclohexan[*b*]indole *N*-β-propionic acid (**1**) and cyclooctan[*b*]indole *N*-β-propionic acid (**2**) have been determined by X-ray methods. The conformational populations of their *N*-β-propionic chains have been determined in solution by ^{1}H nmr analyses. Crystals of **1** are triclinic, space group $P\bar{1}$, with a = 12.3562(4), b = 11.0727(3), c = 10.2050(4) Å, α = 108.519(3), β = 83.941(3), γ = 104.826(3)°, and Z = 4. Crystals of **2** are monoclinic, space group $P2_1/c$, with a = 5.636(1), b = 18.937(3), c = 13.976(4) Å, β = 98.84(3)°, and Z = 4. In both structures, the molecules are linked forming dimers through centrosymmetric H bonds. In solution the *trans* conformation of the chain is the preferred one in both compounds and increases with dilution until a constant value is reached.

CARMEN ESTEBAN-CALDERON, MARTÍN MARTINEZ-RIPOLL, SEVERINO GARCÍA-BLANCO, FERNANDO TEMPRANO et JOSÉ GONZALO RODRIGUEZ. Can. J. Chem. **64**, 1829 (1986).

On a déterminé par cristallographie de rayons-X les structures des acides cyclohexan[*b*]indole (**1**) et cyclooctan[*b*]indole (**2**) *N*-β-propioniques et les populations conformationelles de la chaine *N*-β-propionique en solution par rmn ^{1}H. Les cristaux de l'acide **1** sont tricliniques et appartiennent au groupe d'espace $P\bar{1}$ avec a = 12,3562(4), b = 11,0727(3), c = 10,2050(4) Å, α = 108,519(3), β = 83,941(3), γ = 104,826(3)° et Z = 4. Les cristaux de l'acide **2** sont monocliniques et appartiennent au groupe d'espace $P2_1/c$ avec a = 5,636(1), b = 18,937(3), c = 13,976(4) Å, β = 98,84(3)° et Z = 4. L'empaquetement moleculaire presente des dimeres avec des liaisons hydrogènes vers les centres d'inversion. En solution, la conformation *trans* est la préférée en **1** et **2** et elle augmente avec la dilution jusqu'à un valeur constante.

[Traduit par la revue]

Cycloalkan[*b*]indole *N*-β-propionic acids are potential anti-inflammatory drugs, structurally related to Indomethazin. Moreover, the *N*-γ-aminopropyl derivatives of the cycloalkan[*b*]indoles have antidepressant action.[3] Structures of this type of compound are analyzed to correlate the sizes of the cycloalkane rings with their particular action. The conformational analysis of the *N*-β-propionic acid chain in solution is also interesting, to verify the implication of the bulk of cycloalkane ring versus the conformational equilibrium of the chain.

Experimental

Synthesis

Cyclohexan[b]indole and cyclooctan[b]indole

These compounds were synthesized by thermal reaction (in ethylene glycol) of the phenylhydrazone of the cyclohexanone, 90%, mp 114–115°C, and of the phenylhydrazone of the cyclooctanone, 88%, mp 72–73°C, respectively.

Acids **1** and **2** were prepared by addition of acrylonitrile to an ethereal solution of sodium hydride with the respective cycloalkan[*b*]indole, followed by nitrile hydrolysis and recrystallization; 48%, mp 113–116°C for **1** and 52%, mp 134–135°C for **2**. Crystals of **1** and **2** were formed by slow evaporation at 5°C of an ethanolic solution.

X-ray structure determination

Compound 1

$C_{15}H_{19}O_2N$ Mr = 245.4

V = 1279.4(1) Å^3, D_c = 1.27 g cm^{-3}, $F(000)$ = 527, θ_{max} = 60°, prismatic colorless crystals, 0.25 × 0.20 × 0.10 mm.

Compound 2

$C_{17}H_{21}O_2N$ Mr = 271.4

V = 1474(1) Å^3, D_c = 1.22 g cm^{-3}, $F(000)$ = 584, θ_{max} = 65°, prismatic colorless crystals, 0.20 × 0.15 × 0.10 mm.

A four-circle automatic Pw 1100 diffractometer with graphite monochromated CuKα radiation (λ = 1.5418 Å) and ω/2θ scan were used to collect the intensities of 3792 independent reflections for **1** and 2705 for **2**. Cell constants, as given in the abstract, were obtained by least-squares fit of 30 reflections with high angles, measured for both positive and negative Bragg angles. Two standard reflections, monitored every 90 min, showed no crystal decomposition. In reducing the data, Lorentz and polarization factors were applied, but no corrections for absorption were made. 2639 reflections for **1** and 1658 for **2** were considered as observed with the criterion $I > 3\sigma(I)$.

Both structures were solved using MULTAN (1). The usual sequence of isotropic and anisotropic refinement was followed, after which all H atoms were located on difference maps. A weighting scheme of the type $w = w_1 \cdot w_2$ was used to prevent bias on $\langle w \cdot \Delta^2 F \rangle$ vs. $\langle F_o \rangle$ and vs. $\langle \sin\theta/\lambda \rangle$, with $w_1 = K/(a + b|F_o| + c|F_o|^2)^2$ and $w_2 = 1/(d + e \sin\theta/\lambda)$ (2). Final full-matrix (3) anisotropic weighted refinement (isotropic fixed parameters for H atoms) gave the discrepancy indices R = 0.050, $R\omega$ = 0.054 for **1** and R = 0.047, $R\omega$ = 0.056 for **2**. Scattering factors for neutral atoms (4) were used in both cases. Final atomic parameters are shown in Tables 1 and 2.[4]

Bond lengths, bond angles, least-squares planes, and torsional angles for **1** and **2** are given in Tables 3–10. The atomic labelling for both compounds is shown in Figs. 1((*a*) and (*b*)) and 2.

[1]Author to whom correspondence may be addressed.

[2]Revision received May 7, 1986.

[3]J. G. Rodriguez and F. Temprano, unpublished results.

[4]Tables of observed and calculated structure factors, coefficients of the weighting scheme, atomic and thermal parameters, and the bond angles and bond distances involving H atoms, for **1** and **2**, have been deposited as supplementary material, and may be purchased from the Depository of Unpublished Data, CISTI, National Research Council of Canada, Ottawa, Ont., Canada K1A 0S2.

TABLE 1. Atomic parameters for $C_{15}H_{19}O_2N$

Atom	x/a	y/b	z/c	U_{eq}[a]
N(11)	0.1256(2)	0.4485(3)	0.4147(3)	40(1)
C(12)	0.0648(3)	0.3701(4)	0.2977(4)	42(2)
C(13)	0.0088(3)	0.2541(4)	0.3177(4)	43(2)
C(14)	−0.0020(4)	0.1711(4)	0.5312(5)	58(2)
C(14A)	0.0327(3)	0.2583(4)	0.4530(4)	43(2)
C(15)	0.0386(4)	0.2069(5)	0.6625(5)	68(2)
C(16)	0.1119(4)	0.3291(5)	0.7182(4)	65(2)
C(17)	0.1468(3)	0.4183(4)	0.6439(4)	51(2)
C(17A)	0.1059(3)	0.3811(4)	0.5111(4)	41(2)
C(18)	0.0628(3)	0.4096(4)	0.1718(4)	52(2)
C(19)	−0.0335(4)	0.3120(5)	0.0806(4)	64(2)
C(110)	−0.0370(4)	0.1709(5)	0.0685(5)	68(2)
C(111)	−0.0635(4)	0.1459(4)	0.2088(5)	62(2)
C(112)	0.1924(3)	0.5826(4)	0.4343(4)	47(2)
C(113)	0.3051(3)	0.5881(4)	0.3580(4)	46(2)
C(114)	0.3897(3)	0.5495(3)	0.4217(4)	42(2)
O(115)	0.4761(2)	0.5285(3)	0.3394(3)	59(1)
O(116)	0.3809(2)	0.5404(3)	0.5380(3)	57(1)
N(21)	0.2911(2)	0.0221(3)	0.1568(3)	41(1)
C(22)	0.3192(3)	0.0969(4)	0.0657(4)	41(2)
C(23)	0.3536(3)	0.0244(4)	−0.0581(4)	41(2)
C(24)	0.3688(3)	−0.2187(4)	−0.1423(4)	49(2)
C(24A)	0.3468(3)	−0.1028(4)	−0.0485(4)	40(1)
C(25)	0.3479(4)	−0.3288(4)	−0.0998(4)	58(2)
C(26)	0.3052(4)	−0.3269(4)	0.0336(4)	56(2)
C(27)	0.2839(3)	−0.2139(4)	0.1291(4)	50(2)
C(27A)	0.3067(3)	−0.1024(4)	0.0864(4)	39(1)
C(28)	0.3096(4)	0.2352(4)	0.1000(4)	56(2)
C(29)	0.3378(7)	0.2804(6)	−0.0260(6)	129(4)
C(210)	0.3626(9)	0.2075(6)	−0.1478(7)	165(5)
C(211)	0.3867(4)	0.0765(4)	−0.1799(4)	58(2)
C(212)	0.2396(3)	0.0625(4)	0.2943(4)	50(2)
C(213)	0.3244(4)	0.1510(4)	0.4046(4)	57(2)
C(214)	0.3996(4)	0.0820(4)	0.4438(4)	49(2)
O(215)	0.4988(3)	0.1499(3)	0.4788(3)	64(1)
O(216)	0.3662(3)	−0.0333(3)	0.4449(3)	61(1)

[a]Thermal parameters as: $U_{eq} = (1/3)\Sigma[U_{ij}\cdot a_i^*\cdot a_j^*\cdot a_i\cdot a_j\cdot\cos(a_i\cdot a_j)] \times 10^3$.

TABLE 2. Atomic parameters for $C_{17}H_{21}O_2N$

Atom	x/a	y/b	z/c	U_{eq}
N(1)	0.6158(3)	0.2277(1)	0.0339(1)	444(6)
C(2)	0.3996(4)	0.2088(1)	−0.0231(2)	436(7)
C(3)	0.2919(4)	0.1564(1)	0.0217(2)	432(6)
C(4)	0.4315(5)	0.0944(1)	0.1880(2)	526(8)
C(4A)	0.4444(4)	0.1416(1)	0.1117(2)	420(7)
C(5)	0.6183(5)	0.0928(1)	0.2650(2)	591(9)
C(6)	0.8171(5)	0.1369(1)	0.2667(2)	577(8)
C(7)	0.8332(4)	0.1847(1)	0.1935(2)	516(7)
C(7A)	0.6446(4)	0.1869(1)	0.1168(2)	423(6)
C(8)	0.3251(5)	0.2366(1)	−0.1231(2)	544(8)
C(9)	0.4294(5)	0.1940(2)	−0.2000(2)	620(9)
C(10)	0.4111(6)	0.1128(2)	−0.1911(2)	712(10)
C(11)	0.1572(6)	0.0845(2)	−0.1911(2)	718(10)
C(12)	0.1035(5)	0.0593(1)	−0.0920(2)	605(9)
C(13)	0.0684(4)	0.1175(1)	−0.0200(2)	526(8)
C(14)	0.7689(4)	0.2866(1)	0.0164(2)	486(7)
C(15)	0.6921(5)	0.3545(1)	0.0610(2)	554(8)
C(16)	0.8375(5)	0.4172(1)	0.0395(2)	503(8)
O(17)	0.7539(4)	0.4773(1)	0.0666(2)	804(9)
O(18)	1.0156(4)	0.4131(1)	0.0008(2)	661(7)

[a]Thermal parameters as: $U_{eq} = (1/3)\Sigma[U_{ij}\cdot a_i^*\cdot a_j^*\cdot a_i\cdot a_j\cdot\cos(a_i, a_j)] \times 10^4$.

Discussion

Cyclohexan[b]indole N-*β-propionic acid* ***1***

The bond lengths and bond angles in the two independent molecules can be analyzed together. The average of the C(sp^2)—C(sp^2) indole nucleus distances are 1.398(6) in molecule 1 and 1.397(6) Å in molecule 2. The common fused bonds C(12)—C(13) = 1.361(6) and C(22)—C(23) = 1.357(5) Å are the shortest distances, the C(13)—C(14A) = 1.427(6) and C(23)—C(24A) = 1.423(6) Å being the longest ones within the pyrrole rings. N(11)—C(12) = 1.393(4), N(21)—C(22) = 1.395(5) and N(11)—C(17A) = 1.381(6), N(21)—C(27A) = 1.389(5) Å are between single and double bond lengths, although the latter are slightly shorter than the former. The indole fragment is planar within experimental error, Table 5.

The average of the C(sp^3)—C(sp^3) cyclohexene ring is 1.530(7) (here only molecule 1 is considered), while C(sp^3)—C(sp^2) bond lengths are 1.499(6) Å in molecule 1 and 1.500(6) Å in molecule 2. Moreover, bond lengths C(13)—C(111) = 1.511(5) and C(12)—C(18) = 1.487(7) Å within the cyclohexane ring of molecule 1 are differently affected by the electronegative N(11)—C(12) bond. Similar differences were observed in molecule 2, 1.508(6) vs. 1.492(6) Å.

The cyclohexene ring in molecule 1 is in a half-chair conformation, which seems the most stable from inspection of mechanical models, and it is the only one observed in the crystal structures (5).

Conformation of the cyclohexene ring in molecule 2 cannot be properly analyzed because of a disorder problem affecting the atoms C(29) and C(210). The electron density profiles for C(29) and C(210) are very broad, having maxima corresponding to the coordinates where those atoms were located. The temperature factors of these two atoms and the fact that only one H atom appears attached to each of them, confirms a disorder in which the atomic positions found are actually the average of the positions given by two different "half-chair" conformations.

Conformational site exchange in the liquid state is assumed to proceed via a "boat" intermediate conformation. The energy barrier has been calculated by dynamic nmr to be 22.6 kJ/mol for partially deuterated cyclohexene (6). Cyclohexene on the indole ring should be examined, but care must be exercised in extrapolating the conclusions to cyclohexene derivatives, since the torsional barrier in the C—C bond adjoining the pyrrole ring is close to zero. These energy requirements for the conformational equilibrium through a boat intermediate seem not to be present in 2 in the solid state, and thus alternative "half-chair" conformers in the crystal can be considered as contributing to the disorder.

The *N*-β-propionic chains of both molecules show *gauche* conformations (Fig. 1). The molecules are packed forming dimers through centrosymmetric hydrogen bonds, their geometrical features being presented in Table 3.

Cyclooctan[b]indole N-*β-propionic acid* ***2***

The average of the C(sp^2)—C(sp^2) bond lengths within the indole nucleus is 1.395(3) Å. This molecule shows identical relationships between bond distances, in the pyrrole ring, to the ones reported above for the cyclohexan[*b*]indole. The average of the C(sp^3)—C(sp^3) bond lengths in the cyclooctene ring is

TABLE 3. Bond lengths (Å) for **1**. Standard deviations in parentheses

Bond	Length	
	$X = 1$	$X = 2$
N(X1)—C(X2)	1.393(4)	1.395(5)
N(X1)—C(X7A)	1.381(6)	1.389(5)
N(X1)—C(X12)	1.465(5)	1.461(5)
C(X2)—C(X3)	1.361(6)	1.357(5)
C(X2)—C(X8)	1.487(7)	1.492(6)
C(X3)—C(X4A)	1.427(6)	1.423(6)
C(X3)—C(X11)	1.511(5)	1.508(6)
C(X4)—C(X4A)	1.400(7)	1.407(5)
C(X4)—C(X5)	1.381(7)	1.376(7)
C(X4A)—C(X7A)	1.411(5)	1.412(5)
C(X5)—C(X6)	1.403(6)	1.403(6)
C(X6)—C(X7)	1.388(7)	1.387(6)
C(X7)—C(X7A)	1.394(6)	1.390(6)
C(X8)—C(X9)	1.545(5)	1.500(8)
C(X9)—C(X10)	1.517(8)	1.303(9)
C(X10)—C(X11)	1.529(7)	1.483(10)
C(X12)—C(X13)	1.519(5)	1.532(5)
C(X13)—C(X14)	1.500(7)	1.498(8)
C(X14)—O(X15)	1.308(5)	1.282(5)
C(X14)—O(X16)	1.214(5)	1.240(6)

Hydrogen bonds

A—H....B	A.....B	A—H	H....B	∠A—H....B
O(115)—H(115)...O(116)^{I}	2.651(5) Å	0.81(6) Å	1.84(6) Å	175(4)°
O(215)—H(215)...O(216)^{II}	2.660(5)	0.97(6)	1.69(6)	175(4)

Symmetry operations

I $1 - x, 1 - y, 1 - z$ II $1 - x, -y, 1 - z$

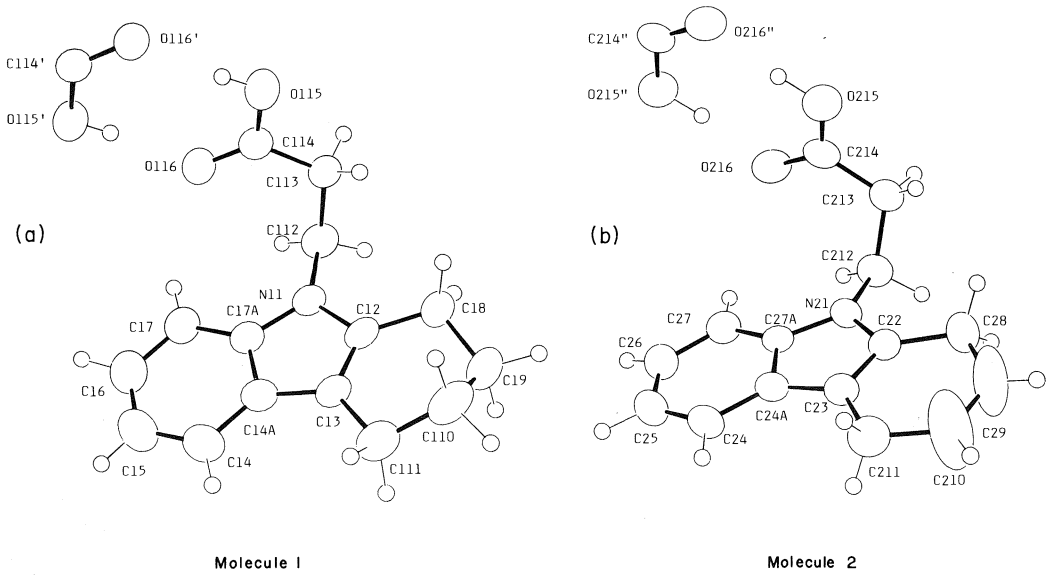

FIG. 1. Atomic labelling (a) for molecule 1; (b) for molecule 2 of compound **1**.

TABLE 4. Bond angles (°) for **1**. Standard deviations in parentheses

Bonds	Angle	
	$X = 1$	$X = 2$
C(X2)—N(X1)—C(X7A)	108.2(3)	107.7(3)
C(X2)—N(X1)—C(X12)	125.3(4)	125.4(3)
C(X7A)—N(X1)—C(X12)	126.3(3)	126.3(3)
C(X3)—C(X2)—N(X1)	109.4(4)	109.9(4)
C(X3)—C(X2)—C(X8)	126.3(3)	125.6(4)
N(X1)—C(X2)—C(X8)	124.3(3)	124.5(3)
C(X2)—C(X3)—C(X4A)	107.6(3)	107.6(4)
C(X2)—C(X3)—C(X11)	122.7(4)	122.8(4)
C(X4A)—C(X3)—C(X11)	129.7(4)	129.6(3)
C(X4A)—C(X4)—C(X5)	118.8(4)	118.5(4)
C(X3)—C(X4A)—C(X4)	133.9(3)	133.7(4)
C(X3)—C(X4A)—C(X7A)	106.8(4)	107.1(3)
C(X4)—C(X4A)—C(X7A)	119.4(4)	119.2(4)
C(X4)—C(X5)—C(X6)	121.0(5)	121.2(4)
C(X5)—C(X6)—C(X7)	121.6(4)	121.7(4)
C(X6)—C(X7)—C(X7A)	117.1(3)	116.9(4)
C(X7)—C(X7A)—C(X4A)	122.2(4)	122.4(3)
N(X1)—C(X7A)—C(X4A)	107.9(3)	107.7(4)
N(X1)—C(X7A)—C(X7)	129.9(3)	129.8(3)
C(X2)—C(X8)—C(X9)	108.5(4)	109.6(4)
CX(8)—C(X9)—C(X10)	112.1(4)	124.8(6)
C(X9)—C(X10)—C(X11)	111.1(4)	126.1(7)
C(X3)—C(X11)—C(X10)	109.7(4)	110.0(4)
N(X1)—C(X12)—C(X13)	112.9(3)	113.0(3)
C(X12)—C(X13)—C(X14)	114.7(4)	114.5(4)
C(X13)—C(X14)—O(X15)	112.9(4)	116.1(4)
C(X13)—C(X14)—O(X16)	124.2(4)	121.4(4)
O(X15)—C(X14)—O(X16)	122.9(4)	122.5(5)

TABLE 5. Atomic deviations (Å) from least-squares planes in **1**[a]

Atom	Deviation	
	$X = 1$	$X = 2$
N(X1)	0.000(3)	−0.015(3)
C(X2)	−0.010(4)	0.028(4)
C(X3)	0.008(4)	0.018(4)
C(X4)	−0.010(5)	−0.017(4)
C(X4A)	0.007(4)	−0.017(4)
C(X5)	−0.002(5)	0.005(5)
C(X6)	0.000(5)	0.032(5)
C(X7)	0.001(4)	0.015(4)
C(X7A)	0.002(4)	−0.027(4)
*C(X8)	−0.035(4)	0.107(5)
*C(X9)	−0.366(5)	0.251(9)
*C(X10)	0.420(5)	0.344(10)
*C(X11)	0.030(5)	0.096(5)
*C(X12)	−0.073(4)	0.124(4)
*C(X13)	1.252(4)	−1.179(5)
*C(X14)	2.279(4)	−2.224(5)
*O(X15)	3.480(3)	−3.443(3)
*O(X16)	2.032(3)	−1.918(3)

[a]Reference 12. Atoms marked with asterisks are not included in the calculations; e.s.d.'s in parentheses.

TABLE 6. Torsional angles (°) for **1**; e.s.d.'s in parentheses

Bonds	Angles	
	$X = 1$	$X = 2$
N(X1)—C(X2)—C(X3)—C(X4A)	1.0(4)	0.7(4)
C(X2)—C(X3)—C(X4A)—C(X4)	178.3(5)	178.6(4)
C(X3)—C(X4A)—C(X4)—C(X5)	179.8(4)	−177.0(4)
C(X4A)—C(X4)—C(X5)—C(X6)	1.0(7)	0.3(6)
C(X4)—C(X5)—C(X6)—C(X7)	−0.3(8)	−1.2(7)
C(X5)—C(X6)—C(X7)—C(X7A)	−0.1(7)	0.2(6)
C(X6)—C(X7)—C(X7A)—N(X1)	179.9(4)	178.0(4)
C(X7)—C(X7A)—N(X1)—C(X2)	−179.5(4)	−175.6(4)
C(X7A)—N(X1)—C(X2)—C(X8)	179.0(4)	177.5(4)
N(X1)—C(X2)—C(X8)—C(X9)	−167.1(3)	−175.3(4)
C(X2)—C(X8)—C(X9)—C(X10)	−44.6(5)	2.4(9)
C(X8)—C(X9)—C(X10)—C(X11)	64.6(5)	−11.1(1)
C(X9)—C(X10)—C(X11)—C(X3)	−47.0(5)	12.6(9)
C(X10)—C(X11)—C(X3)—C(X4A)	−164.0(4)	170.3(5)
C(X2)—N(X1)—C(X12)—C(X13)	−78.3(4)	−81.6(4)
N(X1)—C(X12)—C(X13)—C(X14)	−74.0(4)	−72.1(5)
C(X12)—C(X13)—C(X14)—O(X16)	−14.7(6)	−33.7(6)
C(X9)—C(X8)—C(X2)—C(X3)	12.9(6)	
C(X10)—C(X11)—C(X3)—C(X2)	15.8(6)	

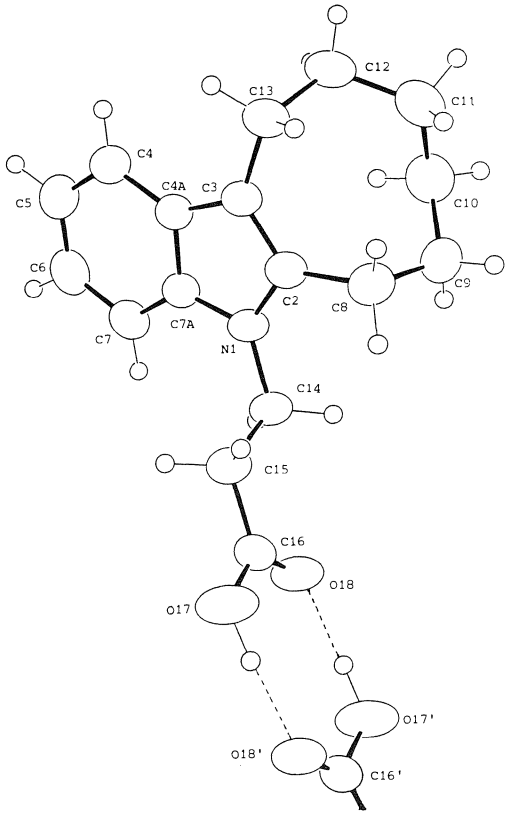

FIG. 2. Atomic labelling of compound **2** showing the *trans* conformation of the *N*-β-propionic chain.

1.534(4) Å, while the C(sp^3)—C(sp^2) are the shortest bond lengths C(2)—C(8) = 1.492(3) and C(3)—C(13) = 1.497(3) Å. The indole fragment is planar within experimental error and atomic deviations from the least-squares plane are given in Table 9. These values from Tables 5 and 9 are in good

TABLE 7. Bond lengths (Å) for **2**; e.s.d.'s in parentheses

Bond	Length	Bond	Length
N(1)—C(2)	1.396(3)	C(6)—C(7)	1.380(4)
N(1)—C(7A)	1.382(3)	C(7)—C(7A)	1.389(3)
N(1)—C(14)	1.454(3)	C(8)—C(9)	1.531(4)
C(2)—C(3)	1.365(3)	C(9)—C(10)	1.549(4)
C(2)—C(8)	1.492(3)	C(10)—C(11)	1.528(5)
C(3)—C(4A)	1.438(3)	C(11)—C(12)	1.537(4)
C(3)—C(13)	1.497(3)	C(12)—C(13)	1.526(4)
C(4)—C(4A)	1.402(3)	C(14)—C(15)	1.522(3)
C(4)—C(5)	1.385(3)	C(15)—C(16)	1.500(4)
C(4A)—C(7A)	1.410(3)	C(16)—O(17)	1.310(3)
C(5)—C(6)	1.394(4)	C(16)—O(18)	1.214(4)

Hydrogen bonds

A—H.....B	A...B	A—H	H...B	∠A—H...B
O(17)—H(17)...O(18)[I]	2.693(3) Å	0.98(4) Å	1.71(4) Å	176(3)°

Symmetry operation
I $2-x, 1-y, -z$

TABLE 8. Bond angles (°) for **2**; e.s.d.'s in parentheses

Bonds	Angle	Bonds	Angle
C(2)—N(1)—C(7A)	108.4(2)	C(6)—C(7)—C(7A)	117.5(2)
C(2)—N(1)—C(14)	126.1(2)	C(4A)—C(7A)—C(7)	122.2(2)
C(7A)—N(1)—C(14)	125.1(2)	C(4A)—C(7A)—N(1)	107.9(2)
C(3)—C(2)—N(1)	109.6(2)	C(7)—C(7A)—N(1)	129.9(2)
C(3)—C(2)—C(8)	127.3(2)	C(2)—C(8)—C(9)	112.9(2)
C(8)—C(2)—N(1)	122.6(2)	C(8)—C(9)—C(10)	115.4(2)
C(2)—C(3)—C(4A)	107.2(2)	C(9)—C(10)—C(11)	115.0(3)
C(2)—C(3)—C(13)	125.9(2)	C(10)—C(11)—C(12)	115.0(2)
C(4A)—C(3)—C(13)	126.8(2)	C(11)—C(12)—C(13)	115.7(2)
C(4A)—C(4)—C(5)	118.9(2)	C(3)—C(13)—C(12)	115.2(2)
C(3)—C(4A)—C(4)	134.1(2)	C(15)—C(14)—N(1)	111.5(2)
C(3)—C(4A)—C(7A)	107.0(2)	C(14)—C(15)—C(16)	112.9(2)
C(4)—C(4A)—C(7A)	118.9(2)	O(17)—C(16)—O(18)	122.9(2)
C(4)—C(5)—C(6)	120.9(2)	O(17)—C(16)—C(15)	113.5(2)
C(5)—C(6)—C(7)	121.6(2)	O(18)—C(16)—C(15)	123.6(2)

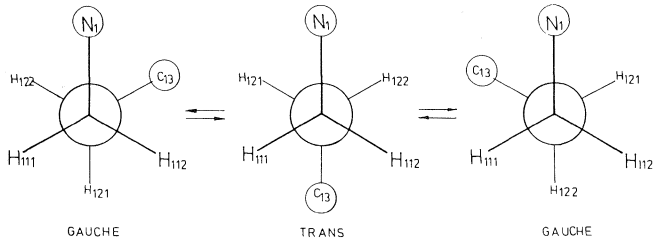

FIG. 3. Newman representations of the staggered conformers.

agreement with those appearing in 3-methylindole (7) and iprindole (8).

While "boat-chair" and "crown" conformations have been experimentally found for the cyclooctane ring in X-ray structure determinations (5), there are only a few examples of a cyclooctene ring in the crystallographic literature. The preferred conformation of a cylooctene system is not known with certainty. The most stable conformation was calculated to be an unsymmetrical structure related to the cylooctane "boat–chair" (9). The *cis* cyclooctene ring shows a twisted boat conformation in this compound under investigation. The torsional angles defining the conformation of this ring are given in Table 10. They are in good agreement with those reported for iprindole (8) and for the *cis*-9,9-dimethyl-9-azoniabicyclo[6,1,0]nonane ion (10).

The *N*-β-propionic chain in Fig. 2 shows the fully extended *trans* conformation. The molecular packing of this compound is also due to centrosymmetric hydrogen bonds, forming dimers (Table 7).

Conformational ^1H nmr analysis

An interesting aspect of the present investigation is the conformational analysis of the *N*-β-propionic chain in **1** and **2**, since this may well be relevant to the mode of action of these compounds.

^1H nuclear magnetic resonance analysis of the cycloalkan[*b*]indole *N*-β-propionic acids has been done, in deuterated

TABLE 9. Atomic deviations from least-squares (Å) plane in **2**[a]

Atom	Deviation
N(1)	−0.006(2)
C(2)	0.007(2)
C(3)	0.016(1)
C(4)	−0.014(3)
C(4A)	−0.007(2)
C(5)	−0.003(3)
C(6)	0.024(3)
C(7)	0.009(3)
C(7A)	−0.017(2)
*C(8)	0.178(3)
*C(9)	1.647(3)
*C(10)	2.585(3)
*C(11)	2.168(3)
*C(12)	1.572(3)
*C(13)	0.150(3)
*C(14)	−0.167(2)

[a]Reference 12. Atoms marked with asterisks are not included in the calculations; e.s.d.'s in parentheses.

TABLE 10. Torsion angles (°) for **2**. e.s.d.'s in parentheses

Bonds	Angle
N(1)—C(2)—C(3)—C(4A)	0.6(3)
C(2)—C(3)—C(4A)—C(4)	179.8(3)
C(3)—C(4A)—C(4)—C(5)	178.4(2)
C(4A)—C(4)—C(5)—C(6)	−0.4(4)
C(4)—C(5)—C(6)—C(7)	1.5(5)
C(5)—C(6)—C(7)—C(7A)	−0.8(4)
C(6)—C(7)—C(7A)—N(1)	−178.3(2)
C(7)—C(7A)—N(1)—C(2)	177.8(2)
C(7A)—N(1)—C(2)—C(8)	−172.8(2)
N(1)—C(2)—C(8)—C(9)	84.8(3)
C(2)—C(8)—C(9)—C(10)	45.8(3)
C(8)—C(9)—C(10)—C(11)	56.1(4)
C(9)—C(10)—C(11)—C(12)	−106.0(3)
C(10)—C(11)—C(12)—C(13)	74.4(3)
C(11)—C(12)—C(13)—C(3)	−71.7(3)
C(12)—C(13)—C(3)—C(4A)	−94.8(3)
C(2)—N(1)—C(14)—C(15)	86.8(3)
N(1)—C(14)—C(15)—C(16)	−176.7(2)
C(14)—C(15)—C(16)—O(18)	−8.4(4)
C(9)—C(8)—C(2)—C(3)	−86.1(3)
C(12)—C(13)—C(3)—C(2)	79.2(3)

TABLE 11. Conformational equilibrium of the *N*-β-propionic acid chain of the cycloalkane[*b*]indoles

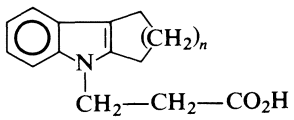

	n = 1			n = 2			n = 3			n = 4		
C (mol L^{-1})	N	n_t (%)	ΔE[a]	N	n_t (%)	ΔE	N	n_t (%)	ΔE	N	n_t (%)	ΔE
0.66	13.84	38	0.15	14.82	55	0.54	14.82	55	0.54	15.27	63	0.73
0.33	14.08	42	0.23	15.08	60	0.65	14.82	55	0.54	15.30	64	0.74
0.16	14.09	42	0.23	15.08	60	0.65	15.07	60	0.64	15.31	64	0.75
0.08	14.33	47	0.33	15.08	60	0.65	15.08	60	0.65	15.32	64	0.75

[a]ΔE in kcal mol^{-1}; $N/2$ (Hz) = J_{AB}.

chloroform solution, to observe the influence of the bulky cycloalkane substitution and of dilution on the conformational equilibrium populations of the *N*-β-propionic acid chain. Thus, cyclopentan-, cylclohexan- (**1**), cycloheptan-, and cyclooctan[*b*]indole (**2**) *N*-β-propionic acids show, in all cases, two triplet signals of A_2B_2 type for the two methylenes of the chain, a complex multiplet of the methylenes of the cycloalkane ring, and a low-field half broadened signal due to the long range coupling with the aromatic protons.

Newman representations of the staggered conformers are shown in Fig. 3. The two *gauche* forms are mirror images and hence of equal energy. The observed value of J_{AB} is then simply obtained as the weighted average of the values in the *trans* (J_t) and *gauche* (J_g) conformations according to a method previously reported (11), with

$$J_{AB} = n_g J_g + n_t J_t$$

$$n_g + n_t = 1$$

$$\Delta E = E_g - E_t = RT \ln 2(J_{AB} - J_g)/(J_t - J_{AB})$$

where n_t and n_g are the populations of the *trans* and *gauche* conformers respectively, ΔE being the excess of energy (strictly free energy) of the *gauche* form. J_t and J_g are experimental values observed in compounds that are entirely in the *trans* (8.68 Hz) and *gauche* (5.38 Hz) conformations, respectively (11). Thus, n_g, n_t, and ΔE can be deduced for the cycloalkan[*b*]indole *N*-β-propionic acids and are given in Table 11. It is remarkable that the conformational equilibrium of the chain of the cycloalkan[*b*]indole *N*-β-propionic acids in solution is displaced to the *trans* conformation, and this is more evident with the bulk of the cycloalkane. Moreover, this equilibrium in all cases remains practically constant with dilution.

1. P. MAIN *et al.* MULTAN 80, A system of computer programs for the automatic solution of the crystal structure from X-ray diffraction data. University of York, England. 1980.
2. M. MARTINEZ-RIPOLL and F. H. CANO. Pesos program, Instituto Rocasolano CSIC, Serrano 119, Madrid-6, Spain.
3. J. M. STEWART *et al.* The XRAY 76 system. Computer Science Center, University of Maryland, College Park, MD. 1976.

4. INTERNATIONAL TABLES FOR X-RAY CRYSTALLOGRAPHY. Vol. IV. Kynoch Press, Birmingham. 1974. p. 72.
5. J. DALES. Stereochemistry and conformational analysis. Verlag Chemie, New York. 1978.
6. F. A. L. ANET and M. Z. HAG. J. Am. Chem. Soc. **87**, 3147 (1965).
7. A. W. HANSON. Acta Crystallogr. **17**, 559 (1964).
8. J. R. RODGERS, O. KENNARD, A. S. HORN, and L. RIVA DI SANSEVERINO. Acta Crystallogr. Sect. B, **30**, 1970 (1974).
9. N. L. ALLINGER and J. T. SPRAGUE. J. Am. Chem. Soc. **94**, 5734 (1972).
10. J. M. TREFONAS and R. MAJESTE. Tetrahedron, **19**, 929 (1963).
11. R. J. ABRAHAM and G. GATTI. J. Chem. Soc. (B), 961 (1969).
12. M. NARDELLI, A. MUSATTI, P. DOMIANO, and G. ANDREETTI. **35**, 807 (1965).

Preparation of 2,2-diaryl-1-picrylhydrazyls using potassium permanganate

K. C. BROWN AND J. A. WEIL[1]

Department of Chemistry, University of Saskatchewan, Saskatoon, Sask., Canada S7N 0W0

Received March 26, 1986

K. C. BROWN and J. A. WEIL. Can. J. Chem. **64**, 1836 (1986).

Potassium permanganate is used as a reagent for the oxidation of various 2,2-diaryl-1-picrylhydrazines to their corresponding hydrazyls. Thin-layer chromatography indicates complete oxidation of the hydrazine to free radical, unlike the case with PbO_2 (the most widely used oxidant for this purpose). Several other advantages over previous oxidants used to produce the hydrazyls are offered.

K. C. BROWN et J. A. WEIL. Can. J. Chem. **64**, 1836 (1986).

On utilise le permanganate de potassium comme réactif pour effectuer l'oxydation de diverses diaryl-2,2 picryl-1 hydrazines en hydrazyles correspondants. La chromatographie en couches minces indique que l'oxydation de l'hydrazine en radical libre est complète; ce résultat diffère de ceux obtenus avec le PbO_2 qui est l'oxydant le plus fréquemment utilisé à cette fin. Cette méthode offre aussi plusieurs autres avantages par rapport aux oxydants utilisés antérieurement pour produire des hydrazyles.

[Traduit par la revue]

As part of our continuing investigations into the chemistry of 2,2-diphenyl-1-picrylhydrazyl radical ($DH_2\cdot$) and related substituted hydrazyl radicals (1), we have found that $KMnO_4$ is very efficient at oxidizing the parent hydrazines to their corresponding hydrazyls. Typically:

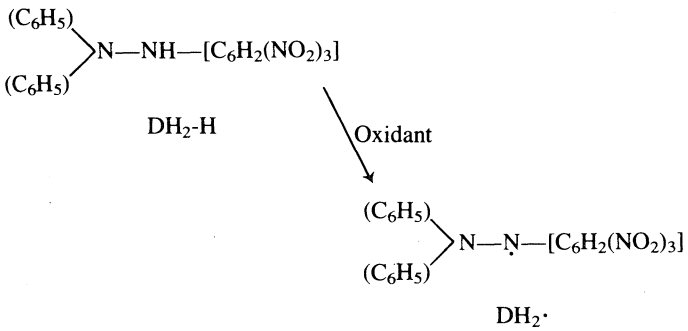

In the past, the most common oxidant for this purpose has been lead dioxide (2). Other oxidants used include benzoyl peroxide (3), oxygen (4), chromium oxides (5), and other radicals (6), although none of these has been used on a preparative scale. $DH_2\cdot$ has also been observed (7) to form electrochemically from DH_2-H. Until now, there appear to have been no reports of the above reaction using $KMnO_4$ as the oxidizing agent.

We have found that, although 2,2-diphenyl-1-picrylhydrazyl is produced in high yield using PbO_2, 2,2-di(*p*-nitrophenyl)-1-picrylhydrazyl ($D(NO_2)_2\cdot$) is not similarly produced in high yield, and that here considerable starting material is left. We attribute this to the fact that $D(NO_2)_2\cdot$ is less stable relative to its hydrazine than is $DH_2\cdot$: a solution of $D(NO_2)_2\cdot$ will revert immediately to $D(NO_2)_2$-H if DH_2-H is added, with formation of $DH_2\cdot$ (8). Moreover, a mixture of $D(NO_2)_2\cdot$ and $D(NO_2)_2$-H is quite difficult to purify. These compounds, unlike $DH_2\cdot$ and DH_2-H, cannot be easily passed through a preparative chromatography column since they are tenaciously adsorbed on the column material even when a highly polar solvent is used as the eluant. It is thus preferable in this case to attempt a crystallization directly from the crude product.

The consequence of these observations was a search for a stronger oxidant for $D(NO_2)_2$-H. Lead tetraacetate was found to be a suitably strong oxidant but presented purification problems. It is highly soluble in most organic solvents and therefore any excess is carried along with the hydrazyl produced, remaining in solution with it. The preparation of specially activated lead dioxide for the purpose of these oxidations is well known (2, 9), but, although it is very efficient at oxidizing hydrazines (2*c*), again this presents problems associated with its preparation and purification.

It was decided that solid $KMnO_4$ used with tetra-*n*-butylammonium bromide (TBAB) phase-transfer catalyst (10) might provide the requisite oxidation power. Here, any excess $KMnO_4$ and the reduced Mn compounds (chiefly MnO_2, presumably) are in the solid phase and therefore easily separated from the products by filtration, and the phase-transfer catalyst is used only in small amounts and is not difficult to separate from the products by crystallization.

Table 1 shows the results of the oxidation of DH_2-H and of some related hydrazines with this method. The extent of reaction can be followed by periodic thin-layer chromatography analysis. Generally only two spots will appear on the plate, those of the hydrazine and the corresponding hydrazyl, making the method simple and useful. Side reactions were noted in some cases but these may be largely avoided by careful attention to the extent of reaction, stopping the reaction when starting material is no longer evident on the tlc plate. The potassium permanganate must be freshly ground, as it was noted that $KMnO_4$ that had been ground and left on the bench for some time lost some of its oxidizing power. This is not surprising since photolytic decomposition of $KMnO_4$ is known to occur (11). There is evidence that $KMnO_4$ will not dissolve unaided in dichloromethane and benzene, the solvents used in this study: when $KMnO_4$ is stirred with dichloromethane or benzene for several hours and then filtered, the solution has no characteristic purple color, indicating that the potassium permanganate does not dissolve. On the other hand, when a small quantity of phase-transfer catalyst is added and the same steps are taken, the filtered solution is deeply purple in color, as with "purple benzene" (10). It was noted, however, that solid $KMnO_4$ alone (no TBAB) will effect oxidation of DH_2-H to $DH_2\cdot$ (Table 1), and presents the added benefit of even easier purification. In this case the reaction is heterogeneous and presumably takes place on the surface of the $KMnO_4$ particles. With or without TBAB present, the rate of oxidation is affected only to a minor extent by stirring; even an unstirred solution of DH_2-H with solid $KMnO_4$ will show complete formation of $DH_2\cdot$, in approximately twice the time observed for a stirred solution. The mole

[1]Author to whom correspondence may be addressed.

TABLE 1. Production of 2,2-diaryl-1-picrylhydrazyls from the corresponding hydrazines

Substrate	Oxidant	Solvent	Yield (%)[b]	Melting point (°C)[b]
DH_2-H	$KMnO_4$/TBAB	CH_2Cl_2	80	132–133.5
$D(NO_2)_2$-H	$KMnO_4$/TBAB	CH_2Cl_2	90[d]	172–182[d]
$D'H_2$-H[a]	$KMnO_4$/TBAB	CH_2Cl_2	81[d]	160–175[d]
DH_2-H	PbO_2/Na_2SO_4	CH_2Cl_2	53	131–133
$D(NO_2)_2$-H	PbO_2/Na_2SO_4	CH_2Cl_2	65[c]	—
$D'H_2$-H[a]	PbO_2/Na_2SO_4	CH_2Cl_2	42[c]	—
DH_2-H	$KMnO_4$	CH_2Cl_2	85 ± 8[e]	130–132
$D(NO_2)_2$-H	$KMnO_4$	CH_2Cl_2	80[d]	178–182[d]
$D'H_2$-H[a]	$KMnO_4$	CH_2Cl_2	70 ± 12[d,e]	170–175[d]
DH_2-H	$KMnO_4$	Benzene	70	131–133.5
DH_2-H	Dry $KMnO_4$	Dry CH_2Cl_2	90	133–135
$DH_2^-K^+$	$KMnO_4$	CH_2Cl_2	59 ± 15[c,e]	—

[a]*N*-Picryl-9-aminocarbazole.
[b]Of corresponding radical.
[c]Determined spectrophotometrically, as noted in Experimental.
[d]Of crude product; see Experimental.
[e]Result of three trials.

ratio of $KMnO_4$ to DH_2-H required for complete oxidation is approximately 3:1, compared to 10:1 for PbO_2 as found by Laederich and Traynard (12).

Usually, when oxidation of a hydrazine is done with PbO_2, anhydrous sodium sulfate is added (2*a*) as a drying agent to prevent reduction of the hydrazyl back to its parent hydrazine by the H_2O produced as a by-product of the reaction:

$$PbO_2 + 2H^+ + 2e^- \rightarrow PbO + H_2O$$

This does not appear to be necessary for oxidations using permanganate. It is known that for the permanganate oxidation of β,γ-unsaturated alcohols (13), water is essential to the reaction: without H_2O in the manganese coordination shell, the oxidation does not proceed. In the present case, however, it was shown that the oxidation proceeds equally well with either off-the-shelf or with dried $KMnO_4$ and solvent. If MnO_2 is formed, then there must be water formed as well:

$$MnO_4^- + 4H^+ + 3e^- \rightarrow MnO_2 + 2H_2O$$

It may be then that any H_2O generated is taken up by the MnO_2 or is in the coordination shell of the excess MnO_4^- present, and is unavailable for reduction of the hydrazyl radicals.

In aqueous solution, the permanganate ion is known to react with atomic hydrogen (14) generated by pulse radiolysis to make MnO_4^{-2} and H^+. The ion $HMnO_4^-$ has been postulated by Webster and Halpern (15) to form during the reaction between permanganate and molecular hydrogen, catalysed by Ag^+. In the present case, a possible first step of the reaction may be abstraction of a hydrogen atom from the hydrazine to form the hydrazyl and hydrogen manganate anion, followed by disproportionation of the latter. That manganate is not likely to be present in large quantities at any stage was shown by an experiment in which finely powdered $BaMnO_4$ in dichloromethane (no TBAB) was found to oxidize DH_2-H to $DH_2\cdot$. This oxidant appears to be virtually as efficient as $KMnO_4$ under the conditions of this study. On the other hand, no oxidation product was observed when DH_2-H was stirred with MnO_2, suggesting that the manganese ends up in the +4 oxidation state. This possibility was investigated by epr (electron paramagnetic resonance) spectroscopy. No signal attributable to manganate or to Mn^{+2} was observed in the frozen reaction vessel containing DH_2-H and $KMnO_4$ in dichloromethane (~30 K); MnO_2, which is antiferromagnetic at this temperature (16), was not observed under these conditions.

It was decided, to further our knowledge about the reaction mechanism, to investigate oxidation of the potassium salt ($DH_2^-K^+$) of DH_2-H with $KMnO_4$. This compound was previously reported to be oxidizable to $DH_2\cdot$ by PbO_2 (17). Using $KMnO_4$, $DH_2\cdot$ was indeed produced (although not in as great yield as for the corresponding hydrazine). This result suggests that, at least here, the first step of the oxidation is a one-electron transfer to permanganate.

Finally, we may note that the use of $KMnO_4$ holds two advantages over PbO_2 and other lead oxidants: its low cost and its relatively low toxicity. The price of potassium permanganate is about one third that of lead dioxide (based on comparable grades of each compound available from Aldrich Chemical Co.) and the acceptable level of manganese in air is approximately 5 mg/m^3 compared with that of 0.2 mg/m^3 for lead (18).

Experimental

2,2-Diphenyl-1-picrylhydrazyl from DH_2-H using $KMnO_4$/TBAB

DH_2-H (1 g) in 100 mL of dichloromethane was oxidized using 5.5 g of $KMnO_4$ and 50 mg of tetra-*n*-butylammonium bromide. The finely ground potassium permanganate was added in increments of 1 g at 15-min intervals with stirring. After each addition of the oxidant, a sample of the solution was taken for tlc analysis on a silica gel 60 plate developed in toluene: DH_2-H, R_f 0.32; $DH_2\cdot$, R_f 0.27.

When DH_2-H was no longer observed, the solution was filtered, the solvent was evaporated, and the crude solid was crystallized from benzene – petroleum ether (1:1). The melting point must be taken carefully since solvent of crystallization is invariably associated with $DH_2\cdot$. The technique used here was to put a sample of the crystals onto a microscope cover plate and then, using a Fisher–Johns melting point apparatus, slowly raise the temperature to ~110°C to drive off the solvent. Then the temperature was slowly raised to 135°C, the melting point being generally observed towards the end of this range. See Table 1 for yield and melting point.

2,2-Diphenyl-1-picrylhydrazyl from DH_2-H using $KMnO_4$

Exactly the same procedure was used as above except that no phase-transfer catalyst was used.

N-Picryl-9-aminocarbazyl from N-picryl-9-aminocarbazole using $KMnO_4$

The procedure was identical to that for $DH_2\cdot$ using $KMnO_4$ without TBAB; however, it was noted that some starting material was left after

the addition of all of the $KMnO_4$. Tetra-*n*-butylammonium bromide (50 mg) was added to the solution of the incompletely oxidized *N*-picryl-9-aminocarbazole and a tlc plate developed after 15 min. All of the starting material was seen to have disappeared. Table 1 gives the yield and melting point of the crude product.

*2,2-Di(*p*-nitrophenyl)-1-picrylhydrazyl from $D(NO_2)_2$-H using $KMnO_4$*

$D(NO_2)_2$-H, prepared by the method of Weil, Sane, and Kinkade (8), was oxidized by $KMnO_4$ in the same way as DH_2-H.

*Preparation of 1-(*N,N*-diphenylhydrazono)-2,4,6-trinitrobenzenide ($DH_2^-K^+$)*

This compound was prepared by the method used by Weil and Janusonis (17).

Calculations of yields for $D(NO_2)_2\cdot$ and $D'H_2\cdot$

$D(NO_2)_2\cdot$ and $D'H_2\cdot$ are unstable in solution and tend to abstract hydrogen from the solvent if left for long periods of time. For this reason, crystallization of these compounds was not attempted. In all cases of reaction of the parent hydrazines of these two compounds with $KMnO_4$, the tlc plate showed no evidence of any hydrazine left after allowing the appropriate time for reaction. Thus the crude yield was reported. However, in the case of the oxidation of these hydrazines by PbO_2, there was always a considerable amount of starting material left over and the yield of radical was determined using the fact that $D(NO_2)_2\cdot$ and $D'H_2\cdot$ will readily and quickly abstract a hydrogen atom from DH_2-H (8) producing $DH_2\cdot$, which may be then determined spectrophotometrically.

Acknowledgements

This research was carried out under the auspices of the Natural Sciences and Engineering Research Council of Canada. We thank Mr. R. S. Dickson for his help with some of the epr experiments and Professor D. G. Lee of the University of Regina for a sample of $BaMnO_4$.

1. (*a*) P. F. Currie, J. W. Quail, and J. A. Weil. Can. J. Chem. **58**, 723 (1980); (*b*) P. F. Currie, J. W. Quail, A. C. M. Rusk, and J. A. Weil. Can. J. Chem. **61**, 1760 (1983).
2. (*a*) S. Goldschmidt and K. Renn. Ber. Dtsch. Chem. Ges. **55**, 628 (1922); (*b*) M. M. Chen, A. F. D'Adamo, and R. I. Walter. J. Org. Chem. **26**, 2721 (1961); (*c*) W. K. Wilmarth and N. Schwartz. J. Am. Chem. Soc. **77**, 4543 (1955).
3. N. I. Budina, O. L. Kaliva, and O. L. Lebedev. J. Org. Chem. USSR (Engl. Trans.), **14**, 2255 (1978).
4. R. B. Moyes, P. B. Wells, K. Baron, and K. Compson. J. Catal. **18**, 224 (1970).
5. M. P. McDaniel and R. L. Burwell. J. Catal. **36**, 404 (1975).
6. R. C. Lamb and C. T. Clark. U.S. Dept. Com. Office Tech. Serv. AD 429279 (1963); Chem. Abstr. **61**, 12699g (1963).
7. A. V. Il'yasov, Y. A. Levin, N. N. Sotnikova, and F. G. Valitova. Teor. Eksp. Khim. **2**, 142 (1966); Chem. Abstr. **65**, 3719f (1966).
8. J. A. Weil, K. V. Sane, and J. M. Kinkade, Jr. J. Phys. Chem. **65**, 710 (1961).
9. J. C. Bailar, Jr. Inorg. Synth. **1**, 47 (1939).
10. W. P. Weber and G. W. Gokel. Phase-transfer catalysis in organic synthesis. Springer Verlag, Berlin. 1977. p. 206.
11. R. Stewart. *In* Oxidation in organic chemistry. Academic Press, New York. 1965. p. 21.
12. T. Laederich and P. Traynard. C. R. Acad. Sci. **254**, 1826 (1962).
13. (*a*) N. A. Noureldin and D. G. Lee. J. Org. Chem. **47**, 2790 (1982); (*b*) D. G. Lee and N. A. Noureldin. J. Am. Chem. Soc. **105**, 3188 (1983).
14. M. Ebert, J. P. Keene, A. J. Swallow, and J. H. Baxendale. Pulse radiolysis. Academic Press, New York. 1965. p. 107.
15. A. H. Webster and J. Halpern. Trans. Faraday Soc. **53**, 51 (1957).
16. J. E. Rives. *In* Transition metal chemistry. Vol. 7. Marcel Dekker, Inc., New York. 1972. p. 142.
17. J. A. Weil and G. A. Janusonis. J. Org. Chem. **27**, 1248 (1962).
18. R. C. Weast (*Editor*). Handbook of chemistry and physics. 56th ed. The Chemical Rubber Company, Cleveland. 1975–1976. p. D108.

Rotations of linear triatomic anions in aqueous solution by nuclear magnetic resonance spectroscopy

A. MARTIN DE P. NICHOLAS AND RODERICK E. WASYLISHEN[1]
Department of Chemistry, Dalhousie University, Halifax, N.S., Canada B3H 4J3

Received November 11, 1985

A. MARTIN DE P. NICHOLAS and RODERICK E. WASYLISHEN. Can. J. Chem. **64**, 1839 (1986).

The temperature dependence of nitrogen-14 nuclear magnetic resonance (nmr) spin-lattice relaxation times (T_1) for dilute aqueous solutions of the linear triatomic anions, $SeCN^-$, SCN^-, OCN^-, and N_3^-, is investigated in the temperature range 3–80°C. These nmr relaxation times (T_1) yield rotational correlation times, τ_{2R}, for the reorientation of the C_∞ symmetry axis in these anions. The observed nonlinear dependence of log $T_1(^{14}N)$ on temperature suggests that the rotations of the anions are coupled to the transport properties of water. For the thiocyanate anion the nmr correlation times are compared with those obtained previously from Raman spectroscopic data and Rayleigh scattering results. ^{17}O T_2 and ^{14}N T_1 measurements for the NCO^- anion are used along with *ab initio* calculations to estimate the ^{17}O nuclear quadrupolar coupling constant in this ion.

A. MARTIN DE P. NICHOLAS et RODERICK E. WASYLISHEN. Can. J. Chem. **64**, 1839 (1986).

Opérant à des températures allant de 3 à 80°C, on a étudié la variation des temps de relaxation spin/réseau (T_1), en rmn du ^{14}N, pour des solutions aqueuses diluées des anions linéaires triatomiques, $SeCN^-$, SCN^-, OCN^- et N_3^-. En utilisant ces temps de relaxation (T_1), on a pu obtenir les temps de corrélation rotationnelle (τ_{2R}) pour la réorientation de l'axe de symétrie C_∞ de ces anions. On a observé que la relation entre la température et le log $T_1(^{14}N)$ n'est pas linéaire et ce résultat suggère que les rotations des anions sont couplées avec les propriétés de transport de l'eau. Dans le cas de l'anion thiocyanate, on a comparé les temps de corrélation rmn avec ceux obtenus antérieurement pour les données de spectrométrie Raman et avec les résultats de diffraction Rayleigh. Dans le but d'évaluer la constante de couplage quadrupolaire nucléaire du NCO^-, on utilise des calculs *ab initio* de concert avec des mesures de $T_2(^{17}O)$ et de $T_1(^{14}N)$ effectuées sur cet ion.

[Traduit par la revue]

Introduction

A variety of spectroscopic techniques have been used to obtain a large body of information on rotations of molecules and ions in condensed phases (1–3). However, relatively little work of this kind has been reported for anions in aqueous solution (4), and in particular for linear ions, where information is available only for the thiocyanate anion (4, 5). Furthermore, the results for SCN^- obtained from Raman spectroscopy and Rayleigh scattering experiments, where the derived correlation times are partly influenced by vibrational relaxation processes and orientational cross-correlations, respectively, are not in agreement (4). Thus it is desirable to obtain nuclear magnetic relaxation data, which are free from such influences (6), in order to investigate further the rotations of linear anions in aqueous solution.

Recently, we have shown the strength of the nmr technique in studying rotations of the nitrate and carbonate anions in aqueous solution (7). Here we apply this method to a group of linear triatomic anions, $SeCN^-$, SCN^-, OCN^-, and N_3^- by studying the temperature dependence of the relaxation rates of the quadrupolar nucleus ^{14}N at anion concentrations of approximately 1 molar. A few ^{14}N T_1 measurements of more dilute solutions are carried out to investigate the importance of ion pairing in these systems. In addition, the rotational correlation times obtained for the dilute solutions are discussed in terms of a hydrodynamic model (7).

Theory

Both ^{14}N ($Q = 0.0195 \times 10^{-28}$ m^2) (8*a*) and ^{17}O ($Q = -0.026 \times 10^{-28}$ m^2) (8*b*) are quadrupolar nuclei that are expected to relax entirely by the quadrupolar mechanism (6). Under conditions of extreme narrowing, the rate of relaxation (R_1) of a quadrupolar nucleus of spin I, in an axially symmetric environment, is given by eq. [1] (6):

$$[1] \quad R_1 = 1/T_1 = \frac{3\pi^2}{10}\,\frac{2I+3}{I^2(2I-1)}(e^2qQ/h)^2\tau_{2R}$$

where e^2qQ/h is the nuclear quadrupolar coupling constant (QCC), and τ_{2R} is the rotational correlation time. Quadrupolar coupling constants for ions in the solid state are available from either nuclear quadrupole resonance (nqr) or nmr experiments (9). Assuming the validity of these values in solution, one can derive rotational correlation times for these ions from the nmr data using eq. [1].

Experimental

All nmr measurements were performed on a Nicolet 360 NB (B_0 = 8.48 T) using a broad-band variable temperature 10-mm probe. The temperature was maintained with an accuracy of ±2 K by a nitrogen gas flow. The transmitter frequency was adjusted so that the transmitter was centred on the resonance of interest and spin-lattice relaxation times were measured by the inversion recovery pulse sequence (IRCA), which uses compensating pulses (10). The $\pi/2$ pulse widths were 50–60 μs. Typically, 16 scans at each variable delay, D_1, in the IRCA experiment were carried out in the ^{14}N relaxation experiments. About 120 000 scans were required in the natural abundance ^{17}O T_2 measurement of the isocyanate anion. The resulting S/N in the $D_1 = \infty$ measurements was about 100:1 for the ^{14}N and approximately 30:1 for the ^{17}O spectrum of the isocyanate anion. All T_1 values were calculated from peak heights obtained at 12 or more different D_1 values, using a nonlinear three-parameter least-squares fitting procedure available on the Nicolet software (11).

Solutions of the chalcogencyanates and the azide were prepared by weighing out appropriate amounts of laboratory reagent grade chemicals and diluting with distilled water volumetrically. The thiocyanate anion concentration was determined by titration with $AgNO_3$ using K_2CrO_4 as indicator (12).

Results and discussion

(a) Temperature dependence of nitrogen-14 T_1 *data*

The temperature dependence of the measured ^{14}N T_1 values for approximately 1 molar aqueous solutions of KSeCN, NaSCN,

[1]Author to whom correspondence may be addressed.

TABLE 1. Temperature dependence of nitrogen-14 nuclear relaxation times and rotational correlation times for the selenocyanate anion in aqueous 0.9 *M* KSeCN solution

T/°C	$T_1(^{14}N)$/ms[a]	τ_{2R}/ps
3	1.53	5.45
10.5	1.88	4.44
15.5	2.16	3.86
23	2.53	3.30
34	3.10	2.69
50	4.09	2.04
64	4.87	1.71
79	5.80	1.44

[a]Error of 3%.

TABLE 2. Temperature dependence of nitrogen-14 nuclear relaxation times and rotational correlation times for the thiocyanate anion in aqueous 0.9 *M* NaSCN solution

T/°C	$T_1(^{14}N)$/ms[a,b]	τ_{2R}/ps
2	2.28	5.01
10.5	2.87	3.98
15.5	3.18	3.59
22	3.83	2.98
34	4.84	2.36
50	6.18	1.85
64	7.60	1.50
80	9.14	1.25

[a]Error of 3%.
[b]$T_1(^{14}N)$ measurements were also performed on a 0.1 *M* solution; in general T_1 values at any given temperature were 10–20% longer than those at 1 *M* (see Fig. 2).

TABLE 3. Temperature dependence of nitrogen-14 nuclear relaxation times and rotational correlation times for the isocyanate anion in aqueous 0.9 *M* NaOCN solution

T/°C	$T_1(^{14}N)$/ms[a]	τ_{2R}/ps
4	38.83	3.45
10	45.33	2.96
15	50.40	2.66
22	59.76	2.24
34	74.44	1.80
50	91.62	1.46
65	112.50	1.19
80	129.00	1.04

[a]Error of 3%.

TABLE 4. Temperature dependence of nitrogen-14 nuclear relaxation times and rotational correlation times for the azide anion in aqueous 1.0 *M* NaN_3 solution

	$T_1(^{14}N)$/ms[a]		
T/°C	Central	Terminal	τ_{2R}/ps[b]
5	18.29	4.82	3.93
10	21.85	5.76	3.30
15.5	24.90	6.49	2.91
24	30.13	7.95	2.38
35.5	38.61	10.11	1.88
51	50.56	13.23	1.42
64	60.27	15.96	1.19
79	74.30	19.35	0.98

[a]Error of 3%.
[b]An average of the values obtained using the T_1's of the central and terminal nitrogens.

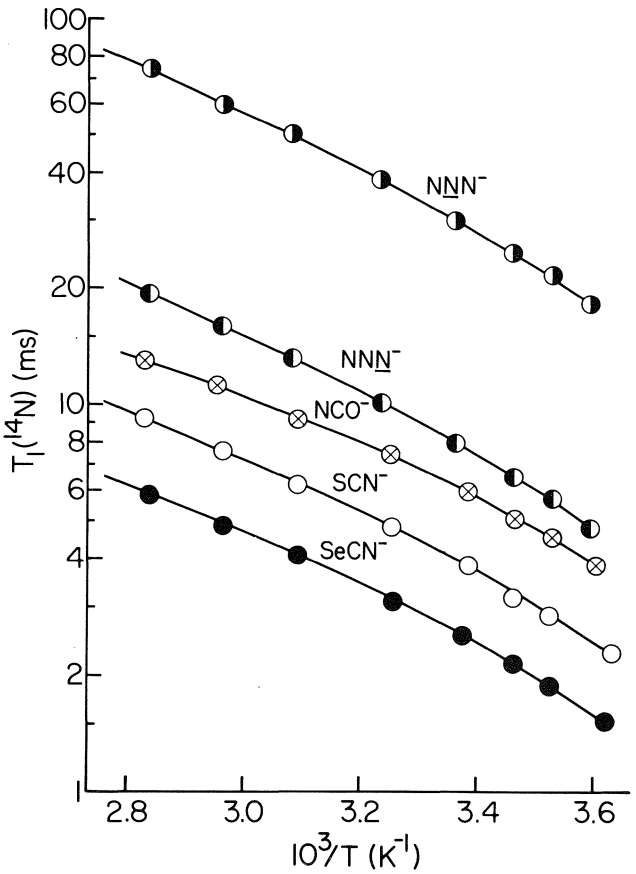

FIG. 1. A. plot of log ($T_1(^{14}N)$) versus $1/T$ for approximately 1 molar aqueous solutions of linear triatomic anions. Note that, for the NCO^- anion, values shown are $T_1/10$.

NaOCN, and NaN_3 are given in Tables 1–4, respectively, and also illustrated in Fig. 1 by a plot of the logarithm of T_1 with the inverse of the absolute temperature.

A comparison of the T_1 values for the chalcogencyanates at any given temperature shows a decrease down the group from OCN^- to $SeCN^-$. This trend is a result of an increase in the ^{14}N QCC and (or) a decrease in the rates of anion reorientation on going from OCN^- to $SeCN^-$. While the order $SeCN^- > SCN^- > OCN^-$ is expected for τ_{2R} on the basis of the size of the anion (*vide infra*), one cannot *a priori* predict the variation of the ^{14}N QCC in these ions because the interpretation of a QCC in terms of the overall electronic distribution is not straightforward (13). Since N_3^- and the NCO^- anions are similar in size, any difference in their T_1's should be predominantly due to the relative magnitude of their respective QCCs.

Rotational correlation times for the $SeCN^-$ and SCN^- were calculated using eq. [1], taking ^{14}N QCC of 2.846 and 2.432 MHz, respectively, obtained from previous nqr results (14). Although the effective values of QCC for $SeCN^-$ and SCN^- in aqueous solution may differ from those obtained in the

TABLE 5. A comparison of correlation times for the rotation of anions in aqueous solution[a]

Anion	Length of axes/Å		$T_1(^{14}N)$/ms	τ_{2R}/ps			C	
	a	b		Nmr	Stick	Slip	Slip	Obs.
$SeCN^{-}$[b]	3.3	1.95	2.76	3.0	15.7	2.6	0.17	0.19
SCN^{-}	3.2	1.85	4.36	2.6	14.0	2.4	0.17	0.19
OCN^{-}	2.8	1.70	70.0	2.0	9.9	1.5	0.15	0.20
N_3^{-}	2.9	1.70	8.3 32.9	2.2	10.5	1.7	0.16	0.21

[a]At a concentration of 0.1 M and a temperature of 23 ± 2°C. Unless stated otherwise the counterion is Na^+.
[b]Counterion is K^+.

TABLE 6. Apparent activation energies for the rotation of anions in aqueous solution[a]

Anion (counterion)	E_a/kcal mol^{-1}	
	0–25°C	35–80°C
0.9 M $SeCN^{-}$ (K^+)	4.1 ± 0.1	3.0 ± 0.1
0.9 M SCN^{-} (Na^+)	4.1 ± 0.2	3.0 ± 0.1
0.9 M OCN^{-} (Na^+)	3.9 ± 0.1	2.6 ± 0.1
1.0 M N_3^{-} (Na^+)	4.2 ± 0.3	3.2 ± 0.1
1.0 M NO_3^{-} (Na^+)	4.6 ± 0.2[b]	2.8 ± 0.1[b]

[a]From eq. [2]. Error limits correspond to the standard deviation.
[b]Reference 7.

solid state by nqr, we anticipate that the solvent effects result in a systematic error in the QCCs. That is, if QCC(SCN^{-}) increases by 5% on going from solid KNCS to aqueous solution, then QCC($SeCN^{-}$) is also expected to increase by approximately the same amount. The implication is that although the τ_{2R} values in Tables 1 and 2 may have significant errors (e.g. ±15%) we expect the relative error to be much smaller (±5%). The consistently larger τ_{2R} values obtained for $SeCN^{-}$ compared to those obtained for SCN^{-} at any given temperature are probably significant. In the absence of an experimental QCC for OCN^{-}, we have used a theoretical value of 0.71 MHz obtained from a high level *ab initio* calculation near the Hartree–Fock limit (13), to derive τ_{2R} values for this ion. In the azide anion two estimates of τ_{2R} were derived from the T_1 data using the QCC values of 1.79 and 1.028 MHz, respectively, for the terminal and central nitrogens; these values were obtained from solid-state nmr experiments (15). The correlation times derived from the nmr T_1 data of the central nucleus were ca. 20% lower than those for the terminal nucleus. These τ_{2R} values were different because the effective QCC values in solution are probably slightly different from those in the solid state. The average of τ_{2R} (terminal) and τ_{2R} (central) at each temperature is given in column 4 of Table 4.

The τ_{2R} values determined by the nmr method are the same rotational correlation times probed previously by Raman spectroscopy and Rayleigh light scattering experiments. For the thiocyanate anion the nmr τ_{2R} values are in good agreement with the corresponding Raman data (4), especially at the higher temperatures. At 30°C, the lowest of these temperatures investigated in the Raman study, τ_{2R} (Raman) = 2.0 ps, while τ_{2R} (nmr) = 2.5 ps; both results pertain to 1 M aqueous solutions of NaSCN. Comparing the nmr results with the Rayleigh scattering data (5), we find the τ_{2R} (nmr) values are slightly shorter (ca. 30%) than the τ_{2R} (Rayleigh) values (e.g., for an infinitely dilute aqueous solution of SCN^{-} at 20°C, τ_{2R} (nmr) = 3.0 ± 0.4 ps, while τ_{2R} (Rayleigh) = 4.2 ± 0.2 ps).

Figure 1 shows that the plot of $\log(^{14}N(T_1))$ versus $1/T$, where T is the absolute temperature, is nonlinear for all the anions studied. As discussed previously in our study of the nitrate anion (7), this behaviour may arise for a variety of reasons. First the equilibrium constant for the association of these anions with the cation may be temperature dependent. However, because a comparison of the correlation times for the 1 M and 0.1 M solutions shows a relatively small variation ranging from 10 to 20% (Tables 1–5), ion pairing does not appear to be important. This is supported by results obtained by other techniques (4, 5).

A second possibility is that the anion rotations are coupled to those of the solvent. It is well known that nmr relaxation data and other transport properties of water can not be fitted to a single exponential (i.e., a single E_a value in eq. [2]) over the

$$[2] \quad \ln T_1 = -(E_a/RT) + \text{constant}$$

entire liquid range (16). In the temperature range 0–25°C and 35–80°C, proton relaxation data for water are well described by eq. [2], with E_a values of 4.6 and 3.3 kcal mol^{-1} respectively for the low and high temperature regions (16*a*, *b*). This is usually ascribed to cooperative behaviour (16*c*). For each of the anions studied here, we have carried out the same arbitrary evaluation of E_a in the low and high temperature regions (see Table 6). Values for the nitrate anion are presented for comparison. From the data in Table 6 it is apparent that the same general behaviour is observed for all ions. This suggests that the anion rotations involve a breaking of the water "structure". Furthermore, the observed linearity in the plots of τ_{2R} vs. η/T (correlation coefficient, r = 0.998–0.999, where η is the solvent viscosity, for the anions considered here) provides evidence for the coupling of the rotations of these linear anions with the transport properties of water (7) (*vide infra*). A plot of τ_{2R} vs. η/T for 0.1 M NaSCN is illustrated in Fig. 2.

For the thiocyanate anion the average activation energy, E_a = 3.6 ± 0.2 kcal mol^{-1}, from the nmr data (1 M NaSCN) is in fair agreement with the value of 3.0 kcal mol^{-1} obtained in the Rayleigh scattering study of 1.8 M NH_4SCN (5). Essentially the same activation energy was determined for a 6.0 M solution of NH_4SCN (5) and τ_{2R} values at any given temperature and solute concentration appeared to be the same for NH_4SCN and KSCN solutions. From the Raman data (4) on 1.0 M NaSCN at

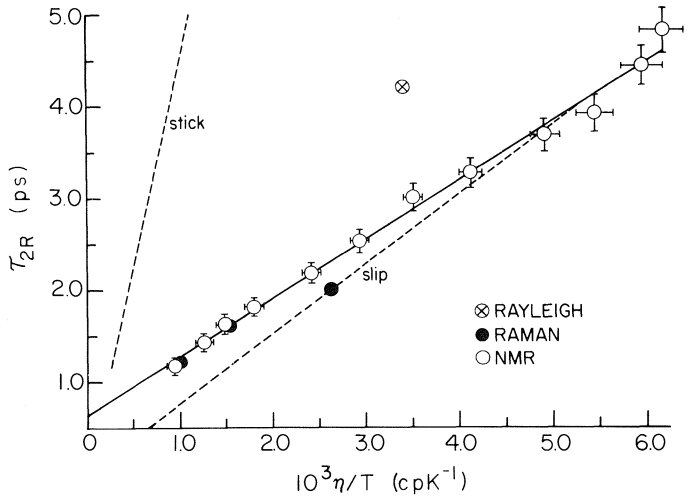

FIG. 2. A plot of τ_{2R} (nmr) versus η/T for an aqueous solution of 0.1 *M* NaSCN ($r = 0.995$). The Raman τ_{2R} values correspond to a 1 *M* solution and the Rayleigh scattering value is at infinite dilution.

30, 55, and 80°C, $E_a = 2.2 \pm 0.3$ kcal mol^{-1}, in fair agreement with the value obtained in this study, 3.0 ± 0.1 kcal mol^{-1}, over the same temperature range.

Finally, we have assumed the QCC to be independent of temperature. Clearly, the vibrationally averaged QCC will be temperature dependent (9); however, such effects are expected to be small in the temperature range investigated. Also we would like to point out that it is not a trivial procedure to correct for such effects in solution.

Next, we investigate further the effect of the medium on the rotation of these ions by considering a hydrodynamic model.

(b) The hydrodynamic rotation of anions

In the hydrodynamic model of molecular rotation (17, 18) the rotational correlation time is given by eq. [3],

$$[3] \quad \tau_{2R} = \eta V f C / k_B T$$

where V is the molecular volume of the anion, f is a shape factor that accounts for the deviation of the ion from spherical symmetry, C is an empirical parameter that accounts for the variable boundary conditions, and k_B is the Boltzmann constant. When the parameters f and C are both set equal to unity, eq. [3] reduces to the familiar Stokes–Einstein–Debye equation originally derived for a sphere (17).

The anions investigated in this study were assumed to be prolate spheroids and the value of f was calculated using eq. [4] (18),

$$[4] \quad f = \frac{(2/3)(1 - x^4)}{[(2 - x^2)x^2 \ln\{(1 + (1 - x^2)^{1/2})/x\}/(1 - x^2)^{1/2}] - x^2}$$

where $x\,(= b/a)$ is the axial ratio of the ellipsoid. For the anions investigated here, the major semiaxis (a) was estimated to be half the total sum of the bond lengths (19) and the van der Waals radii of the terminal atoms. The minor semiaxis (b) was assumed to be equal to the van der Waals radius of the largest atom. The van der Waals radii for Se, S, O, and N were assumed to be 1.95, 1.85, 1.60, and 1.70 Å, respectively. These values are taken to be 0.1 Å larger than the corresponding values in the neutral atoms (20) because of the partial negative charge on the terminal atoms. The assumed values of a and b for each anion are given in Table 5.

The two extreme boundary conditions are the so-called stick boundary condition ($C = 1$) and the slip boundary, where C is a minimum dependent on the shape of the solute (18*a*).

$$[5] \quad C_{slip} = 1 - f^{(-2/3)}$$

For the anions investigated here C_{slip} falls in the range 0.15–0.17; for a perfect sphere $C_{slip} = 0$. An observed "C" value of 1 implies a strong interaction between solute and solvent. For example, recently, Masuda, Sano, and Yamatera (21) have found that rotations of the phosphate anion obey the stick boundary condition. Under the slip boundary condition the only frictional resistance to rotation results from solvent displacement as the solute molecules rotate. Previous workers (4, 5) have found that rotations of the SCN^- anion are best described by the slip boundary condition.

To compare observed nmr rotational correlation times with those calculated under the slip and stick boundary conditions we studied all ions at 0.1 *M*, so that ion pairing will be negligible and the viscosity of the solution can be approximated to that of water. The rotational correlation times derived from the nmr data using eq. [1] are compared with the τ_{2R} values for the "stick" and "slip" boundary conditions in Table 5.

From the data in Table 5 we find that the value of C for all the anions investigated in this study is 0.2, just slightly larger than C_{slip}. The implication is that interactions between these anions and water is rather weak. This statement is not inconsistent with the activation energies reported above in section (*a*). As these prolate ellipsoidal shaped anions rotate they must, because of their shape, displace solvent and, in doing so, break water structure; hence the observed activation energies for anion rotation parallel those observed for water reorientation (i.e., rotations of the solute molecules are coupled to those of the solvent). Rotations of the perchlorate anion in aqueous solution are also described best by the slip boundary condition ($C = 0.03$). However, in this case, since the anion is approximately spherical, rotational correlation times are shorter and the activation energy is only 2.2 kcal mol^{-1} (21). The divalent sulphate anion is also approximately spherical; however, because of its charge it interacts more strongly with water ($C = 0.21$) and $E_a = 3.1$ kcal mol^{-1} (21).

One important basic assumption in applying any hydrodynamic model is that the solvent must appear as a continuum (17); that is, the solute molecule should be large compared to the size of the solvent molecule (18). Also we must assume that the solute molecules undergo small-step rotational diffusion (this assumption appears justified for SCN^- (4)). Because of these assumptions any attempt at interpretation of C values obtained in this and other related studies is at best qualitative. The importance of measuring experimental C values or related empirical parameters to assess solute–solvent interactions has been recently discussed by Zwanzig and Harrison (22).

(c) The ^{17}O quadrupolar coupling constant in the isocyanate anion

(i) The nmr method

In the extreme narrowing limit the spin–spin and spin-lattice relaxation times of quadrupolar nuclei are equal (6):

$$[6] \quad T_1 = T_2 = 1/\pi\nu_{1/2}$$

For the isocyanate anion both ^{17}O and ^{14}N relaxation rates are related to the same correlation time. Hence, by substituting values of $I = 5/2$ and 1, for ^{17}O and ^{14}N, respectively, from eqs. [1] and [6]:

TABLE 7. *Ab initio* calculations of the oxygen-17 nuclear quadrupolar coupling constant in the isocyanate anion

Basis set	EFG/au	QCC/MHz
STO-3G	−1.5280	9.34
4-31G	−1.0191	6.23
6-31G	−1.0460	6.39
6-31G*	−0.8833	5.40
⟨9S,5P⟩	−1.0246	6.26

[7] $1/T_2(^{17}O) = 8(QCC(^{17}O))^2/\{125(QCC(^{14}N))^2T_1(^{14}N)\}$

At 25°C, for a 1.0 *M* NaNCO aqueous solution in 10% D_2O, we find the ^{17}O line width ($\nu_{1/2}$) to be $<40 \pm 3$ Hz, corresponding to $T_2(^{17}O) > 8 \pm 1$ ms. The absence of any previous reports of $\delta(^{17}O)$ for NCO^- (23) may be due to the close proximity of the ^{17}O resonance of this ion to that of water (42.6 ± 1 ppm to high frequency). Substitution of $T_2(^{17}O) > 8 \pm 1$ ms, $T_1(^{14}N) = 62 \pm 3$ ms, and $QCC(^{14}N) = 0.71$ MHz in eq. [7] gives an upper limit of 7.8 ± 1 MHz for the ^{17}O quadrupolar coupling constant in the isocyanate anion.

Next we compare the ^{17}O QCC derived from the nmr relaxation data with the corresponding value obtained using *ab initio* calculations.

(ii) The ab initio *method*

Calculation of nuclear quadrupolar coupling constants from electric field gradients (EFGs) requires a knowledge of the value of the quadrupole moment (Q) of ^{17}O. The uncertainty in this Q value will be one source of error in the derived QCC (8*b*). We have used the $Q(^{17}O)$ value recommended by Fuller (8*b*) after a critical analysis of the available data.

EFGs were computed by performing *ab initio* molecular orbital (MO) calculations at a variety of levels using the program GAUSSIAN 76 (24*a*) appended by a version of the properties package of GAUSSIAN 79 (24*b*) adapted to run on the CDC 170-730 computer at Dalhousie University. The EFGs of NCO^- ($C_{\infty v}$, $r_{NC} = 1.21$ Å, and $r_{CO} = 1.13$ Å) (21) calculated using the STO-3G, 4-31G, 6-31G, and 6-31G* basis sets (25) and the Huzinaga ⟨9S,5P⟩ basis set (26) are given in Table 7. The results in this table indicate that the *ab initio* calculations yield QCCs smaller than those derived from the nmr method for all the extended basis sets. However, previous studies (7, 27) on a variety of molecules indicate that ^{17}O QCCs derived from *ab initio* theory using comparable basis sets are too large by ca. 10–20%. Assuming the calculated values in Table 7 are too large, these calculations suggest an ^{17}O QCC of ca. 5 MHz in NCO^-. From a comparison of the estimates of the QCC by the two methods and a consideration of the uncertainty in the data, we propose a ^{17}O QCC of 6 ± 2 MHz in the isocyanate anion. This estimate is reasonable when compared to the values of 8.1 ± 0.5 and 7 ± 0.5 MHz for oxygen-17 singly coordinated and doubly bonded to carbon in *N*-methylsydnone (28) and the bicarbonate anion (29), respectively, and other reported QCCs (23).

Conclusions

We have applied nmr relaxation techniques to study the temperature dependence of rotations of linear triatomic anions in dilute aqueous solution. Rotational correlation times for the rotation of the C_∞ symmetry axis in the thiocyanate anion are intermediate to those obtained from Rayleigh scattering and Raman spectroscopy. The logarithm of the quadrupolar spin-lattice relaxation time is found to vary nonlinearly with the inverse of temperature. This is attributed to a coupling of the rotations of these linear anions with those of the solvent water. An analysis of these rotations in terms of a hydrodynamic model indicates that anion reorientation is governed by slip boundary conditions in all cases.

We feel that the largest error in the nmr rotational correlation times results from the assumption that solid state and (or) gas phase QCCs are valid in solution. The nmr technique has the advantage in that relatively dilute solutions can be easily studied. Also, for a more accurate description of the temperature dependence of τ_{2R} data the effect of vibrational averaging on EFGs should probably be considered.

The fact that two quadrupolar relaxation rates can be related to the same correlation time in NCO^- without assuming any specific rotational model permits an estimate of the ^{17}O QCC in this ion to be made by nmr spectroscopy. Accurate ^{14}N and (or) ^{17}O nqr data for NCO^- would lead to more reliable rotational correlation times for this ion.

Acknowledgements

All nmr spectra were obtained at the Atlantic Regional NMR centre, Dalhousie University. We are grateful to the Natural Sciences and Engineering Research Council of Canada for financial support in helping establish and maintain this centre and for an operating grant (R.E.W.). We thank Professors R. J. Boyd and B. A. Pettitt and Mr. K. E. Edgecombe for assistance with the MO calculations, and Professors D. E. Irish and M. H. Brooker for helpful suggestions.

1. W. A. STEELE. Adv. Chem. Phys. **34**, 1 (1976).
2. J. E. GRIFFITHS. *In* Vibrational spectra and structrue. Vol. 6. *Edited by* J. R. Durig. Elsevier, New York. 1977. p. 273.
3. (*a*) W. G. ROTHSCHILD. Dynamics of molecular liquids. Wiley, New York, 1984; (*b*) B. BERNE and R. PECORA. Dynamic light scattering. Wiley, New York. 1976.
4. T. KATŌ and T. TAKENAKA. Mol. Phys. **46**, 257 (1982).
5. M. WHITTLE and J. H. R. CLARKE. Mol. Phys. **44**, 1435 (1981).
6. A. ABRAGAM. The principles of nuclear magnetism. Oxford University Press, New York. 1961.
7. A. M. DE P. NICHOLAS and R. E. WASYLISHEN. J. Phys. Chem. **89**, 5446 (1985).
8. (*a*) T.-K. HA. Chem. Phys. Lett. **107**, 117 (1984); (*b*) G. H. FULLER. J. Phys. Chem. Ref. Data, **5**, 835 (1976).
9. (*a*) E. A. C. LUCKEN. Nuclear quadrupole coupling constants. Academic Press, New York. 1969; (*b*) E. R. HENRY and A. SZABO. J. Chem. Phys. **82**, 4753 (1985).
10. R. FREEMAN, S. P. KEMPSELL, and M. H. LEVITT. J. Magn. Reson. **38**, 453 (1980).
11. G. C. LEVY and I. R. PEAT. J. Magn. Reson. **18**, 500 (1975).
12. A. I. VOGEL. Textbook of quantitative inorganic analysis. 4th ed. Longmans, New York. 1978. p. 337.
13. R. BONACCORSI, E. SCROCCO, and J. TOMASI. J. Chem. Phys. **50**, 2940 (1969).
14. (*a*) R. IKEDA, D. NAKAMURA, and M. KUBO. Bull. Chem. Soc. Jpn. **40**, 701 (1967); (*b*) T. ASAJI, R. IKEDA, and D. NAKAMURA. J. Magn. Reson. **31**, 437 (1978).
15. R. A. FORMAN. J. Chem. Phys. **45**, 1118 (1966).
16. (*a*) L. ENDOM, H. G. HERTZ, B. THÜL, and M. D. ZEIDLER. Ber. Bunsenges. Phys. Chem. **71**, 1008 (1967); (*b*) D. EISENBERG and W. KAUZMANN. The structure and properties of water. Oxford University Press, New York. 1969. Chapt. **4**; (*c*) O. CONDE and J. TEIXEIRA. Mol. Phys. **53**, 951 (1984).
17. (*a*) D. KIVELSON and P. A. MADDEN. Ann. Rev. Phys. Chem.

31, 523 (1980); (*b*) R. T. BOERÉ and R. G. KIDD. Ann. Rep. NMR Spectrosc. **13**, 319 (1982).
18. (*a*) J. L. DOTE and D. KIVELSON. J. Phys. Chem. **87**, 3889 (1983); (*b*) J. L. DOTE, D. KIVELSON, and R. N. SCHWARTZ. J. Phys. Chem. **85**, 2169 (1981); (*c*) R. E. WASYLISHEN, B. A. PETTITT, and W. DANCHURA. Can. J. Chem. **55**, 3602 (1977).
19. A. F. WELLS. Structural inorganic chemistry. 5th ed. Clarendon Press, Oxford. 1984. p. 933.
20. (*a*) A. BONDI. J. Phys. Chem. **68**, 441 (1964); (*b*) J. T. EDWARD. J. Chem. Educ. **47**, 261 (1970).
21. Y. MASUDA, M. SANO, and H. YAMATERA. J. Phys. Chem. **89**, 3086 (1985).
22. R. ZWANZIG and A. K. HARRISON. J. Chem. Phys. **83**, 5861 (1985).
23. (*a*) J.-P. KINTZINGER. *In* NMR of newly accessible nuclei. Vol. 2. *Edited by* P. Laszlo. Academic Press, New York. 1983. Chapt. 4; (*b*) J.-P. KINTZINGER. *In* NMR basic principles and progress. Vol. 17. *Edited by* P. Diehl, E. Fluck, and R. KOSFELD. Springer Verlag, New York. 1981. p. 1.
24. (*a*) J. S. BINKLEY, R. A. WHITESIDE, P. C. HARIHARAN, R. SEEGER, and J. A. POPLE. QCPE, **11**, 368 (1978); (*b*) P. MARSH and D. E. WILLIAMS. QCPE Bulletin, **1**, 38 (1981).
25. A. SZABO and N. S. OSTLUND. Modern quantum chemistry, Macmillan Publishing Co., Inc., New York. 1982. Chapt. 3.
26. S. HUZINAGA. J. Chem. Phys. **42**, 1293 (1965).
27. (*a*) J. E. GREADY. Chem. Phys. **55**, 1 (1981); (*b*) J. Am. Chem. Soc. **103**, 3682 (1981).
28. T. T. T. NGUYEN. Thesis, Université de Lausanne, 1978.
29. C. P. CHENG and T. L. BROWN. J. Am. Chem. Soc. **101**, 2327 (1979).

Zn(II)–D-(−)-penicillamine complexes in aqueous solution. Zn-67 nuclear magnetic resonance study

ALFRED DELVILLE[1] AND CHRISTIAN DETELLIER[2]

Ottawa–Carleton Chemistry Institute, University of Ottawa Campus, Ottawa, Ont., Canada K1N 9B4

Received September 4, 1985[3]

ALFRED DELVILLE and CHRISTIAN DETELLIER. Can. J. Chem. **64**, 1845 (1986).

D-(−)-Penicillamine interactions with Zn(II) have been studied in aqueous solutions as a function of pH, penicillamine concentration, and temperature, using Zn-67 nuclear magnetic resonance. Longitudinal and transverse relaxation rate measurements show the presence in solution of complexes in fast exchange with the aquated Zn(II) cation, and belonging to the extreme narrowing regime. Using equilibrium constant values from the literature, the relaxation behaviour was modelled. Characteristic Zn-67 line width values for the two complexes Zn(Pen) (ν = (6200 ± 500) Hz) and $[Zn(Pen\,H)]^+$ (ν = (6000 ± 1000) Hz) were found. Equality of the two values is in agreement with zinc chelation by the sulfhydryl and the amino groups.

ALFRED DELVILLE et CHRISTIAN DETELLIER. Can. J. Chem. **64**, 1845 (1986).

L'étude de la complexation du Zn(II) par la D-(−)-pénicillamine a été effectuée en solutions aqueuses en fonction du pH, de la concentration en pénicillamine et de la température, à l'aide de la résonance magnétique nucléaire du Zn-67. Les mesures des temps de relaxation longitudinal et transverse montrent la présence en solution de complexes en échange rapide avec le cation $Zn(II)_{aq}$. Les résonances de ces complexes obéissent aux conditions de rétrécissement extrême. À l'aide de valeurs de constantes d'équilibre tirées de la littérature, une modélisation de la relaxation observée a fourni des largeurs de raie caractéristiques des complexes Zn(Pen) (ν = (6200 ± 500) Hz) et $[Zn(Pen\,H)]^+$ (ν = (6000 ± 1000) Hz). Ces valeurs sont en accord avec une chélation du zinc par les groupements sulfhydryle et amino.

Introduction

D-(−)-Penicillamine (**1**, H_2Pen) is a powerful ligand for transition metal cations (1–12). It acts as a bidentate or tridentate ligand, taking advantage of the coordination ability of

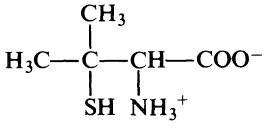

1

its amino, sulfhydryl, and carboxylic groups. The diversity of the possible ligation sites together with their protonation pattern make this small molecule a versatile ligation system. The pK_a values of $(H_3Pen)^+$ are $pK_1 = 1.92$; $pK_2 = 8.00$; $pK_3 = 10.74$ (25.0°C; 0.1 *M* KNO_3) (5), where pK_2 and pK_3 are composite macroscopic constants. These values corroborate previous similar determinations (3). The values of the equilibrium constants for the formation of complexes between the penicillamine dianion and transition metal cations show the effectiveness of this molecule to capture Cd(II) or Hg(II), for example ($\log \beta_1$ = 11.5 and 18.9; $\log \beta_2$ = 19.5 and 25.0 for Cd(II) and Hg(II) respectively) (5). In addition to the 1:1 and 1:2 complexes, diverse protonated complexes or polynuclear species coexist in solution (4, 7). Penicillamine has been used in the treatment of metal poisoning (13–18), can chelate excess copper responsible for the blocking of nerve impulses in Wilson's disease (19, 20), is an effective drug in rheumatoid arthritis (21–23), idiopathic pulmonary fibrosis (24), and scleroderma (25), and its copper complex possesses some anti-inflammatory properties (26).

In that context, the study of the complexes formed between Zn(II) and penicillamine is of interest since, for example, they interfere with the removal of toxic mercury, cadmium, or lead (5). Some unwanted side effects could originate in the complexation of essential zinc (27). X-ray photoelectron spectroscopy results (1) support a structure for the 1:2 complex in the solid state in which one penicillamine moiety acts as a monodentate carboxylate ligand and the second penicillamine is coordinated to zinc through the sulfhydryl and the amino groups. In solution, a structure in which the two penicillamine molecules act as bidentate ligands is more probable, the two sites of ligation being the sulfhydryl and the amino groups (2, 11, 14, 23, 28). The coordination could possibly involve the carboxylic group at lower pH range (6). The X-ray structure of dibromo-bis(D-penicillamine)Zn(II) isolated from an acidic solution (pH 2) has been recently published: penicillamine behaves as a monodentate ligand with the deprotonated carboxylate group as the binding site (29). Formation constants for the Zn(Pen) and $[Zn(Pen)_2]^{2-}$ complexes are $\log \beta_1 = 9.38$ and $\log \beta_2 = 19.39$ respectively (μ = 0.12, 25°C) (3). The order of magnitude of these values is corroborated by other works (4–6). Since $K_2 > K_1$, for a sufficiently high ligand concentration the major species in solution are aquated Zn(II) and $[Zn(Pen)_2]^{2-}$ (4–6). Consequently, until now, the structure of the 1:1 complex in solution has been only rarely discussed.

To better define the nature and the structure of these complexes in solution, we have undertaken a Zn-67 nuclear magnetic resonance study of the system Zn(II)–penicillamine in water at different pH values. The only nmr active isotope of zinc, Zn-67 (spin 5/2) is a quadrupolar nucleus endowed with a poor receptivity (0.665 with respect to C-13) due to its low natural abundance (4.11%) and its low gyromagnetic ratio (1.6737×10^3 rad s^{-1} G^{-1}) (30). So far, only a few studies have involved this nucleus (31–38). Given the high biological importance of zinc, and the inability to use other spectroscopic techniques directly, the development of Zn-67 nmr is of prime significance.

We show in this paper that Zn-67 nmr can be used to study the complexation of Zn(II) by penicillamine in relatively dilute conditions (0.10 *M*). We work in conditions where Zn(II) is in

[1]Chargé de recherches FNRS; usual address: Laboratoire de Chimie Organique Physique, Université de Liège, B-4000, Liège, Belgium.

[2]Author to whom correspondence may be addressed.

[3]Revision received April 11, 1986.

large excess compared to penicillamine and consequently where the 1:1 complex is in excess compared to the 1:2 complex. We give an estimate of the characteristic relaxation rates for the complexes Zn(Pen) and $[Zn(Pen\,H)]^+$.

Experimental

$Zn(NO_3)_2 \cdot 6H_2O$ (Baker) and D-(−)-penicillamine (Aldrich) were used without further purification. The zinc concentration was checked by EDTA titration and the pH was adjusted by addition of small amounts of concentrated NaOH or H_2SO_4. The pH meter (Corning 155) was calibrated with buffer solutions at pH 7.00 ± 0.01 and 4.00 ± 0.01. The precision of the pH measurements was better than 0.02 pH units.

The nmr spectra were recorded on a Varian XL-300 spectrometer operating at the frequency of 18.768 MHz. The 90° pulse width was 91 μs. Typically, the acquisition time was 10 ms for a 1-ms transverse relaxation time. No weighting functions were applied to the FID, which was Fourier transformed with zero filling. All measurements at room temperature were made on 16-mm spinning tubes, and on 10-mm spinning tubes at variable temperatures. Solvent was a mixture of D_2O/H_2O (20:80) to provide a deuterium lock. No correction was made to pH values for the use of 20% D_2O. Chemical shifts were measured with reference to a 1.0 *M* $Zn(NO_3)_2$ solution (pH = 4.47). Sample temperatures were measured with a copper–constantan thermocouple dipped into the non-spinning tube. The precision of the temperature reading was estimated to be ±0.5°C. To attenuate the acoustic ringing of the probe (39) we used the pulse sequence ACOUSTIC (40): —(90°, x – ACQ^+ – Dl – 180°, $x - \tau - 90°$, x – ACQ^- – Dl – 90°, x – ACQ^+ – Dl – 180°, $-x - \tau - 90°$, x – $ACQ^-\rightarrow_n$ (40, 41), which was available as the standard program ACOUST on the XL-300. In the case of a quadrupolar nucleus, the delay D1 can be set to short values or zero, since the acquisition time permits a full relaxation of the magnetization. The delay τ is the crucial parameter for a successful result. With our instrumentation (Varian XL-300) we found 100 μs to be a good compromise, with the use of a delay time (100–200 μs) between the end of the 90° pulse and the beginning of the acquisition. To obtain an acceptable base line in the case of the routine pulse sequence —(90° – $ACQ\rightarrow_n$, this delay would have been 1 ms, an unacceptable value for a rapidly relaxing quadrupolar nucleus. Typical conditions were as follows (given for 0.10 *M* Zn(II) and 0.10 *M* penicillamine at pH 3.0): acquisition time = 0.02 s; delay Dl = 0.01 s; delay between 90° pulse and acquisition = 100 μs; total experiment time was less than 1 h (112 000 transients); signal on noise ratio = 50; line width = (140 ± 10) Hz.

Transverse relaxation times were directly determined from a linewidth measurement. We have checked that the measured line width was independent of the delay time between the 90° pulse and the beginning of the acquisition. All spectra had a Lorentzian line shape. Longitudinal relaxation times were measured with the sequence $-(-180° - \tau - 90° - ACQ\rightarrow_n$, with at least ten τ comprised between 0 and 20 times T_1. T_1 was calculated by a nonlinear regression on three parameters (42). Typical conditions were as follows (given for 0.20 *M* Zn(II), 6×10^{-3} *M* penicillamine, pH 3.5): acquisition time = 0.05 s; delay between 90° pulse and acquisition = 200 μs; ten values of τ between 0.2 ms and 160 ms; the total experiment time was less than 1 h; 3000 transients for each spectrum; T_1^{-1} = (92 ± 5) Hz.

Results

Transverse relaxation times

Table 1 gives the line width at half-height ($\nu_{1/2}$) of the Zn-67 signal as a function of the ratio ρ = $[H_2$ Pen$]/[Zn(II)]$ for different pH, at (21 ± 1)°C. The line width of a 0.1 *M* $Zn(NO_3)_2$ aqueous solution is (25 ± 2) Hz, which is in good agreement with previously published values (31, 33). The line width of the latter solution did not vary significantly with changes in pH. However, small amounts of added penicillamine have a considerable effect on the observed line width: for ρ = 0.1, $\nu_{1/2}$ = 44 Hz (pH = 3.1), 60 Hz (pH = 4.0), 360 Hz (pH = 5.0), 460 Hz[4] (pH = 6.2). This trend corresponds to the diminution of the relative percentage of the aquated Zn(II) cation when the pH increases (6). This is similar to the result obtained recently by Kohnlein *et al.* (33) for a 1 *m* $ZnSO_4$ solution in the presence of increasing amounts of sodium citrate (0–80 m*m*). In the case of a ratio ρ = [citrate]/[Zn(II)] = 0.1, the value of the reported line width was twice that measured from a 1 *m* Zn(II) solution. We have been limited in our investigations by the formation of precipitates for ratios [Pen]/[Zn(II)] bigger than the ones indicated in Table 1.

TABLE 1. Zn-67 bandwidth at half height ($\nu_{1/2}$) as a function of pH and of ρ = [penicillamine]/[Zn(II)] ratios. $[Zn(NO_3)_2]$ = 0.10 *M*

ρ	$\nu_{1/2}$ (Hz)	pH (±0.02)
0	23 ± 3	3.05
0.099	44 ± 6	3.10
0.18	51 ± 6	3.01
0.40	40 ± 10	3.01
0.67	100 ± 10	3.01
1.00	140 ± 10	3.01
2.00	250 ± 15	3.00
0	24 ± 3	4.09
0.020	29 ± 3	4.03
0.053	40 ± 4	3.95
0.10	60 ± 8	3.94
0.18	110 ± 10	4.00
0.30	200 ± 20	4.00
0.44	370 ± 40	4.00
0	25 ± 5	5.0
0.010	37 ± 5	5.04
0.020	66 ± 10	5.08
0.040	125 ± 15	5.02
0.060	190 ± 15	5.01
0.082	260 ± 20	5.00
0.10	360 ± 40	5.00
0	37 ± 4	6.29
0.013	100 ± 10	6.06
0.042	230 ± 20	6.00
0.089	400 ± 60	6.24
0.14	710 ± 150	6.16

Under non-extreme narrowing conditions, the relaxation of a spin 5/2 nucleus is characterized by three exponential decays (43). In all the cases studied here only one Lorentzian line was observed, which can be the result of extreme narrowing conditions, where all three components of the relaxation are identical ($\omega^2\tau_c^2 \ll 1$), or of very fast relaxation for two of the three components. We can simply test which of these two hypotheses is valid by varying the waiting time between the 90° pulse and the acquisition. If the observed resonance were superposed upon one or two other broad resonances, variation of that waiting time should affect the observed line width. This is not observed: the measured line width is independent of the waiting time. A better test is given by the comparison between T_2 and T_1:T_2 = T_1 under extreme narrowing conditions. Moreover, an equality of T_2 and T_1 would show the absence of a chemical exchange contribution to the transverse relaxation time (44–46). This test will be considered in the next section.

Since the observed broadening could be due to an exchange

[4]Interpolated value.

TABLE 2. Zn-67 longitudinal and transverse relaxation rates as a function of pH for different [penicillamine]/[Zn(II)] ratios (ρ). $[Zn(NO_3)_2] = 0.20\ M$

pH (±0.02)	T_2^{-1} (Hz)	T_1^{-1} (Hz)	ρ
3.48	125 ± 10	92 ± 5	0.030
4.02	150 ± 15	130 ± 5	0.030
5.08	480 ± 30	474 ± 10	0.030
6.05	570 ± 40	520 ± 30	0.030
3.42	150 ± 15	110 ± 6	0.050
4.21	310 ± 30	270 ± 15	0.050
5.13	780 ± 40	800 ± 60	0.050
6.16	910 ± 50	870 ± 40	0.050
3.52	220 ± 20	190 ± 10	0.0996
4.19	690 ± 70	680 ± 40	0.0996
5.00	1900 ± 200	1700 ± 200	0.103
5.61	83 ± 10	66 ± 4	0

process between aquated Zn(II) and penicillamine–Zn(II) complexes, we have tested this hypothesis by temperature measurements. Ln (T_2^{-1}) increases linearly with an increase of T^{-1} for 0.2 M $Zn(NO_3)_2$, in the absence of any penicillamine. This behaviour was expected on the basis of the high value of the Zn-67 quadrupole moment (0.15×10^{-28} m^2), which makes the quadrupolar mechanism of relaxation very effective.

In the presence of penicillamine, the order of magnitude of T_2^{-1} does not change dramatically with temperature for a given pH: $4.9 < \ln T_2^{-1} < 5.1$ at pH 3.4; $6.2 < \ln T_2^{-1} < 6.6$ at pH 5.0; $6.4 < \ln T_2^{-1} < 7.3$ at pH 6.4. Line widths in the range 0.7–1.4 kHz are found at pH 5.0 and 6.4. This order of magnitude is accompanied by large errors, precluding any precise analysis of the data. However, the observation that the order of magnitude of the line widths is constant for a given pH is a good indication that there is no chemical exchange contribution to the transverse relaxation time.

Longitudinal relaxation times

Table 2 shows Zn-67 longitudinal and transverse relaxation rates at different pH and for different ratios ρ = [Pen]/[Zn(II)] of 0.2 M zinc nitrate solutions. A measure of the inhomogeneity contribution to T_2 is obtained from the difference between T_2^{-1} and T_1^{-1} for the 0.2 M $Zn(NO_3)_2$ solution (pH = 5.61) and is 17 ± 14 Hz. Given the inhomogeneity contribution, one observes an equality between T_2^{-1} and T_1^{-1} for all the cases studied: the system obeys the extreme narrowing condition. Moreover, the equality of T_2 and T_1 excludes the possibility of an exchange contribution to the transverse relaxation time.

Chemical shifts

Zn-67 chemical shifts are sensitive to the nature of the counterion in concentrated solutions, spanning a range of 300 ppm from iodide to cyanide (34), and are also quite sensitive to the nature of the solvent (31). However, within the limits of experimental error, we did not observe any measurable chemical shifts of the Zn-67 signal with increasing concentrations of penicillamine. We will come back to this point in the discussion.

We have carried out exploratory measurements on a 0.1 M $Zn(NO_3)_2$ solution at pH ≃ 13.5. A single resonance line was observed at (205 ± 5) ppm with reference to 1.0 M $Zn(NO_3)_2$ (pH 4.47); the line width was (200 ± 30) Hz. We attribute this resonance to the zincate anion, $Zn(OH)_4^{2-}$, whose chemical shift is in the range oberved for other tetracoordinated anionic zinc derivatives: $ZnBr_4^{2-}$ (δ = 169 ppm), $ZnCl_4^{2-}$ (δ = 253 ppm) (34).

Modelling

The observed relaxation rate can be described by a fast exchange and is the result of the average of all the possible contributions originating from the different complexes in fast equilibrium. This is reflected in eq. [1], which is valid under the condition that the rate constant for dissociation is small compared to the inverse of the correlation time for the complexed species (47). This condition is fulfilled, given the high values of the equilibrium constants for the formation of the various complexes (see below). To derive the characteristic line widths for some complexes, we have used the formation constants of the Zn(II)–penicillamine complexes that have been determined in the literature (5, 6). The following zinc-containing species have been considered: Zn(Pen) ($\log \beta_{110} = 9.66$); $[Zn(Pen)_2]^{2-}$ ($\log \beta_{120} = 19.39$); $[Zn(Pen\ H)]^+$ ($\log \beta_{111} = 14.8$); $[Zn(Pen)_2H]^-$ ($\log \beta_{121} = 25.23$); $[Zn(Pen)_2H_2]$ ($\log \beta_{122} = 30.65$), in addition to the protonated forms of penicillamine: $(Pen\ H)^-$ ($\log \beta_{011} = 10.658$); $Pen\ H_2$ ($\log \beta_{012} = 7.932 + \log \beta_{011}$); $(Pen\ H_3)^+$ ($\log \beta_{013} = 1.90 + \log \beta_{012}$) (6). For each pH value and total Zn(II) and penicillamine concentrations (Table 1), $[Pen^{2-}]$ was calculated from a third degree equation solved by an iterative Newton–Gauss procedure. The observed line width was then fitted following eq. [1]

$$[1]\quad (\nu_{1/2})_{obs}\cdot[Zn(II)]_T = \nu_0[Zn(II)_{aq}] + \nu_1[Zn(Pen)] + \nu_2[Zn(Pen)_2^{2-}] + \nu_3[Zn(Pen\ H)^+] + \nu_4[Zn(Pen_2H)^-] + \nu_5[Zn(Pen)_2H_2]$$

where $[Zn(II)]_T$ is the total Zn(II) concentration, $[Zn(II)_{aq}]$ the concentration of aquated Zn(II), $[Zn(Pen)_iH_j]$ the concentrations of the different complexes, and ν_0 was experimentally determined (Table 1). Figure 1 shows the result of the fittings. Each fitting was effected independently for each pH value. However, a simultaneous fitting on the four pH curves did not give significantly different results. At pH 6.0, only two species are major: $Zn(II)_{aq}$ and Zn(Pen). We can determine in these conditions a characteristic line width for the complex Zn(Pen) with a good precision: $\nu_{1/2}$ = (6200 ± 500) Hz. At pH = 3.0, two major species are also present: $Zn(II)_{aq}$ and $Zn(Pen\ H)^+$ for which we determine a characteristic line width $\nu_{1/2}$ = (6000 ± 1000) Hz. At intermediate pH, more species strongly influence the fitting procedure and the characteristic line widths for the various complexes could be determined only with large errors. Unfortunately, at the Zn(II) concentrations used we were limited in the quantity of added penicillamine by the insolubility of complexes of the type $Zn(Pen)_2H_j$ (j = 0–2).

Discussion

All the spectra studied belong to the extreme narrowing regime. This is in good agreement with the fact that only monomeric chemical species are formed in the Zn(II)–penicillamine system (4, 7). The equality between T_1 and T_2 rules out the possibility of an exchange contribution to the transverse relaxation rate. Using equilibrium constant data from the literature (6), the characteristic line widths for two complexes were determined: Zn(Pen): (6200 ± 500) Hz and $(Zn\ Pen\ H)^+$: (6000 ± 1000) Hz. The finding of an equality between the two values supports the structure accepted for the solution state: coordination through the sulfhydryl and amino groups (3). The possibility of a coordination involving the carboxylic group in

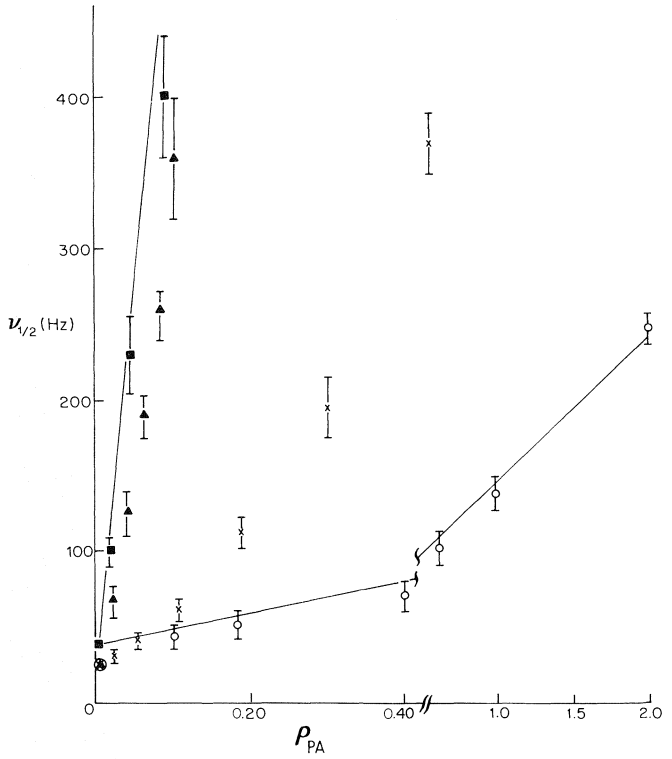

FIG. 1. Zn-67 line width variation as a function of the ratio ρ [penicillamine]/[Zn(II)], at different pH values. $[Zn(NO_3)_2]$ = 0.10 *M*. (○): pH ≃ 3; (×) pH ≃ 4; (▲) pH ≃ 5; (■) pH ≃ 6 (see Table 1 for precise pH values). The points are experimental and the curves are calculated (see text).

the lower pH range had been proposed (6). Our results at pH 3 and 6 strongly suggest a structure involving only sulfhydryl and amino groups in the chelation of Zn(II), in such a manner that the site of protonation of the complex is the non-coordinated carboxylic group. This protonation has a minor influence on the electric field gradient at the Zn(II) site, which is reflected in the similarity of the characteristic relaxation rates for Zn(Pen) and $Zn(Pen\,H)^+$. Of course, these conclusions are valid under the assumption that the equilibrium model used is fully correct. Morever, we have likened proton activities to concentrations. In the case of ionic strength constancy, this approximation results in a systematic error. In the case of our study, the initial ionic strength of the Zn(II) solution (0.3) is progressively reduced with the addition of penicillamine. However, since in our study the population of complexed Zn(II) is always lower than 14%, we have preferred not to introduce any activity correction (48).

A highly asymmetric environment for complexed Zn(II) is suggested by the high value (6000 Hz) of the characteristic line widths of the complexes. Under extreme narrowing conditions, the relaxation rates of a spin 5/2 nucleus is given by:

$$[2]\quad \frac{1}{T_2} = \frac{12\pi^2}{125}\left(\frac{e^2qQ}{h}\right)\tau_q\left(1+\frac{\eta^2}{3}\right)$$

where $\chi = e^2qQ/h$ is the quadrupolar coupling constant (NQCC), η the asymmetry factor, and τ_q the correlation time responsible for the quadrupolar relaxation. A correlation time has been determined by N-14 nmr for penicillamine 0.2 *M* in aqueous solution: τ_q(N-14) = (34 ± 9) ps (49). Knowing that the complex involves only one penicillamine molecule, we make the approximation that τ_q(Zn-67) of Zn(Pen) equals τ_q(N-14) of (Pen) and, neglecting the asymmetry factor η, we obtain an estimate of χ, the quadrupolar coupling constant: χ = (13 ± 5) MHz. This appears to be the first proposed Zn-67 quadrupolar coupling constant value in solution and is valid only under the assumptions of the double nuclear spin method (50, 51). It can be compared with the published value of the Zn-67 quadrupolar coupling constant in Zn metal determined by nuclear quadrupole resonance: 13.620 MHz (52).

Zn-67 chemical shifts are known to span a large range of values and one expects them to be very sensitive to the nature of the first coordination sphere of Zn(II). Consequently, one would expect to observe a large chemical shift variation when Zn(II) is complexed by penicillamine. However, we have an apparent contradiction here since, within the limits of experimental error, the observed Zn-67 chemical shift does not show any variation outside a 1-ppm range. To resolve this apparent contradiction two facts have to be stressed. First, large line width variations are observed: for a ratio ρ = 0.14 and $[Zn(II)]_T$ = 0.10 *M*, $\nu_{1/2}$ = 710 ± 150 Hz. Under these conditions chemical shifts can hardly be measured with a better precision than 3 ppm, and any expected chemical shift variation is accompanied by a large increase of the experimental error on its measurement. Second, in the conditions mentioned of ρ = 0.14 and $[Zn(II)]_T$ = 0.10 *M*, one can calculate (6) that only 9% of the total zinc is the 1:1 complex Zn(Pen), when less than 2% is $[Zn(Pen)_2]^{2-}$ or $[Zn(Pen\,H)]^+$, the quantity of $[Zn(Pen)_2\,H]^-$ being negligible. A chemical shift variation of 3 ppm, the error limit, would correspond to a characteristic chemical shift for the complex of the order of 30 ppm. For a 1 molal $ZnSO_4$ solution in the presence of a 10 m*m* citrate solution a shift of 0.55 ppm to lower frequency has been reported, which would lead to a maximum value of 55 ppm for the complex Zn(II)–citrate (33).

Acknowledgements

This research has been supported by a grant from the Natural Sciences and Engineering Research Council of Canada (NSERCC). A.D. acknowledges a NATO travel grant.

1. C. R. COTHERN, W. E. MODDEMAN, R. G. ALBRIDGE, W. J. SANDERS, P. L. KELLY, W. S. HANLEY, and L. FIELD. Anal. Chem. **48**, 162 (1976).
2. G. A. KHARITONOVA, V. I. NEFEDOV, and L. N. PAWKRATOVA. Russ. J. Inorg. Chem. **17**, 1649 (1972).
3. J. H. RITSMA and F. JELLINEK. Recl. Trav. Chim. Pay-Bas, **91**, 923 (1972).
4. D. D. PERRIN and I. G. SAYCE. J. Chem. Soc. A, 53 (1968).
5. R. STRAND, W. LUND, and J. AASETH. J. Inorg. Biochem. **19**, 301 (1983).
6. I. SOVAGO, A. GERGELY, B. HARMAN, and T. KISS. J. Inorg. Nucl. Chem. **41**, 1629 (1979).
7. A. M. CORRIE, M. D. WALKER, and D. R. WILLIAMS. J. Chem. Soc. Dalton Trans. 1012 (1976).
8. H. C. FREEMAN, C. J. MOORE, W. G. JACKSON, and A. M. SARGESON. Inorg. Chem. **17**, 3513 (1978).
9. M. E. COOKE, M. E. MCDANIEL, S. R. JAMES, S. L. JONES, N. TROBAK, B. C. CRAYTOR, D. R. BUSHMAN, and J. R. WRIGHT. J. Inorg. Biochem. **18**, 313 (1983).
10. H. SAKURAI, S. SHIMOMURA, and T. YOSHIMURA. Biochem. Biophys. Res. Commun. **115**, 618 (1983).
11. E. J. KUCHINSKAS and Y. ROSEN. Arch. Biochem. Biophys. **97**, 370 (1962).
12. A. GERGELY and I. SOVAGO. *In* Metal ions in biological systems. Vol. 9. *Edited by* H. Sigel. M. Dekker, New York. 1979. Chapt. 3. pp. 77–102.
13. J. J. CHISOLM. Pediatr. Clin. North Am. **17**, 591 (1970).

14. D. A. DOORNBOS and J. S. FABER. Pharm. Weekbl. **99**, 289 (1964).
15. R. F. BUTTERWORTH, M. GONCE, and A. BARBEAU. Can. J. Neurol. Sci. **5**, 397 (1978).
16. M. A. BASINGER and A. D. WEATHER. J. Inorg. Nucl. Chem. **43**, 1705 (1981).
17. M. A. BASINGER, M. M. JONES, and S. A. MCCROSKEY. J. Toxicol. Clin. Toxicol. **20**, 159 (1983).
18. D. L. RABENSTEIN, A. A. ISAB, W. KADIMA, and P. MOHANAKRISHNAN. Biochem. Biophys. Acta, **762**, 531 (1983).
19. O. WAWSCHINEK and W. BEYER. J. Clin. Chem. Clin. Biochem. **19**, 541 (1981).
20. I. STERNLIEB and I. H. SCHEINBERG. J. Am. Med. Assoc. **189**, 748 (1964).
21. I. A. JAFFE. Ann. N.Y. Acad. Sci. **256**, 330 (1975).
22. C. J. DUNN, M. PROUTEAU, M. DELAHAYE, T. PURCELL, and C. BRANCENI. Agents Actions, **14**, 269 (1984).
23. J. R. GOLDING, F. M. ANDREWS, A. V. CAMP, A. T. DAY, A. M. FREEMAN, D. N. GOLDING, A. G. S. HILL, W. H. LYLE, and A. G. MOWAT. Ann. Rheum. Dis. **32**, 385 (1973).
24. R. I. HENKIN, H. R. KEISER, I. A. JAFFE, I. STERNLIEB, and I. H. SCHEINBERG. Lancet, **2**, 1268 (1967).
25. E. D. HARRIS, JR. and A. SJOERDSMA. Lancet, **2**, 996 (1966).
26. A. D. SEDGWICK, J. C. W. EDWARDS, and D. A. WILLOUGHBY. Int. J. Tissue React. **5**, 11 (1983).
27. A. CATSCH and A. E. HARMUTH-HOENE. Biochem. Pharmacol. **24**, 1557 (1975).
28. L. FIELD, W. S. HANLEY, P. L. KELLY, W. D. SANDERS, J. E. WHITE, I. A. JAFFE, and P. MERRYMAN. J. Med. Chem. **16**, 1152 (1973).
29. P. BELL and W. S. SHELDRICK. Z. Naturforsch. B: Anorg. Chem. Org. Chem. **39**, 1732 (1984).
30. C. BREVARD and P. GRANGER. Handbook of high resolution multinuclear magnetic resonance. J. Wiley and Sons, New York. 1981. p. 130.
31. Z. F. LI and A. I. POPOV. J. Solution Chem. **11**, 17 (1982).
32. B. W. EPPERLEIN, H. KRUGER, O. LUTZ, and A. SCHWENK. Z. Naturforsch. A: Phys. Phys. Chem. Kosmophys. **29**, 1553 (1974).
33. D. KOHNLEIN, O. LUTZ, and P. RUPPERT. J. Magn. Res. **57**, 486 (1984).
34. G. E. MACIEL, L. SIMERAL, and J. J. H. ACKERMAN. J. Phys. Chem. **81**, 263 (1977).
35. R. E. RICHARDS and N. A. THOMAS. J. Chem. Soc. Perkin Trans. 2, 368 (1974).
36. T. SHIMIZU and M. HATANO. Biochem. Biophys. Res. Commun. **104**, 1356 (1982).
37. T. SHIMIZU and M. HATANO. Inorg. Chim. Acta, **76**, L177 (1983).
38. G. K. LARSON and P. A. W. DEAN. Inorg. Chim. Acta, **66**, 157 (1982).
39. C. BREVARD. *In* NMR of newly accessible nuclei. Vol. 1. *Edited by* P. Laszlo. Academic Press, New York. 1983. Chapt. 1, pp. 12–13.
40. S. L. PATT. J. Magn. Reson. **49**, 161 (1982).
41. D. CANET, J. BRONDEAU, J. P. MARCHAL, and B. ROBIN-LHERBIER. Org. Magn. Reson. **20**, 51 (1982).
42. G. C. LEVY, R. L. LICHTER, and G. L. NELSON. Carbon-13 nuclear magnetic resonance spectroscopy. 2nd ed. John Wiley & Sons, New York. 1980.
43. T. E. BULL, S. FORSEN, and D. L. TURNER. J. Chem. Phys. **70**, 3106 (1979).
44. D. E. WOESSNER. J. Chem. Phys. **35**, 41 (1961).
45. H. D. H. STOVER, A. DELVILLE, and C. DETELLIER. J. Am. Chem. Soc. **107**, 4167 (1985).
46. A. DELVILLE, H. D. H. STOVER, and C. DETELLIER. J. Am. Chem. Soc. **107**, 4172 (1985).
47. J. P. BEHR and J. M. LEHN. J. Am. Chem. Soc. **98**, 1743 (1976).
48. M. S. SUN, D. K. HARRIS, and V. R. MAGNUSON. Can. J. Chem. **58**, 1253 (1980).
49. R. E. RICHARDS and N. A. THOMAS. J. Chem. Soc. Perkin Trans. 2, 368 (1974).
50. J. P. KINTZINGER and J. M. LEHN. J. Am. Chem. Soc. **96**, 3313 (1974).
51. M. BISNAIRE, C. DETELLIER, and D. NADON. Can. J. Chem. **60**, 3071 (1982).
52. E. N. KAUFMANN, J. R. BROOKEMAN, P. C. CANEPA, T. A. SCOTT, D. H. RASMUSSEN, and J. H. PEREPEZKO. Solid State Commun. **29**, 375 (1979).

Properties of a strong intramolecular OHO hydrogen bond in 2-(*N*,*N*-diethylamino-*N*-oxymethyl)-4,6-dichlorophenol

A. KOLL, M. ROSPENK, L. SOBCZYK, AND T. GŁOWIAK
Institute of Chemistry, University of Wrocław, 50-383 Wrocław, Poland

Received September 26, 1985[1]

A. KOLL, M. ROSPENK, L. SOBCZYK, and T. GŁOWIAK. Can. J. Chem. **64**, 1850 (1986).

The crystals of 2-(*N*,*N*-diethylamino-*N*-oxymethyl)-4,6-dichlorophenol chosen as a representative of the Mannich base *N*-oxides were found to be monoclinic, $P2_1/c$ space group, with $a = 11.729(3)$, $b = 16.232(4)$, $c = 13.689(3)$ Å, $\beta = 107.37(3)°$, and $Z = 8$. The structure solved by the direct method was refined to $R = 0.033$ for 3170 independent reflections. Two slightly different molecules denoted as **A** and **B** in the unit cell with very short (2.42 and 2.40 Å) OHO intramolecular hydrogen bonds were detected. Both a X-ray diffraction study and the ir and uv spectra indicate a symmetric type of bridge in this compound.

A. KOLL, M. ROSPENK, L. SOBCZYK et T. GŁOWIAK. Can. J. Chem. **64**, 1850 (1986).

On a trouvé que les cristaux du (*N*,*N*-diéthylamino *N*-oxy méthyl)-2 dichloro-4,6 phénol, qui ont été choisi comme représentatifs des *N*-oxydes des bases de Mannich, sont monocliniques, avec un groupe d'espace $P2_1/c$ et $a = 11,729(3)$, $b = 16,232(4)$ et $c = 13,689(3)$ Å, $\beta = 107,37(3)°$ et $Z = 8$. On a résolu la structure par des méthodes directes et on l'a affinée jusqu'à une valeur de $R = 0,033$ pour 3170 réflexions indépendantes. On a détecté deux molécules légèrement différentes, **A** et **B**, dans chaque maille unitaire; on a aussi noté l'existence de liaisons hydrogènes intramoléculaires OHO très courtes (2,42 et 2,40 Å). Tant l'étude par diffraction des rayons-X que les spectres ir et uv suggèrent la présence d'un pont de type symétrique dans ce composé.

[Traduit par la revue]

Introduction

The *ortho* Mannich bases show an interesting example of intramolecular hydrogen bonds as analogues of intermolecular bonds between parent phenols and amines (1–3). These bonds possess all of the spectroscopic features typical of intermolecular bonds and are characterized by a rigid conformation and high stability. It seemed interesting to undertake a study of the behaviour of *N*-oxides of *ortho* Mannich bases. One could expect that in this case strong intramolecular OH...O hydrogen bonds would be formed. However, in the crystalline state one cannot exclude the possibility of breaking of intramolecular, and the formation of intermolecular bonds as in 2-(*N*,*N*-diethylaminomethyl)-4-nitrophenol where proton transfer and the creation of dimeric ionic structures take place (4). As a subject of our study we selected 2-(*N*,*N*-diethylamino-*N*-oxymethyl)-4,6-dichlorophenol (**1**), in which the proton–donor capability of the phenolic group is distinctly pronounced.

Experimental

The *N*-oxides of *ortho* Mannich bases were synthesized by oxidation of the bases in Perhydrol. The crystals of compound **1** were grown from water–ethanol solutions; mp, 146–147°C. Density of crystals was measured by flotation method in $CCl_4/C_2H_4Cl_2$ solution.

The ir spectra were recorded on a Perkin-Elmer spectrophotometer type 180 and a Carl-Zeiss Jena Specord 75 IR Spectrophotometer. The uv spectra were studied by using a Carl-Zeiss Jena Specord UV Vis Spectrophotometer.

The space group and approximate unit-cell dimensions were determined from rotation and Weissenberg photographs. The diffraction data for a crystal with dimensions 0.45 × 0.50 × 0.50 mm were collected with MoK_α radiation on a Syntex $P2_1$ four-circle diffractometer with a graphite monochromator. The lattice parameters and orientation matrix used from data collection were obtained from the least-squares refinement of 15 reflections ($19° < 2\theta < 29°$). All diffraction data were collected at room temperature by the θ–2θ scan technique, to $2\theta = 50.0°$. Two check reflections measured after each 50 reflections indicated no decomposition. The raw intensity data were corrected for Lorentz and polarization effects, but not for absorption and extinction.

TABLE 1. Summary of data collection and processing parameters

Space group	$P2_1/c$
Cell constants	$a = 11.729(3)$ Å
	$b = 16.232(4)$
	$c = 13.689(3)$
	$\beta = 107.37(3)°$
	$V = 2487.3$ Å^3
Molecular formula	$C_{11}H_{15}NO_2Cl_2$
Molecular weight	264.2
Molecules per cell	$Z = 8$
Density	$D_m = 1.40(1)$ g cm^{-3}
	$D_c = 1.41$
Absorption coefficient (MoK_α)	$\mu = 5.1$ cm^{-1}
Unique data collected	4389
Data with $I > 4\sigma(I)$	3170
Total variables	409
$R = \Sigma(\lvert F_o\rvert - \lvert F_c\rvert)/\Sigma\lvert F_o\rvert$	0.033
$R_w = [\Sigma w(F_o - F_c)^2/\Sigma w(F_o)^2]^{1/2}$	0.032
$S = [\Sigma w(F_o - F_c)^2/(n - p)]^{1/2}$	2.742
Final $\Delta\sigma$	±0.2 eÅ^3
Final $(\Delta/\sigma)_{max}$	0.02 for non-H atoms
	0.13 for H atoms

The structure was solved by the direct phase determination method using the program MULTAN (1974 Syntex version of program in ref. 5) and refined by a full-matrix least-squares technique. The non-hydrogen atoms were recognized from an *E*-map (calculated for the starting set having the highest combined FOM of 3.0) and the Fourier synthesis. The positions of all hydrogen atoms were determined from the difference Fourier synthesis. Several cycles of refinement of coordinates and thermal parameters (anisotropic for non-hydrogen and isotropic for hydrogen atoms) reduced the *R* value to 0.033 and R_w to 0.032 for the 3170 significant independent reflections with $F > 8.0\sigma(F)$. The minimized function was $\Sigma w(\lvert F_o\rvert - \lvert F_c\rvert)^2$ with $w = 1/\sigma^2(F)$. Neutral atomic scattering factors for all atoms were taken from a standard source (6) while all calculations were performed on NOVA 1200 minicomputer with the SYNTEX XTL/STLE struc-

[1]Revision received May 1, 1986.

TABLE 2. Positional parameters and isotropic temperature factors with esd's in parentheses

Atom	x	y	z	B_{eq}/B_{iso}
		Molecule **A**		
Cl(1)	0.1873(1)	0.4492(1)	0.0301(1)	4.96
Cl(2)	0.6555(1)	0.3933(1)	0.0899(1)	4.89
O(1)	0.5809(2)	0.2222(1)	0.0426(2)	4.12
O(2)	0.4984(2)	0.1074(1)	−0.0698(2)	4.04
N	0.3737(2)	0.1145(1)	−0.0925(2)	3.26
C(11)	0.4903(2)	0.2720(2)	0.0400(2)	3.37
C(12)	0.3710(2)	0.2442(2)	0.0148(2)	3.09
C(13)	0.2789(3)	0.2986(2)	0.0122(2)	3.33
C(14)	0.3033(2)	0.3806(2)	0.0348(2)	3.60
C(15)	0.4193(3)	0.4099(2)	0.0607(2)	3.76
C(16)	0.5106(2)	0.3557(2)	0.0624(2)	3.44
C(1)	0.3432(3)	0.1539(2)	−0.0023(2)	3.17
C(2)	0.3228(3)	0.0280(2)	−0.1036(2)	3.61
C(3)	0.3492(4)	−0.0198(2)	−0.1888(3)	5.13
C(4)	0.3299(3)	0.1652(2)	−0.1887(2)	4.04
C(5)	0.1967(3)	0.1761(2)	−0.2281(3)	4.96
H	0.541 (3)	0.163 (2)	−0.010 (3)	7.3
		Molecule **B**		
Cl(1)	0.4253(1)	0.1076(1)	0.2874(1)	4.82
Cl(2)	−0.0405(1)	0.0731(1)	0.2557(1)	6.20
O(1)	−0.0360(2)	−0.0564(1)	0.1084(2)	4.76
O(2)	−0.0037(2)	−0.1901(1)	0.0453(2)	6.19
N	0.1191(2)	−0.1940(1)	0.0550(2)	3.88
C(11)	0.0696(2)	−0.0222(2)	0.1489(2)	3.65
C(12)	0.1726(2)	−0.0470(2)	0.1239(2)	3.12
C(13)	0.2814(2)	−0.0081(2)	0.1674(2)	3.37
C(14)	0.2896(2)	0.0570(2)	0.2347(2)	3.43
C(15)	0.1907(3)	0.0825(2)	0.2614(2)	3.97
C(16)	0.0837(3)	0.0425(2)	0.2196(2)	4.07
C(1)	0.1642(3)	−0.1090(2)	0.0397(2)	3.40
C(2)	0.1302(3)	−0.2479(2)	−0.0325(3)	4.66
C(3)	0.0852(4)	−0.3341(2)	−0.0293(5)	6.87
C(4)	0.1828(3)	−0.2290(2)	0.1588(3)	5.37
C(5)	0.3142(4)	−0.2456(3)	0.1781(3)	5.74
H	−0.023 (3)	−0.117 (2)	0.077 (3)	8.5

ture determination system (7). The data collection and processing parameters are summarized in Table 1. Positional parameters together with the B_{eq} values for non-hydrogen atoms, and B_{iso} for bridge hydrogen atoms for both types of molecules are given in Table 2. The bond lengths, bond angles, and torsion angles are given in Tables 3, 4, and 5, respectively.[2]

Results and discussion

In the unit cell there are two slightly different types of molecules, denoted by **A** and **B**, with very short intramolecular hydrogen bonds, 2.425(3) and 2.407(3) Å, respectively. A drawing of the packing in the unit cell is presented in Fig. 1. The structure of molecules and atom numbering are shown in Fig. 2. The difference between molecules **A** and **B** arises from the packing effects and consists mainly in the torsional angle N—O(2)—H—O(1) and the localization of the bridge hydrogen atom.

One should use some caution about the localization of the hydrogen atoms in the bridges. It seems particularly strange that for a slightly shorter bridge (molecules of type **B**) the refinement gives an asymmetric position of the proton, although it is markedly displaced to the centre of the bridge. Nevertheless, the results obtained seem to confirm very short hydrogen bonds of the symmetric type (8), though from a chemical point of

[2]Supplementary tables containing hydrogen atoms parameters, anisotropic temperature factors and structure factor amplitudes may be purchased from the Depository of Unpublished Data, CISTI, National Research Council of Canada, Ottawa, Ont., Canada K1A 0S2.

TABLE 3. Bond lengths (Å) of the **A** and **B** molecules with esd's in parentheses

Bond	Length **A**	Length **B**
Cl(1)—C(14)	1.745(3)	1.744(3)
Cl(2)—C(16)	1.738(3)	1.745(3)
O(1)—C(11)	1.328(3)	1.319(4)
O(2)—N	1.406(3)	1.407(3)
N—C(1)	1.524(4)	1.514(3)
N—C(2)	1.516(3)	1.519(4)
N—C(4)	1.508(4)	1.506(4)
C(11)—C(12)	1.411(4)	1.409(4)
C(11)—C(16)	1.399(4)	1.403(4)
C(12)—C(13)	1.387(4)	1.389(4)
C(13)—C(14)	1.377(4)	1.386(4)
C(14)—C(15)	1.383(4)	1.379(4)
C(15)—C(16)	1.381(4)	1.378(4)
C(12)—C(1)	1.504(4)	1.511(4)
C(2)—C(3)	1.508(5)	1.502(5)
C(4)—C(5)	1.503(5)	1.508(6)
O(1)—H	1.21 (3)	1.10 (4)
O(2)—H	1.22 (3)	1.31 (4)
O(1)...O(2)	2.426(3)	2.407(3)

TABLE 4. Bond angles (deg) of molecules **A** and **B** with esd's in parentheses

Bonds	Angles **A**	Angles **B**
H—O(1)—C(1)	108 (2)	108 (2)
H—O(2)—N	106 (2)	106 (2)
O(1)—H—O(2)	175 (3)	177 (4)
O(2)—N—C(1)	109.7(2)	109.7(2)
O(2)—N—C(2)	107.4(2)	106.1(2)
O(2)—N—C(4)	107.4(2)	108.2(2)
C(1)—N—C(2)	106.8(2)	107.4(2)
C(1)—N—C(4)	112.2(2)	112.3(2)
C(2)—N—C(4)	113.4(2)	113.0(2)
O(1)—C(11)—C(12)	122.6(2)	122.9(3)
O(1)—C(11)—C(16)	120.2(2)	120.5(3)
C(12)—C(11)—C(16)	117.1(2)	116.6(3)
C(11)—C(12)—C(13)	120.6(2)	120.7(2)
C(11)—C(12)—C(1)	120.2(2)	120.7(2)
C(13)—C(12)—C(1)	119.0(2)	118.2(2)
C(12)—C(13)—C(14)	120.1(3)	120.3(3)
Cl(1)—C(14)—C(13)	120.1(2)	120.5(2)
Cl(1)—C(14)—C(15)	119.1(2)	119.0(2)
C(13)—C(14)—C(15)	120.8(3)	120.6(3)
C(14)—C(15)—C(16)	118.9(3)	118.8(3)
Cl(2)—C(16)—C(11)	118.7(2)	118.2(2)
Cl(2)—C(16)—C(15)	118.9(2)	118.8(2)
C(11)—C(16)—C(15)	122.4(3)	123.0(3)
N—C(1)—C(12)	116.2(2)	166.6(2)
N—C(2)—C(3)	112.9(3)	113.6(3)
N—C(4)—C(5)	115.1(3)	115.2(3)

TABLE 5. Torsion angles (deg) of molecules **A** and **B** with esd's in parentheses

Bonds	Torsion angle A	Torsion angle B
O(1)—C(11)—C(12)—C(1)	5.0(5)	6.6(4)
C(11)—C(12)—C(1)—N	−63.6(4)	−61.9(3)
C(12)—C(1)—N—O(2)	71.7(3)	70.8(3)
C(1)—N—O(2)—H	−28.1(2)	−31.1(2)
N—O(2)—H—O(1)	−79 (10)	−70 (10)
O(2)—H—O(1)—C(11)	67 (10)	62 (10)
H—O(1)—C(11)—C(12)	22.0(16)	19.6(21)
C(3)—C(2)—H—O(2)	−60.9(3)	−61.1(3)
C(3)—C(2)—N—C(1)	−178.4(3)	−178.4(3)
C(3)—C(2)—N—C(4)	57.5(4)	57.2(4)
C(2)—N—C(1)—C(12)	−172.3(3)	−174.3(2)
C(5)—C(4)—N—O(2)	177.1(3)	174.0(3)
C(5)—C(4)—N—C(1)	−62.3(3)	−64.8(4)
C(5)—C(4)—N—C(2)	58.7(4)	56.9(4)
C(4)—N—C(1)—C(12)	−47.5(4)	−49.4(3)

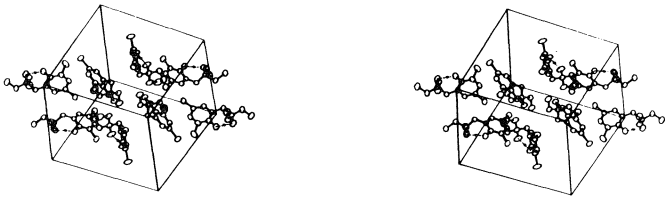

FIG. 1. Stereoview of the packing in the unit cell.

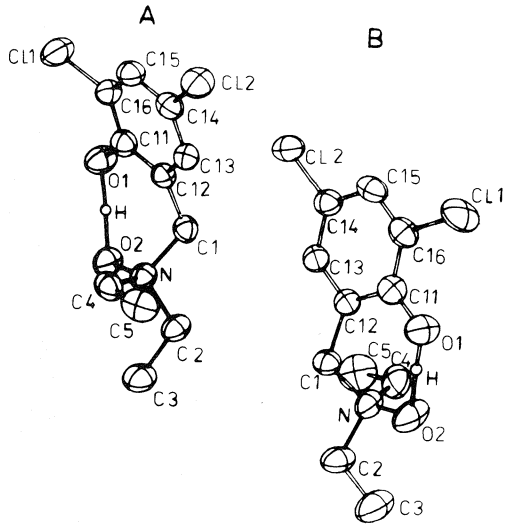

FIG. 2. Schematic representation of molecules **A** and **B**.

view both oxygen bridge atoms possess a different character. Usually, in such situation, asymmetric hydrogen bonds are formed in which the proton is attached to either the proton donor atom or to the proton acceptor (proton transfer ion-pair).

The "symmetric" character of the bridges is clearly reflected in other bond lengths, particularly in the C—O distance. From the Bavoux *et al.* data (9–13) it follows that the average C—O bond length in dichlorophenols equals 1.378(9) Å. In phenolates this bond length undergoes a substantial lowering. Thus, for aniline pentachlorophenolate (14), *N*-methylmorpholine pentabromophenolate (15), and 2-(*N*,*N*-dimethylaminomethyl)-4-nitrophenol (4), it equals to 1.287(13), 1.275(20), and 1.283(3) Å, respectively. In the case of picrates (16) the C—O bond becomes very short, 1.248(1) Å, but this is partly due to a strong mesomeric interaction with nitro groups. Thus, the C—O length of 1.328(3) and 1.319(4) found in this paper for molecules **A** and **B**, respectively, is half-way between the two limited phenolic and phenolate states. Much less sensitive and less informative is the length of N—O bond. For morpholine (17) and trimethylamine (18) *N*-oxides, it is equal to 1.391(3) and 1.388(5) Å, while for trimethylamine *N*-oxide hydrochloride (19) it is 1.425(11) Å. The difference between the two limiting cases, namely, N—O and N—$\overset{+}{O}$H, is reflected in the bond length by 0.04 Å only. Nevertheless, the value of 1.407(3) Å found in this paper could confirm the central proton density distribution within the OHO bridge.

TABLE 6. Position of the long wave-length band of **1** in various solvents (cm^{-1})

Solvent	Wave-length
CCl_4	32 100
Cyclohexane	32 500
Diethyl ether	32 100
DMSO	32 300
Acetonitrile	32 250
$CHCl_3$	32 200
CH_2Cl_2	32 250
Methanol	32 400
Isopenthanol	32 600
Water	33 250
HCl 0.01 *N*	34 000
NaOH 0.01 *N*	31 000

Infrared spectra

The ir spectrum of the investigated compound[2] is typical of very short OHO bridges of the symmetric type (8). One observes a broad intense band over the 400–1800 cm^{-1} frequency range with a maximum at about 900–1000 cm^{-1}. No absorption above 1800 cm^{-1} was found which could be assigned to the bridge protonic vibrations. Also, the isotopic effect seems to confirm very short hydrogen bonds of the symmetric type. The comparison of the ODO and OHO systems shows that the centre of gravity of the broad band in the fingerprint region does not change after deuteration. It means that $\nu_{OHO}/\nu_{ODO} \approx 1$, which is reported for very short OHO bonds (8). One can also notice that the protonic band undergoes some broadening after deuteration without substantial change of the integrated intensity. This is possibly due to some elongation and, thus, to some weakening of the bridge which occurs in the case of short hydrogen bonds (20). In strongly polar solvents the solubility of **1** was high enough to allow the recording of the ir spectra in solution.[2] The position of the maximum of the protonic band was found to remain practically unchanged; however, the long and short wave-length wings appears. This phenomenon seems to be due to both the fluctuations of the bridge conformation (21) and the fluctuations of the electric field around the bridge (22) arising from collisions with the polar solvent molecules.

Ultraviolet spectra

The particular stability of the OHO hydrogen bonds in *N*-oxide of Mannich base is very well reflected in the uv

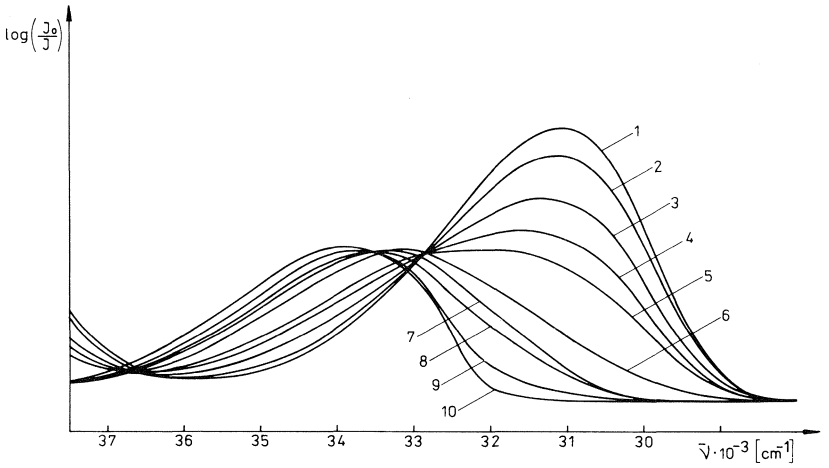

FIG. 3. Ultraviolet absorption spectra of **1** at various pH: 11.1 (*1*), 9.9 (*2*), 9.4 (*3*), 9.0 (*4*), 8.87 (*5*), 8.16 (*6*), 5.14 (*7*), 4.15 (*8*), 2.4 (*9*), and in 1 *N* HCl (*10*).

spectrum of this compound. Firstly, there is well reflected from the position of the long wave-length phenolic band in various solvents. In Table 6 the ν_{max} values are collected for various solvents and compared with those for ionic states in HCl and NaOH solutions. Except in H_2O, ν_{max} remains almost constant, with irregular oscillations depending on the donor–acceptor properties of the solvents. The average ν_{max} value is located exactly at midway between the values for the NaOH (phenolate anion) and HCl (protonized broken bridge) solutions. A special situation occurs in water, where ν_{max} = 33 250 cm^{-1}, i.e. the band is markedly shifted towards the position for protonized species. The results of the effect of the pH on the uv spectra are interesting since they reflect the stability of the intramolecular OHO hydrogen bonds. From the dependence of absorption curves on pH (Fig. 3) and particularly from the dependence of the extinction at 32 000 cm^{-1} (Fig. 4) the following equilibria are clearly visualized:

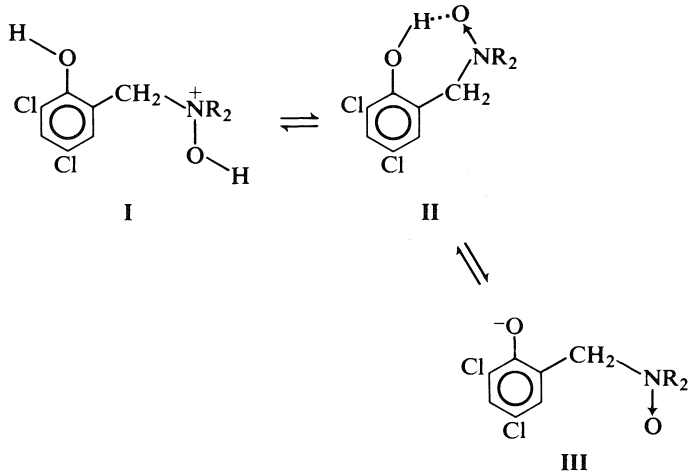

The stabilizing character of the hydrogen bonds causes drastic changes in the acidity and basicity of the interacting groups, as expressed by their pK values. As may be seen in Fig. 4, they undergo a substantial shift in comparison with the respective phenol and *N*-oxide, extending the stability range of the unionized form of Mannich base *N*-oxide. 2,6-Dichlorophenol (pK_a = 7.9 (23)) and tribenzylamine *N*-oxide (pK_a = 4.78 (24)) have been taken as reference compounds. They are

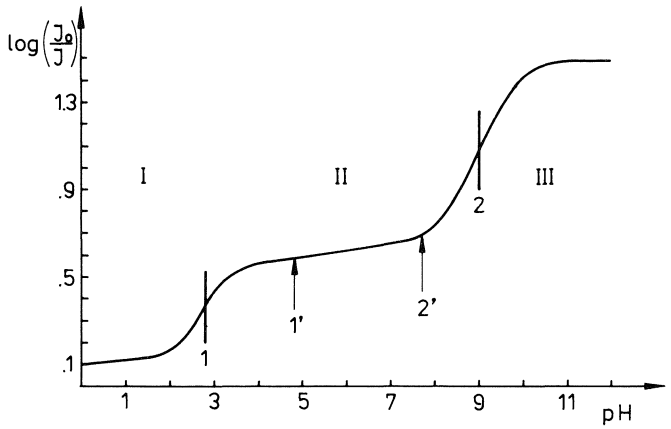

FIG. 4. Dependence of extinction at 3200 cm^{-1} on pH. The arrows correspond to pK_a values for 2,4-dichlorophenol (23) and tribenzylamine *N*-oxide (24).

indicated by arrows in Fig. 4. The hydrogen bond effect is similar here to that observed in dicarboxylic acids and diamines (25).

It is worth noticing that the acid–base behaviour of the Mannich base *N*-oxide is quite different from that of the Mannich base itself, in which the intramolecular OH...N hydrogen bond is formed. In water solution this bond is broken and the hydrated zwitter-ion is formed. The detachment of a proton from the protonized amine group occurs in alkaline solutions. In the Mannich base *N*-oxide the basicity of the *N*-oxide group is much less than for the respective amine group but, in spite of that, the hydrogen bond stability is considerably higher.

1. P. WOLSCHANN and E. HASLINGER. Monatsh. Chem. **111**, 563 (1980).
2. A. KOLL, M. ROSPENK, and L. SOBCZYK. J. Chem. Soc. Faraday Trans. I, **77**, 2309 (1981).
3. A. SUCHARDA-SOBCZYK and L. SOBCZYK. Bull. Acad. Pol. Sci. Ser. Sci. Chim. **26**, 549 (1978).
4. A. KOLL and T. GŁOWIAK. J. Cryst. Spectr. Res. **15**, 411 (1985).
5. G. GERMAIN, P. MAIN, and M. M. WOOLFSON. Acta Crystallogr. A**27**, 368 (1971).
6. International tables for X-ray crystallography. Vol. IV. Kynoch Press, Birmingham. 1974.

7. Syntex XTL/XTLE structure determination system, Syntex Analytical Instruments, Cupertino, CA. 1976.
8. A. NOVAK. *In* Structure and bonding. Vol. 18. Springer. 1974. p. 177.
9. C. BAVOUX and A. THOZET. Acta Crystallogr. B**29**, 2603 (1973).
10. C. BAVOUX and A. THOZET. Cryst. Struct. Commun. **5**, 259 (1976).
11. C. BAVOUX and P. MICHEL. Acta Crystallogr. B**30**, 2043 (1974).
12. C. BAVOUX and M. PERRIN. Acta Crystallogr. B**29**, 666 (1973).
13. C. BAVOUX, M. PERRIN, and A. THOZET. Acta Crystallogr. B**36**, 741 (1980).
14. I. VAN BEELINGEN, G. GERMAIN, P. PIRET, and M. VAN MEERSSCHE. Acta Crystallogr. B**27**, 560 (1971).
15. T. LIS, J. MAJERZ, and Z. MALARSKI. Private communication.
16. E. HOUGH. Acta Crystallogr. B**32**, 1154 (1976).
17. E. MAIA, A. PEQUY, and S. PEREZ. Acta Crystallogr. B**37**, 1858 (1981).
18. A. CARON, G. J. PALENIK, E. GOLDISH, and J. DONOHUE. Acta Crystallogr. **17**, 102 (1964).
19. A. CARON and J. DONOHUE. Acta Crystallogr. **15**, 1052 (1962).
20. M. ICHIKAWA. Acta Crystallogr. B**34**, 2074 (1978).
21. Y. Y. EFIMOV and Y. I. NABERUKHIN. Mol. Phys. **36**, 1973 (1978) and references therein.
22. A. HAYD, E. G. WEIDEMANN, and G. ZUNDEL. J. Chem. Phys. **70**, 86 (1979).
23. E. P. SERJEANT and B. DEMPSEY. Ionisation constants of organic acids in aqueous solutions. Pergamon Press, Oxford. 1979.
24. D. D. PERRIN. Dissociation constants of organic bases in aqueous solution. Butterworths, London. 1965.
25. H. A. STAAB. Einführung in die theoretische organische Chemie. Polish translation, PWN, Warszawa. 1966.

Structural studies of organoboron compounds. XXIV.[1] 5-Methyl-5-nitro-2-phenyl-1,3-dioxa-2-boracyclohexane

W. KLIEGEL AND L. PREU

Institut für Pharmazeutische Chemie, der Technischen Universität Braunschweig, 3300 Braunschweig, Beethovenstraße 55, Bundesrepublik Deutschland

AND

STEVEN J. RETTIG AND JAMES TROTTER

Department of Chemistry, University of British Columbia, 2036 Main Mall, Vancouver, B.C., Canada V6T 1Y6

Received February 12, 1986

W. KLIEGEL, L. PREU, STEVEN J. RETTIG, and JAMES TROTTER. Can. J. Chem. **64**, 1855 (1986).

The title compound was prepared according to the literature in order to determine whether it has a bicyclic cage structure resulting from intramolecular O → B coordination or a monocyclic boronate structure incorporating a trigonal planar boron atom. Crystals of 5-methyl-5-nitro-2-phenyl-1,3-dioxa-2-boracyclohexane are orthorhombic, a = 17.2358(4), b = 6.5007(2), c = 9.9225(3) Å, Z = 4, space group *Pnam*. The structure was solved by direct methods and was refined by full-matrix least-squares procedures to R = 0.064 and R_w = 0.070 for 798 reflections with $I \geq 3\sigma(I)$. The molecule actually has C_1 symmetry but, in the solid state, is located at a site of crystallographic C_s symmetry. In order to maintain the apparent mirror symmetry the nitro oxygen atoms are disordered over two mirror-related rotational positions around the C(2)—N bond. The molecule was found to have a monocyclic boronate structure, in agreement with earlier predictions. The six-membered heterocyclic ring has a "semi-planar" conformation. Bond distances and angles are normal.

W. KLIEGEL, L. PREU, STEVEN J. RETTIG et JAMES TROTTER. Can. J. Chem. **64**, 1855 (1986).

Dans le but de déterminer si le composé mentionné dans le titre possède une structure bicyclique en cage résultant d'une coordination intramoléculaire O → B ou une structure boronate monocyclique incorporant un atome de bore plan trigonal, on a préparé ce composé en suivant les indications fournies dans la littérature. Les cristaux du méthyl-5 nitro-5 phényl-2 dioxa-1,3 bora-2 cyclohexane sont orthorhombiques, avec a = 17,2358(4), b = 6,5007(2) et c = 9,9225(3) Å, Z= 4 et groupe d'espace *Pnam*. On a résolu la structure par des méthodes directes et on l'a affinée par la méthode des moindres carrés (matrice entière) jusqu'à des valeurs de R = 0,064 et R_w = 0,070 pour 798 réflexions avec $I \geq 3\sigma(I)$. La molécule possède une symétrie C_1; toutefois, à l'état solide, elle se situe dans un site cristallographique C_s. Dans le but de maintenir une symétrie apparente dans un miroir, les oxygènes des groupements nitro occupent des positions désordonnées par rapport à deux positions rotationnelles symétriques par rapport à un miroir et résultant d'une rotation autour de la liaison C(2)—N. On a trouvé que la molécule possède une structure boronate monocyclique et ce résultat est en accord avec des prédictions antérieures. L'hétérocycle à six chaînons existe dans une conformation «semi-planaire». Les distances des liaisons ainsi que les angles sont normaux.

[Traduit par la revue]

Introduction

It has been shown by X-ray structure analysis (1) that phenylboronates of bis(hydroxyalkyl)nitrones can have either a bicyclic structure **1** (resulting from intramolecular O → B coordination) or a monocyclic structure **3** (stabilized by O—B $pp(\pi)$ back donation within the trigonal planar boronate system). It was thus of interest to determine whether the phenylboronate of a 2-nitro-1,3-propanediol would possess an analogous bicyclic cage structure **2** or a monocyclic bidentate structure **4**. The "semi-planar" form **4**, with an "axial" nitro group, has been suggested by Urbanski *et al.* (2) for the phenylboronates of 2-alkyl-2-nitro-1,3-propanediols on the basis of calculated and experimentally determined dipole moments. It is noteworthy that these nitro derivatives were found to be more stable than other cyclic phenylboronates with respect to hydrolytic agents (3). This finding would also be consistent with intramolecular O → B coordination leading to a shielded sp^3 boron center. The existence of intramolecular hydrogen bonding in nitroalkanols is well established (4–8). If the "chelated" protons of a nitroalkanol such as 2-methyl-2-nitro-1,3-propanediol were to be replaced by the (formal) dication PhB^{2+} (generated from phenylboronic acid), the chelate **2** could be formed. Similarly, a tridentate nitrone ligand led to the chelate **1** (1) and a tridentate *N*-oxide ligand gave a bicyclic chelate with the same basic ring skeleton (9). For an unambiguous decision between the two possible structures, the phenylboron chelate **2** or the phenylboronate **4**, an X-ray crystallographic analysis of the compound has been carried out.

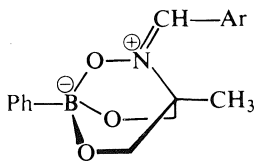

1

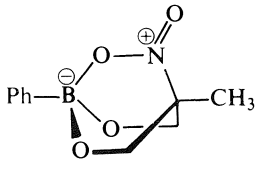

2

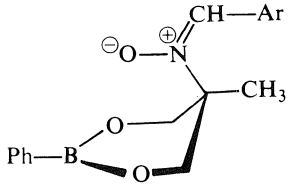

3

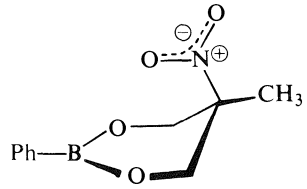

4

Experimental

*5-Methyl-5-nitro-2-phenyl-1,3-dioxa-2-boracyclohexane, **4***

The title compound was prepared according to the literature (ref. 3, method A) and was recrystallized from acetone. Mp. 147–148°C, lit. 148–150°C. *Anal.* calcd. for $C_{10}H_{12}BNO_4$: C 54.34, H 5.47, N 6.34; found: C 53.86, H 5.46, N 6.36. ^{1}H nmr ($CDCl_3$/TMS): δ (ppm) =

[1]Part XXIII, ref. 27.

1.53 (s, CH_3), 4.07 and 4.75 (AB system, J = 11 Hz, 2 OCH_2), 7.15–7.85 (m, C_6H_5).

X-ray crystallographic analysis

A crystal bounded by the seven faces (followed by their distances in mm from a common origin): ±(1 0 0), 0.08, ±(0 0 1), 0.20, (0 1 1), 0.25, (0 1 −1), 0.22, (0 −1 0), 0.25 was mounted in a general orientation. Unit-cell parameters were refined by least-squares on 2 sin θ/λ values for 25 reflections (2θ = 80–100°) measured on a diffractometer with Cu-$K\alpha$ radiation ($\lambda(K\alpha_1)$ = 1.540562, $\lambda(K\alpha_2)$ = 1.544390 Å). Crystal data at 22°C are:

$C_{10}H_{12}BNO_4$ fw = 221.0

Orthorhombic, a = 17.2358(4), b = 6.5007(2), c = 9.9225(3) Å, V = 1111.77(5) Å^3, Z = 4, ρ_c = 1.320 Mg m^{-3}, $F(000)$ = 464, μ(Cu-$K\alpha$) = 7.99 cm^{-1}. Absent reflections: $0kl$, $k + l$ odd, and $h0l$, h odd, space group *Pnam* (non-standard setting of *Pnma*, D_{2h}^{16}, No. 62, equivalent positions: ±(x, y, z; ½ + x, ½ − y, z; −x, −y, ½ + z; ½ − x, ½ + y, ½ + z)) from structure analysis.

Intensities were measured with graphite-monochromated Cu-$K\alpha$ radiation on an Enraf-Nonius CAD4-F diffractometer. An ω–2θ scan at 1.34–10.06° min^{-1} over a range of (0.80 + 0.15 tan θ) degrees in ω (extended by 25% on both sides for background measurement) was employed. Data were measured to 2θ = 150°. The intensities of three check reflections, measured every 3600 s throughout the data collection, remained constant to within 3%. After data reduction,[2] an absorption correction was applied using the Gaussian integration method (10, 11). Transmission factors ranged from 0.742 to 0.880 for 168 integration points. Of the 1213 independent reflections measured, 798 (65.8%) had intensities greater than or equal to 3σ(I) above background where $\sigma^2(I) = S + 2B + (0.04(S - B))^2$ with S = scan count and B = normalized background count.

The systematic absences allow space groups *Pna*2$_1$ or *Pnam*, the latter being indicated by the E-statistics. The structure was solved by direct methods, all non-hydrogen atoms of the molecule (which has crystallographically imposed mirror symmetry) being positioned from an E-map. Hydrogen atoms were positioned from a subsequent difference map. In the final stages of refinement the non-hydrogen atoms were refined with anisotropic, and the hydrogen atoms with isotropic, thermal parameters. The R value at this point was 0.088. The large U_{22} value obtained for the oxygen atom of the nitro group (O(2)) suggested possible disorder or that the actual space group may be *Pna*2$_1$. Attempts to refine the structure in the lower symmetry space group did not resolve this problem and were thwarted by high correlation coefficients. Refinement of the structure was completed with disordered nitro oxygen atoms, O(2) and O(3), being refined with anisotropic thermal parameters and occupancy factors fixed at 0.5. The scattering factors of ref. 12 were used for non-hydrogen atoms and those of ref. 13 for hydrogen atoms. The weighting scheme $w = 1/\sigma^2(F)$, where $\sigma^2(F)$ is derived from the previously defined $\sigma^2(I)$, gave uniform average values of $w(|F_o| - |F_c|)^2$ over ranges of both $|F_o|$ and sin θ/λ and was employed in the final stages of full-matrix refinement of variables. Reflections with $I < 3\sigma(I)$ were not included in the refinement. An isotropic Type I extinction correction (Thornley-Nelmes definition of mosaic anisotropy with a Lorentzian distribution) was applied (14–16). The final value of g was 0.49(23) × 10^4. Convergence was reached at R = 0.064 and R_w = 0.070 for 798 reflections with $I \geq 3\sigma(I)$. For all 1213 reflections R = 0.093. The function minimized was $\Sigma w(|F_o| - |F_c|)^2$, $R = \Sigma||F_o| - |F_c||/\Sigma|F_o|$ and $R_w = (\Sigma w(|F_o| - |F_c|)^2/\Sigma w|F_o|^2)^{1/2}$.

On the final cycle of refinement the mean and maximum parameter shifts corresponded to 0.02 and 0.13σ, respectively. The mean error in an observation of unit weight was 3.044. A final difference map showed maximum fluctuations of −0.35 to +0.22 e Å^{-3}. The final positional and thermal parameters appear in Tables 1 and 5,[3] respectively. Measured and calculated structure factors have been placed in the Depository of Unpublished Data.[3]

TABLE 1. Final positional (fractional × 10^4, H × 10^3) and isotropic thermal parameters (U × 10^3 Å^2) with estimated standard deviations in parentheses

Atom	x	y	z	U_{eq}/U_{iso}
O(1)	8340(1)	2723(3)	1301(2)	69
O(2)†	6651(6)	2043(14)	1496(9)	99
O(3)†	6407(7)	2822(18)	3453(12)	170
N*	6762(2)	3059(5)	2500	63
C(1)	7866(2)	4524(4)	1250(3)	66
C(2)*	7375(2)	4779(5)	2500	55
C(3)*	6946(3)	6835(7)	2500	80
C(4)*	9091(2)	−39(5)	2500	63
C(5)	9327(2)	−938(5)	1292(4)	84
C(6)	9777(2)	−2697(6)	1313(7)	109
C(7)*	9995(3)	−3575(9)	2500	118
B*	8570(2)	1922(6)	2500	55
H(1a)	758(2)	448(5)	32(3)	100(10)
H(1b)	822(2)	573(5)	126(3)	82(8)
H(3a)	661(2)	685(5)	157(3)	104(11)
H(3b)*	727(3)	796(9)	250	129(21)
H(5)	917(2)	−33(5)	46(5)	140(17)
H(6)	985(2)	−310(8)	50(4)	146(19)
H(7)*	1030(5)	−451(11)	250	169(27)

*Multiplicity factor 0.5.
†Occupancy factor 0.5.

The ellipsoids of thermal motion for the non-hydrogen atoms are shown in Fig. 1. The thermal motion has been analysed in terms of the rigid-body modes of translation, libration, and screw motion (17). The rms standard error in the temperature factors σU_{ij} (derived from the least-squares analysis) is 0.0032 and, excluding the nitro oxygen atoms, 0.0017 Å^2. The structural subunits $PhBO_2$ and C(1–3), N, and O(1) (along with their mirror-related counterparts) were analysed separately (rms ΔU_{ij} = 0.0042 and 0.0017 Å^2, respectively). The appropriate bond distances have been corrected for libration (17, 18), using shape parameters q^2 of 0.08 for all atoms involved. Corrected bond lengths appear in Table 2 along with the uncorrected values; corrected bond angles do not differ by more than 1σ from the uncorrected values given in Table 3. Intra-annular torsion angles defining the conformation of heterocyclic ring are listed in Table 4. Bond lengths and angles involving hydrogen and a complete listing of torsion angles (Tables 6–8) are included as supplementary material.

Results and discussion

The crystal structure of 5-methyl-5-nitro-2-phenyl-1,3-dioxa-2-boracyclohexane consists of discrete molecules, all intermolecular distances being greater than the sums of van der Waals radii. The molecule actually has C_1 symmetry but, in the solid state, is located at a site of crystallographic C_s symmetry. In order to maintain the apparent mirror symmetry the nitro oxygen atoms are disordered over two mirror-related rotational positions around the C(2)—N bond.

The observed structure **4** (see Fig. 1) corresponds to that deduced by Urbanski *et al.* (2) as being the most probable one with a calculated dipole moment of μ = 4.35 D in good agreement with the experimental value of 4.25 D. The intra-

[2]The computer programs used include locally written programs for data processing and locally modified versions of the following: MULTAN 80, multisolution program by P. Main, S. J. Fiske, S. E. Hull, L. Lessinger, G. Germain, J. P. Declercq, and M. M. Woolfson; ORFLS, full-matrix least-squares, and ORFFE, function and errors, by W. R. Busing, K. O. Martin, and H. A. Levy; FORDAP, Patterson and Fourier syntheses, by A. Zalkin; ORTEP II, illustrations, by C. K. Johnson.

[3]The structure factor table, Table 5 (anisotropic thermal parameters) and other material mentioned in the text are available, at a nominal charge, from the Depository of Unpublished Data, CISTI, National Research Council of Canada, Ottawa, Ont., Canada K1A 0S2.

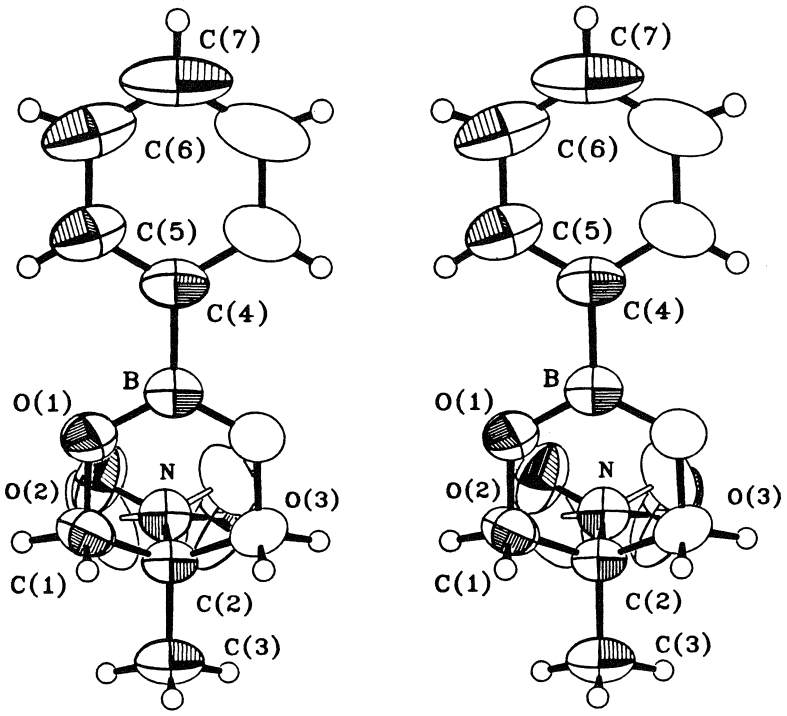

FIG. 1. Stereoscopic view of the 5-methyl-5-nitro-2-phenyl-1,3-dioxa-2-boracyclohexane molecule; 50% probability thermal ellipsoids are shown for the non-hydrogen atoms. Hydrogen atoms have been assigned arbitrary thermal parameters for the sake of clarity. Shaded atoms comprise the asymmetric unit.

TABLE 2. Bond lengths (Å) with estimated standard deviations in parentheses

	Length			Length	
Bond	Uncorr.	Corr.	Bond	Uncorr.	Corr.
O(1)—C(1)	1.428(3)	1.437	C(2)—C(3)	1.528(5)	1.536
O(1)—B	1.358(2)	1.371	C(4)—C(5)	1.394(4)	1.409
O(2)—N	1.210(8)	1.217	C(4)—B	1.559(5)	1.567
O(3)—N	1.137(11)	1.143	C(5)—C(6)	1.382(5)	1.388
N—C(2)	1.539(4)	1.552	C(6)—C(7)	1.362(6)	1.376
C(1)—C(2)	1.510(3)	1.521			

TABLE 3. Bond angles (deg) with estimated standard deviations in parentheses*

Bonds	Angle (deg)	Bonds	Angle (deg)
C(1)—O(1)—B	120.8(2)	C(1)—C(2)—C(1)′	110.4 (3)
O(2)—N—O(3)	121.7(4)	C(5)—C(4)—B	120.7 (2)
O(2)—N—C(2)	120.4(5)	C(5)—C(4)—C(5)′	118.6 (4)
O(3)—N—C(2)	117.9(6)	C(4)—C(5)—C(6)	119.9 (4)
O(1)—C(1)—C(2)	112.4(2)	C(5)—C(6)—C(7)	120.9 (5)
N—C(2)—C(1)	107.8(2)	C(6)—C(7)—C(6)′	119.8 (5)
N—C(2)—C(3)	107.6(3)	O(1)—B—C(4)	118.80(15)
C(1)—C(2)—C(3)	111.5(2)	O(1)—B—O(1)′	122.4 (3)

*Primed atoms have coordinates related to those in Table 1 by the symmetry operation $x, y, \frac{1}{2} - z$.

molecular contacts between the nitro oxygen atoms and the boron atom are clearly too long for coordinative interaction (B—O(2) = 3.46(1), B—O(3) = 3.89(1) Å). The *pp*(π) back donation from the two oxygen atoms to boron in the phenylboronate system is energetically favored over intramolecular O → B coordination involving a nitro group oxygen atom which would force the cycloboronate ring into a boat conformation (formula **2**).

The six-membered heterocyclic ring adopts a "semi-planar" conformation with C(2) displaced from the approximate plane of the other five atoms and the nitro group in a pseudo-axial position. This conformation has been predicted on the basis of nmr (19–22) and dipole moment studies (2, 19), and has been verified by X-ray structure analyses (ref. 1 and references therein). The overall geometry of the 1,3-dioxa-2-boracyclohexane ring in **4** is very similar to that of compound **3** (1). The

TABLE 4. Intra-annular torsion angles (deg) standard deviations in parentheses*

Atoms	Value (deg)
C(1)—O(1)—B—O(1)′	2.8(5)
B—O(1)—C(1)—C(2)	−26.8(4)
O(1)—C(1)—C(2)—C(1)′	48.7(4)

*Symmetry-related torsion angles have the opposite sign.

partial π-bond character of the O—B bonds is demonstrated by the short O—B distance of 1.371(2) Å. The relatively short B—C bond of 1.567(5) Å is indicative of some π-interaction between the sp^2 boron atom and the aromatic system. Both O—B and B—C distances are in good agreement with those observed for **3** and related compounds (ref. 1 and references therein). The C—N bond in **4** (1.552(4) Å) is significantly longer than the corresponding distance of 1.528(3) Å in **3**, whereas the N—O bonds of the nitro group (1.217(8) and 1.143(11) Å) in **4** are considerably shorter than the N—O bond of the nitrone group in **3** (1.291(2) Å). This reflects the more pronounced (partial) double bond character of the N—O bond in the nitro compound **4**. The longer of the two N—O bonds in **4** is in the range 1.190–1.230 Å normally observed for nitro groups (23–25). The anomalously short N—O(3) distance of 1.143(11) Å is most likely an artifact of thermal motion and/or disorder although an inequality of the two N—O bond lengths could arise as a result of differences between the two nitro oxygen atoms with respect to intramolecular non-bonded interactions (O(2)···C(1) = 2.66(1), O(2)···O(1) = 2.95(1), and O(2)···C(3) = 3.31(1) Å vs. O(3)···C(1)′ = 2.76(1), O(3)···O(1)′ = 3.34(1), and O(3)···C(3) = 2.93(1) Å). The geometrical distortion of the phenyl ring is as expected (ref. 26 and references therein). The phenyl ring is planar within experimental error while the boronate and nitro groups are slightly, but significantly, non-planar (B and N are displaced 0.017(4) and 0.015(3) Å, respectively, from the planes of their substituents). The dihedral angle between the normals to the phenyl and boronate mean planes is 1.6(4)°.

Acknowledgments

We thank the Natural Sciences and Engineering Research Council of Canada and the Fonds der Chemischen Industrie, Frankfurt am Main, for financial support and the University of British Columbia Computing Centre for assistance.

1. W. KLIEGEL, L. PREU, S. J. RETTIG, and J. TROTTER. Can. J. Chem. **63**, 509 (1985).
2. T. URBANSKI, D. GÜRNE, R. KOLINSKI, H. PIOTROWSKA, A. JONCZYK, B. SERAFIN, M. SZRETTER-SZMID, and M. WITANOWSKI. Tetrahedron, **20**, Suppl. 1, 195 (1964).
3. H. PIOTROWSKA, B. SERAFIN, and T. URBANSKI. Tetrahedron **19**, 379 (1963).
4. T. URBANSKI. Bull. Acad. Polon. Sci. Cl. III **4**, 87 (1956); **4**, 381 (1956); Roczn. Chem. **31**, 37 (1957); **31**, 53 (1957).
5. T. URBANSKI. *In* Hydrogen bonding. *Edited by* D. Hadzi and H. W. Thompson. Permagon Press, London. 1959. pp. 143–146.
6. E. LIPCZYNSKA-KOCHANY and L. PIELA. Bull. Acad. Polon. Sci. Ser. Sci. Chem. **23**, 895 (1975).
7. E. LIPCZYNSKA-KOCHANY and T. URBANSKI. Can. J. Chem. **55**, 2504 (1977); Roczn. Chem. Ann. Soc. Chim. Polon. **51**, 2349 (1977) and references therein.
8. C. N. R. RAO. *In* The chemistry of the nitro and nitroso groups. *Edited by* H. Feuer. Interscience, New York. 1969. pp. 112–116.
9. W. KLIEGEL and E. AHLENSTIEL. Chem. Ber. **110**, 1623 (1977).
10. P. COPPENS, L. LEISEROWITZ, and D. RABINOVICH. Acta Crystallogr. **18**, 1035 (1965).
11. W. R. BUSING and H. A. LEVY. Acta Crystallogr. **22**, 457 (1967).
12. D. T. CROMER and J. B. MANN. Acta Crystallogr. Sect. A, **24**, 321 (1968).
13. R. F. STEWART, E. R. DAVIDSON, and W. T. SIMPSON. J. Chem. Phys. **42**, 3175 (1965).
14. P. J. BECKER and P. COPPENS. Acta Crystallogr. Sect. A, **30**, 129 (1974); **30**, 148 (1974); **31**, 417 (1975).
15. P. COPPENS and W. C. HAMILTON. Acta Crystallogr. Sect. A, **26**, 71 (1970).
16. F. R. THORNLEY and R. J. NELMES. Acta Crystallogr. Sect. A, **30**, 748 (1974).
17. V. SCHOMAKER and K. N. TRUEBLOOD. Acta Crystallogr. Sect. B, **24**, 63 (1968).
18. D. W. J. CRUICKSHANK. Acta Crystallogr. **9**, 747 (1956); **9**, 754 (1956); **14**, 896 (1961).
19. O. EXNER and R. BOSE. Coll. Czechoslov. Chem. Commun. **39**, 2234 (1974).
20. D. CARTON, A. POITER, M. J. POUET, J. SOULIE, and P. CADIOT. Tetrahedron Lett. 2333 (1975).
21. V. V. KUZNETSOV, A. I. GREN′, A. V. BOGATSKII, S. P. EGOROVA, and V. I. SIDOROV. Khim. Geterotsikl. Soedin. 26 (1978); Chem. Heterocycl. Comp. 19 (1978).
22. B. WRACKMEYER and R. KÖSTER. Chem. Ber. **115**, 2022 (1982).
23. S. SORRISO. *In* The chemistry of amino, nitroso, and nitro compounds and their derivatives. *Edited by* S. Patai. Suppl. F, Part 1. Wiley-Interscience, New York. 1982. p. 32.
24. J. TROTTER. Tetrahedron, **8**, 13 (1960).
25. S. NORDENSON, J. SKRAMSTAD, and E. FLØTRA. Acta Chem. Scand. Ser. B, **38**, 461 (1984).
26. A. DOMENICANO, P. MURRAY-RUST, and A. VACIAGO. Acta Crystallogr. Sect. B, **39**, 457 (1983).
27. W. KLIEGEL, H.-W. MOTZKUS, D. NANNINGA, S. J. RETTIG, and J. TROTTER. Can. J. Chem. **64**, 507 (1986).

The carbonyl group as a reluctant transmitter of hyperconjugative or σ–π spin–spin coupling interactions in derivatives of benzaldehyde, acetophenone, and benzophenone

TED SCHAEFER, JAMES PEELING,[1] GLENN H. PENNER, AND ALBERTA LEMIRE
Department of Chemistry, University of Manitoba, Winnipeg, Man., Canada R3T 2N2

AND

REINO LAATIKAINEN
Department of Chemistry, University of Kuopio, P.O.B. 6, 70211 Kuopio, Finland

Received February 13, 1986

TED SCHAEFER, JAMES PEELING, GLENN H. PENNER, and ALBERTA LEMIRE. Can. J. Chem. **64**, 1859 (1986).

Unlike their counterparts in anisole or toluene derivatives, the six-bond spin–spin coupling constants between *para* ring protons or ^{19}F nuclei and protons or ^{13}C nuclei in the sidechain of derivatives of benzaldehyde, acetophenone, and benzophenone can apparently contain components of opposite sign, at least for the fluorine derivatives. The σ–π components are much smaller in magnitude than in toluene derivatives, leading to very small or unobservable coupling constants. Consequently they are of limited use in conformational analysis. INDO MO FPT computations and their modifications are examined as to the reasons for the small σ–π magnitudes. Although the spin polarizability of the 2*pz* orbital on oxygen appears to play an important role in the transmission of nuclear spin state information, the computations do not account for a ^{19}F coupling mechanism that appears to be significant for planar conformations. On the other hand, spin–spin coupling constants over five formal bonds to *meta* protons are sizeable and stereospecific.

TED SCHAEFER, JAMES PEELING, GLENN H. PENNER et ALBERTA LEMIRE. Can. J. Chem. **64**, 1859 (1986).

Contrairement à leurs contreparties dans les dérivés de l'anisole ou du toluène, les constantes de couplage spin–spin à travers six liaisons, entre les protons du cycle en position *para* ou les noyaux de ^{19}F et les protons ou les noyaux de ^{13}C de la chaîne latérale des dérivés du benzaldéhyde, de l'acétophénone et de la benzophénone peuvent apparemment contenir des composants de signes opposés, au moins dans les dérivés fluorés. Les constituants σ–π ont une intensité inférieure à celle des dérivés du toluène conduisant ainsi à des constantes de couplage très faibles qu'on ne peut observer. En conséquence, ces constantes sont très peu utiles dans l'analyse conformationnelle. On a utilisé des calculs INDO OM FPT ainsi que leurs modifications pour déterminer les causes des faibles intensités des constituants σ–π. Bien que la polarisabilité du spin de l'orbitale 2*pz* de l'oxygène semble jouer un rôle important dans la transmission de l'information sur l'état du spin nucléaire, les calculs ne tiennent pas compte du mécanisme de couplage du ^{19}F qui semble être important dans les conformations planes. Par ailleurs, les constantes de couplage spin–spin à travers cinq liaisons formelles par rapport aux protons en position *meta* sont quantifiables et stéréospécifiques.

[Traduit par la revue]

Introduction

Long-range spin–spin coupling constants between ring protons or fluorine nuclei and α protons on the sidechain in benzene derivatives are valuable indicators of conformational preferences and of the potentials governing internal rotation about the C(1)—X bond in **1** (1–3). In particular, it appears that

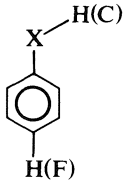

1

$^6J(^1H,^1H)$ and $^6J(^1H,^{19}F)$ are proportional to $\sin^2\theta$, where θ is the angle by which the X—H bond twists out of the benzene plane, as in **2** (1). The proportionality constant is $^6J_{90}$, the value

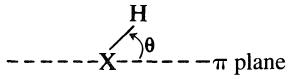

2

of ^6J when θ is 90°. The mechanism of coupling therefore involves the σ–π interaction between the σ electrons in the sidechain and the π electrons of the ring. If $^6J_{90}$ is known, then $\langle\sin^2\theta\rangle$ is derivable from the observed ^6J and this expectation value is related to the preferred conformation and the barrier to rotation about the C—X bond (2).

It also appears that $^6J(^1H,^{13}C)$ and $^6J(^{13}C,^{19}F)$ are σ–π couplings, the ^{13}C nucleus being situated in the sidechain, when $X = CH_2$, CH, or C with sp^2 hybridization (4, 5) or when X = O (6). In such compounds $^6J(^{13}C,^{19}F)$ is particularly easy to measure under conditions of ^1H decoupling and is therefore a convenient conformational indicator.

In this paper, attempts to measure $^6J(^1H,^{13}C) \equiv {}^6J(H,C)$ and $^6J(^{13}C,^{19}F) \equiv {}^6J(C,F)$ are described for compounds in which X is a carbonyl group, C=O. It turns out that the σ–π mechanism is relatively inefficient and some modified INDO MO FPT calculations are examined as to the reasons for its absence. Comparisons are made with $^6J(H,F)$ in 4-fluorobenzaldehyde. These indicate a coupling mechanism giving rise to negative six-bond couplings in planar conformations.

Experimental

All compounds, except for acetophenone-β-^{13}C, 2,6-dichloroacetophenone-β-^{13}C, and 4-fluorophenyl-*tert*-butyl ketone came from Aldrich Chemical Co. The second of these was prepared from 2,6-dichlorobenzaldehyde (Frinton) by treatment with ^{13}C-methyl magnesium iodide in ether (7), prepared from ^{13}C enriched CH_3I (Merck, Sharpe and Dohme), followed by oxidation of the alcohol with pyridinium chlorochromate (Aldrich). The unenriched product followed in the obvious way. Acetophenone-β-^{13}C was prepared from benzaldehyde in a similar way. The 4-fluorophenyl-*tert*-butyl ketone

[1]University of Petroleum and Minerals, Dhahran, Saudi Arabia.

TABLE 1. The ^{1}H nmr spectral parameters for a 5.2 mol% solution of acetophenone-β-^{13}C in acetone-d_6 at 300 K and 300.135$_1$ MHz

Parameter	Value	Parameter	Value
$\nu(CH_3)^a$	771.45[b]	$^4J_{24}$	1.275(2)
$\nu_2 = \nu_6$	2396.568(2)[c]	^4J(H,C)	<0.03[d]
$\nu_3 = \nu_5$	2251.469(1)	^5J(H,C)	±0.220(3)
ν_4	2281.330(2)	$^5J_{25}$	0.617(1)
^1J(H,C)	127.36[b]	^6J(H,C)	<0.03[d]
$^3J_{23}$	7.858(2)	Calcd. transitions	132
$^3J_{34}$	7.449(2)	Assigned trans.	115
$^4J_{26}$	1.914(3)	Largest diff.	0.023
$^4J_{35}$	1.332(3)	Root mean square deviation	0.009

[a]In Hz to high frequency of internal TMS.
[b]Not included in the iterative analysis.
[c]Numbers in parentheses are standard deviations in the last significant figure.
[d]Couplings of 0.06 Hz between methyl and *ortho* ring protons were observed but no couplings from ^{13}C to *ortho* or *para* protons. Line widths for these peaks were no larger than the peaks from the *meta* protons.

was obtained from 1-bromo-4-fluorobenzene (Aldrich) and *tert*-butylcyanide via the Grignard reagent (8). These compounds were identified by means of ^{1}H and ^{13}C nmr spectra.

The ^{13}C nmr spectra for most of the compounds were accumulated on a WH90 FFT nmr spectrometer under conditions of broadband ^{1}H decoupling at a probe temperature of 305 K. The ^{13}C nmr spectra of the methyl carbon nuclei of the acetyl groups in 2,6-dichloroacetophenone and 2,6-dimethoxyacetophenone were acquired with the INEPT (9) pulse sequence, as described recently (4). The ^{1}H nmr spectra of acetophenone-β-^{13}C and of its 2,6-dichloro derivative were recorded on an AM300 nmr spectrometer at a probe temperature of 300 K. All nmr samples were degassed by the freeze–pump–thaw technique and were flame-sealed. Solvents and concentrations are given below.

Molecular orbital computations were performed on an Amdahl 470/V8 computer system and employed MONSTERGAUSS (10), INDO MO FPT (11), and its modified version FINDO (12).

Results and discussion

Spectral data

Table 1 presents the spectral parameters obtained from a NUMARIT (13) analysis of the ^{1}H nmr spectrum of acetophenone-β-^{13}C. A similar analysis of the ^{1}H nmr spectrum of a 5 mol% solution of 2,6-dichloroacetophenone-β-^{13}C in acetone-d_6 gave ^6J(H-4,C) as −0.136(7) Hz and ^5J(H-3,C) as 0.131(5) Hz, the signs being determined by weak multiple irradiation procedures.

In Table 2 are found the ^{13}C chemical shifts and J(C,F) values for 4-fluorophenyl-*tert*-butyl ketone in acetone solution. ^nJ(C,F) for n = 1–4 are very similar for all 4-fluorophenyl compounds and are not reproduced here. Relevant ^6J(C,F) values, those involving the ^{13}C nucleus directly bonded to the carbonyl group, were ±0.132(7) Hz for 4-fluoroacetophenone (25% v/v in acetone-d_6), ±0.087(9) Hz for 4-fluoropropiophenone (30% v/v in acetone-d_6), <0.05 Hz for 4-fluorobenzophenone (25% v/v in acetone-d_6), and <0.07 Hz for 4,4′-difluorobenzophenone (35% v/v in acetone-d_6).

No ^6J(C,F) was observable for 4-fluoro-β-chloroacetophenone nor for pentafluoroacetophenone as a 30% v/v solution in acetone-d_6, although couplings of 2.41(2) and 0.33(2) Hz were measured from the methyl ^{13}C nucleus to the *ortho* and *meta* ^{19}F nuclei, respectively, in the latter compound.

For a 50% v/v solution of 2,6-dimethoxyacetophenone in acetone-d_6, the INEPT spectrum of the acetyl methyl ^{13}C nucleus yielded a ^6J(H-4,C) of ±0.12 ± 0.02 Hz. A similar experiment on unenriched 2,6-dichloroacetophenone gave ^6J(H-4,^{13}C) as ±0.12 ± 0.02 Hz.

TABLE 2. The ^{13}C nmr parameters of 4-fluorophenyl-*tert*-butyl ketone as a 50 v/v% solution in acetone-d_6 at 22.639 MHz and 305 K

Parameter	Value	Parameter	Value
$\delta(CH_3)$	29.08[a]	^1J(C,F)[b]	−250.39
δ(C)	45.21	^2J	21.81
δ(C=O)	207.27	^3J	8.77
δ_1	136.07	^4J	3.31
δ_2	132.32	^5J[c]	<0.05
δ_3	116.44	^6J[c]	<0.05
δ_4	165.62	^7J[c]	<0.04

[a]The chemical shifts were measured relative to the resonance peak of the methyl ^{13}C nuclei in acetone-d_6 and were converted to δ values by addition of 29.8 ppm.
[b]The spin–spin coupling constants have an uncertainty of ca. 0.1 Hz for ^nJ (n = 1–4).
[c]These couplings must be very small, the line width at half height being 0.08 Hz for ^{13}C=O and 0.07 Hz for the methine carbon.

The small magnitudes of ^{6}J(^{1}H,^{13}C) and ^{6}J(^{13}C,^{19}F)

In solution, the free energy of activation for rotation about the exocyclic C_{sp^2}—C_{sp^2} bond in acetophenone is 22.4 kJ/mol (14). Our STO 3G MO computations with geometry optimization indicate a planar ground state and, to within 3%, a twofold barrier to rotation for the acetyl group. Because the barrier to rotation is large compared to thermal energies at 300 K, the absence (Table 1) of ^6J(H,C) is possibly reconcilable with a σ–π mechanism since $\langle \sin^2 \theta \rangle$ is 0.06. If $^6J_{90}$(H,C) is about −0.6 Hz, as in ethylbenzene (4), then the observed ^6J(H,C) should be about −0.04 Hz and may have escaped detection. Some other techniques (15–17) do agree that acetophenone is planar in the ground state.

Turning to 2,6-dichloroacetophenone, ^6J(H,C) is −0.136(7) Hz. Geometry-optimized STO 3G MO computations find the θ = 90° conformation (acetyl plane perpendicular to the benzene plane) as 47.0 kJ/mol more stable than the planar conformation. If this number is correct, then ^6J(H,C) at θ = 90° is −0.14 Hz, compared to (−)0.63 Hz for the corresponding coupling in anisole (6) and (−)0.6$_2$ Hz in ethyl benzene (4). It is true that θ has been estimated as 28° from ^{13}C nmr chemical shifts (18). However, for 2,4,6-trimethylacetophenone a variety of techniques yield various θ values (19, 20), ranging from 50 to 90°. In our opinion, the expectation value of θ cannot be far from 90° in 2,6-dichloroacetophenone. In 2,6-dimethoxyacetophenone,

^6J(H,C) has the same magnitude as in the 2,6-dichloro derivative, the ^{13}C nmr chemical shift suggesting θ as 40° in the former (18).

Because the hyperfine coupling parameter, Q_{CF}, is much larger in magnitude than Q_{CH}, these quantities giving the efficiency of the transfer of spin state information from the π to the σ electrons at the *para* position, measurements of ^6J(C,F) were made on a number of 4-fluorophenyl ketones. In the acetophenone derivative, ^6J(C,F) is ±0.132(7) Hz. The free energy barrier to internal rotation in this compound in solution is 24.7 kJ/mol (14), higher than for acetophenone itself because of increased conjugation across the exocyclic C_{sp^2}—C_{sp^2} bond. In 4-fluoropropiophenone, ^6J(C,F) is ± 0.087(9) Hz and sinks to <0.05 Hz in 4-fluorophenyl-*tert*-butyl ketone (Table 2). In the absence of the fluorine substituent, this compound has been estimated to have $25° \leq \theta \leq 63°$ by different physical techniques (21).

^6J(C,F) at θ = 90° is near 1.5 Hz in anisole derivatives (6) and near 1.3 Hz (5) in 4-fluorophenyl-R (R = CH_2CH_3, $CH(CH_3)_2$, and $C(CH_3)_3$). If ^6J(C,F) at θ = 90° were similar in magnitude in acetophenone derivatives, then a θ of 45° would imply a ^6J(C,F) of at least 0.6 Hz. Yet ^6J(C,F) is absent in 4-fluorophenyl-*tert*-butyl ketone and in pentafluoroacetophenone, for which ⟨θ⟩ may well be as large as 40° (22). Furthermore, ^6J(C,F) is also absent in benzophenone derivatives, for which θ values are about 50° (23). ^6J(C,F) in 4,4′-difluorophenylmethane has a θ dependence very similar to that in 4-fluorophenyl ethane (5), implying similar σ–π parameters for sp^2 and sp^3 carbon atoms at the end of the coupling path.

INDO MO FPT computations

Such computations reproduce the $\sin^2\theta$ dependence of ^6J(H,C) and ^6J(C,F) in anisole derivatives, for example (6). Thus, ^6J(H,C) is computed as $-0.63\sin^2\theta$ in anisole, rather close to the magnitude of 0.62_5 Hz observed in 2,6-dibromoanisole and the 0.64 Hz for ^7J(H,C) in 4-methyl-2,6-dibromoanisole (equality in magnitudes of ^6J(H,C) and ^7J(H,C) is expected for a σ–π mechanism). For ^6J(C,F) the maximum value is computed as too small (6), in line with expectations (1).

In Table 3, computed ^6J(H,C) values as a function of θ are given for a standard geometry (24) of acetophenone. As for similar calculations on anisole (6), the methyl group is rotated as θ increases to keep two H—H_{ortho} distances equal (correlated motion).

When no off-diagonal Fock matrix elements are neglected (3, 12, 25, 26) and no orbitals are restricted (3, 12, 27), the results for ^6J(H,C) indicate a finite value at θ = 0° *and* that its magnitude changes very little as θ goes towards 90° (column A).[2] Qualitatively, the computed increase in magnitude of 0.07 Hz agrees with the −0.14 Hz observed in 2,6-dichloroacetophenone. The finite computed value at 0° then arises from an inadequacy of the INDO MO parameterization.

When the Fock elements between orbitals in the methyl group and the *oxygen* atom and those in the phenyl group are set to zero, the computed ^6J(H,C) values (column B) change very little, implying that such "through-space" or proximate coupling pathways are unimportant.[3] Column B therefore yields the coupling pathway via the orbitals on the carbonyl carbon atom.

If, in addition, the Fock elements involving the 2*pz* orbitals on the carbonyl and the *ipso* carbon atoms are eliminated, ^6J(H,C) drops to zero for all θ. Therefore the implied coupling pathway goes via the partial double bond (conjugation).

On the other hand, restriction of the development of spin polarization in the 2*pz* orbital on oxygen (column D) entails a vanishing ^6J(H,C) for the planar conformer and a maximum magnitude for the perpendicular form. Comparison with column A suggest that the remarkable computed nonzero coupling for the planar conformation arises from an increased polarization of the 2*pz* orbital on the carbonyl carbon atom caused by the spin polarizability of the C=O bond. Note that no such coupling is actually observed in acetophenone (Table 1).

However this may be, in practical terms ^6J(H,C) is not very useful as an indicator of preferred conformations and barriers to rotation about the C_{sp^2}—C_{sp^2}(O) bond in aromatic ketones. Simply put, the carbonyl group acts as a barrier to transfer of nuclear spin state information via a σ–π mechanism.

The INDO MO FPT computations for ^6J(C,F) gave results parallel to those for ^6J(H,C) and are not reproduced here. The theoretical results do not account for the observation of a ^6J(C,F) in acetophenone and its absence in the *tert*-butyl ketone derivative, that is, the decrease in magnitude for nonplanar conformations.

TABLE 3. Some computed $^6J(^1H,^{13}C)$ values in Hz for the methyl ^{13}C nucleus in acetophenone

	$^6J(^1H,^{13}C)$			
θ/deg[a]	A[b]	B[c]	C[d]	D[e]
0	−0.347	−0.360	−0.005	−0.015
7.5	−0.338	−0.357	−0.005	−0.028
15	−0.332	−0.349	−0.004	−0.070
30	−0.336	−0.345	−0.003	−0.191
45	−0.352	−0.341	−0.001	−0.301
60	−0.378	−0.356	0.001	−0.353
75	−0.405	−0.372	0.003	−0.375
90	−0.415	−0.380	0.004	−0.388

[a]The angle of twist about the exocyclic C_{sp^2}—C_{sp^2} bond of length 1.46 Å. The methyl group lies in plane for θ = 0°, one of its C—H bonds lying in plane and pointing away from the benzene ring. As θ increases the methyl group twists so as to keep two of its H—H (*ortho*) distances equal (correlated motion).

[b]A standard INDO MO FPT computation.

[c]All off-diagonal Fock elements are set to zero if they involve interactions between orbitals on the ring and orbitals on the oxygen atom and the methyl group, i.e., "through-space" interactions are minimized.

[d]In addition to footnote *c*, the Fock elements involving the 2*pz* orbitals on the *ipso* and carbonyl carbon atoms are forced to vanish.

[e]In addition to footnote *c*, the 2*pz* orbital on the oxygen atom is restricted, i.e., is not allowed to develop spin polarization.

Comparisons with ^{n}J(*H,CHO*) *in benzaldehyde*

A recent precise and unpublished analysis in this laboratory of the ^{1}H nmr spectrum of benzaldehyde in acetone-d_6 solution yielded ^6J(*H,CHO*) as −0.013(1) Hz. In other words, there was no significant coupling, this number being a consequence of the least-squares analysis procedure. Because the internal barrier to rotation in benzaldehyde in solution is greater than 30 kJ/mol (27–31), this result could again be interpreted as arising from the very small $\langle\sin^2\theta\rangle$. The INDO MO FPT computation gives ^6J(*H,CHO*) as −0.29 Hz for θ = 0° (3), implying that this number represents an inadequacy in the

[2]Use of the geometry-optimized STO 3G MO geometries yielded computed ^6J(H,C) values which changed between −0.22 and −0.30 Hz as θ increased from 0 to 90°.

[3]For a fuller discussion of procedures designed to investigate coupling pathways, see ref. 3.

theory, as apparently is also true for the computation of ^6J(H,C) in acetophenone above.

In 2,6-dichlorobenzaldehyde in acetone-d_6 solution we find $^6J(H,CHO)$ as −0.135(3) Hz. A geometry-optimized STO 3G MO computation of the barrier yields $V(\theta)/\text{kJ mol}^{-1} = 2.7(1)\sin^2\theta - 2.8(1)\sin^2 2\theta$ for the internal rotational potential. In other words, the minimum energy occurs near $\theta = 40°$ and the potential is relatively flat. This potential implies a $\langle\sin^2\theta\rangle$ of 0.41 at 300 K. Then $^6J(H,CHO)$ at $\theta = 90°$ would be −0.33 Hz, very much smaller in magnitude than the ^6J(H,H) of −1.2 Hz at $\theta = 90°$ in toluene (32) or the −1.0 Hz in thiophenol (33). Furthermore, at $\theta = 0°$, ^6J(H,C) in ethylbenzene is near (−)0.6 Hz. The ratio of ^6J(H,H) in toluene and ^6J(H,C) in ethylbenzene is 0.52. If a similar ratio holds for $^6J(H,CHO)$ in benzaldehyde and ^6J(H,C) in acetophenone at $\theta = 90°$, then the latter coupling should be -0.33×0.52 or −0.17 Hz. It is observed as −0.14 Hz in 2,6-dichloroacetophenone. These comparisons again illustrate the ability of the carbonyl group to hinder transmission of spin state information via a σ−π mechanism.

By way of contrast, the σ electron pathways are not hindered, but enhanced. Thus, $^5J(H,CHO)$ is 0.430(1) Hz in benzaldehyde and is the average of *cis* and *trans* coupling paths. If $^5J(H,CHO)$ follows a $\sin^2(\theta/2)$ relationship, then $^5J(trans) \equiv {}^5J_{180} = 0.86$ Hz. This can be compared to a $^5J_{180}$ of 0.32 Hz in toluene (32, 34). Using the factor of 0.52 above, ^5J(H,C) in acetophenone follows as 0.22 Hz, as observed (Table 1). In 2,6-dichlorobenzaldehyde, $^5J(H,CHO)$ is 0.403(2) Hz. If $^5J(H,CHO)$ is a pure σ coupling, then it must be the same in benzaldehyde and its 2,6-dichloro derivative because $\langle\sin^2(\theta/2)\rangle$ will be 0.5 in both molecules. The values differ by 0.03 Hz in the two molecules. The difference between the ^5J(H,C) values in acetophenone and 2,6-dichloroacetophenone is rather larger, however.

^{6}J(CHO,F) in 4-fluorobenzaldehyde

The internal rotational barrier in 4-fluorobenzaldehyde in solution is about 34 kJ/mol (14, 35), so that a σ−π mechanism for $^6J(CHO,F)$ should result in a very small, *positive* number. Instead, it is −0.442(3) Hz (36). The INDO MO FPT values for this coupling are positive (36). Clearly, another mechanism is responsible. In view of the remarks above concerning the non-transmission of spin state information via the σ−π mechanism, the negative $^6J(CHO,F)$ must be attributed to a mechanism represented by ionic structure **3**.

$Q_{C(O)H} < 0$
$Q_{CF} > 0$

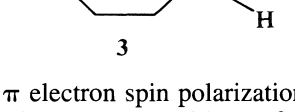

3

In **3** the arrows represent π electron spin polarizations in 2*pz* π-type orbitals on the carbon atoms. Evidence for such a structure comes from hyperfine fields observed in certain paramagnetic nickel(II) aminotropeneimineate derivatives (37), which show that the hyperfine coupling parameter, Q_{CH}, for an aldehydic group attached to a π electron system is negative, unlike the effective Q_{CH} for a methyl group, which is really a Q_{CCH} originating in a θ dependent hyperconjugative interaction.

The fluorine substituent would facilitate the coupling mechanism described by **3** because, being a π electron donor, it would increase the conjugation across the exocyclic C_{sp^2}—C_{sp^2} bond.

This line of evidence implies that ^6J(C,F) in 4-fluoroacetophenone is also negative (a tricky heteronuclear sign determination experiment is implied by the small magnitudes of the couplings). The observed magnitude of 0.13 Hz is qualitatively in agreement with such a mechanism, being smaller than $^6J(CHO,F)$ in the benzaldehyde derivative.

Now, as the carbonyl group twists out-of-plane, the mechanism represented by **3** becomes less effective, perhaps going as $\cos^2\theta$, and the σ−π (hyperconjugative) increases, going as $\sin^2\theta$. The two contributions to ^6J(C,F) are of opposite sign and, depending on their relative magnitudes, can lead to a vanishing coupling for some nonzero θ value, presumably accounting for the vanishing ^6J(C,F) in the nonplanar *tert*-butyl ketone and benzophenone derivatives above. It remains to be seen whether mechanism **3** helps to account for the vanishing ^5J(C,F). It would give a positive contribution to this coupling involving the carbonyl carbon nucleus.[4]

It may be noted that ^6J(C,F) for the ^{13}C nucleus of the methyl group in 4-fluoro-α-methylstyrene appears to be a σ−π coupling and is estimated to have a maximum magnitude of 1.1 Hz at $\sigma = 90°$ (5). Of course, an ionic structure analogous to **3** is not expected to be important for styrene.

If this line of argument is correct, it follows that the INDO MO FPT method does not account for a coupling mechanism of type **3**.

Furthermore, $^6J(H,CHO)$ is of insignificant magnitude in benzaldehyde. Because its internal barrier to rotation is so large, the σ−π mechanism is inoperative ($\langle\sin^2\theta\rangle \sim 0.04$ and ^6J at 90° is perhaps −0.33 Hz). However, mechanism **3**, if as efficient as in 4-fluorobenzaldehyde, would imply a coupling of about +0.2 Hz ($-Q_{CF} \sim 2Q_{CH}$). Its absence in benzaldehyde must then mean that mechanism **3** is not effective because it demands a larger conjugation across the C_{sp^2}—C_{sp^2} double bond, as large as in the 4-fluoro derivative.

Estimates of ^{6}J(CHO,F) and ^{6}J(C,F) at $\theta = 90°$

Assume that these couplings can be written as $^6J_0^\pi\langle\cos^2\theta\rangle + {}^6J_{90}^{\sigma,\pi}\langle\sin^2\theta\rangle$ where $^6J_0^\pi$ is negative and arises from a π mechanism of type **3**, while $^6J_{90}^{\sigma,\pi}$ is the σ−π or hyperconjugative interaction. On the basis of birefringence measurements, θ has been estimated as 28 ± 6° in pentafluorobenzaldehyde. $^6J(CHO,F)$ for the latter is −0.243(5) Hz in acetone solution (38). A barrier of 34 kJ/mol in 4-fluorobenzaldehyde implies a $\langle\sin^2\theta\rangle$ of about 0.045. The actual Kerr constants for the pentafluoro derivative (39) imply a $\langle\sin^2\theta\rangle$ of 0.233. The implied equations in $^6J^\pi$ and $^6J^{\sigma,\pi}$ yield $^6J_{90}^{\sigma,\pi}$ as 0.56 Hz and $^6J_0^\pi$ as −0.49 Hz. In view of the relatively large uncertainties in the $\langle\sin^2\theta\rangle$ values, write $^5J(CHO,F)/\text{Hz} = -0.5 + 1.1\langle\sin^2\theta\rangle$, where the $\cos^2\theta$ term has been absorbed. Note that $^6J_{90}^{\sigma,\pi}(H,CHO)$ was estimated as −0.33 Hz above. The corresponding $^6J_{90}$(H,H) in toluene is −1.20 Hz (32) and $^6J_{90}$(H,F) in 4-fluorotoluene is 2.28 Hz (40), yielding a ratio of −0.53, similar to the ratio (−0.55) of the corresponding numbers here deduced for benzaldehyde and 4-fluorobenzaldehyde.

This treatment implies that $^6J(CHO,F)$ should vanish in 4-fluorobenzaldehyde derivatives when $\langle\sin^2\theta\rangle \sim 0.5$, that is for a zero barrier, and should become positive and sizeable as $\langle\sin^2\theta\rangle$ approaches unity. Unfortunately, it is difficult to twist an aldehydic function substantially out-of-plane, as shown by the θ of 27° in 9-anthracene-carbaldehyde (41). The synthesis of 2,6-diX-4-fluorobenzaldehyde derivatives (X large and polar) is indicated.

Turning to ^6J(C,F) in the fluorophenyl ketone derivatives,

[4]In the 4-fluorophenyl ketones $^5J(C{=}O,F)$ was not observable. In 4-fluorophenyl methane ^5J(C,F) has a magnitude of 0.73 Hz (5) and is 0.59 Hz in 4-fluorostyrene (5). The striking modification of coupling magnitudes caused by the carbonyl moiety is again evident.

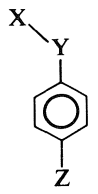

$^6J_{90}^{\sigma,\pi}$/Hz	X	Y	Z
−1.2	H	CH_2	H
−0.3	H	C=O	H
−0.6	C	CH_2	H
-0.1_4	C	C=O	H
2.3	H	CH_2	F
0.6	H	C=O	F
1.3	C	CH_2	F
0.3	C	C=O	F

SCHEME 1

the latest θ value for *tert*-butyl phenyl ketone is 49 ± 5° (21), while that for pentafluoroacetophenone is 41° (22). In both compounds ^6J(C,F) is unobservable. Assume θ as 45°, therefore. Combined with a barrier of 24.7 kJ/mol in 4-fluoroacetophenone, for which $\langle \sin^2 \theta \rangle$ is therefore near 0.05 and ^6J(C,F) is 0.13 Hz, assumed negative here, one derives $^6J_0^{\pi}$ as -0.1_6 Hz and $^6J_{90}^{\pi}$ as 0.3_0 Hz. These are clearly very rough estimates, although it is true that $^6J_{90}^{\sigma,\pi}$, as expected, is roughly twice as large in magnitude as $^6J_{90}^{\sigma,\pi}$ for the ^6J(H,C) in 2,6-dichloroacetophenone above.

Summary and conclusions

The σ−π contributions to spin–spin couplings over six bonds between *para* protons or ^{19}F nuclei, and protons or ^{13}C nuclei, in the sidechain of benzaldehyde and phenyl ketones are only about 25% of those in toluene derivatives. The relative magnitudes are given in Scheme 1. In addition, the six-bond couplings to ^{19}F nuclei contain substantial negative components in planar conformations. In consequence, the utility of these coupling parameters in conformational analysis is very limited as compared with those in toluene, anisole, and thioanisole derivatives. By way of contrast, σ electron couplings over five bonds to *meta* ring protons are not reduced in magnitude by the intervening carbonyl group (36, 42).

As a referee has noted, for a given Y, there is a fairly constant ratio between the above coupling constants that involve protons and those that involve ^{13}C nuclei. This is reasonable if both coupling constants are dependent on a σ−π mechanism. Similar ratios are known for couplings over two, three, and four bonds (43). The $^6J_{90}$ values when Y is C=O are derived on the assumption that the *ortho* substituents do not strongly perturb the σ−π coupling mechanism. This assumption is substantiated for Y = CH_2 (4) and, in view of the data above, appears a sensible one when Y is C=O.

Acknowledgments

We are grateful to the Natural Sciences and Engineering Council of Canada for financial assistance.

1. R. WASYLISHEN and T. SCHAEFER. Can. J. Chem. **50**, 1852 (1972).
2. W. J. E. PARR and T. SCHAEFER. Acc. Chem. Res. **13**, 400 (1980).
3. R. LAATIKAINEN and E. KOLEHMAINEN. J. Magn. Reson. **65**, 89 (1985).
4. T. SCHAEFER, J. PEELING, and G. H. PENNER. Can. J. Chem. **61**, 2773 (1983).
5. T. SCHAEFER, J. PEELING, G. H. PENNER, A. LEMIRE, and R. SEBASTIAN. Can. J. Chem. **63**, 24 (1985).
6. T. SCHAEFER, R. LAATIKAINEN, T. A. WILDMAN, J. PEELING, G. H. PENNER, J. BALEJA, and K. MARAT. Can. J. Chem. **62**, 1592 (1984).
7. G. LOCK and E. BOECK. Chem. Ber. **70**, 921 (1937).
8. E. HARN (*Editor*). Org. Synth. Coll. Vol. III. J. Wiley & Sons, New York. 1955. p. 562.
9. G. A. MORRIS and R. J. FREEMAN. J. Am. Chem. Soc. **101**, 760 (1979).
10. M. R. PETERSEN and R. A. POIRIER. MONSTERGAUSS. Department of Chemistry, University of Toronto, Toronto, Ontario. 1981.
11. P. A. DOBOSH. Quantum Chemistry Program Exchange, **11**, 142 (1979).
12. R. LAATIKAINEN. J. Magn. Reson. **52**, 293 (1983).
13. A. R. QUIRT and J. S. MARTIN. J. Magn. Reson. **5**, 318 (1971); J. S. MARTIN, A. R. QUIRT, and K. E. WORVILL. The NMR program library, Daresbury Laboratory, Daresbury, U.K.
14. T. DRAKENBERG, J. SOMMER, and R. YOST. J. Chem. Soc. Perkin Trans. **2**, 363 (1980).
15. R. J. ABRAHAM, D. J. CHADWICK, and F. A. E. G. SANCASSAN. Tetrahedron, **38**, 3245 (1982).
16. D. MIRARCHI and G. L. D. RITCHIE. Aust. J. Chem. **34**, 1443 (1981); J. Mol. Struct. **118**, 303 (1984).
17. A. GAMBI, S. GIORGIANNI, A. PASSERINI, R. VISINONI, and S. GHERSETTI. Spectrochim. Acta, Part A, **36**, 871 (1980).
18. K. S. DHAMI and J. B. STOTHERS. Can. J. Chem. **43**, 479 (1965).
19. K. S. DHAMI and J. B. STOTHERS. Tetrahedron Lett. 631 (1964).
20. R. J. ABRAHAM, H. A. BERGEN, and D. J. CHADWICK. J. Chem. Soc. Perkin Trans. **2**, 1161 (1983).
21. S. D. BARKER, D. MIRARCHI, R. K. NORRIS, L. PHILLIPS, and G. L. D. RITCHIE. J. Mol. Struct. **75**, 265 (1981), and references therein.
22. T. SCHAEFER, G. H. PENNER, T. A. WILDMAN, and J. PEELING. Can. J. Chem. **63**, 2256 (1985).
23. M. M. GRANGER and M. F. COILLOT. Acta Crystallogr. Part C, **41**, 542 (1985).
24. J. A. POPLE and M. S. GORDON. J. Am. Chem. Soc. **89**, 4253 (1967).
25. M. BARFIELD. J. Am. Chem. Soc. **102**, 1 (1980).
26. M. BARFIELD, E. W. DELLA, and P. E. PIGOU. J. Am. Chem. Soc. **106**, 5051 (1984), and references therein.
27. J. C. FACELLI, C. G. GIRIBET, and R. H. CONTRERAS. Org. Magn. Reson. **19**, 138 (1982), and references therein.
28. F. A. L. ANET and M. AHMAD. J. Am. Chem. Soc. **86**, 119 (1964).
29. T. DRAKENBERG, R. JOST, and J. M. SOMMER. J. Chem. Soc. Chem. Commun. 1011 (1974).
30. L. LUNAZZI, D. MACCIANTELLI, and A. C. BOICELLI. Tetrahedron Lett. 1205 (1975).
31. D. M. DODDRELL, M. R. BENDALL, P. F. BARRON, and T. D. PEGG. J. Chem. Soc. Chem. Commun. 77 (1979).
32. T. SCHAEFER, R. SEBASTIAN, and G. H. PENNER. Can. J. Chem. **63**, 2597 (1985).
33. T. SCHAEFER, T. A. WILDMAN, and S. R. SALMAN. J. Am. Chem. Soc. **102**, 107 (1980).
34. T. SCHAEFER and R. LAATIKAINEN. Can. J. Chem. **61**, 2785 (1983).
35. T. B. GRINDLEY, A. R. KATRITZKY, and R. D. TOPSOM. J. Chem. Soc. Perkin Trans. **2**, 443 (1975).
36. R. WASYLISHEN and T. SCHAEFER. Can. J. Chem. **49**, 3216 (1971).
37. D. R. EATON, A. D. JOSEY, and R. E. BENSON. J. Am. Chem. Soc. **89**, 4040 (1967).
38. T. SCHAEFER and K. MARAT. Org. Magn. Reson. **15**, 294 (1981).
39. M. J. ARONEY. Angew. Chem. Int. Ed. Eng. **16**, 663 (1977).
40. R. WASYLISHEN and T. SCHAEFER. Can. J. Chem. **49**, 94 (1971).
41. J. TROTTER. Acta Crystallogr. **12**, 922 (1959).
42. T. SCHAEFER, J. PEELING, and T. WILDMAN. Org. Magn. Reson. **22**, 477 (1984).
43. J. L. MARSHALL. Carbon–carbon and carbon–proton nmr couplings: applications to organic stereochemistry and conformational analysis. Verlag Chemie International, Deerfield Beach, Florida. 1983.

Oxydoréduction photochimique et thermique entre le chrome(VI) et un acide α aminé (glycine, alanine, hydroxyproline et méthionine)

M. Bolte, B. Robert et J. Lemaire

Laboratoire de photochimie moléculaire et macromoléculaire de l'Université de Clermont-Ferrand II Unité associée au Centre national de la recherche scientifique n° 433 B.P. 45, 63170 Aubière, France

Reçu le 31 janvier 1986

M. Bolte, B. Robert et J. Lemaire. Can. J. Chem. **64**, 1864 (1986).

L'oxydoréduction thermique ou photochimique, qui intervient entre le chrome(VI) et différents acides aminés, conduit quantitativement à la formation de chrome(III), avec apparition intermédiare de chrome(V). Il n'apparaît pas de preuve spectrale de la formation à l'état fondamental d'un complexe entre $HCrO_4^-$ et l'acide aminé. La réduction thermique de $HCrO_4^-$ met en jeu l'acide aminé protoné $NH_3^+—CH(COOH)—R$ et nécessite la présence d'ions H^+. La photo-oxydoréduction fait intervenir $HCrO_4^-$, qui est la seule entité absorbante. $[HCrO_4^-]^*$ réagit ensuite avec l'acide aminé présent dans la solution. Le rendement quantique de réduction du chrome(VI) en chrome(III) est proportionnel à la concentration en acide aminé et indépendant du pH dans le domaine d'existence de $HCrO_4^-$.

M. Bolte, B. Robert, and J. Lemaire. Can. J. Chem. **64**, 1864 (1986).

Photochemical and thermal oxidation that occurs between chromium(VI) and various amino acids leads quantitatively to chromium(III). Spectroscopic studies rule out the formation of a chromium(VI) – amino acid complex in the ground state. Thermal oxidoreduction involves $HCrO_4^-$, the protonated amino acid $NH_3^+—CH(COOH)—R$, and H^+ ions. Chromium(V) appears to be an intermediate species in the reaction. $HCrO_4^-$ is the only absorbing compound and the photochemical chromium(VI) reduction proceeds through a reaction between $[HCrO_4^-]^*$ and the amino acid. Chromium(V) is the primary product of the charge transfer reaction. Reduction quantum yields are proportional to the amino acid concentration and pH independent in the $HCrO_4^-$ existence range.

Introduction

La modification de réseaux macromoléculaires par l'introduction de composés de coordination et leur exposition à la lumière est une technique couramment utilisée en photogravure. Ainsi, l'insolubilisation de la gélatine (1), de la cellulose (1) ou de l'alcool polyvinylique (2) peut être provoquée par des réticulations photo-induites par du bichromate de potassium. Une revue complète sur la gélatine bichromatée, matériau photosensible, et ses applications a été faite par D. Meyerhofer (3). Il nous est apparu important d'essayer d'élucider les mécanismes mis en jeu lors de la photo-oxydoréduction, qui intervient entre le chrome(VI) et un substrat réducteur. Dans un premier travail, l'acrylamide a été la substance oxydable étudiée (4). Ainsi, alors qu'il n'apparaît pas de complexation entre $HCrO_4^-$ et l'acrylamide à l'état fondamental, on provoque par excitation dans une transition propre de $HCrO_4^-$ la polymérisation du monomère vinylique. La réaction entre le chrome(VI) et l'acrylamide, qui intervient à l'état excité, conduit à la formation de chrome(V) et d'un radical amorceur de polymérisation.

Dans le présent travail, nous avons examiné les processus d'oxydoréduction photochimique et thermique, intervenant entre le chrome(VI) et différents acides aminés, principaux constituants de la chaîne peptidique de la gélatine : la glycine, l'alanine, l'hydroxyproline et la méthionine. L'étude préliminaire concernant la glycine et le chrome(VI) a fait l'objet d'une note (5).

Partie expérimentale

I. Réactifs utilisés

Le chromate de potassium, le bichromate d'ammonium ou de potassium sont des produits Fluka purum.

$CrCl_3 \cdot 6H_2O$, la glycine, l'alanine, l'hydroxyproline et la méthionine sont des produits Fluka puriss.

II. Préparation des solutions

Les solutions de sels de chrome(VI) ont une concentration en chrome comprise entre 5×10^{-4} *M* et 10^{-3} *M*. Elles sont extrêmement stables à l'inverse des solutions d'acide aminé, dont la durée d'utilisation ne peut excéder quelques jours.

Le pH, ajusté au moyen de HCl ou $HClO_4$, est mesuré avec un pH mètre Orion 811.

La désoxygénation des solutions est réalisée par un bullage d'argon pendant 30 min.

Les irradiations à 365 nm ont été réalisées à l'aide d'une lampe à vapeur de mercure «haute pression» associée à un monochromateur Bausch et Lomb. Le faisceau obtenu est parallèle et le réacteur est une cuve de quartz ronde de trajet optique 1 cm. L'intensité incidente, déterminée par actinométrie avec le ferrioxalate de potassium, est de l'ordre de 3×10^{15} photons $cm^{-2}\,s^{-1}$.

III. Méthodes d'analyse

Les spectres d'absorption uv–visible ont été enregistrés sur un spectrophotomètre Cary 118 C et sur un spectrophotomètre Perkin Elmer 554. La correction de l'effet thermique a été faite en analysant simultanément une solution irradiée et la même solution gardée à l'obscurité.

Les mesures rpe (résonance paramagnétique électronique) ont été réalisées sur un spectromètre Bruker ER 200 D bande X (ν = 9,21 GHz), fréquence des modulations 100 kHz, phase 90°. Les irradiations polychromatiques dans la cavité du spectromètre rpe ont été faites au moyen d'une lampe Hanovia Xe–Hg 1000 W. Le facteur de Landé *g* a été déterminé par rapport au DPPH (diphényl picryl hydrazyle) utilisé comme standard.

Résultats expérimentaux

Le chrome(VI), dans une solution aqueuse de bichromate d'ammonium de concentration comprise entre 10^{-3} et 10^{-4} *M* à pH inférieur à 5 se trouve à 85% sous forme $HCrO_4^-$ (6). Son spectre d'absorption uv–visible présente deux maximums à 263 et 352 nm et un épaulement à 440 nm. L'addition à une solution aqueuse de $HCrO_4^-$ de quantités croissantes de glycine,

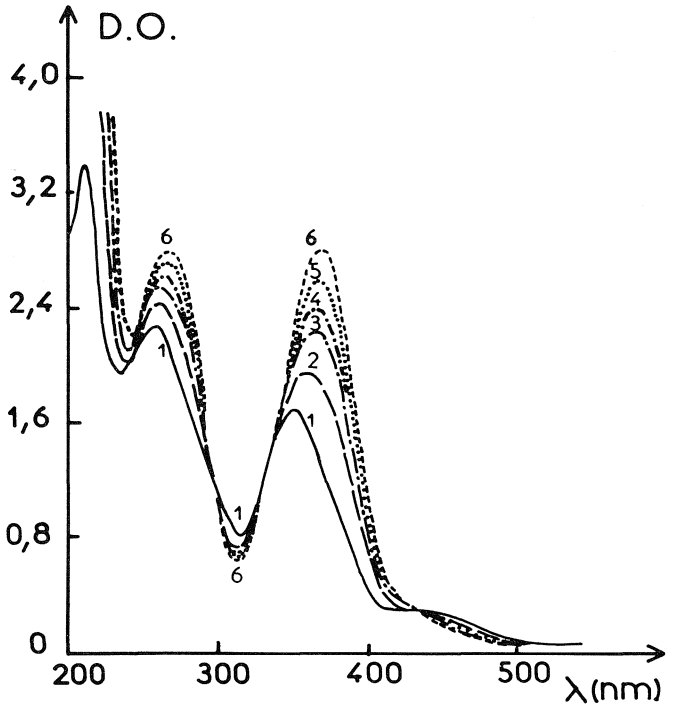

FIG. 1. Spectres d'absorption uv–visible de solutions de bichromate ((Cr(VI) = $10^{-3}M$) en présence de glycine en concentration c croissante (1, c = 0; 2, c = 0,35 M; 3, c = 0,75 M; 4, c = 1 M; 5, c = 1,3 M; 6, c = 1,68 M).

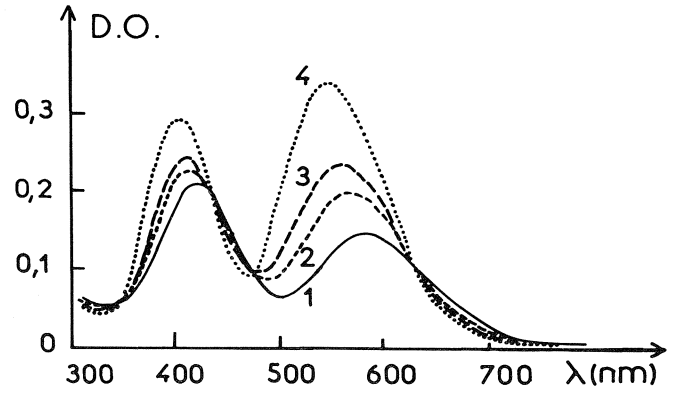

FIG. 2. Évolution spectroscopique d'une solution de chrome(III) ($c = 10^{-2}M$) et de glycine (c = 1 M) en fonction du temps (1, t = 0; 2, t = 1 jour; 3, t = 2 jours; 4, t = 8 jours).

alanine, hydroxyproline ou méthionine, provoque le déplacement vers le rouge du maximum à 352 nm, ainsi que la diminution de l'absorption à 440 nm (fig. 1). Cette modification spectrale est accompagnée d'une augmentation de pH. Si le pH est maintenu inférieur ou égal à 4, l'addition d'acide aminé ne modifie pas le spectre uv–visible de $HCrO_4^-$.

Le chrome(III), sous forme $Cr(H_2O)_6^{3+}$, stable dans l'eau dans le domaine 1,5 < pH < 5, présente deux maximums dans le visible à 415 et 582 nm (ε = 13 M^{-1} cm^{-1}). L'addition d'acide aminé provoque un lent déplacement des maximums vers les courtes longueurs d'onde (fig. 2). En fin de réaction, pour une solution molaire en glycine et $10^{-2}M$ en chrome(III), on observe deux maximums à 390 et 526 nm ($\varepsilon = 80\,M^{-1}$ cm^{-1}). Cette évolution traduit la substitution progressive de l'eau par l'acide aminé.

À 350 nm, le coefficient d'extinction molaire du chrome(III) est négligeable devant celui du chrome(VI). Les cinétiques de disparition du chrome(VI) peuvent être suivies par spectroscopie uv–visible à 352 nm, maximum d'absorption de l'espèce $HCrO_4^-$.

TABLEAU 1. Constantes de vitesse de réduction du chrome(VI) en fonction du pH

	pH	k_0 (min^{-1})
[Méthionine]	1,1	0,344
0,05 M	1,5	0,155
[Cr(VI)]	1,65	0,087
7,25 × $10^{-4}M$	1,83	0,057
	2,27	0,015
	2,80	0,006

Evolution thermique

Laissées à l'obscurité et à température ordinaire, des solutions aqueuses de chrome(VI) et d'acide aminé peuvent évoluer avec le temps. Ainsi, en milieu acide, on note la disparition de la couleur jaune de départ et l'apparition en fin de réaction d'une très faible coloration violette. L'absorption à 350 et 440 nm, due à $HCrO_4^-$, décroît régulièrement, tandis qu'apparaissent deux maximums à 390 et 525 nm. La vitesse de ce phénomène, observée pour tous les acides aminés, dépend de l'acide aminé étudié et du pH. Très lente avec la glycine, la disparition du chrome est beaucoup plus rapide avec la méthionine. L'influence des différents paramètres, pH, concentration en acide aminé et chrome(VI), a été étudiée dans le cas de la méthionine.

Les réactions ont systématiquement été réalisées avec un excès de méthionine par rapport au chrome(VI). La disparition du chrome(VI) à pH = 2,8 suit une loi du premier ordre en fonction du temps, si le rapport méthionine/Cr(VI) est supérieur ou égal à 15. De plus, à cette condition, la vitesse initiale est proportionnelle à la concentration en méthionine. La disparition du chrome(VI) est également du premier ordre par rapport au temps dans un domaine de pH compris entre 1 et 3. À pH supérieur, il apparaît une déviation.

Nous avons également calculé les valeurs de vitesse initiale lorsque le pH varie en dessous de la valeur du pK_I de la méthionine égal à 2,28 (7). Il apparaît une relation de proportionnalité directe entre la vitesse initiale et la concentration en ions H^+. Le tableau 1 regroupe les constantes de vitesse à différents pH. Dans nos conditions expérimentales, il n'y a pas de modification notable de pH en cours de réaction.

Dans le cas de la glycine, les constantes de vitesse sont extrêmement faibles, souvent difficilement déterminables avec une bonne précision. Nous avons cependant évalué la valeur de la constante de vitesse en milieu relativement acide et en présence d'un très gros excès de glycine. Soit :

$$[\text{glycine}] = 0{,}5\,M$$
$$\text{pH} = 1{,}5$$
$$[\text{Cr(VI)}] = 7{,}25 \times 10^{-4}\,M$$
$$k_0 \simeq 1{,}5 \times 10^{-4}\ \text{min}^{-1}$$

Considérant la proportionnalité qui existe entre k_0 et la concentration en acide aminé, le rapport des constantes de vitesse entre la méthionine et la glycine est de l'ordre de 10^4. La réaction thermique en présence d'alanine est du même ordre que

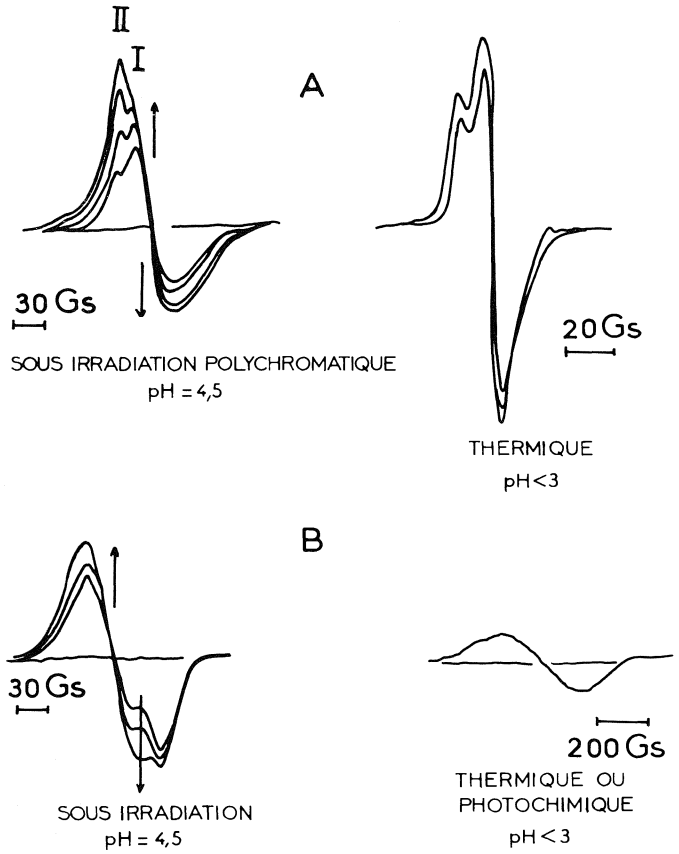

FIG. 3. Spectres rpe de solutions congelées (−30°C) de : A : glycine + chrome(VI); B : méthionine + chrome(VI).

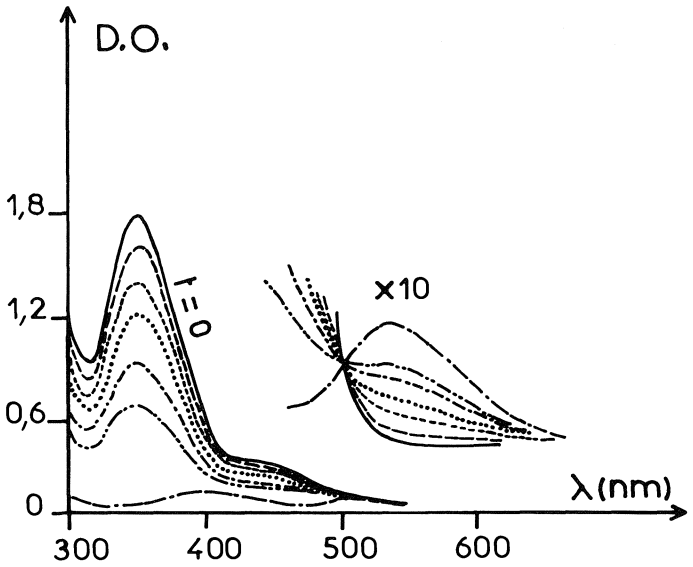

FIG. 4. Évolution du spectre uv–visible d'une solution de bichromate en présence de glycine, pH = 4, sous irradiation à 365 nm.

TABLEAU 2. Rendement quantique de réduction du chrome(VI) en présence de méthionine à λ = 365 nm

Méthionine pH = 4	$\phi^0_{Cr(VI)\rightarrow Cr(III)}$	
0,0125 *M*	$3,9 \times 10^{-3}$	
0,025 *M*	$6,4 \times 10^{-3}$	
0,05 *M*	13×10^{-3}	Cr(VI) = $7,25 \times 10^{-4}$ *M*
0,115 *M*	28×10^{-3}	
0,166 *M*	48×10^{-3}	

celle observée en présence de glycine, tandis que l'hydroxyproline possède un caractère réducteur intermédiaire.

Étude en résonance paramagnétique électronique

À température ordinaire, on n'observe aucun signal pour des solutions aqueuses Cr(VI)–glycine ou méthionine. C'est également le cas en matrice solide (solution congelée à −30°C) à pH supérieur à 3,5. Par contre, à pH inférieur, un ou plusieurs signaux apparaissent, caractéristiques du système étudié : avec la glycine, il apparaît deux signaux intenses de largeur respective 7,5 et 15 Gs (g = 1,9795 et g = 1,9824) et dont les intensités augmentent, puis diminuent avec la même vitesse. Par contre, leur intensité relative dépend des conditions expérimentales. Après complète transformation, on observe un signal faible et de grande largeur de bande ($\Delta G \simeq 160$ Gs).

Avec la méthionine, on observe directement un signal faible de grande largeur de bande ($\Delta G \simeq 320$ Gs). Ce signal augmente très lentement à −30°C. La figure 3 regroupe l'ensemble des signaux rpe étudiés.

Comportement photochimique

L'irradiation d'une solution [Cr(VI)] = $7,25 \times 10^{-4}$ *M* et [acide aminé] = 1 *M*, dont le pH est environ 5, provoque une augmentation de pH. La photoréaction est pratiquement arrêtée dès que le pH atteint une valeur de 6,5. La consommation d'ions H^+ ne peut être imputée à la réaction thermique, car la vitesse d'une telle réaction est nulle dans cette zone de pH. Les manipulations ont donc été réalisées à pH compris entre 1,5 et 4,5, le pH étant ajusté avec $HClO_4$ ou HCl. Au delà de pH = 1,5, la réaction thermique devient trop importante et rend imprécise la détermination des rendements quantiques. Les expériences faites en milieu aéré ou désoxygéné montrent que l'oxygène n'a pas d'influence sur les valeurs des rendements quantiques.

Les rendements quantiques de réduction du chrome(VI) sous excitation à 365 nm ont été déterminés en présence de glycine, alanine, hydroxyproline et méthionine à pH = 4. Lors de l'irradiation, on observe la diminution de l'absorption à 352 et 440 nm, la présence d'un point isobestique à 500 nm, ainsi que l'apparition de deux absorptions à 390 et 525 nm (fig. 4). La diminution de densité optique est parfaitement linéaire en début de photoréaction. Lorsque l'irradiation est maintenue, on observe la disparition presque complète du chrome(VI) : il reste en fin d'expérience environ 2% du chrome(VI) de départ.

Les courbes A de la figure 5 donnent la variation du rendement quantique initial de réduction en fonction du pH. Après correction de l'oxydoréduction thermique, réalisée pour la glycine et la méthionine, le rendement quantique apparaît indépendant du pH dans le domaine 1,5–4,5 (courbes B de la figure 5). Dans ce domaine de pH, le rendement quantique est directement proportionnel à la concentration en acide aminé. Les tableaux 2 et 3 regroupent l'ensemble des rendements quantiques obtenus.

Spectroscopie rpe sous irradiation

L'étude a été faite sous irradiation polychromatique avec des

TABLEAU 3. Rendement quantique de réduction du chrome(VI) par excitation à 365 nm

[Acide aminé] = 0,1 *M*, pH = 4	Structure	$\Phi_{Cr(VI)\rightarrow Cr(III)}$
Glycine	$NH_2—CH_2COOH$	$0{,}24 \times 10^{-3}$
Alanine	$CH_3CH(NH_2)—COOH$	$0{,}36 \times 10^{-3}$
Hydroxyproline	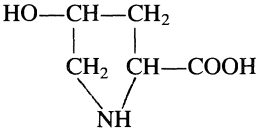	$2{,}40 \times 10^{-3}$
Méthionine	$CH_3—S—(CH_2)_2—CH(NH_2)COOH$	25×10^{-3}

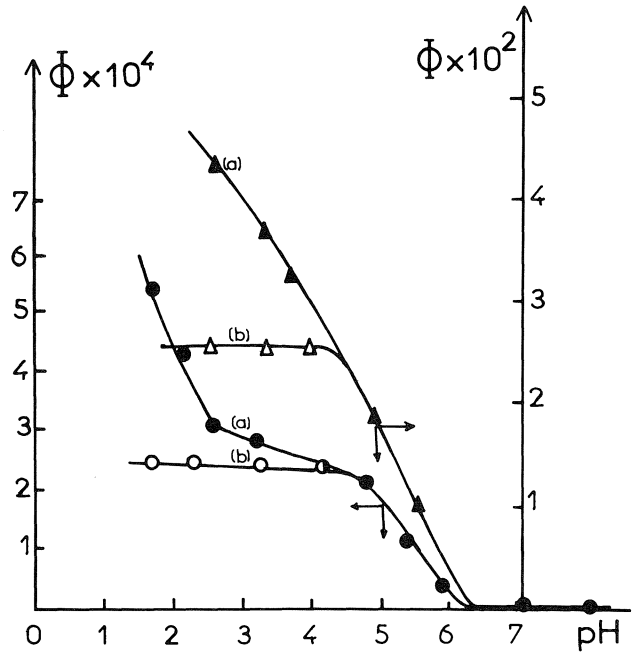

FIG. 5. Rendements quantiques de réduction du chrome(VI) par la glycine (0,1 *M*) et la méthionine (0,1 *M*) (○ : glycine; △ : méthionine); a : ϕ apparent; b : Φ corrigé de l'effet thermique.

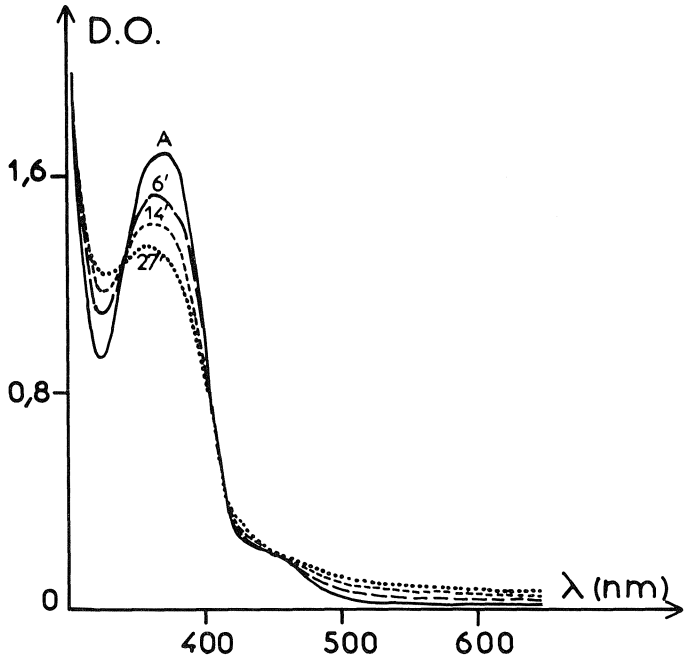

FIG. 6. Évolution spectrale d'un film de gélatine imprégné de bichromate sous irradiation à 365 nm.

solutions liquides (23°C) ou congelées (−30°C) de chrome(VI) en présence de méthionine (0,1 *M*) ou de glycine (1 *M*). À température ordinaire, on observe uniquement et pour de longues irradiations un signal faible et de très grande largeur de bande ($\Delta G \simeq 160$ Gs). En matrice solide, à −30°C, il faut différencier les systèmes et les conditions :

(*i*) Pour le système chrome(VI)–glycine et à pH = 4,5, deux signaux apparaissent à $g = 1{,}9765$ et $g = 1{,}9746$. Leur intensité relative varie avec le temps d'irradiation (fig. 3), le signal I ($\Delta G = 23$ Gs) apparaît dans un premier temps, puis décroît tandis que le signal II ($\Delta G = 30$ Gs) augmente, atteint un maximum, puis décroît très lentement. À pH inférieur à 3, on observe dès le début les deux signaux décrits lors de l'étude thermique ($g = 1{,}9795$ et $g = 1{,}9824$). L'irradiation provoque leur disparition au profit de deux autres signaux analogues ($g = 1{,}9765$ et $g = 1{,}9746$) déplacés vers les champs forts. Pour des irradiations prolongées, on voit apparaître un très faible signal de $\Delta G = 160$ Gs.

(*ii*) Pour le système chrome(VI)–méthionine à pH = 4,5, pH auquel le phénomène thermique ne masque pas le phénomène photochimique, on a, sous irradiation, un spectre rpe analogue à celui obtenu avec la glycine : deux signaux de largeur respective 13 et 26 Gs, dont l'intensité relative varie en cours d'irradiation. À pH inférieur à 3, la réaction thermique provoque l'apparition d'un signal faible et de très grande largeur de bande ($\Delta G = 300$ Gs). L'irradiation en accélère la formation.

Cas particulier de la gélatine

Un film de gélatine, d'épaisseur environ 40 μm, est trempé dans une solution de bichromate de potassium à 5% en poids, pendant 5 min. L'imprégnation de chrome(VI) conduit à une concentration de l'ordre de 0,35 *M*, déterminée par spectroscopie uv–visible. Le spectre rpe d'un film fraîchement préparé ne présente aucun signal. Par contre, avec le temps, il apparaît un signal intense ($\Delta G = 17{,}5$ Gs). Photochimiquement, il apparaît également un signal analogue, mais déplacé vers les champs forts. Pour des irradiations prolongées, on a également apparition d'un signal faible de $\Delta G = 160$ Gs. L'évolution du spectre d'absorption d'un film imprégné de chrome(VI) a été suivie sous irradiation à 365 nm (fig. 6). Il apparaît deux points isobestiques à 340 et 432 nm. Le spectre ΔD.O. $= f(\lambda)$ présente deux maximums à 320 et 424 nm, et un à environ 520 nm (fig. 7).

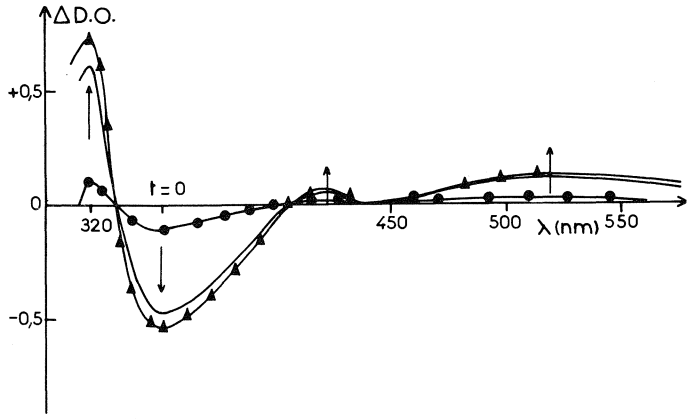

FIG. 7. $\Delta D.O. = f(\lambda)$: variation de la densité optique du film de gélatine imprégné de bichromate sous irradiation à 365 nm.

Discussion

Un certain nombre de résultats et les considérations qui en découlent concernent à la fois les phénomènes thermiques et photochimiques. Nous présentons donc dans la première partie de la discussion un ensemble de points communs aux deux types d'activation.

La méthionine $NH_2—CH(COOH)—(CH_2)_2—S—CH_3$ existe sous forme protonée $NH_3^+—CH(COOH)—(CH_2)_2—S—CH_3$ à pH inférieur à pK_I, ou zwitterionique $NH_3^+—CH(COO^-)—(CH_2)_2—S—CH_3$ à pH supérieur à pK_I, avec $pK_I = 2{,}28$ (7). Le pK de déprotonation du groupement NH_3^+ est en dehors de notre domaine d'études ($pK_{II} = 9$).

Il n'y a apparemment pas de complexation entre Cr(VI) et l'acide aminé à l'état fondamental. La réduction thermique ou photochimique de $HCrO_4^-$ par les acides aminés conduit au chrome(III), comme le montre l'évolution spectrale. La présence de maximums à 390 et 525 nm implique que le complexe obtenu soit, non pas le chrome(III) hexahydraté $Cr(H_2O)_6^{3+}$, mais le chrome(III) complexé par l'acide aminé. Étant donné la faible vitesse de substitution de l'eau par un acide aminé, le complexe chrome(III) – acide aminé s'établit obligatoirement au cours du processus d'oxydoréduction. À pH supérieur, CrO_4^{2-} est la seule espèce présente en solution. Le dianion s'avère une espèce non réductible par les acides aminés dans nos conditions expérimentales.

Les signaux obtenus en rpe dépendent des conditions expérimentales, quel que soit le type d'activation, thermique ou photochimique. Si l'acide aminé est très réducteur, si le milieu est très acide et (ou) à température ordinaire, l'oxydoréduction est très rapide et on observe seulement le stade ultime de la réaction, le chrome(III) hexacoordonné caractérisé par un signal faible et de très grande largeur de bande. Dans des conditions moins favorables à l'oxydoréduction (pouvoir réducteur inférieur, pH supérieur ou milieu rigide ...), on observe un signal intense que, parmi les états de valence du chrome, seul le chrome(V) en d^1 peut présenter. Le chrome(VI) est diamagnétique, le chrome(IV) avec deux électrons non appariés ne présente un signal qu'à très basse température et le chrome(III) présente un signal faible déjà décrit. Les différents signaux observés thermiquement ou photochimiquement correspondent à des environnements du chrome(V) différents selon les conditions (nature de l'acide aminé, concentrations respectives et pH).

Les expériences réalisées avec la gélatine nous ont permis de corréler le signal rpe et le spectre uv. On observe une espèce dont le spectre d'absorption est analogue à celui calculé par Srinivasan et Rocek (8), pour le complexe de chrome(V) résultant de la réduction thermique du chrome(VI) par l'acide oxalique. Ces auteurs observent un maximum à 320 nm et une différence d'absorption ($\varepsilon Cr(V) - \varepsilon Cr(VI)$) maximum à 425 nm et importante au delà de 520 nm. Par ailleurs, ils signalent l'apparition de deux signaux rpe analogues aux signaux que nous observons.

Le chrome(V) apparaît donc comme un produit primaire de l'oxydoréduction thermique ou photochimique entre le chrome(VI) et les acides aminés étudiés. En effet, l'hypothèse souvent admise (9–11), selon laquelle le chrome(V) résulte de la réaction du chrome(VI) de départ sur le chrome(IV), produit primaire d'une oxydation à deux électrons est hautement

[1] $Cr(VI) + Cr(IV) \rightleftharpoons 2Cr(V)$

improbable. Rahman et Rocek (12) ont montré que la constante de vitesse de la réaction [1] en solution aqueuse est très faible. L'équilibre est donc très fortement déplacé vers la gauche.

Il est à remarquer que la gélatine support solide permet de mettre en évidence le chrome(V) dans des conditions de température où, en solution, seul le chrome(III) final peut être observé.

Oxydoréduction thermique chrome(VI) – acide aminé

L'étude de la réduction thermique du chrome(VI) montre que la constante de vitesse dépend de la concentration en ions H^+ et en méthionine. La disparition du chrome(VI) ne suit plus une loi du premier ordre si le pH est trop élevé et (ou) si la concentration en réducteur est faible. Par ailleurs, dans ces conditions, la réduction est extrêmement lente donc difficilement analysable avec une bonne précision.

À $pH < pK_I$ où la méthionine est majoritairement sous forme protonée, la constante de vitesse varie proportionnellement à la concentration en ions H^+. La réduction du chrome(VI) par la méthionine est donc une réaction faisant intervenir trois composants $HCrO_4^-$, H^+ et $NH_3^+—CH(COOH)—(CH_2)_2—S—CH_3$; étant donné l'excès de méthionine présent dans la solution, la réaction est en fait contrôlée par les ions H^+. Les conclusions sont analogues avec les autres acides aminés étudiés.

Réaction photochimique

Comme indiqué précédemment, l'unique espèce absorbante est $HCrO_4^-$: une excitation à 365 nm correspond à une transition à caractère de transfert de charge du ligand oxygène vers le chrome(VI). $[HCrO_4^-]^*$ réagit ensuite avec l'acide aminé présent sous forme zwitterionique; la vitesse de réaction contrôle l'ensemble du mécanisme comme le prouvent les rendements quantiques proportionnels à la concentration en acide aminé. Le chrome(V) formé par transfer puis séparation des charges est réduit en chrome(III) par un mécanisme de réaction en cage qui maintient la complexation entre le centre métallique et l'acide aminé. On ne note aucune influence du pH sur le rendement quantique dans le domaine d'existence de $HCrO_4^-$, alors que la photoréduction consomme des ions H^+.

La photoréaction peut être schématisée de la façon suivante :

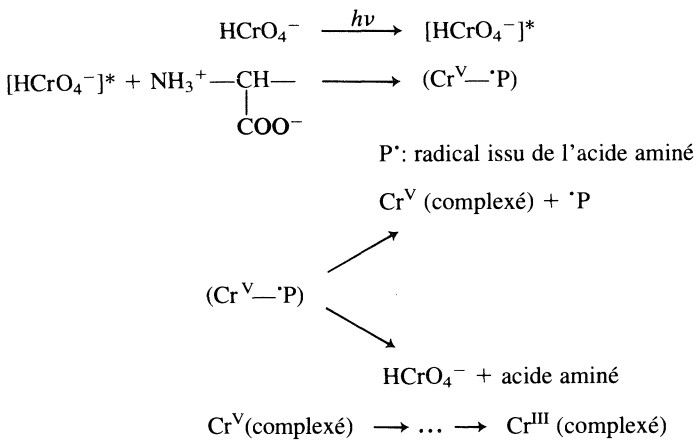

La formation d'un radical a été mise en évidence lors de l'étude de l'oxydation de l'acide oxalique par le chrome(VI) (10), ainsi que par nous-mêmes lors de l'étude de la polymérisation de l'acrylamide photo-amorcée par $HCrO_4^-$ (4).

Étant donné que nous travaillons à faible degré d'avancement (<10%), nous négligeons l'absorption de la lumière par le chrome(V) qui conduirait au chrome(III).

En conclusion, thermiquement ou photochimiquement, la vitesse de la réaction d'oxydoréduction entre le chrome(VI) et la glycine, l'alanine, l'hydroxyproline ou la méthionine est proportionnelle à la concentration en réducteur. Cependant, les résultats divergent quant à l'influence du pH. La réaction thermique nécessite un milieu relativement acide, afin de fournir les ions H^+ nécessaires à la réaction et à la protonation de l'acide aminé; elle est pratiquement inexistante à pH = 4. Au contraire, la réaction photochimique possède un rendement quantique indépendant du pH dans le domaine d'existence de $HCrO_4^-$ et permet ainsi de travailler à des pH où la réaction thermique est inefficace. La réaction est ainsi contrôlée par la lumière sans réaction thermique parasite, ce qui rend possible la photogravure.

1. P. Glafkides. Chimie et physique photographiques. P. Monte, Paris. 1976.
2. W. H. Fonger. J. Electrochem. Soc. **128**, 213 (1981).
3. D. Meyerhofer. Top. Appl. Phys. **20**, 75 (1977).
4. B. Robert, M. Bolte et J. Lemaire. J. Chim. Phys. **82**, 361 (1985).
5. B. Robert, M. Bolte et J. Lemaire. C. R. Acad. Sci. Paris, **301**, Série II, 881 (1985).
6. J. Y. P. Tong et E. L. King. J. Am. Chem. Soc. **75**, 6180 (1953).
7. J. P. Greenstein et M. Winitz. John Wiley and Sons, New York, London. 1961.
8. V. Srinivason et J. Roček. J. Am. Chem. Soc. **96**, 127 (1974).
9. J. Roček et A. E. Radkowsky. J. Am. Chem. Soc. **95**, 7123 (1973).
10. P. M. Nave et W. J. Trahanovsky. J. Am. Chem. Soc. **92**, 1120 (1970).
11. K. B. Wiberg et S. K. Mukherjee. J. Am. Chem. Soc. **93**, 2593 (1971).
12. M. Rahman et J. Roček. J. Am. Chem. Soc. **93**, 5462 (1971).

Synthesis and structural studies of rhodium complexes of phosphorus—sulfur ligands

DAVID G. DICK AND DOUGLAS W. STEPHAN[1]
Department of Chemistry, University of Windsor, Ont., Canada, N9B 3P4

Received October 1, 1985[2]

DAVID G. DICK and DOUGLAS W. STEPHAN. Can. J. Chem. **64**, 1870 (1986).

Rhodium complexes of the phosphorus—sulfur ligands, 2-diphenylphosphinoethyl methyl sulfide (MeSP), **1**, and 2-diphenylphosphinothiophene (PTH), **2**, have been prepared and studied by single crystal X-ray diffraction methods. $[Rh(MeSP)_2]BF_4 \cdot H_2O$, **3**, crystallizes in the space group $P2_1/n$ with a = 16.939(6) Å, b = 17.152(5) Å, c = 12.049(9) Å, β = 106.50(4)°, and Z = 4. The MeSP ligands chelate to Rh yielding a distorted square-planar geometry. The disposition of the methyl groups on the *cis* sulfur atoms is transoid. Average Rh—P and Rh—S bond distances were found to be 2.225(3) and 2.347(3) Å, respectively. $[Rh(PTH)_2(COD)]BF_4$, **4**, crystallizes in the space group Cc with a = 15.862(2) Å, b = 15.112(3) Å, c = 16.029(3) Å, β = 103.32(1)°, and Z = 4. The Rh atom in **4** also has essentially a square-planar coordination geometry. **2** does not chelate but rather is monohapto through phosphorus. Rh—P distances of 2.319(3) and 2.378(3) Å and Rh—C distances of 2.17(1), 2.22(1), 2.24(1), and 2.27(1) Å were found. The small variations in the Rh—P and Rh—C bonds distances appear to be a result of steric interactions between **2** and the COD ligand.

DAVID G. DICK et DOUGLAS W. STEPHAN. Can. J. Chem. **64**, 1870 (1986).

On a préparé des complexes de rhodium des ligands phosphore–soufre : le diphényl-2 phosphinoéthyle sulfure de méthyle (PSMe), **1** et le diphényl-2 phosphinothiophène (PTH) **2**, et on les a étudiés par diffraction de rayons X sur un monocristal. Le complexe de $[Rh(PSMe)_2]BF_4 \cdot H_2O$, **3**, cristallise dans le groupe d'espace $P2_1/n$ avec a = 16,939(6) Å, b = 17,152(5) Å, c = 12,049(4) Å, β = 106,50(9)° et Z = 4. Le ligand PSMe chélaté au Rh donne une géométrie carré plan déformée. Les groupes méthyle situés sur l'atome de soufre en position *cis* sont transoides. On a trouvé des distances moyennes de liaison Rh—P et Rh—S de 2,225(3) et 2,347(3) Å respectivement. Le complexe $[Rh(PTH)_2(COD)]BF_4$, **4** cristallise dans le groupe d'espace Cc avec a = 15,862(2) Å, b = 15,112(3) Å, c = 10,029(3) Å, β = 103,32(1)° et Z = 4. L'atome de Rh du composé **4** également a essentiellement une géométrie de coordination carré-plan. Le composé **2** ne chélate pas mais il est plutôt monohapto à travers l'atome de phosphore. Les longueurs de liaison Rh—P sont de 2,319(2) et 2,378(3) Å et celles de la liaison Rh—C sont de 2,17(1), 2,22(1), 2,24(1) et 2,27(1) Å. Les faibles variations observées dans les longueurs de liaison Rh—P et Rh—C se révèlent être le résultat d'interactions stériques entre le composé **2** et le ligand COD.

[Traduit par la revue]

Introduction

Over the past ten years increasing attention has focused on ligands containing both phosphorus and sulfur (1–18). Such ligands are of interest because they can exist in either monohapto or dihapto forms. For example, in Mo, Rh, and Ir complexes (7–12), the ligand 2-diphenylphosphinoethyl methyl sulfide (MeSP), **1**, exhibits dihapto coordination. However, reactivity studies of the complex $[Rh(MeSP)_2]BF_4$ suggest that the sulfur end of **1** is easily displaced yielding a monohapto ligand (10, 12). In comparison, Rh, Co, and Ni complexes of the ligand, 2-diphenylphosphinothiophene (PTH), **2**, have been reported in which **2** is proposed to coordinate only through phosphorus (15, 16). In our continuing interest (17–19) in such dissymmetric ligands, we have prepared and characterized by X-ray crystallography Rh complexes of both **1** and **2**. These structural studies confirm the dihapto and monohapto coordination modes of **1** and **2** in the complexes $[Rh(MeSP)_2]BF_4$, **3**, and $[Rh(PTH)_2(COD)]BF_4$, **4**, respectively. The results of these studies are presented and discussed herein.

Experimental

All preparations were done under an atmosphere of dry O_2-free N_2. Solvents were reagent grade and were degassed by the freeze–thaw method at least three times prior to use. $^{31}P\{^1H\}$ nmr spectra were recorded on a Nicolet GN-300 spectrometer located at Wayne State University, operating at 121.5 MHz with broad band proton decoupling. The ^{31}P chemical shifts are reported relative to external 85% H_3PO_4. Combustion analyses were performed by Guelph Chemical Laboratories, Guelph, Ontario. $[(COD)_2Rh]BF_4$, diphenylphosphinoethanethiol and 2-diphenylphosphinothiophene (PTH), **2**, were prepared by literature methods (20–22). Chlorodiphenylphosphine and 2-iodothiophene were purchased from the Aldrich Chemical Co.

Preparation of 2-diphenylphosphinoethyl methyl sulfide, (MeSP), 1

A solution consisting of 4.33 g (17.6 mmol) of the phosphine thiol, $HSCH_2CH_2PPh_2$, was prepared using 150 mL of THF. A solution of 1.6 *M* *n*-butyl lithium (11.0 mL, 17.6 mmol) in anhydrous diethyl ether was then added followed by dropwise addition of iodomethane (2.50 g, 17.6 mmol). The lithium iodide was extracted from the reaction mixture with water. The THF layer was dried over $MgSO_4$ and the solvent removed under vacuum, leaving a pale yellow oil. This subsequently crystallized *in vacuo* to give white needles (2.43 g, 53% yield). The product may be recrystallized from methanol by addition of diethyl ether. Comparison of the ^{31}P and ^1H nmr parameters to those already reported for **1** confirm the formulation of this product (9, 13).

Preparation of $[Rh(MeSP)_2]BF_4 \cdot H_2O$, 3

A solution of $[Rh(COD)_2]BF_4$ (0.334 g, 0.823 mmol) was prepared in approximately 15 mL of CH_2Cl_2. The ligand, **1** (0.430 g, 1.65 mmol), was dissolved in a small amount (approximately 3 mL) of the same solvent and added to the Rh complex. *n*-Hexane was allowed to diffuse into the yellow reaction mixture. The product, $[Rh(MeSP)_2]BF_4 \cdot H_2O$, crystallized as yellow needles (0.44 g, 70% yield). $^{31}P\{^1H\}$ nmr (CH_2Cl_2) δ (ppm): 65.4 (d) $J_{Rh—P}$ = 160.5 Hz. *Anal.* calcd. for $C_{30}H_{36}BF_4OP_2RhS_2$: C 49.47, H 4.98; found: C 50.59, H 4.92.

Preparation of $[Rh(PTH)_2(COD)]BF_4$, 4

A solution of $[Rh(COD)_2]BF_4$ (60 mg, 0.148 mmol) was prepared in approximately 5 mL of CH_2Cl_2. To this was added **2** (79 mg, 0.295 mmol) in 1 mL of the same solvent. The solution immediately takes on a yellow–orange color. Diffusion of *n*-hexane into this solution precipitated an orange crystalline product (93 mg, 75% yield). $^{31}P\{^1H\}$ nmr (CH_2Cl_2) δ (ppm): 17.7 (d), $J_{Rh—P}$ = 147.1 Hz. *Anal.* calcd. for $C_{40}H_{38}BF_4P_2RhS_2$: C 57.57, H 4.59; found: C 56.82, H 4.78.

[1]Author to whom correspondence should be addressed.
[2]Revision received April 28, 1986.

TABLE 1. Crystallographic parameters

Parameter	Value	
	3	**4**
Formula	$RhS_2P_2C_{30}H_{34}BF_4 \cdot H_2O$	$RhS_2P_2C_{40}H_{38}BF_4$
Crystal color, form	Yellow needles	Orange needles
a (Å)	16.936(6)	15.862(2)
b (Å)	17.152(5)	15.112(3)
c (Å)	12.049(9)	16.029(3)
β (deg)	106.50 (4)	103.32 (1)
Crystal system	Monoclinic	Monoclinic
Space group	$P2_1/n$	Cc
Vol. (Å^3)	3356(3)	3739(1)
Density (g cm^{-3})	1.44	1.48
Z	4	4
Crystal dimension (mm)	0.58 × 0.17 × 0.29	0.92 × 0.21 × 0.21
Crystal faces		(1 1 0), ($\bar{1}$ $\bar{1}$ 0), ($\bar{1}$ 1 0) (1 $\bar{1}$ 0), (1 1 1), ($\bar{1}$ $\bar{1}$ 1)
Absorption coefficient, μ (cm^{-1})	6.87	6.23
Radiation, λ (Å)	Mo Kα (0.71069)	Mo Kα (0.71069)
Temperature (°C)	24	24
Scan speed (deg/min)	2.0–5.0 (θ/2θ scan)	2.0–5.0 (θ/2θ scan)
Scan range (deg)	1.0 below $K\alpha_1$, 1.1 above $K\alpha_2$	1.0 below $K\alpha_1$, 1.1 above $K\alpha_2$
B_{kgd}/scan time ratio	0.5	0.5
Data collected	4830	5335
No. of unique data $F_o > 3\sigma(F_o^2)$	2950	2459
No. of variables	193	216
R (%)	6.88	6.82
R_w (%)	7.67	7.54

X-ray data collection and reduction

Yellow crystals of **3** were obtained by vapor diffusion of diethyl ether into a CH_2Cl_2 solution of **3**. Orange crystals of **4** were obtained by diffusion of *n*-hexane into a CH_2Cl_2 solution of **4**. Diffraction experiments were performed on a four-circle Syntex $P2_1$ diffractometer with graphite-monochromatized Mo Kα radiation. The initial orientation matrix for each crystal was obtained from 15 machine-created reflections selected from rotation photographs. These data were used to determine the crystal systems. Partial rotation photographs around each axis were consistent with a monoclinic crystal system in each case. Ultimately, 40 high-angle reflections ($15° < 2\theta < 31°$) for **3** and 30 high-angle reflections for **4** ($15° < 2\theta < 36°$) were used to obtain the final lattice parameters and the orientation matrices. Machine parameters, crystal data, and data collection parameters are summarized in Table 1. The observed extinctions were consistent with the space group $P2_1/n$ for **3** and Cc or $C2/c$ for **4**. Successful refinement later confirmed the space group as Cc for **4**. $\pm h, +k, +l$ data were collected in one shell ($4.5° < 2\theta < 45°$) for both **3** and **4**. Three standard reflections were recorded every 197 reflections. Their intensities showed no statistically significant change over the duration of data collection. The data were processed using the SHELX-76 program package on the computing facilities at the University of Windsor. A total of 2950 reflections for **3** and 2459 reflections for **4** with $F_o^2 > 3\sigma F_o^2$ were used in the refinements. In both cases the absorption coefficients were small ($\mu < 7$ cm^{-1}). The complexity of the crystal faces of **3** precluded accurate indexing. To check for absorption effects psi-scans were recorded for **3**. The average deviation from the mean intensity was less than 2.0% of the mean thus no absorption correction was applied to the data for **3**. For **4**, in which the crystal dimensions were distinctly anisotropic, the crystal faces were indexed, measured and an analytical absorption correction applied to the data. The maximum and minimum absorption corrections applied were 1.247 and 1.578, while the average correction was 1.343.

Structure solutions and refinements

Non-hydrogen atomic scattering factors were taken from the literature (23). The Rh atom positions were determined using the heavy atom (Patterson) method. The remaining non-hydrogen atoms were located from successive difference Fourier map calculations. Refinement was carried out by using full-matrix least-squares techniques on F, minimizing the function $\Sigma w(|F_o| - |F_c|)^2$ where the weight, w, is defined as $4F_o^2/\sigma^2(F_o^2)$ and F_o and F_c are the observed and calculated structure factor amplitudes. The refinement of **4** confirmed the space group as Cc. In the final cycles of refinement for each structure, the Rh, S, and P atoms were assigned anisotropic temperature factors. The methylene and methyl carbon atoms of **3** and the COD carbon atoms of **4** were also assigned anisotropic thermal parameters. The remaining non-hydrogen atoms were described by isotropic temperature factors. The phenyl-ring geometries were constrained to those of regular hexagons with C—C bond lengths of 1.39 Å. Hydrogen atom positions were allowed to ride on the carbon to which they are bonded assuming a C—H bond length of 0.95 Å. Hydrogen atom temperature factors were fixed at 1.10 times the isotropic temperature factor of the carbon atom to which the hydrogen is bonded. The hydrogens of the methyl groups of **3** were treated as rigid rotors. In all cases the hydrogen atom contributions were calculated but not refined. In both refinements disorder of the BF_4 moieties were apparent thus the geometries of BF_4 groups were constrained to those of tetrahedra with B—F bond distances of 1.28 Å. Difference map calculations suggested the presence of a two orientation disorder of the BF_4 group in **3**. After refinement of positional and site occupancy factors the best model for **3** was found to involve two orientations of the BF_4, centered at the same site, each with a 0.5 occupancy. For **4**, no simple multi-site disorder model was evident from the difference map analyses, thus a single constrained group with isotropic atoms was ultimately used. The final values of $R = \Sigma||F_o| - |F_c||/\Sigma|F_o||$ and $R_w = (\Sigma w(|F_o| - |F_c|)^2/\Sigma wF_o^2)^{1/2}$ are given in Table 1. Refinement of the inverted

TABLE 2. Positional parameters*

(*a*) $[Rh(MeSP)_2]BF_4 \cdot H_2O$

Atom	*x*	*y*	*z*	Atom	*x*	*y*	*z*
Rh	1533(1)	4275(1)	3908(1)	S1	492(2)	5517(2)	2852(3)
S2	2174(2)	5324(2)	5060(3)	P1	714(2)	3323(2)	2977(3)
P2	2613(2)	3570(2)	4864(3)	C1	934(10)	5573(9)	1814(15)
C2	−280(7)	4499(7)	1869(11)	C3	52(8)	3758(8)	1603(11)
C4	1583(9)	5375(8)	6078(12)	C5	3157(8)	4944(8)	5964(12)
C6	3108(9)	4081(8)	6241(12)	C12	−768(5)	2684(5)	3242(5)
C13	−1302(5)	2483(5)	3890(5)	C14	−1088(5)	2648(5)	5072(5)
C15	−341(5)	3014(5)	5605(5)	C16	192(5)	3215(5)	4957(5)
C11	−21(5)	3049(5)	3776(5)	C22	1555(5)	2427(4)	1781(8)
C23	1857(5)	1741(4)	1431(8)	C24	1662(5)	1022(4)	1825(8)
C25	1166(5)	0989(4)	2570(8)	C26	864(5)	1674(4)	2921(8)
C21	1059(5)	2394(4)	2527(8)	C32	3230(5)	3767(5)	2972(8)
C33	3832(5)	3731(5)	2389(8)	C34	4622(5)	3467(5)	2963(8)
C35	4809(5)	3239(5)	4119(8)	C36	4206(5)	3274(5)	4702(8)
C31	3417(5)	3538(5)	4128(8)	C42	2802(5)	1931(5)	4812(7)
C44	2306(5)	1049(5)	6027(7)	C45	2032(5)	1682(5)	6544(7)
C46	2143(5)	2439(5)	6194(7)	C41	2528(5)	2564(5)	5328(7)
B	3305(6)	8691(5)	5907(8)	F1	2675(9)	8998(11)	5185(15)
F2	3953(9)	8847(10)	5598(15)	F3	3383(12)	8970(9)	6920(10)
F4	3210(11)	7950(5)	5924(16)	F1B	2837(10)	8147(9)	5352(15)
F2B	3520(14)	9137(9)	5188(13)	F3B	2914(13)	9092(10)	6479(19)
F4B	3948(10)	8390(13)	6608(18)	O	4597(7)	4876(10)	8858(11)

(*b*) $[Rh(PTH)_2(COD)]BF_4$

Atom	*x*	*y*	*z*	Atom	*x*	*y*	*z*
Rh	0000	2044(1)	2500	P1	794(2)	1351(2)	3771(2)
P2	−489(2)	3167(2)	3254(2)	S1	1401(4)	−602(3)	3835(3)
S2	230(5)	4379(5)	4838(5)	C1	−907(10)	2524(9)	1316(9)
C2	−133(10)	2793(9)	1319(9)	C3	445(11)	2442(12)	757(10)
C4	1021(13)	1726(16)	1094(11)	C5	652(9)	1133(9)	1744(8)
C6	−163(10)	814(8)	1668(9)	C7	−836(12)	900(11)	860(11)
C8	−1389(11)	1734(13)	825(12)	C11	−1074(4)	4084(6)	2622(7)
C12	−595(4)	4747(6)	2338(7)	C13	−1019(4)	5415(6)	1801(7)
C14	−1921(4)	5421(6)	1548(7)	C15	−2400(4)	4758(6)	1832(7)
C16	−1976(4)	4089(6)	2369(7)	C21	360(8)	3738(9)	4005(9)
C22	1168(10)	3817(10)	3863(10)	C23	1724(12)	4400(12)	4442(12)
C24	1262(9)	4774(20)	5058(20)	C31	660(6)	1620(7)	4876(7)
C32	1215(6)	2253(7)	5342(7)	C33	1122(6)	2509(7)	6153(7)
C34	474(6)	2131(7)	6496(7)	C35	−81(6)	1498(7)	6029(7)
C36	12(6)	1242(7)	5219(7)	C41	603(8)	166(9)	3731(9)
C42	−225(9)	−231(10)	3610(10)	C43	−207(12)	1155(13)	3548(12)
C44	699(16)	−1466(20)	3695(17)	C51	1971(5)	1452(6)	3889(5)
C52	2521(5)	1008(6)	4564(5)	C53	3413(5)	1005(6)	4627(5)
C54	3755(5)	1445(6)	4015(5)	C55	3206(5)	1888(6)	3339(5)
C56	2314(5)	1892(6)	3276(5)	C61	−1298(8)	2669(7)	3811(7)
C62	−1498(8)	2985(7)	4560(7)	C63	−2104(8)	2543(7)	4914(7)
C64	−2512(8)	1784(7)	4519(7)	C65	−2312(8)	1467(7)	3770(7)
C66	−1705(8)	1910(6)	3416(7)	B	2491(9)	4282(9)	2178(8)
F1	2768(11)	4062(11)	2966(8)	F2	1666(9)	4186(15)	1963(12)
F3	2845(16)	3787(18)	1705(13)	F4	2684(14)	5093(12)	2078(14)

*Multiplied by 10^4.

model was of **4** performed. The R and R_w increased to 0.0688 and 0.0756, respectively. Using the Hamilton R factor test, the initial solution was confirmed to be the correct enantiomorph at a greater than 95% confidence level. The maximum Δ/σ on any of the parameters in the final cycles of refinement was 0.005 for **3** and 0.008 for **4**. Final difference Fourier map calculations showed no peaks of chemical significance; the largest peak was 1.35 electrons/Å^3 for **3** and was associated with the water molecule, while the largest peak for **4** was 1.5 electrons/Å^3 associated with C62. The following data are tabulated: positional parameters (Table 2); selected bond distances and angles (Table 3). Thermal parameters (Table S1), Hydrogen atom parameters (Table S2), and values of $10|F_o|$ and $10|F_c|$ (Table S3) have been deposited as supplementary material.[3]

Results and discussion

Reaction of CH_3I with the thiolate anion, $Ph_2PCH_2CH_2S^-$, yielded the previously reported ligand, **1** (10). This synthetic method is a convenient alternative to the known route. The

[3]Complete set of data may be purchased from the Depository of Unpublished Data, CISTI, National Research Council of Canada, Ottawa, Ont., Canada K1A 0S2.

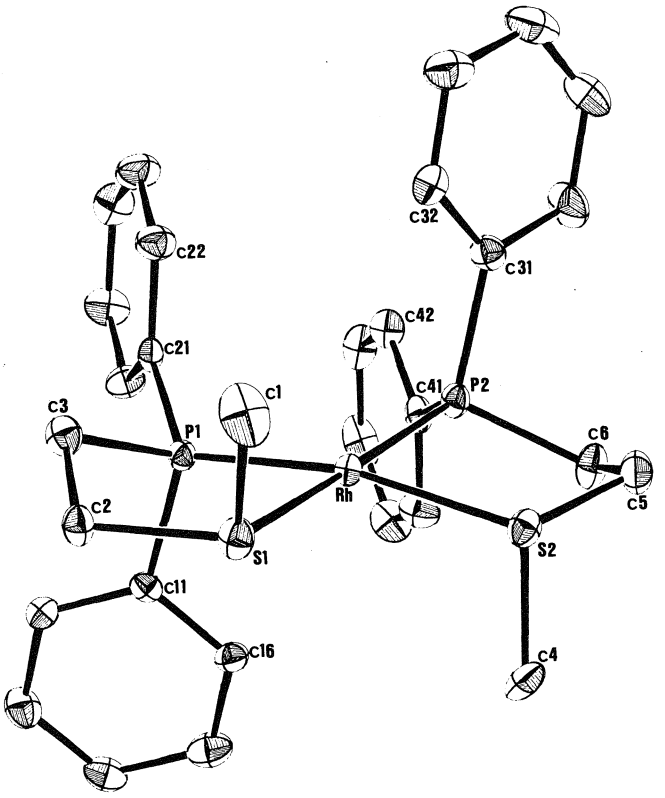

FIG. 1. ORTEP drawing of the cation of **3**, 30% thermal ellipsoids are shown.

second P—S ligand, **2**, was prepared by the published method (17). Reaction of the ligands, **1** and **2**, with $[Rh(COD)_2]BF_4$ gave yellow and orange rhodium complexes, respectively. In the case of **1**, the $^{31}P\{^1H\}$ nmr spectrum of the complex shows a doublet at 65.4 ppm. The Rh—P coupling constant is 160.5 Hz. These data were identical to those recently reported for the complex, $[Rh(MeSP)_2]BF_4$, **3** (9). Analytical data suggest that there is a molecule of H_2O per Rh atom in the crystal lattice. A similar reaction with ligand **2** gives an orange rhodium complex. $^{31}P\{^1H\}$ nmr as well as analytical data are consistent with the formulation $[Rh(PTH)_2(COD)]BF_4$, **4**. The upfield shift of the phosphorus resonance (17.7 ppm) and the Rh—P coupling constant of 147.1 Hz are consistent with phosphorus nuclei *trans* to COD (24).

Structural studies

Confirmation of the formulation as well as structural details of the Rh complexes **3** and **4** are obtained from crystallographic investigations. The study of compound **3** clearly shows that the crystal lattice is built from unit cells each containing discrete cations, anions, and waters of crystallization. The closest non-bonded approach between anion and cation is 2.501 Å (F3···H1C), while the closest approach between adjacent cations is 2.612 Å (H1A···H2B). The closest approach between the water molecule of crystallization and either the cation or the anion is 2.967 Å (O···H5A). Selected bond distances and angles are given in Table 3. An ORTEP drawing of the cation of **3** is shown in Fig. 1. The geometry of the Rh is essentially square planar with two phosphorus and two sulfur atoms comprising the coordination sphere. The Rh—P and Rh—S

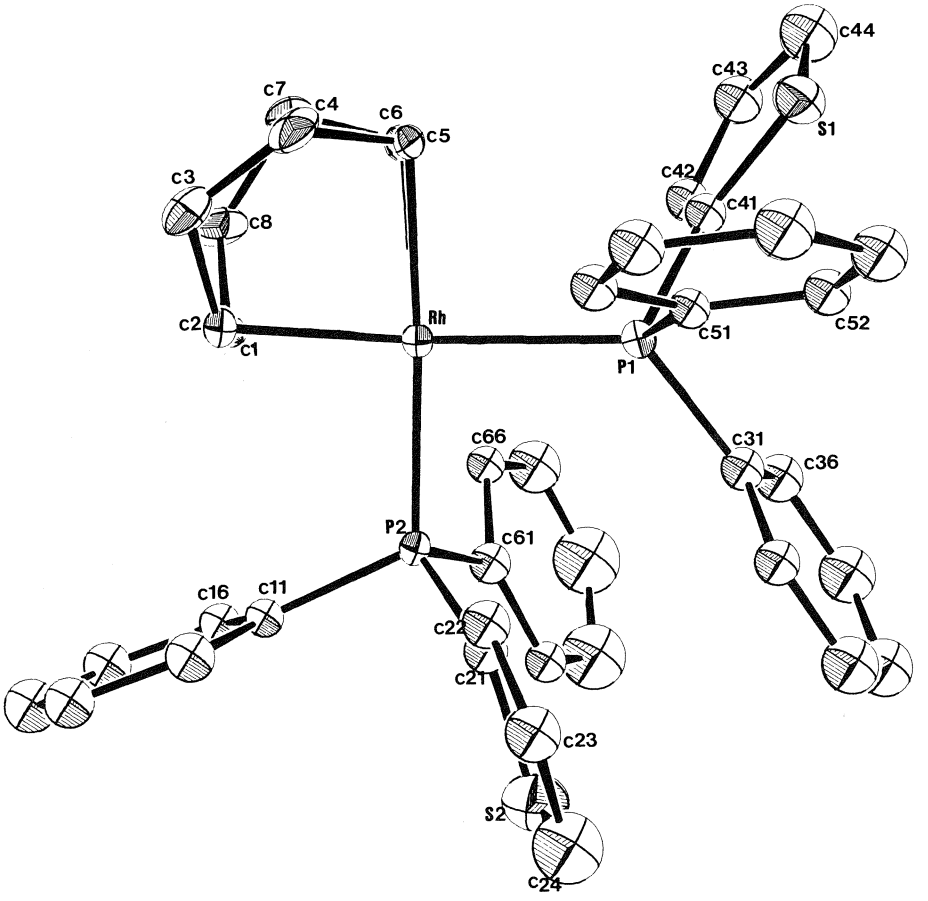

FIG. 2. ORTEP drawing of the cation of **4**, 30% thermal ellipsoids are shown.

TABLE 3. Selected bond distances and angles
(*a*) $[Rh(MeSP)_2]BF_4 \cdot H_2O$

Bond	Distance (Å)	Bond	Distance (Å)
Rh—S1	2.353(3)	P1—C3	1.87 (1)
Rh—S2	2.342(3)	P1—C11	1.839(8)
Rh—P1	2.227(3)	P1—C21	1.832(8)
Rh—P2	2.223(3)	P2—C6	1.85 (1)
S1—C1	1.81 (2)	P2—C31	1.82 (1)
S1—C2	1.83 (1)	P2—C41	1.832(9)
S2—C4	1.79 (1)	C2—C3	1.46 (2)
S2—C5	1.83 (1)	C5—C6	1.52 (2)

Bonds	Angle (deg)	Bonds	Angle (deg)
S1—Rh—P1	85.1(1)	C3—P1—C21	104.2(5)
S2—Rh—P1	168.2(1)	C11—P1—C21	104.6(4)
S1—Rh—P2	173.7(1)	C11—P1—Rh	109.9(2)
S2—Rh—P2	86.3(1)	C21—P1—Rh	125.6(3)
P1—Rh—P2	99.5(1)	C6—P2—Rh	107.5(4)
S1—Rh—S2	90.0(1)	C6—P2—C31	103.8(6)
C1—S1—C2	99.4(7)	C6—P2—C41	103.1(5)
C1—S1—Rh	104.2(5)	C31—P2—C41	104.7(4)
C2—S1—Rh	106.4(4)	C31—P2—Rh	112.5(3)
C4—S2—C5	101.6(6)	C41—P2—Rh	123.1(3)
C4—S2—Rh	100.8(4)	C5—C6—P2	107.5(9)
C5—S2—Rh	105.6(5)	S2—C5—C6	112.3(9)
C3—P1—Rh	106.6(4)	C2—C3—P1	108.9(9)
C3—P1—C11	103.9(5)	S1—C2—C3	113.4(8)
P1—C11—C12	122.3(2)	P1—C11—C16	117.7(2)
P1—C21—C22	117.1(2)	P1—C21—C26	122.9(2)
P2—C31—C32	119.2(2)	P2—C31—C36	120.8(2)
P2—C41—C42	122.1(2)	P2—C41—C46	117.8(2)

(*b*) $[Rh(PTH)_2(COD)]BF_4$

Bond	Distance (Å)	Bond	Distance (Å)
Rh—C1	2.22 (1)	Rh—C2	2.17 (1)
Rh—C5	2.24 (1)	Rh—C6	2.27 (1)
Rh—P1	2.378(3)	Rh—P2	2.319(3)
P1—C41	1.82 (1)	P1—C31	1.88 (1)
P1—C51	1.840(8)	P2—C11	1.836(9)
P2—C21	1.81 (1)	P2—C61	1.88 (1)
C1—C41	1.70 (1)	S1—C44	1.70 (3)
S2—C21	1.70 (1)	S2—C24	1.70 (2)
C21—C22	1.36 (2)	C22—C23	1.43 (2)
C23—C24	1.47 (4)	C41—C42	1.42 (2)
C42—C43	1.40 (2)	C43—C44	1.48 (3)
C1—C2	1.29 (2)	C2—C3	1.52 (2)
C3—C4	1.44 (3)	C4—C5	1.59 (3)
C5—C6	1.36 (2)	C6—C7	1.48 (2)
C7—C8	1.53 (3)	C8—C1	1.53 (2)

Bonds	Angle (deg)	Bonds	Angle (deg)
P1—Rh—P2	92.9(1)	C1—Rh—P1	170.6(4)
C1—Rh—P2	88.7(3)	C1—Rh—C2	34.2(6)
C1—Rh—C6	78.6(5)	C2—Rh—P1	154.4(4)
C2—Rh—P2	95.5(4)	C2—Rh—C5	79.2(5)
C5—Rh—P1	88.5(3)	C5—Rh—C6	35.1(6)
C5—Rh—P2	169.8(4)	C6—Rh—P1	96.3(3)
C6—Rh—P2	154.2(3)	Rh—P1—C31	124.1(4)
Rh—P1—C41	110.7(5)	Rh—P1—C51	112.1(2)
C31—P1—C41	101.2(5)	C31—P1—C51	102.6(4)
C41—P1—C51	104.0(5)	P1—C31—C32	117.4(2)
P1—C31—C36	122.5(2)	P1—C51—C52	118.5(2)

TABLE 3. (*concluded*)
(*b*) $[Rh(DPPT)_2(COD)]BF_4$

Bonds	Angle (deg)	Bonds	Angle (deg)
P1—C51—C56	121.2(2)	C11—P2—C21	102.3(5)
C11—P2—C61	104.6(4)	C61—P2—C21	111.1(5)
P2—C11—C12	118.6(2)	P2—C11—C16	120.0(2)
P2—C61—C62	125.9(3)	P2—C61—C66	114.1(3)
P1—C41—S1	123.8(8)	P1—C41—C42	124 (1)
C42—C41—S1	112 (1)	C41—S1—C44	94 (1)
S1—C44—C43	111 (2)	C42—C43—C44	110 (2)
C41—C42—C43	113 (1)	P2—C21—S2	126.1(7)
P2—C21—C22	121.2(8)	S2—C21—C22	112 (1)
C21—C22—C23	114 (1)	C22—C23—C24	110 (2)
C23—C24—S2	109 (2)	C21—S2—C24	95 (1)
C1—C2—C3	126 (1)	C2—C3—C4	117 (1)
C3—C4—C5	112 (1)	C4—C5—C6	129 (1)
C5—C6—C7	122 (1)	C6—C7—C8	113 (1)
C7—C8—C1	114 (1)	C8—C1—C2	128 (1)

bond distances average 2.225(3) and 2.348(3) Å and are typical (25, 26). The MeSP ligands form puckered five-membered chelate rings with the Rh. The bite angles average 85.8(6)°, a typical value for five-membered chelate rings (27). The disposition of the methyl groups on the *cis* sulfur atoms is transoid. The phenyl rings on the phosphorus atom adopt pseudo-axial and pseudo-equatorial positions. The two equatorial phenyl rings (C21—C26 and C41—C46) are almost parallel as the angle between the planes is only 8.16°. The average distance between these phenyl rings is 3.39 Å. This type of phenyl ring alignment for adjacent phenyl—phosphine groups has been observed in other structures (28).

The crystallographic study of **4** shows that the crystal is made up of unit cells containing discrete anions and cations. The closest non-bonded approach between anion and cation is 2.483 Å (F2···H24). The closest approach between adjacent cations is 2.389 Å (H14···H63). The interatomic distances and angles are included in Table 3. An ORTEP drawing of the cation of **4** is shown in Fig. 2. The geometry of the Rh is essentially square planar; two phosphorus atoms and the midpoints of the two carbon—carbon double bonds of the COD moiety complete the coordination sphere. The COD moiety binds to the Rh such that the Rh—C1 and Rh—C6 distances average 2.19(2) Å while Rh—C2 and Rh—C5 distances average 2.26(2) Å. In addition, the Rh—P1 bond length (2.378 Å) is slightly longer than the Rh—P2 bond length (2.319 Å). It is noteworthy that the closest approach of H5 or H6 to any of the rings on P1 is 2.357 Å (H5···H56), while for H1 or H2, the closest approach to the rings on P2 is 2.396 Å (H1···C11). Thus the slight lengthening of the Rh—C5, Rh—C6, and Rh—P1 bond lengths may serve to alleviate some of the steric interactions between the phosphine substituents and the COD ligand. The S atoms of the thiophene groups are not oriented to allow coordination to Rh. The intramolecular Rh···S distances are 4.828 and 5.099 Å while the closest intermolecular Rh···S distance is 7.085 Å (Rh···S1), thus confirming the monohapto nature of **2** in **4**. Once again, the phenyl groups on the adjacent phosphines are oriented such that two of the rings (C31—C36 and C61—C66) are almost parallel; the angle between the planes is 12.47°. The average distance between these phenyl rings is 3.45 Å. This situation is similar to that observed in **3** and other species (28).

The structures of the complexes described herein confirm two

possible coordination modes for phosphorus—sulfur ligands. The MeSP ligands in **3** form chelate rings (dihapto), while the PTH ligands in **4** coordinate only through phosphorus (monohapto). These modes of coordination have been proposed for **1** and **2** as well as related ligands (7–16). The monohapto nature of **2** may be attributed to the substantial strain involved in the formation of a four-membered chelate ring. In addition, the donor capability of the thiophene sulfur atom of **2** is certainly poorer than that of the thioether sulfur in **1**.

Acknowledgements

NSERC of Canada is thanked for financial support of this work. D.D. is grateful for the award of a NSERC postgraduate scholarship. Lucio Gelmini and Hilde Berends are thanked for the ligand syntheses. Drs. O. Mols and R. Hood of Wayne State University are thanked for use of the nmr facilities.

1. E. P. Kyba and C. N. Clubb. Inorg. Chem. **23**, 4766 (1984).
2. V. K. Issleib and W. Gans. Z. Anorg. Allg. Chem. **491**, 163 (1982).
3. G. R. Clark and J. D. Orbell. J. Organomet. Chem. **215**, 121 (1981).
4. P. G. Eller, J. M. Riker, and D. W. Meek. J. Am. Chem. Soc. **95**, 3540 (1973).
5. T. N. Lockyer. Aust. J. Chem. **27**, 259 (1974).
6. M. Savignac, P. Cadiot, and F. Mathey. Inorg. Chim. Acta, **45**, L43 (1980).
7. G. Doyle. J. Organomet. Chem. **101**, 85 (1975).
8. M. Bressan, F. Morandini, and P. Rigo. J. Organomet. Chem. **247**, C8 (1983).
9. M. Bressan, F. Morandini, and P. Rigo. Inorg. Chim. Acta, **77**, L139 (1983).
10. M. Bressan, F. Morandini, A. Morvillo, and P. Rigo. J. Organomet. Chem. **280**, 139 (1985).
11. M. Bressan, C. Furlani, and G. Polzonetti. Polyhedron, **2**, 523 (1983).
12. M. Bressan, F. Morandini, A. Morvillo, and P. Rigo. J. Organomet. Chem. **280**, 3538 (1983).
13. P. Rigo and M. Bressan. Inorg. Chem. **14**, 1491 (1975).
14. A. R. Sanger. Can. J. Chem. **61**, 2214 (1983).
15. A. R. Sanger. Can. J. Chem. **62**, 2168 (1984).
16. D. W. Allen and D. F. Ashford. J. Inorg. Nucl. Chem. **38**, 1953 (1976).
17. D. W. Stephan. Inorg. Chem. **23**, 2207 (1984).
18. G. S. White and D. W. Stephan. Inorg. Chem. **24**, 1499 (1985).
19. G. S. White and D. W. Stephan. Unpublished results.
20. R. S. Giorgano and R. H. Crabtree. Inorg. Synth. **19**, 218 (1979).
21. J. Chatt, J. R. Dilworth, J. A. Schmutz, and J. A. Zubieta. J. Chem. Soc. Dalton Trans. 1595 (1979).
22. D. W. Allen, J. R. Charlton, and B. G. Hutley. Phosphorus, **6**, 191 (1976).
23. D. T. Cromer and J. B. Mann. Acta Crystallogr. Sect. A, (*a*) A**24**, 321 (1968); (*b*) A**24**, 390 (1968).
24. N. C. Payne and D. W. Stephan. Inorg. Chem. **21**, 182 (1982).
25. J. Halpern, D. P. Riley, A. S. C. Chan, and J. J. Pluth. J. Am. Chem. Soc. **99**, 8055 (1977).
26. (*a*) C. Bianchini, C. Mealli, A. Meli, and M. Sabat. Inorg. Chem. **23**, 4125 (1984); (*b*) A. M. Mueting, P. Boyle, and H. Pignolet. Inorg. Chem. **23**, 44 (1984).
27. N. C. Payne and D. W. Stephan. J. Organomet. Chem. **221**, 203 (1981) and references therein.
28. D. H. Farrar and N. C. Payne. Inorg. Chem. **20**, 821 (1981).

Interaction of the methylmercury cation with glycine and alanine: a vibrational and X-ray diffraction study

MARIE-CLAUDE CORBEIL AND ANDRÉ L. BEAUCHAMP[1]
Département de Chimie, Université de Montréal, C.P. 6128, Succ. A, Montréal, Qué., Canada H3C 3J7

AND

SERGE ALEX AND RODRIGUE SAVOIE[1]
Département de Chimie, Université Laval, Cité Universitaire, Québec, Qué., Canada G1K 7P4

Received November 15, 1985[2]

MARIE-CLAUDE CORBEIL, ANDRÉ L. BEAUCHAMP, SERGE ALEX, and RODRIGUE SAVOIE. Can. J. Chem. **64**, 1876 (1986).

The complexes $(CH_3Hg)Gly$, (CH_3Hg)(L-Ala), and (CH_3Hg)(DL-Ala) were prepared by reacting CH_3HgOH with glycine (HGly) and alanine (HAla). Crystals of (CH_3Hg)(DL-Ala) are monoclinic, space group $P2_1/c$, $a = 9.460(2)$, $b = 8.794(2)$, $c = 8.723(2)$ Å, $\beta = 97.49(2)°$, $Z = 4$. The structure was refined on 935 MoKα reflections to $R = 0.042$. The complex results from displacement of an alanine NH_3^+ proton by the CH_3Hg^+ ion, which is linearly bonded to the $—NH_2$ group. An intramolecular Hg...O contact of 2.63 Å is also formed with a carboxylate oxygen. The Raman and infrared spectra of solid $(CH_3Hg)Gly$ and (CH_3Hg)(L-Ala) are compared with those of the ligands. Raman spectra of aqueous solutions at different pH indicate that the NH_2-bonded structure is retained in solution, although no complexation via the carboxylate occurs.

MARIE-CLAUDE CORBEIL, ANDRÉ L. BEAUCHAMP, SERGE ALEX et RODRIGUE SAVOIE. Can. J. Chem. **64**, 1876 (1986).

Les complexes $(CH_3Hg)Gly$, (CH_3Hg)(L-Ala) et (CH_3Hg)(DL-Ala) ont été préparés par réaction de CH_3HgOH avec la glycine (HGly) et l'alanine (HAla). Les cristaux de (CH_3Hg)(DL-Ala) sont monocliniques, de groupe spatial $P2_1/c$, $a = 9{,}460(2)$, $b = 8{,}794(2)$, $c = 8{,}723(2)$ Å, $\beta = 97{,}49(2)°$, $Z = 4$. La structure a été affinée au moyen de 935 réflexions MoKα jusqu'à $R = 0{,}042$. Dans ce complexe, un proton du groupement NH_3^+ de l'alanine est déplacé par l'ion CH_3Hg^+, qui se trouve linéairement coordonné au groupe NH_2. Un oxygène du groupe carboxylate établit également un contact intramoléculaire Hg...O de 2,63 Å. Les spectres Raman et infrarouges de $(CH_3Hg)Gly$ et (CH_3Hg)(L-Ala) à l'état solide sont comparés à ceux des ligands libres. Les spectres Raman de solutions aqueuses à différents pH indiquent que la liaison avec le groupe NH_2 persiste en solution, aucune complexation avec le groupe carboxylate n'ayant cependant pu être décelée.

Introduction

Our laboratories have undertaken a series of studies on the interaction of the CH_3Hg^+ ion with amino acids and small peptides, both in the solid state and in solution, with the aim of better understanding the behaviour of this cation with respect to polypeptides and proteins. In a recent paper (1), we have reported that the CH_3Hg^+ ion coordinates first to the $—NH_2$ lone pair of glycylglycine, in agreement with earlier observations by Rabenstein and co-workers (2) for other amino acids. We have also found that a second CH_3Hg^+ ion binds to a carboxylate oxygen in solid $[(CH_3Hg)_2Glygly]ClO_4$ (1). The very intense Raman bands observed between 450 and 575 cm^{-1} for the Hg—ligand stretching vibrations were particularly useful in distinguishing between these two different types of bonding.

Concurrently with the above study, 1:1 complexes with glycine (HGly) and alanine (HAla) were isolated which, judging from the Hg—ligand stretching regions in Raman, seemed to show different binding sites.[3] Indeed, whereas $(CH_3Hg)Gly$ produced a strong signal at the position expected for the Hg—N stretching vibration, the analogous band for $(CH_3Hg)Ala$ occurred in the region where the ν(Hg—O) band had been observed for the glycylglycine compound (1). As these amino acids were not expected to react differently, we decided to examine these two systems in greater detail.

[1]To whom correspondence may be addressed.

[2]Revision received April 25, 1985.

[3]Symbols for the various forms of the ligands are as follows: neutral zwitterionic forms: HGly and HAla; monoanions, Gly^- and Ala^-; monocations, H_2Gly^+ and H_2Ala^+.

Experimental section

Reagents and techniques

Glycine and alanine (both from Fisher Scientific) were used without further purification. The source of CH_3Hg^+ ions was the hydroxide CH_3HgOH (1 *M* aqueous solution from Alfa Inorganics).

The CH_3Hg^+ ion was analyzed potentiometrically by titration with KCl in ethanol (Ag/AgCl indicator electrode) (3). The concentrations of the solutions studied by Raman spectroscopy (4–16% w/w) are indicated for each of the spectra presented below, the pH being adjusted in each case with either NaOH or HNO_3 (4 *N*).

Raman spectroscopy

The Raman spectra, generally excited by the 514.5 nm line from a Spectra Physics Model 165 argon ion laser, were recorded on a Spex Model 1400 microcomputer-controlled spectrometer. The 488.0 nm line was used for the $(CH_3Hg)Gly$ crystals. The samples were contained in capillary tubes which, in the case of the highly light-sensitive solid complexes, were mounted on a motor shaft and rotated at high speed in the laser beam. Even so, the laser power at the sample had to be kept very low (~25 mW) in order to prevent sample decomposition. The various solutions, contained in sealed capillaries mounted in a copper block maintained at 10°C, were studied at a laser power of 200 mW at the sample. The spectra were typically recorded at 5 cm^{-1} spectral slit width, with a 2 s integration time at each 2 cm^{-1} frequency increment.

Infrared spectroscopy

The ir spectra were recorded as KBr pellets with a Digilab FTS-15 C/D Fourier-transform spectrophotometer equipped with a Globar source and a wide-band mercury cadmium telluride detector (Infrared Associates, New Brunswick, NJ). Typically, 100 interferograms of 4096 points recorded with an optical velocity of 1.2 cm s^{-1} and maximum optical retardation of 0.5 cm were co-added, apodized with a boxcar function, and Fourier transformed with four levels of zero filling

resulting in a spectral resolution of 2 cm^{-1}. The apparatus was purged with nitrogen during the experiment.

Nuclear magnetic resonance spectroscopy

The ^1H nmr spectra were obtained with a Bruker WH-90 spectrometer. The internal references used ($\delta = 0$) were TMS for DMSO-d_6 solutions or DSS for D_2O solutions. The solvents used were Silanor DMSO-d_6 (Merck, Sharp and Dohme Canada, 99.5% isotopic purity) and D_2O (Cambridge Isotope Lab., 99.83% isotopic purity).

Preparations

[(CH$_3$Hg)Gly]

Glycine (1 mmol, 75 mg) was dissolved in 1.0 mL of 1 *M* aqueous CH_3HgOH. Absolute ethanol (1 mL) and dimethylformamide (9 mL) were added. After a few hours at room temperature and in open air (hood), thin colorless platelets were obtained. Yield: 100 mg (33%). *Anal.* calcd. for $C_3H_7HgNO_2$: C 12.44, H 2.44, N 4.84; found: C 12.55, H 2.57, N 4.86. ^1H nmr (in D_2O): 3.69 (2H, s, CH_2), 0.86 (3H, s, CH_3Hg), $^2J(^1H—^{199}Hg)$ = 216 Hz; (in DMSO-d_6): 5.09 (2H, s, br, NH_2), 3.26 (2H, s, CH_2), 0.60 (3H, s, CH_3Hg), $^2J(^1H—^{199}Hg)$ = 208 Hz.

[(CH$_3$Hg)(DL-Ala)]

Prepared from DL-alanine by the same method as above, with addition of 2 mL of absolute ethanol and 8 mL of dimethylformamide. Colorless platelets precipitated after a few days. Yield: 100 mg (30%). ^1H nmr (in D_2O): 4.17 (1H, q, CH), 1.45 (3H, d, CH_3), 0.89 (3H, s, CH_3Hg), $^2J(^1H—^{199}Hg)$ = 215 Hz; (in DMSO-d_6): 5.05 (2H, s, br, NH_2), 3.70 (1H, q, CH), 1.24 (3H, d, CH_3), 0.63 (3H, s, CH_3Hg), $^2J(^1H—^{199}Hg)$ = 207 Hz. A crystal from this homogeneous crystalline sample was used for X-ray work.

[(CH$_3$Hg)(L-Ala)]

Prepared as above from L-alanine. The ^1H nmr data were identical with those of the DL-isomer. *Anal.* calcd. for $C_4H_9NO_2Hg$: C 15.82, H 2.99, N 4.61; found: C 16.04, H 3.01, N 4.60.

Crystal data

$C_4H_9HgNO_2$ fw = 303.71

Monoclinic, $P2_1/c$, $a = 9.460(2)$, $b = 8.794(2)$, $c = 8.723(2)$ Å, $\beta = 97.49(2)°$, $V = 719.2$ Å^3, $Z = 4$, $D_c = 2.804$ g cm^{-3}, λ(MoK$\bar{\alpha}$) = 0.71069 Å (graphite monochromator), μ(MoKα) = 213.0 cm^{-1}, T = 293 K.

Crystallographic measurements and structure determination

The crystal used for X-ray work had dimensions 0.045 × 0.188 × 0.168 mm^3. The space group and initial cell parameters were determined from precession and cone-axis photographs. Space group $P2_1/c$ was uniquely defined from the systematic absences ($0k0$, $k \neq 2n$; $h0l$, $l \neq 2n$). Accurate cell parameters and intensity data were obtained with an Enraf-Nonius CAD4 diffractometer, as described elsewhere (4). Three standard reflections monitored during the experiment showed that the crystal slowly decomposed in the X-ray beam, their intensities having decreased by 15% over the 2½ days of data collection. This decay was considered at the data reduction stage. A total of 1015 hkl and hkl reflections were measured, within a sphere limited by 2θ = 45°. After rejection of 80 systematic absences, the data set consisted of 935 independent reflections, of which 660 were used to solve the structure ($I > 3.0\sigma(I)$). The data were corrected for absorption (Gaussian integration, grid 8 × 8 × 8, transmission range: 0.074–0.392), polarization, and the Lorentz effect.

The structure was solved by the heavy-atom and refined on $|F_o|$ by full-matrix least squares. The Hg atom was located from a Patterson map and the remaining non-hydrogen atoms were found on the difference Fourier (ΔF) map phased on Hg. Isotropic refinement converged to $R = \Sigma||F_o| - |F_c||/\Sigma|F_o| = 0.052$ and $R_w = [\Sigma w(|F_o| - |F_c|)^2/\Sigma w|F_o|^2]^{1/2} = 0.064$. The hydrogen atoms on the amino and methine groups were fixed at ideal positions (C—H = 0.95 Å, N—H = 0.87 Å, B_{iso} = 4 Å^2). Their parameters were not refined, but the coordinates were recalculated after each cycle. The hydrogens of the methyl groups were neglected. Anisotropic refinement of all non-hydrogen atoms converged to $R = 0.042$ and $R_w = 0.049$. The goodness-to-fit ratio was 1.82. The highest residuals on the final ΔF map (±|1.2–2.0| e Å^{-3}) were all around the Hg atom. The general background was below ±1.0 e Å^3. The refined coordinates and equivalent isotropic temperature factors are listed in Table 1.[4] The temperature factor of C(1) is relatively large. Mercury-bound methyl groups often exhibit high thermal motion, which sometimes includes rotational disordering of the methyl group about the Hg—CH_3 bond. This results in larger esd's for C(1), but does not affect the overall structure.

The scattering curves were from standard sources (5). The f' and f'' contributions of Hg to anomalous dispersion were included in structure factor calculation (6). The programs used are listed elsewhere (7).

TABLE 1. Coordinates ($\times 10^3$, Hg $\times 10^5$) and equivalent temperature factors ($\times 10^3$) of the non-hydrogen atoms

Atom	X	Y	Z	U_{eq}
Hg(1)	22899(9)	20989(9)	15189(10)	56
O(6)	−181(2)	−29(2)	131(2)	69
O(7)	18(1)	65(1)	256(1)	47
N(2)	27(2)	302(1)	58(2)	45
C(1)	427(3)	139(4)	244(3)	102
C(3)	−93(2)	198(2)	32(2)	42
C(4)	−236(2)	288(2)	29(3)	71
C(5)	−86(2)	68(2)	149(2)	44

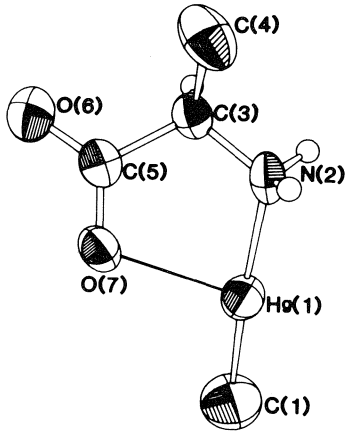

FIG. 1. Drawing of the (CH_3Hg)(DL-Ala) molecule, with the numbering scheme used. Thermal ellipsoids correspond to 50% probability. The methyl hydrogens were not found, the others are shown as small spheres of arbitrary size. The single line corresponds to the intramolecular Hg...O contact.

Results and discussion

Description of the structure

The [(CH_3Hg)Ala] complex is represented in Fig. 1 with the atom symbols used. Interatomic distances and bond angles are listed in Table 2.

The CH_3Hg^+ ion has replaced one of the ammonium protons of alanine, as anticipated from the higher affinity of mercury for amino than carboxylate groups. The Hg atom shows a

[4]The supplementary material includes lists of refined temperature factors, coordinates of hydrogen atoms, atom-to-plane distances and structure factor amplitudes. Complete set of material may be purchased from the Depository of Unpublished Data, CISTI, National Research Council of Canada, Ottawa, Ont., Canada K1A 0S2.

TABLE 2. Interatomic distances and bond angles

Bond	Distance (Å)	Bond	Distance (Å)
C(1)—Hg(1)	2.04(3)	C(3)—C(5)	1.53(2)
Hg(1)—N(2)	2.14(2)	C(5)—O(6)	1.23(2)
N(2)—C(3)	1.45(2)	C(5)—O(7)	1.26(2)
C(3)—C(4)	1.56(3)		

Bonds	Angle (deg)	Bonds	Angle (deg)
C(1)—Hg(1)—N(2)	175.6(9)	C(4)—C(3)—C(5)	111(1)
Hg(1)—N(2)—C(3)	117(1)	C(3)—C(5)—O(6)	118(2)
N(2)—C(3)—C(4)	110(1)	C(3)—C(5)—O(7)	118(2)
N(2)—C(3)—C(5)	114(1)	O(6)—C(5)—O(7)	124(2)

TABLE 3. Distance and angles in the hydrogen bonds and Hg...O contacts

Bond	Distance (Å)	Bonds	Angle (deg)
(*a*) Hydrogen bonds			
N(2)—H(21)...O(7)[a]	2.87(2)	C(3)—N(2)—O(7)[a]	101(1)
N(2)—H(22)...O(7)[b]	2.89(2)	C(5)[a]—O(7)[a]—N(2)	126(1)
		C(3)—N(2)—O(7)[b]	115(1)
		C(5)[b]—O(7)[b]—N(2)	106(1)
(*b*) Hg...O contacts			
Hg(1)...O(7)	2.63(1)	Hg(1)—O(7)—C(5)	107(1)
Hg(1)...O(6)[c]	2.92(1)	C(1)—Hg(1)—O(7)	114.6(9)
Hg(1)...O(6)[b]	3.05(1)	N(2)—Hg(1)—O(7)	68.6(5)
		Hg(1)—O(6)[c]—C(5)[c]	120(1)
		C(1)—Hg(1)—O(6)[c]	101.6(9)
		N(2)—Hg(1)—O(6)[c]	81.4(5)
		Hg(1)—O(6)[b]—C(5)[b]	127(1)
		C(1)—Hg(1)—O(6)[b]	100.9(9)
		N(2)—Hg(1)—O(6)[b]	75.8(5)
		O(7)—Hg(1)—O(6)[c]	89.2(4)
		O(7)—Hg(1)—O(6)[b]	88.2(4)
		O(6)[b]—Hg(1)—O(6)[c]	156.3(4)

[a] $x, \frac{1}{2} - y, -\frac{1}{2} + z$.
[b] $-x, \frac{1}{2} + y, \frac{1}{2} - z$.
[c] $-x, -y, -z$.

linear coordination (C(1)—Hg(1)—N(2) = 175.6(9)°), and the Hg—N(2) distance (2.14(2) Å) is similar to those reported for this type of complex (1, 8–10). Besides the strong Hg—CH_3 and Hg—NH_2 bonds, there is an intramolecular contact between mercury and the carboxylate oxygen O(7) at 2.63(1) Å (Table 3). Contacts of this type have been found for other compounds, namely in the 1:1 tyrosine (8) and the 1:1 methionine (10) complexes. In the 1:1 and 2:1 complexes with glycylglycine (1), the amino-bonded CH_3Hg^+ group also establishes a contact with the amide oxygen, but the distances (2.71(1) and 2.82(2) Å, respectively) are greater.

Light-atom positions cannot be determined precisely in the presence of the heavy atom. Considering the high esd's, complexation seems to leave the bond lengths and angles of DL-alanine unchanged (11), although the conformation is modified. In free alanine, the chain is not planar, the N—C—C—O torsion angle being 17°. In the complex, this same angle is 2(2)°, and the $NCCO_2$ chain is nearly planar. However, the CH_3Hg^+ group does not lie in this plane. The Hg—N(2)—C(3)—C(5) torsion angle of 33(2)° probably results from the intramolecular Hg—carboxylate contact mentioned above.

Each molecule is held in the lattice by six neighbors with which it forms hydrogen bonds and Hg...O contacts (Fig. 2 and Table 3). Both amino hydrogens participate in moderately strong N—H...O(7) hydrogen bonds of 2.88(2) Å with two different complex molecules (12). On the other hand, each Hg atom forms intermolecular contacts of 2.92(1) and 3.05(1) Å, respectively, with free carboxylate oxygens O(6) in two different molecules. These Hg...O(6) contacts are found at 90 ± 22° from the H_3C—Hg and Hg—N bonds, as usual.

The hydrogen bonds and Hg...O contacts generate layers parallel to the *bc* plane, with the complex molecules oriented roughly perpendicular to the layer (Fig. 2). As a result, the layer surface consists mainly of methyl groups from alanine and the CH_3Hg^+ groups. Cohesion between the layers is mainly due to normal van der Waals contacts between these methyl groups.

Vibrational spectroscopy

The vibrational spectra of glycine and alanine are well documented (13–15). Most of the assignments used in this work for the free ligands are those proposed by Machida and co-workers (13, 14).

The present X-ray work shows that one of the NH_3^+ protons of alanine is displaced by a CH_3Hg^+ ion in the (CH_3Hg)(DL-

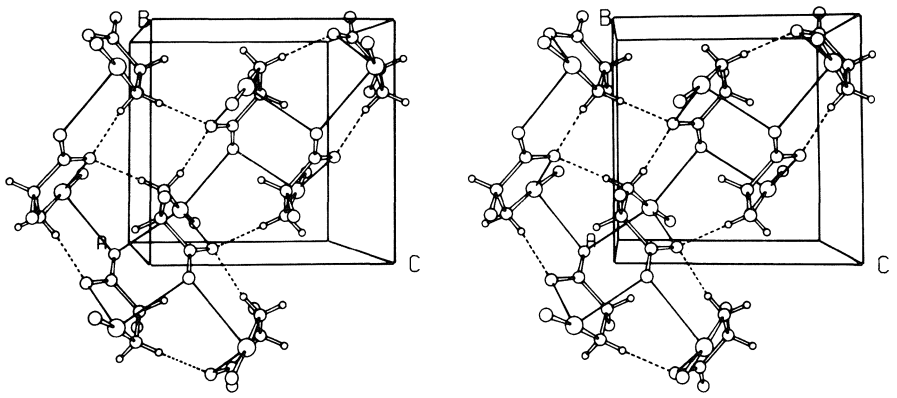

FIG. 2. Stereoview of the unit cell of (CH_3Hg)(DL-Ala). The atoms are shown as spheres of arbitrary sizes (large for Hg), and they can be identified by comparison with Fig. 1. Single lines correspond to Hg...O contacts and dashed lines to hydrogen bonds.

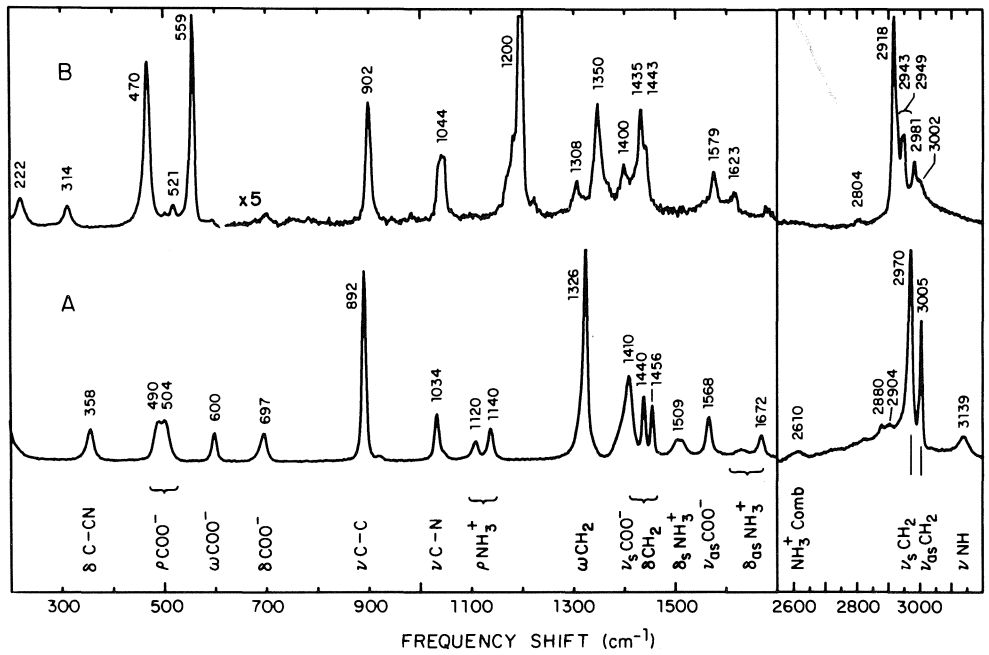

FIG. 3. Raman spectra of glycine (*A*) and its (CH_3Hg)Gly complex (*B*) in the solid state.

Ala) complex, with only secondary interaction between Hg and a carboxyl oxygen. The very close similarity of the Raman and infrared spectra for this compound and (CH_3Hg)(L-Ala) indicates that both have identical structures. The same type of binding probably also occurs in (CH_3Hg)Gly.

Although the vibrational spectra of many glycine and alanine chelates have been analyzed (16–21), the only vibrational study on a complex showing unidentate coordination via $—NH_2$ is that of Kieft and Nakamoto for $Pt(NH_3)_2(Gly)_2$ (22). Our discussion on metal—ligand vibrations is based on earlier work on mercury complexes with amino acids and purines (1, 10, 17, 23).

(CH_3Hg)Gly, solid state

The Raman spectra of glycine and its methylmercury complex, both in the solid state, are compared in Fig. 3. The infrared results are given in Fig. 8 (supplementary material) and Table 4.

The CH_3Hg^+ group in the complex is detected from various characteristic features (1, 10, 24). The $\nu_s(CH_3)$ and $\delta_s(CH_3)$ modes produce strong bands at ~2920 and ~1200 cm^{-1} in the Raman. The broad infrared absorption at ~800 cm^{-1} for the $\rho(CH_3)$ mode is also readily detected. The Hg—C stretching vibration at ~560 cm^{-1}, weak in the infrared, gives rise to the strongest line in the Raman spectrum. This same region contains the Hg—ligand stretching vibration whose high intensity in the Raman is due to the polarizability of mercury. This band and, to a lesser extent, the $\delta(CH_3)$ vibration are sensitive to the type of bonding. They will be used hereafter to identify the coordination site in the amino acid.

The glycine bands arising from the $—NH_3^+$ group are affected by complexation, since proton substitution leads to a $—NH_2(HgCH_3)^+$ unit. The broad ν(N—H) band of glycine at 3139 cm^{-1} disappears in the Raman spectrum for the complex, whereas the infrared counterpart at 3180 cm^{-1} is shifted upward. Complexation also removes from the Raman spectrum of glycine a broad combination band at 2610 cm^{-1} involving the NH_3^+ group (25). The $\delta(NH_3^+)$ bands (1672, 1620, and 1509 cm^{-1}) are replaced by a single $\delta(NH_2)$ mode, which is reported to occur in the 1600–1610 cm^{-1} range for various metal chelates (18). It is probably observed here as a weak band

TABLE 4. Infrared frequencies (cm^{-1}) for HGly and $(CH_3Hg)Gly$[a]

Assignment	Infrared frequency HGly	Infrared frequency $(CH_3Hg)Gly$
$\nu(NH_3^+)$	3180 m, br	—
$\nu(NH_3^+)$	~2900 m, vbr	—
$\nu(NH_2)$	—	~3240 m, br
$\nu(NH_2)$	—	~3100 m, br
$\nu_a(CH_2)$	3055 vw	
$\nu_s(CH_2)$	2980 vw	
$\nu_s(CH_3(Hg))$	—	2916 m
$\delta_a(NH_3^+)$	1610 m, sh	—
$\delta(NH_2)$	—	1606 s, sh
$\nu_a(CO_2^-)$	1597 vs	1581 vs
$\delta_s(NH_3^+)$	1522 vs	—
	1506 vs	—
$\delta(CH_2)$	1457 vw	
	1444 w	1420 w
$\nu_s(CO_2^-)$	1413 vs	1400 m
$\omega(CH_2)$	1333 vs	1356 w
$\tau(CH_2)$	1310 w, sh	1306 w
$\tau(NH_2)$	—	1229 w
$\delta_s(CH_3(Hg))$	—	1204 m
$\omega(NH_2)$	—	1188 m
$\rho(NH_3^+)$	1131 w	—
$\rho(NH_3^+)$	1112 w	—
$\nu(CN)$	1034 w	1051 m
$\rho(CH_2)$	911 m	
$\nu(CC)$	893 m	899 m
$\rho(CH_3(Hg))$	—	794 m
$\rho(NH_2)$	—	753 vw
$\delta(CO_2^-)$	698 m	686 vw
$\omega(CO_2^-)$	608 w	591 vw
$\nu(Hg—C)$	—	~560 vw
$\rho(CO_2^-)$	—	524 vw
		513 vw

[a]Abbreviations: v, very; s, strong; m, medium; w, weak; b, broad. Vibration types: ν, stretching; δ, bending; ω, wagging, ρ, rocking; τ, twisting; s, symmetric; a, antisymmetric.

at 1623 cm^{-1} in the Raman and a shoulder at ~1606 cm^{-1} in the infrared, although band assignments to the $\delta(NH_2)$ and $\nu_a(CO_2^-)$ modes in this region are not unambiguous (20, 26). The τ, ω, and ρ modes of the coordinated NH_2 groups are weak and metal-sensitive (18, 22, 26). The assignments proposed in Table 4 lie in the ranges previously reported.

Deprotonation of the $—NH_3^+$ group also affects vibrations mainly located in the C—H bonds. The Raman spectrum of glycine shows two well-defined ν(C—H) bands at 3005 and 2970 cm^{-1}, which are both shifted by −20 cm^{-1} in $(CH_3Hg)Gly$. The $\omega(CH_2)$ band of glycine at 1326 cm^{-1} occurs at 1350 cm^{-1} in the complex. Similar shifts have been proposed by Krishnan and Plane (16) as diagnostics for the complexation of zinc to the deprotonated form of glycine.

The $(CH_3Hg)Gly$ bands at 902 (ν(C—C)) and 1044 cm^{-1} (ν(C—N)) are shifted by +10 cm^{-1} with respect to free glycine. These bands are sensitive to perturbations in charge distribution caused by changes of ionization or substitution on terminal groups. In the case of glycine, for instance, they occur at 899/968 cm^{-1} for Gly^-, 896/1027 cm^{-1} for HGly, 869/1042 cm^{-1} for H_2Gly^+ (27), and 912/1048 cm^{-1} for glycylglycine (28). As to the vibrations originating from the

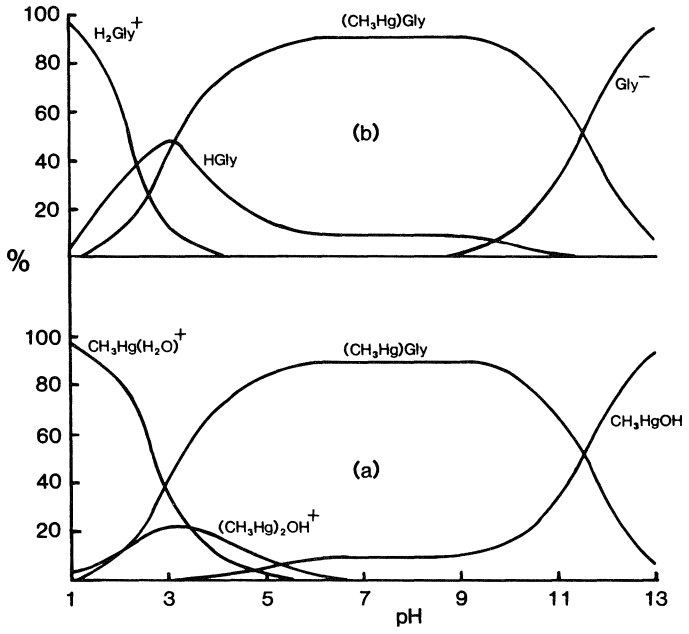

FIG. 4. Distribution curves of CH_3Hg^+ (*a*) and glycine (*b*) as a function of pH for a mixture of CH_3Hg^+ (0.2 *M*) and glycine (0.2 *M*). Calculated from literature values of equilibrium constants (see text).

$—CO_2^-$ group, they are not greatly modified in the complex, in agreement with the absence of strong coordinative Hg—O interactions.

Although the spectral modifications discussed so far indicate that the CH_3Hg^+ group is present and the $—NH_3^+$ group of glycine is deprotonated, they provide only indirect evidence that mercury is actually bound to nitrogen. In this respect, the 400–600 cm^{-1} region of the Raman spectrum is more informative. The two strongest Raman signals are observed at 559 cm^{-1} (ν(Hg—C) band mentioned above) and at 470 cm^{-1}. The latter is assigned to the ν(Hg—N) vibration. It occurs at the same position in the Raman spectra of CH_3Hg^+ complexes of glycylglycine (1) and at 464 cm^{-1} for the Hg^{2-}–glycine system (17). The relatively strong Raman line at 222 cm^{-1} is probably due to a C—Hg—N deformation motion.

$(CH_3Hg)Gly$, aqueous solutions

The equilibrium constant for the formation of $(CH_3Hg)Gly$ has been determined by Rabenstein and co-workers (2):

$$CH_3Hg^+ + Gly^- \rightleftharpoons (CH_3Hg)Gly \qquad \log K = 7.88\ (2)$$

In addition, glycine participates in two acid–base equilibria,

$$H_2Gly^+ \rightleftharpoons HGly + H^+ \qquad \log k_a = -2.35\ (29)$$

$$HGly \rightleftharpoons Gly^- + H^+ \qquad \log k_a = -9.78\ (29)$$

where the CH_3Hg^+ cation can be involved in two acid–base and condensation reactions:

$$CH_3Hg^+ \overset{H_2O}{\rightleftharpoons} CH_3HgOH + H^+ \qquad \log K = -4.63\ (2)$$

$$2CH_3Hg^+ \overset{H_2O}{\rightleftharpoons} (CH_3Hg)_2OH^+ + H^+ \qquad \log K = -2.37\ (2)$$

These constants were used to calculate the distribution curves represented in Fig. 4. The trimer $(CH_3Hg)_3O^+$ known to exist at high concentrations (30) can be neglected at the concentration level used here.

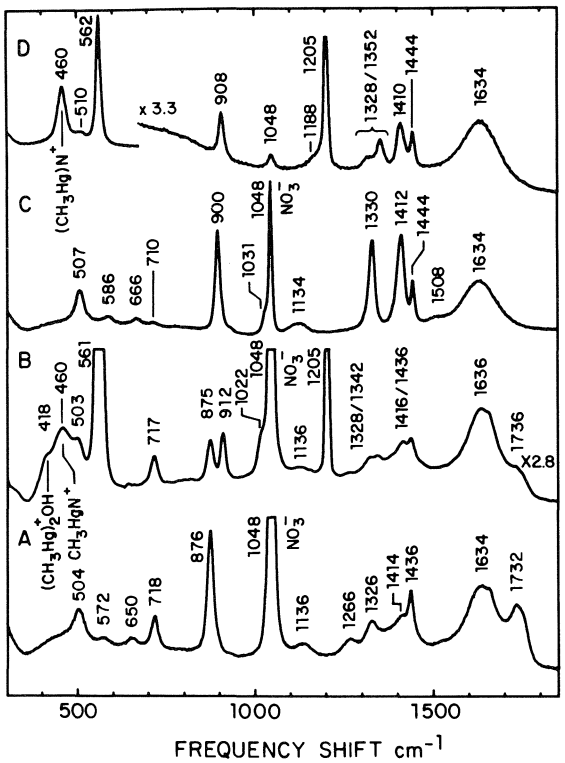

FIG. 5. Raman spectra of glycine and the (CH_3Hg)Gly complex in aqueous solutions: glycine 8% (w/w), pH 1 (*A*); (CH_3Hg)Gly 4% (w/w), pH 2 (*B*); glycine 8% (w/w), pH 7.8 (*C*); (CH_3Hg)Gly 4% (w/w), dissolved in H_2O (*D*).

These curves indicate that dissociation of (CH_3Hg)Gly should be <5% between pH 5 and 10.5. Accordingly, no free glycine can be detected from the Raman spectra of a water solution of solid (CH_3Hg)Gly or of a 1:1 mixture of CH_3HgOH and glycine at pH 7 (Fig. 5, spectra *C* and *D*). For instance, only one strong band is observed for the ν(C—C) mode at 908 cm^{-1}, whereas free HGly, which possesses a strong and sharp band at 900 cm^{-1}, should show a shoulder or even a resolved peak if it were present in appreciable amounts. The presence of large quantities of free methylmercury can also be discarded. At pH 7, free methylmercury would consist of ~50% of CH_3HgOH, which should produce a strong band at 510 cm^{-1} due to ν(Hg—OH) and a shoulder on the ν(Hg—C) band at 560 cm^{-1}.

Furthermore, the spectra at pH 7 and 10 are found to be identical, and in the latter case, the 510 cm^{-1} band should be very strong, since free methylmercury should exist completely as CH_3HgOH molecules. The strong bands assigned to the CH_3Hg^+ group for the solid complex occur at almost the same positions for the solution (ν(Hg—N) = 460 cm^{-1}, ν(Hg—C) = 562 cm^{-1}, $\delta(CH_3)$ = 1205 cm^{-1}), in agreement with the same binding being present in solution and in the solid state. It is noteworthy that the $\nu_s(CO_2^-)$ and $\rho(CO_2^-)$ bands (1410 and 510 cm^{-1}, respectively) occur at the same position as for aqueous HGly, which is consistent with the presence of a free carboxylate group in both cases. This holds true even in the presence of a two-fold excess of CH_3Hg^+, thereby indicating that a second CH_3Hg^+ ion does not coordinate to the free carboxylate end of the NH_2-bonded (CH_3Hg)Gly complex.

Acidic solutions (1:1 and 2:1 CH_3Hg^+:Gly ratios) were also examined for possible binding to the carboxylate end of glycine.

TABLE 5. Infrared frequencies (cm^{-1}) for L-HAla and (CH_3Hg)(L-Ala)

Assignment	Infrared frequency	
	L-HAla	(CH_3Hg)(L-Ala)
$\nu(NH_2)$	—	~3200 m, br
$\nu(NH_3^+)$	3086 s, br	—
$\nu(CH_3)$	2999 m	2989 m
ν(CH)		2963 m
$\nu(CH_3(Hg))$	—	2920 m
$\delta_a(NH_3^+)$	~1650 w, sh	—
$\delta_a(NH_3^+)$	1621 vs	—
$\nu_a(CO_2^-)$	1594 vs	1584 vs
$\delta(NH_2)$	—	1558 vs
$\delta_s(NH_3^+)$	1521 m	—
	1506 m	—
$\delta_a(CH_3)$	1455 m	1459 m
$\nu_s(CO_2^-)$	1413 s	1406 s
$\delta_s(CH_3)$	1363 s	1373 w
		1353 s
δ(CH)	1307 s	1297 w
$\tau(NH_2)$	—	1253 w
		1226 w
$\rho(NH_3^+)$	1236 w	—
$\rho(CH_3(Hg))$	—	1198 w
$\rho(NH_3^+)$	1152 w	—
ν(CN)	1114 m	1115 m
$\rho(CH_3)$	1014 m	1072 w
$\omega(NH_2)$	—	1032 w
ν(C—CO_2)	919 w	929 w
ν(C—CH_3)	851 w	852 m
$\rho(NH_2)$	—	809 m
$\rho(CH_3(Hg))$	—	792 m, sh
$\omega(CO_2^-)$	773 w	766 w, sh
$\delta(CO_2^-)$	649 w	618 vw
$\rho(CO_2^-)$	541 m	573 vw
ν(Hg—C)	—	534 m

The spectra of glycine and of a 1:1 CH_3Hg^+:glycine mixture are shown in Fig. 5 (spectra *A* and *B*). The Raman lines for H_2Gly^+ have been listed earlier (31). The ν(C—C) band for the H_2Gly^+ form occurs at 876 cm^{-1}. A band is also observed at this position for the 1:1 mixture, together with the sharp (CH_3Hg)Gly peak at 912 cm^{-1} discussed above. Therefore, H_2Gly^+ and (CH_3Hg)Gly appear to be the only forms of glycine present in appreciable amounts under these conditions. According to the distribution curves (Fig. 4), complexation to an extent of ~20% should occur at pH 2. The free methylmercury should exist as monomeric CH_3Hg^+ and dimeric $(CH_3Hg)_2OH^+$ in roughly equal amounts. These two species and (CH_3Hg)Gly have their ν(Hg—C) and $\delta(CH_3(Hg))$ bands almost at the same positions, but they show differences in the 450–500 cm^{-1} region. The observed spectrum (Fig. 5, spectrum *B*) is consistent with the presence of some (CH_3Hg)Gly, characterized by a sharp ν(Hg—N) band at 460 cm^{-1}, whereas the uncomplexed methylmercury as monomer and dimer produces much weaker and broader bands at 455 and 418 cm^{-1}, respectively.

There is no evidence for species with the CH_3Hg^+ ion bonded to glycine via the carboxylate group. This type of coordination was found to produce ν(Hg—O) and ν(Hg—C) bands at 536 and 572 cm^{-1}, respectively, for $[(CH_3Hg)_2Glygly]ClO_4$ (1).

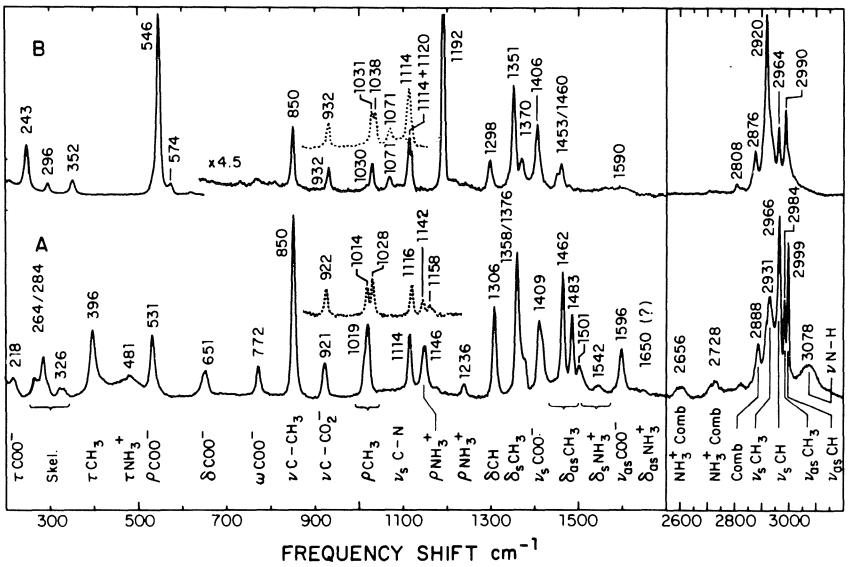

FIG. 6. Raman spectra of L-alanine (*A*) and its CH_3Hg^+ complex (*B*) in the solid state. The dotted lines correspond to the compounds with DL-alanine.

The very weak band at 503 cm^{-1} in the spectrum of the 1:1 mixture (Fig. 5, curve *B*) originates from $\rho(CO_2^-)$ motion of H_2Gly^+ (31), and the absence of nearby bands for ν(Hg—O) and of splitting in the ν(Hg—C) band indicates that no O-bonded complexes are appreciably formed.

(CH_3Hg)(L-Ala), solid state

The Raman spectra of solid L-alanine and (CH_3Hg)(L-Ala) are shown in Fig. 6 (spectra A and B). The infrared results are provided in Fig. 9 (supplementary material) and Table 5.

The spectra of (CH_3Hg)(L-Ala) include the characteristic bands of the CH_3Hg^+ unit, namely at 2920 (ν, ir, R), 1195 (δ, ir, R), and 809 cm^{-1} (ρ, ir) (1, 24). The strong Raman line observed at 546 cm^{-1} could be due to the ν(Hg—C) vibration, but assignment is not so straightforward as for the glycine complex (*vide infra*).

Evidence for $—NH_3^+$ deprotonation arises, as in the case of glycine, from the disappearance of the bands originating from this group, to be replaced by those of the coordinated $—NH_2$ group. The $\delta(NH_2)$ and $\nu_a(CO_2)$ vibrations are close together at ~1575 cm^{-1} and they cannot be individually assigned with certainty (19–21). Segnini and co-workers (21) have reported that the bands at 1230 and 1120 cm^{-1}, removed by NH_2 deuteration for a number of alanine complexes, originate from the twisting and wagging modes, respectively. By comparison, the broad absorption at ~1226 cm^{-1} in infrared is assigned to the NH_2 twisting mode, whereas the wagging mode is believed to produce the sharp infrared peak at 1032 cm^{-1}. According to the same authors, the NH_2 rocking mode occurs at ~780 cm^{-1} in several complexes. It is probably located at ~809 cm^{-1} here.

The carboxylate ν_a, ν_s, ω, and ρ modes undergo only minimal shifts by complexation, whereas the $\delta(CO_2^-)$ band at 650 cm^{-1} is displaced by −32 cm^{-1} in (CH_3Hg)(L-Ala). This reflects changes in the environment of the $—CO_2^-$ group, which remains uncoordinated in the complex. Several other shifts of 5–15 cm^{-1} are found for bands located in the C—C(CH_3)—N portion of the ligand, namely for the δ(C—H), ν(C—CO_2^-) and $\rho(CH_3)$ modes (Table 5).

On the basis of the results obtained with (CH_3Hg)Gly, we

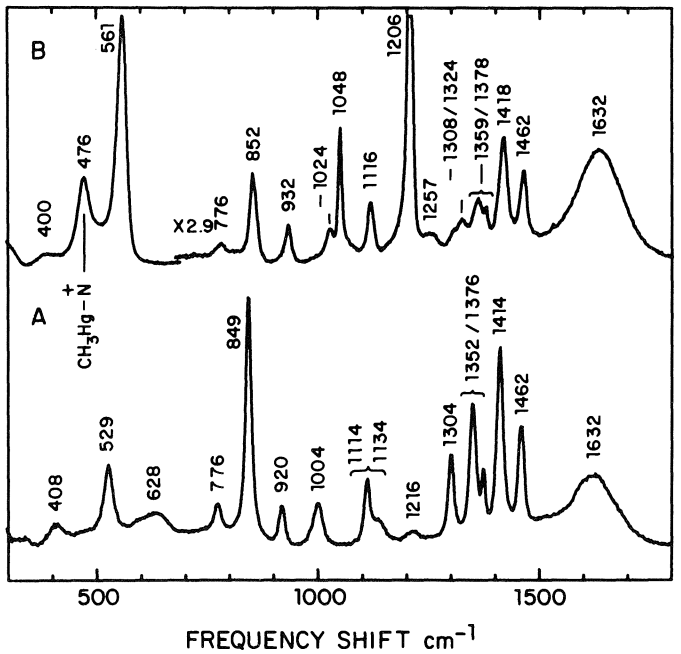

FIG. 7. Raman spectra of aqueous solutions of L-alanine, 16% (w/w), pH 6 (*A*) and (CH_3Hg)(L-Ala), 8% (w/w), pH 6 (*B*).

anticipated that the ν(Hg—N) and ν(Hg—C) vibrations would produce strong Raman lines at ~460 and ~560 cm^{-1}, respectively. However, the solid showed only one strong line at 546 cm^{-1} and a very weak band at 574 cm^{-1}. If we dissolve this neutral (CH_3Hg)Ala complex in water, we effectively obtain the expected pair of strong Raman lines (*vide infra*). When the solvent is then removed, the initial solid spectrum (Fig. 6) is restored.

We were first tempted to conclude that the CH_3Hg^+ group could be both amino- and carboxylate-bonded in this compound, as we had already observed for $[(CH_3Hg)_2Glygly]ClO_4$ a vibration at 536 cm^{-1} which was assigned to ν(Hg—O) motion (1). However, since it is known from the X-ray work

that the metal is bonded only to the nitrogen end, we assume that no discrimination can be made in this case between ν(Hg—N) and ν(Hg—C) for the solid, probably because of specific intra- and intermolecular interactions. A similar behavior has been noted by Wong and co-workers (10) for (DL-methioninato)methylmercury(II), in which the contacts with Hg are comparable with those found here for the alanine complex. However, the lack of crystal structures on a large enough sample of related systems precludes further discussion for the moment.

(CH_3Hg)(L-Ala), aqueous solutions

The pk_a values of alanine (2.35, 9.87) (29) are close to those of glycine, and both amino acids should form CH_3Hg^+ complexes of comparable stability. Therefore, the distribution curves of Fig. 4 should also apply to the CH_3Hg^+–alanine system.

A series of Raman spectra at various pH is consistent with the same reaction pattern found for glycine. The spectra of a solution of (CH_3Hg)(L-Ala) and of a 1:1 mixture of CH_3HgOH and alanine at pH 7 (which are identical) (Fig. 7, spectrum *B*) provide no evidence for appreciable dissociation of the complex. The presence of free ligand would be detectable in the ν(C—CO_2) region, where the band appears at 932 cm^{-1} for the complex and at 920 cm^{-1} for HAla. The complex and the free ligand also differ in two other regions: the $\rho(CO_2)$ mode produces a medium band at 529 cm^{-1} for HAla, but no detectable band for the complex, whereas the δ(C—H) band at 1304 cm^{-1} is strong for HAla, but much weaker for the complex. No free ligand could be detected from these three regions. The presence of significant amount of free methylmercury is also ruled out by inspection of the 450–500 cm^{-1} region, as in the case of glycine. On the other hand, the presence of (CH_3Hg)Ala is deduced from the clear ν(Hg—N) band observed at 476 cm^{-1}.

In acidic media (pH < 3.5), the complex is progressively destroyed as the pH is decreased, while the cationic H_2Ala^+ species becomes increasingly important (31). In all these cases, the spectra (not shown) could be satisfactorily explained by assuming superposed contributions from HAla and H_2Ala^+ (whose proportions depend on pH), (CH_3Hg)Ala and free methylmercury (as monomeric and dimeric species). Even with excess CH_3Hg^+ and at any pH, it has not been possible to detect binding to the carboxylate group in this system.

Conclusion

The crystal structure of (CH_3Hg)(DL-Ala) shows that the soft Hg atom binds to the NH_2 end of this amino acid, in preference to the carboxylate oxygens, which are much harder sites. Raman spectroscopy provides evidence that the metal is also bonded to the NH_2 lone pair in the solid (CH_3Hg)Gly complex. Raman studies in aqueous solutions show that the NH_2-bonded structure is retained in solution in the pH interval 3.5–10. Rabenstein and co-workers (2) also interpreted their ^1H nmr data for the CH_3Hg–glycine system in terms of a similar amino-bonded complex. However, the presence of a minor carboxylate-bonded species and tautomeric equilibrium between these two isomeric forms could not be dismissed, since fast exchange in this system would lead to signal averaging in nmr. Our results in Raman spectroscopy, which has a much faster time scale, indicate that such an equilibrium does not exist to any appreciable extent, and that (CH_3Hg)Gly and (CH_3Hg)Ala are the only species present under these conditions.

Acknowledgments

We wish to thank M. J. Olivier who collected the X-Ray data. The financial supports of the Natural Sciences and Engineering Research Council of Canada and the Ministère de l'Éducation du Québec are gratefully acknowledged.

1. S. Alex, R. Savoie, M. C. Corbeil, and A. L. Beauchamp. Can. J. Chem. **64**, 148 (1986).
2. D. L. Rabenstein. Acc. Chem. Res. **11**, 100 (1978); D. L. Rabenstein, R. Ozubko, S. Libich, C. A. Evans, M. T. Fairhurst, and C. Suvanprakurn. J. Coord. Chem. **3**, 263 (1974).
3. F. Allaire and A. L. Beauchamp. Can. J. Chem. **62**, 2249 (1984).
4. F. Bélanger-Gariépy and A. L. Beauchamp. J. Am. Chem. Soc. **102**, 3461 (1980).
5. D. T. Cromer and J. T. Waber. Acta Crystallogr. **18**, 104 (1965); R. F. Stewart, E. R. Davidson, and W. T. Simpson. J. Chem. Phys. **42**, 3175 (1965).
6. D. T. Cromer. Acta Crystallogr. **18**, 17 (1965).
7. M. Authier-Martin and A. L. Beauchamp. Can. J. Chem. **55**, 1213 (1977).
8. N. W. Alcock, P. A. Lampe, and P. Moore. J. Chem. Soc. Dalton Trans. 1324 (1978).
9. Y. S. Wong, A. J. Carty, and C. Chieh. J. Chem. Soc. Dalton Trans. 1801 (1977); Y. S. Wong, N. J. Taylor, C. Chieh, and A. J. Carty. J. Chem. Soc. Chem. Commun. 625 (1974); Y. S. Wong, P. C. Chieh, and A. J. Carty. Can. J. Chem. **51**, 2597 (1973).
10. Y. S. Wong, A. J. Carty, and C. Chieh. J. Chem. Soc. Dalton Trans. 1157 (1977).
11. J. Donohue. J. Am. Chem. Soc. **72**, 949 (1950).
12. G. H. Stout and L. H. Jensen. X-ray structure determination, a practical guide. Macmillan, London. 1968. p. 303.
13. K. Machida, A. Kagayama, Y.Saito, and T. Uno. Spectrochim. Acta, **34**A, 909 (1978); K. Machida, A. Kagayama, and Y. Saito. J. Raman Spectrosc. **7**, 188 (1978).
14. K. Machida, A. Kagayama, and Y. Saito. J. Raman Spectrosc. **8**, 133 (1979); K. Machida, A. Kagayama, Y. Saito, Y. Kuroda, and T. Uno. Spectrochim. Acta, **33**A, 569 (1977).
15. R. K. Khanna, M. Horak, and E. R. Lippincott. Spectrochim. Acta, **22**, 1759 (1966); H. Stenback. J. Raman Spectrosc. **5**, 49 (1976); R. F. Adamowicz and M. L. Sage. Spectrochim. Acta, **30**A, 1007 (1974); J. Herranz and J. M. Delgado. Spectrochim. Acta, **32**A, 821 (1976); H. S. Randhawa and C. N. R. Rao. J. Cryst. Mol. Struct. **3**, 309 (1973).
16. K. Krishnan and R. A. Plane. Inorg. Chem. **6**, 55 (1967).
17. T. V. Long, II, and C. M. Yoshida. Inorg. Chem. **6**, 1754 (1967).
18. G. C. Percy and H. S. Stenton. J. Chem. Soc. Dalton Trans. 1466 (1976); Y. Y. Kharitonov, H. Bissinger, E. Ambach, and W. Beck. Z. Naturforsch. **37**B, 1034 (1982); M. L. Niven and D. A. Thornton. Inorg. Chim. Acta, **32**, 205 (1979); R. A. Condrate and K. Nakamoto. J. Chem. Phys. **42**, 2590 (1965); J. R. Kincaid and K. Nakamoto. Spectrochim. Acta, **32**A, 277 (1976); T. J. Lane, J. A. Durkin, and R. J. Hooper. Spectrochim. Acta, **20**, 1013 (1964); G. W. Watt and J. F. Knifton. Inorg. Chem. **7**, 1159 (1968).
19. J. F. Jackovitz, J. A. Durkin, and J. L. Walter. Spectrochim. Acta, **23**A, 67 (1967).
20. B. Dupuy and C. Garrigou-Lagrange. J. Chim. Phys. **62**, 1359 (1965); B. Dupuy, C. Castinel, and C. Garrigou-Lagrange. Spectrochim. Acta, **25**A, 571 (1969).
21. D. Segnini, C. Curran, and J. V. Quagliano. Spectrochim. Acta, **16**, 540 (1960).
22. J. A. Kieft and K. Nakamoto. J. Inorg. Nucl. Chem. **29**, 2561 (1967).
23. R. Savoie, J.-J. Jutier, L. Prizant, and A. L. Beauchamp.

Spectrochim. Acta, **38**A, 561 (1982); R. SAVOIE, D. POIRIER, L. PRIZANT, and A. L. BEAUCHAMP. J. Raman Spectrosc. **11**, 481 (1981); Y. K. SZE, A. R. DAVIS, and G. A. NEVILLE. Inorg. Chem. **14**, 1969 (1975).
24. J. H. S. GREEN. Spectrochim. Acta, **24**A, 863 (1968); J. H. R. CLARKE and L. A. WOODWARD. Trans. Faraday Soc. **62**, 3022 (1966); D. L. RABENSTEIN, M. C. TOURANGEAU, and C. A. EVANS. Can. J. Chem. **54**, 2517 (1976).
25. C. BRISSETTE and C. SANDORFY. Can. J. Chem. **38**, 34 (1960).
26. Y. INOMATA, T. TAKEUCHI, and T. MORIWAKI. Spectrochim. Acta, **40**A, 179 (1984).
27. S. A. S. GHAZANFAR, D. V. MYERS, and J. T. EDSALL. J. Am. Chem. Soc. **86**, 3439 (1964).
28. A. M. DWIVEDI and V. D. GUPTA. Biopolymers, **11**, 2091 (1972).
29. Handbook of chemistry and physics. The Chemical Rubber Co. 1979–1980, p. C-757.
30. J. H. R. CLARKE and L. A. WOODWARD. Trans. Faraday Soc. **64**, 1041 (1968); Spectrochim. Acta, **23**A, 2077 (1967).
31. M. TAKEDA, R. E. S. IAVAZZO, D. GARFINKEL, I. H. SCHEINBERG, and J. T. EDSALL. J. Am. Chem. Soc. **80**, 3813 (1958); J. L. KOENIG. Macromol. Rev. **6**, 59 (1972).

Acyclic nucleoside analogues: methods for the preparation of 2′,3′-secoguanosine, 5′-deoxy-2′,3′-secoguanosine, and (*R*,*S*)-9-[1-(2-hydroxyethoxy)-2-hydroxyethyl]guanine[1]

DANNY P. C. MCGEE[2] AND JOHN C. MARTIN
Syntex Research, Institute of Bio-Organic Chemistry, 3401 Hillview Avenue, Palo Alto, CA 94304, U.S.A.

Received January 27, 1986

DANNY P. C. MCGEE and JOHN C. MARTIN. Can. J. Chem. **64**, 1885 (1986).

A high yielding, one-pot method for the preparation of 2′,3′-secoguanosines **5** and **6** by treatment of 5′-deoxyguanosine (**4**) and guanosine (**2**), respectively, with sodium periodate and then sodium borohydride is described. The final products **5** and **6** were purified from contaminating salts by passage of the reaction mixture over a column of activated charcoal. An additional acyclic derivative **14** was prepared in racemic form by an approach involving a novel condensation reaction. Alkylation of N^2,9-diacetylguanine (**8**) with 2,3-dichlorotetrahydrofuran (**7**) resulted in selective *N*-9 alkylation to give adduct **9***a*. Compound **9***a* was deacylated with ammonium hydroxide to give **10**, which was monomethoxytritylated to **11**. Elimination of hydrogen chloride from **11** using potassium *tert*-butoxide afforded **12**, which was reacted with OsO_4–$NaIO_4$ followed by treatment with $NaBH_4$ to give **13**, which was then deprotected with acid to **14**. Compounds **5**, **6**, **14**, and **16** were tested in vitro against herpes simplex virus types 1 and 2 and were found to be inactive.

DANNY P. C. MCGEE and JOHN C. MARTIN. Can. J. Chem. **64**, 1885 (1986).

On décrit une méthode de préparation dans un récipient unique qui conduit aux séco-2′,3′ guanosines **5** et **6** avec d'excellents rendements. Cette méthode utilise respectivement la déoxy-5′ guanosine (**4**) et la guanosine (**2**) que l'on traite successivement par le périodate de sodium et le borohydrure de sodium. Le désalage sur une colonne de charbon actif conduit aux produits **5** et **6** à l'état pur. On a en outre préparé un dérivé acyclique racémique **14** en faisant appel à une nouvelle réaction de condensation. L'alkylation sélective de la N^2-diacétyl-9 guanine (**8**) avec le dichloro-2,3 tétrahydrofuranne (**7**) conduit au produit d'addition **9***a* alkylé sélectivement sur l'azote en position 9. La désacylation du composé **9***a* par l'hydroxyde d'ammonium conduit au composé **10** qui, par monométhoxytritylation, donne le composé **11**. Ce dernier, traité par le *tert*-butylate de potassium, libère du chlorure d'hydrogène et conduit au composé **12** dont la réaction avec le mélange OsO_4–$NaIO_4$, suivie d'un traitement par le $NaBH_4$, conduit au composé **13** que l'on déprotège avec de l'acide pour obtenir le composé **14**. On a effectué des essais in vitro avec les composés **5**, **6**, **14** et **16** sur les virus simplex de l'herpes de type 1 et 2. Ces composés sont inactifs.

[Traduit par la revue]

Investigators faced with the task of discovering effective antiviral agents have often turned to nucleosides and analogues thereof for solutions (1). One such compound recently reported by several groups (2), 9-[(1,3-dihydroxy-2-propoxy)methyl]guanine (**1**, DHPG), is visualized as an acyclic analogue of 2′-deoxyguanosine and is highly effective against herpes simplex virus types 1 (HSV-1) and 2 (HSV-2), as well as Epstein–Barr virus and human cytomegalovirus (3).

As a result of the demonstrated activity of DHPG (**1**), we elected to synthesize a number of related acyclic nucleoside analogues that retain a 2′-hydroxymethyl group and thus more closely resemble guanosine in structure. We selected as represented members of this class 2′,3′-secoguanosine (**6**), 5′-deoxy-2′,3′-secoguanosine (**5**), (*R*,*S*)-9-[1-(2-hydroxyethoxy)-2-hydroxyethyl]guanine (**14**), and 9-(β-(D,L)-*erythro*-furanosyl)guanine (**16**). It should be noted that a cursory disclosure of the antiherpes virus activity of compounds **6** and **14** has previously appeared (2*e*).

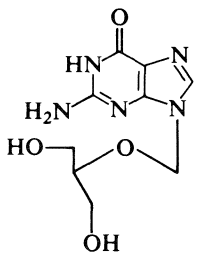

1

Results and discussion

As a general approach to the acyclic analogues **5**, **6**, and **14** we wished to make use of a one-pot reaction sequence using $NaIO_4$ and then $NaBH_4$ on suitably derivatized 2′,3′-dihydroxypentofuranosyl guanines (**2**, **4**, **15**). The action of $NaIO_4$ on unprotected nucleosides is well known; the resulting dialdehydes (4) exist as a complex mixture of hydrates, and are generally not isolated as such but converted to the respective acylic triols by the action of $NaBH_4$. The purification of the acyclic triols from the residual salts is difficult and has usually been limited to the use of ion-exchange chromatography (4) from which the acyclic nucleosides are often obtained as foams or lyophilized powders. Thus, difficulty in obtaining reasonable quantities of acyclic nucleosides via these procedures has generally limited their use to biochemical/enzymatic studies (5), leaving the chemistry (6) of such derivatives relatively untouched. Alternatively, the synthesis of a few acyclic derivatives in this system has been accomplished using 5′-protected nucleosides as starting material (6).

Recently, two improved approaches to secoguanosines have been published (7). Lerner has described a procedure in which the crude product reaction mixture, after treatment with $NaIO_4$ and then $NaBH_4$, is exhaustively acetylated and a triacetate derivative is isolated in 38% yield. Deacetylation gave **6** (7*a*). Alternatively, Bessodes and Antonakis (7*b*) have used polymer bound reagents so that reagent salts are simply removed by filtration. We have found, *inter alia*, that activated charcoal can be used to desalt the final reaction mixture, effectively removing the iodate and borate salts, to afford crystalline **6** directly in 67% yield. This was accomplished by neutralization of the crude reaction mixture to pH 7 and then passing the resulting solution

[1]Contribution 221 from the Institute of Bio-Organic Chemistry.

[2]Author to whom correspondence may be addressed. Present address: Bristol-Myers Co., P.O. Box 5100, Wallingford, CT 06492, U.S.A.

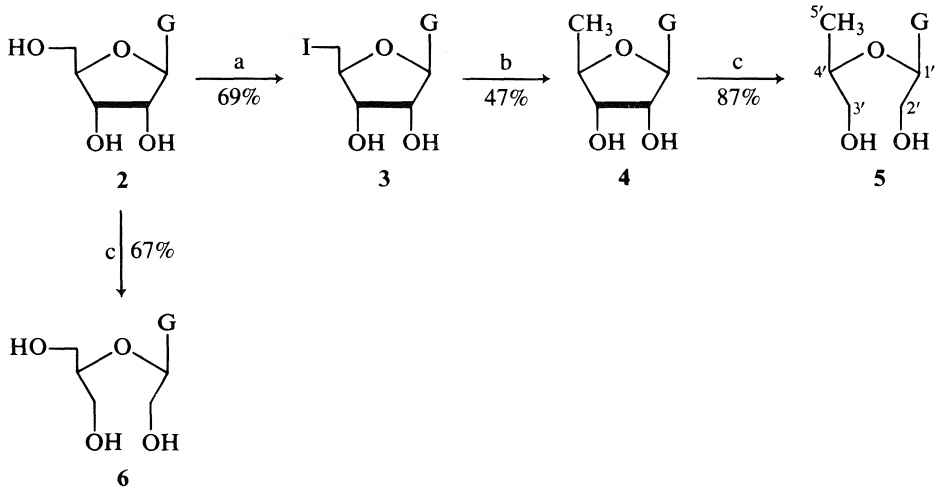

G = 9-guaninyl; (a) $P(Ph)_3$, I_2, imidazole, *N*-methyl-2-pyrrolidinone; (b) 10% Pd/C, H_2, 60°C, in H_2O/EtOH; (c) $NaIO_4$, 3 h, then $NaBH_4$, charcoal chromatography

SCHEME 1

over a column of the charcoal.[3] The column was first eluted with water to remove the salts. The desired product **6** was then eluted with 3% NH_4OH in 1:1 ethanol/water.

With this method in hand our approach to **5** (Scheme 1) proceeded in a straightforward manner. Iodination of unprotected guanosine using triphenylphosphine–iodine–imidazole (8) proceeded exceptionally well in *N*-methyl-2-pyrrolidinone as solvent to afford crystalline 5′-deoxy-5′-iodoguanosine (**3**) in 69% yield after simple dilution of the reaction mixture with dichloromethane and water. The high selectivity of this reaction is attributable both to the *in situ* protection of the 2′- and 3′-hydroxyls as a cyclic oxyphosphorane intermediate (9) and to the rate enhancement associated with the use of *N*-methyl-2-pyrrolidinone as reaction solvent. The iodide **3** was catalytically reduced with 10% Pd/C to give 5′-deoxyguanosine (**4**) (10) in 47% yield. The vicinal diol functionality of **4** was oxidized using sodium periodate and the resulting dialdehyde was reduced directly to **5** using sodium borohydride. The above reaction mixture was then desalted using activated charcoal to afford 5′-deoxy-2′,3′-secoguanosine (**5**) in 87% yield.

The initial steps in the synthesis of analogue **14** (Scheme 2) are conceptually similar to an approach taken by others for the synthesis of substituted tetrahydro-2-furanyl analogues of 5-fluorouracil (11) (Ftorafur) and guanine (12). The preparation of a similar analogue of adenine, (*R*,*S*)-9-[1-(2-hydroxyethoxy)-2-hydroxyethyl]adenine, has been described (13) via the reaction of 2-alkyl-1,3-dioxolane with trimethylsilyl iodide, and subsequent coupling of the resultant alkyl iodide with a purine base. A number of thio analogues related to **14** and **16** have also been reported (14).

The outcome of the coupling of N^2,9-diacetylguanine (**8**) (15) with *trans*-2,3-dichlorotetrahydrofuran[4] (**7**) (16) in a fusion reaction was variable, resulting in the production of either a mixture of *N*-9 and *N*-7 alkylated guanines (**9***a*, *b*) in low yield or, in other cases, a near quantitative conversion to the *N*-9 isomer (**9***a*). The position of alkylation of the guanine nucleus for adducts **9***a*, *b* was determined on the basis of their characteristic uv spectra. The assigned 1′,2′-*trans* relative stereochemistry[5] (17) is consistent with the small coupling constants in the ^1H nmr ($J_{1',2'} = 1.7$ Hz) and is circumstantially corroborated by the subsequent transformation of derivative **11** to afford **12**. Due to the poor solubility of adduct **9** it was generally more convenient to treat the crude reaction mixture containing only **9***a* directly with methanolic ammonium hydroxide to obtain **10** in 59% yield from diacetylguanine. Reaction of **10** with monomethoxytrityl chloride in pyridine gave **11**, which was freely soluble in several organic solvents. Heating a toluene–pyridine solution of **11** with potassium *tert*-butoxide at 75°C for 1 h gave **12** in 92% yield. The elimination proved sensitive to both solvent and temperature where, for example, the reaction of **11** with potassium *tert*-butoxide in tetramethylene sulfone at 100°C quickly led to elimination of the purine to produce N^2-monomethoxytritylguanine. This alternative product is a useful form of protected guanine and is currently being studied in our laboratory as a building block for nucleoside synthesis.

The *cis* hydroxylation of **12** using potassium permanganate afforded **15** in 25% yield, which we assume had a 1′,2′-*trans* orientation due to steric hindrance (18) associated with a β face approach. Deprotection of **15** with aqueous acetic acid gave analogue **16** in 34% yield. The 1′,2′-*trans* orientation assigned to analogues **15** and **16** is consistent with the small coupling ($J_{1',2'} < 0.3$ Hz) observed for the 2′,3′-isopropylidene of **16**. The observed $\Delta\delta$ of 0.13 ppm for the methyls of the isopropylidene of **16** falls short of the generalizations proposed by Imbach and co-workers for ribonucleosides (19). Alternatively, analogue **14** can best be prepared directly from **12** by reaction with catalytic osmium tetroxide and sodium periodate to produce the dialdehyde intermediate, which was reduced with sodium borohydride to give **13** in 64% yield after silica gel chromatography. Deprotection of **13** with acid afforded analogue **14** in 53% yield.

[3]Neutralization to pH 7 prior to charcoal chromatography is not deemed essential. For example, reaction of adenosine as described above, with omission of the neutralization step, afforded 2′,3′-secoadenosine, which crystallized from ethanol, 2.65 g (53%); mp 139–140°C.

[4]The 2,3-dichlorotetrahydrofuran produced by the action of chlorine gas on tetrahydrofuran at 0–10°C was a single isomer; ^1H nmr δ: 6.23 (s, 1H, H-2), 4.64 (ddd, J = 0, 1, 5.6 Hz, 1H, H-3), 4.35 (dd, J = 5.4, 9.1 Hz, 2-H, H-5), 2.83, 2.25 (m, 2H, H-4).

[5]For convenience, we adopted a "ribose-like" numbering of the tetrahydrofuranyl moiety when said is coupled to a purine base, i.e., structure **16**.

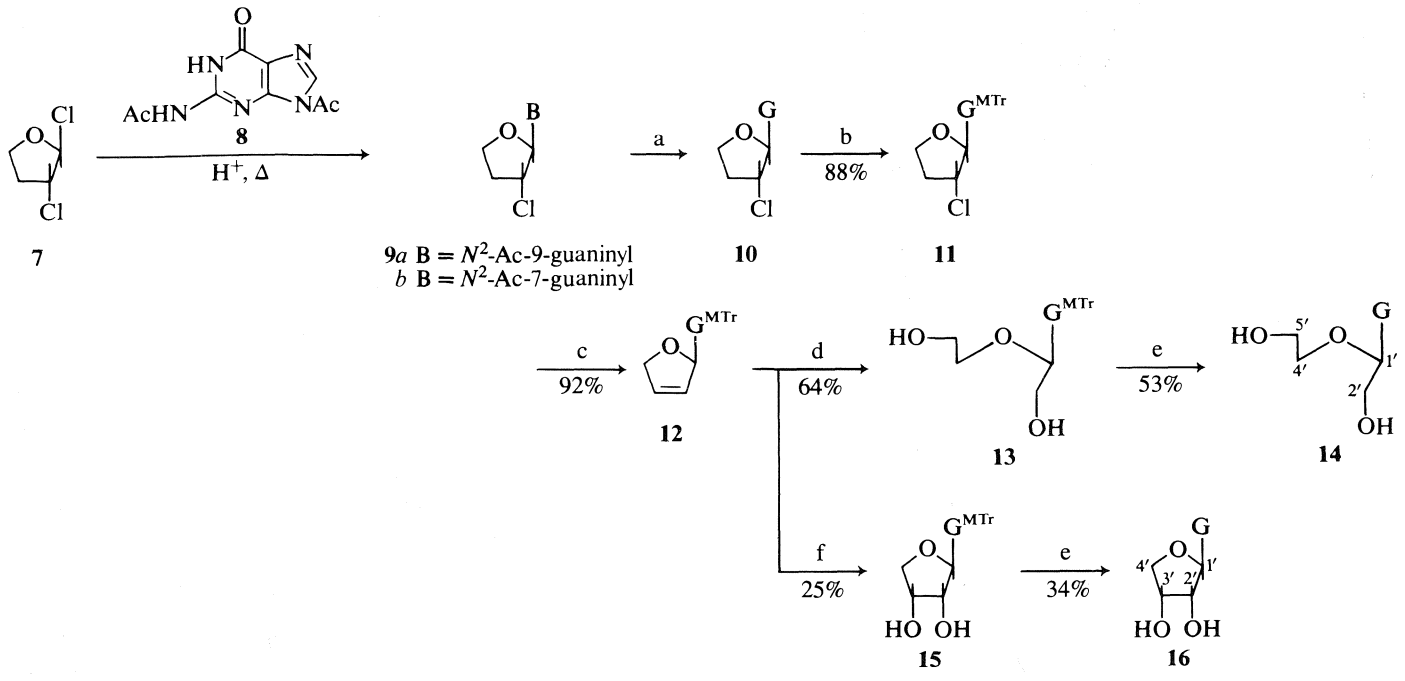

(a) NH_4OH, MeOH; (b) MTr-Cl, TEA, pyridine; (c) *t*-BuOK, pyridine, toluene, 80°C, 1 h; (d) OsO_4, $NaIO_4$, MeOH, then $NaBH_4$; (e) 80% aqueous HOAc, 50°C, 16 h; (f) $KMnO_4$, H_2O, acetone

SCHEME 2

Preliminary in vitro testing of compounds **5**, **6**, **14**, and **16** showed them to be inactive against herpes simplex virus types 1 and 2.

Experimental

Nuclear magnetic resonance spectra were recorded on samples dissolved in deuteriodimethyl sulfoxide unless otherwise stated and chemical shifts are reported in parts per million downfield from internal tetramethylsilane. The compounds described are viewed as nucleoside analogues and for convenience the peak assignments are numbered according to a ribose-like representation. Spectroscopic data and elemental analyses were obtained by Syntex Analytical Research. All chromatographic purifications were carried out on Merck Silica Gel 60. Charcoal used was commercially available from Aldrich (nucleotide desalting grade). Alternatively, Sigma charcoal C-3014 could be used with a resultant small decrease in product recovery. Melting points were determined on a hot stage microscope and are corrected.

*5′-Deoxy-5′-iodoguanosine (**3**)*

Iodine (40.2 g, 158 mmol) was added over 5 min to a magnetically stirred suspension of guanosine hydrate (15.0 g, 50 mmol), triphenylphosphine (43.2 g, 165 mmol), and imidazole (22.5 g, 331 mmol) in *N*-methyl-2-pyrrolidinone (200 mL) at room temperature. During the addition complete dissolution occurred and the solution warmed to 60°C. The solution cooled back to room temperature and after 3 h was diluted with dichloromethane (2 L) and water (0.6 L). A white crystalline solid separated from solution and was collected by filtration to give 13.53 g (69%) of **3**: mp 190–200°C (dec.) (lit. (8*b*) mp 192–216°C (dec.); $[\alpha]_D$ −26.9° (*c* 1.1, Me_2SO); uv λ_{max} (0.1 *N* HCl): sh 278 nm (ε 7 320), 258 (10 800); (0.1 *N* NaOH): 266 (11 800), 260 (11 500); ^1H nmr δ: 10.67 (s, br, 1H, NH), 7.93 (s, 1H, H-8), 6.50 (s, br, 2H, NH_2), 5.72 (d, J = 6 Hz, 1H, H-1′), 5.56 (s, br, 1H, OH), 5.38 (s, br, 1H, OH), 4.63 (m, 1H, H-2′), 4.08 (s, br, 1H, H-3′), 3.95 (m, 1H, H-4′), 3.57 and 3.42 (ABX, J_{AB} = 10 Hz, J_{AX} = 6 Hz, J_{BX} = 7 Hz, 2H, H-5′); ^{13}C nmr (75.453 MHz) δ: 156.63 (C-6), 153.59 (C-2), 151.32 (C-4), 135.74 (C-8), 116.70 (C-5), 86.57 (C-1′), 83.62 (C-4′), 73.02 (C-2′), 72.65 (C-3′), 7.91 (C-5′). *Anal.* calcd. for $C_{10}H_{12}N_5O_4I$ (393.14): C 30.55, H 3.08, N 17.81; found: C 30.38, H 2.97, N 17.62.

*5′-Deoxyguanosine (**4**)*

A magnetically stirred suspension of **3** (12.83 g, 32.6 mmol) and 10% Pd/C (10 g) in water (300 mL) plus ethanol (300 mL) was heated at 60°C under 1 atm (1 atm = 101.3 kPa) of hydrogen gas for 8 h, filtered through Celite, and then evaporated to a volume of 400 mL. The solution was applied to a charcoal column (100 g) and eluted with water (3.5 L). The product was then eluted with 2% NH_4OH in 1:1 water/ethanol. Selected fractions were evaporated to dryness and the solid residue crystallized from water to give 4.14 g (47%) of **4**: mp 222–223°C (lit. (9) mp 226–228°C uncorrected); $[\alpha]_D$ −42.5 (*c* 1.4, Me_2SO); uv λ_{max} (0.1 *N* HCl): sh 278 nm (ε 8 200), 257 (12 000); (0.1 *N* NaOH): 267 (10 200), 257 (10 000); ^1H nmr δ: 10.73 (s, br, 1H, NH), 8.02 (s, 1H, H-8), 6.53 (s, br, 2H, NH_2), 5.67 (d, J = 5 Hz, 1H, H-1′), 4.46 (dd, J = 5 Hz, 1H, H-2′), 3.90 (m, 2H, H-3′, H-4′), 1.29 (d, J = 6 Hz, 3H, H-5′). *Anal.* calcd. for $C_{10}H_{13}N_5O_4$ (267.25): C 44.94, H 4.90, N 26.21; found: C 44.66, H 4.94, N 26.11.

*5′-Deoxy-2′,3′-secoguanosine (**5**)*

$NaIO_4$ (3.12 g, 14.6 mmol) was added to a mechanically stirred suspension of **4** (3.0 g, 11.2 mmol) in water (150 mL) at room temperature. After 3 h, $NaBH_4$ (0.70 g, 18.5 mmol) was added. After an additional 1.5 h, the pH was reduced from 9.5 to 7.0 with concentrated HCl. The solution was applied to a carbon column (30 g), and the column was eluted with water (2.5 L). The product was eluted with 3% NH_4OH in 1:1 water/ethanol. Selected fractions were concentrated to a yellow solid, which was crystallized from water/ethanol to give 2.63 g (87%) of **5**: mp >300°C; $[\alpha]_D$ 31.3 (*c* 1, Me_2SO); uv λ_{max} (0.1 *N* HCl): sh 278 nm (ε 8 050), 256 (11 900); (0.1 *N* NaOH), 266 (10 700), 257 (10 500); ^1H nmr δ: 10.6 (s, br, 1H, NH), 7.79 (s, 1H, H-8), 6.46 (s, br, 2H, NH_2), 5.63 (t, 1H, H-1′), 5.14 (t, br, 1H, OH), 4.74 (t, br, 1H, OH), 3.83, 3.79 (ABX, after D_2O, J = 6, 11 Hz, 2H, H-2′), 3.55 (tq, 1H, H-4′), 3.39 (d, J = 5.1 Hz, 2H, H-3′), 0.82 (d, J = 6.8 Hz, 3H, CH_3); ^{13}C nmr (22.62 MHz) δ: 156.89 (C-6), 153.67 (C-2), 151.49 (C-4), 135.66 (C-8), 116.48 (C-5), 83.51 (C-1′), 75.65 (C-4′), 64.62 (C-3′), 62.22 (C-2′), 17.36 (C-5′). *Anal.* calcd. for $C_{10}H_{15}N_5O_4 \cdot 0.33\,H_2O$ (275.20): C 43.63, H 5.74, N 25.44; found: C 43.74, H 5.74, N 25.48.

*2′,3′-Secoguanosine (**6**)*

$NaIO_4$ (5.56 g, 26 mmol) was added to a mechanically stirred

suspension of guanosine hydrate (6.03 g, 20 mmol) in water (200 mL) at room temperature. After 2 h, $NaBH_4$ (2.0 g, 53 mmol) was added. After an additional 1 h, the pH was reduced from 8.5 to 7.0 with concentrated HCl. The solution was applied to a carbon column (50 g), and the column was eluted with water (2 L). The product was then eluted with 3% concentrated NH_4OH in 1:1 water/ethanol. Selected fractions were concentrated to a yellow solid, which was crystallized from water/ethanol to give 3.82 g (67%) of **6**: mp 263–265°C (lit. (*7a*) mp 215–220°C); $[\alpha]_D$ 31.4° (*c* 1, 0.1 *N* NaOH); uv λ_{max} (0.1 *N* HCl): sh 277 nm (ε 8 200), 255 (12 200); (0.1 *N* NaOH): 266 (11 200), 257 (11 000); ^{1}H nmr δ: 7.70 (s, 1H, H-8), 6.94 (s, br, 2H, NH_2), 5.65 (t, 1H, J = 5.6 Hz, H-1′), 4.60 (br, 3H, OH), 3.80, 3.77 (ABX, 2H, J = 5, 11 Hz, H-2′), 3.56, 3.47 (ABX, 2H, J = 4, 12 Hz, H-5′), 3.42 (m, 1H, H-4′), 3.24, 3.22 (ABX, 2H, J = 6, 12 Hz, H-3′); ^{13}C nmr (22.62 MHz) δ: 163.16 (C-6), 158.02 (C-2), 151.88 (C-4), 134.26 (C-8), 116.90 (C-5), 83.06 (C-1′), 79.61 (C-4′), 62.35 (C-2′), 60.82, 60.56 (C-3′, C-5′). *Anal.* calcd. for $C_{10}H_{15}N_5O_5$ (285.26): C 42.11, H 5.30, N 24.55; found: C 42.20, H 5.35, N 24.45.

trans-N^2-*Acetyl-9-(3-chlorotetrahydofuran-2-yl)guanine (**9**a)*

A mixture of freshly distilled **7** (9.6 g, 68 mmol), N^2,9-diacetylguanine (**8**) (13 g, 55 mmol), bis(*p*-nitrophenyl)phosphate (120 mg, 0.35 mmol), and dimethylformamide (10 mL) was heated for 1 h at 90–95°C, then left for 16 h at room temperature. The reaction mixture was then suspended in 12% methanol/dichloromethane and filtered free of insolubles. The filtrate was evaporated to a dark oil, which was chromatographed (5% methanol/dichloromethane) to give, in order of elution, 2.2 g (10.9%) of the N-7 isomer, **9***b*, obtained as a powder: mp 200–202°C; uv λ_{max} (methanol): 264 nm (ε 13 600); ^{1}H nmr δ: 12.2 (s, br, 1H, NH), 11.64 (s, br, 1H, NH), 8.29 (s, 1H, H-8), 6.36 (d, J = 1.8 Hz, 1H, H-1′), 4.96 (m, 1H, H-2′), 4.55, 4.22 (ABXY, 2H, J_{AB} = J_{AX} = 8.2 Hz, J_{AY} = 3.2 Hz, J_{BX} = 7.6 Hz, J_{BY} = 8.2 Hz, H-4′), 2.51, 2.26 (m, 2H, H-3′), 2.17 (s, 3H, $COCH_3$); ^{13}C nmr (22.62 MHz) δ: 173.50 (*C*OCH_3), 157 (C-6), 152.57 (C-2), 147.30 (C-4), 141.68 (C-8), 110.50 (C-5), 92.68 (C-1′), 68.50 (C-4′), 32.41 (C-3′), 23.67 (CO*C*H_3). *Anal.* calcd. for $C_{11}H_{12}N_5O_3Cl$ (297.70): C 44.38, H 4.06, N 23.52, Cl 11.91; found: C 44.38, H 4.09, N 23.32, Cl 11.83, followed by 2.4 g (11%) of the N-9 isomer **9***a*, which was crystallized from dimethylformamide: mp 205–206°C; uv λ_{max} (methanol): sh 278 nm (ε 9 800), 259 (13 600); ^{1}H nmr δ: 12.07, 11.71 (s, br, 2H, NH), 8.09 (s, 1H, H-8), 6.12 (d, J = 1.7 Hz, 1H, H-1′), 5.01 (m, 1H, H-2′), 4.47, 4.19 (ABXY, 2H, J_{AB} = J_{AX} = 8.2 Hz, J_{AY} = 2.4 Hz, J_{BX} = 6.8 Hz, J_{BY} = 8.4 Hz, H-4′), 2.73, 2.29 (m, 2H, H-3′), 2.19 (s, 3H, $COCH_3$); ^{13}C nmr (22.62 MHz) δ: 173.66 (*C*OCH_3), 154.81 (C-6), 147.95, 147.85 (C-2, C-4), 137.19 (C-8), 120.51 (C-5), 90.77 (C-1′), 68.30 (C-4′), 60.76 (C-2′), 33.41 (C-3′), 23.73 (CO*C*H_3). *Anal.* calcd. for $C_{11}H_{12}N_5O_3Cl$ (297.70): C 44.38, H 4.06, N 23.52, Cl 11.91; found: C 44.36, H 4.26, N 23.72, Cl 11.99.

trans-*9-(3-Chlorotetrahydrofuran-2-yl)guanine (**10**)*

A mixture of freshly distilled **7** (13 g, 92.3 mmol), N^2,9-diacetylguanine (20 g, 85.1 mmol), bis(*p*-nitrophenyl)phosphate (30 mg), and sulfolane (25 mL) was heated for 16 h at 100°C, then cooled. The resultant mass was treated with concentrated NH_4OH (50 mL) in methanol (170 mL) for 21 h and the solid that had formed was isolated by filtration, washed twice with acetone, and dried to give 13 g (59.7%) of **10**. An analytical sample was obtained by crystallization from DMSO/ethanol: mp >300°C (dec.); uv λ_{max} (0.1 *N* HCl): sh 278 nm (ε 9 000), 255 (11 700); (0.1 *N* NaOH): 265 (11 300), 257 (11 100); ^{1}H nmr δ: 10.94 (s, br, 1H, NH), 8.06 (s, 1H, H-8), 6.25 (s, br, 2H, NH_2), 6.25 (d, J = 1.9 Hz, 1H, H-1′), 4.94 (m, 1H, H-2′), 4.40, 4.16 (ABXY, 2H, H-4′), 2.48, 2.23 (m, 2H, H-3′); ^{13}C nmr (22.62 MHz) δ: 156.79 (C-6), 153.87 (C-2), 150.58 (C-4), 134.88 (C-8), 116.94 (C-5), 90.31 (C-1′), 67.94 (C-4′), 60.56 (C-2′), 33.65 (C-3′). *Anal.* calcd. for $C_9H_{10}N_5O_2Cl$ (255.66): C 42.28, H 3.94, N 27.39, Cl 13.87; found: C 42.38, H 3.90, N 27.20, Cl 13.62.

trans-N^2-(p-*Anisyldiphenylmethyl)-9-(3-chlorotetrahydrofuran-2-yl)guanine (**11**)*

A mixture of **10** (14.7 g, 57.5 mmol), *p*-anisylchlorodiphenylmethane (19.5 g, 63.1 mmol), and triethylamine (20 mL) in pyridine (100 mL) was stirred for 16 h at room temperature, then evaporated to a slurry. The residue was redissolved in dichloromethane and partitioned twice with H_2O; the organic phase was dried over $MgSO_4$ and evaporated to a foam. Redissolution in ethyl acetate deposited 26.8 g (88.7%) of **11** as a white crystalline mass: mp 183–184°C; uv λ_{max} (methanol): sh 277 nm (ε 13 100), 261 (14 800); ^{1}H nmr δ: 10.67 (s, br, 1H, NH), 7.74 (s, br, 1H, NH), 7.69 (s, 1H, H-8), 7.25–7.15, 6.98 (m, 14H, aromatic), 5.53 (d, J = 3.1 Hz, 1H, H-1′), 4.42 (m, 1H, H-2′), 3.82 (m, 2H, H-4′), 3.73 (s, 3H, CH_3), 2.07, 1.89 (m, 2H, H-3′); ^{13}C nmr (75.453 MHz) δ: 157.80 (C-6), 156.26 (MTr), 150.85 (C-2), 148.39 (C-4), 144.78, 144.54, 136.49, 129.65, 128.32, 127.59, 126.61, 112.92 (MTr), 136.56 (C-8), 117.99 (C-5), 90.98 (C-1′), 69.84 (MTr), 67.36 (C-4′), 58.67 (C-2′), 54.95 (OCH_3), 33.83 (C-3′). *Anal.* calcd. for $C_{29}H_{26}N_5O_3Cl$ (528.01): C 65.97, H 4.96, N 13.26, Cl 6.71; found: C 65.94, H 5.08, N 13.41, Cl 6.79.

(R,S)-N^2-(p-*Anisyldiphenylmethyl)-9-(2,5-dihydrofuran-2-yl)guanine (**12**)*

To **11** (20.2 g, 38.4 mmol) and potassium *tert*-butoxide (19.5 g, 173.7 mmol) was added a mixture of pyridine (10 mL), 1,2-dimethoxyethane (10 mL), and toluene (180 mL). The resulting mixture was heated for 1 h at 75°C (monitored with $KMnO_4$ spray), then cooled and partitioned directly with H_2O (1×), and the aqueous phase was back washed with dichloromethane (800 mL). The combined organic phase was washed with H_2O (1×), dried ($MgSO_4$), and then evaporated to give 17.4 g (92%) of **12** as a yellow foam. An analytical sample was obtained as a white powder by precipitating a dichloromethane solution of **12** with ether: mp 203–205°C; uv λ_{max} (methanol): sh 276 nm (ε 14 000), 261 (15 700), 234 (16 300); ^{1}H nmr δ: 10.63 (s, br, 1H, NH), 7.63 (s, br, 1H, NH), 7.54 (s, 1H, H-8), 7.29–7.33 (m, 10H, aromatic), 7.30, 6.87 (AB, J = 8.9 Hz, 4H, aromatic), 6.23 (dd, $J_{1',2'}$ = 6.1 Hz, $J_{1',3'}$ = 1.5 Hz, 1H, H-1′), 6.12 (m, 1H, H-3′), 5.56 (m, 1H, H-2′), 4.53, 4.46 ($J_{4',4''}$ = 11 Hz, $J_{4',3'}$ = 5 Hz, $J_{4'',3'}$ = 1.9 Hz, $J_{4',2'}$ = 1.5 Hz, $J_{4'',2'}$ ≃ 0, 2H, H-4′), 3.71 (s, 3H, OCH_3); ^{13}C nmr (75.453 MHz) δ: 157.69 (C-6), 156.38 (MTr), 150.84 (C-2), 148.83 (C-4), 144.90, 144.77, 136.74, 129.80, 128.41, 128.35, 127.51, 126.44, 112.84 (MTr), 135.33 (C-8), 132.57 (C-2′), 123.53 (C-3′), 117.27 (C-5), 88.40 (C-1′), 74.88 (C-4′), 69.82 (MTr), 54.93 (OCH_3). *Anal.* calcd. for $C_{29}H_{25}N_5O_3$ (491.55): C 70.86, H 5.12, N 14.25; found: C 70.98, H 5.13, N 14.04.

N^2-(p-*Anisyldiphenylmethyl)-9-(β-(DL)*-erythro-*furanosyl)guanine (**15**)*

A solution of $KMnO_4$ (3.4 g, 21.5 mmol) in H_2O (mL) was added over 5 min with vigorous stirring to a solution of **12** (10.8 g, 21.9 mmol) in acetone (100 mL): H_2O (40 mL). The reaction mixture was then filtered through Celite and partially evaporated. The residue was redissolved in CH_2Cl_2 and washed with H_2O (2×), the organic phase dried over $MgSO_4$ and evaporated. The resulting oil was chromatographed (5% methanol/CH_2Cl_2) to give 2.85 g (25%) of **15** as a powder from ether: mp 180–181°C; uv λ_{max} (methanol): sh 278 nm (ε 10 300), 260 (11 300); ^{1}H nmr δ: 10.64 (s, br, 1H, NH), 7.68 (s, 1H, H-8), 7.62 (s, br, 1H, NH), 7.31–7.2 (m, 10H, aromatic), 7.27, 6.87 (AB, 4H, J = 8.9 Hz, aromatic), 5.28 (d, J = 6.6 Hz, 1H, H-1′), 4.94, 4.90 (d, J = 6.9, 3.5 Hz, 2H, OH), 4.03 (after D_2O added, dd, J = 6.6, 4.4 Hz, 1H, H-2′), 3.72 (s, 3H, OCH_3), 3.61 (s, br, 1H, H-3′), 3.29 (s, br, 1H, H-4′); ^{13}C nmr (75.453 MHz) δ: 157.74 (C-6), 156.36 (MTr), 150.59 (C-2), 148.87 (C-4), 138.39 (C-8), 144.86, 144.64, 136.62, 129.60, 128.22, 127.61, 126.56, 112.94 (MTr), 118.72 (C-5), 89.06 (C-1′), 73.23, 73.13 (C-2′, C-4′), 70.38 (C-3′), 69.81 (MTr), 54.95 (OCH_3). *Anal.* calcd. for $C_{29}H_{27}N_5O_5$ (525.56): C 66.27, H 5.18, N 13.32; found: C 66.33, H 5.20, N 13.48.

9-(β-(DL)-erythro-*furanosyl)guanine (**16**)*

A solution of **15** (400 mg, 0.76 mmol) in 80% acetic acid was heated for 16 h at 50°C, then evaporated. The residue was first triturated with acetone and then crystallized from ethanol/H_2O to afford **16** (65 mg, 34%). Recrystallization from hot H_2O gave the analytical sample: mp >230°C (dec.); uv λ_{max} (H_2O): sh 274 nm (ε 8 190), 253 (11 700); ^{1}H nmr δ: 10.62 (s, br, 1H, NH), 7.89 (s, 1H, H-8), 6.44 (s, br, 2H, NH_2), 5.66 (d, J = 6.7 Hz, 1H, H-1′), 5.41 (d, J = 6.3 Hz, 1H, OH),

5.12 (d, J = 3.7 Hz, 1H, OH), 4.63 (after D_2O added, dd, J = 4.7, 6.7 Hz, 1H, H-2′), 4.30, 3.75 (ABX, J_{AB} = 10 Hz, J_{AX} = 3.6 Hz, J_{BX} = 1.6 Hz, 2H, H-4′), 4.20 (m, 1H, H-3′). *Anal.* calcd. for $C_9H_{11}N_5O_4 \cdot H_2O$ (271.23): C 39.85, H 4.83, N 25.82; found: C 39.79, H 4.85, N 25.82.

*(R,S)-N²-(p-Anisyldiphenylmethyl)-9-[1-(2-hydroxyethoxy)-2-hydroxyethyl]guanine (**13**)*

To a solution of **12** (6.3 g, 12.8 mmol) in methanol (150 mL)/H_2O (20 mL) was added $NaIO_4$ (6 g, 28 mmol) followed by a solution of OsO_4 (5 mL) (0.5 g OsO_4 in 100 mL *tert*-butanol). The suspension was stirred for 3 h at room temperature, after which time $NaBH_4$ (1.7 g, 44.9 mmol) was added, stirring was continued for 10 min, and then the reaction mixture was partially evaporated. The resulting residue was redissolved in chloroform and washed with H_2O (1×) followed by dilute Na_2CO_3 (1×), and the organic phase was dried over $MgSO_4$ and evaporated to a brown oil. The oil was chromatographed (5–10% methanol/dichloromethane) to afford 4.3 g (64%) of **13** as a foam: uv λ_{max} (methanol): sh 277 nm (ϵ 14 500), 261 (16 000), 235 (16 900); ^{1}H nmr δ: 10.57 (s, br, 1H, NH), 7.69 (s, 1H, H-8), 7.63 (s, br, 1H, NH), 7.29 (m, 10H, aromatic), 7.19, 6.86 (AB, 4H, J = 8.9 Hz, aromatic), 4.97 (t, J = 5 Hz, 1H, OH), 4.79 (t, J = 6 Hz, 1H, H-1′), 3.72 (s, 3H, OCH_3), 3.48 (dd, J = 5, 6 Hz, 2H, H-2′), 3.24 (dt, 2H, H-5′), 2.93 (t, J = 4 Hz, 2H, H-4′); ^{13}C nmr (75.453 MHz) δ: 159.12 (C-6), 157.48 (MTr), 152.59 (C-2), 150.14 (C-4), 145.49, 145.38, 137.26, 129.90, 128.45, 127.30, 126.12, 112.64 (MTr), 134.86 (C-8), 116.78 (C-5), 83.37 (C-1′), 70.30 (MTr), 69.52 (C-4′), 61.67, 59.60 (C-2′, C-5′), 54.87 (OCH_3). *Anal.* calcd. for $C_{29}H_{29}N_5O_5 \cdot H_2O$ (545.59): C 63.84, H 5.72, N 12.84; found: C 63.83, H 5.77, N 12.80.

*(R,S)-9-[1-(2-Hydroxyethoxy)-2-hydroxyethyl]guanine (**14**)*

A solution of **13** (4.3 g, 8.1 mmol) in 80% aqueous acetic acid (50 mL) was heated for 4.5 h at 70°C, then cooled to room temperature (1 h) and evaporated. The residue was co-evaporated with ethanol (2×) and crystallized from methanol/H_2O to afford in 2 crops 1.1 g (53%) of **14**: mp >300°C; uv λ_{max} (0.1 *N* HCl): sh 278 nm (ϵ 8 020), 255 (12 100); (0.1 *N* NaOH): 265 (10 800), 254 (10 600); ^{1}H nmr δ: 10.61 (s, br, 1H, NH), 7.79 (s, 1H, H-8), 6.46 (s, br, 2H, NH_2), 5.46 (t, J = 5.9 Hz, 1H, H-1′), 5.16 (t, J = 6 Hz, 1H, 2′-OH), 4.63 (t, J = 5.2 Hz, 1H, 3′-OH), 3.81 (dd, 2H, J = 5.9, 4.8 Hz, H-2′), 3.46 (dt, 2H, H-5′), 3.32 (t, J = 6 Hz, 2H, H-4′); ^{13}C nmr (75.453 MHz) δ: 156.78 (C-6), 153.58 (C-2), 151.60 (C-4), 135.60 (C-8), 116.32 (C-5), 83.97 (C-1′), 70.12 (C-4′), 61.88, 59.68 (C-5′, C-2′). *Anal.* calcd. for $C_9H_{13}N_5O_4$ (255.23): C 42.35, H 5.13, N 27.44; found: C 42.07, H 4.98, N 27.46.

Acknowledgement

We appreciate the assistance of Syntex Analytical Research and especially that of Dr. M. L. Maddox, Mrs. J. Nelson, and Mrs. L. Kurz in obtaining and interpreting spectroscopic data.

1. (*a*) T. Hovi. Med. Biol. **61**, 196 (1983); (*b*) Ann. N.Y. Acad. Sci. 284 (1977).
2. (*a*) J. C. Martin, C. A. Dvorak, D. F. Smee, T. R. Matthews, and J. P. H. Verheyden. J. Med. Chem. **26**, 759 (1983); (*b*) J. P. H. Verheyden and J. C. Martin. U.S. Patent No. 4,355,032. October 19, 1982; (*c*) W. T. Ashton, J. D. Karkas, A. K. Field, and R. L. Tolman. Biochem. Biophys. Res. Commun. **108**, 1716 (1982); (*d*) K. K. Ogilvie, U. O. Cheriyan, B. K. Radatus, K. O. Smith, K. S. Galloway, and W. L. Kennell. Can. J. Chem. **60**, 3005 (1982); (*e*) H. J. Schaeffer. *In* Nucleosides, nucleotides and their biological applications. *Edited by* J. L. Rideout, D. W. Henry, and L. M. Beacham. Academic Press, New York. 1983.
3. (*a*) D. F. Smee, J. C. Martin, J. P. H. Verheyden, and T. R. Matthews. Antimicrob. Agents Chemother. **23**, 676 (1983); (*b*) Y.-C. Cheng, E.-S. Huang, J.-C. Lin, E.-C. Mar, J. S. Pagano, G. E. Dutschman, and S. P. Grill. Proc. Natl. Acad. Sci. U.S.A. **80**, 2767 (1983).
4. (*a*) J. X. Khym and W. E. Cohn. J. Am. Chem. Soc. **82**, 6380 (1960); (*b*) A. J. Grant and L. M. Lerner. J. Med. Chem. **23**, 39 (1980); (*c*) L. M. Lerner. Carbohydr. Res. **13**, 465 (1970); (*d*) F. Hansske and F. Cramer. Carbohydr. Res. **54**, 75 (1977).
5. (*a*) A. J. Grant and L. M. Lerner. Biochemistry, **18**, 2838 (1979); (*b*) R. T. Borchardt, Y. S. Wu, and B. S. Wu. J. Med. Chem. **21**, 1307 (1978).
6. (*a*) A. J. Grant and L. M. Lerner. J. Med. Chem. **23**, 795 (1980); (*b*) M. Vuilhorgne, P. Blanchard, C. J. R. Hedgecock, F. Lawrence, M. Robert-Gero, and E. Lederer. Heterocycles, **11**, 495 (1978); (*c*) J. M. J. Tronchet and D. Schwarzenback. Carbohydr. Res. **99**, 78 (1982); (*d*) W. A. Szarek, B. M. Pinto, and M. Iwakawa. Can. J. Chem. **63**, 2149 (1985); **63**, 2162 (1985); (*e*) S. N. Mikhailov, V. L. Florentiev, and W. Pfleiderer. Synthesis, 399 (1985); (*f*) A. S. Jones, M. J. McClean, H. Tanaka, R. T. Walker, J. Balzarini, and E. De Clercq. Tetrahedron, **41**, 5965 (1985).
7. (*a*) L. M. Lerner. Carbohydr. Res. **127**, 141 (1984); (*b*) M. Bessodes and K. Antonakis. Tetrahedron Lett. **26**, 1305 (1985); (*c*) Biologicals Inc., U.S. Patent No. 4,460,690. 1983.
8. (*a*) J. G. Moffatt. *In* Nucleoside analogues. *Edited by* R. T. Walker, E. DeClercq, and F. Eckstein. Plenum Press, New York. 1979. pp. 71–164; (*b*) S. D. Dimitrijevich, J. P. H. Verheyden, and J. G. Moffatt. J. Org. Chem. **44**, 400 (1979); (*c*) P. J. Garegg and B. Samuelson. J. Chem. Soc. Perkin Trans. 1, 2866 (1980).
9. I. Nakagawa, K. Aki, and T. Hata. J. Chem. Soc. Perkin Trans. 1, 1315 (1983).
10. (*a*) E. J. Reist, P. A. Hart, L. Goodman, and B. R. Baker. J. Org. Chem. **26**, 1557 (1961); (*b*) M. Ikehara, H. Tada, and K. Muneyama. Chem. Pharm. Bull. **13**, 639 (1965).
11. S. Ueda, S. Takeda, I. Yamawaki, J. I. Yamashita, M. Yasumoto, and S. Hashimoto. Chem. Pharm. Bull. **30**, 125 (1982).
12. W. A. Bowles, F. H. Schneider, L. R. Lewis, and R. K. Robins. J. Med. Chem. **6**, 471 (1963).
13. J. D. Bryant, G. E. Keyser, and J. R. Barrio. J. Org. Chem. **44**, 3733 (1979).
14. J. E. McCormick and R. S. McElhinney. Proc. R. Ir. Acad. Sect. B, **83**, 125 (1983); J. Chem. Res. Miniprint, 256 (1981).
15. Y. Ishido, A. Hosono, S. Isome, A. Maruyama, and T. Sato. Bull. Chem. Soc. Jpn. **37**, 1389 (1964).
16. W. Reppe. Justus Liebigs Ann. Chem. **596**, 1 (1955).
17. A. J. Lin, R. S. Benjamin, P. N. Rao, and T. L. Loo. J. Med. Chem. **22**, 1096 (1979).
18. T. Mukaiyama, F. Tabusa, and K. Suzuki. Chem. Lett. 173 (1983).
19. B. Rayner, C. Tapiero, and J.-L. Imbach. Carbohydr. Res. **47**, 195 (1976).

Catalysis of ring expansion of 1-methylcyclopropylmethanol to 1-methylcyclobutanol by rhodium(I)

J. Thomas Burton and Richard J. Puddephatt[1]

Department of Chemistry, University of Western Ontario, London, Ont., Canada N6A 5B7

Received January 14, 1986

J. Thomas Burton and Richard J. Puddephatt. Can. J. Chem. **64**, 1890 (1986).

Stoichiometric reaction between $[Rh_2(\mu\text{-}Cl)_2(CO)_4]$ and $CH_2CH_2CHCMe_2OPNB$, OPNB = 4-nitrobenzoate, gave $[Rh_2(\mu\text{-}OPNB)_2(CO)_4]$ and $Me_2C{=}CHCH_2CH_2Cl$. The complex $[Rh_2(\mu\text{-}Cl)_2(CO)_4]$ in acetone solution catalyzes the ring expansion of $CH_2CH_2CMeCH_2OH$ to give $CH_2CH_2CH_2CMeOH$, and experiments with labelled derivatives indicate that the rhodium complex acts as a Lewis acid. The reaction is zero order in cyclopropyl derivative but second order in catalyst concentration. The equilibrium constant for the reaction is 21 at 40°C and a mechanism is proposed.

J. Thomas Burton et Richard J. Puddephatt. Can. J. Chem. **64**, 1890 (1986).

La réaction stoïchiométrique du $[Rh_2(\mu\text{-}Cl)_2(CO)_4]$ et du $CH_2CH_2CHCMe_2OPNB$ (OPNB = nitro-4 benzoate) conduit au $[Rh_2(\mu\text{-}OPNB)_2(CO)_4]$ et au $Me_2C{=}CHCH_2CH_2Cl$. En solution dans l'acétone, le complexe $[Rh_2(\mu\text{-}Cl)_2(CO)_4]$ catalyse l'extension de cycle du $CH_2CH_2CMeCH_2OH$ qui conduit au $CH_2CH_2CH_2CMeOH$; des expériences avec des dérivés marqués indiquent que le complexe de rhodium agit comme un acide de Lewis. La réaction est d'ordre zéro en dérivé cyclopropyle; toutefois, elle est d'ordre deux par rapport au catalyseur. A 40°C, la constante d'équilibre de la réaction est égale à 21 et on propose un mécanisme.

[Traduit par la revue]

Introduction

We have been interested in the reactions of cyclopropylmethanol and its derivatives with platinum complexes (1–3). In favorable cases, platinacyclobutanes have been isolated and subsequent solvolysis gave platinacyclopentanols (for example, reaction [1], OMs = mesylate, py = pyridine)

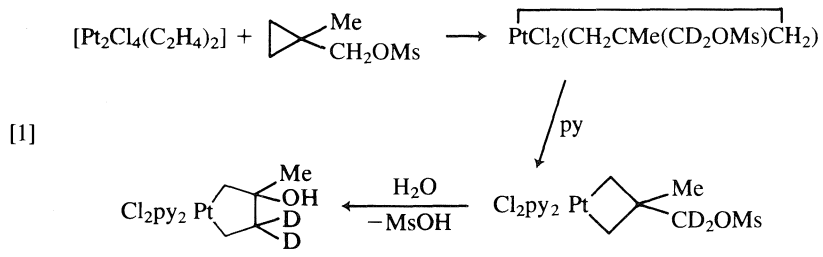

[1]

Since $[Rh_2(\mu\text{-}Cl)_2(CO)_4]$ is known to react with cyclopropanes to give rhodacyclobutanes (4), which may then undergo further interesting reactions (5–7), attempts were made to develop rhodium chemistry analogous to reaction [1]. The results of this study are described below.

Results

In no case did reaction of a derivative of cyclopropylmethanol give organorhodium complexes of the type expected by analogy with reaction [1]. However, new reactions were observed in two cases.

*Reaction with 2-cyclopropyl-2-propyl-*p*-nitrobenzoate*

In this case a stoichiometric reaction occurred according to reaction [2] (OPNB = *p*-nitrobenzoate)

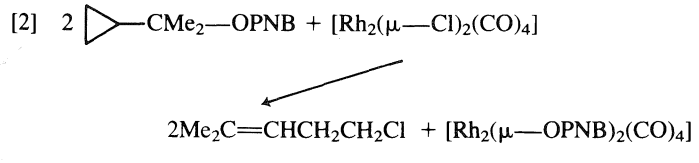

The rhodium complex precipitated from the reaction mixture as a blue–black crystalline solid, which dissolves in organic solvents such as dichloromethane to give orange solutions. Similar carboxylate bridged complexes are known and are also dichroic (8, 9). They have the structure **1**. The organic product was identified by its ^1H and ^{13}C nmr spectra and was formed quantitatively. The reaction is stoichiometric and the rhodium-containing product did not react with $c\text{-}C_3H_5CMe_2OPNB$.

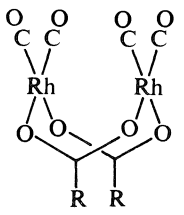

1

This organic product is not expected on the basis of the solvolysis of the cyclopropyl precursor which gives only unrearranged 2-cyclopropyl-2-propanol and no alkene products (11). However, it is known that magnesium halides in refluxing ether can effect a similar reaction to that in reaction [2] (10). These precedents do not aid an understanding of the mechanism of reaction [2], in particular whether the rhodium centre is involved in the cyclopropyl ring opening step.

[1]To whom all correspondence should be addressed.

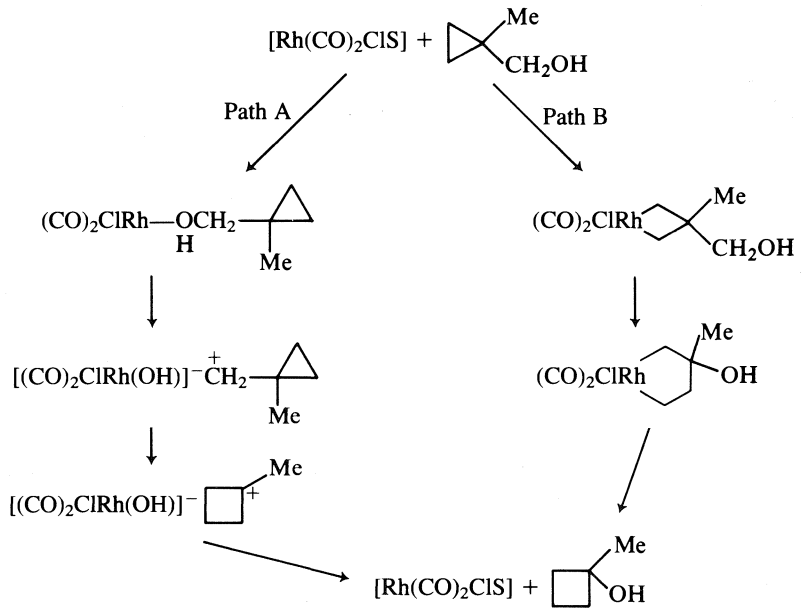

SCHEME 1

Reaction with 1-methylcyclopropylmethanol

It was found that $[Rh_2(\mu\text{-}Cl)_2(CO)_4]$ in acetone solution at 40°C catalyzes the ring expansion of 1-methylcyclopropylmethanol according to reaction [3].

[3] 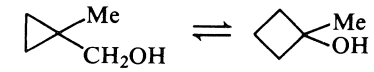

This ring expansion occurred under mild conditions and was easily monitored by nmr in acetone-d_6 solution. The reaction did not proceed to completion but reached an equilibrium with the equilibrium constant at 40°C for reaction [3] equal to 21. This corresponds to a free energy change, ΔG, of -1.9 kcal mol^{-1} for the reaction. This is fairly close to the value expected from the difference in ring strain between cyclopropane and cyclobutane, which would predict $\Delta H = 26.4\text{–}27.6 = -1.2$ kcal mol^{-1}. We have not measured the changes in K for reaction [3] with temperature and so ΔH for reaction [3] is not known. Despite the large numbers of studies of ring expansions analogous to reaction [3], there appear to be very few systems where it is possible to determine the equilibrium constants (12). In this case, integration of the signals due to the methyl protons of starting material and product, at $\delta = 1.22$ and 1.40 ppm, respectively, when the reaction had reached equilibrium gave an accurate measure of K. No other compounds could be detected by nmr in these reactions. The ring expansion can be catalyzed by acid at 100°C (12), but no ring expansion occurred using acid catalysts CF_3CO_2H or HCl at 40°C. The catalyst is therefore clearly the rhodium complex, which could be recovered unchanged at the end of the reaction.

Two possible mechanisms for the rhodium-catalyzed reaction are shown in Scheme 1. In path A, which has many precedents in organic systems (13), the rhodium acts only as a Lewis acid and the ring expansion involves carbocation intermediates whereas, path B, rhodacyclobutane intermediates are proposed and the mechanism is based on the platinum chemistry of reaction [1] (1, 2).

It has been shown that hydrolysis of $[Cl_2py_2\overline{PtCH_2CMe(CD_2OMs)CH_2}]$ is selective and gives very largely $[Cl_2py_2\overline{PtCH_2CMe(OH)CD_2CH_2}]$, reaction [1] (1, 2, 13), whereas general methylene scrambling occurs within the cyclopropylmethyl cation (14). It seemed likely therefore that different distributions of deuterium label would be seen between the products of hydrolysis of $\overline{CH_2CH_2CMe(CD_2OMs)}$ and rhodium-catalyzed ring expansion of $\overline{CH_2CH_2CMe(CD_2OH)}$ if path B was correct whereas the same distribution of deuterium label would be observed if path A was correct. When these experiments were carried out, the same distribution of deuterium label was observed, the products being $\overline{CH_2CH_2CD_2CMe(OH)}$, 65%, and $CH_2CD_2CH_2CMe(OH)$, 35%, in each case. This strongly suggested that path A, or some similar pathway in which the rhodium acts as a powerful Lewis acid, was correct. Further evidence against path B was obtained by conducting the isomerization reaction under CO pressure. Rhodacyclobutanes are known to undergo rapid CO insertion, and any such intermediates should therefore be trapped under these conditions (15). However, the reaction proceeded in the usual way under these conditions (reaction [3]), the only complication being the conversion of some of the catalyst to $[Rh_6(CO)_{16}]$.

The complex $[Rh_2(\mu\text{-}Cl)_2(CO)_4]$ in acetone solution is very largely present as the acetone complex (reaction [4], S = acetone) (16).

[4] $[Rh_2(\mu\text{-}Cl)_2(CO)_4] + 2S \rightleftharpoons 2cis\text{-}[RhCl(CO)_2S]$

The reaction according to path A should therefore follow overall second order kinetics, first order in both $[RhCl(CO)_2S]$ and in cyclopropane derivative. A kinetic study was carried out at 40°C, with monitoring by ^{1}H nmr. Unexpectedly, for a given kinetic run, the order with respect to cyclopropane derivative was close to zero, and the zero order rate constants for runs with varying concentrations of $[RhCl(CO)_2S]$ were approximately proportional to $[RhCl(CO)_2S]^2$, Fig. 1.

The kinetic data are interpreted in terms of the mechanism of reactions [5] and [6]

[5] $2cis\text{-}[RhCl(CO)_2S] \xrightarrow{\text{slow}}$ "A"

[6] "A" + $\overline{CH_2CH_2CMe(CH_2OH)} \xrightarrow{\text{fast}} 2cis\text{-}[RhCl(CO)_2S] + \overline{CH_2CH_2CH_2CMe(OH)}$

The nature of the species "A" is obscure since it is not formed in spectroscopically detectable concentration. One possibility is

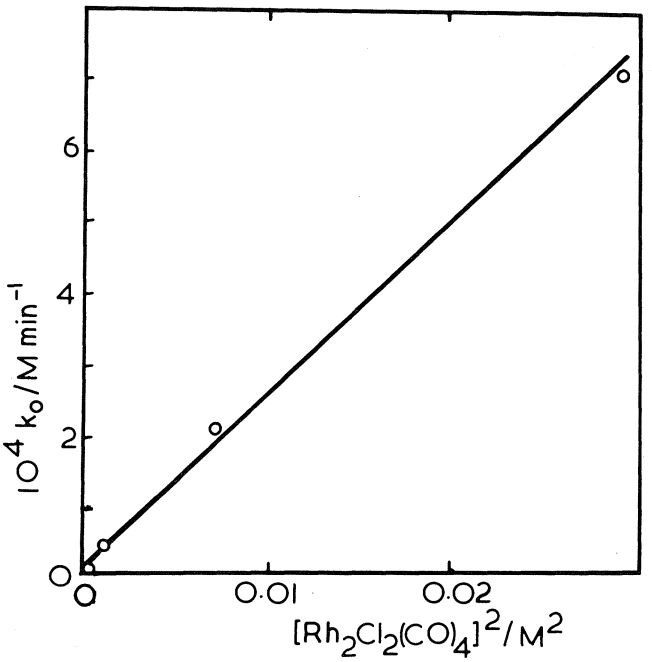

FIG. 1. Plot of observed zero order rate constants ($k_0/M\ min^{-1}$) for the rhodium-catalyzed ring expansion versus the square of the catalyst concentration.

that it might be *cis*-$[Rh(CO)_2S_2]^+$ *cis*-$[RhCl_2(CO)_2]^-$, with the cation acting as a strong Lewis acid. Alternatively it could be a dinuclear complex with a single μ-Cl bridge, which should also be a stronger Lewis acid than *cis*-$[RhCl(CO)_2S]$. Such complexes with two labile centres, could also interact with the cyclopropyl group and facilitate ring expansion. The ability of $[Rh_2(\mu\text{-}Cl)_2(CO)_4]$ to act as a Lewis acid, including its use in catalysis of other reactions of strained ring compounds, has been noted previously (17–19).

The observed kinetic behaviour was unexpected but may be used to rationalize the fact that the catalyzed ring expansion of reaction [3] is very sensitive to solvent. Thus effective catalysis was not observed using chloroform solvent, when the catalysis is present as the dimer $[Rh_2(\mu\text{-}Cl)_2(CO)_4]$, or in neat 1-methylcyclopropylmethanol, when the catalyst is probably present as *cis*-$[RhCl(CO)_2S]$, S = 1-methylcyclopropylmethanol.

Experimental

^1H and ^{13}C nmr spectra were recorded using a Varian XL100 or Varian XL200 spectrometer, and chemical shifts are quoted with respect to TMS. $[Rh_2(\mu\text{-}Cl)_2(CO)_4]$ was prepared by the literature method and was purified by vacuum sublimation (20), and cyclopropane derivatives were prepared as described previously (13).

Reaction with $CH_2CH_2CHCMe_2CH_2O_2CC_6H_4NO_2$

2-Cyclopropyl-2-propyl-4-nitrobenzoate (0.258 mmol) was added to a solution of $[Rh_2(\mu\text{-}Cl)_2(CO)_4]$ (0.129 mmol) in acetone-d_6 (2 mL). The solution became dark red in colour and a blue–black precipitate formed. This was removed by filtration, dried under a vacuum, and identified as $[Rh_2(\mu\text{-}O_2CC_6H_4NO_2)_2(CO)_4]$. Yield 70%; mp 209–210°C; ir (Nujol): 2076, 2021 (ν(CO)); 1605, 1555 ($\nu(CO)_2$). ^1H nmr: δ = 8.34 (*m*, C_6H_4). *Anal.* calcd. for $C_{18}H_8N_2O_{12}Rh_2$: C 33.25, H 1.2, N 4.3. Found: 33.5, H 1.9, N 4.2. The organic product was identified as $(C^1H^1{}_3)_2C^2{=}C^3H^3C^4H^4{}_2C^5H^5{}_2Cl$ by comparison of the ^1H and ^{13}C nmr spectra with those of an authentic sample (21). ^1H: δ = 1.63 (*s*, H^1); 1.69 (*s*, H^1); 5.17 (*t*, $J(H^3H^4)$ = 7, H^3); 2.44 (*q*, $J(H^3H^4) = J(H^4H^5)$ = 7, H^4); 3.53 (*t*, $J(H^4H^5)$ = 7, H^5). ^{13}C: δ = 25.8, 17.8 (C^1H_3); 135.1 (C^2); 121.2 (C^3H); 32.2 (C^4H_2); 45.1 (C^5H_2).

Reaction with $CH_2CH_2CMeCH_2OH$

In a typical experiment, a solution of $[Rh_2(\mu\text{-}Cl)_2(CO)_4]$ (1.71×10^{-2} *M*) and $CH_2CH_2CMeCH_2OH$ (1.71×10^{-1} *M*) in acetone-d_6 (0.6 mL) in an nmr tube was thermostated at 40°C and nmr spectra were recorded periodically until no further change occurred. The product was identified as $C^1H_2C^2H_2C^3H_2C^4Me^5OH$ by its ^1H and ^{13}C nmr spectra (18). ^1H: δ = 1.40 (*s*, CH_3); 1.5–2.3 (*m*, cyclobutyl CH_2 protons). ^{13}C: δ = 38.4 (C^1, C^3); 12.2 (C^2); 72.5 (C^4); 27.2 (C^5). The rate was monitored by integration of the resonances due to the CH_3 groups of the starting material and product. At the end of the reaction, $[Rh_2(\mu\text{-}Cl)_2(CO)_4]$ was recovered from the solution and identified by ir.

Reaction with $CH_2CH_2CMeCD_2OH$

A solution of $[Rh_2(\mu\text{-}Cl)_2(CO)_4]$ (0.103 mmol) and CH_2CH_2C-$MeCD_2OH$ (0.556 mmol) in acetone-d_6 (0.6 mL) was allowed to react until there was no further change in the nmr spectrum. The volatiles were then distilled on the vacuum line into a clean nmr tube and the ^{13}C nmr spectrum of the 1-methylcyclobutanol-d_6 was recorded. The residue was identified as $[Rh_2(\mu\text{-}Cl)_2(CO)_4]$ by ir.

For comparison, a sample of $CH_2CH_2CMe(CD_2OMs)$, OMs = methanesulfonate (3.41 mmol), was hydrolyzed in aqueous acetone (15 mL), 60% v/v) at 40°C in the presence of $CaCO_3$ (34 mmol) for 90 min. The mixture was extracted with pentane (10 mL) and then pentane–ether (3 × 3 mL, 1:1 mixture). The solvent was removed from the dried combined organic extracts to give 1-methylcyclobutanol-d_2, and the ^{13}C nmr spectrum of this product (50 mg) in acetone-d_6 (0.6 mL) was recorded.

The relative intensities of ^{13}C resonances in the above two samples were the same, and both were estimated to contain $CH_2CH_2CD_2CMe(OH)$, 65%, and $CH_2CD_2CH_2CMe(OH)$, 35%, by comparison of the spectra with that of $CH_2CH_2CH_2CMe(OH)$, recorded using identical conditions.

Acknowledgements

We thank Natural Sciences and Engineering Research Council of Canada for financial support.

1. J. T. BURTON and R. J. PUDDEPHATT. J. Am. Chem. Soc. **104**, 4242 (1982).
2. R. J. PUDDEPHATT. Inorganic chemistry toward the 21st century. *Edited by* M. H. Chisholm. Am. Chem. Soc. Symposium Series, **211**, 353 (1983).
3. J. T. BURTON, R. J. PUDDEPHATT, N. L. JONES, and J. A. IBERS. Organometallics, **2**, 1487 (1983).
4. B. F. G. JOHNSON, J. LEWIS, and S. W. TAM. J. Organomet. Chem. **105**, 271 (1976).
5. F. J. MCQUILLIN and K. G. POWELL. J. Chem. Soc. Dalton Trans. 2129 (1972).
6. K. C. BISHOP, III. Chem. Rev. **76**, 461 (1976).
7. R. B. TAYLOR and P. W. JENNINGS. Inorg. Chem. **20**, 3997 (1980).
8. R. P. HUGHES. *In* Comprehensive organometallic chemistry. *Edited by* G. Wilkinson, F. G. A. Stone, and E. W. Abel. Pergamon, Oxford. 1982. Chapt. 35.
9. D. N. LAWSON and G. WILKINSON. J. Chem. Soc. 1900 (1965).
10. C. A. GROB and A. WALDNER. Helv. Chim. Acta, **62**, 1854 (1979).
11. J. P. MCCORMICK and D. L. BARTON. J. Org. Chem. **45**, 2566 (1980).
12. M. C. CASERIO, W. H. GRAHAM, and J. D. ROBERTS. Tetrahedron, **11**, 171 (1960).
13. J. T. BURTON and R. J. PUDDEPHATT. Organometallics. To be published.

14. H. G. RICHEY, JR. *In* Carbonium ions. Vol. 3. *Edited by* G. A. Olah and P. v. R. Schleyer. Wiley, New York. 1972. p. 1201.
15. F. J. MCQUILLIN and K. G. POWELL. J. Chem. Soc. Dalton Trans. 2129 (1972).
16. M. HIDAI, M. ORISAKU, and Y. UCHIDA. Chem. Lett. 753 (1980).
17. P. G. GASSMAN and R. R. REITZ. J. Am. Chem. Soc. **95**, 3057 (1973).
18. R. V. HOFFMAN. Tetrahedron Lett. 2415 (1974).
19. G. ADAMES, C. BIBBY, and R. GRIGG. J. Chem. Soc. Chem. Commun. 491 (1972).
20. J. A. MCCLEVERTY and G. WILKINSON. Inorg. Synth. **8**, 211 (1966).
21. K. L. SERVIS and F.-F. SHUE. J. Am. Chem. Soc. **102**, 7233 (1980).

Iodo-bridged complexes of platinum(II) and synthesis of *cis* mixed-amine platinum(II) compounds

F. D. ROCHON AND P. C. KONG

Département de chimie, Université du Québec à Montréal, C.P. 8888, succ. A, Montréal, Qué., Canada H3C 3P8

Received October 1, 1985[1]

F. D. ROCHON and P. C. KONG. Can. J. Chem. **64**, 1894 (1986).

Iodo-bridged platinum(II) dimers, $[Pt(L)I_2]_2$ with ligands (L) containing nitrogen as the donor atom, have been synthesized from the reactions of *cis*-$[Pt(L)_2I_2]$ with perchloric acid. The dimers can be cleaved in aqueous media by a second nitrogen ligand to produce isometrically pure *cis*-$[Pt(L)(L')I_2]$. These compounds can finally be converted to the chloro or carboxylato compounds by precipitating the iodo ligands with a silver salt and adding KCl or a carboxylate salt. Several compounds of the types *cis*-$[Pt(L)(L')Cl_2]$ and *cis*-[Pt(L)(L')(dicarboxylate)] were thus prepared. A few dimers of the type [(L)(L')Pt(tetracarboxylate)Pt(L)(L')] were also synthesized.

F. D. ROCHON et P. C. KONG. Can. J. Chem. **64**, 1894 (1986).

Des complexes de platine(II) à ponts iodés $[Pt(L)I_2]_2$ avec des ligands à atomes donneurs azotés, ont été synthétisés par la réaction entre *cis*-$[Pt(L)_2I_2]$ et l'acide perchlorique. L'ouverture des dimères a été réalisée en milieu aqueux par un autre ligand azoté (L') et des complexes isomériquement purs, *cis*-$[Pt(L)(L')I_2]$ ont été isolés. Ces derniers composés peuvent être transformés en composés chlorés ou carboxylates, par précipitation des ligands iodés avec un sel d'argent et l'ajout de KCl ou un sel carboxylate. Plusieurs complexes de types *cis*-$[Pt(L)(L')Cl_2]$ et *cis*-[Pt(L)(L')(dicarboxylate)] ont ainsi été préparés. De plus, quelques dimères de type [(L)(L')Pt(tétracarboxylate)Pt(L)(L')] ont été synthétisés.

Introduction

Iodo-bridged platinum(II) dimers $[Pt(L)I_2]_2$ containing nitrogen as the donor atom are not known and there are no methods in the literature that could lead to their synthesis. Iodo dimers with phosphine (1) or sulfoxide (2) ligands have been reported, but these two methods cannot be used to prepare amine iodo dimers.

Chloro-bridged dimers of piperidine, aniline, and pyridine derivatives have been reported (3–7). Courtot *et al.* (5) synthesized a chloro-bridged dimer with a very bulky amine, *t*-butylamine but were unable to prepare dimers with smaller amines since their method of synthesis is limited. They used the following photochemical method:

$$[Pt(L)(olefin)Cl_2] \xrightarrow[\substack{CHCl_3 \text{ or} \\ CHCl_3/\text{pentane}}]{h\nu} [Pt(L)Cl_2]_2$$

When L = is a simple amine R—NH_2 (R ≠ *t*-butyl) the starting material $[Pt(L)(olefin)Cl_2]$ is not soluble in $CHCl_3$ or $CHCl_3$/pentane and the dimers cannot be synthesized.

The halide dimers are important compounds because they can be the starting material for the preparation of mixed-ligand complexes, $[Pt(L)(L')X_2]$. Indeed, the dimers can be cleaved with several types of molecules (L') and depending on L, L', and the conditions of reactions, will produce *cis* or *trans* compounds. We have been trying for several years to prepare mixed-amine compounds of the type *cis*-$[Pt(L)(L')X_2]$ in view of increasing the screening range for antitumor properties of platinum compounds. We have now developed a general method to synthesize iodo-bridged dimers with amines. The method can also be used to prepare dimers with NH_3, pyridine derivatives, and probably any nitrogen ligand. This method will be discussed below.

The iodo dimers can be cleaved by several type of ligands (L'). The results obtained when L' = amine ≠ L will be discussed, along with the experimental conditions which are important for obtaining isomerically pure *cis* isomers.

Very few mixed-amine Pt(II) compounds have been reported. Braddock *et al.* (8) and Hydes (9) prepared a few compounds by the following method:

$$K[Pt(NH_3)Cl_3] + \text{amine} \rightarrow \textit{cis}\text{-}[Pt(NH_3)(am)Cl_2]$$

The method is limited to L = NH_3 and the yields are very low (<8%). $K[Pt(amine)Cl_3]$ cannot be prepared with the presently published method. We have published a method to produce $K[Pt(py)Cl_3]$ where py = pyridine derivatives (10), but the method cannot be used with amines. We have tried reacting $K[Pt(py)Cl_3]$ with amines in order to obtain *cis*-$[Pt(am)(py)Cl_2]$. But the yields are very low because of the formation of several ionic by-products and decomposed products.

The synthesis of mixed-amine compounds from the cleavage of the iodo dimers is a very important method at the moment, since *cis*-$[Pt(L)(L')I_2]$ can be the starting material for several other mixed-amine complexes. We have synthesized several chloro compounds, *cis*-$[Pt(L)(L')Cl_2]$, eight of which were sent to the National Cancer Institute (U.S.A.) for antitumor testing (11). Carboxylate (especially bidentate) compounds, *cis*-$[Pt(L)(L')(carboxylate)_2]$, have also been synthesized. Carboxylate platinum(II) compounds are less toxic and more soluble than the corresponding chloro analogues. Therefore they seem to be quite promising, since these compounds also have good antitumor activities. We have also synthesized carboxylate dimers by the same method, using a tetracarboxylate salt. These will be discussed below.

Experimental

Microanalyses were done by Galbraith Laboratories Inc., Knoxville. Melting points were measured on a Fisher-Johns apparatus. Infrared spectra were measured in Nujol on a P.E. 621 spectrometer.

K_2PtCl_4 was purchased from Strem Chemicals and Johnson Matthey Inc. and recrystallized from water. Most chemicals were bought from Aldrich. All the platinum complexes were dried at 60°C under vacuum in the presence of P_2O_5.

Synthesis of cis-*[Pt(L)$_2$I$_2$]*

A K_2PtI_4 solution was obtained by mixing K_2PtCl_4 (0.415 g in 5 mL H_2O) and KI (0.67 g in 5 mL H_2O) for 5 min. *cis*-$[Pt(L)_2I_2]$ (L = amine or other nitrogen ligand) was synthesized according to

[1]Revision received April 29, 1986.

Dhara's method (12) from the aqueous reaction of K_2PtI_4 and L. Yield: quantitative. A table of the elemental analysis of a few compounds has been deposited.[2]

Iodo-bridged complexes [Pt(L)I$_2$]$_2$

cis-[Pt(L)$_2$I$_2$] (2 mmol) was mixed with 10 mL of perchloric acid 0.67 *M*. Water (30 mL) was added to the mixture which was left at room temperature overnight. (Ethanol (30 mL) can also be added, instead of water, to the mixture which is left at room temperature for 4–6 h.) When L = pyridine derivative, slight heating to ~50°C is necessary. The reddish or brownish precipitate is filtered off, washed with water or 1:1 mixture of ethanol–water, and dried under vacuum. Yield: 80–90%, except for L = NH_3 (60%).

Compounds with NH_3, methylamine, ethylamine, isopropylamine, *t*-butylamine, dimethylamine, diethylamine, cyclopropylamine, cyclobutylamine, cyclopentylamine, pyridine, and ethanolamine have been synthesized and characterized.[2]

cis-*[Pt(L)(L′)I$_2$]$_2$*

The iodo dimer [Pt(L)I$_2$]$_2$ (1 mmol) was mixed with an excess of L′ (1.5–2.5×) (or 4 mL of 1 *M* ammonium hydroxide for L′ = NH_3) in 25 mL of water. The mixture was left at room temperature for about 6 h or overnight. The colour of the resulting mixture was bright yellow. The precipitate *cis*-[Pt(L)(L′)I$_2$] was filtered, washed with water, and dried under vacuum over P_2O_5. Yield: almost quantitative.[2]

cis-*[Pt(L)(L′)Cl$_2$]*

cis-[Pt(L)(L′)I$_2$] (1 mmol) was stirred with 1.8 mmol of $AgNO_3$ in 20 mL of water for 10 h or overnight in the dark. The AgI precipitate was removed by filtration and 1–2 drops of NaCl (0.5 *M*) was added to the filtrate. If a precipitate (AgCl) appeared immediately it was filtered out after 10 min and again 1 drop of NaCl was added to the filtrate. The procedure was repeated until there was no immediate precipitate after adding one drop of NaCl solution. When all the silver ions have been removed, solid NaCl or in aqueous solution was added to the filtrate. After a few hours, the mixture was evaporated to dryness, washed with a great quantity of cold water to remove $NaNO_3$ and NaCl completely. The pale yellow compounds, *cis*-[Pt(L)(L′)Cl$_2$] were dried under vacuum over P_2O_5. Yield: ~80%.

cis-*[Pt(L)(L′)(carboxylate)$_2$]*

cis-[Pt(L)(L′)I$_2$] (1 mmol) was reacted with $AgNO_3$ exactly as in the above procedure to prepare *cis*-[Pt(L)(L′)Cl$_2$]. When all the silver ions have been removed a slight excess of the sodium salt of the carboxylic acid was added to the filtrate. After 3–4 h, the mixture was evaporated to dryness and washed a few times with a minimum quantity of very cold water, since the product is slightly soluble in water. The white product was dried under vacuum over P_2O_5. Yield: ~80%.

Compounds with 1,1′-cyclobutanedicarboxylate, *trans*-1,2-cyclobutanedicarboxylate, *cis*- and *trans*-1,2-cyclohexanedicarboxylate were characterized.

[(L)(L′)Pt(tetracarboxylate)Pt(L)(L′)]

cis-[Pt(L)(L′)I$_2$] (1 mmol) was treated with $AgNO_3$ exactly as in the procedure to prepare *cis*-[Pt(L)(L′)Cl$_2$]. After the complete removal of the silver ions, slightly more than 0.5 mmol of the tetracarboxylate sodium salt was added to the clear filtrate. After 3–4 h, the mixture was evaporated to dryness and washed with cold water. The white product was dried under vacuum over P_2O_5. Yield: ~80%.

Compounds with 1,2,4,5-benzenetetracarboxylate and 1,1′,3,3′-cyclobutanetetracarboxylate were characterized.[2]

Results and discussion

The general method which we have developed to synthesize *cis* mixed-amine platinum(II) compounds is shown below.

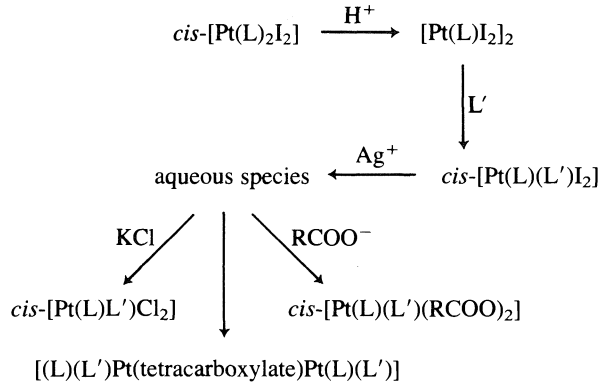

The complexes *cis*-[Pt(L)$_2$I$_2$], where L = amine, were first prepared according to Dhara's method (12) who synthesized *cis*-[Pt(NH_3)$_2$I$_2$] from the reaction of K_2PtI_4 and NH_3 in water. Since *cis*-[Pt(L)$_2$I$_2$] is completely insoluble in water, it will precipitate immediately, preventing the formation of by-products. The yields are quantitative.

Iodo-bridged dimers were then synthesized from the reaction of *cis*-[Pt(L)$_2$I$_2$] with perchloric acid. In these conditions, one amine is protonated. The formation of aquo species is limited because of the strength of the Pt—I bonds and the equilibrium is shifted towards the formation of the iodo-bridged compound since the dimer is insoluble in the reaction medium.

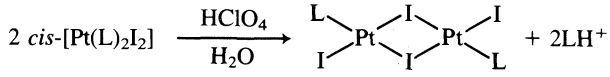

Other acids can be used, but for most amines, perchloric acid was found preferable. The dimerisation reaction was done for most amines, at room temperature in aqueous media, overnight. For some ligands like isopropylamine, the reaction is slower, and it can be accelerated by the addition of ethanol. For the pyridine derivatives, heating at ~50°C is necessary to obtain good yields. The formation of the dimer can be seen by the appearance of a reddish or brownish precipitate, which can then be removed by filtration and washed with water or ethanol. The yields are almost quantitative except for L = NH_3 (60%). Compounds with NH_3, with primary, secondary, and tertiary amines, with pyridine and with 2-aminoethanol were synthesized.[2]

Results of the chemical analyses carried out on some of the compounds have shown the composition [Pt(L)I$_2$]$_2$.[2] The infrared spectra were measured between 4000 and 200 cm^{-1} and confirmed the presence of coordinated amines. The stretching ν(Pt—I) vibrations absorb below 200 cm^{-1} and were not observed as expected. Thus, the configuration of the dimer could not be determined although platinum(II) dimers are very often centrosymmetric. The *trans* configuration is therefore expected as in the chloro-bridged dimer [Pt(2,6-lutidine)Cl$_2$]$_2$ (7). We have tried to prepare adequate crystals for X-ray diffraction, in order to determine the crystal structure of one of the iodo-bridged dimers but have not been successful as yet.

The iodo-bridged dimers can be cleaved with a second nitrogen ligand (L′) in aqueous media to give bright yellow *cis*-[Pt(L)(L′)I$_2$]. Under theses conditions, no isomerisation occurs, since *cis*-[Pt(L)(L′)I$_2$] is very insoluble in water.

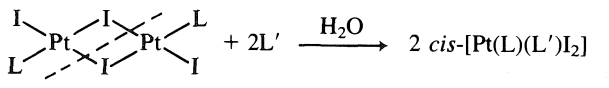

[2]Lists of the results of the elemental analysis, the decomposition points, and the main infrared bands of all the different types of platinum(II) complexes may be purchased from the Depository of Unpublished Data, CISTI, National Research Council of Canada, Ottawa, Ont., Canada K1A 0S2.

Since only *cis*-[Pt(L)(L′)I_2] is obtained from the bridge splitting of the dimer, we can come to the conclusion that the dimer was the *trans* isomer, since the cleavage of a *cis* isomer would produce a mixture of isomers [Pt(L)(L′)I_2]. The cleaved Pt—I bonds are those in *trans* position to the iodide ligands, as predicted by the *trans* effect ($I^- > RNH_2$).

The yield of the reaction is almost quantitative. This reaction cannot be done in organic solvents, since *cis*-[Pt(L)(L′)I_2] may dissolve and isomerise to produce the *trans* compounds, as already observed for the complexes *cis*-[Pt(L)$_2X_2$] (13–17). The results of the chemical analyses on a few iodo compounds have confirmed the expected composition. The ir spectra were measured but again do not give much information on the structure of the compounds.

When synthesizing compounds of the type *cis*-[Pt(amine)-(NH_3)I_2], it is preferable to start with the amine (L = amine, L′ = NH_3) since the NH_3 dimer is slightly more difficult to obtain and the yield is lower.

The synthesis of mixed-amine compounds *cis*-[Pt(L)(L′)I_2] is important especially in relation to the synthesis of potential new platinum anti-cancer drugs. Compounds with almost any combination of nitrogen ligands can now be synthesized and tested systematically for antitumor acivity. These iodo compounds can be converted to the more active chloro or carboxylato complexes by the following reactions:

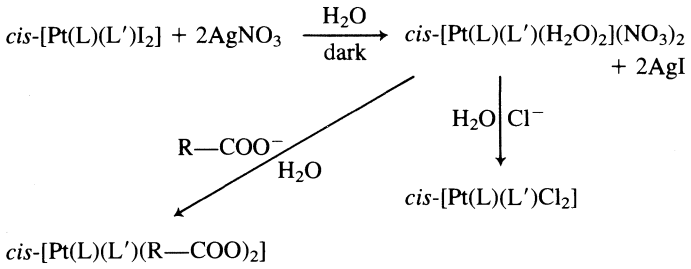

This is a modification of Dhara's method to synthesize *cis*-[Pt(NH_3)$_2Cl_2$] from *cis*-[Pt(NH_3)$_2I_2$] (12). The iodide ions are removed by precipitating with a silver salt in the dark. A slight excess of the platinum compound is used in order to prevent an excess of silver ions. The latter has to be completely removed before the precipitation of the platinum complex. After the complete removal of the silver ions, the sodium salt of the carboxylic acid or NaCl is added to the filtrate to precipitate the appropriate complex. The results of the chemical analysis done on the synthesized compounds have confirmed the expected composition.[2]

Dimeric species were also prepared with tetracarboxylate ligands by adding the sodium salt of the ligand to the aqueous species as follows:

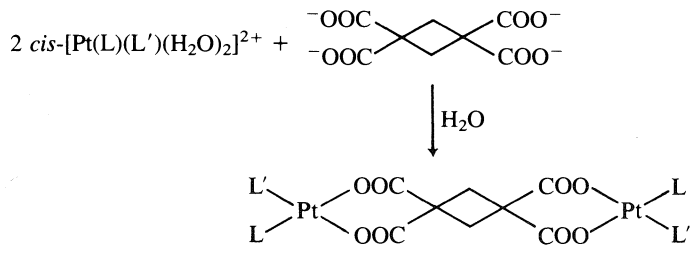

Compounds with 1,1′,3,3′-cyclobutanetetracarboxylate, *cis,cis,cis,cis*-1,2,3,4-cyclopentanetetracarboxylate and 1,2,4,5-benzenetetracarboxylate were prepared.

Usually, infrared spectroscopy is a good method to identify the configuration of the dichloro platinum(II) compounds. Both symmetric and asymmetric ν(Pt—Cl) are active in ir for the *cis* compound, while only the asymmetric mode of the *trans* compound is active in ir. But sometimes there is coincidence of the two bands in the Pt—Cl stretch region for the *cis* isomer. For example, *cis*-[Pt(cyclobutylamine)$_2Cl_2$] showed one ν(Pt—Cl) at 311 cm^{-1}, while the *trans* isomer showed also one band but at slightly higher wave number (333 cm^{-1}). These assignments were confirmed by structure determination of the two compounds (14). These authors suggested that for this type of compounds, band position is more important for determining the configuration of the compound than the number of bands.

For the mixed amines compounds, we have observed that depending on the ligands, some compounds show two bands while others show only one large band. For example, *cis*-[Pt(cyclopropylamine)(NH_3)Cl_2] and *cis*-[Pt(cyclopropylamine)(CH_3NH_2)Cl_2] showed two ν(Pt—Cl) bands at 327, 316 and 312, 308 cm^{-1}, respectively, while *cis*-[Pt(L)(NH_3)Cl_3] where L = isopropylamine (310 cm^{-1}), cyclobutylamine (320 cm^{-1}), and cyclopentylamine (318 cm^{-1}) showed only one ν(Pt—Cl) band. More than one ν(Pt—Cl) was also observed for *cis*-[Pt(cyclopropylamine)$_2Cl_2$] (18). Therefore infrared spectroscopy should be used with great care when determining the configuration of the dichloroplatinum(II) compounds. The configuration of *cis*-[Pt(cyclobutylamine)(NH_3)Cl_2] and *cis*-[Pt(cyclopentylamine)(NH_3)Cl_2] were confirmed by crystal structure determinations (19, 20).

Acknowledgments

The authors are grateful to the Natural Sciences and Engineering Research Council of Canada and to the Ministère de l'Education (FCAR) for financial support.

1. J. Chatt. J. Chem. Soc. 652 (1951).
2. P. C. Kong and F. D. Rochon. Inorg. Chim. Acta, **37**, L457 (1979).
3. J. Chatt and L. M. Venanzi. J. Chem. Soc. 2787 (1955).
4. P. Courtot, A. Peron, R. Rumin, J. C. Chottard, and D. Mansuy. J. Organomet. Chem. **99**, C59 (1975).
5. P. Courtot, R. Rumin, and A. Peron. J. Organomet. Chem. **144**, 357 (1978).
6. P. C. Kong and F. D. Rochon. Can. J. Chem. **57**, 682 (1979).
7. F. D. Rochon and R. Melanson. Acta Crystallogr. B**37**, 690 (1981).
8. P. D. Braddock, T. A. Connors, M. Jones, A. R. Khokhar, D. H. Melzack, and M. L. Tobe. Chem. Biol. Interact. **11**, 145 (1975).
9. P. C. Hydes. U.S. Patent No 4,329,299 (1982).
10. P. C. Kong and F. D. Rochon. Can. J. Chem. **56**, 441 (1978).
11. F. D. Rochon and P. C. Kong. J. Clin. Hem. Onc. To be published.
12. S. C. Dhara. Indian J. Chem. **8**, 193 (1970).
13. P. C. Kong and F. D. Rochon. Inorg. Chim. Acta, **83**, 65 (1984).
14. C. J. L. Lock and M. Zvagulis. Inorg. Chem. **20**, 1817 (1981).
15. P. C. Kong and F. D. Rochon. Can. J. Chem. **57**, 526 (1979).
16. C. J. L. Lock and M. Zvagulis. Acta Crystallogr. B**36**, 2140 (1980).
17. P. C. Kong and F. D. Rochon. Inorg. Chim. Acta, **61**, 269 (1982).
18. H. E. Howard-Lock, C. J. L. Lock, G. Turner, and M. Zvagulis. Can. J. Chem. **59**, 2737 (1981).
19. F. D. Rochon and R. Melanson. Acta Crystallogr. In press.
20. F. D. Rochon, C. Dion, and A. L. Beauchamp. Acta Crystallogr. To be published.

Reactions of *cis*-[Pt(sulfoxide)$_2$Cl$_2$] with silver salts and synthesis of hydroxo-bridged platinum(II) complexes with sulfoxides

FERNANDE D. ROCHON, PI-CHANG KONG, AND LOUISE GIRARD

Département de chimie, Université du Québec à Montréal, C.P. 8888, succ. A, Montréal (Qué.), Canada H3C 3P8

Received August 8, 1985[1]

FERNANDE D. ROCHON, PI-CHANG KONG, and LOUISE GIRARD. Can. J. Chem. **64**, 1897 (1986).

Platinum(II) compounds of the type *cis*-[Pt(L)$_2$X$_2$] where L = tetramethylenesulfoxide (TMSO), ethylmethylsulfoxide (EMSO), di-*n*-propylsulfoxide (DPSO), benzylmethylsulfoxide (BMSO), and dibenzylsulfoxide (DBSO) and X = Cl^- and I^- have been synthesized. The reactions of these compounds with a silver salt were studied in aqueous solution. Monomers of the type *cis*-[Pt(L)$_2$(ClO$_4$)$_2$] (L = TMSO, EMSO, and DBSO), *cis*-[Pt(EMSO)$_2$(SO$_4$)] and hydroxy-bridged oligomers were isolated. Dimers, *cis*-[Pt(L)$_2$(OH)]$_2$(NO$_3$)$_2$ (L = TMSO, DPSO), and *cis*-[Pt(EMSO)$_2$(OH)]$_2$SO$_4$ and possibly a trimer (*cis*-[Pt(EMSO)$_2$(OH)]$_3$)$_2$(SO$_4$)$_3$ were characterized. The compounds were studied by infrared spectroscopy and by ^{1}H nmr.

FERNANDE D. ROCHON, PI-CHANG KONG et LOUISE GIRARD. Can. J. Chem. **64**, 1897 (1986).

Des complexes de platine(II), *cis*-[Pt(L)$_2$X$_2$] où L = tétraméthylènesulfoxyde (TMSO), éthylméthylsulfoxyde (EMSO), di-*n*-propylsulfoxyde (DPSO), benzylméthylsulfoxyde (BMSO) et dibenzylsulfoxyde (DBSO) et X = Cl^- et I^- ont été synthétisés. La réaction de ces composés avec un sel d'argent a été étudiée en solution aqueuse. Des monomères de types *cis*-[Pt(L)$_2$(ClO$_4$)$_2$] (L = TMSO, EMSO et DBSO), *cis*-[Pt(EMSO)$_2$(SO$_4$)] ainsi que des oligomères à ponts hydroxo ont été isolés. Les dimères *cis*-[Pt(L)$_2$(OH)]$_2$(NO$_3$)$_2$ (L = TMSO, DPSO) et *cis*-[Pt(EMSO)$_2$(OH)]$_2$SO$_4$ et possiblement un trimère (*cis*-[Pt(EMSO)$_2$(OH)]$_3$)$_2$(SO$_4$)$_3$ ont été caractérisés. Les complexes ont été étudiés par spectroscopie infrarouge et par rmn protonique.

Introduction

Sulfoxide ligands have two potential donor sites but the preference of Pt(II) for the sulfur donor site is well known and all reported neutral complexes are exclusively sulfur bonded in the solid state (1). Platinum, being a soft metal, does not form strong bonds with oxygen unless it is deprotonated or partly ionized as in DMF.

When K_2PtCl_4 reacts with a sulfoxide ligand (L), *trans*-[Pt(L)$_2$Cl$_2$] is probably first formed and is eventually isomerized to the *cis* configuration (2). There are three factors affecting the formation and the stability of the two isomers. First, the *trans* effect of sulfoxide ligands is fairly large. Therefore the *trans* isomer should be first formed. The second factor is the enhanced $(d-d)\pi$ bonding which is more effective in the *cis* geometry (1) and finally the steric hindrance between two large ligands in *cis* position. In the Pd(II) complexes, the enhanced $(d-d)\pi$ bonding in the *cis* geometry is probably not sufficient to overcome the interligand repulsions which are larger in the *cis* configuration, and all the compounds have the *trans* structure. In the corresponding Pt(II) complexes $(d-d)\pi$ bonding is apparently more effective and *cis* structures are obtained for all the complexes except with a very sterically demanding ligand like diisoamylsulfoxide (1).

The synthesis of *cis*-[Pt(L)$_2$Cl$_2$] where L = tetramethylenesulfoxide (TMSO), di-*n*-propylsulfoxide (DPSO), benzylmethylsulfoxide (BMSO), and dibenzylsulfoxide (DBSO) has been reported (1, 3). But we have found that the published method does not produce isomerically pure compounds especially for bulky groups like DPSO, BMSO, and DBSO. For example, the aqueous reaction between K_2PtCl_4 with DPSO will produce in the first 10 min yellow insoluble *trans*-[Pt(DPSO)$_2$Cl$_2$] which has to be filtered out in order to obtain isomerically pure, very pale yellow coloured *cis*-[Pt(DPSO)$_2$Cl$_2$]. The formation of *trans*-[Pt(DPSO)$_2$Cl$_2$] in the few first minutes has already been observed (2). We have therefore modified the published methods in order to obtain pure *cis*-[Pt(L)$_2$Cl$_2$]. *Cis* and *trans*-compounds can be identified by their stretching Pt—Cl vibrations. Since some of the ligands (L) absorb in this region the corresponding iodo compounds were synthesized to confirm the ν(Pt—Cl) assignments. Compounds with ethylmethylsulfoxide (EMSO) were also synthesized since *cis*-[Pt(EMSO)$_2$Cl$_2$] has not yet been reported.

These compounds were well characterized since they were the starting material for a study of their reactions with a silver salt to prepare oligomeric species. Dimeric species of DMSO has been recently synthesized (4). The crystal structure of a hydroxo-bridged platinum compounds [(DMSO)$_2$Pt(OH)$_2$Pt(DMSO)$_2$](ClO$_4$)$_2$, isolated from an aqueous solution of *cis*-[Pt(DMSO)$_4$](ClO$_4$)$_2$ (two O-bonded and two S-bonded DMSO (1)) was recently reported (4). However, this method was found to be inadequate for the synthesis of dimers with other sulfoxides. We have developed a new method involving the precipitation of the chloride ligands of *cis*-[Pt(L)$_2$Cl$_2$] with a silver salt. The method is similar to the one used to prepare amine hydroxo-bridged oligomers (5, 6). Usually, sulfoxide and amine platinum complexes behave quite differently. But we found that in this case, reactions were very similar. This study of the reactions of *cis*-[Pt(L)$_2$X$_2$] (X = Cl^- or I^-) with several silver salts is described below.

Experimental

Elemental analyses were done by Galbraith Inc. The infrared spectra were measured as Nujol mulls on a P.E. 621 spectrometer. A 60 MHz Varian EM 360C was used to record the ^{1}H nmr spectra. The reactions with silver salts were done in the dark. Special care was taken with silver perchlorate, since it is explosive when mixed with combustible material. However, it was not considered a potential hazard when used in the following experiments.

cis-*[Pt(EMSO)$_2$Cl$_2$]*

An aqueous solution (volume 15 mL) containing 3 mmol of purified K_2PtCl_4 and 9 mmol EMSO was stirred overnight. The white precipitate was filtered, washed with water, ethanol, and ether, and then dried. The yield can be increased by concentrating the filtrate to 10 mL and letting the solution stand at room temperature. After a few days, the crystals were filtered, washed with water, ethanol, ether, and then dried. Total yield: 67%, mp 126°C. *Anal.* calcd.: C 16.00, H 3.58; found: C 16.26, H 3.83.

[1]Revision received May 6, 1986.

cis-*[Pt(DPSO)$_2$Cl$_2$]*

A 40 mL aqueous solution containing 2 mmol of K_2PtCl_4 and 4.4 mmol DPSO was stirred for 15 min. The mixture was filtered and the filtrate was stirred overnight at room temperature. The very pale yellow precipitate was filtered, washed with hot water, ethanol, and ether, and then dried. Yield: 70%, mp 105°C. *Anal.* calcd.: C 26.97, H 5.28; found: C 27.07, H 5.25.

cis-*[Pt(TMSO)$_2$Cl$_2$]*

An aqueous solution (15 mL) containing 3 mmol of purified K_2PtCl_4 and 6.6 mmol TMSO was stirred at room temperature for 18 h. The white precipitate was filtered, washed with a great quantity of hot water, and dried. Yield: 90%, mp 194°C. *Anal.* calcd.: C 20.26, H 3.40; found: C 20.33, H 3.39.

cis-*[Pt(BMSO)$_2$Cl$_2$]*

Method 1: BMSO (6 mmol, finely powdered) were added to an aqueous solution containing 3 mmol of K_2PtCl_4. The mixture was stirred at room temperature for 48 h and then filtered. The precipitate was washed with hot water, ethanol, and ether, and then dried. The yellow compound was dissolved in DMF and stirred for 3–4 days. The DMF was then evaporated, and the residue dissolved in acetone. Ether was added to the solution and the pale yellow precipitate filtered and dried. Yield: 67%, mp 140°C (lit. (3) 141–143°C). *Anal.* calcd.: C 33.45, H 3.51; found: C 33.41, H 3.58.

Method 2: BMSO (6 mmol) and K_2PtCl_4 (3 mmol) were dissolved in 40 mL of DMF. The mixture was stirred for 3 days and heated at 70°C for 5 h each day. The DMF was evaporated at reduced pressure at 40°C. The product was washed with ether, ethanol, and water, and then dried. Yield: 60%.

cis-*[Pt(DBSO)$_2$Cl$_2$]*

This compound was prepared by the methods described for *cis*-[Pt(BMSO)$_2$Cl$_2$]. Yield: 70% (method 1), mp 141°C (lit. (3) 142°C). *Anal.* calcd.: C 46.28, H 3.88, Cl 9.76; found: C 45.92, H 3.86, Cl 10.09.

cis-*[Pt(L)$_2$I$_2$] L = TMSO, EMSO, DBSO*

KI (4 mmol) was added to 1 mmol of K_2PtCl_4 dissolved in 15 mL H_2O. After stirring for 4 min, 2 mmol of L were added and the mixture was stirred in the dark for 24 h. The compound was filtered, washed with hot water, ethanol, ether, and then dried. Yield: ~80%. *Anal.* calcd. for *cis*-[Pt(EMSO)$_2$I$_2$]: C 11.38, H 2.55; found: C 11.26, H 2.64.

cis-*[Pt(EMSO)$_2$(ClO$_4$)$_2$]·2H$_2$O*

cis-[Pt(EMSO)$_2$Cl$_2$] (1.325 mmol) and $AgClO_4$ (2.650 mmol) were mixed together in 15 mL H_2O. After 24 h of stirring, AgCl was filtered out. The pH of the filtrate which was about 1.5 was raised to 6.5 with NaOH. The solution was concentrated avoiding precipitation of the products. The solution was then passed through "Sephadex G-25" in order to eliminate $NaClO_4$. The solution was then evaporated to dryness and the product dissolved in acetone. Ether was then added to precipitate the compound which was filtered and dried to yield a white hygroscopic compound. Yield: 30%, mp 160°C. *Anal.* calcd.: C 11.73, H 3.26, S 10.42; found: C 11.56, H 2.92, S 9.93.

cis-*[Pt(TMSO)$_2$(ClO$_4$)$_2$]·H$_2$O*

cis-[Pt(TMSO)$_2$Cl$_2$] (0.752 mmol) and $AgClO_4$ (1.504 mmol) were stirred together in water for 24 h and then filtered to remove AgCl. The filtrate was neutralized with KOH and evaporated to dryness. The residue was dissolved in acetone and filtered to remove $KClO_4$. The acetone filtrate was evaporated to dryness, washed with ether, and dried. A pale yellow hygroscopic compound was obtained. Yield: 30%, mp 100°C. *Anal.* calcd.: C 15.05, H 3.13, S 10.03; found: C 15.46, H 2.77, S 9.97.

cis-*[Pt(BMSO)$_2$(ClO$_4$)$_2$]*

cis-[Pt(BMSO)$_2$I$_2$] (0.263 mmol) and $AgClO_4$ (0.526 mmol) were mixed together in a H_2O–ethanol mixture. After stirring for 4 days, ethanol was evaporated and AgI filtered out. The filtrate was concentrated and refrigerated. The white precipitate was filtered, washed with very cold water, and dried. Yield: 30%, mp 135–140°C. *Anal.* calcd.: C 27.35, H 2.85, S 9.12; found: C 27.62, H 2.89, S 8.76.

cis-*[Pt(EMSO)$_2$SO$_4$]*

cis-[Pt(EMSO)$_2$Cl$_2$] (1.870 mmol) and Ag_2SO_4 (1.870 mmol) were mixed together in 15 mL H_2O. The mixture was stirred overnight and filtered to remove AgCl. Ethanol (5 mL) was added to the filtrate which was then evaporated to dryness. The white product was washed with ethanol, ether, and dried. Yield: 90%, mp 125°C.

cis-*[(TMSO)$_2$Pt(OH)$_2$Pt(TMSO)$_2$](NO$_3$)$_2$*

cis-[Pt(TMSO)$_2$Cl$_2$] (3 mmol) was suspended in 20 mL of water. Slightly less than 6 mmol of $AgNO_3$ dissolved in water were added to the above suspension and the mixture was stirred in the dark for 24 h. The precipitate (AgCl) was filtered and the excess $AgNO_3$ (if present) was precipitated with 0.5 *M* NaCl. The pH of the filtrate (about 1.5) was increased to 6.5 with a 1 *M* NaOH. The solution was maintained at 40°C for a few days until crystallization occurred. Very pale yellow crystals were obtained upon filtration. Yield: 30%, mp 170°C. *Anal.* calcd.: C 19.92, H 3.55, O 19.90, N 2.90; found: C 19.87, H 3.72, O 19.25, N 2.58.

cis-*[(DPSO)$_2$Pt(OH)$_2$Pt(DPSO)$_2$](NO$_3$)$_2$*

The above method was used. The mixture was stirred in the dark for 48 h (instead of 24 h). Yield: 83%, mp 145°C. *Anal.* calcd.: C 26.56, H 5.39, O 17.69; found: C 26.24, H 5.17, O 17.29.

cis-*[(EMSO)$_2$Pt(OH)$_2$Pt(EMSO)$_2$]SO$_4$ and* (cis-*[Pt(EMSO)$_2$(OH)]$_3$)$_2$-(SO$_4$)$_3$*

cis-[Pt(EMSO)$_2$Cl$_2$] (4 mmol) was mixed with slightly less than 4 mmol of Ag_2SO_4 in 15 mL H_2O. The mixture was stirred for 24 h and the AgCl formed was then filtered. The pH of the solution (1.4) was raised to 6.5 with $Ba(OH)_2$. The mixture was stirred at room temperature overnight. (Heating at 40°C overnight will increase the proportion of the trimer.) The precipitate ($BaSO_4$) was then filtered and the filtrate evaporated to dryness under vacuum at 40°C. About 5–10 mL of absolute ethanol were added to the dry product to dissolve the yellow trimer. The white dimer, insoluble in ethanol, was filtered and dried. Yield: 33%, mp 115°C.

The ethanol filtrate was evaporated to dryness. Ether was added to the product which was filtered and dried. The yellow compound is believed to be a trimer. Yield: 32%, mp 195°C (dec.).

The yield of the dimer can be increase by reducing the heating to a minimum throughout the preparation procedure while the yield of the trimer can be increased by heating the aqueous mixture for several hours at 40°C. *Anal.* calcd. for [(EMSO)$_2$Pt(OH)$_2$Pt(EMSO)$_2$]SO$_4$: C 16.22, H 3.85, O 18.00; found: C 15.48, H 4.17, O 17.39. *Anal.* calcd. for ([Pt(EMSO)$_2$OH]$_3$)$_2$(SO$_4$)$_3$: C 16.22, H 3.85, S 18.04; found: C 15.70, H 3.74, S 18.84.

Results and discussion

Complexes cis-*[Pt(L)$_2$X$_2$]*

Five complexes of this type were synthesized. Four of these compounds (L = TMSO, DPSO (1), BMSO, and DBSO (3)) have been reported as yellow crystals. We have modified the method used by these authors and we have isolated pure *cis* compounds which are white or very pale yellow in colour. The yellow compounds are believed to be the *trans* complexes which are formed at the beginning of the reaction. If the *trans* compounds stay in solution, they will isomerize to give the thermodynamically more stable *cis* species. If they precipitate, a mixture of *cis* and *trans* compounds will be obtained. To obtain pure *cis*-compounds, the reaction can be done in a solvent like DMF (BMSO and DBSO) or the first formed *trans* compounds can be filtered out. We were able to isolate pure *trans*-[Pt(BMSO)$_2$Cl$_2$] which is yellow. The infrared spectrum showed one ν(Pt—Cl) at 349 cm^{-1}. All *cis* compounds showed two ν(Pt—Cl) vibrations (Table 1).

All *cis*-[Pt(L)$_2$Cl$_2$] compounds showed a ν(S—O) vibration

TABLE 1. Main infrared bands of the $[Pt(L)_2X_2]$ complexes (cm^{-1})

Compound	ν(S—O)	ν(Pt—Cl)	Other bands (500–300 cm^{-1})
TMSO	1020s		326m
cis-$[Pt(TMSO)_2Cl_2]$	1150s, 1134s, 1119s	336s, 320s	515m, 368s, 335sh
cis-$[Pt(TMSO)_2I_2]$	1135s, 1125s		368m
EMSO	1048s, 1015s		395w, 372w, 347w, 310w
cis-$[Pt(EMSO)_2Cl_2]$	1140s, 1121s	339s, 317s	439s, 418s
DPSO	1010s		450w, 395w
cis-$[Pt(DPSO)_2Cl_2]$	1120s	349m, 324m	510s, 456m, 440s
BMSO	1038s		464m, 394m, 335m
cis-$[Pt(BMSO)_2Cl_2]$	1116s	331s, 311m	477s, 440s, 381m, 364m
cis-$[Pt(BMSO)_2I_2]$	1115s		478s, 419m, 388m
trans-$[Pt(BMSO)_2Cl_2]$	1110s	349s	480s, 430s, 383m, 370w
DBSO	1015s		460s, 366m, 327m
cis-$[Pt(DBSO)_2Cl_2]$	1125s	328m, 311m	480s, 476s, 419m, 411m, 394w
cis-$[Pt(DBSO)_2I_2]$	1100s		476s, 410m, 405m, 353w

at a frequency higher than that in the free ligand, confirming that the binding site is the sulfur atom (3) (Table 1). The infrared spectra of the iodo compounds confirmed the ν(Pt—Cl) assignments since some of the ligands absorb in that region.

A crystal structure determination of *cis*-$[Pt(TMSO)_2Cl_2]$ (7) and *cis*-$[Pt(DPSO)_2Cl_2]$ (8) confirmed the configuration of the complexes and the binding site of the ligands.

Reactions of cis-*[Pt(L)$_2$Cl$_2$] with AgClO$_4$*

Rochon, Kong, and Melanson (4) have synthesized a DMSO dimer by the following method:

$$cis\text{-}[Pt(DMSO)_2Cl_2] + 2AgClO_4 \xrightarrow{DMSO} cis\text{-}[Pt(DMSO)_4](ClO_4)_2 + 2AgCl\downarrow$$
$$\xrightarrow{H_2O\downarrow} [(DMSO)_2Pt(OH)_2Pt(DMSO)_2](ClO_4)_2$$

DMSO was used as solvent and as ligand. We have tried this method with other sulfoxides (L) using DMF as solvent. But we have found the method inadequate. We have then tried the reaction in aqueous medium. Compounds of the type $[Pt(L)_2(ClO_4)_2]$ were isolated (L = EMSO, TMSO, and BMSO).

$$cis\text{-}[Pt(L)_2Cl_2] + 2AgClO_4 \xrightarrow{H_2O} cis\text{-}[Pt(L)_2(ClO_4)_2] + 2AgCl\downarrow$$

The results of the elemental analyses showed that some of the compounds were hydrated even after drying under vacuum (see Experimental section). The coordination of the perchlorate ion to the platinum atom in the solid state can be determined by infrared spectroscopy. Group theory predicts one large band ν_3(Cl—O) in the region 1150–1030 cm^{-1} for ionic ClO_4^- (T_d) and two bands for coordinated monodentate ClO_4^- (C_{3v}) (9). *cis*-$[Pt(DMSO)_2(OH)]_2(ClO_4)_2$ showed one ν_3 at 1076 cm^{-1} while $[Pt(BMSO)_2(ClO_4)_2]$ showed two bands at 1130 and 1094 cm^{-1}. The infrared spectra of $[Pt(TMSO)_2(ClO_4)_2].2H_2O$ and $[Pt(EMSO)_2(ClO_4)_2].H_2O$ showed the presence of water.

Conductivity measurements of *cis*-$[Pt(EMSO)_2(ClO_4)_2].2H_2O$ showed that the compound is hydrolyzed in aqueous solution. The value found immediately after dissolving the compound in water was 182 and 229 Ω^{-1} cm^2 mol^{-1} after 24 h, indicating the presence of close to three ions (10). The different hydrolysed species could be *cis*-$[Pt(EMSO)_2(H_2O)_2](ClO_4)_2$, *cis*-$[Pt(EMSO)_2(H_2O)(OH)](ClO_4)$, and possibly some dimeric species *cis*-$[Pt(EMSO)_2(OH)]_2(ClO_4)_2$. Perchlorate in aqueous solution does not coordinate to platinum as shown by ^{195}Pt nmr (11).

Attempts to isolate oligomeric species by neutralizing the resulting aqueous solution of *cis*-$[Pt(L)_2(ClO_4)_2]$ were not successful.

Reactions with AgNO$_3$

The reactions between *cis*-$[Pt(L)_2Cl_2]$, (where L = TMSO and DPSO) and $AgNO_3$ produced dimeric species $[Pt(L)_2(OH)]_2(NO_3)_2$. Nitrate dimers seem easier to crystallize than perchlorate dimers. The synthetic method is shown in Fig. 1. The reaction is slower for L = DPSO but the yield is higher (80% and 35% for L = TMSO).

The quantity of $AgNO_3$ is critical since an excess will decompose the complexes. The mixture of *cis*-$[Pt(L)_2Cl_2]$ and $AgNO_3$ in water is stirred for 24 h (48 h for DPSO) in the dark before filtering the AgCl. The pH is then about 1.5. NaOH (1 *M*) is added until the pH is 6.5 to increase the proportion of monoaquo–monohydroxo species in order to favor dimerisation. The solution is kept at 40°C for 3–4 days and crystallization occurs. The method of separation is based on solubility differences of the species in solution. The dimer crystallizes first, but it is quite soluble in water. The dimer containing DPSO is less soluble and is therefore easier to separate than the TMSO analogue. A series of forced crystallizations can increase the yield of the TMSO dimer. During this process, a very pale yellow compound is first obtained. Later, a darker compound believed to be a trimer can be isolated. The crystal structure analysis of *cis*-$[Pt(TMSO)_2OH]_2(NO_3)_2$ has confirmed the structure (12). The cation contains a centre of symmetry.

The molar conductivities were measured in aqueous solutions. The results showed the presence of three ionic species. The experimental values were 238 Ω^{-1} cm^2 for *cis*-$[Pt(TMSO)_2OH]_2(NO_3)_2$ and 236 Ω^{-1} cm^2 for *cis*-$[Pt(DPSO)_2OH]_2(NO_3)_2$.

The nitrate salt of the EMSO dimer could not be isolated. This compound is very soluble and could not be separated from $NaNO_3$ produced upon neutralisation with NaOH.

The reactions of *cis*-$[Pt(BMSO)_2Cl_2]$ and *cis*-$[Pt(DBSO)_2Cl_2]$ with $AgNO_3$ are very different probably for steric reasons. The reaction is very slow ($\approx$1 week) and must be initiated by heating. The product of the reaction is also different from the expected dimer. About half of the sulfoxide molecules were found free after the reaction. The pH of the solution after the reaction was acidic indicating the presence of deprotonated hydroxo species. The product is very soluble in acidic media but precipitates when the solution is neutralized. Therefore the complex is probably ionic in acidic media but neutral at pH > 7. The preliminary results seem to suggest the following reactions:

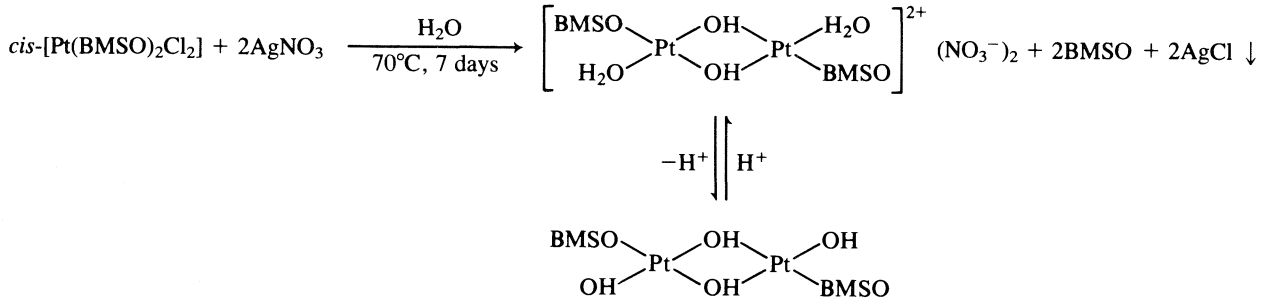

The infrared spectrum of the neutral compound showed the presence of O—H vibrations but no ionic or coordinated NO_3^-.

Several attempts to synthesize dimers *cis*-$[Pt(BMSO)_2(OH)]_2^{2+}$ were not successful. The close proximity of two very bulky sulfoxide ligands which contain phenyl groups situated above and below the platinum plane, might prevent the expected dimerisation. The platinum atom will prefer to lose a sulfoxide ligand to reduce the steric hindrance and dimerisation can then occur. The complex *cis*-$[Pt(DBSO)_2Cl_2]$, which is even more bulky, will react similarly with $AgNO_3$, but slower.

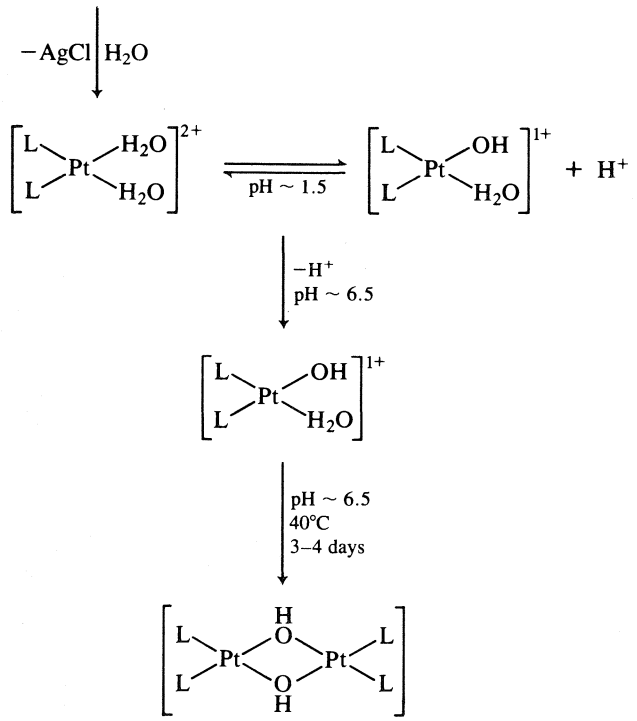

FIG. 1. Synthetic method for hydroxy-bridged dimers.

Reactions with Ag_2SO_4

The method developed to synthesize the EMSO dimer involve the following reactions:

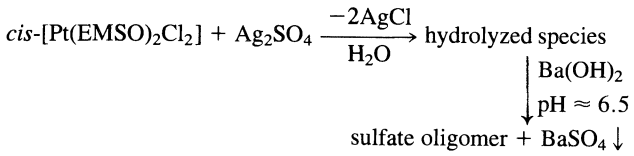

The complex *cis*-$[Pt(EMSO)_2Cl_2]$ reacts in water with Ag_2SO_4. After 24 h, AgCl is filtered out. The pH of the solution is 1.4 and is raised to 6.5 with $Ba(OH)_2$. The next day, the barium sulfate is filtered out. The filtrate contains the hydroxo dimer and probably some trimeric species. If it is desired to increase the proportion of the trimer, the mixture can be heated at 40°C for several hours before filtering the $BaSO_4$. The dimer and the trimer can be separated with ethanol. The white dimer is insoluble in ethanol while the trimer is soluble. After evaporating the ethanol, the trimer can be recovered with ether. This complex is dark yellow. The dimer can be obtained pure, while the trimer is more difficult to purify. Both compounds are very soluble in water and are difficult to recrystallize. The results of the element analyses of the two compounds are shown in the Experimental section. The trimer might contain some higher oligomers.

Conductance measurements do not give any informations on the different oligomeric species for this type of compounds. The molar conductivities depend on the molecular weights which change with the different oligomers.

The dimeric species were confirmed by ^{195}Pt nmr which gave a signal at $\delta = -2887$ ppm which is 259 ppm higher (lower field) than *cis*-$[Pt(EMSO)_2(H_2O)_2]$ as expected. The trimer showed a weak and broad signal at −2906 ppm (13).

^1H nmr and ir spectra

The ^1H nmr spectra of the oligomeric species were measured in D_2O. The results are shown in Table 2. The α protons in the complexes have been shifted to lower field by 0.56 to 0.73 ppm

TABLE 2. ^{1}H nmr of the oligomers (δ(ppm))

Compound	Hα	Hβ	Hγ	Hα′(CH$_3$SO)
TMSO	2.97m	2.22m		
[(TMSO)$_2$Pt(OH)]$_2$(NO$_3$)$_2$	3.65m	2.25m		
Δδ	0.68	0.03		
DPSO	2.88t ^3J = 8 Hz	1.74m	1.02t ^3J = 8 Hz	
[(DPSO)$_2$Pt(OH)]$_2$(NO$_3$)$_2$	3.44m	2.07m	1.15t ^3J = 8 Hz	
Δδ	0.56	0.33	0.13	
EMSO	2.92m	1.30t ^3J = 8 Hz		2.70s
[(EMSO)$_2$Pt(OH)]$_2$SO$_4$	~3.55m	1.47t ^3J = 8 Hz		3.40, 3.42 ^3J(^{195}Pt—H) = 25 Hz
Δδ	~0.6	0.17		0.70, 0.72
([(EMSO)$_2$Pt(OH)]$_3$)$_2$(SO$_4$)$_3$	~3.55m (wide)	1.51 (wide)		3.43, 3.45
Δδ	~0.6	0.21		0.73, 0.75
[Pt(EMSO)$_2$(SO$_4$)]*	~3.6 (wide)	1.55t ^3J = 8 Hz		3.57 ^3J(^{195}Pt—H) = 26 Hz
Δδ	~0.7			

*See text.

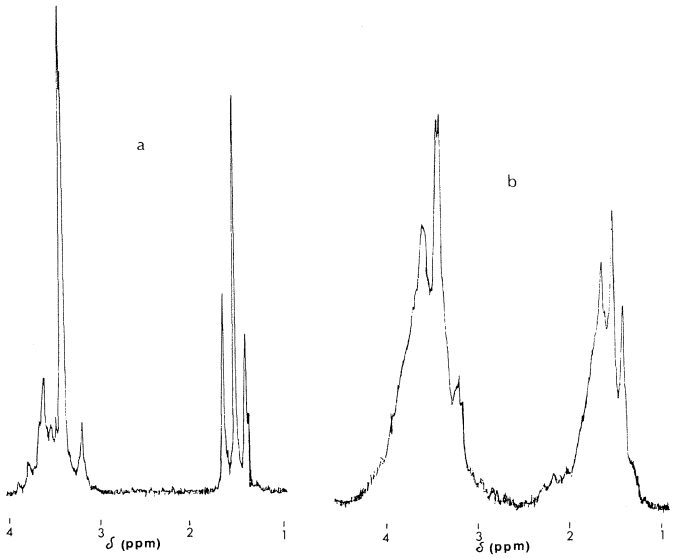

FIG. 2. ^{1}H nmr spectra of (*a*) the dimer [Pt(EMSO)$_2$OH]$_2$SO$_4$ and (*b*) the trimer.

upon complexation. These values show the great influence of Pt on its environment. This influence is still important on the protons in β and even γ (DPSO) positions. The smaller influence of Pt on Hβ of TMSO (Δδ = 0.03 ppm) can be explained by the cyclic nature of the ligand, since the β protons cannot approach the Pt atom as much as those in aliphatic ligands.

The dimer and trimer of EMSO have similar chemical shifts, but the peaks are much broader for the trimer (Fig. 2). The widening of the peaks can be explained by different conformations of the cation which is stereochemically non-rigid in solution as observed for the ammine trimer [(NH$_3$)$_2$Pt(OH)]$_3^{3+}$ (6). The EMSO trimer might contain some small quantities of the dimeric compound.

The EMSO complexes contain chiral sulfur centers, so that diastereoisomers may coexist as oberved for *cis*-[Pt(CH$_3$SOCH$_2$C$_6$H$_5$)$_2$Cl$_2$] (3) which showed, in chloroform solution, two CH$_3$—S resonances separated by 0.14 ppm. There seem to be two very close CH$_3$—S resonances for the EMSO dimer and trimer (Fig. 2). The separation between the two peaks is only 0.02 ppm. Therefore, two forms might coexist in aqueous solution. The ^{195}Pt—H^1 satellites of the CH$_3$—S resonances are well defined in the spectrum of the dimeric compound (Fig. 2*a*). The ^{195}Pt—H^1 coupling constant is 26 Hz and compares well with the values found in *cis*-[Pt(DMSO)$_2$Cl$_2$] (23 Hz), in *cis*-[Pt(CH$_3$SOCH$_2$C$_6$H$_5$)$_2$Cl$_2$] (22.5 Hz), and in [Pt(CH$_3$SOCH(CH$_3$)$_2$)$_2$Cl$_2$] (23 Hz) (3).

The monomeric compound *cis*-[Pt(EMSO)$_2$SO$_4$] also contains two chiral centers with the possibility of the coexistence of *dl* and *meso* forms. But the nmr spectrum of the compound is consistent with the presence of one form, since a single CH$_3$—S resonance was observed. Only one CH$_3$—S resonance was also observed for *cis*-[Pt(CH$_3$SOCH(CH$_3$)$_2$)$_2$Cl$_2$] in chloroform solution (3). The ^{195}Pt nmr spectrum of *cis*-[Pt(EMSO)$_2$SO$_4$] showed that the compound is hydrolysed in aqueous solution (13). The two main species are *cis*-[Pt(EMSO)$_2$(SO$_4$)(H$_2$O)] and *cis*-[Pt(EMSO)$_2$(H$_2$O)$_2$]$^{2+}$. A small quantity of the dimeric compound was also observed.

Infrared spectroscopy is an important method to identify the different synthesized species. Monomers are characterized in the solid state by coordinated NO_3^- or SO_4^{2-}, while these are ionic in oligomers. Ionic NO_3^- (D_{3h}) has four vibrational modes, three are ir active, two of which are more intense (9). These were observed at 1360 and ≈825 cm^{-1} (Table 3) for the TMSO and DPSO dimers. Therefore these two compounds contain ionic nitrate ions. Ionic SO_4^{2-} (T_d) has two vibrations active in infrared (ν_3 and ν_4) while chelating bidentate sulfate with lower symmetry (C_{2v}) has all degenerated modes separated (9). All the modes are infrared-active. The main bands of the three EMSO sulfate compounds are listed in Table 3. These results show that the dimer and the trimer contain ionic sulfate ions while the monomer contains coordinated SO_4^{2-}. Three ν_3 and three ν_4 bands have been identified indicating C_{2v} symmetry for the monomer. The ν_3 vibrations appear at higher frequencies indicating chelating bidentate SO_4^{2-} rather than a bridged bidentate complex (9). A unidentate SO_4^{2-} (C_{3v}) complex would show two ν_3 and two ν_4 vibrations. Therefore

TABLE 3. Mean infrared bands of the bridged-hydroxy oligomers

Assignment	TMSO	DPSO
ν_2 ionic nitrate	826s	822m
ν_3 ionic nitrate	1355vs	1360vs
ν(S—O)	1138vs	1140vs
ν(Pt—O), ν(Pt—S), and skeletal vibrations below 600 cm^{-1}	568s	537s
	534m	512s
	374s	442s
	346w	392w
	272w	285m
	257m	

	EMSO		
Assignment	Monomer	Dimer	Trimer
$\nu_3SO_4^{2-}$ ionic + ν(S—O)		1125s,br	1100s,br
$\nu_4SO_4^{2-}$ ionic		620s	615s
$\nu_1SO_4^{2-}$ bidentate	940s		
$\nu_2SO_4^{2-}$ bidentate	512m		
$\nu_3SO_4^{2-}$ bidentate	1265vs		
	1130vs		
	1050s		
$\nu_4SO_4^{2-}$ bidentate	663m		
	622m		
	586m		
ν(Pt—O), ν(Pt—S), and skeletal vibrations below 600 cm^{-1}	430m	550s	540m
	376w	505m	505m
	300w	425s	430s
		380m	375m
		292m	305w

we can conclude that the structure of the monomer is *cis*-[Pt(EMSO)$_2$(SO$_4$)] and the dimer and trimer contain ionic sulfates.

Acknowledgments

The authors are grateful to the Natural Sciences and Engineering Research Council of Canada and to the Ministère de l'Education (FCAR) for financial support.

1. J. H. PRICE, A. N. WILLIAMSON, R. F. SCHRAMM, and B. B. WAYLAND. Inorg. Chem. **11**, 1280 (1972).
2. R. H. PRICE, J. P. BIRK, and B. B. WAYLAND. Inorg. Chem. **17**, 2245 (1978).
3. W. KITCHING, C. J. MOORE, and D. DODDRELL. Inorg. Chem. **9**, 541 (1970).
4. F. D. ROCHON, P. C. KONG, and R. MELANSON. Acta Crystallogr. C**41**, 1602 (1985).
5. J. A. STANKO, L. S. HOLLIS, J. A. SCHREIFELS, and J. D. HOESCHELE. J. Clin. Hem. Onc. **7**, 138 (1977).
6. C. J. L. LOCK, J. BRADFORD, R. FAGGIANI, R. A. SPERANZINI, G. TURNER, and M. ZVAGULIS. J. Clin. Hem. Onc. **7**, 63 (1977).
7. R. MELANSON, C. DE LA CHEVROTIÈRE, and F. D. ROCHON. Acta Crystallogr. C**41**, 1428 (1985).
8. R. MELANSON and F. D. ROCHON. Acta Crystallogr. To be published.
9. K. NAKAMOTO. Infrared and Raman spectra of inorganic and coordination compounds. 3rd ed. John Wiley and Sons. 1978.
10. R. J. ANGELICI. Synthesis and technique in organic chemistry. 2nd ed. W. B. Saunders Company. 1977. p. 18.
11. T. G. APPLETON, R. D. BERRY, C. A. DAVIS, J. R. HALL, and H. A. KIMLIN. Inorg. Chem. **23**, 3514 (1984).
12. F. D. ROCHON and F. GUAY. Acta Crystallogr. In press.
13. F. D. ROCHON and L. GIRARD. Can. J. Chem. In press.

Ligand properties of phosphinito platinum complexes: ^{31}P and ^{195}Pt nuclear magnetic resonance studies and the crystal and molecular structure of $[Cl(Et_3P)Pt(\mu\text{-}PPh_2O)_2Pt(PEt_3)_2][BF_4]$

DAVID ERIC BERRY, KATHRYN ANNE BEVERIDGE, JANE BROWNING, GORDON WILLIAM BUSHNELL, AND KEITH ROGER DIXON[1]

Department of Chemistry, University of Victoria, Victoria, B.C. Canada V8W 2Y2

Received February 25, 1986

DAVID ERIC BERRY, KATHRYN ANNE BEVERIDGE, JANE BROWNING, GORDON WILLIAM BUSHNELL, and KEITH ROGER DIXON. Can. J. Chem. **64**, 1903 (1986).

Reaction of sodium hydride in tetrahydrofuran with the hydrogen-bonded phosphinito complex, $[PtCl(PEt_3)\{(PPh_2O)_2H\}]$, gives a solution of the salt, $[PtCl(PEt_3)\{(PPh_2O)_2Na\}]$, which is a precusor to synthesis of other bimetallic derivatives, $[PtCl(PEt_3)\{(\mu\text{-}PPh_2O)_2Q\}]^{n+}$: n = 0, Q = Rh(COD) or Ir(COD); n = 1, Q = $Pd(PEt_3)_2$ or $Pt(PEt_3)_2$. Detailed ^{31}P and ^{195}Pt nmr studies are reported for these and related examples including a titanium complex (n = 0, Q = $Ti(acac)Cl_2$) synthesised by direct reaction of $[PtCl(PEt_3)\{(PPh_2O)_2H\}]$ with $[TiCl_2(acac)_2]$. The diplatinum complex, $[Cl(PEt_3)Pt(\mu\text{-}PPh_2O)_2Pt(PEt_3)_2][BF_4]$ crystallizes in the monoclinic space group $P2_1/n$, with a = 13.018(2), b = 34.205(9), c = 11.279(2) Å, β = 91.71(2)°. A complete X-ray diffraction study shows that the two platinum centres are significantly non-planar and are linked by the phosphinito ligands to form a six-membered ring in a boat conformation with phosphorus and oxygen atoms forming the prows of the boat.

DAVID ERIC BERRY, KATHRYN ANNE BEVERIDGE, JANE BROWNING, GORDON WILLIAM BUSHNELL et KEITH ROGER DIXON. Can. J. Chem. **64**, 1903 (1986).

La réaction de l'hydrure de sodium, dans le tétrahydrofuranne, avec les complexes phosphinito suivants ayant des liaisons hydrogènes $[PtCl(PEt_3)\{(PPh_2O)_2H\}]$ conduit à une solution de sel de $[PtCl(PEt_3)\{(PPh_2O)_2Na\}]$ qui est un précurseur dans la synthèse d'autres dérivés bimétalliques comme $[PtCl(PEt_3)\{(\mu\text{-}PPh_2O)_2Q\}]^{n+}$ dans lesquels n = 0, Q = Rh(COD) ou Ir(COD); n = 1, Q = $Pd(PEt_3)_2$ ou $Pt(PEt_3)_2$. On rapporte les études détaillées de la rmn du ^{31}P et du ^{195}Pt de ces complexes et des complexes apparentés, y compris un complexe de titane (n = 0, Q = $Ti(acac)Cl_2$) préparé par la réaction directe du $[PtCl(PEt_3)\{(PPh_2O)_2H\}]$ avec le $[TiCl_2(acac)_2]$. Le double complexe de platine $[Cl(PEt_3)Pt(\mu\text{-}PPh_2O)_2Pt(PEt_3)_2][BF_4]$ cristallise dans le groupe d'espace monoclinique $P2_1/n$ avec a = 13,018(2), b = 34,205(9), c = 11,279(2) Å et β = 91,71(2)°. Les études par diffraction des rayons X révèlent que les deux centres Pt ne sont pas plans et se lient aux ligands phosphinito pour former un cycle à six chaînons dans une conformation bateau avec les atomes d'oxygène et de phosphore en positions de proue.

[Traduit par la revue]

Introduction

The coordination chemistry of organophosphites is notable for the large variety of possible products occasioned by the reactivity of the P—OR bond. We have summarized the literature relating to this area in two recent papers and have also discussed the formation of P—O complexes via hydrolysis of coordinated chlorophosphines (1, 2). A particularly interesting and widely studied class of complexes is exemplified by structure **I**.

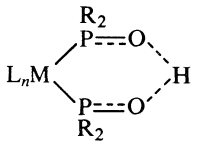

I

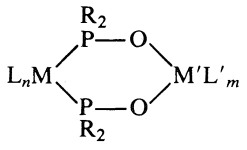

II

Hydrogen bonded ring systems of this type are formed in many reactions of secondary phosphites and are also the most usual final outcome of hydrolyses of *cis*-$M(PR_2Cl)_2$ fragments. They have been studied by many research groups (3) and examples are known for a wide range of transition metals including Mn (4), Cr (5), Mo (5–7), W (5), Ru (8, 9), Rh (10), Ir (11), Ni (12), Pd (13–16), and Pt (13–15). X-ray diffraction studies (4, 7, 9, 10, 17–19) have shown O---O distances in the range 2.38–2.43 Å and the hydrogen bonds have been generally assumed to be symmetrical. However, it is interesting that the only two crystal structures (4, 9) which explicitly locate the hydrogen atom have shown asymmetrical hydrogen bonds despite the short O—O distances. Values less than 2.5 Å are normally considered indicative of symmetrical hydrogen bonds (19).

The hydrogen bonded proton of structure **I** is readily removed by a variety of bases and this leads to an extensive coordination chemistry in which the anion derived from **I** may be regarded as an analogue of acetylacetonate (acac). Coordination compounds have been reported in which the proton is replaced by the non-metals B (6, 8, 11, 20–22), Si (20), and P (5), and by a wide range of metals, including Na (6), Zn (12, 21, 22), Al, Tl (12), V (11, 12, 20, 23), Mn (23), Co (11, 12, 21–24), Ni, Cu (21–23), U (21, 22, 25), and Th (21, 22). The chemistry is interesting as a potential route to mixed metal chain oligomers having different metal ions in specific sites (21, 22), one site being "soft" in character and the other "hard", and also as a route to studies of reactivity of proximate metal centres. As we have noted above, the hydrogen bonded ring systems **I** are structurally well-characterized but despite the large number of known metal derivatives only two X-ray diffraction studies are available, the uranium complex, $[(\eta\text{-}C_5H_5)Ni\{\mu\text{-}P(OMe)_2O\}_2)_4U]$ (25) and, very recently, a relatively low accuracy (R_w = 11.4%) cobalt structure, $[\{(Et_2NS_2)Pt(\mu\text{-}PPh_2O)_2\}_2Co]$ (24, 26).

In the present paper we describe syntheses and ^{31}P and ^{195}Pt nmr studies of Ti, Pd, Pt, Rh, and Ir complexes of the type I ligand $[(Et_3P)ClPt(PPh_2O)_2]^-$. With the exception of the Ti complex, these differ from previous examples in that M′ in structure **II** is a "soft" metal. A structural study of

[1]To whom all correspondence should be addressed.

the platinum complex, $[(Et_3P)ClPt(\mu\text{-}PPh_2O)_2Pt(PEt_2)_2][BF_4]$ (**III**) is reported.

Results and discussion

(A) Synthesis

The complexes discussed below were characterized primarily by the ^{31}P nmr spectra discussed in the next section. ^{195}Pt spectra were also recorded as given in the Experimental section and in all cases show coupling constants and multiplicities as expected from the ^{31}P spectra. ^1H spectra served mainly to confirm the ratios of aryl, alkoxy, and alkyl protons.

If complexes of type **I** are regarded as analogues of acetylacetone (acacH) then two simple routes to their coordination complexes are available.

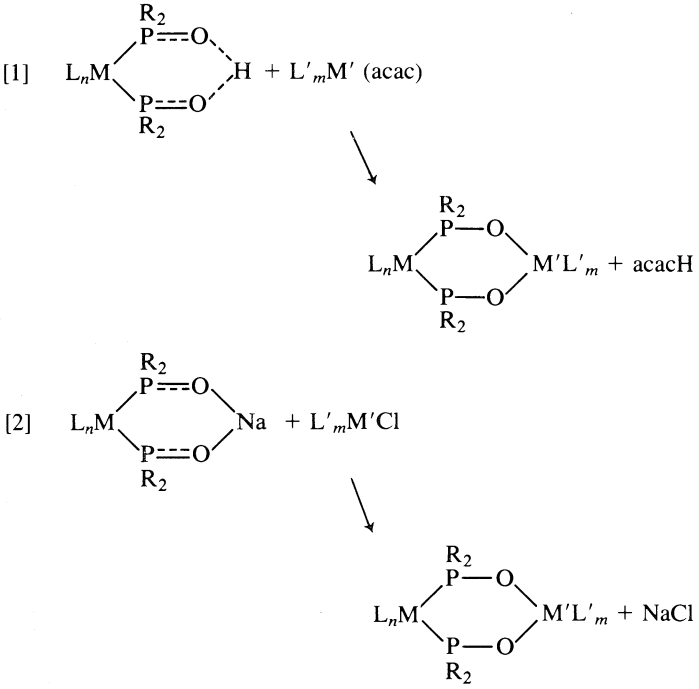

In practice, since reaction [2] requires an expansion of the coordination shell of M′, we have found a variant using cleavage of a double chloride bridge to be more useful. Thus:

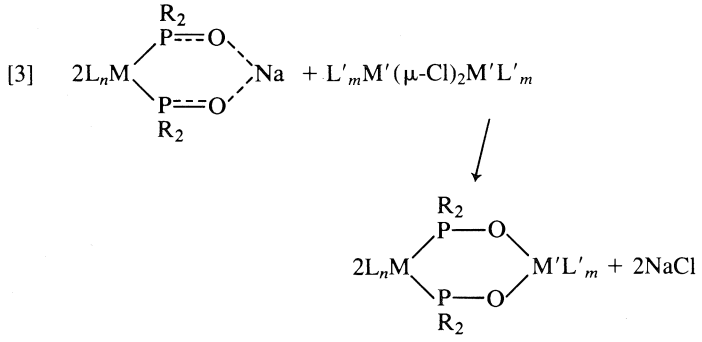

Solutions of $[PtCl(PEt_3)\{(PPh_2O)_2Na\}]$ are readily prepared by heating the known complex, $[PtCl(PEt_3)\{(PPh_2O)_2H\}]$ (15), with excess sodium hydride under reflux in tetrahydrofuran. Reactions of this solution with the chloride bridged complexes, $[Pt_2Cl_2(PEt_3)_4]^{2+}$ or $[Rh_2Cl_2(COD)_2]$ proceed under mild conditions according to reaction [3] to give, respectively, $[Cl(Et_3P)Pt(\mu\text{-}PPh_2O)_2Pt(PEt_3)_2]^+$ or $[Cl(Et_3P)Pt(\mu\text{-}PPh_2O)_2Rh(COD)]$. Palladium and iridium analogues, $[Cl(Et_3P)Pt(\mu\text{-}PPh_2O)_2Pd(PEt_3)_2]^+$ or $[Cl(Et_3P)Pt(\mu\text{-}PPh_2O)_2Ir(COD)]$ can be similarly prepared. As a check on the analogy with acetylacetone we also reacted $[Pt_2Cl_2(PEt_3)_4]^{2+}$ with Na(acac) to give $[Pt(acac)(PEt_3)_2]^{2+}$, the expected product according to reaction [3].

The products from an acac displacement reaction similar to reaction [1] were more problematical. Reaction of $[PtCl(PEt_3)\{(PPh_2O)_2H\}]$ with $[TiCl_2(acac)_2]$ gave a principal product analysing as $[Cl(Et_3P)Pt(\mu\text{-}PPh_2O)_2TiCl_2(acac)]$.

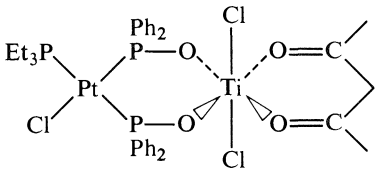

IV

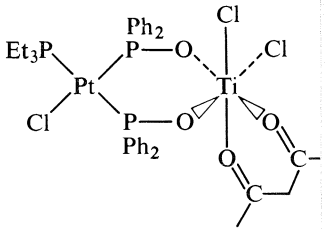

V

There are five possible isomers of this formulation since the complex can be *trans* (structure **IV**) or *cis* (structure **V**). There are two possible *cis* structures (with transposition of the Cl and PEt_3 ligands) and each of these is chiral. The ^{31}P nmr of the main product is very similar to that of the other complexes described above except that the resonances for the bridging PPh_2O resonances are doubled indicating the presence of two isomers. The centreband resonances for the PEt_3 ligands of the two isomers are not resolved but some resolution is seen in the ^{195}Pt sidebands. A third product showing another very similar spectrum but in which the PEt_3 resonances were also significantly chemically shifted was observed in the supernatant liquids from the reaction. These observations suggest that the principal (less soluble) product consists of a racemic mixture of the two possible *cis* isomers (**V**), and the other (more soluble) product is probably the *trans* isomer (**IV**), but it is clear that we cannot be certain of these assignments. Data for all three products are given in Table 1 but spectra for the more soluble component were poor and only the parameters for the PEt_3 group could be determined with confidence.

In the course of our preliminary studies for the above work we also prepared several analogues of $[PtCl(PEt_3)\{(PPh_2O)_2H\}]$. Bridge cleavage reactions of $[Pt_2(\mu\text{-}Cl)_2\{(PPh_2O)H\}_2]$ with tertiary phosphines and phosphites gave $[PtCl(L)\{(PPh_2O)_2H\}]$, L = PBu^n_3, $P(OMe)_3$, or $P(OPh)_3$, and reaction of $(EtO)_2P(O)H$ with $[Pt_2Cl_4(PEt_3)_2]$ gave $[PtCl(PEt_3)\{(P(OEt)_2O)_2H\}]$.

In their 1978 review of phosphinite and phosphite chemistry (3), Roundhill, Sperline, and Beaulieu noted an unusual and little studied substitution reaction in which $[Pt\{(PPh_2O)_2H\}_2]$ is converted to $[Pt\{(PPh_2O)(P(OPh)_2)H\}_2]$ by reaction with $P(OPh)_3$. The reaction of $P(OMe)_3$ with $[Pt_2(\mu\text{-}Cl)_2\{(PPh_2O)H\}_2]$ provides a further example of this type of process. As noted above, use of two molar equivalents of $P(OMe)_3$ gives $[PtCl\{P(OMe)_3\}\{(PPh_2O)_2H\}]$, but if excess phosphite is used then the product is complex **VI**. In contrast to the example reported previously (3), we found no evidence for a corresponding reaction with excess $P(OPh)_3$.

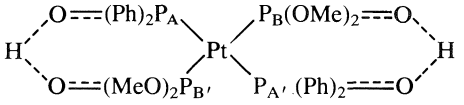

VI

TABLE 1. Phosphorus-31 nuclear magnetic resonance parameters[o] for complexes

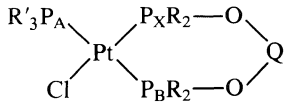

M	R	R'3	Q	Notes	δ(PA)	δ(PB)	δ(PX)	J(PA—PB)	J(PA—PX)	J(PB—PX)	J(Pt—PA)	J(Pt—PB)	J(Pt—PX)
Pt	Ph	Et_3	H	*a, f*	12.59	76.31	58.52	397.7	−17.3	−20.3	2123	2730	3835
Pt	Ph	Et_3	H	*b*	12.0	76.5	58.3	397	17	21	2129	2726	3833
Pt	Ph	Et_3	BF_2	*a, e, h*	13.34	79.49	65.72	392.1	−17.0	*i*	2132	2661	3911
Pt	Ph	Et_3	BF_2	*b*	14.0	81.7	67.7	393	17	*i*	2139	2654	3882
Pt	Ph	Et_3	$SiMe_3$	*b*	14.5	82.6	58.8	412	19	21	2151	2766	3960
Pt	Ph	Et_3	Na	*a, g*	15.55	59.49	29.66	430.6	−20.2	−19.3	1960	3142	4085
Pt	Ph	Et_3	$TiCl_2$(acac)	*a, f, n*	13.51	106.48	85.69	400.8	−17.2	−12.2	2165	2785	4089
					13.38	110.71	89.07	402.5	−17.5	−11.9	2175	2796	4100
					16.75			402.5			2175		
Pt	Ph	Et_3	Rh(COD)	*a, f*	16.35	72.55	46.95	409.4	−19.0	−19.1	2040	2942	4033
Pt	Ph	Et_3	Ir(COD)	*a, g*	16.67	73.66	46.83	412.4	−19.2	−20.4	2062	2903	3958
Pt	Ph	Et_3	$Pd(PEt_3)_2$	*a, g, j, k*	17.08	74.87	55.72	416.2	−18.0	−23.2	2063	2879	4021
Pt	Ph	Et_3	$Pt(PEt_3)_2$	*a, e, g, j, l*	17.09	75.60	56.44	415.4	−17.5	−24.8	2079	2848	3994
Pt	Ph	Bu^n_3	H	*a, e, f*	5.33	76.20	58.43	399.3	−17.4	−20.6	2120	2719	3849
Pt	Ph	Bu^n_3	$Pd(PEt_3)_2$	*a, e, h, j, m*	15.91	74.61	56.30	413.3	−17.7	−22.5	2059	2870	4073
Pt	Ph	$(MeO)_3$	H	*a, e, h*	110.20	74.16	56.23	618.3	−24.9	−20.2	3857	2744	3595
Pt	Ph	$(PhO)_3$	H	*a, e, h*	98.43	73.02	56.93	634.8	−22.4	−20.6	3825	2881	3592
Pt	MeO	Et_3	H	*c*	18.9	94.9	55.4	542	25	35	2144	3872	5276
Pt	MeO	Et_3	BF_2	*c*	19.2	88.6	58.0	545	24	41	2103	3880	5520
Pt	MeO	Et_3	Th	*c*	19.4	82.6	45.9	560	24	32	2034	3701	5624
Pt	MeO	Ph_3	H	*c*	29.1	89.4	60.1	567	25	36	2179	4110	5209
Pt	EtO	Et_3	H	*a, h*	17.63	90.77	51.31	540.2	−24.4	−33.6	2121	3909	5298
Pt	PhO	Et_3	H	*d*	18.6	87.7	48.7	547	23.4	36.8	2217	3818	5469
Pt	PhO	Bu^n_3	H	*d*	12.1	88.5	48.8	539	23.9	35.8	2220	3806	5519
Pd	Ph	Et_3	H	*a, f*	13.06	84.01	85.16	424.5	−23.9	0			
Pd	Ph	Et_3	BF_2	*a, h*	14.56	89.57	94.13	429.9	−25.4	0			
Pd	PhO	Me_2Ph	H	*d*	−2.9	95.7	75.2	630	*i*	*i*			
Pd	PhO	Ph_3	H	*d*	24.4	92.0	74.4	600	*i*	*i*			

[a]Present work.
[b]Data from ref. 20.
[c]Data from ref. 29.
[d]Data from ref. 14. These workers used P_4O_6 as a phosphorus reference and we have converted the shifts assuming that P_4O_6 is at +113 ppm relative to 85% H_3PO_4.
[e]Platinum-195 parameters for this complex are given in the Experimental section.
[f]24.3 MHz in dichloromethane solution.
[g]24.3 MHz in tetrahydrofuran solution.
[h]101.3 MHz in deuterochloroform solution.
[i]Not resolved.
[j]The *cis*-PEt_3 groups in "Q" appeared as an NM quartet. All P—P and Pt—P couplings through the oxygen were smaller than the instrument resolution.
[k]δ(N) 41.65, δ(M) 39.43 ppm; ^2J(NM) −26.6 Hz.
[l]δ(N) 8.28, δ(M) 5.51 ppm; ^2J(NM) −25.2, ^1J(Pt—P_N) 3683, ^1J(Pt—P_M) 3716 Hz.
[m]δ(N) 39.44, δ(M) 38.00 ppm; ^2J(NM) −27.4 Hz.
[n]Three isomers were observed for this complex. Their significance is discussed in the text.
[o]Chemical shifts (δ) are quoted in parts per million relative to 85% H_3PO_4. Except as indicated, all shifts were positive. Coupling constants (*J*) are in Hz and their signs are discussed in the text.

(B) ^{31}P nuclear magnetic resonance spectra

Most of the complexes studied in this work are of the general type illustrated by structure **VII**:

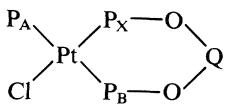

VII

Proton decoupled ^{31}P nmr spectra of these complexes can usually be analyzed in the ABX spin system as defined in **VII**, and exhibit ^{195}Pt sidebands belonging to the ABMX spin system. This designation is somewhat unusual in that the chemical shift difference between A and B is often greater than that between B and X; but it is the large *trans* coupling between A and B which determines the spin system. Most of the spectra are sufficiently close to first order that the analyses present no special problems and a typical spectrum has been illustrated in a previous paper (20). However, in the present work we have improved the reliability of the parameters by computer simulation and refinement of all spectra, thereby avoiding the assumption of first order character made by previous authors.

For many of the complexes, we had available spectra at both 24.3 and 101.3 MHz and the non-first order character of the lower frequency spectra provided some information on signs of coupling constants. The details varied from compound to compound, but the procedure adopted for $[PtCl\{P(OMe)_3\}\{(PPh_2O)_2H\}]$ is illustrative of the internal checks for consistency which were applied in all cases. At 101.3 MHz the spectrum of $[PtCl\{P(OMe)_3\}\{(PPh_2O)_2H\}]$ was essentially first order. At 24.3 Mz the centre bands were an ABC spin system but the ^{195}Pt sidebands allowed ABMX analysis. Refinement of the sidebands with all possible sign combinations for J_{AX} and J_{BX} showed that only like signs gave satisfactory refinements with magnitudes in agreement with those obtained from the 101.3 MHz spectrum. Moreover, only negative signs for these parameters were able to predict the appearance of the ABC centre bands. The large *trans* coupling, J_{AB}, and all the platinum–phosphorus coupling were assumed to be positive on the basis of previous literature results (27, 28).

The parameters derived from these analyses are collected in Table 1 together with literature data for comparison. In general the parameters follow well established trends and require little comment. Thus $J(Pt—P_B)$ and $J(Pt—P_X)$ reflect the *trans*-influences of the Et_3P and Cl ligands; a difference which is also apparent in the Pt—P bonds lengths discussed below. Also the various coupling constants depend as expected on the electronegativity of the substituents, with larger magnitudes where either or both atoms carry alkoxy or aryloxy substituents. There is, however, one interesting trend associated with the variation of the group Q. Changing from a hydrogen bonded proton to a sodium ion causes shielding of P_B and P_X and increases in $J(Pt—P_B)$, $J(Pt—P_X)$, and $J(P_A—P_B)$. All of these changes are consistent with greater electron density in the sigma bonds of the $Pt(PR_2O)_2$ unit. At the same time the slightly strengthened $Pt—P_B$ bond exerts an increased *trans* influence causing a decrease in $J(Pt—P_A)$ and deshielding of P_A. When Q is a group containing a less electropositive metal (Rh, Ir, Pd, or Pt) the changes relative to the protonated species are similar but generally smaller in magnitude than those for sodium. When Q contains boron or silicon the changes are of small magnitude and erratic in direction. These trends can all be rationalised by increasing polarising power of the group Q in the sequence: electropositive metals < electronegative metals < non-metals and hydrogen. The data for the titanium complexes fit into this sequence (assuming Ti(IV) to be strongly polarising) except for a large deshielding of P_B and P_X, a perturbation which could be a result of the very different six-coordinate geometry of these complexes.

$[Pt\{(PPh_2O)(P(OMe)_2O)H\}_2]$

In principle the ^{31}P spectrum of this complex should belong to the AA′BB′ spin system as shown in structure **VI**, but in practice $J(AA')$ and $J(BB')$ are both *trans* phosphine couplings which are expected to be large and significantly different in magnitude because of the different substituents. Also it is likely that $J(AB) \simeq J(AB')$ since *cis* couplings show very little variation (see Table 1). Either of these two conditions could lead to the deceptively simple A_2B_2 spectrum (30) shown in Fig. 1. Computer refinement and simulation gave the following parameters:

$\delta(P_A)$ +82.11, $\delta(P_B)$ +85.14 ppm. $J(Pt—P_A)$ 2463, $J(Pt—P_B)$ 3324 Hz. $(1/2)\{J(AB) + J(AB')\}$ 38.4 Hz.

Comparison of these parameters with those for $[Pt\{(PPh_2O)_2H\}_2]$, $\delta(P)$ +72.5 ppm, $J(Pt—P)$ 2467 Hz (25), and $[Pt\{(P(OMe)_2O)_2H\}_2]$, $\delta(P)$ +89.2 ppm, $J(Pt—P)$ 3456 Hz (24), makes it clear that P_A above is the PPh_2O group and P_B is $P(OMe)_2O$ as shown in **VI**.

The spectrum of **VI** is also interesting as a further example showing significantly different centre bands and ^{195}Pt sidebands (31). As Figure 1 shows, the low field sideband is first order A_2X_2, the centre band is a weakly coupled A_2B_2 pattern, and the upfield sideband is strongly coupled A_2B_2. These differences are caused by the effective chemical shifts introduced into the sidebands by the different magnitudes of $J(Pt—P_A)$ and $J(Pt—P_B)$ (31).

*(c) Structure of $[Cl(Et_3P)Pt(\mu\text{-}PPh_2O)_2Pt(PEt_3)_2][BF_4]$ (**III**)*

The atomic labelling scheme and the structure of a single molecule are shown in Fig. 2. Fractional atomic coordinates and isotropic temperature parameters, bond lengths, and bond angles are collected in Tables 2–4, and the following tables have been deposited: anisotropic temperature factors, structure factors, selected intermolecular distances, and mean plane information.[2]

The structure of $[Cl(Et_3P)Pt(\mu\text{-}PPh_2O)_2Pt(PEt_3)_2][BF_4]$ consists of two nominally square-planar platinum centres linked by a pair of P—O bridges to form a six-membered ring. There is asymmetry at both ends of the molecule, Cl versus PEt_3 at Pt(1) and differing conformations of PEt_3 at Pt(2), and the coordination geometry around both platinums is considerably distorted. The angles seem to reflect the most obvious considerations of ligand size and the constraints imposed by the ring structure. Thus, around Pt(1) all the angles are compressed (84.1–88.6°) except for P(2)—Pt(1)—P(3) (102.0(2)°), whereas around Pt(2) it is the angle between the terminal PEt_3 groups which is opened (98.5(2)°) and the others compressed (85.2–90.4°). Both sets of atoms bonded to Pt are distinctly non-planar ($\chi^2 = \Sigma p^2/\sigma(p)^2 = 7906$ at Pt(1), 116 at Pt(2)), but the distortion at Pt(1) is much larger and may be due to a significant intramolecular interaction between PEt_3 containing P(3) and the adjacent phenyl ring.

[2]Copies of these tables may be purchased from the Depository of Unpublished Data, CISTI, National Research Council of Canada, Ottawa, Ont., Canada K1A 0S2.

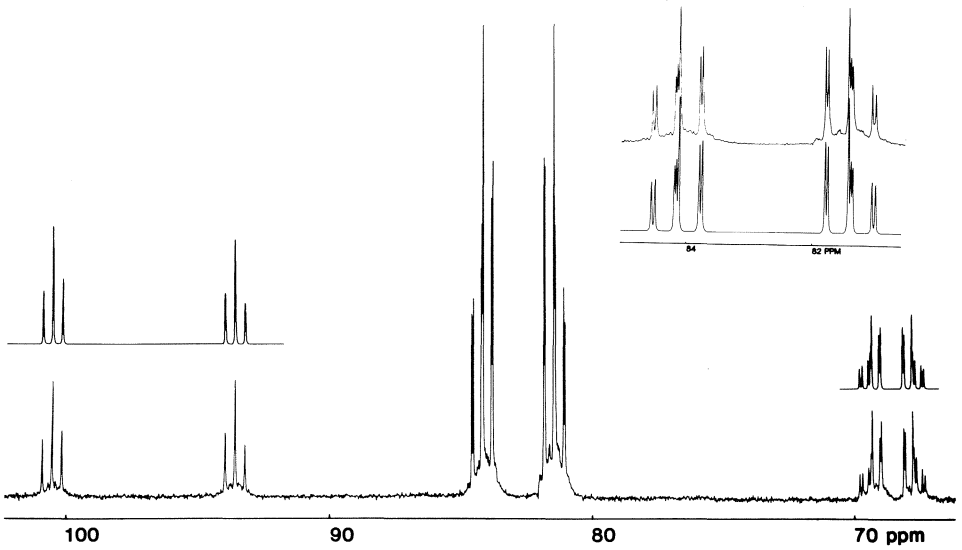

FIG. 1. $^{31}P\{^1H\}$ nuclear magnetic resonance spectrum of $[Pt\{(PPh_2O)(P(OMe)_2O)H\}_2]$. The main figure shows the complete spectrum with computer simulations of the ^{195}Pt sidebands (upper traces). The inset is an expansion of the centre band with a computer simulation (lower trace).

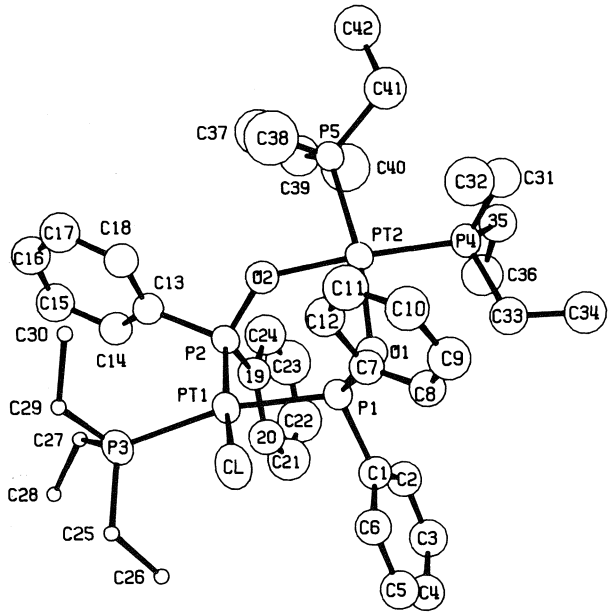

FIG. 2. ORTEP plot of compound **III**, $[Cl(Et_3P)Pt(\mu\text{-}PPh_2O)_2Pt(PEt_3)_2][BF_4]$. Thermal ellipsoids scaled to enclose 50% probability.

The bond lengths involving Pt(1) and the P—O lengths in the six-membered ring are all closely similar to those observed previously in $[Pt\{(P(OMe)_2O\}_2)BF_2\}_2]$ (32) and $[Cl(Et_3P)Pt(PPh_2O)_2BF_2]$ (33). The Pt(2)—P(4), 2.226(5) Å, and Pt(2)—P(5), 2.253(5) Å, bonds are relatively short (34, 35), consistent with the expected small *trans*-influence of oxygen ligands. The shorter length is similar to the Pt—P bonds (ave. 2.235 Å) in the dihydroxy bridged cation, $[Pt_2(OH)_2(PEt_3)_4]^{2+}$ (36). The Pt(2)—O lengths in **III**, 2.057(10) and 2.087(11) Å, are also close to those in the hydroxy bridged cation, ave. 2.133 Å.

The most interesting structural feature concerns the conformation of the six-membered ring. Our previous study of $[Pt\{(P(OMe)_2O\}_2)BF_2\}_2]$ showed a chair conformation, with a roughly planar P_2O_2 unit forming the seat, and we noted that the geometry of the MP_2O_2 fragment was relatively unaffected by substitution of BF_2 for H (32). In the present structure substitution by platinum changes the ring to a boat conformation, either because of the P(3)Et_3---phenyl interaction or because of the need to accommodate a second ~90° angle within the ring. Also the non-bonded O(1)---O(2) distance increases from the 2.38–2.43 Å in the BF_2 and H derivatives (4, 7, 9, 10, 17–19, 32) to 2.822(14) Å in **III**. The boat is not the obvious one having the Pt atoms at the prows, but rather that with P(2) and O(1) at the prows. Referring to Fig. 2, the Pt(1)—P(1) and O(2)—Pt(2) vectors are approximately parallel and the four atoms involved are all within 0.061 Å of the unweighted least-squares plane through the four atoms. The prows of the boat, P(2) and O(1), are, respectively, −0.780(4) and −0.658(9) Å below this plane. The torsion angle across the ring, O(1)—P(1)---P(2)—O(2) is 47.6(5)°. The coordination planes of Pt(1) and Pt(2) are incorporated into the ring in similar ways, being set at respective dihedral angles of 26.4 and 18.4° to the Pt(1), P(1), Pt(2), O(2) plane. It is interesting that the only other related structure involving two metal centres, compound **VIII** (24, 26), can be described in a similar way.[3]

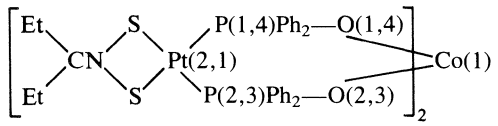

VIII

Using the revised coordinates given by Marsh (26),[3] we calculate that the unweighted least-squares plane through Pt(2,1), Co(1), O(2,3), and P(1,4) has a maximum perpendicular deviation of 0.153 Å leaving O(1,4) and P(2,3), respectively, 0.14(2) and 0.825(8) Å out-of-plane in boat conformation. The phenyl ring positions on P(2,3) resemble those on our P(2). The more obvious unweighted least-squares plane through P(1,4), P(2,3), O(1,4), and O(2,3), has a marginally worse maximum

[3]The double numbering in **VIII** results from the fact that the structure was refined in a less symmetric space group (24).

TABLE 2. Fractional atomic coordinates and temperature parameters[a]

Atom	x/a	y/b	z/c	U_{iso}	Atom	x/a	y/b	z/c	U_{iso}
Pt(1)	30321(5)	29929(2)	43240(5)	404(3)′	C(20)	5556(13)	3323(6)	3906(15)	63(5)
Pt(2)	27322(5)	41600(2)	27620(5)	416(3)′	C(21)	6611(16)	3463(7)	4009(20)	93(7)
Cl	2051(3)	2778(1)	5953(4)	65(2)′	C(22)	7017(18)	3692(8)	3132(22)	104(7)
P(1)	2895(3)	3612(1)	5087(4)	41(2)′	C(23)	6473(18)	3777(8)	2135(22)	109(8)
P(2)	3664(3)	3254(1)	2684(4)	42(2)′	C(24)	5392(15)	3643(7)	1967(18)	83(6)
P(3)	3291(4)	2320(2)	4008(4)	72(2)′	C(25)	3601(13)	2059(6)	5373(11)	78(6)
P(4)	2514(4)	4757(1)	3501(4)	54(2)′	C(26)	4410(20)	2243(8)	6177(24)	125(9)
P(5)	2240(4)	4283(2)	867(4)	63(2)′	C(27)	4307(14)	2203(4)	2992(16)	337(31)
O(1)	3283(7)	3966(3)	4386(8)	45(3)	C(28)	5223(19)	1947(9)	3328(28)	156(11)
O(2)	3022(7)	3594(3)	2164(9)	50(3)	C(29)	2163(10)	2064(4)	3413(20)	270(22)
C(1)	3715(11)	3637(5)	6416(14)	48(4)	C(30)	1391(18)	2260(8)	2571(22)	136(10)
C(2)	4620(12)	3858(5)	6349(15)	57(5)	C(31)	1269(13)	4994(6)	3334(16)	69(5)
C(3)	5322(13)	3866(6)	7325(16)	66(5)	C(32)	369(17)	4697(7)	3671(20)	100(7)
C(4)	5078(12)	3654(5)	8385(15)	59(5)	C(33)	2744(12)	4754(6)	5146(15)	63(5)
C(5)	4231(13)	3444(6)	8468(16)	65(5)	C(34)	2746(14)	5171(6)	5722(18)	79(6)
C(6)	3500(12)	3437(5)	7465(15)	56(5)	C(35)	3425(13)	5110(6)	2929(16)	68(5)
C(7)	1587(11)	3716(5)	5508(14)	50(4)	C(36)	4556(15)	4984(6)	3183(18)	85(6)
C(8)	1335(12)	3933(5)	6493(14)	53(5)	C(37)	1450(16)	3887(7)	290(20)	93(7)
C(9)	252(14)	4013(6)	6692(17)	72(5)	C(38)	518(20)	3839(8)	1133(24)	127(9)
C(10)	−483(14)	3877(6)	5906(17)	74(6)	C(39)	3327(15)	4241(6)	−104(18)	80(6)
C(11)	−259(14)	3663(6)	4949(18)	79(6)	C(40)	4117(19)	4549(8)	50(23)	119(8)
C(12)	810(13)	3584(6)	4698(15)	63(5)	C(41)	1546(15)	4731(6)	455(18)	81(6)
C(13)	3668(11)	2931(5)	1414(14)	46(4)	C(42)	1417(16)	4780(7)	−913(20)	95(7)
C(14)	4554(12)	2756(5)	986(14)	52(4)	B(1)	798(3)	418(1)	−80(4)	129(13)
C(15)	4484(14)	2493(6)	−21(17)	73(6)	F(1)	884(1)	437(1)	−92(1)	150(6)
C(16)	3522(14)	2443(6)	−578(17)	71(5)	F(2)	719(1)	439(0)	−48(1)	131(5)
C(17)	2646(14)	2613(6)	−209(17)	75(6)	F(3)	807(2)	384(1)	−21(2)	222(10)
C(18)	2716(12)	2863(5)	819(15)	54(5)	F(4)	783(2)	409(1)	−200(2)	210(9)
C(19)	4964(12)	3413(5)	2876(14)	52(4)					

[a]Estimated standard deviations are given in parentheses. Coordinates $\times 10^n$ where $n = 5, 3, 3$ for Pt, B, F and $n = 4$ ortherwise. Temperature parameters $\times 10^n$ where $n = 4$ for Pt and $n = 3$ otherwise. U_{eq} (the equivalent isotropic temperature parameter) $= (1/3)\Sigma_i\Sigma_j U_{ij} a_i^* a_j^* (a_i \cdot a_j)$. Primed values indicate that U_{eq} is given. $T = \exp[-(8\pi^2 U_{iso} \sin^2\theta/\lambda^2)]$.

deviation of 0.174 Å, passes almost exactly through Co(1), and leaves Pt(2,1) 0.957 Å out-of-plane. The transannular torsion angle O(1,4)—P(1,4)---P(2,3)—O(2,3) is 25(1)°.

We conclude that the less obvious description brings out the structural similarity between the two compounds well, and is a better description in both cases although only marginally so for the cobalt compound. In agreement with this, the possible causative steric interactions are less severe in the cobalt case and there is also no need to accommodate a second small angle since the cobalt is tetrahedral.

Experimental section

(a) Synthetic and spectroscopic studies

Data relating to the characterization of the complexes are given in the tables, the Results section, and in the preparative descriptions below. Microanalysis was by the Canadian Microanalytical Service, Vancouver, B.C., Canada. ^{31}P nuclear magnetic resonance spectra were recorded in appropriate solvents (Table 1) at either 24.3 MHz using a Nicolet TT14 Fourier transform spectrometer with a Varian HA60 magnet and an external C_6D_6 lock signal or at 101.3 MHz using a Bruker WP250 Fourier transform spectrometer locked to the solvent deuterium resonance. ^{195}Pt spectra were recorded at 53.5 MHz in $CDCl_3$ solution using the Bruker instrument. For both nuclei protons were decoupled by broad band ("noise") irradiation at appropriate frequencies. ^{31}P chemical shifts were measured relative to external $P(OMe)_3$ and are reported in ppm relative to 85% H_3PO_4 using a conversion factor of +141 ppm. ^{195}Pt chemical shifts are reported in ppm relative to $\Xi(^{195}Pt) = 21.4$ MHz (37). Positive values are downfield of the references. ^1H spectra were recorded at 60 MHz in $CDCl_3$ solution using the Nicolet instrument and chemical shifts were measured relative to internal $Si(CH_3)_4$ reference. Simulated nmr spectra were calculated on an IBM 3031 computer and plotted on a Calcomp 1039 plotter. The programs used were a locally constructed package based on the UEAITR and NMRPLOT programs from the literature (38, 39).

All operations were carried out at ambient temperature (ca. 25°C) under an atmosphere of dry nitrogen using standard Schlenk tube techniques. Solvents were dried by reflux over appropriate reagents (calcium hydride for dichloromethane, molecular sieves for acetone, and potassium/benzophenone for diethyl ether, tetrahydrofuran, toluene, benzene, and hexane) and were distilled under nitrogen prior to use. Recrystallizations from solvent pairs were by dissolution of the complex in the first solvent (using about double the volume required for complete solution) followed by dropwise addition of sufficient second solvent to cause turbidity at ambient temperature. Crystallization was then completed either by continued very slow dropwise addition of the second solvent or, in those cases where a temperature is indicated in the detailed descriptions below, by setting the mixture aside at a reduced temperature.

Sodium acetylacetonate (40), $[Ti(acac)_2Cl_2]$ (41), $[Pt_2Cl_2\{(PPh_2O)H\}_2]$ (15), $[Pt_2Cl_4(PEt_3)_2]$ (42), $[Pt_2Cl_2(PEt_3)_4][BF_4]_2$ (43), $[Pd_2Cl_2(PEt_3)_4][ClO_4]_2$ (43), $[Rh_2Cl_2(COD)_2]$ (44), $[Ir_2Cl_2(COD)_2]$ (45), $[PdCl(PEt_3)\{(PPh_2O)_2H\}]$ (15), and $[PdCl(PEt_3)\{(PPh_2O)_2BF_2\}]$ (20), were prepared as previously described.

[Pt(acac)(PEt$_3$)$_2$][BF$_4$]

A slurry of sodium acetylacetonate (0.036 g, 0.30 mmol) in acetone was added to a stirred solution of $[Pt_2Cl_2(PEt_3)_4][BF_4]_2$ (0.163 g, 0.15 mmol) in acetone (20 mL). After 15 min the solvent was removed *in vacuo* and the residue dissolved in dichloromethane and stirred vigorously with an aqueous solution of $NaBF_4$. The organic layer was separated, the solvent removed *in vacuo* and the residue recrystallized from tetrahydrofuran/diethyl ether at −20°C to yield

TABLE 3. Interatomic distances* (Å)

Atoms	Distance	Atoms	Distance
Cl—Pt(1)	2.385(4)	C(12)—C(7)	1.42(2)
P(1)—Pt(1)	2.294(4)	C(9)—C(8)	1.46(2)
P(2)—Pt(1)	2.233(4)	C(10)—C(9)	1.37(2)
P(3)—Pt(1)	2.355(5)	C(11)—C(10)	1.34(3)
P(4)—Pt(2)	2.226(5)	C(12)—C(11)	1.45(2)
P(5)—Pt(2)	2.253(5)	C(14)—C(13)	1.40(2)
O(1)—Pt(2)	2.057(10)	C(18)—C(13)	1.41(2)
O(2)—Pt(2)	2.087(11)	C(15)—C(14)	1.45(2)
O(1)—P(1)	1.541(11)	C(16)—C(15)	1.40(2)
C(1)—P(1)	1.816(15)	C(17)—C(16)	1.36(2)
C(7)—P(1)	1.816(15)	C(18)—C(17)	1.44(2)
O(2)—P(2)	1.539(11)	C(20)—C(19)	1.41(2)
C(13)—P(2)	1.809(16)	C(24)—C(19)	1.42(3)
C(19)—P(2)	1.785(16)	C(21)—C(20)	1.46(3)
C(25)—P(3)	1.815(14)	C(22)—C(21)	1.38(3)
C(27)—P(3)	1.82	C(23)—C(22)	1.34(3)
C(29)—P(3)	1.82	C(24)—C(23)	1.49(3)
C(31)—P(4)	1.817(18)	C(26)—C(25)	1.51(3)
C(33)—P(4)	1.871(17)	C(28)—C(27)	1.52
C(35)—P(4)	1.825(19)	C(30)—C(29)	1.52
C(37)—P(5)	1.811(23)	C(32)—C(31)	1.61(3)
C(39)—P(5)	1.821(21)	C(34)—C(33)	1.57(3)
C(41)—P(5)	1.832(21)	C(36)—C(35)	1.55(3)
C(2)—C(1)	1.40 (2)	C(38)—C(37)	1.57(3)
C(6)—C(1)	1.40 (2)	C(40)—C(39)	1.48(3)
C(3)—C(2)	1.41 (2)	C(42)—C(41)	1.56(3)
C(4)—C(3)	1.44 (2)	F(1)—B(1)	1.32(4)
C(5)—C(4)	1.32 (2)	F(2)—B(1)	1.32(4)
C(6)—C(5)	1.46 (2)	F(3)—B(1)	1.35(4)
C(8)—C(7)	1.38 (2)	F(4)—B(1)	1.40(4)

*Estimated standard deviations are given in parentheses.

$[Pt(acac)(PEt_3)_2][BF_4]$ as colourless crystals (0.165 g, 0.27 mmol). *Anal.* calcd. for $C_{17}H_{37}BF_4O_2P_2Pt$: C 33.1, H 6.04; found: C 33.1, H 5.99; nmr: $\delta(^{31}P)$ +5.33 ppm in CH_2Cl_2, ^1J(Pt—P) 3586 Hz; $\delta(^{195}Pt)$ +407.78 ppm (t, Ξ 21.408726 MHz).

[PtClL{(PPh$_2$O)$_2$H}], L = PEt$_3$, PBu$^n_3$, P(OMe)$_3$, or P(OPh)$_3$

These complexes were prepared by similar methods to that described previously for the L = PEt_3 complex (15). For example; PBu^n_3 (0.08 mL, 0.32 mmol) was added dropwise to a stirred suspension of $[Pt_2Cl_2\{(PPh_2O)H\}_2]$ (0.20 g, 0.16 mmol) in acetone (20 mL). A clear solution resulted almost immediately and the solvent was removed *in vacuo* to leave a colourless oil which was crystallized from benzene/pentane. Recrystallization by the same method gave $[PtCl(PBu^n_3)\{(PPh_2O)_2H\}]$ (0.223 g, 0.27 mmol) as white crystals. *Anal.* calcd. for $C_{36}H_{48}ClO_2P_3Pt$: C 51.7, H 5.79; found: C 51.8, H 5.63. ^{195}Pt nmr: δ −70.75 ppm (ddd, Ξ 21.398486 MHz).

L = P(OMe)$_3$. Anal. calcd. for $C_{27}H_{30}ClO_5P_3Pt$: C 42.8, H 3.99; found: C 42.7, H 3.83. mp 163–166°C; nmr: $\delta(^1H)$ ~7.5 (m, 20H, Ph), 3.48 ppm (d with ^{195}Pt sidebands, ^3J(PH) 11 Hz, ^4J(PtH) 112 Hz, 9H, Me); $\delta(^{195}Pt)$ −54.29 ppm (ddd, Ξ 21.398838 MHz).

L = P(OPh)$_3$. Anal. calcd. for $C_{42}H_{36}ClO_5P_3Pt$: C 53.4, H 3.84; found: C 52.5, H 3.81. ^{195}Pt nmr: δ −56.43 ppm (ddd, Ξ 21.398792 MHz).

[Pt{(PPh$_2$O)(P(OMe)$_2$O)H}$_2$]

This complex was prepared as colourless crystals by the same procedure described above for $[PtCl\{P(OMe)_3\}\{(PPh_2O)_2H\}]$ except that an excess of $P(OMe)_3$ (ca. 0.5 mmol) and an extended reaction time (18 h) were employed. It could also be made by reaction of equimolar quantities of $P(OMe)_3$ and $[PtCl\{P(OMe)_3\}\{(PPh_2O)_2H\}]$ in acetone. *Anal.* calcd. for $C_{28}H_{34}O_8P_4Pt$: C 41.1, H 4.19; found: C 41.1, H 4.20. mp 216–218°C; nmr: $\delta(^1H)$ ~7.5 (m, 20H, Ph), 2.94 ppm (t with ^{195}Pt sidebands, $(1/2)\{^3J(PH) + {}^5J(PH)\}$ 5.5 Hz, ^5J(PtH) 66 Hz, 12H, Me); $\delta(^{195}Pt)$ −492.25 ppm (tt, Ξ 21.398466 MHz).

[PtCl(PEt$_3$){(P(OEt)$_2$O)$_2$H}]

A slight excess of $(EtO)_2P(O)H$ (0.4 mL, 3 mmol) was added dropwise to a stirred solution of $[Pt_2Cl_4(PEt_3)_2]$ (0.5 g, 0.65 mmol) in dichloromethane (20 mL). The reaction mixture was warmed to 50°C for 2 h and then stirred at 25°C for 18 h. Removal of solvent and excess diethylphosphite *in vacuo* gave $[PtCl(PEt_3)\{(P(OEt)_2O)_2H\}]$ as yellowish crystals which were identified by ^{31}P nmr spectroscopy (see Table 1).

[Cl(Et$_3$P)Pt(PPh$_2$O)$_2$BF$_2$]

This complex was prepared for nmr experiments by the reaction of $BF_3 \cdot OEt_2$ with $[PtCl(PEt_3)\{(PPh_2O)_2H\}]$ as previously described (5). ^{195}Pt nmr: δ −134.93 ppm (ddd, Ξ 21.397113 MHz).

[Cl(Et$_3$P)Pt(μ-PPh$_2$O)$_2$Ti(acac)Cl$_2$]

A solution of $[Pt_2Cl_2\{(PPh_2O)_2H\}_2]$ (0.10 g, 0.13 mmol) in dichloromethane (10 mL) was added dropwise to a stirred solution of $[Ti(acac)_2Cl_2]$ (0.04 g, 0.13 mmol) in the same solvent (10 mL). After 2 h the solvent was removed *in vacuo*. The residue was washed with diethyl ether followed by toluene and recrystallized from dichloromethane/diethyl ether to give $[Cl(Et_3P)Pt(\mu\text{-}PPh_2O)_2Ti(acac)Cl_2]$ as orange–yellow crystals. *Anal.* calcd. for $C_{35}H_{42}Cl_3O_4P_3PtTi.(1/2)CH_2Cl_2$: C 42.2, H 4.29; found: C 42.4, H 4.19. mp 227–228°C.

^{31}P nmr spectra of this product showed the presence of two isomers and a third isomer was seen in the spectrum of the toluene extract (see Results and discussion section).

[PtCl(PEt$_3$){(PPh$_2$O)$_2$Na}]

$[PtCl(PEt_3)\{(PPh_2O)_2H\}]$ (ca. 0.2 mmol) was heated under reflux in tetrahydrofuran (20 mL) for 15 min with a 2–3 fold excess of NaH (ca. 0.5 mmol as a dispersion in mineral oil). The mixture was filtered to yield a clear yellow solution of $[PtCl(PEt_3)\{(PPh_2O)_2Na\}]$. The solution was then used as a reagent in the following four preparations:

1. [Cl(Et$_3$P)Pt(μ-PPh$_2$O)$_2$Pt(PEt$_3$)$_2$][BF$_4$]

A suspension of $[Pt_2Cl_2(PEt_3)_4][BF_4]_2$ (0.10 g, 0.09 mmol) in tetrahydrofuran (10 mL) was added dropwise to a solution of $[PtCl(PEt_3)\{(PPh_2O)_2Na\}]$ (0.18 mmol) in the same solvent (20 mL) and the mixture was stirred for 3 h to give a clear, colourless solution. The solvent was removed *in vacuo* and the residue washed with diethyl ether and recrystallized from tetrahydrofuran/diethyl ether to give $[Cl(Et_3P)Pt(\mu\text{-}PPh_2O)_2Pt(PEt_3)_2][BF_4]$ (0.16 g, 0.12 mmol) as colourless crystals. *Anal.* calcd. for $C_{42}H_{65}BClF_4O_2P_5Pt_2$: C 39.7, H 5.16; found: C 39.7, H 5.24. mp 223–225°C (dec.). ^{195}Pt nmr: δ +48.94 (ddd, Ξ 21.401047 MHz), +354.20 ppm (t, 21.407580 MHz).

2. [Cl(Et$_3$P)Pt(μ-PPh$_2$O)$_2$Pd(PEt$_3$)$_2$][ClO$_4$]

A procedure identical to *1* above but using $[PtCl(PEt_3)\{(PPh_2O)_2Na\}]$ (0.20 mmol) and $[Pd_2Cl_2(PEt_3)_4][ClO_4]_2$ (0.095 g, 0.10 mmol) gave $[Cl(Et_3P)Pt(\mu\text{-}PPh_2O)_2Pd(PEt_3)_2][ClO_4]$ (0.14 g, 0.12 mmol) as colourless crystals. *Anal.* calcd. for $C_{42}H_{65}Cl_2O_6P_5PdPt$: C 42.3, H 5.49; found C 42.6, H 5.59.

The analogous compound, $[Cl(Bu^n_3P)Pt(\mu\text{-}PPh_2O)_2Pd(PEt_3)_2][BF_4]$, was prepared on a small scale for nmr experiments by a similar procedure. ^{195}Pt nmr: δ +43.00 ppm (ddd, Ξ 21.400920 MHz).

3. [Cl(Et$_3$P)Pt(μ-PPh$_2$O)$_2$Rh(COD)]

A solution of $[Rh_2Cl_2(COD)_2]$ (0.049 g, 0.10 mmol) in tetrahydrofuran (10 mL) was added to a solution of $[PtCl(PEt_3)\{(PPh_2O)_2Na\}]$ (0.20 mmol) in the same solvent (20 mL). The reaction mixture was stirred for 8 h before filtration through Celite and removal of the solvent *in vacuo*. Extraction of the residue with diethyl ether and addition of hexane to the extract gave $[Cl(Et_3P)Pt(\mu\text{-}PPh_2O)_2Rh(COD)]$ (0.06 g, 0.06 mmol) as yellow crystals. *Anal.* calcd. for $C_{38}H_{47}ClO_2P_3PtRh$: C 47.4, H 4.92; found: C 47.6, H 4.37. Dec. > 184°C.

4. [Cl(Et$_3$P)Pt(μ-PPh$_2$O)$_2$Ir(COD)]

A procedure identical to *3* above but using $[Ir_2Cl_2(COD)_2]$ in place of the Rh analogue gave an orange solution which was shown by ^{31}P nmr to contain mainly $[Cl(Et_3P)Pt(\mu\text{-}PPh_2O)_2Ir(COD)]$. Attempts to isolate a solid product resulted in decomposition.

(b) X-ray data collection

$[Cl(Et_3P)Pt(\mu\text{-}PPh_2O)_2Pt(PEt_3)_2][BF_4]$ (**III**) was prepared as des-

TABLE 4. Bond angles* (deg)

Atoms	Angle	Atoms	Angle
P(1)—Pt(1)—Cl	86.9(2)	C(3)—C(2)—C(1)	119.5(16)
P(2)—Pt(1)—Cl	168.6(2)	C(4)—C(3)—C(2)	119.0(16)
P(2)—Pt(1)—P(1)	88.6(1)	C(5)—C(4)—C(3)	122.5(16)
P(3)—Pt(1)—Cl	84.1(2)	C(6)—C(5)—C(4)	118.8(17)
P(3)—Pt(1)—P(1)	166.4(2)	C(5)—C(6)—C(1)	120.2(15)
P(3)—Pt(1)—P(2)	102.0(2)	C(8)—C(7)—P(1)	124.2(12)
P(5)—Pt(2)—P(4)	98.5(2)	C(12)—C(7)—P(1)	115.1(12)
O(1)—Pt(2)—P(4)	90.4(3)	C(12)—C(7)—C(8)	120.5(15)
O(1)—Pt(2)—P(5)	170.7(3)	C(9)—C(8)—C(7)	118.6(15)
O(2)—Pt(2)—P(4)	175.8(3)	C(10)—C(9)—C(8)	119.7(18)
O(2)—Pt(2)—P(5)	85.2(3)	C(11)—C(10)—C(9)	122.9(19)
O(2)—Pt(2)—O(1)	85.8(4)	C(12)—C(11)—C(10)	119.4(18)
O(1)—P(1)—Pt(1)	120.2(4)	C(11)—C(12)—C(7)	118.9(16)
C(1)—P(1)—Pt(1)	107.6(6)	C(14)—C(13)—P(2)	123.8(12)
C(1)—P(1)—O(1)	101.1(7)	C(18)—C(13)—P(2)	117.1(12)
C(7)—P(1)—Pt(1)	111.4(6)	C(18)—C(13)—C(14)	119.1(15)
C(7)—P(1)—O(1)	107.7(7)	C(15)—C(14)—C(13)	120.2(15)
C(7)—P(1)—C(1)	107.9(7)	C(16)—C(15)—C(14)	117.7(17)
O(2)—P(2)—Pt(1)	114.1(4)	C(17)—C(16)—C(15)	124.0(19)
C(13)—P(2)—Pt(1)	114.9(5)	C(18)—C(17)—C(16)	117.9(17)
C(13)—P(2)—O(2)	100.1(7)	C(17)—C(18)—C(13)	121.0(15)
C(19)—P(2)—Pt(1)	113.1(6)	C(20)—C(19)—P(2)	121.9(13)
C(19)—P(2)—O(2)	108.6(7)	C(24)—C(19)—P(2)	118.2(13)
C(19)—P(2)—C(13)	104.9(7)	C(24)—C(19)—C(20)	119.9(15)
C(25)—P(3)—Pt(1)	112.4(6)	C(21)—C(20)—C(19)	119.1(17)
C(27)—P(3)—Pt(1)	114.8(5)	C(22)—C(21)—C(20)	120.7(20)
C(27)—P(3)—C(25)	106.2(6)	C(23)—C(22)—C(21)	121.3(23)
C(29)—P(3)—Pt(1)	114.1(5)	C(24)—C(23)—C(22)	121.0(23)
C(29)—P(3)—C(25)	103.5(6)	C(23)—C(24)—C(19)	118.0(18)
C(29)—P(3)—C(27)	104.8(5)	C(26)—C(25)—P(3)	116.1(16)
C(31)—P(4)—Pt(2)	119.6(6)	C(28)—C(27)—P(3)	123.3(17)
C(33)—P(4)—Pt(2)	110.4(6)	C(30)—C(29)—P(3)	122.0(14)
C(33)—P(4)—C(31)	102.8(8)	C(32)—C(31)—P(4)	110.4(14)
C(35)—P(4)—Pt(2)	112.6(6)	C(34)—C(33)—P(4)	113.9(13)
C(35)—P(4)—C(31)	104.7(9)	C(36)—C(35)—P(4)	111.9(14)
C(35)—P(4)—C(33)	105.4(8)	C(38)—C(37)—P(5)	107.5(17)
C(37)—P(5)—Pt(2)	110.1(8)	C(40)—C(39)—P(5)	115.0(17)
C(39)—P(5)—Pt(2)	110.6(7)	C(42)—C(41)—P(5)	112.2(15)
C(39)—P(5)—C(37)	99.6(10)	F(2)—B(1)—F(1)	116 (4)
C(41)—P(5)—Pt(2)	121.4(7)	F(3)—B(1)—F(1)	115 (3)
C(41)—P(5)—C(37)	105.4(10)	F(3)—B(1)—F(2)	113 (3)
C(41)—P(5)—C(39)	107.5(9)	F(4)—B(1)—F(1)	96 (3)
P(1)—O(1)—Pt(2)	126.8(6)	F(4)—B(1)—F(2)	107 (3)
P(2)—O(2)—Pt(2)	132.8(6)	F(4)—B(1)—F(3)	107 (3)
C(2)—C(1)—P(1)	117.0(12)		
C(6)—C(1)—P(1)	123.1(12)		
C(6)—C(1)—C(2)	119.9(14)		

*Estimated standard deviations are given in parentheses.

cribed above and a crystal suitable for study by X-ray diffraction was grown by vapour diffusion of diethyl ether into a solution of the complex in tetrahydrofuran. Preliminary photographic work was carried out with Weissenberg and precession cameras using Cu K_α radiation. After establishment of symmetry and an approximate unit cell the crystal was transferred to a Picker 4-circle diffractometer automated with a PDP11/10 computer and utilising Zr filtered Mo K_α radiation (λ = 0.71069 Å). The unit cell was refined by least-squares methods employing 10 pairs of centering measurements at $\pm 2\theta$ in the range $|2\theta|$ = 10–39°. The crystal was mounted approximately along the c axis. The crystal data at approximately 26°C were as follows:

$C_{42}H_{65}BClF_4O_2P_5Pt_2$ M_r = 1269.3

Monoclinic, space group $P2_1/n$, equivalent positions $x, y, z; -x, -y, -z; \frac{1}{2}+x, \frac{1}{2}-y, \frac{1}{2}+z; \frac{1}{2}-x, \frac{1}{2}+y, \frac{1}{2}-z$; a = 13.018(2), b = 34.205(9), c = 11.279(2) Å; β = 91.71(2)°; V(cell) = 5020(2) Å^3; D_m = 1.66 g cm^{-3} (flotation in $CCl_4/CHBr_3$), D_c = 1.68 g cm^{-3}; Z = 4; asymmetric unit = one molecule.

Intensity measurements were collected for two reciprocal space octants (h unrestricted, $k \geq 0$, $l \geq 0$) up to 2θ = 40°. A $\theta/2\theta$ step scan was used with 104 steps of 0.01° in 2θ, counting for 0.25 s per step. Background measurements were for 13 s at each end of the scan. Each batch of 50 reflections was preceded by the measurement of three standard reflections (0, 0, 6; 4, 0, 0; and 0, 10, 0;). The Lorentz and polarization factors were applied and each batch was scaled to maintain the sum of the standards constant. There was no evidence of sample decomposition during the data collection. Absorption corrections were applied with a numerical integration procedure utilizing a 10 × 8 × 14 Gaussian grid. The crystal shape was defined by perpendicular distances to crystal faces from a central origin as follows: ±{001},

0.2121 mm; ±{100}, 0.1183 mm; ±{010}, 0.0334 mm. The absorption coefficient was 61.18 cm^{-1} and the range of transmission factors 0.23–0.66.

(c) Structure solution and refinement

The structure was found and refined using the SHELX-76 program package (46), and illustrations were drawn using ORTEP (47). The atomic scattering factors used were for neutral atoms, with corrections for anomalous dispersion (48). The structure was solved by direct methods, developed by standard Fourier synthesis procedures using difference maps, and refined by the method of least squares minimising $\Sigma w\Delta^2$ where $\Delta = ||F_o| - |F_c||$. The weights were obtained from counting statistics using $w = 1/(\sigma^2(F) + 0.001F^2)$. Reflections for which $I < 2.5\sigma(I)$ were suppressed from the calculations and reflection (0,2,0), which was intense and at very low angle due to the length of the *b*-axis, was also omitted leaving 3813 of the initial 4680 independent measurements.

The PEt_3 group containing P(3) could not be determined in the same way as the other PEt_3 groups. This was attributed to disorder, but no double imaging of the group was obtained. The difficulty was mainly with two of the ethyl groups, C(27)—C(30), so the well behaved group C(25)—C(26) was used to help locate the other atoms. The following constraints (which did not entirely dominate the X-ray intensities) were applied:

P(3)—C(27), P(3)—C(29) = 1.820(1) Å

C(27)—C(28), C(29)—C(30) = 1.54(1) Å

C(25)—C(27), C(27)—C(29), C(29)—C(25) = 2.88(1) Å

Pt—C(27), Pt—C(29) = 3.517(10) Å

There were 269 parameters to be determined from 3813 independent observations. Hydrogen atoms were not located. All atoms heavier than fluorine were treated as vibrating anisotropically. Convergence was obtained with a maximum shift/esd ratio of 0.12 for the cation excluding the constrained PEt_3 ligand (1.66), and 0.29 for the BF_4^- anion. The residuals were $R = 0.0499$ and $R_w = (\Sigma w\Delta^2/\Sigma wF_o^2)^{1/2} = 0.0707$. The final difference map had a maximum of +1.9 e $Å^{-3}$ close to the disordered group and a minimum of −0.83 e $Å^{-3}$ but gave no indication that any material had been overlooked.

Acknowledgements

We thank the Natural Sciences and Engineering Research Council of Canada and the University of Victoria for research grants, and Mrs. C. Greenwood for recording nmr spectra.

1. D. E. Berry, K. A. Beveridge, G. W. Bushnell, and K. R. Dixon. Can. J. Chem. **63**, 2949 (1985).
2. D. E. Berry, K. A. Beveridge, G. W. Bushnell, K. R. Dixon, and A. Pidcock. Can. J. Chem. **64**, 343 (1986).
3. D. M. Roundhill, R. P. Sperline, and W. B. Beaulieu. Coord. Chem. Rev. **26**, 263 (1978); B. Walther. Coord. Chem. Rev. **60**, 67 (1984).
4. R. Fawzi, W. Hiller, I. P. Lorenz, J. Mohyla, and C. Zeiher. J. Organomet. Chem. **262**, C43 (1984).
5. E. H. Wong, F. C. Bradley, and E. J. Gabe. J. Organomet. Chem. **244**, 235 (1983).
6. G. M. Gray and C. S. Kraihanzel. J. Organomet. Chem. **146**, 23 (1978).
7. F. A. Cotton, L. R. Falvello, M. Tomas, G. M. Gray, and C. S. Kraihanzel. Inorg. Chim. Acta, **82**, 129 (1984).
8. I. W. Robertson and T. A. Stephenson. Inorg. Chim. Acta, **45**, L215 (1980).
9. T. G. Southern, P. H. Dixneuf, J. Y. Le Marouille, and D. Grandjean. Inorg. Chem. **18**, 2987 (1979).
10. J. A. S. Duncan, D. Heddon, D. M. Roundhill, T. A. Stephenson, and M. D. Walkinshaw. Angew. Chem. Int. Ed. Engl. **21**, 452 (1982).
11. J. A. S. Duncan, T. A. Stephenson, W. B. Beaulieu, and D. M. Roundhill. J. Chem. Soc. Dalton Trans. 1755 (1983).
12. H. Werner and T. N. Khac. Inorg. Chim. Acta, **30**, L347 (1979).
13. A. Pidcock and C. R. Waterhouse. J. Chem. Soc. A, 2080 (1970).
14. F. H. Allen, A. Pidcock, and C. R. Waterhouse. J. Chem. Soc. A, 2087 (1970).
15. K. R. Dixon and A. D. Rattray. Can. J. Chem. **49**, 3997 (1971).
16. E. H. Wong and F. C. Bradley. Inorg. Chem. **20**, 2333 (1981).
17. M. C. Cornock, R. O. Gould, C. L. Jones, and T. A. Stephenson. J. Chem. Soc. Dalton Trans. 1307 (1977).
18. D. V. Naik, G. J. Palenik, S. Jacobson, and A. J. Carty. J. Am. Chem. Soc. **96**, 2286 (1974).
19. J. M. Solar, R. D. Rogers, and W. R. Mason. Inorg. Chem. **23**, 373 (1984).
20. K. R. Dixon and A. D. Rattray. Inorg. Chem. **16**, 209 (1977).
21. R. P. Sperline, M. K. Dickson, and D. M. Roundhill. J. Chem. Soc. Chem. Commun. 62 (1977).
22. R. P. Sperline and D. M. Roundhill. Inorg. Chem. **16**, 2612 (1977).
23. J. R. Allan, G. H. W. Milburn, T. A. Stephenson, and P. M. Veitch. J. Chem. Res. (S), **83**, 215 (1983).
24. J. R. Allan, G. H. W. Milburn, L. Sawyer, V. K. Shah, T. A. Stephenson, and P. M. Veitch. Acta Crystallogr. C, **41**, 58 (1985).
25. R. T. Paine, E. N. Duesler, and D. C. Moody. Organometallics, **1**, 1097 (1982).
26. R. E. Marsh. Acta Crystallogr. C **41**, 1383 (1985).
27. R. J. Goodfellow and B. F. Taylor. J. Chem. Soc. Dalton Trans. 1676 (1974).
28. W. McFarlane. J. Chem. Soc. A 1922 (1967).
29. R. P. Sperline, W. B. Beaulieu, and D. M. Roundhill. Inorg. Chem. **17**, 2032 (1978).
30. J. A. Pople, W. G. Schneider, and H. J. Bernstein. High resolution NMR. McGraw-Hill, New York. 1959. p. 139.
31. T. W. Dingle and K. R. Dixon. Inorg. Chem. **13**, 846 (1974).
32. D. E. Berry, G. W. Bushnell, and K. R. Dixon. Inorg. Chem. **21**, 957 (1982).
33. S. G. N. Roundhill and D. M. Roundhill. Acta Crystallogr. B **38**, 2479 (1982).
34. G. G. Mather, A. Pidcock and G. J. N. Rapsey. J. Chem. Soc. Dalton Trans. 2095 (1973).
35. F. R. Hartley. Chem. Soc. Rev. **2**, 163 (1973).
36. G. W. Bushnell. Can. J. Chem. **56**, 1773 (1978).
37. R. G. Kidd and R. J. Goodfellow. *In* NMR and the Periodic Table. *Edited by* R. K. Harris and B. E. Mann. Academic Press, London. 1978. p. 249.
38. R. B. Johannsen, J. A. Ferreti, and R. K. Harris. J. Magn. Reson. **3**, 84 (1970).
39. J. D. Swalen. *In* Computer programmes for chemistry. Vol. I. *Edited by* D. F. Detar. W. A. Benjamin, New York. 1968.
40. L. E. Marchi. Inorg. Synth. **2**, 10 (1946).
41. V. Doron. Inorg. Synth. **7**, 50 (1963); **8**, 8 (1966).
42. R. J. Goodfellow and L. M. Venanzi. J. Chem Soc. 7533 (1965).
43. K. R. Dixon and D. J. Hawke. Can. J. Chem. **49**, 3252 (1971).
44. J. Chatt and L. M. Venanzi. J. Chem. Soc. 4735 (1957).
45. J. L. Herde, J. C. Lambert, and C. V. Senoff. Inorg. Synth. **15**, 18 (1974).
46. G. M. Sheldrick. SHELX-76. A computer program for crystal structure determination. University of Cambridge, Cambridge, England. 1976.
47. C. K. Johnson. ORTEP: A Fortran thermal ellipsoid plot program for crystal structure illustrations. ORNL-3794, Oak Ridge National Laboratory, Oak Ridge, U.S.A. 1965.
48. D. T. Cromer and J. T. Waber. *In* International tables for X-ray crystallography. Vol. 4. *Edited by* J. A. Ibers and W. C. Hamilton. Kynoch Press, Birmingham, England. 1974. pp. 99, 148.

Syntheses of model oligosaccharides of biological significance. 7. Synthesis of a fucosylated *N,N'*-diacetylchitobioside linked to bovine serum albumin and immunochemical characterization of rabbit antisera to this structure[1,2]

HO-HUAT LEE AND DAVID A. SCHWARTZ
Ludwig Institute for Cancer Research, Toronto Branch, 9 Earl Street, Toronto, Ont., Canada M4Y 1M4

JOHN F. HARRIS
London Regional Cancer Centre, 391 South Street, London, Ont., Canada N6A 4G5

JEREMY P. CARVER
Departments of Medical Genetics and Medical Biophysics, University of Toronto, Toronto, Ont., Canada M5S 1A8

AND

JIRI J. KREPINSKY[3]
Ludwig Institute for Cancer Research, Toronto Branch, 9 Earl Street, Toronto, Ont., Canada M4Y 1M4, and Departments of Medical Biophysics and Medical Genetics, University of Toronto, Toronto, Ont., Canada M5S 1A8

Received February 4, 1986

HO-HUAT LEE, DAVID A. SCHWARTZ, JOHN F. HARRIS, JEREMY P. CARVER, and JIRI J. KREPINSKY. Can. J. Chem. **64**, 1912 (1986).

Synthesis of methoxycarbonyloctyl 2-acetamido-4-*O*-[(2′-acetamido-2′-deoxy-β-D-glucopyranosyl)-6-*O*-α-L-fucopyranosyl]-2-deoxy-β-D-glucopyranoside as shown in Scheme 1 is described together with coupling it with bovine serum albumin and poly-L-lysine. Mouse and rabbit antisera to the BSA conjugate were prepared and partially characterized.

HO-HUAT LEE, DAVID A. SCHWARTZ, JOHN F. HARRIS, JEREMY P. CARVER et JIRI J. KREPINSKY. Can. J. Chem. **64**, 1912 (1986).

On décrit la synthèse l'acétamido-2 *O*-4-[(acétamido-2′ déoxy-2′ β-D-glucopyrannosyl) *O*-6-α-L-fucopyrannosyl] déoxy-2 β-D-glucopyrannoside de méthoxycarbonyloctyle, réalisée suivant le schéma 1, ainsi que son couplage avec l'albumine du sérum de boeuf et la poly-L-sérine. On a aussi préparé et partiellement caractérisé des antisérum de souris et de lapin du conjugé du ASB.

[Traduit par la revue]

Any success of contemporary cancer therapy depends heavily on early diagnosis of the disease, i.e. before a widespread invasion and dissemination occurs (1). Since clinical symptoms appear usually when the disease is in a relatively advanced stage, it is of importance to characterize reliable and easily detectable chemical markers (bio-, immuno-) of the onset of neoplasia and malignancy. It has been shown in numerous studies that unusual carbohydrate structures appear both in neoplasia and cancer (2–6). The carbohydrate structures in an appropriate form are usually immunogenic and consequently can be used for the preparation of antibodies which in turn can recognize the original carbohydrate structure. Appropriately modified or as such, the antibodies can serve as diagnostic reagents. The high specificity required can be best achieved by using in the immunization protocol a well-characterized, chemically pure, oligosaccharide antigen. In theory, such an antigen could be available from natural sources. These oligosaccharides are, however, obtainable from natural sources in minute quantities only, and their purity can never be assured entirely even after tedious and time-consuming purification procedures. Chemical synthesis eliminates these problems, and moreover allows to vary structural parameters as necessary for different uses. Since we have centered our attention on large bowel cancer, we have initiated a program of syntheses of oligosaccharide cancer markers associated with this particular site, and of studies of antibodies to these oligosaccharides.

One of the structures of interest is a class of oligosaccharide structures represented certain saccharide moieties of *N*-linked glycoproteins. A characteristic invariant basic structure of this class is portrayed in formula **1**. This structural element has been shown to exist in γ-glutamyltranspeptidase (in liver) and carcinoembryonic antigen (7, 8) in cancer but not in the absence of the disease. The "normal" oligosaccharides lack either *N*-acetylglucosamine or fucose or both (cf. underlined fragments in **1**). We have decided to synthesize **1** in two parts (cf. *a* and *b* in **1**), and investigate the immunochemistry of both fragments separately. This approach will help in the recognition and elimination of antibodies cross-reacting with the small fragments of **1** when the antibodies to the complete **1** are made.

In order to synthesize fragment *a* and link it to bovine serum albumin (and poly-L-lysine as an immunoadsorbent for immunoassays) we have modified a procedure employed previously for the synthesis of a methyl glycoside of the trisaccharide *a* (9). We have chosen to connect the trisaccharide with the carrier, i.e. bovine serum albumine, with a linker proposed by Lemieux *et al.* (10) and successfully used by others as well (11). Ethyl 9-hydroxynonanoate has been used in the first step (ref. 10; cf. Scheme 1) since it was easier to prepare it than a corresponding methyl ester. Its preparation involves diborane reduction of the free carboxyl group in a monoester of azelaic acid, and the methyl carboxylate is reduced to a significant extent whereas ethyl carboxylate is not. In the first Zemplén deacetylation, quantitative exchange to give the methyl ester occurs. Since the linker carries an alkali-labile methoxycarbonyl group, care had

[1]For part 6, see D. M. Whitfield, J. P. Carver, and J. J. Krepinsky, J. Carbohydr. Chem. **4**, 369 (1985).

[2]Presented at 8th International Glycoconjugate Symposium, Houston, TX, September 1985.

[3]Author to whom correspondence should be addressed.

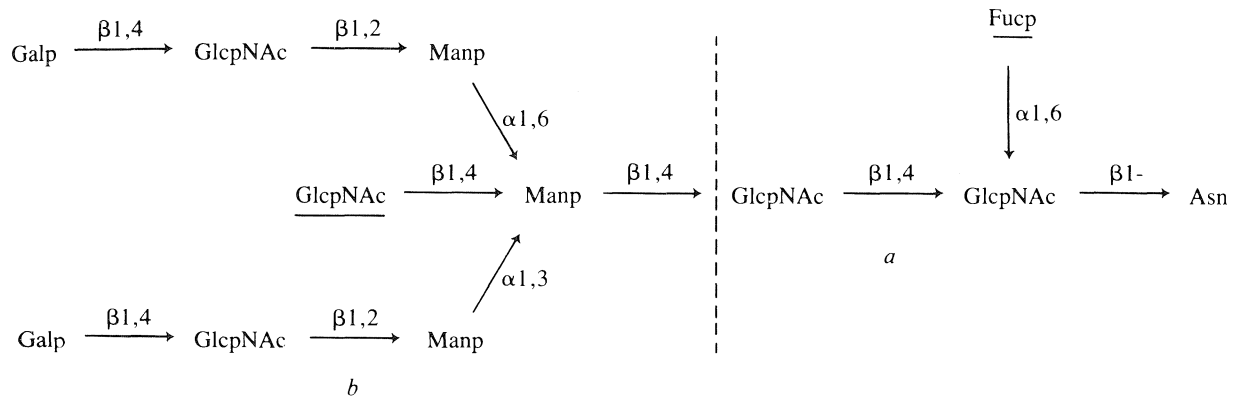

1

to be taken to avoid any condition causing hydrolysis of this ester group. In practice it meant maintaining anhydrous conditions even more carefully than usual in most steps. Particularly difficult was the hydrazinolysis of the phthalimido protective group, since a number of conditions led to the hydrolysis of the ester group. Eventually, hydrazine acetate was found to be compatible with the presence of the ester group. Phthalimido protection of the amino function was used to avoid a potential problem of imidate formation (12) by an acetamido group in glycosylation reactions using strong promoters, as required for the formation of the 1,4 linkage in chitobiose. It has also been found that the simplest approach is to form a chitobiose derivative first, and to connect it with a fucosyl derivative (13) in the second stage. The reaction pathway is depicted in Schemes 1 and 2 which are self-explanatory. Acetylation after complete deprotection was found to be necessary for the purification of the trisaccharide since it allowed for easy chromatographic separation on silica gel. Not only did this chromatography remove unwanted by-products but also inorganic ions introduced during the hydrogenolysis of the benzyl groups. The inorganic ions caused unacceptable broadening of ^{1}H nmr signals (14).

We have found FAB mass spectrometry extremely useful for both identification and purity determination of synthetic intermediates. We report in this article *m/e* values for M-derived ions; the complete analysis, however, of the FAB mass spectra of compounds reported here, together with other carbohydrate intermediates, will be published elsewhere.

Finally, this trisaccharide ester was coupled to two different carrier molecules, bovine serum albumin (BSA) or poly-L-lysine, using a recent modification of the standard procedure (11). The trisaccharide ester **15***a* was first converted into the acyl hydrazide and subsequently, by treatment with dinitrogen tetroxide into the acyl azide which was then attached to BSA or poly-L-lysine. Quantitative determination (16) of incorporation by the colorimetric phenolsulphuric acid method showed incorporation of 10.5 molecules of carbohydrate per molecule of BSA and 1.9 carbohydrate molecules per poly-L-lysine molecule (mw_{ave} 16 000).

The synthetic antigen **15***b* was used to immunize (17) both rabbits and mice. The specificity of binding of rabbit antisera to the trisaccharide determinant **15***a* was determined in a preliminary fashion by competition analysis with various oligosaccharides using a solid-phase immunoassay (18) on the solid state substrate **15***c*. For detection of solid phase binding of the antibodies, ^{125}I-protein A was used. The binding specificity was expressed in terms of the molar concentrations of various oligosaccharides and their derivatives required to inhibit 50% of the binding of a non-saturating concentration of rabbit sera (2×10^{-4}) and the values found are summarized in Table 1. As can be seen from the Table 1, the only effective inhibitors were the trisaccharide derivatives **15**. Other segments of the structure **1** or its variations (cf. Table 1) did not exhibit any binding to the rabbit antibodies. Similar results were obtained with mice. The analysis of rabbit antisera and the biochemical characterization of the purified antibodies is in progress and will be published elsewhere.

Experimental

General methods

Melting points were determined on a Reichert Thermovar melting point apparatus and are uncorrected. Optical rotations were measured with a Perkin-Elmer polarimeter (Model 140) at 26 ± 1°C. Microanalyses were performed by the Microanalytical Laboratory Ltd., Markham, Ont. ^{1}H nmr spectra were recorded at 360 MHz with a Nicolet spectrometer at the Toronto Biomedical NMR Centre, University of Toronto (Director: Dr. A. A. Grey). They were obtained at 23 ± 2°C either in $CDCl_3$ containing 1% TMS as the internal standard or in D_2O (99.996%, Merck, Sharp, and Dohme) with acetone (0.1%, 2.225 ppm relative to internal DSS) as the internal standard. Infrared spectra were recorded with a Perkin-Elmer (Model 1430) Infrared Spectrometer, and calibrated at 1601 cm^{-1} of polystyrene film. FAB mass spectrometry was performed using thioglycerol matrix and ±NaOAc with a VG Analytical ZAB HF reversed geometry instrument (for general conditions, cf. ref. 19, and references therein) at the Institute of Physiological Chemistry, University of Bonn through the courtesy of Dr. H. Egge.

Thin layer chromatography (tlc) was performed on silica gel 60 F_{254} (Merck) plastic plates and visualized by quenching of ultraviolet fluorescence and (or) spraying with 50% aqueous sulfuric acid and heating at 100°C. Silica gel 60 (230–400 mesh; Merck) was used for flash column chromatography. All starting materials were dried overnight over KOH or P_2O_5 *in vacuo* prior to use. All solvents were distilled from appropriate drying agents. Unless stated otherwise, all reactions were carried out under anhydrous conditions and in an argon atmosphere. Solvents were removed at reduced pressures using a rotary evaporator at temperatures not exceeding 40°C.

*8-Ethoxycarbonyloctyl 3,4,6-tri-O-acetyl-2-deoxy-2-phthalimido-β-D-glucopyranoside (**4**a; 15)*

To a mixture of the bromide **2** (1.5 g, 3.01 mmol) and silver zeolite (1.5 g) in dry dichloromethane (9 mL) was added a solution of 8-ethoxycarbonyloctylalcohol (**3***a*; 0.73 g, 3.61 mmol) prepared according to ref. 10 in dichloromethane (9 mL) under stirring and protection from light at room temperature.[4] After 18 h, an additional amount of **3***a* (0.12 g, 0.60 mmol) in dichloromethane (2 mL) was

[4]This compound and some other intermediates were purchased from TRC (Toronto Research Chemicals), 4483 Chesswood Drive, Downsview, Ont., Canada M5J 2C3.

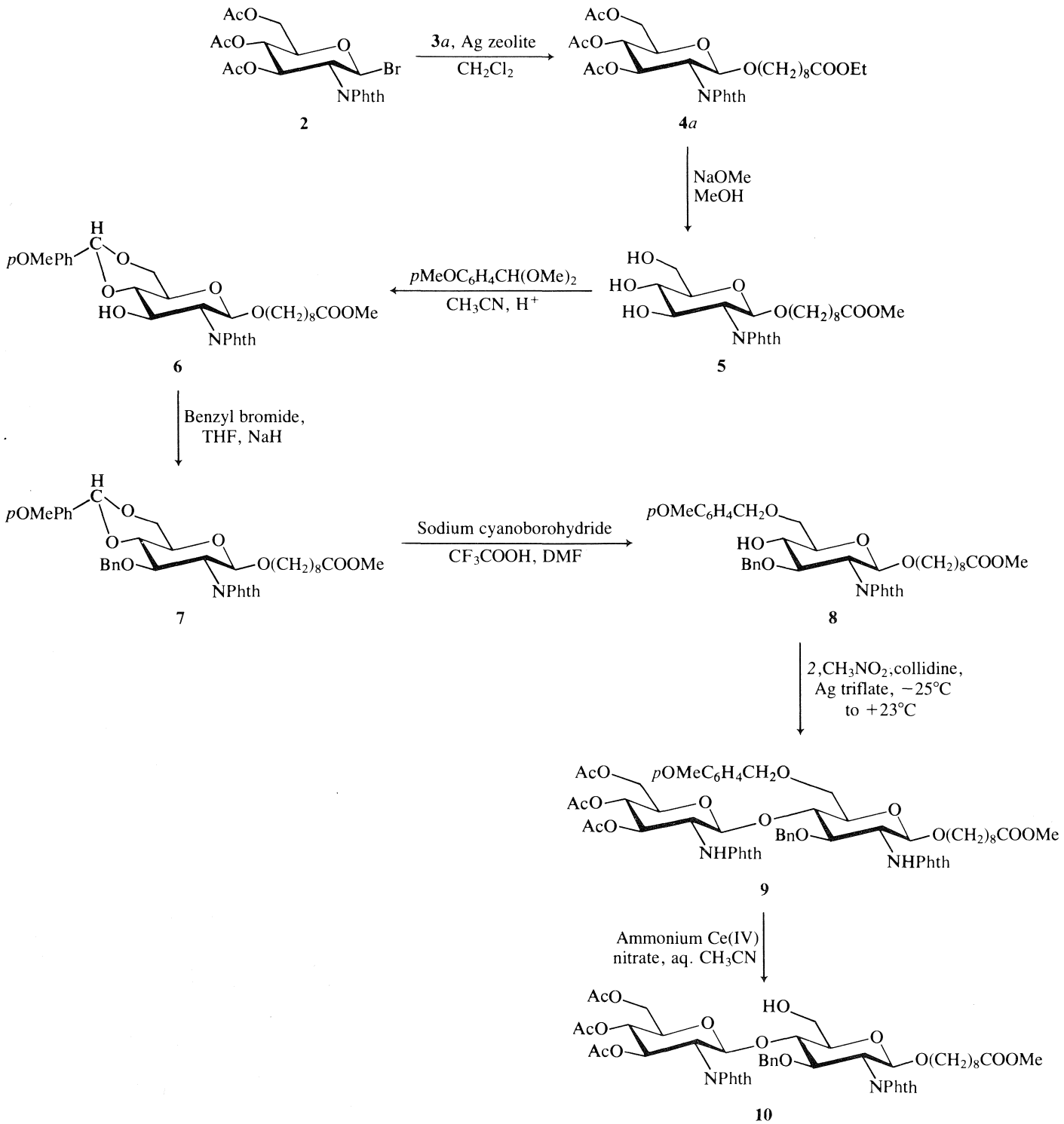

SCHEME 1

added and stirring in the dark was continued for 22 h. The mixture was then filtered through Celite, the Celite was washed with dichloromethane, the combined filtrates and washings (100 mL) were washed with cold aqueous sodium bicarbonate (100 mL) and water (2 × 50 mL), dried over Mg_2SO_4, and concentrated to give a light yellow syrup (2.13 g). The latter was subjected to chromatography on a silica gel column using hexane/ethyl acetate (3:1) to give slightly yellow syrupy **4***a* (1.0 g, 54%), R_f 0.42 (sixfold development in the above solvent mixture); $[\alpha]_D$ +21.2° (c. 1.3, $CHCl_3$); ir (neat) 1780, 1750, 1720 cm^{-1} (CO); ^1H nmr δ: 7.75–7.92 (m, 4H, $N[CO]_2C_6H_4$), 5.80 (dd, 1H, J = 10.7 and 9.1 Hz, H-3), 5.36 (d, 1H, J = 8.5 Hz, H-1), 5.19 (dd, 1H, J = 10.0 and 9.3 Hz, H-4), 4.29–4.37 (m, 2H, H-2 and H-6), 4.18 (dd, 1H, J = 12.3 and 2.3 Hz, H-6′), 4.13 (q, J = 7.1 Hz, OCH_2CH_3), 3.81–3.90 and 3.40–3.47 (2m, 3H, H-5, and $OCH_2(CH_2)_7$), 2.21 (t, 2H, J = 7.4 Hz, CH_2COOEt), 2.12, 2.04, 1.87 (3s, 9H, CH_3COO), 1.26 (t, 3H, J = 7.1 Hz, CH_2CH_3), 1.35–1.58 and 0.90–1.16 (2m, 12H, $[CH_2]_6$). *Anal.* calcd. for $C_{31}H_{41}NO_{12}$ (619.263): C 60.09, H 6.67, N 2.26; found: C 59.83, H 6.42, N 2.18. Molecular ions observed: $[MH]^+$ 620, $[MNa]^+$ 642.

*8-Methoxycarbonyloctyl 3,4,6-tri-*O*-acetyl-2-deoxy-2-phthalimido-β-*D*-glucopyranoside (**4**b)*

To a mixture of the bromide **2** (0.5 g, 1.00 mmol) and silver zeolite (0.5 g) in dry dichloromethane (3 mL) was added a solution of

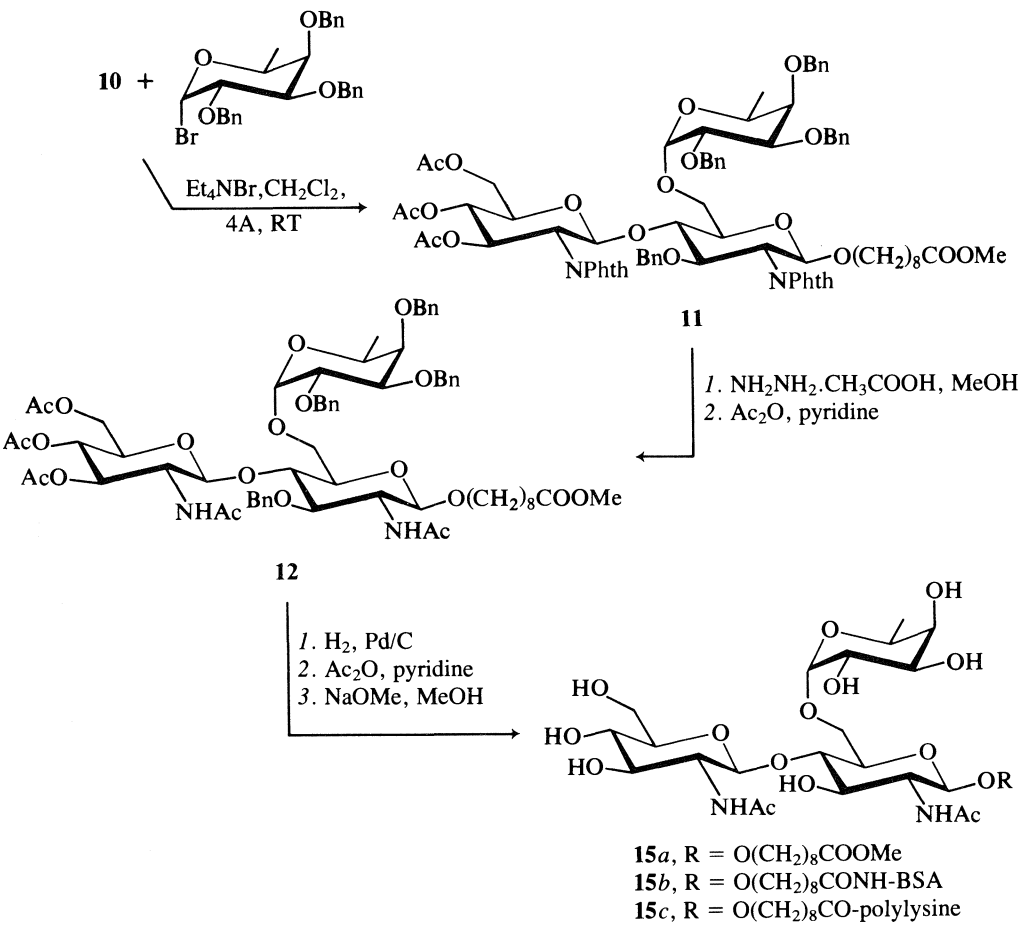

SCHEME 2

TABLE 1. Competition analyses of two rabbit sera raised against **15***b*[a]

Competitor[a]	C_{50} Rabbit 1	C_{50} Rabbit 2
15*b*	5×10^{-9}	7×10^{-9}
15*c*	6×10^{-7}	5×10^{-7}
16	1.4×10^{-5}	4×10^{-4}
17	3×10^{-4}	4×10^{-4}

[a]C_{50} is the molar concentration of carbohydrates and glycoconjugates required to inhibit 50% of the binding of a non-saturating concentration of rabbit sera (2×10^{-4}) using a solid phase immunoassay. The solid phase substrate was **15***c* and the detection of solid phase binding of antibodies was with ^{125}I-protein A. Compounds used in competition experiments were preincubated with the dilution of rabbit sera for 16 h in the presence of 1% BSA prior to the assay at 4°C. **16** is GlcNAcβ1,4(Fucα1,6)GlcNaCβ1,OMe; **17** is GlcNAcβ1,BSA. Other compounds tested were not effective competitors with $C_{50} > 10^{-3}$: GlcNAcβ1,4GlcNAcβ1,OBn (**18**); Fucα1,6GlcNAcβ1,OMe; Fucα1,4(Fucα1,6)GlcNAcβ1,OMe; Fucα1,3Galβ1,OMe; Fucα1,OMe; GlcNAcβ1,4GlcNAcβ1,OMe (9); Manα1,3Manα1,OMe; Manα1,6Manα1,OMe; Manα1,3(Manα1,6)Manα1,OMe (21); GlcNAcβ1,2Manα1,3(GlcNAcβ1,2-Manα1,6)Manβ1,4GlcNAcβ1,4GlcNAc; as well as purified oligosaccharides from fetuin, fibrinogen A1, and ovalbumin (these compounds were kindly provided by Dr. D. A. Cumming). Note that 3×10^{-2} of **18** for rabbit 2 was the next most effective concentration.

8-methoxycarbonyloctylalcohol (**3***b*; 0.24 g, 1.28 mmol) prepared according to ref. 10 in dichloromethane (3 mL) under stirring and protection from light at room temperature. After continued stirring for 19 h in dark, the mixture was filtered through Celite, the Celite was washed with dichloromethane, the combined filtrates and washings were washed with water (2 × 50 mL), dried over $MgSO_4$, and concentrated to give a light brown syrup (0.63 g) which was subjected to chromatography on a silica gel column using hexane/ethyl acetate (2:1) giving slightly yellow syrupy **4***b* (0.33 g, 54%), R_f 0.45 (four-fold development in the above solvent mixture); $[\alpha]_D$ +18.5° (c. 1.5, $CHCl_3$); ^{1}H nmr δ: 7.75–7.92 (m, 4H, N[CO]$_2$C$_6$*H*$_4$], 5.79 (dd, 1H, *J* = 10.7 and 9.1 Hz, H-3), 5.36 (d, 1H, *J* = 8.5 Hz, H-1), 5.18 (br t, 1H, *J* = 9.5 Hz, H-4), 4.27–4.37 (m, 2H, H-2 and H-6), 4.18 (dd, 1H, *J* = 12.2 and 2.3 Hz, H-6′), 3.80–3.90 and 3.39–3.47 (2m, 3H, H-5, and OC*H*$_2$(CH$_2$)$_7$), 3.68 (s, 3H, OC*H*$_3$), 2.23 (t, 2H, *J* = 7.5 Hz, C*H*$_2$COOMe), 2.12, 2.03, 1.87 (3s, 9H, C*H*$_3$COO), and 0.92–1.57 (m, 12H, [C*H*$_2$]$_6$). *Anal.* calcd. for $C_{30}H_{39}NO_{12}$ (605.247): C 59.50, H 6.49, N 2.31; found: C 59.71, H 6.61, N 2.28. Molecular ions observed: $[MH]^+$ 606, $[MNa]^+$ 628, $[MNH_4]^+$ 623.

*8-Methoxycarbonyloctyl 2-deoxy-2-phthalimido-β-D-glucopyranoside (**5**)*

Treatment of **4***a* (6.15 g, 9.94 mmol) in dry methanol (100 mL) with 1% sodium methoxide in methanol (100 mL) for 30 min, deionization with Dowex-1 (H^+, 37 mL, prewashed with methanol) at 0°C, addition of ethyl acetate (200 mL), filtration, and evaporation of the filtrate and of added toluene (150 mL) gave a thick syrup of **5** (4.77 g, 99%); R_f 0.43 (ethyl acetate); ir (neat): 3430 (OH), 1770, 1735, 1714 cm^{-1} (CO); ^{1}H nmr δ: 7.78 (m, 4H, N[CO]$_2$C$_6$*H*$_4$), 5.20 (d, 1H, *J* = 8.4 Hz, H-1), 3.66 (s, 3H, OC*H*$_3$), 2.22 (t, 2H, *J* = 7.5 Hz, C*H*$_2$COOCH$_3$). This product was used without further purification.

*8-Methoxycarbonyloctyl 2-deoxy-4,6-O-(4-methoxybenzylidene)-2-phthalimido-β-D-glucopyranoside (**6**)*

To a mixture of **5** (4.76 g, 9.94 mmol) and 4-methoxybenzaldehyde dimethyl acetal (3.3 mL, 19.9 mmol) in acetonitrile (150 mL) was added *p*-toluenesulfonic acid monohydrate (120 mg) (20). The reaction mixture was stirred at room temperature and with light exclusion for 50 min, then it was poured into water (300 mL) and the product was

extracted into diethyl ether (3 × 250 mL). The ethereal solution was washed with cold aqueous sodium bicarbonate (200 mL) and water (200 mL), dried over $MgSO_4$, and evaporated to a light brown syrup which was subjected to chromatography on a silica gel column in hexane/ethyl acetate (2:1) yielding **6** (3.81 g, 64%) as a pale yellow syrup, $[\alpha]_D$ −36.2° (c. 0.87, $CHCl_3$), R_f 0.22 (solvent as above); ir (neat): 3487 (OH), 1778, 1735, 1715 cm^{-1} (CO); ^1H nmr δ: 7.89 and 7.75 (m, 4H, $N[CO]_2C_6H_4$), 7.44 and 6.93 (2m, 4H, $C_6H_4OCH_3$), 5.53 (s, 1H, C_6H_5CH), 5.26 (d, 1H, J = 8.5 Hz, H-1), 4.63 (ddd, 1H, J = 10.4, 8.6, and 3.2 Hz, H-3), 4.38 (dd, 1H, J = 10.4 and 4.2 Hz, H-6), 4.24 (dd, 1H, J = 10.5 and 8.5, H-2), 3.81 (s, 3H, $C_6H_4OCH_3$), 3.66 (s, 3H, $COOCH_3$), 3.37–3.87 (m, 5H, H-4, H-5, H-6′, and $OCH_2[CH_2]_7$), 2.44 (d, 1H, J = 3.3 Hz, exchangeable with D_2O, OH), 2.23 (t, 2H, J = 7.4 Hz, CH_2COOMe), 0.90–1.54 (m, 12H, $(CH_2)_6$). *Anal.* calcd. for $C_{32}H_{39}NO_{10}$ (597.369): C 64.31, H 6.58, N 2.34; found: C 64.42, H 6.61, N 2.39. Molecular ions observed: $[MH]^+$ 598, $[MNa]^+$ 620.

8-Methoxycarbonyloctyl 3-O-benzyl-2-deoxy-4,6-O-(4-methoxybenzylidene)-2-phthalimido-β-D-glucopyranoside (7)

A mixture of **6** (3.63 g, 6.07 mmol) and benzyl bromide (14.3 mL, 121 mmol) in dry THF (20 mL) was added to solid sodium hydride (390 mg, 9.71 mmol, prewashed with dry hexane), and the resulting reaction mixture was stirred in the dark at room temperature for 4 h. Additional sodium hydride (180 mg, 4.48 mmol) was added and the reaction mixture stirred for another 17 h. Then it was diluted with ethyl acetate (50 mL), filtered through Celite, washed with ethyl acetate (3 × 50 mL), and the combined filtrate and washings were washed with water (300 mL). The organic layer was separated, the aqueous layer extracted with ethyl acetate, all organic extracts were combined, washed once again with water (200 mL), dried over $MgSO_4$, and evaporated to dryness. The residue was subjected to chromatography on a silica gel column with hexane/ethyl acetate (3:1) to give **7** (3.76 g, 90%) as colorless plates, mp 88–89°C (hexane/ethyl acetate), $[\alpha]_D$ +27.4° (c. 1.0, $CHCl_3$); R_f 0.37 (two-fold development, the same solvent as above); ir (neat): 1778, 1736, and 1716 cm^{-1} (CO); ^1H nmr δ: 5.58 (s, 1H, C_6H_5CH), 5.18 (d, 1H, J = 8.5 Hz, H-1), 4.78 (2d, 2H, J = 12.3 Hz, $C_6H_5CH_2$), 4.49 (2d, 2H, J = 12.3 Hz, $C_6H_5CH_2$), 3.82 (s, 3H, $C_6H_4OCH_3$), 3.66 (s, 3H, $COOCH_3$), 2.22 (t, 2H, J = 7.5 Hz, CH_2COOMe), 0.90–1.54 (m, 12H, $(CH_2)_6$). *Anal.* calcd. for $C_{39}H_{45}NO_{10}$ (687.445): C 68.11, H 6.60, N 2.04; found: C 68.33, H 6.65, N 2.18. Molecular ions observed: $[MH]^+$ 688, $[MNa]^+$ 710.

8-Methoxycarbonyloctyl 3-O-benzyl-2-deoxy-6-O-(4-methoxybenzyl)-2-phthalimido-β-D-glucopyranoside (8) (20)

A mixture of **7** (3.62 g, 5.27 mmol), sodium cyanoborohydride (1.66 g, 26.4 mmol), and powdered molecular sieve 3A (5 g) in *N,N*-dimethylformamide (DMF, 40 mL) was stirred for 15 min at room temperature, and a solution of trifluoroacetic acid (4 mL, 52.7 mmol) in DMF (35.7 mL) was then added; stirring was continued for 19 h and, after addition of further trifluoroacetic acid (3.8 mL, 50 mmol), for an additional 24 h. The mixture was then cooled to 0°C, diluted with ethyl acetate (50 mL) and methanol (5 mL), stirred for 5 min and filtered, and the residue was washed with ethyl acetate (3 × 50 mL). The combined filtrates were washed with cold water (200 mL), cold aqueous sodium bicarbonate (200 mL), and water (2 × 100 mL), dried over $MgSO_4$, and evaporated to dryness. Chromatography of the syrupy residue on a silica gel column with hexane/ethyl acetate (2:1) gave **8** (3.01 g, 83%); $[\alpha]_D$ +16.5° (c. 1.1, $CHCl_3$), R_f 0.36 (same solvent as above); ir (neat): 3487 (OH), 1778, 1737, and 1713 cm^{-1} (CO); ^1H nmr δ: 6.90–7.90 (m, 13H, $N[CO]_2C_6H_4$, $C_6H_4OCH_3$, and $C_6H_5CH_2$), 5.11 (d, 1H, J = 8.3 Hz, H-1), 4.75 (d, 1H, J = 12.2 Hz, C_6H_5CH), 4.50–4.60 (m, 3H, C_6H_5CH), 4.21 (dd, 1H, J = 10.7 and 8.3 Hz, H-3), 4.12 (dd, 1H, J = 10.7 and 8.3, H-2), 3.82 (s, 3H, $C_6H_4OCH_3$), 3.66 (s, 3H, $COOCH_3$), 3.26–3.85 (m, 6H, H-4, H-5, H-6, H-6′, and $OCH_2[CH_2]_7$), 3.02 (d, 1H, J = 2.4 Hz, exchangeable with D_2O, OH), 2.21 (t, 2H, J = 7.6 Hz, CH_2COOMe), 0.85–1.53 (m, 12H, $(CH_2)_6$). *Anal.* calcd. for $C_{39}H_{47}NO_{10}$ (689.320): C 67.91, H 6.87, N 2.03; found: C 67.83, H 6.64, N 1.97. Molecular ions observed: $[MH]^+$ 690, $[MNa]^+$ 712, $[MNH_4]^+$ 707.

8-Methoxycarbonyloctyl 3-O-benzyl-2-deoxy-6-O-(4-methoxybenzyl)-2-phthalimido-4-O-(3′,4′,6′-tri-O-acetyl-2′-deoxy-2′-phthalimido-β-D-glucopyranosyl)-β-D-glucopyranoside (9)

A mixture of **8** (323 mg, 0.469 mmol), collidine (0.26 mL, 1.92 mmol), dry nitromethane (1 mL), and silver triflate (482 mg, 1.87 mmol) was stirred at −25°C, and a solution of **2** (934 mg, 1.87 mmol) in dry nitromethane (1 mL) was added. After 30 min the mixture was warmed up slowly to room temperature, and stirring was continued for 4.5 h. Then the mixture was diluted with ethyl acetate (50 mL) and filtered through Celite, which was washed with ethyl acetate (3 × 20 mL), and the combined filtrates and washings were washed with cold water (100 mL), cold 1 *N* HCl (100 mL), cold aqueous sodium bicarbonate (100 mL), and again cold water (100 mL), and dried over $MgSO_4$. The residue obtained after solvent evaporation was subjected to chromatography on a silica gel column with hexane/ethyl acetate (3:2) and gave **9** (345 mg, 66%) as an amorphous solid, $[\alpha]_D$ +3.3° (c. 0.95, $CHCl_3$); R_f 0.30 (two-fold development in hexane/ethyl acetate 2:1); ir (neat) 1780, 1750, 1717 cm^{-1} (CO); ^1H nmr δ: 6.85–7.90 (m, 17H, $N[CO]_2C_6H_4$, $C_6H_4OCH_3$, and $C_6H_5CH_2$), 5.78 (dd, 1H, J = 10.7 and 9.1 Hz, H-3′), 5.49 (d, J = 8.4 Hz, H-1′), 5.11 (dd, 1H, J = 10.0 and 9.2 Hz, H-4′), 4.92 (d, 1H, J = 8.2 Hz, H-1), 4.82 (d, 1H, J = 12.6 Hz, $C_6H_5CH_2$), 4.46–4.49 (m, 3H, C_6H_5CH), 4.32 (dd, 1H, J = 10.7 and 8.4, H-2′), 3.83 (s, 3H, $C_6H_4OCH_3$), 3.65 (s, 3H, $COOCH_3$), 3.19–4.23 (m, 11H, H-2, H-3, H-4, H-5, 2H-6, H-5′, 2H-6′, and $OCH_2[CH_2]_7$), 2.19 (t, 2H, J = 7.5 Hz, CH_2COOMe), 2.01, 1.97, 1.85 (3s, 9H, CH_3COO), and 0.80–1.50 (m, 12H, $(CH_2)_6$). *Anal.* calcd. for $C_{59}H_{66}N_2O_{19}$ (1106.426): C 64.01, H 6.01, N 2.53; found: C 63.98, H 5.88, N 2.49. Molecular ions observed: $[MH]^+$ 1107, $[MNa]^+$ 1129, $[MNH_4]^+$ 1124.

*8-Methoxycarbonyloctyl 3-O-benzyl-2-deoxy-2-phthalimido-4-O-(3′,4′,6′-tri-O-acetyl-2′-deoxy-2′-phthalimido-β-D-glucopyranosyl)-β-D-glucopyranoside **10** (20)*

To a stirred solution of **9** (419 mg, 0.379 mmol) in acetonitrile/water (9:1, 1.5 mL) at 0°C was added ammonium cerium(IV) nitrate (415 mg, 0.758 mmol) and stirring was continued at 0°C for 10 min and then at room temperature for 45 min. The mixture was diluted with ethyl acetate (100 mL), washed with water (2 × 50 mL), dried with $MgSO_4$, and the solvent evaporated to a syrup which was subjected to chromatography on a silica gel column. Elution with hexane/ethyl acetate (3:1) gave unreacted **9** (24 mg, 6%), followed by **10** (319 mg, 86%) which was a colorless solid, mp 142.5–144.6°C (ethyl ether/hexane); $[\alpha]_D$ +10.3° (c. 1.1, $CHCl_3$); R_f 0.17 (ethyl ether/hexane, 1:1); ir (neat) 3485, 3525 (OH), 1777, 1750, and 1718 cm^{-1} (CO); ^1H nmr δ: 6.80–7.95 (m, 13H, $N[CO]_2C_6H_4$ and $C_6H_5CH_2$), 5.80 (dd, 1H, J = 10.6 and 9.1 Hz, H-3′), 5.65 (d, 1H, J = 8.3 Hz, H-1′), 5.16 (dd, 1H, J = 10.0 and 9.2 Hz, H-4′), 4.99 (d, 1H, J = 8.6 Hz, H-1), 4.86 (d, 1H, J = 12.7 Hz, $C_6H_5CH_2$), 4.46 (d, 1H, C_6H_5CH), 4.35 (dd, 1H, J = 10.6 and 8.3, H-2′), 3.65 (s, 3H, $COOCH_3$), 3.22–4.32 (m, 11H, H-2, H-3, H-4, H-5, 2H-6, H-5′, 2H-6′, and $OCH_2[CH_2]_7$), 2.19 (t, 2H, J = 7.5 Hz, CH_2COOMe), 2.00, 1.99, 1.84 (3s, 9H, CH_3COO), 1.73 (dd, 1H, J = 8.8 Hz and 4.3 Hz, exchangeable with D_2O, OH), and 0.80–1.50 (m, 12H, $(CH_2)_6$). *Anal.* calcd. for $C_{51}H_{58}N_2O_{18}$ (986.368): C 62.06, H 5.92, N 2.84; found: C 62.21, H 6.03, N 2.73. Molecular ions observed: $[MH]^+$ 987, $[MNa]^+$ 1009, $[MNH_4]^+$ 1004.

8-Methoxycarbonyloctyl 4-O-(3′,4′,6′-tri-O-acetyl-2′-deoxy-2′-phthalimido-β-D-glucopyranosyl)-6-O-(2″,3″,4″-tri-O-benzyl-α-L-fucopyranosyl)-3-O-benzyl-2-deoxy-2-phthalimido-β-D-glucopyranoside (11)

A mixture of **10** (312 mg, 0.315 mmol), tetraethylammonium bromide (1.32 g, 6.30 mmol), and powdered molecular sieve 4A (2.33 g) in dry dichloromethane (6 mL) was stirred in the dark at room temperature for 1 h. A solution of freshly prepared tri-*O*-benzyl-α-L-fucopyranosyl bromide (ref. 13*a*; 626 mg, 1.26 mmol) in dry dichloromethane (ref. 13*b*; 5 mL) was then added, and the reaction mixture was slowly stirred for 44 h. It was diluted with dichloromethane (60 mL) and filtered through Celite, which was washed with dichloromethane

(2 × 30 mL), and the combined filtrate and washings were washed with water (2 × 100 mL), dried over $MgSO_4$, and evaporated to give a syrupy residue that was subjected to chromatography on a silica gel column with hexane/ethyl acetate (2:1). Together with unreacted **10** (19 mg, 2%), **11** (347 mg, 79%) was obtained as an amorphous solid, $[\alpha]_D$ −51.9° (c. 1.0, $CHCl_3$); R_f 0.30 (two-fold development in the above solvent); ir (neat) 1779, 1750, and 1718 cm^{-1} (CO); ^1H nmr δ: 6.80–7.95 (m, 28H, $N(CO)_2C_6H_4$ and $C_6H_5CH_2$), 5.72 (dd, 1H, J = 10.7 and 9.2 Hz, H-3′), 5.63 (d, 1H, J = 8.4 Hz, H-1′), 5.09 (d, 1H, J = 3.3 Hz, H-1″), 4.91 (d, 1H, J = 8.3 Hz, H-1), 3.64 (s, 3H, $COOCH_3$), 2.19 (t, 2H, J = 7.5 Hz, CH_2COOMe), 1.91, 1.87, and 1.83 (3s, 9H, CH_3COO), and 1.04 (d, 3H, J = 6.5 Hz, H-6″). *Anal.* calcd. for $C_{78}H_{86}N_2O_{22}$ (1402.567): C 66.75, H 6.18, N 2.00; found: C 66.61, H 6.11, N 1.94. Molecular ions observed: $[MH]^+$ 1403, $[MNa]^+$ 1425, $[MNH_4]^+$ 1420.

*8-Methoxycarbonyloctyl 2-acetamido-4-*O*-(2′-acetamido-3′,4′,6′-tri-*O*-acetyl-2′-deoxy-β-*D*-glucopyranosyl)-3-*O*-benzyl-6-*O*-(2″,3″,4″-tri-*O*-benzyl-α-*L*-fucopyranosyl)-2-deoxy-β-*D*-glucopyranoside (**12**)*

A solution of **11** (591 mg, 0.422 mmol) and hydrazine acetate (1.17 g, 12.7 mmol) in dry methanol (20 mL) was boiled under reflux for 3 h, then another portion of hydrazine acetate (1.17 g, 12.7 mmol) was added and the refluxing continued for 4.5 h. After cooling, the reaction mixture was evaporated to dryness and treated with acetic anhydride (14 mL) in pyridine (15 mL) at room temperature for 19 h. The mixture was diluted with ethyl acetate (200 mL) and washed with cold water (100 mL), 1 *N* HCl (2 × 100 mL), and water (100 mL). The organic layer was dried over $MgSO_4$, the solvent evaporated, and the pale yellow solid residue was subjected to chromatography on silica gel using ethyl acetate/hexane (3:1), to give pure **12** (423 mg, 82%) as a colorless solid, mp 186–188°C; $[\alpha]_D$ −42.5° (c. 0.76, $CHCl_3$); R_f 0.12 (the above solvent); ir (neat) 3305 (NH), 1748 (COOR), and 1662 (CONH); ^1H nmr δ: 7.20–7.50 (m, 20H, $C_6H_5CH_2$), 6.22 (d, 1H, J = 9.4 Hz, N*H*), 5.56 (d, 1H, J = 8.7 Hz, N*H*), 5.00 (d, 1H, J = 9.6 Hz, H-1′), 4.66 (d, 1H, J = 2.5 Hz, H-1″), 4.43 (d, 1H, J = 6.9 Hz, H-1), 3.65 (s, 3H, $COOCH_3$), 2.28 (t, 2H, J = 7.5 Hz, CH_2COOMe), 2.03, 1.98, 1.94, 1.87, and 1.82 (5s, 15H, CH_3COO), 1.20–1.65 (m, 12H, $[CH_2]_6$), and 1.04 (d, 3H, J = 6.4 Hz, H-6″). *Anal.* calcd. for $C_{66}H_{86}N_2O_{20}$ (1226.577): C 64.59, H 7.06, N 2.28; found: C 64.67, H 7.20, N 2.33. Molecular ions observed: $[MH]^+$ 1227, $[MNa]^+$ 1249.

*8-Methoxycarbonyloctyl 2-acetamido-4-*O*-(2′-acetamido-3′,4′,6′-tri-*O*-acetyl-2′-deoxy-β-*D*-glucopyranosyl)-6-*O*-(α-*L*-fucopyranosyl)-2-deoxy-β-*D*-glucopyranoside (**13**)*

Hydrogenolysis of **12** (179 mg, 0.146 mmol) on 10% Pd/C in ethyl acetate/methanol (1:3, 20 mL) gave, after filtration through Celite and evaporation of the solvent, colorless **13** (118 mg, 94%), which was unstable on standing. R_f 0.40 (ethyl acetate/methanol, 5:1); ^1H nmr δ: 5.11 (t, 1H, J = 9.8 Hz, H-3′), 5.02 (t, 1H, J = 9.7 Hz, H-4′), 4.81 (d, 1H, J = 1.8 Hz, H-1″), 4.73 (d, 1H, J = 8.6 Hz, H-1′), 4.39 (d, 1H, J = 7.8 Hz, H-1), 3.67 (s, 3H, $COOCH_3$), 3.40–4.28 (m, 16H, H-2, H-3, H-4, H-5, 2H-6, H-2′, H-5′, 2H-6′, H-2″, H-3″, H-4″, H-5″, $CH_2[CH_2]_7$), 2.30 (t, 2H, J = 7.5 Hz, CH_2COOCH_3), 2.09, 2.02, 2.01, 2.00, and 1.96 (5s, 15H, CH_3COO), and 1.20–1.65 (m, 15H, H-6″ and $CH_2[CH_2]_6COOCH_3$).

*8-Methoxycarbonyloctyl 2-acetamido-4-*O*-(2′-acetamido-3′,4′,6′-tri-*O*-acetyl-2′-deoxy-β-*D*-glucopyranosyl)-6-*O*-(2″,3″,4″-tri-*O*-acetyl-α-*L*-fucopyranosyl)-3-*O*-acetyl-2-deoxy-β-*D*-glucopyranoside (**14**)*

Compound **13** (120 mg, 0.139 mmol) was treated with acetic anhydride (1.5 mL) in dry pyridine (2 mL) for 19 h. The reaction mixture was diluted with ethyl acetate (100 mL), washed with cold water (50 mL), 1 *N* HCl (2 × 50 mL), and water (50 mL), dried ($MgSO_4$), and evaporated to give a colorless, syrupy residue. The latter was subjected to chromatography on a silica gel column using ethyl acetate to give **14** (113 mg, 79%); $[\alpha]_D$ −69.2° (c. 1.0, $CHCl_3$); R_f 0.12 (ethyl acetate), 0.64 (ethyl acetate/methanol 9:1); ^1H nmr δ: 5.68 (d, 1H, J = 7.9 Hz, exchangeable with D_2O, N*H*), 5.60 (d, 1H, J = 8.6 Hz, exchangeable with D_2O, N*H*), 5.07 (d, 1H, J = 3.6 Hz, H-1″), 4.96 (d, 1H, J = 8.4 Hz, H-1′), 4.51 (d, 1H, J = 7.8 Hz, H-1), 4.30 (br, q, 1H, J = 6.2 Hz, H-5″), 3.66 (s, 3H, $COOCH_3$), 2.30 (t, 2H, J = 7.5 Hz, CH_2COOCH_3), 2.18, 2.15, 2.07, 2.01, 2.00, 1.96, and 1.91 (7s, 27H, CH_3COO), 1.28–1.61 (m, 12H, $CH_2[CH_2]_6CH_2COOCH_3$), and 1.13 (d, 3H, J = 6.4 Hz, H-6″). *Anal.* calcd. for $C_{46}H_{70}N_2O_{24}$ (1034.432): C 53.38, H 6.82, N 2.71; found: C 53.46, H 6.91, N 2.83. Molecular ions observed: $[MH]^+$ 1035, $[MNa]^+$ 1057.

*8-Methoxycarbonyloctyl 2-acetamido-4-*O*-(2′-acetamido-2′-deoxy-β-*D*-glucopyranosyl)-6-*O*-α-*L*-fucopyranosyl-2-deoxy-β-*D*-glucopyranoside (**15**a)*

Zemplén deacetylation of **14** (78 mg, 0.075 mmol) in methanol (2 mL) was performed as described for the preparation of **5**. The trisaccharide **15***a* (50 mg, 91%) was obtained as colorless solid, mp 283–286°C (aqueous ethanol), $[\alpha]_D$ −63.5° (c. 0.42, 50% aqueous ethanol); ^1H nmr δ: 4.90 (d, 1H, J = 3.8 Hz, H-1″), 4.64 (d, 1H, J = 8.4 Hz, H-1′), 4.49 (d, 1H, J = 7.8 Hz, H-1), 4.13 (br, t, 1H, J = 6.5 Hz, H-5″), 3.68 (s, 3H, $COOCH_3$), 3.40–3.95 (m, 17H, H-2, H-3, H-4, H-5, 2H-6, H-2′, H-3′, H-4′, H-5′, 2H-6′, H-2″, H-3″, H-4″, $OCH_2[CH_7]$), 2.39 (t, 2H, J = 7.4 Hz, CH_2COOCH_3), 2.08 and 2.03 (2s, 6H, CH_3COO), 1.58 and 1.30 (m, 12H, $CH_2[CH_2]_6CH_2COOCH_3$), and 1.23 (d, 3H, J = 6.6 Hz, H-6″). *Anal.* calcd. for $C_{32}H_{56}N_2O_{17}$ (740.358): C 51.88, H 7.62, N 3.78; found: C 51.92, H 7.83, N 3.88. Molecular ions observed: $[MH]^+$ 741, $[MNa]^+$ 763.

Hydrazide

Compound **15***a* (35 mg, 0.047 mmol) and hydrazine hydrate (1.6 mL) were stirred in dry ethanol (4.6 mL) at room temperature for 24 h. The mixture was evaporated to dryness, and the residue was evaporated from water (2 × 12 mL) to give the hydrazide as a colorless solid (36 mg) that was used in the next step without purification.

Coupling reaction with BSA

To a solution of the hydrazide (21 mg, 0.029 mmol) in DMF (0.4 mL) stirred at −40 to −30°C, was added a solution of dinitrogen tetroxide (11) in dichloromethane (0.46 *M*, 0.08 mL). Stirring was continued at −20 to −10°C for 45 min, then this solution was added to a buffered solution ($KHCO_3/Na_2B_4O_7$; pH 8.93; 9.4 mL) of bovine serum albumin (purified, 94 mg, 0.00145 mmol) under stirring at 0°C, and the stirring was continued for 25 h. The mixture was then dialyzed against water (5 × 100 mL) using an Amicon ultrafiltration cell (Model 402) equipped with a YM-10 membrane. After lyophilization, **15***b* (97 mg) was obtained as a colorless solid. The carbohydrate content was determined according to ref. 16 as 10.5 carbohydrate equiv. per BSA molecule.

Coupling reaction with poly-L-lysine

Hydrazide (17 mg, 0.023 mmol) was treated with dinitrogen tetroxide as in the previous reaction; however, instead of BSA, poly-L-lysine (mw 16 000); 96 mg, 0.006 mmol) in buffer (9.6 mL) at 0°C was used. After 44 h the reaction mixture was dialyzed against water (5 × 100 mL) using a YM-2 membrane, and lyophilized to give **15***c* as a pale yellow solid (47 mg). The incorporation level was determined as above as 1.9 carbohydrate equiv. per poly-L-lysine molecule.

Immunization protocol (17)

Rabbits were immunized subcutaneously with 200 μg of **15***b* (0.2 mL in 0.15 *M* NaCl) and equal volume of Freund's complete adjuvant at four sites at the back of the neck. Boosting immunizations were performed with the same amount of **15***b* and incomplete Freund's adjuvant weekly for 3 weeks. After a resting period of 2 weeks, the animals were again immunized with 400 μg of **15***b* in PBS (0.4 mL) in the ear vein, and blood samples were taken after 1 week.

Solid-phase radioimmunoassay (RIA) and competition analysis

The solid phase RIA was performed using 86-well acrylic plastic plates (Flow laboratories) that were incubated with **15***c* at 20 μg/mL

for 16 h at room temperature. Following washing in ST buffer (0.15 *M* NaCl, 0.01 *M* TRIS, pH 8), the plates were blocked with 0.5% gelatin in ST.

The solid-phase binding of rabbit sera was measured by incubating the plates for 4 h at room temperature with 50 mL rabbit sera diluted in 1% BSA-ST, washing in ST buffer, amplifying for 2 h with ^{125}I-protein A prepared according to ref. 18 (3×10^4 cpm/well). A non-saturating concentration of rabbit sera was determined for use in the competition analysis.

The compounds used in competition experiments prepared in our laboratories (9, 14, 21) were preincubated with this dilution of rabbit sera (2×10^{-4}) in 1% BSA-ST buffer for 16 h at 4°C. The residual activity was determined in the solid phase RIA, and the percent inhibition was calculated for a titration of the competitor.

Acknowledgements

This work was in part supported by a grant from NCI Canada (to J.F.H.). Our thanks are due to Dr. W. R. Bruce, Director of the Toronto Branch of the Ludwig Institute for Cancer Research for continuous encouragement and interest in this work. We thank to Dr. H. Egge for allowing us to record the mass spectra at his instrument, Mr. J. McGoey and Mr. A. Lee for recording the nmr spectra, and Dr. H. Pang for recording mass spectra. We also thank Dr. D. A. Cumming for the generous gift of several competing compounds, Mr. J. Baptista for measuring optical rotations, and Mr. M. Best for technical assistance.

1. J. D. Hardcastle and K. D. Vellacott. Rec. Results Cancer Res. **83**, 86 (1982).
2. S.-I. Hakomori. Cancer Res. **45**, 2405 (1985).
3. T. Feizi. Nature, **314**, 53 (1985).
4. H. Koprowski and M. Herlyn. *In* Molecular biology of tumor cells. *Edited by* B. Wahren. Raven Press, New York, NY. 1985. p. 123.
5. S.-I. Hakomori. *In* Molecular biology of tumor cells. *Edited by* B. Wahren. Raven Press, New York, NY. 1985. p. 139.
6. T. Feizi and R. A. Childs. Trends Biochem. Sci. **10**, 24 (1985).
7. A. Kobata and K. Yamashita. Pure Appl. Chem. **56**, 821 (1984).
8. K. Yamashita, I. Ueda, M. Kuroki, Y. Matsuoka, and A. Kobata. Proc. 8th Int. Symp. Glycoconjugates, Houston, TX. 1985.
9. D. A. Schwartz, H. H. Lee, J. P Carver, and J. J. Krepinsky. Can. J. Chem. **63**, 1073 (1985).
10. R. U. Lemieux, D. R. Bundle, and D. A. Baker. J. Am. Chem. Soc. **97**, 4076 (1975).
11. B. M. Pinto and D. R. Bundle. Carbohydr. Res. **124**, 313 (1983).
12. J.-R. Pougny, U. Kraska, and P. Sinay. Carbohydr. Res. **60**, 383 (1978); **50**, 181 (1976).
13. (*a*) M. Dejter-Juszynski and H. M. Flowers. Carbohydr. Res. **18**, 219 (1971); (*b*) R. U. Lemieux, K. B. Hendricks, R. V. Stick, and K. James. J. Am. Chem. Soc. **97**, 4056 (1975).
14. R. N. Shah, D. A. Cumming, A. A. Grey, J. P. Carver, and J. J. Krepinsky. Carbohydr. Res. In press.
15. (*a*) P. J. Garegg and P. Ossowski. Acta Chem. Scand. B**37**, 249 (1983); (*b*) D. M. Whitfield, R. N. Shah, J. P. Carver, and J. J. Krepinsky. Synth. Commun. **15**, 737 (1985).
16. S. C. Kushawa and M. Kates. Lipids, **10**, 372 (1985).
17. J. H. Pazur. Carbohydr. Res. **107**, 243 (1982).
18. J. J. Langoni, M. D. T. Boyle, and T. Borsos. J. Immunol. Meth. **18**, 281 (1977).
19. H. Egge, J. Peter-Katalinic, J. Paz-Parente, G. Strecker, J. Montreuil, and B. Fournet. FEBS Lett. **156**, 357 (1983).
20. R. Johansson and B. Samuelsson. J. Chem. Soc. Chem. Commun. 201 (1984).
21. F. M. Winnik, J.-R. Brisson, J. P. Carver, and J. J. Krepinsky. Carbohydr. Res. **103**, 15 (1982).

Viscosities of dilute aqueous suspensions of montmorillonite and kaolinite clays[1]

KIM L. KASPERSKI, CHARLES T. HEPLER, AND LOREN G. HEPLER
Department of Chemistry, University of Alberta, Edmonton, Alta., Canada T6G 2G2

Received March 11, 1986

KIM L. KASPERSKI, CHARLES T. HEPLER, and LOREN G. HEPLER. Can. J. Chem. **64**, 1919 (1986).

We have measured viscosities and densities of dilute aqueous suspensions of Na-kaolinite (25°C), of Na-montmorillonite (25–55°C), and of mixtures of Na-kaolinite/Na-montmorillonite (25°C). Results of the measurements at 25°C have been analyzed in terms of the Einstein equation with conclusions that are consistent with previous knowledge that colloidal particles of these clays are non-spherical and that montmorillonite is a swelling clay. Viscosities of mixed clay systems are nearly consistent with a simple additivity model; the small non-additivities are in accord with previous evidence that relatively small montmorillonite particles are adsorbed on the surface of relatively large kaolinite particles. The effect of temperature on the viscosities of suspensions of montmorillonite is consistent with the idea that aggregation of clay particles diminishes with increasing temperature.

KIM L. KASPERSKI, CHARLES T. HEPLER et LOREN G. HEPLER. Can. J. Chem. **64**, 1919 (1986).

On a mesuré les viscosités et les densités de suspensions aqueuses diluées de kaolinite de sodium (25°C), de montmorillonite de sodium (25–55°C) et de mélanges de kaolinite de sodium/montmorillonite de sodium (25°C). On a analysé les résultats des mesures à 25°C en fonction de l'équation de Einstein et les conclusions sont en accord avec nos connaissances antérieures sur le fait que les particules colloïdales de ces argiles ne sont pas sphériques et que la montmorillonite est une argile qui se gonfle. Les viscosités des systèmes mixtes d'argiles sont en accord presque parfait avec un modèle simple d'additivité; les faibles différences à l'additivité sont en accord avec les données antérieures à l'effet que les particules relativement faibles de montmorillonite sont adsorbées sur la surface de particules relativement grosses de kaolinite. L'effet de la température sur les viscosités de suspensions de montmorillonite est en accord avec l'idée que l'aggrégation de particules d'argile diminue avec une augmentation de la température.

[Traduit par la revue]

Introduction

Colloidal suspensions of clays in water and aqueous solutions have been investigated in many ways, including many investigations of rheological properties. Because of applications in such fields as ceramics and drilling muds, most of these investigations have been concerned with concentrated suspensions in which non-Newtonian flow is important. There have been only a few investigations of the viscosities of dilute suspensions, in spite of their general theoretical importance and also their practical importance in such areas as enhanced oil recovery and water treatment. Our particular interest has been in the flow properties of dilute suspensions of clays, including investigations of mixed-clay systems that may be important in connection with problems involving oil sands tailings as well as to problems related to permeabilities in enhanced oil recovery.

As background for our research we cite a few previous investigations of viscosities of dilute suspensions of clays (1–6) and evidence for interesting and potentially important interactions of different kinds of clays with each other in dilute suspensions (7, 8).

Experimental

Materials

Well-characterized clay samples were obtained from the Source Clay Mineral Repository, Department of Geology, University of Missouri, Columbia, MO, U.S.A. The kaolinite (KGa-1) came from Washington County, GA, and the montmorillonite (SWy-1) came from Crook County, WY. Our preparations of Na-kaolinite and Na-montmorillonite for subsequent use followed procedures that have been described previously (9, 10).

Apparatus and methods

Densities of suspensions were obtained with glass pycnometers of 25 cm^3 nominal volume, which we calibrated at each temperature with distilled water. Uncertainties in most of our densities of clay suspensions are less than ± 0.0005 g cm^{-3}.

Cannon-Fenske glass viscometers (ASTM 25 and 50) from Fisher Scientific were calibrated with distilled water and with 0.010 *M* NaOH at each temperature. Flow times ranged from 1 to 20 min, as timed with a stopwatch; total timing uncertainties (due to the stopwatch and our response times) were about ± 0.1 s. At the low flow rates of our measurements, we had no complications due to non-Newtonian flow and were correspondingly unable to investigate the non-Newtonian rheology that becomes important at higher flow rates and for more concentrated suspensions (2, 3, 5, 11).

Particular care was taken with cleaning the viscometers between measurements, because of the tendency of clay particles to adhere to the walls of the capillaries of the viscometers, which was particularly troublesome with our most concentrated suspensions.

All measurements were done with pycnometers and viscometers suspended in a constant temperature water bath with temperature known to ± 0.01°C and stable to ± 0.005°C, as checked with a platinum resistance thermometer.

Results and calculations

Results of our measurements leading to densities and viscosities of suspensions of Na-kaolinite and Na-montmorillonite at 25.00°C are summarized in Tables 1 and 2, respectively, and illustrated in Fig. 1, which is based on eq. [8] that is presented later.

We want to calculate the volume fractions of dry clay in our various suspensions, which requires that we know the density of our solid dry clays. Previous investigations of similar clays have led to reported densities ranging from 2.4 to 2.8 g cm^{-3} for Na-montmorillonite (4, 5, 12, 13) and 2.58 to 2.63 g cm^{-3} for Na-kaolinite (12, 14). Largely because of the substantial range in reported densities for Na-montmorillonite, we use our densities of suspensions to obtain our own values for the densities of the dry clays we have used, as follows.

We begin by assuming that the volumes of clay (V_c) and water (V_w) are additive so that the volumes of suspensions (V_s)

[1]The first part of this research was done in the Department of Chemistry, University of Lethbridge, Lethbridge, Alta.

TABLE 1. Densities and viscosities of suspensions of Na-kaolinite in 0.010 *M* NaOH at 25.00°C

Wt.% clay	Density (g cm^{-3})	Viscosity (mPa s)	ϕ_d	$[(n - n_0)/\phi_d n_0]^a$
1.180	1.005	0.909	0.00453	4.2
2.017	1.010	0.920	0.00778	4.0
2.912	1.016	0.942	0.0113	5.0
3.787	1.021	0.956	0.0148	4.9
3.863	1.022	0.968	0.0151	5.7
5.067	1.030	0.984	0.0199	5.2
6.608	1.039	1.050	0.0262	6.8
7.085	1.042	1.084	0.0282	7.6
7.443	1.045	1.070	0.0297	6.7
8.663	1.052	1.100	0.0347	6.7

[a]The viscotiy of 0.010 *M* NaOH is 0.892 mPa s, as compared with 0.890 mPa s for pure water. Here we use $n_0 = 0.892$ mPa s.

TABLE 2. Densities and viscosities of suspensions of Na-montmorillonite in water at 25.00°C

Wt.% clay	Density (g cm^{-3})	Viscosity (mPa s)	ϕ_d	$[(n - n_0)/\phi_d n_0]$
0.10	0.9976	0.948	3.84×10^{-4}	170
0.20	0.9983	1.007	7.68×10^{-4}	171
0.30	0.9988	1.067	1.15×10^{-3}	173
0.40	0.9997	1.156	1.54×10^{-3}	194
0.50	1.0001	1.220	1.92×10^{-3}	193
0.60	1.0007	1.280	2.31×10^{-3}	190
0.70	1.0014	1.388	2.70×10^{-3}	207
0.90	1.0026	1.630	3.47×10^{-3}	240
1.00	1.0032	1.671	3.86×10^{-3}	227
1.20	1.0045	1.980	4.64×10^{-3}	264
1.40	1.0057	2.311	5.42×10^{-3}	295
1.60	1.0070	2.556	6.20×10^{-3}	302
1.80	1.0083	3.031	6.98×10^{-3}	345
2.00	1.0095	3.622	7.77×10^{-3}	395
2.20	1.0109	4.767	8.55×10^{-3}	509

are given by

[1] $V_s = V_c + V_w$

Very accurate results reported by Low (13) provide support for the validity of eq. [1] to the level of accuracy that we require here. Some algebraic manipulations with eq. [1] and the definition of density lead to

[2] $d_c = [d_w d_s P]/[100(d_w - d_s) + d_s P]$

where d_c, d_s, and d_w represent the densities of dry clay, aqueous suspension, and water, respectively, and P represents the weight percent clay in the suspension. Because of the term $(d_w - d_s)$ in eq. [2] and the ± 0.0005 g cm^{-3} uncertainties in our values of d_s, this equation is useful only when applied to solutions more concentrated than about 1% clay. Our calculations with eq. [2] applied to densities of our suspensions lead to $d_c = 2.6 \pm 0.1$ g cm^{-3} for dry Na-kaolinite and the same value for dry Na-montmorillonite, in which ± 0.1 g cm^{-3} is our estimate of the *total* uncertainty due to our experimental results and the initial assumption that volumes are additive.

There is also another way to calculate d_c from our results. Solution chemists have found it useful to define "apparent molar" properties for solutions of small molecules and "apparent specific" properties for solutions of high molecular weight polymers, with the latter being appropriate to our problem. In similar fashion we define the apparent specific volume of clay (V_ϕ) as

[3] $V_\phi = (V_s - V_w)/m_c$

in which V_s represents the volume of a suspension containing a specified amount of water, V_w represents the volume of that same amount of water, and m_c represents the mass of dry clay in the suspension. Algebraic manipulations similar to those that led to eq. [2] lead to

[4] $V_\phi = [100(d_w - d_s)/(d_s d_w P)] + [1/d_w]$

in which the symbols have already been defined.

In eq. [4], just as in eq. [2], we have a $(d_w - d_s)$ term that limits useful calculations to suspensions containing more than about 1% clay. Calculations with data from Tables 1 and 2 in eq. [4] lead to $V_\phi = 0.387$ cm^3 g^{-1} for each of our clays. Since the reciprocal of V_ϕ is the density, we again obtain $d_c = 2.6$ g cm^{-3} for each of our clays. This value of d_c is *not* an independent confirmation of our identical value based on eq. [2] since our use of eq. [4] is also based on the implied validity of eq. [1].

Now we use the above $d_c = 2.6$ g cm^{-3} for dry clay as follows to obtain the volume fraction of dry clay in water (ϕ_d) that will be used in subsequent calculations with the Einstein equation. Choosing to consider 100 g of suspension, we obtain

[5] $\phi_d = V_c/V_s = P d_s/100 d_c$

Values of ϕ_d, the volume fraction of dry clay, are listed in Tables 1 and 2 for Na-kaolinite and Na-montmorillonite.

A simple way to start the analysis of viscosity data for suspensions is in terms of the Einstein equation, which we write

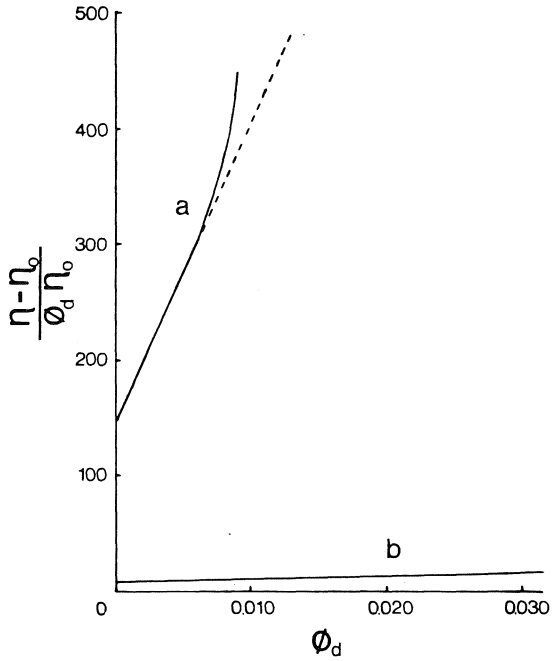

FIG. 1. Graphs of reduced viscosity ($(n - n_0)/\phi_d n_0$) against volume fraction of dry clay (ϕ_d) for montmorillonite (*a*) and kaolinite (*b*). The dashed line for montmorillonite is an extension of the straight line corresponding to $(AS)_m = 148$ and $(BS^2)_m = 2.6 \times 10^4$ and is drawn to show the deviation from linearity above a value of about 0.006 for ϕ_d.

TABLE 3. Densities and viscosities of 0.30 wt.% Na-montmorillonite in water at various temperatures

Temperature (°C)	Density (g cm^{-3})	Viscosity (mPa s)	ϕ_d	$[(n - n_0)/\phi_d n_0]$
25.0	0.9988	1.067	1.15×10^{-3}	173
35.0	0.9959	0.870	1.15×10^{-3}	182
45.0	0.9917	0.721	1.14×10^{-3}	184
55.0	0.9881	0.608	1.14×10^{-3}	181

TABLE 4. Densities and viscosities of 2.20 wt.% Na-montmorillonite in water at various temperatures

Temperature (°C)	Density (g cm^{-3})	Viscosity (mPa s)	ϕ_d	$[(n - n_0)/\phi_d n_0]$
25.0	1.0109	4.767	8.55×10^{-3}	509
35.0	1.0083	4.011	8.53×10^{-3}	536
45.0	1.0044	3.457	8.50×10^{-3}	565
55.0	0.9996	3.020	8.46×10^{-3}	590

as

[6] $(n - n_0)/n_0 = A\phi + B\phi^2 + \ldots$

In this equation n and n_0 represent the viscosities of the suspension and of the pure solvent, ϕ is the volume fraction of the suspended particles, and A and B are constants. It should be emphasized that ϕ refers to the volume fraction of clay particles as they exist in suspension; that is, ϕ refers to the volume fraction of swollen clay particles whereas it is the volume fraction of dry clay (ϕ_d) that we know and have listed in Tables 1 and 2. All we can do now is recognize that ϕ and ϕ_d are related by a "swelling factor" that we denote by S so that

[7] $\phi = S\phi_d$

Substitution of eq. [7] into eq. [6] and rearrangement leads to

[8] $(n - n_0)/\phi_d n_0 = (AS) + (BS^2)\phi_d + \ldots$

As suggested by this equation, we have calculated the values of the reduced viscosities, $[(n - n_0)/\phi_d n_0]$, that are listed in Tables 1 and 2 and have constructed graphs of these reduced viscosities against ϕ_d as in Fig. 1. Least-squares fits of eq. [8] to our experimental results lead to $(AS)_m = 148$ and $(BS^2)_m = 2.6 \times 10^4$ for Na-montmorillonite and to $(AS)_k = 3.5$ and $(BS^2)_k = 1.1 \times 10^2$ for Na-kaolinite, where the subscripts m and k refer to montmorillonite and kaolinite, respectively.

Einstein's original calculations showed that $A = 2.5$ for spherical particles. Subsequent calculations by others have shown that $A > 2.5$ for particles of non-spherical shape, such as the clays of present interest. Since it is known that montmorillonite is a swelling clay (14), we also know that $S_m > 1$. On the basis that $A_m > 2.5$ and $S_m > 1$, it is expected that $(AS)_m$ should be substantially greater than 2.5, as has indeed been found. Kaolinite, however, is not a swelling clay (15), so we expect the difference between $(AS)_k$ and 2.5 to be determined almost entirely by the non-spherical shape of the kaolinite particles.

More quantitative consideration of the magnitudes of A_m and S_m must be based on detailed considerations of the swelling of montmorillonite and on the related hydration of the clay particles in aqueous suspensions as well as on the shapes of the suspended (hydrated) particles. Although these matters are of general scientific interest and are also important in connection with many questions concerning the colloid chemistry of clays in aqueous systems, they extend beyond the realm of the present investigation and must be left as subjects for future investigations.

TABLE 5. Densities and viscosities of pure water at various temperatures

Temperature (°C)	Density (g cm^{-3})	Viscosity (mPa s)
25.0	0.99707	0.8904
35.0	0.99406	0.7194
45.0	0.99025	0.5960
55.0	0.98573	0.5040

The B term in eq. [6] and thence the BS^2 term in eq. [8] is partly determined by particle–particle interactions. Even allowing for the fact that $S_m > S_k$, the conclusion from our results that $(BS^2)_m \gg (BS^2)_k$ shows that particle–particle interactions are stronger in suspensions of montmorillonite (nearly neutral pH) than in suspensions of kaolinite (high pH) of similar concentrations.

Results obtained for the densities and viscosities of suspensions of Na-montmorillonite at several temperatures are given in Tables 3 and 4. Properties of distilled water used in our calculations are given in Table 5. The viscosities and densities decrease with increasing temperature, as expected. For dilute suspensions (0.30 wt.%) the reduced viscosity does not change significantly with temperature, as was also found by Wood, Granquist, and Krieger (1) for suspensions of attapulgite. However, for more concentrated suspensions (2.20 wt.%), the reduced viscosity increases with increasing temperature, which could be the result of a partial breakdown of relatively large nearly spherical structures to smaller less spherical structures, which can account qualitatively for the observed temperature dependence.

Because many natural environments contain mixtures of clays and earlier investigations (7, 8) have shown that there are specific interactions between different clays in aqueous suspen-

TABLE 6. Viscosities of suspensions of mixtures of Na-kaolinite and Na-montmorillonite in 0.010 *M* NaOH at 25.00°C; total clay concentration = 0.250 wt.%; densities of all suspensions = 0.9991 ± 0.0005 g cm^{-3}

Mass ratio (k/m)	Viscosity (mPa s)	$[(n - n_0)/n_0\phi_d]$	$[(n - n_0)/n_0]_{exp}$	$[(n - n_0)/n_0]_{calcd}$[a]
Pure m[b]	1.040	171	0.164	0.165
0.050	1.024	152	0.146	0.156
0.100	1.031	160	0.154	0.148
0.125	1.015	142	0.136	0.144
0.167	1.024	152	0.146	0.139
0.250	1.021	149	0.143	0.129
0.500	1.007	132	0.127	0.106
1.00	0.972	91	0.088	0.078
2.00	0.952	68	0.065	0.052
4.00	0.942	57	0.054	0.032
6.00	0.922	33	0.032	0.024
8.00	0.928	40	0.038	0.019
10.0	0.930	43	0.041	0.016
20.0	0.914	24	0.023	0.010
Pure k[b]	0.899	6	0.006	0.003

[a]See footnote, Table 1.
[b]Samples of clays used for the series of measurements summarized here were prepared at a different time than those used for the measurements in Tables 1 and 2; hence there are small differences between viscosities reported here and in Tables 1 and 2.

TABLE 7. Viscosities of suspensions of mixtures of Na-kaolinite and Na-montmorillonite in 0.010 *M* NaOH at 25.00°C; total clay concentration = 0.500 wt.%; densities of all suspensions = 1.0006 ± 0.0005 g cm^{-3}

Mass ratio (k/m)	Viscosity (mPa s)	$[(n - n_0)/n_0\phi_d]$	$[(n - n_0)/n_0]_{exp}$	$[(n - n_0)/n_0]_{calcd}$[a]
Pure m[b]	1.351	267	0.513	0.375
0.050	1.197	177	0.340	0.354
0.100	1.178	166	0.320	0.334
0.125	1.200	179	0.344	0.325
0.167	1.229	196	0.376	0.312
0.250	1.219	190	0.365	0.287
0.500	1.541	378	0.726	0.232
1.00	1.167	160	0.307	0.168
2.00	1.090	115	0.222	0.109
4.00	1.045	89	0.170	0.066
6.00	0.977	49	0.094	0.048
8.00	0.953	35	0.067	0.039
10.0	0.944	30	0.058	0.033
20.0	0.925	18	0.036	0.020
Pure k[b]	0.894	1	0.002	0.007

[a]See footnote, Table 1.
[b]See footnote, Table 6.

sions, we have measured viscosities of some dilute mixed clay systems. Our densities and viscosities of suspensions of mixtures of Na-kaolinite and Na-montmorillonite at five different total clay concentrations (0.25, 0.50, 0.75, 1.00, and 3.00 wt.%) were measured at 25.00°C, with results given in Tables 6–10.

We investigate the possible effects of kaolinite–montmorillonite specific interactions on viscosities by comparing our measured viscosities with those that can be predicted on the basis of a simple additivity principle. This comparison can be done in two ways.

One way to express additivity of viscosity effects is by way of

$$[9]\quad [(n - n_0)/n_0]_{mixture} = [(n - n_0)/n_0]_k + [(n - n_0)/n_0]_m$$

in which $[(n - n_0)/n_0]_k$ and $[(n - n_0)/n_0]_m$ are obtained from eq. [8] multiplied through by ϕ_d, using values of (AS), (BS^2), and ϕ_d appropriate to each component of the mixture. Comparison of results of these calculations with the measured viscosities shows that there are small (relative to uncertainties) deviations from additivity.

The other (effectively equivalent) way of testing our results for additivity is to use the viscosities of mixtures having the same ratio of (kaolinite/montmorillonite) in eq. [8] to permit

TABLE 8. Viscosities of suspensions of mixtures of Na-kaolinite and Na-montmorillonite in 0.010 *M* NaOH at 25.00°C; total clay concentration = 0.750 wt.%; densities of all suspensions = 1.0022 ± 0.0005 g cm^{-3}

Mass ratio (k/m)	Viscosity (mPa s)	$[(n - n_0)/n_0\phi_d]$	$[(n - n_0)/n_0]_{exp}$	$[(n - n_0)/n_0]_{calcd}$[a]
Pure m[b]	1.364	182	0.526	0.633
0.050	1.381	189	0.546	0.594
0.100	1.347	176	0.508	0.559
0.125	1.336	171	0.495	0.543
0.167	1.325	167	0.483	0.518
0.250	1.339	172	0.499	0.475
0.500	1.313	162	0.470	0.379
1.00	1.229	130	0.376	0.270
2.00	1.234	132	0.382	0.172
4.00	1.082	73	0.211	0.102
6.00	1.028	52	0.150	0.074
8.00	0.991	41	0.118	0.060
10.0	0.962	26	0.077	0.050
20.0	0.941	18	0.053	0.031
Pure k[b]	0.916	9	0.025	0.011

[a]See footnote, Table 1.
[b]See footnote, Table 6.

TABLE 9. Viscosities of suspensions of mixtures of Na-kaolinite and Na-montmorillonite in 0.010 *M* NaOH at 25.00°C; total clay concentration = 1.00 wt.%; densities of all suspensions = 1.0037 ± 0.0005 g cm^{-3}

Mass ratio (k/m)	Viscosity (mPa s)	$[(n - n_0)/n_0\phi_d]$	$[(n - n_0)/n_0]_{exp}$	$[(n - n_0)/n_0]_{calcd}$[a]
Pure m[b]	1.782	258	0.996	0.937
0.050	1.742	246	0.951	0.876
0.100	1.856	279	1.078	0.822
0.125	1.844	276	1.065	0.797
0.167	1.706	236	0.910	0.759
0.250	2.04	333	1.28	0.692
0.500	2.40	437	1.69	0.546
1.00	2.260	396	1.530	0.383
2.00	1.340	130	0.501	0.240
4.00	No measured viscosity			
6.00	No measured viscosity			
8.00	0.971	23	0.087	0.081
10.0	0.950	17	0.064	0.068
20.0	0.910	12	0.045	0.042
Pure k[b]	0.910	5	0.019	0.015

[a]See footnote, Table 1.
[b]See footnote, Table 6.

TABLE 10. Viscosities of suspensions of mixtures of Na-kaolinite and Na-montmorillonite in water at 25.00°C; total clay concentration = 3.00 wt.%; densities of all suspensions = 1.0157 ± 0.0005 g cm^{-3}

Mass ratio (k/m)	Viscosity (mPa s)	$[(n - n_0)/n_0]_{exp}$	$[(n - n_0)/n_0]_{calcd}$
9.00	1.54	0.73	0.252
5.67	1.70	0.91	0.375
3.00	2.4	1.7	0.672
2.33	2.8	2.1	0.845
1.86	3.7	3.2	1.036

evalution of $(AS)_{mix}$ and $(BS^2)_{mix}$ for each (k/m) ratio. To the extent that a simple additivity principle is valid, these $(AS)_{mix}$ and $(BS^2)_{mix}$ values should vary linearly with composition from the values for pure kaolinite to those for pure montmorillonite. We have also found in this way that there are small (relative to uncertainties) deviations from additivity.

The deviations (just barely statistically significant) of viscosities of dilute suspensions of mixed clays from simple additivity justify a brief summary as follows. First, viscosities of dilute suspensions with (k/m) ratios larger than about 0.5 are slightly larger than predicted on the basis of additivity, while viscosities of suspensions with smaller (k/m) ratios are close to those

predicted on the basis of additivity. These observations are consistent with the idea that there are more or stronger particle–particle interactions in the mixed clay suspensions than in corresponding suspensions of single clays, but do not distinguish between adsorption of relatively small montmorillonite particles on the surfaces of relatively large kaolinite particles, as previously suggested (7, 8), and some other kinds of particle–particle interactions. In any case, it should be recognized that the effects of adsorption or other kinds of particle–particle interactions on viscosities of dilute suspensions are less than the effects on electrophoretic mobilities (8) and related ζ potentials.

Acknowledgements

We thank the Alberta Oil Sands Technology and Research Authority for support of this research by way of a Research Agreement and a graduate scholarship.

1. W. H. Wood, W. T. Granquist, and I. M. Krieger. Clays Clay Miner. (Proc. 4th Natl. Conf., 1955) **4**, 240 (1956).
2. H. van Olphen. Clays Clay Miner. (Proc. 4th Natl. Conf., 1955) **4**, 204 (1956).
3. R. B. Langston and J. A. Pask. Clays Clay Miner. (Proc. 5th Natl. Conf., 1956) **5**, 4 (1958).
4. W. T. Granquist. Clays Clay Miner. (Proc. 6th Natl. Conf., 1957) **6**, 207 (1959).
5. I. Shainberg and H. Otoh. Israel J. Chem. **6**, 251 (1968).
6. L. L. Schramm and J. C. T. Kwak. Clays Clay Miner. **30**, 40 (1982).
7. R. K. Schofield and H. R. Samson. Discuss. Faraday Soc. **18**, 135 (1954).
8. N. S. Srinivasan, J. J. Spitzer, and L. G. Hepler. Can. J. Petroleum Tech. **21**, No. 4, 25 (1982).
9. A. P. Ferris and W. B. Jepson. J. Coll. Interf. Sci. **51**, 245 (1975).
10. G. J. Ewin, B. P. Erno, and L. G. Hepler. Can. J. Chem. **59**, 2927 (1981).
11. D. A. Stanley, S. W. Webb, and B. J. Scheiner. U.S. Bur. Mines Rep. Inv. 8895 (1984).
12. C. T. Deeds and H. van Olphen. Clays Clay Miner. (Proc. 10th Natl. Conf., 1961) **10**, 318 (1963).
13. P. F. Low. Adv. Agronomy, **13**, 269 (1961).
14. A. S. Michaels and J. C. Bolger. Ind. Eng. Chem. Fundam. **1**(1), 153 (1962).
15. H. van Olphen. An introduction to clay colloid chemistry. 2nd ed. John Wiley and Sons, New York. 1977.

The relative rate constants of oxygen, $O(^3P)$, atoms with different gaseous unsaturated compounds at room temperature

H. DESLAURIERS AND G. J. COLLIN[1]

Département des sciences fondamentales, Université du Québec à Chicoutimi, Chicoutimi (Qué.), Canada G7H 2B1

Received January 28, 1986

H. DESLAURIERS and G. J. COLLIN. Can. J. Chem. **64**, 1925 (1986).

A simple method is proposed in order to measure the relative rate constants of the interactions between oxygen $O(^3P)$ atoms and unsaturated hydrocarbon. A 147 nm photolysis of air is used to produce the $O(^3P)$ atoms. In the presence of 1,2-butadiene, these oxygen atoms have a very clean reaction that gives rise to propylene formation. By including a suitable additive, and by looking at the formation of propene versus the [additive]/[1,2-butadiene] ratio, the absolute values of the various $O(^3P)$ + unsaturated hydrocarbon interactions can be evaluated. These rate constants increase with the number of substituents attached to the double bond. Moreover, a correlation between the total rate constants and ionization potentials is also observed.

H. DESLAURIERS et G. J. COLLIN. Can. J. Chem. **64**, 1925 (1986).

Une méthode relativement simple est proposée pour mesurer les constantes de vitesse relatives de l'interaction entre les atomes d'oxygène, $O(^3P)$, et une variété d'hydrocarbures insaturés. On utilise la photolyse de l'air à 147 nm pour générer les atomes d'oxygène. En présence de butadiène-1,2 ceux-ci conduisent à la formation de propène dans une réaction considérée comme quantitative. En ajoutant un autre additif, et en suivant la formation de propène avec le rapport [additif]/[butadiene-1,2], on peut estimer les valeurs absolues des différentes constantes de vitesse. Celles-ci ont été mesurées dans le cas de 19 additifs et croissent avec le nombre de substituents attachés à la double liaison. En outre, il existe une bonne corrélation entre les constantes de vitesse et les potentiels d'ionisation.

Introduction

In a recent paper from this laboratory, it was shown that a very clean reaction results from the mixture of oxygen atoms $O(^3P)$ with gaseous 1,2-butadiene: the products are carbon monoxide and propene (1):

[1] $CH_2{=}CH{=}CHCH_3 + O(^3P) \rightarrow CO + C_3H_6$

Thus, if a convenient source of oxygen atoms is available, the monitoring of either carbon monoxide or propene formation may be used to measure the relative rate constants of these atoms with different additives. The 147 nm photolysis of molecular oxygen appears to be a convenient source of such atoms (2). In fact, it is well known that, at this wave-length, molecular oxygen has a fairly high absorption coefficient (3), and the photo-excited molecule decomposes very quickly, giving rise to the formation of two oxygen atoms: one $O(^3P)$ and one $O(^1D)$ atom with a quantum yield of one (2). The fate of the $O(^1D)$ atom is straightforward: at room temperature it is deactivated to the $O(^3P)$ state by collision, provided that a suitable quencher is added to the reaction mixture. For example, molecular oxygen itself is a good quencher, as well as many others such as nitrogen, rare gases ... (4). Conversely, $O(^3P)$ atoms are not known to react or to disappear quickly in the presence of these gases.

[2] $O_2 + h\nu(147\text{ nm}) \rightarrow O(^3P) + O(^1D)$
$\phi = 1.0$

[3] $O(^1D) + O_2 \rightarrow O(^3P) + O_2$
$k_3 = 0.75 \times 10^{-10}\text{ cm}^3\text{ molecule}^{-1}\text{ s}^{-1}$ (4)

[4] $O(^1D) + N_2 \rightarrow O(^3P) + N_2$
$k_4 = 0.55 \times 10^{-10}\text{ cm}^3\text{ molecule}^{-1}\text{ s}^{-1}$ (4)

Thus, it is to be expected that the 147 nm photolysis of molecular oxygen is a clean source of $O(^3P)$ atoms with a quantum yield of 2.0. Since nitrogen is transparent when submitted to the 147 nm wave-length, air is also a good starting source for these $O(^3P)$ atoms. If small amounts of 1,2-butadiene are added to oxygen, a high propene quantum yield is measured: Φ(propene) $\cong$ 1.6–1.8 with a 1,2-butadiene/oxygen ratio lower than 0.05 (1). This paper relies on these interactions to explain the measurements of the relative rate constants of $O(^3P)$ atoms with different hydrocarbon compounds. In fact, by adding a few percentage points of a convenient compound to a mixture of air and 1,2-butadiene, a decrease in the propylene quantum yield may be expected and, from that decrease, one may have access to the relative rate constants. Of course, comparisons with literature values are also in order.

[1]To whom all correspondance should be addressed.

Experimental techniques

Most of the experimental techniques have already been described. In particular, the preparation of samples, photolytic as well as analytic procedures, and also actinometry, have been recently reported (5). Oxygen — research purity (99.98%) — (Matheson Gas Product Canada), and either Air zero — hydrocarbon content < 2 ppm — or extra dry (Liquid Carbonic), are used as received. The origin and the analysis of the starting hydrocarbon materials are indicated in Table 1.

All experiments were done at room temperature (293 ± 2 K) in a 1/2 liter Pyrex bulb. The photolytic times were generally 1 min and in some cases 3 to 5 min. The number of photon entering the cell was between 9 and 35 × 10^{13} photons per s. With these conditions the percentage of transformation of the hydrocarbon is equal to and generally much less than 0.12%.

Results

In all cases, the addition of small amounts of various unsaturated hydrocarbons to air:1,2-butadiene (485:0.75 Torr) mixtures, results in the decrease of propene quantum yield. Conversely, the photolysis of air:hydrocarbon mixtures does not produce propene Φ(propene) < 0.005 except in three cases which will be identified later. In the cases where no propene is formed in the absence of 1,2-butadiene, the following mechanism may be assumed: to reactions [1]–[4], reaction [5] must be added.

[5] $O(^3P) + RH \rightarrow$ products (no propene)

The steady-state approximation leads to the following relationship. Thus, the inverse of propene quantum yield

TABLE 1. Analysis of the starting unsaturated hydrocarbons

Compound	Origin	Stated purity (mol%)	Analysis:[d] main observed impurities: ppm
1,2-Butadiene	A.P.I.[a]	99.94 ± 0.02	Propane:4.54.
1-Butene	Phillips, R. G.[b]	99.92	Propane:7.47.
1-Butene-d_8	M.S.D.[c]	97% D atom	Ethylene + ethane:129; propene:155.
2-Butyne	A.P.I.	99.95 ± 0.04	Isobutene + 1-butene:50; propane:42; ?:13.
1-Butyne	A.P.I.	99.94 ± 0.03	Propane:16.2.
1,3-Butadiene	A.P.I.	99.92 ± 0.04	—
cis-2-Butene	Phillips, R. G.	99.94	Propane:30; *trans*-2-butene:340; 1,3-butadiene:20.
cis-2-Pentene	A.P.I.	99.93 ± 0.02	1-Butene + isobutene:19; ethylene:20; propane:14; 1-pentane:12.
Cyclohexene	A.P.I.	99.977 ± 0.02	Ethylene:67; C_5(?):13; 3,3-dimethyl-1-butene:9.
Cyclopentene	A.P.I.	99.989 ± 0.002	1-Butene + isobutene + 1,3-butadiene:10.4.
3,3-Dimethyl-1-butene	A.P.I.	99.98 ± 0.02	3-Methyl-1-butene:20.
1-Hexene	A.P.I.	99.86 ± 0.08	Propene:12; propane:76; C_5(?):34.
Isobutene	Phillips, R. G.	99.90	Isobutane:830; propane:44.
1,2-Pentadiene	Chem. Sample Co.	99	3-Methyl-1,2-butadiene:790; 1,3-pentadiene:2000; 1,4-pentadiene:80.
Isoprene	A.P.I.	99.96 ± 0.03	3-Methyl-1-butene:47; C_5(?):37; 1-butene + isobutene:17.
2-Methyl-1-butene	A.P.I.	99.90 ± 0.08	Isobutene + 1-butene:12; propane:7.
3-Methyl-1-butene	A.P.I.	99.94 ± 0.05	Isobutene + 1-butene:48; propane:38; 1,2-butadiene:12.
1-Pentene-5-d_1	Chem. Sample Co.	99	Isobutene + 1-butene:13; 3-methyl-1-butene:36.
2,3-Pentadiene	Chem. Sample Co.	99	3-Methyl-1,2-butadiene:700; 1,3-pentadiene:300; ?:280.
3-Methyl-1,2-butadiene	Chem. Sample Co.	99	C_5(?):890; C_5(?):275; C_5(?):280; C_5(?):121.

[a]American Petroleum Institute, Carnegie Mellon Inst.
[b]Phillips, Research Grade.
[c]Merck, Sharp, and Dohme of Canada.
[d]Some of the impurities may come from our analytical system.

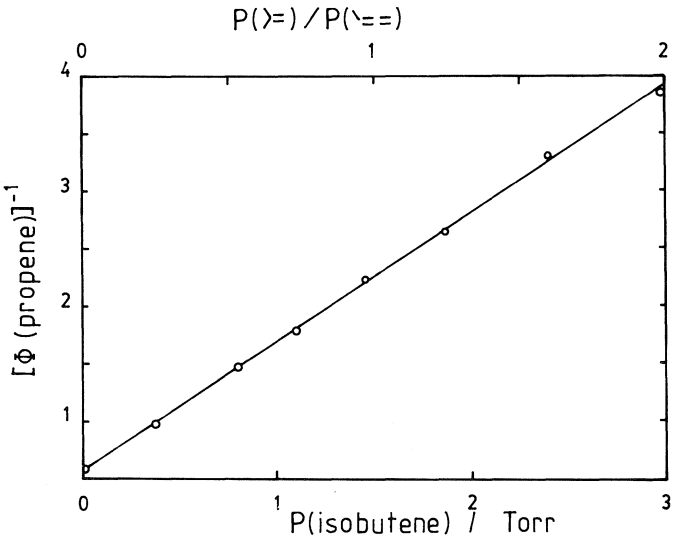

FIG. 1. The 147 nm photolysis of air:1,2-butadiene:isobutene (48:1.5:x Torr) mixtures. The inverse of the propene quantum yield versus the partial pressure of isobutene.

$$[\mathrm{I}] \qquad [\Phi(C_3H_6)]^{-1} = \frac{1}{2\phi} + \frac{k_5}{2k_1\phi}\frac{[RH]}{[1,2\text{-}C_4H_6]}$$

is a linear function of $[RH]/[1,2\text{-}C_4H_6]$ ratio. Figures 1–4 show the plot for expression [I] and for various added compounds. The analytic expressions are given in Table 2, and in each case the slope/intercept ratio gives the pertinent k_5/k_1 one. Using the $k_5[O(^3P)]$ [isobutene] as a standard, the absolute rate constant of $O(^3P)$ + 1,2-C_4H_6 interaction may be calculated (Fig. 1) and through the various k_5/k_1 ratios, each rate constant may be calculated (Table 2 and Fig. 2).

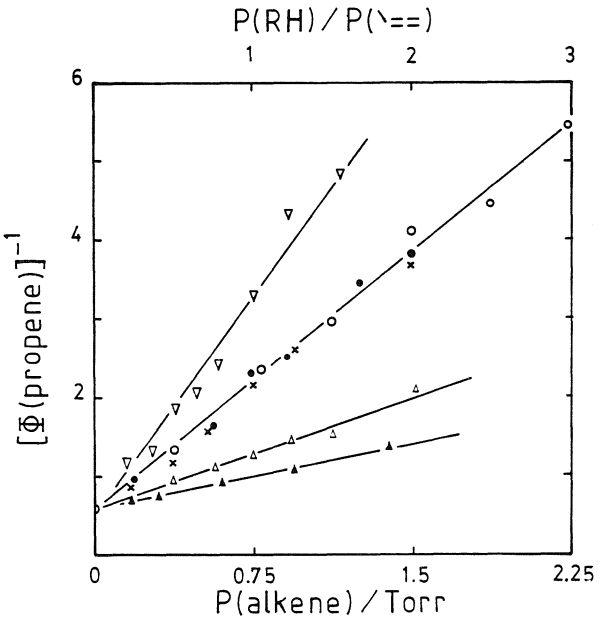

FIG. 2. The 147 nm photolysis of air:1,2-butadiene:alkene (485: 0.74:x Torr) mixtures. The inverse of the propene quantum yield in the presence of 1-pentene-d_1 (▲), 1,2-pentadiene (△), 2,3-pentadiene (×), 2-methyl-1-butene (●), *cis*-2-pentene (○), and 3-methyl-1,2-butadiene (▽).

In cases where the photolysis of air:hydrocarbon mixtures lead to propene, a correction must be applied to the above mechanism and the following process must be added:

[6] $O(^3P) + RH \rightarrow C_3H_6 + X$

In these cases, the steady-state treatment leads to the following equation:

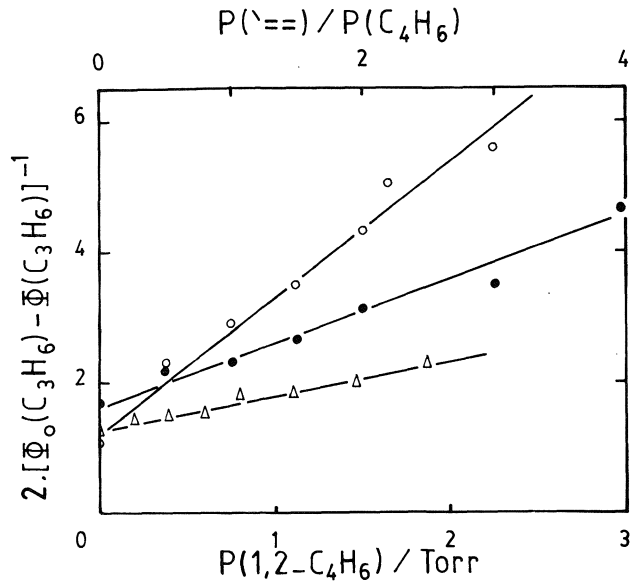

FIG. 3. The 147 nm photolysis of air:1,2-butadiene:C_4H_6 (485: x:0.75 Torr) mixtures. The inverse of the [Φ_0(propene) − Φ(propene)] values versus the 1,2-butadiene pressure in the presence of 1,3-butadiene (△), 2-butyne (●), and 1-butyne (○).

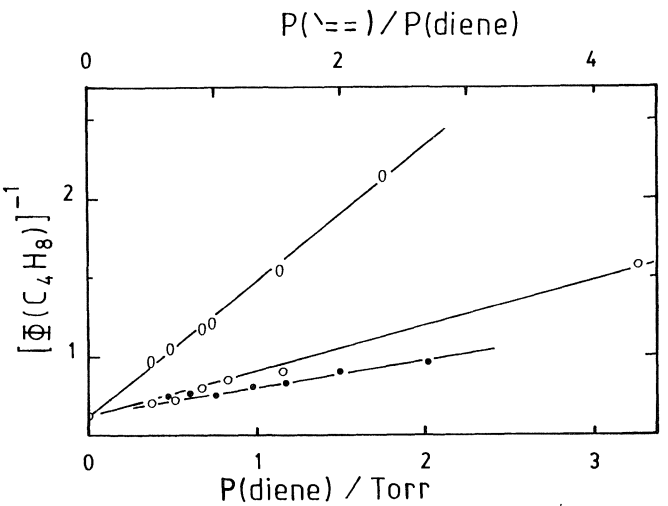

FIG. 4. The 147 nm photolysis of air:1,2-butadiene:C_5H_8 (485: 0.74:x Torr) mixtures. The inverse of Φ(isobutene) in the presence of 3-methyl-1,2-butadiene (●), Φ(2-butene) in the presence of 2,3-pentadiene (○), and Φ(1-butene) in the presence of 1,2-pentadiene (O).

$$[\text{II}] \quad \frac{2\phi}{\Phi_0(\text{Pe}) - \Phi(\text{Pe})} = \frac{k_6 + k_5}{k_5} + \frac{k_1[1,2\text{-}C_4H_6]}{k_5[\text{RH}]}$$

where Φ_O(Pe) is the propene quantum yield measured in the oxygen:1,2-butadiene mixture and Φ(Pe) that measured in various oxygen:1,2-butadiene:RH mixtures. Figure 3 shows the results obtained in the case of the C_4H_6 compounds, namely 1-butyne, 2-butyne, and 1,3-butadiene, and numerical results appear in Table 3.

Finally, some ultimate stable products formed in process [5] have been identified. For example, the photolysis of either the 1,2- and 2,3-pentadienes produce alkenes in a similar way as observed in 1,2-butadiene case.

[7] $O(^3P) + C_5H_8 \rightarrow C_4H_8 + CO$

TABLE 2. Relative rate constants of the $O(^3P)$ + RH reactions

RH	1^a / 2ϕ	k ($\times 10^{12}$ cm^3 molecule^{-1} s^{-1}) Literature (ref.)	This work
Isobutene	—	17.35[b] (6)	—
1,2-Butadiene	0.56_9	7.46 (7)	5.95 (0.25)[c]
1-Butene	0.59_8	3.98–4.00 (6–8)	4.14 (0.13)
1-Butene-d_8	0.59_5		3.93 (0.22)
1-Pentene-5-d_1	0.54_8	4.78 (9)	4.96 (0.28)
1-Hexene	0.66_3	4.51 (10)	4.64 (0.59)
3-Methyl-1-butene	0.57_5	4.25 (6)	3.98 (0.56)
3,3-Dimethyl-1-butene	0.59_6		4.95 (0.39)
2-Methyl-1-butene	0.56_2		18.58 (0.93)
cis-2-Butene	0.64_8	17.65 (6)	13.70 (0.80)
cis-2-Pentene	0.52_0		19.7 (1.85)
Cyclopentene	0.58_8	20.65 (10)	18.6 (1.0)
Cyclohexene	0.64_6	18.74 (10)	16.0 (1.4)
1,2-Pentadiene	0.57_8		7.58 (0.62)
2,3-Pentadiene	0.58_6		16.5 (0.70)
3-Methyl-1,2-butadiene	0.53_1	41.64 (7)	30.4 (2.2)
Isoprene	0.63_5		26.7 (2.2)

[a] The zero intercept of relationship [I]. Each correlation coefficient of the linear regression is higher than 0.988.
[b] This value is taken as a reference in this work.
[c] One standard deviation.

Taking processes [1]–[4] and [7], the steady state treatment leads to a relationship [III] similar to [I]:

$$[\text{III}] \quad \Phi[\text{alkene}]^{-1} = \frac{1}{2\phi} + \frac{k_1[1,2\text{-}C_4H_6]}{2\phi k_7[\text{diene}]}$$

Again the slope/intercept ratio gives the k_1/k_7 ratios (Fig. 4 and Table 4).

Discussion

Results shown in Tables 2–4 are in good agreement with values taken from literature (6–13). In a first approximation, the rate constant of the $O(^3P)$ + alkene interaction increases very quickly with the number of substituents attached to the double bond. However, some remarks must be made on the experimental system in order to determine its value.

The photolytic behavior of molecular oxygen at 147 nm is well established and, as such, does not need to be discussed. The first approximation comes from the conversion of oxygen $O(^1D)$ to $O(^3P)$ atoms. The rate constants for the $O(^1D)$ + alkene interactions are relatively large and larger than that of the $O(^1D)$ + O_2 or $O(^1D)$ + N_2 processes. For example, $k[O(^1D)$ + isobutene] = (4.4 ± 1.2) × 10^{-10} and $k[O(^1D)$ + *cis*-butene] = (8.7 ± 1.8) × 10^{-10} cm^3 molecule^{-1} s^{-1} (14). Thus, in mixtures described in Fig. 1, 25.5 and 70% of $O(^1D)$ atoms react with molecular oxygen and nitrogen, respectively: they are converted to $O(^3P)$ — processes [3] and [4]. Moreover, it may be assumed that the rate constants of the $O(^1D)$ + unsaturated hydrocarbon are not greater than the collision rate constant. Thus, the direct $O(^1D)$ + unsaturated hydrocarbon reactions involve less than 5% of $O(^1D)$ atoms.

Since the primary quantum yield of process [2] is one (2), the total $O(^3P)$ quantum yield must be 2.0. Thus, in the absence of any other additive, from process [1], the expected propene quantum yield must be 2.0. From Table 2, it appears that the inverse of the propene quantum yield at zero concentration of additive (relationship [I]) is 0.59 (σ = 0.04), and the

TABLE 3. Relative rate constants for the $O(^3P)$ + C_4H_6 interactions

RH	$k_5^{-1}(k_5+k_6)^a$	$k_5{}^b$	$(k_5+k_6)^b$	$k_6(k_5+k_6)^{-1}$
1-Butyne	1.16	3.90 (0.30)	4.52	0.14
2-Butyne	1.64	8.65 (0.5)	14.15	0.39
1,3-Butadiene	1.25	15.5 (0.8)	19.4[c]	0.20

[a]Relationship [II]. Each correlation coefficient of the linear regression is higher than 0.98.
[b]10^{-12} cm^3 molecule^{-1} s^{-1}, ( ): one standard deviation.
[c]$(k_5+k_6)_{1,3\text{-butadiene}} = 20.7 \times 10^{-12}$ cm^3 molecule^{-1} s^{-1} (11).

TABLE 4. Products formed in the $O(^3P)$ + 1,2- or 2,3-diene interactions

Diene	Product	$\frac{1^a}{2\phi}$	$k_7{}^b$
1,2-Pentadiene	1-Butene	0.61	5.61 (0.52)
2,3-Pentadiene	2-Butene[c]	0.57	13.8 (1.5)
3-Methyl-1,2-butadiene	Isobutene	0.66	35.5 (3.2)

[a]Relationship [III].
[b]10^{-12} cm^3 molecule^{-1} s^{-1}, ( ): one standard deviation.
[c]*trans*/*cis*: 1.39 ± 0.01; 1-butene is also formed: 1-butene/$C_4H_8 \cong 3 \pm 1\%$.

Φ_0(propene) is rather 1.70. This difference may be explained on the basis of at least four reasons. First, there may be some recombination of the type (O + O + M → O_2 + M) in the reaction chamber, although the intensity of the photon beam is not too high. Moreover, some of the oxygen atoms may be absorbed either by the walls or the window of the reaction chamber. This phenomenon may be non-negligible for the less reactive unsaturated hydrocarbons. Of course part of the $O(^3P)$ + 1,2-butadiene interaction may lead to different compounds than propene + carbon monoxide. For example, traces of buten-2-one (1.7%), crotonaldehyde (1.1%), and methacrylaldehyde (0.3%) are observed (7). Moreover, although molecular oxygen has a high absorption coefficient, a small fraction of the incident beam is absorbed by 1,2-butadiene. In an air:1,2-butadiene (485:0.75 Torr), it may be estimated that 3 to 4% of the incident beam are absorbed directly by 1,2-butadiene (5). Finally, oxygen atoms are known to react with molecular oxygen to form ozone in the presence of a third body:

[8] $$O + O_2 \xrightarrow{(N_2)} O_3$$

and $k_8 = (7.57 \pm 1.72) \times 10^{-15}$ cm^3 molecule^{-1} s^{-1} at 298 K and 400 Torr of added nitrogen (15, 16). With these conditions, in the 1,2-butadiene:air mixtures (1.5:485 Torr), 7.3% of $O(^3P)$ atoms react with O_2. Obviously, this effect is attenuated by the addition of another hydrocarbon. Thus, the two last effects are probably responsible for a 10 ± 1% loss in the original budget of oxygen atoms. Of course a systematic error in the process of actinometry cannot be ruled out.

In the case where propene is also a product of the $O(^3P)$ + additive interaction, the kinetic system may distinguished between propene arising either from 1,2-butadiene or additive interaction (Table 3). From this reaction, the branching ratios have been evaluated in the case of 1-butyne, 2-butyne, and 1,3-butadiene. A branching ratio of 0.32 ± 0.05 has been measured in the case of 2-butyne for the formation of propene, and this value may be higher if carbon monoxide is considered (17).

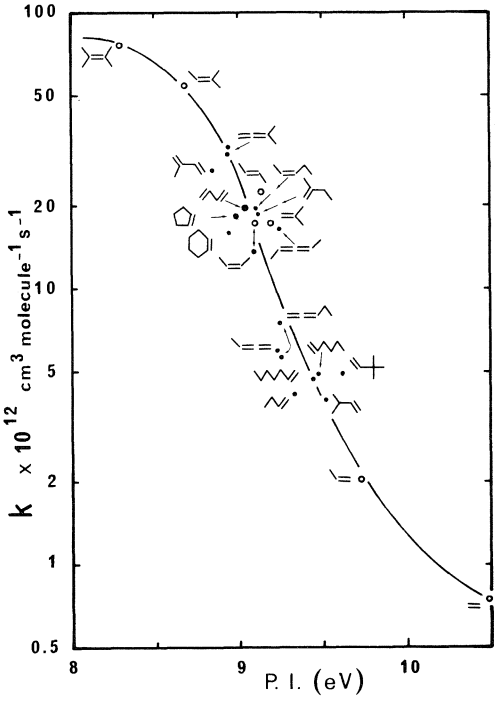

FIG. 5. Rate constants at room temperature as a function of ionization potential (19, 20). ●: this work; ○: ref. 6*b*.

Finally, the relative rate constant measured for processes [5] and [7] and reported in Table 2 and 4 must be compared. Of course process [7] is included in process [5] and k_7 must be smaller or equal to k_5. It may be said that more 60% of the $O(^3P)$ + 1,2-diene interaction results in alkene + carbon monoxyde formation.

Nothing can be said about the mechanism involved in the $O(^3P)$ + alkene reaction. However, the reaction is most likely an addition reaction rather than an abstraction of a hydrogen atom (6). This conclusion is supported by measurements of the relative rates of reaction of $O(^3P)$ atom with 1-butene and 1-butene-d_8 for which k_4/k_D is about 1.05 (Table 2), an isotope effect which is too small to be interpreted on the basis of a primary C—H bond scission. Finally, there is a correlation between the total rate constant and the electron donating property of the alkene molecules, as is illustrated in Fig. 5 where the rate constants are plotted against ionization potential. Similar trend was reported in the case of substituted benzenes (18).

Acknowledgments

The authors would like to express their gratitude to the Natural Sciences and Engineering Research Council of Canada for financial assistance throughout the above research project.

1. G. J. COLLIN and H. DESLAURIERS. J. Photochem. **32**, 9 (1986).
2. L. C. LEE, T. G. SLANGER, G. BLACK, and R. L. SHARPLESS. J. Chem. Phys. **67**, 560 (1977).
3. K. WATANABE, E. C. Y. INN, and M. ZELIKOFF. J. Chem. Phys. **21**, 1026 (1953).
4. H. OKABE. *In* Photochemistry of small molecules. J. Wiley and Sons, New York. 1978. pp. 149–156 and references cited therein.
5. H. DESLAURIERS and G. J. COLLIN. J. Photochem. **32**, 17 (1986).
6. (*a*) D. L. SINGLETON and R. J. CVETANOVIĆ. J. Am. Chem. Soc. **98**, 6812 (1976); (*b*) R. J. CVETANOVIĆ and D. L. SINGLETON. Rev. Chem. Interm. **5**, 183 (1984).
7. J. J. HAVELL. J. Am. Chem. Soc. **96**, 530 (1974).
8. S. FURUYAMA, R. ATKINSON, A. J. COLUSSI, and R. J. CVETANOVIĆ. Int. J. Chem. Kinet. **6**, 741 (1974).
9. H. W. FORD and N. ENDOW. J. Chem. Phys. **27**, 1277 (1957).
10. R. J. CVETANOVIĆ. Adv. Photochem. **1**, 115 (1963).
11. W. S. NIP, D. L. SINGLETON, and R. J. CVETANOVIĆ. Can. J. Chem. **57**, 949 (1979).
12. P. I. ABELL. *In* Comprehensive chemical kinetics. Vol. 18. *Edited by* C. H. Bamford and C. F. H. Tipper. Elsevier Scientific Publishing Co., New York. p. 111 and references therein.
13. J. S. GAFFNEY, R. ATKINSON, and J. N. PITTS, JR. J. Am. Chem. Soc. **97**, 5049 (1975).
14. O. KAJIMOTO and T. FUENO. Chem. Phys. Lett. **64**, 445 (1979).
15. C. L. LIN and M. T. LEU. Int. J. Chem. Kinet. **14**, 417 (1982).
16. A. E. CROCE DE COBOS and J. TROE. Int. J. Chem. Kinet. **16**, 1519 (1984).
17. H. E. AVERY and S. J. HEATH. J. Chem. Soc. Faraday Trans. I, **68**, 512 (1972).
18. R. E. HUIE and J. T. HERRON. Prog. React. Kinet. **8**, 1 (1975).
19. H. M. ROSENSTOCK, K. DRAXL, B. W. STEINER, and J. T. HERRON. J. Phys. Chem. Ref. Data, **6**, suppl. n° 1 (1977).
20. G. BIERI, F. BURGER, E. HEILBRONNER, and J. P. MAIER. Helv. Chim. Acta, **60**, 2213 (1977).

Chiral phosphine ligands in asymmetric synthesis. IV. Hydrosilation of ketones, and the structure of (bicyclo[2.2.1]hepta-2,5-diene)[*N*,*N*-dimethyl-1(*R*)-(*o*-(bis(*tert*-butyl)phosphino)phenyl)ethylamine]rhodium(I) perchlorate

IAN D. MCKAY AND NICHOLAS C. PAYNE[1]

Chemistry Department, University of Western Ontario, London, Ont., Canada N6A 5B7

Received March 7, 1986

IAN D. MCKAY and NICHOLAS C. PAYNE. Can. J. Chem. **64**, 1930 (1986).

The crystal structure and absolute configuration of (bicyclo[2.2.1]hepta-2,5-diene)[*N*,*N*-dimethyl-1(*R*)-(*o*-(bis(*tert*-butyl)phosphino)phenyl)ethylamine]rhodium(I) perchlorate, [Rh(*R*-dibutphos)(C_7H_8)]ClO_4, have been determined from three-dimensional X-ray data collected by counter methods. The complex crystallizes in the orthorhombic space group $P2_12_12_1$ with four formula units in a cell of dimensions a = 15.773(3), b = 18.660(4), and c = 8.990(3) Å. Full-matrix least-squares techniques on F, using 2257 reflections with $F > 1.5\sigma(F)$, were used to refine the structure to a final agreement factor of R_1 = 0.042. The cation displays a small tetrahedral distortion from square planar geometry (if the diene is viewed as a bidentate ligand) with Rh—P and Rh—N distances of 2.398(2) and 2.212(6) Å, respectively. The absolute configuration of the aminophosphine ligand was determined to be *R* by the Bijvoet method. The six-membered chelate ring adopts a δ twist-boat conformation with the methyl substituent of the chiral C atom axially disposed. Rh complexes of the aminophosphine ligand were shown to catalyze the homogeneous hydrosilation of prochiral ketones, but failed to produce an optical bias in any of systems investigated.

IAN D. MCKAY et NICHOLAS C. PAYNE. Can. J. Chem. **64**, 1930 (1986).

En se basant sur des données de diffraction des rayons-X tridimensionnelles, on a déterminé la structure cristalline et la configuration absolue du perchlorate du (bicyclo[2.2.1]heptadiène-2,5) [*N*,*N*-diméthyl (*o*-(bis(*tert*-butyl)phosphino)phényl)-1(*R*) éthylamine] rhodium(I), [Rh(*R*-dibutphos)(C_7H_8)]ClO_4. Le complexe cristallise dans le groupe d'espace orthorhombique $P2_12_12_1$, avec quatre molécules par cellule dont les dimensions sont a = 15,773(3), b = 18,660(4) et c = 8,990(3) Å. On a résolu la structure par la méthode des moindres carrés (matrice entière sur F) et on l'a affinée jusqu'à une valeur de R_1 = 0.042 en se basant sur 2257 réflexions avec $F > 1{,}5\sigma(F)$. Le cation existe dans un forme tétraédrique légèrement déformée de la géométrie plan carré (si l'on considère le diène comme un ligand bidentate) et les distances Rh—P et Rh—N sont respectivement égales à 2,398(2) et 2,212(6) Å. Utilisant la méthode de Bijvoet, on a déterminé que la configuration absolue du ligand aminophosphie est *R*. Le chélate à six chaînons adopte une conformation δ bateau déformé dans lequel le substituant méthyle de l'atome de carbone chiral est disposé dans la position axiale. On a démontré que les complexes de Rh avec l'aminophosphine catalysent l'hydrosilation homogène des cétones prochirales; toutefois, dans les systèmes étudiés, il n'y a pas de formation préférentielle de l'un des isomères optiques.

[Traduit par la revue]

Introduction

The use of chiral transition metal catalysts in the asymmetric, homogeneous hydrosilation of prochiral ketones to produce chiral silyl ethers is a topic which has been of interest to others (1–15) as well as ourselves (16, 17) in the last few years. Chiral silyl ethers can subsequently be hydrolyzed to the corresponding chiral alcohols.

In previous work (16), the ligand amphos (E = P) and its analog, amars (E = As), were prepared, and Rh(I) complexes of these species were investigated as possible hydrosilation catalysts (16, 17). Both complexes catalyzed the reaction, but whereas the amphos complex gave encouraging optical yields

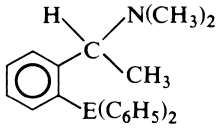

(up to 72%), the amars analog showed no such optical induction. X-ray crystal structure analyses of the complexes [Rh(*S*-amars)(C_7H_8)]ClO_4 (16) and [Rh(*S*-amphos)(C_7H_8)]ClO_4 (17) were completed, and conformational analyses of the solution species were conducted (17) using variable temperature ^1H nmr spectroscopy and energy minimization calculations (Molecular Mechanics II, MM2) (18). An explanation for the observed difference in optical selectivity was suggested.

To further our work in this area we have synthesized the chiral ligand *N*,*N*-dimethyl-1-(*o*-(bis(*tert*-butyl)phosphino)phenyl)ethylamine, dibutphos, and prepared Rh complexes of dibutphos for use as hydrosilation catalysts. We report herein the results of these studies, and describe the single crystal X-ray structure determination of [Rh(*R*-dibutphos)(C_7H_8)]ClO_4, **I**.

[1]To whom correspondence should be addressed.

Experimental

All syntheses and hydrosilation reactions were performed under a dry, O_2-free Ar atmosphere. ^1H nmr spectra were recorded on a Varian XL-200 spectrometer using $Si(CH_3)_4$ as a reference. ^{31}P nmr spectra were recorded on a Varian XL-300 spectrometer with $OP(OCH_3)_3$ as the reference. Rotations were recorded with a Rudolph polarimeter, model 80, at the sodium D line. Concentrations are given in g 100 mL^{-1}, path lengths in dm. Chemical analyses were performed by Guelph Chemical Laboratories, Guelph, Ont., Canada. $RhCl_3 \cdot xH_2O$ was purchased from Johnson Matthey Ltd. [$RhCl(C_2H_4)_2]_2$ (19) and [$Rh(C_7H_8)_2$] (20) were prepared via published routes.

Synthesis of (R)-o-(($t\text{-}C_4H_9)_2P)C_6H_4CHCH_3N(CH_3)_2 \cdot HCl$, (R-*dibutphos·HCl)*

(*R*)-*N*,*N*-Dimethyl-1-phenylethylamine was prepared from (*R*)-1-phenylethylamine by reaction with formaldehyde and formic acid (21). (*R*)-*N*,*N*-Dimethyl-1-phenylethylamine (20.0 mL) was dissolved in freshly distilled diethyl ether (50 mL) and cooled in a dry ice/acetone bath. *n*-BuLi (47.5 mL) in hexanes (2.6 *M*) was added, the cooling bath was removed and the mixture was stirred for 18 h. The mixture was cooled again and ($t\text{-}C_4H_9)_2PCl$ (22.0 mL) was added slowly. After removal of the cooling bath and stirring for 6 h, 50 mL of H_2O was added and the stirring continued for 1 h. The organic layer was separated and the aqueous phase extracted with diethyl ether (2 × 50 mL). The combined organic phases were dried over $MgSO_4$,

TABLE 1. ^1H and ^{31}P nmr spectral data for ligands and complex

Compound	^1H nmr data		^{31}P nmr data	
	δ^a	J, Hz	$\delta^{b,c}$	J, Hz
dibutphos·HCl	8.86–8.76(m), 7.96–7.78(m), 7.70–7.56(m), 5.75(d of q), 3.25(d), 2.61(d), 1.69(d), 1.48(d), 1.40(d)	$^3J(CH_3—CH) = 7.0$ $^4J(P—CH) = 9.0$ $^3J(HN—CH_3) = 5.0$ $^3J(P—CH_3) = 22.0$	11.56	
dibutphos	7.88–7.70(m), 7.50–7.36(m), 7.32–7.18(m), 4.65(d of q), 2.31(s), 1.35(d), 1.28(d), 1.24(d)	$^3J(CH_3—CH) = 7.0$ $^4J(P—CH) = 9.0$ $^3J(P—CH_3) = 12.0$	8.64	
Compound **I**	7.92–7.80(m), 7.58–7.40(m), 7.26–7.18(m), 5.00(br), 4.89(br), 4.68(br), 4.54(br), 4.02(br), 3.93(br), 3.50(d of q), 2.43(s), 2.31(d), 2.27(s), 1.62(d), 1.68–1.48(m,sh), 1.18(d)	$^3J(CH_3—CH) = 6.0$ $^4J(P—CH) = 2.0$ $^3J(PC—CH_3) = 14.0$	35.29	$^1J(Rh—P) = 156.5$

[a] ^1H nmr spectra were recorded using d-$CHCl_3$ solutions and TMS as a reference.
[b] ^{31}P nmr spectra for dibutphos·HCl and dibutphos were recorded using $CHCl_3$ solutions and $OP(OCH_3)_3$ as a reference. The spectrum of the Rh complex was recorded using CH_2Cl_2 as the solvent.
[c] Small amounts of deuterated solvents were added to serve as lock signals.

filtered, and excess gaseous HCl added. The white precipitate formed was washed with diethyl ether, and recrystallized from CH_2Cl_2/acetone to give 8.3 g (19%) of product. $[\alpha]_D^{20} = 7.4°$ ($CHCl_3$, $c = 0.53$, $l = 2.0$); mp = 241°C, dec. Elemental analyses were variable.

Synthesis of (S)-o-*((*t-$C_4H_9)_2P)C_6H_4CHCH_3N(CH_3)_2$·*HCl, (*S-*dibutphos·HCl)*

S-Dibutphos·HCl was prepared in an analogous fashion. $[\alpha]_D^{20} = 7.8°$ ($CHCl_3$, $c = 1.4$, $l = 2.0$); mp = 240°C, dec. Elemental analyses were variable.

Synthesis of (R)-o-*((*t-$C_4H_9)_2P)C_6H_4CHCH_3N(CH_3)_2$, (R-*dibutphos)*

R-Dibutphos·HCl (5.0 g) was stirred with excess NaOH in ethanol for 15 min. After filtration and solvent removal, the residue was dissolved in diethyl ether and filtered. The solvent was removed and the product was distilled under reduced pressure to yield 2.0 g of viscous liquid. $[\alpha]_D^{20} = 116.0°$ ($CHCl_3$, $c = 0.61$, $l = 2.0$); bp 140°C/1 mm. *Anal.* calcd. for $C_{18}H_{32}NP$: C 73.68, H 10.99, N 4.77; found: C 73.94, H 11.12, N 4.89.

Synthesis of (S)-o-*((*t-$C_4H_9)_2P)C_6H_4CHCH_3N(CH_3)_2$, (S-*dibutphos)*

In the same manner *S*-dibutphos was prepared. $[\alpha]_D^{20} = 119.6°$ ($CHCl_3$, $c = 0.93$, $l = 2.0$); bp 140°C/1 mm. *Anal.* calcd. for $C_{18}H_{32}NP$: C 73.68, H 10.99, N 4.77; found: C 74.41, H 11.15, N 5.84.

*Synthesis of [Rh(*R-*dibutphos)C*$_7H_8$*]ClO*$_4$*, I*

$[Rh(C_7H_8)_2]ClO_4$ (100 mg) and *R*-dibutphos (76 mg) were dissolved in 15 mL of 50/50 $CH_2Cl_2/CHCl_3$ and stirred for 15 min. After filtration and addition of several mL of hexanes, the mixture was left to stand at room temperature. Crystals formed rapidly and were recovered from solution within 4 h of reaction; mp 180–182°C dec. *Anal.* calcd. for $C_{25}H_{40}ClNO_4PRh$: C 51.07, H 6.86, N 2.38; found: C 50.13, H 6.78, N 2.37.

^1H and ^{31}P nmr data for the species above are summarized in Table 1.

Procedure for hydrosilation of ketones

The hydrosilation reactions were all performed as described below for acetophenone, with appropriate modifications. $[RhCl(C_2H_4)_2]_2$ (19) (20 mg) was dissolved in degassed benzene (3 mL). A solution of *R*-dibutphos in benzene (1.95 mL, 0.053 *M*) was then added from a syringe. $C_6H_5SiH(CH_3)_2$ (5.0 mL) was then added, followed by acetophenone (2.92 mL). The mixture was stirred for 7 days. Chemical yields were measured by ^1H nmr spectroscopy. The benzene was removed by distillation and the silyl-ether $(C_6H_5)CHCH_3OSi(CH_3)_2C_6H_5$ distilled under vacuum (127°C/2 mm). A total of 3.8 g of product was isolated. In each of the trials with 3,3-dimethyl-2-butanone and 2-butanone, using the silane $C_6H_5SiH(CH_3)_2$, the amount of product isolated was too small for an optical rotation measurement. In the remaining trials all optical rotations were zero within experimental error.

X-ray data collection and reduction

Orange crystals of **I** were prepared as described above. A photographic examination using Weissenberg and precession techniques showed the crystals to be orthorhombic, Laue symmetry *mmm*. Observation of the systematic absences $h00$ for h odd, $0k0$ for k odd, and $00l$ for l odd led to an unambiguous assignment of the acentric space group $P2_12_12_1$ (22). The crystal density was determined by neutral buoyancy in a mixture of 1,2-dibromoethane and hexanes.

A crystal, cleaved from a long needle, of approximate dimensions $0.36 \times 0.16 \times 0.07$ mm^3 was chosen for data collection. Eight crystal faces were identified by optical goniometry, and indices (001) assigned to the broken face. Faces {100} were prominent. The crystal dimensions were carefully measured with a filar microscope.

Intensity data were recorded on an Enraf-Nonius CAD4F diffractometer using an incident beam graphite monochromator. Cell parameters and an orientation matrix were obtained from refinement of 23 reflections with $15 < 2\theta < 25°$. ω-Scans of several intense, low angle reflections, recorded with a wide open counter, had an average width at half height of 0.16°. Crystal data and experimental conditions are summarized in Table 2. Variable scan rates within a maximum time per datum of 75 s were used in order to optimize counting statistics. A Zr foil attenuator was used for extremely strong reflections and three standard reflections were recorded every 2 h of X-ray exposure time. On average, the standard intensities decreased in a nearly linear fashion by 3.9% during the 66 h required to record 3408 reflections. Corrections for background, monochromator polarization, Lorentz, and polarization effects were applied to the data using the Enraf-Nonius Structure Determination Package running on a DEC PDP11/23+ computer (23). Standard deviations were assigned, based on counting statistics, and a linear decay correction and a Gaussian absorption correction were applied to the data (23). In all, 2075 reflections with $F > 3\sigma(F)$ were available.

TABLE 2. Summary of crystal data and experimental conditions

Compound	$C_{24}H_{40}ClNO_4PRh$ f.w. 587.93
Unit cell dimensions (Å)	a = 15.773(3) Å, b = 18.660(4) Å, c = 8.990(3) Å, T = 18°C
Cell volume (Å^3)	2645(2) Z = 4
Density (g cm^{-3})	Obsd. 1.508(1), calcd 1.476
Space group	$P2_12_12_1$ (D_2^4, No. 19)
Absorption coefficient (cm^{-1})	μ(Mo Kα) = 8.26 μ(Cu Kα) = 66.59
Radiation, wavelength (Å)	MoKα, λ = 0.71073
Crystal faces	{1 1 0}, {1 0 0}, ($\bar{1}$ 1 $\bar{1}$), (1 $\bar{1}$ $\bar{1}$), (0 0 1)
Crystal volume (mm^3)	0.00286
Absorption correction grid	6 × 12 × 26
Transmission coefficients	max. 0.961, min. 0.889
Crystal-detector, take-off angle	205 mm 2.7°
Receiving aperture	4 mm vertical, 5.00 + 0.35 tan θ mm horizontal
Scan mode and range	ω−2θ 0.60 + 0.35 tan θ
Background	At 25% scan extensions
Data collected	$0 \leq h \leq 20$, $0 \leq k \leq 24$, $0 \leq l \leq 11$, for $0 \leq 2\theta \leq 55°$
Standard reflections	200, 080, 002

Structure solution and refinement

Positional parameters for the Rh and P atoms were obtained from a three dimensional Patterson sythesis. A series of least-squares refinements and difference Fourier syntheses were used to locate the remaining 31 non-H and 25 H atoms of the cation and anion. Refinement of atomic parameters was by full-matrix least-squares techniques on F, minimizing the function $\Sigma w(|F_o| - |F_c|)^2$, where F_o and F_c are the observed and calculated structure factor amplitudes and w, the weighting factor, is given by $w = 4F_o^2/\sigma^2(F_o^2)$. Scattering factors used for non-H atoms were those for neutral atoms calculated by Cromer and Waber (22), those for H by Stewart *et al.* (24). The real and imaginary components of anomalous dispersion of Cromer (22) were included for all atoms.

In the final model the 26 non-H atoms, excluding those in the norbornadiene ligand, were refined with anisotropic thermal parameters. The seven C atoms in the norbornadiene ligand were refined with isotropic Debye factors. All 25 H atoms were located in a difference Fourier with peak heights ranging from 0.16(11) to 0.46(11) e Å^{-3}, and included in ideal positions (C—H = 0.90 Å; methyl C atoms, C—H = 0.95 Å) in calculations of F_c. H atom thermal parameters were 110% of the isotropic equivalent of those of the atoms to which they are bonded. No H parameters were refined, but all values were updated as refinement continued.

Since the absolute configuration of the ligand was known, the correct choice of hand could be made at the beginning of the analysis. In the final cycles of refinement, 2257 reflections with $F > 1.5\sigma(F)$ were used to refine 263 variables, with convergence at residuals of R_1 = 0.0420 and R_2 = 0.0494. In the final cycle all parameter shifts were less than 0.01σ, and, with a p value of 0.08 (25), the error in an observation of unit weight was 1.03 e. A total difference Fourier synthesis showed that the highest peak, at fractional coordinates (0.437, 0.328, 0.531), with an electron density of 0.61(9) e Å^{-3} is situated 0.72 Å from the Rh atom. A statistical analysis of R_1 and R_2 in terms of F_o, λ^{-1} sin θ, and classes of indices showed no unusual trends, indicating a satisfactory weighting scheme and the absence of significant secondary extinction.

Final positional and U equivalent thermal parameters are given in Table 3 for the non-H atoms. H atom parameters, anisotropic thermal parameters, root-mean-square amplitudes of vibration and structure amplitudes have been deposited.[2]

Confirmation of absolute configuration

The absolute configuration of the cation was confirmed by the Bijvoet absorption edge technique (26) using Cu Kα radiation (λ = 1.5418 Å), and the same crystal. Friedel pairs were recorded for a selection of structure amplitudes calculated from the final model and its enantiomorph for which $F_c(h\,k\,l)$ and $F_c(\bar{h}\,\bar{k}\,\bar{l})$ differed by more than 15%. The results are presented in Table SIV,[2] and indicate that the assignment based upon the ligand synthesis was correct.

TABLE 3. Atomic positional (×10^4) and thermal (×10^3) parameters

Atom	x	y	z	U_{eq} (Å^2)
Rh	4400.2(3)	3121.2(3)	4588.9(7)	37.6(1)
Cl	7708(2)	7154(1)	5861(2)	59.3(6)
P	5148(1)	4166.6(9)	5417(2)	32.6(4)
O(1)	6592(7)	7766(5)	5448(16)	184(4)
O(2)	7398(5)	6892(5)	4590(10)	134(3)
O(3)	7614(5)	7355(4)	6930(9)	114(3)
O(4)	6497(6)	6633(5)	6501(12)	169(3)
N	3190(3)	3718(3)	4492(8)	47(2)
C(1)	4719(6)	1698(5)	5383(12)	68(2)
C(2)	5322(5)	2318(4)	5122(9)	53(2)
C(3)	5354(6)	2435(4)	3615(10)	57(2)
C(4)	4756(7)	1890(6)	2895(12)	82(3)
C(5)	3933(6)	2157(5)	3419(11)	67(3)
C(6)	3886(5)	2048(4)	4923(9)	54(2)
C(7)	4920(8)	1257(6)	3933(14)	93(4)
C(11)	4510(4)	4998(3)	5160(7)	35(2)
C(12)	4835(5)	5633(4)	5742(9)	50(2)
C(13)	4389(6)	6270(4)	5671(12)	59(2)
C(14)	3610(6)	6278(4)	5018(10)	65(3)
C(15)	3286(5)	5670(4)	4426(10)	60(2)
C(16)	3720(4)	5000(4)	4455(9)	41(2)
C(17)	3272(5)	4400(5)	3663(9)	54(2)
C(18)	3661(6)	4274(5)	2133(10)	63(3)
C(19)	2855(5)	3861(5)	6000(10)	60(2)
C(20)	2507(6)	3293(6)	3730(10)	78(3)
C(21)	6162(4)	4348(4)	4311(9)	43(2)
C(22)	6821(5)	3785(4)	4748(12)	61(2)
C(23)	6562(5)	5090(4)	4455(12)	64(2)
C(24)	5913(5)	4265(5)	2675(10)	58(2)
C(31)	5387(5)	4173(4)	7513(9)	50(2)
C(32)	5591(6)	3399(5)	8018(10)	71(3)
C(33)	4605(6)	4395(6)	8376(9)	68(3)
C(34)	6121(6)	4636(5)	8018(10)	72(3)

[a]Anisotropic thermal parameters are given in the form of the isotropic equivalent thermal parameter defined as: $U_{eq} = \frac{1}{3}\Sigma_i\Sigma_j U_{ij} a_i^* a_j^* \boldsymbol{a}_i \cdot \boldsymbol{a}_j$.

Results and discussion

The unit cell contains discrete cations and anions, with short-

[2]Hydrogen atom parameters, anisotropic thermal parameters, root-mean-square amplitudes of vibration, Friedel pairs, supplementary dimensions, selected torsion angles, weighted mean plane calculations, and structure amplitudes are available at a nominal charge from the Depository of Unpublished Data, CISTI, National Research Council of Canada, Ottawa, Ont., Canada, K1A 0S2.

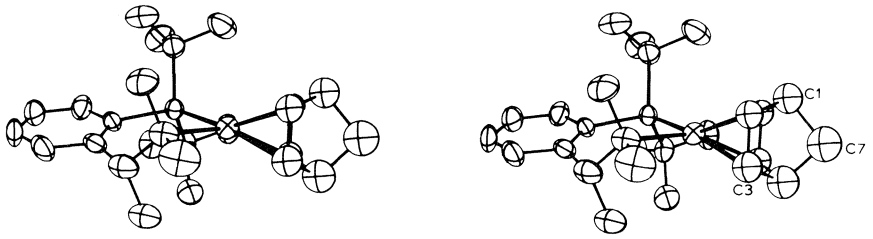

FIG. 1. A stereoview of the cation.

TABLE 4. Selected bond distances (Å) and bond angles (deg)

Atom 1	Atom 2	Distance	Atom 1	Atom 2	Distance	Atom 1	Atom 2	Distance
Rh	P	2.398(2)	N	C(17)	1.480(11)	C(21)	C(24)	1.530(12)
Rh	N	2.212(6)	N	C(19)	1.479(11)	C(31)	C(32)	1.548(12)
Rh	C(2)	2.143(8)	N	C(20)	1.503(12)	C(31)	C(33)	1.515(12)
Rh	C(3)	2.161(9)	C(11)	C(12)	1.392(10)	C(31)	C(34)	1.514(12)
Rh	C(5)	2.210(9)	C(11)	C(16)	1.398(10)	C(1)	C(2)	1.516(12)
Rh	C(6)	2.181(8)	C(12)	C(13)	1.383(10)	C(1)	C(6)	1.524(12)
Cl	O(1)	1.368(11)	C(13)	C(14)	1.362(13)	C(1)	C(7)	1.574(15)
Cl	O(2)	1.386(9)	C(14)	C(15)	1.353(11)	C(2)	C(3)	1.373(12)
Cl	O(3)	1.406(9)	C(15)	C(16)	1.427(11)	C(3)	C(4)	1.531(14)
Cl	O(4)	1.389(10)	C(16)	C(17)	1.504(11)	C(4)	C(5)	1.468(14)
P	C(11)	1.864(7)	C(17)	C(18)	1.524(12)	C(4)	C(7)	1.527(15)
P	C(21)	1.914(7)	C(21)	C(22)	1.529(10)	C(5)	C(6)	1.369(13)
P	C(31)	1.921(9)	C(21)	C(23)	1.526(10)			

Atom 1	Atom 2	Atom 3	Angle	Atom 1	Atom 2	Atom 3	Angle	Atom 1	Atom 2	Atom 3	Angle
P	Rh	N	91.6(2)	C(11)	P	C(31)	102.9(3)	P	C(21)	C(24)	105.5(5)
P	Rh	C(2)	99.6(2)	C(21)	P	C(31)	110.2(3)	C(22)	C(21)	C(23)	108.7(6)
P	Rh	C(3)	105.4(2)	C(17)	N	C(19)	109.8(6)	C(22)	C(21)	C(24)	110.6(7)
P	Rh	C(5)	166.8(3)	C(17)	N	C(20)	106.7(7)	C(23)	C(21)	C(24)	106.2(7)
P	Rh	C(6)	152.5(2)	C(19)	N	C(20)	104.9(6)	P	C(31)	C(32)	108.8(6)
N	Rh	C(2)	161.2(3)	P	C(11)	C(12)	117.5(5)	P	C(31)	C(33)	110.2(6)
N	Rh	C(3)	152.0(3)	P	C(11)	C(16)	122.6(5)	C(32)	C(31)	C(33)	106.0(7)
N	Rh	C(5)	95.9(3)	C(12)	C(11)	C(16)	119.8(6)	C(32)	C(31)	C(34)	106.7(7)
N	Rh	C(6)	98.4(3)	C(11)	C(12)	C(13)	121.7(7)	C(33)	C(31)	C(34)	108.4(7)
C(2)	Rh	C(3)	37.2(3)	C(12)	C(13)	C(14)	119.2(7)	C(2)	C(1)	C(6)	99.9(7)
C(2)	Rh	C(6)	65.1(3)	C(13)	C(14)	C(15)	120.1(7)	C(2)	C(1)	C(7)	98.3(8)
C(3)	Rh	C(5)	63.7(3)	C(14)	C(15)	C(16)	123.1(8)	C(6)	C(1)	C(7)	100.0(8)
C(5)	Rh	C(6)	36.3(3)	C(11)	C(16)	C(15)	116.0(7)	C(1)	C(2)	C(3)	107.3(8)
O(1)	Cl	O(2)	106.5(7)	C(11)	C(16)	C(17)	129.2(7)	C(2)	C(3)	C(4)	106.8(8)
O(1)	Cl	O(3)	106.9(6)	C(15)	C(16)	C(17)	114.7(7)	C(3)	C(4)	C(5)	100.6(8)
O(1)	Cl	O(4)	114.7(6)	N	C(17)	C(16)	116.3(7)	C(3)	C(4)	C(7)	98.7(8)
O(2)	Cl	O(3)	110.9(5)	N	C(17)	C(18)	110.9(7)	C(5)	C(4)	C(7)	102.5(9)
O(2)	Cl	O(4)	110.5(6)	C(16)	C(17)	C(18)	110.7(7)	C(4)	C(5)	C(6)	108.3(8)
O(3)	Cl	O(4)	107.3(6)	P	C(21)	C(22)	108.2(5)	C(1)	C(6)	C(5)	106.6(8)
C(11)	P	C(21)	103.9(3)	P	C(21)	C(23)	117.5(5)	C(1)	C(7)	C(4)	93.9(8)

est Rh...Rh and Cl...Cl distances of 8.253(1) and 8.140(3) Å respectively. The shortest Rh...Cl distance is 4.992(2) Å. The shortest non-bonded cation–anion contacts are O(3)...H3C(19) $(1 - x, \frac{1}{2} + y, \frac{3}{2} - z)$ of 2.51 Å and O(4)...HC(12) (x, y, z) of 2.62 Å. Between cations the closest contacts are H1C(7)...H1C(24) $(1 - x, -\frac{1}{2} + y, \frac{1}{2} - z)$ at 2.50 Å and H2C(23)...H2C(34) $(\frac{3}{2} - x, 1 - y, -\frac{1}{2} + z)$ at 2.56 Å. The perchlorate anions are well ordered, with Cl—O distances ranging from 1.368(11) to 1.406(9) Å and angles from 106.5(7) to 114.7(6)°.

A stereoview of the cation showing the atom numbering scheme for the norbornadiene ligand is given in Fig. 1 and a perspective drawing of the cation, less the norbornadiene ligand and showing the remainder of the numbering scheme, is presented in Fig. 2. Atoms are drawn as 50% probability thermal ellipsoids in both figures. Selected bond distances and bond angles are given in Table 4, and others have been deposited.[2]

The Rh atom is coordinated in a square-planar environment, with a slight tetrahedral distortion. The angle between the plane formed by the Rh, P, and N atoms and that formed by the Rh atom and M23 and M56, which are the midpoints of the alkene bonds, is 9.8°. The six-membered chelate ring adopts a twist boat conformation of absolute configuration δ, and the configuration of C(17) has been confirmed as *R*, as expected from the synthesis. The methyl substituent, C(18), is axially disposed with respect to the chelate ring. This arrangement has been shown to occur in order to minimize steric interactions between the methyl substituent, C(18), and H(15), the nearest neighbour

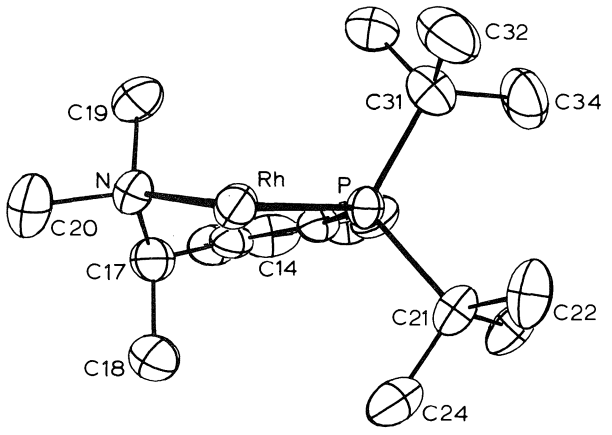

FIG. 2. A perspective view of the cation.

TABLE 5. Asymmetric hydrosilation of ketones as catalysed by L—L + $[RhCl(C_2H_4)_2]_2$

R	R^1	$[\alpha]_D^{20}$	Chem. yield, %[a]	Opt. yield, %
$C_6H_5SiH(CH_3)_2$[c]		L—L = *R*-dibutphos		
Ph	Me	0	61	0
Ph	Et	0	50	0
t-Bu	Me	[b]	25	—
Et	Me	[b]	15	—
		L—L = *S*-dibutphos		
Ph	Me	0	57	0
Ph	Et	0	53	0
t-Bu	Me	[b]	18	—
Et	Me	[b]	21	—
$(C_6H_5)_2SiH_2$[c]		L—L = *R*-dibutphos		
Ph	Me	0	68(18)[d]	0
Ph	Et	0	71(17)[d]	0
t-Bu	Me	0	85(10)[d]	0
Et	Me	0	91(5)[d]	0
		L—L = *S*-dibutphos		
Ph	Me	0	64(23)[d]	0
Ph	Et	0	75(13)[d]	0
t-Bu	Me	0	83(11)[d]	0
Et	Me	0	92(3)[d]	0

[a]Based on ^1H nmr of the reaction mixture after 7 days of stirring for trials with $C_6H_5SiH(CH_3)_2$ and 3 days of stirring for trials with $(C_6H_5)_2SiH_2$.
[b]Not measured due to insufficient chemical yield.
[c]Silane used for these trials.
[d]Number in parentheses indicates the percentage of olefin formed due to β-elimination of siloxyalkyl intermediate.

on the phenyl ring in the chelate backbone (17). The N-methyl substituents then adopt corresponding staggered dispositions. All dimensions within the dibutphos ligand are normal, and they and other dimensions in the cation correspond well with those in related complexes (17, 27, 28). The geometry of the norbornadiene ligand is unexceptional (29–44). Weighted least-squares planes and selected torsion angles have been deposited as Tables SVI and SVII.[2]

Hydrosilation reactions

The results of hydrosilation reactions performed using the silanes dimethylphenylsilane and diphenylsilane, with each of the four ketones, acetophenone, 3,3-dimethyl-2-butanone, propiophenone, and 2-butanone, are presented in Table 5. Some trends are evident. The reactions in which diphenylsilane was used produced greater chemical yields in a shorter period of time than did those with dimethylphenylsilane. Use of dimethylphenylsilane resulted in the formation of only a silyl-ether as the product in each case, whereas trials with diphenylsilane produced two products, one being the silyl-ether (major product), and the other, an olefin, presumably resulting from β-elimination of a siloxyalkyl intermediate. We also note that, when dimethylphenylsilane was used, reactions with the dialkyl ketones gave markedly lower chemical yields than the reactions with the alkylaryl ketones. When diphenylsilane was used the reverse was seen, with the dialkyl ketones giving slightly higher chemical yields. In contrast to the results reported for catalytic systems based on the ligand amphos (16), the reactions described herein produced no measurable optical bias in the products. A possible explanation may be proposed from an examination of the structure of $[Rh(dibutphos)(C_7H_8)]ClO_4$ in the solid state. The *tert*-butyl groups on the dibutphos complex cannot produce an asymmetric coordination environment through a face-edge arrangement of phenyl rings, as was seen for the amphos complex. We had hoped that an equivalent asymmetric environment could result from a pseudo-axial/equatorial arrangement of the bulky *tert*-butyl groups in the metal-chelate unit, but such was not observed in the solid state. The tertiary C atoms of the *tert*-butyl groups, C(21) and C(31), are displaced from the plane of the Rh, P, and N atoms to a similar extent, by −1.331(8) and 1.716(8) Å, respectively. Thus, although the complex catalyzes the hydrosilation reaction, the dibutphos ligand does not induce an asymmetric environment for the incoming substrate molecule, and hence no optical induction results.

Acknowledgments

We thank the Natural Sciences and Engineering Research Council of Canada for financial support of this work, through grants to N.C.P. and a scholarship to I.D.M.

1. H. MATSUMOTO, Y. YOSHINO, and Y. NAGAI. Bull. Chem. Soc. Jpn. **54**, 1279 (1981).
2. T. HAYASHI, K. YAMAMOTO, K. KASUGA, H. OMIZU, and M. KUMADA. J. Organomet. Chem. **113**, 127 (1976).
3. D. WANG, and T. H. CHAN. Tetrahedron Lett. **24**, 1573 (1983).
4. I. OJIMA, T. KOGURE, and M. KUMAGAI. J. Org. Chem. **42**, 1671 (1977).
5. T. HAYASHI, K. YAMAMOTO, and M. KUMADA. J. Organomet. Chem. **112**, 253 (1976).
6. I. OJIMA, T. KOGURE, M. KUMAGAI, S. HORIUCHI, and T. SATO. J. Organomet. Chem. **122**, 83 (1976).
7. I. OJIMA, and Y. NAGAI. Chem. Lett. 191 (1975).
8. R. J. P. CORRIU and J. J. E. MOREAU. J. Organomet. Chem. **64**, C51 (1974).
9. R. J. P. CORRIU and J. J. E. MOREAU. J. Organomet. Chem. **85**, 19 (1975).
10. T. HAYASHI, K. YAMAMOTO, and M. KUMADA. Tetrahedron Lett. 4405 (1974).
11. I. KOLB, J. HETFLEJS. J. Coll. Czech. Chem. Commun. **45**, 2224 (1980).
12. H. BRUNNER and G. RIEPL. Angew. Chem. Int. Ed. Engl. **21**, 377 (1982).
13. H. BRUNNER. Angew. Chem. Int. Ed. Engl. **22**, 897 (1983).
14. H. BRUNNER, R. BECKER, and G. RIEPL. Organometallics, **3**, 1354 (1984).
15. H. BRUNNER, G. RIEPL, and H. WEITZER. Angew. Chem. Int. Ed. Engl. **22**, 331 (1983).
16. N. C. PAYNE and D. W. STEPHAN. Inorg. Chem. **21**, 182 (1982).

17. I. D. McKay and N. C. Payne. Organometallics. To be published.
18. S. Profeta, Jr., N. L. Allinger, and Y. H. Yuh. QCPE 423, Indiana University.
19. D. W. Stephan. Ph.D. Thesis. The University of Western Ontario, London, Ont. 1980.
20. R. Cramer. Inorg. Chem. **1**, 722 (1962).
21. F. Klages, G. Nober, F. Kircher, and M. Bock. Justus Liebigs Ann. Chem. **547**, 1 (1947).
22. International Tables for X-ray Crystallography, Kynoch Press, Birmingham, England. Vol. I, 1969; Vol. IV, 1974.
23. Enraf-Nonius Structure Determination Package. SDP-PLUS, Version 1.0. 1982.
24. R. F. Stewart, E. R. Davidson, and W. T. Simpson. J. Chem. Phys. **42**, 3175 (1965).
25. W. R. Busing and H. A. Levy. J. Chem. Phys. **26**, 563 (1957).
26. A. F. Peerdeman, A. J. Van Bommel, and J. M. Bijvoet. Proc. Acad. Sci. Amst. B**54**, 16 (1951).
27. I. D. McKay and N. C. Payne. Acta Crystallogr. C**42**, 304 (1986).
28. I. D. McKay and N. C. Payne. Acta Crystallogr. C**42**, 307 (1986).
29. W. R. Cullen, F. W. B. Einstein, C. H. Huang, A. C. Willis, and E. S. Yeh. J. Am. Chem. Soc. **102**, 988 (1980).
30. H. J. Langenbach, E. Keller, and H. J. Varenkamp. J. Organomet. Chem. **171**, 259 (1979).
31. K. Itoh, N. Oshima, G. B. Jameson, H. C. Lewis, and J. A. Ibers. J. Am. Chem. Soc. **103**, 3014 (1981).
32. S. Swaminathan and L. Lessinger. Cryst. Struct. Commun. **7**, 621 (1978).
33. S. A. Bezman, P. H. Bird, A. R. Fraser, and J. A. Osborn. Inorg. Chem. **19**, 3755 (1980).
34. E. P. Kyba, R. E. Davis, P. N. Kuri, and K. R. Shirley. Inorg. Chem. **20**, 3616 (1981).
35. I. L. C. Campbell and F. S. Stephens. J. Chem. Soc. Dalton Trans. 226 (1975).
36. M. Cocivera, G. Ferguson, B. Kaitner, F. J. Lalor, D. J. O'Sullivan, M. Parvez, and B. Ruhl. Organometallics, **1**, 1132 (1982).
37. A. H. Reis, C. Willi, S. Siegel, and B. Tani. Inorg. Chem. **18**, 1859 (1979).
38. F. P. Boer and J. J. Flynn. J. Am. Chem. Soc. **93**, 6495 (1971).
39. C. Potvin, J. M. Manoli, G. Pannatier, R. Chevalier, and N. Platzer. J. Organomet. Chem. **113**, 273 (1976).
40. P. J. P. Declercq, G. Germain, M. Van Meerssche, and S. A. Chawdhury. Acta Crystallogr. B**31**, 2896 (1975).
41. J. Antony, J. Jarvis, and R. Whyman. J. Chem. Soc. Chem. Commun. 562 (1975).
42. M. R. Churchill and K. K. G. Lin. J. Am. Chem. Soc. **96**, 76 (1974).
43. W. R. Cullen, T. J. Kim, F. W. B. Einstein, and T. Jones. Organometallics, **2**, 704 (1983).
44. R. E. Davis, B. B. Meyer, K. L. Hassett, P. N. Juri, and E. P. Kyba. Acta Crystallogr. C**40**, 21 (1984).

The oxidation of hydrogen peroxide by tris(polypyridine) complexes of osmium(III), iron(III), ruthenium(III), and nickel(III) in aqueous media

DONAL H. MACARTNEY

Department of Chemistry, Queen's University, Kingston, Ont., Canada K7L 3N6

Received November 5, 1985

DONAL H. MACARTNEY. Can. J. Chem. **64**, 1936 (1986).

The stoichiometry and kinetics of the oxidation of hydrogen peroxide by tris(2,2′-bipyridine) and tris(4,4′-dimethyl-2,2′-bipyridine) complexes of osmium(III), iron(III), ruthenium(III), and nickel(III) were studied in acidic and neutral aqueous media at 25°C and $I = 0.50\ M$ ($LiCF_3SO_3$). The reaction $2M(bpy)_3^{3+} + H_2O_2 \rightarrow 2M(bpy)_3^{2+} + O_2 + 2H^+$ is observed with quantitative yields of dioxygen gas. The observed rate constants displayed an inverse acid dependence over the pH range 6.0–8.5; $k_{obsd} = k_1 + k_2K_1/[H^+]$, attributed to the oxidations of H_2O_2 (k_1) and HO_2^- (k_2). An application of the Marcus theory relationship to the cross-reaction data gave a self-exchange rate constant of 10^{-2}–$10^{-1}\ M^{-1}\ s^{-1}$ for the HO_2^-/HO_2 couple. The electron exchange rate constant is evaluated in terms of the inner-sphere and solvent reorganizational barriers and is compared to values reported for other small molecule couples. Rate and activation parameters for the reduction of the nickel(III) complexes by the hydroxide ion have been determined and are compared with the corresponding values for other metal tris(polypyridine) complexes.

DONAL H. MACARTNEY. Can. J. Chem. **64**, 1936 (1986).

Opérant en milieu aqueux acide ou neutre, à 25°C et à $I = 0{,}50\ M$ ($LiCF_3SO_3$), on a étudié la stoéchiométrie et la cinétique de l'oxydation du peroxyde d'hydrogène par les complexes de tris(bipyridine-2,2′) et tris(diméthyl-4,4′ bipyridine-2,2′) d'osmium(III), de fer(III), de ruthénium(III) et de nickel(III). On a observé que la réaction $2M(bpy)_3^{3+} + H_2O_2 \rightarrow 2M(bpy)_3^{2+} + O_2 + 2H^+$ se produit avec des rendements quantitatifs en dioxygène gazeux. Il existe une corrélation inverse entre les constantes de vitesse observées et la concentration d'acide dans l'intervalle de pH allant de 6,0 à 8,5; $k_{obs} = k_1 + k_2K_1/[H^+]$ et on attribue k_1 et k_2 respectivement à l'oxydation du H_2O_2 (k_1) et du HO_2^- (k_2). L'application de la relation de la théorie de Marcus aux données de la réaction d'échange donne une constante de vitesse d'auto-échange de 10^{-2}–$10^{-1}\ M^{-1}\ s^{-1}$ pour le couple HO_2^-/HO_2. On évalue la constante de vitesse d'échange de l'électron en fonction de la sphère interne et des barrières de réorganisation du solvant et on la compare aux valeurs rapportées pour d'autres couples de petites molécules. On a déterminé la vitesse et les paramètres d'activation de la réduction des complexes de nickel(III) par l'ion hydroxyde et on les compare aux valeurs correspondantes pour d'autres complexes tris(polypyridine) de métal.

[Traduit par la revue]

Introduction

The oxidation water to molecular oxygen involves the overall transfer of four electrons and four protons.

$$2H_2O \rightarrow O_2 + 4H^+ + 4e^-$$

This reaction represents the net oxidation process in green plant photosynthesis (1) and is important in the transfer and storage of energy in many chemical and biochemical systems. The successive addition of electrons to molecular oxygen generates dioxygen intermediates such as the superoxide, $H_nO_2^{(n-1)+}$, and the peroxide, $H_nO_2^{(n-2)+}$, ions. The interconversions of the various dioxygen species and their affinities for metal complexes have been studied in considerable detail (2–5).

Hydrogen peroxide is usually regarded as an oxidant but may itself be oxidized by species such as Ce(IV), MnO_4^-, and Cl_2. With metal aquo ions such as Ce^{4+}(aq) (6), Tl^{3+}(aq) (7), Mn^{3+}(aq) (8), Ag^{3+}(aq) (9), and Co^{3+}(aq) (10) as oxidants the electron transfers occur by inner-sphere processes, involving $MOOH^{n+}$ intermediates and complicated by the proton dissociation equilibria of the metal ions. Outer-sphere oxidations of H_2O_2 by $Ag(bpy)_2^{2+}$ (11), $Ru(bpy)_3^{3+}$ (12), $(bpy)_2pyRuO^{2+}$ (13), and $Ni(bpy)_3^{3+}$ (14) have also been observed.

In this paper the results of systematic kinetic investigation of the oxidation of H_2O_2 and its conjugate base HO_2^- by tris(2,2′-bipyridine) and tris(4,4′-dimethyl-2,2′-bipyridine) complexes of osmium(III), iron(III), ruthenium(III), and nickel(III) in aqueous media are reported. These species are well characterized one-electron outer-sphere oxidants and the lack of proton equilibria associated with these complexes permits a differentiation between H_2O_2 and HO_2^- pathways. The Marcus relationship (15) has been employed to correlate the cross-reaction data and provide an estimate of the electron exchange rate constant for the HO_2^-/HO_2 couple. This exchange rate constant may be compared with values reported for other small molecule couples, such as O_2^-/O_2. A semi-classical model (16) for bimolecular electron transfer is used to evaluate the rate of electron exchange in HO_2^-/HO_2 in terms of inner-sphere and solvent reorganizational barriers. Kinetic and activation parameters are also reported for the spontaneous reduction of the nickel(III) complexes in basic aqueous solution and are compared with corresponding values for the Os(III), Fe(III), and Ru(III) complexes.

Experimental

Reagents

Trifluoromethanesulphonic acid (CF_3SO_3H, 3M Co.) was purified by distillation at reduced pressure. Dilute stock solutions of CF_3SO_3H were standardized by titration with sodium hydroxide. Solutions of $LiCF_3SO_3$ were prepared by the neutralization of CF_3SO_3H with recrystallized lithium carbonate. An aliquot of the solution was passed through a Dowex 50W-X2 column in the H^+ form and titrated with standardized base. Solutions of hydrogen peroxide (Mallinckrodt or Fisher, 30%, stabilizer free) were prepared with doubly distilled water, analyzed by titration with standardized permanganate, and used promptly.

The tris(2,2′-bipyridine) and tris(4,4′-dimethyl-2,2′-bipyridine) complexes of osmium(II) (17), iron(II) (18), ruthenium(II) (18), and nickel(II) (19) were prepared as perchlorate salts by reported procedures. The corresponding metal(III) complexes for Os, Fe, and Ru were synthesized by PbO_2 oxidation in 1 M H_2SO_4 followed by precipitation with excess sodium perchlorate. The nickel(III) complexes were prepared by electrochemical oxidation of the correspond-

ing nickel(II) salts in anhydrous acetonitrile (19, 20). The reactions of $M(bpy)_3^{3+}$ and $M(4,4'\text{-}(CH_3)_2bpy)_3^{3+}$ with H_2O_2 were studied in 0.50 *M* CF_3SO_3H and in the pH range of 6.0 to 8.5. The pH was controlled by the use of 0.10 *M* tris and 0.025 *M* phosphate buffers with the ionic strength maintained at 0.50 *M* with $LiCF_3SO_3$. The buffered H_2O_2 solutions were mixed with metal complex solutions kept at pH 2 and the pH of the reaction mixture was measured immediately following the reaction. The spontaneous reductions of the nickel(III) complexes in basic aqueous solution were studied by mixing solutions of the Ni(III) complex in 10^{-3} *M* CF_3SO_3H with solutions of various $[OH^-]$, at an ionic strength of 0.50 *M* maintained using $LiCF_3SO_3$.

Kinetic experiments

Kinetic measurements were made using a Durrum D-110 stopped-flow apparatus or with slower reactions, Cary 17 and 210 spectrophotometers. All experiments were performed under pseudo-first-order conditions of an excess of hydrogen peroxide or hydroxide ion. The reactions involving the Os(III), Fe(III), Ru(III), and Ni(III) complexes were monitored at 480, 510, 460, and 400 nm, respectively. Plots of $\ln(A_t - A_\infty)$ or $\ln(A_\infty - A_t)$ against time were linear for at least three half-lives with first-order rate constants reproducible to within 5%. The temperature was maintained to within 0.1°C by means of an external water bath.

Oxygen analysis

Gas chromatography (Varian Series 1400 gas chromatograph, 2 m × ⅛ cm Molecular Sieve 5A column, argon carrier gas) was used to analyze for O_2 in the gas phase above a helium saturated reaction mix- as described previously (21). Equal volumes of 3×10^{-3} *M* H_2O_2 phosphate buffer and 2×10^{-3} *M* $M(bpy)_3^{3+}$ in 10^{-2} *M* H_2SO_4 mixed and stirred for 20 min before sampling. The observed peak ıts were corrected for any air leakage using the N_2 peak produced.

Results

The addition of an excess of hydrogen peroxide to neutral solutions of OsL_3^{3+}, FeL_3^{3+}, RuL_3^{3+}, and NiL_3^{3+} (L = bpy or $4,4'\text{-}(CH_3)_2bpy$) result in the rapid formation of products whose visible spectra resemble those of the corresponding ML_3^{2+} species. The expected stoichiometry for the two electron oxidation of hydrogen peroxide to molecular dioxygen by ML_3^{3+} was observed.

$$[1] \quad 2ML_3^{3+} + H_2O_2 \rightarrow 2ML_3^{2+} + O_2 + 2H^+$$

The yields of dioxygen gas based on this stoichiometry were as follows: for $Ni(bpy)_3^{3+}$, 98 ± 10%; $Ru(bpy)_3^{3+}$, 94 ± 10%; $Fe(bpy)_3^{3+}$, 95 ± 10%; and $Os(bpy)_3^{3+}$, 104 ± 10%.

Kinetic measurements of the oxidation of hydrogen peroxide by the ML_3^{3+} complexes were performed in acidic solution (0.5 *M* CF_3SO_3H) and in solutions buffered between pH 6.0 and 8.5 (I = 0.50 *M* $LiCF_3SO_3$). The reactions in 0.5 *M* CF_3SO_3H were slow and followed the rate law in eq. [2]

$$[2] \quad \frac{-d[ML_3^{3+}]}{2dt} = k_a[ML_3^{3+}][H_2O_2]$$

with the pseudo-first-order rate constant k_{obsd} displaying a first-order dependence on $[H_2O_2]$. The rate constants k_a are presented in Table 1. In the $Fe(bpy)_3^{3+}/H_2O_2$ reaction, the redox step is followed by acid hydrolysis of $Fe(bpy)_3^{2+}$. No reactions of H_2O_2 were observed at 25°C with the weaker oxidants $Os(4,4'\text{-}(CH_3)_2bpy)_3^{3+}$, $Os(bpy)_3^{3+}$, or $Fe(4,4'\text{-}(CH_3)_2bpy)_3^{3+}$. Rate constants have been reported previously for the oxidation of H_2O_2 by $Ru(bpy)_3^{3+}$ (4.2 M^{-1} s^{-1}, pH = 3, I = 1.00 *M* Na_2SO_4 (12)) and by $Ni(bpy)_3^{3+}$ (0.34 M^{-1} s^{-1}, I = 2.00 *M* $LiClO_4$ (14)). The discrepancies between these values and the present results are likely due to the different media and acid and ionic strengths employed in the kinetic experiments.

TABLE 1. Rate constants for the oxidation of H_2O_2 by ML_3^{3+} complexes at 25°C, I = 0.50 *M* ($LiCF_3SO_3$)

Oxidant	pH	k_{obsd} (M^{-1} s^{-1})	k_b (s^{-1})
$Os(4,4'\text{-}(CH_3)_2bpy)_3^{3+}$	7.37	0.0322	1.42×10^{-9}
	7.71	0.0644	
	8.02	0.142	
	8.19	0.211	
	8.39	0.346	
$Os(bpy)_3^{3+}$	7.06	0.870	8.31×10^{-8}
	7.52	2.27	
	7.95	6.92	
	8.16	11.3	
	8.31	16.9	
$Fe(4,4'\text{-}(CH_3)_2bpy)_3^{3+}$	7.50	1.46	3.73×10^{-8}
	7.80	2.92	
	7.97	3.80	
	8.20	6.29	
	8.45	10.9	
$Fe(bpy)_3^{3+}$	7.34	22.7	9.83×10^{-7}
	7.55	33.4	
	7.80	60.7	
	8.03	102	
	8.22	164	
$Ru(4,4'\text{-}(CH_3)_2bpy)_3^{3+}$	0.30	0.0017	
	7.27	29.7	1.78×10^{-6}
	7.62	66.7	
	7.91	143	
	8.13	240	
	8.39	420	
$Ru(bpy)_3^{3+}$	0.30	0.333	
	5.98	31.3	3.24×10^{-5}
	6.76	109	
	7.30	612	
	7.58	1190	
	7.81	2030	
$Ni(4,4'\text{-}(CH_3)_2bpy)_3^{3+}$	0.30	0.105	
	6.77	298	4.49×10^{-5}
	7.16	895	
	7.43	1140	
	7.66	2370	
	7.87	3350	
$Ni(bpy)_3^{3+}$	0.30	2.75	
	6.82	1750	3.34×10^{-4}
	6.89	2240	
	7.17	4280	
	7.62	13600	
	7.86	23700	

At higher pH the oxidation of hydrogen peroxide by ML_3^{3+} is more rapid. Between 6.0 and 8.5 the observed rate constants (Table 1) displayed an inverse first-order dependence on the acid concentration as illustrated in Fig. 1 for the bipyridine complexes.

$$[3] \quad \frac{-d[ML_3^{3+}]}{2dt} = k_b[ML_3^{3+}][H_2O_2]/[H^+]$$

The negligible intercepts are consistent with the small rate constants observed in acidic solution. The rate constants k_b derived from the slopes of k against $[H^+]^{-1}$ are presented in Table 1.

Spontaneous reduction of tris(polypyridine)metal(III) com-

TABLE 2. Rate and activation parameters for the reduction of metal(III) tris(polypyridine) complexes by OH^-; ionic strength given in parentheses

Oxidant	T (°C)	k (M^{-1} s^{-1})	$\Delta H^{\ddagger}$ (kcal mol^{-1})	$\Delta S^{\ddagger}$ (cal K^{-1} mol^{-1})
$Ni(bpy)_3^{3+}$	3.9	490 (0.50)	11.5 ± 1.0	−4 ± 3
	11.6	748 (0.50)		
	18.5	1210 (0.50)		
	25.0	1320 (1.00)		
		1960 (0.50)		
		4640 (0.20)		
		11500 (0.10)		
$Ni(4,4'\text{-}(CH_3)_2bpy)_3^{3+}$	4.1	30.9 (0.50)	15.1 ± 1.0	3 ± 3
	11.7	55.6 (0.50)		
	18.2	111 (0.50)		
	25.0	199 (0.50)		
$Ru(bpy)_3^{3+}$	25.0	148 (1.00)[a]	15.3 ± 1.0	7 ± 3
$Fe(bpy)_3^{3+}$	25.0	15.8 (1.00)[b]	14.9 ± 0.2	−4 ± 1
$Os(bpy)_3^{3+}$	25.0	4.66(1.00)[c]	15.6 ± 0.4	−3 ± 5

[a]Reference 12.
[b]Reference 22.
[c]Reference 23.

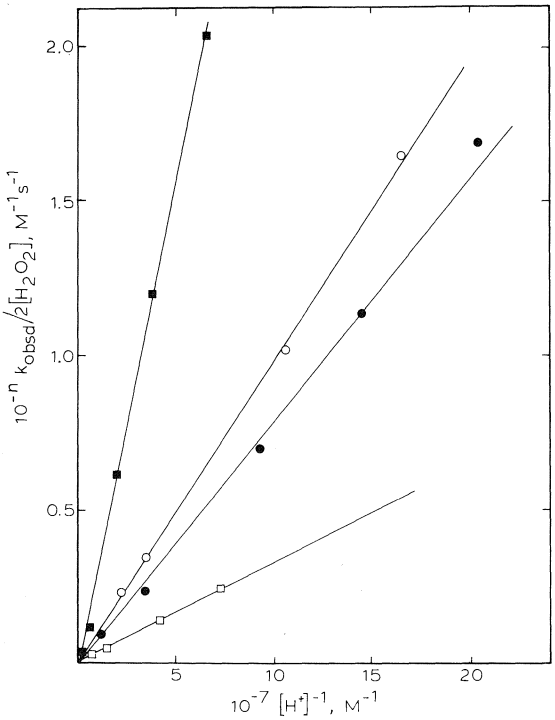

FIG. 1. Dependence of the observed rate constant on $[H^+]^{-1}$ for the reactions of $M(bpy)_3^{3+}$ with hydrogen peroxide: M = Os (n = 1) (●); M = Fe (n = 2) (○); M = Ru (n = 3) (■); M = Ni (n = 4) (□).

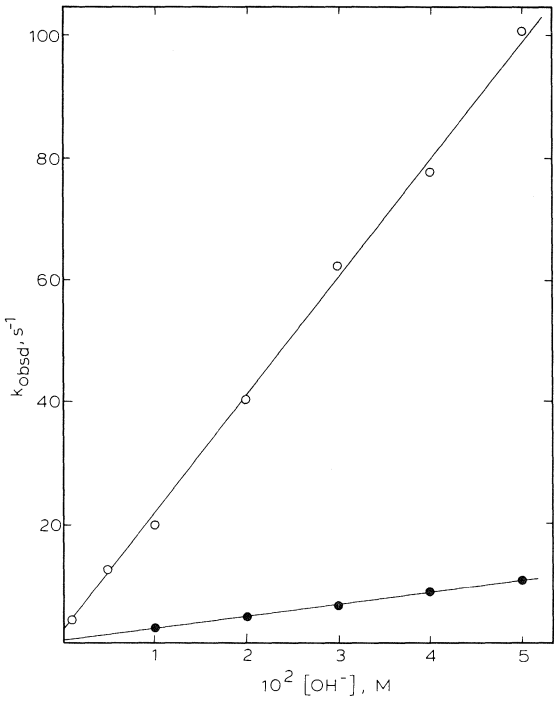

FIG. 2. Dependence of the observed rate constant on $[OH^-]$ for the reductions of $Ni(bpy)_3^{3+}$ (○) and $Ni(4,4'\text{-}(CH_3)_2bpy)_3^{3+}$ (●) at 25°C and I = 0.50 M.

plexes also occurs in aqueous solution in the absence of hydrogen peroxide. The kinetics of the reduction of $Ni(bpy)_3^{3+}$ and $Ni(4,4'\text{-}(CH_3)_2bpy)_3^{3+}$ in basic solution were studied at several temperatures. The pseudo-first-order rate constants were observed to have a first-order dependence on hydroxide ion concentration over the range $[OH^-]$ = 0.001–0.050 M, with small intercepts in plots of k against $[OH^-]$ (Fig. 2). The variation of k with ionic strength (Table 2) is consistent with the reaction between +3 and −1 charged species. The second-order rate constants and activation parameters for these reactions are presented in Table 2, along with the corresponding values (12, 22, 23) for $M(bpy)_3^{3+}$ complexes of Os(III), Fe(III), and Ru(III). The rate of reduction of these complexes by hydroxide ion is negligible compared to the rate of reduction by hydrogen peroxide in the pH range 6–9.

Discussion

The kinetic data for the reactions of metal(III) tris(polypyridine) complexes with hydrogen peroxide are consistent with a mechanism involving the reduction of ML_3^{3+} by both the

TABLE 3. Acid dissociation constants and reduction potentials for peroxide and superoxide ions

Proton equilibria	pK
$H_2O_2 \rightleftharpoons HO_2^- + H^+$	$pK_1 = 11.86^a$
$HO_2^- \rightleftharpoons O_2^{2-} + H^+$	$pK_2 = 20^b$
$H_2O_2^+ \rightleftharpoons HO_2 + H^+$	$pK_{r1} < -10^c$
$HO_2 \rightleftharpoons O_2^- + H^+$	$pK_{r2} = 4.69^d$
Redox couples	**E^0 (vs. NHE) (V)**
$HO_2 + e^- + H^+ \rightleftharpoons H_2O_2$	1.45^e
$O_2^- + e^- + H^+ \rightleftharpoons HO_2^-$	1.03^e
$H_2O_2^+ + e^- \rightleftharpoons H_2O_2$	$>2.0^f$
$HO_2 + e^- \rightleftharpoons HO_2^-$	0.75^f
$O_2^- + e^- \rightleftharpoons O_2^{2-}$	-0.15^f
$O_2 + e^- \rightleftharpoons O_2^-$	-0.15^g

[a]Reference 24.
[b]Reference 25.
[c]Reference 26.
[d]Reference 27.
[e]Reference 28.
[f]Calculated using pK and E^0 values as described in text.
[g]At $[O_2(aq.)] = 1\ M$, ref. 29.

undissociated H_2O_2 and the peroxide anion HO_2^- (pK_1 = 11.86, $I = 0.50\ M$ (24)).

[4] $$H_2O_2 \overset{K_1}{\rightleftharpoons} HO_2^- + H^+$$

[5] $$M(bpy)_3^{3+} + H_2O_2 \xrightarrow{k_1} M(bpy)_3^{2+} + H_2O_2^+$$

[6] $$M(bpy)_3^{3+} + HO_2^- \xrightarrow{k_2} M(bpy)_3^{2+} + HO_2$$

The one-electron oxidation products, $H_2O_2^+$ and HO_2, are both acidic (Table 3) such that in the pH range 6–9, the superoxide ion would exist in the form O_2^-.

[7] $$M(bpy)_3^{3+} + O_2^- \xrightarrow{\text{fast}} M(bpy)_3^{2+} + O_2$$

The rate law for the one-electron oxidations of H_2O_2 and HO_2^- is given by eq. [8].

[8] $$-\frac{d[M(bpy)_3^{3+}]}{2dt} = \left(\frac{k_1 + k_2K_1/[H^+]}{1 + K_1/[H^+]}\right)[M(bpy)_3^{3+}][H_2O_2]$$

In the pH range 6–9 employed in this study $K_1 \ll [H^+]$ such that the observed second-order rate constant may be expressed as $k_{obsd} = 2\{k_1 + k_2K_1/[H^+]\}$ where $k_1 = k_a$ and $k_2 = k_b/K_1$ (eq. [3]). For the oxidants employed in this study reaction [5] is thermodynamically very unfavourable because of the high reduction potential of $H_2O_2^+$ (Table 3). The acid-independent pathway is likely more complicated than represented by k_1 and these values will not be used in further calculations. The rate constants specific to the HO_2^- pathway are presented in Table 4. A rate constant of $2.7 \times 10^7\ M^{-1}\ s^{-1}$ ($I = 1.00\ M\ Na_2SO_4$) has been reported for the $Ru(bpy)_3^{3+}/HO_2^-$ reaction (12), in good agreement with value from this study.

In the absence of hydrogen peroxide the nickel(III) tris(polypyridine) complexes are spontaneously reduced in aqueous solution, with a rate that is first-order in hydroxide ion concentration. Similar processes are observed with the analogous complexes of Os(III) (23), Fe(III) (22, 23), and Ru(III) (12, 21), and these reactions, especially with $Ru(bpy)_3^{3+}$, have been of much interest in regards to the catalysis of water photooxidation. There have been several mechanisms proposed for the $M(bpy)_3^{3+}/OH^-$ reactions (21, 30) and the products of reduction depend on a number of factors including pH, photocatalysis, and added cayalysts such as $Co^{2+}(aq)$. In the noncatalyzed thermal reductions of the $Ni(bpy)_3^{3+}$ complexes in basic solution there are two mechanisms which are suggested by the kinetic data: (*a*) the nucleophilic addition of H_2O or OH^- to a bipyridine carbon to form a pseudobase species and (*b*) formation of a free hydroxyl radical OH· and $Ni(bpy)_3^{2+}$. Both mechanisms are consistent with the $[OH^-]$ rate dependence and the increase in the rate constant as the oxidizing power of $M(bpy)_3^{3+}$ is increased. The latter mechanism may be more favourable with the nickel(III) complexes as the reduction potential of 1.89 V for the $OH\cdot/OH^-$ couple (31) would render the reaction energetically unfavourable for the complexes of the other metals. The former mechanism has received much support in the reactions of $Ru(bpy)_3^{3+}$ with OH^-, but further studies are clearly required to establish its applicability to the $Ni(bpy)_3^{3+}$ complexes. It is unlikely, owing to the lability of the $Ni(bpy)_3^{2+}$, that this complex would find use in the catalysis of water oxidation.

The rate constants for the oxidation of HO_2^- increase as the reduction potentials of the oxidants in the series is increased (Table 4). This trend is consistent with the Marcus theory relationship (15) for outer-sphere electron transfer reactions. The Marcus equation, which relates the rate and equilibrium constants for a cross-reaction to the self-exchange rate constants for the component reactants is given, in a modified form (16), by eqs. [9]–[12].

[9] $$k_{12} = (k_{11}k_{22}K_{12}f_{12})^{1/2}W_{12}$$

where

[10] $$\ln f_{12} = \frac{[\ln K_{12} + (w_{12} - w_{21})/RT]^2}{4\left[\ln\left(\frac{k_{11}k_{22}}{A_{11}A_{22}}\right) + \left(\frac{w_{11} + w_{22}}{RT}\right)\right]}$$

[11] $$W_{12} = \exp\left[-(w_{12} + w_{21} - w_{11} - w_{22})/2RT\right]$$

[12] $$w_{ij} = \frac{z_iz_je^2}{D_s\sigma_{ij}(1 + \beta\sigma_{ij}I^{1/2})}$$

In these expressions w_{ij} is the work required to bring ions i and j (charges z_i and z_j) to the separation distance σ_{ij} (taken equal to the sum of a_i and a_j, the radii of ions i and j), $\beta = (8\pi Ne^2/1000D_skT)^{1/2}$, and D_s is the dielectric constant of the medium. The value of $A_{11}A_{22}$ for the ML_3^{3+}/HO_2^- reactions is $2 \times 10^{24}\ M^{-2}\ s^{-2}$, taking the radii of the metal tris(bipyridine) complexes and the peroxide anion to be 6.8 Å and 1.6 Å, respectively.

Equation [9] was used to determine the self-exchange rate constant for the HO_2^-/HO_2 couple from the cross-reaction data in Table 4. In order to calculate the constants K_{12} for the equilibria in eq. [6], the reduction potential of the HO_2/HO_2^- couple must be determined. This potential may be calculated (eq. [13]) using the proton equilibrium constants and formal electrode potentials found in Table 3.

[13] $$E^0(HO_2/HO_2^-) = E^0(O_2^-/HO_2^-) - 0.059pK_{r2}$$

The reduction potential of HO_2 from this calculation is 0.75 V. The reduction potential of the $H_2O_2^+$ is calculated to be ≥ 2.0 V using the HO_2/H_2O_2 potential and the value of $pK_{r1} < -10$

TABLE 4. Cross-reaction and self-exchange rate constants for reactions involving the HO_2^-/HO_2 couple; ionic strength in parentheses

Oxidant[a]	Reductant[a]	$E^{0\,b}$ (V)	$k_{22}{}^c$ (M^{-1} s^{-1})	k_2 (M^{-1} s^{-1})	$k_{11}{}^c$ (M^{-1} s^{-1})
$Os(dmbpy)_3^{3+}$	HO_2^-	0.66	$4.2 \times 10^8(0.1)^d$	$1.0 \times 10^3(0.5)$	1.1×10^{-2}
$Os(bpy)_3^{3+}$	HO_2^-	0.81	$4.2 \times 10^8(0.1)^d$	$6.0 \times 10^4(0.5)$	1.0×10^{-1}
$Fe(dmbpy)_3^{3+}$	HO_2^-	0.81	$3 \times 10^8(5.5)^e$	$2.7 \times 10^4(0.5)$	7.5×10^{-2}
$Fe(bpy)_3^{3+}$	HO_2^-	1.05	$3 \times 10^8(5.5)^e$	$7.1 \times 10^5(0.5)$	0.9×10^{-2}
$Ru(dmbpy)_3^{3+}$	HO_2^-	1.06	$4.2 \times 10^8(0.1)^f$	$1.3 \times 10^6(0.5)$	0.6×10^{-2}
$Ru(bpy)_3^{3+}$	HO_2^-	1.26	$4.2 \times 10^8(0.1)^f$	$2.4 \times 10^7(0.5)$	0.4×10^{-2}
$Ni(dmbpy)_3^{3+}$	HO_2^-	1.59	$1.5 \times 10^3(1.0)^g$	$3.3 \times 10^7(0.5)$	1.5×10^{-1}
$Ni(bpy)_3^{3+}$	HO_2^-	1.72	$1.5 \times 10^3(1.0)^g$	$2.4 \times 10^8(0.5)$	2.9×10^{-1}
$(bpy)_2pyRuOH^{2+}$	HO_2^-	0.85[h]	$10^7(0.1)^i$	$2.9 \times 10^3(0.1)^j$	0.4×10^{-2}
HO_2	O_2^-	−0.15	$10^2(1.0)^k$	$1.0 \times 10^8(0.1)^l$	6.3
HO_2	$Ru(NH_3)_5isn^{2+}$	0.39[m]	$4.7 \times 10^5(0.1)^n$	$9.1 \times 10^6(0.1)^o$	2.0
HO_2	$KFe(CN)_6^{3-}$	0.42[p]	$2.2 \times 10^3(0.02)^p$	$3.3 \times 10^4(0.02)^q$	3.2×10^{-1}
HO_2	$Mo(CN)_8^{4-}$	0.75[r]	$3 \times 10^4(0.0)^s$	$5.7 \times 10^4(0.5)^t$	53

[a]dmbpy = 4,4′-$(CH_3)_2$bpy, py = pyridine, isn = isonicotinamide.
[b]E^0 values for $ML_3^{3+/2+}$ measured in 0.50 M CF_3SO_3H.
[c]Self-exchange rate constants: k_{22} is for partner of HO_2^- or HO_2 in cross-reaction; k_{11} is for HO_2^-/HO_2 using eq. [9].
[d]k_{22} for $OsL_3^{2+/3+}$ is assumed to be the same as for $Ru(bpy)_3^{2+/3+}$.
[e]Reference 33.
[f]Reference 34.
[g]Reference 35.
[h]Calculated from data in ref. 36.
[i]Calculated from k_{22} of related couples reported in ref. 37.
[j]Reference 38.
[k]References 5 and 39.
[l]Reference 27.
[m]Reference 39.
[n]Reference 40.
[o]Reference 41.
[p]Reference 42.
[q]Reference 43.
[r]Reference 44.
[s]Reference 45.
[t]Reference 46.

suggested by Schwarz (26) for the $H_2O_2^+$ ion. The very high reduction potential for $H_2O_2^+$ explains the much reduced rate constantes for the oxidations of H_2O_2 compared with the rate constants for HO_2^-. The reduction potentials of the metal(III) polypyridine complexes were measured in trifluoromethanesulphonate media at an ionic strength of 0.50 M. The E^0 values, similar to the reported potentials in sulphate and perchlorate media (32), are presented in Table 4 along with the self-exchange rate constants for the $ML_3^{2+/3+}$ couples.

The application of eq. [9] to the cross-reaction data yields a k_{11} value for the HO_2^-/HO_2 couple in the range of 10^{-2}–10^{-1} M^{-1} s^{-1}. The plot of log $(k_{12}/(k_{11}k_{22})^{1/2}W_{12})$ against log $(K_{12}f_{12})^{1/2}$ in Fig. 3, with $k_{11} = 5 \times 10^{-2}$ M^{-1} s^{-1}, indicates that the Marcus correlation is applicable over a wide range of thermodynamic driving forces. Also included in Table 4 and Fig. 3 are data for several reactions involving the reduction of the HO_2 radical. The calculated k_{11} values for the HO_2^-/HO_2 couple determined from these systems are for the most part larger than the estimates from the HO_2^- reactions. A much larger variation in self-exchange rate constants derived from the application of the Marcus equation is seen in the O_2^-/O_2 couple, with values spread over the range 10^{-7}–10^6 M^{-1} s^{-1}. Espenson and co-workers (47) have suggested that this variation results from the considerable differences in the solvation characteristics of the superoxide anion and the dioxygen molecule. With the variety, in terms of size and charge, of the cross-reactants employed, the transition stat would vary substantially in regard to the extent of desolvatior the superoxide anion. The same behaviour, perhaps to a les extent, would thus be expected in other small molecule coupl such as HO_2^-/HO_2.

Considerable success in predicting the electron exchange ra constant for transition metal complex (48) and small molecu (49) couples has been achieved using a semi-classical model fo outer-sphere electron exchange reactions (16). In this model the rate constant for a bimolecular exchange k_{11} may be expressed as the product of a pre-equilibrium constant K_A, an effectiv nuclear frequency ν_n, and electronic and nuclear factors, and κ_n, respectively.

$$[14] \quad k_{11} = K_A \nu_n \kappa_{el} \kappa_n$$

The nuclear factor is related to the reorganization barrier t electron exchange and is comprised of terms for the inne sphere reorganization bond distances and angles (ΔG_{in}^*) and the outer-sphere reorganization of solvent polarization (ΔG_{out}^*),

$$[15] \quad \kappa_n = \Gamma_n \exp\left[-(\Delta G_{in}^* + \Delta G_{out}^*)/RT\right]$$

where Γ_n is the inner-sphere nuclear tunneling factor. The inner-sphere reorganization energy may be derived from a knowledge of the change in the equilibrium bond distances between the reduced and oxidized states (Δd_0) and the reduced force constants (f_i) of the intramolecular vibrations.

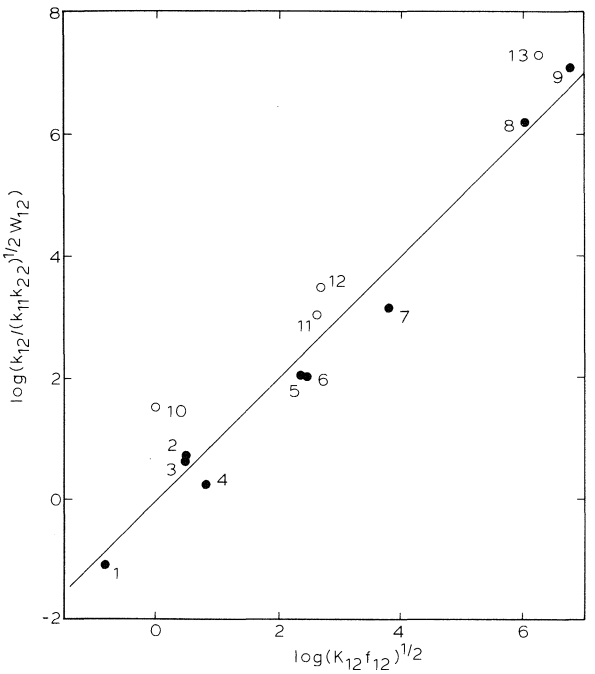

FIG. 3. Plot of log $(k_{12}/(k_{11}k_{22})^{1/2}W_{12})$ against log $(K_{12}f_{12})^{1/2}$ for the oxidation of HO_2^- by: (*1*) $Os(4,4'\text{-}(CH_3)_2bpy)_3^{3+}$; (*2*) $Os(bpy_3^{3+}$; (*3*) $Fe(4,4'\text{-}(CH_3)_2bpy)_3^{3+}$; (*4*) $(bpy)_2pyRuOH^{2+}$; (*5*) $Fe(bpy)_3^{3+}$; (*6*) $Ru(4,4'\text{-}(CH_3)_2bpy)_3^{3+}$; (*7*) $Ru(bpy)_3^{3+}$; (*8*) $Ni(4,4'\text{-}(CH_3)_2bpy)_3^{3+}$; (*9*) $Ni(bpy)_3^{3+}$; and for the reduction of HO_2 by: (*10*) $Mo(CN)_8^{4-}$; (*11*) $KFe(CN)_6^{3-}$; (*12*) $Ru(NH_3)_5isn^{2+}$; (*13*) O_2^-. The points are calculated using k_{11} for $HO_2^-/HO_2 = 5 \times 10^{-2}\ M^{-1}\ s^{-1}$. Solid line has the theoretical slope of unity.

$$[16]\quad \Delta G_{in}^{*} = (1/2)\Sigma f_i(\Delta d_0/2)_i^2$$

The solvent reorganization energy may be calculated using eq. [17],

$$[17]\quad \Delta G_{out}^{*} = \frac{(\Delta e)^2}{4}\left(\frac{1}{2a_1}+\frac{1}{2a_2}-\frac{1}{r}\right)\left(\frac{1}{D_{op}}-\frac{1}{D_s}\right)$$

where r is the radius of the activated complex ($r = a_1 + a_2$), and D_{op} and D_s are the optical and static dielectric constants of the medium.

The addition of an electron to a π^* orbital in HO_2 to form HO_2^- increases the O—O bond distance from 1.33 Å to 1.49 Å (50, 51). Using O—O stretching force constants of 610 Nm^{-1} ($\nu_{O—O}$ = 1138 cm^{-1}) (52) for HO_2 and 360 Nm^{-1} ($\nu_{O—O}$ = 836 cm^{-1}) (53) for HO_2^-, an inner-sphere reorganization barrier of 4.2 kcal mol^{-1} is obtained. The radius of the HO_2^-/HO_2 activated complex is estimated to be ~3.2 Å, giving a solvent reorganization barrier of 14.1 kcal mol^{-1}. The nuclear tunneling factor (16) in most transition metal complex couples is close to unity as the M—L stretching frequencies are low. When $h\nu > kT$ (as in HO_2^-/HO_2, where ν = 964 cm^{-1}) the vibration modes which allow for nuclear reorganization cannot be fully populated by thermal excitations and electron exchange occurs to some degree by nuclear tunneling. Using Holstein's expression (54) a value of 8 for Γ_n was calculated for the HO_2^-/HO_2 couple. The estimate of ΔG_{in}^{*} is based on negligible contributions from changes in the O—H bond distance (<0.02 Å) and the OOH bond angle (~4°) in the HO_2^-/HO_2 couple (50). The nuclear factor (eq. [15]) is calculated to be 3.1×10^{-13}, and the nuclear frequency is $1.4 \times 10^{13}\ s^{-1}$. The pre-equilibrium constant is estimated to be 0.062 M^{-1} using a radius of 3.2 Å. For an adiabatic electron exchange ($\kappa_{el} = 1$) the semi-classical model predicts an exchange rate constant of $2.7 \times 10^{-1}\ M^{-1}\ s^{-1}$. This value is in reasonably good agreement with the rate constants derived from the cross-reaction data, although it is subject to the uncertainties associated with the assumptions made in its determination. One of these assumptions is that the radius of the activated complex is the sum of the hard-sphere radii of HO_2^- and HO_2. Estimates of the self-exchange rate constants or other small molecule couples, such as ClO_2^-/ClO_2 ($k_{11} = 1.6 \times 10^2\ M^{-1}\ s^{-1}$ (53)), NO_2^-/NO_2 ($k_{11} = 8.1 \times 10^{-3}\ M^{-1}\ s^{-1}$ (55)), and Br_2^-/Br_2 ($k_{11} = 10^2\ M^{-1}\ s^{-1}$ (29, 47, 56)), have been made from cross-reaction kinetic studies. Applications of classical and semi-classical models to these couples have invariably led to calculated radii which are ~1 Å larger than is predicted from the hard-sphere radii. This may imply an activated complex in which the reactants are not in close contact but are separated by solvent molecules originating from solvation of the anionic species in the couple. The variations in k_{11} for diatomic and triatomic molecules from cross-reaction data also suggest that the solvent reorganization barrier associated with the cross-reaction may differ substantially (higher or lower) from an average of the individual solvent reorganization barriers for the self-exchange reactions. Kinetic studies of the reactions of HO_2^- and HO_2 with additional outer-sphere cross reactants may help to clarify the energetics of electron exchange in this and other small molecule couples.

Acknowledgements

Financial support from the Natural Sciences and Engineering Research Council of Canada is acknowledged. This work was done in part at the Brookhaven National Laboratory and Dr. Norman Sutin is thanked for helpful discussions.

1. G. RENGER. *In* Photosynthetic oxygen evolution. *Edited by* H. Metzner. Academic Press, New York. 1978. p. 229.
2. H. A. D. HILL. *In* New trends in bio-inorganic chemistry. *Edited by* R. J. P. Williams and J. R. R. F. Silva. Academic Press, New York. 1978. p. 173.
3. J. WILSHIRE and D. T. SAWYER. Acc. Chem. Res. **12**, 105 (1979).
4. A. B. P. LEVER and H. B. GRAY. Acc. Chem. Res. **11**, 348 (1978).
5. J. F. ENDICOTT and K. KUMAR. Am. Chem. Soc. Symp. Ser. **198**, 425 (1982), and references therein.
6. A. SAMUNI and G. CZAPSKI. J. Chem. Soc. Dalton Trans. 487 (1973).
7. Z. BOTI, I. HORVATH, Z. SZIL, and L. J. CSANYI. J. Chem. Soc. Dalton Trans. 1012 (1978).
8. C. F. WELLS and D. MAYS. J. Chem. Soc. A, 665 (1968).
9. E. T. BORISH and L. J. KIRSCHENBAUM. J. Chem. Soc. Dalton Trans. 749 (1983).
10. G. DAVIES and K. O. WATKINS. J. Phys. Chem. **74**, 3388 (1970).
11. M. P. HEYWARD and C. F. WELLS. J. Chem. Soc. Dalton Trans. 1863 (1981).
12. C. CREUTZ and N. SUTIN. Proc. Natl. Acad. Sci. USA, **72**, 2858 (1975).
13. J. A. GILBERT, S. W. GERSTEN, and T. J. MEYER. J. Am. Chem. Soc. **104**, 6872 (1982).
14. C. F. WELLS and D. FOX. J. Chem. Soc. Dalton Trans. 1498 (1977).
15. R. A. MARCUS. Ann. Rev. Phys. Chem. **15**, 155 (1964).
16. N. SUTIN. Acc. Chem. Res. **15**, 275 (1982); Prog. Inorg. Chem. **30**, 441 (1983).
17. C. CREUTZ, M. CHOU, T. L. NETZEL, M. OKUMURA, and N. SUTIN. J. Am. Chem. Soc. **102**, 1309 (1980).

18. C.-T. LIN, W. BOTTCHER, M. CHOU, C. CREUTZ, and N. SUTIN. J. Am. Chem. Soc. **98**, 6384 (1976).
19. J. C. BRODOVITCH, R. I. HAINES, and A. MCAULEY. Can. J. Chem. **59**, 1610 (1981).
20. D. J. SZALDA, D. H. MACARTNEY, and N. SUTIN. Inorg. Chem. **23**, 3473 (1984).
21. P. K. GHOSH, B. S. BRUNSCHWIG, M. CHOU, C. CREUTZ, and N. SUTIN. J. Am. Chem. Soc. **106**, 4772 (1984).
22. G. NORD and O. WERNBERG. J. Chem. Soc. Dalton Trans. 866 (1972).
23. G. NORD and O. WERNBERG. J. Chem. Soc. Dalton Trans. 845 (1975).
24. M. G. EVANS and N. URI. Trans. Faraday Soc. **45**, 224 (1949).
25. D. DOLPHIN and B. R. JAMES. Am. Chem. Soc. Symp. Ser. **211**, 99 (1983).
26. H. A. SCHWARZ. J. Chem. Ed. **58**, 101 (1981).
27. J. WEINSTEIN and B. H. J. BIELSKI. J. Am. Chem. Soc. **101**, 58 (1979).
28. A. O. ALLEN and B. H. J. BIELSKI. *In* Superoxide dismutase. *Edited by* L. W. Oberley. CRC Press, Cleveland. 1982. Chapt. 7.
29. D. M. STANBURY, O. HAAS, and H. TAUBE. Inorg. Chem. **19**, 518 (1980).
30. N. SERPONE, G. PONTERINI, M. A. JAMIESON, F. BOLLETTA, and M. MAESTRI. Coord. Chem. Rev. **50**, 209 (1983), and references therein.
31. H. A. SCHWARZ and R. W. DODSON. J. Phys. Chem. **88**, 3643 (1984).
32. C. CREUTZ and N. SUTIN. Adv. Chem. Ser. **168**, 1 (1978).
33. I. RUFF and M. ZIMONYI. Electrochim. Acta, **18**, 515 (1973).
34. R. C. YOUNG, R. F. KEENE, and T. J. MEYER. J. Am. Chem. Soc. **99**, 2468 (1977).
35. D. H. MACARTNEY and N. SUTIN. Inorg. Chem. **22**, 3530 (1983).
36. R. A. BINSTEAD, B. A. MAYER, G. J. SAMUELS, and T. J. MEYER. J. Am. Chem. Soc. **103**, 2897 (1981).
37. G. M. BROWN and N. SUTIN. J. Am. Chem. Soc. **101**, 883 (1979).
38. J. A. GILBERT, S. W. GERSTEN, and T. J. MEYER. J. Am. Chem. Soc. **104**, 6873 (1982).
39. D. M. STANBURY, D. GASWICK, G. M. BROWN, and H. TAUBE. Inorg. Chem. **22**, 1975 (1983).
40. G. M. BROWN, H. J. KRENTZIEN, M. ABE, and H. TAUBE. Inorg. Chem. **18**, 3374 (1979).
41. D. M. STANBURY, W. A. MULAC, J. C. SULLIVAN, and H. TAUBE. Inorg. Chem. **19**, 3735 (1979).
42. S. WHERLAND and H. B. GRAY. *In* Biological aspects of inorganic chemistry. *Edited by* A. W. Addison, W. R. Cullen, D. Dolphin, and B. R. James. Wiley-Interscience, New York. 1977. p. 289.
43. D. ZEHAVI and J. RABANI. J. Phys. Chem. **76**, 3703 (1972).
44. W. V. MALIK and S. I. ALI. Ind. J. Chem. **1**, 347 (1963).
45. R. J. CAMPION, N. PURDIE, and N. SUTIN. Inorg. Chem. **3**, 1091 (1964).
46. M. FARAGGI. J. Phys. Chem. **80**, 2316 (1976).
47. M. S. MCDOWELL, J. H. ESPENSON, and A. BAKAC. Inorg. Chem. **23**, 2232 (1984).
48. B. S. BRUNSCHWIG, C. CREUTZ, D. H. MACARTNEY, T. K. SHAM, and N. SUTIN. Discuss. Faraday Soc. **74**, 113 (1982).
49. D. M. STANBURY and L. A. LEDNICKY. J. Am. Chem. Soc. **106**, 2847 (1984).
50. D. COHEN, M. BASCH, and R. OSMAN. J. Chem. Phys. **80**, 5684 (1984).
51. Y. BEERS and C. J. HOWARD. J. Chem. Phys. **64**, 1541 (1976).
52. R. S. DRAGO. Inorg. Chem. **18**, 1409 (1979).
53. O. KNOP and P. A. GIGUERE. Can. J. Chem. **37**, 1794 (1959).
54. T. HOLSTEIN. Philos. Mag. **37**, 49 (1978).
55. W. K. WILMARTH, D. M. STANBURY, J. E. BYRD, H. N. PO, and C. P. CHUA. Coord. Chem. Rev. **51**, 155 (1983).
56. W. H. WOODRUFF and D. W. MARGERUM. Inorg. Chem. **13**, 2578 (1974).

Synthesis of some ring-substituted ruthenocenes and their use in the preparation of Ru/ZSM-5 catalysts

G. LEMAY, S. KALIAGUINE, A. ADNOT, S. NAHAR, AND D. COZAK
Departments of Chemistry and Chemical Engineering and GRAPS, Laval University, Québec, P.Q., Canada G1K 7P4

AND

J. MONNIER
CANMET Energy Research Laboratories, Energy, Mines and Resources Canada, Ottawa, Ont., Canada

Received February 4, 1986

G. LEMAY, S. KALIAGUINE, A. ADNOT, S. NAHAR, D. COZAK and J. MONNIER. Can. J. Chem. **64**, 1943 (1986).

A method is proposed for the preparation of Ru/ZSM-5 catalysts using substituted and non-substituted ruthenocenes. To this end, the following complexes have been synthesized and characterized: dimethyl-1,1′; diphenyl-1,1′; dibenzoyl-1,1′, and monobenzoyl ruthenocene. Results of ESCA intensity ratio and ir of adsorbed pyridine show differences in the surface segregation of Ru as well as in the cationic exchange of Ru with Brønsted acid sites of the zeolite, when the catalyst is prepared using ring-substituted ruthenocene instead of ruthenocene itself. The binding energies of Ru $3d_{5/2}$ measured by ESCA are discussed.

G. LEMAY, S. KALIAGUINE, A. ADNOT, S. NAHAR, D.COZAK et J MONNIER. Can. J. Chem. **64**, 1943 (1986).

On propose une méthode de préparation des catalyseurs de type Ru/ZSM-5 utilisant des ruthenocènes substitués ou non. A cette fin, on a fait la synthèse et la caractérisation des complexes suivants: dimethyl-1,1′, dipenyl-1,1′, dibenzoyl-1,1′ et monobenzoyl ruthenocène. Des données sur les rapports d'intensités ESCA et sur l'analyse infrarouge de la pyridine adsorbée indiquent des différences relatives à la ségrégation superficielle du Ru ainsi qu'à l'échange de cations ruthenium avec les sites acides de Brønsted de la zéolithe, lorsque le catalyseur est préparé à l'aide de ruthenocène substitué au lieu de ruthenocène. Les énergies de liaisons de Ru $3d_{5/2}$ déterminées par ESCA sont discutées.

Organometallic complexes of transition metals have been systematically utilized in the preparation of model catalysts in which the transition metal is deposited on a support and the supported species retains some desirable properties of the complex (1). Among the properties being controlled are the state of dispersion and the size of metallic clusters (2), the oxidation state of the metal (3), the nature and number of organic ligands retained on the species (4), the number of its bonds to the support and to surrounding atoms like oxygen or sulfur, and its state of coordination (5).

In this paper, complexes of ruthenium have been used in an effort to control yet another property, namely the spatial distribution of the metal in a particle of zeolite used as the support. The ZSM-5 type zeolite used in this work has near-circular ten-oxygen ring pore openings with diameters in the 5.1 to 5.7 Å range (6). It is therefore expected that ruthenocene (ruthenium biscyclopentadienyl) with 4.6 Å ring diameter and 3.2–3.6 Å ring interplanar distance would diffuse freely in the ZSM-5 pores (7). However, 1,1′-disubstitution of bulky functional groups like phenyl or benzoyl should yield complexes with kinetic diameters higher than 5–6 Å, and diffusion in the ZSM-5 pores should be limited by steric constraints.

Therefore the following series of organometallic compounds have been synthesized and used in the preparation of ZSM-5 supported ruthenium catalysts: ruthenocene, dimethyl-1,1′ ruthenocene, diphenyl-1,1′ ruthenocene, and dibenzoyl-1,1′ ruthenocene.

This paper will be divided in two parts dealing, respectively, with the synthesis of these ring-substituted ruthenocenes and with the preparation and characterization of the Ru/ZSM5 catalysts.

Part I. Synthesis of ring-substituted ruthenocenes

Ruthenocene is known to have chemical properties and a structure similar to ferrocene. A preparative procedure for the synthesis of ruthenocene was proposed in 1961 by Bublitz, McEwen, and Klemberg (8). A much simpler procedure, giving a quantitative yield of ruthenocene was, however, suggested more recently by Pertici *et al.* (9). Based on this last method, we have been successful in synthesizing with improved yields two ruthenocene-derived compounds: dimethyl-1,1′ ruthenocene and diphenyl-1,1′ ruthenocene.

[1] $RuCl_3 \cdot 3H_2O$ —(R, ethanol)→ Ru(R)(R)

with (*a*) R = CH_3, (*b*) R = C_6H_5.

Dimethyl-1,1′ ruthenocene has been synthesized by Hofler and Schlögl (10). This procedure however is time consuming and complex, whereas with Pertici *et al.*'s technique the product is obtained in only one step in quantitative yield.

Before using this method for the preparation of diphenyl-1,1′ ruthenocene, we tried the reaction used by Pauson (11) for the production of diphenyl-1,1′ ferrocene. For this, we utilized anhydrous ruthenium trichloride ($RuCl_3$) instead of $FeCl_3$. No product was obtained after stirring for 24 h and therefore this technique was abandoned. Perhaps anhydrous ruthenium trichloride is too insoluble in organic solvents for this type of reaction.

The method of Pertici *et al.* requires, however, a large excess of phenylcyclopentadiene (PCP). The yield is high but a large excess of PCP with respect to hydrated ruthenium trichloride must be used.

No synthesis procedure could be found in the literature for dibenzoyl-1,1′ ruthenocene. Rosenblum and Woodword (12) in 1958, proposed a Friedel–Craft synthesis for dibenzoyl-1,1′ ferrocene. We therefore tried to apply this technique, starting from ruthenocene, and the results were satisfactory:

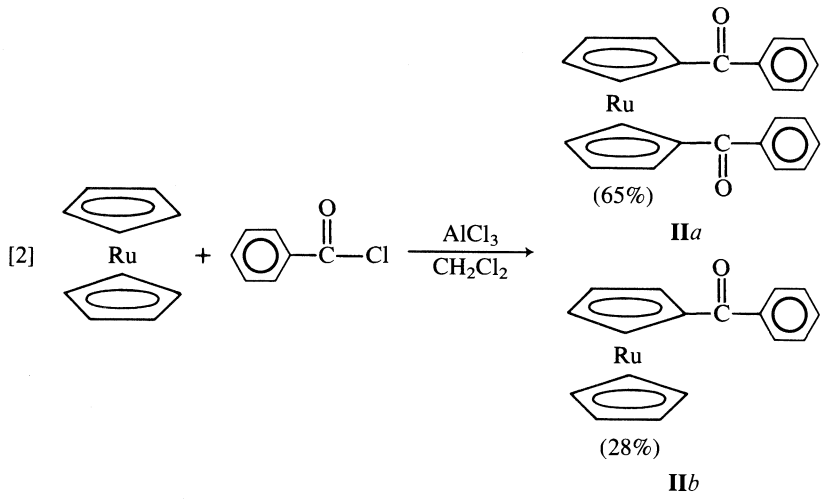

Some monobenzoyl ruthenocene (**II***b*) is necessarily produced in the course of this reaction since too large an excess of benzoyl chloride results in the formation of other nondesirable impurities. Ruthenocene, benzoyl ruthenocene (**II***b*), and dibenzoyl-1,1′ ruthenocene (**II***a*) can be well separated by column chromatography on silica gel. These ruthenocene compounds are air stable at room temperature. Davis and O'Reardon (13) have synthesized monobenzoyl ruthenocene (**II***b*) in order to perform a mass spectrometric comparative study with monobenzoyl ferrocene. They applied Hofler and Schlög's method, monobenzoyl ruthenocene being prepared by a technique similar to the one proposed for monoacetyl ruthenocene. This method involves several steps with the Friedel–Craft technique, the main product (**II***a*) can be obtained with a high yield by using 2 mol of benzoyl chloride per mole of ruthenocene. The technique is fast and simple.

It may be mentioned that Davis and O'Reardon did not give the characteristics of benzoyl ruthenocene except for the mass spectrum. We therefore report both nmr and ir spectra for this compound.

Experimental

Melting points were determined in capillary tubes using a Thomas–Hoover melting point apparatus and were not corrected. Infrared spectra were recorded with KBr wafers using a Beckman IR-4250 spectrometer calibrated with the 2851 and 1602 cm^{-1} bands of polystyrene. Samples for mass spectrometric analysis were prepared under purified nitrogen in sealed capillaries. Mass spectra (ms) were determined using a Hewlett-Packard 5992 GC/MS system. Proton nuclear magnetic resonance spectra were recorded using a 90 MHz Brucker HX-90 spectrometer or a 60 MHz Varian A60 instrument. Elemental C, H, N analyses were performed using a Hewlett-Packard F and M Scientific 185 analyzer.

Starting materials

Ruthenocene was synthesized using the method of Pertici *et al.* Phenylcyclopentadiene was produced according to the method of Pauson and purified by vacuum distillation. Methylcyclopentadiene was distilled immediately prior to use. Hydrated 2-cyclopentenone (lot No 8024 KL), metallic lithium (lot No 5320 LK), and anhydrous ruthenium trichloride (lot No 4431 KL) were from Aldrich chemicals and hydrated ruthenium chloride from Aesar Johnson Mattey Inc. (lot No 122783). Aluminium chloride (lot No 710047), benzoyl chloride (lot No 716475), and powdered zinc (lot No 733421) were bought from Fisher Scientific Ltd. All solvents were purified by distillation under purified nitrogen (Cu + molecular sieves).

*Preparation of dimethyl-1,1′ ruthenocene (**I**a)*

Hydrated ruthenium trichloride (5.00 g, 0.019 mol) is dissolved absolute ethanol (100 mL) under purified nitrogen and cooled to −70°C. Freshly distilled methylcyclopentadiene (100 mL) and powdered zinc (50 g) are then added to the solution. This mixture is slowly warmed up to room temperature while stirring. The reaction starts at −40°C. The mixture is stirred for 30 min after it reaches room temperature and is filtered in air. The solvent is then evaporated to dryness and dimethyl-1,1′ ruthenocene is extracted with pentane. The product is purified by column chromatography (silica gel, activity I, 20 cm) and eluted with pentane. Evaporation of the solvent yields light yellow crystals (4.9 g). Melting point: 56–57.5°C [lit. (3): 61–63°C]. *Anal.* calcd. for $C_{12}H_{14}Ru$: C 55.58, H 5.44, mw 259.32; found: C 55.28, H 5.83, ms 259 *m/z*. Ir (KBr): 1465 or 1445, 990 and 803 cm^{-1} (C_5H_4). ^1H nmr (60 MHz, CCl_4): δ 1.96 ppm (6H, s) CH_3, 4.4 ppm (8H, m) C_5H_4.

Preparation of diphenyl-1,1′ ruthenocene (***I***b)

Hydrated ruthenium trichloride (2.91 g, 0.0111 mol) is dissolved in absolute ethanol (60 mL) under purified nitrogen. The solution is cooled down to −70°C.

Freshly distilled phenylcyclopentadiene (9.50 g, 0.0668 mol) is dissolved in ethanol (125 mL) and added to the solution along with powdered zinc (29 g). With stirring, the mixture is slowly warmed to room temperature and kept stirring for 1 h. The mixture is then filtered in air and the solvent is evaporated to dryness. Diphenyl-1,1′ ruthenocene is extracted with cyclohexane (1.5 L) and purified by column chromatography (silica gel, activity I, 150 g) and eluted with cyclohexane. Evaporating the solvent yields 3.23 g of pure diphenyl-1,1′ ruthenocene which corresponds to a yield of 76%. The product can be purified either by recrystallization or by sublimation at 150°C, 10.01 Torr. Melting point: 162°C (benzene/petroleum ether). *Anal.* calcd. for $C_{22}H_{18}Ru$: C 68.91, H 4.73, mw 383.43; found: C 67.66, H 4.45, ms 384 *m/z*. Ir (KBr): 1603 [ν(C=C) of Ph], 1445, 995, and 800 cm^{-1} (C_5H_4). ^1H nmr (90 MHz, $CDCl_3$): δ 4.66 ppm (4H, m) and 5.0 ppm (4H, m) C_5H_4, 7.24 ppm (10H, s) C_6H_5.

*Preparation of dibenzoyl-1,1′ ruthenocene (**II**a)*

Ruthenocene (3 g, 0.013 mol) is added to a suspension of benzoyl chloride (3.66 g, 0.026 mol) and aluminum chloride (3.81 g, 0.0285 mol) in anhydrous dichloromethane (75 mL) under purified nitrogen. The mixture is heated to reflux for 2 h, hydrolyzed over ice, and extracted three times with dichloromethane. The extract is then washed with water and dried over magnesium sulfate. The solvent is then evaporated. Dibenzoyl-1,1′ ruthenocene crystallizes and is purified by recrystallization from a benzene/petroleum ether solution. **II***b* can be easily separated from **II***a* by column chromatography of the mother liquor over 100 g of silica gel by elution with benzene. Yields of

TABLE 1. Binding energies from XPS spectra (eV)

Organometallic compound	Sample designation	Δ_c	Si 2*p*	O 1*s*	Al 2*p*	Ru $3d_{5/2}$	Ru $3d_{3/2}$
Ruthenocene	129-A	6.3	103.3	532.6	75.5	280.6	284.6
	129-B	6.3	103.3	532.5	75.2	279.7	284.3
	129-C	6.3	103.3	532.5	75.5	279.8	284.1
	129-D	4.8	103.3	—	76.1	280.0	284.2
Dimethyl ruthenocene	124-A	6.1	103.3	532.6	74.9	280.5	284.6
	124-B	6.1	103.3	532.6	74.9	279.9	284.5
	124-C	6.1	103.3	532.7	74.9	280.2	284.5
	124-D	6.1	103.3	532.7	75.2	280.2	284.5
Diphenyl ruthenocene	133-A	6.6	103.3	532.5	75.4	280.3	284.5
	133-B	5.3	103.3	532.6	75.6	280.7	285.0
	133-C	6.7	103.3	532.4	75.4	280.2	284.2
	133-D	6.3	103.3	532.6	75.1	280.8	284.8
Dibenzoyl ruthenocene	132-A	6.4	103.3	532.5	75.5	280.2	284.5
	132-B	6.3	103.3	532.6	75.3	280.1	284.3
	132-C	6.1	103.3	532.6	75.3	280.4	284.5
	132-D	6.0	103.3	532.5	75.2	280.3	284.4

65% and 28% were obtained, respectively, for dibenzoyl-1,1′ ruthenocene (4.9 g) and monobenzoyl-1,1′ ruthenocene (1.6 g).

Dibenzoyl-1,1′ ruthenocene (**II***a*): mp: 121–122°C (benzene/petroleum ether). *Anal.* calcd. for $C_{24}H_{18}Ru$: C 65.59, H 4.10, mw 439.45; found: C 64.59; H 4.39, ms 440 *m/z*. Ir (KBr): 1635 [ν(C=O)], 1598 [ν(C=C) of Ph], 1438 or 1448, 1024 and 820 cm^{-1} (C_5H_4). ^1H nmr (90 MHz, $CDCl_3$): δ 4.89 ppm (4H, t) and 5.24 ppm (4H, t) C_5H_4, 7.11–8.11 ppm (10H, m) C_6H_5.

Monobenzoyl ruthenocene (**II***b*): mp 110°C (benzene/petroleum ether). *Anal.* calcd. for $C_{17}H_{14}ORu$: C 60.88, H 4.20, mw 335.35; found: C 60.58, H 4.25, ms 336 *m/z*. Ir (KBr): 1632 [ν(C=O)], 1595 [ν(C=C) of Ph], 1439 or 1446, 1020 and 800 cm^{-1} (rings). ^1H nmr (90 MHz, $CDCl_3$): δ 4.62 ppm (5H, s) C_5H_5, 4.85 ppm (2H, t) and 5.17 ppm (2H, t) C_5H_4, 7.27–8.03 ppm (5H, m) C_6H_5.

Part II. Preparation and characterization of Ru/ZSM-5

Experimental procedures

The catalysts reported in this study were prepared using ZSM-5 samples from the same batch as a support. This zeolite was synthesized according to the procedure described as method B′ by Gabelica *et al.* (14).

The sodium precursor was thoroughly washed under flowing distilled water and dried overnight at 130°C. It was then slowly heated under static air up to 500°C and maintained at this temperature for 15 h in order to decompose the organic base [TPA]Br. Then the Na^+ counter ions were exchanged with NH_4^+ ions in 1 *M* ammonium nitrate solution at 80°C, this operation being repeated three times. The ammonium form was then again thoroughly washed with distilled water, dried, and calcined at 550°C yielding the H form which was used as the support. This H-ZSM-5 has a Si/Al ratio of 36 and a sodium content lower than 0.01 wt%. Its X-ray diffraction pattern in characteristic of the ZSM-5 lattice (15) and shows a crystallinity very close to 100%.

The Ru/ZSM-5 catalysts were prepared according to the following original procedure: the zeolite and the solid ruthenocene compound were mixed in calculated proportions, ground in an agate mortar and introduced into a Pyrex tube. This tube was evacuated, sealed, and introduced in a furnace in which it was slowly heated to 500°C and kept for 24 h at this temperature. The recovered material was placed in a crucible and calcined for 5 h in air at 550°C. The ruthenium content of these solids was determined by X-ray fluorescence. X-ray diffraction spectra showed the pattern of RuO_2 superimposed on the one of ZSM-5. The ZSM-5 spectrum showed no alteration of the ZSM-5 crystallinity. The RuO_2 lines, even though not very intense, especially in the low Ru samples, showed almost no broadening over the experimental lines of a stoichiometric RuO_2 sample. This observation indicates the presence in all samples of RuO_2 particles larger than 300 Å.

The photoelectron spectra were recorded using a Vacuum Generators ESCALAB mark II instrument using an Al K_α X-ray source (1486.6 eV). The base pressure of the instrument is 5×10^{-11} Torr and during experiments the pressure was less than 10^{-8} Torr. The spectrometer energy scale was calibrated using both Au $4f_{7/2}$ (84.0 eV) and Ag $3d_{5/2}$ (368.3 eV). The Si 2*p* (103.3 eV) line was systematically used as an internal standard in obtaining the binding energies of ruthenium and other elements. The Ru/ZSM-5 samples were introduced in the spectrometer as powders pressed onto indium disks. No flood gun was utilized.

Infrared spectra of adsorbed pyridine were shown by Stencel *et al.* (16) to be of special value for Fe and Co/ZSM5 catalysts. The technique employed in this study involves preparing very thin wafers (10 mg in 13 cm wafers) and the use of a special movable ir cell which can be connected to a vacuum line. The wafer is preheated to 450°C in vacuum. Pyridine is adsorbed at room temperature and the wafer is heated overnight at 150°C in a vacuum better than 10^{-4} Torr in order to eliminate physisorbed pyridine. The ir spectrum is then recorded at room temperature on a Beckman model IR-4250 instrument.

Results and discussion

Table 1 shows results for the binding energies of several elements in our Ru/ZSM5 samples, calculated from the experimental values of the kinetic energy of photoelectrons E_k as:

$$[1] \quad E_B = h\nu - E_k - \Delta_c$$

where $h\nu$ is the energy of the incident photons and Δ_c a correction including the charging effect and calculated by referencing the energy scale to some known standard value. Table 1 gives the values of Δ_c obtained by adjusting the Si 2*p* level to a binding energy of 103.3 eV. A lower value is often

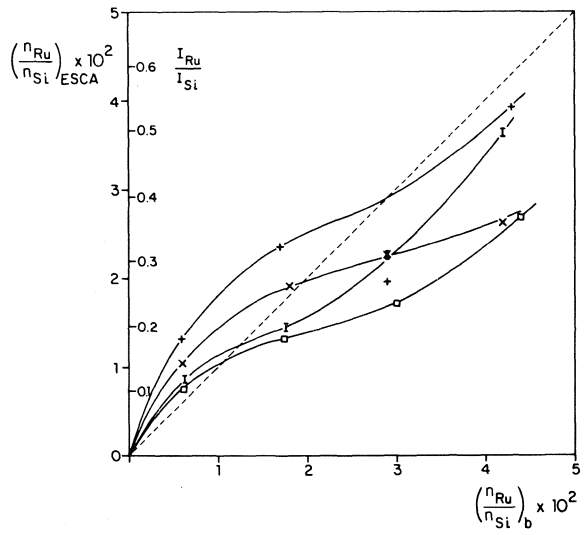

FIG. 1. ESCA intensity ratio (I_{Ru3d}/I_{Si2p}) and atomic ratio $(n_{Ru}/n_{Si})_{ESCA}$ as a function of bulk atomic ratio. □ ruthenocene, × dimethyl ruthenocene, + diphenyl ruthenocene, I dibenzoyl ruthenocene.

reported in the literature, for example 102.7 eV for Si $2p$ in silica gel, but it is our experience that for Si $2p$ in ZSM-5, the value of 103.3 eV is more appropriate. This is confirmed here by the correct position of the O_{1s} line obtained (532.55 ± 0.15 eV). The Al $2p$ line shows more scatter (74.9 to 75.6 eV and one point at 76.1 eV). The average value close to 75.2 eV is higher than the value quoted for Al $2p$ in Al_2O_3 (74.5 eV) but such a difference would be compatible with a more ionic character of the links of Al^{3+} to the zeolite lattice. The Ru $3d$ binding energy results will be discussed later on.

Figure 1 shows the results for the XPS intensity ratio Ru $3d$/Si $2p$ plotted as a function of the bulk atomic ratio $(n_{Ru}/n_{Si})_b$ calculated from X-ray fluorescence analytical results.

According to Kerkhoff and Moulijn (17) the XPS intensity ratio is given by

$$[2] \quad \left(\frac{I_{Ru}}{I_{Si}}\right)_{mono} = \left(\frac{n_{Ru}}{n_{Si}}\right)_b K$$

in the case of Ru being uniformly distributed within the pore lattice of the support. Moreover, for a monolayer dispersion of ruthenium, K can be calculated as:

$$[3] \quad K = \frac{D(E_{kRu})}{D(E_{kSi})} \frac{\sigma_{Ru}}{\sigma_{Si}} \frac{\beta_1}{2} \frac{(1 + e^{-\beta_2})}{(1 - e^{-\beta_2})}$$

In our case K was estimated using

$$[4] \quad \frac{D(E_{kRu})}{D(E_{kSi})} = \left(\frac{E_{kSi}}{E_{kRu}}\right)^{1/2}$$

σ_{Ru} and σ_{Si} being the photoelectron cross sections, as given by Scofield (18), and

$$[5] \quad \beta_1 = 2/\rho_s S_0 \lambda_{Si}$$
$$\beta_2 = 2/\rho_s S_0 \lambda_{Ru}$$

ρ_s and S_o are respectively the density and specific surface area of the support and λ_{Si}, λ_{Ru} the escape depths of Si and Ru photoelectrons from the support.

Deviations from the hypothesis of eq. [2] can be shown by comparing to $(n_{Ru}/n_{Si})_b$ the calculated values of:

$$[6] \quad (n_{Ru}/n_{Si})_{ESCA} = \left(\frac{I_{Ru}}{I_{Si}}\right)_{expt} \frac{1}{K}$$

Such a comparison is made in Fig. 1. When, as found for the lower Ru loadings, $(n_{Ru}/n_{Si})_{ESCA} > (n_{Ru}/n_{Si})_b$, the Ru content of the surface layers sensed by ESCA is higher than the average value. It can therefore be concluded from the results of Fig. 1 that superficial segregation is already present at Ru contents as low as 1%, and is more important for samples prepared from substituted than for non-substituted ruthenocene. At higher loadings the dispersion of Ru is decreased, K is no longer represented by eq. [3] and, as shown in ref. 17, mus decrease, yielding

$$\left(\frac{I_{Ru}}{I_{Si}}\right)_{expt} < \left(\frac{I_{Ru}}{I_{Si}}\right)_{mono}$$

or

$$\left(\frac{n_{Ru}}{n_{Si}}\right)_{ESCA} < \left(\frac{n_{Ru}}{n_{Si}}\right)_b$$

Nevertheless, ruthenocene-prepared catalysts show the lowest $(I_{Ru}/I_{Si})_{expt}$ whereas for diphenyl ruthenocene-prepared samples this ratio is the highest, indicating as expected, mor surface segregation in this last case.

Table 2 gives results for ir of adsorbed pyridine and in particular the ir absorbance ratio A_B/A_L, A_B and A_L corresponding to pyridine adsorbed on Brønsted and Lewis acid sites, respectively. This ratio is related to (B/L), the ratio of Brønsted to Lewis sites per unit cell:

$$[7] \quad (A_B/A_L) = (B/L) \times (\epsilon_B/\epsilon_L)$$

where ϵ_b and ϵ_L are extinction coefficients.

The ratio (ϵ_L/ϵ_B) has been measured in silica–alumina (19) and zeolites (20) and from the trend of these data with increasing Si/Al, it was suggested (21) that the value of $(\epsilon_L/\epsilon_B) = 1.5$ is appropriate for high silica zeolites. Applying eq. [7] to the support yields:

$$[8] \quad (B_z/L_z) = 3.75$$

Because the unit cell of the support is expressed as $Al_{2.6}Si_{93.4}O_{192}$, and the Lewis site in the zeolite is generated by dehydroxylation of two Brønsted sites:

$$[9] \quad B_z = 2.6 - 2L_z$$

Combining eqs. [8] and [9] yields $B_z = 1.7$, $L_z = 0.45$.

A rough estimate of the number of ruthenium ions exchanged per unit cell (Ru) can be obtained by combining eq. [7] with balances of acid sites, which, assuming arbitrarily the valence 2 for the exchanged ruthenium, may be written as:

$$[10] \quad L = 2(\text{Ru}) + L_z$$

$$[11] \quad B = B_z - 2(\text{Ru})$$

$$[12] \quad (\text{Ru}) = \frac{B_z - (\epsilon_L/\epsilon_B)(A_B/A_L)L_z}{2[1 + (\epsilon_L/\epsilon_B)(A_B/A_L)]}$$

These results expressed either as the number of unexchanged Brønsted sites or as the weight percent of exchanged ruthenium are given in Table 2.

Although these figures are not definitely established due to uncertainties in the valence state of exchanged ruthenium, they can nevertheless be used for comparison between the various catalysts.

Figure 2 allows such a comparison by showing the uncon-

TABLE 2. Infrared results of adsorbed pyridine

Sample designation	Ru wt%	ν cm^{-1} Brønsted	ν cm^{-1} Lewis	A_B/A_L	Brønsted/ u.c	Ru exchanged wt%
HZSM5	—	1545	1444	2.5	1.7	—
129-A	0.96	1538	1445	1.14	1.36	0.30
B	2.65	1539	1445	1.63	1.53	0.15
C	4.50	1538	1445	1.46	1.48	0.20
D	6.40	1538	1445	1.01	1.30	0.35
124-A	0.93	1538	1445	1.73	1.55	0.13
B	2.73	1538	1445	2.15	1.64	0.05
C	4.30	1538	1445	1.24	1.40	0.26
D	6.15	1539	1447	1.2	1.38	0.28
133-A	0.93	1542	1448	1.16	1.37	0.29
B	2.63	1540	1448	1.72	1.55	0.13
C	4.40	1540	1448	1.63	1.53	0.15
D	6.26	1540	1448	1.32	1.43	0.24
124-A	0.98	1542	1445	1.83	1.58	0.11
B	2.68	1540	1446	0.99	1.28	0.36
C	4.33	1540	1446	1.53	1.50	0.18
D	6.17	1540	1445	1.12	1.35	0.31

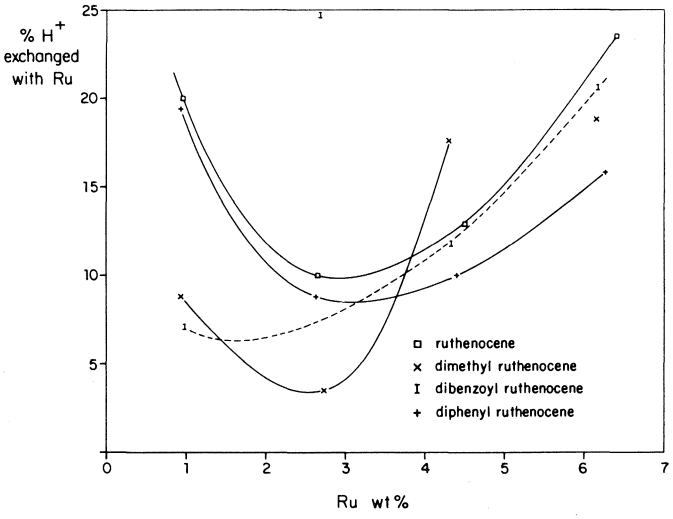

FIG. 2. Percent of Brønsted acid sites exchanged with Ru cations, as measured by ir of adsorbed pyridine.

verted percentage of Brønsted acid sites as a function of bulk ruthenium loadings.

The general trend of these curves shows a higher exchange of ruthenium when ruthenocene is used in the preparation, indicating more metal has penetrated the pore lattice in this case. This result is in agreement with the ESCA results reported in Fig. 1. Figure 2 shows that increasing the size of the ring substituent does not completely avoid the penetration of ruthenium. The curve for diphenyl ruthenocene for example is almost as high as the ruthenocene one. The initial decrease in exchanged Brønsted sites with increasing ruthenium loading may be explained by restrictions to the inward diffusion of ruthenium compounds due to an early formation of ruthenium plugs. This lower dispersion of the inside ruthenium is indeed compatible with the ESCA results in Fig. 1 at these low Ru loadings.

We may now proceed to the discussion of the Ru ESCA data of Table 1.

ESCA data for stoichiometric ruthenium compounds have been reported by Kim and Winograd (22) and by Folkesson (23). These data are presented in Table 3. Both authors agree on a value close to 280.0 eV for the binding energy of Ru $3d_{5/2}$ in Ru^0. Folkesson (23), however, mentions that this is about 1 eV higher than the values reported by Siegbahn. There is, however, a clear disagreement on the RuO_2 value. Kim and Winograd (22) discuss in details the difficulties in obtaining this value. They explain that the surface of a RuO_2 sample may contain species of higher oxides (RuO_3 and RuO_4) which are volatile. They show by ESCA that this species can be eliminated by heating at temperatures as low as 220°C and that in this process ruthenium metal appears on the surface. We believe that this process must be quite common on RuO_2 surfaces. We produced a sample of ruthenium oxide by calcination of $RuCl_3$ in air at 900°C. The X-ray diffraction pattern showed this sample was essentially RuO_2 but the spectrum of Ru metal was definitely apparent. The ESCA spectrum of this sample showed essentially a Ru^0 covered surface with a Ru $3d_{5/2}$ binding energy of 279.8 eV, with only a shoulder at 281.7 eV corresponding to RuO_2.

Therefore we believe that the ESCA data of Table 1 showing that for a large proportion of our samples the binding energy of Ru $3d_{5/2}$ is in the range 280.0 ± 0.3 eV correspond to a similar situation. Most of the ruthenium would therefore be in the form of RuO_2 microcrystals of diameter larger than 300 Å (as shown by XRD) located at the external surface of the ZSM-5 crystal, and having their surface covered with metallic ruthenium.

It is interesting to note in this regard that both Pedersen and Lunsford (24) and Tkatchenko *et al.* (25) find low Ru $3d_{5/2}$ binding energies for oxygen- or air-calcined samples of Ru Y catalysts. The last author reports for example values of 280.6, 280.7, 280.8, and 280.6 eV, respectively, for Ru metal and Ru Y heated at 400°C, 500°C in O_2 for 2.5 h and at 500°C in H_2 for 1.5 h. Therefore on these catalysts, just like on ours, it seems

TABLE 3. Binding energies of Ru $3d_{5/2}$ in ruthenium compounds

Oxidation state	Compound	Reference line	B.E. Ru $3d_{5/2}$ (eV)	Reference
0	Ru metal	Au $4f_{7/2}$ = 84.0 eV	280.0	22
4	RuO_2		280.7	22
4	RuO_2,XH_2O		281.4	22
6	RuO_3		282.5	22
8	RuO_4		283.3	22
0	Ru metal	Pt $4f_{7/2}$ = 71.1 eV	279.9	23
2	$Ru(NH_3)_5N_2Cl_2$		282.5	23
2	$Ru(NH_3)_5N_2Br_2$		280.5	23
2	$Ru(NH_3)_5N_2I_2$		282.2	23
3	$RuCl_3$		281.8	23
4	RuO_2		282.1	23

that Ru is essentially in the zero valence state in the surface zone sensed by ESCA, even in the calcined samples.

As shown by the ir results of Table 2, the exchanged ruthenium is only a minor fraction of total supported ruthenium in our samples. It is therefore not surprising that the ruthenium ions that exchanged with protons do not have a major effect on the ESCA spectra. It may at most be conjectured that the 0.5–0.6 eV higher Ru $3d_{5/2}$ binding energies observed for samples 129-A and 124-A compared to samples with higher loadings reflect the presence of cationic species with charges between 0 and +4.

Conclusion

Our investigation of the synthesis of ring-substituted ruthenocenes allowed us to propose improved methods for the syntheses of dimethyl and diphenyl-1,1′ ruthenocene which are derived from the procedure reported by Pertici *et al.* (9) for the synthesis of ruthenocene. An original method is also proposed for the synthesis of dibenzoyl-1,1′ ruthenocene in which monobenzoyl ruthenocene is obtained as a by-product. Complete chemical identifications of these four ruthenocenes are reported.

A new method based on the gas–solid interaction of these compounds with the H form of the zeolithe ZSM-5 has been used for the preparation of ZSM-5 supported ruthenium catalysts. The addition of ring substituents allows some control of the spatial distribution of ruthenium with respect to the limits of the ZSM-5 crystal. From the characterization of the catalysts by ESCA, XRD, and ir of adsorbed pyridine, three forms of ruthenium may be present in the calcined samples.

(*1*) RuO_2 particles with diameter larger than 300 Å, located on the external surface of the ZSM-5 crystals. Unexpectedly, the surface of these particles is covered with Ru^0.

(*2*) Ruthenium ions located in the ZSM-5 pore lattice and having partially exchanged the Brønsted acid sites. ESCA did not allow for a determination of the valence state of these ions which could be 1+, 2+, or 3+.

(*3*) Ruthenium oxide (likely RuO_2) with a particle size in the 5–10 Å range may also be present in the pore lattice. The presence of such plugging material is inferred from the variations in the content of exchanged ruthenium ions with bulk ruthenium loading.

1. YU. I. YERMAKOV, B. M. KUZNETSOV, and V. A. ZAKHAROV. Catalysis by supported complexes. Elsevier, Amsterdam. 1981.
2. B. C. GATES. *In* Chemistry and chemical engineering of catalytic processes. *Edited by* R. Prins and G. C. A. Schuit. Nato Advanced Study Institutes Series, Sijthoff and Noordhoff, Germantown. 1980. p. 427.
3. R. L. BURWELL. *In* Catalysis on the energy scene. Studies in surface science and catalysis. Vol. 19. Elsevier, Amsterdam. 1984. p. 45.
4. D. D. WHITEHURST. Proc. 5th Can. Symp. Catal. Calgary, 1977. p. 182.
5. Y. IWASAWA and S. OGASAWARA. J. Chem. Soc. Faraday Trans. 1, **75**, 1465 (1979).
6. E. G. DEROUANE. *In* Intercalation Chemistry. *Edited by* M. S. Whittingham and A. J. Jackson. Academic Press, New York. 1982. p. 101.
7. A. MAHAY. Ph.D. Thesis, Université Laval. 1986.
8. D. E. BUBLITZ, W. E. MCEWEN, and J. KLEINBERG. Org. Synth. **41**, 96 (1961).
9. P. PERTICI, G. VITULLI, M. PACI, and L. PORRI. J. Chem. Soc. Dalton Trans. 1961 (1980).
10. O. HOFLER and K. SCHLÖGL. J. Organomet. Chem. **13**, 443 (1968).
11. P. L. PAUSON. J. Am. Chem. Soc. **76**, 2187 (1954).
12. M. ROSENBLUM and R. B. WOODWORD. J. Am. Chem. Soc. **80**, 5443 (1958).
13. R. DAVIS and D. J. O'REARDON. J. Indian Chem. Soc. **59** (11-12), 1270 (1982).
14. Z. GABELICA, N. BLOM, and E. G. DEROUANE. Appl. Catal. **5**, 227 (1983).
15. A. ERDEM and L. B. SAND. J. Catal. **60**, 241 (1979).
16. J. M. STENCEL, V. U. S. RAO, J. R. DIEHL, K. H. RHEE, A. G. DHERE, and R. J. DE ANGELIS. J. Catal. **84**, 109 (1983).
17. F. P. J. M. KERKHOF and J. A. MOULIJN. J. Phys. Chem. **83**, 1612 (1979).
18. J. H. SCOFIELD. J. Electron. Spectrosc. Relat. Phenom. **8**, 129 (1976).
19. J. A. SCHWARTZ. J. Vac. Sci. Technol. **12**, 321 (1975).
20. M. LEFRANÇOIS and G. HALBOIS. J. Catal. **20**, 350 (1971).
21. K. H. RHEE, V. U. S. RAO, J. M. STENCEL, G. A. MELSON, and J. E. CRAWFORD. Zeolites, **3**, 337 (1983).
22. K. S. KIM and N. WINOGRAD. J. Catal. **35**, 66 (1974).
23. B. FOLKESSON. Acta Chem. Scand. **27**, 287 (1973).
24. L. A. PEDERSEN and J. H. LUNSFORD. J. Catal. **61**, 39 (1980).
25. O. P. TKATCHENKO, E. S. SHPIRO, G. V. ANTOSHIN, and KH. M. MINATCHEV. IZV. Akad. Nauk SSSR, Sci. Khim. No 6, 1249 (1980).

COMMUNICATION

Photochemical retro-aldol type reactions of nitrobenzyl derivatives. Mechanistic variations in the elimination of nitrobenzyl carbanions from nitrobenzyl derivatives on photolysis

PETER WAN[1] AND S. MURALIDHARAN
Department of Chemistry, University of Victoria, Victoria, B.C., Canada V8W 2Y2

Received March 4, 1986

PETER WAN and S. MURALIDHARAN. Can. J. Chem. **64**, 1949 (1986).

The photochemical retro-aldol type reactions of several nitrobenzyl derivatives are reported. The reactions are observed only in aqueous solution with quantum efficiencies being pH dependent for several derivatives, consistent with the existence of several mechanistic pathways for reaction. The primary photochemical event is believed to involve the generation of a nitrobenzyl carbanion, which acts as a photolabile leaving group in these reactions, and the generation of an oxocarbocation (or oxocarbocation-derived) fragment.

PETER WAN et S. MURALIDHARAN. Can. J. Chem. **64**, 1949 (1986).

On a étudié les réactions photochimiques de type rétro-aldol de plusieurs dérivés nitrobenzyles. On n'a observé ces réactions qu'en solution aqueuse et les rendements quantiques dépendent souvent du pH. Ceci témoigne de l'existence de divers chemins réactionnels. On pense que la première réaction photochimique implique la formation d'un carbanion nitrobenzyle, agissant comme groupe photolabile ainsi que celle d'un fragment oxocarbocation (ou d'un dérivé d'oxocarbocation).
[Traduit par la revue]

The photochemistry of nitroaromatic compounds has been a topic of continued interest and several reviews (1–4) summarize the photochemical behaviour of this functional group in solution. Many photoreactions of nitro compounds are known to proceed via radical intermediates which in many examples (e.g., photoreduction) are formed via initial hydrogen transfer to the photoexcited nitro group, consistent with the notion of an electrophilic n,π^* reactive state of the nitro group (5). In this work, we report several closely related photochemical reactions of appropriately substituted nitroaromatic compounds which are observed only in aqueous solution and are best explained by proposing the formation of nitrobenzyl carbanion and oxocarbocation (or oxocarbocation-derived) intermediates, via an excited state configuration other than the usual n,π^*. One of these reactions appears suited for direct photogeneration of a variety of dioxocarbocations and hemi-orthoesters in aqueous solution, which is amenable for flash-photolysis study. These results provide new insights into the intriguing photobehaviour of nitroaromatic compounds in aqueous solution (6–9).

	R^1	R^2	X	Y
1	H	H	NO_2	H
2	H	H	H	NO_2
3	H	Ph	H	NO_2
4	H	Ph	NO_2	H
5	CH_3	Ph	H	NO_2
6	H	H	H	H

Whereas nitroaromatic compounds **1**–**4** are photostable in a variety of organic solvents (e.g., CH_3CN, MeOH, diethyl ether, benzene), they react with moderate efficiencies (*vide infra*) in aqueous solution in a manner suggestive of a retro-aldol pathway, as shown in Scheme 1 for the reaction of 2-(*p*-nitrophenyl)-1-phenylethanol **3**. In a typical experiment, 100 mg of the substrate is dissolved in aqueous CH_3CN (100 mL; 10–30% CH_3CN; pH 1–14) and saturated with oxygen-free argon. Photolyses were carried out using quartz vessels in a Rayonet photochemical reactor (300 nm lamps). The photolyzed solutions were worked up by CH_2Cl_2 extraction, after adding NaCl. Typical photolysis times were 20–60 min, which gave conversions of 20–50%, depending on the substrate. Mass balances were >90%, except for experiments carried out at high pH, where some decomposition of benzaldehyde product (from **3** and **4**) was observed. However, under dilute conditions (10^{-4} *M*), the benzaldehyde product was found to be stable for several days at high pH. The structures of the products were characterized via standard spectroscopic techniques. The formation of *p*,*p*′-dinitrobibenzyl as a product is evidence for a *p*-nitrobenzyl carbanion intermediate on photolysis, since Russell and Buncel and their respective co-workers have shown in earlier work (10–13) that this compound is formed via the *p*-nitrobenzyl carbanion generated under more strongly basic conditions. The mechanism for the formation of *p*,*p*′-dinitrobibenzyl from the *p*-nitrobenzyl carbanion has been studied in some detail (10–12) in which the first step is believed to involve the ejection of an electron from the carbanion to give *p*-nitrobenzyl radical. The electron acceptor may be a molecule of substrate or *p*-nitrotoluene product (10–12). The reaction conditions employed for the photolysis (maximum pH = 14) do not permit any significant deprotonation of *p*-nitrotoluene,

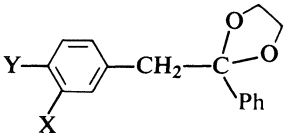

7 X = NO_2; Y = H
8 X = H; Y = NO_2

[1]NSERC University Research Fellow. Author to whom correspondence should be addressed.

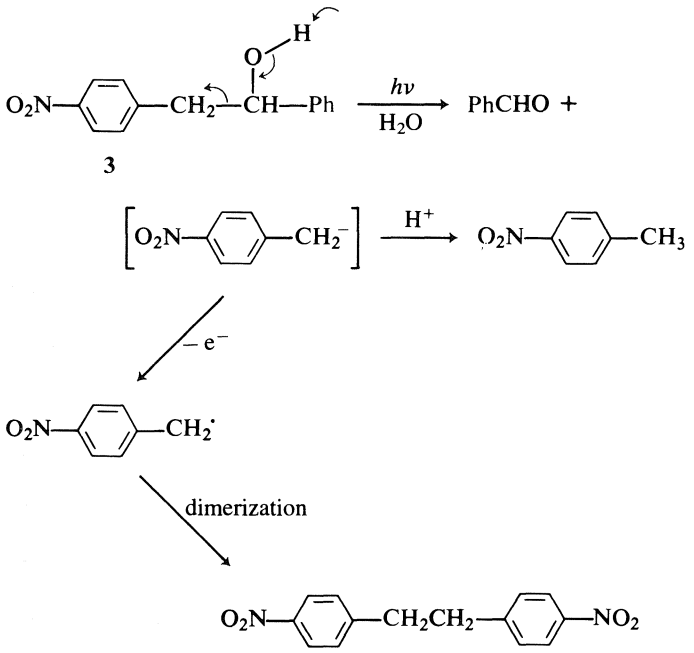

SCHEME 1

as shown by control experiments. In addition, *p*-nitrotoluene is photostable under the reaction conditions. Thus the *p*-nitrobenzyl carbanion is generated photochemically and reacts in a similar manner as the species generated under much more basic conditions. For example, in addition to dimerization to give *p,p'*-dinitrobibenzyl, we have found that if the photolysis is run under the presence of oxygen, the major product is *p*-nitrobenzoic acid, which is the known oxygenation product of the *p*-nitrobenzyl carbanion (11). The relative amounts of *p*-nitrotoluene vs. *p,p'*-dinitrobibenzyl formed (i.e., the relative rates of partitioning of the photogenerated *p*-nitrobenzyl carbanion by protonation (to give *p*-nitrotoluene) and by electron ejection (to give *p,p'*-dinitrobibenzyl)) is under study. Initial results indicate that the relative rates of the above two competing processes are dependent on the basicity of the medium. Additional evidence for a retro-aldol pathway (Scheme 1) is the observation that compound **3** reacts more efficiently in H_2O than in D_2O, as measured by relative quantum yields for benzaldehyde formation ($\Phi_{H_2O}/\Phi_{D_2O} = 1.3 \pm 0.05$). This observation is consistent with a primary isotope effect for deprotonation of the O—H(D) bond in the retro-aldol-type transition state. Successful triplet sensitization experiments using sodium benzophenone-2-carboxylate (λ_{excit} = 350 nm) for several compounds would suggest triplet state reactivity for these reactions, which is usually the norm for many nitroaromatic compounds (3).

Photolysis of the *meta*-isomer **4** in the absence of oxygen gave only benzaldehyde and *m*-nitrotoluene as the products, which indicates that the photogenerated *m*-nitrobenzyl carbanion does not react via the Russell mechanism (10–12). Compounds **1** and **2** react in an analogous manner as above but both **5** and **6** failed to react. These results indicate that a nitro group is necessary, in addition to the presence of a hydroxyl group at the 1-position for reaction in structures of the type **1**–**6**. However, both acetals **7** and **8** were found to react to give the nitrobenzyl carbanion-derived products (as above) and hydroxy ester **11**. The formation of **11** is best explained by reaction [1], in which the photoreaction initially generates a highly stabilized

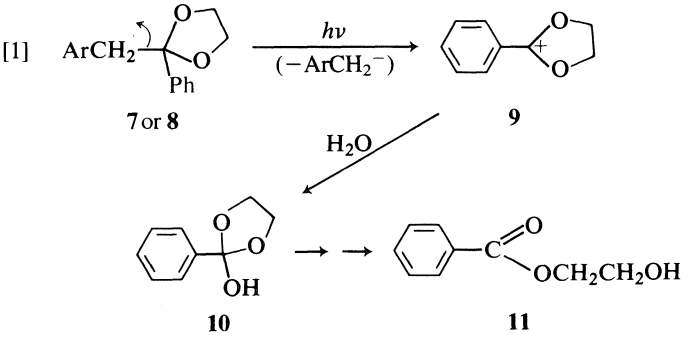

dioxocarbocation **9** (and the corresponding nitrobenzyl carbanions). Carbocation **9** subsequently reacts with water to give hemi-orthoester **10**, which on further hydrolysis gives hydroxyester **11**. Thus the availability of two oxygens to stabilize the incipient carbocation is sufficient to cause reaction whereas one oxygen (in **5**) was insufficient. This observation clearly demonstrates that the reaction proceeds via a heterolytic mechanism. Additional evidence for a heterolytic retro-aldol type pathway is suggested by the variation of quantum yields for reaction (product formation) as a function of pH of the solution. Quantum yields were measured via uv spectrophotometry, by monitoring the formation of benzaldehyde (for **3** and **4**) at 252 nm or hydroxyester **11** at 230 nm (for **9** and **10**). For compounds **1** and **2**, small scale preparative photolyses were used. Potassium ferrioxalate actinometry was employed in all cases for the measurement of light intensity (λ_{excit} = 300 nm). The results are shown in Fig. 1 for several derivatives. The striking variations in quantum efficiencies observed with pH suggest a variety of mechanistic possibilities of reaction. For example, for the acetal derivative **8**, where no pH dependence was observed, a mechanism involving unimolecular heterolytic cleavage of the benzylic C—C bond is suggested. However, for alcohol **3**, there are distinctly two mechanistic regimes: one at high pH and the other below pH 11. In high pH, hydroxide ion catalysis of reaction (first step in Scheme 1) is important and at lower pH, water replaces hydroxide ion as the deprotonating base. For alcohol **2**, reaction is not observed below pH 11 which indicates that water is ineffective as the deprotonating base for

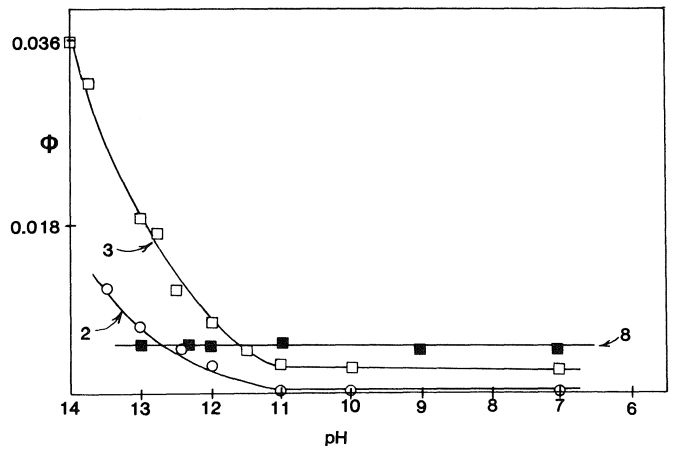

FIG. 1. Product quantum yields for retro-aldol reactions of compounds **2**, **3**, and **8** (λ_{excit} = 300 nm; 10% CH_3CN as cosolvent except for **8**, where 30% CH_3CN was used). The quoted pH is the basicity of the aqueous portion). Selected quantum yields at pH 7: 0.000 for **2**, 0.0025 for **3**, and 0.005 for **8**; at pH 12: 0.003 for **2**, 0.0072 for **3**, and 0.005 for **8**; at pH 13: 0.007 for **2**, 0.018 for **3**, and 0.006 for **8**.

this compound. Not shown in Fig. 1 is the observation that the *meta* isomers are about two times more reactive than the corresponding *para* isomers, as indicated by their quantum yields. This is suggestive of a selective *meta* transmission of ionic charge of photoexcited nitroaromatic compounds, initially reported by Zimmerman and Somasekhara (14).

Although the decarboxylation of several (nitrophenyl)acetic acids has been reported by Margerum and Petrusis (15), the present study indicates that this type of chemistry — in which the nitrobenzyl carbanion acts as photolabile leaving group in aqueous solution — is quite general for suitably substituted nitroaromatic compounds, which are amenable for detailed mechanistic studies.

Acknowledgment

The authors are grateful to the Natural Sciences and Engineering Research Council of Canada and the Research Corporation for support of this work.

1. H. A. Morrison. *In* The chemistry of the nitro and nitroso groups. *Edited by* H. Feuer. Wiley, New York. 1969. Chapt. 4.
2. Y. L. Chow. *In* The chemistry of the amino, nitro and nitroso compounds and their derivatives. *Edited by* S. Patai. Wiley, New York. 1982. Chapt. 6.
3. D. Döpp. Top. Curr. Chem. **55**, 49 (1975).
4. A. N. Frolov, N. A. Kuznetsova, and A. V. El'tsov. Russ. Chem. Rev. Engl. Trans. **45**, 1024 (1976).
5. R. W. Yip, D. K. Sharma, R. Giasson, and D. Gravel. J. Phys. Chem. **89**, 5328 (1985).
6. P. Wan and K. Yates. J. Org. Chem. **48**, 136 (1983).
7. P. Wan and K. Yates. J. Chem. Soc. Chem. Commun. 1023 (1981).
8. P. Wan and K. Yates. J. Chem. Soc. Chem. Commun. 275 (1982).
9. G. G. Wubbels, T. F. Kalhorn, D. E. Johnson, and D. Campbell. J. Org. Chem. **47**, 4664 (1982).
10. G. A. Russell and E. G. Janzen. J. Am. Chem. Soc. **89**, 300 (1967).
11. G. A. Russell, A. J. Moye, E. G. Janzen, S. Mak, and E. R. Talaty. J. Org. Chem. **32**, 137 (1967).
12. E. Buncel and B. C. Menon. J. Am. Chem. Soc. **102**, 3499 (1980).
13. E. Buncel, T. K. Venkatachalam, and B. C. Menon. J. Org. Chem. **49**, 413 (1984).
14. H. E. Zimmerman and S. Somasekhara. J. Am. Chem. Soc. **85**, 922 (1963).
15. J. D. Margerum and C. T. Petrusis. J. Am. Chem. Soc. **91**, 2467 (1969).

ADDITIONS AND CORRECTIONS/AJOUTS ET CORRECTIONS

F. Brisse, D. Thoraval, and T. H. Chan. Can. J. Chem. **64**, 739 (1986). The crystal structure of an enol silyl ether.

Page 739. The date of receipt of the manuscript by the editor should read September 27, 1985.

High-performance liquid chromatography of some bis(ethylenediamine)cobalt(III) complexes

MOUSTAFA H. M. ABOU-EL-WAFA, HESHAM MANSOUR, AND G. A. NOUBI
Department of Chemistry, Faculty of Science at Qena, Qena, Egypt

Received November 4, 1985[1]

MOUSTAFA H. M. ABOU-EL-WAFA, HESHAM MANSOUR, and G. A. NOUBI. Can. J. Chem. **64**, 1953 (1986).

Chromatographic separation of the complexes *cis*- and *trans*-$Co(en)_2(S_2O_3)_2^-$, *cis*- and *trans*-$Co(en)_2(SO_3)_2^-$, *cis*- and *trans*-$Co(en)_2Cl_2^+$, *cis*-$Co(en)_2(N_3)_2^+$, *cis*-$Co(en)_2(SO_3)(N_3)^0$, $Co(en)_2(S_2O_3)(N_3)^0$, and $Co(en)_2(S_2O_3)(OH_2)^+$ (en = ethylenediamine) was carried out by high-performance liquid chromatography. Good separations were achieved on a μ-Bondapak C_{18} reversed-phase octadecyldimethylsilane (ODS) column using tributylmethylammonium cations and octylsulphonate anions. The efficiency and speed of the separations were superior to those obtained on a Partisil SCX ion exchange column.

MOUSTAFA H. M. ABOU-EL-WAFA, HESHAM MANSOUR et G. A. NOUBI. Can. J. Chem. **64**, 1953 (1986).

Les complexes *cis*- et *trans*-$Co(en)_2(S_2O_3)_2^-$ (en = éthylènediamine), *cis*- et *trans*-$Co(en)_2(SO_3)_2^-$, *cis*- et *trans*-$Co(en)_2Cl_2^+$, *cis*-$Co(en)_2(N_3)_2^+$, *cis*-$Co(en)_2(SO_3)(N_3)^0$, $Co(en)_2(S_2O_3)(N_3)^0$ et $Co(en)_2(S_2O_3)(OH_2)^+$ ont été préparés par chromatographie en phase liquide à haute performance. Une bonne résolution a été obtenue sur colonne d'octadécyldiméthylsilane à phase inversée C-18-μ-Bondapak, en utilisant des cations de tributyl méthyl ammonium et des anions d'octyl sulfonate. L'efficacité et la vitesse de résolution étaient supérieures à celles obtenues sur colonne échangeuse d'ions Partisil SCX.
[Traduit par la revue]

Introduction

The separation of neutral and cationic Co(III) complexes of the type $[Co(en)_2X,Y]^{n+}$ (n = 0, 1, 2) by reversed-phase high-performance liquid chromatography (rp-hplc) and high-performance ion exchange chromatography (hpiec) have been reported (1–6).

The use of rp-hplc for the separation of $[Co(en)_2X,Y]^n$ complexes with n = 0, 1−, 1+ has not been reported before. We chose to investigate these compounds because of our interest in the kinetic and mechanistic aspects of Co(III) complexes in general (7). An hplc technique was used here because the compounds (e.g. *trans*-$Co(en)_2(S_2O_3)_2^-$, $Co(en)_2(S_2O_3)(N_3)^0$, and $Co(en)_2(S_2O_3)(OH_2)^+$) have generally similar physical and spectral properties and half-lives of the order of 10^2 min.

Experimental

Materials and apparatus

Analar grade perchloric acid was used to adjust the eluent pH to 5 using a Pye Unicam pH meter fitted with a glass electrode. G.P. grade tributylmethylammonium bromide, lithium perchlorate, sodium perchlorate and octylsulphonate were used as received. Separations were carried out on a μ-Bondapak C_{18} reversed-phase column (25 × 0.5 cm) which was end-capped with trimethylsilane. Some experiments were carried out using a Partisil μm SCX ion exchange column. The columns were equilibrated for at least 15 min with the required eluent. All runs were carried out using a constant eluent composition. The columns when not in use were thoroughly flushed with methanol.

The chromatograms were recorded with a Perkin-Elmer Model 3B chromatograph with flow rate of 1 cm^3 min^{-1}. Samples of 20-μL volume (10^{-3} M) were introduced by a Rheodyne valve and the peaks detected by uv spectroscopy at 254 nm and integrated with a Hewlett-Packard integrator. The eluents were made up in water or in methanol–water mixtures and filtered through Millipore 1.2-μm porosity filters before use.

Complexes

All bis(ethylenediamine)cobalt(III) complexes were prepared by standard procedures; their elemental analyses are given in Table 1. All microanalyses were performed by analytical services in the Department of Chemistry at Queen University of Belfast (N. Ireland). The compounds are *cis*-$Li[Co(en)_2(S_2O_3)_2]$ (8), *trans*-$Na[Co(en)_2(S_2O_3)_2]$ (9), *cis*-$Na_2[Co(en)_2(SO_3)_2]$ $ClO_4.3H_2O$ (10), *trans*-$Na[Co(en)_2(SO_3)_2].3H_2O$ (10), *cis*-$[Co(en)_2(N_3)_2]$ NO_3 (11), *cis*-$[Co(en)_2Cl_2]$ $Cl.H_2O$ (10), *trans*-$[Co(en)_2Cl_2]Cl$ (12), and *cis*-$[Co(en)_2(N_3)(SO_3)]$ (10).

A solution of the complex $[Co(en)_2(S_2O_3)(OH_2)]$ was prepared using Deutsch's method (9). In a typical preparation 0.04 M *trans*-$Na[Co(en)_2(S_2O_3)_2]$ was oxidized with 0.06 M I_3^- (pH = 5, $HClO_4$) in 2 mL of water. The reaction mixture was loaded onto a sephadex sp-25 cation exchange column (Na^+ form, 2 cm id × 25 cm), and the bands eluted with 0.25 M $NaClO_4$. The required green band of the complex $[Co(en)_2(S_2O_3)(OH_2)]$ was collected and its concentration calculated, allowing for dilution. The agreement between the obtained and reported (9) absorptivity values (Table 2) suggest that conversion is practically stoichiometric.

A solution of the complex $[Co(en)_2(S_2O_3)(N_3)]$ was prepared by allowing 10^{-3} M *trans*-$[Co(en)_2(S_2O_3)_2]$ or $[Co(en)_2(S_2O_3)(OH_2)]$ to react with 0.1 M NaN_3 at 25°C for 24 h. High-performance liquid chromatography was used to monitor the percentage of the reactant and the product during the course of the reaction until the reactant peak disappeared. The spectrum of the product was recorded and its molar absorptivity values obtained (Table 2). On the other hand, reaction of the product with $S_2O_3^{2-}$ ions regenerated the complex $[Co(en)_2(S_2O_3)_2]$, which indicates that the product in solution is actually $[Co(en)_2(S_2O_3)(N_3)]$.

Results and discussion

The octahedral complexes reported here exist as cations, anions, and uncharged species in solution. Most are stable towards dissociation (14*a*, 15). However, some are more labile. A kinetic study (16) of *trans*-$Co(en)_2(SO_3)_2^-$ established that the complex ion undergoes rapid acid or base hydrolysis to form the $Co(en)_2(SO_3)(OH_2)^+$ ion. In contrast to *trans*-$Co(en)_2(SO_3)_2^-$, *cis*-$Co(en)_2(SO_3)_2^-$ is not labile with respect to hydrolysis and exchange reactions (16). On the other hand, it is reported (17) that the *cis* form of the complex $Co(en)_2(S_2O_3)_2^-$ isomerizes to the *trans* form in neutral aqueous medium (pH ~ 6–6.3), as shown by a change in the spectrum from the *cis* to the *trans* form after 2–3 days at room temperature. The *trans* form isomerizes to the *cis* in basic solution only (8) (pH ~ 7–11), and above pH 11 base hydrolysis becomes prominent. The

[1]Revision received May 29, 1986.

TABLE 1. Elemental analyses of bis(ethylenediamine)cobalt(III) complexes

Complex	%C		%H		%N	
	Calcd.	Found	Calcd.	Found	Calcd.	Found
trans-$Na[Co(en)_2(S_2O_3)_2]$	11.27	11.42	3.78	3.71	13.14	12.95
cis-$Li[Co(en)_2(S_2O_3)_2]$	8.21	8.50	4.83	4.71	9.57	9.46
trans-$Na[Co(en)_2(SO_3)_2].3H_2O$	13.26	13.12	4.45	4.54	15.47	15.78
cis-$Na_2[Co(en)_2(SO_3)_2]ClO_4.3H_2O$	8.9	8.91	4.1	3.98	10.40	10.19
trans-$[Co(en)_2Cl_2]Cl$	16.83	16.29	5.65	5.40	19.63	18.85
cis-$[Co(en)_2Cl_2]Cl.H_2O$	15.83	16.15	5.98	5.75	18.46	18.83
cis-$[Co(en)_2(N_3)_2]NO_3$	14.78	14.76	4.96	4.75	47.38	47.46
cis-$[Co(en)_2(N_3)(SO_3)]$	15.95	14.68	5.35	5.72	32.55	31.53

TABLE 2. Molar absorptivities[a] of bis(ethylenediamine)cobalt(III) complexes

Complex	Molar absorptivity at				
	216 nm	289 nm	333 nm	390 nm	545 nm
trans-$[Co(en)_2(S_2O_3)_2]^-$	12925 (11900)[b]	2632	30025 (27700)[b]	—	91 (85.5)[b]
$[Co(en)_2(S_2O_3)(OH_2)]^+$	13734 (12600)[b]	8572 (9500)[c]	—	164 (188)[c]	45
$[Co(en)_2(S_2O_3)(N_3)]^0$	—	3415	17280	1930	237

[a]In $dm^3\ mol^{-1}\ cm^{-1}$ (literature values in parentheses).
[b]From ref. 9.
[c]From ref. 13.

conclusion from these observations is that the complexes under investigation are quite stable at pH 5, so that the hplc technique can be utilized for their separation from the complex *trans*-$Co(en)_2(SO_3)_2^-$ and to a lesser extent from its derivative *trans*-$Co(en)_2(SO_3)(N_3)^0$.

A complete analysis using an ion exchange or ion pair column would require one portion for the anion and a second for the cation separation. The positively charged complexes were ion-paired with octylsulphonate anions ($C_8H_{17}SO_3^-$), while the negatively charged complexes were paired with tributylmethylammonium cations ($NMeBu_3^+$) to provide suitable retention for separation on a C_{18} bonded (ODS) column. Some complexes were eluted from a Partisil SCX ion exchange column with ClO_4^- anions. The data presented in Table 3 are representative of the performance of the columns in use. Results obtained using 0.3% by weight tributylmethylammonium cation as pairing ion and a reverse phase ODS column are given in Fig. 1. The void volume of the column was about 2.2 cm^3. The cation complexes (*a*) and (*b*) eluted at about 3 cm^3, a volume slightly exceeding the void volume. This indicates that hydrophobic interactions between these complexes and the C_{18} layer are insignificant. The unexpected order of the negatively charged complex (c) may be due to rapid hydrolysis into $[Co(en)_2(SO_3)(OH_2)]^+$ as mentioned before. The bonded hydrocarbon surface layer and the eluent electrolyte have the effect of reducing the column's capacity for uncharged hydrophilic complexes. This leads to the early separation shown in Fig. 1.

The separation of the negatively charged complexes (e) or (f) from (g) has been achieved. The separation of (e) from (f) is poor. Both possess the *cis* form and a single negative charge. Retention times follow the order e < f < g i.e.: *cis*-$Co(en)_2(SO_3)_2^-$ < *cis*-$Co(en)_2(S_2O_3)_2^-$ < *trans*-$Co(en)_2(S_2O_3)_2^-$.

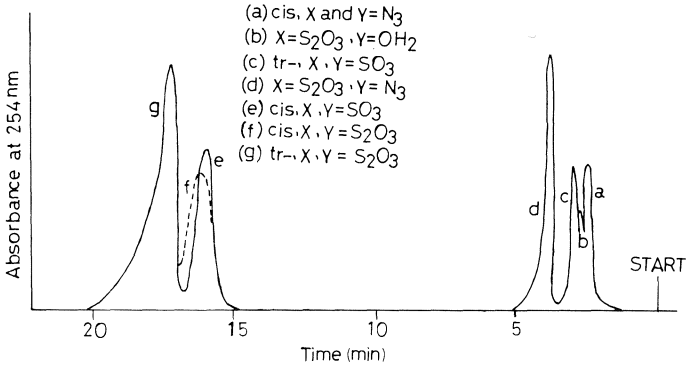

FIG. 1. Chromatogram of a mixture of $[Co(en)_2XY]^n$ complexes (ODS column, 0.3% $NMeBu_3^+$ in water, flow rate 1 $cm^3\ min^{-1}$, chart speed 0.5 cm min^{-1}).

The basicity of SO_3^{2-} ($pK = 7.2$) (18) is much greater than that of $S_2O_3^{2-}$ ($pK = 2.5$) (18). Consequently, the reactivity of SO_3^{2-} far exceeds that of $S_2O_3^{2-}$, giving a fast rate of retention in comparison with $S_2O_3^{2-}$. On the other hand, the order of the size of the stability constants (14*a*) of the complexes of the nucleophiles SO_3^{2-} and $S_2O_3^{2-}$ with the soft acid CH_3Hg^+ is $S_2O_3^{2-} > SO_3^{2-}$, which is in accord with the retention shown above.

Figure 2 shows the separation of the complexes using an ODS column and octylsulphonate in 10% MeOH as eluent. Each complex is clearly separated from the others. The negatively charged complex (a) is eluted at the void volume of the column followed by the uncharged compounds (b) and (c). Compound (b) shows another unidentified small peak at 4.7 cm^3. The positively charged complexes elute in the order d < e < f < g, i.e.: $Co(en)_2(S_2O_3)(OH_2)^+$ < *cis*-$Co(en)_2Cl_2^+$ < *cis*-$Co(en)_2(N_3)_2^+$ < *trans*-$Co(en)_2Cl_2^+$.

TABLE 3. Retention volumes of bis(ethylenediamine)cobalt(III) complexes

Complex	ODS column[a]		SCX column[b]	
	O.3% $NMeBu_3^+$	0.2% $C_8H_{17}SO_3^-$ 10% MeOH	0.1 *M* ClO_4^-	0.2 *M* ClO_4^-
trans-$[Co(en)_2(S_2O_3)_2]^-$	17.4	2.8	3.6	3.7
cis-$[Co(en)_2(S_2O_3)_2]^-$	16.4	—	3.4	3.5
cis-$[Co(en)_2(SO_3)_2]^-$	16.2	—	—	—
$[Co(en)_2(S_2O_3)(N_3)]^0$	4.0	4.4 4.7	4.7	4.5
trans-$[Co(en)_2(SO_3)_2]^-$	3.0	—	—	—
$[Co(en)_2(S_2O_3)(OH_2)]^+$	2.8	18	10.7	7.4
cis-$[Co(en)_2(N_3)_2]^+$	2.6	48	9.9	7.3
trans-$[Co(en)_2Cl_2]^+$	—	60.4	—	—
cis-$[Co(en)_2Cl_2]^+$	—	42.2	—	—
cis-$[Co(en)_2(SO_3)(N_3)]^0$	—	5.8	—	—

[a]Chart speed 0.5 cm min^{-1}.
[b]Chart speed 1.0 cm min^{-1}.

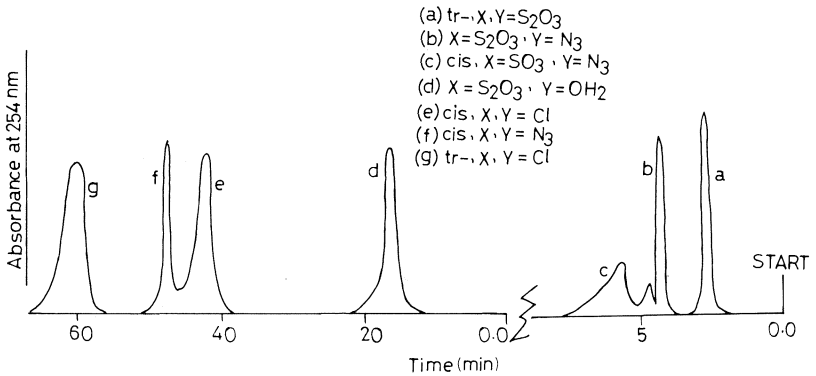

FIG. 2. Chromatogram of a mixture of $[Co(en)_2XY]^n$ complexes (ODS column, 0.2% $C_8H_{17}SO_3^-$ in 10% MeOH, flow rate 1 cm^3 min^{-1}, chart speed 0.5 cm min^{-1}).

This order is consistent with the hydrophobicity order of these compounds and with the ability of the added anion to interact with the C_{18} stationary phase and to form an ion pair with the cation complex. Such interactions have been discussed by Bidlingmeyer *et al.* (19), and may lead to the formation of species of different counter-ion stoichiometry which have sufficient lifetime on the matrix of the stationary phase to allow separation. Moreover, the basicity of N_3^- ($pK = 4.7$) (14*b*) is greater than Cl^- and H_2O ($pK = -4$ and -1.7, respectively) (14*b*). This is in agreement with the elution order of $Co(en)_2(S_2O_3)(OH_2)^+$ and *cis*-$Co(en)_2Cl_2^+$ but not with that of *trans*-$Co(en)_2Cl_2^+$. The difference between *cis*- and *trans*-$Co(en)_2Cl_2^+$ may be due to electrostatic repulsion of the negative ligand Cl^-, which would appear to be greater in the *cis* position than in the *trans* because of the smaller distance of separation (14*c*).

The sharpness observed for the peak of compound (f) is difficult to rationalize on steric ion pairing or stationary phase interaction grounds and a complex set of parameters probably combine. This requires more investigation for clarification. In an attempt to reduce the retention time of the cationic complexes (Fig. 2), the percentage of MeOH was raised to 30%, but this tended to dwarf the differences between the complexes and the extent of separation declined.

Use of a partisil high performance ion exchange column and aqueous ClO_4^- as anion gave in general poor results. Elution times were shorter than for those obtained by rp-hplc, with broad peaks and poor resolution. The elution order was the same as observed using an ODS column. On increasing the anion concentration from 0.1 to 0.2 *M*, the negatively charged complexes *cis*- and *trans*-$Co(en)_2(S_2O_3)_2^-$ eluted with somewhat longer retention times and the uncharged complex $Co(en)_2(S_2O_3)(N_3)^0$ eluted in a shorter time, but the discrimination between the three complexes was not as good. The positively charged complexes *cis*-$Co(en)_2(N_3)_2^+$ and $Co(en)_2(S_2O_3)(OH_2)^+$ had smaller retention times than were observed with 0.1 *M* ClO_4^- and the peaks overlapped. This phenomenon was noted before (2), and was found to be due to interactions between the different complexes, the reagent, and the stationary phase.

Overall, the results obtained may be of value to those contemplating the use of rp-hplc for separating complexes similar to those investigated here.

1. Y. YOSHIKAWA, M. KOJIMA, M. FUJITA, M. IIDA, and H. YAMATERA. Chem. Soc. J. Chem. Lett. 1163 (1974).
2. D. A. BUCKINGHAM, C. R. CLARK, R. F, TASKER, and M. T. W. HEARN. J. Liq. Chromatogr. **4**, 689 (1981).
3. D. A. BUCKINGHAM, D. M. FOSTER, and A. M. SARGESON. J. Am. Chem. Soc. **91**, 4102 (1969).
4. G. GRASSINI-STRAZZA and C. M. POLCARO. J. Chromatogr. **147**, 516 (1978).

5. D. A. BUCKINGHAM, C. R. CLARK, M. M. DEVA, and R. F. TASKER. Inorg. Chem. **22**, 2754 (1983).
6. C. R. CLARK, R. F. TASKER, P. SUTTON, and D. A. BUCKINGHAM. J. Chromatogr. **93**, 313 (1984).
7. M. H. M. ABOU-EL-WAFA and M. G. BURNETT. J. Chem. Soc. Chem. Commun. 833 (1983); Polyhedron Commun. **3**, 895 (1984).
8. P. R. RAY and S. N. MAULIK. J. Ind. Chem. Soc. **10**, 655 (1933).
9. J. N. COOPER, J. D. MCCOY, M. G. KATZ, and E. DEUTSCH. Inorg. Chem. **19**, 2265 (1980).
10. J. SPRINGBØRG and C. E. SCHAFFER. Inorganic synthesis. Vol. XIV. McGraw Hill, New York. 1973. p. 79.
11. P. J. STAPLES and M. L. TOBE. J. Am. Chem. Soc. 4812 (1963).
12. J. C. BAILAR, JR. Inorganic synthesis. Vol. II. McGraw Hill, New York. 1946. p. 233.
13. J. N. COOPER, J. G. BENTSEN, T. M. HANDEL, K. M. STROHMAIER, W. A. PORTER, B. C. JOHNSON, A. M. CARR, D. A. FARNATH, and S. L. APPLETON. Inorg. Chem. **22**, 3060 (1983).
14. F. BASOLO and R. G. PEARSON. Mechanisms of inorganic reactions. 2nd ed. J. Wiley, New York. (*a*) p. 171; (*b*) p. 140; (*c*) p. 175.
15. C. H. LANGFORD and H. B. GRAY. Ligand substitution processes. W. A. Benjamin, Inc., New York. 1965. p. 66.
16. D. R. STRANKS and J. K. YANDELL. Inorg. Chem. **9**, 751 (1970).
17. B. CHAKRAVARTY and P. K. DAS. Trans. Met. Chem. **7**, 340 (1982).
18. A. I. VOGEL. A textbook of quantitative inorganic analysis. 4th ed. Longman, London. p. 889.
19. B. A. BIDLINGMEYER, S. N. DEMINY, W. P. PRICE, B. SACHAK, and M. PETRUSEK. J. Chromatogr. **186**, 419 (1979).

On why some low-energy decomposition pathways of simple ketone molecular ions do not give rise to metastable peaks. A reappraisal

PETER J. DERRICK AND STEEN HAMMERUM

School of Chemistry, University of New South Wales, Kensington NSW 2033, Australia, and Department of General and Organic Chemistry, University of Copenhagen, The H.C. Ørsted Institute, DK-2100 Copenhagen Ø, Denmark

Received November 21, 1985

PETER J. DERRICK and STEEN HAMMERUM. Can. J. Chem. **64**, 1957 (1986).

The concept of minimum rate constants, $k(E)_{min}$, for unimolecular decompositions does not, according to the quasi equilibrium theory (QET), provide a rationalisation of the occurrence of the higher energy reaction, loss of methyl, rather than the more favorable process, loss of methane, from metastable butanone and 3-methylbutanone molecular ions.

PETER J. DERRICK et STEEN HAMMERUM. Can. J. Chem. **64**, 1957 (1986).

En se basant sur la théorie des quasi-equilibres le concept des constantes de vitesses minimales ($k(E)_{min}$) appliqué aux décompositions unimoléculaires ne fournit pas de rationalisation pour l'existence de la réaction de la perte d'un radical méthyle, qui demande plus d'énergie que la réaction plus favorable impliquant la perte d'une molécule de méthane, à partir des ions moléculaires métastables de la butanone et de la méthyl-3 butanone.

[Traduit par la revue]

In 1976 Cooks *et al.* (1) pointed out that some ketone molecular ions eliminate simple alkanes in the microsecond time-domain, because, they suggested, these are decomposition pathways with low energy requirements and such decompositions predominate at these times. The loss of alkane molecules from certain ketones had been noted previously (2), but many small ketone radical cations react predominantly by the loss of alkyl radicals through α-cleavage. The loss of an alkyl is not always straightforward, as demonstrated by McAdoo, McLafferty, and Smith (3), who proposed that the loss of $CH_3^{\bullet}$ from certain $(C_3H_6O)^{+\bullet}$ ions constituted an example of non-ergodicity. The decomposing $(C_3H_6O)^{+\bullet}$ ions were said to have the acetone structure having been formed by isomerization of the enol ions, $(CH_3C(OH)=CH_2)^{+\bullet}$, and the loss of $CH_3^{\bullet}$ gave rise to the only significant metastable peak. The extensive discussion over the next fourteen years of this proposed example of non-ergodicity has been reviewed recently (4), and the conclusion reached that there is no reasonable alternative explanation for the particular characteristics of the $(C_3H_6O)^{+\bullet}$ system. However, the $(CH_3COCH_3)^{+\bullet}$ ion formed by electron ionization of acetone exhibits only one significant metastable peak, which is due to the loss of CH_4 (1, 5). The apparent contradiction has been resolved on the basis of the different internal energy contents (5). The $(CH_3COCH_3)^{+\bullet}$ ions formed by the isomerization of $(CH_3C(OH)=CH_2)^{+\bullet}$ have more internal energy, and they decompose by losing $CH_3^{\bullet}$. The acetone molecular ions that remain undecomposed after microseconds have less internal energy, and they decompose by losing CH_4. That is to say, the $k(E)$ vs. E curves cross. An analogous situation arises with the $(C_5H_{10}O)^{+\bullet}$ system (6–8), where the $(CH_3CH_2COCH_2CH_3)^{+\bullet}$ ions formed by electron ionization of 3-pentanone lose C_2H_6, while the $(CH_3CH_2COCH_2CH_3)^{+\bullet}$ ions formed by isomerization of its enol lose $C_2H_5^{\bullet}$. The latter reaction has also been suggested (7) to exhibit non-ergodic behaviour, but this claim has been shown (8) to be without substance.

$$CH_3^{\bullet} + CH_3CO^+ \leftarrow CH_3COCH_3^{+\bullet} \rightarrow CH_4 + CH_2{=}C{=}O^{+\bullet}$$

$$C_2H_5^{\bullet} + CH_3CH_2CO^+ \leftarrow CH_3CH_2COCH_2CH_3^{+\bullet} \rightarrow C_2H_6 + CH_3CH{=}C{=}O^{+\bullet}$$

The $(C_4H_8O)^{+\bullet}$ ion differs from $(C_3H_6O)^{+\bullet}$ and $(C_5H_{10}O)^{+\bullet}$ in metastable ion characteristics (9). The $(C_4H_8O)^{+\bullet}$ keto-ion formed by the isomerization of 2-butanone enol ions loses both CH_3 and $C_2H_5^{\bullet}$ (10), and it has been suggested (11, 12) on the basis of energy release that these reactions are also non-ergodic. The $(C_4H_8O)^{+\bullet}$ ions formed by electron ionization of 2-butanone also lose both $CH_3^{\bullet}$ and $C_2H_5^{\bullet}$ in the microsecond time-frame. What is remarkable is that the 2-butanone molecular ion loses neither CH_4 nor C_2H_6, even though the loss of CH_4 is endoergic by only 30 kJ mol^{-1} (cf. the loss of $CH_3^{\bullet}$, 60 kJ mol^{-1}; the loss of $C_2H_5^{\bullet}$, 100 kJ mol^{-1}) (see Appendix). A similar situation arises with the 3-methyl-2-butanone molecular ion (13, 14), which also does not lose CH_4. This reaction should be approximately thermoneutral (cf. the loss of $CH_3^{\bullet}$, 65 kJ mol^{-1}; the loss of $C_3H_7^{\bullet}$, 100 kJ mol^{-1}) (see Appendix).

$$CH_3^{\bullet} + CH_3CH_2CO^+ \leftarrow CH_3COCH_2CH_3^{+\bullet} \not\rightarrow CH_4 + CH_3CH{=}C{=}O^{+\bullet}$$

$$CH_3^{\bullet} + (CH_3)_2CHCO^+ \leftarrow CH_3COCH(CH_3)_2^{+\bullet} \not\rightarrow CH_4 + (CH_3)_2C{=}C{=}O^{+\bullet}$$

An explanation involving the idea of minimum rate constants, $k(E)_{min}$, has been advanced (14) to account for the absence of the loss of CH_4 from the molecular ions of 2-butanone and 3-methyl-2-butanone. Consider the QET expression,

$$k(E) = \sigma G^*(E - E_0)/(hN(E))$$

$k(E)$ assumes a near-minimum but non-zero value, $k(E)_{min}$, at the threshold when $\sigma G^*(E - E_0) = 1$. The explanation (14) supposes that the $k(E)$ vs. E curves for the loss of CH_4 and the loss of $CH_3^{\bullet}$ from either the 2-butanone or 3-methyl-2-butanone molecular ions are as shown in Fig. 1. Curve *A* representing the loss of $CH_3^{\bullet}$ has $k(E)_{min} < 10^6$ s^{-1}; curve *B* representing the loss of CH_4 has $k(E)_{min} > 10^6$ s^{-1}. The argument (14) upon which the explanation rested was that, if $k(E)_{min}$ is greater than 10^6 s^{-1} for a decomposition, no metastable peak will be observed for that decomposition, because no ions will react at the appropriate rates. If this argument were valid, it would follow directly from Fig. 1 that the loss of CH_4 ought not be observed. We wish to point out that this argument is incorrect when a metastable peak is observed for some competing reaction whose $k(E)$ curve lies below that of the non-observed process, as in Fig. 1. Figure 1 shows that molecular ions with internal energies E_1 to $E_1 + \Delta E$, corresponding to rate constants $k(E) = 10^5$ s^{-1} and 10^6 s^{-1} on curve *A*, would largely

Printed in Canada

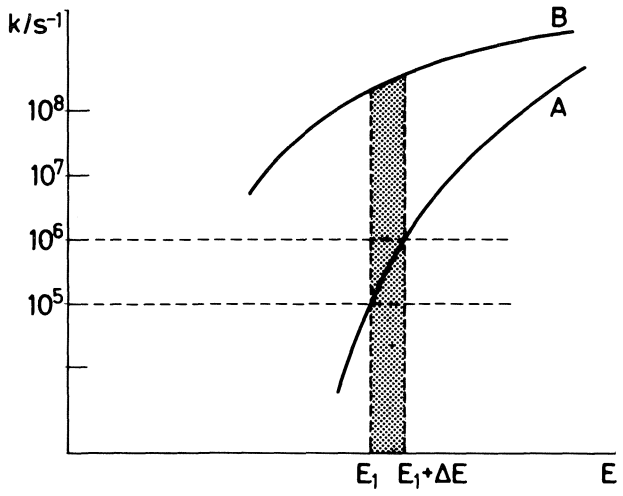

FIG. 1. Schematic representation of the variation of $k(E)$ with E for a situation where two competing reactions have $k(E)_{min} < 10^6\ s^{-1}$ (curve A) and $k(E)_{min} > 10^6\ s^{-1}$ (curve B), respectively; ions with internal energies E_1 to $E_1 + \Delta E$ will decompose predominantly by the path represented by curve B.

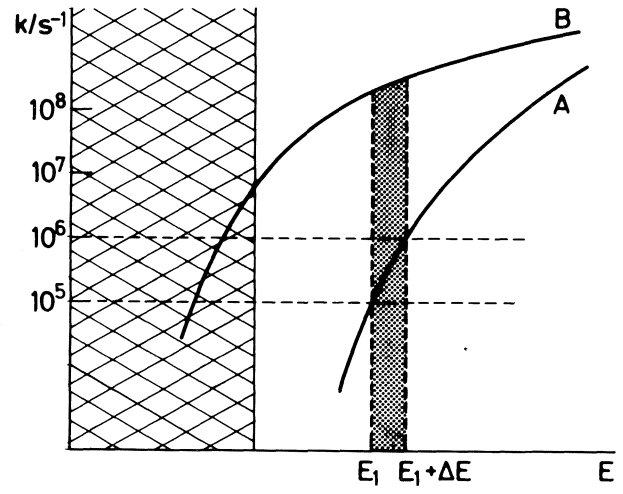

FIG. 2. Schematic representation of the variation of $k(E)$ with E for two competing reactions for a situation where no molecular ions have internal energies in the shaded energy region; ions with internal energies E_1 to $E_1 + \Delta E$ will decompose predominantly by the path represented by curve B.

decompose in times of the order of nanoseconds by losing CH_4 (curve B). Only a very small proportion of such molecular ions would survive long enough to enter the field-free region of the mass spectrometer (i.e., be undecomposed after microseconds), but *these would still decompose predominantly by losing CH_4*.

To demonstrate this point, it is sufficient to consider ions with a discrete energy E_1 (Fig. 1). Let the rate constants for losing $CH_3^\bullet$ and CH_4 at this energy be $k(E_1)_A$ and $k(E_1)_B$, respectively, and let the metastable time-window be from, say, $t_1 = 1\ \mu s$ to $t_2 = 10\ \mu s$. The number of ions, N_A and N_B, decomposing to lose $CH_3^\bullet$ and CH_4, respectively, in this time-window are (15):

$$N_A = \int_{t_1}^{t_2} k(E_1)_A N_0 \{\exp -[k(E_1)_A + k(E_1)_B]t\}dt$$

and

$$N_B = \int_{t_1}^{t_2} k(E_1)_B N_0 \{\exp -[k(E_1)_A + k(E_1)_B]t\}dt$$

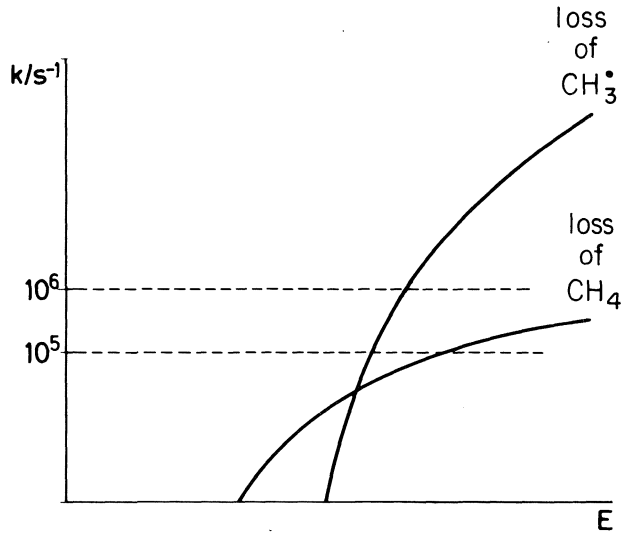

FIG. 3. Schematic representation of the variation of $k(E)$ with E for the competing reactions of $(CH_3COCH_2CH_3)^{+\bullet}$, showing presumed crossing below $10^5\ s^{-1}$.

where N_0 is the original number of molecular ions formed at $t = 0$. Other decomposition pathways can be neglected. The ratio of the number of ions decomposing by losing $CH_3^\bullet$ to those by losing CH_4 is then

$$\frac{N_A}{N_B} = \frac{k(E_1)_A}{k(E_1)_B}$$

and in Fig. 1, $k(E_1)_A/k(E_1)_B < 10^{-2}$. Therefore the intensity for the loss of CH_4 should exceed that for the loss of $CH_3^\bullet$ by a factor greater than 10^2. The $k(E)$ curves in Fig. 1 may be used to estimate relative metastable peak intensities by locating the energy range corresponding to $k(E) = 10^5\ s^{-1}$ or $10^6\ s^{-1}$ (depending on the time-window) for the lowest energy curve, i.e., the curve which crosses the $k = 10^5\ s^{-1}$ and $k = 10^6\ s^{-1}$ lines at the lowest energy. Approximate relative metastable intensities are then obtained by making *vertical* comparisons on the $k(E)$ diagram. That is to say, compare the $k(E)$ values for different decompositions at the energy range located.

A variation of this explanation has also been discussed (14). Here curve B continues below $k(E) = 10^5/10^6\ s^{-1}$, but there are no molecular ions in the shaded energy region (Fig. 2). In this case, the proposal (14) that the loss of $CH_3^\bullet$ would give rise to a metastable peak is unsound for the same reasons as before.

There are two plausible lines of explanation within the framework of the QET for why the loss of $CH_3^\bullet$ is observed but the loss of CH_4 is not with 2-butanone molecular ions. One is that the energies (heats) of reaction do not accurately reflect the critical energies. Thus if the critical energy for the loss of CH_4 were greater than that for the loss of $CH_3^\bullet$, the observations would be readily explained. This would mean that there was a significant reverse critical energy for the loss of CH_4. There could also be a reverse critical energy for the loss of $CH_3^\bullet$, but it would need to be much smaller than that for the loss of CH_4.

There is no evidence that the loss of CH_4 from the acetone molecular ion would have a significantly greater reverse critical energy that the loss of $CH_3^\bullet$. Baer[1] has found that the loss of CH_4 has a slightly lower onset than does the loss of $CH_3^\bullet$. It thus seems unlikely that the loss of CH_4 from 2-butanone molecular ion has a significant reverse critical energy.

[1]T. Baer. Private communication to C. Lifshitz (16).

The other explanation would be that the $k(E)$ curves for the loss of $CH_3^{\bullet}$ and the loss of CH_4 cross below about $k(E) = 10^5\ s^{-1}$. With both $(CH_3COCH_3)^{+\bullet}$ and $(CH_3CH_2COCH_2CH_3)^{+\bullet}$, it is generally believed that the $k(E)$ curves for the loss of alkyl and the loss of alkane do cross. It is, therefore, not unreasonable to consider that there is a similar crossing of $k(E)$ curves for $(CH_3COCH_2CH_3)^{+\bullet}$. In this case, however, the crossing would be below rather than above $10^5\ s^{-1}$ (see Fig. 3).

Acknowledgements

The authors are indebted to T. Bjørnholm and T. Vulpius for many stimulating discussions. The financial support from Statens Naturvidenskabelige Forskningsraad and Carlsbergfondet is gratefully acknowledged.

1. J. F. Litton, T. L. Kruger, and R. G. Cooks. J. Am. Chem. Soc. **98**, 2011 (1976).
2. R. G. Cooks, A. N. H. Yeo, and D. H. Williams. Org. Mass Spectrom. **2**, 985 (1969).
3. (*a*) D. J. McAdoo, F. W. McLafferty, and J. S. Smith. J. Am. Chem. Soc. **92**, 6343 (1970); (*b*) F. W. McLafferty, D. J. McAdoo, J. S. Smith, and R. Kornfeld. J. Am. Chem. Soc. **93**, 3720 (1971).
4. F. Turecek and F. W. McLafferty. J. Am. Chem. Soc. **106**, 2525 (1984).
5. (*a*) D. J. McAdoo and D. N. Witiak. J. Chem. Soc. Perkin 2, 770 (1981); (*b*) C. Lifshitz and E. Tzidony. Int. J. Mass Spectrom. Ion Phys. **39**, 181 (1981).
6. A. N. H. Yeo and D. H. Williams. J. Chem. Soc. Chem. Commun. 956 (1969).
7. D. J. McAdoo, W. Farr, and C. E. Hudson. J. Am. Chem. Soc. **102**, 5165 (1980).
8. G. Depke and H. Schwarz. Org. Mass Spectrom. **16**, 421 (1981).
9. D. J. McAdoo and M. P. Barbalas. Int. J. Mass Spectrom. Ion Phys. **36**, 281 (1980).
10. D. J. McAdoo, F. W. McLafferty, and T. E. Parks. J. Am. Chem. Soc. **94**, 1601 (1972).
11. D. J. McAdoo and C. E. Hudson. J. Phys. Chem. **87**, 2451 (1983).
12. C. Lifshitz, P. Berger, and E. Tzidony. Chem. Phys. Lett. **95**, 109 (1983).
13. S. Hammerum, K. F. Donchi, and P. J. Derrick. Int. J. Mass Spectrom. Ion Phys. **47**, 347 (1983).
14. (*a*) G. Bouchoux and Y. Hoppilliard. Can. J. Chem. **60**, 2107 (1982); (*b*) Y. Hoppilliard and G. Bouchoux. Int. J. Mass Spectrom. Ion Phys. **47**, 109 (1983).
15. P. J. Derrick and K. F. Donchi. Compr. Chem. Kinet. **24**, 53 (1983).
16. C. Lifshitz. Int. J. Mass Spectrom. Ion Phys. **43**, 179 (1982).
17. H. M. Rosenstock, K. Draxl, B. W. Steiner, and J. T. Herron. J. Phys. Chem. Ref. Data, **6**, suppl. 1 (1977).
18. J. B. Pedley and J. Rylance. Sussex-NPL computer analysed thermochemical data: organic and organometallic compounds. University of Sussex. 1977.
19. A. L. Castelhano and D. Griller. J. Am. Chem. Soc. **104**, 3655 (1982).
20. J. C. Traeger, R. G. McLoughlin, and A. J. C. Nicholson. J. Am. Chem. Soc. **104**, 5318 (1982).
21. J. C. Traeger. Org. Mass Spectrom. **20**, 223 (1985).
22. H. Bock, T. Hirabayashi, S. Mohmand, and B. Solouki. Angew. Chem. **89**, 106 (1977).

Appendix

Heats of formation employed (all numbers are 298 K values). $\Delta H_f(CH_3COCH_3^{+\bullet})$, $\Delta H_f(CH_3CH_2COCH_3^{+\bullet})$, $\Delta H_f((CH_3)_2CHCOCH_3^{+\bullet})$, and $\Delta H_f(CH_3CH_2COCH_2CH_3^{+\bullet})$ have been taken as 719, 676, 635, and 640 kJ mol^{-1}, respectively (17). $\Delta H_f(CH_4)$ and $\Delta H_f(C_2H_6)$ are taken to be -75 and -84 kJ mol^{-1}, respectively (18). $\Delta H_f(CH_3^{\bullet})$, $\Delta H_f(C_2H_5^{\bullet})$, and $\Delta H_f(C_3H_7^{\bullet})$ are taken to be 144, 117, and 80 kJ mol^{-1}, respectively (19). $\Delta H_f(CH_3CO^+)$ has been taken as 657 kJ mol^{-1} (20), and $\Delta H_f(CH_2CO^{+\bullet})$ has been placed at 870–880 kJ mol^{-1}, on the basis that the adiabatic IE is 9.61 eV (17) and $\Delta H_f(CH_2CO)$ is -48 kJ mol^{-1} (18). $\Delta H_f(CH_3CH_2CO^+)$ and $\Delta H_f((CH_3)_2CHCO^+)$ have been taken as 591 (21) and 554 kJ mol^{-1} (17). $\Delta H_f(CH_3CHCO^{+\bullet})$ has been estimated to be 775–785 kJ mol^{-1} on the basis that the adiabatic IE is 8.95 eV (22) and that $\Delta H_f(CH_3CHCO)$ is -86 kJ mol^{-1} (21). $\Delta H_f((CH_3)_2CCO^{+\bullet})$ has been estimated to be 700–710 kJ mol^{-1} on the basis that the adiabatic IE is 8.38 eV (22) and that $\Delta H_f((CH_3)_2CCO)$ is -105 kJ mol^{-1} (estimated).

Ion–ion–solvent interactions in aqueous ionic cosolvent systems. I. Transfer thermodynamics of hydrogen chloride in aqueous sodium nitrate solutions from emf measurements

SIBAPRASAD RUDRA, HIMANSU TALUKDAR, BIJOY P. CHAKRAVARTI, AND KIRON K. KUNDU[1]
Physical Chemistry Laboratories, Jadavpur University, Calcutta-700 032, India

Received May 29, 1985[2]

SIBAPRASAD RUDRA, HIMANSU TALUKDAR, BIJOY P. CHAKRAVARTI, and KIRON K. KUNDU. Can. J. Chem. **64**, 1960 (1986).

Standard potentials (E^0) of the Ag–AgCl electrode have been determined in 1, 2, and 4 *m* $NaNO_3$ + water mixtures at five equidistant temperatures ranging from 15–35°C from the emf measurements of the cell: Pt, H_2 (g, 1 atm)/HCl (*m*) $NaNO_3$ + water/AgCl–Ag. These values have been used to evaluate the transfer energetics (ΔG_t^0, $T\Delta S_t^0$, and ΔH_t^0) accompanying the transfer of 1 mole of HCl from the standard state in water to the standard state in each of the $NaNO_3$ + water mixtures. Transfer free energies ΔG_t^0 of HCl and that of the individual ions obtained from a separate study, and those obtained after correcting the "cavity effect" and Born-type electrostatic effect, as estimated tentatively by the scaled-particle theory (SPT) and simple Born equation respectively, have been discussed in the light of ion–ion–solvent interactions. The observed $T\Delta S_t^0$–composition profile as well as that obtained after correcting for the "cavity effect" were examined in the light of semiquantitative theory proposed by Kundu *et al.* earlier and are found to substantiate this theory.

SIBAPRASAD RUDRA, HIMANSU TALUKDAR, BIJOY P. CHAKRAVARTI et KIRON K. KUNDU. Can. J. Chem. **64**, 1960 (1986).

Opérant avec des mélanges 1, 2 et 4 m de $NaNO_3$ dans de l'eau et à cinq températures équidistantes allant de 15 à 35°C et en se basant sur des mesures de fem de la cellule |Pt, H_2(g, 1 atm)/HCl(*m*) $NaNO_3$ + eau/AgCl–Ag|, on a déterminé les potentiels standards (E^0) de l'électrode Ag–AgCl. On a utilisé ces valeurs pour évaluer les énergies de transfert (ΔG_t^0, $T\Delta S_t^0$ et ΔH_t^0 qui accompagnent le transfert de 1 mole de HCl de son état standard dans l'eau vers l'état standard de chacun des mélanges $NaNO_3$ + eau. A la lumière d'interactions ion–ion–solvant, on discute des énergies libres de transfert ΔG_t^0 du HCl ainsi que de celles des ions individuels qui ont été obtenues au cours d'une étude séparée de même que celles obtenues après avoir corrigé les valeurs pour l'«effet de cavité» et pour l'effet électrostatique du type de Born qui ont respectivement été évalués sur une base préliminaire en faisant appel d'une part à la théorie des particoles et d'autre part à une équation de Born simple. A la lumière de la théorie de Kundu et de ses associés qui a été proposée antérieurement, on a examiné les corrélations qui existent entre la composition et les valeurs de $T\Delta S_t^0$ ainsi que celles obtenues après avoir apporté des corrections pour l'«effet de cavité»; on a trouvé que les résultats sont en accord avec la théorie.

[Traduit par la revue]

Introduction

It is well recognized that thermodynamic quantities, especially transfer enthalpies and entropies of electrolytes and non-electrolytes, often provide useful information regarding the structuredness of solvents (1–12). There have been extensive studies (9–14) on the thermodynamics of hydrogen halides (HX), alkali halides (MX), and the related ion–solvent interactions, solvent structuredness, etc., in a host of aquo-organic solvent systems. However, apart from a few studies (15) by Bates and co-workers in synthetic sea water systems, parallel studies on aquo-ionic cosolvent systems are yet a fairly untrodden field, although a number of studies have been made from the point of mixed electrolyte properties (16, 17). In fact, it would be highly interesting and useful to treat aqueous electrolyte solutions of any molality as an individual solvent and the infinitely dilute solution of the solute in that solvent as the standard state, exactly similar to what is being done in aquo-organic solvent systems. It is hoped that the transfer free energies derived in this way will help show the ion–ion–solvent interactions from a new angle and the transfer entropies will help show solvent structuredness with extra confidence as hydrophilic ions are well known three dimensional (3D) structure breakers of water (18, 19), although ions with larger ionic force field induce overall structural order round them and hence are tacitly designated as "structure makers" (18, 19).

Moreover, simple aquo-ionic cosolvent systems are also likely to serve as precursors to suitable model systems of highly complex physiological fluids (20*a*) on the one hand and sea water (20*b*) on the other. So, comprehensive studies on different physico-chemical properties including transfer thermodynamics of HX, MX, and other selected electrolytes and non-electrolytes etc. in different aquo-ionic cosolvent systems should prove immensely useful, particularly in imparting far-reaching implications which will help us to understand the complex processes in bio-fluids or in sea water.

Therefore, as part of the systematic studies that have been taken up for the first time, we are now reporting transfer thermodynamics of HCl in the aquo-ionic solvent system comprising 1, 2, and 4 *m* $NaNO_3$. This has been determined from emf measurements of the cell [A]

[A] Pt, H_2 (g, 1 atm)/HCl (*m*), $NaNO_3$ + water/AgCl–Ag

at five equidistant temperatures ranging from 15–35°C.

The choice of NaCl instead of $NaNO_3$ as the ionic cosolvent would have been more useful from the point of physiological fluid/sea water. But the response of Ag–AgX (X = Cl, Br or I) electrodes to the small concentration of solute halide ions in presence of overwhelming concentration of solvent Cl^- is likely to be rather sluggish. Secondly, the behaviour of HCl or other chlorides even in the assumed standard state in each cosolvent mixtures is likely to be complicated by the common-ion type effects. On the other hand, structural characteristics of aqueous solutions of various nitrate salts including $NaNO_3$ are fairly well known (21, 22). Studies in nitrate solutions should thus help us to understand the behaviour of HCl and other solutes in this aquo-ionic cosolvent system. More importantly, systematic studies on the activity coefficients of HCl or other halides in this

[1]Author to whom all correspondence should be addressed.
[2]Revision received May 7, 1986.

type of aquo-ionic system but based on water as the standard state, are likely to initiate a new series of studies on Harned's rule (16) involving quarternary ionic mixtures.

Experimental

Sodium nitrate (A.R., B.D.H.) was used after drying at 150°C and then cooled in a vacuum desiccator. Water used was triply distilled. Solvents of various molalities were prepared by mixing the components by weight. Cell design, electrode and solution preparation and experimental procedures were similar to those described earlier (7, 23). Equilibrium at the lowest temperature was reached within 3–4 h of the commencement of hydrogen bubbling after which emf data at successively higher temperatures were recorded. The criterion of equilibrium in each case was ±0.2 mV per h. The equilibrium emf data at 25°C agreed within ±0.3 mV of the previous data when tested back at the end of the experiment.

Solvent densities (d_s) at different temperatures were measured with a pyknometer of 15 cm^3 capacity, having a 15 cm long neck made up of 1 mm bore capillary tubing and graduated into 1 mm divisions. The values thus obtained are listed in Table 1. The vapour pressure (p_s/mm Hg) of the different solvent mixtures at different temperatures were obtained with the help of the approximate relation [1] (24)

$$[1] \quad \log (p_s)_t = \log (p_w)_t - \frac{M_w}{1000}\frac{m\phi}{2.303}$$

where $(p_w)_t$ is the vapour pressure of pure water (25) at the temperature, M_w the molecular weight of pure water, and ϕ is the osmotic coefficient of $NaNO_3$ solution of molality m, the required values of ϕ being obtained from literature (26). The values so obtained are given in Table 1. The dielectric constant (ϵ_s) values of the solvents (27) are known only at 25°C as are given in Table 1. The values of mean molar mass (M_s) of the solvents are also given in Table 1.

Results

The emf (E) values of the cell (A) (corrected for pH_2 = 1 atm) for molality m of HCl are given elsewhere.[3] As in pure water and aquo-organic solvents these values are related to the standard potential of the cell on molal scale E^0_m by eq. [2]

$$[2] \quad E = E^0_m - 2k \log m - 2k \log (\gamma_\pm)_{HCl}$$

where $(\gamma_\pm)_{HCl}$ is the mean molal activity coefficient of HCl and $k = 2.303\,RT/F$. The E^0_m values at different temperatures in each solvent were determined by use of curve fitting technique of Sen *et al.* (28) with the polynomial [3]

$$[3] \quad E + 2k \log m = E^{0\prime}_m = E^0_m + 2k \log (\gamma_\pm)_{HCl} = E^0_m + Am^{1/2} + B(m^{1/2})^2 + C(m^{1/2})^3$$

using a FORTRAN program and a B 6700 computer. Notably, as in aquo-organic solvents, the standard state is so chosen that at infinitely dilute solution of HCl in each of the solvent compositions of the mean activity coefficient $(\gamma_\pm)_{HCl}$ is taken to be unity. The values of E^0_m (molal scale) and the coefficients A, B, and C as obtained are listed in Table 2. The average standard deviation of these values is ±0.3 mV.

The E^0_m values at different temperatures for each of the solvent mixtures were then fitted into E^0_m–temperature quadratic equation [4]

$$[4] \quad E^0_m = a + b(t - 25) + c(t - 25)^2$$

by the method of least squares, where t is the temperature in °C. The coefficients a, b, and c for different ($NaNO_3$ + water) solvents are given in Table 3. The coefficients of eq. [4] for water were obtained by using the data of Bates *et al.* (29) and are listed in Table 3.

Standard free energy (ΔG^0_t), entropy (ΔS^0_t), and enthalpy (ΔH^0_t) changes accompanying the transfer of 1 mole of HCl from the standard state in water (w) is that in each of the ionic cosolvent compositions (s), i.e. of the process HCl (w) → HCl (s) were computed on the mole fraction scale at 25°C by the usual relations [5]–[7]

$$[5] \quad \Delta G^0_t = -F[(E^0_m)^{25}_s - (E^0_m)^{25}_w] - 2RT \ln M_s/M_w$$

[3] A complete set of the data referred to above may be purchased from the depository of Unpublished Data, CISTI, National Research Council of Canada, Ottawa, Ont., Canada K1A 0S2.

TABLE 1. Some properties of $NaNO_3$ + water mixtures at different temperatures

T (°C)	d_s (kg dm^{-3})	p_s (mm Hg)	ϵ_s
	1 *m* $NaNO_3$ + water, M_s = 19.20		
15	1.0538	13.59	—
20	1.0515	17.27	—
25	1.0492	23.39	68.4
30	1.0472	31.34	—
35	1.0454	41.53	—
	2 *m* $NaNO_3$ + water, M_s = 20.35		
15	1.1037	12.41	—
20	1.1000	17.02	—
25	1.0968	23.05	60.2
30	1.0941	30.88	—
35	1.0931	40.93	—
	4 *m* $NaNO_3$ + water, M_s = 22.52		
15	1.1894	12.07	—
20	1.1853	16.66	—
25	1.1815	22.42	48.4
30	1.1786	30.04	—
35	1.1764	39.80	—

TABLE 2. E_m (volt) values of cell (A) and the coefficients of eq. [3] in $NaNO_3$ + water solvent system at different temperatures

T (°C)	E^0_m	$A \times 10^3$	$B \times 10^2$	$C \times 10^2$	$(\sigma(E^0_m)) \times 10^4$
			1 *m* $NaNO_3$ + water		
15	0.24013	−7.86	−1.34	1.959	0.5
20	0.23822	−34.90	10.97	−12.684	1.4
25	0.23657	−63.13	22.75	−26.821	1.2
30	0.23384	−72.56	26.34	−31.034	2.0
35	0.23158	−97.67	34.58	−48.055	2.0
			2 *m* $NaNO_3$ + water		
15	0.23076	−24.27	10.45	−14.647	0.3
20	0.22712	−18.11	8.03	−11.786	1.0
25	0.22253	−2.48	0.28	−0.261	0.7
30	0.22094	−29.78	0.89	−16.826	0.9
35	0.21782	−32.62	5.58	−0.440	0.9
			4 *m* $NaNO_3$ + water		
15	0.21191	−3.42	−0.08	−0.181	1.3
20	0.20806	−3.11	−0.61	0.721	1.0
25	0.20461	−6.32	−0.62	1.008	1.4
30	0.20074	−6.72	−1.29	1.860	1.3
35	0.19742	−15.70	−0.46	0.524	1.2

TABLE 3. Coefficients a, b, c of eq. [4] and transfer energetics (ΔG_t^0, ΔH_t^0, and $T\Delta S_t^0$) of HCl and ΔG_t^0 of H^+ and Cl^- from water to aqueous $NaNO_3$ solvents at 25°C (mole fraction scale)[a]

Mole kg^{-1} of $NaNO_3$	a/V	$b \times 10^4$/V $^0C^{-1}$	$c \times 10^6$/V $^0C^{-2}$	ΔG_t^0/kJ mol^{-1} HCl	ΔG_t^0/kJ mol^{-1} H^+ (32)	ΔG_t^0/kJ mol^{-1} Cl^- (32)	$T\Delta S_t^0$/kJ mol^{-1}	ΔH_t^0/kJ mol^{-1}
0.0	0.22246	−6.418	−3.400	—	—	—	—	—
1.0	0.23622	−4.356	−4.229	−1.68	0.6	−2.2	6.27	4.59
2.0	0.22324	−6.492	+12.685	−0.61	1.7	−2.3	0.39	−0.22
4.0	0.20445	−7.260	+1.829	0.62	2.6	−2.0	−1.32	−0.70

[a]The coefficients a, b, and c of eq. [4] for water have been calculated with the help of E_m^0 values at different temperatures taken from ref. 29.

[6] $$\Delta S_t^0 = F(b_s - b_w) + 2F(t - 25)(c_s - c_w) + 2R \ln M_s/M_w$$

[7] $$\Delta H_t^0 = \Delta G_t^0 + T\Delta S_t^0$$

and are listed in Table 3. The estimated uncertainties (30) in ΔG_t^0 and ΔS_t^0 values are ±0.03 kJ mol^{-1} and ± 2 J K^{-1} mol^{-1}, respectively.

Discussion

From Fig. 1 it can be seen that ΔG_t^0–composition profile of HCl exhibits a slight roller-coaster type behaviour. This is possibly due to the involved opposite effects of the constituent ions. That this is partly true is evident from the ΔG_t^0–composition profiles for H^+ and Cl^- (Fig. 1), as obtained by use of the modified form of the widely-used tetraphenylarsonium tetraphenylborate reference electrolyte assumption (31) described in another paper (32).

As these profiles show, while $\Delta G_t^0(H^+)$ values are more or less increasingly positive with a slight hump around 1 m $NaNO_3$, $\Delta G_t^0(Cl^-)$ values decrease sharply till 1 m $NaNO_3$ and then remain almost invariant up to 4 m. Apparently, while H^+ is increasingly destabilized, Cl^- remains stabilized in these solvents compared to that in water. The breaks in destabilization of H^+ or stabilization of Cl^- around 1 m $NaNO_3$ are seemingly the result of change in solvating capacities of the aqueous $NaNO_3$ solutions and the superimposed destabilizing Born-type electrostatic effect on both the ions, because of the difference between the bulk dielectric constants of the solvents concerned.

Notably, as per our assumed standard state, at infinite dilution of HCl in each of the compositions of the ionic cosolvent system $(\gamma_\pm)_{HCl} = 1$. This implies that just as in the aquo-organic cosolvents, the interactions between water and oragnic cosolvents do not influence the ideal behaviour of HCl, so do the interactions of the ionic constituents of the ionic cosolvent among themselves or with water molecules in the respective solvent compositions. Consequently, $\Delta G_t^0(i)$ values accompanying the transfer of either of the ions from the standard state in the reference solvent, water to the corresponding state in any of the cosolvent compositions are likely to be governed by the net effects of attractive ion–ion interactions between the oppositely charged ions of the solute and ionic cosolvent species, viz. H_3O^+ and NO_3^- and Cl^- and Na^+ and the repulsive interactions between the similarly charged ions viz. H_3O^+ and Na^+ and Cl^- and NO_3^-, relative to those in water.

As expected (18–22), due to their small size and large ionic force field, Na^+ ions are to some extent hydrated. But being relatively large in size and having the formal charge delocalized on three O-atoms, NO_3^- ions are comparatively less hydrated (18–22) or even unhydrated as the negative value of the viscosity B-coefficient and the positive value of dB/dT data (18*b*) suggest. The observed increased stabilization of Cl^- therefore suggests that the resulting attractive interaction of Cl^- and $(Na^+)_{aq}$ over the repulsive interaction of Cl^- and NO_3^- exceeds the Cl^-–H_2O interaction in pure water. This is probably due to the fact that H_2O molecules in the hydration cosphere round Na^+ have more protonic character (δ^+) than that in pure water and hence are likely to induce more "acid–base" type (33) short-range attractive interaction with Cl^- than that in pure water. The observed increased destabilization of H^+, on the other hand, suggests that the attractive interaction of H_3O^+ (rather than the bare proton) with delocalized (δ^+) charge on three H atoms, and the NO_3^- with delocalized (δ^-) charge on three O atoms is overcome by the possible larger repulsive interaction between H_3O^+ and $(Na^+)_{aq}$. This is because the repulsive effect of more protonic character of the H_2O molecules in the hydration cosphere of Na_{aq}^+ might exceed the attractive interaction of H_3O^+ with NO_3^-. Besides, the repulsive interaction is also likely to be augmented by the larger stability of H_3O^+ in pure water because of its intrinsic structural propensity towards pure water.

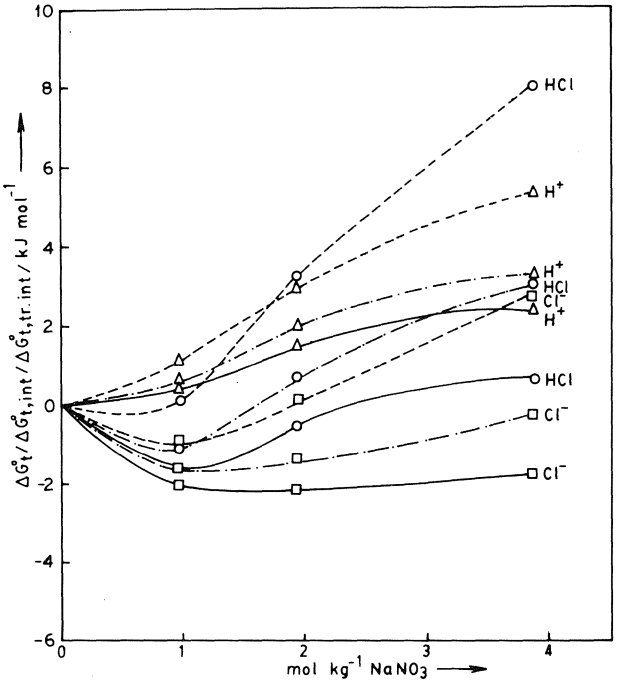

FIG. 1. Variation of ΔG_t^0(—), $\Delta G_{t,int}^0$(---), and $\Delta G_{t,tr.int}^0$ (-·-·-) of HCl (○), H^+ (△), and Cl^- (□) with molality of $NaNO_3$ in aqueous $NaNO_3$ solution.

The observed humps/breaks in ΔG_t^0–composition profiles of H^+ and Cl^- around 1 *m* $NaNO_3$ are possibly associated with the change in solvating species of this ionic solvent system. This is because, as various spectroscopic evidences referred to earlier (21, 22) indicate, around 0–1.5 *m* $NaNO_3$ solution constituent ions mostly exist as Na_{aq}^+ and $(NO_3^-)_{aq}$. But around 1.5 to 6 *m* $NaNO_3$ these ions are increasingly replaced by solvent-separated ion-pairs like $^-O_3N(H_2O)_nNa^+$. Evidently, alteration in the solvating characteristics due to the change in the solvating species is likely to induce some breaks in the relative solvation of the cations and anions, as observed.

Entropies of transfer

Since $T\Delta S_t^0$(HCl) rather than H_t^0(HCl) should be more informative regarding the structuredness of the solvents (2), let us discuss the observed $T\Delta S_t^0$(HCl)–composition profile at 25°C as illustrated in Fig. 2, where ΔH_t^0– and ΔG_t^0–composition profiles are also illustrated for the sake of comparison. Strikingly enough, unlike ΔG_t^0, both $T\Delta S_t^0$– and ΔH_t^0–composition profiles exhibit maxima around 1 *m* $NaNO_3$. This is of course contrary to the smooth downward trends observed in the cases of non-electrolytes like benzoic acid (HBz) in aqueous LiCl and KBr (7*d*) or *p*-nitroaniline (pNA) in aqueous KBr (7*e*) and as expected from the 3D structure breaking propensity of $NaNO_3$ (16, 18*b*) if water would have been the sole solvating species. Evidently, complex structural contributions are involved in the transfer of HCl, unlike that of HBz or pNA where the solvating species are water molecules alone. Thus careful analysis of ΔS_t^0(HCl) is in order.

Following Kundu *et al.*'s (7*a*, 34) four-step transfer process, if we assume that $\Delta S_{t,\text{non-Born}}^0$(HCl) involves (*1*) break down of hydration sphere round H^+ and Cl^- in water with an increase in entropy, ΔS_1^0; (*2*) formation of characteristic 3D structure of water with a decrease to entropy, $-\Delta S_2^0$; (*3*) break down of relevant structure of $NaNO_3$ + water solution or relevant solvation shell round Na^+ or NO_3^- to solvate the transferred ions with an increase in entropy, $+\Delta S_3^0$; and (*4*) formation of solvation spheres round the incoming ions in $NaNO_3$ solutions of the cosolvent and their interactions with oppositely charged ionic constituents with a decrease in entropy, $-\Delta S_4^0$, then

$$[8]\quad \Delta S_{t,\text{non-Born}}(\text{HCl}) = \sum_{i=1}^{i=4} \Delta S_i^0 = \Delta S_1^0 - \Delta S_2^0 + \Delta S_3^0 - \Delta S_4^0$$

Since steps (*1*) and (*2*) refer to water, $(\Delta S_1^0 - \Delta S_2^0)$ should be a constant positive quantity. So, the overall positive or negative magnitudes of $(\Delta S_3^0 - \Delta S_4^0)$ will dictate $\Delta S_{t,\text{non-Born}}^0$(HCl) which again will depend on the relative affinity of H^+ and Cl^- ions towards the solvating components of aqueous $NaNO_3$ solutions, besides the relative structuredness of aqueous $NaNO_3$ solutions.

As indicated earlier, in the lower concentrations of $NaNO_3$ (up to about 1.5 *m*) the prevalent ionic species are free Na^+_{aq} and $(NO^-{}_3)_{aq}$. ΔS_3^0 is likely to be a large positive quantity and consequently the amalgamated effects of $\Delta S_{t,\text{Born}}^0$(HCl) and $(\Delta S_1^0 - \Delta S_2^0 + \Delta S_3^0)$ are likely to be greater than $-\Delta S_4^0$, thus imparting an increasingly positive trend of ΔS_t^0(HCl), as observed. But after 1.5 *m* the prevalent ionic species in $NaNO_3$ solution are solvent-separated ion-pairs such as $^-O_3N(H_2O)_nNa^+$ (21, 22), ΔS_3^0 might be less positive as H^+ and Cl^- are likely to be solvated respectively through NO_3^- and Na^+ of the solvent-separated ion-pairs. Thus $(\Delta S_3^0 - \Delta S_4^0)$ becomes increasingly negative and possibly overcomes the effect of positive magnitudes of $(\Delta S_1^0 - \Delta S_2^0)$, thus resulting in a sharp fall in $T\Delta S_t^0$ after exhibiting a maximum around 1 *m* $NaNO_3$. The observed upward trend beyond 3 *m* $NaNO_3$, however, is possibly attributable to the amalgamated effects of superimposed "cavity effect" (7*d*, 7*e*, 35) and Born-type electrostatic interactions, both of which should be increasingly larger in magnitudes at higher compositions.

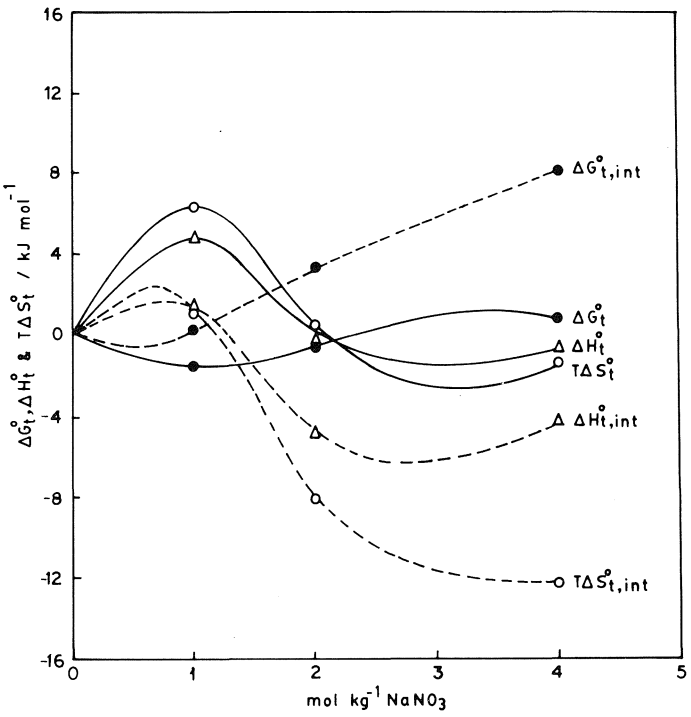

FIG. 2. Variation of ΔG_t^0 (○), ΔH_t^0 (△), and $T\Delta S_t^0$ (○) (all solid lines) and $\Delta G_{t,\text{int}}^0$ (○), $\Delta H_{t,\text{int}}^0$ (△), and $T\Delta S_{t,\text{int}}^0$ (○) (all broken lines) of HCl with molality of $NaNO_3$ in aqueous $NaNO_3$ solutions.

Although computation of Born-type electrostatic contribution for ΔS_t^0 is not feasible at this stage as dielectric constants at different temperatures are not known for this solvent system, that for "cavity effect" is feasible and should be rewarding.

This is because, as indicated by various authors (35–40), ΔP_t^0 (P = G, S, or H) is composed of two parts, where one part ΔP_t^0(cav) is associated with the creation of a cavity of suitable size to accommodate the solute and the other part ΔP_t^0(int) is associated with the interaction of the solvent molecules surrounding the cavity among themselves as well as the solute, both relative to that in water, i.e.

$$[9]\quad \Delta P_t^0 = \Delta P_t^0(\text{cav}) + \Delta P_t^0(\text{int})$$

The scaled particle theory (SPT) (37), though originally used to compute the "cavity effect" of some thermodynamic quantities for some non-ionic apolar solutes in water, is also increasingly used (7*d*, 7*e*, 35–40) for solutes, (apolar (37, 38) and polar (7*d*, 7*e*), and large (13*e*–*h*, 35, 39, 40) and small (13*e*–*h*, 36) ions. It is used not only in water, organic solvents and their aqueous mixtures, but also in aqueous ionic solutions (40). Thus following a procedure exactly similar to that in the cases of HBz and pNA (7*d*,*e*) in various ionic and non-ionic cosolvent systems, we have computed the molar free energy, enthalpy, and entropy of cavity formation for H_3O^+ and Cl^- with the help of SPT relations. The values of ΔG_t^0(cav), $T\Delta S_t^0$(cav), and ΔH_t^0(cav) obtained at T = 298.15 K on mole

TABLE 4. Values of free energy ($\bar{G}_c$) and enthalpy ($\bar{H}_c$) of cavity formation of H^+ and Cl^- and ΔG_t^0(cav) of ΔH_t^0(cav) and $T\Delta S_t^0$(cav) of HCl and the required solvent parameter α and $\Delta G_{t,Born}^0$(i) of H^+ and Cl^- in different $NaNO_3$ + water mixtures at 25°C

Mol kg^{-1} of $NaNO_3$	$10^6\,\alpha/K^{-1}$	$\bar{G}_c$/ kJ mol^{-1} [a]		$\bar{H}_c$/ kJ mol^{-1} [a]		ΔG_t^0(cav)/ kJ mol^{-1} [b]		ΔH_t^0(cav)/kJ mol^{-1}	$T\Delta S_t^0$(cav)/kJ mol^{-1}	$\Delta G_{t,Born}^0$(i)/ kJ mol^{-1} [c]	
		H^+	Cl^-	H^+	Cl^-	H^+	Cl^-	HCl	HCl	H^+	Cl^-
0.0	223 [7d]	13.5	20.7	1.8	2.8	—	—	—	—	—	—
1.0	410	12.8	19.6	3.1	4.8	−0.7	−1.1	3.3	5.1	0.5	0.7
2.0	535	12.1	18.4	3.6	5.7	−1.5	−2.3	4.8	8.6	1.0	1.5
4.0	556	10.7	16.3	2.2	5.0	−2.9	−4.5	3.6	11.0	2.0	3.0

[a]The required diameters of "a" of H_2O, Na^+ and NO_3^- of the solvent constituents are taken to be 0.276 (39), 0.192 (25), and 0.248 (42) nm, respectively, and those of the solute H^+ and Cl^- to be 0.276 (41) and 0.362 (25) nm, respectively. Also vide ref. 7d,e, where $\bar{G}_c$ and $\bar{H}_c$ are denoted as $\bar{G}$(cav) and $\bar{H}$(cav), respectively, and $\alpha = -\mathrm{d} \ln d_s/\mathrm{d}T$.

[b]The required values of the scale effect, i.e., $RT \ln V_w/V_s$ are obtained from density data of the solvents given in Table 1.

[c]The required radii of H^+ and Cl^- are taken as 0.276 and 0.181 nm (41) and the dielectric constant ϵ_s from Table 1.

fraction scale are given in Table 4. The transfer energies ΔG_t^0(int)–, $T\Delta S_t^0$(int)–, and ΔH_t^0(int)–composition profiles of HCl are illustrated in Fig. 2 and the ΔG_t^0(int)–composition profiles for H^+ and Cl^- obtained from another paper (32) in Fig. 1.

Thus it can be seen from Fig. 1 that ΔG_t^0(int)–composition profiles of both H^+ and Cl^- are shifted increasingly upward from the corresponding profiles of ΔG_t^0, which imply that both the ions are relatively more stabilized due to "cavity" effect. Again, if we tentatively compute the Born-type electrostatic effect $\Delta G_{t,Born}^0$ resulting essentially from the difference of dielectric constants of the solvents concerned, using the simple Born equation (41), and subtract from the respective ΔG_t^0(int) values of H^+ and Cl^-, we find that the resulting $\Delta G_{t,tr.int}^0$(i) ($= \Delta G_{t,int}^0$(i) $- \Delta G_{t,Born}^0$(i)) composition profiles are again shifted downward (Fig. 1). This leads us to conclude that in the case of small ions like H^+ and Cl^-, although ΔG_t^0(cav) plays an important role, the opposing Born-type electrostatic interaction nullifies the cavity effect to a large extent, at least where the dielectric constant of the solvents decreases with compositions and that the cavity effect for non-electrolytes in particular, plays a significant role in dictating the observed ΔG_t^0 values.

Again from Fig. 2, it can be observed that $T\Delta S_t^0$(int)–composition profile though still retains the "characteristic maxima" at the lower composition region, after about 1 m $NaNO_3$ the profile takes a more downward trend than the corresponding $T\Delta S_t^0$–composition profile. This indicates that the "cavity effect" plays a fairly important role in dictating the overall transfer entropic behaviour of HCl in this ionic solvent system and possibly in aquo-organic solvent systems as well. The observed downward trend of the profile at higher compositions is consistent with increased order around H^+ and Cl^- with interacting oppositely charged ionic constituents of the ionic cosolvent as well as the expected 3D-structure breaking of water due to packing imbalance. But whether small additions of $NaNO_3$ would break down 3D structure of water will be evident if the Born-type electrostatic effect, $T\Delta S_{t,Born}^0$(HCl) (41) is increasingly positive in this solvent system. Admittedly, since the temperature coefficient of the dielectric constant (ϵ_s) is not known for this salt solution, it is not feasible to compute Born-type electrostatic contributions, $\Delta S_{t,Born}^0$ and hence to predict the real nature of $T\Delta S_{t,tr.int}^0$ ($= T\Delta S_{t.int}^0 - T\Delta S_{t,Born}^0$)–composition profile. However, as per tenets of the four-step transfer process proposed earlier (7*a*) for aquo-organic solvents, the relative order of the corresponding profiles for HX (X = Cl, Br, and I) at least, is likely to reflect the 3D structure breaking/making propensity of $NaNO_3$.

Thus, just as $\Delta S_{t,int}^0$ rather than ΔS_t^0 for a non-electrolyte like HBz (7*d*) or pNA (7*e*) conformed to the dictation of Kundu *et al.*'s theory for solvent structuredness, $\Delta S_{t,tr.int}^0$ rather than $\Delta S_{t,int}^0$ or ΔS_t^0 of ionic solutes, as the present results suggest, should really stand for the overall entropy changes involved in Kundu *et al.*'s four-step transfer process. It is therefore concluded that the "cavity effect" significantly contributes to the observed ΔS_t^0 and the rest ΔS_t^0(int) in the case of non-electrolytes and $\Delta S_{t,tr.int}^0$ in the case of electrolytes, being appertained more to the theory, should give a better reflection of the solvent structural features relative to that in water. Admittedly of course, the magnitudes of both cavity effect and Born-type electrostatic interaction are somewhat tentative because of various limitations and uncertainties. Yet the conclusions based on the relative trends of the different propensities are likely to be meaningful.

Acknowledgement

We wish to thank the University Grants Commission, New Delhi, for financial assistance.

1. F. FRANKS and D. J. G. IVES. Q. Rev. Chem. Soc. **1**, 20 (1966).
2. E. M. ARNETT, C. C. BENTRUDE, J. J. BURKE, and MC. DUGGLEBY. J. Am. Chem. Soc. **87**, 1541 (1965); E. M. ARNETT. *In* Physico-chemical processes in mixed aqueous solvents. *Edited by* F. Franks. Heinemann, London. 1967. p. 105.
3. A. BEN NAIM. J. Phys. Chem. **71**, 4002 (1967); *In* Water and aqueous solutions. *Edited by* R. A. Horne. Wiley Interscience, New York. 1972. p. 425.
4. (*a*) F. FRANKS. *In* Physico-chemical processes in mixed aqueous solvents. *Edited by* F. Franks. Heinemann, London. 1967; (*b*) F. FRANKS and D. S. REID. *In* Water: a comprehensive treatise. Vol. 2. *Edited by* F. Franks. Plenum Press, London. 1974. Chapt. 5.
5. S. RAJENDER and R. LUMRY. Biopolymers, **9**, 1125 (1970).
6. (*a*) W. J. M. HEUVELSLAND, M. BLOEMSDAL, C. DE VISSER, and G. SOMSEN. J. Phys. Chem. **84**, 2391 (1980); (*b*) M. BOOJE and G. SOMSEN. J. Chem. Soc. Faraday Trans. I, **78**, 285 (1982); (*c*) A. C. REUW and G. SOMSEN. J. Chem. Thermodyn. **13**, 67 (1981); (*d*) A. C. REUW and G. SOMSEN. J. Soln. Chem. **10**, 533 (1981); (*e*) C. DE VISSER and G. SOMSEN. Adv. Chem. Ser No. 155 (ACS 1976), p. 289.
7. (*a*) K. BOSE, K. DAS, A. K. DAS, and K. K. KUNDU. J. Chem. Soc. Faraday Trans. I, **74**, 1051 (1978); (*b*) A. K. DAS and K. K. KUNDU. J. Phys. Chem. **79**, 2604 (1975); (*c*) J. DATTA and K. K.

KUNDU. Can. J. Chem. **59**, 3141 (1981); (*d*) J. DATTA and K. K. KUNDU. J. Phys. Chem. **86**, 4055 (1982); (*e*) J. DATTA and K. K. KUNDU. Can. J. Chem. **61**, 625 (1983) and relevant references in all these papers.

8. (*a*) J. JUILLARD. J. Chem. Soc. Faraday Trans. I, **78**, 37 (1982); **78**, 43 (1982); (*b*) Y. POINTUD, J. P. MOREL, and J. JUILLARD. J. Phys. Chem. **80**, 2081 (1976); (*c*) Y. POINTUD and J. JUILLARD. J. Chem. Soc. Faraday Trans. I, **73**, 1907 (1977) and relevant references therein.
9. (*a*) D. FEAKINS and B. E. HICKLEY, J. P. LORIMAR, and P. J. VOICE. J. Chem. Soc. Faraday Trans. I, **71**, 780 (1975); (*b*) D. FEAKINS and C. T. ALLAN. J. Chem. Soc. Faraday Trans. I, **72**, 314 (1976) and relevant references therein.
10. (*a*) C. H. ROCHESTER and D. N. WILSON. J. Chem. Soc. Faraday Trans. I, **73**, 539 (1977); (*b*) C. H. ROCHESTER and S. A. SCLOSA. J. Chem. Soc. Faraday Trans. I, **77**, 575 (1982) and relevant references therein.
11. B. G. COX and W. H. WAGHORNE. Chem. Soc. Rev. **9**, 381 (1980) and relevant references therein.
12. Y. MARCUS. Rev. Anal. Chem. 53 (1980).
13. (*a*) A. K. DAS and K. K. KUNDU. Ind. J. Chem. **16A**, 467 (1978); (*b*) A. K. DAS and K. K. KUNDU. J. Soln. Chem. **8**, 259 (1979); (*c*) I. N. BASU-MULLICK and K. K. KUNDU. Can. J. Chem. **58**, 79 (1980); (*d*) K. DAS, A. DAS, and K. K. KUNDU. Electrochim. Acta, **26**, 471 (1981); (*e*) K. DAS, K. BOSE, and K. K. KUNDU. Electrochim. Acta, **26**, 479 (1981); (*f*) A. BHATTACHARYA, A. K. DAS, and K. K. KUNDU. Ind. J. Chem. **20A**, 347, 353 (1981); (*g*) A. BHATTACHARYA, J. DATTA, K. DAS, and K. K. KUNDU. Ind. J. Chem. **21A**, 9 (1982); (*j*) U. MANDAL, S. BHATTACHARYA, and K. K. KUNDU. Ind. J. Chem. **24A**, 191 (1985).
14. R. SMITS, D. L. MASSART, J. J. JUILLARD, and J. P. MOREL. Electrochim. Acta, (*a*) **21**, 425 (1976); (*b*) **21**, 431 (1976).
15. K. H. KHOO, R. W. RAMATTE, C. B. CULBERSON, and R. G. BATES. Anal. Chem. **49**, 29 (1977); R. W. RAMATTE, C. B. CULBERSON, and R. G. BATES. Anal. Chem. **49**, 867 (1977).
16. H. S. HARNED and B. B. OWEN. Physical chemistry of electrolytic solutions. Reinhold, New York. 1958.
17. K. S. PITZER. *In* Activity coefficients in electrolyte solutions. Vol. 1. *Edited by* R. M. Pytkowicz. C. R. C. Press, Florida. 1979. Chapt. 7 and relevant references therein.
18. (*a*) H. S. FRANK and W. Y. WEN. Discuss. Faraday Soc. **24**, 133 (1957); (*b*) M. KAMINSKI. Discuss. Faraday Soc. **24**, 171 (1957).
19. J. E. DESNOYERS and C. JOLICOEUR. *In* Modern aspects of electrochemistry. *Edited by* J. O'm Bockris and B. E. Conway. Vol. 5. Plenum Press, New York. 1969. p. 1.
20. (*a*) D. A. J. DICK. *In* Water and aqueous solutions. *Edited by* R. A. Horne. Wiley Interscience, New York. 1972. p. 265; (*b*) P. K. PARK. *In* Water and aqueous solutions. *Edited by* Wiley Interscience, New York. 1972. p. 245.
21. D. E. IRISH and A. R. DAVIS. Can. J. Chem. **46**, 943 (1968).
22. R. L. FROST and D. W. JAMES. (*a*) J. Chem. Soc. Faraday Trans. I, **78**, 3223 (1982); **78**, 3235 (1982); **78**, 3263 (1982); (*b*) Aust. J. Chem. **35**, 1793 (1982).
23. K. K. KUNDU, P. K. CHATTOPADHYAY, D. JANA, and M. N. DAS. (*a*) J. Chem. Eng. Data, **15**, 209 (1970); (*b*) J. Phys. Chem. **74**, 2635 (1971).
24. S. GLASSTONE. Thermodynamics for chemists. 1971 Van Nostrand, London. 1978. p. 390.
25. R. C. WEAST. Handbook of chemistry and physics. 52nd ed. The Chemical Rubber Co., Cleveland. 1971–1972.
26. R. A. ROBINSON and R. H. STOKES. Electrolyte solutions. Butterworths, London. 1959.
27. Y. Y. AKHADOV. Dielectric properties of binary solutions. Pergamon Press, 1980.
28. B. SEN, D. A. JOHNSON, and R. N. ROY. J. Phys. Chem. **71**, 1523 (1967).
29. R. G. BATES and V. E. BOWER. J. Res. Natl. Bur. Stand. **53**, 283 (1964).
30. N. W. PLEASE. Biochem. J. 196 (1954).
31. B. G. COX, R. R. HEDWIG, A. J. PARKER, and D. W. WATTS. Aust. J. Chem. **27**, 477 (1974) and relevant references therein.
32. S. RUDRA, H. TALUKDAR, and K. K. KUNDU. Can. J. Chem. To be published.
33. D. FEAKINS. *In* Physico-chemical processes in mixed aqueous solvents. *Edited by* F. Franks. Heinemann, London. 1967.
34. K. K. KUNDU and K. MAZUMDAR. J. Chem. Soc. Faraday Trans. I, **69**, 806 (1973).
35. M. H. ABRAHAM and A. NASEHZADEH. Can. J. Chem. **57**, 2004 (1979).
36. U. SEN. J. Am. Chem. Soc. **101**, 2531 (1979); **102**, 2181 (1980); J. Chem. Soc. Faraday Trans. I, **77**, 2883 (1981).
37. R. A. PIEROTTI. J. Phys. Chem. **67**, 1840 (1963); **69**, 281 (1965); Chem. Rev. **76**, 717 (1976).
38. M. LUCAS. J. Phys. Chem. **80**, 3592 (1976) and relevant references therein.
39. (*a*) C. TREINER, P. TZIAS, and M. CHEMLA. J. Chem. Soc. Faraday Trans. I, **72**, 2007 (1976); (*b*) C. TREINER. Can. J. Chem., **55**, 682 (1977).
40. N. DESROSIERS and J. E. DESNOYERS. Can. J. Chem. **54**, 3800 (1976).
41. U. SEN, K. K. KUNDU, and M. N. DAS. J. Phys. Chem. **71**, 3665 (1967).
42. (*a*) J. V. LEYENDEKKERS. J. Chem. Soc. Faraday Trans. I, **78**, 357 (1982); (*b*) H. L. FRIEDMAN and O. V. KRIESHNAN. *In* Water: a comprehensive treatise. Vol. 3. *Edited by* F. Franks. Plenum Press, New York. 1973.

Excess thermodynamic properties of *n*-pentane + dichloromethane system at 298.15 K[1]

MIGUEL A. POSTIGO, JOSÉ L. ZURITA, MARÍA L. G. DE SORIA, AND MIGUEL KATZ[2]

Cátedra de Fisicoquímica, Instituto de Ingeniería Química e Instituto de Física, Facultad de Ciencias Exactas y Tecnología, U.N. de Tucumán, Avda. Independencia 1800, S. M. de Tucumán(4000), R. Argentina

Received November 22, 1985[3]

MIGUEL A. POSTIGO, JOSÉ L. ZURITA, MARÍA L. G. DE SORIA, and MIGUEL KATZ. Can. J. Chem. **64**, 1966 (1986).

Densities, refractive indices, viscosities, enthalpies, vapor–liquid equilibria, and surface tensions were determined for the *n*-pentane + dichloromethane system at 298.15 K. From the experimental results, excess molar volumes, excess viscosities, excess molar enthalpies, excess molar Gibbs free energies, and excess surface tensions were calculated. From these data, qualitative information could be obtained about the interaction between both chemical species.

MIGUEL A. POSTIGO, JOSÉ L. ZURITA, MARÍA L. G. DE SORIA et MIGUEL KATZ. Can. J. Chem. **64**, 1966 (1986).

Opérant à 298,15 K, on a déterminé les densités, les indices de réfraction, les viscosités, les enthalpies, les équilibres vapeur/liquide et les tensions superficielles du système *n*-pentane + dichlorométhane. A l'aide des données expérimentales, on a calculé les volumes molaires en excès, les viscosités en excès, les enthalpies molaires en excès, les ènergies libres molaires de Gibbs en excès et les tensions superficielles en excès. Sur la base de ces données, on en a déduit des informations qualitatives relativement aux interactions entre les deux espèces chimiques.

[Traduit par la revue]

Introduction

Excess properties such as v^E (excess molar volume); η^E (excess viscosity); h^E (excess molar enthalpy); g^E (excess molar Gibbs free energy), and σ^E (excess surface tension) have been studied to obtain information about the interaction between the molecules of the system *n*-pentane (1) + dichloromethane (2) at 298.15 K.

This work is a continuation of our research on the thermodynamic properties of binary liquid mixtures of non-electrolytes (1–3).

Densities, refractive indices, viscosities, enthalpies, vapor–liquid equilibria, and surface tensions at different mole fractions for this system were measured. In this system component (1) is non-polar and component (2) is highly polar without association in the pure state.

Experimental

The methods used in our laboratory have been described previously (1–3). Densities were determined with a Robertson specific gravity bottle. The total pycnometer volume was about 20 mL; calibration was done with doubly distilled water with an error of ± 0.1 kg m^{-3}. All weighings were made on a H315 Mettler balance. A thermostatically controlled bath (constant to ± 0.01°C) was used. Temperatures were read from calibrated thermometers. Refractive indices for the sodium D line of the pure components and of the mixtures were determined with a Jena dipping refractometer with an estimated error of ± 0.00002.

Viscosities of the pure liquids and of the mixtures were determined with a Cannon-Fenske viscosimeter calibrated with doubly distilled water and benzene. Kinetic energy corrections were applied to viscosity data. The estimated error was ± 0.005 mPa s. During measurements, both the pycnometer and the viscosimeter were maintained in the bath until at least two consecutive values of the liquid height in the capillaries of the flow time, indicated that the sample had reached the temperature of the bath.

The adiabatic calorimeter described by Loiseleur *et al.* (4) was used with some modifications to determine the change of enthalpy. The estimated error was ± 5 J mol^{-1}.

Vapor–liquid equilibria data were determined by using a modified version of the equilibrium still described by Boublik and Benson (5), with an estimate error of ± 0.05 kPa in pressures. Pressures were determined from boiling points of water in a ebulloscope adapted to the equipment. Temperatures were read with a Digitec thermometer to 0.01°C. Compositions of liquid phases and condensed vapor phases were determined by measuring refractive indices. Finally, surface tensions of the pure liquids and their binary mixtures were determined by the maximum bubble pressure method (6). The bubbler was calibrated with benzene (Baker puriss.) assuming a surface tension of 28.10×10^{-3} N m^{-1} for that material at 298.15 K. Values of the surface tension were generally reproducible to $\pm 0.05 \times 10^{-3}$ N m^{-1}.

Materials and solutions

n-Pentane Carlo Erba (puriss.) was distilled over phosphorous pentoxide and the middle fraction was collected and dichloromethane Merck (puriss.) was fractionally distilled over anhydrous calcium chloride and the middle colorless fraction was collected. Mixtures were prepared by mixing weighed amounts of the pure liquids. Caution was taken to prevent evaporation.

Results

The experimental results for the pure liquids are reported in Table 1 together with the values from the literature for comparison.

The excess thermodynamic functions were calculated with the following equations:

$$[1] \quad v^E = v - (x_1 v_1 + x_2 v_2)$$

$$[2] \quad \eta^E = \eta - \exp(x_1 \ln \eta_1 + x_2 \ln \eta_2)$$

$$[3] \quad h^E = h - (x_1 h_1 + x_2 h_2)$$

$$[4] \quad g^E = RT(x_1 \ln \gamma_1 + x_2 \ln \gamma_2)$$

$$[5] \quad \sigma^E = \sigma - (x_1 \sigma_1 + x_2 \sigma_2)$$

where v, v_1, and v_2 are the molar volume of the system and of the pure components; η, η_1, and η_2 are the viscosity of the mixtures and of the pure components; h, h_1, and h_2 are the molar enthalpy of the mixtures and of the pure components; γ_1 and γ_2 are the activity coefficients of the components in the liquid phase, and σ, σ_1, and σ_2 are the surface tension of the mixtures and of the pure components.

The molar volume of the mixtures is defined by:

$$[6] \quad v = (x_1 M_1 + x_2 M_2)/\rho$$

where M_1 and M_2 are the molar weights of the components and ρ the density of the solution.

[1]Presented at the IV Congreso Argentino de Fisicoquímica, Río Cuarto, Córdoba, 1985.

[2]Author to whom correspondence should be addressed.

[3]Revision received June 4, 1986.

TABLE 1. Properties characterizing the pure components at 298.15 K

Property	*n*-Pentane		Dichloromethane	
	Exp.	Lit.	Exp.	Lit.
Density: $\rho \times 10^{-3}$ (kg m^{-3})	0.6219	0.62139[a]	1.3152	1.31618[a]
Refractive index: n_D	1.35466	1.35472[a]	1.42119	1.4211[b]
Viscosity: η (mPa s)	0.218	0.2152[a]	0.419	0.4137[a]
Vapor pressure: p (kPa)	512.0	512.9[c]	57.80	57.36[d]
Surface tension: $\sigma \times 10^3$ (N m^{-1})	15.51	15.54[a](int)	27.36	27.33[a](int)

[a]Reference 10.
[b]Reference 11.
[c]Reference 12.
[d]Reference 13.

TABLE 2. Experimental values of densities, refractive indices, viscosities, enthalpies, and surface tensions for *n*-pentane (1) + dichloromethane (2) system at 298.15 K

x_1	$\rho \times 10^{-3}$ (kg m^{-3})	n_D	η (mPa s)	x_1	h^E (J mol^{-1})	x_1	$\sigma^E \times 10^3$ (N m^{-1})
0.1023	1.1955	1.40861	0.379	0.0521	424	0.0428	26.26
0.1992	1.0977	1.39862	0.345	0.1027	701	0.1162	24.83
0.3043	1.0060	1.38954	0.314	0.1986	1026	0.1934	23.86
0.4032	0.9308	1.38204	0.290	0.2672	1251	0.2875	22.81
0.5097	0.8597	1.37524	0.269	0.3870	1443	0.3615	21.97
0.6030	0.8045	1.37005	0.254	0.5032	1380	0.4573	21.04
0.6984	0.7540	1.36462	0.242	0.6386	1164	0.5387	20.15
0.7991	0.7055	1.36036	0.231	0.7991	774	0.6371	19.13
0.8858	0.6675	1.35468	0.224	0.8965	444	0.7321	18.11
0.9189	0.6538	1.35555	0.221			0.8345	17.10
						0.8999	16.40

Table 2 shows the experimental values of densities, refractive indices, viscosities, enthalpies, and surface tensions for this binary system at various mole fractions in a wide range of concentrations.

The activity coefficients of the components in the liquid phase are related to the vapor–liquid equilibria by the following equation:

$$[7] \quad \ln \gamma_i = \ln \frac{y_i p}{x_i p_i} + (B_{ii} - v_i)(p - p_i)/RT + (1 - y_i)^2 \frac{p\delta}{RT}$$

where x_i and y_i are the mole fractions in the liquid and vapor phase respectively; p_i is the vapor pressure of the component i; p is the total pressure of the mixture, and δ is given by the following equation:

$$[8] \quad \delta = 2B_{12} - B_{11} - B_{22}$$

B_{11} and B_{22} are the virial coefficients of the pure components and B_{12} is the cross virial coefficient. For *n*-pentane, $B_{11} = -1.184 \times 10^{-3}$ m^3 mol^{-1}; for dichloromethane, $B_{22} = -0.862 \times 10^{-3}$ m^3 mol^{-1}, and $B_{12} = -0.920 \times 10^{-3}$ m^3 mol^{-1}. These virial coefficients were estimated by the method of Hayden and O'Connell (7).

Table 3 shows the experimental values of mole fractions, pressures, and activity coefficients for this system.

Each set of results of the excess thermodynamic properties were fitted with a Redlich–Kister form of the type:

$$[9] \quad X^E = x_1(1 - x_1) \sum_{j=1}^{n} a_j (1 - 2x_1)^{j-1}$$

The method of least squares was used to determine the values of the coefficients a_j. In each case, the optimum number of coefficients was ascertained from an examination of the variation of the standard error of estimate with:

$$[10] \quad \epsilon = [\Sigma (X^E_{obs} - X^E_{cal})^2/(n_{obs} - n)]^{1/2}$$

The values adopted for the coefficients and the standard error of the estimate associated with the use of eq. [10] are summarized in Table 4.

Figure 1 shows the experimental values for the v^E, η^E, and σ^E while Fig. 2 shows the experimental values of h^E and g^E. The excess molar entropy is given by the following equation:

$$[11] \quad s^E = (h^E - g^E)/T$$

and the curve Ts^E at 298.15 K is also shown in Fig. 2. The

TABLE 3. Experimental values of moles fractions in the liquid and vapor phases, pressures, and activity coefficients for the *n*-pentane (1) + dichloromethane (2) system at 298.15 K

x_1	y_1	p (kPa)	γ_1	γ_2
0.0369	0.1023	63.30	2.585	1.016
0.0644	0.1592	67.06	2.436	1.040
0.1090	0.2380	70.73	2.264	1.044
0.1606	0.3163	74.45	2.144	1.047
0.2515	0.3870	77.01	1.729	1.088
0.3226	0.4333	79.05	1.553	1.141
0.4208	0.4898	80.78	1.367	1.220
0.5561	0.5593	81.98	1.180	1.380
0.6364	0.6063	81.31	1.127	1.510
0.6517	0.6169	81.18	1.118	1.532
0.7774	0.7046	78.25	1.033	1.784
0.7783	0.7050	78.33	1.033	1.785
0.8448	0.7651	76.11	1.005	1.982

TABLE 4. Coefficients a_j and standard deviation ϵ determined by the method of least squares for *n*-pentane (1) + dichloromethane (2) system at 298.15 K

Function	a_1	a_2	a_3	a_4	a_5	a_6	ϵ
$v^E \times 10^6$ (m^3 mol^{-1})	1.67778	0.132066	−0.945834	−0.310109	0.49599	—	0.008
η^E (mPa s)	−0.116446	−0.046934	−0.0454274	0.0601498	0.0256151	—	0.0008
h^E (J mol^{-1})	5589.21	2342.52	−459.869	−4630.34	2094.79	5754.4	13
g^E (J mol^{-1})	2437.71	149.361	264.75	1109.38	—	—	9
$\sigma^E \times 10^3$ (N m^{-1})	−3.47549	−2.62336	−3.77877	−4.08372	−3.71686	—	0.03

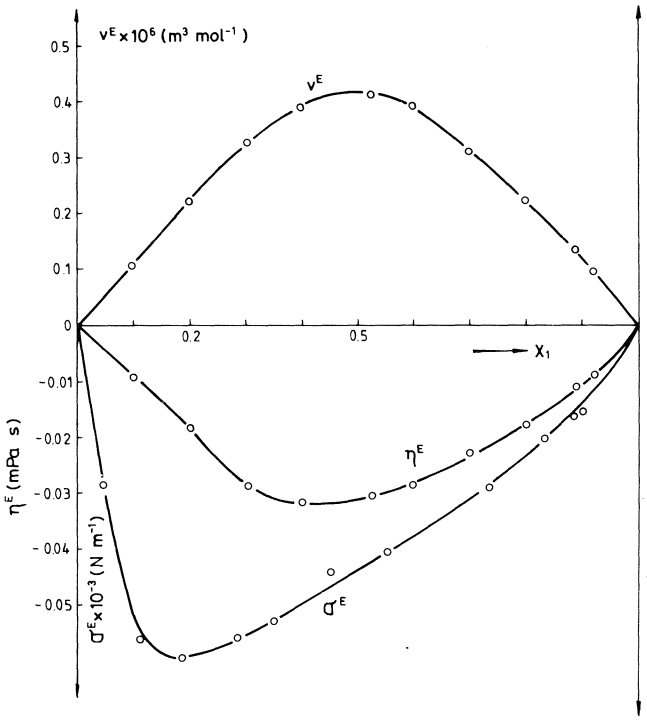

FIG. 1. Excess molar volume, excess viscosity, and excess surface tension for the *n*-pentane (1) + dichloromethane (2) system at 298.15 K.

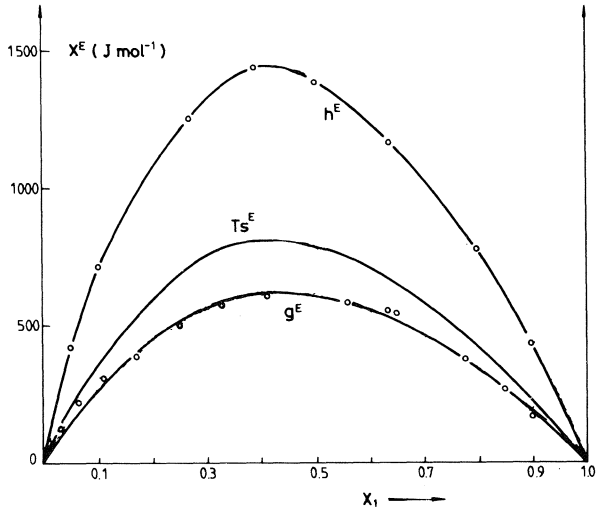

FIG. 2. Excess molar enthalpy, excess molar Gibbs free energy, and excess entropy for the *n*-pentane (1) + dichloromethane (2) system at 298.15 K.

continuous curves were calculated from eq. [9] using these values for the coefficients.

Discussion

Figure 1 shows positive excess volumes over the whole concentration range. Several effects may contribute to the values of v^E, such as the breaking of liquid order on mixing, unfavorable interaction between groups, differences in molecular volumes, and differences in free volumes between liquid components (8). The two first effects produce a positive excess volume and considering that neither of the components exhibits hydrogen bonding in the pure state, dispersion forces must be dominant (9). Generally, a positive excess volume corresponds to a negative excess viscosity as in this system. More qualitative evidence of this interaction is the large excess enthalpy for this system, about 1400 J mol^{-1} at $x_1 \cong 0.4$

Dichloromethane is a polar molecule which induces a dipole moment on non-polar molecules like *n*-pentane, due to the inductive effect of the chloro group. The endothermic effect of rupture of molecular order is corroborated by the excess free energy and molar entropy, both of which are positive, but smaller than h^E.

Normally, due to Gibbsean enrichment of the component with lower surface tension in the surface phase, σ^E is negative for most binary mixtures of non-polar, small sized or non-associated components. In this case, *n*-pentane is non-polar, then, enrichment of the surface area with *n*-pentane produces a negative σ^E.

Acknowledgment

This work was financed by a SUBCYT grant.

1. H. N. SÓLIMO, S. V. ALONSO, and M. KATZ. Can. J. Chem. **57**, 678 (1979).
2. G. C. PEDROSA, F. DAVOLIO, M. F. DE JAPAZE, and M. KATZ. Rev. latinoam. quím. quím. apl. **14**, 103 (1984).
3. G. C. PEDROSA, J. A. SALAS, F. DAVOLIO, and M. KATZ. Anal. Asoc. Quím. Argentina, **72**, 541 (1984).
4. A. LOISELEUR, J. C. MERLIN, and R. A. PARIS. J. Chim. Phys. **62**, 1380 (1965).
5. T. BOUBLIK and G. C. BENSON. Can. J. Chem. **47**, 539 (1969).
6. A. J. ARÁOZ, B. O'DONELL, and M. KATZ. Anal. Asoc. Quím. Argentina, **71**, 987 (1983).
7. J. G. HAYDEN and J. P. O'CONNELL. Ind. Eng. Chem. Process Des. Dev. **14**, 209 (1975).
8. M. G. PROLONGO, R. M. MASEGOSA, and I. HERNÁNDEZ-FUENTES. J. Phys. Chem. **88**, 2163 (1984).
9. R. J. FORT and W. R. MOORE. Trans. Faraday Soc. **62**, 1112 (1966).
10. A. WEISSBERGER. Technique of organic chemistry. Vol 7. Organic solvents. 2nd ed. Interscience Publishers, New York. 1955.
11. Eastman organic bulletin 45, N° 3. 1973.
12. R. C. REID, J. M. PRAUSNITZ, and T. K. SHERWOOD. The properties of gases and liquids. 3rd ed. McGraw-Hill Book Co., 1977.
13. O. VILIM and J. SZLAUR. Coll. Czech. Chem. Commun. **29**, 1878 (1964).

Azides. Part VI. Thermolysis of ethyl azidoformate in dimethyl terephthalate; formation of a diazabicyclooctadiene heterocycle[1]

N. R. AYYANGAR,[2] R. B. BAMBAL, K. V. SRINIVASAN, T. N. GURU ROW,[3] V. G. PURANIK,[3] S. S. TAVALE,[3] AND P. S. KULKARNI[4]

National Chemical Laboratory, Pune 411 008, India

Received February 7, 1986

N. R. AYYANGAR, R. B. BAMBAL, K. V. SRINIVASAN, T. N. GURU ROW, V. G. PURANIK, S. S. TAVALE, and P. S. KULKARNI. Can. J. Chem. **64**, 1969 (1986).

Thermal decomposition of ethyl azidoformate in excess of dimethyl terephthalate (DMT) (**1**) in acetic anhydride as solvent results in the formation of *N*,*N*-dicarbethoxy-4,8-dicarbomethoxy-2,6-diazabicyclo[3.3.0]octa-3,7-diene (**3**) in addition to *N*-carbethoxy-2,5-dicarbomethoxy-1*H*-azepine (**2**) and ethyl *N*-(2,5-dicarbomethoxyphenyl)carbamate (**4**). The structure of the diazabicyclooctadiene (**3**) was established on the basis of spectral, elemental, and X-ray crystallographic analyses.

N. R. AYYANGAR, R. B. BAMBAL, K. V. SRINIVASAN, T. N. GURU ROW, V. G. PURANIK, S. S. TAVALE et P. S. KULKARNI. Can. J. Chem. **64**, 1969 (1986).

La décomposition thermique de l'azidoformiate d'éthyle dans un excès de téréphtalate de diméthyle (TDM) (**1**) et dans l'anhydride acétique comme solvant conduit à la formation de *N*,*N*-dicarbéthoxy dicarbométhoxy-4,8 diaza-2,6 bicyclo[3.3.0]octadiène-3,7 (**3**) aux côtés de la *N*-carbéthoxy dicarbométhoxy-2,5 1*H*-azépine (**2**) et du *N*-(dicarbométhoxy-2,5 phényl) carbamate d'éthyle (**4**). On a déterminé la structure du diazabicyclooctadiène (**3**) en se basant sur des données spectrales, sur des analyses élémentaires et sur la diffraction des rayons-X.

[Traduit par la revue]

Introduction

The thermal decomposition of ethyl azidoformate in benzene, toluene, chlorobenzene, biphenyl, *o*-, *m*-, and *p*-xylenes has been shown to form the corresponding *N*-carbethoxy-1*H*-azepine (1, 2). The synthesis of azepines using the nitrene generated from azidoformate has also been reported by Hafner and Konig (3) and Lwowski *et al.* (4). These authors have mainly dealt with the nitrene insertion into aromatic substrate bearing electron-donating substituents. Formation of *N*-(*p*-toluenesulphonyl)-1*H*-azepine by the thermolysis of *p*-toluenesulphonylazide in benzene and the kinetic study of the reaction were reported by us (5*a*, 5*b*). The nitrene generated by the thermolysis of *p*-toluenesulphonylazide has been shown to react with dimethyl terephthalate (DMT) resulting in the formation of *N*-*p*-toluenesulphonyl-2,5-dicarbomethoxy-1*H*-azepine (5*c*). It has been indicated that the stabilising influence of the electron-withdrawing carbomethoxy substituent on the benzaziridine intermediate complex, leads preferentially to the formation of the *N*-sulphonyl-1*H*-azepine (6*a*). In this paper, the formation of a new heterocyclic compound *N*,*N*-dicarbomethoxy-2,6-diazabicyclo[3.3.0]octa-3,7-diene (3) by the thermolysis of ethyl azidoformate in DMT has been described.

Results and discussion

Thermolysis of ethyl azidoformate was initially carried out in molten DMT (**1**) at 160°C at atmospheric pressure which resulted in an *explosive reaction* with visible flame (6*b*). Thermolysis was therefore carried out in acetic anhydride, apparently a good solvent for this reaction. Acetic anhydride not only absorbed the heat of the reaction but also provided the critical reaction temperature. Thus, the reaction of ethyl azidoformate with DMT (1) in refluxing acetic anhydride yielded in addition to *N*-carbethoxy-2,5-dicarbomethoxy-1*H*-azepine (**2**) and ethyl *N*-(2,5-dicarbomethoxyphenyl)carbamate (**4**), a bicyclic heterocycle containing two nitrogen atoms, the structure of which has been established as *N*,*N*-dicarbethoxy-4,8-dicarbomethoxy-2,6-diazabicyclo[3.3.0]octa-3,7-diene (**3**) on the basis of spectral, elemental, and X-ray crystallographic analyses. The identity of the carbamate (**4**) was confirmed by an unambiguous synthesis from dimethyl amino terephthalate. A similar observation involving the formation of diazabicyclo-octadienes by the reaction of a nitrene with 1,4-di-*tert*-butyl or 1,4-di-isopropyl benzenes has been reported recently (7*a*). In a more recent work, the synthesis of dihydropyrrolo[3,2-*b*] pyrrole starting from 1,4-bis(trimethylsilyl)benzene, a 10π-aromatic compound which incorporates the diazabicyclo[3.3.0] framework, has been reported (7*b*).

The uv spectrum of azepine (**2**) shows a low intensity broad band at 350 nm, which extends into the visible region giving the compound its yellow colour. The ir absorption bands at 1470 cm^{-1} (strong) and 1640 cm^{-1} (weak) for **2** are characteristic of cyclic conjugated double bonds of the azepine ring. In the ir spectrum of **3**, the C=C and C—H stretching vibrations are manifested as sharp absorptions at 1610 cm^{-1} and 3100 cm^{-1}, respectively. In the ^{1}H-nmr spectrum, the azepine ring protons of **2** appear as a multiplet at 6.0 to 7.2 ppm. The alternative azepine, **5**, which should have highly symmetrical ^{1}H-nmr pattern (two singlet peaks appearing for protons at C(2)/C(7) and C(4)/C(5), respectively) could not be isolated from the reaction mixture in spite of several careful attempts to do so. ^{1}H-nmr spectrum of **3** shows a sharp singlet at 5.6 ppm integrating for two protons at 1,5-*cis* junction whereas those at C(3) and C(7) are seen as a sharp singlet at 7.3 ppm. The down-field shift into the aromatic region is caused by the presence of the electron-withdrawing carbomethoxy substituents.

The X-ray crystallographic data show that molecule **3** is under steric strain, since the two five-membered dihydropyrrole rings are inclined at an angle of 66.9°. Apparently, this strain is released during the mass spectral fragmentation of **3** with the formation of aromatic product ions. The mass spectrum of **3** shows strong molecular ion at m/z 368 (Scheme 1). The steric strain in the molecular ion is released by homolytic cleavage of C(1)—C(5) bond which is β to the ionised nitrogen atom at 2

[1]NCL Communication No. 3673. For Part V, see ref. 5*b*.
[2]To whom all correspondence should be addressed.
[3]Performed work on X-ray crystallography.
[4]Performed work on mass spectral analysis.

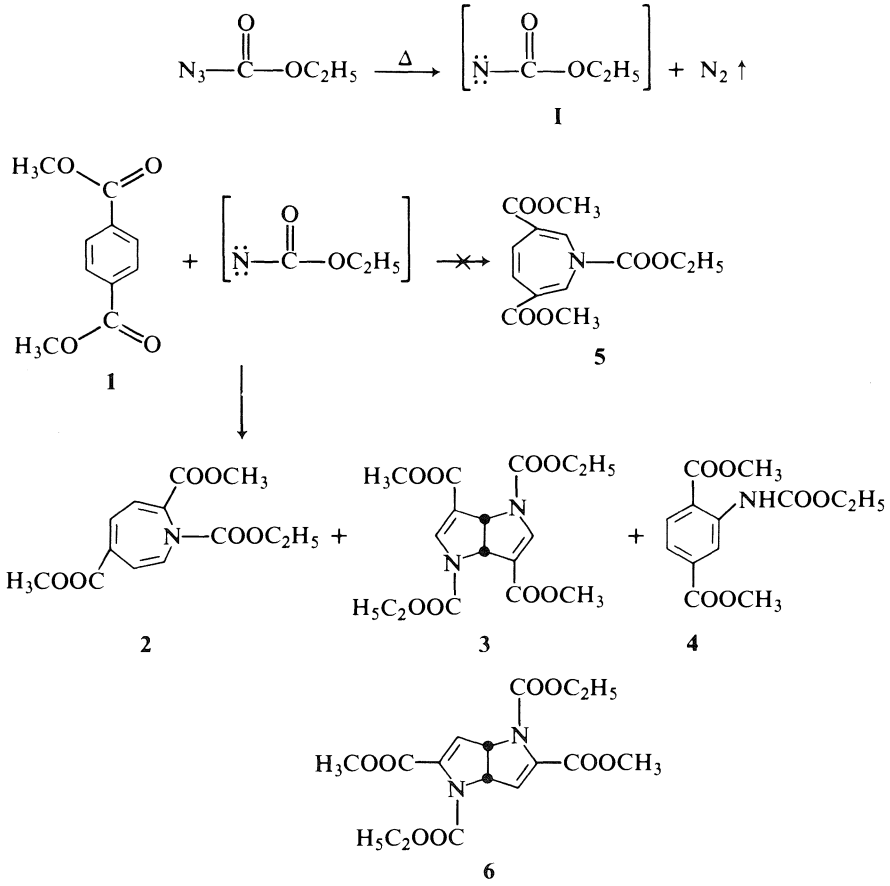

I

1 5

2 3 4

6

(or 6) position, generating radical centre at C(5) (or C(1)) carbon atom (**3***a*). Loss of carbethoxy radical from **3***a* generates a strong peak at *m/z* 295, attributable to the cation **3***b*. The elimination of hydrogen cyanide from **3***b* gives rise to radicals at C(4) and C(7), respectively. Subsequent bond formation generates the *N*-substituted pyridinium cation **3***c* (*m/z* 268). The stepwise loss of carbon dioxide and ethylene molecules results in the formation of strong 3,5-dicarbomethoxy pyridinium cation at *m/z* 196.

The 2,6-diazabicyclo[3.3.0] framework, the 1,5-*cis* junction, and the positions of the two carbomethoxy substituents in **3** were firmly established by X-ray crystallographic analysis.

X-ray crystallography

Crystal data

$C_{16}H_{20}N_2O_8$ fw = 368.35

Monoclinic, a = 15.976(1), b = 4.561(1), c = 28.024(3) Å, β = 120.30(1)°, V = 1763.07 Å^3, $A2/a$ (standard $C2/c$), Z = 4, ρ_c = 1.39, ρ_o = 1.39 mg M^{-3} (flotation in KI solution), MoKα (λ = 0.7107 Å), T = 293 K, $F(000)$ = 776.0.

Crystals of **3** were found to be very soft and tend to bend on cutting. It is interesting to note that these bent crystals diffracted weakly and also indicated reflections which otherwise are systematically absent for the monoclinic ($A2/a$) space group. However, it was possible to procure an uncut crystal of size 0.06 × 0.1 × 0.6 mm which diffracted well and showed no "unusual" reflections.

Data collection was done on an Enraf-Nonius CAD4F-11M diffractometer. The intensity data (1545 reflections were measured, 883 of which were judged significant $|F_o| \geq 3\sigma|F_o|$) were collected with ω/2θ scan technique, scan speed 1°/min up to θ = 23.5°. During the data collection, three standard reflections (6 0 0, $\bar{4}\,\bar{2}\,\bar{2}$, 0 0 10) showed statistical variation within ±2% in intensity, *hkl* range *h*, 0 to 17; *k*, 0 to 5; *l*, −31 to 31; data were not corrected for absorption (μ = 1.21 cm^{-1}). The lattice parameters were refined using 25 reflections (12° ≤ θ ≤ 21°).

The structural aspects were studied by direct methods using MULTAN-78 (Main *et al.*, 1978) (8). A full-matrix least-squares refinement of a scale factor, positional and anisotropic thermal parameters (isotropic thermal parameters for H atoms; located from a difference map) using program LALS (Gantzel *et al.*, 1961) (9*a*) resulted in a final R ($R = \Sigma(|F_o| - |F_c|)/\Sigma|F_o|$) of 0.032 for 883 reflections with $|F_o| \geq 3\sigma|F_o|$. A Cruickshank type weighting scheme was used with $W = (7.0 + 1.0|F_o| \pm 0.009|F_o|^2)^{-1}$. The final difference Fourier map has $\Delta\rho < |0.3|$ e Å^{-3} and thus is of no chemical significance. The atomic parameters with their esd's and equivalent isotropic temperature factors for non-hydrogen atoms are listed in Table 1. Table 2 gives the bond length and bond angles involving non-hydrogen atoms. List of structure factors, anisotropic thermal parameters, H atom positions with isotropic temperature factor tables are in the Depository of Unpublished Data.[5] Atomic scattering factors are taken from the International tables for X-ray crystallography (9*b*).

Each half of the molecule (x, y, z) is related by symmetry to the other half ($\frac{1}{2} - x$, y, z). Figure 1 gives a perspective view of the molecule along with crystallographic numbering. The dihydropyrrole rings of the diazabicyclo[3.3.0]octa-3,7-diene adopt an "envelope" conformation. The dihedral angle between the best planes through the two five-membered rings is 66.9°. The molecules are held together in the crystal structure by pure van der Waals interactions.

The singlet carbethoxy nitrene (**I**) generated by thermolysis of ethyl azidoformate adds to the aromatic double bond of DMT to produce a benzaziridine intermediate (**I′**) (Scheme 2). The attack preferentially takes place at the carbon atom bearing the carbomethoxy substituent. The benzaziridine intermediate (**I′**) undergoes sigmatropic ring opening to give rise to the azepine (**2**). The C—N bond fission followed by aromatisation yielded the carbamate (**4**). The alternative structure (**5**) for the azepine (**2**) has been ruled out on the basis of the ^{1}H-nmr spectrum, as discussed earlier. The azepine (**5**) could neither be

[5]Complete set of data may be purchased from the Depository of Unpublished Data, CISTI, National Research Council of Canada, Ottawa, Ont., Canada K1A 0S2.

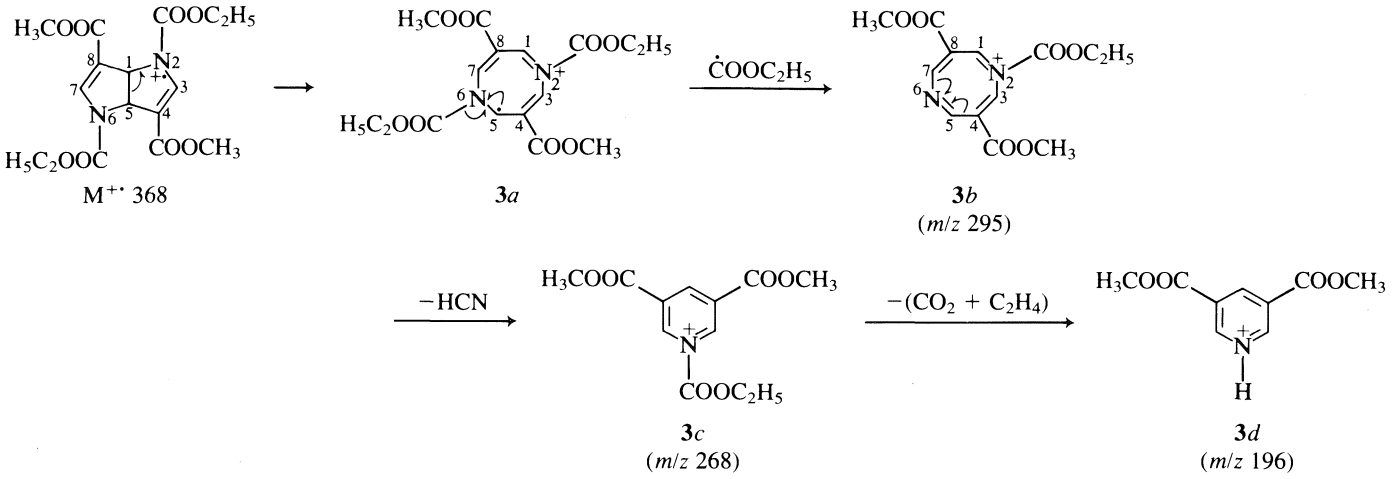

SCHEME 1

TABLE 1. Atomic coordinates ($\times 10^4$) and equivalent isotropic thermal parameters for non-hydrogen atoms with esd's in parentheses

Atom	X	Y	Z	B_{eq} (Å^2)[a]
C(1)	2583(1)	4640(5)	298(1)	2.97
C(2)	1165(1)	2075(5)	−280(1)	3.20
C(3)	1151(1)	2604(5)	−596(1)	3.02
C(4)	1155(1)	1665(5)	−1167(1)	3.59
C(5)	−19(2)	−1272(8)	−1886(1)	6.31
C(6)	1272(1)	3927(5)	553(1)	3.40
C(7)	1492(2)	6503(7)	1341(1)	5.85
C(8)	2310(3)	7280(10)	1854(1)	8.01
N	1673(1)	3406(4)	230(1)	3.33
O(1)	1435(1)	2441(5)	−1468(1)	6.22
O(2)	422(1)	−245(4)	−1326(1)	5.13
O(3)	556(1)	2721(4)	493(1)	5.06
O(4)	1786(1)	5907(4)	939(1)	4.38

[a] $B_{eq} = (8/3)\pi^2\Sigma_i\Sigma_j v_{ij} a_i^* a_j^* \cdot \boldsymbol{a}_i \cdot \boldsymbol{a}_j$.

TABLE 2. Bond distances (Å) and bond angles (deg) with esd's in parentheses

Bond	Distance	Bonds	Angle
C(1′)—C(1)	1.554(3)		
C(1′)—C(3)	1.520(3)		
		C(1)—C(1′)—C(3)	102.0(2)
C(1)—N	1.479(3)		
		C(1′)—C(1)—N	103.7(2)
C(2)—C(3)	1.332(3)	N—C(1)—C(3′)	113.7(2)
C(2)—N	1.380(2)		
		C(3)—C(2)—N	112.5(2)
C(3)—C(4)	1.445(3)		
		C(1′)—C(3)—C(2)	110.0(2)
		C(1′)—C(3)—C(4)	123.8(2)
		C(2)—C(3)—C(4)	125.9(2)
C(4)—O(1)	1.192(3)		
C(4)—O(2)	1.343(3)		
		C(3)—C(4)—O(1)	125.5(2)
		C(3)—C(4)—O(2)	112.3(2)
		O(1)—C(4)—O(2)	122.2(2)
C(5)—O(2)	1.435(3)		
C(6)—N	1.369(3)		
C(6)—O(3)	1.202(3)		
C(6)—O(4)	1.328(3)		
		N—C(6)—O(3)	123.9(2)
		N—C(6)—O(4)	110.7(2)
		O(3)—C(6)—O(4)	125.3(2)
C(7)—C(8)	1.416(4)		
C(7)—O(4)	1.447(4)		
		C(8)—C(7)—O(4)	109.9(3)
		C(1)—N—C(2)	109.1(2)
		C(1)—N—C(6)	127.3(2)
		C(2)—N—C(6)	122.4(2)
		C(4)—O(2)—C(5)	116.2(2)

detected nor isolated in spite of several careful attempts to do so. The thermolysis of *p*-toluenesulphonylazide in DMT under nitrogen pressure of 62 atm yielded *N*-(*p*-toluenesulphonyl)-2,5-dicarbomethoxy-1*H*-azepine in 71% yield. Formation of 3,6-dicarbomethoxy isomer was not detected (6*b*). Further, the diazabicyclooctadiene (**3**) cannot be a product of reaction of carbethoxy nitrene with the azepine (**2**). The mechanistic considerations would have given rise to the structure (**6**) starting from **2** whereas the positions of the carbomethoxy substituents were firmly established as in **3** by X-ray analysis. The diazabicyclooctadiene (**3**) could not be detected in the products resulting from the reaction of the azepine (**2**) with equimolar proportion of ethyl azidoformate under identical reaction conditions.

In light of the above comments, a probable reaction pathway for the formation of **3** has been shown in Scheme 2. The approach of the carbethoxy nitrene to the benzaziridine intermediate (**I′**) triggers a nitrogen walk from bond *a* to bond *b* and the nitrene adds across double bond *c* in a concerted manner. The concerted sequence of reactions is also accompanied by a simultaneous ring opening, eventually giving rise to the azahomoazepine intermediate (**I″**). The diazabicyclooctadiene (**3**) is then formed from a 1,3-carbon migration of (**I″**).

Experimental

Melting points were recorded in capillary tubes. Ultraviolet spectra were recorded on a Perkin-Elmer 350 spectrophotometer, ir spectra on a Perkin-Elmer 221 spectrophotometer, ^{1}H-nmr spectra on a Varian T-60 spectrometer using TMS as the internal standard, and mass spectra on a CEC-21-110-B double focussing spectrometer using direct inlet gas system. Petroleum ether used was of the boiling range 60–80°C. Ultraviolet wavelength maxima are in nm, ir frequencies are in cm^{-1}, and chemical shifts are in δ ppm.

Ethyl azidoformate

An aqueous solution of sodium azide (25 g, 0.38 mol) in water (70 mL) was added gradually over 1 h to ethyl chloroformate (17 g, 0.11 mol) under stirring, at room temperature. The reaction mixture was stirred further for 3 h. The organic layer was separated, washed with water, and distilled carefully under reduced pressure at 50°C to obtain ethyl azidoformate as a colourless liquid, in quantitative yield.

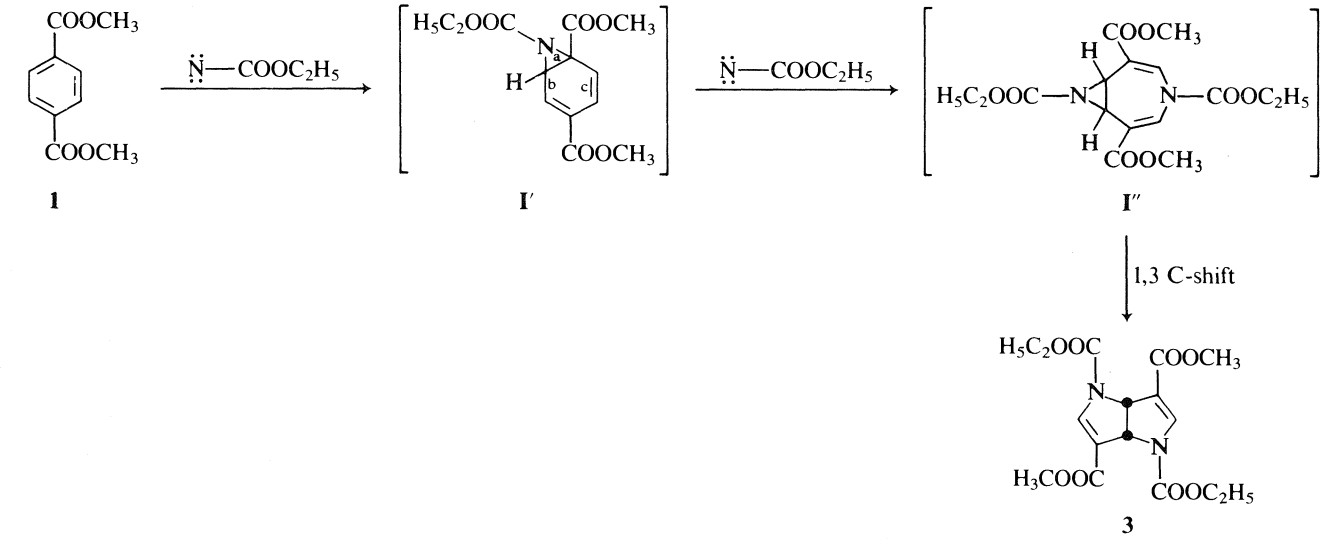

SCHEME 2

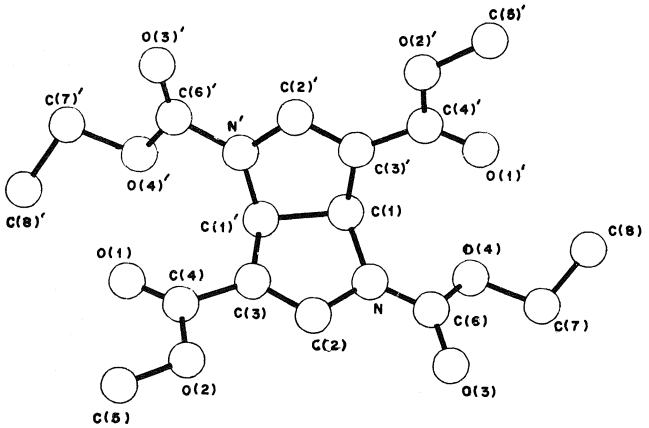

FIG. 1. A perspective view of diazabicyclooctadiene **3**.

N-*Carbethoxy-2,5-dicarbomethoxy-1* H-*azepine* (**2**)

A mixture of DMT (**1**) (40 g, 0.20 mol) and acetic anhydride (140 mL) was heated to reflux temperature (135°C) under stirring. Ethyl azidoformate (4 g, 0.034 mol) was added gradually over a period of 0.5 h. The reaction mixture was maintained at reflux for 2 h. At the end of the reaction, the acetic anhydride was removed under reduced pressure. The residual mass was subjected to fractional crystallisation in benzene, when the less soluble DMT crystallised out. In this manner, 30 g of unreacted DMT was recovered. The residual liquor from the crystallisations was adsorbed on silica gel and chromatographed through a silica gel column. Initial elution with petroleum ether gave more of the unreacted DMT (0.5 g). Next elution with petroleum ether – benzene (1:1) and recrystallisation from petroleum ether yielded deep yellow crystals of **2** (0.1 g, 1%) mp 93°C; uv (MeOH): 230 (log ϵ, 4.38) and 350 (3.28); ir (Nujol): 3000, 1701, 1640, 1587, 1450, 1316, 1268, 1180, 1130; ^{1}H-nmr ($CDCl_3$): 1.3 (t, 3H, —CH_3 of COOEt), 3.7 (s, 6H, $COOCH_3$), 4.3 (q, 2H, CH_2), 6.0 (d, 2H, C_3—H and C_6—H), 6.7 (m, 1H, C_4—H), and 7.2 (m, 1H, C_7—H); ms: m/z 281 (M^+, 100%), 250 (58), 208 (72), 207 (85), 180 (32), 178 (58), 149 (59), 122 (22). *Anal.* calcd. for $C_{13}H_{15}NO_6$: C 55.5, H 5.3, N 4.9; found: C 55.4, H 5.4, N 4.8.

N,N-*Dicarbethoxy-4,8-dicarbomethoxy-2,6-diazabicyclo[3.3.0]octa-3,7-diene* (**3**)

The chromatography of the reaction mass was continued with petroleum ether – benzene (1:1) as eluent. The compound **3** eluted out and was recrystallized from petroleum ether to yield colourless needles of **3** (0.15 g, 2.2%), mp 103°C; uv (MeOH): 260 (log ϵ, 3.55); ir (Nujol): 3100, 1710, 1620, 1460, 1250, 1030; ^{1}H-nmr ($CDCl_3$): 1.3 (t, CH_3 of COOEt), 3.7 (s, 6H, $COOCH_3$), 4.2 (q, 4H, CH_2 of COOEt), 5.6 (s, 2H, C_1-H and C_5-H) and 7.3 (s, 2H, C_3-H and C_4-H); ms: m/z 368 (M^+, 100%), 337 (55), 295 (28), 268 (48), 250 (18), 196 (55), 193 (58), 192 (59), 164 (58), 163 (42), 159 (50), 149 (35), 137 (38), 132 (39), 77 (25). *Anal.* calcd. for $C_{16}H_{20}N_2O_8$: C 52.2, H 5.4, N 7.6; found: C 52.3, H 5.6, N 7.5.

Ethyl N-*(2,5-dicarbomethoxyphenyl)carbamate* (**4**)

The chromatography was continued with benzene as eluent. The carbamate (**4**) eluted out and was recrystallised from petroleum ether to yield colourless needles of **4** (0.03 g, 0.33%), mp 134°C; ir (Nujol): 3300, 1750, 1730, 1710, 1600, 1450, 1320, 1250; ^{1}H-nmr ($CDCl_3$): 1.3 (t, 3H, CH_3 of COOEt), 4.0 (s, 6H, CH_3 of COOMe), 4.3 (q, 3H, Ar-H); ms: m/z 281 (M^+, 100%), 250 (92), 208 (95), 192 (92), 181 (88), 180 (92), 149 (78), 122 (20), 129 (98). *Anal.* calcd. for $C_{13}H_{15}NO_6$: C 55.5, H 5.3, N 4.9; found: C 55.4, H 5.4, N 5.0.

Dimethyl nitroterephthalate

DMT was nitrated by a procedure already reported (10). The dimethyl nitroterephthalate was recrystallised from ethanol as a white solid, mp 76°C (lit. (11) mp 76°C).

Dimethyl aminoterephthalate

The nitro derivative (10 g, 0.04 mol) was taken in methanol (200 mL) contained in a glass bottle mild pressure reactor. Palladium on carbon (12% w/w) (0.5 g) as catalyst was added to the mixture. The reactor was pressurised to 3 atm with hydrogen and maintained at room temperature with shaking for 2 h. The reaction mixture was filtered to remove the catalyst and methanol was removed by distillation. The crude reaction mixture was taken in benzene (300 mL) and extracted with dilute hydrochloric acid (20% w/w). The aqueous layer was separated out and neutralised with sodium carbonate solution (20% w/v). The amino derivative precipitated out and was crystallised from ethanol to yield pale yellow needles of dimethyl aminoterephthalate, (3.5 g, 40%), mp 134°C (lit. (12) mp 134°C).

Ethyl N-*(2,5-dicarbomethoxyphenyl)carbamate* (**4**)

A mixture of dimethyl aminoterephthalate (0.1 g, 0.00048 mol), ethyl chloroformate (100 mL) and sodium carbonate (0.1 g) was refluxed for 16 h. Excess ethyl chloroformate was distilled off under reduced pressure. The residue was recrystallised from petroleum ether to yield colourless needles of the carbamate (**4**), (0.05 g, 43%), mp 134°C.

1. R. J. COTTER and W. F. BEACH. J. Org. Chem. **29**, 751 (1964).
2. J. M. PHOTIS. J. Heterocycl. Chem. 1249 (1970).
3. K. HAFNER and C. KONIG. Angew. Chem. **75**, 89 (1963).
4. W. LWOWSKI, T. J. MARICICH, and T. W. MATTINGLY. J. Am. Chem. Soc. **85**, 1200 (1963).

5. (*a*) N. R. AYYANGAR, R. B. BAMBAL, and A. G. LUGADE. J. Chem. Soc. Chem. Commun. 790 (1981); (*b*) N. R. AYYANGAR, R. B. BAMBAL, D. D. NIKALJE, and K. V. SRINIVASAN. Can. J. Chem. **63**, 887 (1985); (*c*) N. R. AYYANGAR, M. V. PHATAK, and B. D. TILAK. Indian J. Chem. **16B**, 547 (1978).
6. (*a*) N. R. AYYANGAR, M. V. PHATAK, A. K. PUROHIT, and B. D. TILAK. Chem. Ind. London, 853 (1979); (*b*) N. R. AYYANGAR, R. B. BAMBAL, and A. G. LUGADE. Heterocycles, **18**, 77 (1983).
7. (*a*) T. KUMAGAI, K. SATAKE, K. KIDUORA, and T. MUKAI. Tetrahedron Lett. **24**, 2275 (1983); (*b*) T. KUMAGAI, S. TANAKA, and T. MUKAI. Tetrahedron Lett. **25**, 5669 (1984).
8. P. MAIN, S. E. HULL, L. LESSINGER, G. GERMAIN, J. P. DECLERCQ, and M. M. WOOLFSON. MULTAN 78. A system of computer programs for the automatic solution of crystal structures from X-ray diffraction data. Universities of York, England and Louvain, Belgium. 1978.
9. (*a*) P. K. GANTZEL, R. A. SPARKS, and K. N. TRUEBLOOD. LALS. A program for the full matrix least squares refinement positional and thermal parameters and scale factors. 1961; (*b*) International tables for X-ray crystallography. Vol. IV. Kynoch Press, Birmingham. 1974.
10. G. A. BURKHARDT. Chem. Ber. **10**, 145 (1877).
11. Dictionary of organic compounds. Vol. 4. Chapman and Hall, New York. 1982. p. 4225.
12. Dictionary of organic compounds. Vol. 1. Chapman and Hall, New York. 1982. p. 145.

Étude par résonance magnétique nucléaire du platine-195 de la réaction de *cis*-[Pt(éthylméthylsulfoxyde)$_2$Cl$_2$] avec un sel d'argent

F. D. Rochon et Louise Girard

Département de chimie, Université du Québec à Montréal, C.P. 8888, succursale A, Montréal (Qué.), Canada H3C 3P8

Reçu le 18 juillet 1985[1]

F. D. Rochon et Louise Girard. Can. J. Chem. **64**, 1974 (1986).

Les produits de la réaction du *cis*-[Pt(EMSO)$_2$Cl$_2$] (EMSO = éthylméthylsulfoxyde) avec le sulfate d'argent, ont été étudiés par la résonance magnétique nucléaire du ^{195}Pt. Les résultats ont mis en évidence l'existence de plusieurs espèces en solution aqueuse. L'étude a porté sur des réactions effectuées dans différentes conditions de pH et sur des produits de réaction neutralisés à différents degrés. De plus, les spectres de deux oligomères isolés ont été enregistrés. Le dimère et le trimère à ponts hydroxo produisent un signal autour de −2900 ppm tandis que les espèces monomériques hydrolysées ont des signaux autour de −3200 ppm. Cette étude a permis d'établir un profil semi-quantitatif des différents équilibres en solution.

F. D. Rochon and Louise Girard. Can. J. Chem. **64**, 1974 (1986).

The products of the reaction of *cis*-[Pt(EMSO)$_2$Cl$_2$] (EMSO = ethylmethylsulfoxide) with Ag_2SO_4 were studied by ^{195}Pt nuclear magnetic resonance. The results have shown the presence of several species in aqueous solution. The reactions were done at different conditions of pH. The spectra of two isolated oligomers were also measured. The hydroxy-bridged dimer and trimer show a signal around −2900 ppm while the hydrolyzed monomers have signals around −3200 ppm. A semi-quantitative profile of the different equilibria in solution is suggested.

Introduction

Les ligands sulfoxydes possèdent deux sites donneurs, mais dans le cas du platine, un métal mou, la coordination s'effectue exclusivement par l'atome de soufre.

Nous avons récemment étudié les réactions des complexes de platine de type *cis*-[Pt(L)$_2$X$_2$] (L = sulfoxyde et X = Cl ou I) avec des sels d'argent (1). Des monomères *cis*-[Pt(L)$_2$(ClO$_4$)$_2$] et *cis*-[Pt(L)$_2$SO$_4$], des dimères à ponts hydroxo, *cis*-[(L)$_2$Pt(OH)$_2$Pt(L)$_2$]$^{2+}$, et possiblement un trimère ont été isolés et caractérisés par spectroscopie infrarouge et par résonance magnétique nucléaire du proton. Afin de confirmer les différentes espèces oligomériques, nous avons entrepris une étude par rmn du platine-195. La bonne sensibilité de ce noyau, combinée à une haute fréquence de résonance et une bonne abondance naturelle, facilite l'étude par rmn de cet isotope.

Nous avons étudié les produits de la réaction entre *cis*-[Pt(EMSO)$_2$Cl$_2$] (EMSO = éthylméthylsulfoxyde) et Ag_2SO_4 dans D_2O. Les résultats ont montré la présence de plusieurs espèces en solution. Plusieurs facteurs tels que pH, concentration, température et temps de réaction ont une influence très importante sur les différents équilibres et sur la vitesse d'oligomérisation des complexes. La rmn du ^{195}Pt a permis de mieux visualiser ces équilibres qui seront discutés plus bas.

Partie expérimentale

Les spectres rmn du platine-195 ont été mesurés sur un spectromètre Bruker WH400. Les spectres ont été découplés du proton, utilisant un découplage à deux niveaux. Les spectres ont été obtenus à différentes largeurs spectrales 31 250–50 000 Hz avec une durée d'impulsion de 40 μs et un nombre d'accumulations de 400 à 3281. Les concentrations des solutions étaient d'environ 0,3 *M* en platine. Une solution de K_2PtCl_4 (0,415 g dans 3 mL D_2O) a servi de référence externe. Les déplacements chimiques rapportés dans cette publication sont relatifs à Na_2PtCl_6 (K_2PtCl_4 : δ = −1628 ppm (2)).

Les complexes *cis*-[Pt(EMSO)$_2$Cl$_2$], *cis*-[(EMSO)$_2$Pt(OH)$_2$Pt(EMSO)$_2$](SO$_4$) et (*cis*-[Pt(EMSO)$_2$(OH)]$_3$)$_2$(SO$_4$)$_3$ ont été préparés par la méthode décrite précédemment (1).

Résultats et discussion

Un complexe binucléaire à ponts hydroxo a été isolé selon les réactions suivantes:

cis-[Pt(EMSO)$_2$Cl$_2$] + Ag_2SO_4

↓ H_2O

espèces ioniques hydrolysées

↓ pH ≈ 6,5, $Ba(OH)_2$

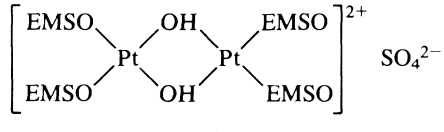

Ce complexe est blanc et insoluble dans l'éthanol. Lors de la synthèse, un autre composé, de couleur jaune et soluble dans l'éthanol, a été isolé. L'analyse élémentaire a montré la même composition. Mais les propriétés physiques et les spectres infrarouges des deux composés sont différents. Les spectres rmn protoniques des deux produits montrent les mêmes déplacements chimiques mais les pics du composé jaune sont beaucoup plus larges. Nous avons émis l'hypothèse que le composé jaune était un trimère à ponts-hydroxo (*cis*-[Pt(EMSO)$_2$(OH)]$_3$)$_2$(SO$_4$)$_3$) (1). L'élargissement des pics en rmn protonique serait causé par un processus de réarrangement du cation qui est stéréochimiquement non rigide en solution comme observé pour le complexe *cis*-[Pt(NH$_3$)$_2$(OH)]$_3^{3+}$ (3).

Les spectres rmn du ^{195}Pt des deux oligomères isolés sont montrés à la figure 1 (a et b). Un seul signal apparaît dans chacun des cas : à −2891 ppm pour le dimère et −2906 ppm pour le trimère. La proximité de ces deux pics pourrait mettre en doute l'existence de deux espèces différentes. Cependant, d'une part, les propriétés caractéristiques différentes (solubilité, point de fusion, couleur et spectre infrarouge) des deux complexes, et d'autre part, l'absence de tout autre signal dans le spectre rmn, semblent suggérer la présence de deux composés distincts. Le signal du trimère est très large probablement à cause du processus de réarrangement du cation mentionné plus haut. Il est également possible que le petit signal observé pour le trimère

1. Revision reçue le 14 avril 1986.

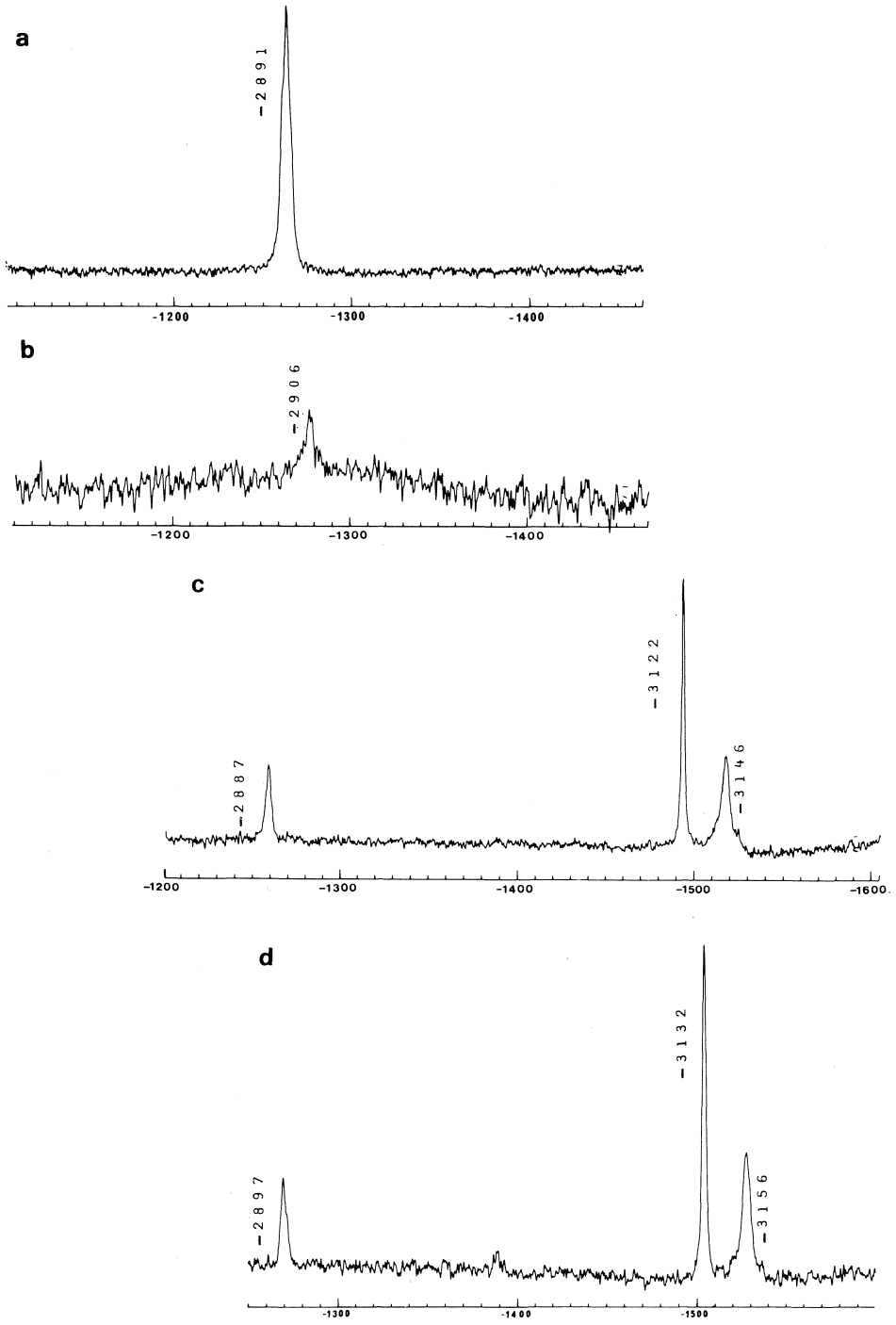

FIG. 1. Spectres rmn ^{195}Pt; (a) dimère isolé et redissous dans D_2O; (b) trimère isolé et redissous dans D_2O; (c) $[Pt(EMSO)_2Cl_2]$ + Ag_2SO_4 dans D_2O fraîchement préparé, sans ajustement de pD (~1,9); (d) réaction dans H_2SO_4 pD = 1.

soit causé par une petite quantité de dimère dans le trimère et que le signal de ce dernier soit trop large pour être détecté.

Une étude de la réaction entre *cis*-$[Pt(EMSO)_2Cl_2]$ et Ag_2SO_4 (rapport 1:1), en milieu D_2O, a ensuite été entreprise directement dans le tube de rmn. Le pD obtenu lors du mélange des deux réactifs est d'environ 1,9. Le spectre d'une solution fraîchement préparée est montré à la figure 1c. Ce spectre met en évidence la formation de plusieurs espèces lors de la réaction. Après sept jours à la température ambiante, le spectre avait peu changé, montrant ainsi la stabilité des espèces dans ces conditions. Seul le pic à −2887 ppm semble avoir augmenté. Ce signal correspond au dimère, tandis que les pics à −3122 et −3146 ppm sont attribués à des espèces monomériques. Le monomère *cis*-$[Pt(EMSO)_2SO_4]$ est probablement hydrolysé en solution aqueuse sous les formes *cis*-$[Pt(EMSO)_2(H_2O)SO_4]$, *cis*-$[Pt(EMSO)_2(H_2O)_2]^{2+}$ et *cis*-$[Pt(EMSO)_2(H_2O)(OH)]^{+}$. L'espèce monoaquo-monohydroxo s'oligomérise en dimère et éventuellement en trimère (1). L'oligomérisation est plus importante après quelques jours même en pH acide.

Il est difficile d'attribuer sans ambiguïté les signaux des espèces monomériques. Gill et Rosenberg (4) ont observé un seul signal pour les trois espèces monomériques hydrolysées $[Pt(dach)(H_2O)_2]^{2+}$, $[Pt(dach)(H_2O)(OH)]^{+}$ et $[Pt(dach)(OH)_2]$ (dach = *trans*-diamino-1,2 cyclohexane, et l'anion = NO_3^-).

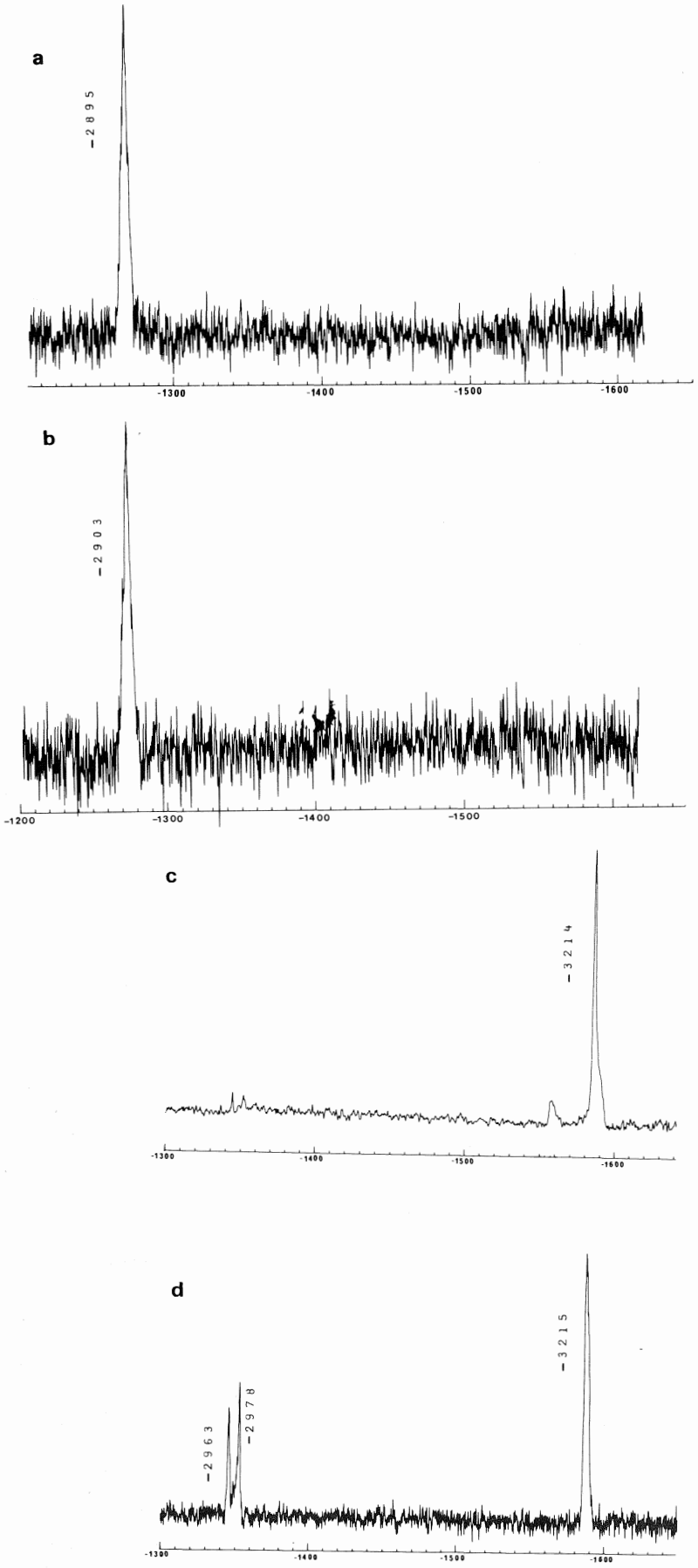

FIG. 2. Spectres rmn ^{195}Pt; (a) réaction dans D_2O, pD ajusté à 3,9 avec KOH; (b) réaction dans D_2O, pD ajusté à 5,0 avec KOH; (c) réaction dans KOH pD = 9–10; (d) *cis*-$[Pt(EMSO)_2Cl_2]$ hydrolysé dans une solution fraîchement préparée KOH pD = 10–12.

TABLEAU 1. Déplacements chimiques en rmn du ^{195}Pt des différentes espèces en solution aqueuse

Espèce	δ (ppm)
K_2PtCl_4	−1628[a]
$[Pt(EMSO)_2OH]_2^{2+}$	−2887
$[Pt(EMSO)_2OH]_3^{3+}$	−2906
$[Pt(EMSO)_2(H_2O)_2]SO_4$	−3146
$[Pt(EMSO)_2(OH)_2]$	−3213
$[Pt(EMSO)_2(H_2O)(SO_4)]$	−3122
cis-$[Pt(EMSO)Cl(OH)_2]$[b]	−2978
trans-$[Pt(EMSO)Cl(OH)_2]$[b]	−2963

[a]Référence 2.
[b]Voir texte.

Ces espèces participent à un équilibre acide–base par échange de proton (ou D^+ dans D_2O) et un seul signal est observé en rmn du ^{195}Pt. Ces auteurs ont observé une variation de la position du signal selon le pH. Ils ont assumé qu'à des pH extrêmes (2,5 et >9), les espèces présentes sont l'espèce protonée $[Pt(dach)(H_2O)_2]^{2+}$ observée à −1898 ppm et déprotonée $[Pt(dach)(OH)_2]$ observée à −1796 ppm. Dabrowiak *et al.* (5) ont fait une étude par rmn du ^{195}Pt de l'hydrolyse (pD = 3) d'un complexe sulfato avec le di(aminométhyl)-1,1 cyclohexane (A). Ils ont attribué un pic à −1835 ppm à l'espèce partiellement hydrolysée, $[Pt(A)(H_2O)SO_4]$, et celui à −1860 ppm à $[Pt(A)(H_2O)_2]^{2+}$. Appleton *et al.* (6) ont également attribué un pic à −1550 ppm à l'espèce *cis*-$[Pt(NH_3)_2(H_2O)SO_4]$ à un champ légèrement plus bas que le signal de *cis*-$[Pt(NH_3)_2(H_2O)_2]^{2+}$ observé à −1584 ppm. Ce même groupe de chercheurs a aussi observé un pic à 74 ppm attribué à l'espèce $[Pt(H_2O)_3SO_4]$, c'est à dire à un champ un peu plus bas que le signal de $[Pt(H_2O)_4]^{2+}$ (7). En nous basant sur ces travaux, nous avons attribué le signal observé à −3122 ppm, pour nos complexes, à l'espèce $[Pt(EMSO)_2(H_2O)SO_4]$ et celui à −3146 ppm, à $[Pt(EMSO)_2(H_2O)_2]^{2+}$.

Afin de confirmer cette hypothèse, des spectres de réactions effectuées dans différentes conditions de pH ont été mesurés. La réaction effectuée en milieu acide pD = 1 (fig. 1d) ne montre pas de variation dans les proportions des différentes espèces. Les spectres des produits de réaction amenés à des pD de 3,9 et 5,0 (fig. 2 (a et b)) avec KOH, montrent un seul signal aux environ de −2898 ppm, indiquant ainsi une oligomérisation complète. La dimérisation de l'espèce monohydroxo-monoaquo semble donc trés rapide. Le spectre de la réaction effectuée en solution basique (KOH) à un pD de 9–10, montre un seul pic à −3214 ppm (fig. 2c) dû à l'espèce déprotonée dihydroxo, *cis*-$[Pt(EMSO)_2(OH)_2]$. Ce complexe peut aussi être préparé à partir de *cis*-$[Pt(EMSO)_2Cl_2]$ dissous dans une solution de KOH 1*M* (fig. 2d). En effet ce complexe s'hydrolyse et donne une espèce dihydroxo à −3215 ppm et deux autres espèces à −2963 et −2978 ppm. Ces pics, n'apparaissant dans aucun autre spectre, ont été attribués à des espèces chlorées déprotonées, soit *cis*- et *trans*-$[Pt(EMSO)Cl(OH)_2]$. Le spectre rmn protonique du composé *cis*-$[Pt(EMSO)_2Cl_2]$ dissous dans KOH a montré la présence de EMSO libre en plus du ligand lié. La proportion de EMSO libre est d'environ 25–30% pour une solution fraîchement préparée et environ 50% pour une solution vieille de 24 h. L'espèce $[Pt(EMSO)Cl(OH)_2]$ devrait montrer un signal en rmn du platine-195 à un champ plus faible que $[Pt(EMSO)_2(OH)_2]$. En effet, dans une série semblable, la résonance métallique bouge vers les hauts champs selon l'ordre $S > N > Cl^- > O$ (8). Donc lorsqu'un ligand lié par le soufre dans $[Pt(EMSO)_2(OH)_2]$ est remplacé par un ligand chlorure, le signal devrait apparaître à un champ plus faible, ce que nous avons observé.

Les deux signaux observés à −2963 et −2978 ppm sont donc attribués aux deux isomères $[Pt(EMSO)Cl(OH)_2]$, mais il est difficile de savoir avec exactitude quel isomère correspond à chaque signal. Kerrison et Sadler (9) ont mesuré le spectre rmn du platine-195 des deux paires d'isomères *cis*- et *trans*-$[Pt(DMSO)(NH_3)Cl_2]$ ($\Delta\delta$ = 21 ppm) et *cis*- et *trans*-$[Pt(DMSO)(NH_3)_2Cl]$ ($\Delta\delta$ = 21 ppm). Ces auteurs ont attribué le signal observé à plus bas champ à l'isomère où le ligand DMSO est en position *trans* du ligand chlorure. En se basant sur ces résultats, nous pouvons suggérer que le signal observé à −2963 ppm correspond à la résonance de l'isomère *trans*-$[Pt(EMSO)Cl(OH)_2]$, tandis que le signal à plus haut champ (−2978 ppm) correspond à la résonance de l'isomère *cis*-$[Pt(EMSO)Cl(OH)_2]$.

Le tableau 1 montre de façon globale les déplacements chimiques des différentes espèces. Ces valeurs sont régies par la dominance du terme σ sur les déplacements chimiques. La principale contribution à la constante de blindage d'un noyau de métal lourd tel que le platine englobe 2 termes ($\sigma = \sigma_p + \sigma_d$) où σ_p et σ_d sont les contributions paramagnétiqes et diamagnétiques au blindage. Pour un noyau lourd σ_p est prédominant. Ramsey (10) a défini ce terme, qui a été évalué pour ^{195}Pt par Dean et Green (11). À l'aide de cette relation, Gill et Rosenberg (4) ont interprété le déplacement chimique des espèces diaquo (−1898 ppm) et dihydroxo (−1796 ppm) en terme de degré de convalence de la liaison Pt—OD_2 et PT—OD. D_2O étant plus polarisable que OD^-, l'accroissement du degré de covalence du lien Pt—OD_2 résulte en une diminution de δ. Cependant, nos observations des signaux pour $[Pt(EMSO)_2(H_2O)_2]^{2+}$ (δ = −3146 ppm) et $[Pt(EMSO)_2(OH)_2]$ (δ = −3214) montrent un déplacement inversé du complexe dihydroxo relativement au complexe diaquo. Par contre, nos résultats sont en accord avec ceux obtenus par Gröning, Drakenberg et Elding (12), qui ont observé un signal pour *trans*-$[PtCl_2(H_2O)_2]$ à δ = −630 ppm et pour *trans*-$[PtCl_2(OH)_2]^{2-}$ à δ = −675 ppm. Ce phénomène suggère donc une explication plus complexe que celle suggérée par Gill et Rosenberg (4) et tenant compte de l'influence du second ligand.

Le signal du dimère $[Pt(EMSO)_2OH]_2$ apparaît à un champ plus bas (259 ppm) que celui du monomère $[Pt(EMSO)_2(H_2O)_2]^{2+}$ comme observé dans les complexes avec NH_3 (431 ppm (13)) et *trans*-dach (436 ppm (4)). Par contre, contrairement à nos résultats, ces auteurs ont observé un trimère à 78 ppm (13) et 141 ppm (4) du monomère diaquo.

La rmn du ^{195}Pt a permis de mieux visualiser les équilibres en jeu lors de la réaction entre les complexes *cis*-$[Pt(EMSO)_2Cl_2]$ avec Ag_2SO_4. Plusieurs auteurs (4, 13–15) ont étudié les différents équilibres du système *cis*-$[Pt(L)_2Cl_2]$ (L = amine) avec un sel d'argent en solution aqueuse et ont mis en évidence une variété d'espèces mononucléaires et polynucléaires. À ce jour, les complexes avec les sulfoxydes n'ont pas encore fait l'objet d'une telle étude.

Pour les complexes avec des amines, l'espèce diaquo *cis*-$[Pt(L)_2(H_2O)_2]^{2+}$ est prédominante à des petits pH, tandis que l'espèce dihydroxo *cis*-$[Pt(L)_2(OH)_2]$ apparaît en forte proportion à pH élevé. La molécule d'eau est un excellent groupe sortant et la formation de l'espèce monoaquo-monohydroxo, *cis*-$[Pt(L)_2(H_2O)(OH)]$, est prédominante à un pH intermédiaire entre pK_{a1} et pK_{a2} qui se situent pour différentes amines à 5,56–6,14 et 7,32–7,56 (4, 10, 16) respectivement. L'espèce monoaquo-monohydroxo est l'intermédiaire dans la formation d'oligomères à ponts hydroxo. En effet, la réaction

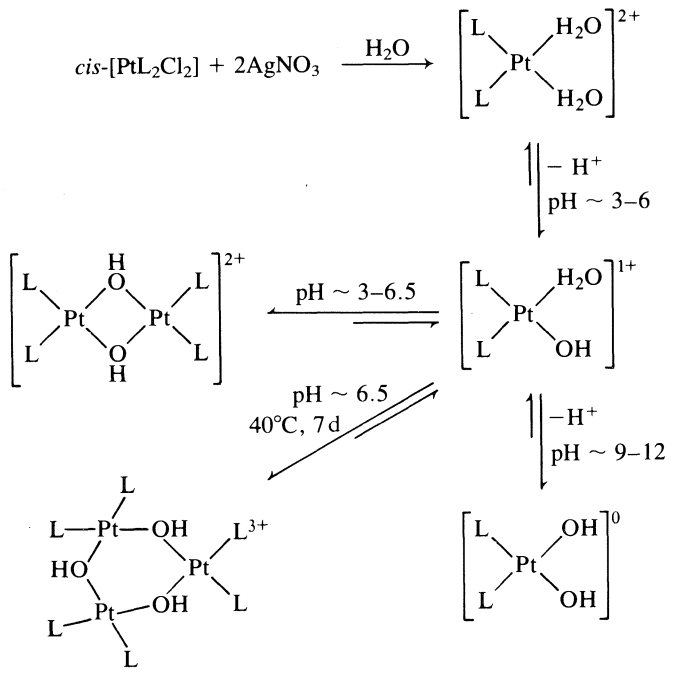

FIG. 3. Profil semi-quantitatif des différents équilibres en solution.

d'oligomérisation est plus rapide dans la région de pH neutre. L'ion hydroxo lié au platine, est encore un bon nucléophile et peut agir comme ligand ponté formant ainsi un complexe binucléaire ponté par deux ligands hydroxo.

Les équilibres des complexes avec des sulfoxydes semblent être semblables à ceux des complexes avec des amines. Lors de la mise en réaction du complexe *cis*-[Pt(sulfoxyde)$_2$Cl$_2$] avec un sel d'argent, le pH de la solution décroît immédiatement de façon radicale de 6,5 à environ 1,5. Ce pH acide indique la formation d'espèces déprotonées telles que le monomère monoaquo-monohydroxo et des oligomères à ponts hydroxo. Ces espèces ont été observées dans le spectre rmn du ^{195}Pt (fig. 1c sans ajustement de pH). Le dimère se forme spontanément et sa proportion augmente en neutralisant la solution. Aprés environ une heure à des pH de 3,9 à 6, la proportion de dimère est près de 100% (figures 2a, 2b).

La formation du trimère est favorisée à haute concentration, à pH neutre, à température plus élevée (40°C) et à un plus long temps de réaction (1 semaine). La figure 3 montre schématiquement l'influence de différents paramètres sur les proportions des différentes espèces en solution. La molécule H_2O est un excellent groupement sortant, mais l'hydroxyde ponté ne l'est pas. Dans les complexes hydroxo pontés, l'affinité de l'hydroxyde pour le platine(II) est approximativement celle de NH_3 (17).

La préparation sélective des complexes est basée sur leur différence de solubilité et sur des conditions de réaction appropriées (1). De façon générale, les dimères avec sulfoxydes sont moins solubles dans l'eau que les trimères. La même tendance a été observée pour le dimère et le trimère avec NH_3 (18), alors qu'avec *trans*-diamino-1,2 cyclohexane (4), des solubilités inverses ont été observées.

Avec le sulfate comme contre-ion, les complexes dimériques et trimériques avec des sulfoxydes sont formés, mais contrairement aux nitrates, la proportion de trimère est importante (1). Faggiani *et al.* (19) ont observé le même phénomène pour les sels de sulfate et de nitrate des trimères avec NH_3. Ils ont attribué cette différence à l'arrangement différent des deux cations trimériques. En effet, à l'état solide l'arrangement stérique du cation dans le sel nitrate semble plus tendu que dans le sel sulfate. Nous croyons également que dans les complexes avec des sulfoxydes, le cation du trimère dans le sel sulfate serait moins tendu et plus facile à isoler que le sel nitrate ou perchlorate. Nous avons tenté de préparer des monocristaux des trimères afin d'en déterminer la structure cristalline, mais sans succès jusqu'à maintenant. Par contre, nous avons déterminé la structure cristalline de deux dimères, *cis*-[Pt(DMSO)$_2$(OH)]$_2$(ClO$_4$)$_2$ (20) et *cis*-[Pt(TMSO)$_2$(OH)]$_2$(NO$_3$)$_2$ (TMSO = tétraméthylènesulfoxyde) (21). Le cation des deux dimères est très semblable mais contrairement aux ions perchlorates, les ions NO_3^- sont très désordonnés. De plus, le système de ponts hydrogènes impliquant les anions est différent.

Remerciements

Nous remercions le Conseil de recherches en sciences naturelles et en génie du Canada et le Ministère de l'Education (FCAR) pour l'aide financière apportée à ce projet.

1. F. D. ROCHON, P. C. KONG et L. GIRARD. Can. J. Chem. **64**, 1897 (1986).
2. W. FREEMAN, P. S. PREGOSIN, S. N. SZE et L. M. VENANZI. J. Mag. Reson. **22**, 473 (1976).
3. C. J. L. LOCK, J. BRADFORD, R. FAGGIANI, R. A. SPERANZINI, G. TURNER et M. ZVAGULIS. J. Clin. Hematol. Oncol. **7**, 63 (1977).
4. D. S. GILL et B. ROSENBERG. J. Am. Chem. Soc. **104**, 4598 (1982).
5. J. C. DABROWIAK, M. S. BALAKRISHMAN, J. CLARDY, G. D. VAN DUYNE et L. SILVIERA. Platinum coordination complexes in cancer chemotherapy. Martinus Nijhoff Publishing, Boston. 1984. p. 63.
6. T. G. APPLETON, R. D. BERRY, C. A. DAVIS, J. R. HALL et H. A. KIMLIN. Inorg. Chem. **23**, 3514 (1984).
7. T. G. APPLETON, J. R. HALL, S. F. RALPH et G. M. THOMPSON. Inorg. Chem. **23**, 3521 (1984).
8. P. S. PREGOSIN. Coord. Chem. Rev. **44**, 247 (1982).
9. S. J. S. KERRISON et P. J. SADLER. J. Chem. Soc. Chem. Commun. 861 (1977).
10. N. F. RAMSEY. Phys. Rev. **78**, 6, 699 (1950).
11. R. R. DEAN et J. C. GREEN. J. Chem. Soc. (A), 3048 (1968).
12. Ö. GRÖNING, T. DRAKENBERG et L. I. ELDING. Inorg. Chem. **21**, 1820 (1982).
13. C. J. BOREHAM, J. A. BROOMHEAD et D. P. FAIRLIE. Aust. J. Chem. **34**, 659 (1981).
14. B. ROSENBERG. Biochimie, **60**, 859 (1978).
15. M. C. LIM et R. B. MARTIN. J. Inorg. Nucl. Chem. **38**, 1911 (1976).
16. R. FAGGIANI, B. LIPPERT, C. J. L. LOCK et B. ROSENBERG. J. Am. Chem. Soc. **99**, 3, 777 (1977).
17. H. SIGEL. Metal ions in biological systems. Vol. 11. Metal complexes as anticancer agents. Marcel Dekker Inc., New York. 1980. Chapt. 2.
18. R. FAGGIANI, B. LIPPERT, C. J. L. LOCK et B. ROSENBERG. Inorg. Chem. **16**, 1192 (1977).
19. R. FAGGIANI, B. LIPPERT, C. J. L. LOCK et B. ROSENBERG. Inorg. Chem. **17**, 1941 (1978).
20. F. D. ROCHON, P. C. KONG et R. MELANSON. Acta Crystallogr. Sect. C, **41**, 1602 (1985).
21. F. D. ROCHON et F. GUAY. Acta Crystallogr. Sous presse.

A comparative ion chemistry study of acetone, diacetone alcohol, and mesityl oxide

AFAF KAMAR,[1] ALEXANDER BALDWIN YOUNG, AND RAYMOND EVANS MARCH[2]
Department of Chemistry, Trent University, Peterborough, Ont., Canada K9J 7B8

Received June 17, 1985[3]

AFAF KAMAR, ALEXANDER BALDWIN YOUNG, and RAYMOND EVANS MARCH. Can. J. Chem. **64**, 1979 (1986).

The evolution of ion species by unimolecular and bimolecular reactions, both concurrent and sequential, has been investigated for each of 2-propanone, d_6-2-propanone, 4-hydroxy-4-methyl-2-pentanone, and 4-methyl-3-penten-2-one. Infrared multiphoton dissociation (IRMPD) has been used in order to differentiate between gaseous ionic isomers. It is concluded that the isomeric species, protonated 2-propanone dimer and protonated 4-hydroxy-4-methyl-2-pentanone, both of m/z 117, are of different structures. The ion species $C_6H_{11}O^+$ of m/z 99, and its perdeuterated analogue, which is observed in all three systems, may exist in two forms, one of which is unique to 2-propanone while an alternative form appears to be common to 4-hydroxy-4-methyl-2-pentanone and 4-methyl-3-penten-2-one. The ion species of m/z 83 ($C_5H_7O^+$) which is observed only in the latter two systems only could not be differentiated and may have a common structure. In the protonated dimers of 2-propanone and 4-hydroxy-4-methyl-2-pentanone, evidence obtained by IRMPD indicates that the activation energy for dedimerization (134 kJ mol^{-1}) is less than that for the dehydration process.

AFAF KAMAR, ALEXANDER BALDWIN YOUNG et RAYMOND EVANS MARCH. Can. J. Chem. **64**, 1979 (1986).

On a étudié l'évolution des espèces ioniques provenant de réactions unimoléculaires ainsi que bimoléculaires, tant des réactions qui se produisent d'une façon concurente que séquentielle, de la propanone-2, de la propanone-2-d_6, de l'hydroxy-4 méthyl-4 pentanone et de la méthyl-4 pentène-3 one-2. Dans le but de distinguer les divers isomères ioniques gazeux, on a fait appel à la dissociation multiphotonique infrarouge (DMPIR). On en conclut que les espèces isomères dimères protonés de la propanone-2 et de l'hydroxy-4 méthyl-4 pentanone-2 protonée, de m/z = 117, possèdent deux structures différentes. L'espèce ionique $C_6H_{11}O^+$, de m/z = 99, et celle de son analogue perdeutéré qui est observée dans les trois systèmes peut exister sous deux formes; l'une est unique à la propanone-2 alors qu'une autre forme semble être commune à l'hydroxy-4 méthyl-4 pentanone-2 et à la méthyl-4 pentène-3 one-2. Les espèces ioniques de m/z = 83 ($C_5H_7O^+$), qui ne sont observées que dans les deux derniers systèmes, ne présentent pas de différences et possèdent peut être la même structure. Dans le cas des dimères protonés de la propanone-2 et de l'hydroxy-4 méthyl-4 pentanone-2, on a obtenu des données à l'aide de la DMPIR à l'effet que l'énergie d'activation pour la dédimérisation (134 kJ mol^{-1}) est plus faible que celle requise pour le processus de deshydratation.

[Traduit par la revue]

Introduction

Previous studies employing slow Infrared Multiphoton Dissociation (IRMPD), as a probe of activation energy hierarchies in the gas phase photolysis of proton-bound dimers, have been carried out with each of 2-propanol (1–4), ethanol (5), 1-butanol (6), and deuterated propanols (7). With proton-bound alcohol dimers it is possible to determine in some degree the hierarchy of activation energies among the reaction channels leading to loss of alkene, water, and monomer or parent molecule. With the proton-bound dimers of 2-propanone and 4-hydroxy-4-methyl-2-pentanone studied here, it is possible to assess the activation energy hierarchy for loss of water and monomer. IRMPD may be used also to differentiate between isomeric ion species in the gas phase. The distinguishing criteria for photochemical differentiation are relative absorptivity at the wavelength available for laser irradiation and, of greater importance, the photoproduct distribution, i.e. the ionic species produced and their relative intensities. In some cases it is informative to photolyze the species of interest in both the ground state and in its nascent state; nascent ion internal excitation is enhanced by multiple photon absorption to access reaction channels of higher activation energy, limited in practice, by competition between laser fluence and collision frequency.

The ion-chemistry for each of 2-propanone, 4-hydroxy-4-methyl-2-pentanone, and 4-methyl-3-penten-2-one is presented here. These three compounds are related in the following ways: the proton-bound dimer of 2-propanone is isomeric with protonated 4-hydroxy-4-methyl-2-pentanone and the ion structures could be identical if aldol condensation occurs in the gas phase; an ion species of m/z 99 ($C_6H_{11}O^+$) is produced in both of the above systems and is isomeric with protonated 4-methyl-3-penten-2-one; and lastly an ion species of m/z 83 ($C_5H_7O^+$) is observed only with 4-hydroxy-4-methyl-2-pentanone and 4-methyl-3-penten-2-one and is conspicuously absent in 2-propanone. Thus these three compounds present an opportunity for isomer differentiation using the techniques of ion storage and IRMPD.

Experimental

Although the basic apparatus has been described previously (1–3), a brief description of the technique used in this work is presented here. A three-dimensional quadrupole ion store (QUISTOR) mounted in place of the ion source of a conventional quadrupole mass filter (Vacuum Generators QXK 400), serves as the reactor in which ion/molecule reactions take place over the period 0–200 ms. The ring electrode of the QUISTOR has two central perforations diametrically opposed. A low power CW CO_2 laser beam is directed through a sodium chloride window and through the first ring perforation, of diameter 3 mm. The beam passes radially through the centre of the QUISTOR and totally illuminates the ion cloud which rapidly becomes tightly focused at the centre of the device. A portion of the beam passes through the perforation at the opposite side of the ring electrode and is monitored externally through a second sodium chloride window. The remainder of the beam is thought to undergo multiple reflections within the QUISTOR. The laser beam is chopped mechanically and phase-locked with the pulsing sequence as shown in Fig. 1.

The repetition rate of the pulse sequence is controlled by a square-wave generator (Heathkit SG 18A). The laser beam is interrupted by a PAR 222 chopper phase-locked to the square-wave generator. A range

[1]Registered in the Ph.D. programme in Chemistry Department, Queen's University.

[2]Adjunct Professor, Department of Chemistry, Queen's University, Kingston.

[3]Revision received February 21, 1986.

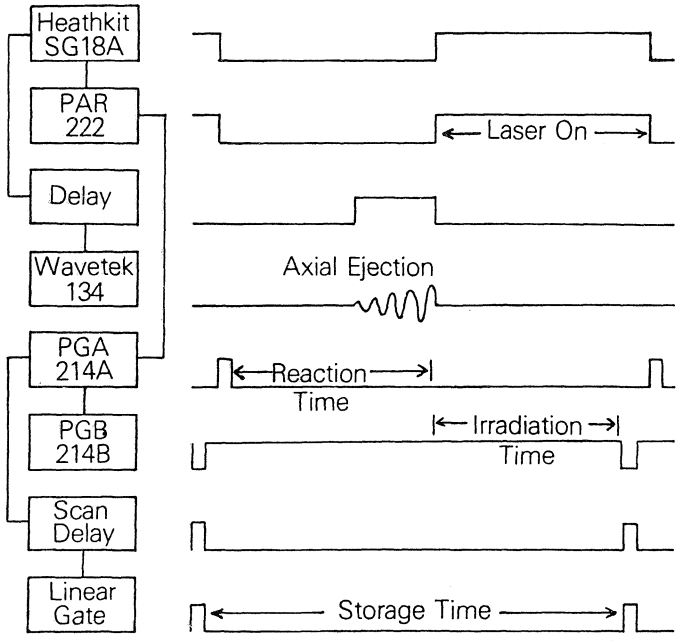

FIG. 1. Pulse sequence used in IRMPD with axial ejection employed to isolate an ionic species of interest by removal of all lower m/z ions prior to laser irradiation.

of total storage times was effected using chopper wheels with a variety of wheel apertures, while variation of the laser irradiation period within a fixed total storage time was achieved with chopper wheels of different light-to-dark ratio. The mechanical chopper triggers the creation pulse (Hewlett Packard pulse generator 214B, PGA) which triggers in turn the extraction pulse (PGB) and a Brookdeal scan delay generator (9425) which provides a detection pulse to drive a linear gate (Brookdeal 9415). The square-wave generator also drives a delay pulse generator which triggers in turn a Sweep Generator (Wavetek 134) which is then used to remove, by axial ejection (8), ions of mass-to-charge ratio less than that of protonated dimer prior to laser irradiation.

The ion abundances are obtained by recording mass spectra at zero storage (electron impact) and at a variety of storage times; the relative ion intensities are calculated for each species at each storage time to yield the data points shown in the figures. The temporal variation of the intensity of each ion species was checked by single ion monitoring over the storage period employed.

2-Propanone (acetone)

Ion/molecule chemistry

The ion chemistry of 2-propanone has been studied previously by Munson (9) and by Blair and Harrison (10), and is re-examined here both to resolve the minor differences between the findings of these two groups and to provide a basis for explanation of our photodissociation results obtained with proton-bound dimers of 2-propanone and 4-hydroxy-4-methyl-2-pentanone. Munson employed a variable pressure source and reported on secondary ion intensities as a function of pressure only. Blair and Harrison, in an electron beam trapping study with a trapping period of 3 ms, used an ionizing electron energy sufficient to produce only $(CH_3)_2CO^{+\cdot}$ and CH_3CO^+ as primary ions, with the former comprising 70% of the primary ion abundance. Protonated parent molecules, m/z 59, are produced by reactions of the primary ions

$$[1]\quad \underset{m/z\ 58}{(CH_3)_2CO^{+\cdot}} + (CH_3)_2CO \rightarrow \underset{m/z\ 59}{(CH_3)_2\overset{+}{C}OH} + CH_3\dot{C}OCH_2$$

$$[2]\quad \underset{m/z\ 43}{CH_3CO^+} + (CH_3)_2CO \rightarrow \underset{m/z\ 59}{(CH_3)_2\overset{+}{C}OH} + CH_2CO$$

The proton-bound dimer m/z 117 is produced continuously with either increasing pressure or increasing storage time by reaction with parent neutrals

$$[3]\quad \underset{m/z\ 59}{(CH_3)_2COH^+} + (CH_3)_2CO \rightleftharpoons \underset{m/z\ 117}{[(CH_3)_2CO]_2H^+}*$$

where * denotes a degree of internal excitation. The nascent proton-bound dimer may then be either collisionally deactivated

$$[4]\quad \underset{m/z\ 117}{[(CH_3)_2CO]_2H^+}* \xrightarrow{M} \underset{m/z\ 117}{[(CH_3)_2CO]_2H^+} + M$$

or may dissociate

$$[5]\quad \underset{m/z\ 117}{[(CH_3)_2CO]_2H^+}* \rightarrow \underset{m/z\ 101}{CH_3CO(CH_3COCH_3)^+} + CH_4$$

$$[6]\quad \underset{m/z\ 117}{[(CH_3)_2CO]_2H^+}* \rightarrow \underset{m/z\ 99}{C_6H_{11}O^+} + H_2O$$

An alternative and preferred mechanism for the formation of m/z 101, is the clustering reaction

$$[7]\quad \underset{m/z\ 43}{CH_3CO^+} + (CH_3)_2CO \rightarrow \underset{m/z\ 101}{(CH_3)_2CO\text{---}\overset{+}{H}\text{---}OCCH_2}*$$

which is then collisionally stabilized. This species may be regarded as the product of a mixed associative ion (or a heterogeneous proton-bound dimer) of ketene proton-bridged to 2-propanone. Mixed associative ions of ketene with methanol, ethanol, and 2-propanol have been reported previously (11). The stabilization of this mixed associative ion, m/z 101, may require a reactant CH_3CO^+ of modest internal excitation only, which would account for the fact that it was observed by Blair and Harrison under their conditions of low ionizing electron energy, but not by Munson who employed ionizing electrons of 70 eV and a high pressure source. The $CH_3CO(CH_3COCH_3)^+$ product reacts slowly at longer reaction times to produce the proton-bound dimer ion in a ligand replacement reaction

$$[8]\quad \underset{m/z\ 101}{CH_3CO(CH_3COCH_3)^+} + CH_3COCH_3 \rightarrow \underset{m/z\ 117}{[(CH_3)_2CO]_2H^+} + CH_2CO$$

The species of m/z 99 formed by loss of water in the dissociation of the protonated dimer, reaction [6], was tentatively identified by Munson as protonated 4-methyl-3-penten-2-one. Since the proton-bound dimer of 2-propanone is isomeric with protonated 4-hydroxy-4-methyl-2-pentanone, it was plausible to propose that gaseous ion reactions may be observed which correspond with solution ionic reactions in which the acid-catalyzed formation of 4-hydroxy-4-methyl-2-pentanone and 4-methyl-3-penten-2-one is observed from 2-propanone. The requirement of reactant excitation in order for reaction [6] to proceed in a manner which is endothermic for ground state reactants would explain the observation of m/z 99 by Munson but not by Blair and Harrison.

In the work reported here and shown in Fig. 2, both species of m/z 99 and m/z 101 were observed as the ions were created with ionizing electrons of 70 eV and the reactions of both excited and ground state (collisionally cooled) CH_3CO^+ ions were monitored.

Perdeuterated 2-propanone was investigated also as there was some interest in the infrared relative absorptivity of deuteron-bound deuterated dimer ions $[(CD_3)_2CO]_2D^+$, m/z 130.

The ion profiles obtained with 2-propanone and d_6-2-propanone are similar in general form as shown in Figs. 2 and 3.

In 2-propanone, the ions of m/z 99 may be formed by the loss of water, reaction [6], while ions of m/z 101 may be formed by reaction [5] and/or reaction [7] to yield $C_6H_{11}O^+$ and $C_5H_9O_2^+$, respectively. The corresponding product ions in d_6-2-propanone will be $C_6D_{11}O^+$ and $C_5D_9O_2^+$, respectively, formed in reactions [9], and [10] and/or [11] to produce isobaric species of m/z 110.

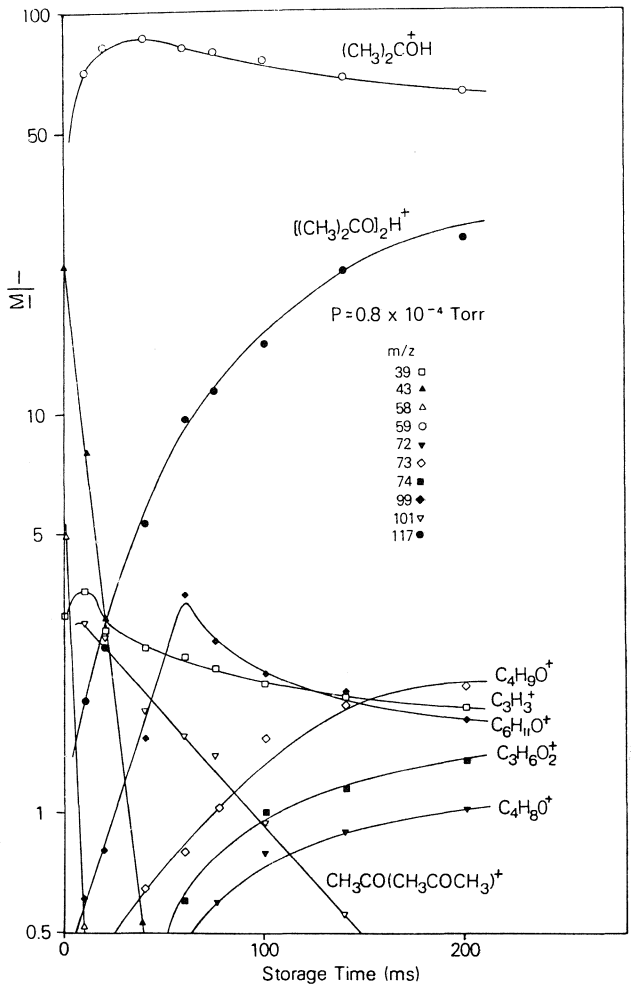

FIG. 2. Variation in the logarithm of normalized ion abundances in 2-propanone with storage time 0–200 ms, 0.8×10^{-4} Torr.

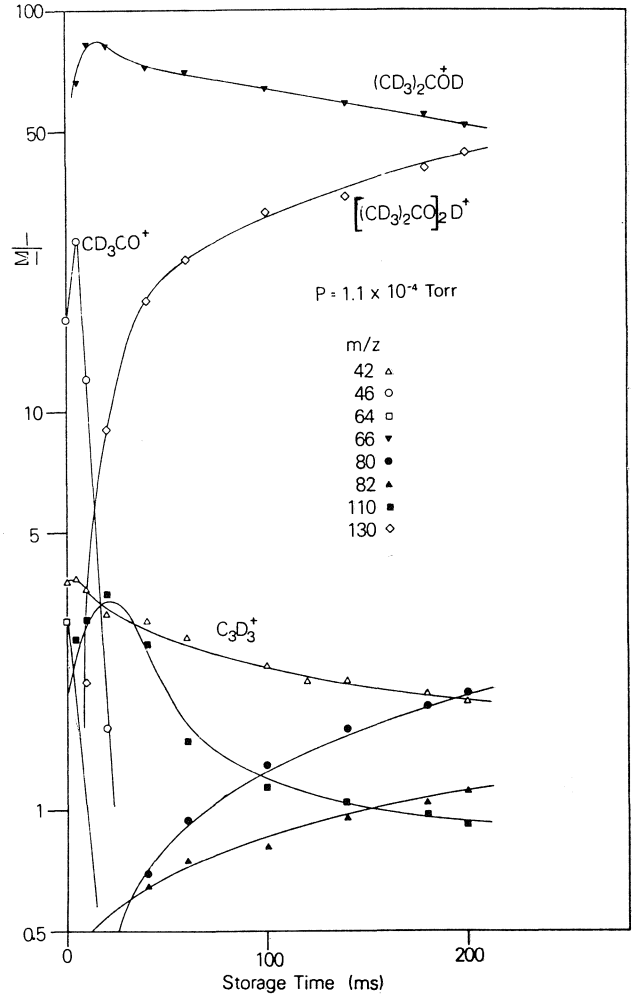

FIG. 3. Variation in the logarithm of normalized ion abundances in perdeutero-2-propanone with storage time 0–200 ms, 1.1×10^{-4} Torr.

[9] $[(CD_3)_2CO]_2D^+* \rightarrow C_6D_{11}O^+ + D_2O$
m/z 130 m/z 110

[10] $[(CD_3)_2CO]_2D^+* \rightarrow C_5D_9O_2^+ + CD_4$
m/z 130 m/z 110

[11] $CD_3CO^+ + (CD_3)_2CO \rightarrow (CD_3)_2CO\text{---}\overset{+}{D}\text{---}OCCD_2$
m/z 46 m/z 110

Thus the ion profile for m/z 110 in Fig. 3 is a composite of the two isobaric ions.

While the ions of m/z 80 and m/z 82 observed in d_6-2-propanone were of low relative intensity, they can be reconciled with the observation of ions of m/z 72, 73, and 74 in 2-propanone as shown in Fig. 2.

(*i*) Let us examine the possible origin for m/z 82 in d_6-2-propanone. The $C_5D_9O_2^+$ species may lose CO or C_2D_2 to produce $C_4D_9O^+$ and $C_3D_7O_2^+$, respectively. The corresponding ions in 2-propanone would be $C_4H_9O^+$, m/z 73 and $C_3H_7O_2^+$, m/z 75. The latter species was not observed therefore $C_5D_9O_2^+$ does not lose C_2D_2.

The isobaric $C_6D_{11}O^+$ ion may lose CO to produce $C_5D_{11}^+$ or lose C_2D_2 to produce $C_4D_9O^+$. The corresponding ions in 2-propanone would be $C_5H_{11}^+$, m/z 71, which was not observed, and $C_4H_9O^+$, m/z 73, which was observed. Thus we conclude that either reaction [12]

[12] $C_5D_9O_2^+* \rightarrow C_4D_9O^+ + CO \qquad \Delta H_{12}$

or reaction [13]

[13] $C_6D_{11}O^+* \rightarrow C_4D_9O^+ + C_2D_2 \qquad \Delta H_{13}$

occurs or both occur, where ΔH_{12} and ΔH_{13} are the enthalpy changes for reaction [12] and [13], respectively. As either reaction [12] or reaction [13] may account for the observations, it is appropriate to consider the energetics of the processes bearing in mind that a small fraction of stored ions may acquire translational energy from the three-dimensional quadrupole field and produce minor amounts of fragment ions in super-thermal collisions. As reactions [12] and [13] produce a common daughter ion with an assumed common structure, and the heats of formation of CO and C_2H_2 are -110 and 227 kJ mol^{-1}, respectively, then for reaction [13] to occur the heat of formation of $C_6D_{11}O^+$ plus internal excitation must exceed the heat of formation of $C_5D_9O_2^+$ plus internal excitation of 337 kJ mol^{-1}, provided that $\Delta H_{12} = \Delta H_{13}$. Thus the occurrence of reaction [13] is less probable than reaction [12].

(*ii*) In a similar examination of the origin of m/z 80 in d_6-2-propanone, the $C_5D_9O_2^+$ may lose $C_2D_3^\bullet$ or $CDO^\bullet$ to produce $C_3D_6O_2^{+\bullet}$ or $C_4D_8O^{+\bullet}$, respectively. The corresponding product ions in 2-propanone are $C_3H_6O_2^{+\bullet}$, m/z 74, and $C_4H_8O^{+\bullet}$, m/z 72, both of which were observed.

Thus as m/z 74 was observed in 2-propanone, we conclude that reaction [14] occurs

[14] $C_5D_9O_2^+* \rightarrow C_3D_6O_2^{+\bullet} + C_2D_3^\bullet$

The observation of m/z 72 in 2-propanone may be explained by the analogous reactions to either

[15] $C_5D_9O_2^+* \rightarrow C_4D_8O^{+\bullet} + CDO^\bullet$

or

[16] $C_6D_{11}O^+* \rightarrow C_4D_8O^{+\cdot} + C_2D_3^{\cdot}$

or both.

The heats of formation of $HCO^{\cdot}$ and $C_2H_3^{\cdot}$ are reported as 33.9 and 332 kJ mol^{-1}, respectively (12). The observation of m/z 74 infers that the heat of formation of $C_3D_6O_2^+$ is some 332 kJ mol^{-1} less than the heat of formation of $C_5D_9O_2^+$ plus internal excitation when reaction [14] is thermoneutral. By an argument similar to that presented above for reactions [12] and [13], it can be shown that for reaction [16] to occur the heat of formation of $C_6D_{11}O^+*$ must exceed that of $C_5D_9O_2^+*$ by some 298 kJ mol^{-1} again provided that the enthalpy changes for reactions [15] and [16] are similar. Thus the occurrence of reaction [16] is less probable than reaction [15].

The observation of $C_3H_3^+$ as a persistent ion species in each of the systems studied here is in keeping with previous observations of this species wherever the parent molecule has a 2-propyl grouping. The reactivity of $C_3H_3^+$ is discussed elsewhere (13).

Photochemical studies

The IRMPD of the collisionally relaxed proton-bound dimer of 2-propanone yielded but a single photodissociative channel, as is

[17] $\underset{m/z\ 117}{[(CH_3)_2CO]_2H^+} \xrightarrow{nh\nu} \underset{m/z\ 59}{(CH_3)_2\overset{+}{C}OH} + (CH_3)_2CO$

shown in Fig. 4, that of protonated 2-propanone.

In this figure, two sets of experiments are shown; the first experiment employing an initial ionization period followed by 45 ms of ion–molecule reaction time, wherein the proton-bound dimer ion is produced. Axial ejection removes all ionic species of $m/z < 117$, isolating the dimer in the trap. These isolated dimers possess a range of internal energies and some undergo thermal unimolecular dissociation to produce the protonated parent m/z 59 during the 80 ms following isolation and prior to ejection and mass analysis. In the second experiment shown as solid lines in Fig. 4, the dimer is irradiated at 944 cm^{-1} for the 80 ms period following its isolation in the QUISTOR, then the trap population is ejected and mass analyzed.

The period of laser irradiation was varied from 50 to 100 ms, that is one half the total storage time, and in each case greater than 90% of the proton-bound dimers were dissociated. As proton-bound dimers are being produced continually, the ions irradiated will have a range of ages and internal energies. As but a single photoproduct was obtained we conclude that the energies of activation for reactions [5] and [6] exceed that of reaction [17] which is reported to be 134 kJ mol^{-1} (14). While precise measurements of the cross-section for photodissociation (σ_D) were not made, the high absorptivity at 944 cm^{-1} of proton-bound dimers of 2-propanone is comparable to that of 2-d_1-2-propanol (7). This high absorptivity is remarkable as neutral 2-propanone has negligible absorption in the vicinity of 944 cm^{-1}.

In contrast the deuteron-bound dimer of d_6-2-propanone exhibited somewhat lower absorptivity in that approximately 40% only of this species was photodissociated under similar conditions; reduced absorptivity in perdeutero-2-propanol has been observed (7) also. As expected, a single photoproduct, deuteron-bound d_6-2-propanone, was observed upon IRMPD.

4-Hydroxy-4-methyl-2-pentanone (diacetone alcohol)

Ion/molecule chemistry

The ion chemistry of 4-hydroxy-4-methyl-2-pentanone obtained at a pressure of 6×10^{-5} Torr is depicted in Fig. 5 where it is seen that the predominant second order product ion at long storage times is the protonated parent molecule, $(CH_3)_2C(OH)CH_2\overset{+}{C}OHCH_3$, m/z 117. Of the two possible structures for the m/z 117 ion structure **II** is

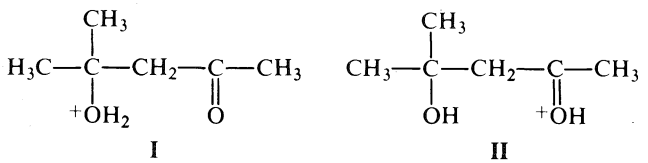

I **II**

recommended by Parker *et al.* (15) on the basis of collisionally activated dissociation (CAD) studies. The base peak in the electron impact mass spectrum, i.e. 38% relative ion intensity at zero storage time, is due to CH_3CO^+, m/z 43; this primary ion reacts rapidly along with other minor primary ions during the first 20 ms principally by proton transfer reactions such as

[18] $\underset{m/z\ 43}{CH_3CO^+*} + (CH_3)_2C(OH)CH_2COCH_3 \rightarrow (CH_3)_2C(OH)CH_2\overset{+}{C}OHCH_3* + CH_2CO$
$m/z\ 117$

where * denotes a degree of internal excitation.

At this juncture, it is appropriate to consider the nature of the $C_2H_3O^+$ species which is observed in the electron impact fragmentations of simple oxygen-containing molecules. In the 2-propanone system discussed above, it was suggested that the stabilization and subsequent observation of the ion of m/z 101 may require a reactant CH_3CO^+ of but modest internal excitation, while in the 4-hydroxy-4-methyl-2-pentanone system it is evident from Fig. 5 that two forms of $C_2H_3O^+$ exist which differ in reactivity. The temporal variation of the ion abundance of m/z 43 in Fig. 5 clearly shows two linear components in the decay curve; the bimolecular rate constant derived from the steep component is almost an order of magnitude greater than that derived from the shallow component. While one form of $C_2H_3O^+$ may derive its greater reactivity by virtue of internal energy, it is improbable that the internal energy of some 90% of the initial $C_2H_3O^+$ abundance would survive the many collisions by which deactivation could occur. The co-existence of $C_2H_3O^+$ in three structures from a single precursor has been reported (16). While as many as eleven possible isomeric structures for $C_2H_3O^+$ have been examined recently, only five structures will be considered here.

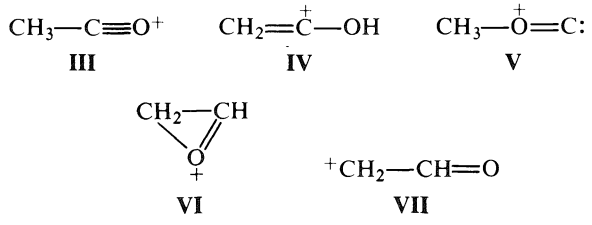

III **IV** **V**

VI **VII**

Of the potential $C_2H_3O^+$ above, the acetyl cation (**III**), 1-hydroxyvinyl cation (**IV**) and oxiranyl cation (**VI**) have been well characterized as being stable, observable species (16–18); the acetyl cation is the lowest energy isomer. The 1-hydroxyvinyl cation (**IV**) was found to lie 181 kJ mol^{-1} above **III**, with a barrier to rearrangement by

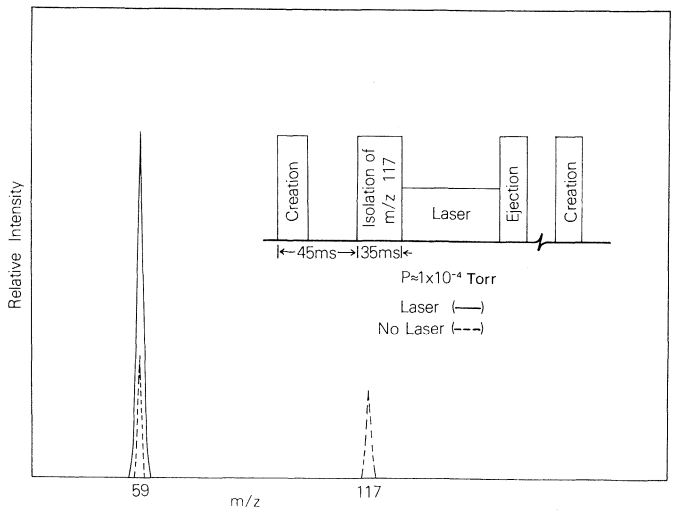

FIG. 4. Experimental sequence and results from IRMPD of 2-propanone protonated dimers at 1.0×10^{-4} Torr. Dashed lines correspond to the ion intensities in an experiment wherein the laser was blocked, solid lines correspond to ion intensities obtained with laser irradiation at 944 cm^{-1} for the latter 80 ms of the experimental period.

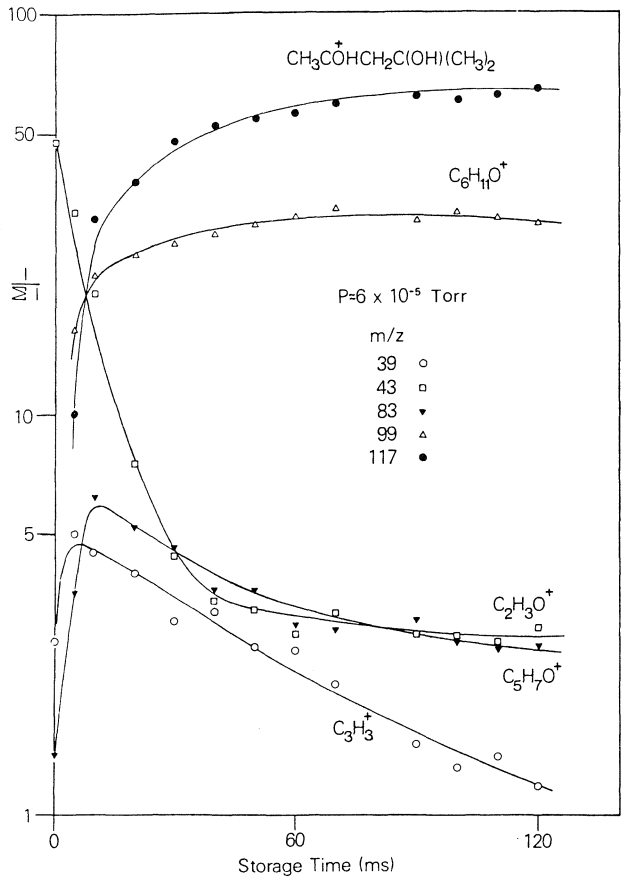

FIG. 5. Variation in the logarithm of normalized ion abundances in 4-hydroxy-4-methyl-2-pentanone with storage time 0–120 ms, 6×10^{-5} Torr.

successive 1,2-hydrogen shifts of 287 kJ mol^{-1} (19). CH_3OC^+ (**V**) was found to be the third lowest isomer in energy of the $C_2H_3O^+$ ions examined, lying 216 kJ mol^{-1} above CH_3CO^+ (**III**) (19). There appears to be no experimental study of CH_3OC^+. The results of a recent study (16) of metastable peak intensities and shapes and collision induced processes over a range of pressures provide unequivocal evidence for identification of the acetyl (**III**), 1-hydroxyvinyl (**IV**) and oxiranyl (**VI**) cations. The oxiranyl cation was predicted (19) to be 244 kJ mol^{-1} above **III** with a barrier to rearrangement of 85 kJ mol^{-1}, while **VII** was predicted to collapse without activation energy to either **VI** or **III**.

The acetyl cation **III** is known to react rapidly with oxygen-containing molecules such as 2-propanone (20). In previous studies we have noted the rapid reaction of primary $C_2H_3O^+$ cations in 1- and 2-propanol and in tetrahydrofuran (unpublished work by the authors) and conclude that this ion must be of structure **III**. However, the ion chemistry of the 1- and 2-propanol and tetrahydrofuran systems, following the initial decay of the acetyl cation, is characterized by a steady accumulation of a $C_2H_3O^+$ cation which is presumed to be of a different but unspecified structure.

While it is proposed that $(CH_3)_2C(OH)CH_2COHCH_3^+$, m/z 117, is formed with excess internal excitation in reaction [18] from an excited acetyl ion in order to explain the subsequent unimolecular dissociation of m/z 117, some discussion of the proton affinities of 4-hydroxy-4-methyl-2-pentanone and ketene would be useful here. The proton affinity of the former does not appear in the literature (22) but has been determined in this laboratory (23) to be 831 ± 0.8 kJ mol^{-1} (198.7 ± 0.2 kcal mol^{-1}), while the proton affinity for ketene is 828 kJ mol^{-1} (22). Thus for ground state acetyl ions from which a proton is transferred and ketene remains, the reaction is virtually thermoneutral.

The excited protonated parent molecules formed may then be collisionally deactivated.

[19] $(CH_3)_2C(OH)CH_2COHCH_3^{+*}$ (m/z 117) $\xrightarrow{M}$ $(CH_3)_2C(OH)CH_2\overset{+}{C}OHCH_2 + M$ (m/z 117) **II**

where M represents a collision partner, or may dissociate

[20] 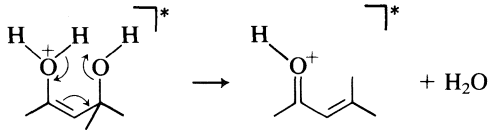 + H_2O

(m/z 117 → m/z 99) **VIII**

to give m/z 99 of structure **VIII** which is that of protonated mesityl oxide (4-methyl-3-penten-2-one). The excited **VIII** may then either be collisionally deactivated or eject CH_4 to produce an ion of m/z 83

[21] 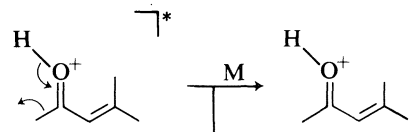

(m/z 99 → m/z 99)

[22] 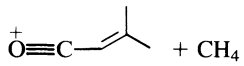 + CH_4

(m/z 83) **IX**

The possibility of CH_4 loss occurring initially from m/z 117 followed by loss of H_2O to produce m/z 83 is rejected as no species of m/z 101 was detected. Although the species of m/z 99 and m/z 83 have been observed previously (15), neither the structures of these ions nor the identities of the neutral fragments ejected have been investigated further except for an attempt to photodissociate m/z 99 by multiphoton absorption as discussed below.

The principal minor primary ions, m/z 57, 59, 98, and 101 reacted rapidly during the first 10 ms and linear plots of the logarithm of ion intensities with time have been omitted from Fig. 5 so that the ion profiles of the more stable ions may be portrayed clearly. After the first 20 ms of reaction time, the remaining unreacted m/z 43 ions isomeric with CH_3CO^+ reacted slowly along with ions of m/z 83 and 99 in proton transfer reactions to produce the protonated parent molecule, m/z 117. At pressures higher than 6×10^{-5} Torr, proton-bound dimers of 4-hydroxy-4-methyl-2-pentanone of m/z 233 were observed.

Photochemical studies

IRMPD of $(CH_3)_2C(OH)CH_2\overset{+}{C}OHCH_3$, m/z 117, was carried out as described earlier. Two photoproducts as depicted in Fig. 6 were observed.

[23] $(CH_3)_2C(OH)CH_2\overset{+}{C}OHCH_3$ (m/z 117) $\xrightarrow{nh\nu\ 10\%}$ $C_2H_3O^+ + C_4H_{10}O$ (m/z 43)

[24] $\xrightarrow{n'h\nu\ 90\%}$ $C_6H_{11}O^+ + H_2O$ (m/z 99)

where n and n' are the minimum number of photons ($h\nu$) necessary to overcome the activation energy barriers for reactions [23] and [24], respectively. IRMPD has been shown to be a useful probe of activation energy hierarchies when ground state reactants are irradiated. It is concluded from the observed ratio of photoproducts obtained with 33 ms of laser irradiation that the activation energy for reaction [24] is less than that for reaction [23]; this conclusion is supported by the observation that with prolonged laser irradiation, the fractional yield of reaction [23] can be increased.

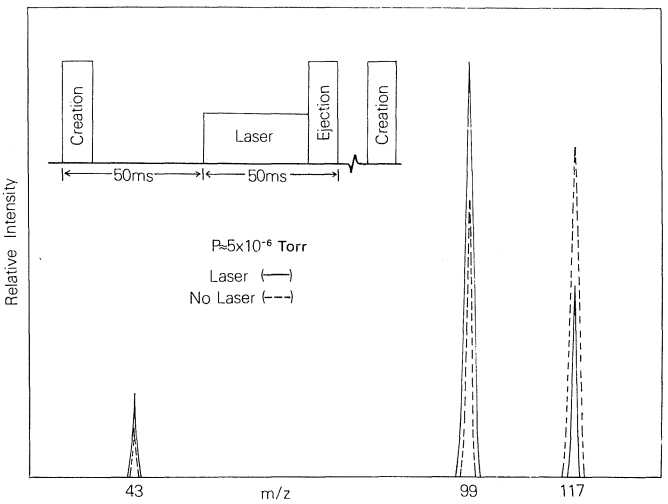

FIG. 6. Experimental sequences and results from IRMPD of protonated 4-hydroxy-4-methyl-2-pentanone at 6×10^{-5} Torr. Dashed lines correspond to the ion intensities obtained in an experiment wherein the laser was blocked, solid lines correspond to ion intensities obtained with laser irradiation at 944 cm^{-1} for the latter 50 ms of the experimental period.

In the discussion above of the ion chemistry of 4-hydroxy-4-methyl-2-pentanone, it was assumed that the unreactive form of $C_2H_3O^+$ had been produced as a fragment ion upon electron impact. However, during experiments using axial ejection in which all ion species of $m/z < 117$ are ejected from the QUISTOR, it was observed that a relatively unreactive form of $C_2H_3O^+$ was generated by dissociation of protonated parent molecules, as shown in reaction [25] which is the thermal analogue of the photochemical process, reaction [23].

It is of interest to speculate on the possibility that the products of reactions [23] and [25] are derived from the protonated keto form via a 4-centred elimination

[25] 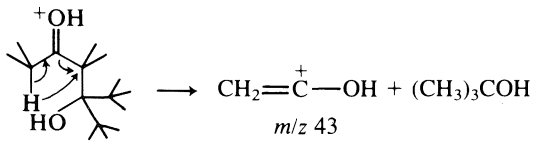

$\longrightarrow CH_2{=}\overset{+}{C}{-}OH + (CH_3)_3COH$
m/z 43

whereas the products of reaction [24] are derived from the protonated enol form via a 6-centred elimination as depicted in reaction [20]. As activation energies for 6-centred rearrangements are generally lower than those for 4-centred, then the above speculative mechanistic argument is consistent with the IRMPD results.

Let us consider now the structures of protonated 4-hydroxy-4-methyl-2-pentanone and the isomeric cation formed by the addition of 2-propanone to protonated 2-propanone which has been identified in reaction [3] as a proton-bound dimer. Parker *et al.* (15) found a qualitative similarity between the relative ion abundances in the self-chemical ionization mass spectrometry (self-CIMS) of 2-propanone and that of 4-hydroxy-4-methyl-2-pentanone; the relative ion abundances are tabulated in ref. 15 and reproduced here as stick form mass spectra in Fig. 7. Furthermore, the same workers found that the CAD spectrum of the m/z 117 ion, obtained with the magnetic (B) and electric (E) sectors linked so as to maintain a constant B/E value, gave the same daughter ions for both 2-propanone and 4-hydroxy-4-methyl-2-pentanone although no spectra were given. On the basis of the self-CIMS spectra and the CAD B/E linked-scan spectra, Parker *et al.* concluded that the two species of m/z 117 had a common structure and that protonated 2-propane must undergo an aldol condensation with 2-propanone in the gas phase identical with that of the acid-catalyzed condensation of 2-propanone in the solution phase.

Relative ion intensities obtained by self-CIMS should be comparable with those of a particular storage time as obtained in this work.

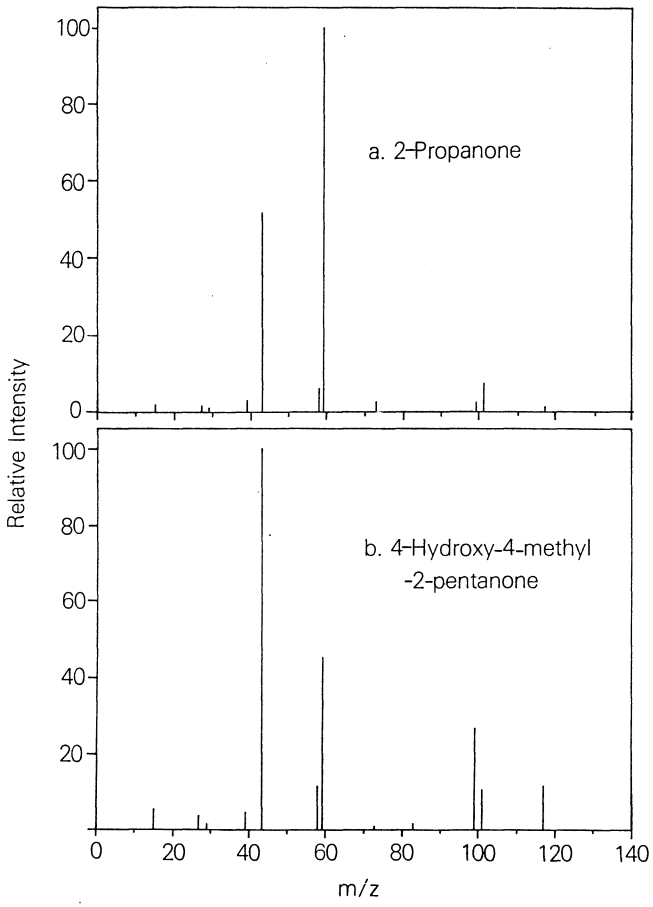

FIG. 7. Relative abundances for self-CIMS of (*a*) 2-propanone and (*b*) 4-hydroxy-4-methyl-2-pentanone.

Although the pressures and residence times in various sources may differ, the dependence of ion intensities on the product of pressure (raised to the power of the reaction order) and time permit a ready comparison. Thus the relative ion intensities shown in Fig. 7*a* and *b* correspond to a storage time of ~5 ms in each of Figs. 2 and 5, respectively. There is, however, a disparity in the ion abundances of m/z 58 and m/z 59 in Fig. 7*b*; only negligible abundances of these ions were observed in our QUISTOR studies.

We are not convinced that an aldol condensation occurs in the gas phase with 2-propanone on the basis of the evidence shown in Fig. 7. On the contrary it has been shown that IRMPD of protonated 4-hydroxy-4-methyl-2-pentanone, m/z 117, isolated in the QUISTOR yielded two photoproducts m/z 43 and m/z 99 (reactions [23] and [24]), whereas IRMPD of proton-bound 2-propanone dimers, m/z 117, carried out under identical conditions, yielded but the single photoproduct, m/z 59 (reaction [17]).

Thus we conclude that the structures of the ion species of m/z 117 obtained in these two systems are different, and that an aldol condensation does not occur with 2-propanone in the gas phase.

The species of m/z 99 was irradiated by the laser for periods of 33 ms, 50 ms, and 100 ms which is the entire period of its genesis yet no photodissociation products were observed. Thus it is concluded that the m/z 99 species is virtually transparent to the laser irradiation at the wavelength employed. It had been anticipated that photodissociation of the m/z 99 species would lead to the formation of the m/z 83 species by the photochemical reaction similar to reaction [22]. As no such species as m/z 83 was observed even from nascent m/z 99 ions it was concluded that the m/z 99 species is transparent at the laser wavelength.

At higher pressure, protonated 4-hydroxy-4-methyl-2-pentanone reacts with parent neutrals to form the proton-bound dimer, m/z 233.

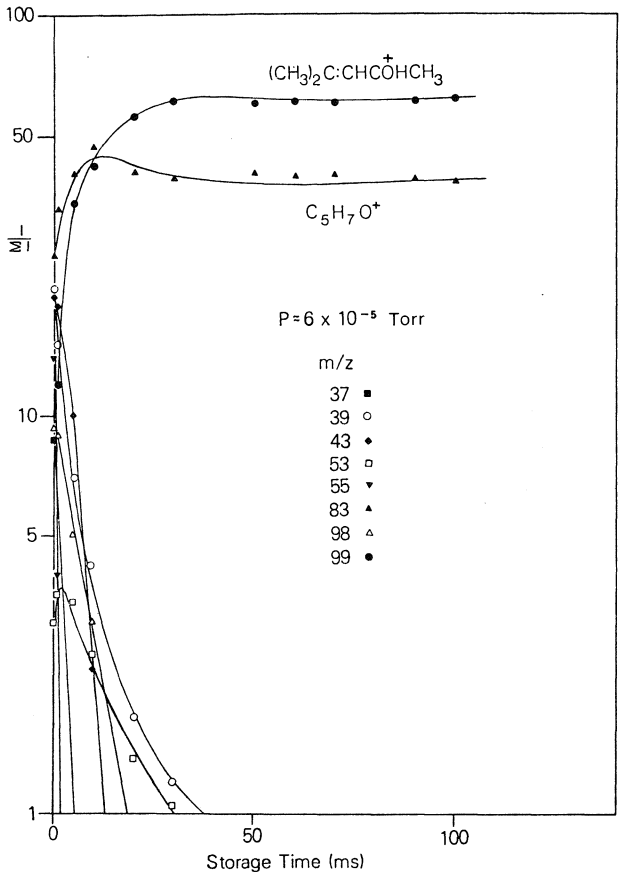

FIG. 8. Variation in the logarithm of normalized ion abundances in 4-methyl-3-penten-2-one with storage time 0–100 ms, 6×10^{-5} Torr.

In addition, ions were observed at m/z 215 $[2M + 1 - H_2O]^+$, m/z 175 $[2M + 1 - 58]^+$, and m/z 157 $[2M + 1 - H_2O - 58]^+$. Isolation of the proton-bound dimer was beyond the limit of the ramped rf sweep for axial ejection, thus it was not possible to isolate m/z 233 for irradiation. The intensities of all of the above species were diminished by IRMPD. As the fractional dissociation of the $[2M + 1 - H_2O]^+$ species exceeded that of the $[2M + 1]^+$ species, we conclude that the former is a mixed associative dimer and the activation energy for dehydration of $[2M + 1]^+$ exceeds that for the dedimerization process.

[26] $[(CH_3)_2C(OH)CH_2COCH_3]_2H^+ \xrightarrow{nh\nu}$
$(CH_3)_2C(OH)CH_2\overset{+}{C}OHCH_3 + (CH_3)_2C(OH)CH_2COCH_3$

The thermal and photochemical reactions of $[2M + 1]^+$ will be compared with those in the α,ω-hydroxy thiols in a forthcoming publication in this journal.

4-Methyl-3-penten-2-one (mesityl oxide)

Ion/molecule reactions

It was decided to investigate the ion chemistry of 4-methyl-3-penten-2-one (mesityl oxide) as the structure of protonated 4-methyl-3-penten-2-one was proposed for the major unimolecular product of protonated 4-hydroxy-4-methyl-2-pentanone and for the ion formed by loss of water from the proton-bound dimer of 2-propanone [9]. Furthermore the ion chemistry of this compound is not evident in the literature. The temporal variation of ion intensities of 4-methyl-3-penten-2-one at a pressure of 6×10^{-5} Torr is shown in Fig. 8.

The base peak in the electron impact mass spectrum is due to m/z 83 while the other major ions were observed at m/z 39, 43, and 55 in order of decreasing relative intensity. Minor ions (<10%) which were observed were the molecular ion of m/z 98, and m/z 53.

The molecular ion reacted rapidly and completely within 10 ms presumably by proton transfer to form protonated 4-methyl-3-penten-2-one

[27] $(CH_3)_2C{=}CHCOCH_3^{+\bullet} + (CH_3)_2C{=}CHCOCH_3$
m/z 98
$\rightarrow (CH_3)_2C{=}CH\overset{+}{C}OHCH_3 + C_6H_9O$
m/z 99

Within 40 ms of storage all primary ions save m/z 83 reacted completely also presumably to form m/z 99. Only the reactive form of $C_2H_3O^+$, CH_3CO^+, was observed in this system. The species of m/z 53, $C_4H_5^+$, rose slightly in intensity during the rapid decay of the molecular ion then reacted slowly and completely.

The intensity due to the protonated 4-methyl-3-penten-2-one rose rapidly during the first 20 ms of storage (or reaction) time to become the dominant ion in the system. It reached a maximum intensity after 40 ms and proved unreactive for the duration of the storage time. The intensity of another ion, m/z 83, increased initially, then after 40 ms of storage, remained constant. The behaviour of m/z 99 and m/z 83 suggests that the proton affinity of the neutral species C_5H_6O (82 mu) must be greater than that of 4-methyl-3-penten-2-one. The proton affinity of the latter compound also is not in the literature, but has been determined in this laboratory (23). Proton-bound dimer ions of m/z 197 were not observed.

Photochemical studies

The protonated molecule, m/z 99, was isolated and subjected to laser irradiation but no photoproducts were observed; this species is thought also to be transparent at the laser wavelength.

Discussion

The structure of m/z 99 in 2-propanone constitutes a problem. The loss of H_2O from a proton-bridged 2-propanone dimer of m/z 117 must be explained. It has been demonstrated earlier by IRMPD that the structure of the proton-bound dimer of 2-propanone must differ from that of protonated 4-hydroxy-4-methyl-2-pentanone, m/z 117. It is significant here that the dehydration channel for the proton-bound 2-propanone dimer is not accessed by laser irradiation. In an attempt to explain the dehydration channel in the 2-propanone dimer which is observed thermally only, we have considered the keto and enol forms of protonated 2-propanone. MINDO/3 calculations show the latter to be less stable by 110 kJ mol^{-1} (15), hence relaxed protonated 2-propanone is expected to exist as the keto form, structure **X**, as opposed to the isomeric enol, structure **XI**.

X **XI**

It is important to recognize that nascent proton-bound 2-propanone dimers contain a minimum of 134 kJ mol^{-1} (14) excess internal energy if formed from fully relaxed neutrals and protonated monomers.

As the protonated monomers, m/z 59, are formed via exothermic proton transfer reactions, the nascent dimers may contain more than 134 kJ mol^{-1} and may isomerize to form a mixed keto–enol species of structure **XII** as opposed to the anticipated fully relaxed structure **XIII**.

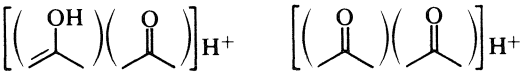

XII **XIII**

While either isomer may dedimerize to produce m/z 59, the elimination of water is more easily rationalized from the high energy structure, **XII**, as shown in reaction [28].

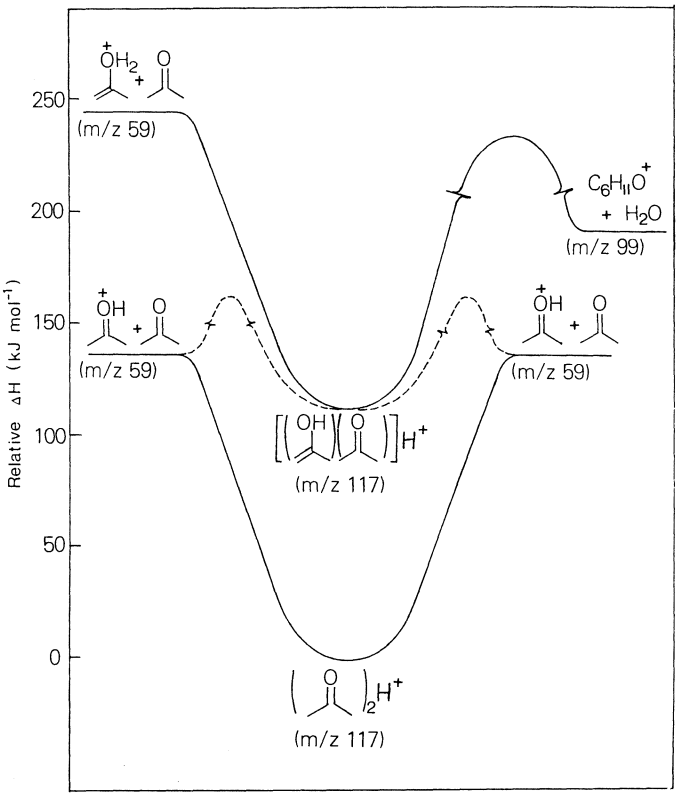

FIG. 9. Schematic energy profile for rearrangements involving the proton-bound dimer of 2-propanone.

[28] 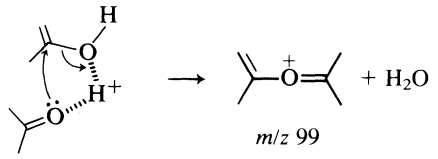

XII

In Fig. 9, the relative enthalpies (ΔH) of the major ionic species derived from 2-propanone are shown. The height of the barrier leading to the formation of the dehydration product, m/z 99, is unknown, as is the activational energy requirement to form the enol.

The apparent difference between the observed products of thermal and photolysis reactions, as shown in Figs. 2 and 4, respectively, may be explained by noting that in the photolysis experiment, all ions of $m/z < 117$ were removed, leaving "aged" or partially relaxed dimer ions at 80 ms of storage time which were subsequently photolyzed. In Fig. 2 it is apparent that thermal genesis of m/z 99 reaches a maximum at ~70 ms storage time, hence the "aged" dimers photolyzed at the onset of laser irradiation in the IRMPD study contain insufficient internal energy for the dehydration process. It has been demonstrated that in slow IRMPD, laser pumping of vibrational states is slower than the rate of unimolecular dissociation (7), hence solely the reaction channel of lowest activation energy will be accessed if relaxed species are irradiated and the activation energy requirements for competing channels differ by at least the energy of the photon employed. The IRMPD results demonstrate that the dedimerization reaction is of lower E_a than dehydration in proton-bound 2-propanone dimers.

The structure of m/z 99 in 4-methyl-3-penten-2-one may be either that of the keto, **XIV** or the enol **XV**. Structure **XIV** is the

XIV **XV**

preferred form as it is presumably the more stable of the two and it lacks a β-hydrogen. The presumption of greater stability of **XIV** relative to **XV** is based on a comparison of the energies of protonated acetaldehyde, **XVI** and protonated vinyl alcohol, **XVII**

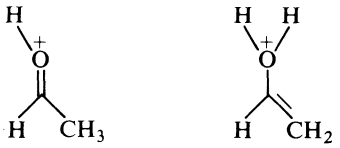

XVI **XVII**

The heat of formation of protonated acetaldehyde is given by

[29] $\Delta H_f(\mathbf{XVI}) = \Delta H_f(CH_3CHO) + \Delta H_f(H^+) - PA(CH_3CHO)$

where PA is the proton affinity. Similarly

[30] $\Delta H_f(\mathbf{XVII}) = \Delta H_f(CH_2{=}CHOH) + \Delta H_f(H^+) - PA(CH_2{=}CHOH)$

Thus for **XVI** to be thermodynamically more stable than **XVII** and, by analogy, **XIV** to be more stable than **XV**, $\Delta H_f(\mathbf{XVII}) - \Delta H_f(\mathbf{XVI})$ should be greater than zero, that is

[31] $\Delta H_f(CH_2{=}CHOH) + PA(CH_3CHO) - \Delta H_f(CH_3CHO) - PA(CH_2{=}CHOH) > 0$

$\Delta H_f(CH_2{=}CHOH)$ lies in the range $-(111\text{–}125)$ kJ mol^{-1} (24)

$PA(CH_3CHO) = 781$ kJ mol^{-1} (22)

$\Delta H_f(CH_3CHO) = -166$ kJ mol^{-1} (25)

The $PA(CH_2{=}CHOH)$ is reported (26) as 47–54 kJ mol^{-1} less than $PA(C_2H_5OH)$ which is given (22) as 788 kJ mol^{-1}; hence $PA(CH_2{=}CHOH)$ lies in the range 734–741 kJ mol^{-1}. As the sum of the thermodynamic quantities in eq. [31] lies in the range 81–102 kJ mol^{-1}, structure **XIV** is probably more stable than **XV**. The presence of a β-hydrogen is required for the elimination of water from protonated ketones (27) and, since neither structure **XIV** nor **XV** has a β-hydrogen, dehydration is not expected and no dehydration product (m/z 81) was observed. Apart from the energy consideration discussed above, no distinction may be made at this time between the keto and enol tautomers for the identity of m/z 99.

The identity of m/z 99 derived via dehydration of protonated 4-hydroxy-4-methyl-2-pentanone, m/z 117, was proposed earlier as **XIV** above, and as such further dehydration was neither expected, nor observed.

The structure of m/z 83 produced from protonated 4-methyl-3-penten-2-one is proposed as **IX** as shown in the alkane elimination reaction [22].

[22] 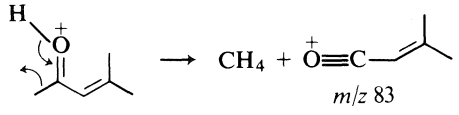

XIV **IX**

TABLE 1. Activation energies for α-cleavage reactions of ionized methyl ketones estimated from the appearance energy of the α-cleavage product and the ionization energy of the methyl ketone

α-Cleavage reaction	AE (eV)	1E[a] (eV)	AE − 1E ~ E_a
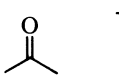 → ·CH_3 + $C_2H_3O^+$	10.3–10.4[a]	9.7	0.6–0.7
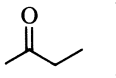 → ·CH_3 + $C_3H_5O^+$	10.22[a]	9.5	0.7
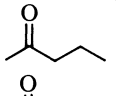 → ·CH_3 + $C_4H_7O^+$	10.03[b]	9.40	0.63
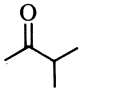 → ·CH_3 + $C_4H_7O^+$	9.94[a]	9.30	0.64
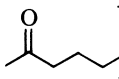 → ·CH_3 + $C_5H_9O^+$	9.4[a]	9.2–9.4	0–0.2
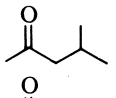 → ·CH_3 + $C_5H_9O^+$	9.8[b]	9.30	0.50
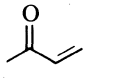 → ·CH_3 + $C_3H_3O^+$	10.4[a]	10.1–9.6	0.3–0.8

[a]Reference 28.
[b]Reference 21.

The protonated ketone, **XIV**, may also eliminate isobutene, as shown in reaction [32];

[32] 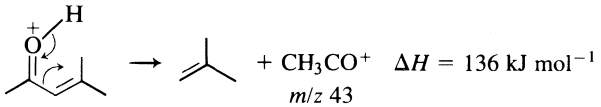 + CH_3CO^+ ΔH = 136 kJ mol^{-1} (m/z 43)

XIV

however, no trace of m/z 43 was observed, thus reaction [32] is of higher E_a than reaction [22]. The enthalpy change for reaction [22] is not known as the heat of formation of m/z 83 of structure **IX** is not available. However, an estimate of the activation energy may be obtained by examination of the ionization energy (IE) of a number of ketones and the appearance energy (AE) for the α-cleavage reaction

[33] 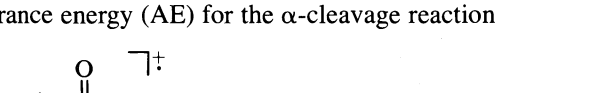

As the energy of activation may be approximated by the expression

[34] $E_a \approx$ AE − IE

it is apparent from Table 1 that as the alkyl (or alkenyl) group, R, is extended the activation energy of the reaction is diminished. Thus it seems probable that the heat of formation of m/z 83 is less than that for CH_3CO^+ in reaction [32]; however, it has been brought to our attention that such may not be the case as $\Delta H_f^0(CH_3CO^+)$ in some 240 kJ mol^{-1} less than $\Delta H_f^0(CH_2{=}CHCO^+)$ although the AE − IE values in Table 1 suggest otherwise. Therefore, despite a lower ΔH_f^0 for methane than for isobutene in reaction [32], the enthalpy hierarchy between reactions [22] and [32] may not be satisfactorily established.

The structure of m/z 83 formed from protonated 4-hydroxy-4-methyl-2-pentanone is also proposed as **IX** above. Although m/z 43 was observed both thermally and photolytically from the protonated hydroxy ketone, m/z 117, IRMPD of the isolated m/z 117 demonstrated that m/z 43 was derived directly from the protonated parent, rather than from its dehydration product, m/z 99.

Acknowledgements

The authors acknowledge with thanks the financial support of the Natural Sciences and Engineering Research Council of Canada, Trent University, and Queen's University for a Graduate Student Assistantship to A. Kamar. We acknowledge also the technical assistance of W. King and J. A. Tomlinson. We are greatly appreciative of the co-operation of Drs. C. W. Willis and D. Rayner of the National Research Council of Canada for the loan of the CO_2 laser. The constructive comments of the referees are much appreciated.

1. R. J. HUGHES, R. E. MARCH, and A. B. YOUNG. Int. J. Mass Spectrom. Ion Phys. **42**, 255 (1982).
2. R. J. HUGHES, R. E. MARCH, and A. B. YOUNG. Int. J. Mass Spectrom. Ion Phys. **47**, 85 (1983).
3. R. J. HUGHES, R. E. MARCH, and A. B. YOUNG. Can. J. Chem. **61**, 834 (1983).
4. R. E. MARCH. Ionic processes in the gas phase. *Edited by* M. A. Almoster-Ferreira. D. Reidel Publishing. 1984. p. 359.
5. R. E. MARCH, R. J. HUGHES, and A. B. YOUNG. Proc. 13th Conf. British Mass Spec. Soc., Warwick Univ. U.K. Sept. 19–22, 1983.
6. R. J. HUGHES, R. E. MARCH, and A. B. YOUNG. Proc. 31st Ann. Conf. Am. Soc. Mass Spec. Boston. 1983. p. 747.
7. A. B. YOUNG, R. E. MARCH, and R. J. HUGHES. Can. J. Chem. **63**, 2324 (1985).
8. R. E. MARCH, A. B. YOUNG, R. J. HUGHES, A. KAMAR, and M. BARIL. Spectrosc. Int. J. **3**, 17 (1984).
9. M. S. B. MUNSON. J. Am. Chem. Soc. **87**, 5313 (1965).
10. A. S. BLAIR and A. G. HARRISON. Can. J. Chem. **51**, 703 (1973).

11. G. B. DEBROU, J. E. FULFORD, E. G. LEWARS, and R. E. MARCH. Int. J. Mass Spectrom. Ion Phys. **26**, 345 (1978).
12. J. L. HOLMES and F. P. LOSSING. Int. J. Mass Spectrom. Ion Processes, **58**, 113 (1984).
13. J. L. HOLMES and F. P. LOSSING. Can. J. Chem. **57**, 249 (1979).
14. J. W. LARSON and T. B. MCMAHON. J. Am. Chem. Soc. **104**, 6255 (1982).
15. J. A. HUNTER, C. A. JOHNSON, J. E. PARKER, and G. P. SMITH. 14th Meeting of the British Mass Soc., Heriot-Watt Univ., Edinburgh, U.K. Sept. 18–21, 1984. Abstr. p. 24.
16. P. C. BURGERS, J. L. HOLMES, J. E. SZULEJKO, A. A. MOMMERS, and J. K. TERLOUW. Org. Mass Spectrom. **18**, 254 (1983).
17. J. VOGT, A. D. WILLIAMSON, and J. L. BEAUCHAMP. J. Am. Chem. Soc. **100**, 3478 (1978).
18. J. K. TERLOUW, W. HEERMA, and G. DIJKSTRA. Org. Mass Spectrom. **15**, 660 (1980).
19. R. H. NOBES, W. J. BOUMA, and L. RADOM. J. Am. Chem. Soc. **105**, 309 (1983).
20. K. A. MCNEIL and J. H. FUTRELL. J. Phys. Chem. **76**, 409 (1972).
21. H. M. ROSENSTOCK, K. DRAXL, B. W. STEINER, and J. T. HERRON. J. Phys. Chem. Ref. Data, 6, Suppl. 1 (1977).
22. S. G. LIAS, J. F. LIEBMAN, and R. D. LEVIN. J. Phys. Chem. Ref. Data, **13**(3), 695 (1984).
23. A. KAMAR, R. E. MARCH, and A. B. YOUNG. Can. J. Chem. To be published.
24. W. J. BOUMA, J. K. MACLEOD, and L. RADOM. J. Am. Chem. Soc. **101**, 5540 (1979); J. L. HOLMES, J. K. TERLOUW, and F. P. LOSSING. J. Phys. Chem. **80**, 2860 (1976); J. L. HOLMES and F. P. LOSSING. J. Am. Chem. Soc. **104**, 2648 (1982).
25. J. F. COX and D. PILCHER. Thermochemistry of organic and organometallic compounds. Academic Press, New York. 1970.
26. W. J. BOUMA, R. N. NOBES, S. SAEBO, and L. RADOM. Chem. Phys. Lett. **99**(2), 112 (1983).
27. M. L. SIGSBY, R. J. DAY, and R. G. COOKS. Org. Mass Spectrom. **14**, 273 (1979).
28. R. D. LEVIN and S. G. LIAS. Natl. Stand. Ref. Data Ser. 71 (1982).

The Claisen rearrangement of 1,4-bis(*m*-methoxyphenoxy-)2-butyne

E. KIEHLMANN,[1] E. P.-M. LI, AND J. G. MILLAR[2]

Department of Chemistry, Simon Fraser University, Burnaby, B.C., Canada V5A 1S6

Received December 2, 1985

E. KIEHLMANN, E. P.-M. LI, and J. G. MILLAR. Can. J. Chem. **64**, 1989 (1986).

The Claisen rearrangement of 1,4-bis(*m*-methoxyphenoxy-)2-butyne (**1***b*) gives four isomeric dimethoxy-6*H*-benzofuro[3,2-*c*]-6a,11a-dihydro-11a-methylbenzopyrans (**3**), three dimethoxy-4b,9b-dihydro-4b,9b-dimethylbenzofuro[3,2-*b*]benzofurans (**4**), and, in the presence of acid, three dimethoxy-5a,10b-dihydro-5a,10b-dimethylbenzofuro[2,3-*b*]benzofurans (**5**), which have been separated and identified by proton and ^{13}C nmr spectroscopy. Based on the isolation of two chromene intermediates and their conversion to **3** and **4**, as well as the isomerization of **3** to **4** and **4** to **5**, a "double Claisen" mechanism is proposed. The reaction is not regiospecific but the two [3,3] sigmatropic shifts occur preferentially to the *para* positions of the methoxy substituents.

E. KIEHLMANN, E. P.-M. LI et J. G. MILLAR. Can. J. Chem. **64**, 1989 (1986).

La transposition de Claisen appliquée au bis(*m*-méthophénoxy)-1,4 butyne-2 (**1***b*) conduit à quatre diméthoxy 6*H*-benzofuro[3,2-*c*] dihydro-6a,11a méthyl-11a benzopyrannes isomères (**3**), à trois diméthoxy dihydro-4b,9b diméthyl-4b,9b benzofuro[3,2-*b*] benzofurannes (**4**) et, en présence d'acides, à trois diméthoxy dihydro-5a,10b diméthyl-5a,10b benzofuro[2,3-*b*] benzofurannes (**5**) qui ont été séparés et identifiés par spectroscopie rmn ^1H et ^{13}C. En se basant sur le fait que l'on a isolé deux chromènes intermédiaires, que ceux-ci ont pu être transformés en **3** et **4** et que l'on a pu réaliser les isomérisations **3** → **4** et **4** → **5**, on propose un mécanisme impliquant un «double Claisen». La réaction n'est pas régiospécifique; toutefois les deux déplacements sigmatropiques [3,3] se produisent préférentiellement vers les positions *para* des substituants méthoxy.

[Traduit par la revue]

Introduction

The Claisen rearrangement of aryl propargyl ethers is a convenient route for the preparation of chromenes (1, 2). With 1,4-bis(aryloxy-)2-butynes it yields 6*H*-benzofuro[3,2-*c*]-6a,11a-dihydro-11a-methylbenzopyrans (short: 11a-methylpterocarpans **3**) and varying amounts of isomeric 4b,9b-dihydro-4b,9b-dimethylbenzofuro[3,2-*b*]benzofurans (short: benzofuro[3,2-*b*]benzofurans **4**) and 5a,10b-dihydro-5a,10b-dimethylbenzofuro[2,3-*b*]benzofurans (short: ketals **5**). Mechanistic studies have demonstrated the intermediacy of chromenes (3–5) in the formation of 11a-methylpterocarpans, and the high thermodynamic stability of the cyclic ketals **5**, which are generally isolated as end products after long reaction times at high temperatures (4–8), especially in the presence of acid catalysts (Scheme 1).

In view of the occurrence of pterocarpans in various plant tissues and of their antifungal activities (9, 10), we were primarily interested in adapting this reaction to the synthesis of 11a-methyl analogs of natural phytoalexins, such as 11a-methylhomopterocarpin (**3***b*), in order to study their chemical and biological properties. Since the 1,3-dioxygenated aromatic substitution pattern (resorcinol type) is typical of all natural pterocarpans, we selected as starting material 1,4-bis(*m*-methoxyphenoxy-)2-butyne (**1***b*), which is readily obtained from 1,4-dichloro-2-butyne and *m*-methoxyphenol (11). In contrast to the *ortho*- and *para*-disubstituted aryloxy-2-butynes used by all previous investigators, *meta*-disubstituted compounds can give two regioisomers (*ortho* or *para* to the methoxy substituent) in each of the two [3,3] sigmatropic shifts (Scheme 2), leading to the possibility of formation of four isomeric 11a-methylpterocarpans **3**, three isomeric benzofuro[3,2-*b*]benzofurans **4**, and (or) three isomeric cyclic ketals **5**, unless one or both steps are regiospecific. Therefore, the main goals of our project were the determination of the product distribution, identification of each isomer formed, and the optimization of reaction conditions (time, temperature, solvent, and catalyst) in favor of one or two isomers of the desired structure **3**. Recent publications on the proton and ^{13}C magnetic resonance parameters of a series of *ortho*- and *para*-substituted benzofurobenzofurans **4** and **5** (12), on an efficient procedure for their synthesis (5), and on the regiochemistry of the Claisen rearrangement of several *meta*-substituted allyl and propargyl ethers (13, 14) prompt us now to report our results.

Results

Preliminary experiments established that, on reflux in *N*,*N*-diethylaniline for several hours, 1,4-bis(*m*-methoxyphenoxy-)2-butyne (**1***b*) rearranges to six heterocyclic isomers (subsequently identified as **3***b*, **3***c*, **3***d*, **3***e*, **4***b*, and **4***c*, see Scheme 1) whose ratio is a function of reaction time and temperature. Although some of the starting material (approximately 20%) reacted during passage through the capillary column, the rearrangement products were found to be stable to the conditions employed for gas chromatographic analysis. At 225°C, all four dimethoxy-11a-methylpterocarpans (**3**) and smaller amounts of the two dimethoxybenzofuro[3,2-*b*]benzofurans **4***b* and **4***c* were present after 1.5 h, and **4***b* and **4***c* constituted the major products at the time of complete consumption of **1***b* (2.5 h). Continued monitoring revealed a gradual increase in the **4**/**3** ratio as the reaction progressed, leading to a mixture containing approximately equal quantities of **3***b*, **3***c*, and **4***b* in addition to the minor components **3***d*, **3***e*, and **4***c* after 6.5 h. The predominance of **4***b*, reduced percentages of **3***c*, **3***d*, and **3***e*, and the complete absence of **3***b* at the end of the reaction (29 h) indicate that all pterocarpans isomerize gradually to benzofuro[3,2-*b*]benzofurans, with the rate of the **3***b* → **4***b* interconversion being particularly rapid. Lowering the temperature from 225 to 210°C slowed down this process but gave otherwise similar results: six major isomers after 4.5 h, with **3***b* and **4***b* as main components, and a final product mixture containing **3***b*, **3***c*, **3***d*, **3***e*, **4***b*, and **4***c* in the approximate molar ratio 2:2:2:1:4:2. The individual components were isolated by liquid chromatography, as described in the experimental section, and the composition was verified by integration of the peak areas of the methoxy and angular methyl protons (3.8 and 1.7 ppm, respectively) in the nmr spectrum.

Gas chromatographic analysis of an aliquot withdrawn after

[1]Author to whom correspondence may be addressed.

[2]Present address: National Research Council of Canada, Plant Biotechnology Institute, 110 Gymnasium Road, University of Saskatchewan, Saskatoon, Sask., Canada S7N 0W9.

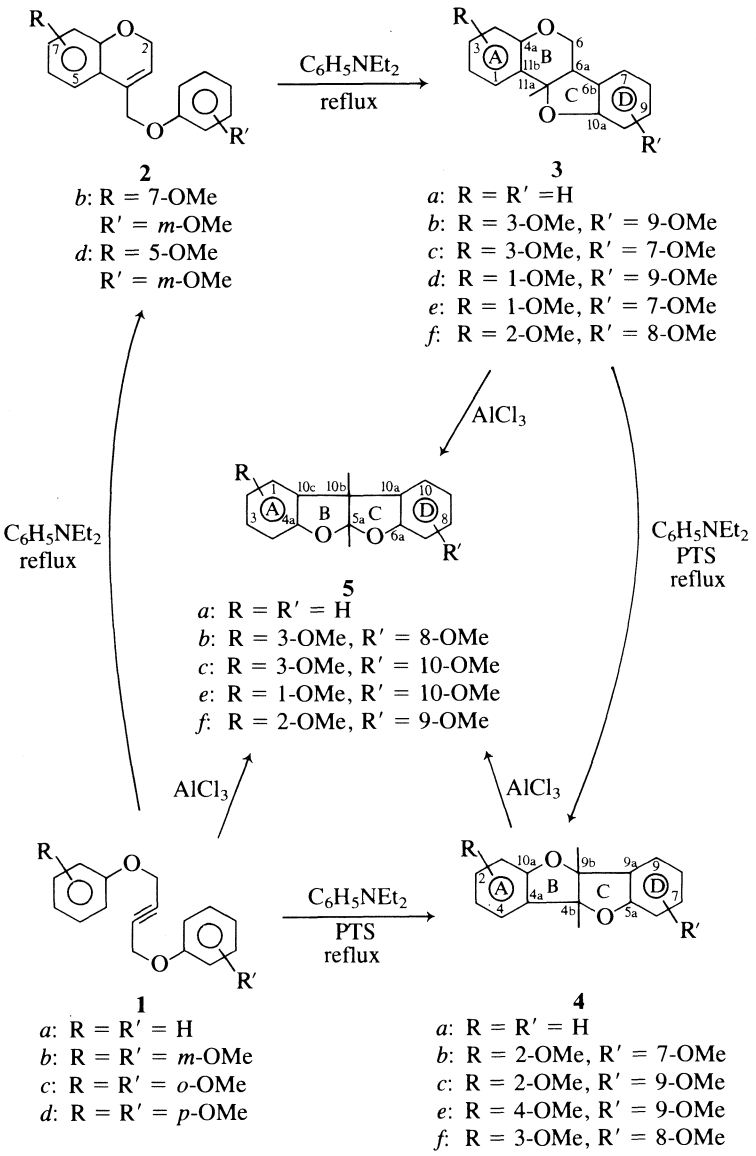

2
b: R = 7-OMe, R′ = *m*-OMe
d: R = 5-OMe, R′ = *m*-OMe

3
a: R = R′ = H
b: R = 3-OMe, R′ = 9-OMe
c: R = 3-OMe, R′ = 7-OMe
d: R = 1-OMe, R′ = 9-OMe
e: R = 1-OMe, R′ = 7-OMe
f: R = 2-OMe, R′ = 8-OMe

5
a: R = R′ = H
b: R = 3-OMe, R′ = 8-OMe
c: R = 3-OMe, R′ = 10-OMe
e: R = 1-OMe, R′ = 10-OMe
f: R = 2-OMe, R′ = 9-OMe

1
a: R = R′ = H
b: R = R′ = *m*-OMe
c: R = R′ = *o*-OMe
d: R = R′ = *p*-OMe

4
a: R = R′ = H
b: R = 2-OMe, R′ = 7-OMe
c: R = 2-OMe, R′ = 9-OMe
e: R = 4-OMe, R′ = 9-OMe
f: R = 3-OMe, R′ = 8-OMe

SCHEME 1

15 min at 210°C revealed the presence of three intermediates (in addition to 34% starting material and 4% **4***b*), which were identified as 5- and 7-methoxy-4-(*m*-methoxyphenoxymethyl-)2*H*-chromene **2***b* and **2***d* (14% each) and a mixture of several isomeric dimethoxy-4b,5,10b,11-tetrahydrobenzopyrano[4,3-*c*]benzopyrans **11** (6%). Chromene **2***b* was found to rearrange cleanly to a mixture of **3***b*, **3***c*, **4***b*, and **4***c* (molar ratio 3:2:3:1) within 4 h (210°C), thus confirming its true intermediacy in the reaction (3, 4) and the irreversibility of the first Claisen rearrangement step.

The addition of *p*-toluenesulfonic acid (PTS) to a mixture of approximately equimolar quantities of 11a-methylpterocarpans (**3***b*, **3***c*, **3***d*, and **3***e*) and benzofuro[3,2-*b*]benzofurans (**4***b* and **4***c*) in refluxing *N*,*N*-diethylaniline leads to rapid conversion of the former to the latter, reaching constant composition (40% **4***b* and 35% **4***c*) after 2.5 h at 225°C or 6.5 h at 210°C. As in the absence of acid, **3***b* was observed to rearrange most rapidly and **3***e* most slowly. Adding the acid catalyst to the 1,4-diaryloxy-2-butyne at the beginning of the reaction and monitoring the composition over a 13-h period (210°C) gave similar results: after 1.5 h, before complete consumption of the starting material, **2***b* constituted the main product and the three benzofuro[3,2-*b*]benzofurans outweighed the four methylpterocarpan isomers by a factor of four. By the end of the reaction (13 h), the chromene and the pterocarpans had all but disappeared while the percentages of **4***b*, **4***c*, and **4***e* had increased substantially. The slow buildup of the **4***e* concentration at the expense of **3***e* was particularly noticeable. As expected, the chromene **2***b* rearranged to **4***b* and **4***c* (2:1) under acid-catalyzed conditions, while pure **3***d* yielded only **4***c*. The latter observation represents the first direct experimental evidence for the previously postulated (4, 5) isomerization of **3** to **4**, probably via a 2-aryl-3-exomethylene-2,3-dihydro-benzofuran (**15**). The gas chromatograms of the mixtures formed in the presence of *p*-toluenesulfonic acid exhibited an unexpected small peak, possibly due to this elusive intermediate; however, all our attempts to isolate a pure sample by liquid chromatography or to trap it in the form of its acetate by performing the reaction in quinoline/acetic anhydride (5) failed.

In refluxing *N*-methylaniline (bp 196°C) the rearrangement proceeded much more slowly, with the product distribution being virtually identical to that observed in *N*,*N*-diethylaniline.

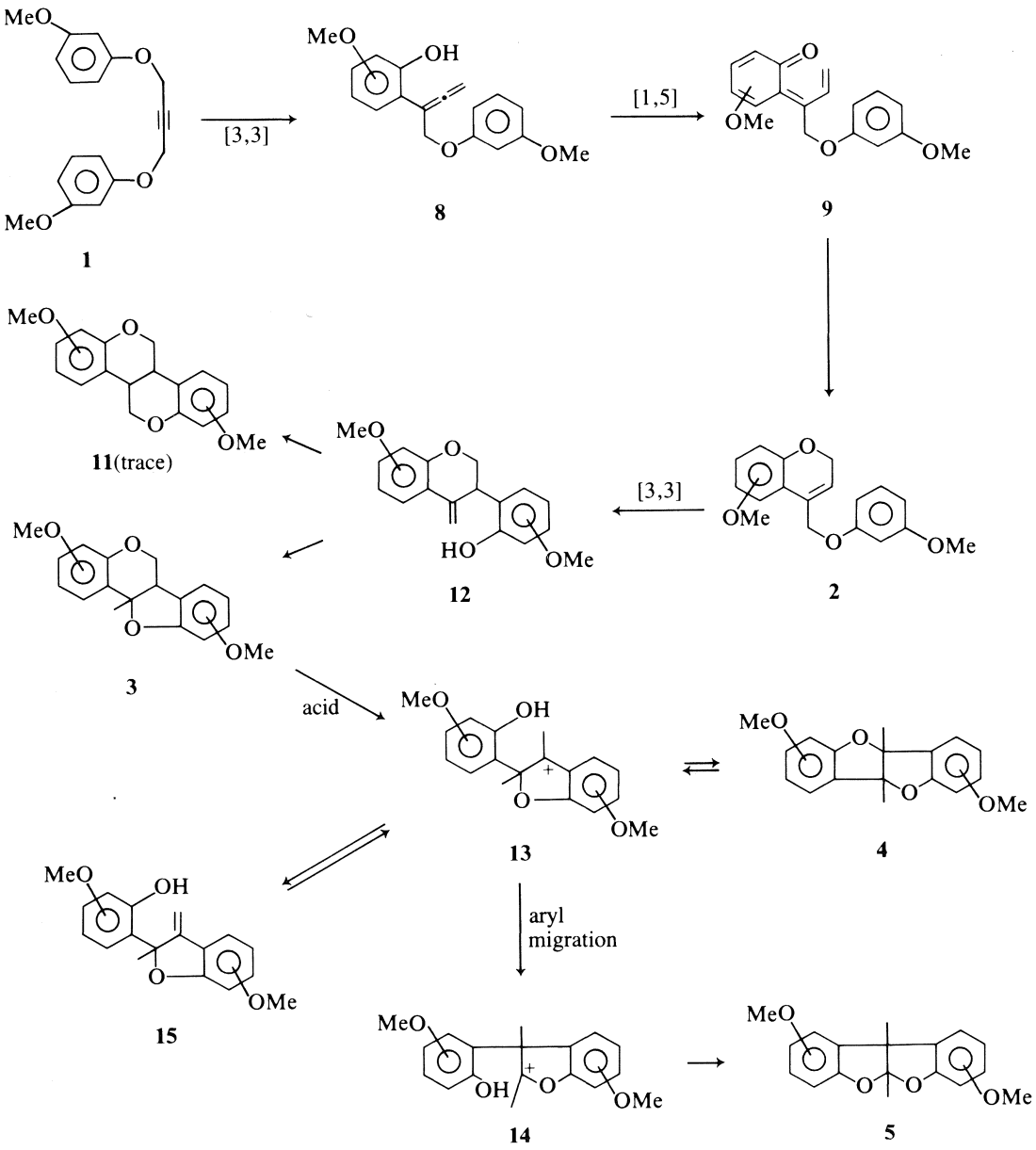

SCHEME 2

Similar results were obtained in decalin (bp 190°C) except that the proportion of methylpterocarpans during the early stages of the reaction was larger than in the other two solvents. Heating **1** to 200°C in the absence of solvent led to rapid formation of **4***b* and **4***c* without accumulation of significant quantities of **3** at an intermediate stage. Most of the starting material was recovered when silver tetrafluoroborate was used in place of *p*-toluenesulfonic acid under mild conditions (CH_2Cl_2, 7 h). Bates and Jones (4) found 1,4-bis(*o*-methoxyphenoxy-)2-butyne to be similarly inert, in sharp contrast to the high reactivity of the corresponding *para* isomer. With aluminum chloride as catalyst, **1***b* rearranged smoothly (in refluxing dichloromethane) to a mixture of **4***b*, **4***c*, and the corresponding ketals **5***b* (major product) and **5***c*. To test whether the latter two compounds are formed from **4***b* and **4***c*, respectively, by a pinacole-type rearrangement (5–7), we subjected each of the three benzofuro[3,2-*b*]benzofuran isomers separately to the same reaction conditions and observed no reaction with **4***b*, partial conversion of **4***c* to **5***c*, and complete conversion of **4***e* to **5***e*; the reactions were accompanied by some ether cleavage, as noted previously (4). The unsubstituted 4b,9b-dihydro-4b,9b-dimethylbenzofuro[3,2-*b*]benzofuran (**4***a*) was also found to isomerize to the corresponding ketal (**5***a*) with aluminum chloride.

Discussion

Our results show that the Claisen rearrangement of 1,4-bis(*m*-methoxyphenoxy-)2-butyne (**1***b*) proceeds by a mechanism very similar to that of the previously studied *ortho*- and *para*-substituted 1,4-diaryloxy-2-butynes. However, the simple sequential pathway **1** → **2** → **3** → **4** → **5** established by Balasubramanian and co-workers (5) for the latter must be modified for the analogous isomerization of **1***b* because it does not explain the direct conversion of **3** to **5**, bypassing **4**, nor does it account for the important role played by acid catalysts in the ring contraction of **3**. We believe that Lewis acids are essential for the formation of the ketals **5**. Various free phenolic intermediates (e.g., **8**, **12**) may act as proton source and *N*,*N*-diethylaniline or polyethylene glycol PEG-200 (5) as

efficient proton carriers when no catalyst is added. The relatively large proportion of methylpterocarpans **3** formed in decalin, a nonpolar solvent, appears to support this conclusion. In contrast to the results reported by Bates and Jones (4) for **1***c* and **1***d*, we have found that **1***b* yields substantial quantities of benzofuro[3,2-*b*]benzofurans under virtually all thermal and catalyzed reaction conditions, even during the initial phase without added catalyst and at the end of the reaction with aluminum chloride. Therefore, we feel that intermediates such as **9** or **10** cannot be excluded (although they could not be

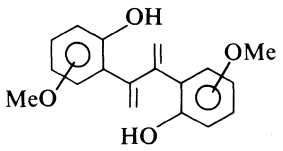

10

isolated), and that the observed products result from several competing pericyclic and ionic pathways (Scheme 2).

In the first step, a concerted [3,3] sigmatropic shift leads to the formation of an allene as postulated by Schmid and coworkers (in ref. 15). Though unstable, such structures have actually been isolated (2) in the Claisen rearrangement of several aryl propargyl ethers to chromenes. The presence of large quantities of chromenes (**2**) shortly after the start of the reaction indicates that the second step involves a rapid [1,5] hydrogen shift, to yield the ω-vinylquinone methide **9**, and subsequent electrocyclic ring closure. As an alternate possibility, **8** may undergo another Claisen rearrangement to a 2,3-diarylbutadiene (**10**) from which **3**, **4**, and the minor by-product **11** could be formed directly by two successive cyclizations (16).

The further course of the reaction depends to a large extent on the availability of protons. Chromene **2** is converted to methylpterocarpan **3** (and traces of **11**) via a 3-aryl-4-exomethylenebenzopyran (**12**) by a second [3,3] sigmatropic shift (normal Claisen rearrangement) and a homodienyl [1,5] sigmatropic shift (abnormal Claisen rearrangement) (10), and the latter undergoes irreversible ring contraction to a benzofurobenzofuran (**4** and (or) **5**). The rate acceleration observed on addition of Lewis acids suggests the formation of a common resonance-stabilized benzylic carbocation intermediate (**13**) by acid-catalyzed cleavage of the pyran ring of **3** (4). The pronounced dependence of the **3** → **4** and **4** → **5** interconversion rates on the positions of the methoxy groups may be due to a combination of steric and electronic substituent effects on the lifetime of this cation and the migratory aptitude of the disubstituted aryl group in the pinacole-type rearrangement leading to ketal **5**. We hope that molecular energy and charge density calculations currently in progress will lead to a better understanding of the driving forces for these two isomerizations. The 2-aryl-3-exomethylene-2,3-dihydrobenzofuran **15** is probably the unidentified intermediate detected in all reactions catalyzed by *p*-toluenesulfonic acid (5). Benzofurobenzofuran ring systems (**4** and **5**) are apparently more stable than benzofurobenzopyrans (**3**), and the unusual thermodynamic and chemical stabilities of **4***b* and **5***e* are particularly noteworthy.

Because of our interest in the synthesis of analogs of specific naturally occurring pterocarpans, we carefully analyzed variations in the product distribution as a function of solvent, catalyst, reaction time, and temperature. Unfortunately we could not identify a single set of conditions producing a specific 11a-methylpterocarpan isomer (**3***b*, **3***c*, **3***d*, or **3***e*) in high yield and purity such as to obviate elaborate chromatographic separation procedures. The Claisen rearrangement of **1***b* is clearly not regiospecific, in agreement with the widely fluctuating isomer ratios reported in the literature for the chromanes and chromenes formed in the corresponding reactions of other *meta*-substituted allyl and propargyl aryl ethers (13, 14, 17). However, it can be stated that the two [3,3] sigmatropic shifts occur preferentially to the aromatic carbon *para* to the methoxy group, i.e., the sterically least crowded isomers **3***b* and **4***b* constitute the major portion of the product mixture in all experiments.

The nmr spectra of the heterocyclic Claisen rearrangement products exhibit several interesting features. Complete analysis of the aromatic proton region has generally not been possible before the advent of high resolution spectroscopy at high frequencies (200–400 MHz), explaining the scarcity of literature data on di- and trisubstituted benzenes. Tables 1 and 2 summarize the proton chemical shifts and coupling constants of the 13 compounds prepared in our laboratory and include the spectral parameters of 3,8-dimethoxy-4b,9b-dihydro-4b,9b-dimethylbenzofuro[3,2-*b*]benzofuran **4***f* (12), 2,9-dimethoxy-5a,10b-dihydro-5a,10b-dimethylbenzofuro[2,3-*b*]benzofuran **5***f* (4), homopterocarpin **6***a* (18), and variabilin **6***b* (19) for comparison.

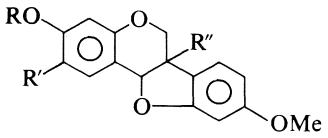

6

a: R = Me, R′ = R″ = H
b: R = Me, R′ = H, R″ = OH
c: R = R′ = R″ = H
d: R—R′ = —CH:CH—, R″ = H

Focussing first on the clearly recognizable and well-separated methoxy and angular methyl singlets, we found that a methoxy group *ortho* to the point of attachment of the benzylic carbon (e.g., in **3***e*, **4***e*, **5***e*) invariably resonates at lower field (by 0.10–0.18 ppm) than the corresponding *para*-methoxy protons (e.g., in **3***b*, **4***b*, **5***b*), and that in **5** the angular methyl group attached at the ketal carbon (Me-5a) resonates at lower field strength than Me-10b. The aromatic *meta* protons (relative to the position of MeO attachment) absorb considerably downfield (by 0.6–0.8 ppm) from the corresponding *ortho* and *para* protons in all compounds while the latter were frequently difficult to distinguish from each other. To determine their chemical shifts, we ran several spectra in acetone-d_6, which gave a better separation of their peaks and permitted measurement of their coupling constants. In the unsubstituted compounds (**3***a*, **4***a*, **5***a*), saturation of the angular methyl protons (nuclear Overhauser effect) identified the lowfield multiplet as belonging to the proton adjacent to the position of attachment of the benzylic carbon, and decoupling experiments established that the resonance shifts gradually upfield in the order H-1/H-3/H-2/H-4 (H-1 arbitrarily defined as the proton absorbing at lowest field). This general trend and the close agreement of our chemical shifts with those reported by Ramah *et al.* (12) prompt us to propose a correction of the H-2 (from δ 7.25 to δ 6.95) and H-3 assignments (from δ 6.95 to δ 7.25) for 4b,9b-dihydrobenzofuro[3,2-*b*]benzofuran (20).

Comparing the substituted heterocycles with their unsubsti-

TABLE 1. Proton chemical shifts

Compound	H-1	H-2	H-3	H-4	H-6ax	H-6eq	H-6a	H-75	H-8	H-9	H-10	MeO[a]	Ang.Me[a]
A. Benzofuro[3,2-*c*]benzopyrans(pterocarpans)													
3*a*	7.63	7.06	7.22	6.89	3.85[b]	4.32[b]	3.52[b]	7.26	6.90	7.17	6.81	—	1.72[b]
3*b*	7.49	6.64	—	6.40	3.82	4.26	3.40	7.11	6.43	—	6.39	3.77/3.75	1.69
3*c*	7.50	6.64	—	6.43	3.87	4.38	3.58	—	6.43	7.10	6.44	3.77/3.85	1.67
3*d*	—	6.59	7.16	6.55	3.64	4.22	3.36	7.12	6.43	—	6.51	3.95/3.75	1.80
3*e*	—	6.57	7.16	6.57	3.64	4.38	3.54	—	6.43	7.12	6.43	3.95/3.85	1.78
6*a* (ref. 18)	7.40	6.61	—	6.45	3.60	4.20	3.44	7.10	6.42	—	6.43	3.74, 3.72	—
6*b* (ref. 19)	7.33	6.61	—	6.37	3.98	4.12	—	7.17	6.46	—	6.35	3.72	—
B. Benzofuro[3,2-*b*]benzofurans													
	H-4	H-3	H-2	H-1				H-9	H-8	H-7	H-6		
4*a*	7.44	6.96	7.23	6.80	—	—	—	7.44	6.96	7.23	6.80	—	1.78[c]
4*b*	7.30	6.50	—	6.33	—	—	—	7.30	6.50	—	6.33	3.74	1.73
4*c*	7.29	6.50	—	6.42	—	—	—	—	6.43	7.16	6.41	3.74/3.91	1.73/1.89
4*e*	—	6.43	7.15	6.49	—	—	—	—	6.43	7.15	6.49	3.91	1.89
4*f* (ref. 12)		6.6–6.8			—	—	—		6.6–6.8			3.8	1.73
C. Benzofuro[2,3-*b*]benzofurans(ketals)													
	H-1	H-2	H-3	H-4				H-10	H-9	H-8	H-7		
5*a*	7.28	6.92	7.12	6.84	—	—	—	7.28	6.92	7.12	6.84	—	1.78/1.69[d]
5*b*	7.11	6.46	—	6.41	—	—	—	7.11	6.46	—	6.41	3.73	1.75/1.63
5*c*	7.38	6.45	—	6.39	—	—	—	—	6.44	7.06	6.49	3.73/3.87	1.74
5*e*	—	6.45	7.08	6.48	—	—	—	—	6.45	7.08	6.48	3.85	1.78/1.70
5*f* (ref. 4)		6.63–6.73			—	—	—		6.63–6.73			3.7	1.72/1.63[e]

[a]Listed in numerical order of position, e.g., MeO-3/MeO-9.
[b]H-6ax/H-6eq/H-6a/Me 3.8/4.3/3.45/1.74 (ref. 3).
[c]Me 1.70 (ref. 8), 1.73 (ref. 12).
[d]Me 1.7/1.6 (ref. 6), 1.77/1.65 (ref. 8), 1.72/1.62 (ref. 12).
[e]Me 1.65/1.60 (ref. 12).

TABLE 2. Proton coupling constants[a] (Hz)

	R ring		R′ ring			
Compound	J_{ortho}	J_{meta}	J_{ortho}	J_{meta}	J_{66}	J_{66a}
3*a*[b]	7.8/7.3/8.2	1.7/1.3	7.3/7.5/8.0	1.4/1.0	11.3	4.9/9.3
3*b*	8.7	2.6	8.2	2.3	11.3	4.7/9.2
3*c*[c]	8.7	2.6	8.2	[h]	11.0	4.9/9.5
3*d*[d]	8.3	1.1	8.1	2.3	11.0	5.0/10.7
3*e*	8.3	[h]	8.2	[h]	10.7	4.8/10.7
6*a* (ref. 18)	8.5	2.4	8.8	2.7	11.1	5.5/10.8
6*b* (ref. 19)		2.5	8.5	2.5	12	—
4*a*[e]	7.5/7.4/8.1	1.4/0.9	7.5/7.4/8.1	1.4/0.9	—	—
4*b*	8.4	2.3	8.4	2.3	—	—
4*c*	8.4	2.3	8.2	0.6	—	—
4*e*[f]	8.2	0.6	8.2	0.6	—	—
5*a*[g]	7.4/7.4/8.0	1.3/1.0	7.4/7.4/8.0	1.3/1.0	—	—
5*b*	8.3	2.3	8.3	2.3	—	—
5*c*	8.3	2.3	8.1	[h]	—	—
5*e*	8.2	0.7	8.2	0.7	—	—

[a]Listed in numerical order of position, e.g., $J_{12}/J_{23}/J_{34}$.
[b]J_{para} 0.3/0.5 Hz, J_{76a} 0.8 Hz, J_{86a} 0.3 Hz, J_{96a} 0.6 Hz, $J_{10.6a}$ 0.5 Hz.
[c]J_{96a} 0.4 Hz.
[d]J_{76a} 0.5 Hz.
[e]J_{ortho} 8/—/7.5, J_{meta} —/1 (ref. 12).
[f]J_{para} 0.5 Hz.
[g]J_{ortho} 7.5/—/8, J_{meta} 1.0/— (ref. 12).
[h]Not measurable due to peak overlap.

tuted counterparts, MeO substitution can be seen to have little effect on the δ values of the nonaromatic protons except that an upfield shift of H-6a (**3***d* and **3***e*) and H-6 (**3***b* and **3***d*) is observed on introducing a methoxy group at C-1 and C-9 (of **3***a*), respectively. Unsymmetrical MeO substitution separates the originally degenerate angular methyl resonances of **4***a* (1.78 ppm) by 0.16 ppm (**4***c*), with the upfield singlet (1.73 ppm) being due to Me-4b as proved by nOe enhancement of H-4. Interestingly, the methyl protons of the unsubstituted ketal **5***a* (6, 8, 12) and its 1,10-dimethoxy derivative (**5***e*) absorb at nearly identical field strengths. Analysis of the changes in the aromatic proton signal positions induced by methoxy substitution reveals a remarkably good agreement with published additivity parameters (12, 21): an upfield shift of 0.06 ± 0.01 or 0.15 ± 0.01 ppm (depending on whether MeO is *ortho* or *para* to the benzylic carbon) for *meta*, 0.45 ± 0.05 for *ortho*, and 0.35 ± 0.03 for *para* protons.

Focussing on the splitting patterns (Table 2), the two vicinal coupling constants (5 and 10 Hz) of the methylene group of **3** identify the upfield proton as axial and the downfield proton as equatorial, with the C—H_6/C—H_{6a} dihedral angle approaching 180° (18). We attribute the increase in J_{6ax-6a} from 9.3 to 10.7 Hz on MeO substitution at C-1 to rotation around the C_{6a}—C_6 bond leading toward a half-chair conformation, caused by van der Waals repulsions between ring C and the bulky methoxy group. With regard to the stereochemistry at the B/C ring junction, we concur with the conclusion of previous authors (4, 22) that the *cis* structures are less strained than their *trans* isomers and are formed exclusively, i.e., the cyclization steps of the Claisen rearrangement and the aryl migration leading to **5** are stereospecific. This interpretation is supported by the X-ray crystallographic determination of the structures of phaseolin (23), 1,3,4b,6,8,9b-hexamethyl-4b,9b-dihydrobenzofuro[3,2-*b*]benzofuran (24), and 5a,10b-dihydrobenzofuro[2,3-*b*]benzofuran (25). Table 2 shows that *ortho* coupling constants are generally large (8.0–8.5 Hz), and *para* coupling is negligible (<0.2 Hz) except for **3***a* and **4***a* (0.3–0.5 Hz). *Meta* coupling across a methoxy-substituted carbon is considerably stronger (2.3–2.7 Hz) than across an unsubstituted carbon (0.6–0.7 Hz). In the unsubstituted heterocycles, one can clearly distinguish three *ortho* and two *meta* couplings, three of which we have assigned to different proton pairs (J_{12} and J_{34} of **4***a*, J_{13} of **5***a*) than Ramah *et al.* (12). The long-range benzylic coupling (26) between H-6a and the four aromatic hydrogens of ring D (0.3–0.8 Hz) was particularly useful for the assignment of the proton signals in the spectrum of **3***a*. Among the four methoxy-substituted 11a-methylpterocarpans, only H-7 of **3***d* and H-9 of **3***c* were similarly split by the benzylic hydrogen.

Though the proton nmr spectra permitted unambiguous identification of the 12 major Claisen rearrangement products of 1,4-bis(*m*-methoxyphenoxy-)2-butyne, we also examined the ^{13}C spectra of those compounds that could be readily obtained in high yield and purity to verify our structural assignments and to generate additional reference data for the structure elucidation of natural and synthetic pterocarpans. The ^{13}C chemical shifts of 11 compounds prepared in our laboratory and 8 closely related compounds reported in the literature (8, 10, 12, 27, 28) are listed in Table 3.

It can be seen that the heterocyclic ring carbons resonate at frequencies that are characteristically different for the three ring systems under investigation, thus permitting a clear distinction. The C-6, C-6a, C-11a, and Me-11a signals of the methylpterocarpans **3** appear at 66.5 ± 0.5, 48.0 ± 1.0, 83.9 ± 0.7, and 26.2 ± 1.4 ppm, respectively, the angular methyl peaks of the benzofurobenzofurans at 19.5 ± 1.4 ppm, and the benzylic carbons of **4** and **5** at 96.8 ± 0.9 and 56.7 ± 0.7 ppm, respectively. The latter resonance is close to but not overlapping with the methoxy peaks (55.5 ± 0.4 ppm), which can also be readily distinguished from it by their higher intensity. Similarly, the ketal carbon of **5** gives rise to a low-intensity, substituent-independent singlet between 124.0 and 125.0 ppm while the high-intensity peaks due to the unsubstituted aromatic carbons (97.0–132.8 ppm) appear as doublets in the off-resonance decoupled spectra.

Although the ^{13}C spectra of the unsubstituted compounds have been reported before, we recorded them again in order to verify the peak assignments. In the event, our values agree well with those listed by Ramah *et al.* (12) for **4***a* and **5***a* (except for a small deviation of 0.4 ppm for C-5a and C-10b of **5***a*), but the previously published ^{13}C assignments for **3***a* (10) were found to be incorrect. As expected, the oxygen-substituted carbons resonate farthest downfield (154.5 and 158.4 ppm), with the higher value most likely due to C-10a on the basis of a comparison to the corresponding carbon in the structurally similar **4***a* (158.5 ppm). C-6b and C-11b resonate at 125.5 and 126.5 ppm; their individual assignments, however, remain uncertain. The unsubstituted aromatic carbons are readily recognized by their high intensities, and the D-ring signals by the excellent match of their absorption positions with those of the comparable benzofuran carbons of **4***a* and **5***a*. Confirmation of the CH assignments was obtained by correlation of the proton and carbon chemical shifts. Based on this analysis of the 11a-methylpterocarpan spectrum, we propose a similar revision (as listed in Table 3) of the previously reported (10) peak assignments for 6a-hydroxy-11a-methylpterocarpan (**7***a*).

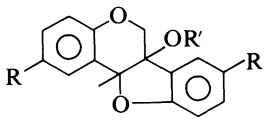

7

a: R = R′ = H
b: R = OMe, R′ = Ac

Analysis of the spectra of the methoxy-substituted compounds was considerably aided by the independence of the ring A and ring D carbon signals, i.e, variation of the substitution pattern in one ring has little, if any, effect on the carbon chemical shifts of the other. The virtual identity of the D-ring chemical shifts measured for the substrate pairs **3***b* and **3***d*, **4***c* and **4***e*, **5***c* and **5***e*, and for the A-rings of **4***b* and **4***c* illustrates this point. In conjunction with the experimentally determined substituent increments discussed below, it permitted us to assign the peaks with reasonable confidence. It is well known (29) that in simple benzene derivatives a methoxy group strongly deshields the directly attached aromatic carbon (±30.2 ppm), shields the *ortho* and *para* positions (by −15.5 and −8.9 ppm, respectively), and has little effect on the *meta* position. In more complex molecules, methoxy groups have been observed to induce different shifts of the resonance signals of two nonequivalent *ortho* (or *meta*) carbons (28). Therefore, indiscriminate application of the average additivity parameters may lead to erroneous conclusions unless the model compounds are chosen carefully.

We have found that the methoxy-substituted carbon is deshielded by 31.5 ± 0.5 ppm if located *para*, and by 33.8 ± 1.0 ppm (except C-1 of **3***d*) if located *ortho* to the benzylic

TABLE 3. Carbon chemical shifts

A. Benzofuro[3,2-*c*]benzopyrans(pterocarpans)

Compound	C-1	C-2	C-3	C-4	C-7	C-8	C-9	C-10	C-4a	C-11b	C-10a	C-6b	C-11a	C-6a	Me	C-6	MeO
3*a*[a]	128.3	121.9	129.2	117.2	124.7	120.6	129.0	110.3	154.5	125.5[f]	158.4	126.5[f]	83.2	47.8	27.6	66.6	—
3*b*	129.1	109.3	160.4	101.5	124.7	106.2	161.1	97.0	155.7	117.9	159.8	118.6	84.3	47.0	27.4	66.9	55.2/55.3
3*c*	129.0	109.1	160.2	101.5	157.5	103.5	129.9	102.9	155.9	118.0	159.8	113.2	83.6	46.2	27.6	66.0	55.1
3*d*	159.9	104.9	129.4	110.4	124.7	106.2	161.1	97.3	156.3	113.9	160.1	118.0	84.6	48.9	24.8	66.8	55.4/55.9
3*f*[b] (ref. 10)	119.1	154.4	115.9	118.0	111.1	154.4	113.8	110.2	148.4	126.1	152.3	127.4	83.6	48.0	27.7	66.7	55.8
6*a* (ref. 28)	131.7	109.0	160.8	101.5	124.5	106.2	160.9	96.8	156.5	112.3	160.5	119.0	78.5	39.5	—	66.5	55.3/55.4
6*c*[c] (ref. 27)	132.0	109.7	158.7	102.9	125.0	106.0	160.6	96.3	156.4	111.3	160.4	119.4	78.1	39.3	—	65.5	55.3
6*d*[c] (ref. 27)	123.1	110.4	154.8	99.0	124.9	106.1	160.5	96.2	153.3	117.2	160.2	119.7	78.5	39.4	—	66.5	55.2
7*a*[b] (ref. 8)	129.4	122.0	130.9	116.8	123.9	121.2	128.7	111.1	153.6	125.6	158.3	128.1	87.5	77.4	21.4	67.9	—
7*b*[b] (ref. 10)	116.2	154.5	117.7	117.3	112.2	153.9	113.3	111.1	147.4	125.3	153.6	125.3	87.7	85.3	22.3	64.3	55.7/55.8

B. Benzofuro[3,2-*b*]benzofurans

Compound	C-4	C-3	C-2	C-1	C-9	C-8	C-7	C-6	C-10a	C-4a	C-5a	C-9a	C-4b	C-9b	Me-4b	Me-9b	MeO
4*a*[a,d]	124.7	120.9	130.8	110.6	124.7	120.9	130.8	110.6	158.5	128.8	158.5	128.8	95.9	95.9	20.2	20.2	—
4*b*	124.7	107.4	162.5	96.1	124.7	107.4	162.5	96.1	160.0	121.0	160.0	121.0	96.8	96.8	20.3	20.3	55.3
4*c*	124.8	107.5	162.5	96.4	158.1	103.7	131.7	103.2	160.0	121.0	159.9	115.3	96.1	97.6	20.5	19.4	55.4/55.6
4*e*	158.1	103.9	131.6	103.2	158.1	103.9	131.6	103.2	159.9	115.3	159.9	115.3	96.8	96.8	19.4	19.4	55.6
4*f*[d,e] (ref. 10)	109.1	154.4	117.0	110.9	109.1	154.4	117.0	110.9	152.2	129.4	152.2	129.4	96.4	96.4	20.4	20.4	55.7

C. Benzofuro[2,3-*b*]benzofurans(ketals)

Compound	C-1	C-2	C-3	C-4	C-10	C-9	C-8	C-7	C-4a	C-10c	C-6a	C-10a	C-10b	C-5a	Me-10b	Me-5a	MeO
5*a*[d]	122.7	121.7	128.6	110.1	122.7	121.7	128.6	110.1	156.6	132.8	156.0	132.8	56.3	124.5	20.2	20.9	—
5*c*	124.7	107.1	160.5	96.1	156.5	104.4	129.3	103.3	157.6	125.0	157.8	119.3	56.3	125.0	19.3	20.2	55.2/55.3
5*e*	157.5	104.7	129.4	103.2	157.5	104.7	129.4	103.2	158.3	118.7	158.3	118.7	56.0	124.6	18.1	19.1	55.4
5*f* (ref. 12)	109.4	155.2	113.5	110.2	109.4	155.2	113.5	110.2	150.0	133.5	150.0	133.5	57.3	124.1	20.1	20.6	55.9

[a]Aromatic CH assignments differ from ref. 10.
[b]Revised assignments.
[c]In DMSO-d_6.
[d]See also ref. 12.
[e]C-2/C-4 assignments exchanged.
[f]Assignments uncertain.

carbon. The former value is in excellent agreement with the shift of 31.5–32.5 ppm reported for the natural pterocarpans **6** (27, 28) relative to their unsubstituted 11a-methyl analog. Good agreement with **6** is also observed for the methoxy-induced *ortho* shift, which varies between −11.7 and −15.7 ppm in the benzopyran ring system (ring A of **3**) but remains in the narrower range of −13.0 to −14.6 ppm in all benzofurans. When an MeO group is introduced at the sterically less accessible peri position (next to the benzylic carbon), the resonance signal of the adjacent unsubstituted carbon is shifted upfield by 17.0–17.3 ppm. Unsubstituted *meta* carbons are weakly affected (−0.2 – +1.1 ppm) by the introduction of a methoxy group, while the absorption of oxygen-substituted *meta* carbons is shifted downfield by 1.0–1.8 ppm. *Para*-methoxy substitution leads to a downfield shift of the peaks due to absorption by both unsubstituted (6.8–7.4 ppm) and alkyl-substituted carbons (7.5–8.5 ppm). Using these refined shift parameters, we have obtained reasonable agreement between calculated and experimental values only by revising several assignments made by Donnelly (10) for **3***f* and **7***b*; analogous reassignments have already been proposed by Ramah *et al.* (12) for **4***f*.

Thus the structures of the isomeric rearrangement products isolated in our laboratory are firmly supported by their nmr spectra. Their mass spectra feature prominent molecular ion and methyl cleavage ($M - 15$) peaks but no significant differences in the fragmentation patterns that would allow a distinction between the different heterocyclic ring systems. In conclusion, the dimethoxy-11a-methylpterocarpans formed by Claisen rearrangement of 1,4-bis(*m*-methoxyphenoxy-)2-butyne are accompanied by and readily converted to more stable dimethoxybenzofurobenzofurans. Since the reaction cannot be stopped at the benzofurobenzopyran stage and the isomeric products are difficult to separate, it is not considered as a convenient route for the synthesis of 11a-methyl analogs of natural pterocarpans.

Experimental

Melting points (uncorrected) were recorded on a Fisher–Johns melting point apparatus, mass spectra (70 eV) on an HP-5985 quadrupole instrument, and nmr spectra on a Bruker spectrometer (400 MHz); chemical shifts were referenced to the center solvent (chloroform) line and corrected (+7.258 ppm for ^{1}H, +77.0 ppm for ^{13}C) to TMS. Gas chromatographic analyses were carried out on a Hewlett–Packard instrument (model HP-5890A) with integrator (model HP-3392A) and 15-m DB-1 capillary column (temperature programmed to increase from 150 to 250°C at 20°/min, carrier gas helium). For other chromatographic separations we used the following systems: (a) analytical tlc in toluene/ethyl acetate (49:1, solvent A), dichloromethane, hexanes/ether/methanol (96:10:4, solvent B), or dichloromethane/hexanes (85:15, solvent C) on Merck Kieselgel 60F-254 (0.2 mm) DC-Plastikfolien; (b) preparative tlc on Merck Silica Gel 60HF254+366; (c) flash chromatography on Kieselgel 60 (230–400 mesh) with the same solvents; and (d) hplc on Partisil-M9/ODS-2 with methanol/water/acetic acid (85:15:0.6) at a flow rate of 4.0 mL/min. Elemental analyses were performed on a Carlo Erba Elemental Analyzer Model 1106; $C_{18}H_{18}O_4$ requires 72.47% C and 6.08% H.

1,4-Bis(m-*methoxyphenoxy-)2-butyne* (**1**b)

Into a 500-mL three-necked round-bottom flask equipped with reflux condenser and mechanical stirrer were placed 150 mL reagent-grade acetone (dried over K_2CO_3 and freshly distilled), 57.9 g (0.419 mol) anhydrous potassium carbonate, and 43.4 g (0.350 mol) freshly distilled (bp 126–128°C/14 Torr; 1 Torr = 133.3 Pa) *m*-methoxyphenol (Aldrich, technical, purified as described in ref. 30). A solution of 16.05 g (0.1305 mol) freshly distilled (bp 72°C/23 Torr) 1,4-dichloro-2-butyne (Aldrich) in 50 mL acetone was added with stirring, and the dark-colored reaction mixture was stirred and refluxed for 25 h. The product mixture obtained after cooling, filtration, and evaporation of the solvent was dissolved in 125 mL ether, washed with 2 *M* KOH (3 × 50 mL) and water (2 × 50 mL), and dried ($MgSO_4$). Evaporation of the ether yielded 15.19 g of dark brown liquid which was fractionated at 0.05–0.10 Torr to give 12.05 g (40.5 mmol, 31%) 1,4-bis(*m*-methoxyphenoxy-)2-butyne boiling at 170–180°C; nmr (ppm): 7.17 (t, *J* 8.3 Hz, H-5), 6.53 (m, H-2,4,6), 4.71 (s, CH_2), and 3.77 (s, OMe). *Anal.* found: 72.29% C, 6.25% H. A small amount of 1-chloro-4-(*m*-methoxyphenoxy-)2-butyne was isolated from the low-boiling fraction (1.16 g) collected at 90–165°C/0.1 Torr; nmr (ppm): 7.17 (t, *J* 8 Hz, H-5), 6.49–6.62 (m, H-2,4,6), 4.71 (t, *J* 2 Hz, $ArOCH_2$), 4.15 (t, *J* 2 Hz, CH_2Cl), and 3.77 (s, OMe). *Anal.* calcd. for $C_{11}H_{11}ClO_2$: C 62.72, H 5.26; found: C 62.95, H 5.42. Unreacted *m*-methoxyphenol (28.9 g, 233 mmol) was recovered from the alkaline washings by acidification (concentrated HCl) and ether extraction.

11a-Methylpterocarpan (**3**a) *and 4b,9b-dihydro-4b,9b-dimethylbenzofuro[3,2-*b*]benzofuran* (**4**a)

These two compounds were prepared from 1,4-diphenoxy-2-butyne (11) as described in the literature (8, 22) and separated by fractional crystallization from ethanol, yielding pure **3***a*, mp 126–128°C (lit.(8) mp 124–125°C) and **4***a*, mp 128–129°C (lit.(8) mp 126–129°C).

*Rearrangement of 1,4-bis(*m*-methoxyphenoxy-)2-butyne* (**1**b)

(*a*) Without acid: In a 200-mL three-necked round-bottom flask fitted with nitrogen inlet tube, condenser, and thermometer, a solution of 8.69 g (29.1 mmol) 1,4-bis(*m*-methoxyphenoxy-)2-butyne (**1***b*) in 63 mL freshly distilled *N*,*N*-diethylaniline was heated under nitrogen at 210°C for 24 h. The originally yellow solution turned orange after one hour. Eight 50-μL samples were withdrawn at suitable time intervals for gc analysis. After cooling and addition of 200 mL ether, the solvent was removed by acidification and extraction with 10% HCl (3 × 200 mL) and water (5 × 50 mL), the organic layer was dried ($MgSO_4$), and the solvent evaporated to give 7.42 g (86%) of a brown viscous liquid. Gas chromatographic separation and mass spectrometric analysis showed the presence of six major components: 12.8% **3***b* (*m*/*z* 298 (35), 283 (100)), 11.0% **3***c* (*m*/*z* 298 (42), 283 (100), 267 (21)), 12.1% **3***d* (*m*/*z* 298 (46), 283 (100), 267 (14)), 6.9% **3***e* (*m*/*z* 298 (33), 283 (76), 267 (14), 162 (100)), 25.9% **4***b* (*m*/*z* 298 (32), 283 (100)), and 14.6% **4***c* (*m*/*z* 298 (47), 283 (100), 267 (32)). The composition was verified by integration of the methoxy and angular methyl peak areas in the ^{1}Hmr spectrum: 14% **3***b*, 13% **3***c*, 11% **3***d*, 7% **3***e*, 23% **4***b*, 10% **4***c*, and 2% **4***e*. Flash chromatography (solvent A) separated the mixture into four fractions (in order of elution): (*1*) a small quantity of material tentatively identified as a mixture of several isomeric dimethoxy-4b,5,10b,11-tetrahydrobenzopyrano[4,3-*c*]benzopyrans (**11**) on the basis of the absence of angular methyl protons in its ^{1}Hmr spectrum and the appearance of resonance signals (at 4.21, 4.28, 4.38, 2.56, 2.79, and 2.86 ppm) characteristic of the methylene and benzylic protons of this rare class of compounds (20, 31); (*2*) **3***c* (*Anal.* 72.35% C, 5.85% H), which was further purified by hpcl; (*3*) the major fraction from which **3***b* (*Anal.* 72.55% C, 6.23% H), **3***e* (contaminated with **4***c*), **4***b*, and **4***c* were obtained by repeated flash chromatography (solvent C); and (*4*) **3***d*, which was purified by preparative tlc (solvent A) and recrystallized from methanol (mp 110–113°C; *Anal.* 72.33% C, 5.91% H). Work-up of a large aliquot after 15 min reflux, followed by flash chromatography (solvent A) and preparative tlc (solvent B), yielded samples of 7-methoxy-4-(*m*-methoxyphenoxymethyl-)2*H*-chromene (**2***b*): *m*/*z* 298 (38), 191 (23), 161 (52), 77 (100); nmr (ppm): 3.78 and 3.79 (2s, OMe), 4.78 (q, *J* 1.3 Hz, $ArOCH_2$), 4.82 (dt, *J* 1.3 and 3.6 Hz, 2-CH_2), 5.80 (tt, olefinic CH), 7.11 (d, *J* 8.4 Hz, H-5), 7.21 (t, *J* 8.4 Hz, H-5′), 6.54–6.60 (m, H-2′,4′,6′), 6.43 (d *J* 2.5 Hz, H-8), and 6.46 (dd, H-5), and its 5-methoxy isomer **2***d* (contaminated with **11** and **3***c*); nmr (ppm): 3.76 and 3.79 (2s, OMe), 4.63 (dt, *J* 1.8 and 4.2 Hz, 2-CH_2), 5.04 (q, *J* 1.8 Hz, $ArOCH_2$), 5.97 (septet, olefinic H), and 6.3–7.4 (m, aromatic H).

(b) With *p*-toluensesulfonic acid (PTS): Repetition of the Claisen rearrangement in the presence of 10 mol% PTS gave a product mixture containing (time:%) **4***c* (1.5 h:14, 6 h:30, 13 h:31), **4***b* (1.5 h:16, 6 h:33, 13 h:36), **2***b* (1.5 h:31, 6 h:11, 13 h:4), an unidentified intermediate (1.5 h:8, 6 h:7, 13 h:8), **4***e* (1.5 h:3, 6 h:5, 13 h:6), and minor quantities of the four pterocarpan isomers **3** (1.5 h:9, 6 h:7, 13 h:4). Pure **4***e* (mp 187–190°C from methanol; *Anal.* 72.69% C, 6.19% H) was isolated from the final mixture (86% crude yield) by flash chromatography with dichloromethane.

(c) With aluminum chloride: In a two-necked 50-mL round-bottom flask fitted with condenser, drying tube, and nitrogen inlet tube, a solution of 250 mg (8.38 mmol) 1,4-bis(*m*-methoxyphenoxy-)2-butyne in 10 mL dichloromethane was mixed with an equimolar amount of aluminum chloride and magnetically stirred for 3 h at 25°C. After another 5 h reflux, washing with 3 *N* HCl, 1 *N* NaOH, and water, drying ($MgSO_4$), and solvent evaporation, 165 mg (66%) of a viscous brown oil remained, which was found (by gc analysis) to contain 25% **5***b*, 15% **4***b*, 8% **4***c*, and 17% unreacted starting material, together with small quantities of isomers. Gas chromatographic monitoring showed a gradual increase of the (**4** + **5**)/**3** ratio with time. Flash chromatography (dichloromethane) gave **4***b* and **5***b* (71.98% C, 6.55% H) for spectroscopic identification.

*Rearrangement of 7-methoxy-4-(*m*-methoxyphenoxymethyl-)2*H*-chromene (**2**b)*

A solution of 20 mg **2***b* in 1 mL *N*,*N*-diethylaniline was heated under nitrogen to 210°C, and its composition was monitored by gc over a period of 6 h. After 4 h the mixture contained 24% **4***b*, 22% **3***b*, 15% **3***c*, 10% of an unidentified by-product, and 7% **4***c*. On addition of a few milligrams PTS and another 2 h reflux, **3***b* and **3***c* disappeared and the percentages of **4***b* and **4***c* increased to 36% and 19%, respectively.

*2,9-Dimethoxy-4b,9b-dihydro-4b,9b-dimethylbenzofuro[3,2-*b*]benzofuran (**4**c) from 1,9-dimethoxy-11a-methylpterocarpan (**3**d)*

The thermal stability of **3***d* in the absence of acid was tested by subjecting a 30-mg sample, dissolved in 1.0 mL *N*,*N*-diethylaniline, to the Claisen rearrangement conditions (210°C/50 min); no reaction was observed (gc analysis). One hour after the addition of 5 mg PTS, more than half of the starting material had been converted to **4***c*, and after another 21 h at 190–210°C the reaction mixture contained 79% **4***c* and small amounts of two unidentified compounds (9 and 4% respectively). The structure of the major product (**4***c*: 72.26% C, 6.01% H) was confirmed by ^{1}Hmr after work-up (as described above) and purification by preparative tlc (solvent B).

*5a,10b-Dihydro-5a,10b-dimethylbenzofuro[2,3-*b*]benzofuran (**5**a) from 4b,9b-dihydro-4b,9b-dimethylbenzofuro[3,2-*b*]benzofuran (**4**a)*

An equimolar quantity of aluminum chloride was added to a solution of 83 mg (0.35 mmol) **4***a* in 4.0 mL dichloromethane. After 24 h of magnetic stirring at 25°C the purple solution was extracted with 1 *N* HCl and water, dried ($MgSO_4$), and distilled to obtain 80 mg (96%) of a beige solid that yielded pure **5***a*, mp 135–136°C (previously reported (8) as 195–196°C), on recrystallization from ethanol.

*Rearrangement of dimethoxy-4b,9b-dihydro-4b,9b-dimethylbenzofuro[3,2-*b*]benzofurans (**4**) to dimethoxy-5a,10b-dihydro-5a,10b-dimethylbenzofuro[2,3-*b*]benzofurans (**5**)*

Reflux of a solution of 27 mg (0.09 mmol) **4***e* in 1.5 mL dichloromethane (under nitrogen) with 0.12 mmol aluminum chloride for one hour, extraction with 1 *N* HCl, 1 *N* NaOH, and water, drying ($MgSO_4$), and solvent evaporation gave 23 mg (85%) of a semisolid residue containing 67% **5***e* and 20% unreacted starting material (by gc and ^{1}Hmr analysis). Continued reflux in chloroform (5 h) with fresh aluminum chloride raised the **5***e*/**4***e* ratio to 4:1 while further extension of the reaction time (69 h) resulted in partial ether cleavage (4). Similar treatment of **4***c* (70 h at 25°C in dichloromethane) yielded a viscous brown oil (77% yield) containing more than 80% **5***c*, while **4***b* did not react.

Acknowledgement

The financial support of these investigations by the Natural Sciences and Engineering Research Council is gratefully acknowledged.

1. J. Hlubucek, E. Ritchie, and W. Taylor. Aust. J. Chem. **24**, 2347 (1971); **24**, 2355 (1971).
2. U. Koch-Pomeranz, H. J. Hansen, and H. Schmid. Helv. Chim. Acta, **56**, 2981 (1973).
3. B. S. Thyagarajan, K. K. Balasubramanian, and R. B. Rao. Tetrahedron, **23**, 1893 (1967).
4. D. K. Bates and M. C. Jones. J. Org. Chem. **43**, 3856 (1978).
5. S. Ramakanth, K. Narayanan, and K. K. Balasubramanian. Tetrahedron, **40**, 4473 (1984).
6. B. S. Thyagarajan, K. K. Balasubramanian, and R. B. Rao. Tetrahedron, **21**, 2289 (1965).
7. M. Ramah and B. Laude. Bull. Soc. Chim. Fr. 2655 (1975).
8. D. M. X. Donnelly, P. J. Gunning, and M. J. Meegan. Proc. Ir. Acad. Sect. B, **77**, 435 (1977).
9. D. R. Perrin and I. A. M. Cruickshank. Phytochemistry, **8**, 971 (1969).
10. D. M. X. Donnelly. Proceedings of the Fifth Hungarian Bioflavonoid Symposium, Matrafured, Hungary. 1977. p. 15.
11. A. W. Johnson. J. Chem. Soc. 1009 (1946).
12. M. Ramah, J. Vebrel, and B. Laude. Spectrochim. Acta, Part A, **40**, 189 (1984).
13. J. M. Bruce and Y. Roshan-Ali. J. Chem. Soc. Perkin Trans. 1, 2677 (1981).
14. U. Rao and K. K. Balasubramanian. Heterocycles, **22**, 1351 (1984).
15. H. J. Hansen. Mechanisms of molecular migrations. Vol. 3. Wiley–Interscience, New York. 1971. p. 177.
16. J. Borgulya, R. Madeja, P. Fahrni, H. J. Hansen, H. Schmid, and R. Barner. Helv. Chim. Acta, **56**, 14 (1973).
17. (*a*) I. Iwai and J. Ide. Chem. Pharm. Bull. (Tokyo), **11**, 1042 (1963); (*b*) W. K. Anderson and E. J. LaVoie. J. Org. Chem. **38**, 3832 (1973).
18. K. G. R. Pachler and W. G. E. Underwood. Tetrahedron, **23**, 1817 (1967).
19. K. Kurozawa, W. D. Ollis, I. O. Sutherland, and O. R. Gottlieb. Phytochemistry, **17**, 1417 (1978).
20. B. Cardillo, M. Cornia, and L. Merlini. Gazz. Chim. Ital. **105**, 1151 (1975).
21. L. M. Jackman and S. Sternhell. Applications of nuclear magnetic resonance spectroscopy in organic chemistry. Pergamon Press, Oxford. 1969. p. 202.
22. K. C. Majumdar and B. S. Thyagarajan. J. Heterocycl. Chem. **10**, 159 (1973).
23. C. DeMartinis, M. F. Mackay, and B. J. Poppleton. Tetrahedron, **34**, 1849 (1978).
24. R. Mercier, M. Ramah, B. Laude, R. Faure, and H. Loiseleur. Acta Crystallogr. Sect. C, Cryst. Struct. Commun. **40**, 1208 (1984).
25. G. D. Andreetti, G. Bocelli, L. Cavalca, and P. Sgarabotto. Gazz. Chim. Ital. **104**, 1127 (1974).
26. M. Barfield, C. J. Fallick, K. Hata, S. Sternhell, and P. W. Westerman. J. Am. Chem. Soc. **105**, 2178 (1983).
27. A. A. Chalmers, G. J. H. Rall, and M. E. Oberholzer. Tetrahedron, **33**, 1735 (1977).
28. A. Pelter, R. S. Ward, and T. I. Gray. J. Chem. Soc. Perkin 1, 2475 (1976).
29. J. B. Stothers. Carbon-13 NMR spectroscopy. Academic Press, New York. 1972.
30. W. H. Perkin, J. N. Ray, and R. Robinson. J. Chem. Soc. 941 (1926); 2097 (1927).
31. M. Cornia, L. Merlini, and A. Zanarotti. Gazz. Chim. Ital. **107**, 299 (1977).

Proton magnetic resonance spectra of catechin and bromocatechin derivatives: C_6- vs. C_8-substitution

E. KIEHLMANN AND A. S. TRACEY
Department of Chemistry, Simon Fraser University, Burnaby, B.C., Canada V5A 1S6

Received February 18, 1986

E. KIEHLMANN and A. S. TRACEY. Can. J. Chem. **64**, 1998 (1986).

The ^{1}Hmr spectra of 20 catechin derivatives substituted at C-6/C-8 by bromine and/or hydrogen and at oxygen by methyl, acetyl, and/or hydrogen have been analyzed in deuterated acetone, acetonitrile, and chloroform. Because of its dependence on the nature of the solvent and of the oxygen substituent, the difference between H-6 and H-8 chemical shifts has been found to be an unreliable criterion for the distinction between 8-bromo and 6-bromo isomers. In methylated catechins, double irradiation of H-8 and H-6 enhances one (MeO-7) and two (MeO-5 and MeO-7) methoxy signals, respectively, via the nuclear Overhauser effect. This permits unambiguous assignment of chemical shifts to all ring A protons. The H-6 and H-8 resonance frequencies of catechin have been determined by decoupling of the OH-5 and OH-7 protons.

E. KIEHLMANN et A. S. TRACEY. Can. J. Chem. **64**, 1998 (1986).

Utilisant l'acétone deutériée, l'acétonitrile et le chloroforme comme solvants, on a analysé les spectres de rmn du ^{1}H des dérivés de la catéchine substitués en position C-6/C-8 par le brome et/ou l'hydrogène et sur l'oxygène par des groupes méthyle, acétyle et/ou hydrogène. La différence entre les déplacements chimiques des protons H-6 et H-8 ne constitue pas un critère valable de distinction entre les isomères bromo-6 et bromo-8 puisqu'elle dépend de la nature du solvant et des substituants fixés sur l'oxygène. L'irradiation double des protons H-8 et H-6 des catéchines méthylés augmente respectivement les signaux d'un groupe méthoxy (MeO-7) et de deux groupes méthoxy (MeO-5 et MeO-7) via l'effet Overhauser nucléaire. Ceci permet d'identifier sans ambiguïté les déplacements chimiques de tous les protons du cycle A. On a déterminé les fréquences de résonance des protons H-6 et H-8 de la catéchine en découplant les protons OH-5 et OH-7.

[Traduit par la revue]

Introduction

Ever since the isolation and structure elucidation of the first dimeric procyanidins by Weinges *et al.* (1) and their first synthesis (2, 3), unambiguous determination of the position of the interflavanoid linkage, i.e., the carbon atom of ring A of the terminal catechin or epicatechin unit (C-6 or C-8) that is bonded to C-4 of a second flavanoid, has remained problematic. This applies even to simple monoflavanoids such as monobromotetra- and penta-*O*-methylcatechin, for which Weinges (1, 3) postulated the 8-bromo structure on the basis of the greater steric accessibility of C-8 relative to C-6 in electrophilic aromatic substitution. It was not until 1977 (4) and 1985 (5) that the configurations of 8-bromo-3′,4′,5,7-tetra-*O*-methylcatechin (**3***d*) and 6-bromo-3,3′,4′,5,7-penta-*O*-methylcatechin (**4***c*) were proven by X-ray structure analysis. Due to the difficulty of obtaining di- and oligomeric flavanoids in crystalline form (6), this technique is clearly inconvenient for routine application to proanthocyanidins. Chemical correlation with authentic samples and nmr spectroscopy have, therefore, been most widely used to establish the substitution pattern in new natural and synthetic products.

Hundt and Roux (7, 8) derived several empirical nmr parameters from the proton spectra of 11 pairs of simple 6- and 8-monosubstituted tetra-*O*-methylcatechins (**1**) and established characteristic non-overlapping regions for the H-8 (6.32–6.47) and H-6 (6.10–6.22) resonance signals in chloroform. Carbon-13 and various different proton chemical shifts (9–12) and coupling constants (13) have been used by other researchers to identify the position of flavanyl and benzyl substituents in ring A of catechin derivatives. However, the observed chemical shift differences are usually small and the ^{1}Hmr parameters of most diflavanoid methyl ether acetates do not fall inside the relative and absolute ranges determined for monoflavanoids (8) if one assumes (14–16) that assignment of the position of the interflavanoid linkage can be based *solely* on the downfield chemical shift of H-8 of one regioisomer relative to H-6 of the other. Since the validity of this basic assumption has not been proved for diflavanoids by independent structure determination, e.g., X-ray diffraction or unambiguous synthesis, and the successful application of this comparative technique depends critically on the availability of the twin regioisomer of any new natural or synthetic procyanidin, the development of absolute distinction criteria appears prudent. With this goal in mind, we decided to synthesize all 15 6-bromo-, 8-bromo-, and 6,8-dibromo derivatives of catechin, 3′,4′,5,7-tetra-*O*-methylcatechin, 3,3′,4′,5,7-penta-*O*-methylcatechin, 3-acetyl-3′,4′,5,7-tetra-*O*-methylcatechin and catechin pentaacetate (eq. [1]), and the 4 non-brominated parent compounds, determine their structures by chemical correlation with authentic samples of **3***d* (4) and **4***c* (5), and record, analyze, and correlate their ^{1}Hmr spectra at 400 MHz in three different solvents.

Results and discussion

The ^{1}Hmr data listed in Tables 1–4 confirm the validity of the empirical rules proposed by Hundt and Roux (8) for the distinction between 6- and 8-substituted tetra-*O*-methylcatechins. However, we found that these criteria cannot be applied without modification to the corresponding peracetates in chloroform (17) or free phenols in acetone. For example, while the trends in the chemical shift difference $\Delta\delta$(H-2/6 or 8) and in the ratio $\Delta\delta$(H-2/4a)/$\Delta\delta$(H-2/6 or 8) are the same as for the corresponding methylated compounds, their magnitudes are considerably reduced, viz., from $\Delta\delta$(H-2/8) − $\Delta\delta$(H-2/6) = 0.41–0.52 for **3***c*/**4***c*/**5***c* vs. **3***d*/**4***d*/**5***d* to 0.24 for **6***c* vs. **6***d* and only 0.04 for **2***c* vs. **2***d*, and from $\Delta\delta$(H-2/4a)/$\Delta\delta$(H-2/6) − $\Delta\delta$(H-2/4a)/$\Delta\delta$(H-2/8) = 0.62–1.63 for **3***d*/**4***d*/**5***d* vs. **3***c*/**4***c*/**5***c* to 0.41 for **6***d* vs. **6***c* and 0.19 for **2***d* vs. **2***c*. The H-2 protons of 6-bromocatechin (**2***c*) and its pentaacetate (**6***c*) resonate slightly upfield (4.61 and 5.16 ppm) relative to the corresponding protons of the 8-bromo isomers **2***d* (4.77 ppm)

[1]

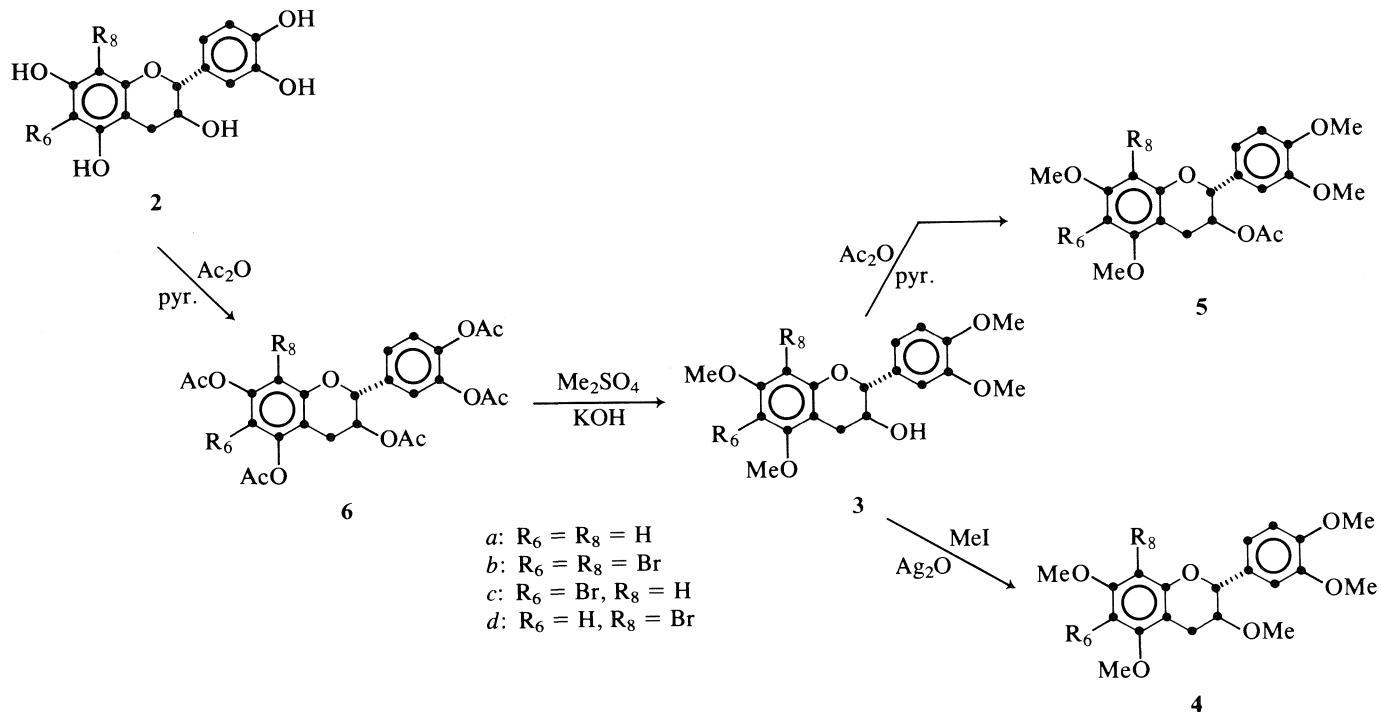

and **6***d* (5.33 ppm), and the H-4a signals are shifted slightly downfield (2.91 and 2.88, respectively, for **2***c* and **6***c* vs. 2.84 for **2***d* and **6***d*), as observed with greater magnitude for the methylated compounds, but the positions of the signals for the residual ring A protons are nearly identical for the acetates **6***c* (6.75 ppm) and **6***d* (6.69 ppm) and actually reversed for the free phenols, i.e., H-8 of **2***c* absorbs *upfield* (6.11 ppm) from H-6 of **2***d* (6.23 ppm). Changing the solvent from chloroform to acetone generally reduces the magnitude of the chemical shift differences between C_6- and C_8-substituted isomers. It is concluded that both the absolute and relative ^{1}Hmr parameters depend not only on the position of the bromine substituent (C-6 vs. C-8) but also on the solvent and the nature of the substituent attached to the phenolic oxygens. Magnetic anisotropy effects caused by a second flavanoid unit linked to C-6 or C-8 of catechin would make the chemical shift of the remaining ring A proton even less predictable. As all of these factors must be taken into account, great caution is advisable in making structural assignments based solely on chemical shift criteria.

While the coupling constants J_{23} and J_{34b} are seen to be larger for the 6- than for the 8-bromocatechins (Table 4), their predictive power for the differentiation between regioisomeric flavanoids is also questionable. The high degree of conformational flexibility of the heterocyclic ring (18) leads to J variations that depend not only on the nature and position of the substituents attached at C-3 and at the ring A carbons but also on the solvent used in the nmr experiment.

We therefore concentrated our efforts on a search for spectral parameters that could serve as absolute criteria for unambiguous structure assignments to single compounds, without the need for comparative data of their regioisomers. For example, the shift of the residual ring A proton signal on changing the nmr solvent may be of diagnostic value if it can be demonstrated to be equally applicable to catechin derivatives containing substituents other than bromine. The replacement of chloroform by acetone results in a large downfield shift (by 0.23–0.28 ppm) of the H-6 singlet of all three methylated 8-bromocatechins (**3***d*, **4***d*, and **5***d*) but only a small downfield shift (by 0.01–0.07 ppm) of the H-8 singlet of the corresponding 6-bromo isomers (**3***c*, **4***c*, and **5***c*). The same phenomenon is observed to a lesser degree for the non-brominated parent compounds (**3***a*, **4***a*, and **5***a*) for which the corresponding solvent change induces a small downfield shift (0.02–0.06 ppm) of the H-6 and a small upfield shift (0.05–0.10 ppm) of the H-8 signal. This indicates a preferred orientation of the acetone molecules with respect to the bromine, leading to more effective paramagnetic deshielding of H-6 in 8-bromocatechins than of H-8 in 6-bromocatechins. Such anisotropic solvent shifts are known to be a function of the distance between the nucleus under observation and the polar substituent, and of the dipole moment of the solute as well as the shape and dielectric constant of the solvent (19), and have aided previous investigators (20), mainly using chloroform and benzene, in the assignment of methoxy proton resonances.

Studies of the nuclear Overhauser effect (nOe) suggest a convenient method for the distinction between 6- and 8-substituted isomers, which should be of general applicability and independent of the nature of the substituent (Table 5). Double irradiation of the H-6 resonance frequency of any C_8-substituted 5,7-di-*O*-methylcatechin derivative increases the intensities of both methoxy signals, while H-8 irradiation of a C_6-substituted compound enhances only the one methoxy signal (MeO-7) positioned in its close physical proximity. The same phenomenon is observed for the C_6/C_8-unsubstituted derivatives **3***a*, **4***a*, and **5***a*, in which case H-6 saturation is found to enhance the MeO-5 more than the MeO-7 signal. These differences in the magnitude of the nOe effect confirm that the 5-methoxy group is preferentially oriented toward H-6 to minimize steric interactions with the C-4 hydrogens, and that in the monobromo compounds the 7-O-methyl group points away from the bulky bromine substituent (5). Chloroform was chosen as solvent for these experiments since it provides the best resolution of the methoxy signals. We have thereby firmly established

TABLE 1. Proton chemical shifts: aromatic rings A and B[a]

		Catechin derivatives					6,8-Dibromocatechin derivatives				
Proton	Compound: 3,5,7,3′,4′-Substituents:	**2***a* -(OH)$_5$	**3***a* -(OMe)$_4$ 3-OH	**4***a* -(OMe)$_5$	**5***a* -(OMe)$_4$ 3-OAc	**6***a* -(OAc)$_5$[b]	**2***b* -(OH)$_5$	**3***b* -(OMe)$_4$ 3-OH	**4***b* -(OMe)$_5$	**5***b* -(OMe)$_4$ 3-OAc	**6***b* -(OAc)$_5$
H-6		6.011	6.124	6.122	6.149	6.597	—	—	—	—	—
		5.921	6.124	6.118	6.139	6.551	—	—	—	—	—
		—	6.107	6.089	6.094	6.592	—	—	—	—	—
H-8		5.860	6.034	6.055	6.117	6.663	—	—	—	—	—
		5.824	6.050	6.072	6.139	6.650	—	—	—	—	—
		—	6.138	6.143	6.168	6.654	—	—	—	—	—
H-2′		6.882	7.022	7.017	6.994	7.284	6.859	7.029	7.013	7.004	7.308
		6.817	6.966	6.930	6.914	7.203	6.781	6.949	6.894	6.897	7.194
		—	6.972	6.932	6.886	7.165	—	6.970	6.895	6.857	7.140
H-5′		6.767	6.910	6.916	6.910	7.266	6.792	6.930	6.919	6.935	7.298
		6.781	6.916	6.880	6.872	7.211	6.768	6.932	6.899	6.898	7.228
		—	6.899	6.869	6.826	7.191	—	6.896	6.866	6.829	7.21
H-6′		6.767	6.948	6.916	6.910	7.347	6.725	6.930	6.877	6.891	7.355
		6.714	6.916	6.880	6.872	7.288	6.674	6.898	6.828	6.845	7.281
		—	7.002	6.967	6.912	7.252	—	6.971	6.866	6.829	7.21
Ar-OR			3.72–3.80	3.73–3.79	3.75–3.78	2.23–2.26		3.79–3.83	3.77–3.84	3.76–3.85	2.25–2.40
			3.72–3.79	3.72–3.78	3.74–3.77	2.22–2.23		3.76–3.81	3.74–3.82	3.72–3.83	2.23–2.37
			[c]	[c]	[c]	2.27–2.28		3.82–3.89	3.79–3.88	3.76–3.90	2.28–2.41

[a]Solvents: acetone-d_6 (top), CD_3CN (center; with trace D_2O for **2***a* and **2***b*), $CDCl_3$ (bottom). Coupling constants: J_{68} = 2.2–2.4 Hz, $J_{2',6'}$ = 1.8–2.1 Hz, $J_{5',6'}$ = 8.1–8.4 Hz, $J_{26'}$ = 0.5–0.7 Hz.

[b]H-6/H-8 assignments uncertain; the spectrum of partially deuterated **6***a* indicates that in all three solvents H-8 resonates downfield from H-6 (added in proof).

[c]See Table 5.

TABLE 2. Proton chemical shifts: aromatic rings A and B[a]

		6-Bromocatechin derivatives					8-Bromocatechin derivatives				
Proton	Compound: 3,5,7,3′,4′-Substituents:	**2***c* -(OH)$_5$	**3***c* -(OMe)$_4$ 3-OH	**4***c* -(OMe)$_5$	**5***c* -(OMe)$_4$ 3-OAc	**6***c* -(OAc)$_5$	**2***d* -(OH)$_5$	**3***d* -(OMe)$_4$ 3-OH	**4***d* -(OMe)$_5$	**5***d* -(OMe)$_4$ 3-OAc	**6***d* -(OAc)$_5$
H-6		—	—	—	—	—	6.230	6.399	6.396	6.427	6.776
		—	—	—	—	—	6.127	6.305	6.303	6.324	6.705
		—	—	—	—	—	—	6.165	6.145	6.151	6.690
H-8		6.111	6.383	6.409	6.477	6.857	—	—	—	—	—
		6.062	6.382	6.404	6.467	6.813	—	—	—	—	—
		—	6.367	6.379	6.406	6.752	—	—	—	—	—
H-2′		6.859	7.020	7.013	6.995	7.285	6.891	7.040	7.024	7.008	7.302
		6.804	6.957	6.916	6.906	7.197	6.807	6.966	6.919	6.914	7.201
		—	6.962	6.895	6.857	7.151	—	6.990	6.946	6.893	7.153
H-5′		6.783	6.933	6.934	6.932	7.273	6.794	6.907	6.902	6.905	7.293
		6.782	6.923	6.903	6.895	7.213	6.784	6.903	6.882	6.876	7.226
		—	6.917	6.874	6.834	7.194	—	6.881	6.843	6.858	7.196
H-6′		6.722	6.933	6.907	6.903	7.343	6.751	6.945	6.902	6.905	7.360
		6.705	6.923	6.867	6.868	7.279	6.702	6.903	6.822	6.831	7.290
		—	7.005	6.942	6.891	7.234	—	6.970	6.919	6.805	7.238
Ar-OH			3.77–3.82	3.76–3.83	3.74–3.86	2.25–2.34		3.78–3.87	3.77–3.87	3.76–3.89	2.26–2.32
			3.76–3.80	3.73–3.80	3.71–3.82	2.23–2.31		3.77–3.85	3.75–3.86	3.74–3.87	2.23–2.30
			[b]	[b]	[b]	2.28–2.34		[b]	[b]	[b]	2.26–2.35

[a]Solvents: acetone-d_6 (top), CD_3CN (center; with trace D_2O for **2***c* and **2***d*), $CDCl_3$ (bottom). Coupling constants: $J_{2'6'}$ = 1.8–2.1 Hz, $J_{5'6'}$ = 8.1–8.4 Hz, $J_{26'}$ = 0.5–0.7 Hz.
[b]See Table 5.

TABLE 3. Proton chemical shifts and coupling constants: heterocyclic ring C[a]

Proton	Compound: 3,5,7,3′,4′-Substituents:	Catechin derivatives					6,8-Dibromocatechin derivatives				
		2*a* -(OH)$_5$	**3***a* -(OMe)$_4$ 3-OH	**4***a* -(OMe)$_5$	**5***a* -(OMe)$_4$ 3-OAc	**6***a* -(OAc)$_5$	**2***b* -(OH)$_5$	**3***b* -(OMe)$_4$ 3-OH	**4***b* -(OMe)$_5$	**5***b* -(OMe)$_4$ 3-OAc	**6***b* -(OAc)$_5$
H-2		4.554	4.630	4.833	5.052	5.264	4.858	4.978	5.263	5.366	5.494
		4.525	4.638	4.896	5.057	5.231	4.726	4.898	5.205	5.288	5.37(m)
		—	4.660	4.821	5.014	5.143	—	4.839	5.170	5.350	5.341
H-3		3.973	4.044	3.742	5.284	5.305	4.113	4.202	3.952	5.436	5.399
		3.954	4.048	3.75	5.324	5.320	4.034	4.129	3.897	5.402	5.37(m)
		—	4.061	3.680	5.344	5.248	—	4.055	3.736	5.434	5.278
3-OR				3.204	1.903	1.914			3.314	1.960	1.941
				3.235	1.889	1.911			3.301	1.930	2.144
				3.246	1.948	1.995			3.318	2.034	2.032
H-4a		2.912	2.895	2.813	2.779	2.842	2.862	2.992	2.87(m)	2.96(m)	2.90(m)
		2.796	2.837	2.740	2.729	2.775	2.802	2.966	2.83(m)	2.91(m)	2.80(m)
		—	3.073	2.993	2.901	2.860	—	3.179	2.933	2.89(m)	2.85
H-4b		2.497	2.503	2.509	2.613	2.715	2.692	2.825	2.87(m)	2.96(m)	2.90(m)
		2.414	2.445	2.514	2.607	2.683	2.556	2.746	2.83(m)	2.91(m)	2.80(m)
			2.588	2.593	2.664	2.658	—	2.818	2.861	2.89(m)	2.72
Coupling constant											
	J_{23}	7.7	8.4	7.6	6.8	6.2	6.6	7.8	5.9	4.8	5.1
	J_{34a}	5.4	5.7	5.2	5.4	5.1	5.2	5.3	4.8		
	J_{34b}	8.4	9.1	8.1	6.9	6.4	7.2	8.7	6.0	Σ = 10.0	
	J_{44}	16.1	16.3	16.4	16.7	17.0	16.3	16.6	16.8		

[a]Solvents: acetone-d_6 (top), CD_3CN (center; with trace D_2O for **2***a* and **2***b*), $CDCl_3$ (bottom). Coupling constants (Hz) measured in $CDCl_3$, except for **2***a* and **2***b* (acetone-d_6).

TABLE 4. Proton chemical shifts and coupling constants: heterocyclic ring C[a]

Proton	Compound: 3,5,7,3′,4′-Substituents:	6-Bromocatechin derivatives					8-Bromocatechin derivatives				
		2*c* -(OH)$_5$	**3***c* -(OMe)$_4$ 3-OH	**4***c*[b] -(OMe)$_5$	**5***c*[b] -(OMe)$_4$ 3-OAc	**6***c* -(OAc)$_5$	**2***d* -(OH)$_5$	**3***d* -(OMe)$_4$ 3-OH	**4***b*[b] -(OMe)$_5$	**5***d*[b] -(OMe)$_4$ 3-OAc	**6***d* -(OAc)$_5$
H-2		4.613	4.742	4.978	5.148	5.33(m)	4.770	4.860	5.135	5.298	5.446
		4.572	4.726	4.992	5.119	5.257	4.691	4.815	5.127	5.243	5.38(m)
		—	4.675	4.890	5.072	5.158	—	4.878	5.134	5.338	5.333
H-3		4.027	4.106	3.81(m)	5.322	5.33(m)	4.058	4.133	3.787	5.416	5.380
		3.978	4.076	3.81(m)	5.333	5.323	4.004	4.107	3.885	5.416	5.38(m)
		—	4.070	3.688	5.355	5.245	—	4.081	3.731	5.448	5.281
3-OR				3.244	1.913	1.919			3.280	1.956	1.941
				3.258	1.896	1.911			3.287	1.930	1.919
				3.251	1.965	1.997			3.317	2.026	2.033
H-4a		2.910	3.002	2.907	2.930	2.79(m)	2.837	2.841	2.697	2.72(m)	2.889
		2.832	2.966	2.865	2.892	2.75(m)	2.756	2.798	2.64(m)	2.708	2.821
		—	3.229	3.051	2.977	2.876	—	2.982	2.819	2.74(m)	2.840
H-4b		2.600	2.712	2.739	2.836	2.79(m)	2.598	2.595	2.640	2.72(m)	2.796
		2.500	2.661	2.721	2.807	2.75(m)	2.476	2.517	2.64(m)	2.685	2.749
		—	2.759	2.768	2.829	2.673	—	2.658	2.710	2.74(m)	2.710
Coupling constant											
	J_{23}	7.5	8.5	7.2	6.4	6.0	7.0	7.4	6.3	5.4	5.3
	J_{34a}	5.4	5.5	5.0	5.1	3.9	5.3	5.4	5.0	5.2	4.8
	J_{34b}	8.1	9.4	7.7	6.6	6.1	7.7	8.0	6.5	5.4	5.6
	J_{44}	16.2	16.2	16.3	16.7	17.0	16.2	16.5	16.6	17.3	16.9

[a]Solvents: acetone-d_6 (top), CD_3CN (center; with trace D_2O for **2***c* and **2***d*), $CDCl_3$ (bottom). Coupling constants (Hz) measured in $CDCl_3$, except for **5***d* (in CD_3CN), **2***c* and **2***d* (in acetone-d_6).
[b]J_{24b} = 0.7–0.9 Hz.

TABLE 5. Nuclear Overhauser enhancements[a]

Compound	Frequency (ppm) of saturation	Frequency (ppm) of enhancement	Compound	Frequency (ppm) of saturation	Frequency (ppm) of enhancement
2*a*[b]	8.280[c]	6.011	**2***a*[b]	8.096[c]	6.011, 5.860
3*a*	6.138	3.750	**3***a*	6.107	3.802, 3.750
4*a*	6.143	3.746	**4***a*	6.089	3.793, 3.746
5*a*	6.168	3.766	**5***a*	6.094	3.776, 3.766
3*c*	6.367	3.827	**3***d*	6.165	3.835, 3.901
4*c*	6.379	3.828	**4***d*	6.145	3.818, 3.893
5*c*	6.406	3.854	**5***d*	6.151	3.795, 3.907

[a]Solvent: $CDCl_3$.
[b]Solvent acetone-d_6 [+100 ppm $Cd(NO_3)_2$].
[c]Gated decoupling.

TABLE 6. Methoxy proton chemical shifts[a]

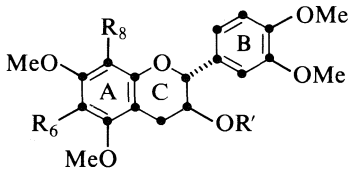

1
R′ = H, Ac or $CH_2C_6H_5$
R_6 or R_8 = Br, OH, OAc, or COOMe

Compound, including 3,5,6,7,8,3′,4′-substituents	Methoxy protons MeO-5	MeO-7	MeO-3′,4′
3*a*: -$(OMe)_4$, 3-OH	3.802	3.750	3.893
4*a*: -$(OMe)_5$	3.793	3.746	3.875/3.880
5*a*: -$(OMe)_4$, 3-OAc	3.776	3.766	3.848/3.864
3*c*: 6-Br, -$(OMe)_4$, 3-OH	3.841	3.827	3.906
4*c*: 6-Br, -$(OMe)_5$	3.817	3.828	3.875/3.887
5*c*: 6-Br, -$(OMe)_4$, 3-OAc	3.786	3.854	3.854/3.872
3*d*: 8-Br, -$(OMe)_4$, 3-OH	3.835	3.901	3.881/3.873
4*d*: 8-Br, -$(OMe)_5$	3.818	3.893	3.848/3.865
5*d*: 8-Br, -$(OMe)_4$, 3-OAc	3.795	3.907	3.821/3.845

[a]Solvent: $CDCl_3$.

that in all methylated catechins, whether monobrominated or unsubstituted at C-6/C-8, H-6 resonates upfield from H-8 in chloroform, as proved for penta-*O*-methylcatechin (**4***a*) by regiospecific deuteration by Weinges *et al.* (21) and postulated for the structurally closely related tetra-*O*-methyl derivatives **3***a* and **5***a* by Haslam and co-workers (22) and Roux (14). To determine the ring A aromatic proton chemical shifts of **3***a*, **4***a*, and **5***a* in acetone and acetonitrile, we calculated the shift increments for H-6 and H-8 due to monobromination at C-8 and C-6, respectively. Due to the structural rigidity of the aromatic ring, the effect of replacing one hydrogen by bromine (e.g., H-8) on the chemical shift of the other (e.g., H-6) should be the same for all three compounds in a given solvent. In the event, 8-bromination was found to shift the H-6 resonance downfield by 0.06 ppm in $CDCl_3$, 0.18 ppm in CD_3CN, and 0.27–0.28 ppm in acetone-d_6, while 6-bromination shifts the H-8 resonance downfield by 0.23–0.24, 0.33, and 0.35–0.36 ppm, respectively, in the same three solvents. Thus a bromine substituent at C-6 has a larger deshielding effect on H-8 than 8-Br on H-6. The proton assignments based on this concept of additivity of substituent effects (23) are readily verifiable by nOe experiments or by running the ^{1}Hmr spectra in binary mixtures of acetonitrile or acetone with chloroform and plotting the H-6/H-8 chemical shift differences as a function of solvent composition. It is noteworthy that in acetone solution, in contrast to chloroform, H-6 of all three non-brominated methyl derivates of catechin resonates *downfield* from H-8.

As a corollary of the nOe studies, the frequencies of enhancement define the resonance positions of the 5- and 7-methoxy protons of the non-brominated compounds **3***a*, **4***a*, and **5***a* and the 7-methoxy protons of the 6-bromo derivatives **3***c*, **4***c*, and **5***c* (see Table 6). The 5-methoxy protons of the latter give rise to characteristically narrow lines, due to the absence of weak long-range *ortho* coupling (24), and are thereby distinguishable from the two methoxy groups of ring B. Finally, a distinction between the 5- and 7-methoxy singlets of the 8-bromocatechins **3***d*, **4***d*, and **5***d* is possible by calculation of the substituent increments relative to their non-brominated

analogs. A bromine atom at C-8 deshields the adjacent 7-methoxy protons more strongly (by 0.14–0.15 ppm) than 6-Br (0.08–0.09 ppm), while neither C_6- nor C_8-bromination has much effect (0.01–0.04 ppm downfield shift) on the absorption position of the 5-methoxy group. The close proximity of the latter to the C-4 hydrogens makes it more sensitive than MeO-7 to conformational changes in the heterocyclic ring caused by different C-3 substituents (OH vs. OMe vs. OAc). The ring B methoxy protons were found to resonate consistently in the narrow range between 3.84 and 3.91 ppm.

The assignment of specific resonance frequencies to H-6 and H-8 of catechin presented a particularly challenging problem because rapid chemical exchange gives rise to a broad OH absorption peak (near 8.0 ppm) that is ill-suited for nOe or decoupling experiments. However, a trace of cadmium nitrate added to the substrate solution in acetone reduces the exchange rate (25) to such an extent that the phenolic protons appear as four sharp, well-separated lines (8.280, 8.096, 7.984, and 7.928 ppm). Thus, gated decoupling of OH-5 (8.280 ppm) becomes possible and, if limited to only one second during each eight-second scan, permits the buildup of an nOe factor for the adjacent H-6 resonance signal (6.011 ppm) before any significant exchange with the other hydroxy protons has occurred. Since, under the same conditions, saturation of the OH-7 proton at 8.096 ppm increases the intensities of *both* the H-6 and the H-8 doublet, the chemical shifts of these two protons are clearly identified. The previously published assignments of 5.88 ppm to H-6 and 6.02 ppm to H-8 (22) must therefore be reversed. The readily observable faster decrease of the upfield signal intensity on exposure of catechin solutions to D_2O in the presence of acid or base catalysts shows that electrophilic substitution occurs preferentially at C-8, in agreement with the results of bromination studies (8, 9, 26).

In catechin pentaacetate (**6***a*) the aromatic ring A protons resonate at 6.592 and 6.654 ppm (in $CDCl_3$). The assignments of the downfield doublet to H-6 and the upfield doublet to H-8 reported in the literature (22, 27) are not supported by experimental evidence and remain uncertain. We have been unable to duplicate the stronger nOe effect of H-6 relative to H-8 on H-4 claimed by Outtrup and Schaumburg (28). However, lineshape analysis before and after decoupling indicates weak long-range coupling between H-6 and H-4 in **3***d* and between H-8 and H-4 in **4***c* and **5***c*.

In summary, nOe difference spectra are eminently suitable for the distinction between 6- and 8-substituted catechin derivatives. The applicability of this technique to the structure elucidation of natural procyanidins and their degradation products awaits testing on authentic samples of regiospecifically synthesized diflavanoids. Synthetic work toward this goal is currently in progress.

Experimental

Catechin (**2***a*) and its three bromination products **2***b*, **2***c*, and **2***d* (26) were derivatized by standard literature procedures (29). Under the neutral or alkaline conditions employed, no bromine migration by Wessely–Moser rearrangement or reversed electrophilic aromatic substitution (8) was observed. The complete spectral identity of the tetra-*O*-methyl derivatives **3***a* and **3***c* obtained by our procedure and the more commonly employed methylation with diazomethane (9, 30) proved that the acetate hydrolysis in strong alkaline medium is not accompanied by epimerization (5). Anhydrous catechin (**2***a*) was obtained by drying commercial catechin hydrate (Sigma) under vacuum (110°C/12 h). The catechin derivatives were identified by chemical correlation (eq. [1]), ^{1}Hmr (Tables 1–4), X-ray diffraction (compound **4***c* (5)), carbon/hydrogen analysis (agreement with calculated values within ±0.3%), and melting points (agreement with literature values within ±2°): **3***a*, **4***a*, **5***a*, **6***a* (29*c*), **2***b*, **2***c*, **2***d* (26), **3***b*, **3***d*, **4***b*, **4***d* (21), **6***b*, **6***c*, **6***d* (9), and **3***c*, **5***b* (mp 145–148°C), **5***c* (mp 106–108°C), **5***d* (mp 165–167°C) (8).

Nuclear magnetic resonance spectra of 0.03 *M* substrate solutions in acetone-d_6, chloroform-*d*, and acetonitrile-d_3 were recorded on a Bruker 400-MHz FT spectrometer at a probe temperature of 30°C. Chemical shifts are reported in ppm (±0.005) downfield from TMS. Samples for nOe difference spectra were degassed immediately prior to the experiment. Cadmium nitrate monohydrate (approximately 100 ppm) was added to a 0.10 *M* solution of catechin in acetone-d_6 to resolve the OH signals; the cadmium salt concentration had no effect on the chemical shifts of other protons. To correlate H-6 and H-8 resonance frequencies of non-brominated catechins in different solvents, substrate solutions were prepared in binary solvent mixtures and the chemical shift differences $\Delta\delta$(H-6/8) plotted versus solvent composition. The free phenolic compounds **2***a*, **2***b*, **2***c*, and **2***d* were found to be insoluble in chloroform and sparingly soluble in acetonitrile; their solubilities in acetonitrile, as well as spectral resolution, were improved by addition of 10% D_2O (by volume).

Acknowledgements

We wish to thank D. Cherniwchan, R. Chan, T. Starr, and H. Harris for technical assistance, Professor D. G. Roux for valuable discussions, and the Natural Sciences and Engineering Research Council of Canada for the financial support of these investigations.

1. K. Weinges, W. Kaltenhauser, H.-D. Marx, E. Nader, F. Nader, J. Perner, and D. Seiler. Liebigs Ann. Chem. **711**, 184 (1968).
2. T. A. Geissmann and N. N. Yoshimura. Tetrahedron Lett. **24**, 2669 (1966).
3. K. Weinges, J. Perner, and H.-D. Marx. Chem. Ber. **103**, 2344 (1970).
4. D. W. Engel, M. Hattingh, H. K. L. Hundt, and D. G. Roux. J. Chem. Soc. Chem. Commun. 695 (1978).
5. F. W. B. Einstein, E. Kiehlmann, and E. K. Wolowidnyk. Can. J. Chem. **63**, 2176 (1985).
6. P. H. van Rooyen and H. J. P. Redelinghuys. S. Afr. J. Chem. **36**, 49 (1983).
7. H. K. L. Hundt and D. G. Roux. J. Chem. Soc. Chem. Commun. 696 (1978).
8. H. K. L. Hundt and D. G. Roux. J. Chem. Soc. Perkin. Trans. **1**, 1227 (1981).
9. G. W. McGraw and R. W. Hemingway. J. Chem. Soc. Perkin Trans. **1**, 973 (1982).
10. A. C. Fletcher, L. J. Porter, E. Haslam, and R. K. Gupta. J. Chem. Soc. Perkin Trans. **1**, 1628 (1977).
11. (*a*) G. Nonaka and I. Nishioka. Chem. Pharm. Bull. **28**, 3145 (1980); (*b*) G. Nonaka, F. Hsu, and I. Nishioka. J. Chem. Soc. Chem. Commun. 781 (1981).
12. L. J. Porter, R. H. Newman, L. Y. Foo, H. Wong, and R. W. Hemingway. J. Chem. Soc. Perkin Trans. **1**, 1217 (1982).
13. Y. Shirataki, I. Yokoe, M. Endo, and M. Komatsu. Chem. Pharm. Bull. **33**, 444 (1985).
14. J. A. Delcour, D. Ferreira, and D. G. Roux. J. Chem. Soc. Perkin Trans. **1**, 1711 (1983).
15. J. J. Botha, D. Ferreira, and D. G. Roux. J. Chem. Soc. Perkin Trans. **1**, 1235 (1981).
16. P. M. Viviers, H. Kolodziej, D. A. Young, and D. G. Roux. J. Chem. Soc. Perkin Trans. **1**, 2555 (1983).
17. H. Kolodziej, D. Ferreira, and D. G. Roux. J. Chem. Soc. Perkin Trans. **1**, 343 (1984).
18. (*a*) F. R. Fronczek, G. Gannuch, W. Mattice, R. W. Hemingway, G. Chiari, F. L. Tobiason, K. Houglum, and A. Shanafelt. J. Chem. Soc. Perkin Trans. **2**, 1383 (1985); (*b*)

L. J. PORTER, R. Y. WONG, M. BENSON, B. G. CHAN, V. N. VISHWANADHAN, R. D. GANDOUR, and W. L. MATTICE. J. Chem. Research (S), 86 (1986).
19. J. B. LAMBERT, H. F. SHURVELL, L. VERBIT, R. G. COOKS, and G. H. STOUT. Organic structural analysis. Collier MacMillan, London. 1976. p. 43.
20. (*a*) A. PELTER, P. I. AMENECHI, R. WARREN, and S. H. HARPER. J. Chem. Soc. C, 2572 (1969); (*b*) R. G. WILSON, D. H. WILLIAMS, and J. H. BOWIE. Tetrahedron, **24**, 1407 (1968).
21. K. WEINGES, W. EBERT, D. HUTHWELKER, H. MATTAUCH, and J. PERNER. Liebigs Ann. Chem. **726**, 114 (1969).
22. R. S. THOMPSON, D. JACQUES, E. HASLAM, and R. J. N. TANNER. J. Chem. Soc. Perkin Trans. **1**, 1387 (1972).
23. L. M. JACKMAN and S. STERNHELL. Applications of nuclear magnetic resonance spectroscopy in organic chemistry. Pergamon Press, Oxford. 1969. p. 202.
24. G. SCHILLING. Liebigs Ann. Chem. **1975**, 1822.
25. Y. SUZUKI and I. ANAZAWA. Bunseki Kagaku, **31**, 498 (1982).
26. E. KIEHLMANN, P. J. VAN DER MERWE, and H. K. L. HUNDT. Org. Prep. Proc. Int. **15**, 341 (1983).
27. L. Y. FOO and L. J. PORTER. J. Chem. Soc. Perkin Trans. **1**, 1535 (1983).
28. H. OUTTRUP and K. SCHAUMBURG. Carlsberg Res. Commun. **46**, 43 (1981).
29. (*a*) T. PURDIE and J. C. IRVINE. J. Chem. Soc. **83**, 1021 (1903); (*b*) K. FREUDENBERG. Liebigs Ann. Chem. **433**, 230 (1923); (*c*) K. FREUDENBERG and L. PURRMANN. Liebigs Ann. Chem. **437**, 274 (1924).
30. J. W. SWEENY and G. A. IACOBUCCI. J. Org. Chem. **44**, 2298 (1979).

Mobilities of thermal cations in argon and xenon gases: temperature and field dependence

NORMAN GEE AND GORDON R. FREEMAN
University of Alberta, Edmonton, Alta., Canada T6G 2G2

Received February 11, 1986

NORMAN GEE and GORDON R. FREEMAN. Can. J. Chem. **64**, 2006 (1986).

In argon at $n = (2–6) \times 10^{24}$ molecules/m^3, the density-normalized mobility $n\mu$ of argon cations at low electric field strengths E/n is constant from 150 to 300 K; at >300 K $n\mu$ increases. The increase was smaller when the "effective" temperature T_{eff} of the ions was increased by applying higher E/n at 300 K. At 630 K, $(n\mu)_T/(n\mu)_{T_{\text{eff}}} = 1.6$, whereas in xenon it was 2.7, and in helium 1.0. The difference in behavior is attributed to the main ions being dimers Y_2^+; in argon and xenon collision-induced dissociation can occur:

$$Y^+ + 2Y \rightarrow Y_2^+ + Y$$

$$Y_2^+* + Y \rightarrow Y^+ + 2Y$$

where * indicates excess kinetic energy acquired by acceleration in the electric field. The dissociation energies of He_2^+, Ar_2^+, and Xe_2^+ are 2.3, 1.3, and 0.7 eV, respectively. Dissociation of He_2^+ is negligible because of its large dissociation energy. Dissociation of Y_2^+* and reformation of Y_2^+ is equivalent to the inelastic de-excitation of Y_2^+*.

NORMAN GEE et GORDON R. FREEMAN. Can. J. Chem. **64**, 2006 (1986).

Dans l'argon, à des valeurs de n = (2 à 6) $\times 10^{24}$ molecules/m^3 et à de faibles champs électriques (E/n), la mobilité normalisée pour la densité ($n\mu$) des cations d'argon est constante de 150 à 300 K; à des températures >300 K, la valeur de $n\mu$ augmente. L'augmentation est plus faible lorsqu'on augmente la température "effective" (T_{eff}) des ions en appliquant des valeurs de E/n à 300 K. A 630 K, $(n\mu)_T/(n\mu)_{T_{\text{eff}}} = 1{,}6$ alors que dans le xénon cette valeur était égale à 2,7 et que dans l'hélium elle est égale à 1,0. On attribue cette différence de comportement au fait que les ions principaux seraient des dimères Y_2^+; dans l'argon et le xénon, il peut se produire une dissociation induite par des collisions:

$$Y^+ + 2Y \rightarrow Y_2^+ + Y$$

$$Y_2^+* + Y \rightarrow Y^+ + 2Y$$

dans lesquelles * indique l'énergie cinétique en excès qui est acquise par l'accélération dans le champ électrique. Les énergies de dissociation de He_2^+, Ar_2^+ et Xe_2^+ sont respectivement 2,3, 1,3 et 0,7 eV. A cause de son énergie de dissociation élevée, la dissociation du He_2^+ est négligeable. La dissociation du Y_2^+* et la reformation de Y_2^+ est équivalente à une dé-excitation inélastique du Y_2^+*.

[Traduit par la revue]

Introduction

Collisions between noble gas dimer cations Y_2^+ and atoms Y are not purely elastic (1). It has been suggested that cation–atom exchange occurs, which causes the ion mobility at low energies to be smaller than the polarization limit. Such exchange was originally proposed for the drift of H_3^+ in H_2 (2), where the temperature dependence was much different from that expected in the absence of exchange (3*a*).

The ion–molecule collision energy can be varied by increasing the gas temperature T while keeping the density-normalized field strength E/n small, or by sufficiently increasing E/n while holding T constant. For simple systems such as potassium ions in argon gas, where the collisions are elastic, the mobility is the same when the low field T equals the high field T_{eff} (4). However, when inelastic collisions occur, the mobility at a high field T_{eff} is lower than that at the equivalent low field T (5, 6). Such a mobility difference might result from cation–atom exchange ($Y_2^+ + Y \rightarrow Y + Y_2^+$) or inelastic collisions in the drift of Y_2^+ through Y.

Mobility values have been reported for Ar_2^+ in Ar (1, 7) and for Xe_2^+ in Xe (1) against T_{eff}, where the gas temperature was constant. This work reports mobility values obtained at low E/n where the cations are in thermal equilibrium with the gas, and T was increased.

Experimental

A. Materials

The argon was Matheson Ultra High Purity (≥99.999%). The xenon (≥99.995%) was from the Gas Dynamics Division of Liquid Carbonic Canada Ltd. Samples were transferred into a grease-free vacuum rack through a vacuum-tight valve that was welded to a flexible stainless steel tube, which was in turn welded to a Kovar seal. Further purification of the gases was effected by passage through freshly activated silica gel, followed by exposure to a series of freshly generated potassium mirrors in 2-L bulbs at room temperature for at least one month.

B. Production of cations

Cations were generated in parallel plate conductance cells by bombarding the samples with 100 ns pulses of X-rays from a 1.7 MeV Van de Graaff accelerator. The simultaneously generated electrons were removed with a collecting field (8). Drift distances of 4.80 to 10.58 mm were used.

Cations were not mass identified in the present work, but previous mass identified measurements in argon (1), and a non-mass identified ion study in xenon at different densities (9), concluded that at higher T the cations are Y_2^+. At the densities used in our work, $0.97 \leq n/10^{24}$ molecules m$^{-3} \leq 14.2$, the Ar^+ or Xe^+ initially formed would attach other molecules (1, 9*a*).

The dimer cation is thermally stable with a binding energy ~1 eV (1, 10). The Ar_2^+ cation dominates at $T_{\text{eff}} \gtrsim 194$ K and $0.7 \leq n/10^{24} \leq 4$, but multimers form by reaction [1] at lower temperatures; the exchange rate is rapid compared to drift times (1).

[1] $\quad Ar_j^+ (j \geq 2) + 2Ar \rightleftharpoons Ar_{j+1}^+ + Ar$

Multimers in xenon gas persist to higher T and lower n than in argon (11): at 4×10^{24} molecules/m^3 Xe_2^+ cations do not dominate the mobility until $T_{\text{eff}} \gtrsim 304$ K (9), which is 110 K higher than was needed in argon.

Hence, in this work the mobility measured at $n < 4 \times 10^{24}$ molecules/m^3 and at $T \gtrsim 194$ K in argon, or at $T \gtrsim 304$ K in xenon, is

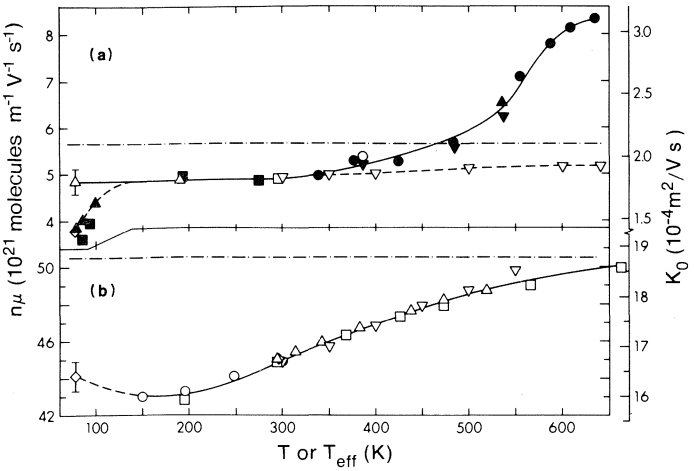

FIG. 1. Density-normalized mobilities of ions as a function of temperature at ($n/10^{24}$ molecules m^{-3}, reference). (*a*) *Argon*: ● (2.39, this work); ▲ (3.08, this work); ▼ (3.17, this work); ■ (4.68, this work); ○ (5.77, this work); △ (0.028 to 0.10, 1); ◇ (1.9, 1); ▽ (<1, 7*a*). □, average of six present measurements (4.85 ± 0.05) 10^{21} molecules m^{-1} V^{-1} s^{-1} at $2.39 \leq n/10^{24} \leq 4.68$ at 295 ± 1 K. Present ions and those of ref. 7 not mass identified, but ref. 7*a* considered them to be established as Ar_2^+. Reference 7*a* measurements were at 300 K, and T_{eff} calculated from eq. [2]. Mass spectral study (1) indicated that Ar_2^+ dominates at $T > 178$ K. △, Ar_2^+ at $T_{eff} \doteq 190$ K ($T = 77$ K, 55 Td) and 9.4×10^{22} molecule/m^3, and at 77 K as estimated from the density dependence of μ measured at ~10 Td. ▲, ■, and ◇ at $T \leq 100$ K are Ar_j^+ ($j > 2$). (*b*) *Helium*: △ (0.075 to 2.0, 1); ▽ (<1, 7*a*); □ (0.13 to 0.40, 13); ○ (0.8, 14); ◇ (0.097 to 12.6, 15). ◇, mass identified as He_2^+ in some runs. Other measurements not mass identified, but He_2^+ considered as established. ▽ and △, $T_{eff} > 300$ K calculated from eq. [2]. ·····, $n\mu_{pol}$ (eq. [3]) for Ar_2^+ in Ar and He_2^+ in He.

attributed to the dimer cations. At lower T, multimer formation occurs and the mobility is due to a mixture Y_j^+ ($j \geq 2$).

C. Methods

The conductance cells were similar to the low pressure cells described earlier (8*b*). Temperature control and measurement (8), voltage source and signal amplifier (8*a*), and the time of flight method for obtaining the mobility μ (8*a*) were described in the references indicated. The current-time signals are like that in Fig. 1 of ref. 8*a*.

At pressures used in this work, densities were calculated by assuming the ideal gas law. Checks using the van der Waals equation (12) showed no deviation from ideality.

The cells were baked under vacuum at $T > 650$ K prior to each experiment, but the possibility of further outgassing during measurements, or of other contamination of the samples, was checked for by the method of ref. 8.

Results

Ion flight times were measured with positive and then negative applied voltages, to check for effects of strain voltage in the cell. The values obtained were the same within ~3%, and the average was used at each field strength.

A. Field independence

The cation mobilities were independent of field strength over the range used, which was 0.36–26 Td in argon, and 0.9–37 Td in xenon (Td = 10^{-21} V m^2/molecule). At these fields the cations are essentially in thermal equilibrium with the gas.

The effective temperature of ions that have drift velocity $v_d = \mu E$ and undergo only elastic collisions with the molecules is (7):

$$[2] \quad T_{eff} = T + Mv_d^2(1 + \beta)/3k_B$$

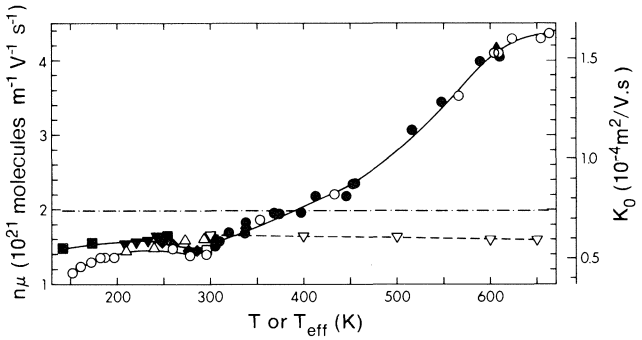

FIG. 2. Density-normalized mobility of ions in xenon as a function of temperature at ($n/10^{24}$ molecules m^{-3}, reference). ◆ (0.97, this work); ■ (1.33, this work); ▼ (1.89, this work); ▲ (2.00, this work); ● (3.09, this work); ○ (11.5, this work); ▽ (<0.1, 1); △ (1.33, 9*a*). □, average of 13 present measurements, (1.46 ± 0.02)10^{21} molecules m^{-1} V^{-1} s^{-1} at $0.97 \leq n/10^{24} \leq 3.09$ at 296 ± 1 K. At $T >$ 300 K the ions were probably predominantly Xe_2^+ (see text). At $T <$ 300 K the ions were probably mixtures of Xe_j^+ ($j \geq 2$). ·····, $n\mu_{pol}$ (eq. [3]) for Xe_2^+ in Xe.

where M is the molecular mass of the gas, β is a correction (often set to zero) based on d ln $(n\mu)$/d ln (E/n), and k_B is Boltzmann's constant. Equation [2] predicts that $T_{eff} = 1.05T$ at ~20 Td in argon and ~35 Td in xenon. The occurrence of inelastic collisions would increase the field necessary to achieve $T_{eff} = 1.05T$. The observed results are therefore consistent with eq. [2].

B. Temperature dependence

Each reported value of $n\mu$ is the average of at least ten measurements at different positive and negative applied voltages.

The value of $n\mu$ in argon decreased from 8.3×10^{21} molecules m^{-1} V^{-1} s^{-1} at 634 K towards a constant value 4.9×10^{21} molecules m^{-1} V^{-1} s^{-1} at $T \leq 300$ K (Fig. 1*a*). At $T \leq$ 100 K, $n\mu$ decreased further; the gas densities were 3.1 and 4.6×10^{24} molecules/m^3. Values from refs. 1 and 7 are included for comparison. The present value at 295 K agrees within 1% with that reported for Ar_2^+ in Ar at that temperature (7).

Mobilities of ions in the gas phase are commonly reported as K_0 (m^2 V^{-1} s^{-1}), which corresponds to μ at a density of 1 atm at STP (1 amagat, $n = 2.69 \times 10^{25}$ molecules/m^3). Values of K_0 are displayed on the right side of the figure for comparison.

In xenon the variation of $n\mu$ with temperature (Fig. 2) is qualitatively similar to that in argon. Values from refs. 1 and 9*a* are within about 10% of the present ones at $T \lesssim 300$ K.

The increase of $n\mu$ with T in helium (13–15) is shown in Fig. 1*b* for comparison. The relative variation decreases in the order Xe > Ar > He.

Discussion

A. Polarization limit

When scattering is dominated by the polarization potential, as in the case when $T_{eff} \rightarrow 0$, the value of $n\mu$ is determined by the polarizability α of the scatterer and the reduced mass M_r of the collision pair (3*b*). Expressed in SI units it reduces to

$$[3] \quad n\mu_{pol} = 1.60 \times 10^{-11}/(\alpha M_r)^{1/2}$$

where the units are $n\mu_{pol}$ (molecules m^{-1} V^{-1} s^{-1}), α (C m^2 V^{-1}), and M_r (kg/molecule). The commonly listed values of polarizability in units of cm^3 correspond to the SI quantity $\alpha/4\pi\epsilon_0$ (17), where ϵ_0 is the electric permittivity of

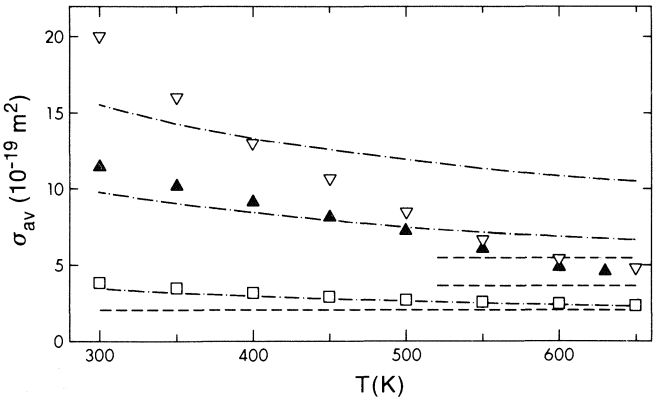

FIG. 3. Average cross sections of Y for scattering Y_2^+, estimated from the full lines in Figs. 1 and 2. □, He; ▲, Ar; ▽, Xe. ·····, σ_{pol} calculated from eqs. [5] and [3]. ---, neutral hard sphere cross sections σ_{hs}, calculated from Lennard–Jones collision radii (16). In all cases He has the lowest cross section and Xe the highest.

vacuum; the conversion factor $cm^3 \rightarrow C\,m^2\,V^{-1}$ is $1.11 \times 10^{-16} C\,m^2\,V^{-1}\,cm^{-3}$.

The values of α ($10^{-40} C\,m^2\,V^{-1}$) are 0.228, 1.82, and 4.49 for He, Ar, and Xe, respectively (18), and the corresponding values of $n\mu_{pol}$ (10^{21} molecules $m^{-1}\,V^{-1}\,s^{-1}$) for Y_2^+ in Y are 50, 5.7, and 2.0. These values are shown as dash–dot lines in Figs. 1 and 2.

As previously noted (1), the observed $n\mu$ at ~300 K is smaller than $n\mu_{pol}$ in all three gases (Figs. 1 and 2). The low mobility was attributed to resonant ion–atom exchange (14, 19), as was postulated for H_3^+ in H_2 (2).

B. Effect of temperature

In Ar and Xe the value of $n\mu$ for thermal ions increased above the value of $n\mu_{pol}$ at $T > 500$ and 400 K, respectively (Figs. 1*a* and 2). When the ion temperature T_{eff} was increased by increasing E/n (and hence v_d, eq. [2]), the value of $n\mu$ remained below $n\mu_{pol}$ (Figs. 1*a* and 2). In He the value of $n\mu$ approached that of $n\mu_{pol}$ when either T or T_{eff} approached 700 K (Fig. 1*b*), so the crossover temperature increases in the order Xe < Ar < He.

The product $n\mu$ is related to the average momentum transfer cross section (3*c*, 21):

$$[4] \quad \sigma_{ave} = \langle v^3 \sigma_m \rangle / \langle v^3 \rangle,$$

where σ_m is the momentum transfer cross section and v is the relative velocity of the ions with respect to the molecules;

$$[5] \quad n\mu = \left(\frac{3e}{4M_r}\right) \frac{1}{\langle v \rangle \sigma_{ave}}$$

where e is the protonic charge, and for a Maxwellian distribution of velocities $\langle v \rangle = (8k_B T/\pi M_r)^{1/2}$.

The value of σ_{ave} decreases with increasing T (Fig. 3). The experimental values of σ_{ave} are compared with those expected from the polarization potential, σ_{pol}, and the hard sphere potential, σ_{hs}. The latter are approximated by the Lennard–Jones neutral atom collision cross sections (16).

At 650 K σ_{ave} is similar to σ_{hs} in all three gases. In helium, which has a relatively small polarizability, σ_{pol} is only 11% greater than σ_{hs}; the difference increases to 67% at 300 K. The value of σ_{ave} in helium is nearly equal to σ_{pol} at all temperatures.

As T is decreased below 650 K, in argon and xenon σ_{ave} increases towards σ_{pol} and crosses above it below 500 K in argon, and below 400 K in xenon. The rate of increase at $T <$ 500 K is greater in xenon than in argon. At 300 K the ratio $\sigma_{ave}/\sigma_{pol}$ equals 1.10 in helium, 1.16 in argon, and 1.29 in xenon (Fig. 3). The increase in σ_{ave} is not caused by clustering, because in xenon at 278 K a 12-fold increase of n caused only a 5% decrease of $n\mu$ (Fig. 2). The ions can be assumed to be Y_2^+ in each of the gases at 300–600 K.

The dimer ion probably dominates down to at least 150 K in the gases at $n = 1 \times 10^{24}$ molecules/m^3. The values of the ratio $\sigma_{ave}/\sigma_{pol}$ at 150 K are 1.17, 1.17, and 1.32 in helium, argon, and xenon, respectively, similar to those at 300 K.

C. Inelastic collisions

When T_{eff} was increased by increasing E/n in helium, $n\mu$ had the same value as when the gas T was increased the same amount (Fig. 1*b*). However, when the field was used to increase T_{eff} in argon, $n\mu$ increased more slowly than when the gas T was increased (Fig. 1*a*). In xenon, increasing T_{eff} with the field actually caused $n\mu$ to decrease slightly (Fig. 2). These results indicate that, although inelastic processes can be ignored in He_2^+–He collisions, they become progressively more important on going to argon and xenon.

The Y—Y^+ dissociation energy is 2.3 eV in helium (10*a*), 1.3 eV in argon (10*c*), and ~0.7 eV in xenon (10*b*). While the He_2^+ is stable under all the conditions used in the mobility experiments, it seems that when the argon and xenon ions were heated above the gas temperature by applying a high electric field, some collision-induced dissociation occurred.

$$[6] \quad Ar_2^+* + Ar \rightarrow Ar^+ + 2Ar$$

$$[7] \quad Xe_2^+* + Xe \rightarrow Xe^+ + 2Xe$$

where the asterisk designates excess translational energy. The mobilities of the monomer cations are 20–30% lower than those of the dimers (7*a*, 9*b*). The dimers would form again,

$$[8] \quad Y^+ + 2Y \rightarrow Y_2^+ + Y$$

so a major effect of reactions [6] and [7] would be deenergization of Y_2^+, which means the reduction of T_{eff}. Reactions [6]–[8] are inelastic processes which invalidate eq. [2]. As process [8] is a three body reaction $n\mu$ might not be independent of n if a wider range of density than that in the present study is used.

This de-energization does not occur when the cation energy is increased by increasing T, although dissociation/association can occur. Increasing T increases the energy of both Y_2^+ and Y, whereas a high E/n increases only the energy of the ions. The relative collision energy is increased in both cases but the average energy transfer depends on the average energy difference between cation and molecule. At low E/n and a given T the average cation energy and the average molecule energy both equal thermal energy; the average net energy transfer is zero (6, 20).

In argon the value of $d(n\mu)/dT_{eff}$ remains positive, so the contribution of the monomer ions to the measured mobility can be neglected. It is assumed that the inelastic collisions simply have the effect of reducing T_{eff} towards the gas temperature T. Then the ratio ζ of the collision integral for inelastic energy loss to that for momentum transfer can be obtained from (6, 20):

$$[9] \quad \zeta = \frac{m}{M}\left(\frac{T_{eff}}{T} - 1\right)$$

where m is the ion mass, M the neutral atom mass, T_{eff} is

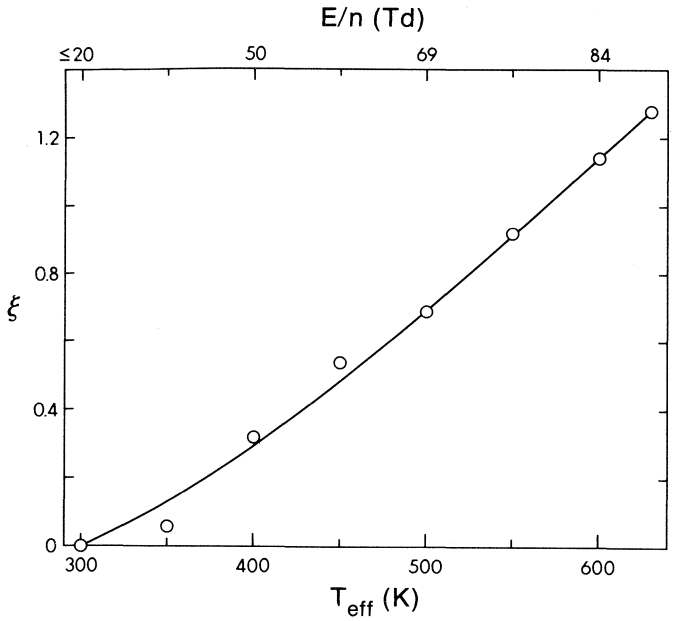

FIG. 4. Ratio of collision integral for inelastic energy loss to that for momentum transfer for Ar_2^+ in Ar at $T = 300$ K. T_{eff} was calculated from eq. [2]. Data from Fig. 1*a*.

calculated from eq. [2] for the observed $n\mu$ and E/n, and T is the gas temperature at which the same $n\mu$ is obtained at low fields. The value of ζ characterizes (but does not equal) the fractional energy loss due to inelastic collisions (6). For Ar_2^+ in Ar at 300 K, $\zeta = 0.0$ at $E/n \leq 20$ Td and increased to 1.28 at 88 Td (Fig. 4). For $T_{eff} = 630$ K the actual equivalent thermal ion temperature was 384 K.

Acknowledgements

We thank the Natural Sciences and Engineering Research Council of Canada for financial support, and the staff of the Radiation Research Center for construction and maintenance of apparatus.

1. H. HELM and M. T. ELFORD. J. Phys. B, **11**, 3939 (1978).
2. R. N. VARNEY. Phys. Rev. Lett. **5**, 559 (1960).
3. E. W. MCDANIEL and E. A. MASON. The mobility and diffusion of ions in gases. Wiley, New York. 1973. (*a*) p. 230; (*b*) p. 146; (*c*) p. 140.
4. L. A. VIEHLAND and E. A. MASON. Ann. Phys. (N.Y.), **91**, 499 (1975).
5. M. D. PERKINS, F. L. EISELE, and E. W. MCDANIEL. J. Chem. Phys. **74**, 4206 (1981).
6. L. A. VIEHLAND and D. W. FAHEY. J. Chem. Phys. **78**, 435 (1983).
7. (*a*) H. W. ELLIS, R. Y. PAI, E. W. MCDANIEL, E. A. MASON, and L. A. VIEHLAND. At. Data Nucl. Data Tables, **17**, 177 (1976); (*b*) L. A. VIEHLAND and E. A. MASON. Ann. Phys. (N.Y.), **91**, 499 (1975).
8. (*a*) N. GEE, M. A. FLORIANO, and G. R. FREEMAN. Z. Naturforsch **39a**, 1225 (1984); (*b*) N. GEE and G. R. FREEMAN. J. Chem. Phys. **81**, 3194 (1984).
9. H. HELM. (*a*) Phys. Rev. A, **14**, 680 (1976); (*b*) J. Phys. B, **9**, 2931 (1976).
10. (*a*) M. L. GINTER and R. BATTINO. J. Chem. Phys. **52**, 4469 (1970); (*b*) R. S. MULLIKEN. J. Chem. Phys. **52**, 5170 (1970); (*c*) J. T. MOSELEY, R. P. SAXON, B. A. HUBER, P. C. COSBY, R. ABOUAF, and T. TADJEDDINE. J. Chem. Phys. **67**, 1659 (1977).
11. J. L. MAGEE and K. FUNABASHI. Rad. Res. **10**, 622 (1959).
12. R. C. WEAST (*Editor*). Handbook of chemistry and physics. 57th ed. Chemical Rubber, Cleveland OH. 1978. p. D-178.
13. O. J. ORIENT. Can. J. Phys. **45**, 3915 (1967).
14. P. L. PATTERSON. Phys. Rev. A, **2**, 1154 (1970).
15. H. HELM. J. Phys. B, **9**, 1171 (1976).
16. J. O. HIRSCHFELDER, C. F. CURTISS, and R. B. BIRD. Molecular theory of gases and liquids. Wiley, New York. 1964. p. 1212.
17. J. R. REITZ, F. J. MILFORD, and R. W. CHRISTY. Foundations of electromagnetic theory. 3rd ed. Addision-Wesley, Reading, MA. 1979. p. 105.
18. R. R. TEACHOUT and R. T. PACK. At. Data, **3**, 195 (1971).
19. E. C. BEATY, J. C. BROWNE, and A. DALGARNO. Phys. Rev. Lett. **16**, 723 (1966).
20. L. A. VIEHLAND, S. L. LIN, and E. A. MASON. Chem. Phys. **54**, 341 (1981).
21. N. GEE and G. R. FREEMAN. Can. J. Chem. **59**, 2988 (1981).

Cobalt carbonyl catalyzed reaction of mercaptans with Schiff bases and carbon monoxide

SHLOMO ANTEBI AND HOWARD ALPER[1]

Ottawa–Carleton Chemistry Institute, Department of Chemistry, University of Ottawa, Ottawa, Ont., Canada K1N 9B4

Received February 5, 1986

SHLOMO ANTEBI and HOWARD ALPER. Can. J. Chem. **64**, 2010 (1986).

Thiophenols and *p*-methylbenzyl mercaptan react with Schiff bases and carbon monoxide in benzene, in the presence of cobalt carbonyl, to give amides as the principal products. These amides arise from cleavage of the carbon–nitrogen double bond of the reactant imine. The reaction is applicable to a variety of Schiff bases (i.e. aliphatic, benzylic, aromatic). Thioesters and olefins are usually obtained as reaction by-products.

SHLOMO ANTEBI et HOWARD ALPER. Can. J. Chem. **64**, 2010 (1986).

Les thiophénols et les *p*-méthylbenzyles mercaptans réagissent avec les bases de Schiff et le monoxyde de carbone dans le benzène, en présence de cobalt carbonyle pour donner des amides comme produits majoritaires. Ces amides proviennent du clivage de la double liaison carbone–azote de l'imine. La réaction peut s'appliquer à différentes bases de Schiff (i.e. aliphatique, aromatique, benzylique). On obtient habituellement des thioesters et des oléfines comme produits secondaires.

[Traduit par la revue]

Mercaptans have been employed as substrates in several metal-catalyzed carbonylation reactions. Benzylic mercaptans and thiophenols can be carbonylated to carboxylic esters, with concurrent desulfurization, by means of cobalt carbonyl in aqueous alcohol (1, 2). However, if the latter reaction is conducted in the presence of a conjugated diene, then thioesters are formed in good yields. While the diene has a significant

$$RSH + CO \xrightarrow[Co_2(CO)_8,\ C_6H_6/H_2O]{\text{diene, 185–190°C}} RCOSR + COS$$

55–61 atm.

influence on the course of the mercaptan – carbon monoxide reaction, the hydrocarbon is not incorporated in the product (3). However, the diene does participate when thiophenols are treated first with synthesis gas and then with carbon monoxide, in the presence of cobalt carbonyl and pyridine, the heterocyclic base being essential for this reaction. In this manner, 1,3-butadiene reacts with thiophenol and carbon monoxide to give isomeric pentenoic acid phenyl thioesters (4). Thioesters are also obtained by treatment of a monoolefin with mercaptan, carbon monoxide, and a palladium(II) catalyst (5).

Since a conjugated diene had an important influence on the course of the cobalt carbonyl catalyzed carbonylation of mercaptans, it was of interest to determine the effect of other unsaturated moieties on this reaction. We now wish to report that Schiff bases undergo interesting reactions with thiols and carbon monoxide, in the presence of the cobalt catalyst.

Results and discussion

Treatment of *p*-thiocresol (**1**, R = *p*-$CH_3C_6H_4$) with *N*-benzylidenemethylamine (**2**, R′ = Ph, R″ = CH_2), carbon monoxide, and a catalytic amount of cobalt carbonyl in benzene, at 850 psi and 170–180°C, afforded *N*-methyl-*p*-toluamide **3**, R = *p*-$CH_3C_6H_4$, R″ = CH_3, as the major product. This product results from carbon–nitrogen double bond cleavage of the Schiff base. One of the by-products is the amide **4**, R = *p*-$CH_3C_6H_4$, R′ = Ph, R″ = CH_3 containing all of the former Schiff base unit. Other by-products are formed, the most noteworthy being stilbene (**5**, R′ = Ph) and carbonyl sulfide (ms: *m*/*e* 60). The product yields for this and for other

$$\underset{\mathbf{1}}{RSH} + CO + \underset{\mathbf{2}}{R'CH{=}NR''} \xrightarrow[850\ \text{psi}]{Co_2(CO)_8/C_6H_6/H_2O,\ 170\text{–}180°C} \underset{\mathbf{3}}{RCONHR''} + \underset{\mathbf{4}}{RCONR''(CH_2R')} + \underset{\mathbf{5}}{R'CH{=}CHR'} + COS$$

Schiff base-mercaptan reactions are listed in Table 1. Amides were not formed in the absence of the metal catalyst.

The carbonylation reaction is applicable to a variety of Schiff bases including those bearing primary, secondary, and tertiary alkyl, as well as benzylic groups, and affords amides (**3**) in moderate yields. Methoxy and bromine substituents on the benzene ring of the thiophenol do not interfere with the reaction. While the reaction does not proceed when an aliphatic mercaptan is used, it does occur using a benzylic mercaptan (**1**, R = *p*-$CH_3C_6H_4CH_2$) as the reactant. The optimum ratio of Schiff base to mercaptan is 1.0–1.2/1.0 while that of **1**/$Co_2(CO)_8$ is 6–10/1.

Several types of thioesters are formed as by-products in most of these reactions. One class of thioester, RCOSR, is the anticipated product assuming that the Schiff base functions in an analogous manner to that observed using a conjugated diene (3). However, thioesters of type $RCOSCH_2R'$ are also formed, where CH_2R' arises from the Schiff base. It is interesting to note that aromatic hydrocarbons (2) are not detected in any of these reactions. While most of the R group of the thiol is generally accounted for in these reactions, the fate of some of the Schiff base — particularly the NR″ portion — is unknown. It has previously been reported that Schiff bases, **2**, where R′ is aromatic, experience carbonylation to phthalimidines when **2** is exposed to a catalytic quantity of $Co_2(CO)_8$ in benzene at 100–200 atom and 200–230°C (6). Phthalimidines were not formed in any Schiff base – mercaptan carbonylation reaction catalyzed by $Co_2(CO)_8$.

A possible mechanism for the formation of the amide **3** is outlined in Scheme 1. The initial steps of the proposed pathway — i.e. reaction of mercaptan with cobalt carbonyl

[1]Fellow of the John Simon Guggenheim Memorial Foundation, 1985–1986. To whom all correspondence should be addressed.

TABLE 1. Mercaptan/Schiff base/CO/$Co_2(CO)_8$ reactions

1, R =	2, R′ =, R″ =	Products (%)[a] 3	4	Other
p-$CH_3C_6H_4$	Ph, CH_3	59	7	PhCH=CHPh, 22 p-$CH_3C_6H_4COSC_6H_4CH_3$-p, 10 p-$CH_3C_6H_4COCH_2Ph$, 7 p-$CH_3C_6H_4SCH_2Ph$, 6
	Ph, CH_2Ph	56	4	PhCH=CHPh, 14 p-$CH_3C_6H_4SCH_2Ph$, 17 p-$CH_3C_6H_4COSCH_2Ph$, 22
	C_3H_7, $CH(CH_3)Ph$	65		n-C_3H_7CH=CHC_3H_7-n, 18 p-$CH_3C_6H_4SSC_6H_4CH_3$-p, 7 p-$CH_3C_6H_4COSC_4H_9$, trace
	$(CH_3)_2CH$, $C(CH_3)_3$	38		p-$CH_3C_6H_4COSCH_2CH(CH_3)_2$, 16 p-$CH_3C_6H_4COSC_6H_4CH_3$-p, 15
	$(CH_3)_2CH$, n-C_4H_9	40		p-$CH_3C_6H_4COSCH_2CH(CH_3)_2$, 20 $(p$-$CH_3C_6H_4S)_2$, 7
	R′CH=⟨⟩=, $CH(CH_3)Ph$	52	6	p-$CH_3C_6H_4COSC_6H_{11}$, 21 p-$CH_3C_6H_4SCH(CH_3)Ph$, 10 p-$CH_3C_6H_4COSC_6H_4CH_3$-p, 6
p-$CH_3OC_6H_4$	Ph, CH_3	62	11	p-$CH_3OC_6H_4COSC_6H_4OCH_3$-$p$, 10
p-BrC_6H_4	Ph, CH_3	43	8	p-$BrC_6H_4SCH_2Ph$, 5 $(p$-$BrC_6H_4S)_2$, 6
Ph	2-Furyl CH=CH, p-$CH_3C_6H_4$	33		PhSCOPh, 46 PhSSPh, 15
2-Naphthyl	Ph, CH_3	57	8	2-$C_{10}H_7COSC_{10}H_7$-2, 5 2-$C_{10}H_7SCH_2Ph$, 20 PhCH=CHPh, 26
p-$CH_3C_6H_4CH_2$	Ph, CH_3	34	2	$(p$-$CH_3C_6H_4CH_2)_2S$, 43 p-$CH_3C_6H_4CH_2SCH_2Ph$, 6

[a]Yields are of *pure* materials.

to give **6** and $HCo(CO)_4$, as well as the carbonylation of **6** to **7**, followed by elimination of carbonyl sulfide (**8**) and carbonylation to **9** — are identical to those postulated in the conversion of mercaptans to thioesters (3). Complex **11** may arise from **2** either by direct addition of **9** (7) or by a two-step pathway as illustrated in Scheme 1. It is conceivable that the hydridotetracarbonylcobalt can react in two different ways. It may protonate **11** affording **12** with subsequent carbon–nitrogen bond cleavage giving the amide **3**, which is the major product, and a binuclear cobalt complex **13**. The latter may serve as the source of the olefin **5**, either via a free or a complexed carbene. The cobalt hydride, $HCo(CO)_4$, can alternatively cleave the carbon–cobalt bond of **11**, affording the amide **4**.

In conclusion, carbonyl-containing compounds (amides, thioesters) are obtained in good combined yields from the cobalt carbonyl catalyzed reaction of thiophenols and p-methylbenzyl mercaptan with Schiff bases and carbon monoxide.

Experimental section

General

All of the mercaptans, and *N*-benzylidenemethylamine, were commercial materials and were distilled or recrystallized prior to use. The other Schiff bases were synthesized from the appropriate carbonyl compounds and amines following standard methodology (8). Cobalt carbonyl was obtained from Strem Chemical Co. and was used as received. Solvents were dried by standard methods (e.g. benzene was dried using sodium benzophenone ketyl).

Melting point determinations were made using a Fisher-Johns apparatus. Infrared spectra were recorded on a Perkin Elmer 783 spectrometer, and mass spectral determinations were made using a VG 5050 micromass spectrometer. Nuclear magnetic resonance spectra were recorded on Varian EM-360 and/or XL-300 spectrometers. Gas chromatographic determinations were made on a Varian Vista 6000 gas chromatograph (flame ionization detector) equipped with a 3% OV-17 on Chromosorb W column (110°C; 10°/min to 300°C).

Representative procedure for the reaction of mercaptans with Schiff bases and carbon monoxide

A 125 mL stainless steel autoclave (Parr Instrument Co.) was charged with 1.24 g (10 mmol) of p-thiocresol (**1**, R = p-$CH_3C_6H_4$), cobalt carbonyl (0.45 g, 1.33 mmol), **2**, R′ = $(CH_3)_2CH$, R″ = n-C_4H_9 (1.52 g, 12.0 mmol), and 30 mL of anhydrous benzene. The bomb was filled and evacuated three times with carbon monoxide, and then pressurized with CO to 850 psi. The reaction mixture was stirred overnight at 180°C (pressure increased to 1100–1300 psi), and then cooled to room temperature. The gas was evacuated, the reaction mixture was filtered, and the filtrate was concentrated using a rotary evaporator. Separation of the products was achieved by preparative thin layer chromatography with silica gel, using 3:1 hexane – ethyl acetate as the developer. The first fraction was the amide **3**, R = p-$CH_3C_6H_4$, R″ = n-C_4H_9, obtained in 40% yield (0.763 g). Ir ν(NH) 3420 cm^{-1}, ν(CO) 1660 cm^{-1}; nmr δ ($CDCl_3$) 1.0–1.5 (m, 7H, C_3H_7), 2.32 (s, 3H, CH_3), 3.30 (m, 2H, CH_2), 6.58 (s (br), 1H, NH), 7.1–7.5 (AB quartet, 4H, aromatic protons); ms (m/e) 191 $[M]^+$, 176 $[M - CH_3]^+$, 119 $[p$-$CH_3C_6H_4CO]^+$; the gc retention time was 10.44 — spiking with an authentic sample provided further evidence for the assigned structure. The thioester p-$CH_3C_6H_4COSCH_2CH(CH_3)_2$, was isolated in 20% yield (0.42 g) from the second band. Ir ν(CO) 1665 cm^{-1}; nmr δ ($CDCl_3$) 1.20 (d, 6H, CH_3), 1.80 (m, 1H, CH), 2.32 (s, 3H, CH_3), 2.94 (d, 2H, CH_2), 7.50 (AB quartet, 4H,

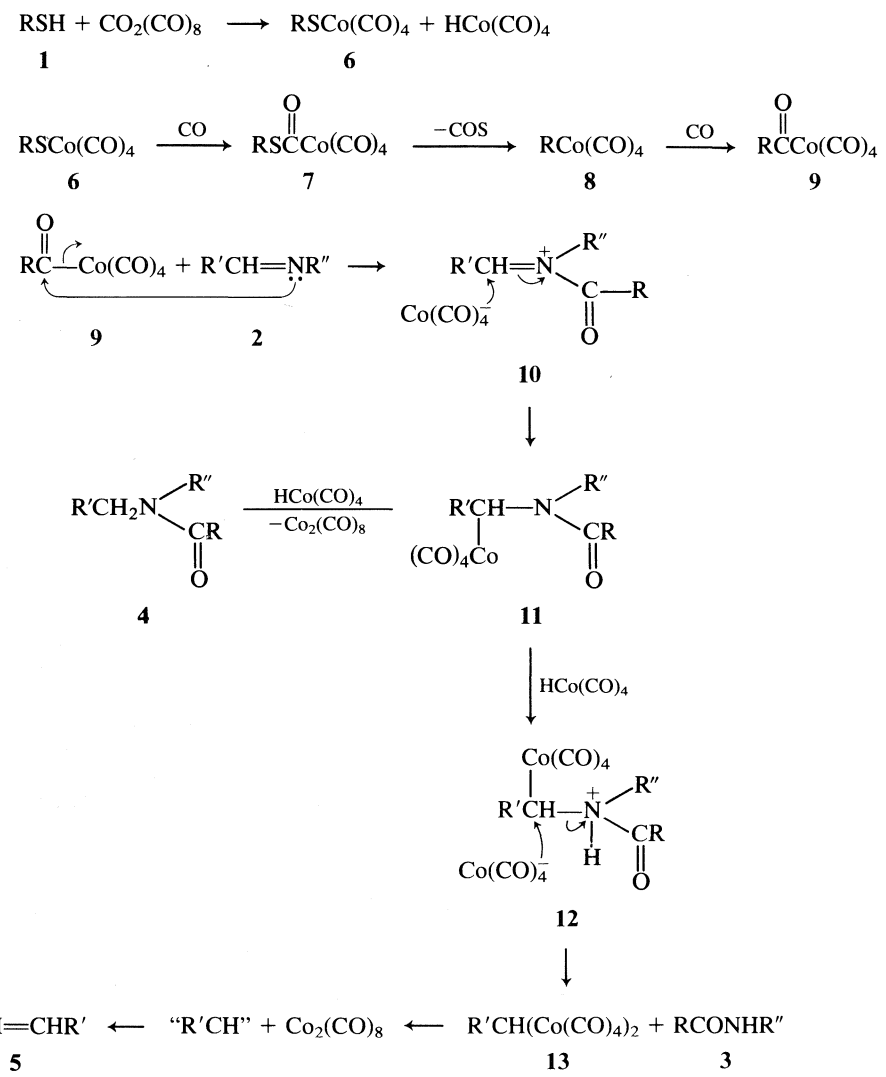

SCHEME 1

aromatic protons); ms (*m/e*) 208 $[M]^+$, 152 $[M - C_4H_8]^+$, 119 $[p\text{-}CH_3C_6H_4CO]^+$. The third fraction was identified as *p*-tolyl disulfide, by comparison of spectral data and gc retention time with an authentic sample. Yield: 0.081 g (7%).

The same reaction and work-up procedure was used in the other cases, with product identification and purity ascertained by comparison of spectral data and retention times with those of authentic materials.

The optimum ratios of reactants and catalyst were determined from numerous experiments covering a Schiff base to mercaptan ratio ranging from 1.0/2.0 up to 2.0/1.0, and a ratio of **1**/$Co_2(CO)_8$ ranging from 1–100/1.

Acknowledgements

We are grateful to British Petroleum and the Natural Sciences and Engineering Research Council of Canada for support of this research.

1. S. C. SHIM, S. ANTEBI, and H. ALPER. J. Org. Chem. **50**, 147 (1985).
2. S. C. SHIM, S. ANTEBI, and H. ALPER. Tetrahedron Lett. **26**, 1935 (1985).
3. S. ANTEBI and H. ALPER. Organometallics, **5**, 596 (1986).
4. T. KADELKA and H. H. SCHWARZ. Ger. Offen. DE 3,246,149 (14 Jun 1984); Chem. Abstr. **102**, 5914k (1985).
5. P. FOLEY. U.S. 4,422,977 (27 Dec 1983); Chem. Abstr. **100**, 102773*e* (1984).
6. A. ROSENTHAL and I. WENDER. Organic syntheses via metal carbonyls. Vol. 1. *Edited by* I. Wender and P. Pino. Wiley-Interscience, New York. 1968. pp. 405–566 and references cited therein.
7. H. ALPER and S. AMARATUNGA. Can. J. Chem. **61**, 1309 (1983).
8. R. R. FRASER and T. S. MANSOUR. J. Org. Chem. **49**, 3442 (1984).

Mechanisms of $^1H,^1H$; $^1H,^{13}C$; and $^{13}C,^{13}C$ spin–spin coupling constants in benzyl cyanide and some derivatives. Experimental and theoretical estimates of internal rotational potentials

TED SCHAEFER AND GLENN H. PENNER[1]

Department of Chemistry, University of Manitoba, Winnipeg, Man., Canada R3T 2N2

Received March 10, 1986

TED SCHAEFER and GLENN H. PENNER. Can. J. Chem. **64**, 2013 (1986).

The mechanisms of long-range spin–spin coupling constants involving the methylene protons and the ^{13}C nucleus of the cyano group are discussed for benzyl cyanide. Analysis of the ^1H nmr spectrum of benzyl cyanide-8-^{13}C in benzene-d_6 solution yields $^nJ(H,CH_2)$ and $^nJ(H,^{13}CN)$ for $n = 4$–6. Similar data are reported for the 2,6-dichloro and 2,6-difluoro derivatives, together with some sign determinations. $^nJ(^{13}C,^{13}CN)$, $n = 1$–5, are given for the three compounds. It is shown that all these parameters are consistent with a small barrier to internal rotation about the C_{sp^2}—C_{sp^3} bond in benzyl cyanide in solution. Computations at various levels of molecular orbital theory agree that this barrier is small. The $^nJ(^{13}C,^{13}CN)$ imply a stabilization in polar solvents of the conformation in which the cyano group of benzyl cyanide lies in a plane perpendicular to the benzene plane. The molecular orbital calculations indicate a predominantly twofold nature of the internal barrier, although a significant fourfold component is also present. The coupling constants cannot discern the presence of the fourfold component for benzyl cyanide nor for its 2,6-difluoro derivative. $^1J(^{13}C,^{13}CN)$ is solvent dependent. A table of the computed sidechain geometries is appended.

TED SCHAEFER et GLENN H. PENNER. Can. J. Chem. **64**, 2013 (1986).

On discute du mécanisme des constantes de couplage spin–spin à longue distance impliquant les protons méthyléniques et le noyau de ^{13}C du groupe cyano du cyanure de benzyle. L'analyse du spectre de rmn du ^1H du cyanure ^{13}C-8 de benzyle en solution dans le benzène-d_6 donne des constantes $^nJ(H,CH_2)$ et $^nJ(H,^{13}CN)$, $n = 4$–6. On rapporte des données semblables dans le cas des dérivés dichloro-2,6 et difluoro-2,6 ainsi que quelques déterminations de signes. On donne les valeurs de $^nJ(^{13}C,^{13}CN)$, $n = 1$–5 de ces trois composés. On montre que tous ces paramètres correspondent à une faible barrière interne à la rotation autour de la liaison C_{sp^2}—C_{sp^3} du cyanure de benzyle en solution. Les calculs à différents niveaux de la théorie des orbitales moléculaires confirment cette faible barrière. La constante $^nJ(^{13}C,^{13}CN)$ implique dans les solvants polaires, une stabilisation de la conformation dans laquelle le groupe cyano du cyanure de benzyle se situe dans un plan perpendiculaire a celui du benzène. Les calculs d'orbitales moléculaires indiquent que la barrière interne est double de façon prédominante, en dépit de l'existence d'un constituant quaternaire important. Les constantes de couplage ne permettent pas de discerner la présence d'un constituant quaternaire dans le cyanure de benzyle et dans son dérivé difluoro-2,6. La constante de couplage $^1J(^{13}C,^{13}CN)$ dépend du solvant. On ajoute une table contenant les géométries théoriques des chaînes latérales.

[Traduit par la revue]

Introduction

The motion of the cyanomethyl group about the sp^2–sp^3 carbon–carbon bond in benzyl cyanide or its derivatives has been investigated by measurements of birefringence, spin-lattice relaxation rates, and of long-range spin–spin coupling constants (1–5). The Kerr constant of benzyl cyanide in CCl_4 solution (1) is consistent with a conformational angle, θ, of 44° (see **1**) or with essentially free internal rotation. The temperature

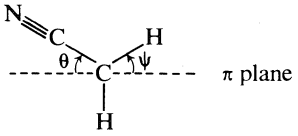

1

dependence of the spin-lattice relaxation rate of ^{14}N in neat 4-methylbenzyl cyanide has been interpreted to give an activation energy of 6.3 kJ/mol for the internal reorientational motion of the cyanomethyl group (2). A similar experiment for a 50 mol% solution in *m*-xylene gives an activation energy of 5.0 kJ/mol. The spin-lattice relaxation rates of ^2H in neat α,α-dideuterobenzyl cyanide yield about 10 kJ/mol for this activation energy (3). These numbers are probably sensitive to the details of the model employed to separate the contributions of internal and overall molecular reorientational motions to the relaxation rates; a study of ^{13}C relaxation rates in benzyl cyanide does not attempt such a separation (4).

The long-range spin–spin coupling constant over six formal bonds between methylene protons and *para* ring protons in 3,5-dichlorobenzyl cyanide, dissolved in a mixture of C_6D_6, $CDCl_3$, and CS_2, yields an apparent twofold internal rotational potential of 1.0 ± 0.8 kJ/mol (5). The bottom of the potential lies at θ = 90° in **1**. If a value of $^6J(H,CH_2)$ of −1.20 Hz is taken, as deduced later in the present paper, the barrier is essentially zero in this compound. Again, the six-bond coupling involving ^{19}F in 4-fluorobenzyl cyanide in CS_2 solution has been taken to mean that V_2 is 1.9 ± 0.8 kJ/mol, also with a θ of 90° at the minimum (5). These small barriers are consistent with the Kerr effect measurements, but not with those of spin-lattice relaxation rates.

However, the dipole moment of benzyl cyanide in benzene solution is 3.5 D (6) and, although that of methyl cyanide is also 3.5 D (7), therefore suggesting very small perturbations of the π electrons in the former, the presence of polar aromatic C–halogen bonds might cause appreciable perturbations of the phase or magnitude of the internal rotational potential. Furthermore, it is not known that the latter is purely twofold, while the model used to derive the barriers from the long-range spin–spin interactions assumed (5) a twofold potential. The presence of a 300-MHz spectrometer in this laboratory now allows the analysis of the ^1H nmr spectrum of benzyl cyanide itself, at least in benzene solution.

Accordingly, we report the analysis of the ^1H nmr spectrum of benzyl cyanide-8-^{13}C, yielding long-range $^1H,^1H$ and $^1H,^{13}C$ coupling constants. Together with the corresponding $^{13}C,^{13}C$ coupling parameters, they provide a data set amenable to a

[1]Holder of an NSERC graduate scholarship, 1985–1986.

TABLE 1. The ^{1}H nmr parameters for a 7.0 mol% solution of benzyl cyanide-8-^{13}C in benzene-d_6 at 300 K and 100.1351 MHz

Parameter	Value	Parameter	Value
$\nu(CH_2)$	825.339(2)[a,b]	$^4J_{26}$	2.042(3)
ν_2	2057.339(2)	$^4J_{24}$	1.213(3)
ν_3	2093.550(2)	$^4J_{35}$	1.449(3)
ν_4	2088.929(3)	$^5J_{25}$	0.594(2)
^2J(H,C)	−10.580(4)[c,d]	^4J(H,CH$_2$)	−0.740(2)
		^5J(H,CH$_2$)	0.302(2)
^4J(H,C)	−0.479(3)	^6J(H,CH$_2$)	−0.585(3)
^5J(H,C)	0.230(4)	Calculated transitions (^{1}H)	620
^6J(H,C)	−0.364(4)	Assigned transitions	458
$^3J_{23}$	7.762(2)	Largest difference	0.049
$^3J_{34}$	7.499(3)	Root mean square deviation	0.019

[a]In Hz to high frequency of internal tetramethylsilane.
[b]Numbers in parentheses are the standard deviations in the last significant figure.
[c]This coupling is negative (15) and the signs of $^{4,5,6}J$(H,C) are assumed to be those determined for $^{5,6}J$(H,C) in 2,6-dichlorobenzylcyanide-8-^{13}C (Table 3) and calculated for ^4J(H,C) by INDO MO FPT (see text).
[d]^1J(^{13}C,^{14}N) could not be determined (4) because the ^{13}C peak is broad (quadrupolar ^{14}N relaxation rate).

discussion of coupling mechanisms, guided by the results of INDO MO FPT computations. Corresponding measurements on 2,6-dichloro- and 2,6-difluorobenzyl cyanide-8-^{13}C yield estimates of the extrema in the angle dependence of the long-range coupling constants. These are combined with extensive molecular orbital calculations of the nature of the internal rotational potentials to provide a description of the reorientational motion of the cyanomethyl group in the three compounds.

Experimental

Benzyl cyanide-8-^{13}C (99 at.% ^{13}C) came from MSD Isotopes, as did KCN enriched to 99 at.% in ^{13}C. The latter was used to prepare 2,6-difluoro- and 2,6-dichlorobenzyl cyanide-8-^{13}C from the corresponding bromide (Aldrich). The bromide was dissolved in acetone and warmed to 50°C. An aqueous solution of the potassium cyanide was slowly added while stirring the acetone solution. The mixture was held at 50°C for 1 h, was diluted with water, and extracted with ether. The product gave characteristic ^{1}H and ^{13}C nmr spectra, displaying splittings arising from the ^{13}C nucleus of the cyano group.

Degassed samples for nmr measurements were prepared in a manner recently described in detail (8). The ^{1}H and ^{13}C nmr spectra were accumulated on a 300-MHz Bruker spectrometer, also in the way described before (8). Relative signs of some coupling constants were obtained via partial decoupling procedures (9).

INDO MO FPT (10, 11) computations of coupling constants were performed on an AMDAHL V8 system. Geometry-optimized energies as a function of θ utilized the computer programs MONSTERGAUSS (12) and GAUSSIAN 80 (13).

Results and discussion

Spectral analyses

The ^{1}H nmr spectra were analyzed with the computer program NUMARIT (14) and the ensuing spectral parameters appear in Tables 1 and 2. The chemical shift dispersion for benzyl cyanide-8-^{13}C was large enough for a reasonably reliable analysis only in benzene-d_6. ^{13}C{^{1}H} experiments yielded the signs of ^nJ(H,^{13}CN) parameters in Table 3. Figure 1 demonstrates the partial decoupling experiments, leading to the sign of ^4J(^{13}C,^{13}CN) in 2,6-dichlorobenzyl cyanide-8-^{13}C.

INDO MO FPT computations

For long-range spin–spin coupling constants, ^nJ, where n represents the formal number of bonds intervening between the coupled nuclei, the INDO MO FPT formulation usually gives the correct qualitative θ dependence when $n \geq 3$. Quantitative reproduction of the magnitudes of $^{4,5,6}J$ is not expected for coupling between sidechain nuclei and nuclei in the benzene moiety because of the parameterization of this semiempirical method and because the geometry assumed in the computation may well be different from the true geometry.

Nevertheless, $^6J(H,CH_3)$ in toluene is very nearly quantitatively reproduced by such calculations (16). For this molecule, $^{5,6}J$(H,CH$_3$) have been written (17) as eqs. [1] and [2].

$$[1]\quad {}^6J(H,CH_3)/\text{Hz} = -1.20\sin^2\psi = {}^6J^{\pi}_{90}\sin^2\psi$$

$$[2]\quad {}^5J(H,CH_3)/\text{Hz} = 0.336\sin^2\psi + 0.322\sin^2(\psi/2) = {}^5J^{\pi}_{90}\sin^2\psi + {}^5J^{\sigma}_{180}\sin^2(\psi/2)$$

In eq. [1], $^6J^{\pi}_{90}$ is the magnitude of $^6J(H,CH_3)$ when the C—H bond of the sidechain lies in a plane perpendicular to the ring. Accordingly, $^6J(H,CH_3)$ is a σ–π coupling constant and arises from a hyperconjugative interaction between the σ electrons in the C—H bonds of the sidechain and the π electrons in the phenyl group. Similar remarks apply to $^5J^{\pi}_{90}$ in eq. [2]. $^5J^{\sigma}_{180}$ arises from a σ electron mechanism and has a maximum for an all-*trans* arrangement of the intervening bonds.

Equation [3] has been proposed (18) for $^4J(H,CH_3)$.

$$[3]\quad {}^4J(H,CH_3)/\text{Hz} = -1.08\sin^2\psi - 0.32\cos^2\psi$$

INDO MO FPT computations (17) agree that $^4J(H,CH_3)$ is indeed dominated by a σ–π mechanism. Equation [4] indicates a small σ electron component, varying as $\cos^2\psi$.

In a benzyl derivative, an electronegative substituent (19) will polarize the C—H bonds in the methylene group, thereby decreasing the hyperconjugative interaction and reducing the magnitude of $^6J^{\pi}$. Qualitatively, the INDO MO FPT formulation agrees with this reduction (19). It is interesting, therefore, that for benzyl cyanide our calculations indicate *no* reduction of $^6J^{\pi}$ relative to toluene, perhaps an increase of 0.005 Hz at θ = 90°. Confirmatory evidence comes from a plot (20) of $^6J(H,CH_2)$ against the electronegativity of the substituent, X, in a series of 2,6-dichlorobenzyl X compounds. For X = CN, the smallest deviation from the roughly linear plot occurs if the cyano group is taken to have the same electronegativity as hydrogen. One might speculate as to the reason for these results;

TABLE 2. ^1H and ^{19}F nmr spectral parameters for a 3.0 mol% solution in benzene-d_6 of 2,6-difluorobenzylcyanide-8-^{13}C at 300 K

Parameter	Value	Parameter	Value
$\nu(CH_2)$	848.112(2)[a]	^3J(H,F)	8.928(1)
ν_2	13753.679(1)[b,c]	^4J(H,F)	6.519(1)
ν_3	1898.320(1)	^5J(H,F)	−1.362(2)
ν_4	1953.362(1)	^3J(H,H)	8.475(1)
^2J(H,C)	−11.027(4)	^4J(H,H)	1.065(2)
^4J(F,C)	±1.045(2)	^4J(F,F)	4.373(2)
^5J(H,C)	0.329(2)	Calculated transitions (^1H and ^{19}F)	640
^6J(H,C)	−0.656(2)	Assigned transitions	383
$^4J(CH_2, F)$	1.045(2)	Root mean square deviation	0.012
$^5J(H,CH_2)$	0.328(1)	Largest difference	0.033
$^6J(H,CH_2)$	−0.390(2)		

[a]In Hz at 300.1351 MHz to high frequency of internal TMS.
[b]In Hz at 282.363 MHz to high frequency of internal C_6F_6.
[c]Numbers in parentheses are standard deviations in the last significant figure.

TABLE 3. The ^1H nmr spectral parameters of 2,6-dichlorobenzyl cyanide-8-^{13}C as a 2.8 mol% solution in benzene-d_6 at 300 K and 200.1351 MHz

Parameter	Value	Parameter	Value
$\nu(CH_2)$	952.972(2)[a]	$^5J(H,CH_2)$	0.337(2)
ν_3	2005.825(2)	$^6J(H,CH_2)$	−0.334(3)
ν_4	1900.541(2)	^3J(H,H)	9.132(2)
^2J(H,C)	−11.114(3)[b]	Calculated transitions (^1H)	96
^5J(H,C)	0.311(3)[c]	Assigned transitions	77
^6J(H,C)	−0.718(5)[c]	Root mean square deviation	0.009
		Largest difference	0.029

[a]In Hz to high frequency of internal TMS.
[b]Numbers in parentheses are standard deviations in the last significant figure.
[c]The signs of ^5J(H,C) and ^6J(H,C) are given relative to ^2J(H,C) which is negative (15), and were determined by $^{13}C\{^1H\}$ experiments in which the methylene protons were decoupled in turn for the two spin states of ^{13}C.

the discussion below assumes the empirical and semiempirical results above.

Turning to $^{4,5,6}J(H,^{13}CN) \equiv {}^{4,5,6}J$(H,C), the INDO MO FPT numbers display a dependence entirely similar to that for $^{4,5,6}J(H,CH_3)$ in toluene (16) and hence are not tabulated here. For the STO 3G MO geometry (see below), $^6J_{90}$(H,C) is computed as −0.756 Hz and happens to agree quantitatively with the estimate arrived at below. Furthermore, ^5J(H,C) can be shown to obey an equation of type [2] in the manner discussed for $^5J(H,CH_3)$ previously (17, 21). It is unlikely that the theoretical values of $^5J^{\pi}_{90}$ and $^5J^{\sigma}_{180}$ are quantitatively correct (17, 21). Empirical estimates are given below.

The INDO MO FPT computations imply that $^{4,5,6}J(H,CH_2)$ and $^{4,5,6}J$(H,C) in benzyl cyanide have the same angle dependence, although naturally the coefficients of $\sin^2\theta$ and $\sin^2(\theta/2)$ will be different for the two kinds of coupling constants. The experimental data support this conclusion, as discussed below.

Turning to $^{3,4,5}J(^{13}C,^{13}CN) \equiv {}^{3,4,5}J$(C,C), using the STO 3G MO geometries for benzyl cyanide, the INDO MO FPT computations can be reproduced by eqs. [4]–[6], errors at the 95% confidence interval.

$$[4]\quad {}^3J(C,C)/Hz = 3.07(1) - 1.04(2)\sin^2\theta + 2.54(2)\sin^2(\theta/2)$$

$$[5]\quad {}^4J(C,C)/Hz = -0.32(4) - 2.19(6)\sin^2\theta + 0.51(6)\sin^2(\theta/2)$$

$$[6]\quad {}^5J(C,C)/Hz = 0.18(1) + 2.30(3)\sin^2\theta$$

Normally, the Karplus equation (22) for a vicinal coupling constant is written as $^3J = A\cos 2\theta + B\cos\theta + C$, in which θ is zero for an eclipsed arrangement of the end-bonds. Of course, eq. [4] is equivalent to the usual Karplus formulation because of trigonometrical identities. In this discussion the formulation used in eq. [4] is more convenient. For free rotation about the C_{sp^2}—C_{sp^3} bond, $\langle\sin^2\theta\rangle$ and $\langle\sin^2(\theta/2)\rangle$ are both 0.5 and eq. [4] suggests 3.8 Hz for such a situation. If $\langle\sin^2(\theta/2)\rangle$ approaches unity, corresponding to θ approaching 90°, then ^3J should decrease to 3.3 Hz, according to eq. [4]. Of course, this prediction depends crucially on the true values of the coefficients in eq. [4], assuming that the functional form is correct. Apparently, the noncontact contributions to ^3J(C,C) in a molecule of this kind are rather small (23) and will not much alter the general form of eq. [4].

In contrast, the angle-independent terms in eqs. [5] and [6] are probably artifacts of the computations, as discussed before for a variety of long-range coupling constants (16, 19, 24). ^4J(C,C) appears to have a negative σ–π component, proportional to $\sin^2\theta$, and a small, positive σ component. ^5J(C,C)

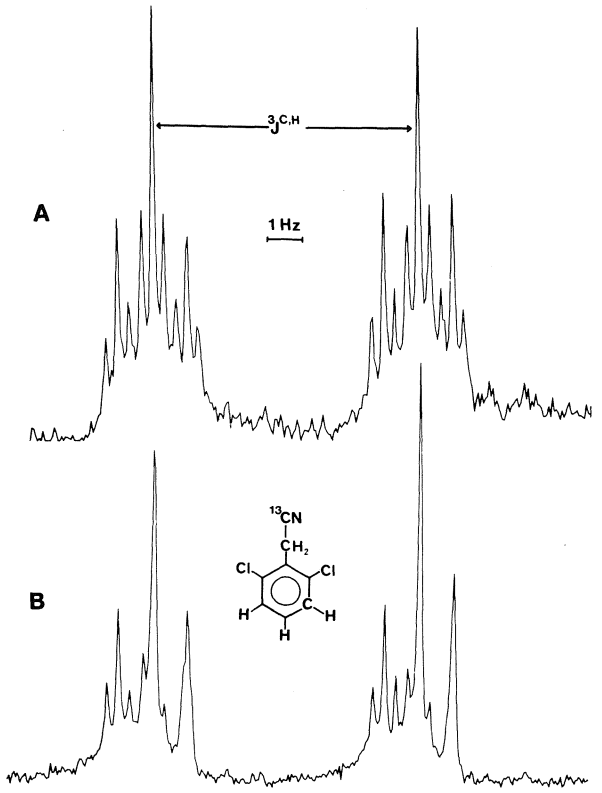

FIG. 1. Half of the ^{13}C nmr spectrum of C-3 in 2,6-dichlorobenzyl cyanide-8-^{13}C, as a 7.1 mol% solution in acetone-d_6, is shown in A. The oscillator frequency is 75.486 MHz and the probe temperature is 300 K. The pair of multiplets is separated by 8 Hz, due to a coupling interaction with H-5. The dominant triplet structure arises from the near equality in the magnitudes of ^2J(H-4,C-3) and ^4J(C-3,^{13}CN). The small triplet spacings of about 0.35 Hz are caused by ^4J(C-3,CH_2). In B the low frequency multiplet of the methylene protons is being irradiated (^2J(CH_2,^{13}CN) is −11.1 Hz). The ^{13}C triplets at low frequency collapse (partial decoupling experiment). Hence ^2J(CH_2,^{13}CN)/^4J(C-3,^{13}CN) > 0.

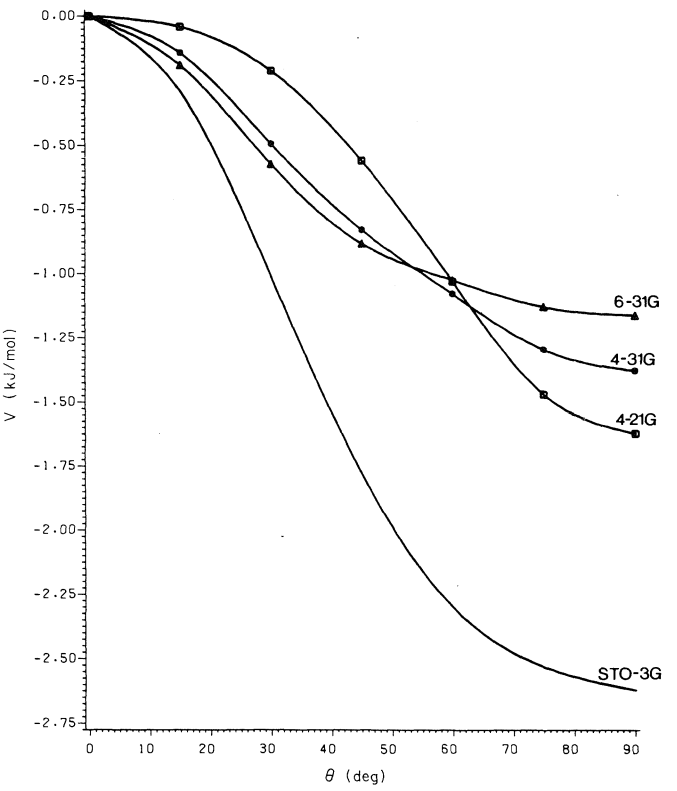

FIG. 2. The relative energies of the optimized geometries of benzyl cyanide are plotted against the dihedral angle θ, which is zero when the cyano group lies in the benzene plane. The calculated internal rotational potentials are discussed in the text. The larger basis sets yield the lower internal barriers. For 6-31G, $V(\theta)$/kJ mol^{-1} = $-1.076(3)\sin^2\theta - 0.293(3)\sin^2 2\theta - 0.084(3)\sin^2 3\theta$, the minimum energy being −361.327 917 au. The barrier height is 1.16(1) kJ/mol.

is computed to be a σ−π coupling constant, analogous to $^5J(C,CH_3)$ in toluene (25–27), but with a magnitude too large at θ = 90° (see below). It is noted that similar computations of ^nJ(C,C) are available for phenylacetic acid (28).

These theoretical considerations provide a guide to the use of $^nJ(H,CH_2)$, $^nJ(H,^{13}CN)$, and $^nJ(^{13}C,^{13}C)$ in the conformational deductions below.

Molecular orbital computations

With rather extensive geometry-optimization procedures, but constraining the carbon framework of the phenyl group to a regular hexagon, the energies of benzyl cyanide as a function of θ yield eq. [7] at the STO 3G level of molecular orbital theory.

$$[7]\quad V(\theta)/\text{kJ mol}^{-1} = -2.597(6)\sin^2\theta - 0.477(6)\sin^2 2\theta = V_2\sin^2\theta + V_4\sin^2 2\theta$$

The energies were computed at intervals of 15° (−357.018 970 au at θ = 0°) and the seven values gave a best fit to a potential containing twofold and fourfold components. The numbers in parentheses in eq. [7] represent the uncertainties at the 95% confidence level. The term in V_4 amounts to nearly 20% of V_2 and the conformation of minimum energy has the cyano group lying in a plane perpendicular to the benzene plane. For a complete geometry optimization, carried out at 0° and 90°, the amplitude of $V(\theta)$ becomes 2.51 kJ/mol, insignificantly different from eq. [7].

Repetition of the computations with the 4-21G basis set gave V_2 and V_4 as −1.634(4) and 0.266(4) kJ/mol, respectively, while the 4-31G basis set yielded a set of energies which were best fit with V_2, V_4, and V_6 as −1.312(5), −0.131(5), and −0.62(2) kJ/mol. Finally, the 6-31G basis predicted V_2, V_4, and V_6 as −1.076(3), −0.293(3), and −0.084(3) kJ/mol, respectively. The minimum energies for the 4-21G, 4-31G, and 6-31G bases were −360.709 315, −360.944 650, and −361.327 917 au, respectively. Apparently the internal rotational barrier in benzyl cyanide is rather small and contains an appreciable fourfold, in addition to the dominant twofold, component. Figure 2 displays the computed rotational potentials.

As expected, the computed barrier in 2,6-difluorobenzyl cyanide at the STO 3G level increases in magnitude relative to benzyl cyanide, V_2 and V_4 being −9.86(3) and −2.35(3) kJ/mol, respectively. The minimum energy is −551.934 111 au. In the presence of two *ortho* chlorine substituents, the best fit to the STO 3G MO energies has V_2 as −29.6(5) kJ/mol and a minimum energy of −1265.009258 au. Inclusion of a fourfold component does not improve the fit, but it must be stated that the smooth curve through the computed energies displays a somewhat "flat top" near 90°.

Computations with other basis sets were not done for the two benzyl cyanide derivatives because they were too expensive.

In the discussion below, the presence of a fourfold term in the internal rotational potential modifies the experimental estimates

of the conformational potential deduced from the long-range coupling constants.

Internal barriers in solution based on ^{6}J(H,CH$_2$) and ^{6}J(H,C)

In 2,6-dichlorobenzyl cyanide, V_2 is calculated as 29.6(5) kJ/mol. At 300 K a hindered rotor model (29) yields $\langle\sin^2\theta\rangle$ as 0.955 for a V_2 of 29.6 kJ/mol (51 free rotor basis functions). A harmonic oscillator basis has $\langle\sin^2\theta\rangle$ as 0.957. A V_2 as high as 38 kJ/mol corresponds to a $\langle\sin^2\theta\rangle$ of 0.965 and this drops to 0.934 for a V_2 of 21 kJ/mol. It will be assumed that $\langle\sin^2\theta\rangle$ in this compound is 0.955. ^6J(H,C) is −0.718(5) Hz, corresponding to a $^6J_{90}$ of −0.752(5) Hz. In benzyl cyanide-8-^{13}C, ^6J(H,C) is −0.364(4) Hz. It follows that $\langle\sin^2\theta\rangle$ is 0.484(8). This number implies that the conformer of lowest energy has a θ of 0°. If the internal barrier were purely twofold, it would be only 0.3(1) kJ/mol, a zero barrier corresponding to 0.5 for $\langle\sin^2\theta\rangle$. A fourfold component amounting to 20% of the twofold magnitude and of the same sign (see eq. [7]), will alter $\langle\sin^2\theta\rangle$ insignificantly for such a small barrier. In view of the possible error in $^6J_{90}$(H,C), which is not known but must be finite, it is concluded that essentially free internal rotation occurs in benzyl cyanide-8-^{13}C in benzene-d_6 solution. If, for example, it is assumed that the barrier in 2,6-dichlorobenzyl cyanide is very large indeed, so that $\langle\sin^2\theta\rangle$ is effectively unity, then its value in benzyl cyanide becomes 0.507 and corresponds to a θ of 90° for the conformation of lowest energy in benzene-d_6 solution. The apparent twofold barrier is then 0.1 kJ/mol.

This conclusion can be checked by means of ^6J(H,CH$_2$), which is −0.585(3) Hz in the same solution. Based on the discussion in a previous section, $^6J_{90}$(H,CH$_2$) is −1.20(2) Hz. Hence $\langle\sin^2\psi\rangle$ is 0.488(10) Hz, confirming the very flat internal rotational potential, but implying a minimum energy at θ = 90° and a V_2 of 0.4(4) kJ/mol. For the 3,5-dichlorobenzyl cyanide, dissolved in a mixture of C_6D_6, $CDCl_3$, and CS_2, ^6J(H,CH$_2$) is −0.60(1) Hz (5), implying only a small perturbation of the potential by the *meta* substituents. This result contrasts with those found for benzyl fluoride and 3,5-dichlorobenzyl fluoride (19).

In the 2,6-dichloro derivative, ^6J(H,CH$_2$) is −0.334(3) Hz, corresponding to a $\langle\sin^2\theta\rangle$ of 0.278(7) if $^6J_{90}$(H,CH$_2$) is −1.20(2) Hz. Because $\langle\sin^2\theta\rangle = 1.5 - 2\langle\sin^2\psi\rangle$ (see **1**), the $\langle\sin^2\theta\rangle$ of 0.955 Hz, deduced above, yields $\langle\sin^2\psi\rangle$ as 0.273(3). However, a careful analysis of the ^{1}H nmr spectrum of 2,6-dichlorotoluene in CS_2 solution gave ^6J(H,CH$_3$) as −0.630(1) Hz, implying $^6J_{90}$(*H*,C*H*$_3$) as −1.26(2) Hz in the presence of two *ortho* chlorine substituents. Then $\langle\sin^2\psi\rangle$ becomes 0.263(7), now somewhat lower than deduced from $\langle\sin^2\theta\rangle$. Better agreement is perhaps not to be expected in view of measurement and other errors.

All these comparisons suggest that a barrier in 2,6-difluorobenzyl cyanide is derivable from ^6J(H,C) and ^6J(H,CH$_2$), which are −0.656(2) Hz and −0.390(2) Hz, respectively. Hence $\langle\sin^2\theta\rangle$ is 0.872(8) and $\langle\sin^2\psi\rangle$ is 0.325(7). These numbers correspond to apparent twofold barriers of 11.8(6) and 10.3(9) kJ/mol, respectively. In 2,6-difluorotoluene in CS_2 solution, ^6J(H,CH$_3$) is −0.623(5) Hz (30), implying a $^6J_{90}$(H,CH$_2$) of −1.25(2) Hz, a $\langle\sin^2\psi\rangle$ of 0.312(7), and an apparent V_2 of 12.1(9) kJ/mol. Although this value of $\langle\sin^2\theta\rangle$ is in better agreement with $\langle\sin^2\theta\rangle \equiv 1.5 - 2\langle\sin^2\psi\rangle$ than that deduced from $^6J_{90}$(H,CH$_2$) = −1.20(2) Hz, one might also expect an *ortho* substituent perturbation of ^6J(H,C). There is no clear way to establish such a perturbation. The MO barrier implies a V_4/V_2 ratio 0.24. Such a ratio and a $\langle\sin^2\theta\rangle$ of 0.87(1) correspond to a V_2 of 19.5(5) and a V_4 of 4.5(4) kJ/mol, quite different from the magnitude indicated by the MO computations. One might note that one of the larger basis set calculations for benzyl cyanide itself has a different sign of V_4/V_2 than does the STO 3G, minimal basis computation. Suppose, for example, that V_4/V_2 is −0.24 for the 2,6-difluoro derivative. Then a $\langle\sin^2\theta\rangle$ of 0.872(8) fits V_2 and V_4 of 9.0(3) and −2.2(3) kJ/mol, respectively, implying a barrier *height* of 9.0(3) kJ/mol (the fourfold component is zero at θ = 90°). On the other hand, if V_4/V_2 is positive, then the height of the barrier is 19.5(5) kJ/mol.

Unfortunately, these two combinations of V_2 and V_4 cannot be distinguished on the basis of $\langle\sin^2\psi\rangle$. The C—H and C—C bonds do sample different regions of the internal rotational potential. However, at least for the present situation, the sampling leads to a $\langle\sin^2\psi\rangle$ of 0.315 for $V_4/V_2 > 0$ and to 0.314 for $V_4/V_2 < 0$. Furthermore, the numbers are not sufficiently different from the experimental value of 0.325(7) so as to provide evidence for the absence of V_4.

^{5}J(C,C) as a conformational indicator

Equation [6] is taken as theoretical support for a σ–π mechanism for ^5J(C,C). Then its value of 1.08(1) Hz for 2,6-dichlorobenzylcyanide-8-^{13}C in benzene-d_6 solution implies ^5J(C,C) = $^5J_{90}\langle\sin^2\theta\rangle$ where $^5J_{90}$ is 1.08(1)/0.955 or 1.13(1) Hz. It follows that $\langle\sin^2\theta\rangle$ for benzyl cyanide in benzene solution is 0.51(1)/1.13(1) or 0.45(1), corresponding to an apparent twofold barrier of 1.0(3) kJ/mol. Furthermore, the conformer of lowest energy has θ = 0°, as indicated by ^6J(H,C) but not by ^6J(H,CH$_2$). If the barriers indicated by the three coupling constants are treated on an equal footing, then it follows that the barrier in benzyl cyanide in benzene-d_6 solution at 300 K is 0.3(3) kJ/mol, the in-plane conformer having the lowest energy.

For the 2,6-difluoro derivative, ^5J(C,C) corresponds to an apparent V_2 of 9.6 ± 1.2 kJ/mol, but again its value cannot discriminate between this estimate and a combination of V_2 and V_4.

Concerning ^{4,5}J(H,CH$_2$) and ^{4,5}J(H,C) in benzyl cyanide-8-^{13}C

Because $\langle\sin^2\theta\rangle$ and $\langle\sin^2\psi\rangle$ are so very near 0.5 in benzyl cyanide, it should be possible to rationalize all the observed long-range couplings involving the ring protons and the side-chain methylene protons or ^{13}C nucleus in terms of equations of type [1]–[3]. This statement follows because the INDO MO FPT computations strongly imply that these couplings have the same qualitative conformational dependence. On the assumption that, as discussed in previous sections, ^6J(H,CH$_2$) is −1.20(2) Hz at θ = 90° and that ^6J(H,C) is −0.752(5) Hz, their ratio follows as 0.627(15). Hence, the ratio of the observed coupling constants (Table 1) should be the same and is indeed 0.622(10).

Again, because ^4J is dominated by the σ–π electron term, the ratio for ^4J(H,C) to ^4J(H,CH$_2$) is expected to be similar to the ratio of the ^6J values. The observed ratio is 0.647(8). The discrepancy can be attributed to differing σ electron components, which become $-0.40\langle\cos^2\psi\rangle$ and $-0.29\langle\cos^2\theta\rangle$ for ^4J(H,CH$_2$) and ^4J(H,C), respectively (use eq. [3] and experimental values, assuming $\langle\sin^2\theta\rangle = \langle\sin^2\psi\rangle = 0.5$).

By way of contrast, ^5J consists of σ and σ–π contributions of similar magnitude. The latter can be taken as that in toluene for ^5J(H,CH$_2$) and as 0.622 of this for ^5J(H,C). Consequently, ^5J(H,CH$_2$) becomes (Table 1) 0.134 Hz, while ^5J(H,C) is

TABLE 4. The ^{13}C nmr chemical shifts and $^{13}C,^{13}C$ coupling constants at 75.486 MHz and 300 K for benzyl cyanide-8-^{13}C and its derivatives

Parameter	Compound					
	2,6-diH			2,6-diCl		2,6-diF
δ(CN)	116.54[a]	117.86[b]	119.06[c]	114.99[d]	116.33[e]	115.76[f]
$\delta(CN_2)$	23.437	22.840	23.335	19.268	20.08	10.239
δ_1	130.578	130.802	132.261	127.532	128.73	107.464
δ_2	127.887	128.000	128.908	135.262	136.26	160.851
δ_3	129.103	129.082	129.831	128.145	129.67	111.478
δ_4	127.863	127.830	128.528	129.735	131.63	130.263
^1J	58.33	57.8	57.0	58.9	58.2	59.3
^2J	(−)3.52	(−)3.53	(−)3.65	(−)4.82	(−)4.83	(−)4.41
^3J	(+)3.51	(+)3.45	(+)3.31	(+)2.27	(+)2.28	(+)2.26
^4J	(−)0.17	(−)0.19	(−)0.29	(−)1.02	(−)1.03[g]	(−)0.87
^5J	(+)0.50	(+)0.51	(+)0.58	(+)1.08	(+)1.10[g]	(+)0.95

[a]For a 5 mol% solution in CS_2 solution containing ca. 30 vol% of C_6D_{12}.
[b]For an 11 mol% solution in benzene-d_6 in ppm relative to internal TMS. The shifts are reproducible to 1 ppb and the coupling constants to within 0.01 Hz.
[c]For a 3.0 mol% solution in acetone-d_6.
[d]3.0 mol% in benzene-d_6.
[e]7.1 mol% in acetone-d_6.
[f]5.0 mol% in benzene-d_6. The couplings in Hz to ^{19}F are $^1J(C,F) = -250.04$, $^2J(C\text{-}1,F) = 19.29$, $^3J(CH_2,F) = \pm 4.41$, $^3J(C\text{-}2,F) = 6.90$, $^2J(C\text{-}3,F) + {}^4J(C\text{-}3,F) = 25.02$, $^3J(C\text{-}4,F) = 10.12$, $^4J(CN,F) = \pm 1.01$ Hz.
[g]These signs, see Fig. 1, are assumed also for those given in other columns and agree with theoretical calculations.

0.126 Hz. Accordingly, for benzyl cyanide one has eqs. [8] and [9].

$$[8]\quad {}^5J(H,CH_2)/Hz = 0.336\langle \sin^2 \psi\rangle + 0.268\langle \sin^2 (\psi/2)\rangle$$

$$[9]\quad {}^5J(H,C)/Hz = 0.209\langle \sin^2 \theta\rangle + 0.252\langle \sin^2 (\theta/2)\rangle$$

A test of such equations can be had from, for example, 2,6-difluorobenzyl cyanide-8-^{13}C. However, it is known that *ortho* fluorine substituents increase the σ component of $^5J(H,CH_2)$, it being 0.270 Hz in 2,6-difluorotoluene compared to 0.161 Hz in toluene (17, 21). If this increase is factored into eq. [8], then $^5J(H,CH_2)$ is computed as 0.334 Hz, the observed value being 0.328(1) Hz. The $\langle \sin^2 \psi\rangle$ is taken from Table 5 and $\langle \sin^2 (\psi/2)\rangle$ is 0.5, the value for twofold and fourfold barriers of any magnitudes. It is not known how the substituents would alter the components of $^5J(H,C)$. Equation [9] yields $^5J(H,C)$ as 0.308 Hz, while 0.329(2) Hz is observed, perhaps implying an increased σ component. On the other hand, $^5J(H,C)$ in the 2,6-dichloro derivative is calculated as 0.326 Hz, whereas the observed value is 0.331(3) Hz. Rather more data are needed to reach firm conclusions, although most of the increase of 0.1 Hz in $^5J(H,C)$ observed in going from benzyl cyanide to its two derivatives is reproduced by the implied coupling mechanism.

$^{2,3,4}J(^{13}C,^{13}CN)$ mechanisms

In toluene, $^2J(C\text{-}1,CH_3)$ is −5.97 Hz (25) and INDO MO FPT values (26) for this coupling are reproduced by $-5.93 - 2.21 \sin^2 \psi$. Of course, $\langle \sin^2 \psi\rangle$ is 0.5 in toluene and hence the theoretical numbers overestimate the magnitude of the coupling constant by 1.06 Hz. The present INDO values for $^2J(C,C)$ obey $^2J(C,C)/Hz = -7.16 - 1.31 \sin^2 \theta$. For the benzene solutions in Table 4, and from the values of $\langle \sin^2 \theta\rangle$ in Table 5, the empirical equation for $^2J(C,C)$ is $|^2J(C,C)/Hz| = 2.2(1) + 2.7(1) \sin^2 \theta$.

The theoretical numbers for $^3J(C,C)$ are fit by $3.1(1) - 1.0(2) \sin^2 \theta + 2.5(2) \sin^2 (\theta/2)$, a Karplus equation, just as in toluene the $^3J(C\text{-}2,CH_2)$ values given by theory (26) are reproduced by $4.89(3) - 1.44(4) \sin^2 \theta + 3.18(4) \sin^2 (\theta/2)$. The experimental numbers in Tables 4 and 5 for benzene solutions cannot yield the coefficients of $\sin^2 (\theta/2)$ because the latter is 0.5 for any combinations of V_{2n}, where n is an integer. However, they yield $^3J(C,C)/Hz = 4.3(2) - 2.3(1) \sin^2 \theta$,

TABLE 5. Internal rotational potentials in benzylcyanide-8-^{13}C and its two derivatives in benzene-d_6 solution

Parameter	2,6-diCl	2,6-diH	2,6-diF
$^6J(H,C)/Hz$	−0.718(5)	−0.364(4)	−0.656(2)
$^6J_{90}(H,C)$	−0.752(5)[a]	−0.752(5)	−0.752(5)
V_2/kJ mol^{-1}	29.6(5)[a]	0.3(1)[d]	11.8(6)
$\langle \sin^2 \theta\rangle_H^C$	0.955[a]	0.484(8)[d]	0.872(8)
$^6J(H,CH_2)$	−0.334(3)	−0.585(3)	−0.390(2)
$^6J_{90}(H,CH_2)$	−1.20(2)	−1.20(2)	1.20(2)
$\langle \sin^2 \psi\rangle_H^H$	0.278(7)	0.488(10)[e]	0.325(7)
			0.213(7)[f]
V_2/kJ mol^{-1}	24(6)[b]	0.4(4)[e]	10.3(0.9)
			12.1(0.9)[f]
$^5J(C,C)$	1.08(1)	0.51(1)	0.95(1)
$^5J_{90}(C,C)$	1.13(1)[c]	1.13(1)	1.13(1)
$\langle \sin^2 \theta\rangle_C^C$	0.955[c]	0.45(1)[d]	0.84(2)
V_2/kJ/mol	29.6(5)[c]	1.0(3)[d]	9.6 ± 1.2

[a]The theoretical value of V_2 is used to derive $^6J_{90}(H,C)$ and $\langle \sin^2 \theta\rangle_H^C$. See text.
[b]The value of V_2 obtained from $^6J(H,CH_2)$ assuming a $^6J_{90}(H,CH_2)$ of −1.20(2) Hz.
[c]The theoretical value of V_2 is used to find $^5J_{90}(C,C)$ and $\langle \sin^3 \theta\rangle_C^C$.
[d]Implying that in the conformation of lowest energy, the cyano group lies in the benzene plane.
[e]Implying that the cyano group prefers the plane perpendicular to the benzene ring. To obtain agreement with $\langle \sin^2 \theta\rangle^C = 1.5 - 2\langle \sin^2 \psi\rangle_H^H$, one needs $\langle \sin^2 \psi\rangle_H^H$ as 0.508 or $^6J_{90}(H,CH_2)$ as 1.15(2) Hz. See text for a fuller discussion.
[f]With a $^6J_{90}(H,CH_2)$ of −1.25(2) Hz. See text.

implying rather minor intrinsic perturbations from the ring substituents attached to the coupled carbon nucleus.

Turning to ^4J(C,C) in benzyl cyanide-8-^{13}C, the INDO numbers are represented by ^4J(C,C)/Hz = $-0.32(4) - 2.19(6)\sin^2\theta + 0.51(6)\sin^2(\theta/2)$, implying a positive coupling only when θ is 180°, that is, for an all-*trans* arrangement of the intervening bonds. It is conceivable that the constant term in this equation is an artifact of the computation, as found for $^5J(H,CH_3)$ in toluene (16). The data in Tables 4 and 5 cannot be used to rule out a constant term. They do yield $0.5 - 1.6\sin^2\theta$ for the behaviour of ^4J(C,C), a result perhaps most consistent with a vanishing ^4J(C,C) at $\theta = 0°$ (all-*cis*). The best fit is obtained for a negative value of ^4J(C,C), −0.19 Hz, in benzyl cyanide itself in benzene-d_6 solution.

The solvent dependence of the internal barrier in benzyl cyanide

In benzyl fluoride (19) the perpendicular conformer ($\theta = 90°$ for C—F) is stabilized by approximately 2 kJ/mol when the solvent is changed from CS_2 to acetone, qualitatively as expected from electrostatic considerations because this conformer has a higher computed dipole moment than the one with $\theta = 0°$. The internal rotational barrier in benzyl fluoride is small, comparable in magnitude with that computed for benzyl cyanide, except that the most stable conformer has $\theta = 0°$ in the former for the isolated molecule. In benzyl fluoride, all the long-range coupling constants, J(C,F), J(H,F), and $J(H,CH_2)$, are in agreement as to the solvent-induced change in the internal rotational potential (19). Unfortunately, the ^{1}H nmr spectrum of benzyl cyanide at 300 MHz yields to analysis only in benzene-d_6 solution. Therefore $^nJ(H^{13}CN)$ and $^nJ(H,CH_2)$ are not available for other solvents, leaving only ^nJ(C,CN) as indicators of the conformational changes induced by solvents.

The dipole moments of benzyl cyanide are computed as 3.17 and 3.26 D for $\theta = 0$ and 90°, respectively, at the STO 3G level of MO theory. The observed dipole moment in benzene solution is 3.50 D at 298 K, that of methyl cyanide also being 3.5 D in the same solvent. Qualitatively, then, the perpendicular conformer should be more stable in acetone that in CS_2 solution.

The ^nJ(C,CN) of benzyl cyanide in CS_2/C_6D_{12}, benzene-d_6, and acetone-d_6 solutions are given in Table 4. Qualitatively, their values do indeed indicate increased stability of the more polar conformer in acetone-d_6. In terms of the discussion in the previous section, ^2J(C,C) and ^3J(C,C) should decrease in magnitude when the perpendicular conformer is stabilized by solvent, while $^{4,5}J$(C,C) should increase, in congruence with observation.

Quantitatively, based on ^5J(C,C), $\langle\sin^2\theta\rangle$ changes from 0.44(1) in CS_2/C_6D_{12} to 0.51(1) in acetone-d_6 solutions. Therefore the apparent V_2 changes from 1.3(4) kJ/mol, the in-plane conformer being of lowest energy in the nonpolar solvent mixture, to 0.2(2) kJ/mol in acetone-d_6 solution with a possibly slight preference for the perpendicular conformer.

On the assumption that the two conformers differ in their dipole moments by a maximum of 0.2 D, the perpendicular conformer having one of 3.6 D, the reaction field model (31) implies that the perpendicular conformer is stabilized by 0.5 kJ/mol in the CS_2 solution and by 0.8 kJ/mol in acetone-d_6 solution. More than semiquantitative agreement with the measurements above is not expected (31), nor was it found for benzyl fluoride (19). What is certain from the measurements of ^5J(C,C) is the increased stability of the perpendicular conformer in the more polar solvent by 1.5(3) kJ/mol, this number being insensitive to the error in $^5J_{90}$(C,C).

Intrinsic solvent perturbations of $^nJ(C,C)$

Comparison of ^nJ(C,C) values, $n = 2$–5, for 2,6-dichlorobenzyl cyanide-8-^{13}C in benzene-d_6 and acetone-d_6 solutions in Table 4 suggests their insensitivity to solvent polarity. The barrier to internal rotation in this molecule is very high relative to benzyl cyanide, so that significant differences in the magnitudes of these coupling constants in the two solvents would be attributable to an intrinsic perturbation of coupling mechanisms by solvent molecules. Consequently, the solvent dependence of these coupling constants in benzyl cyanide can be assigned to conformational changes, that is, to perturbations of the internal rotational potential.

However, ^1J(C,C) does evince an intrinsic solvent dependence as well as a sensitivity to the presence of *ortho* substituents (Table 4). The original INDO MO FPT computations (4) of ^1J(C,C) predict a smaller value for the conformer defined by $\theta = 90°$. In that event, the decrease of 1.3 Hz in ^1J(C,C) in benzyl cyanide on moving from nonpolar to polar solutions is in qualitative agreement with conclusions in the previous section. However, much of this decrease may well arise from an intrinsic solvent perturbation because ^1J(C,C) decreases by 0.7 Hz between benzene-d_6 and acetone-d_6 solutions for the 2,6-dichloro derivative. Furthermore, the values are larger than for benzyl cyanide in the same solvents, presumably a substituent perturbation. Its presence is emphasized by the value of ^1J(C,C) in the 2,6-difluoro derivative, being larger than any other in Table 4. The present solvent perturbations of $^1J(CH_2, C{\equiv}N)$ join those known for a variety of other one-bond coupling constants (32–37).

Conclusions

Ab initio molecular orbital calculations and long-range ^{1}H,^{1}H; ^{1}H,^{13}C; and ^{13}C,^{13}C spin–spin coupling constants agree that the internal barrier to rotation about the C_{sp^2}—C_{sp^3} bond in benzyl cyanide is small relative to kT at ambient temperatures. The molecular orbital calculations have the conformer of lowest energy as that with the cyano group perpendicular to the benzene plane, whereas in benzene solution the coupling constants imply that this conformer has the cyano group in the benzene plane. The coupling parameters indicate a stabilization of the perpendicular conformer by polar solvents. For 2,6-difluorobenzyl cyanide the coupling constants cannot discriminate between a purely twofold barrier and one containing an additional fourfold component, as computed by molecular orbital methods. However, they do indicate a substantial barrier and the conformer of lowest energy.

1. K. E. Calderbank, R. J. W. LeFèvre, and R. Pierens. J. Chem. Soc. B, 1463 (1970).
2. D. Wallach. J. Phys. Chem. **73**, 307 (1969).
3. J. DeZwaan and J. Jonas. J. Phys. Chem. **77**, 1768 (1973).
4. R. E. Wasylishen and B. A. Pettitt. Can. J. Chem. **57**, 1274 (1979).
5. T. Schaefer, W. Danchura, W. Niemczura, and J. Peeling. Can. J. Chem. **56**, 2442 (1978).
6. C. P. Smyth and W. S. Walls. J. Am. Chem. Soc. **54**, 1854 (1932).
7. J. R. Partington and E. G. Cowley. Nature, **135**, 474 (1935).
8. T. Schaefer, J. Peeling, and R. Sebastian. Can. J. Chem. **63**, 3219 (1985).
9. J. P. Maher and D. F. Evans. Proc. Chem. Soc. (London), 208 (1961).
10. J. A. Pople, J. W. McIver, and N. S. Ostlund. J. Chem. Phys. **49**, 2965 (1968).

11. P. DOBOSH and N. S. OSTLUND. QCPE, **11**, 281 (1975).
12. M. R. PETERSEN and R. A. POIRIER. MONSTERGAUSS. Department of Chemistry, University of Toronto, Toronto, Ontario. 1981.
13. J. S. BINKLEY, R. A. WHITESIDE, R. KRISHNAN, R. SEEGER, D. J. DEFREES, H. B. SCHLEGEL, S. TOPIOL, L. R. KAHN, and J. A. POPLE. QCPE, **12**, 406 (1980).
14. J. S. MARTIN, A. R. QUIRT, and K. E. WORVILL. The nmr program library. Daresbury Laboratory, Daresbury, U.K.
15. W. MCFARLANE. Mol. Phys. **10**, 603 (1966).
16. R. WASYLISHEN and T. SCHAEFER. Can. J. Chem. **50**, 1852 (1972).
17. T. SCHAEFER, R. SEBASTIAN, and G. H. PENNER. Can. J. Chem. **63**, 2597 (1985).
18. M. BARFIELD, C. S. FALLICK, K. HATA, S. STERNHELL, and P. W. WESTERMAN. J. Am. Chem. Soc. **105**, 2178 (1983).
19. T. SCHAEFER, J. PEELING, and R. SEBASTIAN. Can. J. Chem. **63**, 3219 (1985).
20. A. F. JANZEN and T. SCHAEFER. Can. J. Chem. **49**, 1818 (1971).
21. T. SCHAEFER and R. LAATIKAINEN. Can. J. Chem. **61**, 2785 (1983).
22. M. KARPLUS. J. Am. Chem. Soc. **85**, 2870 (1965).
23. M. L. SEVERSON and G. E. MACIEL. J. Magn. Reson. **57**, 248 (1984).
24. T. SCHAEFER, K. MARAT, J. PEELING, and R. P. VEREGIN. Can. J. Chem. **61**, 2779 (1983).
25. M. HANSEN and H. J. JAKOBSEN. J. Magn. Reson. **20**, 520 (1975).
26. L. ERNST, V. WRAY, V. A. CHERTKOV, and N. M. SERGEYEV. J. Magn. Reson. **25**, 123 (1977).
27. T. SCHAEFER, J. PEELING, and G. H. PENNER. Can. J. Chem. **61**, 2773 (1983).
28. J. L. MARSHALL, L. G. FAEHL, A. M. IHRIG, and M. BARFIELD. J. Am. Chem. Soc. **98**, 3406 (1976).
29. W. J. E. PARR and T. SCHAEFER. Can. J. Chem. **13**, 400 (1980).
30. T. SCHAEFER, R. SEBASTIAN, R. P. VEREGIN, and R. LAATIKAINEN. Can. J. Chem. **61**, 29 (1983).
31. R. J. ABRAHAM and E. BRETSCHNEIDER. *In* Internal rotation in molecules. *Edited by* W. J. Orville-Thomas. J. Wiley and Sons, New York. 1974. Chapt. 13.
32. S. L. SMITH. Top. Curr. Chem. **27**, 117 (1972).
33. M. BARFIELD and M. D. JOHNSTON. Chem. Rev. **73**, 53 (1973).
34. J. KOWALEWSKI. Prog. Nucl. Magn. Reson. Spectrosc. **11**, 1 (1977).
35. M. KONDO, S. WATANABE, and I. ANDO. Mol. Phys. **37**, 1521 (1979).
36. I. ANDO, Y. INOUE, S. WATANABE, Y. SAKAMOTO, and G. A. WEBB. J. Mol. Liq. **27**, 179 (1984).
37. J. C. FACELLI, C. G. GIRIBET, and R. H. CONTRERAS. Int. J. Quantum Chem. **25**, 515 (1984).
38. C. C. COSTAIN. J. Chem. Phys. **29**, 864 (1958).

Appendix

A referee requested some computed geometrical data and these are given in Table A1. The sidechain geometry is characterized for the most stable conformations, those in which the cyano group lies in a plane perpendicular to the benzene plane. As expected, the bond lengths and angles are somewhat basis dependent. For comparison, the C—C bond length in methyl cyanide is 1.458 Å and that of the C≡N bond is 1.157 Å (38). According to the STO 3G MO computations, the *ortho* halogen substituents cause rather small changes in the sidechain geometry.

TABLE A1. Computed bond lengths and angles for the sidechain of benzyl cyanide and two of its derivatives[a]

X[b]	Basis set	C_1C_α[c]	$C_\alpha C$	CN	$C_\alpha H_\alpha$	$C_1C_\alpha H_\alpha$	$C_1C_\alpha C$
H	STO-3G	1.5363	1.4952	1.1546	1.0905	110.38	111.79
H	4-21G	1.5258	1.4650	1.1404	1.0836	110.33	111.44
H	4-31G	1.5196	1.4631	1.1421	1.0830	110.35	112.46
H	6-31G	1.5211	1.4670	1.1467	1.0836	110.36	112.66
F	STO-3G	1.5363	1.4951	1.1546	1.0908	110.00	112.11
Cl	STO-3G	1.5386	1.4934	1.1547	1.0894	109.93	111.43

[a]For the conformation of lowest energy, that in which the cyano group lies in a plane perpendicular to that of the ring.
[b]The two *ortho* substituents.
[c]Bond lengths in angstroms, angles in degrees.

A high pressure mass spectrometric study of proton transfer between tri-, tetra-, penta-, and hexamethylbenzene

JOHN ALFRED STONE, XIAOPING LI, AND PATRICIA ANNE TURNER
Chemistry Department, Queen's University, Kingston, Ont., Canada K7L 3N6

Received April 9, 1986

JOHN ALFRED STONE, XIAOPING LI, and PATRICIA ANNE TURNER. Can. J. Chem. **64**, 2021 (1986).

The proton affinities (PA) of some methylaromatic compounds and the rates of proton transfer reactions have been measured using high pressure mass spectrometry. The equilibria studied were of the form $B_1H^+ + B_2 \rightleftharpoons B_1 + B_2H^+$. Van't Hoff plots yielded the following PA values (kcal mol^{-1}) relative to PA(ethylacetate) = 200.7 as standard: mesitylene 201.0, 1,2,3,5-tetramethylbenzene 203.2, pentamethylbenzene 204.4, hexamethylbenzene 206.6. ΔS^0 values for the proton transfer equilibria are not fully determined by changes in rotational symmetry numbers and it is suggested that vibrational and torsional changes must be considered. Proton transfer is slow in both the forward (exothermic) and reverse (endothermic) directions and, in addition, for all except the most endothermic reaction studied (1,2,3,5-tetramethylbenzene + protonated hexamethylbenzene) the rate constants for proton transfer increase with decreasing temperature. Such behaviour can be associated with the potential energy profile along the reaction coordinate for the reaction. A limited number of charge transfer experiments involving molecular ions ($B_1^+ + B_2 \rightleftharpoons B_1 + B_2^+$) showed that reaction occurs at every collision in the forward (exothermic) direction and the reaction efficiency in the reverse (endothermic) direction is small but increases with increasing temperature.

JOHN ALFRED STONE, XIAOPING LI et PATRICIA ANNE TURNER. Can. J. Chem. **64**, 2021 (1986).

On a mesuré les affinités pour le proton (AP) de quelques composés aromatiques méthylés ainsi que les vitesses des réactions de transfert de proton, en utilisant la spectrométrie de masse à haute pression. Les équilibres étudiés sont de la forme $B_1H^+ + B_2 \rightleftharpoons B_1 + B_2H^+$. Les courbes de Van't Hoff donnent les valeurs suivantes des AP (kcal mol^{-1}) par rapport à celle de l'acétate d'éthyle = 200,7 utilisé comme standard : mésithylène = 201,0; tétraméthyl-1,2,3,5 benzène = 203,2; pentaméthylbenzène = 204,4; hexaméthylbenzène = 206,6. Les variations des nombres de symétrie rotationnelle ne déterminnent pas complètement les valeurs de ΔS^0 des équilibres de transfert du proton et on suggère que les changements dans la vibration et la torsion doivent être pris en considération. Le transfert du proton est lent dans la réaction directe (exothermique) et inverse (endothermique) et de plus dans tous les cas étudiés, à l'exception de la réaction la plus endothermique (tétraméthyl-1,2,3,5 benzène + hexaméthylbenzène protoné), les constantes de vitesse de transfert du proton augmentent lorsque la température diminue. On peut associer un tel comportement à l'allure de la courbe d'énergie potentielle en fonction de la progression de la réaction. Un nombre limité d'expériences de transfert de charges impliquant les ions moléculaires ($B_1^+ + B_2^+ \rightleftharpoons B_1 + B_2^+$) montre que la réaction se produit pour chaque collision dans la réaction directe (exothermique) et l'efficacité de la réaction inverse (endothermique) est faible, mais elle augmente quand la température augmente.

[Traduit par la revue]

Introduction

Many proton affinity (PA) values for neutral molecules have been obtained in the last fifteen years, usually by proton-transfer equilibrium techniques. The majority of the measurements have been made using either ion cyclotron resonance (icr) or pulsed electron beam, high pressure mass spectrometry (HPMS) (1). Icr is limited in temperature range and most measurements are made at an ambient temperature of about 320 K which is determined by the heating effect of an electron emitting filament. The pressures in icr studies are in the range 10^{-5}–10^{-6} Torr (1 Torr = 133 Pa). HPMS studies are usually conducted over a range of pressures (0.5–5 Torr) and a range of temperatures (300–600 K).

The equilibria studied by both techniques are of the form

[1] $$B_1H^+ + B_2 \rightleftharpoons B_1 + B_2H^+$$

B_1 and B_2 are gas phase bases. It is assumed that the measured equilibrium ion currents $i_{B_1H^+}$ and $i_{B_2H^+}$ are proportional to the respective ion concentrations and hence, knowing the ratio of neutral concentrations from the sample composition, the equilibrium constant K is obtained where K is defined as

[2] $$K = \frac{i_{B_2H^+}[B_1]}{i_{B_1H^+}[B_2]}$$

The standard free energy change at the temperature of measurement (T) is

[3] $$\Delta G^0 = -RT \ln K = \Delta H^0 - T\Delta S^0$$

ΔH^0, the standard enthalpy change for reaction [1] is, by definition, the difference in proton affinities of B_1 and B_2, i.e., $\Delta H^0 = PA(B_1) - PA(B_2)$ where PA(B) is ΔH^0 for the reaction

[4] $$BH^+ \rightarrow B + H^+$$

In icr studies, ΔH^0 must be obtained from ΔG^0 using calculated ΔS^0 values because the temperature range available is usually very small. The usual simplifying assumption made in such calculations is that only changes in rotational symmetry numbers (σ) are important and ΔS^0 is adequately approximated by (2)

[5] $$\Delta S^0 = R \ln \frac{\sigma_{B_1H^+}\sigma_{B_2}}{\sigma_{B_2H^+}\sigma_{B_1}}$$

This equation may not be adequate for some systems such as those in which internal rotations are lost or gained upon protonation and those for which there are significant changes in moments of inertia or vibrational frequencies (3).

Although HPMS does not suffer from a limited temperature range, the tendency of protonated bases to solvate at the high pressures employed requires that many equilibrium measurements be carried out at high temperature (often ~600 K) when solvation is minimal. For such studies the entropy changes must also be calculated and it is gratifying that low temperature icr and high temperature HPMS results using calculated entropies usually yield proton affinities in good agreement with each other.

Proton transfer equilibria can be studied over a large temperature range by HPMS only for systems in which solvation of ions is not a problem at lower temperatures. Such measurements have been made for benzene and halogenated benzenes using both HPMS (4, 5) and icr (6), the latter over a more limited temperature range. All the measured ΔS^0 values are in good agreement with each other and with the ones calculated from eq. [5] when "reasonable" assumptions are made regarding the sites of protonation. Some fairly small differences between experimental and calculated values were ascribed to the possibility of protonation at more than one site (5).

A recent investigation (7) has presented evidence for very large entropy changes in proton transfer equilibria involving monohalogenated toluenes. The idea of localized protonation sites was not sufficient to explain these values and the authors proposed that "dynamic" protonated structures may be present in certain of the systems (1,2- and 1,4-halotoluenes), the hydrogen atom being shared by two or more of the adjacent ring carbon atoms which bear no substituents. Such "dynamic" structures have been postulated to be present when aromatics are dissolved in super-acid media (8, 9).

When such "dynamic" structures are possible or when more than one protonation site is present in an aromatic base, it is not possible to check the adequacy of eq. [5] for aromatic compounds in particular and bases in general. This paper reports the results of a study of proton transfer equilibria involving some of the higher methylbenzenes, mesitylene to hexamethylbenzene, in which the sites of protonation should be unambiguous. The equilibria have been studied over as wide a temperature range as possible and in addition the rate constants for proton tranfer reactions in both forward and reverse directions have been measured. Since methane chemical ionization yields not only protonated methylbenzenes but also methylbenzene molecular ions, it has been possible in a few cases to also measure differences in ionization energies and rate constants for electron transfer.

Experimental

All experiments were carried out using the pulsed electron beam, high pressure ion source mass spectrometer which has been described in detail elsewhere (10). All the required compounds were available from commercial sources and were used without further purification. The 1,2,3,5-tetramethylbenzene (TMB) and 1,3,5-trimethylbenzene (MES) could have been contaminated with small amounts (<2 mol%) of structural isomers but since it was determined that both compounds were much more basic than any of their isomers, the presence of such impurities at these concentrations is not of significance. Pentamethylbenzene (PMB) and hexamethylbenzene (HMB) contain no structural isomers.

Samples of two bases were made up by weighing and where necessary were dissolved in benzene as solvent. The temperatures of the sample oven and its connecting line to the ion source were raised to 420 K to prevent problems with sample condensation. Most experiments were carried out at ion source pressures of 4–5 Torr, the bulk of the gas being methane.

Results and discussion

Methane chemical ionization spectra

The major ions in methane at pressures in the range 1–5 Torr are CH_5^+ and $C_2H_5^+$. Both react with aromatic hydrocarbons by proton transfer and $C_2H_5^+$ can also add to the aromatic ring (11). The chemical ionization (CI) spectra of alkyl aromatics (M) contain not only MH^+ and $MC_2H_5^+$ but also significant peaks due to $(M - 1)^+$ and M^+. As the number of alkyl groups on the ring increases the relative intensity of MH^+ decreases while that of $(M - 1)^+$ increases (12). We confirm these results and also find that the intensity of M^+, always small (less than 5% of the base peak), does increase slightly with an increase in the number of methyl groups on the aromatic ring. The origin of this ion is not known; its relative intensity appears to be independent of the concentration of aromatic.

In order to reduce the rate of positive ion diffusion to the ion source walls it was found advantageous to use an electron capture reagent to set up a positive–negative ion plasma rather than work with the positive ion – electron plasma formed by electron impact. The use of SF_6 yielded an enhanced ion signal and also considerably increased the average residence time of ions in the source. SF_6 was the agent of choice but its presence did affect the spectra by increasing the relative intensity of M^+, mainly at the expense of MH^+. In addition, benzene was used as solvent for PMB and HMB and this also affected the initial intensity ratios of $(M - 1)^+$, M^+, and MH^+.

SF_6 is rapidly protonated by CH_5^+ yielding SF_5^+

$$[6] \quad CH_5^+ + SF_6 \rightarrow CH_4 + (SF_6H^+)^*$$

$$[7] \quad (SF_6H^+)^* \rightarrow SF_5^+ + HF$$

The ionization energy of SF_5 is 10.5 eV (13) so that charge transfer to benzene (IP = 9.24 eV) and all the methylbenzenes (IP < 9.24 eV) (14) is exothermic. For example, TMB in CH_4 yields $(M - 1)^+$ (25%), M^+ (5%), and MH^+ (70%) at 464 K. These values are independent of ion source pressure (1–5.5 Torr) but $(M - 1)^+$ does increase slightly with increasing temperature. In the presence of 1 mol% SF_6, the spectrum changes to $(M - 1)^+$ (20%), M^+ (30%), and MH^+ (50%). $(M - 1)^+$ arises from protonation of a methyl substituent of the aromatic ring followed by loss of H_2. Benzene, having no methyl groups, yields no $(M - 1)^+$ peak and when present due to use as a solvent for the methylbenzenes, diminishes the $(M - 1)^+$ and increases the MH^+ intensity of the methylbenzenes. CH_5^+ reacts mainly with solvent C_6H_6 which is present in greater concentrations than the alkyl aromatics. Proton transfer from $C_6H_7^+$ to the methylbenzenes gives MH^+ in a process of much lower exothermicity than that involving CH_5^+ and protonation of methyl does not occur. For example HMB in benzene as solvent and in the presence of SF_6 yields $(M - 1)^+$ (2%), M^+ (11%), and MH^+ (87%) at 465 K. A typical CIMS spectrum is shown in Fig. 1.

Equilibrium measurements

Proton transfer was found to occur at less than the collision rate in all the methylbenzene binary mixtures studied. In order to achieve proton transfer equilibrium in the available ion residence time it was necessary to use relatively large concentrations of the alkyl benzenes in the ion source and this necessitated making up relatively high concentrations of these compounds in methane in the sample reservoir. The least volatile of the alkyl benzenes studied, HMB, is calculated to have a vapour pressure of ~0.9 Torr at 370 K (15) and in order to obtain a sufficient safety margin and prevent condensation in the reservoir and lines, the latter were kept at 420 K and the minimum ion source temperature employed was 370 K.

Figure 2 shows a typical plot of normalized ion intensity versus time for a mixture of HMB and PMB in methane at 601 K and 4.1 Torr. There are three pairs of ions to consider viz. $(M - 1)^+$, M^+, and MH^+ and in the figure both M^+ and MH^+ have been corrected for isotopic contributions from $(M - 1)^+$ and M^+, respectively.

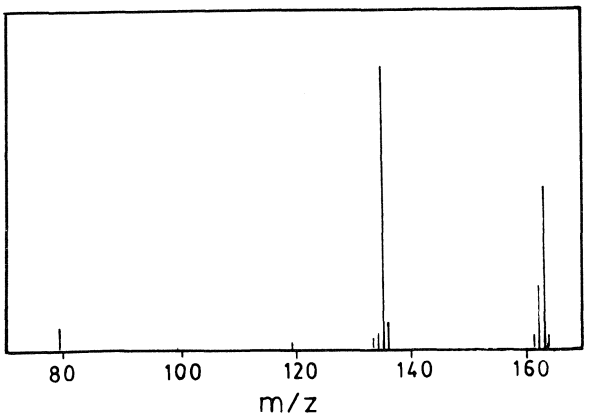

FIG. 1. Mass spectrum of TMB/HMB/SF_6/CH_4 ($1.7 \times 10^{-4}/3.6 \times 10^{-5}/10^{-3}/1$) at 4.22 Torr and 598 K. The major peaks and their m/z values are $C_6H_7^+$ (79), $TMBH^+$ (135), HMB^+ (162), $HMBH^+$ (163).

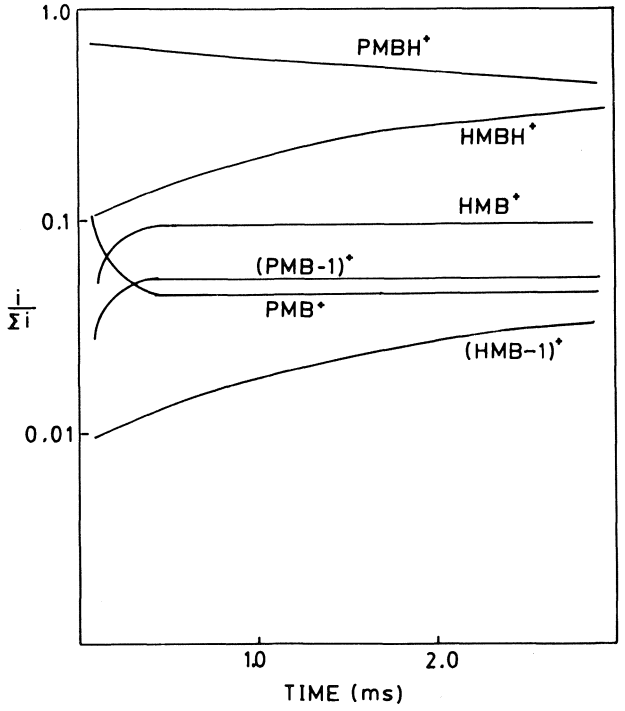

FIG. 2. Normalized ion intensities as functions of time after a 50 μs ionizing pulse of electrons for a mixture of composition PMB/HMB/C_6H_6/SF_6/CH_4 ($8 \times 10^{-4}/1 \times 10^{-4}/5 \times 10^{-3}/10^{-3}/1$) at 3.8 Torr and 602 K.

After a very short time (~0.5 ms) the normalized intensities of HMB^+ and PMB^+ are independent of time, suggesting that charge transfer equilibrium has been attained.

[8] $C_6H(CH_3)_5^+ + C_6(CH_3)_6 \rightleftharpoons C_6H(CH_3)_5 + C_6(CH_3)_6^+$

This was confirmed in the usual manner by determining that the calculated equilibrium constant K was independent of ion source pressure and of the ratio of concentrations of PMB and HMB.

$$[9] \quad K = \frac{[C_6(CH_3)_6^+][C_6H(CH_3)_5]}{[C_6H(CH_3)_5^+][C_6(CH_3)_6]} = \frac{i_{C_6(CH_3)_6^+}[C_6H(CH_3)_5]}{i_{C_6H(CH_3)_5^+}[C_6(CH_3)_6]}$$

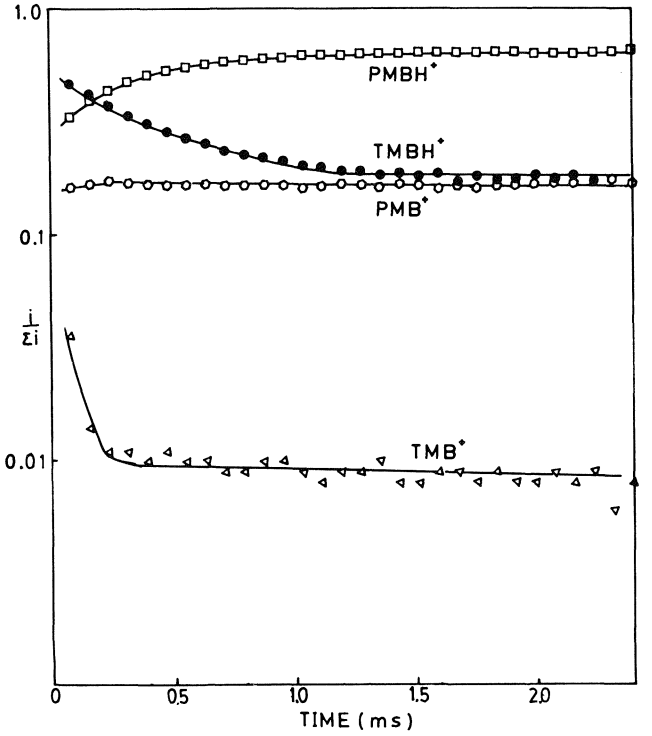

FIG. 3. Normalized ion intensities as functions of time after a 50 μs ionizing pulse of electrons for a mixture of TMB/PMB/C_6H_6/SF_6/CH_4 ($1.2 \times 10^{-4}/5.8 \times 10^{-4}/5 \times 10^{-3}/10^{-2}/1$) at 3.9 Torr and 586 K.

In the expression for K, i is a normalized ion current.

Although the M^+ ions in Fig. 2 rapidly come into equilibrium with each other, the $(M - 1)^+$ ion intensities are apparently approaching equilibrium values only at the longest time shown (3 ms), while the MH^+ ions are not in equilibrium even at this long time. $(M - 1)^+$ ions, because of their low intensity, were not studied further. Proton transfer equilibria could be studied by the judicious choice of relative and total ion-source concentrations of alkylbenzenes. Figure 3 shows one such run involving TMB and PMB when equilibrium (reaction [10]) is achieved after ~1.6 ms.

[10] $C_6H_3(CH_3)_4^+ + C_6H(CH_3)_5 \rightleftharpoons C_6H_2(CH_3)_4 + C_6H_2(CH_3)_5^+$

It is to be noted that the equilibrium between $(M - 1)^+$ ions is not shown and that the charge transfer reaction involving M^+ ions has essentially achieved equilibrium at all but the shortest recorded reaction time.

Equilibrium constants for equilibria of the form

[1] $B_1H^+ + B_2 \rightleftharpoons B_1 + B_2H^+$

were measured over the temperature range 400–600 K. The equilibrium constants at a given temperature were independent of both the ratios of base concentrations over at least a variation of a factor of five and of ion source pressures in the range 2–5 Torr.

A typical van't Hoff plot of ln K vs. $1/T$ is shown in Fig. 4. The slope of such a plot has the value $-\Delta H^0/R$ and the intercept yields $\Delta S^0/R$. The results obtained for the four methylbenzenes are shown in Table 1. In order to more securely tie the results to standard proton affinity tabulations, the equilibrium between MES and ethylacetate was examined and the resulting thermodynamic data for this equilibrium are also shown.

The internal consistency of the ladder of ΔH^0 values is very good and well within the experimental precision. These results

TABLE 1. Standard enthalpy and standard entropy changes for proton transfer

Compound	$-\Delta H^0$ (kcal mol^{-1})[a]	ΔS^0 (cal K^{-1} mol^{-1})[a]	proton affinity[b]
Hexamethylbenzene			206.6 (207.3)[d]
	2.10 ± 0.14[c]	1.84 ± 0.30 (4.92)[e]	
	3.49 ± 0.16	3.85 ± 0.35 (3.55)	
Pentamethylbenzene			204.4
	1.24 ± 0.13	1.28 ± 0.25 (−1.37)	
	3.54 ± 0.10	0.27 ± 0.21 (−2.17)	
1,2,3,5-Tetramethylbenzene			203.2
	2.20 ± 0.04	−1.07 ± 0.09 (−0.81)	
Mesitylene			201.0 (200.7)[d]
	0.35 ± 0.10	2.67 ± 0.20 (2.17)	
Ethylacetate			200.7 (200.7)[d]

[a]Obtained from experimental van't Hoff plots for the reaction $B_1H^+ + B_2 \rightleftharpoons B_1 + B_2H^+$. B_2 is above B_1 in the table.
[b]Proton affinity values are relative to PA(ethyl acetate) = 200.7 kcal mol^{-1}, evaluated in ref. 3.
[c]Uncertainty is one standard deviation from a linear least squares analysis.
[d]Evaluated data from ref. 3.
[e]Data in parentheses calculated from eq. [5] assuming all methyl carbons are in the plane of the aromatic ring.

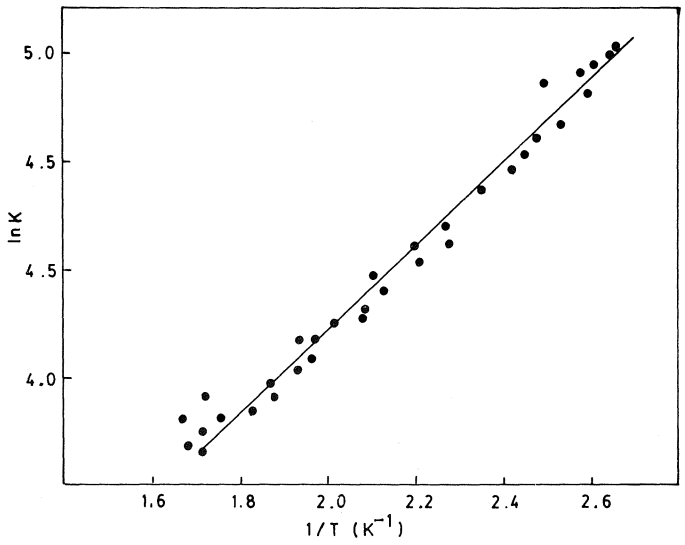

FIG. 4. The van't Hoff plot for the proton transfer equilibrium $MESH^+ + PMB \rightleftharpoons MES + PMBH^+$. A least-squares analysis yields $\Delta H^0 = -3.54 \pm 0.10$ kcal mol^{-1} and $\Delta S^0 = 0.27 \pm 0.21$ cal K^{-1} mol^{-1}.

confirm that proton affinity does increase with increase in the number of methyl groups on the aromatic ring. In the course of this work some experiments were performed with 1,2,4-trimethylbenzene and with 1,2,4,5- and 1,2,3,4-tetramethylbenzenes. We choose not to report the results of these experiments because the samples were impure and equilibria were not sufficiently clearly defined but we did find that, as for the isomeric xylenes (16), proton affinity is a function of both the number and the position of the methyl groups. Suffice to say, the proton affinity of 1,2,4-trimethylbenzene is ~2.4 kcal mol^{-1} less than that of MES and the above-mentioned tetramethylbenzenes have proton affinities lower than that of TMB.

The proton affinities of MES and HMB have been measured by Taft and co-workers; their values are cited in ref. 3. The measurements were made by icr techniques at a temperature which was initially stated to be 300 K but is to be corrected to 320 K. The corrected proton affinity difference obtained by Taft using a value of ΔS^0 calculated according to eq. [5] is PA(HMB) − PA(MES) = 6.15 kcal mol^{-1}. There is therefore good agreement with the value of 5.6 kcal mol^{-1} in Table 1.

Taft and co-workers (16) also suggested that the effects of methyl groups in stabilizing the proton on the ring depend on position and are additive and calculable since protonation always occurs at the most favourable site. For example, since the difference between the proton affinities of benzene and toluene is 7.6 kcal mol^{-1} and on the assumption that protonation occurs *para* to methyl, a *p*-methyl group is stabilizing to this extent. Similarly, since the proton affinity of *m*-xylene is 14.0 kcal mol^{-1} greater than that of benzene and the proton will be most effectively stabilized by one methyl at the *para* position and one at the *ortho* position relative to the site of protonation then an *o*-methyl stabilizes to the extent of 14.0 − 7.6 = 6.4 kcal mol^{-1}. Using data for *p*-xylene, it is readily shown that the stabilization afforded by a *m*-methyl is 2.6 kcal mol^{-1}. The stabilization afforded by an *ipso*-methyl was assigned a value of less than or equal to 1.2 kcal mol^{-1}, this value being based on calculation. In Table 2 we have used the upper limit of 1.2 kcal mol^{-1} in a comparison of experimental and calculated proton affinity values, all relative to benzene. For internal consistency the experimental result are referenced to PA(MES) being 19.4 kcal mol^{-1} greater than that of benzene (3).

The calculated results are all slightly higher than the experimental values by 1–1.7 kcal mol^{-1}. The calculated order of PA values is certainly in agreement with experiment and the additivity principle is certainly a reasonable method for the prediction of proton affinities of the methylbenzenes. It is also to be noted that the PA values which may be calculated but which

TABLE 2. Experimental and estimated proton affinities relative to benzene

Compound	Δ(PA)(expt)	Δ(PA)(est)[a]
Hexamethylbenzene	25.1	26.8
Pentamethylbenzene	24.9	25.6
Tetramethylbenzene	21.6	23.0
Mesitylene	19.4[b]	20.4

[a]Estimated as described in text.
[b]PA(mesitylene) − PA(benzene) = 19.4 kcal mol^{-1} from ref. 3.

are not shown, for 1,2,3,4- and 1,2,4,5-tetramethylbenzene correctly predict values lower than that of TMB while 1,2,4-trimethylbenzene is correctly predicted to have a lower PA value than that of MES.

PA(HMB) − PA(PMB) = 2.2 kcal mol^{-1} shows a significant stabilization afforded by an *ipso*-methyl. Protonation of HMB to give a localized, tetrahedral $HCCH_3$ group, for which nmr evidence has been found at 190 K in super acids, leads to a distorted structure (8). At higher temperature the nmr studies suggested that there was a rapid H transfer amongst ring positions so that all sites became equivalent. Later studies confirmed this finding (9). Protonation of PMB in HF/BF_3 yielded only one isomeric $C_6(CH_3)_5H_2^+$ at temperatures from 213 to 293 K. This showed that the added proton is indeed localized at the only available C—H site yielding what is essentially a methylene group with charge delocalization over the rest of the ring (18). These studies suggest that the basicity of a ring carbon is considerably decreased by a CH_3 substituent and that the favoured sites of protonation will always be unsubstituted ones. Fernandez, Jennings, and Mason have taken this idea one step further and produced some evidence that "dynamic" ion structures are present in the gas phase (7). They found anomalously high entropy changes for proton transfer reactions involving, 1,2 and 1,4 halotoluene isomers, the extreme example cited being a value of −13.4 cal K^{-1} mol^{-1} for transfer from *p*-chlorotoluene to *o*-fluorotoluene. This value is to be compared with the value of −1.4 cal K^{-1} mol^{-1} calculated from rotational symmetry changes. They suggest that for the 1,4 compound in particular, no available (i.e. unsubstituted) protonation site is strongly favoured over any other and that there are relatively high energy barriers at the unfavoured carbon atoms. The low energy barrier between adjacent unsubstituted sites allows "internal translation" of H and hence a substantial decrease in entropy when this translational mode is lost.

Should such internal translation effects be expected in the present study? Each of MES, TMB, and PMB has only one type of preferred site for protonation and in TMB and MES in which there are respectively two and three equivalent sites, these sites are separated by unfavoured sites. HMB has six equivalent sites and it could be argued that internal translation should therefore be facile and anomalous entropy effects should be observed. Alternatively, it could be argued that the H should be localized since the adjacent methyls block movement from the site of protonation. Table 1 confirms that there are no anomalously high values of ΔS^0 for any of the equilibria studied and therefore that hydrogen translation is not a factor in these systems. Moreover, if "internal translation" can occur then it should surely be most improtant for benzene. However, we known of no experimental results showing anomalous entropy effects in proton transfer equilibria involving this molecule.

The ladder of standard entropy differences is internally self consistent and in some cases the ΔS^0 values are reasonably close to those calculated using rotational symmetry numbers (eq. [5]). Symmetry numbers were chosen using the assumption that all methyl group are in the plane of the aromatic ring except when an *ipso* H is present ($HMBH^+$). The precision quoted for the experimental results is one standard deviation and even allowing for this optimistic precision it is seen that some results (e.g. $MESH^+$ + PMB) are not adequately described by eq. [5]. The applicability of non-planar structures was considered since calculation has shown that in HMB alternate methyls are slightly above and below the ring which is also slightly puckered (19). Such puckering probably occurs whenever there are adjacent methyls. The agreement between experimental and calculated ΔS^0 values was even poorer when such distorted structures were used.

TABLE 3. Enthalpy and entropy changes for the charge transfer reaction $B_1^+ + B_2 \rightleftharpoons B_1 + B_2^+$

B_1	B_2	$-\Delta H^0$ (kcal mol^{-1})	$-\Delta S^0$ (cal K^{-1} mol^{-1})	Δ(IP)[a] (kcal mol^{-1})
TMB	HMB	6.6 ± 1.0	1.4 ± 2.2	10.6
PMB	HMB	4.1 ± 0.2	1.0 ± 0.3	6.7

[a]Calculated difference in ionization energy from ref. 14.

The total entropy change, ΔS^0, in a proton transfer reaction has four contributions if the proton is always localized at the most favourable site and "internal translation" need not be considered

$$[11] \quad \Delta S^0 = \Delta S^0_{elec} + \Delta S^0_{vib} + \Delta S^0_{rot} + \Delta S^0_{trans}$$

ΔS^0_{elec} is zero for the reactions studied and the calculated ΔS^0_{trans} is negligibly small for these relatively massive molecules. The addition of a proton to any of the molecules leads to only small geometry changes and will not significantly change the moments of inertia; ΔS^0_{rot} will therefore be given by eq. [5]. The differences between the experimental entropies and calculated ΔS^0_{rot} values must therefore be due to non-zero values of ΔS^0_{vib}. The methylbenzenes with adjacent methyl groups will, like HMB (19), have some low frequency torsional and puckering modes which are strongly coupled in the neutral molecule and which will be altered upon protonation when tetrahedral geometry is approximated at one of the ring carbons. Insufficient information is available to prove that the resulting changes in vibrational frequencies together with rotational symmetry number changes do indeed account for the entropy charges observed. It is apparent, however, that calculations of ΔS^0 for the methylbenzenes using eq. [5] above are not adequate.

Data for charge transfer are in Table 3. There are insufficient results to obtain good thermodynamic data since, as noted before, the reactions were very fast and precision was not as good as for proton transfer. The two ΔH^0 values obtained correspond to the difference in vertical ionization energies between PMB and HMB and between TMB and HMB. The ionization potentials for the higher methylbenzenes are not known with precision. Calculation suggests that the ionization energy decreases linearly with the number of methyl groups on the ring, with energy differences of 10.6 kcal mol^{-1} between PMB and HMB and 6.7 kcal mol^{-1} between TMB and PMD (14). These values are almost a factor of two greater than the present ones. We are carrying out further experiments on these charge transfer reactions to determine whether these initial values are reliable.

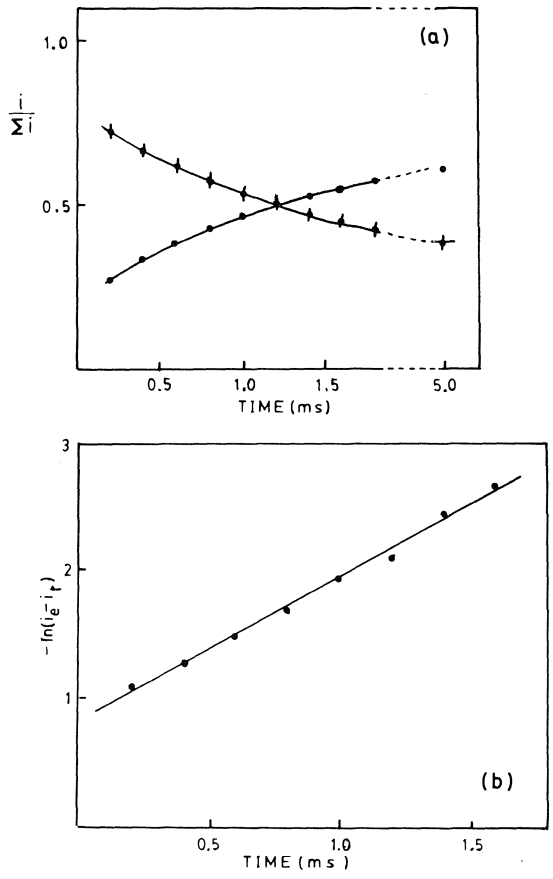

FIG. 5. Kinetic data for the proton transfer reaction $TMBH^+ + PMB \rightleftharpoons TMB + PMBH^+$ at 571 K and an ion source pressure of 3.99 Torr: (*a*) The normalized ion intensities ● $TMBH^+$, ● $PMBH^+$; (*b*) kinetic data plotted according to eq. [14]. Sample composition $TMB/PMB/C_6H_6/CH_4$ ($2.9 \times 10^{-4}/1.8 \times 10^{-4}/5 \times 10^{-3}/10^{-2}/1$).

The kinetics of proton and charge transfer

Proton transfer between the methylaromatics was found to be slow, especially at the higher temperatures. Such was not the case for charge transfer involving the molecular ions which were generated mainly by electron transfer to SF_5^+. The kinetics of charge transfer between the aromatics was studied, when possible, under experimental conditions which were optimized for proton transfer studies. In such circumstances charge transfer equilibrium was often set up too rapidly for meaningful kinetic data to be obtained since relatively high concentrations of the aromatics were used in the proton transfer studies.

Rate constants for proton transfer

Both the forward and reverse rate constants were determined for proton transfer reactions of the form of reaction [1]. A typical graph of the pertinent normalized data for such a system is shown in Fig. 5*a* for the reaction

$$[12] \quad TMBH^+ + PMB \underset{k_-}{\overset{k_+}{\rightleftharpoons}} TMB + PMBH^+$$

Since the concentrations of PMB and TMB are very much greater than those of $TMBH^+$ and $PMBH^+$ they remain constant and the reaction may be written as a reversible reaction which is first order in each direction

$$[13] \quad TMBH^+ \underset{k_-'}{\overset{k_+'}{\rightleftharpoons}} PMBH^+$$

where $k_+' = k_+[PMB]$ and $k_-' = k_-[TMB]$. This form is treated by the standard method for reversible first order reactions (20) to yield the integrated form

$$[14] \quad \ln \frac{i_e - i_0}{i_e - i_t} = -(k_+' + k_-')t$$

where i_e, i_0, and i_t are respectively the normalized $TMBH^+$ or $PMBH^+$ ion currents at equilibrium and at times zero and t. The approach to equilibrium is a first order process with pseudo rate constant $(k_+' + k_-')$. Since the equilibrium constant is equal to k_+'/k_-' then each of k_+' and k_-' may be determined and from the known concentrations of neutrals in the ion source, k_+ and k_- may be calculated. Figure 5*b* shows the linear plot of $-\ln(i_e - i_t)$ against t for the data in 5*a* which has slope $(k_+' + k_-')$. Such an analysis was also carried out for the charge transfer reactions when data were available. The results from this method of deriving rate constants were compared with those from the more usual method which employs the slope of the linear decay obtained from a plot of the logarithm of the normalized ion intensity versus time e.g. for reaction [12].

$$[15] \quad \frac{i_t}{i_0} = -k_+[PMB]t = -k_+'t$$

This method could only be applied satisfactorily to the fastest, most exothermic proton transfer reactions under conditions when the reverse reactions were not significant. The results obtained by the two methods are in reasonable agreement. For the TMB/PMB system for which the measured exothermicity is low ($\Delta H^0 = -1.24$ kcal mol^{-1}) the back reaction was obviously of significance and the linear decay method yielded somewhat lower values.

The results obtained for the five systems studied are shown in Figs. 6–10 in which reaction efficiency is plotted against the logarithm of the absolute temperature. The reaction efficiency is defined as k/k_c where k is the measured rate constant and k_c is the rate constant for collision as calculated by the Average Dipole Orientation (ADO) theory of Su and Bowers (21). The proton transfer reactions under study involve molecules with quite large polarizabilities and very small or no dipole moments. k_c values are therefore all in the range 1.15–1.28×10^{-9} cm^3 molecule^{-1} s^{-1} with very little temperature dependence.

Several generalizations can be made regarding these kinetic results. The difference between the forward and the reverse rate constants is greatest for the reactions with highest exothermicity as expected, since

$$\frac{k_+}{k_-} = K = \exp\left[-\frac{\Delta G^0}{RT}\right]$$

and ΔG^0 is roughly proportional to ΔH^0 when ΔS^0 is small. In no case is proton transfer efficient, the maximum reaction efficiencies in the forward direction being for the two most exothermic reactions at the lowest temperature employed. All reactions, both forward and reverse, with the exception of $TMBH^+ + HMB$, show a negative coefficient of reactivity, i.e., the rate constant increases with decrease of temperature. The plots of log k vs. log T are linear as are plots of ln k vs. $1/T$. The latter Arrhenius type plots yield small (~2 kcal mol^{-1}) negative "activation" energies, the one exception being $TMBH^+ + HMB$ with a positive activation energy of 0.76 kcal mol^{-1}. The efficiencies of proton transfer at 400 K and 600 K are plotted against the overall change in free energy for reaction, ΔG^0, in Fig. 11. The two curves are

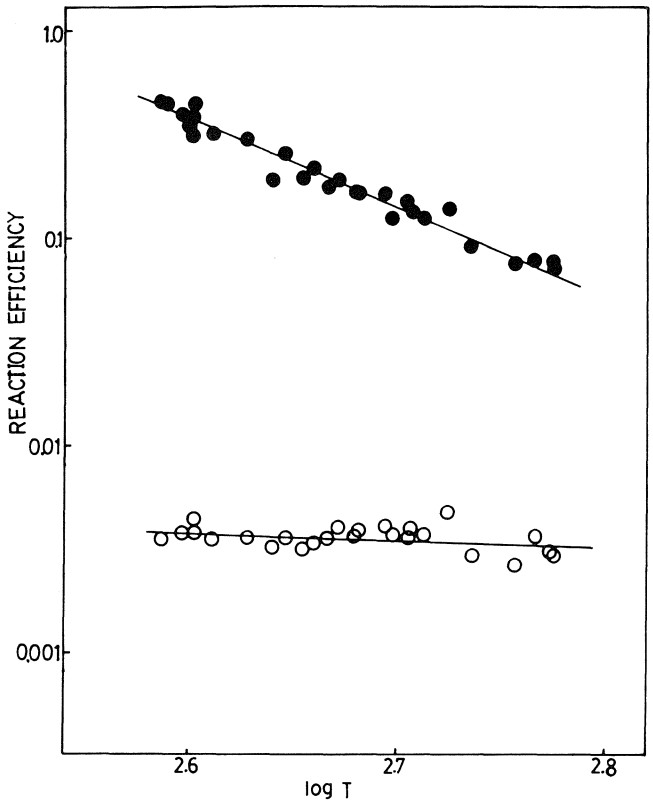

FIG. 6. The variation of reaction efficiency with temperature for the reaction $MESH^+ + PMB \rightleftharpoons PMBH^+ + MES$. ● Forward reaction, ○ reverse reaction.

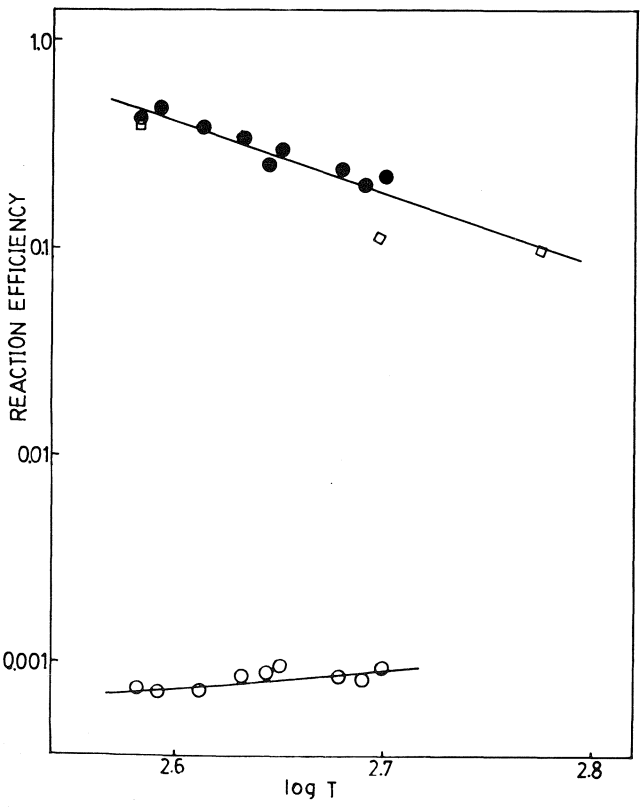

FIG. 7. The variation of reaction efficiency with temperature for the reaction $TMBH^+ + HMB \rightleftharpoons HMBH^+ + TMB$. ● Forward reaction, ○ reverse reaction, □ forward reaction determined using eq. [15].

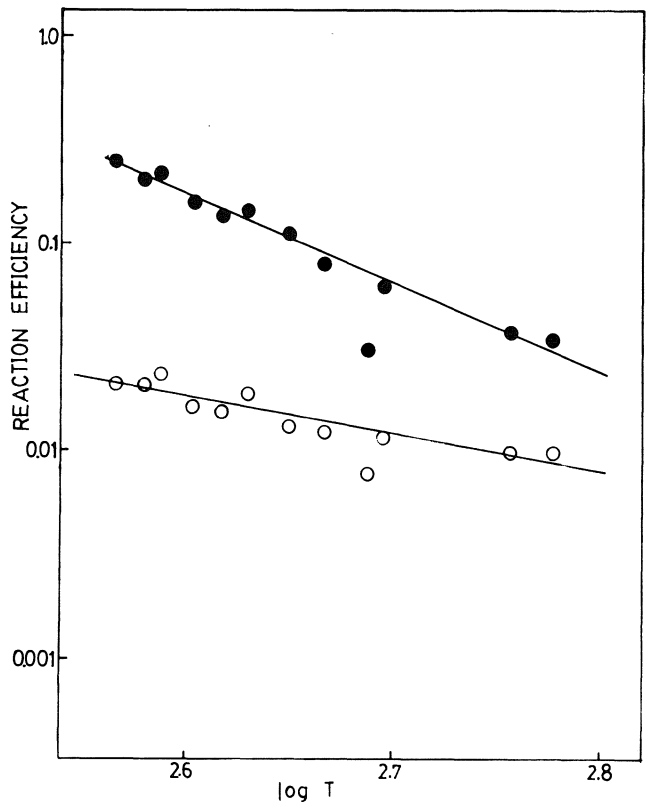

FIG. 8. The variation of reaction efficiency with temperature for the reaction $MESH^+ + TMB \rightleftharpoons TMBH^+ + MES$. ● Forward reaction, ○ reverse reaction.

similar to the one obtained at 298 K by Bohme and co-workers (22) for a series of proton transfer reactions encompassing a much wider range of ΔG^0 in the negative direction and approximately the same range in the positive direction. They found that the reactions were 100% efficient when $\Delta G^0 \leqq -10$ kcal mol^{-1}. We have no data for 298 K but extrapolation of the plots of log (k_f/k_c) vs. log T to log 298 for the two most exothermic reactions yields efficiencies very close to unity. Obviously efficiency will not be unity at higher temperatures until ΔG^0 is considerably more negative than the values for any of the reactions studied in this work. Figure 11 emphasizes that a positive temperature coefficient of reaction efficiency (k/k_c increasing with increasing temperature) occurs only when ΔG^0 (and ΔH^0) is significantly positive.

Slow, exothermic proton transfer reactions have been described by Brauman and co-workers (23, 24) and Meot-Ner (25). The latter demonstrated negative temperature coefficients for the forward (exothermic) rate constants. Kebarle (26) has succinctly outlined the basic types of reactions in which such behaviour should be observed and has discussed briefly the theory of such reactions. Central to the theory is a model involving the formation of an ion–molecule collision complex which is sufficiently long-lived that its energy is completely randomized over all accessible levels. The total energy includes the excitation energy generated by the ion–molecule interactions. The inefficiency of the reactions is due to the rate of dissociation of the excited complex to regenerate reactants being greater than chemical reorganization to give products. The explanation for this behaviour is based on the shape of the potential energy profile along the reaction coordinate. In order to make quantitative predictions about such reactions this profile and the characteristics of the complex at pertinent points on the

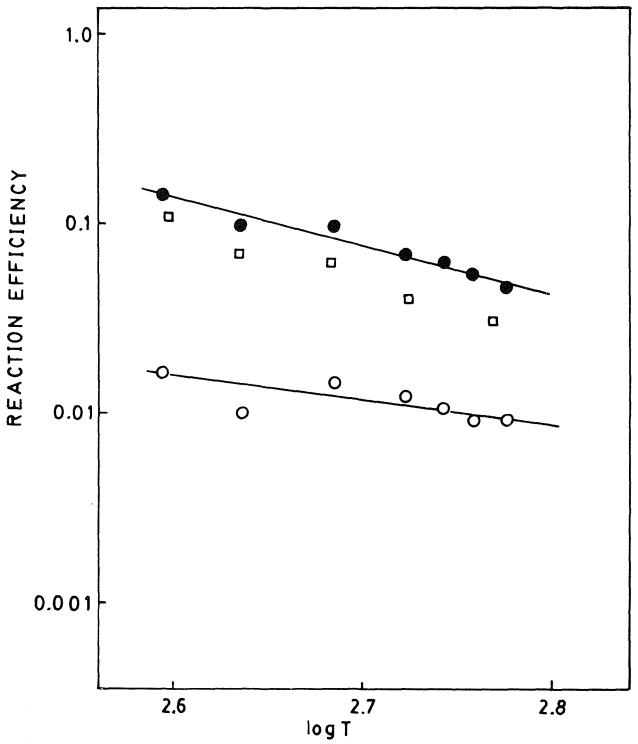

FIG. 9. The variation of reaction efficiency with temperature for the reaction $MESH^+ + TMB \rightleftharpoons TMBH^+ + MES$. ● Forward reaction, ○ reverse reaction, □ forward reaction determined using eq. [15].

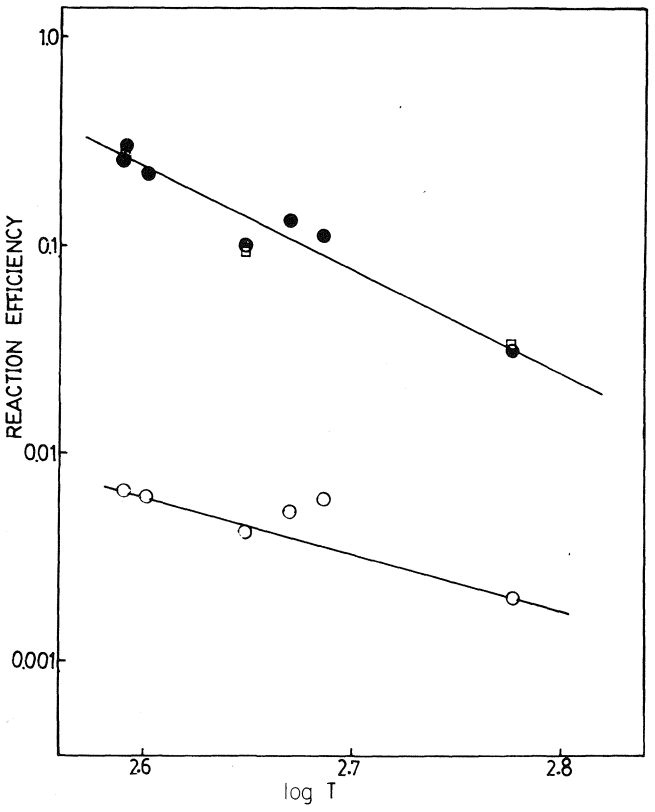

FIG. 10. The variation of reaction efficiency with temperature for the reaction $PMBH^+ + HMB \rightleftharpoons HMBH^+ + PMB$. ● Forward reaction, ○ reverse reaction, □ forward reaction determined using eq. [15].

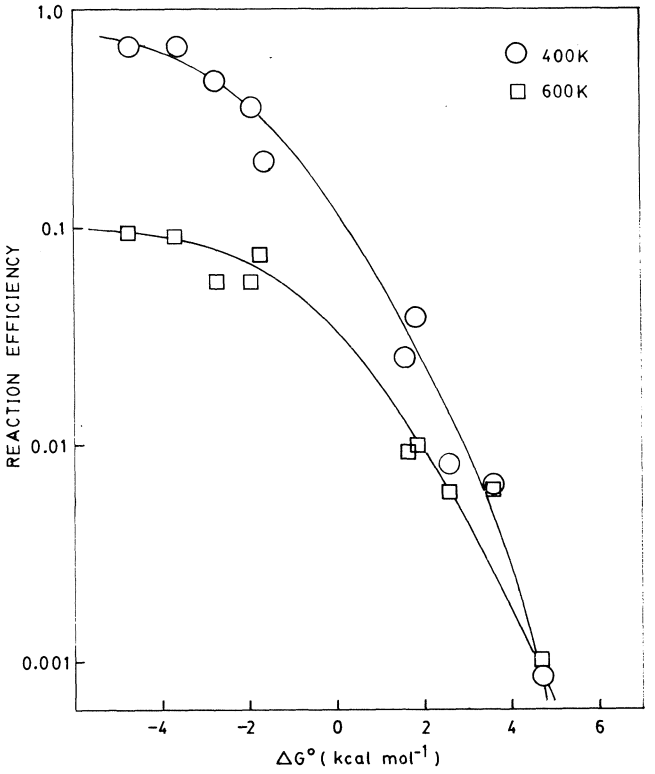

FIG. 11. The variation of reaction efficiency with standard free energy change for proton transfer reactions.

profile must be known. Since the reactions under study involve relatively complex ions and molecules whose mode of association is not known, only qualitative arguments in support of the proposed reaction mechanism can be made.

The potential energy profile along the reaction coordinate (Fig. 12) is for the generalized proton transfer reaction.

[16] $B_1H^+ + B_2 \rightleftharpoons B_1H^+\cdots B_2 \rightleftharpoons B_1\cdots{}^+HB_2 \rightleftharpoons B_1 + HB_2^+$

The two potential wells correspond to the two ion–neutral association complexes $B_1H^+\cdots B_2$ and $B_1\cdots{}^+HB_2$. The central maximum corresponds to a chemical transition state of the form $B_1\cdots\overset{+}{H}\cdots B_2$ for the proton transfer step. Although the potential profile cannot be described with any exactitude, its qualitative features are known. The ions involved, protonated aromatics, have considerable charge delocalization and indeed the CH_2 or $CHCH_3$ group formed by the addition of a proton to the aromatic ring will have some tetrahedral character with little of the charge present at this site (27, 28). There will be a significant fraction of the charge on the methyl groups as was calculated for the toluenium ion (27). This charge delocalization will lead to a very low stability for the ion-molecule association complexes, i.e., both potential wells are very shallow. No stabilized complexes ($B_1\cdots HB_2^+$ or $B_2\cdots HB_1^+$) were observed with these protonated aromatics, even at temperature as low as 298 K. An enthalpy of dissociation of 11.0 kcal mol^{-1} has been reported for $C_6H_7^+\cdot C_6H_6$ which suggested that in such aromatic dimers the binding is purely electrostatic (29). The association complexes formed in the present case will probably be more weakly bound since the methyl groups will inhibit close approach of ion and neutral and negate the increased polarizability due to methyl groups. The geometry of the entities $B_1H^+\cdots B_2$ and $B_1\cdots HB_2^+$ are open to conjecture. If the charge remains delocalized over much of the ion then although the maximum

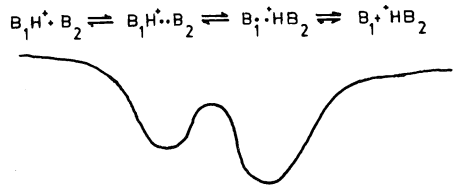

FIG. 12. The reaction coordinate for proton transfer between polymethyl aromatics.

polarizability of aromatic molecules is in the plane of the ring (30), the maximum electrostatic interaction energy will be obtained if the aromatic rings can form a sandwich even though the methyl groups will sterically hinder anything but a very loose association. Interaction of the two rings via a proton bridge would lead to loss of charge delocalization on one ring with little compensating stabilizing delocalization on the other. Such a geometry, although not likely for $B_1 \cdots {}^+HB_2$, would of necessity be the transition state for proton transfer. The proton is probably transferred via a transition state involving interaction with the π orbitals of the rings. A π complex has been suggested as the transition state for intramolecular proton transfer with a calculated activation energy of 8 kcal mol^{-1} (28). The central ptoential barrier in Fig. 12 corresponds to the activation barrier for transfer of a proton, from an essentially sp^3 carbon in $B_1H^+ \cdots B_2$ via the π bound state $B_1 \cdots \overset{+}{H} \cdots B_2$. The height of the barrier will probably be less than that for intramolecular transfer because of the participation of the second aromatic ring but the zero point energies associated with the new vibrations or severely hindered methyl rotations replacing free rotations will increase the fixed energy and raise the energy level of the reaction coordinate at the barrier maximum.

Proton transfer between the methyl benzenes satisfies more than one of the criteria for slow proton transfer, viz., very low exothermicity, a decrease of rotational freedom on complex formation, and a central chemical barrier (26). The initially formed chemically activated complexes, in both the forward direction, $(R_1H^+ \cdots R_2)$, and the reverse direction, $(R_1 \cdots {}^+HR_2)$ may either cross the central barrier or return to reactants by crossing the centrifugal barrier. The much higher density of states of the complex at the latter barrier favours dissociation to the reactants. Increasing temperature increases the importance of this density of states relative to those at the central barrier and hence the rate constants show a negative temperature dependence. This is also apparently true in the endothermic direction as well for all but one ion–molecule reactant pair. This is one of the two most endothermic reactions, viz. TMB + $PMBH^+$, the other, MES + $PMBH^+$ having only a very slightly negative temperature dependence. For TMB + $HMBH^+$ the activation energy, obtained from an Arrhenius plot is 0.76 kcal mol^{-1}, a value considerably lower than the measured enthalpy change for the reaction (3.5 kcal mol^{-1}). It is obvious from these results that an endothermic reaction does not necessarily have a rate constant which increases with increasing temperature, when the endothermicity is small the shape of the potential energy profile is equally important.

The two forward (exothermic) charge transfer reactions studied are more exothermic than the corresponding proton transfer reactions involving the same neutrals and all proceed with close to 100% efficiency and with very little if any, temperature dependence. This is in accord with the results of Meot-Ner and Field using a variety of lower alkylbenzenes (17). The two reverse reactions show a normal, positive temperature dependence, i.e., the rate increases with increasing temperatures. Since electron transfer can occur over a much greater distance than proton transfer, a long-lived complex is not necessary and considerations applied to the proton transfer reactions are not appropriate to charge transfer. The data are typical of fast charge transfer reactions which lends credence to the validity of the proton transfer data.

Conclusions

The relative basicities of methylbenzenes increase with increasing number of methyl groups. The relative proton affinities determined using van't Hoff plots are not in agreement with those obtained using calculated entropy differences based only on changes in rotational symmetry numbers. Although such calculations are usually found to be adequate for less complex bases, the results obtained here suggest that acceptable calculated ΔS^0 values will only be obtained when changes in molecular vibrational levels and the coupled methyl torsional levels are included.

The measured rate constants show that proton transfer is inefficient except at low temperatures and when ΔG^0 is negative by $\geqq 4$ kcal mol^{-1}. A negative temperature coefficient of the reaction efficiency is observed for both the exothermic forward direction and the endothermic reverse direction. There is only one exception to the latter; the most endothermic reaction studied (TMB + $HMBH^+$) shows a slight positive temperature coefficient. Such behaviour in near thermoneutral proton transfer reactions may not be exceptional and we are presently investigating whether it is the rule rather than the exception.

Acknowledgement

The authors thank the Natural Sciences and Engineering Research Council of Canada for financial assistance.

1. D. H. AUE and M. T. BOWERS. *In* Gas phase ion chemistry. Vol. 2. *Edited by* M. T. Bowers. Academic Press, New York. 1979. p. 1.
2. P. KEBARLE. Ann. Rev. Phys. Chem. **28**, 445 (1977).
3. S. G. LIAS, J. F. LIEBMAN, and R. D. LEVIN. J. Phys. Chem. Ref. Data, **132**, 695 (1984).
4. Y. K. LAU and P. KEBARLE. J. Am. Chem. Soc. **98**, 7452 (1976).
5. D. K. BOHME, J. A. STONE, R. S. MASON, R. S. STRADLING, and K. R. JENNINGS. Int. J. Mass Spec. Ion. Phys. **37**, 283 (1981).
6. K. G. HARTMANN and S. G. LIAS. Int. J. Mass Spec. Ion Phys. **28**, 213 (1978).
7. M. T. FERNANDEZ, K. R. JENNINGS, and R. S. MASON. Presented at 33rd Annual Conference on Mass Spectrometry and Allied Topics. San Diego. 1985.
8. G. A. OLAH, R. H. SCHLOSBERG, R. D. PORTER, Y. K. MO, D. P. KELLY, and G. D. MATEESAU. J. Am. Chem. Soc. **94**, 2034 (1972).
9. D. FARCASIU. Acc. Chem. Res. **15**, 46 (1982).
10. J. A. STONE and D. E. SPLINTER. Can. J. Chem. **59**, 1779 (1981).
11. A. G. HARRISON. Chemical ionization mass spectrometry. C.R.C. Press Inc., Boca Raton. 1982.
12. K. ISEDA. Bull. Chem. Soc. Jpn. **51**, 2167 (1978).
13. L. M. BABCOCK and G. E. STREIT. J. Chem. Phys. **74**, 5700 (1981).
14. E. HEILBRONNER and J. P. MAIER. *In* Electron spectroscopy, theory, technique and application. V1. *Edited by* C. R. Brundle and A. D. Baker. Academic Press, London. 1977.
15. D. AMBROSE, I. J. LAWRENSEN, and C. H. S. SPRAKE. J. Chem. Thermodyn. **8**, 503 (1976).
16. J. L. DEVLIN, J. F. WOLF, R. W. TAFT, and W. J. HEHRE. J. Am. Chem. Soc. **98**, 1990 (1976).

17. M. MEOT-NER and F. H. FIELD. Chem. Phys. Lett. **44**, 484 (1976).
18. D. M. BROUWER, E. L. MACKOR, and C. MACLEAN. Rec. Trav. Chim. **84**, 1564 (1985).
19. V. MELISSAS, K. FAEGRI, and J. ALMLOF. J. Am. Chem. Soc. **107**, 4640 (1985).
20. J. W. MOORE and R. G. PEARSON. Kinetics and mechanism. 3rd ed. John Wiley and Sons, New York. 1981.
21. T. SU and M. T. BOWERS. Int. J. Mass Spectrom. Ion Phys. **17**, 211 (1975).
22. D. K. BOHME, G. I. MACKAY, and H. I. SCHIFF. J. Chem. Phys. **73**, 4976 (1980).
23. W. E. FARNETH and J. I. BRAUMAN. J. Am. Chem. Soc. **98**, 7891 (1976).
24. J. M. JASINSKI and J. I. BRAUMAN. J. Am. Chem. Soc. **102**, 2906 (1980).
25. M. MEOT-NER. Presented at 30th Annual Conference on Mass Spectrometry and Allied Topics; Honolulu 1982.
26. P. KEBARLE. *In* Ionic processes in the gas phase. *Edited by* M. A. Almoster-Ferreira. NATO ASI Series V 118. 1984.
27. W. C. ERMLER and R. S. MULLIKEN. J. Am. Chem. Soc. **100**, 1647 (1978).
28. T. SORDO, J. BERTRAN, and E. CANADELL. J. Chem. Soc. Perkin 2, 1486 (1979).
29. M. MEOT-NER, P. HAMLET, E. P. HUNTER, and F. H. FIELD. J. Am. Chem. Soc. **100**, 5466 (1978).
30. M. J. ARONEY, H. H. HUANG, R. J. W. LEFEBRE, and G. L. D. RITCHIE. J. Chem. Soc. B, 416 (1966).

Janovsky reactions between cyclopentadienyliron complexes of substituted benzenes and carbanions derived from ketones[1]

RONALD G. SUTHERLAND, RATAN L. CHOWDHURY, ADAM PIÓRKO, AND CHOI CHUCK LEE
Department of Chemistry, University of Saskatchewan, Saskatoon, Sask., Canada S7N 0W0

Received December 20, 1985

RONALD G. SUTHERLAND, RATAN L. CHOWDHURY, ADAM PIÓRKO, and CHOI CHUCK LEE. Can. J. Chem. **64**, 2031 (1986).

Janovsky reactions were carried out between various η^6-substituted benzene-η^5-cyclopentadienyliron cations containing at least one electron-withdrawing substituent in the complexed arene and the enolate-carbanion derived from acetone, butanone, or 3-pentanone. Highly colored adducts were obtained from reactions of the cyclopentadienyliron (CpFe) complexes of nitrobenzene, cyanobenzene, *p*-tolylsulfonylbenzene, benzoylbenzene, *o*-, *p*-, or *m*-nitrotoluene, and *o*-, *p*-, or *m*-dichlorobenzene with acetone in aqueous KOH, the products being derived from *exo*-addition of the acetonyl anion regioselectively at a position *ortho* to an electron-withdrawing substituent. For example, reaction of the η^6-nitrobenzene-η^5-cyclopentadienyliron cation (**1***a*) with acetone in aqueous KOH gave (*R*,*S*)-(1-5-η^5-1-nitro-6-*exo*-(2-oxo-1-propyl)-cyclohexadienyl)(η^5-cyclopentadienyl)iron (**2***a*), isolated as a purple solid. Similarly, reaction of the nitrobenzene complex **1***a* with 3-pentanone in aqueous KOH gave two diastereomeric adducts, (*R*,*R*-*S*,*S*)- and (*R*,*S*-*S*,*R*)-(1-5-η^5-1-nitro-6-*exo*-(3-oxo-2-pentyl)-cyclohexadienyl)(η^5-cyclopentadienyl)iron (**11***a*, *b*). Reactions of the CpFe complexes of chlorobenzene and *o*- or *p*-dichlorobenzene with butanone in aqueous KOH were also investigated. In each case, three Janovsky adducts, two being diastereomers, were obtained from addition of the two carbanions derived from loss of either α-proton of butanone. Potential synthetic applications via these Janovsky adducts are pointed out since their treatment with ammonium ceric nitrate could lead to demetallation–oxidation; for example, (2,5-dichlorophenyl)propanone, a new compound, was obtained from the adduct formed between the *p*-dichlorobenzene complex and the acetonyl anion.

RONALD G. SUTHERLAND, RATAN L. CHOWDHURY, ADAM PIÓRKO et CHOI CHUCK LEE. Can. J. Chem. **64**, 2031 (1986).

On a effectué la réaction de Janovsky entre divers cations benzène η^6-substitués cyclopentadiényl-η^5 de fer contenant au moins un substituant électro-attracteur dans le complexe arène et les carbanions énoliques dérivés de l'acétone, de la butanone ou de la pentanone-3. On obtient des adduits fortement lors des réactions des complexes cyclopentadiényles de fer (CpFe) et du nitrobenzène, du cyanobenzène, du *p*-tolylsulfonylbenzène, du benzoylbenzène des *o*-, *p*- ou *m*-nitrotoluène et des *o*-, *p*- ou *m*-dichlorobenzène avec l'acétone dans du KOH aqueux. Les produits proviennent d'une addition *exo* régiosélective de l'anion acétonyle en position *ortho* d'un substituant électro-attracteur. Par exemple, la réaction du cation nitro-η^6 benzènecyclopentadiényle-η^5 de fer (**1***a*) avec l'acétone dans du KOH aqueux donne du (nitro-1 (oxo-2 propyl-1)-*exo*-6 cyclohexadienyl-η^5-1,5) (cyclopentadiényl-η^5) de fer (*R*,*S*) (**2***a*) qui a été isolé sous la forme d'un solide de couleur pourpre. Le complexe **1***a* du nitrobenzène réagit de la même façon avec la pentanone-3 dans du KOH aqueux pour donner deux adduits diastéréoisomères soit les nitro-1 (oxo-3 pentyl-2)-*exo*-6 (cyclohexadiényl-η^5-1,5) (cyclopentadiényl-η^5) de fer (*R*,*R*-*S*,*S*) et (*R*,*S*-*S*,*R*) (**11***a*, *b*). On a également étudié les réactions des complexes de CpFe du chlorobenzène et du *o*- ou du *p*-dichlorobenzène avec la butanone dans du KOH aqueux. Dans chaque cas, on obtient trois adduits de Janovsky, dont deux sont des diastéréoisomères, qui proviennent de l'addition de deux carbanions provenant de la perte de l'un des protons en α de la butanone. On met en évidence les possibilités de synthèse à partir des adduits de Janovsky puisque leur réaction avec le nitrate d'ammonium cérique peut conduire à une démétallation oxydante. Par exemple, on obtient la (dichloro-2,5 phényl)propanone, un nouveau composé, à partir de l'adduit formé entre le complexe du *p*-dichlorobenzène et l'anion acétonyle.

[Traduit par la revue]

The reactions of nitroarenes with nucleophiles continue to be the topic of many investigations and these reactions have been the topic of several recent reviews (2–4). One of the more intriguing of such reactions is the Janovsky reaction,[2] which involves the addition of a carbanion derived from ketones, such as acetone, to polynitro derivatives of arenes, such as *m*-dinitro- or 1,3,5-trinitrobenzene, leading to the formation of a carbon–carbon bond at the position *ortho* to a nitro group (7). In the present paper, the ready formation of Janovsky adducts is described for reactions between a number of η^6-substituted benzene-η^5-cyclopentadienyliron cations and a carbanion derived from acetone, butanone, or 3-pentanone.

In Janovsky reactions with substituted benzenes, two or more electron-withdrawing substituents have to be present before the reaction can take place (7). Complexation to the cyclopentadienyliron (CpFe) moiety apparently has a similar effect as a second electron-withdrawing substituent, and thus the η^6-nitrobenzene-η^5-cyclopentadienyliron cation (**1***a*), prepared as its hexafluorophosphate (8), could react readily under very mild conditions with the enolate-carbanion derived from acetone to give the Janovsky adduct, (1-5-η^5-1-nitro-6-*exo*-(2-oxo-1-propyl)-cyclohexadienyl)(η^5-cyclopentadienyl)iron, a complex resulting from *exo*-addition of the acetonyl anion regioselectively at a position *ortho* to the nitro substituent (eq. [1]).

[1] 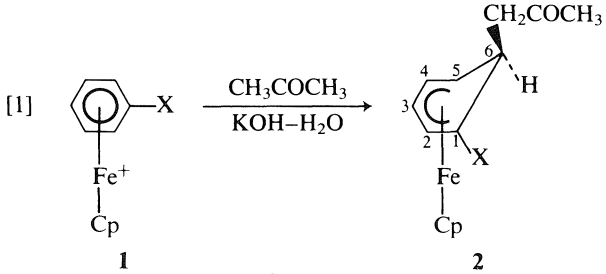

1 **2**

a, X = NO_2
b, X = CN
c, X = *p*-$SO_2C_6H_4CH_3$
d, X = COC_6H_5
e, X = Cl

[1]For a preliminary communication, see ref. 1.

[2]Named for the Czech chemist, J. V. Janovsky, but also translated as the Yanovsky or Yanovskii reaction (1, 5, 6) for a more appropriate English pronounciation.

TABLE 1. Data from the ^{1}H nmr spectra of Janovsky adducts from cyclopentadienyliron complexes of monosubstituted benzenes

	δ ($CDCl_3$), (ppm from TMS)								
	Cyclohexadienyl protons								
Adduct	C-2	C-3	C-4	C-5	C-6	Cp	CH_2[a]	CH_3	Ar
2*a*	5.79(d)	6.25(t)	4.71(t)	3.66(t)	3.81(m)	4.35(s)	1.20, 1.51	1.87(s)	—
2*b*	4.78(d)	6.10(t)	4.47(t)	3.09(t)	2.48(m)	4.41(s)	1.26, 1.43	1.83(s)	—
2*c*	5.07(d)	6.02(t)	4.44(t)	3.07(t)	3.05(m)	4.52(s)	0.38, 0.64	1.52(s)	7.12–7.14(d, 2H)
								2.26(s, tolyl-CH_3)	7.39–7.60(d, 2H)
2*d*[b]	5.28(d)	6.16(t)	4.68(t)	3.22(t)	3.43(d)	4.17(s)	—	—	7.36–7.41(m, 3H)
									7.65–7.68(m, 2H)

[a]The chemical shifts of the two diastereotopic protons of the methylene group were determined by a 360-MHz spectrometer. The other spectral data were obtained by a 60-MHz spectrometer. More detailed splitting patterns for the cyclohexadienyl protons obtained by the 360-MHz spectrometer will be reported later.

[b]Adduct formed from reaction with acetone-d_6.

Similar results were obtained when the nitro group in **1***a* was replaced by another electron-withdrawing substituent. Thus the CpFe complex of cyanobenzene (**1***b*), *p*-tolylsulfonylbenzene (phenyl *p*-tolyl sulfone) (**1***c*), or benzoylbenzene (benzophenone) (**1***d*) gave the same reaction with the acetonyl anion, resulting in the formation of Janovsky adducts **2***b*, **2***c*, or **2***d*, respectively (eq. [1]). In all of these cases, since C-6 is a chiral carbon, the products would be *R*,*S* pairs.

exo-Addition of nucleophiles to CpFe complexes of arenes is well known (9–13), and by analogy the acetonyl groups in these adducts are assigned the *exo*-configuration. Data from the ^{1}H nmr spectra of Janovsky adducts **2***a*–**2***d* are summarized in Table 1, and these results are consistent only with an attack by the acetonyl anion at a position *ortho* to the electron-withdrawing substituent. It may also be noted that in the reaction with **1***d*, acetone-d_6 in KOD–D_2O was employed with the resulting deuterated adduct showing a simpler spectrum. Some observations from the ir and ms spectra of these adducts, which are also consistent with the structures assigned, are given in Table 2 together with the physical appearance, yields, and analytical data.

In the Janovsky reaction with *m*-dinitrobenzene, for example, the acetonyl anion adds to the C-4 position, *ortho* to one and *para* to the other NO_2 group, and the resulting negative charge in the ring can be shown as being delocalized over both NO_2 groups (7). The present finding of regiospecific addition only to the *ortho* position and not to the *para* position may suggest that the electron-withdrawing inductive effect of substituent X in cations **1***a*–**1***d* may play a more important role than resonance delocalization in controlling the regiospecificity. In contrast to this regiospecificity, reaction of the CpFe complex of toluene (**1**, X = CH_3) with the hydride ion gave a 1:1:1 mixture of products derived from additions at the *o*-, *m*-, and *p*-positions (14). On the other hand, a similar reaction with the CpFe complex of chlorobenzene (**1***e*) or of methyl benzoate (**1**, X = $COOCH_3$), respectively, gave a 4:1:0 or 12.7:1:1.1 mixture of products derived from hydride additions at the *o*-, *m*-, and *p*-positions (14), the major product being derived from *o*-addition, and probably also indicating an important role for the inductive effect of the electron-withdrawing substituent.

It is of interest to note that in Meisenheimer or Janovsky type of adducts of nitroarenes such as 1,3,5-trinitrobenzene, from the ir spectra, it was found that there was a lowering of the asymmetric and symmetric stretching vibrational frequencies of the NO_2 group when compared with the analogous frequencies in the nitroarene, and this finding was attributed to a decrease in the N—O bond order because of the transfer of negative charge to the nitro groups in the adduct (15, 16).[3] A similar lowering in NO_2 stretching frequencies was observed in the presently prepared Janovsky adducts; for example, the ir frequencies for the NO_2 group of **2***a* are lower than the corresponding frequencies for the NO_2 group of cation **1***a* (Table 2) from which **2***a* was prepared. Apparently, such a decrease in bond order also occurred in the CN, SO_2, or CO substituent directly attached to the complexed cyclohexadienyl ligand in adduct **2***b*, **2***c*, or **2***d*, with the corresponding ir absorptions in cation **1***b*, **1***c*, or **1***d*, respectively, appearing at higher frequencies (Table 2).

When the hexafluorophosphate salts of the η^6-benzene-η^5-cyclopentadienyliron or similar CpFe complexes of substituted benzenes including toluene, cumene, anisole, *N*,*N*-dimethylaniline, (*p*-tolylthio)benzene, tetralin, and biphenyl were treated with acetone in aqueous KOH, no Janovsky adduct was obtained and the complex used as reactant was recovered unchanged. Thus a strong electron-withdrawing substituent on the complexed arene is required for the Janovsky reaction. Similar attempts to prepare the Janovsky adduct with the CpFe complex of azidobenzene or fluorobenzene resulted in a nucleophilic aromatic substitution to give a CpFe complex of phenol that in the basic medium led to the formation of a known complex, η^5-cyclohexadienone-η^5-cyclopentadienyliron (**3**) (17). When the hexafluorophosphate of the η^6-chlorobenzene-η^5-cyclopentadienyliron cation (**1***e*) was treated with acetone in aqueous KOH, a mixture of Janovsky adduct **2***e* and the cyclohexadienone complex **3** was formed and a pure sample of **2***e* was not obtained.

Although the chlorobenzene complex **1***e* failed to give a pure Janovsky adduct, CpFe complexes of dichlorobenzenes readily undergo the Janovsky reaction. With the *o*- or *p*-dichlorobenzene complex **4***a* or **6***a*, reaction with the acetonyl anion gave only one product, **5***a* or **7***a*, respectively, again derived from regioselective *exo*-addition at a position *ortho* to a chloro substituent (eqs. [2] and [3]). With the *m*-dichlorobenzene complex **8***a*, two Janovsky products, **9***a* and **10***a*, were obtained (eq. [4]), the ratio of **9***a*:**10***a* being about 9:1 based on the

[3]See also ref. 4, p. 31.

TABLE 2. Data on yields and analyses and some infrared and mass spectral results for Janovsky adducts

Adduct	Appearance	Yield (%)	Analysis, found (calcd) (%)			Infrared (cm^{-1})		Mass spectrum (m/e (relative abundance))	
			C	H	N	CO	Others[a]	M^+	$(M - acetonyl)^+$
2*a*	Purple solid	55	56.34(55.86)	4.67(4.98)	5.13(4.65)	1710	1290; 1490(NO_2) (1340); (1560)	301(6.40)	244(100.00)
2*b*	Red oil	58	64.53(64.12)	5.69(5.38)	4.91(4.98)	1700	2190(2245)(CN)	281(4.60)	244(52.60)
2*c*[b]	Red oil	70	—	—	—	1700	1080; 1285(SO_2) (1150); (1325)	410(trace)	353(15.30)
2*d*	Red solid	77	68.60(69.10)	6.60(6.85)	—	1700	1600(1600)(PhCO)	365(2.41)	303(88.81)
5*a*	Orange red oil	60	51.55(51.74)	4.29(4.39)	—	1700	—	324(4.65); 326(2.94)	267(100.00); 269(61.31); 271(9.99)
7*a*	Orange red oil	65	51.49(51.74)	4.18(4.39)	—	1700	—	324(3.74); 326(2.32)	267(100.00); 269(62.12); 271(10.42)
9*a* + **10***a*[c]	Orange red oil	55	—	—	—	1710	—	—	—
5*b*	Purple solid	50	57.45(57.14)	5.51(5.40)	4.47(4.44)	1710	1300; 1490(NO_2) (1340); (1560)	315(5.69)	258(100.00)
7*b*	Purple solid	65	56.52(57.14)	4.89(5.40)	4.21(4.44)	1710	1300; 1490(NO_2) (1345); (1565)	315(6.16)	258(58.20)
9*b* + **10***b*	Purple solid	45	57.98(57.14)	5.81(5.40)	4.39(4.44)	1710	1300; 1485(NO_2) (1340); (1560)	315(7.45)	258(100.00)
11*a*, *b*[b]	Purple oil	20	—	—	—	1700	1300; 1490(NO_2) (1340); (1560)	3.29(1.10)	244(100.00)[d]
12*a*, *b*, *c*[e]	Orange red oil	20	—	—	—	—	—	—	—
13*a*, *b*, *c*	Red oil	70	52.75(53.14)	4.66(4.75)	—	1700	—	338(trace)	267(100.00);[f] 269(63.00);[f] 271(1140)[f]
14*a*, *b*, *c*	Red oil	60	53.04(53.14)	4.59(4.75)	—	1700	—	338(trace)	267(100.00);[f] 269(63.30);[f] 271(10.50)[f]

[a]The numbers in the parentheses are the corresponding ir absorptions in the η^6-substituted benzene-η^5-cyclopentadienyliron cation from which the Janovsky adduct was prepared.
[b]Difficult to purify; no analysis for C, H, and N.
[c]Decomposes slowly, no analytical or ms data.
[d]$(M - CH_3CHCOCH_2CH_3)^+$.
[e]Contaminated by cyclohexadienone complex **3**; structures assigned on the basis of ^1H nmr data only (Table 4).
[f]$(M - CH_3CHCOCH_3)^+$ or $(M - CH_2COCH_2CH_3)^+$.

[2] 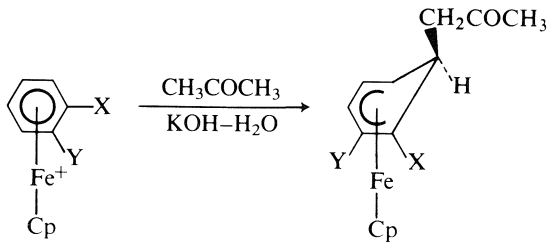

4

a, X = Y = Cl
b, X = NO_2, Y = CH_3

[3] 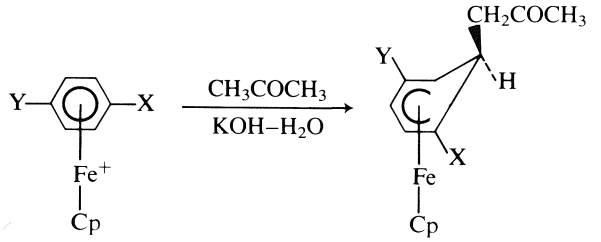

6 7

a, X = Y = Cl
b, X = NO_2, Y = CH_3

relative intensities of the Cp absorptions in the ^{1}H nmr spectra. Thus the major product, **9***a*, was derived from reaction at the position *ortho* to both electron-withdrawing chloro substituents.

In a similar way, the CpFe complex of *o*- or *p*-nitrotoluene (**4***b* or **6***b*) gave only one Janovsky adduct, **5***b* or **7***b*, respectively, with the acetonyl anion reacting regioselectively at the position *ortho* to the nitro substituent. In the reaction with the *m*-nitrotoluene complex **8***b*, two Janovsky adducts, **9***b* and **10***b*, were obtained in a relative ratio of about 3:2 for **9***b*:**10***b* (eq. [4]). Both **9***b* and **10***b* are derived from regioselective reaction at a site *ortho* to the electron-withdrawing nitro group, but the reason for the somewhat higher amount of **9***b* than **10***b* is not apparent. Data from the ^{1}H nmr spectra of these Janovsky adducts obtained from CpFe complexes of disubstituted benzenes are given in Table 3, and these results are consistent with the assigned structures. The yields, analytical data, and some ir and ms results for these adducts are included in Table 2.

When the nitrobenzene complex **1***a* was treated with 3-pentanone, instead of acetone, in aqueous KOH, the Janovsky adduct obtained, (1-5-η^5-1-nitro-6-*exo*-(3-oxo-2-pentyl)-cyclohexadienyl)(η^5-cyclopentadienyl)iron (**11***a*, *b*), would have two chiral centers (C-2 of the 3-oxo-2-pentyl side chain and C-6 of the cyclohexadienyl ring), thus giving rise to two diastereomeric products, the *R*,*R* + *S*,*S* enantiomeric pair and the *R*,*S* + *S*,*R* enantiomeric pair. The 360-MHz nmr spectrum of the product mixture, as given in Table 4, confirms the formation of two diastereomeric products, **11***a* and **11***b*, present in a ratio of about 5:4. It is, however, not possible to decide whether **11***a* or **11***b* is *R*,*R*-*S*,*S* or *R*,*S*-*S*,*R*.

[4] 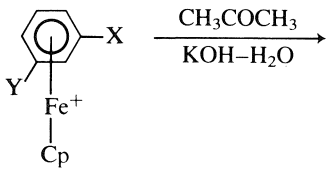

8

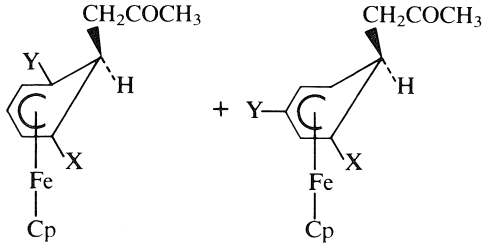

9 10

a, X = Y = Cl
b, X = NO_2, Y = CH_3

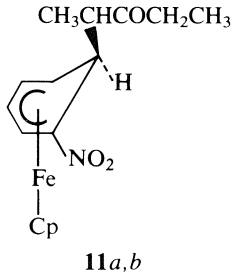

11*a*,*b*

On treatment of the chlorobenzene complex **1***e* with butanone in aqueous KOH, high resolution ^{1}H nmr (Table 4) showed that although the product mixture was contaminated with a small amount of the cyclohexadienone complex **3**, three Janovsky products were obtained from *exo*-addition at the position *ortho* to the chloro substituent of the two carbanions derived from removal of a proton from either α-position of butanone to give **12***a*, **12***b*, and **12***c*, with **12***a* and **12***b* as diastereomers. In an analogous way, reaction of *o*- or *p*-dichlorobenzene complex **4***a* or **6***a* with butanone in aqueous KOH gave Janovsky adducts **13***a*, **13***b*, and **13***c* or **14***a*, **14***b*, and **14***c*, respectively. The ^{1}H nmr data for these adducts are given in Table 4 and other relevant observations are included in Table 2.

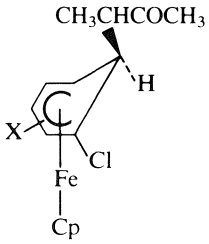

12*a*,*b*, X = H
13*a*,*b*, X = Cl at C-2
14*a*,*b*, X = Cl at C-4

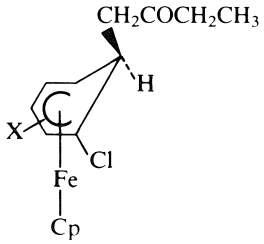

12*c*, X = H
13*c*, X = Cl at C-2
14*c*, X = Cl at C-4

It has been noted earlier that treatment of the chlorobenzene complex **1***e* with acetone in aqueous KOH gave a mixture of the Janovsky adduct **2***e* and the cyclohexadienone complex **3**. The relative amounts of these two products were found to be dependent on reaction time, increasing amounts of **3** being formed with longer reaction times. Similarly, when the nitrobenzene complex **1***a* was stirred with acetone in aqueous KOH at room temperature for about 20 min, the product obtained was the Janovsky adduct **2***a*. If the stirring was extended to 4–6 h, the major product became the cyclohexadienone complex **3**. These observations suggest that the Janovsky reaction with the chlorobenzene complex **1***e* or the nitrobenzene complex **1***a*, and nucleophilic aromatic substitution of the chloro group of **1***e* or the nitro group of **1***a* by hydroxide ion may be competing reactions and, probably, the Janovsky adduct is the kinetically controlled product, while with prolonged reaction time, more nucleophilic aromatic substituion would occur to give rise to the

TABLE 3. Data from the ^{1}H nmr spectra of Janovsky adducts from cyclopentadienyliron complexes of disubstituted benzenes

	δ ($CDCl_3$), (ppm from TMS)							
	Cyclohexadienyl protons							
Adduct	C-2	C-3	C-4	C-5	C-6	Cp	CH_2[a]	CH_3
5*a*	—	6.16(d)	4.14(d)	2.92(t)	3.36(m)	4.34(s)	1.22, 1.76	1.84(s)
7*a*	4.48(d)	6.04(d)	—	3.30(d)	3.35(m)	4.36(s)	1.30, 1.72	1.86(s)
9*a*[b]	4.46(d)[c]	5.72(t)	4.46(d)[c]	—	3.87(s)	4.37(s)	1.55(d)	1.98(s)
10*a*[b]	4.92(s)	—	4.51(d)	2.86(t)	3.18(m)	4.35(s)	1.23, 1.76	1.86(s)
5*b*	—	6.59(d)	4.59(t)	3.56(t)	3.55(m)	4.25(s)	1.06, 1.38	1.84(s), 2.35(s)
7*b*	5.77(d)	6.12(d)	—	3.63(d)	3.73(m)	4.24(s)	1.17, 1.50	1.81(s), 1.86(s)
9*b*[d]	5.76(d)	6.10(t)	4.53(d)	—	3.87(m)	4.24(s)	1.32, 1.41	1.79(s), 1.94(s)
10*b*[d]	5.75(s)	—	4.66(d)	3.60(t)	3.77(m)	4.27(s)	1.20, 1.53	1.89(s), 2.56(s)

[a]As in Table 1 except that the methylene protons of **9***a* are not diastereotopic and appear as a doublet.
[b]Data from the spectrum of a mixture of **9***a* and **10***a*; relative intensities of the Cp peaks in the 360-MHz spectrum gave a ratio of about 9:1 for **9***a*:**10***a*.
[c]The C-2 and C-4 protons of **9***a* are equivalent.
[d]Data from the spectrum of a mixture of **9***b* and **10***b*; relative intensities of the Cp peaks in the 360-MHz spectrum gave a ratio of about 3:2 for **9***b*:**10***b*.

TABLE 4. Data from ^{1}H nmr spectra of Janovsky adducts from reactions with butanone and 3-pentanone[a]

	δ ($CDCl_3$), (ppm from TMS)						
	Cyclohexadienyl protons						
Adduct	C-2	C-3	C-4	C-5	C-6	Cp	Others
11*a*[b]	5.87(d)	6.16(t)	4.69(t)	3.50(t)	3.67(m)	4.30(s)	0.47(d)(CH_3CH); 0.89(t)(CH_3CH_2); 1.24(m)(C*H*CH_3); 2.15(q)(CH_2CH_3)
11*b*[b]	5.89(d)	6.20(t)	4.78(t)	3.50(t)	3.55(m)	4.32(s)	0.58(d)(CH_3CH); 0.83(t)(CH_3CH_2); 1.14(m)(C*H*CH_3); 2.17(q)(CH_2CH_3)
12*a*[c]	5.10(d)	5.46(t)	4.10(t)	3.10(t)	3.55(m)	4.33(s)	0.52(d)(CH_3CH); 1.20(m)(C*H*CH_3); 2.00(s)(CH_3CO)
12*b*[c]	4.85(d)	5.35(t)	4.20(t)	3.05(t)	3.36(m)	4.32(s)	0.76(d)(CH_3CH); 1.20(m)(C*H*CH_3); 1.88(s)(CH_3CO)
12*c*[c]	4.89(d)	5.30(t)	4.30(t)	3.20(t)	3.30(m)	4.325(s)	0.89(t)(CH_3CH_2); 2.14(q)(CH_2CH_3); 1.40, 1.72(CH_2)[d]
13*a*[e]	—	6.09(d)	4.17(t)	2.77(t)	3.06(m)	4.29(s)	0.42(d)(CH_3CH); 1.37(m)(C*H*CH_3); 1.91(s)(CH_3CO)
13*b*[e]	—	6.03(d)	4.08(t)	2.77(t)	3.06(m)	4.28(s)	0.67(d)(CH_3CH); 1.36(m)(C*H*CH_3); 1.78(s)(CH_3CO)
13*c*[e]	—	6.10(d)	4.09(t)	2.85(t)	3.30(m)	4.285(s)	0.80(t)(CH_3CH_2); 2.04(q)(CH_2CH_3); 1.15, 1.65(CH_2)[d]
14*a*[f]	4.52(d)	5.97(d)	—	3.22(s)	3.08(m)	4.32(s)	0.51(d)(CH_3CH); 1.39(m)(C*H*CH_3); 1.91(s)(CH_3CO)
14*b*[f]	4.53(d)	5.95(d)	—	3.20(s)	3.00(m)	4.31(s)	0.68(d)(CH_3CH); 1.40(m)(C*H*CH_3); 1.84(s)(CH_3CO)
14*c*[f]	4.44(d)	6.00(d)	—	3.27(s)	3.29(m)	4.315(s)	0.82(t)(CH_3CH_2); 2.07(q)(CH_2CH_3); 1.25, 1.63(CH_2)[d]

[a]All spectral data were obtained by a 360-MHz spectrometer; the splitting patterns given for the cyclohexadienyl protons are rough approximations and more detailed analyses of these patterns will be reported later.
[b]Data from the spectrum of a mixture of **11***a* and **11***b*, the ratio of **11***a*:**11***b* being about 5:4 based on the relative intensities of the Cp absorptions.
[c]Data from the spectrum of a mixture of **12***a*, **12***b*, and **12***c*, the ratio of **12***a*:**12***b*:**12***c* being about 7:6:4 based on the relative intensities of the Cp absorptions.
[d]Diastereotopic C-1 methylene protons of the side chain coupled with the C-6 proton of the cyclohexadienyl ring to give two sets of AB splitting patterns.
[e]Data from the spectrum of a mixture of **13***a*, **13***b*, and **13***c*, the ratio of **13***a*:**13***b*:**13***c* being about 3:2:1 based on the relative intensities of the Cp absorptions.
[f]Data from the spectrum of a mixture of **14***a*, **14***b*, and **14***c*, the ratio of **14***a*:**14***b*:**14***c* being about 9:6:4 based on the relative intensities of the Cp absorptions.

CpFe complex of phenol, which in the basic medium would be irreversibly converted to the cyclohexadienone complex **3**.

The present work may also have potential for applications in organic synthesis. We have found that when the Janovsky adduct **7***a*, obtained from the *p*-dichlorobenzene complex **6***a*, was treated with ammonium ceric nitrate in wet acetone in the presence of NaOAc as described by Pearson *et al.* (18), demetallation together with oxidation took place to give a 50% yield of (2,5-dichlorophenyl)propanone (erroneously stated as (2,4-dichlorophenyl)propanone in ref. 1), a compound that has not been previously reported. RajanBabu *et al.* (19) have recently studied the addition of silyl enol ethers to aromatic nitro compounds, followed by oxidation to give α-nitroaryl carbonyl compounds. These workers (19) have also pointed out that "even though α-anionic complexes between aromatic polynitro compounds and enolates (Janovsky complexes) have been known for over 90 years, these have found no application in synthesis." As in the present preparation of (2,5-dichlorophenyl)propanone, it appears that similar demetallation–oxidation of Janovsky adducts of CpFe complexes of substituted arenes may provide a method for the introduction of alkyl side chains bearing a useful oxo function into the *ortho* position of substituted benzenes with an electron-withdrawing substituent such as nitrobenzene.

Experimental

η^6-Substituted benzene-η^5-cyclopentadienyliron cations

The η^6-substituted benzene-η^5-cyclopentadienyliron cations employed in the present study were prepared as their hexafluorophosphate salts utilizing known procedures. The CpFe complexes of nitrobenzene (**1***a*) and *o*-, *p*-, or *m*-nitrotoluene (**4***b*, **6***b*, or **8***b*, respectively) were obtained as described by Lee *et al.* (8). Similar complexes of chlorobenzene (**1***e*) and *o*-, *p*-, or *m*-dichlorobenzene (**4***a*, **6***a*, or **8***a*, respectively) were prepared by ligand exchange reactions as reported by Khand *et al.* (20). The cyanobenzene complex **1***b* was obtained by a nucleophilic substitution reaction between cyanide ion and the chlorobenzene complex **1***e* (21). The sulfone complex **1***c* was prepared by oxidation of the η^6-(*p*-tolylthio)benzene-η^5-cyclopentadienyliron cation, while the benzophenone complex **1***d* was obtained from the $KMnO_4$ oxidation of the η^6-diphenylmethane-η^5-cyclopentadienyliron cation (22). The CpFe complex of (*p*-tolylthio)benzene (**15**) was prepared from a nucleophilic aromatic substitution reaction between the nitrobenzene complex **1***a* and 4-methylbenzenethiol in the presence of K_2CO_3 (23). Oxidation of **15** by *m*-chloroperbenzoic acid gave the sulfone complex **1***c* as its hexafluorophosphate (24).

Besides cation **15**, which did not give the Janovsky reaction, other complexes that also failed to give the Janovsky adduct, including the CpFe complexes of benzene, toluene, cumene, anisole, *N*,*N*-dimethylaniline, tetralin, biphenyl, and fluorobenzene, were all prepared from ligand exchange reactions between the arene and ferrocene as reviewed by Sutherland (25). Finally, the azidobenzene complex, which, like the fluorobenzene complex, gave the cyclohexadienone complex **3** under the Janovsky reaction conditions, was prepared from the nucleophilic aromatic substitution reaction between chlorobenzene complex **1***e* and NaN_3 (26).

Janovsky reactions

Described below is the general procedure for the preparation of Janovsky adducts formed from reactions between the various η^6-substituted benzene-η^5-cyclopentadienyliron cations and acetone, butanone, or 3-pentanone.

To a stirred solution of 3.0 mmol of the hexafluorophosphate salt of an η^6-substituted benzene-η^5-cyclopentadienyliron cation in 15 mL of the ketone, 5.0 mL of a 20% solution of KOH in H_2O was added. An intense color developed immediately and the solution was stirred at room temperature for about 20 min. The reaction mixture was then extracted with $CHCl_3$ (3 × 25 mL) and the extract washed with H_2O (3 × 50 mL). After drying over $MgSO_4$, the $CHCl_3$ was removed in a rotary evaporator. The residue was then purified by passage through a short column (5 cm) packed with F-20 alumina (Alcoa Chemical Co.) that had been deactivated by exposure to air for 48 h. Any impurities that may have been present were first removed by elution with pentane and the Janovsky adduct was then eluted with $CHCl_3$. Upon evaporation to dryness at room temperature, the highly colored product was obtained either as an oil or recrystallized from $CHCl_3$–pentane.

2,5-Dichlorophenylpropanone

To a stirred solution of 800 mg (2.47 mmol) of Janovsky adduct **7***a* ((1-5-η^5-1,4-dichloro-6-*exo*-(2-oxo-1-propyl)-cyclohexadienyl)(η^5-cyclopentadienyl)iron) in 15 mL of acetone and 0.5 mL of H_2O containing 2.0 g of NaOAc, $(NH_4)_2Ce(NO_3)_6$ (Aldrich Chemical Co.) was added at room temperature and with stirring in ten 200-mg portions over a period of 2.5 h. Ether (200 mL) was then introduced and the resulting solution was washed with H_2O (3 × 50 mL). After drying over $MgSO_4$, removal of the solvent in a rotary evaporator gave an oil that, upon analysis by gc–ms, showed a 50% yield of 2,5-dichlorophenylpropanone; ^1H nmr ($CDCl_3$) δ: 2.33 (s, 3H, CH_3), 3.95 (s, 2H, CH_2), 7.36 (br s, 3H, Ar). Its ir spectrum showed a carbonyl absorption at 1710 cm^{-1}. In its mass spectrum, the molecular ion region showed *m*/*e* 202, 204, and 206 with relative abundances of 37.16, 23.20, and 4.05%, respectively, in agreement with the expected relative ratio of about 9:6:1 for two Cl atoms in the molecule with an approximate ^{35}Cl:^{37}Cl ratio of 3:1.

Acknowledgement

The financial support given by the Natural Sciences and Engineering Research Council of Canada is sincerely acknowledged.

1. R. G. Sutherland, R. L. Chowdhury, A. Piórko, and C. C. Lee. J. Chem. Soc. Chem. Commun. 1296 (1985).
2. F. Terrier. Chem. Rev. **82**, 77 (1982).
3. M. Makosza. *In* Current trends in organic synthesis. *Edited by* H. Nozaki. Pergamon Press, Oxford. 1983. pp. 401–412.
4. E. Buncel, M. R. Crampton, M. J. Strauss, and F. Terrier. Electron deficient aromatic heteroaromatic-base interactions. Elsevier, Amsterdam. 1984.
5. A. Ya. Kaminskii and S. S. Gitis. Zh. Org. Khim. **4**, 1826 (1968); J. Org. Chem. USSR, **4**, 1763 (1968).
6. I. M. Sosonkin, A. Ya. Kaminskii, and G. N. Strogov. Zh. Obshch. Khim. **45**, 482 (1975); J. Gen. Chem. USSR, **45**, 475 (1975).
7. S. S. Gitis and A. Ya. Kaminskii. Russ. Chem. Rev. **47**, 1061 (1978).
8. C. C. Lee, U. S. Gill, M. Iqbal, C. I. Azogu, and R. G. Sutherland. J. Organometal. Chem. **231**, 151 (1982).
9. I. U. Khand, P. L. Pauson, and W. E. Watts. J. Chem. Soc. (C), 2024 (1969).
10. S. G. Davies, M. L. H. Green, and D. M. P. Mingos. Tetrahedron, **34**, 3047 (1978).
11. P. L. Pauson. J. Organometal. Chem. **200**, 207 (1980).
12. J. C. Boutonnet and E. Rose. J. Organometal. Chem. **221**, 157 (1981).
13. C. C. Lee, U. S. Gill, and R. G. Sutherland. J. Organometal. Chem. **267**, 157 (1984).
14. S. L. Grundy and P. M. Maitlis. J. Organometal. Chem. **272**, 265 (1984).
15. A. R. Norris and H. F. Shurvell. Can. J. Chem. **47**, 4267 (1969).
16. E. G. Kaminskaya, S. S. Gitis, and A. Ya. Kaminskii. Dokl. Akad. Nauk SSSR, **221**, 617 (1975).
17. J. F. Helling and W. A. Hendrickson. J. Organometal. Chem. **168**, 87 (1979).
18. A. J. Pearson, P. R. Bruhn, and I. C. Richards. Isr. J. Chem. **24**, 93 (1984).

19. T. V. RAJANBABU, G. S. REDDY, and T. FUKUNAGA. J. Am. Chem. Soc. **107**, 5473 (1985).
20. I. U. KHAND, P. L. PAUSON, and W. E. WATTS. J. Chem. Soc. (C), 2261 (1968).
21. E. I. SIROTKINA, A. N. NESMEYANOV, and N. A. VOL'KENAU. Izv. Akad. Nauk SSSR, Ser. Khim. 1524 (1969).
22. C. C. LEE, K. J. DEMCHUK, U. S. GILL, and R. G. SUTHERLAND. J. Organometal. Chem. **247**, 71 (1983).
23. R. L. CHOWDHURY, C. C. LEE, A. PIÓRKO, and R. G. SUTHERLAND. Synth. React. Inorg. Met.-Org. Chem. **15**, 1237 (1985).
24. C. C. LEE, R. L. CHOWDHURY, A. PIÓRKO, and R. G. SUTHERLAND. J. Organometal. Chem. In press.
25. R. G. SUTHERLAND. J. Organometal. Chem. Library, **3**, 311 (1977).
26. C. C. LEE, C. I. AZOGU, P. C. CHANG, and R. G. SUTHERLAND. J. Organometal. Chem. **220**, 181 (1981).

Aqueous solution interaction of the methylmercuric cation with the dinucleotides CpG and dCpdG as studied by carbon-13 nuclear magnetic resonance spectroscopy[1]

G. W. BUCHANAN AND M. J. BELL

Ottawa–Carleton Institute for Research and Graduate Studies in Chemistry, Department of Chemistry, Carleton University, Ottawa, Ont., Canada K1S 5B6

Received December 30, 1985

G. W. BUCHANAN and M. J. BELL. Can. J. Chem. **64**, 2038 (1986).

^{13}C nuclear magnetic resonance chemical shifts and ^{13}C–^{31}P coupling constants are reported for the self-complementary dinucleotides CpG and dCpdG in aqueous solution. The influence of methylmercuration at pH 6.0 on these spectral parameters has been examined. Results are interpreted in terms of preferential methylmercuration at the N-7 site of the guanine base of each dinucleotide with concomitant base destacking.

G. W. BUCHANAN et M. J. BELL. Can. J. Chem. **64**, 2038 (1986).

On rapporte les déplacements chimiques en rmn du ^{13}C et les constantes de couplages ^{13}C–^{31}P des dinucléotides autocomplémentaires CpG et dCpdG en solution aqueuse. On a examiné l'influence de la méthylmercuration à pH 6,0 sur ces paramètres spectraux. On interpréte les résultats en fonction d'une méthylmercuration préférentielle au niveau de l'azote en position 7 du site de la guanine de chaque nucléotide avec un désentassement concomitant de la base.

[Traduit par la revue]

Introduction

Chromosomal damage caused by some organomercurials appears to be due in part to the consequences of "secondary" interactions between the heavy metal ion and DNA constituents (1–3). A number of attempts have been made to "model" such interactions between the methylmercuric cation, CH_3Hg^+, and nucleotide components. The earliest work utilized uv difference spectra to examine CH_3Hg^+–nucleoside interactions as a function of pH (4). Subsequently, Raman difference spectroscopy was employed to probe purine and pyrimidine mononucleotide interactions with CH_3Hg^+ (5). More recently, ^1H and ^{13}C nmr were applied in this area involving complexes of the nucleosides guanosine and inosine (6).

To date, no nmr studies on these interactions have proceeded beyond the mononucleotide level. There is, therefore, a clear need to examine systems that more closely approximate the DNA and RNA structures in solution. To this end, we report herein the results of a ^{13}C nmr investigation of the interaction of CH_3Hg^+ with the self-complementary dinucleotides cytidylyl-(3′-5′)-guanosine (CpG, **1**) and its deoxy counterpart dCpdG **2**. These dinucleotides are known to form base-stacked dimers that are mini-helices in aqueous solution (7) and thus they constitute reasonable structural models for RNA and DNA respectively.

Results and discussion

^{13}C chemical shift assignments

The structure and numbering scheme for CpG, **1**, is depicted in Fig. 1. Since 13 of the 19 carbons of this molecule are protonated, our initial strategy was to check the literature ^1H assignments and then use the ^1H shifts along with selective ^1H decoupling in the ^{13}C spectrum to identify directly bonded carbons.

The published 270-MHz ^1H spectrum of **1** contains some resonance overlap, but was successfully analyzed by spectral simulation (8). In the present work the earlier assignments have been verified by 2-D spectroscopy via the ^1H–^1H COSY (9) experiment at 500 MHz.

With the ^1H assignments in hand, selective ^1H decoupling in the ^{13}C spectra readily furnished the protonated carbon assignments for CpG. In Table 1 are presented the complete ^{13}C shift data for CpG along with those for the related mononucleotide models 3′-CMP and 5′-GMP. For 3′-CMP there has been a recent report (10) of the ^{13}C–^{31}P couplings, but no ^{13}C shift data were included. Our results for 5′-GMP are in good agreement with the literature (11), with the appropriate reversal (12) of the original (11) assignments for the 2′ and 3′ carbon resonances.

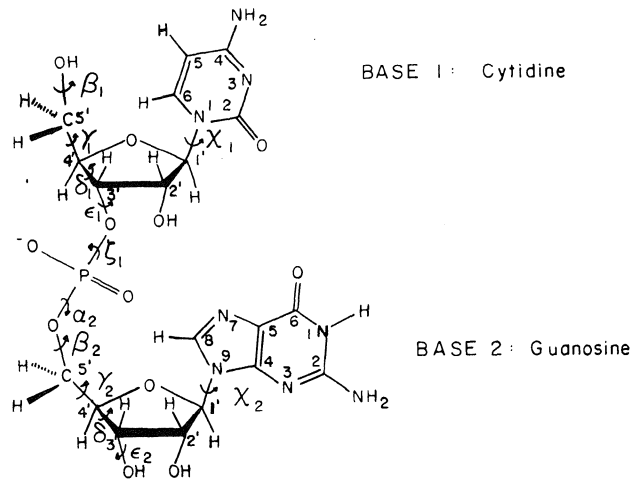

FIG. 1. Structure, numbering scheme, and some appropriate torsional angles for CpG **1**.

Several methods were used to assign the 6 quaternary carbon resonances of CpG. Examination of data in Table 1 shows that the resonance at $\delta_C = 115.82$ if CpG is separated by more than 20 ppm from any other. It can therefore, by analogy with the results for 5′ GMP, be confidently assigned to the 5 position of the guanosine residue.

The totally coupled ^{13}C spectrum of CpG revealed several $^2J_{CH}$ and $^3J_{CH}$ interactions that could be selectively removed by low power ^1H decoupling, leading to assignment of 3 quaternary carbons. Specifically, the cytidine 4 position (via $^2J_{CH}$ to H-5 of cytidine and $^3J_{CH}$ to H-6 of cytidine), the guanosine 4 position (via $^3J_{CH}$ to H-1′ of guanosine), and the cytidine 2 position (via $^3J_{CH}$ to H-6 of cytidine and $^3J_{CH}$ to H-1′ of cytidine) were assigned in this manner.

The remaining two resonances of CpG appear at $\delta_C = 153.63$

[1]Taken in part from the Ph.D. thesis of M. J. Bell, Carleton University, Ottawa, June 1985.

TABLE 1. ^{13}C chemical shifts (δ_C from TMS ± 0.01)* for CpG and mononucleotide models

Site	CpG	3′-CMP	5′-GMP
C-2	151.52	156.93	
C-4	161.50	165.60	
C-5	95.06	96.18	
C-6	142.29	141.65	
C-1′	90.28	89.81	
C-2′	73.06	73.53	
C-3′	72.01	72.06	
C-4′	82.68	83.17	
C-5′	59.55	60.56	
G-2	153.63		153.49
G-4	151.16		150.95
G-5	115.82		115.46
G-6	158.37		158.29
G-8	136.98		137.05
G-1′	87.56		86.80
G-2′	73.49		74.02
G-3′	69.47		70.22
G-4′	82.71		83.88
G-5′	64.46		63.35

*0.1 *M* in D_2O with external TMS reference.

TABLE 2. ^{13}C shift data (δ_C from TMS ± 0.01)* for dCpdG (**2**) and mononucleotide models

Site	dCpdG	3′-dCMP	5′-dGMP
C-2	155.29	157.27	
C-4	164.28	166.09	
C-5	96.12	96.29	
C-6	140.77	141.70	
C-1′	85.29	86.08	
C-2′	37.55	38.71	
C-3′	75.37	73.22	
C-4′	85.51	86.17	
C-5′	60.91	61.42	
G-2	153.63		153.67
G-4	151.28		150.72
G-5	115.63		115.65
G-6	158.54		158.48
G-8	137.08		137.08
G-1′	82.76		83.05
G-2′	38.06		38.83
G-3′	70.43		71.28
G-4′	85.12		86.08
G-5′	64.76		63.82

*0.1 *M* in D_2O with external TMS reference.

and 158.37 respectively and they show no appreciable splittings in the ^1H coupled ^{13}C spectrum in D_2O. This is consistent with expectations for the 2 and 6 positions of guanosine, the only 2 unassigned carbons. Specific designation of these two resonances was made using 5′-GMP as a model and the agreement is excellent.

A similar strategy was employed to assign the ^{13}C signals for the deoxy analog of **1**, namely dCpdG (**2**). Although no ^{13}C data for **2** are in the literature, the experimental 270-MHz ^1H spectrum has been published, as well as the computer simulated version. Using these available proton data (13), the protonated carbon assignments were obtained directly and the remaining carbon resonances were assigned in ways totally analogous to those for **1**. The resulting data are presented in Table 2. Included in this table are chemical shifts for the related mononucleotide models 3′-dCMP and 5′-dGMP. No ^{13}C shift data for 3′-dCMP have been reported previously, although the $^{13}C-^{31}P$ couplings have been studied (10). Our results for 5′-dGMP are in good accord with literature values (11).

TABLE 3. $^{13}C-^{31}P$ couplings (Hz) ± 0.1

Compound	Path	^2J	^3J
1	(G-4′)-5′-O-P		9.2
5′-GMP	(G-4′)-5′-O-P		8.8
2	(G-4′)-5′-O-P		8.9
5′-dGMP	(G-4′)-5′-O-P		8.8
1	(G-5′)-O-P	5.5	
5′-GMP	(G-5′)-O-P	2.8	
2	(G-5′)-O-P	3.6	
5′-dGMP	(G-5′)-O-P	3.8	
1	(C-4′)-3′-O-P		6.0
3′-CMP	(C-4′)-3′-O-P		4.6
2	(C-4′)-3′-O-P		7.4
3′-dCMP	(C-4′)-3′-O-P		Peak overlap*
1	(C-2′)-3′-O-P		2.4
3′-CMP	(C-2′)-3′-O-P		4.8
2	(C-2′)-3′-O-P		1.9
3′-dCMP	(C-2′)-3′-O-P		2.9
1	(C-3′)-O-P	3.0	
3′-CMP	(C-3′)-O-P	4.6	
2	(C-3′)-O-P	5.9	
3′-dCMP	(C-3′)-O-P	4.3	

*With C-1′ resonance.

$^{13}C-^{31}P$ couplings

These data for **1** and **2**, along with those for the corresponding mononucleotides, are presented in Table 3. Our data for the mononucleotides are in good agreement with published results (10, 11).

Effects of methylmercuration on ^{13}C chemical shifts

These results are depicted in graphical form in Figs. 2 and 3 for **1** and **2** respectively. Experiments were limited to 0.5 molar equivalents of added CH_3HgOH for reasons of solubility at pH 6.0. Of the ribose and deoxyribose carbons only C-1′ is affected to any extent by methylmercuration and thus data for C-2′ to C-5′ are not included. For both **1** and **2** the major result of CH_3HgOH addition in the cytidylyl region is the substantial deshielding of the C-2 and C-4 resonances. In fact the chemical shifts for these carbons of the "complexes" approach those for the mononucleotide models 3′-CMP and 3′-dCMP respectively.

Interestingly, in **1** and **2**, which are self-complementary and base-stacked (see Fig. 4), the ring current of the purine moiety will cause the carbons of the pyrimidine base to be shielded relative to the corresponding carbons of the 3′-CMP and 3′-dCMP systems, which do not base-stack. Due to the preferred conformations of **1** and **2** these effects are most pronounced at the C-2 and C-4 sites.

The ^{13}C shifts indicate no apparent mercury binding to the N-3 site of the cytidine moiety in either **1** or **2**. Such a conclusion can be made by noting that the presently observed ^{13}C shift changes are different from those previously found for the nucleoside cytosine, upon Hg coordination to N-3 (14).

The nearly identical nature of the cytidine ring carbon shifts for the methylmercuric adducts of **1** and **2** with the isolated mononucleotides 3′-CMP and 3′-dCMP suggests that a major

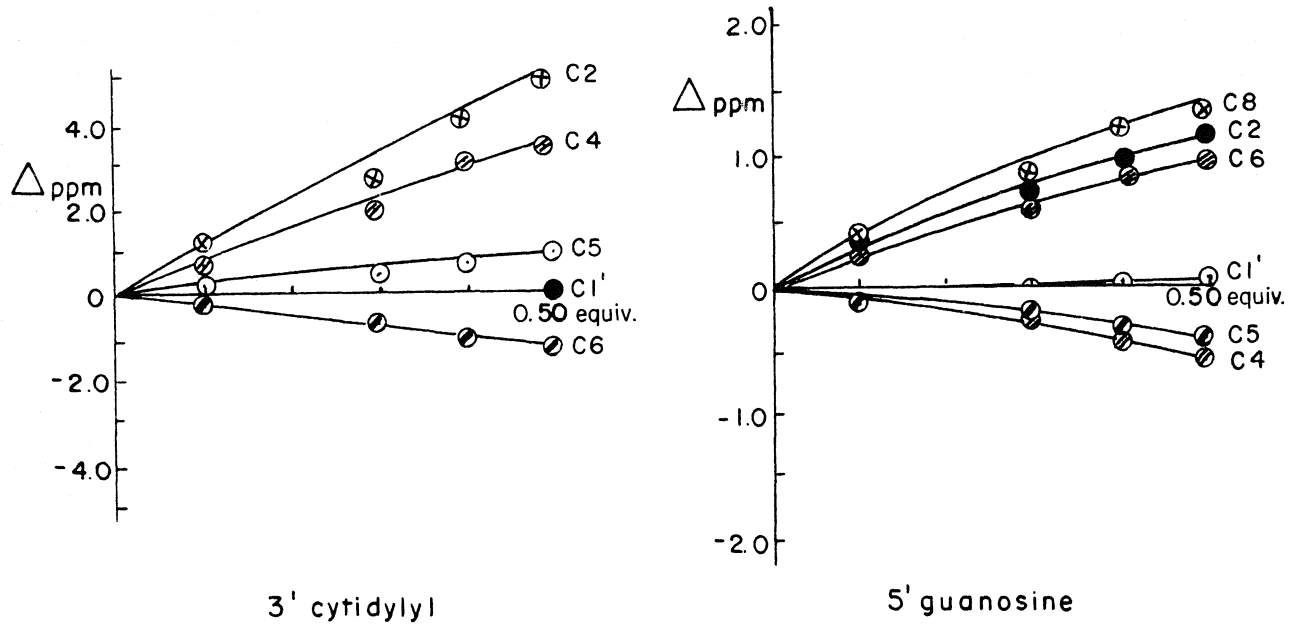

FIG. 2. Effects of methylmercuration on ^{13}C shifts of CpG **1**. Positive values denote downfield shifts.

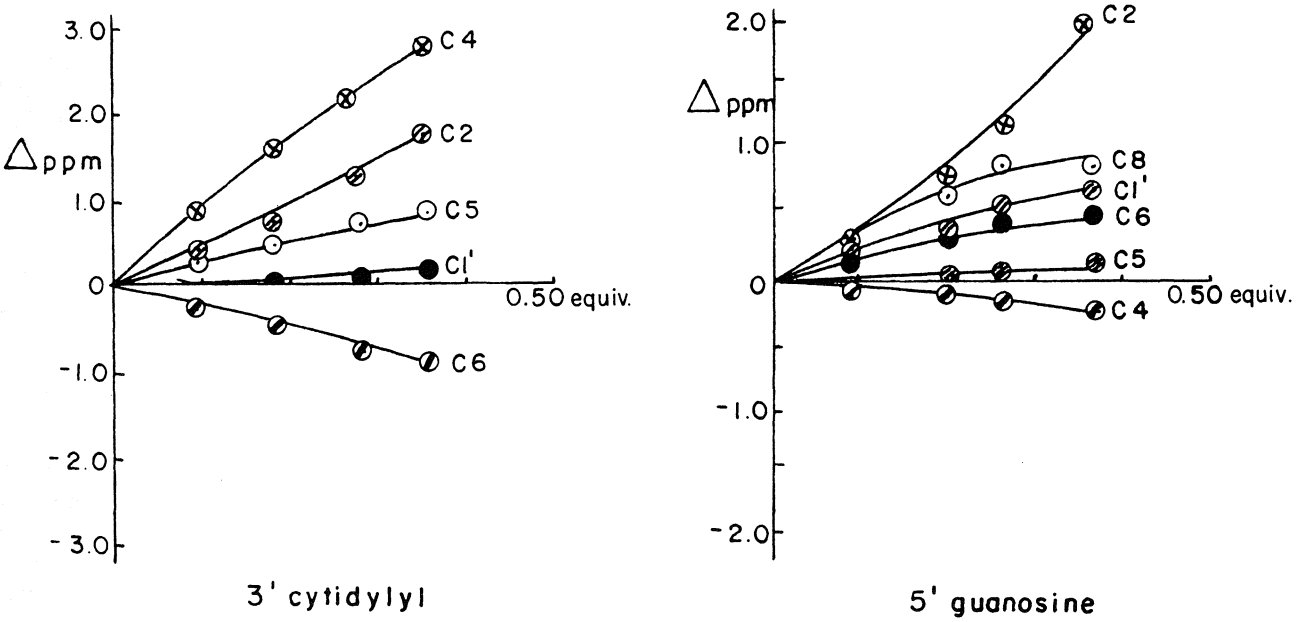

FIG. 3. Effects of methylmercuration on ^{13}C shifts of dCpdG **2**. Positive values denote downfield shifts.

result of CH_3HgOH addition is to disrupt the base-stacking phenomena.

The induced ^{13}C shifts in the guanine rings of **1** and **2** are indicative of CH_3Hg^{II} interactions at the N-7 site in rapid equilibrium with binding at the N-1 site. This conclusion is based primarily on the induced downfield shifts of the C-2 and C-8 sites of the guanine rings of **1** and **2** (6).

It is well known (4) that the nature of CH_3Hg^{II} species in solution depends greatly on the pH. At pH 6.0 (i.e., the present work) the charged $(CH_3Hg)_2\overset{+}{O}H$ species exists in an equilibrium with CH_3HgOH, in which the two moieties are almost equally prevalent (4). The cationic species can bind directly at the N-7 site of guanine while the CH_3HgOH can bind at N-1 in a two-step process involving deprotonation at N-1. This latter process becomes more likely as the pH increases. Indeed for 5′-GMP we have confirmed recently via ^{15}N nmr (15) that at pH 8.0 this N-1 binding completely dominates.

At pH 6.0, however, it is likely that N-7 is the preferred binding site for the methylmercuric ion. The consequences of this binding could be twofold in their influence on the structure of the self-complementary systems **1** and **2** in solution. Initially the hydrogen bonding possibilities at N-7 of the guanine ring are removed. This will destabilize the mini-helix and lead to destacking phenomena. An increase in the acidity of the N1-H proton should also accompany N-7 mercuration (16).

Effects of methylmercuration on ^{13}C–^{31}P coupling constants

For mononucleotides 3′-CMP, 3′-dCMP, 5′-GMP, and

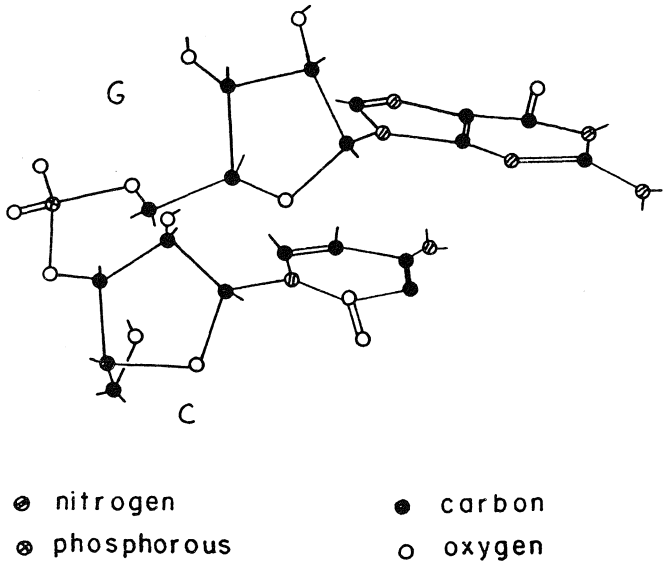

FIG. 4. Base stacked mini-helix structure of CpG **1**.

5′-dGMP no substantial change (i.e., above 0.2 Hz) was noted for any of the geminal or vicinal $^{13}C-^{31}P$ couplings upon CH_3HgOH addition.

By contrast, significant changes in two of the vicinal $^{13}C-^{31}P$ couplings were noted for **1** upon methylmercuration. Specifically, these involved 2′ and 4′ ribose carbons attached to the cytidine base. Before complexation, $^3J_{C4'-C-O-P}$ is 6.0 Hz while $^3J_{C2'-C-O-P}$ is 2.4 Hz. After complexation these couplings become nearly equal, with values of 4.6 and 4.2 Hz respectively. This result suggests a substantial increase in the amount of the ε_{tg} conformation (below) relative to the ε_{gt} conformation upon methylmercuration.

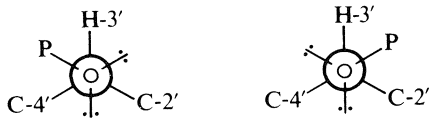

ε_{tg} ε_{gt}

Such a change in these vicinal coupling constants would be an expected consequence of the destacking process. In the base-stacked (uncomplexed) case, the ε_{gt} conformer dominates, as evidenced by the larger vicinal coupling from ^{31}P to C-4′ than to C-2′. This is consistent with expectations, by analogy with results for other cytidine polynucleotides (17) in which stacking occurs.

A further point of interest here is that $^3J_{C2'-C-O-P}$ and $^3J_{C4'-C-O-P}$ in the methylmercuric adduct of **1** are almost identical to the corresponding couplings in 3′-CMP, which also lacks base-stacking.

By contrast, complexation of CH_3HgOH with dCpdG **2** produces no significant changes in $^3J_{C4'-C-O-P}$ or $^3J_{C2'-C-O-P}$. It has been noted previously (13) that there is a much wider conformational spread for the pentose ring in deoxyriboses relative to riboses. As a result, attempts to translate time-averaged nmr coupling constants into conformer populations is much more difficult than in the ribose systems.

Thus it appears from ^{13}C chemical shift results for **2** that the methylmercuric ion does induce destacking, but that the more flexible pentose ring in **2** prevents monitoring of this destacking via vicinal $^{13}C-^{31}P$ coupling constants that necessarily invoke the pentose carbons.

Experimental

Materials

All nucleotides were purchased as their sodium salts from Sigma Chemical Company and were used without further purification. The source of methylmercury was $[(CH_3Hg)_3O]OH$, which was available from Alpha Products Ltd.

The initial pH of the sodium salts of the nucleotides in aqueous solution was 6.0. No substantial change in pH was noted after addition of 0.5 equivalents of mercuric salt. A 20-min shaking period was needed for complete dissolution of the salt.

Spectra

^{13}C spectra were obtained using 0.1 *M* solutions in D_2O with a Varian XL-200 nmr spectrometer. Normally 5-mm sample tubes were employed with spectral widths of 10 kHz and 32K data points. Pulse widths were 45° with repetition rates of 2 s. For measurement of $^{13}C-^{31}P$ couplings spectral widths of 2 kHz were commonly employed with retention of 32K data points.

The 500 MHz ^1H-COSY spectrum of **1** was obtained on a Bruker WH500 spectrometer using a sample that had been lyophilized five times from D_2O. The sweep width was 625 Hz in both dimensions and this was centered in the ribose proton region between 3.6 and 6.2 ppm. A data matrix of 256 × 512 data points was transformed to yield the final 2-D spectrum.

Acknowledgements

We thank the Natural Sciences and Engineering Research Council of Canada for financial support (to G.W.B.) and acknowledge an Ontario Graduate Fellowship to M.J.B. The 500 MHz COSY spectrum of **1** was carried out courtesy of Dr. D. R. Bundle of the National Research Council.

1. C. RAVEL. Hereditas, **61**, 208 (1968).
2. J. J. MULVIHILL. Science, **176**, 132 (1972).
3. C. MATTHEW and Z. AL-DOORI. Mutat. Res. **40**, 31 (1976).
4. R. B. SIMPSON. J. Am. Chem. Soc. **86**, 2059 (1964).
5. S. MANSY, T. E. WOOD, J. C. SPROULES, and R. S. TOBIAS. J. Am. Chem. Soc. **96**, 1762 (1974).
6. E. BUNCEL, A. R. NORRIS, W. J. RACZ, and S. E. TAYLOR. Inorg. Chem. **20**, 98 (1981).
7. P. O. P. TS'O, N. S. KARDO, M. P. SCHWEIZER, and D. P. HOLLIS. Biochemistry, **8**, 997 (1969).
8. F. S. EZRA, C.-H. LEE, N. S. KONDO, S. S. DANYLUK, and R. H. SARMA. Biochemistry, **16**, 1977 (1977).
9. A. BAX and R. FREEMAN. J. Magn. Reson. **42**, 164 (1981).
10. W. J. P. BLONSKI, R. E. HRUSKA, K. L. SADANA, and P. C. LOWEN. Biopolymers, **22**, 605 (1983).
11. D. E. DORMAN and J. D. ROBERTS. Proc. Natl. Acad. Sci. U.S.A. **65**, 19 (1970).
12. H. H. MANTSCH and I. C. P. SMITH. Biochem. Biophys. Res. Commun. **46**, 808 (1972).
13. D. M. CHENG and R. H. SARMA. J. Am. Chem. Soc. **99**, 7333 (1977).
14. L. G. MARZILLI, B. DE CASTRO, J. P. CARADONNA, R. C. STEWART, and C. P. VAN VUUREN. J. Am. Chem. Soc. **102**, 916 (1980).
15. G. W. BUCHANAN and M. J. BELL. Magn. Reson. Chem. **24**, 493 (1986).
16. B. LIPPERT. J. Am. Chem. Soc. **103**, 5691 (1981).
17. P. P. LANKHORST, C. A. G. HAASNOOT, C. ERKELENS, and C. ALTONA. J. Biomol. Struct. Dyn. **1**, 1387 (1984).

Analysis of intramolecular hydrogen bonding in terms of the topological properties of the charge density. The protonated fluoroacetones

SAI CHENG CHOI AND RUSSELL J. BOYD[1]

Department of Chemistry, Dalhousie University, Halifax, N.S., Canada B3H 4J3

Received March 27, 1986

SAI CHENG CHOI and RUSSELL J. BOYD. Can. J. Chem. **64**, 2042 (1986).

A new method for the analysis of intramolecular hydrogen bonding is proposed and applied to the equilibrium structures of the protonated fluoroacetones. The method, based on a theory of molecular structure due to Bader, uses the topological properties of the charge density to elucidate the types of interactions within a molecule of interest. The calculations show a strong basis set dependence. In particular, the STO-3G optimized geometries exhibit intramolecular hydrogen bonding between a fluorine substituent and the carbonyl proton, whereas some calculations with geometries optimized at the 4-31G and 6-31G* levels indicate a direct bonding interaction between the fluorine and oxygen atoms. Two types of catastrophe point, namely conflict and bifurcation, are possible in protonated monofluoroacetone. Only the latter was located in the present calculations.

SAI CHENG CHOI et RUSSELL J. BOYD. Can. J. Chem. **64**, 2042 (1986).

On propose une nouvelle méthode pour analyser les liaisons hydrogènes intramoléculaires et on l'applique aux structures en équilibre dans les fluoroacétones protonées. La méthode, qui est basée sur une théorie de structure moléculaire due à Bader, fait appel aux propriétés topologiques de la densité de charge pour élucider les divers types d'interactions à l'intérieur d'une molécule présentant de l'intérêt. Les calculs démontrent qu'il existe une grande dépendance sur l'ensemble de base choisi. En particulier, des calculs à l'aide de l'ensemble STO-3G avec des géométries optimisées démontre l'existence de liaisons hydrogènes moléculaires entre un substituant fluor et le proton d'un carbonyle; par ailleurs, des calculs aux niveaux 4-31G et 6-31G* avec des géométries optimisées indiquent la présence d'une interaction directe de liaison entre les atomes de fluor et d'oxygène. Les deux types de point de catastrophe, soit le conflit et la bifurcation, sont possibles dans la monofluoroacétone protonée. Seulement le dernier point a pu être localisé dans les calculs effectués jusqu'à maintenant.

[Traduit par la revue]

Introduction

Numerous experimental and theoretical methods exist for the direct investigation of intermolecular hydrogen bonding, whereas evidence for internal or intramolecular hydrogen bonding is generally obtained indirectly. For example, an ion cyclotron resonance study (1) of the gas-phase basicities of six fluorinated acetones has revealed a very regular decrease of 6.1 ± 0.4 kcal/mol in the proton affinity for each successive fluorine substituent. Furthermore, the 2–3 kcal/mol departure from linearity for acetone has been attributed to the formation of an intramolecular hydrogen bond within each of the protonated fluoroacetones.

Previous theoretical studies have used the energy difference between *syn* and *anti* conformations to estimate the intramolecular hydrogen bond energy of selected systems (2–4).

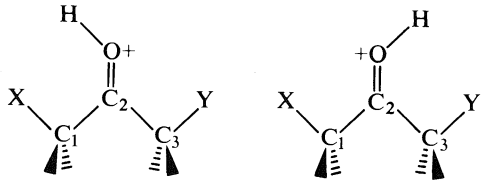

syn *anti*

This method has a number of shortcomings, not the least of which is the fact that application of the method is limited because it is not always possible to choose appropriate *syn* and *anti* conformations. For example, in the protonated form of hexafluoroacetone, positions X and Y are both occupied by fluorine atoms and, therefore, the distinction between the *syn* and *anti* conformations disappears. Moreover, where two appropriate conformations are possible, the energy difference is the net result of all interactions and not simply due to intramolecular hydrogen bonding. Such calculations provide only indirect evidence for hydrogen bonding. As an aside, we note that the two conformations have been detected in some protonated carbonyl compounds (5). In this paper we propose a direct theoretical method for the investigation of intramolecular hydrogen bonding and we apply the method to the protonated fluoroacetones.

The main focus of this paper is on analysis of intramolecular hydrogen bonding in terms of the topological properties (6, 7) of the charge density $\rho(\boldsymbol{r})$. Specifically, the sign of the Laplacian of the charge density, $\nabla^2\rho(\boldsymbol{r})$, is used to determine the existence of local concentrations of charge between two atoms within the molecule of interest. Particular attention is paid to the properties of the bond critical points and the bond paths defined in terms of the gradient of $\rho(\boldsymbol{r})$. The magnitude of the charge density at a bond critical point, $\rho(\boldsymbol{r}_c)$, provides a measure of the bond strength (8). In fact, Bader *et al.* (9) have shown that the bond-length – bond-order relationship of CC bonds in Hückel theory may be generalized to include a variety of hydrocarbons. Their conclusion is based on the observation that the value of the total charge density at a bond critical point is characteristic of a bond of a given formal order. Thus, they observed a linear relationship between $\rho(\boldsymbol{r}_c)$ and the CC bond length. Recently we have shown (10) that there exists a similar relationship between the charge density of the hydrogen-bond critical point of RCN---HF complexes and the NH internuclear distances of the complexes. Moreover, we have some additional calculations which indicate that bond-length – bond-order relationships based on the topological properties of the charge density exist for other examples of intermolecular interactions.

Method

In addition to the MO calculations described previously (11), some supplementary calculations were performed on a Perkin-Elmer 3230 by use of the GAUSSIAN 80 series of programs (12). The bond critical points and bond paths were computed by use of program EXTREM

[1]Author to whom all correspondence should be addressed.

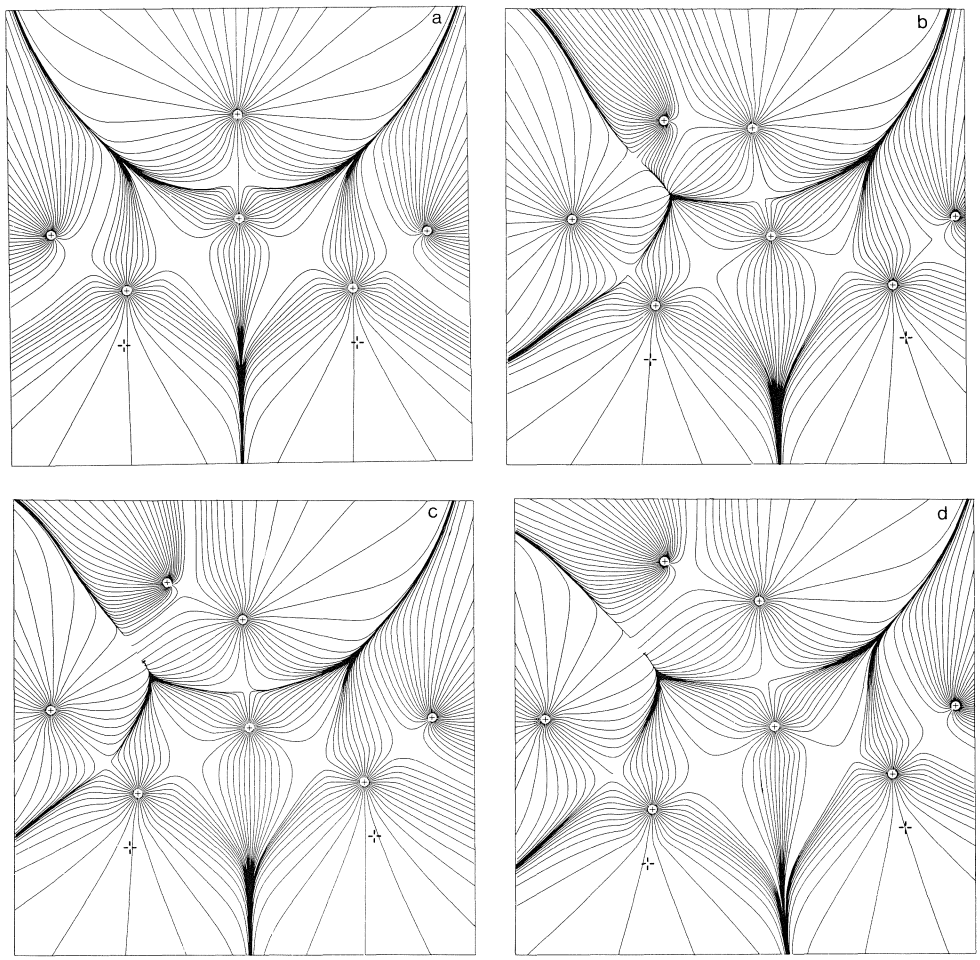

FIG. 1. Gradient vector field of the charge densities: (*a*) acetone, (*b*) $CH_2FCOHCH_3^+$, (*c*) $CH_2FCOHCH_3^+$, (*d*) bifurcation of $CH_2FCOHCH_3^+$. Both (*a*) and (*b*) are at the STO-3G equilibrium geometries while (*c*) is at the 4-31G geometry. Nuclei on the molecular plane are denoted by + while the projections of the out-of-plane nuclei are denoted by -|-.

(13), while plots of the charge density and its Laplacian were obtained by use of program PLOTDEN (13) and a Nicolet Zeta 8 plotter attached to the PE-3230. Program SCHUSS (13) was used to obtain plots of the trajectories or gradient vector field of the charge densities and the molecular graphs.

Results and discussion

Figure 1 shows the gradient vector field of the charge density in a few representative cases, while Fig. 2 displays the corresponding contour maps of the Laplacian of the charge density, $\nabla^2\rho(\boldsymbol{r})$. The cross sign (+) in a gradient vector field diagram refers to the nuclei on the molecular plane while the out-of-plane nuclei are denoted by -|-. Positive values of $\nabla^2\rho(\boldsymbol{r})$ are denoted by solid contours, negative values by dashed contours. The former indicates a depletion of charge density while the latter is just the reverse (14). The molecular graphs of many of the molecules studied are given in Fig. 3 where the bond critical points are denoted by solid circles. Properties at the critical points are listed in Table 1, where the notation A//B indicates that the properties have been calculated at the level of basis set A with the geometry optimized at the level of basis set B.

Figure 1 shows that none of the gradient paths (trajectories) cross zero-flux surfaces and that all trajectories terminate at nuclei. Each atom in a molecule is governed by an interatomic surface which separates neighbouring atoms (7). Furthermore, when two atoms are bonded to each other, a (3, −1) critical point exists between the atoms. The STO-3G calculations for $CH_2FCOHCH_3^+$, $CH_2FCOHCH_2F^+$, and $CF_3COHCH_3^+$ exhibit (3, −1) critical points between fluorine and the carbonyl proton (Fig. 3(*c*), 3(*f*), and 3(*g*), respectively). A F---H bond interaction is also observed (Fig. 3(*h*)) for $CF_3COHCH_3^+$ at the "4-31G" geometry (11). These F---H—O intramolecular hydrogen bonds are consistent with the interpretation of the gas-phase basicities of the protonated fluoroacetones (1). Further insight can be gained by examining the properties of the bond critical point. In particular, the charge density of the F---H bond critical point at the 4-31G//STO-3G level decreases as the number of F atoms increases (Table 1). This indicates a weakening of the bond, which is reflected by the increase in the F—H distance in going from the protonated mono- to trifluorinated acetones. This is similar to the relationship, noted above, between $\rho(\boldsymbol{r}_c)$ and the CC bond length (9). Note that for a X—Y bond where X ≠ Y, the bond critical point (solid circle) in a molecular graph is shifted in accord with the transfer of electrons between atoms (7). In short, the bond critical point of each bond lies nearer to the less electronegative atom of each bonded pair. The relationship between the position of the bond critical point and the polarity of bonds will be discussed in other papers from this laboratory (15, 16).

The 4-31G and 6-31G* basis sets give equilibrium geo-

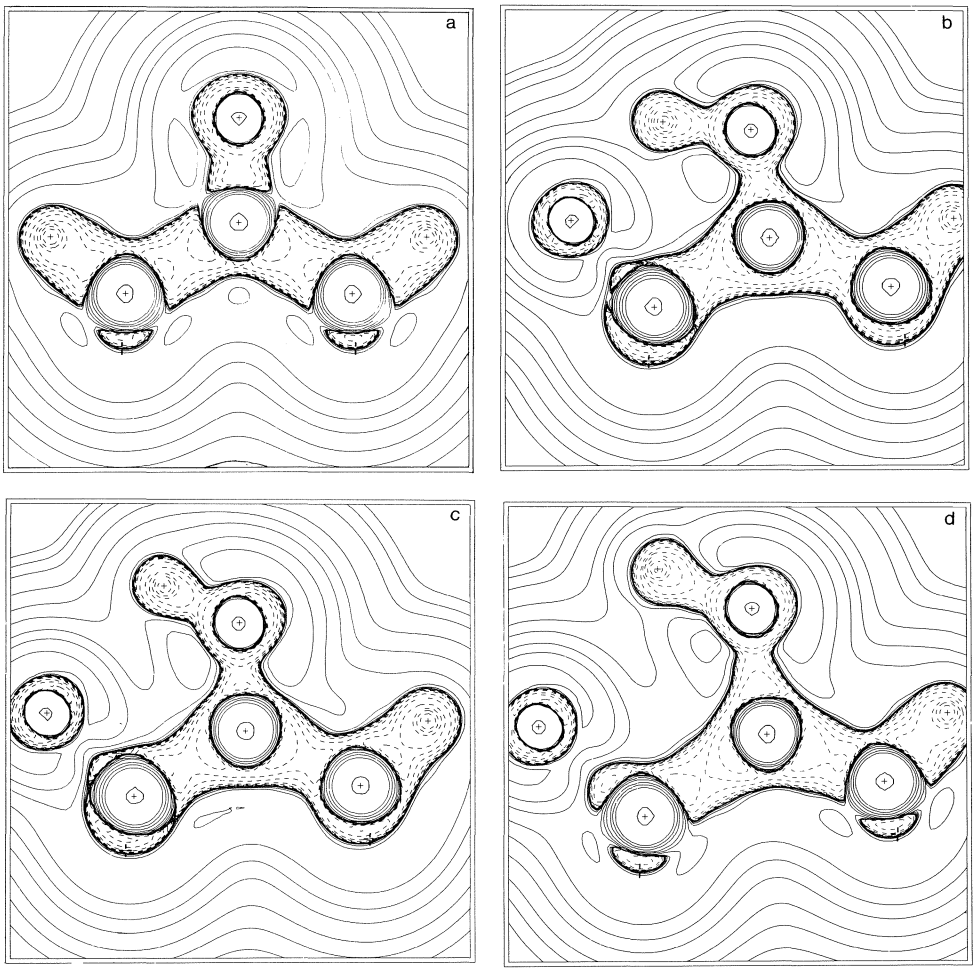

FIG. 2. Contour maps of the Laplacian of atomic densities. The molecules shown are the same as in Fig. 1. The contour values in au are ±0.002, ±0.004, and ±0.008 increasing in powers of 10. The orientations are as shown in the Introduction section. Nuclei on the molecular plane are denoted by + while the projections of the out-of-plane nuclei are denoted by -|-.

metries that show intramolecular bonding between the fluorine and the carbonyl oxygen in $CH_2FCOHCH_3^+$. In order to assess the effect of the choice of basis set on the intramolecular bonding interaction in protonated fluoroacetones, both $CH_2FCOHCH_2F^+$ and $CF_3COHCH_3^+$ were optimized at the 4-31G level. Table 2 summarizes the types of interactions and the bond distances between fluorine and oxygen, and between fluorine and the carbonyl proton. These data suggest that: (*i*) a F---H interaction is observed if the F—H separation is less than about 1.6 Å; and (*ii*) a F---O interaction is observed if the F—H separation is about 2.0 Å and the F—O separation is about 2.5 Å or less. With F—H and F—O separations of 2.1 Å and 2.5 Å, or greater, respectively, no F---H or F---O interactions are observed. To test these conclusions, we carried out STO-3G//STO-3G and 4-31G//4-31G calculations on *o*-fluorophenol. The optimized structures are shown in Fig. 4. No F---H and F---O intramolecular bonding interactions were observed. Moreover, the F---H and F---O internuclear separations are greater than the values for which intramolecular bonding interactions are observed in the protonated fluoroacetones (Table 2). Our calculations support the claim (17) that there is no hydrogen bonding in *o*-fluorophenol due to the larger internuclear separation between fluorine and the carbonyl proton. It is interesting to note that in the case of $CH_2FCOHCH_3^+$, $\rho(\boldsymbol{r}_c)$ of the F---H interaction at the 4-31G//STO-3G level is more than double that of the F---O interaction at the 4-31G//4-31G level. Clearly this indicates a significant bond interaction in the former.

The charge densities of the *syn* and *anti* conformers of $CH_2FCOHCH_3^+$ at the C=O, C_1—F, and O—H bond critical points show considerable differences (Table 1). The decrease in the C=O $\rho(\boldsymbol{r}_c)$ value of the *anti* conformer indicates a weakening of the bond relative to the *syn* conformer. In contrast both the C_1—F and O—H bonds show an increase for $\rho(\boldsymbol{r}_c)$ upon going from the *syn* to the *anti* conformation. Clearly, the substantial changes in $\rho(\boldsymbol{r}_c)$ in the above three bonds should cast doubt on the validity of evaluating the intramolecular hydrogen bond energy by the energy difference between the *syn* and *anti* conformations.

Protonation at the carbonyl oxygen results in a considerable reorganization of charges. As shown in Table 3, the carbonyl oxygen remains negatively charged, and electron transfer to the carbonyl proton decreases as the number of fluorine substituents increases. This is consistent with the inverse dependence of the proton affinity on the number of fluorine substituents (11). The contour maps for $\nabla^2\rho(\boldsymbol{r})$ exhibit noticeable changes within the carbonyl group relative to $CH_3COHCH_3^+$. In addition, replacement of the H at C_1 by F reduces the covalent nature of the C_1—H bond.

Two types of catastrophe point are possible in $CH_2FCOHCH_3^+$,

TABLE 1. Critical point properties[a]

Molecule/bond	$\rho(r_c)^a$	$\nabla^2\rho(r_c)^a$	Molecule/bond	$\rho(r_c)^a$	$\nabla^2\rho(r_c)^a$
CH_3COCH_3			$CH_2FCOHCH_2F^{+\,b}$		
C═O	0.3837	−0.0879	C═O	0.3410	0.0819
C_1–C_2	0.2247	−0.4138	C_1—C_2	0.2511	−0.5430
C_1—H	0.2621	−0.7562	C_2—C_3	0.2524	−0.5599
			C_1—F	0.2176	−0.0928
$CH_3COHCH_3^+$			C_3—F	0.2366	−0.1713
C═O	0.3161	−0.2004	O—H	0.3146	−1.6842
C_1—C_2	0.2274	−0.4326			
C_2—C_3	0.2282	−0.4443	$CF_3COHCH_3^+$		
C_1—H	0.2631	−0.7704	C═O	0.3344	−0.3271
C_3—H	0.2659	−0.8153	C_1—C_2	0.2072	−0.3693
O—H	0.3023	−1.4460	C_2—C_3	0.2241	−0.4354
			C_1—F	0.2362	−0.3365
$CH_2FCOHCH_3^+$			C_3—H	0.2659	−0.8331
C═O	0.3318	−0.3023	O—H	0.2785	−1.3021
C_1—C_2	0.2241	−0.4214	F---H	0.0517	0.2071
C_2—C_3	0.2274	−0.4449			
C_1—F	0.2110	0.0874	$CF_3COHCH_3^{+\,d}$		
C_3—H	0.2657	−0.8249	C═O	0.3357	−0.3288
O—H	0.2768	−1.2747	C_1—C_2	0.2224	−0.4257
F---H	0.0573	0.2247	C_2—C_3	0.2243	−0.4368
			C_1—F	0.2341	−0.3324
$CH_2FCOHCH_3^{+\,b}$			C_3—H	0.2659	−0.8338
C═O	0.3352	0.0607	O—H	0.2775	−1.2914
C_1—C_2	0.2510	−0.5414	F---H	0.0539	0.2104
C_2—C_3	0.2537	−0.5762			
C_1—F	0.2139	−0.0467	$CF_3COHCH_3^{+\,b}$		
C_3—H	0.2658	−0.8216	C═O	0.3391	0.0747
O—H	0.3170	−1.6910	C_1—C_2	0.2439	−0.5128
O---F	0.0251	0.1259	C_2—C_3	0.2527	−0.5847
			C_1—F	0.2589	−0.3631
$CH_2FCOHCH_3^{+\,c}$			C_3—H	0.2660	−0.8276
C═O	0.3737	0.4341	O—H	0.3135	−1.6736
C_1—C_2	0.2834	−0.8841			
C_2—C_3	0.2785	−0.8960	$CH_2FCOHCH_3^+$ (*anti*)		
C_1—F	0.2445	0.4641	C═O	0.3194	−0.2247
C_3—H	0.2826	−1.0644	C_1—C_2	0.2205	−0.4144
O—H	0.3336	−2.1942	C_2—C_3	0.2258	−0.4528
O---F	0.0251	0.1260	C_1—F	0.2320	−0.1781
			C_3—H	0.2634	−0.7806
$CH_2FCOHCH_2F^+$			O—H	0.3003	−1.4410
C═O	0.3343	−0.3234			
C_1—C_2	0.2221	−0.4126			
C_2—C_3	0.2193	−0.4114			
C_1—F	0.2126	0.0528			
C_3—F	0.2333	−0.2198			
O—H	0.2756	−1.2715			
F---H	0.0561	0.2198			

[a]In atomic units at the 4-31G//STO-3G level, except where noted otherwise.
[b]4-31G//4-31G level.
[c]6-31G*//6-31G* level.
[d]4-31G//"4-31G" level, where "4-31G" refers to the partial optimizations described in ref. 11.

namely, the conflict and the bifuraction types (18) from the STO-3G and 4-31G geometries, respectively. A catastrophe point can be defined as a point in control space where a discontinuous change in the molecular behaviour is observed (8). The difference between conflict and bifurcation catastrophe points is that the former is one in which a bond switches from one nucleus to another nucleus, while the latter is due to the formation of a singularity in the charge density. Needless to say both types of catastrophe points are structurally unstable. A bifurcation catastrophe point can be obtained by elongation of the F—O distance of $CH_2FCOHCH_3^+$ from its 4-31G equilibrium value of 2.454 Å (see Fig. 1(*d*)). The coalescence of the bond and ring critical points occurs at an O—F distance of about 2.819 Å, as illustrated in Fig. 3(*i*). The exact location of the bifurcation point cannot be located due to the low symmetry (C_s) of the molecule. Even in water, which is a simpler molecule of higher symmetry, the position of the coalescence of the bond and ring critical points can only be determined to within ±0.03 Å (19). A conflict catastrophe point can be observed when the F—H distance is increased from the

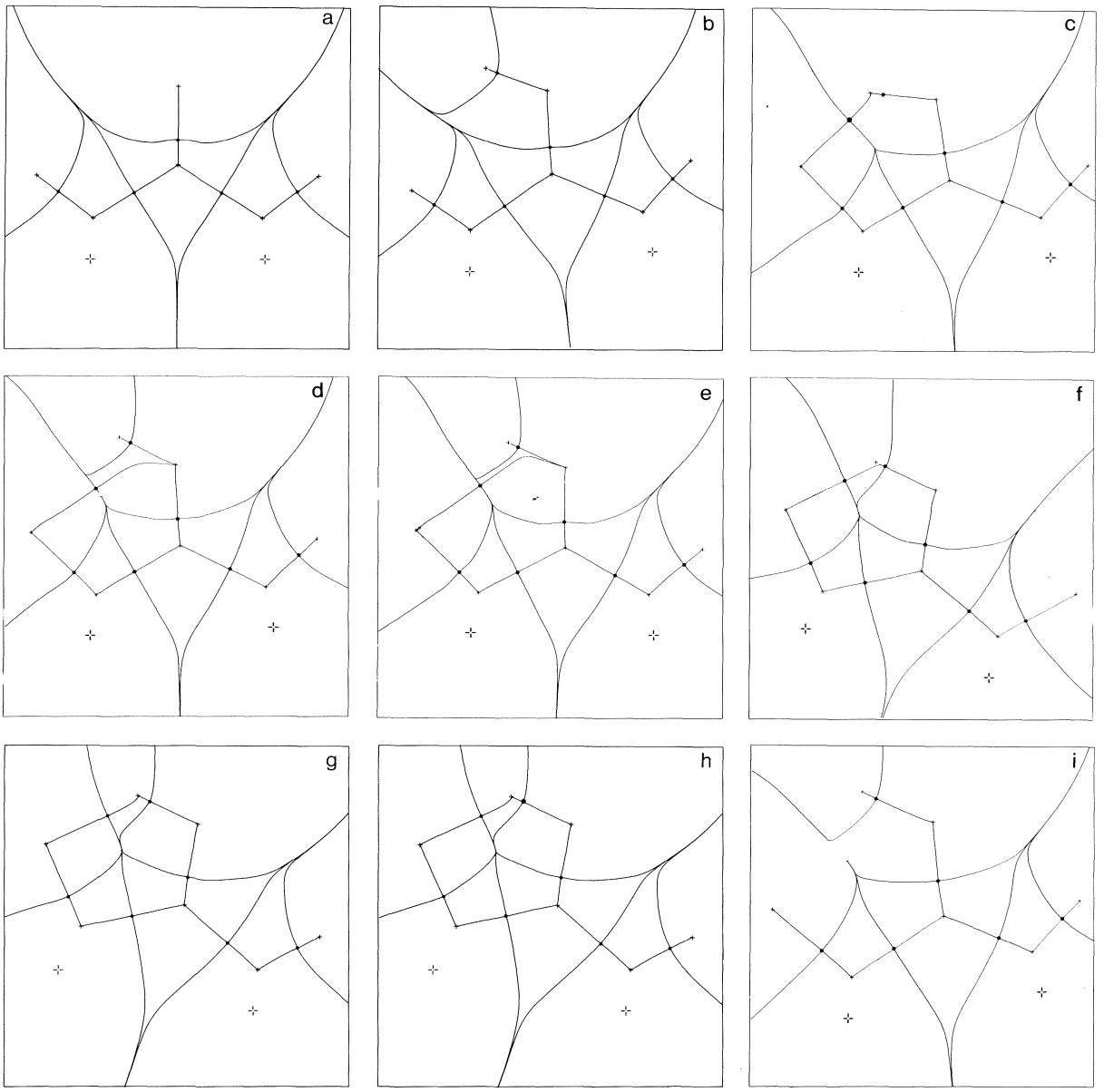

FIG. 3. Molecular graphs: (*a*) acetone, (*b*) $CH_3COHCH_3^+$, (*c*)–(*e*) $CH_2FCOHCH_3^+$, (*f*) $CH_2FCOHCH_2F^+$, (*g*)–(*h*) $CF_3COHCH_3^+$, (*i*) bifurcation of $CH_2FCOHCH_3^+$. All molecules are at the STO-3G equilibrium geometries except for (*d*), (*e*), and (*h*) which are at the 4-31G, 6-31G*, and "4-31G" equilibrium geometries, respectively. Nuclei on the molecular plane are denoted by + while the projections of the out-of-plane nuclei are denoted by ⊹.

TABLE 2. Selected internuclear distances and types of interaction

Species	Method	Internuclear distance[a] F---H	Internuclear distance[a] F---O	Type of interaction
$CH_2FCOHCH_3^+$	4-31G//STO-3G	1.563	2.334	F---H
	4-31G//4-31G	2.004	2.454	F---O
	6-31G*//6-31G*	1.959	2.487	F---O
$CH_2FCOHCH_2F^+$	4-31G//STO-3G	1.571	2.339	F---H
	4-31G//4-31G	2.107	2.515	None
$CF_3COHCH_3^+$	4-31G//STO-3G	1.602	2.357	F---H
	4-31G//"4-31G"	1.584	2.343	F---H
	4-31G//4-31G	2.190	2.573	None
o-Fluorophenol	STO-3G//STO-3G	2.158	2.747	None
	4-31G//4-31G	2.306	2.724	None

[a]In Å.

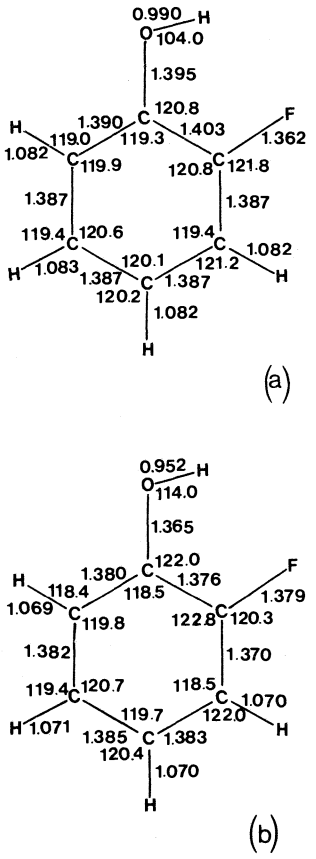

FIG. 4. Optimized C_s equilibrium geometry of *o*-fluorophenol: (*a*) STO-3G level, (*b*) 4-31G level.

TABLE 3. Mulliken population data for $RCOR'H^+$ at 4-31G//STO-3G

R	R′	Oxygen electron population[a]	e^- transfer to H^+	e^- loss by CO	π–e^- gain by CO
CH_3	CH_3	8.603 (8.561)	0.498	0.073	0.113
CH_2F	CH_3	8.586 (8.526)	0.453	0.023	0.099
CH_2F	CH_2F	8.557 (8.491)	0.450	0.007	0.097
CHF_2	CH_3	8.569 (8.522)	0.448	0.021	0.084
CF_3	CH_3	8.562 (8.484)	0.446	0.054	0.087
CHF_2	CH_2F	8.557 (8.488)	0.436	−0.032	0.070
CHF_2	CHF_2	8.539 (8.480)	0.429	−0.041	0.046
CF_3	CH_2F	8.561 (8.500)	0.436	0.008	0.081
CF_3	CHF_2	8.518 (8.441)	0.424	−0.026	0.041
CF_3	CF_3	8.510 (8.402)	0.424	0.010	0.038

[a]Values in parentheses are those of the bases RCOR′.

STO-3G value of 1.563 Å to not more than the 4-31G value of 2.004 Å in $CH_2FCOHCH_3^+$. Unfortunately the low symmetry of this molecule hindered efforts to locate this unstable structure.

Acknowledgements

The authors are grateful to Professor R. F. W. Bader for many helpful discussions and the hospitality extended to one of us (S.C.C.) during visits to McMaster University. The financial support of the Natural Sciences and Engineering Research Council of Canada is gratefully acknowledged.

1. D. F. DRUMMOND and T. B. MCMAHON. J. Phys. Chem. **85**, 3746 (1981).
2. R. JOST, J. SOMMER, and G. WIPFF. Nouv. J. Chim. **2**, 63 (1977).
3. R. L. DEKOCK, C. P. JASPERSE, and M. S. KONINGS. J. Mol. Struct. (THEOCHEM). **94**, 343 (1983).
4. P. GEORGE, C. W. BOCK, and M. TRACHTMAN. J. Mol. Struct. (THEOCHEM). **92**, 109 (1983).
5. G. A. OLAH and D. H. O'BRIEN. J. Am. Chem. Soc. **89**, 3582 (1967).
6. R. F. W. BADER, Y. TAL, S. G. ANDERSON, and T. T. NGUYEN-DANG. Israel J. Chem. **19**, 8 (1980).
7. R. F. W. BADER, T. T. NGUYEN-DANG, and Y. TAL. Rep. Prog. Phys. **44**, 893 (1981).
8. R. F. W. BADER, T. H. TANG, Y. TAL, and F. W. BIEGLER-KONIG. J. Am. Chem. Soc. **104**, 940 (1982).
9. R. F. W. BADER, T. H. TANG, Y. TAL, and F. W. BIEGLER-KONIG. J. Am. Chem. Soc. **104**, 946 (1982).
10. R. J. BOYD and S. C. CHOI. Chem. Phys. Lett. **120**, 80 (1985).
11. S. C. CHOI and R. J. BOYD. Can. J. Chem. **63**, 836 (1985).
12. J. S. BINKLEY, R. A. WHITESIDE, R. KRISHNAN, R. SEEGER, D. J. DEFREES, H. B. SCHLEGEL, S. TOPIOL, L. R. KAHN, and J. A. POPLE. GAUSSIAN 80. Department of Chemistry, Carnegie-Mellon University, Pittsburgh, PA, USA.
13. R. F. W. BADER. Department of Chemistry, McMaster University, Hamilton, Ont., Canada L8S 4M1.
14. R. F. W. BADER and H. ESSEN. J. Chem. Phys. **80**, 1943 (1984).
15. K. E. EDGECOMBE and R. J. BOYD. Int. J. Quantum Chem. **29**, 959 (1986).
16. R. J. BOYD and K. E. EDGECOMBE. J. Comput. Chem. To be published.
17. E. A. ALLAN and L. W. REEVES. J. Phys. Chem. **66**, 613 (1962).
18. Y. TAL, R. F. W. BADER, and J. ERKKU. J. Phys. Rev. A, **21**, 1 (1980).
19. R. F. W. BADER, T. T. NGUYEN-DANG, and Y. TAL. J. Chem. Phys. **70**, 4316 (1979).

Motional and conformational dynamics in a homologous series of smooth muscle relaxing agents

GIANNI VALENSIN,[1] ELENA GAGGELLI, AND ANDREA LEPRI
Department of Chemistry, University of Siena, Pian dei Mantellini 44, 53100 Siena, Italy

AND

ALESSANDRO SEGA
Institute of Organic Chemistry, University of Siena, Pian dei Mantellini 44, 53100 Siena, Italy

Received January 16, 1986

GIANNI VALENSIN, ELENA GAGGELLI, ANDREA LEPRI, and ALESSANDRO SEGA. Can. J. Chem. **64**, 2048 (1986).

Dynamic features were investigated in a homologous series of synthesized drugs having pharmacologic activity, with particular emphasis on relative motions of the two side chains anchored to a backbone of two aromatic rings linked by an amide bridge. A general and deep insight was reached by using a model-free approach. Conformational and motional dynamics within the compound exhibiting maximum activity were delineated and the most relevant parameters for pharmacologic action were defined.

GIANNI VALENSIN, ELENA GAGGELLI, ANDREA LEPRI et ALESSANDRO SEGA. Can. J. Chem. **64**, 2048 (1986).

On a étudié les caractéristiques dynamiques d'une série homologue de médicaments synthétiques ayant une activité pharmacologique en insistant particulièrement sur les mouvements relatifs des deux chaînes latérales attachées au squelette de deux cycles aromatiques liés par un pont amide. L'utilisation de l'approche du modèle libre a permis d'avoir une connaissance générale et profonde de ces substances. On a délimité les dynamiques conformationnelles et les dynamiques du mouvement dans le composé qui a une activité maximale et on a défini les paramètres les plus significatifs de l'action pharmacologique.
[Traduit par la revue]

Introduction

p(*o*-Alkyloxybenzamido)benzoate diethyl(2-hydroxyethyl)-methylammonium halides (see formula) are synthesized drugs that exhibit a smooth muscle relaxing property (1). Investigations of their pharmacologic activities demonstrated a striking dependence upon length and position of the alkyloxy sidechain. The *ortho*-substituted compounds were by far the most effective and a sharp maximum of activity could be shown for the octyloxy (n = 7) derivative; this derivative is moreover almost completely devoid of central ocular and cardiovascular atropine-like side effects when administered in doses producing spasmolytic effects comparable with those of *N*-butylscopolammonium bromide (2, 3).

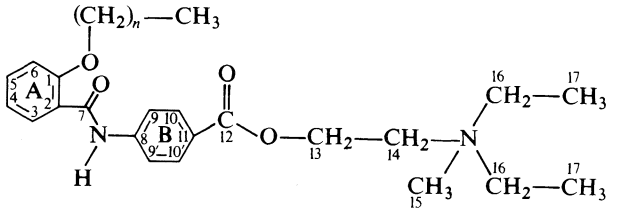

We have previously delineated the first term of the series (n = 2) for conformation and dynamics of the two aromatic moieties by exploiting ^{1}H nmr selective and nonselective relaxation rate measurements, ^{1}H–^{1}H intramolecular nOes (nOe, nuclear Overhauser effect), and ^{13}C nmr relaxation rate measurements (4, 5). The preferred conformations of the two aromatic rings were inferred by evaluating proton–proton distances, and a molecular model was built in which complete motional freedom was allowed for the two hydrocarbon side chains.

In a first attempt to correlate pharmacologic activity and conformational features, calculations were extended to other alkyloxy derivatives (n = 3, n = 7, n = 9) (6). Substantial differences in the spatial arrangement of the two aromatic moieties at increasing length of the alkyloxy chain were inferred: the most active octyloxy derivative was shown to assume a configuration in which the angles between each aromatic ring and the plane of the amide unit were almost equal (±55° and ±53°). Moreover, ^{1}H 2D-magnetization transfer experiments (6) demonstrated that, in the case of the octyloxy derivative only, an intramolecular dipolar connectivity exists between methyl groups of the two side chains. Also in agreement with these findings, X-ray analysis of single crystals suggested folding of the alkyloxy side chain towards the diethylmethylammonium moiety, but only in the case of the most active compound was a "closed" structure found (7).

We present hereafter the whole picture of nmr data for the four compounds of the series, from which a complete dilineation of motional and conformational dynamics is reached. Besides the aromatic backbone already investigated, attention is focussed on the hydrocarbon side chains in order to arrive at a thorough understanding of structural parameters relevant for biological activity.

Results and discussion

The ^{13}C spin-lattice relaxation rates (R_1's) are almost exclusively determined by dipolar interactions with directly bonded or nearby protons (8) thus allowing suitable delineation of the molecular dynamics. ^{13}C R_1 values are summarized in Table 1 for the four compounds. We first considered motional features of aromatic carbons that have fewer degrees of freedom with respect to the two side chains, as in the analysis previously carried out for compound **1** (n = 2) (4). The relaxation rate of C5 (the carbon *para* to the amide bridge) is always faster than those of the other aromatic carbons; it follows that C2—C5 is always the main rotation axis for ring A despite the increasing length and weight of the alkyloxy chain in the *ortho* position. Passing from n = 2 to n = 3 to n = 9, this motion slows down, which is very likely due to the effect of the alkyloxy chain. The

[1]Author to whom correspondence may be addressed.

TABLE 1. ^{13}C spin-lattice relaxation rates (R_1) for *p*(*o*-alkyloxybenzamido)benzoate diethyl(2-hydroxyethyl)methylammonium halides 0.2 mol dm^{-3} in DMSO-d_6 at 298 K[a]

	R_1			
Carbon	$n = 2$	$n = 3$	$n = 7$	$n = 9$
C1	0.18	0.22	0.22	0.31
C2	0.14	0.19	0.17	0.20
C3	3.00	3.37	4.37	5.18
C4	2.77	3.73	4.06_5	4.83
C5	4.93	6.71	6.02	7.19
C6	3.11	3.86	4.93	4.97_5
C7	0.17	0.19	0.22	0.23
C8	0.30	0.37	0.42	0.46
C9,9′	2.86	4.11_5	3.66	3.85
C10,10′	2.72_5	3.51	3.68	3.94
C11	0.21	0.27	0.26	0.25
C12	0.16	0.24	0.26	0.30
C13	5.92	5.71	6.41	6.41
C14	4.63	4.59	5.46	4.93
C15	2.69_5	3.62	3.69	3.30
C16	3.73	4.40_5	5.18	4.06_5
C17	0.81	1.12	1.39_5	1.03
C18	2.62_5	2.86	4.78_5	4.65
C19	1.13	1.67	0.94	0.74
C20	0.38	0.77	1.88	2.37_5
C21		0.46	1.66	0.90
C22			1.47	1.85_5
C23			0.94	1.53
C24			0.63	1.90
C25			0.33	0.74
C26				0.50
C27				0.28

[a]Errors ranged between 4 and 6%.

matter is, however, not simple since the motion around the C2—C5 axis reaches a relative minimum for $n = 7$ (6.02 s^{-2} against 6.71 s^{-1} for $n = 3$). The relaxation rates of the other carbons in ring A steadily increase along the series with increasing length of the alkyloxy chain, from a mean value of 2.97 s^{-1} ($n = 2$) to 3.67 s^{-1} ($n = 3$), 4.47 s^{-1} ($n = 7$), and 5.00 s^{-1} ($n = 9$). Consequently, the librational motions of ring A, accompanying the main rotational motion around the C2—C5 axis, are slowed down by the increasing size of the substituent. It should be observed that, as a consequence of the relative minimum reached in the relaxation rate of C5 for $n = 7$, this compound exhibits the lowest difference between the rates of the main rotational motion and librational motions. In fact the ratio between R_1 (*para*) and the average R_1 of the other protonated ring carbons (9) is 1.66, 1.84, 1.35, and 1.44 for $n = 2$, 3, 7, and 9 respectively.

The C8—C11 axis is naturally the main rotational axis for ring B. The relaxation rates of C9,9′ and C10,10′ steadily increase along the series from $n = 2$ to $n = 9$; the overall increment (1.0 s^{-1}) is, however, much less pronounced than that observed for ring A (2.0 s^{-1}), the former being one-half of the latter. Clearly, motions of ring B are less markedly affected by the alkyloxy chain. Librational motions of ring B therefore become faster than those of ring A: for $n = 2$, $n = 3$, and, to a lesser extent, $n = 7$, the two librational motions occur at the same or at very similar velocities, whereas dephasing is accomplished for $n = 9$. The relaxation data can be rationalized in terms of an anisotropic model made by rotational reorientation around the two molecular axes with some degrees of internal motion (8), as already done for the first term of the series (4). The values of the calculated correlation times are reported in Table 2. The most important feature to be inferred is the matching of librational motions with the main rotational motion for $n = 7$, while librational motions of the two rings are still governed by approximately the same correlation time (see Table 2).

Motional delineation of the side chains was then attempted in the light of the surprising intramolecular dipolar connectivity between protons of the terminal methyl of the octyloxy chain and protons of the methyls of the ethyl groups bonded to the quaternary nitrogen (6). When analyzing ^{13}C R_1's of the compound with $n = 2$, it was noticed that C13 was undergoing a reorientational motion very close to that of the aromatic rings while, on the contrary, the ^{13}C R_1 of C18 suggested that motions of the propyloxy chain were faster than those in the backbone.

Quantitative evaluation of motional features within the four compounds was approached in terms of the model-free approach of Lipari and Szabo (10, 11). According to these authors, dynamic information on fast internal motions in an nmr relaxation experiment on molecules in solution can be specified by a "generalized" order parameter, ζ^2, and an effective correlation time, τ_e, that can be calculated either by ^{13}C R_1's and ^{13}C–{^1H} nOes at one frequency or by ^{13}C R_1's at two frequencies. Instead of assuming any given model of molecular motion, such an approach allows immediate inference on local steric hindrances experienced by molecular motions and on the way such hindrances develop along any hydrocarbon chain. It therefore appeared to be the most suitable method for pointing out eventual differences in local order parameters for homologous compounds, where the length of one side chain exclusively determines the conformation assumed in solution.

Following the procedure presented by Lipari and Szabo we selected C6 as the carbon atom of the backbone to which motional features of carbon atoms in the side chains refer. In fact, the alkyloxy chain is motionally linked to ring A, as suggested by the strong ^1H–^1H dipolar connectivity between H6 and H18 shown by all the compounds (the ^1H–^1H H18–{H6} nOe ranges from 0.072 ($n = 2$) to 0.038 ($n = 9$)) (5, 6). Such connectivity was already explained in terms of folding of the initial segments of the alkyloxy chain towards ring A. The decreasing nOe is again a consequence of slowing down motions with increasing chain length. If the ^{13}C–{^1H} nOes of the four compounds (Table 3) are considered and compared to the R_1 values (Table 1), it is apparent that, while all the aromatic protonated carbons of ring A but C5 exhibit the same relaxation behavior, the nOe is similar for C3 and C4 but much lower for C6. The ^{13}C relaxation rates, under broadband proton decoupling and in the extreme narrowing region, are mainly determined (12, 13) by single-quantum (W_1) and double-quantum (W_2) relaxation transition probabilities among the four energy levels of the AX spin system. Thus only fast motions are relevant for spin-lattice relaxation, and slow superimposed motions, if any, cannot be detected. On the contrary the ^{13}C–{^1H} nOe also includes a contribution, to a variable extent, by the zero-quantum (W_0) relaxation transition probability and it is therefore more suited to detect eventual slow-motion components. The lower nOe for C6 was, as a consequence, thought to result from the presence of a slowly modulated ^{13}C–^1H interaction, the observed nOe being proportional to $W_2 - W_0$. To further support such an interpretation, the

TABLE 2. Correlation times (s) for the main rotational motion (τ_R) and for internal motions (τ_G) of selected carbons of *p*(*o*-alkyloxybenzamido)benzoate diethyl(2-hydroxyethyl)methylammonium halides 0.2 mol dm^{-3} in DMSO-d_6 at 298 K

Motion	Correlation times (s)			
	$n = 2$	$n = 3$	$n = 7$	$n = 9$
τ_R(C5)	2.17×10^{-10}	2.96×10^{-10}	2.60×10^{-10}	3.17×10^{-10}
τ_G(C3, C4, C6)	7.26×10^{-11}	7.78×10^{-11}	1.84×10^{-10}	1.62×10^{-10}
τ_G(C9, C10)	6.22×10^{-11}	8.51×10^{-11}	0.97×10^{-10}	7.96×10^{-11}

TABLE 3. ^{13}C–{^{1}H} nOes for *p*-(*o*-alkyloxybenzamido)benzoate diethyl(2-hydroxyethyl)methylammonium halides 0.2 mol dm^{-3} in DMSO-d_6 at 298 K

Carbon	nOe			
	$n = 2$	$n = 3$	$n = 7$	$n = 9$
C1	1.30	1.58	1.55	2.00
C2	1.75	1.77	1.80	1.67
C3	2.41	2.89	2.64	2.87
C4	2.30	2.92	2.33	2.96
C5	2.74	2.98	2.52	2.64
C6	1.74	1.70	1.86	2.23
C7	1.52	1.62	1.72	1.45
C8	1.79	1.94	1.71	2.13
C9,9′	2.08	2.26	2.42	2.75
C10,10′	2.84	2.64	2.92	2.98
C11	1.17	1.54	1.25	1.72
C12	1.56	1.83	1.56	2.24
C13	2.35	2.51	2.41	2.93
C14	2.77	2.85	2.98	2.83
C15	2.98	2.49	2.43	2.93
C16	2.23	2.18	2.11	2.53
C17	2.63	2.75	2.53	2.98
C18	1.53	1.73	1.96	2.32
C19	2.80	2.82	2.68	2.98
C20	2.28	2.87	2.98	2.86
C21		2.41	2.98	2.98
C22			1.79	2.79
C23			2.68	2.98
C24			2.65	2.98
C25			2.24	2.98
C26				2.60
C27				2.38

spin–spin relaxation rates (R_2's) of aromatic protonated carbons of ring A (Table 4) demonstrated that (*i*) $R_1 \ll R_2$, such that a single correlation time cannot account for modulation of the whole motional features of the various ^{13}C—^{1}H vectors; (*ii*) R_2 of C6 is faster than those of C3 and C4, demonstrating that slow-motion components are much more effective for C6 than for the other two carbons.

According to one of the possible procedures, the measured ^{13}C R_1's (Table 1) and ^{13}C–{^{1}H} nOes (Table 3) at 50.3 MHz were used in the following equations whereby ζ^2 and τ_e were directly extracted:

$$\zeta^2 = \frac{R_1(2.988 - \mathrm{nOe})}{R_{1_0}(2.988 - \mathrm{nOe}_0)}$$

and

TABLE 4. ^{13}C spin–spin relaxation rates for selected carbons of *p*-(*o*-octyloxybenzamido) benzoate diethyl(2-hydroxyethyl)methylammonium bromide 0.2 mol dm^{-3} in DMSO-d_6 at 298 K

Carbon	R_2 (s^{-1})
C3	11.76
C4	12.99
C5	10.99
C6	13.89

$$\frac{\hbar^2 \gamma_C^2 \gamma_H^2}{r_{CH}^6} \tau_e = \frac{\mathrm{nOe} - \mathrm{nOe}_0}{R_1^{-1}(2.988 - \mathrm{nOe}_0) - R_{1_0}^{-1}(2.988 - \mathrm{nOe})}$$

where R_{1_0} and nOe_0 are the relaxation parameters describing the main isotropic motion to which the actual internal motion is referred. This is not apparently our case; however, since the aim is the comparison among relative motions of homologous side chains, we used the isotropic expressions referring the internal motion to the slowest reorienting C—H vector, that is, to C6. The values of ζ^2 and τ_e calculated in such a way are reported in Tables 5 and 6 respectively.

According to Lipari and Szabo, ζ, the "generalized" order parameter, is a model-independent measure of the degree of spatial restriction of the motion, such that

$$0 \leq \zeta^2 \leq 1$$

If the internal motion of any particular C—H vector is isotropic, $\zeta^2 = 0$, while if the same motion is completely restricted, $\zeta^2 = 1$. Inspection of Table 5 shows that very high values of ζ^2 are found for C18, in agreement with the already mentioned motional connection between the C18 methylene and ring A, thus ratifying the interpretation of restricted motion for the first segment of the alkyloxy chain. A very interesting feature is the large value of ζ^2 for C22 within the octyloxy chain in the compound with $n = 7$ ($\zeta^2 = 0.316$). This value is much greater than that corresponding to the Woessner model ($\zeta^2 = 0.111$, for axially symmetric motion) (14). If it is considered that C22 has a middle chain position relatively far from the almost anchored C18, it may be stated that the conformational freedom of the octyloxy chain ($n = 7$) is somehow reduced with respect to the decyloxy chain ($n = 9$). This is further ratified by the fact that for the least restricted carbon atom for $n = 7$ (C21) ζ^2 is more than one order of magnitude greater than for the least restricted

TABLE 5. Comparison of the generalized order parameter ζ^2 for selected carbons of *p*-(*o*-alkyloxybenzamido)benzoate diethyl(2-hydroxyethyl)methylammonium halides 0.2 mol dm^{-3} in DMSO-d_6 at 298 K[a]

	ζ^2			
Carbon	$n = 2$	$n = 3$	$n = 7$	$n = 9$
C13	0.966	0.545	0.661	0.097
C14	0.261	0.125	0.008	0.200
C15	0.005	0.362	0.366	0.052
C16	0.730	0.711	0.815	0.489
C17	0.075	0.052	0.114	0.002
C18	0.984	0.720	0.880	0.826
C19	0.048	0.057	0.051	0.002
C20	0.181	0.019	0.030	0.079
C21		0.054	0.026	0.004
C22			0.316	0.099
C23			0.051	0.003
C24			0.038	0.004
C25			0.044	0.002
C26				0.051
C27				0.045

[a]Errors were ranged between 12 and 16%.

TABLE 6. Comparison of effective correlation times τ_e (ns) for selected carbons of *p*-(*o*-alkyloxybenzamido)benzoate diethyl(2-hydroxyethyl)methylammonium halides 0.2 mol dm^{-3} in DMSO-d_6 at 298 K

	τ_e			
Carbon	$n = 2$	$n = 3$	$n = 7$	$n = 9$
C13	0.417	0.390	0.458	0.323
C14	0.254	0.231	0.269	0.242
C15	0.132	0.172	0.146	0.158
C16	0.267	0.282	0.310	0.157
C17	0.031	0.047	0.046	0.050
C18	0.014	0.013	0.184	0.153
C19	0.050	0.075	0.036	0.036
C20	0.009	0.035	0.092	0.106
C21		0.013	0.081	0.093
C22			0.007	0.074
C23			0.036	0.075
C24			0.023	0.093
C25			0.006	0.036
C26				0.013
C27				0.003

carbon atoms for $n = 9$ (C19) and C25). In general the ζ^2 values for $n = 7$ are of the same order of magnitude as those for $n = 2$ and $n = 3$ (with the remarkable exception of C22). Then only for $n = 9$ is the alkyloxy chain characterized by a certain degree of conformational freedom.

The same analysis has been extended to the quaternary nitrogen side chain, maintaining C6 as the reference carbon atom. In fact, although the activity depends on the length of the alkyloxy chain, an interaction between the terminal methyls of the two side chains was strongly suggested by ^{1}H 2D nOe measurements (6), indicating that a "loop" conformation could be the most important or, at least, one of the most important conformational features. It is therefore relevant to delineate motions within the quaternary nitrogen side chain in connection with motions within the alkyloxy side chain.

For $n = 2$, $\zeta^2 = 0.966$ was found for C13, a value that confirms what had been already interpreted on the basis of ^{13}C R_1's (R_1(C6) = 3.11 s^{-1} as compared with $\frac{1}{2}R_1$(C13) = 2.96 s^{-1}). C—H vectors within the C13 methylene are reorienting in close connection with librational motions of aromatic rings; thus selecting C6 as a motional reference brings about a value of ζ^2 close to 1 for C13. For $n = 3$ and also for $n = 7$, motions of C13 are still spatially restricted, whereas for $n = 9$ such motions are far less hindered. By considering all ζ^2 values for these side chains it is apparent that the most restricted motions belong to the $n = 7$ compound where, in particular, the alkyl substituents undergo very hindered reorientations. It is worth stating again that terms such as "spatially restricted" or "hindered" must be taken on a relative scale, the calculated order parameter being referred to the motion of the alkyloxy chain. It can be concluded that the octyloxy derivative (the most active compound) displays the lowest conformational freedom, which can explain the detection of the otherwise surprising dipolar connectivity between the terminal methyls.

The effective correlation times, τ_e (see Table 6), depend on both the microscopic diffusion constants and the spatial nature of the motion. As a consequence, the interpretation of τ_e values is more complicated than that of ζ^2 values; in fact, while ζ^2 is a model-free parameter by definition, the effective correlation times can be related to microscopic rate constants only within the framework of a particular dynamic model (14–18). Generally speaking, any such model contains at least one adjustable rate parameter that is intrinsically flexible, making it possible to reproduce the τ_e values in any model. Since simple models are not suitable for the complete analysis of our data, we preferred not to introduce any motional model and limited ourselves to a qualitative discussion of dynamic features. It should in any case be noticed that ζ^2 and τ_e values exhibit different trends such that spatial restriction of the motion does not always correspond to lengthening of effective correlation times.

By considering the ζ^2 values and the conformational features previously established, a consistent picture of motional and conformational dynamics of the four molecules can be obtained. The following results are a consequence of increasing length of the alkyloxy chain.

(*i*) The preferred conformations of the benzanilide moiety change: the angle between ring A and the plane of the amide bridge steadily increases from ±15° ($n = 2$) to ±75° ($n = 9$) while the angle between ring B and the same plane steadily decreases from ±60° ($n = 2$) to ±48° ($n = 9$) (6). In the biologically most active compound ($n = 7$), the two dihedral angles have very similar values (±55° and ±53° respectively) yielding conformations having the two rings either parallel or nearly perpendicular to each other.

(*ii*) The mean rotational correlation time of the rings increases (the motion slows down), with the exception of the $n = 7$ compound. The librational motions of the two rings follow the same trend: they increase from $n = 2$ to $n = 7$ and decrease for $n = 9$. The whole motional picture of the aromatic moieties is such that the most active compound is characterized by librational motions of the two rings still very close to each other and also close to the main rotational motion; as a consequence this compound exhibits the most limited internal motions.

(*iii*) The analysis of ζ^2 values points out the overall greater

spatial constraints presented by the two side chains in the case of $n = 7$ as compared to the other terms of the homologous series; this loss of conformational freedom could explain the ^{1}H 2D nOe between the terminal methyls (6), and it is, at the same time, in agreement with the restriction of internal motions within the aromatic moieties.

As far as the relationship between pharmacologic activity and position and length of the alkyloxy chain is concerned, the following general conclusion can be reached: intramolecular interaction between the ends of the two side chains must be important. This being the case, as strongly suggested by present and previous results, the sharp decrease of activity in the case of *meta*- or *para*-substituted molecules (whatever the length of the alkyloxy chain) could also be explained.

Experimental

The compounds investigated were synthesized as already described (1). Solutions were made in 99.96% DMSO-d_6 and were carefully deoxygenated. The nmr spectra were registered on a Varian XL-200 spectrometer in the pulse FT mode at probe temperatures of 25 ± 1°C; chemical shifts were referenced to internal TMS.

Spin-lattice relaxation rates were measured with the inversion recovery pulse sequence $(t-\pi-\tau-\pi/2)_n$; spin–spin relaxation rates were measured with the Carr–Purcell–Meiboom–Gill pulse sequence; 100 FIDs were collected in both cases. R_1 and R_2 values were calculated from exponential regression analysis of the recovery or decay curves of longitudinal or transverse magnetization components respectively by using the computer of the spectrometer.

The ^{13}C–{^{1}H} nOes were calculated by comparing peak intensities measured on fully relaxed ^{13}C spectra obtained under conditions of continuous and gated broadband decoupling.

1. M. Ghelardoni, V. Pestellini, N. Pisanti, and G. Volterra. J. Med. Chem. **16**, 1063 (1973).
2. C. A. Maggi, G. Grimaldi, G. Volterra, and A. Meli. Drugs Exp. Clin. Res. **9**, 235 (1983).
3. C. A. Maggi and A. Meli. Arch. Int. Pharmacodyn. **264**, 305 (1983).
4. G. Valensin, L. Pogliani, M. Ghelardoni, V. Pestellini, and A. Sega. Can. J. Chem. **62**, 2131 (1984).
5. A. Sega, M. Ghelardoni, V. Pestellini, L. Pogliani, and G. Valensin. Org. Magn. Reson. **22**, 649 (1984).
6. A. Sega, E. Gaggelli, and G. Valensin. Magn. Reson. Chem. **23**, 649 (1985).
7. P. Dapporto and A. Sega. Acta Crystallogr. Ser. C. In press.
8. A. Allerhand, D. Doddrell, and R. Komoroski. J. Chem. Phys. **55**, 189 (1971).
9. G. C. Levy, J. D. Cargioli, and F. A. L. Anet. J. Am. Chem. Soc. **95**, 1527 (1973).
10. G. Lipari and A. Szabo. J. Am. Chem. Soc. **104**, 4546 (1982).
11. G. Lipari and A. Szabo. J. Am. Chem. Soc. **104**, 4559 (1982).
12. J. H. Noggle and R. E. Schirmer. The nuclear Overhauser effect. Academic Press, New York. 1971.
13. I. D. Campbell and R. Freeman. J. Chem. Phys. **58**, 2666 (1973).
14. D. E. Woessner. J. Chem. Phys. **36**, 1 (1962).
15. R. J. Wittebort and A. Szabo. J. Chem. Phys. **69**, 1722 (1978).
16. R. E. London and J. Avitabile. J. Am. Chem. Soc. **100**, 7159 (1978).
17. D. Wallach. J. Chem. Phys. **47**, 5258 (1967).
18. R. M. Levy, M. Karplus, and P. G. Wolynes. J. Am. Chem. Soc. **103**, 5998 (1981).

Pyridoxal and pyridoxal 5′-phosphate catalyzed β-deuteration of α-aminobutyric acid and homoserine. I. Metal-free systems

KUNIYASU TATSUMOTO, RABINDRA P. REDDY, AND ARTHUR E. MARTELL[1]
Department of Chemistry, Texas A&M University, College Station, TX 77843, U.S.A.

Received April 17, 1985[2]

KUNIYASU TATSUMOTO, RABINDRA P. REDDY, and ARTHUR E. MARTELL. Can. J. Chem. **64**, 2053 (1986).

As the initial step in the investigation of metal ion- and vitamin B_6-catalyzed, β,γ-elimination in α-amino acids, the pyridoxal- and pyridoxal 5′-phosphate-catalyzed β-deuteration of α-aminobutyric acid and homoserine in D_2O in metal-free systems has been studied by nuclear magnetic resonance. The reaction kinetics of α-H, β-H, and 4′-CH exchange rates were measured by following the rates of deuteration of these positions. The kinetic data obtained for these reactions lead to a proposed mechanism for β-deuteration. The relative rates of the deuteration reactions observed, and the order in which deuteration products were obtained are: α-H exchange > transamination (4′-CH exchange) > β-H exchange. The observed rates of β-proton exchange exhibit specific base catalysis and are dependent on the activation of the α-hydrogen of the amino acid moiety in the aldimine, and on the activation of the β-hydrogens of the amino acids in the ketimine.

KUNIYASU TATSUMOTO, RABINDRA P. REDDY et ARTHUR E. MARTELL. Can. J. Chem. **64**, 2053 (1986).

Dans le cadre de la recherche sur les éliminations β,γ dans les acides α aminés, catalysées par les ions métalliques et par la vitamine B-6, on a fait appel à la rmn pour étudier la deutération β de l'acide α-aminobutyrique et de l'homosérine, catalysée par le pyridonal et le phosphate-5′ de pyridonal, dans le D_2O dans des systèmes ne contenant pas de métal. On a mesuré les cinétiques des vitesses d'échange des protons: H-α, H-β et CH-4′, en examinant les vitesses de deutération en ces positions. Les données cinétiques obtenues permettent de proposer un mécanisme réactionnel. Les vitesses relatives de deutération observées et l'ordre dans lequel on obtient les produits sont les suivants : échange du H en α > transamination (échange CH-4′) > échange H en β. Les vitesses observées pour les échanges du proton H en β montrent une catalyse basique spécifique et dépendent de l'activation de l'hydrogène en position α du fragment d'acide aminé de l'aldimine et également de l'activation des hydrogènes β de l'acide aminé de la cétimine.

[Traduit par la revue]

Introduction

The general mechanism suggested for β-proton exchange (1, 2) as a preliminary step in the elimination of electronegative groups in the γ-positions of amino acids is one of the recognized vitamin B_6-catalyzed reactions (3, 4). Somewhat earlier, β-proton exchange was observed for leucine at pH 5 in the presence of pyridoxal (5). More recently, some initial studies of the rates and mechanism of β-proton exchange of α-amino acids and α-keto acids in the presence and in the absence of metal ions have been carried out (3). The generally accepted mechanism of β-proton exchange involves the formation of ketimine Schiff base, followed by preliminary β-proton labilization to produce an intermediate ketimine-stabilized carbanion. Reprotonation at the β position regenerates the ketimine Schiff base.

The purpose of the present work is to undertake a kinetic study of the reaction sequences of β-proton exchange as an aid in elucidating the reaction mechanism, and thus to contribute to the understanding of the nature of the related enzymatic reactions. In this paper, nmr measurements are employed under β-proton exchange conditions in the presence of pyridoxal or pyridoxal 5′-phosphate. The use of these two forms of vitamin B_6 makes it possible to overcome the difficulties encountered because of limited solubilities of each catalyst at various but different pH ranges, thus greatly expanding the range of pH available for kinetic studies. The results of the present study provide a baseline for comparison with subsequent work on metal-ion catalysis of these reaction systems.

Experimental

Pyridoxal hydrochloride and pyridoxal 5′-phosphate, obtained from Sigma Chemical Company, and DL-α-aminobutyric acid and DL-homoserine from Mann Laboratories, were of sufficiently high quality to be used without further purification. NaOD and D_2O were obtained from Diaprep Corporation, and the purity of D_2O was 99.7%. NaOD (40% in D_2O) was diluted to the appropriate concentration under dry nitrogen.

The pH values of the solutions were measured by using a Corning Model 101 digital electrometer fitted with a Beckman miniature combination glass electrode and pH values were adjusted by the addition of NaOD solution in D_2O. The instrument was calibrated before and after each kinetic run by the use of standard buffers and corrected by the use of activity coefficients to read $-\log [H^+]$ directly. In D_2O solution, the deuterium ion concentration was computed by adding 0.41 (6) to the observed reading. The temperature was maintained at 25.0 ± 0.1°C and the ionic strength was maintained at 1.0 *M* (KNO_3). In the binary systems studied, the analytical concentrations of amino acid, pyridoxal, and pyridoxal phosphate were 0.10 *M*.

The nmr spectra were obtained with a Varian HA-100 nuclear magnetic resonance spectrometer. The chemical shifts (ppm) are reported relative to tetramethylsilane (Me_4Si), which was inserted in the reaction mixture in a coaxial tube. All kinetic runs were carried out on homogeneous systems. Before each spectrum was taken, the instrument was readjusted and five integrals were taken of the resonances used for following kinetics, and at least three integrals were taken for other peaks. The integral values were then averaged for further calculation and normalized relative to spectra based on unreactive protons. The fraction of Schiff base in the experimental solution was determined by taking ratios of the sums of the integrals of the 6H and $2CH_3$ resonances of the pyridoxal and pyridoxal phosphate Schiff bases and the γ-CH_3 of 2-aminobutyric acid. Since the resonances for the β-protons of the Schiff base and of the free amino acid overlap considerably, the integral values for Schiff base β-protons were obtained from the differences between the total integrals for the β-protons and the corresponding normalized values of the free amino acids. The constants were determined from the slope of the line obtained by plotting the appropriate values versus time. The reliabilities of the measurements were determined from the variations of the concentrations from the expected values based on the least-squares treatment. Since most of the kinetic runs were repeated, the results of these runs are reported with the estimated deviations.

[1]Author to whom correspondence may be addressed.
[2]Revision received March 4, 1986.

Printed in Canada

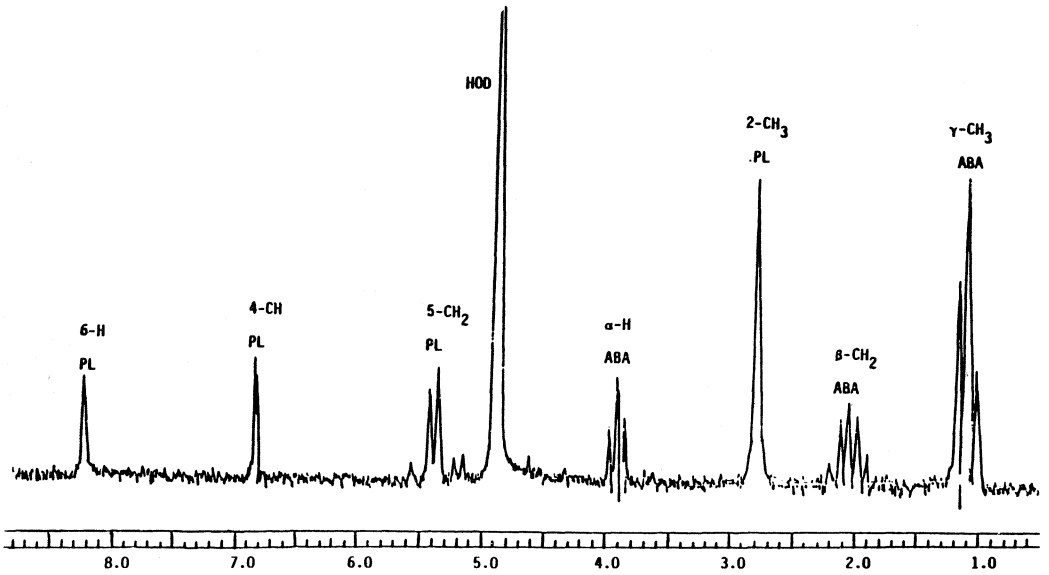

FIG. 1. The 100-MHz nmr spectrum of 0.10 *M* pyridoxal and 0.10 *M* α-aminobutyric acid at pD 5.40; chemical shifts are reported in ppm with respect to Me_4Si. PL = pyridoxal; α-ABA = α-aminobutyric acid.

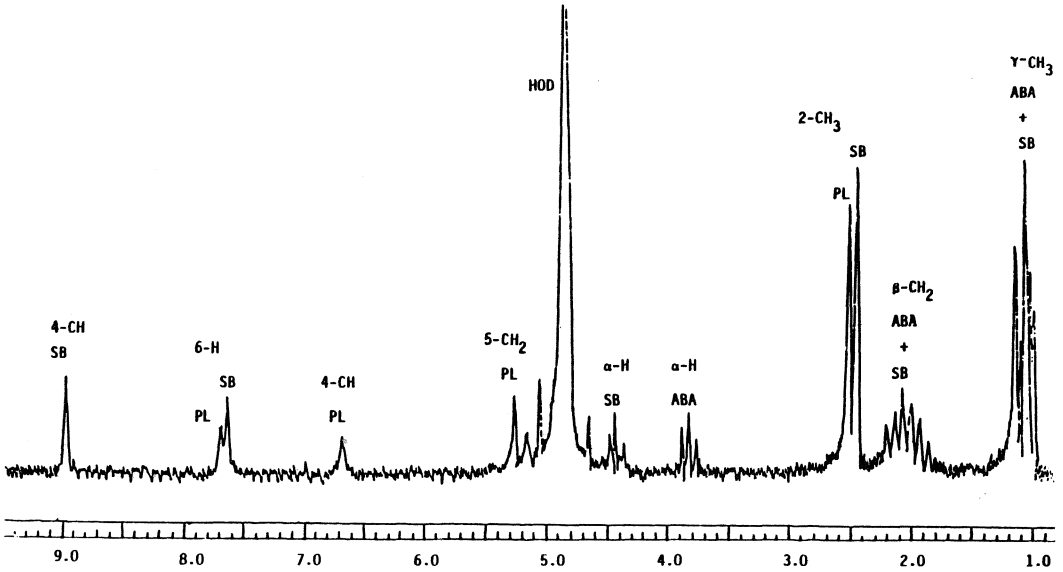

FIG. 2. The 100-MHz nmr spectrum of 0.10 *M* pyridoxal and 0.10 *M* α-aminobutyric acid at pD 8.67 showing the formation of pyridoxylidene-α-aminobutyrate; chemical shifts are reported in ppm with respect to Me_4Si. PL = pyridoxal, α-ABA = α-aminobutyric acid, and SB = Schiff base.

Results and treatment of data

Nuclear magnetic resonance spectra

The pyridoxal (PL) and pyridoxal 5′-phosphate (PLP) resonances have been assigned previously (7, 8). In this study, the resonances of α-aminobutyric acid (α-ABA) at pD 7.15 consist of a triplet near 1.05 ppm (CH_3), a multiplet near 2.00 ppm (β-CH_2), and a triplet near 3.80 ppm (α-CH). At pD values less than 6 in the absence of metal ion, the nmr spectra of equimolar solutions of pyridoxal and α-aminobutyric acid consist of resonances attributable entirely to the components as shown in Fig. 1 (pD 5.40). As the pD is raised, the resonances of the Schiff base become apparent and are labelled as SB in Fig. 2 (pD 7.97). In the case of the pyridoxal 5′-phosphate system, Schiff base formation becomes apparent at pD 4.82 (15%). This indicates that at a given pD in acid solution the degree of Schiff base formation is considerably higher for PLP than for PL. This behavior is expected since PL exists predominantly in the hemiacetal form, tending to inhibit Schiff base formation, whereas for PLP, in which the phosphate group precludes hemiacetal formation, the concentration of the free aldehyde is approximately 50 times higher (9). In pH or pD ranges in which the Schiff bases are minor species, the concentration of the PLP Schiff base should be nearly two orders of magnitude higher than that of the PL Schiff base. All resonances shift to higher field with increasing pD of the solution, as would be expected from the increasing negative charge on the Schiff base anion as protons are dissociated in a stepwise fashion from the pyridine and azomethine nitrogen atoms. Figure 3 presents the 100-MHz nmr spectrum of the pyridoxal–α-aminobutyric acid Schiff base, showing the decrease of β-CH_2 resonances of α-ABA with time, and Fig. 4 is the 100-MHz nmr spectrum of pyridoxal 5′-phosphate-α-aminobutyric acid Schiff base, also

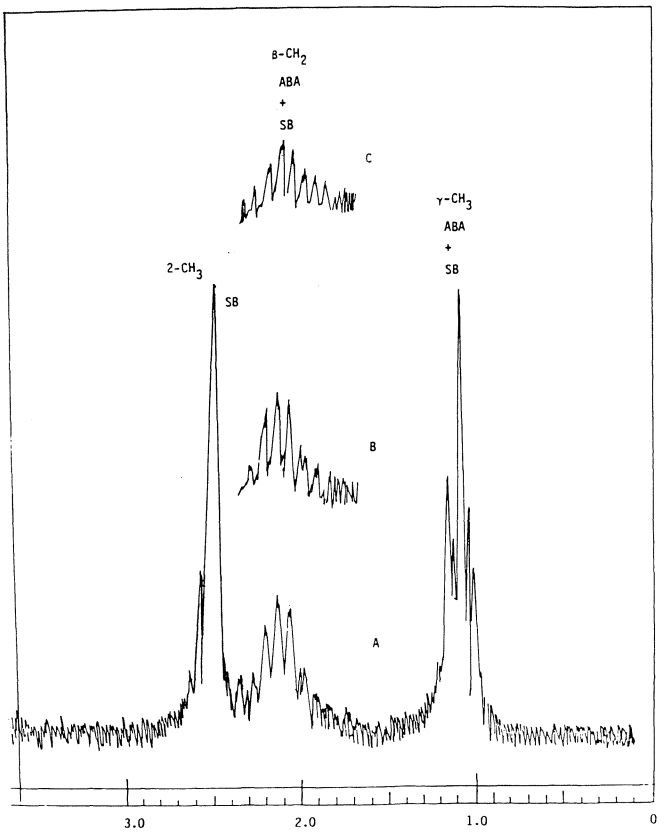

FIG. 3. The 100-MHz nmr spectrum of 0.10 *M* pyridoxal and 0.10 *M* α-aminobutyric acid at pD 9.95 showing the decrease of β-CH_2 signal of α-ABA. PL = pyridoxal, α-ABA = α-aminobutyric acid, and SB = Schiff base. A: after 1 h 22 min; B: 24 h 40 min; and C: 120 h 38 min. Chemical shifts are reported in ppm with respect to Me_4Si.

showing the decrease in β-proton resonances. The results are summarized in Table 1 for 4′-CH and α-H exchange rates.

Kinetic treatment

For the α-amino acid – PL and α-amino acid – PLP systems, the rate equations are based on the simple α- and β-proton exchange reactions:

α-Proton exchange

The removal or exchange of the α-proton is expressed by:

$$[1] \quad \alpha\text{-HSB} \xrightarrow{k'} \alpha\text{-DSB}$$

where α-HSB is α-amino acid Schiff base **1** with a hydrogen at the α-position and α-DSB is the corresponding α-deuterated Schiff base. The first-order rate equation

$$[2] \quad \frac{d[\alpha\text{-DSB}]}{dt} = k'_{obs}[\alpha\text{-HSB}]$$

may be employed directly if the concentration of α-HSB in solution can be determined, and the first-order rate constant k'_{obs} is then found from the slope of the line by plotting ln [α-HSB] vs. time.

4′-CH Exchange

The reactions controlling the rate of 4′-CH exchange in D_2O involve forward and reverse transamination steps (aldimine $\rightleftharpoons$ ketimine) and may be expressed by the following equations:

$$[3] \quad 4\text{CHSB} \underset{k_r}{\overset{k_f}{\rightleftharpoons}} 4\text{CHDSB} \xrightarrow{k_t} 4\text{CDSB}$$

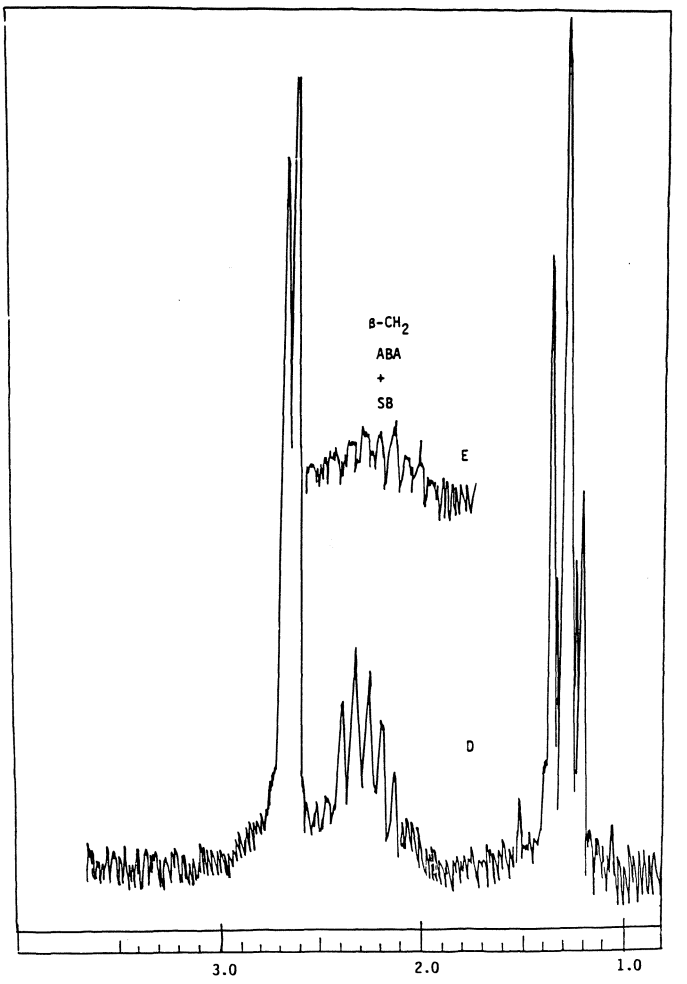

FIG. 4. The 100-MHz nmr spectrum of 0.10 *M* pyridoxal phosphate and 0.10 *M* α-aminobutyric acid at pD 8.47 showing the decrease of the β-CH_2 signal of α-ABA. PLP = pyridoxal phosphate, α-ABA = α-aminobutyric acid, and SB = Schiff base. D: after 1 h; E: 88 h. Chemical shifts are reported in ppm with respect to Me_4Si.

TABLE 1. Observed rate constants* for the α-H and 4′-CH exchange of Schiff bases (1:1)

[PL–α-ABA]			[PLP–α-ABA]	
pD	$k'_{obs}\cdot s^{-1} \times 10^6$ α-H	$k''_{obs}\cdot s^{-1} \times 10^6$ 4′-CH	pD	$k''_{obs}\cdot s^{-1} \times 10^6$ 4′-CH
8.67	4.8	3.4	5.88	6.4
9.25	6.2	3.8	6.93	4.5
9.46	7.6	4.5	7.34	3.9
9.93	8.7	6.5	7.97	1.3
10.26	9.4	6.2	8.47	0.94
			9.35	0.56

*Repeated measurements indicate that constants reported are reliable to ±5%.

$$[4] \quad 4\text{CDSB} \underset{k'_r}{\overset{k'_f}{\rightleftharpoons}} 4\text{CD}_2\text{SB}$$

where 4CHSB is the α-amino acid (aldimine) Schiff base **1**, with a hydrogen atom at the 4′ (α′) position of the pyridine ring, 4CDSB is the same Schiff base with a deuterium at the 4 position, and 4CHDSB is the intermediate half-deuterated ketimine, **3**.

The rate of disappearance of **1** is expressed by:

$$[5] \quad -\frac{d[4CHSB]}{dt} = k_f[4CHSB] - k_r[4CHDSB]$$

The rate of change in concentration of the intermediate ketimine, 4CHDSB, is expressed by:

$$[6] \quad \frac{d[4CHDSB]}{dt} = k_f[4CHSB] - k_r[4CHDSB] - k_t[4CHDSB]$$

The rate of change in concentration of the fully deuterated ketimine is expressed by:

$$[7] \quad \frac{d[4CD_2SB]}{dt} = k'_f[4CDSB] - k'_r[4CD_2SB]$$

The steady-state assumption is applied to the ketimine intermediate 4CHDSB, which is formed in undetectable concentrations in the experimental solution.

$$[8] \quad \frac{d[4CHDSB]}{dt} = k_f[4CHSB] - k_r[4CHDSB] - k_t[4CHDSB] = 0$$

To a first approximation, it may be assumed that $k_f = k'_f$ since these reactions both involve the transfer of D^+ from solution to α'-CH and α'-CD of the aldimine to form a C—D covalent bond. Similarly, $2k_r = k'_r$ because the reaction steps being compared both involve the breaking of a C—D covalent bond and transfer of D^+ to a base in solution, and differ only in the presence of adjacent C—H and C—D bonds, respectively. The rate constants k_t and k_r, however, should reflect a primary isotope effect resulting from the breaking of C—H and C—D bonds for the transfer of protons to a base in solution, so that $k_t = \alpha k_r$, where α is the kinetic deuterium isotope effect. Therefore:

$$[9] \quad k_r[4CHDSB] = \frac{k_f}{1+\alpha}[4CHSB]$$

and substituting the above relationship (9) into eq. [5]:

$$[10] \quad -\frac{d[4CHSB]}{dt} = \frac{\alpha}{1+\alpha}k_f[4CHSB] = k''_{obs}[4CHSB]$$

where the factor $\alpha/(1+\alpha)$ varies from $\frac{1}{2}$ for a minimal isotope effect, to nearly unity for a large isotope effect.

The only isotope effect that has been reported for pyridoxal Schiff bases in D_2O is 2.7, by Blake *et al.* (10), for the rate-determining transfer of a proton from the α-CH to the solvent. Assuming a value of similar magnitude for the α'-CH, the ratio of k_{obs} (i.e., k''_{obs}) to k_f would be about 0.74.

Thus the rate of 4′-CH exchange is also based on the concentration of Schiff base in solution, and the first-order constant k''_{obs} may be found from the slope of the plot of ln [4CHSB] vs. time.

β-CH exchange

With two hydrogen atoms in the β position, the rate of β-CH exchange is dependent on the sequential reaction steps:

$$[11] \quad \beta\text{-}CH_2SB \xrightarrow{k_1} \beta\text{-}CHDSB \xrightarrow{k_2} \beta\text{-}CD_2SB$$

where β-CH_2SB is the α-amino acid Schiff base with both hydrogens on the β position of the amino acid moiety, β-CHDSB is the same Schiff base with one hydrogen and one deuterium on the β position, and β-CD_2SB is the Schiff base with both hydrogens replaced by deuterium atoms. The following rate equations apply to this system:

$$[12] \quad \frac{d[\beta\text{-}CH_2SB]}{dt} = -k_1[\beta\text{-}CH_2SB]$$

$$[13] \quad \frac{d[\beta\text{-}CHDSB]}{dt} = k_1[\beta\text{-}CH_2SB] - k_2[\beta\text{-}CHDSB]$$

The stoichiometric relationships are:

$$[14] \quad T_c = [\beta\text{-}CH_2SB] + [\beta\text{-}CHDSB] + [\beta\text{-}CD_2SB]$$

$$[15] \quad T_p = 2[\beta\text{-}CH_2SB] + [\beta\text{-}CHDSB]$$

where T_c is total concentration of the species and T_p is total proton count. The following rate equation is obtained for total proton count.

$$[16] \quad \frac{dT_p}{dt} = 2\frac{d[\beta\text{-}CH_2SB]}{dt} + \frac{d[\beta\text{-}CHDSB]}{dt}$$

Substituting the variables from eqs. [12] and [13] into eq. [16]

$$[17] \quad \frac{dT_p}{dt} = -2k_1[\beta\text{-}CH_2SB] + k_1[\beta\text{-}CH_2SB] - k_2[\beta\text{-}CHDSB]$$

By substituting relationship [15] into eq. [17], and with the assumption $k_1 = 2k_2$ (i.e., the isotope effect here would also be minimal because both reactions involve the breaking of a C—H bond, and differ only in having adjacent C—H or C—D bonds),

$$[18] \quad \frac{dT_p}{dt} = -k_2T_p = -k'''_{obs}T_p$$

Thus the rate of proton exchange is directly proportional to the total concentration of the protonated Schiff base species in solution. This first-order rate constant k_2 is then found from the slope of the line by plotting ln $[T_p]$ vs. time.

The β-deuteration rate constants obtained for the PL and PLP Schiff bases are presented in Table 2. The values for these constants are reported to only two significant figures because of the difficulty encountered in determining precise integral values for these protons located adjacent to the intense HOD resonance. The spinning side-band encountered from the large HOD resonance complicated the integration of these resonances in some cases.

Mechanistic considerations

The proposed β-exchange mechanism is outlined in Scheme 1. The final product, assuming no side reactions, is the deuterated aldimine Schiff base species, **9**. Since no transamination reaction products (the keto acid and pyridoxamine or pyridoxamine-5′-phosphate) were found even after four half-lives of β-deuteration, the reaction is expected to go through two successive (forward and reverse) transamination steps. The first transamination involves the formation of the ketimine Schiff base **3**, which initiates the β-deuteration reaction, and the final transamination step is conversion of the ketimine to the aldimine Schiff base (**5** → **10** → **11** and **5** → **6** → **7** → **8** → **9**). Since the aldimine form is more stable than the ketimine form in these systems, it would be expected to predominate in the reaction mixture. Thus intermediates **3**, **5**, and **7** are not formed in sufficient quantities to be detected by nmr, but are essential for the sequential eliminations of the α- and β-protons.

TABLE 2. Observed rate constants* for the β-deuteration of α-aminobutyric acid Schiff base (1:1) and the homoserine Schiff base (1:1)

PL–α-ABA		PLP–α-ABA		PLP–homoserine	
pD	$K'''_{obs}\cdot s^{-1} \times 10^7$	pD	$K'''_{obs}\cdot s^{-1} \times 10^7$	pD	$K'''_{obs}\cdot s^{-1} \times 10^7$
8.67	5.8	4.82	4.2	4.39	4.8
9.46	5.8	5.88	5.8	5.37	6.2
9.93	6.1	7.34	6.0	5.92	7.4
10.26	6.2	7.97	5.8	6.61	12.0
		8.47	5.5	7.46	13.0
		9.35	5.3	8.46	16.0
				8.99	19.0
				10.33	18.0
				11.24	17.0

*Values reported are reproducible to about ±5%.

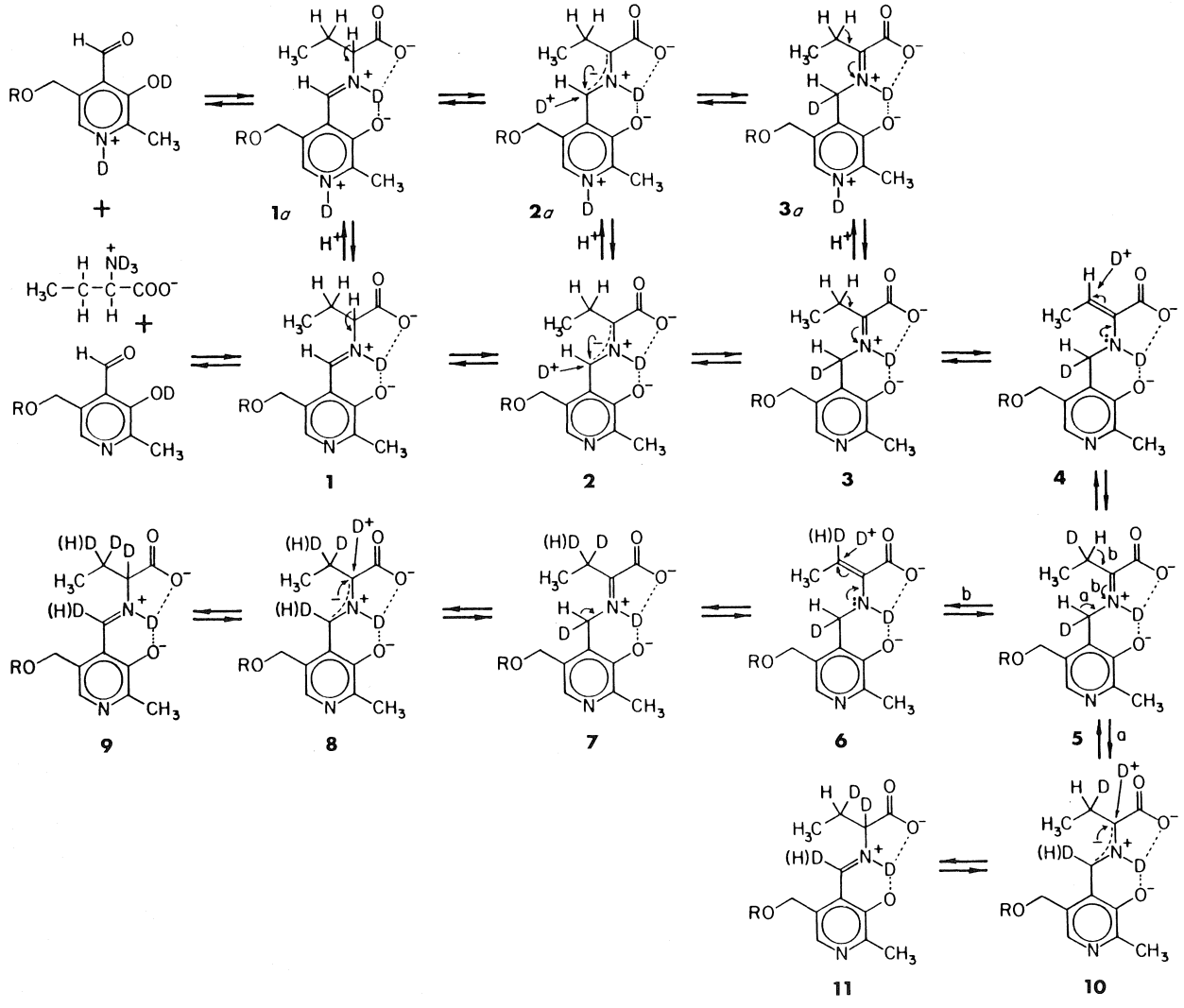

SCHEME 1. Metal free pyridoxal (R = H) or pyridoxal phosphate (R = PO_3H^-) catalyzed mechanism of β-proton exchange of α-aminobutyric acid.

Discussion

The rates of α′(4′-CH) exchange and α-H exchange of α-amino acid Schiff bases in the absence of metal ions are influenced by the ability of the Schiff base to labilize the protons at the α and α′ positions, which in turn is directly influenced by the protonation of the Schiff base at the azomethine and pyridine nitrogen atoms. The ability of the Schiff base to labilize α- and α′-protons should be greater for the doubly protonated form, since the negative charge of the active deprotonated intermediates **2** and **2***a* can then be distributed throughout the

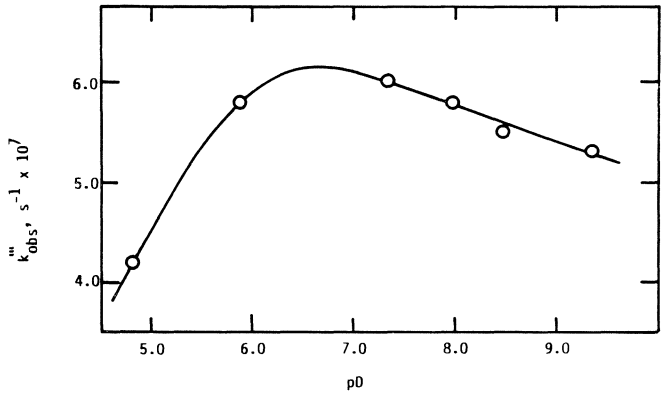

FIG. 5. The observed rate constants for the β-deuteration of α-aminobutyric acid and pyridoxal 5′-phosphate in D_2O solution at μ = 1.00 *M* (KNO_3); *t* = 25.0°C.

conjugated π-bond system of the Schiff base. Thus the electron-withdrawal effect in **2** is less than in **2***a*, and the rate of transamination would be expected to decrease with increasing pH, on the basis of these factors alone.

As pD increases, the diprotonated species **2***a* disappears first, and finally the monoprotonated species **2** becomes converted to the completely deprotonated Schiff base (not shown), which does not have an activating positive charge on the azomethine nitrogen. The lowered reactivity of this species toward α and α′ exchange would be counterbalanced by base (hydroxide ion)-catalyzed activation of the exchange process. This type of catalysis would also occur with **2**, so that the effect of its deprotonation at high pH would be balanced by increased hydroxide ion catalysis. Thus the base-catalyzed rate assigned to **2** would be kinetically indistinguishable from the exchange rate attributed to the fully deprotonated Schiff base.

In the pyridoxal – aminobutyric acid system, the values for the rate constants of α and α′ exchange, as functions of pD, show interesting trends. The α exchange shows the effect of base catalysis since the rates increase with increasing pD, while α′ exchange shows the effect of base as well as of protonation. Since the pK_a of the monoprotonated Schiff base is ≈10, the fact that the values for the rate constants are equivalent within the standard deviation range at pD 9.93 and pD 10.26 suggests that the decrease in the concentration of **2** is approximately balanced by increased hydroxide concentration.

In the pyridoxal phosphate – aminobutyric acid system, the trend of decreasing rate constants with increasing pD was observed (Fig. 5). The trend was as predicted on the basis of the factors previously mentioned for transamination, as well as by the fact that the phosphate group would be expected to sterically and electrostatically hinder base catalysis in the abstraction of a proton from the α′(4′-CH_2) position. Thus the effect of the degree of protonation of the Schiff base would predominate. The marked difference between the pyridoxal and pyridoxal phosphate trends must be due to steric and electrostatic effects on the phosphate anion and on the hydroxymethyl group. The phosphate hydroxyl group at the 5′ position may hydrogen bond with the azomethine nitrogen (11) of the pyridoxamine Schiff base, thus increasing the reactivity of the α′-hydrogen toward base catalysis. In view of these factors the observed difference between the trends for α and α′ exchange becomes reasonable.

The rate constants for β-deuteration for the α-ABA Schiff base and for D,L-homoserine – pyridoxal 5′-phosphate, presented in Table 2, also indicate interesting trends. The factors that influence the rate of the β-deuteration of the amino acid moiety in the absence of the metal ion are analogous to those suggested for the α and α′ exchange. After transamination takes place to form the ketimine Schiff base, the conjugation of π-bonds between the aromatic ring and the azomethine nitrogen is eliminated. Thus the Schiff base influences the labilization of β-protons through the positive charge on the azomethine nitrogen in the protonated form and through inductive forces exerted by the substituents on the amino acid. The effect of substituents is applicable only when comparing the rates of different amino and keto acids. Electron-withdrawing substituents are expected to increase the rate while the reverse is true for the electron-donating substituents. The influence of protonation of the imine nitrogen is restricted to the pD range below the pK_a (12–14) of the azomethine nitrogen atom (~10–11), and the effect on rate of this factor is expected to decrease above this pD. Base catalysis of β-proton exchange is expected to show an increase in rate with increase in pH. In the pyridoxal system the trends expected in the β-exchange rate constants were not so clearly discernable for the pD range studied since the accuracy of the values of the constants was somewhat limited, and the pD range was too narrow to observe the effect of the diprotonated form of the Schiff bases.

In the pyridoxal phosphate system as well as in other similar systems the following trends are expected: (*a*) if the rates were dependent on the degree of the Schiff base imine nitrogen protonation, the observed trend would be an increase or decrease depending on the relative amounts of protonated and deprotonated species present, as predicted by the pK_a of the imine nitrogen (~11). In the corresponding species distribution curve, the amount of the monoprotonated Schiff base maximizes around pD 8.5–9.0, giving a bell-shaped curve for the relative population of catalytic species. Also (*b*) if the rates were dependent on hydroxide ion catalysis, then the rate would increase with increasing pH. In the α-ABA system the values of the rate constants show a bell-shaped curve with a shallow maximum at pD 7.34. Although this is somewhat lower than the expected maximum it is not much different from the rate constant at pD ~7.97, which is much closer to the pD of the maximum degree of formation of the monoprotonated species. The increasing effect of hydroxide ion catalysis with pH is observed in the lack of a sharp decrease in the rate constants above pD 8.0. The considerable decrease in rate constants observed at pD 4.82 is probably due in part to dissociation of the Schiff base. The homoserine system also shows a bell-shaped rate curve, but with a maximum at pD ~9.0. This system shows the effect of Schiff base protonation and hydroxide ion catalysis more clearly than does the α-ABA Schiff base. Comparison of the values of the rate constants of homoserine and α-ABA indicates the effect, on the exchange rate, of the substituent on the amino acid moiety. The methoxy group has higher electron-withdrawing effect than does the methyl group, weakening the bonding of the β-hydrogen and increasing the exchange rate.

Additional studies of metal-ion catalysis of β-proton exchange and elimination of γ-electronegative substituents are now being carried out in this laboratory.

Acknowledgement

This research was supported by a grant, No. AM-11694, from the National Institute of Arthritis, Diabetes, Digestive and Kidney Diseases, U.S. Public Health Service.

1. E. H. ABBOTT and A. E. MARTELL. J. Chem. Soc. Chem. Commun. **23**, 1502 (1968).
2. E. H. ABBOTT and A. E. MARTELL. J. Am. Chem. Soc. **91**, 6931 (1969).
3. S. W. TENENBAUM, T. H. WITHERUP, and E. H. ABBOTT. Biochem. Biophys. Acta, **362**, 308 (1974).
4. A. E. BRAUNSTEIN and M. M. SHEMYAKIN. Biokhimiya, **18**, 393 (1953).
5. C. A. JUNK and J. H. SVEC. J. Org. Chem. **29**, 947 (1964).
6. A. K. COVINGTON, M. PAABO, R. A. ROBINSON, and R. G. BATES. Anal. Chem. **40**, 700 (1968).
7. O. A. GANSOW and R. H. HOLM. J. Am. Chem. Soc. **90**, 5699 (1968); **91**, 571 (1969).
8. W. KORYTNYK and H. AHRENS. Methods Enzymol. **18**, 574 (1980).
9. C. M. HARRIS, R. J. JOHNSON, and D. E. METZLER. Biochim. Biophys. Acta, **421**, 181 (1976).
10. M. I. BLAKE, F. P. SIEGLE, J. J. KATZ, and M. KILPATRICK. J. Am. Chem. Soc. **85**, 294 (1963).
11. C. M. METZLER, A. CAHILL, and D. E. METZLER. J. Am. Chem. Soc. **102**, 6075 (1980).
12. K. NAGANO and D. E. METZLER. J. Am. Chem. Soc. **89**, 2891 (1967).
13. W. L. FELTY, C. G. EKSTROM, and D. L. LEUSSING. J. Am. Chem. Soc. **92**, 3006 (1970).
14. K. TATSUMOTO and A. E. MARTELL. J. Am. Chem. Soc. **99**, 6082 (1977).

Ionic dissociation in pyridine–iodine solutions

SEYMOUR ARONSON, STUART BRYAN WILENSKY, TAUN-IUAN YEH, DARNEL DEGRAFF, AND GRACE MARILYN WIEDER

Department of Chemistry, City University of New York, Brooklyn College, Brooklyn, NY, U.S.A. 11210

Received January 28, 1986

SEYMOUR ARONSON, STUART BRYAN WILENSKY, TAUN-IUAN YEH, DARNEL DEGRAFF, and GRACE MARILYN WIEDER. Can. J. Chem. **64**, 2060 (1986).

An electrochemical technique has been employed to study the ionization of the pyridine–iodine complex in pure pyridine and in 1,2-dichloroethane. A mechanism for the ionization in accord with the experimental data is proposed. The results indicate that, for wide ranges of iodine and pyridine concentration, one quarter of the I_2 is dissociated into ionic species.

SEYMOUR ARONSON, STUART BRYAN WILENSKY, TAUN-IUAN YEH, DARNEL DEGRAFF et GRACE MARILYN WIEDER. Can. J. Chem. **64**, 2060 (1986).

Opérant dans la pyridine pure ainsi que dans le dichloro-1,2 éthane, on a utilisé une technique électrochimique pour étudier l'ionisation du complexe pyridine/iode. On propose un mécanisme pour l'ionisation qui est en accord avec les données expérimentales. Les résultats indiquent que, pour des concentrations très variables d'iode et de pyridine, 25% du I_2 est dissocié en espèces ioniques.

[Traduit par la revue]

Introduction

The pyridine–iodine system has been the subject of intensive investigation (1–10). Mulliken (4) suggested the following complexation and ionization sequence for the reaction between pyridine and iodine.

[1] $Py + I_2 = PyI_2$

[2] $PyI_2 = PyI^+I^-$

[3] $PyI^+I^- = PyI^+ + I^-$

Reaction [1], whose product Mulliken called an "outer complex", occurs in both polar and nonpolar solvents. Reaction [2] produces an "inner complex" PyI^+I^-. Reaction [3] takes place only in polar organic solvents (1, 4, 5). One evidence for the ionization process in reaction [3] is the relatively high electrical conductivity observed in pyridine–iodine solutions in polar solvents (1, 5). On the basis of experimental evidence, Mulliken (3) suggested that reactions [1] and [3] reach equilibrium rapidly. He further suggested that reaction [2] involves an activation barrier of considerable height and that equilibrium is approached slowly.

Equilibrium constants for reaction [1] have been determined in a number of solvents (10). Experimental evidence indicates that reaction [2] requires a period of days or weeks for equilibrium to be attained (3, 7). Ionization reactions which yield the I_3^- ion as well as the I^- ion formed in reaction [3] have only been studied at short reaction times during which period reaction [2] has not reached equilibrium. Ionization constants which have been determined (8, 9, 11, 12) are, therefore, of questionable value.

In the present study, an electrochemical technique (12) has been used to investigate the ionization process in the pyridine–iodine complex. Quantitative information has been obtained on solutions of iodine in pyridine and solutions of pyridine and iodine in 1,2-dichloroethane.

Experimental

Chemicals

Fisher certified ACS grade pyridine was allowed to stand over solid potassium hydroxide for several days, then refluxed over calcium hydride for several hours, and then repeatedly distilled from fresh portions of the hydride with a boiling point 115–116°C at 760 Torr. This procedure sufficed to give a highly purified and anhydrous pyridine whose specific conductivity was below 1×10^{-7} (ohm-cm)$^{-1}$. Fisher certified ACS grade 1,2-dichloroethane was dried over calcium hydride for several days, then refluxed over calcium hydride for one day and repeatedly distilled from fresh portions of this hydride. A middle fraction was collected. This gave a pure, anhydrous product with a normal boiling point of 82.9–83.1°C. Fisher laboratory grade resublimed iodine was resublimed twice and kept in a dessicator over anhydrous copper sulfate. Reagent grade sodium iodide and tetraethylammonium iodide, obtained from Alpha Products, were used as received.

Electrochemical, conductivity, and spectrophotometric measurements

The electrochemical measurements were made in a 2-compartment "H" cell in which separation of the compartments was effected by a fine-frit disk. Both compartments were filled to the same level. Pieces of platinum foil attached to platinum wire leads were inserted into each compartment to serve as electrodes. Voltage measurements were made with a Keithley Model 160B digital multimeter. All measurements were made in a constant temperature water bath regulated to 25.0 ± 0.1°C. The platinum electrodes and cells were cleaned by immersion in hot concentrated nitric acid, and then in cleaning solution for several days. The electrodes were then repeatedly rinsed with distilled water and left standing in distilled water for several days.

Conductivity measurements were made using a standard conductivity cell with platinum electrodes and a YSI Model 31 conductivity bridge. The cell constant was determined to be 0.1037 cm^{-1} using a 0.0200 *N* solution of potassium chloride at 25.0°C.

In addition to the electrical measurements, ultraviolet–visible absorption measurements were made with a Cary 17 spectrophotometer using quartz cells of 10 mm and 2 mm thickness.

All solutions of iodine and pyridine were freshly prepared just before the first measurement of a property. Subsequent measurements were then made at intervals of one day, three to four days, one week, two weeks, three weeks, etc., for a total time of one month. All stored solutions were protected by sealing stoppered flasks with Parafilm.

Mathematical treatment

Reaction mechanism

The reaction sequence we will employ utilizes reactions [1] and [2] above as proposed by Mulliken. In place of reaction [3], we employ the following reaction

[4] $2PyI^+I^- = Py_2I^+ + I_3^-$

The ionic species Py_2I^+ and PyI^+ have been postulated and observed (6, 8, 9, 13). We postulate the formation of Py_2I^+

Printed in Canada

because the experimental data presented below will be shown to be independent of pyridine concentration. This observation is in accord with the formation of Py_2I^+, as in reaction [4], but not with the formation of PyI^+. The I_3^- ion rather than the I^- ion is postulated to form because the concentrations of iodine used in this investigation are high enough to favor the stable I_3^- ion (14). Experimental verification for the presence of I_3^- are the very strong absorption bands observed at 365 nm and 295 nm which are the locations of the I_3^- peaks (14, 15).

The equilibrium constant for reaction [4] is

$$[5] \quad K_4 = \frac{[Py_2I^+][I_3^-]}{[PyI^+I^-]^2}$$

We will assume that concentration can be substituted for activity in all the equilibrium expressions. For the autoionization of PyI^+I^- in reaction [4], we can write

$$[6] \quad [Py_2I^+] = [I_3^-] = x$$

An additional assumption we make is that the ratio of pyridine to iodine is sufficiently high (>10:1) so that all the iodine is in complex form, i.e., reaction [1] goes all the way to the right. This assumption is experimentally verified by the absence of an I_2 peak in the visible region of the spectrum.

Using the symbol, b, for the nominal[1] concentration of iodine, we can write

$$[7] \quad b = [PyI_2] + [PyI^+I^-] + 2x$$

From reaction [2], we obtain

$$[8] \quad [PyI_2] = [PyI^+I^-]/K_2$$

Substituting in eq. [7], we get

$$[9] \quad b = (1 + 1/K_2)[PyI^+I^-] + 2x$$

and

$$[10] \quad [PyI^+I^-] = (b - 2x)/(1 + 1/K_2)$$

Substituting in eq. [5], we obtain

$$[11] \quad K_4 = \frac{x^2}{\left(\frac{b - 2x}{1 + 1/K_2}\right)^2}$$

and finally

$$[12] \quad \frac{[Py_2I^+]}{[PyI_2] + [PyI^+I^-]} = \frac{K_2}{K_2 + 1}(K_4)^{1/2} = K$$

Thus, the ratio of the concentrations of charged complex, Py_2I^+, to neutral complexes, PyI_2 and PyI^+I^-, should be independent of the nominal iodine and pyridine concentrations.

Electrochemical equations

We have employed electrochemical cells of the following types

$$[13] \quad Pt|I_2, NaI(c) \text{ in } Py\|I_2, NaI(c') \text{ in } Py|Pt$$

and

$$[14] \quad Pt|I_2, Py, TEAI(c) \text{ in DCE}\|I_2, Py \text{ in DCE}|Pt$$

where TEAI and DCE refer to tetraethylammonium iodide and 1,2-dichloroethane, respectively. The c and c' values represent nominal concentrations. The nominal I_2 and Py concentrations are the same in both half-cells.

We will assume that added NaI or TEAI, represented by the term MI, is completely ionized according to the reactions

$$[15] \quad MI + PyI^+I^- \rightarrow I_3^- + Py + M^+$$

and

$$[16] \quad MI + Py_2I^+ \rightarrow PyI^+I^- + Py + M^+$$

complete ionization of MI appears reasonable on the basis of the known information about the ionization of NaI and TEAI and the stability of I_3^- (11, 14). The species PyI^+I^-, Py_2I^+, and I_3^- rapidly resume thermodynamic equilibrium on the basis of reaction [4]. We assume the following virtual electrode reactions corresponding to Line-diagrams 13 and 14.

$$[17] \quad 3Py(1) + PyI^+I^-(1) - 2e = 2Py_2I^+(1)$$

$$[18] \quad 2Py_2I^+(2) + 2e = 3Py(2) + PyI^+I^-(2)$$

Half-cell 1 in Line-diagram 13 has more NaI than half-cell 2. Half-cell 1 in Line-diagram 14 contains TEAI while half-cell 2 contains no TEAI.

We will make the reasonable assumption that, for small additions of MI, the concentration of PyI^+I^- does not depend significantly on the quantity of added MI. We can then write for the emf, E, of the cell at room temperature

$$[19] \quad E = -0.0591 \log \frac{[Py_2I^+(2)]}{[Py_2I^+(1)]}$$

We have already used the symbol, x, for $[Py_2I^+]$ in a solution without added MI. In the presence of nominal concentration of MI designated as c, the concentration of Py_2I^+ is designated as y. The equilibrium expression corresponding to Line-diagram 14 is

$$[20] \quad y(y + c) = x^2$$

We can solve for x and y using eqs. [19] and [20].

When MI is present in the half-cell on the right in concentration, c', as well as on the left in concentration, c, which corresponds to Line-diagram 13, we can use the equation

$$[21] \quad y(y + c) = y'(y' + c') = x^2$$

y, y', and x can be determined.

The value of x and the nominal concentration of iodine, b, yield the constant K in eq. [12] corresponding to the ratio of the concentrations of charged to neutral complexes.

Results and discussion

The acquisition of equilibrium data for the ionization process in reaction [4] requires that reactions [1], [2], and [4] all be at equilibrium. Reaction [1] reaches equilibrium rapidly (3, 10). On the basis of the electrochemical data presented below, reaction [4] also approaches equilibrium rapidly. The slow approach to equilibrium of reaction [2] is indicated in Fig. 1. In the upper graph, the conductivity of a pyridine–iodine solution in dichloroethane reaches a plateau in about one week. The absorptivity of a pyridine–iodine solution in dichloroethane, shown in the lower graph in Fig. 1 also reaches a plateau in about one week. The explanation for these phenomena is that the concentrations of Py_2I^+ and I_3^- continue to increase until reaction [2] reaches equilibrium. The absorption maximum at 365 nm is primarily due to the presence of the I_3^- ion with a

[1]The nominal concentration of iodine is the number of moles of I_2 dissolved in a litre of solution. The value is not effected by the dissociation and interaction of iodine in solution which yields new iodine species.

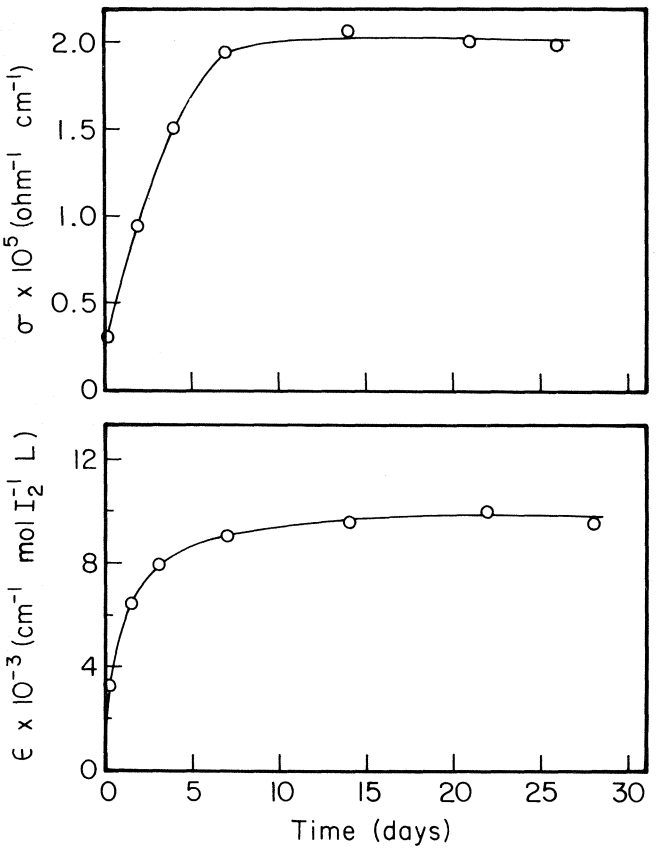

FIG. 1. The upper curve shows the variation of conductivity with time for nominal concentrations of 0.0903 *M* Py and 0.00101 *M* I_2. The lower curve shows the variation of absorptivity at 365 nm with time for nominal concentrations of 0.0496 *M* Py and 0.000492 *M* I_2.

small contribution from the PyI_2 "outer complex" (10). PyI^+I^- does not absorb in this region of the spectrum (4). Conductivity and absorptivity data on samples with other pyridine–iodine concentrations gave similar results.

We used the electrochemical cell, in dichloroethane,

$$\text{Pt}|\text{I}_2\ (2.98 \times 10^{-3}\ M),\ \text{Py}\ (0.297),$$
$$\text{TEAI}\ (3.12 \times 10^{-5}\ M)\|\text{I}_2\ (2.98 \times 10^{-3}\ M),\ \text{Py}\ (0.297\ M)|\text{Pt}$$

to determine the value of x, the concentration of Py_2I^+, as a function of time on the basis of eqs. [19] and [20]. The data obtained, shown in Fig. 2, confirm the approach to equilibrium in about one week.

Electrochemical data were obtained at 25°C for solutions of pyridine and iodine in dichloroethane. The solutions were stored for two weeks prior to measurement. The electrochemical cells used were of the type shown in Line-diagram 14. Data obtained on a typical cell are presented in Table 1. The nominal iodine concentration in both half-cells was 2.00×10^{-3} *M*. One half-cell contained a nominal concentration of TEAI of 2.20×10^{-5} *M*. The emf was measured over a period of 1 h and was found to have a steady value of 1.25 ± 0.05 mV. The TEAI concentration was increased in steps four times and emf measurements were made. The calculated value of x was constant to within experimental error.

Values of the ionization constant, K, in eq. [12], were calculated from electrochemical data on solutions with nominal I_2 concentrations ranging from 2.56×10^{-4} *M* to 2.98×10^{-3} *M*. In each case, the nominal Py concentration was 100 times higher than the nominal I_2 concentration. The values

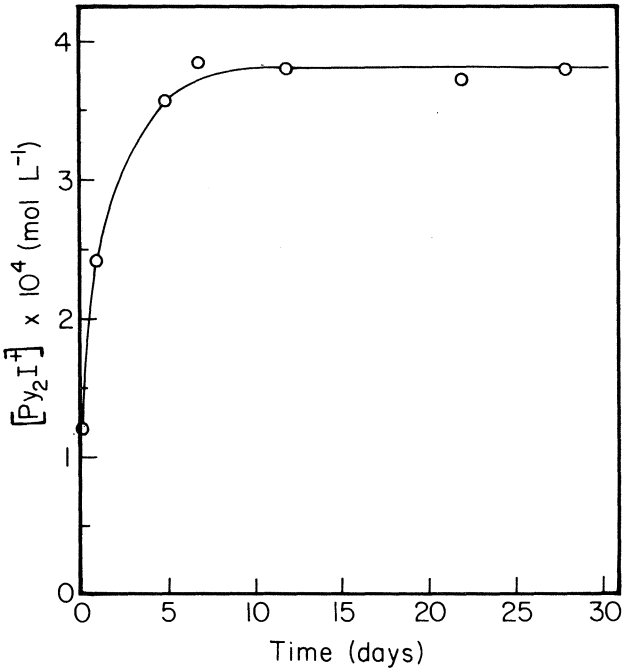

FIG. 2. Variation of Py_2I^+ concentration, x, with time for nominal concentrations of 0.297 *M* Py and 0.00298 *M* I_2.

TABLE 1. Emf data on the cell, in dichloroethane, $\text{Pt}|\text{I}_2$ $(2.00 \times 10^{-3}\ M)$, TEAI (c), Py (0.199 *M*)$\|\text{I}_2$ $(2.00 \times 10^{-3}\ M)$, Py (0.199 *M*)|Pt

c, $M \times 10^5$	E, mV*	y, $M \times 10^4$	x, $M \times 10^4$
2.20	1.25	2.15	2.26
4.32	2.46	2.05	2.25
6.35	3.60	1.96	2.26
8.31	4.67	1.90	2.27
10.2	5.85	1.77	2.22

*Oxidation occurs on side of cell containing TEAI.

TABLE 2. Summary of data from electrochemical cells of the type described by Line-diagram 14, in dichloroethane

Py conc. $M \times 10^2$	I_2 conc. $M \times 10^4$	x, $M \times 10^4$	K
2.48	2.56	0.340	0.179
4.96	4.92	0.546	0.143
9.03	10.1	1.21	0.157
19.9	20.0	2.20	0.141
29.7	29.8	3.80	0.171

of x and K are shown in Table 2. For the ten-fold range of iodine and pyridine concentrations, the value of K is reasonably constant, 0.158 ± 0.014.

Solutions of iodine in pure pyridine were also investigated. Spectrophotometric and Py_2I^+ concentration data of the type shown in Figs. 1 and 2 again indicated the attainment of equilibrium in about one week. Electrochemical data were obtained at 25°C for solutions of iodine in pyridine stored for two weeks. The electrochemical cells were of the type shown in Line-diagram 13. Data obtained on a typical cell are shown in Table 3. In this case, NaI was added to both half-cells as indicated by the initial values of c and c'. Additional aliquots

TABLE 3. Emf data on the cell, in pyridine, Pt | I_2 (0.0772 *M*), NaI (*c*) ‖ I_2 (0.0772 *M*), NaI (*c'*) | Pt

$c, M \times 10^3$	$c', M \times 10^3$	E, mV*	$y, M \times 10^3$	$y', M \times 10^3$	$x, M \times 10^3$
2.80	1.40	1.85	8.34	8.96	9.63
4.03	1.34	3.50	7.94	9.10	9.75
5.17	1.29	4.99	7.56	9.19	9.81
6.22	1.24	6.45	7.07	9.09	9.69
7.20	1.20	7.71	6.76	9.13	9.71

*Oxidation occurs on the side of the cell containing a higher NaI concentration.

TABLE 4. Summary of data from electrochemical cells of the type described by Line-diagram 13, in pyridine

I_2 conc., *M*	*x*, *M*	*K*
0.0411	0.0052	0.169
0.077	0.0097	0.168
0.157	0.0179	0.147
0.310	0.0353	0.147
0.628	0.0745	0.155
1.26	0.152	0.160

of NaI in pyridine–iodine solution were added in increments to one half-cell. Equal aliquots of pyridine–iodine solution were added in increments to the other side to avoid hydrostatic pressure. The calculated value of x was constant to within experimental error.

Values of the ionization constant, K, were calculated from data on solutions with nominal I_2 concentrations ranging from 0.0411 to 1.26 *M*. A value of K of 0.158 ± 0.008 was obtained for the thirty-fold variation in iodine concentration.

It is interesting that the interaction of iodine with pyridine is the same over wide ranges of iodine concentration in pure pyridine and in solutions in dichloroethane. The difference in dielectric constant between pyridine, 12.3, and dichloroethane, 10.4, is apparently not sufficient to effect the degree of ionization of the pyridine–iodine complexes. In nonpolar solvents such as heptane and benzene, with dielectric constants in the range of 2, no ionization is expected to occur (4).

When the concentration ratio of pyridine to iodine in dichloroethane is close to unity, the behavior of the system is more complex. Uncomplexed I_2 is observed spectrophotometrically and the I_3^- concentration continues to increase for more than 4 weeks.[2] This behavior can be qualitatively explained on the assumption that, in this case, reaction [1] does not proceed all the way to the right.

1. L. F. AUDRIETH and E. J. BIRR. J. Am. Chem. Soc. **55**, 668 (1933).
2. R. S. MULLIKEN. J. Am. Chem. Soc. **74**, 811 (1952).
3. R. S. MULLIKEN. J. Phys. Chem. **56**, 801 (1952).
4. C. REID and R. S. MULLIKEN. J. Am. Chem. Soc. **76**, 3869 (1954).
5. G. KORTUM and H. WILSKI. Z. Physik. Chem. **202**, 35 (1953).
6. R. ZINGARO, C. A. VANDER-WERF, and J. KLEINBERG. J. Am. Chem. Soc. **73**, 88 (1951).
7. J. KLEINBERG, E. COLTON, J. SATTIZAHN, and C. A. VANDER-WERF. J. Am. Chem. Soc. **75**, 442 (1953).
8. G. PEZZATINI and R. GUIDELLI. Electrochim. Acta, **16**, 1415 (1971).
9. J. M. NIGRETTO and M. JOSEFOWICZ. Electrochim. Acta, **19**, 809 (1974).
10. W. J. MCKINNEY and A. I. POPOV. J. Am. Chem. Soc. **91**, 5215 (1969).
11. J. M. NIGRETTO and M. JOSEFOWICZ. *In* The chemistry of nonaqueous solvents. *Edited by* J. J. Lagowski. Academic Press, New York. 1978. Chapt. 5.
12. S. ARONSON, P. EPSTEIN, D. B. ARONSON, and G. WIEDER. J. Phys. Chem. **86**, 1035 (1982).
13. O. HASSEL and H. HOPE. Acta Chem. Scand. **15**, 407 (1961).
14. L. I. KATZIN and E. GEBERT. J. Am. Chem. Soc. **76**, 2049 (1954).
15. R. E. BUCKLES, J. P. YUP, and A. I. POPOV. J. Am. Chem. Soc. **74**, 4379 (1952).

[2]S. Aronson *et al.*, unpublished data.

Structure and reactions of 4-(2,4,6-trimethyl)benzylidene-2-phenyloxazolin-5-one[1]

MIROSLAW CYGLER AND CAROL P. HUBER[2]
Division of Biological Sciences, National Research Council of Canada, Ottawa, Ont., Canada K1A 0R6

AND

JAMES R. P. GODIN AND DAVID J. PHELPS
Department of Chemistry, St. Mary's University, Halifax, N.S., Canada B3H 3C3

Received January 10, 1986

MIROSLAW CYGLER, CAROL P. HUBER, JAMES R. P. GODIN, and DAVID J. PHELPS. Can. J. Chem. **64**, 2064 (1986).

The crystal structure of 4-(2,4,6-trimethyl)benzylidene-2-phenyloxazolin-5-one has been determined. Crystals of $C_{19}H_{17}NO_2$, fw 291.35, are monoclinic, $P2_1/c$, a = 10.207(2), b = 8.977(2), c = 17.123(4) Å, β = 92.66(1)°. For 2435 observed independent reflections the final R = 0.039 and R_w = 0.042. The molecule has Z configuration about the exocyclic double bond, and the benzylidene ring is twisted 61.3° out of the oxazoline ring plane, thus relieving the overcrowding caused by the two *ortho*-methyl substituents. The reaction of this compound with benzylamine in acetonitrile occurs almost four times as fast as predicted using model reactions.

MIROSLAW CYGLER, CAROL P. HUBER, JAMES R. P. GODIN et DAVID J. PHELPS. Can. J. Chem. **64**, 2064 (1986).

On a déterminé la structure cristalline de la triméthyl-2,4,6 benzylidène-4 phényl-2 oxazolinone-5. Les cristaux de $C_{19}H_{17}NO_2$, m.f. 291.35, sont monocliniques, $P2_1/c$, avec a = 10,207(2), b = 8,977(2) et c = 17,123(4) Å et β = 92,66(1)°. En se basant sur 2435 réflexions indépendantes observées, les valeurs finales de R et R_w sont respectivement de 0,039 et 0,042. La molécule adopte une configuration Z autour de la double liaison exocyclique et le cycle benzylidène forme un angle de 61,3° avec le plan du cycle oxazoline; cette déviation élimine l'encombrement stérique causé par les deux substituants méthyles en positions *ortho*. La vitesse de la réaction de ce composé avec la benzylamine dans l'acétonitrile est pratiquement quatre fois plus rapide que celle qui pourrait être prédite en utilisant des réactions modèles.

[Traduit par la revue]

Introduction

The 4-benzylidene-2-phenyloxazolin-5-one molecule (**1**) and its substituted analogues[3] can exist in two configurations, *E* and *Z*, about the exocyclic double bond. In the cases studied to date (1–5) the Plöchl azlactone synthesis (6), or modifications of it (7) used in the synthesis of oxazolinones, gave the *Z* isomer, obviously the more thermodynamically stable form. It is, however, possible to effect *Z* to *E* isomerization (8). Infrared, Raman, and absorption spectra of the two isomers are quite similar (4), but more fine structure has been noted (1, 4) in the absorption spectrum of the *Z* isomer. A study of fifteen methyl- and dimethyloxazolinones, all in the *Z* form (7), found no significant changes in absorption maximum, extinction coefficient, or fine structure over the series, even for the relatively hindered di-*ortho* derivative, **2**. But in the reaction of benzylamine with *ortho*-substituted oxazolinones, a quantitative effect is exerted by *ortho* substituents (9). *Ortho* substitution in the benzylidene ring, e.g. **3**, leads to acceleration of the ring-opening reaction by a factor of ca. 2, while *ortho* substitution in the phenyl ring, e.g. **4**, retards the reaction by a factor of ca. 2. A possible explanation for this is that steric strain is released if **3** is ring-opened, whereas **4** presents steric hindrance to the approach of the nucleophile. In order to investigate further the effects of *ortho* substitution on the absorption spectra and reactivity of oxazolinones, compounds **5**–**7** were synthesized. In this paper, the physical properties and reactivity of **5**–**7** and the crystal structure of **5**, 4-(2,4,6-trimethyl)benzylidene-2-phenyloxazolin-5-one, will be discussed.

Experimental

All oxazolinones were synthesized by a previously described method (7). Kinetic studies of the reaction with benzylamine were carried out as before (9). Compounds **5**, **6**, and **7** were prepared for the first time for this study. Their physical properties are reported in Table 1. Yields are based on recrystallized (ethanol/water), analytically pure material. Melting points are uncorrected. Elemental analyses were performed by Mr. Hector Seguin, NRCC.

Crystals of **5** were obtained from 95% ethanol as yellow prisms. The specimen used for data collection had maximum dimensions 0.30 × 0.35 × 0.25 mm. Crystal data are as follows:

$C_{19}H_{17}NO_2$ fw = 291.35

Monoclinic, $P2_1/c$, a = 10.207(2), b = 8.977(2), c = 17.123(4) Å, β = 92.66(1)°, V = 1567.3 Å^3, (based on λ(Cu Kα_1) = 1.54056 Å), Z = 4, D_x = 1.235 Mg m^{-3}, μ(Cu) = 0.65 mm^{-1}, F(000) = 616, T = 293 K.

Measurements were made on a CAD-4 diffractometer. The cell dimensions were determined from the angular settings of 22 carefully centered reflections with 45° < θ < 58°. Relative intensities were measured using $\omega/2\theta$ scans for ω ranges of 1.50 (0.85 + 0.20 tan θ) at scan speeds of 0.65–5.0°/min in ω. All 3219 independent reflections in the hkl and $\bar{h}kl$ octants with θ = 0–75° were recorded, and 2435 of these were considered observed at the 1.0$\sigma(I)$ level. The others were assigned zero weights during least-squares refinement. Three standard reflections were monitored after every 6000 s exposure time. Their intensities showed only minor fluctuations, within ±2% of their respective means. Lorentz and polarization corrections were applied, and a correction for secondary extinction ($g/\mu = 0.185 \times 10^{-6}$) was made during the refinement stage. Absorption corrections were considered unnecessary because of the small value of μR and the nearly equidimensional specimen.

The structure was solved by direct methods, using the MULTAN 78 program (10). Refinement was by block-diagonal least-squares calculations, minimizing $\Sigma w(\Delta F)^2$. All hydrogen atoms were located on a difference map, and were refined isotropically while non-hydrogen atoms were refined anisotropically. The weighting scheme was of the form $w = P_1/|F_o|$ if $|F_o| > P_1$, and $w = 1$ otherwise, with P_1 = 25.0 e. Scattering factor values for O, N, C, and H were taken from International tables for X-ray crystallography (11). Convergence was attained at R = 0.039, R_w = 0.042 (for all observed reflections). During the final cycle of refinement the mean (shift/esd) was 0.057 and $(\Delta/\sigma)_{max}$ was 0.27. A difference map was calculated from the

[1]NRC No. 26013.
[2]To whom all correspondence should be addressed.
[3]Hereinafter referred to as oxazolinones.

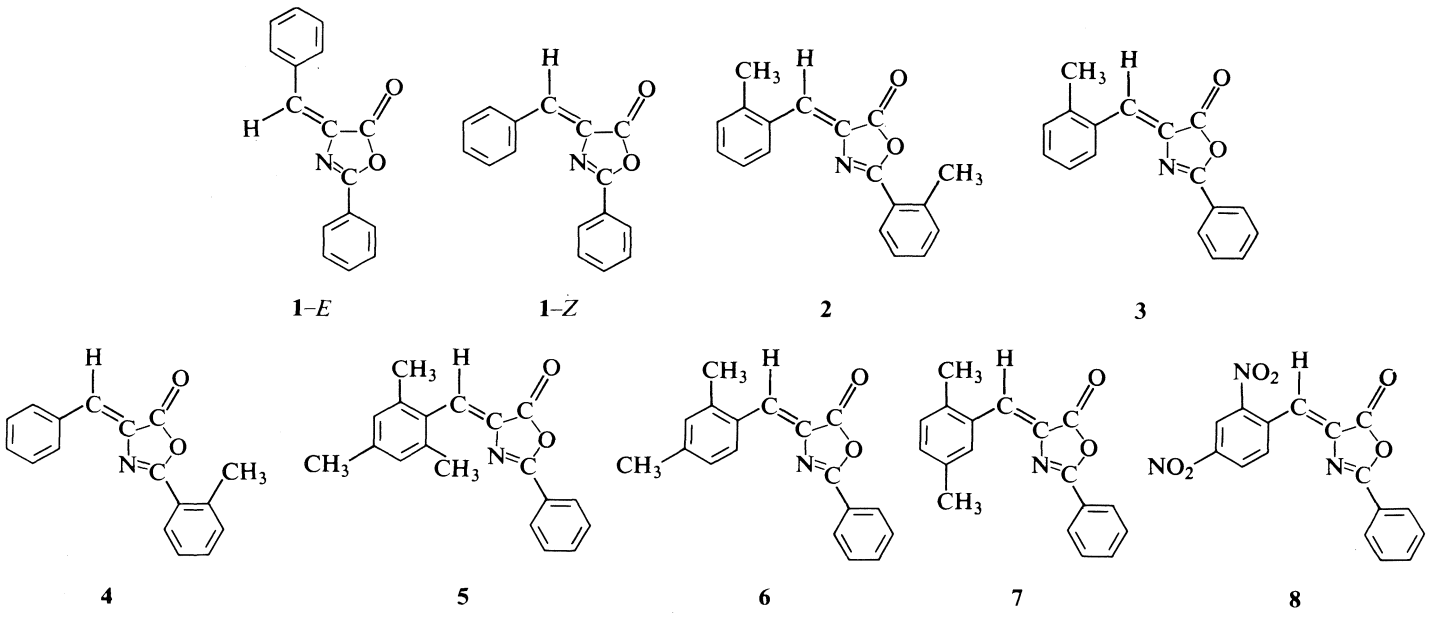

final structure factors[4] and showed no residual density outside the limits −0.12 to 0.12 e Å^{-3}. Computer programs of Ahmed *et al.* (12), Main *et al.* (10), and Johnson (13) were used.

Results and discussion

Final coordinates for the non-hydrogen atoms obtained from the X-ray analysis are listed in Table 2. A perspective view of the molecule with the numbering scheme used in this analysis is shown in Fig. 1 and bond distances and angles are given in Fig. 2. The X-ray analysis has established that the molecule has the *Z* configuration, with C(8) *cis* to N(3).

Comparison of the bond lengths found here with those in a closely-related dinitro oxazolinone, **8** (3), suggests that there is less conjugation in the present compound. Bonds C(2)—N(3) and C(4)—C(7) are slightly shorter and N(3)—C(4) and C(7)—C(8) slightly longer here. While the individual differences are not significant, the overall pattern is consistent with the fact that the trisubstituted benzylidene ring is twisted 61.3° out of the oxazoline ring plane, whereas in the dinitro compound the rings are approximately coplanar. The large twist in the present compound avoids too-close contact of C(14) and N(3), here 3.180(2) Å, and of C(16) and H(7), 2.81(2) Å.

Each of the three rings separately is planar within ±0.011 Å, although the deviations from planarity are statistically significant for each ring. Substituents on the rings show displacements from the mean planes of up to 0.089(2) Å; interestingly, the two *ortho*-methyl carbon atoms do not show the largest deviations. The unsubstituted phenyl ring is twisted 15.0° out of the plane of the oxazoline ring. Agreement of the bond angles in this structure with those in the dinitro compound is very good, especially for the oxazolinone system. Few other crystal structures containing an oxazolin-5-one group have been reported (14–17), and because they each show important differences in the immediately adjacent bonding, detailed comparisons would be meaningless.

The packing arrangement is shown in Fig. 3. The pair of

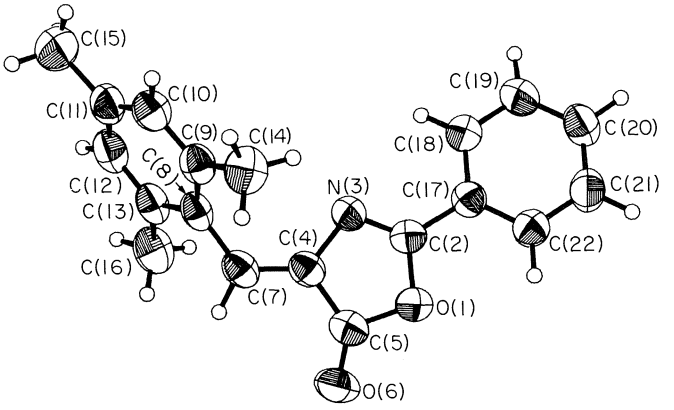

FIG. 1. A perspective view of the molecule showing the numbering scheme. Hydrogen atoms are shown as spheres of 0.1 Å radius, while the anisotropic ellipsoids enclose 50% probability.

lactone groups related by the centre of symmetry at $\frac{1}{2}$, $\frac{1}{2}$, 0 show C···C and C···O contacts of about 3.3 Å; however, stacking of the oxazoline rings is only marginal. A distance of about 5.6 Å along *b* separates such pairs of lactone groups. The pair of head-to-tail trimethylbenzene groups related by a centre of symmetry at 0, $\frac{1}{2}$, 0 show a ring spacing of about 3.64 Å. Overlap is at the C(8) end of the rings, such that the C(8)—C(7) bond of one molecule is superimposed on the benzene ring of the other molecule, and there is considerable overlap of the C(14)—C(9), C(9)—C(8), C(8)—C(13), C(13)—C(16) bonds of one molecule with the opposite sequence of bonds in the other molecule.

The absorption spectra of **5**, **6**, and **7** are shown in Fig. 4. The absorption maximum is shifted significantly for **5**, while its extinction coefficient is less by a factor of ca. 2, and no fine structure can be seen in its spectrum. Such fine structure *is* evident in the spectra of **6** and **7** and in other published examples (4, 5).

Second order rate constants for the reaction of benzylamine with compounds **5**–**7** are reported in Table 3. Each is an average of three determinations. For comparison, and to obtain "calculated" rate constants for **5**, **6**, and **7**, data for **1**-Z, **3**, 4-(3-methyl)benzylidene-2-phenyloxazolin-5-one, and 4-(4-

[4]Tables of observed and calculated structure factors, of refined parameters for the hydrogen atoms and of anisotropic displacement parameters for the non-hydrogen atoms are available at a nominal charge from the Depository of Unpublished Data, CISTI, National Research Council of Canada, Ottawa, Ont., Canada K1A 0S2.

TABLE 1. Physical characteristics of oxazolinones

Compound	Yield %	m.p. °C	Elemental analysis (% C, H, N) Calcd	Found	λ_{max} (nm) (CH_3CN)	Molar extinction coefficient
5	21	167–169	78.32, 5.88, 4.81	78.18, 5.73, 4.96	348	19700
6	28	150–151	77.96, 5.45, 5.05	77.75, 5.31, 4.88	376	36200
7	31	123–125	77.96, 5.45, 5.05	77.77, 5.33, 5.15	372	35100

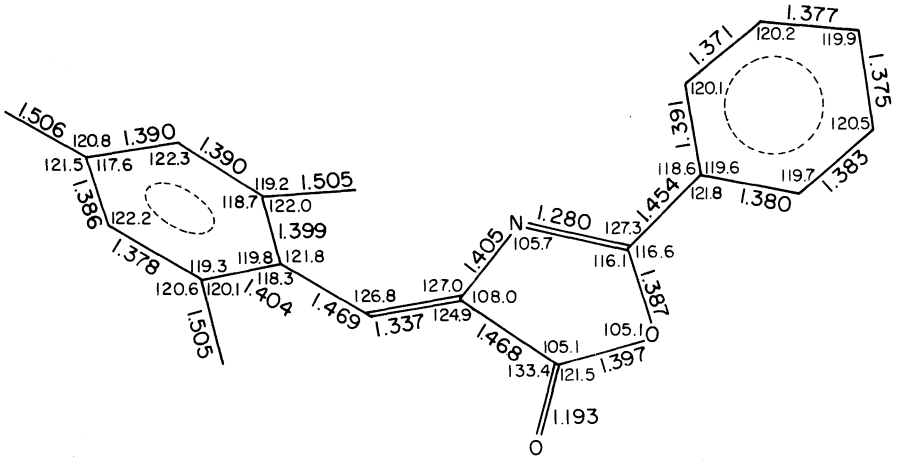

FIG. 2. Bond lengths (Å) and bond angles (deg); esd's are 0.002–0.003 Å and 0.1–0.2°.

TABLE 2. Fractional atomic coordinates ($\times 10^4$) and equivalent isotropic thermal parameters ($Å^2$)[a]

Atom	x	y	z	B_{eq}($Å^2$)
O(1)	5317(1)	2412(1)	35(1)	4.8
C(2)	4842(2)	1973(2)	745(1)	4.2
N(2)	3718(1)	2490(2)	907(1)	4.3
C(4)	3332(2)	3418(2)	277(1)	4.3
C(5)	4368(2)	3381(2)	−289(1)	4.8
O(6)	4511(1)	3992(2)	−898(1)	6.5
C(7)	2250(2)	4255(2)	208(1)	4.6
C(8)	1201(2)	4347(2)	765(1)	4.3
C(9)	473(2)	3095(2)	967(1)	4.6
C(10)	−544(2)	3275(2)	1471(1)	5.2
C(11)	−851(2)	4650(2)	1788(1)	5.5
C(12)	−96(2)	5863(2)	1588(1)	5.5
C(13)	906(2)	5745(2)	1079(1)	4.8
C(14)	722(2)	1579(2)	629(1)	5.9
C(15)	−2004(2)	4818(3)	2299(1)	7.9
C(16)	1707(2)	7088(2)	880(1)	6.5
C(17)	5682(2)	1001(2)	1228(1)	4.2
C(18)	5408(2)	821(2)	2011(1)	5.4
C(19)	6186(2)	−77(3)	2485(1)	6.0
C(20)	7236(2)	−817(2)	2188(1)	5.7
C(21)	7507(2)	−646(2)	1414(1)	5.7
C(22)	6740(2)	271(2)	932(1)	4.9

[a] $B_{eq} = \frac{8}{3}\pi^2 \Sigma_i \Sigma_j U_{ij} a_i^* a_j^* \mathbf{a}_i \cdot \mathbf{a}_j$.

methyl)benzylidene-2-phenyloxazolin-5-one are included (9). The positional effect of methyl substitution in the benzylidene ring can be calculated by subtracting rate constants obtained for the *ortho*-, *meta*-, or *para*-methyl analogues from the value for the unsubstituted compound **1**-Z. Assuming that the effects of methyl groups are additive, subtraction of the values for each

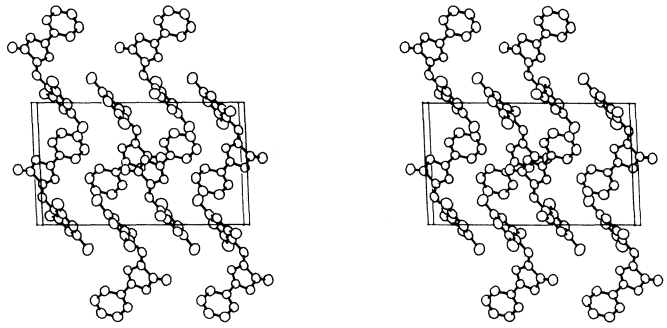

FIG. 3. A stereoview down the *b* axis of the packing arrangement. The *c* axis is horizontal and *a* is vertical.

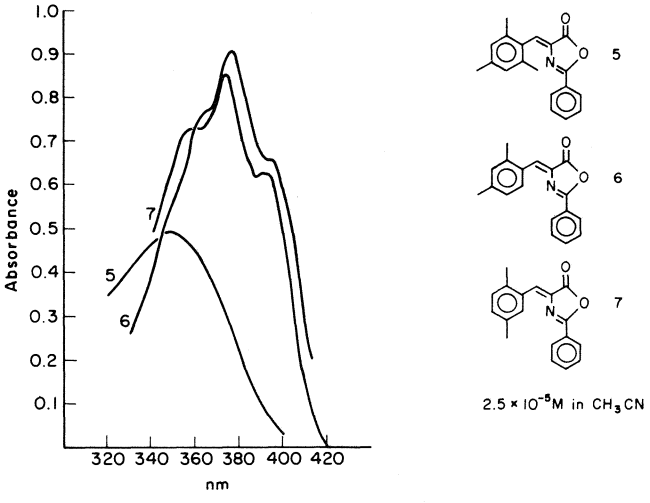

FIG. 4. Absorption spectra of compounds **5**, **6**, and **7**.

TABLE 3. Second order rate constants for the reaction of oxazolinones with benzylamine in acetonitrile solution at 25°C

Compound	k	
	Expl.	Calcd
5	3.86 ± 0.10	0.98
6	1.58 ± 0.03	1.62
7	2.64 ± 0.09	2.22
1-*Z*	4.80 ± 0.12 (9)	—
3	4.16 ± 0.17 (9)	—
4-(*m*-CH_3)	2.86 ± 0.04	—
4-(*p*-CH_3)	2.26 ± 0.06 (9)	—

methyl substituent allows an estimate of the rate constants for compounds **5**, **6**, and **7**. From Table 3 the experimentally obtained values for **6** and **7** are in reasonable agreement with the calculated values while the respective rate constants for **5** are very different.

Compound **5** differs from the two isomeric dimethylated oxazolinones **6** and **7** in four major regards: (*1*) There is no fine structure in the absorption spectrum of **5** while there is such structure in other alkyl- or unsubstituted *Z*-oxazolinones (4, 7, Fig. 4). (*2*) The λ_{max} value of **5** is about 30 nm lower than those of **6** and **7**. (*3*) The molar extinction coefficient is reduced about two-fold for **5**. (*4*) The reaction of **5** with benzylamine in acetonitrile occurs about four times as fast as predicted using model reactions.

The lack of fine structure might be consistent with an isomerization of the usual *Z* isomer to the *E* form. The other points, however, are consistent with a lack of resonance between π electrons of the benzylidene ring and the remainder of the 2-phenyloxazolin-5-one structure. The finding that the benzylidene ring conformation is greatly removed from co-planarity with the oxazolinone portion satisfactorily explains the absorption spectrum and the reduced inductive effect of the methyl groups in **5**. An earlier study of oxazolinone ring opening by benzylamine concluded that *o*-substitution in the 4-benzylidene ring actually enhanced reactivity, probably by release of strain upon ring opening (9). In the present case, due to non-planarity, this argument need not be called upon. It is interesting, and yet another indication that the *Z* isomer is the preferred form, that the di-*ortho*-substituted compound **5** takes up this configuration.

1. K. BROCKLEHURST and K. WILLIAMSON. Tetrahedron, **30**, 351 (1974).
2. P. O. LARSEN and E. WIECZORKOWSKA. Acta Chem. Scand. B, **28**, 92 (1974).
3. A. W. HANSON. Acta Crystallogr. Sect. B, **33**, 594 (1977).
4. K. KUMAR, D. J. PHELPS, and P. R. CAREY. Can. J. Chem. **56**, 232 (1978).
5. D. J. PHELPS, R. G. CARRIERE, K. KUMAR, and P. R. CAREY. Can. J. Chem. **56**, 240 (1978).
6. J. PLÖCHL. Ber. **16**, 2815 (1883).
7. E. S. NICHOLAS and D. J. PHELPS. J. Chem. Eng. Data, **25**, 89 (1980).
8. Y. S. RAO and R. FILLER. Synthesis, 749 (1975).
9. D. J. PHELPS, P. V. GODREAU, and E. S. NICHOLAS. J. Chem. Soc. Perkin Trans. II, 140 (1981).
10. P. MAIN, S. E. HULL, L. LESSINGER, G. GERMAIN, J.-P. DECLERCQ, and M. M. WOOLFSON. MULTAN 78. A system of computer programs for the automatic solution of crystal structures from X-ray diffraction data. University of York, York, England, and University of Louvain, Louvain, Belgium. 1978.
11. International tables for X-ray crystallography. Vol. IV. Kynoch Press, Birmingham. 1974.
12. F. R. AHMED, S. R. HALL, M. E. PIPPY, and C. P. HUBER. J. Appl. Crystallogr. **6**, 309 (1973).
13. C. K. JOHNSON. ORTEP, Report ORNL-3794, 2nd rev. Oak Ridge National Laboratory, Oak Ridge, TN. 1970.
14. H.-D. STACHEL and H. ERHARDT. Arch. Pharm. 968 (1979).
15. S. MOHR. Tetrahedron Lett. 3139 (1979).
16. M. VAN MEERSSCHE, G. GERMAIN, J. P. DECLERCQ, H. G. VIEHE, and E. FRANCOTTE. Acta Crystallogr. B**33**, 668 (1977).
17. P. A. C. GANE and M. O. BOLES. Acta Crystallogr. B**35**, 2664 (1979).

Synthesis of 9- and 10-membered rings by the intramolecular Michael addition of malonate on enone and ynone

PIERRE DESLONGCHAMPS AND BERNARD L. ROY[1]

Laboratoire de synthèse organique, Département de chimie, Faculté des sciences, Université de Sherbrooke, Sherbrooke (Qué.), Canada J1K 2R1

Received April 29, 1986

PIERRE DESLONGCHAMPS and BERNARD L. ROY. Can. J. Chem. **64**, 2068 (1986).

The base-catalyzed (Cs_2CO_3 in THF/DMF) intramolecular Michael addition of β-ketoester-ynones **7**–**10** and -enone **11** is reported. Macrocyclization (Table 1), which produces the corresponding medium rings, was observed in 25–50% yield.

PIERRE DESLONGCHAMPS et BERNARD L. ROY. Can. J. Chem. **64**, 2068 (1986).

On rapporte l'addition Michael intramoléculaire baso-catalysée (Cs_2CO_3, THF/DMF) des β-cétoesters-ynones **7**–**10** et -énone **11**. La réaction conduit aux cycles moyens correspondants avec des rendements de 25–50% (Tableau 1).

The study of medium and large carbocyclic rings containing several substituents and functional groups has not yet received much attention (1) and one of the main reasons is the lack of direct reliable synthetic methods. Our laboratory has recently reported (2) that 10-membered rings were accessible by using a simple irreversible process, i.e., the SN_2 displacement of a leaving group by malonate anion under medium diluted conditions. The success of this approach relied upon the choice of aliphatic precursors that have two unsaturations (*cis* and *trans* double or triple bonds) in the chain. These unsaturations eliminate most of the transannular steric interactions and diminish, at the same time, the number of degrees of freedom in the chain. More recently, we have also shown that 11-, 12-, 13-, and 14-membered rings can also be successfully constructed by this approach, and in very good yield (13).

In principle, any factor that will appropriately restrict the conformational mobility of a chain and lower transannular steric interactions should favor macrocyclization reaction. For instance, conjugation between sp_2 type functional groups and use of reactions that have a high degree of stereochemical control at the transition state level should promote these cyclizations. For these reasons, the internal Michael reaction of a nucleophile on enone and ynone appears to be an attractive route, because stereoelectronic effects predict a high degree of conformational restriction at the transition state level in the first step of these reactions (4). Indeed, it is expected that the intramolecular addition of a nucleophile on enone **1** and ynone **4** (Scheme 1) will produce an enolate intermediate having a structure and conformation close to **2** and **5** respectively, which by protonation will then lead to the reaction products, i.e., the cyclic ketone **3** and conjugated ketone **6**. Our previous studies (2, 3) indicated that two unsaturations in the chain are necessary for a successful macrocyclization; it was therefore planned to study the cyclization of enone and ynone of types **1** and **4**, which possess a second unsaturation site in the chain. Following this idea, we wish to report a study on the cyclization of ynones **7**–**10** and enone **11** (Scheme 2). Compound **7** can theoretically give a nine-membered ring while the others can lead to a ten-membered ring.

Results and discussion

Compounds **7**–**11** were prepared following standard procedures of known reactions. The synthesis of compound **7** is illustrated in Scheme 3, and syntheses of compounds **8**–**11** are shown in Scheme 4. Both schemes are self-explanatory. One element that is worth mentioning is the temporary transformation of the malonate group into a triester (cf. **18** → **19** and **25** → **26**) and, at a later stage, the reconversion of the triester into the malonate group (**20** → **21**, **28** → **29**, **28** → **30**, **32** → **33**, **32** → **34**) by reactions with organometallic reagents (5).

The cyclization of the acyclic precursors **7**–**11** was carried out with cesium carbonate in a 1:1 mixture of tetrahydrofuran and *N*,*N*-dimethylformamide at room temperature. The results are summarized in Table 1 and the structure of the cyclic monomers and (or) dimers obtained are shown in Scheme 5. The cyclizations were carried out at 2×10^{-3} *M*. In some cases, a pseudo high dilution technique (slow addition of the substrate in the medium with a syringe pump (6, 7)) was used to increase the quantity of cyclic monomer and (or) dimer.

The structures of the monomers and dimers were established spectroscopically (ir, ^1H and ^{13}C nmr, and ms). The configuration of the olefin of the conjugated enones was assigned *cis* for the monomers **35**, **36**, and **38** and *trans* for the dimer **39**. This assignment is based on the coupling constant ($J_{H,H}$(*cis*) ≅ 13 Hz and $J_{H,H}$(*trans*) ≅ 17 Hz) observed for the olefinic hydrogens of the enone.

Compound **37** with an exocyclic olefin must be formed via the isomerization of conjugated enone **42** under basic conditions. Such deconjugation of a 10-membered ring enone has literature precedent (8). The structure of enone **38** was further established by its conversion into bicyclic dienone **43** under acidic conditions. This type of transannular reaction between a ketone and an acetylene in a 10-membered ring yielding a bicyclic enone has been previously observed by Weiler and co-workers (9).

The aliphatic precursors **7**, **8**, and **9**, which contain a *cis* olefin, gave the corresponding cyclic monomers **35**, **36**, and **37** respectively in moderate yield, but no dimer was observed. Cyclization of enone **10**, which contains an isolated triple bond, gave a mixture of monomer **38** and dimer **39** at medium dilution, and only monomer **38**, in 50% yield, at pseudo high dilution. The enone **11** gave at medium dilution a low yield of dimer **41** and no monomer. At pseudo high dilution, both monomer **40** and dimer **41** were observed.

Nine and ten-membered rings are the most difficult ones to be produced by a direct cyclization method. For instance, the internal displacement of bromide by malonate anion in C-9 and C-10 saturated chains gave the corresponding cyclic monomer under high dilution in 3 and 0.1% yield respectively (10). It can therefore be concluded that, although the yields are moderate

[1]NSERCC and FCAC predoctoral fellowships (1980–1984).

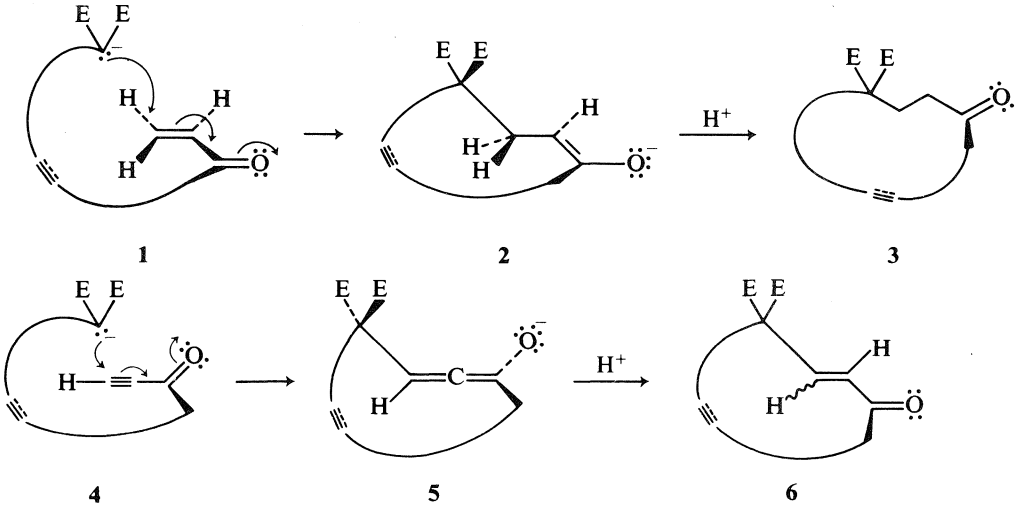

1 2 3

4 5 6

SCHEME 1 (E = $COOCH_3$)

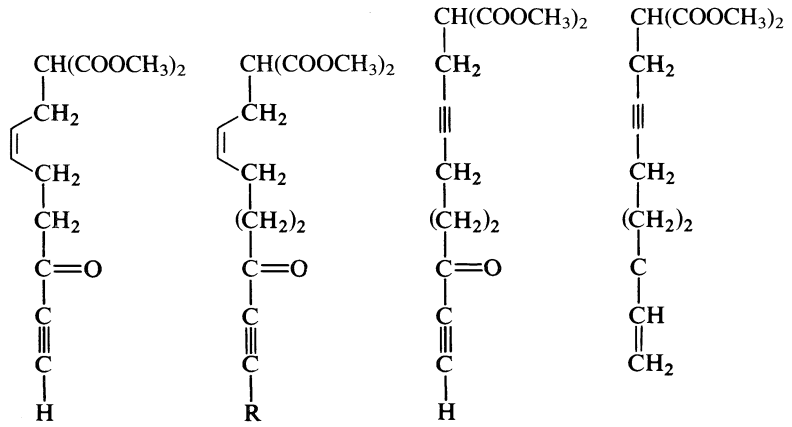

7 8 R = H 9 R = CH_3 10 11

SCHEME 2

TABLE 1. Cyclization products of acyclic precursors **7–11**

Starting material	Time (h)	*M*	Cyclic products: Monomer (%)	Cyclic products: Dimer (%)
7	48	2×10^{-3}	**35** (35)	—
8	48	2×10^{-3}	**36** (29)	—
9	48	p.h.d.[a]	**37** (27)	—
10	36	2×10^{-3}	**38** (31)	**39** (13)
10	36	p.h.d.[a]	**38** (50)	—
11	60	2×10^{-3}	—	**41** (20)
11	60	p.h.d.[a]	**40** (27)	**41** (56)

[a]Pseudo high dilution.

(25–50%), the intramolecular addition of malonate on enone and ynone is an interesting method to produce medium rings directly. This synthetic strategy may eventually lead to excellent yield (≥80%) in macrocyclization provided that transannular steric interactions and conformational mobility can be further decreased. Work in this direction is in progress in our laboratory.

Experimental

The infrared (ir) spectra were taken on a Perkin–Elmer 681 spectrophotometer. Proton nmr spectra were recorded on a Bruker WP-60, WP-80, or a Bruker WM-250 instrument. Carbon-13 nmr spectra were recorded on a Bruker WM-250 instrument. The following abbreviations have been used: s, singlet; d, doublet; t, triplet; q, quadruplet; m, multiplet; b, broad. Deuterated chloroform was used as the solvent and internal standard unless indicated otherwise. The mass spectra (ms) were recorded on a VG Micromass ZAB-1F mass spectrometer.

Reactions were carried out under argon. Anhydrous magnesium sulfate was used as the drying agent in work-up of reactions.

Dioloxane ***14***

n-Butyllithium (3.7 mL of 1.7 *M* in hexane, 6.3 mmol) was added to a solution of acetylene **13** (850 mg, 6.1 mmol) in dimethoxyethane (10 mL) at −78°C. The solution was stirred for 15 min, after which hexamethylphosphoramide (3 mL) was added. The mixture was stirred at −78°C for an additional 5 min, then warmed to 0°C. The bromide **12** (1.0 g, 5.52 mmol) was then added, the mixture was stirred at 0°C for 1 h, and the reaction was quenched with a saturated solution of ammonium chloride (4 mL). The resulting mixture was extracted with ether–hexane ((1:1, 3 × 50 mL). The organic layer was washed with a solution of lithium chloride (10% weight/vol, 2 × 100 mL) and the solvent was evaporated. The residue was purified by flash chromatog-

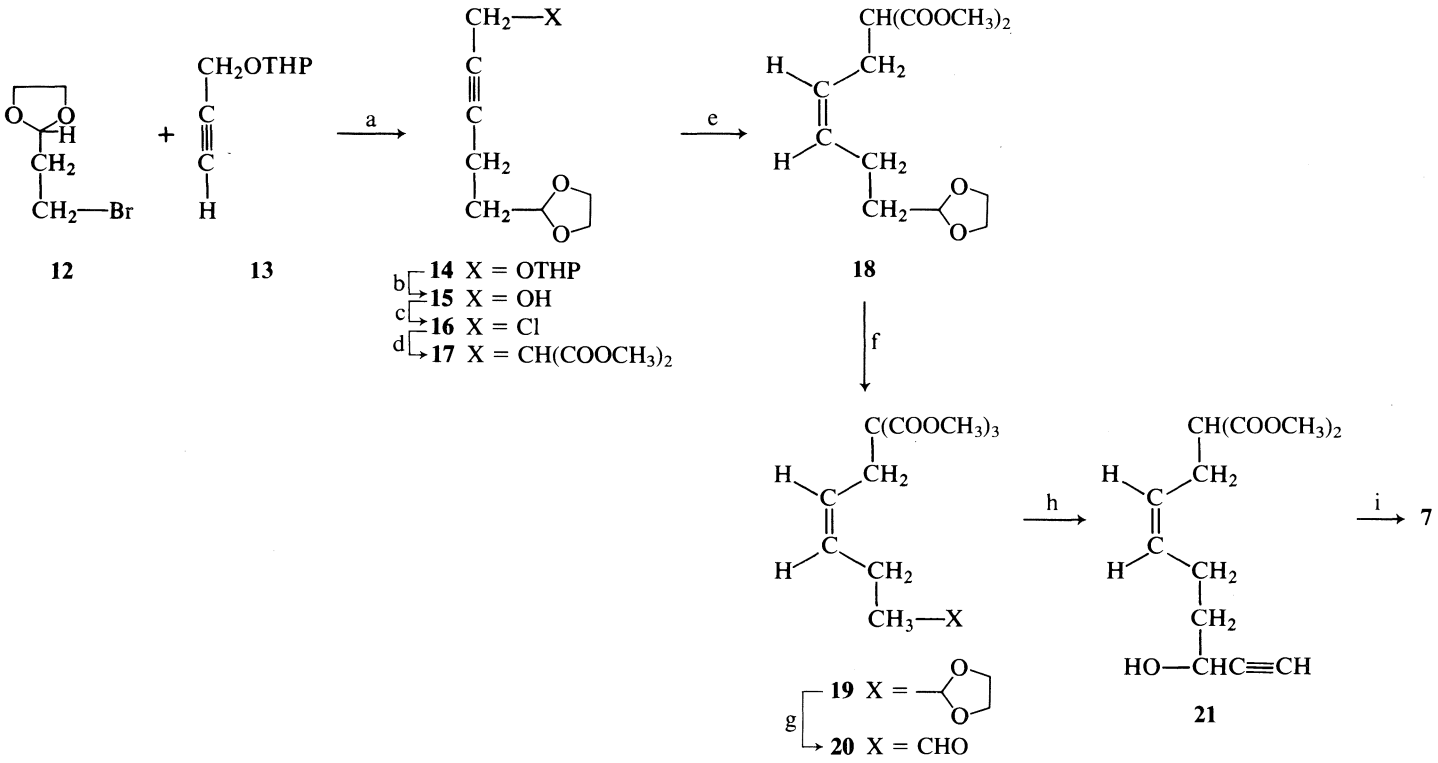

(a) *n*-BuLi, DME, HMPA, −30 → 0°C, 81%
(b) pyridinium *p*-toluenesulfonate (PPTS), CH_3OH, room temp., 90% (ref. 11)
(c) CH_3SO_2Cl, LiCl, collidine, DMF, 0°C → room temp., 85% (ref. 12)
(d) $CH_2(COOCH_3)_2$, K_2CO_3, THF:DMF (1:1), reflux, 82%
(e) H_2, $Pd/BaSO_4$ 5%, quinoline, benzene, 99%
(f) NaH, $ClCOOCH_3$, THF, 0°C → room temp., 88% (ref. 5)
(g) PTSA, H_2O, acetone, reflux, 83% (ref. 13)
(h) HC≡C—MgBr, THF, −30°C, 34% (ref. 14)
(i) CrO_3, acetone, H_2SO_4, room temp., 95% (ref. 15)

SCHEME 3

raphy with hexane – ethyl acetate (4:1) as the eluent to afford pure dioxolane **14** (1.074 g, 81%); ir ($CHCl_3$): 2940 (C—H), 1150 (C—O); nmr ($CDCl_3$) δ: 4.96 (1H, t, J = 5.1 Hz, CH of the dioxolane), 4.80 (1H, bs, CH of the tetrahydropyran), 4.23 (2H, t, J = 2.1 Hz, —C≡CCH_2O—), 3.93 (2H, s, —CH_2O— of the dioxolane), 3.89 (2H, s, —CH_2O— of the dioxolane), 3.58 (2H, m, —CH_2O— of the tetrahydropyran), 2.37 (2H, m, —CH_2—C≡C—), 2.00–1.40 (8H, m, —CH_2CH_2—C≡C—, 3 × CH_2 of the tetrahydropyran); ms *m/e*: 240 (M^+), 239 (M^+ − H).

Alcohol ***15***

Pyridinium *p*-toluenesulfonate (PPTS) (111 mg, 0.446 mmol) was added to a solution of dioxolane **14** (1.07 g, 4.46 mmol) in methanol (10 mL). The solution was stirred at room temperature for 30 h, after which the methanol was evaporated and ether (10 mL) was added to the residue to precipitate the PPTS. The ether solution was filtered and evaporated to afford pure alcohol **15** (626 mg, 90%); ir: 3620 (OH), 3450 (OH); nmr δ: 4.96 (1H, t, J = 4.6 Hz, CH of the dioxolane), 4.21 (2H, t, J = 2.1 Hz, —C≡CCH_2O—), 3.91 (2H, s, —CH_2O— of the dioxolane), 3.88 (2H, s, —CH_2O— of the dioxolane), 2.40 (3H, m, —CH_2—C≡C—, —O*H*), 1.88 (2H, m, —CH_2—CH_2—C≡C—); ms *m/e*: 155 (M^+ − H). *Exact Mass* calcd. for $C_8H_{12}O_3$: 155.0708; found: 155.0707.

Chloride ***16***

To a solution of alcohol **15** (2.5 g, 16 mmol), lithium chloride (1.0 g, 23.8 mmol), and s-collidine (2.3 g, 19 mmol) in *N*,*N*-dimethylformamide (96 mL) maintained at 0°C was added mesyl chloride (2.2 g, 19.2 mmol). The solution was stirred for 20 min at 0°C, warmed to room temperature, and stirred for an additional 4 h. Water (100 mL) was then added and the mixture was extracted with ether–hexane ((1:1), 3 × 100 mL). The organic layer was dried and evaporated. The residue was purified by flash chromatography with hexane – ethyl acetate (2:1) as the eluent to afford pure chloride **16** (2.39 g, 85%); ir: 1420 (CH_2), 1260 (C—O), 750 (C—Cl); nmr δ: 4.96 (1H, t, J = 4.8 Hz, CH of the dioxolane), 4.13 (2H, t, J = 2.3 Hz, —CH_2Cl), 3.92 (2H, s, —CH_2O—), 3.90 (2H, s, —CH_2O—), 2.40 (2H, m, —CH_2—C≡C—),1.88 (2H, m, —CH_2—CH_2—C≡C—).

Diester ***17***

A solution of chloride **16** (916 mg, 5.2 mmol), dimethylmalonate (3.45 mg, 26 mmol), and potassium carbonate (5.82 g, 42 mmol) in tetrahydrofuran (30 mL) and *N*,*N*-dimethylformamide (30 mL) was refluxed for 13 h. The mixture was then cooled to room temperature, filtered, and the solvents were removed under reduced pressure. The residue was purified by flash chromatography with hexane – ethyl acetate (4:1) as the eluent to afford pure diester **17** (1.16 g, 82%); ir: 1740 (C=O); nmr δ: 4.92 (1H, t, J = 5.1 Hz, CH of the dioxolane), 3.90 (2H, s, —CH_2O—), 3.88 (2H, s, —CH_2O—), 3.75 (6H, s, 2 × —$COOCH_3$), 3.43 (1H, t, J = 7.2 Hz, —CH—$(COOCH_3)_2$), 2.73 (2H, dd, J = 2.1 Hz, 7.6 Hz, —C≡C—CH_2—CH—), 2.25 (2H, m, —CH_2—C≡C—), 1.84 (2H, m, —CH_2—CH_2—C≡C—); ms *m/e*: 270 (M^+). *Exact Mass* calcd. for $C_{13}H_{16}O_6$: 270.1103; found: 270.1097.

Olefin diester ***18***

A solution of diester **17** (562 mg, 2.08 mmol) in benzene (25 mL) was added to a suspension of palladium (5%) on barium sulfate in

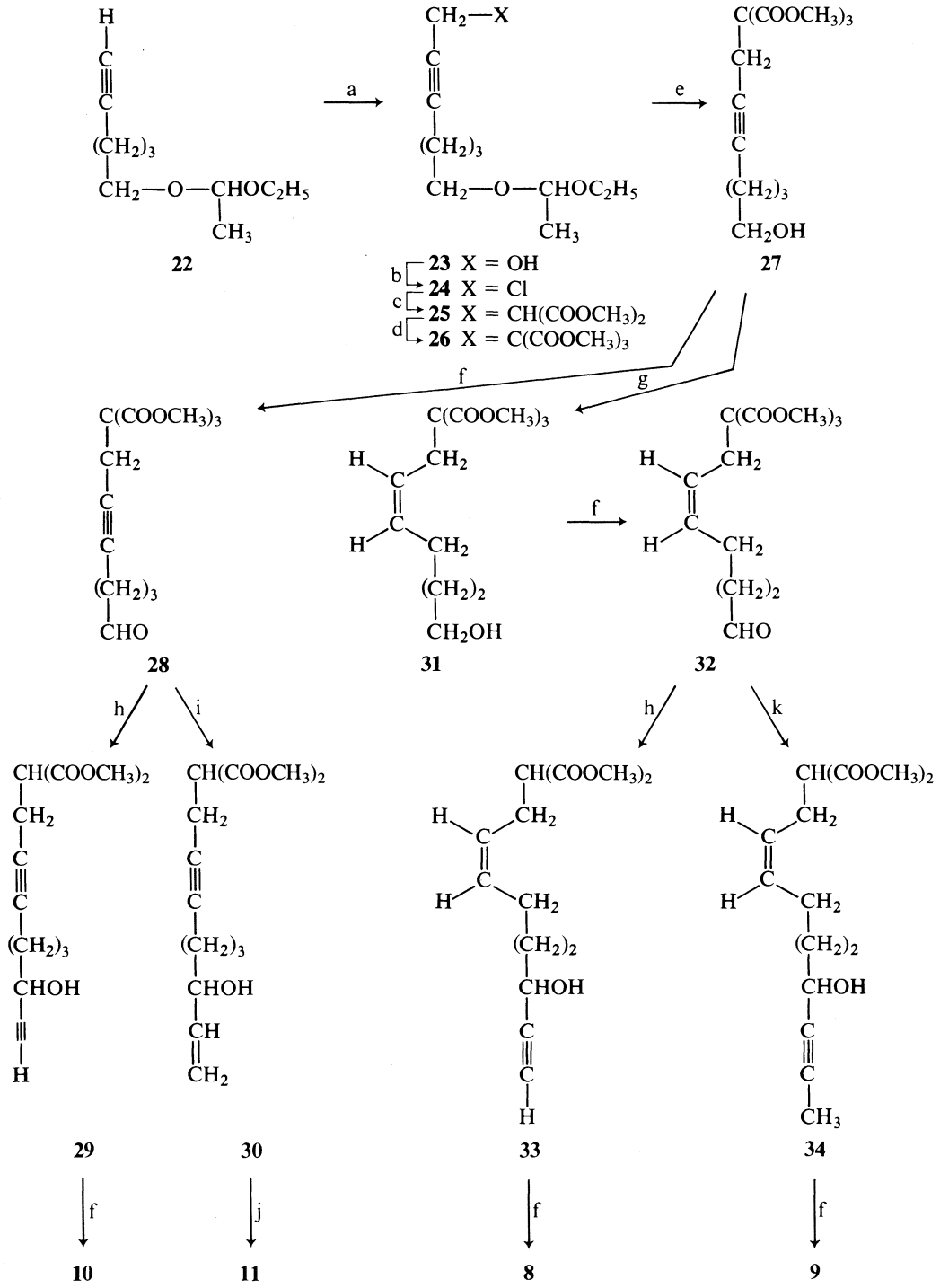

(a) *n*-BuLi, $(CH_2O)_n$, Et_2O:THF (1:1), − 30°C → room temp., 46% (ref. 14)
(b) CH_3SO_2Cl, LiCl, s-collidine, DMF, 0°C → room temp., 87% (ref. 12)
(c) $CH_2(COOCH_3)_2$, K_2CO_3, THF:DMF (1:1), reflux, 99%
(d) NaH, CH_3OCOCl, THF, 0°C → room temp., 99% (ref. 5)
(f) PCC, molecular sieve, 3Å, CH_2Cl_2, room temp., >85% (ref. 16, 17)
(g) H_2, Pd/$BaSO_4$ 5% quinoline, benzene, 86%
(h) HC≡C—MgBr, THF, −30°C, 59% (ref. 14)
(i) CH=CHMgBr, THF, −20°C, 58%
(j) MnO_2, $CHCl_3$, hexane, room temp., 73%
(k) CH_3—C≡C—MgBr, THF, −30°C, 58%

SCHEME 4

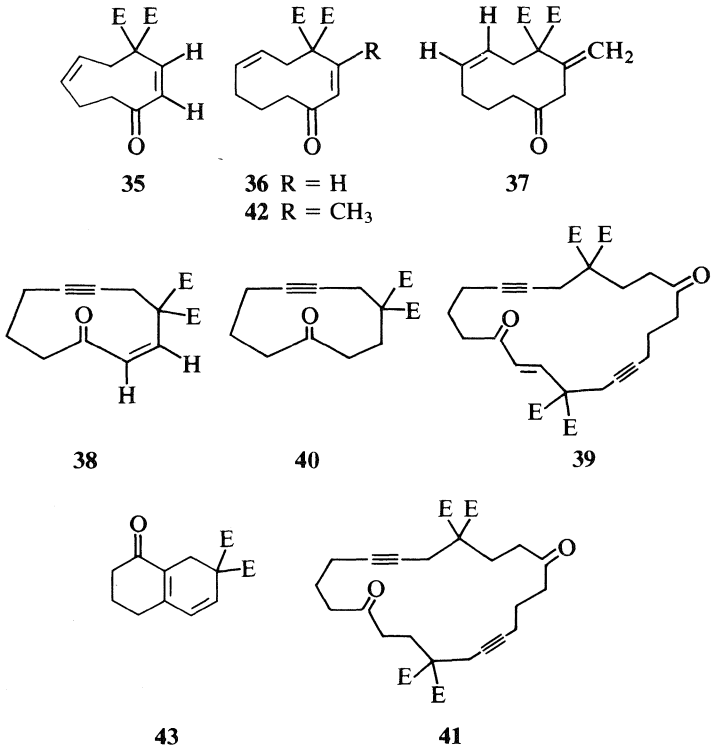

SCHEME 5

benzene (1 mL) and quinoline (50 μL). The mixture was shaken under a hydrogen atmosphere until all uptake of hydrogen had ceased. The mixture was then filtered on Celite and the solution was washed with a solution of hydrochloric acid (10 mL, 1 *N*). The organic layer was dried and evaporated, affording pure olefin diester **18** (558 mg, 99%); ir: 1740 (C=O); nmr δ: 5.37 (2H, m, —*H*C=C*H*—), 4.76 (1H, t, *J* = 4.5 Hz, CH of the dioxolane), 3.83 (2H, s, —CH_2O—), 3.80 (2H, s, —CH_2O—), 3.64 (6H, s, 2 × —COOCH_3), 3.31 (1H, t, *J* = 6.9 Hz, —C*H*—(COOCH_3)$_2$), 2.60 (2H, m, —CH=CH—CH_2—CH—), 2.06 (2H, m, —CH_2—CH=CH—), 1.68 (2H, m, —CH_2—CH_2—CH=CH—); ms *m/e*: 272 (M^+), 241 ($M^+ - OCH_3$).

*Triester **19***

Sodium hydride (90 mg, 3.73 mmol) was added to a solution of olefin diester **18** (562 mg, 2.07 mmol) in tetrahydrofuran (1.6 mL) at 0°C. The solution was stirred at room temperature for 45 min, methyl chloroformate (293 mg, 3.10 mmol) was then added, and the solution was stirred for one extra hour. A saturated solution of ammonium chloride (5 mL) was then added to the cooled solution (0°C). The mixture was extracted with ether (3 × 20 mL), and the organic layer was dried and evaporated. The residue was purified by flash chromatography with hexane – ethyl acetate (2:1) as the eluent to afford pure triester **19** (600 mg, 88%); ir: 1740 (C=O); nmr δ: 5.52 (2H, m, —C*H*=C*H*—), 4.85 (1H, t, *J* = 4.5 Hz, CH of the dioxolane), 3.91 (2H, s, —CH_2O—), 3.89 (2H, s, —CH_2O—), 3.76 (9H, s, 3 × —COOCH_3), 2.90 (2H, d, *J* = 4.9 Hz, —CH_2—C—(COOCH_3)$_3$), 2.12 (2H, m, —CH_2—CH=CH—), 1.67 (2H, m, —CH_2—CH_2—CH=CH—).

*Aldehyde triester **20***

To a solution of ketal **19** (322 mg, 0.976 mmol) in acetone (10 mL) was added water (20 μL) and *p*-toluenesulfonic acid (50 mg). The solution was refluxed for 48 h, after which the acetone was evaporated and the residue was taken up in methylene chloride (20 mL). The solution was then washed with a saturated solution of sodium bicarbonate (10 mL), the organic layer was dried, and the solvent was evaporated to afford pure aldehyde **20** (230 mg, 83%); ir: 1730 (C=O); nmr δ: 9.75 (1H, bs, *H*C=O), 5.50 (2H, m, —C*H*=C*H*—), 3.75 (9H, s, 3 × —COOCH_3), 2.90 (2H, d, *J* = 5.0 Hz, —CH_2—C—(COOCH_3)$_3$), 2.40 (2H, m, —CH_2—CH_2—CH=CH—), 2.12 (2H, m, —CH_2—CH=CH—).

Ethynylmagnesium bromide

Ethyl bromide (1.27 g, 11.6 mmol) was added in 100-μL portions to a suspension of magnesium (310 mg, 12.8 at.-g) in tetrahydrofuran (12 mL). The internal temperature was monitored to maintain a maximum of 45°C. After the addition of ethyl bromide was completed the solution was stirred at room temperature for 20 min. Acetylene was purified by flowing the gas through two cold traps (−78°C), concentrated sulfuric acid, and potassium hydroxide and copper sulfate. The purified acetylene was then bubbled into the ethyl magnesium bromide solution at such a rate as to maintain a maximum internal temperature of 36°C. After the exothermic reactions had subsided, the acetylene was bubbled another 5 min. The solution was used as such.

*Alcohol diester **21***

Ethynylmagnesium bromide (2.58 mL of a 0.95 *M* solution in tetrahydrofuran, 2.45 mmol) was added to a solution of aldehyde triester **20** (139 mg, 0.49 mmol) in tetrahydrofuran (3 mL) maintained at −35°C. The solution was stirred at −35°C for an additional 30 min and then quenched with a saturated solution of ammonium chloride (10 mL). The mixture was extracted with ether (3 × 30 mL), the organic layer was dried, and the solvent was evaporated. The residue was purified by flash chromatography with hexane – ethyl acetate (2:1) as the eluent to afford pure alcohol diester **21** (43 mg, 34%); ir: 3610, 3480 (OH), 3310 (—C≡C—H), 1730 (C=O); nmr δ: 5.45 (2H, m, —C*H*=C*H*), 4.37 (1H, m, —C*H*OH), 3.74 (6H, s, 2 × —COOCH_3), 3.42 (1H, t, *J* = 7.4 Hz, —C*H*—(COOCH_3)$_2$), 2.45 (1H, d, *J* = 2.1 Hz, —C≡C—*H*), 2.68 (2H, m, —CH_2—CH—(COOCH_3)$_2$), 2.20 (3H, m, —CH$_2$—CH_2—CH=CH—, O*H*), 1.82 (2H, m, —CH_2—CH$_2$—CH=CH—); ms *m/e*: 255 (MH^+), *m/e*: 237 (M^+ − OH), and *m/e*: 223 ($M^+ - OCH_3$).

*Ynone **7***

To a solution of alcohol diester **21** (14.7 mg, 0.057 mmol) in acetone (2 mL) was added dropwise a solution of Jones reagent until persistence of a reddish colour. Ethanol (3 mL) was then added to the solution, which was thereafter neutralized with solid sodium bicarbonate, filtered, and the solvent evaporated. The residue was taken up in a saturated solution of sodium bicarbonate (3 mL) and the mixture was extracted with ether (3 × 20 mL). The organic layer was then washed with brine (30 mL), dried, and the solvent evaporated to afford pure ynone **7** (14 mg, 95%); ir: 3310 (C≡CH), 2110 (C≡C), 1730 (C=O, ester), 1680 (C=O, ynone); nmr δ: 5.41 (2H, m, —C*H*=C*H*—), 3.74 (6H, s, 2 × —COOCH_3), 3.41 (1H, t, *J* = 7.1 Hz, —C*H*—(COOCH_3)$_2$), 3.22 (1H, s, C≡C—*H*), 2.75–2.40 (6H, m, 3 × CH$_2$); ms *m/e* 253 (MH^+) and *m/e*: 221 ($M^+ - OCH_3$).

*Monomer **35***

Cesium carbonate was added to a solution of ynone **7** (7.5 mg, 0.030 mmol) in tetrahydrofuran (11 mL) and *N*,*N*-dimethylformamide (4 mL). The solution was stirred for 48 h at room temperature. The solution was then filtered, and the solvents were removed by distillation under reduced pressure. The residue was purified on a small column of silica gel with hexane – ethyl acetate (3:1) as the eluent to afford pure monomer **35** (2.6 mg, 35%); ir: 1735 (C=O, ester), 1690 (C=O, enone), 1650 (C=C); nmr δ: 6.36 (1H, d, J_{AB} = 15 Hz, —C*H*=CH—C(O)—), 6.09 (1H, d, J_{AB} = 15 Hz, —CH=C*H*—C(O)—), 5.36 (2H, m, —C*H*=C*H*—), 3.79 (6H, s, 2 × —COOCH_3), 2.90 (2H, d, *J* = 8.6 Hz, —CH_2—C—(COOCH_3)$_2$), 2.45 (2H, s, —CH_2—), 2.41 (2H, s, —CH_2—); ms *m/e*: 252 (M^+), *m/e*: 224 (M^+ − C=O), *m/e*: 221 ($M^+ - OCH_3$). *Exact Mass* calcd. for $C_{13}H_{16}O_5$: 252.0998; found: 252.0993.

*Alcohol **23***

A solution of ketal acetylene **22** (10 g, 59 mmol) and triphenylmethane (25 mg) in tetrahydrofuran (125 mL) and ether (125 mL) was treated with *n*-butyllithium (44 mL of 1.6 *M* in hexane, 70 mmol) at

−30°C. The reddish solution was then treated with dry paraformaldehyde (6.2 g, 206 mmol), warmed to room temperature (the reddish colour disappeared), and stirred for 16 h. Water (250 mL) was then added and the layers were separated. The aqueous layer was extracted with water (3 × 250 mL). The combined organic layers were dried and evaporated. The residue was then purified by flash chromatography with hexane – ethyl acetate (3:1) as the eluent to afford pure alcohol **23** (5.4 g, 46%); ir: 3610, 3450 (OH); nmr δ: 4.67 (1H, q, J = 5.1 Hz, CH of the ketal), 4.21 (2H, s, —C≡C—CH_2O—), 3.53 (4H, m, 2 × —CH_2O—), 2.23 (3H, m, —CH_2—C≡C—, OH), 1.67 (4H, m, —CH_2—CH_2—), 1.28 (3H, d, J = 5.3 Hz, CH_3—CH—), 1.18 (3H, t, J = 7.0 Hz, CH_3—CH$_2$—); ms m/e: 199 (M^+ − H), m/e: 183 (M^+ − OH). *Exact Mass* calcd. for $C_{11}H_{20}O_3$: 199.1334; found: 199.1331.

Chloride ***24***

To a solution of alcohol **23** (11 g, 55 mmol), lithium chloride (4.66 g, 110 mmol), and s-collidine (10.6 g, 88 mmol) in *N,N*-dimethylformamide (600 mL) maintained at 0°C was added mesyl chloride (9.4 g, 82 mmol). The solution was stirred for 20 min at 0°C, warmed to room temperature, and stirred for an additional 3 h. A saturated solution of sodium bicarbonate (600 mL) was then added and the mixture was extracted with ether–hexane ((1:1), 3 × 500 mL). The organic layer was dried and evaporated. The residue was purified by flash chromatography with hexane – ethyl acetate (4:1) to afford pure chloride **24** (10.4 g, 87%); ir: 2240 (C≡C); nmr δ: 4.53 (1H, q, J = 5.1 Hz, CH of the ketal), 4.14 (2H, t, J = 2.3 Hz, —C≡C—CH_2Cl), 3.54 (4H, m, 2 × —CH_2O—), 2.27 (2H, m, —CH_2—C≡C—), 1.63 (4H, m, —CH_2—CH_2—), 1.30 (3H, d, J = 5.3 Hz, CH_3—CH—), 1.20 (3H, t, J = 6.9 Hz, CH_3—CH$_2$—); ms m/e: 203, 205 (M^+ − OCH_3). *Exact Mass* calcd. for $C_{11}H_{19}O_2Cl$: 203.0838; found: 203.0832.

Diester ***25***

A solution of chloride **24** (217 mg, 1.0 mmol), dimethylmalonate (661 mg, 5.0 mmol), and potassium carbonate (690 mg, 5.0 mmol) in tetrahydrofuran (5 mL) and *N,N*-dimethylformamide (5 mL) was refluxed for 18 h. The mixture was then cooled to room temperature, filtered, and the solvents were removed under reduced pressure. The residue was purified by flash chromatography with hexane – ethyl acetate (3:1) as the eluent to afford pure diester **25** (310 mg, 99%); ir: 1740 (C=O); nmr δ: 4.66 (1H, q, J = 5.3 Hz, CH of the ketal), 3.75 (6H, s, 2 × —COOCH_3), 3.53 (5H, m, 2 × —CH_2O—, —CH—(CO_2CH_3)$_2$), 2.73 (2H, d of t, J = 7.8 Hz, 2.3 Hz, —CH_2—CH—(CO_2CH_3)$_2$), 2.13 (2H, m, —CH_2—C≡C—), 1.62 (4H, m, —CH_2—CH_2—), 1.29 (3H, d, J = 5.1 Hz, CH_3—CH—), 1.19 (3H, t, J = 7.0 Hz, CH_3—CH$_2$—); ms m/e: 299 (M^+ − CH_3), m/e: 269 (M^+ − OCH_2CH_3). *Exact Mass* calcd. for $C_{16}H_{26}O_6$: 299.1494; found: 299.1494.

Triester ***26***

Sodium hydride (96.6 mg, 4.0 mmol) was added to a solution of diester **25** (812 mg, 2.6 mmol) in tetrahydrofuran (2.0 mL) at 0°C. The solution was stirred at room temperature for 1 h, methyl chloroformate (368 mg, 3.9 mmol) was then added, and the solution was stirred for an extra hour. A saturated solution of ammonium chloride (10 mL) was then added to the cooled solution (0°C). The mixture was extracted with ether (3 × 20 mL), and the organic layer was dried and evaporated. The residue was purified by flash chromatography with hexane – ethyl acetate (3:1) as the eluent to afford pure triester **26** (962 mg, 99%); ir: 2300 (C≡C), 1745 (C=O); nmr δ: 4.65 (1H, q, J = 5.3 Hz, CH of the ketal), 3.80 (9H, s, 3 × —COOCH_3), 3.52 (4H, m, 2 × —CH_2O—), 2.97 (2H, t, J = 2.5 Hz, —CH_2—($COOCH_3$)$_3$), 2.15 (2H, m, —CH_2—C≡C—), 1.62 (4H, m, —CH_2—CH_2—), 1.31 (3H, d, J = 5.3 Hz, CH_3—CH—), 1.18 (3H, t, J = 6.9 Hz, CH_3—CH$_2$—).

Alcohol triester ***27***

Trifluoroacetic acid (2 drops) was added to a solution of triester **26** (962 mg, 2.6 mmol) in methanol (8 mL). The solution was stirred at room temperature for 2.5 h. The methanol was evaporated and the residue was taken up in methylene chloride (5 mL), which was then evaporated. The residue was purified by flash chromatography with hexane – ethyl acetate (1:1) as the eluent to afford pure alcohol triester **27** (769 mg, 99%); ir: 3610, 3560 (OH), 1745 (C=O); nmr δ: 3.81 (9H, s, 3 × —COOCH_3), 3.64 (2H, m, —CH_3OH), 2.98 (2H, t, J = 2.7 Hz, —CH_2—C—($COOCH_3$)$_3$), 2.28 (3H, m, —CH_2—C≡C—, —OH), 1.53 (4H, m, —CH_2—CH_2); ms m/e: 301 (MH^+), m/e: 283 (M^+ − OH), and m/e: 269 (M^+ − OCH_3). *Exact Mass* calcd. for $C_{14}H_{20}O_7$: 283.1181; found: 283.1181.

Aldehyde triester ***28***

Pyridinium chlorochromate (453 mg, 2.1 mmol) was added to a solution of alcohol **27** (208 mg, 0.70 mmol) in methylene chloride (5 mL) containing crushed 3 Å molecular sieves (400 mg). The solution was stirred for 10 min at room temperature, and ether (20 mL) was then added to precipitate the chromium salts. The solution was then filtered on silica gel with ether as the eluent. The solvents were evaporated to afford pure aldehyde **28** (175 mg, 85%); ir: 2840, 2720 (CHO), 1740 (C=O); nmr δ: 9.76 (1H, t, J = 2.0 Hz, HC=O), 3.78 (9H, s, 3 × —COOCH_3), 2.96 (2H, t, J = 2.5 Hz, —CH_2—C—($COOCH_3$)$_3$), 2.55 (2H, t, J = 6.7 Hz, —CH_2—CHO), 2.20 (2H, d of t, J = 7.0 Hz, 2.5 Hz, —CH_2—C≡C—), 1.80 (2H, bq, J = 6.7 Hz, —CH$_2$—CH_2—CH$_2$—).

Alcohol diester ***29***

Alcohol diester **29** was prepared in the same manner as alcohol diester **20**, from aldehyde **28** (96 mg, 0.32 mmol), to afford after purification pure alcohol **29** (50 mg, 59%); ir: 3600, 3520 (OH), 3310 (C≡CH), 1740 (C=O); nmr δ: 4.40 (1H, m, —CH≡C—CHOH—), 3.68 (6H, s, 2 × —COOCH_3), 3.43 (1H, t, J = 7.2 Hz, —CH—($COOCH_3$)$_2$), 2.72 (2H, d of t, J = 7.0 Hz, 1.9 Hz, —CH_2—CH—($COOCH_3$)$_2$), 2.45 (1H, d, J = 2.1 Hz, —C≡CH), 2.17 (2H, m, —CH_2—C≡C—), 1.73 (4H, m, —CH_2—CH_2—).

Ynone ***10***

Pyridinium chlorochromate (215 mg, 1.0 mmol) was added to a solution of alcohol **29** (67 mg, 0.25 mmol) in methylene chloride (5 mL) containing crushed 3 Å molecular sieves (125 mg). The solution was stirred for 60 min at room temperature, and ether (10 mL) was then added to precipitate the chromium salts. The solution was then filtered on silica gel with ether as the eluent. The solvents were evaporated to afford pure ynone **10** (59 mg, 89%); ir: 3295 (C≡CH), 2100 (C≡C), 1740 (C=O, ester), 1685 (C=O, ynone); nmr δ: 3.74 (6H, s, 2 × —COOCH_3), 3.43 (1H, t, J = 7.2 Hz, —CH—($COOCH_3$)$_2$), 3.24 (1H, s, —C≡C—H), 2.73 (2H, d of t, J = 6.6 Hz, 2.0 Hz, —CH_2—CH(CO_2CH_3)$_2$), 2.57 (2H, t, J = 5.0 Hz, —CH_2—C(O)—C≡C—H), 2.11 (2H, m, —CH_2—C≡C—), 1.77 (2H, m, —CH$_2$—CH_2—CH$_2$—); ms m/e: 264 (M^+), m/e: 265 (MH^+), and m/e: 233 (M^+ − OCH_3). *Exact Mass* calcd. for $C_{14}H_{16}O_5$: 264.0998; found: 264.0991.

Monomer ***38*** *and dimer* ***39****:* direct cyclization

Cyclization of ynone **10** (27 mg, 0.103 mmol) was done in the same manner as for ynone **7** to afford, after purification, pure monomer **38** (8.2 mg, 31%) and dimer **39** (3.5 mg, 13%).

Monomer ***38****:* ir: 1740 (C=O, ester), 1690 (C=O, enone), 1630 (C=C); uv λ_{max} (CH_3CN): 227 (ε 1600); nmr δ: 6.46 (2H, s, —CH=CH—), 3.81 (6H, s, 2 × —COOCH_3), 2.76 (2H, t, J = 2.1 Hz, —CH_2—C—($COOCH_3$)$_2$), 2.44 (2H, m, —CH$_2$—C(O)—), 2.21 (2H, m, —CH_2—C≡C—), 2.07 (2H, bq, J = 5.4 Hz, —CH$_2$—CH_2—CH$_2$—); nmr (benzene-d_6) δ: 6.60 (1H, d, J_{AB} = 12.6 Hz, —CH=CH—C(O)—), 5.90 (1H, d, J_{AB} = 12.6 Hz, —CH=CH—C(O)—), 3.48 (6H, s, 2 × —COOCH_3), 2.81 (2H, m, —CH_2—C—($COOCH_3$)$_2$), 1.80 (6H, m, 3 × —CH_2—); nmr (^{13}C) δ: 202 (C=O, enone), 170 (C=O, ester), 134 (C=C, β of enone), 131 (C=C, α of enone), 86, 80 (C≡C), 53.2 (C, α of esters), 53 (CH_3O), 42 (CH_2, α of enone), 27 (CH_2, β of esters), 25 (—CH_2—C≡C—), 19 (CH_2, β of enone); ms m/e: 264 (M^+), m/e:

265 (MH^+), and *m/e*: 247 ($MH^+ - H_2O$). *Exact Mass* calcd. for $C_{14}H_{16}O_5$: 264.0998; found: 264.0998.

Dimer ***39****:* ir: 1740 (C=O, ester), 1660 (C=O, enone), 1630 (C=C); uv λ_{max} (CH_3CN): 227 nm (ε 13 000); nmr δ: 7.29 (2H, d, J_{AB} = 16.8 Hz, 2 × —C*H*=CH—C(O)—), 6.20 (2H, d, J_{AB} = 16.8 Hz, 2 × —CH=C*H*—C(O)—), 3.78 (12H, s, 4 × —COOCH_3), 3.00 (4H, t, *J* = 2.4 Hz, 2 × —CH_2—C—(COOCH_3)$_2$), 2.78 (4H, t, *J* = 5.2 Hz, 2 × —CH_2—C(O)—), 2.23 (4H, m, 2 × —CH_2—C≡C—), 1.74 (4H, large quintuplet, *J* = 5.5 Hz, 2 × —CH$_2$—CH_2—CH$_2$—); nmr (^{13}C) δ: 199 (C=O, enone), 169 (C=O, esters), 140 (C=C, β of enone), 132 (C=C, α of enone), 84, 74 (C≡C), 59 (C, α of ester), (53 (CH_3 of esters), 37 (CH_2, α of enone), 25 (CH_2, β of esters), 22 (—CH_2—C≡C—), 17 (CH_2, β of enone); ms *m/e*: 528 (M^+), *m/e*: 497 ($M^+ - OCH_3$). *Exact Mass* calcd. for $C_{28}H_{32}O_{10}$: 528.1966; found: 528.1996.

Monomer ***38****:* "pseudo" high dilution

To a solution of cesium carbonate (2 mg, 0.009 mmol) in tetrahydrofuran (50 mL) and *N*,*N*-dimethylformamide (50 mL) was added, via a syringe pump, a solution of ynone **10** (54 mg, 0.21 mmol) in tetrahydrofuran (5 mL) and *N*,*N*-dimethylformamide (5 mL) at room temperature over a period of 10 h. The mixture was stirred for an additional 2 h, after which the mixture was filtered and the solvents were removed by distillation under reduced pressure. The residue was purified on a small column of silica gel with hexane – ethyl acetate (3:1) as the eluent to afford pure monomer **38** (27 mg, 50%).

Triester ***31***

A solution of alcohol triester **27** (600 mg, 2.0 mmol) and quinoline (45 μL) in benzene (5 mL) was added to a suspension of palladium 5% on barium sulfate (130 mg) in benzene (2 mL). The solution was stirred under a hydrogen atmosphere until the hydrogen uptake had ceased (8 h). The solution was filtered and the solvent evaporated. The residue was purified by flash chromatography with hexane – ethyl acetate (2:1) to afford starting material (187 mg) and triester **31** (387 mg, 86% based on recovered starting material); ir: 3610, 3500 (OH), 1740 (C=O); nmr δ: 5.52 (2H, m, —C*H*=C*H*—), 3.78 (9H, s, 3 × —COOCH_3), 3.65 (2H, m, —CH_2OH), 2.90 (2H, d, *J* = 8.0 Hz, —CH_2—C—(COOCH_3)$_3$), 2.04 (2H, m, —CH_2—CH=CH—), 1.51 (5H, m, —CH_2—CH_2—, OH); ms *m/e*: 303 (MH^+), *m/e*: 285 ($M^+ - OH$).

Aldehyde ***32***

Oxidation of alcohol **31** (115 mg, 0.38 mmol) was done in the same manner as for alcohol **27** to afford pure aldehyde **32** (101 mg, 88%); ir: 2720 (HC=O), 1740 (C=O); nmr δ: 9.76 (1H, m, *H*C=O), 5.52 (2H, m, —C*H*=C*H*—), 3.78 (9H, s, 3 × —COOCH_3), 2.85 (2H, m, —CH_2—C—(COOCH_3)$_3$), 2.43 (2H, m, —CH_2—CHO), 2.20 (2H, m, —CH_2—CH=CH—), 1.66 (2H, m, —CH$_2$—CH_2—CH$_2$—).

Alcohol diester ***33***

Alcohol diester **33** was prepared in the same manner as alcohol diester **21** from aldehyde **32** (101 mg, 0.34 mmol) to afford after purification pure alcohol **33** (28 mg, 31%); ir: 3600, 3500 (OH), 3310 (C≡CH), 1740 (C=O); nmr δ: 5.44 (2H, m, —C*H*=C*H*—), 4.36 (1H, m, —C*H*OH), 3.73 (6H, s, 2 × —COOCH_3), 3.40 (1H, t, *J* = 8.2 Hz, —C*H*—(COOCH_3)$_2$), 2.78 (2H, m, —CH_2—CH—(COOCH_3)$_2$), 2.47 (1H, d, *J* = 2.0 Hz, —C≡C*H*), 2.03 (2H, m, —CH_2—CH=CH—), 1.64 (3H, m, —CH_2—CHOH, —O*H*), 1.32 (2H, m, —CH$_2$—CH_2—CH$_2$); ms *m/e*: 268 (M^+), *m/e*: 237 ($M^+ - OCH_3$).

Ynone ***8***

Ynone **8** was prepared in the same manner as ynone **10** from alcohol **33** (28 mg, 0.104 mmol) to afford pure ynone **8** (24 mg, 86%); ir: 3300 (C≡CH), 2100 (C≡C), 1735 (C=O, ester), 1670 (C=O ynone); nmr δ: 5.44 (2H, m, —C*H*=C*H*—), 3.73 (6H, s, 2 × —COOCH_3), 3.41 (1H, t, *J* = 6.0 Hz, —C*H*—(COOCH_3)$_2$), 3.21 (1H, s, —C≡C—*H*), 2.80 (4H, m, —CH_2—C(O)—, —CH_2—CH—(COOCH_3)$_2$), 2.03 (2H, m, —CH_2—CH=CH—), 1.60 (2H, m, —CH$_2$—CH_2—CH$_2$—); ms *m/e*: 266 (M^+), *m/e*: 235 ($M^+ - OCH_3$).

Monomer ***36***

Cyclization of ynone **8** (21 mg, 0.079 mmol) was done in the same manner as for ynone **7** to afford after purification pure monomer **36** (6 mg, 29%); ir: 1735 (C=O, ester), 1680 (C=O, enone), 1650 (C=C, enone); uv λ_{max} (CH_3CN): 227 nm (ε 3000); nmr δ: 6.35 (1H, d, J_{AB} = 13 Hz, —C*H*=CH—C(O)—), 6.05 (1H, d, J_{AB} = 13 Hz, —CH=C*H*—C(O)—), 5.48 (1H, m, —CH=C*H*—), 5.12 (1H, m, —C*H*=CH—), 3.78 (6H, s, 2 × —COOCH_3), 2.60 (4H, m, —CH_2—C—(COOCH_3)$_2$), —CH_2—C(O)—), 2.16 (2H, m, —CH_2—CH=CH—), 1.93 (2H, m, —CH$_2$—CH_2—CH$_2$—); nmr (^{13}C) δ: 205 (C=O, enone), 134 (C=C, β of enone), 132 (C=C, α of enone), 130, 125 (C=C), 58 (C, α of esters), 53 (CH_3 of esters), 39 (CH_2, α of enone), 29 (CH_2, β of esters), 23 (—CH_2—C≡C—), 22 (CH_2, β of enone); ms *m/e*: 266 (M^+), 231 ($M^+ - OCH_3$). *Exact Mass* calcd. for $C_{14}H_{18}O_5$: 266.1154; found: 266.1154.

Propynylmagnesium bromide

A solution of propyne (6.3 g, 158 mmol) in tetrahydrofuran (9.3 g) was prepared by distilling liquified propyne over calcium hydride. The distillate was collected in a round-bottom flask containing dry tetrahydrofuran at −78°C. This solution was then added via a cannula to a solution of ethylmagnesium bromide (50 mL of 1.2 *M* in tetrahydrofuran, 60 mmol) at −78°C. The solution was warmed to 0°C and kept at this temperature until the evolution of ethane had ceased; the solution was then heated to 40°C to get rid of any excess gas. A concentration of 0.55 *M* was estimated by gas-volume displacement.

Alcohol diester ***24***

To a solution of aldehyde triester **32** (32 mg, 0.106 mmol) in tetrahydrofuran (2 mL) was added a solution of propargylmagnesium bromide (1.16 mL of 0.55 *M* in tetrahydrofuran, 0.64 mmol). The mixture was stirred for 1 h at −30°C, after which a saturated solution of ammonium chloride (5 mL) was added. The mixture was then extracted with ether (3 × 15 mL), and the organic layer was dried and evaporated. The residue was purified by flash chromatography with hexane – ethyl acetate (3:1) as the eluent to afford pure alcohol **34** (17.4 mg, 58%); ir: 3600 (OH), 1735 (C=O); nmr δ: 5.36 (2H, m, —C*H*=C*H*—), 4.34 (1H, m, —C*H*OH), 3.73 (6H, s, 2 × —COOCH_3), 3.41 (1H, t, *J* = 7.4 Hz, —C*H*—(COOCH_3)$_2$), 2.65 (2H, m, —CH_2—CH—(COOCH_3)$_2$), 2.11 (2H, m, —CH_2—CH=CH—), 1.80 (2H, m, —CH_2—CH(OH)—), 1.90 (3H, d, *J* = 2.1 Hz, CH_3—C≡C—), 1.61 (2H, m, —CH$_2$—CH_2—).

Ynone ***9***

Pyridinium chlorochromate (247 mg, 1.15 mmol) was added to a solution of alcohol **34** (69 mg, 0.24 mmol) in methylene chloride (5 mL) containing sodium acetate (94 mg, 1.15 mmol) and crushed 3 Å molecular sieves (150 mg). The mixture was stirred for 1 h at room temperature, after which ether (20 mL) was added; the mixture was then filtered over silica gel with ether as the eluent to afford pure ynone **9** (59 mg, 89%); ir: 2210 (C≡C), 1735 (C=O, ester), 1660 (C=O, ynone); nmr δ: 5.42 (2H, m, —C*H*=C*H*—), 3.74 (6H, s, 2 × —COOCH_3), 3.42 (1H, t, *J* = 7.0 Hz, —C*H*—(COOCH_3)$_2$, 2.65 (2H, m, —CH_2—CH—(COOCH_3)$_2$), 2.53 (2H, t, *J* = 6.6 Hz, —CH_2—C(O)—), 2.10 (2H, m, —CH_2—CH=CH—), 2.02 (3H, s, CH_3—C≡C—), 1.70 (2H, m, —CH$_2$—CH_2—CH$_2$—); ms *m/e*: 281 (MH^+), *m/e*: 249 ($M^+ - OCH_3$).

Monomer ***37****:* "pseudo" high dilution

Cyclization of ynone **9** (7 mg, 0.021 mmol) was done in the same manner as for ynone **10** at "pseudo" high dilution to afford after purification pure monomer **37** (4 mg, 27%); ir: 1735 (C=O), 1680 (C=C); nmr δ: 5.50 (2H, m, —C*H*=C*H*—), 5.33 (1H, bs, *exo* olefin), 5.28 (1H, bs, *exo* olefin), 3.78 (6H, s, 2 × —COOCH_3), 3.25 (2H, CH$_2$=C—CH_2), 2.72 (2H, d, *J* = 6 Hz, —CH_2—C—(COOCH_3)$_2$), 2.49 (2H, m, —CH$_2$—CH_2—C(O)—), 2.10 (2H, m, —CH_2—

CH=CH—), 1.80 (2H, m, —CH_2—CH_2—CH_2—); ms *m/e*: 280 (M^+), *m/e*: 249 ($M^+ - OCH_3$). *Exact Mass* calcd. for $C_{15}H_{20}O_5$: 280.1311; found: 280.1319.

Allylic alcohol ***30***

To a solution of aldehyde **28** (65.6 mg, 0.22 mmol) in tetrahydrofuran (4 mL) was added a solution of vinylmagnesium bromide (412 μL of 1.6 *M* in tetrahydrofuran, 0.66 mmol) at −30°C. The solution was stirred for 15 min, after which a saturated solution of ammonium chloride (10 mL) was added. The mixture was extracted with ether (3 × 20 mL), the organic layer was then dried and evaporated, and the residue was purified by flash chromatography with hexane – ethyl acetate (3:1) as the eluent to afford pure alcohol **30** (34 mg, 58%); ir: 3600–3500 (OH), 1740 (C=O); nmr δ: 5.75 (1H, ddd, *J* = 9.8 Hz, 5.9 Hz, 1.0 Hz, CH_2=C*H*—), 5.20 (2H, ddd, *J* = 10.0 Hz, 4.0 Hz, 1.0 Hz, CH_2=CH—), 4.15 (1H, m, —C*H*OH), 3.75 (6H, s, 2 × —COOCH_3), 3.56 (1H, t, *J* = 7.2 Hz, —C*H*—$(COOCH_3)_2$), 2.70 (2H, d of t, *J* = 7.8 Hz, 2.5 Hz, —CH_2—CH—$(COOCH_3)_2$), 2.23 (2H, m, —CH_2—C≡C—), 1.81 (1H, s, —O*H*), 1.60 (4H, m, —CH_2—CH_2—).

Enone ***11***

Manganese dioxide (220 mg, 2.54 mmol) was added to a solution of allylic alcohol **30** (34 mg, 0.127 mmol) in chloroform (1 mL) and hexane (1 mL). The mixture was stirred at room temperature for 1 h, after which ether (20 mL) was added and the solution was filtered over silica gel with ether as the eluent. The solvents were evaporated to afford pure enone **11** (25 mg, 73%); ir: 1740 (C=O, ester), 1660 (C=O, enone), 1620 (C=C); nmr δ: 6.35 (2H, dd, *J* = 7.0 Hz, 4.5 Hz, CH_2=CH—), 5.85 (1H, dd, *J* = 7.0 Hz, 4.5 Hz, CH_2=C*H*—), 3.75 (6H, s, 2 × —COOCH_3), 3.54 (1H, t, *J* = 7.0 Hz, —C*H*—$(COOCH_3)_2$), 2.75 (2H, d of t, *J* = 7.0 Hz, 2.0 Hz, —CH_2—CH—$(COOCH_3)_2$), 2.59 (2H, t, *J* = 3.0 Hz, —CH_2—C(O)—), 2.18 (2H, m, —CH_2—C≡C—), 1.75 (2H, m, —CH_2—CH_2—CH_2—); ms *m/e*: 266 (M^+), *m/e*: 235 ($M^+ - OCH_3$). *Exact Mass* calcd. for $C_{14}H_{18}O_5$: 266.1154; found: 266.1159.

Dimer ***41****: direct cyclization*

Cyclization of enone **11** (25 mg, 0.094 mmol) was done in the same manner as for ynone **7** (*vide supra* monomer **35**) to afford, after purification, pure dimer **41** (5.2 mg, 20%).

Monomer ***40*** *and dimer* ***41****:* "pseudo" high dilution

To a solution of cesium carbonate (10 mg, 0.032 mmol) in tetrahydrofuran (18 mL) and *N*,*N*-dimethylformamide (18 mL) was added, via a syringe pump, a solution of enone **11** (19 mg, 0.071 mmol) in tetrahydrofuran (2 mL) and *N*,*N*-dimethylformamide (2 mL) at room temperature over a period of 10 h. The mixture was stirred for an additional 3 h, after which it was filtered and the solvents were removed by distillation under reduced pressure. The residue was purified on a small column of silica gel with hexane – ethyl acetate (3:1) as the eluent to afford pure monomer **40** (5.1 mg, 27%) and dimer **41** (10.7 mg, 56%).

Monomer ***40****:* ir: 1735 (C=, ester), 1710 (C=O, ketone); nmr δ: 3.75 (6H, s, 2 × —COOCH_3), 2.89 (2H, m, —C(O)—CH_2—CH_2—), 2.77 (2H, t, *J* = 2.0 Hz, —CH_2—C—$(COOCH_3)_2$), 2.50 (2H, m, —C(O)—CH_2—CH_2—C—$(COOCH_3)_2$), 2.35 (2H, m, —CH_2—CH_2—CH_2—C(O)—), 2.16 (2H, m, —CH_2—C≡C—), 2.11 (2H, m, —CH_2—CH_2—CH_2—); ms *m/e*: 266 (M^+), *m/e*: 235 ($M^+ - OCH_3$). *Exact Mass* calcd. for $C_{14}H_{18}O_5$: 266.1154; found: 266.1156.

Dimer ***41****:* ir: 1735 (C=O, ester), 1715 (C=O, ketone); nmr δ: 3.73 (12H, s, 4 × —COOCH_3), 2.80 (4H, t, *J* = 2.4 Hz, 2 × —CH_2—$(COOCH_3)_2$), 2.59 (4H, t, *J* = 7.1 Hz, 2 × —CH_2—CH_2—CH_2—C(O)—), 2.50 (4H, m, 2 × —C(O)—CH_2—CH_2—$(COOCH_3)_2$, 2.35 (4H, m, 2 × —C(O)—CH_2—CH_2—C$(COOCH_3)_2$), 2.21 (4H, m, 2 × —CH_2—C≡C—), 1.74 (4H, quintuplet, *J* = 6.9 Hz, 2 × —CH_2—CH_2—CH_2—); ms *m/e*: 532 (M^+), *m/e*: 501 ($M^+ - OCH_3$). *Exact Mass* calcd. for $C_{28}H_{36}O_{10}$: 532.2309; found: 532.2306.

Dienone ***43***

Two drops of hydrochloric acid (12 *N*) were added to a solution of cyclic monomer **38** (10 mg, 0.038 mmol) in *tert*-butanol. The mixture was left under argon for 30 h at room temperature. Solvent was evaporated and the residual material was purified by column chromatography with silica gel and a mixture of ethyl acetate – hexane (1:2) to give pure dienone **43** (4.2 mg, 42%); ir: 1735 (C=O, ester), 1660 (C=O, enone), 1590 (C=C), 1150 (C—O); nmr δ: 6.35 (1H, d, *J* = 9.7 Hz, CH=C*H*—C$(COOCH_3)_2$, 6.15 (1H, d, *J* = 9.7 Hz, C*H*=CH—C$(COOCH_3)_2$), 3.74 (6H, s, 2 × $COOCH_3$), 3.09 (2H, m, CH_2—C$(COOCH_3)_2$, 2.45 (2H, m, —CH_2—CO—), 2.06 (2H, q, *J* = 6.8 Hz, —CH_2—CH=C—), 1.64 (2H, m, CH_2—CH_2—CH_2); ms *m/e*: 265 (MH^+) and *m/e*: 205 ($M^+ - COOCH_3$). *Exact Mass* calcd. for $C_{14}H_{16}O_5$: 265.1076; found: 265.1076.

Acknowledgements

Support for this work by the Natural Sciences and Engineering Research Council of Canada (NSERCC) and by the "Ministère de l'Éducation (FCAR)," Quebec, is gratefully acknowledged.

1. P. Deslongchamps. Aldrichimica Acta, **17**, 59 (1984); Bull. Soc. Chim. Fr. II, **9–10**, 349 (1984).
2. P. Deslongchamps, S. Lamothe, and H.-S. Lin. Can. J. Chem. **62**, 2395 (1984).
3. D. Brillon and P. Deslongchamps. Tetrahedron Lett. **27**, 1131 (1986).
4. P. Deslongchamps. *In* Stereoelectronic effects in organic chemistry. Vol. 1: Organic Chemistry Series. *Edited by* J. E. Baldwin. Pergamon Press, Oxford, England. 1983. pp. 221–242.
5. D. Brillon. Synth. Commun. **16**, 291 (1986).
6. T. Kitahara and K. Mori. J. Org. Chem. **49**, 3281 (1984).
7. T. Katahashi, T. Nagashima, and J. Tsuji. Tetrahedron Lett. 1359 (1981).
8. M. Niwa, A. Nishiyama, M. Iguchi, and S. Yamamura. Bull. Chem. Soc. Jpn. **48**, 2930 (1975).
9. R. J. Balf, B. Rao, and L. Weiler. Can. J. Chem. **49**, 3135 (1971).
10. M. A. Casadei, C. Galli, and L. Mandolini. J. Org. Chem. **46**, 3127 (1981).
11. M. Miyashita, A. Yoshikoshi, and P. A. Grieco. J. Org. Chem. **42**, 3772 (1977).
12. E. W. Colington and A. I. Meyers. J. Org. Chem. **36**, 3044 (1971).
13. G. Bauduin, D. Bondon, Y. Pietrasanta, and B. Pucci. Tetrahedron, **34**, 3269 (1978).
14. L. Bransdma. *In* Preparative acetylenic chemistry. Elsevier Publishing Company, New York, NY. 1971.
15. K. Bowden, I. M. Heilbrown, E. R. H. Jones, and B. C. L. Weedon. J. Chem. Soc. 39 (1946).
16. E. J. Corey and W. J. Suggs. Tetrahedron Lett. 2547 (1975).
17. J. Herscovici and K. Antonakis. J. Chem. Soc. Chem. Commun. 561 (1980).

Photoredox chemistry of nitrobenzyl alcohols in aqueous solution. Acid and base catalysis of reaction

PETER WAN[1]
Department of Chemistry, University of Victoria, Victoria, B.C., Canada V8W 2Y2

AND

KEITH YATES
Department of Chemistry, University of Toronto, Toronto, Ont., Canada M5S 1A1

Received February 26, 1986

PETER WAN and KEITH YATES. Can. J. Chem. **64**, 2076 (1986).

The photochemistry of several *m*- and *p*-nitrobenzyl alcohols (**1**–**5**) has been studied in aqueous solution. These compounds react via an intramolecular photoredox pathway to give reduced and oxidized moieties of the substituent groups. The reaction is an example of a new type of photoreaction of nitro-substituted aromatic derivatives that is not observed in organic solvents, the presence of water being essential. This effect is exemplified by measuring the quantum efficiency as a function of mol% water in aqueous acetonitrile, methanol, and formamide: the reaction efficiency decreases rapidly as water is depleted in the mixture. Catalytic effects due to the hydronium and hydroxide ions were studied: the *para* derivatives exhibited hydroxide ion catalysis; the *meta* derivatives exhibited hydronium ion catalysis. Quantum yields, solvent isotope effects, and α-deuterium isotope effects are reported for the parent derivatives.

PETER WAN et KEITH YATES. Can. J. Chem. **64**, 2076 (1986).

On a étudié la photochimie de plusieurs alcools *m*- et *p*-nitro benzyliques (**1**–**5**) en solution aqueuse. Ces composés réagissent selon un processus photoredox intermédiaire pour donner des fragments de groupes substitués oxydés et réduits. C'est un exemple d'un nouveau type de réactions photochimiques des dérivés aromatiques nitrés que l'on n'observe pas dans des solvants organiques. L'eau est donc indispensable. On a mis en évidence le rôle de l'eau en mesurant le rendement quantique de la réaction en fonction du pourcentage molaire d'eau dans des solutions aqueuses d'acétonitrile, de méthanol et de formamide. Le rendement de la réaction diminue rapidement lorsque la teneur en eau du mélange diminue. On a étudié les effets catalytiques dus aux ions hydronium et hydroxydes. Les réactions des dérivés *para* sont catalysés par les ions hydroxydes tandis que celles des dérivés substitués en *méta* sont catalysées par les ions hydroniums. On rapporte les rendements quantiques, les effets isotopiques du solvant et les effets isotopiques du deutérium en α des dérivés apparentés.

[Traduit par la revue]

Introduction

The photochemistry of the nitro group has been a topic of continued interest although it has not been as extensively studied as the carbonyl group. Four reviews (1–4) summarize the present understanding of the photochemistry of the nitro group in solution. Aromatic nitro compounds undergo a variety of intriguing photoreactions that are initiated by five known primary photochemical processes (1–4). The vast majority of these reactions are known to proceed via the triplet excited state, of either π,π^* or n,π^* configuration. The intramolecular photoredox reactions of nitrobenzenes comprise a class of reactions of interest in this work since the reactions to be reported here can be classified under this category. The intramolecular photoredox reaction of a nitroaromatic compound may be defined as a reaction resulting in the overall reduction of the nitro group (usually to nitroso) concurrent with the oxidation of another functional group in the same molecule (eq. [1]).

[1] 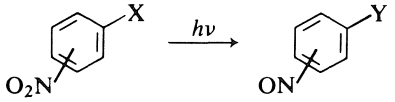

(X $\xrightarrow{[O]}$ Y)

All the known intramolecular redox reactions (1–5) (with one exception, *vide infra*) involve *ortho*-substituted nitrobenzenes. Mechanistically related to these reactions is the photochromic behaviour exhibited by some *ortho*-substituted alkyl nitrobenzenes (6). The primary photochemical event in all the above intramolecular reactions is believed to be hydrogen atom abstraction by the excited nitro group (usually triplet n,π^*, but not restricted to this reactive state (5)), to give a biradical. Subsequent transformation of the biradical results in overall reduction of the nitro group and oxidation of the other substituent (eq. [1]). An example of this type of mechanism is shown in eq. [2] for the well-known reaction of *o*-nitrobenzaldehyde, to give *o*-nitrosobenzoic acid (1–4, 7). Prior to our investigations, the only known example of a nitroaromatic compound reacting via an intramolecular redox-type pathway that was not *ortho*-substituted is that of *p*-nitrobenzaldehyde, to give *p*-nitrosobenzoic acid (8–10). We report in this paper a new class of intramolecular redox-type reactions of *meta*- and *para*-substituted nitroaromatic compounds discovered by us recently (11, 12), which exhibit novel pH effects. These reactions appear to be general for appropriately substituted nitrobenzene derivatives.

[2] 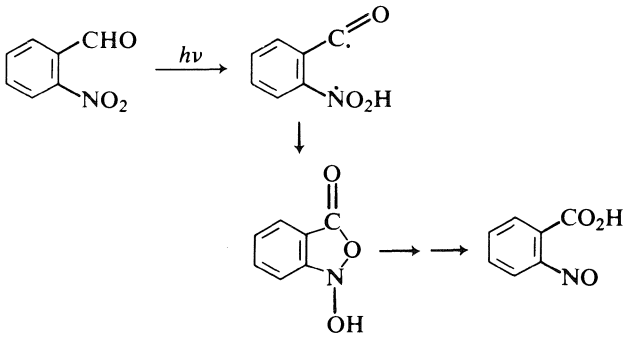

[1]NSERC University Research Fellow. Correspondence may be addressed to either author.

Results

Materials

para-Substituted nitrobenzyl alcohols **1** and **2** and *meta*-substituted nitrobenzyl alcohols **3–5** were studied in this work. *o*-Nitrobenzyl alcohol **6** was used as the model for the photochemical behaviour of the *ortho*-substituted isomers. These materials were either purchased or obtained via $NaBH_4$ reduction of the corresponding ketones or aldehydes.

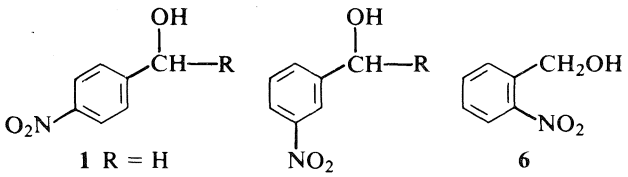

1 R = H
2 R = CH_3

3 R = H
4 R = CH_3
5 R = Ph

6

Product studies

Irradiation of argon-purged 10^{-4} *M* quartz cuvette solutions of *meta*-substituted alcohols **3–5** in neutral water (1% CH_3CN as cosolvent) at 254, 300, or 350 nm in a Rayonet photochemical reactor (merry-go-round apparatus) resulted in large changes in the uv spectrum (see Fig. 1 for *m*-nitrobenzyl alcohol **3**). Loss of the substrate absorption band at 268 nm is accompanied by growing bands at 233 nm and at 330 nm. Photolysis under identical conditions as above, but in MeOH, CH_3CN, 95% EtOH, and cyclohexane, resulted in no observable change in the uv spectrum. Irradiation of **1** and **2** at pH's > 11 resulted in loss of the absorption band at 278 nm accompanied by an increasing absorption band at 340 nm. These absorption changes are not observed when the alcohol is photolyzed in organic solvents or at pH's < 11. *o*-Nitrobenzyl alcohol **6** is known to react to give *o*-nitrobenzaldehyde (13) on photolysis, neat or in organic solvents. Using uv spectrophotometry to monitor the reaction, we found no observable differences in efficiency of photoreaction of **6** in a variety of solvents (neutral water, aqueous H_2SO_4, MeOH, and CH_3CN). Thus the *ortho* isomer **6** reacts according to the known intramolecular pathway regardless of solvent, while significant photochemistry is observed for the *meta* and *para* isomers only when photolysis is carried out in aqueous solution.

Product studies were carried out using 10^{-3} *M* solutions. In a typical run for the *para* isomers, 100 mg of the alcohol was dissolved in 200 mL of aqueous CH_3CN (80% H_2O; pH of the aqueous portion > 11) and photolyzed at 254 or 300 nm after saturating the solution with argon. The *para*-substituted alcohols **1** and **2** gave the corresponding nitrosocarbonyl compounds (dimeric form, see Experimental) as the only product in conversions of up to 40% (eq. [3]). When the solutions were

[3] 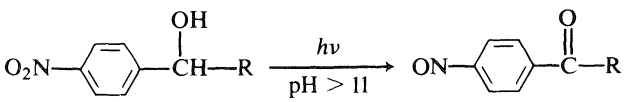

1 R = H
2 R = CH_3

1*a* R = H (nitroso dimer)
2*a* R = CH_3 (nitroso dimer)

photolyzed for extended periods, highly colored material was formed, in addition to the nitrosocarbonyl products. After chromatographic separation, the structures of all the products were fully characterized by standard spectroscopic techniques. In solutions of pH < 11 or in strongly acidic medium

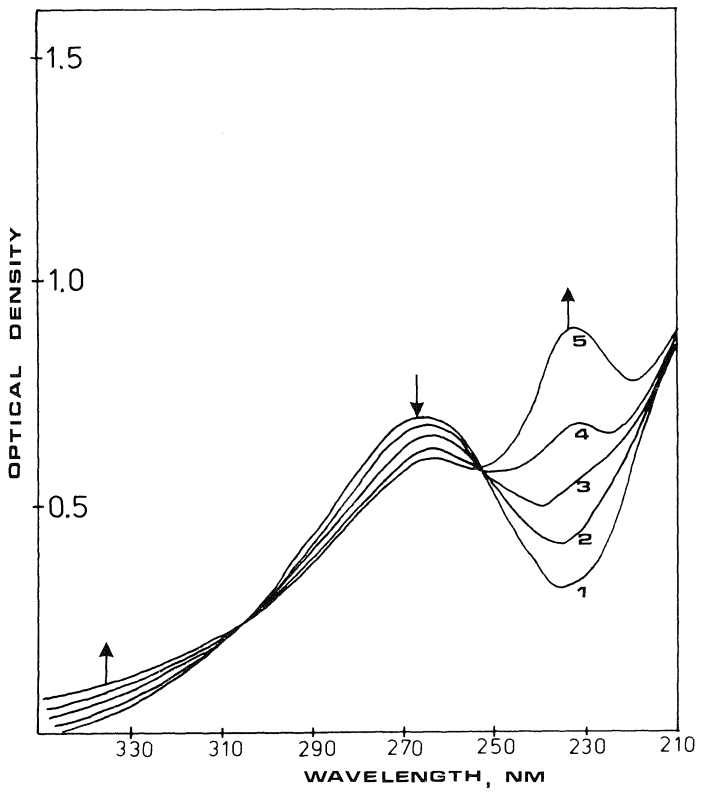

FIG. 1. Photochemical uv traces for *m*-nitrobenzyl alcohol **3** in neutral water (λ_{excit} = 254 nm; 3 min irradiation time per trace).

($H_0 \simeq -2$), complete recovery of the substrate was possible after photolysis. Additionally, no photoreaction was observed when photolysis was carried out in a number of organic solvents (pure CH_3CN, 0.1 *M* NaOMe/MeOH, pure MeOH, EtOH, and diethyl ether). The *meta*-substituted alcohols **3–5** gave two products (10–100% conversion) in basic (pH 12), neutral, or acidic medium (up to $H_0 = -4$): nitroketones (or aldehyde) **7** and azoxyketones (or azoxyaldehyde) **8** in the quoted isolated weight ratios (eq. [4]). The total yield of **7** and **8** is about 50%.

[4] 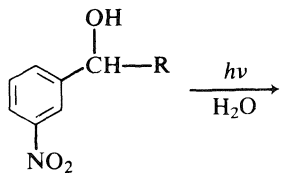

3 R = H
4 R = CH_3
5 R = Ph

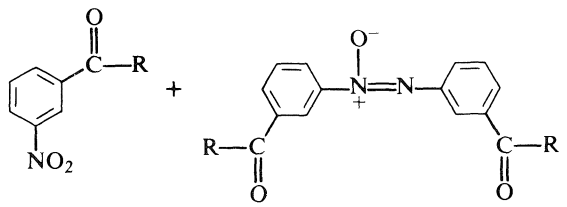

7*a* (60–70%)
7*b*
7*c*

8*a* (40–30%)
8*b*
8*c*

Substrates **3–5** were unreactive when photolyzed in organic solvents under similar conditions. Photolysis of *m*-nitrobenzaldehyde or *m*-nitroacetophenone under the above conditions

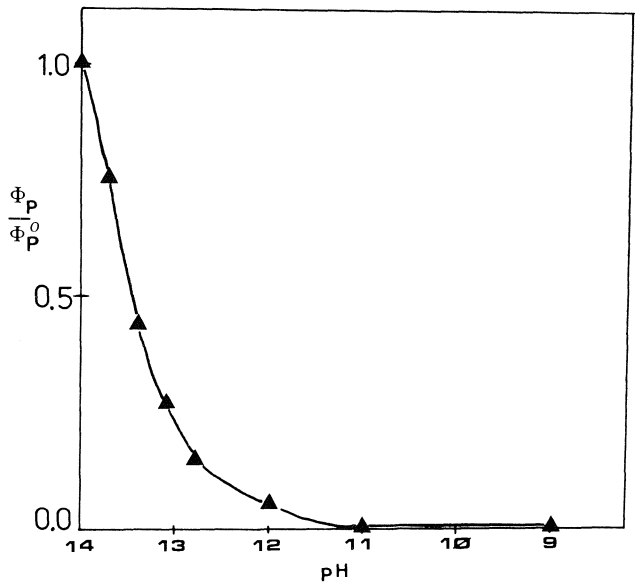

FIG. 2. Variation of Φ_p/Φ_p^0 as a function of pH for the photoredox reaction of *p*-nitrobenzyl alcohol **1** (Φ_p^0 = quantum yield at pH 14).

resulted in no observable reaction and hence demonstrates that **8** does not arise via secondary photochemistry of **7**. The fact that both **7** and **8** are observed as products at low conversions (down to 5%) suggests that they are either primary products or are formed via a number of very fast dark reactions after the primary photochemical step.

Product quantum yields and pH effects

Relative quantum yields (Φ_p/Φ_p^0) for reaction of **1**, where Φ_p^0 is the quantum yield of product formation in 1.0 *M* NaOH, were measured as a function of pH via preparative photolysis and also via uv spectrophotometry (λ_{excit} = 254 nm). The results are shown in Fig. 2. The efficiency of the photoreaction was found to depend strongly on the hydroxide ion concentration. Nearly identical results were observed for **2**. The absolute quantum yield for reaction at pH 14 was below 0.01 and an accurate measurement was not obtainable using the apparatus available. The photoredox chemistry of the *meta* isomers **3–5** was also subject to pH effects. The effect of medium acidity (aqueous H_2SO_4) on the total quantum yield for formation of **7** and **8** (Φ_m, defined as $\Phi_m = \Phi(\mathbf{7}) + \Phi(\mathbf{8})$, *vide infra*) was determined by monitoring for the increase in absorbance at 233 nm (λ_{max}) due to both **7** and **8** (Fig. 1), using a merry-go-round apparatus at 254 nm. The results are shown in Fig. 3. The efficiency of the photoreaction was found to depend strongly on the acidity of the medium, reaching a maximum efficiency at $H_0 \simeq -2$, and decreases significantly on going to higher acidity. There is no base catalysis of reaction since photolysis at pH 9 and 12 resulted in no observable increase in reaction efficiency, compared to a solution at pH 7. However, in contrast to the *para* isomers, the *meta* isomers react in neutral solution with moderate efficiencies.

The absolute quantum yields for formation of **7** ($\Phi(\mathbf{7})$) and of **8** ($\Phi(\mathbf{8})$) were calculated by partitioning the total quantum yield for these derivatives (Φ_m) into a $\Phi(\mathbf{7})$ and a $\Phi(\mathbf{8})$ component, using eq. [5], where the ratio 0.76:0.24 is the isolated mole ratio

$$[5] \quad \Phi_m = 0.76\Phi(\mathbf{7}) + 0.24\Phi(\mathbf{8})$$

(averaged) of products **7** and **8**, respectively. The results are given in Table 1.

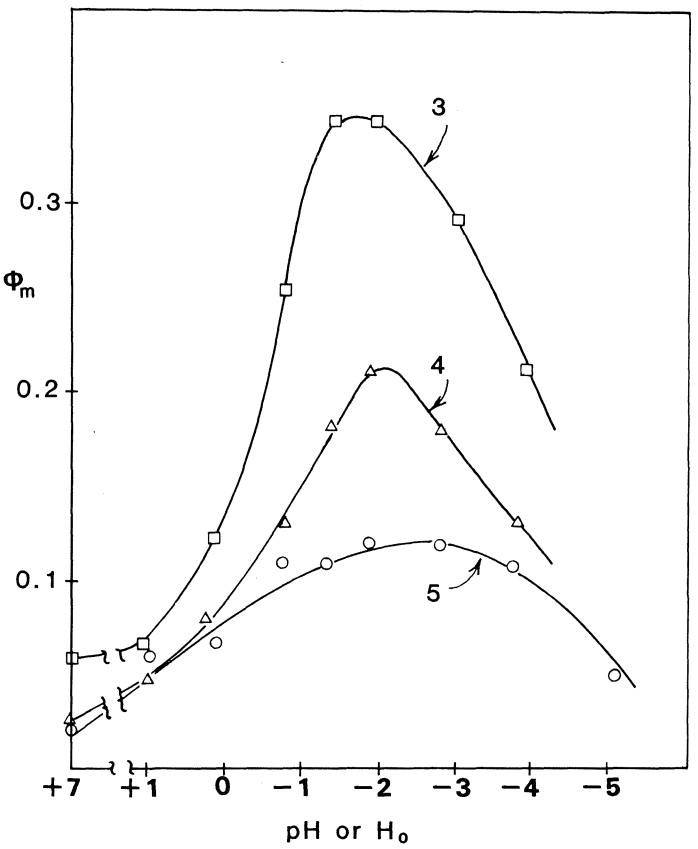

FIG. 3. Variation of Φ_m^0 (= $\Phi(\mathbf{7}) + \Phi(\mathbf{8})$) as a function of medium acidity for the photoredox reaction of *meta* isomers **3–5**.

TABLE 1. Quantum yields for formation of **7** and **8** as a function of medium acidity for *meta* isomers **3–5**[a]

	3		4		5	
pH or H_0	$\Phi(\mathbf{7})$	$\Phi(\mathbf{8})$	$\Phi(\mathbf{7})$	$\Phi(\mathbf{8})$	$\Phi(\mathbf{7})$	$\Phi(\mathbf{8})$
pH 7	0.042	0.013	0.014	0.0044	0.013	0.0041
pH 3	0.042	0.013	0.014	0.0044	0.013	0.0041
pH 1	0.049	0.015	0.036	0.011	0.045	0.014
−0.18	0.092	0.029	0.043	0.014	0.062	0.019
−0.74	0.19	0.060	0.099	0.031	0.084	0.026
−1.40	0.25	0.079	0.14	0.044	0.084	0.026
−1.90	0.25	0.079	0.16	0.050	0.091	0.029
−2.95	0.22	0.069	0.14	0.044	0.091	0.029
−3.95	0.12	0.038	0.099	0.031	0.084	0.026
−5.20	—	—	—	—	0.031	0.0098

[a]Determined spectrophotometrically. Estimated error 10%.

The effect of substrate concentration on the efficiency of the photoredox reaction of **3** was studied via uv spectrophotometry in the $10^{-3} - 10^{-5}$ *M* concentration range. The total quantum efficiency (Φ_m) for formation of **7** and **8** as a function of initial substrate concentration is given in Table 2. The observation of no change in reaction efficiency over a tenfold change in initial substrate concentration suggests that the mechanism for reaction involves a single substrate molecule in the primary photochemical step. Due to the relative inefficiency of the reaction for the *para* isomers (**1** and **2**), a study of the variation of quantum efficiency with substrate concentration has not been carried out. However, studies at 10^{-5} *M* initial substrate

TABLE 2. Dependence of quantum efficiency (Φ_m) on initial substrate concentration for the photoredox reaction of *m*-nitrobenzyl alcohol **3**[a]

Initial substrate concentration (M)	Φ_m[b]
5.52×10^{-5}	0.060
1.10×10^{-4}	0.052
1.65×10^{-4}	0.047
1.97×10^{-4}	0.055
2.19×10^{-4}	0.054
3.31×10^{-4}	0.045
8.55×10^{-4}	0.055[c]
1.42×10^{-3}	0.052[c]

[a]Measured spectrophotometrically in neutral water (pH 7); λ_{excit} = 248 nm; estimated error 10%.
[b]Total quantum yield for formation of **7***a* and **7***b*.
[c]λ_{excit} = 254 nm.

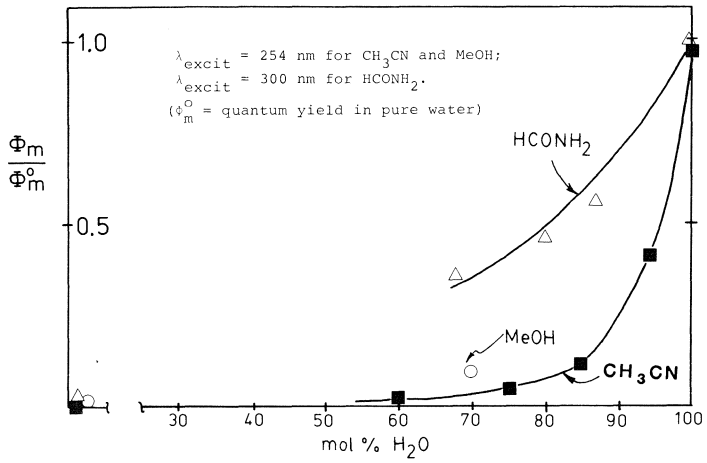

FIG. 4. Effect of added H_2O to CH_3CN, CH_3OH, and $HCONH_2$ on the photoredox efficiency of *m*-nitrobenzyl alcohol **3** (λ_{excit} = 254 nm; results determined spectrophotometrically). The quantum yield (Φ^0_m) in 100 mol% water was normalized to unity.

concentration (via uv spectrophotometry, monitoring for the product λ_{max} at 340 nm) indicates that the reaction proceeds with comparable efficiency to that carried out with uv studies at 10^{-3} *M*. Additional evidence for a unimolecular primary photochemical step in these reactions is the finding that irradiation of an equimolar (10^{-4} *M*) mixture of nitrobenzene and benzyl alcohol (20% H_2SO_4 or pH 12) results in no observable reaction, as indicated by uv spectrophotometry and via preparative photolysis.

Medium and isotope effects

The requirement of water in the photoreaction of these substrates is exemplified by the effect of added H_2O to CH_3CN, MeOH, and $HCONH_2$ on the photoredox efficiency of *m*-nitrobenzyl alcohol **3** (Fig. 4). In this plot, the ratio Φ_m/Φ^0_m represents the relative reaction efficiency of **3**, as organic solvent is added to the pure water solution (pH 7). Φ^0_m is the total quantum yield for formation of **7***a* and **8***a* in pure water (at pH 7), normalized to unity at 100 mol% water. In CH_3CN and MeOH, the reaction is not observed below 60 mol% water. In $HCONH_2$, the decrease in reaction efficiency is more gradual. The reaction efficiency is also sensitive to added electrolytes (Fig. 5). In the solvent system 30% CH_3CN/H_2O (v/v), the efficiency of the reaction nearly doubles on the addition of 0.6 *M* LiCl (or $NaClO_4$), relative to a solution without added salt (at pH 7). In pure water, much higher salt concentrations are required ($\simeq$2 *M*) to give an observable salt effect. For the *para* isomer **1**, the presence of 1.0 *M* NaCl in pH 13 failed to enhance the efficiency. However, since the medium at pH 13 is already quite polar, the amount of enhancement may be insignificant. The observation of a salt effect for the *meta* isomers would favour a mechanism involving polarized or ionic species.

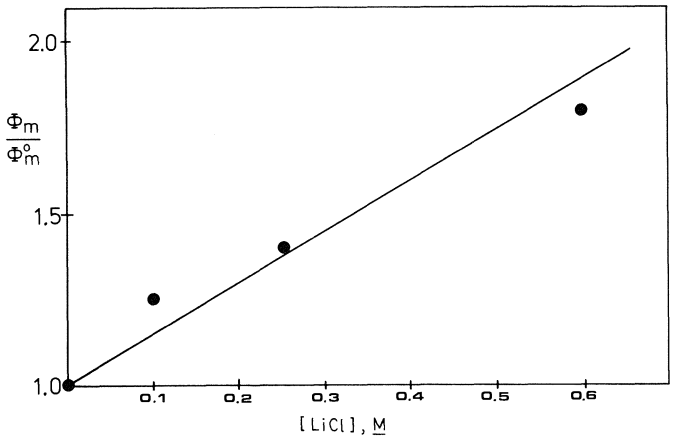

FIG. 5. Effect of added LiCl in 30% CH_3CN/H_2O (pH 7) on the photoredox efficiency of *m*-nitrobenzyl alcohol **3** (λ_{excit} = 254 nm; results determined spectrophotometrically). The quantum yield (Φ^0_m) in the absence of LiCl was normalized to unity.

Solvent isotope effects on the efficiency of the photoredox reaction were measured for **1** and **3**. For the *meta* isomer **3**, the experiment was performed using pure H_2O vs. pure D_2O, and the relative quantum efficiency (as monitored by uv spectrophotometry at 233 nm) in these two solvents (Φ_H/Φ_D) was 1.40 ± 0.05. For **1**, 0.1 *M* NaOH/H_2O and 0.1 *M* NaOD/D_2O solutions were used, and the relative efficiency (Φ_H/Φ_D) was 1.09 ± 0.05. These observations suggest that the solvent is involved chemically in the reaction, perhaps providing a source of available protons to mediate these reactions, as suggested by the values (greater than unity) of the solvent isotope effects.

α-Deuterium isotope effects were studied using compounds **9–11** under several different medium basicities or acidities.

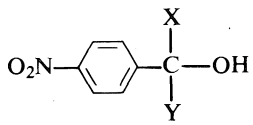

9 X = H; Y = D
10 X = Y = D

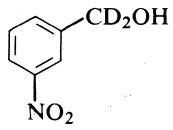

11

Compound **9** (mono-α-deuterated analog of **1**) can be studied by noting the relative amounts of *p*-nitrosobenzaldehyde-α-H vs. α-D product formed in the ^1H nmr spectrum of the product mixture. The amount of α-D product formed was deduced by noting the ratio of the integrated areas of the formyl proton of the α-H product vs. total aromatic protons. A preference for abstracting the proton over the deuteron in **9** would give more *p*-nitrosobenzaldehyde-α-D product vs. the α-H product. This was in fact observed, and the isotope effect (Φ_H/Φ_D), which measures the preference for α-H vs. α-D, was 6.1 ± 0.6 at pH 14 and 4.6 ± 0.7 in 0.25 *M* NaOH. A different approach for measuring this type of isotope effect is to compare the relative reaction efficiencies of **10** vs. the parent compound **1**, under

identical reaction conditions. Surprisingly, however, **10** failed to react in pH 14, whereas **1** gave 54% conversion, both under identical photolysis conditions. This would give an estimated isotope effect of about 10, by assuming an upper limit of 5% conversion for **10**.

The corresponding isotope effect for the *meta* isomer **3** was studied by comparing the difference in reaction efficiency between **3** and **11** under identical conditions, using uv spectrophotometry to monitor the reaction. As was observed for the *para* isomer, there is again a preference for the undeuterated compound, and the isotope effects Φ_H/Φ_D (as defined above) were 2.4 ± 0.2 in pH 7, 1.4 ± 0.1 in $H_0 = -0.60$, and 1.3 ± 0.1 in $H_0 = -1.3$. These observations suggest that deprotonation (or removal in the form of hydrogen atom) of the α-proton is involved in the primary step of the reaction mechanism. To test whether the α-hydrogens of **1–5** are exchangeable in recovered starting material, a number of exchange experiments were performed using labelled **11** in H_2O (model for the *meta* isomers) and *p*-nitrobenzyl alcohol **1** in 0.10 *M* NaOD/D_2O (model for the *para* isomers). At conversions of 8–62%, no exchange of α-D or α-H in **11** and **1**, respectively, was detected, as indicated by ^1H nmr and mass spectrometry. Since these two techniques can detect a minimum of ≃3% exchange, we conclude that at most 3% of the "deprotonated" substrate molecules returns to starting material without going on to form product.

Triplet sensitization and quenching studies

The photoredox reactions of **1** and **3** can be sensitized by sodium benzophenone-2-carboxylate **12** ($E_T \simeq 69$ kcal mol^{-1}) (14) in 0.1 *M* NaOH and neutral water, respectively, using 350 nm irradiation. Both reactions can be quenched by 2,4-cyclohexadiene-1,6-dicarboxylic acid (monosodium salt) **13**

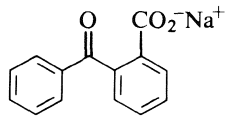

12

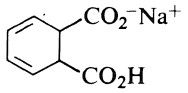

13

($E_T \simeq 50$ kcal mol^{-1}, based on the known value for 1,3-cyclohexadiene (14)). At a quencher concentration of 0.02 *M*, the photoreaction was quenched to the extent of ≃70%, compared to a sample without added quencher, in neutral water for **3** and in 0.1 *M* NaOH for **1**. These results imply that the major part of the reaction proceeds from the triplet state.

The quantum efficiency via S_1 (Φ_S) was estimated via the following analysis for "bracketing" Φ_S (15). The quantum yield for reaction on direct irradiation (Φ_D) is given by eq. [6], where

$$[6] \quad \Phi_D = \Phi_S + \Phi_{ST}\Phi_T$$

$$[7] \quad \Phi_{sens} = \Phi_{ET}\Phi_T$$

Φ_{ST} is the quantum yield for intersystem crossing from the singlet to the triplet state, and Φ_T is the fractional efficiency of triplets undergoing reaction. The sensitized quantum yield (Φ_{sens}) is given by eq. [7], where Φ_{ET} is the quantum efficiency of energy transfer between the sensitizer and the substrate. Assuming 100% efficient energy transfer, we have $\Phi_{sens} = \Phi_T$. This condition is met if E_T(sens) > E_T(substrate), and the substrate concentration is sufficiently high to intercept all the excited sensitizer triplets. Employing compound **12** as the sensitizer in 0.1 *M* NaOH and a substrate (compound **1**) concentration of 10^{-3} *M*, it was found that $\Phi_{sens}/\Phi_D = 1.5 \pm 0.3$. Since E_T(**12**) ≃ 69 kcal mol^{-1} (14) and the triplet energy of **1** ≃ 60 kcal mol^{-1} (3, 16), and because the triplet lifetime of **12** is ≃10^{-6} s (14), we have $\Phi_{sens} = \Phi_T$ (i.e., $\Phi_{ET} \simeq 1$; every excited triplet of **12** is intercepted by **1**). Therefore, we can write $\Phi_T/\Phi_D = 1.5 \pm 0.2$. Equation [6] can be rearranged as eq. [8]. Substituting the inverse value of Φ_T/Φ_D in eq. [7] and

$$[8] \quad \Phi_D/\Phi_T = (\Phi_S/\Phi_T) + \Phi_{ST}$$

$$[9] \quad \Phi_S/\Phi_T = (0.69 \pm 0.09) - \Phi_{ST}$$

rearranging, we obtain eq. [9]. Since Φ_{ST} for simple nitrobenzenes is ≃0.7 (3, 16, 17), we find that $\Phi_T \gg \Phi_S$. That is, reaction via Φ_S is insignificant, if not completely absent. Although Φ_{sens}/Φ_D for the *meta* isomer **3** has not been measured as accurately as for **1**, a value of ca. 1.6 has been observed, and a similar conclusion regarding the insignificance of the S_1 pathway can be made.

Discussion

The proposed mechanism for the photoredox reaction of the *para* isomers (**1** and **2**) is shown in Scheme 1 for *p*-nitrobenzyl alcohol **1**, which is consistent with all the available experimental data. The k_{OH} step is presumed to involve hydroxide ion deprotonation of the benzylic proton concerted with proton transfer from solvent water to the nitro group oxygen. Although a two-step sequence would be kinetically distinguishable from this concerted step, the one-step process was chosen based on its kinetic simplicity. The mechanism involves a highly polarized intermediate in **14**, consistent with the observed solvent effect and base catalysis of reaction. The triplet reactive state is also presumed to be highly polarized, to facilitate the α-deprotonation (*vide infra*). The expression for product quantum yield can be derived by assuming a steady state for intermediate **14** and the singlet and triplet excited states of the substrate. The resulting expression is given by eq. [10],

$$[10] \quad \Phi_p = \Phi_{ST}\left(\frac{k_1}{k_1 + k_2}\right)\left(\frac{k_{OH}[OH^-] + k_{H_2O}[H_2O]}{\Sigma k_d + k_{OH}[OH^-] + k_{H_2O}[H_2O]}\right)$$

$$[11] \quad \Phi_p = \Phi_{ST}\left(\frac{k_{OH}[OH^-]}{\Sigma k_d + k_{OH}[OH^-]}\right)$$

$$[12] \quad \Phi_p^0 = \Phi_{ST}\left(\frac{k_{OH}}{\Sigma k_d + k_{OH}}\right)$$

$$[13] \quad \Phi^0/\Phi_p = \left(\frac{1}{\Sigma k_d + k_{OH}}\right)k_{OH} + \left(\frac{\Sigma k_d}{\Sigma k_d + k_{OH}}\right)[OH^-]^{-1} = \tau_p^0 k_{OH} + (\tau_p^0/\tau_p')[OH^-]^{-1}$$

where Σk_d represents all triplet decay processes that do not lead to product and k_{H_2O} and k_{OH} are the water and hydroxide ion catalyzed rate constants for the primary photochemical step (leading to intermediate **14**). However, since it was observed that water is ineffective as a catalyzing base (no reaction in neutral solution), we have $k_{H_2O}[H_2O] \ll k_{OH}[OH^-]$. In addition, based on the exchange experiments, we know that intermediate **14** does not return to starting material efficiently. Kinetically this implies that $k_1 \gg k_2$. Therefore, eq. [10] simplifies to eq. [11]. We define the quantity Φ_p^0 as the quantum yield of reaction in 1.0 *M* NaOH, which can be written as eq. [12]. A simple division of eq. [12] by eq. [11] results in an expression for Φ_p^0/Φ_p, which after simplification is given by eq. [13], where τ_p^0 and τ_p' are the triplet lifetimes of the molecule in 1.0 *M* NaOH and in neutral water, respectively.

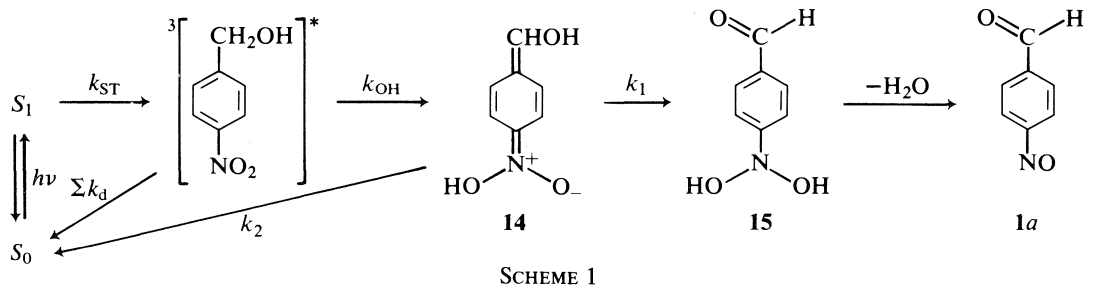

SCHEME 1

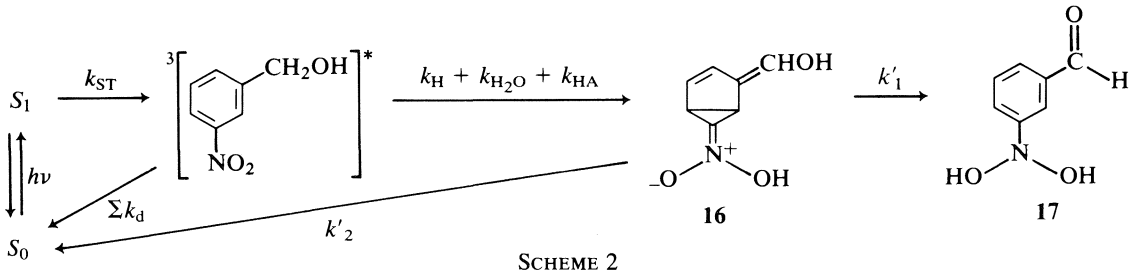

SCHEME 2

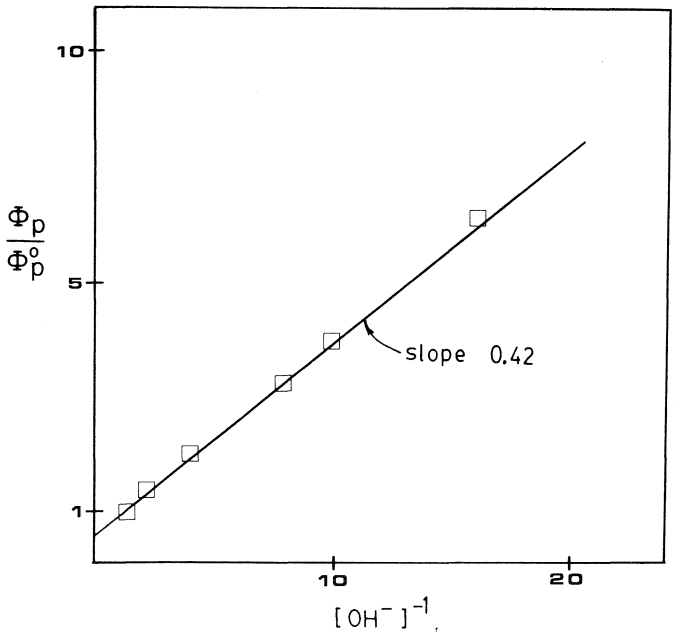

FIG. 6. Plot of Φ_p^0/Φ_p vs. $[OH^-]^{-1}$ for the photoredox reaction of *p*-nitrobenzyl alcohol **1** (Φ_p^0 = quantum yield at pH 14).

In this way, the kinetic equation presented by eq. [10] can be linearized. Using data presented in Fig. 2, a plot of Φ_p^0/Φ_p^0 vs. $[OH^-]^{-1}$ (Fig. 6) gave a good straight line, with a slope of 0.42 and an intercept of 0.6. This result gives kinetic support to the proposed mechanism presented in Scheme 1. Simple nitrobenzenes are known to have characteristically short triplet lifetimes of $\simeq$1 ns (3, 16, 17), which has been attributed to rapid radiationless decay to S_0. Assuming that $\tau'_p = 1 \times 10^{-9}$ s, then we calculate $\tau_p^0 = 0.42 \times 10^{-9}$ s and $k_{OH} = 1 \times 10^9\ M^{-1}\ s^{-1}$. However, as the triplet lifetimes of the molecules studied in this work are not available, we can calculate that intercept/slope = $k_{OH}/\Sigma k_d \simeq 1.4$, indicating that k_{OH} and Σk_d are similar in magnitude.

The mechanism for the photoredox reaction of the *meta* isomers appears to be somewhat more complicated: the *meta* isomers do not react via an overall simple intramolecular reduction–oxidation process. However, it seems clear that the initial steps should be similar to the mechanism proposed for the *para* isomers (Scheme 1), since the evidence accumulated does not require a completely different mechanism. By analogy with Scheme 1, the proposed sequence of events for the *meta* isomers is shown in Scheme 2 for *m*-nitrobenzyl alcohol **3**. The "$k_H + k_{H_2O} + k_{HA}$" step in Scheme 2 involves abstraction of the benzylic proton by solvent water concerted with protonation at the nitro group by protonating agents H_2O, H_3O^+, and general acid HA, respectively. The proposed highly polarized nature of the reactive triplet state facilitates protonation at the nitro group. Acid catalysis due to initial protonation of the nitro group in the ground state can be ruled out since the nitro group is an extremely weak base in S_0 ($pK_{SH^+} < -10$) (18). The quantum yield expression for loss of substrate (Φ_L) or formation of **17** is given by eq. [14]. However, experimentally the quantum yields for formation of **7** and **8** (i.e., Φ_m) were measured, where these products are believed to be derived from **17** via secondary dark reactions (*vide infra*). Therefore, we can write eq. [15], which gives the relationship between Φ_L and Φ_m, where $\beta < 1$. The value of β is not unity since the reaction is not 100% clean. Intermediate **16** does not return to starting material to any significant extent, based on the results of the exchange experiments (*vide supra*). Kinetically this implies that $k'_1 \gg k'_2$. In the pH region and in the absence of general acids, eqs. [14] and [15] can be simplified to give eq. [16].

$$[14]\quad \Phi_L = \Phi_{ST}\left(\frac{k'_1}{k'_1 + k'_2}\right) \times \left(\frac{k_H[H^+] + k_{H_2O}[H_2O] + k_{HA}[HA]}{\Sigma k_d + k_H[H^+] + k_{H_2O}[H_2O] + k_{HA}[HA]}\right)$$

$$[15]\quad \Phi_m = \beta \times \Phi_L$$

$$[16]\quad \Phi_m = \beta\Phi_{ST}\left(\frac{k_{H_2O}[H_2O]}{\Sigma k_d + k_{H_2O}[H_2O]}\right)$$

In stronger acids (pH < 1), the proton-catalyzed reaction dominates ($k_H[H^+] \gg k_{H_2O}[H_2O]$), resulting in a rapid increase in Φ_m with increasing medium acidity. The maximum in reaction

efficiency is observed at $H_0 \simeq -2$, followed by a decrease in reaction efficiency at higher acidities. It is proposed that this decrease at higher acidities is due to static quenching effects by hydronium ion, as the hydroxyl group can be protonated significantly at these acidities (estimated $pK_{SH^+} \simeq -2$ to -4). The exact nature of this quenching mechanism has not been delineated and is a topic for future studies.

The proposed mechanism in Scheme 2 predicts general acid catalysis of photoreaction. We have observed general acid catalysis of reaction for compound **3** at pH 1.5 using H_3PO_4/NaH_2PO_4 as the buffer, at pH 4.2 using NaH_2PO_4/K_2HPO_4 as the buffer. These experiments were carried out relative to a solution of the same pH and ionic strength, but without added general acid. Typically, $\Phi(0.44\ M\ [HA])/\Phi(0\ M[HA]) = 1.22 \pm 0.05$ at pH 4.2, where NaH_2PO_4 is the general acid, and a value of 1.5 ± 0.01 at pH 1.5, where H_3PO_4 is the general acid. These results corroborate the proposed mechanism requiring proton assistance in the primary photochemical step.

The problem of proposing a viable route from intermediate **17** (Scheme 2) to the observed reaction products **7** and **8** (eq. [4]) will now be addressed. Compound **17**, on dehydration, gives *m*-nitrosobenzaldehyde. However, this compound is not observed in the photoreaction. To examine the possibility that the observed photoproducts are due to a secondary photoreaction (or dark reaction) of *m*-nitrosobenzaldehyde, attempts were made to synthesize this compound independently and study its chemical and photochemical behaviour. After a number of unsuccessful attempts at preparing *m*-nitrosobenzaldehyde, we decided to make *m*-nitrosoacetophenone **18** instead, since it is the analogous product for reaction of alcohol **4**. Compound **18** (in the dimeric form) was readily prepared via *m*-chloroperoxybenzoic acid oxidation of *m*-aminoacetophenone. The results for **18** should be equally valid for the other *meta* alcohols

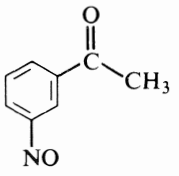

18

(**3** and **5**). Compound **18** was found to be stable in the dark indefinitely in aqueous solution (pH 7–0). It could be recovered unchanged as the dimeric form. Since the color remained yellow in solution, there is no evidence to suggest that significant amounts of monomeric **18** are formed on dissolution. Photolysis of **18** in aqueous solution (neutral or acidic) failed to give rise to the observed photoproducts, and only resulted in decomposition to give highly colored material that was not characterized. These observations rule out **18**, at least in the dimer form, as a discrete intermediate in the reaction pathway. We present two possible reaction schemes to account for the reaction products. The first involves a dark disproportionation reaction of two molecules of **17** (or some structurally equivalent species, which may be in a hot ground state), to give *m*-nitrobenzaldehyde and hydroxylamine derivative **19**. Subsequent reaction of **19** with **17** results in *m*-azoxybenzaldehyde, via the known condensation reaction of hydroxylamines and nitroso groups, to give azoxy compounds (19). However, it is not clear at this time why the primary nitroso carbonyl products (eq. [3]) are isolable for the *para* isomers and not so for the *meta* isomers. It would appear that this difference in reaction products observed between the

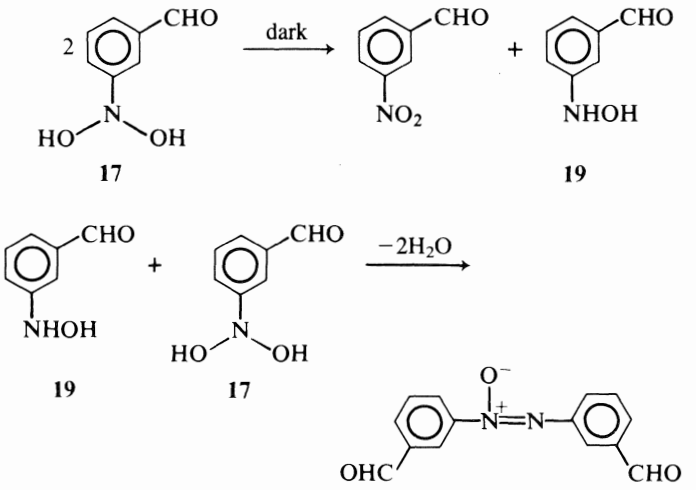

SCHEME 3

meta and *para* alcohols, which otherwise complement each other, reflects a fundamental difference in their photochemical behaviour.

An alternative explanation[2] to account for the fact that the primary nitroso products are not observed for the *meta* alcohols is that the initially formed *m*-nitrosobenzaldehyde *monomer* (from reaction of **3**) may react with a molecule of starting material in a redox fashion, to give *m*-nitrobenzaldehyde and **19**. Subsequent reaction of **19** with *m*-nitrosobenzaldehyde leads to azoxy compound **8***a*. This alternative pathway seems plausible considering the fact that nitrosobenzene monomer itself is known to oxidize certain benzylic amines (20), to give azoxybenzene and the corresponding carbonyl compound derived from the benzyl amine. As we have no viable way of making monomeric **18**, this possible pathway remains to be explored.

The isolated mole ratios of **7** and **8** (average ratio 1:0.33) do not represent redox material balance. For redox balance, one requires a 1:1 mole ratio of **7** to **8**. In other words, 0.67 equivalents of oxidized material is missing, or an excess of 0.67 equivalents of oxidized material is formed. Such a large discrepancy cannot adequately be accounted for by the presence of adventitious oxygen since >90% of dissolved oxygen can be removed by saturating the solution with argon. A reasonable explanation to account for this discrepancy is the observation that products **7***a–c* are photostable, while products **8***a–c* are photolabile under the photolysis conditions. For example, photolysis of **8***a* in aqueous solution quickly results in decomposition of the azoxy compound, as followed by tlc. The products are highly colored materials that failed to elute on preparative tlc and are believed to be phenolic dyes (see Experimental).

The proposed initial sequence of events (Schemes 1 and 2) represents a new type of photoreaction of nitroaromatic compounds. The overall result is a redox reaction. The reaction mechanism proposed has as its key step the substrate acting as a carbon acid. It is known that the pK_a values of common carbon acids are generally much greater than 20, particularly for those compounds without adjacent groups that can stabilize the negative charge of the conjugate base. For example, the ground state pK_a of toluene has been estimated to be about 41 (21). The introduction of two nitro groups at the *ortho* and *para* positions increases the acidity by 24 log units, to give a pK_a value of 17

[2]We thank Prof. D. Gravel for suggesting this possibility to us.

(22). The pK_a of *p*-nitrotoluene (23) and that of the α-cyano derivative (22) have been estimated to be 20 and 13, respectively. Based on these values, the pK_a of *p*-nitrobenzyl alcohol **1** for deprotonation of the benzylic proton should be in the range 17–19 in the ground state since the α-hydroxyl group can stabilize the anion to some extent by an inductive effect. The pK_a of the *meta* isomer (*m*-nitrobenzyl alcohol **3**) should be greater than the range 17–19 since resonance stabilization of the α-anion is not available. A reasonable pK_a range for **3** in the ground state is 19–22. On excitation to the triplet state, it would appear that the acidities of the α-protons of **1–5** increase dramatically. For the *para* isomers (**1** and **2**), it is estimated that $pK_a(T_1) \simeq 13$–15, as suggested by Fig. 2, an increase in acidity of 3–6 log units. For the *meta* isomers, the increase in acidity appears to be more dramatic; the $\Delta pK = pK(S_0) - pK(T_1)$ is probably greater than 20 log units since even water can deprotonate the molecule in T_1. The observed increase in acidity of the α-proton of these compounds can be interpreted as being due to the enhanced electron-withdrawing effect of aromatic nitro groups in T_1. This phenomenon has been well documented by Zimmerman and Somasekhara (24) and Cornelisse and Havinga (25) in their studies of nucleophilic aromatic substitutions of nitroaromatic derivatives. That the *meta* nitro group has a better electron-withdrawing effect has also been observed previously (24, 25) and lends support to the interpretation offered above.

A comment regarding the configuration of the T_1 reactive state is warranted. Simple nitrobenzenes, without strongly electron-donating groups, are believed to have n,π^* lowest triplets (1–4, 16, 17) in the commonly employed organic solvents. This is consistent with the observation that simple nitrobenzenes react via characteristic n,π^* triplet state reactions, in close analogy with many carbonyl n,π^* triplets. However, the photoredox reactions reported in this work do not take place in organic solvents and appear to be inconsistent with the assumption that these molecules have n,π^* lowest triplet reactive states, since the redox reactions clearly must involve activation of the benzene ring. n,π^* Triplets are not known to activate the benzene ring in photochemical reactions (1–4). It is well known that solvents of high dielectric constant stabilize π,π^* and destabilize n,π^* configurations (26). It is proposed that in water ($\varepsilon = 80$), either the lowest triplet is π,π^* or that the two configurations are very close in energy, thus allowing for a significant thermal population of π,π^* triplets and hence the observed reaction. In the commonly employed organic solvents (typically $\varepsilon < 40$), the lowest triplet configuration is n,π^* in character and no reaction is observed. In pure formamide ($\varepsilon = 110$) these reactions are also not observed. This can be explained by noting that formamide cannot catalyze the reactions as can water, that is, functioning as a weak base and also as a source of protons.

The only other photoredox reaction of a nitroaromatic compound that does not involve an *ortho*-substituted nitro group, known prior to this work, is that of the water-catalyzed reaction of *p*-nitrobenzaldehyde, to give *p*-nitrosobenzoic acid, reported by Wubbels *et al.* (8, 9). The primary photochemical event proposed by Wubbels for this reaction involves electron transfer from water to the n,π^* triplet of the nitro group. The results of our work suggest that the reaction reported by Wubbels (8, 9), although chemically similar, is fundamentally different from the reactions reported in this work with respect to the nature of the primary photochemical event. For example, *m*-nitrobenzaldehyde does not react at any pH. Interestingly, no additional examples of the reaction reported by Wubbels (8, 9) have been discovered whereas the photoredox reactions of **1–5** appear to be quite general for structurally related systems. However, additional work is required to fully delineate the difference between the above two types of photoredox reactions with respect to the primary photochemical event.

In summary, the photochemistry of a number of *meta* and *para* nitro-substituted benzyl alcohols, previously believed to be photochemically unreactive, has been investigated in some detail. Interesting catalytic effects due to hydronium and hydroxide ions were observed. The *para* isomers react via a simple photoredox mechanism whereas the *meta* isomers give rise to products that are believed to be due to secondary dark reactions of the initially photogenerated intermediate.

Experimental

General

Ultraviolet spectra were recorded in 95% EtOH (unless otherwise noted) on either a Cary 14 or a Unicam SP 1800 instrument. The ^{1}H nmr spectra were recorded on a Varian T60 spectrometer in $CDCl_3$. The ir spectra were obtained on a Unicam SP 1025 instrument in chloroform solution. Mass spectra were taken on a CEC 21-490 single-focussing magnetic sector instrument operating at 70 eV. Preparative photolyses were carried out using a Rayonet RPR 100 photochemical reactor.

Materials

Nitrobenzyl alcohols **1**, **3**, and **6** were purchased from Aldrich, while **2** and **4** were prepared via $NaBH_4$ reduction of the corresponding ketones in MeOH. These were either distilled or recrystallized prior to use. Compound **12** was purchased from Aldrich and **13** was a gift from BASF Wyandotte.

m-*Nitrosoacetophenone* ***18*** *(dimer)*

A solution of 3.1 g (18 mmol) of *m*-chloroperoxybenzoic acid in 50 mL CH_2Cl_2 was added dropwise over a 20-min period to a boiling solution of 1.0 g (7.4 mmol) of *m*-aminoacetophenone (Aldrich) in 100 mL CH_2Cl_2. After one minute the solution turned green, indicative of the formation of a monomeric nitroso compound. After refluxing for an additional 15 min, the solution was quenched by adding 200 mL 3% NaOH. The CH_2Cl_2 layer was separated (the solution was now yellow rather than green) and washed with additional aliquots of 3% NaOH, and finally with 5% HCl. Evaporation of the solvent gave 300 mg of a yellow solid, which was recrystallized twice from pentane/CH_2Cl_2, mp 134–135°C; ir ($CHCl_3$): 1275 (s), 1360 (s), 1465 (s), 1490 (m), 1695 (vs); uv (80% H_2O/EtOH): 238 nm (ε 20 000), 310 nm (ε 10 000), no absorption >400 nm; ^{1}H nmr δ: 2.6 (s, 3H, $COCH_3$), 2.65 (s, 3H, $COCH_3$), 7.2–9 (m, 8H, arom.); mass spectrum (*m/e*): 119 (100), 163 (10), 264 (15) ($M^+ - 32$), 282 (40) ($M^+ - 16$). *Anal.* calcd. for $C_8H_7NO_2$: C 64.42, H 4.73, N 9.93%; found: C 64.23, H 4.62, N 9.21%.

p-*Nitrosoacetophenone* ***2a*** *(dimer)*

In a similar procedure as described for *m*-nitrosoacetophenone, use of *p*-aminoacetophenone gave a yellow solid that on recrystallization from acetone gave mp 190–191°C; ir ($CHCl_3$): 955 (m), 1010 (w), 1270 (s), 1310 (m), 1355 (s), 1410 (m), 1465 (s), 1600 (w), 1690 (s); uv (95% EtOH): 340 nm (ε 10 000); ^{1}H nmr δ: 2.7 (s, 3H, $COCH_3$), 2.75 (s, 3H, $COCH_3$), 8.1–8.8 (m, 8H, arom.); mass spectrum (*m/e*): 91 (59), 119 (100), 126 (13), 135 (12), 147 (13), 169 (13), 211 (10), 267 (10), 168 (13) ($M^+ - 32$), 282 (65) ($M^+ - 16$). *Anal.* calcd. for $C_8H_7NO_2$: C 64.42, H 4.73, N 9.39%; found: C 64.62, H 4.81, N 9.42%. The spectral data (uv, mass spectra, and ^{1}H nmr) indicate that both **18** and ***2a*** exist in the dimeric form:

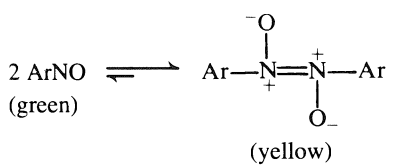

A large number of nitroso compounds are known to exist in the form of the dimer (27). Doubling-up of the ^{1}H nmr peaks due to restricted rotation about the Ar—N bond has been reported for aromatic nitroso compounds with electron-donating groups (28), which are known to be monomeric in solution. We believe the nitroso dimers reported here also have restricted rotation about the Ar—N bond in solution, although this phenomenon to our knowledge has not been documented for these types of nitroso dimers.

α-Deuterio-*p*- and *m*-nitrobenzyl alcohols (**9** and **11**) were prepared via $NaBD_4$ reduction of the corresponding aldehydes. α,α-Dideuterio-*p*-nitrobenzyl alcohol **10** was prepared via LAD reduction of methyl *p*-nitrobenzoate in THF. The deuterated alcohols were spectroscopically identical (except for the absence or reduced absorption of the α-H in the ^{1}H nmr) with the parent compounds.

Preparative photolyses

Dark reactions of ***1–6***

Alcohols **1–6** are stable in the dark in pure H_2O, 10% H_2SO_4, 40% H_2SO_4, and at pH 14, with or without argon saturation, for an indefinite period at room temperature. A typical experiment involves dissolving 100 mg of the substrate in 250 mL solution (no cosolvent required for **1–4** and **6** since these are sufficiently water soluble) and leaving it for the required time in the dark.

Preparative photolysis of m-*nitrobenzyl alcohol* ***3***

A solution of 100 mg of **3** in 500 mL distilled water was placed in a 0.67-L quartz vessel and saturated with argon for 30 min using a fritted-glass dispersion tube. A cold finger was placed inside the vessel along with a long syringe needle connected to the argon line. A stream of argon was allowed to enter the vessel continuously. The solution was then irradiated for 2 h at 254 nm (Rayonet reactor; 300- or 350-nm lamps were also used and gave the same result). The standard work-up procedure involves saturating the aqueous solution with NaCl and extracting with 2 × 100 mL CH_2Cl_2. The above photolysis was repeated four times, the crude isolated materials combined, and the products separated on preparative tlc plates (silica gel; CH_2Cl_2). An ^{1}H nmr spectrum was recorded of the product mixture before separation was carried out, to ensure that no new products were formed during the preparative tlc procedure. In this way, it was shown that the products recovered from prep. tlc were the primary products observed after photolysis. There was isolated 120 mg (40% isolated yield; R_f 0.45) of *m*-nitrobenzaldehyde **7***a* as identified by spectroscopic comparison with the authentic material, and 50 mg (17% isolated yield; R_f 0.30) of a yellow solid identified as *m*-azoxybenzaldehyde **8***a*, mp 103–106°C; ir ($CHCl_3$): 1140 (m), 1320 (w), 1470 (w), 1490 (w), 1590 (w), 1620 (w), 1710 (s); uv (95% EtOH): 235 nm (ε 22 000), 320 nm (ε 9 800); ^{1}H nmr δ: 7–9 (8H, arom.), 10.1 and 10.15 (2s, 2H, non-equiv. CHO); mass spectrum (*m*/*e*): 254 (M^+). *Anal.* calcd. for $C_{14}N_{10}N_2O_3$: C 66.14, H 3.96, N 11.02%; found: C 66.22, H 4.16, N 10.96%. Relative yield experiments (prep. scale) were performed in H_2O (pH 7, pH 9, pH 13), 10% and 20% H_2SO_4 with 100-mg samples in 400 mL of the appropriate solvent. The irradiation time was 20 min at 254 nm, which gave a conversion of 20% at pH 7, as calculated by ^{1}H nmr integration (C*H*O vs. CH_2OH peaks). An increase in conversion was observed only in the 10% and 20% H_2SO_4 samples, and the relative increase calculated agrees with those reported in Fig. 3, which were calculated via uv spectrophotometry.

Preparative photolysis of α-*methyl*-m-*nitrobenzyl alcohol* ***4***

The procedure for **4** is identical to that described for **3**. The products were isolated via preparative tlc (silica gel; CH_2Cl_2) and were *m*-nitroacetophenone **7***b* and *m*-azoxyacetophenone **8***b* in the quoted isolated weight ratios (eq. [4]). *m*-Azoxyacetophenone **8***b*: mp 100–103°C; ir ($CHCl_3$): 900 (m), 960 (m), 1080 (m), 1115 (m), 1165 (m), 1290 (s), 1360 (s), 1465 (s), 1545 (m), 1620 (s), 1700 (s), 2940 (s); uv (95% EtOH): 227 nm (ε 23 000), 315 nm (ε 10 000); ^{1}H nmr δ: 2.7 and 2.8 (2s, 6H, non-equiv. $COCH_3$), 7–9 (8H, arom.); mass spectrum (*m*/*e*): 282 (M^+). *Anal.* calcd. for $C_{16}H_{14}N_2O_3$: C 68.08, H 4.99, N 9.92%; found: C 67.89, H 4.89, N 9.88%.

Preparative photolysis of α-*phenyl*-m-*nitrobenzyl alcohol* ***5***

Employing the above procedure, *m*-nitrobenzophenone **7***c* and *m*-azoxybenzophenone **8***c* were isolated. The former was identified by comparison with the authentic material. *m*-Azoxybenzophenone **8***c*: mp 170–171°C; ir ($CHCl_3$): 1120 (m), 1290 (s), 1320 (s), 1450 (m), 1600 (s), 1660 (s); uv (95% EtOH): 253 nm (ε *25 000), 320 (*ε 10 000); ^{1}H nmr δ: 7–9 (arom.); mass spectrum (*m*/*e*): 406 (M^+). *Anal.* calcd. for $C_{26}H_{18}N_2O_3$: C 76.83, H 4.46, N 6.89%; found: C 77.04, H 4.62, N 6.64%.

Photolysis of m-*azoxybenzaldehyde* ***8***a

m-Azoxybenzaldehyde **8***a* is photochemically labile when irradiated at 254 nm in aqueous solution, as exemplified by the following experiment. A solution of 50 mg of **8***a* (100 mL CH_3CN and 400 mL H_2O) was irradiated in a quartz vessel for 45 min at 254 nm in a Rayonet reactor. The color of the solution changes from light yellow to deep yellow. Upon basification to pH 10, the solution turns to a deep orange, indicative of the presence of phenolic material. The ^{1}H nmr of the recovered material showed broad absorption peaks and could not be characterized. We presume **8***a* (and also **8***b* and **8***c*) photodecomposes to give azophenols, which is a known reaction pathway of aromatic azoxy compound (the photo-Wallach rearrangement) (29).

Preparative photolysis of p-*nitrobenzyl alcohol* ***1***

A solution of 200 mg of **1** in 25 mL CH_3CN and 300 mL pH 13 (NaOH) was prepared in a 0.67-L quartz vessel and saturated with argon. The solution was photolyzed at 254 nm for 10 h in a Rayonet reactor. After irradiation, the solution was neutralized with concentrated HCl, saturated with NaCl, and extracted with 2 × 100 mL CH_2Cl_2. Evaporation of the solvent gave 170 mg of a yellow solid. The tlc of this material showed two spots (silica gel, CH_2Cl_2): R_f 0.2 (substrate) and R_f 0.3 (product; yellow in color). The above photolysis was done in triplicate and the crude materials combined and separated via prep. tlc. There was obtained 180 mg (30% overall isolated yield) of fraction #2 (R_f 0.3), identified as *p*-nitrosobenzaldehyde **1***a* (dimer): mp 185–187°C; ir ($CHCl_3$): 1180 (s), 1460 (m), 1600 (m), 1710 (s), 2740 (w), 2840 (w); uv (95% EtOH): 340 nm (ε 12 000); ^{1}H nmr δ: 10.1 and 10.15 (2s, 2H, non-equiv. CHO), 7.8–8.7 (8H, arom.); mass spectrum (*m*/*e*): 254 (M^+ − 16). *Anal.* calcd. for $C_7H_5NO_2$: C 62.22, H 3.73, N 10.36%; found: C 62.10, H 3.80, N 10.21%. As was observed for **2***a*, **1***a* also exists as a dimer.

Preparative photolysis of α-*methyl*-p-*nitrobenzyl alcohol* ***2***a

The procedure employed for **2** is identical to that for **1** described above. The isolated product was identified as *p*-nitrosoacetophenone **2***a* (dimer), by comparison with the authentic material synthesized in a previous section above.

Relative quantum yields for reaction of ***1*** *and* ***2*** *via preparative photolyses*

The general procedure is described as follows: A solution of 100 mg of the substrate is dissolved in 140 mL aqueous NaOH (6% CH_3CN) and irradiated in a Rayonet reactor for 6 h at 254 nm. After work-up (described above), the extent of reaction was calculated by integrating the aldehyde resonance of **1***a* (or $COCH_3$ resonance of **2***a*) relative to the methylene signal of the substrate at δ 4.8.

Reactions of m-*nitrosoacetophenone* ***18*** *(dimer)*

A solution of 100 mg of **18** was prepared in 50 mL CH_3CN and 200 mL H_2O (pH 7) and left in the dark overnight. The color of the solution was a light yellow during the whole period and therefore suggests that little, if any, monomeric nitroso compound exists in solution. After work-up, **18** was recovered unchanged (as the dimer). When an identical solution was photolyzed at 254 nm for 1 h, an intense orange color developed. After work-up, the tlc (CH_2Cl_2; silica gel) of this material showed a single orange spot at R_f 0.25; no trace of *m*-nitroacetophenone or *m*-azoxyacetophenone was observed. The ^{1}H nmr of the reaction mixture showed a new singlet at δ 2.7, along with the "doublet" at δ 2.6 and 2.65 characteristic of **18** (ratio of product to **18** is about 2:1). We have tentatively identified this product as the corresponding nitroxide of **18**, a known photoproduct of aromatic nitroso compounds (30).

Spectrophotometric studies

Solutions for spectrophotometric studies were prepared in 1.00-cm quartz cuvettes (3.0 mL) by injecting a solution of the substrate (dissolved in CH_3CN) into the solution of appropriate pH via a

microlitre syringe. After purging with argon for 5 min, the cuvette was photolyzed in a merry-go-round apparatus placed inside a Rayonet reactor. The pH solutions were made from aqueous NaOH or phosphate buffer; neither of these absorb significantly above 230 nm. After photolysis, uv spectra were recorded and the increase in OD at λ_{max} of the product was measured. The λ_{max} of the products are given in the above sections dealing with product isolation. An example of a typical uv trace of the photochemical reaction is given in Fig. 1 for *m*-nitrobenzyl alcohol **3**. For relative quantum determinations, care was taken not to irradiate beyond 20% conversion.

Absolute quauntum yield measurements

Malachite green leucocyanide (MGL) in acidic ethanol was employed for chemical actinometry (31). The material was synthesized according to the method of Calvert and Rechen (32), mp 174–176°C (lit. (32) mp 176–177°C). The actinometer is best suited for low light intensities ($\simeq 10^{-9}$ einsteins min^{-1}), which was the situation encountered in these measurements. The actinometer solution was prepared by mixing 0.50 mL acidic aqueous ethanol ($\simeq 10^{-3}$ *M* HCl) with 2.50 mL of a 10^{-3} *M* stock of MGL in 95% EtOH in a quartz cuvette (1.00 cm). The OD at 622 nm was measured prior to and after photolysis (typical irradiation time 3–10 min), and the change in OD (ΔA) at 622 nm was then used to calculate the light intensity of the source via the equation:

$$I(\text{einsteins min}^{-1}\text{ cm}^{-3}) = 10^{-3}\,\Delta A/(\varepsilon_{622}\Phi_{MGL}\Delta t)$$

where ε_{622} is the extinction coefficient of the blue dye produced at 622 nm (1.063×10^5 cm M^{-1}) (31), Φ_{MGL} is the quantum yield for dye formation (0.91) (31), and Δt the elapsed irradiation time in minutes. The light source employed was a 200-W Hg lamp filtered through a Bausch and Lomb monochromator and a 240–420 nm bandpass (Corning 7–54). Ultraviolet spectrophotometry was also employed to monitor the extent of conversion of photoreaction of the substrates. In this method, the product quantum yield (Φ_m), under low conversions, is given by the equation:

$$\Phi_m = \Delta A_\lambda/(10^3\,\varepsilon_\lambda \Delta I_a)$$

where ΔA_λ is the change in OD at the monitored wavelength (λ_{max} of the product) and ε_λ is the corresponding extinction coefficient, and ΔI_a the number of quanta absorbed by the compound during the photolysis time. For compounds **3–5**, the excitation wavelength was 254 nm. The λ_{max} of **7** and **8** (the products) are the same and the extinction coefficients differ by less than 5% at this wavelength. Therefore the above equation can be employed to calculate the total quantum yield for formation of **7** and **8**. Since the mole ratio of **7** and **8** could be determined experimentally (0.76:0.24, respectively; averaged value), we have:

$$\Phi_m = 0.76\Phi(\mathbf{7}) + 0.24\Phi(\mathbf{8})$$

where $\Phi(\mathbf{7})$ and $\Phi(\mathbf{8})$ represent the quantum yield for formation of **7** and **8**, respectively. Individual values for $\Phi(\mathbf{7})$ and $\Phi(\mathbf{8})$ determined via the above method are tabulated in Table 1.

Triplet sensitization

Sodium benzophenone-2-carboxylate **12** was employed as the water-soluble triplet sensitizer. A typical experiment is described as follows. A 10-g solution of **12** was first prepared in the appropriate pH and 100 mg of the substrate dissolved in 50 mL CH_3CN was added with vigorous stirring. The solution was photolyzed at 350 nm, where **12** absorbs >95% of the exciting light. The solution was worked up by first extracting with 2 × 100 mL ether and then back-washing several times with bicarbonate solution to remove residual sensitizer. The extent of reaction could be determined by ^{1}H nmr spectroscopy, by integrating the CHO resonance of the products (for **3**) vs. the methylene protons of the substrate.

Triplet quenching experiments

Diene **13** was used as the water-soluble triplet quencher. A typical experiment is described as follows. A 250-mg solution of **1** and **2** was first prepared in the appropriate pH (100 mL) and a sufficient amount of **13** was added to give a quencher concentration of 0.02 *M*. An identical sample of **1** or **2** was prepared but without added quencher. These two solutions were photolyzed at 350 nm (where the quencher absorbs negligibly) under identical conditions (typically 20–40 min). Both solutions were worked up and the extent of reaction compared via ^{1}H nmr.

General acid catalysis experiments

Two solutions (200 mL) each of 100 mg of **3** were prepared. One solution was made up in 1.0 *M* NaH_2PO_4 and the pH adjusted to 4.2 with dilute $HClO_4$, while the other, of 1.0 *M* NaCl, was also adjusted to pH 4.2. After the photolysis, the percentage conversion was determined via ^{1}H nmr integration as described above. By this method, it was found that $\Phi(1.0\ M\ [HA])/\Phi(1.0\ M\ NaCl) = 1.22 \pm 0.05$ (error is standard deviation), which is indicative of general acid catalysis. The same result was obtained by monitoring the reaction spectrophotometrically at λ_{max} of the product. Using H_3PO_4 (a stronger general acid), at pH 1.5, a value of 1.5 ± 0.1 was obtained and suggests that additional studies are warranted to delineate this effect, which is suggestive of a Brønsted catalysis law of photochemical reaction.

Acknowledgments

The authors are grateful to the Natural Sciences and Engineering Research Council of Canada for continued support. P.W. thanks the Research Corporation and the University of Victoria for additional support.

1. H. A. Morrison. *In* The chemistry of the nitro and nitroso groups. *Edited by* H. Feuer. Wiley, New York. 1969.
2. Y. L. Chow. *In* The chemistry of the amino, nitro, and nitroso compounds and their derivatives. *Edited by* S. Patai. Wiley, New York. 1982. Chapt. 6.
3. D. Döpp. Top. Curr. Chem. **55**, 49 (1975).
4. A. N. Frolov, N. A. Kuznetsova, and A. V. El'tsov. Russ. Chem. Rev. Engl. Trans. **45**, 1024 (1976).
5. R. W. Yip, D. K. Sharma, R. Giasson, and D. Gravel. J. Phys. Chem. **89**, 5328 (1985).
6. J. D. Margerum and L. J. Miller. *In* Techniques of organic chemistry. Vol. III. *Edited by* G. H. Brown. Wiley–Interscience, New York. 1971. pp. 557–626.
7. G. Ciamician and P. Silber. Chem. Ber. **34**, 2040 (1901).
8. G. G. Wubbels, R. R. Hautuala, and R. L. Letsinger. Tetrahedron Lett. 1689 (1970).
9. G. G. Wubbels, T. F. Kalhorn, D. E. Johnson, and D. Campbell. J. Org. Chem. **47**, 4664 (1982).
10. J. Reich and K. G. Weidmann. Arch. Pharm. (Weinheim, Ger.), **304**, 906 (1971).
11. P. Wan and K. Yates. J. Org. Chem. **48**, 136 (1983).
12. P. Wan and K. Yates. J. Chem. Soc. Chem. Commun. 1023 (1981).
13. E. Bamberger. Chem. Ber. **51**, 606 (1918).
14. S. L. Murov. Handbook of photochemistry. Marcel Dekker, New York. 1973.
15. H. E. Zimmerman and D. J. Kreil. J. Org. Chem. **47**, 2060 (1982).
16. R. W. Yip, D. K. Sharma, R. Giasson, and D. Gravel. J. Phys. Chem. **88**, 5770 (1984).
17. R. Hurley and A. C. Testa. J. Am. Chem. Soc. **90**, 1949 (1968).
18. E. M. Arnett. Prog. Phys. Org. Chem. **1**, 223 (1963).
19. J. March. Advanced organic chemistry. 3rd ed. McGraw–Hill, New York. 1977. pp. 531–582.
20. K. Suzuki and E. K. Weisburger. J. Chem. Soc. (C), 199 (1968).
21. A. Streitwieser, Jr., M. R. Granger, F. Mares, and R. A. Wolf. J. Am. Chem. Soc. **95**, 4257 (1973).
22. R. Schaal. J. Chim. Phys. (Paris), **52**, 796 (1955).
23. F. G. Bordwell, D. Algrim, and N. R. Vanier. J. Org. Chem. **42**, 1817 (1977).
24. H. E. Zimmerman and S. Somasekhara. J. Am. Chem. Soc. **85**, 922 (1963).
25. J. Cornelisse and E. Havinga. Chem. Rev. **75**, 353 (1975).

26. N. J. TURRO. Modern molecular photochemistry. Benjamin–Cummings, Menlo Park, California. 1978. p. 107.
27. (*a*) B. G. GOWENLOCK, H. SPEDDING, J. TROTMAN, and D. H. WHIFFEN. J. Chem. Soc. 3927 (1957); (*b*) C. K. INGOLD and H. A. PIGGOTT. J. Chem. Soc. 125 (1924); 169 (1924); (*c*) W. LUTTKE and B. G. GOWENLOCK. Q. Rev. (London), **12**, 321 (1958).
28. I. C. CALDER and P. J. GARRATT. Tetrahedron, **25**, 4023 (1969).
29. (*a*) R. H. SQUIRE and H. H. JAFFE. J. Am. Chem. Soc. **95**, 8188 (1973); (*b*) D. J. W. GOON, N. G. MURRAY, J.-P. SCHOCH, and N. J. BUNCE. Can. J. Chem. **51**, 3827 (1973).
30. C. CHATGILIALOGLU and K. U. INGOLD. J. Am. Chem. Soc. **103**, 4833 (1981).
31. G. J. FISCHER, J. C. LEBLANC, and H. E. JOHNS. Photochem. Photobiol. **6**, 757 (1967).
32. J. G. CALVERT and H. J. L. RECHEN. J. Am. Chem. Soc. **74**, 2101 (1952).

A C-13 nuclear magnetic resonance study of the pyrimidine synthesis by the reactions of 1,3-dicarbonyl compounds with amidines and ureas

ALAN R. KATRITZKY[1] AND TAHER I. YOUSAF
Department of Chemistry, University of Florida, Gainesville, FL 32611, U.S.A.

Received April 14, 1986

ALAN R. KATRITZKY and TAHER I. YOUSAF. Can. J. Chem. **64**, 2087 (1986).

The detailed mechanistic pathways are elucidated for the reactions of acetylacetone, methyl acetoacetate, and dimethyl malonate with a variety of amidines and ureas. In many cases the identification of a single intermediate allows the definition of the reaction path and identification of two slow steps. Intermediates characterized include ring-closed dihydroxytetrahydropyrimidines, dihydrohydroxypyrimidinones, open-chain enamides, and carbonyl addition compounds.

ALAN R. KATRITZKY et TAHER I. YOUSAF. Can. J. Chem. **64**, 2087 (1986).

On a élucidé le mécanisme détaillé des réactions de l'acétylacétone, de l'acétoacétate de méthyle et du malonate de méthyle avec diverses amidines et urées. Dans plusieurs cas, l'identification d'un seul intermédiaire permet de définir le chemin réactionnel et l'identification de deux étapes lentes. Les intermédiaires caractérisés comprennent les dihydroxytétrahydropyrimidines et les dihydrohydroxypyrimidinones cycliques ainsi que les énamides en chaîne ouverte et les composés provenant d'une addition sur le groupement carbonyle.

[Traduit par la revue]

Introduction

Pyrimidines are widely distributed in nature (1*a*), and include many synthetic drugs (1*b*). An important principal synthesis of pyrimidines is the reaction of a 1,3-dicarbonyl compound with amidines or ureas, the Traube synthesis (2*a*,*b*, 3*a*,*b*). The older (4*a*,*b*,*c*) and the more recent (5*a*,*b*,*c*) literature on this reaction give preparative details for the synthesis of literally thousands of pyrimidines, but surprisingly little is known of its mechanism. Thus, neither of the two definitive monographs on the subject (6*a*,*b*), nor a recent review by Brown (1*c*), discuss the mechanism. Just two papers published in the last decade have dealt with limited aspects of this question: a ^{14}C and ^{15}N labeling study (7) of the formation of 4-amino-5-aminomethyl-2-methylpyrimidine **2** from two specifically labeled 2-(diethoxymethyl)-3-ethoxypropionitriles **1** and acetamidine showed that the labels were incorporated as indicated: two alternative reaction pathways via a bicyclic intermediate were postulated. An ^1H nmr kinetic study (8) of the formation of trimethroprim **3**

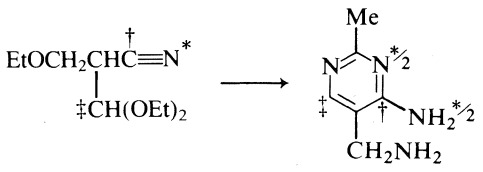

1 **2**

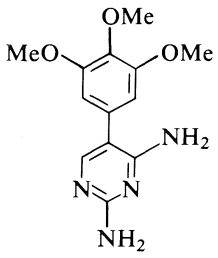

3

from the reaction of various precursor α,β-unsaturated nitriles with guanidine disclosed no intermediates, and was interpreted to show that the initial, and rate-determining, step was attack of the guanidine nitrogen on the nitrile carbon, followed by a fast intramolecular Michael addition to give product.

The present work examines the reactions of acetylacetone **4** (Schemes 1 and 2), methyl acetoacetate **18** (Schemes 3 and 4), and dimethyl malonate **27** (Schemes 5 and 6) with the amidines **5** and ureas **11** by ^{13}C nmr spectroscopy. It was undertaken with a view to identify the intermediates on the reaction pathways, and represents a continuation of our earlier studies of the mechanisms of heterocyclic ring formation (9, 31).[2]

Results and discussion

Basis of investigation

The reactions were carried out in the spectrometer cavity in 5-mm nmr tubes using deuterated solvents. They were all followed by observing in the nmr spectrum the decay of peaks due to starting material, the formation and decay of peaks due to an intermediate, and the concomitant formation of product peaks. The assignments of all starting materials and some product pyrimidines were in accord with the literature. Authentic values for chemical shifts of those pyrimidines not reported in the literature were obtained by appropriate syntheses using literature procedures (6*a*,*b*) and subsequent ^{13}C nmr characterization. Intermediate peaks were assigned by reference to tables of published values for the appropriate open chain compounds (10–13, 14, 15). All assignments were supported using the two INEPT(D) pulse sequences previously described (9).

C-13 assignments and identification of intermediates

Table 1 gives the chemical shifts and assignments of the 1,3-dicarbonyl compounds used in the present study; similar data for amidines **5** (*a*–*d*) are given in the Experimental; they are in broad agreement with the literature values (12, 13), as are the chemical shifts and assignments of the pyrimidines **9** (Table 2), formed from the reactions of the amidines **5** (*a*–*c*) with acetylacetone **4** (Scheme 1) (16).

A maximum of one intermediate was observed in each of the reactions studied, and this was identified on the basis of the evidence discussed below as either the diol **7** (Table 3, Scheme 1) (in reactions with amidines) or as the enamide **17** (Scheme 2) (in reactions with ureas).

[1]Author to whom correspondence may be addressed.

[2]A. R. Katritzky, P. Barczynski, and D. Ostercamp. Manuscript in preparation.

TABLE 1. C-13 nmr chemical shifts and assignments[a] of acetylacetone **4** (Scheme 1), methyl acetoacetate **18** (Scheme 3), and dimethyl malonate **27** (Scheme 5)

R	R′	Compound	C1	C2	C3	R	R′	Reference
Me	Me	**5***a*[b]	204.0	58.0	204.0	30.8	30.8	14*e*
		5*b*[c]	191.5	100.8	191.5	24.6	24.6	14*e*
Me	OMe	**18***a*[b]	202.3	51.4	168.3	30.3	49.7	14*f*
		18*b*[c]	[d]	89.6	[d]		21.1[e]	14*f*
OMe	OMe	**27**	167.7	41.4	167.7	52.6	52.6	14*g*

[a]Chemical shifts in ppm relative to internal DMSO-d_6 at 39.5 ppm.
[b]Keto form.
[c]Enol form.
[d]Concentration of enol form too low to detect quaternary carbons.
[e]Overlapping into methoxy peak of the keto form.

TABLE 2. C-13 nmr chemical shifts and assignments[a] of 2-substituted-4,6-dimethylpyrimidines **9** (Scheme 1) and 4,6-dimethylpyrimidin-2-ones **15** (Scheme 2)

R	Compound	C2	C (4,6)	C5	Me (4,6)	Reference
NH_2	**9***a*	163.2	169.6	111.6	23.9	17
H	**9***b*	155.2	165.4	119.2	22.7	17
Me[b]	**9***c*	164.1	167.6	118.7	24.1	17
Ph[c]	**9***d*	165.3	167.1	118.7	24.1	—
O	**15***a*	153.8	168.4	105.1	21.0	—
S	**15***b*	173.9	169.5	111.4	20.7	—

[a]Chemical shifts in ppm relative to internal DMSO-d_6 at 39.5 ppm.
[b]26.4.
[c]Ph: *o*, 128.5; *m*, 129.4; *p*, 132.8; *i*, 134.8; *ortho* and *meta* assignments are interchangeable.

TABLE 3. C-13 nmr chemical shifts and assignments[a] of the intermediate diols **7** (Scheme 1)

R	Compound	C2	C (4,6)	C5	Me (4,6)
NH_2	**7***a*	161.8	80.2	44.2	29.1
H	**7***b*	150.9	79.4	43.6	28.2
Me	**7***c*	161.6	80.3	43.5	29.4[b]

[a]Chemical shifts in ppm relative to DMSO-d_6 at 39.5 ppm.
[b]2-Me s at 26.3 ppm.

The peak most characteristic of the diols **7** is that due to the two equivalent sp^3 carbons, C(4,6), at ca. 80 ppm (Table 3). Given that an sp^3 carbon attached to one oxygen resonates at ca. 50–56 ppm (11*a*), and when attached to a nitrogen at ca. 27–45 ppm (11*b*), and assuming the additivity of substituent effects (11*c*), it follows that the hemiaminal carbons C(4,6) should resonate in the region 77–110 ppm, as observed above and in the literature (15*b*). A similar approach rationalizes the chemical shifts of the methylene (5-CH_2) and methyl (4,6-CCH_3) carbons, which resonate characteristically at ca. 44 ppm and 28–29 ppm, respectively (Table 3). The C=N carbons (C2) resonate in the intermediate ca. 7–8 ppm upfield of the corresponding carbons in the parent amidine (cf. C2, Table 3 and Experimental) with the exception of R = NH_2, where the value in the intermediate is ca. 2 ppm downfield of that in the amidine. Notably, replacement of hydrogen by methyl at C2 has a *deshielding* effect: thus, C2 (R = Me) is ca. 10 ppm downfield of C2 (R = H) in the intermediates **7** (Table 3), products **9** (Table 2), and amidines **5** (cf. Experimental). A similar effect is observed at carbons 4 and 6 of the product: in the dimethyl derivatives these carbons resonate at ca. 167–170 ppm (Table 2), whereas in the parent compounds (16, 17) they resonate in the region 157–162 ppm.

The diols **7** (Scheme 1) may, in principle, be formed as mixtures of three enantiomers, having the configurations *RR*, *SS*, or *RS* at C4 and C6. As the first two enantiomers are diastereomerically related to the third, *two* peaks may, in principle, be observed for the atoms C(4,6) (which are otherwise identical due to rapid proton exchange between the two nitrogens at the medium pH of 10–12). In practice, only one peak was observed (Table 3; C4,6).

No intermediate was observed in the reaction of benzamidine **5***d* with acetylacetone **4**; this reaction goes smoothly to product **9***d* (Table 2). Lowering of the reaction temperature merely slowed the rate of product formation and led, ultimately, to precipitation of the amidine.

In none of the above reactions was the intermediate enamide **10** (Scheme 1) observed. In particular, none of the three characteristic peaks (the key enamine carbon C4 (expected in the range 135–165 ppm) (15*a*), the methine carbon C5 (92–110 ppm) (15*a*), and the conjugated carbonyl C6 (190–200 ppm) (12*a*)) were observed in reactions of the amidines **5** (*a*–*d*) with acetylacetone **4**.

In stark contrast, in reactions of urea **11***a* and thiourea **11***b* with acetylacetone **4** in acidic media (pH 1–2) the enamide **17** (Scheme 2) is the *only* intermediate seen; it is formed immediately upon mixing and slowly decays to give product **15** (Table 2). All three key enamide **17** carbons, C4 (δ 148.7), C5 (δ 102.7), and C6 (δ 198.2) of **17***a* and C4 (149.0), C5 (101.5), and C6 (197.1) of **17***b*, resonate in the expected regions (see above). Only the (*Z*) isomer is seen in both reactions, although in principle, both the (*E*) and the (*Z*) isomers could be formed. The C2 carbons resonate at 157.0 and 183.9 ppm for **17***a* and **17***b*, respectively, differing little from the resonances of the starting materials (cf. Experimental); the chemical shifts of the methyls C4-Me (21.3) and C6-Me (29.8) of **17***a* and C4-Me (22.8) and C6-Me (29.4) of **17***b* parallel those of the atoms C4 and C6 to which they are attached: the mechanistic interpretations of these observations are discussed later.

Table 4 gives the chemical shifts and assignments of the pyrimidin-ones **21** and -diones **25** formed in the reactions of methyl acetoacetate **18** with the amidines **5** (*a*–*d*) (Scheme 3) and with the ureas **11***a* and **11***b* (Scheme 4). Their values are not recorded in the pyrimidine nmr literature (1*d*, 12*e*), although those of the parent compounds are known (12*f*, 14). Again, replacement of hydrogen by methyl or phenyl at C2 has a

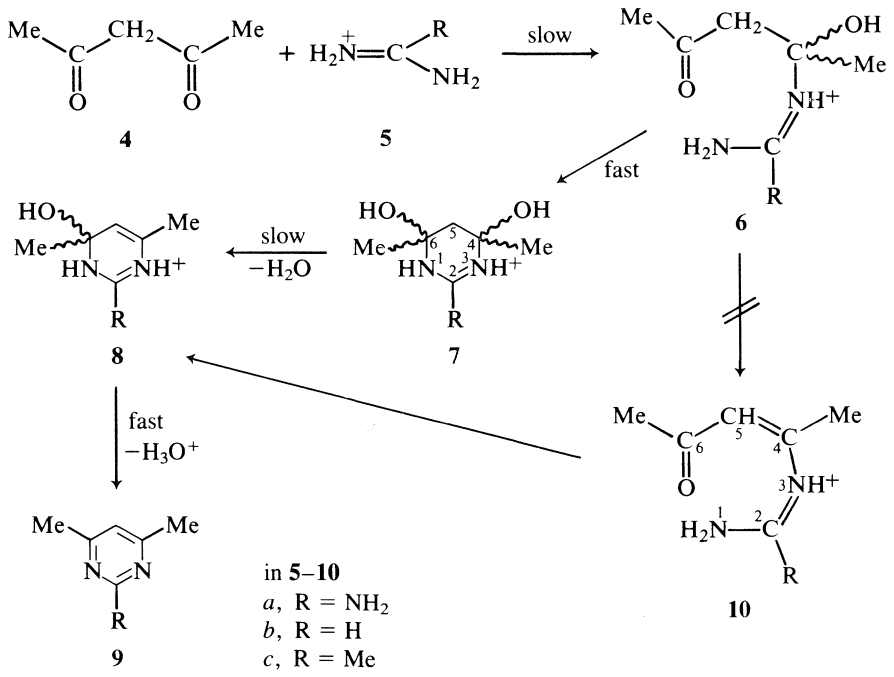

SCHEME 1. Mechanism of reaction of acetylacetone **4** with the amidines **5**.

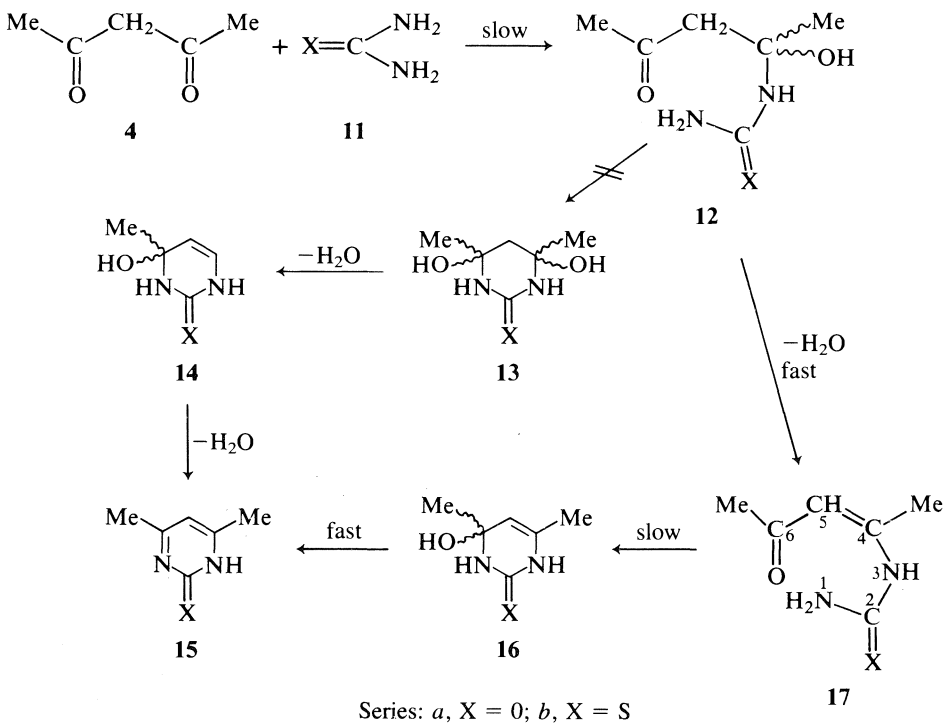

SCHEME 2. Mechanism of reaction of acetylacetone with urea **11***a* and thiourea **11***b*.

deshielding effect: thus, for R = Me or Ph, C2 resonates ca. 14 ppm downfield of R = H (Table 4). Substitution at C2 has a small effect on the chemical shifts of carbons 4 and 6, which resonate in the regions 161–171 ppm and 153–162 ppm, respectively (Table 4), and a somewhat larger effect on the chemical shift of the methine carbon C5, which resonates at ca. 99–113 ppm (Table 4).

Table 5 gives the chemical shifts and assignments of the intermediates **19** and **20**, seen in the reactions of the amidines **5** (*a*–*d*) with methyl acetoacetate **18** (Scheme 3); for guanidine **5***a* and formamidine **5***b*, the peaks were assigned to the intermediate ester **19**, and for acetamidine **5***c* and benzamidine **5***d*, they were assigned to the hydroxydihydropyrimidinone **20**. In all cases, the characteristic HN—C—OH sp^3 carbons (C-4) (Scheme 3) resonate in the region 80–84 ppm (Table 5), ca. 2–4 ppm downfield of the analogous carbons in the intermediate diol **7** (Scheme 1, Table 3). Both the ester and lactam carbonyls of the intermediates **19** and **20**, respectively (Scheme 3), resonate in the region 172–176 ppm (Table 5), within the literature values (12*b*, *c*). No difference is observed between the

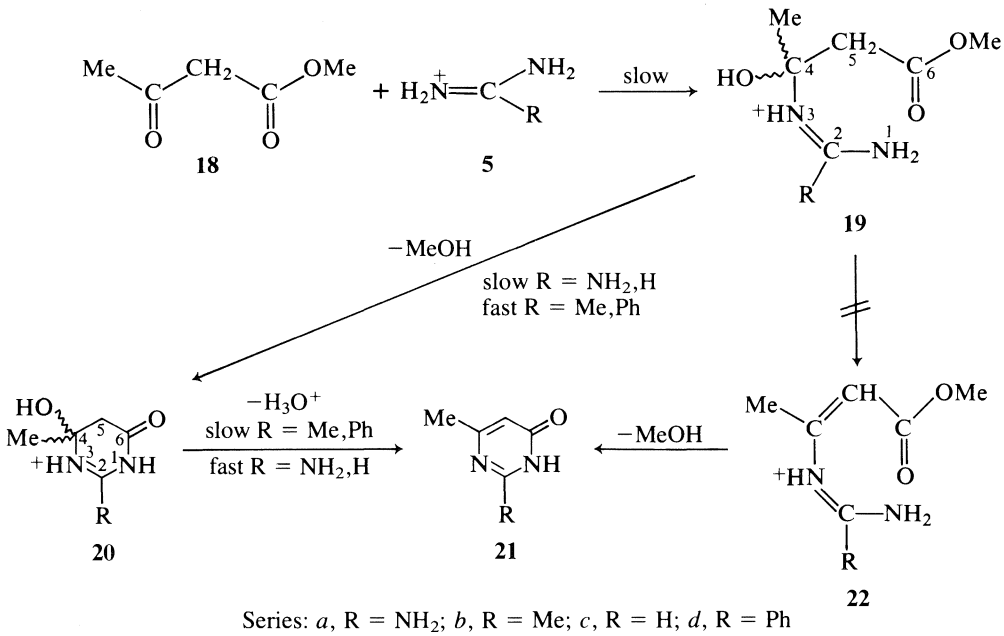

18 5 19 20 21 22

Series: *a*, R = NH_2; *b*, R = Me; *c*, R = H; *d*, R = Ph

SCHEME 3. Mechanism of reaction of methyl acetoacetate **18** with the amidines **5**.

TABLE 4. C-13 nmr chemical shifts and assignments[a] of 2-substituted-6-methylpyrimidin-4-ones **21** (Scheme 3) and 6-methylpyrimidin-2,4-diones **25** (Scheme 4)

R	Compound	C2	C4	C5	C6 (6-Me)
NH_2	**21***a*	153.0[c]	160.9	103.0	153.1[c] (18.7)
H	**21***b*	149.7	164.0[d]	112.6	162.3[d] (23.1)
Me[b]	**21***c*	163.8[d]	171.2	108.2	163.1[d] (22.0)[e]
Ph[g]	**21***d*	163.5[f]	164.2[f]	109.2	156.9 (23.1)
O	**25***a*	151.7	164.2	98.8	153.0 (18.1)
S	**25***b*	175.9	161.1	103.7	153.2 (18.2)

[a]Chemical shifts in ppm relative to internal DMSO-d_6 at 39.5 ppm.
[b]2-Me: 23.1.
[c]C2 and C6 assignments are interchangeable.
[d]C4 and C6 assignments are interchangeable.
[e]C-Me and R assignments are interchangeable.
[f]C2 and C4 assignments are interchangeable.
[g]Ph: *o*, 128.1; *m*, 127.4; *p*, 130.9; *i*, 132.8; *ortho* and *meta* assignments are interchangeable.

TABLE 5. C-13 nmr chemical shifts and assignments[a] of the intermediates **19** and **20** (Scheme 3)

R	Compound	C2	C4 (4-Me)	C5	C6 (OMe)
NH_2	**19***a*	163.4	81.6 (29.5)	45.2	171.9 (52.6)
H	**19***b*	[b]	80.2 (29.3)	48.0	[b] (51.6)
Me[c]	**20***b*[d]	165.8	82.1 (28.3)	43.2	175.6 (—)
Ph[e]	**20***d*	158.1	83.7 (27.8)	43.7	176.3 (—)

[a]Chemical shifts in ppm relative to internal methanol-d_4 at 49.0 ppm unless otherwise stated.
[b]Concentration of intermediate too low for sp^2 carbons to be observed.
[c]19.0.
[d]Chemical shifts in ppm relative to internal DMSO-d_6 at 39.5 ppm.
[e]Phenyl carbons of intermediate overlapping with those of starting material and product.

chemical shifts of the methylene carbons C5 in the intermediates **19** and **20** (Table 5) and those in the diol **7** (C5, Table 3), all resonating at ca. 43–45 ppm (with the exception of C5 in **19***b*, which resonates at 48.0 ppm). The amidine-like carbons C2 in the intermediates **19** and **20** resonate in the region 158–166 ppm (Table 5), downfield of the corresponding carbons in the diol **7**, which resonate in the region 151–162 ppm (C2; Table 3).

The only intermediate observed in the reaction of methyl acetoacetate **18** with urea **11***a* is the enamide **26***a* (Scheme 4). Both the (*E*) and (*Z*) isomers are seen, with the latter predominating (*Z*:*E* ca. 10:1 as determined from ^{13}C peak heights). This is in contrast to the reaction of acetylacetone **4** with the ureas **11***a* and **11***b* (Scheme 2), where only the (*Z*) isomer was observed. The key enamide **26***a* carbons C4 and C5 (Scheme 4) resonate at δ 154.2 and 91.5, respectively, for the (*Z*) isomer, and at δ 152.4 and 94.5, respectively, for the (*E*) isomer, and are within the literature range (15*a*). Little change occurs in the chemical shifts of the methoxy carbonyl group in going from starting material **18***a* (C3 and OMe; Table 1) to the intermediate **26***a* (C6 (δ 168.6) and C7 (δ 50.4) for both (*E*) and (*Z*) isomers). A small upfield shift (ca. 5 ppm) is observed in the carbonyl carbon of urea in going from starting material **11***a* (δ 160.7) to the intermediate **26***a* ((*Z*), (δ 156.9); (*E*), (δ 152.4)). A much larger shift (ca. 10 ppm) is observed in the C4 methyl carbon, which resonates at 30.3 ppm in the starting material (Table 1; **18***a*; Me) and at 21.6 ppm ((*Z*) isomer) and 18.1 ppm ((*E*) isomer) in the intermediate **24***a*; this is due to conversion of the ketone carbonyl (C1) of starting material to the enamide carbon C4 of intermediate (Scheme 4).

Table 6 gives the chemical shifts and assignments of the pyrimidinones **29** and **31** formed from the reactions of dimethyl malonate **27** with the amidines **5***a* and **5***d* (Scheme 5) and the ureas **11***a* and **11***b* (Scheme 6).

The chemical shifts of the barbituric acids **31***a* and **31***b* (Scheme 6; Table 6) are in broad agreement with the literature values (12*e*), but those of the pyrimidinones **29***a* and **29***d* (Scheme 5; Table 6) have not been previously reported (10–14, 16, 17). No intermediates were observed in these four reactions, the starting materials going smoothly to product. The mechanistic interpretations of this result are discussed below.

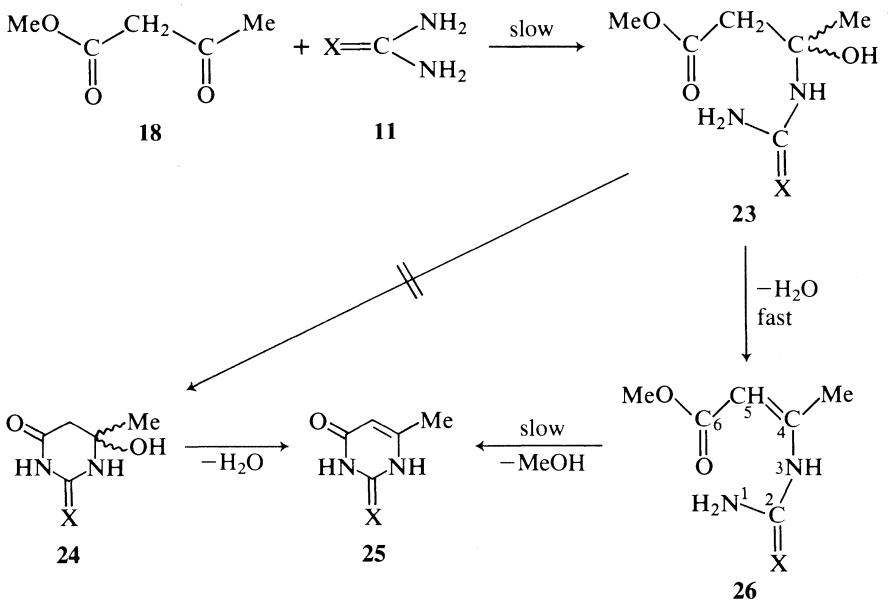

Series: *a*, X = O; *b*, X = S

SCHEME 4. Mechanism of reaction of methyl acetoacetate **18** with urea **11***a* and thiourea **11***b*.

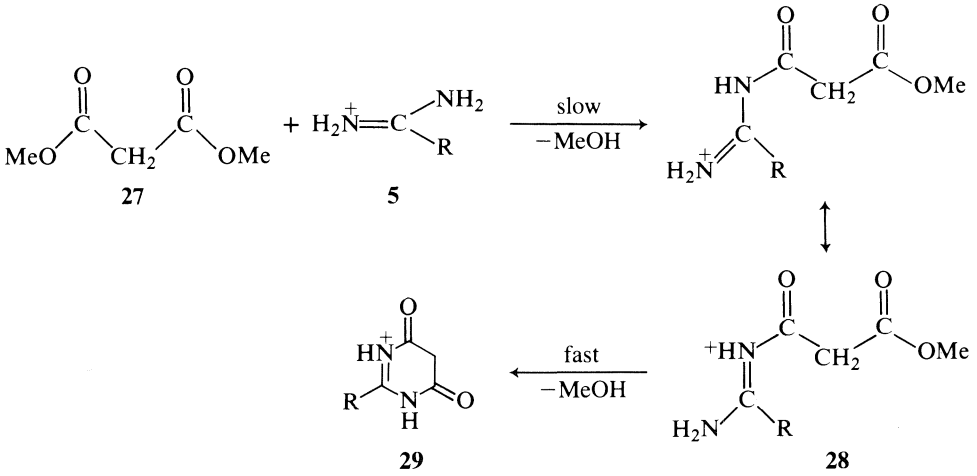

Series: *a*, R = NH_2; *b*, R = Ph

SCHEME 5. Mechanism of reaction of dimethyl malonate **27** with the amidines **5**.

Discussion of mechanistic pathways

The observation of the diol **7** (Scheme 1) as the only intermediate in the reaction of acetylacetone **4** with amidines **5** implies: (*i*) that there are two slow steps in the reaction, one preceding diol **7** formation, and the other succeeding it; (*ii*) that elimination from the intermediate **6** to form the enamide **10** is much slower than ring closure of **6** to the diol **7**. This implies that the initial nucleophilic attack, **4** + **5** → **6**, is the first slow step of the reaction, confirming Todd's earlier speculations (5*b*). Further support for this comes from the fact that the rate of diol **7** formation increases with the pK_a of the amidine (18): thus, guanidine is the most reactive nucleophile, and benzamidine the least reactive. The second slow step of the reaction *must* be the elimination, **7** → **8**, for otherwise the intermediate **7** could not accumulate. The elimination, **8** → **9**, is therefore fast, consistent with the fact that it leads to aromatization (1*e*).

The above mechanism, i.e. **4** —(slow)→ **6** —(fast)→ **7** —(slow)→ **9** is directly analogous to the mechanism of pyrazole formation from 1,3-diketones and hydrazine (19*a*,*b*,*c*), in which the diol **32** and not the hydrazone **33** was observed. It is also analogous to the mechanism of reaction of acetylacetone **4** with hydroxylamine (20) in which the diol **34** (and not the oxime **35**) was the only intermediate observed. However, it is in contrast with the mechanism of pyrrole formation from acetonylacetone and amines (9), where the imine **37** and *not* the diol **36** was the only intermediate observed, and also contrasts with the reaction of hydroxylamine with ethyl acetoacetate (21) in which the oxime **39** and not the isoxazolone **38** was observed. All the above reactions were carried out in basic media and thus these mechanistic differences cannot be ascribed to differences in reaction pH. In reactions of β-dicarbonyl compounds that proceed *via* diols (19, 20), ring closure of the initially formed carbinolamines is faster than elimination; the reverse is true in reactions of β-ketoesters (32), and this difference may be attributed to the greater electrophilicity of a ketone carbonyl vis-à-vis an ester carbonyl: thus Cocivera *et al.* have shown that

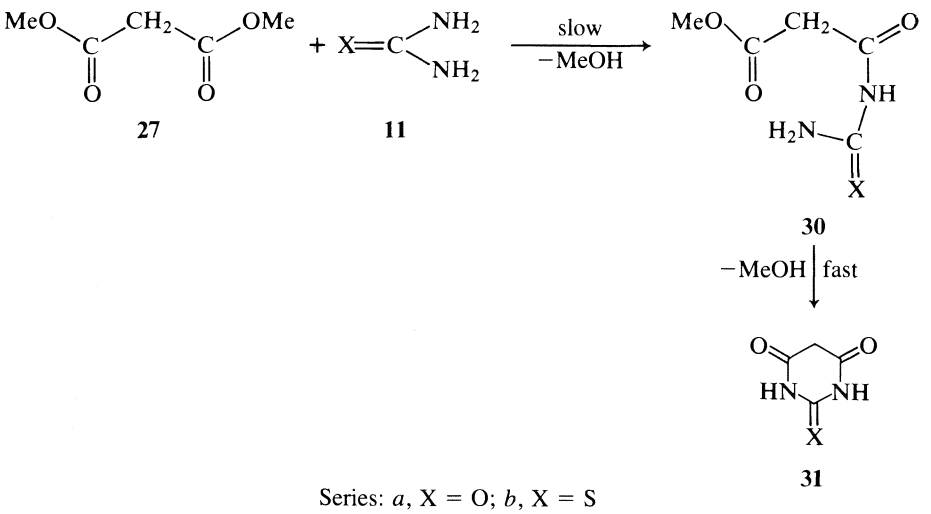

Series: *a*, X = O; *b*, X = S

SCHEME 6. Mechanism of reaction of dimethyl malonate with urea **11***a* and thiourea **11***b*.

TABLE 6. ^{13}C nmr shifts and assignments[a] of 2-substituted-pyrimidin-4,6-diones **29** and **31** (Schemes 5 and 6)

R	Compound	C2	C (4,6)	C5	Reference
NH_2	**29***a*	168.6	175.7	50.3	—
Ph[b]	**29***d*	167.4	157.6	88.3	—
O	**31***a*	151.7	167.8	39.5	13*e*
S	**31***b*	174.3	162.5	82.3	13*e*

[a]Chemical shifts in ppm relative to DMSO-d_6 at 39.5 ppm.
[b]Ph: *o*, 127.8; *m*, 128.9; *p*, 131.7; *i*, 132.3; *ortho* and *meta* assignments are interchangeable.

intramolecular nucleophilic attack at a ketone carbonyl is ca. 10^6 times faster than at an ester carbonyl (21).

The observation of the enamide **17** (Scheme 2) as the *only* intermediate in the reactions of the ureas **11** with acetylacetone **4** under acidic conditions (pH ca. 1–2; no reaction occured at alkaline pH) implies that the elimination **12** → **17** (Scheme 2) is fast compared to the ring closure **12** → **13**, and that the second slow and rate-determining step is ring closure of the enamide **17**, to the hydroxypyrimidinone **16**. The overall mechanistic pathway therefore is **4** —(slow)→ **12** —(fast)→ **17** —(slow)→ **15**, paralleling the mechanism of the Paal–Knorr reaction (9), and the reaction of β-ketoesters with hydroxylamine (21, 32).

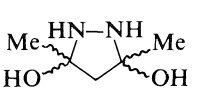

32

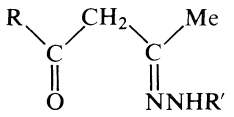

33

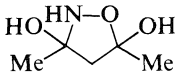

34

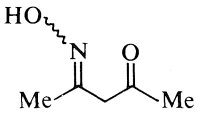

35

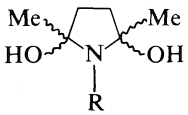

36

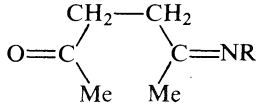

37

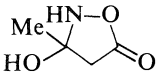

38

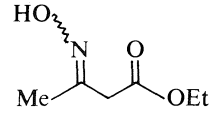

39

In the reactions of methyl acetoacetate **18** with four different amidines **5** (Scheme 3), in each case just one intermediate is seen. However, the nature of this intermediate depends on the structure of the amidine: it is the open chain ester **19** with formamidine **5***b* and guanidine **5***a* and the hydroxypyrimidinone **20** with acetamidine **5***c* and benzamidine **5***d*. In all cases, the initial nucleophilic attack is the first slow step of the reaction as the intermediates are seen in the presence of starting material (paralleling reactions with acetylacetone **4**), but, in the former, the *second* slow step must be the ring closure **19** → **20**, followed by the fast elimination to give product **21**, whereas in the latter it must be the elimination **20** → **21** (with the ring closure **19** → **20** being fast). There appears to be a clear changeover in rate-determining step with the nature of the R group, a result that might be due to the conformational effect of R. The overall mechanistic pathways therefore are **18** —(slow)→ **19** —(fast)→ **20** —(slow)→ **21** for R = Me, Ph; and **18** —(slow)→ **19** —(slower)→ **20** —(fast)→ **21** for R = NH_2, H.

In the reaction of methyl acetoacetate **18** with urea **11***a*, however, only the enamide **26** (Scheme 4) was observed as intermediate, paralleling reactions of acetylacetone **4** with the ureas **11** (Scheme 2), and in accord with earlier isolation of the corresponding enamide from the reaction of ethyl acetoacetate with urea (22). The observation of **26** (Scheme 4) as the only intermediate on the pathway to **25** implies that elimination from the open-chain ester **23** is much faster than ring closure of **23** to **24**; it also implies that the second slow step of the reaction must be the ring closure **26** → **25**, the first slow step being the initial nucleophilic addition, as the intermediate **26** is seen in the presence of starting materials. The overall mechanistic pathway therefore is **18** —(slow)→ **23** —(fast)→ **26** —(slow)→ **25** (Scheme 4) and is analogous to the mechanism in Scheme 2.

No intermediates were observed in reactions of dimethyl malonate **27** with either guanidine **5***a* and benzamidine **5***d* (Scheme 5) or urea **11***a* and thiourea **11***b* (Scheme 6) and this implies that ring closure of the open-chain esters **28** (Scheme 5) and **30** (Scheme 6) is faster than initial nucleophilic attack. This is to be expected when both functional groups have the same reactivity, as was observed previously in reactions with acetyl-

acetone (Scheme 1) where the *intra*molecular nucleophilic attack **6** → **7** was faster than the *inter*molecular nucleophilic attack **4** → **6**.

Experimental

All melting points were determined on a Kofler hot-stage and are uncorrected. Combustion analyses were carried out on a Carlo Erba elemental analyser 1106. All reagents were obtained from Aldrich and characterized by their ^{13}C nmr spectra: guanidine **5***a* (δ 159.8); formamidine **5***b* (δ 158.6); acetamidine **5***c* (δ 169.0) (13*c*); benzamidine **5***d* (δ 163.9) (13*d*); urea, **11***a* (δ 160.7) (12*d*); thiourea, **11***b* (δ 183.7) (12*d*).

General method

Reactions were started by the addition of a concentrated DMSO-d_6 solution of the appropriate amidine or urea (0.01 mol) from a hypodermic syringe to a 5-mm nmr tube containing the β-dicarbonyl compound (0.01 mol); the total volume of the resultant solution was ca. 0.3 mL, giving an initial concentration of reactants of ca. 25–30 mol L^{-1}.

Spectra

C-13 spectra were recorded in the temperature range 22–28°C (unless otherwise stated) on a JEOL FX-100 spectrometer at 25.1 MHz; DMSO-d_6 and methanol-d_4 were both used as internal lock and internal reference. The spectral window was 6 kHz with 8K data points giving a digital resolution greater than 1.5 Hz per point. A pulse width of 19 μs (90°) was used with a 0.5–2.0 s pulse delay (depending upon reaction rates) and an acquisition time of 0.68 s; longer pulse delays (4–6 s) were occasionally used to assign the quaternary carbons of reaction intermediates. Accumulations varied from 500 to 2000 giving a typical signal : noise ratio > 10^2:1.

Syntheses

The following compounds were prepared by literature methods: 2,4,6-trimethylpyrimidine **9***c* (23); 2-phenyl-4,6-dimethylpyrimidine **9***d* (24), mp 83.5–84°C (lit. (24) mp 81–83°C. *Anal.* calcd.: C 78.2, H 6.6, N 15.2; found: C 78.4, H 6.7, N 15.0); 2-amino-4,6-dimethylpyrimidine **9***a* (24), mp 152–153.5°C (lit. (24) mp 152–154°C. *Anal.* calcd.: C 58.5, H 7.4, N 34.1; found: C 58.7, H 7.5, N 33.9); 4,6-dimethylpyrimidin-2-one **15***a* (25), mp 198–199°C (lit. (25) mp 197°C. *Anal.* calcd.: C 58.1, H 6.5, N 22.6; found: C 57.9, N 6.5, H 22.4); 4,6-dimethylpyrimidin-2-thione **15***b* (26), mp 211–211.5°C (lit. (26) mp 210°C. *Anal.* calcd.: C 51.4, H 5.8, N 20.0; found: C 51.6, H 5.9, N 19.8); 6-methylpyrimidin-4-one **21***b* (27), mp 147–148.5°C (lit. (27) mp 148–149°C. *Anal.* calcd.: C 54.4, H 5.5, N 25.5; found: C 54.7, H 5.5, N 25.3); 2-amino-6-methylpyrimidin-4-one **21***a* (28), mp 268–269°C (lit. (28) mp 270°C (dec.). *Anal.* calcd.: C 48.0, H 5.6, N 33.6; found: C 48.3, H 5.6, N 33.4); 2,6-dimethylpyrimidin-4-one **21***c* (29), mp 194.5–195°C (lit. (29) mp 195.5–196.5°C. *Anal.* calcd.: C 58.1, H 6.5, N 22.6; found: C 58.0, H 6.5, N 22.5); 6-methylpyrimidin-2,4-dione **25***a* (22), mp >300°C (lit. (22) mp >300°C. *Anal.* calcd.: C 47.6, H 4.8, N 22.2; found: C 47.3, H 4.6, N 22.1); 2-phenylpyrimidin-4,6-dione **29***d* (30), mp >300°C (lit. (30) mp 325–330°C. *Anal.* calcd.: C 63.8, H 4.3, N 14.9; found: C 63.8, H 4.3, N 14.7).

1. D. J. Brown. *In* Comprehensive heterocyclic chemistry. Vol. 3. *Edited by* A. R. Katritzky and C. W. Rees. Pergamon Press, Oxford. 1984. (*a*) pp. 142–149; (*b*) pp. 150–155; (*c*) pp. 106–118; (*d*) p. 63; (*e*) p. 59.
2. (*a*) W. Traube. Ber. Dtsch. Chem. Ges. **26**, 2551 (1893); (*b*) W. Traube and R. Schwarz. Ber. Dtsch. Chem. Ges. **32**, 3163 (1899).
3. (*a*) W. Traube. Ann. Chem. **331**, 64 (1904); (*b*) W. Traube. Ann. Chem. **432**, 266 (1923).
4. (*a*) T. B. Johnson. J. Ind. Eng. Chem. **10**, 306 (1918); (*b*) V. Meyer and P. Jacobson. Lehrbuch der Organischen Chemie. Vol. 2. part 3. Walter de Gruyter and Co., Berlin. 1920. p. 1172; (*c*) B. Lythgoe. Q. Rev. (London), **3**, 181 (1949).
5. (*a*) G. N. Kenner. *In* Thorpe's Dictionary of Applied Chemistry. 4th ed. Vol. 10. Longmans Green and Co., London. 1950. p. 137; (*b*) G. W. Kenner and A. Todd. *In* Heterocyclic compounds. Vol. 6. *Edited by* R. C. Elderfield. John Wiley and Sons, New York. 1957. p. 234; (*c*) G. R. Ramage and J. K. Landquist. *In* Chemistry of carbon compounds. Vol. IVB. *Edited by* E. H. Rodd. Elsevier, Amsterdam. 1959. p. 1257.
6. D. J. Brown. *In* The chemistry of heterocyclic compounds. *Edited by* A. Weissberger. Wiley–Interscience, Amsterdam. (*a*) Vol. 16. The pyrimidines. 1962; (*b*) Vol. 16 (1st supplement). 1970.
7. H. Morimoto, N. Hayashi, T. Naka, and S. Kato. Chem. Ber. **106**, 893 (1973).
8. J. Paasivirta and T. Asunta. Finn. Chem. Lett. **3**, 90 (1979); Chem. Abstr. **92**, 40882 (1979).
9. A. R. Katritzky, T. I. Yousaf, B. C. Chen, and Z. Guang-Zhi. Tetrahedron, **42**, 623 (1986).
10. L. F. Johnson and W. C. Jankowski. Carbon-13 NMR spectra. Wiley–Interscience, New York. 1972.
11. R. M. Silverstein, G. C. Bassler, and T. C. Morrill. Spectrometric identification of organic compounds. 4th ed. John Wiley and Sons, New York. 1981. (*a*) p. 268; (*b*) p. 270; (*c*) p. 258.
12. G. C. Levy, R. L. Lichter, and G. L. Nelson. Carbon-13 nuclear magnetic resonance spectroscopy. 2nd ed. John Wiley and Sons, New York. 1980. (*a*) p. 141; (*b*) p. 148; (*c*) p. 151; (*d*) p. 165; (*e*) p. 152; (*f*) p. 155.
13. The Sadtler standard C-13 nmr spectra. (*a*) 4651; (*b*) 3104; (*c*) 911; (*d*) 5534; (*e*) 914; (*f*) 1611; (*g*) 677.
14. G. W. H. Cheeseman, C. J. Turner, and D. J. Brown. Org. Magn. Reson. **12**, 212 (1979).
15. M. Shamma and D. M. Hindenlang. Carbon-13 nmr shift assignments of amines and alkaloids. Plenum Press, New York. 1979. (*a*) pp. 47–54; (*b*) pp. 261–287.
16. J. Riand, M. T. Chenon, and N. Lumbroso-Bader. Tetrahedron Lett. 3123 (1974).
17. C. J. Turner and G. W. H. Cheeseman. Org. Magn. Reson. **8**, 357 (1976).
18. D. D. Perrin. Dissociation constants of organic bases in aqueous solution. Butterworths, London. 1965.
19. (*a*) S. I. Selivanov, R. A. Bogatkin, and B. A. Ershov. Zh. Org. Khim. **17**, 886 (1981); (*b*) Zh. Org. Khim. **18**, 909 (1982); (*c*) S. I. Selivanov, K. G. Golodora, Ya. A. Abbasov, and B. A. Ershov. Zh. Org. Khim. **20**, 1494 (1984).
20. M. Cocivera and K. W. Woo. J. Am. Chem. Soc. **98**, 7366 (1976).
21. M. Cocivera, A. Effio, H. E. Chen, and S. Vaish. J. Am. Chem. Soc. **98**, 7362 (1976).
22. J. J. Donleavy and M. A. Kise. Org. Synth. Coll. Volume II, 1943. p. 422.
23. J. C. Roberts. J. Chem. Soc. 3065 (1952).
24. C. A. C. Haley and P. Maitland. J. Chem. Soc. 3155 (1951).
25. W. J. Hale. J. Am. Chem.Soc. **36**, 104 (1914).
26. W. J. Hale and A. G. Williams. J. Am. Chem. Soc. **37**, 594 (1915).
27. H. M. Foster and H. R. Snyder. Org. Synth. Coll. Volume IV, 1963. p. 638.
28. K. Sugino, K. Odo, and T. Sugido. Jap. Pat. No. 180,090 (1949); Chem. Abstr. **46**, 4029g (1952).
29. H. R. Snyder and H. M. Foster. J. Am. Chem. Soc. **76**, 118 (1954).
30. E. L. Pinner. Ber. Dtsch. Chem. Ges. **41**, 3517 (1908).
31. A. R. Katritzky, D. Ostercamp, and T. I. Yousaf. Tetrahedron. In press.
32. A. R. Katritzky, P. Barczynski, D. Ostercamp, and T. I. Yousaf. J. Org. Chem. In press.

COMMUNICATION

Ring inversion in solid fluorocyclohexane

RODERICK E. WASYLISHEN
Department of Chemistry, Dalhousie Univrsity, Halifax, N.S., Canada B3H 4J3

Received March 17, 1986

RODERICK E. WASYLISHEN. Can. J. Chem. **64**, 2094 (1986).

Inversion of the cyclohexane ring system in the solid state has been directly observed in a ^{19}F nmr study of solid fluorocyclohexane. The barrier to ring inversion in the orientationally disordered solid phase, $\Delta G^{\ddagger}_{e\rightarrow a} = 44.1 \pm 0.9$ kJ mol^{-1} at 263 K is found to be only slightly larger than the value previously reported for a $CFCl_3$ solution of fluorocyclohexane. The population of the equatorial conformation is slightly favored over the axial conformation with $K = P_e/P_a = 1.56$ at 281 K; similar values have been obtained in $CFCl_3$ and in the gas phase.

RODERICK E. WASYLISHEN. Can. J. Chem. **64**, 2094 (1986).

Une étude par rmn du ^{19}F du fluorocyclohexane à l'état solide a permis d'observer directement l'inversion du noyau cyclohexane à l'état solide. On a trouvé que, à 263 K, la barrière à l'inversion de cycle, dans le phase solide désordonnée du point de vue de l'orientation, $\Delta G^{\ddagger}_{e\rightarrow a} = 44{,}1 \pm 0{,}9$ kJ mol^{-1}, n'est que légèrement supérieure à la valeur rapportée antérieurement pour une solution de fluorocyclohexane dans le $CFCl_3$. La population de la conformation équatoriale est légèrement favorisée par rapport à la conformation axiale et $K = P_e/P_a = 1{,}56$, à 281 K; des valeurs semblables ont été obtenues pour des solutions dans le $CFCl_3$ ainsi qu'en phase gazeuse.

[Traduit par la revue]

In the gas phase (1, 2) and in solution (3–8) the cyclohexane ring of monosubstituted cyclohexanes is known to undergo rapid ring inversion (**I**). The transition state for this process is

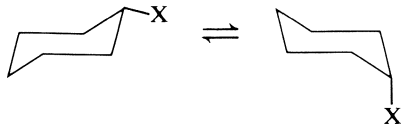

I

thought to involve a half-chair structure with boat and twist-boat forms existing as intermediates along the reaction path (Fig. 1) (3, 8–12). Typical barriers for ring inversion are 40–45 kJ mol^{-1} while the energy differences between the equatorial and axial conformers are generally 0–4 kJ mol^{-1} (3, 7, 8, 13). Although some infrared and Raman evidence exists for ring inversion in solid cyclohexane (11), fluorocyclohexane, and chlorocyclohexane (14, 15), the rates of inversion have not been determined. Here we present preliminary results of a ^{19}F nmr study of *solid* fluorocyclohexane, which clearly demonstrate that the inversion process takes place in the solid state at rates comparable to those reported in $CFCl_3$ solutions (3).

Representative variable temperature ^{19}F nmr spectra of solid fluorocyclohexane are shown in Fig. 2. The spectra were obtained on a commercial sample (Cationics, Inc.) at 339.6736 MHz with ^1H decoupling ($\gamma B_2 \simeq 2$ kHz) using a Nicolet 360 nmr spectrometer. The sample (mp $\simeq$ 285 K) was degassed and sealed under vacuum at 77 K in a 5-mm nmr tube. The relatively narrow ^{19}F nmr lines observed for solid fluorocyclohexane imply that it exists as an orientationally disordered solid between the mp and 183 ± 3 K. Below 183 ± 3 K we were unable to detect a ^{19}F resonance because of dipolar broadening. A similar orientationally disordered solid phase is known to exist for cyclohexane between the mp (279.8 K) and 186.0 (16).

The spectra in Fig. 2 represent a typical example of decoupled two-site exchange between unequally populated sites. In the region of fast exchange ($T > 280$ K) the observed chemical

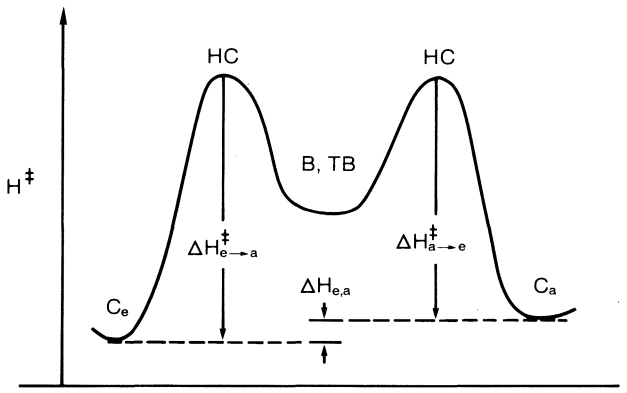

FIG. 1. Energy diagram for ring inversion in a monosubstituted cyclohexane showing the relative energies of the chair (C), half-chair (HC), and twist-boat (TB) conformations.

shift, δ_{obs}, is given by eq. [1],

$$[1] \quad \delta_{obs} = p_e\delta_e + p_a\delta_a$$

where p_e and p_a are the relative populations of the equatorial and axial conformers ($p_e + p_a = 1$) and δ_e and δ_a are the ^{19}F chemical shifts of the two respective conformers. From our data we calculate $p_e = 0.61$ and $p_a = 0.39$ at 281 K, hence $\Delta G^0_{e,a} = 1.045 \pm 0.10$ kJ mol^{-1} (250 ± 25 cal mol^{-1}). This value is within experimental error of the value measured in $CFCl_3$ solution, 242 cal mol^{-1} at 218 K (3), and the value measured in the gas phase, 400 ± 300 cal mol^{-1} (1).

The average lifetime, τ, that the fluorine spends in the equatorial and axial sites can be obtained by visually comparing observed spectra with those calculated for different τ values using standard line-shape computer programs (8, 17). Using this procedure we obtain $\tau = 40 \pm 5$ μs at 263 K, the approximate coalescence temperature. The free energy changes for $\Delta G^{\ddagger}_{e\rightarrow a}$ and $\Delta G^{\ddagger}_{a\rightarrow e}$ were calculated using eq. [2],

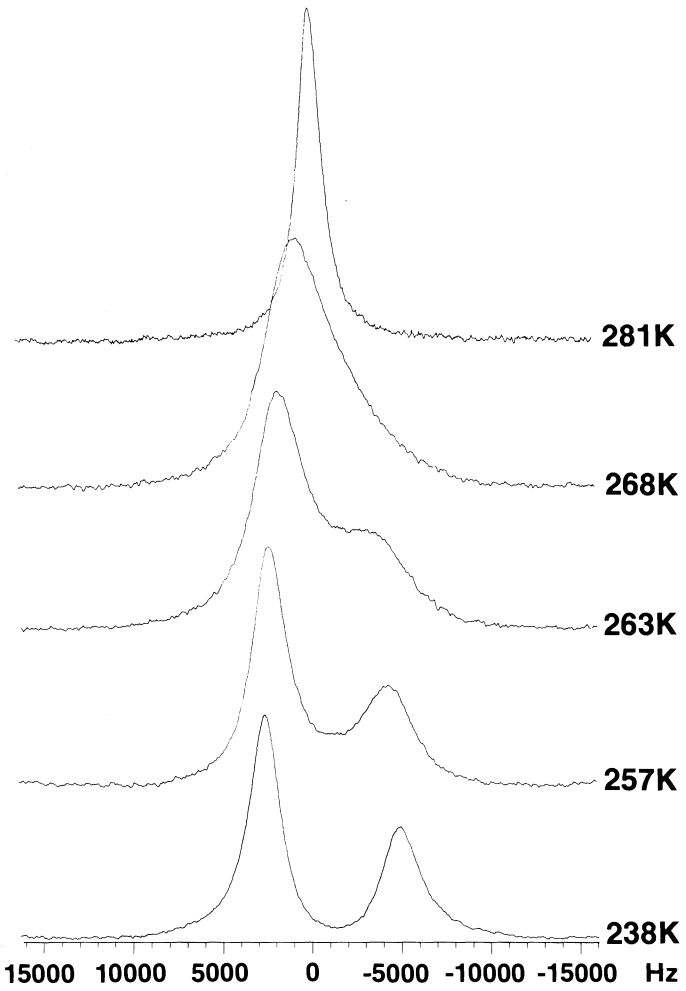

FIG. 2. Fluorine-19 nmr spectra of solid fluorocyclohexane at 339.67 MHz.

$$[2] \quad \Delta G^{\ddagger} = -RT \ln \frac{k_B T}{hk}$$

where k is either $k_{e\to a}$ or $k_{a\to e}$ ($\tau = p_a/k_{e\to a} = p_e/k_{a\to e}$) and all other symbols are standard (8, 15). We obtain $\Delta G^{\ddagger}_{e\to a} = 44.1 \pm 0.9$ kJ mol^{-1} (10.5 ± 0.2 kcal mol^{-1}) and $\Delta G^{\ddagger}_{a\to e} = 43.1 \pm 0.9$ kJ mol^{-1} (10.3 ± 0.2 kcal mol^{-1}). Similar results were obtained using the approximate procedure of Shanan-Atidi and Bar-Eli (18). It is interesting to compare these results with the accurate values obtained in a solution study by Bovey *et al.* (3). In a $CFCl_3$ solution at 218 K they obtained $\Delta G^{\ddagger}_{e\to a} = 10.14 \pm 0.05$ kcal mol^{-1} and $\Delta G^{\ddagger}_{a\to e} = 9.90 \pm 0.05$ kcal mol^{-1}; at 264 K, $\tau = 21.3$ μs. These results indicate that in the case of fluorocyclohexane the barrier to inversion in the high-temperature solid phase is only slightly more hindered than in solution. In fact, the barrier to ring inversion observed here is within experimental error of the value recently measured in the gas phase (19).

Previously Ellett *et al.* (20) found evidence for ring inversion in the plastic crystalline phase of perfluorocyclohexane; however, the barrier to ring inversion was not measured. Further dynamic studies on fluorocyclohexane and related compounds in the solid state are in progress.

Acknowledgement

I wish to thank Mr. J. B. Macdonald for helping obtain some of the preliminary nmr spectra, Mr. Ross Dickson and Dr. T. B. Grindley for assistance with the line-shape calculations, and NSERC for financial support.

1. L. PIERCE and J. F. BEECHER. J. Am. Chem. Soc. **88**, 5406 (1966).
2. W. CAMINATI, D. DAMIANI, and F. SCAPPINI. J. Mol. Spectrosc. **104**, 183 (1984).
3. F. A. BOVEY, E. W. ANDERSON, F. P. HOOD, and R. L. KORNEGAY. J. Chem. Phys. **40**, 3099 (1964).
4. F. R. JENSEN and C. H. BUSHWELLER. J. Am. Chem. Soc. **91**, 3223 (1969).
5. J. REISSE, M.-L. STIEN, J.-M. GILLES, and J. F. M. OHT. Tetrahedron Lett. 1917 (1969).
6. O. A. SUBBOTIN and N. M. SERGEYEV. J. Am. Chem. Soc. **97**, 1080 (1975).
7. D. HÖFNER, S. A. LESKO, and G. BINSCH. Org. Magn. Reson. **11**, 179 (1978).
8. J. SANDSTRÖM. Dynamic NMR spectroscopy. Academic Press Inc., London. 1982.
9. H. M. PICKETT and H. L. STRAUSS. J. Am. Chem. Soc. **92**, 7281 (1970).
10. K. B. WIBERG and R. H. BOYD. J. Am. Chem. Soc. **94**, 8426 (1972).
11. M. SQUILLACOTE, R. S. SHERIDAN, O. L. CHAPMAN, and F. A. L. ANET. J. Am. Chem. Soc. **97**, 3244 (1975).
12. U. BURKERT and N. L. ALLINGER. Molecular mechanics. ACS Monograph 177, American Chemical Society, Washington, DC. 1982. Chapt. 4.
13. J. A. HIRSCH. Concepts in theoretical organic chemistry. Allyn and Bacon Inc., Boston. 1974. Chapt. 12.
14. (*a*) P. KLAEBOE, J. J. LOTHE, and K. LUNDE. Acta Chem. Scand. **10**, 1465 (1956); (*b*) S. D. CHRISTIAN, J. GRUNDNES, P. KLAEBOE, E. TØRNENG, and T. WOLDBAEK. Acta Chem. Scand. Ser. A, **34**, 391 (1980).
15. M. REY-LAFON, C. ROUFFI, M. CAMIADE, and M. T. FOREL. J. Chim. Phys. Phys. Chim. Biol. **67**, 2030 (1967).
16. N. G. PARSONAGE and L. A. K. STAVELEY. Disorder in crystals. Clarendon Press, Oxford. 1978.
17. G. BINSCH. Top. Stereochem. **3**, 97 (1968).
18. H. SHANAN-ATIDI and K. H. BAR-ELI. J. Phys. Chem. **74**, 961 (1970).
19. P.-S. CHU and N. S. TRUE. J. Phys. Chem. **89**, 5613 (1985).
20. J. D. ELLETT, U. HAEBERLEN, and J. S. WAUGH. J. Am. Chem. Soc. **92**, 411 (1970).

Synthesis of amino acid diazoketones[1]

GEORGE R. PETTIT[2] AND PAUL S. NELSON

Cancer Research Institute and Department of Chemistry, Arizona State University, Tempe, AZ 85287, U.S.A.

Received October 2, 1985[3]

GEORGE R. PETTIT and PAUL S. NELSON. Can. J. Chem. **64**, 2097 (1986).

A study of carboxylic acid → diazoketone conversion was pursued employing the γ-carboxyl group of otherwise protected L-glutamic acids. The Arndt–Eistert route employing carboxylic acid chloride intermediates was found best (52% yield, **5***b*), performed at very low temperatures employing oxalyl chloride in dimethylformamide–tetrahydrofuran followed by diazomethane at −23°C. Alternatively, substitution of a mixed carbonic anhydride for the acyl chloride led to very similar yields (57% of **5***b*) of diazoketones (**5**). Among a series of active ester intermediates (**7**) examined, only the ODnp (**7***d*) and SPfp (**7***f*) esters were found to react (23–26% yield), at least partially, with diazomethane. The latter two reactions appear to represent the first such examples employing active esters.

GEORGE R. PETTIT et PAUL S. NELSON. Can. J. Chem. **64**, 2097 (1986).

On a effectué une étude sur la transformation acide carboxylique → diazocétone d'un groupement carboxyle γ d'acides L-glutamiques qui sont par ailleurs protégés. On a trouvé que la réaction de Arndt–Eistert, impliquant un chlorure d'acide comme intermédiaire, conduit aux meilleurs résultats (rendement de 52% en **5***b*) lorsque l'on opère à de très basses températures, avec du chlorure d'oxalyle dans un mélange diméthylformamide et tétrahydrofuranne et que l'on ajoute ensuite le diazométhane à −23°C. Par ailleurs, si l'on substitue un anhydride carbonique mixte pour le chlorure d'acide, on obtient des rendements très semblables (57% de **5***b*) de diazocétones (**5**). Parmi la série d'esters actifs intermédiaires (**7**) qui a été étudiée, on a trouvé que seuls les esters ODnp (**7***d*) et SPfp (**7***f*) réagissent relativement bien (23–26% de rendement) avec le diazométhane. Ces deux dernières réactions semblent représenter les premiers exemples de réactions impliquant des esters actifs.

[Traduit par la revue]

The Streptomyces anticancer antibiotics 6-diazo-5-oxo-L-norleucine (**1**, DON) and azotomycin (**2**) display a broad spectrum of activity against experimental neoplastic diseases and have given evidence of potential clinical utility (2). In 1983 we summarized a new synthesis of DON (3) and more recently completed the first total synthesis of azotomycin (1). For the latter investigation it became necessary to carefully define suitable (very mild) experimental conditions for converting the γ-carboxyl group of glutamic acid to a diazoketone. For that purpose we conducted the present study of carboxylic acid chloride, anhydride, and active ester reactions with diazomethane.

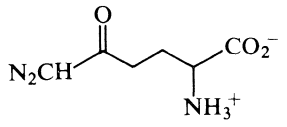

1, DON

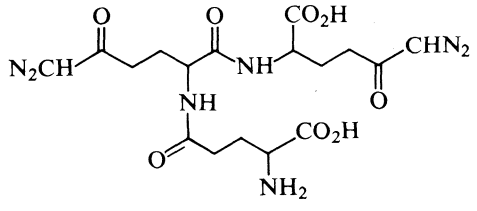

2, Azotomycin

The most common route to α-diazoketones is the Arndt–Eistert method (4) involving reaction of an acid chloride with diazomethane. In early transformations of amino acids to diazoketone derivatives, *N*-monosubstituted glycyl chlorides were found to react with diazomethane to give oxazolones (5) instead of the diazoketones. Later, diazoketone derivatives of *N*-phthaloyl (6) and tosyl (7) protected amino acids were prepared via the Arndt–Eistert method. In respect to diazoketones derived from dicarboxyl amino acids, early studies showed that the γ-carboxyl diazoketone derivative of *N*-Z-Glu-OBzl could be prepared (but not characterized), albeit in low yield (20% based on the α-chloroketone derivative (7*a*)), from its corresponding acid chloride. Later Rudinger and Farkasova (8) showed that a diazoketone could be prepared from an *N*-tosyl oxazolidone protected L-glutamic acid. The β-carboxyl diazoketone derivative of *N*-Tfa-L-Asp-OEt was generated in 82% yield. More recently, using typical Arndt–Eistert conditions, *N*-tosyl-L-glutamic acid was found to give, instead of the expected bisdiazoketone, 5-oxo-1-tosyl-2-(diazoacetyl)pyrrolidine (7*c*). Results of such experiments suggested that synthesis of azotomycin (**2**) would require carefully defined experimental conditions for generating and maintaining the diazoketone groups. Thus we were encouraged to consider alternatives to the acyl halide intermediates, such as carboxylic acid anhydrides, and the previously unexplored possibility of using carboxylic acid active esters.

Previous efforts to employ carboxylic acid anhydrides (9) have included reaction between benzoic acid anhydride and diazomethane to form diazoacetophenone (9*e*) and with cyclic anhydrides to yield mono-diazoketones (9*c*). A more useful diazoketone synthesis has utilized the mixed carbonic anhydride activation of a carboxylic acid (10). And diazoketone derivatives of *N*-phthaloyl, *N*-Boc, and *N*-Z protected amino acids have been obtained from isobutyl- and ethyl-type mixed carbonic anhydrides in 30–70% yields (10).

In the present evaluation of diazoketone formation via an acyl chloride, oxalyl chloride was selected for acid chloride formation in place of, e.g., the more side-reaction-promoting (7*c*) thionyl chloride or phosphorus pentachloride reagents. Three of the most important criteria considered when subjecting the γ-carboxyl group of Glu derivative **3***a* to reaction with oxalyl chloride were low temperature to avoid cyclization, catalytic-type assistance by dimethylformamide, and removal of hydro-

[1]Section 115 of the series Antineoplastic agents; for part 114 refer to ref. 1*a*.

[2]Author to whom correspondence may be addressed.

[3]Revision received June 6, 1986.

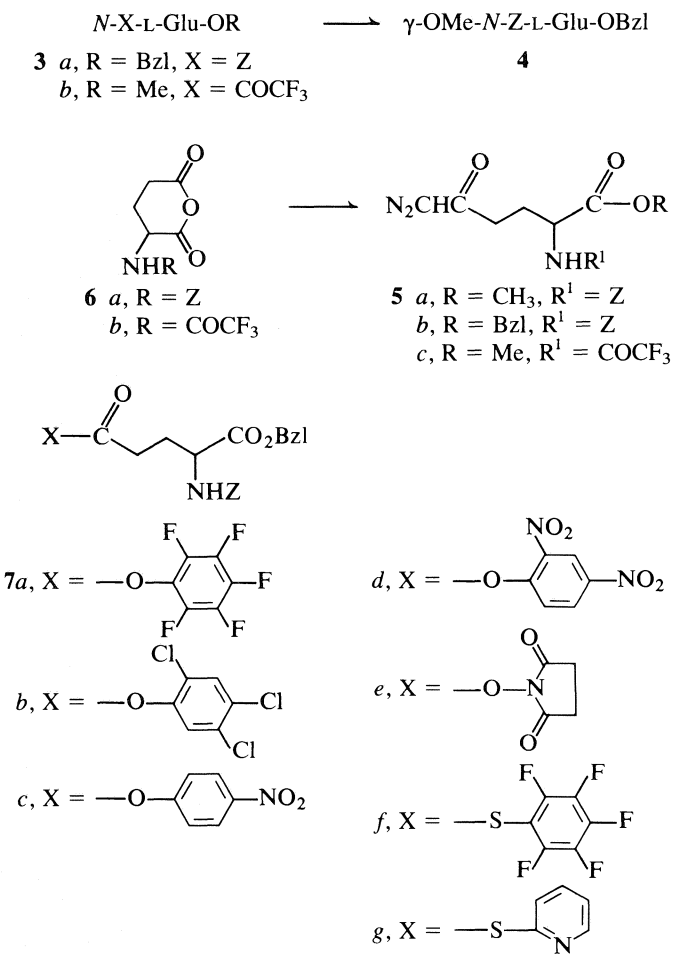

gen chloride with triethylamine. Best results (86% yield of the purified methyl ester derivative **4**, Method A) were obtained employing oxalyl chloride (1 equiv.) in tetrahydrofuran containing triethylamine (1 equiv.) and 2 drops of dimethylformamide near 0°C for 30 min. Application of this procedure to γ-carboxylic acid **3***a* followed by reaction with diazomethane afforded diazoketone **5***b* in 52% yield, as yellow crystals displaying significant antineoplastic activity (1) (e.g., with the MX-3 breast xenograft, 58–84% tumor regression at 150–600 mg/kg). Extension of this diazoketone route to preparation (**3***b* → **5***c*) of the key intermediate, diazoketone **5***c*, used in our synthesis of DON (3, 11) consistently afforded a yield improvement (20% vs. 16% following purification). Earlier we employed oxalyl chloride in methylene chloride for generating the acid chloride.

To ascertain if the yield of diazoketone **5** could be increased by utilizing anhydride or active ester (12) intermediates, attention was redirected to glutamic acid derivatives **6** and **7**. Except for γ-ONp ester **7***c*, all of the active esters are new substances and were obtained (excluding **7***g* prepared using a mixed carbonic anhydride) by condensing acid **3***a*, using dicyclohexylcarbodiimide, with the respective phenol (**7***a–d*), hydroxylamine (**7***e*), or thiophenyl (**7***f*; ref. 12).

Reaction of anhydride **6***a* with diazomethane selectively attacked the γ-carbonyl to afford diazoketone **5***a* in 18% yield. Structure of the product was confirmed by an unambiguous synthesis. For this purpose *N*-Z-L-Glu-α-OMe γ-Dcha salt (13) was converted to the acid chloride, followed by treatment with diazomethane to afford diazoketone **5***a*. Unfortunately, *N*-Tfa-L-Glu-anhydride (**6***b*) proved inert to diazomethane treatment. However, the mixed carbonic anhydride (MCA) approach proved more rewarding. The reactive mixed carbonic anhydride generated *in situ* (at −23°C) from *N*-Z-L-Glu-OBzl (13) or the corresponding dicyclohexylammonium salt (3, 13) and isobutyl chloroformate was allowed to react with diazomethane and warmed to room temperature for 1 h. By this means diazoketone **5***b* was isolated in 55 and 57% yields respectively. This method also proved quite competitive with the improved (see above) acid chloride pathway.

Active esters **7***a–g* proved sluggish or refractory toward reaction with 2 equivalents of diazomethane at room temperature for 1 day. When a significant amount of diazoketone **5***b* was not detectable by tlc analysis, the reaction was terminated. Otherwise the reaction was continued for another day with periodic additions of diazomethane. In only two cases, 2,4-dinitrophenyl ester **7***d* and pentafluorothiophenyl ester **7***f*, were practical amounts (23 and 25% yield respectively) of diazoketone **5***b* isolated. To our knowledge these are the first examples of diazoketones being generated from active esters. Apparently, an even more electron-withdrawing ester than ODnp or SPfp will be required to allow this method of diazoketone formation to more favorably compete with the acyl halide or MCA routes.

A comparison of the acyl chloride and MCA procedures was obtained by parallel syntheses of DON (**1**) precursor diazoketone **5***c*. Reaction of γ-carboxylic acid **3***b* with oxalyl chloride, triethylamine, and dimethylformamide (catalytic amount) at 0°C followed by diazomethane afforded diazoketone **5***c* in 20% yield. Alternatively, reaction of acid **3***b* or its dicyclohexylamine salt (3) with isobutyl chloroformate followed by diazomethane afforded slightly better yields of diazoketone **5***c*, i.e., 21 and 22% respectively. Interestingly, when the acid chloride procedure developed here was employed (dimethoxyethane was substituted for tetrahydrofuran) in our (1) synthesis of azotomycin (**2**), diacid **8** was transformed to the corresponding

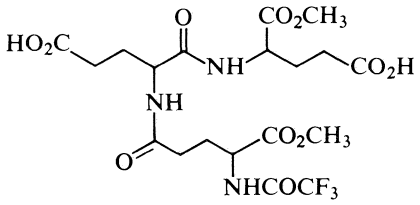

8

bis-diazoketone in 38% yield. Presumably, synthesis of diazoketone **5***c*, the DON precursor, is a quite stringent test of the herein developed acyl chloride and MCA routes to amino acid diazoketones and, under other structural circumstances, should lead to markedly improved yields.

Experimental

Dimethoxyethane and tetrahydrofuran were redistilled from lithium aluminum hydride. Solvent extracts of aqueous solution were dried over sodium sulfate. Analtech Silica Gel GF (0.25 mm) plates were used for thin-layer chromatography (tlc) and viewed with uv light. The thin-layer plates were also developed with concentrated sulfuric acid or a 1% ninhydrin spray. Column chromatography was based on silica gel (70–230 mesh) or neutral alumina supplied by E. Merck (Darmstadt). Ethereal diazomethane solutions (and standardization) used for synthesizing diazoketones were prepared from *N*-nitrosomethylurea by the procedure of Arndt (14). The instrumental methods used in this study have been summarized in the introduction to the experimental of ref. 1.

γ-OMe-N-*Z*-L-*Glu-OBzl* (**4**)

Method A

A solution composed of *N*-Z-L-Glu-OBzl (13) (1.0 g, 2.7 mmol), tetrahydrofuran (25 mL), triethylamine (0.38 mL, 2.7 mmol), and dimethylformamide (2 drops) was cooled (under nitrogen) to −78°C. Oxalyl chloride (0.26 mL, 2.8 mmol) was added and the reaction mixture was warmed to 0°C. After stirring 30 min, absolute methanol (10 mL) was added and the solvent evaporated. The residue was dissolved in chloroform (80 mL) and washed with water (2 × 25 mL), brine (1 × 25 mL), and dried. After evaporating solvent, the oily residue was chromatographed on a column of silica gel (75 g) and the ester was eluted with ethyl acetate – methylene chloride (1:19). The fractions with tlc R_f 0.54 (ethyl acetate – methylene chloride, 1:19) were collected and solvent evaporated to give 0.89 g (86%) of a colorless oil that crystallized on standing (all attempts to recrystallize failed): mp 51–52°C; $[\alpha]_D^{25}$ +1.2 (*c* 1.5, $CHCl_3$); ir (KBr): 3345, 1750, 1732, 1700, 1530, 1457, 1210, 1059, 740, 698 cm^{-1}; ^1H nmr ($CDCl_3$) δ: 1.86–2.58 (m, 4H), 3.74 (s, 3H, -OMe), 4.30–4.68 (m, 1H, asymmetric hydrogen), 5.22 (s, 2H, $-CH_2Ph$), 5.28 (s, 2H, $-CH_2Ph$), 5.59 (d, J = 8 Hz, 1H, -NH-), 7.49[4] (s, 10H, aromatic); and SP-SIMS (15) (solution phase secondary ion mass spectrometry) ms, *m/e*: 406 $(M + Na)^+$ and 386 $(M + H)^+$. *Anal.* calcd. for $C_{21}H_{23}NO_6$: C 65.44, H 6.02, N 3.63; found: C 65.38, H 6.10, N 3.61.

Method B

The preceding reaction was repeated using the exact quantities of reagents except that the dimethylformamide was deleted. Solvent was removed (rotary evaporation) and the resultant oil was purified in the same manner as described in Method A to give 0.85 g (82%) of colorless crystals that melted at 49–51°C, and showed $[\alpha]_D^{25}$ +1.2° ($CHCl_3$).[5]

Method C

A solution of *N*-Z-L-Glu-OBzl-γ-Dcha (13) (1.5 g, 2.7 mmol) in dry methylene chloride (25 mL) – dimethylformamide (2 drops) was cooled to −78°C under nitrogen. Oxalyl chloride (0.26 mL, 2.8 mmol) was added and the reaction mixture was warmed to 0°C. After 30 min of stirring at 0°C, absolute methanol (10 mL) was added and the solvent evaporated. The residue in chloroform (80 mL) was washed with water (2 × 25 mL) and dried. Solvent was removed (rotary evaporation) and the oily residue was purified as described in Method A to give 0.55 g (53%) of colorless crystals that melted at 49–51°C with $[\alpha]_D^{25}$ +1.2° ($CHCl_3$).[5] When this reaction was repeated with omission of the dimethylformamide, the yield of product, mp 49–51°C with $[\alpha]_D^{25}$ 1.2° ($CHCl_3$), rose to 77%.

Method D

In this procedure Method C was repeated employing dry dimethoxyethane (25 mL in place of methylene chloride) and dimethylformamide (2 drops). The yield was 0.70 g (67%) of colorless crystals that melted at 49–51°C and displayed $[\alpha]_D^{25}$ +1.2° ($CHCl_3$).[5]

Method E

To a mixture of sodium hydride (0.12 g of a 53.4% mineral oil dispersion, 2.7 mmol) in dry tetrahydrofuran (10 mL at −78°C), *N*-Z-L-Glu-OBzl (1.0 g, 2.7 mmol) in dry tetrahydrofuran (12 mL) was added (dropwise, under nitrogen). Oxalyl chloride (0.26 mL, 2.8 mmol) was added and the mixture warmed to 0°C for 30 min with stirring. Absolute methanol (10 mL) was added and solvent evaporated. The residue in chloroform (80 mL) was washed with water (2 × 25 mL), dried, and the solvent was removed (rotary evaporation). The resultant oil was purified as summarized in Method A to provide 0.80 g (77%) of colorless crystals that melted at 49–51°C and showed $[\alpha]_D^{25}$ +0.8° ($CHCl_3$).[5]

Method F

A solution of *N*-Z-L-Glu-OBzl (1.0 g, 2.7 mmol) in 0.2 *N* sodium hydroxide (13.5 mL, 2.7 mmol) and tetrahydrofuran (5 mL) was freeze-dried. The solid sodium salt was suspended in dry tetrahydrofuran (25 mL) and dimethylformamide (2 drops) and cooled to −78°C (under nitrogen). Oxalyl chloride (0.27 mL, 2.8 mmol) was added and the reaction performed as described in Method E. The oily product was purified as noted in Method A to afford 0.49 g (47%) of colorless crystals melting at 49–51°C; $[\alpha]_D^{25}$ +1.3° ($CHCl_3$).[5]

γ-Pfp-N-*Z*-L-*Glu-OBzl* (**7**a)

To a solution of *N*-Z-L-Glu-OBzl (13) (2.09 g, 5.6 mmol) and ethyl acetate (35 mL) was added pentafluorophenyl (1.04 g, 5.6 mmol) and dicyclohexylcarbodiimide (1.16 g, 5.6 mmol) at 0°C. The reaction mixture was stirred (magnetically) at 0°C for 1 h, the ice bath was removed, and the mixture was allowed to warm to room temperature overnight (16 h). Dicyclohexylurea was collected and solvent evaporated to a white solid that was dissolved in ethyl acetate (50 mL). The solution was filtered (to remove remaining dicyclohexylurea), and pentane (200 mL) added. After standing 3 h at 0°C, 2.44 g (81%) of the pentafluorophenyl ester was obtained as colorless crystals: mp 60–70°C: $[\alpha]_D^{25}$ +2.8° ($CHCl_3$); ir (KBr): 3355, 1787, 1753, 1697, 1523, 1304, 1295, 1190, 1123, 1095, 996, 751, 738, 700 cm^{-1}; ^1H nmr ($CDCl_3$) δ: 1.90–2.90 (m, 4H), 4.39–4.81 (m, 1H, asymmetric α-H), 5.18 (s, 2H, $-CH_2Ph$), 5.27 (s, 2H, $-CH_2Ph$), 5.33–5.60 (m, 1H, -NH-), 7.43 (12) (s, 10H, aromatic); and SP-SIMS (15) ms, *m/e*: 560 $(M + Na)^+$ and 538 $(M + H)^+$. *Anal.* calcd. for $C_{26}H_{20}F_5NO_6$: C 58.11, H 3.75, N 2.56; found: C 58.27, H 3.75, N 2.53.

γ-OTcp-N-*Z*-L-*Glu-OBzl* (**7**b)

A mixture of *N*-Z-L-Glu-OBzl-γ-Dcha (13) (5.0 g, 9.06 mmol), ethyl acetate (50 mL), and 0.5 *N* citric acid (25 mL) was shaken until only two liquid phases were obtained. The organic phase was separated and washed with water (1 × 25 mL), brine (1 × 25 mL), and dried. The solution was cooled to 0°C and 2,4,5-trichlorophenol (1.79 g, 9.06 mmol) was added, followed by dicyclohexylcarbodiimide (1.87 g, 9.06 mmol). The reaction mixture was stirred for 1 h at 0°C and for 18 h at room temperature. After collecting the dicyclohexylurea, the solution was washed with 5% sodium bicarbonate (1 × 25 mL), brine (1 × 25 mL), and dried. Solvent was evaporated and crystallization induced by addition of ethyl ether followed by hexane. The solid was washed with ethyl ether and recrystallized from ethyl acetate – ethyl ether – hexane to afford 2.03 g (41%) of colorless crystals: mp 118–119°C; $[\alpha]_D^{25}$ +0.3° ($CHCl_3$); ir (KBr): 3335, 1776, 1732, 1695, 1543, 1268, 1280, 1120, 749, 700 cm^{-1}; ^1H nmr ($CDCl_3$) δ: 1.80–2.82 (m, 4H), 4.40–4.94 (m, 1H, asymmetric α-H), 5.17 (s, 2H, $-CH_2Ph$), 5.24 (s, 2H, $-CH_2Ph$), 5.34–5.74 (br m, 1H, -NH-), 7.42[4] (s, 11H, aromatic), 7.60 (s, 1H, aromatic); and SP-SIMS (15) ms, *m/e*: 572 $(M + Na)^+$ and 574 $(M + Na)^+$. *Anal.* calcd. for $C_{26}H_{22}Cl_3NO_6$: C 56.69, H 4.03, N 2.54, Cl 19.31; found: C 56.96, H 4.06, N 2.51, Cl 19.34.

γ-ONp-N-*Z*-L-*Glu-OBzl* (**7**c)

From *N*-Z-L-Glu-α-OBzl-γ-Dcha (13) (5.0 g, 9.06 mmol), *p*-nitrophenol (1.26 g, 9.06 mmol), and dicyclohexylcarbodiimide (1.87 g, 9.06 mmol) ester **7***c* was prepared essentially as described for obtaining ester **7***b* above. Evaporation of solvent yielded a yellow oil, which was chromatographed on a column of silica gel (45 g). The ester was eluted with methylene chloride – ethyl acetate (99:1) as a yellow-green oil (4.0 g, tlc showed only one spot, R_f 0.25, ethyl acetate – methylene chloride, 1:50). Solidification occurred after standing for 2 weeks and recrystallization was accomplished with ethyl ether – hexane to give light yellow crystals melting at 65–67°C; $[\alpha]_D^{25}$ −21.3° (CH_3OH) (lit. (16) mp 64–66°C and $[\alpha]_D^{25}$ −21° in CH_3OH).

γ-ODnp-N-*Z*-L-*Glu-OBzl* (**7**d)

The procedure used for converting *N*-Z-L-Glu-α-OBzl-γ-Dcha (13) (5.0 g, 9.06 mmol) to ester **7***b* was repeated with 2,4-dinitrophenol (1.67 g, 9.06 mmol) and dicyclohexylcarbodiimide (1.87 g, 9.06 mmol). After collecting the dicyclohexylurea the solution was washed with 5% sodium bicarbonate (2 × 25 mL), water (2 × 25 mL), and brine (1 × 25 mL). Solvent was evaporated and the residue dissolved in methanol (25 mL). No precipitation occurred upon addition of ether

[4]Proton resonances superimposed as evidenced by area integration.

[5]Identity was determined by comparison of ^1H nmr and ir spectra and tlc mobilities. Melting points and optical rotations were compared when necessary.

and hexane but addition of acetone caused immediate precipitation. The light yellow solid was recrystallized from acetone–methanol–hexane to yield 2.08 g (43%) of pale yellow crystals: mp 102.5–103.5°C; $[\alpha]_D^{25}$ −2.6° ($CHCl_3$); ir (KBr): 3335, 1780, 1733, 1700, 1615, 1547, 1350, 1280, 1111, 747, 700 cm^{-1}; ^1H nmr ($CDCl_3$) δ: 1.88–2.92 (m, 4H), 4.42–4.90 (m, 1H, asymmetric α-H), 5.18 (s, 2H, -CH_2Ph), 5.25 (s, 2H, -CH_2Ph), 5.36–5.72 (m, 1H, -NH-), 7.43[4] (s, 10H, aromatic), 7.50 (d, J = 9 Hz, 1H, aromatic), 8.50 (dd, J = 9 Hz and J = 1.5 Hz, 1H, aromatic), 9.20 (d, J = 1.5 Hz, 1H, aromatic); and SP-SIMS (15) ms, m/e: 560 $(M + Na)^+$. *Anal.* calcd. for $C_{26}H_{23}N_3O_{10}$: C 58.10, H 4.31, N 7.82; found: C 58.15, H 4.32, N 7.68.

*γ-OSu-*N*-Z-*L*-Glu-OBzl (**7**e)*

By the technique employed with OTcp ester **7***b* (see above), *N*-Z-L-Glu-OBzl-γ-Dcha (13) (5.0 g, 9.06 mmol) was converted to the corresponding carboxylic acid and allowed to react with *N*-hydroxysuccinimide (1.04 g, 9.06 mmol) and dicyclohexylcarbodiimide (1.87 g, 9.06 mmol) for 1 h at 0°C and for 15 h at ambient temperature. Recrystallization was accomplished from methylene chloride – ethyl ether (allowing to stand for 3 h at 0°C) to give 2.5 g (60%) of colorless crystals: mp 105–107°C; $[\alpha]_D^{25}$ +4.7° ($CHCl_3$); ir (KBr): 3325, 1818, 1747 (shoulder), 1698, 1540, 1460, 1288, 1260, 1213, 1083, 732, 696 cm^{-1}; ^1H nmr ($CDCl_3$) δ: 1.94–2.76 (m, 4H), 2.78 (s, 4H, -OSu), 4.35–4.70 (m, 1H, asymmetric α-H), 5.17 (s, 2H, -CH_2Ph), 5.24 (s, 2H, -CH_2Ph), 5.69 (br d, J = 8 Hz, 1H), 7.43[4] (s, 10H, aromatic); and SP-SIMS (15) ms, m/e: 491 $(M + Na)^+$ and 469 $(M + H)^+$. *Anal.* calcd. for $C_{24}H_{24}N_2O_8$: C 61.53, H 5.16, N 5.98; found: C 61.61, H 5.24, N 5.99.

*γ-SPfp-*N*-Z-*L*-Glu-OBzl (**7**f)*

Except for a 7-h period at room temperature, reaction between *N*-Z-L-Glu-OBzl (13) (2.0 g, 5.4 mmol), pentafluorothiophenol (0.72 mL, 5.4 mmol), and dicyclohexylcarbodiimide (1.11 g, 5.4 mmol) in ethyl acetate (35 mL) was conducted as summarized for obtaining OPfp ester **7***a*. The clear oily product solidified on standing overnight (at 5°C) and was dissolved in ethyl ether (40 mL). After filtering the solution, pentane was added until opalescence and the mixture was allowed to stand at 0°C for 2 h. Upon filtration, 1.52 g (51%) of pentafluorothiophenol ester **7***f* was obtained as colorless crystals: mp 58–61°C; $[\alpha]_D^{25}$ +7.6° ($CHCl_3$); ir (KBr): 3330, 1738 br, 1701, 1520, 1500, 1097, 986, 868, 747, 696 cm^{-1}; ^1H nmr ($CDCl_3$) δ: 1.84–2.94 (m, 4H), 4.36–4.76 (m, 1H, asymmetric α-H), 5.18 (s, 2H, -CH_2Ph), 5.25 (s, 2H, -CH_2Ph), 5.32–5.55 (m, 1H, -NH-), 7.44[4] (s, 10H, aromatic); and SP-SIMS (15) ms, m/e: 576 $(M + Na)^+$. *Anal.* calcd. for $C_{26}H_{20}FN_5O_5S \cdot 1/2H_2O$: C 55.52, H 3.58, N 2.49; found: C 55.39, H 3.37, N 2.44.

*γ-SPy-*N*-Z-*L*-Glu-OBzl (**7**g)*

To a solution of *N*-Z-L-Glu-OBzl (13) (1.0 g, 2.7 mmol) in dry tetrahydrofuran (20 mL, with magnetic stirring, under nitrogen at −23°C maintained by Dry Ice/carbon tetrachloride) was added *N*-methylmorpholine (0.30 mL, 2.7 mmol) and isobutyl chloroformate (0.35 mL, 2.7 mmol) by syringe while maintaining the temperature at −23°C. After stirring for 15 min at −23°C, 2-pyridine thiol (0.34 g, 3.1 mmol) in dry tetrahydrofuran (5 mL) was added (addition funnel). The reaction flask was transferred to an ice bath and stirred for 2 h at 0°C followed by 2 h at room temperature. The mixture was filtered (solid rinsed with tetrahydrofuran) and the filtrate evaporated. A solution of the residue in ethyl acetate (80 mL) was washed with brine (1 × 25 mL), 5% sodium bicarbonate (3 × 25 mL), brine (1 × 25 mL), and dried. Solvent was evaporated and the residue allowed to stand overnight at 0°C (no solidification) and dissolved in carbon tetrachloride. Ester **7***g* was induced to crystallize by adding hexane to opalescence, followed by a small amount of acetone. After standing for 2 h at −10°C (freezer), the solid was collected to yield 0.94 g (75%) of pale yellow crystals; mp 84–85°C; $[\alpha]_D^{25}$ +6.3° ($CHCl_3$); ir (KBr): 3345, 1760, 1702, 1533, 1288, 1227, 1174, 1065, 971, 778, 736, 698 cm^{-1}; ^1H nmr ($CDCl_3$) δ: 2.00–2.53 (m, 2H), 2.53–2.93 (m, 2H), 4.31–4.64 (m, 1H, asymmetric α-H), 5.17 (s, 2H, -CH_2Ph), 5.23 (s, 2H, -CH_2Ph), 5.37–5.72 (m, 1H, -NH-), 7.26–7.91[4] (m, 13H; singlet at 7.43, 10H, aromatic), 8.69 (d, J = 5 Hz, 1H aromatic); and SP-SIMS (15) ms, m/e: 487 $(M + Na)^+$. *Anal.* calcd. for $C_{25}H_{24}N_2O_5S$: C 64.64, H 5.21, N 6.03; found: C 64.81, H 5.30, N 6.00.

*6-Diazo-5-oxo-*N*-Z-*L*-norleucine-OMe (**5**a)*

Method A

To a cold (ice bath) solution of *N*-Z-L-Glu-α-OMe-γ-Dcha salt (2.0 g, 4.2 mmol) in dry methylene chloride (30 mL) and pyridine (4 drops) was added (dropwise over 10 min with stirring) oxalyl chloride (4 mL, 47 mmol) in dry methylene chloride (9 mL). Fifteen minutes later the ice bath was removed and the mixture stirred for an additional 5 min. Solvent was evaporated (below 10°C) and cold (and dry) chloroform (10 mL) was added (3 ×) and evaporated. A mixture of dry chloroform (10 mL) and ethyl ether (15 mL, anhydrous) was added, the solution filtered, and the filtrate added dropwise (over 10 min) to an ethereal solution of diazomethane (from 5 g of *N*-nitrosomethylurea) at 0°C. After stirring 0.5 h at 0°C and 1.5 h at room temperature, the solvent was evaporated to give a brown oil (2.5 g). The crude product was purified on a column of silica gel (100 g) using a gradient of 9:1 to 0:1 hexane – ethyl acetate. Fractions with R_f 0.18 (1:2 hexane – ethyl acetate) were collected and solvent evaporated to give 0.5 g (40%) of a yellow oil that crystallized from ether – petroleum ether as light yellow crystals (0.15 g, 12% yield): mp 117–119°C; $[\alpha]_D^{25}$ −14.4° ($CHCl_3$); ir: 3280, 2110, 1746, 1708, 1597, 1535, 1256, 1044, 695 cm^{-1}; ^1H nmr ($CDCl_3$) δ: 1.60–2.20 (m, 4H), 3.65 (s, 3H, -OMe), 4.00–4.61 (m, 1H, asymmetric α-H), 5.10 (s, 2H, -CH_2Ph), 5.50 (s, 1H, -CHN_2), 5.75 (d, 7 Hz, 1H, -NH-), 7.35 (s, 5H, aromatic); SP-SIMS ms, m/e: 326 $(M + Li)^+$, 298 $(M + Li - N_2)^+$. *Anal.* calcd. for $C_{15}H_{17}O_5N_3$: C 56.42, H 5.37, N 13.16; found: C 56.56, H 5.50, N 12.80.

Method B

A solution of *N*-Z-L-Glu anhydride (17) (**6***a*, 1.5 g, 5.3 mmol) in dry tetrahydrofuran (10 mL) was added to a stirred (magnet) ethereal solution of diazomethane (from 5 g of *N*-nitrosomethylurea) cooled in an ice bath. The mixture was stirred at 0°C for 1.5 h and for an additional 2 h at room temperature. Solvent was evaporated to give a yellow oil, which was chromatographed on a column of silica gel (40 g). The fractions with R_f 0.45 and 0.38 (ethyl acetate – methylene chloride, 1:3) eluted with ethyl acetate – methylene chloride (1:6) were combined and solvent removed to give a yellow oil. Crystallization was induced by addition of ethyl ether to yield 0.32 g (18%) of diazoketone **5***a* as light yellow crystals melting at 117°C.

When the reaction was repeated with *N*-Tfa-L-Glu anhydride (17, 18) (**6***b*, 2.0 g) no evidence (ir) was obtained, even following a 24-h reaction period, for production of diazoketone **5***c*.

*6-Diazo-5-oxo-*N*-Z-*L*-norleucine-OBzl (**5**b)*

The acid chloride procedure

A solution of *N*-Z-L-Glu-α-OBzl (13) (1.00 g, 2.7 mmol), dry tetrahydrofuran (25 mL), triethylamine (0.38 mL, 2.7 mmol), and dimethylformamide (2 drops) was cooled to −30°C under argon with mechanical stirring. Oxalyl chloride (0.26 mL, 2.8 mmol) was added (syringe) and the reaction mixture was warmed to 0°C. After stirring for 30 min at 0°C, the mixture was cooled to −78°C and added slowly (over 1 h through a sintered glass filter) into an ethereal solution of diazomethane (0.59 *N*, 15 mL) cooled to −23°C. The temperature was raised to 0°C for 30 min while continuing stirring. Solvent was evaporated (passing through a stream of argon) and the residue was chromatographed on a column of silica gel (65 g). Elution with ethyl acetate – hexane (1:5) and collection of fractions with R_f 0.30 (acetone–hexane, 1:2) gave, upon evaporation of solvent, 0.55 g (52%) of a yellow solid that was recrystallized from methylene chloride – hexane: mp 85–86°C; $[\alpha]_D^{25}$ +0.7° ($CHCl_3$). The product (**5***b*) was found identical[5] to an authentic sample (3).

The mixed carbonic anhydride procedure

A solution of *N*-Z-L-Glu-OBzl-γ-Dcha (13) (2.12 g, 3.84 mmol) in dry methylene chloride (40 mL) was cooled to −23°C, isobutyl

chloroformate (0.50 mL, 3.85 mmol) was added, and stirring was continued for 25 min at −23°C. Ethereal diazomethane (25 mL, 0.4 *M*) was added (dropwise) and immediate precipitation occurred. The mixture was stirred 1 h at 0°C, the solution was filtered (hood), and solvent removed by a stream of nitrogen. The solid yellow residue was chromatographed (attempts to recrystallize failed) on a column of silica gel (45 g) in acetone–hexane (1:5). Elution with acetone–hexane (1:3) and collection of the fractions with tlc R_f 0.30 (1:2 acetone – hexane) followed by crystallization from ethyl ether led to 0.70 g of yellow solid. Hexane was added to the filtrate and, upon standing overnight at −10°C (freezer), an additional 0.14 g was recovered to give an overall yield of 0.85 g (57%) of light yellow crystals that melted at 85–86°C. The specimen of diazoketone **5***b* was identical to an authentic sample (3; see also footnote 5).

The preceding reaction was repeated using *N*-Z-L-Glu-OBzl (13) (1.07 g, 2.88 mmol) in dry methylene chloride (30 mL) – *N*-methylmorpholine (0.32 mL, 2.88 mmol) at −23°C. The isobutyl chloroformate (0.37 mL, 2.88 mmol) and ethereal diazomethane (25 mL, 0.4 *M*) were again added through an addition funnel. Following chromatographic purification (see above) on a column of silica gel, 0.63 g (55%) of light yellow crystals were isolated, melting at 85–86°C and found identical[5] with an authentic sample (3).

The active ester procedure

Each active ester, **7***a–g*, (1.0 g) in dry methylene chloride (30 mL) was cooled to 0°C with magnetic stirring. Two equivalents of diazomethane were added and stirring at 0°C was continued. After 1 h, the reaction was warmed to room temperature and allowed to stir for 16 h. If no significant amount of diazoketone **5***b* was in evidence by tlc, the reaction was terminated. When a promising amount of product was present the reaction was continued for another 24 h with periodic additions of diazomethane. Product isolation and purification were accomplished in the same fashion as described above for the acid chloride procedure. By this means the ODnp (**7***d*) and SPfp (**7***f*) active esters afforded diazoketone **5***b* in 23 and 26% yields respectively. And trace amounts of diazoketone **5***b* were detected (tlc) using esters **7***a*, *e*, and *g*.

N-*Tfa-L-Glu-α-OMe* (**3**b)

To a solution of γ-OBzl-*N*-Tfa-L-Glu-OMe (2.5 g) in 95% ethanol (360 mL) was added 5% palladium-on-carbon (2.0 g). While the mixture was vigorously stirred, a stream of hydrogen was passed through the solution for 1 h. The catalyst was collected and solvent evaporated (*in vacuo*) to give 2.0 g of a pinkish oil (tlc showed only 1 spot at R_f 0.29 using ethyl acetate), which was finally purified by column chromatography (silica gel) with ethyl acetate – methylene chloride (1:1) as eluent to give 1.61 g (88%) of *N*-Tfa-L-Glu-OMe as a colorless oil: $[\alpha]_D^{25}$ +21.0° ($CHCl_3$); ir: 3310 br, 3700–2500, 1720 br, 1557, 1445, 1217, 1180 br cm^{-1}; ^1H nmr ($CDCl_3$) δ: 1.83–2.67 (m, 4H), 3.80 (s, 3H, -OMe), 4.43–4.87 (m, 1H, asymmetric α-H), 7.60 (d, J = 8 Hz, 1H, -NH-), 10.20 (s, 1H, -COOH); ^{13}C nmr ($CDCl_3$) δ: 26.4, 29.7, 52.1, 53.1, 115.7 (q, J = 287.5 Hz, F-coupling), 157.3 (q, J = 38 Hz, F-coupling), 170.9, 177.7; and EI ms, *m/e*: 258 $(M + H)^+$ and 257 M^+.

To a solution of *N*-Tfa-L-Glu-OMe (1.5 g, 5.8 mmol) in tetrahydrofuran (50 mL) was added dicyclohexylamine (1.16 mL, 5.9 mmol). After stirring for 2 h at ambient temperature, and overnight (15 h) in a refrigerator (5°C), the precipitate was collected and washed with tetrahydrofuran to provide 2.4 g (94%) of the Dcha salt[5] as colorless crystals melting at 165–167°C, as we previously reported (3).

6-Diazo 5-oxo-N-*Tfa-L-norleucine-OMe* (**5**c)

Method A

A solution of *N*-Tfa-L-Glu-α-OMe (**3***b*, 1.26 g, 4.9 mmol) prepared as described in the preceding experiment, in dry tetrahydrofuran (25 mL) containing triethylamine (0.68 mL, 4.9 mmol), was cooled (Dry Ice – isopropyl alcohol) to −30°C under argon with mechanical stirring. Oxalyl chloride (0.44 mL, 4.9 mmol) and dimethylformamide (2 drops) were added (syringe). The reaction mixture was warmed to 0°C for 30 min and cooled to −78°C while slowly (30 min) adding it through a sintered glass filter to an ethereal solution of diazomethane (30 mL, 0.51 *M*) cooled to −23°C (Dry Ice – carbon tetrachloride). Following 30 min of stirring at 0°C, solvent was evaporated (by passing through a stream of argon) and the residue was purified as described earlier (3) to yield 0.27 g (20%) of a yellow oil identical[5] to an authentic sample (3) of daizoketone **5***c*.

Method B

A solution of *N*-Tfa-L-Glu-OMe-γ-Dcha salt (2.5 g, 5.7 mmol) prepared in the experiment above, in dry methylene chloride (60 mL), was cooled to −23°C. Isobutyl chloroformate (0.74 mL, 5.7 mmol) was added and the solution stirred for 25 min at −23°C. Ethereal diazomethane (25 mL, 0.4 *M*) was added (dropwise) to the solution and precipitation was immediate. The reaction flask was transferred to an ice bath, the mixture was stirred for 30 min at 0°C, and the solution filtered (hood). Solvent was removed by passing nitrogen above the solution surface. The resulting yellow residue was purified by chromatography as reported (3) to yield 0.35 g (22%) of the diazoketone **5***c* (3; see also footnote 5) as a yellow oil.

When the synthesis was repeated using *N*-Tfa-L-Glu-α-Ome (1.46 g, 5.67 mmol) in dry tetrahydrofuran (30 mL) containing *N*-methylmorpholine (0.63 mL, 5.67 mmol) with isobutyl chloroformate (0.74 mL, 5.67 mmol) and ethereal diazomethane (16.5 mL, 0.52 *M*), the product was again purified by chromatography as described (3) and 0.34 g (21%) of the diazoketone (**5***c*) was isolated as a yellow oil (ref. 3, and footnote 5).

Acknowledgments

With pleasure we thank the following for the financial support necessary to this investigation: Eleanor W. Libby, the Waddell Foundation (Donald Ware), Mary Dell Pritzlaff, the Olin Foundation (Spencer T. and Ann W.), the Fannie E. Rippel Foundation, the Robert B. Dalton Endowment Fund, Virginia L. Bayless, Jack W. Whiteman, Lotte Flugel, Elias M. Romley, and Grants CA-16049-07-09 awarded by the National Cancer Institute, DHHS.

1. (*a*) G. R. PETTIT and P. S. NELSON. J. Org. Chem. **51**, 1282 (1986); (*b*) P. S. NELSON. Ph.D. Thesis. Arizona State University, Tempe, Arizona. May 1983.
2. R. H. EARHART, J. M. KOELLER, and H. L. DAVIS. Cancer Treat. Rep. **66**, 1215 (1982); R. CANTANE, D. D. VON HOFF, D. L. GLAUBINGER, and F. M. MUGGIA. Cancer Treat. Rep. **63**, 1033 (1979).
3. G. R. PETTIT and P. S. NELSON. J. Org. Chem. **48**, 741 (1983).
4. W. E. BACHMAN and W. S. STRUVE. Org. React. **1**, 38 (1948).
5. P. KARRER and G. BUSSMANN. Helv. Chim. Acta, **24**, 645 (1941); K. BALENOVIC, V. THALLER, and L. FILIPOVIL. Helv. Chim. Acta, **34**, 744 (1951); K. BALENOVIC, N. BREGANT, D. CERAR, and M. TKALCIC. J. Org. Chem. **16**, 1308 (1951).
6. (*a*) K. BALENOVIC. Experientia, **3**, 369 (1947); (*b*) K. BALENOVIC and D. FLES. J. Org. Chem. **17**, 347 (1952); (*c*) K. BALENOVIC and D. DVORNIK. J. Chem. Soc. 2976 (1954); (*d*) K. BALENOVIC, D. CERAR, and Z. FUKS. J. Chem. Soc. 3316 (1952); (*e*) K. BALENOVIC *et al.* Croat. Chim. Acta, **28**, 303 (1956); (*f*) Croat. Chim. Acta, **29**, 153 (1957); (*g*) Arh. Kem. **23**, 1 (1951); (*h*) K. BALENOVIC, I. JAMBRESIC, B. GASPERT, and D. CERAR. Recl. Trav. Chim. Pays-Bas, **75**, 1252 (1956).
7. (*a*) C. R. HARRINGTON and R. C. MOGGRIDGE. J. Chem. Soc. 706 (1940); (*b*) G. SCHOELLMANN and E. SHAW. Biochemistry, **2**, 252 (1963); (*c*) Z. SAJADI, M. KASHANI, L. J. LOEFFLER, and I. H. HALL. J. Med. Chem. **23**, 275 (1980).
8. J. RUDINGER and H. FARKASOVA. Collect. Czech. Chem. Commun. **28**, 2941 (1963).
9. (*a*) J. HOOZ and G. F. MORRISON. Org. Prep. Proc. Int. **3**, 227 (1971); (*b*) D. HODSON, G. HOLT, and D. K. WALL. J. Chem. Soc. (C), 971 (1970); (*c*) H. BHATI. J. Org. Chem. **27**, 1138

(1962); (*d*) F. WEYGAND and H. BESTMANN. J. Angew. Chem. **72**, 538 (1960); (*e*) W. BRADLEY and R. ROBINSON. J. Am. Chem. Soc. **52**, 1558 (1930).
10. B. PENKE, J. CZOMBOS, L. BALASPIRI, J. PETRES, and K. KOVACS. Helv. Chim. Acta, **53**, 1057 (1970).
11. F. WEYGAND, H. J. BESTMANN, and E. KLIEGER. Chem. Ber. **91**, 1037 (1958).
12. G. R. PETTIT. Synthetic peptides. Vol. 4. Elsevier Publ. Co., Amsterdam, The Netherlands. 1976.
13. J. S. MORLEY. J. Chem. Soc. 2410 (1967).
14. F. ARNDT. Org. Synth. Collect. Vol. II. 1943. p. 165.
15. G. R. PETTIT, C. W. HOLZAPFEL, G. M. CRAGG, C. L. HERALD, and P. WILLIAMS. J. Nat. Prod. **46**, 917 (1983).
16. E. WUNSCH, A. HOGEL-BETZ, and E. JAEGER. Hoppe-Seylers Z. Physiol. Chem. **352**, 1553 (1971).
17. E. KLIEGER and H. GIBIAN. Annalen, **655**, 195 (1962).
18. F. WEYGAND and E. LEISING. Chem. Ber. **87**, 2488 (1954).

Autoxidation of phosphatidylcholines initiated with dicumylhyponitrite in solution and in bilayers

LAWRENCE ROSS COATES BARCLAY,[1] DAVID KONG, AND JOANN VANKESSEL
Department of Chemistry, Mount Allison University, Sackville, N.B., Canada E0A 3C0

Received March 19, 1986

LAWRENCE ROSS COATES BARCLAY, DAVID KONG, and JOANN VANKESSEL. Can. J. Chem. **64**, 2103 (1986).

Dicumylhyponitrite (DCHN) was used as a thermal initiator of autoxidation of unsaturated phosphatidylcholines in *o*-dichlorobenzene and in mixed bilayers of dilinoleoylphosphatidylcholine (DLPC) with dimyristoylphosphatidylcholine (DMPC). Quantitative studies were made of the products, α,α-dimethylbenzyl alcohol (DMBA), acetophenone (AP), and dicumylperoxide (DCP) from DCHN. The ratio DMBA/Δ2DCHN (37 ± 6%) indicates the effectiveness of cumyloxy in hydrogen abstraction from the phospholipid in solution. The *overall* efficiency (*e*) of DCHN determined by the inhibitor method with α-tocopherol (α-T) was 84 ± 5%, close to the overall ratio (DMBA + AP)/Δ2DCHN (90 ± 6%), and indicates either significant initiation through the methylperoxy radical in *o*-dichlorobenzene solution or that α-tocopherol traps cumyloxy radical before β-scission occurs. The thermal decomposition rate constant of DCHN is greatly reduced in a medium of high viscosity; in DLPC to one-quarter, in Nujol to one-sixth that in isooctane and this is interpreted in terms of a one-bond scission of DCHN. In DLPC + DMPC mixed bilayers the effectiveness of the cumyloxy radical to initiate reaction varied from 30 to 19% depending on the amount of DLPC and in this medium there is little or no initiation by methylperoxy according to product analysis and α-T inhibition studies. In mixed bilayers, the rate of oxidation was directly related to the [DLPC] indicating that the classical rate law applies. The oxidizability of DLPC in mixed bilayers (0.046 $M^{-1/2}$ $s^{-1/2}$) is comparable to that of neat DLPC.

LAWRENCE ROSS COATES BARCLAY, DAVID KONG et JOANN VANKESSEL. Can. J. Chem. **64**, 2103 (1986).

On a utilisé l'hyponitrite de dicumyle (HNDC) comme initiateur thermique pour l'autooxydation de phosphatidylcholines non-saturés dans le *o*-dichlorobenzène et dans des doubles couches mixtes de dilinoléylphosphatidylcholine (DLPC) et de dimyristoylphosphatidylcholine (DMPC). On a réalisé des études quantitatives des produits : l'alcool α,α-diméthylbenzylique (ADMB), l'acétophénone (AP) et le peroxyde de dicumyle provenant du HNDC. Le rapport ADMB/Δ2HNDC (37 ± 6%) est un indicateur de l'efficacité du radical cumyloxy à faire l'abstraction d'un hydrogène du phospholipide en solution. L'efficacité *globale* (*e*) du HNDC, telle que déterminée par la méthode de l'inhibiteur à l'aide de α-tocophérol (α-T), est égale à 84 ± 5%; cette valeur est proche du rapport global (ADMB + AP)/Δ2HNDC (90 ± 6%) et elle indique soit qu'il se produit une initiation importante par le biais du radical méthylperoxy en solution dans le *o*-dichlorobenzène soit que l'α-tocophérol piège le radical cumyloxy avant que la scission β puisse se produire. La constante de vitesse de décomposition du HNDC est grandement réduite dans des milieux de haute densité; dans le DLPC elle est réduite au quart de sa valeur alors que dans le Nujol elle est réduite au sixième et l'on interprète ces résultats en fonction d'une scission d'une liaison du HNDC. Dans des doubles couches de DLPC + DMPC, l'efficacité du radical cumyloxy à initier la réaction varie de 30 à 19% dépendant de la quantité de DLPC et, sur la base d'une analyse des produits ainsi que d'études d'inhibition par α-T, on peut conclure que, dans ce milieu, il ne se produit que peu ou pas d'initiation par le radical méthylperoxy. Dans les doubles couches mixtes, la vitesse d'oxydation peut être reliée directement à la concentration en DLPC et ceci indique que la loi de vitesse classique s'applique. La facilité d'oxyder le DLPC dans des doubles couches mixtes (0,046 $M^{-1/2}$ $s^{-1/2}$ est comparable à celle observée à l'état pur.

[Traduit par la revue]

Introduction

The autoxidation of biological molecules such as phosphatidylcholines organized into bilayers as model biomembranes is relevant to autoxidative disruption of the functions of natural biomembranes leading to important pathological events (1–3). Several groups have recently developed an increased interest in autoxidation of such biologically important molecules. Of particular significance are the application of quantitative kinetic methods (4–8), the mechanism of action and activity of antioxidants (9–21), quantitative product studies (22–25), and the dynamics of free radical initiation, especially in microenvironments (26–29).

Autoxidation of organic substrates in homogenous solution is well known to be a free-radical chain process which follows the classical rate law given by eq. [1] (30–32):

$$[1] \quad -\frac{d[O_2]}{dt} = \frac{k_p}{2k_t^{1/2}}[RH]R_i^{1/2}$$

where RH is the substrate, R_i the rate of chain initiation, k_p the propagation rate constant, and $2k_t$ the termination rate constant. The R_i may be controlled by using a thermal initiator with a known decomposition rate constant, k_i. Because not all of the radicals escape the solvent cage where they are formed, the real R_i must be measured, for example, by the inhibitor method (33) using a phenolic antioxidant such as α-tocopherol (α-T) known to trap two peroxyl radicals (15) so that R_i is given by eq. [2], where τ is the period during which oxidation is suppressed.

$$[2] \quad R_i = 2[ArOH]/\tau$$

Under these conditions, the efficiency (*e*) of chain initiation by a thermal azo initiator, $In \xrightarrow{k_i} 2R\cdot + N_2$, is given by eq. [3].

$$[3] \quad e = R_i/2k_i[In]$$

If the kinetics follows the classical equation [1], the susceptibility of a substrate to undergo autoxidation, the "oxidizability", is given by eq. [4].

$$[4] \quad \frac{k_p}{(2k_t)^{1/2}} = \frac{-d[O_2]/dt}{[RH]R_i^{1/2}}$$

Of the initiators investigated so far for kinetic studies in bilayers, di-*tert*- butylhyponitrite (**1***a*) appeared to be the most useful (5).

R—O—N=N—O—R

1*a* R = $(CH_3)_3C$—

b R = C_6H_5—$C(CH_3)_2$—

[1] Author to whom all correspondence to be addressed.

The diazene, **1***a*, however, has several disadvantages: (*1*) Its low efficiency, *e*, or high cage recombination in bilayer autoxidation (e = 9.1% (5)), means that a relatively high concentration of **1***a* is needed in the bilayer. (*2*) The volatility of the products from **1***a* made it impossible to determine accurately the efficiency of **1***a* by product analyses (5) as a check on the *e* determined by the induction period method with a phenolic inhibitor (33). (*3*) The question of the exact location of **1***a* within the bilayer (5) is further complicated by its partial water solubility (*vide infra*) and this complicates the assessment of the bilayer cage effect on this initiator.

With the above points in mind, we have selected dicumylhyponitrite (DCHN, **1***b*) as a thermal initiator in bilayer autoxidation, anticipating that this more hydrophobic molecule would be wholly sequestered within the bilayer and would also obviate the other limitations of **1***a*. Although the cumyloxy radical (from DCHN) undergoes very rapid cleavage to acetophenone and methyl radical in aqueous solution (34), it is reported to have a higher reactivity in hydrogen abstraction than *t*-BuȮ (34, 35). This current study reports on (*1*) An analysis of the **1***b* decomposition products, α,α-dimethylbenzyl alcohol (DMBA), acetophenone (AP), and dicumylperoxide (DCP) in *o*-dichlorobenzene containing unsaturated phospholipids, and a comparison of the initiator efficiency, *e*, from these product data with the overall *e* measured by a phenolic inhibitor, α-tocopherol (α-T). (*2*) Rate constants for thermal decomposition of **1***b* in bilayers compared to decomposition in organic solvents. (*3*) Analysis of the **1***b* products, DMBA, AP, and DCP in mixed bilayers containing dilinoleoylphosphatidylcholine (DLPC) and comparison of initiator *e* values so obtained with those from inhibition studies with α-T in the bilayer phase and 6-hydroxy-2,5,7,8-tetramethylchroman-2-carboxyl (Trolox) in the aqueous phase. (*4*) The kinetics of DCHN-initiated autoxidation and oxidizability of DLPC in mixed bilayers.

Experimental

1. Materials and preparations

Solvents

ortho-Dichlorobenzene, reagent grade, was dried over calcium chloride and distilled. Other solutions were hplc grade.

Phospholipids

The egg phosphatidylcholine (EPC), dilinoleoylphosphatidylcholine (DLPC), and dimyristoylphosphatidylcholine (DMPC) were obtained from Avanti Polar Lipids. 1-Palmitoyl-2-linoleoylphosphatidylcholine was synthesized in the laboratory of N. A. Porter by known methods (36). The phospholipids were stored in sealed vials in the dark at −30°C.

Inhibitors

α-Tocopherol (α-T) (Eastman-Kodak) was stored in known concentrations in hexane under argon at −30°C. The water-soluble Trolox, a gift from Hoffmann-LaRoche, Nutley, New Jersey, was used in freshly prepared aqueous solutions.

Dicumylhyponitrite (DCHN) was prepared by the procedure of Mendenhall (37) and recrystallized from methanol at low temperatures before use. Commercially available samples of α,α-dimethylbenzyl alcohol, acetophenone, and cumylperoxide were used to prepare standards for hplc analyses.

Bilayers

The multilamellar bilayer dispersions were prepared in 0.1 *M* sodium chloride (Ventron Ultrapure) by vortex stirring as described previously (5). Additives such as DCHN and α-T were introduced with the phospholipids in methylene chloride followed by evaporation of the solvent under reduced pressure. Trolox was added in aqueous solution as inhibitor after initiation of the autoxidations. The amount of DCHN remaining in the bilayer was determined by hplc analysis (*vide infra*).

2. Analyses

The amount of DCHN in each run in *ortho*-dichlorobenzene and incorporated into the phospholipids for the runs in bilayers was determined by hplc analysis. In addition autoxidation runs were continued until the DCHN had decomposed nearly completely into the products: α,α-dimethylbenzyl alcohol (DMBA), acetophenone (AP), and dicumylperoxide (DCP). These compounds were all determined quantitatively by hplc on small aliquots removed from the reactions for purposes of calculating the rate constant for DCHN decomposition and the initiator efficiency. The analyses were carried out on a SP-8000 hplc using a Brownlee RP-8 column operating at 15°C eluted with acetonitrile:water (40:60 for 25 min at 0.5 mL/min and 70:30 at 1.0 mL/min to 45 min). This procedure separated the desired products from solvent and phospholipids and gave the retention times: acetanilide (internal standard) 11.2 min, DMBA (15.7 min), AP (18.3 min), DCHN (38.7 min), and DCP (40.5 min). Three such measurements were made on each sample, the deviations being less than 5% for each compound.

The solubilities of di-*tert*-butylhyponitrite (DBHN) (7) and of DCHN in water were determined by shaking films (from methylene chloride) of these initiators with 2.00 mL of aqueous phase for 2 h at 30°C. The concentration in the filtered aqueous phase was measured by hplc (DBHN) or by ultraviolet analysis (DCHN) (38).

3. Autoxidation procedure

The autoxidations were carried out at 30°C and 760 Torr of O_2 using the sensitive automatic recording gas absorption apparatus and the procedures described earlier (5, 8).

Results and discussion

1. The initiator efficiency of DCHN

(a) In solution in ortho-dichlorobenzene

Results for the analysis of decomposition products from DCHN in the presence of oxygen and oxidizable phospholipids in solution in *o*-dichlorobenzene are summarized in Table 1. The proportion of α,α-dimethylbenzyl alcohol formed as measured by the ratio DMBA/2DCHN varies somewhat with DLPC concentration but the overall number (37 ± 6%) may be taken as an indicator of the effectiveness of the cumyloxy radical to initiate reaction by hydrogen abstraction in this system.

The significant amounts of acetophenone (AP) formed reflects the tendency of cumyloxy to readily undergo β-scission to produce the methyl radical, especially in the absence of an effective hydrogen atom donor (38). This raises the interesting question as to whether the derived methyl peroxy ($CH_3OO\cdot$) radical can also act as an initiator under these conditions. In order to test for this, we carried out some inhibition experiments using α-tocopherol to measure the efficiency of DCHN by the induction period method. The results of these experiments are given in Table 2. The efficiency so determined (e = 84 ± 5%)[2] is much higher than that accounted for by initiation via the cumyloxy radical alone. The *e* determined by product studies agrees with this value by the inhibitor method, within experimental error, if one includes the amount of acetophenone in the ratio and calculates *e* from the ratio: (DMBA + AP)/2DCHN (90 ± 6%). This indicates that the eliminated methyl radical, through the formation of $CH_3OO\cdot$, could play a significant role in initiating these autoxidations in homogeneous solutions. (Compare last columns of Tables 1 and 2.)[3]

[2]The "radical yield" from DCHN is reported to be 84% based on the DMBA yield in the presence of excess hydroquinone (39).

[3]A referee offers an alternative explanation; namely, that α-tocopherol could trap *all* of the cumyloxy radicals before they undergo β-scission.

TABLE 1. Thermal decomposition products of dicumylhyponitrite (DCHN) in *o*-dichlorobenzene at 30°C[a]

Run No.	Substrate[b] (mol × 10^5)	DCHN decomposed (mol × 10^6)	DMBA[c] (mol × 10^6)	AP[c] (mol × 10^6)	DCP[c] (mol × 10^7)	Material[d] balance (mol × 10^6)	DMBA / 2DCHN	DMBA + AP / 2DCHN
1	EPC (2.50)	6.40	4.40	7.73	7.52	6.80	0.344	0.948
2	DLPC (2.33)	5.97	4.79	5.90	7.01	6.05	0.401	0.895
3	DLPC (1.91)	13.8	8.00	14.0	14.9	12.5	0.290	0.797
4	DLPC (2.68)	12.8	8.29	15.5	22.5	14.1	0.324	0.929
5	DLPC (3.68)	3.93	3.39	3.99	6.75	4.37	0.431	0.939
6	PLPC (5.15)	5.27	4.26	5.32	9.80	5.77	0.404	0.909

[a]All runs in 2.00 mL volume and 760 Torr O_2.
[b]EPC, egg lecithin; DLPC, dilinoleoylphosphatidylcholine; PLPC, 1-palmitoyl-2-linoleoylphosphatidylcholine.
[c]DMBA, α,α-dimethylbenzyl alcohol; AP, acetophenone; DCP, dicumylperoxide.
[d]Material balance = the sum of ½DMBA + ½AP + DCP, measurements in moles.

TABLE 2. Determination of R_i and initiator efficiency for DCHN-initiated, α-tocopherol-inhibited autoxidation of phosphatidylcholines in *o*-dichlorobenzene[a]

Run No.	Substrate[b] (mol × 10^5)	DCHN $M \times 10^3$	α-Toc $M \times 10^4$	τ s × 10^{-3}	R_i $M\,s^{-1} \times 10^7$	$2k_i$[DCHN][c] $M\,s^{-1} \times 10^7$	e
1	EPC (2.50)	3.06	3.20	4.573	1.40	1.71	0.819
		2.39	4.00	7.235	1.11	1.34	0.829
2	DLPC (2.33)	2.46	3.20	5.994	1.07	1.38	0.775
3	DLPC (6.39)	6.39	2.89	1.748	3.31	3.58	0.925
		5.94	2.89	1.924	3.00	3.33	0.901
4	PLPC (1.93)	2.31	1.03	1.914	1.08	1.29	0.837
		2.14	1.03	2.003	1.03	1.20	0.858
5	PLPC (5.15)	2.40	1.03	1.929	1.07	1.34	0.799
		2.21	0.825	1.653	0.998	1.24	0.805

[a]See footnote *a*, Table 1.
[b]The same as footnote *b*, Table 1.
[c]$k_i = 2.80 \times 10^{-5}\ s^{-1}$ was used in the calculations (38), see Table 3, footnote *a*.

(b) Effect of phospholipid bilayers on initiator decomposition and efficiency of DCHN

In the course of product analysis from DCHN decomposition in DLPC bilayers, we discovered that nearly half of the DCHN remained after 20 h at 30°C although the rate constant *in solution* at 30°C ($k_i = 2.80 \times 10^{-5}\ s^{-1}$) (38) gives a half-life of only 7 h. This is a completely unexpected result, since the rate of decomposition of di-*tert*-butylhyponitrite was essentially independent of the medium (5), and it prompted us to explore the effect of the medium on the decomposition of DCHN. Some exploratory data are given in Table 3. We find that the k_i for DCHN in a bilayer (DLPC) is substantially less, approximately one-quarter of that in homogeneous solution in organic solvents. There is a similar lowering of the k_i in a viscous homogeneous medium (Nujol) to one-sixth of that in isooctane.

The effect of these media (Nujol and bilayers) on the decomposition rate of DCHN is very surprising. Despite the considerable evidence on the decomposition of organic hyponitrites as a convenient source of alkoxy radicals (40–48), there is no literature report that the decomposition of organic hyponitrites is retarded by high viscosity media. On the contrary, di-*tert*-butylhyponitrite (DBHN), which has been studied extensively, showed a 25% *increase* in k_i in a viscous solvent (Nujol) compared to that in isooctane, and this effect was attributed to "solvent stabilization" of DBHN by isooctane (40). A viscosity effect is more difficult to define when one considers the behaviour of solutes in bilayers. These have a gradation of fluidity as one moves from a region near the head group towards the terminal methyl groups (49). Thus the concept of a *microviscosity* of bilayers has been questioned (50), although there is no doubt that there is restriction of motion of molecules, and presumably of smaller solubilized compounds, when aggregated into bilayers.[4]

We interpret the viscosity effects of Nujol and DLPC bilayers on the rate of decomposition of DCHN in terms of a *one-bond scission* mechanism

$$R{-}O{-}N{=}N{-}OR \rightarrow R{-}O{-}N{=}N\cdot + \cdot OR.$$

Although evidence has been given for a two-bond concerted mechanism for scission of dialkylhyponitrites (42), the matter is not closed, even for di-*tert*-butylhyponitrite (45). It is known that the rate of a one-bond scission may depend on the solvent viscosity whereas two-bond concerted decompositions do not (51). The viscosity effect, found here for DCHN, is presumably due to the effect of high viscosity which retards the diffusion apart of the initially formed radical pair (above).[5] Our findings

[4]DPPC bilayers are reported to exert a "kinetic differentiation" in the k_i between *meso* and ± amphipathic diazenes resulting in a very significant rate ratio of decomposition of over 6 (27). It is possible that DLPC bilayers exert a specific effect on the DCHN decomposition rate; for example, if the two terminal phenyls are in regions of different microviscosities.

[5]The fraction of cage collapse as measured by the ratio DCP/ΔDCHN changed from 0.146 ± 0.035 in *ortho*-dichlorobenzene to 0.781 ± 0.058 in bilayers. The value in Nujol was 0.67, the same as reported for di-*tert*-butylhyponitrite (40).

TABLE 3. Rate constants for the thermal decomposition of DCHN at 30°C

Medium	Viscosity (cP)	[DCHN] (L^{-1})	$10^5 k_i$ (s^{-1})	Method[a]
Isooctane	0.475	—	2.80	Ref. 38
o-Dichlorobenzene	1.324	5.20×10^{-3}	2.21	hplc
DLPC bilayer	—[b]	0.268	0.604	N_2 evolution
DLPC bilayer		0.381	0.843	hplc
		0.193	0.737	hplc
Nujol[d]	79.9 (45°C)	1.80×10^{-2}	0.474[c]	N_2 evolution

[a]Rate constants by N_2 evolution were measured under nitrogen; measurements by hplc were determined on aliquots and are not corrected for DCHN lost during analyses.

[b]Microviscosity values for bilayers vary (e.g. egg lecithin 58–96 cP), according to the probe used for measurement, see ref. 5.

[c]The average of two measurements, 0.486×10^{-5} and 0.461×10^{-5} s^{-1}.

[d]High pressure liquid chromatographic analysis of products from the decomposition of DCHN (3.53×10^{-5} mol) gave DMBA (1.90×10^{-5} mol), AP (0.019×10^{-5} mol), and DCP (2.35×10^{-5} mol). See footnote 4 in text.

TABLE 4. Thermal decomposition products of dicumylhyponitrite (DCHN) in mixed bilayers at 30°C

Run No.	DLPC[b] *M* in bilayer	DCHN decomposed (mol × 10^6)	DMBA (mol × 10^6)	AP (mol × 10^7)	DCP (mol × 10^6)	Material balance (mol × 10^6)	DMBA / 2DCHN	(DMBA + AP) / 2DCHN
1	0.500	6.03	3.67	5.82	[c]	—	0.304	0.353
2	0.495	6.47	3.71	4.33	[c]	—	0.287	0.320
3	0.250	3.06	1.22	1.20	2.32	2.99	0.199	0.219
4	0.248	3.88	1.74	2.40	3.34	4.33	0.224	0.255
5	0.125	4.04	1.52	1.72	2.93	3.78	0.188	0.209
6	0.125	4.58	1.88	2.08	3.57	4.61	0.205	0.228
7	0	4.52	1.68	8.46	[c]	—	0.186	0.279

[a]All runs carried out in 0.1 *M* NaCl, 760 Torr O_2.

[b]Bilayers were prepared from DLPC + dimyristoylphosphatidycholine giving a total 20 mg sample in each run. DLPC concentrations are in *M* of total bilayer using a density of 0.8 (5).

[c]DCP was not completely resolved from bilayer material on hplc.

are fortuitous, especially in view of the various requirements before the viscosity test can be applied (51), and independent evidence is needed on the mechanism of decomposition of DCHN. In any event, this viscosity effect has important practical results; namely, this initiator has a convenient half-life in the hydrophobic phrase of bilayers to be a useful free radical initiator for quantitative autoxidation studies.

Our previous estimate of the solubility of DBHN in water (5) was based on an incorrect molar absorptivity. Therefore, we repeated this measurement here and find the solubility to be significantly higher (2.87×10^{-3} *M*) using a corrected $\epsilon = 5954$ at 227 nm (7). On the other hand, DCHN was found to be insoluble in water,[6] and we assume that it is completely solubilized in the hydrophobic bilayer phase.

Results for the analysis of decomposition products from DCHN in mixed bilayers are given in Table 4. The effectiveness of the cumyloxy radical to initiate reaction by hydrogen abstraction varied from 30 ± 1% to approximately 19% as the amount of readily abstractable hydrogen (e.g. DLPC) decreases. The overall efficiency *e* as determined by the ratio (DMBA + AP)/Δ2DCHN, with DLPC present, is consistently a few percent higher but *generally comparable to the efficiency of cumyloxy alone*. This behaviour is in marked contrast with that in homogeneous solution (Table 1, last column) and indicates that the methylperoxy radical does not contribute significantly to initiation in these bilayer experiments, probably because this small methylperoxy radical could diffuse rapidly out of the bilayer and decompose in the water. To test this idea we carried out some experiments to measure the *e* for DCHN in these bilayers by the inhibitor method with α-tocopherol (in the bilayer phase). These results are shown in Table 5. Now the overall *e* (26–30%) is comparable, within experimental error to the value obtained from products(s) of hydrogen abstraction alone at higher DLPC concentration, DMBA/2DCHN (Table 4), in contrast to the results from the use of α-tocopherol in solution (Table 2).

Some experiments were conducted using the water-soluble inhibitor 6-hydroxy-2,5,7,8-tetramethyl-chroman-2-carboxylate (Trolox) to compare its effectiveness with that of α-tocopherol, to inhibit autoxidation initiated in the hydrophobic bilayer phase by DCHN. We find that Trolox is *not* as effective at stopping the chain reaction as α-tocopherol. The initial rate during the inhibition period with Trolox typically was at least 5% of the uninhibited rate compared to only 2–3% when α-tocopherol was used. This difference in behavior is attributed to the nature of the multilamellar system used. With both DCHN and α-tocopherol uniformly distributed in these bilayers, there is efficient inhibition in all layers. On the other hand, Trolox

[6]Within the detection limit estimated to be $\leq 1.0 \times 10^{-6}$ *M*.

TABLE 5. Autoxidation of dilinoleoylphosphatidylcholine (DLPC) in mixed bilayers initiated by DCHN at 30°C[a]

Run No.	DLPC[b] (M) in bilayer	DCHN (M)	α-Toc ($M \times 10^3$)	τ $\times 10^{-3}$ s	R_i ($M\,s^{-1}\,10^7$)	$2k_i^e$[DCHN] ($M\,s^{-1} \times 10^6$)	e	$-dO_2/dt^f$ ($M\,s^{-1} \times 10^5$)	ν	$\frac{-dO_2/dt}{[RH]R_i^{1/2}}$ ($M^{-1/2}s^{-1/2}$)
1	0.495	0.254	2.40	6.084	7.89	3.07	0.257	2.02	26	0.0459
2	0.248	0.262	4.79	10.296	9.31	3.16	0.295	1.06	11	0.0443
3	0.500	0.219	—	—	7.30[c]	2.65	—	2.06	28	0.0482
4	0.125	0.253	—	—	8.43[c]	3.06	—	0.500	6	0.0436
5	DLPC 5.25×10^{-5} mol	0.193	0.819 Trolox (mol $\times 10^8$)	2.664	6.15[c]	2.33	0.264	3.62	59	0.0462
6	5.25×10^{-5} mol	0.186	4.38	1.854	5.93[d]	2.25	0.400	3.71	41	0.0482
7	5.25×10^{-5} mol	0.183	5.48	2.232	5.84[d]	2.21	0.423	4.21	45	0.0551
8	5.25×10^{-5} mol	0.179	6.57	3.096	5.71[d]	2.16	0.374	4.25	53	0.0562

[a]The same as footnote a, Table 4.
[b]See footnote b, Table 4. In runs 5–8 42 mg (5.25×10^{-5} mol) DLPC was used.
[c]An average $e = 0.276$ was used to calculate R_i.
[d]The $e = 0.264$ determined with α-Toc (Run 5) was used to calculate R_i.
[e]The k_i determined by N_2 evolution ($0.604 \times 10^{-5}\ s^{-1}$) was used (see Table 3 and Text).
[f]Rates are corrected for nitrogen evolution from the initiator, oxygen absorbed by the initiating radicals and evolved in chain termination by adding $(1 - e)k_i$[In] to the measured rate. Experimental errors in the rate measurements are estimated as ≤20%.

apparently can only effectively access the outer layers while some oxidation continues in the inner layers (52). Thus the apparent efficiency of DCHN as measured by Trolox *appears* to be higher than that measured by α-tocopherol.

2. The kinetics of autoxidation in mixed bilayers

The earlier conclusion that the classical rate law (eq. [1]) applied to the kinetics of autoxidation in bilayers was based only on the variation of the rate of oxygen uptake with the initiator (DBHN) concentration in egg lecithin bilayers and the near constancy of the resulting oxidizability. Results shown in Table 5 now provide important evidence on *the effect of oxidizable (DLPC) bilayer concentration* in mixed bilayers on the rate of oxygen uptake. Thus for approximately the same DCHN concentration in the bilayers, the rates are directly proportional to the DLPC concentration (Runs 1–4). This provides confirmation that the classical rate law is applicable to mixed bilayers. The oxidizability of DLPC in mixed bilayers ($0.046 \pm 0.002\ M^{-1/2}\ s^{-1/2}$) is the same, within experimental error, to that of neat DLPC ($0.051 \pm 0.005\ M^{-1/2}\ s^{-1/2}$), and the value is in agreement with previous reported results (6). A more detailed kinetic analysis and product studies on mixed bilayers for reactions initiated in either the aqueous phases or the bilayer phase is in progress.

Acknowledgements

Financial assistance provided by the Natural Sciences and Engineering Research Council of Canada is gratefully acknowledged. We thank Hoffmann-Laroche, Nutley, New Jersey for a sample of Trolox.

We are indebted to Steven Locke for his helpful technical assistance.

1. B. HALLIWELL and J. M. C. GUTTERRIDGE. Free radicals in biology and medicine. Oxford Science Publication. 1985.
2. W. BORS, M. SARAN, and D. TART (*Editors*). Oxygen radicals in chemistry and biology. 3rd International Conf., Neuherberg, Germany. W. de Gruyter, New York. 1984.
3. A. L. TAPPEL. *In* Free radicals in biology. Vol. IV. *Edited by* W. A. Pryor. Academic Press, New York. 1980. Chapt. 1, pp. 1–47.
4. L. R. C. BARCLAY and K. U. INGOLD. J. Am. Chem. Soc. **102**, 7792 (1980).
5. L. R. C. BARCLAY and K. U. INGOLD. J. Am. Chem. Soc. **103**, 6478 (1981).
6. L. R. C. BARCLAY, S. J. LOCKE, J. M. MACNEIL, J. VANKESSEL, G. W. BURTON, and K. U. INGOLD. J. Am. Chem. Soc. **106**, 2479 (1984).
7. L. R. C. BARCLAY, S. J. LOCKE, and J. M. MACNEIL. Can. J. Chem. **63**, 366 (1985).
8. L. R. C. BARCLAY, S. J. LOCKE, J. M. MACNEIL, and J. VANKESSEL. Can. J. Chem. **63**, 2633 (1985).
9. Y. YAMAMOTO, E. NIKI, and Y. KAMIYA. Bull. Chem. Soc. Jpn. **55**, 1548 (1982).
10. E. NIKI, R. TANIMURA, and Y. KAMIYA. Bull. Chem. Soc. Jpn. **55**, 1551 (1982).
11. Y. YAMAMOTO, E. NIKI, and Y. KAMIYA. Lipids, **17**, 870 (1982).
12. J. TSUCHIYA, E. NIKI, AND Y. KAMIYA. Bull. Chem. Soc. Jpn. **56**, 229 (1983).
13. E. NIKI, J. TSUCHIYA, R. TANIMURA, and Y. KAMIYA. Chem. Lett. 789 (1982); E. NIKI *et al.* Bull. Chem. Soc. Jpn. 631 (1983).
14. E. NIKI, T. SAITO, A. KAWAKAMI, and Y. KAMIYA. J. Biol. Chem. **259**, 4177 (1984).
15. G. W. BURTON and K. U. INGOLD. J. Am. Chem. Soc. **103**, 6472 (1981).
16. G. W. BURTON, L. HUGHES, and K. U. INGOLD. J. Am. Chem. Soc. **105**, 5950 (1983).
17. T. DOBA, G. W. BURTON, and K. U. INGOLD. J. Am. Chem. Soc. **105**, 6505 (1983).
18. G. W. BURTON and K. U. INGOLD. Protective agents in cancer. Academic Press, London. 1983.
19. G. W. BURTON and K. U. INGOLD. Science, **224**, 569 (1984).
20. J. W. WINTERLE, D. DULIN, and T. MILL. J. Org. Chem. **49**, 491 (1984).
21. L. R. C. BARCLAY, A. M. H. BAILEY, and D. KONG. J. Biol. Chem. **260**, 15809 (1985).
22. N. A. PORTER, B. A. WEBER, H. WEENEN, and J. A. KHAN. J. Am. Chem. Soc. **102**, 5597 (1980).
23. N. A. PORTER, L. S. LEHMAN, B. A. WEBER, and K. J. SMITH. J. Am. Chem. Soc. **103**, 6447 (1981).
24. H. WEENEN and N. A. PORTER. J. Am. Chem. Soc. **104**, 5216 (1982).
25. N. A. PORTER and D. G. WUJEK. J. Am. Chem. Soc. **106**, 2626 (1984).

26. J. S. WINTERLE and T. MILL. J. Am. Chem. Soc. **102**, 6336 (1980).
27. R. C. PETTER, J. C. MITCHELL, W. J. BRITTAIN, T. J. MCINTOSH, and N. A. PORTER. J. Am. Chem. Soc. **105**, 5700 (1983).
28. N. A. PORTER, R. C. PETTER, and W. J. BRITTAIN. J. Am. Chem. Soc. **106**, 803 (1984).
29. W. J. BRITTAIN, N. A. PORTER, and P. J. KREBS. J. Am. Chem. Soc. **106**, 7652 (1984).
30. F. R. MAYO. Acc. Chem. Res. **1**, 193 (1965).
31. K. U. INGOLD. Acc. Chem. Res. **2**, 1 (1969).
32. J. A. HOWARD. *In* Free radicals. Vol. II. *Edited by* J. K. Kochi. Wiley, New York. 1973. Chapt. 12, pp. 3–62; Adv. Free Radical Chem. **4**, 49 (1972).
33. C. E. BOOZER, G. S. HAMMOND, C. E. HAMILTON, and J. N. SEN. J. Am. Chem. Soc. **77**, 3233 (1955).
34. P. NETA, M. DIZDAROGLU, and M. G. SIMIC. Israeli J. Chem. **24**, 25 (1984).
35. A. BAIGNÉE, J. A. HOWARD, J. C. SCAIANO, and L. C. STEWART. J. Am. Chem. Soc. **105**, 6120 (1983).
36. N. A. PORTER, R. A. WOLF, and H. WEENEN. Lipids, **15**, 163 (1980).
37. C. A. OGLE, S. W. MARTIN, M. P. DZIOBAK, M. S. URBAN, and G. D. MENDENHALL. J. Org. Chem. **48**, 3728 (1983).
38. L. DULOG and P. KLEIN. Chem. Ber. **104**, 895 (1971).
39. L. DULOG and P. KLEIN. Chem. Ber. **104**, 902 (1971).
40. H. KIEFER and T. G. TRAYLOR. J. Am. Chem. Soc. **89**, 6667 (1967).
41. R. C. NEUMAN. J. Org. Chem. **37**, 495 (1972).
42. R. C. NEUMAN and R. J. BUSSEY. J. Am. Chem. Soc. **92**, 2440 (1970).
43. G. D. MENDENHALL, L. C. STEWART, and J. C. SCAIANO. J. Am. Chem. Soc. **104**, 5109 (1982).
44. E. M. Y. QUINGA and G. D. MENDENHALL. J. Am. Chem. Soc. **105**, 6520 (1983).
45. H. T. E. CHEN and G. D. MENDENHALL. J. Am. Chem. Soc. **106**, 6375 (1984).
46. E. M. Y. QUINGA and G. D. MENDENHALL. J. Org. Chem. **50**, 2836 (1985).
47. J. PROTASIEWICZ and G. D. MENDENHALL. J. Org. Chem. **50**, 3220 (1985).
48. C. A. OGLE, K. A. VANDERKOOI, G. D. MENDENHALL, V. LORPRAYOON, and B. C. CORNILSEN. J. Am. Chem. Soc. **104**, 5114 (1982).
49. W. L. HUBBELL and H. M. MCCONNELL. J. Am. Chem. Soc. **93**, 314 (1971).
50. B. L. SILVER. The physical chemistry of membranes. The Soloman Press, New York. 1985.
51. W. A. PRYOR and K. SMITH. J. Am. Chem. Soc. **92**, 5403 (1970).
52. T. DOBA, G. W. BURTON, and K. U. INGOLD. Biochim. Biophys. Acta, **835**, 298 (1985).

Acyl migration from N^6 to $N7$ of a 2′,3′-*O*-isopropylideneadenosine derivative accompanied by cyclonucleoside formation

KENTARO ANZAI[1] AND JUN UZAWA

The Institute of Physical and Chemical Research, Wako-shi, Saitama 351, Japan

Received December 24, 1985

KENTARO ANZAI and JUN UZAWA. Can. J. Chem. **64**, 2109 (1986).

Reaction of 2′,3′-*O*-isopropylideneadenosine (**1**) with *p*-NCC_6H_4COCl in 1:6 Et_3N–CH_2Cl_2 afforded the cyanoimidazole nucleoside **8** (53%) and the 8,5′-*O*-cycloadenosine derivative **7** (29%). Treatment of N^6,N^6-di-*p*-toluyl-2′,3′-*O*-isopropylideneadenosine (**23**) with $ZnBr_2$ in *p*-dioxane resulted in acyl migration from N^6 to $N7$ to give the cycloadenosine derivative **4**. The coordination site of the zinc cation on the base moiety of adenosine derivatives was determined by ^{15}N nmr spectra.

KENTARO ANZAI et JUN UZAWA. Can. J. Chem. **64**, 2109 (1986).

La réaction, dans un mélange 1:6 de Et_3N–CH_2Cl_2, du *O*-isopropylidène-2′,3′ adénosine (**1**) avec le *p*-NCC_6H_4COCl conduit au nucléoside du cyanoimidazole (**8**) (53%) ainsi qu'au dérivé *O*-cycloadénoside-8,5′ (**7**) (29%). Si l'on traite le N^6,N^6-di-*p*-toluyl *O*-isopropylidène-2′,3′ adénosine (**23**) par du $ZnBr_2$ dans du *p*-dioxanne, il en résulte une migration de l'acyle du N^6 vers le $N7$ ainsi que la formation du dérivé cycloadénosine **4**. On a fait appel à la rmn du ^{15}N pour déterminer le site de coordination du zinc sur la portion basique des dérivés de l'adénosine.

[Traduit par la revue]

Introduction

We reported previously (1) that reaction of 2′,3′-*O*-isopropylideneadenosine (**1**) with *p*-toluyl chloride in pyridine afforded 2′,3′-*O*-isopropylidene-N^6,N^6,5′-*O*-tri-*p*-toluyladenosine (**2**) as the main product (70%), as well as the tri-*p*-toluyl-8,5′-*O*-cycloadenosine derivative **3** as the minor one (6%). On the other hand, when the reaction was carried out in a mixture of methylene chloride and triethylamine (6:1), cyclonucleoside formation was the main reaction path, thus giving **2** (30%), **3** (34%), the di-*p*-toluyl-8,5′-*O*-cycloadenosine derivative **4** (11%), and the cyanoimidazole nucleoside **5** (12%), the formation of which was explained by initial acylation at $N1$ followed by $N1$—$C2$ elimination.

The present paper is an extension of the study on acylation of adenosine derivatives, which has led to the finding of acyl migration from N^6 to $N7$.

Results and discussion

Several *p*-substituted derivatives of benzoyl chloride were used in acylation of **1** in a mixture of methylene chloride and triethylamine (6:1), and the reaction products are listed in Table 1. The results showed that, in the methylene chloride – triethylamine solvent, cyclonucleoside formation predominated over the conventional acylation reaction and, in the case of reaction with *p*-cyanobenzoyl chloride (Entry 2), production of the cyanoimidazole nucleoside **8**, i.e. acylation at $N1$ of **1**, was the main reaction course. The ester bond in **8** was selectively cleaved to give **6**.

Reaction of **1** with excess *p*-toluyl chloride in a mixture of methylene chloride and pyridine (3:1) gave **2** (32%) and **3** (41%) without formation of **5** and, with a limited amount of the acid chloride in the same solvent, **1** was converted to **4** as the main reaction path as well as **21** as the minor one.

These results showed that, in the reaction of **1** with the substituted derivatives of benzoyl chloride, the product distribution, i.e. the position of attack on the base moiety of **1** by acyl groups (N^6, $N7$ or $N1$), seemed to be determined by several factors, i.e. solvent polarities, base species, and acylating reagents.

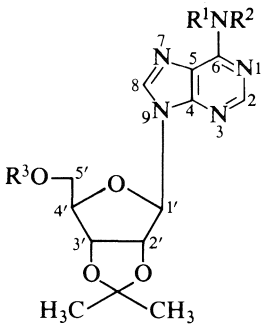

1 R^1,R^2,R^3 = H
2 R^1,R^2,R^3 = *p*-$CH_3C_6H_4CO$
9 R^1,R^2,R^3 = *p*-$CH_3OC_6H_4CO$
13 R^1,R^2,R^3 = *p*-BrC_6H_4CO
17 R^1,R^2,R^3 = *p*-ClC_6H_4CO
21 R^1 = H, R^2,R^3 = *p*-$CH_3C_6H_4CO$
23 R^1, R^2 = *p*-$CH_3C_6H_4CO$, R^3 = H
24 R^1, R^2 = *p*-$CH_3C_6H_4CO$
R^3 = $(p\text{-}CH_3OC_6H_4)_2C_6H_5C$
25 R^1, R^2 = *p*-$CH_3C_6H_4CO$, R^3 = CH_3COO
26 R^1 = *p*-$CH_3C_6H_4CO$, R^2, R^3 = H
27 R^1, R^2 = H, R^3 = *p*-$CH_3C_6H_4CO$
28 R^1, R^2 = H, R^3 = $(p\text{-}CH_3OC_6H_4)_2C_6H_5C$

Rearrangement of the N^6,N^6,5′-*O*-triacyladenosine compound **2** to its 8,5′-*O*-cycloadenosine isomer **3** was investigated under both acid and alkaline conditions. With zinc bromide as the acid catalyst, **2** was converted to **3** in low yield (18%), the main reaction path being hydrolysis to give **21** (54%). Another minor product (10%) was identified as the 4,5,6-triaminopyrimidine nucleoside **22**, based on the fact that the H-8 and C-8 signals of adenosine were missing on the ^1H nmr and ^{13}C nmr spectra of **22**. The assignment of the three carbonyl groups in the ^{13}C nmr spectrum was accomplished with help of selective $^{13}C\{^1H\}$ nOe (nuclear Overhauser enhancement) (2): δ 165.0 ($^{13}COOCH_2$, $^{13}C\{CH_2\}$ 50%), δ 164.5 ($^{13}CONH$, $^{13}C\{NH\}$ 50%), δ 166.0 ($^{13}CONH$, $^{13}C\{NH\}$ 60%).

Acyl migration from N^6 to $N7$ accompanied by cyclonucleoside formation as the sole reaction path was achieved using, as the starting material, N^6,N^6-di-*p*-toluyl-2′,3′-*O*-isopropyli-

[1]Author to whom correspondence may be addressed.

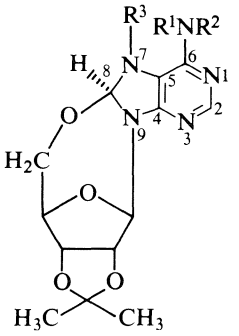

3 $R^1,R^2,R^3 = p\text{-}CH_3C_6H_4CO$
4 $R^1 = H, R^2, R^3 = p\text{-}CH_3C_6H_4CO$
7 $R^1,R^2,R^3 = p\text{-}NCC_6H_4CO$
10 $R^1,R^2,R^3 = p\text{-}CH_3OC_6H_4CO$
11 $R^1 = H, R^2,R^3 = p\text{-}CH_3OC_6H_4CO$
14 $R^1,R^2,R^3 = p\text{-}BrC_6H_4CO$
18 $R^1,R^2,R^3 = p\text{-}ClC_6H_4CO$
19 $R^1 = H, R^2,R^3 = p\text{-}ClC_6H_4CO$

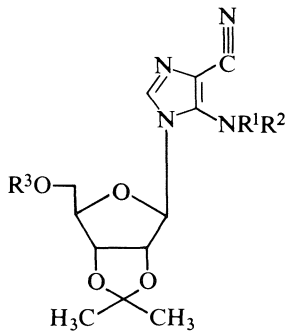

5 $R^1 = H, R^2,R^3 = p\text{-}CH_3C_6H_4CO$
6 $R^1,R^3 = H, R^2 = p\text{-}NCC_6H_4CO$
8 $R^1 = H, R^2,R^3 = p\text{-}NCC_6H_4CO$
12 $R^1 = H, R^2,R^3 = p\text{-}CH_3OC_6H_4CO$
15 $R^1,R^2,R^3 = p\text{-}BrC_6H_4CO$
16 $R^1 = H, R^2,R^3 = p\text{-}BrC_6H_4CO$
20 $R^1 = H, R^2,R^3 = p\text{-}ClC_6H_4CO$

deneadenosine (**23**), which was prepared by three different routes: (*1*) hydrolysis of the dimethoxytrityl derivative **24** in aqueous acetic acid, (*2*) hydrolysis of the acetyl derivative **25** in aqueous sodium hydrogen carbonate, and (*3*) hydrolysis attending rearrangement of the cyclonucleoside **3** in aqueous sodium hydrogen carbonate. Thus, reaction of **23** with zinc bromide in *p*-dioxane proceeded without hydrolysis to give the N^6,7-diacyl-8,5′-*O*-cycloadenosine derivative **4**.

The necessity of the N^6,N^6-diacyl structure in **23** for this

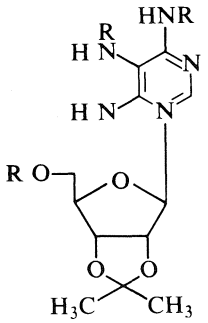

22 R = $p\text{-}CH_3C_6H_4CO$

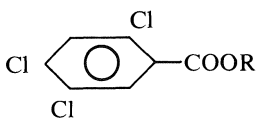

29 R = $p\text{-}CH_3C_6H_5$
30 R = C_6H_5

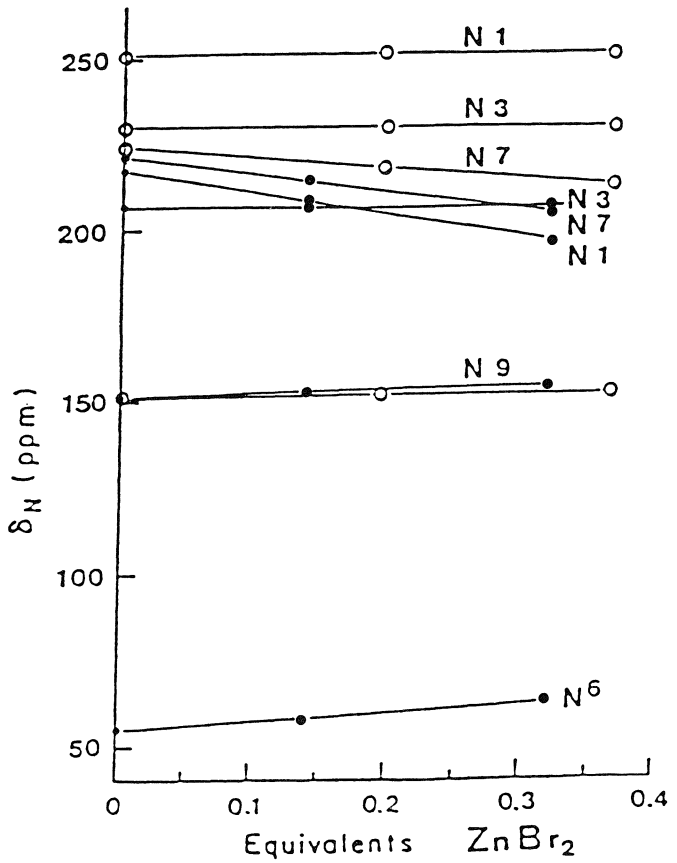

FIG. 1. The ^{15}N nmr chemical shifts of compound **2** (—○—) and compound **27** (—●—) in the presence of $ZnBr_2$.

rearrangement reaction was shown by the fact that 2′,3′-*O*-isopropylidene-N^6-*p*-toluyladenosine (**26**) was stable under the same conditions. The N^6-acyl compound **26** for this experiment was prepared by treatment with 2,4,5-trichlorophenyl-*p*-toluate (**29**). 2,4,5-Trichlorophenyl benzoate (**30**) had been used to acylate N^4 of cytidine selectively (3). In the present case the N^6,5′-*O*-di-*p*-toluyl compound **21** was also obtained as the minor product. Ammonium hydrolysis of **25** also gave **26**.

To learn something about the mechanism of the zinc bromide catalyzed conversion of **2** to **3** or **23** to **4**, we investigated how zinc bromide coordinated to the adenine ring. The ^{15}N nmr spectrum of the N^6,N^6,5′-*O*-tri-*p*-toluyl compound **2**[2] as well as that of 2′,3′-*O*-isopropylidene-5′-*O*-*p*-toluyladenosine (**27**) (1) were taken at the natural abundance level based on INEPT (4–6) in the presence and absence of zinc bromide (Fig. 1).[3] We found that the coordination site was *N*7 in the case of **2** and both *N*1 and *N*7 in the case of **27**, being shown by upfield shifts of the ^{15}N nmr signals on addition of zinc bromide (Δ 3 ppm for 0.1 equiv. of $ZnBr_2$). The coordination site of zinc cation on guanosine had been investigated using the ^{15}N nmr chemical shift (7).

In the ^1H nmr spectrum of **2** only the *H*-8 signal suffered a downfield shift to a considerable extent (Δ 0.2 ppm for 0.5 equiv. $ZnBr_2$). Coordination of zinc cation at *N*7 in **23**

[2]Determination of the coordination site of $ZnBr_2$ on the adenine ring of **23** using ^{15}H nmr spectra could not be accomplished, because cyclonucleoside formation proceeded during the period of taking the spectrum.

[3]The same experiment was run with the N^6-*p*-toluyladenosine compound **21**. The result was almost the same as was obtained for **2**.

TABLE 1. The reaction products from 2′,3′-*O*-isopropylideneadenosine and some *p*-substituted derivatives of benzoyl chloride in 1:6 Et_3N–CH_2Cl_2[a]

Entry	Acylating reagents	Products	Type of reaction[b] (number of acyl groups introduced)	Yields (%)
1	*p*-$CH_3C_6H_4COCl$	**2**	Non-cyclo (3)	30
		3	Cyclo (3)	34
		4	Cyclo (2)	11
		5	Ring cleavage (2)	12
2	*p*-NCC_6H_4COCl	**7**	Cyclo (3)	29
		8	Ring cleavage (2)	53
3	*p*-$CH_3OC_6H_4COCl$	**9**	Non-cyclo (3)	15
		10	Cyclo (3)	29
		11	Cyclo (2)	21
		12	Ring cleavage (2)	23
4	*p*-BrC_6H_4COCl	**13**	Non-cyclo (3)	7
		14	Cyclo (3)	33
		15	Ring cleavage (3)	11
		16	Ring cleavage (2)	36
5	*p*-ClC_6H_4COCl	**17**	Non-cyclo (3)	15
		18	Cyclo (3)	35
		19	Cyclo (2)	6
		20	Ring cleavage (2)	20

[a]Reaction conditions: room temperature, overnight. See also Experimental.
[b]Non-cyclo: conventional acylating reaction; cyclo: cyclonucleoside formation; ring cleavage: formation of cyanoimidazole nucleoside.

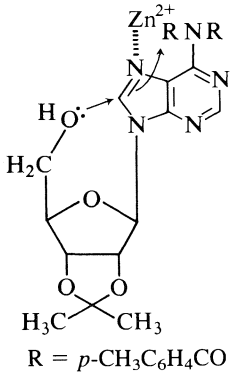

FIG. 2. Mechanistic drawing of the conversion of **23** to **4**.

would result in the decrease of π-electron density at *C*8, thus rendering possible attack of 5′-*O* at *C*8, accompanying acyl migration from N^6 to *N*7 (Fig. 2).

The mechanism of the conversion of **2** to **3** in the presence of zinc bromide is presumably a variation of that depicted in Fig. 2. The same conversion under alkaline conditions was also observed: i.e. **2** was treated in a mixture of propanol and 0.25 *M* $NaHCO_3$ (2:1) for 10 days, giving 30% of **3** with a 50% recovery of the starting material. To the best of our knowledge, acyl migration onto the basic moiety of adenosine compounds has not been reported previously.

Experimental

Measurement of ^{15}N nmr spectra

The ^{15}N nmr spectra were recorded using a JEOL FX-100 spectrometer with multinuclear observed system and PG-200 pulse programmer based on INEPT. Chemical shifts were measured relative to external aqueous NH_4NO_3 ($\delta_{NH_4^+}$ = 0). As the refocussed INEPT sequence (8, 9) gave a poor S/N ratio because of the presence of zinc bromide, which caused shortening of T_2, the measurement was carried out based on the non-refocussed INEPT sequence (4, 5). It was also useful to observe $^2J_{N,H}$, thus making it possible to establish the chemical shift assignment, i.e. selective low power irradiation ($\gamma B_2/2\pi$ = 25 Hz) on proton signals resulted in enhancement of nitrogen signals: τ = 16 ms ($1/4J$); ^1H 90° pulse, 11 ms; repetition time, 1.8 s.

General procedure for acylation of 2′,3′-O-isopropylideneadenosine (1)

To an ice-cooled solution of **1** in pyridine or a mixture of CH_2Cl_2 and an organic base (pyridine or Et_3N) was added an acyl chloride and, after the mixture was stirred at room temperature overnight, it was evaporated to dryness. The pyridine was removed as the toluene azeotrope. The residue was distributed between aqueous $NaHCO_3$ and $CHCl_3$ and, after the organic layer was washed with water and concentrated, it was applied to a silica gel column. Eluting solvents were, in most cases, mixtures of C_6H_6 and EtOAc, gradually increasing the latter content.

7,8-Dihydro-2′,3′-O-isopropylidene-N^6,N^6,7-tri-p-toluyl-8,5′-O-cycloadenosine (3)

The previous method (1) was modified to increase the yield of **3** and avoid the ring-cleavage reaction. Thus, **1** (921 mg, 3 mmol) was treated with *p*-toluyl chloride (4 g, 26 mmol) in a mixture of CH_2Cl_2 (30 mL) and pyridine (10 mL) following the general procedure for acylation. Silica gel chromatography (4:1 C_6H_6–EtOAc) afforded two compounds, the less polar one being **3**, mp 205–208°C (MeOH) (lit. (1) mp 182–185°C (toluene–hexane)); uv λ_{max} (MeOH): 253 nm (ε 47 000), 310 nm (sh) (ε 12 600). The more polar one was *2′,3′-O-isopropylidene-N^6,N^6,5′-O-p-toluyladenosine* (**2**), yield 630 mg (32%), mp 188–189°C (MeOH) (lit. (1) mp 189–190°C (MeOH)); uv λ_{max} (MeOH): 243 nm (ε 35 000), 275 nm (sh) (ε 27 000).

7,8-Dihydro-N^6,7-di-p-toluyl-2′,3′-O-isopropylidene-8,5′-O-cycloadenosine (4)

Treatment of **1** (921 mg, 3 mmol) with *p*-toluyl chloride (1.8 g, 11.8 mmol) in a mixture of CH_2Cl_2 (30 mL) and pyridine (2 mL) afforded, as was shown on tlc, four products, which were separated on

a silica gel column by eluting with a mixture of C_6H_6 and EtOAc (4:1), gradually increasing the latter content. Thus, **3** (120 mg, 6%) and **2** (70 mg, 4%) were eluted with 4:1 to 2:1 C_6H_6–EtOAc, **4** (810 mg, 50%) with 2:1 to 1:1 C_6H_6–EtOAc, and **21** (280 mg, 17%) with EtOAc; **4**: mp 229–230°C (C_6H_6) (lit. (1) mp 229–230°C (C_6H_6)); uv λ_{max} (MeOH): 240 nm (ε 28 800), 285 nm (ε 15 200); **21**, glassy solid from toluene–ligroin (1).

*4-Cyano-1-(2,3-O-isopropylidene-β-D-ribofuranosyl)-5-(*p*-cyanobenzoylamino)imidazole (**6**)*

(*a*) A solution of **8** (1) (1 g, 1.86 mmol) in a mixture of MeOH (20 mL) and 1 *M* NaOH (5 mL) was left standing at room temperature overnight and neutralized with AcOH to pH 5. The product was, after the methanol was removed by evaporation, extracted with $CHCl_3$ and separated by silica gel chromatography (EtOAc), yield 680 mg (89%), mp 191–192°C (BuOAc); ir ν_{max} (KBr) cm^{-1}; 2250 (m, CN), 1670 (s, NH_2CO); uv λ_{max} (MeOH): 235 nm (ε 25 400), 285 (sh) (ε 4100); ^1H nmr data (100 MHz, $CDCl_3$) δ: 5.78 (s, 1H, H-1′, $J_{1',2'}$ = 2 Hz), 7.76 (s, 1H, H-2), 7.81 and 8.10 (2d, 4H, *p*-cyanobenzoyl, J_o = 7 Hz). *Anal.* calcd. for $C_{20}H_{19}O_5N_5$: C 58.67, H 4.68, N 17.11; found: C 58.90, H 4.57, N 17.25.

(*b*) A solution of **8** (269 mg, 0.5 mmol) in a mixture of EtOH (10 mL) and concentrated NH_4OH (1 mL) was left standing at room temperature for one week. After ammonia was removed by evaporation, the product was isolated as mentioned in (*a*), yield 190 mg (93%).

*Reaction of **1** with* p*-cyanobenzoyl chloride*

Compound **1** (3.07 g, 10 mmol) was treated with *p*-cyanobenzoyl chloride (7.8 g, 47 mmol) in a mixture of CH_2Cl_2 (150 mL) and Et_3N (25 mL). *7,8-Dihydro-2′,3′-*O*-isopropylidene-*N^6,N^6,*7-tri-*p*-cyanobenzoyl-8,5′-*O*-cycloadenosine (**7**)* was eluted from a silica gel column with 4:1 C_6H_6–EtOAc, yield 2.04 g (29%), mp 236.5–237.5° (MeOH); uv λ_{max} (MeOH): 243 nm (ε 47 900); ^1H nmr data (100 MHz, $CDCl_3$) δ: 3.30 (dd, 1H, H-5′a, J_{gem} = 12 Hz, $J_{4,5'a}$ = 2 Hz), 3.94 (d, 1H, H-5′b, J_{gem} = 12 Hz), 5.81 (s, 1H, H-1′), 6.08 (s, 1H, H-8), 8.16 (s, 1H, H-2). *Anal.* calcd. for $C_{37}H_{26}O_7N_8 \cdot 1/2\ H_2O$: C 63.16, H 3.74, N 15.93; found: C 63.14, H 3.74, N 15.79.

*4-Cyano-5-*p*-cyanobenzoylamino-1-(5-*O*-*p*-cyanobenzoyl-2,3-*O*-isopropylidene-β-D-ribofuranosyl)imidazole (**8**)* was eluted with 1:1 C_6H_6–EtOAc, yield 2.87 g (53%), mp 139–143°C (toluene); ir ν_{max} (KBr): 2250 cm^{-1} (m, CN); uv λ_{max} (MeOH): 247 nm (ε 37 800); ^1H nmr data (100 MHz, $CDCl_3$) δ: 5.88 (d, 1H, H-1′, $J_{1',2'}$ = 2 Hz), 7.68 (s, 1H, H-2); ms *m/e*: 538 (M^+). *Anal.* calcd. for $C_{28}H_{22}O_6N_6$: C 62.45, H 4.12, N 15.61; found: C 62.43, H 4.26, N 15.39.

*Reaction of **1** with* p*-anisoyl chloride*

Compound **1** (1.54 g, 5 mmol) was treated with *p*-anisoyl chloride (5 g, 29 mmol) in a mixture of CH_2Cl_2 (150 mL) and Et_3N (25 mL). *7,8-Dihydro-2′,3′-*O*-isopropylidene-*N^6,N^6,*7-tri-*p*-anisoyl-8,5′-*O*-cycloadenosine (**10**)* was eluted from a silica gel column with 4:1 C_6H_6–EtOAc, yield 1.04 g (29%), mp 167–170°C (MeOH); uv λ_{max} (MeOH): 278 nm (ε 45 000); ^1H nmr data (100 MHz, $CDCl_3$) δ: 3.42 (dd, 1H, H-5′a, J_{gem} = 14 Hz, $J_{4,5'a}$ = 2 Hz), 3.94 (d, 1H, H-5′b, J_{gem} = 14 Hz), 5.80 (s, 1H, H-1′), 6.08 (s, 1H, H-8), 8.21 (s, 1H, H-2). *Anal.* calcd. for $C_{37}H_{35}O_{10}N_5$: C 62.61, H 4.97, N 9.87; found: C 62.38, H 4.92, N 9.64.

*2′,3′-*O*-Isopropylidene-*N^6,N^6,*5′-*O*-tri-*p*-anisoyladenosine (**9**)* was eluted with 2:1 to 1:1 C_6H_6–EtOAc, yield 540 mg (15%), mp 144.5–145.5°C (MeOH). **Notice**: the solubility of this compound in MeOH at room temperature is lower than that in a refrigerator; uv λ_{max} (MeOH): 260 nm (sh) (ε 39 000), 272 nm (ε 41 100), 290 nm (ε 37 600); ^1H nmr data (100 MHz, $CDCl_3$) δ: 4.56 (br, 3H, H-4′ and H-5′), 6.14 (d, 1H, H-1′, $J_{1',2'}$ = 3 Hz), 8.16 (s, 1H, H-8), 8.64 (s, 1H, H-2). *Anal.* calcd. for $C_{37}H_{35}O_{10}N_5$: C 62.61, H 4.97, N 9.87; found: C 62.64, H 4.94, N 9.90.

*5-*p*-Anisoylamino-1-(5-*O*-*p*-anisoyl-2,3-*O*-isopropylidene-β-D-ribofuranosyl)-4-cyanoimidazole (**12**)* was eluted with 1:1 C_6H_6–EtOAc and obtained as a glassy solid from toluene, yield 630 mg (23%); ir ν_{max} (KBr): 2250 cm^{-1} (m, CN); uv λ_{max} (MeOH): 259 (ε 34 400); ^1H nmr data (100 MHz, $CDCl_3$) δ: 5.84 (d, 1H, H-1′, $J_{1',2'}$ = 3 Hz), 7.64 (s, 1H, H-2); ms *m/e*: 548 (M^+). *Anal.* calcd. for $C_{28}H_{28}O_8N_4$: C 61.31, H 5.15, N 10.21; found: C 61.16, H 5.10, N 10.35.

*N^6,7-di-*p*-Anisoyl-7,8-dihydro-2′,3′-*O*-isopropylidene-8,5′-*O*-cy*cloadenosine (**11**) was eluted with EtOAc and obtained as a glassy solid from toluene, yield 610 mg (21%); uv λ_{max} (MeOH): 266 nm (ε 39 100); ^1H nmr data (100 MHz, $CDCl_3$) δ: 3.48 (dd, 1H, H-5′a, J_{gem} = 14 Hz, $J_{4',5'a}$ = 2 Hz), 3.92 (d, 1H, H-5′b, J_{gem} = 14 Hz), 5.83 (s, 1H, H-1′), 6.07 (s, 1H, H-8), 8.52 (s, 1H, H-2). *Anal.* calcd. for $C_{29}H_{29}O_8N_5$: C 60.51, H 5.08, N 12.17; found: C 60.50, H 5.12, N 11.96.

*Reaction of **1** with* p*-bromobenzoyl chloride*

Compound **1** (1.54 g, 5 mmol) was treated with *p*-bromobenzoyl chloride (8 g, 36.4 mmol) in a mixture of CH_2Cl_2 (150 mL) and Et_3N (25 mL). *7,8-Dihydro-2′,3′-*O*-isopropylidene-*N^6,N^6,*5′-*O*-tri-*p*-bromobenzoyl-8,5′-*O*-cycloadenosine (**14**)* was eluted first from a silica gel column with 4:1 C_6H_6–EtOAc, yield 1.41 g (33%), mp 197–199°C (EtOH); uv λ_{max} (MeOH): 254 nm (ε 41 900), 315 nm (sh) (ε 6800); ^1H nmr data (100 MHz, $CDCl_3$) δ: 3.37 (dd, 1H, H-5′a, J_{gem} = 13 Hz, $J_{4',5'a}$ = 2 Hz), 3.94 (d, 1H, H-4, J_{gem} = 13 Hz), 5.80 (s, 1H, H-1′), 6.07 (s, 1H, H-8), 8.20 (s, 1H, H-2). *Anal.* calcd. for $C_{34}H_{26}O_7N_5Br_3$: C 47.68, H 3.06, N 8.18, Br 28.00; found: C 47.57, H 2.97, N 8.03, Br 27.90.

*2′,3′-*O*-Isopropylidene-*N^6,N^6,*5′-*O*-tri-*p*-bromobenzoyladenosine (**13**)* was eluted with 4:1 C_6H_6–EtOAc contaminated by **14**. However, an analytically pure sample of **13** was obtained by crystallization from BuOH, yield 360 mg (7%), mp 214–215°C; uv λ_{max} (MeOH): 242 nm (ε 67 600), 275 nm (sh) (ε 18 500); ^1H nmr data (100 MHz, $CDCl_3$) δ: 6.16 (d, 1H, H-1′, $J_{1',2'}$ = 2 Hz), 8.16 (s, 1H, H-8), 8.61 (s, 1H, H-2). The isolated sample was found to be a *p*-bromobenzoic acid adduct. *Anal.* calcd. for $C_{34}H_{26}O_7N_5Br_3 \cdot BrC_6H_4CO_2H$: C 46.57, H 2.96, N 6.62, Br 30.23; found: C 46.80, H 2.84, N 6.55, Br 30.54.

*1-(5-*O*-p-bromobenzoyl-2,3-*O*-isopropylidene-β-D-ribofuranosyl)-4-cyano-5-di-*p*-bromobenzoylaminoimidazole (**15**)* was eluted with 4:1 to 2:1 C_6H_6–EtOAc and obtained as a glassy solid from toluene–ligroin, yield 450 mg (11%); ir ν_{max} (KBr): 2250 cm^{-1} (m, CN); uv λ_{max} (MeOH): 248 nm (ε 35 900); ^1H nmr data (100 MHz, $CDCl_3$) δ: 1.32 and 1.44 (2s, 6H, 2 isopropylidene methyls), 4.5 (br, 2H, H-5′), 4.68 (complex, 1H, H-4′), 4.84 (dd, 1H, H-3′, $J_{3',4'}$ = 2 Hz, $J_{2',3'}$ = 6 Hz), 5.02 (dd, 1H, H-2′, $J_{2',3'}$ = 6 Hz, $J_{1',2'}$ = 3 Hz), 5.78 (d, 1H, H-1′, $J_{1',2'}$ = 3 Hz), 7.3–7.8 (aromatic protons and H-2). *Anal.* calcd. for $C_{33}H_{25}O_7N_4Br_3$: C 47.79, H 3.04, N 6.76, Br 28.91; found: C 48.09, H 3.07, N 6.78, Br 28.79.

*5-*p*-Bromobenzoylamino-1-(5-*O*-*p*-bromobenzoyl-2,3-*O*-isopropylidene-β-D-ribofuranosyl)-4-cyanoimidazole (**16**)* was eluted with 1:1 C_6H_6–EtOAc, yield 1.17 g (36%), mp 114–115°C (toluene); uv λ_{max} (MeOH): 244 nm (ε 36 100); ^1H nmr data (100 MHz, $CDCl_3$) δ: 1.32 and 1.44 (2s, 6H, 2 isopropylidene methyls), 4.5 (br, 2H, H-5′), 4.68 (complex, 1H, H-4′), 4.76 (dd, 1H, H-3′, $J_{3',4'}$ = 2 Hz, $J_{2',3'}$ = 6 Hz), 4.92 (dd, 1H, H-2′, $J_{2',3'}$ = 6 Hz, $J_{1',2'}$ = 3 Hz), 5.85 (d, 1H, H-1′, $J_{1',2'}$ = 3 Hz), 7.64 (s, 1H, H-2), 8.84 (br s, 1H, NH). *Anal.* calcd. for $C_{26}H_{22}O_6N_4Br_2$: C 48.31, H 3.43, N 8.67, Br 24.73; found: C 48.14, H 3.36, N 8.57, Br 24.73.

*Reaction of **1** with* p*-chlorobenzoyl chloride*

Compound **1** (3.07 g, 10 mmol) was treated with *p*-chlorobenzoyl chloride (14 g, 80 mmol) in a mixture of CH_2Cl_2 (300 mL) and Et_3N (50 mL). *7,8-Dihydro-2′,3′-*O*-isopropylidene-*N^6,N^6,*7-tri-*p*-chlorobenzoyl-8,5′-*O*-cycloadenosine (**18**)* was eluted from a silica gel column with 9:1 to 4:1 C_6H_6–EtOAc, yield 2.5 g (35%), mp 184–186°C (EtOH); uv λ_{max} (MeOH): 248 nm (ε 39 700), 310 nm (sh) (ε 7900); ^1H nmr data (100 MHz, $CDCl_3$) δ: 3.37 (dd, 1H, H-5′a, J_{gem} = 13 Hz, $J_{4',5'a}$ = 2 Hz), 3.96 (d, 1H, H-5′b, J_{gem} = 13 Hz), 5.82 (s, 1H, H-1′), 6.07 (s, 1H, H-8), 8.19 (s, 1H, H-2); ms *m/e*: 727, 725, 723 (a cluster of parent ions). *Anal.* calcd. for $C_{34}H_{26}O_7N_5Cl_3$: C 56.48, H 3.63, N 9.69, Cl 14.71; found: C 56.37, H 3.62, N 9.64, Cl 14.85.

*2′,3′-*O*-Isopropylidene-*N^6,N^6,*5′-*O*-tri-*p*-chlorobenzoyladenosine (**17**)* was eluted with 4:1 C_6H_6–EtOAc, yield 1.6 g (15%), mp 180–181°C (toluene); uv λ_{max} (MeOH): 237 nm (ε 80 800), 275 nm (sh)

(ε 41 400); ^{1}H nmr (100 MHz, $CDCl_3$) δ: 6.19 (d, 1H, H-1′, $J_{1',2'}$ = 3 Hz), 8.21 (s, 1H, H-8), 8.64 (s, 1H, H-2); ms *m/e*: 727, 725, 723 (a cluster of parent ions). The isolated sample was found to contain two moles of *p*-chlorobenzoic acid as the adduct. *Anal.* calcd. for $C_{34}H_{26}O_7N_5Cl_3 \cdot 2ClC_6H_4CO_2H$: C 55.64, H 3.50, N 6.76, Cl 17.11; found: C 55.49, H 3.49, N 6.64, Cl 17.10.

N^6,*7-Dichlorobenzoyl-7,8-dihydro-2′,3′-*O*-isopropylidene-8,5′-*O*-cycloadenosine (**19**)* was eluted with 4:1 C_6H_6–EtOAc and obtained as a glassy solid from toluene–hexane, yield 370 mg (6%); uv λ_{max} (MeOH): 242 nm (ε 31 800), 265 nm (ε 30 000); ^{1}H nmr data (100 MHz, $CDCl_3$) δ: 3.36 (dd, 1H, H-5′a, J_{gem} = 13 Hz, $J_{4',5'a}$ = 3 Hz), 3.88 (d, 1H, H-5′b, J_{gem} = 13 Hz), 5.80 (s, 1H, H-1′), 6.04 (s, 1H, H-8), 8.02 (s, 1H, H-2). *Anal.* calcd. for $C_{27}H_{23}O_6N_5Cl_2$: C 55.48, H 3.97, N 11.99, Cl 12.14; found: C 55.59, H 4.05, N 11.62, Cl 11.93.

*5-*p*-Chlorobenzoylamino-1-(5-*O*-*p*-chlorobenzoyl-2,3-*O*-isopropylidene-β-*D*-ribofuranosyl)-4-cyanoimidazole (**20**)* was eluted with 2:1 C_6H_6–EtOAc, yield 1.1 g (20%), mp 118–120°C (toluene); ir ν_{max} (KBr): 2250 cm^{-1} (m, CN); uv λ_{max} (MeOH): 239 nm (ε 32 400); ^{1}H nmr data (100 MHz, $CDCl_3$) δ: 5.83 (d, 1H, H-1′, $J_{1',2'}$ = 3 Hz), 7.83 (s, 1H, H-2), 9.90 (br s, 1H, NH); ms *m/e*: 560, 558, 556 (a cluster of parent ions). *Anal.* calcd. for $C_{26}H_{22}O_6N_4Cl_2$: C 56.02, H 3.98, N 10.05, Cl 12.72; found: C 56.22, H 4.02, N 9.92, Cl 12.66.

*Treatment of **2** with $ZnBr_2$ in* p*-dioxane*

A solution of **2** (935 mg, 1.41 mmol) and $ZnBr_2$ (10 g) in *p*-dioxane (100 mL) was left standing at room temperature for 4 days. Aqueous $NaHCO_3$ was added and, after the precipitate of $Zn(OH)_2$, was removed by centrifugation; the products were extracted with $CHCl_3$. Thin-layer chromatography (1:1 C_6H_6–EtOAc) showed the presence of three uv-absorbing compounds, which were separated by silica gel chromatography. Compound **3** was eluted with 2:1 C_6H_6–EtOAc, yield 170 mg (18%).

N^5,N^6-*di*-*p*-*toluylamino*-N^4-*(2,3-*O*-isopropylidene-5-*O*-*p*-toluyl-β-*D*-ribofuranosyl)-4,5,6-triaminopyrimidine (**22**)* was eluted with 1:1 C_6H_6–EtOAc and obtained as a glassy solid from toluene, yield 90 mg (10%); uv λ_{max} (MeOH): 240 nm (ε 39 400); ^{1}H nmr data (100 MHz, $CDCl_3$) δ: 1.36 and 1.58 (2s, 6H, 2 isopropylidene methyls), 2.32, 2.36, and 2.40 (3s, 9H, *p*-toluyl methyls), 6.73 (s, 1H, H-1′, $J_{1',2'}$ = 4 Hz), 8.16 (s, 1H, H-1′), 9.00 and 9.60 (2s, 2H, 2NH, collapsed on addition of D_2O); ^{13}C nmr data ($CDCl_3$, TMS) δ: 159.6 (C4), 155.1 (C2, ^1J = 201.4 Hz), 153.1 (C6), 108.9 (C5), 87.6 (C1′), 83.6 (C2′), 81.6 (C4′), 81.2 (C3′), 64.6 (C5′); ms *m/e*: 651 (M^+), 636 ($M^+ - CH_3$), 532 ($M^+ - CH_3C_6H_4CO$), 516 ($M^+ - CH_3C_6H_4CONH_2$). *Anal.* calcd. for $C_{36}H_{37}O_7N_5 \cdot 1/4H_2O$: C 65.89, H 5.76, N 10.67; found: C 65.91, H 5.78, N 10.66.

N^6,*5′-*O*-Di-*p*-toluyl-2′,3′-*O*-isopropylideneadenosine (**21**)* was eluted with EtOAc, yield 380 mg (54%).

*Treatment of **2** with aqueous $NaHCO_3$*

A solution of **2** (500 mg, 0.76 mmol) in a mixture of PrOH (100 mL) and 0.25 *M* $NaHCO_3$ (50 mL) was left standing at room temperature for 10 days. The propanol was removed by evaporation and the products were extracted with EtOAc. Thin-layer chromatography (4:1 C_6H_6–EtOAc) showed the presence of two uv-absorbing compounds, which were separated by silica gel chromatography eluting with 4:1 C_6H_6–EtOAc. The less polar compound was **3**, yield 150 mg (30%). The more polar compound was the starting material with a recovery of 250 mg (50%).

N^6,N^6-*di*-*p*-*toluyl-2′,3′-*O*-isopropylideneadenosine (**23**)*

(*1*) A solution of **24** (350 mg, 0.41 mmol) in 70% AcOH (10 mL) was left standing at room temperature for 1 h and concentrated to dryness keeping the temperature below 40°C. After the residue was distributed between EtOAc and aqueous $NaHCO_3$, the organic layer was applied to silica gel chromatography (1:1 C_6H_6–EtOAc followed by EtOAc) to obtain a glassy solid (C_6H_6–ligroin), yield 160 mg (72%); uv λ_{max} (MeOH): 260 nm (ε 27 700), 275 nm (sh) (ε 25 500); ^{1}H nmr data (100 MHz, $CDCl_3$) δ: 1.42 and 1.68 (2s, 6H, 2 isopropylidene methyls), 2.40 (s, 6H, 2 *p*-toluyl methyls), 5.96 (d, 1H, H-1′, $J_{1',2'}$ = 4 Hz), 8.18 (s, 1H, H-8), 8.66 (s, 1H, H-2). *Anal.* calcd. for $C_{29}H_{29}O_6N_5$: C 64.08, H 5.38, N 12.89; found: C 63.99, H 5.45, N 12.75.

(*2*) A solution of **25** (7.5 g, 12.8 mmol) in a mixture of 0.25 *M* $NaHCO_3$ (1 L) and EtOH (1 L) was left standing for 6 days. After the ethanol was removed by evaporation, the product was extracted with $CHCl_3$. Silica gel chromatography (1:1 C_6H_6–EtOAc) afforded 5.95 g (86%) of **23**.

(*3*) A solution of **3** (1.32 g, 2 mmol) in a mixture of acetone (100 mL), MeOH (80 mL), and 0.25 *M* $NaHCO_3$ (20 mL) was refluxed for 3 h. The organic solvent was removed by evaporation and the product was extracted with $CHCl_3$. Silica gel chromatography (1:1 C_6H_6–EtOAc) afforded 770 mg (71%) of **23**.

*5′-*O*-(4,4′-dimethoxytrityl)-*N^6,N^6-*di*-*p*-*toluyl-2′,3′-*O*-isopropylideneadenosine (**24**)*

Compound **28** (981 mg, 1.61 mmol) was treated with *p*-toluyl chloride (800 mg, 5.18 mmol) in pyridine (10 mL). Silica gel chromatography (4:1 C_6H_6–EtOAc) afforded 860 mg (63%) of a glassy solid (ligroin); uv λ_{max} (MeOH): 234 nm (ε 33 800), 260 nm (ε 29 600), 275 nm (sh) (ε 27 000); ^{1}H nmr data (100 MHz, $CDCl_3$) δ: 1.39 and 1.63 (2s, 6H, 2 isopropylidene methyls), 2.32 (s, 6H, 2 *p*-toluyl methyls), 3.74 (s, 6H, $2CH_3O$), 6.14 (d, 1H, H-1′, $J_{1',2'}$ = 3 Hz), 8.16 and 8.49 (2s, 2H, H-8 and H-2). *Anal.* calcd. for $C_{50}H_{47}O_8N_5$: C 70.99, H 5.60, N 8.28; found: C 71.10, H 5.68, N 8.08.

*5′-*O*-acetyl-*N^6,N^6-*di*-*p*-*toluyl-2′,3′-*O*-isopropylideneadenosine (**25**)*

5′-O-Acetyl-2′,3′-*O*-isopropylideneadenosine (1.745 g, 5 mmol) was treated with *p*-toluyl chloride (3 g, 19 mmol) in pyridine (50 mL). Silica gel chromatography (2:1 C_6H_6–EtOAc) afforded 2.75 g (94%) of a glassy solid (C_6H_6–ligroin); uv λ_{max} (MeOH): 260 nm (ε 29 000), 275 nm (sh) (ε 27 000); ^{1}H nmr data (100 MHz, $CDCl_3$) δ: 1.40 and 1.63 (2s, 6H, 2 isopropylidene methyls), 1.98 (s, 3H, acetyl), 2.36 (s, 6H, 2 *p*-toluyl methyls), 6.16 (d, 1H, H-1′, $J_{1',2'}$ = 3 Hz), 8.17 (s, 1H, H-8), 8.68 (s, 1H, H-2). *Anal.* calcd. for $C_{31}H_{31}O_7N_5$: C 63.58, H 5.34, N 11.96; found: C 63.63, H 5.39, N 11.71.

*2′,3′-*O*-isopropylidene-*N^6-*p*-*toluyladenosine (**26**)*

(*1*) A solution of **1** (767.5 mg, 2.5 mmol) and 2,4,5-trichlorophenyl *p*-toluate (945 mg, 3 mmol) in pyridine (30 mL) was refluxed for one week. Thin-layer chromatography (EtOAc) showed the presence of two products as well as the starting material in the reaction mixture. The solution was concentrated to dryness and the residue was applied to a silica gel column. Elution with EtOAc afforded 220 mg (16%) of **21**. Compound **26** was eluted with 9:1 EtOAc–MeOH, yield 510 mg (48%), mp 170–171°C (toluene); uv λ_{max} (MeOH): 255 nm (ε 15 700), 279 nm (ε 21 900); ^{1}H nmr data (100 MHz, $CDCl_3$) δ: 1.40 and 1.66 (2s, 6H, 2 isopropylidene methyls), 2.44 (s, 3H, *p*-toluyl methyl), 6.06 (d, 1H, H-1′, $J_{1',2'}$ = 4 Hz), 8.19 (s, 1H, H-8), 8.76 (s, 1H, H-2). *Anal.* calcd. for $C_{21}H_{23}O_5N_5$: C 59.28, H 5.45, N 16.46; found: C 59.26, H 5.40, N 16.33.

(*2*) A solution of **25** (500 mg, 0.85 mmol) in a mixture of EtOH (40 mL) and concentrated NH_4OH (20 mL) was left standing at room temperature for 1.5 h. The main product was isolated by silica gel chromatography (EtOAc), yield 210 mg (58%). Other minor products, which were eluted with 19:1 to 9:1 EtOAc–MeOH, were 5′-*O*-acetyl-2′,3′-*O*-isopropylideneadenosine (30 mg, 10%) and **1** (20 mg, 8%).

*5′-*O*-(4,4′-dimethoxytrityl)-2′,3′-*O*-isopropylideneadenosine (**28**)*

To an ice-cooled solution of **1** (1.04 g, 5 mmol) in pyridine (50 mL) was added 4,4′-dimethoxytrityl chloride (1.8 g, 5.3 mmol) portionwise during a period of 5 h, and the reaction mixture was left standing at 0°C overnight. An ice-cooled aqueous solution of $NaHCO_3$ was added and the products were extracted with $CHCl_3$.

Thin-layer chromatography showed the formation of one main product, which was separated by silica gel chromatography (19:1 EtOAc–MeOH), and obtained as a glassy solid from C_6H_6–ligroin, yield 1.6 g (53%), uv λ_{max} (MeOH): 234 nm (ε 25 000), 257 nm (ε 15 800); ^{1}H nmr data (100 MHz, $CDCl_3$) δ: 1.41 and 1.63 (2s, 6H, 2 isopropylidene methyls), 3.78 (s, 6H, $2CH_3O$), 6.11 (d, 1H, H-1′, $J_{1',2'}$ = 3 Hz), 7.90 (s, 1H, H-8), 8.23 (s, 1H, H-2). *Anal.* calcd. for

$C_{34}H_{35}O_6N_5$: C 66.98, H 5.79, N 11.49; found: C 66.61, H 5.77, N 11.36.

Reaction of ***23*** *with* $ZnBr_2$ *in* p-*dioxane*

A solution of **23** (1.63 g, 3 mmol) and $ZnBr_2$ (6.75 mmol, 30 mmol) in *p*-dioxane (75 mL) was left standing at room temperature overnight. Aqueous $NaHCO_3$ was added and, after the precipitate of $Zn(OH)_2$ was removed by centrifugation, the product was extracted with $CHCl_3$. The solution was concentrated to dryness and the residual material was crystallized from *p*-dioxane and ligroin to give 1.15 g (71%) of **4**.

2,4,5-Trichlorophenyl p-*toluate* (***29***)

To a solution of 2,4,5-trichlorophenol (3.95 g, 20 mmol) in pyridine (50 mL) cooled at −15°C was added *p*-toluyl chloride (3.5 g, 23 mmol) and the mixture was stirred at room temperature overnight. The pyridine was removed by evaporation and the residue was distributed between aqueous $NaHCO_3$ and EtOAc. After the organic layer was washed with water, it was concentrated to dryness. From EtOH 6 g (95%) of **29** melting at 120–121°C was obtained. *Anal.* calcd. for $C_{14}H_9O_2Cl_3$: C 53.28, H 2.87, Cl 33.71; found: C 53.10, H 2.85, Cl 33.69.

1. K. Anzai and J. Uzawa. J. Org. Chem. **49**, 5076 (1984).
2. J. Uzawa and S. Takeuchi. Org. Magn. Reson. **11**, 502 (1978).
3. M. Finlay, J. P. Debiard, A. Guy, D. Molko, and R. Teouk. Synthesis, 303 (1983).
4. G. A. Morris and R. Freeman. J. Am. Chem. Soc. **101**, 760 (1979).
5. K. Anzai and J. Uzawa. Nucleic Acids Symp. Ser. **15**, 49 (1984).
6. G. A. Morris. J. Am. Chem. Soc. **102**, 428 (1980).
7. G. W. Buchanan and M. J. Bell. Can. J. Chem. **61**, 2445 (1983).
8. A. Bax. J. Magn. Reson. **57**, 314 (1984).
9. A. Bax, C. Niu, and D. Live. J. Am. Chem. Soc. **106**, 1150 (1984).

Studies of azo and azoxy dyestuffs. Part 18.[1] Kinetics and mechanism of the hydrolysis of 3- and 4-(*p'*-methoxyphenylazo)pyridines in aqueous sulfuric acid media

ERWIN BUNCEL
Department of Chemistry, Queen's University, Kingston, Ont., Canada K7L 3N6

AND

IKENNA ONYIDO
Department of Chemistry, University of Ibadan, Ibadan, Nigeria

Received November 20, 1985

ERWIN BUNCEL and IKENNA ONYIDO. Can. J. Chem. **64**, 2115 (1986).

The kinetics of hydrolysis of 4-(*p'*-methoxyphenylazo)pyridine, **1**, and its 3-isomer, **2**, have been studied in moderately concentrated sulfuric acid media at 25°C. In all the acid solutions investigated, **1** reacted faster than **2**; rate differences between the two compounds varied from ca. 1000-fold in the dilute region of acidity to ca. 250-fold in the more concentrated acid solutions. The observed first-order rate constants, k_ψ, for both substrates exhibit a maximum, at ca. 42% H_2SO_4 and 47% H_2SO_4 for **1** and **2** respectively. Activation parameters have also been determined. The pK_a values for the second protonation equilibria of **1** and **2** have been evaluated and structures of the diprotonated species are discussed. Hydrolysis is shown to occur from the diprotonated substrates and two main mechanisms are operative. The first is an A-2 type mechanism, which involves rate-limiting attack of H_2O on the aryl carbon center giving delocalized transition states and intermediates in which the pyridinium and azonium functions are involved in charge delocalization. Subsequent transfer of a proton and detachment of the leaving group are fast processes. In the second A-S_E2 type mechanism, nucleophilic attack and transfer of the proton are fast steps preceding the slow general acid catalyzed separation of the leaving group. The difference in reactivity of the two compounds is attributed to differences in extent of charge delocalization in the transition states of the reactions: for **1** both the pyridinium and protonated azonium functions are involved whereas for **2** only the azonium function participates in charge delocalization.

ERWIN BUNCEL et IKENNA ONYIDO. Can. J. Chem. **64**, 2115 (1986).

Opérant à 25°C, dans un milieu modérément concentré en acide sulfurique, on a mesuré la cinétique de l'hydrolyse du (*p*-méthoxyphénylazo)-4 pyridine (**1**) et de son isomère en position 3 (**2**). Dans tous les milieux acides étudiés, le composé **1** réagit plus rapidement que le composé **2**; les vitesses de réaction des deux composés sont dans un rapport d'environ 1000 en milieu acide dilué et d'environ 250 dans des solutions acides plus concentrées. Les constantes de vitesse du premier ordre qui sont observées pour chacun des deux substrats (**1** et **2**) présentent respectivement un maximum à environ 42% et 47% en H_2SO_4. On a aussi déterminé les paramètres d'activation. On a évalué les valeurs de pK_a pour le deuxième équilibre de protonation des espèces **1** et **2** et on discute de la nature des espèces diprotonées. On démontre que l'hydrolyse se produit à partir des substrats diprotonés et que deux mécanismes principaux sont en opération. Le premier est un mécanisme principaux sont en opération. Le premier est un mécanisme du type A-2 impliquant une attaque, qui détermine la vitesse de la réaction, de H_2O sur le carbone de l'aryle conduisant à des états de transition délocalisés et à des intermédiaires dans lesquels les fonctions pyridinium et azonium sont impliquées dans la délocalisation de la charge. Un transfert subséquent d'un proton ainsi que le détachement du groupement nucléofuge sont des processus rapides. Dans le deuxième mécanisme de type A-S_E2, une attaque nucléophile et un transfert de proton sont deux étapes rapides précédant la séparation lente, soumise à une catalyse acide générale, du groupement nucléofuge. On attribue les différences de réactivité des deux composés à des différences dans l'étendue de la délocalisation de la charge dans les états de transition des réactions : dans le cas du composé **1**, tant le pyridinium que l'azonium protoné sont impliqués dans cette délocalisation alors que, dans le cas du composé **2**, seule la fonction azonium participe à la délocalisation de la charge.

[Traduit par la revue]

The relative insensitivity of alkyl aryl ethers towards hydrolysis in acid media is well known. Interestingly, however, when the aromatic ring is activated through phenylazo substitution, these ethers become susceptible to hydrolysis in acidic media. Following earlier observations of this phenomenon (2–4), Bunnett *et al.* (5–7) reported kinetic and mechanistic studies of such cleavages for several azo aryl ethers. There have been no studies reported so far in which the effect of pyridyl substitution on these processes has been examined, which is the subject of the present paper.

Our original interest was the investigation of the spectroscopic properties and protonation equilibria of some phenylazopyridines, in connection with studies of the mechanism of the acid catalyzed Wallach rearrangement of azoxyarene compounds (8). We observed, as part of another study (8*e*), that 4-(*p'*-methoxyphenylazo)pyridine, **1**, underwent hydrolysis even in mild acid at room temperature. We thought that a more detailed study of this system would add to information available regarding the mechanism of such ether cleavages. As well, it was of interest to evaluate the effect of an additional protonation equilibrium, which could be anticipated in this and related processes. Accordingly we undertook a kinetic study of **1** in aqueous sulfuric acid media, as well as that of its isomer, 3-(*p'*-methoxyphenylazo)pyridine, **2**, which we report herein.

[1]Part 17: ref. 1.

Results

Kinetics

The kinetics of the hydrolysis of **1** and **2** were followed by monitoring spectrophotometrically the appearance of the products, 4- and 3-(*p*-hydroxyphenylazo)pyridines. These products were formed quantitatively. The kinetic data, along with other relevant information, are assembled in Table 1 and presented graphically in Fig. 1. The pseudo first-order rate constants, k_ψ, for both substrates pass through a maximum, at ca. 42 wt.% and 47 wt.% H_2SO_4 for **1** and **2** respectively.

TABLE 1. Rate, equilibrium, and other relevant data for the hydrolysis of **1** and **2** in aqueous sulfuric acid media at 25°C

Substrate	H_2SO_4 (wt.%)	H_0[a]	a_{H_2O}[b]	$\frac{C_{SH^+}}{C_S + C_{SH^+}}$[c]	$\frac{C_{SH^+}}{C_{SH^+} + C_{SH_2^{2+}}}$[d]	$\frac{C_{SH_2^{2+}}}{C_{SH^+} + C_{SH_2^{2+}}}$[d]	C_{H^+}[e] (M)	X[e]	k_ψ (s^{-1})
1	1.80	0.56	0.994	0.9999	0.9998	0.0002	0.25	0.04	0.82×10^{-4}
	5.88	0.02	0.977	1.0	0.9994	0.0006	0.73	0.14	3.27×10^{-4}
	10.12	−0.36	0.947	1.0	0.9986	0.0014	1.30	0.25	7.87×10^{-4}
	16.25	−0.82	0.914	1.0	0.9958	0.0042	2.27	0.44	2.13×10^{-3}
	23.37	−1.30	0.844	1.0	0.9876	0.0124	3.50	0.71	5.58×10^{-3}
	25.56	−1.44	0.817	1.0	0.9829	0.0171	3.85	0.81	7.64×10^{-3}
	27.90	−1.60	0.783	1.0	0.9755	0.0245	4.30	0.94	1.07×10^{-2}
	35.33	−2.10	0.660	1.0	0.9264	0.0736	5.80	1.33	2.63×10^{-2}
	38.27	−2.32	0.599	1.0	0.8835	0.1165	6.40	1.51	3.40×10^{-2}
	42.02	−2.60	0.522	1.0	0.7992	0.2008	7.18	1.75	3.77×10^{-2}
	46.40	−2.98	0.426	1.0	0.6240	0.3760	8.10	2.07	3.60×10^{-2}
	48.00	−3.12	0.395	1.0	0.5459	0.4541	8.40	2.18	2.95×10^{-2}
	52.06	−3.52	0.307	1.0	0.3237	0.6763	9.25	2.50	1.72×10^{-2}
	55.70	−3.89	0.236	1.0	0.1696	0.8304	10.00	2.82	9.81×10^{-3}
	60.09	−4.40	0.161	1.0	0.0594	0.9406	10.85	3.23	3.11×10^{-3}
2	8.27	−0.24	0.966	0.9999	0.9993	0.0007	1.00	0.20	0.05×10^{-5}
	17.11	−0.84	0.907	1.0	0.9971	0.0029	2.43	0.47	0.20×10^{-5}
	28.37	−1.62	0.776	1.0	0.9829	0.0171	4.40	0.96	0.85×10^{-5}
	36.36	−2.16	0.640	1.0	0.9432	0.0568	6.03	1.40	2.24×10^{-5}
	38.27	−2.32	0.599	1.0	0.9199	0.0801	6.40	1.51	3.17×10^{-5}
	42.02	−2.60	0.522	1.0	0.8576	0.1424	7.18	1.75	4.66×10^{-5}
	46.40	−2.98	0.426	1.0	0.7153	0.2847	8.10	2.07	6.38×10^{-5}
	48.00	−3.12	0.395	1.0	0.6454	0.3546	8.40	2.18	6.85×10^{-5}
	50.40	−3.34	0.341	1.0	0.5230	0.4770	8.90	2.38	6.49×10^{-5}
	52.06	−3.52	0.307	1.0	0.4201	0.5799	9.25	2.50	6.23×10^{-5}
	53.60	−3.66	0.276	1.0	0.3442	0.6558	9.55	2.62	5.80×10^{-5}
	55.70	−3.89	0.236	1.0	0.2361	0.7639	10.00	2.82	3.86×10^{-5}
	65.17	−5.06	0.091	1.0	0.0205	0.9795	11.75	3.82	0.96×10^{-5}

[a]Values taken from the data of ref. 26.
[b]Values taken from the data of ref. 27.
[c]pK_{SH^+} for **1** = 4.53 and **2** = 3.88 (see text).
[d]$pK_{SH_2^{2+}}$ for **1** = −3.20 and **2** = −3.38 (see text).
[e]Values taken from the data of ref. 21.

Similar maxima in moderately concentrated acid solutions were reported by Bunnett and Buncel (6) in their study of the acid catalyzed hydrolysis of 4-(*p'*-sulfophenylazo)-1-naphthyl methyl ether, **3**, and 4-(*p'*-sulfophenylazo)anisole, **4**, in hydrochloric and perchloric acid solutions. In all the acid solutions investigated, **1** reacted faster than **2**. A rate difference of ca. 10^3-fold was observed in the more dilute acid solutions but this difference decreased as the acidity of the medium increased. Activation parameters were also determined for some of the acid solutions. Rate data at various temperatures as well as the corresponding activation parameters are given in Table 2.

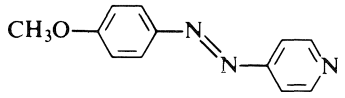

1

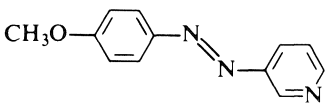

2

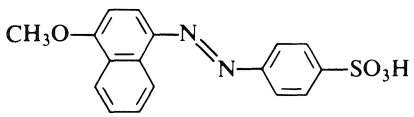

3

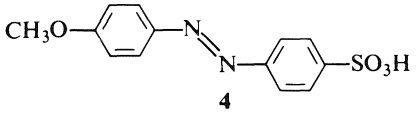

4

*p*K$_{SH_2^{2+}}$ *Determination*

The basicity of the ring nitrogen in **1** and **2** ensures that these substrates are already fully monoprotonated in the pH range of acidity and hence the pK determination of interest in the present study was for the second protonation equilibrium:

$$SH^+ + H^+ \underset{}{\overset{K_{SH_2}^{2+}}{\rightleftharpoons}} SH_2^{2+}$$

where SH^+ and SH_2^{2+} represent the mono- and diprotonated forms of the substrates.

A study of the protonation behaviour of the conjugate acid of **2** gave the following results. Compound **2** has an absorption maximum (λ_{max}) at 351 nm in ethanol. In dilute aqueous acid, e.g. 2 wt.% H_2SO_4, this maximum shifts to 367 nm and we ascribe this λ_{max} to the species **7**. Between 2.0 and 28.4 wt.% H_2SO_4 there were small changes in absorbance and in λ_{max} that

TABLE 2. Rate data at different temperatures and activation parameters[a] for the hydrolysis of **1** and **2** in different sulfuric acid media

Substrate	H_2SO_4 (wt.%)	$k_\psi^{13.8°}$ (s^{-1})	$k_\psi^{25°}$ (s^{-1})	$k_\psi^{34°}$ (s^{-1})	$k_\psi^{45.6°}$ (s^{-1})	$\Delta G^{\ddagger}$ (kcal mol^{-1})	$\Delta H^{\ddagger}$ (kcal mol^{-1})	$\Delta S^{\ddagger}$ (eu)
1	10.12		7.87×10^{-4}		1.03×10^{-2}	21.7	23.0	4.4
	25.56		7.64×10^{-3}	2.24×10^{-2}	5.53×10^{-2}	20.4	17.4	−9.9
	42.02	1.73×10^{-2}	3.77×10^{-2}	8.58×10^{-2}		19.4	13.2	−20.8
	55.70		9.81×10^{-3}	2.17×10^{-2}	5.48×10^{-2}	20.2	15.2	−16.7
	60.09		3.30×10^{-3}	1.01×10^{-2}	2.32×10^{-2}	20.8	17.1	−12.5

Substrate	H_2SO_4 (wt.%)	$k_\psi^{25°}$ (s^{-1})	$k_\psi^{34°}$ (s^{-1})	$k_\psi^{43.3°}$ (s^{-1})	$\Delta G^{\ddagger}$ (kcal mol^{-1})	$\Delta H^{\ddagger}$ (kcal mol^{-1})	$\Delta S^{\ddagger}$ (eu)
2	17.11	2.02×10^{-6}		1.73×10^{-5}	25.2	21.5	−12.5
	29.32	8.91×10^{-6}		7.27×10^{-5}[b]	24.3	19.2	−17.2
	42.02	4.66×10^{-5}	1.27×10^{-4}	2.81×10^{-4}	23.3	17.8	−18.6
	50.40	6.49×10^{-5}	1.78×10^{-4}	4.41×10^{-4}	23.2	19.0	−14.0
	55.70	3.86×10^{-5}	1.18×10^{-4}	3.17×10^{-4}	23.4	21.0	−8.0

[a]At 25°C.
[b]Data obtained at 45°C.

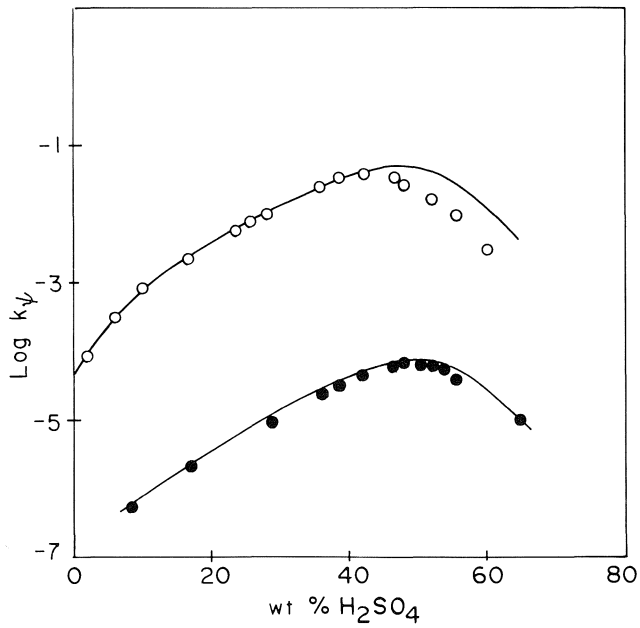

FIG. 1. Plots of log k_ψ versus % H_2SO_4 for the hydrolysis of **1** (○) and **2** (●) at 25°C. Points are experimental; lines are calculated from eq. [7] with $r = 3$ using log k_2 values derived from plots in Fig. 5.

could not readily be correlated with the acidity of the medium. This may be due to a medium effect, as such effects have been noted previously (6, 9, 10). In the region 36.4–65.2 wt.% H_2SO_4, the spectra (not shown) showed regular behaviour consistent with decreasing concentration of the species with λ_{max} at 367 nm and increasing concentration of a new species with λ_{max} 465 nm. The peak at 465 nm is attributed to the diprotonated substrate, **8**. The $pK_{SH_2^{2+}}$ was evaluated using the Davis–Geissman method (12). The relevant data are presented in Table 3. A plot of $A_{465} - A_{367}$ versus H_0 (not shown) gives the usual sigmoid curve from which the $pK_{SH_2^{2+}}$ value of −3.38 was obtained. It is interesting to note that this value is similar to the value of −3.35 obtained by the same procedure for 3-(*p'*-hydroxyphenylazo)pyridine (11), the hydrolysis product of **2**. It should also be noted, however, that the H_0 function may

TABLE 3. Absorbance data for **2** as a function of H_0 for determination of $pK_{SH_2^{2+}}$

H_0	A_{367}[a]	A_{465}[b]	$(A_{465} - A_{367})$[c]
−2.16	0.675	0.097	−0.578
−2.60	0.600	0.192	−0.408
−2.83	0.552	0.315	−0.237
−3.12	0.458	0.576	0.118
−3.34	0.365	0.876	0.520
−3.38	0.335	0.952	0.617
−3.65	0.226	1.214	0.988
−3.73	0.198	1.296	1.098
−4.73	0.103	1.584	1.481
−5.10	0.086	1.639	1.553

[a]Absorbance at λ_{max} of monoprotonated species, **7**.
[b]Absorbance at λ_{max} of diprotonated species, **8**.
[c]Absorbance differences used to determine $pK_{SH_2^{2+}}$ value by the Davis–Geissman method (see ref. 12).

not strictly be applicable to this protonation equilibrium (*vide infra*), although its use is not expected to lead to a significant error while facilitating comparison with previous studies.

The $pK_{SH_2^{2+}}$ of **1** was not measured as it hydrolysed much more rapidly than **2** in acidic solutions. Although an extrapolation procedure could perhaps be used to estimate its $pK_{SH_2^{2+}}$ value, this was not attempted; rather the close similarity between the $pK_{SH_2^{2+}}$ value of **2** and that of its phenolic product led us to assume that the $pK_{SH_2^{2+}}$ of **1** would be very similar to that of 4-(*p'*-hydroxyphenylazo)pyridine, i.e. −3.20 (11). Such an assumption seemed quite reasonable, as the replacement of H by a CH_3 group would not be expected to have a profound effect on the second protonation equilibrium of 4-(*p'*-hydroxyphenylazo)pyridine.

The $pK_{SH_2^{+}}$ of **1** was measured to be 4.53 (8*e*), and the $pK_{SH_2^{+}}$ of **2** was estimated to be 3.88 by analogy with the $pK_{SH_2^{+}}$ of 3-(*p'*-hydroxyphenylazo)pyridine (11).

Discussion

In this study, the rate of hydrolysis of **1** was determined in the region 1.80–60.09 wt.% H_2SO_4, while **2** was studied in the range 8.27–65.17 wt.% H_2SO_4. The $pK_{SH_2^{2+}}$ values of these

[1] 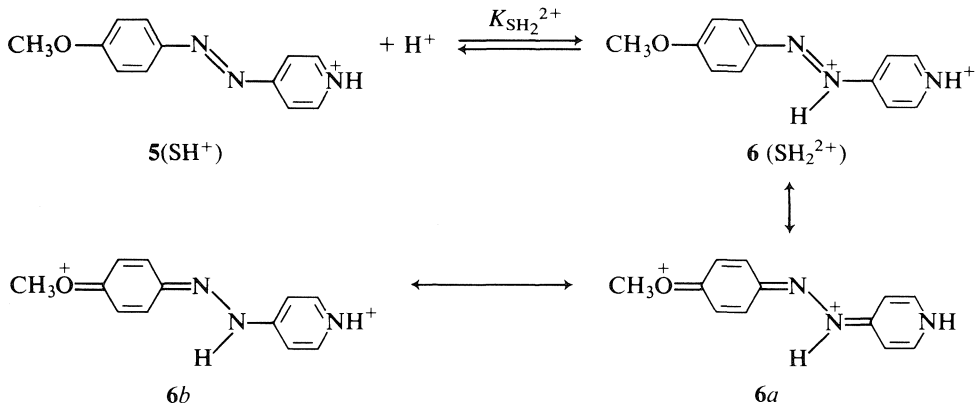

[2] 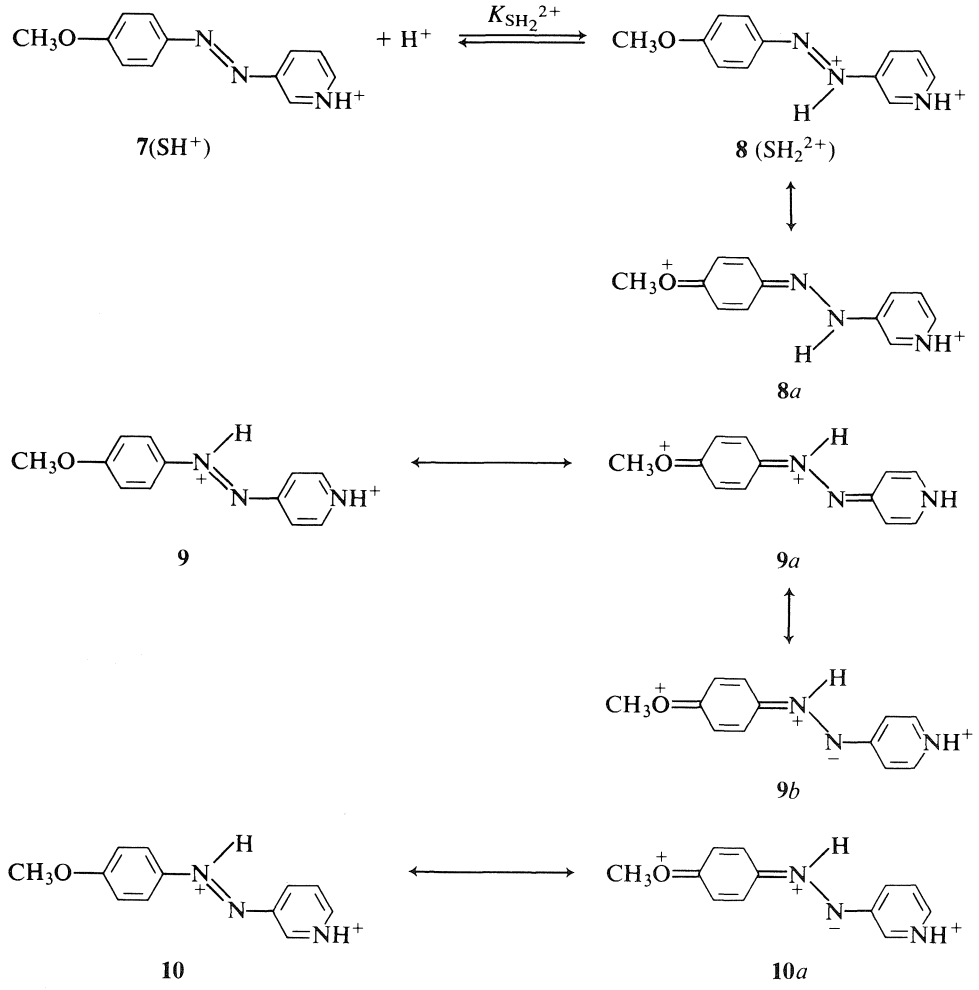

substrates indicate that in this region of acidity, substantial amounts of the substrates exist in their diprotonated forms. Any mechanism that is proposed for the hydrolysis must therefore include consideration of such diprotonated species.

Protonation equilibria

The equilibria for the second protonation of **1** and **2** are given in eqs. [1] and [2], which include the principal resonance structures of the various species involved for purposes of subsequent discussion. It is noted that in principle the second protonation could occur on either nitrogen of the azo function and hence **9** and **10** may be envisaged as alternatives to the structures of the diprotonated species of the substrates represented as **6** and **8**. However, the resonance forms **9***b* and **10***a*, corresponding to **6***b* and **8***a* respectively, are deemed to be destabilizing due to accumulation of charges, and hence **6** and **8** are preferred. The ensuing discussion will thus consider the involvement of the latter species in the various mechanistic schemes.

The pK values for the protonation of the azo nitrogen in **1**–**4** are listed in Table 4, with the value for *p*-hydroxyazobenzene, **11**, (eq. [3]) being given for comparison. One would not expect a large effect on the basicity of the azo function when a CH_3 group replaces H; thus introduction of the pyridinium function

[3] 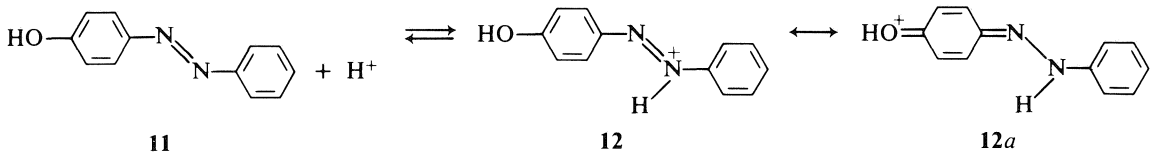

11 12 12*a*

into **11** lowers the basicity of the azo nitrogen by ca. 2.5 pK units. This difference, representing a $\Delta\Delta G^0$ value of 3.4 kcal, reflects the effect of protonation of an azo nitrogen when this is linked to an aromatic ring that already bears a positive charge.

Mechanism of hydrolysis

Hydrolysis of diverse substrates in acid solutions has generally been discussed in terms of three mechanisms, as follows. 1. The A-1 mechanism involves equilibrium protonation of the substrate S to give the protonated substrate SH^+, which decomposes unimolecularly in the rate-limiting step to give an intermediate X^+; this intermediate reacts rapidly with water to give the products. 2. The A-2 mechanism involves again a rapid pre-equilibrium to give SH^+ but this is attacked by water in the rate-limiting step. 3. In the A-S_E2 mechanism, transfer of the proton either to the substrate or from the protonated substrate constitutes the rate-determining step.

In the systems under investigation, some of these mechanisms can be rejected or favoured on theoretical grounds and (or) other considerations. Thus the A-1 mechanism of hydrolysis is untenable for our substrates on energetic grounds in view of the fact that the CH_3^+ cation that would result in the rate-limiting step is a very high energy species. This leaves the A-2 and A-S_E2 mechanisms for further consideration.

Secondly, the reactive species could in theory be the monoprotonated substrates **5** and **7**, the diprotonated substrates **6** and **8**, or even triprotonated species involving O-protonation as well. Reaction from the monoprotonated substrates cannot account for the increase in rate observed with increasing acidity, since the substrates are already fully monoprotonated in the pH region. On the other hand, reaction from a triprotonated species is unlikely on the following grounds. (*i*) Normal ether hydrolysis proceeds by way of a pre-equilibrium oxygen protonation and one might reasonably assume that the substrates **1** and **2** would hydrolyse in a similar way. The $pK_{SH_2^{2+}}$ measurements discussed above provide experimental evidence for the existence of diprotonated species in which the two protons are attached to the pyridine and azo nitrogens. The structures contributing to the diprotonated species for the two substrates are shown in eqs. [1] and [2] and it is evident that the ether oxygen is depleted of charge density through resonance so that further protonation on oxygen is unlikely. (*ii*) A three-proton mechanism would demand rates of reaction that would increase throughout the entire range of acidity studied; this is contrary to the kinetic results, which actually show a downturn in k_ψ in the higher acid concentration range.

A third question that should be addressed is whether attack by water as the nucleophile occurs on the alkyl or on the aromatic carbon center. We favour attack on the aromatic carbon on the following grounds. (*i*) There is experimental evidence from ^{18}O studies that the aryl-oxygen bond is the one broken in the hydrolysis of **4** in HCl solutions (7), and since **1** and **2** are structurally similar to **4**, it is reasonable to assume that they undergo the same kind of bond rupture. (*ii*) Attack on the aryl carbon is actually an activated aromatic nucleophilic substitution (S_NAr) reaction and would involve structurally favoured intermediates (as shown in Schemes 1 and 2) with the azonium and pyridinium functions providing the activation by serving as electron sinks. Our discussion of mechanism will therefore focus on A-2 and A-S_E2 mechanisms of the S_NAr type involving diprotonated substrates. These mechanisms are given in Schemes 1 and 2 and are considered in detail below in terms of rate correlations that can be derived using established criteria of mechanism.[2]

Rate correlations

(a) Edward–Meacock acidity function correlations

Rate maxima of the type observed in the present study have been reported in the acid hydrolysis of amides, for which the mechanism is believed to be of the A-2 type (14). Edward and Meacock (14*c*) utilized the expression of eq. [4] to draw theoretical curves correlating rates with acidities and these showed satisfactory fit with experimental data for the hydrolysis of benzamide, *p*-methoxybenzamide, and *p*-nitrobenzamide.

$$[4] \quad k_\psi = k_2K[H_3O^+]/(K + h_0)$$

They also found that the acid concentrations corresponding to the maximum rates were in accord with the pK_a values of the amides. However, our attempts to employ this method to test for the A-2 mechanism with our substrates led to theoretical curves that deviated considerably from experimental data, although the acid concentrations corresponding to the maximum rates were coincident for the experimental and theoretical curves. The Hammett acidity function is included in eq. [4] and it is possible that the inherent assumption about the activity coefficient behaviour of the monoprotonated substrates and transition states (15) does not hold in our system, which involves attack by H_2O on diprotonated species.

TABLE 4. pK_a values for the protonation of the azo function in compounds **1**–**4** and **11**

Compound	pK_a
1	−3.20[a]
2	−3.38, −3.35[b]
3	−0.74[c]
4	−1.56[c], −1.45[d]
11	−0.93[d]

[a]This is an estimate of the $pK_{SH_2^{2+}}$ of **1**, based on an analogy with the $pK_{SH_2^{2+}}$ of 4-(*p*′-hydroxyphenylazo)pyridine, taken from ref. 11.

[b]Value for the hydrolysis product of **2**, taken from ref. 11.

[c]Values taken from ref. 6.

[d]Values taken from ref. 13.

[2]It has been pointed out by a referee that, in Scheme 2, the addition of H_2O to **6** might be subject to general base catalysis, analogous to the general acid catalyzed detachment of CH_3OH from **15**. This has not been included in Scheme 2 owing to the difficulty of establishing satisfactory criteria for such a process in moderately concentrated acid solutions. We thank the referee for drawing attention to this possible ambiguity.

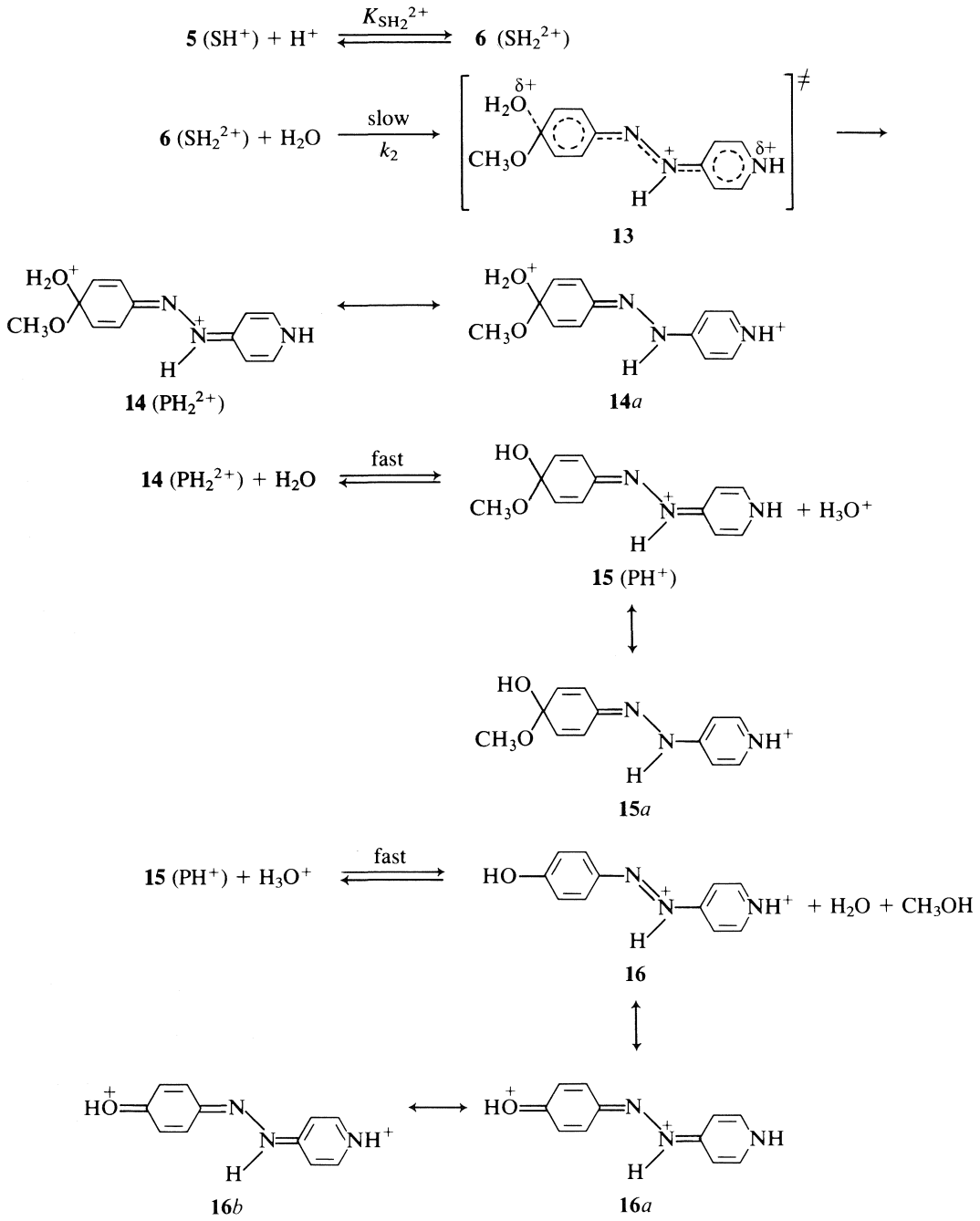

SCHEME 1. A-2 mechanism for azo ether hydrolysis.

(b) Bunnett–Olsen ϕ parameter treatment

The Bunnett–Olsen linear free energy relationship (LFER) method for correlating rates in moderately concentrated mineral acids (16–18) has been used successfully by various workers, although the method was subsequently modified by Lucchini *et al.* (19). In its original form, for moderately basic substrates the relevant expression for an A-2 reaction is given by eq. [5].

$$[5] \quad \log k_\psi - \log \frac{C_{SH_2^{2+}}}{C_{SH^+} + C_{SH_2^{2+}}} = \log k_2 + \phi(H_0 + \log C_{H^+})$$

Plots according to eq. [5] shown in Fig. 2 are curved, with initial slopes of 0.2 for both substrates increasing to 1.1 and 0.7 for **1** and **2** respectively. These plots deserve further consideration. It has been pointed out by Lucchini *et al.* (19) that eq. [5] does not include the nucleophile activity, as would be required in an A-2 type reaction. However, the plot involving one molecule of water is also curved, as shown in Fig. 3. Cox and Yates (20) have pointed out that such a modification of the Bunnett–Olsen LFER as suggested by Lucchini *et al.* (19) closely resembles their excess acidity method, and further showed that $H_0 + \log C_{H^+} \approx -X$. This is considered further below.

(c) The Cox–Yates excess acidity method

The Cox–Yates method for correlating rates using the concept of "excess acidity" or X-functions (21) has been employed to establish the mechanisms of the acid hydrolysis of diverse substrates (20–22). This method has not so far been

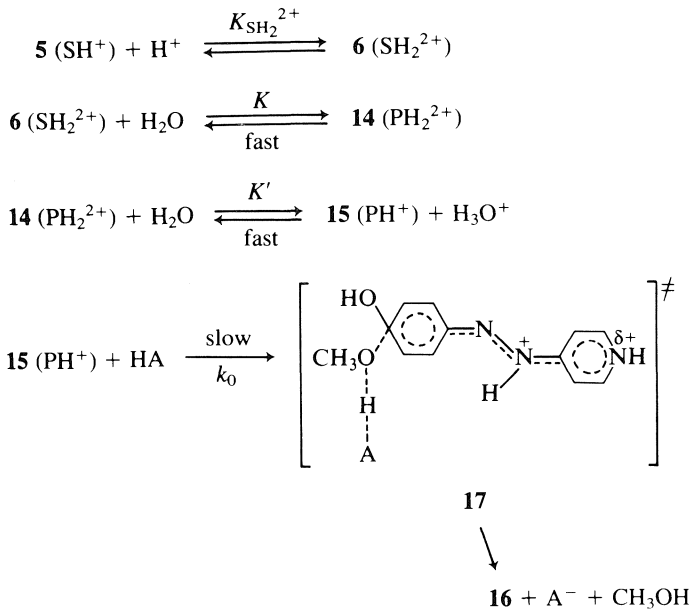

SCHEME 2. A-S_E2 mechanism for azo ether hydrolysis.

extended to the hydrolysis of alkyl aryl ethers and it is of interest to employ the method for our substrates **1** and **2** and also to check its validity for the substrates **3** and **4** whose mechanism of hydrolysis has been established by Bunnett and Buncel (6, 7).

For the A-2 mechanism of Scheme 1, eq. [6] is derived. One would expect that on plotting the LHS of [6] against X for an A-2 process, a downward curve would result (20). Such curves are indeed obtained for **1** and **2**, as shown in Fig. 4. Different r log a_{H_2O} values are then subtracted from the LHS until linearity is achieved, such that eq. [6] transforms to [7].

$$[6]\quad \log k_\psi - \log \frac{C_{SH_2^{2+}}}{C_{SH^+} + C_{SH_2^{2+}}} = (m^\ddagger - 1)m^*X + r \log a_{H_2O} + \log k_2$$

$$[7]\quad \log k_\psi - \log \frac{C_{SH_2^{2+}}}{C_{SH^+} + C_{SH_2^{2+}}} - r \log a_{H_2O} = (m^\ddagger - 1)m^*X + \log k_2$$

The resulting plots are shown in Fig. 5. Linearity is achieved with $r = 3$ over the entire range of acidity for **2**, while a break occurs at ca. 42 wt.% H_2SO_4 for **1**. The magnitude of the slope parameter $m^\ddagger$ offers mechanistic information; in particular, for the A-2 mechanism presently under consideration, $m^\ddagger \approx 1$ is expected (20). Values of $m^\ddagger$ calculated from the slopes by using m^* values obtained from protonation data indicate that **2** ($m^\ddagger = 1.3$) reacts by the A-2 mechanism over the entire range of acidity, whereas **1** ($m^\ddagger = 1.1$) reacts by the same mechanism up to ca. 42 wt.% H_2SO_4 where there is a break in the plot. Using the values of log k_2 derived from the plots in Fig. 5, log k_ψ can be calculated for both substrates. The theoretical curves obtained from such calculations are shown in Fig. 1 and it is clear that there is agreement between the theoretical and experimental curves for **2** over the entire range of acidity studied. The deviation of the theoretical curve from the experimental for **1** in the more concentrated acid solutions suggests that this substrate reacts by a different mechanism in this region of acidity.

In their study of the hydrolysis of **3** and **4**, Bunnett and Buncel (6, 7) showed that attack by water occurs on the aromatic carbon and that the substrates react by an A-S_E2 mechanism involving general acid catalysis of leaving group departure. The reaction sequence for compounds **3** and **4** differs from the mechanism of Scheme 2 applicable to **1** and **2** in the sense that reaction occurs from the monoprotonated forms of these substrates. For the mechanism of Scheme 2, eq. [8] is derived for **3** and **4**. Since $a_{SH^+} = a_S a_{H^+}/K_{SH^+}$, eqs. [9] and [10] result and hence a plot of the LHS against X should be linear with slope $= m^\ddagger m^*$. Values of m^* have been calculated from the original data (6, 7) of these workers to be ca. 0.9.

$$[8]\quad k_\psi(C_S + C_{SH^+}) = k_0 \cdot a_{PH^+} \cdot a_{H_3O^+}/f^\ddagger = k_0 K K' a_{SH^+} \cdot a_{H_2O^+}{}^2/f^\ddagger$$

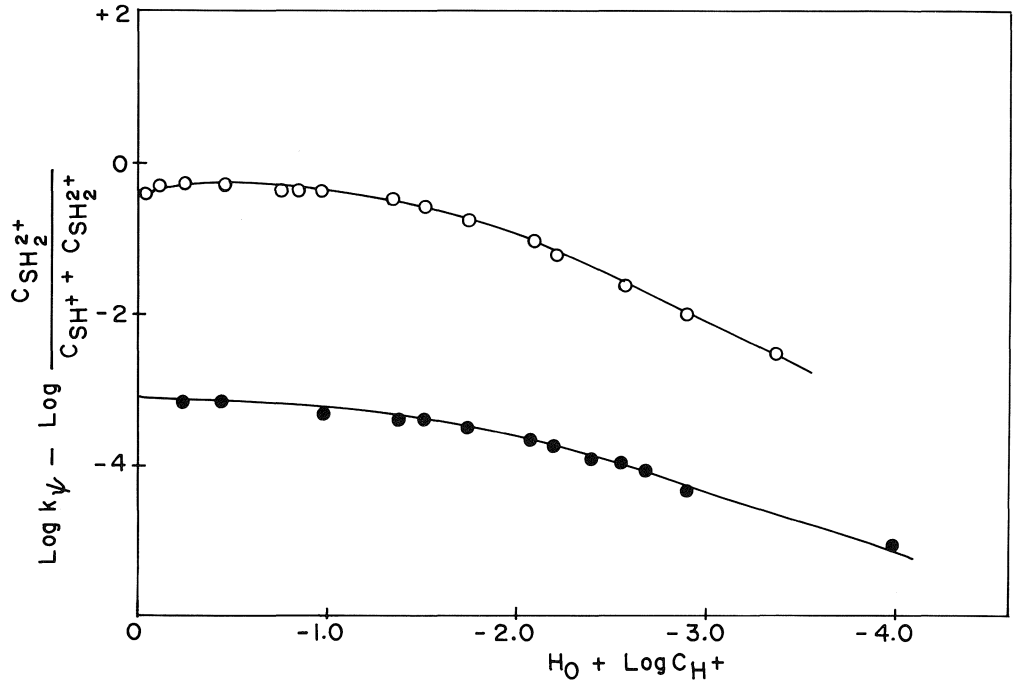

FIG. 2. Bunnett–Olsen plots for the hydrolysis of **1** (○) and **2** (●).

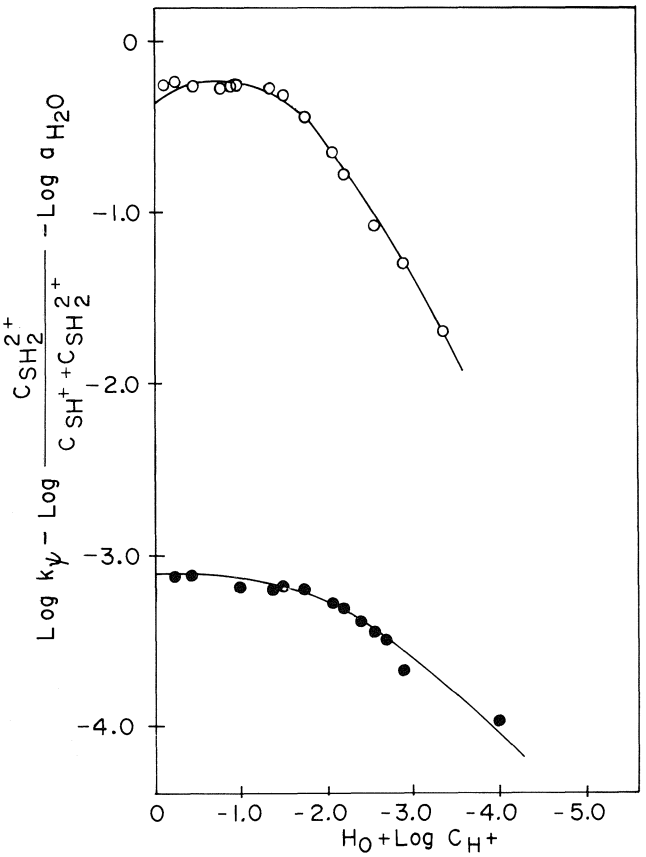

FIG. 3. Bunnett–Olsen plots for the hydrolysis of **1** (○) and **2** (●) assuming an A-2 mechanism involving one H_2O molecule.

$$[9] \quad k_\psi(C_S + C_{SH^+}) = \frac{k_0 KK'}{K_{SH^+}} \cdot a_S \cdot a_{H^+} \cdot a_{H_2O^+}{}^2/f^{\neq} = k' \cdot C_S \cdot C_{H^+} \cdot a^2{}_{H_2O} f_S f_{H^+}/f^{\neq}$$

$$[10] \quad \log k_\psi - \log \frac{C_S}{C_S + C_{SH^+}} - \log C_{H^+} - 2\log a_{H_2O} = \log k' + m^{\neq} m^* X$$

Application of eq. [10] to the data for **3** and **4** gives reasonably good straight lines, as shown in Fig. 6, and values of $m^{\neq}$ of 0.5 and 0.8 for **3** and **4**, respectively, lie within the limits of 0 and 1 expected for rate-limiting proton transfer (20). The agreement of the conclusions obtained from these plots with the mechanism proposed by Bunnett and Buncel (6, 7) based on ω-values gives further confidence to the conclusion that the Cox–Yates method is a valid criterion of mechanism in azoether hydrolysis.

Similar plots for the A-S_E2 mechanism can be made for our substrates **1** and **2** allowing for a second protonation equilibrium, and hence eq. [10] transforms to [11].

$$[11] \quad \log k_\psi - \log \frac{C_{SH^+}}{C_{SH^+} + C_{SH_2^{2+}}} - \log C_{H^+} - 2\log a_{H_2O} = \log k' + m^{\neq} m^* X$$

The plots are displayed in Fig. 7. The plot for **2** is linear over the entire range of acidity with $m^{\neq} = 1.1$. For **1** there is a break in the plot with an initial value of $m^{\neq} = 1.1$, which then changes to 0.6. These values of $m^{\neq}$ suggest that **2** does not react by an A-S_E2 mechanism over the entire range of acidity, whereas **1** reacts by this mechanism beyond 42 wt%. H_2SO_4.

The M_c function of Marziano, Passerini, and co-workers (23) is analogous to the X function of Cox and Yates (20) and the same mechanistic conclusions as drawn by use of X can also be reached using M_c values.

Evaluation of mechanisms

Having applied several mechanistic criteria in relation to the present study, we can now evaluate the results of these treatments. In the A-2 mechanism, if the involvement of 3 water molecules as indicated by the Cox–Yates excess acidity method is assumed, then the Bunnett–Olsen LFER method leads to eq. [12] as the relevant expression. Plots (not shown) according to eq. [12] closely parallel the plots of Fig. 5 and the same mechanistic conclusions can be reached. If an A-S_E2 mechanism is assumed, the relevant expression is eq. [13] and once again the plots (not shown) obtained according to these

$$[12] \quad \log k_\psi - \log \frac{C_{SH_2^{2+}}}{C_{SH^+} + C_{SH_2^{2+}}} - 3\log a_{H_2O} = (\phi_{\neq} - \phi_e)(H_0 + \log C_{H^+}) + \log k_2$$

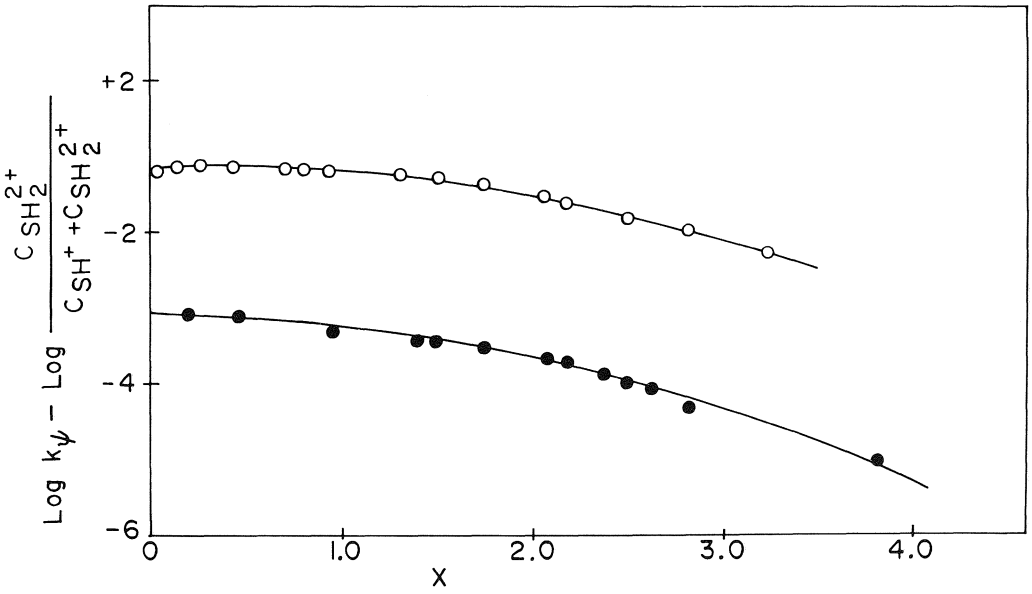

FIG. 4. Cox–Yates plots for the A-2 mechanism of hydrolysis for **1** (○) and **2** (●).

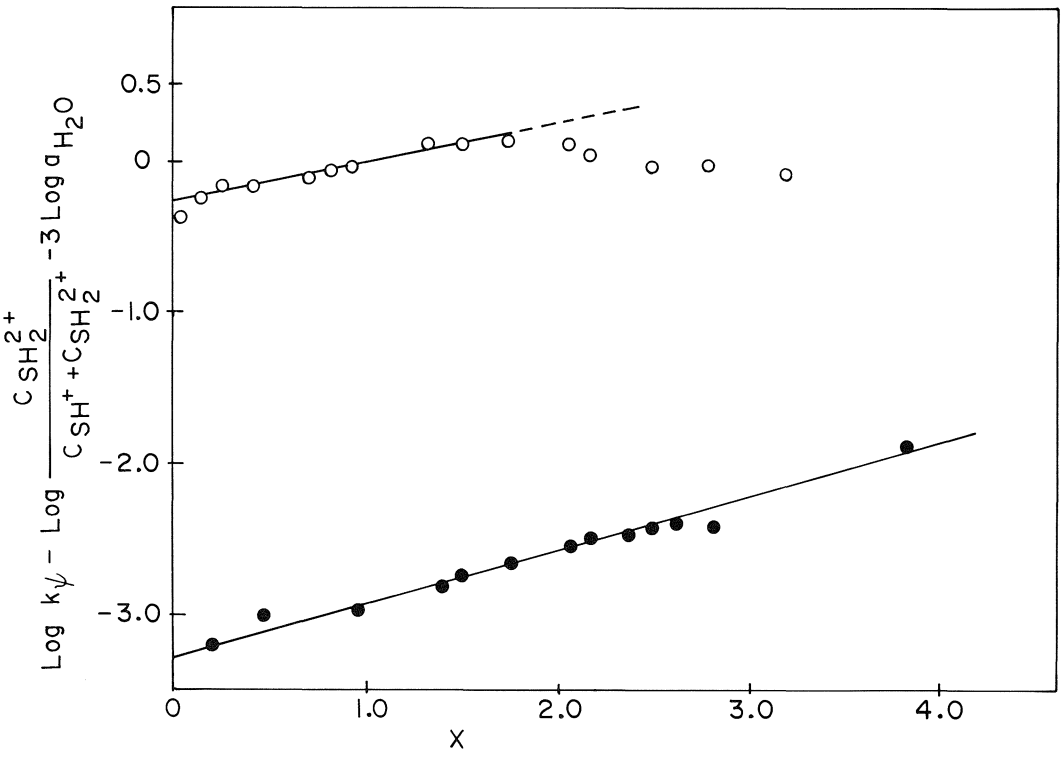

FIG. 5. Cox–Yates plots for the A-2 mechanism of hydrolysis involving 3 H_2O molecules for **1** (○) and **2** (●).

$$[13]\quad \log k_\psi - \log \frac{C_{SH^+}}{C_{SH^+} + C_{SH_2^{2+}}} - \log C_{H^+} - 2\log a_{H_2O} = (\phi_\pm - \phi_e)(H_0 + \log C_{H^+}) + \log k'$$

equations are similar to the plots of Fig. 7 (eq. [11]). We infer that the breaks in the plots for **1** imply a change of mechanism in the reaction of this substrate, from A-2 to A-S_E2.

Values of the slope parameters ($\phi_\pm - \phi_e$) for both substrates are set out in Table 5, along with those for **3** and **4**, whose reactions are known to proceed by the A-S_E2 mechanism. According to Arnett and Scorrano (24) and Modena and co-workers (25), ϕ_e values range from +1.0 to −1.6 depending on the type of cationic species formed on protonation and the degree of interaction with the solvent, particularly when the cation is small and the positive charge is localized. The negative values of the slope parameters ($\phi_\pm - \phi_e$) for all the substrates indicate that the transition states are in all cases less solvated than the initial states.

The detailed mechanism for the A-2 reaction as set out in Scheme 1 would involve 3 molecules of water as indicated by the Cox–Yates excess acidity method demonstrated above. This is best represented by the transition states, **18** and **19**, for the reactions of **1** and **2**, respectively. In **18**, the electrons from the incoming nucleophile are delocalized into the pyridinium moiety. As this is not possible in **19**, the transition state for the reaction of **1** is better stabilized than that for **2**. The requirement for three water molecules stems from the need for one to act as nucleophile and two to provide solvation as the nucleophilic water acquires a positive charge. It can be pointed out that the idea of 3 H_2O molecules being involved in hydrolysis reactions has precedent. Thus Cox and Yates have shown that the A-2 reaction of benzamide and some benzimidium ions in dilute acid involves 3 H_2O molecules (14*d*). Similarly, an A-2 mechanism involving 3 H_2O molecules has also been implicated in the hydrolysis of thioacids (21).

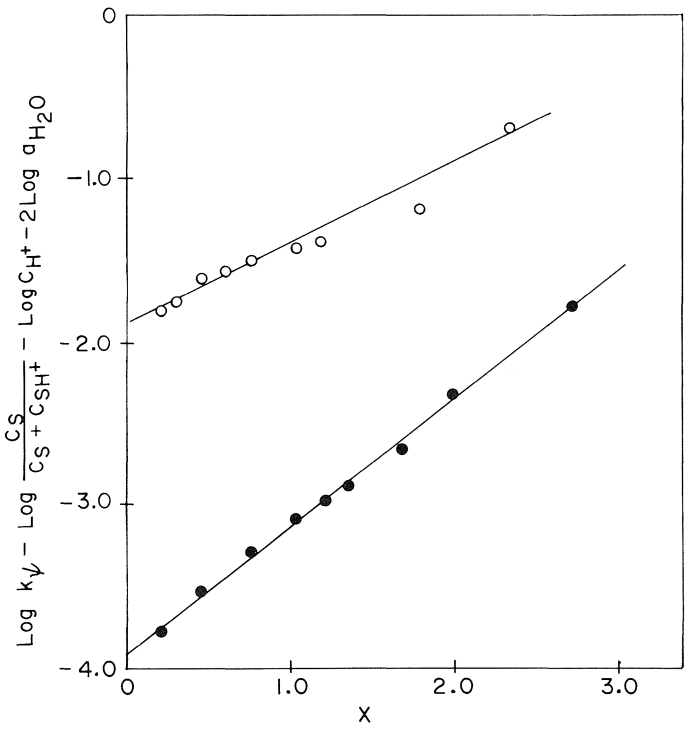

FIG. 6. Cox–Yates plots for the A-S_E2 mechanism of hydrolysis of **3** (○) and **4** (●).

Scheme 2 gives the A-S_E2 mechanism that is believed to hold for **1** in media >42 wt.% H_2SO_4. This is essentially a general acid catalyzed detachment of the leaving group in which the catalytic entities are the various acidic species present in solution.

The activation parameters displayed in Table 2 show that in all cases $\Delta H^\ddagger$ for **1** is less than that for **2**. This reflects the lower

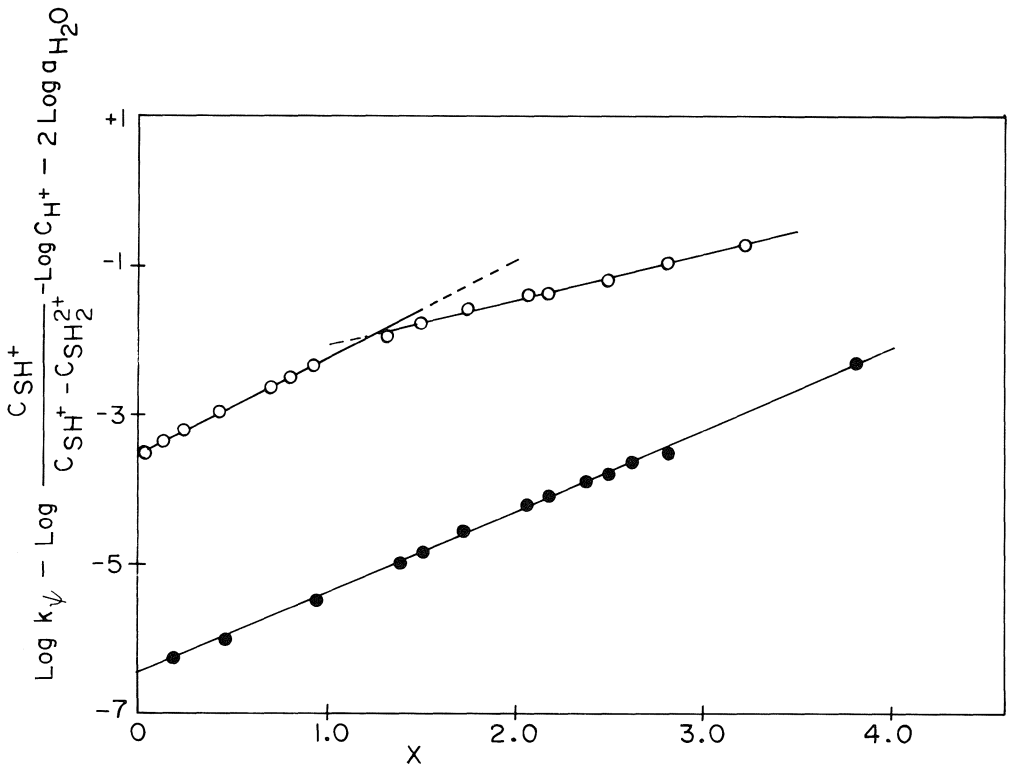

FIG. 7. Cox–Yates plots for the A-S_E2 mechanism of hydrolysis of **1** (○) and **2** (●).

TABLE 5. Summary of the slope parameters ($\phi_{\neq} - \phi_e$) for hydrolysis of the azoaryl ethers **1**–**4**

	Substrate			
Parameter	**1**	**2**	**3**[a]	**4**[a]
($\phi_{\neq} - \phi_e$)	−0.25[b] −0.56[c]	−0.34[b]	−0.54[c,d]	−0.84[c,d]

[a]Calculated from the original data given in ref. 6.
[b]Values for A-2 mechanism.
[c]Values for A-S_E2 mechanism.
[d]In aqueous HCl media.

activation provided by a 3-azopyridinium function compared with a 4-azopyridinium group. Comparison of the contributing resonance structures of **8** for the 3-isomer with those for **6** for the 4-isomer clearly shows that there is charge delocalization into the pyridinium moiety for the 4-isomer that is not readily available for the 3-isomer. Both $\Delta H^{\neq}$ and $\Delta S^{\neq}$ vary in a more or less compensating manner. The large negative values of $\Delta S^{\neq}$ indicate ordered transition structures for the reactions of both substrates in accord with charge development in the transition state and the consequent electrostriction of solvent molecules.

Finally, it would be of interest to compare reactivity in the pyridinylazo and phenylazo series. Such comparison should be meaningfully restricted to **1** and **2** versus **4** since replacement of a phenyl group by naphthyl is known to have a large effect on reactivity (6). A strict comparison is difficult since reactions in the two series were studied in different acid media and at widely different temperatures, and in all cases reaction rates vary with medium acidity. These restrictions are further heightened by sulfo substitution in **4**, which is absent in the pyridinylazo compounds. However, an estimate of reactivity differences can be made after extrapolation of data to $C_{H^+} = 1\,M$

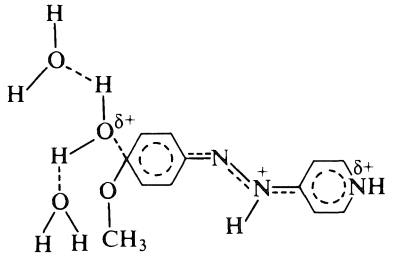

18

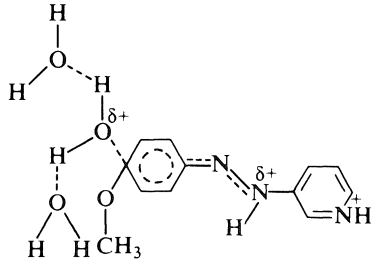

19

and a common temperature. Under these conditions, **1** reacts ca. 10^4 times faster than **4** while **2** reacts only 20 times faster, thereby highlighting the powerful activating influence of an aza substituent when situated in a position where it can conjugatively interact with the reaction centre.

Conclusions

The main conclusions that can be drawn from the above discussion are as follows:

1. Compound **1** reacts by the A-2 mechanism (Scheme 1) in acidities less than 42% H_2SO_4, while at higher acidities the mechanism changes to A-S_E2 involving general acid catalysis of leaving group departure (Scheme 2). Compound **2**, on the other hand, reacts by the A-2 mechanism over the entire range of acidity studied.

2. The A-2 reactions of these substrates involve 3 H_2O molecules in the transition state.

3. Introduction of a protonated azopyridinyl moiety decreases the basicity of the azo nitrogen relative to an azophenyl group by ca. 2.5 pK units.

4. An estimate of reactivity differences indicates that **1** reacts ca. 10^4 times faster than **4** while **2** reacts only 20 times faster.

Experimental

p$K_{SH_2^{2+}}$ Determination

The p$K_{SH_2^{2+}}$ of **2** was determined as follows. Aliquots of 3 μL of a stock solution of **2** in ethanol (2.89×10^{-2} M) were injected into 2.5 mL of the different acid solutions contained in a 1-cm cuvette and the spectra were recorded with distilled water as the reference on a Perkin–Elmer Lambda-5 spectrophotometer. Results are given in Table 3. An estimate of the p$K_{SH_2^{2+}}$ of **1** was made by analogy with the close similarity of the p$K_{SH_2^{2+}}$ of **2** and its hydrolysis product.

Materials

Sulfuric acid solutions were made up with distilled water and concentrated sulfuric acid (Fisher Reagent Grade) and standardized by titration.

Compound **2** was prepared by diazotization of 3-aminopyridine and coupling with phenol. The yellow precipitate of 3-(*p'*-hydroxyphenylazo)pyridine was washed thoroughly with water and recrystallized from ethanol, mp 220°C (lit. (11) mp 222°C). The compound was methylated by dissolving 0.65 g in 60 mL of 2 M methanolic H_2SO_4 and refluxing under N_2 for 30 h. Progress of methylation was followed through uv–visible spectroscopy by withdrawing samples of the reaction mixture at various intervals, quenching in excess NaOH, and observing the disappearance of the peak at 443 nm (λ_{max} of the conjugate base of the azophenol) and the growth of the peak at 353 nm (λ_{max} of **2** in basic solution). The reaction mixture was neutralized by addition of 120 mL of ice-cold 10% NaOH solution and extracted with three 100-mL portions of ether. The ether was distilled off and the resulting material purified by preparative tlc (benzene:acetonitrile 24:1). The orange solid was recrystallized from methanol and dried *in vacuo*, mp 69–70°C, yield 0.40 g (62%); $\lambda_{max}(\varepsilon)$ in EtOH: 351 nm (27 600 M^{-1} cm^{-1}). *Anal.* calcd. for $C_9H_{11}ON_3$: C 67.59, H 5.20, N 19.27%; found: C 67.20, H 5.21, N 19.40%.

Although **1** was previously prepared in low (5%) yield from *p*-nitroanisole and 4-aminopyridine (8*a*), we have since found that by employing the method given for **2** above, with the modifications of keeping the reaction mixture at 60°C and using 0.1 M methanolic H_2SO_4 as the methylating medium, the reaction was complete in 4 h with 67% yield.

Kinetics

The rates of formation of products were monitored spectrophotometrically. Slow reactions were followed mainly by the "indirect method," as follows. The substrate (ca. 1.5–2 mg) was weighed into a 25-mL volumetric flask and 50 μL of ethanol was added to aid solubility. Both the acid solution and the volumetric flask were placed in a thermostat to attain temperature equilibrium. Reaction was initiated by introducing 25 mL of the acid solution by means of a rapid delivery pipette. Aliquots (1 mL) were withdrawn at various intervals by means of a rapid delivery pipette and quenched in 20 mL of ca. 3 M NaOH solution containing ethanol in a 25-mL volumetric flask previously cooled in ice. At the end of the kinetic run the flasks were made up to mark and spectra of the quenched solutions were recorded by the overlay method on a Beckman DU-8 spectrophotometer.

For faster reactions the "direct method" of following the reaction was employed. A sample of the acid solution was placed in a 1-cm cuvette and thermostatted in the cell compartment of either a Beckman DU-8 or Beckman Acta IV spectrophotometer. Reaction was initiated by injecting 3–6 μL of the stock solution of the substrate (ca. $(2.75–3.0) \times 10^{-2}$ M in ethanol) into the acid solution, and the cuvette was shaken to ensure homogeneity. Depending on the rate of the reaction, data were collected either by the overlay method or at a fixed wavelength.

All rate constants were calculated by plotting $\ln(A_\infty - A_t)$ versus time. Excellent linearity was obtained in all cases.

Acknowledgements

We thank the Natural Sciences and Engineering Research Council of Canada for a grant and a CIDA/NSERC Research Associateship to one of us (I.O.). Preliminary experiments by S. R. Keum and S. Rajagopal and discussions with Dr. R. A. Cox are also acknowledged.

1. E. Buncel, S. R. Keum, M. Cygler, K. I. Varughese, and G. I. Birnbaum. Can. J. Chem. **62**, 1628 (1984).
2. O. N. Witt and C. Schmidt. Ber. **25**, 1013 (1892).
3. (*a*) W. Borsche, W. Muller, and C. A. Bodenstein. Ann. **472**, 201 (1929); (*b*) K. H. T. Pfister. J. Am. Chem. Soc. **54**, 1521 (1932).
4. J. B. Muler, L. Blangey, and H. E. Fierz-David. Helv. Chim. Acta, **35**, 2579 (1952).
5. J. F. Bunnett and G. B. Hoey. J. Am. Chem. Soc. **80**, 3142 (1958).
6. J. F. Bunnett and E. Buncel. J. Am. Chem. Soc. **83**, 1117 (1961).
7. J. F. Bunnett, E. Buncel, and K. V. Nahabedian. J. Am. Chem. Soc. **84**, 4136 (1962).
8. (*a*) E. Buncel. Acc. Chem. Res. **8**, 132 (1975); (*b*) R. A. Cox and E. Buncel. J. Am. Chem. Soc. **97**, 1871 (1975); (*c*) E. Buncel and S. R. Keum. J. Chem. Soc. Chem. Commun. 578 (1983); (*d*) E. Buncel, S. R. Keum, M. Cygler, K. I. Varughese, and G. I. Birnbaum. Can. J. Chem. **62**, 1628 (1984); (*e*) E. Buncel and S. R. Keum. Tetrahedron, **39**, 1091 (1983).
9. L. A. Flexser, L. P. Hammett, and A. Dingwall. J. Am. Chem. Soc. **57**, 2103 (1935).
10. H. H. Jaffe and R. W. Gardner. J. Am. Chem. Soc. **80**, 319 (1958).
11. S. R. Keum. Ph.D. Thesis. Queen's University, Kingston. 1982.
12. C. T. Davies and T. A. Geissman. J. Am. Chem. Soc. **76**, 3507 (1954).
13. W. M. J. Strachan, A. Dolenko, and E. Buncel. Can. J. Chem. **47**, 3631 (1969).
14. (*a*) V. K. Krieble and K. A. Holst. J. Am. Chem. Soc. **60**, 2976 (1938); (*b*) J. T. Edward, H. P. Hutchison, and S. C. R. Meacock. J. Chem. Soc. 2520 (1955); (*c*) J. T. Edward and S. C. R. Meacock. J. Chem. Soc. 2000 (1957); (*d*) R. A. Cox and K. Yates. Can. J. Chem. **59**, 2853 (1981).
15. K. Yates. Acc. Chem. Res. **4**, 136 (1971).
16. J. F. Bunnett. J. Am. Chem. Soc. **83**, 4956 (1961); **83**, 4968 (1961); **83**, 4973 (1961); **83**, 4978 (1961).
17. (*a*) D. S. Noyce and M. J. Jorgenson. J. Am. Chem. Soc. **85**, 2427 (1963); (*b*) J. R. Buchholz and R. E. Powell. J. Am. Chem. Soc. **85**, 509 (1963).
18. J. F. Bunnett and F. P. Olsen. Can. J. Chem. **44**, 1917 (1966).
19. V. Lucchini, G. Modena, G. Scorrano, and U. Tonellato. J. Am. Chem. Soc. **99**, 3387 (1977).
20. R. A. Cox and K. Yates. Can. J. Chem. **57**, 2944 (1979).
21. R. A. Cox and K. Yates. J. Am. Chem. Soc. **100**, 3861 (1978).

22. R. A. Cox and K. Yates. Can. J. Chem. **60**, 3061 (1982).
23. (*a*) N. C. Marziano, G. M. Cimino, and R. C. Passerini. J. Chem. Soc. Perkin Trans. 2, 1915 (1973); (*b*) N. C. Marziano, P. G. Traverso, and R. C. Passerini. J. Chem. Soc. Perkin Trans. 2, 306 (1977); (*c*) N. C. Marziano, P. G. Traverso, A. Tomasin, and R. C. Passerini. J. Chem. Soc. Perkin Trans. 2, 309 (1977).
24. E. M. Arnett and G. Scorrano. Adv. Phys. Org. Chem. **13**, 83 (1976).
25. A. Levi, G. Modena, and G. Scorrano. J. Am. Chem. Soc. **96**, 6585 (1974).
26. C. D. Johnson, A. R. Katritzky, and S. A. Shapiro. J. Am. Chem. Soc. **91**, 6654 (1969).
27. W. G. Giauque, E. W. Hornung, J. E. Kunzler, and T. R. Rubin. J. Am. Chem. Soc. **82**, 62 (1960).

Dissolution enthalpy of NaCl in aqueous nonelectrolyte solutions at 298.15 K. Analysis of electrolyte–nonelectrolyte enthalpic pair interaction coefficients in aqueous solution

HENRYK PIEKARSKI

Department of Physical Chemistry, University of Lódź, ul. Nowotki 18, Lódź, 91-416 Poland

Received January 20, 1986

HENRYK PIEKARSKI. Can. J. Chem. **64**, 2127 (1986).

Enthalpies of solution of NaCl in aqueous solutions of isopropanol, *s*-butanol, 2-methoxyethanol, 2-ethoxyethanol, acetone, and *N*,*N*-dimethylformamide were measured. The results of enthalpy measurements were analyzed from the point of view of the effect of added nonelectrolyte on water structure, and enthalpic pair interaction coefficients $h_{xy}\{(Na^+ + Cl^-)$–nonelectrolyte$\}$ were calculated and compared with appropriate data for $(Na^+ + I^-)$–nonelectrolyte pairs. The group additivity concept appeared to be useful for the analysis of calculated h_{xy} coefficients. The correlations between h_{xy} and the functions characterizing different properties of the solutes under study were examined. It was shown that the correlation with the heat capacity of transfer of the nonelectrolyte molecule from the vapour phase to high dilution in water was the most promising. The interpretation of observed correlations was proposed.

HENRYK PIEKARSKI. Can. J. Chem. **64**, 2127 (1986).

On a mesuré les enthalpies de solution du NaCl dans des solutions aqueuses d'isopropanol, de *s*-butanol, de méthoxy-2 éthanol, d'éthoxy-2 éthanol, d'acétone et de *N*,*N*-diméthylformamide. On a analysé les résultats des mesures d'enthalpies en fonction de l'effet de l'addition d'électrolytes sur le structure de l'eau; de plus, on a calculé les coefficients d'interaction entre les paires enthalpiques $[h_{xy}\{(Na^+ + Cl^-)$–nonelectrolyte$\}]$ et on les a comparés avec les données appropriées relatives aux paires $(Na^+ + I^-)$–nonelectrolyte. Le concept d'additivité de groupe semble utile pour l'analyse des coefficients h_{xy} calculés. On a examiné les corrélations qui existent entre h_{xy} et les fonctions qui caractérisent les diverses propriétés des solutés étudiés. On a démontré que la corrélation avec la capacité calorifique de transfert de la molécule nonélectrolyte de la phase vapeur à une grande dilution dans l'eau est celle qui offre le plus de promesses. On propose une interprétation des corrélations observées.

[Traduit par la revue]

Introduction

Thermochemical properties of electrolyte solutions in the mixtures of water with nonelectrolytes are frequently studied in many scientific centres. The obtained results are explained from the point of view of mixed solvent structure as well as solute – mixed solvent interactions. Enthalpic pair interaction coefficients between the solute and cosolvent in solvent water are often regarded as a measure of the interactions that can appear in these systems (1). As it is known the above mentioned coefficients can be calculated among others from experimentally determined enthalpy of transfer of the solute from water to water–cosolvent mixture (2, 3). From the numerous papers devoted to the analysis of the pair interaction coefficients, the most refer to the nonelectrolyte–nonelectrolyte pairs. Only a few papers concern the interactions between an electrolyte and a nonelectrolyte. One of them is a previous publication, prepared in our laboratory, that presents the systematic investigations of enthalpic pair interaction coefficients between NaI and different nonelectrolytes (4). The data related to other electrolytes (e.g. NaCl (5), Bu_4NBr (6), $CaCl_2$ (7)) are only fragmentary. Such situation hampers explicit interpretation of discussed coefficients and drawing of more general conclusions concerning the impact of different factors on h_{xy} values.

In order to fill this gap at least partly, there were performed thermochemical investigations of NaCl solution in mixtures of water with isopropanol, *s*-butanol, 2-methoxyethanol, 2-ethoxyethanol, acetone, and *N*,*N*-dimethylformamide, within the range of small organic component content. The above mentioned systems have not been examined calorimetrically till now. This set of water–organic mixtures together with data concerning dissolution enthalpy of NaCl in other nonelectrolyte–water mixtures, taken from the literature, made it possible to carry out more complete analysis of interactions occurring in NaCl–nonelectrolyte–water system and their comparison with interactions observed in the NaI–nonelectrolyte–water system.

Experimental

Materials

Sodium chloride, suprapur (Merck, FRG), was dried for several days at 393 K. Isopropanol and acetone, both analytically pure (POCh Gliwice, Poland), *s*-butanol A.R. (Reanal, Hungary), and *N*,*N*-dimethylformamide for spectroscopy (Fluka, FRG) were purified and dried using standard procedures (8). 2-Methoxyethanol and 2-ethoxyethanol, pure (Loba Chemie), were fractionally distilled. All solvents were stored over 4A molecular sieves. The water–organic mixtures were prepared by weight.

Apparatus and method of measurements

The measurements of solution enthalpies were made up using an "isoperibol" calorimeter. The calorimeter and the method of measurements were described in an earlier paper (9).

Results

The measured enthalpies of NaCl solution in the mixtures of water with isopropanol, *s*-butanol, 2-methoxyethanol, 2-ethoxyethanol, acetone, and *N*,*N*-dimethylformamide were extrapolated to an infinitely dilute solution, using the method introduced by Criss and Cobble (10). The standard enthalpies of NaCl solution in all investigated mixtures determined in this way are presented in Table 1 and Fig. 1. The complete set of experimental data is available elsewhere upon request.[1]

The standard solution enthalpy of NaCl in water at 298.15 K

[1]Values of $\Delta_{sol}H$ of NaCl in all investigated mixtures may be purchased from the Depository of Unpublished Data, CISTI, National Research Council of Canada, Ottawa, Ont., Canada K1A 0S2.

TABLE 1. Standard enthalpies of solution of NaCl in mixtures of the nonelectrolytes with water at 298.15 K

	$\Delta_{sol}H^{\infty}$ (kJ mol^{-1})					
ω_y[a]	*i*-PrOH	*s*-BuOH	MEtOH	EEtOH	ACT	DMF
0.025	—	4680	3975	—	—	—
0.05	5375	5500	4080	4330	3905	3575
0.10	6880	7195	4110	4710	3915	3430
0.15	8370	8995	4015	5060	3935	3395
0.20	9790	—	3515	5335	3955	3385
0.25	10980	—	—	5520	3975	3335
0.30	10900	—	—	5400	3995	3300
0.35	10420	—	—	5120	3975	—

[a]Mass fraction of the nonelectrolyte. Estimated uncertainty is ±20 J mol^{-1}.

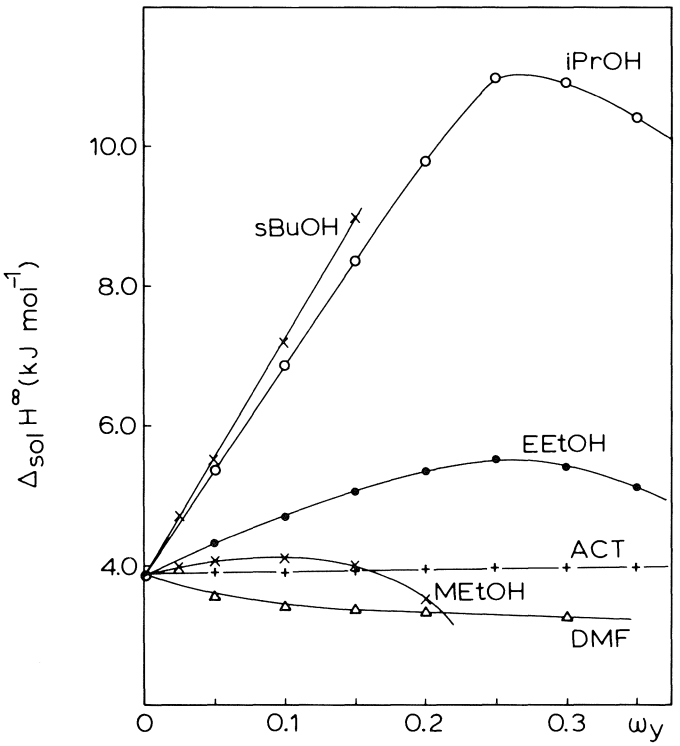

FIG. 1. Standard enthalpies of solution of NaCl in mixtures of water with isopropanol (*i*-PrOH), *s*-butanol (*s*-BuOH), 2-methoxyethanol (MEtOH), 2-ethoxyethanol (EEtOH), acetone (ACT), and *N*,*N*-dimethylformamide (DMF) vs. mass fraction of the organic component ω_y.

found in this work $\Delta_{sol}H^{\infty} = 3875$ J mol^{-1} is fully compatible with literature data (e.g. 3.82 kJ mol^{-1} (10), 3.88 kJ mol^{-1} (11)).

Discussion

Enthalpy of solution

As it can be seen in Fig. 1 enthalpy of NaCl solution in water mixtures of isopropanol, 2-methoxyethanol, 2-ethoxyethanol shows a maximum analogous to that observed in other water–alcohol mixtures hitherto analyzed (4, 12–23). It is generally accepted that this maximum is connected with the structure-making or -stabilizing effect of the added alcohol on water (24–28). In the case of *s*-butanol, the maximum is nonvisible, most probably due to limited solubility of this alcohol in water. The enthalpy of solution of NaCl in the mixtures of water with acetone grows quite insignificantly along with growing acetone content, without showing any maximum within the examined area of the mixed solvent composition. In the mixtures of DMF with water, unlike the previously discussed systems a drop of dissolution enthalpy of NaCl with growth of DMF content can be observed.

Enthalpic pair interaction coefficients

Enthalpic pair interaction coefficients $h_{xy}\{(Na^+ + Cl^-)$–nonelectrolyte$\}$ in water were estimated on the basis of dissolution enthalpy of NaCl in water–organic mixtures measured in this work. In order to calculate the h_{xy} coefficients, the method similar to that described by Heuvelsland *et al.* (6) was used. The standard enthalpy of solution $\Delta_{sol}H^{\infty}$ of NaCl in water–organic mixtures was presented as a function:

$$[1]\quad \Delta_{sol}H^{\infty}(\text{NaCl in W} + \text{Y}) = \Delta_{sol}H^{\infty}(\text{NaCl in W}) + b\omega_y + c\omega_y^2$$

where $\Delta_{sol}H^{\infty}$(NaCl in W) denotes standard enthalpy of solution of NaCl in pure water, ω_y is mass fraction of cosolvent Y, and b and c are coefficients that can be determined by the least-squares method. Parameter b in eq. [1], which represents limiting slope of function $\Delta_{sol}H$(NaCl in W + Y) is connected with McMillan–Mayer interaction coefficient h_{xy}:

$$[2]\quad b = 2\nu h_{xy}(\delta m_y/\delta\omega_y)_{\omega_y\to 0}$$

Denoting the molecular mass of cosolvent by M_y, we have for dilute solutions:

$$[3]\quad (\delta m_y/\delta\omega_y)_{\omega_y\to 0} = 1/M_y$$

where m_y is in mol kg^{-1}, M_y in kg mol^{-1}. Hence:

$$[4]\quad h_{xy} = bM_y/2\nu$$

where ν is the number of ions. The pair interaction coefficients defined as above constitute, for the systems containing an electrolyte of the 1–1 type, a half of the sum of the enthalpic effect of the interaction between molecule of a given nonelectrolyte and cation C^+ and anion A^-:

$$[5]\quad h_{xy} = \tfrac{1}{2}h\{(C^+ + A^-)\text{–nonelectrolyte}\} = \tfrac{1}{2}\{h(C^+\text{–nonelectrolyte}) + h(A^-\text{–nonelectrolyte})\}$$

The values of h_{xy} obtained this way can be found in Table 2. The same table shows also the $h_{xy}\{(Na^+ + Cl^-)$ – nonelectrolyte$\}$ values referring to other nonelectrolytes not examined in this work. These values were taken from literature (5), or estimated on the basis of enthalpies of NaCl solution found in the literature (29–35). Moreover, for comparison, Table 2 gives h_{xy} values for interactions $(Na^+ + I^-)$–nonelectrolyte determined in earlier work (4) as well as estimated on the basis of literature data (29, 31, 34–38).

The data presented in Table 2 show that the enthalpic pair interaction coefficients assume different values according to the kind of nonelectrolyte: positive for aliphatic alcohols, cellosolves, and THF and negative for the others. It is worth noting here that h_{xy} coefficients concerning the interactions of $(Na^+ + I^-)$ with aprotic nonelectrolyte have more negative (for DMF, DMSO, acetone, dioxane, sulfolane, acetonitrile) or less positive (for THF) values than analogous coefficients for $(Na^+ + Cl^-)$ interactions with the same nonelectrolytes. The cause of the observed differences should be sought in a different interaction of both anions with molecules of the above mentioned nonelectrolytes. In the case of the remaining nonelectro-

TABLE 2. Enthalpic pair interaction coefficients h_{xy} for $(Na^+ + Cl^-)$–nonelectrolyte and $(Na^+ + I^-)$–nonelectrolyte pairs at 298.15 K

Nonelectrolyte	h_{xy} (J kg mol^{-2}) $(Na^+ + Cl^-)$	$(Na^+ + I^-)$
MeOH	150[a]	157[c]
EtOH	290[a]	298[c]
PrOH	370[a]	395[c]
i-PrOH	450[b]	509[c]
s-BuOH	590[b]	643[c]
t-BuOH	490[a]	720[c]
MEtOH	95[b]	97[c]
EEtOH	210[b]	195[k]
Ethylene glycol	−43[d]	−45[d]
Glycerol	−30[d]	−60[l]
Urea	−245[e]	−262[k]
Formamide	—	−348[c]
DMF	−125[b]	−175[c]
THF	202[f]	172[f]
Dioxane	−145[g]	−440[m]
Acetone	10[b]	−46[c]
Acetonitrile	−143[h]	−247[n]
DMSO	−101[i]	−314,[c] −208[i]
Sulpholane	−336[j]	−542[j]

[a]Reference 5.
[b]This paper.
[c]Reference 4.
[d]Calculated from ref. 29.
[e]Calculated from ref. 30.
[f]Calculated from ref. 31.
[g]Calculated from ref. 32.
[h]Calculated from ref. 33.
[i]Calculated from ref. 34.
[j]Calculated from ref. 35.
[k]Calculated from ref. 36.
[l]Calculated from ref. 37.
[m]Calculated from ref. 38.
[n]Calculated from ref. 39.

lytes (apart from *t*-butanol) h_{xy} coefficients referring to NaCl and NaI have similar values.

Having at our disposal the values of enthalpic pair interaction coefficients for $(Na^+ + Cl^-)$–nonelectrolyte pairs it seemed interesting to check whether the group additivity concept can be applied for analysis of the system examined in this work. As it is known the group additivity concept was introduced by Savage and Wood (40) to correlate the pair interaction coefficients for a number of nonelectrolyte pairs, mainly alcohols, polyols, and amides in aqueous solutions. This concept was applied successfully to the systems containing both organic $\{(R_4N^+ + Br^-)$–DMF in water (41)$\}$ and inorganic $\{(Na^+ + I^-)$–alkanols in water (4)$\}$. Basing on the model described in the work already mentioned (4) three interaction types in the system analyzed can be distinguished here: $\frac{1}{2}\{(Na^+ + Cl^-)$–$CH_2\}$, $\frac{1}{2}\{(Na^+ + Cl^-)$–OH$\}$, and $\frac{1}{2}\{(Na^+ + Cl^-)$–O$\}$. In this case h_{xy} may be denoted as a sum:

$$[6] \quad h_{xy} = \sum^{i} n_{yi} h_{yi}$$

where n_{yi} is the number of group "*i*" in molecule Y, and h_{yi} is a characteristic contribution to h_{xy} of an average ionic interaction with a selected "*i*" type group in molecule Y. Following other authors it can be accepted that CH_3 group corresponds to $1.5CH_2$ while CH corresponds to $\frac{1}{2}CH_2$ (40, 41). Applying the method of multiple linear regression to solve eq. [6] for h_{xy} values for nine nonelectrolytes having in their molecule the distinguished groups (methanol, ethanol, propanol, isopropanol, *s*-butanol, 2-methoxyethanol, 2-ethoxyethanol, THF, dioxane) the group contributions collected in Table 3 were calculated. Table 3 also shows analogous group contributions referring to $(Na^+ + I^-)$–nonelectrolyte systems described in a previously cited work (4). In order to compare both data series, values concerning the $(Na^+ + I^-)$–nonelectrolyte systems were recalculated taking additional h_{xy} coefficients for $(Na^+ + I^-)$–THF and $(Na^+ + I^-)$–2-ethoxyethanol (36) pairs. The enthalpic pair interaction coefficients $h_{xy}\{(Na^+ + Cl^-)$–nonelectrolyte$\}$ calculated on the basis of the group additivity concept and determined experimentally are compared in Fig. 2. The slope and the regression coefficient for the function:

$$[7] \quad h_{xy}^{exp} = \alpha h_{xy}^{calc} + \beta$$

are equal to 1.003 ± 0.007 and 0.9933, respectively.[2]

This correlation visualised in Fig. 2 shows, that despite simplicity of the model its application both for nonelectrolytes with linear (alcohols) and cyclic (THF, dioxane) structure of molecule yields fully satisfactory results.

TABLE 3. Functional group interaction parameters h_{yi} with their standard deviations in water at 298.15 K

Functional group combinations "i"	h_{yi} (J kg mol^{-2}) $(Na^+ + Cl^-)$	$(Na^+ + I^-)$
$\frac{1}{2}\{(C^+ + A^-)$–$CH_2\}$	+138 ± 8	+145 ± 11
$\frac{1}{2}\{(C^+ + A^-)$–OH$\}$	−55 ± 25	−48 ± 36
$\frac{1}{2}\{(C^+ + A^-)$–O$\}$	−347 ± 20	−394 ± 34
Standard error of fit	28.0	40.7
Regression coefficient r^2	0.9948	0.9928

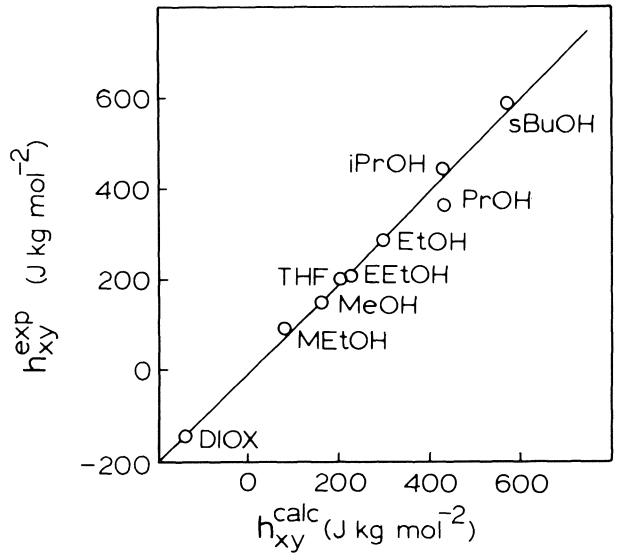

FIG. 2. A comparison of the enthalpic pair interaction coefficients $(Na^+ + Cl^-)$–nonelectrolyte determined experimentally (h_{xy}^{exp}) and calculated from group contributions (h_{xy}^{calc}). DIOX = dioxane, THF = tetrahydrofurane.

[2]Analogous data for the pairs containing NaI as an electrolyte are $\alpha = 1.016 \pm 0.007$, $r^2 = 0.9908$.

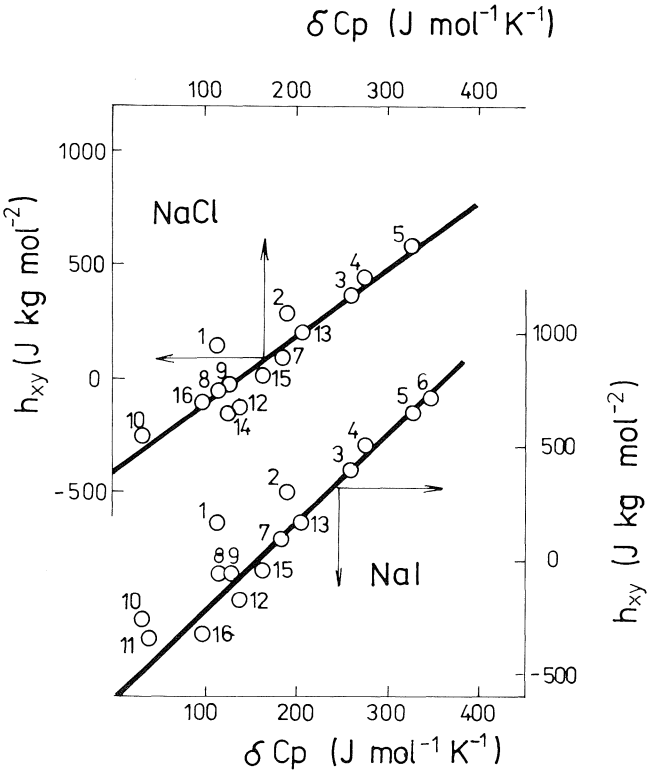

FIG. 3. The dependence of the enthalpic pair interaction coefficients h_{xy} for $(Na^+ + Cl^-)$–nonelectrolyte and $(Na^+ + I^-)$–nonelectrolyte interactions on the heat capacity of transfer of the nonelectrolyte from gas phase to high dilution in water: $\delta C_p = (\bar{C}^{\infty}_{p,2} - C^{g}_{p,m})$ at 298.15 K. The numbers denote the following: *1*, methanol; *2*, ethanol; *3*, propanol; *4*, isopropanol; *5*, *s*-butanol; *6*, *tert*-butanol; *7*, 2-methoxyethanol; *8*, ethylene glycol; *9*, glycerol; *10*, urea; *11*, formamide; *12*, *N*,*N*-dimethylformamide; *13*, tetrahydrofurane; *14*, dioxane; *15*, acetone; *16*, dimethylsulfoxide.

Comparison of h_{yi} group contributions concerning NaCl and NaI indicates that interaction of both electrolytes with CH_2 as well as OH group is similar. In the case of their interaction with aprotic ether group the value h_{yi} for NaI is more negative than h_{yi} for NaCl. This confirms an earlier observation concerning more negative interaction coefficients of aprotic nonelectrolytes with NaI than with NaCl (Table 2).

The enthalpy effect of the interaction between the ions and CH_2 group is positive due to the breaking of the structured water around the methylene group. The interactions of the ions with the polar group in a nonelectrolyte molecule is negative. A comparison of these results with the analogical data concerning the nonelectrolyte–nonelectrolyte interactions (42) indicates that the ion behaves similarly to polar group in the nonelectrolyte molecule, when it interacts with any distinguished group in other nonelectrolyte molecule. The functional group interaction parameters have respectively the same signs. These observations confirm the conclusions presented in the paper of Okamoto *et al.* that "... an exothermic enthalpy of interaction does not necessarily depend on hydrogen bonding between polar group" (42).

Very recently it has been found that enthalpic pair interaction coefficients h_{xy}(DMF–nonelectrolyte) for 16 nonelectrolytes of different type, depended linearly on heat capacity of transfer of the nonelectrolyte molecule from gas phase to high dilution in water (9).

[8] $\delta C_p = \bar{C}^{\infty}_{p,2} - C^{g}_{r,m}$

The h_{xy} values for interactions of 13 nonelectrolytes with urea gave similar correlation (9). It seemed interesting to verify whether a similar relation could be found also in the case of electrolyte–nonelectrolyte interactions in water solution. Figure 3 presents the dependence of h_{xy} for $(Na^+ + Cl^-)$–nonelectrolyte and $(Na^+ + I^-)$–nonelectrolyte pairs on δC_p of the nonelectrolyte in water. The values of $\bar{C}^{\infty}_{p,2}$ and $C^{g}_{p,m}$ are taken from compilation of Cabani *et al.* (43). As it can be seen from the Fig. 3 the analyzed functions correlate well with each other. The slope of the line correlating δC_p with h_{xy} values for pairs $(Na^+ + Cl^-)$–nonelectrolyte is 2.99 ± 0.25 kg mol^{-1} K^{-1}; that for pairs $(Na^+ + I^-)$–nonelectrolyte amounts to 3.28 ± 0.21 kg mol^{-1} K^{-1}. It is worth noting that neither $\bar{C}^{\infty}_{p,2}$ (partial molal heat capacity of nonelectrolyte in infinitely diluted aqueous solution) nor $C^{g}_{p,m}$ (molal heat capacity of nonelectrolyte in gas phase) correlate with h_{xy}.

The observed dependences strongly suggest that for a given X (NaCl or NaI, respectively), the effect of hydration of nonelectrolyte Y is more important than the direct interaction between particles X and Y when they approach each other (see also ref. 9). However, in some cases the latter effect can be more significant and then the deviations of the h_{xy} values from linear relation are observed — just as it happens for $(Na^+ + Cl^-)$–methanol and $(Na^+ + I^-)$–methanol pairs (Fig. 3).

The above observations together with conclusions provided by earlier work concerning the nonelectrolyte–nonelectrolyte–water systems (9) allowed us to suppose that the correlation of enthalpic pair interaction coefficients in water and δC_p can be of a general character. Now it seems interesting to check whether this correlation can find its application also in the case of solution in nonaqueous media. Appropriate studies are under way at the present time.

1. W. G. McMillan, Jr. and J. E. Mayer. J. Chem. Phys. **13**, 276 (1945).
2. J. E. Desnoyers, G. Perron, L. Avedikian, and J.-P. Morel. J. Solution Chem. **5**, 631 (1976).
3. H. L. Friedman and C. V. Krishnan. J. Solution Chem. **2**, 119 (1973).
4. H. Piekarski. Can. J. Chem. **61**, 2203 (1983).
5. G. Perron, D. Joly, J. E. Desnoyers, L. Avedikian, and J.-P. Morel. Can. J. Chem. **56**, 552 (1978).
6. W. J. M. Heuvelsland, C. de Visser, and G. Somsen. J. Chem. Soc. Faraday Trans. I, **77**, 1191 (1981).
7. S. Taniewska-Osińska and J. Barczyńska. J. Chem. Soc. Faraday Trans. I, **80**, 1409 (1984).
8. A. Weissberger, E. S. Proskauer, J. A. Riddick, and E. E. Toops, Jr. Organic solvents. Interscience Publishers Inc., New York. 1955.
9. H. Piekarski and G. Somsen. Can. J. Chem. **64**, 1721 (1986).
10. C. M. Criss and J. W. Cobble. J. Am. Chem. Soc. **83**, 3223 (1961).
11. V. B. Parker. Thermal properties of aqueous uni-univalent electrolytes. Natl. Stand. Ref. Data, N.B.S. 2, 1965.
12. R. L. Moss and J. H. Wolfenden. J. Chem. Soc. London, 118 (1939).
13. C. M. Slansky. J. Am. Chem. Soc. **62**, 2430 (1940).
14. G. V. Karpenko, K. P. Mishchenko, and G. M. Poltoratskii. Zhur. Strukt. Khim. **8**, 416 (1967).
15. S. Taniewska-Osińska and H. Piekarski. J. Solution Chem. **7**, 891 (1978).
16. H. Piekarski, A. Piekarska, and S. Taniewska-Osińska. Can. J. Chem. **62**, 856 (1984).
17. R. K. Mohanty, T. S. Sarma, S. Subramanian, and J. C. Ahluvalia. Trans. Faraday Soc. **67**, 305 (1971).

18. R. K. MOHANTY, S. SUNDER, and J. C. AHLUVALIA. J. Phys. Chem. **76**, 2577 (1973).
19. L. AVEDIKIAN, J. JUILLARD, J.-P. MOREL, and M. DUCROS. Thermochim. Acta, **6**, 283 (1973).
20. Y. POINTUD, J. JUILLARD, L. AVEDIKIAN, J.-P. MOREL, and M. DUCROS. Thermochim. Acta, **8**, 423 (1974).
21. N. DOLLET and J. JUILLARD. J. Solution Chem. **5**, 77 (1976).
22. G. A. KRESTOV. Thermodynamics of ionics processes in solution (in Russian). *Edited by* Khimiya, Leningrad. 1973.
23. B. G. PERELYGIN, YU. A. BYVALCEV, and A. F. VOROB'EV. Zhur. Fiz. Khim. **52**, 484 (1978); **52**, 1836 (1978).
24. G. NEMETHY and H. A. SCHERAGA. J. Phys. Chem. **66**, 1773 (1962).
25. M. N. BUSLAEVA and O. YA. SAMOILOV. Zhur. Strukt. Khim. **4**, 502 (1963).
26. O. YA. SAMOILOV. Zhur. Strukt. Khim. **7**, 15 (1964); **7**, 175 (1964).
27. G. NEMETHY. Ann. Ist. Super. Sanita, **6**, 487 (1970).
28. K. P. MISHCHENKO and G. M. POLTORATSKII. Problems of thermodynamics and structure of aqueous and nonaqueous electrolyte solutions. Plenum Publishing Corp., New York. 1972.
29. V. D. SOROKIN, Y. I. CHISTIAKOV, I. V. EGOROVA, and G. A. KRESTOV. Izv. Vyssh. Ucheb. Zaved. Khim. Khim. Tekhnol. **20**, 139 (1977).
30. Y. POINTUD and J. JUILLARD. J. Chem. Soc. Faraday Trans. I, **73**, 1048 (1977).
31. S. TANIEWSKA-OSIŃSKA, B. PIESTRZYŃSKA, and R. ŁOGWINIENKO. Can. J. Chem. **58**, 1584 (1980).
32. D. FEAKINS and C. T. ALLAN. J. Chem. Soc. Faraday Trans. I, **72**, 314 (1976).
33. B. G. COX, R. NATARAJAN, and W. E. WAGHORNE. J. Chem. Soc. Faraday Trans. I, **75**, 86 (1979).
34. A. F. VOROB'EV, A. S. MONAENKOVA, and J. D. PADUNOVA. Izv. Vyssh. Ucheb. Zaved. Khim. Khim. Tekhnol. **20**, 1641 (1977).
35. M. CASTAGNOLO, G. PETRELLA, M. DELLA MONICA, and A. SACCO. J. Solution Chem. **8**, 501 (1979).
36. H. PIEKARSKI. To be published.
37. S. TANIEWSKA-OSIŃSKA, J. WOŹNICKA, and L. BARTEL. Thermochim. Acta, **47**, 65 (1981).
38. K. P. MISHCHENKO and S. V. SHADSKII. Teor. Eksp. Khim. **1**, 60 (1965).
39. M. F. STENNIKOVA. Thesis, Technical Institute of Industry. Leningrad, USSR. 1971.
40. J. J. SAVAGE and R. H. WOOD. J. Solution Chem. **5**, 733 (1976).
41. C. DE VISSER, W. J. M. HEUVELSLAND, and G. SOMSEN. J. Solution Chem. **7**, 193 (1978).
42. B. Y. OKAMOTO, R. H. WOOD, J. E. DESNOYERS, G. PERRON, and L. DELORME. J. Solution Chem. **10**, 139 (1981).
43. S. CABANI, P. GIANNI, V. MOLICA, and L. LEPORI. J. Solution Chem. **10**, 563 (1981).

A ^{1}H and ^{13}C nuclear magnetic resonance study of carnosine

JAN O. FRIEDRICH[1] AND RODERICK E. WASYLISHEN[2]
Department of Chemistry, Dalhousie University, Halifax, N.S., Canada B3H 4J3

Received January 10, 1986

JAN O. FRIEDRICH and RODERICK E. WASYLISHEN. Can. J. Chem. **64**, 2132 (1986).

The proton and carbon-13 resonance signals of carnosine (β-alanyl-L-histidine) were unambiguously assigned using a variety of nmr techniques including proton–carbon chemical shift correlations, titrations of nmr chemical shifts, coupling constants, and isotope shifts. From the ^{13}C nmr titration, carnosine's three pK_a values were estimated to be 2.7, 7.1, and 10.6, and it was found that the imidazole ring existed predominantly as the 3-H tautomer in basic solution. Conformational information about the C_α—C_β bond and about the N—C_α bond was deduced from observed ^3J(C,H) and ^3J(H,H) values. The ^{13}C nmr spectrum of carnosine in solution is also compared with that obtained for a solid sample.

JAN O. FRIEDRICH et RODERICK E. WASYLISHEN. Can. J. Chem. **64**, 2132 (1986).

Faisant appel à diverses techniques de rmn, incluant les corrélations de déplacements chimiques proton–carbone, les titrations des déplacements chimiques en rmn, les constantes de couplage ainsi que les déplacements dus aux isotopes, on a attribué sans ambiguïtés les signaux observés dans les spectres rmn du ^{1}H et du ^{13}C de la carnosine (β-alanyl L-histidine). En se basant sur la titration en rmn du ^{13}C, on a évalué que les trois constantes de pK_a de la carnosine sont respectivement égales à 2,7, 7,1 et 10,6; de plus, on a aussi trouvé que, en solution aicaline, le cycle imidazole existe principalement sous le forme du tautomère 3-H. À l'aide des valeurs observées pour les constantes de couplage ^3J(C,H) et ^3J(H,H), on a déduit des informations relatives à la conformation autour des liaisons C_α—C_β et N—C_α. On a aussi comparé le spectre rmn du ^{13}C de la carnosine en solution avec celui obtenu à l'aide d'un échantillon à l'état solide.

[Traduit par la revue]

Introduction

Carnosine (**1**), a dipeptide consisting of L-histidine and β-alanine, was discovered at about the beginning of the century (1). Although it is present in relatively high concentrations in skeletal muscle it can be found in a variety of other animal tissues as well. Various suggestions have been made (2) as to its role in living organisms but its precise function is not well understood. Carnosine has been the subject of numerous ^{1}H and ^{13}C nmr investigations, even being detected with ^{1}H nmr in intact muscle (3–5). However, there still seems to be ambiguity over some of the proton and carbon-13 assignments. For example, the ^{1}H nmr signals of the two pairs of methylene protons of the β-alanine group, which have similar chemical shifts, have been assigned in both possible ways (6–9). In this paper the proton and carbon resonance signals were unambiguously assigned using a variety of nmr techniques. These techniques involved a ^{13}C nmr titration, which also yielded estimates of carnosine's pK_a values and the site of protonation on the imidazole ring. Conclusions regarding the conformation of carnosine in aqueous solution were deduced from measured three-bond ^{1}H–^{1}H and ^{13}C–^{1}H spin–spin coupling constants. Finally, carbon-13 chemical shifts of solid carnosine were measured using cross-polarization and magic-angle spinning techniques and the solid (10, 11) and solution structures were compared.

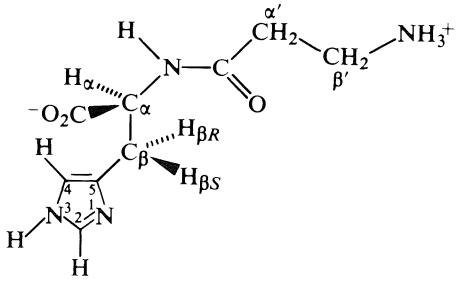

1

Experimental

L-carnosine (β-alanyl-L-histidine) was obtained from Sigma Chemical Company and used without further purification. The concentrations of carbon-13 and proton nmr samples were approximately 0.5 *M* and 0.1 *M* respectively in D_2O or H_2O. The values of pH (uncorrected for deuterium) were obtained at 25 ± 1°C with an Orion model 601A digital Ionalyzer pH meter. The meter was calibrated with two buffers: a 0.05 *M* phosphate buffer (pH 6.865) and a 0.05 *M* phthalate buffer (pH 4.008) at pH readings below pH 7; the phosphate buffer and a 0.01 *M* borax buffer (pH 9.18) were used at pH readings above 7.

Proton-decoupled carbon-13 nmr spectra were recorded on a Varian CFT-20 with data acquisition times of at least 1.023 s (1 data point every 0.98 Hz). Sensitivity enhancements were always 0.3 s thus ensuring that the line widths were not broadened by more than about 1 Hz. All chemical shifts are reported with respect to external TMS and are accurate to 0.05 ppm except where noted. Proton spectra and proton coupled ^{13}C nmr spectra were obtained at 21°C on a Nicolet 360 NB operating at 361.06 MHz and 90.81 MHz, respectively. The 1331 sequence (12) was used to suppress the solvent signal for spectra obtained in H_2O.

The ^{1}H–^{13}C chemical shift correlations (13) were obtained on a Bruker MSL-300, where ^{1}H and ^{13}C resonated at 300.13 and 75.47 MHz, respectively.

Carbon-13 spectra of solid samples were obtained on a Bruker MSL-200 using ^{1}H cross-polarization (CP) and magic-angle spinning (MAS) techniques (14–16). The contact and recycle times were 1 ms and 5 s, respectively, and the MAS spinning rates were 5.0 kHz. An aluminum oxide rotor of volume 0.35 cm^3 was used. The quaternary carbon resonances were assigned using the pulse sequence of Opella and Frey (17). Chemical shifts were referenced to external adamantane (18).

Results and discussion

^{1}H and ^{13}C nuclear magnetic resonance spectra of carnosine in solution

^{13}C chemical shifts as a function of pH

As mentioned above, some ambiguity existed over the

[1]Holder of a 1985 NSERC Summer Undergraduate Research Award.

[2]Author to whom correspondence may be addressed.

TABLE 1. Acid dissociation constants of carnosine

Reference	pK_1	pK_2	pK_3	Temperature (°C)
This work[a]	2.73 ± 0.07[b]	7.06 ± 0.13[c]	10.55 ± 0.03[d]	25
Tanokura *et al.*[e]	2.77	6.83	9.66	37
Bradbury *et al.*[f]	7.4	7.6	10.0	—
Ihnat and Bersohn[g]	—	7.0	9.6	27

[a]Errors were estimated assuming chemical shift measurements were accurate to ±0.05 ppm and pH measurements to ±0.1 of a pH unit, and from the standard deviations of the average pK_a values obtained from eq. [2].
[b]Using chemical shifts from CO_2^-, C5, C_α, and C_β.
[c]Using chemical shifts from CO_2^-, C2, C5, C_α, and C_β.
[d]Using chemical shifts from C(O)NH, $C_{\alpha'}$, and $C_{\beta'}$.
[e]Reference 20.
[f]Reference 21, temperature not reported.
[g]Reference 9 (the authors corrected for deuterium using pD = pH + 0.4).

assignment of the $C_{\alpha'}$ and $C_{\beta'}$ signals in the carbon-13 spectrum and their respective pairs of attached protons in the ^1H spectrum. To determine whether any carbon-13 resonance signals cross over the entire pH range, a ^{13}C nmr titration of carnosine was carried out in which the resonance signals were recorded at increments of 0.5 pH units. As expected, the ^{13}C chemical shifts exhibited typical titration curves as an amino, imidazole, or carboxyl group in the vicinity was titrated (for example, see Fig. 1). From these titration curves it is possible to calculate acid dissociation constants (19, 20). The average values for the three acid dissociation constants of carnosine obtained from the ^{13}C chemical shifts are shown in Table 1, as are values obtained from previous ^1H nmr titrations (9, 20, 21). Although these experiments were all carried out in deuterium oxide, the pK_a values obtained in this study are within 0.2 units of the values in H_2O (22).

Assignment of ^{13}C and ^1H resonances of the β-alanyl group

Table 2 lists the chemical shifts of the carbon signals for the various species obtained from the nmr titration while Table 3 lists the corresponding proton chemical shifts. From the ^{13}C data it appears that the signals for $C_{\alpha'}$ and $C_{\beta'}$ do indeed cross around pH 11.5 (see Fig. 2). This was verified using proton–carbon correlation two-dimensional nmr (13) and using isotope effects as explained below.

At pH 7.0, the proton–carbon correlation spectra indicated that the protons at 2.5 ppm were bonded to the carbon resonating at 33.5 ppm, and the protons at 3.0 ppm were bonded to the carbon resonating at 37.2 ppm. At pH 13.4, the 2D spectra also indicated that the low frequency (upfield) protons were bonded to the carbon resonating at 40.3 ppm and the high frequency (lowfield) protons to the carbon resonating at 39.0 ppm. Thus, since the chemical shift difference between the corresponding proton triplets remains fairly constant over the pH range (i.e., they do not cross), the carbon signals must have crossed.

Another method for confirming that the two carbon resonance signals crossed and also to unambiguously assign them is to use H/D isotope effects (23–25). It has been demonstrated (25) that carbons directly bonded to an amino group (that is, a two-bond isotope effect) experience a low frequency shift of approximately 0.055–0.097 ppm/deuteron while carbons two bonds from an amino group (a three-bond isotope effect) experience a low frequency shift of approximately 0.025–0.051 ppm/deuteron. The results obtained for two 0.5 *M* samples of carnosine, one dissolved in H_2O and the other in D_2O, are summarized in Table 4. The isotope shift data confirm that the $C_{\alpha'}$ and $C_{\beta'}$ signals cross because at low pH the high frequency ^{13}C resonance signal has the larger isotope shift while at high pH the low frequency peak has the larger shift. The isotope shift data also allow one to assign the two resonance signals since $C_{\beta'}$, which is directly bonded to the nitrogen atom, should experience a larger isotope shift than the more distant $C_{\alpha'}$. Finally returning to the proton–carbon chemical shift correlation spectra, it is possible to assign the proton signals as well. These assignments can be found in Tables 2 and 3.

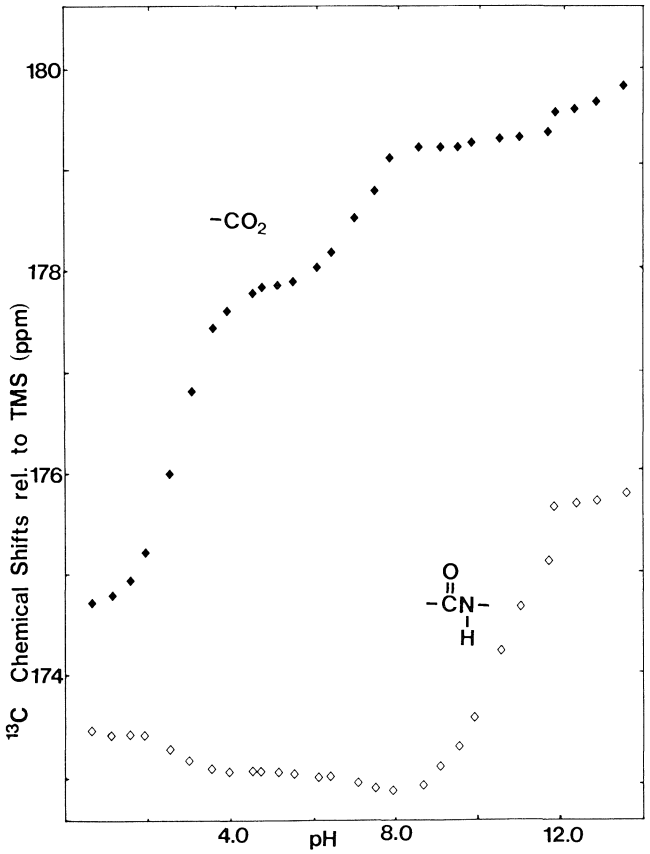

FIG. 1. Chemical shifts of the carbonyl and carboxyl ^{13}C nuclei as a function of pH.

Further support for this carbon-13 assignment comes from the

TABLE 2. Carbon-13 chemical shifts relative to external TMS[a]

Species	pH[b]	CO_2^-	C(O)NH	C2	C5	C4	C_α	$C_{\beta'}$	$C_{\alpha'}$	C_β
$ND_3^+ImD^+COOD$	0.6	174.7	173.5	135.0	130.0	118.7	53.2	37.1	33.2	27.5
$ND_3^+ImD^+COO^-$	4.7	177.8	173.1	134.8	131.1	118.2	55.5	37.2	33.4	28.5
$ND_3^+ImCOO^-$	8.0	179.1	172.9	137.0	134.5	118.7	56.5	37.2	33.7	30.2
ND_2ImCOO^-	13.1	179.8	175.7	137.8	134.9	119.4	56.6	39.0	40.3	30.7

[a]Shifts are accurate to ±0.1 ppm.
[b]pH meter readings are accurate to ±0.1 pH units.

TABLE 3. Proton chemical shifts relative to external TMS[a]

Species	pH[b]	H2	H4	H_α	$H_{\beta S}$	$H_{\beta R}$	$H2_{\beta'}$	$H2_{\alpha'}$
$HD_3^+ImD^+COOD$	0.0	8.37	7.08	4.51	3.07	2.95	2.96	2.46
$ND_3^+ImD^+COO^-$	4.8	8.45	7.12	4.32	3.09	2.95	3.07	2.54
$ND_3^+ImCOO^-$	8.3	7.38	6.63	4.15	2.82	2.65	2.90	2.35
ND_2ImCOO^-	13.3	7.36	6.64	4.21	2.87	2.66	2.50	2.08

[a]Shifts are accurate to ±0.01 ppm; shifts were also measured with respect to internal 0.01 *M* DSS (add 0.28 ppm to each of the above values to obtain the chemical shift with respect to internal DSS).
[b]pH meter readings are accurate to ±0.1 pH units.

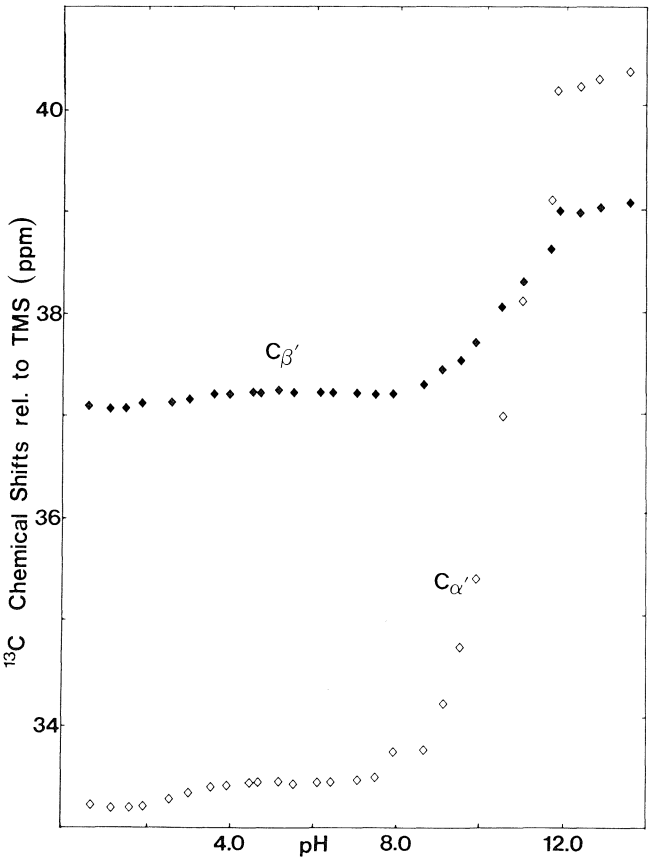

FIG. 2. Chemical shifts of $^{13}C_{\alpha'}$ and $^{13}C_{\beta'}$ as a function of pH.

changes in the chemical shifts of $C_{\alpha'}$ and $C_{\beta'}$ upon amino protonation (26, 27). Also, the smaller value of $^1J(C_{\alpha'},H_{\alpha'})$, 129.6 Hz, compared to $^1J(C_{\beta'},H_{\beta'})$, 145.5 Hz, is consistent with our assignment since $CH_3NH_3^+$, $^1J(C,H) = 145$ Hz (28), and in CH_3CONH_2, $^1J(C,H) = 129$ Hz (29).

Site of imidazole ring protonation

The behavior of the chemical shifts of the three carbon atoms C2, C4, and C5 upon protonation of the imidazole ring can provide some information on which of the two nitrogen atoms is protonated and hence which tautomer predominates in basic solution. Comparing previous results (26, 30) on histidine and methylhistidines to the carnosine results (Table 5), one comes to the same conclusion for carnosine as Reynolds *et al.* (26, 30) did for histidine. That is, protonation occurs predominantly at the N1 position because the change in chemical shift of C4 is relatively small and close to zero while that of C5 is larger in magnitude and to lower frequency. These shifts are similar to those in 3-methylhistidine, which must of course protonate at the N1 position. Therefore the neutral ring exists predominantly as the N3—H tautomer. However, this does not rule out the presence of some of the N1—H tautomer since the carbon shifts are intermediate between those of the two methylhistidines. In fact if one assumes that the shifts of the N1—H and N3—H forms of carnosine are similar to the 1-methyl- and 3-methylhistidines one obtains a 2:1 ratio of the N3—H:N1—H tautomers. This estimate is only approximate in view of the above assumption.

Application of coupling constants to determine the conformations about the C_α—C_β bond and assign $H_{\beta R}$ and $H_{\beta S}$

Because of the chiral centre at C_α the two H_β protons are nonequivalent in carnosine, thus, the methine and methylene protons attached to C_α and C_β respectively form an approximate AMX spin system (see Fig. 3). The assignment of $H_{\beta R}$ and $H_{\beta S}$ is not immediately obvious; however, from observed $^3J(H,H)$ and $^3J(^{13}C,H)$ values this assignment can be made (31–33). The conformation about the C_α—C_β bond axis is generally described in terms of the fractional populations P_I, P_{II}, and P_{III} of the rotamers I–III (34). Assuming that the vicinal coupling constants are functions only of dihedral angle, $^3J(H_\alpha,H_{\beta R})$ and $^3J(H_\alpha,H_{\beta S})$ can be expressed in terms of the *gauche* ($J_g(H,H)$) and *trans* ($J_t(H,H)$) coupling constants (31–34). Of particular interest is the difference and sum of the two observed vicinal proton–proton coupling constants

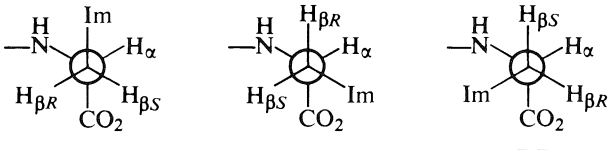

TABLE 4. Deuterium induced isotope shifts

	Chemical shift,[a] δ, relative to external TMS $C_{\alpha'}$	$C_{\beta'}$	Species present
pH = *1.96* ± 0.05			
H_2O	33.25 ± 0.01	37.14 ± 0.01	$-NHC(O)CH_2CH_2NH_3^+$
D_2O	33.03	36.84	$-NDC(O)CH_2CH_2ND_3^+$
Δδ[b]	0.22 ± 0.02	0.30 ± 0.02	
Δδ/deuteron	0.07_3 ± 0.01	0.10 ± 0.01	
pH = 12.32 ± 0.05			
H_2O	40.28 ± 0.01	39.07 ± 0.01	$-NHC(O)CH_2CH_2NH_2$
D_2O	40.15	38.79	$-NDC(O)CH_2CH_2ND_2$
Δδ[b]	0.13 ± 0.02	0.28 ± 0.02	
Δδ/deuteron	0.06_5 ± 0.01	0.14 ± 0.01	

[a]Acquisition time = 4.095 s (one point per 0.25 Hz = 0.012 ppm).
[b]Positive isotope shifts correspond to low frequency (upfield) shifts.

TABLE 5. Changes in ^{13}C chemical shifts of imidazole ring carbons upon ring protonation[a]

	3-Methyl histidine[b]	1-Methyl histidine[b]	Histidine[b]	Carnosine[c]
C2	−3.5	−3.4	−2.4	−2.44 ± 0.14
C4	+2.1	−7.1	+0.7	−0.74
C5	−6.8	+2.3	−4.8	−3.60

[a]Positive shift is to higher frequency (downfield).
[b]From ref. 26.
[c]This work.

(eqs. [1] and [2]) (31, 32, 35).

$$[1]\quad {}^3J(H_\alpha,H_{\beta R}) - {}^3J(H_\alpha,H_{\beta S}) = (P_I - P_{II})(J_t(H,H) - J_g(H,H))$$

$$[2]\quad {}^3J(H_\alpha,H_{\beta R}) + {}^3J(H_\alpha,H_{\beta S}) = J_g(H,H)(1 + P_{III}) + J_t(H,H)(1 - P_{III})$$

Although P_{III} can be determined from eq. [2] it is impossible to determine P_I and P_{II} from eq. [1] unless $H_{\beta R}$ and $H_{\beta S}$ are correctly assigned. Further information about P_I and P_{II} can be obtained from the observed values of ${}^3J({}^{13}CO_2^-,H_\beta)$. Again averaging the observed coupling constants over the fractional populations one obtains, after rearrangement,

$$[3]\quad {}^3J({}^{13}CO_2^-,H_{\beta R}) - {}^3J({}^{13}CO_2^-,H_{\beta S}) = (P_{II} - P_{III})(J_t(C,H) - J_g(C,H))$$

$$[4]\quad {}^3J({}^{13}CO_2^-,H_{\beta R}) + {}^3J({}^{13}CO_2^-,H_{\beta S}) = J_g(C,H)(1 + P_I) + J_t(C,H)(1 - P_I)$$

Given the *trans* and *gauche* proton–carbon coupling constants, one can uniquely determine P_I from eq. [4], which can then be used to unambiguously determine ${}^3J(H_\alpha,H_{\beta R})$ and ${}^3J(H_\alpha,H_{\beta S})$.

Using eqs. [2] and [4] and taking $J_g(H,H)$ = 2.4 ± 0.3 Hz, $J_t(H,H)$ = 13.3 ± 0.3 Hz, $J_g(C,H)$ = 1.2 ± 0.2 Hz, and $J_t(C,H)$ = 10.0 ± 0.2 Hz (35),[3] and our measured coupling constants (see Table 6), gives P_{III} = 0.20 ± 0.06, and P_I = 0.68 ± 0.08. Since $P_I > P_{II}$ it is apparent from eq. [1] that ${}^3J(H_\alpha,H_{\beta R})$ = 8.7 ± 0.3 Hz and ${}^3J(H_\alpha,H_{\beta S})$ = 4.8 ± 0.3 Hz, thus the signal at 2.82 ppm (see Table 1) corresponds to $H_{\beta S}$ while the lower frequency signal corresponds to $H_{\beta R}$. Similar observations on the relative chemical shifts of the two β protons have been observed for several amino acids (33, 34*b*, and 35). From the ${}^3J(H,H)$ values, P_I = 0.58 ± 0.04 and P_{II} = 0.22 ± 0.04.

Our conclusion that $P_I \cong 0.6 > P_{II} = P_{III}$ for carnosine is in excellent agreement with results obtained in two independent studies of the related dipeptide Gly-L-His (31, 37). It is interesting to note that the conformation about the C_α—C_β bond of carnosine in the solid state is best described by rotamer II (10, 11).

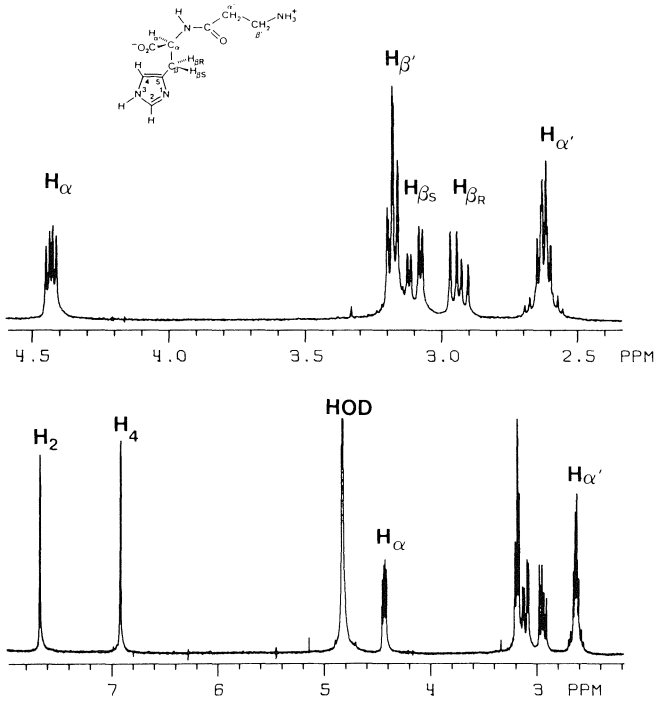

FIG. 3. Proton nmr spectrum of 0.1 *M* carnosine in D_2O at pH 8.0. Chemical shifts are relative to internal DSS. The upper spectrum is an expansion of the region between δ = 2.4 and 4.5 ppm.

[3]Using different *gauche* and *trans* proton–proton coupling constants (determined using cyclic amines) that are rotamer dependent (36) gives almost identical results for ${}^3J(H_\alpha,H_{\beta R}) > {}^3J(H_\alpha,H_{\beta S})$: P_I = 0.63, P_{II} = 0.23, P_{III} = 0.14.

TABLE 6. Spin–spin coupling constants for aqueous solutions of carnosine

	Coupling constant (Hz)	
	pH 4[a]	pH 8.5[a]
Proton–proton[b]		
$^3J(H_\alpha,H_{\beta R})$	8.4 ± 0.3	8.7 ± 0.3
$^3J(H_\alpha,H_{\beta S})$	5.2	4.8
$^3J(H_{\beta R},H_{\beta S})$	−15.4	−15.0
$^3J(H_\alpha,HN)$	7.5	—
$^3J(H_{\alpha'},H_{\beta'})$	6.7	6.7
One-bond carbon–proton		
$^1J(C_\alpha,H_\alpha)$	141.8 ± 0.5	142.1 ± 0.5
$^1J(C_\beta,H_\beta)$	133.0	130.5
$^1J(C_{\alpha'},H_{\alpha'})$	129.6	129.6
$^1J(C_{\beta'},H_{\beta'})$	146.0	145.5
^1J(C2,H2)	221.1	209.1
^1J(C4,H4)	201.0	190.3
Two-bond carbon–proton[c]		
$^2J(C_\alpha,H_{\beta R})$	4.5	4.1
$^2J(C_\alpha,H_{\beta S})$	4.5	4.1
$^2J(C_{\alpha'},H_{\beta'})$	3.5	3.4
$^2J(C_{\beta'},H_{\alpha'})$	4.7	4.8
$^2J(CO_2^-,H_\alpha)$	5.7	5.2
^2J(C(O)N,$H_{\alpha'}$)		5.0
Three-bond carbon–proton		
^3J(C2,H4)	6.5	8.4
$^3J(CO_2^-,H_{\beta R})$	2.8 ± 0.4	2.6 ± 0.4
$^3J(CO_2^-,H_{\beta S})$	2.8 ± 0.4	2.6 ± 0.4
^3J(C(O)N,$H_{\alpha'}$)	3.4 ± 0.7	2.7 ± 0.3
^3J(C(O)N,$H_{\beta'}$)		5.0 ± 0.5

[a] ±0.5 of a pH unit.
[b] Small additional long-range coupling for H2, H4, $H_{\alpha'}$, $H_{\beta'}$, and $H_{\beta S}$ was also observed at several pH's.
[c] Sign not determined.

Dihedral analysis of the N—C_α bond

It is well known that the peptide fragment (**2**), is essentially

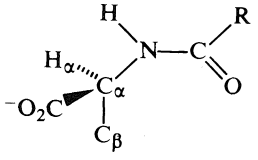

2

planar and that the barrier to internal rotation about the N—C amide bond exceeds 80 kJ mol^{-1} (38). Information concerning the conformation about the N—C_α bond is potentially available from observed values of $^3J(^1H–N—C_\alpha–^1H_\alpha)$, $^3J(^1H–N—C_\alpha–^{13}CO_2^-)$, $^3J(^1H–N—C_\alpha–^{13}C_\beta)$, and $^3J(^{13}C(O)–N—C_\alpha–^1H_\alpha)$. The dependencies of these coupling constants on the torsional angle (the torsional angle, ϕ, is defined using IUPAC rules (39)) have been extensively investigated using empirical (40–44) and theoretical (45, 46) data, which are summarized in ref. 47. Our measured value of $^3J(^1H–N—C_\alpha–^1H)$ = 7.5 Hz at pH 4.3 and at pH 0.2 is similar to $^3J(^1H–N—C_\alpha–^1H)$ = 8 Hz observed from pH 1.0 to 4.5 (10) and gives possible dihedral angles, ϕ, of −150°, −80°, and 30–90° (47). The measured value of $^3J(^{13}C(O)–N—C_\alpha–H_\alpha)$ = 3.4 Hz at pH 4.3 gives dihedral angles of −150°, −80°, 0°, and 120° (47). Thus the two dihedral angles of −150° (**3**) and −80° (**4**) are both consistent with the observed coupling constants $^3J(^1H–N—C_\alpha–^1H_\alpha)$ and $^3J(^{13}C(O)–N—C_\alpha–^1H_\alpha)$. It is interesting to note that the X-ray diffraction data indicate that the torsional angles about the N—C_α bonds of various histidine residues may be classified into two groups of about −80° and −150°. Our inability to observe $^3J(^1H–N—C_\alpha–^{13}CO_2^-)$ and $^3J(^1H–N—C_\alpha–^{13}C_\beta)$ in aqueous solution suggests that the relative energies of **3** and **4** are comparable to or less that *kT*; hence one is measuring an average coupling constant, which to a first approximation can be described as a weighted average of **3** and **4**. If either rotamer existed alone in solution it should be possible to measure $^3J(^1H–N—C_\alpha–^{13}CO_2^-)$ for **3** and $^3J(^1H–N—C_\alpha–^{13}C_\beta)$ for **4** since the relevant Karplus angles are 30° and −20° respectively. In the solid state the conformation about the N—C_α bond is best described by **4** with ϕ = −93° (10, 11).

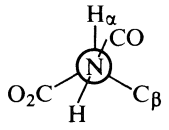

3

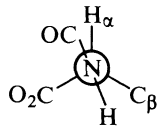

4

Solid ^{13}C spectrum of carnosine

In Fig. 4, the CP/MAS ^{13}C nmr spectrum of solid carnosine is compared with the spectrum obtained in aqueous solution (pH = 8). The three carbon nuclei not directly bonded to protons (C(O)N, C5, and CO_2^-) were distinguished from the other carbons by turning the ^1H rf power off for 40 μs just prior to data acquisition (17). Other assignments in the solid spectrum were made by assuming that the chemical shifts are similar in the solid and in aqueous solution (see Table 7). In contrast to the solution spectrum, the chemical shifts of C2 and C5 coincide in the solid spectrum; this can be qualitatively explained as follows. Using ^{13}C solution chemical shift data for pyrrole and 2-methylpyrrole (48), one calculates an α-effect of +8.7 ppm, a β-effect of −2.3 ppm, and a γ-effect (across the nitrogen) of −1.8 ppm upon methyl substitution. Assuming these methyl group substituent effects are valid for the imidazole ring and using the ^{13}C chemical shifts for imidazole in the solid state (49), one calculates the ^{13}C chemical shifts depicted below for the N3—H (**5**) and N1—H (**6**) tautomers. The observed ^{13}C

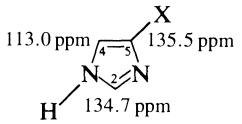

5

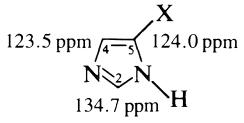

6

chemical shifts for C2, C4, and C5 in the solid state are in good agreement with those calculated assuming N3 is protonated (which is the nitrogen protonated in the solid state (10, 11)). Notice that while the C4 and C5 resonances differ by more than 20 ppm in the solid state, in aqueous solution (pH = 8) their resonances move closer together (separation 15.8 ppm) indicating the presence of some of the N1—H tautomer (**6**). Carbon-13 nmr spectra of solid histidine and histamine appear to support this qualitative explanation; the resonance signals for C2 and C5 of histidine, which also crystallizes as the N3—H tautomer in the solid (50), were found to almost overlap while those of histamine, which crystallizes as the N1—H tautomer (51), were found to be separated by 8 ppm.

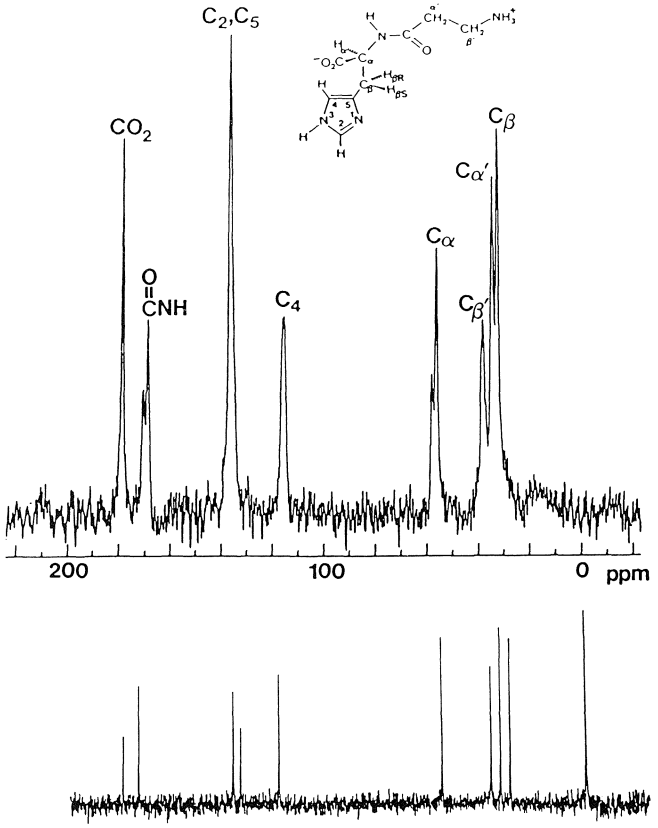

FIG. 4. Solid-state carbon-13 spectrum of carnosine using ^1H cross-polarization and magic angle spinning compared to solution spectrum at pH 8.

TABLE 7. Comparison of solution and solid carbon-13 chemical shifts in carnosine

	Chemical shifts (ppm)		
Carbon	Solution (pH = 8)	Solid state	Difference
CO_2^-	179.1	178.7	0.4
CONH	172.9	169.4	3.5
C2	137.0	136.5	0.5
C5	134.5	136.5	−2.0
C4	118.7	116.0	2.7
C_α	56.5	57.0	−0.5
$C_{\beta'}$	37.2	38.0	−0.8
$C_{\alpha'}$	33.7	34.6	−0.9
C_β	30.2	32.6	−2.4

In contrast to the solution spectra, the resonances due to C(O)NH and C_α were split into unsymmetrical doublets and the C4 resonance was significantly broadened. Brown (52) was unable to resolve these splittings in his reported ^{13}C nmr spectra of solid carnosine. In two independent X-ray crystallography studies (10, 11) it was determined that carnosine crystallizes in the monoclinic *C*2 space group which indicates that all carnosine molecules are equivalent in the solid. We attribute the doublets to ^{14}N–^{13}C dipolar coupling, which is not averaged to zero because the ^{14}N quadrupolar interaction is comparable in magnitude to the ^{14}N Zeeman interaction (53–56). The magnitude of the apparent splitting is proportional to the dipolar interaction, $\gamma_C\gamma_N h/4\pi^2(r_{CN})^3$, the quadrupolar interaction, e^2qQ/h, its orientation with respect to r_{CN}, and the magnitude of the Zeeman interaction, B_o. No attempt will be made to analyze these line shapes at this time; details for related compounds are presented in refs. 54–57.

One final point: the spectrum of solid carnosine in Fig. 4 was obtained using only 148 acquisitions; clearly paramagnetic doping is unnecessary (52).

Conclusions

The results of this nmr study of carnosine may be summarized as follows:

1. All ^1H and ^{13}C nmr resonances of carnosine have been unambiguously assigned as a function of pH, and the following pK_a's have been measured: 2.7, 7.1, and 10.6.
2. The N3—H tautomer predominates in aqueous solution.
3. The conformation about the C_α—C_β bond in aqueous solution can be described in terms of three rotamers with relative populations, $P_I = 0.58 \pm 0.04$, $P_{II} = 0.22 \pm 0.04$, and $P_{III} = 0.20 \pm 0.06$. Interestingly, in the solid state the conformation about C_α—C_β corresponds to rotamer II.
4. The conformation about the N—C_α bond in solution is best described by an average of at least two rotamers with potential minima near $\phi = -150°$ (**3**) and $\phi = -80°$ (**4**), whereas in the solid state $\phi = -93°$.
5. In spite of the conformational differences in solution and the solid state, all ^{13}C nmr chemical shifts in these two phases differ by less than 4 ppm. This suggests that it may be dangerous to assume that similar ^{13}C shifts in the solid and solution states imply identical conformations in these phases.

Acknowledgements

We wish to thank Dr. J. A. Walter, Dr. S. Peris, and Mr. B. J. Macdonald for their assistance in obtaining some of the nmr spectra, and Professor T. P. Forrest and Dr. Martin Nicholas for several helpful suggestions. Proton measurements with respect to internal DSS were carried out by Mr. Bill Power. This research was supported by generous NSERC operating and equipment grants.

1. W. GULEWITSCH and S. AMIRADZIBI. Ber. Dtsh. Chem. Ges. **33**, 1902 (1900).
2. A. BEZDOROVAINY. J. Chem. Educ. **51**, 652 (1974).
3. C. ARUS, M. BARANY, W. M. WESTLER, and J. L. MARKLEY. FEBS Lett. **165**, 231 (1984).
4. C. ARUS, M. BARANY, W. M. WESTLER, and J. L. MARKLEY. J. Magn. Reson. **57**, 519 (1984).
5. K. YOSHIZAKI, Y. SEO, and H. NISHIKAWA. Biochim. Biophys. Acta, **678**, 283 (1981).
6. C. E. BROWN, F. L. MARGOLIS, T. H. WILLIAMS, R. G. PITCHER, and G. ELGAR. Neurochem. Res. **2**, 555 (1977).
7. C. E. BROWN. *In* Biomembranes. Vol. 11. *Edited by* A. Nowotny. Plenum Publishing Corp., New York. 1983. Chapt. 16. p. 439.
8. C. E. BROWN, F. L. MARGOLIS, T. H. WILLIAMS, R. G. PITCHER, and G. J. ELGAR. Archiv. Biochem. Biophys. **193**, 529 (1979).
9. M. IHNAT and R. BERSOHN. Biochemistry, **9**, 4555 (1970).
10. Y. BARRANS, A. M. BELLOCQ, M. CORTRAIT, and H. RICHARD. J. Mol. Struct. **30**, 225 (1976).
11. H. ITOH, T. YAMANE, T. ASHIDA, and M. KAKUDO. Acta Crystallogr. Sect. B, **33**, 2959 (1977).
12. (*a*) D. L. TURNER. J. Magn. Reson. **54**, 146 (1983); (*b*) P. J. HORE. J. Magn. Reson. **55**, 283 (1983).
13. A. BAX. Two dimensional nuclear magnetic resonance in liquids. Delft University Press. Delft. 1982.
14. R. E. WASYLISHEN and C. A. FYFE. Annu. Rep. NMR Spectrosc. **12**, 1 (1982).

15. M. MEHRING. Principles of high resolution NMR in solids. 2nd ed. Springer Verlag, New York. 1983.
16. J. SCHAEFER and O. E. STEJSKAL. J. Am. Chem. Soc. **98**, 1031 (1976).
17. S. J. OPELLA and M. H. FREY. J. Am. Chem. Soc. **101**, 5854 (1979).
18. W. L. EARL and D. L. VANDERHART. J. Magn. Reson. **48**, 35 (1982).
19. (*a*) J. L. MARKLEY. Acc. Chem. Res. **8**, 71 (1975); (*b*) D. L. RABENSTEIN, M. S. GREENBERG, and C. A. EVANS. Biochemistry, **16**, 977 (1977).
20. M. TANOKURA, M. TASUMI, and T. MIYAZAWA. Biopolymers, **15**, 393 (1976).
21. J. H. BRADBURY, B. E. CHAPMAN, and F. A. PELLEGRINO. J. Am. Chem. Soc. **95**, 6139 (1973).
22. M. TANOKURA, M. TASUMI, and T. MIYAZAWA. Chem. Lett. 739 (1978).
23. J. REUBEN. J. Am. Chem. Soc. **105**, 3711 (1983).
24. J. C. CHISTOFIDES and D. B. DAVIES. J. Am. Chem. Soc. **105**, 5099 (1983); J. Chem. Soc. Chem. Commun. 324 (1983); J. Chem. Soc. Perkin Trans. 2, 481 (1984).
25. J. REUBEN. J. Am. Chem. Soc. **107**, 1433 (1985).
26. W. F. REYNOLDS and C. W. TZENG. Can. J. Biochem. **55**, 576 (1977).
27. A. R. QUIRT, J. R. LYERLA, JR., I. R. PEAT, J. S. COHEN, W. F. REYNOLDS, and M. H. FREEDMAN. J. Am. Chem. Soc. **96**, 570 (1974).
28. G. BINSCH, J. B. LAMBERT, B. W. ROBERTS, and J. D. ROBERTS. J. Am. Chem. Soc. **86**, 5564 (1964).
29. R. L. MIDDAUGH and R. S. DRAGO. J. Am. Chem. Soc. **85**, 2575 (1963).
30. W. F. REYNOLDS, I. R. PEAT, M. H. FREEDMAN, and J. R. LYERLA, JR. J. Am. Chem. Soc. **95**, 328 (1975).
31. W. G. ESPERSEN and R. B. MARTIN. J. Phys. Chem. **80**, 741 (1976).
32. P. E. HANSEN, J. FEENEY, and G. C. K. ROBERTS. J. Magn. Reson. **17**, 249 (1975).
33. M. C. REDDY, B. P. N. REDDY, K. R. SRIDHARAN, and J. RAMAKRISHNA. Org. Magn. Reson. **22**, 464 (1984).
34. (*a*) J. R. CAVANAUGH. J. Am. Chem. Soc. **89**, 1558 (1967); **90**, 4533 (1968); (*b*) A. J. FISCHMAN, H. R. WYSSBROD, W. C. AGOSTA, F. H. FIELD, W. A. GIBBONS, and D. COWBURN. J. Am. Chem. Soc. **99**, 2953 (1977).
35. R. B. MARTIN. J. Phys. Chem. **83**, 2404 (1979).
36. J. FEENEY. J. Magn. Reson. **21**, 473 (1976).
37. B. PERLY and C. CHACHATY. J. Magn. Reson. **49**, 397 (1982).
38. T. DRAKENBERG and S. FORSEN. J. Chem. Soc. Chem. Commun. 1404 (1971).
39. IUPAC–IUB COMMISSION ON BIOCHEMICAL NOMENCLATURE RULES. Pure Appl. Chem. **40**, 292 (1974).
40. A. DEMARCO, M. LLINAS, and K. WUETHRICH. Biopolymers, **17**, 637 (1978).
41. V. F. BYSTROV, Y. D. GAVRILOV, and V. N. SOLKAN. J. Magn. Reson. **19**, 123 (1975).
42. M. T. CUNG, M. MARRAUD, and J. NEEL. Macromolecules, **7**, 606 (1974).
43. V. F. BYSTROV, V. T. IVANOV, S. L. PORTNOVA, T. A. BALASHOVA, and Y. A. OVCHINNIKOV. Tetrahedron, **29**, 873 (1973).
44. G. N. RAMACHANDRAN and R. CHANDRASEKARAN. Biopolymers, **10**, 2113 (1971).
45. V. N. SOLKAN and V. F. BYSTROV. Tetrahedron Lett. 2261 (1973).
46. M. BARFIELD and H. L. GEARHART. J. Am. Chem. Soc. **95**, 641 (1973).
47. V. F. BYSTROV, A. S. ARSENIEV, and Y. D. GAVRILOV. J. Magn. Reson. **30**, 151 (1978).
48. G. C. LEVY and G. L. NELSON. Carbon-13 nuclear magnetic resonance for organic chemists. John Wiley & Sons, Inc., New York. 1972. p. 97.
49. J. ELGUERO. J. Chem. Soc. Chem. Commun. 1208 (1981).
50. J. J. MADDEN, E. L. MCGANDY, and N. C. SEEMAN. Acta Crystallogr. Sect. B, **28**, 2377 (1972).
51. J. J. BONNET and J. A. IBERS. J. Am. Chem. Soc. **95**, 4829 (1973).
52. C. E. BROWN. J. Am. Chem. Soc. **104**, 5608 (1982).
53. S. J. OPELLA, M. H. FREY, and T. A. CROSS. J. Am. Chem. Soc. **101**, 5856 (1979).
54. J. G. HEXEM, M. H. FREY, and S. J. OPELLA. J. Am. Chem. Soc. **103**, 224 (1981).
55. N. ZUMBULYADIS, P. M. HENRICHS, and R. H. YOUNG. J. Chem. Phys. **75**, 1603 (1981).
56. A. NAITO, S. GANAPATHY, and C. A. MCDOWELL. J. Magn. Reson. **48**, 367 (1982).
57. M. H. FREY and S. J. OPELLA. J. Magn. Reson. **66**, 144 (1986).

Heat capacities of binary mixtures of *n*-octane with each of the hexane isomers at 298.15 K[1]

GEORGE C. BENSON[2] AND PATRICK J. D'ARCY
Division of Chemistry, National Research Council of Canada, Ottawa, Ont., Canada K1A 0R6

Received April 17, 1986

GEORGE C. BENSON and PATRICK J. D'ARCY. Can. J. Chem. **64**, 2139 (1986).

Volumetric heat capacities for binary mixtures of *n*-octane with *n*-hexane, 2-methylpentane, 3-methylpentane, 2,2-dimethylbutane, and 2,3-dimethylbutane were measured at 298.15 K in a Picker flow microcalorimeter. The results were combined with previously published excess molar volumes to obtain excess molar isobaric heat capacities. Interpretation of the results in terms of the Flory theory of mixtures is discussed.

GEORGE C. BENSON et PATRICK J. D'ARCY. Can. J. Chem. **64**, 2139 (1986).

Opérant à 298,15 K et utilisant un microcalorimètre à écoulement de Picker, on a mesuré les capacités calorifiques volumétriques des mélanges binaires du *n*-octane avec le *n*-hexane, le méthyl-2 pentane, le méthyl-3 pentane, le diméthyl-2,2 butane et le diméthyl-2,3 butane. En combinant les résultats obtenus avec ceux publiés antérieurement pour les volumes molaires en excès, on a pu déterminer les capacités molaires calorifiques isobariques en excès. On discute de l'interprétation de nos résultats en fonction de la théorie de Flory des mélanges.

[Traduit par la revue]

Recent papers from our laboratory reported excess molar enthalpies (1) and excess molar volumes (2) for binary mixtures of *n*-octane with the five isomeric hexanes: *n*-hexane (*n*-C_6), 2-methylpentane (2-MP), 3-methylpentane (3-MP), 2,2-dimethylbutane (2,2-DMB), and 2,3-dimethylbutane (2,3-DMB). As an extension of those investigations, we have determined the excess molar isobaric heat capacities of the same set of mixtures.

Experimental

Component liquids

The *n*-octane was Aldrich Chemical Co. Gold Label reagent with a specified purity of 99+ mol%. The isomeric hexanes were Phillips Research Grade reagents with purities of 99.88 mol% or greater. The component liquids were stored over molecular sieve pellets (BDH Type 4A) and partially degassed prior to their use. Densities of the liquids, determined at 298.15 K in an Anton-Paar densimeter (Model DMA 02C) are listed in Table 1, where the values compiled by the TRC (3) are given for comparison.

Calorimetric measurements

Heat capacities per unit volume were obtained from comparisons between pairs of liquids flowing in the test and reference cell of a Picker microcalorimeter (4, 5). A temperature interval of 1.5 K centred on 298.15 K was used.

The initial reference liquid was Pure Grade *n*-heptane from the Phillips Petroleum Co., and a value of 226.764 J K^{-1} mol^{-1} was adopted for its molar isobaric heat capacity at 298.15 K (6). The molar isobaric heat capacity of *n*-octane was then determined to be 254.11 J K^{-1} mol^{-1} by comparison with *n*-heptane.

Mixtures were prepared by weighing, and corrections for the effect of buoyancy were included in calculating their mole fractions. The error of the mole fractions is estimated to be less than 5×10^{-5}. Starting with *n*-octane as the reference liquid, the volumetric heat capacities of the mixtures were determined by the stepwise procedure (5). Molar isobaric heat capacities, $C_{p,m}$, were obtained from the volumetric heat capacities, $C_{p,m}/V_m$, using molar volumes, V_m, estimated from the densities of the components and the excess molar volumes, V_m^E, of their mixtures (2). Excess molar isobaric heat capacities, $C_{p,m}^E$, were then calculated from the relation:

$$[1] \quad C_{p,m}^E = C_{p,m} - xC_{p,1}^* - (1 - x)C_{p,2}^*$$

where x is the mole fraction of *n*-octane, and $C_{p,1}^*$ and $C_{p,2}^*$ are the molar isobaric heat capacities of the pure liquids, *n*-octane and hexane isomer, respectively. The error of $C_{p,m}^E$ is estimated to be less than 0.05 J K^{-1} mol^{-1}.

TABLE 1. Densities, ρ, and molar isobaric heat capacities, $C_{p,m}$, of the component liquids at 298.15 K

	ρ/(kg m^{-3})		$C_{p,m}$/(J K^{-1} mol^{-1})	
Component	Obs.	Lit.	Obs.	Lit.
n-Octane	698.62	698.62[a]	254.11	254.15[b]
n-C_6	654.90	654.84[a]	195.84	195.48[c]
2-MP	648.57	648.52[d]	193.96	193.91[c]
3-MP	659.81	659.76[d]	190.99	190.67[c]
2,2-DMB	644.47	644.46[d]	189.44	188.7[c]
2,3-DMB	657.08	657.02[d]	189.04	188.7[c]

[a]Reference 3, see Table 23-2-(1.101)-a, dated October 31, 1977.
[b]Reference 3, see Table 23-2-(1.203)-vc, dated October 31, 1976.
[c]Reference 3, see Table 23-2-(1.201)-vc, dated October 31, 1975.
[d]Reference 3, see Table 23-2-(1.201)-a, dated October 31, 1952.

Results and discussion

The molar isobaric heat capacities of the component liquids are listed in Table 1. The results for each of the hexane isomers are averages of the values obtained from three or more stepwise runs involving an indirect comparison of the isomer with *n*-octane. In most cases, these agree reasonably (within 0.2%) with the literature values (3) given in the last column of the table.

Values of $C_{p,m}^E$ measured for $\{xn\text{-}C_8H_{18} + (1 - x)C_6H_{14}\}$ mixtures are summarized in Table 2. The smoothing equation:

$$[2] \quad C_{p,m}^E/(\text{J K}^{-1}\,\text{mol}^{-1}) = x(1 - x)\sum_{j=1}^{n} c_j(1 - 2x)^{j-1}$$

was fitted to each set of results by the method of least-squares with all points weighted equally. Values of the coefficients c_j are listed in Table 3 together with the standard deviations s of the representations.

The experimental results and their representations by eq. [2] are plotted in Fig. 1. In all cases, $C_{p,m}^E$ is negative and nearly symmetric about $x = 0.5$. We are not aware of any directly

[1]NRC No. 26086.

[2]Present address: Department of Chemical Engineering, University of Ottawa, 770 King Edward Avenue, Ottawa, Ont., Canada K1N 9B4.

TABLE 2. Excess molar isobaric heat capacities $C^E_{p,m}$ for $\{xn\text{-}C_8H_{18} + (1 - x)C_6H_{14}\}$ at 298.15 K

x	$C^E_{p,m}$ / J K^{-1} mol^{-1}	x	$C^E_{p,m}$ / J K^{-1} mol^{-1}	x	$C^E_{p,m}$ / J K^{-1} mol^{-1}	x	$C^E_{p,m}$ / J K^{-1} mol^{-1}	x	$C^E_{p,m}$ / J K^{-1} mol^{-1}
				n-Octane + *n*-C$_6$					
0.02204	−0.017	0.15305	−0.110	0.33018	−0.196	0.65469	−0.186	0.85057	−0.091
0.04565	−0.032	0.17348	−0.143	0.35407	−0.201	0.70209	−0.193	0.85089	−0.098
0.05052	−0.028	0.20118	−0.156	0.50632	−0.226	0.74748	−0.163	0.89955	−0.104
0.07703	−0.062	0.25111	−0.150	0.54967	−0.214	0.75613	−0.150	0.94790	−0.044
0.10439	−0.093	0.25472	−0.157	0.60707	−0.222	0.77756	−0.174	0.95074	−0.039
0.15094	−0.101	0.30025	−0.195	0.65219	−0.188	0.80134	−0.159	0.95202	−0.028
				n-Octane + 2-MP					
0.04760	−0.091	0.19827	−0.320	0.40060	−0.444	0.70522	−0.373	0.82661	−0.267
0.09901	−0.186	0.25476	−0.374	0.46067	−0.453	0.73050	−0.331	0.90124	−0.157
0.12911	−0.239	0.27035	−0.390	0.55296	−0.429	0.74670	−0.322	0.92519	−0.150
0.14992	−0.264	0.29837	−0.395	0.60456	−0.413	0.81079	−0.263		
				n-Octane + 3-MP					
0.07153	−0.155	0.25439	−0.430	0.43052	−0.552	0.65387	−0.499	0.83274	−0.297
0.13261	−0.279	0.32488	−0.509	0.49864	−0.576	0.70432	−0.445	0.88118	−0.229
0.15193	−0.301	0.35895	−0.506	0.54914	−0.559	0.75746	−0.399	0.90316	−0.195
0.15747	−0.289	0.39937	−0.552	0.60919	−0.506	0.79892	−0.334	0.95308	−0.093
0.20032	−0.376								
				n-Octane + 2,2-DMB					
0.02585	−0.158	0.20308	−0.784	0.39805	−1.009	0.60258	−0.987	0.80953	−0.599
0.04946	−0.310	0.24943	−0.933	0.45601	−1.084	0.65293	−0.901	0.85169	−0.489
0.09914	−0.540	0.30147	−0.984	0.50347	−1.085	0.66835	−0.929	0.90267	−0.330
0.14404	−0.645	0.35567	−1.083	0.54927	−1.069	0.75580	−0.727	0.94776	−0.179
				n-Octane + 2,3-DMB					
0.04676	−0.151	0.25269	−0.548	0.45538	−0.703	0.60916	−0.592	0.80394	−0.354
0.07801	−0.236	0.30130	−0.625	0.49811	−0.694	0.65072	−0.569	0.93022	−0.137
0.15457	−0.414	0.35192	−0.674	0.51239	−0.671	0.69969	−0.495	0.94677	−0.114
0.19698	−0.507	0.39513	−0.676						

TABLE 3. Coefficients c_j and standard deviation s for representations of $C^E_{p,m}$/(J K^{-1} mol^{-1}) for $\{xn\text{-}C_8H_{18} + (1 - x)C_6H_{14}\}$ at 298.15 K by eq. [2]

Parameter	Value for hexane isomer				
	n-C$_6$	2-MP	3-MP	2,2-DMB	2,3-DMB
c_1	−0.881	−1.774	−2.232	−4.326	−2.701
c_2		−0.210	−0.140	−1.011	−0.712
c_3		−0.328		−0.543	
s	0.012	0.010	0.011	0.024	0.012

TABLE 4. Parameters used in calculations for (*n*-octane + hexane isomer) mixtures at 298.15 K by the Flory theory[a]

Component	p^* / J cm^{-3}	V^* / cm^3 mol^{-1}	T^* / K	X_{12}	$(\partial X_{12}/\partial T)_p$ / J cm^{-3} K^{-1}
n-C$_8$H$_{18}$	436.9	127.70	4827.0		
n-C$_6$	424.2	99.52	4436.1	0.3382	−0.00444
2-MP	408.3	99.99	4380.8	0.9996	−0.01354
3-MP	424.2	98.68	4423.0	0.8284	−0.01949
2,2-DMB	389.0	100.07	4324.8	1.6123	−0.04062
2,3-DMB	405.3	99.16	4430.2	0.8391	−0.02508

[a]Values of p^*, V^*, T^*, and X_{12} are taken from ref. 2.

comparable studies of these mixtures. However, in previous papers, we have reported $C^E_{p,m}$ for (*n*-heptane + hexane isomer) mixtures (7) and for (*n*-dodecane + hexane isomer) mixtures (8). Comparison of the results for the three sets of mixtures shows that at a fixed value of x, $|C^E_{p,m}|$ increases in the order:

$$n\text{-}C_6 < \text{2-MP} < \text{3-MP} < \text{2,3-DMB} < \text{2,2-DMB}$$

and that for the same hexane isomer $|C^E_{p,m}|$ increases with increasing size of the *n*-alkane.

Previous work (2) has shown that the excess enthalpies and excess volumes of (*n*-octane + hexane isomer) mixtures can be correlated satisfactorily by means of the Flory theory (9, 10). Analysis of $C^E_{p,m}$ in terms of the Flory theory follows the treatment described for other (*n*-alkane + hexane isomer) mixtures (7, 8). Differentiation of the Flory expression for the excess molar enthalpy (9) with respect to the temperature, T, leads to the relation[3]:

$$[3]\quad C^E_{p,m} = -(x_1p_1^*V_1^*/\tilde{v}_1^2)(\partial\tilde{v}_1/\partial T)_p - (x_2p_2^*V_2^*/\tilde{v}_2^2)(\partial\tilde{v}_2/\partial T)_p + \tilde{v}^{-2}(x_1p_1^*V_1^* + x_2p_2^*V_2^* - x_1V_1^*\theta_2X_{12})(\partial\tilde{v}/\partial T)_p + (x_1V_1^*\theta_2/\tilde{v})(\partial X_{12}/\partial T)_p$$

where, in the present application, the subscripts 1 and 2 refer to *n*-octane and a hexane isomer, respectively. The characteristic pressures p^*, molar volumes V^*, and temperatures T^* for

[3]In refs. 7 and 8, the term in $(\partial X_{12}/\partial T)_p$ is misprinted. The correct formula was used in all of the calculations.

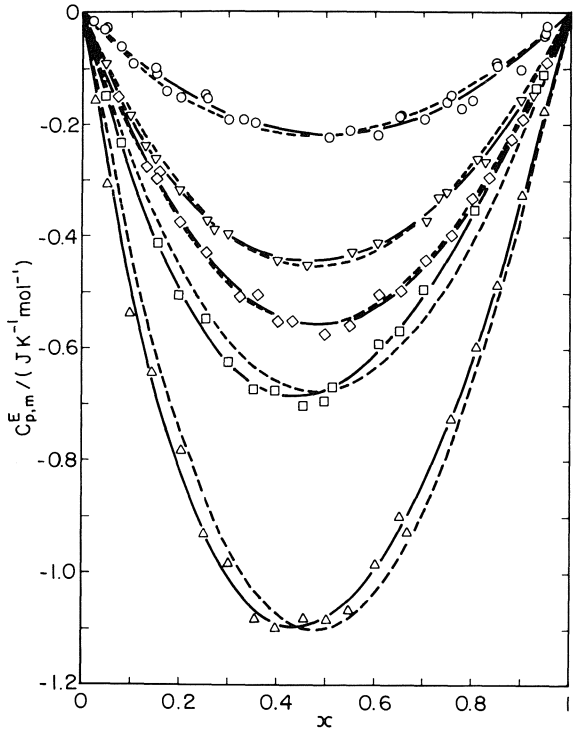

FIG. 1. Excess molar isobaric heat capacities, $C^E_{p,m}$, for $\{xn\text{-}C_8H_{18} + (1 - x)C_6H_{14}\}$ at 298.15 K. Experimental results: ○, n-C_6; ▽, 2-MP; ◇, 3-MP; △, 2,2-DMB; □, 2,3-DMB. Curves: —, calculated from eq. [2] with coefficients from Table 3; ----, calculated from the Flory theory.

the components, and the interchange energy parameters X_{12} have already been evaluated (2), and are summarized for convenience in Table 4. In eq. [3], $\tilde{v}$ denotes the reduced volume (V_m/V^*), and the derivatives $(\partial\tilde{v}/\partial T)_p$ can be calculated from Flory's equation of state (9). As in our previous work, it is assumed that the site fraction, θ_2, for species 2 can be approximated by the relation:

$$[4] \quad \theta_2 = x_2/[x_2 + x_1(V_1^*/V_2^*)^{2/3}]$$

In Flory's original formulation, X_{12} was considered to be independent of T. However, our previous work (7, 8) has shown that the magnitude of $C^E_{p,m}$ is underestimated if the last term in eq. [3] is neglected, and that it is necessary to treat $(\partial X_{12}/\partial T)_p$ as an adjustable parameter. Values of $(\partial X_{12}/\partial T)_p$, determined by a least-squares procedure in which eq. [3] was fitted to the representations of the $C^E_{p,m}$ results by eq. [2], are given in Table 4. The broken curves in Fig. 1 were calculated from eq. [3] with the parameters from Table 4 and agree well with the curves representing the smoothed experimental results. If the term in $(\partial X_{12}/\partial T)_p$ is omitted, the curves calculated for the five systems fall above the experimental curve for the (n-octane + n-C_6) mixtures and the estimates of $C^E_{p,m}$ at $x = 0.5$ are limited to the narrow range between -0.11 and -0.19 J K^{-1} mol^{-1}. Thus the calculations again indicate the importance of the last term in eq. [3].

1. S. E. M. HAMAM, M. K. KUMARAN, and G. C. BENSON. Fluid Phase Equilib. **18**, 147 (1984).
2. M. K. KUMARAN and G. C. BENSON. Can. J. Chem. **62**, 2369 (1984).
3. TRC thermodynamic tables — hydrocarbons. Thermodynamics Research Center, The Texas A&M University System, College Station, TX.
4. J.-L. FORTIER, G. C. BENSON, and P. PICKER. J. Chem. Thermodyn. **8**, 289 (1976).
5. J.-L. FORTIER and G. C. BENSON. J. Chem. Thermodyn. **8**, 411 (1976).
6. F. KIMURA, A. J. TRESZCZANOWICZ, C. J. HALPIN, and G. C. BENSON. J. Chem. Thermodyn. **15**, 503 (1983).
7. G. C. BENSON, P. J. D'ARCY, and M. K. KUMARAN. Thermochim. Acta, **75**, 353 (1984).
8. G. C. BENSON and P. J. D'ARCY. Thermochim. Acta, **102**, 75 (1986).
9. P. J. FLORY. J. Am. Chem. Soc. **87**, 1833 (1965).
10. A. ABE and P. J. FLORY. J. Am. Chem. Soc. **87**, 1838 (1965).

High-field proton and carbon-13 nuclear magnetic resonance studies of the conformational dynamic properties of seven-membered rings. 1,5-Benzodithiepin and 3-substituted derivatives

D. MÉNARD AND M. ST-JACQUES

Département de chimie, Université de Montréal, C.P. 6210, Succ. A, Montréal (Qué.), Canada H3C 3J7

Received June 4, 1986

D. MÉNARD and M. ST-JACQUES. Can. J. Chem. **64**, 2142 (1986).

The conformational and dynamic properties of 1,5-benzodithiepin (**1**), its 3,3-dimethyl (**2**), 3-methyl (**3**), and 3-methoxy (**4**) derivatives have been investigated by high-field ^1H and ^{13}C dynamic nuclear magnetic resonance methods. Analyses of the spectra at low temperatures indicate that, in CS_2, both **1** and **2** exist as a mixture of C and TB forms (97:3 for **1**; 63:37 for **2**). In contrast, both **3** and **4** exist as a mixture of three equilibrating conformations C_e, C_a, and TB in ratios of 55:25:20 and 88:8:4 respectively. Comparison with analogues derived from 1,5-benzodioxepins (**1***a*–**4***a*) indicates that the replacement of O by S decreases the amount of the TB form for all four compounds studied. The observation that C_e is the most abundant form for **4** while it is not observed for **4***a* can be explained by a repulsive S/O *gauche* interaction in **4** compared to an attractive O/O interaction in **4***a*.

D. MÉNARD et M. ST-JACQUES. Can. J. Chem. **64**, 2142 (1986).

Faisant appel à des méthodes de rmn du ^1H et du ^{13}C à hauts champs, on a étudié les propriétés dynamiques et conformationelles de la benzodithiépine-1,5 (**1**) et de ses dérivés diméthyl-3,3 (**2**), méthyl-3 (**3**) et méthoxy-3 (**4**). L'analyse des spectres mesurés dans le CS_2, à basse température, indiquent que les composés **1** ainsi que **2** existent à l'état de mélange des formes C et TB (97:3 dans le cas du composé **1** et 63:37 dans le cas du composé **2**). Par ailleurs, les composés **3** and **4** existent tous les deux à l'état de mélange des trois conformations à l'équilibre, C_e, C_a et TB dans des proportions respectives de 55:25:20 et 88:8:4. Une comparaison avec des analogues provenant des benzodioxépines (**1***a*–**4***a*) indique que, dans chacun des composés étudiés, le remplacement d'un oxygène par un soufre diminue la proportion de la forme TB. Le fait que la forme C_e soit la forme la plus abondante dans le composé **4** alors que l'on n'observe pas sa présence dans le cas du composé **4***a* pourrait être expliqué par la présence d'un interaction *gauche* S/O répulsive dans le composé **4** alors que, dans le composé **4***a*, il existerait une interaction O/O attractive.

[Traduit par la revue]

Pursuing our study of seven-membered heterocyclic compounds related to the 1,5-benzodioxepin (**1***a*) family, which recently revealed novel and diversified conformational features for some 3-substituted derivatives (1, 2), we have sought to identify the conformational preferences of analogous compounds derived from 1,5-benzodithiepin (**1**). Comparison of the results from the two series should provide valuable information on the origin of the underlying forces, which appear to involve strong electrostatic interactions in addition to steric ones. Indeed, it has been pointed out that the substitution of oxygen by sulfur significantly modifies the *gauche* effect in six-membered heterocycles so that the O/O *gauche* interaction present in **4***a* should be attractive (2) while the O/S interaction that would exist in **4** should be repulsive (3).

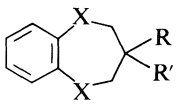

1: X = S; R = R′ = H
1*a*: X = O; R = R′ = H
2: X = S; R = R′ = CH_3
3: X = S; R = CH_3, R′ = H
4: X = S; R = OCH_3, R′ = H

We therefore wish to report the results of a high-field ^1H and ^{13}C dynamic nmr study of 1,5-benzodithiepin together with its 3,3-dimethyl (**2**), 3-methyl (**3**), and 3-methoxy (**4**) derivatives. The significant conformational differences brought about by sulfur shed more light on the many forces governing the conformational features of seven-membered heterocycles.

Results

All four compounds investigated (**1**–**4**) gave dynamic ^1H and ^{13}C spectral changes at low temperatures. Spectral parameters for these compounds are listed in Tables 1 and 2.

The three aromatic signals observed in the 100.62-MHz ^{13}C spectrum of **1** in THF-d_8 at 22°C (Fig. 1) (142.72, 134.47, and 128.88 ppm) broaden noticeably near −10°C to sharpen again at lower temperatures with the appearance of two additional smaller signals at 131.6 and 126.6 ppm at −90°C. These minor signals (labelled TB) have intensities of 3–4% relative to the intensity of the larger signals (labelled C). The three aliphatic carbons show one signal at 34.02 ppm at +22°C, because of accidental equivalence. It has separated into two signals (34.53 and 33.95 ppm) at −90°C with relative intensities of 1:2 assigned to C-3 and C-2,4 respectively. Minor peaks in the aliphatic region are not observed clearly in the low temperature spectrum owing to the solvent and impurity signals nearby. The quaternary carbon line C-6,7 is also assigned on the basis of reduced intensity, as was C-3 above.

The lines belonging to the four protonated C-8 to C-11 aromatic carbons are assigned tentatively on the basis of analogies with chemical shifts determined for benzocycloheptene (4) and other related compounds (5). For all the compounds studied, the equivalent C-8 and C-11 carbons (referred to as C-8,11) appear at lower field than the C-9,10 carbons. Furthermore, a comparison of the substituent effects of the methyl and the thiomethyl groups, as in toluene and thioanisole, show relatively small differences (**5***b*). Unfortunately the AA′XX′ pattern of the ^1H aromatic signals precludes correlations of ^{13}C signals with ^1H assignments. The above tentative assignment is adequate for our purpose since a reversal

TABLE 1. ^{1}H nuclear magnetic resonance spectral parameters[a,b] for **1–4**

Compound	Temperature (°C)	Conformation[c]	Aromatic protons	H-2,4	H-3	Substituent on C-3
1	25		7.48, 7.05 (AA′XX′)	2.83 (s)	2.26 (quint)	—
					($^3J_{HH} \simeq 5$ Hz)	—
(H,H)	−70	C	7.62, 7.20	2.98 (d; H-2,4e)	2.47 (d; H-3e)	
				$^2J_{HH} = -13.2$ Hz		
				2.47 (t; H-2,4a)	2.15 (q; H-3a)	
				($^3J_{HH} \simeq 13$ Hz)	($^3J_{HH} \simeq 13$ Hz)	—
		TB	6.99, 6.93	3.47		
2	18		7.3[d] 6.98	2.74 (s, br)		1.15 s
	−70	C	7.60, 7.18	2.51 (H-2,4e) AB quartet;		1.31 (s; CH_3 ax)
(CH_3,CH_3)				2.43 (H-2,4a) $^2J_{HH} = -14.5$ Hz		1.02 (s; CH_3 eq)
		TB	6.95, 6.91	—		1.14 (s; TB)
3	20		7.47, 7.08	3.0 (d; $^3J_{HH} \simeq 13$ Hz)	2.30 m	1.11 (d; CH_3)
				2.57 (s; br)		($^3J_{HH} = 4.6$ Hz)
(H,CH_3)	−100	C_e		2.87 (t; H-2,4a)		1.04 (d)
				(sep. $\simeq 12.2$ Hz)		($^3J_{HH} = 3.7$ Hz)
			7.61, 7.20			
				2.23 (d; H-2,4e)		
				(sep. $\simeq 12.9$ Hz)		1.33 (d)
		C_a		2.18		($^3J_{HH} = 6.3$ Hz)
		TB	6.99, 6.93	3.48 (d × d)		
				($^2J_{HH} = -14.5$, $^3J_{HH} = 3.9$ Hz)		1.09 (d)
				3.12 (d × d)		($^3J_{HH} = 6.4$ Hz)
				($^2J_{HH} = -14.5$, $^3J_{HH} = 6.4$ Hz)		
4	+14		7.47, 7.08	3.1 (d)	3.65 (m)	3.4 (s)
				(sep. = 12.9 Hz)		
(H,OCH_3)				2.55 (s, br)		
	−65	C_e		3.02 (d; H-2,4e)	3.62 (t × t)	3.38 (s)
				($^2J_{HH} = -12$ Hz)	($^3J_{HH} = 11$ Hz)	
			7.68, 7.25	2.18 (t; H-2,4a)		
				($^2J_{HH} = -12$ Hz)		
		C_a		2.62 (d; H-2,4e)	3.8 (d, br)	
				($^2J_{HH} = -15$ Hz)		
				3.14 (d × d; H-2,4a)		
				($^2J_{HH} = -15$ Hz, $^3J_{HH} = 5$ Hz)		
		TB	7.03, 6.96	2.75 (d)		
				($^2J_{HH} = -14$ Hz)		

[a]Chemical shifts are in ppm downfield from TMS. Solvent: CS_2 with 19% CD_2Cl_2 added for field locking purpose.
[b]The meaning of the symbols used is: a: axial; e: equatorial; s = singlet; d = doublet; t = triplet; quint = quintuplet; m = multiplet; sep. = separation.
[c]At high temperature the various conformations are averaged.
[d]This line is very broad.

does not alter the conformational conclusions formulated later in the text.

The aliphatic proton signals in the 400.13-MHz ^{1}H nmr spectrum of the same compound in CS_2 (Fig. 2) undergo important changes when the temperature is lowered from 25 to −100°C. At 25°C, the spectrum shows two slightly broadened signals at 2.83 ppm (H-2,4) and 2.26 ppm (H-3). Maximum broadening occurs near −20°C, below which three intense signals are observed at 2.98, 2.47, and 2.15 ppm while, below −50°C, another small signal (4%; labelled TB) appears at 3.47 ppm.

At −100°C, the three intense signals are better resolved and proton decoupling experiments were carried out at that temperature. The doublet at 2.98 ppm (separation = 13 Hz) collapses into a singlet when the quartet (separation ~ 13 Hz) at 2.15 ppm is selectively irradiated. This decoupling also causes the triplet (separation = 13 Hz) at 2.47 ppm to become a large singlet overlapping a smaller signal. Homonuclear decoupling of the doublet at 2.98 also perturbs the central peaks while selective irradiation of the signals at 2.47 ppm collapses both signals at 2.98 ppm and 2.15 ppm into broad singlets. These experiments therefore show that the H-3e signal is actually a broadened doublet superimposed on that of H-2,4a, which is a broadened triplet. Finally, irradiation at 3.47 ppm produces no change in the other three signals. These experiments lead to the assignments shown in Fig. 2 and summarized in Table 1. The aromatic ^{1}H spectral region of **1** also shows a change whereby weak additional signals appear slightly above 7.0 ppm as summarized in Table 1.

The 100.62-MHz ^{13}C nmr spectrum of **2** (dimethyl derivatives) in CHF_2Cl (Fig. 3) shows broadening at 20°C arising from an appreciable slowing down of a conformational process. Maximum broadening occurs near 10°C and, at −100°C, the spectrum consists of 7 well-resolved lines in the aliphatic region and 5 lines in the aromatic region. Figure 3 shows that the C-2,4 signal (46.05 ppm at 20°C) has split into two components

TABLE 2. Carbon-13 chemical shifts for **1**–**4** at high and low temperatures[a]

Compound	Solvent	Temperature (°C)	Conformation[b]	C-6,7	C-8,11[c]	C-9,10	C-2,4	C-3	Substituent on C-3
1	THF-d_8	22		142.72	134.47	128.88	34.02	34.02	—
		−90	C	143.69	135.10	128.96	33.95	34.53	—
(H,H)			TB	—	131.60	126.61	—	—	—
2	CHF_2Cl	20		—	133.93	128.40	46.15	36.30	~28
		−100	C	143.83	135.15	129.67	46.10	35.47	31.34(e)[e]
(CH_3,CH_3)									23.82(a)
			TB	—	131.61	126.93	43.11	35.18	26.43
3	CS_2	20		140.13	133.08	127.05	39.57	36.92	20.45
		−40	C_e	142.18	134.11	127.89	39.94	36.86	22.85
(H,CH_3)			C_a	142.18	134.11	127.90	39.82	31.44	16.18
			TB	142.76	130.48	125.33	40.17	34.53	19.31
4	CHF_2Cl	0		141.94	135.02	129.39	37.31	84.51	57.14
		−120	C_e	142.23	135.78	130.22	36.77	84.77	57.45
			C_a	143.10	135.60	129.88	36.77	74.82	56.63
(H,OCH_3)			TB	—	131.90	127.15	33.47	79.23	60.82

[a]Solutions containing internal Me_4Si and CD_2Cl_2 (20%) for field lock purpose.
[b]The letters C_a, C_e, and TB refer to the conformations described in the text.
[c]Tentative assignment only; see text for details.
[d]These letters identify the equatorial and axial methyl signals.

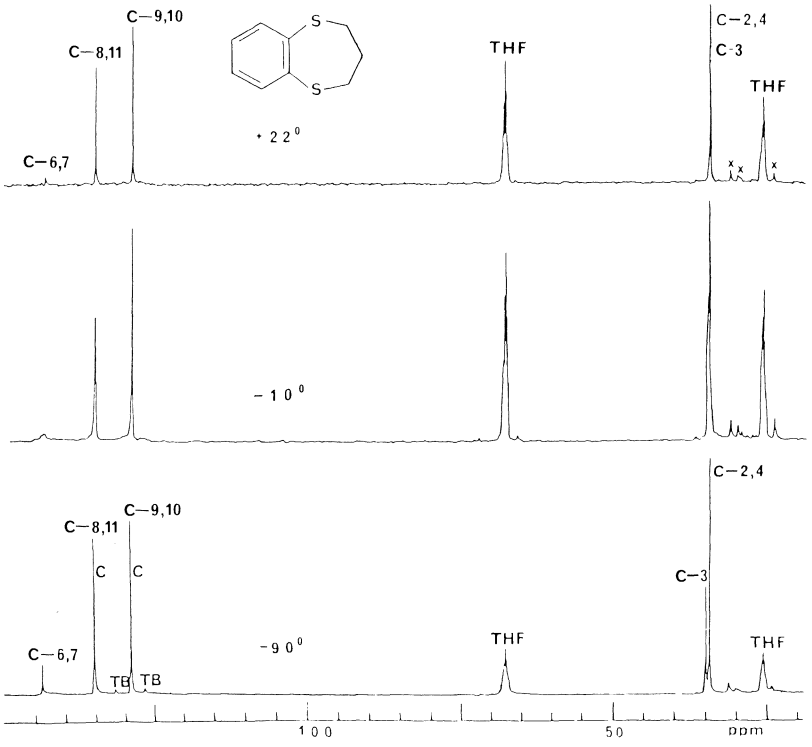

FIG. 1. 100.62-MHz ^{13}C nmr spectrum of **1** in THF-d_8 at several temperatures. The small signals denoted by X arise from impurities. The symbols C and TB refer to conformations described in the text.

at 46.10 and 43.11 ppm (labelled C and TB) with relative intensities of 82:18 respectively. The line labels C and TB in this figure (and in others) indicate the conformations (to be identified later) responsible for the various signals. The methyl signal (~28 ppm at 20°C) splits into three components at 31.34, 26.43, and 23.82 ppm (labelled CH_{3e}, TB, and CH_{3a}) with relative intensities of 41:18:41 at −100°C. At this temperature, the quaternary C-3 carbon appears as two small and close signals at 35.47 (C) and 35.18 ppm (TB). The aromatic region of the spectrum undergoes similar changes whereby the two intense C-8,11 and C-9,11 signals at 133.94 and 128.40 ppm split into intense components at 135.15 and 129.67 ppm (labelled C) and minor ones at 131.61 and 126.93 ppm (labelled TB). The C-6,7 signal shows no visible evidence of splitting.

The partial 400.13-MHz ^1H nmr spectrum of **2** in CS_2 (Fig. 4) is similar to that reported earlier (6) at 60 MHz. The

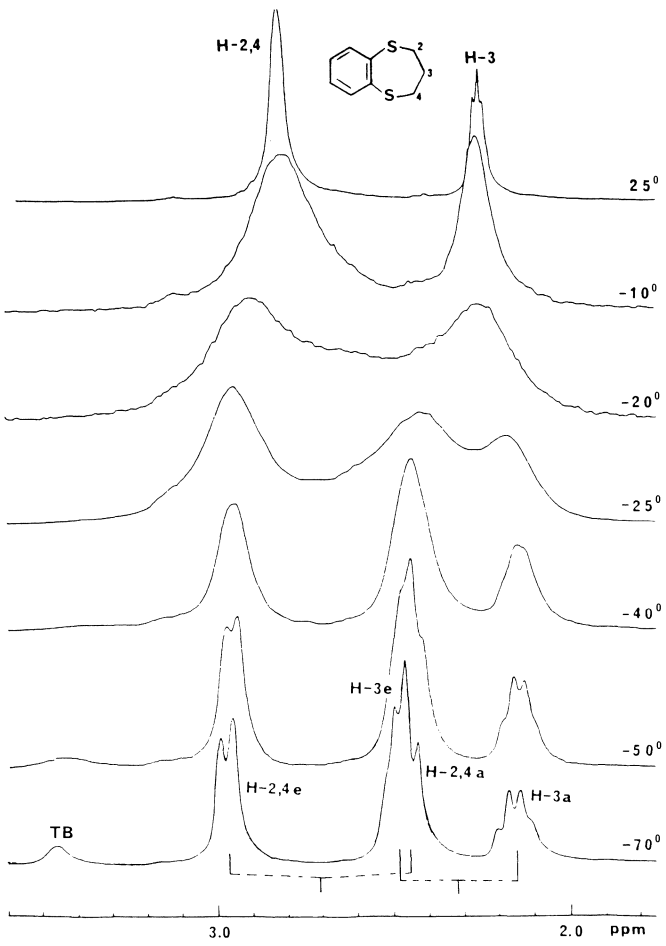

FIG. 2. Partial 400.13-MHz ^{1}H nmr spectrum of **1** in CS_2 at several temperatures.

methyl signal (1.15 ppm), already broadened at about 18°C, splits into a triplet below −10°C with components at 1.31, 1.14, and 1.02 ppm having relative intensities 31:37:32 at −60°C. The H-2,4 signal (2.74 ppm) experiences maximum broadening near 0°C and splits into two components consisting of a quartet at 2.4 ppm, arising from nonequivalent H-2,4 methylene protons in the C form, and a broad singlet at 3.1 ppm attributed to TB. The intensities of these two signals are in a 62:38 ratio at −40°C. When the temperature is further lowered, the lower field singlet (3.1 ppm) broadens further, possibly indicating the slowing down of a second conformational process. At −125°C, the lowest temperature reached, this signal is very broad and does not show resolved lines as would be expected from the nonequivalent H-2,4 methylene protons of the TB form. Additional aromatic signals also appeared at low temperature, as summarized in Table 1.

The 100.62-MHz ^{13}C nmr spectrum of the methyl derivative **3** in CS_2 is illustrated in Fig. 5 with the exception of the C-6,7 signal, which is not detected at 0°C under the conditions used at the higher temperatures. At 0°C the C-8,11 and C-9,10 signals are observed at 133.08 and 127.05 ppm while the C-6,7 signal was found at 140.13 ppm using a longer pulse delay. In the upfield region, the intense signal at 39.57 ppm is attributed to C-2,4 while two smaller and already broad signals at 36.92 and 20.45 ppm are assigned to C-3 and the CH_3 carbon respectively. All these lines split at lower temperature: the C-3 and the methyl signals each show three well-resolved components (labelled C_e, TB, and C_a) at −40°C with intensities in a 55:20:25 ratio. The other 4 signals each give rise to only two components with intensities in an 80:20 ratio (labelled C and TB). In THF-d_8 the ratio of the three conformations is found to be similar to CS_2 (i.e. 54:23:23) whereas in the more polar solvent CHF_2Cl, the intensities of the three components of the C-3 and CH_3 signals are in a 60:11:20 ratio while those for the two-component signals are 88:12.

Figure 6(*a*) shows the changes observed in the upfield part of the 400.13-MHz ^{1}H nmr spectrum of **3** in CS_2. Again all the lines show broadening at 20°C. Maximum broadening occurs near −10°C for the methyl signal and the high-field component of the H-2,4 signal (2.57 ppm) and near −20°C for the H-3 signal and the low-field component of H-2,4. At −60°C the methyl signal shows three components (labelled C_a, TB, and C_e). Additional aromatic signals also appeared, as summarized in Table 1. At −100°C (Fig. 6*b*) most lines in the spectrum are better resolved. The three components of the methyl signal now appear as doublets with coupling constants reported in Table 1. The high-field portion of the major component of the H-2,4 signal is a doublet (separation = 12.9 Hz) that appears to overlap a smaller signal seen as a shoulder while the low-field portion appears as a triplet (separation ≈ 14 Hz). Smaller signals with various multiplicities are seen at 3.48, 3.12, 2.4, and 2.3 ppm. Figure 6(*b*) also shows the results of selective homonuclear decoupling experiments performed at −100°C. These will be discussed in the next section of this text.

Figure 7 illustrates that 100.62-MHz ^{13}C nmr spectral modifications observed for the methoxy derivative **4** in CHF_2Cl. As was the case for the methyl derivative, all lines observed in the spectrum at 0°C have split into two or three components at lower temperatures. The relative intensities of the three components (labelled C_e, C_a, and TB) of the C-3 and methoxy signals are 61:33:6 while the two components (labelled C and TB) of the remaining signals give a 94:6 intensity ratio.

The 400.13-MHz ^{1}H nmr spectrum of **4** in CF_2Cl_2 is partially illustrated in Fig. 8. Here, as in the case of the methyl derivative **3**, complex changes are observed as the temperature is lowered. The H-2,4 signal, which appears as a doublet at 3.1 ppm (separation = 12.9 Hz) and a broad line at 2.55 ppm, experiences maximum broadening near −9°C. Below this temperature, two intense signals (88%) sharpen into a triplet (separation = 12–13 Hz) at 2.18 ppm (C_e) and a doublet (separation = 12–13 Hz) at 3.02 ppm (C_e). Smaller doublets also appear at 2.62 ppm (8%; C_a) and 2.75 ppm (4%; TB). Additional aromatic signals have also appeared at low temperature as summarized in Table 1. Homonuclear selective decoupling of the triplet at 2.18 ppm collapses both the intense doublet at 3.02 ppm and the H-3 triplet at 3.62 ppm into singlets while irradiation of the small C_a doublet at 2.62 ppm has a similar effect on the other small doublet of doublets at 3.14 ppm, also assigned C_a. Such decouplings help assigning the signals belonging to each of the C_e and C_a forms whose geometries will be defined in the next section.

Discussion

Spectral interpretation and the conformations of the seven-membered rings

The spectral modifications observed in the ^{1}H and ^{13}C nmr spectra of compound **1** (Figs. 1 and 2) reveal that this compound exists predominantly in one conformation in both CS_2 and THF-d_8. The presence of weak aromatic signals noted in both of the ^{1}H (Table 1) and ^{13}C (Fig. 1) low temperature spectra,

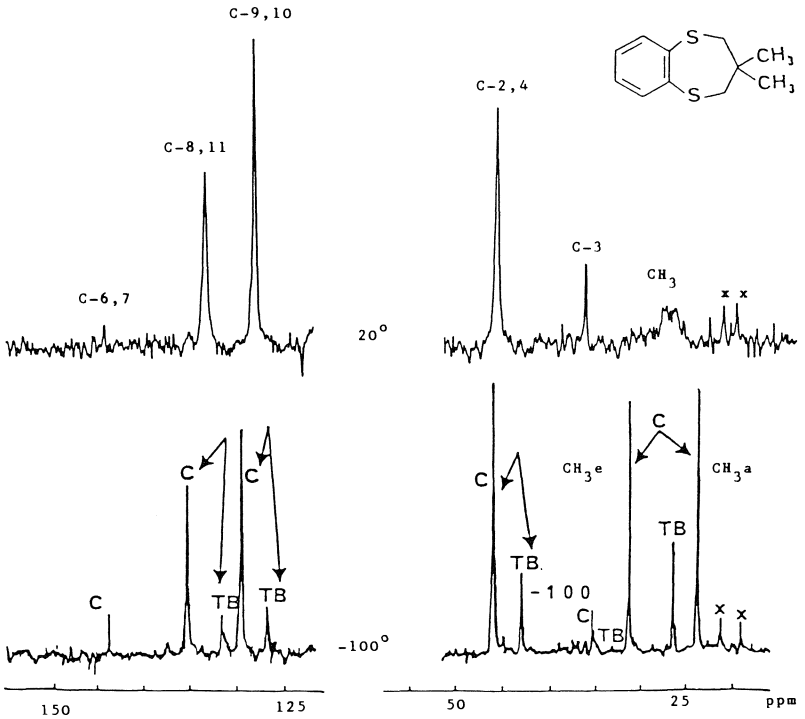

FIG. 3. 100.62-MHz ^{13}C nmr spectrum of **2** in CHF_2Cl at several temperatures.

however, shows that a minor conformer (about 3%) is also present.

The nature of the major conformation is identified as a chair form (C) from the chemical nonequivalence of the two H-3 protons observed in the ^1H spectrum at $-70°C$ and below (Fig. 2). The nature of the minor conformation is thought to be the twist-boat (TB) for energetic reasons discussed previously (1, 2) and by analogy with **1***a*.

The splitting of signals in the ^{13}C nmr spectrum of **2** in CHF_2Cl (Fig. 3) indicates that this compound exists in a mixture of two conformers in an 82:18 ratio at $-100°C$. The nature of these two conformers is easily deduced from the three-line pattern of the methyl carbon signals for which the two intense components of equal intensity at 31.34 and 23.82 ppm are assigned to the equatorial and axial methyl group of the C form while the third line identifies a second less intense component that is characterized by the two equivalent methyl positions of the TB conformation. This conclusion is confirmed by the ^1H spectrum of **3** in CS_2 at $-60°C$ (Fig. 4). The methyl proton signal shows a similar pattern to that just described for the methyl carbons with the exception that, because of the solvent change, the total relative intensity of the two components of the C form is 63% with respect to the single component of the TB form. The identification of the minor conformer as the TB form is compatible with the broadening of the H-2,4 signal at 3.1 ppm below $-40°C$, resulting from the slowing down of the TB inversion on the nmr time scale.

The analysis of the ^{13}C spectrum of **3** at $-40°C$ in CS_2 (Fig. 5) clearly reveals, as was the case in the benzodioxepin analog (**3***a*), the presence of three stable conformers. The pattern observed in the methyl region indicates that these conformers are the chair with equatorial methyl group (C_e, 55% in CS_2; 69% in CHF_2Cl), the chair with an axial methyl group (C_a, 25%; 20% in CHF_2Cl), and the TB form (20%; 11% in CHF_2Cl). This assignment is suggested by the fact that in the dithiane-1,3 system the signal of an axial methyl group appears at higher field than an equatorial one (7).

Confirmation is provided by the analysis of the ^1H spectrum at $-100°C$ (Fig. 6(*b*)), which shows that one of the two components of the H-2,4 signal of the major conformation (labelled H-2,4a) appears as a triplet. This pattern can only arise from large coupling of the axial H-2,4 protons with the axial H-3 proton and with the geminal H-2,4 equatorial protons. The H-2,4e protons, on the other hand, appear as a doublet due to the effect of the large geminal coupling with H-2,4a. It is pertinent to point out that, as was observed for some derivatives of 1,3-dithiane (8), the axial H-2,4 protons appear at lower field than the equatorial ones.

Having established that C_e is the major form for **3**, it now remains to confirm that C_a exists in a larger amount than TB. Because the C-8,11 and C-9,10 signals are very distant from the site of substitution, chemical shifts are not expected to be appreciably influenced by the axial or equatorial nature of the substituent and hence both C_e and C_a signals should coincide. On the other hand, changing the ring conformation from C to TB is expected to produce a significant change in these chemical shifts. Integration of the two lines for each of the C-8,11 and C-9,10 signals at $-40°C$ (Fig. 5) shows an 80:20 ratio, indicating that the weaker signals belong to the TB form. Thus observations for **1**, **2**, and **3** in Table 2 show that the presence or not of a 3-substituent does not significantly perturb the chemical shifts of these aromatic carbons, so that their signals constitute convenient conformational probes.

Finally, the three components observed for most signals of the ^{13}C spectrum of **4** at $-120°C$ indicate that this compound also exists as a mixture of three stable conformations at this temperature. Comparing the chemical shifts of the components of the C-3 signal with those observed for **3** suggests that these three conformations are C_e (61%), C_a (33%), and TB (6%). This suggestion is confirmed by the triplet multiplicity of the

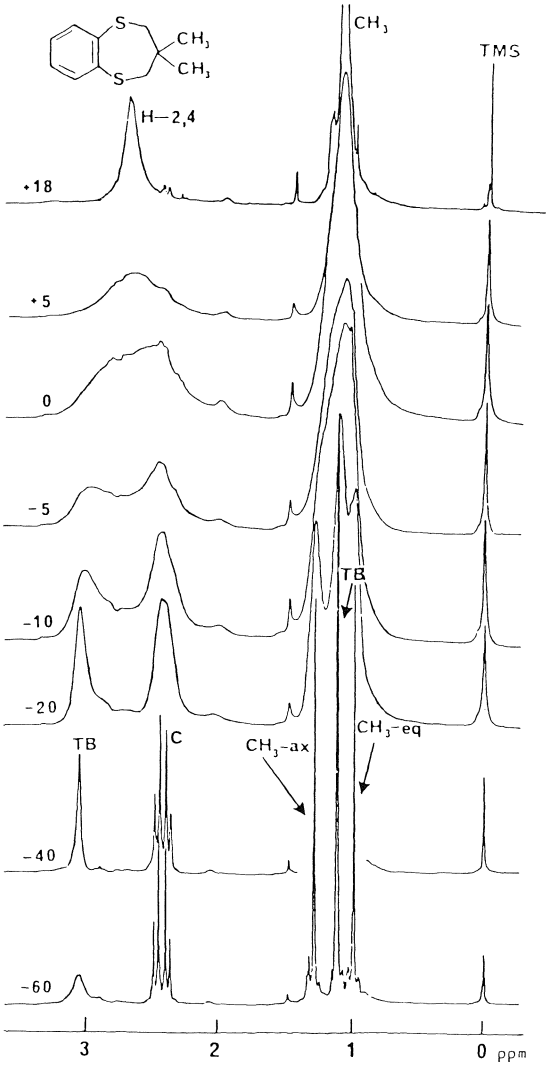

FIG. 4. Partial 400.13-MHz ^{1}H nmr spectrum of **2** in CS_2 at several temperatures.

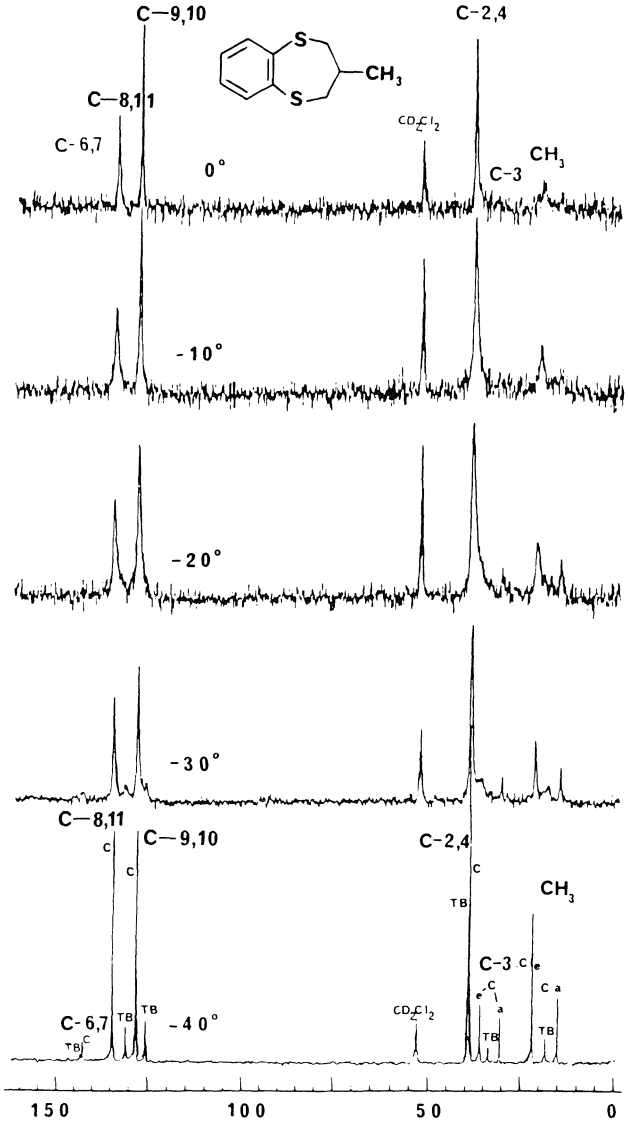

FIG. 5. 100.62-MHz ^{13}C nmr spectrum of **3** in CS_2 at several temperatures.

most intense H-2,4 signal at 2.18 ppm (Fig. 7), which, as in **3**, is assigned to the axial H-2,4 protons. Finally, analysis of the C8–C11 region of the low temperature ^{13}C spectrum shows that TB is the least abundant form.

Table 3 summarizes the relative populations of the various conformers adopted by compounds **1**–**4** and the corresponding dynamic parameters characterizing the conformation equilibria exhibited by each of these compounds.

Conformational averaging processes

Although Friebolin and co-workers (6) studied the parent compound 1,5-benzodithiepin (**1**), they were not able to determine the nature of its stable conformation nor its kinetic parameters.

The information derived from the ^{1}H nmr spectra of **1**, namely T_c = 20°C, $\Delta\nu$ = 204 Hz, and $^2J_{HH}$ = −13.2 Hz for the H-2,4 protons of the major conformation, enables us to calculate a free energy of activation ($\Delta G^{\ddagger}$) of 11.3 ± 0.3 kcal/mol for the chair inversion process using a transmission coefficient of one-half. No detailed information can be deduced for the pseudorotation process of the minor TB conformation.

An average $\Delta G^{\ddagger}$ of 12.9 ± 0.5 kcal/mol is estimated for the C → TB interconversion of the dimethyl derivative **2** from the coalescence temperature of +10°C observed for the ^{13}C nmr signals of the C-2,4 and C-8,11 carbons, using a two-site approximation (9) and a transmission coefficient of one. A slightly lower value of 12.4 ± 0.5 kcal/mol is obtained when using the ^{1}H coalescence temperature of 0°C and $\Delta\nu$ = 280 Hz for the H-2,4 proton signals of both conformers at −20°C. Finally, a value of 12.1 ± 0.5 kcal/mol is obtained for the chair inversion process when using a T_c = −10°C and $\Delta\nu$ = 116 Hz for the methyl protons of the chair form or T_c = +10°C and $\Delta\nu$ = 762 Hz for the methyl carbons and a transmission coefficient of one-half. These values are similar to that of 12.6 kcal/mol reported by Friebolin (6).

The free energy of activation of the C → TB transformation in the monomethyl derivative **3**, is estimated from the ^{13}C coalescence temperature of −20°C observed for the two components of the C-8,11 and C-9,10 carbons. A value of 11.4 ± 0.5 kcal/mol is obtained. The coalescence of the methyl carbon signals of the chair form of this compound (−10°C) yields a value of 12.1 ± 0.5 kcal/mol for the chair inversion process.

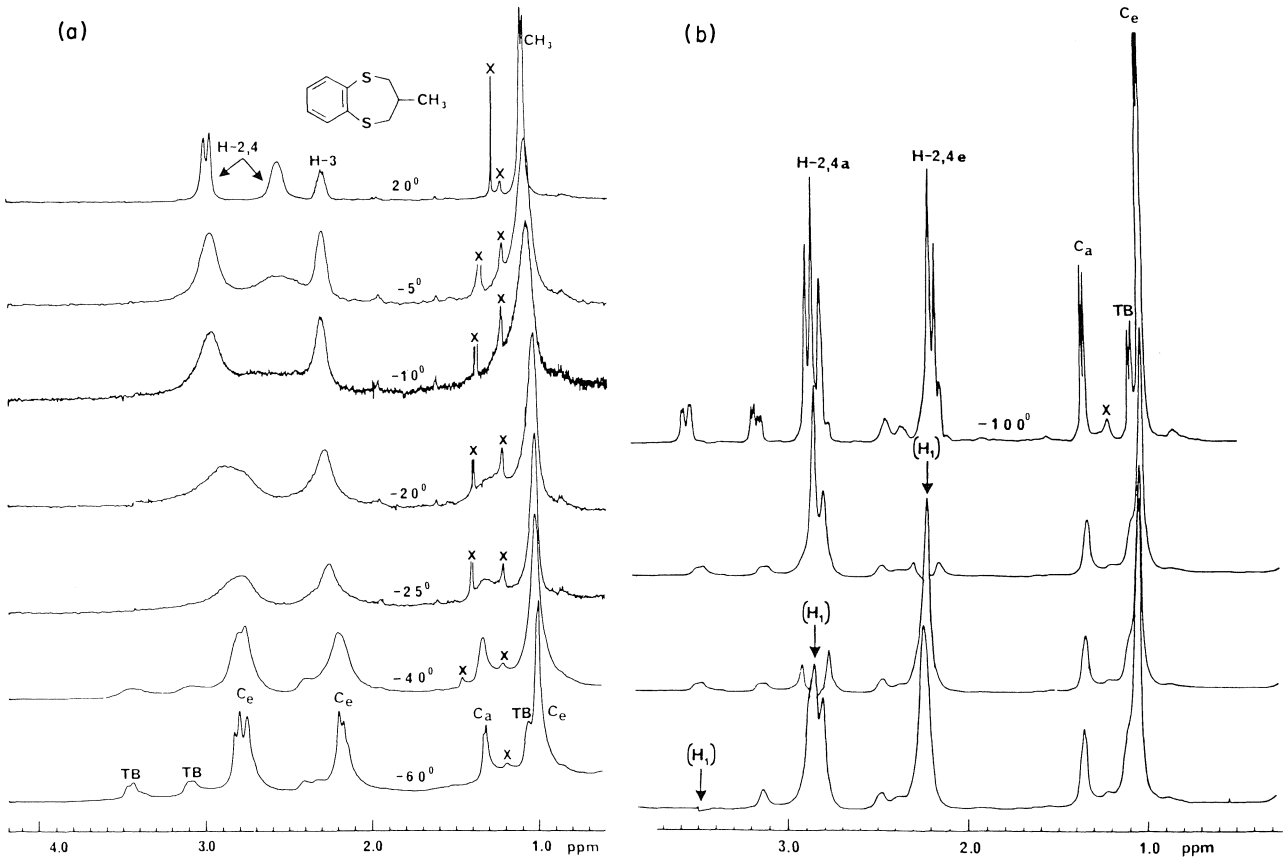

FIG. 6. (*a*) Partial 400.13-MHz ^{1}H nmr spectrum of **3** in CS_2 at several temperatures (X denotes impurities). (*b*) Homonuclear selective decoupling experiments on the 400.13-MHz ^{1}H nmr spectrum of **2** in CS_2 at −100°C.

Finally, a value of 10.9 ± 0.5 kcal/mol is derived for the C → TB interconversion of **4** using a ^{13}C coalescence temperature of −30°C and a $\Delta\nu$ = 332 Hz between the signals of the C-1,4 carbons of both forms. The chair inversion process involves a $\Delta G^{\ddagger}$ of 11.4 ± 0.5 kcal/mol as calculated from the following parameters: T_c = 0°C, $\Delta\nu$ = 1001 Hz for C-3 or T_c = −30°C, $\Delta\nu$ = 82.5 Hz for the methoxy carbon.

These results, summarized in Table 3, indicate that the presence of substituents at the 3-position of the seven-membered ring has little influence on the energy barrier for chair inversion, somewhat like analogous results for 1,3-dithianes substituted at the 5-position (10).

Origin of the conformation preferences

We have previously (2, 11) explained the conformational behavior of seven-membered carbocyclic and heterocyclic molecules in a framework combining such effects as steric, electrostatic (12), and bond–antibond interactions (13–15).

Because it has been estimated that the chair–TB energy difference is less for 1,3-dithiane than for 1,3-dioxane (16), it is most surprising to observe the opposite with regard to the conformation preferences of 1,5-benzodioxepin and 1,5-benzodithiepin. Indeed, the replacement of the ring oxygens in 1,5-benzodioxepins by sulfur leads to a larger amount of the C form(s) for all four compounds studied. A brief explanation of the results for each compound is given next in light of the above broadly applicable generalization, together with refinements arising from specific effects associated with each of the substituents.

The parent compound, 1,5-benzodithiepin (**1**), exists predominantly in the chair conformation and the free energy difference ($-\Delta G^0$) between this form and the TB conformation at −90°C is 1.1 kcal/mol. It would then appear that the stabilization of the TB form through electronic factors, as noted for the oxygen analog **1***a*, is attenuated when sulfur has replaced oxygen (2). Possibly the two-electron stabilizing interactions (17) stabilizing the TB arrangement becomes less important when oxygen is replaced by sulfur.

The shift in population observed for **1** by changing the solvent from CS_2 to THF is negligible, as would be expected from the similarly weakly polar nature of both solvents. The effect of CHF_2Cl was not investigated because the anticipated reduction of the already small amount of TB would not have permitted detection.

Dimethyl substitution in **2** causes a shift favoring TB, as similarly observed (2) for **1***a* and **2***a*. Table 3 shows that an increase in solvent polarity favors the C form, probably because of better solvation of the more polar chair form (2).

The data in Table 3 show that, in CS_2, the C_a form of **3** is more abundant (C_e:C_a:TB = 55:25:20) than for **3***a* in CH_3OCH_3 (C_e:C_a:TB = 42:9:49) (2), most probably because of reduced steric interaction between the axial methyl group and the sulfur lone pair owing, in part, to the larger C—S bond length. An increase in solvent polarity (CS_2 to CHF_2Cl) favors the C_e form of **3** at the expensve of C_a, whereas for **3***a*, C_e is also favored but at the expense of TB, since the amount of C_a is rather small for **3***a*.

Furthermore, the $-\Delta G^0$ value[1] between the axial and equatorial methyl groups of **3** in both solvents (0.27 kcal/mol in

[1]The use of ΔG^0 implies the equilibrium between the two conformers is viewed as axial conformer ⇌ equatorial conformer.

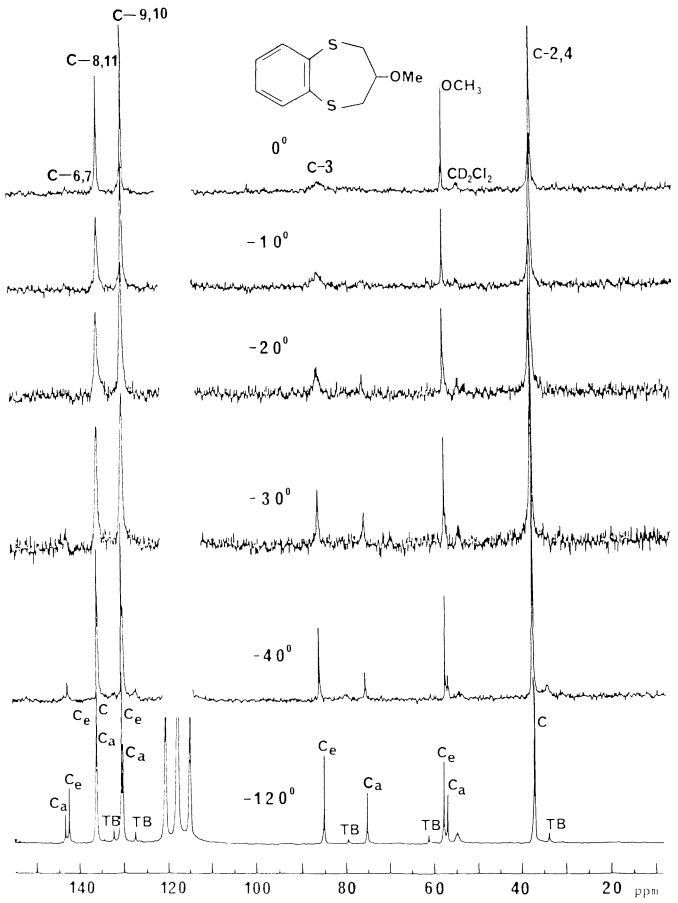

FIG. 7. 100.62-MHz ^{13}C nmr spectrum of **4** in CHF_2Cl at several temperatures.

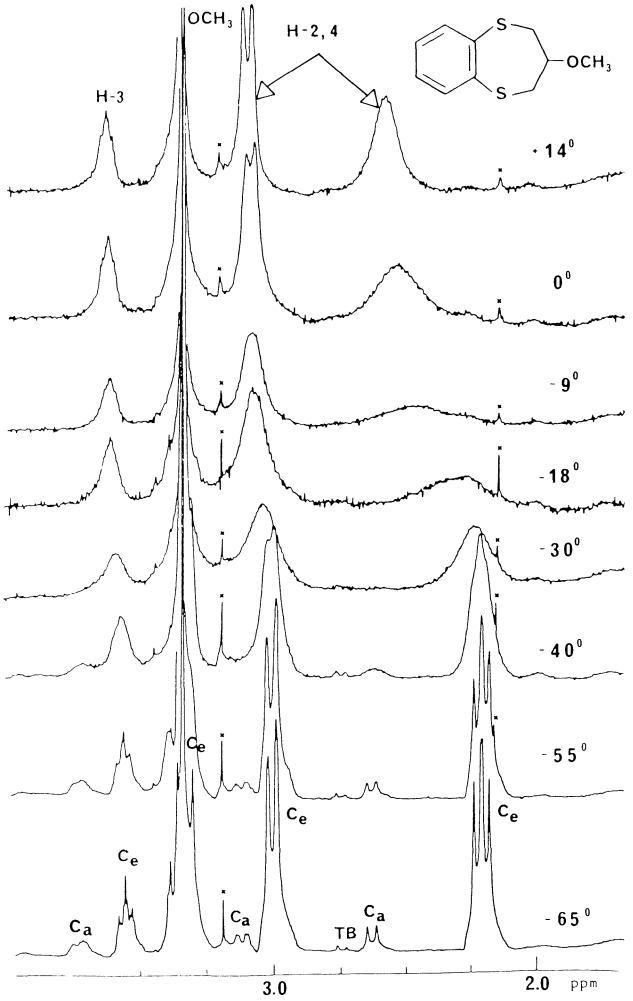

FIG. 8. Partial 400.13-MHz ^1H nmr spectrum of **4** in CHF_2Cl at several temperatures.

CS_2 and 0.63 kcal/mol in CHF_2Cl) is lower than that reported for 5-methyl-1,3-dithiane in $CHCl_3$ (1.05 kcal/mol) (16). This suggests that steric interactions are indeed weaker in the present seven-membered ring, as is also the case in the analogous oxa-pair (2).

Finally, the methoxy derivative **4** exists predominantly in the C_e form in CS_2. The great importance of the C_e form for **4**, contrary to **4***a*, can be explained in terms of bond–antibond interactions (13–15) that act in a totally reverse manner when oxygen is replaced by sulfur. Indeed, it has been reported that the O/S *gauche* "conformation effect" is repulsive whereas the O/O *gauche* effect is attractive (3, 15). Thus, the C_a conformer of **4**, possessing the largest number of *gauche* arrangements for the $S—CH_2CH—OCH_3$ fragments, should be destabilized relative to C_e. On the other hand, the absence of the C_e form noted for **4***a* would then result from the fact that the O/O *gauche* interaction is attractive.

An increase in solvent polarity (as in CHF_2Cl) increases the amount of the C_a conformer of **4** at the expense of C_e, keeping the amount of TB essentially unchanged. In contrast, only the TB conformation of **4***a* is observed in the less polar solvent (2) (CH_3OCH_3 or CS_2) while the increase in polarity leads to a mixture of TB and C_a. If we consider that the TB preference is stronger in the oxa family because of electronic factors (17), then the solvent effect, increasing the amount of the more polar C_a conformation through better solvation in the more polar solvent (12), is similar for both **4** and **4***a*.

Experimental

The vapor phase chromatographic (vpc) analyses and separations were carried out on a Varian-Aerograph Model 920 instrument using helium as carrier gas.

The variable temperature ^1H and ^{13}C nmr spectra were recorded in the FT mode with a Bruker WH-400 instrument operating at 400.13 and 100.62 MHz respectively and equipped with a standard Bruker variable temperature accessory. Temperatures were read off the B-VT-1000 control unit and compared to a calibration curve previously established by using a Fluka Model 2165A digital display thermometer, equipped with a copper constantan thermocouple placed inside a solvent containing a dummy nmr tube inserted in the probe. A precision of ±3°C is expected.

All ^{13}C nmr spectra were recorded with broad-band proton decoupling and the following instrumental parameters are typical: SW = 52 215 Hz; flip angle = 15 μs; data size = 16 K; AQ = 0.4 s; pulse delay = 0.2 s. For proton spectra, the typical instrumental parameters used are as follows: flip angle = 50 μs; SW = 20 000 Hz; data size = 8 K; AQ = 0.2 s; pulse delay = 0.3 s. The ^1H spectra were resolution enhanced by exponential and (or) gaussians multiplication.

All variable temperature studies were performed on CHF_2Cl and CS_2 or THF-d_8 solutions of the sample containing Me_4Si and about 18% of CD_2Cl_2 (for field locking purposes) in standard 5-mm (^1H) and 10-mm (^{13}C) nmr tubes that had been degassed and sealed. The ^1H nmr tubes contained 5–10 mg of the sample in 0.5 mL of solvent while the ^{13}C nmr tubes contained 60–120 mg of the sample in 2.2 mL of the solvent.

Some rate constants were estimated at the coalescence temperature with the equations $k = \pi\Delta\nu/2^{1/2}$ for singlet to doublet splitting and $k = \pi(\Delta\nu^2 + J^2)^{1/2}/2^{1/2}$ for singlet to AB quartet splitting (9). The free energies of activation values ($\Delta G^{\pm}$) were calculated from standard

TABLE 3. Thermodynamic and kinetic parameters characterizing compounds **1**–**4**

Compound	Solvent	Conformation	Relative populations	$-\Delta G^0$ (°C)	T_c (°C)	$\Delta G^{\ddagger}$ C → TB	$\Delta G^{\ddagger}$ C → C*
1	CS_2	C	97	1.19	−20 (H-2,4)[b]		11.3
		TB	3[a]	(−100)			
(H,H)	THF-d_8	C	95	1.07			
		TB	5	(−90)			
2	CS_2	C	63	0.23			
		TB	37	(−60)			
(CH_3,CH_3)	CHF_2Cl	C	82	0.50	+10 (C-2,4)	12.9	
		TB	18	(−100)	+10 (H_3C)		12.0
3	CS_2	C_e	55	0.59 (C_e/TB)[c]	−20 (C-8,11)	11.3	
		C_a	25	0.31 (C_a/TB)	−10 (CH_3)		12.1
		TB	20	0.27 (C_e/C_a)			
(H,CH_3)				(−100)			
	CHF_2Cl	C_e	69	0.66 (C_e/TB)			
		C_a	20	−0.03 (C_a/TB)			
		TB	11	0.63 (C_e/C_a)			
				(−100)			
4	CS_2	C_e	88	1.56 (C_e/TB)			
		C_a	8	0.57 (C_a/TB)			
		TB	4	0.99 (C_e/C_a)			
(H,OCH_3)				(−65)			
	CHF_2Cl	C_e	61	0.92 (C_e/TB)	−30 (C-2,4)	10.9	
		C_a	33	0.73 (C_a/TB)	0 (C-3)		11.4
		TB	6	0.19 (C_e/C_a)			
				(−120)			

[a]The uncertainty in the integration results is about ±2%.

[b]The identity of nucleus and signal whose parameters are used to calculate $\Delta G^{\ddagger}$ is given in brackets next to the coalescence temperature. For the methyl group, CH_3 refers to the ^{13}C spectra whereas H_3C refers to the ^1H data.

[c]The ΔG^0 values referring to the TB form are corrected (2) for statistical effects owing to the existence of two equivalent TB forms for **3** and **4**.

equations using a transmission coefficient of 1 (for chair to twist-boat transformation) and of ½ (for chair inversion and TB inversion) (18).

o-*Benzenedithiol*

This compound was prepared by a three-step procedure described in the literature (19, 20) starting from butanethiol and *o*-dibromobenzene. Quantities of this compound were also purchased from Aldrich.

1,5-Benzodithiepin (ref. 6)

A suspension of 0.80 g of K_2CO_3 in 3 mL of *n*-pentanol was refluxed under vigorous stirring and a solution of 218 mg (1 mmol) of 1,3-dibromopropane and 142 mg (1 mmol) of *o*-benzenedithiol in 3 mL of *n*-pentanol was added dropwise. The mixture was refluxed for 10 h, then cooled and filtered. The filtrate was washed with water, dried over $MgSO_4$, and the solvent was evaporated. The residue was dissolved in benzene, treated with activated charcoal, and distilled. The colorless liquid obtained was purified by gas chromatography on a SE-30 5% column (150 cm × 6.4 mm, T = 140°C) yielding 85 g (47%) of 1,5-benzodithiepene, characterized by its ^1H nmr spectrum described in Table 1 and its comparison with that reported in the literature (6).

3-Methyl-1,5-benzodithiepene

A solution of 145 mg of *o*-benzenedithiol (1 mmol) and 342 mg of ditosylate of 2-methyl-1,3-propanediol (described elsewhere (2)) was added to a suspension of 0.78 g of K_2CO_3 in 3 mL of DMSO. The mixture was heated at 110°C for 20 h. After cooling at room temperature, water and benzene were added and the phases were separated. The aqueous layer was extracted with benzene (2 × 20 mL) and the combined organic fractions were washed with water and dried over $MgSO_4$. The solvent was evaporated and the residue purified by gas chromatography on a SE-30, 5% column (150 cm × 6.4 mm, T = 140°C). Thus 107 mg (64%) of a colorless liquid was obtained. *Exact Mass* calcd. for $C_{10}H_{12}S_2$: 196.0380; found (ms, m/e): 196.0365 $(M)^+$, 180 $(M - CH_4)^+$, 153 $(C_7H_5S_2)^+$, 140 $(C_6H_4S_2)^+$.

3,3-Dimethyl-1,5-benzodithiepene

This compound was prepared from 0.28 g (2 mmol) of *o*-benzenedithiol and 0.51 g of 1,3-dibromo-2,2-dimethylpropane according to a procedure already described (3). Distillation yielded 105 g (25%) of a colorless liquid whose ^1H nmr spectrum was identical to that already known (6).

3-Methoxy-1,5-benzodithiepene

A solution of 190 mg (1.3 mmol) of *o*-benzenedithiol and 392 mg (1.8 mmol) of 1,3-dibromo-2-propanol in 4 mL of pentanol was slowly added to a refluxing and vigorously stirred mixture of 1.11 g of K_2CO_3 in 4 mL of pentanol. After refluxing overnight, the mixture was cooled and filtered. The filtrate was washed with water and dried over $MgSO_4$. The solvent was evaporated and the remaining yellow oily product was dissolved in 3 mL of diglyme and cooled in an ice bath. CH_3I (12.15 g, 15 mmol) was added and then slowly 0.375 g (16 mmol) of NaH suspended in 3 mL of diglyme. The mixture was stirred at room temperature overnight and the excess of hydride was destroyed by slowly adding 2 mL of methanol. Water and ether were added, the phases were then separated, and the aqueous layer was extracted with ether (3 × 20 mL). The combined organic fractions were washed with water (3 × 20 mL) and dried over $MgSO_4$. The solvent was evaporated and the resulting yellow oil was purified by gas chromatography using a SE-30, 5% column (150 cm × 6.4 mm, T = 140°C). A colorless liquid (98 mg, 36%) was recovered. *Exact Mass* calcd. for $C_{10}H_{12}S_2O$: 212.0330; found (ms, m/e): 212.0316 $(M)^+$, 180 $(M - CH_3OH)^+$, 153 $(M - C_3H_3O)^+$.

Acknowledgements

We wish to acknowledge the technical contribution of Robert Mayer and Sylvie Bilodeau and the assistance of Dr. Phan Viet Ninh Tan of the "Laboratoire Régional de RMN à haut champ" in Montréal. We thank Alain Lachapelle for his collaboration

in recording some of the nmr spectra. We thank the Natural Sciences and Engineering Research Council of Canada and the Ministère de l'Éducation du Québec for financial assistance.

1. D. MÉNARD and M. ST-JACQUES. Can. J. Chem. **59**, 1160 (1981).
2. D. MÉNARD and M. ST-JACQUES. J. Am. Chem. Soc. **106**, 2055 (1984).
3. (*a*) E. L. ELIEL and E. JUARISTI. J. Am. Chem. Soc. **100**, 6114 (1978); (*b*) N. S. ZEFIROV, L. G. GURVICH, A. S. SHASHKOV, M. Z. KRIMER, and E. A. VORBEVA. Tetrahedron, **32**, 1221 (1976).
4. W. ADCOCK, B. D. GUPTA, T. C. KHOR, D. DODDRELL, and W. KITCHING. J. Org. Chem. **41**, 751 (1976).
5. G. W. BUCHANAN, M. E. ISABELLE, and R. H. WIGHTMAN. Org. Magn. Reson. **16**, 156 (1981); (*b*) E. BREITMAIER and W. VOELTER. ^{13}C nmr spectroscopy. Verlag Chemie, New York. 1978.
6. K. VON BREDOW, H. FRIEBOLIN, and S. KABUSS. Org. Magn. Reson. **2**, 43 (1970).
7. E. L. ELIEL, V. S. RAO, and F. G. RIDDELL. J. Am. Chem. Soc. **98**, 1583 (1976).
8. J. B. LAMBERT and J. E. GOLDSTEIN. J. Am. Chem. Soc. **99**, 5689 (1977).
9. D. KOST, E. H. CARLSON, and M. RABAN. J. Chem. Soc. D, 656 (1971).
10. H. FRIEBOLIN, H. G. SCHMID, S. KABUSS, and W. FAISST. Org. Magn. Reson. **1**, 67 (1969).
11. D. MÉNARD and M. ST-JACQUES. Tetrahedron, **39**, 1041 (1983).
12. M. K. KALOUSTIAN. J. Chem. Educ. **51**, 777 (1974).
13. T. K. BRUNCK and F. WEINHOLD. J. Am. Chem. Soc. **101**, 1700 (1979).
14. W. K. OLSON. J. Am. Chem. Soc. **104**, 278 (1982).
15. E. JUARISTI. J. Chem. Educ. **56**, 438 (1979).
16. E. L. ELIEL and R. O. HUTCHINS. J. Am. Chem. Soc. **91**, 2703 (1969).
17. G. M. ANDERSON, P. A. KOLLMAN, L. N. DOMELSMITH, and K. N. HOUK. J. Am. Chem. Soc. **101**, 2344 (1979).
18. F. A. L. ANET, P. J. DEGER, and J. KRANE. J. Am. Chem. Soc. **98**, 2059 (1976).
19. R. ADAMS, W. REILSCHNEIDER, and A. FERRETTI. Org. Synth. Coll. Vol. **V**, 107 (1973).
20. A. FERRETTI. Org. Synth. Coll. Vol. **V**, 419 (1973).

The visible absorption spectrum of 1,2-cyclobutanedione in the gas phase[1]

R. A. Back and J. M. Parsons

Division of Chemistry, National Research Council of Canada, 100 Sussex Drive, Ottawa., Ont., Canada K1A 0R6

Received February 27, 1986

R. A. Back and J. M. Parsons. Can. J. Chem. **64**, 2152 (1986).

The visible absorption spectrum of 1,2-cyclobutanedione has been measured in the gas phase at wavelengths between 4000 and 5100 Å. The absorption is attributed to the allowed $\pi^* \leftarrow n_+$, $^1B_1 \leftarrow {}^1A_1$ transition corresponding to the first excited singlet state. The spectrum shows a complex well-resolved vibrational structure which has been analysed, with some 125 bands measured and assigned. The bands at the longer wavelengths show sharp rotational fine structure, not yet analysed. The strongest band in the spectrum at 4933 Å has been assigned as the 0–0 band, while a band almost as strong at 4820 Å is attributed to excitation of one quantum of ν'_{12}, the a_2 out-of-plane carbonyl bending vibration, and it is suggested that this band owes its intensity to vibronic coupling. A number of symmetric vibrations are also excited in the spectrum, but with no long progressions. Sequence bands running to the blue with an interval of about 72 cm^{-1} are prominent throughout the spectrum, and are assigned to ν_{13}, the a_2 ring-twisting vibration. Other hot bands were also observed involving ν_{13} which permitted estimation of energy levels for this vibration both in the ground state and the excited state. The infrared spectrum was also measured and analysed in the gas phase between 600 and 4000 cm^{-1}, and 14 bands were assigned to fundamental vibrations; some of these assignments, at the lower frequencies, are uncertain.

R. A. Back et J. M. Parsons. Can. J. Chem. **64**, 2152 (1986).

Opérant en phase gazeuse, on a mesuré le spectre d'absorption visible de la cyclobutanedione-1,2 à des longueurs d'onde allant de 4000 à 5100 Å. L'absorption est attribuée à une transition $\pi^* \leftarrow n_+$, $^1B_1 \leftarrow {}^1A_1$ qui est permise et qui correspond au premier état singulet excité. Le spectre présente une structure vibrationnelle complexe et bien résolue que l'on a analysé; on a mesuré et attribué quelques 125 bandes. Les bandes aux longueurs d'onde les plus élevées présentent une structure fine rotationnelle qui est bien définie; on ne les a toutefois pas analysées. La bande la plus intense du spectre apparaît à 4933 Å et on l'a attribuée à la bande 0–0; par ailleurs, une bande qui est pratiquement aussi intense et qui apparaît à 4820 Å est attribuée à l'excitation d'un quantum de ν'_{12}, la vibration a_2 de déformation angulaire hors-plan du carbonyle; on suggère que cette bande doit son intensité à un couplage vibronique. Un certain nombre de vibrations symétriques sont aussi excitées dans ce spectre; elles ne présentent toutefois pas de longues progressions. Des séquences de bandes allant jusqu'au bleu, avec un intervalle d'environ 72 cm^{-1}, sont en évidence dans tout le spectre et on les attribue à ν_{13}, la vibration a_2 de déformation du cycle. On a aussi observé d'autres bandes chaudes impliquant ν_{13} qui permettent d'évaluer les niveaux d'énergie de cette vibration tant à l'état fondamentale qu'à l'état excité. On a aussi mesuré le spectre infrarouge en phase gazeuse entre 600 et 4000 cm^{-1}, on l'a analysé et on a attribué 14 bandes à des vibrations fondamentales; toutefois quelques-unes de ces attributions, aux fréquences les plus basses, sont incertaines.

[Traduit par la revue]

Introduction

The spectroscopy of α-dicarbonyl compounds shows many interesting features. The two lone-pair orbitals interact strongly, splitting into n_+ and n_- components, raising the energy of the former enough to shift the $\pi^* \leftarrow n_+$ transition into the near ultraviolet or visible region. The spectroscopy of glyoxal, the prototype α-dicarbonyl compound, has been very thoroughly studied (1). The ultraviolet spectrum of oxalic acid has recently been analysed in this laboratory (2), and those of pyruvic (3) and glyoxylic acid (4) briefly reported. All these compounds exist almost entirely as the *trans* isomer; only with glyoxal has the *cis* isomer been detected and its absorption spectrum observed, and this only with difficulty because of overlapping absorption by the *trans* isomer which is present in about a thousand-fold excess (5). With 1,2-cyclobutanedione (hereafter CBD), in contrast, the molecule is locked in a *cis* configuration. It is a yellow solid, and visible absorption bands have been observed in solution (6), but no gas-phase spectra appear to have been measured. In conjunction with photochemical studies of CBD (7), we have measured the visible absorption spectrum, which we now report in detail in the present paper. To aid in the vibrational analysis, the infrared absorption spectrum, not previously reported, was also measured.

Experimental

Absorption spectra were first measured in a 1-m single-pass quartz cell, heated to temperatures up to about 50°C, using a Spex 1-m grating spectrometer with a resolution of about 0.1 Å. Spectra were also photographed at medium resolution using an Eagle spectrograph in the 1st and 2nd order, using a multi-pass 2-m White cell at room temperature. High resolution spectra of some bands were photographed using the 12th order of an Ebert spectrograph.

The infrared spectrum of the vapor was measured from 600 to 4000 cm^{-1} with a path length of about 60 cm and a pressure of 0.5 Torr, using a Bomem F.T. spectrometer at a resolution of about 1 cm^{-1}.

Cyclobutanedione was prepared by M. Hrytsak and his colleagues at the University of Ottawa, using methods in the literature (8, 9). The vapor was admitted to the absorption cell after simple degassing, keeping exposure to visible light and to water vapor at a minimum. The sample was replaced frequently as some loss by photolysis was observed, but the products, chiefly C_2H_4 and CO, are transparent in the region of interest.

Results

The absorption spectrum between 5100 and 4000 Å, measured in the Spex spectrometer, is shown in Fig. 1. No absorption could be observed at longer wavelengths or at wavelengths between 3900 and 2200 Å. Medium-resolution photographic spectra from 5100 to 4780 Å are shown in Fig. 2. In Table 1 are listed the vibrational bands observed, their wavelengths in air, and their wavenumbers *in vacuo*. Bands evident in the spectrometer trace (Fig. 1) are designated by upper-case letters, while other bands seen only in photographs are labelled with lower-case letters. Numerical subscripts refer to members of ν_{13} sequences, discussed below. The wavelengths and wavenumbers shown were measured from the photographic spectra using iron-arc lines as references in the usual way, and refer to

[1]NRC No. 25309.

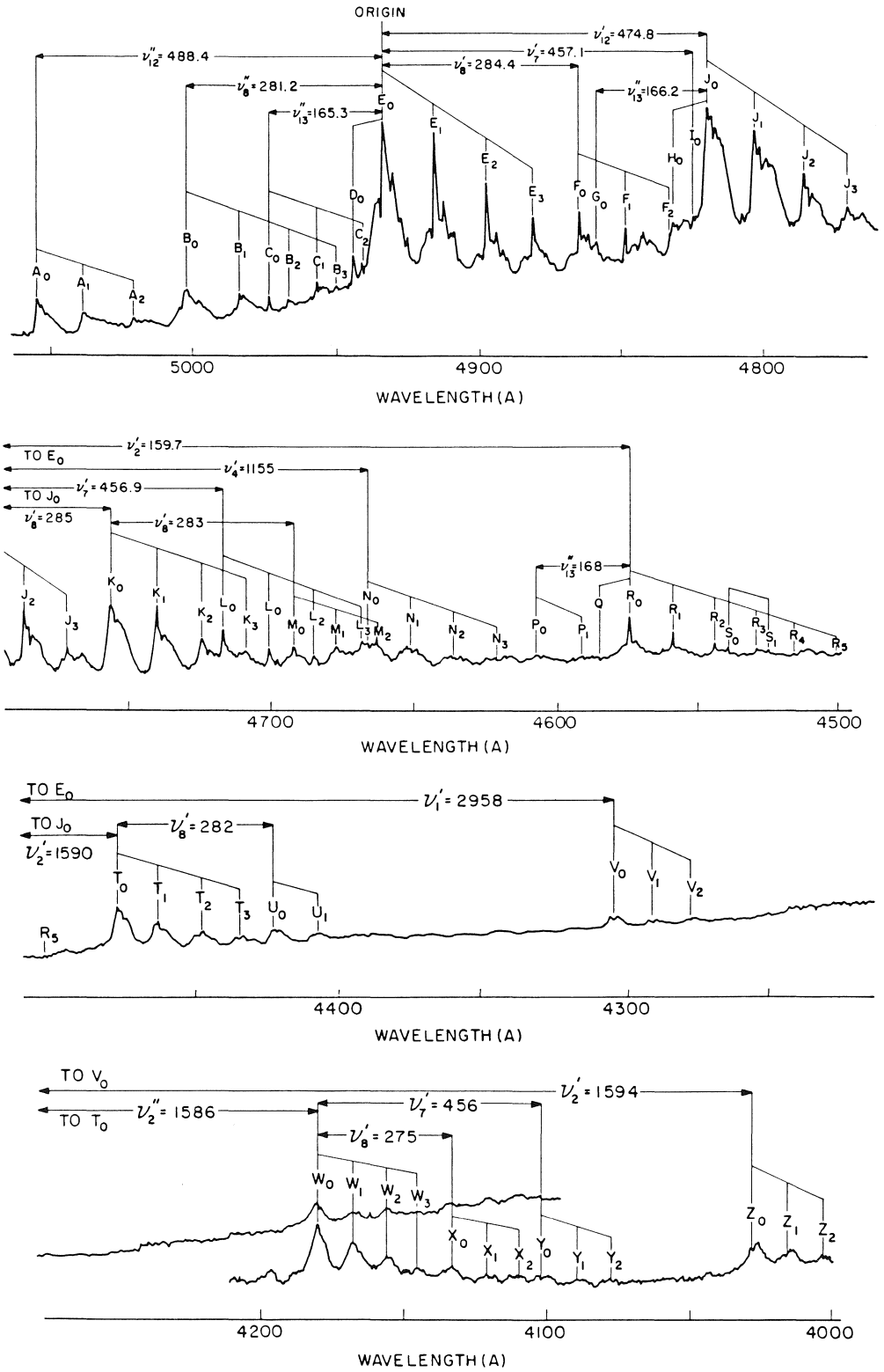

FIG. 1. Low-resolution absorption spectrum of 1,2-cyclobutanedione, measured with a Spex 1-m grating spectrometer. No correction was made for the wavelength response of the photomultiplier. See text and Table 1 for band assignments, wavelengths, and meaning of symbols.

the band heads, degraded to the blue, evident in the spectrum (Fig. 2). At the lower wavelengths, these band heads are very sharp, and measurements were made from these sharp edges (e.g. bands labelled A_0, B_0, E_0, E_1, E_2, J_0, J_1 in Fig. 2). With decreasing wavelength generally, and within ν_{13} sequences, band heads tend to become more diffuse, and measurements were made from estimated points of maximum intensity. At the shortest wavelengths, the band heads become quite diffuse, and some bands become distinctly double (e.g., V_0, Y_0, and Z_0 in Fig. 1), and in these cases measurements refer to the intensity maximum of the longest-wavelength member of each pair. Frequencies are reported to the nearest cm^{-1} or the nearest $0.1\,cm^{-1}$, depending on the sharpness of the band. The accuracy of the measurements varies considerably from band to

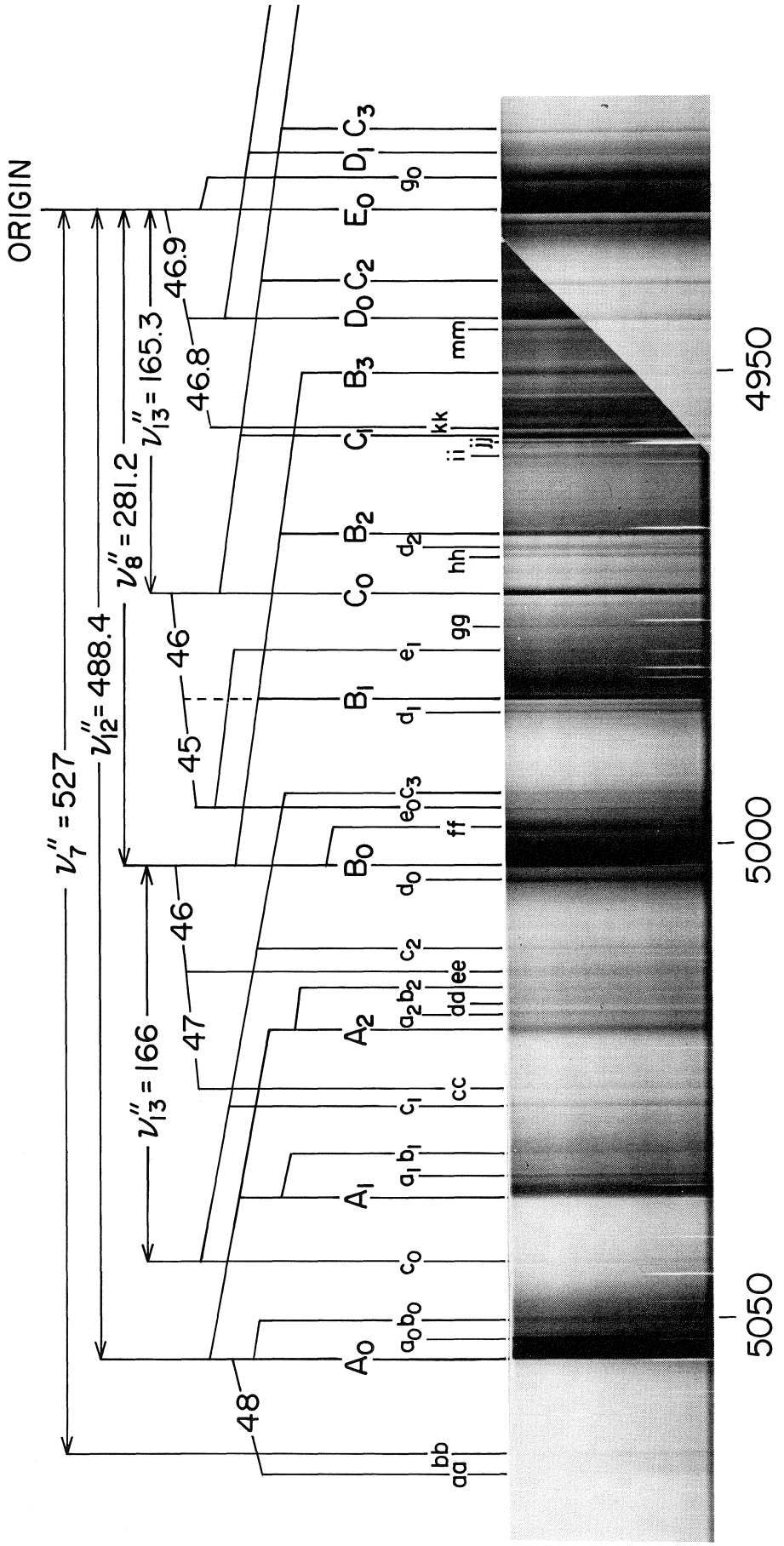

FIG. 2. Medium-resolution absorption spectrum of 1,2-cyclobutanedione photographed in the 1st order of an Eagle 6.65-m grating spectrograph. See text and Table 1 for band assignments, wavelengths and meaning of symbols.

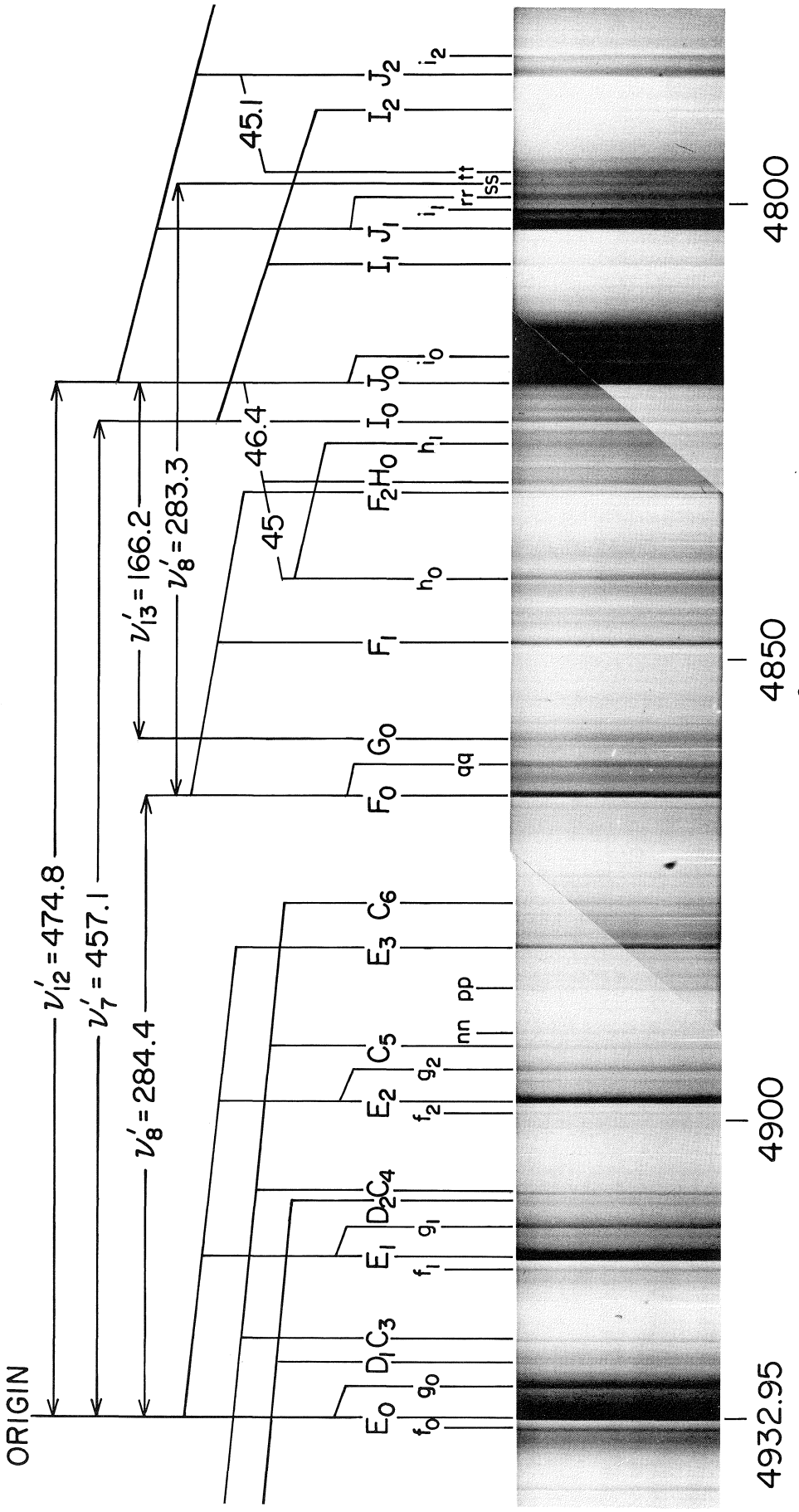

FIG. 2. (*concluded*)

TABLE 1. Band heads in the absorption spectrum of 1,2-cyclobutanedione (all frequencies and frequency differences in cm^{-1} *in vacuo*)*

Band symbol	Wavelength (Å, in air)	ν	ν_{13} sequence intervals	Vibrational assignment	Comments
aa	5067.00	19730	—	$12_1^0 24_1^1$	df, wk, $A_1 - aa = 48 = \nu''_{24} - \nu'_{24}$
bb	5064.71	19739	—	7_1^0	sh, wk, $E_0 - bb = 527 = \nu''_7$
A_0	5054.76	19777.8	—	12_1^0	sh, st, $E_0 - A_0 = 488.4 = \nu''_{12}$
a_0	5051.92	19789	—		df, st, $A_0 + 11$, rf?
b_0	5050.39	19795	—	$12_1^0 X_1^1$	df, $b_0 - A_0 = 17 = \nu'_X - \nu''_X$
c_0	5044.21	19819	—	$8_1^0 13_1^0$	df, wk, $B_0 - c_0 = 166 = \nu'_{13}$
A_1	5037.11	19847.1	69.3	$12_1^0 13_1^1$	sh, st
a_1	5035.14	19854.9	65		sh, $A_1 + 8$, rf?
b_1	5032.73	19864	69	$12_1^0 X_1^1 13_1^1$	df, $b_1 - A_1 = 17 = \nu'_X - \nu''_X$
c_1	5027.68	19884.4	65	$8_1^0 13_2^1$	sh
cc	5025.71	19892	—	$8_1^0 24_2^2$	df, wk, $ee - cc = 47 = \nu'_{24} - \nu''_{24}$
A_2	5019.48	19916.8	69.7	$12_1^0 13_2^2$	sh, st
a_2	5017.84	19923.3	68.4		sh, st, $A_2 + 7$, rf?
dd	5017.08	19926.3	—	?	sh
b_2	5015.58	19932	68	$12_1^0 X_1^1 13_2^2$	df, wk
ee	5013.77	19939	—	$8_1^0 24_1^1$	df, $B_0 - ee = 46 = \nu''_{24} - \nu'_{24}$
c_2	5011.01	19950.5	66.1	$8_1^0 13_3^2$	sh, wk
d_0	5003.80	19979	—	?	df, $B_0 - 6$
B_0	5002.37	19985.0	—	8_1^0	sh, st, $E_0 - B_0 = 281.2 = \nu''_8$
ff	4998.44	20001	—	$8_1^0 X_1^1$	df, st, $ff - B_0 = 16 = \nu'_X - \nu''_X$
e_0	4996.09	20010.0	—	$13_1^0 24_2^2$	sh, $C_0 - e_0 = 91 = 2\nu''_{24} - 2\nu'_{24}$
c_3	4994.45	20017	66.1	$8_1^0 13_4^3$	df, wk
d_1	4985.86	20051.1	72	?	sh, $B_1 - 5.5$
B_1	4984.50	20056.6	71.6	$8_1^0 13_1^1$	
e_1	4979.36	20077.3	67.3	$13_2^1 24_2^2$	sh, wk
gg	4976.79	20087.7	—	?	sh
C_0	4973.51	20100.9	—	13_1^0	sh, st, $E_0 - C_0 = 165.3 = \nu''_{13}$
hh	4969.25	200118.2	—	?	sh, st, $B_2 - 8.5$
d_2	4968.37	20121.7	70.6	?	$B_2 - 5.0$
B_2	4967.15	20126.7	70.1	$8_1^0 13_2^2$	sh, st
ii	4958.88	20160	—	?	df, wk, $C_1 - 7.8$
jj	4957.31	20166.6	—	?	sh, wk, $kk - 5.9$
C_1	4957.01	20167.8	66.9	13_2^1	sh
kk	4955.88	20172.5	—	24_2^2	sh, $D_0 - kk = 46.8 = \nu''_{24} - \nu'_{24}$
B_3	4950.14	20195.8	69.1	$8_1^0 13_3^3$	sh
mm	4945.34	20215.5	—	?	$D_0 - 3.8$
D_0	4944.38	20219.3	—	24_1^1	sh, st, $E_0 - D_0 = 46.9 = \nu''_{24} - \nu'_{24}$
C_2	4940.62	20234.7	66.9	13_3^2	sh
f_0	4934.06	20261.6	—	?	sh, st, $E_0 - 4.6$
E_0	4932.95	20266.2	—	origin	sh, st
g_0	4929.47	20280.5	—	X_1^1	sh, st, $g_0 - E_0 = 14.3 = \nu'_X - \nu''_X$
D_1	4926.90	20291	71.7	$13_1^1 24_1^1$	df
C_3	4924.27	20301.9	67.2	13_4^3	sh
f_1	4916.57	20333.7	72.1	?	df, $E_1 - 4.1$
E_1	4915.57	20337.8	71.6	13_1^1	sh, st
g_1	4911.98	20352.7	72.2	$X_1^1 13_1^1$	sh, st
D_2	4909.26	20364	73	$13_2^2 24_1^1$	df, wk
C_4	4908.15	20368.6	66.7	13_5^4	sh
f_2	4899.41	20404.9	71.2	?	df, $E_2 - 4.1$
E_2	4898.42	20409.0	71.2	13_2^2	sh, st
g_2	4894.70	20424.6	71.9	$X_1^1 13_2^2$	sh
C_5	4892.39	20434.2	65.6	13_6^5	df, wk
nn	4890.59	20441.7	—	?	
pp	4886.00	20460.9	—	?	
E_3	4881.49	20479.8	70.8	13_3^3	sh, st
C_6	4876.73	20499.8	65.6	13_7^6	df, wk
F_0	4864.69	20550.6	—	8_0^1	sh, st, $F_0 - E_0 = 284.4 = \nu'_8$
qq	4861.48	20564	—	$8_0^1 X_1^1$	df, $qq - F_0 = 13.6 = \nu'_X - \nu''_X$
G_0	4858.98	20574.8	—	$12_0^1 13_1^0$	df, $J_0 - G_0 = 166.2 = \nu''_{13}$
F_1	4848.33	20619.9	69.3	$8_0^1 13_1^1$	sh
h_0	4841.36	20649.6	—	$12_0^1 13_1^1 24_2^2$	sh, $H_0 - h_0 = 45.0 = \nu''_{24} - \nu'_{24}$
F_2	4831.79	20690.4	70.5	$8_0^1 13_2^2$	sh
H_0	4830.84	20694.6	—	$12_0^1 24_1^1$	sh, $J_0 - H_0 = 46.6 = \nu''_{24} - \nu'_{24}$

TABLE 1. (*continued*)

Band symbol	Wavelength (Å, in air)	ν	ν_{13} sequence intervals	Vibrational assignment	Comments
h_1	4825.38	20718.0	68.4	$12_0^1 13_3^2 24_2^2$	sh
I_0	4824.14	20723.3	—	7_0^1	sh, $I_0 - E_0 = 457.1 = \nu_7'$
J_0	4820.01	20741.0	—	12_0^1	sh, st, $J_0 - E_0 = 474.8 = \nu_{12}'$
i_0	4818.10	20749.3	—		sh, $J_0 + 8.3$, rf?
I_1	4807.28	20796.0	72.7	$7_0^1 13_1^1$	sh
J_1	4803.36	20812.9	71.9	$12_0^1 13_1^1$	sh, st
i_1	4801.31	20821.8	72.5		sh, $J_1 + 8.9$, rf?
rr	4799.87	20828.1	—	$12_0^1 13_1^1 X_1^1$	sh, $rr - J_1 = 15.2 = \nu_X' - \nu_X''$
ss	4798.52	20833.9	—	8_0^2	df, $ss - F_0 = 283.3 = \nu_8'$
tt	4797.42	20838.7	—	$12_0^1 13_2^2 24_1^1$	df, $J_2 - tt = 45.1 = \nu_{24}'' - \nu_{24}'$
I_2	4790.90	20867.1	71.1	$7_0^1 13_2^2$	sh
J_2	4787.07	20883.8	70.9	$12_0^1 13_2^2$	sh
i_2	4784.84	20893.5	71.7		sh, $J_2 + 9.7$, rf?
I_3	4774.66	20938.1	71.0	$7_0^1 13_3^3$	sh
J_3	4770.76	20955.1	71.3	$12_0^1 13_3^3$	sh
K_0	4754.78	21026	—	$8_0^1 12_0^1$	df, $K_0 - J_0 = 285 = \nu_8'$
K_1	4738.94	21096	70	$8_0^1 12_0^1 13_1^1$	df
K_2	4723.25	21166	70	$8_0^1 12_0^1 13_2^2$	df
L_0	4716.13	21197.9	—	$7_0^1 12_0^1$	sh, $L_0 - J_0 = 456.9 = \nu_7'$
K_3	4707.30	21238	72	$8_0^1 12_0^1 13_3^3$	df
L_1	4700.44	21269	71	$7_0^1 12_0^1 13_1^1$	df
M_0	4691.59	21308.8	—	$8_0^2 12_0^1$	sh, $M_0 - K_0 = 283 = \nu_8'$
L_2	4684.07	21343	74	$7_0^1 12_0^1 13_2^2$	df
M_1	4676.15	21379.1	70.3	$8_0^2 12_0^1 13_1^1$	sh
L_3	4668.42	21415	72	$7_0^1 12_0^1 13_3^3$	df
N_0	4666.97	21421	—	4_0^1	df, $N_0 - E_0 = 1155 = \nu_4'$
M_2	4661.09	21448	69	$8_0^2 12_0^1 13_2^2$	df
N_1	4651.06	21495	74	$4_0^1 13_1^1$	df
N_2	4636.14	21564	69	$4_0^1 13_2^2$	df
N_3	4620.57	21636	72	$4_0^1 13_3^3$	df
P_0	4608.93	21691	—	$2_0^1 13_1^0$	df, $R_0 - P_0 = 168 = \nu_{13}''$
P_1	4594.00	21761.4	70	$2_0^1 13_2^1$	sh
Q_0	4584.54	21806.3	—	$2_0^1 24_1^1$	sh, $R_0 - Q_0 = 52.6 = \nu_{24}'' - \nu_{24}'$
R_0	4573.51	21858.9	—	2_0^1	sh, $R_0 - E_0 = 1592.7 = \nu_2'$
R_1	4558.43	21931.2	72.3	$2_0^1 13_1^1$	sh
R_2	4543.59	22002.9	71.7	$2_0^1 13_2^2$	sh
S_0	4538.78	22026.2	—	?	sh
R_3	4528.90	22074.2	71.3	$2_0^1 13_3^3$	sh
S_1	4524.66	22094.9	68.7	?	sh
j_0	4515.83	22138.1	—	$2_0^1 8_0^1$	sh, $j_0 - R_0 = 279.2 = \nu_8'$
R_4	4514.38	22145.2	71.0	$2_0^1 13_4^4$	sh
S_2	4510.79	22162.0	68.0	?	sh
j_1	4501.21	22210.0	71.9	$2_0^1 8_0^1 13_1^1$	sh
j_2	4486.95	22281	71	$2_0^1 8_0^1 13_2^2$	df
T_0	4476.80	22331	—	$2_0^1 12_0^1$	df, $T_0 - J_0 = 1590 = \nu_2'$
T_1	4462.00	22405	74	$2_0^1 12_0^1 13_1^1$	df
T_2	4447.21	22480	75	$2_0^1 12_0^1 13_2^2$	df
T_3	4433.40	22550	70	$2_0^1 12_0^1 13_3^3$	df, db
U_0	4421.03	22613	—	$2_0^1 8_0^1 12_0^1$	df, db, $U_0 - T_0 = 282 = \nu_8'$
U_1	4407.42	22683	70	$2_0^1 8_0^1 12_0^1 13_1^1$	df, db
U_2	4392.09	22762	79	$2_0^1 8_0^1 12_0^1 13_2^2$	df, db
k_0	4386.15	22793	—	$2_0^1 7_0^1 12_0^1$	df, $k_0 - T_0 = 462 = \nu_7'$
k_1	4372.47	22864	71	$2_0^1 7_0^1 12_0^1 13_1^1$	df
m_0	4357.28	22944	—	$1_0^1 8_1^0$	df, $V_0 - m_0 = 280 = \nu_8''$
m_1	4344.50	23011	67	$1_0^1 8_1^0 13_1^1$	df
n_0	4333.42	23067	—	$2_0^1 7_0^1 8_0^1 12_0^1$	df, $n_0 - U_0 = 454 = \nu_7'$
n_1	4319.80	23143	76	$2_0^1 7_0^1 8_0^1 12_0^1 13_1^1$	df
V_0	4304.69	23224	—	1_0^1	df, db, $V_0 - E_0 = 2958 = \nu_1'$
V_1	4291.27	23297	73	$1_0^1 13_1^1$	df, db
V_2	4278.25	23368	71	$1_0^1 13_2^2$	df, db
V_3	4264.94	23440	72	$1_0^1 13_3^3$	df, db
p_0	4253.06	23506	—	$1_0^1 8_0^1$	df, db, $p_0 - V_0 = 282 = \nu_8'$
p_1	4239.95	23579	73	$1_0^1 8_0^1 13_1^1$	df, db
p_2	4227.39	23649	70	$1_0^1 8_0^1 13_2^2$	df, db

TABLE 1. (*concluded*)

Band symbol	Wavelength (Å, in air)	ν	ν_{13} sequence intervals	Vibrational assignment	Comments
q_0	4221.26	23683	—	$1_0^1 7_0^1$	df, db, $q_0 - V_0 = 459 = \nu_7'$
p_3	4215.12	23717	68	$1_0^1 8_0^1 13_3^3$	df, db
q_1	4208.51	23755	72	$1_0^1 7_0^1 13_1^1$	df, db
p_4	4202.00	23792	75	$1_0^1 8_0^1 13_4^4$	df, db
q_2	4195.70	23827	72	$1_0^1 7_0^1 13_2^2$	df, db
r_0	4187.95	23871	—	$2_0^2 12_0^1 24_1^1$	df, $W_0 - r_0 = 46 = \nu_{24}'' - \nu_{24}'$
W_0	4179.90	23917	—	$2_0^2 12_0^1$	df, db, $W_0 - T_0 = 1586 = \nu_2'$
W_1	4167.40	23989	72	$2_0^2 12_0^1 13_1^1$	df, db
W_2	4156.08	24054	65	$2_0^2 12_0^1 13_2^2$	df
W_3	4144.40	24122	68	$2_0^2 12_0^1 13_3^3$	df
X_0	4132.40	24192	—	$2_0^2 8_0^1 12_0^1$	df, db, $X_0 - W_0 = 275 = \nu_8'$
X_1	4120.80	24260	68	$2_0^2 8_0^1 12_0^1 13_1^1$	df, db
X_2	4109.40	24328	68	$2_0^2 8_0^1 12_0^1 13_2^2$	df
Y_0	4101.80	24373	—	$2_0^2 7_0^1 12_0^1$	df, db, $Y_0 - W_0 = 456 = \nu_7'$
Y_1	4089.43	24446	73	$2_0^2 7_0^1 12_0^1 13_1^1$	df, db
Y_2	4077.33	24519	73	$2_0^2 7_0^1 12_0^1 13_2^2$	df
Z_0	4028.16	24818	—	$1_0^1 2_0^1$	df, db, $Z_0 - V_0 = 1594 = \nu_2'$
Z_1	4016.50	24890	72	$1_0^1 2_0^1 13_1^1$	df, db
Z_2	4005.00	24962	72	$1_0^1 2_0^1 13_2^2$	df, db
s_0	3983.50	25097	—	$1_0^1 2_0^1 8_0^1$	df, $s_0 - Z_0 = 279 = \nu_8'$
s_1	3971.90	25170	73	$1_0^1 2_0^1 8_0^1 13_1^1$	df, db

*sh = sharp, df = diffuse, st = strong, wk = weak, rf = rotational feature, db = double.

band, but should be adequate for vibrational analysis. High-resolution spectra show sharp, partially resolved rotational structure in most bands at longer wavelengths. This structure is complex and overlapped and has not yet been analysed, but it appears that the true vibronic band origins probably lie from 5 to 10 cm^{-1} to the blue of the values listed in Table 1.

Table 2 lists and describes the bands observed in the infrared spectrum between 600 and 4000 cm^{-1}, and their assignments; some of the latter are obviously uncertain, especially some of the weaker bands and those at the lower frequencies. Where the band types are clear, they are all in accord with the vibrational assignment, with consideration of the permanent dipoles associated with the C—O and C—H bonds. Of the 24 fundamentals, 14 are assigned to observed bands, 4 should be infrared inactive or very weakly active (ν_4, ν_9, ν_{10}, ν_{11}), and the other 6 are expected to lie below 600 cm^{-1}. This spectrum will not be discussed further.

Discussion

The electronic transition

The microwave spectrum (10) and electron diffraction measurements (11) have shown that the carbon—oxygen skeleton of CBD is planar in the ground state, with C_{2v} geometry; like glyoxal, it probably also remains planar in the excited state. From the photoelectron spectrum (12) and by analogy with other α-dicarbonyl compounds, the highest occupied molecular orbital is the $a_1(n_+)$ component of the n_+–n_- pair formed by interaction of the two carbonyl lone-pair orbitals. The observed spectrum is undoubtedly due to the allowed $\pi^* \leftarrow n_+$, $^1B_1 \leftarrow {}^1A_1$ transition, entirely analogous to the similar visible absorption spectrum of *cis*-glyoxal (5). The O–O bands are quite close (4933 vs. 4875 Å in *cis*-glyoxal) and the value (7) of $\epsilon_{max} \approx 20\ M^{-1}\ cm^{-1}$ is about that expected for a $\pi^* \leftarrow n_+$ transition.

Vibrational analysis

The 24 normal-mode vibrations of CBD are listed and approximately described in Table 3. Lacking well-established ground-state frequencies, the numbering of several of these is uncertain. Ground-state values for ν_1'', ν_8'', ν_{12}'', and ν_{13}'' have been obtained from hot-bands in the visible absorption spectrum and from the fluorescence spectrum (13), while other values are taken from the ir spectrum, or estimated.

The strongest band in the spectrum at 4933 Å, labelled E_0, has been assigned as the 0—0 band. Obvious sequence bands, labelled E_1, E_2, and E_3 run towards shorter wavelengths with an interval of about 70 cm^{-1}. Similar sequences can be seen throughout the spectrum (denoted by subscripts) and are all assigned as $\Delta v = 0$ sequences in ν_{13}. Similar sequences, running to the blue, are prominent in the spectra of glyoxal (1) and oxalic acid (2), where they involve the torsional vibration around the C—C bond, which becomes shorter and stronger in the excited state. The analogous vibration in CBD is the a_2 out-of-plane ring-twisting mode, ν_{13}, which is also expected to have the lowest frequency in the molecule, and has been observed in the form of vibrational satellites in the microwave spectrum (10). The role of ν_{13} in the spectrum will be discussed further at a later stage.

The second strongest band in the spectrum, J_0, 475 cm^{-1} above E_0 at 4820 Å, is assigned to excitation of one quantum of ν_{12}', the a_2 out-of-plane C=O bending vibration. We suggest that this band owes its strength to Herzberg–Teller intensity borrowing through vibronic coupling to a strong, higher-energy electronic transition. The lowest π^*–π state, which probably corresponds to the next allowed transition of CBD and can be expected to lie around 2000 Å, is a likely candidate for such coupling, and a consideration of the orbitals involved shows that this will be a $^1B_2$ state. Vibronic coupling with this state requires an a_2 vibration which combines with the $^1B_1$ upper state of the π^*–n_+ transition to give a vibronic state of the same B_2 symmetry species. The only a_2 vibrational mode of the right frequency for the J_0 band appears to be ν_{12}'.

Support for this assignment for J_0 comes from the absence of

TABLE 2. Infrared spectrum of 1,2-cyclobutanedione

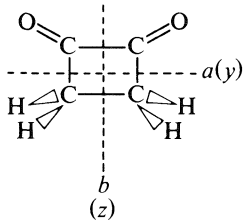

ν (cm^{-1})	Band type	Strength	Assignment
~3630	?	Weak	$2\nu_{19}$
~3575	*B*	Weak	$2\nu_2$
3005	*A*	Medium	ν_{18}, asym. C—H stretch (b_2)
2956	*C*	Medium	ν_{14}, asym. C—H stretch (b_1)
~2865	*B*(?)	Weak	$2\nu_3$ (or ν_1, sym. C—H stretch (a_1))
~1960	?	V. weak	
~1920	?	Weak	
1881	*B* or *C*	Weak	
1821	*A*	Strong	ν_{19}, asym. C=O stretch (b_2)
1787	*B*	V. strong	ν_2, sym. C=O stretch (a_1)
1427	*B*	Medium	ν_3, sym. C—H scissors (a_1)
~1260	?	Weak	ν_{20}, asym. C—H scissors (b_2) (?)
~1101	*B*(?)	Weak	ν_5 + 49 (?)
1052	*B*	Strong	ν_5, ring distortion (a_1)
~1013	*C*	Weak	ν_{15} + 51 (?)
962	*C*	Medium	ν_{15}, sym. C—H wag (b_1)
918	*B*	Medium	ν_6, sym. CH_2 rock (a_1)
~854	*C*(?)	Weak	ν_{16}, CH_2 wag + C=O wag (b_1)
~756	?	Weak	ν_{21}, ring distortion (b_2)
702	*A*	Medium	ν_{22}, ring distortion (b_2)
~637	*A*(?)	Weak	ν_{23}, asym. CH_2 rock (b_2)

strong bands corresponding to $v'_{12} = 2$, 3, etc., expected if J_0 were simply the first member of a progression in a symmetric mode. (A weak band, P_0, may correspond to $v'_{12} = 3$, in which ν_{12} would again act as an inducing mode; there is no band at the wavelength expected for $v'_{12} = 2$, where it would not.) Further evidence that J_0 is induced by vibronic coupling is the distinctly different band profile, compared to E_0, which is expected from the different vibronic symmetry of the excited state (Figs. 1, 2). It is interesting that the spectrum of *trans*-glyoxal (1) and probably of *cis*-glyoxal (5, 14) also show strong bands induced by vibronic coupling involving an out-of-plane bending vibration.

The band designated F_0 at 4865 Å, 284.4 cm^{-1} above the origin, has been assigned to ν'_8, the symmetric, in-plane carbonyl bending mode; in *cis*-glyoxal the corresponding ν''_5 is 284.5 cm^{-1} in the ground state (5). The same vibration is also active in a number of combination bands, K_0, M_0, j_0, U_0, p_0, X_0, and s_0, and in the band *ss* assigned as 8_0^2.

The band I_0, 457.1 cm^{-1} above the origin, is attributed to ν'_7, an in-plane ring distortion that might be expected to be excited by a change in the C_1—C_2 bond length. The same vibration shows up more clearly in L_0 in combination with ν'_{12}, and in the other combination bands k_0, n_0, q_0, and Y_0. A weak broad band, N_0, 1155 cm^{-1} above the origin, has been assigned to a second in-plane ring vibration, ν'_4, the symmetric breathing mode.

The band R_0, 1592.7 cm^{-1} above the origin, is assigned to ν'_2, the symmetric C=O stretching vibration, which is also excited in the combination bands T_0, W_0, and Z_0 and is a common feature of most $\pi^* \leftarrow$ n transitions. The band V_0 is assigned to ν'_1, the symmetric C—H stretching vibration, with a frequency of 2958 cm^{-1}.

It remains to discuss the bands observed to the red of the origin, and related bands throughout the spectrum. The band A_0, 488.4 cm^{-1} from the origin, has been assigned to absorption from the $v''_{12} = 1$ level in the ground state. This is supported by the frequency (close to ν'_{12}), by the band profile, which resembles that of J_0, and by its strength, which is greater than predicted from the Boltzmann factor but can be explained by the action of ν_{12} as a vibronic coupling mode as discussed earlier.

The band B_0 is assigned to ν''_8, a symmetric vibration also actively excited in the upper state. The band m_0, lying 280 cm^{-1} to red of V_0, is also assigned to ν''_8. The band C_0 has been assigned to ν''_{13} (165.3 cm^{-1}), the ring-twisting vibration so prominent in many sequences throughout the spectrum, while it is also involved in the combination bands c_0, G_0, and P_0. The band D_0, 46.9 cm^{-1} from the origin, has been assigned as a 1,1 sequence band of ν_{24}, the asymmetric in-plane carbonyl bend, chosen chiefly because of its probable low frequency, but a sequence in some other vibration is almost equally possible. The same sequence seems to be involved in a dozen other combination bands listed in Table 1. The band g_0, 14.3 cm^{-1} to the blue of E_0, has been assigned as a sequence band of an unknown vibration X, and a number of similar bands lying about the same distance to the blue of other strong features have been given similar assignments. A number of other features even closer to several of the stronger bands are probably rotational structure. Finally, a very weak band, *bb*, 527 cm^{-1} to the red of E_0, is assigned to ν''_7, a ring-distortion vibration; the

TABLE 3. Fundamental vibrations of 1,2-cyclobutanedione*

C_{2v} species	No.	Description	ν (cm^{-1})	Source
a_1	1	Sym. C—H stretch	~3000	Estimate, cf. ν_{14}, ν_{18}
	2	Sym. C=O stretch	1787	Infrared
	3	Sym. C—H bend, ⊥, scissors	~1427	Infrared
	4	Sym. C—C stretch, breathing	~1152	Fluorescence
	5	Ring distortion, //, 	1052	Infrared
	6	Sym. CH_2 rock, // 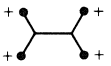	918	Infrared
	7	Ring distortion, //, 	527	Fluorescence
	8	Sym. C—C=O bend, //	281	B_0 hot band, visible
a_2	9	Asym. C—H stretch 	~3000	Estimate, cf. ν_{14}, ν_{18}
	10	Asym. CH_2 wag, ⊥ 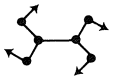	~1230	Estimate cf. cyclobutane
	11	C—H bend 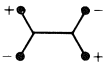	~1220	Estimate (1234, 1225)
	12	Asym. C—C=O bend, ⊥, wag	488	A_0 hot band, visible
	13	Ring twist 	165	C_0 hot band, visible
b_1	14	Asym. C—H stretch 	2956	Infrared
	15	Sym. CH_2 wag, ⊥ 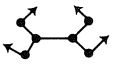	962	Infrared
	16	CH_2 wag + C—C=O wag, ⊥	~854	Infrared
	17	Sym. C—C=O wag, ⊥	~500	Estimate, cf. ν_{12}
b_2	18	Asym. C—H stretch 	3005	Infrared
	19	Asym. C=O stretch	1821	Infrared
	20	C—H bend, asym. scissors, ⊥	~1260	Infrared
	21	Ring distortion, // 	~756	Infrared
	22	Ring distortion, // 	~702	Infrared (uncertain)
	23	Asym. CH_2 rock, // 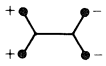	~637	Infrared
	24	Asym. C—C=O bend //	250	Estimate, cf. ν_8

*Symbols ⊥ and // refer to molecular (skeletal) plane. Infrared and visible spectra data from present work, fluorescence data from ref. 13.

same band has also been observed in the emission spectrum of CBD (13) where it is much stronger. Many of the other bands to the red of the origin have also been seen in emission.

The role of the ν_{13} ring-twisting vibration in the spectrum requires some further comment. There is little doubt about the assignment of the many regular sequences throughout the spectrum to this vibration. There is some doubt, however, about the assignment of C_0 as 13_1^0, with $\nu''_{13} = 165.3\,cm^{-1}$, and the alternative assignment of D_0 as 13_1^0, with $\nu''_{13} = 46.9\,cm^{-1}$, was given serious consideration. In favour of the D_0 assignment was the approximate agreement with a value of about $50\,cm^{-1}$ for ν''_{13} that can be obtained from a Boltzmann factor estimated from the ratio of intensities E_1/E_0 or J_1/J_0, and with a value of 68 (±30) estimated in a similar way from microwave "satellite" bands (10). On the other hand, 46.9 cm^{-1} seems very low for the observed sequence interval of 72 cm^{-1}, which would lead to an exceptionally large percentage change in frequency between the ground and excited states. This frequency also seems low for the relatively stiff ring expected in CBD, planar in both states, not much higher than the frequency of 36 cm^{-1} found in the

TABLE 4. Energy levels of ν_{13} (cm^{-1}) derived from E_0–E_3 and C_0–C_3 sequences

1	165.3		236.9	
		(170.0)		(241.2)
2	335.3		478.1	
		(174.3)		(245.1)
3	509.6		723.2	
		(117.9)		
4	687.5			

TABLE 5. Vibrational frequencies (cm^{-1}) obtained from visible spectrum*

Vibration	Ground state	Excited state
ν_1 (C—H stretch)	—	2958 (V_0)
ν_2 (C=O stretch)	(1787)†	1592.7 (R_0)
ν_4 (ring breathing)	(1152)‡	1155 (N_0)
ν_7 (ring distortion)	527 (bb)	457.1 (I_0)
ν_8 (C=O in-plane bend)	281.2 (B_0)	284.4 (F_0)
ν_{12} (asym. C=O wag)	488.4 (A_0)	474.8 (J_0)
ν_{13} (ring twist)	165.3 (C_0)	236.9 (C_0–E_1)

*Bands from which data were obtained in parentheses.
†From ir spectrum.
‡From fluorescence (13).

much less rigid ring in cyclobutanone (15). A more convincing piece of evidence favoring the C_0 assignment for 13_1^0 is the significantly lower sequence interval in the C_0–C_5 sequence, compared with the E_0–E_3 sequence; the former sequence would then be 0,1, 1,2, etc., rather than 0,0, 1,1, etc., and a different interval is not unexpected. The D_0–D_2 sequence, on the other hand, shows the same sequence interval as the E_0–E_3 sequence. A second sequence, based on c_0, which we have assigned as $8_1^0 13_1^0$, also shows a reduced interval, close to that of the C_0–C_5 sequence, as expected from this assignment. From these observations, and the fact that frequencies based on Boltzmann factors can be notoriously unreliable, we have chosen to assign C_0 as 13_1^0 and D_0 as a 1,1 sequence band of ν_{24}. A low-frequency infrared spectrum would obviously be useful to confirm this assignment. From the two sequences, E_0–E_3 and C_0–C_5, energy levels for ν_{13} for both excited and ground states can be calculated and are shown in Table 4. Both states showed a modest regular negative anharmonicity, compatible with a relatively stiff ring structure in CBD, probably planar rather than quasi-planar in both states.

Finally, in Table 5 are summarized the fundamental vibrational frequencies of both excited and ground states determined in this study and in the recent measurement of the emission spectrum in this laboratory (13).

Acknowledgements

We are grateful to Dr. D. A. Ramsay of the Herzberg Institute of Astrophysics for use of the spectrographic equipment and for helpful discussions of the spectra, and to Mr. M. Barnett for photographing the visible spectrum. We also wish to thank Mr. D. J. Moffatt for assistance with the infrared measurements, and are grateful to Dr. J. M. Hollas of the University of Reading for useful discussions and advice on the interpretation of the visible spectrum.

1. G. HERZBERG. Electronic structure of polyatomic molecules. Van Nostrand, Reinhold, New York. 1966; F. W. BIRSS, D. B. BRAUND, A. R. H. COLE, R. ENGLEMAN, JR., A. A. GREEN, S. M. JAPAR, R. NANES, B. J. ORR, D. A. RAMSAY, and S. SZYSZKA. Can. J. Phys. **55**, 390 (1977) and references therein.
2. R. A. BACK. Can. J. Chem. **62**, 1414 (1984).
3. S. YAMAMOTO and R. A. BACK. Can. J. Chem. **63**, 549 (1985).
4. R. A. BACK and S. YAMAMOTO. Can. J. Chem. **63**, 542 (1985).
5. W. HOLZER and D. A. RAMSAY. Can. J. Phys. **48**, 1759 (1970); G. N. CURRIE and D. A. RAMSAY. Can. J. Phys. **49**, 317 (1971); R. Y. DONG and D. A. RAMSAY. Can. J. Phys. **51**, 1491 (1973).
6. J. M. CONIA and J. M. DENIS. Tetrahedron Lett. 2845 (1971).
7. R. A. BACK and J.-R. CAO. J. Photochem. **33**, 161 (1986).
8. J.-R. CAO and R. A. BACK. Can. J. Chem. **63**, 2945 (1985).
9. J. M. DENIS, J. CHAMPION, and J. M. CONIA. Org. Synth. **60**, 18 (1980).
10. A. C. LEGON. J. Chem. Soc. Faraday II, **75**, 651 (1979).
11. K. HAGEN and K. HEDBERG. J. Am. Chem. Soc. **103**, 5360 (1981).
12. P. SCHANG, R. GLEITER, and A. RIEKER. Ber. Bunsenges. Phys. Chem. **82**, 629 (1978).
13. R. A. BACK and J. M. PARSONS. Chem. Phys. Lett. **125**, 38 (1986).
14. D. A. RAMSAY. Private communication.
15. D. C. MOULE. J. Chem. Phys. **64**, 3161 (1976).

The mechanisms of long-range $^{13}C,^{19}F$ and $^{19}F,^{19}F$ coupling constants in derivatives of biphenyl and fluorene. Differential isotope shifts

TED SCHAEFER, JAMES PEELING,[1] AND GLENN H. PENNER
Department of Chemistry, University of Manitoba, Winnipeg, Man., Canada R3T 2N2

Received February 12, 1986

TED SCHAEFER, JAMES PEELING, and GLENN H. PENNER. Can. J. Chem. **64**, 2162 (1986).

$^{13}C,^{19}F$ and $^{19}F,^{19}F$ nuclear spin–spin coupling constants over n formal bonds, n = 1–9, are reported for 4-fluorobiphenyl, 4,4′-difluorobiphenyl, 4,4′-difluoro-2,2′,6,6′-tetramethylbiphenyl, 2,7-difluorofluorene, 2-fluoro-9-fluorenone, and 2,7-difluoro-9-fluorenone in acetone solutions. The signs of many of the coupling constants are deduced from second-order spectral phenomena caused by differential ^{13}C isotope effects on the ^{19}F nmr chemical shifts. Theoretical potentials, based on geometry-optimized STO 3G MO computations for 4-fluorobiphenyl and 4,4′-difluorobiphenyl, yield expectation values for the torsion angles about the exocyclic C—C linkage that are very close to those deduced from electron diffraction patterns. These potentials and INDO MO FPT computations of the long-range coupling constants allow a discussion of the coupling mechanisms. In Hz, $^9J(F,F) = 1.3(1)\cos^2\theta$, where θ is zero for a planar biphenyl, while $^8J(C,F) = 0.8(1)\cos^2\theta$ and $^7J(C,F) = -0.43(5)\cos^2\theta$. $^6J(C,F)$ is a composite of $\sigma-\pi$ and π electron coupling components and is written in Hz as $0.57(1) + 0.29(1)\sin^2\theta$. The corresponding coupling constants in the fluorene and 9-fluorenone derivatives are enhanced in magnitude relative to a hypothetical planar biphenyl derivative. It is tentatively suggested that $^5J(C,F)$ consists of three coupling components, one negative and proportional to $\cos^2\theta$, the other two positive and independent of θ. $^4J(C,F)$ is suggested to consist of a σ component of -1.0 Hz and a π component proportional to the atom–atom polarizability for the parent hydrocarbon.

TED SCHAEFER, JAMES PEELING et GLENN H. PENNER. Can. J. Chem. **64**, 2162 (1986).

Opérant dans des solutions dans l'acétone, on a mesuré les constantes de couplage nucléaires $^{13}C,^{19}F$ et $^{19}F,^{19}F$ à travers n liaisons (n = 1–9) dans le fluoro-4 biphényle, le difluoro-4,4′ biphényle, le difluoro-4,4′ tétraméthyl-2,2′,6,6′ biphényle, le difluoro-2,7 fluorène, la fluoro-2 fluorénone-9 et la difluoro-2,7 fluorénone-9. On a déduit les signes de plusieurs des constantes de couplage à partir d'un phénomène spectral du deuxième ordre qui est causé par des effets isotopiques ^{13}C différentiels sur les déplacements chimiques rmn du ^{19}F. Les potentiels théoriques, basés sur des calculs d'orbitales molécules STO 3G optimisés pour la géométrie, conduisent à des valeurs attendues pour les angles de torsion autour de la liaison C—C exocyclique qui sont en accord avec celles que l'on peut déduire à partir de données de diffraction des rayons-X. Sur la base de ces potentiels ainsi que sur la base de calculs d'orbitales moléculaires INDO FPT des constantes de couplage à longue distance, on peut discuter des mécanismes de couplage. Si l'on exprime les constantes de couplage en Hz, $^9J(F,F) = 1{,}3(1)\cos^2\theta$ (θ est égal à zéro dans un biphényle plan) alors que $^8J(C,F) = 0{,}8(1)\cos^2\theta$ et $^7J(C,F) = -0{,}43(5)\cos^2\theta$. Le couplage $^6J(C,F)$ est composé de couplages $\sigma-\pi$ ainsi que de couplages d'électrons π et il est égal à $0{,}57(1) + 0{,}29(1)\sin^2\theta$. Les amplitudes des constantes de couplage correspondantes dans les dérivés du fluorène et de la fluorénone-9 sont plus grandes que celles qui sont prévues en faisant l'hypothèse qu'il s'agit de dérivés biphénylés plans. On suggère que le couplage $^5J(C,F)$ comporte trois composantes : une serait négative et proportionnelle à $\cos^2\theta$ alors que les deux autres seraient positives et indépendantes de θ. On suggère que $^6J(C,F)$ comporte une composante σ de $-1{,}0$ Hz et une composante π qui est proportionnelle à la polarisabilité atome–atome de l'hydrocarbure de base.

[Traduit par la revue]

Introduction

The form of the potential governing the hindered rotation about the carbon–carbon bond linking the benzene rings in biphenyl has been investigated extensively by theory and experiment. Recent reviews are available (1, 2), so that a compilation of references is unnecessary here. Briefly, biphenyl is nearly planar in the crystal below 40 K and twists about the linking C—C bond by about 44° in the vapor phase. The hindering potential certainly contains twofold and fourfold components, but sixfold and eightfold components may also be present (3). In the presence of substituents *ortho* to the linking C—C bonds, the angle of twist increases. Sufficiently bulky substituents lead to a perpendicular arrangement of the two phenyl planes (4–11).

Although ^1H and ^{13}C nmr chemical shifts (12–20), dipolar couplings in ordered solvents (8, 9, 21), and multiple quantum nmr spectra (22) have been studied as indicators of the conformations of biphenyl and its derivatives in solution, little or no use has been made of long-range spin–spin couplings as conformational indicators in such compounds. Long-range $^{13}C,^{19}F$ couplings are informative about the conformational preferences of 4-fluorophenyl derivatives of methane, ethene, and other compounds (23). Their precise measurement is relatively easy.

In this study, the long-range couplings $^nJ(C,F)$ over six to eight bonds (n = 6, 7, 8) in 4-fluorobiphenyl, 4,4′-difluorobiphenyl, and in 4,4′-difluoro-2,2′,6,6′-tetramethylbiphenyl are investigated as to their dependence on the twist angle, θ, about the linking C—C bond. Because the θ dependence of the hindering potential is not simple, the measurement of $J(C,F)$ is combined with extensive geometry-optimized STO 3G MO calculations. These yield potential functions that can be used to compute average or expectation values of θ and of functions of θ. INDO MO FPT computations of the long-range $J(C,F)$ values, and of $^9J(F,F)$ in 4,4-difluorobiphenyl, indicate the form of their θ dependence, if not their correct extrema. A combination of the experimental and theoretical data allows reasonable semiquantitative deductions about the coupling mechanisms.

Measurements of chemical shifts in fluorene have been taken to mimic those in planar biphenyl (12, 15). We report values for $^nJ(C,F)$ in 2,7-difluorofluorene, the corresponding

[1]University of Petroleum and Minerals, Dhahran, Saudi Arabia.

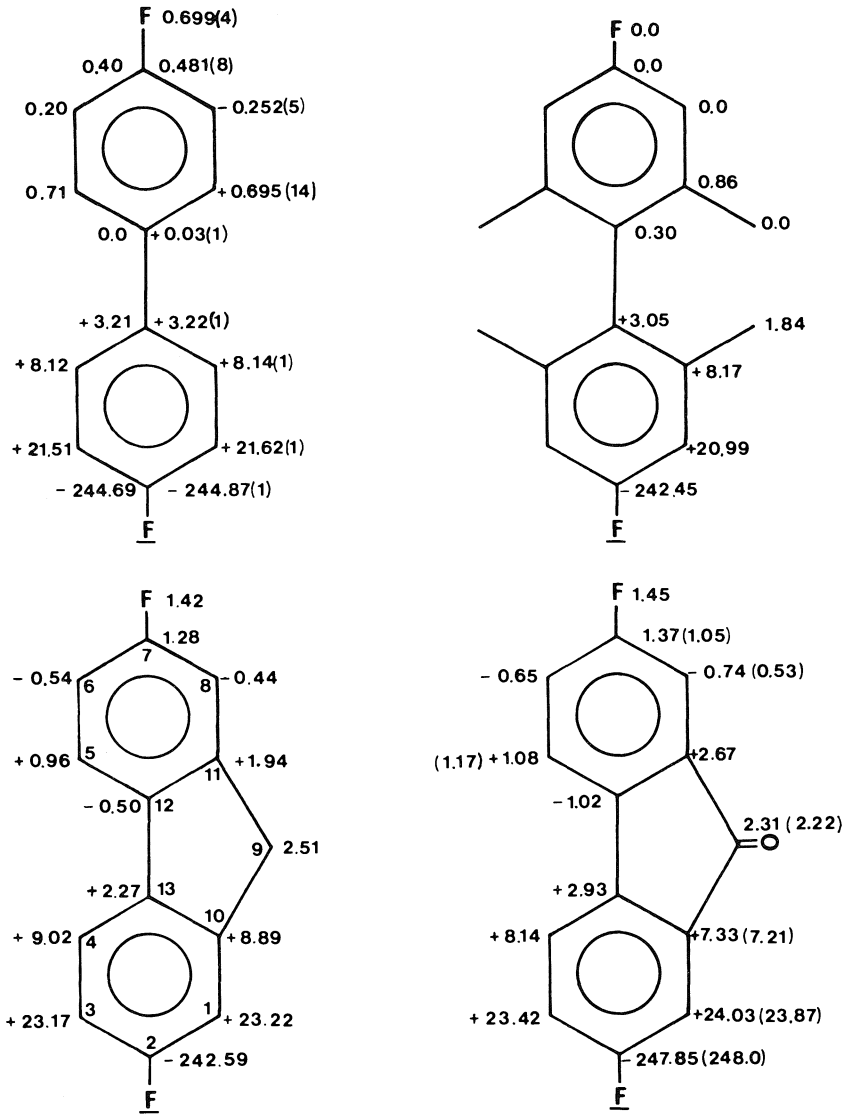

SCHEME 1. The coupling constants to ^{13}C and ^{19}F in Hz are given for the underlined ^{19}F nucleus. The signs are given when known. For the 4,4′-difluorobiphenyl the coupling constants are given on the right and, on the same structure, are given on the left for 4-fluorobiphenyl. The atoms in 2,7-difluorofluorene are numbered in the same way as for 2-fluorofluorene (29). The coupling constants in the latter (29) differ very little from those in the difluoro derivative. One significant difference is that to C-7, being 1.01 Hz in the former. Similarly, in the 2-fluoro-9-fluorenone, this coupling is 1.05 Hz and that to C-8 is 0.53 Hz. For the latter, the coupling constants are given in parentheses if they differ by more than 0.03 Hz from those in the difluoro derivative.

9-fluorenone, and in 2-fluoro-9-fluorenone. The presence of differential ^{13}C isotope effects on ^{19}F chemical shifts allows the determination of the signs of many of the $^{n}J(C,F)$.

Experimental

4-Fluorobiphenyl, 4,4′-difluorobiphenyl, 2,7-difluorofluorene, and 2-fluoro-9-fluorenone came from Aldrich. The 2,7-difluoro-9-fluorenone was prepared from the fluorene derivative, of which 2 g in 10 mL of benzene were stirred at room temperature for 36 h with 10 mL of a 50 wt.% aqueous NaOH solution containing 0.1 g of benzyltriethylammonium chloride. A green precipitate formed, which was extracted with CH_2Cl_2 and evaporated to dryness, yielding 1.7 g of a yellowish green, fluffy powder. The ^{13}C nmr spectrum was consistent with the desired product. The 4,4′-difluoro-2,2′,6,6′-tetramethylbiphenyl was prepared (24) via the 3,3′,5,5′-tetramethylhydrazobenzene (obtained from 5-nitro-*m*-xylene) by rearrangement to 4,4-diamino-2,2′,6,6′-tetramethylbiphenyl, followed by the usual diazotization procedures.

Because of limited solubility the nmr samples were prepared as saturated solutions in acetone-d_6.

The ^{13}C and ^{19}F spectra were accumulated on WH-90 and AM-300 FFT Bruker spectrometers at a probe temperature of 300 K in a manner described previously (23).

Geometry-optimized STO 3G MO (25) computations employed the program MONSTERGAUSS (26) on an Amdahl 470/V8 system. This computer was also used for the INDO MO FPT computations (27, 28) of $^{n}J(C,F)$ and $J(F,F)$.

Results and discussion

The $^{n}J(C,F)$ values and $^{9}J(F,F)$ are given in Scheme 1, which presents the data in the most easily comprehensible form (note that n is determined by counting via the C_{sp^2}—C_{sp^2} linkage). The coupling magnitudes for 2-fluorofluorene were determined elsewhere (29). The signs of $^{5,6,7}J(C,F)$ were determined for the difluoro derivatives relative to $^{2,3,4}J(C,F)$, the latter being positive (29). The sign determination depended on $^{13}C/^{12}C$ isotope shifts for ^{19}F, $^{n}\Delta$. From the ^{19}F spectra, $^{n}\Delta$ (n = 1, 2, 3) were typically obtained as 80, 25, and 5 ppb, respectively. In

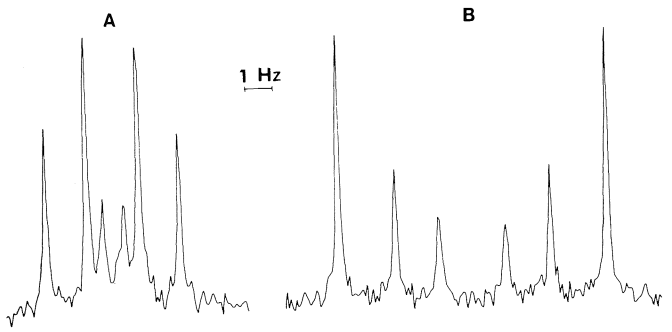

FIG. 1. In (A) is shown the $^{13}C\{^1H\}$ nmr spectrum of C-12 and C-13 in 2,7-difluoro-9-fluorenone as a saturated solution in acetone-d_6. The spectrometer frequency is 75.477 MHz and the probe temperature is 300 K. The difference in resonance frequencies of the ^{19}F nuclei is 0.478 Hz (1.69 ppb); $^9J(F,F)$ is $\pm 1.45(3)$ Hz. The six peaks of the ^{13}C nmr spectrum show that $^4J(C,F)$ and $^5J(C,F)$ are of opposite sign, as given in Scheme 1. Similarly, in (B) the six peaks of the ^{13}C nmr spectrum of C-10 and C-11 are consistent with equal signs of $^3J(C,F)$ and $^6J(C,F)$, the difference in resonance frequencies of the ^{19}F nuclei (differential isotope shift) being 1.55_6 Hz (5.51 ppb). The relative signs follow from an ABX analysis (52). Note also that the separation between the most intense peaks is equal to $^4J(C,F) + {}^5J(C,F)$ in (A) and $^3J(C,F) + {}^6J(C,F)$ in (B). $^4J(C,F)$ and $^3J(C,F)$ are of known sign and their magnitudes in the monofluoro derivative must be almost the same as in the difluoro derivative. Therefore the relative signs here follow by inspection.

the difluoro derivatives, a differential isotope shift gives rise to an ABX spectrum, the ^{19}F nuclei being represented as AB with an AB spin–spin coupling constant. If J_{AB}/ν_{AB} has the appropriate value, six peaks appear in the $^{13}C(X)$ nmr spectrum. The relative signs of J_{AX} and J_{BX}, that is, of the $^nJ(C,F)$ values, follow in a straightforward analysis. Their magnitudes can also be checked against the first-order splittings observed in the monofluoro derivatives. Figure 1 displays two typical ^{13}C nmr spectral patterns, from which relative signs can be deduced. The sign of $^8J(C,F)$ could not be determined in this way, nor could that of the coupling to ^{13}C in the CH_2 or C=O groups (symmetry).

The signs of the coupling constants are useful in the discussion of coupling mechanisms below. In addition, computations of the internal rotational potential in biphenyl and its derivatives, as well as of long-range $^nJ(C,F)$ values, are helpful and these are given next.

Theoretical internal barriers and $^{6,7,8}J(C,F)$

Geometry-optimized STO-3G MO computations of the internal rotational potential in biphenyl (3) yield $V(\theta) = \sum_{i=1}^{n} V_{2i} \sin^2 i\theta$ where n is the foldedness of the barrier component. A best fit (3) to the computed energies gave V_2, V_4, V_6, and V_8 as $-1.60(4)$, $-10.93(4)$, $-2.25(4)$, and $-0.43(4)$ kJ/mol, respectively. $\theta = 0$ corresponds to a planar molecule. For this potential, the classical expectation value, $\langle\theta\rangle$, is 43.8° at 300 K and $\langle\sin^2\theta\rangle$ is 0.447_5. As it happens, the latter is nearly the same as $\sin^2\langle\theta\rangle$ in this instance. In the gas phase, the best value of θ deduced from electron diffraction patterns is 44.4°, apparently the angle of maximum probability (1, 2).

A similar computation for 4-fluorobiphenyl, done at 15° intervals of the torsion angle, θ, gave a set of energies that could be best fit (judging by standard errors at the 95% confidence level) to a potential consisting of $-1.14(13)$, $-10.93(13)$, and $-2.34(13)$ kJ/mol for V_2, V_4, and V_6, respectively. Similarly, V_2, V_4, and V_6 were -0.62, -10.82, and -2.29 kJ/mol for 4,4′-difluorobiphenyl, again with an error of 0.13 kJ/mol. For 4-fluorobiphenyl the potential yields $\langle\sin^2\theta\rangle$ as 0.471 at 300 K, while it is 0.464 for the difluoro derivative. These potentials correspond to $\langle\theta\rangle$ values of 43°, compared to 45° from electron diffraction studies (2).

The INDO MO FPT numbers for $^{6,7,8}J(C,F)$ are given in Table 1, computed for the optimized STO 3G MO geometries. In view of previous experience with computed long-range H,F and C,F coupling constants (23, 30), it is anticipated that the form of their θ dependence will be reproduced by the theory, but that their magnitudes will be underestimated. The variation with θ of $^{6,8}J(C,F)$ appears to go roughly as $\sin^2\theta$ or $\cos^2\theta$ in Table 1.

The conformational implications of $^9J(F,F)$

In the difluorofluorene, $^9J(F,F)$ is $\pm 1.42(1)$ Hz and is $\pm 1.45(1)$ Hz in the corresponding fluorenone derivative, consistent with a coupling pathway over nine bonds via the C_{sp^2}—C_{sp^2} bond, unless the CH_2 and C=O groups are equally efficient as transmitters of spin-state information.

For 4-fluorobiphenyl, INDO MO FPT computations give $^9J(F,F)$ as positive, decreasing to zero as θ goes to 90° and varying approximately as $\cos^2\theta$ (footnote in Table 1). The theoretical values are much too small, as is often found for long-range couplings involving a C_{sp^2}—F bond (23, 30), but their qualitative θ dependence is indicative of an electron mechanism depending on $2p\pi$ overlap at the exocyclic C—C bond. This indication is confirmed by the vanishing $^9J(F,F)$ in 4,4′-difluoro-2,2′,6,6′-tetramethylbiphenyl, for which all available evidence suggests a θ of very near 90° and a large barrier to internal rotation, that is, that $\langle\cos^2\theta\rangle \sim 0$ (4, 8, 9, 11, 17, 31, 32).

Now, in 4,4′-difluorobiphenyl, $^9J(F,F)$ is 0.699(4) Hz. The theoretical potential implies a $\langle\cos^2\theta\rangle$ of 0.536 and therefore that $^9J(F,F)$ can be written as $^9J_0\langle\cos^2\theta\rangle$, where $^9J_0$ is ± 1.30 Hz. The $^9J(F,F)$ values for the fluorene derivatives imply $^9J_0$ as $\pm 1.4_3$ Hz. The magnitudes of $^9J_0$ in these compounds will presumably depend on the mobile bond orders ($2p\pi$ overlap) of the exocyclic C_{sp^2}—C_{sp^2} bonds and these need not be identical in biphenyl and fluorene.

The observed $^9J(F,F)$ values are consistent with $\langle\theta\rangle$ of 43–45° in 4,4′-difluorobiphenyl. Of course, the measurements are for acetone solutions.[2] Nevertheless, it appears that $^9J(F,F)$ is a π-electron transmitted coupling constant, going as $\cos^2\theta$, and that it is therefore a convenient conformational indicator. $^9J(F,F)$ is obtainable by procedures much less tedious than those presently employed in solution.

The mechanisms of $^nJ(C,F)$ for n = 6–8

For a π-electron mechanism the signs of $^{6,7,8}J(C,F)$ are expected to alternate. Then (Scheme 1) $^8J(C,F)$ is positive, as also indicated by the INDO MO results in Table 1. It follows that $^9J(F,F)$ is also positive because the hyperfine coupling parameter, which measures the spin polarization transfer from π to σ electrons, is positive (30, 35), in agreement with the theoretical sign. If $^9J(F,F)$ is proportional to $\cos^2\theta$, then

[2]A series of 4,4′-disubstituted biphenyls have θ values between 39.4 and 42.4° in their crystals (33), but θ cannot be determined accurately for 4,4-difluorobiphenyl (33, 34) because of disorder. The electron diffraction data (2) for the latter suggest about 45°, as noted above.

TABLE 1. INDO MO FPT values for $^{6,7,8}J$(C,F) in 4-fluoro- and 4,4′-difluorobiphenyl[a]

	^6J(C,F)/Hz		^7J(C,F)/Hz		^8J(C,F)/Hz	
θ/deg	4-F		4-F		4-F	
0	0.395	0.410	−0.297	−0.322	0.382	0.410
15	0.401	0.417	−0.268	−0.292	0.350	0.374
30	0.419	0.435	−0.196	−0.213	0.274	0.291
45	0.449	0.466	−0.101	−0.111	0.177	0.186
60	0.479	0.497	−0.006	−0.008	0.082	0.086
75	0.499	0.521	−0.066	−0.070	0.013	0.013
90	0.506	—	0.093	—	−0.013	—

[a] ^9J(F,F) varies from 0.12 to 0.00 Hz, approximately as $\cos^2\theta$ between 0 and 90°; θ = 0 for the planar form.

$^{7,8}J$(C,F) should also depend on $\cos^2\theta$.

Indeed, $^{7,8}J$(C,F) vanish in 4,4′-difluoro-2,2′,6,6′-tetramethylbiphenyl. In terms of the theoretical potentials, $^7J_0$ and $^8J_0$ are then −0.38 and 0.75 Hz in 4-fluorobiphenyl, respectively, and −0.48 and 0.90 Hz in 4,4′-difluorobiphenyl. The larger magnitudes in the latter compound can be attributed to the perturbation caused by a fluorine substituent near the end of the coupling path.[3]

However, these $^{7,8}J_0$ numbers are smaller in magnitude than those in the fluorene derivatives. If the latter are taken as correct for planar biphenyl, then $\langle\theta\rangle$ becomes about 39° for the biphenyl derivatives. That the presence of the CH_2 and C=O groups does alter the observed couplings, is clear from their values in Scheme 1. The idea that fluorene and perhaps fluorenone mimic a planar biphenyl is not quantitative. Nevertheless, it is very probable that $^{7,8}J$(C,F) are π-electron coupling constants and vary as $\cos^2\theta$ in biphenyl derivatives.

Turning to ^6J(C,F), it is known that, for sp^3 carbon atoms in the sidechain containing the coupled ^{13}C nucleus, ^6J(C,F) arises from a σ−π mechanism, proportional to $\sin^2\theta$ and involving hyperconjugation with the electron system of the aromatic moiety (23). If the sidechain carbon atom is sp^2 hybridized, then a π-electron mechanism can exist, depending on $2p\ldots2p\pi$ electron conjugation across the exocyclic bond, and proportional to $\cos^2\theta$. Accordingly, write eq. [1].

$$[1]\quad {}^6J(\mathrm{C,F})/\mathrm{Hz} = {}^6J_{90}^{\sigma,\pi}\langle\sin^2\theta\rangle + {}^6J_0^{\pi}\langle 1-\sin^2\theta\rangle = {}^6J_0^{\pi} + ({}^6J_{90}^{\sigma,\pi} - {}^6J_0^{\pi})\langle\sin^2\theta\rangle$$

If the numbers in Table 1 for 4,4′-difluorobiphenyl were correct, then $^6J_0^{\pi}$ would be 0.41 Hz and $^6J_{90}^{\sigma,\pi}$ would be 0.52 Hz. As noted above, their magnitudes are most likely too small.

Now, in the tetramethyl compound, ^6J(C,F) is 0.856(2) Hz. Because $\langle\sin^2\theta\rangle$ must be near unity, $^6J_{90}^{\sigma,\pi}$ is near 0.86 Hz in eq. [1]. Further, if the computed internal rotational potential holds for 4,4′-difluorobiphenyl, then the observed ^6J(C,F) of 0.70 Hz and the $\langle\sin^2\theta\rangle$ of 0.464 imply a $^6J^{\pi}$ of 0.56 Hz, yielding eq. [2] for ^6J(C,F).

$$[2]\quad {}^6J(\mathrm{C,F})/\mathrm{Hz} = 0.86\langle\sin^2\theta\rangle + 0.56\langle\cos^2\theta\rangle = 0.56 + 0.30\langle\sin^2\theta\rangle$$

[3] For ^8J(C,F) the attached fluorine atom contracts the 2*s* orbital on the carbon, increasing the contact contribution to the coupling constant, while for ^7J(C,F) the π donation by fluorine increases the π-electron density at carbon.

For 4-fluorobiphenyl the same reasoning yields eq. [3].

$$[3]\quad {}^6J(\mathrm{C,F})/\mathrm{Hz} = 0.86\langle\sin^2\theta\rangle + 0.58\langle\cos^2\theta\rangle = 0.58 + 0.28\langle\sin^2\theta\rangle$$

It seems certain that $^6J_{90}^{\sigma,\pi} > {}^6J_0^{\pi}$, the reverse of the situation in styrene (23) and probably sensible because, in contrast to biphenyl, in styrene the pathway for $^6J^{\pi}$ involves a sidechain C=C bond with a mobile bond order of very near unity. The ratio of the computed $^6J_{90}^{\sigma,\pi}$ in Table 1 to that in eq. [3] is 0.59, almost exactly that for the corresponding numbers for 4-fluorophenylethane (23). Because of the interference between the two coupling mechanisms, the change in ^6J(C,F) caused by rotation about the exocyclic C—C bond is small, varying between 0.6 and 0.9 Hz as θ goes from 0 to 90°.

^nJ(C,F) in the fluorene derivative

While the θ dependence of $^{6,7,8}J$(C,F) and ^9J(F,F) in the biphenyl derivatives is rather simple and the magnitudes of these couplings at 90° can be reasonably inferred from the tetramethyl derivative, their magnitudes at 0° are somewhat uncertain. The latter are estimated above from the theoretical potentials. Suppose, however, that in acetone solution $\langle\theta\rangle$ is rather less than in the gas phase. Intramolecular magnetic dipolar splittings for 4,4′-dichlorobiphenyl dissolved in anisotropic media (8) imply a θ of 31.8°, actually smaller than the 39.4° found in the solid (33). The vibrational spectra of 4,4′-difluorobiphenyl indicate that θ is much the same as in biphenyl, 35–40°, both in solution (36).

Suppose now that $\langle\theta\rangle$ is as low as 30° for the two fluorine derivatives of biphenyl in solution and suppose that $\langle\cos^2\theta\rangle$ is near 0.75. Then ^9J(F,F) at 0° is 0.93 Hz while ^6J(C,F), ^7J(C,F), and ^8J(C,F) become 0.65, −0.27, and 0.53 Hz, respectively, at 0° for 4-fluorobiphenyl. These numbers deviate markedly from those measured in 2-fluorofluorene and 2,7-difluorofluorene (Scheme 1). The deviations are larger than those obtained with the theoretical internal rotational potentials.

Indeed, if the fluorene derivatives are taken as planar biphenyls, then the mechanism for ^6J(C,F) as given by eqs. [1]–[3] is incorrect; yielding $\langle\sin^2\theta\rangle$ as greater than unity in 4-fluorobiphenyl, for example, when the coupling constant to C-5 is employed.

This discussion implies that, for C,F coupling constants, the fluorene derivatives do not mimic planar biphenyl. The exocyclic C_{sp^2}—C_{sp^2} bond lengths in biphenyl, fluorene, and 9-fluorenone are 1.494(3), 1.486(6), and 1.475(5) Å, respectively (4, 37–39), in the solid state. If the $^{6,7,8}J$(C,F) depend on the mobile bond order of this linkage, then their apparent increase in magnitude in going from "planar" biphenyl to fluorene and 9-fluorenone is rationalized. Of course, this rationalization does not prove that the CH_2 and C=O groups are non-transmitters of π-electron spin-state information in these molecules (see below). Note, however, that coupling to C-5, formally a ^6J(C,F) if considered as transmitted via the C_{sp^2}—C_{sp^2} linkage, becomes a ^7J(C,F) or a ^9J(C,F) if the π-electron coupling goes via the C=O or CH_2 moieties. Presumably these pathways should provide a negative contribution to this coupling constant. Yet the coupling is large and positive. Similar remarks apply to the coupling constants involving C-6 and C-7.

Turning to the coupling constants involving the nonprotonated carbon atoms, note first that ^4J(C,F) in fluorobenzene is 3.20 Hz and has a large positive π-electron component (40). ^4J(C,F) has the same values in the two biphenyl derivatives

TABLE 2. Differential isotope shifts for ^{19}F caused by ^{13}C, in Hz at 282.363 MHz

Compound	$^1\Delta \pm {}^8\Delta$[a]	$^2\Delta \pm {}^7\Delta$	$^3\Delta \pm {}^6\Delta$		$^4\Delta \pm {}^5\Delta$
4,4′-DiF-biphenyl	23.77	6.62	1.309		0.679
2,7-DiF-fluorene	23.03	6.14[d]	1.134[b]	1.484[c]	0.698
2,7-Di-F-9-fluorenone	24.47	7.63[d]	1.002[b]	1.556[c]	0.478

[a] $^n\Delta$ is the shift to low frequency (high field) cause by ^{13}C situated n bonds away from ^{19}F counting via the C_{sp^2}—C_{sp^2} linkage. If all $^n\Delta$ have the same sign as $^1\Delta$, then the negative sign applies.
[b] For C-4 in Scheme 1.
[c] For C-10 in Scheme 1.
[d] These are the averages for C-1 and C-3. $^1\Delta \pm {}^8\Delta$ and $^2\Delta \pm {}^7\Delta$ are determined from the ^{19}F nmr spectra. The other shifts are obtained from the analysis of the ^{13}C nmr spectra.

above and in derivatives of 4-fluorotoluene (23), and changes by less than 0.1 Hz in 4-fluorostyrene (23). Yet in the fluorene derivatives ^4J(C,F) drops to 2.3 Hz. In the tetramethylfluorene compound, ^4J(C,F) is 3.05 Hz.

It is interesting, therefore, that 13 values of ^4J(C,F) in alternant and nonalternant hydrocarbon derivatives (29) correlate significantly with the mutual atom–atom polarizabilities computed (41) for the parent hydrocarbons, as in eq. [4]. A

$$[4] \quad {}^4J(\mathrm{C,F}) = -0.98 + 40.24\,\pi_{pp'} \quad (r = 0.922)$$

precedent for such a correlation between the π-electron contribution to a coupling constant and the atom–atom polarizability, $\pi_{pp'}$, exists for the orthobenzylic coupling constant, $^4J(\mathrm{H,CH_3})$, in toluene derivatives (42). Equation [4] includes the diphenyl derivatives in this paper. The value of −0.98 Hz is then an estimate of the σ-electron contribution to ^4J(C,F). Now, if fluorene is conceived as an analog of the nonalternant hydrocarbon, dibenzofulvene (take the carbon atom of the methylene group as sp^2 hydridized and take appropriate linear combinations of the hydrogen orbitals to simulate a π-type orbital on the exocyclic methylene carbon atom of fulvene), then $\pi_{pp'}$ is 0.083 (41). Equation [4] yields ^4J(C,F) as 2.36 Hz compared with the observed value of 2.27 Hz (29).

In terms of this model, the methylene moiety in fluorene hyperconjugates with the aromatic π-electron system[4] and is therefore not a good mimic of planar biphenyl.

Unpublished work in this laboratory on long-range ^nJ(C,F) in derivatives of 4-fluoroacetophenone strongly implies that the carbonyl group is a relatively weak transmitter of π-electron spin-state information. In that event the ^4J(C,F) of 2.92 Hz in the 9-fluorenone derivatives is reasonable. On the other hand, the carbonyl moiety definitely enhances σ-electron coupling magnitudes and hence the ^5J(C,F) of 2.65 Hz to C-11 in these compounds is expected and observed to be larger than the corresponding ^5J(C,F) of 1.99 Hz in the fluorene compounds in Scheme 1. These ^5J(C,F) values, of course, also contain positive six-bond π-electron contributions via the C_{sp^2}—C_{sp^2} linkage. The notation, ^5J(C,F), used for C-11 coupling constants, forms an exception to the notation used elsewhere in this paper and is meant to emphasize the likelihood of a large positive σ-electron component.

The ^5J(C,F) values for the carbon-13 nucleus in the C_{sp^2}—C_{sp^2} linkage can be discussed as follows. The π-electron contribution to ^5J(C,F) is negative, being positive for ^4J(C,F) above. Schematically, as in **1**, it is known that the signs of the hyperfine interaction constants are $Q^F_{CF} > 0$, $Q^C_{CC} > 0$, and $Q^C_{C'C} < 0$ (44). Hence the indicated π-electron spin polarizations caused by

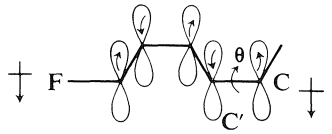

1

the ^{19}F magnetic moment all result in a negative $^5J^\pi$. The σ-electron contribution to ^5J(C,F) will be positive, as, for example, for ^5J(H,F) in fluorobenzene (29, 45). In the fluorene and fluorenone derivatives, ^5J(C,F) is indeed negative, implying that $|^5J^\pi| > |^5J^\sigma|$ when $\theta = 0°$. Assume that this relationship holds for biphenyl derivatives.

Now, as θ increases, the $2p\ldots2p\pi$ overlap decreases. The π-electron contribution originating in Q^C_{CC} will diminish, probably as $\cos^2\theta$. If $^5J^\sigma$ does not change, then ^5J(C,F) will decrease in magnitude. Indeed, ^5J(C,F) is +0.03 Hz in 4,4′-difluorobiphenyl, implying a near cancellation of the composite $^5J^\pi$ and the $^5J^\sigma$ near 45°. In the tetramethyl derivative, ^5J(C,F) is ±0.30 Hz. Unfortunately its sign is unknown and cannot be determined via differential isotope shifts because ^9J(F,F) vanishes in this compound. The model implies that ^5J(C,F) is positive, assuming that the methyl substituents do not alter the individual components except via their determination of θ as near 90°.

The model implies eq. [5]

$$[5] \quad {}^5J(\mathrm{C,F}) = {}^5J^\pi_0\langle\cos^2\theta\rangle + {}^5J^\pi_0 + {}^5J^\sigma$$

in which $^5J^\pi_0$ is the coupling constant arising from Q^C_{CC}, that is, from the π-electron density centered on the atom containing the coupled nucleus (see **1**). $^5J^\pi_1$ arises from $Q^C_{C'C}$. In the fluorene derivative $\langle\cos^2\theta\rangle$ is unity, whereas it is near zero in the tetramethyl compound. Taking $^5J^\pi_1 + {}^5J^\sigma$ as +0.30 Hz, yields $^5J^\pi_0$ as −0.80 Hz. Application of eq. [5] to 4,4′-difluorobiphenyl implies a $\langle\cos^2\theta\rangle$ of 0.41 or a $\langle\theta\rangle$ of 50°, instead of the 43° derived from the STO 3G MO computations.

Alternatively, the theoretical potential for 4,4′-difluorobiphenyl implies $^5J^\pi_0$ as −0.50 Hz and ^5J(C,F) in the planar form as −0.20 Hz. A plot of ^5J(C,F) versus the length of the C_{sp^2}—C_{sp^2} linkage in biphenyl, fluorene, and 9-fluorenone, assuming linearity over such a small change in length (see values above), yields ^5J(C,F) as −0.10 to −0.20 Hz, depending on how near planarity biphenyl is in the crystal (46). This rationalization is consistent with the apparently enhanced magnitudes of the long-range ^nJ(C,F) and J(F,F) values in the fluorene and 9-fluorenone derivatives, as discussed above. Clearly, the available structural information is insufficient to settle the coupling mechanism and eq. [5] remains tentative. Ideally, a series of 4,4-difluorobiphenyl derivatives with a range of θ values are needed.

[4] See a similar treatment of cyclopentadiene by Mulliken (43).

Finally, ^4J(C,F) for the methyl groups is ± 1.84 Hz. Because of the zigzag or omega (ω) arrangement of the intervening bonds, this coupling is probably dominated by a σ-electron mechanism. This could also be true for the ^4J(C,F) of 2.51 Hz in the fluorene derivative. The vanishing ^7J(C,F) in the tetramethyl derivative reflects a θ near 90° and a $\sigma-\pi$ (hyperconjugative) coupling interaction with the contiguous ^{13}C nucleus in the benzene ring as described in eq. [3]. Hence no ^7J(C,F) is expected, just as in 4-fluoro-*n*-propylbenzene, for example (23), and its absence can be taken as confirmation of the model represented by eq. [3].

Differential isotope shifts

$^1\Delta$ lies between 81 and 93 ppb in the mono and poly fluorobenzenes (47–51) and $^1\Delta \pm {}^8\Delta$ in Table 2 falls into this range, as expected. $^2\Delta \pm {}^7\Delta$ in Table 2 varies from 21.7 to 27.0 ppb, also within the reported range of the seven values found for $^2\Delta$ in the fluorobenzenes. Again, $^3\Delta$ in the difluorobenzenes samples values between 1.4 and 6 ppb, whereas $^3\Delta \pm {}^6\Delta$ brackets 3.5 and 5.5 ppb in Table 2. In 1,3-difluorobenzene, $^4\Delta$ is 4 ppb and is as large as 8 ppb in 1,3,5-trifluorobenzene. $^4\Delta \pm {}^5\Delta$ in Table 2, however, ranges from only 1.7 to 2.5 ppb, suggesting a $^5\Delta$ of the same sign as $^4\Delta$. No $^5\Delta$ numbers appear to be available. Finally, the differential isotope shifts in Table 2 appear not to depend on θ.

Acknowledgements

We thank Dr. Alberta Lemire for the synthesis of 4,4′-difluoro-2,2′,6,6′-tetramethylbiphenyl and the Natural Sciences and Engineering Research Council of Canada for financial assistance.

1. A. Almenningen, O. Bastiansen, L. Fernholt, B. N. Cyvin, S. J. Cyvin, and S. Samdal. J. Mol. Struct. **128**, 59 (1985).
2. O. Bastiansen and S. Samdal. J. Mol. Struct. **128**, 115 (1985).
3. G. H. Penner. J. Mol. Struct. Theochem. **137**, 191 (1986).
4. G. Häfelinger and J. Strahle. Z. Naturforsch. B: Anorg. Chem. Org. Chem. Biochem. Biophys. Biol. **31**, 1155 (1976).
5. A. J. Grumadas, D. P. Poshkus, and A. V. Kiselev. J. Chem. Soc. Faraday Trans. 2, **78**, 2013 (1982).
6. L. D. Field, B. W. Skelton, S. Sternhell, and A. H. White. Aust. J. Chem. **38**, 391 (1985).
7. P. Singh and J. D. McKinney. Acta Crystallogr. Part B, **35**, 259 (1979).
8. L. D. Field, S. Sternhell, and A. S. Tracey. J. Am. Chem. Soc. **99**, 5249 (1977).
9. L. D. Field and S. Sternhell. J. Am. Chem. Soc. **103**, 738 (1980).
10. H. Suzuki. Bull. Chem. Soc. Jpn. **32**, 1340 (1959).
11. A. Modelli, G. Distefano, and D. Jones. Chem. Phys. **82**, 489 (1983).
12. W. Kitching, I. deJonge, W. Adcock, and A. N. Abeywickrema. Org. Magn. Reson. **14**, 502 (1980).
13. E. M. Schulman, K. A. Cristensen, D. M. Grant, and C. Walling. J. Org. Chem. **39**, 2686 (1974).
14. W. F. Reynolds and G. K. Hamer. J. Am. Chem. Soc. **98**, 7296 (1976).
15. R. M. G. Roberts. Magn. Reson. Chem. **23**, 52 (1985).
16. Y. Nomua and Y. Takeuchi. J. Chem. Soc. B, 956 (1970).
17. G. Häfelinger, M. Beyer, P. Burry, B. Eberle, G. Ritter, G. Westermayer, and M. Westermayer. Chem. Ber. **117**, 895 (1984).
18. R. E. Mayo and J. H. Goldstein. Mol. Phys. **10**, 301 (1966).
19. A. R. Tarpley, Jr. and J. H. Goldstein. J. Phys. Chem. **75**, 421 (1971).
20. T. Schaefer, T. A. Wildman, R. Sebastian, and D. M. McKinnon. Can. J. Chem. **62**, 2692 (1984).
21. W. Niederberger, P. Diehl, and L. Lunazzi. Mol. Phys. **26**, 571 (1973).
22. S. W. Sinton, D. B. Zan, J. B. Murdoch, and A. Pines. Mol. Phys. **53**, 333 (1984).
23. T. Schaefer, J. Peeling, G. H. Penner, A. Lemire, and R. Sebastian. Can. J. Chem. **63**, 24 (1985).
24. R. B. Carlin. J. Am. Chem. Soc. **67**, 928 (1945).
25. W. J. Hehre, R. Ditchfield, R. F. Stewart, and J. A. Pople. J. Chem. Phys. **52**, 2769 (1970).
26. M. R. Petersen and R. A. Poirier. MONSTERGAUSS. Department of Chemistry, University of Toronto, Toronto, Ontario. 1981.
27. J. A. Pople, J. W. McIver, and N. S. Ostlund. J. Chem. Phys. **49**, 2965 (1968).
28. P. Dobosh and N. S. Ostlund. QCPE, **11**, 281 (1975).
29. P. E. Hansen, A. Berg, H. J. Jakobsen, A. P. Manzara, and J. Michl. Org. Magn. Reson. **10**, 179 (1977).
30. R. Wasylishen and T. Schaefer. Can. J. Chem. **50**, 1852 (1972).
31. J. J. Dynes, F. L. Baudais, and R. K. Boyd. Can. J. Chem. **63**, 1292 (1985).
32. G. Bott, L. D. Field, and S. Sternhell. J. Am. Chem. Soc. **102**, 5618 (1980).
33. C. Pratt Brock, M.-S. Kuo, and H. A. Levy. Acta Crystallogr. Sect. B: Struct. Crystallogr. Cryst. Chem. **34**, 981 (1978).
34. T. K. Halstead, H. W. Spiess, and U. Haeberlen. Mol. Phys. **31**, 1569 (1976).
35. D. R. Eaton, A. D. Josey, W. D. Phillips, and R. E. Benson. Mol. Phys. **5**, 407 (1962).
36. R. J. Pulham and D. Steele. J. Raman Spectrosc. **15**, 217 (1984).
37. A. Hargreaves and S. H. Rivi. Acta Crystallogr. **15**, 365 (1962).
38. D. M. Burns and J. Iball. Proc. R. Soc. London, Ser. A, **227**, 200 (1955).
39. H. R. Luss and D. L. Smith. Acta Crystallogr. Sect. B: Struct. Crystallogr. Cryst. Chem. **28**, 884 (1972).
40. W. S. Brey, L. W. Jaques, and H. J. Jakobsen. Org. Magn. Reson. **12**, 243 (1979).
41. C. A. Coulson and A. Streitwieser, Jr. Dictionary of π-electron calculations. W. H. Freeman and Company, San Francisco. 1965.
42. M. Barfield, C. J. Fallick, K. Hata, S. Sternhell, and P. W. Westerman. J. Am. Chem. Soc. **105**, 2178 (1983).
43. R. S. Mulliken. J. Chem. Phys. **7**, 339 (1939).
44. M. Karplus and G. K. Fraenkel. J. Chem. Phys. **35**, 1312 (1961).
45. R. Wasylishen and T. Schaefer. Can. J. Chem. **49**, 94 (1971).
46. C. Pratt Brock and K. L. Haller. J. Phys. Chem. **88**, 3570 ((1984).
47. V. Wray, L. Ernst, and E. Lustig. J. Magn. Reson. **27**, 1 (1977).
48. W. S. Brey, K. H. Ladner, R. E. Block, and W. A. Tallon. J. Magn. Reson. **8**, 406 (1972).
49. P. E. Hansen. Annu. Rep. NMR Spectrosc. **15**, 105 (1983).
50. L. Ernst, D. N. Lincoln, and V. Wray. J. Magn. Reson. **21**, 115 (1976).
51. V. A. Chertkov and N. M. Sergeev. Zh. Strukt. Khim. **19**, 613 (1977).
52. R. J. Abraham. Analysis of high resolution nmr spectra. Elsevier, Amsterdam. 1971. pp. 58–83.

The pressure dependence of rates of homolytic fission of metal–ligand bonds in aqueous solution

KOJI ISHIHARA AND THOMAS WILSON SWADDLE
Department of Chemistry, The University of Calgary, Calgary, Alta., Canada T2N 1N4

Received May 13, 1986

KOJI ISHIHARA and THOMAS WILSON SWADDLE. Can. J. Chem. **64**, 2168 (1986).

The volume of activation for the exclusively homolytic decomposition of protonated 4-pyridylmethylchromium(III) ion in aqueous $HClO_4$ at 63.4°C is $+19\ cm^3\ mol^{-1}$, with negligible dependence on pressure up to 350 MPa at least. The origins of the strongly positive volumes of activation that characterize homolysis of complex cations in aqueous solution are examined.

KOJI ISHIHARA et THOMAS WILSON SWADDLE. Can. J. Chem. **64**, 2168 (1986).

Le volume d'activation uniquement de la décomposition homolytique de l'ion méthyl-4 pyridyl chrome(III) protoné, à 63,4°C et en solution dans du $HClO_4$ aqueux, est égal à $+19\ cm^3\ mol^{-1}$; cette valeur ne varie pratiquement pas avec la pression jusqu'à 350 MPa. On discute des origines des valeurs extrèmement positives des volumes d'activation qui caractérisent l'homolyse des cations complexes, en solutions aqueuses.

[Traduit par la revue]

Introduction

There are relatively few authenticated cases of homolytic fission of metal–ligand bonds in aqueous coordination chemistry, and most of them involve Cr—C σ-bonds in organochromium complexes of the type $(H_2O)_5CrR^{2+}$, the chemistry of which has been reviewed by Espenson (1). There are two primary mechanisms for the decomposition of these complexes in acidic aqueous solution: heterolysis, which would in principle give initially $Cr^{3+}(aq)$ and the carbanion R^- but actually seems to produce RH together with the conjugate base of $Cr^{III}(aq)$:

$$[1]\quad (H_2O)_5CrR^{2+} + H_2O \xrightarrow{k_A} Cr(H_2O)_5OH^{2+} + RH,$$

and homolysis which gives initially chromium(II) and the organic free radical R•:

$$[2]\ (H_2O)_5CrR^{2+} + H_2O \underset{k_{-H}}{\overset{k_H}{\rightleftharpoons}} Cr(H_2O)_6^{2+} + R^\bullet \rightarrow \text{etc.}$$

Homolytic decomposition can be suppressed by addition of sufficient chromium(II) ion, or it can be driven at the limiting rate set by the first-order rate constant k_H by adding a scavenger such as O_2 or Cu^{2+} to eliminate $Cr^{2+}(aq)$ and (or) R• (2, 3). Reaction [1], however, cannot be suppressed, and turns out to be important in the decompositions of most CrR^{2+} species in acidic aqueous solution (indeed, it is usually acid-catalyzed).

In two suitable cases (R = $CH(CH_3)_2$ and $C(CH_3)_2OH$) in which k_H and the rate constant k_A for reaction [1] are similar under ambient conditions, it proved to be possible to measure the pressure dependence of the rate constants to obtain the corresponding volumes of activation ΔV_H^* and ΔV_A^* (Table 1) (4). This is intriguing inasmuch as ΔV_H^* and ΔV_A^* refer to isomeric transition states (in essence, $\{(H_2O)_6Cr^{2+}\ldots R^\bullet\}^*$ and $\{(H_2O)_5CrOH^{2+}\ldots HR\}^*$) for the decomposition of a given species. As Table 1 shows, activation via the homolytic pathway involves a remarkable expansion whereas heterolysis does not, and this was attributed (4) to the necessity of breaking up the solvent cage in homolysis to separate Cr^{2+} from R• if recombination is to be avoided and net reaction observed — a restriction that is irrelevant to heterolysis, which forms the product RH directly and irreversibly.

The measured volume of activation for homolytic decomposition of $(H_2O)_5CrCH(CH_3)_2^{2+}$, however, decreased significantly with increasing pressure beyond 100 MPa (4), i.e., the plot of ln k_H against pressure was curved. Such curvature is a common phenomenon, and is often associated with solvational change in the activation process (5), which in this case could be related to break-up of the solvent cage (4). Nevertheless, data from the 100–300 MPa region which defined this curvature were susceptible to systematic errors because the fraction $k_H/(k_H + k_A)$ of the total rate constant for decomposition that was due to homolysis became small at high pressures.

We have therefore measured k_H over a wide range of pressure for a reaction for which k_A is negligible (i.e., for which homolysis is the only detectable reaction pathway), namely, the decomposition of the protonated 4-pyridylmethylchromium(III) aqua-ion, $(H_2O)_5CrCH_2C_5H_4NH^{3+}$, in oxygenated aqueous $HClO_4$ (2, 3, 6).

Experimental

The general preparative and kinetic procedures have been described elsewhere (2, 3, 6). Rate constants were measured *in situ* with a Cary Model 17H spectrophotometer at 308 nm and 63.4°C; the light beam was allowed to pass through the sample only long enough to make intermittent absorbance measurements, so as to avoid possible photolysis of the organochromium complex (although there was no indication that this was ever significant). Samples were saturated with pure oxygen gas at 0°C before each kinetic run. For runs at high pressure, the samples were contained in a le Noble-Schlott cell (7) and pressurized with water in an Aminco high-pressure optical cell.

Because the reactions were slow, especially at the higher pressures, the first-order rate constants k_H were calculated by the Kedzy–Swinbourne method (8) from optical absorbance data collected over the first four half-lives; standard deviations were typically about 0.3%, and values of k_H obtained at atmospheric pressure were in excellent agreement with published data (2, 3).

Results

Two to four measurements of k_H were made at each of ten pressures P ranging from 0.1 to 350 MPa. The results are summarized in the semilogarithmic plot (Fig. 1) in which the error bars show the *range* in ln k_H values. Clearly, ln k_H is quite adequately represented by the linear relationship

$$[3]\quad \ln k_H = \ln k_H^0 - (\Delta V_H^*/RT)P$$

which gives $\Delta V_H^* = +18.9 \pm 0.3\ cm^3\ mol^{-1}$ and the zero-pressure rate constant $k_H^0 = 1.50 \times 10^{-4}\ s^{-1}$ (±1.6%), with a

TABLE 1. Volumes of activation for heterolytic and homolytic decomposition of $(H_2O)_5CrR^{(2+x)+}$ in aqueous $HClO_4$

R^{x+}	$\Delta V_A^*/cm^3\ mol^{-1}$	$\Delta V_H^*/cm^3\ mol^{-1}$	$\Delta\beta_H^*/10^{-2}\ cm^3\ mol^{-1}\ MPa^{-1}$
$CH(CH_3)_2$[a]	-0.2 ± 0.2	$+24.2 \pm 1.8$[b]	$+5.9 \pm 1.4$
$C(CH_3)_2OH$[a]	$+0.3 \pm 0.2$[c]	$+15.1 \pm 1.6$	———
$CH_2C_5H_4NH^+$[d]	———	$+20.0 \pm 0.9$[b]	$+0.7 \pm 0.6$

[a]Reference 4; $[HClO_4] = 1.0–1.1\ mol\ L^{-1}$; 25.0°C except as stated.
[b]Low-pressure asymptotic value from quadratic fit (eq. [4]).
[c]15.0°C.
[d]This work; $[Cr] = 5.2 \times 10^{-5}\ mol\ L^{-1}$; $[HClO_4] = 0.026\ mol\ L^{-1}$; 63.4°C.

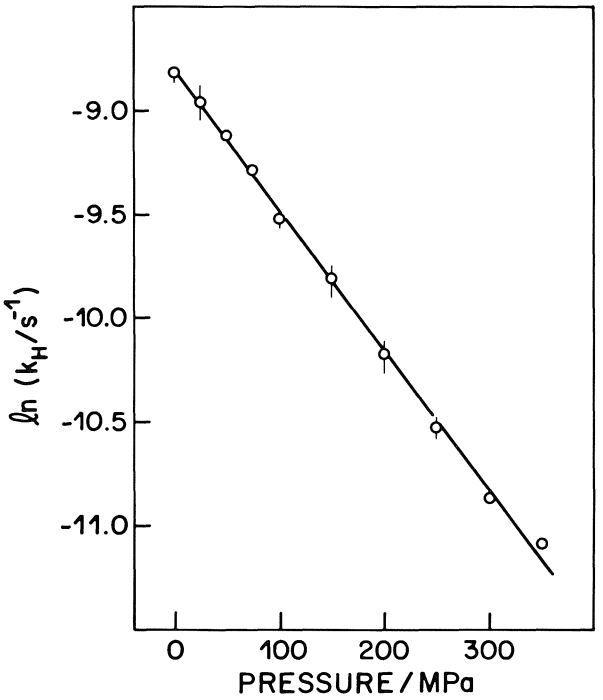

FIG. 1. Pressure dependence of ln k_H for the decomposition of 4-pyridylmethylchromium(III) ion in aqueous $HClO_4$ (0.026 mol L^{-1} at ambient conditions) at 63.4°C. Line represents linear fit of data (eq. [3]).

residual sum of squares of 0.0954. Only a minor improvement in fit (residual sum of squares = 0.0905) is achieved by going to a quadratic in pressure

$$[4] \quad \ln k_H = \ln k_H^0 - (\Delta V_H^{0*}/RT)P + (\Delta\beta_H^*/2RT)P^2$$

in which the zero-pressure volume of activation $\Delta V_H^{0*} = +20.0 \pm 0.9\ cm^3\ mol^{-1}$ and the mean compressibility coefficient of activation $\Delta\beta_H^* = -(\partial\Delta V_H^*/\partial P)_T$ for this pressure range is $(6.8 \pm 5.6) \times 10^{-3}\ cm^3\ mol^{-1}\ MPa^{-1}$. These uncertainty limits are standard deviations, so $\Delta\beta_H^*$ is not really significant at the 95% confidence level, but in any event it is only about one-tenth of that reported (4) for the 2-propylchromium(III) ion ($+(5.9 \pm 1.4) \times 10^{-2}\ cm^3\ mol^{-1}\ MPa^{-1}$).

Discussion

Table 1 shows that a large, positive volume of activation is characteristic of the homolytic pathway for decomposition of aqueous organochromium(III) complexes, regardless of the charge on the leaving organic radical, R•.

The $\Delta\beta_H^*$ data, however, raise the question as to whether ΔV_H^* is, in the general case, significantly pressure-dependent. When $^\bullet CH(CH_3)_2$ is the leaving group, the measured $\Delta\beta_H^*$ is large, but is derived from rate data at the higher pressures where k_H makes only a minor contribution and may therefore be subject to large systematic errors. For cationic $^\bullet CH_2C_5H_4NH^+$ as the leaving-group, k_H values at the higher pressures are more reliable than for the 2-propyl analogue because heterolysis is absent, and here $\Delta\beta_H^*$ is negligible. It is likely, however, that the marked curvature of the plot of ln k_H vs. P for the 2-propylchromium(III) case is real, and originates in a desolvation effect associated with neutral hydrocarbon radical release that may be minimized when *both* of the separating fragments (Cr^{2+} and $R^{+\bullet}$) are cations. In other words, solvent cage break-up need not imply desolvation, at least not when the escaping fragments are both cationic.

It is not feasible at present to attempt to account in a quantitative, absolute way for the large, positive values that are found for ΔV_H^*, but a crude estimate of $\Delta\Delta V^* = (\Delta V_H^* - \Delta V_A^*)$, i.e., the volume of activation for homolysis relative to heterolysis for the decomposition of a given aqueous organochromium(III) complex, can be made. A model introduced previously (9, 10) allows us to estimate that the (presently unmeasured) absolute molar volume of $Cr(H_2O)_6^{2+}(aq)$ is 20.7 $cm^3\ mol^{-1}$ larger than that of $Cr(H_2O)_6^{3+}(aq)$, and so, from the known volume of hydrolysis of the latter ion (11), 19.1 $cm^3\ mol^{-1}$ larger than that of $Cr(H_2O)_5OH^{2+}(aq)$. The contribution of a covalent hydrogen atom to the molar volume of an alkyl group is about 5.5 $cm^3\ mol^{-1}$ (12), and so, *solvation apart*, the radical R• should occupy that much less volume than RH. Thus, if the activation processes of heterolysis and homolysis can be approximated to the generation of the intermediates shown in reactions [1] and [2], $\Delta\Delta V^*$ should be about 14 $cm^3\ mol^{-1}$ if solvation of R and RH is ignored (solvation of the chromium ions is already taken into account). Table 1 indicates that this is a reasonable estimate; the excess in the experimental $\Delta\Delta V^*$ values probably reflects contributions from desolvation, and indeed is largest where $\Delta\beta_H^*$ is significant.

Finally, we consider other possible homolyses involving inorganic complexes in aqueous solution for which volumes of activation are available. It has been proposed (13) that the internal redox decomposition of the O-bonded sulfitopentaamminecobalt(III) ion in water involves a rate-determining initial step in which the $SO_3^{\bullet-}$ radical is created along with cobalt(II) — i.e., that the Co—OSO_2 bond undergoes homolysis:

$$[5] \quad Co(NH_3)_5OSO_2^+ \xrightarrow{\text{slow}} Co(NH_3)_5^{2+} + SO_3^{\bullet-} \rightarrow \text{etc.}$$

Our present study lends support to this interpretation, since the volume of activation is strongly positive ($+35\ cm^3\ mol^{-1}$ (13);

the pressure range was only 100 MPa, so experimental uncertainty may have obscured any curvature of the ln k vs. P plot). This volume of activation is unusually large by the standards set by Table 1, and may reflect homolysis with a change of spin state on going from cobalt(III) (singlet) to cobalt(II) (quartet), as this would be accompanied by substantial changes in metal–ligand bond lengths (14).

It might be thought that the markedly positive and pressure-dependent volume of activation ($\Delta V^{0*} = +16.0\,cm^3\,mol^{-1}$, $\Delta\beta^* = +2.1 \times 10^{-2}\,cm^3\,mol^{-1}\,MPa^{-1}$) for the acid-independent pathway for hydrolysis of azidopentaamminecobalt(III) ion (15) is indicative of a very plausible homolytic mechanism producing initially $Co(NH_3)_5^{2+}$ and the familiar $N_3^{\bullet}$ radical, with $Co^{2+}(aq)$ and gaseous nitrogen among the final products. The products of hydrolysis in dilute aqueous acid, however, appear to be exclusively $Co(NH_3)_5OH_2^{3+}$ and HN_3 (16), and certainly the reverse reaction in azide/hydrazoic acid buffer goes to at least 99% completion with very little reduction of cobalt(III) (17). The heterolytic interpretation advanced previously (15, 17) therefore remains appropriate.

We therefore conclude that a strongly positive volume of activation provides a valuable piece of confirmatory evidence in the assignment of homolytic mechanisms of decomposition of metal complexes in aqueous solution. Caution, however, must be exercised in the use of ΔV^* as a *prima facie* criterion of a homolysis mechanism, however plausible such a process may seem, unless there is supporting chemical evidence.

Acknowledgement

We thank the Natural Sciences and Engineering Research Council of Canada for financial support.

1. J. H. Espenson. Adv. Inorg. Bioinorg. Mech. **1**, 1 (1982).
2. A. R. Schmidt and T. W. Swaddle. J. Chem. Soc. A, 1927 (1970).
3. R. G. Coombes and M. D. Johnson. J. Chem. Soc. A, 177 (1966).
4. M. J. Sisley, W. Rindermann, R. Van Eldik, and T. W. Swaddle. J. Am. Chem. Soc. **106**, 7432 (1984).
5. T. W. Swaddle. *In* Mechanistic aspects of inorganic reactions. *Edited by* D. B. Rorabacher and J. F. Endicott. Am. Chem. Soc. Symp. Ser. **198**, 39 (1982).
6. A. R. Schmidt. M. Sc. Thesis, The University of Calgary. 1970.
7. W. Le Noble and R. Schlott. Rev. Sci. Instrum. **47**, 770 (1976).
8. J. H. Espenson. Chemical kinetics and reaction mechanisms. McGraw-Hill, New York, 1981. p. 25.
9. T. W. Swaddle and M. K. S. Mak. Can. J. Chem. **61**, 473 (1983).
10. T. W. Swaddle. Inorg. Chem. **22**, 2663 (1983).
11. T. W. Swaddle and P.-C. Kong. Can. J. Chem. **48**, 3223 (1970).
12. B. E. Conway and J. C. Currie. J. Chem. Soc. Faraday Trans. I, **74**, 1390 (1978).
13. R. Van Eldik. Inorg. Chem. **22**, 353 (1983).
14. H. C. Stynes and J. A. Ibers. Inorg. Chem. **10**, 2304 (1971).
15. W. E. Jones, L. R. Carey, and T. W. Swaddle. Can. J. Chem. **50**, 2739 (1972).
16. G. C. Lalor and E. A. Moelwyn-Hughes. J. Chem. Soc. 1560 (1963).
17. T. W. Swaddle and G. Guastalla. Inorg. Chem. **8**, 1604 (1969).

Influence of alkene structure on the formation constants of alkene–ICl molecular complexes

GEORGE H. SCHMID AND JAMES W. GORDON
Department of Chemistry, University of Toronto, Toronto, Ont., Canada M5S 1A1

Received April 14, 1986

GEORGE H. SCHMID and JAMES W. GORDON. Can. J. Chem. **64**, 2171 (1986).

The experimentally determined rate law for the addition of ICl to 22 alkenes in CCl_4 at 25°C under conditions of $(alkene)_0 \gg (ICl)_0$ is $-d(ICl)/dt = k_{exp}(alkene)_0(ICl)^3/\{1 + C_2(alkene)_0\}^3$. The constant C_2 is shown to be equal to K_{app} which is a measure of the formation constant or constants of the molecular complexes in this system. Under the experimental conditions used, C_2 is a good approximation of the formation constant of the 1:1 alkene–ICl molecular complex. Thus the values of C_2 obtained allow an estimate of the effect of alkene structure on the formation constant of the first molecular complex involved in this addition reaction. The contribution of the effect of substituents on C_2 is estimated to be approximately 24% of the overall change in rate due to change in the alkene structure.

GEORGE H. SCHMID et JAMES W. GORDON. Can. J. Chem. **64**, 2171 (1986).

Opérant dans le CCl_4, à 25°C et dans des conditions où la $(alcène)_0 \gg (ICl)_0$, on a déterminé expérimentalement que la loi de vitesse pour l'addition du ICl sur 22 alcènes est définie par l'équation $-d(ICl)/dt = k_{exp}(alcène)_0(ICl)^3/\{1 + C_2(alcène)_0\}^3$. On démontre que la constante C_2 est égale à K_{app} qui est une mesure de la constante de formation ou des constantes des complexes moléculaires impliqués dans ce système. Dans les conditions expérimentales utilisées, C_2 est une bonne approximation de la constante de formation du complexe moléculaire 1:1 alcène/ICl. Les valeurs de C_2 obtenues permettent donc d'évaluer l'effet de la structure de l'alcène sur la constante de formation du premier complexe moléculaire impliqué dans cette réaction d'addition. On a évalué que la contribution de l'effet des substituants sur C_2 est égale à environ 24% du changement global dans la vitesse du à un changement dans la structure de l'alcène.

[Traduit par la revue]

There is ample evidence in the literature (1–3) that molecular complexes or charge transfer complexes (CTC) as they are also called are involved on the reaction pathway prior to the rate determining step in electrophilic additions of bromine, chlorine, and iodine monochloride to alkenes. These complexes are defined according to Mulliken as σ–π CTC (4).

The existence of one or more complexes prior to the rate determining step introduces a complication in the interpretation of linear free energy relationships in electrophilic additions of bromine to alkenes because a change in alkene structure affects not only the rate determining step but also the value of the formation constant of the CTC. Thus the value of ρ obtained from such rate data is the sum of ρ for the formation of the complex or complexes and ρ for the rate determining step.

Based upon data from CTC formed between ketones and bromine, it was concluded that the effect of structure on the formation constants of the CTC is much smaller than the kinetic substituent effect. Consequently, it was assumed that ρ for the formation constant of the CTC is negligible as compared to ρ for the rate determining step (5). While values of formation constants have been measured for complexes of alkenes with bromine (6), ICl (7), and chlorine (8), the variation of alkene structure has not been sufficiently large to be able to verify this conclusion.

We have previously studied the rate of addition of ICl to a limited number of alkenes in CCl_4 at 25°C and have determined the experimental rate law (9). In this paper, we wish to show that from this rate law it is possible to extract a value of the formation constant of the ICl–alkene complex. In this way, we can for the first time determine the effect of substituents on this formation constant. We report these data in this paper.

Results and discussion

The rates of addition of ICl to the 22 alkenes listed in Table 1 were measured by monitoring the disappearance with time of the ICl absorption at 460 nm by means of a Durrum–Gibson stopped-flow spectrometer. The rate measurements were made with $(alkene)_0 \gg (ICl)_0$. All data were treated in the same way as previously described (9) for addition to 2,3-dimethyl-2-butene. Treatment of the data in this way allows the reactivity of all alkenes to be described by the experimental rate law given in eq. [1].

$$[1] \quad -d(ICl)/dt = k_{exp}(alk)_0(ICl)^3/[1 + C_2(alk)_0]^3$$

The values of k_{exp} and C_2 from analysis of the rate law for all the alkenes are summarized in Table 1.

The addition of ICl to alkenes is a simple irreversible addition reaction (10) whose stoichiometry is shown in eq. [2].

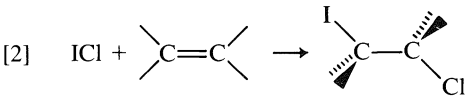

From the rate data in Table 1, it is clear that this reaction is a typical electrophilic addition reaction.

While the stoichiometry of this reaction is simple, the experimental rate law, as given in eq. [1], is not. Furthermore, immediately upon mixing ICl and an alkene in CCl_4 at 25°C a new absorption band, absent in either reactant or product, appears in the ultraviolet region of the spectrum and decreases with time. This new band is assigned to the presence of an intermediate ICl-alkene molecular complex (9).

Based on evidence of a CTC, the rate law, and the experimentally determined enthalpy change during the reaction, the mechanism shown in Scheme 1 was proposed in a previous publication (9). This mechanism involves both 1:1 and 2:1 ICl–alkene complexes.

The value of formation constants of donor–acceptor complexes can be determined by a number of standard techniques (11). In our previous publication (9), we applied the Benesi–Hildebrand method to the variation of the initial absorbance values at 300 nm with varying initial concentrations of alkene where $(alkene)_0 \gg (ICl)_0$ in order to determine the value of

TABLE 1. Rates of addition and C_2, for addition of ICl to various alkenes in CCl_4 at 25°C

Alkene	R	$k_{exp} \times 10^{-6}$ (M^{-3} s^{-1})	C_2 (M^{-1})	$k_{res} \times 10^{-6}$ (M^{-2} s^{-1})
$CH_2=CH_2$	—	0.0555 ± 0.0038	—	—
$CH_2=CHR$	CH_3	0.983 ± 0.050	1.76 ± 0.10	0.558 ± 0.043
	C_2H_5	2.43 ± 0.12	1.61 ± 0.05	1.51 ± 0.09
	i-C_3H_7	4.62 ± 0.30	1.86 ± 0.06	2.48 ± 0.18
	t-C_4H_9	1.58 ± 0.06	1.67 ± 0.04	0.946 ± 0.040
$CH_2=CR$	CH_3	27.2 ± 1.9	5.81 ± 0.22	4.68 ± 0.37
$\vert$	C_2H_5	51.9 ± 8.0	5.52 ± 0.41	9.40 ± 1.61
CH_3	i-C_3H_7	37.7 ± 9.1	5.56 ± 0.50	6.79 ± 1.75
	t-C_4H_9	33.1 ± 7.5	5.04 ± 0.42	6.56 ± 1.58
Z-$CH_3CH=CHR$	CH_3	70.7 ± 7.5	5.81 ± 0.14	12.2 ± 0.8
	C_2H_5	101 ± 14	5.19 ± 0.29	19.5 ± 2.8
	i-C_3H_7	55.2 ± 8.4	4.30 ± 0.26	12.9 ± 2.1
	t-C_4H_9	112 ± 18	4.67 ± 0.30	23.9 ± 4.2
E-$CH_3CH=CHR$	CH_3	22.7 ± 0.6	3.73 ± 0.06	6.08 ± 0.20
	C_2H_5	43.8 ± 2.7	3.56 ± 0.09	12.3 ± 0.8
	i-C_3H_7	26.7 ± 3.3	1.86 ± 0.13	14.3 ± 2.0
	t-C_4H_9	1.23 ± 0.07	1.64 ± 0.05	0.746 ± 0.046
$(CH_3)_2C=CHCH_3$	—	458 ± 10	9.90 ± 0.86	46.3 ± 1.8
$(CH_3)_2C=C(CH_3)_2$	—	908 ± 12	17.84 ± 0.76	50.9 ± 6.6
Z-$C_6H_5CH=CHCH_3$	—	3.11 ± 0.13	1.39 ± 0.05	2.25 ± 0.13
E-$C_6H_5CH=CHCH_3$	—	5.22 ± 0.19	1.40 ± 0.08	3.73 ± 0.26
E-4-$CH_3OC_6H_4CH=CHCH_3$	—	52300 ± 1100	—	—

the formation constant for the ICl–alkene complex. Linear plots of $1/(\text{alkene})_0$ against the apparent extinction coefficient were obtained.

A major problem with this and other methods of determining values of the formation constants of donor–acceptor complexes is that it is difficult to establish the stoichiometry of the complex. The Benesi–Hildebrand method assumes a 1:1 stoichiometry for the complex. In theory, if a 2:1 complex is present in the system in appreciable amounts, nonlinearity of the Benesi–Hildebrand plot is predicted. However, in practice a linear plot can be obtained even in systems where both 1:1 and 2:1 complexes are present. This occurs under the following circumstances. Firstly, if the range of saturation fraction is low, a linear plot can be obtained.[1] Secondly, in the particular case where $K_1 = 4K_2$ (K_1 and K_2 are the formation constants for 1:1 and 2:1 complexes, respectively), a Benesi–Hildebrand plot will be exactly linear over the entire saturation range.

In our previous work (9), we found that the absorbance values at 300 nm disappear rapidly with time and follow a third order rate law. In order to obtain initial absorbance values, it was necessary to extrapolate back to zero time. This was possible as long as the rates of disappearance of the band at 300 nm could be measured by stopped-flow technique. At saturation fractions above 0.29, it was impossible to follow the rate and consequently, no initial absorbance values could be obtained. This means that our Benesi–Hildebrand plots are linear only at the low saturation fraction and no conclusion can be reached about the stoichiometry of the CTC observed in the reaction.

Deranleau (13, 14) has shown that the value of the formation constant obtained from the slope and intercept of the Benesi–Hildebrand plot at low saturation fraction is given by eq. [3].

$$\text{A} + \text{D} \underset{}{\overset{K_1}{\rightleftharpoons}} \text{AD}$$

$$\text{AD} + \text{A} \overset{K_2}{\rightleftharpoons} \text{A}_2\text{D}$$

$$\text{A}_2\text{D} + \text{A} \xrightarrow{k} \text{product}$$

A = ICl

D = 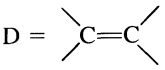

SCHEME 1

[3] $$K_{app} = K_1\{1 - [(K_2)(E_2)/(K_1)(E_1)]\}$$

The quantities E_1 and E_2 are the extinction coefficients of the 1:1 and 2:1 complexes, respectively. We have followed the proposal of Deranleau and have given this formation constant the designation K_{app} (14). A K_{app} value of 19 ± 6 M^{-1} was obtained by this method for the addition of ICl to 2,3-dimethyl-2-butene (9).

A value of the formation constant of the complex or complexes can be obtained independently from the rate law derived from the mechanism in Scheme 1. For convenience, the following abbreviations are used. A = ICl; D = alkene. When $(\text{alkene})_0 \gg (\text{ICl})_0$, the following mass balance equations can be written.

$$(\text{A})_t = [\text{A}]_t + [\text{AD}]_t + [\text{A}_2\text{D}]_t$$

$$(\text{D})_0 = [\text{D}]_t$$

where $(\text{X})_t$ equals total concentration and $[\text{X}]_t$ equals free concentration of a reagent at time t. From these equations and

[1]The saturation fraction is defined according to ref. 13 as $s = K[\text{alkene}]/(1 + K[\text{alkene}])$, $0 < s < 1$.

the equilibrium constant expression, eq. [4] can be derived.

[4] $[AD] + K_1(D)[AD] + K_2[AD]^2 = K_1(A)(D)$

If we make the reasonable assumption,[2] that $K_2[AD]^2 \ll K_1(D)[AD] + [AD]$, then

[5] $[AD] = K_1(D)(A)/[1 + K_1(D)]$

and

[6] $[A_2D] = K_1K_2(D)(A)[A]/[1 + K_1(D)]$

From the mass balance equation, we can obtain the following equation for [A].

[7] $[A] = (A)/[1 + K_1(D) + K_1K_2(D)(A)]$

Since $-d(A)/dt = kK_1K_2[D][A]^3$, it follows that

[8] $$\frac{-d(ICl)}{dt} = \frac{kK_1K_2(alkene)_0(ICl)^3}{\{1 + K_1[1 + K_2(ICl)](alkene)_0\}^3}$$

Comparing eqs. [1] and [8], it follows that $kK_1K_2 = k_{exp}$ and $C_2 = K_1[1 + K_2(ICl)]$.

We know that for the addition of ICl to 2,3-dimethyl-2-butene $C_2 \approx K_{app}$. For this to be true, $K_2(ICl) < 1$ and $K_2E_2/K_1E_1 < 1$. Therefore C_2, obtained from the kinetic data, or K_{app}, obtained from data extrapolated to time zero, *while not exactly equal to* K_1, are both a good approximation of the formation constant of the first molecular complex involved in this reaction. Thus, it is possible to estimate the effect of alkene structure on K_1 from the value of C_2 obtained from the rate of addition of ICl to a series of alkenes.

It is clear from the values of C_2 given in Table 1 that the alkene–ICl complex stability increases as the hydrogen atoms on ethylene are successively replaced by alkyl groups. In two of the four series of alkenes, the nature of the alkyl substituent has little effect on the value of C_2. Thus the values of C_2 for propene, 1-butene, 3-methyl-1-butene, and 3,3-dimethyl-1-butene are the same within experimental error. In the other series the introduction of bulky substituents such as isopropyl and *tert*-butyl groups decreases the stability of the complex. These data are in accord with previous work by Dubois (16) who established a spectroscopic measure of CTC stability called Γ. Values of Γ determined in Freon 112 show a similar variation with alkyl substituents within a particular alkene type.

One way to estimate the steric effects within the ICl–alkene CTC is to compare their values of C_2 with a series of complexes in which there is little or no steric hindrance. Such a system is a series of phenol–alkene complexes whose stabilities have been determined by the frequency shift, $\Delta\nu$, of the OH stretching frequency of the complexes in CCl_4 (17). ICl and phenol are similar in that both are σ acceptors but they differ greatly in their steric requirements for complex formation. Since phenol has a low steric requirement for complex formation, it is assumed that in the reaction of phenol and alkenes the only change in entropy is the loss of translational entropy which is constant for the series. Therefore it is possible to compare $\Delta\nu$, a measure of enthalpy change, with C_2, a measure of the free energy change in the system. The plot of ΔG (which is equal to $RT \ln C_2$) vs. $\Delta\nu$ is given in Fig. 1.

[2]When concentrations of [ICl] and $(D)_0$ in the range used experimentally and reasonable values of K_1 and K_2 are chosen, this condition is fulfilled. For example: if $[ICl] = [AD] = 10^{-3}$; $K_1 = K_2 = 20$; and $(D)_0 = 10^{-2}$, then $K_2[AD]^2 = 2 \times 10^{-5}$ and $K_1(D)_0[AD] + [AD] = 10^{-3}$.

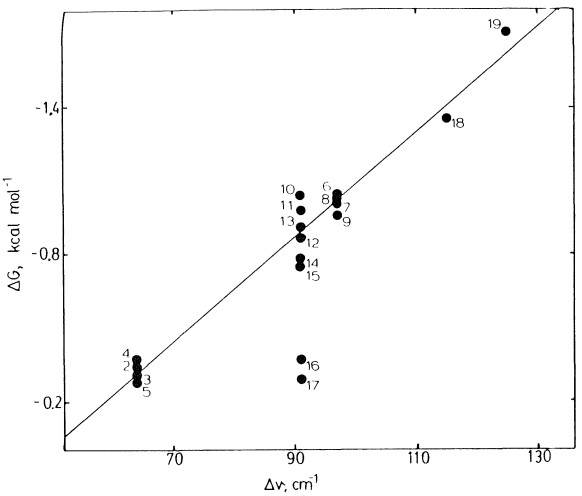

FIG. 1. Correlation of alkene–ICl complex stability, ΔG, with the numbers and the corresponding alkenes are **2**, propene; **3**, butene-1; **4**, 3-methylbutene-1; **5**, 3,3-dimethylbutene-1; **6**, methylpropene; **7**, 2-methylbutene-1; **8**, 2,3-dimethylbutene-1; **9**, 2,3,3-trimethylbutene-1; **10**, *Z*-butene-2; **11**, *Z*-pentene-2; **12**, *Z*-4-methylpentene-2; **13**, *Z*-4,4-dimethylpentene-2; **14**, *E*-butene-2; **15**, *E*-pentene-2; **16**, *E*-4-methylpentene-2; **17**, *E*-4,4-dimethylpentene-2; **18**, 2-methylbutene-2; **19**, 2,3-dimethylbutene-2.

The values of $\Delta\nu$ are insensitive to the steric bulk of the substituent within a given alkene type. This is shown in the value of $\Delta\nu$ which is the same for compounds **2**, **3**, **4**, and **5**, all monsubstituted terminal alkenes.

If there were no steric effects in the ICl–alkene complexes, a good linear correlation between log C_2 and $\Delta\nu$ would be expected. The points in Fig. 1 do follow a general linear trend with a few notable exceptions. The points for all the alkenes except the 1,2-disubstituted alkenes fit reasonably well on the line. The two alkenes *E*-4-methylpentene-2 (**16**) and *E*-4,4-dimethylpentene-2 (**17**) deviate markedly from the line. Furthermore, while there is no difference in the stability of complexes formed between isomeric *E*- and *Z*-alkenes and phenol, a *Z*-alkene complexes more strongly with ICl than does the isomeric *E*-alkene. This difference between *E*- and *Z*-isomeric alkenes is also found in their rates of addition of Br_2 (18), arenesulfenyl chlorides (19), Cl_2 (20), and areneselenenyl chlorides (21). From our data, we can conclude that the cause of this difference in rates of additions to isomeric *Z*- and *E*-alkenes is present also in their molecular complexes prior to the rate determining step.

Several explanations have been advanced to explain this reactivity difference. Dubois originally postulated that relief of some of the ground state steric strain present in the *Z*-alkene was occurring in the transition state (22). However, the lack of correlation of *E*/*Z* reactivity with the difference in ground state strain of isomeric alkenes has been cited as evidence against such an explanation (23). Steric interaction between electrophile and alkene in which approach to the *Z*-alkene is less sterically hindered relative to the corresponding *E*-alkene has been postulated to explain the large rate difference in the addition to *E*- and *Z*-1,2-di-*tert*-butylethylenes (24).

A more likely general explanation is that there is less entropy loss on activation of the *Z*-alkene. Since there is more rotational entropy available in the *E*-alkene than in the corresponding *Z*-alkene, there will be a greater loss of entropy in the *E*-alkene

upon complex formation and subsequent reaction. This results in a lower complex stability and a slower rate. The effect is more marked as the alkyl group becomes more complex in the 1,2-disubstituted series as shown by the $C_2(Z)/C_2(E)$ ratios for the series $CH_3CH{=}CHR$: CH_3, 1.6; C_2H_5, 1.5; $CH(CH_3)_2$, 2.3; $C(CH_3)_3$, 2.9.

While it is possible to determine how substituents affect C_2, the effect of such substitution on the rate of addition of ICl to alkenes cannot be exactly determined from our data in Table 1. The reason for this is clear from the rate law (eq. [8]) derived from Scheme 1. The experimentally obtained rate constant k_{exp} is the product of the rate constant of the slow step, k, and two equilibrium constants, $C_2 \approx K_1$ and K_2. The quantity k_{res}, obtained by dividing k_{exp} by C_2 is equal to kK_2. It is impossible from our data to determine values of K_2 and consequently the effect of alkene structure on values of K_2.Thus it is impossible to obtain values of k from kK_2.

However, it is possible to estimate the contribution of the effect of substituents on C_2 to the overall value of ρ simply by considering the effect on C_2, k_{exp}, and k_{res} of replacing the hydrogens of propene by methyl groups. Plots of log C_2, log k_{exp}, and log k_{res} vs. the number of methyl groups are all linear giving the following Taft ρ values. For C_2, -0.67 ± 0.09; k_{exp}, -2.8 ± 0.2; k_{res}, -2.0 ± 0.3. Thus the effect of alkene structure on the value of C_2 contributes approximately 24% of the overall change in rate due to changes in the alkene structure. This is a substantial amount even without considering structural effects on the value of K_2. While we do not have the data, we can make an estimate from data in the literature. In cases where both 1:1 and 1:2 molecular complexes have been shown to exist and their values have been determined, K_2 is usually less than K_1 (15). In addition it would be expected that due to saturation, the effect of substituents on K_2 would be smaller. If we assume that as a maximum, the value of ρ for K_2 would be equal to that for K_1, then almost half of the overall change in rate would be due to substituent effects in the equilibrium reaction occurring prior to the rate determining step.

From this analysis of our data, we caution that comparing ρ values of even similar kinds of reactions may lead to erroneous mechanistic conclusions. For example, the first step is rate determining in the mechanism of the addition of arenesulfenyl chlorides with alkenes in nonpolar solvents (12). Thus a value of ρ obtained from these rate data is a true measure of substituent effects on an elementary reaction. This value of ρ cannot be compared with that obtained from experimental rate constants for the addition of ICl to alkenes in nonpolar solvents because the latter value of ρ measures the effect of substituents not on a single elementary reaction but on the sum of three consecutive reactions.

Experimental

All of the liquid alkenes were commercially available from Chemical Samples Co. Gaseous alkenes were obtained from Matheson Co. Iodine monochloride (Sargent-Welch) was purified by fractional crystallization from the melt, discarding the remaining liquid portion. ACS grade carbon tetrachloride was found to be satisfactory without further purification. Use of dried and carefully fractionated carbon tetrachloride did not affect the rates of addition. Solutions were prepared by weight. The concentration of propene in solution was determined by titration with bromine. The concentration of ethylene in solution was determined by titration with iodine monochloride. In both cases the amount of excess halogen was determined spectrophotometrically. All solutions were prepared at room temperature.

The rate of addition of iodine monochloride to the alkenes was determined by monitoring the disappearance with time of the iodine monochloride absorption at 460 nm by means of a Durrum–Gibson stopped-flow spectrometer. The rate measurements were made with $(\text{alkene})_0 \gg (\text{ICl})_0$.

The high reactivity of *E*-1-(4-methoxyphenyl)propene limited the concentration of alkene to the range 0.002 *M* to 0.015 *M* with an iodine monochloride concentration of about 3×10^{-4} *M*. Under these dilute conditions, k_{app}, when plotted against $(\text{alkene})_0$, gave a straight line described by a zero intercept and slope equal to k_{exp}.[3] With ethylene, the highest concentration obtainable was only 0.055 *M*. The low reactivity did not permit working with dilute solutions as in the case of *E*-1-(4-methoxyphenyl)propene. The initial absorbance readings agreed with the values predicted by assuming that none of the iodine monochloride was complexed. Thus k_{exp} was obtained as the average value of $k_{app}/(\text{ethylene})_0$.

Acknowledgement

Continued financial support from the Natural Sciences and Engineering Research Council is gratefully acknowledged.

1. P. B. D. De la Mare. Electrophilic halogenations. Cambridge University Press, Cambridge. 1976.
2. G. H. Schmid and D. G. Garratt. Chemistry of the functional groups, double bonded functional groups. *Edited by* S. Patai. Wiley, New York. 1977. Suppl. A. p. 725.
3. G. Bellucci, R. Bianchini, and R. Ambrosetti. J. Am. Chem. Soc. **107**, 2464 (1985).
4. R. S. Mulliken. J. Phys. Chem. **56**, 801 (1952).
5. M. F. Ruasse and J. E. Dubois. J. Am. Chem. Soc. **106**, 3230 (1984).
6. G. B. Sergev and C. Tan-kha. Theoret. Exptl. Chem. **5**, 240 (1970).
7. N. Amirtha, S. Viswanathan, and R. Gamesan. Bull. Chem. Soc. Jpn. **56**, 314 (1983).
8. G. B. Sergeev and Yu A. Serguchev. Theoret. Exptl. Chem. **4**, 258 (1968).
9. G. H. Schmid and J. W. Gordon. Can. J. Chem. **62**, 2526 (1984).
10. L. F. Fieser and M. Fieser. Reagents for organic synthesis. John Wiley and Sons Inc., New York. 1967. p. 502.
11. R. Foster. Organic charge-transfer complexes. Academic Press, London and New York. 1969.
12. M. Kanska and A. Fry. J. Am. Chem. Soc. **104**, 5512 (1982).
13. D. A. Deranleau. J. Am. Chem. Soc. **91**, 4044 (1969).
14. D. A. Deranleau. J. Am. Chem. Soc. **91**, 4050 (1969).
15. B. Dodson, R. Foster, A. A. S. Bright, M. I. Foreman, and J. Gordon. J. Chem. Soc. B, 1283 (1971).
16. J. E. Dubois and F. Garnier. Spectrochimica Acta, **23**A, 2279 (1967).
17. (*a*) Z. Yoshida and E. Osawa. J. Am. Chem. Soc. **87**, 1467 (1965). (*b*) L. P. Kuhn and R. E. Bowman. Spectrochimica Acta, **23**A, 189 (1967).
18. J. E. Dubois and G. Mouvier. Bull. Soc. Chim. Fr. 1426 (1968).
19. G. H. Schmid and D. G. Garratt. Can. J. Chem. **51**, 2463 (1973).
20. M. Poutsma. J. Am. Chem. Soc. **87**, 4285 (1965).
21. G. H. Schmid and D. G. Garratt. Tetrahedron, **34**, 2869 (1978).
22. J. E. Dubois and G. Mouvier. Tetrahedron Lett. 1629 (1965).
23. (*a*) G. H. Schmid, C. L. Dean, and D. G. Garratt. Can. J. Chem. **54**, 1253 (1976); (*b*) K. Izawa, T. Okuyama, and T. Fueno. Bull. Chem. Soc. Jpn. **47**, 1477 (1974).
24. C. L. Dean, D. G. Garratt, T. T. Tidwell, and G. H. Schmid. J. Am. Chem. Soc. **96**, 4958 (1974).

[3] k_{app} is defined by the following: $-\text{d(ICl)}/\text{d}t = k_{app}(\text{ICl})^3$.

Thermolysis of *N*-alkylated ethylenediamines: an ultraviolet photoelectron spectroscopy study

N. H. WERSTIUK

Department of Chemistry, McMaster University, Hamilton, Ont., Canada L8S 4M1

Received May 8, 1986

N. H. WERSTIUK. Can. J. Chem. **64**, 2175 (1986).

Thermolyses of *N,N,N',N'*-tetramethylethylenediamine (**1***a*), *N,N,N',N'*-tetraethylethylenediamine (**1***b*) and *sym-N,N'*-dimethylethylenediamine (**1***c*) at 760–825°C have been studied by ultraviolet photoelectron spectroscopy. Although the corresponding *N*-alkylated aminomethylene radicals were not observed, this study establishes that thermolysis of **1***a* is an efficient route to *N*-methylenimine (**3***a*); methane, ethane, and ethene are the other major products. Diamine **1***b* yields, besides ethane, ethene, and propane, heretofore unreported *N*-ethylmethylenimine (**3***b*). Diamine **1***c* yields imine **3***a* and methylenimine (**3***c*), as well as hydrogen, methane, ethane, and ethene. Molecular orbital eigenvalues of the imines are calculated using HAM/3, MNDO, HF/STO-3G, HF/3-21G, and HF/6-31G* methods.

N. H. WERSTIUK. Can. J. Chem. **64**, 2175 (1986).

Faisant appel à la spectroscopie photoélectronique ultraviolette et opérant entre 760 et 825°C, on a étudié la thermolyse de la *N,N,N',N'*-tétraméthylènediame (**1***a*), de la *N,N,N',N'*-tétraéthylènediamine (**1***b*) et de la *N,N'*-diméthylènediamine symétrique (**1***c*). Même si l'on n'observe pas la formation des radicaux aminométhylènes *N*-alkylés correspondants, cette étude a permis d'établir que la thermolyse du composé **1***a* est une méthode efficace d'obtenir la *N*-méthylèneimine (**3***a*); le méthane, l'éthane et l'éthylène sont les autres produits majeurs. La diamine **1***b* conduit, aux côtés de l'éthane, de l'éthylène et du propane, à la *N*-éthylméthylèneimine (**3***b*) qui n'avait pas été décrite jusqu'à maintenant. La diamine **1***c* conduit à l'imine **3***a* et à la méthylèneimine (**3***c*) ainsi qu'à de l'hydrogène, du méthane, de l'éthane et de l'éthylène. On a calculé les valeurs de eigen des orbitales moléculaires des imines en faisant appel à des méthodes HAM/3, MNDO, HF/STO-3G, HF/3-21G et HF/6-31G*.

[Traduit par la revue]

Introduction

Over the last decade uv photoelectron spectroscopy has been used extensively to study transient species in the gas phase. A variety of highly reactive molecules and free radicals have been generated and their p.e. spectra recorded for identification and to study bonding. This unconventional use of p.e. spectroscopy yields information about electronic structure of transients which can be obtained by no other technique. To assist in the identification of species and to assign the ionization energies (IEs) to specific molecular orbitals these studies are usually accompanied by calculations of molecular orbital eigenvalues (MOEs).

This publication documents an attempt to determine the IEs of the *N,N*-dimethylaminomethylene radical ($(CH_3)_2NCH_2\cdot$) — two different values (5.7 and 5.35 eV) have been reported (1, 2) — by using gas phase thermolysis of *N,N,N',N'*-tetramethylethylenediamine (TMEDA) (**1***a*) at 790°C as its source. Accounts of the thermolyses of *N,N,N',N'*-tetraethylethylenediamine (TEEDA) (**1***b*) and *sym-N,N'*-dimethylethylenediamine (*s*-DMEDA) (**1***c*) are given as well, along with the MOEs calculated for *N*-methylmethylenimine (**3***a*), *N*-ethylmethylenimine (**3***b*), and methylenimine (**3***c*) using HAM/3 (3), MNDO (4), HF/STO-3G (5), HF/3-21G (5), and HF/6-31G* (5) methods.

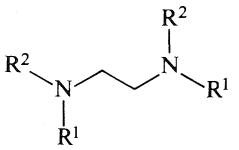

1

a, $R^1 = R^2 = CH_3$
b, $R^1 = R^2 = CH_2CH_3$
c, $R^1 = H$; $R^2 = CH_3$

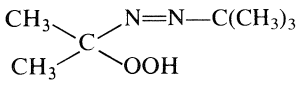

2

$R—N{=}CH_2$

3

a, R = CH_3
b, R = CH_2CH_3
c, R = H

Experimental

The spectrometer used in this study is described elsewhere (6). Spectra were calibrated by N_2 or Ar. Temperature was measured by a digital thermometer using a type-K thermocouple located mid-way along the hot zone of the furnace. Thermolyses were carried out at $>1 \times 10^{-5}$ Torr[1] in a silica tube heated to 760–825°C depending on the substrate used. Two furnaces were used for thermolyzing TMEDA. For thermolysis of TMEDA, TEEDA, and *s*-DMEDA, a 40-cm furnace with a hot zone of approximately 20 cm was used with a 10-cm "U"-trap located between the pyrolysis tube and the spectrometer. That the furnace had no effect on the count rate and resolution was established by comparing the spectra of air obtained with the furnace off and with the furnace on. To maximize the probability of detecting the *N,N*-dimethylaminomethylene radical, several thermolyses of TMEDA were also carried out by a 3-cm non-inductively wound furnace located in a housing 2 cm above the ionization cup of the spectrometer and the system was fast-pumped. To calibrate the spectrometer with respect to the detection of radicals with this furnace, azohydroperoxide **2**, a source of *t*-butyl radicals,[2] was thermolyzed at 350°C. To separate the products of the diamines, the "U"-trap was cooled with liquid nitrogen and the thermolysis was carried out for 1–2 h as 200–300 scans were accumulated. The flow of substrate was stopped, most of the liquid nitrogen was blown away with a stream of air, and, as the trap was allowed to warm up gradually, the low-temperature distillation was monitored by recording p.e. spectra. Bock *et al.* (7) have used this method to detect 2*H*-azirine. When possible, at least 20 scans were accumulated for each species obtained from the distillation. In all cases, the products exhibited sufficiently different volatilities making analysis of the products an easy matter. In the case of TEEDA, the yield of highly reactive **3***b* was reduced because it was necessary to warm the trap more than in the case of

[1] The pressure was measured below the analyzer. The pressure in the thermolysis tube is expected to be substantially higher.

[2] The author thanks Professor J. Warkentin for a sample of **2**. Studies of other azohydroperoxides are planned.

TMEDA and *s*-DMEDA. Where spectrum stripping was necessary, VISICHARTAD, a program for the APPLE II+ available from Interactive Microware was used. Spectra of methane, ethane, propane, butane, and ethene were obtained and used as standards.

Results

Thermolysis of N,N,N′,N′-*tetramethylethylenediamine (TMEDA)* (*1*a)

The p.e. spectra of TMEDA and its thermolysate produced at 790°C are given in Fig. 1 as 1*A* and 1*B*, respectively. From 1*B* it is seen that thermolysis is essentially complete at a pressure $>1 \times 10^{-5}$ Torr and that the spectrum is dominated by four peaks; at 9.8, 11.3, 13.4, and 15.9 eV.[3] During the trapping with liquid nitrogen, spectrum 1*C* was obtained. After 2 h, the flow of TMEDA was stopped, the trap was allowed to warm up slowly and p.e. spectra were obtained as the pressure was maintained roughly constant by opening and closing the fast-pumping valve. Spectrum 1*D* was obtained first, followed by spectra 1*E* and 1*F*. Spectrum 1*C* collected during the thermolysis identifies methane as one of the products, in keeping with the fact that it is not trapped at −196°C. It is established from the bands of spectrum 1*D*, a composite of ethene and ethane, that ethene is a minor product. This result identifies the small peaks at 10.5–10.7 eV of spectrum 1*B*. This is also in accord with the fact that this product distills after a slight warming of the trap. Spectrum 1*E* identifies ethane as a major product of thermolysis and spectrum 1*F* corresponds to the p.e. spectrum of *N*-methylmethylenimine (**3***a*) reported previously (8). When the trap was warmed to ambient temperature a spectrum of TMEDA was obtained. By warming the viscous liquid remaining in the trap, a spectrum corresponding to the trimer of *N*-methylmethylenimine was obtained (8). Analysis of this residue by ^{1}H nmr yielded a spectrum consistent with assignment of the p.e. spectrum.

When TMEDA was thermolyzed by the 3-cm furnace with fast pumping and with scanning beginning 4 eV below the lowest IE of TMEDA, no peak was detected in the region where the radical was expected. To "calibrate" the system with respect to the detection of radicals, azohydroperoxide **2** was thermolyzed at 350°C with fast pumping and the *t*-butyl radical was detected by its IE at 7 eV (9).

Thermolysis of N,N,N′,N′-*tetraethylethylenediamine (TEEDA)* (*1*b)

The p.e. spectra of TEEDA and its thermolysate, obtained at 760°C, are given in Fig. 2 as 2*A* and 2*B*, respectively. Spectrum 2*B* is dominated by peaks at 9.7, 11.1, 12.3, 13.3, 14.0, 15.0, and 16.0 eV.[3] When the products were trapped by liquid nitrogen and a spectrum acquired over the 2-h period, no significant features above background were evident. This indicates that unlike the case of TMEDA, methane is not a major product of thermolysis. When the trap was warmed slowly, a spectrum of ethene shown as 2*C* is obtained indicating that it is a major product of thermolysis. In fact, the peak of lowest binding energy of ethene is seen at 10.4 eV of 2*B*. As the trap was warmed slowly a "transition" spectrum was obtained that appeared to be predominately due to ethane. Furthermore, the broad peak with an on-set at approximately 10.5 eV of 2*C* is consistent with the presence of a small amount of ethane. As the trap was warmed further, spectrum 2*D* corresponding to propane was obtained. In several runs, a "transition" spectrum that appeared to be *N*-methylmethylenimine (**3***a*) was observed as well. Finally spectrum 2*E* was obtained. Some difficulty was experienced in obtaining a good spectrum of this product even though it is clear, by comparison to 2*B*, that it is one of the major products of thermolysis. When the trap was allowed to warm to ambient temperature, a viscous film remained. Further warming of the trap to 30°C yielded a spectrum of TEEDA, in keeping with the fact that thermolysis is incomplete.

Thermolysis of sym-N,N′-*dimethylethylenediamine (s-DMEDA)* (*1*c)

Unlike the thermolyses of TMEDA and TEEDA, a temperature of 825°C was required to achieve significant conversion of *s*-DMEDA to products. The spectra of *s*-DMEDA and its thermolysate are given in Fig. 3 as 3*A* and 3*B*(1), respectively. Although spectrum 3*B*(1) is rather featureless except for the band between 8–9 eV, considered to be due to *s*-DMEDA, this component was selectively trapped by solid Dry Ice, yielding 3*B*(2). The peaks at 13.7–14 eV of 3*B*(2) are due to HCN (10, 11) and the peaks at 15.6–17 eV are due to N_2 used as the calibrant. Application of the method — trapping followed by low temperature distillation — used successfully in this study yields a remarkable resolution of the spectrum. Spectrum 3*C*, acquired as the products were trapped by liquid nitrogen, establishes that methane, and hydrogen — identified by the group of sharp peaks at 15.5–18 eV — are products of thermolysis. When the trap was allowed to warm up slowly over a period of 1.5 h, 3*C*, 3*D*, 3*E*, and 3*F* as well as several "transition" spectra were obtained, one of which, after spectrum stripping, established that propane is a minor product. Spectra 3*D* — the shoulder at 11.5 eV is due to ethane — and 3*E* identify ethene and ethane as major products. Aside from including a small amount 3*G* that was stripped to yield 3*F*(2), 3*F*(1) is the spectrum of *N*-methylmethylenimine (**3***a*). The low-intensity, sharp peaks at 10.5 of 3*F*(1) and 3*F*(2) could be due to ammonia (10). Spectrum 3*G*(2), obtained after 3*G*(1) was stripped of 3*F*(2), is the best spectrum of methylenimine (**3***c*) reported to date (11, 12). The distillation also established that *N*-methylmethylenimine has a lower boiling point than methylenimine.

Discussion

It is clear from this study that thermolysis of TMEDA in a silica tube at 790°C provides a simple, one-step, high-yield route to highly reactive *N*-methylmethylenimine (**3***a*). In Table 1 are listed the experimental IEs as well as the molecular orbital eigenvalues (MOEs) calculated using MNDO, HF/3-21G, and HF/6-31G* methods. The results complement the calculations already carried out on this molecule (13). That **3***a* is one of the major products is consistent with cleavage of the C—C bond to form the dimethylaminomethylene radical (pathway *a*, Scheme 1). However, under the conditions required to cleave the bond, the life-time of the radical is expected to be short because β-scission to **3***a* and a methyl radical is fast. Subsequently, the methyl radical abstracts hydrogen to form methane and dimerizes to ethane. Although it is possible that ethene is formed by dehydrogenation of ethane at 790°C, an alternative route to this product, along with **3***a* and a methyl radical, is shown as pathway *b*. It will be of interest to carry out the thermolysis of TMEDA on a larger scale and establish by suitable experiments whether or not **3***a* is a useful synthon.

From the products, it appears that thermolysis if TEEDA proceeds via a mechanism (pathway *a*, Scheme 2) similar to the one proposed for TMEDA, and, *N*-ethylmethyleneimine (**3***b*),

[3]Due to the broadness of the bonds the errors in the IEs are estimated to be in the region of ±0.1 eV.

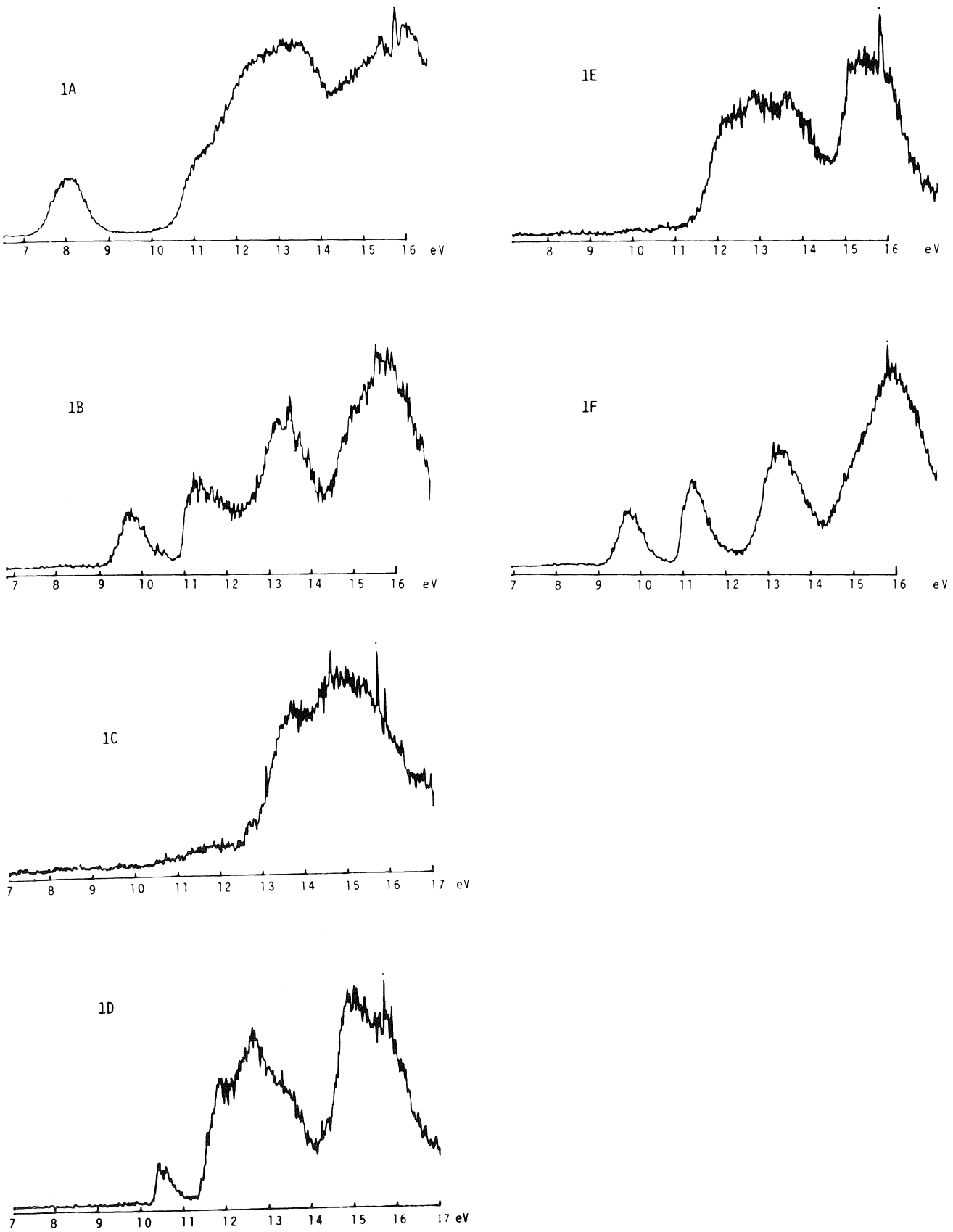

FIG. 1. 1*A*, p.e. spectrum of **1***a*. 1*B*, p.e. spectrum of thermolysate of **1***a*. 1*C*, p.e. spectrum of methane. 1*D*, p.e. spectrum of ethene and ethane. 1*E*, p.e. spectrum of ethene. 1*F*, p.e. spectrum of *N*-methylenimine (**3***a*).

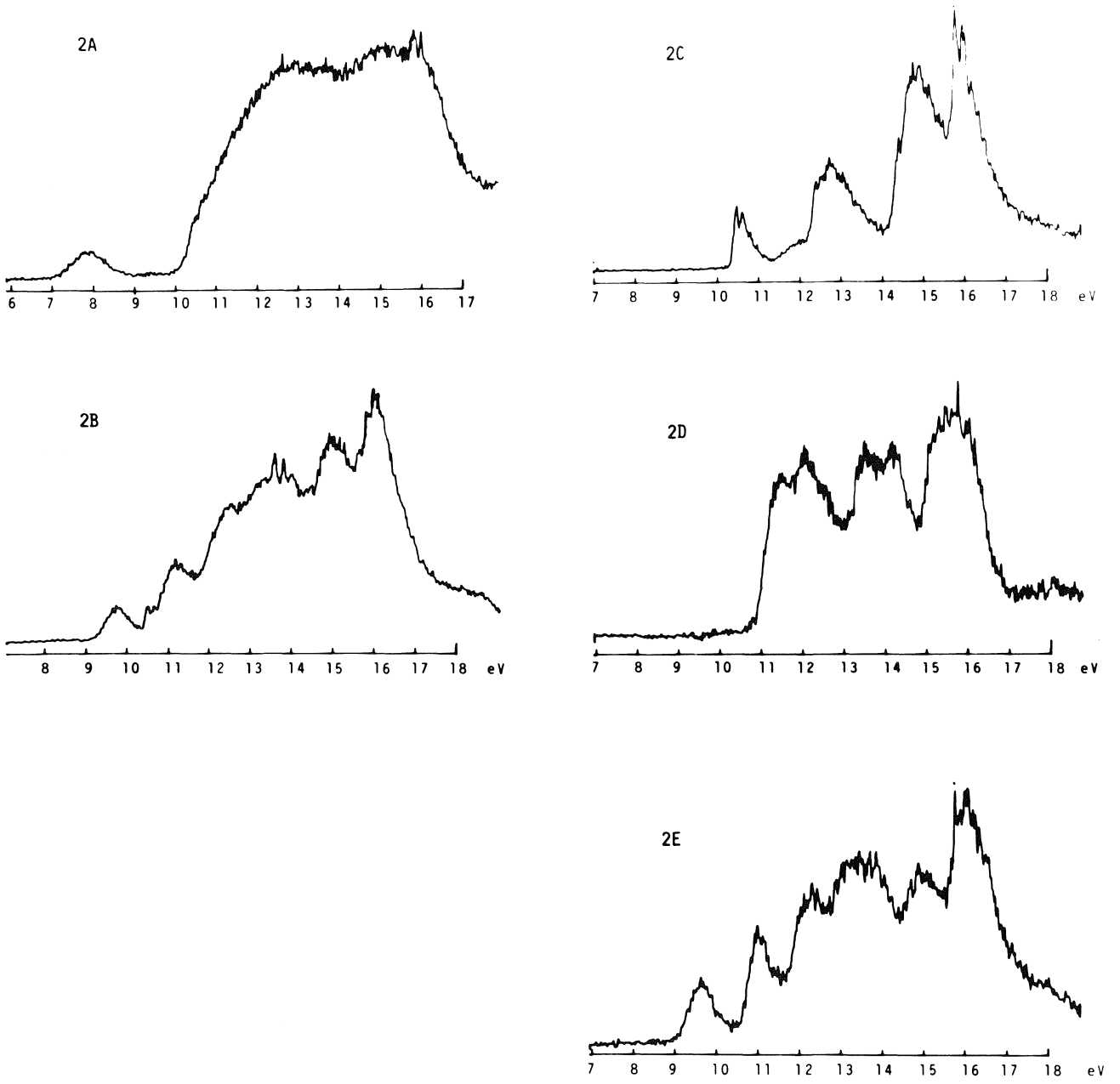

FIG. 2. 2*A*, p.e. spectrum of **1***b*. 2*B*, p.e. spectrum of thermolysate of **1***b*. 2*C*, p.e. spectrum of ethene. 2*D*, p.e. spectrum of propane. 2*E*, p.e. spectrum of *N*-ethylmethylenimine (**3***b*).

TABLE 1. Experimental ionization energies and molecular orbital eigenvalues of *N*-methylmethylenimine

Expt.[a]	MNDO[b,c]	MNDO[b,c] opt.	3-21G[b,c]	6-31G*[b,c]
9.8	10.87	10.64	10.78 (9.91)[d]	(10*a'*)[e] 11.04 (10.16)[d]
11.3	11.36	11.43	11.02 (10.14)	(2*a''*) 11.05 (10.17)
13.4	13.62	13.47	14.54 (13.38)	(9*a'*) 14.52 (13.35)
	15.08	14.94	16.30 (15.00)	(8*a'*) 16.16 (14.86)
15.9	16.11	15.87	16.88 (15.52)	(1*a''*) 16.89 (15.53)
	16.58	16.69	17.89 (16.45)	(7*a'*) 17.84 (16.41)

[a]Maxima taken as vertical IEs are reported in electron volts; ±0.1 eV.
[b]The experimental geometry was used.
[c]Only the MOEs which are <21 eV are reported.
[d]92% of Koopmans' theorem.
[e]Orbital symmetry.

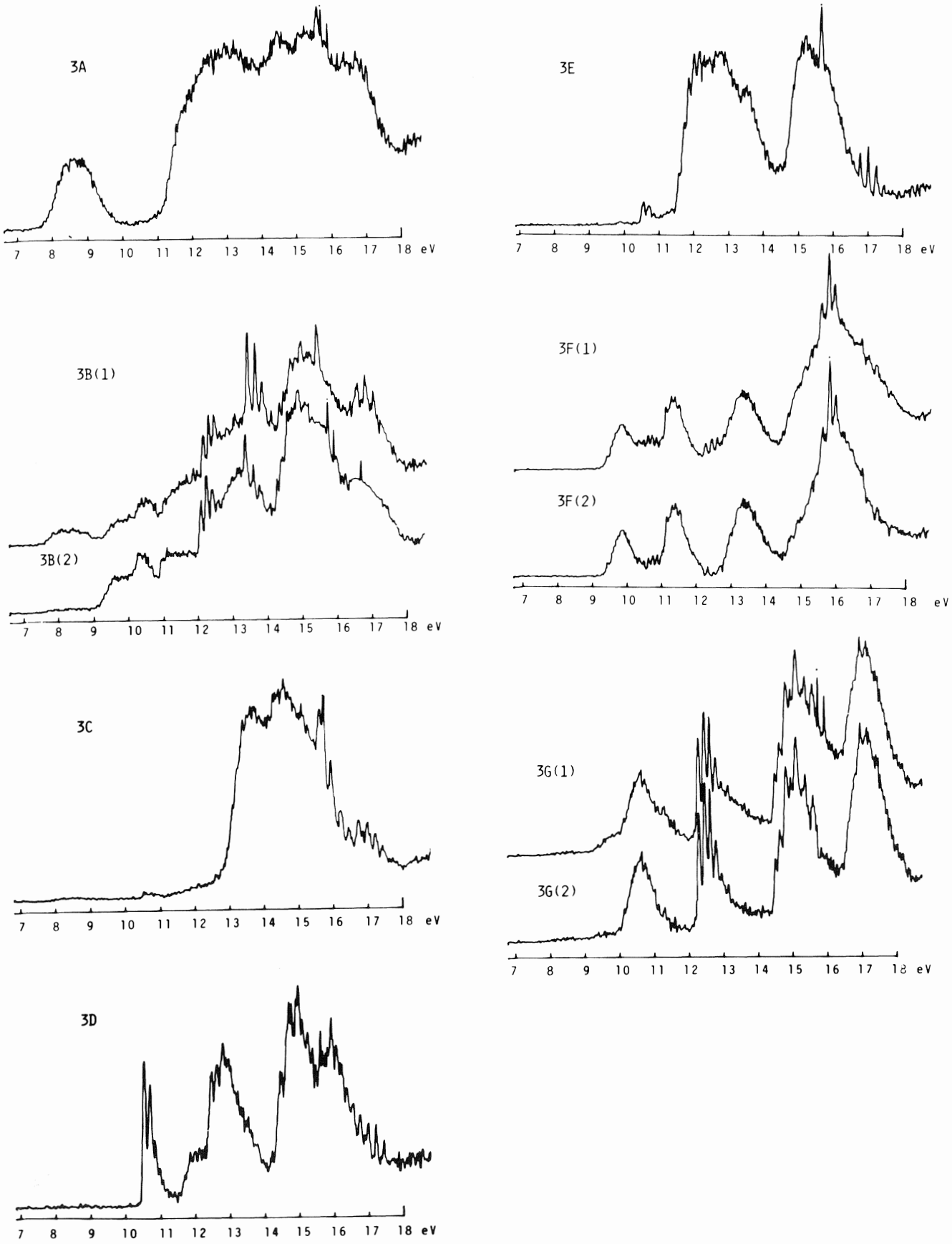

FIG. 3. 3*A*, p.e. spectrum of **1***c*. 3*B*(1), p.e. spectrum of thermolysate of **1***c*. 3*B*(2), p.e. spectrum of thermolysate of **1***c* passed through solid Dry-Ice trap. 3*C*, p.e. spectrum of methane and hydrogen. 3*D*, p.e. spectrum of ethene. 3*E*, p.e. spectrum of ethane. 3*F*(1), p.e. spectrum of *N*-methylenimine (**3***a*) and methylenimine (**3***c*). 3*F*(2), p.e. spectrum of 3*F*(1) minus p.e. spectrum 3*G*(1). 3*G*(1), p.e. spectrum of methylenimine (**3***b*) and *N*-methylenimine (**3***a*). 3*G*(2), p.e. spectrum 3*G*(1) minus p.e. spectrum 3*F*(2).

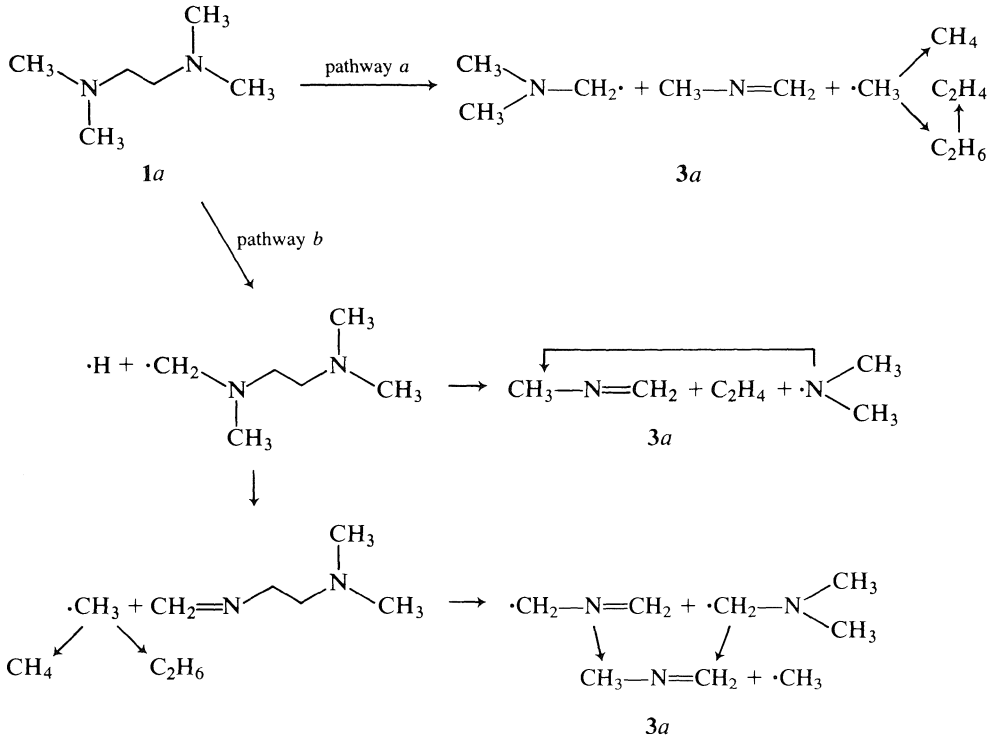

SCHEME 1

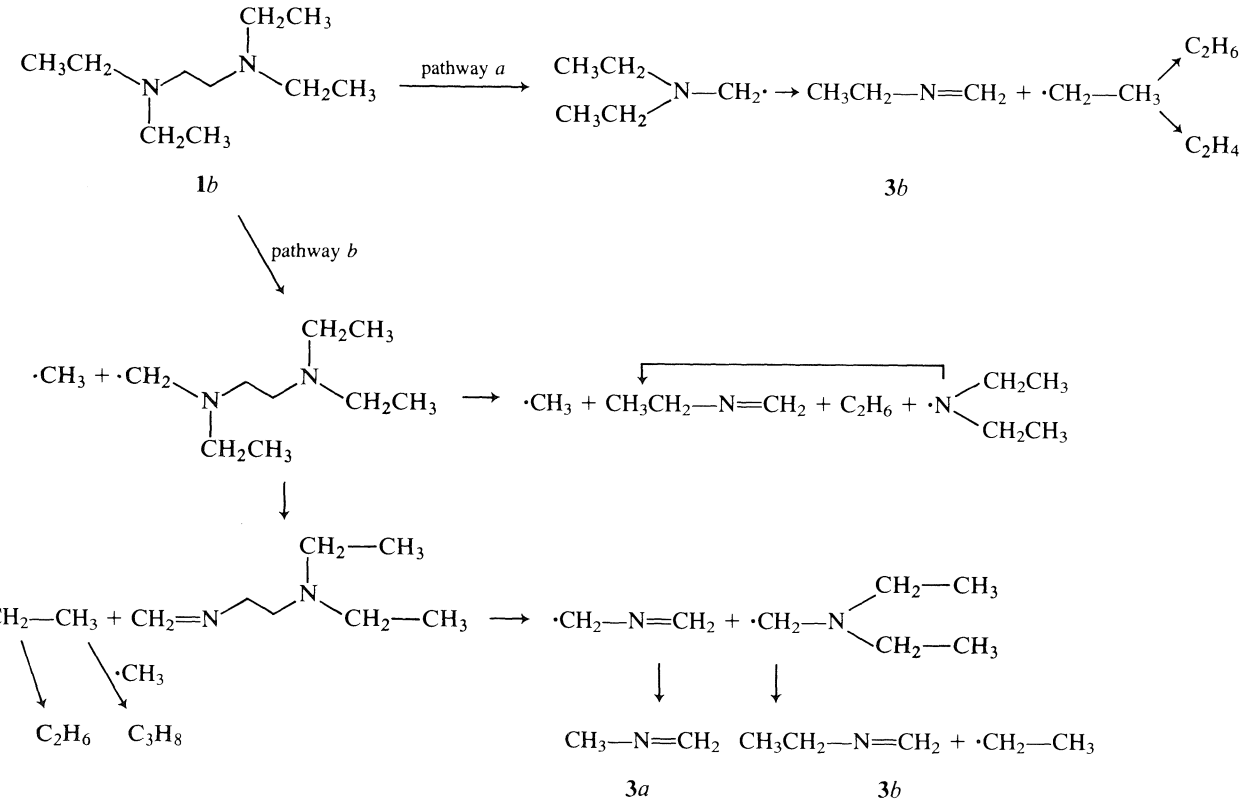

SCHEME 2

heretofore unreported, is a major product. Ethene, also a major product, could result from loss of a hydrogen atom from the ethyl radical formed by β-scission of the *N*,*N*-diethylaminomethylene radical. Unlike the case of TMEDA where R· dimerizes, the dimer of $CH_3—CH_2·$ is not observed presumably because loss of a hydrogen atom is fast. However, this mechanism does not account for the formation of propane, also a major product. An attractive alternative is shown as pathway *b*. Cleavage of a C—C bond of an ethyl group followed by further bond cleavages yields **3***a*, ethene, methyl radicals, and ethyl radicals which lead to the other products. That methane is not formed in significant amount may be a consequence of the

TABLE 2. Experimental ionization energies and molecular orbital eigenvalues of *N*-ethylmethylenimine

Expt.[a]	HAM/3[b]	MNDO[b]	MNDO[b] opt.	STO-3G[b,c]	3-21G[b,c]	6-31G*[b,c]
9.7	9.35	10.70	10.45	8.75	10.39 (9.56)[d]	(13*a*')[e] 10.43 (9.50)[d]
11.1	11.08	11.28	11.36	9.45	10.99 (10.11)	(3*a*") 11.13 (10.24)
12.3	12.89	13.42	12.94	13.00	14.12 (12.99)	(12*a*') 13.56 (12.47)
13.4	12.99	13.54	13.41	13.35	14.12 (12.99)	(2*a*") 13.88 (12.77)
14.0	13.24	13.69	14.12	13.47	14.48 (13.32)	(11*a*') 14.94 (13.74)
15.0	14.27	15.47	15.45	14.88	16.31 (15.01)	(10*a*') 16.48 (15.16)
16.0	15.69	16.05	15.81	16.62	17.50 (16.10)	(9*a*') 17.03 (15.67)
	16.10	17.29	16.86	17.25	18.49 (17.01)	(1*a*") 17.75 (16.33)
	18.40	21.30	21.76	19.61	20.75	(8*a*') 20.86

[a]Maxima taken as vertical IEs are reported in electron volts; ±0.1 eV.
[b]Only the MOEs which are <22 eV are reported.
[c]The MNDO optimized geometry was used.
[d]92% of Koopmans' theorem.
[e]Orbital symmetry.

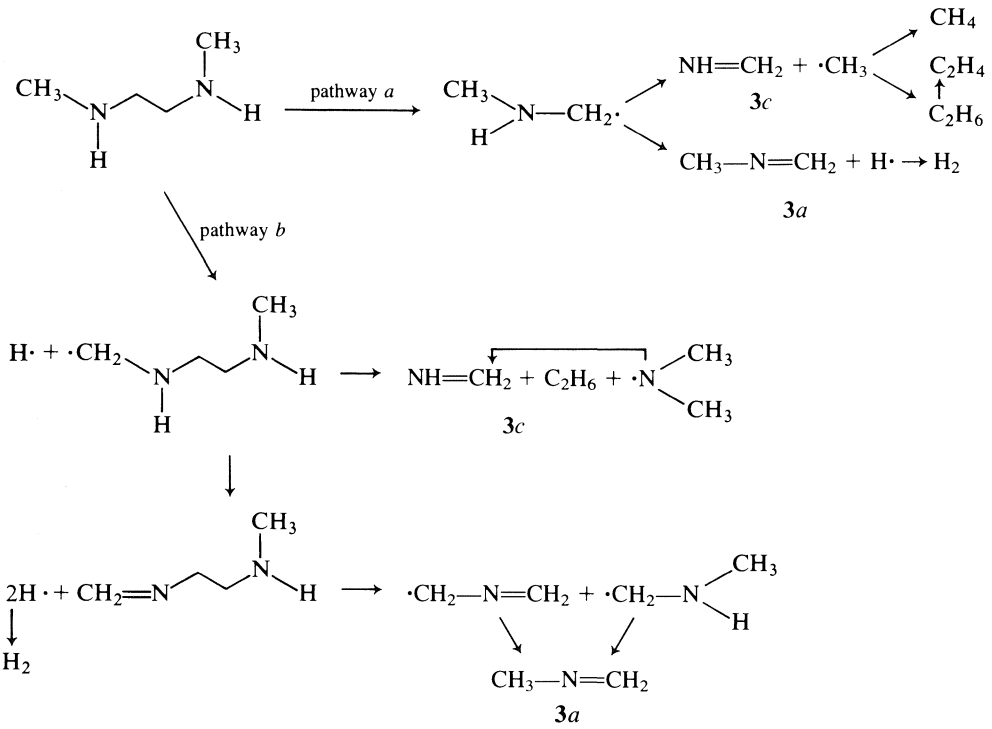

SCHEME 3

fact that methyl radicals are scavenged by ethyl radicals. The small amount of **3***a* observed in "transition" spectra in several thermolyses could result from decomposition of **3***b* to the 2-azaallyl radical (CH_2=N—CH_2·) or from decomposition of the intermediate CH_2=N—CH_2—CH_2R shown in pathway *b*. Whatever the route to propane and **3***a*, thermolysis of TEEDA appears to be more complex than thermolysis of TMEDA. Nevertheless, that **3***b* is a major product is clear from spectra 2*B* and 2*E*, the nature of the other products, its volatility in the low temperature distillation — it distilled after propane — and by the fact the IEs of the "lone-pair" and the "π-system" are slightly lower (~0.1 eV) than the IEs of **3***a*. These differences are comparable to the small differences in IEs reported for *N*-methyl- and *N*-ethylimines **5** (14) and **6** (15). The results of calculations listed in Table 2 also support the assignment of spectrum 2*E* to **3***b*.

Thermolysis of *s*-DMEDA can also be rationalized on the basis of a mechanism (Scheme 3) that is identical to the one suggested for TMEDA (Scheme 1). That a higher temperature is required to achieve significant conversion of *s*-DMEDA is in keeping with an expected lower stability of the *N*-methylaminomethylene radical — relative to its fully alkylated analogue — which is reflected in the C—C dissociation energy. That imines **3***a* and **3***c* are obtained in roughly equal yields, based on the number of scans which were acquired at the same pressure, indicates that cleavage of the C—H and C—C bonds is equally likely. However, this pathway does not account for the formation of ethene, a major product, unless it is formed by dehydrogenation of ethane. An alternative mehanism, shown as pathway *b*, which leads to ethene, **3***c* and H_2 involves initial cleavage of a C—H bond to yield an *N*-alkylaminomethylene radical that undergoes further decomposition.

CH_3—CH=N—CH_3
5
(n, 9.5; π, 10.67)

CH_3—CH_2—CH=N—CH_2—CH_3
6
(n, 9.45; π, 10.35)

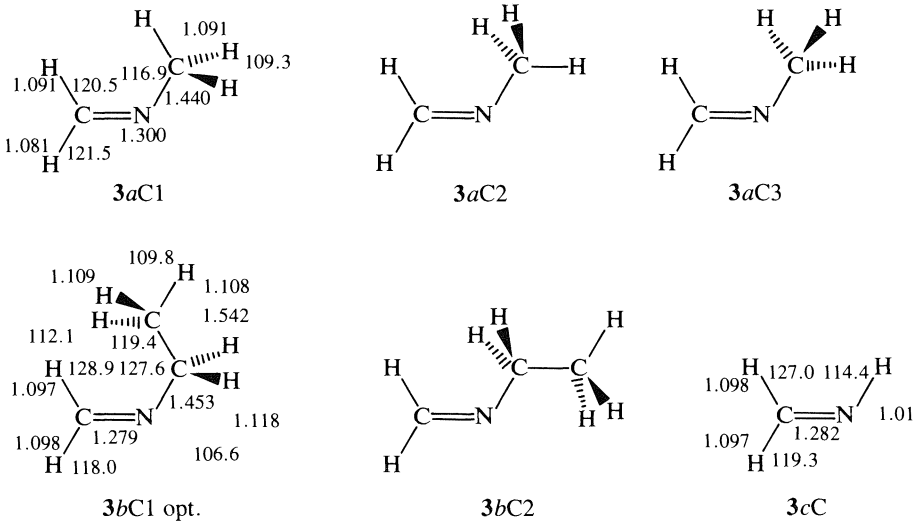

FIG. 4. Structural parameters and conformations of methylenimines.

TABLE 3. Experimental ionization energies and molecular orbital eigenvalues of methylenimine

Expt.[a]	MNDO[b,c]	MNDO opt. trial. geom.	MNDO opt. expt. geom.	STO-3G[b,c]	6-31G*[b,c]
10.6	11.37	11.19	11.19	9.50	(7a')[d] 11.63 (10.70)[e]
12.4	12.10	12.13	12.13	10.25	(1a") 12.09 (11.12)
15.1	15.03	15.07	15.07	15.26	(6a') 16.31 (15.01)
17.2	17.14	17.70	17.70	17.00	(5a') 18.57 (17.08)

[a]Maxima taken as vertical IEs and reported in electron volts; ±0.1 eV.
[b]Calculated using the experimental geometry.
[c]Only the MOEs which are <21 eV are reported.
[d]Orbital symmetry.
[e]92% of Koopmans' theorem.

Calculation of molecular orbital eigenvalues (MOEs)

The geometry used in the calculations on **3***a*, shown as **3***a*Cl (Fig. 4), was obtained by microwave spectroscopy (16, 17). It is seen in Table 1 that MNDO yields MOEs which closely parallel the experimental IEs although the binding energy of the "lone-pair" is somewhat high. That the calculations yield MOEs — especially those obtained by MNDO optimization of the experimental geometry — which closely approximate the IEs, indicates that this method can be used to identify simple imines with some degree of confidence. Hence the data in Table 2 provide support that **3***b* is indeed a product of thermolysis of TEEDA. Although the geometry of **3***b* is unknown, calculations were initially carried out on a geometry based on **3***a*Cl, a NCC bond angle of 109.3°, CCH angles of 109.3°, and C—C and C—H bond lengths of 1.540 and 1.091 Å, respectively. The good correlation between the experimental IEs and the calculated MOEs (column 2, Table 2) validates this assumption and supports the conclusion that **3***b* is a product of thermolysis of TEEDA. MNDO optimization (see **3***b*Cl, Fig. 4) of the trial geometry yields a better fit of the MOEs (column 3, Table 2) and the experimental IEs. The same general trends in the MOEs are observed for **3***b* as are observed for **3***a*. Both 3-21G and 6-31G* bases yield MOEs which are reasonably close to the IEs although the fit is not quite as good at higher energies. However, if 92% of the Koopmans' values are used (18), the fit is improved. Although the fit at higher IEs is reasonably good when the STO-3G basis is used, the MOEs for the "lone pair" and the "π-system" are somewhat low. Optimizations using 3-21G and 6-31G* bases was not carried out because of the cpu time required relative to MNDO.

MOEs were also obtained for two other conformations of **3***a*: **3***a*C2 (MNDO opt.; 10.62, 11.43, 13.47, 14.95, 15.87, and 16.69) and **3***a*C3 (MNDO; 10.84, 11.37, 13.76, 15.13, 16.09, and 16.58). MOEs (10.60, 11.40, 13.07, 13.09, 13.47, 15.63, 15.64, 16.80) were also calculated for the zig–zag conformation of **3***b* shown as **3***b*C2 (Fig. 4) using MNDO with optimization.

Calculations carried on the experimental geometry[4] (19) of **3***c* complement the calculations carried out previously (10). In this connection it is useful to point out, once again, the utility of MNDO. The experimental geometry of the CH_2=N— fragment of **3***a* (see **3***a*Cl, Fig. 4), was used with an assumed =N—H bond length of 0.99 Å (20) and the parameters optimized using MNDO (see **3***c*C, Fig. 4) to calculate the MOEs (column 1, Table 3). The correlation between the parameters obtained by optimization and the experimental values is good. The MOEs obtained by optimizing the experimental geometry[4] (column 2, Table 3) are identical to the values obtained by optimizing the trial geometry. This indicates that accurate experimentally-obtained geometries will not be required to obtain MOEs which will be useful for identifying other, as yet unknown, imines.

[4]Geometry: *r*CN = 1.273, *r*NH = 1.021, *r*CH = 1.09 Å, ∠HNC = 110.4, ∠HCH = 117.0, and ∠NCH(*cis*) = 125.1, ∠NCH(*trans*) = 117.9°.

Acknowledgements

The author thanks the Natural Sciences and Engineering Research Council of Canada for financial support, Dr. D. Griller for helpful discussions, Mr. F. Ramelan for invaluable assistance in constructing the p.e. spectrometer, and Mr. P. Nicholas Werstiuk for assistance in the theoretical calculations.

1. D. GRILLER and F. P. LOSSING. J. Am. Chem. Soc. **103**, 1586 (1981).
2. Y. LOGUINOV, V. V. TAKHISTOV and L. P. VATLINA. Org. Mass. Spectrosc. **16**, 239 (1981).
3. L. ASBRINK, C. FRIDH, and E. LINDHOLM. HAM/3, OCPE. No. 393, Bloomington, IN.
4. J. P. STEWART. MOPAC. QCPE. No. 455, Bloomington, IN.
5. J. S. BINKLEY, M. FRISCH, K. RAGHAVACHIRI, D. DEFREES, H. B. SCHLEGEL, R. WHITESIDE, E. FLUDER, R. SEEGER, and J. A. POPLE. Gaussian 82. Release H. Department of Chemistry. Carnegie-Mellon University, Pittsburgh (1984).
6. N. H. WERSTIUK, D. N. BUTLER, and E. SHAHID. Can. J. Chem. **65**, 760 (1986).
7. H. BOCK, R. DAMMEL, and S. AYGEN. J. Am. Chem. Soc. **105**, 7681 (1983).
8. D. C. FROST, B. MACDONALD, C. A. MCDOWELL, and N. P. C. WESTWOOD. J. Electron Spectrosc. Relat. Phenom. **14**, 379 (1976).
9. F. HOULE and J. L. BEAUCHAMP. J. Am. Chem. Soc. **101**, 4067 (1979).
10. K. KIMURA, S. KATSUMATA, Y. ACHIBA, T. YAMAZAKI, and S. IWATA. Handbook of HeI photoelectron spectra of fundamental organic molecules. Japan Scientific Societies Press, Tokyo. 1981.
11. J. B. PEEL and G. D. WILLETT. J. Chem. Soc. Faraday Trans. II, **71**, 1799 (1975).
12. D. C. FROST, S. T. LEE, C. A. MCDOWELL, and N. P. C. WESTWOOD. J. Electron Spectrosc. Relat. Phenom. **12**, 95 (1977).
13. D. C. FROST, W. M. LAU, C. A. MCDOWELL, and N. P. C. WESTWOOD. J. Mol. Struct. **90**, 283 (1982).
14. E. HASELBACH and E. HEILBRONNER. Helv. Chim. Acta, **53**, 684 (1970).
15. A. DARGELOS, R. POTTIER, and C. SANDORFY. J. Chem. Phys. **66**, 2860 (1977).
16. K. V. L. N. SASTRY and R. F. CURL. J. Chem. Phys. **41**, 77 (1964)
17. J. T. YARDLEY, J. HINZE, and R. F. CURL. J. Chem. Phys. **41**, 2562 (1964); **86**, 5068 (1964).
18. C. R. BRUNDLE, M. B. ROBIN, N. A. KUEBLER, and H. BASCH. J. Am. Chem. Soc. **94**, 1451 (1972).
19. R. PEARSON, JR., and F. J. LOVAS. J. Chem. Phys. **66**, 6904 (1977).
20. A. D. MITCHELL and L. C. CROSS (*Editors*). Tables of interatomic distances and configuration in molecules and ions. The Chemical Society, London. Special Publication No. 11. 1953. p. S7.

Synthesis and in vitro activity of several new carbapenems

YASUTSUGU UEDA[1] AND VIVIANE VINET

Antiinfective Chemistry Department, Pharmaceutical Research and Development Division, Bristol-Myers Co., 100 Industrial Blvd., Candiac (Qué.), Canada J5R 1J1

Received March 12, 1986

YASUTSUGU UEDA and VIVIANE VINET. Can. J. Chem. **64**, 2184 (1986).

The synthesis and in vitro activity of several new carbapenems, 2-(3-*cis*-substituted cyclopentylthio)- and 2-(4-*cis*-substituted cyclohexylthio)-(6*S*)-[(1′*R*)-hydroxyethyl]-(5*R*)-carbapen-2-em-3-carboxylic acids **7** and **8**, are described. The synthesis involves the stereospecific preparation of *cis*-substituted cyclopentyl- and cyclohexylthiols **2** and **3** by the hetero Diels–Alder reaction followed by some chemical manipulations.

YASUTSUGU UEDA et VIVIANE VINET. Can. J. Chem. **64**, 2184 (1986).

On décrit la synthèse et l'activité in vitro de plusieurs nouveaux carbapénèmes, soit les acides (X-3-*cis* cyclopentylthio)-2 et (X-4-*cis* cyclohexylthio)-2 [hydroxy-1′*R* éthyl]-6*S* carbapène-2 ème-2 carboxyliques-3 (**7** et **8**). La synthèse implique la préparation stéréospécifique des cyclopentyl- et cyclohexylthiols, **2** et **3**, portant des substituants en position *cis*; cette synthèse implique une réaction hétérocyclique de Diels–Alder qui est suivie de quelques manipulations chimiques.

[Traduit par la revue]

Since the discovery of thienamycin (**1**), a potent and broad spectrum antibiotic, extensive efforts have been directed toward the chemical modification at the 2-position of the carbapenem ring system, to improve the undesirable characteristics associated with this antibiotic, that is, chemical and metabolic instability (1). The 6*S*-(1*R*-hydroxyethyl) group has been left unchanged, since it was reported to be responsible for the β-lactamase stability of thienamycin (2).

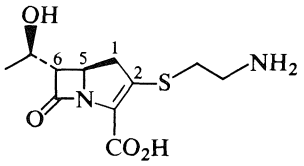

1

As part of our program directed toward the synthesis of thienamycin analogs, we designed novel side chains, 3-substituted cyclopentylthio- and 4-substituted cyclohexylthio groups, at the 2-position of the carbapenem ring system. Unlike the thioethyl chain in thienamycin, these cyclic rings will provide a more rigid spacing between the terminal functionality (e.g., amino group in thienamycin) and the nucleus. Thus the effect of the ring vs. the flexible ethyl chain on the antibacterial potency might be observed.

In this paper, we wish to describe (*1*) the stereospecific preparation of 3-*cis*-substituted cyclopentylthiols **2** and 4-*cis*-substituted cyclohexylthiols **3** by applying an hetero Diels–Alder reaction of cyclic dienes **4**, and **5**, with 1,1′-thiocarbonylbis(1,2,4-triazole), **6**, which was recently developed by Larsen and Harpp (3) and (*2*) the subsequent synthesis and the in vitro antibacterial activity of 2-(3-*cis*-substituted cyclopentylthio)- and 2-(4-*cis*-substituted cyclohexylthio)carbapenems, **7** and **8**.

Thiabicyclo compounds **9** and **10**, prepared by the method of Larsen and Harpp (3) from cyclopentadiene (**4**) and 1,3-cyclohexadiene (**5**) respectively, with thiocarbonylbis-triazole **6** were hydrogenated in the presence of 10% Pd–carbon in ethyl acetate to give thiabicycloheptane **11** and thiabicyclooctane **12**

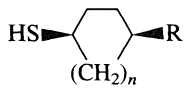

2, $n = 1$
3, $n = 2$

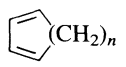

4, $n = 1$
5, $n = 2$

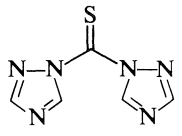

6

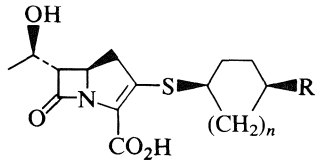

7, $n = 1$
8, $n = 2$

in 84.7 and 86.8% yield respectively. The partial hydrolysis of the bis-triazolyl moiety was successfully achieved by treatment with two equivalents of *p*-toluenesulfonic acid monohydrate in acetone to produce bicyclic thiolactones **13** and **14**[2] in 66.3 and 89.8% yield respectively (Scheme 1). These bicyclic thiolactones served as our common synthetic intermediates for the stereospecific preparation of several 3-*cis*-substituted cyclopentylthiols **2** and 4-*cis*-substituted cyclohexylthiols **3**.

It has been recognized that a strongly basic functionality, such as an amino or a formimidoyl group, in the side chain at the 2-position of the carbapenem ring system confers antibacterial activity, particularly antipseudomonal activity (2*b*). Therefore we were primarily interested in introducing a strongly basic group in the cyclopentyl- and cyclohexylthiols.

The stereospecific preparation of *cis*-3-(*p*-nitrobenzyloxycarbonylamino)cyclopentylthiol **2***a* and *cis*-4-(*p*-nitrobenzyloxycarbonylamino)cyclohexylthiol **3***a* from bicyclic thiolactones **13** and **14** is outlined in Scheme 2.

Bicyclic thiolactone **13** was hydrolyzed in refluxing 4 *N* HCl to produce *cis*-3-mercaptocyclopentyl carboxylic acid (**15**) in quantitative yield. *cis*-4-Mercaptocyclohexyl carboxylic acid (**16**) was more conveniently prepared, in 70.3% yield, from bis-triazolylthiabicyclooctane **12** by refluxing in 6 *N* HCl. However, this same treatment on thiabicyclopentane **11** often

[1]To whom all correspondence should be addressed: Antiinfective Chemistry Department, Pharmaceutical Research and Development Division, Bristol-Myers Co., P.O. Box 5100, Wallingford, CT 06492, U.S.A.

[2]Bicyclic thiolactone **14** was also prepared by a partial hydrolysis of **10** to thiolactone **i** followed by hydrogenation. However, the hydrogenation was much slower than that on **12**, requiring a large amount of the catalyst (10% Pd–C, three times by weight).

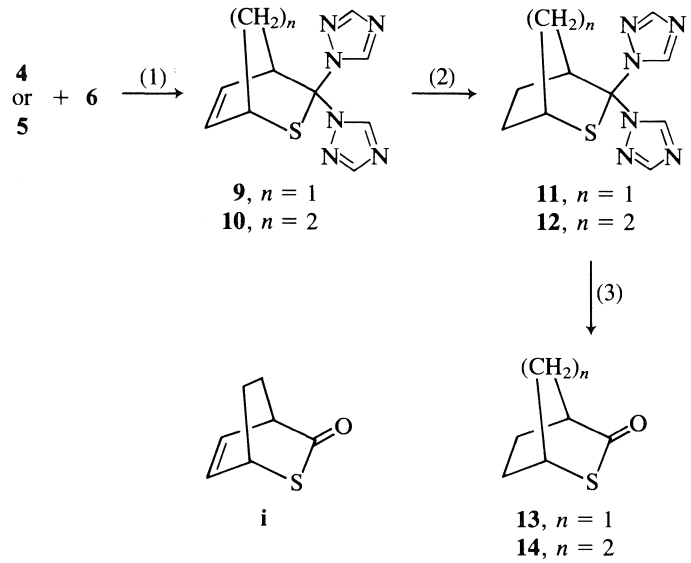

(1) Δ, CH_2Cl_2 or benzene
(2) H_2/Pd–C, EtOAc
(3) *p*-TsOH·H_2O, acetone

SCHEME 1

produced a mixture of thiolactone **13** and carboxylic acid **15**. The thiol group was readily protected by treatment with triphenylmethyl chloride (trityl chloride) and pyridine in $CHCl_3$, which produced tritylthio derivatives **17** and **18** in 72 and 63% yield respectively. These carboxylic acids were converted to acyl azides **19** and **20** in 98 and 90% yield respectively by activation with ethyl chloroformate followed by reaction with NaN_3. Refluxing with *p*-nitrobenzyl alcohol in toluene furnished bis-protected *cis*-amino cyclic thiols **21** and **22** in 63 and 84% yield respectively. The *cis* stereochemistry was maintained, since the Curtius rearrangement is known to proceed with retention of configuration. Finally the trityl group was removed (4) by treatment with mercuric acetate followed by reaction with H_2S, yielding the desired N-protected *cis*-3-aminocyclopentylthiol **2***a* as an oil and *cis*-4-aminocyclohexylthiol **2***b* as white crystals in quantitative yields.

The preparation of a few other *cis*-substituted cyclopentyl- and cyclohexylthiols, **2***b* and **3***b*–**3***e*, is outlined in Scheme 3. The nonbasic carbamyl and cyano groups were introduced into the ring for comparison of the antibacterial activity. The ring opening of bicyclic thiolactones **13** and **14** by ammonium hydroxide in methanol cleanly produced *cis*-carbamylcyclopentylthiol **2***b* and *cis*-carbamylcyclohexylthiol **3***b* in 88 and 90% yield respectively. The carbamyl derivative **3***b* was converted to 4-cyanocyclohexylthiol **3***c* in 52.5% yield by reaction with titanium tetrachloride in the presence of *N*-methylmorpholine (5). *cis*-Aminomethyl cyclohexylthiol hydrochloride (**3***d*) was prepared in 77% yield from **3***b* by lithium aluminum hydride reduction. Treatment with trimethylsilyl chloride followed by reaction with *p*-nitrobenzyl chloroformate (6) furnished N-protected *cis*-4-(aminomethyl)cyclohexylthiol **3***e*, which is a homolog of **3***a*, as white crystals in 57% yield.

The 2-(*cis*-substituted cyclopentylthiol and *cis*-substituted cyclohexylthiol)carbapenems **7***a*, **7***b* and **8***a*–**8***e* were prepared from the thiols described above, following essentially the same method developed by Salzmann *et al.* (7*a*) and Sletzinger *et al.* (7*b*) (Scheme 4).

Thus, the chiral 2-ketocarbapenam ester **23**, derived from diazoazetidinone **24** (7*a*, 8) was reacted with diphenyl chlorophosphate in the presence of diisopropylethylamine, then with *cis*-cyclopentyl- and cyclohexylthiols **2***a*, **2***b*, **3***a*, **3***b*, **3***c*, and **3***e* to furnish carbapenem esters **25***a*, **25***b*, and **26***a*–**26***d*. The hydrogenolysis over 10% Pd–C in the presence of pH 7.0 phosphate buffer produced *cis*-substituted cyclopentylthiol- and cyclohexylthiocarbapenem carboxylic acids or their salts **7***a*, **7***c*, **8***a*, and **8***c*–**8***e*. At this stage, two diastereomers in the cyclopentyl series **7***a* and **7***c* were successfully separated by hplc (high pressure liquid chromatography) on a reverse phase silica gel. No attempt was made to determine the absolute configuration of each diastereomer. The *N*-formimidolyl derivatives **7***b* and **8***b* were also prepared from the corresponding amino compounds **7***a* and **8***a* by treatment with benzyl formimidate hydrochloride in water at pH 8.5 (9).

In vitro antibacterial activities of the new carbapenems were tested and the minimum inhibitory concentrations (MIC) against a variety of Gram-positive and Gram-negative bacteria are listed in Table 1, which includes those of imipenem (*N*-formimidoyl thienamycin) for comparison.

The carbapenems having a strongly basic group, **7***a*, **7***b*, **8***a*, **8***b*, and **8***c*, generally exhibited better antibacterial activity than those having a nonbasic group, **7***c*, **8***c*, and **8***d*, although the latter also had good activity against Gram-positive and Gram-negative organisms. In the cyclopentyl series, two diastereomers did not show a significant difference in their antimicrobial potency. The aminomethyl derivative **8***d*, a homolog of **8***a*, was found to be less active against Gram-positive organisms than **8***a*. Among them, the most active carbapenem was one of the diastereomers of the *cis*-aminocyclopentylthio derivative **7***a*,

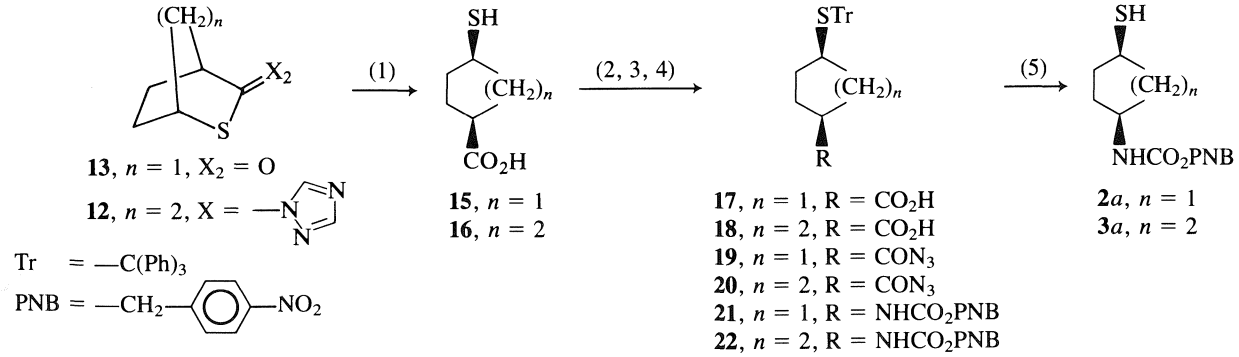

(1) 4–6 *N* HCl/H_2O, Δ; (2) $(Ph)_3CCl$, pyr/$CHCl_3$; (3) $ClCO_2Et$, Et_3N/aqueous acetone, then NaN_3; (4) PNB—OH/toluene, Δ; (5) $Hg(OAc)_2/CH_2Cl_2$–EtOH, then H_2S/CH_2Cl_2

SCHEME 2

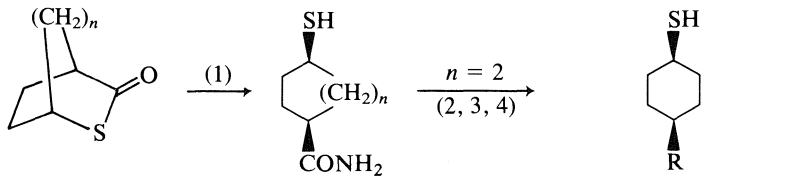

13, $n = 1$
14, $n = 2$

2*b*, $n = 1$
3*b*, $n = 2$

3*c*, R = CN
3*d*, R = $CH_2NH_2 \cdot HCl$
3*e*, R = CH_2NHCO_2PNB

(1) $NH_4OH/MeOH$; (2) $TiCl_4$, *N*-methylmorpholine/THF; (3) $LiAlH_4$/THF; (4) Me_3Si Cl, $(iPr)_2NEt/CH_3CN$, then $ClCO_2PNB$

SCHEME 3

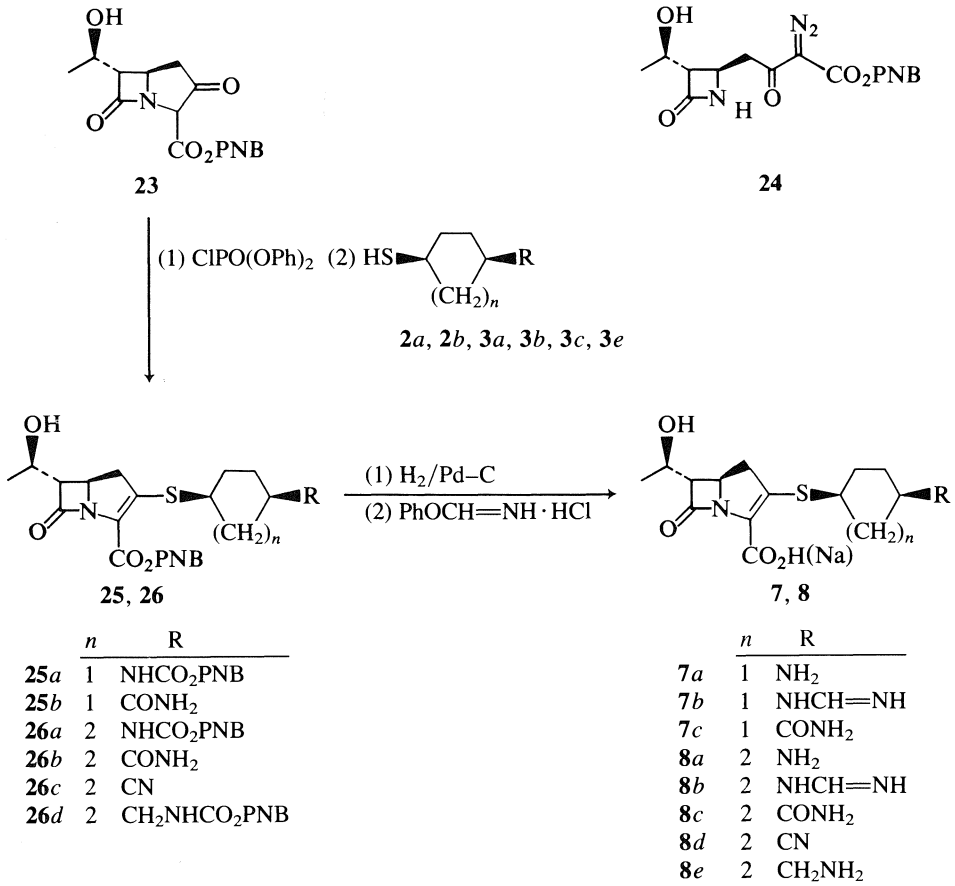

23

24

(1) $ClPO(OPh)_2$ (2) HS—(cyclohexyl)—R

2*a*, **2***b*, **3***a*, **3***b*, **3***c*, **3***e*

25, **26**

	n	R
25*a*	1	$NHCO_2PNB$
25*b*	1	$CONH_2$
26*a*	2	$NHCO_2PNB$
26*b*	2	$CONH_2$
26*c*	2	CN
26*d*	2	CH_2NHCO_2PNB

(1) H_2/Pd–C
(2) $PhOCH{=}NH \cdot HCl$

7, **8**

	n	R
7*a*	1	NH_2
7*b*	1	NHCH=NH
7*c*	1	$CONH_2$
8*a*	2	NH_2
8*b*	2	NHCH=NH
8*c*	2	$CONH_2$
8*d*	2	CN
8*e*	2	CH_2NH_2

SCHEME 4

which had comparable activities to imipenem, except against pseudomonas aeruginosa. Overall, the introduction of the rigid ring system between the nucleus and the strongly basic functionality did not significantly change the antibacterial potency.

Experimental

Melting points were determined on a Gallenkamp melting point apparatus and are not corrected. The infrared spectra were recorded on a Perkin–Elmer 267 grating infrared spectrometer. The ^1H nuclear magnetic resonance spectra were taken with either a Varian EM-360 (60 MHz), unless specified, or a Varian CFT-20 (80 MHz) nmr spectrometer. Tetramethylsilane was used as an internal standard and chemical shifts were reported in parts per million (δ) relative to the internal standard. The ultraviolet spectra were recorded on an Unicam SP8-100 uv spectrophotometer. Optical rotations were measured with a Perkin–Elmer Model 141 polarimeter. Tetrahydrofuran was freshly distilled from lithium aluminum hydride. All other solvents, with the exception of absolute EtOH, were reagent grade and had been stored over molecular sieves before use. Triethylamine, pyridine, and diisopropylethylamine were distilled from CaH_2 and stored over NaOH. Compounds **9** and **10** were prepared from cyclopentadiene and 1,3-cyclohexadiene respectively by the method of Larsen and Harpp (3). Compound **23** was obtained by the rhodium acetate catalyzed cyclization (7*a*) of diazoazetidinone **24**, which was in turn prepared as described in ref. 8. Analytical thin-layer chromatography (tlc) was conducted on either precoated plates (Silica Gel 60F-254, E. Merck) unless specified or reverse phase silica plates (Analtech), to obtain R_f values. High pressure column chromatography (hplc) was conducted on reverse phase silica gel, C_{18} μ Bondapak (Waters Associate). Column chromatography was carried out on Silica Gel 60 (70–230 mesh, E. Merck) unless specified. For purification of carbapenem esters **25** and **26**, Silica Gel 60 pure (70–230 mesh, E. Merck #7754) was used. The analyses were performed by Micro-Tech Laboratories, Skokie, Illinois, U.S.A.

*3,3-Bis(1,2,4-triazol-1-yl)-2-thiabicyclo[2.2.1]heptane (**11**)*

A solution of 3,3-bis(1,2,4-triazol-1-yl)-2-thiabicyclo[2.2.1]hept-5-ene (**9**) (3) (30.0 g, 0.122 mol; material recrystallized from *i*-PrOH/hexanes; mp 126–128°C) in EtOAc (800 mL) was mixed with 10% Pd–C (22.5 g, Engelhard). This mixture was hydrogenated in a Parr hydrogenation apparatus (H_2, 50 psi) at room temperature for 20 h. After filtration of the catalyst over Celite, the filtrate was evaporated to obtain 30.0 g of a green oil. This oil was purified by column chromatography (900 g, EtOAc:acetone 1:1) to obtain 25.6 g (0.103 mol, yield 84.4%) of the title compound **11** as a light yellow oil: R_f 0.49 (50% EtOAc/acetone); ir (neat) ν_{max}: 3130 (triazole-CH) and 1500 (C=N) cm^{-1}; ^{1}Hmr ($CDCl_3$) δ: 2.08 (6H, m, CH_2), 3.85 (1H, m, 4-H), 4.12 (1H, m, 1-H), 7.93 (2H, s, N=CH), 8.63 (1H, s, N=CH), and 8.67 (1H, s, N=CH) ppm.

*2-Thiabicyclo[2.2.1]heptan-3-one (**13**)*

A solution of 3,3-bis(1,2,4-triazol-1-yl)-2-thiabicyclo[2.2.1]heptane (**11**) (4.30 g, 17.3 mmol) in acetone (105 mL) was treated at room temperature with *p*-toluenesulfonic acid monohydrate (6.57 g, 34.6 mmol) for 1 h. After filtration of the precipitate, the filtrate was evaporated to yield 2.40 g of an oily solid, which was purified by column chromatography (72 g, 20% Et_2O/hexanes) to obtain 1.459 g (11.4 mmol, yield 65.9%) of the title compound **13** as a white solid: mp 88–89°C (sublime); R_f 0.40 (20% Et_2O/hexanes); ir (film) ν_{max}: 1710 (C=O) cm^{-1}; ^{1}Hmr ($CDCl_3$, CFT-20) δ: 1.5–2.4 (6H, m, CH_2), 3.00 (1H, m, 4-H), and 3.97 (1H, m, 1-H) ppm.

*2-Thiabicyclo[2.2.2]oct-5-en-3-one (**i**)*

The title compound **i** was prepared in 91.0% yield as white crystals from 3,3-bis(1,2,4-triazol-1-yl)-2-thiabicyclo[2.2.2]oct-5-ene (**10**) by the method described for the preparation of **13**: mp 61–63°C (lit. (10) mp 65–67°C, lit. (11) mp 73–74°C); R_f 0.31 (20% Et_2O/hexanes); ir (film) ν_{max}: 1680 (C=O) and 1615 (C=C) cm^{-1}; ^{1}Hmr ($CDCl_3$) δ: 1.5–2.4 (4H, m, CH_2), 3.63 (1H, m, 4-H), 4.20 (1H, m, 1-H), 6.32 (1H, td, J = 8 Hz, J = 2 Hz, 5-H), and 6.68 (1H, td, J = 8 Hz, J = 2 Hz, 6-H) ppm.

cis-*3-Mercaptocyclopentanecarboxylic acid (**15**)*

A suspension of 2-thiabicyclo[2.2.1]heptan-3-one (**13**) (4.50 g, 35.1 mmol) in 4 *N* HCl (22 mL) was heated at reflux under a nitrogen atmosphere for 4.5 h. This was extracted with EtOAc and the ethyl acetate extracts were washed with brine, dried ($MgSO_4$), and then evaporated to yield 5.09 g (34.8 mmol, yield 99.3%) of the title compound **15** as a colourless oil: R_f 0.20 (20% Et_2O/toluene). An analytical sample was obtained by purification on preparative silica gel plate (Schleicher and Schnell) eluting with 40% Et_2O in toluene to obtain the title compound as an oil: ir (neat) ν_{max}: 1700 (CO_2H) cm^{-1}; ^{1}Hmr ($CDCl_3$, CFT-20) δ: 1.70 (1H, d, J = 6.5 Hz, SH), 1.7–3.2 (8H, m, CH_2), and 9.2 (1H, br, CO_2H) ppm. *Anal.* calcd. for $C_6H_{10}O_2S$: C 49.29, H 6.89, S 21.93; found: C 49.49, H 6.89, S 22.04.

cis-*4-Mercaptocyclohexanecarboxylic acid (**16**)*

A suspension of 3,3-bis(1,2,4-triazol-1-yl)-2-thiabicyclo[2.2.2]octane (**12**) (1.04 g, 3.96 mmol) in 6 *N* HCl (10 mL) was heated at reflux under a nitrogen atmosphere for 2 h. This was extracted with EtOAc and the ethyl acetate extracts were washed with brine, dried ($MgSO_4$), and then evaporated to yield 580 mg of off-white solid. This was crystallized from boiling water (12 mL) to obtain 446 mg (2.79 mmol, yield 70.4%) of the title compound **16** as white crystals: mp 58–60°C; ir (film) ν_{max}: 1690 (CO_2H) cm^{-1}; ^{1}Hmr ($CDCl_3$, CFT-20) δ: 1.51 (1H, d, J = 6.7 Hz, SH), 1.5–2.4 (8H, m, CH_2), 2.5 (1H, m, $CHCO_2$), 3.1 (1H, m, CHS), and 8.0 (br, CO_2H) ppm. *Anal.* calcd. for $C_7H_{12}O_2S$: C 52.47, H 7.55; found: C 52.33, H 7.54.

It should be noted that when less concentrated hydrochloric acid (4 *N* or 1 *N*) was used, the reaction was slower and, in some cases, produced bicyclothiolactone **14** as a by-product.

cis-*3-(Triphenylmethylthio)cyclopentanecarboxylic acid (**17**)*

To a solution of *cis*-3-mercaptocyclopentanecarboxylic acid (**15**) (4.94 g, 33.8 mmol) in $CHCl_3$ (156 mL; purified by passing through

TABLE 1. Antibacterial activity of new synthetic carbapenems and imipenem, MIC (μg/mL)*

Organisms (strain no.)	Imipenem	7a†		7b†		7c†		8a	8b	8c	8d	8e
		A	B	A	B	A	B					
Str. pneumoniae (A-9585)	0.001	0.001	0.001	0.001	0.002	0.004	0.008	0.0002	0.002	0.004	0.004	0.002
Str. pyogenes (A-9604)	0.001	0.001	0.002	0.002	0.002	0.016	0.03	0.0005	0.002	0.008	0.008	0.004
Staph. aureus (A-9537)	0.002	0.002	0.004	0.004	0.004	0.06	0.13	0.008	0.008	0.06	0.03	0.008
Escherichia coli (A15119)	0.016	0.008	0.016	0.008	0.016	0.016	0.06	0.16	0.03	0.03	0.03	0.03
K. pneumoniae (A-9664)	0.03	0.03	0.06	0.03	0.03	0.06	0.13	0.03	0.06	0.06	1.	0.13
Pr. mirabilis (A-9900)	0.06	0.008	0.13	0.03	0.06	0.06	0.13	0.06	0.06	0.03	0.06	0.06
Ps. aeruginosa (A-9843A)	1	8	8	8	8	32	>63	16	8	8	16	16

*Determined by 2-fold serial broth dilution assay (data from Microbiology Dept., Bristol-Myers, Syracuse, N.Y. U.S.A.). Str. = Streptococcus, Staph. = Staphylococcus, K. = Klebsiella, Pr. = Proteus, Ps. = Pseudomonas.
†MIC of two diastereomers (A and B) in this series is shown.

Merck Silica Gel 60) were added triphenylmethyl chloride (10.4 g, 37.3 mol) and pyridine (5.45 mL, 67.7 mmol) and the mixture stirred at room temperature under a nitrogen atmosphere for 72 h. This was washed with 1 *N* HCl (34 mL), then with brine, dried (Na_2SO_4), and evaporated, yielding yellow oil that was purified by column chromatography (580 g, 20% Et_2O/toluene) to obtain 9.77 g of white solid. This was crystallized from Et_2O–hexanes, yielding 9.17 g (23.6 mmol, yield 69.8%) of the title compound **17** as white crystals: mp 153–154°C; R_f 0.55 (20% Et_2O/toluene); ir (film) ν_{max}: 1700 (CO_2H) cm^{-1}; ^{1}Hmr ($CDCl_3$, CFT-20) δ: 1.5–2.1 (6H, m, CH_2), 2.3–2.8 (2H, m, CH), and 7.1–7.6 (15H, m, ArH's) ppm. *Anal.* calcd. for $C_{25}H_{24}O_2S$: C 77.28, H 6.23, S 8.25; found: C 77.16, H 6.24, S 8.27.

cis-*3-(Triphenylmethylthio)cyclopentanecarbonyl azide (**19**)*

To a solution of *cis*-3-(triphenylmethylthio)cyclopentanecarboxylic acid (**17**) (28.0 g, 72.1 mmol) in acetone (1.5 L) and H_2O (237 mL) was added triethylamine (12.2 mL, 87.7 mmol) followed by ethyl chloroformate (9.09 mL, 95.1 mmol). The mixture was stirred for 2 min and then to this mixture was added a solution of sodium azide (7.42 g, 0.114 mol) in H_2O (237 mL) at 0–5°C. This was stirred for 4 min and then poured into cold water (1.5 L) and extracted with Et_2O (700 mL × 3). The ether extracts were washed with water, dried ($MgSO_4$), and evaporated to yield 29.5 g (71.3 mmol, crude yield 98.9%) of the title compound **19** as a crude oil: R_f 0.70 (Et_2O); ir (neat) ν_{max}: 2270 (NCO), 2140 (N_3), and 1710 (C=O) cm^{-1}. The ir spectrum indicated the presence of the isocyanate as an impurity. This crude material was immediately used in the subsequent reaction.

cis-*3-(Triphenylmethylthio)-1-(*p*-nitrobenzyloxycarbonylamino)cyclopentane (**21**)*

A mixture of *cis*-3-(triphenylmethylthio)cyclopentylcarbonyl azide (**19**) (10.89 g, 26.3 mmol; crude) and *p*-nitrobenzylalcohol (19.8 g, 120 mmol; the material purchased from Aldrich Chem. Co. was triturated with Et_2O) in toluene (270 mL) was heated at gentle reflux for 20 h, by which time the ir spectrum indicated the absence of the peaks at 2140 and 2270 cm^{-1}. After evaporation of the solvent, the residual solid was purified by column chromatography (700 g, 10% Et_2O/CH_2Cl_2) to obtain 13.0 g of foam, which was crystallized from Et_2O to yield 9.22 g (17.1 mmol, yield 65.1% of the title compound **21** as off-white crystals. An analytical sample was obtained by recrystallization from Et_2O–EtOAc: mp 128–130°C; R_f 0.62 (Et_2O); ir (film) ν_{max}: 3320 (NH), 1715, 1695 (C=O), 1515 and 1350 (NO_2) cm^{-1}; ^{1}Hmr ($CDCl_3$, CFT-20) δ: 1.0–2.2 (6H, m, CH_2), 2.69 (1H, m, CHS), 3.7 (1H, m, CHN), 4.7 (1H, br, NH), 5.15 (2H, s, CH_2CO_2), 7.1–7.5 (17H, m, ArH's), and 8.20 (2H, "d", J = 8.7 Hz, ArH's) ppm. *Anal.* calcd. for $C_{32}H_{30}N_2O_4S$: C 71.35, H 5.61, N 5.20; found: C 71.35, H 5.56, N 5.32.

cis-*3-Mercapto-1-(*p*-nitrobenzyloxycarboxylamino)cyclopentane (**2**a)*

A solution of *cis*-3-(triphenylmethylthio)-1-(*p*-nitrobenzyloxycarbonylamino)cyclopentane (**21**) (27.2 g, 50.5 mmol) in CH_2Cl_2 (715 mL) was diluted with absolute EtOH (715 mL). To this solution was added mercuric acetate (16.1 g, 50.5 mmol) at once and the mixture stirred at room temperature for 15 min, by which time the tlc (Et_2O) indicated the reaction was complete. The resulting clear solution was evaporated and the solid residue was triturated with Et_2O (300 mL × 2), yielding 30.0 g of the intermediate, mercuric salt, as a white solid: ir (film) ν_{max}: 1720 cm^{-1}.

This solid (30.0 g) was dissolved in CH_2Cl_2 (250 mL) and the solution was saturated with H_2S by bubbling through at 0–5°C for 1 h. The resulting black precipitate was filtered over Celite and the clear filtrate was treated with Norite (activated carbon). Evaporation of the filtrate and trituration of the residue with Et_2O gave 15.34 g (51.8 mmol, crude yield >100%) of the title compound (**2***a*) as white crystals. This crude material was used in the subsequent reaction without further purification. An analytical sample was obtained by recrystallization from EtOAc–Et_2O–hexanes: mp 87–88°C; R_f 0.68 (Et_2O); ir (film) ν_{max}: 3320 (NH) and 1685 (C=O) cm^{-1}; ^{1}Hmr ($CDCl_3$, CFT-20) δ: 1.4–2.8 (7H, m, CH_2, SH), 3.3 (1H, m, CHS), 4.1 (1H, m, CHN), 5.18 (2H, s, CH_2CO_2), 7.50 (2H, "d", J = 8.7 Hz, ArH's), and 8.20 (2H, "d", J = 8.8 Hz, ArH's) ppm. *Anal.* calcd. for $C_{18}H_{16}N_2O_4S$: C 52.69, H 5.44, N 9.45; found: C 52.38, H 5.32, N 9.21.

cis-*3-Mercaptocyclopentanecarboxamide (**2**b)*

A solution of 2-thiabicyclo[2.2.1]heptan-3-one (**13**) (2.56 g, 20.0 mmol) in MeOH (80 mL; deoxygenated by bubbling through nitrogen gas) was mixed with concentrated ammonium hydroxide (39.94 mL), and stirred at room temperature under a nitrogen atmosphere for 20 h. The solvent was evaporated to dryness and the solid residue was triturated with Et_2O to obtain 2.55 g (17.6 mmol, yield 88.2%) of the title compound **2***b* as a white solid. An analytical sample was obtained by crystallization from *iso*-propanol–hexanes: mp 138–140°C; ir (Nujol) ν_{max}: 3360, 3190 (NH), 2550 (SH), 1660 (sh), and 1635 ($CONH_2$) cm^{-1}; ^{1}Hmr ($CDCl_3$, CFT-20) δ: 1.5–2.9 (8H, m, CH_2, CHCO, SH), 3.2 (1H, m, CHS), and 5.4 (br, NH_2) ppm. *Anal.* calcd. for $C_6H_{11}NOS$: C 49.62, H 7.63, N 9.65; found: C 49.52, H 7.43, N 9.57.

cis-*1-Cyano-4-mercaptocyclohexane (**3**c)*

A solution of $TiCl_4$ (1.1 mL, 10 mmol) in CCl_4 (2.5 mL) was injected, at 0–5°C under a nitrogen atmosphere, into THF (20 mL). To the resulting yellow mixture was added a suspension of *cis*-4-mercaptocyclohexanecarboxamide (**3***b*) (800 mg, 5.02 mmol) in THF (20 mL), followed by a solution of *N*-methylmorpholine (2.2 mL) in THF (2.0 mL). After stirring at 0–5°C under a nitrogen atmosphere for 1 h, to this mixture was added H_2O (30 mL) and EtOAc (30 mL). The ethyl acetate extract was washed with H_2O, brine, and dried (Na_2SO_4). Evaporation of the solvent *in vacuo* gave 623 mg of an oily solid, which was purified by column chromatography (30 g, EtOAc) to collect 495 mg of an oil. The corresponding disulfide, 4-cyanocyclohexyl disulfide (125 mg), crystallized out by addition of Et_2O–hexanes to this oil: mp 103–115°C; R_f 0.39 (Et_2O). The filtrate was evaporated to yield 370 mg (2.62 mmol, yield 52.2%) of the title compound **3***c* as a clear oil that crystallized on standing: mp 42–44°C; R_f 0.58 (Et_2O); ir (film) ν_{max}: 2560 (SH) and 2240 (CN) cm^{-1}; ^{1}Hmr ($CDCl_3$) δ: 1.63 (1H, d, J = 7 Hz, SH), 1.5–2.3 (8H, m, CH_2), and 2.85 (2H, br, CH) ppm.

cis-*4-Aminomethylcyclohexylthiol hydrochloride (**3**d)*

A suspension of lithium aluminum hydride (800 mg, 21.1 mmol) in THF (100 mL) was heated at reflux through a pressure-equalized dropping funnel where *cis*-4-mercaptocyclohexanecarboxamide (**3***b*) (795 mg, 5 mmol) was placed with a cotton plug. After 24 h, all of the amide **3***b* dissolved into the reaction flask and tlc (acetone:EtOAc 1:1) indicated the completion of the reaction. After cooling, the excess lithium aluminum hydride was destroyed by slow addition of H_2O (3 mL). This was slowly diluted with EtOAc (150 mL), and the precipitate was filtered over Celite and washed with hot EtOH (150 mL × 2). The filtrate and washings were combined and evaporated to yield 664 mg of a crude oil. This was dissolved in absolute EtOH (20 mL) and treated with HCl gas. The solvent was evaporated to yield white solid, which was rinsed with Et_2O to obtain 699 mg (3.85 mmol, yield 77.0%) of the title compound (**3***d*) as white solid: R_f 0.43 (CH_2Cl_2:1 *M* NH_4OH/MeOH 4:1); ir (Nujol) ν_{max}: 2550 (SH) cm^{-1}; ^{1}Hmr ($CDCl_3$, CFT-20) δ: 1.54 (1H, d, J = 6.4 Hz, SH), 1.73 (9H, br, CH_2, CH), 2.95 (2H, br, CH_2N), 3.35 (1H, br, CHS), and 8.35 (br, $^+NH_3$) ppm.

cis-*4-(*p*-Nitrobenzyloxycarbonylaminomethyl)cyclohexylthiol (**3**e)*

To a suspension of *cis*-4-aminomethylcyclohexylthiol hydrochloride (**3***d*) (190 mg, 1.05 mmol) in CH_3CN (10 mL) was added at 0–5°C, trimethylsilyl chloride (0.15 mL, 1.18 mmol) followed by diisopropylamine (0.42 mL, 2.42 mmol), under a dry nitrogen atmosphere. The mixture was stirred (0–5°C, N_2) for 30 min, and to this cloudy solution was added *p*-nitrobenzyl chloroformate (226 mg, 1.05 mmol) in CH_3CN (3 mL), followed by diisopropylethylamine (0.18 mL, 1.05 mmol). The mixture was stirred at 0–5°C for 3 h and diluted with EtOAc (30 mL). This was washed with brine, with 1 *N* HCl, and then with brine again, dried (Na_2SO_4), and evaporated to yield 341 mg of a crude oil. This oil was purified by column chromatography (20 g, CH_2Cl_2) to obtain 194 mg (0.60 mmol, yield 57%) of the title

compound **3***e* as an oil that crystallized on standing: mp 61–63°C; R_f 0.29 (CH_2Cl_2); ir (neat) ν_{max}: 3420, 3350 (CONH), 1720 (C=O), 1520 and 1350 (NO_2) cm^{-1}; ^{1}Hmr ($CDCl_3$) δ: 1.50 (1H, d, J = 5 Hz, SH), 1.56 (9H, br, CH_2, CH), 3–3.5 (3H, m, CH_2N, CHS), 5.17 (2H, s, CO_2CH_2), 5.35 (br, NH), 7.43 (2H, "d", J = 9 Hz, ArH's), and 8.13 (2H, "d", J = 9 Hz, ArH's) ppm.

Thiabicyclo[2.2.2]octane series **12** and **14**, and cyclohexyl series **18**, **20**, **22**, **3***a*, and **3***b* were prepared by the method described for the preparation of the corresponding 2-thiabicyclo[2.2.1]heptane series and cyclopentyl series respectively.

*3,3-Bis(1,2,4-triazol-1-yl)-2-thiabicyclo[2.2.2.]octane (**12**):* yield 86.8%; mp 139–141°C; R_f 0.67 (20% EtOAc/acetone); ir (film) ν_{max}: 3130 (triazole-CH) and 1500 (C=N) cm^{-1}; ^{1}Hmr ($CDCl_3$) δ: 1.2–2.2 (8H, m, CH_2), 3.22 (1H, br s, 4-H), 3.58 (1H, br s, 1-H), 7.92 (2H, s, N=CH), and 8.77 (2H, s, N=CH) ppm. *Anal.* calcd. for $C_{11}H_{14}N_6S$: C 50.36, H 5.38, N 32.04, S 12.22; found: C 50.54, H 5.48, N 32.41, S 12.19.

*2-Thiabicyclo[2.2.2.]octan-3-one (**14**):* yield 89.8%; mp 174–175°C (Et_2O–hexanes); R_f 0.31 (20% Et_2O/hexanes); ir (film) ν_{max}: 1675 (C=O) cm^{-1}; ^{1}Hmr ($CDCl_3$) δ: 2.0 (8H, m, CH_2), 2.37 (1H, m, 4-H), and 3.50 (1H, m, 1-H) ppm. *Anal.* calcd. for $C_7H_{10}OS$: C 59.12, H 7.09, S 22.55; found: C 59.23, H 6.99, S 22.37.

cis-*4-(Triphenylmethylthio)cyclohexanecarboxylic acid (**18**):* yield 62.9%; mp 172–174°C (EtOAc/hexane); R_f 0.44 (20% Et_2O/toluene); ir (film) ν_{max}: 1705 (CO_2H) cm^{-1}; ^{1}Hmr ($CDCl_3$) δ: 1.2–2.5 (10H, m, CH, CH_2) and 7.1–7.6 (15H, m, ArH's) ppm. *Anal.* calcd. for $C_{26}H_{26}O_2S$: C 77.58, H 6.51, S 7.97; found: C 77.61, H 6.57, S 7.94.

cis-*4-(Triphenylmethylthio)cyclohexanecarbonyl azide (**20**):* crude yield 89.4%; oil R_f 0.7 (Et_2O); ir (neat) ν_{max}: 2260 (NCO), 2140 (N_3), and 1720 (C=O) cm^{-1}.

cis-*4-(Triphenylmethylthio)-1-(*p*-nitrobenzyloxycarbonylamino)cyclohexane (**22**):* yield 84.2%; mp 184–186°C (CH_2Cl_2–pentane); R_f 0.72 (10% Et_2O/CH_2Cl_2); ir (film) ν_{max}: 3340 (NH), 1720, 1695 (C=O), 1520, and 1350 (NO_2) cm^{-1}; ^{1}Hmr ($CDCl_3$, CFT-20) δ: 1.2–1.8 (8H, m, CH_2), 2.49 (1H, q, J = 4.5 Hz, CHS), 3.45 (1H, br, $W_{1/2}$ = 20 Hz, CHN), 4.65 (1H, d, J = 8 Hz, NH), 5.16 (2H, s, CH_2CO_2), 7.1–7.6 (17H, m, ArH's), and 8.19 (2H, "d", J = 8.8 Hz, ArH's) ppm. *Anal.* calcd. for $C_{33}H_{32}N_2O_4S$: C 71.71, H 5.84, N 5.07, S 5.80; found: C 71.80, H 5.85, N 5.03, S 5.82.

cis-*4-Mercapto-1-(*p*-nitrobenzyloxycarbonylamino)cyclohexane (**3**a):* R_f 0.45 (Et_2O); ir (film) ν_{max}: 3400, 3340 (NH), and 1710 (C=O) cm^{-1}; ^{1}Hmr ($CDCl_3$, CFT-20) δ: 1.49 (1H, d, J = 6.1 Hz, SH), 1.5–2.0 (8H, m, CH_2), 3.15 (1H, m, $W_{1/2}$ = 16 Hz, CHS), 3.61 (1H, m, $W_{1/2}$ = 19 Hz, CHN), 4.76 (1H, br, NH), 5.18 (2H, s, CH_2CO_2), 7.49 (2H, "d", J = 8.8 Hz, ArH's), and 8.21 (2H, "d", J = 8.8 Hz, ArH's) ppm.

cis-*4-Mercaptocyclohexanecarboxamide (**3**b):* yield 90.1%; mp 198–200°C (*i*-PrOH–hexanes); R_f 0.46 (acetone:EtOAc 1:1); ir (Nujol) ν_{max}: 3370, 3200 (NH), 1665 and 1625 ($CONH_2$) cm^{-1}; ^{1}Hmr ($CDCl_3$, CFT-20) δ: 1.53 (1H, d, J = 6.8 Hz, SH), 1.5–2.2 (8H, m, CH_2), 2.17 (1H, m, CHCO), 3.23 (1H, br, CHS), and 5.3 (2H, br, NH_2) ppm. *Anal.* calcd. for $C_7H_{13}NOS$: C 52.79, H 8.23, N 8.80, S 20.13; found: C 52.75, H 8.13, N 8.57, S 20.17.

*General procedure for the preparation of carbapenem esters **25** and **26***

To a solution of *p*-nitrobenzyl (6*S*)-[(1*R*)-hydroxyethyl]-2-oxo-(5*R*)-carbapenam-(3*R*)-carboxylate (**23**) (1 mmol) and diisopropylethylamine (1.1 mmol) in CH_3CN (20 mL) was added at 0–5°C under a dry nitrogen atmosphere diphenyl chlorophosphate (1.1 mmol). The mixture was stirred for 1 h and to this was added at 0–5°C a solution of thiol **2** or **3** (1 mmol) in CH_3CN (5 mL), followed by diisopropylethylamine (1 mmol). For thiols **2***b* and **3***b*, the solution was made in DMF (5 mL). The mixture was stirred at room temperature under a nitrogen atmosphere; reaction time: 20 h for **25***a* and **26***c*, 3 days for **25***b* and **26***b*, 6 days for **26***a* and **26***d*. For **25***a*, the mixture was cooled to 0–5°C, and the crystals were collected. For others, the mixture was diluted with EtOAc, washed with H_2O (×2), then with brine, dried (Na_2SO_4), and evaporated. The crude material was purified by column chromatography (50% acetone/EtOAc for **25***b* and **26***b*; EtOAc for others).

p-*Nitrobenzyl(6*S*)-[(1*R*)-hydroxyethyl]-2-[*cis*-3-(*p*-nitrobenzyloxycarbonylamino)cyclopentylthio]-(5*R*)-carbapen-2-em-3-carboxylates (diastereomeric mixture) (**25**a):* yield 78.3%; mp 159–161°C (Et_2O–MeOH); R_f 0.35 (EtOAc); $[\alpha]_D^{22°}$ +29.7° (*c* 0.50, MeOH); ir (Nujol) ν_{max}: 3500, 3340, 1775 (β-lactam), 1700 (ester), 1520 and 1345 (NO_2) cm^{-1}; uv (EtOH) λ_{max}: 324 (ε 15 300) and 267 nm (ε 22 900); ^{1}Hmr ($CDCl_3$, CFT-20) δ: 1.37 (3H, d, J = 6.3 Hz, 1′-Me), 1.5–2.9 (6H, m, CH_2), 3.1–3.3 (3H, m, 1-H_2, 6-H), 3.5 (1H, m, CHS), 3.9–4.4 (3H, m, 1′-H, 5-H, CHN), 4.85 (1H, br, NH), 5.12–5.29–5.43–5.61 (2H, Abq, CH_2CO_2), 5.18 (2H, s, CH_2CO_2), 7.50 (2H, "d", J = 8.8 Hz, ArH's), 7.65 (2H, "d", J = 8.8 Hz, ArH's), and 8.22 (4H, "d", J = 8.8 Hz, ArH's) ppm. *Anal.* calcd. for $C_{29}H_{30}N_4O_{10}S$: C 55.58, H 4.83, N 8.94; found: C 54.86, H 4.84, N 8.90.

p-*Nitrobenzyl(6*S*)-[(1*R*)-hydroxyethyl]-2-[*cis*-3-carbamylcyclopentylthio]-(5*R*)-carbapen-2-em-3-carboxylates (diastereomeric mixture) (**25**b):* yield 31.7%; mp 164–166°C (isopropanol–hexanes); R_f 0.17 (EtOAc:acetone 1:1); $[\alpha]_D^{22°}$ +2.4° (*c* 0.6, MeOH); ir (Nujol) ν_{max}: 3490, 3450, 3430, 3210, 1765 (β-lactam), 1700 (ester), and 1665 ($CONH_2$) cm^{-1}; uv (EtOH) λ_{max}: 322 (ε 13 100) and 267 nm (ε 11 200); ^{1}Hmr (acetone-d_6, CFT-20) δ: 1.28 (3H, d, J = 6.1 Hz), 1.5–3.0 (7H, m), 3.1–3.8 (4H, m), 3.9–4.4 (2H, m), 5.15–5.34–5.44–5.63 (2H, ABq), 7.80 (2H, "d", J = 8.8 Hz), and 8.25 (2H, "d", J = 8.8 Hz) ppm.

p-*Nitrobenzyl(6*S*)-[(1*R*)-hydroxyethyl]-2-[*cis*-4-(*p*-nitrobenzyloxycarbonylamino)cyclohexylthio]-(5*R*)-carbapen-2-em-3-carboxylate (**26**a):* yield 30.3%; oil; R_f 0.23 (EtOAc); $[\alpha]_D^{22°}$ +51.8° (*c* 0.875, CH_2Cl_2); ir (film) ν_{max}: 3400 (OH), 1775 (β-lactam), 1705 (ester), 1525 and 1350 (NO_2) cm^{-1}; uv (EtOH) λ_{max}: 267 (ε 23 300) and 323 nm (ε 15 300); ^{1}Hmr ($CDCl_3$, CFT-20) δ: 1.35 (3H, d, J = 6.2 Hz, 1′-Me), 1.81 (8H, br s, CH_2), 3.04 (1H, dd, J = 17.5 Hz, J = 7.5, 1-H), 3.19 (1H, dd, J = 4.7 Hz, J = 2 Hz, 6-H), 3.3 (1H, m, CHS), 3.44 (1H, dd, J = 17.5 Hz, J = 7.6 Hz, 1-H), 3.7 (1H, m, CHN), 4–4.4 (2H, m, 5-H, 1′-H), 4.75 (1H, br, NH), 5.11–5.28–5.42–5.60 (2H, ABq, 3-CH_2CO_2), 5.17 (2H, s, CH_2CO_2), 7.49 (2H, "d", J = 8.8 Hz, ArH's), 7.64 (2H, "d", J = 8.8 Hz, ArH's), and 8.20 (4H, "d", J = 8.8 Hz, ArH's) ppm.

p-*Nitrobenzyl(6*S*)-[(1*R*)-hydroxyethyl]-2-[*cis*-4-(carbamyl)-cyclohexylthio]-(5*R*)-carbapen-2-em-3-carboxylate (**26**b):* yield 30%; mp 172–174°C; R_f 0.24 (EtOAc:acetone 1:1); ir (Nujol) ν_{max}: 3460 (OH), 3370, 3200 (NH), 1740 (β-lactam) 1700 (ester), and 1650 ($CONH_2$) cm^{-1}; uv (EtOH) λ_{max}: 324 (ε 12 800) and 267 nm (ε 10 600) nm; ^{1}Hmr (acetone-d_6, CFT-20) δ: 1.27 (3H, d, J = 6.2 Hz, 1′-Me), 1.6–2.1 (8H, m, CH_2), 2.35 (1H, m, CHCO), 3.2–3.6 (3H, m, 1-H, 6-H), 3.55 (1H, m, CHS), 4–4.5 (2H, m, 5-H, 1′-H), 5.16–5.34–5.44–5.62 (2H, ABq, CH_2CO_2), 7.81 (2H, "d", J = 8.8 Hz, ArH's), and 8.26 (2H, "d", J = 8.8 Hz, ArH's) ppm.

p-*Nitrobenzyl(6*S*)-[(1*R*)-hydroxyethyl]-2-[*cis*-4-cyanocyclohexylthio]-(5*R*)-carbapen-2-em-3-carboxylate (**26**c):* yield 43.5%; mp 167–169°C (CH_2Cl_2–EtOAc); $[\alpha]_D^{22°}$ +61.8° (*c* 0.57, CH_2Cl_2); ir (film) ν_{max}: 3400 (OH), 2240 (w, CN), 1770 (β-lactam), and 1700 (ester) cm^{-1}; uv (EtOH) λ_{max}: 267 (ε 11 000) and 322 nm (ε 13 000); ^{1}Hmr ($CDCl_3$, CFT-20) δ: 1.37 (3H, d, J = 6.3 Hz), 1.5–2.2 (8H, m), 2.8 (2H, m), 2.8–3.5 (4H, m), 4–4.4 (2H, m), 5.12–5.31–5.44–5.61 (2H, ABq), 7.65 (2H, "d", J = 8.8 Hz), and 8.22 (2H, "d", J = 8.8 Hz) ppm.

p-*Nitrobenzyl(6*S*)-[(1*R*)-hydroxyethyl]-2-[*cis*-4-(*p*-nitrobenzyloxycarbonylaminomethyl)cyclohexylthio]-(5*R*)-carbapen-2-em-3-carboxylate (**26**d):* yield 54%; yellow foam; R_f 0.37 (EtOAc); $[\alpha]_D^{21°}$ +51° (*c* 0.71, CH_2Cl_2); ir (film) ν_{max}: 3400 (OH), 1770 (β-lactam), 1720, 1700 (C=O), 1520 and 1350 (NO_2) cm^{-1}; uv (EtOH) λ_{max}: 268 (ε 21 100) and 323 nm (ε 12 900); ^{1}Hmr ($CDCl_3$, CFT-20) δ: 1.38 (3H, d, J = 6.2 Hz), 1.5–2.0 (9H, m), 3–3.4 (4H, m), 3.18 (1H, dd, J = 6.9 Hz, J = 2.5 Hz, 6-H), 3.47 (1H, m, CHS), 4–4.5 (2H, m), 4.9 (br), 5.12–5.29–5.45–5.62 (2H, ABq), 5.18 (2H, s), 7.50 (2H, "d", J = 8.8 Hz), 7.65 (2H, "d", J = 8.8 Hz), and 8.22 (4H, "d", J = 8.8 Hz) ppm.

*(6S)-[(1R)-Hydroxyethyl]-2-(*cis*-3-aminocyclopentylthio)-(5R)-carbapen-2-em-3-carboxylic acid (diastereomers A and B) (7a)* (Procedure A)

A solution of *p*-nitrobenzyl (6*S*)-[(1*R*)-hydroxyethyl]-2-[*cis*-3-(*p*-nitrobenzyloxycarbonylamino)cyclopentylthio]-(5*R*)-carbapen-2-em-3-carboxylates (**25***a*) (1.00 g, 1.60 mmol; diastereomeric mixture) in THF (173 mL) was mixed with Et_2O (173 mL), H_2O (173 mL), phosphate buffer (64 mL, pH 7.0, 0.05 *M*), and 10% Pd–C (1.00 g, Engelhard). The mixture was hydrogenated in a Parr apparatus (H_2, 50 psi) at room temperature for 5 h. The aqueous layer was filtered over Celite to remove the catalyst and the filtrate washed with Et_2O. This aqueous layer was lyophilized to obtain 1.08 g of yellow solid, which was purified by hplc (3% CH_3CN/H_2O) to yield 108 mg (0.343 mmol, yield 21.5%) of the title compound **7***a* (diastereomer A) as a yellowish powder; hplc, fast moving peak; $[\alpha]_D^{22°}$ +48.5° (*c* 0.3, H_2O); ir (KBr disc) ν_{max}: 3400 (OH), 1770 (β-lactam), and 1580 (CO_2) cm^{-1}; uv (H_2O) λ_{max}: 300 nm (ε 7400); ^{1}Hmr (D_2O, CFT-20) δ: 1.47 (3H, d, *J* = 6.4 Hz, 1′-Me), 1.5–3.0 (6H, m, CH_2), 3.4 (2H, m, 1-H), 3.57 (1H, dd, *J* = 6.1 Hz, *J* = 2.6 Hz, 6-H), 3.8 (2H, m, CHN, CHS), and 4.2–4.5 (2H, m, 1′-H, 5-H) ppm; and 83 mg (0.27 mmol, yield 16.7%) of the title compound **7***a* (diastereomer B) as a yellowish powder; hplc, slow moving peak; $[\alpha]_D^{22°}$ +46.9° (*c* 0.30, H_2O); ir (KBr disc) ν_{max}: 3400, 1750, and 1550 cm^{-1}; uv (H_2O) λ_{max}: 300 nm (ε 6800); ^{1}Hmr (D_2O, CFT-20) δ: 1.48 (3H, d, *J* = 6.3 Hz), 1.6–3.0 (6H, m), 3.27 (1H, dd, *J* = 17 Hz, *J* = 9.3 Hz, 1-H), 3.49 (1H, dd, *J* = 17 Hz, *J* = 8.8 Hz, 1-H), 3.58 (1H, dd, *J* = 6.1 Hz, *J* = 2.6 Hz), 3.85 (2H, m), and 4.3–4.5 (2H, m) ppm.

*(6S)-[(1R)-Hydroxyethyl]-1-[*cis*-3-(formimidoylamino)cyclopentylthio]-(5R)-carbapen-2-em-3-carboxylic acid (diastereomers A and B) (7b)* (Procedure B)

A solution of (6*S*)-[(1*R*)-hydroeyethyl]-1-(*cis*-3-aminocyclopentylthio)-(5*R*)-carbapen-2-em-3-carboxylic acid (**7***a*) (60 mg, 0.19 mmol; diastereomer A or B) in H_2O (140 mL) was cooled to 0–5°C and the pH was adjusted to 8.5 by the addition of a 0.06 *N* KOH solution. To this mixture was added at 0–5°C, portionwise and alternately, benzylformimidate hydrochloride (182 mg, 1.15 mmol) and a 0.06 *N* KOH solution, while maintaining the pH of the reaction mixture at 8.5 ± 0.3. After 15 min, the pH was adjusted to 7.0 by the dropwise addition of a 1 *N* HCl solution. The mixture was washed with Et_2O (150 mL × 2) and the aqueous layer was purified by column chromatography (10 g, Waters Assoc. $C_{18}\mu$ Bondapak reverse phase, 5% CH_3CN/H_2O) to obtain a yellow solid after lyophilization. This was purified by hplc (5% CH_3CN/H_2O) to yield the title compound **7***b* as off-white powder. Diastereomer A: yield 61 mg (0.18 mmol, yield 93%); R_f 0.45 (RP silica plate, 5% CH_3CH; H_2O); $[\alpha]_D^{22°}$ −31.0° (*c* 0.55, H_2O); ir (KBr disc) ν_{max}: 3000–3400 (br, OH, NH), 1750 (β-lactam), 1700 (C=N), and 1580 (CO_2) cm^{-1}; uv (H_2O) λ_{max}: 303 nm (ε 9500); ^{1}Hmr (D_2O, CFT-20) δ: 1.25 (3H, d, *J* = 6.4 Hz, 1′-Me), 1.5–2.3 (4H, m, CH_2), 2.3–2.8 (2H, m, CH_2), 3.04 (1H, dd, *J* = 19 Hz, *J* = 9 Hz, 1-H), 3.31 (1H, dd, *J* = 19 Hz, *J* = 9 Hz, 1-H), 3.35 (1H, dd, *J* = 6.1 Hz, *J* = 2.6 Hz, 6-H), 3.4–3.8 (2H, m, CHN, CHS), 4–4.3 (2H, m, 1′-H, 5-H), and 7.66–7.67–7.78 (1H, 3s, HC=N) ppm. Diastereomer B: yield 57 mg (0.17 mmol, yield 88%); R_f 0.40 (RP silica plate, 5% CH_3CH/H_2O); $[\alpha]_D^{22°}$ +100° (*c* 0.55, H_2O); ir (KBr disc) ν_{max}: 3000–3400 (br), 1750, 1700, and 1565 cm^{-1}; uv (H_2O) λ_{max}: 302 nm (ε 8300); ^{1}Hmr (D_2O, CFT-20) δ: 1.25 (3H, d, *J* = 6.4 Hz), 1.5–2.3 (4H, m), 2.3–2.8 (2H, m), 3.04 (1H, dd, *J* = 17.5 Hz, *J* = 9.6 Hz), 3.30 (1H, dd, *J* = 17.5 Hz, *J* = 8.8 Hz), 3.36 (1H, dd, *J* = 6.0 Hz, *J* = 2.7 Hz), 3.4–3.8 (2H, m), 3.9–4.3 (2H, m), and 7.64–7.65–7.78 (1H, 3s) ppm.

*Sodium (6S)-[(1R)-hydroxyethyl]-2-[*cis*-3-carbamylcyclopentylthio]-(5R)-carbapen-2-em-3-carboxylates (diastereomers A and B) (7c)* (Procedure C)

A suspension of *p*-nitrobenzyl (6*S*)-[(1*R*)-hydroxyethyl]-2-[*cis*-3-carbamylcyclopentylthio]-(5*R*)-carbapen-2-em-3-carboxylate (**25***b*) (235 mg, 0.494 mmol) in THF (60 mL) was mixed with Et_2O (60 mL), phosphate buffer (9.90 mL, pH 7.0, 0.05 *M*), a solution of $NaHCO_3$ (41.9 mg, 0.494 mmol) in H_2O (60 mL), and 10% Pd–C (235 mg, Engelhard). The mixture was hydrogenated (H_2, 32 psi) in a Parr apparatus at room temperature for 1 h. The same work-up and purification procedure as described for **7***a* gave 17.3 mg (0.048 mmol, yield 9.7%) of the title compound **7***c* (diastereomer A) as an orange powder; hplc, fast moving peak; ir (KBr disc) ν_{max}: 3300 (br, OH, NH_2), 1740 (β-lactam), 1660 ($CONH_2$), and 1580 (CO_2) cm^{-1}; uv (H_2O) λ_{max}: 300 nm (ε 8300); ^{1}Hmr (D_2O, CFT-20) δ: 1.44 (3H, d, *J* = 6.4 Hz, 1′-Me), 1.5–3.2 (7H, m), 3.4 (2H, 2dd, 1-H), 3.57 (1H, dd, *J* = 6.2 Hz, *J* = 2.6 Hz, 6-H), 3.7 (1H, CHS), and 4.2–4.5 (2H, m, 1′-H, 5-H) ppm; and 43.3 mg (0.119 mmol, yield 24.4%) of the title compound **7***c* (diastereomer B) as an orange powder; hplc, slow moving peak; ir (Nujol) ν_{max}: 3400 (br), 1750, 1670, and 1590 cm^{-1}; uv (H_2O) λ_{max}: 300 nm (ε 8000); ^{1}Hmr (D_2O, CFT-20) δ: 1.49 (3H, d, *J* = 6.3 Hz), 1.5–3.2 (7H, m), 3.42 (2H, 2dd), 3.57 (1H, dd, *J* = 6.1 Hz, *J* = 2.6 Hz), 3.75 (1H, m), and 4.2–4.6 (2H, m) ppm.

The cyclohexyl series, compounds **8**, were prepared by one of the procedures described above for the preparation of the cyclopentyl series, **7**.

*(6S)-[(1R)-Hydroxyethyl]-2-(*cis*-4-aminocyclohexylthio)-(5R)-carbapen-2-em-3-carboxylic acid (8a)* (Procedure A): yield 11%; ir (KBr disc) ν_{max}: 3420 (OH), 1755 (β-lactam), and 1580 (CO_2) cm^{-1}; uv (H_2O) λ_{max}: 303 nm (ε 6750); ^{1}Hmr (D_2O, CFT-20) δ: 1.45 (3H, d, *J* = 6.3 Hz, 1′-Me), 2.06 (8H, br s, CH_2), 3.20 (1H, dd, *J* = 17.3 Hz, *J* = 9.1 Hz, 1-H), 3.48 (1H, dd, *J* = 17.3 Hz, *J* = 9.1 Hz, 1-H), 3.55 (1H, dd, *J* = 6.1 Hz, *J* = 2.6 Hz, 6-H), 3.75 (1H, m), and 4.2–4.6 (2H, m, 1′-H, 5-H) ppm.

*(6S)-[(1R)-Hydroxyethyl]-2-[*cis*-4-(formimidoylamino)cyclohexylthio]-(5R)-carbapen-2-em-3-carboxylic acid (8b)* (Procedure B): yield 82%; R_f 0.13 (RP silica plate, 5% CH_3CN/H_2O); ir (KBr disc) ν_{max}: 3100–3400 (br), 1750, 1710, and 1580 cm^{-1}; uv (H_2O) λ_{max}: 307 nm (ε 9000); ^{1}Hmr (D_2O, CFT-20) δ: 1.25 (3H, d, *J* = 6.4 Hz), 1.81 (8H, br s, CH_2), 3.02 (1H, dd, *J* = 17.5 Hz, *J* = 9.5 Hz, 1-H), 3.29 (1H, dd, *J* = 17.5 Hz, *J* = 9.0 Hz, 1-H), 3.35 (1H, dd, *J* = 6.0 Hz, *J* = 2.5 Hz, 6-H), 3.65 (1H, m), 4.0–4.4 (2H, m, 1′-H, 5-H), and 7.66–7.77–7.80 (1H, 3s, HC=N) ppm.

*Sodium (6S)-[(1R)-hydroxyethyl]-2-[*cis*-4-(carbamyl)cyclohexyl]-(5R)-carbapen-2-em-3-carboxylate (8c)* (Procedure C): yield 57%; R_f 0.63 (RP silica plate, 10% CH_3CN/H_2O); ir (KBr disc) ν_{max}: 3400, 1750, 1650, and 1590 cm^{-1}; uv (H_2O) λ_{max}: 303 nm (ε 8700); ^{1}Hmr (D_2O, CFT-20) δ: 1.44 (3H, d, *J* = 6.8 Hz), 2.0 (8H, br s), 2.5 (1H, m, CHCO), 3.20 (1H, dd, *J* = 17.5 Hz, *J* = 9.2 Hz, 1-H), 3.48 (1H, dd, *J* = 17.5 Hz, *J* = 9.0 Hz, 1-H), 3.53 (1H, dd, *J* = 6.1 Hz, *J* = 2.5 Hz, 6-H), 3.65 (1H, m, CHS), and 4.15–4.5 (1H, m) ppm.

*Sodium (6S)-[(1R)-hydroxyethyl]-2-(*cis*-4-cyanocyclohexylthio)-(5R)-carbapen-2-em-3-carboxylate (8d)* (Procedure C): yield 14%; R_f 0.37 (RP silica plate, 5% CH_3CN/H_2O); ir (KBr disc) ν_{max}: 3400, 1745, and 1570 cm^{-1}; uv (H_2O) λ_{max}: 305 nm (ε 8000); ^{1}Hmr (D_2O, CFT-20) δ: 1.47 (3H, d, *J* = 6.3 Hz), 1.6–2.3 (8H, m, CH_2), 3.1–3.5 (2H, m, CHS, CHCN), 3.23 (1H, dd, *J* = 17.2 Hz, *J* = 9.2 Hz, 1-H), 3.49 (1H, dd, *J* = 17.2 Hz, *J* = 9.0 Hz, 1-H), 3.55 (1H, dd, *J* = 6.2 Hz, 6-H), and 4.1–4.5 (2H, m) ppm.

*(6S)-[(1R)-Hydroxyethyl]-2-[*cis*-4-(aminomethyl)cyclohexylthio]-(5R)-carbapem-2-em-3-carboxylic acid (8e)* (Procedure A): yield 44%; $[\alpha]_D^{22°}$ +29° (*c* 0.11, H_2O); ir (KBr disc) ν_{max}: 3450, 1735, and 1565 cm^{-1}; uv (H_2O) λ_{max}: 303 nm (ε 5400); ^{1}Hmr (D_2O, CFT-20) δ: 1.26 (3H, d, *J* = 6.4 Hz), 1.5–1.9 (9H, m, CH_2, CH), 2.92 (2H, d, *J* = 5.9 Hz, CH_2N), 3.03 (1H, dd, *J* = 17.5 Hz, *J* = 9.0 Hz, 1-H), 3.31 (1H, dd, *J* = 17.5 Hz, *J* = 9.0 Hz, 1-H), 3.36 (1H, dd, *J* = 6.1 Hz, *J* = 2.6 Hz, 6-H), 3.5 (1H, m, CHS), and 4.0–4.4 (2H, m, 1′-H, 5-H) ppm.

Acknowledgements

We would like to thank Professor B. Belleau of McGill University and Dr. M. Menard for their advice during the

course of this work. We also thank the Microbiology Department, Bristol-Myers, Syracuse, N.Y. for the antibacterial tests.

1. (*a*) R. W. RATCLIFFE and G. ALBERS-SCHONBERG. *In* Chemistry and biology of β-lactam antibiotics. Vol. 2. *Edited by* R. B. Morin and M. Gorman. Academic Press, New York, NY. 1982. pp. 227–313; (*b*) L. D. CAMA, K. J. WILDONGER, R. GUTHIKONDA, R. W. RATCLIFFE, and B. G. CHRISTENSEN. Tetrahedron, **15**, 2531 (1983), and references therein.
2. (*a*) D. H. SHIH, J. HANNAH, and B. G. CHRISTENSEN. J. Am. Chem. Soc. **100**, 8004 (1978); (*b*) W. J. LEANZA, K. J. WILDONGER, J. HANNAH, D. H. SHIH, R. W. RATCLIFFE, L. BARASH, E. WALTON, R. A. FIRESTONE, G. F. PATEL, F. M. KAHAN, J. S. KAHAN, and B. G. CHRISTENSEN. *In* Recent advances in the chemistry of β-lactam antibiotics. *Edited by* G. I. Gregory. The Royal Society of Chemistry, London. 1981. pp. 240–254, and references therein.
3. C. LARSEN and D. N. HARPP. J. Org. Chem. **45**, 3713 (1980).
4. (*a*) F. I. CARROLL, H. M. DICKSON, and M. E. WALL. J. Org. Chem. **30**, 33 (1965); (*b*) R. LATTRELL. Angew. Chem. Int. Ed. Engl. **12**, 925 (1973).
5. W. LEHNERT. Tetrahedron Lett. **19**, 1501 (1971).
6. I. SHINKAI, T. LIU, R. REAMER, and M. SLETZINGER. Synthesis, 924 (1980).
7. (*a*) T. N. SALZMANN, R. W. RATCLIFFE, B. G. CHRISTENSEN, and F. A. BOUFFARD. J. Am. Chem. Soc. **102**, 6161 (1980); (*b*) M. SLETZINGER, T. LIN, R. A. REAMER, and I. SHINKAI. Tetrahedron Lett. **21**, 4221 (1980).
8. Y. UEDA, G. ROBERGE, and V. VINET. Can. J. Chem. **62**, 2936 (1984).
9. (*a*) W. J. LEANZA, K. J. WILDONGER, T. W. MILLER, and G. G. CHRISTENSEN. J. Med. Chem. **22**, 1435 (1979); (*b*) F. M. KAHAN and H. KROPP. European Patent Application 0007614 (1980).
10. H. J. REICH and J. E. TREND. J. Org. Chem. **38**, 2637 (1973).
11. D. N. HARPP, J. G. MACDONALD, and C. LARSEN. Can. J. Chem. **63**, 951 (1985).

An electron spin resonance study of the reactions of hydrogen atoms with halocarbons

WILLIAM E. JONES AND JOSEPH L. MA
Department of Chemistry, Dalhousie University, Halifax, N.S., Canada B3H 4J3

Received May 26, 1986

WILLIAM E. JONES and JOSEPH L. MA. Can. J. Chem. **64**, 2192 (1986).

The absolute rate constants for the reaction of H atoms with methyl- and vinyl-halides have been determined using esr spectroscopy and a conventional gas flow system. The rate constants determined at 298 ± 2 K at a pressure of 0.55 Torr are methane, $(1.7 \pm 0.3) \times 10^{-17}$; ethane, $(2.3 \pm 0.5) \times 10^{-17}$; methylfluoride, $(4 \pm 3) \times 10^{-15}$; methylchloride, $(8 \pm 2) \times 10^{-16}$; methylbromide, $(2.1 \pm 0.6) \times 10^{-14}$; vinylfluoride, $(1.47 \pm 0.02) \times 10^{-13}$; vinylchloride, $(1.66 \pm 0.08) \times 10^{-13}$; and vinylbromide $(4.07 \pm 0.73) \times 10^{-13}$ in units of cm^3 $molecule^{-1}$ s^{-1}.

WILLIAM E. JONES et JOSEPH L. MA. Can. J. Chem. **64**, 2192 (1986).

Faisant appel à la rpe et un système conventionnel d'écoulement des gaz, on a mesuré les constantes absolues des vitesses de réaction des atomes H avec les halogénures de méthyle et de vinyle. On a déterminé que, à 298 ± 2 K et à une pression de 0,55 Torr, les constantes sont les suivantes (en cm^3 $molécule^{-1}$ s^{-1}) : méthane, $(1,7 \pm 0,3) \times 10^{-17}$; éthane, $(2,3 \pm 0,5) \times 10^{-17}$; fluorométhane, $(4 \pm 3) \times 10^{-15}$; chlorométhane, $(8 \pm 2) \times 10^{-16}$; bromométhane, $(2,1 \pm 0,6) \times 10^{-14}$; fluorure de vinyle, $(1,47 \pm 0,02) \times 10^{-13}$; chlorure de vinyle, $(1,66 \pm 0,08) \times 10^{-13}$ et bromure de vinyle, $(4,07 \pm 0,73) \times 10^{-13}$.

[Traduit par la revue]

Introduction

While much work has been reported on the reactions of H atoms with the hydrocarbons; methane, ethane, and ethylene (1, 2), there have been few reports of studies of the reactions of H atoms with halo-substituted hydrocarbons (1, 3).

The reactions with saturated hydrocarbons are very slow and approach the limit of measurement in the normal vacuum flow system. The initial step in the reaction is the abstraction of a hydrogen atom, or in halo-substituted hydrocarbons a halogen atom. This initial reaction would be followed by a series of radical reactions. Since the reactions with methane and ethane are so slow, measurements have been usually made at elevated temperatures (4–14). However, these measurements provide Arrhenius parameters from which estimates of rate constants at room temperature may be predicted.

The reactions with CH_3F, CH_3Cl, and CH_3Br were first studied by Chadwell and Titani (15) and by Cremer, Curry, and Polanyi (16) in 1933. No further measurements were reported on these reactions until 1967, when Parsamyan *et al.* (17) reported their results on the reaction with CH_3F. In 1969, Seidel (18) reported results from a crossed molecular beam study on the reaction with CH_3Cl and CH_3Br. In 1970, Davis *et al.* (19) also gave values for the Arrhenius parameters for the reaction with CH_3Br.

The recent paper by Ahmed and Jones (3) summarizes the previous work (20–24) on the reactions of hydrogen atoms with the mono-halo-substituted ethylenes.

In this article we report on a study of the kinetics of the reaction of hydrogen atoms with mono-halo-substituted methanes and ethylenes using esr spectrometry as a detector for H atoms. In the course of this work, we also measured the kinetics of the reactions with methane and ethane for comparison purposes.

Experimental

The reactions were studied in a conventional fast flow vacuum system coupled to a Varian E109-B electron spin resonance spectrometer. The design of the reaction zone was similar to that described by Westenberg and DE Haas (25). The reaction tube which passed through the esr cavity was made of 19 mm i.d. quartz tubing having a low dielectric constant. The main reaction tube was 1 m long and 20 mm i.d. Mixtures of hydrogen and helium could be admitted to the reaction tube through three side tubes situated at varying distances from the esr cavity. Each of these entry tubes was made of quartz to allow production of H atoms by a microwave discharge sustained by a 2450 MHz (200 W) microwave generator. The reactant gas was admitted to the stream of H atoms through a gas inlet tube which could be moved axially within the reaction tube. This allowed admittance of the reactant to the H atom stream at various distances (various reaction times) from the esr cavity. The flow system was connected to two large mechanical vacuum pumps which maintained a pumping speed of 450 L min^{-1} at a pressure of 1 Torr, giving a linear velocity of 40 m s^{-1} in the reaction zone.

Hydrogen atoms were produced by passing a mixture of molecular hydrogen and helium through a 2450 MHz electrodeless discharge. Typical flow conditions were He, 8.7×10^{-5} mol s^{-1}; H_2, 3.1×10^{-7} mol s^{-1}. The surface of the reaction tube and the moveable inlet probe were coated with phosphoric acid to inhibit recombination of H atoms.

Helium and molecular hydrogen were obtained from Linde. Methane, ethane, halo-substituted methanes and ethylenes and nitrogen dioxide were obtained from Matheson of Canada Ltd. All condensable gases were purified by bulb-to-bulb distillation. Nitrogen dioxide was treated with molecular oxygen and purified by trap-to-trap distillation *in vacuo*.

The concentration of atomic hydrogen was determined by titration with NO_2. This determination was made by observation of the H atom signal as the flow rate of NO_2 was gradually increased. A plot of a typical result is shown in Fig. 1. In this figure the end point was located at a NO_2 flow rate of 2.1×10^{-6} mol s^{-1}. The flow rate of H atoms was thus determined on the assumption that $[H]/[NO_2] = 1/1.5$ at the end point (26). The usual correction for the NO_2/N_2O_4 equilibrium was applied to the calculation of the flow rate of NO_2.

All experiments were performed at room temperature, 298 ± 2 K, and a pressure of 0.55 Torr as measured by a mercury McLeod gauge. The axial pressure gradient in the reactor was less than 2% of the total pressure. The reaction time was calculated from the distance between the point of mixing of the reactants and the centre of the esr cavity. Under the experimental conditions used, a plug flow condition could be assumed and the time was calculated as $t = d/v$, where d is the distance from the point of mixing and the centre of the esr cavity and v is the linear flow velocity of reactant gases. The progress of the reaction was monitored by esr detection of the remaining H atoms

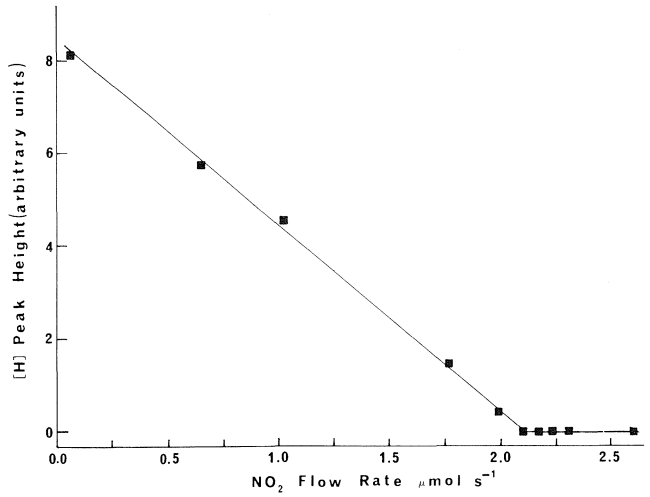

FIG. 1. A typical titration curve for the determination of the concentration of atomic hydrogen with NO_2. The curve indicates the decay of the H atom signal as the flow of NO_2 is increased.

after the specified reaction time. The concentration of the reactant gas was maintained at least 100-fold greater than the atomic hydrogen concentration allowing calculation of the rate constants to be made on the basis of pseudo-first order conditions.

Results

A simplified scheme for the bimolecular reaction between hydrogen atoms and reactants, RX, may be represented as

[1] $H + RX = \text{products}$

On the assumption that the concentration of the reactant is constant, the integrated rate expression for this reaction is given by

[2] $\ln [H]_t = -k[RX]t + \ln [H]_0$

where k is the apparent bimolecular rate constant, and $[H]_t$ and $[H]_0$ are the concentrations of H atoms at time t and 0, respectively, and [RX] is the concentration of reactant which is assumed to remain constant. Under pseudo-first-order conditions, i.e., $[RX] \gg [H]$, the integrated equation becomes

[3] $\ln [H]_t = -k_{obs}t + \ln [H]_0$

where k_{obs} is the pseudo-first-order rate constant. For the present study, it has been assumed that the reduction of H atom concentration is entirely due to reaction with the hydrocarbon or halo-hydrocarbon reactant and that homogeneous and heterogeneous recombination of H atoms are negligible. It has been also assumed that reaction of H atoms with radicals are not significant. These reactions would not be expected to be important relative to the primary step since the concentration of H atoms and radicals are extremely low compared to the concentration of major reactant.

The slope of a plot of $-\ln [H]$ vs. time t gives the pseudo-first-order rate constant k_{obs}. The value of the bimolecular rate constant k is then calculated from the value of [RX].

Methane and ethane

Although the reaction of H atoms with methane and ethane have been well studied and the rate constants determined many times, it was decided to measure these rates with the present system as a test for the apparatus and the overall procedure. As

TABLE 1. Rate constants for the reaction of hydrogen atoms with CH_4 and C_2H_6 (k in units of cm^3 molecule^{-1} s^{-1}) $\times 10^{17}$

Temperature (K)	k		Reference
	CH_4	C_2H_6	
298	1.7 ± 0.3^a	—	This work
372	0.22	—	4
500	1.6	—	5
372	3.5	—	6
426	2.4	—	7
372	1.5	—	8
298	—	2.3 ± 0.5^a	This work
298	—	2.0	9
298	—	2.7	10
353	—	0.45	11
323	—	1.6	12
303	—	2.4	13
304	—	3.6	14

[a]Average of six independent determinations.

TABLE 2. Rate constants for the reaction of hydrogen atoms with CH_3F, CH_3Cl, and CH_3Br (temperature 298 K, k in units of cm^3 molecule^{-1} s^{-1} $\times 10^{15}$)

Reactant	k	Reference
CH_3F	4 ± 3^a	This work
	5.8	17
CH_3Cl	0.8 ± 0.2^b	This work
	0.7	23
CH_3Br	21 ± 6^c	This work
	5.0	23

[a]Average of twelve independent measurements.
[b]Average of three independent measurements.
[c]Average of eight independent measurements.

can be seen in Table 1, the values obtained are in reasonable agreement with those of previous studies. These reactions are extremely slow at room temperature and represent a lower limit for determination by the flow technique used here. In fact, the reaction with methane may be too slow to provide reliable data (27). The main reason for measuring the kinetics of the reactions with methane was to assure that the apparatus could provide information that was in agreement with previous measurements. In so far as the previous measurements (4–14) are comparable, the current values are satisfactory.

Methylfluoride, methylchloride, and methylbromide

These reactions have received very little attention to date (1), and with the exception of the work by Chadwell and Titani (15), studies have been reported only at high temperature. However, it is possible using the Arrhenius parameters given by Parsamyan *et al.* (17) for methylfluoride and Seidel (28) for methylchloride and methylbromide, to predict the rate constants at room temperature as given in Table 2. It may be seen that the values for CH_3F and CH_3Cl in the present study are in reasonable agreement with the calculated values while the value determined here for CH_3Br is greater than the calculated value by a factor of four.

TABLE 3. Rate constants for the reaction of hydrogen atoms with C_2H_3F, C_2H_3Cl, and C_2H_3Br (temperature 298 K, k in units of cm^3 molecule^{-1} $s^{-1} \times 10^{14}$)

Pressure (Torr)	k			Reference
	C_2H_3F	C_2H_3Cl	C_2H_3Br	
0.55	14.7 ± 0.2[a]	16.6 ± 0.8[a]	40.7 ± 7.3[a]	This work
0.70	7.64 ± 0.78	21.1 ± 1.6	24.6 ± 1.4	3
1.00	8.86 ± 1.12	27.0 ± 0.5	27.8 ± 2.5	3
1.30	10.80 ± 0.90	30.3 ± 3.9	38.3 ± 1.8	3
1.20	4.7	—	—	20
305	7.3	—	—	21
700	13.1	—	—	22
180–900	52.0	—	—	23
1.1	—	0.7	—	24
20	—	6.8	—	20

[a]Average of four independent measurements.

Vinylfluoride, vinylchloride, and vinylbromide

Several studies have reported values for the rate constants for the reaction of H atoms with C_2H_3F and C_2H_3Cl, the most recent by Ahmed and Jones (3), in which they followed the reactions by mass spectroscopy. They also reported the rate constant for the reaction of H atoms with C_2H_3Br for the first time. Table 3 presents the values obtained in the present work and compares them with values determined by other methods.

Discussion

Two quite different types of reaction have been studied in this work. The first is the reaction of H atoms with saturated hydrocarbons and saturated mono-halo-substituted hydrocarbons. These reactions are extremely slow and difficult to measure by normal flow techniques. However, we have been able to obtain values of the room temperature rate constants which are in reasonable agreement with previously reported values or those calculated from previously reported Arrhenius data. These measurements give us reasonable confidence in both the present apparatus and procedures.

For the reaction H + CH_3X = products, where X may be H, F, Cl, or Br, the rate constants k_X follow the order $k_H < k_{Cl} < k_F < k_{Br}$. Two reactions have been proposed as possible initial steps in these reactions. Chadwell and Titani (15) suggested the abstraction of the halogen atom by H as in the reaction:

[4] $H + CH_3X = HX + CH_3$

while Cremer *et al.* (16) proposed the abstraction of an H atoms by H as in the reaction:

[5] $H + CH_3X = H_2 + CH_2X$

If we estimate the enthalpy for the reaction [4] from available bond energies (29), we obtain the values $\Delta H^0 = -9$, -92, -113, and -153 kJ mol^{-1} for H, Cl, F, Br, respectively. Thus the relative values obtained for the rate constants appear to fit well with the relative order of the enthalpies of reaction [4], i.e., $k_H = 1.7 \times 10^{-17}$, $k_{Cl} = 8 \times 10^{-16}$, $k_F = 4 \times 10^{-15}$, and $k_{Br} = 2 \times 10^{-14}$ cm^3 molecule^{-1} s^{-1}.

Since reaction [5] involves the breaking of a C—H bond and formation of H—H bond for each of the halo-substituted hydrocarbons, the enthalpies would not differ as significantly as in reaction [4]. Further, based on the fact that the rate constant for the reaction with methane is extremely small, reaction [5] would be expected to be unimportant relative to reaction [4].

The second type of reaction, that of H atoms with the vinyl-halides, have a larger rate constant than those of reactions with the methyl halides by at least an order of magnitude. In these reactions, the initial step is the addition of H atoms to the double bond of the vinyl-halide;

[6] $H + RX = RHX^*$

The values determined for the rate constants in the present study are in good agreement with the values determined by Ahmed and Jones (3), for H + C_2H_3Cl, but are about a factor of two greater for the reactions with C_2H_3F and C_2H_3Br. Ahmed and Jones (3) found a slight dependence on pressure and a gradual increase in the value of the rate constants from H + C_2H_3F through H + C_2H_3Cl to H + C_2H_3Br. They explained this dependence on halogen by considering two opposing influences created by the substituted halogen atom on the reactivity of the olefin. The influences were the strong negative inductive effect (−I) due to the electronegativity of the halogen, and the positive inductive effect (+I) as a result of the repulsion of electrons present in the p orbitals of the halogen atom and the mesomeric (+M) effect. The results presented here confirm the earlier results obtained by a different method of measurement (mass spectroscopy).

Acknowledgements

We acknowledge financial support from the Natural Sciences and Engineering Research Council of Canada in the form of an operating grant to W.E.J. and from the Faculty of Graduate Studies of Dalhousie University for a fellowship to J.L.M. We thank Dr. D. R. Arnold for permission to use the Varian E-109B ESR spectrometer.

1. W. E. JONES, S. D. MCKNIGHT, and L. TENG. Chem. Rev. **73**, 407 (1973).
2. C. A. COWFER and J. V. MICHAEL. J. Chem. Phys. **62**, 3504 (1975).
3. M. G. AHMED and W. E. JONES. Can. J. Chem. **63**, 2127 (1985).
4. M. R. BERLIE and D. J. LEROY. Can. J. Chem. **32**, 650 (1954).
5. J. W. S. JAMIESON and G. R. BROWN. Can. J. Chem. **42**, 1638 (1964).
6. R. R. BALDWIN, D. E. HOPKINS, A. C. NORRIS, and R. W. WALKER. Combust. Flame, **15**, 33 (1970).
7. M. J. KURYLO and R. B. TIMMONS. J. Chem. Phys. **50**, 5076 (1969).
8. R. W. WALKER. J. Chem. Soc. A, 2391 (1968).
9. V. V. AZATYAN, S. B. FILIPPOV, A. B. NALBANDYAN, and L. B. ROMANOVICH. Arm. Khim. Zh. **22**, 193 (1969); Chem. Abstr. **71**, 90606v (1969).
10. V. V. AZATYAN, and S. B. FILIPPOV. Dokl. Akad. Nauk. SSSR. **184**, 625 (1969); Chem. Abstr. **70**, 91193z (1969).
11. M. R. BERLIE and D. J. LEROY. Discuss. Faraday Soc. **14**, 50 (1953).
12. K. YANG. J. Phys. Chem. **67**, 562 (1963).
13. R. R. BALDWIN. Symp. (Int.) Combust. Proc. 9th. 1962, 604 (1963).
14. R. R. BALDWIN and A. MELVIN. J. Chem. Soc. 1785 (1964).
15. H. M. CHADWELL and T. TITANI. J. Am. Chem: Soc. **55**, 1363 (1933).
16. E. CREMER, J. CURRY, and M. POLANYI. Z. Phys. Chem. Abt. B, **23**, 445 (1933).
17. N. I. PARSAMYAN, V. V. AZATYAN, and A. B. NALBANDYAN.

Arm. Khim. Zh. **20**, 950 (1967); Chem. Abstr. **69**, 76218x (1968).
18. W. SEIDEL. Z. Physik. Chem. Frank. **65**, 95 (1969).
19. P. B. DAVIS, B. A. THRUSH, and A. F. TUCK. Trans. Faraday Soc. **66**, 886 (1970).
20. A. M. RENNERT and M. H. J. WIJNEN. Ber. Bunsenges. Phys. Chem. **72**, 22 (1969).
21. J. P. KILCOYNE and K. R. JENNINGS. J. Chem. Soc. Faraday I, **70**, 379 (1974).
22. R. D. PENZHORN and H. L. SANDOVAL. J. Phys. Chem. **74**, 2065 (1970).
23. K. SUGAWARA, K. OKAZAKI, and S. SATO. Bull. Chem. Soc. Jpn. **54**, 358 (1981).
24. J. S. TANNER and J. W. S. JAMIESON. Can. J. Chem. **49**, 1023 (1971).
25. A. A. WESTENBERG and N. DE HAAS. J. Chem. Phys. **47**, 1393 (1967).
26. L. F. PHILLIPS and H. I. SCHIFF. J. Chem. Phys. **37**, 1233 (1962).
27. W. R. TROST and E. W. R. STEACIE. J. Chem. Phys. **16**, 361 (1962).
28. W. SEIDEL. Ber. Bunsenges. Phys. Chem. **72**, 978 (1968).
29. T. L. COTTRELL. The strength of chemical bonds. 2nd ed. Butterworths Scientific Publications, London. 1958.

Formation of blue diquinolinyl methine dyes by irradiation of N-acylated primaquine in chloroform solution with ultraviolet light

WIESLAW P. GESSNER,[1] BINDUMADHAVAN VENUGOPALAN,[2] AND ARNOLD BROSSI[3]

Section on Medicinal Chemistry, Laboratory of Chemistry, National Institute of Diabetes, and Digestive and Kidney Diseases, National Institutes of Health, Bethesda, MD 20892, U.S.A.

AND

ALEX R. JURGENS AND CHARLES D. HUFFORD

Department of Pharmacognosy, School of Pharmacy, University of Mississippi, University, MI 38677, U.S.A.

Received April 1, 1986

WIESLAW P. GESSNER, BINDUMADHAVAN VENUGOPALAN, ARNOLD BROSSI, ALEX R. JURGENS, and CHARLES D. HUFFORD. Can. J. Chem. **64**, 2196 (1986).

Irradiation of N-acylated primaquines **1***b–d* in chloroform solution with ultraviolet light afforded blue diquinolinyl methine dyes **3***b–d*. The structures of compounds **3***b–d* are supported by spectral data, synthesis of **3***c* from **1***c* with orthoformate, and chemical reduction of **3***d* affording known dimer **5***d*.

WIESLAW P. GESSNER, BINDUMADHAVAN VENUGOPALAN, ARNOLD BROSSI, ALEX R. JURGENS et CHARLES D. HUFFORD. Can. J. Chem. **64**, 2196 (1986).

Lorsqu'on soumet des solutions chloroformiques de primaquines N-acétylées (**1***b–d*) à une irradiation par de la lumière ultraviolette, on obtient les colorants bleus (**3***b–d*) de la famille des diquinolinylméthines. On a déduit les structures des composés **3***b–d* de leurs données spectrales, de la synthèse du composé **3***c* à partir du composé **1***c* et de l'orthoformiate ainsi que de la réduction chimique de **3***d* qui conduit au dimère **5***d* qui est connu.

[Traduit par la revue]

The antimalarial primaquine (**1***a*) is the most widely used tissue schizonticide and the drug of choice in the treatment of vivax malaria (1). *N*-Ethoxyacetylprimaquine (**1***b*), prepared from primaquine base and ethoxyacetic anhydride, and chosen to study the importance of the primary amino group for antimalarial activity, formed a blue color on tlc plates upon irradiation with ultraviolet light of 254 nm while still wet after development with chloroform–methanol. Formation of this blue color was also observed when **1***b* was irradiated with uv light in chloroform solution, but not in dichloromethane or carbon tetrachloride solution, suggesting that chloroform played a role in this reaction. The blue dye, when extracted from tlc plates and rechromatographed with **1***b*, was found to be more polar, and its uv maximum of 618 nm (MeOH) was different from that of 589 nm (MeOH) of a blue dye obtained by Strother *et al.* by base-catalyzed air oxidation of primaquine and 5-hydroxyprimaquine in aqueous solution (2).

The structure of the blue dye formed from **1***b* was of interest, and the results of the investigation which led to the diquinolinyl methine structure **3***b* will be reported. The molecular ion at *m/z* 701 for **3***b* as determined by the Californium plasma desorption ms, the uv maximum at 618 nm, and the involvement of chloroform in its formation suggested the diquinolinyl methine dye **3***b*, formed probably by dichlorocarbene (or dichloromethyl radical) addition to **1***b*, and further reaction of the hypothetical adduct **2** with another molecule of **1***b*. Blue dye **3***b* was a gum that was difficult to handle and for this reason did not give a good elemental analysis. The *p*-nitrobenzoyl analog **1***c*, prepared from primaquine and *p*-nitrobenzoyl chloride, seemed a better compound and its photoreaction afforded the blue dye **3***c* as an amorphous solid. Blue dye **3***c* gave good spectral data, and the results of its combustion analysis supported the structure of an imine hydrochloride salt. The compound **3***c* could alternatively be obtained by treating the hydrochloride of **1***c* with trimethylorthoformate in refluxing methanol.

Photoreaction of known *N*-acetylprimaquine (3) **1***d* in chloroform solution yielded the blue dye **3***d*, fully characterized by ms, uv, ^{1}H nmr, and ^{13}C nmr spectral data. Good support for the diquinolinylmethine structure **3***d* was obtained by chemical reduction with zinc dust in dilute hydrochloric acid, leading to the known microbial metabolite **5***d*, obtained also by synthesis (4). Oxidation of **5***d* in chloroform solution by air under uv light led to the blue dye **3***d*.

Compounds **3***b–d* can in principle exist as two geometrical isomers, convertible throughout deprotonation and reprotonation, but they are most likely present as *E*-isomers (twisted around the C5=CH—C5′ axis) to avoid interaction of the two bulky 6,6′-positioned methoxy groups (based on the inspection of Dreiding models). Blue dyes **3***b–d* behave as indicators, undergoing color change from blue to colorless at pH 11.2, a behavior best explained with the formation of carbinol bases **4***b–d* and reminiscent of properties of polymethine and triphenylmethane dyes (5).

Experimental

Melting points were determined on a Fisher–Johns apparatus and are corrected. The ^{1}H nmr spectra were recorded using a Varian XL-300, JEOL FX-100, or Varian EM-390 spectrometer with TMS as the internal reference. The ^{13}C nmr spectra were recorded using a JEOL FX-100 or JEOL FX-60 spectrometer with TMS as the internal reference. Chemical ionization mass spectra (cims) were obtained on a Finnigan 1015D spectrometer with ammonia as the reagent gas and a Model 6000 data collection system. Californium-252 plasma desorption mass spectra were recorded as described previously (6), at an acceleration voltage of 10 kV. Ultraviolet–visible spectra were measured using a Hewlett–Packard 8450A uv–vis spectrometer. Elemental analyses were performed by the Instrumentation Section, Laboratory of Analytical Chemistry, NIDDK, National Institutes of Health, Bethesda, Maryland or by the Atlantic Microlab Inc., Atlanta, Georgia.

[1] Visiting Scientist from A. Mickiewicz University, Poznan, Poland.
[2] Guest Scientist from Hoechst India Ltd., Bombay, India.
[3] Author to whom correspondence may be addressed.

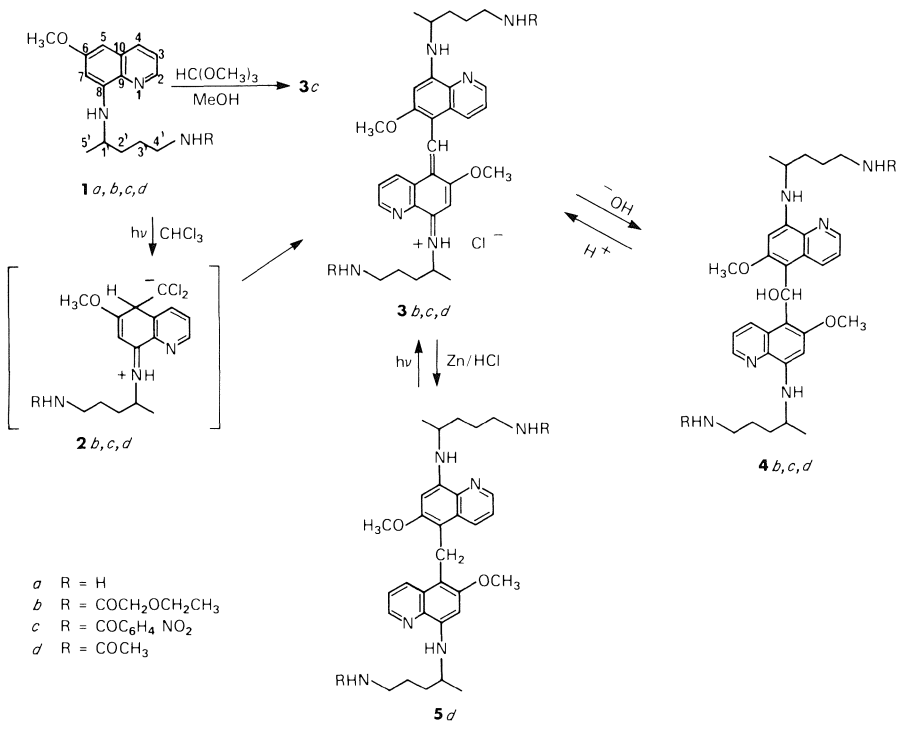

Thin-layer chromatography (tlc) plates (silica gel GHLF analytical and GF preparative) were purchased from Analtech, Inc. and silica gel 60 for short column flash chromatography (0.015–0.040 mm) was from E.M. Reagents.

N-*Ethoxyacetylprimaquine (**1**b)*

Primaquine diphosphate (4.55 g, 10 mmol) was converted to the free base by dissolving in 2 *N* NaOH and extracting with ethyl ether. The ether extract was evaporated to dryness, the residue was dissolved in 50 mL of dry pyridine, then 2.0 g (11 mmol) of ethoxyacetic anhydride and 100 mg of 4-(*N*,*N*-dimethylamino)pyridine were added, and the reaction mixture was kept at room temperature overnight. It was evaporated to dryness, dissolved in methylene chloride, washed with dilute HCl and water, dried with Na_2SO_4, and evaporated to dryness to yield 3.25 g (94%) of *N*-ethoxyacetylprimaquine as a yellow gum. This product was used in the next step without further purification.

An analytical sample was prepared as the phosphate salt and crystallized from 90% ethanol in the form of yellow crystals, mp 145–147°C; uv (free base, $CHCl_3$), λ_{max}: 364 nm; ^{1}H nmr (free base, $CDCl_3$, 100 MHz), δ: 1.20 (m, 6H, C5′CH_3-H, OCH_2CH_3), 1.64 (m, 4H, C2′-H, C3′-H), 3.10–3.70 (m, 4H, C1′-H, C4′-H, NH), 3.48 (q, J = 7.0 Hz, 2H, OCH_2CH_3), 3.84 and 3.86 (2s, 5H, OCH_3, OCH_2CO), 6.28 and 6.22 (2d, J_{5-7} = 3.0 Hz, 2H, C5-H, C7-H), 6.55 (br s, 1H, NHCO), 7.24 (dd, J_{2-3} = 5.0 Hz, J_{3-4} = 8.0 Hz, 1H, C3-H), 7.86 (dd, J_{2-4} = 1.5 Hz, J_{3-4} = 8.0 Hz, 1H, C4-H), 8.46 (dd, J_{2-3} = 5.0 Hz, J_{2-4} = 1.5 Hz, 1H, C2-H); ^{13}C nmr, see Table 1; cims (free base) m/z: 346 (M^+ + 1). *Anal.* calcd. for $C_{19}H_{30}N_3O_7P$: C 51.46, H 6.82, N 9.48, P 6.98; found: C 51.56, H 7.12, N 9.32, P 6.68.

*Photosynthesis of **3**b*

Ethoxyacetylprimaquine (1.5 g) was dissolved in 80 mL of chloroform, placed in a quartz photoreactor, and irradiated at 254 nm (model UVG-11 Mineralight lamp, Ultra-violet Products, Inc.) for 3 h, with stirring, under an argon atmosphere. The deep-green reaction mixture was then evaporated to dryness and chromatographed over a SiO_2 column (CH_2Cl_2, then CH_2Cl_2–MeOH 9:1) to yield first the unchanged starting material, then the deep-blue compound (150 mg). This was rechromatographed on a preparative SiO_2 tlc plate to yield 75 mg of blue compound **3***b* as an amorphous solid, which was homogeneous on tlc (R_f 0.35, CH_2Cl_2–MeOH 9:1); uv–vis ($CHCl_3$, MeOH, H_2O), λ_{max}: 618 nm; uv (MeOH + KOH), λ_{max}: 385 nm; ^{1}H nmr (CD_3OD, 100 MHz), δ: 1.18 (2t, J = 6.5 Hz, 6H, CH_3CH_2O), 1.40 (d, J = 7 Hz, 6H, C5′-H), 1.74 (m, 8H, C2′-H, C3′-H), 3.50 (m, 4H, CH_3CH_2O), 3.85 (2s, 4H, $COCH_2O$), 4.00 (s, 6H, OCH_3), 4.20 (m, 2H, C1′-H), 6.56 (s, 2H, C7-H), 7.32 (dd, J_{2-3} = 4.5 Hz,

TABLE 1. ^{13}C nuclear magnetic resonance[a]

	Compound		
Carbon no.	**1***b*	**3***b*	**3***d*
2	145.3 d	147.9 d	147.9 d
3	122.8 d	126.2 d	126.2 d
4	136.2 d	134.9 d	134.8 d
5	93.0 d	112.8 s	112.8 s
6	160.9 s	172.6 s	173.2 s
7	98.3 d	91.3 d	91.4 d
8	146.0 s	156.3 s	156.3 s
9	136.4 s	136.5 s	136.4 s
10	131.5 s	130.3 s	130.3 s
1′	48.8 d	49.2 d	49.9 d
2′	34.8 t	34.4 t	34.6 t
3′	27.1 t	27.2 t	27.0 t
4′	39.8 t	39.4 t	40.1 t
5′	20.7 q	20.5 q	20.6 q
OCH_3	55.6 q	57.6 q	57.8 q
$COCH_3$	172.6 s	168.6 s	168.5 s
$COCH_3$	—	—	22.7 q
$CH_2OCH_2CH_3$	70.6 t	70.6 t[b]	—
$CH_2OCH_2CH_3$	68.0 t	68.0 t[b]	—
$CH_2OCH_2CH_3$	15.2 q	15.2 q	—
—C=CH—Ar	—	142.6 s[b]	142.6 s[b]

[a]All spectra taken in CD_3OD solution using 15 MHz (compounds **3***b* and **3***d*) or 25 MHz (compound **1***b*) ^{13}C nmr instruments. Multiplicities were confirmed by SFORD. Assignments were based on previously reported ^{13}C nmr assignments for primaquine and derivatives (7–10).

[b]Selective SFORD irradiation was used to confirm these assignments.

J_{3-4} = 9.0 Hz, 2H, C3-H), 7.90 (br d, J_{3-4} = 9.0 Hz, 2H, C4-H), 8.58 (br d, J_{2-3} = 4.5 Hz, 2H, C2-H), 8.90 (s, 1H, =CH—); ^{13}C nmr, see Table 1; Californium plasma desorption ms, *m/z*: 701 (positive molecular ion).

N-p-*Nitrobenzoyl primaquine* (**1***c*)

The free base was generated from primaquine diphosphate (9.10 g, 20 mmol) using 50 mL of 2 *N* NaOH followed by extraction with $CHCl_3$. The organic layer was washed with water, dried, and evaporated to dryness. The free base was dissolved in 100 mL of dry benzene, then triethylamine (3.5 mL) was added, followed by *p*-nitrobenzoyl chloride (4.0 g) while keeping the reaction mixture at 0–5°C. The reaction mixture was brought to room temperature and stirred for 3 h, then the solvent was removed and the reaction product extracted with methylene chloride. The organic layer was washed with aqueous $NaHCO_3$ and water, dried, and concentrated to furnish a viscous gum. The product was converted into a hydrochloride salt and crystallized from methanol–ether to yield 7.0 g (86%) of **1***c*·HCl, mp 143–145°C; uv (MeOH), λ_{max}: 206 nm, 266 nm, 360 nm; ^{1}H nmr (CD_3OD, 300 MHz), δ: 1.37 (d, 3H, C5′-H), 1.70–1.90 (m, 4H, C2′-H, C3′-H), 3.45 (m, 2H, C4′-H), 3.85 (m, 1H, C1′-H), 3.95 (s, 3H, OCH_3), 6.95 and 7.01 (2d, J_{5-7} = 2.5 Hz, 2H, C5-H, C7-H), 7.85 (dd, J_{2-3} = 5.0 Hz, J_{3-4} = 8.0 Hz, 1H, C3-H), 7.95 (dd, J_1 = 9.0 Hz, J_2 = 1.5 Hz, 2H, ar.), 8.30 (dd, J_1 = 9.0 Hz, J_2 = 1.5 Hz, 2H, ar.), 8.72 (d, J_{3-4} = 8.0 Hz, C4-H), 8.78 (dd, J_{2-3} = 5.0 Hz, J_{2-4} = 1.5 Hz, C2-H); cims *m/z*: 409 (M^+ + 1). *Anal.* calcd. for $C_{22}H_{25}N_4O_4Cl$: C 59.38, H 5.66, N 12.59, Cl 7.97; found C 59.30, H 5.67, N 12.54, Cl 8.00.

Photosynthesis of **3**c

To a suspension of **1***c*·HCl in 300 mL of $CHCl_3$ was added aqueous NH_3 to adjust the pH to 7.0. The organic layer was washed with water and dried. The solution of the free base **1***c* in $CHCl_3$ was then photolysed as described for the preparation of **3***b*. The crude material was chromatographed on a silica gel column. Elution with methylene chloride gave the starting material first, while further elution with methylene chloride – methanol (9:1) gave the blue material (600 mg), which was again chromatographed on a silica gel column using methylene chloride – methanol (9:1) to yield a blue solid (500 mg). Attempted recrystallization from chloroform–ether gave an amorphous blue solid of mp 140–143°C (dec.); uv–vis (MeOH), λ_{max}: 620 nm; uv (MeOH + NaOH, pH 11.2), λ_{max}: 388 nm; ^{1}H nmr ($CDCl_3$, 300 MHz), δ: 1.45 (d, 6H, C5′-H), 1.95 (m, 8H, C2′-H, C3′-H), 3.55 (m, 4H, C4′-H), 4.05 (s, 6H, OCH_3), 4.30 (m, 3H, C1′-H, NH), 6.50 (2s, 2H, C7-H), 7.29 (m, 2H, C3-H), 7.80 (2d, *J* = 9.0 Hz, 2H, C4-H), 8.05–8.25 (m, 10H, ar., NHCO), 8.53 (m, 2H, C2-H), 8.90 (s, 1H, —CH=); Californium plasma desorption ms, *m/z*: 828.0 (positive molecular ion), calcd. 827.9. *Anal.* calcd. for $C_{45}H_{46}N_8O_8$·1.3 HCl: C 61.82, H 5.45, N 12.81, Cl 5.27; found: C 62.00, H 5.97, N 12.32, Cl 5.27.

Preparation of blue dye **3** d *from methylene dimer* **5** d

The solution of methylene dimer **5***d* (0.51 g), prepared as described previously (6), in 150 mL of chloroform was placed in a 250-mL round bottom flask equipped with a magnetic stirrer. The yellow nondegassed solution was irradiated externally at a distance of 6 in. with a Pyrex-filtered Hanovia mercury lamp.

After 3.5 h of irradiation the solution was evaporated to dryness and the dark green-blue residue was subjected to column chromatography on silica gel 60 (6 g), eluting wih methanol–chloroform mixtures of increasing polarity ($CHCl_3$ to 4:1 $CHCl_3$–MeOH). The "blue band" that eluted last was collected and evaporated to dryness, affording a deep blue-mauve residue (63 mg). Thin-layer chromatography of this material (silica gel 60; $CHCl_3$–MeOH 85:15) and ^{13}C nmr (CD_3OD) showed the presence of minor impurities. The material was once again subjected to column chromatography as before, this time yielding an intense blue solid (25 mg), pure by tlc and hplc. The material was stored in a desiccator where it remained as a solid residue. It quickly became a gummy residue upon exposure to moisture; uv–vis (MeOH), λ_{max}: 618 nm; ^{1}H nmr (CD_3OD, 90 MHz), δ: 1.53 (d, *J* = 6.0 Hz, 6H, C5′-H), 2.03 (s, 6H, $COCH_3$), 4.13 (s, 6H, OCH_3), 6.70 (s, 2H, C7-H), 7.39 (dd, J_{2-3} = 4.5 Hz, J_{3-4} = 9.0 Hz, C3-H), 8.10 (br d, *J* = 9.0 Hz, 2H, C4-H), 8.73 (br d, *J* = 4.5 Hz, 2H, C2-H), 9.07 (s, 1H, —CH=); ^{13}C nmr, see Table 1; Californium plasma desorption ms, *m/z*: 613 (positive molecular ion).

Preparation of blue dye **3** d *from* N-*acetylprimaquine* **1** d

The solution of *N*-acetylprimaquine (1.0 g), prepared as described previously (2), in chloroform (250 mL) was placed in a 500-mL round bottom flask equipped with a magnetic stirrer. Photolysis of the solution was carried out as above. After a total of 5.5 h of irradiation the solution was evaporated to dryness. Chromatography as above gave pure blue dye **3***d* (67.5 mg), which was identical (^{1}H and ^{13}C nmr, tlc, hplc) to that prepared above.

Reduction of blue dye **3** d *to methylene dimer* **5** d

Zinc dust (200 mg) was added to a stirring solution of blue dye **3***d* (30 mg) in 20 mL of methanol–water 1:1. To this deep blue solution was added 50 drops of 10% HCl. (**Note**: the solution must at no time be allowed to become basic.) After 10 min the green solution was filtered and concentrated to ca. 10 mL on the rotary evaporator. This solution was transferred to a separatory funnel and extracted with diethyl ether (4 × 30 mL). The organic layer was dried ($MgSO_4$) and evaporated to dryness, affording a yellow material (5 mg) that was shown to be *N*-acetylprimaquine (^{1}H nmr, tlc).

The aqueous layer was reextracted with chloroform (3 × 20 mL), the organic layer was dried ($MgSO_4$) and evaporated to dryness, affording a yellow material (15 mg) that was shown by ^{1}H nmr and tlc to consist mainly of methylene dimer **5***d* with a trace of *N*-acetylprimaquine. Preparative tlc (silica gel G-200, 2.0 mm, double run with $CHCl_3$–MeOH 95:5) gave a band (R_f ca. 0.2) that, after extraction with methanol–chloroform 1:1, afforded a residue (7 mg). This residue was shown (^{1}H nmr, ir, tlc, hplc) to be identical to the authentic methylene dimer **5***d*.

Preparation of blue dye **3**c *from* **1**c

To a solution of **1***c*·HCl (150 mg) in 5 mL of methanol was added 1 mL of trimethylorthoformate, and the reaction mixture was refluxed for 18 h. During this period the color of the reaction mixture changed from yellow to blue-green. The solvent was then removed and the crude product was passed down a column of silica gel. Elution with $CHCl_3$–MeOH (99:1) gave the starting material first, while further elution with $CHCl_3$–MeOH (97:3) gave the blue dimer **3***c* (30 mg), which was found to be identical (tlc, uv–vis, ms) with that obtained from the direct photolysis of **1***c*.

Acknowledgements

We thank Dr. Louis Pannel from the Laboratory of Bio-organic Chemistry and Mr. Noel Whittaker from the Laboratory of Analytical Chemistry, NIDDK, National Institutes of Health, Bethesda, Maryland for the recording of mass spectra.

1. L. T. Webster, Jr. *In* The pharmacological basis of therapeutics. 7th ed. *Edited by* L. S. Goodman and A. Gilman. Macmillan Publishing Co., Inc., New York. 1985. pp. 1038–1041.
2. A. Strother, R. Allahyari, J. Buchholz, I. M. Fraser, and B. E. Tilton. Drug Metab. Dispos. **12**, 35 (1984).
3. A. M. Clark, C. D. Hufford, and J. D. McChesney. Antimicrob. Agents Chemother. **19**, 337 (1981).
4. A. M. Clark, S. L. Evans, C. D. Hufford, and J. D. McChesney. J. Nat. Prod. **45**, 574 (1982).
5. P. Karrer. Organic chemistry. 4th English ed. Elsevier, New York. 1950. pp. 606–608.
6. L. K. Pannel, E. A. Sokoloski, H. Fales, and R. L. Tate. Anal. Chem. **57**, 1060 (1985).
7. A. M. Clark, C. D. Hufford, R. C. Gupta, R. K. Puri, and J. D. McChesney. Appl. Environ. Microbiol. **47**, 537 (1984).
8. C. D. Hufford, J. D. McChesney, and J. K. Baker. J. Heterocycl. Chem. **20**, 273 (1983).
9. A. M. Clark, J. K. Baker, and J. D. McChesney. J. Pharm. Sci. **73**, 502 (1984).
10. C. D. Hufford, A. M. Clark, I. N. Quinones, J. K. Baker, and J. D. McChesney. J. Pharm. Sci. **72**, 92 (1983).

Ion/molecule reactions in allene. IV. Kinetic considerations

FRANÇOIS HAMON, DANIELLE CARRIER, AND JAN A. HERMAN
Centre de recherche sur les atomes et les molécules et le département de chimie, Université Laval, Québec (P.Q.), Canada G1K 7P4

Received January 27, 1986

FRANÇOIS HAMON, DANIELLE CARRIER, and JAN A. HERMAN. Can. J. Chem. **64**, 2199 (1986).

An analysis of the kinetic rate constants for ion/molecule reactions of allene by use of the Laplace–Carson transform is performed and the results are compared with experimental data.

FRANÇOIS HAMON, DANIELLE CARRIER et JAN A. HERMAN. Can. J. Chem. **64**, 2199 (1986).

On a effectué une analyse des constantes de vitesse des réactions ion/molécule de l'allène en faisant appel à la transformation de Laplace–Carson; on compare les résultats avec les données expérimentales.

[Traduit par la revue]

Introduction

In a previous paper we presented a mechanism for ion/molecule reactions of gaseous allene in the pressure range 0.02 to 3.5 Torr (1). This reaction mechanism was deduced from results obtained in a high pressure mass-spectrometer equipped with a photoionization source operating at 10 eV (krypton resonance line). At this energy only parent ions of allene are formed, therefore all daughter and subsequent generations of ions must be traced to the $C_3H_4^+$ primary species. At that time no attempt was made to calculate rate constants of the successive reaction steps. In another paper we considered the collisional stabilization by non-polar gases of the dimer-ion species, $C_6H_8^+$, which was assumed to play an important role in the overall reaction scheme (2). Other studies of the ion/molecule reaction of allene at low pressure (<0.01 Torr) have not indicated the presence of the $C_6H_8^+$ ion species, but the formation of $C_6H_7^+$ and of $C_7H_7^+$ species have been observed (3–6). Obviously, the presence of the $C_6H_8^+$ ion species at high pressure, even at low fractional intensity (<1%), is an indication that this species has to be stabilized by collision in order to be observed.

The reaction scheme for ion/molecule reactions in allene is shown below in which only the two most important reaction channels are considered.

[1] $C_3H_4^+ + C_3H_4 \xrightarrow{k_1} C_6H_7^+ + H^\cdot$

[2] $C_3H_4^+ + 2C_3H_4 \xrightarrow{k_2} C_7H_7^+ + C_2H_5^\cdot$

[3] $C_6H_7^+ + C_3H_4 \underset{k_{-3}}{\overset{k_3}{\rightleftharpoons}} C_6H_7^+\cdot C_3H_4$

[4] $C_6H_7^+\cdot C_3H_4 + C_3H_4 \underset{k_{-4}}{\overset{k_4}{\rightleftharpoons}} C_6H_7^+(C_3H_4)_2$

[5] $C_6H_7^+(C_3H_4)_2 + C_3H_4 \underset{k_{-5}}{\overset{k_5}{\rightleftharpoons}} C_6H_7^+(C_3H_4)_3$

[6] $C_7H_7^+ + C_3H_4 \underset{k_{-6}}{\overset{k_6}{\rightleftharpoons}} \alpha\text{-}C_{10}H_{11}^+$

[7] $C_6H_7^+\cdot C_3H_4 + C_3H_4 \xrightarrow{k_7} \beta\text{-}C_{10}H_{11}^+ + C_2H_4$

[8] $\beta'\text{-}C_{10}H_{11}^+ + C_3H_4 \xrightarrow{k_8} \beta\text{-}C_7H_7^+ + 2C_3H_4$

These species account for around 90% of the total ion intensities (1). The question which could not have been answered at that time concerned the mechanism of formation of the $C_6H_7^+$ species at high pressure, either through the long-lived ion complex ($C_3H_4^+\cdot C_3H_4$) requiring a reactive collision with a neutral allene molecule, or simply through an unimolecular fragmentation of the excited collisional complex: $(C_3H_4)_2^+ * \rightarrow C_6H_7^+ + H\cdot$ (6, 7). In both cases the reaction processes are exothermic. Another problem which could not be settled was the unexpected behaviour at high pressure (>0.1 Torr) of the $C_{10}H_{11}^+$ and $C_7H_7^+$ ion species (1). We assumed that at least two isomeric $C_7H_7^+$ and $C_{10}H_{11}^+$ ion species have to be formed through different reaction channels accounting for the steady build up of the concentrations of these species with increasing pressure.

In order to test the proposed reaction scheme and to get a better insight we present the calculation of the rate constants of the various steps of the ion/molecule reactions and we compare the numerical results with the experimental data published in ref. 1.

Kinetic model

In order to calculate the rate coefficients of the elementary steps in the sequence of ion/molecule reactions of allene, one has to know the mean residence time, t_R, of ion species in the collision cell. The cylindrical ion source of our experimental setup is not equipped for residence time or ion mobility measurements (1). However, for the present purposes it may be assumed on the basis of ion mobility theory (8) and some experimental data (9–13) that the residence time at pressures above a few tenths of a Torr is proportional to the pressure and to the length of the path between the site of formation of the ion and the exit slit. Under vanishing electric field conditions the diffusion of ions is isotropic and one can show that the average path length of ions can be correlated to the distance, l, between the plane of ion formation by incident photons, and the exit slit. In the case of a cylindrical cavity of radius r_0 and length l the residence time is given by (14):

$$t_R = D[(2.045/r_0)^2 + (\pi/2l)^2]$$

where D is the diffusion coefficient which can be calculated from the Einstein relation, $D = KT \times 8.6 \times 10^{-5}$. The ion mobility, K, can be evaluated at the temperature and the pressure of the experiments from the reduced mobility, $K_0 = 35.9\,(\alpha\mu)^{-1/2}$, where α is the polarizability and μ is the reduced mass of the system, both expressed in atomic units. This expression of the reduced mobility applies only to an ion diffusing in a bath gas of different nature, in order to avoid resonant charge transfer, and in a vanishing field. Both conditions are met in the present case. Strictly speaking, one

should use the ambipolar coefficient of diffusion to calculate the residence time of ions, but this is very difficult to take into account in a simple manner. In any case the dominant effect of the ambipolar diffusion will involve the velocity distribution of ions rather than the average drift velocity (15).

Following these expressions, the average residence time is calculated to be $t_R = 80$ μs at 0.1 Torr and at the distance $l = 2.2$ mm for the cylindrical source used in the present experiments ($r_0 = 9.52$ mm). The average reduced mass $\mu = 30.9$ amu was used which gives a difference of 10% between the average residence time and the individual residence time values for each ion/molecule system.

The ion source used in this study (16) is not suited to residence time measurements, therefore it was difficult to verify experimentally the above calculated relation of t_R. However, at the lowest pressure ($P < 0.015$ Torr) and at the shortest path length[1] ($l = 2.2$ mm) we could roughly estimate the variation of the fractional intensities of the $C_6H_7^+$ species, which is the most important abundant ion (~60%) in this pressure range. From these data we found a residence time, $t_R = 87 \pm 17$ μs at $P = 0.1$ Torr, which compares reasonably well with the residence time calculated from the simplified model using the transport properties of gases (8). Therefore, in all subsequent calculations we used the pressure-dependent average residence time, $t_R = 0.80 \times 10^{-3} P$ (s Torr^{-1}) for all experimental data obtained for the length 2.2 mm in the collision cell.

In the kinetic model discussed below we assume that the disappearance of the primary ion species, $C_3H_4^+$, proceeds through two channels leading to $C_6H_7^+ \cdot (C_3H_4)_n$ (with $n = 0$–3) and $C_7H_7^+ \cdot (C_3H_4)_m$ (with $m = 0$, 1) ion species, respectively. We also assume that the rate constant for disappearance of the primary ion species, $C_3H_4^+$, is given by $k = (6.4 \pm 0.5) \times 10^{-10}$ cm^3 molecule^{-1} s^{-1} as measured by Lifshitz in a trapped-ion mass spectrometer (5). Moreover, we will neglect in our calculations the very weak reaction channel (around 2%) leading to $C_6H_9^+$ ion species.

In order to fit the calculated fractional intensities of ion species with experimental data, we have to assume two additional processes besides the reactions [1]–[8]:

$$[9] \quad \beta'\text{-}C_{10}H_{11}^+ + C_3H_4 \xrightarrow{k_9} \beta\text{-}C_7H_7^+ + 2C_3H_4$$

$$[10] \quad \alpha\text{-}C_{10}H_{11}^+ + C_3H_4 \xrightarrow{k_{10}} \text{unidentified products}$$

Reaction [9] might be an isomerization process or a stabilization reaction giving unreactive $C_{10}H_{11}^+$ species toward allene molecule. The relative positions of processes [9] and [10] in the sequence of ion/molecule reactions of allene are shown in Fig. 1.

For the sake of clarity we will present first the kinetics of the $C_6H_7^+ \cdot (C_3H_4)_n$ formation channel, and then the kinetics of $C_7H_7^+ \cdot (C_3H_4)_m$ channel.

The $C_6H_7^+ \cdot (C_3H_4)_n$ species formation channel

The following rate equations describe the formation of the above mentioned species

$$[11] \quad d[C_3H_4^+]/dt = -(k_1 + k_2)[C_3H_4^+]P$$

$$[12] \quad d[C_6H_7^+]/dt = k_1[C_3H_4^+]P - k_3[C_6H_7^+]P^2 + k_{-3}[C_6H_7^+ \cdot C_3H_4]P$$

[1]The photoionization collision cell is equipped with several slits whose distances vary from 2.2 to 13.2 mm from the site of primary ion formation to the exit orifice (16).

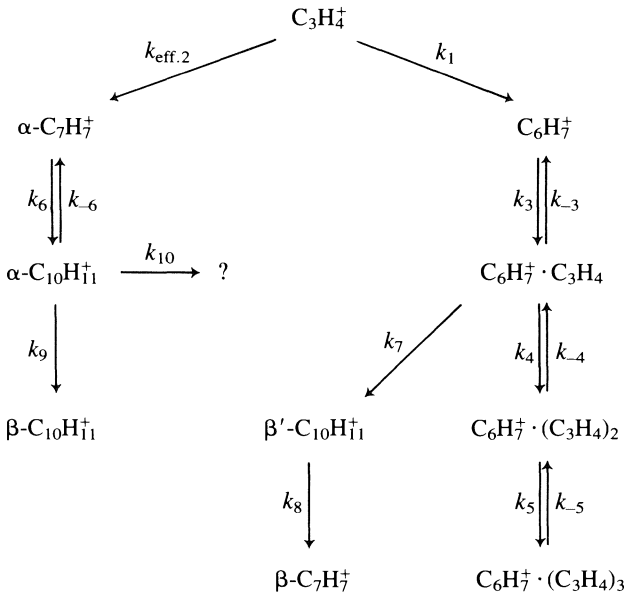

FIG. 1. The proposed reaction scheme for ion/molecule reactions in allene.

$$[13] \quad d[C_6H_7^+ \cdot C_3H_4]/dt = k_3[C_6H_7^+]P^2 + k_{-4}[C_6H_7^+ \cdot (C_3H_4)_2]P - (k_4P + k_8 + k_{-3})[C_6H_7^+ \cdot (C_3H_4)]P$$

$$[14] \quad d[C_6H_7^+ \cdot (C_3H_4)_2]/dt = k_4[C_6H_7^+ \cdot C_3H_4]P^2 + k_{-5}[C_6H_7^+ \cdot (C_3H_4)_3]P - (k_{-4} + k_5P)[C_6H_7^+ \cdot (C_3H_4)_2]P$$

$$[15] \quad d[C_6H_7^+ \cdot (C_3H_4)_3]/dt = k_5[C_6H_7^+ \cdot (C_3H_4)_2]P^2 - k_{-5}[C_6H_7^+ \cdot (C_3H_4)_3]P$$

In these equations P (Torr) stands for the concentration of the neutral allene.

The additional reaction channel characterised by rate coefficient k_8 in eq. [13] relates the experimentally established absence of thermodynamic equilibrium between the $C_6H_7^+ \cdot C_3H_4$ species and the $C_6H_7^+$ precursor ion on one side and the $C_6H_7^+ \cdot (C_3H_4)_2$ species on the other side (1). However, starting from the $C_6H_7^+ \cdot (C_3H_4)_2$ species and higher order clusters the chemical equilibrium is achieved as shown experimentally by varying the residence time of these species in the collision cell (1).

Within this kinetic scheme we assumed the generally accepted mechanisms of solvation processes, namely, that the forward reaction requires a stabilization collision and the backward or declustering reaction an activation step (17). This introduces a third order forward reaction step and a reverse bimolecular dissociation process.

Another important comment concerns the formation of $C_7H_7^+$ species in reaction [2]. The best fit of the rate coefficients with experimental data requires that $C_7H_7^+$ species to be formed in an *apparent second order reaction*. Any attempt to introduce a third order formation process of $C_7H_7^+$ species from primary $C_3H_4^+$ ions and allene neutrals leads to rate coefficients for both channels, $C_6H_7^+$ and $C_7H_7^+$, which is experimentally not supported. In the next section we will discuss this behaviour in more detail.

Keeping these remarks in mind we used the Laplace–Carson transform method for the solution of these simultaneous

TABLE 1. List of rate constants

Reaction	Rate coefficient
$C_3H_4^+[C_3H_4, H^\cdot]C_6H_7^+$	$k_1 = 4.33 \times 10^{-10}$ [a]
$C_3H_4^+[2C_3H_4, C_2H_5']\alpha\text{-}C_7H_7^+$	$k_{2,\text{eff}} = 2.16 \times 10^{-10}$ [a]
$C_6H_7^+[2C_3H_4, C_3H_4]C_6H_7^+C_3H_4$	$k_3 = 1.1 \times 10^{-27}$ [b]
$C_6H_7^+C_3H_4[C_3H_4, 2C_3H_4]C_6H_7^+$	$k_{-3} = 1.5 \times 10^{-12}$ [a]
$C_6H_7^+C_3H_4[2C_3H_4, C_3H_4]C_6H_7^+(C_3H_4)_2$	$k_4 = 9.6 \times 10^{-29}$ [b]
$C_6H_7^+(C_3H_4)_2[C_3H_4, 2C_3H_4]C_6H_7^+C_3H_4$	$k_{-4} = 1.2 \times 10^{-11}$ [a]
$C_6H_7^+(C_3H_4)_2[2C_3H_4, C_3H_4]C_6H_7^+(C_3H_4)_3$	$k_5 = 9.6 \times 10^{-30}$ [b]
$C_6H_7^+(C_3H_4)_3[C_3H_4, 2C_3H_4]C_6H_7^+(C_3H_4)_2$	$k_{-5} = 4.6 \times 10^{-13}$ [a]
$\alpha\text{-}C_7H_7^+[2C_3H_4, C_3H_4]\alpha\text{-}C_{10}H_{11}^+$	$k_6 = 1.9 \times 10^{-27}$ [b]
$\alpha\text{-}C_{10}H_{11}^+[C_3H_4, 2C_3H_4]\alpha\text{-}C_7H_7^+$	$k_{-6} = 1.9 \times 10^{-12}$ [a]
$C_6H_7^+\cdot C_3H_4[C_3H_4, C_2H_4]\beta'\text{-}C_{10}H_{11}^+$	$k_7 = 3.1 \times 10^{-15}$ [a]
$\beta'\text{-}C_{10}H_{11}^+[C_3H_4, 2C_3H_4]\beta\text{-}C_7H_7^+$	$k_8 = 6.2 \times 10^{-15}$ [a]
$\alpha\text{-}C_{10}H_{11}^+[C_3H_4, C_3H_4]\beta\text{-}C_{10}H_{11}^+$	$k_9 = 9.3 \times 10^{-13}$ [a]
$\alpha\text{-}C_{10}H_{11}^+[C_3H_4, ?]I^+$ [c]	$k_{10} = 2.2 \times 10^{-12}$ [a]

[a] Units: cm^3 $molecule^{-1}$ s^{-1}.
[b] Units: cm^6 $molecule^{-2}$ s^{-1}.
[c] Unidentified ion products.

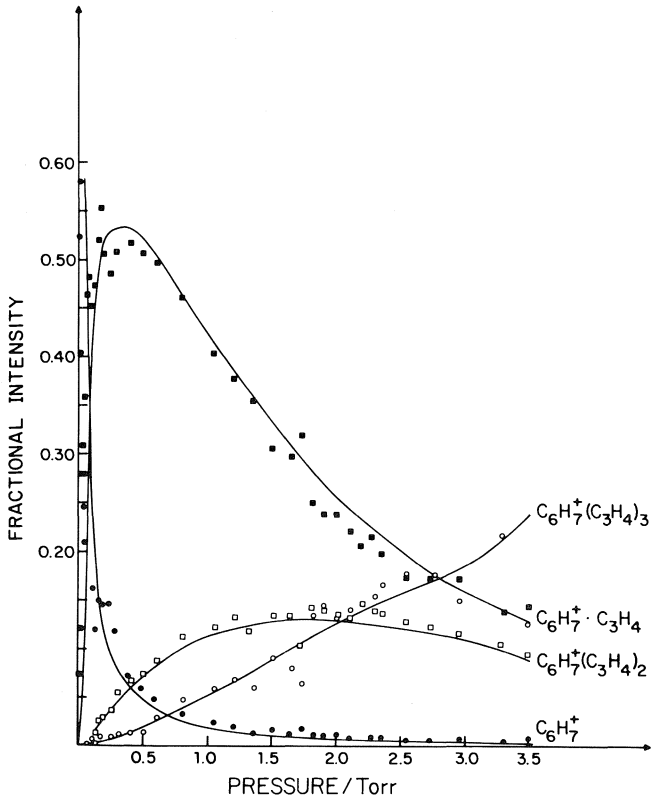

FIG. 2. Calculated fractional intensity curves (solid lines) as a function of the pressure for the $C_6H_7^+\cdot(C_3H_4)_n$ family of ions.

differential equations as a function of time. Some details of the solutions are presented in Appendix 1. The rate coefficients for the $C_6H_7^+(C_3H_4)_n$ species channel formation are presented in Table 1, and in Fig. 2 the calculated corresponding fractional intensities curves are shown.

The $C_7H_7^+$ and $C_{10}H_{11}^+$ species formation channel

First, let us look into the apparent anomaly, mentioned in the previous section, of the experimental second order rate of formation of the $C_7H_7^+$ ion species instead of a third order process which would normally be expected. Indeed, if one tries to fit the $C_7H_7^+$ ion formation to a third order process, the best calculated rate coefficient is around 10^{-25} cm^6 $molecule^{-2}$ s^{-1}, which is physically not acceptable and, moreover, the rate of formation of $C_6H_7^+$ species has to be compensated also by a third order contribution also having an unlikely high rate coefficient of the order of 10^{-24} cm^6 $molecule^{-2}$ s^{-1}. However, the *pseudo second order* mechanism of $C_7H_7^+$ formation is explained by assuming the formation of a $C_4H_4^+$ intermediate ion species, which reacts very efficiently with neutral allene to form the $C_7H_7^+$ species:

$$[16]\quad C_3H_4^+ + C_3H_4 \underset{k_r}{\overset{k_f}{\rightleftharpoons}} (C_3H_4)_2^+{}^*$$

$$[17]\quad (C_3H_4)_2^+{}^* \xrightarrow{k_1} C_6H_7^+ + H^\cdot$$

$$[18]\quad (C_3H_4)_2^+{}^* \xrightarrow{k_d} C_4H_4^+ + C_2H_4$$

$$[19]\quad (C_3H_4)_2^+{}^* + C_3H_4 \xrightarrow{k_s} C_6H_8^+ + C_3H_4$$

$$[20]\quad C_4H_4^+ + C_3H_4 \xrightarrow{k_2'} \alpha\text{-}C_7H_7^+ + H^\cdot$$

In our experiments the pressure is too high to allow the detection of the $C_4H_4^+$ species, but at lower pressure ($P < 10^{-3}$ Torr) it was observed experimentally (3), and reaction [20] was definitely established in double resonance I.C.R. experiments (4, 5). We assume that the $C_4H_4^+$ species is very reactive and reacts at almost every collision with neutral allene in process [20], which might explain its absence in the mass spectrum, even at the lowest pressure of our experiments. Applying the steady state assumption to the collisional complex, $(C_3H_4)_2^+$, and to the $C_4H_4^+$ species, one gets the following order dependence for the formation of $C_7H_7^+$

$$[21]\quad d[C_7H_7^+]/dt = \left(\frac{k_f k_d}{k_r + k_1 + k_d + k_s P}\right)[C_3H_4^+]P$$

The relative stabilization rate coefficient, k_s, was measured by Nagase *et al.* (18), and is at least two orders of magnitude smaller than the sum $(k_r + k_1 + k_d) \simeq k_f$, and at low pressure it can be neglected in eq. [21]. Consequently, eq. [21] takes

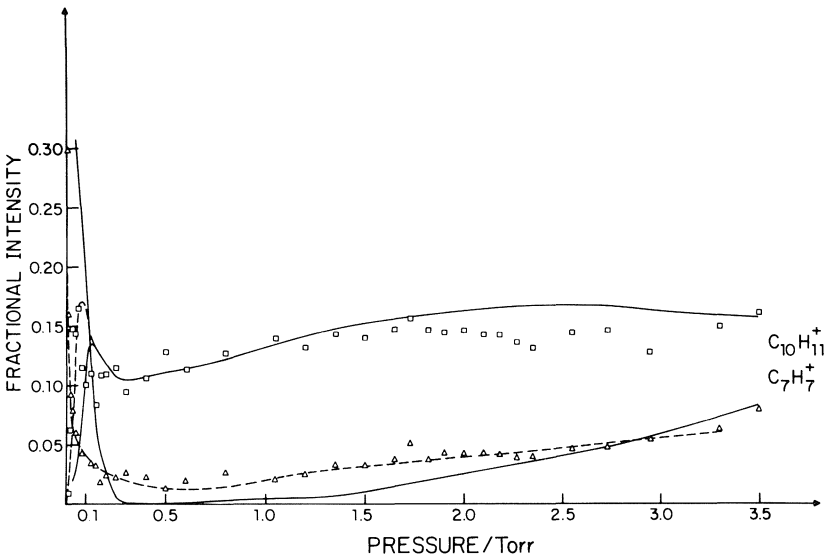

FIG. 3. Calculated fractional intensity curves (solid lines) as a function of the pressure for the $C_7H_7^+$ and $C_{10}H_{11}^+$ species. The broken lines are the experimental curves.

the experimentally required kinetic order dependence:

$$[22]\quad d[C_7H_7^+]/dt \simeq \left(\frac{k_f k_d}{k_r + k_1 + k_d}\right)[C_3H_4^+]P = k_{2,\text{eff}}[C_3H_4^+]P$$

Assuming that the rate coefficient, k_f, can be calculated from the "average dipole orientation" collision rate theory (ADO), and is equal to $k_f = k_{ADO} = 12.9 \times 10^{-10}$ cm^3 molecule^{-1} s^{-1} [7], one can use this value to estimate the ratio $(k_r + k_1)/k_d$ in eq. [22]. Substituting the experimental value for $k_{2,\text{eff}} = 2.2 \times 10^{-10}$ cm^3 molecule^{-1} s^{-1} (Table 1) one finds $(k_r + k_1)/k_d \simeq 5.9$.

As shown previously the $C_7H_7^+$ and $C_{10}H_{11}^+$ ion formation channel displays a complex behaviour (1). At low pressure and short residence time the fractional intensity of $C_{10}H_{11}^+$ species reaches a sharp maximum at $P \sim 0.05$ Torr, passes through a minimum at $P = 0.2$ Torr, and then rises slowly with pressure to a plateau. Concurrently the fractional intensity of the $C_7H_7^+$ species drops to 0.03 at low pressure <0.4 Torr, and then slowly rises with increasing pressure to around 0.06 at 3.5 Torr. At longer residence time of ion species in the collision cell this behaviour is enhanced. In order to explain this complex behaviour we have assumed that the $C_7H_7^+$ and $C_{10}H_{11}^+$ ion species are formed in at least two different reaction channels leading to isomer species of different structures, as shown by their different reactivities toward the neutral allene. There is also the possibility that these isomeric species of $C_7H_7^+$ and $C_{10}H_{11}^+$ general formula, are converted through collisionally induced isomerization processes.

Several kinetic schemes were tested and the best results were obtained for the reaction sequence:

$$[23]\quad d[\alpha\text{-}C_7H_7^+]/dt = k_{2,\text{eff}}[C_3H_4^+]P + k_{-6}[\alpha\text{-}C_{10}H_{11}^+]P - k_6[\alpha\text{-}C_7H_7^+]P^2$$

$$[24]\quad d[\beta\text{-}C_7H_7^+]/dt = k_9[\beta'\text{-}C_{10}H_{11}^+]P$$

$$[25]\quad d[\alpha\text{-}C_{10}H_{11}^+]/dt = k_6[\alpha\text{-}C_7H_7^+]P^2 - (k_{-6} + k_7 + k_{10})[\alpha\text{-}C_{10}H_{11}^+]P$$

$$[26]\quad d[\beta'\text{-}C_{10}H_{11}^+]/dt = k_8[C_6H_7^+\cdot C_3H_4]P - k_9[\beta'\text{-}C_{10}H_{11}^+]P$$

In the expressions [23]–[26] the reaction processes and the corresponding rate coefficients are numbered according to the overall reaction scheme in Fig. 1.

The α-, β-, and β′- species are identified in Fig. 1. The α-$C_7H_7^+$ and α-$C_{10}H_{11}^+$ ion species seems to be related by a solvation process and are formed preferentially at low pressure. The β-$C_7H_7^+$, β-$C_{10}H_{11}^+$, and β′-$C_{10}H_{11}^+$ species are most probably a mixture of unreactive isomers formed at high pressure which accumulate in the system. The experimental fractional intensities of $C_7H_7^+$ and $C_{10}H_{11}^+$ as a function of the pressure are, of course, the sum of these processes and the solutions of corresponding differential equations are shown in the Appendix (eqs. [34], [35]). The numerical solutions are presented in Table 1 and the calculated curves are shown in Fig. 3.

Discussion

The Laplace–Carson transform method applied to a scheme of elementary reactions such as shown in Fig. 1, is sensitive to the assumed order of the reactions and to the number of elementary steps involved in the formation of each species. In such a way a number of kinetically plausible combinations of elementary reactions can be eliminated, because they do not fit the experimental intensities. However, it should be pointed out that the rate coefficient values of the first steps are critical, allowing only a small variation in order to reproduce the experimental curves. On the other hand, the rate coefficient values of the last steps are less sensitive.

The calculated curves of fractional intensities as a function of the pressure using the rate coefficients obtained by the Laplace–Carson transform method fit the experimental data satisfactorily (Figs. 2, 3). The precision expected in these calculations for the $C_6H_7^+\cdot(C_3H_4)_n$ ion formation channel is estimated to be around 30% if one takes into account the approximate values of the mean residence time of ions in the collision cell and the use of an average value for the reduced mass of all ions in the system. In the case of this reaction channel the thermodynamic equilibrium relations impose supplementary constraints on the choice of possible combinations of rate coefficient values describing the experimental curves. The value of the third-order rate coefficient for the forward reaction forming the $C_6H_7^+\cdot C_3H_4$

species (reaction [3]) of approximately 10^{-27} cm^6 molecule^{-2} s^{-1} is a fairly large value. However, the value for a third-order rate coefficient depends primarily on the lifetime of the excited complex which must be collisionally deactivated. The further solvation processes (reactions [4] and [5] proceed much slower, as indicated by the corresponding rate coefficients, and this may be due to a decrease in the energy of association as the size of the cluster increases.

The overall precision in the calculations of the $C_7H_7^+$ and $C_{10}H_{11}^+$ formation channel is lower than that for the $C_6H_7^+ \cdot (C_3H_4)_n$ reactions sequence. Especially in the case of $C_7H_7^+$ the precision seems to be poor.

The calculated curves for the $C_7H_7^+$ and $C_{10}H_{11}^+$ species formation involve several contributions from different sources (Fig. 1), therefore their fit to experimental data is more complex. At low pressure both calculated curves diverge from the experimental points. In the case of $C_7H_7^+$ species the disagreement is sufficiently pronounced to consider the existence of another process consuming the precursor of the $C_7H_7^+$ species. However, we have not succeeded in reproducing such a reaction channel in our calculations. Moreover, we have to assume an additional second order reaction channel consuming the α-$C_{10}H_{11}^+$ species (reaction [10]) in order to account for the shape of the curve. In fact, this second order reaction is relatively slow ($k_{10} = 2.2 \times 10^{-12}$ cm^3 molecule^{-1} s^{-1}) and it could also be responsible for the formation of minor ion species, i.e. $C_9H_9^+$ whose origin is difficult to assess with certainty.

The contribution to the β-$C_{10}H_{11}^+$ and β'-$C_7H_7^+$ formation through reactions [7] and [8] accounts for >50% at high pressure. It seems that the slow decomposition reaction [7] with a rate coefficient $k_7 \sim 10^{-15}$ cm^3 molecule^{-1} s^{-1} is the rate-determining step at pressures above 1 Torr. For the olefin systems studies in this laboratory we have found that there are slow ion/molecule reactions which take place at high pressure. The origin of these reactions is not very clear owing to the numerous steps preceding the formation process of the species accumulated in the gas phase.[2] This may also be the case for reactions [7] and [8], which albeit slow are determinant for the formation of the unreactive $C_7H_7^+$ and $C_{10}H_{11}^+$ species.

The kinetic analysis of ion/molecule reactions of allene suggests two mechanisms for the disappearance of $C_3H_4^+$ primary ions through an excited complex $(C_3H_4^+)^{2*}$: (*a*) dissociating into $C_6H_7^+$ and a hydrogen atom, which is the main reaction channel [7], and (*b*) dissociating into $C_4H_4^+$ ion species, which on collision with neutral allene form the $C_7H_7^+$ species (reaction [20]). It is possible that the long-lived dimer-ion is formed by a partial deactivation of the excited loose complex $(C_3H_4^+)^{2*}$ preventing further dissociation into $C_6H_7^+$, but transforming it into a tighter configuration.

The discrepancy between the rate coefficients for the disappearance of the primary ion species, $C_3H_4^+$, measured by ICR mass-spectrometry (19) and in photoionization high-pressure mass-spectrometry (5–7) is probably due to the differences of internal energies in the primary ion species. The ion–molecule reaction cross-section of allene decreases with increasing photon energy and was observed to decrease by ~70% of the initial value for $C_6H_7^+$ production upon increasing the internal vibrational energy by 1.0 eV, [7]. In the ICR mass-spectrometry experiments the rate coefficient for $C_6H_7^+$ formation was measured to be 9.6×10^{-10} cm^3 molecule^{-1} s^{-1} (19), which is 2.2 times higher than the calculated rate constant for the same reaction in the present experiments (Table 1). For the time being we have no explanation for this apparently contradictory result, unless some deactivation and stabilization processes have to be accounted for in experiments at high pressure ($>10^{-3}$ Torr).

[2]Unpublished results from this laboratory.

Acknowledgements

The authors are indebted to the Natural Sciences and Engineering Research Council of Canada for financial support. D.C. acknowledges a fellowship from the same Institution.

1. D. Carrier and J. A. Herman. Int. J. Mass Spectrom. Ion Proc. **59**, 49 (1984).
2. K. Nagase and J. A. Herman. Can. J. Chem. **62**, 2364 (1984).
3. J. J. Myher and A. G. Harrison. J. Phys. Chem. **72**, 1905 (1968).
4. M. T. Bowers, D. D. Elleman, R. M. O'Malley, and K. R. Jennings. J. Phys. Chem. **74**, 2583 (1970).
5. C. Lifshitz, Y. Gleitman, S. Gefen, U. Shainok, and I. Dotan. Int. J. Mass Spectrom. Ion Phys. **40**, 1 (1981).
6. C. Lifshitz and Y. Gleitman. Int. J. Mass Spectrom. Ion Phys. **40**, 17 (1981).
7. C. Lifshitz and Y. Gleitman. J. Chem. Phys. **77**, 2383 (1982).
8. E. W. McDaniel. Collision phenomena in ionized gases. J. Wiley and Sons. New York. 1964. p. 426.
9. R. N. Varney. Phys. Rev. **89**, 708 (1953).
10. M. Saporoshenko. Phys. Rev. **139**A, 352 (1961); J. Phys. Chem. **42**, 768 (1968).
11. S. F. Kasper and J. L. Franklin. J. Chem. Phys. **56**, 1156 (1972).
12. G. Sroka, C. Chang, and G. G. Meisels. J. Chem. Phys. **94**, 1052 (1972).
13. H. Wincel and J. A. Herman. Int. J. Mass Spectrom. Ion Phys. **14**, 139 (1974).
14. E. W. McDaniel and E. A. Masson. The mobility and diffusion of ions in gases. J. Wiley and Sons, New York. 1973. p. 24.
15. C. Chang, G. J. Sroka, and G. G. Meisels. Int. J. Mass Spectrom. Ion Phys. **11**, 367 (1973).
16. Z. Łuczynski and J. A. Herman. Int. J. Mass Spectrom. Ion Phys. **31**, 237 (1979).
17. P. Kebarle. Ion–molecule reaction. *Edited by* J. L. Franklin. Plenum Press, New York. 1972. Chapt. 7.
18. K. Nagase and J. A. Herman. Can. J. Chem. **64**, 192 (1986).
19. V. G. Anicich, G. A. Blake, J. K. Kim, M. J. McEwan, and W. T. Huntress, Jr. J. Phys. Chem. **88**, 4608 (1984).
20. N. M. Rodiguin and E. N. Rodiguina. Consecutive chemical reactions, D. Van Nostrand Co., Princeton, NJ. 1964.

Appendix

The system of linear differential equations for the rates of consecutive, reverse, or parallel reactions can be solved using the Laplace–Carson method

$$F(L) = L\int_0^\infty e^{-Lt} f(t)dt$$

as described by Rodiguin and Rodiguina (20). In the present case of a complex ion/molecule reactions sequence one obtains transforms whose originals have to be separately evaluated. The general procedure is to decompose the transform

$$[27] \quad \frac{F_1(L)}{F_2(L)} = \frac{a_0L^m + a_1L^{m-1} + \ldots + a_m}{b_0L^n + b_1L^{n-1} + \ldots + b_n}$$

where the multinomials $F_1(L)$ and $F_2(L)$ have no common roots, into a sum of partial fractions:

$$[28]\quad \frac{F_1(L)}{F_2(L)} = \sum_{j=1}^{n} \frac{A_j}{L - L_j}$$

where L_j are the roots of the equation $F_2(L) = 0$. The decomposition coefficients A_j, given by

$$[29]\quad A_j = \frac{F_1(L_j)}{F_2'(L_j)}$$

are substituted into [28]:

$$[30]\quad \frac{F_1(L)}{F_2(L)} = \sum_{j=1}^{n} \frac{F_1(L_j)}{F_2'(L_j)}\left(\frac{1}{L - L_j}\right)$$

in which the original of $F_1(L)/F_2(L)$ can be readily determined, since each term of the sum of the right-hand portion of the equation is a constant multiplied by the factor $\{1/(L - L_j)\}$, the original of which is known. The final expression of the ratio is:

$$[31]\quad \frac{F_1(L)}{F_2(L)} = \sum_{j=1}^{n} \frac{F_1(L_j)}{F_2'(L_j)} \frac{1}{L_j} [\exp(L_j t) - 1]$$

Suitable computer programs were developed in order to solve eq. [31] for each ion species.

The application of this method to the simultaneous differential equations as a function of the residence time yields the following solution for the primary ions:

$$[32]\quad [C_3H_4{}^+] = \frac{\exp\{-(k_1 + k_2)\mathrm{Pt}\} - 1}{-(k_1 + k_2)P}$$

and four equations of the form:

$$[33]\quad [S^+] = \sum_{j}^{1-5} {}_sA_j[\exp(L_j t) - 1]/L_j$$

for $C_6H_7{}^+$ and its clustered species, where $[S^+]$ stands for the concentration of $C_6H_7{}^+\cdot(C_3H_4)_n$ ion species with $n = 0$, 1, 2, 3, respectively. The superscripts of the sum symbol [33] are related to the kinetic rate equations characterized by the rate coefficients, $k_{\pm j}$ (Fig. 1). The real roots, L_j, of the multinomial of the denominator in expression [33] are the same, and only the coefficients ${}_sA_j$ obtained from the decomposition of the ratio of multinomials into simple fractions are different for each species, S^+. Obviously, at the initial time, $t_0 = 0$, the fractional intensity of the primary ions $[C_3H_4{}^+]_0 = 1$.

In the case of the $C_7H_7{}^+$ formation channel we get the following solutions:

$$[34]\quad [C_7H_7{}^+] = \sum_{j}^{2,6} \frac{{}_\alpha B_j}{L_j} [\exp(L_j t) - 1] + \sum_{j}^{1,3-5,7,8} \frac{{}_\beta B_j}{L_j} [\exp(L_j t) - 1]$$

$$[35]\quad [C_{10}H_{11}{}^+] = \sum_{j}^{2,6,9,10} \frac{{}_\alpha C_j + {}_\beta C_j}{L_j} [\exp(L_j t) - 1] + \sum_{j}^{1-5,7} \frac{{}_{\beta'} C_j}{L_j} [\exp(L_j t) - 1]$$

where ${}_\alpha B_j$, ${}_\beta B_j$, ${}_\alpha C_j$, ${}_\beta C_j$, and ${}_{\beta'} C_j$ are the coefficients of the simple fractions and L_j are the real roots of the multinomials of the denominator in [28].

Enantioselective synthesis of isoquinoline alkaloids[1]

ZBIGNIEW CZARNOCKI AND DAVID B. MACLEAN[2]
Department of Chemistry, McMaster University, Hamilton, Ont., Canada L8S 4M1

AND

WALTER A. SZAREK[2]
Department of Chemistry, Queen's University, Kingston, Ont., Canada K7L 3N6

Received April 8, 1986

ZBIGNIEW CZARNOCKI, DAVID B. MACLEAN, and WALTER A. SZAREK. Can. J. Chem. **64**, 2205 (1986).

The utility of the Pictet–Spengler condensation of (*R*)-(+)-glyceraldehyde with dopamine hydrochloride in the enantioselective synthesis of isoquinoline alkaloids is demonstrated by the preparation of (*S*)-(−)-carnegine, (*R*)-(−)-calycotomine, and (*S*)-(+)-laudanosine.

ZBIGNIEW CZARNOCKI, DAVID B. MACLEAN et WALTER A. SZAREK. Can. J. Chem. **64**, 2205 (1986).

On démontre l'utilité de la condensation de Pictet–Spengler du (*R*)-(+)-glycéraldéhyde avec le chlorhydrate de la dopamine dans la synthèse énantiosélective des alcaloïdes de l'isoquinoléine en préparant la (*S*)-(−)-carnégine, la (*R*)-(−)-calycotomine et la (*S*)-(+)-laudanosine.

[Traduit par la revue]

Introduction

The asymmetric synthesis of isoquinoline alkaloids has been investigated widely in recent years because of the importance of these alkaloids in medicine and pharmacology (1). A variety of approaches have been explored to achieve the synthesis of the alkaloids in high optical purity.

Reduction of imines **I** using a chiral sodium prolinate – borane complex afforded products in enantiomeric excess (ee) up to 60% (2). A chiral rhodium complex as a homogeneous hydrogenation catalyst also has been used (3) to give products in optical yields in the range of 15–99%. Moderate optical yields were observed in reduction of chiral 3,4-dihydroisoquinolinium salts **II** (4). Several methods, other than reductive, have been used successfully. A compound of type **III**, formed by Bischler–Napieralski cyclization of an optically active amino acid of type **IV**, has been elaborated to the protoberberine alkaloid, xylopinine, in a photochemical enamide cyclization (5). The alkylation of carbanions **V** derived from chiral amidines has yielded products in high optical yields (90–99% ee) (6), and enantiomerically pure amino acids such as **IV** have been used to advantage in Pictet–Spengler condensations (7). A recent report has described the application of optically active *N*-oxyacyliminium salts **VI** for the enantioselective synthesis of 1-(α-hydroxyalkyl)-1,2,3,4-tetrahydroisoquinolines (8). In this article we describe the application of the Pictet–Spengler condensation in the enantioselective synthesis of isoquinoline alkaloids.

The ready availability of carbohydrates in pure enantiomeric form prompted us to investigate their use as chiral starting materials in alkaloid synthesis. Although the Pictet–Spengler condensation has been widely used in the synthesis of isoquinoline alkaloids, only a few examples of this reaction involving carbohydrates and other polyhydroxy compounds have been reported (9–11). In the present study the reaction of dopamine hydrochloride (**1**) and (*R*)-(+)-glyceraldehyde (**2**) has been studied.

Results and discussion

The Pictet–Spengler condensation of **1** and **2** in boiling methanol gave a mixture of diastereomers, **3***a* and **3***b*, in 93% yield. Treatment of the mixture with an excess of ethyl chloroformate converted the NH group into a carbamate and the OH groups into carbonates. The major component, designated **4***a*, was isolated by chromatography in 56% yield; however, the minor component (**4***b*) could not be obtained in a homogeneous state. Nevertheless, it was possible to estimate the relative proportions of **4***a* and **4***b* (~9:1) by comparing the specific rotation and ^{1}Hmr spectrum of **4***a* with those of the mixture. The stereoselectivity of the reaction may be ascribed to the influence of the chiral centre present in the intermediate iminium ion on the direction of nucleophilic attack by the aromatic ring. The observed stereochemical result (see below) can be rationalized on the basis of an analogy to Cram's rule (see ref. 12) (see Fig. 1). All of the carbonic ester functions were removed from **4***a* by treatment with methanolic ammonia, and the product **5** was then methylated at the phenolic hydroxyls with methyl

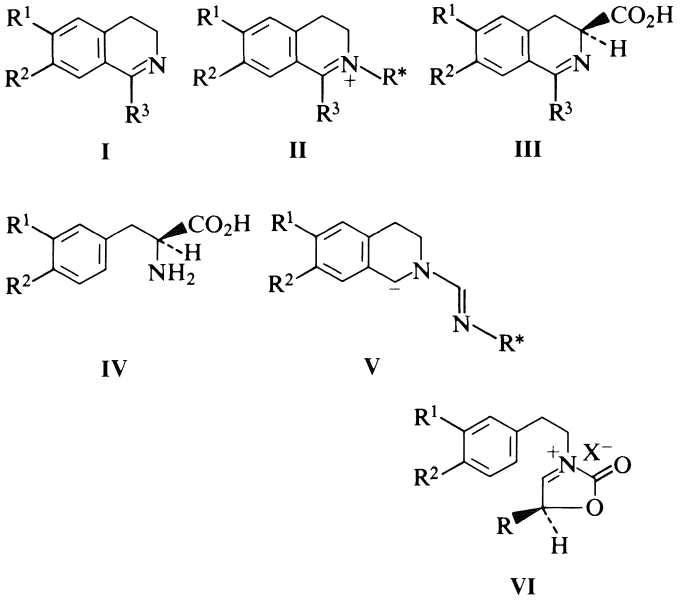

R^1 and R^2: H or alkoxy groups
R^3: alkyl, aryl, or aralkyl group
R*: a suitable, enantiomerically pure chiral group

[1]A preliminary account of part of this work has appeared in J. Chem. Soc. Chem. Commun. 1318 (1985).

[2]Authors to whom correspondence may be addressed.

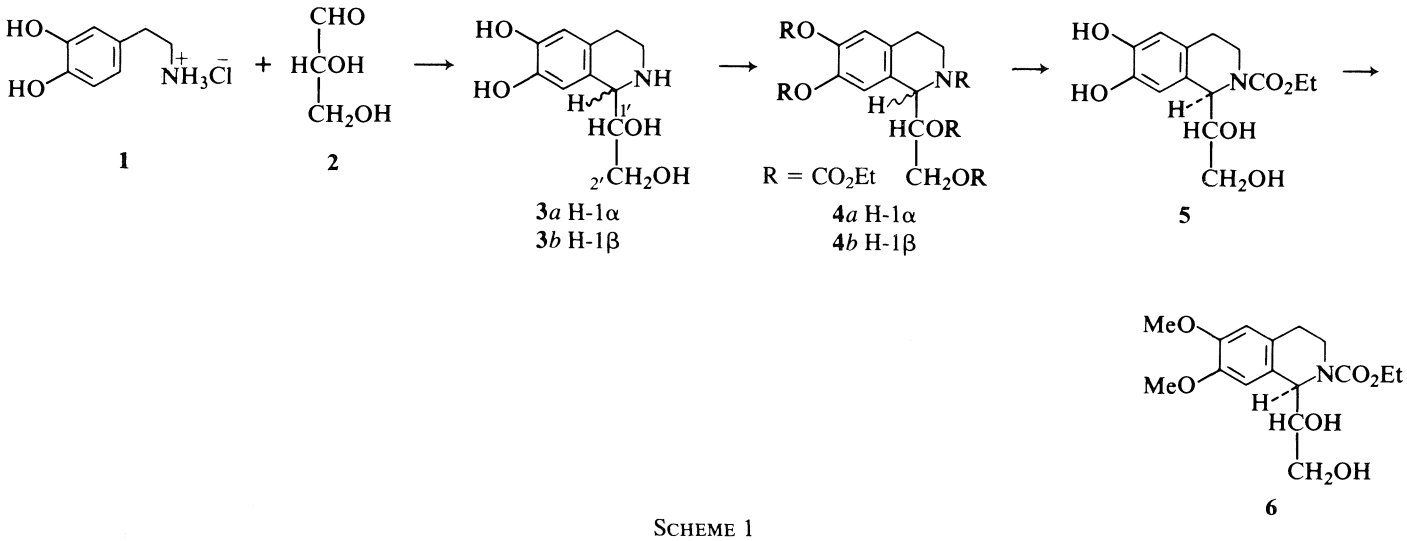

SCHEME 1

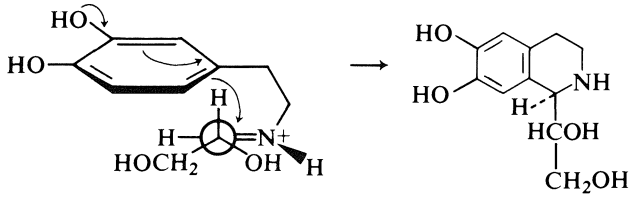

FIG. 1. Orientation of iminium-salt intermediate for formation of the tetrahydroisoquinoline in the Pictet–Spengler condensation of **1** and **2**.

iodide in the presence of potassium carbonate to give **6** in 44% yield from **1** (see Scheme 1).

In our initial attempts to synthesize simple 1-alkylisoquinoline alkaloids we investigated the cleavage of the glycol system of amine **7**, which had been obtained by reduction of **6** using lithium aluminum hydride. Treatment of **7** with sodium periodate followed by reduction of the reaction mixture with sodium borohydride gave compound **8**. A possible mechanism for the formation of compound **8** is shown in Scheme 2.[3] In contrast, cleavage of the glycol system in the carbamate **6**, followed by reduction of the intermediate with sodium borohydride, afforded the *N*-ethoxycarbonyl derivative **10** in 86% yield (see Scheme 3). In this experiment the intermediate aldehyde[4] was used without purification; however, its chromatographic and mass spectral properties were identical with those of the racemate, which had been prepared separately. If the periodate oxidation of **6** were performed under slightly basic conditions, then part of the starting material was converted into the tricyclic derivative **11**, (1*S*,11b*R*)-1,6,7,11b-tetrahydro-1-hydroxy-9,10-dimethoxy-2*H*,4*H*-[1,3]oxazino[4,3-*a*]isoquinolin-4-one.

Treatment of the *N*-ethoxycarbonyl derivative **10** with lithium aluminum hydride afforded our first target material, namely (*R*)-(−)-*N*-methylcalycotomine (**12**) (see ref. 14) in 82% yield. (*R*)-(−)-Calycotomine (**14**) itself was prepared by treatment of **10** with 10% potassium hydroxide in methanol to give the oxazolo[4,3-*a*]isoquinoline **13**, in 98% yield, which, when subjected to the conditions of Kano *et al.* (8, 15), afforded **14** of known absolute configuration (see ref. 1) in 95% yield and 80.1% ee (based on published data (13)). The *N*-ethoxycarbonyl derivative **10** was transformed also into (*S*)-(−)-carnegine (**16**); (±)-carnegine is the major alkaloid of the giant cactus, *Carnegiea gigantea* (16*a*). Compound **16** was obtained by reduction of the intermediate *O*-tosyl derivative **15** using lithium aluminum hydride; the chemical yield was 87% and the ee was 92.8% (based on published data (16*b*)).

In the present work a convenient route to the synthesis of 1-benzylisoquinolines has also been developed. Attempts to utilize the *O*-tosyl derivative **15** in reactions with a variety of organometallic reagents were unsuccessful. However, aldehyde **9** proved to be a suitable starting material for elaboration to the 1-benzylisoquinoline system. Thus, treatment of **9** with 3,4-dimethoxyphenyllithium afforded a product from which the *threo* isomer (+)-**17** was isolated in 64% yield (see Scheme 4); the presence of the *erythro* isomer was not detected by thin-layer chromatographic examination. The formation of the *threo* isomer can be rationalized on the basis of Cram's rule as shown in Fig. 2. The assignment of the relative stereochemistry of **17** was confirmed by the transformation of (±)-**9** into (±)-**17** by a procedure identical with that used in the preparation of (+)-**17**; subsequent reduction of (±)-**17** with lithium aluminum hydride afforded the previously described (17) (±)-*threo*-hydroxylaudanosine (**18**). Compound (+)-**17** was converted into (*S*)-(+)-laudanosine (**19**) by treatment with equimolar amounts of thionyl chloride and pyridine in tetrahydrofuran at −10°C followed by the direct addition of lithium aluminum hydride; (*S*)-(+)-**19** was obtained in 88% chemical yield and in 78.9% ee (based on published data (18)). The process employed for the removal of the hydroxyl group is noteworthy, since a variety of other attempted procedures failed to effect the desired transformation. The generality of the process is currently being investigated.

The work described in this article clearly demonstrates the usefulness of the aldehyde **9** as an intermediate in the enantioselective synthesis of 1-substituted 1,2,3,4-tetrahydroisoquinolines. The 1-benzylisoquinolines in particular are known to be precursors of many more-complicated ring systems amongst the isoquinoline family of alkaloids in both chemical and biochemical pathways. Other synthetic applications are currently under investigation to explore the versatility of **9** and its enantiomer.

[3]We acknowledge the suggestion made by a referee that the reaction may proceed by way of the cyclic intermediate shown in Scheme 2.

[4]The *N*-acetyl analog of **9** was an unisolated intermediate in the conversion of dehydromethopholine into *N*-acetylcalycotomine (13).

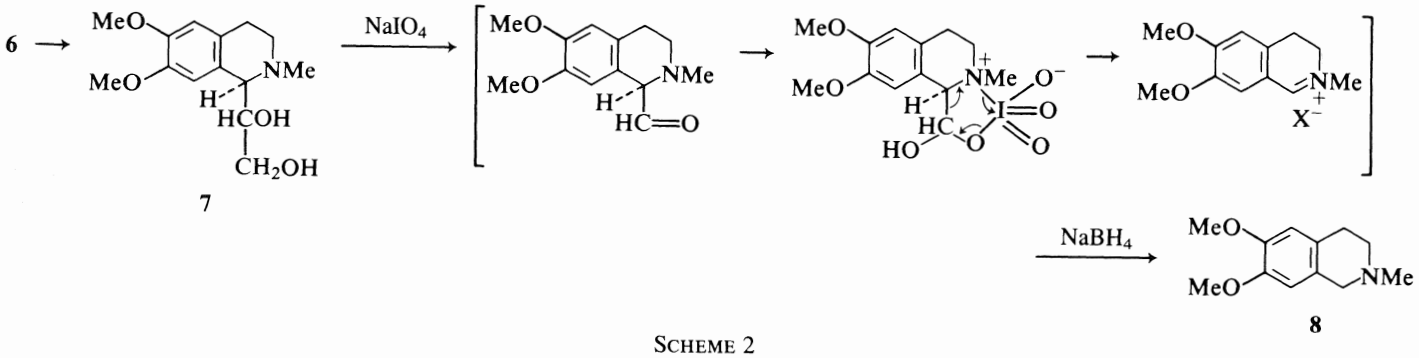

SCHEME 2

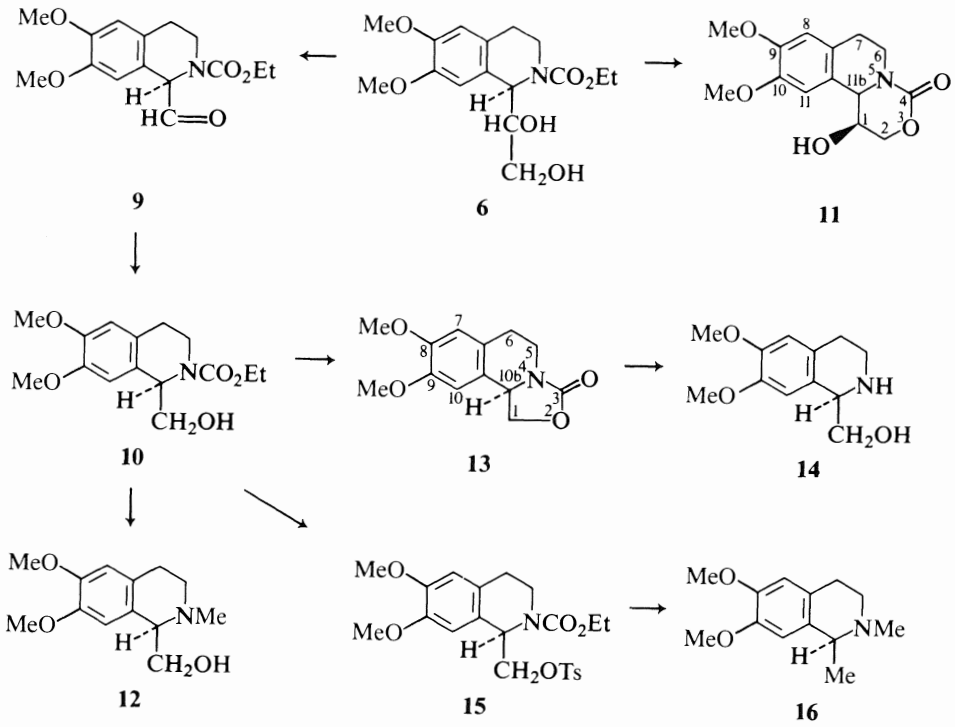

SCHEME 3

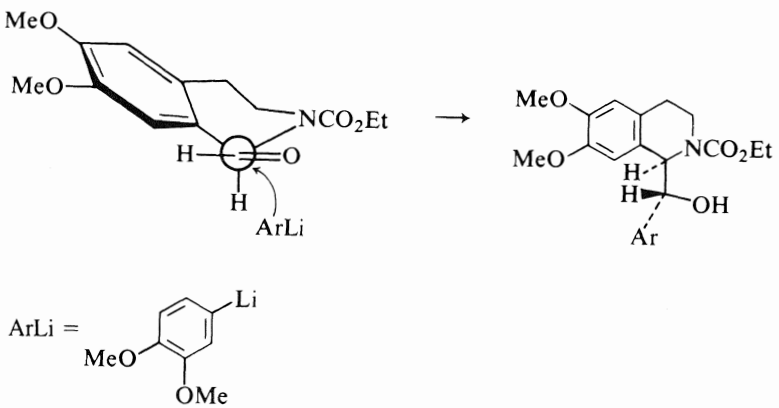

FIG. 2. Attack of 3,4-dimethoxyphenyllithium on the (*R*)-aldehyde **9**.

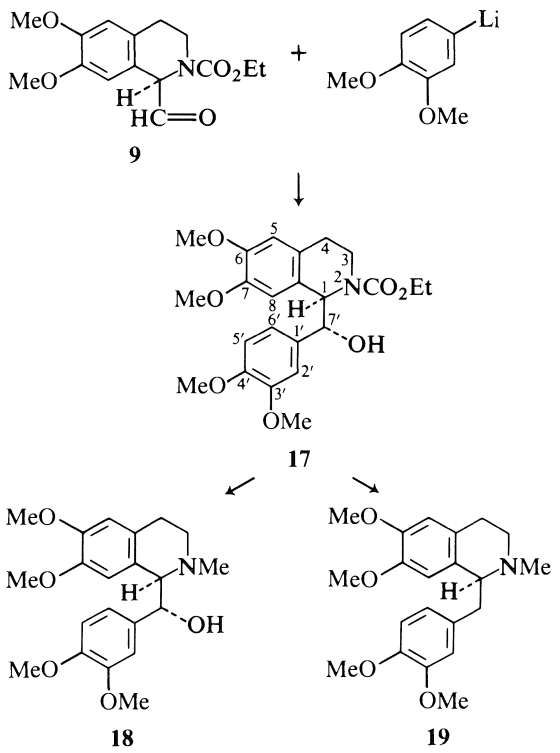

SCHEME 4

Experimental

The ^{1}Hmr spectra were recorded on a Varian EM390 spectrometer at 90 MHz, unless otherwise stated. Tetramethylsilane (TMS) was used as the internal standard for samples examined in organic solvents, and 1,4-dioxane for samples examined in aqueous solutions; chemical shifts are reported in ppm (δ) downfield from the signal of TMS. The symbols, s (singlet), d (doublet), t (triplet), q (quartet), m (multiplet), and br (broadened), are used to report the multiplicity and shape of signals. EI mass spectra were recorded on a VG Micromass 7070F mass spectrometer at an ionizing voltage of 70 eV, and CI spectra were recorded on the same instrument using NH_3 at ~1 Torr (1 Torr = 133.3 Pa) as reagent gas; data are given as m/z (% relative intensity). Infrared (ir) spectra were recorded on a Perkin–Elmer 283 spectrophotometer.

Melting points were determined using a Gallenkamp apparatus and are uncorrected. Optical rotations were measured using a Perkin–Elmer 247MC polarimeter in a 1-mL microcell that is 1 dm in length. The values for ee were calculated as described by Andersen *et al.* (19), and differ from those given in the preliminary account; in the latter, the values were actually enantiomeric percentages. Flash chromatography was performed on Kieselgel 60 (230–400 mesh). (+)-Glyceraldehyde and (±)-glyceraldehyde were purchased from the Aldrich Chemical Co.

The homogeneity of the products was established on the basis of chromatographic and spectroscopic (^{1}Hmr and mass spectral) examination. It is known that 1-substituted 1,2,3,4-tetrahydroisoquinolines of the type studied in this investigation fragment readily when examined by EI mass spectrometry and seldom show a molecular ion; consequently, most of the compounds studied were examined by CI mass spectrometry using ammonia as the reagent gas. In all cases except that of **4***a* satisfactory $(M + 1)^{+\cdot}$ ions were observed, which served as a measure of the molecular weights of the compounds. Fragmentation often accompanied the formation of the adduct ion and the patterns were sometimes useful in corroborating the assigned structures.

*Condensation of (*R*)-(+)-glyceraldehyde (**2**) with dopamine hydrochloride (**1**)*

A mixture of (*R*)-(+)-glyceraldehyde (2.00 g) and dopamine hydrochloride (1.36 g) in methanol (100 mL) was stirred overnight and heated at reflux temperature for 2 days. The solvent was evaporated and the residue was fractionated by column chromatography on silica gel, using 10% methanol in chloroform to remove unreacted dopamine and nonpolar impurities, and then 20% methanol in chloroform to obtain the condensation product; the fractions were monitored by ^{1}Hmr spectroscopy. The mixture of diastereomers **3***a* and **3***b* was obtained as a brown foam (1.50 g, 93% based on dopamine hydrochloride); ^{1}Hmr (D_2O) δ: 6.70 and 6.68 (two 1H s's, H-5 and H-8), 4.52 (1H, d, J = 6.0 Hz, H-1), 4.25–3.96 (1H, d of t, J = 4.5 Hz and 6.0 Hz, H-1′), 3.80 (2H, d, J = 4.5 Hz, 2H-2′), 3.68–3.46 (2H, m, 2H-3), 2.95 (2H, apparent t, J = 6 Hz, 2H-4); ms (CI): 226 $(M + 1)^+$ (100), 208 (28), 192 (36).

*Preparation of carbonate **4**a*

To a solution of **3***a* and **3***b* (316 mg) in 1% aqueous sodium hydroxide (50 mL) was added 1,2-dichloromethane (50 mL), and the mixture was stirred vigorously while ethyl chloroformate (3 mL) was added gradually over a period of 1 h. Stirring was continued for a further 0.5 h while the mixture was kept alkaline by the addition of 10% aqueous sodium hydroxide. The organic layer was then separated and washed twice with an aqueous solution of sodium chloride. The solution was dried over magnesium sulfate, and evaporation of the solvent afforded the mixture of diastereomers **4***a* and **4***b* (780 mg, 95%), $[\alpha]_D^{20}$ +28.5° (*c* 1.23, chloroform). The major component (**4***a*) was isolated as a colorless oil (56% based on the starting material) by flash chromatography on silica gel using 2% methanol in chloroform as the eluant; $[\alpha]_D^{23}$ +76.4° (*c* 1.61, chloroform); ^{1}Hmr ($CDCl_3$) δ: 7.30 and 7.17 (two 1H s's, H-5 and H-8), 5.27 (1H, br s, H-1), 4.50–4.07 (13H, m, 5CH_2CH$_3$, C*H*OR, CH_2OR), 3.77–3.45 (2H, m, 2H-3), 2.86 (2H, br t, 2H-4), 1.50–1.23 (15H, m, 5CH$_2$CH_3).

*Preparation of carbamate **5***

A sample of compound **4***a* (818 mg) was stirred overnight in 2% ammonia in methanol. The solvent was evaporated and the residue was chromatographed on silica gel using 7% methanol in chloroform as the eluant to afford **5** as a slightly brown oil (388 mg, 93%); ^{1}Hmr (CD_3OD) δ: 6.79 and 6.72 (two 1H s's, H-5 and H-8), 5.05 (1H, d, J = 6.0 Hz, H-1), 4.25 (2H, q, J = 7.5 Hz, CH_2CH$_3$), 4.17–3.55 (5H, m, 2H-3, H-1′, 2H-2′), 2.73 (2H, br t, J = 6.7 Hz, 2H-4), 1.28 (3H, t, J = 7.5 Hz, CH$_2$CH_3); ms (CI): 298 $(M + 1)^+$ (60), 280 (20), 236 (100).

*Preparation of **6***

A solution of compound **5** (388 mg) in dry acetone (50 mL) was treated overnight at reflux temperature with potassium carbonate (3.0 g) and methyl iodide (4 mL). The reaction mixture was cooled, the inorganic salts were removed by filtration, and the filtrate was evaporated under reduced pressure. The residue was dissolved in chloroform, and the solution was washed with an aqueous solution of sodium chloride, dried over magnesium sulfate, and evaporated to afford **6** as a colorless oil (369 mg, 86%), $[\alpha]_D^{23}$ +72.8° (*c* 0.61, chloroform); ^{1}Hmr ($CDCl_3$) δ: 6.76 and 6.62 (two 1H s's, H-5 and H-8), 5.18 (1H, d, J = 5.0 Hz, H-1), 4.37–3.97 (7H, m, D_2O exchange caused the disappearance of signals corresponding to 2H, CH_2CH$_3$, 2H-3, H-1′, 2OH), 3.83 (6H, s, 2OCH$_3$), 3.60 (2H, d, J = 7.5 Hz, 2H-2′), 2.80 (2H, m, 2H-4), 1.27 (3H, t, J = 8.0 Hz, CH$_2$CH_3); ms (CI): 326 $(M + 1)^+$ (100), 264 (75). High-resolution measurements were performed on the ion resulting from C-1—C-1′ fission in the EI mass spectrum. *Mol. Wt.* calcd. for $C_{14}H_{18}NO_4$: 264.1235; found (m/z): 264.1233.

*Preparation of amine **7***

A solution of compound **6** (150 mg) in tetrahydrofuran was heated at reflux temperature for 1 h in the presence of lithium aluminum hydride (100 mg), and to the reaction mixture were then added successively water (0.1 mL), 15% aqueous sodium hydroxide solution (0.1 mL), and water (0.3 mL). The reaction mixture was filtered, the residue was washed three times with dry ethanol, and the combined filtrate and washings were evaporated. Chromatography of the residue on silica gel using 10% methanol in chloroform as the eluant afforded **7** as a colorless oil (97 mg, 79%); ^{1}Hmr ($CDCl_3$) δ: 6.83 and 6.66 (two

1H s's, H-5 and H-8), 4.25 (2H, br s, 2OH), 3.84 (6H, s, $2OCH_3$), 3.93–3.50 (4H, m, H-1, H-1′, 2H-2′), 3.25–2.55 (4H, m, 2H-3, 2H-4), 2.46 (3H, s, NCH_3).

*Formation of 6,7-dimethoxy-2-methyl-1,2,3,4-tetrahydroisoquinoline (**8**) by way of periodate oxidation of amine **7***

A solution of compound **7** (90 mg) in methanol (10 mL) was treated with a solution of sodium periodate (150 mg) in methanol (10 mL) at 5°C for 1 h; sodium borohydride (150 mg) was then added in small portions over a period of 0.5 h and the reaction mixture was left for 0.5 h. The reaction mixture was filtered, the residue was washed with cold methanol, and the combined filtrate and washings were evaporated. Chromatography of the residue on silica gel using 10% methanol in chloroform as the eluant afforded **8** as a colorless oil (74%) that solidified on standing; ^{1}Hmr (250 MHz, $CDCl_3$) δ: 6.58 and 6.49 (two 1H s's, H-5 and H-8), 3.82 and 3.81 (6H, $2OCH_3$), 3.48 (2H, s, 2H-1), 2.82 (2H, t, J = 5.8 Hz, 2H-3), 2.64 (2H, t, J = 5.8 Hz, 2H-4), 2.43 (3H, s, NCH_3); ^{13}Cmr data are identical with those reported by Hughes *et al.* (20); ms (EI): 207 (40), 206 (60), 164 (100). The product formed a picrate, mp 160–162°C (lit. (21) mp 161–162°C).

Preparation of N*-ethoxycarbonyl derivative **10***

A solution of compound **6** (122 mg) in methanol (20 mL) was treated with a solution of sodium periodate (160 mg) in water (2 mL) at 5°C for 1 h; sodium borohydride (80 mg) was then added in small portions over a period of 0.5 h and the reaction mixture was left for 0.5 h. The reaction mixture was filtered, the residue was washed with cold methanol, and the combined filtrate and washings were evaporated. Chromatography of the residue on silica gel using 1.5% methanol in chloroform as the eluant afforded **10** as a colorless oil (96 mg, 86%), $[\alpha]_D^{23}$ +88.8° (*c* 2.08, chloroform); ^{1}Hmr ($CDCl_3$) δ: 7.03 and 6.98 (two 1H s's, H-5 and H-8), 5.16 (1H, t, J = 6.0 Hz, H-1), 4.20 (2H, q, J = 7.0 Hz, CH_2CH_3), 3.78 (6H, s, $2OCH_3$), 3.60–3.15 (4H, m, 2H-3, 2H-1′), 2.90–2.52 (2H, m, 2H-4), 1.26 (3H, t, J = 7.0 Hz, CH_2CH_3); ms (CI): 296 $(M + 1)^+$ (100), 264 (38), 192 (7).

*Preparation of tricyclic derivative **11***

Compound **6** was treated as described in the preceding experiment, except that the reactions were performed in the presence of sodium hydroxide (200 mg) in the reaction mixture, to afford the *N*-ethoxycarbonyl derivative **10** (65%), and also the tricyclic derivative **11** as a colorless oil (25%), $[\alpha]_D^{23}$ −152° (*c* 1.13, chloroform); ^{1}Hmr ($CDCl_3$) δ: 6.63 (2H, s, H-9, H-10), 4.87 (1H, d, J = 5 Hz, H-11b), 4.53–4.38 (1H, m, H-6_{eq}), 4.25–3.95 (3H, m, H-1, 2H-2), 3.86 (6H, s, $2OCH_3$), 3.35–2.53 (3H, m, H-6, 2H-7), 2.38 (1H, br s, exchanged with D_2O, OH); ms (CI): 280 $(M + 1)^+$ (100), 279 (32).

*Preparation of (*R*)-(−)-*N*-methylcalycotomine (**12**)*

A solution of compound **10** (80 mg) in tetrahydrofuran (30 mL) was treated with lithium aluminum hydride (50 mg) for 1 h at reflux temperature. The reduction product, *N*-methylcalycotomine (**12**), was obtained, after chromatography on silica gel using 11% methanol in chloroform as the eluant, as a colorless oil (82%), $[\alpha]_D^{23}$ −48.3° (*c* 2.8, chloroform) (lit. (14) for the enantiomer, $[\alpha]_D$ +55° (*c* 0.4, chloroform)); ^{1}Hmr ($CDCl_3$) δ: 6.56 (2H, s, H-5, H-8), 3.83 (6H, s, $2OCH_3$), 3.80–3.53 (3H, m, H-1, 2H-1′), 3.25–2.63 (4H, m, 2H-3, 2H-4), 2.56 (3H, s, NCH_3); ms (CI): 238 $(M + 1)^+$ (100), 206 (80). The ^{1}Hmr data are in agreement with those reported for the enantiomer by Kerekes *et al.* (14). The product formed a picrate, mp 216°C (dec.).

*Formation of (*R*)-1,5,6,10b-tetrahydro-8,9-dimethoxy-3*H*-oxazolo[4,3-a]isoquinolin-3-one (**13**)*

Compound **10** (55.8 mg) was treated with 10% potassium hydroxide in methanol for 6 h at reflux temperature. The solvent was evaporated; water (5 mL) was added to the residue and the mixture was extracted with chloroform. The product **13** (15) was obtained, after chromatography on silica gel using 4% methanol in chloroform as the eluant, as a colorless oil (43 mg, 98%), $[\alpha]_D^{23}$ −154.3° (*c* 0.9, chloroform); ν_{max} (neat): 1750 cm^{-1} (lactone); ^{1}Hmr ($CDCl_3$) δ: 6.70 and 6.53 (two 1H s's, H-7 and H-10), 5.08–4.73 (2H, m), 4.30–4.08 (2H, m), 3.91 (6H, s, $2OCH_3$), 3.30–2.65 (3H, m, H-5_{ax}, 2H-6); ms (EI): 249 $(M)^+$ (100), 248 $(M - 1)^+$ (60), 218 (18), 191 (63).

*(*R*)-(−)-Calycotomine (**14**)*

Compound **13** was treated with 10% sodium hydroxide in ethanol for 6 h at reflux temperature, conditions described by Kano *et al.* (8, 15). The reaction mixture was processed as described in the preceding experiment, and chromatography on silica gel using 20% methanol in chloroform as the eluant afforded crystalline **14** (95%), mp 145–148°C, $[\alpha]_D^{22}$ −28.9° (*c* 1.05, water) (lit. (13) mp 149–150°C, $[\alpha]_D^{23}$ −36° (water)); ^{1}Hmr ($CDCl_3$) δ: 6.36 (2H, s, H-5, H-8), 3.88 (6H, s, $2OCH_3$), 3.80–3.66 (3H, m, H-1, 2H-1′), 3.10 (2H, apparent t, $J \simeq$ 6 Hz, 2H-4), 2.70 (2H, apparent t, $J \simeq$ 6 Hz, 2H-3), 2.36 (2H, br s, exchanged with D_2O, OH, NH); ms (CI): 224 $(M + 1)^+$ (100), 206 (25), 192 (65). The ^{1}Hmr data are in agreement with those reported by Rozwadowska and Brózda (22).

Conversion of N*-ethoxycarbonyl derivative **10** into (*S*)-(−)-carnegine (**16**)*

Compound **10** (38 mg) was treated with a solution of *p*-toluenesulfonyl chloride (49 mg) in pyridine (5 mL) for 12 h at 5°C. The solvent was evaporated under reduced pressure at ambient temperature to yield an oil, which was dissolved in chloroform; the solution was washed with a 2% aqueous solution of sodium carbonate and then with an aqueous solution of sodium chloride, dried ($MgSO_4$), and evaporated. A solution of the residue in tetrahydrofuran was treated with lithium aluminum hydride (100 mg) for 1.5 h at reflux temperature. The reduction product, (*S*)-(−)-carnegine (**16**), was obtained, after chromatography on silica gel using 7% methanol in chloroform as the eluant, as an oil (87% based on **10**), $[M]_D^{23}$ −106.7° (*c* 1.05, benzene) (lit. (16*b*) $[M]_D^{22}$ −115° (*c* ~4.5, benzene)); ^{1}Hmr ($CDCl_3$) δ: 6.60 (2H, s, H-5, H-8), 3.86 (6H, s, $2OCH_3$), 3.68 (1H, q, J = 6.5 Hz, H-1), 3.23–2.56 (4H, m, 2H-3, 2H-4), 2.50 (3H, s, NCH_3), 1.38 (3H, d, J = 6.5 Hz, $CHCH_3$); ms (CI): 222 $(M + 1)^+$ (100), 206 (20). The ^{1}Hmr data are in agreement with those reported by Rozwadowska and Brózda (22). The product formed a picrate, mp 228–230°C (lit. (16*b*) mp 233–234°C).

*Preparation of aldehyde **9** by periodate oxidation of **6***

To a solution of compound **6** (210 mg) in methanol (10 mL) was added sodium periodate (138 mg) in water (1 mL), and the mixture was stirred at 0°C for 1.5 h. The reaction mixture was filtered, the residue was washed with cold methanol, and the combined filtrate and washings were evaporated at ambient temperature. The residue was dissolved in dichloromethane, and the solution was dried ($MgSO_4$) and evaporated; this residue was dissolved in dry benzene, and the solution was evaporated to remove traces of water. The syrupy product (176 mg, 93%) was chromatographically homogeneous (thin-layer chromatography, 2% methanol in chloroform) and was used in the following step without further purification; ms (CI): 294 $(M + 1)^+$ (100), 264 (43), 248 (18), 192 (17). A sample of (±)-**9** was obtained from (±)-**6**, and its mass spectrum showed the same fragment ions as did that of **9**; ^{1}Hmr ($CDCl_3$) δ: 9.40 (1H, s, HC=O), 6.85 and 6.68 (two 1H s's, H-5 and H-8), 5.33 (1H, br s, H-1), 4.20 (2H, q, J = 7.5 Hz, CH_2CH_3), 3.85 (6H, s, $2OCH_3$), 3.75–3.61 (2H, m, 2H-3), 2.75 (2H, apparent t, J = 6 Hz, 2H-4), 1.27 (3H, t, J = 7.5 Hz, CH_2CH_3).

*Reaction of **9** with 3,4-dimethoxyphenyllithium*

A solution of bromoveratrole (725 mg) in tetrahydrofuran (20 mL) was treated with a 2.4 *M* solution of *n*-butyllithium in *n*-hexane (1.5 mL) at −78°C (Dry Ice – methanol) for 15 min. A solution of compound **9** (255 mg) in tetrahydrofuran (5 mL) was then added slowly, and the mixture was kept at −78°C for 30 min. Water (0.5 mL) was added, and the mixture was warmed to room temperature and evaporated. The residue was dissolved in chloroform, and the solution was washed with a 20% aqueous solution of ammonium chloride and then with an aqueous solution of sodium chloride; the solution was dried ($MgSO_4$) and evaporated. Chromatography of the residue on silica gel using 1% methanol in chloroform as the eluant afforded compound **17** as a viscous, colorless oil (240 mg, 64% based on **9**), $[\alpha]_D^{22}$ +29.9° (*c* 2.57, chloroform); ^{1}Hmr ($CDCl_3$) δ: 6.72–6.47 (4H, m, H-5, H-2′, H-5′, H-6′), 5.88 (1H, br s, H-8), 5.05 (1H, d, J = 7.0 Hz, H-1), 4.66

(2H, m, d after addition of D_2O, J = 7.0 Hz, H-7′, OH), 4.33–3.87 (4H, m, 2H-3, CH_2CH_3), 3.75 (6H, s, $2OCH_3$), 3.65 (3H, s, OCH_3), 3.38 (3H, s, OCH_3 at C-7),[5] 2.63–2.40 (2H, m, 2H-4), 1.11 (3H, t, J = 7.5 Hz, CH_2CH_3); irradiation at δ 5.05 caused collapse of the doublet at δ 4.66 to a singlet; ms (EI): 413 (20), 385 (25), 264 (100).

*(S)-(+)-Laudanosine (**19**)*

To a solution of compound **17** (120 mg) in tetrahydrofuran (25 mL) were added, under dry nitrogen and at −10°C, dry pyridine (0.024 mL) and then thionyl chloride (0.020 mL), and the reaction mixture was stirred for 45 min. Solid lithium aluminum hydride (200 mg) was then added in small portions, and the mixture was stirred at room temperature for 15 min and then heated at reflux temperature for 30 min. The reaction mixture was cooled and decomposed in the usual manner; the mixture was filtered, the residue was washed three times with hot chloroform, and the combined filtrate and washings were evaporated. Chromatography of the residue on silica gel using 5% methanol in chloroform as the eluant afforded **19** as a colorless oil (88%), $[\alpha]_D^{22}$ +78.9° (*c* 1.55, ethanol) (lit. (18) $[\alpha]_D$ +100° (ethanol)); ^{1}Hmr ($CDCl_3$) δ: 6.80–6.56 (4H, m, aromatic H's), 6.12 (1H, s, H-8), 3.86 (6H, s, $2OCH_3$), 3.80 (3H, s, OCH_3), 3.60 (3H, s, OCH_3 at C-7), 3.50–2.63 (7H, m, 2H-7′, H-1, 2H-3, 2H-4), 2.55 (3H, s, NCH_3); ms (CI): 358 $(M + 1)^+$ (100), 206 (21). The ^{1}Hmr data are in agreement with those reported by Konda *et al.* (23). The product formed a methiodide, mp 213–215°C (lit. (18) mp 215–217°C).

*Formation of (±)-*threo*-hydroxylaudanosine (**18**)*

A sample of (±)-**17** (241 mg, 0.56 mmol), obtained from (±)-glyceraldehyde by the same sequence of reactions as had been employed for the preparation of (+)-**17**, was treated with lithium aluminum hydride (1.8 g) in tetrahydrofuran (75 mL) for 1 h at reflux temperature. The reduction product, (±)-**18**, was obtained, after chromatography on silica gel using 5% methanol in chloroform as the eluant, in crystalline form (88%) and recrystallized from methanol–ether, mp 137–138°C (lit. (24) mp 138°C); ^{1}Hmr ($CDCl_3$) δ: 6.95–6.59 (4H, m, aromatic H's), 5.43 (1H, s, H-8), 4.38 (1H, d, J = 9 Hz, C*H*OH), 4.06 (1H, br s, OH), 3.85 (9H, s, $3OCH_3$), 3.33 (1H, d, J = 9 Hz, H-1), 3.30 (3H, s, OCH_3 at C-7), 3.16–2.73 (4H, m, 2H-3, 2H-4), 2.57 (3H, s, NCH_3); ms (CI): 374 $(M + 1)^+$ (100), 206 (17), 167 (4).

Acknowledgements

We thank the Natural Sciences and Engineering Research Council of Canada for financial support of this research in the form of grants to WAS and DBM.

1. M. Shamma. The isoquinoline alkaloids, chemistry and pharmacology. Academic Press, New York. 1972; M. Shamma and J. L. Moniot. Isoquinoline alkaloid research 1972–1977. Plenum Press, New York. 1978.
2. K. Yamada, M. Takeda, and T. Iwakuma. J. Chem. Soc. Perkin Trans. 1, 265 (1983).
3. H. B. Kagan, W. Langlois, and T. Phat Dang. J. Organometal. Chem. **90**, 353 (1975).
4. T. Kametani and T. Okawara. J. Chem. Soc. Perkin Trans. 1, 579 (1977).
5. T. Kametani, N. Takagi, M. Toyota, T. Honda, and K. Fukumoto. Heterocycles, **16**, 591 (1981).
6. A. I. Meyers, L. M. Fuentes, and Y. Kubota. Tetrahedron, **40**, 1361 (1984).
7. (*a*) R. T. Dean and H. Rapoport. J. Org. Chem. **43**, 4183 (1978); (*b*) M. Konda, T. Oh-Ishi, and S.-I. Yamada. Chem. Pharm. Bull. **25**, 69 (1977).
8. S. Kano, Y. Yuasa, and S. Shibuya. Heterocycles, **23**, 395 (1985).
9. I. M. Piper, D. B. Maclean, I. Kvarnström, and W. A. Szarek. Can. J. Chem. **61**, 2721 (1983); I. M. Piper, D. B. Maclean, R. Fagianni, C. J. L. Lock, and W. A. Szarek. Can. J. Chem. **63**, 2915 (1985); T. Severin and K.-H. Bräutigam. Chem. Ber. **106**, 2943 (1973); T. Severin and K.-H. Bräutigam. Z. Lebensm. Unters. Forsch. **154**, 80 (1974).
10. D. Soerens, J. Sandrin, F. Ungemach, P. Mokry, G. S. Wu, E. Yamanaka, L. Hutchins, M. Dipierro, and J. M. Cook. J. Org. Chem. **44**, 535 (1979).
11. H. Bieräugel, R. Plemp, and U. K. Pandit. Tetrahedron, **39**, 3987 (1983).
12. J. D. Morrison and H. S. Mosher. Asymmetric organic reactions. Prentice Hall, London. 1971. p. 40. E. L. Eliel. *In* Asymmetric synthesis. Vol. 2. *Edited by* J. D. Morrison. Academic Press, Inc., New York. 1983. Chapt. 5.
13. A. Brossi and F. Burkhardt. Helv. Chim. Acta, **44**, 1558 (1961).
14. P. Kerekes, P. N. Sharma, A. Brossi, and J. L. McLaughlin. J. Nat. Prod. **48**, 142 (1985).
15. S. Kano, Y. Yuasa, T. Yokomatsu, and S. Shibuya. Chem. Lett. 1475 (1983).
16. (*a*) S. D. Brown, J. E. Hodgkins, J. L. Massingill, Jr., and M. G. Reinecke. J. Org. Chem. **37**, 1825 (1972); (*b*) A. R. Battersby and T. P. Edwards. J. Chem. Soc. 1214 (1960).
17. R. M. McMahon, C. W. Thornber, and S. Ruchirawat. J. Chem. Soc. Perkin Trans. 1, 2163 (1982).
18. T. Kametani. The chemistry of the isoquinoline alkaloids. Elsevier, Amsterdam. 1969. p. 35.
19. K. K. Andersen, D. M. Gash, and J. D. Robertson. *In* Asymmetric synthesis. Vol. 1. *Edited by* J. D. Morrison. Academic Press, Inc., New York. 1983. p. 45.
20. D. W. Hughes, H. L. Holland, and D. B. MacLean. Can. J. Chem. **54**, 2252 (1976).
21. J. Knabe. Arch. Pharm. **292**, 652 (1959).
22. M. D. Rozwadowska and D. Brózda. Pharmazie, **39**, 387 (1984).
23. M. Konda, T. Shioiri, and S.-I. Yamada. Chem. Pharm. Bull. **23**, 1025 (1975).
24. K. L. Wert, S. Chackalamannil, E. Miller, D. R. Dalton, D. E. Zacharias, and J. P. Glusker. J. Org. Chem. **47**, 5141 (1982).

[5]Shielding of H-8 and of the OCH_3 group at C-7 has been observed also in the ^{1}Hmr spectra of *N*-methyl-1-benzylisoquinolines (see ref. 1).

Benzoyl phenyl 1-methylpyrazoles. Synthesis, characterization, and spectra[1]

KUNIO KANO, DAVID SCARPETTI, JOHN C. WARNER, AND JEAN-PIERRE ANSELME[2]
Department of Chemistry, University of Massachusetts at Boston, Harbor Campus, Boston, MA 02125, U.S.A.

AND

JAMES P. SPRINGER[3] AND BYRON H. ARISON[3]
Research Laboratory, Merck, Sharpe and Dohme, Rahway, NJ 07065, U.S.A.

Received April 8, 1986

KUNIO KANO, DAVID SCARPETTI, JOHN C. WARNER, JEAN-PIERRE ANSELME, JAMES P. SPRINGER, and BYRON H. ARISON. Can. J. Chem. **64**, 2211 (1986).

The synthesis and unequivocal characterization of all six isomers of benzoyl phenyl 1-methylpyrazole (**2**) are described. The isomer of **2** isolated as one of the products of the reaction of 1,1-dimethyl-1-phenacylhydrazinium bromide (**1**) with base was shown to be the only previously reported isomer, 5-benzoyl-3-phenyl-1-methylpyrazole (**2***b*).

KUNIO KANO, DAVID SCARPETTI, JOHN C. WARNER, JEAN-PIERRE ANSELME, JAMES P. SPRINGER et BYRON H. ARISON. Can. J. Chem. **64**, 2211 (1986).

On décrit la synthèse et la caractérisation non-équivoque des six isomères du benzoyl phényl méthyl-1 pyrazole (**2**). On a isolé un isomère de **2** lors de la réaction du bromure de diméthyl-1,1 phénacyl-1 hydrazinium (**1**) avec de la soude; on a identifié ce produit comme étant le benzoyl-5 phényl-3 méthyl-1 pyrazole (**2***b*), le seul isomère rapporté jusqu'à maintenant.

[Traduit par la revue]

Introduction

In the context of another investigation (1), the synthesis of all six isomers of benzoyl phenyl 1-methylpyrazole (**2**) was

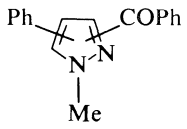

2

a 3-Ph, 4-PhCO; *b* 3-Ph, 5-PhCO
c 4-Ph, 3-PhCO; *d* 4-Ph, 5-PhCO
e 5-Ph, 3-PhCO; *f* 5-Ph, 4-PhCO

undertaken. At the outset of this study, only one isomer of **2** had been reported (2). We now describe the preparation and characterization of all the isomers of **2**.

Results and discussion

3-Phenyl isomers

The few reported investigations of the Friedel–Crafts acylation of pyrazoles (3) indicate that reaction occurs at the 4-position (4, 5). This was confirmed in the present work by the benzoylation of 3-phenyl- and 4-phenyl-1-methylpyrazoles (6). While the open 4-position of the 3-phenyl isomer indeed underwent benzoylation to yield **2***a*, albeit in only 6% yield (eq. [1]), several attempts to introduce the benzoyl group into the pyrazole ring of 4-phenyl-1-methylpyrazole by various modifications of the Friedel–Crafts procedure resulted in benzoylation at the *p*-position of the phenyl substituent rather than the open 3- or 5-positions, as shown by nmr analysis and by the authentic synthesis of **2***c* and **2***d* (*vide infra*). An improved synthesis of **2***a*, starting from 4-bromo-3-phenyl-1-methylpyrazole, was achieved by the sequence shown in eq. [1].

The benzoyl phenyl 1-methylpyrazole isolated from the

[1]

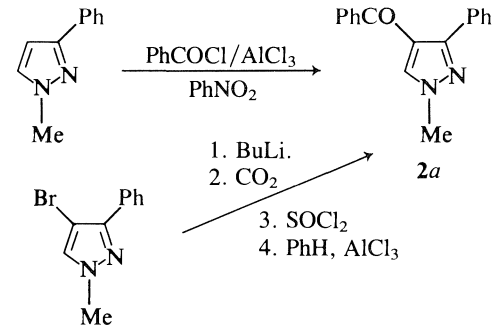

action of base on 1,1-dimethyl-1-phenacylhydrazinium bromide (**1**) (eq. [3]) (1) turned out to be identical to the compound obtained by Heine *et al.* from the reaction of methylhydrazine on dibenzoylacetylene (eq. [2]) (2). The assignment of structure

[2]

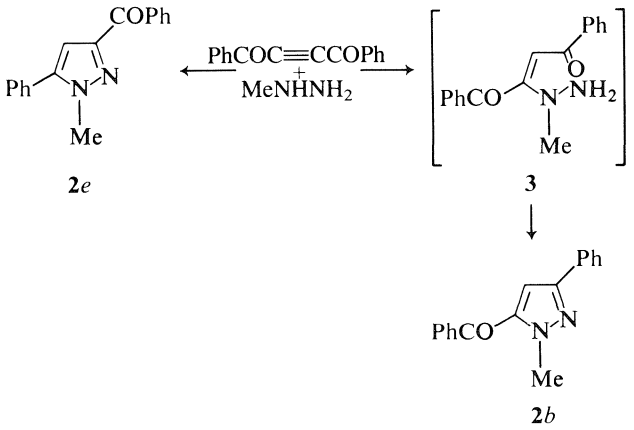

as **2***b* appeared secure since Heine also obtained **2***b* from alternate routes, and our rationale to explain the formation of **2***b* from **1** and base (1) (eq. [3]) postulates the same intermediate **3**. A careful reexamination of the reaction product of Heine *et al.* (2) did reveal the presence of a small amount of the isomeric pyrazole **2***e* whose authentic synthesis is described later in this paper (eq. [9]).

[1]Taken in part from the M.Sc. Thesis of K. Kano, University of Massachusetts at Boston, June 1980, and in part from the B.Sc. Theses of D. Scarpetti, University of Massachusetts at Boston, June 1986, and of J. C. Warner, University of Massachusetts at Boston, June 1984.

[2]Author to whom inquiries may be directed.

[3]Authors to whom inquiries regarding the high resolution nmr spectra and X-ray analysis may be directed.

[3] 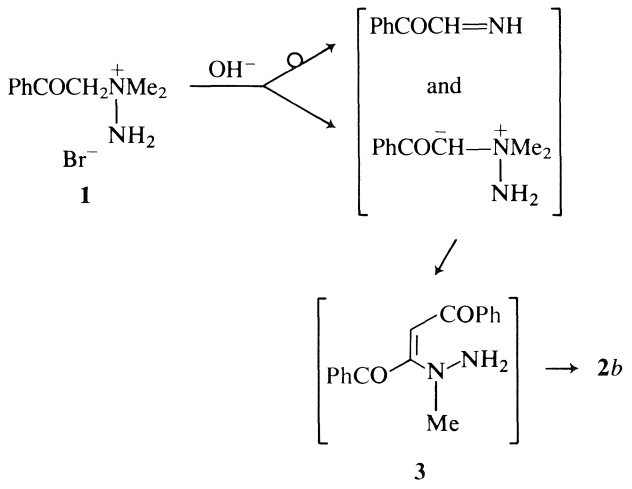

4-Phenyl isomers

Our initial approach to the 4-phenyl isomers (**2***c* and **2***d*) was predicated on the reported cyclization of monohydrazones of α-diketones. In 1958, Domnin *et al.* (7) had described the presumed cyclization of benzil monodimethylhydrazone to a compound purported to be 1-methyl-3,4-diphenylpyrazole; subsequent and apparently independent reports of related cyclizations were disclosed by two other groups (8).

The preparation of the required *N*-methyl-*N*-phenacylhydrazone of phenylglyoxal was initially attempted by alkylation of the methylhydrazone of phenylglyoxal (obtained by controlled condensation of phenylglyoxal with methylhydrazine; compound **6** may also be a product of this reaction) was unsuccessful. This failure led to the synthesis of 5-benzoyl-4-phenyl-1-methylpyrazole (**2***d*) illustrated in eq. [4]. Treatment of **5** with sulfuric acid led to 3-benzoyl-4-phenyl-1-methylpyrazole (**2***c*) rather than **2***d*, which would have been the expected product on the basis of the literature precedents cited above. Indeed, three alternate routes, one involving the dehydrogenation of 3-benzoyl-4-phenyl-1-methyl-2-pyrazoline (**7**) (eq. [5]), a second proceeding via the cycloaddition of 3-methylsydnone to benzoylphenylacetylene (eq. [6]), and a third using the decarboxylation of 3-benzoyl-4-phenyl-1-methylpyrazole-5-carboxylic acid (**10**) (eq. [7]) (9), each afforded the same product, which was identical to that obtained from the reaction described in eq. [4]. The confirmation of the structure of this compound as 3-benzoyl-4-phenyl-1-methylpyrazole (**2***c*),

[4] 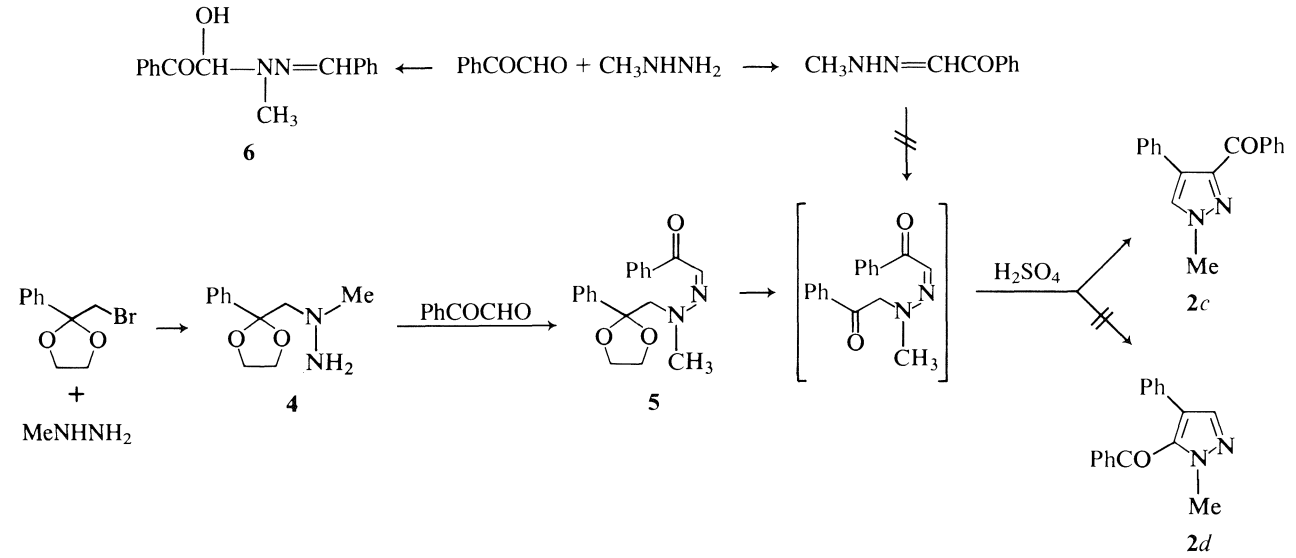

obtained by an X-ray crystallographic structure determination (10), raised doubt (11) regarding the validity or at least the generality of the purported cyclization described by Domnin *et al.* Authentic 5-benzoyl-4-phenyl-1-methylpyrazole (**2***d*) was obtained by the decarboxylation of 5-benzoyl-4-phenyl-1-methylpyrazole-3-carboxylic acid (**11**) (9), which in turn was obtained along with, and isolated from the isomeric acid **10** by the sequence shown in eq. [7]. The unequivocal assignment of the structure of **2***c* by X-ray crystallography thus establishes the structure of the product obtained by the decarboxylation of **11** as **2***d*; by the same token the original assignment of the structure of the precursor acids **10** and **11**, which was based solely on difference in their rates of esterification (9), was confirmed beyond doubt. These results also agreed with the structure of the 2-pyrazoline (see eq. [5]) originally assigned by Smith and Pings (12).

[5] 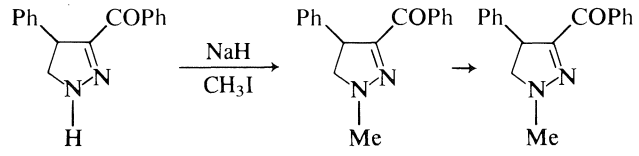

[6] 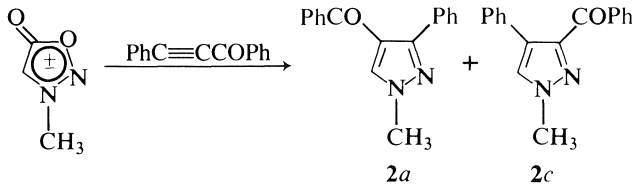

Kohler and Steele (13) had described the formation of ethyl 4-phenyl-5-benzoyl-2-pyrazoline-3-carboxylate (**12**) from the addition of ethyl diazoacetate to benzalacetophenone. Though it was somewhat surprising to us that the carbon–nitrogen bond should have entered into conjugation with the ester function to give **12** rather than with the ketone group (to give **13**), the ease of preparation of **12** suggested that, if the original assignment was correct, **12** would constitute an ideal starting material for

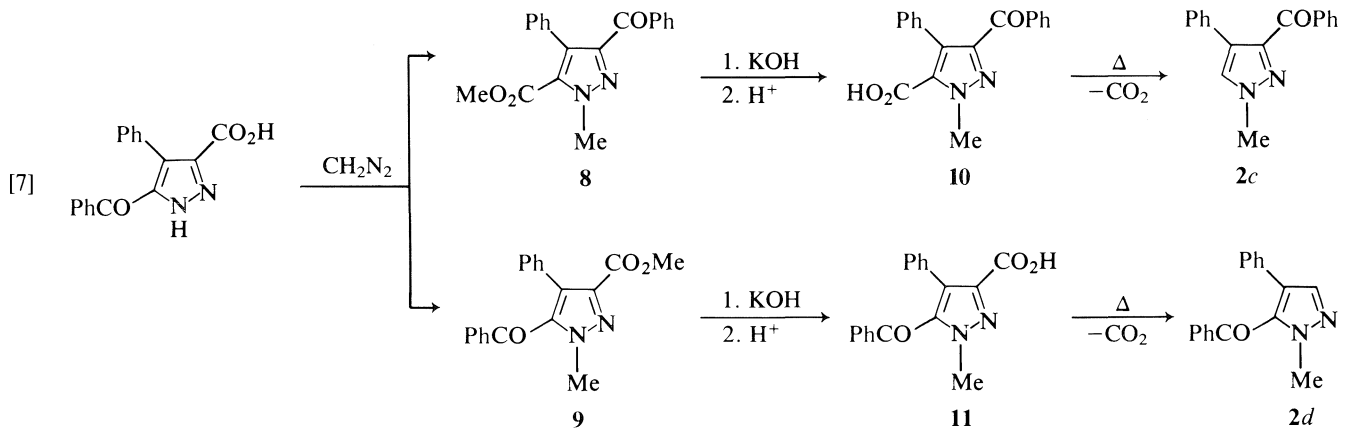

the preparation of **2***d*. However, methylation of putative **12** followed by oxidation and hydrolysis gave acid **10**, thus demonstrating that the product of the cycloaddition was **13** and not **12** as previously reported (eq. [8]) (14).

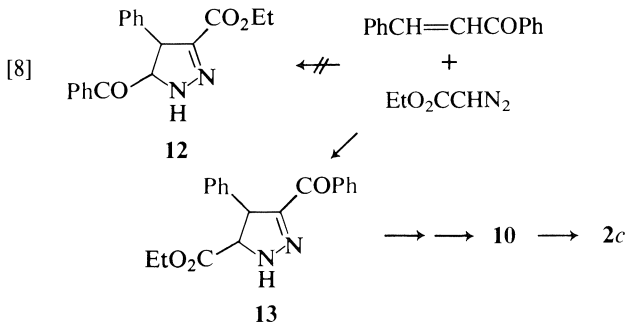

5-Phenyl isomers

The 5-phenyl isomers (**2***e* and **2***f*) were obtained as shown in eqs. [9] and [10]. 1,3-Cycloaddition of phenyldiazomethane to

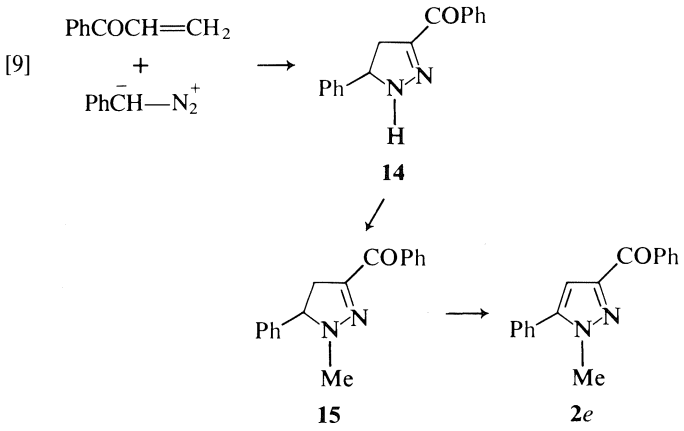

acrylophenone provided the expected 3-benzoyl-5-phenyl-2-pyrazoline (**14**) whose extremely low carbonyl absorption (1605 cm^{-1}) prompted us to confirm its structure by an X-ray crystal structure. Methylation of the anion of **14** followed by oxidation with sulfur led to 3-benzoyl-5-phenyl-1-methylpyrazole (**2***e*). The last isomer **2***f* was obtained by the Friedel–Crafts acylation of benzene with the acid chloride of 4-carboxy-5-phenyl-1-methylpyrazole (eq. [10]). The required acid **16** was obtained by the cycloaddition of 3-methyl-4-phenylsydnone to dimethyl acetylenedicarboxylate followed by hydrolysis of the diester and selective decarboxylation (14) of the 3-carboxy group of the resulting diacid to acid **16**, which was identified by conversion to its methyl ester (15). Although the complete decarboxylation of 5-phenyl-1-methylpyrazole-3,4-dicarboxylic acid provides an easy access to pure 5-phenyl-1-methylpyrazole, which is otherwise tedious to obtain (16), the experimental difficulties encountered in the clean selective decarboxylation of the diacid to **16** led us to develop another synthesis, involving bromination of 5-phenyl-1-methylpyrazole (3–5) followed by

lithiation, carbonation, and finally Friedel–Crafts acylation of benzene (eq. [11]).

Spectra and X-ray data

X-ray crystal structure analysis of 3-benzoyl-4-phenyl-1-methylpyrazole (2c)

Suitable crystals for X-ray diffraction studies formed with space group symmetry of $P2_1/c$ and cell constants of a = 12.088(2) Å, b = 11.219(1) Å, c = 10.949(2) Å, and β = 106.27(1)° for Z = 4 and a calculated density of 1.222 g/cm^3. Of the 1900 reflections measured with an automatic four-circle diffractometer equipped with Cu radiation, 1623 were observed ($I > 3\sigma I$). The structure was solved with a multi-solution tangent formula approach and difference Fourier analysis and

TABLE 1. Melting points and ^{1}H nuclear magnetic resonance and infrared data of compounds **2***a*–**2***f*

Compound	Melting point (°C)	C=O (cm^{-1})	^{1}H nmr (δ) C_6H_5[a] *o*	*m*	*p*	C_6H_5CO[a] *o*	*m*	*p*	PyH	NCH_3
2*a*	85.5–86.5	1650	7.65	7.32	7.32	7.80	7.39	7.51	7.29	4.00
2*b*	65–67[b]	1650	7.80	7.41	7.31	7.93	7.53	7.64	6.93	4.27
2*c*	92–93	1645	7.45	7.32	7.28	8.08	7.45	7.54	7.56	4.02
2*d*	Liquid[c]	1660	6.97–7.04			7.59	7.13	7.30	7.59	3.97
2*e*	57–57.5	1640	7.44–7.50			8.25	7.50	7.58	6.98	4.00
2*f*	Liquid[c]	1645	7.34	7.38	7.38	7.75	7.34	7.47	7.87	3.81

[a]Geometric center of multiplet.
[b]Literature (2) mp 52–57°C.
[c]Thick liquid.

TABLE 2. Relevant ^{13}C parameter of compounds **2***a*–**2***f*[a]

Carbon	**2***a*	**2***b*	**2***c*	**2***d*	**2***e*	**2***f*
CH_3N	39.3	39.3	39.6	38.8	38.3	37.3
C-3	153.2 dt (7.5, 4)	149.5 q (4)	146.4 d (8)	137.1 (187)	149.3 d (5)	141.8 d (188)
C-4	119.5 d (8.2)	110.2 d (177.1)	126.3 dt (7.5, 4)	126.1 dt (10, 5)	109.3 d (179.5)	120.2 d (10)
C-5	136.4 dq (188, 4)	139.5 dq (9, 2)	130.3 dq (188, 3)	136.0 qn (~3)	144.9 br s[b]	142.2 br s[c]
PhC-1[d]	132.4 t (7.5)	132.4 t (7.5)	131.8 t (7.5)	131.8 t (6.5)	129.8 t (7.5)	128.9 t (7.5)
PhCO-C-1[d]	139.2 t (7.5)	138.2 t (7.5)	137.8 t (7.5)	136.6 t (7.5)	137.5 t (7.5)	138.9 t (7.5)
CO	189.8 t (4.5)	185.9 t (4)	189.5 t (4)	188.6 t (4.5)	187.9 t (4)	189.4 t (4.5)

[a]Run in $CDCl_3$; chemical shifts relative to internal TMS.
[b]Width at half-height: 18 Hz.
[c]Width at half-height: 13 Hz.
[d]Assignment may be interchanged.

refined using full-matrix least-squares techniques (17). Hydrogens were assigned isotropic temperature factors corresponding to their attached atoms. The function $\Sigma w(|F| - |F|)^2$ with $w = 1/(\sigma F_o)^2$ was minimized to give an unweighted residual of 0.042. No abnormally short intermolecular contacts were noted. Tables I, II, and III containing the final fractional coordinates, temperature parameters, bond distances, and bond angles are available upon request from the authors.

^{1}H and ^{13}C nuclear magnetic resonance analysis

Chemical shifts of the six isomeric benzoyl phenyl 1-methylpyrazoles are listed in Table 1. Since all aromatic signals are multiplets, the usual multiplicity designations are omitted. Although the pattern shifts are by and large unexceptional, a few comments on trends are in order. The absence of an aromatic substituent at the pyrazole C-4 position can always be inferred from the distinctive high-field shift of the pyrazole C4-H. A comparison of the two 3,4- and the two 4,5-disubstituted analogues indicates that the nuclear pyrazole proton resonates about 0.25 ppm downfield in the isomer having an adjacent benzoyl group.

The *N*-methyl signal can be perturbed by a substituent at C-5 although the effect can be modified significantly if the second aromatic group is located at C-4. This can be seen by comparing **2***b*, in which the *N*-methyl peak is displaced 0.25 ppm downfield by the C-5 benzoyl, with **2***d*, in which the deshielding influence of the benzoyl group is completely nullified by the neighboring C-4 phenyl. This compensating property can be attributed to the steric hindrance that forces the aromatic substituents out of planarity with the pyrazole ring. The fact that the chemical shifts of the benzoyl protons in **2***d* are approximately 0.2 ppm upfield from their typical values is consistent with the hindrance hypothesis. These findings thus indicate that, apart from identifying a C-4 pyrazole proton, the assignment of the individual isomers by proton nmr would be risky.

In contrast to the proton data, all six isomers could be assigned unambiguously from the proton decoupled and gated decoupled ^{13}C spectra by taking advantage of both chemical shifts and long-range proton ^{13}C couplings (Table 2). The C-4 pyrazole carbon, whether substituted or unsubstituted, could always be identified because of its high-field chemical shift (18). The distinctively large pyrazole one-bond coupling constants (J_{CH}: C-4, ca. 178 Hz; C-3 and C-5, ~188 Hz) distinguish the pyrazole proton-bearing carbon from the aro-

matic resonances, which all have a J_{CH} value close to 160 Hz (19, 20). Differences in the multiplicities of the substituted pyrazole carbons arising from two- and three-bond coupling with protons (J_{C-C-H} and $J_{C-C-C-H}$) could be used to locate the position of the aromatic substituents on the pyrazole ring. This approach appeared feasible for the present series since long-range couplings exhibited by the pyrazole carbons would result from interaction with the *ortho* protons of the phenyl ring, the lone nuclear proton, and the *N*-methyl, the latter affecting only the pyrazole C-5. The *ortho* benzoyl protons were not expected to contribute to the multiplicities since four-bond couplings ($J_{C-C-C-C-H}$) are normally very small. Based on this analysis, a doublet for a substituted pyrazole carbon would be diagnostic for either C-3 or C-4 bearing a benzoyl substituent, as seen in Table 2 for **2***a* (C-4), **2***c* (C-3), **2***e* (C-3), and **2***f* (C-4). Further, the substituted pyrazole C-5 can always be distinguished from C-3 because of its higher multiplicity, since it is coupled with the *N*-methyl as well as the nuclear proton and with the *ortho* phenyl protons when this group is located at C-5.

Experimental

Elemental analyses were carried out by the Microanalysis Laboratories of the University of Massachusetts at Amherst. The infrared spectra were recorded on a Perkin–Elmer model 137B spectrophotometer (Infracord) and the nmr spectra were obtained in $CDCl_3$ (except as may be noted otherwise) on a Hitachi–Perkin–Elmer R-24 (60 MHz) and Varian XL-400 MHz spectrometer using tetramethylsilane as an internal standard.

4-Bromo-3-phenyl-1-methylpyrazole

A solution of bromine (2.88 g, 20.5 mmol) in 2.5 mL of chloroform was added dropwise over a period of 10 min to a stirred solution of 3-phenyl-1-methylpyrazole (3.0 g, 20.5 mmol) in 5.0 mL of chloroform cooled in an ice bath, and the mixture was allowed to stir overnight. It was then washed with saturated sodium bicarbonate solution (4 × 25 mL) and the chloroform was evaporated *in vacuo* to yield 3.6 g (78%) of a brown liquid; ^{1}H nmr δ: 3.55 (s, 3H, CH_3), 7.10 (s, 1H, PyH), 7.50 (m, 5H, ArH).

3-Phenyl-1-methylpyrazole-4-carboxylic acid

To a solution of crude 4-bromo-3-phenyl-1-methylpyrazole (2.0 g, 7.0 mmol) in 20 mL of anhydrous ether cooled to −30°C in a Dry Ice – acetone bath, was added dropwise a 1.7 *M* solution of *n*-butyllithium in hexane (9.0 mL, 15.3 mmol) through a syringe and the solution was allowed to stir at that temperature for a period of 1 h. The solution was then cooled to −60°C in a Dry Ice – acetone bath and gaseous carbon dioxide was bubbled through for a period of 1 h. The solution was then stirred overnight and the temperature allowed to become ambient. The precipitated solid was collected; it was then suspended in 15 mL of water, acidified, filtered, and air-dried to give 1.6 g (95%) of the acid, mp 93–99°C.

*4-Benzoyl-3-phenyl-1-methylpyrazole (***2**a)

A solution of 3-phenyl-1-methylpyrazole-4-carboxylic acid (0.2 g, 1.0 mmol) in 5.0 mL of thionyl chloride was heated to reflux for 1.5 h. The excess thionyl chloride was evaporated *in vacuo*, to the residue was added benzene (3.0 mL), and the solution was evaporated again to remove any remaining thionyl chloride; this process was repeated. To the crude acid chloride obtained as a brown oil was added 10 mL of benzene and aluminum chloride (0.4 g, 3.0 mmol) and the solution was heated at reflux overnight. The benzene was evaporated *in vacuo* to yield a residue that was dissolved in ether and washed with saturated aqueous sodium bicarbonate (4 × 25 mL) and dried. The ethereal solution was evaporated to give 0.25 g (81%) of **2***a* as an oil. This sample was identical by tlc, ir, and nmr to **2***a* obtained below.

*4-Benzoyl-3-phenyl-1-methylpyrazole (***2**a)

A solution of 1.58 g (10 mmol) of 3-phenyl-1-methylpyrazole, 1.68 g (12 mmol) of benzoyl chloride, and 0.13 g (1 mmol) of aluminum chloride in 20 mL of nitrobenzene was heated to reflux for 2 days. The nitrobenzene was distilled *in vacuo* and the residue was dissolved in 30 mL of ether. The ethereal layer was washed with saturated sodium bicarbonate and water, dried over $MgSO_4$, and the ether was evaporated to give a viscous oil. It was purified by column chromatography (silica gel, benzene) to give 0.15 g (6%) of **2***a* as a very viscous oil, which was triturated with ether – petroleum ether to give a white solid; recrystallization from ethanol yielded white crystals, mp 85.5–86.5°C. *Anal.* calcd. for $C_{14}H_{14}N_2O$: C 77.84, H 5.38, N 10.68; found: C 77.62, H 5.31, N 10.71.

*4-(*p*-Benzoylphenyl)-1-methylpyrazole*

A solution of 4-phenyl-1-methylpyrazole (316 mg, 2 mmol), benzoyl chloride (350 mg, 2.5 mmol), and anhydrous aluminum chloride (27 mg, 0.2 mmol) in 5 mL of nitrobenzene was heated to reflux for 2 days. The solvent was distilled *in vacuo* and the residue was dissolved in 30 mL of ether. The ethereal solution was washed with 10% NaOH and water, dried over $MgSO_4$, and evaporated *in vacuo*. The residue was chromatographed on 15 g of silica gel (60–200 mesh) using a 1:1 mixture of benzene–hexanes as eluent. The solid obtained from the second fraction was recrystallized from ether – petroleum ether to give 0.05 g (10%) of white crystals, mp 161–163°C; ir (KBr): 1655 (C=O) cm^{-1}; ^{1}H nmr δ: 3.94 (s, 3H, CH_3), 7.65 (m, 11H, ArH, PyH). *Anal.* calcd. for $C_{17}H_{14}N_2O$: C 77.84, H 5.38, N 10.68; found: C 77.59, H 5.32, N 10.68.

*5-Benzoyl-3-phenyl-1-methylpyrazole (***2**b)

A solution of 5 g (20 mmol) of dibenzoylacetylene, 1 drop of concentrated sulfuric acid, and 1 g (20 mmol) of methylhydrazine in 150 mL of ethanol was stirred at room temperature for 2 h and heated to reflux overnight. Ethanol was removed and ether was added to the residue. The ethereal solution was washed with water, dried, and the solvent was evaporated. The residue was recrystallized from ether – petroleum ether to give 1.5 g (30%) of **2***b*, mp 64–66°C, lit. (2) mp 52–57°C.

In a separate run, the filtrate of the crystallized residue was concentrated and chromatographed on silica gel (70–230 mesh; elution with chloroform). One of the less mobile fractions, obtained as an oil, was identified as 3-benzoyl-5-phenyl-1-methylpyrazole (**2***e*) by ir, nmr (spiking with an authentic sample), and tlc; the yield of this isomer was not determined but was very small.

Phenylglyoxal N*-methylhydrazone*

To methylhydrazine (1.84 g, 40 mmol) and two drops of acetic acid in 20 mL of ethanol was added a solution of phenylglyoxal monohydrate (3.04 g, 20 mmol) in 30 mL of ethanol; the mixture was stirred at room temperature for 24 h. Ethanol was evaporated and 30 mL of ether was added to the residue. The ethereal layer was washed with water, dried, and the ether was evaporated to give a pale yellow oil, which was chromatographed on silica gel to give 2.7 g (83%) of product; ^{1}H nmr δ: 7.57 (m, 7H, ArH, CH=N, NH), 2.83, 3.05, 3.20 (d, d, d, 3H, CH_3).

*Addition product of phenylglyoxal methylhydrazone with phenylglyoxal (***6**)

A solution of phenylglyoxal monohydrate (0.45 g, 3 mmol), methylhydrazine (0.14 g, 3 mmol), and a drop of acetic acid in 20 mL of ethanol was stirred overnight at room temperature. Ethanol was evaporated *in vacuo* and the residue was dissolved in ether. The ethereal solution was washed with water, dried over anhydrous $MgSO_4$, and the ether was evaporated. The residue was recrystallized from methylene chloride – petroleum ether to yield 0.43 g (99%) of product, mp 112–113.5°C; ir (KBr): 3490, 1699, 1640 cm^{-1}; ^{1}H nmr δ: 2.98 (s, 3H, CH_3), 4.83 (d, 1H, OH exchangeable with D_2O), 6.1 (d, 1H, O—CH), 7.05 (s, 1H, CH), 7.60 (m, 10H, ArH). *Anal.* calcd. for $C_{17}H_{16}N_2O_3$: C 68.90, H 5.44, N 9.46; found: C 68.93, H 5.38, N 9.49.

1-Methyl-1-phenacylhydrazine ethylene glycol ketal

A solution of 17 g (70 mmol) of phenacyl bromide ethylene glycol

ketal (19) in 50 mL of methylhydrazine was heated to reflux for 4 days. The excess methylhydrazine was distilled and ether was added to the residue. The ethereal solution was washed with water, dried over $MgSO_4$, and the ether was evaporated. The white solid obtained, mp 46–65°C (dec.), may be recrystallized from ether – petroleum ether (11.5 g, 76%), but was used for the next step without purification; ^{1}H nmr δ: 7.37 (m, ArH, 5H), 3.94 (m, CH_2CH_2, 4H), 3.30 (s, NH_2, 2H), 2.89 (s, CH_2, 2H), 2.47 (s, CH_3, 3H).

Hydrazone **5**

A mixture of 11.5 g (53 mmol) of the ketal hydrazine obtained above, 8.1 g (53 mmol) of phenylglyoxal monohydrate, and 0.05 mL of acetic acid in 120 mL of ethanol was stirred at room temperature. After 20 min, a solid had precipitated and the solution was stirred for an additional period of 3 h; it was then stored in the refrigerator overnight. The solid was collected and the filtrate was concentrated to give additional product. The two crops were combined and recrystallized from ethanol to give 11.4 g (65%) of the hydrazone as white crystals, mp 108–109°C; ^{1}H nmr δ: 7.53 (m, 10H, ArH), 6.95 (s, 1H, CH=N), 3.94 (m, 4H, CH_2CH_2), 3.89 (s, 2H, CH_2), 3.11 (s, 3H, CH_3). *Anal.* calcd. for $C_{19}H_{20}N_2O_3$: C 70.35, H 6.22, N 8.64; found: C 70.44, H 6.31, N 8.69.

*3-Benzoyl-4-phenyl-1-methylpyrazole (***2***c)*

A solution of 3.24 g (10 mmol) of phenylglyoxal hydrazone **5** in 75 mL of 75% H_2SO_4 was stirred for 2 weeks at room temperature. It was then diluted with 100 mL of water, neutralized with solid $NaHCO_3$, and extracted with ether. The ethereal layer was dried over anhydrous $MgSO_4$ and ether was evaporated. The resulting yellow solid was recrystallized from ethanol to give 1.48 g (56%) of **2***c* as white crystals, mp 92.5–93.5°C. *Anal.* calcd. for $C_{17}H_{14}N_2O$: C 77.84, H 5.38, N 10.68; found: C 77.70, H 5.40, N 10.67.

3-Benzoyl-1-methyl-4-phenyl-2-pyrazoline

To 0.27 g (11 mmol) of *dry* sodium hydride was added dropwise 8 mL of dry DMSO at 18–20°C and the mixture was stirred at ambient temperature for 20 min. The mixture was then cooled to 18°C and a solution of 3-benzoyl-4-phenyl-2-pyrazoline (12) (1.6 g, 6.4 mmol) in 14 mL dry DMSO was added dropwise at 18–20°C; the color changed from yellow to green. The green reaction mixture was stirred at ambient temperature for 20 min and cooled to 18°C. Then a solution of 1.6 g (11 mmol) of methyl iodide in 2 mL of dry DMSO was added dropwise to the reaction mixture at 18–20°C; the color changed from green to yellow and the mixture was stirred at ambient temperature for 1 h, after which it was poured into 100 mL of ice water and extracted with 30 mL of ether. The ethereal layer was washed with water, dried over $MgSO_4$, and the solvent was evaporated *in vacuo* to yield 1.34 g (79%) crude product, mp 131–137°C; ir (KBr): 1615 (C=O) cm^{-1}; ^{1}H nmr δ: 3.05 (s, 3H, CH_3), 3.50 (t, 2H, CH_2), 4.55 (q, 1H, CH), 7.50 (m, 10H, ArH).

*3-Benzoyl-4-phenyl-1-methylpyrazole (***2***c) by sulfur dehydrogenation of 3-benzoyl-4-phenyl-1-methyl-2-pyrazoline*

A mixture of 1.1 g (4.2 mmol) of 3-benzoyl-4-phenyl-1-methyl-2-pyrazoline and 0.14 g (4.4 mmol) of sulfur was gently heated with a flame; the two solids melted and heating was continued until gas evolution subsided. Ether was added and the ethereal solution was washed with water, 10% NaOH, water, and dilute HCl. After a final wash with water, the solution was dried over $MgSO_4$ and concentrated to yield 0.45 g (41%) of a yellow solid, mp 92–93°C, identical in all respects with authentic **2***c* (*vide supra*), mp 92.5–93.5°C.

Other oxidations of 3-benzoyl-4-phenyl-1-methyl-2-pyrazoline. General procedure

A stirred solution of the 2-pyrazoline (0.2 g, 1.0 mmol) and an equimolar amount of the oxidizing agent in the appropriate solvent (25 mL) were heated to reflux. Upon cooling, the precipitate (if any) was removed by filtration. Evaporation of the filtrate left a residue (which solidified in some cases) whose ir and nmr spectra indicated 3-benzoyl-4-phenyl-1-methylpyrazole (**2***c*) to be the product of the oxidation. The product was induced to crystallize by trituration with ether – petroleum ether at low temperature, or by chromatography on silica gel (70–230 mesh) by elution with a benzene–chloroform (5:2) mixture. Recrystallization may be effected from anhydrous ethanol, mp 90–92.5°C.

Oxidant	Solvent	Heating time (h)	Crude yield (%)
$Pb(OAc)_4$[a]	Acetic acid[b]	2	60
DDQ	Benzene	15	>95
NBS	CCl_4	3.5	95
NCS	CH_2Cl_2	7	20
10% Pd/C	*m*-Xylene	24	—[c]

[a]Reference 27.
[b]Volume of glacial acetic acid was 3.8 mL.
[c]Although the yield was not recorded, it is not negligible.

Photolysis of 3-benzoyl-4-phenyl-1-methyl-2-pyrazoline

A solution of the 2-pyrazoline (1.0 g, 3.8 mmol), AIBN (0.31 g, 1.9 mmol),[4] and cumene (280 mL), under a nitrogen atmosphere, was irradiated overnight by a Hanovia high pressure mercury immersion lamp (Pyrex filter). The cumene was removed by distillation under reduced pressure. The nmr spectrum of the residue showed the presence of the starting pyrazoline as well as of **2***c* (spiking with an authentic sample).

syn-N-*Nitrososarcosine*

To a stirred solution of sarcosine (35.6 g, 0.40 mol), 67 mL of concentrated hydrochloric acid, and 100 mL of water at 0°C was added dropwise a solution of sodium nitrite (55.2 g, 0.80 mol) in water (200 mL) over a period of 40 min. The solution warmed gradually to ambient temperature. The aqueous solution was then extracted continuously with ether (ca. 300 mL) for 48 h and the ethereal extract was dried ($MgSO_4$). Evaporation of the ether *in vacuo* below 35°C afforded 44 g (93%) of yellow viscous liquid (^{1}H nmr δ: 3.20, 3.90 (3H, s, NCH_3), 4.40, 5.10 (2H, s, NCH_2), 5.70 (1H, s, OH)). To this viscous liquid was added ether (ca. 10 mL) and the solution was stored in a freezer overnight, whereupon the *syn* isomer crystallized. The colorless solid was collected by filtration and washed several times with small portions of ether – petroleum ether (1:1). The *syn-N*-nitrososarcosine should be stored in a freezer until use. The filtrate was concentrated carefully (because of the instability of nitroso acid) and the procedure above repeated twice, converting nearly all of the mixture to *syn-N*-nitrososarcosine; ir (neat): 1725 (C=O) cm^{-1}; ^{1}H nmr δ: 3.85 (3H, s, NCH_3), 4.30 (2H, s, NCH_2), 10.1 (1H, s, OH).

3-Methylsydnone

A solution of acetic anhydride (70 mL) and *syn-N*-nitrososarcosine (20.0 g, 0.169 mol) was heated to reflux for 5 min; color changes from colorless to green and eventually yellow were observed during this period. The reaction mixture was cooled and acetic acid and the excess acetic anhydride were removed by distillation (aspirator). The remaining orange liquid was distilled twice under reduced pressure (lit. (20) bp 125–128°C) to afford 9.28 g (56%) of pure 3-methylsydnone as a deliquescent solid, which was stored in a refrigerator; ir (neat): 1735 (sh 1775) (C=O) cm^{-1}; ^{1}H nmr δ: 4.15 (3H, s, NCH_3), 6.60 (1H, s, CH).

Reaction of 3-methylsydnone with benzoylphenylacetylene

A stirred solution of 3-methylsydnone (1.10 g, 11.0 mmol) and benzoylphenylacetylene (21) (2.06 g, 10.0 mmol) in *o*-dichlorobenzene (50 mL) was heated to reflux for 6 days under an atmosphere of nitrogen. The solvent was removed by distillation under reduced pressure. The dark viscous residue was chromatographed on silica gel (70–230 mesh) and eluted with benzene–chloroform (5:2); evaporation of the solvents afforded a mixture whose nmr spectrum (by spiking with authentic samples of **2***a* and **2***c*) showed that 3-benzoyl-4-phenyl-

[4]α,α′-Azobisisobutryonitrile.

1-methylpyrazole (**2***c*) and 4-benzoyl-3-phenyl-1-methylpyrazole (**2***a*) were formed (ratio of 1:2.2) in a nearly quantitative yield (2.6 g, 99%).

Cycloaddition of 3-benzylsydnone with benzoylphenylacetylene

A solution of 3-benzylsydnone (0.88 g, 5.3 mmol) (22) and benzoylphenylacetylene (1.03 g, 5.00 mmol) in *o*-dichlorobenzene (20 mL) was heated to reflux under nitrogen for 72 h. The solvent was removed by distillation *in vacuo* leaving a brown residue, which was chromatographed on silica gel (70–230 mesh) and eluted with benzene. Based on recovered benzoylphenylacetylene (0.14 g), the yield of the dark residue was nearly quantitative (1.46 g). The residue was shown to be a mixture of 3-benzoyl-4-phenyl-1-benzylpyrazole and 4-benzoyl-3-phenyl-1-benzylpyrazole in a ratio of 5:1 as determined by nmr integration. Further chromatography of this mixture as described above allowed the separation of these isomers as solids after evaporation of the solvent. The more mobile fraction was a yellow solid, mp 100–104°C; ir (KBr): 1650 (C=O) cm^{-1}; ^1H nmr δ: 5.23 (2H, s, NCH_2), 7.20 (14H, m, ArH, CH), 7.65 (2H, m, ArH). The other isomer crystallized as off-white crystals, mp 93–94.5°C; ir (KBr): 1650 (C=O) cm^{-1}; ^1H nmr δ: 5.25 (2H, s, NCH_2), 7.30 (14H, m, ArH, CH), 8.05 (2H, m, ArH).

Esterification and methylation of 5-benzoyl-4-phenylpyrazole-3-carboxylic acid

To a suspension of 5-benzoyl-4-phenylpyrazole-3-carboxylic acid (6.6 g, 22.6 mmol) in an ice bath was added dropwise an ethereal solution of diazomethane (50 mmol, 170 mL); the mixture was stirred at ambient temperature overnight. The ethereal solution was washed with water, aqueous sodium bicarbonate, and water, followed by the usual work-up to give 7.5 g of a crude solid, shown by nmr to be a mixture of the two esters. The solid was recrystallized from ethanol twice to give a white solid mixture of the two esters; the filtrate was concentrated to give a white solid, shown by nmr to be one isomer of the esters (nmr δ: 4.10 (s, 3H, N-CH_3), 3.83 (s, 3H, O-CH_3)), mp 118–119°C. The original solid (mixture) obtained was recrystallized from ethanol twice to give 2.86 g (40%) of isomeric ester (nmr ($CDCl_3$) δ: 4.21 (s, 3H, N-CH_3), 3.62 (s, 3H, O-CH_3)) as colorless needles, mp 121–122°C, and concentration of the filtrate gave the ester of mp 118–119°C; further concentration of the filtrates and crystallization (from ethanol) afforded additional amounts of the lower melting ester and the total yield was 1.45 g (20%). The residue, consisting of a mixture of the two esters, amounted to 1.8 g (25%). The melting point of a mixture of the two pure esters was depressed (95–100°C).

*3-Benzoyl-4-phenyl-1-methylpyrazole-5-carboxylic acid (**10**)*

A mixture of pyrazole ester (1.28 g, 4 mmol), mp 121–122°C, and aqueous potassium hydroxide (1 g in 5 mL of water) was heated to reflux for 4 h and some of the water and methanol produced were removed by distillation; 5 mL of water was added to the residue and it was heated to reflux overnight. The cooled mixture was washed with ether and then acidified with concentrated HCl to give a white solid, which was collected and washed with water. Recrystallization from aqueous ethanol afforded 1.06 g (87%) of colorless needles, mp 178–179°C, decomposition at 210°C (lit. (9) mp 181–182°C). The filtrate was extracted with ether followed by the usual work-up to give a white solid, which was then combined with the residue from the filtrate of the recrystallization and recrystallized from aqueous ethanol to yield 0.08 g (7%) of off-white crystals, mp 172–176°C; the total yield was 94%.

*5-Benzoyl-4-phenyl-1-methylpyrazole-3-carboxylic acid (**11**)*

A mixture of pyrazole ester (0.64 g, 2 mmol), mp 118–119°C, and aqueous potassium hydroxide (0.5 g in 3 mL of water) was heated to reflux overnight and 1 mL of a mixture of the water and the methanol formed as by-product was removed by distillation. Upon acidification of the residue with 10% hydrochloric acid, a white solid precipitated immediately; it was collected, washed with water until neutral, and air-dried. Recrystallization from aqueous ethanol yielded 0.48 g (78%) of white needles, mp 213–213.5°C (lit. (9) mp 213°C). Although the sample melted at 212–213°C (with some gas evolution at 218°C), the cooled sample melted at 212–213°C. This observation suggests that complete decomposition requires much higher temperatures.

*5-Benzoyl-4-phenyl-1-methylpyrazole (**2** d) by decarboxylation of pyrazole acid **11***

Pyrazole acid **11** (0.30 g, 1 mmol), mp 212–213°C, was heated at 280°C for 3 min and at 310°C for 15 min to yield 0.26 g of crude product; its tlc (SiO_2/$CHCl_3$) showed one major product and one small spot on the original starting point. Purification by column chromatography (SiO_2, $CHCl_3$) gave 0.24 g (94%) of 5-benzoyl-4-phenyl-1-methylpyrazole (**2***d*) as a thick oil.

*3-Benzoyl-4-phenyl-1-methylpyrazole by decarboxylation of acid **10***

Similar decarboxylation of pyrazole acid **10** gave a nearly quantitative yield of **2***c*, mp 91–93°C.

Ethyl 3-benzoyl-4-phenyl-1-methyl-2-pyrazoline-5-carboxylate

To 0.43 g (18 mmol) of sodium hydride (dry) was added dry DMSO (12 mL) dropwise under N_2. The suspension was stirred for 20 min at 20–22°C. To this suspension was added dropwise ethyl 3-benzoyl-4-phenyl-2-pyrazoline-5-carboxylate (5.0 g, 15 mmol) (13) in dry DMSO (40 mL), while the temperature was kept at 20–22°C. The solution turned blood-red in color and stirring was continued for an additional 20 min. Then, a solution of iodomethane (2.5 g, 18 mmol) in dry DMSO (10 mL) was added dropwise and a gradual color change from red to yellow was observed. The yellow solution was stirred at ambient temperature overnight and was then poured into vigorously stirred ice water (200 mL). The product was extracted into ether (2 × 100 mL). The combined ethereal extracts were washed twice with water, dried over $MgSO_4$, and the ether evaporated, leaving 5.03 g (99%) of a residue whose ir and nmr spectra indicated it to be the desired methylated pyrazoline. It was used without further purification; ir (neat): 1740, 1720 (C=O) cm^{-1}; ^1H nmr ($CDCl_3$) δ: 1.30 (t, 3H, C-CH_3), 3.30 (s, 3H, N-CH_3), 4.20 (q, 2H, C-CH_2), 7.60 (m, 11H, ArH, PyH).

Ethyl 3-benzoyl-4-phenyl-1-methyl-5-pyrazolecarboxylate

To a stirred solution of ethyl 3-benzoyl-4-phenyl-1-methyl-2-pyrazoline-5-carboxylate (1.0 g, 3.0 mmol) in CCl_4 (10 mL) chilled in an ice bath was added dropwise a solution of bromine (0.64 g, 3.6 mmol) in CCl_4 (6 mL). After the addition, the solution was allowed to warm to ambient temperature and subsequently heated to reflux for 2 days. The solvent was removed by distillation and the residue was dissolved in ether (25 mL). The ethereal solution was washed successively with saturated aqueous sodium bicarbonate, water, saturated aqueous sodium thiosulfite, and water, then dried over $MgSO_4$ and evaporated *in vacuo* to give a quantitative yield of the pyrazole as a brown residue; ir (neat): 1720 (C=O) cm^{-1}; ^1H nmr δ: 0.97 (t, 3H, C-CH_3), 4.10 (q, 2H, C-CH_2), 4.22 (s, 3H, N-CH_3), 7.53 (m, 10H, ArH, PyH).

3-Benzoyl-4-phenyl-1-methyl-5-pyrazolecarboxylic acid

A solution of potassium hydroxide (0.67 g, 12 mmol) in water (6 mL) was added to ethyl 3-benzoyl-4-phenyl-1-methyl-5-pyrazolecarboxylate (1.00 g, 3.00 mmol) and the mixture was heated to reflux with stirring overnight. Excess water and ethanol (2 mL) were removed by distillation *in vacuo*. An additional portion of water was then added to the solution, which was subsequently washed twice with small portions of ether. The basic solution was then acidified with concentrated hydrochloric acid and extracted with ether (2×). The ethereal solution was washed with water until neutral, dried over $MgSO_4$, and concentrated to give 0.50 g (54%) of a tan colored solid, mp 165–167°C, which was identical in all respects (tlc, ir, and nmr) to the acid (**10**) obtained above.

Acrylophenone

β-Dimethylaminopropiophenone hydrochloride (88.0 g, 0.41 mol) was placed into a 1-L 3-necked round-bottomed flask and steam distilled. The distillate was extracted with ether, washed with water, and filtered. The ethereal extract was dried over magnesium sulfate and the solvent was evaporated *in vacuo* to yield 24.1 g (45%) of a pale

golden oil (23), used without further purification. The infrared and nmr spectra confirmed its structure.

*3-Benzoyl-5-phenyl-2-pyrazoline (**14**)*

To 13.2 g (0.10 mol) of acrylophenone in 100 mL of anhydrous ether in a 500-mL 3-necked round-bottomed flask fitted with a magnetic stirring bar, a reflux condenser, drying tube, and an addition funnel, and cooled to 0°C, was added dropwise a solution of phenyldiazomethane (24). When the addition was complete the mixture was stored in the freezer overnight. The precipitated yellow crystals were collected and recrystallized from anhydrous ether to yield 14.8 g (60%) of pale yellow crystals, mp 81–83°C; its *N*-acetyl derivative, mp 113–114.5°C (from ethanol) was prepared and analyzed. *Anal.* calcd. for $C_{18}H_{16}N_2O_2$: C 73.95, H 5.52, N 9.58; found: C 73.84, H 5.47, N 9.79.

*3-Benzoyl-5-phenyl-1-methyl-2-pyrazoline (**15**)*

To 0.27 g (11 mmol) of *dry* sodium hydride was added dropwise 8 mL of dry DMSO at 18–20°C and the mixture was stirred at ambient temperature for 20 min. The mixture was then cooled to 18°C and a solution of 3-benzoyl-5-phenyl-2-pyrazoline (1.6 g, 6.4 mmol) in 14 mL of dry DMSO was added dropwise at 18–20°C; the color changed from yellow to green. The green reaction mixture was stirred at ambient temperature for 20 min and cooled to 18°C. Then, a solution of 1.6 g (11 mmol) of methyl iodide in 2 mL of dry DMSO was added dropwise to the reaction mixture at 18–20°C; the color changed from green to yellow and the mixture was stirred at ambient temperature for 1 h. It was then poured into 100 mL of ice water and extracted with 30 mL of ether. The ethereal layer was washed with water, dried over $MgSO_4$, and the solvent was evaporated *in vacuo* to yield 1.77 g of a yellow oil; the oil solidified upon standing at room temperature. The solid was recrystallized from ether – petroleum ether to give an analytical sample, mp 79.5–81°C. The solid from the evaporation of the filtrate was recrystallized; the combined yield of recrystallized product was 1.02 g (60%). *Anal.* calcd. for $C_{17}H_{16}N_2O$: C 77.25, H 6.10, N 10.60; found: C 76.98, H 6.09, N 10.60.

Evaporation of the filtrate from the recrystallization of the second crop afforded a residual oil whose nmr spectrum showed, in addition to **15**, the presence of 3-benzoyl-5-phenyl- and 5-benzoyl-3-phenyl-1-methylpyrazoles.

*3-Benzoyl-5-phenyl-1-methylpyrazole (**2**e)*

A mixture of 1.0 g (3.8 mmol) of 3-benzoyl-5-phenyl-1-methyl-2-pyrazoline and 0.13 g (94 mmol) of sulfur was gently heated with flame. Two solids melted and two layers were observed. Heating was continued until the mixture became homogeneous. After cooling, ether was added and the ethereal solution was washed with water, 10% aqueous NaOH, water, dilute HCl (2 drops in 30 mL of water), and water. The dried ethereal solution was concentrated to dryness *in vacuo* to give 0.91 g of an oil. Column chromatography (silica gel, benzene) of the mixture gave 0.86 g (96%) of an oil (single spot by tlc), which was triturated with ether – petroleum ether and crystallized to give white crystals, mp 57–57.5°C. *Anal.* calcd. for $C_{17}H_{14}N_2O$: C 77.84, H 5.38, N 10.68; found: C 77.69, H 5.15, N 10.82.

3-Methyl-4-phenylsydnone

A mixture of *N*-nitroso-*N*-methyl-*C*-phenylglycine (4.0 g, 20.6 mmol) and acetic anhydride (15 mL) was stirred on a steam bath overnight (25). The mixture was cooled to room temperature and poured slowly into a mixture of ice and water with vigorous stirring to give 3.6 g (99%) of a tan precipitate, mp 126–130°C. Recrystallization from an ether–benzene mixture afforded colorless crystals, mp 130.5–131.5°C. *Anal.* calcd. for $C_9H_8N_2O_2$: C 61.35, H 4.58, N 15.92; found: C 61.33, H 4.55, N 15.94.

Dimethyl 1-methyl-5-phenylpyrazole-3,4-dicarboxylate

A mixture of 3-methyl-4-phenylsydnone (5.0 g, 28.0 mmol) and dimethyl acetylenedicarboxylate (8.0 g, 56.0 mmol) in 100 mL *p*-xylene was heated at reflux overnight. The *p*-xylene was distilled under vacuum (aspirator). Ether – petroleum ether was added to the residue to precipitate 5.9 g (77%) colorless crystals, mp 82–83°C.

1-Methyl-5-phenylpyrazole-3,4-dicarboxylic acid

A mixture of dimethyl 1-methyl-5-phenylpyrazole-3,4-dicarboxylate (12.0 g, 44 mmol) and 10% NaOH (480 mL) was heated at reflux for 14 h. The cooled solution was acidified with concentrated HCl and the precipitate was collected and washed with water to give 10.0 g (93%) of colorless crystals, mp 266°C (dec.); NE (neutralization equivalent): 125.75.

*1-Methyl-5-phenylpyrazole-4-carboxylic acid (**16**)*

A 1.0 g (4 mmol) sample of the diacid was heated in an oil bath at ~280°C. The acid melted, with gas evolution. After cooling, the residue was shaken with 2.5 *N* NaOH and 0.37 g (45%) of white crystals, mp 215–216°C. It was converted to the known methyl ester as described below.

Methyl 1-methyl-5-phenyl-4-pyrazolecarboxylate

A solution of 1-methyl-5-phenylpyrazole-4-carboxylic acid (0.2 g, 1 mmol), methanol (1 mL), and H_2SO_4 (0.5 mL) was heated at reflux for 1 h. After cooling to room temperature, the reaction mixture was extracted with CH_2Cl_2, washed with water, and then with aqueous $NaHCO_3$. After drying over $MgSO_4$, the mixture was evaporated to yield 0.14 g (65%) of the methyl ester as yellow crystals, mp 105.5–107°C. The melting point and spectra were identical to literature values (15).

5-Phenyl-1-methylpyrazole was obtained by heating a solution of 1-methyl-5-phenylpyrazole-3,4-dicarboxylic acid (4.0 g) in 12 g of diphenyl ether at reflux overnight. The brown oil was acidified with concentrated HCl, extracted with water, neutralized with 2.5 *N* NaOH, extracted with ether, and dried over $MgSO_4$. The ether was evaporated to yield 2.6 g (96%) of a yellow oil, identical in all respects (tlc, ir, and nmr) to an authentic sample (17).

Preparation of 5-phenyl-1-methylpyrazole

An approximately 1:1 mixture (32 g) of 3-phenyl-1-methyl-2-pyrazoline and 5-phenyl-1-methyl-2-pyrazoline (26) (bp 137–138°C/30 Torr; 1 Torr = 133.3 Pa) and sulfur (7 g) was heated to 230°C overnight. To the cooled reaction mixture was added 100 mL of 10% NaOH and it was stirred overnight. It was extracted with ether and the ethereal solution was washed with water, dried over $MgSO_4$, and the ether was evaporated. The mixture of pyrazoles was carefully distilled at 0.75 Torr three times to yield 16 g (51%) of a mixture, bp 105°C/0.75 Torr, which contained 80% of 5-phenyl-1-methylpyrazole (by nmr). To a solution of this mixture (16 g) in ethanol (20 mL) was added a saturated solution of picric acid in ethanol to precipitate the picrate, which was collected. The filtrate was treated in the same fashion and the process repeated until no more picrate formed. The precipitates were combined and recrystallized from ethanol to give 25 g of the picrate of 5-phenyl-1-methylpyrazole, mp 143–144°C, as yellow crystals (lit. (16) mp 142–143°C). A solution of the picrate (16.5 g, 0.043 mmol) in benzene (100 mL) was shaken with 10% NaOH and then with water. The benzene solution was dried over $MgSO_4$ and benzene was evaporated *in vacuo* to give an oil. It was distilled under vacuum to yield 5.3 g (82%) of 5-phenyl-1-methylpyrazole, bp 105°C/1.0 Torr (lit. (16) bp 118–119°C/12 Torr).

4-Bromo-5-phenyl-1-methylpyrazole

A solution of bromine (7.21 g, 45.1 mmol) in chloroform (10 mL) was added dropwise to a stirred solution of 5-phenyl-1-methylpyrazole (6.49 g, 41.10 mmol) in chloroform (7 mL) cooled in an ice bath. The mixture was then allowed to warm to room temperature and stirring continued overnight. The red reaction mixture was washed successively with a saturated aqueous solution of sodium bicarbonate, water, saturated aqueous sodium thiosulfite, and finally water. The organic phase was dried over $MgSO_4$ and concentrated, to afford a yellow liquid that solidified on standing to give 9.27 g (95%) of a yellow solid. Recrystallization from petroleum ether afforded pale yellow crystals of 4-bromo-5-phenyl-1-methylpyrazole, mp 51.5–52.5°C; ^{1}H nmr δ: 3.72 (s, 3H, CH_3), 7.35 (s, 5H, ArH), 7.45 (s, 1H, PyH).

*5-Phenyl-1-methyl-4-pyrazolecarboxylic acid (**16**)*

To a stirred solution of 4-bromo-5-phenyl-1-methylpyrazole (5.95 g, 25.1 mmol) in anhydrous ether (10 mL) under N_2 at −30°C was

added dropwise a solution of *n*-butyllithium in hexanes (31.4 mL, 50.2 mmol); the temperature was maintained between −30 and −35°C throughout the addition; during the addition, dry THF (20 mL) was added to prevent the mixture from freezing. After the addition, the mixture was allowed to warm to 0°C for a short while, and eventually to room temperature. Stirring at room temperature continued for 1.5 h. The resulting yellow suspension was then cooled back to −30 to −35°C and dry carbon dioxide was bubbled through the solution while the temperature was allowed to increase to 25°C. This process took a total of 2 h; stirring was continued overnight. The yellow solid that had formed was collected and it was immediately dissolved in 50 mL of water and acidified with concentrated hydrochloric acid, causing a precipitation of a cream colored solid, which was collected and washed with small portions of cold water. The carboxylic acid (3.6 g, 71%) was allowed to air-dry, mp 214–215°C, identical in all respects to the previous sample (*vide supra*); ir (KBr) 1700 cm^{-1}; ^1H nmr (DMSO-d_6) δ: (3H, s, NCH_3), 7.30 (6H, br s, ArH, CH), 7.80 (1H, br s, OH).

*4-Benzoyl-5-phenyl-1-methylpyrazole (**2**f)*

A solution of 5-phenyl-1-methyl-4-pyrazolecarboxylic acid (2.00 g, 10.0 mmol) in thionyl chloride (18 mL) was heated to reflux for 24 h. After removal of excess thionyl chloride by distillation (aspirator), benzene was added and the solution was evaporated; this procedure was repeated to insure the complete removal of any residual thionyl chloride. The resulting dark residue was dissolved in dry benzene (20 mL), treated with aluminum chloride (2.70 g, 20 mmol), and heated gently for 36 h. The reaction mixture was washed successively with a saturated aqueous solution of sodium bicarbonate (3 × 25 mL) and water (2 × 25 mL). The organic phase was dried (Na_2SO_4) and concentrated to afford a brown oil, 2.59 g (99%). The oil was chromatographed on silica gel (70–230 mesh) eluted with benzene (and gradually changed to chloroform) to yield an orange oil (2.25 g). All attempts to induce crystallization of the oil, including Kugelrohr distillation (bp 175–180°C), failed and only a viscous yellow oil was obtained. *Anal.* calcd. for $C_{17}H_{14}N_2O$: C 77.84, H 5.38, N 10.68; found: C 77.93, H 5.54, N 10.58.

Acknowledgements

The authors thank Mrs. Ruth Elsbree Newman, Messrs. C. H. Rosansky, W. A. Manganiello, and P. T. Anastas for some experiments. The support of the Polaroid Corporation, of the Shell Company, and of the University of Massachusetts at Boston is hereby gratefully acknowledged.

1. K. Kano and J.-P. Anselme. Bull. Chem. Soc. Jpn. **57**, 905 (1984).
2. H. W. Heine, T. R. Hoye, P. G. Williard, and R. C. Hoye. J. Org. Chem. **38**, 2984 (1973).
3. A. N. Kost and I. I. Grandberg. *In* Advances in heterocyclic chemistry. Vol. 6. *Edited by* A. R. Katritzky. Academic Press, New York, NY. p. 347 ff.
4. I. I. Grandberg, L. G. Vasina, A. S. Volkova, and A. N. Kost. J. Gen. Chem. USSR, **31**, 1765 (1961).
5. T. L. Jacobs. *In* Heterocyclic compounds. Vol. 5. *Edited by* R. C. Elderfield. John Wiley and Sons, New York, NY. p. 45; R. Fusco. *In* Heterocyclic compounds. Vol. 22. *Edited by* A. Weissberger. Interscience Publishers, New York. NY. 1967. p. 1.
6. E. K. Fields. J. Am. Chem. Soc. **77**, 4255 (1955); E. Klingsberg. J. Am. Chem. Soc. **83**, 2394 (1961).
7. N. A. Domnin, V. I. Diurnbaum, and V. A. Cherkasova. J. Gen. Chem. USSR, **28**, 1520 (1958).
8. (*a*) I. Fabra and V. Sprio. Atti Accad. Sci. Lett. Arti Palermo, **21**, 129 (1962); Chem. Abstr. **59**, 1617g (1963); (*b*) A. Alemagna, T. Bacchetti, and S. Rossi. Gazz. Chim. Ital. **93**, 748 (1963).
9. I. L. Finar and B. H. Walter. J. Chem. Soc. 1588 (1960).
10. D. Scarpetti, K. Kano, and J.-P. Anselme. Tetrahedron Lett. **26**, 6151 (1985).
11. W. L. Collibee and J.-P. Anselme. Tetrahedron Lett. **26**, 1595 (1985).
12. L. I. Smith and W. B. Pings. J. Org. Chem. **2**, 23 (1937).
13. E. P. Kohler and L. L. Steele. J. Am. Chem. Soc. **41**, 1043 (1919).
14. C. Bülow and A. Schlesinger. Ber. **33**, 3362 (1900).
15. A. Padwa, E. M. Burgess, H. L. Gingrich, and D. M. Rousch. J. Org. Chem. **47**, 786 (1982).
16. K. von Auwers and W. Schmidt. Ber. **58**, 528 (1925).
17. P. Main *et al.* MULTAN 80, University of York, York, England (1980); C. K. Johnson. ORTEP-II, Oak Ridge National Laboratory, Oak Ridge, Tennessee (1970); Y. Okaya *et al.* SDP Plus. Vol. 1. B. A. Frenz and Associates, College Station, Texas (1984).
18. J. B. Stothers. ^{13}C NMR spectroscopy. Academic Press, New York, NY. 1972. pp. 254, 343, and references cited therein; G. Levy. ^{13}C NMR spectroscopy. 2nd ed. J. Wiley and Sons Inc., New York, NY. 1980. pp. 119, 129, and references cited therein.
19. E. F. Godefroi, J. Heeres, J. van Cutsem, and P. A. J. Janssen. J. Med. Chem. **12**, 784 (1969); S. Vineswariah, G. Prakash, V. Bhushan, and S. Chandrasekaran. Synthesis, 309 (1982).
20. D. L. Hammick and D. J. Voaden. J. Chem. Soc. 3303 (1961).
21. Y. Tohda, K. Sonogashira, and N. Hagihara. Synthesis, 777 (1977).
22. M. Nakajima and J.-P. Anselme. J. Org. Chem. **48**, 1444 (1983).
23. C. Mannich and G. Heilner. Ber. **55**, 356 (1922).
24. J.-P. Anselme. Org. Prep. Proced. **1**, 73 (1969).
25. J. C. Earl and A. W. Mackney. J. Chem. Soc. 899 (1935).
26. K. von Auwers and P. Heinke. Ann. **458**, 176 (1927).
27. G. F. Duflin and J. D. Kendall. J. Chem. Soc. 408 (1954).

A proton spin-lattice relaxation pathway analysis of conformational preferences of aryl and enol ethers in some cinchona and morphine alkaloids

WALTER J. CHAZIN AND LAWRENCE D. COLEBROOK[1]

Department of Chemistry, Concordia University, 1455 de Maisonneuve Blvd., West, Montreal (Que.), Canada H3G 1M8

Received April 29, 1986

WALTER J. CHAZIN and LAWRENCE D. COLEBROOK. Can. J. Chem. **64**, 2220 (1986).

The spin-lattice relaxation rates of protons adjacent to hydroxyl and methoxy groups in aryl and enol ethers are dependent on the orientation of the alkyl group. This property has been employed to identify preferred conformations of these groups in some cinchona and morphine group alkaloids.

WALTER J. CHAZIN et LAWRENCE D. COLEBROOK. Can. J. Chem. **64**, 2220 (1986).

On a observé que les taux de relaxation spin-réseau des protons adjacents des groupements hydroxyles et méthoxyles des éthers aryliques et énoliques dépendent de l'orientation des groupements alkyles. On a utilisé cette propriété pour identifier les conformations privilégiées de ces groupements dans quelques alcaloïdes des familles de la cinchona ainsi que de la morphine.

[Traduit par la revue]

Introduction

Conformational preferences of enol ethers, in particular, aromatic methoxy groups, have been a subject of interest to organic chemists for many years. These preferences have been observed by a number of experimental techniques, and investigated by a range of computational methods (1, 2). In general, it has been found that in alkyl enol ethers there is a decided preference for the *s–cis* conformation, where the alkyl group is coplanar and *syn* to the bond of higher order (1, 3). Recently, corresponding preferences in aromatic ethers have also been discussed (1, 2, 4, 5).

Nuclear magnetic resonance (nmr) has proven to be a very powerful technique for determination of the conformational bias of enols (6) and enol ethers (3–5, 7). Using a method that is closely related to techniques utilizing $^1H\{^1H\}$ nuclear Overhauser effects (nOe) (8), as reported by Sanders and co-workers (9) and Kruse *et al.* (5), the spin-lattice relaxation of vinylic, allylic, and ring protons of enol and aromatic ethers in some cinchona and morphine alkaloids[2] has been examined to gain insight into specific conformational preferences of the ether function.

For organic molecules of molecular weight less than about 1000, proton spin-lattice relaxation in a dilute solution of a nonviscous solvent is usually dominated by intramolecular dipolar interactions between protons. The rate equation for dipolar relaxation of a proton, j, is given by:

$$[1] \quad R_{1_j} = 1/T_{1_j} = K\sum_i (1/r_{ij})^6 \tau_{c_{ij}} \qquad (i \neq j)$$

where K is a product of constants, r_{ij} is the distance between proton j and proton i, and $\tau_{c_{ij}}$ is the rotational correlation time for the r_{ij} interproton vector. Each term in eq. [1] represents the relative magnitude of the dipolar interaction between j and i, and is referred to as a specific relaxation pathway. Direct nuclear Overhauser effects are proportional to the relative weight of each relaxation pathway to the overall sum.

The strong inverse sixth power dependence on interproton distance implies that R_1 values and nOe enhancements can be useful for the determination of details of local structure. The method used in these studies involves detailed analysis of ^1H spin-lattice relaxation pathways based on calculation, followed by fitting to experimentally observed nonselective relaxation rates (10, 11). The interproton distances required for calculations are obtained from a structural model (e.g., crystal structure coordinates from diffraction data, molecular mechanics calculations, or Dreiding molecular models).

This approach can be understood by considering a simple example, 2-methylanisole, **1**. The conformational bias of the methoxy group in this, and related derivatives, is well characterized (1–5, 7); due to steric hindrance in 6-*trans* conformations, **A**, 6-*cis* conformations, **B**, are greatly favored. An examination of spin-lattice relaxation of the adjacent proton at C-6 was made, relative to the other ring protons. First, calculations of R_1 values were carried out for the molecule with various methoxy group conformations. If only 6-*trans* conformations were populated, the ^1H R_1 value of H-6 would be expected to be about 50% lower than the R_1 value for all other ring protons, because H-3, H-4, and H-5 all have two nearby neighbours giving significant relaxation contributions, whereas H-6 has only one. On the other hand, if only 6-*cis* conformations were populated, H-6 would have a significantly larger R_1 value than other ring protons due to the efficient relaxation pathway from the methoxyl protons, about 2.5 Å away in a standard (2) conformation.

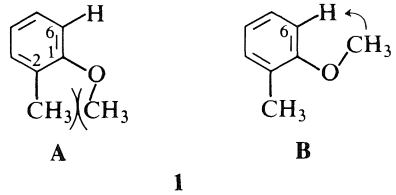

A **B**

1

The experimentally observed ^1H R_1 value of H-6 is ~50% higher than those of the other ring protons, reflecting the strong preference for conformation **B**.

Results and discussion

The conformational bias of ether functions in the cinchona alkaloids quinine, **2**, and quinidine, **3**, and in the morphine alkaloids morphine, **6**, codeine, **7**, diacetylmorphine (heroin), **8**, and thebaine, **9**, have been determined using this ^1H R_1 method. The pertinent experimental ^1H R_1 values for quinine, **2**, and quinidine, **3**, are given in Table 1, and for the morphine alkaloids morphine, **6**, codeine, **7**, thebaine, **9**, and diacetylmorphine (heroin), **8**, in Table 2. Since the calculations of R_1 values play a key role in the method demonstrated here, a brief

[1]Author to whom correspondence may be addressed.

[2]A comprehensive discussion of the ^1H R_1 values of these and other alkaloids has been presented elsewhere (10).

TABLE 1. Normalized experimental R_1 values for cinchona alkaloids[a]

H	R_1 (s^{-1})			
	2	**3**	**4**	**5**
5′	0.52 (2.56)	0.52 (2.77)	0.48 (2.39)	0.49 (2.62)
7′	0.09 (0.60)	0.09 (0.62)	0.17 (0.96)	0.16 (0.96)
8′	0.10 (0.64)	0.08 (0.59)	0.09 (0.61)	0.09 (0.60)

[a]All measurements obtained from 0.1 *M* solutions of HCl salts in DMSO-d_6 at 20°C. The observed R_1 values (s^{-1}), given in parentheses, were corrected for the contribution from dissolved oxygen, and normalized to H-5ex. Estimated precision and accuracy are ±5% and ±10%, respectively.

TABLE 2. Normalized experimental R_1 values of morphine alkaloids[a]

H	R_1 (s^{-1})			
	Morphine, **6**	Codeine, **7**	Heroin, **8**	Thebaine, **9**
1	1.00 (1.05)	1.00 (0.83)	1.00 (0.91)	1.00 (0.96)
2	0.96 (1.02)	1.00 (0.83)	0.57 (0.59)	1.10 (1.03)
5	1.90 (1.82)	2.00 (1.51)	1.80 (1.47)	0.97 (0.94)
7	0.96 (1.02)	0.99 (0.82)	0.97 (0.89)	1.50 (1.36)

[a]All values obtained from 0.1 *M* DMSO-d_6 solutions of HCl salts, except for codeine as the phosphate salt, at 20°C. The observed R_1 values (s^{-1}), given in parentheses, were corrected for the contribution from dissolved oxygen, and normalized to H-1. Estimated precision and accuracy are ±5% and ±10%, respectively.

description of the analysis of cinchona alkaloids **2** and **3** is given below.

The methoxy group in the cinchona alkaloids is located at C-6′, thus we shall examine in detail the ^{1}H R_1 values of H-5′ and H-7′, to demonstrate that they indicate conformational preferences. Initially, interproton distances were obtained by generating proton coordinates using standard geometries from published X-ray crystal structures of cinchonine (12) and quinidine (13). These calculations served as a guide to understanding the relative importance of various relaxation pathways, but contained a number of unrealistic interproton distances, due to the inaccuracies inherent in *generating* H atom coordinates. Past experiences suggested that a more reliable set of interproton distances for protons within rigid substructures (in this case, the quinoline and quinuclidine rings) could be obtained from molecular models, so a second set of calculations was carried out using standard distances measured on Dreiding models.

A third set of calculations used a slightly different comparative approach, wherein it was assumed that **4** and **5** are good models for analyzing relaxation in **2** and **3**. Relaxation pathways involving protons within the quinoline ring were calculated using interproton distances from Dreiding models for all appropriate model substructures, while pathways from outside the ring were determined from comparisons of calculated and experimental data for **2** and **3** with **4** and **5**, respectively. The "internal" and "external" calculated results for **2** and **3** were then normalized, combined, and compared to the experimental data, to determine the presence or absence of conformational bias.

We now examine the spin-lattice relaxation of specific protons in detail. H-7′, rather isolated from the rest of the molecule, is relaxed primarily by protons at the 6′ and 8′

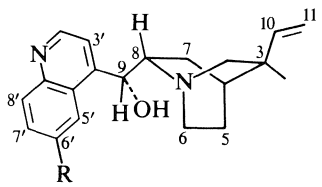

2 R = OCH_3
4 R = H

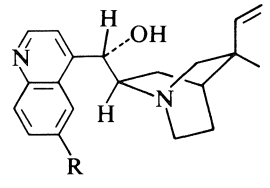

3 R = OCH_3
5 R = H

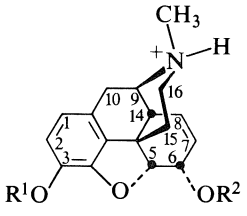

6 R^1 = R^2 = H
7 R^1 = CH_3, R^2 = H
8 R^1 = R^2 = $COCH_3$

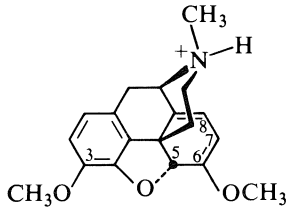

9

positions (98%, calculated) in **4** and **5**, with a much smaller contribution from the proton at 5′ (2%, calculated). R_1 values for H-7′ in **2** and **3** are expected to be substantially different from those in **4** and **5** if the methoxy group at 6′ in **2** and **3** has a large preference for either the 5′-*cis* or 7′-*cis* conformation. In the 7′-*cis* orientation, the relaxation pathway from the methoxy group to H-7′ will be very efficient, so, if only these conformations are populated, the H-7′ R_1 values should be higher (up to a maximum of 55%, calculated) than the corresponding values in **4** and **5**. Alternatively, if the 5′-*cis* orientation is greatly preferred, the H-7′ R_1 values should be lower (by as much as 45%, calculated) than those in **4** and **5**. The lower H-7′ R_1 values for **2** and **3** (Table 1) indicate a bias of the methoxy group towards H-5′.

This conclusion can also be drawn from a comparison of the H-7′ R_1 values with those of H-8′. Calculations show that H-8′ is relaxed almost exclusively (>90%) by interaction with H-7′ in all four compounds, hence its R_1 value is relatively insensitive to modifications at C-6′. In **4** and **5**, H-8′ has a substantially lower R_1 value than H-7′ because H-7′ has two near neighbours (6′ and 8′), but H-8′ has only one (H-7′), yet in **2** and **3**, the R_1 values of H-7′ and H-8′ are nearly equivalent. This indicates that the major relaxation pathway to H-7′ from the 6′ proton(s) has been lost, and, in turn, implies that the 5′-*cis* methoxy conformation is preferred.

Whereas analysis of the relaxation of H-7′ and H-8′ is relatively straightforward because these protons are relaxed via dipolar interactions with protons within the rigid quinoline ring, analysis of H-5′ relaxation is complicated by the presence of several efficient relaxation pathways to protons outside the ring that may have additional degrees of motional freedom (e.g. H-8, H-9). These "external" relaxation pathways are evident upon inspection of model structures, and are the reason for the substantially greater magnitude of the R_1 values for H-5′ (relative to the other quinoline ring protons) in all four compounds.

In **4** and **5**, the C-6′ proton contribution to H-5′ relaxation is ~20% (calculated using crystal structure coordinates). Almost all of the other contributions are from protons outside the quinoline ring. If the methoxy group at C-6′ in **2** and **3** populates only those conformations with 5′-*cis* orientation, a greater contribution from C-6′ protons is expected. Using a model with a standardized methoxyl group conformation (2) (see

Experimental for further details), an increase in the H-5′ R_1, by as much as 21%, was calculated for **2** and **3**, relative to **4** and **5**. If the methoxy group populates only 5′-*trans* orientations, then the calculations predict a *decrease* of as much as 17% in the H-5′ R_1. The larger R_1 values observed for H-5′ in **2** and **3**, relative to the 6′-H analogues (**4** and **5**, respectively), are consistent with the H-7′ data in indicating a preference for the 5′-*cis* conformation.

As a check on the results obtained by our method, the combined R_1 and nOe method (5, 9) was used to determine the presence or absence of a specific methoxy conformational preference. This involves the determination of the OCH_3 conformational bias by comparing the nOe observed at adjacent protons (in this case, H-5′ and H-7′) upon presaturation of the CH_3 protons. We emphasize that a thorough relaxation pathway analysis is a prerequisite for proper interpretation of the nOe data. The ratio of the H-5′ to the H-7′ nOe enhancements upon presaturation of the 6′-OCH_3 was calculated to be <0.03 for 7′-*cis* only, 3.5 for 5′-*cis* only, and approximately 0.44 for a 1:1 equilibrium of 5′-*cis*:7′-*cis*. The observed ratios of 3 for both **2** and **3** confirmed that a significant preference for the 5′-*cis* orientation is present in these molecules. It is of interest to note that this particular conformation is observed in the X-ray crystal structure (13).

Working in a similar manner, the conformational bias of the 3-OH in morphine, **6**, the 3-OCH_3 in codeine, **7**, and thebaine, **9**, and the 3-acetoxyl group in diacetylmorphine (heroin), **8**, have been determined. We make note here of the observation of two species in solution for several morphine alkaloids, as has been reported by others (14). Data are reported only for the major isomer, that which is observed in X-ray crystallographic studies (15–17). Since a detailed analysis has already been given for **2** and **3**, only a summary of results for **6**–**9** will be presented.

To determine 3-OH and 3-OCH_3 conformational bias in these morphine alkaloids, the relaxation pathways for H-2 were analyzed in detail, by comparing experimental and calculated R_1 values. These comparisons were made relative to the values of H-1, for which previous calculations (X-ray crystal coordinates) had shown that the ^{1}H R_1 value would be insensitive to the C-3 substituent. In morphine, calculations indicated that if only the conformation with planar 2-*cis* OH orientation were populated, then the ^{1}H R_1 value of H-2 would be 20% higher than that for H-1. If only the conformation with the planar 2-*trans* OH orientation were populated, then the ^{1}H R_1 value of H-2 would be 50% lower than that for H-1. The close similarity in the experimentally observed ^{1}H R_1 values for H-1 and H-2 indicated a small preference for the 2-*cis* orientation.

In **7** and **9**, a methoxyl group is substituted at the C-3 position. Calculations indicated that for populations of conformations with standard (2) 2-*cis* orientations, the H-2 R_1 values should be higher (to a maximum of 26%) than those for H-1, whereas for 2-*trans* orientations, the H-2 R_1 values should be lower (by as much as 52%). The observed R_1 values of H-2 (Table 2) for **7** and **9** both indicate a preference for the 2-*cis* conformation.

The same basic approach was used for detection of conformational bias of the 3-acetoxy group in heroin, **8**. The substantially slower relaxation of H-2 relative to H-1 (H-2:H-1 ratio of 0.57) indicated that the C-3 substituent relaxation pathway is greatly reduced, relative to **6**. This was also readily apparent from the normalized R_1 value of H-2 in **8**, $>\frac{1}{3}$ lower than the other morphine alkaloids.

Since an appreciable amount of motional freedom about the single bonds of the acetoxy group can be expected in solution, a detailed conformational analysis was not possible. The relaxation data do indicate that there is little or no population of conformations where the methyl group comes into close dipolar contact with the H-2 proton. In the solid state (17), the 3-(O-acetyl) group of **8** adopts a 2-*cis* orientation, but with the carbonyl oxygen in plane and facing H-2, and the methyl group turned away. Such a conformation is compatible with the ^{1}H R_1 data.

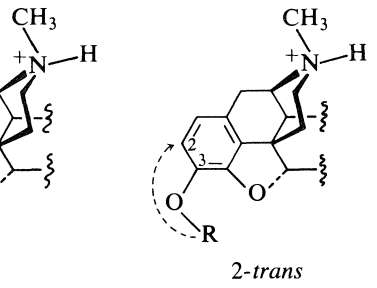

2-*cis* 2-*trans*

R = H, CH_3, acetyl

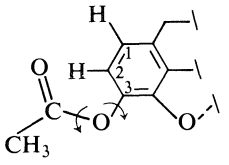

8

The conformational preference of the 6-OCH_3 group in thebaine, **9**, has also been determined. In morphine, **6**, calculations of H-5 relaxation, using X-ray coordinates, predict that the total contribution from H-6 and 6-OH is approximately 50%. A similar percentage contribution is predicted for relaxation of H-7. In **9**, the C-6 proton contributions to H-5 and H-7 relaxation are replaced by relaxation pathways to 6-OCH_3. On comparing the normalized experimental R_1 values of H-5 and H-7 in **9** to those in **6** (Table 2), a very substantial decrease in H-5 (~50%) and a significant increase in H-7 (~50%) are observed. These data can be interpreted in the following manner: in **9**, H-5 has lost nearly all contributions from the C-6 proton of the substituent, whereas H-7 has acquired a more efficient relaxation pathway from the C-6 protons. A 7-*cis* conformational bias for the 6-OCH_3 group is, therefore, clearly indicated.

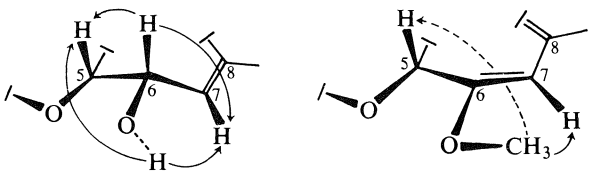

6 **9**

A preference for the *s*–*cis* conformation has been observed in several enol ethers; the conformational preference observed in **9** is consistent with the previous observations that alkyl enol ethers prefer a conformation where the alkyl group is coplanar and *syn* to the double bond (3).

Conclusions

A method for determining conformational bias of aryl and enol ethers, in a qualitative manner, has been demonstrated. It has the advantages of being simple and efficient, because all ^{1}H

R_1 values can be obtained from a single set of nonselective inversion–recovery experiments, measured under standard ^{1}H nmr conditions. A second important aspect, which adds to the appeal of this ^{1}H R_1 method, is the *a priori* focus on the analysis of the complete set of relaxation pathways. This global approach is required for unambiguous qualitative or quantitative interpretation of all relaxation data. The method described here is generally applicable for studies of conformational preferences of enol ethers, and is complementary to previously reported methods.

Experimental

All spectra were measured at 400 MHz at ambient temperature (about 20°C) using a Bruker WH-400 spectrometer at the Montreal Regional High Field NMR Laboratory. Spectra (eight transients) were acquired into 32K (standard spectra and R_1 measurements) or 16K (nOed spectra) data blocks over a spectral range of 3900 Hz. Solutions were 0.1 *M* in deuterated solvent, and were not degassed, since highly accurate experimental R_1 values were not required. All relaxation data were, however, corrected for contributions from dissolved oxygen.

The basis for the method of oxygen correction is that the contribution from dissolved oxygen to proton relaxation is nonspecific, i.e. the contribution is equivalent for all of the protons in a molecule. This has been demonstrated for molecules similar in size and type to the alkaloids used in this study (18), and for other classes of compounds (19, 20).

The correction relies on a previous determination of the "degassed" R_1 value of TMS in the specific solvent, over the temperature range of interest. R_1 (degassed) of TMS in 99.8% $CDCl_3$ over the range 291–295 K was found to be 0.075 ± 0.005 s^{-1} (0.075 ± 0.002 s^{-1} at 293 K). The correction for the oxygen contribution was determined by subtracting the known R_1 for a degassed solution from the R_1 value measured for TMS in the solution that was not degassed. A direct comparison of results obtained by this method and from degassed solutions is given in refs. 19 and 20. In general, it was found that this method was adequate for *qualitative* analysis of relaxation parameters, of the type carried out in these studies. We note that this method is very useful for R_1 measurements of small molecules where relaxation times are long and, therefore, the total time for acquisition of a degassed R_1 data set is rather considerable (6–8 h) (20).

The ^{1}H R_1 values were measured by the standard inversion–recovery technique (21). The 180° pulse length was checked at the beginning of each experiment. R_1 data were obtained using the null point method (18). The absolute accuracy of R_1 measurements is typically ±10% but, within a single experiment, the relative R_1 values can be determined to a precision of better than ±5%. The nOe enhancements were measured by the difference technique (22), as described elsewhere (11).

Interproton distances for calculations of relaxation pathways were obtained from crystal structure coordinates of cinchonine (12), quinidine (13), morphine (15), codeine (16), and heroin (17), and from Dreiding molecular models. For calculating the relaxation contributions from methoxyl groups to adjacent ring protons, it was necessary to examine results from a number of models for methoxy conformation and dynamics. The best fit to the experimental data was obtained with a model in which the dihedral angle (C—O—C) is set to ~30°C and the rotation of the methyl group is described by a three-site jump model (23) between the three equivalent conformations, with the methyl protons staggered with respect to the adjacent ring proton.

Samples used in this study were obtained from the following suppliers: Baker, quinine; BDH, codeine; F. E. Cornell, heroin, morphine; Fisher, cinchonine; Sigma, cinchonidine, quinidine; T. and H. Smith, thebaine, and were dried before use.

Acknowledgments

This work was supported by an operating grant from the Natural Sciences and Engineering Research Council of Canada (NSERC), which also supplied funding towards the purchase of the 400-MHz spectrometer. We thank the Ministry of Education, Province of Quebec, and NSERC for post-graduate fellowships (to W.J.C.). The authors are indebted to Dr. Z. Amit and Mr. F. Rogan, Centre for Studies in Behavioral Neurobiology, Concordia University, for their collaboration.

1. G. M. Anderson III, P. A. Kollman, R. M. Domelsmith, and K. N. Houk. J. Am. Chem. Soc. **101**, 2344 (1979); N. L. Owen and R. E. Hester. Spectrochim. Acta Part A, **25**, 343 (1979); D. J. Lister and N. L. Owen. J. Chem. Soc. Faraday Trans. 2, 1304 (1973); D. J. Lister. J. Mol. Struct. **68**, 33 (1980); H. Tylli and H. Konschin. J. Mol. Struct. **42**, 7 (1977); G. J. Karabatsos and D. J. Fenoglio. Top. Stereochem. **5**, 167 (1970); J. R. Larson, N. D. Epiotis, and F. Bernardi. J. Am. Chem. Soc. **100**, 5713 (1978); J. Hine and S. M. Linden. J. Org. Chem. **46**, 1635 (1981); J. D. Dunitz and P. Strickler. *In* Structural chemistry and molecular biology. *Edited by* A. Rick and N. Davidson. Freeman, London. 1968. p. 595; A. J. Pearson, E. Mincioni, M. Chandler, and P. R. Raithly. J. Chem. Soc. Perkin Trans. 1, 2774 (1980); H. Hope and A. T. Christensen. Acta Crystallogr. Sect. B, **24**, 375 (1968); M. J. Aroney, M. G. Cornfield, and R. J. W. LeFevre. J. Chem. Soc. 2954 (1964); M. J. Aroney, R. J. W. LeFevre, R. K. Pierens, and M. G. N. The. J. Chem. Soc. (B), 666 (1969).
2. N. L. Allinger, J. L. Maul, and M. J. Hickey. J. Org. Chem. **36**, 2747 (1971).
3. J. D. Mersh and J. K. M. Sanders. Tetrahedron Lett. **22**, 4029 (1981).
4. T. Schaefer, J. Peeling, and T. A. Wildman. Org. Magn. Reson. **22**, 477 (1984); T. Schaefer, T. A. Wildman, and J. Peeling. Org. Magn. Reson. **56**, 144 (1984); T. Schaefer and J. Peeling. J. Magn. Reson. **64**, 131 (1985); W. J. P. Blonski, F. E. Hruska, and T. A. Wildman. Org. Magn. Reson. **22**, 505 (1984); A. Sega, M. Ghelardoni, V. Pestellini, L. Pogliani, and G. Valensin. Org. Magn. Reson. **22**, 649 (1984); G. Valensin, L. Pogliani, M. Ghelardoni, V. Pestellini, and A. Sega. Can. J. Chem. **62**, 2131 (1984); A. Sega, E. Gaggelli, and G. Valensin. Magn. Reson. Chem. **23**, 649 (1985).
5. L. I. Kruse and J. K. Cha. J. Chem. Soc. Chem. Commun. 1329 (1982); L. I. Kruse, C. W. DeBrosse, and C. H. Kruse. J. Am. Chem. Soc. **107**, 5435 (1985).
6. T. Schaefer, R. Sebastian, and S. R. Salman. Can. J. Chem. **62**, 113 (1981); B. Capon and A. K. Siddhanta. J. Org. Chem. **49**, 255 (1984); S. E. Biali and Z. Rappoport. J. Am. Chem. Soc. **106**, 5641 (1984); P. E. Balonga, C. Vasquez, R. H. Contreras, V. J. Kowalewski, and D. G. de Kowalewski. J. Magn. Reson. **59**, 58 (1984).
7. H. A. Gaur, J. Vriend, and W. G. B. Huysmans. Tetrahedron Lett. 1999 (1969); W. M. M. J. Bovee and J. Smidt. Mol. Phys. **28**, 1617 (1974); A. Makriyannis and S. Fesik. J. Am. Chem. Soc. **104**, 6462 (1982); J. J. Knittel and A. Makriyannis. J. Med. Chem. **24**, 906 (1981); K. E. Kover and J. Borbely. Magn. Reson. Chem. **23**, 90 (1985).
8. J. H. Noggle and R. E. Schirmer. The nuclear Overhauser effect. Academic Press, New York. 1971.
9. J. D. Mersh, J. K. M. Sanders, and S. I. Matlin. J. Chem. Soc. Chem. Commun. 306 (1983); J. K. M. Sanders and J. D. Mersh. Progr. NMR Spectrosc. **15**, 353 (1982).
10. W. J. Chazin and L. D. Colebrook. J. Org. Chem. **51**, 1243 (1986).
11. W. J. Chazin, L. D. Colebrook, and J. T. Edward. Can. J. Chem. **61**, 1749 (1983).
12. B. Oleksyn, L. Lebioda, and M. Ciechanowicz-Rutkowska. Acta Crystallogr. Sect. B, **35**, 440 (1979).
13. R. Doherty, N. R. Benson, M. Maienthal, and J. Stewart. J. Pharm. Sci. **76**, 1698 (1978).
14. J. A. Glasel. Biochem. Res. Commun. **102**, 703 (1981); J. G.

HEXEM, M. H. FREY, and S. J. OPELLA. J. Am. Chem. Soc. **105**, 5717 (1983); C. E. BROWN, S. C. ROERIG, J. M. FUJIMOTO, and V. T. BURGER. J. Chem. Soc. Chem. Commun. 1506 (1983); E. L. ELIEL, S. MORRIS-NATSCHKE, and V. M. KOLB. Org. Magn. Reson. **22**, 258 (1984).
15. L. GYLBERT. Acta Crystallogr. Sect. B, **29**, 1630 (1973).
16. G. KARTHA, F. R. AHMED, and W. H. BARNES. Acta Crystallogr. **15**, 326 (1962).
17. D. CANFIELD, J. BARRICK, and B. C. GIESSEN. Acta Crystallogr. Sect. B, **35**, 2806 (1979); **37**, 1800 (1981).
18. L. D. COLEBROOK and L. D. HALL. Can. J. Chem. **58**, 2016 (1980).
19. W. J. CHAZIN and L. D. COLEBROOK. Magn. Reson. Chem. **23**, 597 (1985).
20. W. J. CHAZIN and L. D. COLEBROOK. 23rd ENC, Madison, Wisc. 1981; W. J. CHAZIN. Ph.D. Thesis, Concordia University, Montreal. 1983.
21. R. L. VOLD, J. S. WAUGH, M. P. KLEIN, and D. E. PHELPS. J. Chem. Phys. **48**, 3831 (1968).
22. L. D. HALL and J. K. M. SANDERS. J. Am. Chem. Soc. **102**, 5703 (1980).
23. D. E. WOESSNER and B. S. SNOWDEN, JR. Adv. Mol. Relaxation Processes, **3**, 181 (1972).

An INDO investigation of the bonding modes occurring in five-membered heterocyclic thiones

GEORGE KAPSOMENOS AND PERICLES AKRIVOS

Department of Chemistry, Aristotelian University of Thessaloniki, P.O.B. 125, GR-540 06, Thessaloniki, Greece

Received January 28, 1986

GEORGE KAPSOMENOS and PERICLES AKRIVOS. Can. J. Chem. **64**, 2225 (1986).

A group of five-membered heterocyclic thioketo-compounds is studied by using results derived from the semi-empirical INDO method. The interest of these compounds from a theoretical point of view is the simultaneous presence of both sulfur and nitrogen in active positions so that a diversity of bonding schemes with metal ions could be encountered. The prediction of these coordination aspects are here explained quite satisfactorily by means of the computed HOMO eigenvalues of the ligands and by application of the energy-based HSAB criterion. This criterion is applied in cases where the coordination is not strongly pH dependent and the appropriate ligand form is considered. The straightforward derivation of the conclusions allows predictions of the bonding subtleties to be made in cases where experimental data are lacking or insufficient for clear conclusions.

GEORGE KAPSOMENOS et PERICLES AKRIVOS. Can. J. Chem. **64**, 2225 (1986).

On étudie toute une série de composés heterocycliques pentatomiques contenant un groupe latéral thionique par la méthode semi-empirique de calcul INDO. L'intérêt de ces composés du point de vue théorique consiste à la présence simultanée d'atomes de soufre et d'azote en positions actives, ce qui entraîne la possibilité de différents modes de coordination. Cet effet est expliqué ici d'une façon satisfaisante au moyen de valeurs propres HOMO des ligands et par l'application du critère énergétique HSAB. Ce critère peut être appliqué dans le cas ou la coordination n'est pas fortement dépendante du pH et quand le ligand approprié est considéré. La dérivation directe des conclusions donne le moyen par lequel on peut faire des prédictions pour la préférence de positions d'attaque dans le cas où les données expérimentales sont absentes ou insuffisantes pour soutenir des conclusions solides.

Introduction

Heterocyclic keto and thioketo compounds have attracted much interest in the past and have been the subject of numerous investigations covering practically every area of applied spectroscopy. Such compounds possess active sites closely resembling those of uracil, lumazine, and the flavins, this similarity challenging experimentalists to investigate their spectroscopic and redox properties in detail (1). These studies have been mainly based on the perspective of studying reactions of biological interest on small model compounds. Five-membered heterocyclic thiones form a subseries of the above-mentioned series of compounds. The combination of a thioketo group and an heteroatom, mainly N, O, or S, in the α-position results in considerable coordination ability. Thus, pentatomic heterocyclic thione coordination chemistry has been extensively studied and the main investigations of this field have appeared recently in an interesting review article (2).

In the present study we investigate the degree of electron delocalization from the thioketo group toward the α-heteroatoms in pentatomic thiones in which one α-atom is nitrogen and the other is nitrogen, oxygen, or sulfur. The effect of the hetero-atom occupying the 1-position and the influence of the C—C bond in the ring have been investigated. Both saturated and unsaturated systems have been considered, the series of compounds studied being completed by the benzo-analogues. The three classes under study are presented in Fig. 1.

Computational details

In the solid state the thione form of the compounds studied is the dominant one as has been experimentally verified. However, the tendency of π- and total electron population to diffuse toward the α-heteroatoms should be evident even if we base our considerations on the uncoordinated ligand geometry. Thus we use as sources of geometry data the references presenting X-ray results for a number of the studied compounds (3–6). The phenyl rings in the benzo-derivatives, while slightly distorted, were assumed to be strictly planar, while the C—C

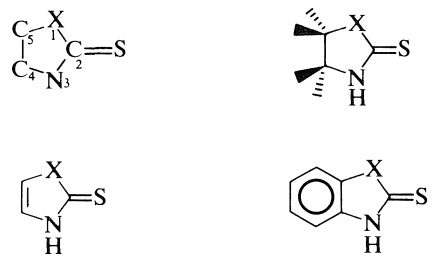

FIG. 1. The five-membered ring numbering and the three types of thione ligands considered within each class, possessing a single (*a*), double (*b*), or aromatic (*c*) C_4—C_5 bond. X stands for NH (class 1), S (class 2), or O (class 3).

bond distances in the pentatomic ring were modified when necessary in order to account for a single, double, or aromatic bond according to the molecule considered. We did not attempt to alter simultaneously the C=S bond length. In the case of saturated carbon atoms, a strict tetrahedral environment was assumed around them, the C—H bond distance set equal to 1.05 Å. In each case the pentatomic ring is placed in the *xy* plane while the C=S bond is along the *x* axis. The calculations were carried out by the semi-empirical INDO approximation (7), using the GEOMO program (8) with the appropriate corrections already proposed (9). A similar series of calculations have also been performed using the CNDO/2 option of the program. These results did not deviate significantly from the INDO ones as far as the MO's symmetry, ordering and atomic participation is considered, though changes up to 10% resulted in the corresponding energy eigenvalues. Thus the results presented and discussed herein emerged from INDO type calculations.

Discussion

Experimentation of varying degree has been carried out on the ligands considered, the most general conclusion drawn being the proposed bonding scheme toward metal centres and its verification by spectroscopic and in a few cases by X-ray

diffraction results. We therefore focus our interest on the determination of the site bonding effects that are important in the formation of the coordination compounds. The energy and constitution of a set of frontier molecular orbitals and a few reactivity indices derived from the Fock–Dirac density matrix are used to describe the donor–acceptor properties of the ligands considered. A common computational feature of the three classes of heterocyclic thiones examined must be noted here, since in all our calculations $3d$ functions for sulfur atoms are present in the basis set. This allows the importance of electron promotion from sulfur $3s$ and $3p$ orbitals toward $3d$ orbitals to be probed. The phenomenon is most clearly shown in the case of heterocyclic sulfur containing ligands (class 2), on the sulfur heteroatom. In this case the d-functions "are forced" to take part in the linear combination of atomic functions that produce the best-fit hybrid orbitals which overlap with the neighbouring atomic centres hybrids.

Since no geometry optimization has been carried out in those cases where structural data were not available, one does not hope to detect any significant change on going from the saturated through the unsaturated to the aromatic analogue in each class of thiones. Minor changes on level ordering and detectable energy differences do of course occur, and these are discussed presently for each group of compounds. One point of attention is that the conclusions drawn can not, without consideration, be valid in the case where the ligands form coordination compounds in strongly acidic or alkaline media or in the presence of strong reducing or oxidizing agents. It is obvious that since the protonated or deprotonated forms of the α-imidothiones have not been dealt with we are only discussing those cases where the complexes have been formed in neutral pH or non-polar solvents.

Within the above-mentioned limitations, both S- and N- or even simultaneous S- and N-donation have been detected toward metal ion coordination spheres. Our purpose is to deal with these bonding schemes by means of an HSAB (Hard and Soft Acids and Bases) treatment (10), considering the relative "softness" of the thione molecules as expressed by their frontier molecular orbital energies. Though it is not easy to draw a borderline between hard and soft metal ions, especially when other ligands occupying different sites in the coordination sphere perturb the initial "hard" or "soft" metal ion character, it is apparent that the lower the HOMO energy of the thione ligand, the more easily hard metals will react toward the α-nitrogen atom. In a similar way, as the ligand HOMO energy increases more metals will prefer to predominantly attack the sulfur site. According to the existing literature (2), no N-coordination has yet been reported for the soft metals of the third transition series, while S-donation has been established by X-ray data for the hard cations belonging to the first row. Intermediate bonding involving both S- and N-sites simultaneously is expected for the second transition series, the former playing the dominant role.

Class 1. Nitrogen-containing thiones

These belong to the most widely studied class of those discussed. Complexes with the most usual coordination numbers (4 and 6) have been reported (2) with practically every transition metal.

The HOMO eigenvalues of the three members of the series range from −0.3161 au for imidazoline-2-thione to −0.3477 au for imidazolidine-2-thione (au = Hartree). These values are high enough so as to classify the three ligands as soft donors. So far only sporadic cases are reported where N-donation

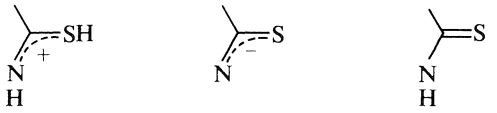

FIG. 2. The protonated (*a*), deprotonated (*b*), and neutral (*c*) forms of the thiones, occurring in acidic, alkaline, and neutral solutions respectively.

accompanies the well-established sulfur coordination and this only for **1***a*, which possesses the lowest HOMO eigenvalue. Crystal structure determinations and X-ray PES data confirm the above statement (11, 12). For the other two members there exists practically no evidence for N-participation in the metal coordination sphere. Besides the HOMO constitution presented in Table 1, which implies that S-donation is favoured, the virtual orbitals available for π-back bonding practically rule out every other possible coordination scheme as they are local to the C═S bond. The LUMO is not the appropriate MO for back donation as it is mainly localized on the carbon double bond or the aromatic ring when present, while for imidazolidine-2-thione it is distributed all over the five-membered ring. We have therefore to look further up (see Table 1) toward the next LUMOs for the appropriate MOs to take part in the π-back donation from the metal.

Class 2. Nitrogen- and sulfur-containing thiones

The degree of the exocyclic sulfur atom participation in the HOMOs of this group is significant though not as important as that occurring in class 1 members. Considerable contribution from the heterocyclic sulfur atom is present in both frontier MOs but this is partly due to the incorporation of d-orbitals in the basis set, that has been already discussed.

The computed HOMO eigenvalues range from −0.3373 au to −0.3634 au, the lower one corresponding to the saturated member (**2***a*) in analogy to the observation in class 1. The relative low HOMO eigenvalues imply that these compounds approach or even cross the borderline between soft and hard thiones and they are therefore expected to express a slight preference for N-participation in the coordination scheme they adopt. Naturally for thiazolidine-2-thione numerous cases are mentioned where coordination occurs mainly through nitrogen, though initial sulfur "attack" has been proposed in many cases. Sulfur donation has been confirmed in the crystal structure of $PdCl_2$(1,3-thiazolidine-2-thione)$_2$ (13), in accordance with the HSAB rule and our proposition is that, though certainly "harder" than the other members of this class, the saturated one must not be classified as "definitely" hard.

A few examples of coordination through nitrogen for **2***b* and **2***c* that are softer than the above-mentioned saturated ligand, should not be regarded as exceptions to the HSAB rule but have to be understood as the result of hydrogen migration from the nitrogen atom to the thione sulfur. Such a transfer has been assumed to take place either prior to or even after the initial coordination (14). Computational work has already been performed on analogous systems, namely the cyclic form of the CHS_2N_3 acid where the thiol-structure has been found to be more stable than its thione tautomer (15), but only by 2.4 kcal/mol, implying that both forms co-exist in solution.

Thiazoline-2-thione closely resembles its class 1 analogue since it is found to act as a sulfur-donating ligand in most of the few complexes reported. On the basis of our results we must express some scepticism about the proposition (16) that nitrogen coordination occurs in a complex with the formula $CdCl_2$(1,3-thiazoline-2-thione)$_2$. We tend to believe that in this case a four-membered ring is more likely to be formed involving

TABLE 1. Energy and constitution of the HOMO and NLUMO orbitals of the compounds studied*

	Value					
	1a		*1b*		*1c*	
Parameter	HOMO	NNLUMO	HOMO	NLUMO	HOMO	NNLUMO
Energy	−0.3477	0.1347	−0.3161	0.1365	−0.3273	0.1404
S%	85.89	31.34	80.11	24.67	79.38	33.16
C%	1.71	17.11	0.16	35.73	0.79	15.76
N%	5.04	20.44	6.73	13.02	6.23	16.49
X%	4.98	2.23	5.59	14.50	5.83	6.15

	Value					
	2a		*2b*		*2c*	
Parameter	HOMO	LUMO	HOMO	LUMO	HOMO	LUMO
Energy	−0.3634	0.0309	−0.3415	0.0236	−0.3373	0.0343
S%	70.36	33.19	55.40	32.90	54.71	34.51
C%	3.41	28.26	0.90	28.42	1.42	28.68
N%	10.00	12.15	10.10	8.58	10.89	9.02
X%	14.43	24.11	23.61	25.70	21.30	31.44

	Value					
	3a		*3b*		*3c*	
Parameter	HOMO	NLUMO	HOMO	NLUMO	HOMO	NLUMO
Energy	−0.3688	0.1387	−0.3543	0.1331	−0.3572	0.1378
S%	75.77	71.51	64.47	69.94	64.20	72.19
C%	0.02	16.67	0.91	17.21	1.79	16.91
N%	5.24	2.75	13.93	2.47	14.02	2.90
X%	5.63	3.98	8.43	2.53	7.41	2.09

*Energy values in au; X stands for the heteroatom at the 1-position.

TABLE 2. Net atomic charges and the calculated values of the HOMO superdelocalizability and local anisotropy indices*

	Value								
Parameter	*1a*	*1b*	*1c*	*2a*	*2b*	*2c*	*3a*	*3b*	*3c*
Q_S	−0.521	−0.571	−0.546	−0.365	−0.361	−0.367	−0.427	−0.436	−0.431
Q_C	0.366	0.318	0.350	0.222	0.191	0.204	0.387	0.362	0.374
Q_N	−0.221	−0.153	−0.199	−0.066	−0.063	−0.104	−0.195	−0.115	−0.164
Q_X	−0.099	−0.064	−0.107	−0.104	−0.065	−0.127	−0.249	−0.177	−0.225
$S_{HOMO}(S)$	−2.4703	−2.5343	−2.4253	−1.9362	−1.6223	−1.6217	−2.0545	−1.8196	−1.7973
$S_{HOMO}(N)$	−0.1450	−0.2129	−0.1904	−0.2752	−0.2958	−0.3232	−0.1420	−0.3932	−0.3919
ΔS_{HOMO}	−2.3253	−2.3214	−2.2349	−1.6610	−1.3265	−1.2985	−1.9125	−1.4264	−1.4054
L_S	1.317	1.336	1.240	1.183	1.172	1.170	1.219	1.222	1.216
L_N	0.318	0.220	0.282	0.201	0.141	0.159	0.214	0.142	0.164
L_X	0.228	0.140	0.190	1.256	1.142	1.128	0.502	0.430	0.438

*The quantity ΔS_{HOMO} represents the difference of the two individual S_{HOMO} values tabulated for each compound. The compounds are numbered according to the notation used in Fig. 1 and X stands for the heteroatom at the 1-position.

simultaneous sulfur and nitrogen coordination, but the available experimental data are not sufficient for a further discussion.

As for benzothiazoline-2-thione, the corresponding anion has received much more attention than the neutral ligand. The pK_a value of the compound and the less pronounced contribution of thione sulfur to the frontier MOs with respect to the other members of the class, leads us to suggest that hydrogen migration to the thione sulfur is facilitated, giving rise to the thiol-form. The experimentally confirmed observation that even in neutral media nitrogen coordination occurs (17) must therefore be understood on the basis of the above arguments.

Class 3. Nitrogen- and oxygen-containing thiones

The degree of thione sulfur participation in the HOMOs of this class is intermediate between the previous two groups (Table 2). The saturated compound is again predicted to be the

hardest of the class, while every specific member is harder than its class 1 and 2 analogues.

As for **3***c*, with a pK_a value of 6.58 it is easily converted to the corresponding anion and acts therefore as a nitrogen donor even in neutral media. Thus no firm conclusion can be drawn on its bonding ability as a neutral ligand. However, on the basis of its HOMO eigenvalue one could assume that N-coordination will predominantly occur when the ligand is present in complexes in its neutral form.

Oxazolidine-2-thione is predicted to be the hardest of all the studied ligands, and is for this reason, expected to coordinate via the imido-nitrogen. Unfortunately the conclusions drawn from the few studies of its coordination compounds are not so firm as to establish either sulfur or nitrogen or intermediate mode of bonding (18).

Lack of experimental data on oxazoline-2-thione allows us to make predictions only and hope to see them tested by experimentalists. On the grounds of the INDO calculations performed and on the arguments presented at the beginning of the discussion, we may assume that this ligand will act in a way quite similar to its benzo-analogue. It is thus expected to be readily converted to its anionic form in solution, giving rise to a through-nitrogen bonding scheme. Even as a neutral ligand, hydrogen migration must be favourable enough to lead to the tautomer form which would provide both nitrogen and sulfur sites for metal chelation. Our prediction therefore is that regarding first row transition elements, both sulfur- and nitrogen-donating must be expected, while sulfur coordination must be the dominant bonding scheme with soft metals such as Pd, Pt, Au, Hg etc.

Reactivity indices

Several sets of indices derived from the density matrix have been proposed in the literature (19–21) to act as reactivity representatives when using semi-empirical methods of calculation, such as

$$B_{AA}^{tot} = \Sigma P_{\mu\nu}^2 \qquad |\ \mu, \nu \text{ on A}$$

$$L_A = \sum\sum P_{\mu\nu}^2 - \sum_{l=0}\left(\sum_{\mu=l^2+1}^{\nu=(l+1)^2} P_{\mu\mu}\right)^2 \frac{1}{2l+1} \qquad |\ \mu, \nu \text{ on A}$$

$$S_E(A) = 2\sum_{j=1}^{occ}\sum_{m=1}^{N_A}\frac{(C_{mj}^A)^2}{\epsilon_j} \qquad |\ N_A \text{ number of AOs on A}$$

Here the symbols have their usual meaning, μ,ν running over all AOs and i,j over all occupied (for S_E) or virtual MOs (for S_N). Though such static indices are not universally accepted, we tried during this study to use their values for predictive purposes in comparison with directly derived quantities (HOMO eigenvalues and atomic participation). One of them, the superdelocalizability index is probably the most interesting one proposed so far since it succeeds in relating site occupancy with energy. From this, cancelling the summation over all occupied MOs, a certain MO superdelocalizability can be defined. Our goal is to obtain in this way a quantity related to the electron donor–acceptor properties of similar sites in different molecules. The HOMO resident fraction of the original S_E (21) which we indicate as $S_{HOMO}(A)$, is computed for both imido-nitrogen and exocyclic sulfur atoms and presented in Table 2. The difference of the two values also listed in the table is quite interesting as it succeeds in relating the sulfur-preferred bonding ability of the three groups of thiones to the electron-withdrawing ability of the heteroatom (N, O, S) at the 1-position of the ring. The more electron withdrawing the heteroatom is, the more nitrogen coordination is gaining importance relative to the existing sulfur donation.

Of the other indices known, B_{AA}^{tot} has been found to vary as the total charge on each atom and is therefore not listed in our table.

The local anisotropy L_A, which represents the deviation from an ideal spherical distribution of the electrons around each centre, is also computed and presented in the table. The values of this index indicate that the heterocyclic sulfur atom in the members of class 2 competes strongly with the thione sulfur in coordinating the metal. We believe therefore, that, in such a case, this index is misleading so that it has to be eventually replaced by a more appropriate one, like the free valence (22) or the net electron population of each atom.

Acknowledgment

The authors wish to express their thanks to a referee for his useful comments and suggestions on the manuscript.

1. L. Sestili, C. Cauletti, and C. Furlani. Inorg. Chim. Acta, **102**, 55 (1985).
2. E. S. Raper. Coord. Chem. Rev. **61**, 115 (1985) and references therein.
3. J. P. Chesick and J. Donohue. Acta Crystallogr. **27B**, 1441 (1971).
4. P. Groth, K. Davidkov, and D. Simov. Acta Chem. Scand. **26**, 1931 (1972).
5. E. S. Raper, R. E. Oughtred, and I. W. Nowell. Inorg. Chim. Acta, **77**, L89 (1983).
6. E. S. Raper, A. R. W. Jackson, and D. J. Gardiner. Inorg. Chim. Acta, **84**, L1 (1984).
7. J. A. Pople and D. L. Beveridge. Approximate molecular orbital theory. McGraw-Hill, New York. 1970.
8. QCPE program No 290, Indiana University, Bloomington Indiana.
9. I. Mayer and M. Révész. Comput. Chem. **6**, 155 (1982).
10. R. G. Pearson. J. Am. Chem. Soc. **85**, 3533 (1963).
11. E. M. Holt, S. L. Holt, and K. J. Watson. J. Am. Chem. Soc. **92**, 2721 (1970).
12. F. A. Devillanova, C. Furlani, G. Mattogno, G. Verani, and R. Zaconi. Gazz. Chim. Ital. **110**, 19 (1980).
13. M. Fabiak and T. Glowiak. Acta Crystallogr. **38B**, 2031 (1982).
14. J. Dehand and J. Jordanov. Inorg. Chim. Acta, **17**, 37 (1976).
15. M. Conti, D. W. Franco, and M. Trsic. Inorg. Chim. Acta, **113**, 71 (1986).
16. K. Geertharani and D. N. Sathyanarayana. Indian J. Chem. **14A**, 925 (1976).
17. R. F. Wilson and P. Merchant. J. Inorg. Nucl. Chem. **29**, 1993 (1967).
18. (*a*) C. Preti and G. Tosi. Can. J. Chem. **54**, 85 (1976); (*b*) **55**, 1409 (1977).
19. D. R. Armstrong, P. G. Perkins, and J. P. Stewart. J. Chem. Soc. Dalton, 836 (1972).
20. M. I. Bán, I. Balint, M. Révész, and M. T. Beck. Inorg. Chim. Acta, **57**, 119 (1982).
21. R. A. Brown and A. M. Simas. Theoret. Chim. Acta, **62**, 1 (1982).
22. I. Mayer. Chem. Phys. Lett. **97**, 270 (1983).

Light-promoted catalysis of nickel hydride complexes in the isomerization and hydrogenation of *cis,cis*-1,5-cyclooctadiene: mechanistic studies

YUAN L. CHOW[1] AND HUALI LI[2]

Department of Chemistry, Simon Fraser University, Burnaby, B.C., Canada V5A 1S6

Received May 30, 1986

YUAN L. CHOW and HUALI LI. Can. J. Chem. **64**, 2229 (1986).

Xanthone-sensitized photoreduction of $Ni(acac)_2$ in benzene under hydrogen, in the presence of *cis,cis*-1,5-cyclooctadiene (1,5-COD), causes isomerization and hydrogenation of the diene according to the consecutive transformation 1,5-COD → 1,4-COD → 1,3-COD → cyclooctene → cyclooctane. Evidence was provided that (*i*) a nickel hydride complex was generated, (*ii*) the sensitized excitation of this complex caused addition to the double bond, (*iii*) subsequent elimination caused isomerization, and (*iv*) triplet excited xanthone sensitized the transformations.

YUAN L. CHOW et HUALI LI. Can. J. Chem. **64**, 2229 (1986).

La photoréduction du $Ni(acac)_2$, sensibilisée par la xanthone du $Ni(acac)_2$ et effectuée dans le benzène, sous un atmosphère d'hydrogène et en présence de cyclooctadiène-1-*cis*,5-*cis* (COD-1,5), conduit à une isomérisation et une hydrogénation du diène impliquant la série de transformations suivantes : COD-1,5 → COD-1,4 → COD-1,3 → cyclooctène → cyclooctane. On a obtenu des indications à l'effet que (*i*) il y a génération d'un complexe d'hydrure de nickel; (*ii*) l'excitation sensibilisée de ce complexe est la cause de l'addition à la double liaison; (*iii*) l'élimination subséquente est la cause de l'isomérisation et (*iv*) la xanthone excitée au niveau triplet sensibilise les transformations.

[Traduit par la revue]

Nickel hydride complexes are good homogeneous catalysts (1–5) for isomerization (6–8), oligomerization (9–11), and hydrogenation (12, 13) of olefins under moderate pressures and temperatures. The mechanism of isomerization and hydrogenation by these and other (14–17) transition metal complexes has been generally interpreted in terms of reversible addition of a metal hydride to coordinated olefins. Examples of light-promoted hydrogenation of olefins catalysed by other metal complexes are known (2, 4, 5). We wish to report (*i*) the generation of the transient Ni(I) complex by aromatic ketone sensitized photoreduction of bis(acetylacetonato)nickel(II), $Ni(acac)_2$, using hydrogen as a H-atom donor, (*ii*) the interaction of hydrogen with the transient complex to form a nickel hydride complex in the dark, and (*iii*) *in situ* utilization of the Ni—H complex in light-promoted catalytic isomerization and hydrogenation of *cis,cis*-1,5-cyclooctadiene (1,5-COD). The whole reaction is carried out at room temperature and atmospheric pressure in one operation. While this system is not necessarily the most efficient reaction it is an ideal one for mechanistic studies. The details of the pathway are summarized in Scheme 1, where Ni—H represents a hydride complex of an unknown structure. The pertinent evidence in support of the mechanistic proposal is discussed below.

Xanthone-sensitized photoreduction of $Ni(acac)_2$ has been demonstrated to generate coordinatively unsaturated Ni(acac) and acetylacetonyl radicals (18). The latter is trapped by H-atom donors (e.g., methanol used as solvent) to give acetylacetone.[3]

$$Ni(acac)_2 + H_2 \xrightarrow[C_6H_6]{h\nu,\ \text{xanthone}} Ni(acac)L_x + acacH$$

$$\xrightarrow{H_2} \text{H—Ni complexes} \quad L = 1,5\text{-COD, THF}$$

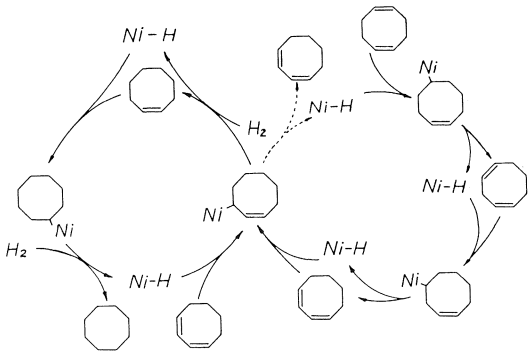

SCHEME 1

It is now shown that the same photoreduction occurs in benzene (or THF) under hydrogen which acts as a H-atom donor (Scheme 1). In THF, in the presence of 1,5-COD under nitrogen, the esr signal (6, 18) of $Ni(acac)L_x$ (*g*-value 2.183, ΔH_{pp} 25 G) was generated in a brief irradiation and decayed in the dark with double exponential decays of a fast second order reaction, $k_2 = (1.07 \pm 0.15) \times 10^{-2}$ unit^{-1} s^{-1}, followed by a slow first order reaction, $k_1 = (1.32 \pm 0.09) \times 10^{-2}$ s^{-1}. Similar esr signals generated *under hydrogen* also decayed with double exponential decays, but the slow pseudo-first order rate constant (k_1) decreased as hydrogen concentrations were reduced (Fig. 1): the fast second order rate constants, $k_2 = (1.10 \pm 0.13) \times 10^{-2}$ unit^{-1} s^{-1}, were very similar to those obtained under nitrogen. The kinetic pattern in Fig. 1 shows that the Ni(I) complex, assumed to be $Ni(acac)(THF)_x$, does react with hydrogen. The yellow photolysate under these conditions exhibited a singlet in the ^{1}H nmr spectrum at −15.7 ppm,

[1]Author to whom correspondence may be addressed.

[2]On study leave from Shanghai Institute of Organic Chemistry, People's Republic of China.

[3]Appropriate solution placed in a Quartz tube was saturated with hydrogen or nitrogen and sealed. The tube was irradiated in the cavity of a Varian E-4 spectrometer with >314 nm light. The conditions of esr spectroscopy and irradiation are described (19). At intervals the light passage was blocked and the decay was followed at the peak of the Ni(I) signal (18). As the net irradiation time accumulated, hydrogen was consumed to give lower concentration.

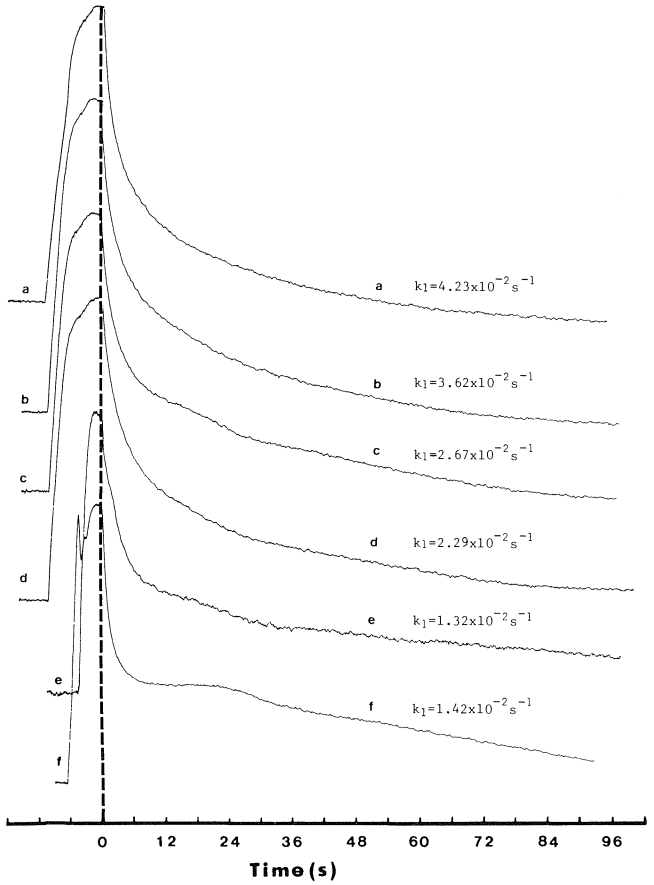

FIG. 1. Decay profiles of the Ni(I) complex, under hydrogen (*a–e*) and nitrogen (*f*), generated by photolysis of a sealed tube containing $Ni(acac)_2$ (1×10^{-2} *M*), xanthone (1.3×10^{-2} *M*), and 1,5-COD (6×10^{-2} *M*) in THF. Curves *a–e* were decays in the presence of hydrogen recorded after the net irradiation time of 10, 10, 10, 20, and 300 s; curve *f* was an example of decays under nitrogen (see ref. 19 for experimental conditions).

which was assigned to Ni—H (11) of the unknown complex[4] tentatively represented as a Ni—H complex which is sensitive to the air and has not been isolated.

Xanthone-sensitized photoreduction of $Ni(acac)_2$ under H_2 purging in benzene and in the presence of 1,5-COD caused isomerization of the diene to 1,4-COD and 1,3-COD, and hydrogenation to cyclooctene (COE) and cyclooctane (COA). These transformations are presumably catalyzed by nickel hydride complex. Since the composition of the products ceases to change in the dark (Fig. 2),[5] light energy is required for photoexcitation of xanthone which, in turn, induces the transformations (*vide infra*). Addition of xanthone to the olefins also occurs slowly to give the corresponding oxetanes as an

[4]The structures of η^1,η^2-cyclooctenyl(β-diketonato)nickel(II) complexes are well established and, together with H—Ni(acac), have been suggested as the intermediates in olefin oligomerization (9–11). We are not able to establish these species as intermediates in the present experiments.

[5]In a typical experiment, a benzene solution (50 mL) containing $Ni(ACAC)_2$ (5×10^{-3} *M*), xanthone (1×10^{-2}), and 1,5-COD (1×10^{-7} *M*) was irradiated through a Pyrex filter under a slow stream of hydrogen (1 bubble per second) with a Hanovia Medium Pressure mercury lamp (200 W). At intervals a sample of the photolysate was worked up and the organic products were analyzed by gc. When a Pyrex filter was replced by a GWV filter (cut off <380 nm) the variation of product yields also ceased.

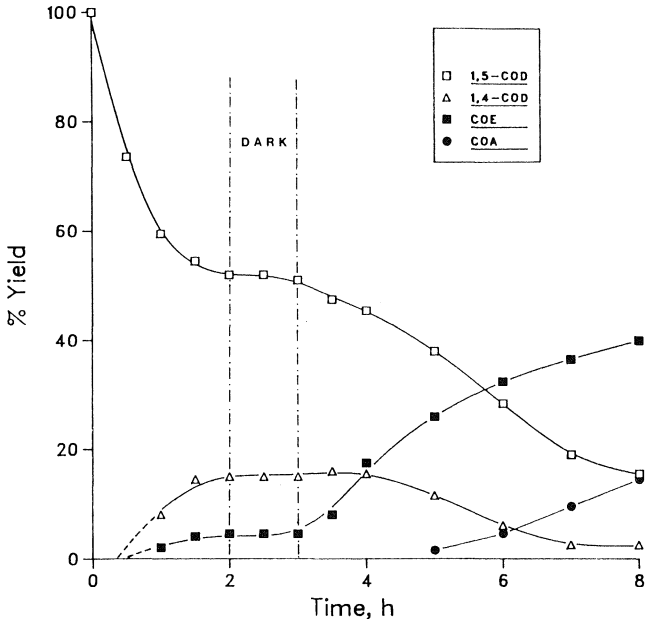

FIG. 2. The variation of C-8 hydrocarbon yields in irradiation at room temperature of a benzene solution containing $Ni(acac)_2$ (5.6×10^{-3} *M*), xanthone (8.3×10^{-3} *M*), and 1,5-COD (4.4×10^{-2} *M*) through a Pyrex filter under hydrogen purging; irradiation was interrupted in the 1.5–3 h period.

undesirable side reaction. The details of the photoprocesses remain to be investigated further.

The profiles of the product variations (Fig. 2) obviously indicate the sequential formation of 1,5-COD → 1,4-COD → COE → COA, on the basis of the consecutive appearance of the products as photolysis proceeds. That 1,3-COD was a part of the reaction sequence was demonstrated by subjecting 1,4-COD to similar reactions conditions to generate 1,3-COD in 3.1% in 15 min and <1% yields thereafter. The rapid hydrogenation of 1,3-COD → COE was also demonstrated by the addition of *a small amount* of 1,3-COD (2 m*M*) to a pre-photolyzed mixture of 1,5-COD, whereby, on continued irradiation, 1,3-COD quickly diminished to insignificant percentages and COE increased equally rapidly. Both observations indicate that the interaction of 1,3-COD with the Ni—H complex and the subsequent hydrogenation were much faster than other comparable processes. However, 1,3-COD added in a large concentration (≈10 m*M*) efficiently quenched triplet excited xanthone by energy transfer and was isomerized to *cis,trans*-1,3-COD (22); the changes in the yields of other products also stopped concurrently. This observation shows that triplet excited xanthone sensitizes the nickel–hydride complex causing addition to the double bonds of the olefins (*vide supra*).

Light-promoted transformations of 1,5-COD under D_2 gave partially deuterated products as determined by gc–ms: 1,5-COD-d_0, 100%; 1,4-COD-d_0, 43.5%; $-d_1$, 56.5%; COE-d_0, <2%; $-d_1$, 10%; $-d_2$, 45%; $-d_3$, 28%; $-d_4$, 14%; d_5, <1%; COA-d_2, <2%; $-d_3$, 23%; $-d_4$, 45%; $-d_5$, 30%; $-d_6$, 0%. The high deuterium incorporation in the products further along in the reaction sequence suggests that the isomerization pathway is addition–elimination. The recovery of undeuterated 1,5-COD indicates that either the elimination step is regiospecific to give 1,4-COD, or, addition of Ni—H to

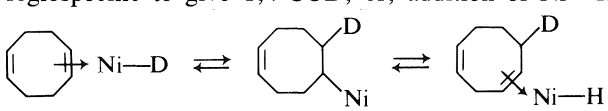

1,5-COD and the subsequent reverse elimination to give 1,5-COD are both stereospecific. In the reaction, acetylacetone-d_1 (100% purity) was also identified, thereby unambiguously showing that hydrogen is the H-atom donor to the acetylacetonyl radical.

Acknowledgement

The authors thank the Natural Sciences and Engineering Research Council of Canada for generous financial support of this project.

1. G. W. PARSHALL. Homogeneous catalysis. Wiley-Interscience, New York. 1980. Chapt. 3.
2. B. R. JAMES. (*a*) Adv. Organomet. Chem. **17**, 319 (1979); (*b*) Compr. Organomet. Chem. **8**, 285 (1982).
3. P. W. JOLLY and G. WILKE. The organic chemistry of nickel. Vol. II. Academic Press, New York. 1975. Chapt. 1.
4. R. G. SOLOMON. Tetrahedron, **39**, 575 (1983).
5. L. MAGGI, A. JURIS, D. SANDRINI, and M. F. MANFRIN. Rev. Chem. Interm. **4**, 171 (1981).
6. M. J. D'ANIELLO, JR. and E. K. BARFIELD. J. Am. Chem. Soc. **100**, 1474 (1978).
7. H. KANI, K. KUSHI, K. SAKANOUE, and N. KISHIMOTO. Bull. Chem. Soc. Jpn. **53**, 2711 (1980).
8. H. TAKAYA, T. SUZUKI, Y. KUMAGAI, M. YAMAKAWA, and R. NOYORI. J. Org. Chem. **46**, 2846 (1981).
9. B. BOGDANOVIC, M. KRÖNER, and G. WILKE. Liebigs Ann. **699**, 1 (1966).
10. W. KEIM, B. HOFFMANN, R. LODEWICK, M. PEUCKERT, G. SCHMITT, J. FLEISCHHAUER, and U. MEIER. J. Mol. Catal. **6**, 79 (1979).
11. W. KEIM, A. BEHR, and G. KRAUS. J. Organomet. Chem. **251**, 377 (1983).
12. H. ITATANI, and J. C. BAILAR, JR. Ind. Eng. Chem. Prod. Res. Develop. **11**, 146 (1972).
13. L. W. GOSSER and G. W. PARSHALL. Tetrahedron Lett. 2555 (1971).
14. F. PINNA, G. STRUKUL, R. PASSERINI, and A. ZINGALES. J. Mol. Catal. **24**, 79 (1984).
15. M. GARGANO, P. GIANNOCCARO, and M. ROSSI. J. Organometal. Chem. **84**, 389 (1975).
16. J. TSUJI and H. SUZUKI. Chem. Lett. 1083 (1977).
17. M. AIROLDI, G. DEGANELLO, G. DIA, and G. GUENNARO. Inorg. Chim. Acta, **68**, 179 (1983).
18. Y. L. CHOW and G. E. BUONO-CORE. J. Chem. Soc. Chem. Commun. 592 (1985).
19. Y. L. CHOW and G. E. BUONO-CORE. J. Am. Chem. Soc. **108**, 1234 (1986).
20. R. S. H. LIU. J. Am. Chem. Soc. **89**, 112 (1986).

A highly convergent and enantiospecific synthesis of acyclic subunits of ionomycin from a single chiral progenitor

STEPHEN HANESSIAN AND P. J. MURRAY

Department of Chemistry, Université de Montréal, Montréal, P.Q., Canada H3C 3J7

Received June 12, 1986

STEPHEN HANESSIAN and P. J. MURRAY. Can. J. Chem. **64**, 2231 (1986).

The C_2–C_{10} and C_{11}–C_{22} subunits of ionomycin were synthesized from a chiron derived from L-glutamic acid or D-ribonolactone. A strategy is presented in which *C*-methyl and hydroxyl groups are introduced on appropriate carbon frameworks in a completely predictable fashion based on the replicating lactone method, thus chemically matching any substitution pattern arising from the propionate biosynthetic pathway.

STEPHEN HANESSIAN et P. J. MURRAY. Can. J. Chem. **64**, 2231 (1986).

Les sous-unités C_2–C_{10} et C_{11}–C_{22} de l'ionomycine ont été synthetisées à partir d'un chiron qui provient de l'acide L-glutamique ou de la D-ribonolactone. Une stratégie est présentée dans laquelle des groupements *C*-méthyle et hydroxyle sont introduits sur des chaînes carbonées avec un élément de prévision totale, donnant ainsi un contrôle stéréochimique sur la voie propionate.

The calcium selective ionophore antibiotic ionomycin (1) represents a rather novel structural type among this class of ion-binding natural products (for recent reviews see ref. 2). The acyclic C_1–C_{22} polyfunctional carbon chain, consisting of several alternating arrangements of *C*-methyl groups, presents a formidable challenge in design and stereocontrolled methods of assembly. Several innovative approaches that generate 1,3-relationships of *C*-methyl groups have been recently reported in connection with synthetic efforts directed at ionomycin (3). The asymmetric synthesis of the C_1–C_{10} and C_{11}–C_{16} subunits of ionomycin based on chiral enolate technology was recently reported by Evans and Dow (4), while the synthesis of the bis-furanoid segment had been disclosed earlier (5).

Although a symmetrical *C*-methyl substitution pattern is evident in the C_1–C_{22} acyclic segment of ionomycin, careful scrutiny reveals antithetic relationships in which the seemingly different left C_{17}–C_{22}, middle C_{11}–C_{16}, and right-hand C_1–C_{10} segments can be related to the inherent asymmetry of hidden chirons (6*a*).[1]

We demonstrate such an analysis in Scheme 1, and we further highlight how practically the entire acyclic subunit can be derived from a single chiral progenitor. In this paper, we report on the total synthesis of optically pure C_2–C_{10} and C_{11}–C_{22} subunits of ionomycin from a chiral butenolide that is readily available from D-ribonolactone (7, 8) or L-glutamic acid (9, 10).

The C_{11}–C_{16} subunit

Conjugate addition of lithio tris(trimethylthio) methane to the butenolide **1** (7–9)[2] gave a single crystalline adduct, mp 140–

[1]For another example of the use of the term "hidden symmetry" see ref. 6*b*, as quoted in section 5.3.2 under "Stereochemical considerations."

[2]For a preferred synthesis, see ref. 8 as modified in this laboratory.

1,5-COD and the subsequent reverse elimination to give 1,5-COD are both stereospecific. In the reaction, acetylacetone-d_1 (100% purity) was also identified, thereby unambiguously showing that hydrogen is the H-atom donor to the acetylacetonyl radical.

Acknowledgement

The authors thank the Natural Sciences and Engineering Research Council of Canada for generous financial support of this project.

1. G. W. PARSHALL. Homogeneous catalysis. Wiley-Interscience, New York. 1980. Chapt. 3.
2. B. R. JAMES. (*a*) Adv. Organomet. Chem. **17**, 319 (1979); (*b*) Compr. Organomet. Chem. **8**, 285 (1982).
3. P. W. JOLLY and G. WILKE. The organic chemistry of nickel. Vol. II. Academic Press, New York. 1975. Chapt. 1.
4. R. G. SOLOMON. Tetrahedron, **39**, 575 (1983).
5. L. MAGGI, A. JURIS, D. SANDRINI, and M. F. MANFRIN. Rev. Chem. Interm. **4**, 171 (1981).
6. M. J. D'ANIELLO, JR. and E. K. BARFIELD. J. Am. Chem. Soc. **100**, 1474 (1978).
7. H. KANI, K. KUSHI, K. SAKANOUE, and N. KISHIMOTO. Bull. Chem. Soc. Jpn. **53**, 2711 (1980).
8. H. TAKAYA, T. SUZUKI, Y. KUMAGAI, M. YAMAKAWA, and R. NOYORI. J. Org. Chem. **46**, 2846 (1981).
9. B. BOGDANOVIC, M. KRÖNER, and G. WILKE. Liebigs Ann. **699**, 1 (1966).
10. W. KEIM, B. HOFFMANN, R. LODEWICK, M. PEUCKERT, G. SCHMITT, J. FLEISCHHAUER, and U. MEIER. J. Mol. Catal. **6**, 79 (1979).
11. W. KEIM, A. BEHR, and G. KRAUS. J. Organomet. Chem. **251**, 377 (1983).
12. H. ITATANI, and J. C. BAILAR, JR. Ind. Eng. Chem. Prod. Res. Develop. **11**, 146 (1972).
13. L. W. GOSSER and G. W. PARSHALL. Tetrahedron Lett. 2555 (1971).
14. F. PINNA, G. STRUKUL, R. PASSERINI, and A. ZINGALES. J. Mol. Catal. **24**, 79 (1984).
15. M. GARGANO, P. GIANNOCCARO, and M. ROSSI. J. Organometal. Chem. **84**, 389 (1975).
16. J. TSUJI and H. SUZUKI. Chem. Lett. 1083 (1977).
17. M. AIROLDI, G. DEGANELLO, G. DIA, and G. GUENNARO. Inorg. Chim. Acta, **68**, 179 (1983).
18. Y. L. CHOW and G. E. BUONO-CORE. J. Chem. Soc. Chem. Commun. 592 (1985).
19. Y. L. CHOW and G. E. BUONO-CORE. J. Am. Chem. Soc. **108**, 1234 (1986).
20. R. S. H. LIU. J. Am. Chem. Soc. **89**, 112 (1986).

A highly convergent and enantiospecific synthesis of acyclic subunits of ionomycin from a single chiral progenitor

STEPHEN HANESSIAN AND P. J. MURRAY

Department of Chemistry, Université de Montréal, Montréal, P.Q., Canada H3C 3J7

Received June 12, 1986

STEPHEN HANESSIAN and P. J. MURRAY. Can. J. Chem. **64**, 2231 (1986).

The C_2–C_{10} and C_{11}–C_{22} subunits of ionomycin were synthesized from a chiron derived from L-glutamic acid or D-ribonolactone. A strategy is presented in which *C*-methyl and hydroxyl groups are introduced on appropriate carbon frameworks in a completely predictable fashion based on the replicating lactone method, thus chemically matching any substitution pattern arising from the propionate biosynthetic pathway.

STEPHEN HANESSIAN et P. J. MURRAY. Can. J. Chem. **64**, 2231 (1986).

Les sous-unités C_2–C_{10} et C_{11}–C_{22} de l'ionomycine ont été synthetisées à partir d'un chiron qui provient de l'acide L-glutamique ou de la D-ribonolactone. Une stratégie est présentée dans laquelle des groupements *C*-méthyle et hydroxyle sont introduits sur des chaînes carbonées avec un élément de prévision totale, donnant ainsi un contrôle stéréochimique sur la voie propionate.

The calcium selective ionophore antibiotic ionomycin (1) represents a rather novel structural type among this class of ion-binding natural products (for recent reviews see ref. 2). The acyclic C_1–C_{22} polyfunctional carbon chain, consisting of several alternating arrangements of *C*-methyl groups, presents a formidable challenge in design and stereocontrolled methods of assembly. Several innovative approaches that generate 1,3-relationships of *C*-methyl groups have been recently reported in connection with synthetic efforts directed at ionomycin (3). The asymmetric synthesis of the C_1–C_{10} and C_{11}–C_{16} subunits of ionomycin based on chiral enolate technology was recently reported by Evans and Dow (4), while the synthesis of the bis-furanoid segment had been disclosed earlier (5).

Although a symmetrical *C*-methyl substitution pattern is evident in the C_1–C_{22} acyclic segment of ionomycin, careful scrutiny reveals antithetic relationships in which the seemingly different left C_{17}–C_{22}, middle C_{11}–C_{16}, and right-hand C_1–C_{10} segments can be related to the inherent asymmetry of hidden chirons (6*a*).[1]

We demonstrate such an analysis in Scheme 1, and we further highlight how practically the entire acyclic subunit can be derived from a single chiral progenitor. In this paper, we report on the total synthesis of optically pure C_2–C_{10} and C_{11}–C_{22} subunits of ionomycin from a chiral butenolide that is readily available from D-ribonolactone (7, 8) or L-glutamic acid (9, 10).

The C_{11}–C_{16} subunit

Conjugate addition of lithio tris(trimethylthio) methane to the butenolide **1** (7–9)[2] gave a single crystalline adduct, mp 140–

[1]For another example of the use of the term "hidden symmetry" see ref. 6*b*, as quoted in section 5.3.2 under "Stereochemical considerations."

[2]For a preferred synthesis, see ref. 8 as modified in this laboratory.

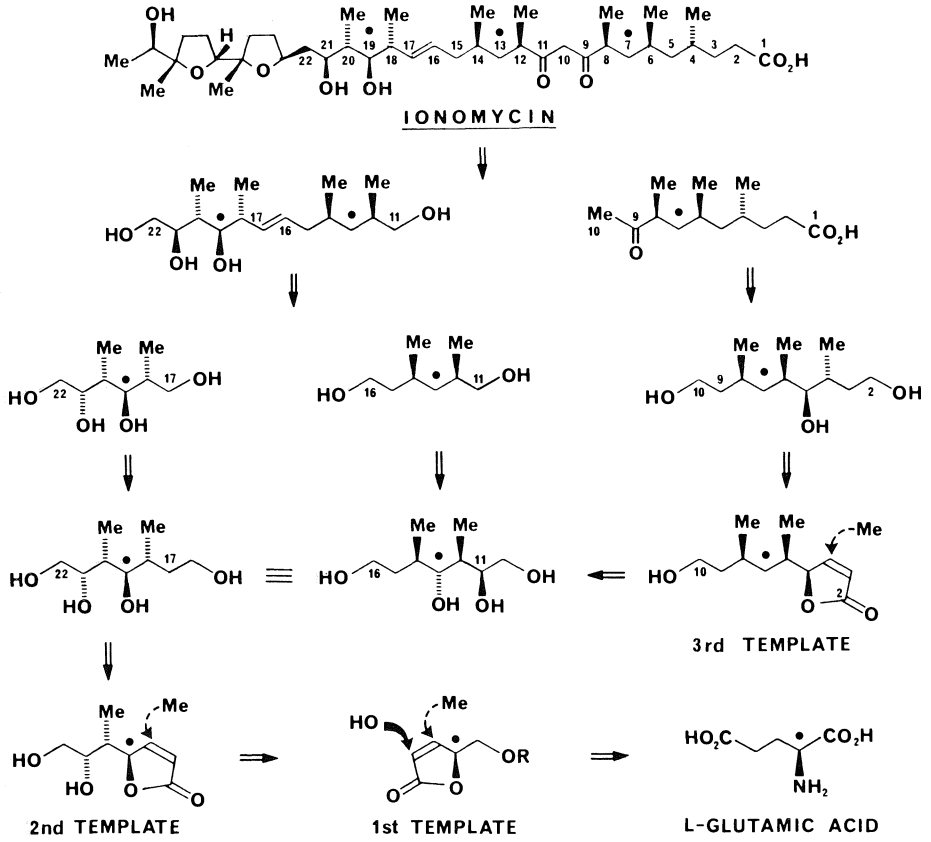

SCHEME 1

142°C, $[\alpha]_D$ 20.5° (*c* 1.1).[3] Hydroxylation of the corresponding enolate with the Vedejs reagent (10, 11) afforded only the hydroxy lactone **2**, $[\alpha]_D$ 8.1° (*c* 1.3), by virtue of the bulk of the vicinal substituent. Desulfurization led to the *C*-methyl derivative **3**, $[\alpha]_D$ 12.5 (*c* 2.2), which was reduced and protected as the acetonide derivative, **4**, $[\alpha]_D$, −0.3° (*c* 3.3). This polyol was then subjected to a two-carbon homologation and lactone replication process (10, 12) to give **6**. Oxidative elimination led to the crystalline butenolide **7**, mp 78–79°C, $[\alpha]_D$ 91.3° (*c* 6.3). Conjugate addition of lithium dimethylcuprate proceeded with anticipated stereocontrol to give the lactone **8**, $[\alpha]_D$ −32° (*c* 2.1). The template effect of the original and replicated butanolide had thus been fully exploited, and the required complement of functional groups was introduced with complete regio- and stereocontrol.

Reduction of **8**, followed by selective silylation, gave **9**, $[\alpha]_D$ 5.5° (*c* 1.9), which was deoxygenated to **10**, $[\alpha]_D$ 21.6° (*c* 2.1). Further manipulation and cleavage of the vicinal diol unit gave **11**, $[\alpha]_D$ 1.9° (*c* 1.8), which was finally transformed into the sulfone derivative **12**, $[\alpha]_D$ 6.7° (*c* 3.7). Compound **10** serves as a precursor not only to the C_{11}–C_{16} subunit, but it is utilized as a starting material for the C_2–C_{10} subunit as well, since C_5–C_{10} is functionally and configurationally identical to C_{11}–C_{16}.

The C_2–C_{10} subunit

The seven-carbon chiron **10** was homologated via the epoxide **13**, to give the replicated butenolide **14** (Scheme 3). With the side chain properly oriented vis-à-vis the enone system, it was possible to effect conjugate addition of lithium dimethyl cuprate with complete stereocontrol giving lactone **15**, $[\alpha]_D$ −8.4° (*c* 0.5). Reduction and deoxygenation at the secondary hydroxyl position gave the selectively protected trisubstituted diol **17**, which corresponds to the C_2–C_{10} subunit of the intended target after adjustment of the oxidation state at C_9.

The C_{11}–C_{22} subunit

The common intermediate **8** (Scheme 1), in which all the required substituents for the C_{17}–C_{22} segment are in place, was hydroxylated to give **9** as an epimeric mixture of lactones (Scheme 4). A one-carbon excision was now possible, via cleavage of the diol **19**. Selective protection and oxidation then provides the aldehyde **20**.

With the required optically pure chirons **12** and **20** in hand, we next addressed their coupling. Thus, reaction of the anion resulting from the sulfone **12** with aldehyde **20**, followed by acetylation and reductive elimination (13), gave **21** as a 9:1 mixture of *E*/*Z* olefins. There now remained the problem of adjusting the configuration at the carbon atom that corresponds to C_{21} in the target. This was accomplished by an inversion via epoxide formation to give the advanced C_{11}–C_{22} intermediate **22**, $[\alpha]_D$ −9.4° (*c* 0.51).

The five-carbon framework of the original L-glutamic acid or D-ribonolactone can be found hidden in the C_4–C_8, C_{10}–C_{14}, and C_{18}–C_{22} segments of ionomycin. Furthermore, the single asymmetric center present in L-glutamic acid (Scheme 1, black dot) dictates the stereochemical events that led to the elaboration of all other asymmetric centers in the acyclic subunits of ionomycin.[4]

[3]Optical rotations were measured in chloroform at room temperature.

[4]Efficient and expeditious access to advanced intermediates needed for the synthesis of the three fragments is now possible, based on our lactone enolate and replication methodology (ref. 10).[5] The overall yields are high, and the number of steps can be effectively halved compared to the conjugate addition–replication technology.

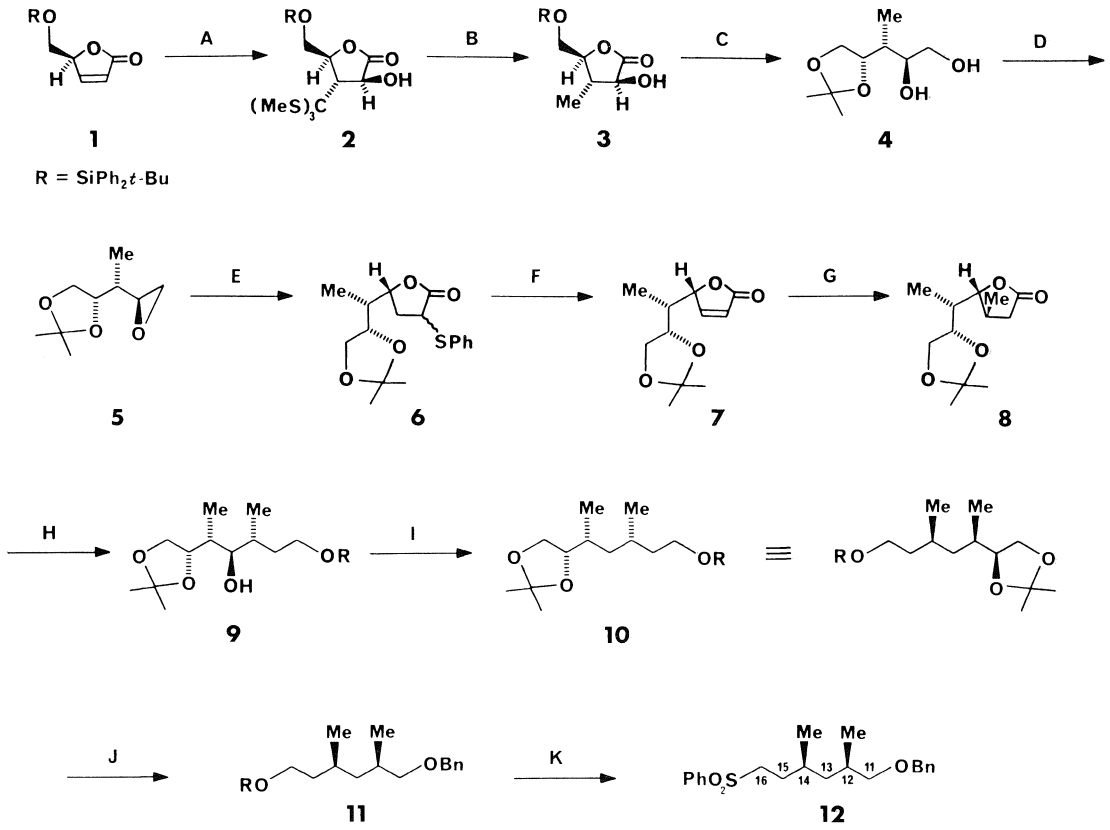

A. *i.* $(MeS)_3CLi$, THF, −78°C, 86%; *ii.* MoOPH, THF, −78°C, 85%; B. Raney nickel, THF, 65%; C. *i.* $NaBH_4$, THF, H_2O; *ii.* acetone, dimethoxypropane, H^+; *iii.* $Bu_4N^+F^-$, THF, 62% (3 steps); D. *i.* 2,4,6-triisopropylbenzenesulfonyl chloride, pyridine, 0°C, 92%; *ii.* NaOMe, MeOH, 85%; E. *i.* dilithio phenylthioacetate, THF, 0–25°C; *ii.* EDAC·HCl, DMAP, CH_2Cl_2, 77% (2 steps); F. *i.* *m*-CPBA, CH_2Cl_2, −23°C; *ii.* toluene, $CaCO_3$, reflux, 89% (2 steps); G. Me_2CuLi, Et_2O, −23°C, 91%; H. $LiAlH_4$, Et_2O, 90%; *tert*-butyldiphenylsilyl chloride, pyridine, DMAP, CH_2Cl_2, 96%; I. *i.* MsCl, Et_3N, CH_2Cl_2; *ii.* $LiAlH_4$, Et_2O, 75% (2 steps); J. *i.* AcOH, H_2O, quant.; *ii.* $NaIO_4$, aqueous MeOH, then $NaBH_4$; *iii.* benzyl bromide, KH, DMF, THF, 61% (4 steps); K. *i.* H^+, MeOH, quant.; *ii.* MsCl, Et_3N, CH_2Cl_2; *iii.* lithium thiophenoxide, THF, 0°C; *iv.* *m*-CPBA, CH_2Cl_2, 73% (4 steps).

SCHEME 2

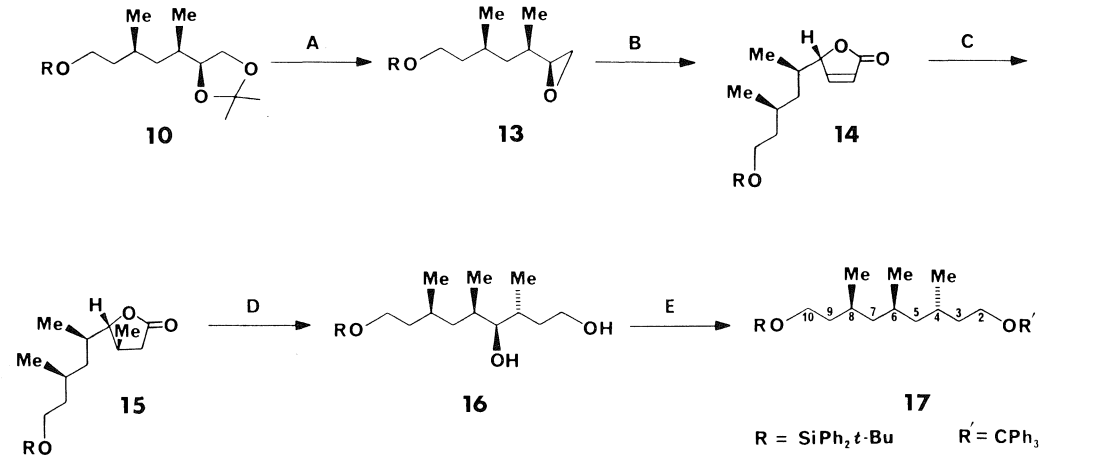

A. *i.* AcOH, H_2O; *ii.* 2,4,6-triisopropylbenzenesulfonyl chloride, pyridine; *iii.* NaOMe, MeOH, 70% (3 steps); B. *i.* dilithio phenylthioacetate, THF, 0–25°C, RT; *ii.* EDAC·HCl, DMAP, CH_2Cl_2; *iii.* H_2O_2, CH_2Cl_2, 0°C; *iv.* toluene, $CaCO_3$, reflux, 69% (4 steps); C. Me_2CuLi, Et_2O, −23°C, 90%; D. $LiAlH_4$, Et_2O, 88%; E. *i.* tritylpyridinium tetrafluoroborate, CH_3CN; *ii.* MsCl, Et_3N, CH_2Cl_2; *iii.* $LiAlH_4$, Et_2O, 51% (3 steps).

SCHEME 3

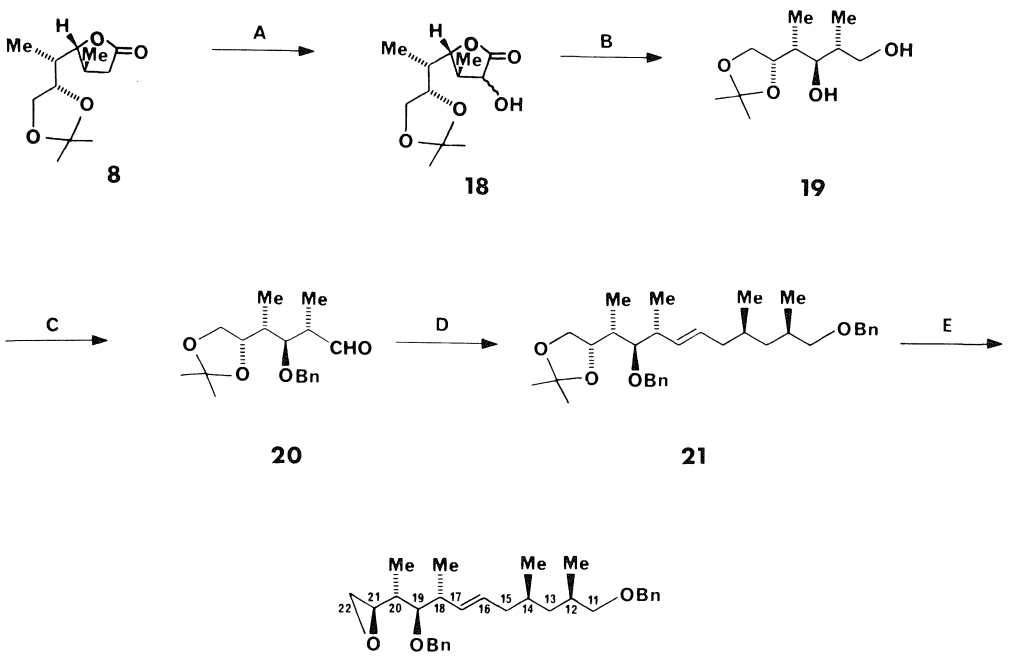

A. LiHMDS, THF, −78°C, then MoOPH, 77%; B. *i*. $NaBH_4$, THF, H_2O; *ii*. $NaIO_4$, MeOH, H_2O, then $NaBH_4$, 53% (3 steps); C. *i*. *tert*-butyldiphenylsilyl chloride, pyridine, DMAP, CH_2Cl_2; *ii*. benzyl bromide, KH, DMF, THF; *iii*. $Bu_4N^+F^-$, THF, 76% (3 steps); *iv*. PCC, CH_2Cl_2, 86%; D. *i*. **12** plus *n*-BuLi, THF, −78°C; add **20**, −78°C, 78%; *ii*. Ac_2O, pyridine, DMAP; *iii*. Na/Hg, MeOH, THF, 76% (2 steps); E. *i*. H^+, MeOH; *ii*. *tert*-butyldiphenylsilyl chloride, pyridine, DMAP, CH_2Cl_2, 95%; *iii*. MsCl, Et_3N, CH_2Cl_2; *iv*. $Bu_4N^+F^-$, THF, 70% (2 steps).

SCHEME 4

Our strategy for the regio- and stereocontrolled sequential functionalization of butenolide-type templates (9, 12, 14), coupled with the possibility of reiterating the process through replication (10, 12), offers a powerful and predictable tool for the total synthesis of a variety of other natural products. In effect, any stereochemical combination generated by nature via its obiquitous propionate biosynthetic pathway can now be directly addressed and chemically reproduced using the methodology described herein and variants thereof.[5]

1. B. K. TOEPLITZ, A. I. COHEN, P. T. FUNKE, W. L. PARKER, and J. Z. GOUGOUTAS. J. Am. Chem. Soc. **101**, 3344 (1979).
2. J. W. WESTLEY (*Editor*). Polyether antibiotics: naturally occurring acid ionophores. Vols. 1, 2. Marcel Dekker, New York, NY. 1982; W. WIERENGA. *In* The total synthesis of natural products. Vol. 4. *Edited by* J. ApSimon. Wiley–Interscience, New York, NY. 1981. p. 263.
3. D. A. EVANS, M. M. MORRISSEY, and R. L. DOW. Tetrahedron Lett. **26**, 6005 (1985); D. A. EVANS. Aldrichimica Acta, **15**, 23 (1982); S. L. SCHREIBER and Z. WANG. J. Am. Chem. Soc. **107**, 5303 (1985); D. NICOLL-GRIFFITH and L. WEILER. J. Chem. Soc. Chem. Commun. 659 (1984).
4. D. A. EVANS and R. L. DOW. Tetrahedron Lett. **27**, 1007 (1986).
5. P. G. M. WUTS, R. D'COSTA, and W. BUTLER. J. Org. Chem. **49**, 2582 (1984).
6. (*a*) S. HANESSIAN. *In* The total synthesis of natural products; the CHIRON approach. *Edited by* J. E. Baldwin. Pergamon Press, Oxford, U.K. 1983; (*b*) S. MASAMUNE, G. S. BATES, and J. W. CORCORAN. Angew. Chem. Int. Ed. Engl. **16**, 585 (1977).
7. P. CAMPS, J. CARDELLACH, J. FONT, R. M. ORTUNO, and O. PONSATI. Tetrahedron, **38**, 2395 (1982); K. L. BHAT, S. Y. CHAN, and M. M. JOUILLÉ. Heterocycles, **23**, 691 (1985).
8. R. E. IRELAND, R. C. ANDERSON, R. BADOUD, B. J. FITZSIMMONS, G. J. MCGARVEY, S. THAISRIVONGS, and C. S. WILCOX. J. Am. Chem. Soc. **105**, 1988 (1983).
9. O. H. GRINGARE and F. P. RONESSAC. Org. Synth. **63**, 121 (1984); J. P. VIGNERON, R. MERIC, M. LARCHEVEQUE, A. DEBAL, J. Y. LALLEMAND, G. JUNESCH, P. TAGATTI, and M. GALLOIS. Tetrahedron, **40**, 3521 (1984); M. TANIGUCHI, K. KOGA, and S. YAMADA. Tetrahedron, **30**, 3547 (1970).
10. S. HANESSIAN, P. J. MURRAY, and S. P. SAHOO. Tetrahedron Lett. **26**, 5623 (1985); **26**, 5627 (1985).
11. E. VEDEJS, D. A. ENGLER, and J. E. TELSCHOW. J. Org. Chem. **43**, 188 (1978).
12. S. HANESSIAN, S. P. SAHOO, and P. J. MURRAY. Tetrahedron Lett. **26**, 5631 (1985).
13. P. KOCIENSKI. Phosphorus Sulfur, **24**, 97 (1985); M. JULIA and J.-M. PARIS. Tetrahedron Lett. 4833 (1973).
14. T. K. CHAKRABORTY and S. CHANDRASEKARAN. Tetrahedron Lett. **25**, 2891 (1985); K. TOMIOKA, T. ISHIGURO, and K. KOGA. Tetrahedron Lett. **21**, 2973 (1980).

[5]S. Hanessian, G. McCraw, P. J. Murray, S. P. Sahoo, and P. Hodges. Unpublished results.

A high temperature, pressure study of the comparative rates of enolization and oxidation of acetone in aqueous solution

JOHN W. THOMAS[1] AND JAY E. TAYLOR[2]
Department of Chemistry, Kent State University, Kent, OH 44242, U.S.A.

Received June 11, 1986

JOHN W. THOMAS and JAY E. TAYLOR. Can. J. Chem. **64**, 2235 (1986).

The rate of enolization and acetone has been determined as 6.6×10^{-4} s^{-1} at 193.5°C under nitrogen at 136 atm total pressure via isotopic exchange. The rate of oxidation was determined to be 8.8×10^{-6} s^{-1} at 193.5°C in 123 atm partial pressure of oxygen (136 atm total pressure). In a previous study it was shown that the rates of oxidation of several ketones correlated with the extents of enolization at room temperature. This prompted the suggestion that the enol is an intermediate in the oxidation. Since the rate of enolization exceeded the rate of oxidation by a factor of 75, this suggestion is further supported. A dependence of the rate of oxidation of acetone on oxygen concentration was also demonstrated.

JOHN W. THOMAS et JAY E. TAYLOR. Can. J. Chem. **64**, 2235 (1986).

Opérant à 193,5°C et sous une pression totale de 136 atm d'azote et se basant sur l'échange isotopique, on a déterminé que la vitesse d'énolisation de l'acétone est égale à $6{,}6 \times 10^{-4}$ s^{-1}. A 193,5°C et sous une pression partielle d'oxygène de 123 atm (pression totale de 136 atm), on a déterminé que la vitesse d'oxydation est égale à $8{,}8 \times 10^{-6}$ s^{-1}. Dans une étude antérieure, il a été démontré qu'il existe une corrélation entre les vitesse d'oxydation et les taux d'énolisation de plusieurs cétones. Cette observation suggère que l'énol est un intermédiare dans l'oxydation. Puisque la vitesse d'oxydation de l'acétone est 75 fois plus grande que la vitesse d'oxydation, on peut en déduire que cette hypothèse est supportée. On a aussi démontré qu'il existe une corrélation entre la vitesse d'oxydation de l'acétone et la concentration d'oxygène.

[Traduit par la revue]

Introduction

In an introductory study of the aqueous reactions of oxygen with a variety of organic compounds pressurized at high temperatures, it was suggested that the enol may be an intermediate in the oxidation of simple ketones (1). This conclusion was based on the observed correlation between the rates of oxidation of several ketones and their projected extents of enolization.

The purpose of this paper is to determine the validity of this hypothesis for acetone by determining the relative rates of oxidation and enolization at an elevated temperature. Thus, if the rate of oxidation exceeds the rate of enolization, the above proposal is obviously invalid but, if the reverse is true, then it remains acceptable.

Experimental

This investigation was done in an apparatus similar in principle to that previously described (1), but with a number of alterations to improve accuracy and reliability of the data. In particular there were changes in the stirring and temperature control systems and related equipment.

A vapor pressure bath greatly increased the accuracy of temperature control over the previously used air bath (1) (see Fig. 1). Bath G contained a refluxing liquid whose temperature was controlled by a mercury manostat with an adjustable mercury contact. This in turn activated a relay and air inlet valve (not shown). Thus, a selected temperature could be maintained at ±0.05°C. Refluxing liquids which were found to be stable and convenient to use were ethanediol, 193–197°C; 1-heptanol, 171–175°C; 2-heptanone, 142–147°C; and 1-butanol 115–118°C.

To initiate a reaction the ketone was sealed under vacuum at ~ −80°C in a 10 mm glass sphere, designed to implode at 136 atm or lower, and placed in reactor E along with a stirring bar and solvent water. E was pressurized to 17 atm, and then sealed inside bath G which was then warmed to the desired temperature with the internal pressure at 17 atm (250 psi). About one hour was required. The pressure was then increased to 136 atm (2000 psi) using O_2 or N_2, effecting rupture of the bulb and instantaneous initiation of isotope exchange or oxidation. Stirring was immediately started via the magnet I. Samples were removed at appropriate times by opening valve P, permitting the liquid to enter PQ. P was then closed and Q opened, releasing the sample for analysis. The major disadvantage of this technique was the low success rate (25–30%) in fabricating bulbs which would reliably perform as indicated. Also the fine particles of glass sometimes clogged the outlet tube.

The change in molarity of the oxidizing substrate was followed using a gas chromatograph. The relative standard deviation was ±2% with an external standard. Oxygen pressure was determined by subtracting the vapor pressure of water from the total pressure.

The determination of the rate of isotope exchange was done under a nitrogen atmosphere (136 atm) at 193.5°C and was followed by gas chromatograph – mass spectrometric analyses of the samples collected. The rates of enolization were evaluated by determining the rate of isotopic substitution of ^1_1H for ^2_1D in aqueous solutions of acetone-D_6. The data were corrected for the natural abundances of interfering C and O isotopes and for those fragmentation patterns observed in the spectral analysis of neat acetone $(M - D \text{ or } H)^+$ and $(M - 3D \text{ or } 3H)^+$ which would contribute ions in the mass range of 58–64. Thus the substitution of a proton for a deuteron was directly followed. The reverse reaction was neglected because of the excess of water. Since the plots of $\ln (M_{64}/M_{58-64})$ versus time were linear, the reactions were first order, and the slopes were equal to the rate constants.

Data and discussion

The enolization of acetone-D_6, as determined by the isotope exchange procedure, was shown to be first order. The data from three exchange runs are plotted in Fig. 2. The calculated values of the rate constants are 2.24×10^{-4}, 2.06×10^{-4}, 2.30×10^{-4} with a mean value of $2.2 \pm 0.1 \times 10^{-4}$ at 193.5°C and 136 atm pressure.

In order to relate the enolization of acetone-D_6 to that of acetone-H_6, it was necessary to estimate the kinetic isotope effect, KIE (i.e., k_H/k_D) since this has not been determined at

[1]Present address: Pfizer, Inc., Terre Haute, IN 47808, U.S.A.
[2]Author to whom correspondence should be addressed.

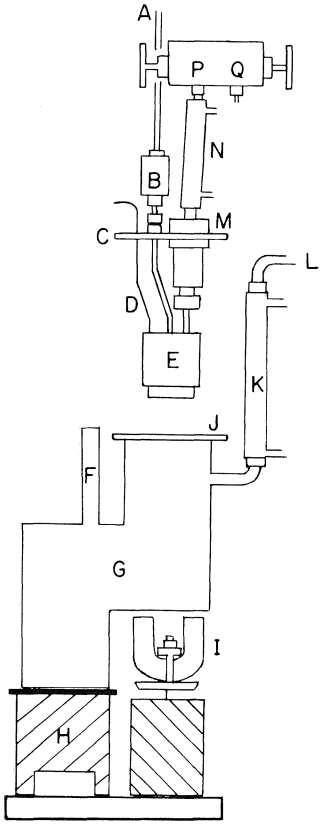

FIG. 1. Revised high pressure oxidation apparatus. A, oxygen inlet which leads to a shut-off valve, high pressure filter, pressure gauge, and oxygen tank with pressure regulator, not all shown; B, rupture disk; C—M copper plate to form a gas-tight seal on J; D, thermocouple lead; E, heavy steel reactor containing a Teflon liner and lid, magnetic stirring bar, glass bulb containing the ketone, sampling tube and thermocouple inside the reactor wall (the lower section of E was fabricated of nonmagnetic stainless steel); F, thermoregulator well; G, copper vapor pressure bath; H, heater; I, large rotating magnet; J, flange to accommodate the plate C—M; K, condenser; L, tube leading to the pressure control system, not shown; M, bulkhead union for sampling tube; N, cooling tube for samples taken from E; P, double valve for sampling; Q, sample outlet.

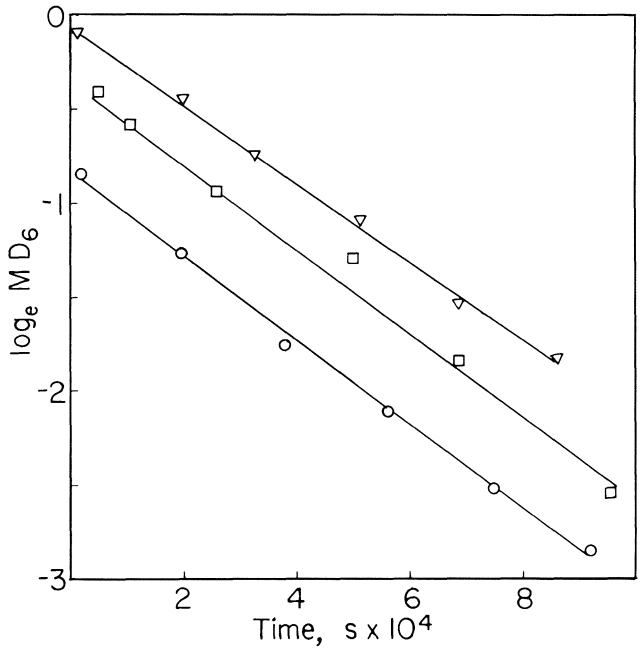

FIG. 2. Graphs of the first order of deuterium exchange of acetone-D_6 with water. M_{D_6} represents the effective molarity of acetone-D_6 remaining at the specified time. M_{D_6} was calculated from the initial molarity of acetone-D_6 multiplied by the relative ion abundance (M_{64}/M_{58-64} corrected as indicated).

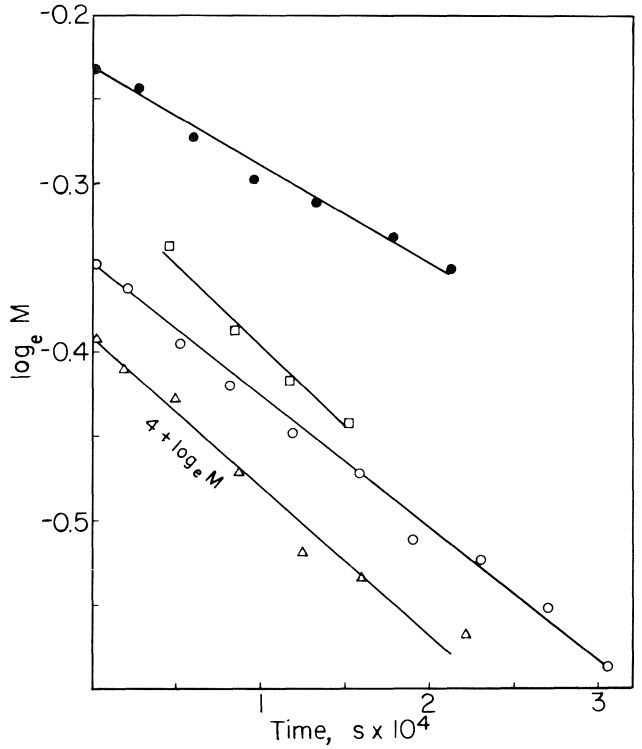

FIG. 3. The oxidation of acetone at 193.5°C and 123 and 56.4 atm partial pressure of oxygen. A plot of ln (acetone concentration) versus time. ●, ■, and ○ 123 atm oxygen partial pressure; △ 56.4 atm oxygen partial pressure.

elevated temperatures. Hine, Kaufman, and Cholod (2) have reported a KIE of 6.5 at 25°C, and this is deemed to follow the equation:

[1] $\text{KIE} = \exp(\Delta E_0/RT)$

Using E_0 = 1100 cal, the value of KIE (193°C) should be roughly 3.0. Thus the enolization rate for acetone-H_6 was estimated as $6.6 \times 10^{-4}\,s^{-1}$.

Three determinations of the rate of oxidation of acetone were performed at 193.5°C/123 atm O_2 and one at 193.5°C/56.4 atm O_2 (136 and 68 atm total pressure). These data are graphed in Fig. 3, and the calculated values for the rate constants at 123 atm (partial pressure O_2) are $8.0 \pm 0.25 \times 10^{-6}$, $9.5 \pm 0.4 \times 10^{-6}$, and $8.8 \pm 0.4 \times 10^{-6}\,s^{-1}$ giving a mean value of $8.8 \pm 0.5 \times 10^{-6}\,s^{-1}$. The value at 56.4 atm O_2 is calculated as $5.7 \pm 0.4 \times 10^{-6}\,s^{-1}$.

In keeping with the conclusion of the earlier paper (1), there appears to be a dependence of the rate of oxidation of acetone on oxygen concentration. Although the previous estimate was unity for both the ketone and oxygen kinetic dependencies (with some deviation), the present data indicate the oxidation to be first order in acetone and roughly one-half order in oxygen.

Comparison of the rates of enolization and oxidation demonstrates that enolization is much faster than oxidation by the factor $6.6 \times 10^{-4}/8.8 \times 10^{-6} = 75$. Thus it appears that the enolization of acetone is sufficiently rapid at this temperature to maintain an equilibrium enol concentration despite con-

sumption of the enol in the oxidation process. Hence the keto–enol reaction can justifiably be treated as a precursor to the final oxidation, and the previous suggestion to this effect is supported.

The equilibrium constant for the enolization of acetone was previously estimated (1) at 200, 220, and 240°C using the method of Benson (3). These calculations have been extended to 193.5°C giving a value of $K = 0.0022$. Based on this, the forward and reverse rates of enolization are $k_1 = 6.6 \times 10^{-4}\,s^{-1}$ and $k_{-1} = 0.3\,s^{-1}$ at 193.5°C.

In summary, the oxidation of acetone may be represented at this time by two equations:

[2] $CH_3COCH_3 \rightleftharpoons CH_2{=}COHCH_3$

[3] $CH_2{=}COHCH_3 + 2O_2 \rightarrow CH_3CO_2H + CO_2 + H_2O$

In keeping with reaction [3], oxygen must then interact with the enol by a series of reactions as yet undefined. Studies on the oxygenation of acetone and other ketones in the liquid phase are few in number and most have been done with neat ketones plus additives (see Denison (4) or Rouchad and Lutete (5)). Further, Zaikov *et al.* (6), have reported that 2-butanone is appreciably slower in aqueous solutions than in the pure state, and they explain this on the basis of hydration of the intermediate radicals. Rif *et al.* (7) reported that 6-undecanone was oxidized in a nonspecific manner with only partial regard for the positioning of the keto group. Since the keto group was in the center of a long chain, it is our conjecture that it may be relatively unavailable for reaction, and the reported oxidation was largely equivalent to that of a hydrocarbon.

1. J. E. Taylor and J. C. Weygandt. Can. J. Chem. **52**, 1925 (1974).
2. J. Hine, J. C. Kaufman, and M. S. Cholod. J. Am. Chem. Soc. **94**, 4590 (1972).
3. S. W. Benson. Thermochem. Kinet. Wiley, New York. 1968. p. 18.
4. E. T. Denison. Kinet. Katal. Akad. Nauk SSSR, Sb. Stat. 95 (1960); cf. Chem. Abstr. **57**, 8421*c* (1962).
5. J. Rouchad and B. Lutete. Can. J. Chem. Eng. **47**, 157 (1969).
6. G. E. Zaikov, A. A. Vichutinskii, and Z. K. Maizus. Kinet. Katal. **8**, 675 (1967).
7. I. I. Rif, V. M. Potekhin, V. A. Proskuryakov, and T. Mikheenko. Zh. Prikl. Khim. Leningrad, **43**, 372 (1970).

Cation–anion combination reactions. 26.[1] A review

CALVIN D. RITCHIE
Department of Chemistry, State University of New York at Buffalo, Buffalo, NY, 14214, U.S.A.

Received July 11, 1986

CALVIN D. RITCHIE. Can. J. Chem. **64**, 2239 (1986).

Rate and equilibrium constants for reactions of carbocations, and a few other electrophiles, with anionic and neutral nucleophiles in several solvents are summarized. Equilibrium constants for such reactions are a measure of the carbon basicities of the nucleophiles, and are discussed in the context of differences in proton and carbon basicities. The factors affecting the kinetic reactivities of nucleophiles are not well understood, even though the reactivity patterns are frequently the same toward widely different electrophiles.

CALVIN D. RITCHIE. Can. J. Chem. **64**, 2239 (1986).

On présente un résumé des constantes de vitesses et d'équilibre des réactions de carbocations ainsi que de quelques autres électrophiles avec des nucléophiles anioniques et neutres, dans plusieurs solvants. Les constantes d'équilibre pour de telles réactions servent de mesure pour la basicité des nucléophiles vis-à-vis les carbones et on en discute dans le contexte de différences dans les basicités des protons et des carbones. Les facteurs affectant les réactivités cinétiques des nucléophiles ne sont pas très bien comprises, même si les réactivités, par rapport à des électrophiles forts différents, sont fréquemment très semblables.

[Traduit par la revue]

Introduction

The formation of a covalent bond between a Lewis acid and a Lewis base, and the reverse reaction, heterolytic dissociation of a covalent bond, are among the most fundamental of chemical reactions. Fundamental, unfortunately, does not imply simple. Nearly all of the "effects", steric, polar, resonance, solvent, etc., of chemistry are encountered in these reactions.

The well known fact that the order of acidities of Lewis acids depends on the reference base, and vice versa, immediately implies that at least two properties of each acid and of each base are operative in determining reactivities in the Lewis acid–base reactions. The Edwards equation (26), the Drago equation (27), and Pearson's concept of hardness and softness of acids and bases (28) are familiar attempts to correlate reactivities, quantitatively or qualitatively, in terms of the minimal four parameters.

The two parameters for each acid and two for each base do not allow for variable steric, resonance, polar, or solvent effects. Neither do they accommodate the special effect, pointed out by Edwards and Pearson (29), which appears to be associated with the existence of a lone pair of electrons on an atom adjacent to the reacting atom; the "α-effect". In addition, if one wishes to consider kinetic reactivity, the possible operation of reactivity–selectivity relationships must be taken into account (30).

Against this background of complexity, the simplicity of behavior which we initially observed for several anionic nucleophiles (Lewis bases) reacting with several triarylmethyl cations, aryldiazonium ions, and aryltropylium cations, in several solvents, was truly astounding (1–8). The rate constants for these reactions were correlated by a two parameter equation:

$$[1] \quad \log k = \log k_0 + N_+$$

in which $\log k_0$ is a parameter depending only on the identity of the cation, and N_+ is a parameter depending on the identity of the nucleophile and the solvent (9). Equation [1], the N_+ equation, has now been tested for a wide variety of Lewis acid–base reactions (10–25). Although it is far from being general, and fails badly in some specific cases without apparent cause, it is probably as good as most of the more complex equations when applied to electrophile–nucleophile combination reactions. Within this class of reactions, it is not often that one encounters reactivities that are qualitatively different from expectations based on N_+ values.

There is no general theory of nucleophilic reactivity which anticipates the existence of the N_+ relationship, and most theories cannot even accommodate it (31). One of the major purposes of the present review is to present the body of experimental data now available on "simple" electrophile–nucleophile combination reactions in a summarized fashion to challenge theorists to think about this important area of chemistry.

Reactions of cations with water

The reactions of an electrophile (Lewis acid) with water and hydroxide ion must be fully characterized before the study of reactions with other nucleophiles can be attempted. The equilibrium constants for reactions of cations with water:

$$[2] \quad R^+ + H_2O \rightleftarrows ROH + H^+$$

$$[3] \quad K_R = \{ROH\}\{H^+\}/\{R^+\}$$

are frequently used measures of the "stabilities" of cations. In eq. [3], the quantities in brackets are activities of the indicated species, and the activity of water is defined as unity in dilute solution. For cations with pK_R's in the range from ca. 0–14, K_R is usually determined by measurement of pH and of the concentrations of alcohol and cation in dilute solution (7).

For cations having pK_R lower than zero, the H_R acidity function (32) is generally employed for determination of K_R. In special cases, such as *p*-dimethylamino triphenylmethyl cation, where water can add to the cation to form the alcohol protonated on the dimethylamino group, combinations of acidity functions are useful (12).

[1]For Parts 1 to 25, see refs. 1 to 25.

Printed in Canada / Imprimé au Canada

TABLE 1. Electrophile reactions in water[a]

Electrophile	pK_R	log k_w (s^{-1})	log k_{OH} ($M^{-1}\,s^{-1}$)
Tri-(*p*-$N(CH_3)_2$) trityl cation	9.39	−4.71	−0.70
Bis-(*p*-$N(CH_3)_2$) trityl cation	6.94	−3.68	0.34
Bis-(*p*-$N(CH_3)_2$), *p*-CF_3trityl cation	6.07	−3.70	0.52
Bis-(*p*-$N(CH_3)_2$), *p*-NO_2trityl cation	5.24	−3.74	0.75
Bis-(*p*-OCH_3), *p*-$N(CH_3)_2$trityl cation	5.75	−2.64	1.11
p-$N(CH_3)_2$, *p*-OCH_3trityl cation	4.86	−2.34	1.20
p-$N(CH_3)_2$, *p*-CH_3trityl cation	4.40	−2.26	1.25
p-$N(CH_3)_2$trityl cation[b]	3.88	−2.02	
Tris-(*o*-CH_3, *p*-OCH_3) trityl cation	3.80	−2.00	1.00
Tris-(*o*,*p*-$(OCH_3)_2$) trityl cation	3.24	0.30	1.24
Bis-(*p*-OCH_3), *o*-SO_3^-trityl cation	1.31	−1.55	1.77
Tris-(*p*-OCH_3) trityl cation[c]	0.81	1.17	3.91
Bis-(*p*-OCH_3), *o*-SO_2CH_3trityl cation	0.55	−1.06	2.65
Bis-(*p*-OCH_3) trityl cation[b]	−1.14	1.98	
p-OCH_3trityl cation[b]	−3.4	3.0	
Trityl cation[d]	−6.63	5.18	6.72
p-$N(CH_3)_2$phenyltropylium cation	7.35	−1.78	3.23
p-OCH_3phenyltropylium cation	5.75	−0.50	4.60
Phenyltropylium cation	4.84	0.00	4.90
Tropylium cation	4.76	0.41	5.49
p-Cl phenyltropylium cation	4.55	0.08	5.15
Benzenediazonium cation[e]	15.1		3.65
Trifluoroacetophenone[f]	8.1	0.51	5.70
Ferrocenyl, *p*-anisylmethyl cation	1.39	1.64	4.56
N,*O*-Trimethylenephthalimidium cation[h]	−0.15	1.75	6.60
3,6-Bis-$N(CH_3)_2$ xanthylium cation	11.52		1.61
1,3,6,8-Tetra-OCH_3 xanthylium cation[i]	6.00	0.74	5.1
3,6-Bis-OCH_3 xanthylium cation[i]	4.40	1.15	6.0
9-CH_3, 3,6-bis-OCH_3 xanthylium cation[i]	4.30	0.34	4.34
9-CH_3, 1,3,6,8-tetra-OCH_3 xanthylium cation[i]	4.03	0.40	3.68
9-Phenylxanthylium cation[j]	1.8	1.36	4.78
Xanthylium cation[j]	−0.2	4.34	7.56
3,6-Bis-$N(CH_3)_2$ thioxanthylium cation	11.56		0.97

[a]Data from papers in this series, refs. 1–25, unless otherwise noted.
[b]Data from ref. 34.
[c]Data from ref. 35.
[d]Data from ref. 36.
[e]The pK_R is calculated from data given in ref. 33.
[f]Data from ref. 37.
[g]Data from ref. 38.
[h]Data from ref. 39.
[i]Unpublished work from this laboratory.
[j]Data from ref. 40.

Aryldiazonium ions react in basic aqueous solutions to form, in the first observable reactions, the *syn*-diazotates (2). Special techniques must be used (33) to obtain K_R values in these cases. Neutral electrophiles, such as carbonyl compounds, react with water in a reaction analogous to eq. [2]. For carbonyl compounds, the product of reaction is the conjugate base of a *gem*-diol. If the equilibrium constant for hydration of the carbonyl compound, and the acidity constant of the *gem*-diol, are known, the K_R value can be calculated.

The equilibrium constant, K_{OH}, for reaction of an electrophile with hydroxide ion:

[4] $R^+ + OH^- \rightleftarrows ROH$

is directly related to K_R:

[5] $K_{OH} = K_R/K_w$

where K_w is the ion-product of water ($K_w = 1.0 \times 10^{-14}\,M^2$ at 25°C).

Kinetically, the formation of alcohol from cation occurs simultaneously by reactions [2] and [4], with the pseudo-first-order forward rate constant in buffered solution, k_f, given by:

[6] $k_f = k_w + k_{OH}(OH^-)$

Note particularly that k_w, the forward rate constant for reaction [2], is given as a pseudo-first-order rate constant throughout the current series of papers. Many other authors, however, report a "second-order" rate constant obtained by dividing k_w by 55.5 *M*.

Reaction [2] is further complicated by being subject to general-acid–base catalysis (10, 12), so that eq. [6] strictly applies only with very dilute buffer solutions.

Rate and equilibrium constants for the reactions of several types of carbocations, and a few miscellaneous electrophiles, with water and hydroxide ion are shown in Table 1. The range of pK_R values included spans 21 units; rivalling, if not exceeding,

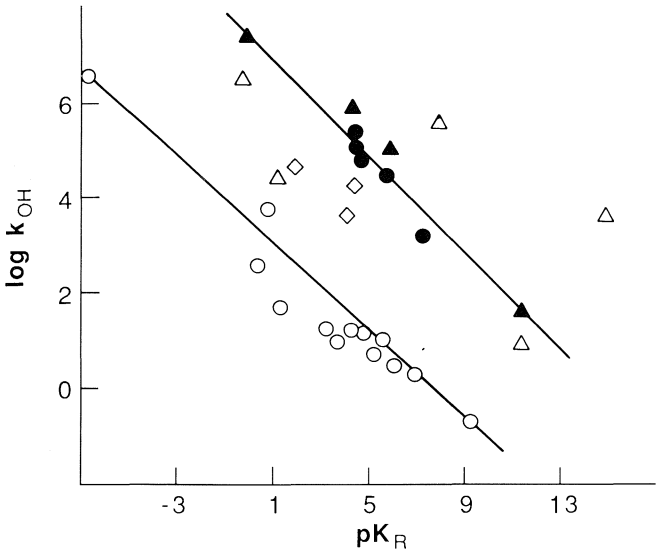

FIG. 1. log k_{OH} vs. pK_R. Open circles, Ar_3C^+; closed circles, $ArTr^+$; closed triangles, xanthylium cations; open triangles, miscellaneous; diamonds, 9-substituted xanthylium cations.

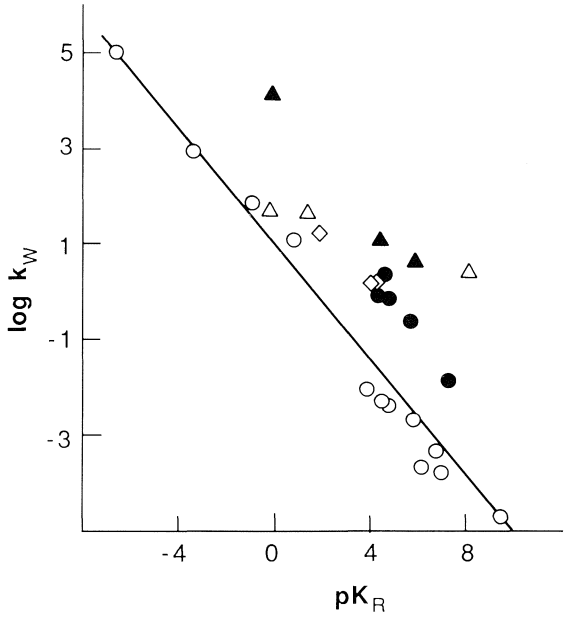

FIG. 2. log k_w vs. pK_R. Symbols are as in Fig. 1.

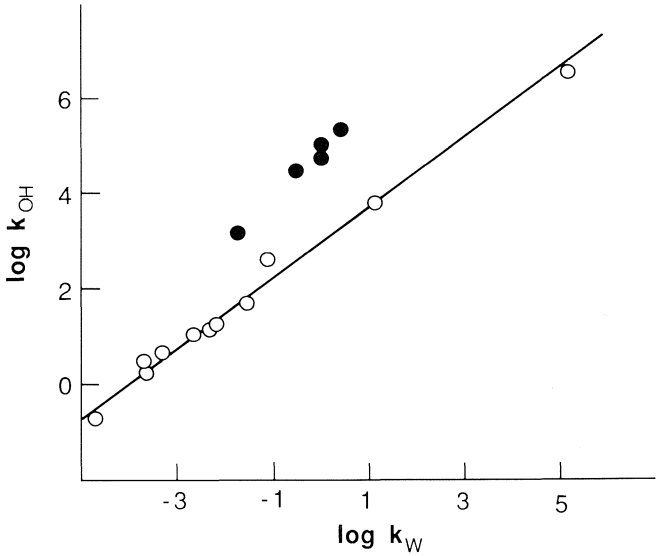

FIG. 3. log k_w vs. log k_{OH} for triarylmethyl and aryltropylium cations.

the range included in any other study of both rate and equilibrium constants for a single reaction type.

Figure 1 shows a plot of log k_{OH} vs. pK_R for all of the electrophiles in Table 1. The lower line in Fig. 1 is arbitrarily drawn through the extreme points for triarylmethyl cations and has a slope of 0.47. The upper line is arbitrarily drawn through the extreme points for xanthylium cations, has a slope of 0.51, and, interestingly, passes very close to the points for aryltropylium cations. Whether or not one attaches any significance to these lines, it is clear that, for a given pK_R, the order of reactivity of cation types is aryldiazonium > xanthylium $\simeq$ aryltropylium > triarylmethyl cations. This is what one might expect from either simple steric, or least-motion (41), considerations.

Figure 2 shows a plot of log k_w vs. pK_R. The line shown is arbitrarily drawn through the extreme points for triarylmethyl cations, and makes the point, contrary to Taft's early conclusion (34), that there is a rough correlation between log k_w and pK_R for the entire range of triarylmethyl cations. One could, however, draw "better" lines through selected groups of points as suggested by Taft (34).

There are differences and similarities in Figs. 1 and 2 which may be seen more clearly in Fig. 3 where log k_w is plotted against log k_{OH} for the triarylmethyl and aryltropylium cations. The line through the points for the triarylmethyl cations has a slope of 1.33 ($\Delta\log k_w/\Delta\log k_{OH}$). Although this non-unit slope has been interpreted (42) as an example of the operation of the reactivity–selectivity relationship, I think it is more likely to be due to a complete difference in the mechanisms of the water and hydroxide ion reactions.

It was noted above that the reactions of water with cations are subject to general-base catalysis. The existence of such catalysis has been confirmed for the least reactive (Crystal Violet) and the most reactive (triphenylmethyl cation) (36) of the triarylmethyl cations, and several of the other types of cations (13, 14, 37, 39) shown in Table 1. The reactions are believed to involve simultaneous carbon–oxygen bond formation and proton transfer to the base catalyst (12). Richard and Jencks (43) have discussed factors influencing the disappearance of the general-base catalysis for extremely reactive cations reacting with water and alcohols.

Although possible, it appears unlikely that the reactions of hydroxide ion with cations actually involve catalysis of the water reactions by hydroxide ion. Alkoxide ions, such as trifluoroethoxide ion, react with cations in aqueous solution to form ethers (23, 39). Hydroxide ion reacts more slowly than alkoxides of similar basicity. These facts indicate that hydroxide ion reacts in a direct cation–anion combination.

A difference in mechanism of the water and hydroxide ion reactions is also indicated by the results of a study of the α-deuterium isotope effect on the reactions of di-ferrocenylmethyl cation (38). The k_w shows $k_H/k_D = 0.91$, k_{OH} shows $k_H/k_D = 0.99$, and K_R shows $K_H/K_D = 0.85$. According to this measure, the water reaction has a transition state in which the cationic carbon has progressed well toward the carbinol carbon, while the hydroxide ion reaction has a transition state in which the cationic carbon has hardly changed from reactant state. This is consistent with the slope of greater than unity found in Fig. 3 for the triarylmethyl cations.

The mechanism of the reaction of water with carbonyl compounds has been discussed by Guthrie (44). Unfortunately, the conclusions were based on an unjustified (22) use of Marcus theory. There appear, however, several similarities between the carbonyl reactions and the cation reactions discussed here. It is particularly interesting that a plot of log k_w vs. log k_{OH} for the carbonyl reactions (not shown by Guthrie) has a slope of ca. 1.4, and that the water reactions are subject to general-base catalysis (45).

Gandler (46) has studied the general-base catalysis by substituted quinuclidines of the reactions of a series of triarylmethyl cations with water. Brønsted slopes of 0.33 to 0.52 are found, with, perhaps, a slight tendency for the slope to decrease with decreasing pK_R of the cations. It should be noted, however, that the log k_{Dab}/k_w, where k_{Dab} is the second-order rate constant for catalysis of the water reaction by Dabco (1,4-diazabicyclo[2.2.2]octane) and k_w is the first-order rate constant for the un-catalyzed (or water-catalyzed) water reaction, is 0.78 for Crystal Violet (46), 0.60 for tri-*p*-anisylmethyl cation (47), and 0.71 for triphenylmethyl cation (36). There is no appreciable change in this value as the pK_R of the cation changes from 9.39 to −6.63.

The relative reactivities of hydroxide ion and water, as given by k_{OH}/k_w, vary considerably for the cations shown in Table 1, ranging from a low of 8 for tris-(2,4-dimethoxyphenyl)methyl cation to ca. 10^5 for the aryltropylium cations. Values slightly greater than 10^7 have been reported for reactions of some quinolinium cations (48). The variations follow no obvious pattern, and the extremely low value for the tris-(2,4-dimethoxyphenyl)methyl cation is not found for the similarly substituted xanthylium cation.

In the initial paper on the N_+ relationship (9), log k_0 was defined as the logarithm of the rate constant for reaction of the given cation with water. The later finding of the difference in mechanism between water reactions and others (10–14) led to the suggestion (13) that water reactions not be included in the N_+ correlations, and that log k_0 be based on reactions of other nucleophiles. From a purely empirical standpoint, k_{OH}/k_w seldom varies outside the range of 10^3 to 10^5 and is only slightly more poorly behaved than some other relative reactivities which we have encountered in later work (17).

Equilibrium reactivities of nucleophiles

Parker suggested (49) and Hine developed (50) the concept of "carbon basicity", realizing that the common practice of comparing basicities of nucleophiles toward the proton with kinetic reactivities toward carbon compounds was not a proper rate-equilibrium comparison. The equilibrium constants, K^{RX}_{HX}, for the exchange reactions:

[7] $\quad R—OH + H—X \rightleftarrows R—X + H—OH$

were suggested by Hine (50) to be particularly appropriate for measuring the differences between proton and carbon basicities of various X^- bases. In an attempt to place water on the same basis as dilute solutes, HX, in aqueous solution, it is common to define the activity of water to be 55.5 *M* in dilute aqueous solutions. This definition will be used in the following discussion of reaction [7].

Equilibrium constants for reaction [7] can be calculated from those of simpler reactions in several ways. The most convenient method for the present purposes considers reaction [4] for OH^-, the corresponding reaction for X^-:

[8] $\quad R^+ + X^- \overset{K_X}{\rightleftharpoons} R—X$

TABLE 2. Values of log K^{RX}_{HX}

Nucleophile[a]	pK_a	log K^{RX}_{HX} Pyr[b]	Ar_3C^+	CH_3^+(gas)
$CF_3CH_2O^-$	12.4	−0.3		
CO_3^{2-}	10.3	0.2		
HOO^-	11.6	4.1		(6.6)[c]
n-PrS^-	10.8	7.6		9.6[d]
$HOCH_2CH_2S^-$	9.5	7.2	4.6	
$CH_3O_2CCH_2S^-$	8.0	7.6	4.9	
$C_6H_5S^-$	6.5	7.7		9.3
CN^-	9.1	(17.0)[e]		18.0
SO_3^{2-}	7.2	12.7	7.8	
N_3^-	4.0		3.4	
n-$BuNH_2$	10.5	3.0	0.2	18.6[f]
$^-O_2CCH_2NH_2$	9.8	2.1	0.5	
$CH_3OCH_2CH_2NH_2$	9.7	2.4		
$CF_3CH_2NH_2$	5.6	1.9	−0.1	
H_2NNH_2	8.1	4.7	1.2	
CH_3ONH_2	4.6	4.0	3.0	
$H_2NCONHNH_2$	3.9	3.2	2.6	
Piperidine	11.4	3.2		
Morpholine	8.5	2.8		

[a]In water at 20–25°C.
[b]For Pyronin-Y or aryltropylium cations.
[c]This value is for R^+ = *t*-Bu^+ from ref. 50.
[d]This value is actually for CH_3S^-.
[e]This is an estimated value; see ref. 52.
[f]This value is actually for CH_3NH_2. The value for CH_3NH^- is 6.5; the remaining 12.1 units comes from the differences in basicities of CH_3NH_2 and $(CH_3)_2NH$ in the gas phase. Thus, the value for CH_3NH_2 in water is ca. 6.5.

and the acid ionizations of the acids HX and HOH. The equilibrium constants for reaction [7] are then calculated as:

[9] $\quad \log K^{RX}_{HX} = \log K_X - \log K_{OH} - pK_{a(HX)} + pK_{a(HOH)}$

where the acid ionization constant for water is defined as the ion product of water, K_w, divided by 55.5 *M* (i.e.: at 25°C, $pK_{a(HOH)}$ = 15.74). For neutral nucleophiles such as primary and secondary amines, the reaction analogous to reaction [8] is

[10] $\quad R^+ + BH \rightleftarrows R—BH^+$

and the pK_a in eq. [9] is that for BH_2^+.

Values of log K^{RX}_{HX} for several types of R and for a range of nucleophiles are shown in Table 2. Since relative equilibrium reactivities of nucleophiles are the same toward Pyronin-Y and aryltropylium cations (22), the values of K^{RX}_{HX} are the same for the two types of cations and are shown in a single column of Table 2. Similarly, relative equilibrium reactivities are the same for all of the triarylmethyl cations, excepting the *ortho*-substituted ones, and a single column is needed in Table 2. For a few nucleophiles, data are given for R = CH_3 in the gas phase. These data are calculated from bond dissociation energies (51) as described by Hine (50).

It may be useful to note that the data in Tables 1 and 2 used in eq. [9] allow the solution for log K_X for specific cations and nucleophiles. Values thus obtained are expected to be very good estimates.

The value of log K^{RX}_{HX} for trifluoroethoxide ion reacting with Pyronin-Y or aryltropylium cations is precisely the value expected from symmetry if our standard state definition of water has accomplished its aim, and if the relative basicities of trifluoroethoxide and hydroxide ions are the same toward the proton and carbon, except for the symmetry of HOH. Similarly,

the basicity of carbonate ion, relative to hydroxide ion, is only marginally greater toward carbon than toward the proton.

None of the values of log K^{RX}_{HX} shown in Table 2 are significantly negative, indicating that none of the nucleophiles considered here, relative to hydroxide ion, are significantly more basic toward the proton than toward carbon. Hine and Weimer (50) have pointed out that this is consistent with expectations based on electronegativity if carbon is more electronegative than hydrogen. Hydrogen would then preferentially bond to the more electronegative X. The value of log K^{RX}_{HX} for X = F and R = isopropyl, in the gas phase, is −2.3. The absence of negative values in Table 2, according to this argument, is due to the fact that none of the X included there are more electronegative than OH.

It is interesting to note that in every case where comparisons are possible the value of log K^{RX}_{HX} is smaller for triarylmethyl cations than for Pyronin-Y cation, and, in the few cases available, is smaller for Pyronin-Y than for methyl cation. This is what would be expected from a simple steric argument based on OH being sterically smaller than any of the other X considered. A steric effect is also likely involved in the reactions of azide ion with *ortho*-substituted triarylmethyl cations (18). The value of log K^{RX}_{HX} for azide ion with tri-*p*-anisylmethyl cation is 3.4. Smaller values of 1.3 and 2.3 are found for *ortho*-SO_2CH_3 and *ortho*-SO_3^- compounds, respectively.

Dixon and Bruice (53) first pointed out that "α-effect" nucleophiles show large equilibrium constants for reactions with triarylmethyl cations. Peroxide ion, hydrazine, methoxylamine, and semicarbazide all show larger values of log K^{RX}_{HX} than do alkoxides or primary amines. This is not likely to be a steric effect since the values for secondary amines are also larger than those for primary amines, and, in the case of peroxide ion, it would be difficult to argue that peroxide is smaller than hydroxide ion.

There appears to be a trend for values of log K^{RX}_{HX} to decrease with decreasing pK_a of the conjugate acids of primary amines. This is consistent with the above arguments that the R's are more electronegative than hydrogen. It is also consistent with the fact that the pK_a's of the RBH^+ products of reaction [10] are lower than the pK_a's of the corresponding BH_2^+ ions (11, 22).

The largest values of log K^{RX}_{HX} are for thiolate and sulfite ions. It is even possible that the values for sulfite ion are higher than those reported in Table 2. The products of reaction of sulfite ion with cations almost certainly involve bond formation between carbon and sulfur. If the stable form of bisulfite ion in water is the isomer with a hydrogen–sulfur bond, then the values given in Table 2 are proper ones. If, however, the stable isomer is the one with a hydrogen–oxygen bond, then the measured pK_a is greater than the pK_a for the unstable isomer, which is the one which should be used in the calculation from eq. [9]. Guthrie (54) has argued that the stable isomer in aqueous solution is the H—S bonded form. If that is correct, then the values in Table 2 are the proper ones.

Arnett *et al.* have recently reported (56) studies of the reactions of carbocations with carbanions. Heats of reactions for trimethyl- and triphenylcyclopropenium cations with a series of substituted arylmalononitrile anions in acetonitrile solution, and for triphenylmethyl cation with a series of 9-substituted fluorenide ions in benzonitrile solution were measured. The pK_R's of the cations are known in aqueous acid, and the pK_a's of the conjugate acids of the carbanions are known in dimethyl sulfoxide solution. A plot of the molar heats of reactions vs. (pK_a − pK_R), amazingly, gave a reasonably good single straight line for all of the reactions in both solvents:

$$[11] \quad -\Delta H_{rxn} = 11.98 + 1.18(pK_a - pK_R)$$

Arnett *et al.* call this the "Master Equation" for the carbocation–carbanion reactions. They point out that relative pK_a's and pK_R's for delocalized ions such as those involved in the study are not sensitive to solvent, so that the use of values measured in solvents different from those used in the heat measurements is justified. In earlier work (57), it was found that the free energies are linearly related to the enthalpies for some of these reactions, with a slope of 1.16. If this relationship holds for all of the reactions obeying eq. [11], then the slope of a plot of the standard free energies vs. (pK_a − pK_R) will be 1.16 × 1.18 = 1.37, which is precisely (embarrasingly so) equal to 2.3RT at 25°C. This implies a constant value of log K^{RX}_{HX} for all of the carbocations and carbanions studied. It is very difficult to understand this constancy, particularly for the reactions of triphenylmethyl cation with fluorenides where steric effects would be expected to be huge.

In addition to the data shown in Table 2, values of log K^{RX}_{HX} are available for a good range of X for R = CH_3CO, mostly from Jencks' laboratory (55), and for α-hydroxy groups, R = R′CHOH, from studies of carbonyl addition reactions (52).

Although values of log K^{RX}_{HX} are not expected to be very solvent sensitive, the equilibrium constants for reaction [8] should vary tremendously with change of solvent from water to non-hydroxylic polar solvents. Some of these changes for solvents water, methanol, and dimethyl sulfoxide are shown in Table 3. If the free energies of transfer of the cations, nucleophiles, and products of reactions were determined by additive contributions of groups, it is easy to show (21) that:

$$[12] \quad \Delta\log K_X - \Delta pK_{a(HX)} = \text{constant} \equiv \Pi$$

where $\Delta\log K_X$ is the change in log K_X, and $\Delta pK_{a(HX)}$ is the change in the pK_a of HX, on changing solvent, and Π is defined by the equation and is expected to be independent of R^+ and X^-. For the change from water to methanol or to dimethyl sulfoxide, the values of Π are shown in Table 3 (23).

For the change from water to methanol solvent, values of Π range from −1.7 to +0.9, and for the change from water to dimethyl sulfoxide, values range from 2.5 to 4.3. Although the ranges are disappointingly large, indicating the breakdown of additivity, the average values of −0.4 for methanol and 3.3 for dimethyl sulfoxide allow reasonable estimates of equilibrium constants in these solvents if values are known in water. It is also interesting to note that the average value of Π for dimethyl sulfoxide solutions is equal to the negative of the logarithm of the activity coefficient of the proton in dimethyl sulfoxide relative to a standard state in water (52). This implies that the free energies of transfer from water to dimethyl sulfoxide of the cations considered here are all close to zero. This follows from the fact that:

$$[13] \quad \Delta\log K_X - \Delta pK_{a(HX)} = \log \gamma_R\gamma_{HX}/\gamma_H\gamma_{RX}$$

where the γ's are activity coefficients of the subscripted species (charges omitted) in dimethyl sulfoxide relative to a standard state in water, since the activity coefficients of HX and RX are expected to be close to unity (52).

Kinetic reactivities of nucleophiles

Relative reactivities of nucleophiles toward several different types of cations and a neutral electrophile are shown in Table 4. In the triarylmethyl cation series, relative reactivities of nucleophiles, with the exception of water, are independent of

TABLE 3. Solvent effects on equilibria (24)[a]

Reaction	log K_w	log K_M	Π_M	log K_D	Π_D
CV^{+}[b] + $HOCH_2CH_2S^-$	2.85			11.00	2.5
Pyronin-Y^+ + *n*-PrS^-	5.10			14.64	3.3
$DMAPTr^{+}$[c] + $C_6H_5S^-$	5.10	8.96	−0.9		
p-$ClC_6H_4N_2^+$ + CN^-	2.65			9.40	3.0
p-$CH_3C_6H_5N_2^+$ + CN^-	1.18			8.15	3.2
p-$NCC_6H_5N_2^+$ + CN^-	4.15	7.34	−0.7		
Pyronin-Y^+ + *n*-$BuNH_2$	−0.24	−0.25	−1.7	4.00	3.8
Pyronin-Y^+ + $CH_3OCH_2CH_2NH_2$	−1.17			3.26	3.6
MG^{+}[d] + $CF_3CH_2NH_2$	−2.89			0.00	2.7
MG^+ + $EtO_2CCH_2NH_2$	−1.30	−0.80	−0.8		
$DMAPTr^+$ + $EtO_2CCH_2NH_2$	1.10	1.39	−1.0		
$DMAPTr^+$ + $CF_3CH_2NH_2$	−1.69	−0.39	0.2		
$DMAPTr^+$ + $H_2NCONHNH_2$	−2.00	0.80	0.9		
$DMAPTr^+$ + Morpholine	2.30	3.30	−0.1		
Pyronin-Y^+ + Morpholine	−2.00			2.47	4.3
Pyronin-Y^+ + Piperidine	1.35			4.35	3.5

[a]Subscripts w, M, and D refer to solvents water, methanol, and dimethyl sulfoxide, respectively.
[b]CV^+ is Crystal Violet, tris-(*p*-dimethylaminophenyl)methyl, cation.
[c]$DMAPTr^+$ is the *p*-dimethylaminophenyltropylium cation.
[d]MG^+ is Malachite Green, bis-(*p*-dimethylaminophenyl)phenylmethyl, cation.

TABLE 4. log k_{nuc}/k_{OH} in water[a]

Nucleophile	log k_{nuc}/k_{OH}				
	Ar_3C^+	$ArTr^+$	Pyr-Y^+	ArF	ϕ_3C^+
CH_3O^-		2.20			
$HC{\equiv}CCH_2O^-$	1.1[b]				
$(CH_3)_3^+NCH_2CH_2O^-$	1.0[b]				
$CF_3CH_2O^-$	0.31	0.91		0.95	0.09[c]
CO_3^{2-}		−0.20			
SO_3^{2-}	3.26	2.75	3.16		1.66[c]
CN^-	−0.63	−1.70	−1.60	−1.88	0.02[c]
N_3^-	2.79[d]			−0.80	2.87[c]
RS^-[e]	4.01	4.95	4.99	3.2	1.70[c]
HOO^-	3.77	2.45	2.58	2.74	
n-$BuNH_2$	0.53	0.41	1.36	0.91	0.39[c]
$CF_3CH_2NH_2$	−1.30	−1.62		−1.89	−0.29[c]
Piperidine		1.77	2.83	1.91	0.30[c]
Morpholine		1.05	2.24	0.93	0.23[c]
H_2NNH_2	1.26	0.25	0.97	0.53	0.60[c]
CH_3ONH_2	−0.38	−1.59		−1.67	
$HONH_2$	0.30	−0.93			0.39[c]

[a]ArF is 2,4-dinitrofluorobenzene. Data are from refs. 1–25 unless otherwise indicated.
[b]Data from ref. 58.
[c]Data from ref. 35.
[d]Data are for *n*-propanethiolate where available. Since thiolates all show essentially the same rate toward a given electrophile (see ref. 17), some of the data are for other thiolates.

the pK_R of the cation from 0.81 for tri-*p*-anisylmethyl cation to 9.39 for Crystal Violet (16, 42). Similar behavior is found for tropylium and aryltropylium cations (11, 14), although the pK_R range is only 4.7–7.3.

Comparisons of one cation type with another show substantial variations in relative reactivities of the nucleophiles, and, therefore, breakdowns of the N_+ relationship. The variations in relative kinetic reactivities, usually, are smaller than the variations in relative equilibrium reactivities discussed above. For example, sulfite ion gave log K^{RX}_{HX} of 12.7 for Pyronin-Y and of 7.8 for triarylmethyl cations, while log $k_{sulfite}/k_{OH}$ is 3.26 for triarylmethyl cations, 2.75 for aryltropylium cations, and 3.16 for Pyronin-Y cation. Similarly, for thiolate ions, log K^{RX}_{HX} varies by nearly 3 units while log k_{RS}/k_{OH} varies by ca. 1 unit for the change from triarylmethyl to Pyronin-Y cations.

In the comparison of Pyronin-Y with aryltropylium cations, however, substantial differences in relative kinetic reactivities are shown, while, as already remarked, the relative equilibrium reactivities are the same for the two types (22). Amines, particularly the secondary amines morpholine and piperidine, are more reactive, relative to other nucleophiles, toward Pyronin-Y than toward the aryltropylium cations. There are no obvious reasonable rationalizations of this behavior.

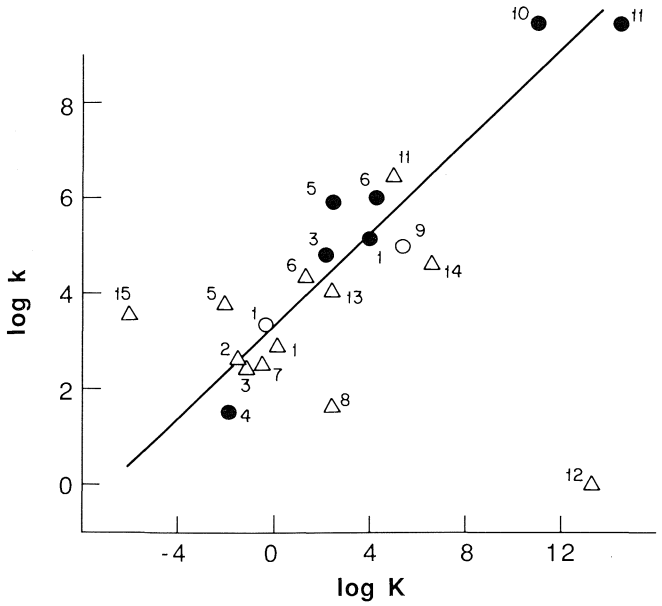

FIG. 4. Rate–equilibrium plot for pyronin-Y cation reactions. Triangles, aqueous solution; open circles, methanol solution; closed circles, dimethyl sulfoxide solution. Nucleophiles are identified as follows: 1-*n*-$BuNH_2$; 2-glycinate; 3-2-methoxyethylamine; 4-2,2,2-trifluoroethylamine; 5-morpholine; 6-piperidine; 7-hydrazine; 8-hydroxide ion; 9-methoxide ion; 10-methyl thioglycollate ion; 11-*n*-PrS^-; 12-CN^-; 13-HOO^-; 14-SO_3^{2-}; 15-N_3^-. Data for azide and cyanide ions estimated as described in ref. 52.

It is clear that there is no general correlation of the rates and equilibria of the reactions (22). A plot of log k vs. log K for reactions of nucleophiles with Pyronin-Y cation is shown in Fig. 4. The line shown is an arbitrary one having a slope of 0.5 and passing close to the points for reactions of primary amines. Azide ion and thiolate ions have much greater rate constants than do other nucleophiles with similar equilibrium constants, while sulfite ion, hydroxide ion, and cyanide ion have much smaller rate constants than other nucleophiles with similar equilibrium constants.

Relative kinetic reactivities are surprisingly similar toward aryltropylium cations and the neutral 2,4-dinitrohalobenzenes (15). Data are given in Table 4 for 2,4-dinitrofluorobenzene. Only thiolate ions and azide ion show significantly different relative reactivities toward the aryl halides than toward aryltropylium cations. The thiolate ion relative reactivities, log k_{RS}/k_{OH}, also vary with the halogen of the aryl halide, being 3.2 for F, 4.5 for Cl, 4.7 for Br, and 5.1 for I (15). The increasing value for increasing size of the halide is what one might expect from polarizability arguments (59), but it is the values for the Cl, Br, and I that are most "normal" when compared with those for cations. In a comparison of Pyronin-Y cation and its thio-analog, log k_{RS}/k_{OH} values were 4.9 and 5.9, respectively (22). The increase by one unit on substitution of S for O at the remote site is very nearly as large as the 1.3 unit change on substitution of Cl for F at the reaction site for the aryl halides.

For "families" of nucleophiles, values of log K_x are linearly related to pK_a's of the conjugate acids of the nucleophiles with slopes not far from unity, as we discussed in the earlier section of this paper. For such families, Brønsted slopes are nearly equal to slopes of log K vs. log k plots, and are frequently interpreted in terms of the extents of bond formation at transition states. For the reactions of a series of primary amines with any of the cations which we have studied, Brønsted slopes of ca. 0.4 are found (11, 13). The Brønsted slopes for reactions of thiolates with cations are all very close to zero (17), and the slopes for alkoxide ions (58) are ca. 0.2 to 0.3. These differences in slopes for the different families would be expected to be reflected in differences in relative rates of reactions of the cations if the interpretation in terms of bond formation is correct. The clearest comparisons are for Crystal Violet (pK_R = 9.39) and tri-*p*-anisylmethyl cation (pK_R = 0.81). The rate constant ratios, log k_{TAM}/k_{CV}, are 4.66 for ammonia, 4.61 for hydroxide ion, and 4.50 for 2-hydroxyethanethiolate ion. Since the difference in pK_R values is 8.6 units, the values of log k_{TAM}/k_{CV} indicate approximately 0.5 (i.e.: 8.6/4.5) "extent of reaction" for all of the nucleophiles, counter to the conclusion from differing Brønsted slopes.

Another measure of "extent of reaction" is furnished by the secondary α-isotope effects reported by Bunton *et al.* (38) for reactions of di-ferrocenylmethyl cation. Values of k_H/k_D of 1.00 ± 0.01 for reactions of all anionic nucleophiles, and of 0.96 for reactions of amines, compared with the equilibrium isotope effect K_H/k_D for reaction of hydroxide ion of 0.85, indicate no "progress" at the transition states for reactions of anions, and very little progress for reactions of amines.

It is obvious that interpretation of any of these measures in terms of a simple "extent of reaction" parameter (22) is not possible. These types of "imbalances" in various measures of extent of reaction have been discussed for several other reaction types (17, 55*a*, 60).

The constancy of the values of log k_{TAM}/k_{CV} remarked above for several nucleophiles is quite pertinent to the question of the operation of a reactivity-selectivity relationship in these reactions (42). The value of log k_{RS}/k_{OH} is 4.05 for Crystal Violet and 3.94 for tri-*p*-anisylmethyl cation. Thus, a difference of 10^4 in nucleophilic reactivity does not influence appreciably the difference of 10^4 in electrophilic reactivity, and vice versa. Other examples abound in our studies (9, 13), and were the basis of the N_+ relationship, which contains no cross terms, and, therefore, no allowance for change in selectivity.

The actual value of the rate constant for reaction of 2-hydroxyethanethiolate ion with tri-*p*-anisylmethyl cation is $7.1 \times 10^7\ M^{-1}\ s^{-1}$ in water at 25°C (17). This value is within two orders of magnitude of that expected for a diffusion-controlled reaction (Richard and Jencks (61) take $k_{DC} = 5 \times 10^9\ M^{-1}\ s^{-1}$), yet k_{RS}/k_{OH} is essentially the same as for Crystal Violet, for which $k_{RS} = 2.2 \times 10^3\ M^{-1}\ s^{-1}$. An even closer approach of rates to diffusion control occurs for the reactions of sulfite ion with aryldiazonium ions in water. For *p*-nitro- and *p*-cyanobenzenediazonium ions, $k_{SO_3} = 4. \times 10^8\ M^{-1}\ s^{-1}$, and log k_{SO_3}/k_{OH} = 3.0. For Crystal Violet, $k_{SO_3} = 5. \times 10^2\ M^{-1}\ s^{-1}$, and log k_{SO_3}/k_{OH} = 3.4. The selectivity for Crystal Violet is insignificantly greater than that of the aryldiazonium ions where the rate for sulfite is within an order of magnitude of diffusion control. In non-aqueous solutions, greater rate constants are frequently observed. In methanol solution, the *p*-nitro- and *p*-cyanobenzenediazonium ions react with thiophenoxide ion with rate constants slightly greater than $5 \times 10^9\ M^{-1}\ s^{-1}$; the unsubstituted benzenediazonium ion has $k_{PhS} = 1.4 \times 10^9\ M^{-1}\ s^{-1}$. Yet the value of log k_{PhS}/k_{OH} for benzenediazonium ion (5.5) is scarcely different from that for Malachite Green (5.7) which reacts more than 10^3 more slowly with either nucleophile (9).

This type of behavior led Jencks and co-workers (61, 62) to

use the reactions of the very reactive sulfite ion and azide ion in water with very reactive cations as "clocks" for the rates of reactions of the cations with solvent. The cations were generated as reactive intermediates in the presence of the reactive nucleophile. The product ratio resulting from trapping by solvent and by the reaction nucleophile then gives the rate ratio. In cases where this ratio is much less than those found for our "stable" cations, Jencks assumes that the rate constant for reaction of the reactive nucleophile is diffusion-controlled, with a value of $5 \times 10^9\ M^{-1}\ s^{-1}$, allowing the calculation of the rate constant for reaction of solvent.

The technique was first used in the acid-catalyzed breakdown of substituted acetophenone dimethyl ketals to give rate constants ranging from 7×10^6 to $4 \times 10^8\ s^{-1}$ for reactions of water with the intermediate oxocarbonium ions (62). More recently, rate constants up to $4 \times 10^9\ s^{-1}$ for reaction of water with aryl-substituted 1-phenylethyl cations generated as intermediates in solvolysis reactions have been calculated (61). Ta-Shma and Rappoport (63) have re-examined the trapping studies which have been carried out for solvolysis reactions by many workers and conclude that the results can most reasonably be interpreted in terms of diffusion-controlled trapping of intermediate cations and changes in mechanism from S_N1 to S_N2.

There is some question concerning the exact magnitudes of diffusion-controlled reaction rates in water for electrophile–nucleophile combination reactions (64). In the series of increasingly reactive 1-arylethyl cations (65), the rate ratios for two different anionic nucleophiles do not always level out at close to unity. For azide and acetate, for example, the rate constant ratio seems to level at $k_{az}/k_{ac} = 10$. Jencks suggests that basic oxyanions, such as acetate and alkoxide ions, have a barrier to desolvation which causes rate constants for their reactions to level at ca. $5 \times 10^8\ M^{-1}\ s^{-1}$. It is not obvious, however, why oxyanions differ in this respect from azide or thiolate ions. The change in pK_a on changing from water to dimethyl sulfoxide is ca. 7 units for acetic acid and ca. 6 units for 2-hydroxyethanethiol (21). If this change results largely from hydrogen bonding in water, as usually believed (66), then acetate and thiolate ions must have comparable hydrogen bonding stabilization in water.

In the studies of "stable" cations, the fastest rates measured in water give values of log k as follows: tri-*p*-anisylmethyl cation + 2-hydroxyethanethiolate (17), 7.85; tri-*p*-anisylmethyl cation + thiophenoxide ion (67), 8.26; *p*-dimethylaminophenyltropylium cation + thiophenoxide ion (23), 8.80; Pyronin-Y cation + *n*-propanethiolate ion (22), 6.60. There is no indication in any of these reactions that the rates have levelled off, causing a decrease in selectivity.

McClelland's very recent results for reactions of triphenylmethyl cation are particularly interesting (36). Although this study was actually carried out in 1:2 acetonitrile:water solvent, it does not seem likely that the results would be appreciably different in pure water (see, for example, the study by Bunton *et al.* (38) in a very comparable solvent). The rate constant for reaction of azide ion with the trityl cation, $k_{az} = 4 \times 10^9\ M^{-1}\ s^{-1}$, is very close to the value estimated by Richard and Jencks (61) for a diffusion-controlled reaction. For thioglycollate and sulfite dianions, both of which are more reactive than azide ion toward tri-*p*-anisylmethyl cation, the rate constants for reactions with trityl cation are $2. \times 10^8$ and $2.4 \times 10^8\ M^{-1}\ s^{-1}$, respectively. The rate constant for reaction of thioglycollate dianion with tri-*p*-anisylmethyl cation is expected (17) to be the same as that for reaction of 2-hydroxyethanethiolate, $k = 7. \times 10^7\ M^{-1}\ s^{-1}$, which is only a factor of three smaller than that for trityl cation, whose pK_R is 7 units below tri-*p*-anisylmethyl cation. This seems to indicate that, at least for the thioglycollate ion, the rate constant has levelled off below the diffusion-controlled limit for trityl cation reaction.

From the data given in Table 4, it is evident that reactions of trityl cation do not obey the N_+ relationship. This could conceivably be due to a levelling of rates at below diffusion control, as discussed above, or to the incursion of the reactivity–selectivity relationship in its originally conceived form (30). As McClelland *et al.* point out (36), the reactions of amines, with rate constants on the order of $10^7\ M^{-1}\ s^{-1}$ and an appreciable, although small, Brønsted slope, appear more consistent with the reactivity–selectivity relationship. The thioglycollate and sulfite reactions, however, seem more consistent with the levelling out postulate, possibly having to do with desolvation requirements (55*a*, 61, 68).

In this latter connection, it should be noted that thiolates of widely differing equilibrium reactivities have essentially identical kinetic reactivities toward cations both in water (17) and in dimethyl sulfoxide (21) solutions. The essentially zero Brønsted slopes for the thiolate reactions are not, therefore, due to hydrogen bonding of water as has been postulated for oxyanions (55*a*, 68).

Solvent effects on kinetics

One of the primary reasons for beginning the study of cation–anion combination reactions was the possibility that these reactions might be particularly susceptible of the types of solvent effects suggested by Caldin (69). The essential idea is that the solvation of transition states need not be analogous to that of stable species having the same structure (70). For cation–anion combination reactions, the transition states are expected to have structures which are in all senses intermediate between reactants and products. If the transition states were solvated as stable species, the solvation would also be expected to be intermediate between that of reactants and products. Quite specifically, the effect of changing solvent on the rate constant for such a reaction would be expected to be smaller than the effect of the equilibrium constant (1).

There are some indications that the transition states for cation–anion combinations are solvated in an unusual manner. For the reaction of Malachite Green cation with hydroxide ion in aqueous solution (12), $\Delta S^0 = -2.0$ eu, and $\Delta S^\dagger = -14.0$ eu. The entropy of the transition state is more negative than that of the reactants or the products. LeNoble *et al.* (71) find a similar situation for the volume of activation of the same reaction. The ΔV^0 is estimated to be $+15.0\ cm^3/mol$, and $\Delta V^\dagger$ is $+30.0\ cm^3/mol$.

In spite of some excitement based on limits (1) and estimates (21), however, no spectacular solvent effects on rates and equilibria have been found. In all cases where both rates and equilibria have been determined in more than one solvent, the solvent effects on rates are either smaller than the effects on equilibria, or are very small (23).

For the change of solvent from water to dimethyl sulfoxide, very large effects on both rates and equilibria are observed (1, 9, 21, 23). For cations reacting with cyanide ion (9), rate constants are ca. 10^5, and equilibrium constants ca. 10^7, greater in dimethyl sulfoxide than in water. Even for cations reacting with neutral amines, increases of ca. 10^2 in rate constants and of ca. 10^4 in equilibrium constants occur on going from water to dimethyl sulfoxide (23). In all cases actually measured,

however, the effect of solvent on log k is 0.3 to 0.8 times the effect on log K, as expected for "normal" solvation of transition states.

For the solvent change from water to methanol, there are a few reactions, all involving carbocations reacting with primary amines, for which the rate constants are affected more than, or even in the opposite direction from, the equilibrium constants (23). Only four of the nine reactions of carbocations with primary amines studied in both solvents show this unusual effect, and, in all of the reactions, the effect of changing from water to methanol solvent is small, producing a maximum of a factor of ten change in rate constant.

Even though there is, then, some evidence for an "unusual" solvent effect on some of the reactions, the "non-classical" solvation of transition states seems to have a minor effect, at most, on the rate constants. Kurz *et al.* (72) have discussed similar types of solvent effects in solvolyses of methyl compounds, and van der Zwan and Hyne (73) have developed a general theory of such effects.

General patterns of nucleophilic reactivity

The N_+ relationship, eq. [1], was first formulated (9) to describe the behaviors of reactions of carbocations and aryldiazonium ions with a few anionic nucleophiles in several solvents (31). The relationship was then found to apply reasonably well to the reactions of the carbocations with neutral amine nucleophiles (11). The next obvious step was to see if the relationship applies to reactions of neutral electrophiles.

Jencks and co-workers (74, 75) had reported rate constants for reactions of a good variety of nucleophiles with aryl acetates and with some very reactive acetyl- and acetoxypyridinium ions. The absence of selectivity–reactivity relationships in the reactions had been particularly noted (75). The data for the reactions were found to fit reasonably well to the N_+ relationship when allowance was made for changes in rate-determining step in some of the reactions (13). Some severe failures of the N_+ relationship were found for specific cases, however. In particular, azide ion, fluoride ion, and aryloxide ions could not be accommodated. Later work by Hupe and Jencks (55*a*) on reactions of oxyanions and thiolates with esters and our work (17) on reactions of thiolates with carbocations showed a particularly serious failure of the N_+ relationship for reactions of thiolates with esters. More recently, Palling and Jencks (76) have reported a study of reactions of nucleophiles with acetyl chloride and conclude that the N_+ relationship does not apply to these reactions.

As already mentioned in earlier sections, the reactions of nucleophiles with 2,3-dinitrohalobenzenes in water correlate very well with the reactions of the nucleophiles with aryltropylium cations (15). Some of the features of those reactions are also found in the reactions of nucleophiles with *trans*-3-methoxyacrylophenone and its thiomethyl analog (20). In comparing these reactions of neutral electrophiles with those of *p*-dimethylaminophenyltropylium cation, separate lines are generated by reactions in water and those in methanol solutions. That this is caused by a difference in free energy of transfer of the cationic and neutral electrophiles is indicated by a comparison of the reactions of *trans*-3-methoxyacrylophenone with those of 2,4-dinitrophenyl acetate in the two solvents; a single correlation line is found (20).

In connection with the interpretations of studies of trapping of solvolysis intermediates (6, 63), it seemed important to establish the patterns of reactivity of nucleophiles toward ion-pairs. This was accomplished by synthesizing and studying reactions of an intramolecular ion-pair, an *ortho*-sulfonate substituted triarylmethyl cation (18). The relative reactivities of positive, neutral, anionic, and di-anionic nucleophiles were not affected by the presence of the *ortho*-sulfonate group. This study and that of the neutral electrophiles demonstrate an absence of any significant electrostatic effects on the rates of electrophile–nucleophile combination reactions.

Bunton *et al.* (38, 67) have extended the N_+ relationship to reactions of ferrocenyl-substituted methyl cations, and to a few nucleophiles, such as borohydride ion, which are not simple Lewis bases. His studies of the α-isotope effects on the reactions have been discussed in earlier sections of this paper. Alavosus and Sweigart (77) have gone considerably farther into the organometallic area by showing that the N_+ relationship works remarkably well for the reactions of nitrogen and phosphorus nucleophiles with metal-complexed Π-hydrocarbons.

McClelland and co-workers' recent studies of very reactive cations (36, 40), and Richard and Jencks' studies of the 1-arylethyl cations (43, 61, 65) clearly indicate the need for more studies of cations less stable than the tri-*p*-anisylmethyl cation ($pK_R = 0.81$). As discussed above, the point to be established is whether or not limiting rates below diffusion control are common, and whether or not reactivity–selectivity relationships become operable for very reactive species.

The N_+ relationship is certainly not the final word on nucleophilic reactivity. It fails badly in some instances for no apparent reasons, and it may not apply to extremely reactive carbocations. It is, however, about as good as one can do at the present time in attempts to predict or correlate rates of electrophile–nucleophile combination reactions. Several sets of N_+ values are given in Table 5.

Theories of nucleophilic reactivity

Swain and Scott (78) were certainly among the very first to attempt an understanding of nucleophilic reactivity, at least in the empirical sense of correlating such reactions. The focus of their attention, however, was on S_N2 substitution and S_N1 and S_N2 solvolysis reactions. Edwards (26) gave attention to more general types of nucleophilic reactivity. Following an earlier suggestion by Foss (79), Edwards examined the possible relationship between oxidation potentials and nucleophilicity. The oxidation potentials considered were those for the oxidative dimerizations:

$$[14] \quad X^- \rightleftarrows \tfrac{1}{2}X_2 + e^-$$

The four parameter equation:

$$[15] \quad \log k/k_0 = AE + BH$$

was proposed, in which k and k_0 are rate constants for reactions of the given electrophile with the given nucleophile and with water, respectively, E is the oxidation potential (reaction [14]) of the nucleophile, relative to water, H is the pK_a of the conjugate acid of the nucleophile, relative to hydronium ion, and A and B are parameters giving the sensitivity of the electrophile to oxidation potential and basicity of the nucleophile.

Edwards was bothered by eq. [15] in that some reactions required negative values of the parameter A (80). Other authors (81) had expressed doubt about the appropriateness of reaction [14] as a "model process" for nucleophilic reactivity, since the potentials contain a large contribution from the X—X bond energies. The parameter E was then redefined by Edwards (80) as the polarizability of the nucleophile. Edwards and Pearson

TABLE 5. N_+ values[a]

Nucleophile	Solvent	N_+ Ar_3C^+[b]	N_+ Pyr-Y[c]	N_+ $ArTr^+$[d]
H_2O	Water	0.73		−0.26
NH_3	Water	3.89		
n-$BuNH_2$	Methanol	6.16	6.54	
$EtNH_2$	Water	5.28	6.11	4.97
$H_2NCH_2CH_2NH_2$	Water	5.44		5.09
$EtO_2CCH_2NH_2$	Water	4.40		4.25
$EtO_2CCH_2NH_2$	Methanol	5.13		5.13
$EtO_2CCH_2NH_2$	DMSO	6.54		
$H_3^+NCH_2CH_2NH_2$	Water	4.35		3.84
$^-O_2CCH_2NH_2$	Water	5.36	5.79	5.23
Glycylglycinate	Water	4.69		4.63
$CH_3OCH_2CH_2NH_2$	Water	5.07	5.57	
$CH_3OCH_2CH_2NH_2$	DMSO	7.56	8.12	
n-$PrNH_2$	DMSO	7.88	8.40	
$CF_3CH_2NH_2$	Water	3.45		3.13
$CF_3CH_2NH_2$	DMSO	4.86	4.70	
H_2NNH_2	Water	6.01	5.71	5.00
H_2NNH_2	Methanol	6.89		5.93
H_2NNH_2	DMSO	8.17		
$HONH_2$	Water	5.05		3.82
CH_3ONH_2	Water	4.37		3.16
CH_3ONH_2	DMSO	6.38		
$C_6H_5NHNH_2$	Water	4.77		4.28
$H_2NCONHNH_2$	Water	3.73		3.42
$H_2NCONHNH_2$	DMSO	6.22		
Morpholine	Water		6.99	5.80
Morpholine	DMSO		9.17	
Piperidine	Water		7.58	
Piperidine	DMSO		9.32	
OH^-	Water	(4.75)	(4.75)	(4.75)
CH_3O^-	Methanol	7.51	8.32	7.88
$HC{\equiv}CCH_2O^-$	Water	5.84		
$CF_3CH_2O^-$	Water	5.06		5.66
CN^-	Water	4.12	3.15	3.05
CN^-	DMF	9.44		
CN^-	DMSO	8.64		
N_3^-	Water	7.54		
N_3^-	Methanol	8.78		
ClO^-	Water	7.41		
HOO^-	Water	8.52	7.33	7.20
SO_3^{2-}	Water	8.01	7.91	7.50
BH_4^-	Water	6.95		
$C_6H_5S^-$	Water	9.10		10.32
$C_6H_5S^-$	Methanol	10.41		>11.3[e]
EtS^-	Water	8.76		9.7
$HOCH_2CH_2S^-$	Water	8.87		9.24
$HOCH_2CH_2S^-$	DMSO	12.71		
$CH_3O_2CCH_2S^-$	Water	8.89		9.29
$CH_3O_2CCH_2S^-$	DMSO	12.71	>13.0[e]	
n-PrS^-	Water	8.93	9.74	
$^-O_2CCH_2S^-$	Water	9.09		9.26

[a]All values are relative to $N_+ = 4.75$ for hydroxide ion in water. See ref. 13.
[b]Values based on reactions of Malachite Green or tri-*p*-anisylmethyl cation.
[c]Values based on reactions of Pyronin-Y cation.
[d]Values based on reactions of *p*-dimethylaminophenyltropylium cation.
[e]The rates measured were at the diffusion-controlled limit.

(29) discussed the applications of the modified eq. [15] to a wide range of reactions, considerd how the parameters A and B vary with the nature of the electrophile, and pointed out the existence of the "α-effect", which is not included in the equation.

One of the difficulties of the Edwards equations is that neither oxidation potentials nor polarizabilities, particularly anisotropic ones, are known for very many nucleophiles. In actual practice, the parameter E was "evaluated" by fitting eq. [15] to experimental data. Pearson *et al.* (82) attempted to solve this problem by using "model" reactions in which factors other than basicity are dominant in determining reactivity. He reached the conclusion that equations such as eq. [15] have very limited ranges of applicability and that the qualitative concept of "hardness and softness", which he had earlier introduced (28), was about all that one could hope for.

The concepts of hardness and softness are loosely (no pun intended) related to proton basicity and polarizability, but are defined in terms of empirical reactivities (28). Klopman (83) has attempted to relate these properties to quantum mechanical concepts.

Albery and Kreevoy (85) showed that the Marcus theory (84), which began as a theory for electron transfer reactions (84), could be applied reasonably to S_N2 reactions of nucleophiles. Lewis *et al.* (86) have provided an impressive body of supporting data for application of the Marcus equation to the specific case of methyl transfers in sulfolane solution. Albery (87) has applied the Marcus equations to cation–nucleophile combination reactions, but there appears to be no justification for the application (22), and the results cannot be taken seriously.

One of the interesting features of cation–anion combination reactions is that the reverse reactions, heterolytic dissociation of covalent bonds, take place frequently in solution, but not in the gas phase. In the gas phase, the dissociation of a covalent bond is almost always homolytic. In solution, as a bond begins to stretch, it probably follows a homolytic pathway for some distance before solvent can lower the energy of the heterolytic pathway sufficiently for it to be followed. In the combination reactions, two ions must come together to some critical distance, then an electron-transfer must occur as the distance shortens to that of the bond. For some extreme cases, the combination reaction can obviously become a two-step process in which an electron transfer precedes bond formation (88).

For the reactions discussed here, there is no evidence for a separate electron-transfer step. For some reactions of carbocations with carbanions, however, Arnett and co-workers have observed (57) major, or exclusive, side reactions resulting from electron transfer. For the reactions considered in the present paper, it is almost certain that the electron transfer and bond formation are simultaneous (24). Pross (89) has discussed such "electron shift" processes, and Hoz and Speizman (90) have pointed out the role of the LUMO of the electrophile in these reactions.

These considerations led to an examination of the possible relationship between nucleophilic reactivity and one-electron oxidation potentials for the half-cells:

[16] $X^- \rightleftarrows X\cdot + e^-$

Note that the half-cell in reaction [16] is quite different from that in reaction [14] used by Edwards. Although very few of the potentials for reaction [16] have been measured in solution, it was possible to devise a thermodynamic cycle (24, 90) from which the potentials can be estimated from bond-dissociation energies in the gas phase and acidities in solution of the HX molecules. Some pertinent data for potentials and related solvation energies are shown in Table 6.

Although a surprisingly good correlation of potentials for reaction [16] with reactivities of nucleophiles was originally

TABLE 6. Oxidation potentials and solvation energies of nucleophiles in water[a]

Nucleophile	B.D.E.[b]	E^0, eq. 16[c]	ΔG^{0d}_{sol}
HOO^-	88.6	20.5	−95.0
$C_6H_5O^-$	86.5	20.7	−74.0
NO_2^-	78.0	21.5	
n-PrS^-	88.6	21.7	−78.0
$C_6H_5S^-$	83.3	22.3	−68.0
CH_3O^-	102.0	27.3	−93.0
$CF_3CH_2O^-$	102.0	32.9	−84.0
N_3^-	92.5	34.	−75.0
ClO^-	98.0	35.6	−74.0
CH_3COO^-	106.0	47.5	−67.0
CN^-	123.8	59.1	−74.0
OH^-	119.3	45.7	−105.0
NH_2NH_2	80.0	16.1	(−72.0)[e]
Piperidine	94.0	26.7	(−56.0)[e]
n-$PrNH_2$	103.0	36.5	(−63.0)[e]
H_2O	141.0	89.3	(−103.0)[e]

[a]Data are from ref. 52. Original references to literature are in ref. 24.
[b]Enthalpy of bond dissociation of H-nucleophile in the gas phase, at 25°C.
[c]Standard oxidation potentials relative to N.H.E. at 25°C.
[d]Free energies of transfer of the anions from dilute gas to dilute aqueous solution at 25°C.
[e]The values given are for the radical cations of the neutral nucleophiles. See ref. 24.

found (24), later data for more systems, and particularly for non-aqueous solutions, do not confirm the correlation (52). It was pointed out in the original paper (24) that the correlation is not expected on the basis of any of the quantum mechanical theories (90–94) of the reactions. These theories must deal with vertical transitions between states, while the potentials for reaction [16] are for non-vertical, adiabatic, processes.

The fact that solvation energies of ions are frequently on the order of bond energies (see Table 6), and that molecular orbital theories are poorly suited to the problem of such solvation has probably been responsible for the slow development of reasonable quantum mechanical theories of cation–anion reactions. Warshel and Weiss (91) cast the problem in valence bond formalism and presented an approximate treatment for handling the solvation energies. Shaik (92) generalized the valence bond curve crossing model, Pross and Shaik (93) have discussed qualitative features of the model, and Shaik (94) has presented quantitative details of the application of the model to S_N2 reactions. The latter paper by Shaik (94) also details how one may obtain the contributions of solvation in an approximate form. Thus, a quantum mechanical theory of the reactions discussed in this review exists. We may confidently look forward to seeing the details of its application.[2]

Acknowledgements

The work presented here has, continuously since its inception, been supported by grants from the Natural Science Foundation, most recently by Grant CHE 8205767. Less continuous, but significant, support has been provided by NIH-GMS and by PRF-ACS. Initial support was provided by AROD. I am grateful to these agencies.

Professors R. McClelland and S. Shaik have provided me with copies of manuscripts and outlines of ideas before publication. I am grateful for these and for several informative discussions.

[2]S. Shaik. Private communications. 1985–1986.

1. C. D. RITCHIE, G. A. SKINNER, and V. G. BADDING. J. Am. Chem. Soc. **89**, 2063 (1967).
2. C. D. RITCHIE and D. J. WRIGHT. J. Am. Chem. Soc. **93**, 2425 (1971).
3. C. D. RITCHIE and D. J. WRIGHT. J. Am. Chem. Soc. **93**, 2429 (1971).
4. C. D. RITCHIE and D. J. WRIGHT. J. Am. Chem. Soc. **93**, 6574 (1971).
5. C. D. RITCHIE and P. O. I. VIRTANEN. J. Am. Chem. Soc. **94**, 1589 (1972).
6. C. D. RITCHIE and P. O. I. VIRTANEN. J. Am. Chem. Soc. **93**, 7324 (1971).
7. C. D. RITCHIE and H. FLEISCHHAUER. J. Am. Chem. Soc. **94**, 3481 (1972).
8. C. D. RITCHIE and P. O. I. VIRTANEN. J. Am. Chem. Soc. **94**, 4963 (1972).
9. C. D. RITCHIE and P. O. I. VIRTANEN. J. Am. Chem. Soc. **94**, 4966 (1972).
10. C. D. RITCHIE. J. Am. Chem. Soc. **94**, 3275 (1972).
11. C. D. RITCHIE and P. O. I. VIRTANEN. J. Am. Chem. Soc. **95**, 1882 (1973).
12. C. D. RITCHIE, D. J. WRIGHT, D.-S. HUANG, and A. A. KAMEGO. J. Am. Chem. Soc. **97**, 1163 (1975).
13. C. D. RITCHIE. J. Am. Chem. Soc. **97**, 1170 (1975).
14. C. D. RITCHIE, R. J. MINASZ, A. A. KAMEGO, and M. SAWADA. J. Am. Chem. Soc. **99**, 3747 (1977).
15. C. D. RITCHIE and M. SAWADA. J. Am. Chem. Soc. **99**, 3754 (1977).
16. C. D. RITCHIE. Pure Appl. Chem. **50**, 1281 (1978).
17. C. D. RITCHIE and J. GANDLER. J. Am. Chem. Soc. **101**, 7318 (1979).
18. C. D. RITCHIE and T. C. HOFELICH. J. Am. Chem. Soc. **102**, 7039 (1980).
19. C. D. RITCHIE, A. A. KAMEGO, P. O. I. VIRTANEN, and C. KUBISTY. J. Org. Chem. **46**, 1957 (1981).
20. C. D. RITCHIE and A. KAWASAKI. J. Org. Chem. **46**, 4704 (1981).
21. C. D. RITCHIE, J. E. VANVERTH, and P. O. I. VIRTANEN. J. Am. Chem. Soc. **104**, 3491 (1982).
22. C. D. RITCHIE, C. KUBISTY, and G. Y. TING. J. Am. Chem. Soc. **105**, 279 (1983).
23. C. D. RITCHIE. J. Am. Chem. Soc. **105**, 3573 (1983).
24. C. D. RITCHIE. J. Am. Chem. Soc. **105**, 7313 (1983).
25. C. D. RITCHIE and Y. TANG. J. Org. Chem. To be published.
26. J. O. EDWARDS. J. Am. Chem. Soc. **76**, 1540 (1954).
27. R. S. DRAGO, G. C. VOGEL, and T. E. NEEDHAM. J. Am. Chem. Soc. **93**, 6014 (1971), and earlier references cited there.
28. R. G. PEARSON and J. SONGSTAD. J. Am. Chem. Soc. **89**, 1827 (1967).
29. J. O. EDWARDS and R. G. PEARSON. J. Am. Chem. Soc. **84**, 16 (1962).
30. G. S. HAMMOND. J. Am. Chem. Soc. **77**, 334 (1955).
31. C. D. RITCHIE. Acc. Chem. Res. **5**, 348 (1972).
32. N. C. DENO, J. J. JARUZELSKI, and A. SCHRIESHEIM. J. Am. Chem. Soc. **77**, 3044 (1955); N. C. DENO, H. E. BERKHEIMER, W. L. EVANS, and H. J. PETERSON. J. Am. Chem. Soc. **81**, 2344 (1959).
33. P. D. GOODMAN, T. J. KEMP, and P. P. DEMOIRA. J. Chem. Soc. Perkin II, 1221 (1981).
34. R. A. DIFFENBACH, K. SANO, and R. W. TAFT. J. Am. Chem. Soc. **88**, 4747 (1966).
35. C. A. BUNTON and S. K. HUANG. J. Am. Chem. Soc. **94**, 3536 (1972); **95**, 2701 (1973); **96**, 515 (1974).
36. R. A. MCCLELLAND, N. BANAIT, and S. STEENKEN. J. Am. Chem. Soc. To be published.
37. C. D. RITCHIE. J. Am. Chem. Soc. **106**, 7187 (1984).

38. C. A. BUNTON, N. CARRASCO, F. DAVOUDZADEH, and W. C. WATTS. J. Chem. Soc. Perkin II, 1520 (1980).
39. N. GRAVITZ and W. P. JENCKS. J. Am. Chem. Soc. **96**, 489 (1974); **96**, 499 (1974); **96**, 507 (1974).
40. R. A. MCCLELLAND and S. STEENKEN. J. Chem. Soc. Chem. Commun. To be published.
41. J. HINE. J. Am. Chem. Soc. **88**, 5525 (1966).
42. K. HILLIER, J. M. W. SCOTT, D. J. BARNES, and F. J. P. STEELE. Can. J. Chem. **54**, 3312 (1976).
43. J. P. RICHARD and W. P. JENCKS. J. Am. Chem. Soc. **106**, 1396 (1984).
44. J. P. GUTHRIE. J. Am. Chem. Soc. **100**, 5892 (1978).
45. V. GOLD, D. G. OAKENFULL, and T. RILEY. J. Chem. Soc. B, 515 (1968).
46. J. GANDLER. J. Am. Chem. Soc. **107**, 8218 (1985).
47. J. N. RIDE, P. A. H. WYATT, and Z. ZOCHOWSKI. J. Chem. Soc. Perkin II, 1188 (1974).
48. J. W. BUNTING and D. J. NORRIS. J. Am. Chem. Soc. **99**, 1189 (1977).
49. A. J. PARKER. Proc. Chem. Soc. 371 (1961).
50. J. HINE and R. D. WEIMAR, JR. J. Am. Chem. Soc. **87**, 3387 (1965).
51. D. F. MCMILLEN and D. M. GOLDEN. Ann. Rev. Phys. Chem. **33**, 493 (1982).
52. C. D. RITCHIE. Nucleophilicity Symposium, Sept. 1985, Natl. Am. Chem. Soc. Meeting, to be published as an "Advances in Chemistry" volume edited by M. Harris and S. McManus.
53. J. E. DIXON and T. C. BRUICE. J. Am. Chem. Soc. **93**, 3248 (1971); **93**, 6592 (1971).
54. J. P. GUTHRIE. Atual. Fisico-Quim. Org. 35 (1983) (Proceedings of 2nd Conference on Physical Organic Chemistry, Florianopolis, Brazil, April 6–8, 1983).
55. (*a*) D. J. HUPE and W. P. JENCKS. J. Am. Chem. Soc. **99**, 451 (1977); (*b*) J. GERSTEIN and W. P. JENCKS. J. Am. Chem. Soc. **86**, 4655 (1964).
56. E. M. ARNETT, B. CHAWLA, K. MOLTER, K. AMARNATH, and M. HEALY. J. Am. Chem. Soc. **107**, 5288 (1985).
57. E. B. TROUTON, K. E. MOLTER, and E. M. ARNETT. J. Am. Chem. Soc. **106**, 6726 (1984).
58. C. A. BUNTON and C. H. PAIK. J. Org. Chem. **41**, 40 (1976).
59. G. BARTOLI and P. E. TODESCO. Acc. Chem. Res. **10**, 125 (1977).
60. D. A. JENCKS and W. P. JENCKS. J. Am. Chem. Soc. **100**, 6544 (1978); C. F. BERNASCONI. Tetrahedron, **41**, 3219 (1985); C. F. BERNASCONI, J. P. FOX, A. KANAYARIOTI, and M. PANDA. J. Am. Chem. Soc. **108**, 2372 (1986).
61. J. P. RICHARD and W. P. JENCKS. J. Am. Chem. Soc. **106**, 1361 (1984).
62. P. R. YOUNG and W. P. JENCKS. J. Am. Chem. Soc. **98**, 8238 (1977).
63. R. TA-SHMA and Z. RAPPOPORT. J. Am. Chem. Soc. **105**, 6082 (1983).
64. J. P. GUTHRIE, J. COSAR, and A. KLYM. J. Am. Chem. Soc. **106**, 1351 (1984).
65. J. P. RICHARD and W. P. JENCKS. J. Am. Chem. Soc. **106**, 1373 (1984).
66. A. J. PARKER. Chem. Rev. **69**, 1 (1969).
67. C. A. BUNTON, S. K. HUANG, and C. H. PAIK. Tetrahedron Lett. 1445 (1976).
68. E. R. POHL and D. J. HUPE. J. Am. Chem. Soc. **102**, 2763 (1980).
69. E. F. CALDIN. J. Chem. Soc. 3345 (1959).
70. C. D. RITCHIE. Pure Appl. Chem. **51**, 153 (1979).
71. W. J. LENOBLE, E. GEBICKA, and S. SRIVASTA. J. Am. Chem. Soc. **104**, 3153 (1982); Errata, **104**, 6167 (1982).
72. J. L. KURZ, L. LEE, M. E. LOVE, and S. RHODES. J. Am. Chem. Soc. **108**, 2960 (1986).
73. G. VAN DER ZWAN and J. T. HYNE. J. Chem. Phys. **76**, 2993 (1982); **78**, 4174 (1983).
74. M. GILCHRIST and W. P. JENCKS. J. Am. Chem. Soc. **90**, 2622 (1968).
75. A. R. FERSHT and W. P. JENCKS. J. Am. Chem. Soc. **92**, 5442 (1970).
76. D. J. PALLING and W. P. JENCKS. J. Am. Chem. Soc. **106**, 4869 (1984).
77. T. J. ALAVOSUS and D. A. SWEIGART. J. Am. Chem. Soc. **107**, 985 (1985).
78. C. G. SWAIN and C. B. SCOTT. J. Am. Chem. Soc. **75**, 141 (1953).
79. O. Foss. Acta Chim. Scand. **3**, 1385 (1949).
80. J. O. EDWARDS. J. Am. Chem. Soc. **78**, 1819 (1956).
81. M. F. HAWTHORNE, G. S. HAMMOND, and B. M. GRAYBILL. J. Am. Chem. Soc. **77**, 486 (1955).
82. R. G. PEARSON, H. SOBEL, and J. SONGSTAD. J. Am. Chem. Soc. **90**, 319 (1968).
83. G. KLOPMAN. *In* Chemical reactivity and reaction paths. *Edited by* G. Klopman. John Wiley and Sons, Inc., New York. 1974. Chapt. 4.
84. R. A. MARCUS. Discuss. Faraday Soc. **29**, 210 (1960); Ann. Rev. Phys. Chem. **15**, 155 (1964); J. Phys. Chem. **72**, 891 (1968).
85. W. J. ALBERY and M. KREEVOY. Adv. Phys. Org. Chem. **16**, 87 (1978).
86. E. S. LEWIS, M. L. MCLAUGHLIN, and T. A. DOUGLAS. J. Am. Chem. Soc. **107**, 6668 (1985).
87. W. J. ALBERY. Ann. Rev. Phys. Chem. **31**, 227 (1980).
88. L. EBERSON. Adv. Phys. Org. Chem. **18**, 79 (1985).
89. A. PROSS. Acc. Chem. Res. **18**, 212 (1985).
90. S. HOZ and D. SPEIZMAN. J. Org. Chem. **48**, 2904 (1983).
91. A. WARSHEL and R. M. WEISS. J. Am. Chem. Soc. **102**, 6218 (1980); A. WARSHEL. Acc. Chem. Res. **14**, 284 (1981).
92. S. SHAIK. J. Am. Chem. Soc. **103**, 3692 (1981).
93. A. PROSS and S. SHAIK. Acc. Chem. Res. **16**, 363 (1983).
94. S. SHAIK. Prog. Phys. Org. Chem. **15**, 197 (1985).

The photochemical event in rhodopsins

C. SANDORFY
Département de Chimie, Université de Montréal, Montréal (P.Q.), Canada H3C 3J7

AND

D. VOCELLE
Département de Chimie, Université du Québec à Montréal, Montréal (P.Q.), Canada H3C 3P8

Received May 26, 1986

C. SANDORFY and D. VOCELLE. Can. J. Chem. **64**, 2251 (1986).

The photochemical step in the functioning of visual and bacterial rhodopsins entails *cis–trans* or *trans–cis* isomerization and changes in the state of protonation of the retinylidene Schiff base chromophore. In this review our present knowledge on these two events is discussed as well as the role of interactions between the chromophore and the surrounding protein, opsin. The relation between protonation and hydrogen bonding at the Schiff base nitrogen, the problems of stabilization of the proton bridge and charge separation are also discussed. A new proposal is made which implies Schiff base to counter-ion proton translocation with concomitant isomerization and reprotonation of the chromophore.

C. SANDORFY et D. VOCELLE. Can. J. Chem. **64**, 2251 (1986).

L'étape photochimique dans le cycle des rhodopsines visuelles et bactériennes comprend de l'isomérisation *cis–trans* ou *trans–cis* et des changements dans l'état de protonation du chromophore, une base de Schiff du rétinal. Nous passons en revue nos connaissances actuelles relatives à ces deux processus et les interactions entre le chromophore et la protéine opsine. La protonation et la formation d'une liaison hydrogène sur l'azote de la base de Schiff et les problèmes de la stabilisation des ions ainsi formés et de la séparation des charges sont également discutés. On propose un nouveau mécanisme qui impliquerait un transfert de proton de la base de Schiff à son contre-ion qui irait de paire avec l'isomérisation et la reprotonation du chromophore.

Introduction

Only humans and animals can see; plants cannot. What a distressing thought that roses, tulips, anthuria, and all those beautiful flowers cannot see each other or themselves! But we can see them. Light is a decisive factor for life: photosynthesis, germination, and growth regulation of plants, vision and many other functions are initiated or conditioned by light. The light receptors are usually pigments; the chromophore is surrounded by a protein whose field and conformation have a decisive influence on its properties and in which lipids, sugar, water, metals also have roles to play. The principal visual chromophore which is a conjugated olefin containing six double bonds is covalently bound to the apoprotein opsin by a Schiff base linkage, forming rhodopsin.

The eye is a bio-optical device in which light of the appropriate wavelength range is focussed onto the site where the Schiff base of 11-*cis* retinal is located. Photons must be absorbed, initiating a photochemical process which must eventually give a signal to the nervous system; then our brain must somehow form an image which has to be read and interpreted. The field of vision research has been opened by the pioneering work of Wald and Hubbard, and their co-workers (1–16), the spectroscopic part of it by Yoshizawa, Wald, and their co-workers (17–21). The light absorbing molecule in the visual process is the Schiff base of 11-*cis*-retinal, a kin of vitamin-A, formed with lysine, an aminoacid of the protein opsin (Fig. 1). This review is only concerned with the photochemical event on which a great deal of information has been accumulated in recent years. The subsequent events in the mechanism of vision are also the object of intensive research. Exciting new developments can be expected in the coming decades.

Why did creation choose the Schiff base of 11-*cis*-retinal?

Conjugated olefins are known for their tendency to undergo *cis–trans* or *trans–cis* isomerization photochemically. It would be astonishing if nature did not use this property of them.

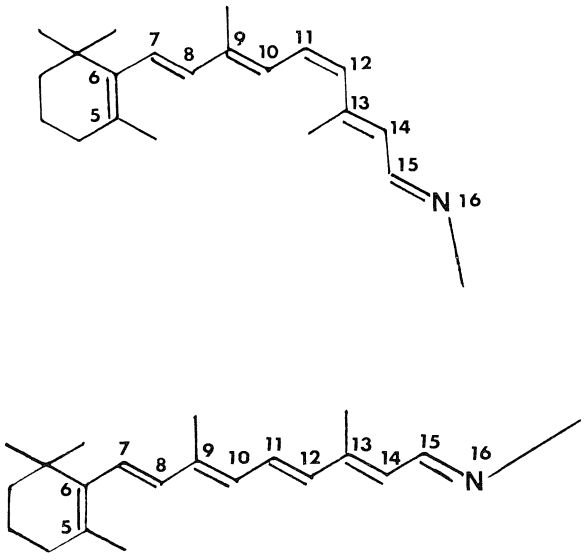

FIG. 1. 11-*cis*-Retinal and all-*trans*-retinal.

The eye is supposed to see light, not heat. Therefore the photochemical event of vision must occur in an excited state which cannot be reached by possible increases in temperature. Retinal derivatives are well suited for this. That *cis–trans* isomerization is the primary step was suggested at an early stage by Yoshizawa and Wald (22).

If this was the only requirement, most conjugated olefins, their aldehydes, alcohols, and other derivatives would be suitable. Why an imine, a Schiff base? The linkup with the protein might be an obvious reason. Another reason might be that nitrogen is needed because it can easily form hydrogen bonds or become protonated. Indeed, Rentzepis and co-workers found evidence for rapid proton transfer in rhodopsin following light absorption (23–25). So both isomerization and proton

transfer can be expected to play an important role in the photochemical event of vision.

A very surprising discovery was made in 1971 by Oesterhelt and Stoeckenius (26, 27). The purple membrane of halobacterium halobium, a bacterium dwelling in salt water, contains a chromophore which turned out to be an isomer of rhodopsin (Rh). Bacteria cannot see; bacteriorhodopsin (bR) functions as a proton pump. It pushes protons across a membrane against a chemical potential gradient using the energy of the absorbed photons. Because of a number of experimental advantages and the possibility of rapid progress much of the present research on rhodopsins is concentrated on bR. During the last few years still other rhodopsins have been discovered and more can be expected. Rhodopsins are devices whose use by nature is more widespread than was originally thought (27–30, 43, and references therein).

Some facts about Rh are intriguing to spectroscopists and photochemists. First, in a test tube in a relatively inert solvent, the Schiff base of retinal has its intense (π,π^*) band of lowest frequency at 370 nm. In human or bovine Rh, however, it is at about 500 nm. Moreover, this wavelength varies from species to species. Some fishes and frogs, for example, can see in the near ultraviolet (up to 350 nm in some cases) (31–35). This amounts to a range of about 350 to 600 nm. In addition to rods which make it possible to see in black and white, the eyes also contain cones which provide for color vision. They contain three or four pigments of different colors in the various animal species.

The remarkable fact is that all these pigments contain Rh as the chromophore. The differences are due to their different conformations and molecular environments, mainly the protein surrounding the chromophore. Only some species contain one more double bond in the β-ionone ring (porphyropsin) conjugated with the six double bonds present in all Rh (30, 36, 37).

Several excellent reviews have been published on rhodopsins (Yoshizawa (20); Honig (38, 39); Ottolenghi (40); Birge (41); Uhl and Abrahamson (42); Stoeckenius and co-workers (43*a*, *b*); Shichi (44); Balogh-Nair and Nakanishi (45); Kliger (46); see also the volume edited by Packer (47)).

The present review does not aim at complete coverage. It is rather intended as a provocative review introducing some unorthodox ideas into the discussion. The problems of isomerization and protonation in rhodopsins are intimately connected. For this reason some repetitions will be inevitable in the following discussions.

The cycles of Rh and bR are known to contain a photochemical primary step leading from Rh to B (bathorhodopsin) and from bR to K, respectively. This is followed by the successive formation of a number of intermediates which differ from one other by isomerism, protonation–deprotonation, and their protein environment. At the end of the cycle, in the visual pigments of vertebrates, the final (all-*trans*) isomer is hydrolyzed down from the apoprotein and is later chemically regenerated. In invertebrates and in bacterial rhodopsins at the end of the cycle the original Rh or bR is regained. The intermediates are usually characterized by the wavelength (in nm) of their visible absorption maxima, and their risetime and lifetime. We reproduce here the schemes relating to Rh and bR based on literature data. The temperatures at which the spectra were taken are also given (Figs. 2, 3).

The initial configuration of the chromophore of Rh is 11-*cis*. In bR it is all-*trans* (light adapted) or about 1:1 all-*trans* and 13-*cis* (dark adapted).

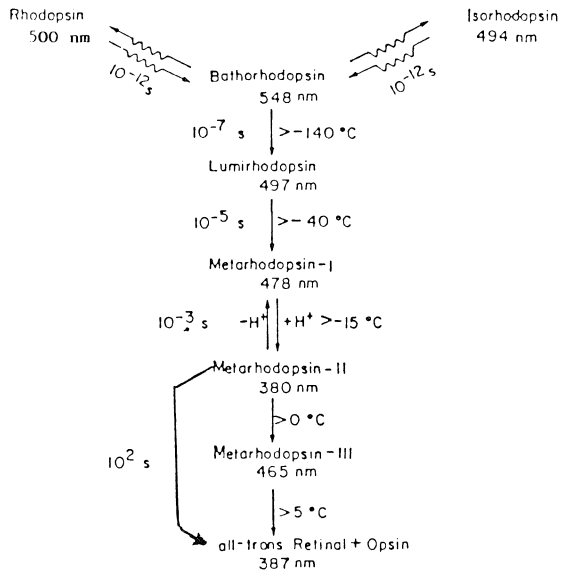

FIG. 2. The photochemically induced cycle of rhodopsin. Adapted from ref. 238. Reproduced with permission of the Elsevier Biomedical Press.

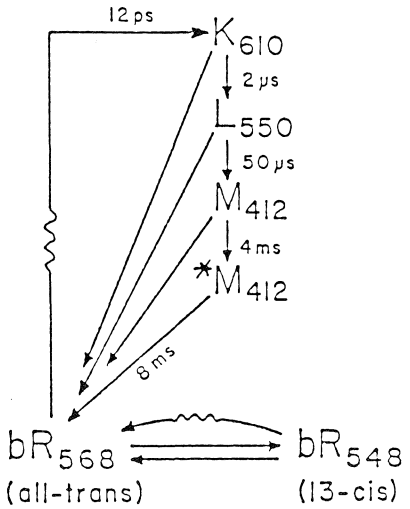

FIG. 3. The photochemically induced cycle of bacteriorhodopsin. Adapted from ref. 239. Reproduced with permission from Annual Review of Biophysics and Bioengineering, **2**, 10 (1981) by Annual Reviews, Inc.

The excited state

The electronic spectra of conjugated polyenes were the object of thorough studies. 1,3-Butadiene can be taken as a school example. In the *trans* conformation which is present in the gas phase, butadiene has a co-planar ground state and C_{2h} symmetry, with a center of inversion. The four π electrons give rise to four π type molecular orbitals. In a first approximation the ground and valence-shell excited states of butadiene are obtained as transitions between these MOs. The ground state is totally symmetrical, ^1A_g while the first excited state is ^1B_u. The $^1A_g \rightarrow {}^1B_u$ transition is allowed and polarized in the molecular plane along the central C—C bond. While the more complicated polyenes present in Rh do not have C_{2h} symmetry this butadiene nomenclature is often used in an approximate sense. The corresponding band has its maximum near 210 nm (about

48000 cm^{-1}) and it is very intense. This preponderance of the first (π,π^*) band is characteristic of the *trans* or approximately *trans* conformation. There is a second $^1A_g \rightarrow {}^1B_u$ band at much higher frequencies. (About 130 nm or 77000 cm^{-1}) (48). The two other (π,π^*) bands correspond to $^1A_g \rightarrow {}^1A_g$ transitions and are forbidden by the Laporte rule for the *trans* polyenes. All this description of the spectrum of *trans*-butadiene is based on the Hückel approximation or SCF MO calculations aimed at the ground state. In 1967, Koutecky (49) drew attention to the fact that when configuration interaction is applied, the two ^1A_g states (obtained in a first approximation) will mix, so that one of them ($^1A_g^-$) moves to lower and the other ($^1A_g^+$) to higher energies. If the mixing is sufficiently large the A_g^- state might become lower in energy than the B_u^+ state and become the first excited singlet state. (The + and − signs refer to the sign in the linear combination resulting from configurational mixing (see refs. 40, 41). Koutecky put forward the idea that this could be so in the case of visual pigments. The photochemical consequences of this can be expected to be very important.

In *cis*-butadiene the situation is different: all four (π,π^*) bands are symmetry allowed, and the one of lowest frequency is no longer the most intense of them.

The importance of the A_g^- problem in the case of butadiene is largely academic. A_g^- does not appear to be the lowest excited state. However, if butadiene has such a low-lying band the higher conjugated polyenes which include retinal derivatives and carotenoids must also have A_g^- type bands. After Hudson and Kohler (50) and Schulten and Karplus (51) a series of investigations were devoted to this problem. It became accessible to experimental research thanks to the rapid development of two photon spectroscopy (see refs. 52–55). Transitions of the g ↔ g type are allowed in two photon absorption spectroscopy. The $^1A_g^-$ state has been shown to be the lowest excited singlet state in long chain linear polyenes (41, 55–65). While actual visual chromophores do not have a center of inversion, they "remember" C_{2h} symmetry sufficiently for transitions from the ground state to $^1A_g^-$-like states to remain weak and transitions to $^1B_u^+$-like states intense in one-photon spectra. On the other hand, the transition from the ground to the $^1A_g^-$ state is the major contributor to the two-photon transition. In EPA (5:5:2 mixture of diethyl ether, isopentane, and ethanol) at 77 K all-*trans*-retinol (61), all-*trans*-retinal (62), and its Schiff base have the $^1A_g^-$-like state at energies lower than the ^1B_u-like state (41, 61–63). The difference is of the order of 2000 cm^{-1}. This seems to apply to both the Franck–Condon maxima and 0–0 bands. Birge and co-workers extended their research to the protonated all-*trans*-retinal Schiff base at room temperature. Then a reversal occurred, the $^1B_u^+$-like state being at slightly lower frequencies. These results, interesting as they are, cannot be directly extended to Rh. Indeed, the order of these bands has been found to be highly sensitive to solvent and environmental conditions. However, Birge, Nakanishi, and their co-workers succeeded in taking the two-photon spectra (in D_2O, at room temperature) of locked-11-*cis*-rhodopsin (64) (Fig. 4). In this molecule the ring introduced at the central double bond makes isomerization impossible, so that this rhodopsin does not bleach. However, the chromophore occupies the same site as in a natural visual pigment with the same counterion environment. The $^1B_u^+$-like band was found to be at significantly lower frequencies than the $^1A_g^-$-like level. This is the opposite trend of what was found for the non-protonated Schiff base or the aldehyde or the alcohol.

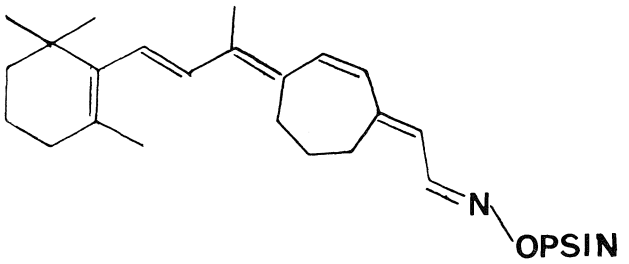

FIG. 4. Locked-11-*cis*-rhodopsin.

Birge *et al.* (64) consider this as a strong indication for the presence of a protonated Schiff base in Rh. It follows that the photochemical cycle of Rh starts in the $^1B_u^+$-like state. Moreover, since the true chromophore does not have C_{2h} symmetry (in a rigorous sense it has no symmetry at all), the excited A_g^- and B_u^+ states might actually mix.

The $^1B_u^+$-like state is a polar state in the valence-bond sense, meaning that resonance structures with large charge separations are predominant in the VB wave function. To the contrary, the $^1A_g^-$-like state is a covalent state (64*a*, 65). This means that the field of the surrounding molecules can affect these two states very differently and that the photochemical reactions occurring in them could also be very different. The $^1A_g^-$ state to which one-photon transitions are rare is a state of long lifetime whereas $^1B_u^+$ is a state corresponding to an intense band with a short lifetime.

As reported above, Birge *et al.* (41, 64*a*) were able to demonstrate that protonation of the Schiff base reverses the order of the lowest excited singlet states, so that $^1B_u^+$ is the lowest. However, according to Murray and Birge (64*b*) hydrogen bonding has the opposite effect; in the presence of methanol, for example, which forms hydrogen bonds with the Schiff base nitrogen the $^1A_g^-$ state is the lowest, actually more so than in retinol or retinal

—CH=N:...H—O—CH_3

(However, Das *et al.* (66) have shown that this H-bond effect is much greater in the excited state than in the ground state.) Since the formation of a hydrogen bond is a situation intermediate between that of the free base and the protonated base, the effect of hydrogen bond formation would also be expected to be intermediate. The reasons why this would not be so in the present case are discussed by Murray and Birge (64*b*) and by Das *et al.* (66).

Birge and Hubbard (67) suggested that the mixing between the $^1B_u^+$ and $^1A_g^-$ states is responsible for producing a barrierless excited state potential energy surface for *cis–trans* isomerization and that the extremely rapid formation of bathorhodopsin may be a consequence of the photochemical lability of the $^1A_g^-$-like state. They used the INDO-CISD method, a semi-empirical molecular orbital technique including a respectable amount of configuration interaction with both singly and doubly excited configurations combined with molecular dynamics calculations to investigate the *cis–trans* isomerization of Rh. They demonstrated that *cis–trans* isomerization around the 11–12 double bond can occur with high quantum efficiency (about 0.6) in approximately 2 ps. The mixing with the A_g^--like state into the largely ionic B_u^+-like state increases the covalent character of the latter. As a consequence, after photon absorp-

tion, a steep potential well with an energy minimum at a dihedral angle $\theta(11,12) = 90°$ is produced during the subsequent isomerization process. This amounts to the formation of an activated complex which preferentially decays to a distorted all-*trans* isomer. The barrier to isomerization is negative in the excited state. Moreover, Birge and Hubbard's calculations have shown that in the photochemical step leading from Rh to B, the lysine residue undergoes a conformational distortion which may distort the chromophore in B, preventing it from reaching a planar all-*trans* conformation. The calculations have also demonstrated the role of the counter-ion (near the C=N bond) in increasing the barrier to thermal ionization in the ground state. Furthermore, the location of the counter-ion is critical and the increase or decrease of the photochemical isomerization time is dependent on it (67).

A different approach was taken by Becker and Freedman (68) who studied photoisomerization quantum yields of 11-*cis*-retinylidene-*n*-butylamine and its protonated counterpart as a function of the nature of the solvent. For the Schiff base the quantum yield (ϕ) varied from 0.01 in hexane to 0.34 in acetonitrile. A hydrogen bonded complex with hexafluoroisopropanol had the high value of 0.31. It is interesting to note that this proton donor has the same effect as acetonitrile, a polar molecule with no hydrogen capable of H-bonding. For the protonated Schiff base they found a quantum yield equal to about 0.24, practically independent of solvent. This shows that protonation is not a prerequisite for *cis–trans* photoisomerization in a polar environment. Only in non-polar solvents does protonation increase the quantum yield. Becker and Freedman (68) interpret these variations in quantum yield by increased $B_u^+ - A_g^-$ mixing as a function of increased polarity of the environment. According to their results A_g^- does not especially promote isomerization; it would seem rather that B_u^+ facilitates it more. Both Birge and Becker agree, however, that the mixing of the two states is essential for promoting *cis–trans* photoisomerization. According to Becker the pK_a of the Schiff base and the negative charge on the nitrogen increase upon excitation with no twist; the charge density decreases upon twisting to 90° (68). Contrary to previous observations they found that the quantum yield (ϕ) for the protonated 11-*cis* Schiff base is independent from the excitation wavelength from 355 to 532 nm. This is the same behavior as that of Rh itself (70–72).

Becker *et al.* (68, 69) made the proposal that "... the primary photostep in vision involves the proton coming off in the excited state during the twisting to ~90° onto one site of the protein and returns from another site of the protein after relaxation to and twisting in the ground state from ~90° to whatever angle is appropriate to B". They also found a non-excited state transient in the photoisomerization reaction of the 11-*cis* Schiff base but not for the protonated Schiff base.

It appears then that the role of protonation (or hydrogen bonding, or a polar environment) is mixing together the $^1A_g^-$-like and $^1B_u^+$-like excited states thereby opening the way to photoisomerization with a high quantum yield.

In a subsequent paper, Freedman and Becker (68*b*) examined the 9-*cis*, 11-*cis*, 13-*cis*, and all-*trans* isomers, both unprotonated and protonated. Their results show that for the protonated species only the 11-*cis* isomer efficiently isomerizes, more than five times than the 9-*cis* or 13-*cis* isomers. This helps in understanding nature's choice of the 11-*cis* isomer. Their results on the unprotonated species show that a polar or hydrogen bonding environment must be provided for efficient isomerization.

An idea which appears to be complementary to the above was put forward by Leclercq and Sandorfy (73). The photochemically active excited state should have an appreciable amount of charge transfer character.

The electron donor is presumed to be a carboxylate group which could be either the primary counter-ion or a secondary counter-ion placed in the vicinity of the chromophore. The HOMO of the carboxylate ion containing the additional electron is a nearly non-bonding orbital while the LUMO is a low-lying empty π^* orbital of the Schiff base. Leclercq's calculations (73) by both the semiempirical CNDO/S and *ab initio* 6-31G methods have shown that upon protonation the lowest unoccupied molecular orbital undergoes a spectacular lowering in energy. (A hydrogen bond at the Schiff base nitrogen would also do this but to a lesser extent.) In consequence a new charge transfer state may exist, the transition to which from the ground state giving rise to absorption at low energies. Much depends on mutual chromophore – counter-ion separation and other geometrical and environmental conditions. It is also possible that without having a separate charge transfer state, the existing excited states acquire a significant CT character. Since no CT band has been identified so far this latter possibility is more likely. The problem should be further explored.

Triplet excited states do not seem to play any role in the photochemistry of vision. The reason that can be given for this is the low yield of singlet–triplet internal conversion. (For a discussion of this problem see Ottolenghi's review (40) and references therein.) The same seems to apply to the (n,π^*) and Rydberg excited states which are expected to be at frequencies higher than those of the $^1B_u^+$ and $^1A_g^-$ bands (74).

Isomerization

Since Rh uses 11-*cis*-retinal as a chromophore and since all-*trans*-retinal is ultimately obtained in the process of vision, at least one isomerization did occur during the bleaching of the visual pigment. In 1958, Hubbard and Kropf put forward the idea (15) that the isomerization of the 11-*cis* bond of the retinal Schiff base to *trans* occurred in the primary step, at the photochemical stage. The main reason supporting this proposition came from the fact that immediately after the light has struck rhodopsin the following equilibrium is produced (17):

$$\text{Isorhodopsin (9-}cis\text{)} \rightleftharpoons \text{bathorhodopsin} \rightleftharpoons \text{rhodopsin (11-}cis\text{)}$$

More recently it was found that 7-*cis* Rh could be included in the same equilibrium (75).

It was reasoned that since B is an intermediate of both 9-*cis*- and 11-*cis*-retinal derivatives, its structure must be all-*trans*. This became one of the key paradigms regarding the primary event in vision. The conclusion then was that the photoconversion of Rh to B meant the isomerization of the 11-*cis* double bond to a *trans* configuration.

This idea has been supported by data presented by Rosenfeld *et al.* (70), Green *et al.* (77), and Monger *et al.* (78). However, the validity of the argument has been weakened when Spalink *et al.* obtained evidence to the effect that the B formed from 9-*cis*-Rh is not the same as the B of 11-*cis*-Rh (25, 79). For this they used a 25 ps, 532 nm pulse at 85 ps after excitation of the 9- or 11-*cis* Rh sample. This is much more than the time needed for the Rh → B transformation and much more than the time needed for the transformation of B into the next intermediate, lumirhodopsin. The obtained visible absorption spectra are not very different, however, so that the assignment of a distorted all-*trans* configuration to B is still reasonable.

Simultaneously, several research groups used resonance Raman techniques to investigate the structures of Rh, isorhodopsin, and B. Among these, Oseroff and Callender published a work very often cited (76). Using low temperature (80 K) laser irradiation within the visible absorption band, they obtained well-defined photostationary states of Rh, isorhodopsin, and B. In order to distinguish between these three compounds, they used a double wavelength pump–probe technique (one laser creates a resonance Raman effect, the second changes the composition of the photostationary state). By this method, they were able to show that Rh, isorhodopsin, and B were all protonated (the C=N band at 1655 cm^{-1} shifts to 1630 cm^{-1} upon deuteration) and that B had three relatively intense bands at 856, 877, and 920 cm^{-1}. Since the fingerprint region of B differed markedly from that of both all-*trans*-retinylidene and 11-*cis*-retinylidene Schiff bases, they suggested that the retinylidene chromophore assumed some intermediate conformation between a *cis*- and a *trans* configuration (10). In similar works but using deuterated retinal isomers, Eyring *et al.* (80–82) were able to assign these three bands to CH out-of-plane wagging vibrations. They concluded that B had a perturbed all-*trans* configuration and that it is protonated.

The saga of the resonance Raman assault on Rh and bR started with the assignments made for "vitamin-A type molecules", among them *trans*-retinal, by Rimai, Gill, and Parsons in 1971 (83). A rather complete resonance Raman and infrared study was presented in 1978 by Cookingham *et al.* (84) on a number of retinals and their Schiff bases. The knowledge of the spectra of retinals, their Schiff bases and protonated Schiff bases is a prerequisite for the interpretation of the spectra of Rh and bR themselves and those of their intermediates. A representative list of references is found in a recent paper by Smith *et al.* (85), many of them due to the groups of Mathies, Lugtenburg, and Stockburger. We can only quote some of the most recent ones which are of direct importance from the point of view of this review: Eyring *et al.* (80) on the hydrogen out-of-plane vibrations in Rh and bR; Mathies on the conformation of retinal in Rh and in isorhodopsin (86); Eyring *et al.* on B (81); Braiman and Mathies on all-*trans* to 13-*cis* isomerization in bR (87, 88); Curry *et al.* on all-*trans*-retinal (89); and on 13-*cis*-retinal (90); Lugtenburg (91), and Pardoen *et al.* (92, 93) who synthesized series of highly useful labelled molecules; Smith *et al.* on the determination of the retinal Schiff base configuration in bR (85, 94); and Stockburger *et al.* (95) on bR and intermediates in its photochemical cycle, Massig *et al.* on all-*trans*, 13-*cis*, and 3-dehydroretinal (96) and Hildebrandt and Stockburger (97) on the role of water in bR's chromophore.

This list is by no means exhaustive. These investigations have shown that, as stated above, the chromophore of Rh, the protonated Schiff base of 11-*cis*-retinal is photochemically transformed into a distorted all-*trans* isomer in becoming B while the all-*trans* chromophore of light-adapted bR_{568} becomes 13-*cis* in the intermediate K. With the help of detailed normal coordinate analyses very secure assignments were made.

Originally, B was thought to be more unstable than Rh by some 5 to 13 kcal/mol (70). Cooper, in 1979 (98), was able to demonstrate by photocalorimetry that there existed a difference of 35 kcal/mol between B and Rh. Boucher and Leblanc (98*b*) have recently confirmed this value using photoacoustic spectroscopy. Since a simple *cis–trans* isomerization process could not explain such a large energy difference, new mechanisms were proposed (67, 99–101). Important contributions came from Nakanishi and Honig's groups (102–110). After hydrogenating sequentially every double bond of retinal and preparing the related synthetic visual pigments, they were able to show that the 11-*cis*-retinylidene Schiff base was protonated (existence of a salt bridge) and that a second external charge was located near C11–C13. The structure of B consists in a strained all-*trans*-chromophore where the salt bridge was broken and a charge separation had occurred (99). This charge separation is mainly responsible for the high energy of B (see below).

Charge separation without solvent stabilization being unlikely in a polar solvent, a non-polar environment was proposed. This mechanism has been widely acclaimed but criticism came fast also. Warshel in a series of papers (100, 111, 112) argued that the environment surrounding the ion-pair in Rh could not have a low dielectric constant since in such a milieu, a salt bridge should revert to a molecular form.

Since in a medium having a low dielectric constant a salt bridge could not exist between a weak base and a weak acid and since in a polar environment a charge separation is unlikely to occur, Warshel proposed an alternative. In Rh, a salt bridge is present in a polar environment; under the action of light, there is a *cis–trans* isomerization which moves the positive nitrogen of the Schiff base out of the salt bridge and into a non-polar environment so that an effective charge separation has occurred. Based on the works of Blatz's group (113), the increase in the distance between the iminium and its counter-ion should induce a red shift which is in concordance with what is observed.

The *cis–trans* isomerization process in the visual pigments was also proven in a more indirect way. Nakanishi's group synthesized 11-*cis*-locked chromophores such as the aldehyde shown in Fig. 4. This aldehyde (and many others, also locked) could form with opsin a synthetic pigment. This pigment was non-bleachable; that is, it could not be transformed into analogs of B, lumirhodopsin or meta I and meta II, rhodopsins. The conclusion was then given that the 11-*cis* bond is crucial to the visual cycle: it must be able to isomerize to a *trans* entity in order to have a bleachable pigment.

The C=N bond in the chromophore can also exist in a *syn* or *anti* configuration (Fig. 5). This possibility has not been fully exploited and only a few works or ideas have been submitted on the role that this isomerization could play in the mechanism of vision. Oesterhelt in 1973 (114) and Warshel (115) in 1976 have discussed this possibility and so has our group (116). It is important to recognize the role that *syn–anti* isomerization of the imine function could play in the mechanism of vision. As stated earlier, Warshel proposed that there is a charge separation occurring at the photochemical stage because isomerization of the 11-*cis* bond to a transoid configuration transfers the chromophore into a new environment, namely from a polar to a non-polar milieu. If, in addition, the likely *anti* configuration of the Schiff base could isomerize to a *syn* configuration, the environment surrounding the imine bond could well be completely different. Such an isomerization was detected recently by Harbison *et al.* (117). Using ^{13}C solid state nmr and MASS technique, they were able to show that lyophilized dark-adapted bR is composed of a mixture of all-*trans*, 15-*anti* (*E*), and 13-*cis*, 15-*syn* (*Z*) isomers. From this work it appears that the configuration around the C=N bond is of the utmost importance.

Finally the same group has shown (118) that in bR, the chromophore takes a 6-s-*trans* conformation, and that there are possibly three charges which are interacting with the polyenic chain. First, there is the counter-ion of the Schiff base; then

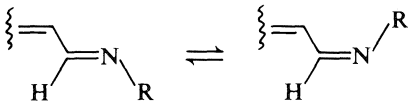

FIG. 5. *Syn–anti* isomerization of Schiff bases.

there is a negative charge near the ionone ring in conformity with the proposal of Nakanishi *et al.* (104). The third charge could be the counter-ion of the negative charge. The positive charge would be located near the C_7—C_8 double bond.

Interactions between opsin and the chromophore

As already stated in the Introduction the frequency of the $^1B_u^+$ band varies a great deal from one animal species to another and between rod and the different cone pigments and it is, in almost all cases, very different from the frequency of the isolated chromophore. This poses the problem of frequency regulation in visual pigments as well as in bacterial Rh. In view of the great importance of the $^1A_g^-$ state for the photochemical reaction of Rh it would be very desirable to know if the species to species changes of the frequency of this state parallel or not those of the $^1B_u^+$ state. However, most of the two-photon work known to us was done on bovine Rh. The knowledge of the $^1A_g^- - ^1B_u^+$ separation could be helpful in assessing the differences in the mechanism of vision from species to species. In the meantime, comparisons between unprotonated and protonated Schiff bases may serve as a guide.

Wavelength regulation can only be achieved by the protein opsin which surrounds the chromophore. (However, the possibility of interaction of the chromophore with the lipid membrane should not be dismissed lightly.) The protein contains a number of ionic and polar groups whose field affects the chromophore. One of them which we call the primary counter-ion, is expected to be hydrogen bonded to the protonated nitrogen of the Schiff base. Protonation alone would explain only a part of the bathochromic shift (see ref. 119 and references therein). So an additional effect is needed. In human or bovine Rh the maximum of the band is near 500 nm.

A fundamental proposal was made at an early stage (1958) by Kropf and Hubbard (15, 16). They suggested that the polar groups of the protein, like COO^-, O^-, S^- could act with their fields upon the Schiff base pushing down the $^1B_u^-$-like state. This idea is at the origin of the external point charge model. In 1968 Wiesenfeld and Abrahamson (120) carried out quantum chemical calculations using a simple model of point charges and the Pariser–Parr–Pople method. They were able to substantiate Kropf and Hubbard's suggestion. Their calculations indicated that the most appropriate place for the polar group is in the vicinity of carbons 5 to 9. We shall call it the secondary counter-ion although it might be actually a properly oriented dipole. Other theoretical results giving strength to Kropf and Hubbard's suggestion came from Abrahamson and Wiesenfeld (121) and Mantione and Pullman (121), Honig *et al.* (123), and Favrot *et al.* (124, 125).

Nakanishi, Honig, and their co-workers (102–110) have greatly developed the external point charge theory. Nakanishi's group prepared a number of synthetic retinals and dihydroretinals in order to secure clues for the location of the point charge. These dihydroretinals can be assumed to bind to the apoprotein in conformations that closely mimic that of the native chromophore (see previous section). Bovine Rh was used in the experiments. The wavelength of their $^1B_u^+$-like absorption maxima was compared to their respective solution values, the difference being the opsin-shift. Methanol was chosen as a solvent (104, 110), since λ_{max} in this solvent is independent from the counter-ion ("levelling effect", Blatz and Mohler (126)). This is not an ideal choice, since methanol as a polar, hydrogen bonding solvent promotes protonation that is, helps to push the proton onto the nitrogen in a salt bridge. However, provided the Schiff bases are 100% protonated anyway this does not make much difference. The opsin shift turned out to be 2700 cm^{-1} for the protonated Schiff base of 11-*cis*-retinal itself, about 1700–2100 cm^{-1} for the 5,6 or 7,8 or 9,10 dihydro compounds and 5300 cm^{-1} for the 11,12 dihydro compound (105, 127). In the latter molecule the insulation effect of the saturated-CH_2—CH_2-group reduces the chromophore to a diene. Thus a point charge placed in proximity of the 11,12 double bond is seen to cause the largest opsin shift. (Interestingly, Honig's calculations show that this can be obtained by a negative charge near C14 or a positive charge near C15). Both the relatively large shift of the 11,12 dihydro derivative and the smaller shift of the native chromophore can be explained by placing a negative charge in the C12—C14 area, 3 Å from C12 and 3.4 Å from C14 (127). This applies to (bovine) visual pigments. Similar data for bR lead to the conclusion that the external negative charge is located in the vicinity of the β-ionone ring. The carboxylate ions which are likely to be the point-charges cannot be considered as exact point charges. They actually contain two negative oxygens and one positive carbon. It is even possible that the primary counter-ion and the external point charge are two oxygen atoms of the same carboxylate ion (127, 128).

Much of our present thinking on the effect of counterions and wavelength regulation goes back to Blatz's pioneering work which will now be reviewed in some detail.

Following initial studies by Morton *et al.* (130–133) Blatz used model compounds (usually all-*trans* retinylidene *n*-butylamine, NRBA), different acids (mostly mineral acids like HCl), and various solvents in order to mimic Rh. For these systems he tried to correlate the variation of the λ_{max} of NRBA with the different acids and to assess solvent effects. In this last respect, using perchlorate salts of NRBA, Blatz *et al.* (113) showed that ion-pairs existed in a non-polar solvent (like chloroform) while in a polar one (like methanol), the cation (the protonated imine) and the anion (ClO_4^-) were fully solvated. With polar solvents, no ion-pairs were present and the λ_{max} of protonated NRBA remains the same irrespective of the polar solvent used (which cause a "levelling effect"). By varying the acid and choosing proper solvents (like 1,2-dichloroethane) Blatz *et al.* were able to obtain uv–visible absorption spectra quite similar to those obtained from a digitonin extract of bovine Rh.

After noting the very important red shift associated with linear conjugated odd-numbered alternant hydrocarbons compared to those which are even numbered (134–137), Blatz and co-workers tried to correlate the λ_{max} of protonated NRBA with some physico-chemical properties of the counterions (113, 138, 139). Using ionic radii, they were able to calculate the ionic electrostatic interaction that existed between the protonated imine function and the counter-ion (viz. —CH=$\overset{+}{N}$—H----X^-). They noted that λ_{max} of NRBA correlates fairly well with the strength of the acids and most importantly that it was the distance from the anion that regulated the λ_{max} of the cation. From this work, Blatz inferred that the protein part of the visual pigments could possibly regulate the absorption wavelength of the chromophore by moving the site of the negative charge density away from or nearer to the cation by conformational change.

Blatz has used systems where the Schiff base is protonated by

very strong acids (like HCl) and only in a few cases did he use a carboxylic acid. The protonating agents in the protein could come from different sources but the terminal carboxylic acids of aspartic and glutamic acids are likely candidates. These are weak acids (pK_a of 3.86 for Asp and 4.25 for Glu) and, in a non-polar environment, protonation of the chromophore could well be different. Furthermore, Rafferty and Shichi (140) and Hildebrandt and Stockburger (97) have shown that water molecules are in the proximity of the azomethine function. It must be said again that in a polar environment, charge separation without solvent stabilization is unlikely. Warshel and Barboy (100) have proposed an interesting alternative. They see the chromophore in a polar milieu but isomerization causes a movement that carries it into a non-polar environment. This would explain the red shift observed when Rh is transformed into B or bR into K. The behavior of weak carboxylic acids toward conjugated Schiff bases has been explored by us since no systematic studies existed on the subject. In works similar to those of Blatz, we tried to evaluate the interaction of several carboxylic acids of pK_as ranging from 0.2 to 4.8. We chose substituted acetic acids (XCH_2CO_2H) as protonating agents, chloroform and methanol as solvents and two different Schiff bases: *trans,trans*-2,4 heptadienylidene *tert*-butylamine (HtBA) and all-*trans* retinylidene *tert*-butylamine (RtBA). In a series of articles (141–143) we have shown that, in a non-polar solvent, weak carboxylic acids are not able to fully protonate a conjugated Schiff base. Actually, with acids in the 4.5 pK_a range, hardly any protonation can be observed. Weak acids can protonate the imine when the solvent is polar but then solvation causes a levelling effect. With moderately strong acids (pK_a = 2–3), only partial protonation is found while with strong acids such as trichloroacetic acid (TCA; pK_a = 0.6), complete protonation is observed. In the last case, in a non-polar solvent, ^1H nmr indicates rapid proton exchange between the Schiff base and the counter-ion. At −40°C, the exchange has stopped and only the protonated imine is obtained. ^{13}C and ^{15}N nmr data (144) indicate that protonation is related directly to the strength of the acids used. Infrared data obtained on the same systems lead to similar results (see below).

In conclusion, no definite answers have been given as to how the protein opsin can shift the λ_{max} of the 11-*cis*-retinylidene chromophore to longer wavelengths and how it can regulate it. But Blatz's observation concerning the salt bridge is pertinent even though the exact nature of the interactions remains to be elucidated. More must be known of the environment surrounding the chromophore for the exact mechanism to be unraveled.

The main problem could be stated in a few words: are point-charges the most important factor for wavelength regulation in Rh or is it the Blatz-effect (regulation by the distance Schiff base – counter-ion) which can govern the distribution of the positive charge in the conjugated system?

Protonation

As mentioned previously, protonation of the Schiff base in Rh has been invoked primarily to give an explanation for the surprising long wavelength absorption of most Rh. But could this shift not be explained otherwise?

Leclercq (see Favrot *et al.* (125)) carried out CNDO/S model calculations on the retinal Schiff base by placing a proton donor at the nitrogen and a carboxylate ion close to the β-ionone ring at C5. The result was that the observed absorption wavelength can be matched by placing the two counter-ions in such a way that the $N_{16}\ldots H^+$ distance is 2.0 Å and the C5—C (carboxylate) distance is about 3.10 Å or shorter. With an $N_{16}\ldots H^+$ distance of 2.0 Å the Schiff base is not protonated but "only" hydrogen bonded. This indicated that outright protonation is not an absolute prerequisite for interpreting the absorption spectra of Rh. The visible absorption spectrum is not, in itself, a proof for protonation.

Moreover, there is at present ample evidence that both protonated and non-protonated Schiff bases can "bleach", that is, undergo photoinduced isomerization yielding a colorless product (see below).

A wealth of infrared spectroscopic data and other physicochemical evidence show that whenever a nitrogen base is protonated the proton remains hydrogen-bonded to the "original" proton donor, or in other words, there must be a counter-ion, X^-:

$$C{=}N^+{-}H{\cdots}X^-$$

or, if the original proton donor was itself protonated:

$$C{=}N^+{-}H{\cdots}X$$

As a consequence of this a tautomeric equilibrium is likely to exist at the Schiff base nitrogen:

$$C{=}N{\cdots}H{-}X \rightleftharpoons C{=}N^+{-}H{\cdots}X^-$$

In the $^1B_u{}^+$ excited state the Schiff base can be expected to be more basic than in its ground state. This expectation is based on Förster's experiments (145), Becker's observation of a large pK_a change in the excited state (69), and on dipole moment measurements in the ground and excited states by Mathies and Stryer (146) and by Corsetti and Kohler (65).

Since this is so, chemical intuition would predict proton transfer in the excited state with only a H-bond on the Schiff base in the ground state. This interpretation could not apply, however, if the Schiff base was initially protonated.

The fact that there must be a counter-ion at the Schiff base nitrogen has been recognized by Schaffer *et al.* (69), Honig *et al.* (147), Peters *et al.* (24), and Favrot *et al.* (124, 125). If the equilibrium is 100% in favor of the $C{=}N^+{-}H$ form one can say that the Schiff base is entirely protonated. Even then the remaining "back-H-bond" (with X being probably a carboxylate ion) is important for shaping the structure and the spectrum of the chromophore. Moreover, even a, say, 10% departure from 100% protonation could have serious consequences for the functioning of the pigment. Protonated amines or imines without a counter-ion, in general, do not exist in nature, except as very short-lived transients. There is little doubt about the existence of what we called a primary counter-ion at the Schiff base nitrogen. The identity of the proton donor is not definitely known, however. It is very likely that it is either aspartic or glutamic acid, since according to our present knowledge on the structure of the protein in bR (148–157) such residues are found close to the chromophore.

That the Schiff base is protonated is, at present, a widely accepted view.

Raman arguments played an important role in the investigations relating to the structure of the chromophore in Rh. The Raman $\nu(C{=}N)$ band is at 1655 cm^{-1} in bovine Rh while the related band of the Schiff base itself is at about 1625 cm^{-1} (76, 158). This increase in frequency is expected if the Schiff base is protonated, not because of the charge displacements connected with protonation but on the ground of mechanical interactions, in particular the mixing of $\nu(C{=}N^+)$ with the NH^+ in-plane bending motion (99, 159). If the NH group is deuterated this mixing is largely reduced and the $\nu(C{=}N^+)$ band shifts downwards to about 1630 cm^{-1} (76). This is usually

taken for a strong indication of protonation. Less direct evidence to this effect comes from the detailed study of the CH and NH out-of-plane bending vibrations (80, 81, 85). The argument would be even more convincing if the bathochromic shifts in the electronic spectrum and the shift towards higher frequencies in the Raman spectrum would show parallelism. Unfortunately, this does not seem to be the case. For example, with visible bands at 568 and 610 nm respectively, bR and K must be assumed to be protonated. However, their ν(C=N) bands are at frequencies as low as 1641 and 1610 cm^{-1}, the latter being lower than that of an unprotonated Schiff base.

Support for protonation came also from infrared investigations. Indeed, since the most characteristic vibrations of the chromophore are due to polar bonds or groups, at first sight infrared spectroscopy should be a better means of gathering information concerning its structure than Raman where intensities are conditioned by the rate of change in polarizability, not that of the dipole moment. However, resonance Raman can, so to say, lift out the chromophore from the protein, an advantage that infrared does not have. In recent years, however, differential infrared techniques have been worked out in the laboratories of Rothschild (160, 161), Siebert (162–164), and Eisenstein (165–167) by which they were able to obtain infrared spectra of the chromophore despite the overwhelming absorption of the surrounding protein. In all cases which were investigated the infrared spectra confirmed the results obtained by resonance Raman spectroscopy.

The question of protonation in Rh and bR has been studied also by ^{13}C and ^{15}N nmr. This form of spectroscopy seems ideally suited for probing the extent of protonation in visual and bacterial pigments since it is a non-destructive method using low excitation energy that permits examination of molecules in their ground state. ^{13}C shifts, it must be remembered, are sensitive to pH variations, to fields induced by charged groups and by steric interactions (168). ^{15}N nmr is even more suited for answering the question at hand since there is a very large upfield shift of some 150 ppm between unprotonated retinal Schiff bases and protonated ones (169, 170).

Mateescu and co-workers using enriched ^{13}C Rh and bR as well as ^{15}N enriched Rh and bR arrived at the conclusion, that with a single exception (the case of ^{13}C-enriched retinal at C14), solubilized Rh and bR had signals close to those of model protonated N-retinylidene alkylamines (ref. 171 and references therein).

Harbison *et al.* also used the same technique of ^{13}C and ^{15}N enriched Rh and bR and by solid-state ^{13}C magic-angle sample spinning (MASS) nmr arrived at the same conclusion (117, 172–175) concerning the protonation of the Schiff base. These studies show that the Schiff base is protonated and that it is hydrogen bonded to the counter-ion, the strength of the hydrogen bond being similar to what a protonated Schiff base would form with an iodide ion (118). One may comment that while this hydrogen bond is weaker than those formed with Cl^- or Br^-, it is much stronger than those which would be formed with carboxylic acids without an additional mechanism of stabilization.

So let us agree that the Schiff base is protonated prior to light absorption. Even then some important questions remain to be answered: (*1*) Is the Schiff base entirely protonated, that is, is the tautomeric equilibrium at the nitrogen 100% in favor of the protonated species? (*2*) How is the ion-pair stabilized in the salt bridge? (*3*) How does the proton translocation observed by Rentzepis occur?

Protonation and hydrogen bonding

The first question entails what, in our opinion, is the fundamental problem: what is the shape of the potential surface governing the motions of the proton on the Schiff base nitrogen? The shape of the potential in hydrogen bonds, in particular those within ion pairs, received a great deal of attention. (For reviews see refs. 176–185). The potential may have one or two minima. It can be asymmetrical single well (as), asymmetrical double well (ad), symmetrical double well (sd), or symmetrical, broad single well (ss). An (as) or (ad) type potential with the proton in the deeper well at covalent distance from the Schiff base nitrogen means protonation. With the proton closer to the original donor (X), the Schiff base would be merely hydrogen bonded. A proton close to the midpoint ($N\cdots H^+\cdots X^-$) with an (sd) or (ss) type potential would mean a nearly symmetrical, usually strong and short hydrogen bond. There are examples for this even in cases where the two end atoms are different (176). It is much more likely, however, that the hydrogen bond is only nearly symmetrical with a double well potential, both wells having significant population. Then this would be the case of a "hesitating" proton with a possibility of rapid exchange between the two wells either thermally or by tunneling. Is such a situation probable in the case of Rh?

Zundel and co-workers (179, 186–191) investigated extensively, by infrared spectroscopy, systems in which the proton is close to the midpoint. They have shown that these "easily polarizable hydrogen bonds" are highly sensitive to environmental effects and since, in a random medium, these are variable, broad areas of continuous absorption are found in their spectra, especially in the O—H or N—H stretching region. This part of the spectrum, together with the NH bending bands, should be of diagnostic value for elucidating the problem of protonation. It is unfortunate that neither the Raman nor the differential infrared spectra make it possible to obtain them. For this reason model studies are of value for gaining knowledge on the protonation of Schiff bases. Certain aspects are seldom discussed in the context of Rh research, so we will go into some detail.

Favrot *et al.* (125, 192) took isobutylidene–isopropylamine, $(CH_3)_2CHCH{=}NCH(CH_3)_2$, a simple non-conjugated Schiff base as their model. This aldimine is stable due to the branched substituents on both the carbon and the nitrogen of the double bond (Thiollais (193)). The free ν(C=N) band is at 1664 in chloroform solution. With a weak acid like CF_3CH_2OH the spectrum was in line with C=N:---HO— association. With an *excess* of $(CF_3)_3COH$, a much stronger acid, the high value of ν(C=N), 1704 cm^{-1} and the low value of the broad ν(OH) stretching band, centered at 2530 cm^{-1}, gives evidence of much stronger association, $C{=}N^+{-}H\ldots{:}O^-$ or $C{=}N\cdots H^+{-}O^-$. However, when the imine was in excess the ν(C=N) band at 1664 cm^{-1} became more intense than the 1704 cm^{-1} band, showing that the equilibrium can be easily tilted in favor of C=N:---H—O—.

Many other examples were given in ref. 125. It is readily demonstrated that if the counter-ion was an aliphatic amine it would take the proton from the Schiff base; if it contains another C=N, like pyridine or the imidazole ring of histidine, for example, it would probably share the proton with the Schiff base; if it was a carboxylic acid, then all will depend on the strength of the acid.

According to our present knowledge, in Rh the proton donor (the primary counter-ion) is probably aspartic or glutamic acid which are somewhat more acid than perfluorotert–butanol in the

above example. Thus Lussier *et al.* (194) have undertaken a systematic study of protonation – hydrogen bonding conditions with a series of carboxylic acids and hydrochloric, hydrobromic, and hydroiodic acids.

The carboxylic acids used were trichloro-, dichloro-, monochloro-, monobromo-acetic acids and 3-chloropropionic- and propionic acid whose pK_a values (in water) are 0.66, 1.26, 2.85, 2.90, 3.99, and 4.87, respectively. (The corresponding pK_a values for aspartic and glutamic acids are 3.86 and 4.25.) All the spectra exhibit Zundel continua in the 2700–2000 cm^{-1} region, except that for the weakest acid (propionic) and the strongest acid (trichloro) they are weak. For non-conjugated Schiff bases the $\nu(C{=}N^+)$ bands are between 1708 and 1712 cm^{-1} and the (non-protonation) $\nu(C{=}N)$ bands are at 1667 cm^{-1}. The relative intensities of these two bands vary with the pK_a of the acid. The estimated percentages of protonation based on the band areas were found to be 90–95% for trichloroacetic acid, 80–90% for dichloroacetic acid, 75–55% for monochloro-, and monobromo acetic acids, and 10–20% for propionic acid. (For 1:1, 0.1 *M* solutions in chloroform.)

Non-conjugated Schiff bases are rather remote models for Rh, however. Thus, subsequently Lussier *et al.* (195) carried out similar infrared investigations on *trans*-retinal in chloroform. The percentages of protonation increased with respect to the non-conjugated imines. The approximate percentages of protonation obtained were 100% for trichloroacetic acid, about 80–90% for monochloroacetic acid, 60–70% for 3-chloropropionic acid, and 10–20% for propionic acid. Thus a significant fraction is still unprotonated. The continua in the 2700–2000 cm^{-1} region indicate that for the medium strong acids the proton is close to the midpoint of the proton bridge.

Previously Zundel and Merz (191) and Rastogi and Zundel (196) considered hydrogen bonds between retinylidene butylamine and various carboxylic acids and in a number of other model systems to see whether such hydrogen bonds show large proton polarizability and to determine the equilibria. If the proton is close to the midpoint, it can be easily shifted by electric fields due to the large proton polarizability of such hydrogen bonds. Zundel suggests (197, 198) that this is the case, among others, of protonated Schiff base/aspartate or phenolate systems. Hydrogen bonded chains with large proton polarizability could be important for the conduction of the positive charge in bR and in the proton pumping mechanism.

Should we definitely admit the 100% initial protonation of the retinal Schiff base chromophore in Rh and in bR?

The agreement of the resonance Raman and differential infrared values for $\nu(C{=}N)$ for all Rh and the results provided by nmr measurements appear to be convincing. In addition, it is noteworthy that the frequencies for Rh, B, and isorhodopsin are essentially the same. These are the three isomers which are in equilibrium when a photostationary state is produced upon illumination of Rh at low temperatures. At first sight this would mean that the state of protonation is the same for the three, that they are all protonated and that the strength of the back-hydrogen bond in the proton bridge is also the same. Caution should be exercised, however. The $\nu(C{=}N^+)$ frequency is obtained by compensation between two main effects. First, upon protonation a new chemical bond is created on the Schiff base nitrogen rendering $\nu(C{=}N)$ a less good "group frequency". This would be expected to *lower* its frequency. Second, the normal coordinate which entails C=N stretching motion as its dominant component will receive N^+—H in-plane bending (and other) admixtures. Since the mainly N^+—H in-plane bending vibration is almost certainly at about 1350 cm^{-1} (85, 96) this would push $\nu(C{=}N)$ to higher frequencies (85, 199). (It is noteworthy that the C_{15}—H rocking band is at almost the same frequency.) Now, since this is so, the uniform $\nu(C{=}N^+)$ might not correspond to the same potential, average proton position and charge distribution in the proton bridge. This is clearly illustrated by the recent differential infrared experiments of Bagley *et al.* (167). These researchers performed experiments on hydrated and deuterated films of native rod outer segment (ROS) and ROS regenerated with retinals with isotopic substitution at C-15. In differential infrared experiments two samples, for example, Rh and B are recorded against each other, so that what the two contain in common cancels out. So did the $\nu(C{=}N^+)$ band between Rh, B, and isorhodopsin. Most significantly, however, the three N-deuterated samples gave three different $\nu(C{=}N^+)$ frequencies (167). They are 1624 for B, 1631 for isorhodopsin, and 1624 cm^{-1} for Rh (164, 200) in agreement with previous results of Siebert *et al.* (164, 200). Since $\nu(C{=}N^+)$ also receives some admixture from C—C and C—H motions involving C-15, Bagley *et al.* (167) also applied ^{13}C labelling at C-15 and deuteration at C-15. The results were, in the above order, 1610, 1603, and 1602 cm^{-1} for $H^{13}C{=}N^2H$ and 1610, 1614, and 1602 cm^{-1} for $^2HC{=}N^2H$. Since the NH and CH bending vibrations shift to about 1000 cm^{-1} or lower upon deuteration, coupling with the C=N motion becomes negligible, so that the results obtained on the sample deuterated on both C-15 and the nitrogen can be considered representative of the purely electronic effect of protonation without mechanical coupling. Thus, while in the hydrated samples all three molecules have the same $\nu(C{=}N^+)$ frequency, in the deuterated samples they do not.

These differences are significant. They mean that the potential governing the motions in the proton bridge, and the average position of the proton are not the same for the three cases. This must be connected with environmental differences around the chromophore. Then the most intriguing question is the following: is the proton closer to the nitrogen in Rh than in B or is the opposite the case? As to bR whose ir $\nu(C{=}N^+)$ frequency is at 1639 cm^{-1} at low temperatures, Bagley *et al.* (201) found 1627 cm^{-1} for $HC{=}N^2H$, 1629 for $H^{13}C{=}NH$, 1610 for $H^{13}C{=}N^2H$, 1632 for $^2HC{=}NH$, and 1614 cm^{-1} for $^2HC{=}N^2H$. The $\nu(C{=}N^+)$ of K is at 1610 cm^{-1}. The low frequencies of (natural) bR and K would themselves require an explanation. Just like Eisenstein's (167, 201) deuteration experiments this can only mean that the role of mechanical coupling in determining the $\nu(C{=}N^+)$ frequency makes the latter an uncertain indicator of protonation. Favrot *et al.* (124) found cases with model Schiff bases where the $\nu(C{=}N)$ only differed from $\nu(C{=}N^+)$ by 7–9 cm^{-1}.

In the differential infrared spectra (167) several bands are found in the 1800–1600 cm^{-1} region which do not belong to the chromophore but to the adjacent protein and some of them, perhaps, to the lipid. This shows that changes occur around the amide carbonyl bands due to the Rh → B transformation. The residue mainly affected is probably lysine-296 which provides for the Schiff base linkage.

The N-deuteration shifts, 30–35 cm^{-1} for Rh and B would seem to be better indicators of protonation than the frequencies themselves. If there is no protonation, why should $\nu(C{=}N^+)$ be affected by changing H to D? However, bR only exhibits a shift of 12 cm^{-1}. Does this mean that the proton is, on the average, closer to the nitrogen for Rh than for bR? The

coupling-free values for $\nu(C{=}N^+)$ for Rh (1602) and for bR (1614 cm^{-1}) point to the same order. The visible band positions would seem to indicate the opposite, however: 500 nm for Rh and 568 nm for all-*trans* bR. In the same way, if we compare Rh to B we find that the ^1B_u-like bands are at 500 and at 543 nm, respectively, indicating closer protonation for B, while the coupling-free C=N frequencies (1602 and 1610 cm^{-1}) seem to indicate closer protonation for Rh.

All what one may conclude from the above reasoning is that neither the visible nor the C=N frequencies are absolute indicators of the degree of protonation. While the balance of evidence is in favor of protonation for Rh, B, I, bR, and K, significant differences might exist in the average position of the proton and the shape of the potential surface governing its motions in the proton bridge.

Now, as has been proposed earlier by Leclercq and Sandorfy (202, 203), this potential is likely to have two minima. This would be in conformity with the pK_a values of the acids available for protonation which are at about the limit of what can be expected to protonate a conjugated Schiff base, with the existence of Zundel continua in the infrared spectra and Lussier *et al.*'s finding (194, 195) that acids even stronger than aspartic or glutamic acids cannot protonate the Schiff base 100%.

The examination of the Raman effect leads, in certain cases to surprising predictions when a vibration is governed by a double well potential (202, 203). Let us suppose that we have two slightly unequal wells, so that both wells have a non-negligible population. Then the Raman lines might correspond to vibrations in one or the other branch of the potential surface. The relative intensities of the two will depend, in a resonance Raman experiment, on the respective Franck–Condon factors with the potential surface of the resonating excited state. This condition may become predominant and it may render the relative populations unimportant. As a consequence it may happen in certain cases that the less populated well becomes the only one to give rise to a band observable in the spectrum. The infrared spectra are not subject to these conditions but the $\nu(C{=}N^+)$ bands are expected to have much greater intensity than $\nu(C{=}N)$. While according to our present knowledge the population of the protonation well (the one closer to the nitrogen) is probably much higher than the population of the non-protonation well, the possibility that a significant fraction of the chromophore molecules are in the non-protonation well cannot be excluded. In ultraviolet pigments which are unlikely to be protonated (λ_{max} about 350 nm) the primary photochemical event might then be proton transfer onto the nitrogen followed by isomerization (see below).

Stabilization of the ion-pair

If we admit that the Schiff base is protonated in both Rh and bR we have to answer the following question: how can the Schiff base be protonated by the relatively weak acids available in the pigments?

In view of the tendency of protonated Schiff bases to hydrolyse in aqueous media it might seem logical to postulate that the chromophore is in a hydrophobic (low dielectric) environment (99). However, as Warshel (100, 111) pointed out, the $C{=}NH^+{---}COO^-$ ion-pair cannot be stable in low dielectric environments. They would be converted into C=N...COOH just as zwitterionic amino acids in non-polar solvents or amine salts in the gas phase. Also, the extensive infrared work by Zundel *et al.* (186–191) demonstrated that under neutral conditions the acids present in the pigment cannot protonate the Schiff base. The ion-pair needs stabilization by polar groups. This stabilization could be obtained in various ways. A simple way would be by a proton relay network often invoked by biochemists. In such a relay the primary counter-ion which is the proton donor with respect to the Schiff base accepts a proton from another donor. As a consequence the primary counter-ion becomes more acid. A suggestion to this effect was made by Khristoforov *et al.* in 1974 (204). The second donor could be another carboxylic acid and more than two may be involved. (See also Denisov and Golubev (205), Zundel and Merz (191), Kristof and Zundel (197, 198), and Rosenbusch (129) for a recent look at the problem.)

The ions could exist in a polar environment created by permanent dipoles of the surrounding protein. Models of this type were given in the literature (Warshel (112); Honig *et al.* (99); Birge *et al.* (64)).

Rafferty and Shichi (140) observed that in a dry nitrogen atmosphere the 500 nm band of bovine Rh underwent a large blue shift to 390 nm. This seems to indicate that the Schiff base lost its proton. The *in vacuo* Raman measurements of Hildebrandt and Stockburger (97) have given strong confirmation for this. Then it is logical to assume that the ion-pair in the proton bridge of the Schiff base is stabilized by water molecules. This goes in the sense of Warshel's suggestion that the local environment of the Schiff base must have a high dielectric constant (ref. 100 and references therein). A few tightly bound water molecules would not hydrolyse the protonated Schiff base.

Dupuis *et al.* (116) suggested that one (or more) water molecules might be intercalated between the carboxylate ion and the iminium ion, so that proton transfer between the two ions would occur via an oxonium ion. In all likelihood other water molecules would form a cluster around the system to lend it more stability. Either of these mechanisms, or a combination of them would make the assumption of a protonated Schiff base credible. The elucidation of this mechanism of stabilization should be, in our opinion, a prime target for future research. Connected to charge separation in the proton bridge is the problem of energy storage after photon absorption, in both Rh and bR.

The energy of a photon with λ = 500 nm (20 000 cm^{-1}) is about 2.5 eV or about 57.5 kcal/mol. Photon absorption leads to the creation of B followed by vibrational relaxation. B is very unstable at room temperature. According to Cooper's photocalorimetric measurements (98) the energy difference between the ground states of Rh and B is still about 35 kcal/mol. This amount of energy is "stored" in B for about 100 ns and is subsequently used to bring about the chemical changes that occur along the remainder of the cycle. Why is B so unstable? According to Honig *et al.* (99) the Schiff base is protonated, hydrogen bonded in a salt bridge to its counter-ion; the isomerization following light absorption breaks the hydrogen bond and twists the Schiff base of Rh into a distorted *trans* configuration. A protonated Schiff base without a counter-ion can only be a short-lived transient at room temperature. (B is stable, however, at liquid nitrogen temperature.) Thus the storage of energy is achieved by charge separation. Since B absorbs at longer waves (543 nm) than Rh (500 nm) this is in agreement with Blatz's original suggestion that pulling away the counter-ion from the chromophore allows a wider distribution of the positive charge in the conjugated double bond system and causes a red shift in the visible spectrum. Subsequently Warshel and Barboy (100) pointed out that it is very difficult to store a

significant amount of energy by charge separation in a *polar environment* which must be assumed in order to have Rh stable. They then suggested that "This dilemma can be resolved if the isomerization takes the protonated Schiff base from a polar environment to a non-polar environment" (100). They then went on to estimate the amount of electrostatic energy that can be stored in this way by microscopic dielectric approaches. It turned out that it can be approximated by the energy change produced by moving the protonated Schiff base from a polar to a non-polar environment and it amounts to about 30 kcal/mol. The Schiff base is contained in a cavity of the protein which has to adjust to the new situation. According to Warshel and Barboy "the relaxation of the protein dipoles can be sufficiently slow to allow for a significant energy storage during times of the order of microseconds at room temperature. At lower temperature, the protein relaxation can be frozen for a much longer period of time. It also follows from these model calculations that B can store a significant part of its excess energy as strain energy. These are then used for the subsequent transformations along the visual cycle." Warshel argues that the proton transfer observed by Rentzepis might occur in the ground state between two groups of the protein as a consequence of pK_a changes caused by the charge separation produced during the primary photochemical event. It "may provide a simple channel for electrostatic energy relaxation". Anyway, the role of the protein in the energy storage process is evident. The basic idea in both Honig's and Warshel's approaches is photo-induced charge separation in the salt bridge due to *cis–trans* isomerization in visual pigments and *trans–cis* isomerization in bR with energy storage in B or K and its transduction into chemical free energy for bringing about the subsequent chemical transformations. The present reviewers believe that this is sound. However, proton translocation is also a part of the photochemical event. Rentzepis and co-workers (23–25) studied the formation of B at temperatures ranging from 300 K to 4 K. The risetime of B was less than 6 ps at 30 K and even at 4 K it was still 36 ps. In view of the very fast risetime of B early doubts as to the possibility for a complete 11-*cis* to all-*trans* isomerization to occur within 6 ps were not without justification. However, detailed comparative studies of the resonance Raman spectra of Rh and B (and of bR and K) together with the attenuation of the all-*trans* requirement to distorted all-*trans* made this credible. On the other hand the more recent results of Rentzepis' group (79) further substantiated the involvement of proton translocation in the photochemical step. They performed measurements on the formation kinetics of B, deuterated on the nitrogen using 6 ps pulses at 530 nm. They observed a pronounced deuterium isotope effect at low temperatures, $k_H/k_D = 7$ for the rate of formation of B. At very low temperatures B exhibited a non-Arrhenius behavior, the rate being independent of temperature. This indicates proton translocation through tunneling, at least at low temperatures. The data made it possible to calculate the distance of the proton translocation, about 0.5 Å. This, together with the fact that with the method used the only exchangeable proton of the chromophore was the one in the proton bridge "provided is the basis for the suggestion that translocation of the Schiff base proton is at least a prominent component of the first event in vision" (25). (But see the next section for another point of view.)

As to bR, Applebury *et al.* (206) found a much more moderate deuterium isotope effect: k_H/k_D 1.6 for the formation of K at 298 K and 2.4 at 4 K. They observed the formation of a transient species (which they called S) between bR and K red shifted with respect to both bR and K. The formation of K from the transient had a (very low) thermal barrier but the rate of formation became practically independent of temperature at very low temperatures. Thus Applebury *et al.* (206) suggested that proton translocation at room temperature occurs mainly thermally but at low temperatures tunneling takes over. (The transient was renamed J by later authors (207).) Recently similar results were published on 11-*cis* and all-*trans*-retinal SB by Huppert and Rentzepis (208).

Some new ideas and developments

After photon absorption the excited molecule may have a great amount of vibrational energy and may start twisting (68, 69) making it possible for the proton to move away from the nitrogen despite its increased basicity. This would remove some of the extra stabilization provided by the proton bridge and give the green light to the Schiff base to isomerize. After twisting, the Schiff base, still in the excited state, would be rapidly reprotonated by a waiting acid. The acid could be Asp_{83}, or Glu_{122}, or Glu_{134} which according to Dratz and Hargrave (154) are in the vicinity of the chromophore. This would explain the rapid proton translocation and kinetic deuteration effect observed by Rentzepis and co-workers. It is believed that this is a more natural explanation than postulating proton transfer from one counter-ion to another. Rentzepis also observed that the quantum yield of the Rh → B transformation is higher at low temperature than at room temperature. This could be linked to the preponderance of transfer by tunneling at low temperature and by passing over the potential barrier at room temperature (Cf. Birge, ref. 67).

An interesting sequel to this hypothesis concerns the intermediates observed by a number investigators (209–215) *between* Rh and B and bR and K. Some of these intermediates like hypsorhodopsins absorb at wavelengths shorter than a protonated Schiff base and nearer to the free base. Now, the above hypothesis would seem to give a natural interpretation for hypsorhodopsins. They would correspond to Schiff bases nearly free from protonation observed between the removal of the "original" proton from the nitrogen and its reprotonation following isomerization.

This could be compatible with the existence of a double well potential governing the motions of the proton in the salt bridge, with both wells having a significant population. Then proton translocation would be possible either onto or away from the nitrogen.

The existence of ultraviolet pigments supplies us an argument in this respect (32–35). Harosi and Hashimoto (34) and Harosi (35) found cone pigments in the eyes of the japanese dace whose absorption maxima are at 350–370 and 405–415 nm. Since all these pigments can bleach, one is led to the idea that in such cases proton transfer onto the Schiff base would precede isomerization. In the above scheme this would correspond to a situation in which the non-protonation well of the double well potential (the one more distant from the nitrogen) is more populated than the protonation well, perhaps much more.

Further indications for this can be found in the experiments of Rafferty and Shichi (140) and Hildebrandt and Stockburger (97). The former observed that under anhydrous conditions the visible absorption maximum shifts hypsochromically from 500 nm to about 390 nm. This very likely is a consequence of deprotonation. Then if they shine light into the 390 band, the absorption maximum goes back to about 480 nm and bleaching occurs. This seems to entail a proton transfer *onto* the Schiff

base, again preceding isomerization. Thus, our original suggestion (116, 125) would correspond to reality in at least certain cases. It is significant that both protonated and non-protonated Schiff bases have a tendency to bleach.

Stoeckenius and co-workers have shown that both acidification and deionization cause color changes in bR (26, 216). Between pH 3 and 1 the color of the membrane changes from purple to blue while the absorption maximum shifts from 568 to 605 nm. The same happens when the membrane is deionized on a cation exchange column or when it is washed first with a sodium chloride solution and then with deionized water. However, the original color of bR can be restored by further lowering the pH to below one or by adding certain metal cations in appropriate concentrations. This phenomenon has been the object of thorough physico-chemical investigations by Kimura *et al.* (217) and, by resonance Raman spectroscopy, Massig *et al.* (218) and Smith and Mathies (219). According to Moore *et al.* (220), Mowery *et al.* (216), Fischer and Oesterhelt (221), and Muccio and Cassim (222) the first color change is due to protonation of a negative charge in the environment of the chromophore and the second one (which is unaffected by deionization) to protonation of another group in the chromophore environment. Kimura *et al.* (217) put forward the idea that the two groups are the two counter-ions near the Schiff base nitrogen and the β-ionone ring. While more detailed investigations are certainly needed at this point, the idea is attractive. At any rate, it is most important to note that the color regulation mechanism in bR (and possibly Rh) is even more refined than was hitherto believed and that metal cations play a role in it. This also makes it very likely for water molecules to be present in the vicinity of the Schiff base nitrogen (Dupuis *et al.* (116), Massig *et al.* (218)); they could be there in hydrated cations and regulate the extent of protonation of the chromophore and the surrounding protein and the conditions for proton translocation.

Recently Sharkov *et al.* (ref. 223 and references therein), Nuss *et al.* (224), and Polland *et al.* (ref. 225 and references therein) reinvestigated the photochemical event in bR. Nuss *et al.* and Polland *et al.* used light pulses as low as 160 fs, a time resolution of 5×10^{-13} s and low intensities. The main results of these investigations were as follows. Photon absorption excites bR to a short-lived excited state S_1. Then a rapid transition occurs into the *J* intermediate (ground state). The rise time of *J* was found to be 430 ± 50 fs (700 according to Sharkov *et al.* (223)). *J* then goes over to *K* which appears with a time constant of 5 ps (3 according to Sharkov). In accordance with the above mentioned work of Applebury *et al.* (206) *J* is red shifted by about 30 nm with respect to bR and *K* by 20 nm. Nuss *et al.* (224) and Polland *et al.* (225) also studied bR deuterated on the nitrogen but found no deuterium isotope effect for either the S_1 to *J*, or the *J* to *K* transformation. Their experiments were carried out at room temperature. An important comment of Polland *et al.* recalls that bR forms a two-dimensional hexagonal lattice (the purple membrane), where "three bR molecules are close enough to form excitonically coupled trimers." So after light absorption excitation is first delocalized for a very short time and then trapped into the S_1 excited state in one of the bR molecules with subsequent transformations into *J* and *K*. These new results would *seem to* exclude the possibility of proton translocation between bR and either *J* or *K*. Moreover, they indicate a large degree of isomerization in less than 1 ps. Before concluding we should like to wait until a consensus is reached in the world of ultrafast spectroscopists. Let us comment, however, that conditions may be different for visual pigments for which a much larger deuterium isotope effect has been found (25).

Concluding remarks

Present trends are directed partly towards the discovery of other bacterial rhodopsins and the study of their properties. They cannot anymore be considered as curiosities but rather as convenient photochemical devices often used by nature. On the other hand, a great deal of effort is deployed on the structure of the intermediates beyond *B* or *K*, the kinetics of their formation, and the concomitant changes in the surrounding protein. Among these we mention the results of Engelhard *et al.* (226), El-Sayed and co-workers (227–230), and Hess *et al.* (231) and a theoretical treatment by Tavan *et al.* (232). Other researchers are looking beyond the photochemical cycles and into the way in which the signal is given to the nervous system in vertebrates. Typical of these is the light scattering work by Abrahamson *et al.* (42, 233) and the electrochemical work by Keszthelyi *et al.* (234–237). The interesting reader might like to consult the volume edited by Packer (47).

A characteristic of publications on rhodopsins is the great number of co-authors on almost all the articles. This is a measure of the hard and diversified work that rhodopsin research entails. Biologists, biochemists, biophysicists, physicochemists, electronic, infrared, Raman, nmr spectroscopists, crystallographers, quantum chemists, are all needed to penetrate into the fascinating secrets of nature which are involved. Pigments are most important instruments in the interactions of light with living matter.

1. G. WALD. J. Gen. Physiol. **21**, 795 (1937–1938).
2. G. WALD. Am. J. Physiol. **133**, 1479 (1941).
3. G. WALD and P. K. BROWN. J. Gen. Physiol. **37**, 189 (1953–1954).
4. G. WALD, J. DURELL, and R. C. C. ST. GEORGE. Science, **111**, 1179 (1950).
5. P. K. BROWN and G. WALD. J. Gen. Physiol. **35**, 797 (1951–1952).
6. G. WALD, P. K. BROWN, and I. R. GIBBONS. J. Opt. Soc. Am. **53**, 20 (1963).
7. G. WALD. Science, **150**, 1028 (1965).
8. W. WRIGHT, P. K. BROWN, and G. WALD. J. Gen. Physiol. **59**, 201 (1972).
9. G. WALD. Exp. Eye. Res. **18**, 333 (1974).
10. G. WALD. *In* Biochemistry and physiology of visual pigments. *Edited by* H. Langer. Springer, Berlin. 1973. p. 1.
11. R. HUBBARD and G. WALD. J. Gen. Physiol. **36**, 269 (1952–1953).
12. R. HUBBARD and R. C. C. ST. GEORGE. J. Gen. Physiol. **41**, 501 (1958).
13. C. M. RADDING and G. WALD. J. Gen. Physiol. **39**, 909a (1955–1956).
14. C. M. RADDING and G. WALD. J. Gen. Physiol. **39**, 923b (1955–1956).
15. R. HUBBARD and A. KROPF. Proc. Natl. Acad. Sci. (USA), **44**, 130 (1958).
16. A. KROPF and R. HUBBARD. Ann. NY Acad. Sci. **74**, 266 (1958).
17. T. YOSHIZAWA and G. WALD. Nature, **197**, 1279 (1963).
18. T. YOSHIZAWA and G. WALD. Nature, **201**, 340 (1964).
19. T. YOSHIZAWA and G. WALD. Nature, **214**, 566 (1967).
20. T. YOSHIZAWA. *In* Photochemistry of vision. *Edited by* H. J. A. Dartnall. Vol. 7/1 of Handbook of Sensory Physiology. Springer, Berlin. 1972. p. 146. Chapt. 5.

21. T. YOSHIZAWA and S. HORIUCHI. *In* Biochemistry and physiology of visual pigments. *Edited by* H. Langer. Springer, Berlin. 1973. p. 69.
22. T. YOSHIZAWA and G. WALD. Nature, **199**, 1279 (1963).
23. G. E. BUSCH, M. L. APPLEBURY, A. A. LAMOLA, and P. M. RENTZEPIS. Proc. Natl. Acad. Sci. **69**, 2802 (1972).
24. K. PETERS, M. L. APPLEBURY, and P. M. RENTZEPIS. Proc. Nat. Acad. Sci. (USA), **74**, 3119 (1977).
25. P. M. RENTZEPIS. *In* Spectroscopy of biological molecules. *Edited by* C. Sandorfy and T. Theophanides. Reidel. 1984. p. 373.
26. D. OESTERHELT and W. STOECKENIUS. Nature New. Biol. **233**, 149 (1971).
27. D. OESTERHELT and W. STOECKENIUS. Proc. Natl. Acad. Sci. (USA), **70**, 2853 (1973).
28. N. A. DENCHER. Photochem. Photobiol. **38**, 753 (1983).
29. R. A. BOGOMOLNI. *In* Information and energy transduction in biological membranes. Alan R. Liss, New York. 1984. p. 5.
30. T. H. GOLDSMITH and G. D. BERNARD. Photochem. Photobiol. **42**, 805 (1985).
31. M. GOGALA. Z. Vgl. Physiol. **57**, 232 (1967).
32. K. HAMDORF, J. SCHWEMER, and M. GOGALA. Nature, **231**, 458 (1971).
33. R. PAULSEN and J. SCHWEMER. Biochem. Biophys. Acta, **283**, 520 (1972).
34. F. I. HAROSI and Y. HASHIMOTO. Science, **222**, 1021 (1983).
35. F. I. HAROSI. *In* The visual system. Alan R. Liss, New York. 1985. p. 41.
36. H. J. A. DARTNALL. Vision Res. **8**, 339 (1968).
37. F. I. HAROSI. J. Gen. Physiol. **66**, 357 (1975).
38. B. HONIG. Ann. Rev. Phys. Chem. **29**, 31 (1978).
39. B. HONIG. Curr. Top. Membr. Transp. **16**, 371 (1982).
40. M. OTTOLENGHI. *In* Advances in photochemistry. Vol. 12. *Edited by* J. N. Pitts, G. S. Hammond, K. Gollnick, and D. Grosjean. Wiley–Interscience, New York. 1980. p. 97.
41. R. R. BIRGE. Ann. Rev. Biophys. Bioeng. **10**, 315 (1981).
42. R. UHL and E. W. ABRAHAMSON. Chem. Rev. **81**, 291 (1981).
43. (*a*) W. STOECKENIUS and R. BOGOMOLNI. Ann. Rev. Biochem. **51**, 587 (1982); (*b*) W. STOECKENIUS, R. H. LOZIER, and R. A. BOGOMOLNI. Biochim. Biophys. Acta, **505**, 215 (1979).
44. H. SHICHI. Biochemistry of vision. Academic Press, New York. 1983.
45. V. BALOGH-NAIR and K. NAKANISHI. *In* New comprehensive biochemistry. Vol. 3. Stereochemistry. *Edited by* C. Tamm. Elsevier Biomedical, Amsterdam. 1982. p. 283.
46. D. S. KLIGER. Intl. J. Quant. Chem. **16**, 809 (1979).
47. L. PACKER (*Editor*). Biomembranes methods in enzymology. Vol. 88. Parts H and I. Academic Press, New York. 1982.
48. C. SANDORFY. J. Mol. Struct. **19**, 183 (1973).
49. J. KOUTECKY. J. Chem. Phys. **47**, 1501 (1967).
50. B. S. HUDSON and B. E. KOHLER. Chem. Phys. Lett. **14**, 299 (1972).
51. K. SCHULTEN and M. KARPLUS. Chem. Phys. Lett. **14**, 305 (1972).
52. R. R. BIRGE. *In* Spectroscopy of biological molecules. *Edited by* C. Sandorfy and T. Theophanides. Reidel, Dordrecht, Holland. 1984. p. 457.
53. W. M. MCCLAIN. Acc. Chem. Res. **7**, 129 (1974).
54. R. R. BIRGE. *In* Biomembranes methods in enzymology. Vol. 88. Parts H and L. *Edited by* L. Packer. Academic Press, New York. 1982.
55. P. R. MONSON and W. M. MCCLAIN. J. Chem. Phys. **53**, 29 (1970).
56. B. S. HUDSON and B. E. KOHLER. Ann. Rev. Phys. Chem. **25**, 437 (1974).
57. R. L. CHRISTENSEN and B. E. KOHLER. J. Chem. Phys. **63**, 1837 (1975).
58. R. R. BIRGE, K. SCHULTEN, and M. KARPLUS. Chem. Phys. Lett. **31**, 451 (1975).
59. R. L. SWOFFORD and W. M. MCCLAIN. J. Chem. Phys. **59**, 10 (1973).
60. G. R. HOLTOM and W. M. MCCLAIN. Chem. Phys. Lett. **44**, 436 (1976).
61. R. R. BIRGE, J. A. BENNETT, B. M. PIERCE, and T. M. THOMAS. J. Am. Chem. Soc. **100**, 1533 (1978).
62. R. R. BIRGE, J. A. BENNETT, L. M. HUBBARD, H. L. FANG, B. M. PIERCE, D. S. KLIGER, and G. E. LEROI. J. Am. Chem. Soc. **104**, 2519 (1982).
63. R. R. BIRGE, D. F. BOCIAN, and L. M. HUBBARD. J. Am. Chem. Soc. **104**, 1196 (1982).
64. (*a*) R. R. BIRGE, L. P. MURRAY, B. M. PIERCE, H. AKITA, V. BALOGH-NAIR, L. A. FINDSEN, and K. NAKANISHI. Proc. Natl. Acad. Sci. USA, **82**, 4117 (1985); (*b*) L. P. MURRAY and R. R. BIRGE. Can. J. Chem. **63**, 1967 (1985).
65. J. P. CORSETTI and B. E. KOHLER. J. Chem. Phys. **67**, 5237 (1977).
66. K. P. DAS, G. KOGAN, and R. S. BECKER. Photochem. Photobiol. **30**, 689 (1979).
67. R. R. BIRGE and L. M. HUBBARD. J. Am. Chem. Soc. **102**, 2195 (1980).
68. (*a*) R. S. BECKER and K. FREEDMAN. J. Am. Chem. Soc. **107**, 1477 (1985); (*b*) K. A. FREEDMAN and R. S. BECKER. J. Am. Chem. Soc. **108**, 1245 (1986).
69. A. M. SCHAFFER, T. YAMAOKA, and R. S. BECKER. Photochem. Photobiol. **21**, 297 (1975).
70. T. ROSENFELD, B. HONIG, and M. OTTOLENGHI. Pure Appl. Chem. **49**, 341 (1977).
71. H. J. A. DARTNALL, C. GOODEVE, and R. LYTHGOE. Proc. R. Soc. London, **97**, 2161 (1975).
72. F. COLLINS, R. LOVE, and R. MARTON. Biochem. J. **51**, 242 (1952).
73. J. M. LECLERCQ and C. SANDORFY. Photochem. Photobiol. **33**, 361 (1981).
74. C. SANDORFY. J. Photochem. **17**, 297 (1981).
75. S. KAWAMURA, S. MUJATANI, T. MATSUMOTO, and R. S. H. LIU. Biochemistry, **19**, 1549 (1980).
76. A. R. OSEROFF and R. H. CALLENDER. Biochemistry, **13**, 4243 (1974).
77. B. K. GREEN, T. G. MONGER, R. R. ALFANO, B. ATON, and R. H. CALLENDER. Nature, **269**, 179 (1977).
78. T. G. MONGER, R. R. ALFANO, and R. H. CALLENDER. Biophys. J. **27**, 105 (1979).
79. J. D. SPALINK, A. H. REYNOLDS, P. M. RENTZEPIS, M. L. APPLEBURY, and W. SPERLING. Proc. Natl. Acad. Sci. USA, **80**, 1887 (1983).
80. G. EYRING, B. CURRY, A. BROEK, J. LUGTENBURG, and R. MATHIES. Biochemistry, **21**, 384 (1982).
81. G. EYRING, B. CURRY, R. MATHIES, R. FRANSEN, I. PALINGS, and J. LUGTENBURG. Biochemistry, **19**, 2410 (1980).
82. G. EYRING, B. CURRY, R. MATHIES, A. BROEK, and J. LUGTENBURG. J. Am. Chem. Soc. **102**, 5290 (1980).
83. L. RIMAI, D. GILL, and J. L. PARSON. J. Am. Chem. Soc. **93**, 1353 (1971).
84. R. E. COOKINGHAM, A. LEWIS, and A. T. LEMLEY. Biochemistry, **17**, 4699 (1978).
85. S. O. SMITH, A. B. MYERS, R. A. MATHIES, J. A. PARDOEN, C. WINKEL, E. M. M. VAN DEN BERG, and J. LUGTENBURG. Biophys. J. **47**, 653 (1985).
86. R. MATHIES. Chem. Biochem. Appl. Lasers, **4**, 55 (1979).
87. M. BRAIMAN and R. MATHIES. Biochemistry, **19**, 5421 (1980).
88. M. BRAIMAN and R. MATHIES. Proc. Natl. Acad. Sci. USA, **79**, 403 (1982).
89. B. CURRY, A. BROEK, J. LUGTENBURG, and R. MATHIES. J. Am. Chem. Soc. **104**, 5274 (1982).
90. B. CURRY, I. PALINGS, A. D. BROEK, J. A. PARDOEN, P. P. J. MULDER, J. LUGTENBURG, and R. MATHIES. J. Phys. Chem. **88**, 688 (1984).

91. J. LUGTENBURG. Pure Appl. Chem. **57**, 753 (1985).
92. J. A. PARDOEN, C. WINKEL, P. P. J. MULDER, and J. LUGTENBURG. Recl. Trav. Chim. Pays-Bas, **103**, 135 (1984).
93. J. A. PARDOEN, H. N. NEIJENESCH, P. P. J. MULDER, and J. LUGTENBURG. Recl. Trav. Chim. Pays-Bas, **102**, 341 (1983).
94. S. O. SMITH, A. B. MYERS, J. A. PARDOEN, C. WINKEL, P. P. J. MULDER, J. LUGTENBURG, and R. MATHIES. Proc. Natl. Acad. Sci. USA, **81**, 2055 (1984).
95. M. STOCKBURGER, W. KLUSSMANN, H. GATTERMANN, G. MASSIG, and R. PETERS. Biochemistry, **18**, 4886 (1979).
96. G. MASSIG, M. STOCKBURGER, W. GAERTNER, D. OESTERHELT, and P. TOWNER. J. Raman Spectrosc. **12**, 287 (1982).
97. P. HILDEBRANDT and M. STOCKBURGER. Biochemistry, **23**, 5539 (1984).
98. (*a*) A. COOPER. Nature, London, **282**, 531 (1979); (*b*) F. BOUCHER and R. M. LEBLANC. Photochem. Photobiol. **41**, 459 (1985).
99. B. HONIG, T. EBREY, R. H. CALLENDER, V. DINUR, and M. OTTOLENGTHI. Proc. Natl. Acad. Sci. USA, **76**, 2503 (1979).
100. A. WARSHEL and N. BARBOY. J. Am. Chem. Soc. **104**, 1469 (1982).
101. B. HONIG. *In* Information and energy transduction in biological membranes. Alan R. Liss, New York. 1984. p. 149.
102. M. A. GAWINOWICZ, V. BALOGH-NAIR, J. S. SABOL, and K. NAKANISHI. J. Am. Chem. Soc. **99**, 7720 (1977).
103. K. NAKANISHI, V. BALOGH-NAIR, M. A. GAWINOWICZ, M. ARNABOLDI, M. MOTTO, and B. HONIG. Photochem. Photobiol. **29**, 657 (1979).
104. M. ARNABOLDI, M. G. MOTTO, K. TSUJIMOTO, V. BALOGH-NAIR, and K. NAKANISHI. J. Am. Chem. Soc. **101**, 7082 (1979).
105. B. HONIG, U. DINUR, K. NAKANISHI, V. BALOGH-NAIR, M. A. GAWINOWICZ, M. ARNABOLDI, and M. G. MOTTO. J. Am. Chem. Soc. **101**, 7084 (1979).
106. M. SHEVES, K. NAKANISHI, and B. HONIG. J. Am. Chem. Soc. **101**, 7086 (1979).
107. R. CROUCH, S. KATZ, K. NAKANISHI, M. A. GAWINOWICZ, and V. BALOGH-NAIR. Photochem. Photobiol. **33**, 91 (1981).
108. K. NAKANISHI, V. BALOGH-NAIR, M. ARNABOLDI, K. TSUJIMOTO, and B. HONIG. J. Am. Chem. Soc. **102**, 7945 (1980).
109. M. G. MOTTO, M. SHEVES, K. TSUJIMOTO, V. BALOGH-NAIR, and K. NAKANISHI. J. Am. Chem. Soc. **102**, 7947 (1980).
110. V. BALOGH-NAIR, J. D. CARRIKER, B. HONIG, V. KAMAT, M. G. MOTTO, K. NAKANISHI, R. SEN, M. SHEVES, M. ARNABOLDI-TANIS, and K. TSUJIMOTO. Photochem. Photobiol. **33**, 483 (1981).
111. A. WARSHEL. Biochemistry, **20**, 3167 (1981).
112. A. WARSHEL. Proc. Natl. Acad. Sci. USA, **75**, 5250 (1978).
113. P. E. BLATZ, J. H. MOHLER, and H. V. NAVANGUL. Biochemistry, **11**, 848 (1972).
114. D. OESTERHELT, M. MEENTZEN, and L. SCHUHMANN. Eur. J. Biochem. **40**, 453 (1973).
115. A. WARSHEL. Nature, **206**, 679 (1976).
116. P. DUPUIS, F. I. HAROSI, C. SANDORFY, J. M. LECLERCQ, and D. VOCELLE. Rev. Ann. Biol. **39**, 247 (1980).
117. G. S. HARBISON, S. O. SMITH, J. A. PARDOEN, C. WINKEL, J. LUGTENBURG, J. HERZFELD, R. MATHIES, and R. G. GRIFFIN. Proc. Natl. Acad. Sci. USA, **81**, 1706 (1984).
118. G. S. HARBISON, S. O. SMITH, J. A. PARDOEN, J. M. L. CURTIN, J. LUGTENBURG, J. HERZFELD, R. A. MATHIES, and R. G. GRIFFIN. Biochemistry, **24**, 6955 (1985).
119. D. S. KLIGER, S. J. MILDER, and E. A. DRATZ. Photochem. Photobiol. **25**, 277 (1977).
120. J. R. WIESENFELD and E. W. ABRAHAMSON. Photochem. Photobiol. **8**, 487 (1968).
121. E. W. ABRAHAMSON and J. R. WIESENFELD. *In* Handbook of sensory physiology. Vol. VII/1. *Edited by* H. J. A. Dartnall. Springer, Berlin. 1972.
122. M. J. MANTIONE and B. PULLMAN. Int. J. Quant. Chem. **5**, 349 (1971).
123. B. HONIG, A. D. GREENBERG, U. DINUR, and T. G. EBREY. Biochemistry, **15**, 4593 (1976).
124. J. FAVROT, J. M. LECLERCQ, R. ROBERGE, C. SANDORFY, and D. VOCELLE. Chem. Phys. Lett. **53**, 433 (1978).
125. J. FAVROT, J. M. LECLERCQ, R. ROBERGE, C. SANDORFY, and D. VOCELLE. Photobiol. **29**, 99 (1979).
126. P. E. BLATZ and J. M. MOHLER. Biochemistry, **14**, 2304 (1975).
127. H. KAKITANI, T. KAKITANI, H. RODMAN, and B. HONIG. Photochem. Photobiol. **41**, 471 (1985).
128. R. R. BIRGE, L. P. MURRAY, B. M. PIERCE, H. AKITA, V. BALOGH-NAIR, L. A. FINDSEN, and K. NAKANISHI. Proc. Natl. Acad. Sci. USA, **82**, 4117 (1985).
129. J. P. ROSENBUSCH. Bulletin de l'Institut Pasteur. **83**, 207 (1985).
130. S. BALL, F. D. COLLINS, P. D. DALVI, and R. A. MORTON. Biochem. J. **45**, 304 (1949).
131. S. BALL, F. D. COLLINS, R. A. MORTON, and A. L. STUBBS. Nature, London, **161**, 424 (1948).
132. G. A. J. PITT, F. D. COLLINS, R. A. MORTON, and P. STOK. Biochem. J. **59**, 122 (1955).
133. R. A. MORTON and G. A. J. PITT. Biochem. J. **59**, 128 (1955).
134. P. E. BLATZ, D. L. PIPPERT, and V. BALASUBRAMANIYAN. Photochem. Photobiol. **8**, 309 (1968).
135. P. E. BLATZ, N. BAUMGARTNER, V. BALASUBRAMANIYAN, P. BALASUBRAMANIYAN, and E. STEDMAN. Photochem. Photobiol. **14**, 531 (1971).
136. P. E. BLATZ, R. H. JOHNSON, J. H. MOHLER, S. K. AL-DILAIMI, S. DEWHURST, and J. O. ERICKSON. Photochem. Photobiol. **13**, 237 (1971).
137. P. E. BLATZ. Photochem. Photobiol. **15**, 1 (1972).
138. P. E. BLATZ and J. H. MOHLER. Biochemistry, **11**, 3240 (1972).
139. P. E. BLATZ and J. H. MOHLER. Biochemistry, **14**, 2304 (1975).
140. C. N. RAFFERTY and H. SHICHI. Photochem. Photobiol. **33**, 229 (1981).
141. M. BISSONNETTE, H. LE THANH, and D. VOCELLE. Can. J. Chem. **62**, 1459 (1984).
142. M. BISSONNETTE, H. LE THANH, and D. VOCELLE. Can. J. Chem. **63**, 1480 (1985).
143. M. BISSONNETTE, H. LE THANH, and D. VOCELLE. Can. J. Chem. **63**, 2298 (1985).
144. D. COSSETTE and D. VOCELLE. To be published.
145. T. FORSTER. Z. Elekrochem. **54**, 42 (1950).
146. R. MATHIES and L. STRYER. Proc. Natl. Acad. Sci. USA, **73**, 2169 (1976).
147. B. HONIG, A. D. GREENBERG, U. DINUR, and T. G. EBREY. Biochemistry, **21**, 4593 (1976).
148. H. G. KHORANA, G. F. GERBER, W. C. HERLIHY, C. P. GRAY, R. J. ANDEREGG, K. NIHEL, and K. BIEMANN. Proc. Natl. Acad. Sci. USA, **76**, 5046 (1979).
149. R. HENDERSON and P. N. T. UNWIN. Nature, **257**, 28 (1975).
150. Y. A. OVCHINNIKOV, N. G. ABDULAEV, M. Y. FIEGINA, A. V. KISELEV, and N. A. LOBANOV. FEBS Lett. **100**, 219 (1979).
151. Y. A. OVCHINNIKOV. FEBS Lett. **148**, 179 (1982).
152. Y. A. OVCHINNIKOV, N. G. ABDULAEV, M. Y. FEIGINA, I. D. ARTAMONOV, A. S. ZOLOTAREV, M. B. KOSTINA, A. S. BOGACHUK, A. I. MOROSHNIKOV, V. I. MARTINOV, and A. B. KUDELIN. Bioorg. Khim. **8**, 1011 (1982).
153. P. A. HARGRAVE, J. H. MCDOWELL, D. R. CURTIS, J. K. WANG, E. JUSZCZAK, S. FONG, J. K. M. RAO, and P. ARGOS. Biophys. Struct. Mech. **9**, 235 (1983).
154. E. A. DRATZ and P. HARGRAVE. Trends Biochem. Sci. **8**, 128 (1983).
155. H. BAYLEY, K. HUANG, R. RADAKRISHNAN, A. H. ROSS, Y. TAKAGAKI, and H. G. KHORANA. Proc. Nat. Acad. Sci. USA, **78**, 2225 (1981).
156. G. E. GERBER, C. P. GRAY, D. WILDENAUER, and H. G. KHORANA. Proc. Natl. Acad. Sci. USA, **74**, 5426 (1977).
157. Y. A. OVCHINNIKOV, N. G. ABDULAEV, M. Y. FEIGINA, A. V. KISELEV, and N. A. LOBANOV. FEBS Lett. **84**, 1 (1977).

158. M. E. HEYDE, D. GILL, R. G. KILPONEN, and L. RIMAI. J. Am. Chem. Soc. **93**, 6776 (1971).
159. B. ATON, A. G. DOUKAS, D. NARVA, R. H. CALLENDER, U. DINUR, and B. HONIG. Biophys. J. **29**, 79 (1980).
160. K. J. ROTHSCHILD and H. MARRERO. Proc. Natl. Acad. Sci. USA, **79**, 4045 (1982).
161. K. J. ROTHSCHILD, W. A. CANTORE, and H. MARRERO. Science, **219**, 1333 (1983).
162. F. SIEBERT and W. MÄNTELE. Biophys. Struct. Mech. **6**, 147 (1980).
163. F. SIEBERT, W. MÄNTELE, and W. KREUTZ. Biophys. Struct. Mech. **6**, 139 (1980).
164. F. SIEBERT and W. MÄNTELE. Eur. J. Biochem. **130**, 565 (1983).
165. K. BAGLEY, G. DOLLINGER, L. EISENSTEIN, A. K. SINGH, and L. ZIMANYI. Proc. Natl. Acad. Sci. USA, **79**, 4972 (1982).
166. K. BAGLEY, G. DOLLINGER, L. EISENSTEIN, J. VITTITOW, L. ZIMANYI, T. G. EBREY, and B. NELSON. Biophys. J. **41**, 337 (1983).
167. K. A. BAGLEY, V. BALOGH-NAIR, A. A. CROTEAU, G. DOLLINGER, T. G. EBREY, L. EISENSTEIN, M. K. HONG, K. NAKANISHI, and J. VITTITOW. Biochemistry, **24**, 6055 (1985).
168. E. BREETMAIER and W. VOELTER. *In* ^{13}C nmr spectroscopy. 2nd ed. Verlag Chemie, New York. 1978. p. 67.
169. D. D. MUCCIO, W. G. COPAN, W. W. ABRAHAMSON, and G. D. MATEESCU. Fed. Proc. Fed. Am. Soc. Exp. Biol. **39**, 2096 (1980).
170. D. D. MUCCIO, W. G. COPAN, W. W. ABRAHAMSON, and G. D. MATEESCU. Org. Magn. Resn. **22**, 121 (1984).
171. G. D. MATEESCU, E. W. ABRAHAMSON, J. W. SHRIVER, W. COPAN, D. MUCCIO, M. IGBAL, and V. WATERHOUS. *In* Spectroscopy of biological molecules. D. Reidel, Boston. 1984.
172. G. S. HARBISON, J. HERZFELD, and R. G. GRIFFIN. Biochemistry, **22**, 1 (1983).
173. G. S. HARBISON, S. O. SMITH, J. A. PARDOEN, P. P. MULDER, J. LUGTENBURG, J. HERZFELD, R. MATHIES, and R. G. GRIFFIN. Biochemistry, **23**, 2662 (1984).
174. G. S. HARBISON, J. HERZFELD, S. SMITH, R. MATHIES, J. A. PARDOEN, J. LUGTENBURG, and R. G. GRIFFIN. Biophys. J. **47**, 92a (1985).
175. G. S. HARBISON, P. P. J. MULDER, J. A. PARDOEN, J. LUGTENBURG, J. HERZFELD, and R. G. GRIFFIN. J. Am. Chem. Soc. **107**, 4809 (1985).
176. D. HADZI and S. BRATOS. *In* The hydrogen bond. *Edited by* P. Schuster, G. Zundel, and C. Sandorfy. Vol. II. North-Holland, Amsterdam. 1976. p. 565.
177. P. SCHUSTER. *In* The hydrogen bond. *Edited by* P. Schuster, G. Zundel, and C. Sandorfy. Vol. I. North-Holland, Amsterdam. 1976. p. 25.
178. J. BRICKMANN. *In* The hydrogen bond. *Edited by* P. Schuster, G. Zundel, and C. Sandorfy. Vol. I. North-Holland, Amsterdam. 1976. p. 217.
179. G. ZUNDEL. *In* The hydrogen bond. *Edited by* P. Schuster, G. Zundel, and C. Sandorfy. Vol. II. North-Holland, Amsterdam. 1976. p. 683.
180. L. SOBCZYK, H. ENGELHARDT, and K. BUNZEL. *In* The hydrogen bond. *Edited by* P. Schuster, G. Zundel, and C. Sandorfy. Vol. III. North-Holland, Amsterdam. 1976. p. 934.
181. P. SCHUSTER, P. WOLSCHANN, and K. TORTSCHANOFF. *In* Molecular biology, biology, biochemistry and biophysics. Vol. 24. *Edited by* I. Pecht and R. Rigler. Springer, Berlin. 1977. p. 107.
182. A. NOVAK. *In* Structure and bonding. Vol. 28. Springer, Berlin. 1974. p. 177.
183. J. L. WOOD. *In* Spectroscopy and structure of molecular complexes. *Edited by* J. Yarwood. Plenum, New York. 1973. p. 303.
184. T. ZEEGERS-HUYSKENS and P. HUYSKENS. *In* Molecular interactions. Vol. 2. *Edited by* H. Ratajczak and W. J. Orville-Thomas. Wiley, Chichester. 1981. p. 1.
185. P. BARCZINSKI, Z. DEGA-SZAFRAN, and M. SZAFRAN. J. Chem. Soc. Perkin Trans. II, 965 (1985).
186. E. G. WEIDEMANN and G. ZUNDEL. Z. Naturforsch. **25**a, 627 (1970).
187. R. JANOSCHEK, E. G. WEIDEMANN, H. PFEIFFER, and G. ZUNDEL. J. Am. Chem. Soc. **94**, 2387 (1972).
188. R. LINDEMANN and G. ZUNDEL. J. Chem. Soc. Faraday Trans. II, **73**, 788 (1977).
189. B. BRZEZINSKI and G. ZUNDEL. Chem. Phys. Lett. **115**, 212 (1985).
190. H. MERZ and G. ZUNDEL. Biochem. Biophys. Res. Commun. **101**, 540 (1981).
191. G. ZUNDEL and H. MERZ. *In* Information and energy transduction in biological membranes. Alan R. Liss, New York. 1984. p. 153.
192. J. FAVROT, D. VOCELLE, and C. SANDORFY. Photochem. Photobiol. **30**, 417 (1979).
193. R. THIOLLAIS. Bull. Soc. Chim. Fr. **14**, 708, 716 (1947).
194. L. S. LUSSIER, A. DION, C. SANDORFY, H. LE THANH, and D. VOCELLE. Photochem. Photobiol. In press.
195. L. S. LUSSIER, C. SANDORFY, H. LE THANH, and D. VOCELLE. To be published.
196. P. P. RASTOGI and G. ZUNDEL. Biochem. Biophys. Res. Commun. **99**, 804 (1981).
197. W. KRISTOF and G. ZUNDEL. Biopolymers, **19**, 1753 (1980).
198. W. KRISTOF and G. ZUNDEL. Biophys. Struct. Mech. **6**, 209 (1980).
199. H. KAKITANI, T. KAKITANI, R. RODMAN, B. HONIG, and R. CALLENDER. J. Phys. Chem. **87**, 3620 (1983).
200. F. SIEBERT, W. MÄNTELE, and K. GERWERT. Eur. J. Biochem. **136**, 119 (1983).
201. K. BAGLEY, G. DOLLINGER, L. EISENSTEIN, M. HONG, J. VITTITOW, and L. ZIMANYI. *In* Information and energy transduction in biological membranes. *Edited by* C. L. Bolis, E. J. M. Helmreich, and H. Passow. Alan H. Liss, New York. 1984. p. 27.
202. J. M. LECLERCQ, P. DUPUIS, and C. SANDORFY. Croat. Chem. Acta, **55**, 105 (1982).
203. J. M. LECLERCQ and C. SANDORFY. J. Raman Spectrosc. **14**, 358 (1983).
204. V. L. KHRISTOFOROV, E. N. ZVONKOVA, and R. P. EVSTIGNEEVA. Zh. Obs. Khim. **44**, 909 (1974).
205. G. S. DENISOV and N. S. GOLUBEV. J. Mol. Struct. **75**, 311 (1981).
206. M. L. APPLEBURY, K. S. PETERS, and P. M. RENTZEPIS. Biophys. J. **23**, 375 (1978).
207. U. DINUR, B. HONIG, and M. OTTOLENGHI. Photochem. Photobiol. **33**, 523 (1981).
208. D. HUPPERT and P. M. RENTZEPIS. J. Phys. Chem. **90**, 2813 (1986).
209. Y. SHICHIDA, T. YOSHIZAWA, T. KOBAYASHI, H. OHTANI, and S. NAGAKURA. FEBS Lett. **80**, 214 (1977).
210. Y. SHICHIDA, T. KOBAYASHI, H. OHTANI, T. YOSHIZAWA, and S. NAGAKURA. Photochem. Photobiol. **27**, 335 (1978).
211. Y. SHICHIDA, F. TOKUNAGA, and T. YOSHIZAWA. Photochem. Photobiol. **29**, 343 (1979).
212. T. KOBAYASHI. FEBS Lett. **106**, 313 (1979).
213. M. TSUDA, F. TOKUNAGA, T. G. EBREY, K. T. YUE, J. MARQUE, and L. EISENSTEIN. Nature, **287**, 461 (1980).
214. C. L. HSIEH, M. NAGUMO, M. NICOL, and M. A. EL-SAYED. J. Phys. Chem. **85**, 2714 (1981).
215. P. ORMOS, L. REINISCH, and L. KESZTHELYI. Biochim. Biophys. Acta, **722**, 471 (1983).
216. P. C. MOWERY, R. H. LOZIER, S. CHAE, Y. W. TSENG, M. TAYLOR, and W. STOECKENIUS. Biochemistry, **18**, 4100 (1979).
217. Y. KIMURA, A. IKEGAMI, and W. STOECKENIUS. Photochem. Photobiol. **40**, 641 (1984).

218. G. MASSIG, M. STOCKBURGER, and T. ALSHUTH. Can. J. Chem. **63**, 2012 (1985).
219. S. SMITH and R. A. MATHIES. Biophys. J. **47**, 251 (1985).
220. T. A. MOORE, M. E. EDGERTON, G. PARR, C. GREENWOOD, and R. N. PERHAM. Biochem. J. **171**, 469 (1978).
221. U. FISCHER and D. OESTERHELT. Biophys. J. **28**, 211 (1979).
222. D. D. MUCCIO and J. Y. CASSIM. J. Mol. Biol. **135**, 595 (1979).
223. A. V. SHARKOV, A. V. PAKULEV, S. V. CHEKALIN, and Y. A. MATVEETZ. Biochim. Biophys. Acta, **808**, 94 (1985).
224. N. C. NUSS, W. ZINTH, W. KAISER, E. KÖLLING, and D. OESTERHELT. Chem. Phys. Lett. **117**, 1 (1985).
225. H. J. POLLAND, M. A. FRANZ, W. ZINTH, W. KAISER, E. KÖLLING, and D. OESTERHELT. Biophys. J. **49**, 651 (1986).
226. M. ENGELHARD, K. GERWERT, B. HESS, W. KREUTZ, and F. SIEBERT. Biochemistry, **24**, 400 (1985).
227. J. M. FUKUMOTO, W. D. HOPEWELL, B. KARVALY, and M. A. EL-SAYED. Proc. Natl. Acad. Sci. USA, **78**, 252 (1981).
228. M. A. EL-SAYED. *In* Proceedings of the VIIth International Conference on Raman Spectroscopy. *Edited by* W. F. Murphy. North-Holland, Amsterdam. 1980. p. 542.
229. B. KARVALY, J. M. FUKUMOTO, W. D. HOPEWELL, and M. A. EL-SAYED. J. Phys. Chem. **86**, 1899 (1982).
230. P. DUPUIS, T. C. CORCORAN, and M. A. EL-SAYED. Proc. Natl. Acad. Sci. USA, **82**, 3662 (1985).
231. B. HESS and D. KUSCHMITZ. FEBS Lett. **100**, 334 (1979).
232. P. TAVAN, K. SCHULTEN, and D. OESTERHELT. Biophys. J. **47**, 415 (1985).
233. E. W. ABRAHAMSON, T. J. BORYS, B. D. GUPTA, R. JONES, R. UHL, A. GEISTEFER, and S. DESHPANDE. *In* Spectroscopy of biological molecules. *Edited by* C. Sandorfy and T. Theophanides. Reidel, Dordrecht, Holland. 1984. p. 385.
234. L. KESZTHELYI. Biochem. Biophys. Acta, **598**, 429 (1980).
235. L. KESZTHELYI and P. ORMOS. FEBS Lett. **109**, 189 (1980).
236. G. VARO and L. KESZTHELYI. Biophys. J. **43**, 47 (1983).
237. K. BARABAS, A. DER, ZS. DANCSHAZY, P. ORMOS, and L. KESZTHELYI. Biophys. J. **43**, 5 (1983).
238. V. BALOGH-NAIR and K. NAKANISHI. New comprehensive biochemistry. Vol. 3. Stereochemistry. *Edited by* Ch. Tamm. Elsevier Biomedical Press, 1982. p. 289.
239. R. R. BIRGE. Ann. Rev. Biophys. Bioeng. **10**, 341 (1981).

Squaraine chemistry. Synthesis of bis(4-dimethylaminophenyl)squaraine from dialkyl squarates. Mechanism and scope of the synthesis

KOCK-YEE LAW[1] AND F. COURT BAILEY
Xerox Corporation, 800 Phillips Road, 0114-39D, Webster, NY 14580, U.S.A.

Received February 18, 1986

KOCK-YEE LAW and F. COURT BAILEY. Can. J. Chem. **64**, 2267 (1986).

The mechanism and the scope of the synthesis of bis(4-dialkylaminoaryl)squaraines from di-*n*-butyl squarate and *N*,*N*-dialkylanilines have been studied. Results show that water and acid are key factors of the synthesis, and these two factors have been optimized. Yields of squaraine are also found to be sensitive to the steric effect provided by the alkyl chain in dialkyl squarates as well as to the concentration of the aniline reagent used in the synthesis. Mechanistic results suggest that alkyl squarate is the precursor of the synthesis, and that squaraine is formed by diarylation of alkyl squarate with an *N*,*N*-dialkylaniline derivative. Under optimized conditions, a number of squaraines have been synthesized. Yields, which are comparable to those synthesized from squaric acid, are obtained. Product analysis with good material balance has been achieved, and results show that arylation and diarylation of the starting di-*n*-butyl squarate are major side reactions in the squaraine synthesis.

KOCK-YEE LAW et F. COURT BAILEY. Can. J. Chem. **64**, 2267 (1986).

On a étudié le mécanisme et la généralité de la synthèse des bis(dialkylamino-4 aryl) squaraïnes à partir du squarate de di-*n*-butyle et des *N*,*N*-dialkylanilines. Les résultats indiquent que l'eau et l'acide sont des facteurs déterminants dans la synthèse et on a optimisé ces deux facteurs. On a aussi trouvé que les rendements en squaraïne sont sensibles aux effets stériques des chaînes alkyles des squarates dialkylés ainsi qu'à la concentration de l'aniline utilisée dans la synthèse. Les résultats mécanistiques suggèrent que le squarate d'alkyle est un précurseur dans la synthèse et que la squaraïne se forme par une diarylation du squarate d'alkyle par un dérivé *N*,*N*-dialkylaniline. Utilisant des conditions optimisées, on a synthétisé un certain nombre de squaraïnes. On a obtenu des rendements qui sont comparables à ceux obtenus lors de la synthèse à partir de l'acide squarique. En se basant sur les produits détectés, on a obtenu une bonne balance des réactifs, et les résultats démontrent que l'arylation et la diarylation du squarate de di-*n*-butyle de départ sont des réactions secondaires importantes dans la synthèse de la squaraïne.

[Traduit par la revue]

Introduction

Bis(4-dialkylaminoaryl)squaraines[2] (for nomenclature, see ref. 1; for reviews on synthesis, see ref. 2) are known to possess photoconductive and semiconductive properties. Although this class of compounds exhibit sharp visible absorption in solution (λ_{max} ~620–670 nm, ε_{max} ~3 × 10^5 cm^{-1} M^{-1}), their absorption in the solid state is panchromatic (400–1000 nm) and is usually very intense (3). These features have made them very attractive for various technological applications in industry, e.g., xerographic photoreceptors (4), organic solar cells (3, 5), and optical recording media (6). Traditionally, these compounds are synthesized by condensing one equivalent of squaric acid (**1**) and two equivalents of *N*,*N*-dialkylaniline

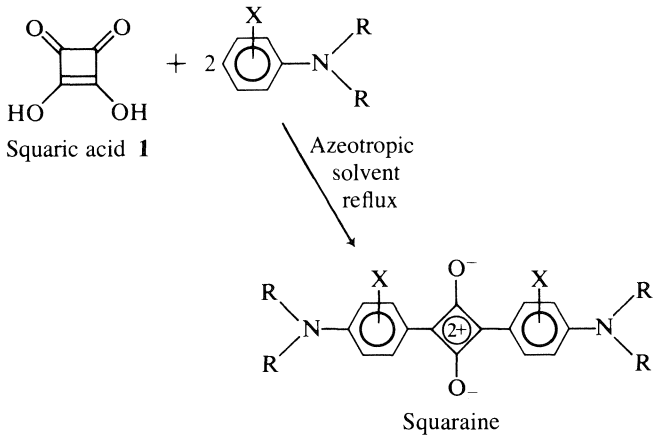

Squaric acid **1**

Squaraine

in an azeotropic solvent (7). Water is the by-product of the synthesis and is removed azeotropically during the squaraine synthesis.

Since the synthesis of squaraine starts with squaric acid, we shall refer to it as the acid route. This synthesis is simple and versatile and a large number of squaraines have been synthesized by this procedure (8). Squaraine pigments synthesized by this procedure are, however, often found to exhibit high dark-conductivity and low charge-acceptance values in

[1]Author to whom correspondence may be addressed.

[2]Squaraines are 1,3-disubstituted compounds derived from the squaric acid structure (1). Bis(4-dialkylaminoaryl)squaraines are a group of squaraine compounds synthesized from squaric acid and *N*,*N*-dialkylanilines (2). Recent single crystal X-ray data[3] and theoretical calculations[4] on the molecular orbitals of model squaraine compounds suggest that the π electrons in squaraine are fully delocalized. The π-orbitals in squaraine can be represented by resonance forms I–V.

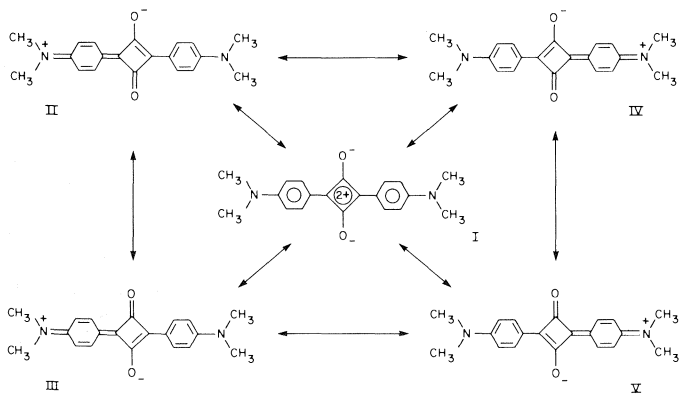

For the purpose of conciseness, resonance form I is used in this paper.

[3]K. Y. Law and R. Ziolo, unpublished results.

[4]Reference 17.

photoreceptor devices (9).[5] Additional purification and processing steps to improve the xerographic properties have yet to be developed.

Earlier, we reported that bis(4-dialkylaminoaryl)squaraines can also be synthesized from dialkyl squarates.[6] Since the squaraine synthesis in this procedure starts with the esters of squaric acid, we refer to the synthesis as the ester route. Xerographic measurements show that squaraines synthesized from dialkyl squarates give consistently better electrical behavior (lower dark conductivity, higher charge acceptance, and higher sensitivity) than those synthesized from squaric acid.[6] Since the improvement in electricals is paralleled by the morphological changes, the enhanced electrical response is attributed to morphological effects. In this paper, we report our investigation on the synthetic aspects of the ester route. The mechanism of squaraine formation and the scope of the synthesis will be presented and discussed.

Experimental

Materials

Squaric acid, *N*,*N*-dimethylaniline, *NN*-diethylaniline, and *N*,*N*-dimethyl-*m*-toluidine were purchased from Aldrich. *N*,*N*-dimethyl-*m*-hydroxyaniline and *N*,*N*-diethyl-*m*-hydroxyaniline were bought from Fisher and were purified by sublimation and recrystallization (from *n*-heptane) before use. Other *N*,*N*-dimethylaniline derivatives were prepared by methylation of an aniline derivative (Aldrich) with trimethyl phosphate as described in the literature (10). Satisfactory elemental analyses and spectroscopic data were obtained for all the anilines synthesized. All solvents were spectro-analyzed grade from Baker and were used without further purification.

General techniques

Melting points were taken on a capillary melting point apparatus (Thomas Hoover) and are uncorrected. Elemental analyses were performed by Galbraith Laboratories. The ir spectra were recorded on a Perkin–Elmer 283 instrument.

Synthesis of dialkyl squarates

Dimethyl squarate was prepared according to the procedure described by Cohen and Cohen (11). Other dialkyl squarates were prepared as follows.

Squaric acid (11.4 g, 0.1 mol) was heated to reflux in a mixture of a 1-alkanol (150 mL) and an azeotropic solvent (150 mL) (benzene for 1-propanol, toluene for 1-butanol, and 1-heptanol). Water was distilled off azeotropically and removed by a Dean–Stark trap. After two equivalents of water were collected, the product mixture was cooled to room temperature. Solvents were removed on a rotatory evaporator. Dialkyl squarate product was then isolated by vacuum distillation.

Di-n-*propyl squarate*, yield 85%, bp ~152°C at 2.1 Torr (1 Torr = 133.3 Pa); ir (CCl_4): 1810 and 1735 (C=O) cm^{-1}; nmr (CD_2Cl_2) δ: 1.03 (t, J = 7 Hz, 6H), 1.6–2.1 (m, 4H), and 4.63 (t, J = 7 Hz, 4H); ms (m/z): 198 (M^+). *Anal.* calcd. for $C_{10}H_{14}O_4$: C 60.59, H 7.12; found: C 60.47, H 7.12.

Di-n-*butyl squarate*, yield 95%, bp ~152°C at 0.13 Torr (lit. (12) bp 139°C at 0.5 Torr); ir (CCl_4): 1808 and 1730 (C=O) cm^{-1}; nmr (CD_2Cl_2) δ: 0.96 (t, J = 7 Hz, 6H), 1.2–2.0 (m, 8H), and 4.66 (t, J = 7 Hz, 4H); ms (m/z): 226 (M^+).

Di-n-*heptyl squarate*, yield 91%, bp ~205°C at 0.19 Torr; ir (CCl_4): 1808 and 1730 (C=O) cm^{-1}; nmr (CD_2Cl_2) δ: 0.7–2.1 (m, 26H) and 4.66 (t, J = 7 Hz, 4H); ms (m/z): 310 (M^+). *Anal.* calcd. for $C_{18}H_{30}O_4$: C 69.64, H 9.74; found: C 69.40, H 9.80.

[5]There are four key steps in xerography, namely charging, photodischarge, image transfer, and development and cleaning. In order to achieve high imaging quality, a photoreceptor device should have high charge-acceptance and low dark-conductivity values. For a discussion on xerography, see ref. 18.

[6]K. Y. Law and F. C. Bailey, manuscript in preparation.

Synthesis of squaraines from di-n-*butyl squarate (general procedure)*

Di-*n*-butyl squarate (1.13 g, 5 mmol), concentrated sulfuric acid (0.1 mL), and water-saturated 1-butanol (5 mL) were discharged in a 100-mL three-neck flask, which was equipped with a magnetic stirring bar and a nitrogen inlet. This mixture was stirred and brought to reflux under a nitrogen atmosphere at an oil-bath temperature of 125–130°C. *N*,*N*-Dialkylaniline derivative (10.2 mmol) was added slowly and evenly in a 6–8 h period (e.g., 2 drops every 30 min) through a pressure equalizing funnel. The addition funnel was washed with 1 mL of 1-butanol when the addition was complete. The product mixture turned from colorless to light green (or yellow green) at the end of the aniline addition. Squaraine product was formed after overnight refluxing and the reaction was allowed to go to completion by further refluxing for 8–24 h. After cooling down the mixture to room temperature, 30 mL methanol was added, and the precipitated product was isolated by filtration. The yields of the squaraines synthesized by this procedure are summarized in Table 4.

Results and discussion

Synthesis

Reaction of di-*n*-butyl squarate, **2**, and *N*,*N*-dimethylaniline in freshly dried 1-butanol at reflux yields no squaraine product. Squaraine formation is found to be effected by the catalytic effects of sulfuric acid[7] and water. Results (Table 1) show that yield of HSq increases monotonically as the water concentration in the reaction medium increases. These results, in conjunction with the acid catalyst required in the synthesis, suggest that the (acid-catalyzed) hydrolyzed product(s) of di-*n*-butyl squarate is the precursor of the squaraine synthesis.

The effect of the concentration of sulfuric acid on the yield of HSq is more interesting (Table 2). At $[H_2SO_4] \leq 0.41 \times 10^{-3}$ M, yield increases as $[H_2SO_4]$ increases, suggesting that more di-*n*-butyl squarate is hydrolyzed and then reacts to form product when the amount of acid catalyst is increased. Yield of HSq, however, decreases at higher sulfuric acid concentrations. The decrease in chemical yield may be attributable to the significant decrease in reactivity of *N*,*N*-dimethylaniline due to its protonation by sulfuric acid at high acid concentrations.

In an independent mechanistic investigation of the reaction of squaric acid (**1**) with *N*,*N*-dimethylaniline, we found that no squaraine is formed when the synthesis is carried out in non-hydroxylic solvents, secondary alcohols, or tertiary alcohols.[8] These findings suggest that **1** is not the precursor of the squaraine. The only candidate for precursor is *n*-butyl squarate, **3**.[8,9] Arylation of **3** by *N*,*N*-dimethylaniline will generate intermediate **4**, which undergoes further arylation to form HSq.

The synthesis reported in this work, which involves partial acid-catalyzed hydrolysis of **2** → **3**, arylation of **3** → **4**, and

[7]In addition to sulfuric acid, trichloroacetic acid, oxalic acid, and toluenesulfonic acid are also found to be effective for the ester route synthesis.

[8]In secondary alcohol such as 2-amyl alcohol, no squaraine is formed when squaric acid is reacted with *N*,*N*-dimethylaniline. On the other hand, HSq can be isolated in 20–30% yield when methyl squarate or di-*n*-butyl squarate (in the presence of H_2SO_4 and water) are allowed to react with *N*,*N*-dimethylaniline in 2-amyl alcohol. These observations strongly suggest that *n*-alkyl squarate is the precursor of the squaraine and the lower yields of HSq in the latter two reactions are due to the transesterification of methyl squarate or *n*-butyl squarate to the unreactive 2-amyl squarate in 2-amyl alcohol (K. Y. Law, unpublished results).

[9]Squaraines can be synthesized from *n*-alkyl squarates (e.g. methyl squarate) in 1-butanol. The yields of squaraine are comparable to those of the acid route and the ester route reported in this work. See K. Y. Law, U.S. Patent 4,524,219.

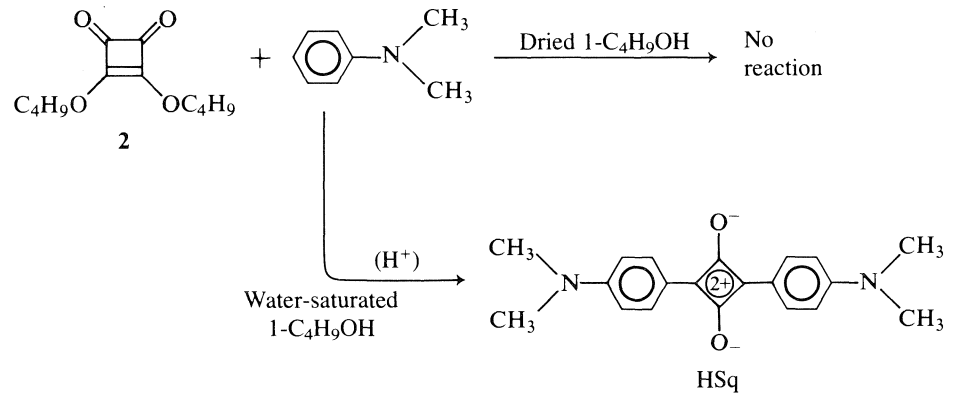

2

SCHEME 1

TABLE 1. Effect of water concentration in 1-butanol on the yield of HSq[a]

Water conc. in 1-butanol (% of vol.)	Yield of HSq (%)
~0[b]	0–3
~0.1[c]	30±3
1[c]	39
16[d]	45±3

[a]Reactant: di-*n*-butyl squarate (1.13 g, 5 mmol), *N*,*N*-dimethylaniline (1.23 g, 10.2 mmol, added in 6–8 h); solvent: 5 mL 1-butanol of specified water concentration; catalyst: H_2SO_4 (0.1 mL).
[b]Freshly distilled over Mg.
[c]Specified amount of water was added to freshly dried 1-butanol.
[d]Water-saturated 1-butanol.

TABLE 2. Effect of sulfuric acid concentration on the yield of HSq[a]

H_2SO_4 ($\times 10^3$ *M*)	Yield of HSq (%)
0.13	30
0.26	38
0.41	45±3
0.51	35

[a]Reactants: di-*n*-butyl squarate (1.13 g, 5 mmol), *N*,*N*-dimethylaniline (1.23 g, 10.2 mmol, added over 6–8 h); solvent: 5 mL water-saturated 1-butanol; catalyst: sulfuric acid of specified concentration.

arylation of **4** → HSq, can be described in three steps, a → c → d, and we refer to the synthesis as the ester route.

Steric effect

As shown in Scheme 2, the ester route synthesis involves steps a → c → d. The acid-catalyzed hydrolysis of **2** → **3** and the arylation of **3** → **4** are expected to be sensitive to the steric factors provided by the alkyl groups in various dialkyl squarates. Table 3 summarizes the results of the effect of chain length of the alkyl group in dialkyl squarates on the yield of HSq. Our results show that yield decreases as the chain length of the alkyl group increases.

The relative rate of hydrolysis of various dialkyl squarates to alkyl squarates is not known. Several attempts have been made to determine this relative rate under the conditions of the squaraine synthesis. Such a study has been difficult due to the very similar retention times of the hydrolyzed products (squaric acid and alkyl squarates) in hplc analyses. On the other hand, assuming that the steric effects of dialkyl squarate to alkyl squarate and alkyl squarate to squaric acid are very similar, the relative rate of dialkyl squarate to alkyl squarate can be estimated by determining the amount of squaric acid formed in the hydrolysis of dialkyl squarate to squaric acid. The relative rate obtained in this fashion is given in Table 3, and results show the hydrolysis rate decreases, as expected, as the chain length of the alkyl group increases. Since this decrease is paralleled by a decrease in yield of HSq, we conclude that the decrease in yield of HSq is primarily a steric effect inherent in the hydrolysis of dialkyl squarate to alkyl squarate.

Thermodynamic estimation shows that hydrolysis of dialkyl squarate to alkyl squarate is endothermic by ~12 kcal/mol and arylation of alkyl squarate to form **4** is exothermic by ~8 kcal/mol. In accordance with Hammond's postulate (13), the hydrolysis reaction should have a later transition state where the impact of steric hindrance will be greater. The dependence of the yield of HSq on the hydrolysis of the starting dialkyl squarate is thus rationalized.

Effect of aniline concentration

Scheme 2 shows that the major side reaction of **3** is to re-esterify to **2**. The conversion of **3** to **4** will drive the reaction in the product-forming direction and will improve the yield of HSq. It is thus almost certain that the squaraine synthesis would be sensitive to the concentration of *N*,*N*-dimethylaniline used in the synthesis. The effect of the concentration of *N*,*N*-dimethylaniline on the yield of HSq was studied and results (Fig. 1) show that optimized yield is obtained when two equivalents of *N*,*N*-dimethylaniline are used. When less than 2 equivalents of *N*,*N*-dimethylaniline is used, yield increases with increasing concentration of *N*,*N*-dimethylaniline, and this can readily be attributed to the increased formation of **4** with increasing concentration of *N*,*N*-dimethylaniline. When more than 2 equivalents of *N*,*N*-dimethylaniline is used, yield decreases rapidly and reaches zero percent at 4 equivalents of *N*,*N*-dimethylaniline. Since optimal amounts of sulfuric acid are used in each experiment, the acidity of the reaction medium is then decreasing as the concentration of *N*,*N*-dimethylaniline increases. While yield of HSq also decreases as the concentration of sulfuric acid decreases when the acid concentration is less than optimal (Table 2), the decrease in yield of HSq observed at high *N*,*N*-dimethylaniline concentrations may be an acidity effect. However, the acidity of the reaction medium should only be decreased by a factor of two when four

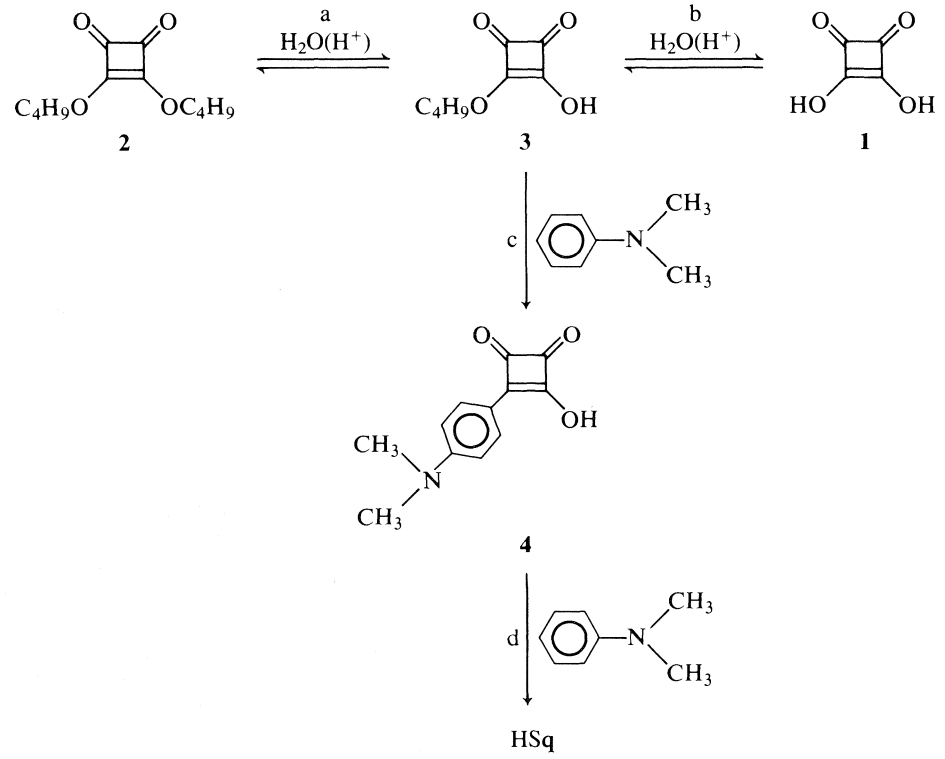

SCHEME 2

TABLE 3. Effect of steric hindrance on the yield of HSq[a]

RO, OR	Yield of HSq (%)	Relative rate[b] of hydrolysis
R = CH_3	52	1
n-C_3H_7	47±1	—
n-C_4H_9	45±3	0.75
n-C_7H_{15}	27±2	0.6

[a]Reactant: specified dialkyl squarate (5 mmol), *N*,*N*-dimethylaniline (1.23 g, 10.2 mmol, added over 6–8 h); solvent: 5 mL water-saturated 1-butanol; catalyst: sulfuric acid, 0.1 mL.
[b]See text for method of estimation.

equivalents of *N*,*N*-dimethylaniline are used. In accordance with Table 2, the yield of HSq should be in the neighborhood of 30–40%; thus, acidity effect alone does not appear to account for the drastic drop in chemical yield. It has been reported in the literature that squaraines can form 1:1 adducts with amines; the significant decrease in yield of HSq is likely due to secondary reactions between HSq and *N*,*N*-dimethylaniline at high *N*,*N*-dimethylaniline concentrations.[10]

The role of water in the synthesis

The necessity of having water in the reacting solvent in the ester route, in contrast to the acid route where water is removed continuously by an azeotropic solvent during the course of the reaction, prompted us to examine the role of water in the synthesis. The water content of the reaction mixture throughout the reaction was monitored by measuring the boiling point of the reacting solvent. The temperature profile in Fig. 2 shows that the boiling point of the reacting solvent increases from the boiling point of the azeotrope of 1-butanol–water at ~96°C to the boiling point of pure 1-butanol at ~118°C as the reaction

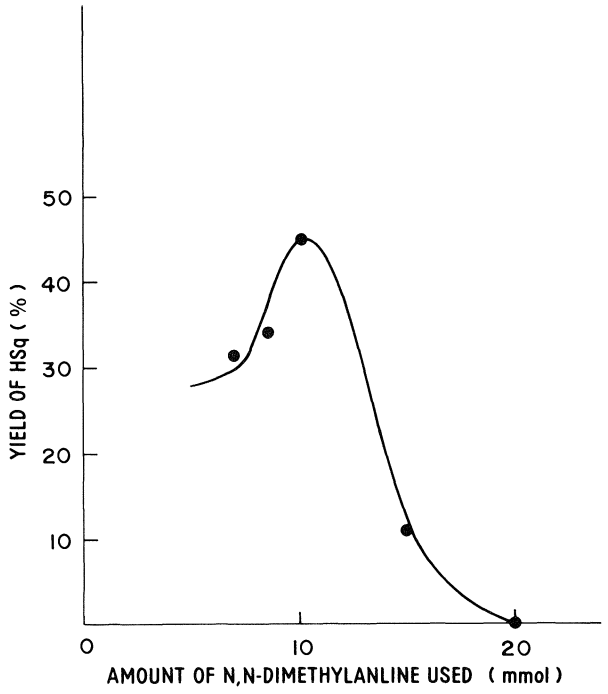

FIG. 1. Plot of yield of HSq as a function of the amount of *N*,*N*-dimethylaniline used (5 mmol scale).

[10]Squaraines are known to react with amines to form adducts. In the case of tertiary aromatic amines, 1:1 squaraine–amine adducts have been isolated and characterized (14). In this work, we have found in controlled experiments that squaraines react with *N*,*N*-dialkylanilines to form colorless products. Although these colorless substances have not yet been characterized, we believe that the decrease in chemical yield of squaraine is the result of the consumption of squaraine in secondary reactions.

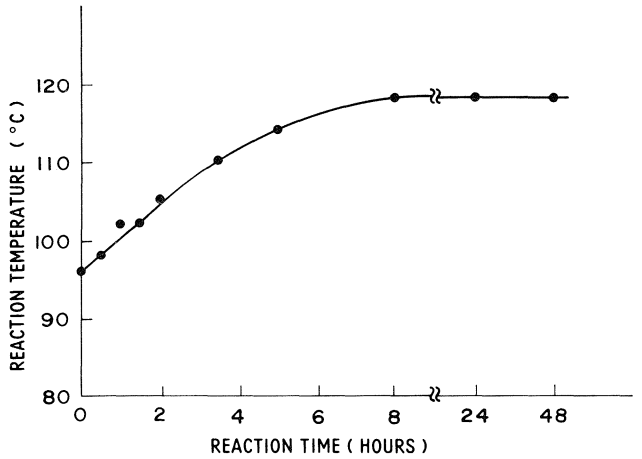

FIG. 2. Plot of reaction temperature as a function of reaction time.

proceeds. The low boiling points observed indicate the presence of water in the reacting solvent; its presence, which is a prerequisite for the occurrence of the synthesis, implies that the starting di-*n*-butyl squarate is hydrolyzing to *n*-butyl squarate, the precursor of the squaraine synthesis, in the initial stage of the reaction.

After ~8 h, the boiling point of pure 1-butanol is reached. This suggests that water is removed during the reaction, presumably by the slow stream of nitrogen under the refluxing condition. At the same time, the color of the reaction mixture turns from light yellow to yellow green (or green). Squaraine starts to precipitate out of the solution several hours later.[11] The necessity of water removal in the later stage of the reaction is consistent with the mechanism proposed in Scheme 2; since water is the by-product of the squaraine formation step (step d), the elimination of water drives the reaction in the product-forming direction.

In the experimental section, *N*,*N*-dimethylaniline derivative is shown to be added slowly in a 6–8 h period. The slow and even addition will permit the selective arylation of *n*-butyl squarate (less steric hindrance), so that side reactions, such as arylation of di-*n*-butyl squarate, can be suppressed. For highly reactive aniline derivatives, e.g., *N*,*N*-dimethyl-3-hydroxyaniline and *N*,*N*-diethyl-3-hydroxyaniline, slow addition is found to be very critical. Due to the slow rate of hydrolysis of di-*n*-butyl squarate relative to arylation reactions in these two cases, yields of squaraine decrease to the 30–50% range when the aniline derivatives are added in a single batch at the beginning of the reaction. The procedure presented in the experimental section is thus a general optimized procedure for squaraine synthesis from di-*n*-butyl squarate.

Scope of the ester route synthesis

A number of squaraines were prepared from di-*n*-butyl squarate using these optimized conditions, and the yields are tabulated in Table 4.[12] The yields of the same set of squaraines synthesized by the traditional acid route are also given for comparison (15). Comparison indicates that very similar chemical yields are obtained from both procedures. The similar synthetic efficiency for both procedures is not unexpected because of the similarity in the squaraine formation step in both procedures (Scheme 2).

TABLE 4. Effect of synthetic route on yields of squaraines

	Yield (%)	
	Ester route[a]	Acid route[b]
Ar: 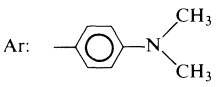	45±3	40–60
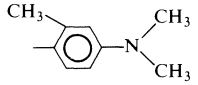	56±2	30
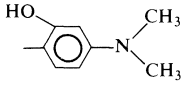	85	~95
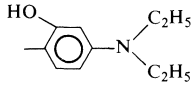	90	~95
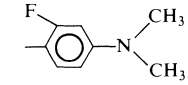	19	23
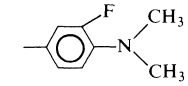	0	0
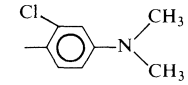	0	0
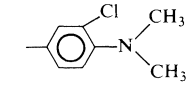	0	0
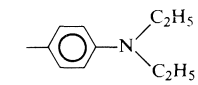	6.7[c]	6
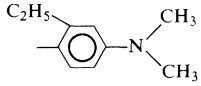	8.3[c,d]	24
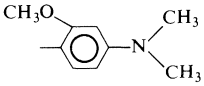	8.1[c]	9.5

[a]Isolated yield, unless specified.
[b]Data taken from ref. 15.
[c]Yield determined by absorption spectroscopy.
[d]Isolated yield was 5.3%.

Product analysis and outlook for further yield improvement

Results in Table 4 show that most of the squaraine syntheses are not quantitative. We felt that mechanistic insight, which usually provides guidance for further yield improvement, may be obtained by analyzing the side products. Using di-*n*-butyl squarate and *N*,*N*-dimethylaniline as reactants, water-saturated 1-butanol as solvent, and sulfuric acid as catalyst, HSq was isolated by filtration in 47% yield in a typical 5-mmol run (see experimental section). The neutral side products in the acidic filtrate solution were isolated by solvent extraction (chloroform–water) techniques. Vacuum bulb-to-bulb distillation yielded two volatile fractions, a light yellow liquid (0.22 g) and an orange solid (0.1 g). The light yellow liquid was found to be di-*n*-butyl squarate by comparing its spectroscopic properties

[11]For more reactive anilines, e.g., *N*,*N*-dimethyl-3-hydroxyaniline, squaraine products precipitate out of the solution even before the completion of the aniline addition.

[12]Satisfactory elemental analyses and spectroscopic data are obtained for all the squaraines isolated in this work.

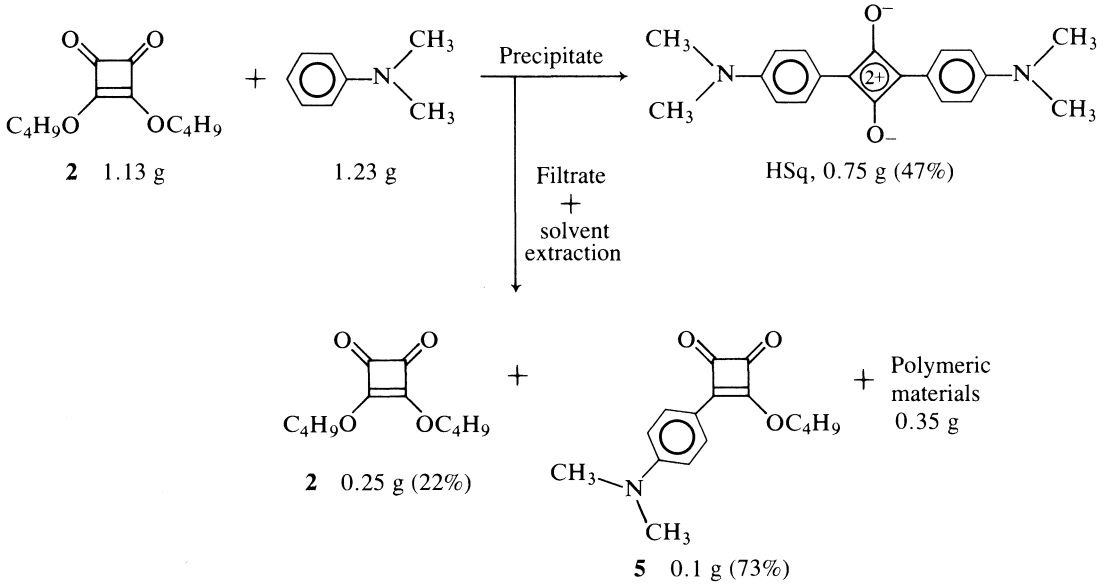

2 1.13 g 1.23 g HSq, 0.75 g (47%)

2 0.25 g (22%) **5** 0.1 g (73%)

SCHEME 3

(ir, nmr, ms) with the starting material. The orange solid was identified as compound **5** (see Scheme 3) by spectroscopic techniques.[13] The residue was a brown solid (0.35 g). The spectroscopic data of this brown solid are ir ($CHCl_3$): 1600 cm^{-1}, no carbonyl bands; nmr (CD_2Cl_2) δ: ~2.8–3.1 (broad multiplets, ~6H, N-CH_3), 6.5–7.3 (very broad doublet, ~4H, aromatic protons). These spectroscopic data suggest that the residue is a polymeric material and has no high frequency C=O functions. The ^1H nmr data strongly suggest that this residue is made up of *N*,*N*-dimethylanilino moieties.

In a parallel experiment, another orange precipitate (~0.16 g) was isolated by adding an appropriate amount of diethyl ether to the acidic filtrate. This orange solid was identified as compound **6** by comparing its spectroscopic properties with those of an authentic sample.[14]

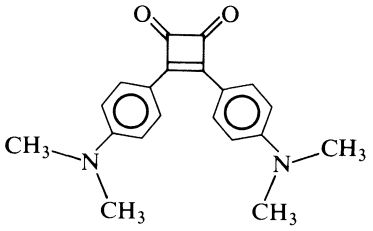

6

In 1961, Blomquist and LaLancette reported that the parent compound of **6**, 1,2-diphenylcyclobutene-3,4-dione (**7**), undergoes a ring-opening reaction at room temperature in ethanol to give diethyl α,α′-diphenylsuccinate (16).

In the present work, it appears that **6** is stable in acidic

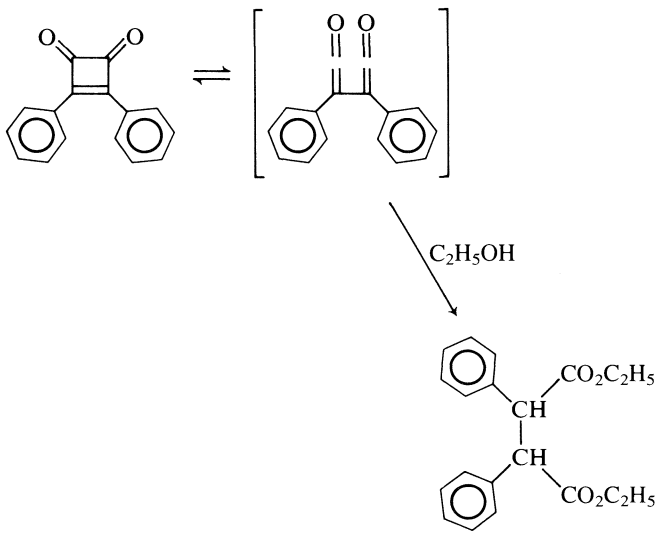

SCHEME 4

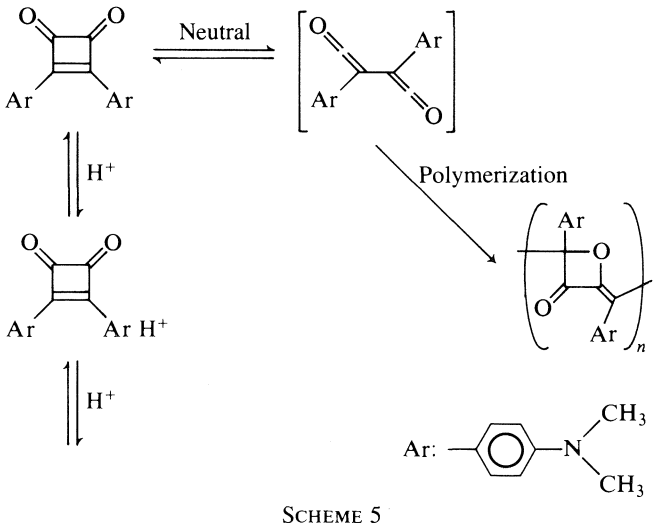

SCHEME 5

[13]The spectroscopic data of **5** are ir ($CHCl_3$): 1782 and 1730 (C=O) cm^{-1}; nmr (CD_2Cl_2) δ: 1.01 (t, J = 6 Hz, 3H), 1.2–2.2 (m, 4H), 3.12 (s, 6H), 4.88 (t, J = 6 Hz, 2H), 6.78 (d, J = 9.2 Hz, 2H), and 7.95 (d, J = 9.2 Hz, 2H); ms (m/z): 273 (M^+) and 217 ($M^+ - 2CO$).

[14]1,2-Bis(*p*-dimethylaminophenyl)cyclobutene-3,4-dione, **6**, was synthesized from squaric acid dichloride and *N*,*N*-dimethylaniline in carbon disulfide, yield ~10%, mp 273–274.5°C; ir (KBr): 1755 and 1735 (C=O) cm^{-1}; nmr (CD_3Cl_2) δ: 3.12 (s, 6H), 6.79 (d, J = 9.5 Hz, 2H), and 8.09 (d, J = 9.5 Hz, 2H); ms (m/z): 320 (M^+) and 264 ($M^+ - 2CO$).

solution, presumably due to the protonation of the nitrogen atoms by sulfuric acid. In neutral chloroform solution, **6** undergoes a ring-opening reaction analogous to its parent compound to give a diketene intermediate that polymerizes to form a polymeric product. The proposed structure of the polymeric product is given in Scheme 5 and its yield was ~22%.

Our product analysis accounts for 98% of the materials. The major side reactions of the squaraine synthesis are arylation and diarylation of **2** to give **5** and **6** respectively. Further yield-improvement experiments should be focussed on the identification of reaction conditions where the competition between hydrolysis and arylation is minimal.

The yield optimization experiments performed in this work are concentrated on the yield of squaraine product isolated in each experiment, and the reaction conditions are not necessarily ideal for individual steps (e.g., steps a, c, and d in Scheme 2). It is anticipated that further yield improvement may be obtained by segmenting the squaraine synthesis into three steps (partial hydrolysis of **2**, arylation of **3**, and arylation of **4**) and optimizing them individually.

1. R. West. Oxocarbons. Academic Press, New York. 1980. Chapt. 10.
2. (*a*) A. H. Schmidt. Synthesis, 961 (1980); (*b*) H. E. Sprenger and W. Ziegenbein. Angew. Chem. Int. Ed. Engl. **7**, 530 (1968); (*c*) G. Maahs and P. Hegenberg. Angew. Chem. Int. Ed. Engl. **5**, 888 (1966).
3. R. O. Loutfy, C. K. Hsiao, and P. M. Kazmaier. Photogr. Sci. Eng. **27**, 5 (1983).
4. (*a*) A. C. Tam and R. D. Balanson. IBM J. Res. Dev. **26**, 186 (1982); (*b*) R. E. Wingard. IEEE Trans. Ind. Appl. 1251 (1982); (*c*) A. C. Tam. Appl. Phys. Lett. **37**, 978 (1980); (*d*) R. J. Melz, R. B. Champ, L. S. Chang, C. Chiou, G. S. Keller, L. C. Liclican, R. B. Neiman, M. D. Shattuck, and W. J. Weiche. Photogr. Sci. Eng. **21**, 73 (1977).
5. (*a*) D. L. Morel, E. L. Stogryn, A. K. Ghosh, T. Feng, P. E. Purwin, R. F. Shaw, C. Fishman, G. R. Bird, and A. P. Piechowski. J. Phys. Chem. **88**, 923 (1984); (*b*) A. P. Piechowski, G. R. Bird, D. L. Morel, and E. L. Stogryn. J. Phys. Chem. **88**, 934 (1984); (*c*) V. Y. Merritt and H. J. Hovel. Appl. Phys. Lett. **29**, 14 (1976).
6. D. J. Gravesteijn, C. Steenbergen, and J. Van der Veen. Proc. SPIE Int. Soc. Opt. Eng. **420**, 327 (1983); V. P. Jipson and C. R. Jones. J. Vac. Sci. Technol. **18**, 105 (1981); V. P. Jipson and C. R. Jones. IBM Tech. Discl. Bull. **24**, 298 (1981).
7. H. E. Spenger and W. Ziegenbein. Angew. Chem. Int. Ed. Engl. **5**, 894 (1966).
8. H. Kampfer and K. E. Verhille. U. S. Patent 3,617,270 (1971); R. B. Champ and M. D. Shattuck. U.S. Patent 3,824,099 (1974); N. F. Haley, J. J. Krutak, and R. J. Ott. U.S. Patent 4,175,956 (1979); J. F. Yanus. U.S. Patent 4,486,520 (1985); K. Y. Law and F. C. Bailey. U.S. Patent 4,508,803 (1985).
9. M. S. H. Chang and P. G. Edelman. U.S. Patent 4,353,971 (1982); M. S. H. Chang and M. F. Berman. U.S. Patent 4,391,888 (1983).
10. A. I. Vogel. Textbook of practical organic chemistry. 4th ed. *Revised by* B. S. Furniss, A. J. Hannaford, V. Roger, P. W. G. Smith, and A. R. Tatchell. Longman, London and New York. 1978. Chapt. IV.
11. S. Cohen and S. G. Cohen. J. Am. Chem. Soc. **88**, 1533 (1966).
12. G. Maahs. Angew. Chem. Int. Ed. Engl. **2**, 690 (1963).
13. G. S. Hammond. J. Am. Chem. Soc. **77**, 334 (1955).
14. A. Treibs and K. Jacob. Justus Liebigs Ann. Chem. **699**, 153 (1966); A. Treibs, K. Jacob, and R. Tribollet. Justus Liebigs Ann. Chem. **741**, 101 (1970).
15. K. Y. Law, F. C. Bailey, and L. J. Bluett. Can J. Chem. **64**, 1607 (1986).
16. A. T. Blomquist and E. A. LaLancette. J. Am. Chem. Soc. **83**, 1387 (1961).
17. R. W. Bigelow and H. J. Freund. Chem. Phys. In press.
18. J. W. Weigl. Angew. Chem. Int. Ed. Engl. **16**, 374 (1977).

Nucleophilic attack on the carbon–carbon double bond. I. Reaction of primary and secondary amines with 2,2-di(4-nitrophenyl)-1,1-difluoroethene

KENNETH T. LEFFEK AND URSZULA MACIEJEWSKA[1]
Department of Chemistry, Dalhousie University, Halifax, N.S., Canada B3H 4H6

Received April 30, 1986

KENNETH T. LEFFEK and URSZULA MACIEJEWSKA. Can. J. Chem. **64**, 2274 (1986).

The reaction of primary and secondary amines with 2,2-di(4-nitrophenyl)-1,1-difluoroethene (**1**) in acetonitrile solvent gives first 2,2-di(4-nitrophenyl)-1-fluoro-1-aminoethene (**2**) and then 2,2-di(4-nitrophenyl)-1,1-difluoro-1-aminoethane (**3**). With excess amine, pseudo-first-order rate constants for the production of **2** were measured, which showed a second-order reaction, together with a catalysed third-order reaction. In addition to the reagent amines, the reaction is also catalysed by tertiary amines and bases such as oxalate and acetate, but not by chloride and perchlorate, nor by ammonium ions. The enthalpy of activation for the reaction of piperidine with **1** in acetonitrile is 3.7 kcal mol^{-1}, but for the catalysed reaction an apparent value of -2.2 kcal mol^{-1} was obtained. It is concluded that the reaction proceeds via a pre-equilibrium to a zwitterion, followed by another equilibrium giving a carbanion that yields the product (**2**) by a rate-determining cleavage of the carbon–fluorine bond.

KENNETH T. LEFFEK et URSZULA MACIEJEWSKA. Can. J. Chem. **64**, 2274 (1986).

Lorsqu'on opère dans l'acétonitrile comme solvant, la réaction des amines primaires ainsi que secondaires avec le di (nitro-4 phényl)-2,2 difluoro-1,1 éthène (**1**) conduit initialement à la formation du di (nitro-4 phényl)-2,2 fluoro-1 amino-1 éthène (**2**) et finalement au di (nitro-4 phényl)-2,2 difluoro-1,1 amino-1 éthane (**3**). Opérant en présence d'un excès d'amine, on a mesuré les constantes de vitesse du premier ordre pour la formation du composé **2**; on a aussi noté la présence d'une réaction du deuxième ordre ainsi qu'une réaction catalysée du troisième ordre. En plus des réactifs aminés, les amines tertiaires et les bases comme l'oxalate et l'acétate catalysent aussi cette réaction; toutefois les ions chlorure, perchlorate ainsi qu'ammonium n'agissent pas comme catalyseurs. Dans l'acétonitrile, l'enthalpie d'activation pour la réaction du composé **1** avec la pipéridine est égale à 3,7 kcal mol^{-1}; toutefois, pour la réaction catalysée, on observe une valeur apparente de $-2,2$ kcal mol^{-1}. On en conclut que la réaction se produit par le biais d'un pré-équilibre conduisant à un zwitterion qui, par un autre équilibre, conduit à un carbanion qui conduit au produit **2** par un clivage de la liaison carbone–fluor qui détermine la vitesse de la réaction.

[Traduit par la revue]

Introduction

In the study of the β-elimination of 2,2-di(4-nitrophenyl)-1,1,1-trifluoroethane promoted by alkoxide bases, it was noted (1) that the first olefin product, 2,2-di(4-nitrophenyl)-1,1-difluoroethene reacted rapidly with the excess base to give further substituted olefins. Nucleophilic attack of fluoroolefins has been known since 1946 (2) and numerous synthetic applications have been reported (3). Koch *et al.* (4) have studied the reactions of *gem*-difluoroethenes with alkoxide bases. With the base in at least 10-fold excess, the major products were alkoxy-substituted ethenes, consistent with a mechanism involving partitioning of a carbanion intermediate.

A number of kinetic studies have also been carried out for nucleophilic additions to olefins, and for substitution via additions to olefins, activated by electron-withdrawing groups other than fluorine (5–8), and different rate-determining steps for the reactions were found under various sets of conditions. The rate-determining step varied from the departure of the leaving group (5), to proton transfer (6, 8), to the nucleophilic attack on the olefin (7). Rappoport *et al.* (9, 10) have studied the attack of primary amines on 1,1-dicyano-2-fluoroolefins, in which the fluorine is replaced to yield a cyanoenamine. The reaction was shown to be base catalysed and a mechanism involving a competition between carbon–fluorine bond cleavage and nitrogen–hydrogen bond cleavage was proposed.

The present study was carried out to determine the products, and the mechanism of their formation, of the reaction of primary and secondary amines with 2,2-di(4-nitrophenyl)-1,1-difluoroethene (**1**), under conditions where the initial products of the reaction were stable.

[1]Postdoctoral Fellow 1984–1985.

Results and discussion

Product analysis

The product of the reaction between amines and the olefin (**1**) in acetonitrile solvent depends on the ratio of the concentration of amine to olefin and also on the type of amine. With the amine in at least a threefold excess over the olefin, the secondary amines morpholine, piperidine, and pyrrolidine gave only the fluoroenamine (**2**) as product (Scheme 1). A separate experiment showed that the fluoroenamine **2** does not react with piperidine. With the primary amines, methoxyethylamine, *n*-propylamine, isobutylamine, benzylamine, and cyclohexylamine, the fluoroenamine was (**2**) produced, together with the saturated compound (**3**).

When the amine-to-olefin ratio was less than 3, all amines, both secondary and primary, gave both products **2** and **3**, with **2** the major product after short reaction times and **3** the major product after long reaction times. Therefore, **3** is interpreted as arising from **2** by the addition of the elements of HF as shown in Scheme 1.

In addition, small amounts of 2,2-di(4-nitrophenyl)-1,1,1-trifluoroethane were produced, which must derive from the addition of HF to the substrate olefin (**1**).

The stability of the fluoroenamine **2** with respect to nucleophilic addition by secondary amines, in contrast to the reactivity of the analogous 2,2-di(4-nitrophenyl)-1-fluoro-1-ethoxyethene towards ethoxide ion (1), makes the reaction of amines with the olefin **1** particularly suitable for a kinetic investigation.

Kinetics

All kinetic runs were carried out with a large excess of amine to give pseudo-first-order kinetics and to ensure that the substrate reacted only with the amine base, so that the initial

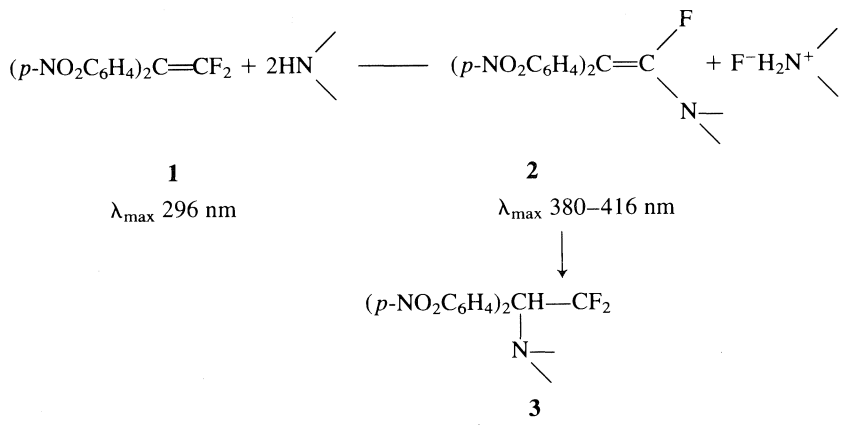

SCHEME 1

product was the enamine **2**. The reaction was followed spectrophotometrically by monitoring the decrease of absorption at 296 nm, the λ_{max} of the olefin substrate, and also the absorption in the visible region due to the enamine (400 nm for the piperidine reaction). The reactions were followed to 70–90% completion in acetonitrile solvent. Pseudo-first-order rate constants were calculated and divided by the amine concentration to obtain the second-order rate constants, $k_{2\,obs}$, which are shown in Table 1. The second-order rate constants increase linearly with the amine concentration and can be fitted to eq. [1].

$$[1] \quad k_{2\,obs} = k'_{2\,obs} + k_{3\,obs}[\text{amine}]$$

A linear least-squares fit of $k_{2\,obs}$ to eq. [1] gives the uncatalysed rate constant $k'_{2\,obs}$ as the intercept and the catalyzed rate constant $k_{3\,obs}$ as the slope. These values are given in Table 2 together with their standard deviations. The pK_a values quoted for the conjugate acids are those of Coetzee (11). It can be seen that, generally, the catalysed reaction accounts for more than half of the reaction at the amine concentrations used. Both $k'_{2\,obs}$ and $k_{3\,obs}$ show a rough correlation with the pK_a of the conjugate acid of the base for the four values of pK_a in acetonitrile shown in Table 2. The uncatalysed reaction gives a correlation coefficient of 0.93 between log $k'_{2\,obs}$ and pK_a with a slope of approximately unity. The catalysed reaction gives a correlation coefficient of 0.965 between log $k_{3\,obs}$ and pK_a with

TABLE 1. Second-order rate constants for the reaction of 2,2-di(4-nitrophenyl)-1,1-difluoroethane* with amines in acetonitrile at 25°C

(a) Pyrrolidine					
10^4[Amine] (M)	1.77	2.65	5.28	7.11	8.75
$k_{2\,obs}$(L mol^{-1} s^{-1}) at λ = 296 nm	1.66	1.88	2.66	3.39	4.00
10^4[Amine] (M)	1.91	2.86	5.69	7.57	9.43
$k_{2\,obs}$(L mol^{-1} s^{-1}) at λ = 416 nm	1.50	1.64	2.42	3.14	3.61
(b) Piperidine					
10^3[Amine] (M)	0.674	1.00	1.34	2.01	3.29
$k_{2\,obs}$(L mol^{-1} s^{-1}) at λ = 296 nm	0.104	0.131	0.165	0.222	0.320
10^3[Amine] (M)	0.660	0.99	1.31	1.95	3.21
$k_{2\,obs}$(L mol^{-1} s^{-1}) at λ = 400 nm	0.096	0.117	0.150	0.200	0.304
(c) Morpholine					
10^3[Amine] (M)	6.02	12.0	17.9	23.7	29.4
$10^3 k_{2\,obs}$(L mol^{-1} s^{-1}) at λ = 296 nm	6.23	11.5	16.9	22.4	27.5
10^3[Amine] (M)	4.57	6.08	9.08	15.7	22.3
$10^3 k_{2\,obs}$(L mol^{-1} s^{-1}) at λ = 390 nm	4.79	7.81	9.02	15.5	21.4
(d) *n*-Propylamine					
10^4[Amine] (M)	3.36	5.03	8.36	10.0	15.0
$k_{2\,obs}$(L mol^{-1} s^{-1}) at λ = 296 nm	0.164	0.184	0.199	0.209	0.237
10^4[Amine] (M)	3.33	6.64	9.93	13.2	16.5
$k_{2\,obs}$(L mol^{-1} s^{-1}) at λ = 380 nm	0.181	0.215	0.235	0.263	0.277
(e) Cyclohexylamine					
10^3[Amine] (M)	3.84	7.63	11.4	15.1	19.3
$k_{2\,obs}$(L mol^{-1} s^{-1}) at λ = 296 nm	0.082	0.122	0.164	0.189	0.216
10^3[Amine] (M)	2.90	11.5	17.1	22.7	28.2
$k_{2\,obs}$(L mol^{-1} s^{-1}) at λ = 390 nm	0.086	0.177	0.234	0.273	0.329

*Initial concentration 5.2×10^{-5} M.

TABLE 2. Rate constants for the uncatalysed and catalysed reactions of 2,2-di(4-nitrophenyl)-1,1-difluoroethene with amines in acetonitrile at 25°C

pK_a CH_3CN/H_2O	Amine	λ (nm)	$k'_{2\,obs}$ ($L\,mol^{-1}\,s^{-1}$)	$k_{3\,obs}$ ($L^2\,mol^{-2}\,s^{-1}$)
19.58±11.27	Pyrrolidine	296	1.00±0.08	3370±150
		416	0.86±0.09	2910±140
18.92/11.12	Piperidine	296	0.051±0.004	82.4±2.1
		400	0.040±0.003	82.2±1.5
16.61/8.33	Morpholine	296	0.00066±0.0001	0.914±0.006
		390	0.0013±0.0006	0.904±0.05
18.22/10.71	*n*-Propylamine	296	0.157±0.13	73.5±12
		380	0.161±0.006	73.5±6
10.66	Cyclohexylamine	296	0.055±0.008	8.74±0.7
		390	0.060±0.006	9.65±0.3

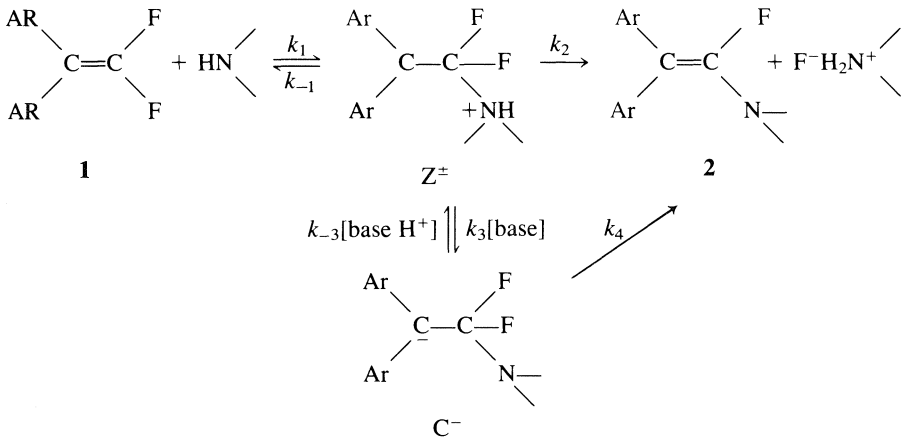

SCHEME 2

a slope of 1.1 ± 0.2. Both of these calculations were based on the four points for which the pK_a values in acetonitrile are quoted in Table 2.

Within the experimental error, both the catalysed and the uncatalysed rate constants show no significant difference between the determination based on the disappearance of the substrate and that based on the appearance of the enamine product **2**. Thus, the substrate is undergoing a reaction in which there is no accumulation of an intermediate between the substrate and the enamine **2**. Scheme 2 shows the probable reaction steps for the reaction.

Rappoport and co-workers (5, 9, 10) and Bernasconi *et al.* (12) proposed a similar mechanism for the reaction of primary and secondary amines to cyano and nitro olefins.

The observed kinetics can be fitted to Scheme 2 in either of two ways. The nucleophilic attack of the amine on the carbon atom of the olefin that bears the fluorine atoms could be the rate-controlling step, followed by a rapid loss of HF in one or two fast steps. On the other hand, there could be a fast pre-equilibrium to yield $Z^{\pm}$ and (or) C^- with a very small equilibrium constant, followed by a slow rate-controlling loss of fluoride. Since fluoride is generally a poor leaving group in nucleophilic substitution reactions, the latter alternative seems to be the more likely mechanism. Since the reaction does not take place with tertiary amines, it is clear that the proton on the nitrogen plays an important role in the departure of the fluoride.

The kinetics of the piperidine reaction were investigated at several temperatures in acetonitrile and tetrahydrofuran solvents. Using the same procedure as before, the uncatalysed and catalysed rate constants were determined and these are collated in Table 3, together with the activation parameters derived from these rate constants. The uncatalysed reaction shows normal activation parameters, but the catalysed reaction gives a negative $\Delta H^{\neq}$ in acetonitrile and a very low $\Delta H^{\neq}$ in tetrahydrofuran, indicating that at least the catalysed reaction involves a pre-equilibrium before the rate-determining step. Both the catalysed and uncatalysed rates are markedly slower in tetrahydrofuran, which may indicate that the solvent effect acts predominantly on the first equilibrium of Scheme 2. However, the experiments in tetrahydrofuran were done primarily to ensure that there was nothing unique about the results in acetonitrile solvent. Very small and negative $\Delta H^{\neq}$ values were also observed by Rappoport and Peled (5) for the catalysed reactions of piperidine and morpholine with fluoro and cyano-olefins in acetonitrile.

To elucidate the nature of the catalysed reaction, the catalytic effects on the piperidine reaction of added alkyl ammonium salts and tertiary amines were studied. The kinetic results were fitted to eq. [2], an extended form of eq. [1].

$$[2]\quad k_{2\,obs} = k'_{2\,obs} + k_{3\,obs}[\text{amine}] + k_{4\,obs}[\text{catalyst}]$$

A plot of $k_{2\,obs}$ vs. catalyst concentration gives ($k'_{2\,obs}$ +

TABLE 3. Rate constants for the uncatalysed and catalysed reactions of 2,2-di(4-nitrophenyl)-1,1-difluoroethene with piperidine at 296 nm

Temperature (°C)	$k'_{2\,obs}$ (L mol^{-1} s^{-1})	$k'_{3\,obs}$ (L^2 mol^{-2} s^{-1})	Uncatalysed reaction $\Delta H^{\neq}$ (kcal mol^{-1})	Uncatalysed reaction $\Delta S^{\neq}$ (cal mol^{-1} deg^{-1})	Catalysed reaction $\Delta H^{\neq}$ (kcal mol^{-1})	Catalysed reaction $\Delta S^{\neq}$ (cal mol^{-1} deg^{-1})
(a) Acetonitrile solvent						
9.5	0.033±0.006	98.5±1.4				
18.0	0.049±0.003	83.4±1.1				
25.0	0.051±0.004	82.4±2.1				
30.0	0.064±0.004	77.6±1.1				
40.0	0.071±0.001	73.1±0.3	3.7±0.7	−51.8±2.3	−2.2±0.3	−57.2±0.9
(b) Tetrahydrofuran solvent						
9.0	0.0033±0.0015	9.3±0.1				
25.0	0.0049±0.0025	8.4±0.3				
40.0	0.0075±0.0008	10.6±0.1	4.0±0.3	−55.5±1.0	0.1±1.1	−53.7±3.8

TABLE 4. Catalytic rate constants for the reaction of 2,2-di(4-nitrophenyl)-1,1-difluoroethene with piperidine* in acetonitrile at 25°C

Catalyst	Catalytic rate constant 10^4[cat. conc.] (M)	Catalytic rate constant $k_{4\,obs}$ (L^2 mol^{-2} s^{-1})
Diazabicyclo[2,2,2]octane (DABCO)	6.7–33.6	80.3±2.6
Piperidinium oxalate	0.67–3.8	454±78
Piperidinium oxalate (296 nm)	1.3–3.3	474±39
Piperdinium acetate	0.43–2.1	173±13
Quinuclidinium oxalate	0.38–7.8	353±10
Piperidinium perchlorate	2.0–10.3	0
Quinuclidinium chloride	1.3–6.7	−31±5†

*Initial concentrations of piperidine were 1.82–1.90 × 10^{-3} M.
†Inhibition rate constant.

$k_{3\,obs}$[amine]) as the intercept and $k_{4\,obs}$ as the slope. For each catalyst a series of runs was carried out at different catalyst concentrations. Values of $k_{2\,obs}$ were obtained by dividing $k_{1\,obs}$ by the piperidine concentration, and $k_{4\,obs}$ was calculated by a least-squares fit to eq. [2]. The results are summarized in Table 4. The reactions were monitored at 400 nm unless otherwise noted.

The results show that the reaction is catalysed by tertiary amines, oxalate and acetate ions, but not by alkyl ammonium ions, perchlorate or chloride ions. Rappoport and Ta-Shma (9) also found that the ammonium ion did not catalyse the reaction of *p*-toluidine with 1,1-dicyano-2-*p*-dimethylaminophenyl-2-fluoroethylene.

Thus, it is clear that the catalysed step is the deprotonation of the zwitterion rather than the departure of the fluoride ion, because fluoride ion departure would be expected to be catalysed by the ammonium ion. It would still be possible to have a rate-determining uncatalysed cleavage of fluoride if it can be assumed that F^- departs more rapidly from C^- than from $Z^{\pm}$. The catalysis would then take place by simply changing the position of the deprotonation equilibrium. This interpretation is supported by the fact that there is a reasonable correlation between log $k_{3\,obs}$ and pK_a for the catalysed reaction for the results shown in Table 2. This means that the sensitivity of the zwitterion $Z^{\pm}$ to deprotonation is essentially the same as that of the amine to protonation.

A steady-state approximation applied to Scheme 2 yields eq. [3], if it is assumed that $k_4 \gg k_{-3}$[base H^+] and $k_{-1} \gg k_2 + k_3$[amine], i.e., that the carbon–fluorine bond cleavage is not rate determining.

$$[3] \quad k_{2\,obs} = \frac{k_1}{k_{-1}} \cdot k_2 + \frac{k_1}{k_{-1}} \cdot k_3[\text{amine}]$$

This predicts that $\Delta H^{\neq}$ should not be dramatically different for the catalysed and uncatalysed reactions. Both would be expected to be positive values, but if one were negative, as a result of an unusual temperature dependence of k_1/k_{-1}, the other would also be negative or a very small positive value. Thus, the results in Table 3 do not fit this assumption.

The alternative assumption, that k_{-3}[base H^+] $\gg k_4$ and that $k_{-1} \gg k_2 + \dfrac{k_3 k_4[\text{amine}]}{k_{-3}[\text{base H}^+]}$, yields eq. [4].

$$[4] \quad k_{2\,obs} = \frac{k_1 k_2}{k_{-1}} + \frac{k_1}{k_{-1}} \frac{k_3 k_4[\text{amine}]}{k_{-3}[\text{amine H}^+]}$$

Equation [4] allows $\Delta H^{\neq}$ for the catalysed reaction to be distinctly different from that for the uncatalysed reaction, by the equilibrium constant k_3/k_{-3} having a different temperature dependence from that of k_1/k_{-1}.

The catalysis of the reaction results from an increase in the rate of the step k_3, in which the zwitterion $Z^{\pm}$ is converted to the carbanion C^-, by virtue of the additional base, relative to the reverse step k_{-3}. This additional base may be a secondary or

tertiary amine or an anion such as acetate or oxalate. Weak bases such as Cl^- and ClO_4^- show little or no catalytic effect. Adding ammonium ion without a moderately strong basic anion increases the rate of the back reaction of the carbanion C^- to the zwitterion and, therefore, retards the overall reaction, in general agreement with the results in Table 4.

Therefore, it is concluded that the reaction takes place by the mechanism in Scheme 2, in which the carbon–fluorine bond breaking is rate determining, but the overall rate is catalysed or retarded by changes in the rates of the steps that interconvert the zwitterion and the carbanion.

Experimental

Materials

2,2-Di(4-nitrophenyl)-1,1,1-trifluoroethane was prepared from α,α,α-trifluoroacetophenone as previously described (1). The substrate 2,2-di(4-nitrophenyl)-1,1-difluoroethene was prepared from this by reaction with excess sodium hydride in very carefully dried tetrahydrofuran. The reaction mixture was refluxed for 10 h protected from atmospheric moisture, during which time about 50% conversion to the ethene took place. After evaporation of the THF, ethyl ether was used to separate the organics from the inorganic residue. The mixture of product and starting material was separated by column chromatography with Kieselgel 60 and a 3:1 mixture of benzene and *n*-hexane as eluent. The ethene product gave mp 129–130°C; λ_{max}: 296 nm in CH_3CN; nmr δ (CD_3CN): 8.22 (d, 4H) and 7.5 (d, 4H).

The reagent amines were dried over KOH and fractionally distilled twice before use of the middle fraction. The concentration of the amine solutions was determined by tiration with standard perchloric acid in acetic acid solvent (13).

The ammonium salts were prepared by reacting the purified piperidine and quinuclidine with the appropriate acid in THF and precipitating the salt with a mixture of ethyl ether and benzene. The salts were washed and dried before use.

The acetonitrile solvent was purified by the method of O'Donnell *et al.* (14) and fractionally distilled first from P_2O_5 and then from CaH_2.

Product analyses

The reaction mixture was separated by column chromatography using Kieselgel 60 and an eluent made up of chloroform, benzene, and *n*-hexane in a ratio 12:3:1. The fractions were analysed by tlc, nmr, and uv spectroscopy.

Kinetics

A fresh 5×10^{-5} *M* solution of the olefin was prepared for each set of runs. Each set consisted of five runs, each with a different amine concentration. The five runs were carried out simultaneously in 1-cm uv cells in a Cary 219 spectrophotometer fitted with a temperature-controlled cell block. Pseudo-first-order rate constants were calculated by a least-squares fit to eq. [5]

$$[5] \quad k_{obs} = 1/t \ln \frac{D_0 - D_\infty}{D_t - D_\infty}$$

where D_0, D_t, and D_∞ represent the optical density of the reaction mixture at time zero, time t, and at infinity, respectively.

Acknowledgment

The authors are grateful for financial support by the Natural Sciences and Engineering Research Council of Canada.

1. A. Jarczewski, G. Schroeder, W. Galezowski, K. T. Leffek, and U. Maciejewska. Can. J. Chem. **63**, 576 (1985).
2. W. E. Hanford and G. W. Rigby. U.S. Pat. 2,409,274 (1946).
3. R. D. Chambers and R. H. Mobbs. Adv. Fluorine Chem. **4**, 50 (1965).
4. H. F. Koch, J. G. Koch, D. B. Donovan, A. G. Toczko, and A. J. Kielbania, Jr. J. Am. Chem. Soc. **103**, 5417 (1981).
5. Z. Rappoport and P. Peled. J. Chem. Soc. Perkin Trans. 2, 616 (1973).
6. Z. Rappoport and P. Peled. J. Am. Chem. Soc. **101**, 2682 (1979).
7. C. F. Bernasconi and D. J. Carre. J. Am. Chem. Soc. **101**, 2698 (1979).
8. C. F. Bernasconi, D. J. Carre, and A. Kanavarioti. J. Am. Chem. Soc. **103**, 4850 (1981).
9. Z. Rappoport and R. Ta-Shma. J. Chem. Soc. (B), 871 (1971).
10. Z. Rappoport and N. Ronen. J. Chem. Soc. Perkin Trans. 2, 955 (1972).
11. J. F. Coetzee. Prog. Phys. Org. Chem. **4**, 45 (1967).
12. C. F. Bernasconi, D. J. Carre, and J. P. Fox. Techniques and applications of fast reactions in solution. *Edited by* W. J. Gettins and E. Wyn-Jones. D. Reidel, Dordrecht. 1979.
13. I. Gyenes. Titrations in non-aqueous media. *Translated by* E. Helevy. Van Nostrand, Princeton. 1967.
14. J. F. O'Donnell, J. T. Ayers, and C. K. Mann. Anal. Chem. **37**, 1161 (1965).

Electrosorption of vinyltriphenyl and propargyltriphenylphosphonium cations from methanolic solutions at the dropping and hanging mercury drop electrodes

ANASTASIA CHRISTODOULOU, ANASTOS ANASTOPOULOS, AND DEMETRIOS JANNAKOUDAKIS
University of Thessaloniki, Thessaloniki 54006, Greece

Received February 19, 1986

ANASTASIA CHRISTODOULOU, ANASTOS ANASTOPOULOS, and DEMETRIOS JANNAKOUDAKIS. Can. J. Chem. **64**, 2279 (1986).

The interfacial behaviour of vinyltriphenyl and propargyltriphenylphosphonium cations at the mercury electrode – methanolic solution interface is studied by phase selective ac polarography using dropping Hg electrodes of short (≤5 s) and long (≃20 s) drop times and the hanging Hg drop electrode.

The various adsorption parameters are determined on the basis of non-ionic adsorption isotherms involving capacitance data independent as well dependent on time.

ANASTASIA CHRISTODOULOU, ANASTOS ANASTOPOULOS et DEMETRIOS JANNAKOUDAKIS. Can. J. Chem. **64**, 2279 (1986).

Faisant appel à la polarographie à ca et à phase sélective et utilisant soit des électrodes à goutte tombante de mercure avec des temps de chute court (≤5 s) et longs (≃20 s) soit une électrode à goutte pendante de mercure, on a étudié le comportement interfacial des cations vinyltriphényl- et propargyltriphenyl-phosphonium.

On a déterminé les divers paramètres d'adsorption en se basant sur des isothermers d'adsorptions non-ioniques impliquant des données de capacitance tant indépendantes que dépendantes du temps.

[Traduit par la revue]

Introduction

Since the pioneering work of Gerovich *et al.* (1), a small but increasing amount of data concerning the adsorption of tetraphenyl and a series of alkyltriphenylphosphonium cations have now appeared in the literature (2–7).

Contrary to many works on the adsorption of quaternary ammonium cations, the interfacial behaviour of phosphonium cations is rarely treated (6) in terms of nonionic isotherms, thus limiting the information available to the characteristics of the development of the adsorption film. Although remarkable efforts have been made by Damaskin and co-workers (8–12) on the development of adsorption isotherms for organic cations, information resulting from non-ionic isotherms, though it will be criticized, may help our understanding on the adsorption behaviour of these substances.

In this work the electrosorption of quaternary phosphonium cations with alkyl groups having multiple bonds are analyzed by means of the Frumkin and Flory–Huggins isotherms to determine the standard free energy of adsorption, the interparticle forces, the maximum surface concentration, and the area per adsorbed particle of vinyltriphenyl- and propargyltriphenyl-phosphonium cations. The adsorption equilibrium of these substances is controlled by their diffusion from the bulk to the inferface and so the use of time-dependent capacitance data, when combined with theoretical adsorption isotherms, allows for a quantitative description of the adsorbed film characteristics.

Experimental

The variation of the differential capacity against the time and the dc polarization potential was recorded by fundamental harmonic phase selective ac polarography, similar to a previous publication (6). The electrochemical system used was the following:

Hg electrode	Phosphonium salt 0.1 *M* CsCl MeOH Working cell	0.1 *M* CsCl MeOH Electrolytic contact	0.1 *M* CsCl H_2O Reference cell	sce with NaCl

The characteristics of the DME with short drop times were 2.235 mg/s (flow rate) and a drop time of 4 s controlled to 2 s by a drop timer system. The DME with large drop times (≃20 s) had a flow rate of 0.35 mg/s and the HMDE was controlled under constant temperature to obtain a radius of 4.27×10^{-2} cm during all measurements.

Methanol (Merck, pro analysi), CsCl (Merck, pro analysi), and propargyltriphenylphosphonium bromide (Fluka, purum 99%) were used without further purification. Vinyltriphenylphosphonium bromide (Fluka, pract. > 95%) was twice recrystallized from water–ethanol solutions, subsequently dried at 140°C under reduced pressure and its melting point was found to be 182–183°C after the recrystallization process.

The solutions were deaerated by a stream of purified nitrogen, previously saturated with vapours of the base solution. All measurements were carried out at 25 ± 0.05°C. The standard deviation of the differential capacity values is less than 2% at the overall potential range studied.

Results and discussion

To study the electrosorption of vinyltriphenyl-, $(VPh_3P)^+$, and propargyltriphenyl-, $(PgPh_3P)^+$, phosphonium cations from methanolic solutions of 0.1 *M* CsCl, capacitance versus potential curves were recorded for various concentrations of the bromide salts of the above cations and they are provided in Figs. 1 and 2.

Capacitance current versus time measurements were also recorded at the DME, at the potentials −0.6, −0.8, −1.05, −1.2, −1.4 V/sce and some of them are shown in Fig. 3.

From the *C–E* curves in Figs. 1 and 2 it is seen that the adsorption of $(VPh_3P)^+$ and $(PgPh_3P)^+$ does not lead to the appearance of capacitance maxima. At the anodic region the lack of maxima must be attributed to the metal–adsorbate interactions between the phenyl groups and the Hg conduction band. At extreme negative polarizations the discharge of the adsorbed cations — occurring at the vicinity of −1.60 V/sce — prior to their complete desorption from the electrode surface, possibly justifies (2) the lack of cathodic adsorption–desorption peaks.

Two potential regions of limiting minimum capacitance were not observed, indicating the absence of condensation effects in the adsorption layer, this was in agreement with the behaviour of the phosphonium cations in non aqueous systems (5, 6).

The absence of discontinuities in the formation of the adsorption layer is also confirmed by the form of the i_c–t curves

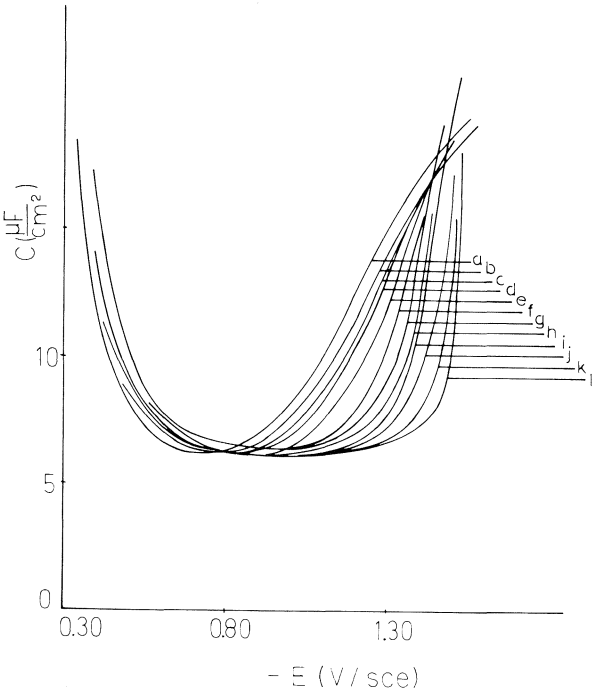

FIG. 1. Differential capacitance of 0.1 *M* CsCl methanolic solutions containing the following VPh_3PBr concentrations: *a*, 0.00; *b*, 2.5×10^{-5} *M*; *c*, 3.75×10^{-5} *M*; *d*, 5×10^{-5} *M*; *e*, 10^{-4} *M*; *f*, 2.5×10^{-4} *M*; *g*, 3.75×10^{-4} *M*; *h*, 5×10^{-4} *M*; *i*, 7.5×10^{-4} *M*; *j*, 10^{-3} *M*; *k*, 1.5×10^{-3} *M*; *l*, 2×10^{-3} *M* at the dme.

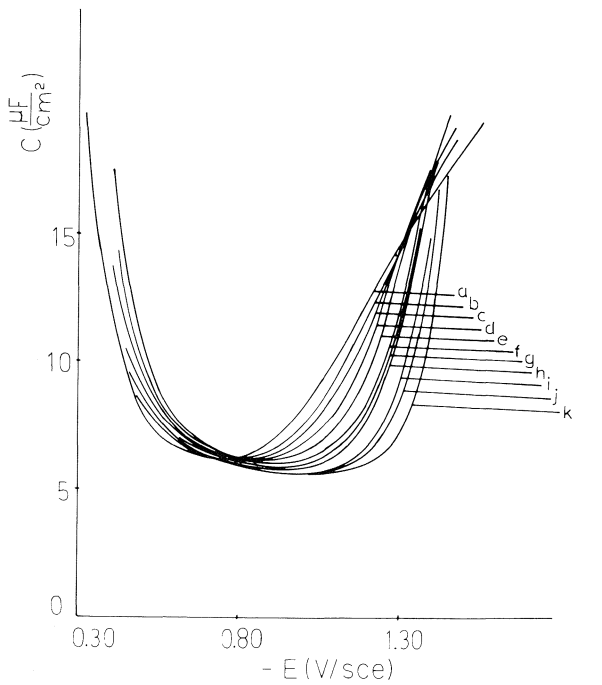

FIG. 2. Differential capacitance curves of 0.1 *M* CsCl methanolic solutions containing the following $PgPh_3PBr$ concentrations: *a*, 0.00; *b*, 2.5×10^{-5} *M*; *c*, 5×10^{-5} *M*; *d*, 10^{-4} *M*; *e*, 1.5×10^{-4} *M*; *f*, 2.5×10^{-4} *M*; *g*, 3.75×10^{-4} *M*; *h*, 5×10^{-4} *M*; *i*, 7.5×10^{-4} *M*; *j*, 10^{-3} *M*; *k*, 2×10^{-3} *M* at the dme.

of Figs. 3. Here a regular development of the adsorbed film is reflected without humps or abrupt changes, thus leading to the conclusion that the presence of methanol prevents the occurrence of surface condensation or other interfacial rearrangement effects.

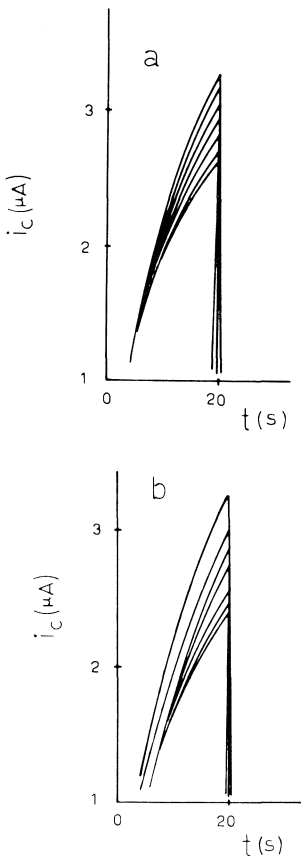

FIG. 3. Capacitance current vs. time curves, at −1.05 V/sce, of 0.1 *M* CsCl methanolic solutions in the presence of the following additions (from top to bottom) of (*a*) VPh_3PBr: 0.0 *M*, 5×10^{-6} *M*, 7.5×10^{-6} *M*, 1.25×10^{-5} *M*, 2.5×10^{-5} *M*, 3.75×10^{-5} *M*, 5×10^{-5} *M*. (*b*) $PgPh_3PBr$: 0.0 *M*, 1.25×10^{-5} *M*, 1.75×10^{-5} *M*, 2.5×10^{-5} *M*, 3.75×10^{-5} *M*, 5×10^{-5} *M*, 7.5×10^{-5} *M*.

The *C*–*E* curves of $(VPh_3P)^+$ and $(PgPh_3P)^+$ cations, in spite of their similar shape, reveal a difference in the adsorbate concentration at which the limiting minimum capacitance, C_{lim}, is attained.

In the presence of $(PgPh_3P)^+$ the increase in concentration causes a gradual depression of the minimum down to a limiting value, 5.30 $\mu F/cm^2$, attained at the concentration 7.5×10^{-4} *M*.

For $(VPh_3P)^+$ cations a limiting value, 5.97 $\mu F/cm^2$, is attained at concentrations $c \geq 10^{-5}$ *M*. This difference can be interpreted in terms of a corresponding difference in their adsorbabilities, which determines the influence of concentration on the formation of a saturation monolayer, as long as all the other characteristics and adsorption parameters do not differ appreciably.

Isotherm analysis

The capacitance potential data in Figs. 1 and 2 were analyzed by means of two well known nonionic isotherms, viz. Frumkin isotherm:

$$[1] \quad \ln \frac{\theta}{(1-\theta)c} = \ln \mathscr{C} + 2a\theta$$

and a type of Flory–Huggins isotherm:

$$[2] \quad \ln \frac{\theta}{(1-\theta)^r c} = \ln \mathscr{C} + 2ar\theta$$

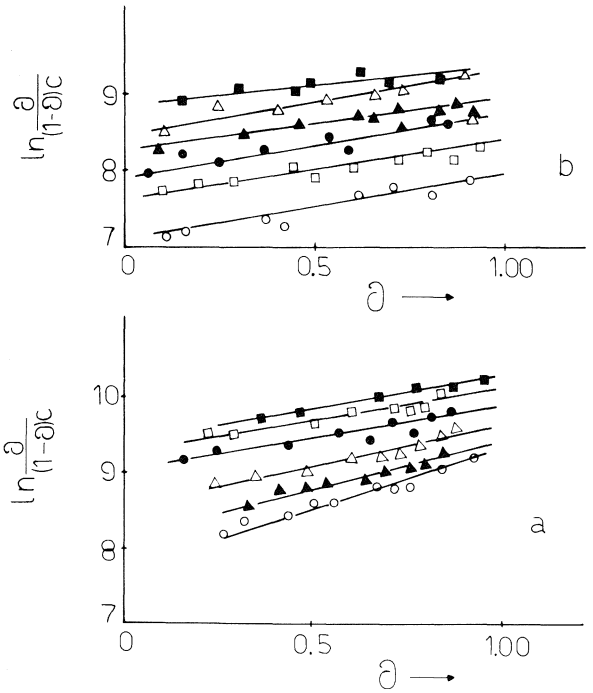

FIG. 4. Test of Frumkin isotherm for VPh_3PBr (*a*) and $PgPh_3PBr$ (*b*) at the following potentials in V/sce: ■ −1.05, △ −1.10, ▲ −1.15, ● −1.20, □ −1.25, ○ −1.30.

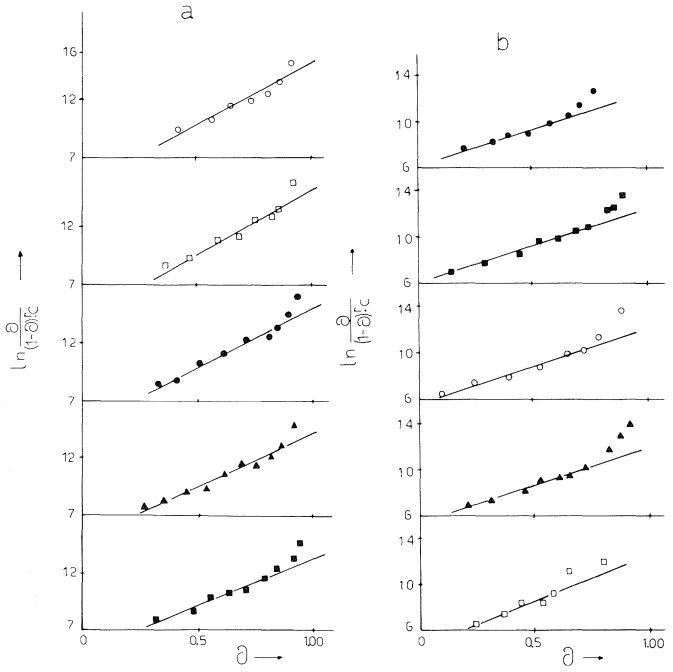

FIG. 5. Test of Flory–Huggins isotherm for VPh_3PBr (*a*) and $PgPh_3PBr$ (*b*) at the following potentials in V/sce: ● −1.00, ■ −1.05, ○ −1.10, ▲ −1.15, □ −1.20.

where θ is the surface coverage calculated by the relation $\theta = (C_0 - C)/(C_0 - C_{lim})$ at the potential region where the condition $d\theta/dE = 0$ is satisfied, C_0 is the capacitance of the base electrolyte, and C_{lim} is the minimum limiting capacitance at maximum coverage, determined by extrapolation of the minimum capacitance vs. concentration plot to high surfactant concentration. In eqs. [1] and [2], c is the bulk concentration, $\mathscr{C}$ is the adsorption equilibrium constant, and a is an interaction parameter. In eq. [2], r is the size ratio which is set equal

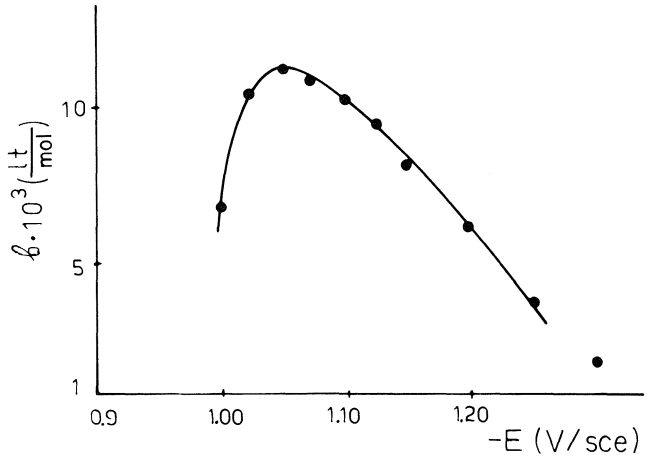

FIG. 6. Variation of the adsorption equilibrium constant of VPh_3PBr with potential.

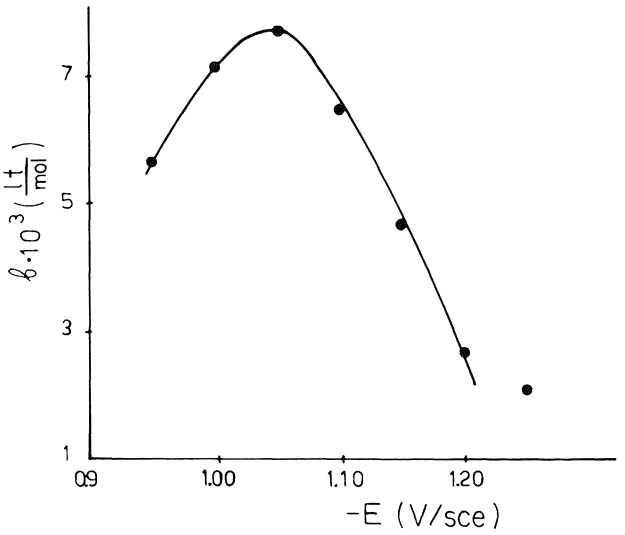

FIG. 7. Variation of the adsorption equilibrium constant of $PgPh_3PBr$ with potential.

to 4, estimated from the area per adsorbed phosphonium cation (approximately 0.75 nm^2) and methanol molecule (0.186 nm^2 according to ref. 13). The results on the test of isotherms [1] and [2] are provided in Figs. 4 and 5, revealing a fair agreement of these isotherms with our experimental data.

The lines in Figs. 4 and 5 have constant positive slopes corresponding to a prevalence of attractive interactions at the interface. However, due to the complex nature of the interaction parameter and the simplicity of the Frumkin and Flory–Huggins models, it is impossible to strictly correlate this parameter to the interactions occurring at the interface. In terms of the solvent–solvent, solvent–adsorbate, and adsorbate–adsorbate interactions, the positive slopes of the plots of Figs. 4 and 5 may be related to positive deviations from Raoult's law (14).

A small variation in slope with potential is only observed in Fig. 6*a* for $(VPh_3P)^+$ cations, where the slope is seen to increase with increasing cathodic potentials. Equations [1], [2], and the plots in Figs. 6, 7 enable the determination of the adsorption equilibrium constant and the potential of maximum adsorption.

The variation in the adsorption equilibrium constant of $(VPh_3P)^+$ and $(PgPh_3P)^+$ cations with potential is shown in Figs. 6 and 7, where it is seen that there is an approximately

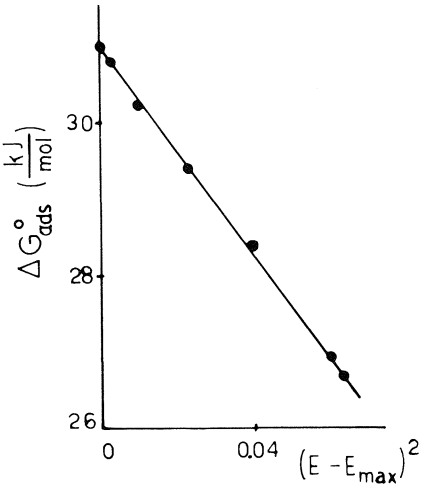

FIG. 8. Variation of the standard free energy of adsorption of VPh_3PBr against the quantity $(E - E_{max})^2$.

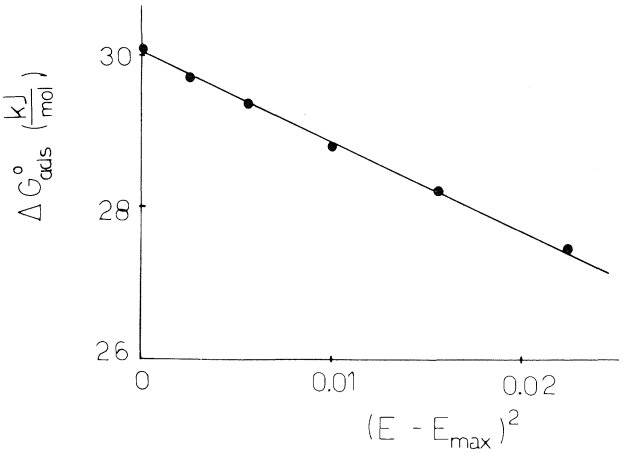

FIG. 9. Variation of the standard free energy of adsorption of $PgPh_3PBr$ against the quantity $(E - E_{max})^2$.

quadratic dependence of $\mathscr{C}$ on E, which reaches a maximum value of 11.2×10^3 and 7.7×10^3 L/mol, respectively.

As long as the value of the adsorption equilibrium constant at a certain potential is a measure of the adsorbability of the substance under examination, we can conclude that in methanol $(VPh_3P)^+$ cations present a moderate adsorbability while the adsorbability of $(PgPh_3P)^+$ is somewhat lower. The potential at which maximum adsorbability is detected can be identified with the potential of maximum adsorption, provided that the interaction parameter does not change significantly with potential.

For both substances examined E_{max} was found at -1.05 V/sce.

From the $\mathscr{C}$–E curves and the equation

$$[3] \quad \mathscr{C} = \frac{1}{24.56} \exp\left(-\frac{\Delta G^0_{ads}}{RT}\right)$$

we calculated the values of the standard free energy of adsorption against the quantity $(E - E_{max})^2$. The resulting plots for $(VPh_3P)^+$ and $(PgPh_3P)^+$ cations are shown in Figs. 8 and 9.

It is seen that there is a linear dependence of ΔG^0_{ads} on $(E - E_{max})^2$, though for a narrow potential range. This feature is not typical of interfacial behaviour of ionic species. The values of ΔG^0_{max} corresponding to E_{max} were found to be -31.00 and -30.10 kJ/mol for $(VPh_3P)^+$ and $(PgPh_3P)^+$ cations, respectively.

Maximum surface concentration of $(VPh_3P)^+$ and $(PgPh_3P)^+$ cations

The kinetics of adsorption of a species at the electrode–solution interface can be used as a means for the determination of its surface concentration. This can be achieved either by examining the dependence of differential capacitance values on the frequency of the ac signal or on the time of exposure of the electrode surface in the electrolyte solution. The latter is suitable for systems without adsorption–desorption maxima, as the C–E curves in Figs. 1 and 2. For this purpose capacitance–time measurements were carried out for $(VPh_3P)^+$ and $(PgPh_3P)^+$ cations both at the DME with long drop times and at the HMDE. In Figs. 10 and 11 we provide the C—$t^{1/2}$ and C–$t^{-1/2}$ curves of $(VPh_3P)^+$ and $(PgPh_3P)^+$ cations, recorded at the potential of maximum adsorption and at the DME and HMDE, respectively.

According to Koryta (15) and Levich (16) the linearity of the experimental plots in Figs. 10 and 11 is evidence for diffusion

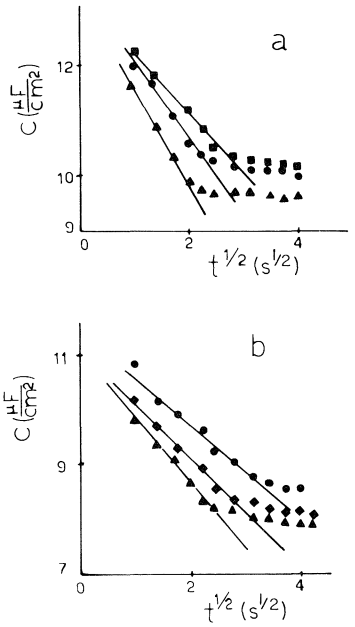

FIG. 10. Variation of the differential capacitance with $t^{1/2}$ at the dme. (*a*) For the following VPh_3PBr concentrations: ● 1.25×10^{-5} *M*, ■ 2.5×10^{-5} *M*, ▲ 3.75×10^{-5} *M*. (*b*) For the following $PgPh_3PBr$ concentrations: ● 2.5×10^{-5} *M*, ■ 3.75×10^{-5} *M*, ▲ 5×10^{-5} *M*.

control of the establishment of the adsorption equilibrium. The C–$t^{1/2}$ curves in Fig. 10 enable the calculation of the maximum surface concentration, Γ_{max}, with the aid (17) of equation

$$[4] \quad C_t = C_0 - 7.36 \times 10^{-4} D^{1/2}(C_0 - C_{lim})c\Gamma^{-1}_{max}t^{1/2}$$

where the symbols C_0 and C_{lim} are previously defined, C_t is the capacity at intermediate surfactant concentrations at time t, c is the phosphonium cation concentration, D is the diffusion coefficient, and Γ_{max} is the maximum surface concentration. The value of the diffusion coefficient was determined by polarographic measurements and was found equal to $(5 \pm 0.2) \times 10^{-6}$ cm^2/s. From eq. [4] the values of 2.05×10^{-10} and 2.11×10^{-10} mol/cm^2 were obtained for the maximum surface concentrations of $(VPh_3P)^+$ and $(PgPh_3P)^+$ cations, respectively.

At the potential of maximum adsorption according to ref. 18,

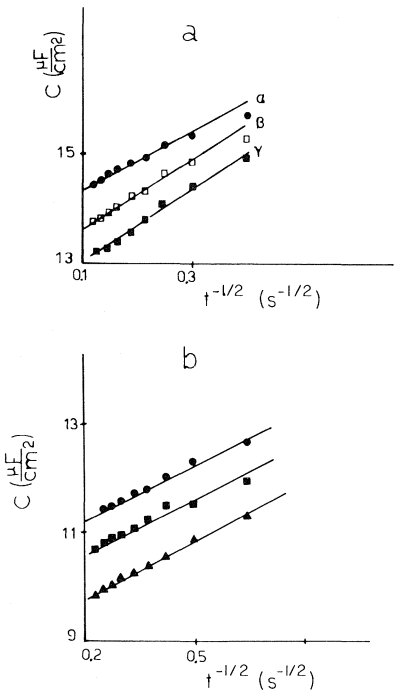

FIG. 11. Variation of the differential capacitance with $t^{1/2}$ at the HMDE. (*a*) For the following VPh_3PBr concentrations: ● 7.5×10^{-6} *M*, ■ 1.25×10^{-5} *M*, ▲ 2.5×10^{-5} *M*. (*b*) For the following $PgPh_3PBr$ concentrations: ● 2.5×10^{-5} *M*, ■ 3.75×10^{-5} *M*, ▲ 5×10^{-5} *M*.

for a system obeying the Frumkin isotherm, the following equation is valid:

$$[5] \quad \left[\frac{dC_t}{dt^{1/2}}\right]_{E=E_{max}} = \frac{(C_0 - C_{lim})\Gamma_{max}\theta_e^2(1-\theta_e)}{2c[1-2a\theta_e(1-\theta_e)]}\left(\frac{\pi}{D}\right)^{1/2}$$

where C_0, C_{lim}, Γ_{max}, c, and D have their usual meaning and $\theta = (C_0 - C_e)/(C_0 - C_{lim})$ is the equilibrium surface coverage, determined at times when the equilibrium value C_e is attained.

The application of eq. [5] to the experimental diagrams of Fig. 11 yields 2.25×10^{-10} and 2.20×10^{-10} mol/cm^2 for the maximum surface concentration of $(VPh_3P)^+$ and $(PgPh_3P)^+$ cations, respectively. When calculating with eqs. [4] and [5], $C_0 = 12.2$ μF/cm^2, $C_{lim}(VPh_3P)^+ = 5.97$ mF/cm^2, $C_{lim}(PgPh_3P)^+ = 5.3$ μF/cm^2, $a(VPh_3P)^+ = 0.45$, $a(PgPh_3P)^+ = 0.6$, $D = 5 \times 10^{-6}$ cm^2/s, $\theta_e \leq 0.5$, were used for low ($c \leq 2.5 \times 10^{-5}$ *M*) surfactant concentrations.

The selection of the most suitable values of Γ_{max} can be facilitated by comparison with theoretical predictions for the possible orientations and the area per adsorbed phosphonium cation. Therefore, taking into account the tetrahedral structure of $(VPh_3P)^+$ and $(PgPh_3P)^+$ cations, two possible orientations can be predicted, viz., two phenyls and the alkyl group or the three phenyl groups oriented towards the Hg surface, the former leading to an approximate area of 0.64 and 0.70 nm^2, respectively, and the latter to an area of 0.77 nm^2 for both substances. Therefore, the experimental values of Γ_{max} determined by means of the HMDE and eq. [5] seem to offer a better approximation to the theoretically predicted value of 0.77 nm^2. The values of area per adsorbed $(VPh_3P)^+$ and $(PgPh_3P)^+$ cations thus obtained are equal to 0.74 and 0.76 nm^2, suggesting that these cations are adsorbed with their three phenyl groups oriented towards the metal surface.

The strong interactions of the π-electrons of the phenyl groups with the conduction band of Hg at positive and small negative polarizations offer support to such an orientation. Nevertheless, since there is no evidence of rearrangement of the adsorption film taking place at higher negative potentials in methanol in the *C–E* and i_c–*t* experimental curves, we can assume that the same orientation is maintained up to the discharge potentials of these cations.

1. V. M. GEROVICH, R. I. KAGANOVICH, and B. B. DAMASKIN. Elektrokhimiya, **12**, 445 (1976).
2. Y. V. MIKHAILIK and B. B. DAMASKIN. Elektrokhimiya, **15**, 478 (1979).
3. H.-D. DÖRFLER and E. MÜLLER. J. Electroanal. Chem. **105**, 383 (1979).
4. H.-D. DÖRFLER and E. MÜLLER. J. Electroanal. Chem. **121**, 153 (1981).
5. E. MÜLLER and H.-D. DÖRFLER. J. Electroanal. Chem. **121**, 169 (1981).
6. A. ANASTOPOULOS, A. CHRISTODOULOU, and D. JANNAKOUDAKIS. Z. Phys. Chem. N.F. **137**, 231 (1983).
7. M. HASSAN SAFFARIAN and R. DE LEVIE. J. Electroanal. Chem. **189**, 325 (1985).
8. B. B. DAMASKIN, U. PALM, M. VÄÄRTNOU, and M. SALVE. J. Electroanal. Chem. **108**, 203 (1980).
9. B. B. DAMASKIN, S. KARPOV, S. DYATKINA, U. PALM, and M. SALVE. J. Electroanal. Chem. **136**, 217 (1982).
10. B. B. DAMASKIN, S. KARPOV, and S. DYATKINA. Elektrokhimiya, **18**, 231 (1982).
11. B. B. DAMASKIN and S. KARPOV. Elektrokhimiya, **18**, 1 (1982).
12. B. B. DAMASKIN, S. KARPOV, S. DYATKINA, U. PALM, and M. SALVE. J. Electroanal. Chem. **189**, 183 (1985).
13. J. LAWRENCE and R. PARSONS. J. Phys. Chem. **78**, 3577 (1969).
14. F. PULIDORI, G. BORGHESANI, R. PEDRIALI, A. DE BATTISTI, and S. TRASATTI. J. Chem. Soc. Faraday I, 74 (1978); 79 (1978).
15. J. KORYTA. Coll. Czech. Chem. Commun. **18**, 206 (1953).
16. V. LEVICH, B. I. KHAIKIN, and E. D. BELOKOLOS. Elektrokhimiya, **11**, 1137 (1965).
17. H. JERING. J. Electroanal. Chem. **20**, 33 (1969).
18. S. SATHYANARAYANA and K. G. BAIKERIKAR. J. Electroanal. Chem. **25**, 209 (1970).

Iodine chemistry in the +1 oxidation state. II. A Raman and uv–visible spectroscopic study of the disproportionation of hypoiodite in basic solutions[1]

J. C. WREN, J. PAQUETTE, S. SUNDER, AND B. L. FORD

Research Chemistry Branch, Atomic Energy of Canada Limited, Whiteshell Nuclear Research Establishment, Pinawa, Man., Canada R0E 1L0

Received March 14, 1986

J. C. WREN, J. PAQUETTE, S. SUNDER, and B. L. FORD. Can. J. Chem. **64**, 2284 (1986).

The kinetics of disproportionation of elemental iodine to iodide and iodate ions has been studied in basic aqueous media using Raman and uv–visible spectroscopy. The IO stretching vibrations for IO^- and I_2OH^- were observed at 430 ± 2 and 560 ± 2 cm^{-1}, respectively. The totally symmetric stretching vibration for IO_2^- was observed at 685 ± 2 cm^{-1}. The Raman results indicate that I_2OH^- is a linear molecule with a stronger I—O bond than IO^-. The rate expression at 25°C in 1 mol dm^{-3} NaOH was found to be

$$-\frac{d\Sigma[I]}{dt} = (0.05 + 2.60[I^-])(\Sigma[I])^2$$

where

$$\Sigma[I] = ([I_2] + [I_3^-] + [IO^-] + [I_2OH^-])$$

The reaction is primarily a reaction of the iodine +1 oxidation-state species IO^- and I_2OH^-. It proceeds through the +3 oxidation-state species IO_2^-. The following equilibrium and rate constants were determined:

$IO^- + I^- + H_2O \rightleftharpoons I_2OH^- + OH^-$	$K = 0.15 \pm 0.01$
$IO^- + IO^- \rightarrow IO_2^- + I^-$	$k \leq 7.2 \times 10^{-2}$ dm^3 mol^{-1} s^{-1}
$IO^- + HOI \rightarrow IO_2^- + I^- + H^+$	$k = 40 \pm 7$ dm^3 mol^{-1} s^{-1}
$IO^- + I_2OH^- \rightarrow IO_2^- + 2I^- + H^+$	$k = 6.0 \pm 0.2$ dm^3 mol^{-1} s^{-1}
$IO^- + IO_2^- \rightarrow IO_3^- + I^-$	$k = 0.5 \pm 0.1$ dm^3 mol^{-1} s^{-1}
$I_2OH^- + IO_2^- \rightarrow IO_3^- + 2I^- + H^+$	$k = 26 \pm 2$ dm^3 mol^{-1} s^{-1}

J. C. WREN, J. PAQUETTE, S. SUNDER et B. L. FORD. Can. J. Chem. **64**, 2284 (1986).

La cinétique de dismutation de l'iode en ions iodure et iodate a été étudiée en milieu aqueux basique, en utilisant la spectroscopie Raman et UV-visible. La vibration d'élongation pour IO^- et I_2OH^- a été observée à 430 ± 2 et 560 ± 2 cm^{-1}, respectivement. La vibration d'élongation totalement symétrique pour IO_2^- a été observée à 685 ± 2 cm^{-1}. Les résultats de la spectroscopie Raman indiquent que I_2OH^- est une molécule linéaire avec un lien I—O plus fort que dans IO^-. La loi cinétique à 25°C, en milieu NaOH 1 mol dm^{-3}, est

$$-\frac{d\Sigma[I]}{dt} = (0.05 + 2.60[I^-])(\Sigma[I])^2$$

où

$$\Sigma[I] = ([I_2] + [I_3^-] + [IO^-] + [I_2OH^-])$$

La réaction est principalement une réaction de l'iode dans l'état d'oxydation +1 et implique les espèces IO^- et I_2OH^-. L'iode dans l'état d'oxydation +3, sous forme de IO_2^-, est un intermédiaire réactif. Les constantes d'équilibre et de vitesse suivantes ont été mesurées :

$IO^- + I^- + H_2O \rightleftharpoons I_2OH^- + OH^-$	$K = 0{,}15 \pm 0{,}01$
$IO^- + IO^- \rightarrow IO_2^- + I^-$	$k \leq 7{,}2 \times 10^{-2}$ dm^3 mol^{-1} s^{-1}
$IO^- + HOI \rightarrow IO_2^- + I^- + H^+$	$k = 40 \pm 7$ dm^3 mol^{-1} s^{-1}
$IO^- + I_2OH^- \rightarrow IO_2^- + 2I^- + H^+$	$k = 6{,}0 \pm 0{,}2$ dm^3 mol^{-1} s^{-1}
$IO^- + IO_2^- \rightarrow IO_3^- + I^-$	$k = 0{,}5 \pm 0{,}1$ dm^3 mol^{-1} s^{-1}
$I_2OH^- + IO_2^- \rightarrow IO_3^- + 2I^- + H^+$	$k = 26 \pm 2$ dm^3 mol^{-1} s^{-1}

I. Introduction

The disproportionation of elemental iodine into iodide and iodate ions is a key reaction controlling the behaviour of iodine in aqueous media:

[1] $3I_2 + 3H_2O \rightleftharpoons 5I^- + IO_3^- + 6H^+$

The thermodynamic parameters for equilibrium [1] are known accurately for temperatures up to 150°C (1). The kinetics of the reverse reaction (Dushman reaction) have also been examined in detail (2–4), but the forward reaction has not been studied so extensively. Thomas *et al.* (5) have investigated its kinetics in neutral to weakly basic media, while other studies (6–11) have been performed in strongly basic media. These authors agree

[1]AECL No. 9037.

that the rate-determining step involves the reactions of the +1 oxidation-state species HOI/IO^-, the hydrolysis and disproportionation of elemental iodine into HOI/IO^- and I^- being a rapid process. However, there is disagreement in the suggested rate laws for further disproportionation to iodide and iodate. Skrabal (9, 10) and Forster (11), as well as Li and White (8), have reported a two-term rate law, with the second term having a first-order dependence on iodide concentration, an effect not observed in the more recent studies of Thomas *et al.* (5) and Haimovich and Treinin (6).

Although some of these studies were done using uv–visible absorption spectroscopy (5, 6), the transient iodine species have never been positively identified. There is no report in the literature on the Raman spectra of any of the intermediates formed during the disproportionation of iodine. For these reasons, we have used the following three reactions to study the kinetics of disproportionation of iodine in basic media, using both Raman and uv–visible spectroscopy:

[2] $I_2 + OH^- \rightleftharpoons IO^- + I^- + H^+$

[3] $HOCl + I^- \rightleftharpoons IO^- + Cl^- + H^+$

[4] $ICl + OH^- \rightleftharpoons IO^- + Cl^- + H^+$

Using Raman spectroscopy, we not only observed the transient iodine species, but also obtained reliable kinetic data for the reaction of these species. We also reinvestigated the kinetics using uv–visible spectrophotometry and iodide-specific electrode measurements to obtain accurate values of the rate constants.

Our interest in aqueous iodine chemistry arises from the importance of iodine compounds in nuclear reactor safety studies. Radioactive isotopes of iodine are among the more radiologically toxic products resulting from the fission of uranium. A knowledge of the aqueous chemistry of iodine is needed to design effective measures to prevent the release of volatile radioactive iodine species into the environment following a serious nuclear reactor accident.

II. Experimental

Reagents

The sodium iodide was of ACS grade and was used without further purification. The hypochlorite was either obtained as a stock solution from the Fisher Scientific Company or generated by slowly bubbling chlorine gas, from Canadian Liquid Air, into a cold 1 mol dm^{-3} NaOH solution. The iodine was resublimed ACS grade and was used as such. The iodine monochloride was obtained from the J. T. Baker Chemical Company and was used as received. Other stock solutions were prepared from ACS-grade chemicals and distilled deionized water.

The experiments at low initial iodide concentration were performed using an ICl_2^- stock solution, prepared by dissolving ICl(s) in 1 mol dm^{-3} HCl. The concentration of the stock ICl_2^- solution was determined from its light absorption at 345 nm (ϵ_{max} = 243 $dm^3\ mol^{-1}\ cm^{-1}$) (12).

The effect of iodide concentration was studied using I_2/I^- solutions prepared by dissolving I_2 in solutions containing various NaI concentrations. For the Raman studies, the I_2 concentration was fixed at 0.1 mol dm^{-3}, and the I^- concentration varied between 0.2 and 2 mol dm^{-3}. Some experiments were performed with added NaCl, to study the effect of the ionic strength. For the uv–visible spectrophotometric experiments, the I_2 concentration was fixed at 0.01 mol dm^{-3} and the I^- concentration varied between 0.1 and 1 mol dm^{-3}; the NaCl concentration was adjusted to provide a constant ionic strength of 1.5 mol dm^{-3}.

For the Raman studies at lower pH (12.0 and 10.5), 0.1 mol dm^{-3} OCl^- and 0.1 mol dm^{-3} I^- solutions were used, in borax buffer for a pH value of 12, and in phosphate buffer for a pH value of 10.5. The hypochlorite stock solutions were analyzed by titration with NaI in 0.01 mol dm^{-3} H_2SO_4, using an Orion iodide-specific electrode (Model 94-53) and an Orion double-junction reference electrode (Model 90-02) as an end-point indicator. The OCl^- absorption band at 290 nm (ϵ = 350 $dm^3\ mol^{-1}\ cm^{-1}$) was also used to analyze for hypochlorite.

Raman spectroscopy

The Raman spectra were obtained using a SPEX 1403 double monochromator equipped with two 1800 grooves/mm gratings, a SPEX 1459 uv–visible illuminator, a RCA C-31034 photomultiplier tube, and photon counting electronics. The spectrometer operates under the control of a SPEX-DATAMATE microcomputer system. The frequency scale was calibrated using the emission lines of a mercury lamp and the ν_1 band of liquid carbon tetrachloride. Most of the Raman spectra were excited using the 514.5-nm radiation from a Spectra-Physics Model 165-09 argon-ion laser. Some of the spectra were also excited with the 488.0-nm radiation, but no difference in the results could be noticed. The laser power at the sample was about 900 mW and the spectra were recorded at a spectral band pass of about 6 cm^{-1}.

The kinetic runs for Raman studies were initiated either by reacting I_2/I^- solutions with an equal volume of a 2 mol dm^{-3} NaOH solution (reaction [2]) or, at pH values of 12 and 10.5, by reacting a 0.1 mol dm^{-3} OCl^- solution with an equal volume of a 0.1 mol dm^{-3} I^- solution (reaction [3]). A flow system was used to observe the Raman spectra of the transient iodine species so obtained. The two reactant solutions were driven by a double-syringe pump into a small Plexiglass mixing chamber. The reacting mixture then travelled down a length of Tygon tubing attached to a fine glass capillary, producing a stable stream of solution in the open air in the sample compartment of the Raman spectrometer. The laser beam was focussed on a point in the stream, about 3 mm from the tip of the glass capillary. Flow rates of the order of 0.1 $cm^3\ s^{-1}$ were used. The spectra of the transient iodine species could be observed at various reaction times by changing the length of the Tygon tubing. The above procedure was necessary since bands due to glass, quartz, or sapphire were found to interfere with the spectra of the transient iodine species. This technique not only removed the extraneous bands, but also enhanced the observed Raman intensities by a factor of about ten compared with those obtained using a glass capillary. The experiments were performed at room temperature (22 ± 1°C).

Each spectrum was obtained by averaging at least five scans from the 300- to 900-cm^{-1} region and subtracting the average background spectra. The background spectra were obtained with a solution containing the same concentration of I^- and NaOH, but without I_2. For the studies done at pH values of 12 and 10.5, the background spectra were obtained with 0.05 mol dm^{-3} I^- in the appropriate buffer solution. Spectra from 50 to 300 cm^{-1} (ν_1 of I_3^- and I_2) and from 2800 to 3800 cm^{-1} (ν_{OH} of H_2O) were also recorded for each run. To compensate for any variation in the optical alignment or laser power, the intensities of the various Raman bands were normalized using the water band (OH stretching vibration) as an internal standard.

Ultraviolet–visible spectrophotometry

The uv–visible spectra were recorded in digital form using a double-beam diode-array spectrophotometer (Hewlett-Packard 8450A) interfaced to a Hewlett-Packard HP-85 microcomputer via a HP-82939A serial interface. Some experiments were also performed using a Cary-17D spectrophotometer interfaced to the HP-85 microcomputer via a HP-82941A BCD interface. The temperature was maintained at 25.0 ± 0.1°C using a recirculating water bath.

Kinetic runs at low iodide concentration were initiated by injecting, with a glass syringe, 1 mL of a NaOH solution into a 1-cm pathlength spectrophotometric cell containing an equal volume of an ICl^-_2/HCl solution (reaction [4]). A NaOH/NaCl solution was used as the reference. The spectrum between 240 and 500 nm was recorded as

a function of time for at least two half-lives. Due to the heat of neutralization, the temperature rose by about 5°C at mixing time; however, the temperature returned to 25.0 ± 0.2°C within 45 s. Since the half-reaction times are of the order of 3000 s, the results were unaffected by the initial temperature transient.

Kinetic runs to study the effect of iodide concentration were initiated by injecting, with a glass syringe, a NaOH solution into an equal volume of an I_2/I^-/NaCl solution contained in a 1-cm pathlength spectrophotometric cell (reaction [2]). A NaOH/I^-/NaCl solution was used as the reference. The absorbance at 363 nm was recorded as a function of time for at least two half-lives.

Iodide-specific electrode

The iodide concentrations were measured with an iodide-specific electrode (Orion 95-53) and a double-junction reference electrode (Orion 90-02) coupled to an Orion Model 701A ionalyzer. The electrode system was calibrated with standard NaI solutions in 1 mol dm^{-3} NaOH, using a 1 mol dm^{-3} NaOH solution in the outer chamber of the double-junction reference electrode. The iodide concentration was calculated from the potential of the electrode system using the relation

$$[5] \quad E = E^0 + B \log_{10} [I^-]$$

where E^0 is a constant that depends on the electrode system, B is the Nernst constant, and E is the measured potential. The experimental value of B, obtained in the I^- concentration range 10^{-2} to 10^{-4} mol dm^{-3}, agreed well with the theoretical value of 59.2 mV at 25°C.

III. Results

Raman spectroscopy

Reaction of I_2/I^-

Figure 1 shows the Raman spectra obtained by reacting an I_2(0.1 mol dm^{-3})/I^-(0.6 mol dm^{-3}) solution with an equal volume of a 2 mol dm^{-3} NaOH solution (reaction [2]). The spectrum of the unreacted I_2/I^- solution showed Raman bands due to I_2 and I_3^-, as expected, including the ν_1 fundamental of I_2 at ~212 cm^{-1} and the ν_1 fundamental of I_3^- at 115 ± 2 cm^{-1}, as well as the overtones of I_3^- ($2\nu_1$ at 235 ± 4, $3\nu_1$ at 352 ± 2, and $4\nu_1$ at 465 ± 2 cm^{-1}) (13). These bands disappeared on mixing, as two new bands, not present in the spectra of the reactants, appeared at 430 and 560 cm^{-1} immediately after mixing. After a short time, bands at 685 and 800 cm^{-1} could also be seen. At long reaction times, the spectra showed only one band at 800 cm^{-1}. The intensity of the 430- and 560-cm^{-1} bands decreased steadily with time, although the I_{560}/I_{430} ratio, where I_ν is the Raman intensity at frequency ν, remained constant throughout the reaction. The intensity of 685-cm^{-1} band increased from zero at short reaction time, went through a maximum, and then decayed to zero at long reaction times. The intensity of the 800-cm^{-1} band, which was initially zero, increased with time but levelled off at long reaction times.

Changing the initial I^- concentration at constant I_2 and OH^- concentrations affected the relative intensity of the 430- and 560-cm^{-1} bands, as well as the time behaviour of all four bands. Although the I_{560}/I_{430} ratio was constant as a function of time for a fixed concentration of I^-, its value increased linearly with the iodide ion concentration, as can be seen from Fig. 2(*a*). Figure 2(*b*) shows that the intensity of the 430-cm^{-1} band at mixing time decreased slightly with an increase in I^- concentration, whereas the intensity of the 560-cm^{-1} band at mixing time increased markedly with an increase in I^- concentration.

Plots of the inverse of the Raman intensities at 560 and 430 cm^{-1} as a function of reaction time for various initial iodide concentrations showed linear relationships (see Fig. 3), indicating that the species responsible for the Raman scattering at 560 and 430 cm^{-1} were decaying by a second-order process. For a second-order process, the slope is k'_ν/α_ν and the intercept is $(\alpha_\nu C^0_\nu)^{-1}$. Here k'_ν, α_ν, and C^0_ν are the apparent second-order rate constant, the Raman scattering probability, and the initial concentration of the species responsible for the Raman band at frequency ν, respectively. The k'_{560}/α_{560} and k'_{430}/α_{430} values are plotted as a function of iodide concentration in Fig. 4. The k'_{560}/α_{560} ratio decreases slightly with an increase in iodide concentration, whereas k'_{430}/α_{430} increases with the iodide concentration. Thus, the rate of decay of the species responsible for the Raman scattering at 560 cm^{-1} is second order in that species and close to zero order in iodide, whereas the rate of decay of the species responsible for the Raman scattering at 430 cm^{-1} is second order in that species and close to first order in iodide. The Raman intensity data are not accurate enough to determine if an iodide-independent term is present in the latter case; however, if such a term exists, it is small.

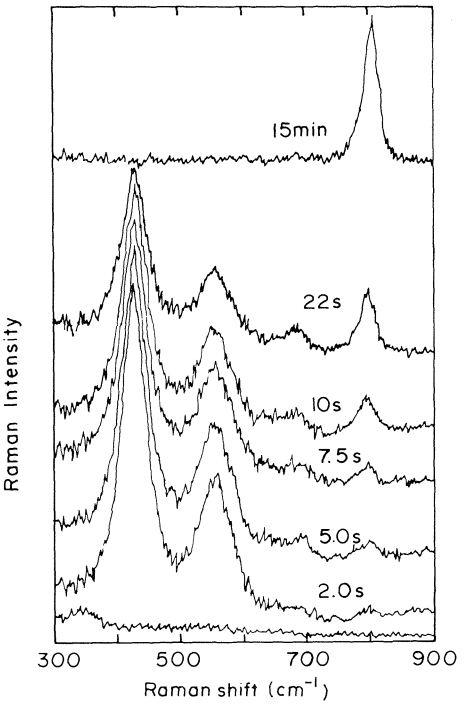

FIG. 1. Raman spectra as a function of time after reacting an I_2 (0.1 mol dm^{-3})/I^- (0.6 mol dm^{-3}) solution with an equal volume of a 2.0 mol dm^{-3} NaOH solution. The bottom spectrum is for the unreacted I_2/I^- solution.

The effect of ionic strength was studied by adding 1.4 and 0.2 mol dm^{-3} NaCl to the I_2/I^- solutions. No significant change was observed in the I_{560}/I_{430} ratio or in the time behaviour of any of the four Raman bands.

Reaction of HOCl/OCl^- with I^- at pH values of 12 and 10.5

The kinetics of iodine disproportionation were also studied at lower pH values using reaction [3]. The reactions at pH values of 12 and 10.5 were initiated by mixing 0.10 mol dm^{-3} HOCl with an equal volume of 0.10 mol dm^{-3} NaI. At a pH of 12, the results were similar to those observed from the reaction of I_2/I^- in 1 mol dm^{-3} NaOH (reaction [2]). Two bands, at 430 ± 2 and 575 ± 5 cm^{-1}, were seen immediately after mixing, and were then the only detectable spectral features. Two additional bands appeared at 685 ± 2 and 800 ± 2 cm^{-1} after a few seconds of reaction time. The intensities of the four bands as a function of time followed a pattern similar to that observed in 1.0 mol dm^{-3}

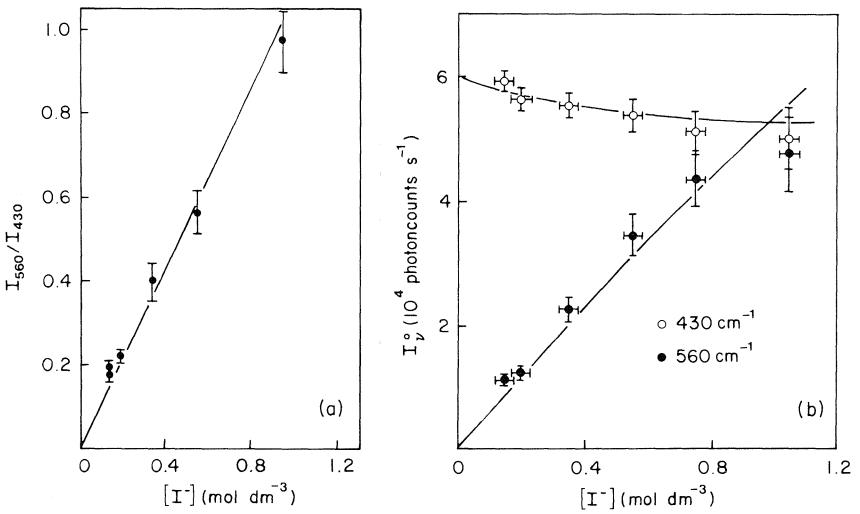

FIG. 2. (*a*) Ratio of the Raman intensity at 560 cm^{-1} to the Raman intensity at 430 cm^{-1}, and (*b*) Raman intensities at mixing time at 560 and 430 cm^{-1}, as a function of the iodide ion concentration, after reacting an I_2 (0.1 mol dm^{-3})/I^- solution with an equal volume of a 2.0 mol dm^{-3} NaOH solution. The solid lines in (*b*) are calculated results from equilibrium [7] and the determined K_7, α_{430}, and α_{560} values.

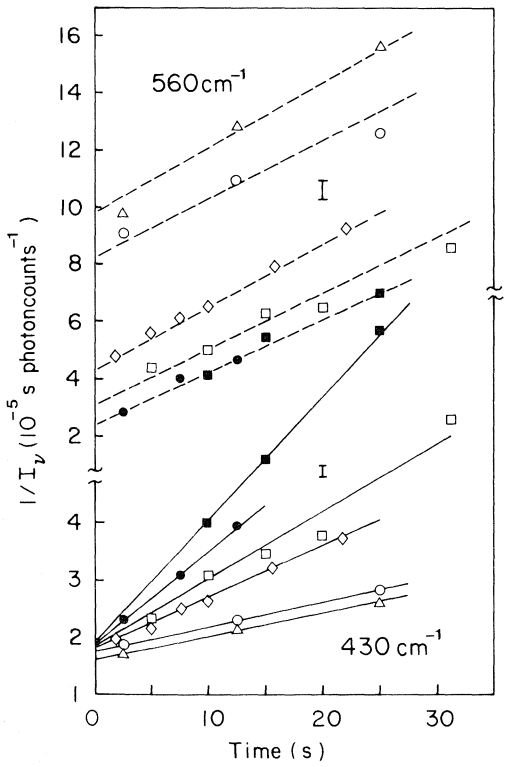

FIG. 3. Second-order plots for the decay of the Raman intensities at 560 and 430 cm^{-1} for various iodide ion concentrations. The reaction was initiated by reacting I_2 (0.1 mol dm^{-3})/I^- solutions with an equal volume of a 2.0 mol dm^{-3} NaOH solution. The I^- concentrations were △ 0.20, ○ 0.40, ◇ 0.60, □ 1.0, ● 1.4, and ■ 2.0 mol dm^{-3}.

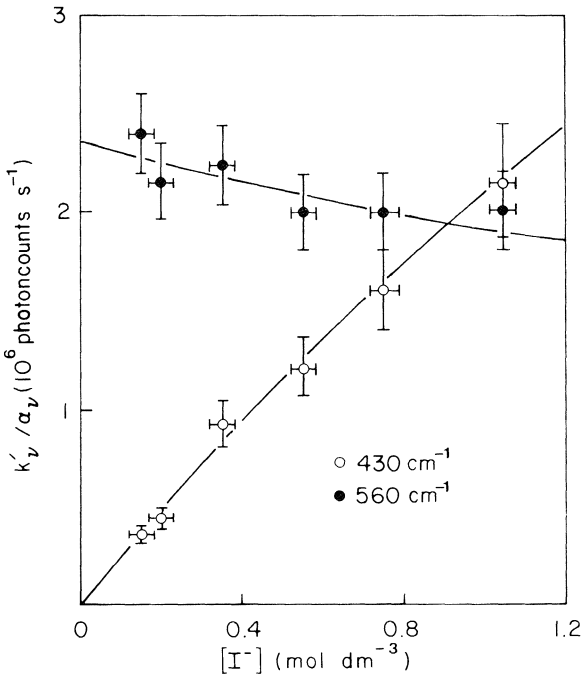

FIG. 4. Apparent second-order rate constants, divided by the Raman scattering probability, for the 430- and 560-cm^{-1} Raman bands, as a function of the iodide ion concentration.

NaOH using reaction [2]. No I_2 or I_3^- peak was observed during the course of the reaction. The differences observed at a pH of 12, compared with reaction [2] in 1 mol dm^{-3} NaOH, were (*1*) the band previously observed at 560 cm^{-1} shifted to 575 cm^{-1}, (*2*) the ratio (I_{575}/I_{430}) was smaller than that observed for all I^- concentrations studied (0.15 to 1.05 mol dm^{-3}) in 1 mol dm^{-3} NaOH, and (*3*) the reaction was faster than the reaction observed in 1 mol dm^{-3} NaOH for comparable I^- concentrations.

At a pH of 10.5, the Raman spectrum became simpler. The band at 430 ± 2 cm^{-1} was still present immediately after mixing, but no band was observed around 560 cm^{-1} or around 685 cm^{-1} during the course of the reaction. The intensity of the 430-cm^{-1} band decreased with time to zero. A band at 800 cm^{-1} appeared within a very short reaction time, increased steadily in intensity with time, and was the only band present at long reaction time. The reaction was much faster than at higher pH values. In addition to the transient iodine bands, an I_3^- band at 110 ± 2 cm^{-1} was also observed. The intensity of the I_3^- band increased from zero at mixing time, went through a maximum, then decayed back to zero at long reaction time. The maximum I_3^- concentration observed was 6.0 ± 5.0 × 10^{-3} mol dm^{-3}. It

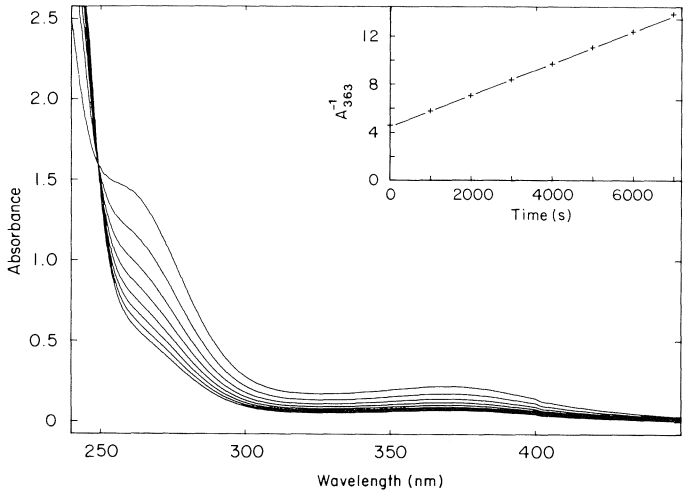

FIG. 5. Ultraviolet–visible spectra obtained as a function of time after reacting an ICl_2^- solution with a NaOH solution. The ICl_2^- and NaOH concentrations were, after mixing, 5×10^{-3} and 1 mol dm^{-3}, respectively. Arrows indicate the direction the absorbance moved with time. The insert is a second-order plot of the absorbance at 363 nm.

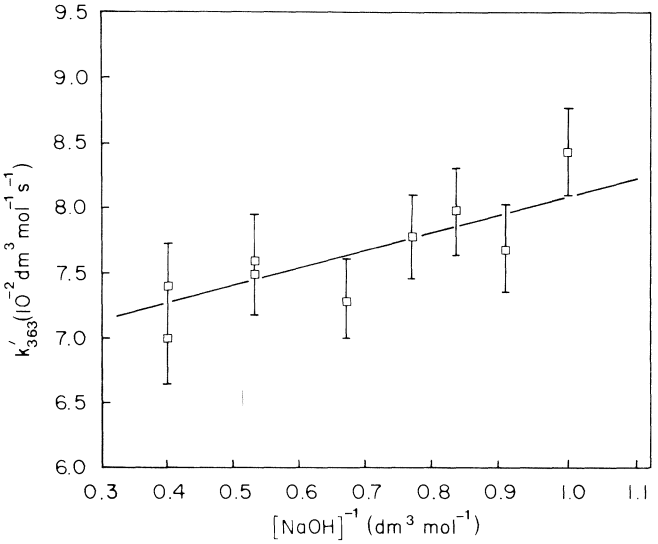

FIG. 6. Apparent second-order rate constant for the decay of IO^- at 363 nm as a function of the reciprocal NaOH concentration. Conditions were the same as those of Fig. 5, except that the NaOH concentration was varied.

was not possible to study the reaction at lower pH values using Raman spectroscopy due to the rapid increase in the rate on lowering the pH.

Ultraviolet–visible spectrophotometry

Reaction of ICl with NaOH

Figure 5 shows a series of uv–visible spectra obtained as a function of time using reaction [4]. The spectrum obtained at times close to mixing is due to the hypoiodite ion, IO^- (14). The spectra as a function of time display an isobestic point at 248 ± 1 nm with the absorbance decreasing with time at wavelengths greater than 248 nm and increasing with time at wavelengths less than 248 nm.

Plots of the inverse of the absorbance at 363 nm, A^{-1}_{363}, as a function of reaction time for various NaOH concentrations showed linear relationships, indicating that the species responsible for the light absorption at 363 nm, IO^-, is decaying by a second-order process. In that case, the slopes are k'_{363}/ϵ_{363} and the intercepts are $(\epsilon_{363}C_0)^{-1}$, where k'_{363} is the apparent second-order rate constant, ϵ_{363} is the molar absorptivity at 363 nm, and C_0 is the initial concentration of the reacting species, IO^-. From the intercepts and the known initial concentrations of IO^-, the molar absorptivity at 363 nm, ϵ_{363}, was found to be 60 ± 3 dm^3 mol^{-1} cm^{-1}, in agreement with the value reported previously (14). A plot of k'_{363} against the inverse of the NaOH concentration (see Fig. 6) or against the inverse of the square of the NaOH concentration is linear, whereas a plot of k'_{363} against the NaOH concentration displays a curvature. Thus, it appears that the rate of decay of the hypoiodite ion is second order in IO^-, and either inverse first order or inverse second order in OH^-. Iodate was found to retard the reaction both at high and at low NaOH concentration, with the reaction remaining second order. This effect has also been noted by Haimovich and Treinin (6).

Reaction of I_2/I^- with NaOH

Ultraviolet–visible spectra obtained using reaction [2] were very similar to the ones in Fig. 5 at wavelengths close to 360 nm. A plot of A^{-1}_{363} against time was also linear, giving an apparent second-order rate constant of (8.5 ± 0.8) × 10^{-2} dm^3 mol^{-1} s^{-1}, in good agreement with the value obtained above (Fig. 6) for the same NaOH concentration.

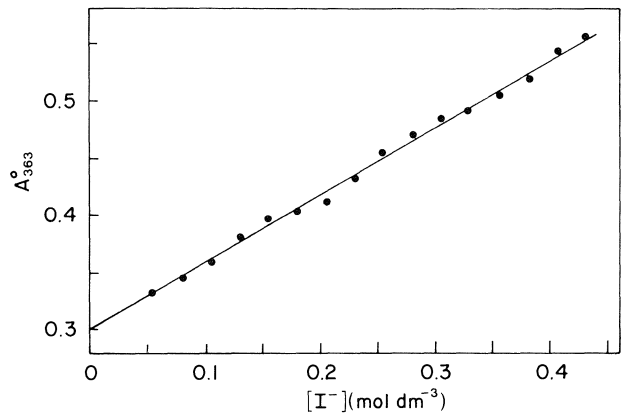

FIG. 7. Absorbance at mixing time at 363 nm as a function of the iodide ion concentration, after reacting an I_2 (5×10^{-3} mol dm^{-3})/I^- solution with an equal volume of a 2.0 mol dm^{-3} NaOH solution.

Varying the initial iodide concentration between 0.1 and 0.8 mol dm^{-3} for a fixed concentration of I_2 of 1×10^{-2} mol dm^{-3} and a fixed NaOH concentration of 1 mol dm^{-3} affected the uv–visible spectra and their time behaviour. The absorbance at 363 nm at the time of mixing, A^0_{363}, increased linearly with the iodide concentration (see Fig. 7). After an initial transient, plots of A^{-1}_{363} against time were linear (see Fig. 8), indicating that the light-absorbing species decay by a second-order process after an initial transient.

Iodide-specific electrode measurements

Reaction of ICl with NaOH

The iodide concentration, monitored using an iodide-specific electrode for reaction [4], is shown in Fig. 9(*a*). The iodide concentration increased steadily with time from zero to 3.2 ± 0.1 × 10^{-3} mol dm^{-3} at long reaction time. A comparison of the concentration of IO^- as a function of time from Fig. 5 and of the concentration of I^- as a function of time from Fig. 9(*a*) shows that the ratio $\Delta[IO^-]/\Delta[I^-]$ is −1.5 ± 0.1 for any given time interval. This confirms that the reaction is a

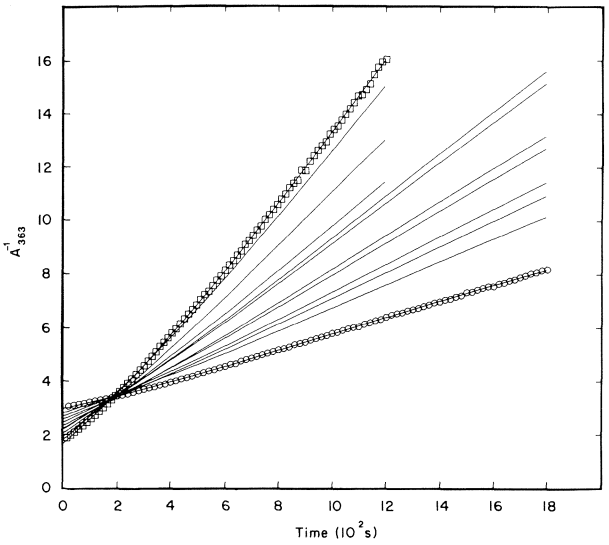

FIG. 8. Second-order plots for the decay of the absorbance at 363 nm for various iodide ion concentrations. The reaction was initiated by reacting an I_2 (5×10^{-3} mol dm^{-3})/I^- solution with an equal volume of a 2.0 mol dm^{-3} NaOH solution. For clarity, only alternate data points are indicated for the highest (□ 0.48 mol dm^{-3}) and the lowest (○ 0.05 mol dm^{-3}) I^- concentration.

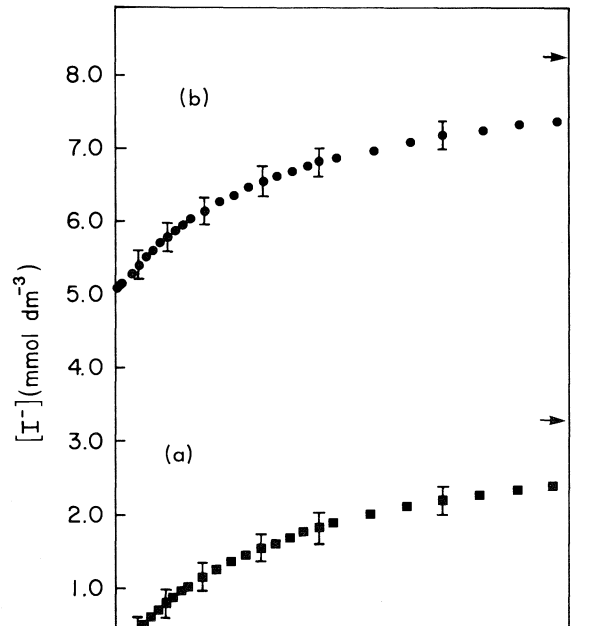

FIG. 9. Iodide ion concentration as a function of time after reacting (*a*), ■: an ICl_2^- solution with a NaOH solution. The concentrations of ICl_2^- and NaOH, after mixing, were 5×10^{-3} and 1 mol dm^{-3}, respectively, and (*b*), ●: a 10^{-2} mol dm^{-3} I_2 solution with an equal volume of a 2 mol dm^{-3} NaOH solution. Arrows indicate final concentrations after 48 h.

disproportionation and has the overall stoichiometry

[6] $3IO^- \rightarrow 2I^- + IO_3^-$

From the constancy of the above ratio and the presence of an isobestic point in the uv–visible spectra (see Fig. 5), any intermediate species besides IO^-, I^-, and IO_3^- must comprise less than 5% of the total iodine in solution at any given time.

Reaction of I_2 with NaOH

Reaction [2] was also monitored using the iodide-specific electrode (see Fig. 9(*b*)). The concentration of I^- very rapidly reached a value equal to the initial I_2 concentration and then increased slowly with time to a limiting value equal to 1.67 times the initial I_2 concentration. This is consistent the known stoichiometry of the overall reaction [1], and with the first step of the reaction being a rapid disproportionation of elemental iodine to the +1 and −1 oxidation states.

IV. Discussion

Raman spectroscopy

Kinetic analysis

The kinetic analysis of the reactions of I_2/I^- in 1 mol dm^{-3} NaOH (reaction [2]) will be considered first. The behaviour of the 685- and 800-cm^{-1} bands as a function of time, and the behaviour of the 430- and 560-cm^{-1} bands as a function of time and as a function of the iodide ion concentration, indicate that these four Raman bands belong to four different species. The band at 800 cm^{-1} can be unambiguously assigned to IO_3^- (15). The final IO_3^- concentration was determined by comparing the Raman intensities with that of standard $NaIO_3$ solutions. For the reactions of solutions 0.05 mol dm^{-3} in I_2 and from 0.1 to 1 mol dm^{-3} in I^- with 1 mol dm^{-3} NaOH, the final concentration of IO_3^- was 0.017 ± 0.002 mol dm^{-3} in all cases. This is consistent with the known stoichiometry of the overall reaction [1], the equilibrium being completely to the right at this low H^+ concentration. The assignment of the bands observed at 430, 560, and 685 cm^{-1} will be discussed later, after analysis of their time and iodide-concentration dependence.

The behaviour of the 560- and 430-cm^{-1} bands as a function of $[I^-]$, (see Fig. 2(*a*)) and as a function of time (see Fig. 3), suggests that these bands are due to two molecules participating in a rapidly established equilibrium involving I^-:

[7] $P_{430} + iI^- \overset{K_7}{\rightleftharpoons} qQ_{560}$

where P_{430} and Q_{560} represent species responsible for the 430- and 560-cm^{-1} bands. Equilibrium [7] implies that the ratio $(I_{560}\alpha_{560})^q/(I_{430}\alpha_{430}[I^-]^i)$ is a constant. Various combinations of q and i were explored. However, only a plot of I_{560}/I_{430} against the iodide concentration gives a straight line (see Fig. 2(*a*)), indicating that the coefficients q and i are unity.

The equilibrium quotient, K_7, can be calculated from the Raman data as follows. Immediately after mixing, only P_{430} and Q_{560} are present. Extrapolation of the Raman intensities at mixing time to zero $[I^-]$ (Fig. 2(*b*)) gives values of 0 and 5.9 ± 0.1 × 10^4 photon counts for I^0_{560} and I^0_{430}, respectively. Since the initial I_2 concentration is 0.05 mol dm^{-3}, α_{430} is found to be 1.2 ± 0.1 × 10^6 photon counts dm^3 mol^{-1} under the experimental conditions used here. The value of α_{560} can then be easily obtained at each $[I^-]$ from mass balance considerations. An average value of 5.5 ± 0.5 × 10^6 photon counts dm^3 mol^{-1} was found for α_{560}. From the slope of the I_{560}/I_{430} vs. $[I^-]$ plot (Fig. 2(*a*)), a value of 0.24 ± 0.07 dm^3 mol^{-1} is obtained for K_7.

The rapidly established equilibrium between P_{430} and Q_{560} has to be considered in the calculation of the rate constants. Since the mixture is ultimately converted to iodate via a second-order process, the rate law can be written as

[8] $$-\frac{d([P_{430}] + [Q_{560}])}{dt} = k_{obs}([P_{430}] + [Q_{560}])^2$$

[9] $$k_{obs} = \sum_i k_i f_i^2$$

TABLE 1. Observed rate constants, k_{obs}, determined from the values of k'_ν obtained using Raman spectroscopy

$[I^-]$/mol dm^{-3}	k_{obs} from k'_{430}	k_{obs} from k'_{560}
0.15	0.41	0.46
0.20	0.52	0.54
0.35	1.02	0.96
0.55	1.27	1.28
0.75	1.63	1.68
1.05	2.06	2.21

where k_i is the actual rate constant for the reaction of the species i and f_i is the fraction of the total iodine concentration for each of the reactive species. In that case, k_{obs} should be related to the apparent rate constants, k'_ν, presented in Fig. 4, by

$$[10] \quad k_{obs} = k'_{560}\left(\frac{K_7[I^-]}{1 + K_7[I^-]}\right)$$

$$[11] \quad k_{obs} = k'_{430}\left(\frac{1}{1 + K_7[I^-]}\right)$$

The k_{obs} values determined from both k'_{560} and k'_{430} values are given in Table 1 as a function of $[I^-]$, and are in good agreement. The k_{obs} increases with an increase in $[I^-]$. These observed rate constants can be used to determine the actual rate constants, k_i, from eq. [9]. If P_{430} was the only reactive species, k_{obs} would be proportional to

$$\left(\frac{1}{1 + K_7[I^-]}\right)^2$$

since $f_{P_{430}}$ is given by

$$\left(\frac{1}{1 + K_7[I^-]}\right)$$

If Q_{560} was the only reactive species, then k_{obs} would be proportional to

$$\left(\frac{K_7[I^-]}{1 + K_7[I^-]}\right)^2$$

since $f_{P_{430}}$ is given by

$$\left(\frac{K_7[I^-]}{1 + K_7[I^-]}\right)$$

These were not found to be the case. However, as can be seen from Fig. 10, a linear relationship is obtained for

$$[12] \quad k_{obs} = \frac{k_{PQ}K_7[I^-]}{(1 + K_7[I^-])^2}$$

indicating that P_{430} and Q_{560} are reacting together according to the rate equation

$$[13] \quad \frac{d}{dt}([P_{430}] + [Q_{560}]) = -k_{PQ}[P_{430}][Q_{560}]$$

with k_{PQ} having a value of 13 ± 1 dm^3 mol^{-1} s^{-1}, which was obtained from the slope in Fig. 10.

The Raman band at 685 cm^{-1} displays a kinetic behaviour typical of a species being formed in an earlier reaction step and destroyed in a subsequent step. This species, R_{685}, is likely the product of the reaction between P_{430} and Q_{560} discussed above, and can itself react to produce iodate. If R_{685} reacts with itself

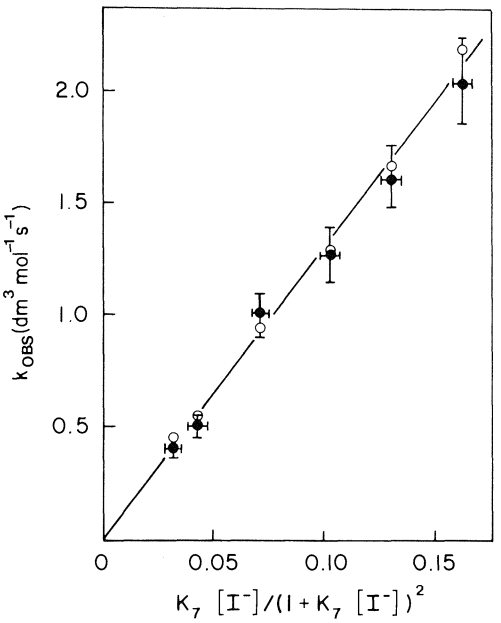

FIG. 10. Correlation of the observed rate constants with the iodide ion concentration for the Raman results in 1 mol dm^{-3} NaOH solutions.

in either a first-order or a second-order reaction, then the final IO_3^- concentration should be $(1/2)([P_{430}]^0 + [Q_{560}]^0)$ or $(1/4)([P_{430}]^0 + [Q_{560}]^0)$, respectively, where $([P_{430}]^0 + [Q_{560}]^0) = 0.05$ mol dm^{-3}. However, the final IO_3^- concentration was 1.7 ± 0.2 × 10^{-2} mol dm^{-3} in all cases, which is $(1/3)([P_{430}]^0 + [Q_{560}]^0)$. If R_{685} reacts with P_{430} and/or Q_{560} to form iodate, then the final concentration of iodate would be 1.67 × 10^{-2} mol dm^{-3}, which is in agreement with the experimental results. The mass balance at any given time after reacting the I_2/I^- solutions with the OH^- solution would then be

$$[14] \quad [P_{430}]_t + [Q_{560}]_t + 2[R_{685}]_t + 3[IO_3^-]_t = [I_2]_{t=0} = 0.05 \text{ mol dm}^{-3}$$

The observed Raman intensities of the four species at any given reaction time can be used to calculate α_{685} from the above mass balance equation and the known values of α_{430} and α_{560}. If the proposed mechanism is correct, then α_{685} obtained at any given reaction time and for any given $[I^-]$ should be constant. The value of α_{685} was found to be in the range (6.6 to 6.9) × 10^5 photon counts dm^3 mol^{-1}, which supports the proposed mechanism. The possibility of forming more than one molecule of R_{685} by reacting P_{430} and Q_{560} can also be rejected on the basis of mass balance.

The Raman results obtained at lower pH values using reaction [3] cannot be directly compared with the results obtained from reaction [2] in 1.0 mol dm^{-3} NaOH. In reaction [3], the I^- concentration is negligible at the time of mixing, but increases as the reaction proceeds, whereas the iodide concentration in the reaction of I_2/I^- in 1 mol dm^{-3} NaOH is nearly constant during the course of the reaction, for a given I_2/I^- solution.

Second-order plots for I_{430} at pH values of 12 and 10.5 are compared with the data obtained for the reaction of 0.05 mol dm^{-3} I_2/0.1 mol dm^{-3} I^- with 1 mol dm^{-3} NaOH in Fig. 11. The figure shows curvatures for pH values of 12 and 10.5, indicating that the iodide concentration is not constant during the reaction. Extrapolating the data to time zero at both

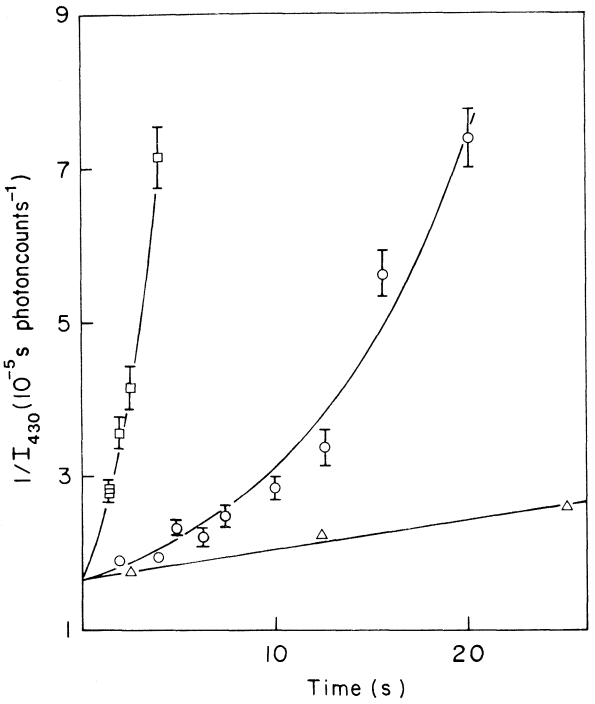

FIG. 11. Second-order plots for the decay of the Raman intensity at 430 cm^{-1} at pH values of 10.5 (□) and 12.0 (○), reaction [3]; and by reacting an I_2 (0.1 mol dm^{-3})/I^- (0.2 mol dm^{-3}) solution with an equal volume of a 2 mol dm^{-3} NaOH solution (△), reaction [2].

pH values gives an I^0_{430} value of $6.1 \pm 0.2 \times 10^4$ photon counts. This corresponds to $[P_{430}]^0 = 0.051 \pm 0.002$ mol dm^{-3} using the α_{430} determined from the data observed using reaction [2]. This indicates that the band observed at 430 cm^{-1} at pH values of 12 and 10.5 belongs to the same species responsible for the 430-cm^{-1} band observed using reaction [2] in 1 mol dm^{-3} NaOH, and that the iodide concentration at the time of mixing is negligible, as expected from reaction [3].

Assignment of Raman bands

The assignment of the band observed at 800 cm^{-1} to the symmetric stretching vibration of IO_3^- (symmetry A_1) is quite obvious, as stated earlier. We assign the band observed at 685 cm^{-1} to the symmetric stretching vibration of IO_2^-. We were unable to find any report in the literature on the Raman spectrum of IO_2^-. However, the Raman spectra of the corresponding chlorine and bromine compounds have been reported. The totally symmetric stretching vibration in ClO_2^- has been observed at 786 cm^{-1} by Tasaka and Toja (16). For BrO_2^-, this vibration has been assigned to the Raman band seen at 710 cm^{-1} by Sombret and Wallart (17) and Evans and Lo (18).

The assignment of the remaining two bands at 560 and 430 cm^{-1} is not so straightforward. These bands are most likely due to IO^- and I_2O^{2-} (or I_2OH^-). In 1 mol dm^{-3} NaOH solution, the equilibrium, $HOI \rightleftharpoons H^+ + IO^-$, is completely to the right. Thus, we will only consider the IO^- contribution in the following analysis. We first attempted to assign the 560-cm^{-1} band to IO^-, based on the literature assignment for the I—O stretch in HOI (the parent acid for the IO^- ion) at 572 cm^{-1} (19–22). Here it should be mentioned that the vibrational (infrared) spectrum for HOI has been reported only for molecules isolated and produced in solid N_2 or Ar matrices. The change in the I—O vibration frequency from 572 to 560 cm^{-1}, in going from the matrix isolated acid state (HOI) to the solution state (IO^-) also seemed typical of that observed for similar halogen systems: ν_{XO} in HOCl and ClO^- is 729 (23) and 713 cm^{-1} (16), and in HOBr and BrO^-, it is 626 (23) and 620 cm^{-1} (17), respectively. Although the assignment of the 560-cm^{-1} band to IO^- stretch would be consistent with the literature assignment for HOI, it makes it very difficult to explain the $[I^-]$ concentration dependence of relative Raman intensities at 560 and 430 cm^{-1} described above, as well as the uv–visible data and ion-specific electrode data. We were unable to arrive at a plausible mechanism that would assign the 560-cm^{-1} band to IO^- and the 430-cm^{-1} band to I_2O^{2-} (or I_2OH^-) and still explain the fact that the I_{560}/I_{430} ratio increases with an increase in iodide ion concentration. Thus, we have assigned the 430-cm^{-1} band to the IO^- stretching vibration and the 560-cm^{-1} band to the I—O stretching vibration in I_2O^{2-} (or I_2OH^-), to explain the intensity dependence on $[I^-]$. The assignment of the Raman band observed at 430 cm^{-1} to IO^- is also supported by the Raman spectra observed using reaction [3]. The reaction of HOCl with I^- is known to produce IO^- (14) and, as there is no excess I^- ions at short reaction times, the observed band at 430 cm^{-1} should be assigned to IO^- rather than I_2O^{2-} (or I_2OH^-).

The assignment suggested above implies that the I—O bond is much weaker for IO^- in aqueous alkaline solution than for HOI in inert matrices. One plausible explanation for this may be found in the description of similar systems by Pimentel (24). He suggested that species isoelectronic with X^- (i.e., OH^-) can combine with groups of electronic character similar to X_2 (i.e., IO^-), where X represents a halogen. According to the above, IO^- in alkaline solution may exist as

$$[15] \quad HO^- + IO^- \rightleftharpoons [HO\text{---}IO]^{2-}$$

The assignment of the I—O stretching vibration to a higher frequency for I_2O^{2-} than that for IO^- may seem unusual at first glance, yet it is not without precedent. The Cl—O stretching vibration has been assigned to a higher frequency for ClClO (962 cm^{-1}) and FClO (1038 cm^{-1}) than for ClO (850 cm^{-1}) by Chi and Andrews (25). These authors attributed the increase in the "Cl—O bond strength" in going from ClO to ClClO or FClO to the removal of the antibonding electron density from ClO, leaving a stronger Cl—O bond. A similar effect can also explain the increase in the I—O stretching vibration frequency in going from IO^- to $[IIO]^{2-}$. In solutions containing iodide ions, I^- may combine with IO^- ions to form I_2OH^-:

$$[16] \quad I^- + IO^- \rightarrow [I\text{---}IO]^{2-} \xrightarrow{H^+} [I_2OH]^-$$

The I_2OH^- would be a linear molecule, in agreement with the simple molecular orbital treatment of the bonding in the trihalide ions by Pimentel (24), which led him to predict that the hydroxide ion should be able to combine with I_2 to form I_2OH^-. Anbar and Taube (26) also proposed that Cl_2OH^- is a possible intermediate in the exchange reaction between Cl^- and HOCl, and suggested that its structure is analogous to that of Br_3^-.

The 560-cm^{-1} band shifted to 575 cm^{-1} at lower pH. We believe that the 560-cm^{-1} band is due to unprotonated I_2O^{2-}, and that the 575-cm^{-1} band is due to partially protonated I_2OH^-. This increase in frequency is consistent with a slight increase in I—O bond strength due to an overall decrease in electron density upon protonation.

Reaction mechanism

With the assignment of IO^-, I_2O^{2-} (or I_2OH^-), and IO_2^-

given to P_{430}, Q_{560}, and R_{685}, respectively, a mechanism can be proposed for the overall disproportionation of iodine in basic solutions. The rate-determining step clearly is the disproportionation of the +1 oxidation-state species (IO^-, I_2OH^-) to iodate and iodide, since the Raman bands due to I_2 and I_3^- disappear instantaneously upon mixing with NaOH. The following mechanism is compatible with all of the Raman results and the overall stoichiometry of reaction [1].

$$[2] \quad I_2 + OH^- \overset{K_2}{\rightleftharpoons} IO^- + I^- + H^+ \qquad K_2 = 1.37 \times 10^{-9}\ dm^3\ mol^{-1}\ (28)$$

$$[17] \quad I_2 + I^- \overset{K_{17}}{\rightleftharpoons} I_3^- \qquad K_{17} = 746\ dm^3\ mol^{-1}\ (29)$$

$$[18] \quad IO^- + I^- + H_2O \overset{K_{18}}{\rightleftharpoons} I_2OH^- + OH^-$$

$$[19] \quad IO^-/HOI + IO^- \xrightarrow{k_{19}} IO_2^- + I^- / + H^+$$

$$[20] \quad IO^- + I_2OH^- \xrightarrow{k_{20}} IO_2^- + 2I^- + H^+$$

$$[21] \quad IO_2^- + IO^- \xrightarrow{k_{21}} IO_3^- + I^-$$

$$[22] \quad IO_2^- + I_2OH^- \xrightarrow{k_{22}} IO_3^- + 2I^- + H^+$$

where equilibria [2], [17], and [18] are established rapidly. The equilibrium [18] is equivalent to equilibrium [7], and thus has a value of 0.24 ± 0.07 $dm^3\ mol^{-1}$. Equilibrium [2] is almost completely to the right at this high pH; thus, the concentrations of I_2 and I_3^- are negligible after mixing with NaOH. Reaction [19] is being considered here for completeness, since it was too slow to be observed in the Raman study (i.e., $k_{19} < k_{20}$). The rate constants, k_{21} and/or k_{22}, are larger than k_{19} and k_{20}. If both k_{21} and k_{22} were smaller than k_{19} and/or k_{20}, then the second-order plots shown in Fig. 4 would display curvature, and a substantial amount of IO_2^- (R_{685}) would accumulate in solution. On the other hand, if k_{21} and/or k_{22} were much larger than k_{19} and k_{20}, virtually no R_{685} would accumulate and k_{obs} would be given by $3k_{19}$ or $3k_{20}$. Since some R_{685} accumulates, the truth is somewhere between these two extremes.

Although we did not obtain enough data at pH 12 and 10.5 to attempt a detailed analysis, some qualitative comments can be made. The reaction was faster at lower pH, which can be explained if the reaction of HOI with HOI or IO^- is faster than the reaction of IO^- with IO^-. Also, the I_2OH^- responsible for the Raman band at 560 cm^{-1} was not observed at a pH of 10.5. At this low pH, equilibrium [2] is not completely to the right and a small amount of I_2 is present, which will react with I^- to form I_3^- according to equilibrium [17]. The values of K_{17} and K_{18} are such that only a small amount of I_2OH^- is expected at this low pH.

Ultraviolet–visible spectrophotometry and iodide-specific electrode measurements

Reaction of ICl with NaOH

The uv–visible and iodide-specific electrode results obtained at low initial iodide concentration for reaction [4] indicate that IO^-, formed by the rapid hydrolysis of ICl_2^-, disproportionates to iodide and iodate at a rate that is second-order in [IO^-] and either inverse first-order or inverse second-order in [OH^-]. These results suggest that both HOI and IO^- participate in the reaction. Since IO^- and HOI are in rapid acid–base equilibrium

$$[23] \quad HOI \overset{K_{23}}{\rightleftharpoons} IO^- + H^+$$

the general rate law for the disproportionation would be

$$[24] \quad -\frac{d[IO^- + HOI]}{dt} = k_{24a}[HOI]^2 + k_{24b}[HOI][IO^-] + k_{24c}[IO^-]^2$$

This can be rewritten in terms of IO^- only as

$$[25] \quad -\frac{d[IO^-]}{dt} = \left[\frac{k_{24a}\frac{[H^+]^2}{K_{23}} + k_{24b}\frac{[H^+]}{K_{23}} + k_{24c}}{1 + \frac{[H^+]}{K_{23}}}\right][IO^-]^2 = k_{obs}[IO^-]^2$$

The rate constant k_{24a} is known to be approximately 200 $dm^3\ mol^{-1}\ s^{-1}$ (5). The contribution from the term in $[HOI]^2$ would thus be quite small at the [OH^-] concentrations used (1 to 2.5 mol dm^{-3}) and can be neglected. The value of k_{24b} can be obtained from the slope of the plot of k_{obs} against $[NaOH]^{-1}$ (Fig. 6) and is 40 ± 7 $dm^3\ mol^{-1}\ s^{-1}$. Not much can be said about the value of k_{24c} except that, from Fig. 6, it is estimated to be less than $7.2 \times 10^{-2}\ dm^3\ mol^{-1}\ s^{-1}$.

Reaction of I_2/I^- with NaOH

The iodide-specific electrode and uv–visible spectroscopy results for reaction [2] are consistent with a rapid hydrolysis and disproportionation of elemental iodine to the +1 and −1 oxidation states, followed by a slower further disproportionation to iodide and iodate with the overall stoichiometry as shown in eq. [6].

For mixtures obtained by reacting I_2/I^- solutions with a NaOH solution, the absorbance at 363 nm at mixing time, A^0_{363}, increases with the initial concentration of iodide, in agreement with the observations of Sigalla (27) and Chia (28). This is likely due to the formation of other iodine compounds besides IO^-, probably I_3^- formed through equilibria [2] and [17]. However, the equilibrium amounts of I_3^- cannot account entirely for the increase in absorbance at mixing time with the iodide ion concentration. An additional light-absorbing species is required.

Both Sigalla (27) and Chia (28) have proposed the involvement of equilibrium [18] in solutions containing hypoiodite and iodide. Since I_2 and I^- have no appreciable light absorption at 363 nm, from equilibria [2], [17], and [18], the absorbance at 363 nm at mixing time would be given by

$$[26] \quad A^0_{363} = \frac{C_0(\epsilon^{IO^-}_{363} + \epsilon^{I_2OH^-}_{363} K_{18}[I^-]/[OH^-] + \epsilon^{I_3^-}_{363}[I^-]^2 K_{17}/K_2[OH^-]^2)}{(1 + K_{18}[I^-]/[OH^-] + [I^-]^2 K_{17}/K_2[OH^-]^2 + [I^-]/K_2[OH^-]^2)}$$

where C_0 is the initial iodine concentration. Here, $\epsilon^{OI^-}_{363}$ is the specific absorptivity for IO^- at 363 nm and has been determined above as being equal to 60 $mol^{-1}\ dm^3\ cm^{-1}$. The specific absorptivity for I_3^- at 363 nm is 19 000 $mol^{-1}\ dm^3\ cm^{-1}$ (29).

A non-linear least-squares fit to eq. [26] was used to determine $\epsilon^{I_2OH^-}_{363}$ and K_{18} from 17 measurements of A^0_{363} as a function of I^- concentration, covering the range from 0.05 mol dm^{-3} to 0.5 mol dm^{-3}. Values of 750 ± 50 $mol^{-1}\ dm^3\ cm^{-1}$ and

$0.15 \pm 0.01\ dm^3\ mol^{-1}$ were obtained, respectively, and could represent the data with an average deviation of 0.6% and a maximum deviation of 1%. Inclusion of additional species having the general formula $H_zO_xI_y$ did not significantly improve the fit, and was deemed unnecessary. The equilibrium constant value agrees well with the K_{18} value calculated from the Raman results.

Although hypoiodite was the predominant form of iodine in these solutions, the equilibria with I_2, I_3^-, and I_2OH^- have to be considered in the calculation of the rate constants. The rate for each experiment was found to obey the following relation after an initial transient:

$$[27] \quad -\frac{d(\Sigma[I])}{dt} = k_{obs}(\Sigma[I])^2$$

where $\Sigma[I]$ is $([I_2] + [I_3^-] + [IO^-] + [I_2OH^-])$, and can be calculated from the absorbance at 363 nm as a function of time using the relation

$$[28] \quad \Sigma[I] = A^t_{363}C_0/A^0_{363}$$

The values of k_{obs} were obtained from plots of the inverse of $\Sigma[I]$ vs. time, and are shown in Fig. 12(*a*). It becomes evident that at 25°C, in 1 mol dm^{-3} NaOH solution, k_{obs} can be written as

$$[29] \quad k_{obs} = k'_{29} + k''_{29}[I^-]$$

with $k'_{29} = 0.05\ dm^3\ mol^{-1}\ s^{-1}$ and $k''_{29} = 2.60\ dm^3\ mol^{-1}\ s^{-1}$.

Since at zero iodide ion concentration only IO^-, and very small amounts of I_3^- and I_2, are present, the first term, k'_{29}, should be equivalent to $k_{24c} + k_{24b}[H^+]/K_{23}$, as can be seen from eq. [25]. The second term would be expected to be composed of a combination of the four equilibrium iodine species, as given in eq. [9] in generalized form. If IO^- was the only reactive species, then the observed rate constant would decrease with an increase in $[I^-]$. If I_2OH^- was the only reactive species, then k_{obs} would be given by

$$[30] \quad k_{obs} = k'_{29} + k_{(I_2OH^-)^2}f^2_{I_2OH^-} = k'_{29} + k_{(I_2OH^-)^2}\left[\frac{1}{1 + [OH^-]/K_{18}[I^-] + K_{17}[I^-][H^+]/K_{18}K_2 + [H^+]/K_{18}K_2}\right]^2$$

where $f_{I_2OH^-}$ can be determined from equilibria [2], [17], and [18]. The terms $K_{17}[I^-][H^+]/K_{18}K_2$ and $[H^+]/K_{18}K_2$ are small. Therefore, $(k_{obs} - k'_{29})$ would be proportional to

$$\left(\frac{1}{1 + 1/K_{18}[I^-]}\right)^2$$

This was not found to be the case. Since neither of these attempts to correlate the data with a single reactive species was successful, various combinations of I_3^-, I_2, IO^-, and I_2OH^- were considered.

Assuming that IO^- and I_2OH^- are reacting together, a linear correlation was obtained for

$$[31] \quad k_{obs} = \frac{k_{IO^-,I_2OH^-}K_{18}[I^-]}{(1 + K_{18}[I^-])^2} + k'$$

as shown in Fig. 12(*b*). From the slope of the line in this figure and the K_{18} values determined above, k_{IO^-,I_2OH^-} is equal to $19.5 \pm 0.05\ dm^3\ mol^{-1}\ s^{-1}$. The rate law can be rewritten as

$$[32] \quad -\frac{d}{dt}([I_2] + [I_3^-] + [IO^-] + [I_2OH^-]) = 0.05[IO^-]^2 + 19.5[IO^-][I_2OH^-]$$

and is valid for 25°C and in 1 mol dm^{-3} NaOH.

Both the rate expression and the value of k_{IO^-,I_2OH^-} are entirely compatible with the mechanism proposed to explain the Raman results (eqs. [2], [17]–[22]). The iodide-independent term is quite small and was not detectable in the Raman experiments, since relatively high concentrations of I^- were required to dissolve a sufficient amount of I_2. According to the uv–visible results, k_{21} and/or k_{22} is larger than k_{19} and k_{20} in eqs. [19]–[22], but not immensely so. If k_{21} or k_{22} was much larger than k_{20}, then the plots of $(\Sigma[I])^{-1}$ against time would be linear with slopes of $3k_{19}[I^-]K_{18}$. Since a curvature is observed at short reaction times, k_{21} and/or k_{22} are somewhat larger than k_{19}.

The differential equations resulting from this mechanism were integrated numerically, using a modified Gear algorithm (30). The values of k_{20}, k_{21}, and k_{22} were obtained by using a non-linear least-squares routine incorporating Marquat's algorithm (31). The objective function was the absorbance of the solutions at 363 nm as a function of time and iodide concentration:

$$[33] \quad A^t_{363} = \epsilon^{IO^-}_{363}[IO^-]_t + \epsilon^{I_2OH^-}_{363}[I_2OH^-]_t + \epsilon^{I_3^-}_{363}[I_3^-]_t$$

where the various concentrations as a function of time were from the numerical integration, assuming that equilibrium between I_3^-, I_2, IO^-, and I_2OH^- is achieved rapidly. Values of 6.0 ± 0.2, 0.5 ± 0.1, and $26 \pm 2\ dm^3\ mol^{-1}\ s^{-1}$ were obtained for k_{20}, k_{21}, and k_{22}, respectively.

Thus, the Raman and the uv–visible spectrophotometric results can be interpreted in terms of a common mechanism. The Raman results provide an unambiguous identification of the species involved, whereas the uv–visible results provide accurate values of the rate constants. It appears that, if the concentration of iodide ions is above 5×10^{-2} mol dm^{-3}, in 1 mol dm^{-3} NaOH, the disproportionation of hypoiodite occurs preferentially through I_2OH^-.

Comparison with the literature

The formation of a weak complex between IO^- and I^- has been proposed in the past by Sigalla (27) and also by Chia (28) to explain the dependence of the uv–visible absorbance of IO^- solutions on the concentration of iodide ions. Chia reported a value of 0.13 for K_{18} at 25°C, whereas Sigalla reported a value of 3×10^{-2} for K_{18} at 25°C, after correction for ionic strength effects. The origin of the discrepancy is unclear. In Chia's experiments, IO^- and I_2OH^- were the dominant species in solution. Due to the large specific absorptivity of I_3^-, these three species contributed to the absorbance in similar proportions. Thus, Chia observed a larger than expected increase in absorbance with an increase in iodide ion concentration. In Sigalla's experiments, I_3^-, IO^-, and I_2OH^- were present in similar proportions. Due to the large specific absorptivity of I_3^-, this species was the only one contributing significantly to the absorbance, and Sigalla observed a lower than expected

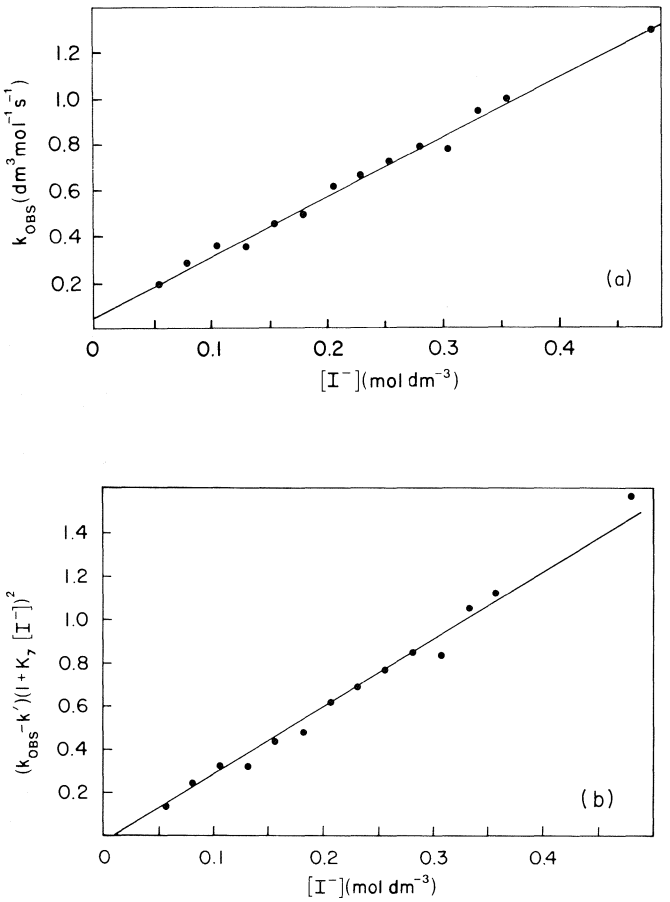

FIG. 12. For the reaction of Fig. 8, (*a*) observed rate constants for the decay of A_{363} as a function of [I^-], and (*b*) correlation of the rate constants with [I^-].

increase in absorbance as the iodide ion concentration was increased. Our experimental conditions were similar to Chia's and our value for K_{18} is in reasonable agreement with hers.

Li and White (8) have obtained, using a titration technique, the following rate law for the decomposition of hypoiodite in basic solutions:

$$[34] \quad -\frac{d[IO^-]}{dt} = k_r[IO^-]^2 + k_s\frac{[IO^-]^2[I^-]}{[OH^-]}$$

with k_r having a value of 5×10^{-2} dm^3 mol^{-1} s^{-1} and k_s having a value of 2.18 dm^3 mol^{-1} s^{-1}. Forster (11) and Skrabal (10) also concluded, using a titration technique, that the rate of reaction at high concentrations of OH^- and I^- ions is proportional to the concentration of IO^- and I^- ions, although they failed to detect the small I^--independent term. Forster (11) found a value of 1.2 for the rate constant k_s, whereas Skrabal (10) reported a value of 1.45. The second term of our rate law and our k''_{29} value of 2.60 dm^3 mol^{-1} s^{-1} agree with the results of these earlier studies.

In later experiments, in the presence of silver oxide and silver iodide, Skrabal and Hohlbaum (9) obtained evidence that the first term of the rate law at 25°C is

$$[35] \quad -\frac{d[IO^-]}{dt} = 0.03\frac{[IO^-]^2}{[OH^-]}$$

although Li and White (8) argued against a reciprocal [OH^-] dependence. Our results at low [I^-], obtained using reaction

TABLE 2. Rate constants for the disproportionation of the hypohalites at 25°C, in dm^3 mol^{-1} s^{-1}

X	k		X^- effect
	$XO^- + XO^-$	$XO^- + XO_2^-$	
Cl[a]	1.1×10^{-8}	1.8×10^{-6}	None
Br[b]	1.0×10^{-6}	1.5×10^{-5}	Slight positive
I[c]	$<7 \times 10^{-2}$	0.5	Marked positive

[a]Value from ref. 32.
[b]Value from ref. 33.
[c]Value from this work.

[2], indicate that the iodide-independent part of the rate law consists of two terms:

$$[36] \quad -\frac{d[IO^-]}{dt} = a[IO^-]^2 + b\frac{[IO^-]^2}{[OH^-]}$$

where a is less than 7×10^{-2} dm^3 mol^{-1} s^{-1} and b is 2×10^{-2} dm^3 mol^{-1} s^{-1}. This seems to reconcile the Li and White (8) and Skrabal and Hohlbaum (9) data.

Haimovich and Treinin (6) have also studied the decomposition of hypoiodite in alkaline solutions at low iodide ion concentrations. They reported a value of $(4.0 \pm 0.4) \times 10^{-2}$ dm^3 mol^{-1} s^{-1} for the rate constant in 4 mol dm^{-3} NaOH, and a value of $(2.7 \pm 0.2) \times 10^{-2}$ dm^3 mol^{-1} s^{-1} in 6 mol dm^{-3} NaOH, which leads to a value of 2×10^{-2} dm^3 mol^{-1} s^{-1} for the $[OH^-]^{-1}$-dependent term, in good agreement with our b value. They also noted that, for I^- concentrations less than 8×10^{-2} mol dm^{-3}, no effect on the rate could be detected and that, on further raising [I^-], the rate increased. This is in qualitative agreement with our observations.

The mechanism for the conversion of hypochlorite or hypobromite to chlorate or bromate ions is well known (32, 33). The reactions consist of two steps:

$$[37] \quad XO^- + XO^- \xrightarrow{\text{slow}} XO_2^- + X^-$$

$$[38] \quad XO^- + XO_2^- \xrightarrow{\text{fast}} XO_3^- + X^-$$

with the formation of the halite ion being the rate-determining step and the subsequent formation of halate ion being rapid. The geometry of the activated complex for the first step is likely

$$[39] \quad \left[\begin{matrix} X\ldots O\text{—}X \\ | \\ O \end{matrix}\right]^{2-} \rightarrow \left[\begin{matrix} X\text{—}O \\ | \\ O \end{matrix}\right]^{-} + X^-$$

The first step is, thus, a nucleophilic displacement of one base (X^-) by another (XO^-).

Using radioactive chlorine, Anbar and Taube (26) have demonstrated that, at least in the chlorine case, the second step involves the formation of a non-symmetrical intermediate in which the chlorine atoms remain distinct, such as

$$[40] \quad \left[\begin{matrix} Cl\text{—}O\ldots Cl\text{—}O \\ \quad\quad\quad\ | \\ \quad\quad\quad O \end{matrix}\right]^{2-} \rightarrow Cl^- + ClO_3^-$$

Presumably, this is also valid for the bromine system.

Our results for the iodine system indicate that the first step of iodine(I) disproportionation at high hydroxide and iodide ion concentrations consists of two parallel reactions: a slow reaction between IO^- (or HOI) and IO^-, and a faster reaction between IO^- (or HOI) and I_2OH^-. The slower path presumably is similar to the chlorine and bromine cases described above (reaction

[39]). The reason that the other path is more rapid can be readily explained. We suggest that IO^- in aqueous solution may exist as a loosely bound complex $[HO....IO]^{2-}$ with a weakened I—O bond, while the I—O bond is strengthened in I_2OH^-. Therefore, if the activated complex and the nucleophilic displacement occur as follows,

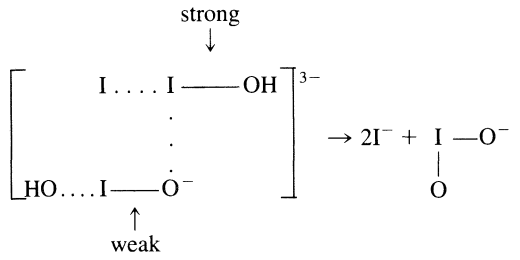

[41]

the activated complex would be more stable than that formed by HOI and $[HO....IO]^{2-}$. The second step in the disproportionation of iodine(I) also consists of two parallel reactions: a slow reaction between IO^- (or HOI) and IO_2^-, and a faster reaction between I_2OH^- and IO_2^-. The slow path likely proceeds by a mechanism similar to the chlorine system (reaction [40]). The other path is more rapid, presumably for the same reasons as in the first step.

A comparison of the rates for the slower paths with the analogous bromine and chlorine reactions can be found in Table 2. The rates increase on going from hypochlorite to hypoiodite. This trend is to be expected since the electronegativity of the halogen is in the order Cl > Br > I. This would cause the partial positive charge on the halogen to increase on going from ClO^- to IO^-, favouring electrostatic interactions. However, the increase on going from the Br to I system is too large to be explained by electrostatic interaction alone. We believe that the weakened O—I bond in $[HO....IO]^{2-}$ favours a more stable activated complex for the reaction of IO^- with IO^- and IO^- and IO_2^-, thus increasing the rate even further.

Chloride has no effect on the rate of disproportionation of hypochlorite. Bromide slightly increases the rate of disproportionation of hypobromite, whereas iodide has a marked accelerating effect on the disproportionation of hypoiodite. Our study indicates that the pronounced effect in the case of hypoiodite comes from the formation of the reactive species I_2OH^-, which is expected to have a structure similar to I_3^-. Since the order of stability for the trihalides is $I_3^- > Br_3^- > Cl_3^-$ (34), the relative effect of the halides on the hypohalites disproportionation can be explained if the X_2OH^- species follow the same order of stability as the trihalides.

It is tempting to try to relate our work to the complex topic of the mechanism of the Dushman reaction (reverse reaction [1]). Our experiments were performed in alkaline solutions whereas most of the studies of the Dushman reactions have been done in acidic media. This precludes quantitative calculations. However, some qualitative comments can be made.

Liebhafsky and Roe (2) have summarized the numerous studies of the Dushman reaction. They concluded that the kinetics of the reaction are best described by a rate law of the form:

$$[42] \quad R = (k_1 + k_2[I^-])([H^+]^2[IO_3^-][I^-])$$

The reaction is first order in iodide at iodide concentrations below 10^{-6} mol dm^{-3} and second order in iodide at higher concentrations. The two-term rate law is accounted for by a mechanism involving the polynuclear iodine species I_2O_2 (or $H_2I_2O_3$). Liebhafsky and Roe (2) state that the existence of such a species is also needed to explain the results of Skrabal (9, 10) on the disproportionation of I_2 into IO_3^- and I^- in alkaline solution. Our study shows that the results of Skrabal can be explained by the presence of the I_2OH^- species, which we have unambiguously identified using Raman spectroscopy. Although I_2OH^- is present in significant concentration at high pH, its concentration would be quite low at low pH. In fact we could not detect any Raman signal due to this species at pH 10 and below. However, Palmer and Van Eldik (35) have recently demonstrated that I_2OH^- plays an important role in the hydrolysis of I_2 to I^- and HOI at low pH, even if it is present in very low concentration. It would be interesting to see if I_2OH^- can be substituted for I_2O_2 in the mechanism of the Dushman reaction.

Acknowledgements

This work was funded jointly by Atomic Energy of Canada Limited and Ontario Hydro under the CANDEV agreement. The assistance of Mr. G. J. Wallace in performing some of the Raman experiments is acknowledged. The authors thank Drs. R. J. Lemire and W. C. H. Kupferschmidt of the Whiteshell Nuclear Research Establishment and Dr. D. A. Palmer of Oak Ridge National Laboratory for helpful comments on the manuscript.

1. P. P. S. Saluja, K. S. Pitzer, and R. C. Phutela. Can. J. Chem. **64**, 1328 (1986).
2. H. A. Liebhafsky and G. N. Roe. Int. J. Chem. Kinet. **11**, 693 (1979).
3. E. Abel and F. Stadler. Z. Phys. Chem. **22**, 49 (1926).
4. S. Dushman. J. Phys. Chem. **8**, 453 (1904).
5. T. R. Thomas, D. T. Pence, and R. A. Hasty. J. Inorg. Nucl. Chem. **42**, 183 (1980).
6. O. Haimovich and A. Treinin. J. Phys. Chem. **71**, 1941 (1967); Nature, **207**, 185 (1965).
7. M. H. Hashmi, A. A. Ayay, A. Rashid, and E. Ali. Anal. Chem. **36**, 1379 (1964).
8. C. H. Li and C. F. White. J. Am. Chem. Soc. **65**, 335 (1943).
9. A. Skrabal and R. Hohlbaum. Monatsh. Chem. **37**, 191 (1916).
10. A. Skrabal. Monatsh. Chem. **33**, 99 (1912); **32**, 185 (1911); **32**, 167 (1911).
11. E. L. C. Forster. J. Phys. Chem. **7**, 640 (1903).
12. D. L. Cason and H. N. Neumann. J. Am. Chem. Soc. **83**, 1822 (1961).
13. W. Kiefer and H. J. Bernstein. Chem. Phys. Lett. **16**, 5 (1972).
14. J. Paquette and B. L. Ford. Can. J. Chem. **63**, 2444 (1985).
15. J. R. Durig, O. D. Bonner, and W. H. Brearzeale. J. Phys. Chem. **69**, 3886 (1965).
16. A. Tasaka and T. Toja. Sci. Eng. Rev. Doshisha Univ. **23**, 14 (1982); Rep. Asahi Glass Found. Ind. Technol. **39**, 103 (1981).
17. B. Sombret and F. Wallart. C. R. Acad. Sci. Paris (Ser. B), **277**, 663 (1973).
18. J. C. Evans and G. Y.-S. Lo. Inorg. Chem. **6**, 1483 (1967).
19. J. F. Ogilvie, V. R. Slares, and M. J. Neulands. Can. J. Chem. **53**, 269 (1975).
20. J. F. Ogilvie. Can. J. Spectrosc. **19**, 171 (1974).
21. N. Walker, D. E. Tevault, and R. R. Smardzewski. J. Chem. Phys. **69**, 564 (1978).
22. J. N. Murrell, S. C. Carter, I. M. Mills, and M. F. Guest. Mol. Phys. **37**, 1199 (1979).
23. I. Schwager and A. Arkell. J. Am. Chem. Soc. **89**, 6006 (1967).
24. G. Pimentel. J. Chem. Phys. **19**, 446 (1951).
25. F. K. Chi and L. Andrews. J. Phys. Chem. **77**, 3062 (1973).

26. M. ANBAR and H. TAUBE. J. Am. Chem. Soc. **80**, 1073 (1958).
27. J. SIGALLA. J. Chim. Phys. **58**, 602 (1961); Nature, **183**, 178 (1959).
28. Y.-T. CHIA. Thesis, UCRL, No. 8311. 1958.
29. T. L. ALLEN and R. M. KEEFER. J. Am. Chem. Soc. **77**, 2957 (1955).
30. M. B. CARVER. *In* Mathematics and computers in simulation. Vol. XXII. North-Holland Publishing Company. 1980. p. 298.
31. D. W. MARQUAT. J. Soc. Ind. Appl. Math. **11**, 431 (1963).
32. M. W. LISTER. Can. J. Chem. **34**, 465 (1956).
33. M. W. LISTER and P. E. MCLEOD. Can. J. Chem. **49**, 1987 (1971).
34. L. PAULING. The nature of the chemical bond. 3rd ed. Cornell University Press, Ithaca. 1960.
35. D. A. PALMER and R. VAN ELDIK. Inorg. Chem. **25**, 928 (1986).

Far ultraviolet induced decomposition of thymine in deaerated and aerated aqueous solutions

BUNSHO OHTANI, HIROSHI NAGASAKI, SEI-ICHI NISHIMOTO, KOICHI SAKANO, AND TSUTOMU KAGIYA
Department of Hydrocarbon Chemistry, Faculty of Engineering, Kyoto University, Sakyo-ku, Kyoto 606, Japan

Received January 2, 1986

BUNSHO OHTANI, HIROSHI NAGASAKI, SEI-ICHI NISHIMOTO, KOICHI SAKANO, and TSUTOMU KAGIYA. Can. J. Chem. **64**, 2297 (1986).

Thymine in aqueous solution was decomposed with quantum yields of 0.3 and 0.4 under N_2-saturated and aerated conditions by far-ultraviolet light (>180 nm, far-uv), and quantum yields of 2×10^{-4} and 3×10^{-4} by near-ultraviolet light (>220 nm, near-uv), respectively. The main photolytic products by far-uv were 5,6-dihydrothymine (DHT) (selectivity: S(DHT) = 0.2) and 5-hydroxymethyluracil (HMU) (S(HMU) = 0.1) under N_2-saturated conditions. *cis*- and *trans*-5,6-Dihydroxy-5,6-dihydrothymine (TG), 6(5)-hydroperoxy-5(6)-hydroxy-5,6-dihydrothymine (HTP) (S(TG) + S(HTP) = 0.2), and N^1-formyl-N^2-pyruvylurea (FPU) (S(FPU) = 0.4) were obtained under aerated conditions. These products were attributed to the reactions of thymine with the ·H and ·OH produced by photolysis of water.

BUNSHO OHTANI, HIROSHI NAGASAKI, SEI-ICHI NISHIMOTO, KOICHI SAKANO et TSUTOMU KAGIYA. Can. J. Chem. **64**, 2297 (1986).

Sous l'influence de la lumière ultraviolette lointaine (>180 nm, uv-lointain), on a mesuré que les solutions aqueuses de thymine se décomposent avec des rendements quantiques de 0,3 et 0,4 suivant que l'on opère sous des conditions saturées en N_2 ou aérées; par ailleurs, dans l'ultraviolet proche (>220 nm, proche-uv), les valeurs sont respectivement 2×10^{-4} et 3×10^{-4}. Dans l'ultraviolet lointain et sous des conditions saturées en N_2, les produits principaux de la photolyse sont la dihydro-5,6 thymine (DHT) (sélectivité; S(DHT) = 0,2) et l'hydroxyméthyl-5 uracile (HMU) (S(HMU) = 0,1). Dans des conditions aérées, les produits principaux sont les dihydroxy-5,6 dihydro-5,6 thymine-*cis* et -*trans* (TG), les hydroperoxy-6(5) hydroxy-5(6) dihydro-5,6 thymines (HTP) (S(TG) + S(HTP) = 0,2) et la N^1-formyl N^2-pyruvylurée (FPU) (S(FPU) = 0,4). On attribue la formation de ces composés aux réactions de la thymine avec les radicaux ·H et ·OH qui sont produits par photolyse de l'eau.

[Traduit par la revue]

Introduction

Photoinactivation of living cells, which is applicable to the sterilization by near-ultraviolet light (near-uv, 240–290 nm) irradiation, is of great interest and has been extensively studied in recent years (1). Among the chemical reactions induced by near-uv, the photoinduced dimerization of pyrimidine bases of DNA likely accounts for such cell inactivation (for a review, see ref. 1).

In contrast, few reports have appeared concerning the far-ultraviolet light (far-uv, >180 nm) induced inactivation and/or chemical reaction of DNA-related compounds. Daniels and Grimison have reported the detailed investigation on far-uv photolysis of thymine under aerated conditions and demonstrated the intermediacy of radical species (2). On the other hand, the fate of such a DNA-related compound under deaerated conditions is of biological and biochemical interests in connection with phototherapy of hypoxic tumor cells. The present paper describes the far-uv induced photolysis of thymine under both deaerated (N_2-saturated) and aerated conditions. Particular emphasis is placed on the comparison of these two photoreaction systems with γ-radiolysis systems. The reaction mechanism is also discussed.

Experimental

Thymine (T), 5-hydroxymethyluracil (HMU), and 5,6-dihydrothymine (DHT) were obtained from Sigma and used as received. *cis*-5,6-Dihydroxy-5,6-dihydrothymine (TG) (3), 6-hydroperoxy-5-hydroxy-5,6-dihydrothymine (HTP) (4), 5-methylbarbituric acid (MBA) (5), 6-hydroxy-5,6-dihydrothymine (HOT) (6), and N^1-formyl-N^2-pyruvylurea (FPU) (7) were prepared by the reported procedures. The chemical structures of these compounds are shown in Fig. 1.

An aqueous solution of thymine (0.5 mmol dm^{-3}) was prepared with twice distilled water and adjusted to pH 7.0 ± 0.1 with phosphate buffer (2 mmol dm^{-3}). The solution (10 cm^3) in a quartz test tube

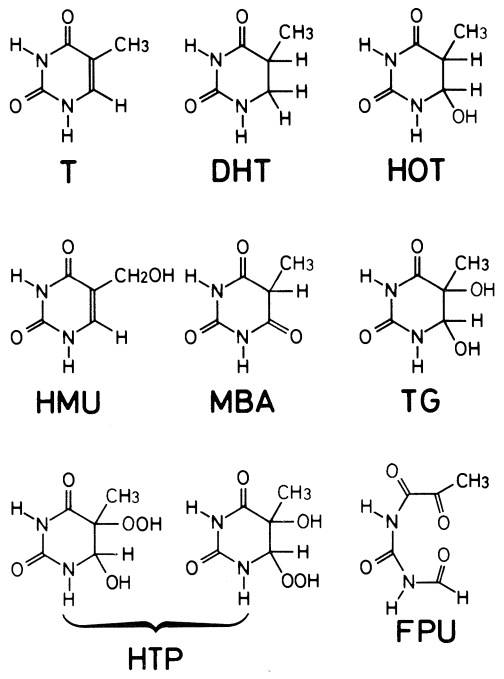

FIG. 1. Chemical structures of thymine and photolytic products.

(17 mm in diameter) was purged with N_2 or air for >15 min, sealed off, and irradiated with a coil-formed low-pressure mercury arc at room temperature. A vycor filter was used to cut off far-uv (<220 nm). The light flux incident upon the reaction vessel was measured to be 4.87×10^{-7} einstein min^{-1} at 185 nm by Farkas actinometry (8) or 1.40×10^{-5} einstein min^{-1} at 254 nm by ferric oxalate actinometry (9).

Typical procedure of γ-radiolysis was as follows. A solution of thymine (0.5 mmol dm^{-3}) was prepared with triply distilled water, buffered at pH 7.0 ± 0.1 with sodium phosphate, and purged with N_2

TABLE 1. Rates ($-\Delta T$) and quantum yields of thymine decomposition ($\phi(-\Delta T)$), and rates[a] and selectivities of products (S)[b] in the uv- and γ-irradiation of aqueous thymine solution in N_2 and air

Conditions	N_2			Air		
	Near-uv (>220 nm)	Far-uv (>180 nm)	γ-Ray[c]	Near-uv (>220 nm)	Far-uv (>180 nm)	γ-Ray[c]
Light flux/einstein min^{-1}	1.40×10^{-5}	4.87×10^{-7}	—	1.40×10^{-5}	4.87×10^{-7}	—
$-\Delta T$/μmol dm^{-3} min^{-1}	0.25	14.7	1.0	0.46	20.7	1.3
$\phi(-\Delta T)$	2×10^{-4}	0.30	—	3×10^{-4}	0.42	—
cis-TG/μmol dm^{-3} min^{-1} (S)	0.0 (0.0)	0.56 (3.8)	(4.0)	0.0 (0.0)	3.82 (18.5)	(45.7)
trans-TG (S)	0.0 (0.0)	0.50 (3.4)	(2.0)	0.0 (0.0)	1.96 (9.49)	(9.6)
HMU (S)	0.0 (0.0)	1.53 (10.4)	(6.0)	0.0 (0.0)	0.41 (2.0)	(1.1)
HOT (S)	0.0 (0.0)	0.52 (3.6)	(4.7)	0.0 (0.0)	0.61 (2.9)	(5.4)
FPU (S)	0.0 (0.0)	0.61 (4.2)	(3.4)	0.0 (0.0)	8.46 (40.9)	(14.7)
MBA (S)	0.0 (0.0)	0.0 (0.0)	(4.0)	0.0 (0.0)	0.99 (4.8)	(7.5)
DHT (S)	0.0 (0.0)	2.94 (20.0)	(21.4)	0.0 (0.0)	0.0 (0.0)	(0.0)
UIC[d] (S)	0.25 (100)[e]	8.04 (54.6)	(54.5)	0.46 (100)[e]	4.45 (22.3)	(16.0)

[a] [Product]/μmol dm^{-3} min^{-1}.
[b] 100 × [product]/[$-\Delta T$].
[c] 760 Gy.
[d] Unidentified products.
[e] Dimeric products.

or air. Irradiation was performed in a Pyrex tube (16 mm in diameter) with a ^{60}Co γ-ray source (380 Gy h^{-1}) at room temperature.

A portion (30 mm^3) of the photo- and γ-irradiated solutions was analyzed by high performance liquid chromatography (hplc), using a Shimadzu LC-3A equipped with a Cosmosil $5C_{18}$ reversed phase column (4.6 × 150 mm). Phosphate buffer containing 5% methanol (pH 2.5) was delivered as the mobile phase at a flow rate of 0.6 cm^3 min^{-1}. The column eluents were monitored with the ultraviolet absorptions at 210 and 260 nm. Products were confirmed by comparison with the authentic samples at both detector wavelengths. Calibration curve for each of the products was obtained at 210 nm.

The amount of peroxides produced in the irradiated solutions was analyzed by iodometry, using the molybdate-catalyzed oxidation of iodide to triiodide anion which was measured spectrophotometrically at 350 nm (10) (the molar extinction coefficient was 5.9×10^3 mol dm^{-3} cm^{-1}). This iodometry responds to both hydrogen peroxide (H_2O_2) and organic peroxides. The amount of H_2O_2 was separately measured by acidic titanium oxysulfate ($TiO(SO_4)$) method (11). These measurements showed the formation of H_2O_2 and organic peroxides only by the far-uv photolysis under aerated conditions. High performance liquid chromatographic separation of *trans*-TG and *trans*-HTP, or *cis*-TG and *cis*-HTP, was not successful. Determination of HTP content in each TG/HTP fraction of hplc was failed because of the unstability of HTP isomers at room temperature. Nevertheless, it seemed most likely that the fractions predominantly consist of HTP, since the amount of organic peroxide was almost equal (110%) to the sum of TG and HOT.

Total amount of some unidentified products listed in Table 1 was obtained as the difference in amount between the converted thymine and the sum of identified products. The products obtained by near-uv photolysis under both deaerated and aerated conditions were not identified. However, comparison of the hplc elution patterns with those obtained by the near-uv photolysis of thymine in ice under the reported conditions (ref. 1 and references therein) suggested that the products consisted mainly of the thymine dimers.

Results and discussion

Ultraviolet-induced decomposition of thymine in aqueous solution in the absence and presence of O_2

Irradiation at >180 nm led to decomposition of thymine (Fig. 2). The amount of the decomposed thymine under aerated conditions was 1.4 times as much as that under N_2-saturated conditions. Linear plots of ln ($[T]_0/[T]$), where $[T]_0$ and [T]

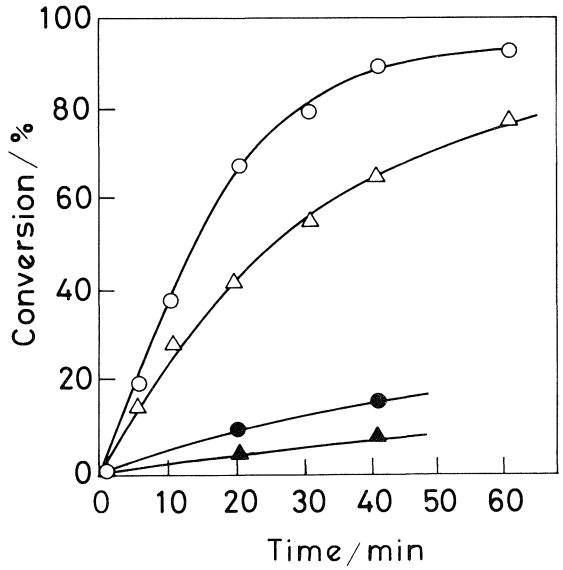

FIG. 2. Time-course of uv-induced decomposition of thymine in aqueous solution. ○ and △: irradiations at >180 nm under aerated and N_2-saturated conditions, respectively. ● and ▲: irradiations at >220 nm under aerated and N_2-saturated conditions, respectively.

refer to concentrations of thymine before and after photoirradiation, respectively, against photoirradiation time demonstrated pseudo-first order kinetics. The apparent rate constants (k), which depend on several terms, e.g., light intensity and quantum efficiency, were evaluated to be 9.4×10^{-4} and 4.4×10^{-4} s^{-1} for aerated and N_2-saturated conditions, respectively.

In both cases cutting off of the shorter wavelength region (<220 nm) by using a vycor filter reduced the apparent reaction rate to ca. 1/10. The low-pressure mercury arc emits photons mainly at 254 nm and 185 nm (Table 1). It follows that the mercury line at 185 nm, rather than 254 nm, is responsible for the decomposition of thymine. The order of quantum efficiency at 254 nm was evaluated as 10^{-4} from the ratio of thymine decomposition rate to the light flux incident upon the reaction

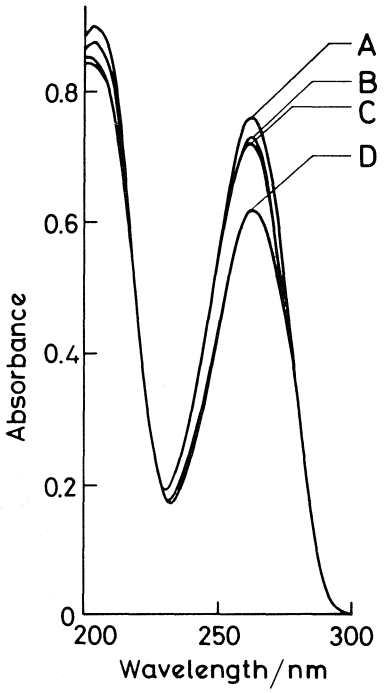

FIG. 3. Electronic absorption spectra of aqueous thymine solutions before (*A*) and after irradiation. *B* and *C*: irradiations of near-uv under N_2-saturated and aerated conditions, respectively, for 1 h. *D*: irradiations of far-uv under N_2-saturated and aerated conditions for 10 and 7 min, respectively.

vessel through a vycor filter (Table 1). This negligibly small efficiency shows that the light at 185 nm induces the reaction of thymine almost exclusively even in the irradiation without a cut-off filter. Thus, the efficiency at 185 nm was estimated to be 0.30 and 0.42 under N_2-saturated and aerated conditions, respectively, which was 200–300 times larger than those at 254 nm.

From the uv-absorption spectra of thymine and water, most of the incident photons at 254 nm were absorbed by thymine in the solution, while photons at 185 nm by not only thymine but also water (2). The fractions of photons of 185 nm absorbed by 0.5 mmol dm^{-3} of thymine and water were evaluated from the reported extinction coefficients (5.75×10^3 mol^{-1} dm^3 cm^{-1} and 1.52 cm^{-1}) (2) to be 66 and 34%, respectively, under the present conditions. Thus, it is suggested that the significantly larger quantum efficiency by 185 nm irradiation is attributed to the water photolysis via homolytic cleavage into hydroxyl radical (·OH) and hydrogen atom (·H) (12) (see Fig. 5).

Photolytic and γ-radiolytic products from thymine

Figure 3 shows the electronic absorption spectra before and after far-uv irradiation of aqueous thymine solution under N_2-saturated and aerated conditions. Characteristic absorption band due to π–π^* transition of *cis* olefinic bond of thymine was observed at 260 nm. The absorbance at this band decreased by photoirradiation, elucidating disappearance of the double bond by the photoirradiation. In accord with these facts the photoproducts under both N_2-saturated and aerated conditions exhibited intense hplc-detector response at 210 nm but negligible at 260 nm (except for the case of HMU) as shown in Fig. 4. Each yield of main photolytic products increased linearly with photoirradiation time within first 5 min. However, prolonged irradiation decreased the product yields to some extent, due to the secondary photolyses. The initial rate (<5 min) and quantum efficiency evaluated for each product were evaluated

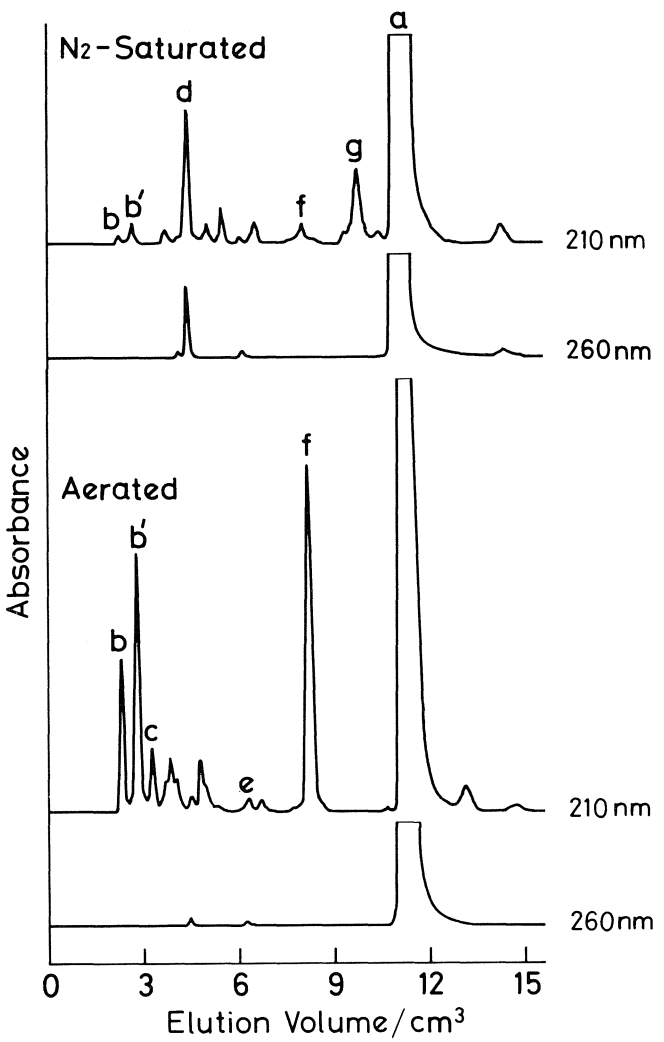

FIG. 4. Typical hplc patterns of far-uv irradiated aqueous thymine solutions.

from the linear portion of the yield–time plot, as listed in Table 1.

It is seen from Table 1 that main photolytic products under N_2-saturated conditions at 185 nm were DHT and HMU, neither of which was produced by the 254 nm irradiation. The selectivities of these products (0.20 and 0.10) were similar to those obtained by γ-radiolysis (0.21 and 0.06, respectively (Table 1)). In the γ-radiolysis, main active species produced in N_2-saturated aqueous solution are ·H (*G*-value (number of molecules per 100 eV-energy absorption at pH 7.0) is 0.55), hydrated electron (e^-_{aq}, $G = 2.7$), and ·OH ($G = 2.7$) (13). Reduction of thymine by e^-_{aq} to thymine anion radical (T·⁻) followed by the addition of H^+ gives hydrothyminyl radicals (·T—H). The addition of ·OH across the C_5—C_6 double bond of thymine produces hydroxythyminyl radicals (·T—OH). Either reduction by e^-_{aq} or recombination with ·OH of ·T—H leads to DHT or HOT.[1]

In the far-uv photolysis, ·H produced via photocleavage of water (see Fig. 5) presumably gives the same intermediate,

[1]The disproportionations among radical intermediates, ·T—H and ·T—OH, are responsible for the formation of DHT, HOT, and TG. Since the formal chemical change can be represented by T + 2·H → DHT and T + ·H + ·OH → HOT, the above processes involving disproportionation are illustrated as T + ·H → ·T—H, ·T—H + ·H → DHT, ·T—H + ·OH → HOT for convenience in Fig. 5.

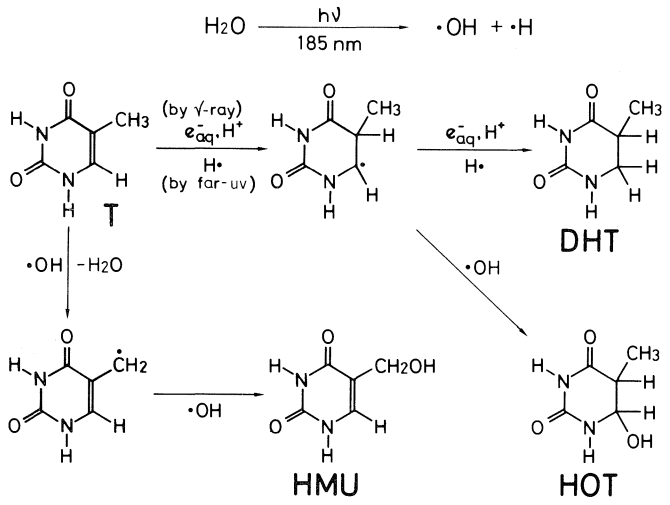

FIG. 5. Scheme of far-uv photolysis of thymine in aqueous solution under N_2-saturated conditions.

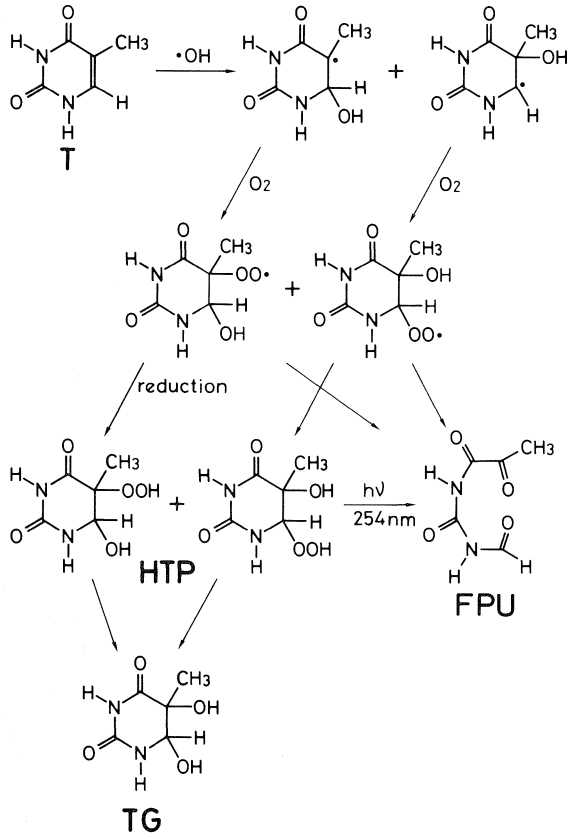

FIG. 6. Scheme of far-uv photolysis of thymine in aqueous solution under aerated conditions.

hydrothyminyl radical. The radical species, ·OH, also abstract hydrogen atom from the methyl group of thymine. The HMU formation is attributable to this hydrogen abstraction followed by the addition of ·OH in both γ-radiolysis and far-uv photolyisis.

In the presence of O_2, the main products were HTP and FPU in the far-uv photolysis (and γ-radiolysis, see Table 1). The peroxide formation is distinct from the N_2-saturated system.

The reduction of thymine to DHT became negligible in the O_2-saturated system, since the reducing species, ·H in both photolysis and γ-radiolysis, and e^-_{aq} in γ-radiolysis, are expected to react with O_2 to produce less active $HO_2\cdot$ and $O_2^{\cdot-}$, respectively. $HO_2\cdot$ is deprotonated to yield $O_2^{\cdot-}$ under neutral conditions. Such trapping of the reducing species with O_2 may also account for the decreased ratio of unidentified products, which would be produced by the reaction at labile N—H bond in thymine. Consequently, the reaction of thymine with ·OH occurs predominantly in both systems under O_2. O_2 addition to the intermediate ·T—OH thus produced leads to HTP and FPU (see Fig. 6).

In the far-uv photolysis the yield ratio of FPU to TG (HTP) was evaluated as 1.5, which is larger than that in the γ-radiolysis (0.5). This enhancement of FPU formation was accounted for by the direct photoreaction of HTP by irradiation at >220 nm, in accord with the observation that authentic sample of HTP in aqueous solution (0.5 mmol dm^{-3}) was photolysed into FPU (and unidentified products) under deaerated conditions.

In conclusion, thymine was decomposed efficiently in aqueous solution by far-uv irradiation. The decomposition was attributed to the active species, ·H and ·OH, produced by the far-uv photolysis of water under both deaerated and aerated conditions.

1. J. JAGGER. *In* Photochemistry and photobiology of nucleic acids. Vol. 2. *Edited by* S. Y. Wang. Academic Press, New York. 1976. p. 147.
2. M. DANIELS and A. GRIMISON. Biochim. Biophys. Acta, **142**, 292 (1967).
3. O. BAUDISH and D. DAVIDSON. J. Biol. Chem. **64**, 233 (1925); J. CADET, J. ULRICH, and R. TEOULE. Tetrahedron, **31**, 2057 (1975).
4. J. CADET and R. TEOULE. Bull. Soc. Chim. Fr. 880 (1975); 883 (1975).
5. C. NOFRE, A. CIER, R. CHAPURLAT, and J. M. MARESCHI. Bull. Soc. Chim. Fr. 332 (1965).
6. B. DOUMAS and H. G. BIGGS. J. Biol. Chem. **237**, 2306 (1962).
7. R. TEOULE, J. CADET, and J. ULRICH. C. R. Acad. Sci. Paris, **270C**, 362 (1970).
8. L. FARKAS and Y. HISHBERG. J. Am. Chem. Soc. **59**, 2450 (1937).
9. C. G. HATCHARD and C. A. PARKER. Proc. Res. Soc. London, A**235**, 578 (1956).
10. C. J. HOCHANADEL. J. Phys. Chem. **56**, 587 (1952).
11. I. R. COHEN and T. C. PURCELL. ANAL. CHEM. **39**, 131 (1967); R. COHEN, T. C. PURCELL, and A. P. ALTSMULLER. Environ. Sci. Technol. **1**, 247 (1967).
12. W. FÜCHTBAUER and P. MAZUR. Photochem. Photobiol. **5**, 323 (1966).
13. G. SCHOLES. *In* Effects of ionizing radiation on DNA. *Edited by* J. Hütterman, W. Kohnlein, and R. Teoule. Springer-Verlag, Berlin. 1978. p. 153.

Fast disproportionation of hexacyanomanganate(III) in acidic solution. Formation of hexacyanomanganate(IV) and kinetics of its decomposition

GUILLERMO LÓPEZ-CUETO[1]

Departamento de Química Analítica, Facultad de Ciencias, Universidad de Alicante, Apdo. 99, 03080 Alicante, Spain

AND

CARLOS UBIDE

Departamento de Química Analítica, Facultad de Química, Universidad del País Vasco, 20017 San Sebastián, Spain

Received March 3, 1986

GUILLERMO LÓPEZ-CUETO and CARLOS UBIDE. Can. J. Chem. **64**, 2301 (1986).

When potassium hexacyanomanganate(III) dissolves in acidic solution it rapidly disproportionates into hexacyanomanganate(IV) and Mn(II). Hexacyanomanganate(IV) then slowly decomposes to yield Mn(II) and $(CN)_2$. Kinetics of the latter reaction has been studied. The reaction is found to be first order with respect to $Mn(CN)_6^{2-}$, H^+, and Mn(II) concentrations and the experimental rate law has the form $v = k_{obs}[Mn(IV)] = (k_a + k_b[H^+] + k_c[Mn(II)])[Mn(IV)]$. At 40°C and ionic strength 2.0, k_a, k_b, and k_c values are $(1.78 \pm 0.01) \times 10^{-4}$ s^{-1}, $(5.97 \pm 0.05) \times 10^{-5}$ s^{-1} M^{-1}, and $(3.40 \pm 0.18) \times 10^{-3}$ s^{-1} M^{-1}, respectively. A mechanism with three parallel pathways is proposed, the deduced rate law being similar to the experimental one. Activation parameters, $\Delta H^{\neq}$ and $\Delta S^{\neq}$ for the rate constants k_a, k_b, and k_c are also reported.

GUILLERMO LÓPEZ-CUETO et CARLOS UBIDE. Can. J. Chem. **64**, 2301 (1986).

Lorsqu'on place l'hexacyanomanganate(III) de potassium en solution acide, il se produit rapidement une réaction de disproportionation conduisant à l'hexacyanomanganate(IV) et au Mn(II); après, l'hexacyanomanganate(IV) se décompose lentement pour donner du Mn(II) et du $(CN)_2$. On a étudié la cinétique de cette dernière réaction. On a trouvé que la réaction est du premier ordre par rapport aux concentrations de $Mn(CN)_6^{2-}$, de H^+ et de Mn(II) et que la loi expérimentale de vitesse se présente sous la forme $v = k_{obs}[Mn(IV)] = (k_a + k_b[H^+] + k_c[Mn(II)])[Mn(IV)]$. A 40°C et à une force ionique égale à 2,0, les valeurs de k_a, k_b et k_c sont respectivement égales à $(1{,}78 \pm 0{,}01) \times 10^{-4}$ s^{-1}, $(5{,}97 \pm 0{,}05) \times 10^{-5}$ s^{-1} M^{-1} et $(3{,}40 \pm 0{,}18) \times 10^{-3}$ s^{-1} M^{-1}. On suggère que la réaction se produit par un mécanisme impliquant trois voies parallèles; la loi de vitesse qui est alors déduite est semblable à celle qui est observée expérimentalement. On rapporte aussi les paramètres d'activation, $\Delta H^{\neq}$ et $\Delta S^{\neq}$, pour les constantes de vitesse k_a, k_b et k_c.

[Traduit par la revue]

Introduction

Two different cyanomanganate(III) complexes have been reported in the literature, hexacyanomanganate(III) and μ-oxo-bis[pentacyanomanganate(III)], and they have mono-and binuclear structures, respectively (1, 2). The uv spectra of $Mn(CN)_6^{3-}$ in acidic and cyanide-containing solutions differ markedly (3); whereas the cyanide-containing solutions are stable, the acidic ones are not, and the absorption bands of their uv spectra slowly fade away because of slow decomposition. On the other hand, clear evidence has been reported that acidic solutions of hexacyanomanganate(III) actually contain hexacyanomanganate(IV), as their uv spectrum is quite similar to that of the $K_2Mn(CN)_6$ solution in DMF (4). Therefore it has been suggested that a disproportionation reaction takes place (5). This paper shows how the uv spectrum of the acidic solutions of $Mn(CN)_6^{3-}$ changes with time during both the disproportionation and the decomposition reactions. The kinetics and mechanism of the decomposition reaction are also studied.

Experimental

Apparatus

A Varian 634-S spectrophotometer with 1.0-cm glass cells and coupled with a Radiometer REC 80 Servograph recorder was used for the kinetic measurements. A water bath circulator Selecta Tectron Digiterm was used for the cells' temperature control.

When pH measurements were required, a Radiometer PHM 82 pH-meter was used.

Reagents

All chemicals were of analytical reagent-grade and doubly distilled water was used throughout.

Potassium hexacyanomanganate(III)

Firstly the potassium salt of the binuclear complex $K_7[(CN)_5MnOMn(CN)_5]CN$ was prepared following a reported procedure (6). $K_3Mn(CN)_6$ was then obtained from the remaining solution as previously described (7). The Mn(III) mononuclear complex in acidic and cyanide-containing media was characterized by uv spectrophotometry and by ir spectroscopy; our results agree with those of the literature (1, 3). Elemental analysis showed a content close to 100%.

Kinetics measurements

Solutions were prepared in a dark 250-mL standard flask by adding the required amounts of $MnSO_4.H_2O$ and $NaNO_3$ to adjust the ionic strength, and sulfuric acid solution of the required concentration to 220–230 mL. The resulting solution was kept in a thermostatic bath for 30 min; $K_3Mn(CN)_6$ was then added (zero time) with stirring and the volume was quickly adjusted to 250 mL by adding some more sulfuric acid solution. The solution was stirred again ($K_3Mn(CN)_6$ dissolves very quickly) and transferred to a spectrophotometric cell. The kinetic curve at 387 nm was recorded for 60 min using water as reference (diluted sulfuric acid of the same concentration was used for measurements in the ultraviolet region).

The temperature in the cell was kept constant within ±0.2°C during each experiment.

The rate constants were calculated by plotting ln A vs. time and linear regression analysis was applied. The temperature was varied between 20 and 50°C, the ionic strength between 0.27 and 2.0, the acidity between 0.08 and 0.75 M, the initial Mn(II) concentration between 0 and 2×10^{-2} M, and the initial $K_3Mn(CN)_6$ concentration between 1 and 6×10^{-4} M.

Results and discussion

Evolution of the uv spectrum in acidic solution

When $K_3Mn(CN)_6$ is dissolved in acidic solution the uv-spectrum that can be scanned at a temperature close to 0°C is similar to the one obtained in a cyanide-containing solution,

[1]To whom correspondence should be addressed.

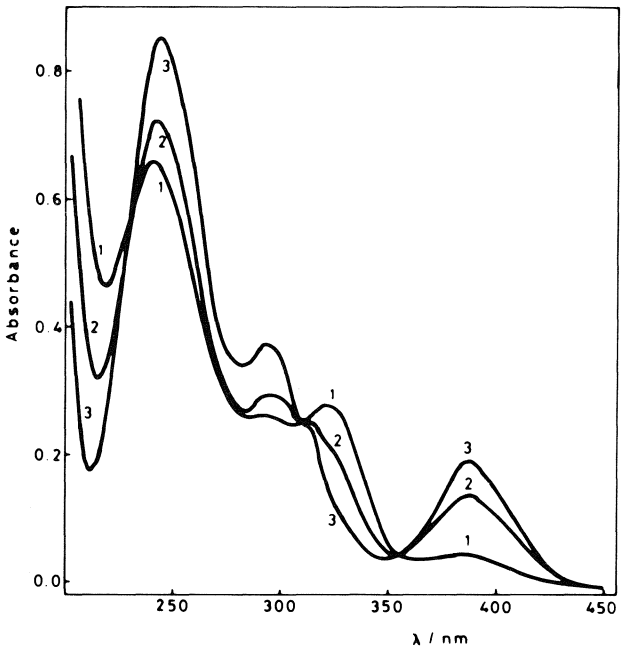

FIG. 1. Evolution of the uv spectrum of hexacyanomanganate(III) in acidic medium with time. Reaction of disproportionation: Mn(III), 10^{-4} *M*; H_2SO_4, 0.25 *M*; *I*, 0.27; *T*, ≅3°C. Scan starting time: (*1*), 0.5 min; (*2*), 3.4 min; (*3*), 12.25 min.

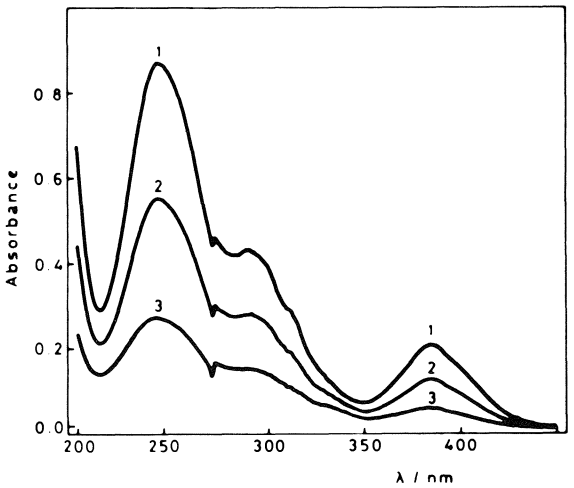

FIG. 2. Evolution of the uv spectrum of hexacyanomanganate(IV) in acidic medium with time. Reaction of decomposition: Mn(IV), 5×10^{-5} *M*; H_2SO_4, 0.25 *M*; *I*, 0.27; *T*, ≅40°C. Scan starting time: (*1*), 10 min; (*2*), 50 min; (*3*), 170 min.

with maxima at 324 and 268 nm. In this acidic medium two consecutive reactions take place. Firstly, the uv spectrum quickly changes to that of $Mn(CN)_6^{2-}$, with absorption maxima at 387, 292, and 244 nm (Fig. 1). This is the disproportionation reaction reported by Trageser and Eysel (5):

$$[1] \quad 2Mn(CN)_6^{3-} + 6H_3O^+ \rightarrow Mn(CN)_6^{2-} + Mn(H_2O)_6^{2+} + 6HCN$$

It is difficult to follow the reaction at room temperature as its rate is rather high (working at 15°C the reaction proceeds to completion in 2–3 min). At 3°C it has been possible to measure the reaction rate spectrophotometrically and its kinetics appears to be close to a pseudo first-order dependence. The reaction product, $Mn(CN)_6^{2-}$, is stable for at least several hours at a

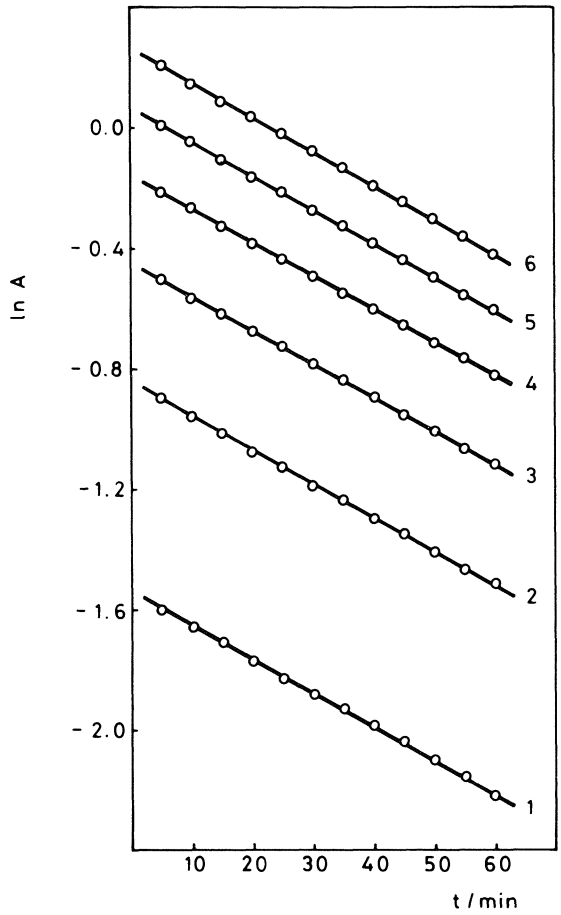

FIG. 3. Plots of ln *A* vs. time for the decomposition of hexacyanomanganate(IV) in acidic solution: H^+, 0.16 *M*; *I*, 2; *T*, 40°C; Mn(IV), $M \times 10^4$: (*1*), 0.5; (*2*), 1.0; (*3*), 1.5; (*4*), 2.0; (*5*), 2.5; (*6*), 3.0.

temperature close to 0°C, but at higher temperatures a slow and uniform fading of the uv-spectrum bands takes place (Fig. 2). This must be the decomposition reaction of the $Mn(CN)_6^{2-}$ species. It has been found in our laboratory that ultraviolet light increases the rate of the latter reaction; nevertheless, we have verified that the reaction proceeded to the same extent both in the spectrophotometric cell and in the flask kept in the dark.

Decomposition of $Mn(CN)_6^{2-}$ in acidic solution

Stoichiometry

If the reaction rate is followed both volumetrically (by adding at fixed times aliquots of the reaction mixture to an excess of Fe^{2+} and estimating the remaining Fe^{2+} with MnO_4^- solution) and spectrophotometrically, it can be proved that the oxidizing capacity of the solution and its absorbance decrease at the same rate. One must therefore conclude that a reduction of Mn(IV) to Mn(II) takes place, the probable stoichiometry being:

$$[2] \quad Mn(CN)_6^{2-} + 4H_3O^+ + 2H_2O \rightarrow Mn(H_2O)_6^{2+} + (CN)_2 + 4HCN$$

Effect of hexacyanomanganate(III) concentration

Reaction order: When Mn(II) is not added initially, plots of ln *A* against time (Fig. 3) are quite linear for at least three half lives, the slope being independent of the initial concentration of $Mn(CN)_6^{2-}$ (which according to [1] will be half the concentration of $Mn(CN)_6^{3-}$ added). This shows a first-order dependence on the hexacyanomanganate(IV) concentration, and hence, the rate law below must be followed:

TABLE 1. Activation parameters for the decomposition reaction of hexacyanomanganate(IV) in sulfuric acid medium at ionic strength 2.0

Parameter	Value at 40°C	$\Delta H^{\ddagger}$/kJ mol^{-1}	$\Delta S^{\ddagger}$/J mol^{-1} K^{-1}
k_a/s^{-1}	$(1.78 \pm 0.01) \times 10^{-4}$	69.5 ± 1.4	−95.3 ± 4.2
k_b/s^{-1} M^{-1}	$(5.97 \pm 0.05) \times 10^{-5}$	119.6 ± 3.2	57.4 ± 2.3
k_c/s^{-1} M^{-1}	$(3.40 \pm 0.18) \times 10^{-3}$	44.8 ± 2.3	−150.1 ± 23.3

$$[3] \quad \text{Rate} = -\frac{d[\text{Mn(IV)}]}{dt} = k_{obs}[\text{Mn(IV)}]$$

The pseudo first-order constant can be evaluated from the slope values. For $T = 40$°C, ionic strength = 2.0, and $[H^+] = 0.16\ M$,

$$k_{obs} = (1.87 \pm 0.01) \times 10^{-4}\ s^{-1}$$

When the concentration of Mn(II) is higher than 8×10^{-3} M, the slope of the logarithmic plot decreases slightly after the reaction has proceeded to a certain extent. In these cases, the values of the pseudo first-order constant were measured before the disturbing effect took place.

Effect of the ionic strength

A very slight positive primary salt effect was found for the reaction but no conclusions can be drawn on the ionic charge of reactants as the minimum amount of acid needed to avoid hydrolysis is too high for the Brønsted–Bjerrum law to apply.

Effect of acidity and Mn(II) concentration

Plots of the pseudo first-order constant, k_{obs}, vs. H^+ concentration give satisfactory straight lines with positive slope and intercept, indicating two parallel pathways for the reaction, one of them being first-order and the other one zero-order with respect to the H^+ concentration. Different initial concentrations of Mn(II) give straight lines with similar slopes but the intercepts get higher as the initial Mn(II) concentration increases, suggesting a third parallel reaction, first-order with respect to Mn(II) concentration but zero-order with respect to H^+ concentration. The obtained results can be described by the following equation:

$$[4] \quad k_{obs} = k_a + k_b[H^+] + k_c[\text{Mn(II)}]$$

From the slopes and intercepts of k_{obs} vs. H^+ concentration plots for different initial Mn(II) concentrations, k_a, k_b, and k_c values can be evaluated (Table 1).

For Mn(II) concentrations ranging from 0.5×10^{-4} to $3.0 \times 10^{-4}\ M$, H^+ concentrations ranging from 0.08 to 0.75 M and initial Mn(II) concentrations ranging from 0 to $2 \times 10^{-2}\ M$, the pseudo first-order constant values calculated from eq. [4] usually agree with the experimental ones, k_{obs}, within ±2%.

Reaction mechanism

The following mechanism, through three parallel pathways, is consistent with the experimental results

$$[5] \quad Mn(CN)_6^{2-} + H_3O^+ \overset{K}{\rightleftharpoons} Mn(CN)_5(CNH)^- + H_2O$$

$$[6] \quad Mn(CN)_6^{2-} \xrightarrow{k_a} Mn(CN)_4^{2-} + (CN)_2$$

$$[7] \quad Mn(CN)_4^{2-} + 4H_3O^+ + 2H_2O \xrightarrow{\text{fast}} Mn(H_2O)_6^{2+} + 4HCN$$

$$[8] \quad Mn(CN)_5(CNH)^- \xrightarrow{k_b'} Mn(CN)_3(CNH)^- + (CN)_2$$

$$[9] \quad Mn(CN)_3(CNH)^- + 3H_3O^+ + 3H_2O \xrightarrow{\text{fast}} Mn(H_2O)_6^{2+} + 4HCN$$

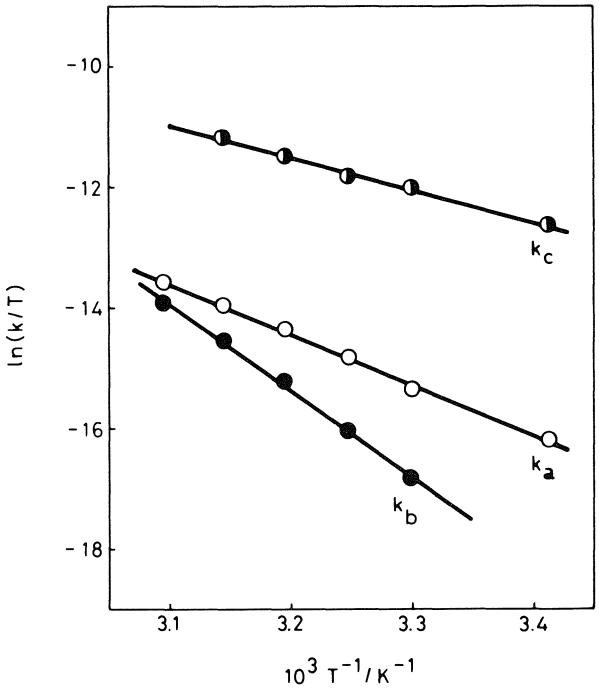

FIG. 4. Plots of ln (k/T) vs. T^{-1} for the decomposition of hexacyanomanganate(IV) in acidic solution. Mn(IV), $2.5 \times 10^{-4}\ M$; H^+, 0.16 M; I, 2.

$$[10] \quad Mn(CN)_6^{2-} + Mn(H_2O)_6^{2+} \xrightarrow{k_c} Mn(CN)_6^{2-}.Mn(H_2O)_6^{2+}$$

$$[11] \quad Mn(CN)_6^{2-}.Mn(H_2O)_6^{2+} + 4H_3O^+ + 2H_2O \xrightarrow{\text{fast}} 2Mn(H_2O)_6^{2+} + (CN)_2 + 4HCN$$

$Mn(CN)_5(CNH)^-$ (reactions [5] and [8]) and $Mn(CN)_3(CNH)^-$ (reactions [8] and [9]) are species partially protonated on the nitrogen of one of the coordinated cyano groups, as reported for some other cyano complexes (8). Reactions [6], [8], and [10] follow the equilibrium step [5] and they are the limiting steps of the three afore-mentioned parallel pathways: (*a*) monomolecular decomposition of the $Mn(CN)_6^{2-}$ ion, (*b*) monomolecular decomposition of the species $Mn(CN)_5(CNH)^-$, and (*c*) bimolecular interaction with Mn(II) ions (adduct formation). Reactions [7], [9], and [11] must proceed through consecutive steps and they are fast, so that none of them exert influence on the rate law.

Participation of Mn(II) ion in path (*c*) must be considered catalytic in nature, as this species remains unaltered at the end of each reaction cycle (reaction sequence [10], [11]). Moreover, since Mn(II) is also a product of the Mn(IV) reduction, the process is actually autocatalytic. Mn(II) appears to be present in the solution as the hexaaquocomplex, $Mn(H_2O)_6^{2+}$, rather than as any other complex with some anionic species; the kind of acid used as reaction medium (H_2SO_4, $HClO_4$, HCl, or HNO_3) shows no effect on the reaction rate.

From the proposed mechanism the following rate law is deduced:

$$[12]\quad \text{Rate} = -\frac{d[Mn(IV)]}{dt} = \left\{\frac{k_a}{1+K[H_3O^+]} + \frac{k'_b}{1+\dfrac{1}{K[H_3O^+]}} + \frac{k_c}{1+K[H_3O^+]}[Mn(H_2O)_6^{2+}]\right\} \times [Mn(IV)]$$

and if $K[H_3O^+] \ll 1$, eq. [12] becomes:

$$[13]\quad \text{Rate} = \{k_a + k_b[H_3O^+] + k_c[Mn(H_2O)_6^{2+}]\}[Mn(IV)]$$

where $k_b = k'_bK$. Equation [13] agrees with the experimental results derived from eq. [4].

Activation parameters

If the k_a, k_b, and k_c values are calculated, as previously stated at different temperatures, activation parameters can be estimated. Figure 4 shows plots of ln (k/T) vs. $1/T$ for the rate constants k_a, k_b, and k_c. The $\Delta H^{\ddagger}$ and $\Delta S^{\ddagger}$ values can be obtained for each constant from the slopes and intercepts (see Table 1).

1. G. Trageser and H. H. Eysel. Inorg. Nucl. Chem. Lett. **14**, 65 (1978).
2. G. Lopez-Cueto and A. Alonso-Mateos. Anal. Lett. **11**, 43 (1978).
3. G. Lopez-Cueto and J. Hernandez-Mendez. Quim. Anal. **28**, 160 (1974).
4. G. Trageser and H. H. Eysel. Z. anorg. allg. Chem. **420**, 273 (1976).
5. G. Trageser and H. H. Eysel. Inorg. Chim. Acta, **26**, L56 (1978).
6. G. Brauer. Química Inorgánica Preparativa. *Edited by* Reverté. Barcelona, Spain. 1958.
7. F. Lucena-Conde, J. Hernandez-Mendez, and G. Lopez-Cueto. Quim. Anal. **28**, 106 (1974).
8. R. J. Gillespie and R. Hulme. J. Chem. Soc. Dalton, 1261 (1973).

An infrared study of the interaction between ethyl *N*-(diphenylmethylene)glycinate with proton donors: comparison with *N*-benzylidenemethylamine

MARLEEN RUYSEN AND THÉRÈSE ZEEGERS-HUYSKENS
Department of Chemistry, University of Leuven, Celestijnenlaan 200F, 3030 Heverlee, Belgium

Received April 25, 1986

MARLEEN RUYSEN and THÉRÈSE ZEEGERS-HUYSKENS. Can. J. Chem. **64**, 2305 (1986).

The interaction between ethyl *N*-(diphenylmethylene)gylcinate (DPG) and hydroxy proton donors or pyrrole has been investigated by ir spectrometry. The equilibrium constants, enthalpies, and entropies of complex formation have been determined in carbon tetrachloride solution and compared with the data obtained for the complexes involving *N*-benzylidenemethylamine and the same proton donors. The ir spectra studied mainly in the ν_{OH}, $\nu_{C=N}$, $\nu_{C=O}$, and ν_{C-O} regions suggest that hydrogen bond formation occurs at the N atom of the imino group and at the O atom of the carbonyl group. The results are discussed in terms of the basicity at the two acceptor sites and of the accessibility of the lone pair of electrons. The ir spectra of the solid adduct of DPG with HCl show that protonation takes place on the N atom. The protonated structure is possibly stabilized by an intramolecular hydrogen bond.

MARLEEN RUYSEN et THÉRÈSE ZEEGERS-HUYSKENS. Can. J. Chem. **64**, 2305 (1986).

Utilisant la spectroscopie infrarouge, on a étudié l'interaction entre le *N*-(diphénylméthlène) glycinate d'éthyle (DPG) et des donneurs de protons hydroxylés ou le pyrrole. Opérant dans le tétrachlorure de carbone, on a déterminé les constantes d'équilibre, les enthalpies et les entropies de formation des complexes et on les a comparées avec les données obtenues pour des complexes impliquant la *N*-benzylidèneméthylamine et les mêmes donneurs de protons. Les spectres ir, qui ont été étudiés principalement dans les régions ν_{OH}, $\nu_{C=N}$, $\nu_{C=O}$ et ν_{C-O}, suggèrent que la liaison hydrogène se forme au niveau de l'atome d'azote de la fonction imino et au niveau de l'atome d'oxygène du groupement carbonyle. On discute des résultats en fonction de la basicité des deux sites accepteurs ainsi que de l'accessibilité de la paire d'électrons libres. Les spectres ir de l'adduit solide de DPG avec du HCl démontrent que la protonation se produit au niveau de l'atome d'azote. Il est possible que la structure protonée soit stabilisée par une liaison hydrogène intramoléculaire.

[Traduit par la revue]

Introduction

In recent years, there has been much interest on the proton acceptor ability of Schiff bases and on the spectroscopic characteristics of these complexes which undergo important changes when the hydrogen bonding in the solvent changes from non-polar to polar. These studies have been done using conventional infrared or Raman spectroscopies (1–5), resonance Raman spectroscopy (6–10), flash induced differential, kinetic infrared spectroscopy (11, 12), ^{13}C (13, 14) and ^{15}N nmr spectroscopy (15), or both nmr and uv spectroscopy (16–18). Recently, the possibility of a double well potential in the proton bridge of visual pigments interacting with proton donors has been discussed (19, 20). In most of these studies, proton donors such as halogenated alcohols, carboxylic acids, or hydrochloric acid have been studied and it was found that the strength of the interaction and the shape of the proton potential depended on their intrinsic acidity.

Despite the biological interest in the Schiff bases and the importance of their interactions with proton donors in biological media, the thermodynamic parameters for hydrogen bond formation have not been reported in the literature. In this work, we report the formation constants, the enthalpies, and entropies of complex formation for the interaction between ethyl *N*-(diphenylmethylene)glycinate (DPG)

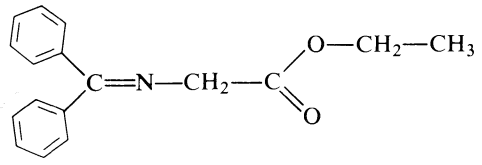

DPG

with 2,2,2-trichloroethanol, phenol derivatives, and pyrrole that are very often taken as reference acids in hydrogen bond studies (21). Owing to the lack of quantitative data for the interaction between proton donors and bases containing an imino nitrogen atom, the results will be compared with those obtained in this work for *N*-benzylidenemethylamine (BMA)

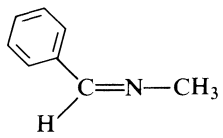

BMA

DPG possesses two interaction sites available for hydrogen bonding formation and the study of the infrared spectrum in the 3500–1000 cm^{-1} region allows one to elucidate the nature of the interaction.

Finally, the infrared spectrum of the solid adduct with HCl will be discussed.

Experimental

The spectra have been recorded on the PE 325 and 580B spectrophotometers.

The equilibrium constants (K) have been calculated from the absorbance of the ν_{OH} band (hydroxylic derivatives) or of the ν_{NH} band (pyrrole). To avoid self-association, the formal concentrations of proton donors (F_A) was kept low and varied between 3 and 10 $\times$ 10^{-3} M. The initial concentrations of base (F_B) ranged between 1 and 3 $\times$ 10^{-2} M. The concentration of free donor C_A has been computed by the expression

$$C_A = A/\epsilon d$$

A, ϵ, and d being the absorbances of the free ν_{OH} (or ν_{NH}) band, ϵ the molar extinction coefficient, and d the cell length. The equilibrium constant was further computed by the expression

$$K = \frac{C_{AB}}{C_A C_B} = \frac{F_A - C_A}{C_A(F_B - C_{AB})}$$

where C_{AB} and C_B are the molar concentrations of the complex and free base, respectively.

TABLE 1. Formation constants (K) at 298 and 323 K, enthalpies, and entropies of formation for complexes between DPG and proton donors*

Proton donor	K^{298K*} (L mol^{-1})	K^{323K*} (L mol^{-1})	$-\Delta H^0$ (kJ mol^{-1})	$-\Delta S^0$ (J mol^{-1} K^{-1})
2,2,2-triCl ethanol	8.5	5.4	14.4	30.6
Phenol	18.5	10.7	17.5	34.5
3,5-DiCl phenol	144	63.8	26.2	46.6
3-CF_3, 4-NO_2 phenol	844	330	30	44.6
Pyrrole	3.8	2.9	8.1	16.1

*Standard deviation lower than 5%. Solvent = carbon tetrachloride.

TABLE 2. Formation constants at 298 and 323 K, enthalpies, and entropies of formation for complexes between BMA and proton donors

Proton donor	K^{298K*} (L mol^{-1})	K^{323K*} (L mol^{-1})	$-\Delta H^0$ (kJ mol^{-1})	$-\Delta S^0$ (J mol^{-1} K^{-1})
2,2,2-triCl ethanol	5.4	2.9	19.4	51.1
Phenol	12.6	5.9	24.4	60.8
3,5-diCl phenol	83	32.7	29.8	63.3
3-CF_3, 4-NO_2 phenol	208	82	30.2	57.1
Pyrrole	1.3	1	8.3	25.7

*Solvent = carbon tetrachloride.

The enthalpies and entropies of complex formation have been calculated from the equilibrium constants determined at 298 and 323 K.

The infrared spectra in the ν_{OH} (ν_{NH}), $\nu_{C=N}$, $\nu_{C=O}$, and ν_{C-O} regions have been recorded at higher concentrations of proton donors (0.01 to 1 M) and proton acceptors (0.03 to 0.20 M) in order to obtain higher complex concentrations in solution. The solvents were CCl_4 (3800–3000 cm^{-1}), CH_2Cl_2 (1800–1600 cm^{-1}), and CS_2 (1250–1100 cm^{-1}).

The solvents were dried by standard methods. DPG was prepared from the corresponding benzophenone imine and the amino ester salt according to published procedure (22); BMA was provided by Professor G. L'abbé. The solid adduct of DPG with HCl was prepared by passing gaseous HCl through a chloroform solution of DPG; the spectrum of the resulting precipitate was taken in a KBr pellet.

Results and discussion

Interaction with hydroxy derivatives and with pyrrole

Table 1 lists the equilibrium constants, the enthalpies and entropies of formation for the complexes between DPG and 2,2,2-trichloroethanol, three phenol derivatives, and pyrrole. The hydroxylic proton donors have been chosen to cover a wide range of pK_a (12 to 6). It is also noteworthy that these phenol derivatives and pyrrole are often taken as reference acids in hydrogen bond studies and as a result their proton donor ability towards a given base can be compared with previously studied systems.

Table 2 gives the values of the same parameters for the BMA complexes.

Comparison of these data shows that the formation constants of the DPG complexes are higher than those reported for complexes involving the same proton donors and aliphatic esters; for the complex between 3,5-diCl phenol and methylacetate the K value is about 40 L mol^{-1} (23) and for the complex between the same ester and pyrrole a K value of 1.3 has been reported in the literature (24). At this stage of the discussion, it is difficult to compare the enthalpies and entropies of complex formation.

As mentioned in the Introduction, DPG has two basic sites

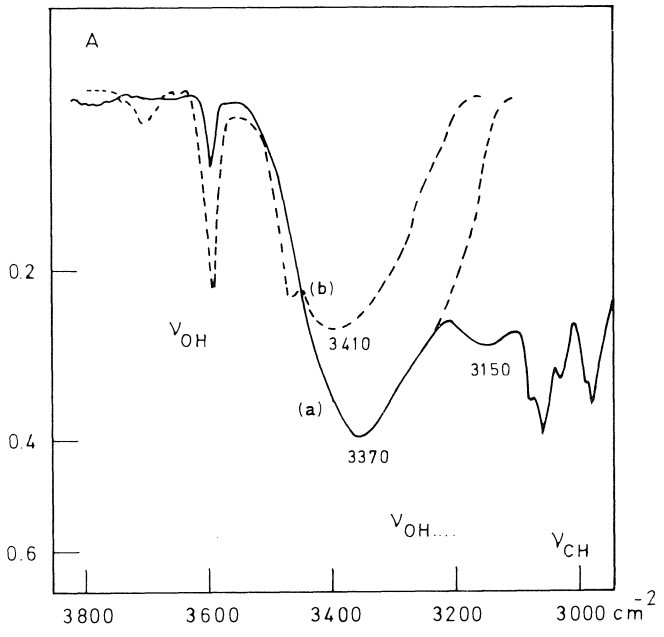

FIG. 1. Infrared spectra (3800–3000 cm^{-1}): (a) DPG (0.14 M) + 3,5-diCl phenol (0.014 M), d = 0.3 cm; (b) methylacetate (0.057 M) + 3,5-diCl phenol (0.06 M). Solvent = CCl_4.

available for hydrogen bonding, the oxygen atom of the carbonyl group and the nitrogen atom of the imino group. As shown in Fig. 1, two complex bands are observed in the ν_{OH} region. For comparison, the spectrum of the complex of methylacetate and the same hydroxylic derivative is also reproduced. For this last complex only one nearly symmetrical band is observed at about the same wavenumber. These two absorptions were observed for the hydroxylic proton donors and the observed wavenumbers depend on their acidity (Table 3). By analogy with the ester complexes having $\nu_{OH...O=C}$ bands

TABLE 3. $\tilde{\nu}/cm^{-1}$ of the bands observed in the $\nu_{OH(NH)}$ region

Proton donor	$\tilde{\nu}^{*}_{OH(NH)}$	$\Delta\tilde{\nu}$†	$\tilde{\nu}_{OH(NH)}$	$\Delta\tilde{\nu}$
2,2,2-triCl ethanol	3450	145	3290	305
Phenol	3440	170	3200	410
3,5-diCl phenol	3370	225	3150	445
3-CF_3, 4-NO_2 phenol	3350	240	3120	470
Pyrrole	3410	82	—	—

*Error on the absorption maxima = $\pm 10\ cm^{-1}$.

†Defined as the wavenumber of the free and complexed $\nu_{OH(NH)}$ band; the free bands ν_{OH} are observed between 3610 and 3595 cm^{-1}; the free ν_{NH} band of pyrrole is observed at 3492 cm^{-1}.

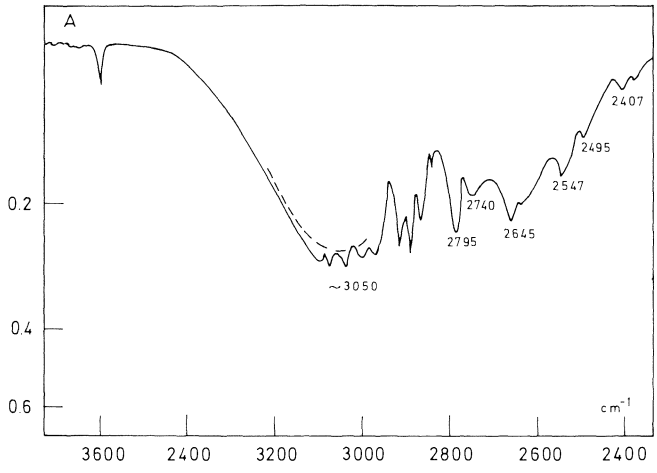

FIG. 2. Infrared spectra in the ν_{OH} range of BMA (0.17 *M*) + 3,5-diCl phenol (0.015 *M*), d = 0.2 cm, solvent = CCl_4.

between 3450 and 3350 cm^{-1} (21), the first band is attributed to hydrogen bonds formed on the ester group in DPG. This assignment is strengthened by the shift of the $\nu_{C=O}$ band to lower wavenumbers ($\Delta\nu_{C=O}$ = −18–20 cm^{-1} for all the complexes) and by the shift of the ν_{C-O} band to higher frequencies ($\Delta\nu_{C-O}$ = +13–15 cm^{-1}); such behaviour is typical for hydrogen bonds formed on an ester group (23). The second band is assigned to complexes formed on the imino nitrogen atom. Frequency shifts of 400–500 cm^{-1} are frequently observed for OH...N(sp^2) hydrogen bonds (21). The spectrum of the BMA complex is shown in Fig. 2 for comparison and a broad band (maximum near 3050 cm^{-1}) with several submaxima is observed; the same spectroscopic behaviour has been noticed for the pyridine–phenol complex and the submaxima have been attributed to a Fermi resonance with the internal modes of the proton donor moiety (25). The $\nu_{C=N}$ band of DPG at 1625 cm^{-1} becomes broader but does not show any shift (Fig. 3). This was also observed by Sandorfy *et al.* (2) who noticed the insensitivity of the $\nu_{C=N}$ band of *N*-benzylideneaniline to hydrogen bonding.

The concentration of OH...O=C complexes was estimated by computing the integrated absorption intensity of the complexes involving the same proton donor and methylacetate. The concentration of OH...O=C complexes was calculated by supposing that this intensity is the same in the DPG complexes. The concentration of OH...N complexes was then computed from the difference between the total concentration of complexes (calculated from *K*) and the concentration of OH...O=C species. It was found that in all the cases, about 60% of OH...O=C complexes are formed.

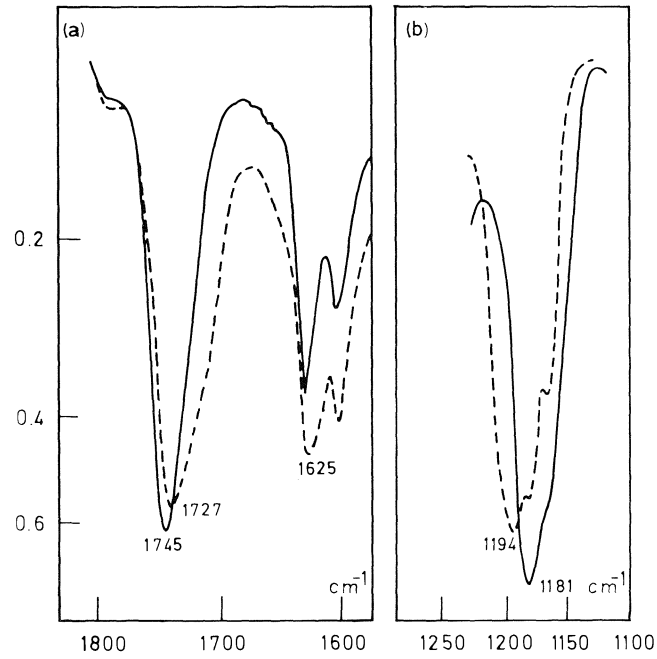

FIG. 3. Infrared spectra in the $\nu_{C=O}$ and $\nu_{C=N}$ region (*a*) and in the ν_{C-O} region (*b*). (*a*) — DPG (0.03 *M*), --- DPG + 2,2,2-triCl ethanol (1 *M*), d = 0.075 cm, solvent = CH_2Cl_2; (*b*) — DPG (0.05 *M*), --- DPG + 3,5-diCl phenol (0.08 *M*), solvent = CS_2.

The $-\Delta H^0$ and $-\Delta S^0$ values reported in Table 1 are in fact the sum of two contributions and the classical correlations $-\Delta H$ vs. $\Delta\nu_{OH}$ could not be discussed in this work. However, we can compare the position of the two complex bands in the 3,5-diCl-phenol. DPG complex (3370 and 3150 cm^{-1}) with that of the complex between the same proton donor complexed with methylacetate (3410 cm^{-1}) and with BMA (3050 cm^{-1}). Although these two last bases do not have exactly the same degree of substitution as DPG, the comparison suggests that in DPG, the carbonyl complex is a little bit stronger than in methylacetate and that the imino complex is somewhat weaker than in BMA. This can be explained by a small delocalization of the electrons from the nitrogen to the carbonyl oxygen atom

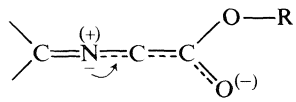

that makes the nitrogen atom less basic and the oxygen atom more basic than in the individual imino- or ester bases; this has been discussed previously for enamino ketones (26).

However, another important factor governing the occupation of the different basic sites of a polyfunctional base (27) is the *accessibility* of the lone pair. It has indeed been found recently that in (diphenylmethylene)amino acetonitrile (28)

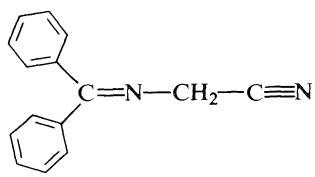

only C≡N...H—O— hydrogen bonds are formed. This violates the general rule that the energy of the hydrogen bond increases with decreasing amount of *s* character in the lone pair (29, 30). This rule predicts a higher hydrogen bond energy for

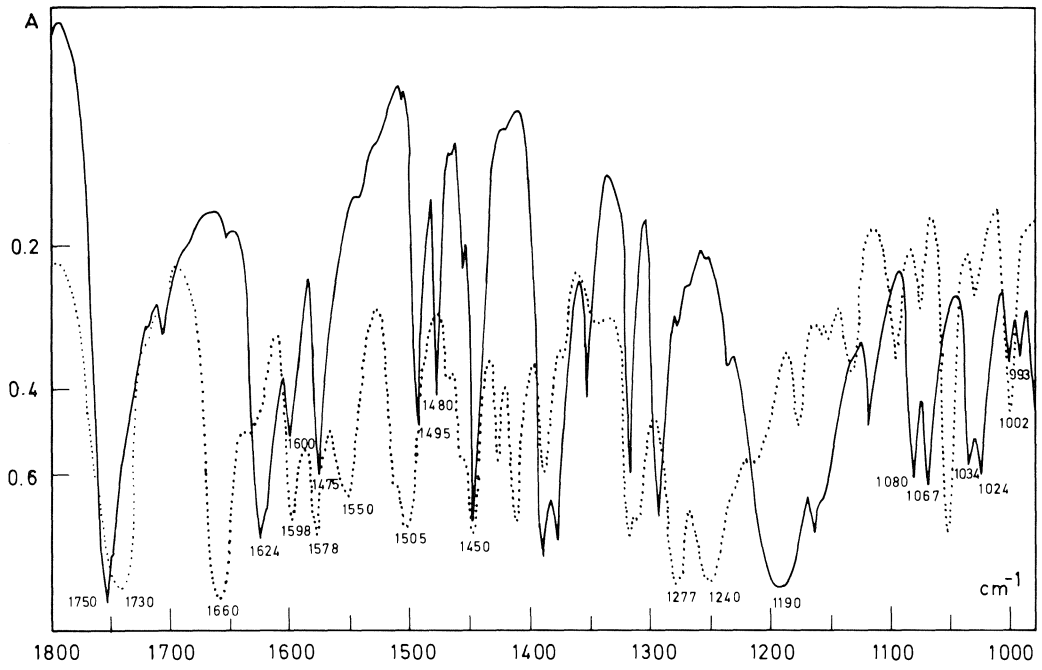

FIG. 4. Infrared spectrum (1800–1000 cm^{-1}), — DPG, --- DPG.HCl adduct (KBr pellet).

the imino nitrogen atom having close to sp^2 hybridization than for the nitrile nitrogen atom having a *sp* geometry. It can thus be concluded that the hydrogen bond interaction site cannot be predicted by energetic considerations alone, but is also governed by the accessibility of the free electron pair(s).

Interaction with HCl

The infrared spectra (1800–1000 cm^{-1}) of DPG and its solid adduct with HCl are reproduced in Fig. 4. Although a complete assignment of the vibrational modes of DPG is difficult, the 1800–1000 cm^{-1} region contains mainly the $\nu_{C=N}$ vibration at 1624 cm^{-1}, the $\nu_{C=O}$ and ν_{C-O} vibrations at 1750 and 1190 cm^{-1}, the ring vibrations R_{8a} and R_{8b} at 1598 and 1578 cm^{-1}, the R_{19b} and R_{19a} vibrations at 1495 and 1480 cm^{-1}, and the in-plane deformations of the CH_2 and CH_3 groups between 1450 and 1350 cm^{-1}. The ring vibrations R_{18b}, R_{12}, and R_1 show in-phase out-of-phase splittings at 1080 and 1067, 1034 and 1024, 1002 and 993 cm^{-1}, respectively.

In the DPG—HCl adduct, the $\nu_{C=N}$ at 1624 cm^{-1} disappears, the R_{8a} and R_{8b} vibrations do not shift appreciably, and two new bands at 1660 and 1550 cm^{-1} are observed. This behaviour is characteristic of nitrogen protonated Schiff bases (2, 3). The $\nu_{C=N}$ band is shifted to higher wavenumbers and in order to explain this apparent anomaly, Aton *et al.* (3) have proposed that upon protonation the C=N—H^+ stretching and the —N—H^+ deformation are coupled. Consequently the ν(C=N—H^+) band occurs at frequencies higher than would otherwise be expected. The spectra thus strongly suggest that protonation occurs at the nitrogen atom of DPG and clearly, nitrogen protonation is favoured over carbonyl protonation, even when in solution, hydrogen bonds are formed on the two sites.

Now, as shown in Fig. 4, the ester vibrations undergo also protonation shifts, the $\nu_{C=O}$ band decreasing by about 25 cm^{-1} and the ν_{C-O} band increasing by more than 50 cm^{-1}. In the absence of secondary effects, protonation should leave the ester vibrations almost unchanged. These important frequency shifts can be explained by an intramolecular NH^+ hydrogen bond that should increase the delocalization in the ester function

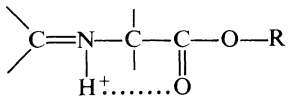

One can also note that the typical $NH^+...Cl^-$ band generally observed between 2600 and 2300 cm^{-1} is absent in the spectrum. A broad band near 3000 cm^{-1} is observed; this absorption could be assigned to water bound to Cl^- anions. This interpretation is supported by the absorption near 1630 cm^{-1} that can be assigned to the in-plane deformation mode of the water moieties. Therefore, it seems possible that the surrounding water molecules stabilize the preceding structure. A somewhat similar structure has been discussed in the Schiff base formation from ω-dimethylamino alkylamines (31).

Acknowledgements

Financial assistance from the University of Leuven and the National Fund of Research of Belgium is gratefully acknowledged.

1. J. W. LEDBETTER, JR. J. Phys. Chem. **81**, 54 (1977).
2. J. W. LEWIS and C. SANDORFY. Can. J. Chem. **60**, 1727 (1982).
3. B. ATON, A. G. DOUKAS, D. NARVA, R. H. CALLENDER, U. DINUR, and G. HONIG. Biophys. J. **29**, 79 (1980).
4. K. J. ROTSCHILD and H. MARRERO. Proc. Natl. Acad. Sci. USA, **79**, 4045 (1982).
5. F. SIEBERT, W. MÄNTELE, and K. GERVERT. Eur. J. Biochem. **136**, 119 (1983).
6. A. R. OSEROFF and R. H. CALLENDER. Biochemistry, **13**, 4243 (1974).
7. R. MATHIES, A. R. OSEROFF, and I. STRYER. Proc. Natl. Acad. Sci. USA, **73**, 1 (1976).
8. B. ATON, A. G. DOUKAS, R. H. CALLENDER, B. BECKER, and T. G. EBREY. Biochemistry, **16**, 2995 (1977).
9. T. DELATOUR, M. H. WARON, J. BELLOC, J. FAVROT, and C. DE LOZÉ. J. Raman Spectrosc. **15**, 147 (1984).
10. G. MASSIG, M. STOCKBURGER, and TH. ASLHUTH. Can. J. Chem. **63**, 2012 (1986).

11. F. SIEBERT and W. MÄNTELE. Biophys. Struct. Mech. **6**, 147 (1980).
12. W. HOFFMAN, F. SIEBERT, K. P. HOFMANN, and W. KREUTZ. Biochim. Biophys. Acta, **503**, 450 (1978).
13. J. SCHRIVER, G. D. MATEESCU, R. FAGER, D. TORCHIA, and E. W. ABRAHAMSON. Nature, **270**, 271 (1977).
14. G. D. MATEESCU, D. D. MUCCIO, W. G. COPAN, and E. W. ABRAHAMSON. J. Photochem. **17**, 63 (1981).
15. M. ALLEN and J. D. ROBERTS. J. Org. Chem. **45**, 130 (1980).
16. H. LE THANH and D. VOCELLE. Chem. Phys. Lett. **111**, 501 (1984).
17. M. BISSONNETTE, H. LE THANH, and D. VOCELLE. Can. J. Chem. **63**, 2298 (1985).
18. M. BISSONNETTE, H. LE THANH, and D. VOCELLE. Can. J. Chem. **63**, 1480 (1985).
19. J. M. LECLERCQ, P. DUPUIS, and C. SANDORFY. Croat. Chem. Acta, **55**, 105 (1982).
20. M. HODOSCEK and D. HADZI. Can. J. Chem. **63**, 1528 (1985).
21. M. D. JOESTEN and L. SCHAAD. Hydrogen bonding. Marcel Dekker Inc., New York. 1974.
22. M. J. O'DONNELL and R. L. POLT. J. Org. Chem. **47**, 2663 (1982).
23. L. VANDERHEYDEN and TH. ZEEGERS-HUYSKENS. J. Mol. Liq. **25**, 1 (1983).
24. J. A. PULLIN and R. L. WERNER. Spectrochim. Acta, **21**, 1257 (1965).
25. A. HALL and J. L. WOOD. Spectrochim. Acta, **23A**, 1257 (1967).
26. P. L. HUYSKENS and H. M. VAN BRABANT-GOVAERTS. J. Mol. Struct. **84**, 141 (1982).
27. O. KASENDE, E. VANDERHEYDEN, and TH. ZEEGERS-HUYSKENS. J. Heterocycl. Chem. **22**, 1647 (1985).
28. C. LAUREYS and TH. ZEEGERS-HUYSKENS. To be published.
29. J. G. VAN DUIJNEVELDT-VAN DE RIJDT and F. B. VAN DUIJNEVELDT. J. Am. Chem. Soc. **93**, 5644 (1971).
30. A. E. LUTSKII, A. I. MITICHKIN, and G. I. SHEREMET'EVA. Zh. Fiz. Khim. **49**, 1374 (1975).
31. T. OKUYAMA, H. SHIBUYA, and T. TUENO. J. Am. Chem. Soc. **104**, 730 (1982).

Basicity of the thionamide group of α-aminothionamides. Attenuation of electrostatic effects by solvation

MARTINO PAVENTI, FENTON HEIRTZLER, AND JOHN T. EDWARD
Department of Chemistry, McGill University, 801 Sherbrooke Street West, Montreal, Que., Canada H3A 2K6

Received March 13, 1986

MARTINO PAVENTI, FENTON HEIRTZLER, and JOHN T. EDWARD. Can. J. Chem. **64**, 2310 (1986).

The first dissociation constants pK_1 of four diprotonated α-aminothionamides, determined spectrophotometrically, are between −8.1 to −8.8; the second dissociation constants pK_2, of three of these compounds, determined titrimetrically, are between 7.3 and 7.7. Both pK_1 and pK_2 values are close to those calculated from current electrostatic theory for equilibria in solutions of zero ionic strength, in spite of the fact that data for pK_1 values were obtained in solutions of high ionic strength. Results indicate a much larger effect of the charged ammonium group on the basicity of the thionamide group than on the basicity of the amide group. A possible explanation based on the greater hydration of the protonated amide group is advanced.

MARTINO PAVENTI, FENTON HEIRTZLER et JOHN T. EDWARD. Can. J. Chem. **64**, 2310 (1986).

Utilisant des méthodes spectrophotométriques on a déterminé les premières constantes de dissociation (pK_1) de quatre α-aminothioamides diprotonés; comme étant entre −8,1 et −8,8; faisant appel à des méthodes titrimétriques, on a aussi déterminé les deuxièmes constantes de dissociation (pK_2) de trois de ces composés comme étant entre 7,3 et 7,7. Les valeurs tant des pK_1 que des pK_2 sont proches des valeurs calculées à partir de la théorie électrostatique actuelle sur les équilibres dans des solutions de force ionique égale à zéro, même si les données relatives aux valeurs de pK_1 sont obtenues dans des solutions de forces ioniques élevées. Les résultats indiquent que le groupement ammonium chargé provoque un effet beaucoup plus important sur la basicité du groupement thionamide que sur la basicité du groupement amide. On propose une explication plausible qui est basée sur une plus grande hydratation du groupement amide protoné.

[Traduit par la revue]

Starting more than 60 years ago with Bjerrum (1), a long succession of investigations has elaborated an electrostatic theory of substitutent effects which is gradually winning general acceptance (2–9). However, the electrostatic effect can be profoundly altered by the presence of a solvent, and although "emphasis has shifted from continuum electrostatics to interactions between specific functionalities in the ions and appropriate sites in a few solvent molecules" (10), a discontinuous solvation model (11) of quantitative (as opposed to qualitative) predictive power has been slow to emerge.

The older continuum solvent model was applied to electrostatic effects by Kirkwood and Westheimer (4) in 1938. As an example, we may consider the fact that the dissociation constant K_2 of monoprotonated glycine **2** would be expected to be higher than K_{AH} of the parent acid, acetic acid, because the substituted acetate ion **3** is stabilized by electrostatic interaction between NH_3^+ and the negatively charged carboxylate group.[1] On the other hand, further dissociation of **3** should be made more difficult than the dissociation of the parent methylammonium ion (K_{BH^+}) by the same electrostatic stabilization, the substituent now being CO_2^-. Classical electrostatic theory shows that both the elevation of K_2 and the depression of K_3 (with respect to K_{AH} and K_{BH^+}) should be given by

$$[1] \quad \Delta pK = \log (K_2/K_{AH}) = -\log (K_3/K_{BH^+}) = e^2/2.3\ kTRD_{eff}$$

where e is the electronic charge, k Boltzmann's constant, T the absolute temperature, R the distance between the charges, and D_{eff} the "effective" dielectric constant. D_{eff} generally lies somewhere between D_e, the dielectric constant of the external solvent, and D_i, the dielectric constant (assumed to be 2.0) of the hydrocarbon framework of the molecule. Kirkwood and Westheimer (4), Ehrenson (5), and others have furnished equations whereby for molecules of spheroidal or ellipsoidal shape D_{eff} can be calculated from D_e and from the shape of the molecule and the location of the charged centres within it.

Values of ΔpK thus calculated are usually in fair agreement with experiment when NH_3^+ and CO_2^- are separated by more than three methylene groups (12), but can be seriously in error for smaller values of R. Thus the experimental ΔpK_2 for **2** is only about half the calculated value, and the experimental ΔpK_3 for **3** has the wrong sign, **3** being a stronger acid than the parent methylammonium ion (12). The reasons for these failures of [1] at smaller distances R are not altogether clear, but may be due to the intrusion of effects other than monopole–monopole interactions: to inductive (13), solvation (12), or monopole–dipole effects (14). The last are given by

$$[2] \quad \Delta pK = e\mu \cos \theta/2.3\ kTR^2D_{eff}$$

where μ is the dipole moment of the substituent and θ is the angle made by the dipole vector and the line joining the mid-point of the dipole to the centre of the charged group (2). They can be ignored for large but not for small values of R.

Equations [1] and [2] apply to reactions or equilibria in solutions of zero ionic strength (13). Sometimes it is possible to extrapolate experimental results to zero ionic strength by use of a modified Debye–Hückel equation, as in the studies of Westheimer *et al.* (15) on the effect of charged substituents on the rates of hydrolysis of esters in very dilute sodium hydroxide solution. However, most chemical reactions require more concentrated solutions of electrolytes for which such an extrapolation is impossible, and so it becomes of interest to discover empirically for such reactions whether the electrostatic effect is still evident. The limited data available at present (e.g. refs. 16, 17) indicate that [1] and [2] may apply moderately well even in unideal situations (contrary to what might be expected (13)). Thus ΔpK_1 for diprotonated glycinamide **5** (parent compound: protonated acetamide) is −2.7 (16), close to ΔpK_2 of −2.31 for protonated glycine **2** (12), in spite of the fact that protonation of the amide group requires moderately concentrated sulfuric acid, so that the H_A acidity function must be used

[1]This exposition differs slightly from that usually given (2, 4), but has been justified previously (6, 10).

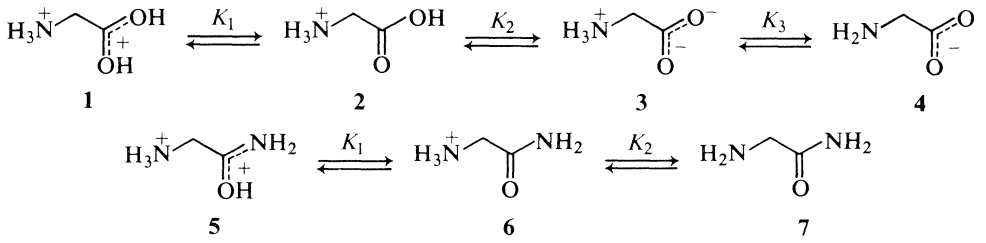

1 2 3 4

5 6 7

in measuring basicities (16). In these solutions the dielectric constant D_e will be reduced (18), and to a lesser extent D_{eff}; this might account for the larger ΔpK (−2.7). On the other hand, 100% sulfuric acid at 25°C has a dielectric constant of 100 (19), 28% higher than the dielectric constant of water, and so electrostatic effects in this solvent should be slightly reduced. The cryoscopic results of O'Brien and Niemann (20) show that the basicity of the carboxyl group in 100% sulfuric acid is decreased (relative to that of acetic acid) by the presence of the $—NH_3^+$ group in the series of protonated amino acids $H_3N^+(CH_2)_nCO_2H^+$, the effect diminishing progressively with increase of n from 1 to 4. A rough-and-ready calculation of ΔpK_1 values for **1** and its homologues from ionization ratios I (20) in 100% sulfuric acid is given in Table 1. Too many assumptions[2] are involved for the absolute values to be taken too seriously but the trend is unmistakable.

Most tests of [1] and [2] have involved compounds having charged or dipolar substituents in the vicinity of ionizable carboxyl or, more rarely, of ammonium groups. It would be useful to test [1] and [2] by observing the effects of charged substituents on the protonation of other groups. According to the continuum solvent model, ΔpK should be about the same for two molecules having different ionizable groups but similar geometry and charge separation R, the solvent attenuation depending only on D_{eff}. According to the newer discontinuous solvent models (10, 11), ΔpK might be different for two such molecules if solvation of the substituents or ionizing groups is grossly different. Accordingly, we have determined ΔpK_1 and ΔpK_2 values for four diprotonated α-aminothionamides of general structure **8**:

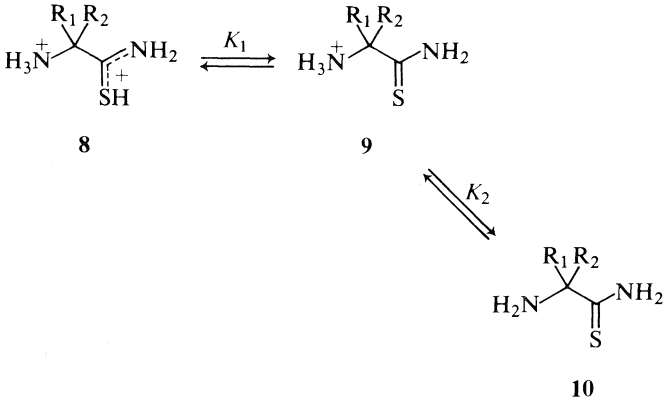

8 9 10

The thionamide grouping has an advantage over the amide grouping in giving more clear-cut changes in ultraviolet absorption spectrum upon protonation (26), which has been shown to follow the H_T acidity function (27). Thionamides, as shown in **8**, are *S*- and not *N*-protonated in strong mineral acid (28–30).

TABLE 1. Dissociation constants of $H_3N^+(CH_2)_nCO_2H_2^+(BH_2^{2+})$ in 100% sulfuric acid and of $H_3N^+(CH_2)_nCO_2H(AH)$ in water (relative to parent compounds)

	BH_2^{2+}			AH
n	I^a	pK^b	ΔpK^c	ΔpK^d
1	0.25	−6.1	−2.3	−2.1
2	2.3	−5.1	−1.3	−1.21
3	9.0	−4.5	−0.7	−0.73

[a]From ref. 20.
[b]See footnote 2 for assumptions in calculations.
[c]Acetic acid (pK_{BH^+} − 3.8) taken as parent acid.
[d]From ref. 12.

Experimental

Materials

2-Aminothionacetamide (**10**; $R_1 = R_2 = H$), 2-amino-2-methylthionpropionamide (**10**; $R_1 = R_2 = Me$), 1-aminocyclohexane-1-thioncarbonamide (**10**; $R_1R_2 = (CH_2)_5$), and 2-amino-3-phenylthionpropionamide (**10**; $R_1 = PhCH_2$, $R_2 = H$) were prepared by modifications (to be published later) of methods in the literature (31, 32). They were stored as the stable hydrochlorides.

Determination of dissociation constants

(a) By spectrophotometry of strongly acid solutions

The 2-aminothionamide hydrochlorides **9** in water or in aqueous sulfuric acid up to 60% w/w concentration all had ultraviolet absorption peaks at about 260 nm, like thionacetamide in water (31). In 96% sulfuric acid these peaks were shifted to about 245 nm, with a drop in intensity, like thionacetamide in 11.9 *M* hydrochloric acid (31), indicating the structure **8** for the diprotonated compounds. Ionization ratios [**8**]/[**9**] in intermediate concentrations (60–96%) of sulfuric acid were determined at 24°C spectrophotometrically, following procedures already described (27), and are available as supplementary material.[3] Plots of log [**8**]/[**9**] against H_T (27)[4] gave straight lines with slopes of 1.00–1.01 (correlation coefficients 0.996 or better), from which the pK_1 values given in Table 2 were obtained in the usual manner.

[2]It was assumed that protonation of the carboxyl group (21) was governed by the H_A function, and that for 100% H_2SO_4 $H_A = -5.5$ (22, 23), so that in this concentration of acid $pK = \log I - 5.5$. I ($\equiv [H_3N^+(CH_2)_nCO_2H_2^+]/[NH_3^+(CH_2)_nCO_2H]$) was obtained from ref. 20. Acetic acid is half-ionized in ca. 75% H_2SO_4 (24, 25), and so has $pK = -3.8$ (22).

[3]A complete set of tabulated data may be purchased from the Depository of Unpublished Data, CISTI, National Research Council of Canada, Ottawa, Ont., Canada K1A 0S2.

[4]A referee has suggested that pK_1 values of **8** should be obtained from plots of [**8**]/[**9**] against H_{T^+}, which should not coincide with H_T. This is not certain. Vetesnik *et al.* (33) established a H_+ scale by the Hammett–Deyrup overlap procedure, based on dilute aqueous solution as the standard state, for sulfuric acid concentrations up to 5.5 *M*; H_+ values do not differ appreciably from H_0 values over this concentration range. Gold (quoted by Brand *et al.* (34)) calculates that in 100% sulfuric acid $H_+ = H_0 - 0.28$. In any case, the evidence to date is that H_+ should differ only slightly from H_0, and presumably H_{T^+} only slightly from H_T.

TABLE 2. Dissociation constants K_1 and K_2 of protonated α-aminothionamides at 24°C

Compound	pK_1	ΔpK_1	pK_2	ΔpK_2
8, $R_1 = R_2 = H$	−8.39 ± 0.02	−5.83[a]	7.27 ± 0.03	−3.33[b]
8, $R_1 = R_2 = Me$	−8.75 ± 0.05	−6.34[a]	7.61 ± 0.02	−3.01[c]
8, $R_1R_2 = (CH_2)_5$	−8.08 ± 0.06	−5.58[a]	7.23 ± 0.03	−3.39[c]
8, $R_1 = PhCH_2$, $R_2 = H$	−8.63 ± 0.04	−6.24[a]	7.15 ± 0.02[d]	−2.68[e]

[a] pK_{BH^+} of parent protonated thionacetamide from ref. 35.
[b] pK_{BH^+} of 10.66 for parent methylammonium ion from ref. 36.
[c] pK_{BH^+} of 10.68 for parent *t*-butylammonium ion from ref. 36.
[d] At 25.0 ± 0.1°C; from ref. 37.
[e] pK_{BH^+} of 9.83 for parent β-phenylethylammonium ion from ref. 36.

(b) By titrimetry in dilute aqueous solution

The α-aminothionamide hydrochloride **8** (100–300 mg) in 10 mL of distilled water was titrated with 2 *N* sodium hydroxide solution at 24°, using a Radiometer (Copenhagen) TTT 80 titrator, ABU 80 auto burette, PHM 63 digital pH meter, and REC 80 servograph. The pK_2 values were obtained from the mid-points of the titration curves. The values recorded in Table 2 are the average of at least six titrations; effects of ionic strength have been taken into account using the Debye–Hückel equation.

(c) By rate measurements

Kinetic data were obtained at 60°C in solutions ranging from 24% to 85% aqueous sulfuric acid, using a Unicam SP-800 spectrophotometer to follow absorbance changes at 243–262 nm. The absorbance at infinite time was assumed to be given by that of a solution heated to 90°C for 2.5 h and then cooled to 60°C. Pseudo-first-order rate constants k_ψ are shown in Fig. 1.

Results and discussion

pK_1 values of diprotonated α-aminothionamides

The pK_1 values of the protonated thionamide groups of the four compounds in Table 2, determined by conventional spectrophotometric means, were much lower than anticipated. Consequently, it was considered worthwhile to confirm one of them by a kinetic method. This method depends on the fact that the pseudo-first-order rate constant k_ψ for the hydrolysis of thionamides (38, 39) (and also amides (40), thio-acids (41), thion-esters (42), and many other compounds) increases with acid concentration up to a maximum and then decreases (illustrated for thionacetamide in excess perchloric at 35°C (38) in Fig. 1). Such a rate – acid concentration profile is indicative of an A-2 mechanism, which for a thionamide is given by [3] and [4]:

[3] $$R{-}C(=S){-}NH_2 + H^+ \underset{}{\overset{K_{BH^+}}{\rightleftharpoons}} R{-}C(SH)=NH_2^+$$

[4] $$R{-}C(SH)=NH_2^+ + rH_2O \xrightarrow{k_2} R{-}C(SH)(NH_2)(O^+H_2) \rightarrow \text{products}$$

with the position of the maximum dependent, *inter alia*, on pK_{BH^+} (40). In fact, for ethyl thionbenzoate and seven substituted derivatives the maximum occurs in acid concentrations at which $H_T \cong pK_{BH^+}$ (43), and for thionacetamide the maximum

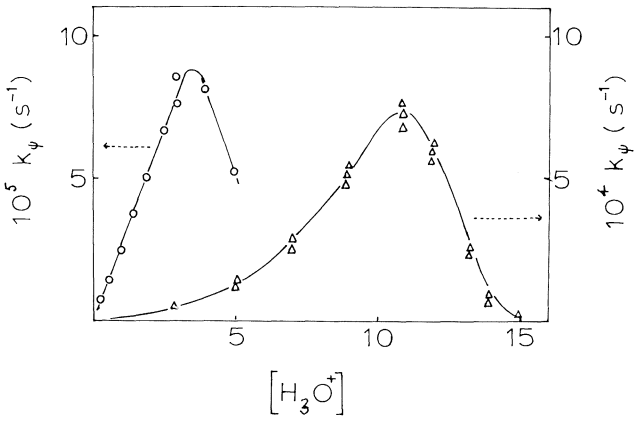

FIG. 1. Variation of pseudo-first-order rate constant k_ψ with molar concentration of acid for thionacetamide in perchloric acid at 35°C (○, ref. 32) and for α-aminothionacetamide in sulfuric acid at 60°C (△).

occurs at $H_T \approx -2.5$,[5] close to −2.56 for pK_{BH^+} (35). Consequently, the rate maximum for α-aminothionacetamide at $H_T = -8.5$ (Fig. 1) supports the pK_{BH^+} of −8.39 determined spectrophotometrically.[6]

Waring (45) has recently shown how pK_{BH^+} values may be obtained from kinetic data by various manipulations of the empirical rate expressions of Bunnett and Olsen (46) and of Yates and McClelland (47), which for moderately basic substrates contain pK_{BH^+} among other terms in the expression. However, the Yates–McClelland equation proved inapplicable to k_ψ for the acid-catalysed hydrolysis of thionacetamide and α-aminothionacetamide, giving curved and not straight-line plots (c.f. ref. 44). On the other hand, the Bunnett–Olsen equation, in the forms

$$[5] \quad \log k_\psi - \log\left(\frac{h_T}{h_T + K_1}\right) = \phi(H_0 + \log [H^+]) + \log k^0$$

$$[5a] \quad \log k_\psi + H_T = \phi(H_0 + \log [H^+]) - \log (h_T + K_1) + \log k^0$$

[5] Thionacetamide was hydrolysed in aqueous perchloric acid (38), for which no H_T scale has yet been determined. However, other acidity function scales almost coincide in perchloric and sulfuric acids of equal weight percent concentration (41), and we have assumed this to be true for H_T also.

[6] The rate curves in Fig. 1 were obtained at temperatures above 25°C, the temperature used for spectrophotometric determination of pK_{BH^+}. However, available evidence indicates that a change in temperature increases rates of hydrolysis but does not affect the rate profile or the position of the maximum (44).

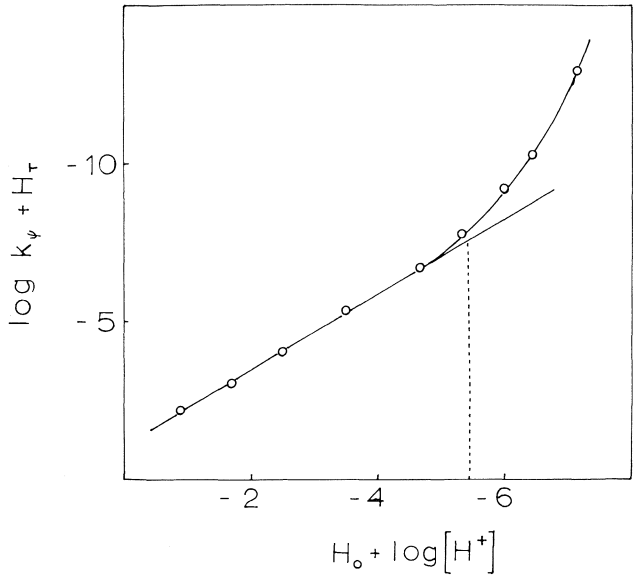

FIG. 2. Bunnett–Olsen plot for hydrolysis of α-aminothionacetamide in sulfuric acid at 60°C.

(see ref. 46 for definition of symbols) proved more useful. At low acidities $h_T \ll K_1$, and [5*a*] simplifies to

[6] $$\log k_\psi + H_T = \phi(H_0 + \log [H^+]) + pK_1 + \log k^0$$

which accounts for the straight-line portion of the experimental curve on the left-hand side of Fig. 2. At high acidities $h_T \gg K_1$, and [5*a*] simplifies to

[7] $$\log k_\psi + H_T = \phi(H_0 + \log [H^+]) + H_T + \log k^0$$

which accounts for the increasing divergence of the experimental curve from a straight line on the right-hand side of Fig. 2. At an acidity where $h_T = K_1$, [5*a*] becomes

[8] $$\log k_\psi + H_T = \phi(H_0 + \log [H^+] + pK_1 + \log k^0 + 0.3$$

and at this acidity the calculated curve should be 0.3 unit above the straight-line curve of [6]. As seen in Fig. 2, this divergence of 0.3 (shown by vertical line) is observed experimentally when $(H_0 + \log [H^+]) = -5.45$ and $H_T = -8.77$, in very rough agreement with the pK_1 value of −8.39 determined spectrophotometrically.

Different effect of the ammonium group on the basicity of the amide and thionamide groups: possible role of hydration in attenuating this effect

A ΔpK_2 of −5.42 may be calculated for protonated glycine **2** in water at 25°C from [1] (12), using D_{eff} according to Kirkwood and Westheimer (4). Since the molecular volume, shape, and intercharge distances of **3**, **5**, and **8** (R = H) are about the same, about the same ΔpK would be expected for all three compounds in a solvent of the same dielectric constant D_e if effects of ionic strength can be ignored. Lower values of D_e (and hence of D_{eff}) should lead to greater values of ΔpK, and so the ΔpK_1 values of Table 2 would appear to be in rough agreement with those calculated from [1]. (An exact comparison is impossible, because D_e values for aqueous sulfuric acid solutions are lacking (18).)

This would seem to indicate that the electrostatic effect of the $—NH_3^+$ group of **8** is not nullified by counter-ions, even in fairly concentrated sulfuric acid, but has about the value expected from [1]. Why, then, is the effect of $—NH_3^+$ group on the ionization of **5** and **2** ($\Delta pK \sim -2$) so much smaller? A partial answer may come from the fact that the protonated thionamide, according to much evidence (27), is less hydrated than the protonated amide group (and presumably than CO_2^-). It has been shown that to the extent that groups are hydrated, their electrostatic interaction with charged or dipolar substituents can be expected to be reduced (11). A difference in hydration would also explain the different Hammett ρ values for the ionization of protonated thionbenzamides (−1.29: ref. 35) and benzamides (−0.92: ref. 16) and the dissociation of benzoic acids (+1.00).

*Effect of the amide and thionamide groups on the acidity of the ammonium groups of **6** and **9** ($R_1 = R_2 = H$)*

We now consider the validity of [2] for explaining the ΔpK_2 values of Table 1. Since the substituent amide and thionamide groups of **6** and **9** ($R_1 = R_2 = H$) do not differ greatly in size or shape, we may expect R, $\cos\theta$, and D_{eff} to be approximately the same in these two compounds, so that the greater acidity of **9** ($R_1 = R_2 = H$) arises from the greater dipole moment of the thionamide group ($\mu = 4.53$ D for thionacetamide (48)) as compared with the amide group ($\mu = 3.8$ D for acetamide (48)):

[9] $$\frac{\Delta pK_1 (\mathbf{9}; R_1 = R_2 = H)}{\Delta pK_1 (\mathbf{6})} = \frac{4.53}{3.8} = 1.19$$

This result is in good agreement with the experimental ratio of 1.22 (49).

Conclusion

The present work indicates that in concentrated aqueous acid solutions the effect of the charged substituent $—NH_3^+$ on the protonation of the thionamide group is not cancelled by the high ionic strength, as might be expected (13), but rather has about the value calculated by [1] for infinitely dilute aqueous solution. In fact, the ionization behaviour of α-aminothionamides conforms better to [1] than does that of the α-aminocarboxylic acids. This suggests that a study of the ionization behaviour of other substituted thionamides in order to test [1] and [2] might be profitable.

Acknowledgment

The financial support of the Natural Sciences and Engineering Research Council of Canada is gratefully acknowledged.

1. N. BJERRUM. Z. Phys. Chem. **116**, 219 (1923).
2. A. EUCKEN. Z. Angew. Chem. **45**, 203 (1932).
3. A. M. SMALLWOOD. J. Am. Chem. Soc. **54**, 3048 (1932).
4. J. G. KIRKWOOD and F. H. WESTHEIMER. J. Chem. Phys. **6**, 506 (1938); F. H. WESTHEIMER, and J. G. KIRKWOOD. J. Chem. Phys. **6**, 513 (1938).
5. S. EHRENSON. J. Am. Chem. Soc. **98**, 7510 (1976).
6. W. F. REYNOLDS. Prog. Phys. Org. Chem. **14**, 165 (1983).
7. S. MARRIOTT and R. D. TOPSOM. J. Am. Chem. Soc. **106**, 7 (1984).
8. Z. FRIEDL. Can. J. Chem. **63**, 1068 (1985).
9. M. G. SIEGEL, C. L. LIOTTA, and D. J. CRAM. J. Am. Chem. Soc. **104**, 1387 (1982).
10. E. M. ARNETT. J. Chem. Educ. **62**, 385 (1985).
11. J. T. EDWARD. J. Chem. Educ. **59**, 354 (1982).
12. J. T. EDWARD, P. G. FARRELL, J. L. JOB, and B.-L. POH. Can. J. Chem. **56**, 1122 (1978).
13. A. J. HOEFNAGEL, M. A. HOEFNAGEL, and B. M. WEPSTER. J. Org. Chem. **43**, 4720 (1978).
14. J. KIRCHNEROVA, P. G. FARRELL, J. T. EDWARD, J.-C. HALLE, and R.SCHAAL. Can. J. Chem. **56**, 1130 (1978).

15. F. H. WESTHEIMER and N. W. SHOOKOFF. J. Am. Chem. Soc. **61**, 555 (1939); F. H. WESTHEIMER, W. A. JONES, and R. A. LAD. J. Chem. Phys. **10**, 468 (1942).
16. K. YATES and J. B. STEVENS. Can. J. Chem. **43**, 529 (1965).
17. J. T. EDWARD, S. C. WONG, A. J. KRESGE, and M. F. POWELL. Can. J. Chem. **62**, 2448 (1984).
18. J. B. HASTED, D. M. RITSON, and C. H. COLLIE. J. Chem. Phys. **16**, 1 (1948).
19. J. C. D. BRAND, J. C. JAMES, and H. RUTHERFORD. J. Chem. Soc. 2447 (1953); R. J. GILLESPIE and R. H. COLE. Trans. Faraday Soc. **52**, 1325 (1956); R. J. GILLESPIE and R. F. M. WHITE. Trans. Faraday Soc. **54**, 1846 (1958).
20. J. L. O'BRIEN and C. NIEMANN. J. Am. Chem. Soc. **73**, 4264 (1951).
21. J. T. EDWARD and S. C. WONG. J. Am. Chem. Soc. **99**, 4229 (1977).
22. J. T. EDWARD and S. C. WONG. Can. J. Chem. **55**, 2492 (1977).
23. R. A. COX and K. YATES. J. Am. Chem. Soc. **100**, 3861 (1978).
24. A. R. GOLDFARB, A. MELE, and N. GUTSTEIN. J. Am. Chem. Soc. **77**, 6194 (1955).
25. N. C. DENO, C. H. PITTMAN, and M. J. WISOTSKY. J. Am. Chem. Soc. **86**, 4370 (1964).
26. M. J. JANSSEN. Rec. Trav. Chim. **79**, 454 (1960).
27. J. T. EDWARD, I. LANTOS, G. D. DERDALL, and S. C. WONG. Can. J. Chem. **55**, 812 (1977).
28. I. C. WANG. Ph.D. Thesis. McGill University, Montreal, Que. 1963.
29. T. BIRCHALL and R. J. GILLESPIE. Can. J. Chem. **41**, 2642 (1963).
30. G. A. OLAH and A. T. KU. J. Org. Chem. **35**, 331 (1970).
31. A. H. COOK, I. HEILBRON, and A. H. MAHADEVAN. J. Chem. Soc. 1061 (1949).
32. F. ASINGER, W. SCHÄFER, M. MEISEL, H. KERSTEN, and A. SAUS. Monatsh. Chem. **98**, 338 (1967).
33. P. VETEŠNÍK, J. BIELARSKÝ, and M. VEČEŘA. Coll. Czech. Chem. Comm. **33**, 1687 (1968).
34. J. C. D. BRAND, W. C. HORNING, and M. B. THORNLEY. J. Chem. Soc. 1374 (1952).
35. J. T. EDWARD, G. D. DERDALL, and S. C. WONG. Can. J. Chem. **55**, 2331 (1977).
36. D. D. PERRIN. Dissociation constants of organic bases in aqueous solution. Butterworths, London. 1965.
37. H. R. ALMOND, R. J. KERR, and C. NIEMANN. J. Am. Chem. Soc. **81**, 2856 (1959).
38. D. ROSENTHAL and T. I. TAYLOR. J. Am. Chem. Soc. **79**, 2684 (1957).
39. J. T. EDWARD, G. D. DERDALL, and S. C. WONG. J. Am. Chem. Soc. **100**, 7023 (1978).
40. J. T. EDWARD, and S. C. R. MEACOCK. J. Chem. Soc. 2000 (1957).
41. J. T. EDWARD, G. WELCH, and S. C. WONG. Can. J. Chem. **56**, 935 (1978).
42. J. T. EDWARD, S. C. WONG, and G. WELCH. Can. J. Chem. **56**, 931 (1978).
43. S. C. WONG. Ph.D. Thesis. McGill University, Montreal, Que. 1974.
44. C. R. SMITH and K. YATES. J. Am. Chem. Soc. **93**, 6578 (1971).
45. A. J. WARING. J. Chem. Soc. Perkin II, 1029 (1979).
46. J. F. BUNNETT and F. P. OLSEN. Can. J. Chem. **44**, 1917 (1966).
47. K. YATES and R. A. MCCLELLAND. J. Am. Chem. Soc. **89**, 2686 (1967).
48. A. L. MCCLELLAN. Tables of experimental dipole moments. Vol. 2. Rahera Enterprises, El Cerrito, CA, U.S.A., 1974.
49. S. P. DATTA and B. R. RABIN. Trans. Faraday Soc. **52**, 1117 (1956); M. ZIEF and J. T. EDSALL. J. Am. Chem. Soc. **59**, 2245 (1937).

Energy partitioning in $O(^1D_2)$ reactions. III.[1] $O(^1D_2) + NH_3 \rightarrow OH(v') + NH_2$

P. M. AKER, J. J. A. O'BRIEN, J. M. PARSONS, AND J. J. SLOAN

Division of Chemistry, National Research Council of Canada, 100 Sussex Drive, Ottawa, Ont., Canada K1A 0R6 and Ottawa–Carleton Chemistry Institute, Carleton University, Col. By Drive, Ottawa, Ont., Canada K1S 5B6

Received June 4, 1986

P. M. AKER, J. J. A. O'BRIEN, J. M. PARSONS, and J. J. SLOAN. Can. J. Chem. **64**, 2315 (1986).

The vibrational distribution in the OH created by the reaction of $O(^1D_2)$ atoms with NH_3 has been recorded directly using low pressure infrared emission spectroscopy. The relative kinetic energy of the reagents is Boltzmann at 300 K. The OH product vibrational levels are populated statistically, indicating that the reaction probably involves a long-lived ONH_3 intermediate. There is some evidence that this may not be the case at higher reagent translational energies.

P. M. AKER, J. J. A. O'BRIEN, J. M. PARSONS et J. J. SLOAN. Can. J. Chem. **64**, 2315 (1986).

Faisant appel à la spectroscopie d'émission infrarouge à basse pression, on a enregistré directement la distribution vibrationnelle du OH qui est créé par la réaction des atomes de $O(^1D_2)$ avec le NH_3. A 300 K, l'énergie cinétique relative des réactifs est celle de Boltzmann. Il y a une distribution statistique des niveaux vibrationnels du produit OH et ceci indique que la réaction implique probablement un intermédiare ONH_3 possédant une longue vie. Quelques données suggèrent que tel ne serait pas le cas à des énergies de translation des réactifs qui seraient plus élevées.

[Traduit par la revue]

Introduction

Reaction of $O(^1D_2)$ with ammonia to produce the OH radical can proceed through two energetically-allowed channels;

[1] $O(^1D_2) + NH_3 \rightarrow OH(X^2\Pi, v) + NH_2(X^2B_1)$
$\Delta H_0^0 = -187.0$ kJ/mol

[2] $O(^1D_2) + NH_3 \rightarrow OH(X^2\Pi, v) + NH_2(A^2A_1)$
$\Delta H_0^0 = -64.4$ kJ/mol

The energy partitioning in reactions [1] and [2] has been measured previously (1–3) by combining laser photolysis of ozone at 266 nm (to generate $O(^1D_2)$) with laser-induced fluorescence detection of the OH product on the $A^3\Sigma \leftarrow X^2\Pi$ transition. The rotational excitation produced in the $v' = 0$ and $v' = 1$ vibrational states of the OH was reported in refs. 1 and 3 and the ratio of the populations in these two vibrational levels was also reported to be 1.0:0.66. In ref. 2, the $P(v' = 1)/P(v' = 0)$ ratio was given as 1.5 and an estimate of the $P(v' = 2)/P(v' = 0)$ ratio was given as 2.1. The exoergicity of the reaction $O(^1D_2) + NH_3 \rightarrow OH(X^2\Pi) + NH_2$ is such that levels up to $v' = 4$ in the OH product can be populated. The complete vibrational distribution for this reaction has not been published, however, as populations in levels greater than $v' = 1$ cannot be measured accurately using the LIF technique, due to predissociation of the $OH(A^2\Sigma)$ state in levels higher than $v' = 1$.

In recent experimental and theoretical work, the hydrogen abstraction reactions of $O(^1D_2)$ (4–7) have been classified into two categories — those which take place via the direct abstraction of a hydrogen atom by the $O(^1D_2)$ atom, and those which proceed by the formation of a highly energetic complex which results from the insertion of the $O(^1D_2)$ into the bond containing the hydrogen. The dynamics and hence the energy partitioned to the product OH would be different for the two mechanisms. For the case of the reactions of $O(^1D_2)$, it has been postulated (6) that abstraction might lead to the formation of a vibrationally hot but rotationally cold product distribution, whereas insertion might lead to a rotationally hot but vibrationally cold product distribution.

In the previous work on reactions [1] and [2], a small shoulder at low J' was observed in the rotational distribution of the $OH(v' = 0)$ level (1, 3). This was attributed to reaction [2]. The remainder of the distribution in the $v' = 0$ level and that in the $v' = 1$ level was assigned to reaction [1]. In a later study of the energy partitioning for the reaction of $O(^1D_2)$ with ND_3, the same authors (3) observed a rotational distribution similar to that found for the NH_3 reaction.

The shape of the rotational distribution which the authors of ref. 3 attributed to reaction [1] was found to agree with that expected from a purely statistical mechanism, in which the reaction proceeds via the formation of a long-lived complex, and the energy of reaction is partitioned among all the degrees of freedom prior to the formation of the product. The statistical energy distribution expected in the case of such a mechanism can be calculated simply by assuming that all product degrees of freedom are formed with equal probability. The statistical vibrational distributions can thus be obtained from a knowledge of the vibrational and rotational state densities of the products. These authors assumed this to be the case and subtracted a calculated statistical rotational distribution from the observed rotation in $v' = 0$, thus obtaining a distribution for the low-J' component. They then compared the population represented by this distribution with the total population, and obtained a branching ratio into the low-J' component of approximately 4% of the reaction. Excited $NH_2(^2A_1)$ was seen in approximately the concentration expected if the low-J' component of the rotational distribution arose from reaction [2]. The authors, however, did not rule out the possibility that this low-J' component could be attributed to an abstraction process with the overall form of reaction [1]. The OH vibrational distribution reported in ref. 3 is $P(v' = 0{:}1) = 1.0{:}0.66$ — a result which is more excited than the statistical case. This seems to be in conflict with the results obtained from the rotational distributions, which indicated statistical energy partitioning. It has been postulated that the modes of the NH_2OH complex which lead to OH vibrational excitation are not randomized, whereas those leading to OH rotation are (9), but the physics leading to such a result is difficult to visualize. The situation with respect to the vibrational distributions is further complicated by the fact that ref. 2 reported the OH vibrational distribution to be $P(v' = 0{:}1{:}2) = 1.0{:}1.5{:}2.1$. The rotational distribution obtained in that case, however, was in broad agreement with that reported in refs. 1 and 3.

In the following, we report a measurement of the complete

[1]NRCC No. 25871.

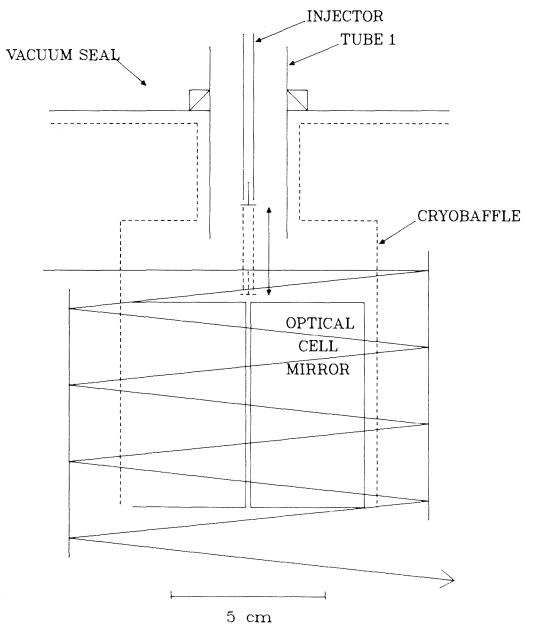

FIG. 1. The configuration of the reagent inlets, the excimer laser multipass mirrors and the Welsh optical cell.

vibrational distribution for reaction [1], obtained by low-pressure infrared emission spectroscopy. We find that the vibrational energy partitioning is statistical, suggesting complete randomization of the reaction exoergicity through the formation of a long-lived NH_2OH complex.

Experimental

The experiments were carried out in a modified version of the apparatus described in ref. 8. The reaction vessel is a stainless steel cylindrical vacuum chamber (25 cm diameter, 25 cm long) which is evacuated by a Varian VHS 400 diffusion pump through a 31 cm gate valve and a 38 cm cryobaffle. The cryobaffle was maintained at a temperature of −80°C throughout the experiments to eliminate backstreaming from the pump.

The reagents are introduced into the reaction chamber by the injector system shown in Fig. 1. The inlet assembly consists of two cylindrical quartz tubes labelled "injector" and "tube 1", located on the central axis of the reaction vessel. The injector, through which the NH_3 enters, can be adjusted vertically over a distance of 3 cm in order to allow variation of the mixing point location. Efficient mixing was ensured by the addition of a small Teflon deflector plate located at the tip of the injector tube (the "T" in Fig. 1). For the present experiments, the injector tip was located about 1 cm below the end of tube 1, in order to reduce the effect of a slow reaction which is known to occur between O_3 and NH_3 (10). This precaution and the short residence time of the reagents in the observation zone (less than 3 ms *vide infra*) reduced this potential interference.

The ozone for these experiments was produced in an ozone generator of conventional ac discharge design. Prepurified oxygen was passed through a type 5A molecular sieve at −80°C; then passed through a 20 kV, 4 amp ac discharge at atmospheric pressure. The ozone was trapped on silica gel which had been cooled to −80°C. After saturation of the silica gel, the ozone was stored under about 500 to 600 Torr of oxygen. Before each experiment, the ozone trap was pumped to a pressure of less than 5 Torr to remove the excess oxygen. The ammonia used for the experiments was obtained from Canadian Liquid Air Co. at a specified purity of 99%; it was used without further purification.

The ozone was photolysed using a KrF laser, operated at a repetition frequency of 360 Hz. The laser energy at this frequency averaged about 10 mJ per pulse. The unfocussed laser beam entered from the left in Fig. 1 and was multipassed through the reagent mixture (indicated by the zig zag lines in the figure) by a pair of dielectric mirrors, coated for maximum reflectance at 248 nm and mounted perpendicular to the axis of the Welsh cell. The infrared emission collected by the Welsh cell was coupled out of the reaction vessel, into a Fourier transform spectrometer, by a 2 inch diameter f/1 CaF_2 lens.

Following each pulse of the excimer laser, a burst of infrared emission having a fast risetime (limited by the detector's electronic bandwidth to about 30 μs and a decay time of about 300–800 μs (depending upon the pressure) was observed from the vibrationally-excited OH. These bursts of emission, in the form of an interferogram generated by the Michelson interferometer, were recorded digitally by the Fourier transform spectrometer. About 500 interferograms were co-added and Fourier transformed to obtain each spectrum. There was no phase relationship between the occurrence of the infrared emission and its digitization by the Fourier transform spectrometer. Consequently, the spectrum represents a time-average of the distribution of spectral intensities over the duration of the emission pulse, weighted by the intensity, which was highest in the early part of the pulse (the first 100–200 μs).

The recorded spectra were corrected for the variation in sensitivity of the detector with wavelength and populations were calculated using the rotationless Einstein transition probabilities of Rosmus (11) and the rotational dependences of Goldman (12). The spectral resolution used for these experiments was 0.48 cm^{-1}, adequate to resolve the rotational structure and spin doublets of OH but not the lambda doublets.

The total pressure in the reaction chamber was in the range of $4–6 \times 10^{-2}$ Torr. In some cases, only the reagents were used while in others, argon was added in order to translationally thermalize the $O(^1D_2)$ atoms, which are produced with some residual translational energy in the photolysis (13). The total pressure in the observation zone was controlled by adjusting the gate valve above the cryobaffle and diffusion pump in order to provide adequate spectral signal-to-noise. For the present experiments, the pumping speed was limited to about 500 L/s, hence the residene time in the effective volume of the Welsh cell (1 L) was about 2×10^{-3} s.

Results

The total energy available to the products of the $O(^1D_2)/NH_3$ reaction is about 188 kJ/mol — enough to populate the fourth vibrational level of the OH produced in reaction [1] but only the ground vibrational state of that created in reaction [2]. The spectra recorded in these experiments contained observable emission from $OH(v' = 1–3)$, which therefore must have come from reaction [1]. The reagent pressures and vibrational distributions for four representative experiments are listed in Table 1. The vibrational distributions for runs 1–3 are reproduced in Fig. 2, which also shows a statistical OH vibrational distribution (the dashed line) calculated for reaction [1]. The uncertainty in the experimental results is estimated to be +0.04 in each population. Although no emission from $v' = 4$ was found, the shape of the observed distributions indicates that this would have been very weak and likely not discernable above the noise.

In experiments 1–3, low partial pressures of reagents were used with a relatively large concentration of Ar. The latter was added to ensure thermalization of the $O(^1D_2)$ prior to reaction. (The probability for $O(^1D_2)$ quenching in collisions with Ar is very small (14).) Experiment 4 shows the result obtained when the Ar is omitted and the difference in pressure is made up by increasing the concentration of ozone. In this case, the product vibrational excitation is slightly higher than that observed for the experiments carried out in the presence of Ar and with a reduced concentration of ozone.

The partial pressure of the reagents in experiments 1–3 is 1.1×10^{-2} Torr while in experiment 4 it is 4.2×10^{-2} Torr. Although the relevant energy transfer rate constants are poorly-

TABLE 1. Vibrational population distributions and reagent partial pressures for four representative experiments

	Reagent partial pressures[a]			Population distributions		
Run	Ozone	Ammonia	Argon	$v' = 1$	$v' = 2$	$v' = 3$
1	8.0	3.0	46.0	0.80	0.15	0.05
2	5.5	5.5	45.0	0.85	0.12	0.03
3	10.0	1.0	48.0	0.83	0.15	0.02
4	36.0	6.0	0.0	0.78	0.20	0.02

[a] Torr $\times 10^{-3}$.

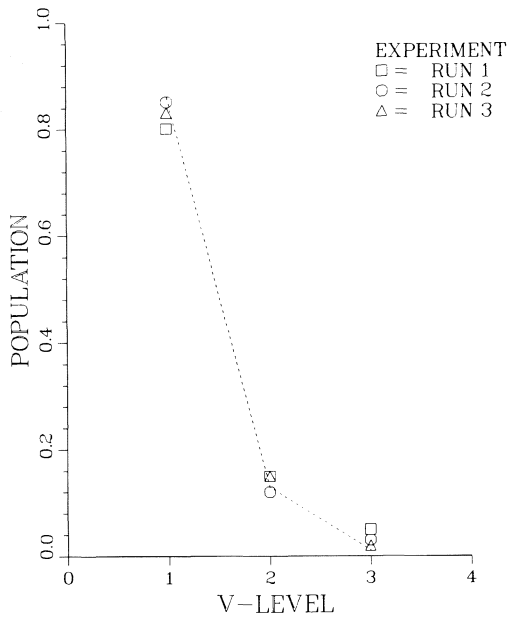

FIG. 2. The vibrational distributions of runs 1–3, Table 1, compared with a statistical vibrational distribution (dashed curve).

known, both ozone and ammonia are thought to be fairly efficient vibrational deactivators of OH (15). The available measurements of these rate constants indicate that both O_3 and NH_3 remove OH($v = 9$) with a probability between 0.05 (15*a*, 15*c*) and 1.0 (15*f*) per gas kinetic collision. If we assume that the rate of removal by NH_3 scales with vibrational level in the same way as that by ozone, the deactivation probabilities for the lower levels OH($v = 1$–3) would be in the range 0.001 to 0.1 per gas kinetic collision. We assume that argon does not deactivate the OH significantly (14, 15*a*). The substantial increase in reagent concentration in experiment 4, therefore, might be expected to cause increased deactivation of the OH vibrational distribution.

In contrast to this expectation, the distribution observed in experiment 4 is slightly *more excited* than those from the experiments using lower reagent concentrations. There could be two possible explanations for this. First, it could be caused by the higher reagent translational energy (created in the photodissociation) which is present in the experiments having no Ar buffer gas. We believe this to be the most likely explanation and will explore it in more detail in the next section. The second (and also possible) explanation is that the increased concentration of $O(^1D_2)$ atoms (due to the increased ozone concentration) results in secondary reactions between these and the radical (NH_2) produced in reaction [1]. If the vibrational distribution created in these secondary reactions were more excited than that of the primary reaction, the result would be an overall increase in the product vibrational excitation, as observed. This effect has been observed, for example, in the reaction of F atoms with NH_3 (16, 17). In that case, for F atom concentrations in substantial excess over the NH_3, the HF vibrational distribution became more excited, as the concentration of F atoms was increased, due to the contribution of the F + NH_2 reaction. It is less likely to have caused the increased vibrational excitation in the present case, however, because it is not possible to sustain a large excess of $O(^1D_2)$ atoms until the necessary concentration of NH_2 radicals has been generated. The rate constants for the reaction of $O(^1D_2)$ with both NH_3 and O_3 are approximately gas kinetic (3×10^{-10} and 2×10^{-10} cm^3 molecule^{-1} s^{-1}, respectively) (2, 18) and thus virtually no $O(^1D_2)$ will remain after the first two or three gas kinetic collisions following the ozone photolysis. Its rapid disappearance while the NH_2 is being formed thus reduces the importance of the secondary reaction.

Using the energy transfer rates quoted above, the vibrational deactivation time for these experiments would be in the range of 10^{-4} to 10^{-3} s. This is of the same order as the estimated residence time of the emitters in the observation zone (2×10^{-3} s) and therefore there remains a possibility that the observed distributions have suffered some vibrational deactivation. The data in Table 1, however, show that the distributions for runs 1–3 and the statistical distribution are all the same within the stated uncertainty. These data cover the range of reagent partial pressures from 5 to 10 $\times 10^{-3}$ Torr for ozone and from 1 to 5 $\times 10^{-3}$ Torr for ammonia. Since changing the partial pressure of a reagent would change the extent of gas phase relaxation caused by that reagent, we conclude from the invariability of the distributions that gas phase deactivation by the unused reagents is not significant in these experiments. From this we conclude that the distribution represented by experiments 1–3 is the initial one created by reaction [1] and hence that the latter creates a statistical vibrational energy distribution.

Discussion

The OH vibrational populations recorded in these experiments decrease rapidly with increasing vibrational level. This result is usually associated with reactions forming a strongly-bound intermediate which lives long enough for the reaction exoergicity to be completely distributed among all product degrees of freedom. This conclusion was indicated by the previously-measured LIF rotational distributions (1–3) but not by the vibrational distributions extracted from those rotational data. It was pointed out in ref. 3 that vibrational distributions extracted from LIF rotational measurements are particularly sensitive to errors introduced by saturation effects and it was further suggested that the unusually high vibrational excitation reported in ref. 2 may have this origin. It is also possible, however, that some of this difference, as well as the smaller difference between the vibrational distribution reported in ref. 3 and that obtained here could be due to the different energetics of the experiments.

The photolysis of ozone at 248 nm (the laser wavelength used in our experiments) generates about 62 kJ/mol of relative translational energy in the $O(^1D_2)/O_2(^1\Delta)$ frame of ref. 13. If, as in the case of experiment 4, no attempt is made to thermalize the $O(^1D_2)$ the $O(^1D_2)/NH_3$ relative translational energy would be about 24.6 kJ/mol. The 300 K thermal translational

energy is only 3.7 kJ/mol. The excess energy might reduce the lifetime of the postulated intermediate ONH_3 species, thereby reducing the extent of energy randomization and increasing the vibrational excitation of the OH product. This is qualitatively consistent with the difference observed between experiment 4 and the other three experiments, where an increase in vibrational excitation was observed under conditions where the relative values of the gas phase energy transfer rate constants would indicate that a decrease should be expected. A similar effect has been suggested in the case of the $O(^1D_2)/H_2$ reaction (19, 20). (We note, however, that the results of the present experiments do not constitute proof of this translational energy effect, since the difference in the vibrational distributions observed here is within the experimental uncertainty.)

The excess translational energy from the photolysis would not have been thermalized before the observations were made in the LIF experiments. In this case, the reagent translational energy for the experiments in ref. 3 would have been approximately 12 kJ/mol, assuming that the proportions of the excess energy partitioned to translation are the same for both the 266 nm photolysis used in the LIF work and the 248 nm photolysis used here. This is substantially greater than the room-temperature energy, 3.7 kJ/mol, and could be expected to have an effect on the lifetime of the intermediate. The statistical $P(v' = 2)/P(v' = 1)$ ratio (0.15), which agrees with our observations, implies a $P(v' = 1)/P(v' = 0)$ ratio of 0.21. The $P(v' = 1)/P(v' = 0)$ ratio reported in ref. 3 is 0.66. It is possible that this difference could represent a translational energy effect on the energy partitioning, as described above. We hope that improvements currently being made to our apparatus will permit the existence of this effect to be confirmed and its quantitative influence measured.

1. C. T. Rettner, J. F. Cordova, and J. L. Kinsey. J. Chem. Phys. **72**, 5280 (1980).
2. N. D. Sanders, J. E. Butler, and J. R. McDonald. J. Chem. Phys. **73**, 5381 (1980).
3. J. F. Cordova, C. T. Rettner, and J. L. Kinsey. J. Chem. Phys. **75**, 2742 (1981).
4. A. C. Luntz. J. Chem. Phys. **73**, 1143 (1980).
5. A. C. Luntz. J. Chem. Phys. **73**, 5393 (1980).
6. A. C. Luntz, R. Schinke, W. A. Lester, Jr., and Hs. H. Gunthard. J. Chem. Phys. **70**, 5908 (1979).
7. R. Schinke and W. A. Lester, Jr. J. Chem. Phys. **72**, 3754 (1980).
8. J. E. Butler, R. G. Macdonald, D. J. Donaldson, and J. J. Sloan. Chem. Phys. Lett. **95**, 183 (1983).
9. W. H. Breckenridge. *In* Reactions of small transient species. *Edited by* M. A. A. Clyne and A. Fontijn. Academic Press, London. 1983. Chapt. 4.
10. K. J. Olszyna and J. Heicklen. Adv. Chem. Ser. **113**, 191 (1972).
11. H.-J. Werner, P. Rosmus, and E. A. Reinsch. J. Chem. Phys. **79**, 905 (1983).
12. (*a*) J. R. Gillis and A. Goldman. J. Quant. Spectrosc. Radiat. Transfer, **26**, 23 (1981); (*b*) A. Goldman. Appl. Opt. **21**, 2100 (1982).
13. R. K. Sparks, L. R. Carlson, K. Shobotake, M. L. Kowlcyzk, and Y. T. Lee. J. Chem. Phys. **72**, 1401 (1980).
14. L. J. Stief, W. A. Payne, and R. B. Klemm. J. Chem. Phys. **62**, 4000 (1975).
15. (*a*) A. E. Potter, R. N. Coltharp, and S. D. Worley. J. Chem. Phys. **54**, 992 (1971); (*b*) R. N. Coltharp, S. D. Worley, and A. E. Potter. Appl. Opt. **10**, 1786 (1971); (*c*) G. E. Streit and H. S. Johnston. J. Chem. Phys. **64**, 95 (1976); (*d*) B. J. Finlayson-Pitts and T. E. Kleindienst. J. Chem. Phys. **74**, 5643 (1981); (*e*) B. J. Finlayson-Pitts, D. W. Toohey, and M. J. Ezell. Int. J. Chem. Kinet. **51**, 151 (1983); (*f*) G. D. Greenblatt and J. R. Wiesenfeld. J. Geophys. Res. **87**, 1145 (1982).
16. D. J. Donaldson, J. Parsons, J. J. Sloan, and A. Stolow. Chem. Phys. **85**, 47 (1984).
17. D. J. Donaldson, J. D. Goddard, and J. J. Sloan. J. Chem. Phys. **82**, 4524 (1985).
18. J. A. Davidson, C. M. Sadowski, H. I. Schiff, G. E. Streit, C. J. Howard, D. A. Jennings, and A. L. Schmeltekopf. J. Chem. Phys. **64**, 57 (1976).
19. P. M. Aker and J. J. Sloan. J. Chem. Phys. **85**, 1412 (1986).
20. P. M. Aker, J. J. Sloan, and J. S. Wright. Chem. Phys. In press.

Study of the CEE mechanism by voltammetry and chronoamperometry

ANDRZEJ LASIA
Department of Chemistry, University of Sherbrooke, Sherbrooke, Que., Canada J1K 2R1

Received June 4, 1986

ANDRZEJ LASIA. Can. J. Chem. **64**, 2319 (1986).

The electroreduction of bivalent metal cations may proceed by a CEE mechanism with a heterogenous chemical reaction on the electrode surface. The applications of the convolutive linear sweep voltammetry and chronoamperometry to study that mechanism are presented. The behaviour of the electrochemical reactions was simulated using an implicit finite difference technique for different values of kinetic parameters. The simulated curves were analysed and an agreement between the introduced and obtained data was found.

ANDRZEJ LASIA. Can. J. Chem. **64**, 2319 (1986).

L'électroréduction de cations bivalents peut procéder par le mécanisme CEE avec une réaction chimique hétérogène à la surface de l'électrode. Les applications de la voltampérométrie à balayage linéaire avec convolution et de la chronoamperométrie aux études de cette réaction sont présentées. Des courbes analytiques ont été simulées par la méthode des différences finies et un accord a été trouvé entre les paramètres introduits et calculés.

Introduction

The electroreduction of metal cations on mercury electrodes often involves a complex reaction mechanism. It was suggested that the electrodeposition proceeds through an adion intermediate which is partially desolvated and adsorbed on the electrode surface (1). The electrochemical reactions of bi- or polyvalent cations are usually more complicated than those of monovalent cations. Different mechanisms were proposed in the literature for the electrode reduction of metal cations, e.g., simple electron transfer process (2, 3), stepwise electron transfer (4), disproportionation (5) or dimerization (6) of the intermediates, adsorption (6), CE or CEE mechanism (7–13), and slow transport across the double layer (14), etc. Some possible mechanisms were discussed by Bongenaar *et al.* (12).

CE mechanisms have been suggested for the electroreduction of cations for which the solvent exchange is slow (7–11). It was also proposed for the electroreduction of alkali metals in HMPA (15, 16) where kinetically limited waves were obtained.

The recent works of Bongenaar *et al.* (12) and Strujis *et al.* (13) show that the electroreduction of Cd(II) in concentrated aqueous solutions of perchlorates and fluorides involves a CEE mechanism with a heterogenous chemical reaction, probably a partial desolvation of the depolarizer at the electrode surface. Alternating current admittance and demodulation technique were applied to study those reactions. Unfortunately the potential range available for the a.c. admittance technique is rather limited. Strujis *et al.* (12) have presented kinetic data in the range of about 130 mV. Larger (~200 mV) potential range is available for the demodulation technique (13) but this method is, up to now, of limited use. If the rate of electroreduction is slower it is possible to use other popular electrochemical techniques. We have attempted to show how linear sweep voltammetry and chronoamperometry are used to determine the kinetics of those reactions.

Theory

The equations presented below hold for the electroreduction of bivalent metal cations according to a CEE mechanism but they may be easily modified for a CE reaction mechanism.

The CEE mechanism for a bivalent metal cation A^{2+} on mercury with the subsequent formation of amalgam may be described as:

$$[1] \quad A^{2+} \overset{k_c}{\rightleftharpoons} B^{2+}$$

$$[2] \quad B^{2+} + e \overset{k_1}{\rightleftharpoons} B^{+}$$

$$[3] \quad B^{+} + e \overset{k_2}{\rightleftharpoons} B(Hg)$$

where B^{2+} is an electroactive form of A^{2+}, k_c is a heterogenous rate constant of the chemical reaction, and k_1 and k_2 are the forward rate constants of the first and second electron transfer.

Since B^{2+} is not detected in the bulk of the solution it is assumed that it is formed at the electrode surface only and that reaction [1] is a heterogenous chemical process. The equilibrium constant of that reaction is defined as:

$$[4] \quad K_c = [A^{2+}]_0/[B^{2+}]_0$$

where subscript "0" indicates surface concentrations.

The rates of reactions [1]–[3] are

$$[5] \quad v_c = k_c\{[A^{2+}]_0 - K_c[B^{2+}]_0\}$$

$$[6] \quad v_1 = k_1\{[B^{2+}]_0 - K_1[B^{+}]_0\}$$

$$[7] \quad v_2 = k_2\{[B^{+}]_0 - K_2[B(Hg)_0]\}$$

where K_1 and K_2 are equilibrium constants of reactions [2] and [3], respectively.

Since both B^{2+} and B^{+} do not exist in the bulk of the solution, one can assume that their surface concentrations are small and their fluxes negligible. Then the concentrations of the unstable intermediates may be eliminated assuming that $v_1 = v_2 = v_3$ and $i = FA(v_2 + v_3)$, where A is the electrode surface area and i is the current.

The solution leads to an equation (12)

$$[8] \quad i = 2FAk_f\{[A^{2+}]_0 - [B(Hg)]_0 \exp(2\phi)\}$$

where

$$[9] \quad \phi = F(E - E^{0\prime})/RT$$

and

$$[10] \quad 1/k_f = 1/k_c + K_cK_1/k_2$$

The last term in the eq. [10] may be written as $K_cK_1K_2/k_2K_2$ and after taking into account the Nernst equation $K_cK_1K_2 = [A^{2+}]/[B(Hg)] = \exp(2\phi)$ one can obtain

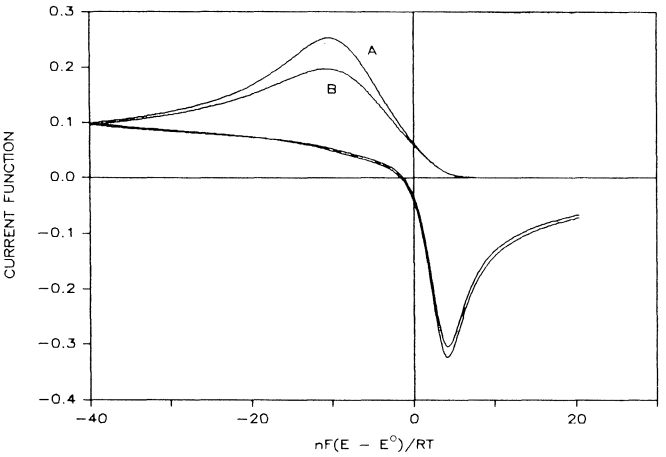

FIG. 1. Cyclic voltammetric curves simulated for EE (*A*) and CEE (*B*) mechanisms. The kinetic parameters are (*A*) $\Lambda_1 = 0.08$, $\Lambda_2 = 10^6$, $\alpha_1 = \alpha_2 = 0.5$; (*B*) $\Lambda_c = 1.0$, $\Lambda_1 = 0.08$, $\Lambda_2 = 10^6$, $\alpha_1 = \alpha_2 = 0.5$.

$$[11]\quad 1/k_f = 1/k_c + \exp(\alpha_1\phi)/(k_{s1}/K_c) + \exp[(1 + \alpha_2)\phi]/k_{s2}$$

where $k_1 = k_{s1}\exp(-\alpha_1\phi)$, $k_2 = k_{s2}\exp(-\alpha_2\phi)$, and k_{s1} and k_{s2} are standard rate constants of transfer of the first and second electron (reactions [2] and [3]).

Thus CEE mechanism is described by a simple Butler–Volmer type equation but k_f is a complex function of the electrode potential and kinetic parameters. Using that equation, the voltammetric and chronoamperometric curves were simulated employing the finite difference technique (17, 18).

Linear sweep voltammetry

The shape of the cyclic voltammetric curves depends strongly on the values of the kinetic parameters of the system, i.e., rate constants and transfer coefficients. For slow simple electron transfer processes with low transfer coefficients the cathodic part of the voltammetric curve is flattened and it is difficult to distinguish between simple charge transfer, EE or CEE mechanisms. This is illustrated in Fig. 1 where cyclic voltammetric curves simulated for EE (curve *A*) and CEE (curve *B*) mechanisms are shown. The following set of kinetic parameters was used in the digital simulations: *A*: $\Lambda_1 = 0.08$, $\Lambda_2 = 10^6$, $\alpha_1 = \alpha_2 = 0.5$; *B*: $\Lambda_c = 1$, $\Lambda_1 = 0.08$, $\Lambda_2 = 10^6$, $\alpha_1 = \alpha_2 = 0.5$. The dimensionless kinetic parameters Λ are defined as follows: $\Lambda_1 = k_{s1}/\sqrt{nFvD_0/RT}$ and $\Lambda_1 = (k_{s1}/K_c)\sqrt{nFvD_0/RT}$ for EE and CEE mechanism, respectively, $\Lambda_2 = k_{s2}/\sqrt{nFAvD_0/RT}$, $\Lambda_c = k_c/\sqrt{nFvD_0/RT}$, D_0 is the diffusion coefficient of A^{2+}, v is the sweep rate, and all other symbols have their usual meaning. A comparison of these two voltammetric curves shows smaller cathodic current for the CEE mechanism while the anodic currents are essentially the same.

It is relatively easy to identify the reaction mechanism by convolutive potential sweep voltammetry (19). The convolution integral (semiintegral) $I\Psi$ is defined as:

$$[12]\quad I\Psi = (1/\sqrt{\pi})\int_u^{\xi} \Psi(\xi)/\sqrt{\xi - v}\,dv$$

where $\Psi = i\Theta/nFAC_0^*D_0^{1/2}$ is the dimensionless current function, $\Theta = RT/nFv$, $\xi = nF(E - E^0)/RT$, $u = nF(E_i - E^0)/RT$, and E_i is the initial potential.

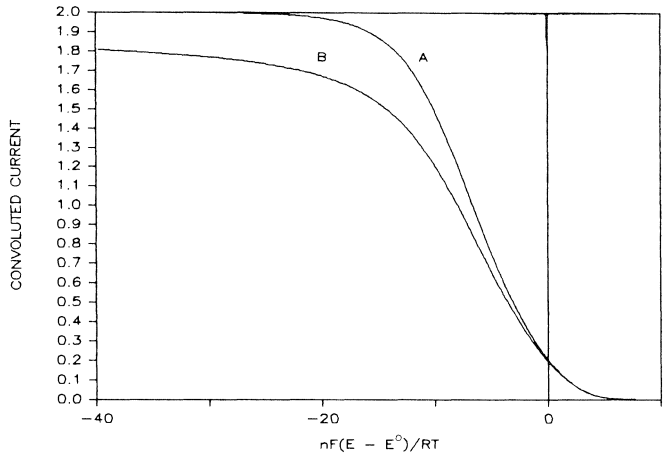

FIG. 2. Convoluted voltammetric curves for EE (*A*) and CEE (*B*) mechanisms. Values of the kinetic parameters are the same as in Fig. 1.

The convoluted current functions $I\Psi$ of the cathodic part of the voltamperometric curves are shown in Fig. 2. It is apparent that in the absence of the chemical step plateau $I\Psi_1 = 2$ is reached for an EE mechanism while for a CEE mechanism $I\Psi$ is always smaller than 2.

More systematic calculations of the influence of the rate constant of the chemical reaction [1] on the shape of the cyclic voltammetric curves were carried out. Figure 3 presents the simulated voltamperometric curves for a reversible electron transfer reaction with $\Lambda_1 = \Lambda_2 = 10^6$ and $\Lambda_c = 0.1, 0.3, 1.0$, and 10^6. When the chemical reaction rate decreases, the cathodic peak current also decreases and the latter is flattened. Semiintegration of the cathodic current (Fig. 4) gives the sigmoidal curves but the theoretical value of the limiting current is obtained only for $\Lambda_c = 10^6$ (which is equivalent to the EE mechanism). For the lower values of Λ_c, at negative potentials, the convoluted current increases with potential and its values are smaller than the theoretical values for the EE mechanism. These curves were further analysed to give the rate constants of the electrochemical process, Λ_f according to the relation (19)

$$[13]\quad \Lambda_f = \Psi/\{I\Psi_1 - I\Psi[1 + \exp(nF(E - E^0)/RT)]\}$$

where $\Lambda_f = k_f/\sqrt{nFvD_0/RT}$, k_f is the forward rate constant of the overall process and $I\Psi_1 = 2$ is limiting value of the convoluted current function in the absence of the chemical step [1].

Using that analysis to the curves presented in Fig. 4 the introduced values of Λ_c parameter were obtained at potentials more negative than the peak current.

The influence of the irreversibility of the electron transfer processes is illustrated in Fig. 5. The voltammetric curves were simulated using $\Lambda_1 = 0.08$, $\Lambda_2 = 10^6$, $\alpha_1 = \alpha_2 = 0.5$, and different values of the kinetic parameter $\Lambda_c = 0.1, 0.3, 1.0$, and 10^6. The corresponding convoluted current functions are shown in Fig. 6. The theoretical value of the limiting convoluted current $I\Psi_1 = 2$ is obtained only for the fast chemical reaction ($\Lambda_c = 10^6$). The analysis using eq. [13] was also performed and the results are presented in Fig. 7. For the fast chemical reaction a linear dependence of $\ln \Lambda_f$ on potential was obtained. In the cases where the kinetics of the process was limited by the rate of the chemical step, constant (independent of the potential) value of Λ_f was obtained at negative potentials, equal to the values introduced in the simulations.

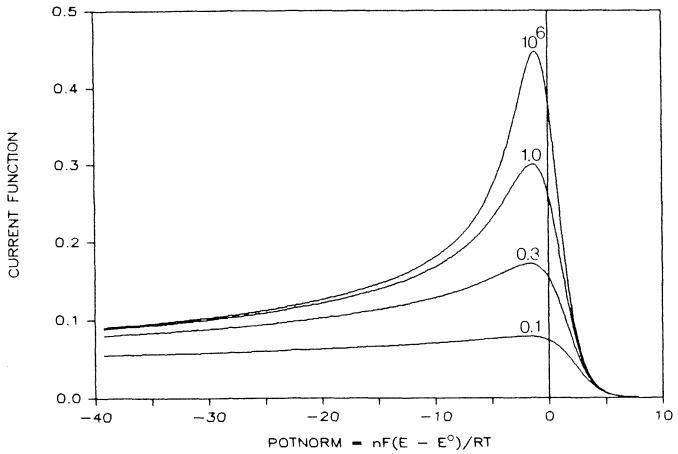

FIG. 3. Voltammetric curves simulated for CEE mechanism with fast electron exchange. The kinetic parameters are $\Lambda_1 = \Lambda_2 = 10^6$, $\alpha_1 = \alpha_2 = 0.5$. The numbers represent the values of the dimensionless rate constant of the chemical reaction Λ_c.

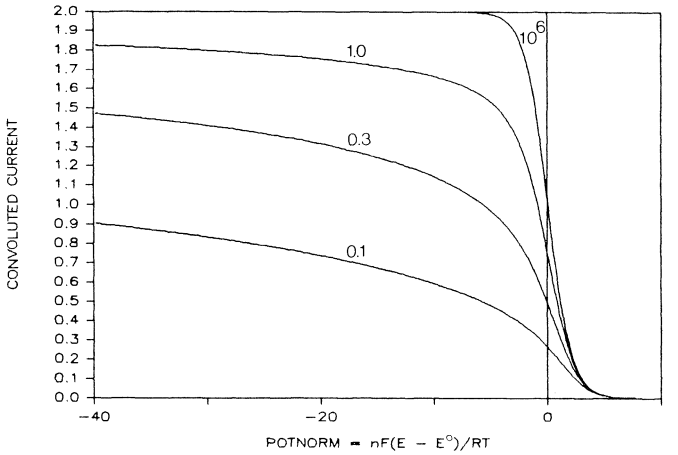

FIG. 4. Convoluted voltammograms of the curves in Fig. 3.

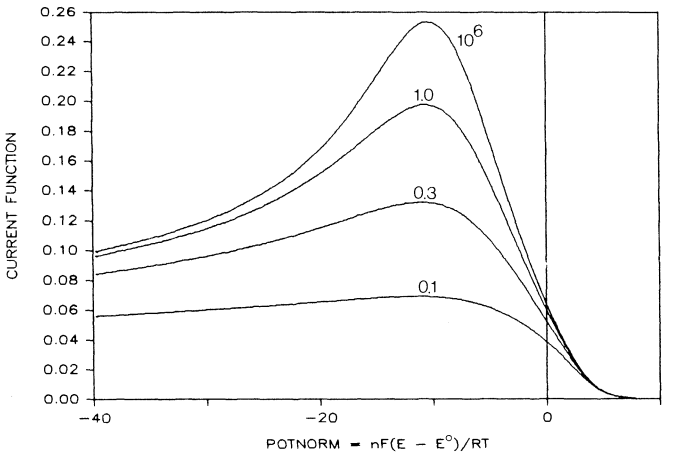

FIG. 5. Voltammetric curves simulated for CEE mechanism with slow electron exchange. The kinetic parameters are $\Lambda_1 = 0.08$, $\Lambda_2 = 10^6$, $\alpha_1 = \alpha_2 = 0.5$. The number on each curve is the value of Λ_c.

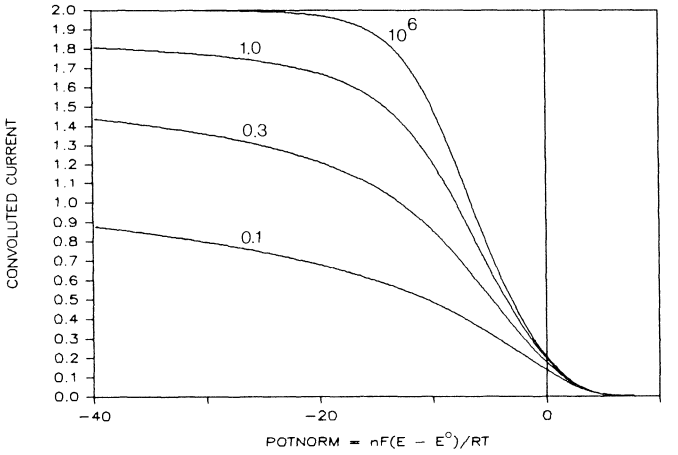

FIG. 6. Convoluted voltammograms of the curves shown in Fig. 5.

The nonlinear analysis of the dependence of the rate constant as a function of the potential according to eq. [11] gives all values for the introduced kinetic parameters Λ and α.

Chronoamperometry

Chronoamperometry has been already applied in the literature to the kinetics of the CE processes with a homogenous chemical reaction (9, 20). The results presented below are for EE and CEE mechanisms with a heterogenous chemical reaction to show the effect of the irreversibility of the electron transfer on the simulated curves. The kinetic parameter Λ was defined as $\Lambda_c = k_c\sqrt{\tau/D_0}$, $\Lambda_1 = (k_{s1}/K_c)\sqrt{\tau/D_0}$, and $\Lambda_2 = k_{s2}\sqrt{\tau/D_0}$, where τ is time at which the current is measured.

Figure 8 shows the simulated chronoamperometric current–potential curves for a reversible electron transfer processes with the dimensionless kinetic parameter Λ_c equal to 0.1, 0.3, 1.0, and 10^6. It is evident that the limiting value of current is quickly established and that it is constant, but its value depends on the rate of the preceding chemical reaction. For the slow electron transfer process (Fig. 9) the plateau is reached at more negative potentials. Its value does not depend on the reversibility of the electrode process.

At negative potentials where the kinetics of the overall process is limited by the rate of the chemical reaction the analytical solution of the problem is given by (20)

$$[14] \quad i/i_l = \pi^{1/2}\Lambda_c \exp(\Lambda_c^2)\,\mathrm{erfc}(\Lambda_c)$$

where i_l is the diffusion-limited current in the absence of the preceding chemical step. The values of the current obtained from simulations are in a very good agreement with the values obtained from eq. [14].

The analysis of the chronoamperometric curves at various potentials for quasi-reversible and irreversible processes was performed by solving the equation:

$$[15] \quad (i/i_l)\{1 + \exp[nF(E - E^0)/RT)]\} = \pi^{1/2}\lambda \exp(\lambda^2)\,\mathrm{erfc}(\lambda)$$

where λ is defined now as

$$[16] \quad \lambda = \Lambda_f[1 + \exp(nF(E - E^0)/RT)]$$

and $\Lambda_f = k_f\sqrt{\tau/D_0}$. The nonlinear approximation of the determined rate constants using eq. [11] gave the introduced kinetic parameters.

TABLE 1. Comparison of the EE and CEE mechanisms for cyclic voltammetry and chronoamperometry

Parameter	EE	CEE
$1/k_f =$	$\exp(\alpha_1\phi)/k_{s1} + \exp[(1+\alpha_2)\phi]/k_{s2}$	$1/k_c + \exp(\alpha_1\phi)/k_{s1}K_c^{-1} + \exp[(1+\alpha_2)\phi]/k_{s2}$
$E \rightarrow -\infty$	$k_f \rightarrow \infty$	$k_f \rightarrow k_c$
Cyclic voltammetry		
i–E curves	Difficult to distinguish	Cathodic part flattened, anodic almost the same
Convoluted curves	Plateau $I\Psi_1 = 2$ $I_l = 2FAD^{1/2}C^*$	Plateau not reached over large potential range $I\Psi_1 < 2$
Chronoamperometry		
Limiting current	$i_{l,EE} = 2FAD_0^{1/2}C^*/\sqrt{\pi t}$	Limiting current smaller than for EE mechanism $i_{l,CEE} = i_{l,EE}\pi^{1/2}\lambda \exp(\lambda^2)\,\mathrm{erfc}(\lambda)$

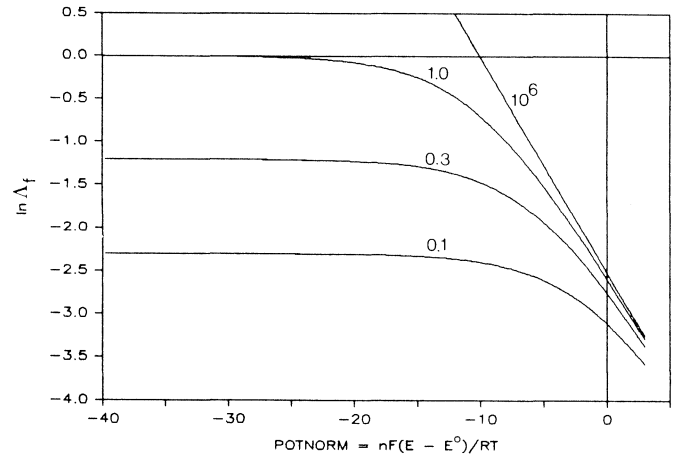

FIG. 7. The dependence of ln Λ_f vs. normalized potential obtained from the analysis of the convoluted curves shown in Fig. 6.

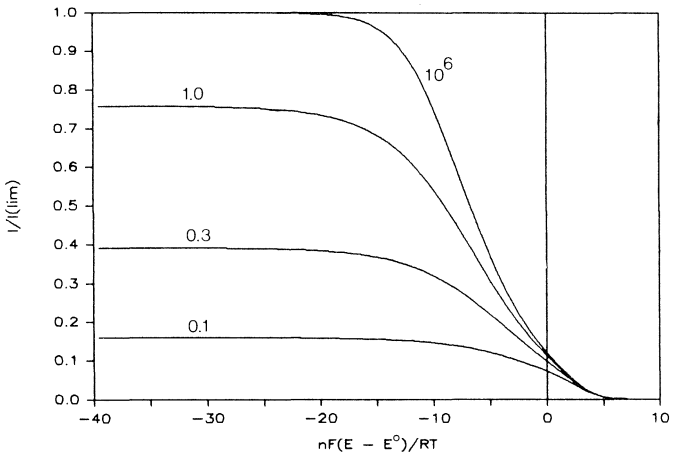

FIG. 9. Chronoamperometric curves i/i_l vs. normalized potential for CEE process with slow electron exchange. Kinetic parameters are the same as in Fig. 5. The number on each curve is the value of Λ_c.

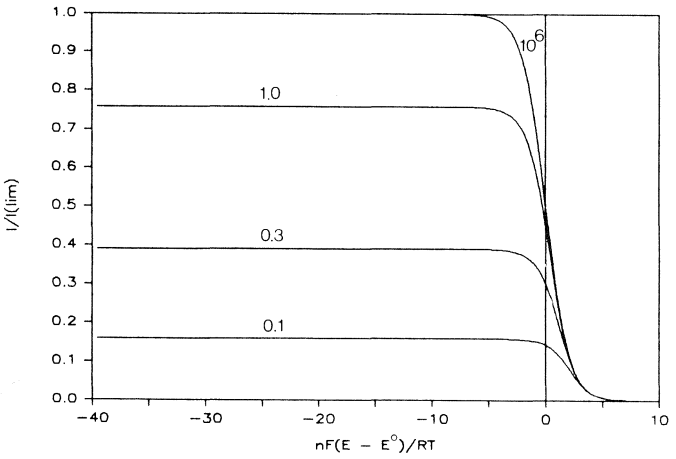

FIG. 8. Chronoamperometric curves i/i_l vs. normalized potential for CEE process with fast electron exchange. Kinetic parameters are the same as in Fig. 3. The number on each curve is the value of Λ_c.

Discussion

The analysis of the voltammetric and chronoamperometric curves for the CE/CEE mechanism gives the possibility of determining the kinetic parameters of that process.

The convolutive linear sweep voltammetry of the CEE process does not produce curves with a plateau. The convoluted current is continually increasing with the potential in a wide potential range even for the fast electron transfer process. However, detailed kinetic analysis gives the correct rate constants.

On the other hand, the chronoamperometric curves of CE/CEE mechanism show a well-established plateau of the limiting current whose value depends on the kinetics of the chemical reaction.

Both techniques may be used in the diagnostics of the electrode processes involved and for the determination of the kinetic parameters. The comparison of the results obtained for the EE and CEE mechanisms and the diagnostic criteria are presented in Table 1. The rate constant of the process may be studied over a wide potential range also at the negative

potentials where the electroreduction process is fast and the kinetics of overall process is limited only by the rate of the chemical reaction [1]. Voltammetric and chronoamperometric techniques have an advantage over a.c. techniques because the presence of a preceding chemical reaction may be confirmed on the basis of the comparison of the calculated and experimentally determined limiting convoluted or chronoamperometric currents, which is a direct evidence of the existence of that mechanism. On the other hand, using a.c. impedance technique one has to apply a nonlinear approximation of the determined k_f values as a function of the electrode potential. The use of convolution voltammetry or chronoamperometry is similar to the classical polarographic study of a slow desolvation of Ni^{2+} in aqueous solutions (see e.g. refs. 7 and 8).

Methods described above will be used for the further study of the kinetics of the electrode process of Cd(II) in DMSO (21).

Acknowledgement

The financial support of the Natural Sciences and Engineering Research Council of Canada is gratefully acknowledged.

1. B. E. Conway and J. O'M. Bockris. Electrochim. Acta, **3**, 340 (1961).
2. A. J. Bard (*Editor*). Encyclopedia of electrochemistry of the elements. Vols. I–IX. Marcel Dekker, New York.
3. K. J. Vetter. Electrochemical kinetics. Academic Press, New York. 1967.
4. V. V. Losev. Modern aspects of electrochemistry. *Edited by* B. E. Conway and J. O'M. Bockris. Butterworths, London. 1972.
5. B. Lovreček and N. Marinčič. Electrochim. Acta, **11**, 237 (1966).
6. T. Biegler, E. R. Gonzalez, and R. Parsons. Collect. Czech. Chem. Commun. **36**, 414 (1971).
7. J. Dandoy and L. Gierst. J. Electroanal. Chem. **2**, 116 (1961).
8. N. S. Hush and J. W. Scarrott. J. Electroanal. Chem. **7**, 26 (1964).
9. W. Górski and J. Lipkowski. J. Electroanal. Chem. **123**, 157 (1981).
10. L. Janiszewska and Z. Galus. Electrochim. Acta, **27**, 1781 (1982).
11. L. Janiszewska and Z. Galus. Electrochim. Acta, **29**, 1419 (1984).
12. C. P. M. Bongenaar, A. G. Remijnse, M. Sluyters-Rehbach, and J. H. Sluyters. J. Electroanal. Chem. **111**, 139 (1980).
13. J. Strujis, M. Sluyters-Rehbach, and J. H. Sluyters. J. Electroanal. Chem. **171**, 177 (1984).
14. W. R. Fawcett and A. Lasia. J. Phys. Chem. **89**, 5695 (1985).
15. K. Izutsu, S. Sakura, K. Kuroki, and T. Fujinaga. J. Electroanal. Chem. **32**, 11 (1971).
16. A. S. Barański and W. R. Fawcett. J. Chem. Soc. Faraday Trans. I, **76**, 1962 (1980).
17. A. Lasia. J. Electroanal. Chem. **146**, 397 (1983).
18. A. Lasia. J. Electroanal. Chem. **191**, 185 (1985).
19. J. C. Imbeaux and J. M. Savéant. J. Electroanal. Chem. **44**, 169 (1973).
20. J. Koutecký and R. Brdička. Collect. Czech. Chem. Commun. **12**, 337 (1947).
21. G. Brisard and A. Lasia. To be published.

Synthesis of the subterminally 6-*O*-phosphorylated trimannosides found on carbohydrate chains of lysosomal enzymes

OM. P. SRIVASTAVA AND OLE HINDSGAUL[1]

Chemistry Department, University of Alberta, Edmonton, Alta., Canada T6G 2G2

Received June 17, 1986

OM. P. SRIVASTAVA and OLE HINDSGAUL. Can. J. Chem. **64**, 2324 (1986).

The three possible subterminally 6-*O*-phosphorylated trimannosides (**2–4**) found on the asparagine-linked carbohydrate chains of lysosomal enzymes have been chemically synthesized as their 8-methoxycarbonyloctyl glycosides, R = $(CH_2)_8COOCH_3$. The key step in the syntheses involves glycosylation of suitably protected α-D-mannopyranosides **5–7** with the phosphorylated mannobiosyl donor 2-*O*-(2,3,4,6-tetra-*O*-acetyl-α-D-mannopyranosyl)-3,4-di-*O*-benzyl-6-*O*-diphenylphosphoryl-α-D-mannopyranosyl chloride (**14**), which produced mixtures of α- and β-linked trisaccharidic products. Compounds **2** (αDMan(1→2)αDMan 6-phosphate(1→2)αDManOR), **3** (αDMan(1→2)αDMan 6-phosphate(1→3)αDManOR), and **4** (αDMan(1→2)αDMan 6-phosphate(1→6)αDManOR) are being used in a study of the targeting of enzymes to the lysosomes by phosphomannosyl receptors.

OM. P. SRIVASTAVA et OLE HINDSGAUL. Can. J. Chem. **64**, 2324 (1986).

On a réalisé la synthèse chimique, sous la forme de glycosides méthoxycarbonyl-8 octyles (R = $(CH_2)_8COOCH_3$), des trois *O*-phosphoryl-6 trimannosides (**2–4**) possibles que l'on retrouve sur les chaînes de carbohydrates liées par l'asparagine dans les enzymes des lysosomes. L'étape clé dans la synthèse implique la glycosylation de α-D-mannopyranosides protégés d'une façon adéquate (**5–7**) avec le donneur mannobiosyle phosphorylé, le chlorure de *O*-(tétra-*O*-acétyl-2,3,4,6 α-D-mannopyrannosyl)-2 di-*O*-benzyl-3,4 *O*-diphénylphosphoryl-6 α-D-mannopyrannosyle (**14**), qui conduit à des mélanges des trisaccharides liés par les positions α et β. On utilise les composés **2** (αDMan(1→2)αDMan 6-phosphate(1→2)αDManOR), **3** (αDMan(1→2)αDMan 6-phosphate(1→3)αDManOR) et **4** (αDMan(1→2)αDMan 6-phosphate(1→6)αDManOR) dans une étude sur la relation des enzymes avec les lysosomes par le biais des récepteurs phosphomannosyles.

[Traduit par la revue]

Introduction

The asparagine-linked oligosaccharide chains of lysosomal enzymes carry a recognition marker required for the translocation of these enzymes from their sites of biosynthesis in the rough endoplasmic reticulum and golgi apparatus to the lysosomes (1–3). D-Mannose 6-phosphate residues are known to be the essential component of this recognition marker and correct intracellular targeting is mediated by specific phosphomannosyl receptors that bind with phosphorylated "high-mannose" oligosaccharides. The carbohydrate chains of lysosomal enzymes have been shown (4–6) to be highly heterogeneous in both size, degree, and type of phosphorylation. Structure **1** shows the mannose residues of the unprocessed high-mannose oligosaccharide chains where 6-*O*-phosphorylation has been found to occur. Smaller structures in which nonphosphorylated outer mannose residues have been enzymatically cleaved have also been identified (4–6).

To clarify the molecular features required for the specific recognition of these phosphorylated oligosaccharides by their receptors we are engaged in a synthetic effort to produce a panel of phosphorylated oligosaccharides, corresponding to partial structures of **1**, which are to be used in systematic binding studies with the purified (7) phosphomannosyl receptors. We have previously reported (8, 9) the syntheses of six phosphorylated di- and trimannosides corresponding to terminii of the composite structure **1**. Here we report the preparation of the 3 possible subterminally phosphorylated oligosaccharides **2**, **3**, and **4**. These structures were prepared as their 8-methoxycarbonyloctyl glycosides (10) to allow the preparation of synthetic glycoconjugates (11) for use in a study (12) of the intracellular transport of lysosomal enzymes.

[1]Author to whom correspondence may be addressed.

Results and discussion

Our strategy for the syntheses of **2–4** centered on the availability, from previous work (9), of the protected 8-methoxycarbonyloctyl α-D-mannopyranosides **5–7** having hydroxyl groups at C-2, C-3, and C-6, respectively, that are free for glycosylation. The most direct route to the target structures **2–4** would then involve glycosylation of **5–7** with a suitable 2-*O*-(α-D-mannopyranosyl)-α-D-mannopyranosyl donor. Although such glycosyl donors have nonparticipating groups at O-2, stereoelectronic (anomeric) (13) effects should favor formation of the α-glycosidic linkage under appropriate conditions (14). Ogawa's group (15–17) has successfully used such mannobiosyl donors in the syntheses of both yeast cell-wall mannan structures and asparagine-linked oligosaccharides and, although α,β mixtures of products may be obtained, the α-linked glycosides were generally the major products. Our synthetic route to **2–4** then required the preparation of the phosphorylated mannobiosyl donor **14** and its coupling with the alcohols **5–7**.

Reaction of the glycosyl bromide **8** (8), readily prepared from 1,2,6-tri-*O*-acetyl-3,4-di-*O*-benzyl-α-D-mannopyranose (18), with allyl alcohol under standard Helferich conditions (14) provided the α-linked glycoside **9** (75%), which was de-*O*-acetylated to produce **10**. Selective phosphorylation of the primary hydroxyl group in **10**, using diphenylphosphoryl chloride (19, 20) gave an α-D-mannopyranose derivative **11** (78%) having the 2-OH group free for glycosylation by 2,3,4,6-tetra-*O*-acetyl-α-D-mannopyranosyl bromide. The α(1→2) linked disaccharide **12** was obtained in 71% yield.

Removal of the allyl protecting group in **12**, using tristriphenylphosphine rhodium(I) chloride followed by mercuric chloride in aqueous acetone (21), gave the reducing disaccharide derivative **13**, which was isolated as an anomeric mixture

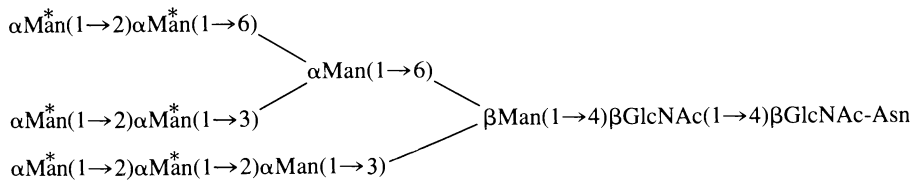

1

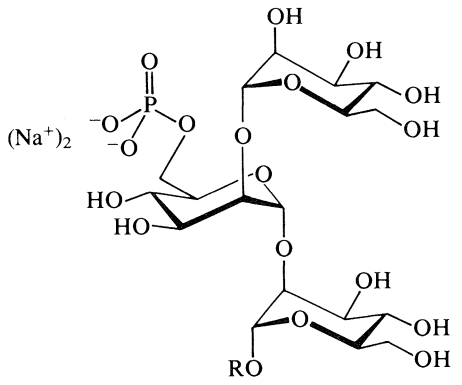

2: αMan(1→2)αMan*(1→2)αManOR

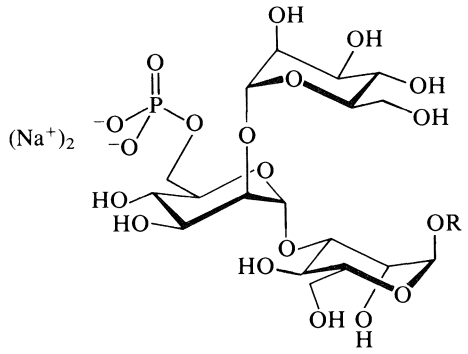

3: αMan(1→2)αMan*(1→3)αManOR

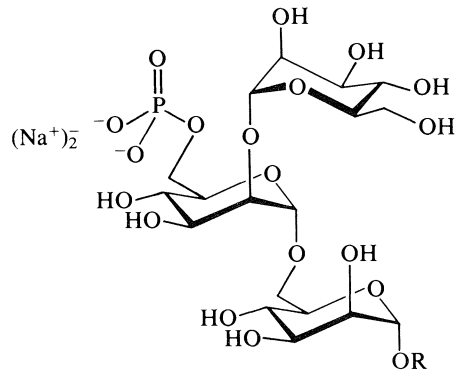

4: αMan(1→2)αMan*(1→6)αManOR

R = —$(CH_2)_8COOCH_3$

(**13**α:**13**β = 4:1) in 83% yield. Reaction of **13**α,β with oxalyl chloride in the presence of *N*,*N*-dimethylformamide (22) then gave the D-mannobiosyl chlorides **14** (59%) and **15** (19%), which could be separated by chromatography on silica gel. The α-anomer (**14**) was stable for weeks on storage, as a solution in dichloromethane at −20°C, and was used in all subsequent glycosylation reactions.

Glycosylation of **5** with **14**, promoted by silver trifluoromethanesulfonate and *sym*-collidine in 1,2-dichloroethane, gave a mixture (82%) of the trisaccharides **16** (α) and **17** (β), in a ratio of 1.2:1, which were readily separable by silica gel chromatography. That all three glycosydic linkages in **16** had the α-configuration was supported by the observation, in its ^{13}C nmr spectrum, of three resolved signals for the anomeric carbons (Table 1) with $^1J_{C,H}$ of 173, 173, and 170 Hz, respectively, in accordance with the empirical rules formulated by Bock and Pedersen (23) for the dependence of one-bond C—H coupling constants on the anomeric configuration of glycopyranosides. The newly formed glycosidic linkage in **17** was assigned the β-configuration based also on its ^{13}C nmr spectrum, which showed a signal for an anomeric carbon having $^1J_{C,H}$ = 156 Hz. Other key spectroscopic data in support of the structural assignments of **16** and **17** are collected in Table 1.

Reaction of **14** with **6** again gave a reasonable yield (73%) of trisaccharidic product, this time in the ratio **18**(α):**19**(β) of 2.3:1. Anomers **18** and **19** comigrated in thin-layer chromatography and their separation required the use of high-pressure liquid chromatography. The assignment of the α-configuration to **18** was based on the characteristic (≈170 Hz) $^1J_{C,H}$ coupling constants for all three anomeric carbons (Table 1). The signal for C-1′ of the β-anomer **19** showed the characteristically smaller ($^1J_{C,H}$ = 155 Hz) one-bond coupling. Other nmr data in support of these structural assignments are also included in Table 1.

Condensation of **14** and **7** also provided a trisaccharidic product (79%), but this time with the β-linked derivative (**21**) as the major component (**20**:**21** = 1:3) as judged by the ^1H nmr spectrum of the chromatographically homogeneous mixture. The loss of α-stereospecificity in the glycosylation of more reactive alcohols has also been observed by Ogawa and Nukuda (17) in comparable reactions with primary alcohols and was therefore not unexpected. The low yield of **20**(α) was nevertheless disappointing, particularly since extensive attempts at separating **20** and **21** chromatographically failed. The mixture of **20** and **21** was therefore hydrogenated over palladium on carbon at atmospheric pressure, which cleaved the benzyl ether

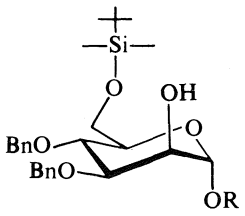

5

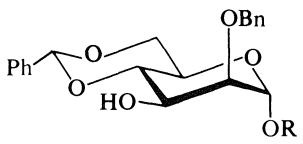

6

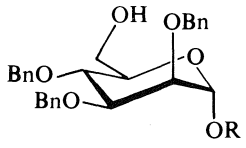

7

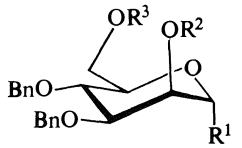

8: R^1 = Br, R^2 = R^3 = Ac
9: R^1 = $OCH_2CH{=}CH_2$, R^2 = R^3 = Ac
10: R^1 = $OCH_2CH{=}CH_2$, R^2 = R^3 = H
11: R^1 = $OCH_2CH{=}CH_2$, R^2 = H, R^3 = $P(OPh)_2O$

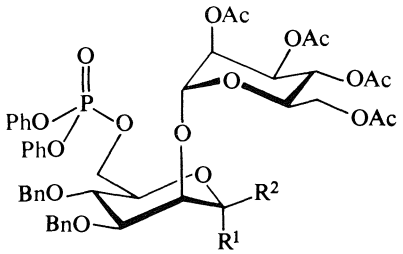

12: R^1 = $OCH_2CH{=}CH_2$, R^2 = H
13α: R^1 = OH, R^2 = H
13β: R^1 = H, R^2 = OH
14: R^1 = Cl, R^2 = H
15: R^1 = H, R^2 = Cl

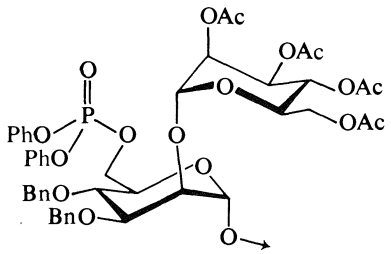

A

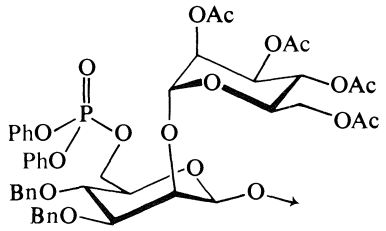

B

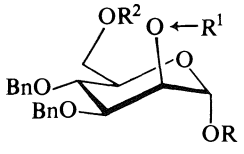

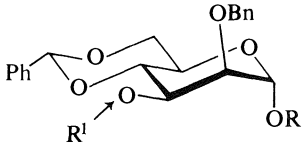

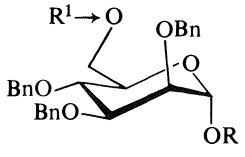

16: R^1 = **A**, R^2 = tBuMe$_2$Si
17: R^1 = **B**, R^2 = tBuMe$_2$Si
24: R^1 = **A**, R^2 = H

18: R^1 = **A**
19: R^1 = **B**

20: R^1 = **A**
21: R^1 = **B**

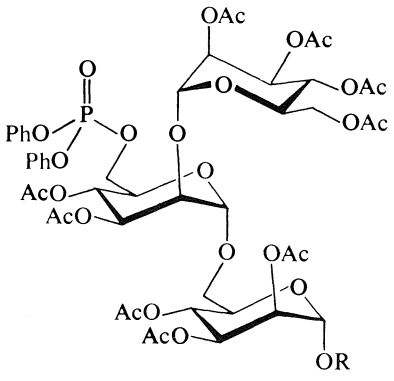

22

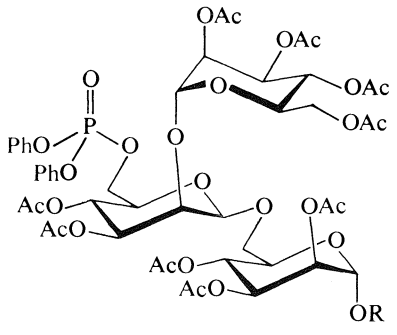

23

groups with only modest (≤20%) loss of the phenyl protecting groups. Acetylation of the resulting material gave a mixture of **22**α (15% from **7**) and **23**β (45% from **7**), which was now readily separated by silica gel chromatography. The anomeric configurations of the glycosidic linkages in **22** and **23** were evident from the nmr data presented in Table 1. Although the overall yield of the required α-linked protected trisaccharide **22** obtained by this route was low, sufficient material was obtained to proceed to the final product (**4**), and other reaction conditions were consequently not explored.

The deprotection of **16**, **18**, and **22** proceeded without complications. Removal of the *tert*-butyldimethylsilyl group from **16** using aqueous acetic acid gave **24** in 85% yield. Hydrogenolysis of the benzyl ethers in **24** over palladium on charcoal followed by deprotection of the phosphate groups using hydrogenolysis over Adams' catalyst (PtO_2) and, finally, removal of the acetates by transesterification with methanol gave **2** (78% from **24**), which was isolated as its disodium salt after chromatography on Bio-Gel P-2 and ion exchange. Similar deprotection of **18** gave trisaccharide **3** in 81% yield. Deprotection of **22** involved only hydrogenation over Adams' catalyst followed by transesterification to produce **4** (81%). Key nmr data for compounds **2**–**4** are presented in Table 1.

Experimental

All solvents and reagents used were reagent grade and, in cases where further purification was required, standard procedures (24) were followed. All solid reactants for glycosylation were dried overnight over phosphorus pentoxide in a high vacuum prior to use. Solution transfers where anhydrous conditions were required were done under nitrogen using standard syringe techniques. Molecular sieves were purchased from BDH Chemicals.

Thin-layer chromatograms (tlc) were performed on precoated silica gel 60-F254 plates (E. Merck, Darmstadt) and visualized by quenching of fluorescence and (or) by charring after spraying with 5% sulfuric acid in ethanol. Unless otherwise stated, chromatography was performed on silica gel 60 (40–63 μm, E. Merck No. 9385). Iatrobeads refer to a beaded silica gel manufactured by Iatron Laboratories, Tokyo (product No. 6RS-8060). The Partisil column was from Waters Associates. Solvents were removed on a rotary evaporator under the vacuum of a water aspirator with bath temperatures of 40°C or lower. For gel filtration, Bio-Gel P-2 (200–400 mesh) (Bio-Rad Laboratories, Richmond, California) was used.

Proton nuclear magnetic resonance (^{1}H nmr) spectra were recorded at either 400 MHz (Bruker WH-400) or 360 MHz (Bruker WM-360) with either tetramethylsilane (δ = 0 in $CDCl_3$) or acetone (δ = 2.225 in D_2O) as internal standard at ambient temperature. Carbon-13 nuclear magnetic resonance (^{13}C nmr) spectra were recorded at either 100.62 MHz (Bruker WH-400) or 90.56 MHz (Bruker WM-360) with either internal tetramethylsilane (δ = 0 in $CDCl_3$) or external 1,4-dioxane (δ = 67.4 in D_2O) as reference standard. Phosphorus-31 nuclear magnetic resonance (^{31}P nmr) spectra were recorded at 145 MHz (Bruker WM-360) with external 85% H_3PO_4 as reference standard (δ = 0) in both $CDCl_3$ and D_2O. Only partial nmr data are reported. Other spectral features were in accord with the proposed structures. The ^{1}H coupling constants are reported as though they were first order. Assignments of ^{13}C resonances are tentative. Additional nmr data for compounds **2**–**4**, **16**–**19**, **22**, and **23** appear in Table 1. Optical rotations were determined on a Perkin–Elmer 241 polarimeter in a 1-dm cell at ambient temperature (23 ± 1°C).

*Allyl 2,6-di-*O*-acetyl-3,4-di-*O*-benzyl-α-*D*-mannopyranoside (**9**)*

To a solution of allyl alcohol (1.22 g, 18 mmol) in dry acetonitrile (5 mL) containing 4Å molecular sieves were added, sequentially, mercuric bromide (7.78 g, 21.6 mmol) and mercuric cyanide (5.45 g, 21.6 mmol), followed by a solution of 2,6-di-*O*-acetyl-3,4-di-*O*-benzyl-α-D-mannopyranosyl bromide (**8**, 21.6 mmol) in acetonitrile

TABLE 1. Selected chemical shifts (ppm) and coupling constants (Hz, in parentheses) for both protected and deprotected synthetic phosphorylated trimannosides[a]

	Compound								
Nucleus[b]	**16**	**17**	**18**	**19**	**22**	**23**	**2**	**3**	**4**
H-1 ($J_{1,2}$)	4.797(—)[c]	4.881(1.5)	4.767(1.5)	4.874(1.5)	4.759(1.8)	4.779(1.7)	5.011(1.6)	4.828(1.8)	4.849(1.6)
H-1′ ($J_{1',2'}$)	5.225(1.5)	4.629(<1)	5.356(1.5)	4.300(<1)	4.912(1.7)	4.535(<1)	5.271(1.8)	5.312(1.6)	5.108(1.6)
H-1″ ($J_{1'',2''}$)	4.899(1.7)	5.243(1.9)	4.847(1.5)	5.085(1.7)	4.893(1.8)	4.901(1.7)	5.041(1.8)	5.049(1.8)	5.029(1.8)
H-2 ($J_{2,3}$)	3.986(—)[c]	4.289(3.2)	3.758(3.2)	3.791(3.2)	5.263(3.0)	5.274(3.4)	3.933(3.2)	4.128(3.2)	3.926(—)[c]
H-2′ ($J_{2',3'}$)	4.064(—)[c]	4.227(2.8)	4.042(2.8)	3.902(2.6)	4.112(3.2)	4.129(2.7)	4.107(3.0)	4.102(3.2)	4.002(3.2)
H-2″ ($J_{2'',3''}$)	5.443(3.2)	5.604(3.5)	5.389(3.2)	5.573(3.2)	5.217(3.0)	5.220(3.0)	4.083(3.2)	4.087(3.4)	4.089(3.4)
C-1 ($^1J_{C,H}$)	98.76(170)	95.94(168)	98.92(169)	98.25(169)	97.35(171)	97.26(172)	98.74(171)	99.26(170)	98.39(172)
C-1′ ($^1J_{C,H}$)	100.26(173)	96.21(156)	99.73(173)	95.60(155)	98.25(172)	100.51(157)	101.24(171)	100.67(172)	99.95(171)
C-1″ ($^1J_{C,H}$)	99.34(173)	98.49(173)	99.08(172)	99.06(169)	99.43(172)	99.03(173)	102.64(170)	101.78(171)	102.35(173)
C-5′ ($^3J_{C,P}$)	71.20(8)	72.91(7)	71.47(8)	74.50(7)	—[c]	73.31(7)	73.10(8)	72.80(6)	72.28(7)
C-6′ ($^2J_{C,P}$)	68.08(6)	67.96(6)	69.90(6)	67.80(6)	67.87(5)	67.89(6)	63.67(4)	63.40(4)	63.27(5)
P	−12.32	−11.86	−11.17	−11.77	−13.91	−14.00	4.03	4.12	4.45

[a]Spectra of **16**–**23** recorded in $CDCl_3$; spectra for **2**–**4** recorded in D_2O. Other experimental conditions and reference standards are described in the experimental section.
[b]Assignments are tentative, but ^{1}H connectivities are confirmed by homonuclear decoupling.
[c]Could not be accurately determined.

(5 mL). The reaction mixture was stirred for 15 h at room temperature, diluted with dichloromethane (25 mL), filtered, and evaporated to dryness. The residue was extracted 3 times with dichloromethane and the extracts were combined and washed with saturated KCl (×3), saturated $NaHCO_3$ (×3), and twice with water, and the solvent was removed by evaporation. Chromatography using hexane – ethyl acetate, (3:1) as eluent provided the title compound as a syrup (6.5 g, 75%); $[\alpha]_D$ +30.9° (*c* 0.69, chloroform); R_f 0.22 (hexane – ethyl acetate, 3:1); ^{1}H nmr ($CDCl_3$) δ: 5.700 (m, 1H, C*H*=CH_2), 2.110 and 1.995 (each s, 3H, $COCH_3$); ^{13}C nmr δ: 170.67 and 170.22 (*C*OCH_3), 138.03 and 137.79 (quat. arom.), 133.25 (*C*H=CH_2), 117.95 (CH=*C*H_2), 96.89 (C-1, $^1J_{C,H}$ = 171 Hz), 63.40 (C-6), 21.00 and 20.80 ($COCH_3$). *Anal.* calcd. for $C_{27}H_{32}O_8$: C 66.93, H 6.66; found: C 66.85, H 6.83.

*Allyl 3,4-di-*O*-benzyl-α-D-mannopyranoside (**10**)*

Compound **9** (6.2 g, 12.8 mmol) was dissolved in dry methanol (50 mL) containing sodium methoxide and left for 15 h at room temperature. After neutralization with IRC-50 (H) and filtration, the solvent was removed and the residue was purified by chromatography using hexane – ethyl acetate (1:1) as eluent, to provide the title compound as a syrup (4.5 g, 88%); $[\alpha]_D$ +56° (*c* 0.45, chloroform); R_f 0.17 (hexane – ethyl acetate, 1:1); ^{1}H nmr ($CDCl_3$) δ: 5.873 (m, 1H, C*H*=CH_2), 4.928 (d, 1H, $J_{1,2}$ = 1.5 Hz, H-1), 2.554 (d, 1H, $J_{OH,2}$ = 1.8 Hz, O*H*$_2$), 2.010 (dd, 1H, $J_{OH,6a}$ = 5.5, $J_{OH,6b}$ = 7.5 Hz, O*H*$_6$); ^{13}C nmr ($CDCl_3$) δ: 138.34 and 137.94 (quat. arom.), 133.57 (*C*H=CH_2), 117.35 (CH=*C*H_2), 98.45 (C-1), 61.59 (C-6). *Anal.* calcd. for $C_{23}H_{28}O_6$: C 68.98, H 7.05; found: C 68.68, H 6.98.

*Allyl 3,4-di-*O*-benzyl-6-*O*-diphenylphosphoryl-α-D-mannopyranoside (**11**)*

Diphenylphosphoryl chloride (2.40 mL, 11.5 mmol) was added to a solution of **10** (4.2 g, 10.5 mmol) in pyridine (20 mL) at 0°C and the reaction mixture allowed to warm to room temperature over 0.5 h. After 15 h, water (20 mL) was added and, after an additional 0.5 h, the reaction was taken to dryness. The residual syrup was dissolved in dichloromethane (150 mL) and washed sequentially with water, 5% HCl, water, saturated $NaHCO_3$, and, finally, water before concentration to a syrup that was purified by chromatography using hexane – ethyl acetate (2:1). Pure **11** was obtained as a syrup (5.2 g, 78.4%); $[\alpha]_D$ +41.8° (*c* 0.79, chloroform); R_f 0.20 (hexane – ethyl acetate, 2:1); ^{1}H nmr ($CDCl_3$) δ: 5.828 (m, 1H, C*H*=CH_2), 4.883 (d, 1H, $J_{1,2}$ = 1.5 Hz, H-1), 2.55 (br, O*H*$_2$); ^{13}C nmr ($CDCl_3$) δ: 137.98 and 137.80 (quat. arom.), 133.47 (*C*H=CH_2), 117.56 (CH=*C*H_2), 98.41 (C-1), 70.27 (C-5, $^3J_{C,P}$ = 7 Hz), 68.06 (C-6, $^2J_{C,P}$ = 6 Hz); ^{31}P nmr ($CDCl_3$) δ: −11.77. *Anal.* calcd. for $C_{35}H_{37}O_9P$: C 66.45, H 5.90; found: C 66.47, H 5.98.

*Allyl 2-*O*-(2,3,4,6-tetra-*O*-acetyl-α-D-mannopyranosyl)-3,4-di-*O*-benzyl-6-*O*-diphenylphosphoryl-α-D-mannopyranoside (**12**)*

A mixture of **11** (1.2 g, 1.90 mmol) and silver trifluoromethanesulfonate (2.9 g, 11.4 mmol) was dried *in vacuo* over phosphorous pentoxide for 5 h at 20°C and dissolved in 1,2-dichloroethane (5 mL) under argon. To this stirring mixture was added *N,N,N′,N′*-tetramethylurea (680 μL, 5.7 mmol) and 2,3,4,6-tetra-*O*-acetyl-α-D-mannopyranosyl bromide (25) (3.8 mmol) in 5 mL of 1,2-dichloroethane. After both 5 h and 20 h, further additions of *N,N,N′,N′*-tetramethylurea (680 μL, 5.7 mmol) and the same glycosyl bromide (3.8 mmol) were made. The reaction was then stirred for an additional 36 h and diluted with 1,2-dichloroethane (50 mL). *Sym*-collidine (1.5 mL, 11.4 mmol) followed by silver trifluoromethanesulfonate (975 mg, 3.8 mmol) were then added to destroy any unreacted glycosyl bromide and, after 0.5 h, excess silver was precipitated by addition of tetraethylammonium bromide (800 mg). Solids were removed by filtration and washed twice with saturated aqueous $NaHCO_3$ (150 mL) and twice with water (150 mL) before evaporation to a syrup. Purification by chromatography (hexane – ethyl acetate 1:1) provided the title compound (1.3 g, 71%) as a syrup; $[\alpha]_D$ +40.5° (*c* 0.60, chloroform); R_f 0.31 (hexane – ethyl acetate, 1:1); ^{1}H nmr ($CDCl_3$) δ: 5.808 (m, 1H, C*H*=CH_2), 4.978 (d, 1H, $J_{1',2'}$ = 1.5 Hz, H-1′), 4.878 (d, 1H, $J_{1,2}$ = 1.2 Hz, H-1), 2.097, 2.069, 1.992, and 1.983 (each s, 3H, $COCH_3$); ^{13}C nmr ($CDCl_3$) δ: 170.54, 169.79, 169.70, and 169.61 (*C*OCH_3), 138.01 and 137.88 (quat. arom.), 133.32 (*C*H=CH_2), 117.60 (CH=*C*H_2), 99.37 (C-1′, $^1J_{C,H}$ = 173 Hz), 97.61 (C-1, $^1J_{C,H}$ = 171 Hz), 71.00 (C-5, $^3J_{C,P}$ = 8 Hz), 68.06 (C-6, $^2J_{C,P}$ = 8 Hz), 62.50 (C-6′), 20.85, 20.71, and 20.65 (2 × C) (*C*O*C*H$_3$); ^{31}P nmr ($CDCl_3$) δ: −11.58. *Anal.* calcd. for $C_{49}H_{55}O_{18}P$: C 61.12, H 5.76; found: C 60.89, H 5.91.

*2-*O*-(2,3,4,6-Tetra-*O*-acetyl-α-D-mannopyranosyl)-3,4-di-*O*-benzyl-6-*O*-diphenylphosphoryl-α,β-D-mannopyranose (**13**α and **13**β)*

A solution of **12** (1.25 g, 1.30 mmol), tristriphenylphosphinerhodium(I) chloride (84.1 mg, 0.09 mmol), and 1,8-diazabicyclo[2.2.2]octane (36.4 mg, 0.33 mmol) in ethanol–benzene–water (7:3:1; 50 mL) was heated at reflux for 36 h. The solvent was removed and the residue dissolved in acetone (50 mL) containing a trace amount of mercuric oxide. To this solution was added a solution of mercuric chloride (1.98 g) in acetone–water (9:1; 30 mL), and the mixture was stirred at room temperature for 2 h. Following evaporation of the solvent, the residue was taken up in dichloromethane (150 mL) and washed with 30% aqueous KBr followed by water. Drying (Na_2SO_4) and evaporation left an oily residue that was purified by chromatography using hexane – ethyl acetate (2:3) as eluent. The title compound was obtained as a syrup (998 mg; 83%); R_f 0.11 (hexane – ethyl acetate 1:1); ^{1}H nmr ($CDCl_3$) δ: 5.140 (br, 0.8 H, H-1α), 4.985 (d, 0.8 H, $J_{1',2'}$ = 1.5 Hz, H-1′β), 3.190 (br, 0.2 H, OHβ), 2.875 (d, 0.8H, OHα), 2.102, 2.077, 1.999, and 1.986 (COC*H*$_3$α), 2.126, 2.085, 2.018 (COC*H*$_3$β). *Anal.* calcd. for $C_{46}H_{51}O_{18}P$: C 59.87, H 5.57; found: C 59.66, H 5.66.

*2-*O*-(2,3,4,6-Tetra-*O*-acetyl-α-D-mannopyranosyl)-3,4-di-*O*-benzyl-6-*O*-diphenylphosphoryl-α-D-mannopyranosyl chloride (**14**) and 2-*O*-(2,3,4,6-tetra-*O*-acetyl-α-D-mannopyranosyl)-3,4-di-*O*-benzyl-6-*O*-diphenylphosphoryl-β-D-mannopyranosyl chloride (**15**)*

A solution of oxalyl chloride (910 μL, 10.4 mmol) in dichloromethane (2 mL) was added to a stirring solution of **13**α and **13**β (3.5 g, 3.79 mmol) and *N,N*-dimethylformamide (47 μL, 0.61 mmol) in dichloromethane (4 mL). The mixture was stirred for 1 h at room temperature and was poured into ice water. The organic layer was washed with cold water (3 × 25 mL), dried (Na_2SO_4), and concentrated to a syrup, which was purified by chromatography using hexane – ethyl acetate (3:2) as eluent. The title compounds **14** (2.10 g, 59%; R_f 0.13 in hexane – ethyl acetate, 3:2) and **15** (680 mg, 19%; R_f 0.27 in hexane – ethyl acetate, 3:2) were obtained as clear syrups.

Compound **14**: ^{1}H nmr ($CDCl_3$) δ: 6.170 (d, 1H, $J_{1,2}$ = 1.8 Hz, H-1), 5.457 (dd, 1H, $J_{1',2'}$ = 1.8 Hz, $J_{2',3'}$ = 3.2 Hz, H-2′), 5.360 (dd, 1H, $J_{3',4'}$ = 9.5 Hz, H-3′), 5.227 (dd, 1H, $J_{4',5'}$ = 10 Hz, H-4′), 4.843 (d, 1H, H-1′), 3.950 (dd, 1H, $J_{2,3}$ = 3.0 Hz, H-2), 2.137, 2.093, 1.997, and 1.967 (each s, 3H, COC*H*$_3$).

Compound **15**: ^{1}H nmr ($CDCl_3$) δ: 5.563 (dd, 1H, $J_{1',2'}$ = 1.8 Hz, $J_{2',3'}$ = 3.0 Hz, H-2′), 5.407 (dd, 1H, $J_{3',4'}$ = 10.0 Hz, H-3′), 5.323 (2H, dd, $J_{4',5'}$ = 10.0 Hz, H-4′ and s, H-1), 5.130 (d, 1H, H-1′), 4.128 (d, 1H, $J_{2,3}$ = 2.3 Hz, H-2), 3.822 (dd, 1H, $J_{3,4}$ = $J_{4,5}$ = 9.5 Hz, H-4), 3.610 (2H, H-5 and H-3), 2.087 (s, 6H, 2 × COC*H*$_3$), 2.027 and 1.983 (each s, 3H, COC*H*$_3$).

*8-Methoxycarbonyloctyl 2-*O*-[2-*O*-(2,3,4,6-tetra-*O*-acetyl-α-D-mannopyranosyl)-3,4-di-*O*-benzyl-6-*O*-diphenylphosphoryl-α-D-mannopyranosyl]-3,4-di-*O*-benzyl-6-*O*-tert-butyldimethylsilyl-α-D-mannopyranoside (**16**) and 8-methoxycarbonyloctyl 2-*O*-[2-*O*-(2,3,4,6-tetra-*O*-acetyl-α-D-mannopyranosyl)-3,4-di-*O*-benzyl-6-*O*-diphenylphosphoryl-β-D-mannopyranosyl]-3,4-di-*O*-benzyl-6-*O*-tert-butyldimethylsilyl-α-D-mannopyranoside (**17**)*

A solution of **14** (298 mg, 0.32 mmol) was added dropwise, over 0.5 h, to a mixture of **5** (120 mg, 0.19 mmol), *sym*-collidine (36.9 μL, 0.28 mmol), silver trifluoromethanesulfonate (81.3 mg, 0.32 mmol), and pulverized 4Å molecular sieves (1.2 g) stirring in 1,2-dichloroethane (1 mL) at room temperature. After 15 h, 1,2-dichloroethane

(20 mL) was added and the sieves were removed by filtration and washed with more 1,2-dichloroethane (20 mL). *Sym*-collidine (37 μL) followed by silver trifluoromethanesulfonate (81 mg) were then added to the filtrate to destroy any unreacted **14** and, after 0.5 h, tetraethylammonium bromide (67 mg) was added to precipitate excess silver. Solids were removed by filtration and the resulting solution was washed twice with saturated $NaHCO_3$ and twice with water and taken to dryness. The residual syrup was purified by chromatography on Iatrobeads using hexane – ethyl acetate (3:2) as eluent. Evaporation of the later fractions provided the α-anomer **16** (131 mg, 45%) as a syrup (R_f 0.30 in hexane – ethyl acetate, 3:2); $[\alpha]_D$ +28° (*c* 0.25, chloroform); ^{1}H nmr ($CDCl_3$) δ: 5.388 (dd, 1H, $J_{3'',4''}$ = 9.5 Hz, H-3″), 5.279 (dd, 1H, $J_{4'',5''}$ = 10 Hz, H-4″), 3.650 (s, 3H, OCH_3), 3.257 (dt, 1H, OCHHCH$_2$), 2.275 (t, 2H, CH_2COO), 2.104, 2.016, 1.985, and 1.967 (each s, 3H, COCH_3), 0.884 (s, 9H, C(CH_3)$_3$), 0.064 and 0.053 (each s, 3H, SiCH_3); ^{13}C nmr ($CDCl_3$) δ: 174.25 (*C*OOCH$_3$), 170.50, 169.76, 169.69, and 169.63 (*C*OCH$_3$), 138.61, 138.37, 138.19, and 138.07 (benzyl. quat. arom.), 62.44 and 62.13 (C-6 and C-6″), 51.42 (OCH$_3$), 34.09 (*C*H$_2$COO), 26.01 (C(*C*H$_3$)$_3$), 20.49, 20.70 (2 × C) and 20.64 (COCH$_3$), 18.33 (*C*(CH$_3$)$_3$), −4.84 and −5.36 (SiCH$_3$). *Anal.* calcd. for $C_{82}H_{105}O_{25}PSi$: C 63.55, H 6.83; found: C 63.41, H 7.05.

The earlier fractions (R_f 0.41 in hexane – ethyl acetate, 3:2) contained the β-anomer **17** (107 mg, 37%); $[\alpha]_D$ +7.0° (*c* 0.18, chloroform); ^{1}H nmr ($CDCl_3$) δ: 5.446 (dd, 1H, $J_{3'',4''}$ = 10.0 Hz, H-3″), 5.376 (dd, 1H, $J_{4'',5''}$ = 10.0 Hz, H-4″), 3.647 (s, OCH$_3$), 3.322 (dt, 1H, OCHHCH$_2$), 2.264 (t, 2H, CH_2COO), 2.107, 2.076, 1.971, and 1.643 (each s, 3H, COCH$_3$), 0.894 (s, 9H, C(CH_3)$_3$), 0.542 (s, 6H, SiCH_3); ^{13}C nmr ($CDCl_3$) δ: 174.24 (*C*OOCH$_3$), 170.70, 169.90, 169.66, and 169.58 (*C*OCH$_3$), 138.73, 138.66, 137.60, and 137.37 (benzyl quat. arom.), 62.93 and 62.36 (C-6 and C-6″), 51.40 (OCH$_3$), 34.06 (*C*H$_2$COO), 25.94 (C(*C*H$_3$)$_3$), 20.95, 20.76, 20.69, and 20.38 (COCH$_3$), 18.33 (*C*(CH$_3$)$_3$), −5.14 and −5.26 (SiCH$_3$). *Anal.* calcd. for $C_{82}H_{105}O_{25}PSi$: C 63.55, H 6.83; found: C 63.67, H 6.80.

*8-Methoxycarbonyloctyl 3-*O*-[2-*O*-(2,3,4,6-tetra-*O*-acetyl-α-D-mannopyranosyl)-3,4-di-*O*-benzyl-6-*O*-diphenylphosphoryl-α-D-mannopyranosyl]-2-*O*-benzyl-4,6-*O*-benzylidene-α-D-mannopyranoside (**18**) and 8-methoxycarbonyloctyl 3-*O*-[2-*O*-(2,3,4,6-tetra-*O*-acetyl-α-D-mannopyranosyl)-3,4-di-*O*-benzyl-6-*O*-diphenylphosphoryl-β-D-mannopyranosyl]-2-*O*-benzyl-4,6-*O*-benzylidene-α-D-mannopyranoside (**19**)*

Reaction of **6** (112 mg, 0.21 mmol) with **14** (339 mg, 0.36 mmol) in the presence of silver trifluoromethanesulfonate and *sym*-collidine, exactly as described for the preparation of **16**, gave a chromatographically homogeneous (R_f 0.23 in hexane – ethyl acetate, 3:2) mixture of **18** and **19**, which could be resolved on a Partisil column using hexane – ethyl acetate 4:1 as eluent. The earlier fractions provided the α-anomer **18** (154 mg, 51%) as a syrup, $[\alpha]_D$ +34.4° (*c* 0.38, chloroform); ^{1}H nmr ($CDCl_3$) δ: 5.575 (s, 1H, C$_6$H$_5$CHOO), 5.356 (dd, 1H, $J_{3'',4''}$ = 10.0 Hz), 5.228 (dd, 1H, $J_{4'',5''}$ = 10.0 Hz, H-4″), 3.650 (s, 3H, OCH_3), 3.325 (dt, 1H, OCHHCH$_2$), 2.272 (t, 1H, CH_2COO), 2.086, 2.025, 1.969, and 1.944 (each s, 3H, COCH_3); ^{13}C nmr ($CDCl_3$) δ: 174.23 (*C*OOCH$_3$), 170.45, 169.76, 169.69, and 169.57 (*C*OCH$_3$), 138.18, 138.01, 137.78, and 137.46 (3 benzyl and benzylidene quat. arom.), 101.63 (C$_6$H$_5$*C*HOO), 61.95 (C-6″), 51.41 (OCH$_3$), 34.07 (*C*H$_2$COO), 20.88, 20.77, 20.67, and 20.59 (COCH$_3$). *Anal.* calcd. for $C_{76}H_{89}O_{25}P$: C 63.68, H 6.26; found: C 63.63, H 6.39.

The later fractions provided the β-anomer **19** (66.3 mg, 22%) as a syrup, $[\alpha]_D$ 0° (*c* 0.89, chloroform); ^{1}H nmr ($CDCl_3$) δ: 5.560 (s, 1H, C$_6$H$_5$CHOO), 5.330 (dd, 1H, $J_{3'',4''}$ = 10.0 Hz, H-3″), 5.291 (dd, 1H, $J_{4'',5''}$ = 10.0 Hz, H-3″), 3.650 (s, OCH_3), 3.308 (dd, $J_{3',4'}$ = 9.5 Hz, H-3′), 2.270 (t, 2H, CH_2COO), 2.083, 2.077, and 1.903 (each s, 3H, COCH_3); ^{13}C nmr ($CDCl_3$) δ: 174.23 (*C*OOCH$_3$), 169.76 (2 × C), 169.63 and 169.36 (*C*OCH$_3$), 137.73 (2 × C), 137.70 and 137.55 (3 benzyl and benzylidene quat. arom.), 100.88 (C$_6$H$_5$*C*HOO), 62.01 (C-6″), 51.41 (OCH$_3$), 34.07 (*C*H$_2$COO), 20.90, 20.82, 20.57, and 20.02 (COCH$_3$). *Anal.* calcd. for $C_{76}H_{89}O_{25}P$: C 63.68, H 6.26; found: C 63.38, H 6.29.

*8-Methoxycarbonyloctyl 6-*O*-[2-*O*-(2,3,4,6-tetra-*O*-acetyl-α-D-mannopyranosyl)-3,4-di-*O*-benzyl-6-*O*-diphenylphosphoryl-α-D-mannopyranosyl]-2,3,4-tri-*O*-benzyl-α-D-mannopyranoside (**20**) and 8-methoxycarbonyloctyl 6-*O*-[2-*O*-(2,3,4,6-tetra-*O*-acetyl-α-D-mannopyranosyl)-3,4-di-*O*-benzyl-6-*O*-diphenylphosphoryl-β-D-mannopyranosyl]-2,3,4-tri-*O*-benzyl-α-D-mannopyranoside (**21**)*

Reaction of **7** (215 mg, 0.35 mmol) with **14** (554 mg, 0.59 mmol) in the presence of silver trifluoromethanesulfonate and *sym*-collidine, exactly as described for the preparation of **16**, gave a chromatographically homogeneous (R_f = 0.23 in hexane – ethyl acetate, 2:1) mixture of **20** and **21** (418 mg, 79%) as a clear syrup, which could not be chromatographically resolved on either Iatrobeads or Partisil. The ^{1}H nmr spectrum of the mixture showed the ratio of **20**:**21** to be 1:3 based on the relative intensities of the following signals:

The minor isomer (**20**): ^{1}H nmr ($CDCl_3$) δ: 5.466 (dd, 1H, $J_{1'',2''}$ = 1.6 Hz, $J_{2'',3''}$ = 3.2 Hz, H-2″), 5.406 (dd, 1H, $J_{3'',4''}$ = 10.0 Hz, H-3″), 5.304 (dd, 1H, $J_{1',2'}$ = 1.8 Hz, H-1′), 4.945 (d, 1H, H-1″), 4.797 (d, 1H, $J_{1,2}$ = 1.8 Hz, H-1), 3.649 (s, OCH_3), 2.095, 2.053, 1.976, and 1.951 (each s, 3H, COCH_3).

The major isomer (**21**): ^{1}H nmr ($CDCl_3$) δ: 5.531 (dd, 1H, $J_{1'',2''}$ = 1.7 Hz, $J_{2'',3''}$ = 3.2 Hz, H-2″), 5.389 (dd, 1H, $J_{3'',4''}$ = 10.0 Hz, H-3″), 5.312 (dd, 1H, $J_{4'',5''}$ = 10.0 Hz, H-4″), 5.033 (d, 1H, $J_{1',2'}$ = 1.6 Hz, H-1′), 4.769 (d, 1H, H-1″), 3.653 (s, OCH_3), 3.424 (dd, 1H, $J_{2',3'}$ = 2.5 Hz, $J_{3',4'}$ = 9.0 Hz, H-3′), 3.351 (m, 1H, H-5′), 2.095, 2.010, 1.946, and 1.939 (each s, 3H, COCH_3).

*8-Methoxycarbonyloctyl 2,3,4-tri-*O*-acetyl-6-*O*-[3,4-di-*O*-acetyl-2-*O*-(2,3,4,6-tetra-*O*-acetyl-α-D-mannopyranosyl)-6-*O*-diphenylphosphoryl-α-D-mannopyranosyl]-α-D-mannopyranoside (**22**) and 8-methoxycarbonyloctyl 2,3,4-tri-*O*-acetyl-6-*O*-[3,4-di-*O*-acetyl-2-*O*-(2,3,4,6-tetra-*O*-acetyl-α-D-mannopyranosyl)-6-*O*-diphenylphosphoryl-β-D-mannopyranosyl]-α-D-mannopyranoside (**23**)*

The mixture of **20** and **21** described above (240 mg, 0.16 mmol) was dissolved in 95% ethanol (4 mL) containing 5% palladium on carbon (120 mg) and stirred under a hydrogen atmosphere (1 atm; 1 atm = 101.3 kPa) for 2 days by which time tlc indicated the presence of a major product (~80%, R_f 0.24 in chloroform–methanol, 9:1) and a more polar product (~20%, R_f 0, presumably the monophenyl phosphate). The catalyst was removed by filtration, washed with 95% ethanol (20 mL), and taken to dryness. The residue (122 mg) was then treated with acetic anhydride – pyridine (1:1, 4 mL) for 18 h at room temperature. Excess acetic anhydride was destroyed by addition of cold water, the mixture was partitioned between dichloromethane (20 mL) and water, and the organic layer was washed sequentially with 1 *N* HCl, saturated $NaHCO_3$, and water, then taken to dryness. The residue was purified by chromatography on Iatrobeads using hexane – ethyl acetate (1:2). The early fractions (R_f 0.27 in hexane – ethyl acetate, 1:2) provided the α-anomer **22** (38.3 mg, 19%) as a syrup, $[\alpha]_D$ +44.2° (*c* 0.53, chloroform); ^{1}H nmr ($CDCl_3$) δ: 3.664 (s, OCH_3), 2.306 (t, 2H, CH_2COO), 2.146, 2.112, 2.074, 2.068, 2.025, 2.021, 2.007, 2.003, and 1.992 (each s, 3H, COCH$_3$); ^{13}C nmr ($CDCl_3$) δ: 174.25 (*C*OOCH$_3$), 66.56 (C-6), 62.39 (C-6″), 51.42 (OCH$_3$), 34.07 (*C*H$_2$COO). *Anal.* calcd. for $C_{58}H_{77}O_{30}P$: C 54.20, H 6.04; found: C 54.25, H 6.07.

The later fractions (R_f 0.21 in hexane – ethyl acetate, 1:2) yielded the β-anomer **23** (115 mg, 57%), $[\alpha]_D$ +16.4° (*c* 0.28, chloroform); ^{1}H nmr ($CDCl_3$) δ: 5.413 (dd, 1H, $J_{3'',4''}$ = 10.0 Hz, H-3″), 5.370 (dd, 1H, $J_{4'',5''}$ = 10.0 Hz, H-4″), 5.331 (dd, 1H, $J_{3,4}$ = 9.5 Hz, H-3), 5.173 (dd, 1H, $J_{4,5}$ = 10 Hz, H-4′), 5.122 (dd, 1H, $J_{3',4'}$ = $J_{4',5'}$ = 10 Hz, H-4′), 5.025 (dd, 1H, H-3′), 3.661 (s, OCH_3), 3.408 (dt, 1H, OCHHCH$_2$), 2.300 (t, 2H, J = 7.5 Hz, CH_2COO), 2.148, 2.121, 2.094, 2.080, 2.022, 2.009, 2.004, 1.998, and 1.978 (each s, 3H, COCH$_3$); ^{13}C nmr ($CDCl_3$) δ: 174.25 (*C*OOCH$_3$), 68.83 (C-6), 67.89, 62.06 (C-6″), 51.40 (OCH$_3$), 34.09 (*C*H$_2$COO). *Anal.* calcd. for $C_{58}H_{77}O_{30}P$: C 54.20, H 6.04; found: C 54.34, H 6.06.

*8-Methoxycarbonyloctyl 2-O-[2-O-(2,3,4,6 tetra-O-acetyl-α-D-mannopyranosyl)-3,4-di-O-benzyl-6-O-diphenylphosphoryl-α-D-mannopyranosyl)-3,4-di-O-benzyl-α-D-mannopyranoside (**24**)*

Compound **16** (83 mg, 0.53 mmol) was dissolved in dichloromethane (1.5 mL) and 80% aqueous acetic acid (15 mL) was added. After 24 h, solvent was evaporated and chromatography of the residue using hexane – ethyl acetate (3:2) as eluent provided the title compound (R_f 0.38 in hexane – ethyl acetate, 1:1) as a syrup (65 mg, 85%); $[\alpha]_D$ 37° (*c* 0.18, chloroform); ^{1}H nmr ($CDCl_3$) δ: 5.448 (dd, 1H, $J_{1'',2''}$ = 1.5 Hz, $J_{2'',3''}$ = 3.0 Hz, H-2″), 5.403 (dd, 1H, $J_{3'',4''}$ = 10.0 Hz, H-3″), 5.295 (dd, 1H, $J_{4'',5''}$ = 10.0 Hz, H-4″), 5.185 (d, 1H, $J_{1',2'}$ = 1.6 Hz, H-1′), 4.893 (d, 1H, H-1″), 4.828 (H-1), 3.655 (s, OCH_3), 2.278 (t, 2H, *J* = 7.5 Hz, CH_2COO), 2.140 (4H, $COCH_3$ and br O*H*), 2.023, 2.005, and 1.980 (each s, 3H, $COCH_3$); ^{13}C nmr ($CDCl_3$) δ: 174.21 ($COOCH_3$), 170.47, 169.73 (2 × C), 169.66 ($COCH_3$), 100.17, 99.19, and 98.72 (C-1, C-1′, and C-1″), 71.51 (C-5′, $^3J_{C,P}$ = 8 Hz), 68.24 (C-6′, $^2J_{C,P}$ = 6 Hz), 62.22 and 62.12 (C-6 and C-6″), 51.39 (OCH_3), 34.06 (CH_2COO), 20.89, 20.68 (2 × C), and 20.62 ($COCH_3$); ^{31}P nmr ($CDCl_3$) δ: −11.42. *Anal.* calcd. for $C_{76}H_{91}O_{25}P$: C 63.59, H 6.39; found: C 63.82, H 6.45.

*8-Methoxycarbonyloctyl 2-O-[2-O-(α-D-mannopyranosyl)-α-D-mannopyranosyl 6-disodiumphosphate]-α-D-mannopyranoside (**2**)*

Compound **24** (38.5 mg, 0.27 mmol) was dissolved in 95% ethanol (3 mL) containing 5% palladium on carbon (40 mg) and stirred under one atmosphere of hydrogen for 36 h. The catalyst was removed by filtration and washed with 95% ethanol (20 mL) and the filtrate was evaporated and redissolved in 95% ethanol (3 mL). Hydrogenation (1 atm) over Adams' catalyst (PtO_2, 5 mg) for 3 h provided a product with R_f 0.25 in chloroform–methanol–water (60:35:6), which was devoid of ultraviolet absorption in tlc. Removal of the catalyst by filtration, followed by evaporation and drying for 15 h over phosphorus pentoxide, left a glass that was dissolved in dry methanol containing sodium methoxide and kept at 0°C until all the material was converted to a single new product with R_f 0.37 in isopropanol–water (4:1). After neutralization with IRC-50 (H^+), removal of the resin, and evaporation, the residue was passed through a column of Bio-gel P-2 (200–400 mesh) (50 × 2.5 cm) using 10% ethanol as eluent. The carbohydrate-containing fractions were pooled, concentrated, and passed through a column of Dowex 50-X8 (Na^+) (10 mL) and the eluate was lyophilized to provide a white powder (16.7 mg, 78%); $[\alpha]_D$ +41.5° (*c* 0.27, water); ^{1}H nmr (D_2O) δ: 3.685 (s, OCH_3), 3.553 (m, $OCHHCH_2$), 2.387 (t, 2H, CH_2COO); ^{13}C nmr (D_2O) δ: 178.42 (*C*O), 79.28, 78.80, 73.76, 73.33, 70.86, 70.75, 70.61, 70.19, 68.70 (OCH_2CH_2), 67.48, 67.38, 66.69, 61.57, and 61.35 (C-6 and C-6″), 52.57 (OCH_3), 34.22 (CH_2COO), 29.04, 28.75, 28.69, 28.63, 25.82, 24.79. *Anal.* calcd. for $C_{28}H_{49}O_{21}Na_2P\cdot 2H_2O$: C 40.29, H 6.40; found: C 39.89, H 6.18.

*8-Methoxycarbonyloctyl 3-O-[2-O-(α-D-mannopyranosyl)-α-D-mannopyranosyl 6-disodiumphosphate]-α-D-mannopyranoside (**3**)*

Compound **18** (50.4 mg, 0.35 mmol) was deprotected as described for the preparation of **2**, using 5% palladium on carbon (50 mg) for 2 days followed by Adams' catalyst (5 mg) for 3 h. After deacylation at 0°C, Bio-gel P-2 chromatography, and Dowex 50-X8 (Na^+) treatment and lyophilization, the product was obtained as a white powder (22.8 mg, 81.2%); $[\alpha]_D$ +60.6° (*c* 0.17, water); R_f 0.39 (isopropanol–water, 4:1); ^{1}H nmr (D_2O) δ: 3.687 (s, OCH_3); 3.530 (m, 1H, $OCHHCH_2$), 2.390 (t, 2H, CH_2COO); ^{13}C nmr (D_2O) δ: 177.44 (*C*O), 79.82, 78.44, 73.37, 72.84, 70.32, 70.15, 69.94, 69.57, 69.14 (OCH_2CH_2), 66.98, 66.58, 65.94, 63.40, 61.09, and 60.94 (C-6 and C-6″), 52.14 (OCH_3), 33.25 (CH_2COO), 28.04, 27.80, 27.73, 27.68, 24.83, 23.82. *Anal.* calcd. for $C_{28}H_{49}O_{21}Na_2P\cdot 2H_2O$: C 40.29, H 6.40; found: C 39.94, H 6.26.

*8-Methoxycarbonyloctyl 6-O-[2-O-(α-D-mannopyranosyl) 6-disodiumphosphate]-α-D-mannopyranoside (**4**)*

Compound **22** (35.4 mg, 0.028 mmol) was deprotected as described for the preparation of **2** but using only Adams' catalyst (8 mg) and sodium methoxide in methanol. The product was isolated as white powder (17.8 mg, 81%) after BioGel P-2 chromatography and ion exchange; R_f 0.41 in isopropanol–water (4:1); $[\alpha]_D$ +53.2° (*c* 0.19, water); ^{1}H nmr (D_2O) δ: 3.688 (s, OCH_3), 3.553 (m, $OCHHCH_2$), 2.393 (t, 2H, CH_2COO); ^{13}C nmr (D_2O) δ: 177.98 (*C*O), 78.65, 73.32, 71.15, 71.02, 70.33, 70.18 (2 × C), 70.10, 68.12 (OCH_2CH_2), 67.07, 66.54, 66.41, 66.06 (C-6), 61.19 (C-6″), 52.15 (OCH_3), 33.80 (CH_2COO), 28.50, 28.27, 28.25, 28.19, 25.35, 24.37. *Anal.* calcd. for $C_{28}H_{49}O_{21}Na_2P\cdot H_2O$: C 41.18, H 6.30; found: C 41.15, H 6.15.

Acknowledgements

The authors gratefully acknowledge the ongoing financial support of the Natural Sciences and Engineering Research Council of Canada and the Alberta Heritage Foundation for Medical Research. The microanalyses and nmr spectra were provided by the Analytical and Spectral Services Laboratory of this department.

1. G. G. Sahagian. Biol. Cell. **51**, 207 (1984).
2. K. E. Creek and W. S. Sly. Lysosomes Biol. Pathol. **7**, 63 (1984).
3. L. Lang, M. Reitman, J. Tang, R. M. Roberts, and S. Kornfeld. J. Biol. Chem. **259**, 14663 (1984).
4. A. Varki and S. Kornfeld. J. Biol. Chem. **255**, 10847 (1980).
5. M. Natowicz, J. U. Baenziger, and W. S. Sly. J. Biol. Chem. **257**, 4412 (1982).
6. A. Varki and S. Kornfeld. J. Biol. Chem. **258**, 2808 (1983).
7. J. Distler and G. W. Jourdian. Proc. 8th Intl. Symp. Glycoconjugates, (Houston, Texas). 1985. p. 139.
8. O. P. Srivastava and O. Hindsgaul. Carbohydr. Res. In press.
9. O. P. Srivastava and O. Hindsgaul. Carbohydr. Res. In press.
10. R. U. Lemieux, D. R. Bundle, and D. A. Baker. J. Am. Chem. Soc. **97**, 4076 (1975).
11. R. U. Lemieux, D. A. Baker, and D. R. Bundle. Can. J. Biochem. **55**, 507 (1977).
12. L. Y. Bourguignon, K. Balazovich, S. J. Suchard, O. Hindsgaul, and M. Pierce. J. Cell. Physiol. **127**, 146 (1986).
13. R. U. Lemieux, K. B. Hendriks, R. V. Stick, and K. James. J. Am. Chem. Soc. **97**, 4056 (1975).
14. H. Paulsen. Angew. Chem. Int. Ed. Engl. **21**, 155 (1982).
15. T. Ogawa and H. Yamamoto. Carbohydr. Res. **104**, 271 (1982).
16. T. Ogawa, H. Yamamoto, T. Nukada, and M. Sugimoto. Pure Appl. Chem. **56**, 779 (1984).
17. T. Ogawa and T. Nukada. Carbohydr. Res. **136**, 135 (1985).
18. M. M. Ponpipom. Carbohydr. Res. **59**, 311 (1977).
19. F. Maley and H. A. Lardy. J. Am. Chem. Soc. **78**, 1393 (1956).
20. C. E. Ballou and D. L. MacDonald. Methods Carbohydr. Chem. **2**, 270 (1963).
21. E. J. Corey and J. W. Sugg. J. Org. Chem. **38**, 3224 (1973).
22. T. Iverson and D. R. Bundle. Carbohydr. Res. **103**, 29 (1982).
23. K. Bock and C. Pedersen. J. Chem. Soc. Perkin Trans. 2, 293 (1974).
24. D. D. Perrin, W. L. Armarego, and D. R. Perrin. Purification of laboratory compounds. 2nd ed. Pergamon Press, London. 1980.
25. W. A. Boomer. J. Am. Chem. Soc. **80**, 3372 (1958).

Configurational assignment of epimeric secondary six-membered allylic alcohols by ^{13}C nuclear magnetic resonance spectroscopy. A new approach

TEODORO S. KAUFMAN, MIRTA P. MISCHNE, MANUEL GONZALEZ-SIERRA, AND EDMUNDO A. RUVEDA

Instituto de Quimica Organica de Sintesis (CONICET–UNR), Facultad de Ciencias Bioquimicas y Farmaceuticas, Casilla de Correo 991, 2000 Rosario, Argentina

Received March 4, 1986

TEODORO S. KAUFMAN, MIRTA P. MISCHNE, MANUEL GONZALEZ-SIERRA, and EDMUNDO A. RUVEDA. Can. J. Chem. **64**, 2331 (1986).

On the basis of the effects of the hydroxyl group on the ^{13}C nuclear magnetic resonance chemical shifts of the olefinic carbons, a new parameter was defined and a new rule was proposed for the assignment of the stereochemistry of secondary six-membered cyclic allylic alcohols.

TEODORO S. KAUFMAN, MIRTA P. MISCHNE, MANUEL GONZALEZ-SIERRA et EDMUNDO A. RUVEDA. Can. J. Chem. **64**, 2331 (1986).

En se basant sur les effets du groupement hydroxyle sur les déplacements chimiques des carbones oléfiniques, en rmn du ^{13}C, on a défini un nouveau paramètre et on propose une nouvelle règle pour attribuer la stéréochimie des alcools allyliques secondaires contenus dans des cycles à six chaînons.

[Traduit par la revue]

In 1979, Schroepfer and co-workers (1) reported that the effect of the introduction of an allylic hydroxyl substituent at C-7 or C-15 on the chemical shifts of the olefinic carbons of $\Delta^{8(14)}$ sterols, relative to the values observed in the parent sterol, is opposite to that observed for the olefinic carbon atoms of acyclic allylic alcohols. Later, Eggert and Djerassi (2), as a result of the analysis of some representative allylic hydroxyl substituted steroids, suggested that the variation of the shifts on the olefinic carbons is related to the conformational class (orientation) of the hydroxyl group as defined in ref. 3, rather than to the acyclic or cyclic structure of the allylic alcohol. They observed that when the hydroxyl group is at an antiperiplanar position, the shifts for the β carbons are larger than those for the γ carbon atoms; a similar effect is observed in acyclic allylic alcohols. However, when the hydroxyl groups are at synclinal or anticlinal positions, the effect is the opposite, that is, larger for the γ carbons than for the β, and, when the oxygenated substituent is at a synperiplanar position, both sp^2 carbons suffer the same downfield shifts.

The application of these simple rules allowed us to predict, by analyzing the ^{13}C nmr reported data (4), that the stereochemistry of the hydroxyl group at C-6 of two natural diterpenes related to grindelic acid (**1***a*) was erroneously assigned (5). In fact, we were able to confirm our predictions by analyzing the ^{13}C nmr spectra of model compounds and by the stereoselective synthesis of both epimers (**1***b* and **1***c*) (6).

To confirm and extend these observations, we analyzed several six-membered allylic alcohols of the diterpene family. We observed the expected shifts of the β and γ sp^2 carbons when the hydroxyl groups are at anticlinal (**2***b* and **3***b*) and antiperiplanar positions (**3***c*). However, we detected deshielding effects for the β carbons and upfield shifts for the γ carbon atoms in those allylic alcohols with hydroxyl groups at synperiplanar positions and carrying hydrogens at the γ carbon atoms (**2***c* and **4***b*) (Table 1).

As we have shown above, the Eggert and Djerassi rules are useful to determine the stereochemistry of allylic alcohols, especially for epimeric pairs. There are, however, a few restrictions on their general use. One of the epimers must always belong to a periplanar conformational class. There are some difficulties whenever there is a discrepancy between the value of the angle that defines the conformational class and that which

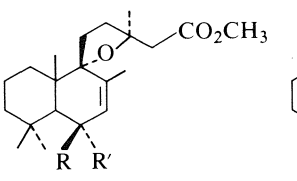

1*a* R = R′ = H
1*b* R = OH; R′ = H
1*c* R = H; R′ = OH

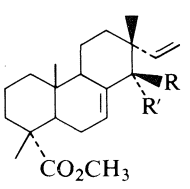

2*a* R = R′ = H
2*b* R = H; R′ = OH
2*c* R = OH; R′ = H

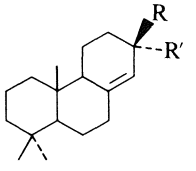

3*a* R = R′ = H
3*b* R = OH; R′ = H
3*c* R = H; R′ = OH

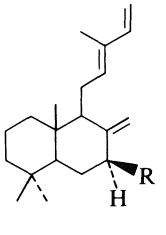

4*a* R = H
4*b* R = OH

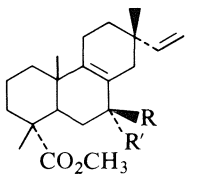

5*a* R = R′ = H
5*b* R = H; R′ = OH
5*c* R = OH; R′ = H

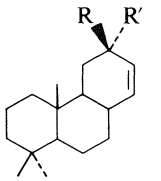

6*a* R = H; R′ = OH
6*b* R = OH; R′ = H

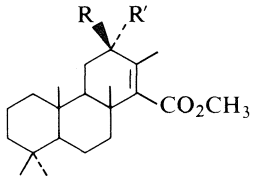

7*a* R = H; R′ = OH
7*b* R = OH; R′ = H

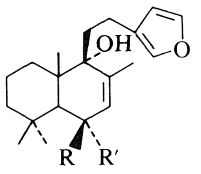

8*a* R = OH; R′ = H
8*b* R = H; R′ = OH

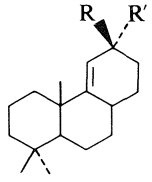

9*a* R = H; R′ = OH
9*b* R = OH; R′ = H

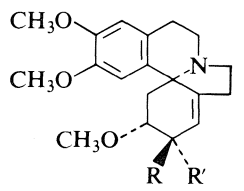

10*a* R = H; R′ = OH
10*b* R = OH; R′ = H

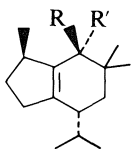

11*a* R = OH; R′ = H
11*b* R = H; R′ = OH

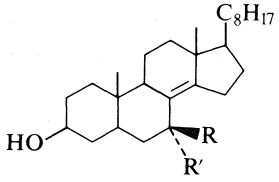

12*a* R = H; R′ = OH
12*b* R = OH; R′ = H

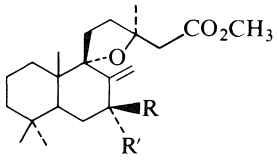

13*a* R = H; R′ = OH
13*b* R = OH; R′ = H

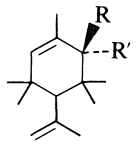

14*a* R = H; R′ = OH
14*b* R = OH; R′ = H

TABLE 1. ^{13}C nuclear magnetic resonance chemical shifts of sp^2 carbons of allylic alcohols relative to the corresponding parent hydrocarbons[a]

Compound	β-Carbon	γ-Carbon	Δδ(β)	Δδ(γ)
1*a*	126.5	134.8	—	—
1*b*	128.3	137.0	1.8	2.2
1*c*	130.4	136.6	3.9	1.8
2*a*	135.6	121.2	—	—
2*b*	137.8	126.9	2.2	5.7
2*c*	136.5	118.7	0.9	−2.5
3*a*	121.4	138.5	—	—
3*b*	122.9	143.9	1.5	5.4
3*c*	126.1	140.3	4.7	1.8
4*a*	148.5	107.3	—	—
4*b*	150.5	104.2	2.0	−3.1
5*a*	124.7	136.6	—	—
5*b*	127.3	141.1	2.6	4.5
5*c*	127.6	140.7	2.9	4.1

[a]The chemical shifts for compound **1***a* were taken from ref. 5, for compounds **1***b* and **1***c* from ref. 6, for compounds **2***a*, **2***b*, and **2***c* from ref. 7, for compounds **4***a* and **4***b* from ref. 8, for compounds **5***a*, **5***b*, and **5***c* from ref. 7. The resonance values for compounds **3***a*, **3***b*, and **3***c* are data from this laboratory.

TABLE 2. ^{13}C nuclear magnetic resonance chemical shifts of epimeric allylic alcohols and their (sp^2) parameters[a]

Compound	β-Carbon	γ-Carbon	Δδ(sp^2)
1*b*	128.3	137.0	8.7
1*c*	130.4	136.6	6.2
2*b*	137.8	126.9	−10.9
2*c*	136.5	118.7	−17.8
3*b*	122.9	143.9	21.0
3*c*	126.1	140.3	14.2
5*b*	127.3	141.1	13.8
5*c*	127.6	140.7	13.1
6*a*	126.7	137.8	11.1
6*b*	129.9	135.0	5.1
7*a*	131.2	142.0	10.8
7*b*	133.0	141.0	8.0
8*a*	128.3	139.0	10.7
8*b*	130.9	137.6	6.7
9*a*	117.4	155.2	37.8
9*b*	119.3	153.1	33.8
10*a*	120.6	145.4	24.8
10*b*	121.3	143.8	22.5
11*a*	138.7	142.1	3.4
11*b*	140.6	141.8	1.2
12*a*	128.1	147.9	19.8
12*b*	127.9	144.2	16.3
13*a*	147.7	111.0	−36.7
13*b*	153.0	103.4	−49.6
14*a*	130.6	136.5	5.9
14*b*	131.2	135.0	3.8

[a]The chemical shifts for compounds **1***b*, **1***c*, and **13***a* were taken from ref. 6, for compounds **2***b*, **2***c*, **5***b*, and **5***c* from ref. 7, for compounds **6***a*, **6***b*, **9***a*, and **9***b* from ref. 9, for compounds **7***a* and **7***b* from ref. 10, for compounds **8***a* and **8***b* from ref. 5, for compounds **10***a* and **10***b* from ref. 11, for compounds **11***a* and **11***b* from ref. 12, for compounds **12***a* and **12***b* from ref. 1, for compounds **14***a* and **14***b* from ref. 13. The resonance values for compounds **3***b*, **3***c*, and **13***b* are data from this laboratory.

is actually responsible for the chemical shift variation of the sp^2 carbons. In every case, the ^{13}C nmr data of the parent hydrocarbon are needed.

As an extension of these rules, and to overcome some of the difficulties mentioned above, we propose a new parameter: Δδ(sp^2), defined for each allylic alcohol as the difference between the chemical shifts of the sp^2 carbons, that is: $\Delta\delta(sp^2) = \delta_{\gamma sp^2C} - \delta_{\beta sp^2C}$.

The correlation[1] of the pseudoaxial vs. pseudoequatorial allylic alcohol parameters allowed us to propose a new empirical rule stating, for any epimeric pair, that the larger Δδ(sp^2) value corresponds to the allylic alcohol with a pseudoaxial hydroxyl group.

In addition to the advantage of using just the ^{13}C nmr data of both epimeric alcohols, generally available by the reduction of the corresponding carbonyl compounds, our proposition establishes unambiguously the pseudoequatorial or pseudoaxial orientation of alcohols such as **5***b* and **5***c*, which, being both anticlinal, can not be solved by using the Eggert and Djerassi rules. The Δδ(sp^2) values are, however, 13.1 and 13.8 and, according to our extension, the hydroxyl group of **5***c* ought to be pseudoaxial (Table 2), as is actually the case.

The precise reason for the different Δδ(sp^2) values is not clear; however, it most probably results from the difference in the through-space effect of the oxygen atom on the resonances of the olefinic carbons, according to the position of the hydroxyl group (14).

[1]The Δδ(sp^2) values for the pseudoaxial allylic alcohols vs. the Δδ(sp^2) for the pseudoequatorial ones, by least-squares analysis, show a linear correlation with a slope of 0.882 and a constant term of 4.94 ($n = 13$; $r = 0.993$; $p < 0.001$).

Acknowledgements

We thank CONICET (Consejo Nacional de Investigaciones Cientificas y Tecnicas) and UNR (Universidad Nacional de Rosario) for financial support and fellowships (T.S.K. and M.P.M.).

1. M. TSUDA, E. J. PARISH, and G. J. SCHROEPFER, JR. J. Org. Chem. **44**, 1282 (1979).
2. H. EGGERT and C. DJERASSI. J. Org. Chem. **46**, 5399 (1981).

3. IUPAC COMMISSION ON NOMENCLATURE OF ORGANIC CHEMISTRY. Pure Appl. Chem. **45**, 13 (1976).
4. A. F. ROSE, K. C. JONES, W. F. HADDON, and D. L. DREYER. Phytochemistry, **20**, 2249 (1981).
5. M. GONZALEZ-SIERRA, M. I. COLOMBO, M. E. ZUDENIGO, and E. A. RUVEDA. Phytochemistry, **23**, 1685 (1984).
6. M. GONZALEZ-SIERRA, M. I. COLOMBO, A. C. OLIVIERI, M. E. ZUDENIGO, and E. A. RUVEDA. J. Org. Chem. **49**, 4984 (1984).
7. B. DELMOND, M. TARAN, J. VALADE, M. PETRAUD, and B. BARBE. Org. Magn. Reson. **17**, 207 (1981).
8. M. NOMA, F. SUZUKI, K. GAMOU, and N. KAWASHIMA. Phytochemistry, **21**, 395 (1982).
9. I. WAHLBERG, S.-O. ALMQVIST, T. NISHIDA, and C. R. ENZELL. Acta Chem. Scand. Ser. B, **29**, 1047 (1975).
10. D. S. DE MIRANDA, G. BRENDOLAN, P. M. IMAMURA, M. GONZALEZ-SIERRA, A. J. MARSAIOLI, and E. A. RUVEDA. J. Org. Chem. **46**, 4851 (1981).
11. A. S. CHAWLA, S. CHUNCHATPRASERT, and A. H. JACKSON. Org. Magn. Reson. **21**, 39 (1983).
12. M. O. STALLARD, W. FENICAL, and J. S. KITTREDGE. Tetrahedron, **34**, 2077 (1978).
13. R. J. GIGUERE, G. VON ILSEMANN, and H. M. R. HOFFMANN. J. Org. Chem. **47**, 4948 (1982).
14. F. S. EL-FERALY, Y.-M. CHAN, G. A. CAPITON, R. W. DOSKOTCH, and E. H. FAIRCHILD. J. Org. Chem. **44**, 3952 (1979), and references cited therein.

Molybdenum(VI) and phenol reactions in concentrated aqueous sulphuric acid[1]

DRAGAN A. MARKOVIĆ AND DRAGAN S. VESELINOVIĆ
Institute of Physical Chemistry, Faculty of Science, University of Belgrade, P.O. Box 550, 11001 Belgrade, Yugoslavia

AND

MIRJANA V. OBRADOVIĆ
Institute of Physics, Faculty of Philosophy, University of Niš, 18000 Niš, Yugoslavia

Received December 9, 1985[2]

DRAGAN A. MARKOVIĆ, DRAGAN S. VESELINOVIĆ, and MIRJANA V. OBRADOVIĆ. Can. J. Chem. **64**, 2334 (1986).

Depending on molybdenum, phenol, and acid concentrations, and time and the method of solution preparation, molybdenum and phenol can react in several ways. In 96% sulphuric acid Mo(VI) can be reduced to Mo(V) by adding solid phenol to the solution. In other cases molybdenum and phenol form stable or unstable complexes which can be in equilibrium with each other. For excess phenol the recorded spectra show two bands at around 600 and 423 nm; the first one, decreasing with time, is ascribed to the formation of an unstable complex of phenol and Mo(VI). At approximately equal concentrations of molybdenum and phenol the band at 423 nm does not appear, but two time-dependent absorption maxima are formed at 600 and 470 nm with a well defined isosbestic point at 505 nm. The complex is unstable because of the sulphonation of phenol. In 80% sulphuric acid molybdenum and phenol form a stable 1:1 complex which absorbs at 480 nm; its pK_s value is 1.44 ± 0.03 at room temperature.

DRAGAN A. MARKOVIĆ, DRAGAN S. VESELINOVIĆ et MIRJANA V. OBRADOVIĆ. Can. J. Chem. **64**, 2334 (1986).

Le molybdène et le phénol réagissent de plusieurs façons différentes suivant soit les concentrations de molybdène, de phénol et d'acide, soit le temps de la réaction ou la méthode utilisée pour préparer la solution. Dans de l'acide sulfurique à 96%, le Mo(VI) peut être réduit en Mo(V) par l'addition de phénol solide à la solution. Dans d'autres cas, le molybdène et le phénol forment des complexes qui peuvent être stables ou instables et qui peuvent être en équilibre les uns avec les autres. Dans les cas où le phénol est en excès, le spectre du mélange présente deux bandes autour de 600 et de 423 nm; la première, dont l'intensité diminue avec le temps, est attribuée à la formation d'un complexe instable entre le phénol et le Mo(VI). A des concentrations approximativement égales de molybdène et de phénol, la bande à 423 nm n'apparaît pas; toutefois, il se forme deux bandes (à 600 et à 470 nm) dont l'absorption varie avec le temps ainsi qu'un point isosbestique bien défini à 505 nm. La raison de l'instabilité du complexe tient son origine dans la sulfonation du phénol. Dans de l'acide sulfurique à 80%, le molybdène et le phénol forment un complexe 1:1 qui est stable et qui absorbe à 480 nm; à la température ambiante, la valeur de son pK_s est égale à 1,44 ± 0,03.

[Traduit par la revue]

Introduction

In concentrated aqueous solutions of strong mineral acids many metals, such as Mo, Ti, Nb, Ta, V, W, Sb, and U, form coloured complexes with hydroxybenzenes (1–13). The absorption of these complexes in the visible region generally decreases with decreasing acid concentration so that colour is rarely observed at an acidity corresponding to 60% sulphuric acid. Their stability constant values are relatively low with pK values for most of the complexes investigated vary between 1 and 5. The most commonly used ligand is 1,4-dihydroxybenzene, but 1,2-, 1,3-, 1,2,3-, and 1,3,5-, di- and trihydroxybenzenes have also been studied.

Spectrophotometric investigation of the reaction of titanium with phenol in 89% sulphuric acid has shown the formation of an unstable complex with an absorbance maximum at 430 nm (14). Instability of the complex has been ascribed to the sulphonation of phenol. A strong dependence of colour intensity on sulphuric acid concentration was observed with molybdenum complexes. For less than 80% sulphuric acid, the colour of the solution fades appreciably, and is completely gone at 60% H_2SO_4. In 90% sulphuric acid the composition of the complex changes with the ligand. Thus, molybdenum forms complexes in the ratio 2:3, 1:2, and 1:4 with 1,2,3-trihydroxybenzene, 1,4-dihydroxybenzene, and 1,2-dihydroxybenzene, respectively (6). The possibility of formation of hydroxybenzenes and metal complexes in other strong mineral acids has also been pointed out (6, 11).

Coloured complexes of metals in concentrated aqueous sulphuric acid solutions can be used for analytical purposes (1, 2, 5, 6). It should also be pointed out that the formation of such complexes is almost certain evidence for oxygen protonation of phenols (14). These complexes can therefore be used as "indicators" for recognizing the protonation of benzene derivatives with hydroxy- or alkoxy-groups in strongly acidic media. On the other hand, the state of metal ions and catalytic effect of metals in strong acidic media has not yet been well defined. The objective of this work is to obtain more information on reactions occurring in the investigated systems.

Experimental

Sulphuric acid solutions of required concentration were prepared by diluting 95–97% H_2SO_4 (d = 1.84) with distilled water. The concentration of these solutions was determined by pH-metric titration, using standard NaOH solution, or by density measurements with a pycnometer. Sodium molybdate solution in 96% sulphuric acid was standardized polarographically (15, 16) using the standard addition method (17). All chemicals used were pure analytical reagent grade.

Spectrophotometric measurements were performed with Specord UV-VIS Carl Zeiss, Unicam SP-600, and Cary 17 D spectrophotometers, at room temperature. Sulphuric acid of the appropriate concentration was used as a blank solution for spectrophotometric work. All measurements were performed using 1-cm quartz cells.

Results and discussion

Molybdenum(VI) reactions with phenol in aqueous sulphuric acid solutions

In the visible region the spectra of phenol and sodium molybdate solution in sulphuric acid depends on both acid

[1]Reaction of hydroxybenzenes in strongly acidic media. VIII. Part VII is ref. 11.

[2]Revision received July 16, 1986.

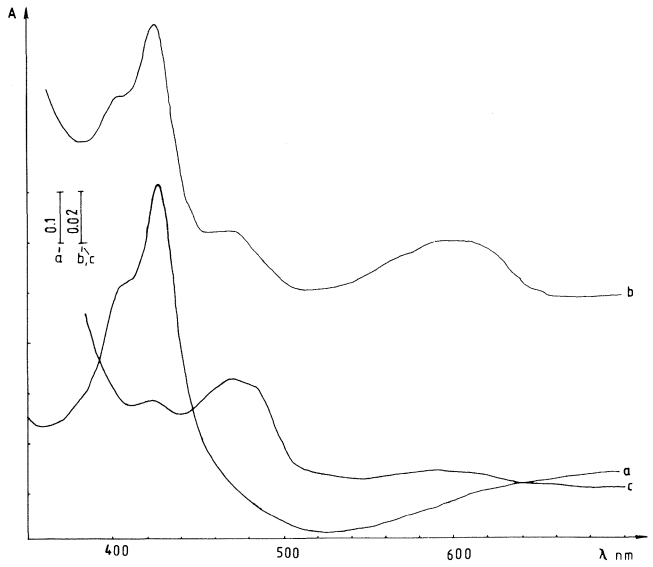

FIG. 1. Absorption spectra recorded in 96% H_2SO_4: *a*, 5.5×10^{-3} mol/dm^3 Na_2MoO_4 and 6×10^{-4} mol/dm^3 phenol 100 min after phenol addition; *b*, 1.20×10^{-2} mol/dm^3 Na_2MoO_4 and 3.50×10^{-2} mol/dm^3 phenol 80 min after preparation of solution; *c*, 2.70×10^{-2} mol/dm^3 Na_2MoO_4 and 2.20×10^{-2} mol/dm^3 phenol 60 min after preparation of solution. The absorbance unit is 0.1 for *a* and 0.02 for *b* and *c*.

concentration and the method of solution preparation. Figure 1 (*a*) shows the spectrum of Na_2MoO_4 solution (5.5×10^{-3} mol/dm^3) in 96% H_2SO_4 after adding sufficient solid phenol for a concentration of 6×10^{-4} mol/dm^3. The spectrum has an absorption band at about 425 nm. Except for a slight absorbance increase in the region 500–700 nm no change with time was observed. Immediately after adding phenol, the molybdate solution becomes dark blue.

In all other cases the form of the spectra depends on the time of contact between acid and phenol, i.e., on the time interval between the dissolution of phenol and its mixing with molybdate solution. Addition of phenol solution, after 15–20 min of standing, to a solution of molybdate in 96% sulphuric acid does not produce absorption in the visible region of the spectrum. A mixture of freshly prepared phenol and molybdate gives a green-blue solution whose spectral characteristics depend on time and reactant concentration. The spectra obtained for a 3:1 phenol to molybdate ratio have two maxima (Fig. 1 *b*). The first, at about 600 nm, decreases with time; the second, at 425 nm, is independent of time. The shorter wavelength maximum is similar in form and position to the maximum in the spectrum of a solution prepared by addition of solid phenol, but its absorbance is 7 to 8 times lower. About 10 min after mixing of the reactants a shoulder appears at the bottom of the shorter wavelength maximum, at 470 nm, which becomes more explicit with time. The spectra become stable within an hour and further changes are very slow.

The spectrum shown in Fig. 1 *c* is obtained at approximately equal molybdenum and phenol concentrations. The maximum at 425 nm, present in the previous cases, does not appear, but is replaced by a shoulder at the same wavelength. Two time-dependent absorption bands are formed, the first having a maximum at about 600 nm and the second a maximum at 480 nm, with a well-defined isosbestic point at 505 nm. The longer wavelength band disappears 2 h after mixing of the reactants, whereas the shorter one increases with time. Spectra

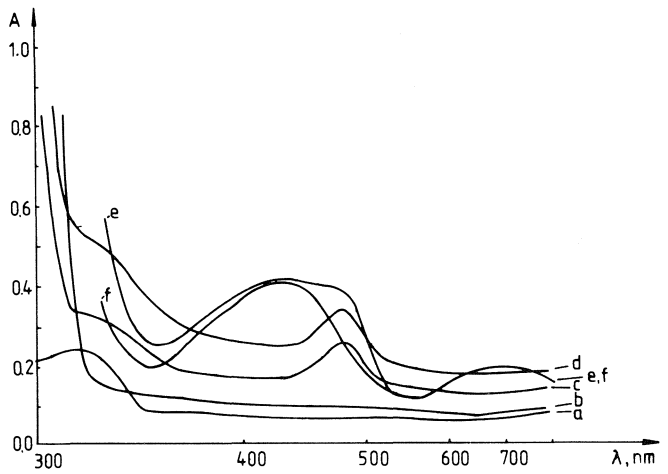

FIG. 2. Absorption spectra recorded in 80% H_2SO_4: *a*, 2.5×10^{-3} mol/dm^3 Na_2MoO_4; *b*, 3.500×10^{-1} mol/dm^3 phenol; *c*, 2.5×10^{-3} mol/dm^3 Na_2MoO_4 and 5.00×10^{-2} mol/dm^3 phenol; *d*, same as *c*, 24 h after preparation of solution; *e*, 2.5×10^{-3} mol/dm^3 Na_2MoO_4 and phenol in the presence of mercury (phenol added to solution 20 min after mercury); *f*, 2.5×10^{-3} mol/dm^3 Na_2MoO_4 24 h in contact with mercury (no change after phenol addition).

of mixtures of freshly prepared phenol and molybdenum solutions in 80% sulphuric acid have only one absorption band at around 480 nm (Fig. 2 *c* and *d*). One absorption band at this wavelength also appears in 96% acid (Fig. 1, *b* and *c*). The position of this band does not change with time, but total absorption in the spectral region from 350–700 nm increases and becomes constant after 4 h (Fig. 2 *d*). The band at 480 nm is assigned to a complex formed between phenol and molybdenum.

Spectra of the system in 71% and 80% acid are similar. In 60% sulphuric acid no colour was observed after mixing of the reactants. Similar results were observed with the other hydroxybenzenes (6).

It is known that the instability of phenol solutions in sulphuric acid is mainly due to sulphonation of phenol (14, 18, 19, 21). However, in spite of the prominent effect of sulphonation on the observed spectral changes in molybdenum–phenol solutions, the effect of a possible change of molybdenum oxidation state on the observed spectra could not be excluded.

In sulphuric acid solutions Mo(VI) can be reduced to Mo(V) by several reducing agents, such as ascorbic acid or 1,4-dihydroxybenzene (15), but we found that reduction can also occur in the presence of elemental mercury (16), whereby solutions take on the blue–green colour characteristic of Mo(V). The presence of Mo(V) has also been demonstrated in the reaction with potassium thiocyanate. In addition to the blue–green solution a gray–white precipitate appeared in molybdate solutions containing mercury and was identified as Hg_2SO_4. This demonstrates that mercury participated in the reaction.

Upon long standing of molybdenum solutions with elemental mercury (24 h or more), further addition of phenol solution did not produce any change in existing Mo(V) bands (Fig. 2*f*). One shoulder appears at 480 nm (Fig. 2*e*) when freshly prepared phenol solution was added to a Mo(VI) solution that only had a short contact time with mercury. This shoulder is produced by a complex between unreduced Mo(VI) and phenol. On this basis it can be concluded that Mo(V) does not form a complex with phenol in sulphuric acid solutions.

The spectra in Figs. 1 *a*, *b* and 2 *f* show absorption maxima at around 420 nm. Since Mo(VI) does not absorb in this region (Fig. 2*a*) and since the spectra in Fig. 1*a* do not contain absorption bands which could be ascribed to a molybdenum–phenol complex, it follows that addition of solid phenol to sodium molybdate solution in 96% sulphuric acid causes reduction of Mo(VI) to Mo(V), as manifested by an intense blue colour in the solution. Metal reduction is possible, since oxidation of phenol in sulphuric acid solutions, in the presence of metals, has been observed (16, 20).

The spectrum in Fig. 1*b* can be explained by postulating that with freshly dissolved phenol one part of the molybdenum is reduced to Mo(V) (spectral band at 425 nm). The spectra indicate that absorption at 425 nm is due to Mo(V). The other part of the metal forms an unstable complex with the as yet unsulphonated phenol which absorbs at around 600 nm.

At equal molybdenum and phenol concentrations in 96% acid the absorption band ascribed to Mo(V) does not appear at 420 nm (Fig. 1*c*). The shoulder at this wavelength is due to the presence of a small amount of reduced metal. The absorption band at 600 nm, which decreases with time, is assigned to an unstable complex of phenol and Mo(VI). This complex is slowly converted to a more stable form, which absorbs at about 480 nm, as is evident from the appearance of a shoulder at 480 nm and an isosbestic point at 505 nm. Molybdenum(VI) does not react with phenol which has been sulphonated by standing in 96% acid for some time. This can be explained by the formation of an intramolecular hydrogen bond between sulpho- and hydroxyl groups in ortho-substituted phenols which prevents the formation of complex (14). Cerfontain *et al.* have provided strong support for the presence of such bonds in phenol – sulphuric acid solutions (21).

Complexation between metals and hydroxybenzenes in aqueous solutions occurs by substitution of one or more hydrogen atoms of the hydroxyl groups by metal ions (6). According to some authors the bonding between metals and hydroxybenzenes in strongly acidic media is due to the presence of protonated OH groups (14). This is based on the fact that coloured complexes with metals are formed only by those benzene derivatives which have substituent groups with oxygen that are capable of being protonated in acid solution. For this reason it seems most probable that metal to ligand bonding can be ascribed to the proton binding oxygen from metal oxy-ions and protonated hydroxyl (alcoxy) groups. This is supported by the recent conclusion that phenol and anisol protonation takes place on oxygen, and at acidities of the medium that are optimal for complexation with metals (14, 21).

Sulphonation of phenol in the *ortho* positions can impede formation or affect the stability of the resulting complex by blocking hydrogen bonding to metal oxy-ions. This might also explain the absence of complexation upon addition of a sulphonated phenol to a molybdate solution, as well as the disappearance of the absorption band of the complex at 600 nm. In our opinion this band is due to the presence of an unsulphonated complex.

Spectral changes in sulphuric acid solutions of lower concentration, 70% and 80%, can also be ascribed to sulphonation. These changes are considerably slower at lower acidities because sulphonation is slower. Lower absorbance values at lower acid concentrations can be attributed to a smaller degree of phenol protonation. The complete absence of absorption between 350 and 700 nm in 60% acid supports the conclusion that complexation is possible only in the presence of protonated phenol. Judging by the pK_{BH^+} value for phenol of −6.4 (21), the concentration of protonated phenol in 60% sulphuric acid is negligible.

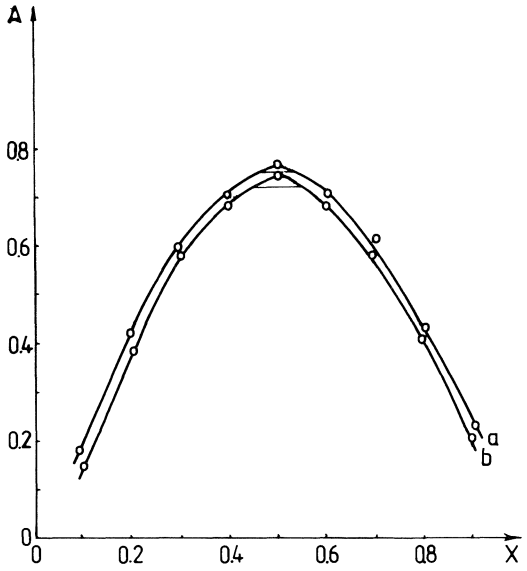

FIG. 3. Job's curves for Mo(VI)–phenol complex in 80% H_2SO_4: *a*, at 490 nm; *b*, at 530 nm; $c_{Mo} + c_{Ph} = 7.00 \times 10^{-2}$ mol/dm^3.

Determination of the composition and stability constant of the Mo(VI)–phenol complex

To investigate the composition and stability constant of a complex it is necessary for the complex to achieve stability with time, to prove the validity of Beer's law, and to determine a molar absorption coefficient. Due to the strong time dependence of complex formation in 96% acid, and due to the dependence on the method of preparation of the solution, it was not possible to satisfy all these conditions. However, an attempt to apply Job's method (22) gave an irregular curve with a maximum at a concentration ratio corresponding to a complex of 1:1 composition.

For the complex in 80% acid a molar absorption coefficient could be determined, and the validity of Beer's law tested, 24 h after mixing the reactants, i.e. after stabilisation of the system. Beer's law was tested at 490 and 530 nm at a constant phenol concentration ($c_{Ph} = 0.15$ mol/dm^3) and over a molybdenum concentration of 0.001 to 0.004 mol/dm^3. Under these conditions Beer's law was found to hold. Assuming that the concentration of complex is equal to that of the molybdenum present, the value obtained for the molar absorption coefficient was 52 cm^{-1} mol^{-1} dm^3 at 490 nm. The composition of the complex in 80% acid was investigated by Job's and Harvey–Manning's method (22); the results, shown in Figs. 3 and 4, indicate formation of a 1:1 complex. Figure 3 shows the Job's curve obtained by using freshly prepared phenol solutions at a total reactant concentration of 0.07 mol/dm^3. Absorbance measurements were performed at 490 nm 24 h after mixing the reactants.

Using Harvey–Manning's method two series of solutions were prepared. In the first the molybdenum concentration was held constant at 0.0025 mol/dm^3 and that of phenol varied from 0.0125 to 0.3000 mol/dm^3. In the second series the concentrations were reversed, i.e., the molybdenum concentration was varied from 0.0012 to 0.0300 mol/dm^3 at a constant phenol concentration of 0.0025 mol/dm^3. The straight lines in Fig. 4 were obtained by plotting the absorbance of the solutions

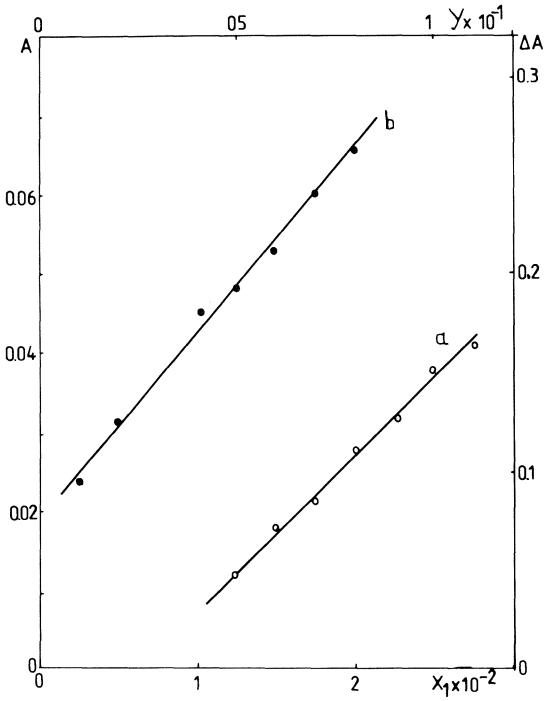

FIG. 4. Harvey–Manning's method for Mo(VI)–phenol complex in 80% H_2SO_4: *a*, 2.5×10^{-3} mol/dm^3 phenol; $c_{Mo} = X_1$; *b*, 2.5×10^{-3} mol/dm^3 Na_2MoO_4, $c_{Ph} = Y$, $\Delta A = A_{complex} - A_{phenol}$.

as a function of concentration. The metal-to-phenol ratio of the complex (1:1) was obtained from the slopes of these linear plots.

The stability constant of the complex formed in 80% sulphuric acid was determined by means of the equation $K_s = [ML]/[M][L]$, where [M] and [L] represent metal and ligand concentrations. The equilibrium concentration of the complex [ML] was calculated from corresponding absorbance values using Beer's law. Equilibrium concentrations of the metal and ligand were obtained by deducing complex concentration value from known initial reactant concentrations. The log stability constant value obtained this way was -1.44 ± 0.03 at room temperature.

The absorption band in the 480 nm region appears in all solutions with different acid concentrations, and is assigned to the 1:1 complex of unchanged composition. The total absorbance of the system, which depends on the time of contact between phenol and acid, actually increases after mixing phenol and molybdenum solutions in 80% and 71% acid. Increased nonselective absorption was also observed between molybdenum and 1,4-dihydroxybenzene complexes (15). A precipitate formed after a long standing of the solutions (several weeks or months). Different reactions (18, 19) may lead to precipitation and may increase nonselective absorption in the investigated system. These slow reactions and their products will be the subject of further studies.

1. L. IKENBERRY, J. L. MARTIN, and W. J. BOYER. Anal. Chem. **25**, 1340 (1953).
2. P. H. CAULFIED and R. J. ROBINSON. Anal. Chem. **25**, 982 (1953).
3. C. E. BRICKER and G. R. WATERBURG. Anal. Chem. **29**, 1093 (1957).
4. S. YA. Shnaiderman. Ukr. Khim. Zh. **23**, 92 (1957).
5. G. R. WATERBURG and C. E. BRICKER. J. Anal. Chem. **30**, 1007 (1958).
6. S. YA. Shnaiderman and G. I. KHRUSTALEV. Zh. Obshchei Khim. **29**, 20 (1959).
7. S. YA. Shnaiderman and A. M. PLESKONOS. Ukr. Khim. Zh. **39**, 641 (1973).
8. G. NORWITZ and H. GORDON. Anal. Chim. Acta, **69**, 59 (1974).
9. F. DZ. BAJRAKTARI, D. A. MARKOVIĆ, and D. S. VESELINOVIĆ. Bull. Soc. Chim. Beograd. **46**, 329 (1981).
10. F. DZ. BAJRAKTARI, D. S. VESELINOVIĆ, and D. A. MARKOVIĆ. Bull. Soc. Chim. Beograd. **46**, 291 (1981).
11. M. V. OBRADOVIĆ, D. S. VESELINOVIĆ, and D. A. MARKOVIĆ. Bull. Soc. Chim. Beograd. **49**, 453 (1984).
12. S. YA. Shnaiderman and A. M. PLESKONOS. Ukr. Khim. Zh. **38**, 1083 (1972).
13. J. P. MCKAVENEY. Anal. Chem. **33**, 744 (1961).
14. D. S. VESELINOVIĆ, D. A. MARKOVIĆ, and D. M. JOVANOVIĆ. Bull. Soc. Chim. Beograd. **43**, 225 (1978).
15. G. EL INANY and D. S. VESELINOVIĆ. J. Electroanal. Chem. **32**, 437 (1971).
16. D. MARKOVIĆ, D. VESELINOVIĆ, and S. MILENKOVIĆ. J. Electroanal. Chem. **73**, 109 (1976).
17. L. MEITES. Polarographic techniques. 2nd ed. John Wiley and Sons, Inc., New York. 1965. p. 398.
18. E. M. ARNETT and C. Y. WU. J. Am. Chem. Soc. **88**, 5660 (1960).
19. B. G. RAMSEY. J. Am. Chem. Soc. **88**, 5358 (1966).
20. K. B. YATSIMIRSKII and G. S. NIKOLOV. Zh. Fiz. Khim. **46**, 1129 (1970).
21. A. KOEBERG-TELDER, H. J. A. LAMBRECHTS, and H. CERFONTAIN. Recl. Trav. Chim. Pays-Bas, **102**, 293 (1983).
22. M. T. BECK. Chemistry of complex equilibria. Van Nostrand-Reinhold, London. 1970. pp. 86–90.

Regioselective reactions of 1,4,5-trihydroxy-9,10-anthraquinone

A. Douglas Broadbent,[1] Wilfred Meschwitz, and John M. Stewart
Department of Chemistry, Mount Allison University, Sackville, N.B., Canada E0A 3C0

Received December 19, 1985[2]

A. Douglas Broadbent, Wilfred Meschwitz, and John M. Stewart. Can. J. Chem. **64**, 2338 (1986).

The regioselective alkylation of 1,4,5-trihydroxy-9,10-anthraquinone via reaction of its leuco compound is significant for the synthesis of anthracyclinones. In the presence of pyrrolidine in toluene solution, the leuco compound **3** selectively forms the 4-pyrrolidino enamine **11**, which undergoes deamination to give 1,5-dihydroxy-9,10-anthraquinone. If an aldehyde is added, however, the enamine is alkylated, eventually yielding the 3-alkyl-1,4,5-trihydroxy-9,10-anthraquinone. Both of the above reactions of **3** give high yields with 100% regioselectivity. The enamine intermediate **11** has been trapped by oxidation to 4-pyrrolidino-1,5-dihydroxy-9,10-anthraquinone, which, after reduction, undergoes the same reactions as **3** giving either the alkylation or deamination product. The selective formation of **11** is explained in terms of an enhancement of carbonyl group electrophilicity by a relay of hydrogen bonds.

A. Douglas Broadbent, Wilfred Meschwitz et John M. Stewart. Can. J. Chem. **64**, 2338 (1986).

L'alkylation régiosélective de la trihydroxy-1,4,5 anthraquinone-9,10, par le biais de la réaction de son composé leuco, est une voie utile pour la synthèse des anthracyclinones. En présence de pyrrolidine, dans une solution dans le toluène, le composé leuco **3** conduit sélectivement à la pyrrolidino-4 ènamine **11** qui subit une déamination pour conduire à la dihydroxy-1,5 anthraquinone-9,10. Toutefois, si on ajoute un aldéhyde, l'aldéhyde est alkylé et il conduit éventuellement à l'alkyl-3 trihydroxy-1,4,5 anthraquinone-9,10. Les deux réactions du composé **3** mentionnées plus haut se produisent avec des rendements élevés et avec 100% de stéréosélectivité. On a piégé l'ènamine intermédiaire **11** grâce à une oxydation conduisant à la pyrrolidino-4 dihydroxy-1,5 anthraquinone-9,10 qui, après réduction, subit les mêmes réactions que le composé **3** en conduisant soit à une alkylation ou à un produit de déamination. On explique la formation sélective du composé **11** en fonction d'une augmentation du caractère électrophile du groupement carbonyle par un relais de liaisons hydrogènes.

[Traduit par la revue]

Introduction

1,4,5-Trihydroxy-9,10-anthraquinone **1** is an obvious starting material for the synthesis of anthracyclinones such as adriamycinone and daunomycinone **2** but necessitates the use of regioselective methods of alkylation because of the dissymmetry of such molecules.

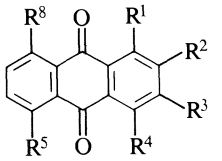

R = H, unless specified otherwise

1 $R^1 = R^4 = R^5 = OH$
4 $R^1 = R^4 = R^5 = OH$, R^2 = propyl
5 $R^1 = R^4 = R^5 = OH$, R^3 = propyl
6 $R^1 = R^4 = OH$
7 $R^1 = OH$
8 $R^1 = R^5 = OH$
10 $R^1 = R^8 = OH$
14 $R^1 = R^5 = OH$, R^2 = propyl
15 $R^1 = R^8 = OH$, R^2 = propyl

Reduction of **1** with tin and HCl in acetic acid (1) gives the leuco compound **3** whose ^{1}Hmr and ir spectra show it to be a keto tautomer of the anthrahydroquinone (2). Recent publications (3–5) have described crossed aldol reactions of **3** with aldehydes, giving 2- or 3-alkyl derivatives of **1** with high regioselectivity. In hot aqueous basic solution, the reaction of **3** with aldehydes, based on the procedure devised by Marschalk *et al.* (6), gives the 2-alkyl derivative of **1** (e.g. **4**) in poor to moderate yields, but with 100% regioselectivity. In hot isopropanol with added piperidinium acetate, alkylation conditions developed by Lewis (7), the 3-alkyl isomer (e.g. **5**) is generated from the same reactants in moderate yield, but the product is contaminated with 10–20% of the 2-alkyl isomer.

We have confirmed the recent report (3) that quinizarins **6** and **1** can be dehydroxylated by reduction to their leuco compounds (**9** and **3** respectively) and by subsequent reaction with pyrrolidine in refluxing toluene to give the 1-hydroxy and 1,5-dihydroxy derivatives (**7** and **8** respectively).

This paper describes our results and conclusions on the origin of the regioselectivity of the above crossed aldol and deoxygenation reactions of **3** in the presence of cyclic secondary amines such as pyrrolidine. In both processes, product formation is controlled by the selective initial reaction of the cyclic amine at the 4-carbonyl group of **3**.

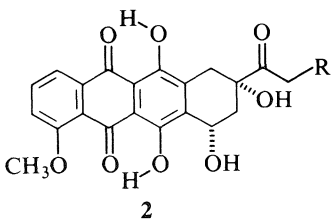

2

R = H, daunomycinone
R = OH, adriamycinone

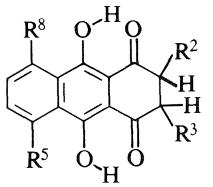

R = H unless indicated otherwise

3 $R^5 = OH$
9
12 $R^5 = OH$, R^2 = propyl
13 $R^5 = OH$, R^3 = propyl
17 $R^5 = R^8 = OH$

[1]Author to whom correspondence should be addressed at: Département de génie chimique, Faculté des sciences appliquées, Université de Sherbrooke, Sherbrooke, Québec J1K 2R1.

[2]Revision received July 28, 1986.

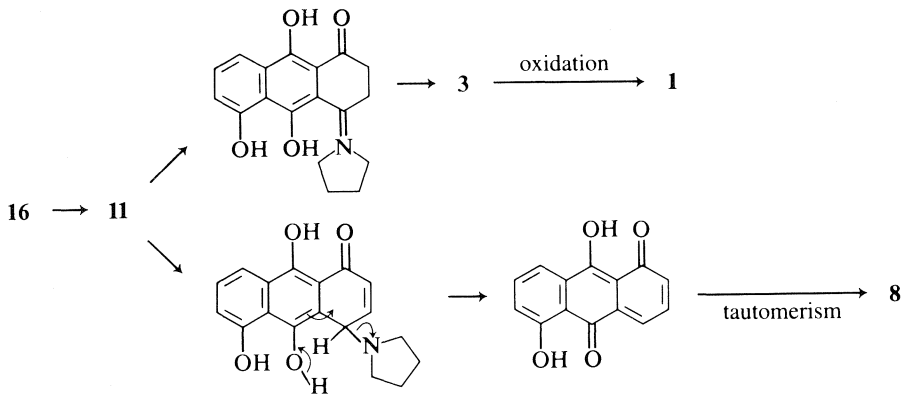

SCHEME 1

Results

Reaction of the leuco compounds **3** or **9** with pyrrolidine in refluxing toluene results in deoxygenation, giving **8** or **7**, respectively. Our study of this reaction established that the product is generated in excellent yield (>90% after chromatographic purification), that azeotropic removal of water is not necessary (3, 8), and that reaction of **3** is completely regioselective, giving only **8** and no 1,8-derivative **10**. Addition of sufficient acetic acid to just neutralize the pyrrolidine solution increased the reaction rate but decreased the selectivity, giving **8** containing a small proportion of **10** (<10%).

The mechanism suggested for this regioselective deoxygenation reaction (8), involving tautomerism of an enamine intermediate **11**, led us to consider that such an intermediate might be responsible for the regioselectivity of both the 3-alkylation of **3** with aldehydes, using piperidinium acetate, as well as its deoxygenation reaction with pyrrolidine, although the same authors have rejected this idea (3). The proposal was supported by our observation that reaction of **3**, in refluxing isopropanol with added piperidium acetate but no aldehyde, resulted in **8** with a little **10**, exactly as for the reaction in toluene with equimolar quantities of pyrrolidine and acetic acid.

Our hypothesis of a common reaction intermediate was confirmed by reactions of **3** with pyrrolidine in boiling toluene, with and without added propanal. In the absence of propanal, **3** reacted smoothly to give a 93% yield of only **8**. An identical reaction with excess propanal gave the 3-propyl derivative **5** in 82% yield. Both these reactions are quantitative, if based on starting material converted. They both proceeded more rapidly, but with lower selectivity, if the pyrrolidine was neutralized with an equimolar quantity of acetic acid.

Although the isomeric 2- and 3-propyl derivatives could not be separated by tlc, the ^{1}Hmr spectra of **4** and **5** showed no cross-contamination with the other isomer, thus confirming the high regioselectivity of the reactions of propanal with **3**. These isomers are readily distinguished by their characteristic pattern of hydroxyl proton resonances. Published ^{1}Hmr spectra indicate that introduction of a 2-alkyl substituent into **1** causes a downfield shift of 0.45 ± 0.02 ppm of the 1-hydroxyl proton resonance, whereas a 3-alkyl substituent gives a downfield shift of 0.46 ± 0.03 ppm of the 4-hydroxyl proton resonance. The chemical shifts of the hydroxyl protons more distant from the alkyl substituent remain very close to the values of **1** (3, 5, 9, 10).

Since the previous distinction of **4** and **5** involved isolation and identification of extremely low yields of chemical degradation products (3), we examined the possibility of a distinction via their leuco compounds **12** and **13**. These were found to have almost identical ^{1}Hmr spectra, but the products of their reaction with pyrrolidine in boiling toluene were quite different. The leuco compound **12** underwent deoxygenation to give 1,5-dihydroxy-2-propyl-9,10-anthraquinone **14**, whereas **13** reacted very slowly to produce a low yield of 1,8-dihydroxy-2-propyl-9,10-anthraquinone **15**. Chromatographic analysis and ^{1}Hmr spectra indicated that both these deoxygenation reactions were highly regioselective. Unfortunately, the low yields of **14** and **15**, caused by the difficulties in separating these products from **4** and **5** respectively, and the very slow reaction of **13**, did not provide the simple, efficient distinction between **4** and **5** that had been anticipated.

Reaction of **3** with pyrrolidine in toluene at room temperature, and subsequent air oxidation, gave about 50% conversion to 1,5-dihydroxy-4-pyrrolidino-9,10-anthraquinone **16**, with an overall 21% yield of the pure compound. The structure was assigned on the basis of the ir and ^{1}Hmr spectra and the fact that reduction by tin and concentrated HCl in acetic acid gave efficient conversion to about equal amounts of **1** from hydrolysis of **11**, and of **8** by deamination. These reactions are shown in Scheme 1. Treatment of **16** with activated Raney nickel in boiling toluene gave a 95% yield of **8**, whereas an identical reaction in the presence of propanal gave 36% conversion to **5**, thus supporting the proposal that the regioselectivity of the 3-alkylation and the deoxygenation reactions of **3** are the result of the regioselective formation of a 4-pyrrolidino substituion product of **3**, such as **11**, in the initial stage of both reactions. Attempts to improve the yield of **5** from the reaction of **16**, at various temperatures, were unsuccessful. Propanal had to be added as soon as deoxygenation of **11** became evident, which deactivated the Raney nickel and limited further formation of **11**.

In the absence of an aldehyde, the reaction may proceed by tautomerism of **11** followed by retro-Michael elimination of pyrrolidine to give **8** via the 1,9-dione tautomer (3, 8). An added aldehyde would react directly with the enamine **11** to give an iminium ion adduct, which, after hydrolysis in the moist toluene, would generate **5** by retro-Michael elimination of hydroxide ion from the 3-(1-hydroxypropyl) side chain. The isolation, identification, and subsequent reactions of **16** provide strong support in favour of the proposed enamine mechanism.

An explanation for the regioselective formation of a 4-pyrrolidino adduct of **3** was then considered, since the formation of this intermediate controls the overall regioselectivity of both the alkylation and deoxygenation reactions. Only the leuco compounds **3**, **12**, and **13** exhibit two closely spaced carbonyl

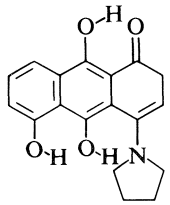

11

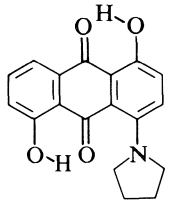

16

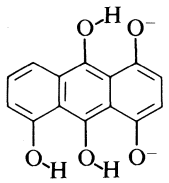

18

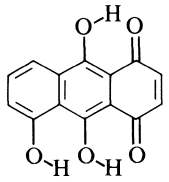

19

absorption bands in the ir spectra of their chloroform solutions. We believe that the selective formation of **11**, or a related derivative, is a consequence of the enhanced electrophilicity of the 4-carbonyl group in **3** brought about by the relay of two hydrogen bonds with that group, and that this is responsible for the regioselectivity of the reactions described and the splitting of the ir carbonyl absorption. Leuco compounds **9** and **17** show only a single carbonyl group absorption. This type of hydrogen bond relay may well be responsible for the regioselectivity of the 2-alkylation reaction of **3** and of the nitronate ion alkylation of **1** (3, 8, 11), the key steps being, respectively, reaction of the more nucleophilic enolate ion centre of **18** (position 2) with an aldehyde, and addition of the nitronate anion to the more electrophilic end of the 2,3-double bond of **19** (position 2) derived from tautomerization of **1**. In support of this idea, destruction of the hydrogen bond relay for a Marschalk reaction of **3** with propanal under more basic conditions (ethanol plus ethoxide) is essentially nonselective, giving about equal yields of **4** and **5**.

The deoxygenation of the leuco compound **13** was unusual in comparison to that of **12** and **3**. The reaction was very slow and gave a poor yield of a product that indicated the loss of the 1- rather than the 4-carbonyl group. This result is probably a consequence of steric hindrance, by the 3-propyl group, of the nucleophilic addition of the cyclic amine at the 4-carbonyl group of **13**, so that reaction occurs at the less hindered and less reactive 1-carbonyl group.

Conclusions

The studies described in this paper have clarified the role of pyrrolidine in the regioselective reactions of the leuco compound **3**. It seems likely that the regioselective alkylation of **3** with aldehydes in isopropanol in the presence of pyridinium acetate (3, 7) also involves the formation of an enamine such as **11**. The formation of 3-alkyl derivatives of **1** by reaction of **3** with aldehydes in toluene with pyrrolidine is, however, completely selective and gives higher yields. It is much more efficient than the method based on the alkylation of 1,5-dimethoxy-4-hydroxy-9,10-anthraquinone (9) and should prove valuable for the synthesis of precursors to anthracyclinones derived from **1**.

Experimental

Leuco compounds

The leuco compounds were prepared by reduction of the corresponding anthraquinones with tin and HCl in boiling glacial acetic acid (1) and crystallized from the reaction solution after addition of water.

1,4-Dioxo-1,2,3,4-tetrahydro-5,9,10-trihydroxyanthracene (leuco 1,4,5-trihydroxy-9,10-anthraquinone), **3**: 80% yield, mp 209–210°C; ir ($CHCl_3$) ν_{max}: 1645, 1630 cm^{-1}; ^{1}Hmr ($CDCl_3$) δ: 15.72 (s, 1H, OH), 13.53 (s, 1H, OH), 9.92 (s, 1H, OH), 7.95 (dd, J = 8 Hz, 1 Hz, 1H, H-8), 7.67 (t, J = 8 Hz, 1H, H-7), 7.18 (dd, J = 8 Hz, 1 Hz, 1H, H-6), 3.07 (s, 4H, CH_2—CH_2). *Anal.* calcd. for $C_{14}H_{10}O_5$: C 65.12, H 3.90; found: C 64.97, H 3.85.

1,4-Dioxo-2-propyl-1,2,3,4-tetrahydro-5,9,10-trihydroxyanthracene (leuco 2-propyl-1,4,5-trihydroxy-9,10-anthraquinone), **12**: 75% yield; ir ($CHCl_3$) ν_{max}: 1648, 1630 cm^{-1}; ^{1}Hmr ($CDCl_3$) δ: 15.73 (s, 1H, OH), 13.38 (s, 1H, OH), 9.86 (s, 1H, OH), 7.93 (dd, J = 8 Hz, 1 Hz, 1H, H-8), 7.63 (t, J = 8 Hz, 1H, H-7), 7.14 (dd, J = 8 Hz, 1 Hz, 1H, H-6), 3.0 (m, 3H, ring CH_2—CH), 1.5 (m, 4H, propyl CH_2—CH_2), 0.9 (m, 3H, propyl CH_3). *Anal.* calcd. for $C_{17}H_{16}O_5$: C 67.99, H 5.37; found: C 67.92, H 5.32.

1,4-Dioxo-3-propyl-1,2,3,4-tetrahydro-5,9,10-trihydroxyanthracene (leuco 3-propyl-1,4,5-trihydroxy-9,10-anthraquinone), **13**: 80% yield; ir ($CHCl_3$) ν_{max}: 1648, 1630 cm^{-1}; ^{1}Hmr ($CDCl_3$) δ: 15.73 (s, 1H, OH), 13.36 (s, 1H, OH), 9.86 (s, 1H, OH), 7.90 (dd, J = 8 Hz, 1 Hz, 1H, H-8), 7.61 (t, J = 8 Hz, 1H, H-7), 7.13 (dd, J = 8 Hz, 1 Hz, 1H, H-6), 3.0 (m, 3H, ring CH_2—CH), 1.5 (m, 4H, propyl CH_2—CH_2), 0.9 (m, 3H, propyl CH_3). *Anal.* calcd. for $C_{17}H_{16}O_5$: C 67.99, H 5.37; found: C 67.88, H 5.31.

Reactions of leuco 1,4,5-trihydroxy-9,10-anthraquinone

Leuco compound **3** (1 mmol) was reacted for 1.5 h with pyrrolidine (5 mmol) in boiling toluene under nitrogen. Evaporation of the reaction solution and column chromatography (SiO_2/toluene) gave **8** (0.93 mmol), identified by comparison of its tlc characteristics and ir spectrum (ν_{max} (C=O): 1630 cm^{-1}) with an authentic sample and literature data (12). It was readily distinguished from **10** (ir ν_{max} (C=O): 1670, 1620 cm^{-1}) by tlc (SiO_2/9:1 v/v petroleum ether – ethyl acetate) and ir spectroscopy (12).

With added excess propanal (10 mmol), an identical reaction procedure produced only **5**.

3-Propyl-1,4,5-trihydroxy-9,10-anthraquinone, **5**: 82% yield, mp 173–174°C (lit. (8) mp 193°C); ir (KBr) ν_{max}: 1605 cm^{-1}; ^{1}Hmr ($CDCl_3$) δ: 13.06 (s, 1H, 1-OH), 12.72 (s, 1H, 4-OH), 12.18 (s, 1H, 5-OH), 7.87 (dd, J = 8 Hz, 1 Hz, 1H, H-8), 7.66 (t, J = 8 Hz, 1H, H-7), 7.28 (dd, J = 8 Hz, 1 Hz, 1H, H-6), 7.13 (s, 1H, H-2), 2.70 (t, J = 7 Hz, 2H, benzylic CH_2), 1.62 (hex, J = 7 Hz, 2H, propyl CH_2), 1.01 (t, J = 7 Hz, 3H, propyl CH_3).

An identical reaction conducted at room temperature for 1.5 h without added propanal gave about a 50% conversion to a major blue product from which **16** was isolated. The initial reaction mixture contained the deoxygenation product **8** and small quantities of two other blue amine substitution products of similar retention to **16**, which hindered the chromatographic purification of the main product.

4-Pyrrolidino-1,5-dihydroxy-9,10-anthraquinone, **16**: 21% yield; ir (KBr) ν_{max}: 1595 cm^{-1}; ^{1}Hmr ($CDCl_3$) δ: 13.75 (s, 1H, OH), 13.45 (s, 1H, OH), 7.83 (dd, J = 8 Hz, 1 Hz, 1H, H-8), 7.59 (t, J = 8 Hz, 1H, H-7), 7.2 (m, 3H, H-6, H-3, H-2), 3.40 (m, 4H, CH_2—N—CH_2), 2.03 (m, 4H, CH_2—CH_2). *Anal.* calcd. for $C_{18}H_{15}O_4N$: C 69.89, H 4.89, N 4.53; found: C 69.81, H 4.79, N 4.58.

2-Propyl-1,4,5-trihydroxy-9,10-anthraquinone was synthesized by literature methods (3).

Deoxygenation reactions of leuco 2- and 3-propyl-1,4,5-trihydroxy-9,10-anthraquinone

The deoxygenation reactions of these compounds with pyrrolidine in toluene were conducted as described above for the reaction of **3**.

Deoxygenation of **12** gave 2-propyl-1,5-dihydroxy-9,10-anthraquinone, **14**: 10% yield. The initial yield was estimated to be 60–70%, but removal of **4** required three chromatographic separations; ir (KBr) ν_{max}: 1620 cm^{-1}; ^{1}Hmr ($CDCl_3$) δ: 13.06 (s, OH), 12.72 (s, OH); remaining multiplets were obscured by noise, a consequence of the very low solubility. *Anal.* calcd. for $C_{17}H_{14}O_4$: C 72.33, H 5.00; found: C 72.06, H 4.82.

Deoxygenation of **13** gave 2-propyl-1,8-dihydroxy-9,10-anthraquinone, **15**: 3% yield. Purification to completely remove **5** required

four chromatographic columns. The initial yield was estimated to be only 10–20% because of the very slow reaction; ir (KBr) ν_{max}: 1670, 1622 cm^{-1}; ^{1}Hmr ($CDCl_3$) δ: 12.42 (s, 1H, OH), 12.09 (s, 1H, OH), 7.8 (m, 2H, H-4, H-5), 7.61 (d, J = 8 Hz, 1H, H-3), 7.56 (t, J = 8 Hz, 1H, H-6), 7.27 (dd, J = 8 Hz, 1 Hz, 1H, H-7), 2.74 (t, J = 7 Hz, 2H, benzylic CH_2), 1.69 (hex, J = 7 Hz, 2H, propyl CH_2), 1.06 (t, J = 7 Hz, 3H, propyl CH_3). Insufficient material for analysis.

Reductions of 4-pyrrolidino-1,5-dihydroxy-9,10-anthraquinone

Reduction of **16** with tin and HCl in glacial acetic acid was carried out as described for the preparation of the leuco compounds above and gave quantitative conversion to about equal yields of **1** and **8**, which were separated by tlc.

The blue **16** was also reduced in boiling toluene using activated Raney nickel. In the absence of propanal, **8** was produced in 95% yield, whereas with added propanal, the reaction gave **5** (38% yield) and some **8**, along with several amine substitution products. Deactivation of the Raney nickel by the propanal prevented any improvement of the yield.

Acknowledgements

This work was supported by grants from the Natural Sciences and Engineering Research Council of Canada. The following students and assistants also contributed to this research: Susan Dickie (Marjorie Young Bell Summer Scholar, Mount Allison University), Paul Johns, and Danny Durant. The authors thank Mr. Michel Trottier and Dr. Esteban Chornet of the Université de Sherbrooke for the elemental analyses.

1. K. H. Meyer and A. Sander. Justus Liebigs Ann. Chem. **420**, 113 (1920).
2. S. M. Bloom and R. F. Hutton. Tetrahedron Lett. 1993 (1963).
3. L. M. Harwood, L. C. Hodgkinson, J. K. Sutherland, and P. Towers. Can. J. Chem. **62**, 1922 (1984).
4. D. T. Davies, P. S. Jones, and J. K. Sutherland. Tetrahedron Lett. **24**, 519 (1983).
5. K. Krohn. Angew. Chem. Int. Ed. Engl. **18**, 621 (1979).
6. C. Marschalk, F. Koenig, and N. Ouroussoff. Bull. Soc. Chim. Fr. 1545 (1936).
7. C. E. Lewis. J. Org. Chem. **35**, 2938 (1970).
8. J. K. Sutherland, P. Towers, and C. W. Greenhalgh. J. Chem. Soc. Chem. Commun. 740 (1981).
9. K. Tolkiehn and K. Krohn. Chem. Ber. **113**, 1575 (1980); K. Krohn and B. Behnke. Chem. Ber. **113**, 2994 (1980); Justus Liebigs Ann. Chem. 1818 (1983).
10. D. J. Mincher, E. DeClercq, and G. Shaw. J. Chem. Soc. Perkin Trans. 1, 613 (1983).
11. A. E. Ashcroft and J. K. Sutherland. J. Chem. Soc. Chem. Commun. 1075 (1981).
12. H. Bloom, L. H. Briggs, and B. Cleverly. J. Chem. Soc. 178 (1959); M. St. C. Flett. J. Chem. Soc. 1441 (1948).

Reduction of carbonyl compounds promoted by silicon hydrides under the influence of trimethylsilyl-based reagents[1]

JESÚS M. AIZPURUA, BEGOÑA LECEA, AND CLAUDIO PALOMO[2]

Departamento de Química Orgánica, Facultad de Químicas, Universidad de País Vasco, Apartado 1072, 20080 San Sebastián, Spain

Received March 25, 1986

JESÚS M. AIZPURUA, BEGOÑA LECEA, and CLAUDIO PALOMO. Can. J. Chem. **64**, 2342 (1986).

The synthetic utility of hydrosilanes under the influence of trimethylsilyl-based reagents as new reducing systems is described. 1,1,3,3-Tetramethyldisiloxane (TMDS) reagent in combination with iodotrimethylsilane or bromotrimethylsilane produces alkyl halides from aldehydes in good to excellent yields. Polymethylhydrosiloxane (PMS) in the presence of iodotrimethylsilane also produces benzyl iodides in excellent yields. On the contrary, PMS reagent was found unsuitable for the synthesis of benzyl bromides. Similarly, TMDS reagent in combination with trimethylsilyl triflate produces symmetrical ethers from aldehydes without concomitant formation of competitive products. Under similar conditions, PMS reagent failed to provide the expected symmetrical ethers and Friedel–Crafts products were formed. Reduction of quinones to hydroquinones is also described.

JESÚS M. AIZPURUA, BEGOÑA LECEA et CLAUDIO PALOMO. Can. J. Chem. **64**, 2342 (1986).

On décrit les avantages que présentent en synthèse les hydrosilanes, sous l'influence de réactifs dérivés du groupement triméthylsilyle, comme systèmes de réduction. Sous l'action du réactif tétraméthyl-1,1,3,3 disiloxane (TMDS), utilisé de concert avec l'iodotriméthylsilane ou le bromotriméthylsilane, les aldéhydes sont transformés en halogénures d'alkyles, avec des rendements qui vont de bons à excellents. On a trouvé que le polyméthylhydrosiloxane (PMS), en présence d'iodotriméthylsilane, conduit aussi aux iodures de benzyles avec d'excellents rendements. Par ailleurs, on a trouvé que le réactif PMS n'est pas approprié pour la synthèse de bromures de benzyles. De la même manière, le réactif TMDS, utilisé de concert avec le triflate de triméthylsilyle, permet de transformer des aldéhydes en des éthers symétriques, sans formation concomitante de produits de compétition. Dans des conditions semblables, le réactif PMS de fournit pas les éthers symétriques attendus; toutefois, il se forme des produits de Friedel–Crafts. On décrit aussi la réduction de quinones en hydroquinones.

[Traduit par la revue]

Although reduction is one of the most widely used and extensively studied methods in organic chemistry, there remains considerable interest in the development of new reagents and synthetic methods for reduction. In recent years, several papers have revealed that silicon hydrides are useful reducing agents for a wide variety of transformations, most of them having been reviewed (1–6). Excluding photochemical reductions (7), four methods—trichlorosilane/tertiary amine reductions (8), Lewis acid catalyzed reductions (9), reductions in trifluoroacetic acid media (10), and potassium or cesium fluoride catalyzed reductions (11)—have received considerable interest for reduction of aldehydes and ketones. Triethylsilane **1** and polymethylhydrosiloxane **2** are the most popular and widely used hydrosilane reagents for these hydrogenation reactions. Recently, we reported the use of iodine together with hydrosilanes in related reactions and found that alkyl iodides were formed in excellent yields (12).

This paper describes a new reduction method for aldehydes and quinones promoted by 1,1,3,3-tetramethyldisiloxane **3** (TMDS) in the presence of the trimethylsilyl-based reagents chlorotrimethylsilane, iodotrimethylsilane, bromotrimethylsilane, and trimethylsilyl trifluoromethanesulfonate.

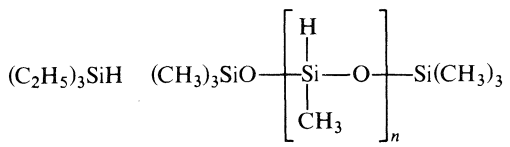

1 **2**

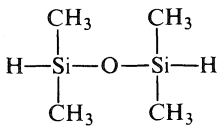

3

Results and discussion

Formation of alkyl halides

The 1,1,3,3-tetramethyldisiloxane reagent **3** has been reported (13) to be quite suitable for the direct reductive halogenation of aromatic aldehydes to benzyl halides in the presence of halosilanes. Thus, the halide groups were smoothly formed in high yields and short reaction times by treatment of benzaldehydes **4** with the reagent **3** and halosilanes, in anhydrous acetonitrile as solvent, in a molar ratio 1:1:1.5 respectively.

Aldehydes, in the absence of solvent, undergo similar reductive iodination with polymethylhydrosiloxane **2** (PMS) and sodium iodide/chlorotrimethylsilane. In contrast, reaction of aldehydes and lithium bromide/chlorotrimethylsilane with PMS reagent failed to provide the corresponding bromides. When benzaldehyde and 4-chlorobenzaldehyde were treated with reagent **2** and bromotrimethylsilane under reflux conditions for 4–6 h, partial halo-reduction took place as detected by tlc analysis; however, when TMDS reagent was added to this reaction mixture, a complete conversion into the corresponding benzyl bromides was accomplished within 30–60 min under reflux conditions. This fact shows that TMDS reagent is probably more active than the PMS reagent.

As shown by the data of Table 1, benzyl halides **5** can be conveniently prepared in good yields by TMDS or PMS reductions under the influence of halosilanes. With the exception of 3-nitrobenzaldehyde, aryl aldehydes form benzyl iodides in yields greater than 80% and benzyl bromides in yields in the range 70–90%. 4-Methoxybenzyl bromide was formed in 90% yield (84% isolated yield) when anisaldehyde was reduced at 80°C by TMDS in acetonitrile with lithium bromide/chlorotri-

[1]Contribution No. 57 in the series Reagents and Synthetic Methods. For part 56 see ref. 24.

[2]Author to whom correspondence may be addressed.

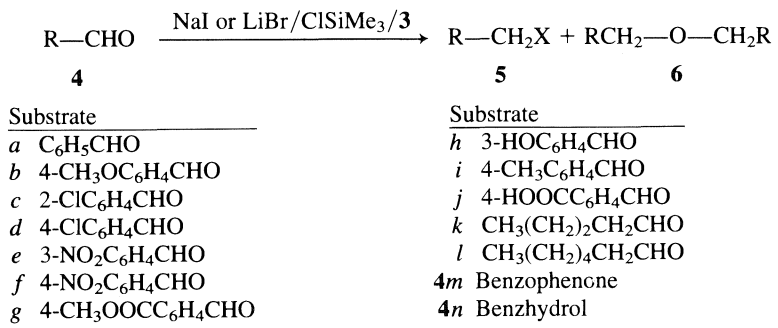

SCHEME 1

TABLE 1. Preparation of benzyl halides **5** by TMDS reduction

Substrate **4**	Product **5** X	T (°C)	Time (min)	Yield of $ArCH_2X$ (%)[a,b]	Boiling point (°C/Torr) or melting point (°C) Found	Literature
a	I	0	30	91,[c] 72[d]	60–62/0.3	24 (22)
	Br	80	30	94	198/760	201/760 (23*a*)
	Cl	70	20	91	175–180/760	179.3/760 (23*a*)
b	I	15	30	89,[c] 90[d]	32–34	27 (23*b*)
	Br	80	15	84	145–148/30	110–113/2 (23*c*)
	Cl	−70	150	60 (40)	145–148/4	100–103/5 (23*d*)
c	I	25	45	86, 70	90/0.05	26–27 (23*e*)
	Br	80	15	64	95–98/0.4	120/10 (23*a*)
	Cl	70	60	55 (45)	140–145/20	94–95/10 (23*a*)
d	I	0	5	95, 90[d]	59–61	63 (23*f*)
	Br	80	20	90	See experimental	
	Cl	70	45	85	150–153/30	117/20 (23*a*)
e	I	80	30	48 (30)	82–85	83.5–85.5 (23*f*)
f	Cl	−70	180	80[e] (20)	68–70	71 (22)
g	Br	80	80	80 (20)	53–55	54–55 (23*g*)
	Cl	−70	180	60[e] (40)	—[h]	160–165/30 (23*h*)
h	Br	80	45	77 (23)	—[i]	
	Cl	−70	195	40[f,g]	105–110/0.1[j]	
i	I	20	30	73[d]	46–47	46 (23*b*)
	Br	80	20	97	106–109/15	218–220/760 (23*a*)
	Cl	70	15	87	See experimental	

[a]Isolated yields; the purity as determined by glc and tlc analysis was ≥97%.
[b]The numbers in parentheses indicate isolated yields of the symmetrical ethers **6**.
[c]These benzyl iodides were unstable compounds, which decompose during storage.
[d]Yield referred to PMS reductions.
[e]After 1 h at −70°C, *N*,*N*-dimethylformamide (10% equiv., catalyst) is added, and the mixture is refluxed for 2 h.
[f]$ZnCl_2$ is used as catalyst instead of ZnI_2.
[g]Friedel–Crafts type compounds were formed as by-products.
[h]Not isolated; percentage determined by nmr analysis.
[i]Percentage determined by nmr ($CDCl_3$); δ: 4.20 (s, CH_2Br), 4.29 (s, CH_2O).
[j]Nuclear magnetic resonance ($CDCl_3$) δ: 4.23 (s, 2H, CH_2), 6.50 (m, 3H, arom.), 6.80 (d, 1H, arom.), 7.01 (s, 1H, OH).

methylsilane; however, under the same conditions, 3-hydroxybenzaldehyde gave the expected 3-hydroxybenzyl bromide in 77% isolated yield and a second compound, which was characterized as the symmetrical ether **6**, in 23% yield.

On the other hand, when benzaldehyde was treated with the hydrosilane **3** under the influence of iodotrimethylsilane in catalytic amount, only traces of benzyl iodide and dibenzyl ether were detected by glc and nmr analysis of the crude reaction mixture, and the starting aldehyde remained intact in the solution after 3.5 h at 0°C. When the reaction mixture was refluxed for 60 min, the isolated products were found to be dibenzyl ether, benzyl iodide, and benzyl chloride in 85, 9, and 6% yield respectively. When the reaction was tested with *n*-pentanal and *n*-heptanal only the corresponding symmetrical ethers were formed. The same result was found when iodotrimethylsilane was used in equimolar amount, without formation of the expected aliphatic iodides.

Reaction between ketones such as 4-methylacetophenone and cyclohexanone, sodium iodide/chlorotrimethylsilane, and TMDS reagent was found troublesome and difficult to control, giving mixtures of products in which we have detected by glc and nmr analysis the corresponding starting materials, alkanes, symmetrical ethers, and traces of the respective iodides.

We next examined the use of chlorotrimethylsilane to obtain the corresponding benzyl chlorides **5** (X:Cl). In a preliminary experiment, we found that under conditions similar to those

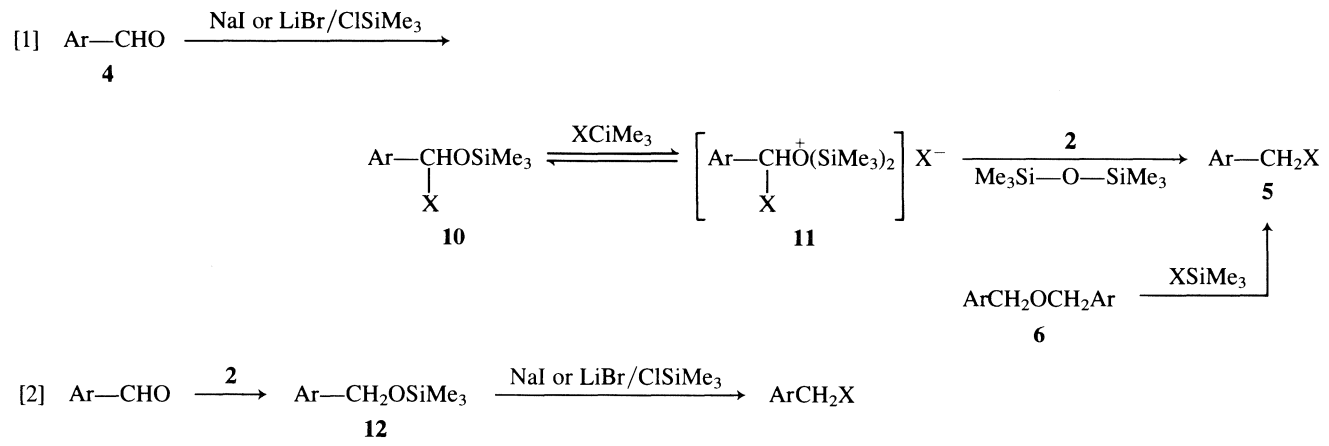

SCHEME 2

used in the formation of benzyl iodides or bromides by TMDS reduction, chlorotrimethylsilane alone failed to provide the corresponding benzyl chlorides. Nevertheless, when the reaction was carried out in the presence of thionyl chloride and zinc iodide as catalyst, the corresponding chlorides were obtained in good yields, even if in some cases the corresponding symmetrical ethers were also formed. For example, whereas benzaldehyde gave only benzyl chloride, 2-chlorobenzaldehyde gave a mixture of 2-chlorobenzyl chloride (55%) and bis(2-chlorobenzyl) ether (45%), which was conveniently analyzed by nmr spectroscopy (Ar-CH_2Cl signal appeared at δ 4.5 ppm and Ar-CH_2O signal appeared at δ 4.56 ppm). On the basis of available data, the ratio of chloride/ether does not appear to be predictable as a function of aromatic ring substituents. In comparison, reaction of aldehydes with iodotrimethylsilane and bromotrimethylsilane gave the respective halides as the only reaction products, except for aromatic aldehydes having electron-withdrawing groups. On the other hand, in the absence of thionyl chloride, 4-chlorobenzaldehyde and 2-chlorobenzaldehyde give the symmetrical ethers **6** instead of the respective benzyl chloride **5**, and in the absence of Lewis acid catalyst, benzaldehyde gave a mixture of benzal chloride and benzyl chloride (molar ratio 57:43) after 3 h reflux. With aromatic aldehydes having electron-withdrawing substituents such as nitro or carbomethoxy groups, the reaction was first carried out at −70°C and then heated to reflux to exclude the formation of symmetrical ethers as major competitive products. For aromatic aldehydes having electron-donating substituents such as 4-methoxybenzaldehyde and 3-hydroxybenzaldehyde, the reaction was achieved in the same way, but using zinc chloride to prevent Friedel–Crafts products as a major competitive reaction.

The halide formation could occur in a number of ways: (*i*) by the reduction of an *O*-silylated halohydrin (18) intermediate **10** (eq. [1]), (*ii*) by the cleavage of an "*in situ*" generated symmetrical ether, or (*iii*) by reduction of the aldehyde into the corresponding alcohol derivative **12** followed by substitution of the hydroxyl function by the halide group (19) (eq. [2]).

Formation of symmetrical ethers

Doyle *et al.* (10) have reported that certain silanes, especially triethylsilane in trifluoroacetic acid, reduce carbonyl compounds to symmetrical ethers[3] with the concomitant formation of a carboxylate ester. An interesting observation of these authors is that increasing basicity of the carboxylic acid also increases the percentage of carboxylate ester to symmetrical ether. This consideration has led us to investigate the behavior of 1,1,3,3-tetramethyldisiloxane (TMDS) reagent **3** in the reduction of aldehydes under the influence of stronger acids than trifluoroacetic acid. As we have mentioned above, the use of iodotrimethylsilane (chlorotrimethylsilane/NaI) in catalytic amount produces the symmetrical ether **6** of the corresponding aldehyde along with the respective iodo and chloro compounds **5**. To avoid this latter reaction, we have examined the reduction of aldehydes under the influence of trimethylsilyl trifluoro-

TABLE 2. Reduction of aldehydes into symmetrical ethers by 1,1,3,3-tetramethyldisiloxane (TMDS) under trimethylsilyl triflate or iodotrimethylsilane catalysis

Substrate **4**	Solvent	*T* (°C)	Time (min)	Yield of RCH_2OCH_2R **6** (%)[a]
a	C_6H_6	30	20	97[b]
c	C_6H_6	80	20	94[c]
d	C_6H_6	80	20	90[d]
	F_3CCOOH	25	30	94(6)[e]
f	CH_2Cl_2	−78	70	9[f]
	CH_2Cl_2	30	120	55[f,g]
j	C_6H_6	80	120	97[h]
	F_3CCOOH	25	240	46(54)[i]
k	C_6H_6	80	30	90[b]
	C_6H_6	30	30	84[j]
l	C_6H_6	80	30	96[k]
	C_6H_6	30	30	90[j]
m	C_6H_6	80	240	95[l]
n	C_6H_6	80	240	91[l]

[a]Yield of isolated pure products; the purity as determined by glc and tlc analysis was ≥97%.
[b]See Experimental.
[c]Nuclear magnetic resonance (CCl_4) δ ppm: 4.53 (s, 2H, CH_2), 7.05 (m, 4H, arom.).
[c]Melting point: 54–55°C, see ref. 9.
[d]Percentage of trifluoroacetate ester determined by nmr analysis; δ: 5.12 (s, CH_2OCO), 4.33 (s, CH_2O).
[f]91% of isolated pure *p*-nitrobenzyl alcohol, see Experimental.
[g]45% of *p*-nitrobenzyl alcohol was formed, based on nmr analysis.
[h]Melting point: 271–272°C; see ref. 26.
[i]Percentage of trifluoroacetate ester determined by nmr analysis.
[j]Iodotrimethylsilane as catalyst was used instead of trimethylsilyl triflate.
[k]Boiling point: 135–138°C (22 Torr); lit. (18) bp 258.8°C (769 Torr).
[l]Diphenylmethane as only reaction product.

[3]While this work was in progress a related paper appeared using trityl perchlorate as catalyst; see ref. 25.

TABLE 3. Alkylation of aromatic compounds by aldehydes

Run	Reactants: Aldehyde	Arene	Conditions: T (°C)	t(h)	Product	Yield (%)[a]
a	Benzaldehyde	Benzene	80	2	Diphenylmethane	92
b		Toluene	110	1	Phenyl-*p*-tolylmethane	95[b]
c					Phenyl-*o*-tolylmethane	
d	*p*-Methylbenzaldehyde	Benzene	80	2.5	Phenyl-*p*-tolylmethane	60
e		Toluene	110	0.5	Di-*p*-tolymethane	80[c]
f					*p*-Tolyl-*o*-tolylmethane	
g	*o*-Chlorobenzaldehyde	Benzene	80	3	Phenyl-*o*-chlorophenylmethane	25
h					Bis(*o*-chlorophenyl)ether	55
i	*p*-Chlorobenzaldehyde	Benzene	80	3	Phenyl-*p*-chlorophenylmethane	65[d]
j					Bis(*p*-chlorophenyl)ether	

[a]Yield of isolated products by fractional reduced pressure distillation; all compounds were characterized by their physical and spectroscopic characteristics (bp, ir, nmr).
[b]Molar ratio **7***b*:**7***c* = 70:30 by nmr spectroscopy.
[c]Molar ratio **7***e*:**7***f* = 90:10 by nmr spectroscopy.
[d]Molar ratio **7***i*:**7***j* = 75:25.

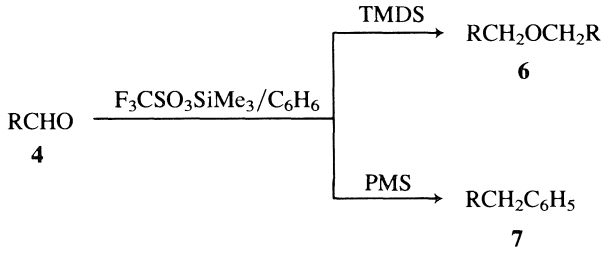

SCHEME 3

methanesulfonate (trimethylsilyl triflate) and have found that the use of this reagent enhances the formation of symmetrical ethers **6** without concomitant formation of competitive products. In the absence of trimethylsilyl triflate, no reaction takes place and the starting aldehyde is completely recovered. We have tested the method with a number of aromatic and aliphatic aldehydes and have found the results (Table 2) to be uniformly good. For aromatic and aliphatic aldehydes, the yields of the symmetrical ethers are in the range 90–97%. Whereas the reduction of 4-nitrobenzaldehyde by the triethylsilane method (10) gives a mixture of 4-nitrobenzyl ether in 33% yield and the corresponding trifluoroacetate in 67% yield, in the method described here only two products are formed depending on the reaction conditions used; thus, when the reaction is carried out at −78°C the major product is the *p*-nitrobenzyl alcohol with 91% yield and the by-product is the corresponding symmetrical ether. Under similar reaction conditions, benzophenone and benzhydrol were reduced at a much slower rate than aromatic and aliphatic aldehydes and only diphenylmethane was obtained from both of them in nearly quantitative yield.

On the other hand, it should be noted that reductions by means of TMDS reagent in trifluoroacetic acid (entries *d* and *j*) as solvent (instead of trimethylsilyl triflate catalysis) also produce symmetrical ethers, but the corresponding trifluoroacetate is formed in a competition process. In a similar manner, from 4-carboxybenzaldehyde, the percentage of the corresponding trifluoroacetate ester was found to be greater than the corresponding symmetrical ether, probably due to the stronger electron-withdrawing group in the *para* position.

Furthermore, we have found that under conditions similar to those used for the formation of symmetrical ethers **6** by TMDS reduction of aldehydes **4**, the reaction between aldehydes and aromatic compounds can take a different course in the presence of polymethylhydrosiloxane (PMS) to produce diphenylmethanes **7**. Thus, when a mixture of an aromatic aldehyde and a catalytic amount of TMS triflate was refluxed in benzene or toluene in the presence of PMS reagent, the corresponding arylmethane was produced in a few hours. As shown in Table 3, from unactivated aldehydes, symmetrical ethers are formed as competitive products. Since condensation of aromatic rings with aldehydes is severely limited by side reactions (14), our procedure constitutes an unusual Friedel–Crafts type alkylation. However, the method reaches a limit with aliphatic aldehydes, from which side products predominated.

Reduction of quinones

The reduction of the carbonyl function of quinones to hydroxyl group has enjoyed wide application in organic synthesis and in many naturally occurring substances (15). Various conventional reducing agents have been employed to convert quinones into hydroquinones (15); however, these procedures are generally accompanied by the formation of a large amount of inorganic salts. Other methods described involve the silylation technique to give, after hydrolysis, the corresponding hydroquinones. Chlorotrimethylsilane (16*a*, *b*), bis(trimethylsilyl)mercury (16*c*, *d*), 1,2-difluorotetramethyldisilane (16*e*), and hexamethyldisilane (16*f*) are silyl reagents used to convert *p*-quinones into bis(trimethylsilyloxy)benzenes. In some of these methods, the reaction takes place only in the presence of metals, involving forceful conditions, and gives yields in the range 40–60%. Some of these reagents are also expensive, and thus their application is limited.

Kursanov and co-workers have reported the reduction of benzoquinone to hydroquinone using triethylsilane in trifluoroacetic acid media (17). Because of the good yield reported for this silane reduction, we expected that TMDS reduction of benzoquinones under the influence of sodium iodide/chlorotrimethylsilane would represent a convenient and synthetically useful method for transforming quinones into hydroquinones.

Reductions were carried out in refluxing dichloromethane for 30–35 min, with TMDS and iodotrimethylsilane as catalyst. Some examples are listed in Table 4 and the results obtained are uniformly good. Triethoxysilane and polymethylhydrosiloxane were also found suitable for such reduction, but they require longer reaction times. Thus, reduction of quinones **8***a* and **8***c* by

TABLE 4. Reduction of benzoquinones

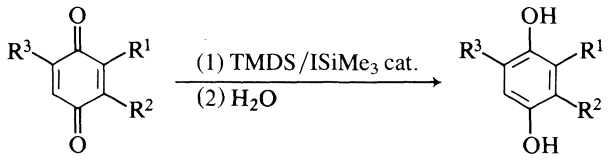

8 9

					Melting point (°C)	
8[a]	R^1	R^2	R^3	Yield (%)[b]	Found	Lit. (22)
a	H	H	H	96	169–171	171
b	CH_3	CH_3	CH_3	90	168–171	169–172[c]
c	CH_3	H	H	90	123–126	124–126
d	Cl	H	H	85	99–102	106
e	CH_3O	H	H	98	88–95	90–92[c]
f	1,4-Naphthoquinone			75	175	176

[a]Molar ratio quinone:TMDS = 1:1.5.
[b]Isolated yields.
[c]These compounds were identified by comparison with authentic samples (Fluka A.G.).

the first reagent under reflux conditions during 3 h gives 66 and 77% yields of the desired hydroquinones **9** and the last reagent reduces **8***a* in 56% yield after 10 h reflux. Indeed, as the results confirm, the method is rather similar to the iodine catalyzed hydrosilane reduction of hydroquinones (12).

Conclusions

In the presence of trimethylsilyl-based reagents, aldehydes are converted by TMDS reduction to alkyl halides and symmetrical ethers in high yields. The reaction product is dependent on the nature of the starting carbonyl compound. From aromatic aldehydes, only benzyl halides were obtained by means of 1,1,3,3-tetramethyldisiloxane TMDS reagent **3**, whereas PMS reagent **2** was found suitable for this transformation only for iodides, but not for bromides. From aliphatic aldehydes, the corresponding symmetrical ethers were formed instead of the respective alkyl halides by TMDS halo-reduction. Similarly, trimethylsilyl triflate catalyzed reductions of aldehydes, producing symmetrical ethers without competitive reactions.

The method described here presents a new reductive halogenation procedure for the direct conversion of benzaldehydes to benzyl halides and a mild catalytic procedure for the selective conversion of carbonyl compounds to symmetrical ethers, as well as hydroquinones from quinones, offering great versatility from the synthetic point of view as demonstrated here by a rather limited number of examples, which may be readily extended to further applications.

Experimental

Melting points were determined on a Büchi SMP-20 melting point apparatus and are uncorrected. Reported boiling points are those observed during distillation with a kugelrohr apparatus and are uncorrected. Proton nmr spectra were measured on a Varian EM-360 A spectrometer and are reported in parts per million downfield from internal tetramethylsilane. All the starting materials used in this work were either commercially available in 98% or higher purity and were used without further purification, or were prepared by standard literature procedures. Acetonitrile was purified (27) and stored over molecular sieves. 1,1,3,3-Tetramethyldisiloxane (TMDS) reagent was obtained from Wacker-Chemie GMBH (München, Germany). Iodotrimethylsilane was formed "*in situ*" from chlorotrimethylsilane and sodium iodide according to the method described by Olah *et al.* (19). Bromotrimethylsilane was also generated "*in situ*" from chlorotrimethylsilane and lithium bromide, similarly to the method reported by Schmidt and Russ (20). Trimethylsilyl triflate was prepared (21*b*) by a modification of the procedure described by Roeski and Giere (21*a*).

Formation of benzyl iodides

General procedure for TMDS reagent

A mixture of the corresponding benzaldehyde (10 mmol), chlorotrimethylsilane (1.92 mL, 15 mmol), and sodium iodide (2.25 mg, 15 mmol) in anhydrous acetonitrile (5 mL) is stirred at room temperature for 10 min and then cooled to 0°C. Immediately after, 1,1,3,3-tetramethyldisiloxane (1.79 mL, 10 mmol) is added dropwise giving an exothermic reaction. Stirring is maintained for 30 min, after which the siloxane products are destroyed with a 2.5 *N* solution of hydrofluoric acid in methanol (15 mL). The mixture is taken up in dichloromethane (30 mL) and washed with cool water (30 mL) and saturated $NaHCO_3$ solution (30 mL). Drying and evaporation of the solvent yields crude benzyl iodide, which is purified by reduced pressure distillation or recrystallization.

General procedure for PMS reagent

A mixture of sodium iodide (2.25 g, 15 mmol) and chlorotrimethylsilane (1.92 mL, 15 mmol) is stirred at room temperature for 10 min; then the corresponding benzaldehyde (10 mmol) is added and stirred for 3 min, after which PMS **2** is added giving an exothermic reaction. Stirring is maintained for 20–40 min. The mixture is taken up in dichloromethane (30 mL) and washed with water (2 × 20 mL) and saturated $NaHCO_3$ solution (2 × 20 mL). Drying and evaporation of solvent yield a crude mixture of the benzyl iodide and siloxane polymer compounds. The upper layer is separated and the lower one is purified by reduced pressure distillation to give the pure benzyl iodide.

Formation of benzyl bromides

4-Chlorobenzyl bromide **5**d*: typical procedure*

A suspension of 4-chlorobenzaldehyde (1.40 g, 10 mmol), lithium bromide (1.5 g, 1.72 mmol), chlorotrimethylsilane (1.92 mL, 15 mmol), and 1,1,3,3-tetramethyldisiloxane (1.79 mL, 10 mmol) in acetonitrile (10 mL) is refluxed with stirring for 20 min. The same work-up used for benzyl iodides is followed, affording crude 4-chlorobenzyl bromide, which is purified by recrystallization from MeOH (1.85 g, 90%); mp 48–50°C (lit. (22) mp 51°C).

Formation of benzyl chlorides

4-Methylbenzyl chloride **5**i*: typical procedure*

A mixture of 4-methylbenzaldehyde (1.18 g, 10 mmol), chlorotrimethylsilane (2.0 mL, 15.7 mmol), 1,1,3,3-tetramethyldisiloxane (1.79 mL, 10 mmol), and thionyl chloride (1.0 mL, 13.7 mmol) is cooled at 0°C. Then ZnI_2 (0.02 g) is added and a very exothermic reaction takes place; when the spontaneous heating has ended, the mixture is refluxed with stirring for 45 min, and a 2.5 *N* solution of hydrofluoric acid in methanol (10 mL) is added. After refluxing for 10 min the solution is cooled at 0°C, filtered, taken up in dichloromethane (30 mL)/water (40 mL), and the aqueous layer extracted with dichloromethane (2 × 10 mL). The combined organic phases are dried (Na_2SO_4) and the solvents evaporated to afford crude 4-methylbenzyl chloride, which is purified by reduced pressure distillation (1.22 g, 87%); bp 190–195°C (lit. (22) bp 192°C/760 Torr) (1 Torr = 133.3 Pa).

Formation of symmetrical ethers

Dibenzylether **6**a*: typical procedure*

Benzaldehyde (1.02 mL, 10 mmol) is added to a mixture of 1,1,3,3-tetramethyldisiloxane (1.79 mL, 10 mmol), trimethylsilyl trifluoromethanesulfonate (0.05 mL, catalyst), and benzene (20 mL). The resulting solution is refluxed for 20 min, until no aldehyde can be detected by tlc analysis (silica gel plates; eluent: EtOAc/hexane 1:3). Upon completion of the reaction, the solvent is evaporated and the residue purified by reduced pressure distillation, yielding dibenzyl ether (0.96 g, 97%); bp 92–94°C/0.3 Torr (lit. (22) 290–300°C/760 Torr).

*Bis(*n*-pentyl) ether* **6**k*: typical procedure*

A mixture of sodium iodide (0.15 g, 1 mmol), valeraldehyde

(1.06 mL, 10 mmol), and chlorotrimethylsilane (2.0 mL, 15.4 mmol) is stirred in acetonitrile (5.0 mL) at room temperature for 10 min, after which 1,1,3,3-tetramethyldisiloxane (1.79 mL, 10 mmol) is added. When the exothermic reaction has ended (30 min), a solution of 2.5 *N* hydrofluoric acid in methanol (30 mL) is added to the reaction mixture, and then refluxed for 5 min. Work-up is carried out by diluting the solution with dichloromethane (40 mL), washing with water (30 mL) and saturated $NaHCO_3$ solution (20 mL), drying, and evaporating the solvents. Crude bis(*n*-pentyl) ether is purified by reduced pressure distillation (0.65 g, 84%); bp 185–189°C/760 Torr (lit. (22) bp 187.5°C/760 Torr).

4-Nitrobenzyl alcohol

A solution of 1,1,3,3-tetramethyldisiloxane (1.79 mL, 10 mmol) and trimethylsilyl triflate (0.05 mL, catalyst) in dichloromethane (20 mL) is added dropwise (30 min) to a cooled solution of 4-nitrobenzaldehyde (0.76 g, 5 mmol) in the same solvent (30 mL) and the reaction mixture is stirred for 70 min. Then the solvent is evaporated and the resulting crude product is purified by column chromatography (silica gel; eluent: hexane/EtOAc 1:1). Yield of 4-nitrobenzyl alcohol: 0.71 g, 91%; mp 92–94°C (lit. (22) mp 93°C).

Diphenylmethane

Benzophenone **4***m* (1.81 g, 10 mmol) is added to a mixture of 1,1,3,3-tetramethyldisiloxane (3.57 mL, 20 mmol), trimethylsilyl triflate (0.05 mL, catalyst), and benzene (20 mL), and the solution is refluxed for 4 h. Then a 2.5 *N* solution of hydrofluoric acid in methanol (30 mL) is added and, after a 5-min reflux, the mixture is taken up over dichloromethane (50 mL) and washed successively with water (30 mL) and saturated $NaHCO_3$ solution (20 mL). Drying and evaporation of the solvent gives crude diphenylmethane, which is purified by reduced pressure distillation (1.59 g, 95%); bp 70–72°C/0.3 Torr (lit. (18) mp 26–27°C). From benzhydrol **4n** (1.8 g, 10 mmol), yield of diphenylmethane: 91%.

Arylmethanes 7 from aldehydes

General procedure

A mixture of the corresponding aromatic aldehyde (10 mmol), PMS reagent (1 mL), and TMS triflate (two drops) in benzene or toluene (20 mL) is refluxed for 2 h and then washed with water (2 × 20 mL). The organic layer is dried over Na_2SO_4. Evaporation of the solvent gives a waxy residue, which is treated with methanol (10 mL). The resulting precipitate of siloxane polymer is filtered off. Evaporation of the solvent gives an oil, which is analyzed by nmr spectroscopy to determine the isomer proportion. Then the crude product is distilled under reduced pressure to afford the corresponding arylmethanes (14*a*).

Reduction of p*-benzoquinones*

General procedure

A mixture of sodium iodide (0.15 g, 1.0 mmol) and chlorotrimethylsilane (0.13 mL, 1.0 mmol) is stirred in acetonitrile (2.0 mL) for 5 min, after which dichloromethane (30 mL), the corresponding *p*-benzoquinone **7** (10 mmol), and 1,1,3,3-tetramethyldisiloxane (2.69 mL, 15 mmol) are successively added. When the spontaneous exothermic reaction has ended, the solution is refluxed for 30 min and then extracted with 1 *N* NaOH (30 mL). The aqueous phase is acidified (HCl aqueous) and extracted with EtOAc (3 × 15 mL). The organic solution is dried (Na_2SO_4) and evaporated to give the respective hydroquinone **9**.

1. D. N. Kursanov, Z. N. Parnes, and N. M. Loim. Synthesis, 633 (1974).
2. E. Lukevics. Russ. Chem. Rev. **46**, 264 (1977).
3. E. Colvin. Silicon in organic synthesis. Butterworths, London. 1981. p. 325.
4. I. Fleming. *In* Comprehensive organic chemistry. Vol. 3. Pergamon Press, New York. 1979. p. 572.
5. M. Hudlický. Reduction in organic chemistry. Ellis Horwood Limited, John Wiley, New York. 1984.
6. W. P. Weber. Silicon reagents for organic synthesis. Springer Verlag, Berlin. 1983. p. 273.
7. V. I. Zdanovich, R. V. Kudryavtser, and D. N. Kursanov. Izv. Akad. Nauk SSSR, 472 (1970).
8. R. A. Benkeser and W. E. Smith. J. Am. Chem. Soc. **91**, 1556 (1969).
9. (*a*) R. Calas, E. Frainnet, and J. Bonastre. C. R. Acad. Sci. **251**, 2987 (1960); (*b*) J. L. Fry, M. Orfanopoulos, M. G. Adlintong, W. P. Dittman, Jr., and S. B. Silverman. J. Org. Chem. **37**, 760 (1972).
10. M. P. Doyle, D. J. DeBruyn, S. J. Donnelly, D. A. Kooistra, A. A. Odubela, Ch. T. West, and S. H. Zonnebelt. J. Org. Chem. **39**, 2740 (1974).
11. (*a*) C. Chuit, R. J. P. Corriu, R. Perz, and R. Réyé. Synthesis, 981 (1982); (*b*) J. Boyer, R. J. P. Corriu, R. Perz, and C. Réyé. J. Chem. Soc. Chem. Commun. 121 (1981); (*c*) R. J. P. Corriu, R. Perz, and C. Réyé. Tetrahedron, **39**, 999 (1983).
12. B. Lecea, J. M. Aizpurua, and C. Palomo. Tetrahedron, **41**, 4657 (1985).
13. J. M. Aizpurua and C. Palomo. Tetrahedron Lett. 1103 (1984).
14. (*a*) C. C. Price. Org. React. **3**, 1 (1946); (*b*) C. A. Buehler and D. E. Pearson. Survey of organic synthesis. Vol. 1. Wiley–Interscience, New York. 1970. p. 38; and Vol. 2. 1977. p. 42; (*c*) J. March. Advanced organic chemistry. 3rd ed. John Wiley, New York. 1985. p. 479.
15. S. Patai (*Editor*). The chemistry of the quinoid compounds. Wiley, New York. 1974.
16. (*a*) H. Bouas-Laurent, R. Lapouyade, C. Brigand, and J. P. Desvergne. C. A. Acad. Sci. Paris. Ser. C, **270**, 2167 (1970); (*b*) T. Murakawa, K. Fuji, S. Murai, and S. Tsutsumi. Bull. Chem. Soc. Jpn. **45**, 2520 (1972); (*c*) A. G. Beaumont, C. Eaborn, and R. A. Jackson. J. Chem. Soc. (B), 1624 (1970); (*d*) W. P. Neumann and G. Neumann. J. Organometal. Chem. **42**, 277 (1972); (*e*) K. Tamao, S. Okazaki, and M. Kumada. J. Organometal. Chem. **146**, 87 (1978); (*f*) H. Matsumoto, S. Koike, I. Matsubara, T. Nakano, and I. Nagai. Chem. Lett. 533 (1982).
17. N. M. Loim, Z. N. Parnes, I. I. Brunovlenskaya, and D. N. Kursanov. Dokl. Akad. Nauk SSSR, **196**, 1361 (1971); Chem. Abstr. **74**, 141369 (1971).
18. M. E. Jung, A. B. Mossman, and M. A. Lyster. J. Org. Chem. **43**, 3698 (1978).
19. (*a*) G. A. Olah, S. C. Narang, B. G. B. Gupta, and R. Malhotra. J. Org. Chem. **44**, 1247 (1979); (*b*) **45**, 1638 (1980); (*c*) T. Morita, Y. Okamoto, and H. Sakurai. J. Chem. Soc. Chem. Commun. 874 (1978).
20. A. H. Schmidt and M. Russ. Chem. Ber. **114**, 1099 (1981), and references cited therein.
21. (*a*) H. W. Roesky and H. H. Giere. Z. Naturforsch. B, **25**, 773 (1970); (*b*) J. M. Aizpurua and C. Palomo. Synthesis, 206 (1985).
22. Z. Rappoport. Organic compounds identification. 3rd ed. C.R.C. Press, Cleveland, Ohio. 1977.
23. (*a*) R. C. Weast (*Editor*). Handbook of chemistry and physics, 57th ed. C.R.C. Press, Cleveland, Ohio. 1977–1978; (*b*) A. Lorenzo, P. Molina, and M. J. Vilaplana. Synthesis, 853 (1980); (*c*) S. T. Feng and K. Y. Chiu. Chem. Abstr. **54**, 17302 (1960); (*d*) M. Sommelet and I. Marszak. Chem. Abstr. **30**, 1185 (1936); (*e*) R. N. Castle and J. L. Riebsomer. J. Org. Chem. **21**, 142 (1956); (*f*) G. H. Daub and R. N. Castle. J. Org. Chem. **19**, 1571 (1954); (*g*) R. C. Fuson and H. G. Cooke, Jr. J. Am. Chem. Soc. **62**, 1180 (1940); (*h*) W. S. Emerson and R. A. Hemsch. J. Am. Chem. Soc. **72**, 5152 (1950).
24. F. Roldán, A. González, and C. Palomo. Carbohydr. Res. **149**, C1 (1986).
25. J. Kato, N. Iwasawa, and T. Mukaiyama. Chem. Lett. 743 (1985).
26. J. N. Ashley, H. J. Barber, A. J. Ewins, G. Newbery, and A. D. H. Self. J. Chem. Soc. 103 (1942).
27. J. A. Riddick and W. Bunger. Organic solvents: Techniques of chemistry. Vol. 2. Wiley–Interscience, New York. 1971.

^1H and ^{13}C nuclear magnetic resonance and ultraviolet studies of the protonation of cytosine, uracil, thymine, and related compounds

ROBERT L. BENOIT AND MONIQUE FRECHETTE

Département de Chimie, Université de Montréal, C.P. 6128, Succ. A, Montréal (Qué.), Canada H3C 3J7

Received April 30, 1986

ROBERT L. BENOIT and MONIQUE FRECHETTE. Can. J. Chem. **64**, 2348 (1986).

The protonation of the three nucleic acid bases, cytosine, uracil, and thymine, and of related 4-amino-2,6-dimethylpyrimidine and 2-hydroxypyridine has been studied by ^1H and ^{13}C nuclear magnetic resonance and ultraviolet spectroscopies mostly in 0.18–18 *M* aqueous sulfuric acid. The experimental data have been interpreted on the basis of the excess acidity method. The pK_n values as well as the assigned protonation sites are discussed and contrasted with other data.

ROBERT L. BENOIT et MONIQUE FRECHETTE. Can. J. Chem. **64**, 2348 (1986).

La protonation des trois bases des acides nucléiques, cytosine, uracil, et thymine, et des composés voisins amino-4 diméthyl-2,6 pyrimidine et hydroxy-2 pyridine a été étudiée par les spectroscopies de rmn du ^1H et ^{13}C principalement dans l'acide sulfurique aqueux 0.18–18 *M*. On a interprété les résultats expérimentaux sur la base de la méthode dite «d'acité en excès». Les valeurs des pK_n ainsi que les attributions des sites de protonation sont examinées et comparées à d'autres données.

Introduction

We have recently reported the results of our research on the protonation of purines (1), important constituents of nucleic acids. Now we have extended our work to study the protonation of that other class of nucleic acid bases, the pyrimidines. We have considered here three biologically important hydroxypyrimidines: cytosine, uracil, and thymine. To assist the identification of the protonated sites of these polyfunctional bases, we have also examined two related compounds, 4-amino-2,6-dimethylpyrimidine (Dap) and 2-hydroxypyridine (Hypy). For this work we used ^1H and ^{13}C nmr spectroscopy as well as uv spectroscopy to confirm our results, since both methods involve widely different base concentrations.

Since the first protonation of cytosine takes place in dilute acid media and the pK_1 value, 4.58 (2), is well established, it was not studied here. Diprotonated cytosine has been identified in both HSO_3F and HSO_3F–SbF_5–SO_2 (3) but no pK_2 value was previously available. Uracil and thymine, which are dihydroxypyrimidines, are much less basic than cytosine and the reported somewhat conflicting pK_1 are −2.2 (4) and −3.0 (5) for uracil and −1.6 to −2.5 (4) for thymine respectively. Diprotonated uracil has been characterized in HSO_3F and HSO_3F–SbF_5–SO_2 (3), and Frederick and Poulter (6), using ^1H nmr, have obtained −7.3 and −6.8 for pK_2 for uracil and thymine respectively.

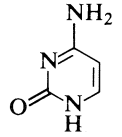

Cytosine (Cyt)

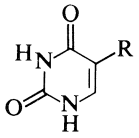

Uracil (Ura), R = H
Thymine (Thy), R = CH_3

We present here the results of our spectroscopic study of the protonation of the three hydroxypyrimidines and two related compounds, mostly in 0.18–18 *M* aqueous sulfuric acid. Our pK values and assigned protonation sites are contrasted with previously published data.

Experimental

Cytosine (Sigma), 1-methylcytosine (Vega Biochemicals, a gift from Prof. A. L. Beauchamp), uracil (Sigma), and thymine (Sigma) were used as received. Their uv spectra were in agreement with those published (7). 2-Hydroxypyridine (Hypy) (Aldrich) was used without purification. 4-Amino-2,6-dimethylpyrimidine (Dap) (Aldrich) was recrystallized in a 2:1 mixture of ethyl acetate and absolute ethanol and dried under vacuum at room temperature for 2 h. Acidimetric titration of the product in acetic acid showed a purity of 99.9 ± 0.3%. Sulfuric acid (BDH), sulfuric acid-d_2 (SIC), and 7% fuming H_2SO_4 (Fisher) were reagent grade. Triple distilled HSO_3F (Aldrich) was also used as received.

Proton nmr spectra were recorded at 28°C on a Bruker WH-90 spectrometer operating at 90 MHz. The ^1H chemical shifts for Ura and Thy were measured relative to internal Et_4NBF_4 and converted to the Me_4Si scale using the relationship $\delta_{Me_4Si} = \delta_{Et_4NBF_4} + 1.27$ ppm (8). The ^1H chemical shifts for Cyt were determined by using as reference external Me_4Si in Me_2SO-d_6. The ^1H nmr spectra in HSO_3F were recorded at −75°C on a Bruker WP-80 spectrometer operating at 80 MHz. The ^1H chemical shifts were measured relative to external acetone-d_6 (coaxial tube) and converted to the Me_4Si scale using $\delta_{Me_4Si} = \delta_{acetone\text{-}d_6} + 2.10$ ppm (8).

Carbon-13 nmr spectra were acquired at 28°C on a Bruker WP-80 spectrometer operating at 20.2 MHz. Proton decoupled spectra were recorded when needed to assist signal assignments. The ^{13}C chemical shifts were measured relative to external dioxane in D_2O (coaxial tube) and converted to the Me_4Si scale using $\delta_{Me_4Si} = \delta_{dioxane} + 67.40$ ppm (9). The nmr samples were prepared by dissolving weighed amounts of the solid bases in known volumes of titrated H_2SO_4 (^{13}C nmr) or D_2SO_4 (^1H nmr) solutions, 7% fuming H_2SO_4, and HSO_3F.

The ^1H nmr spectra were recorded for Cyt with 0.18–18 *M* H_2SO_4 solutions, and for Ura and Thy with 4.0–18 *M* D_2SO_4. The base concentrations were 0.16 *M* for Cyt and 0.12 *M* (0.04 *M* at low acid concentration) for Ura and Thy. The non-exchanging protons were assigned by using literature data (10) and by taking the C-6 (adjacent to N-1) proton to be less shielded than the C-5 proton. The Me protons of Thy appeared at high field and integrated 3 times the C-6 proton. The ^1H shifts of Cyt were corrected for bulk magnetic susceptibility (11) while those of Ura and Thy were not corrected since the internal reference used, Et_4NBF_4, is satisfactory in the range of acid concentrations used (11). The ^{13}C spectra were taken with H_2SO_4 solutions. For Hypy, H_2SO_4 was varied from 0 to 7.72 *M*. Dap was studied between 0 and 18 *M* H_2SO_4. For Cyt, the H_2SO_4 range was 0.18–18 *M* and for Ura and Thy, it was 6.3–18 *M*. For MeCyt two spectra were recorded, one in 1.8 *M* H_2SO_4 and the other in HSO_3F. The base concentrations were 0.30 *M* for Hypy, Ura, and Thy, 0.42 *M* for Dap, and 0.16 *M* for Cyt and MeCyt. The carbons of the bases were assigned by using off-resonance spectra and literature data on related compounds (9, 12).

The uv spectra were recorded on a 545 Perkin–Elmer spectrophotometer, and absorbances at a fixed wavelength were measured at 25°C on a PMQ II Zeiss spectrophotometer. Values were measured within 10 min of preparing the solutions because absorbances increased somewhat on standing. The uv samples were prepared by dissolving the

TABLE 1. Ultraviolet spectral data of uracil, thymine, and Dap

Base	$[H_2SO_4]$ (M)	λ_{max} (nm)	log ϵ_{max}
Ura	0	258, (258),[a] (259)[b]	3.92, (3.91),[a] (3.92)[b]
$UraH^+$	14.4, (10.3)[a]	276, (272)[a]	3.90, (3.82)[a]
Thy	0	263, (264)[b]	3.90 (3.89)[b]
$ThyH^+$	15.3	286.5	3.84
$DapH^+$	0.18	247.5	4.11
$DapH_2^{2+}$	10.1	244	4.08

[a]Reference 11.
[b]Reference 21.

solid bases in titrated acid solutions and diluting aliquots with the same titrated acid to give (1–2) $\times 10^{-4}$ M base concentrations.

Results

Chemical shifts

To illustrate the variations of the ^1H and ^{13}C shifts of the bases with increasing acidity and to discuss qualitatively the protonation reactions, the ^1H and ^{13}C shifts of Cyt, Ura, Thy, and Dap were initially plotted against H_0 (1). While all protons move downfield with increasing acidity, the carbons move either upfield or downfield. The plots of the ^1H chemical shifts against H_0 are for the most part sigmoid curves, indicative of base protonation. For Ura and Thy, which are present as the neutral bases in the more dilute acid solutions, the ^1H plots then correspond to the first protonation step when H_0 passes from −2.5 to −9.0, with half protonation H_0 values of −4.0 for Ura and −5.0 for Thy respectively. The ^{13}C plots generally confirm these results, though the initial part of the curves is missing because Ura and Thy are too weakly soluble below 6.3 M H_2SO_4 to record their ^{13}C spectra. The ^{13}C data further indicate for both bases the beginning of a second protonation step for H_0 below −8. Additional ^{13}C spectra of Ura and Thy, taken in 7% fuming H_2SO_4 ($H_0 = -12.7$) and HSO_3F ($H_0 = -14.2$), show large shifts and confirm the presence of $UraH_2^{2+}$ and $ThyH_2^{2+}$. For Cyt, which is present as $CytH^+$ at the lowest acid concentration used, the ^1H and ^{13}C shifts show the onset of a second protonation step for H_0 lower than −6.0 but no plateau is reached in 18 M H_2SO_4 ($H_0 = -10$), while the spectra for the ^{13}C shifts in 7% fuming H_2SO_4 and HSO_3F are identical and thus are likely to correspond to full protonation. Finally, for Dap, which is monoprotonated in the most dilute H_2SO_4 solutions used, the ^{13}C plot indicates a second protonation step with an H_0 value at half protonation of −1.5. Additional ^1H spectra were taken at −75°C on HSO_3F solutions of Cyt, Ura, and Thy. The NH_2 protons of Cyt as well as the NH protons of all hydroxypyrimidines were now observed but no OH signals corresponding to C=O protonation could be detected. The values obtained for the chemical shifts in these HSO_3F solutions differ from those reported by Wagner and von Philipsborn (3) by 2.5 ppm, probably because of different references.

Ultraviolet spectra

The H_2SO_4 concentrations corresponding to the spectra of the various neutral and protonated species of Ura, Thy, and Dap are given in Table 1 together with λ_{max}, the wavelengths of maximum absorption, and ϵ_{max}, the corresponding molar absorptivities. For Ura and Thy, our spectra are similar to those reported by Gukovskaya *et al.* (4) who, however, give no ϵ_{max} values. The λ_{max} and ϵ_{max} for $UraH^+$ given in ref. 7 differ slightly from ours because, for the medium used, 10.3 M H_2SO_4, formation of $UraH^+$ is not complete. The absorbances of Ura, Thy, and Dap solutions were determined between 0 and 18 M H_2SO_4. The plots of the absorbances, measured at 8 selected wavelengths, against H_0 also gave sigmoid curves. The shorter plateaus at high acidities for Ura and Thy suggest the onset of the second protonation.

TABLE 2. Protonation data for uracil and thymine

Base	pK_n (H_0)	pK_n m_0	pK_n (H_A)	pK_n m_A
	−3.97	2.33	−2.87	1.12
$UraH^+$	−3.50[a]	1.92[a]	−2.20[a]	1.39[a]
	−3.38[b]	1.89[b]	−2.98[c]	1.14[c]
$ThyH^+$	−5.47	2.12	−3.60	0.99
	−2.50[a]	2.13[a]	−1.90[a]	1.43[a]

[a]Reference 4.
[b]Reference 7.
[c]Reference 5.

Calculation of pK_n

Initially, to compare our data with the published data (4, 5, 7), values of pK_n for the various protonated species BH^{n+} were calculated for the acidity functions H_0 and H_A using the standard equations (1). Values for pK_n of $UraH^+$ and $ThyH^+$ for the H_0 and H_A acidity functions are presented in Table 2 together with the corresponding slopes m_0 and m_A. Subsequently, the values of pK_n were obtained by the excess acidity method (13). The program developed by Cox was used, as we described previously (1), to calculate the pK_n values given in Table 3[1] with their standard deviations and the refined values of δ_{n+} and $\delta_{(n-1)^+}$ listed in Tables 4 (^1H nmr) and 5 (^{13}C nmr) respectively. The uv data (absorbances A or molar absorptivities ϵ) were similarly treated. To check the absence of medium effect, pK values were also calculated from values of ΔA or $\Delta\epsilon$ corresponding to pairs of wavelengths (14). Both sets of pKs, calculated from A (or ϵ) and ΔA (or $\Delta\epsilon$) were identical within experimental error, so that large medium effects can be ruled out. This point is further strengthened by the good agreement between pK values obtained from uv and nmr data (Table 3).

Discussion

Ionization constants

First, let us compare our protonation data for $UraH^+$ and

[1]Complete sets of nmr, uv, and program data have been deposited and may be purchased from the Depository of Unpublished Data, CISTI, National Research Council of Canada, Ottawa, Ont., Canada K1A 0S2.

TABLE 3. pK_n and m^* values[1] and protonation sites for cytosine, uracil, thymine, and related bases

Base	pK_n (nmr) (m^*)	pK_n (uv) (m^*)	pK_n (lit.)	Protonation site
$CytH^+$	—	—	4.58[a]	N-3
$CytH_2^{2+}$	~ -6.4[b]	—	—	O-2
$UraH^+$	-2.35 ± 0.25 (0.45 ± 0.07)	-2.38 ± 0.08 (0.46 ± 0.05)	-2.07[c]	O-4
$UraH_2^{2+}$	—	—	-7.3[d]	O-2
$ThyH^+$	-3.08 ± 0.13 (0.45 ± 0.05)	-3.02 ± 0.06 (0.45 ± 0.05)	-1.60[c]	O-4
$ThyH_2^{2+}$	—	—	-6.8[d]	O-2
$DapH^+$	—	—	6.85[e]	N-1
$DapH_2^{2+}$	-1.58 ± 0.03 (0.83 ± 0.03)	-1.73 ± 0.13 (1.05 ± 0.15)	—	N-3
$HypyH^+$	0.77 ± 0.07	—	0.75,[f] 1.25[g]	O-2

[a]Reference 2.
[b]See text.
[c]Reference 4; pK calculated by the Bunnett–Olsen method (13).
[d]Reference 6; pK based on H_A acidity scale.
[e]Reference 1.
[f]Reference 22.
[g]Reference 23.

TABLE 4. ^1H shift values[a] (ppm) of neutral and protonated cytosine, uracil, and thymine

Base	N(1)H	N(3)H	C(5)H	C(6)H	CH_3(5)	NH_2(4)
$CytH^+$			6.53	7.90		
$CytH_2^{2+}$[b]	10.66	10.81	7.14	8.11		8.32
(−75°C)						
Ura			5.87	7.61		
$UraH^+$			6.70	8.30		
$UraH_2^{2+}$	11.60	12.34	7.50	8.84		
(−75°C)						
Thy				7.38	1.89	
$ThyH^+$				7.82	2.09	
$ThyH_2^{2+}$	?	12.29		8.66	2.63	
(−75°C)						

[a]Standard deviation usually better than 0.02 ppm.
[b]Estimated values; evidence of a large medium effect.

$ThyH^+$ with previous data (4, 5, 7). We note that the pK_1 values in Table 2 vary not only according to the acidity function selected but also according to the data used. For H_A, which on the basis of the slope m_A appears here to be the best acidity function, our pK_1 value of -2.9 for $UraH^+$ is in good agreement with -3.0, that of Poulter and Frederick (5), but in only passable agreement with -2.2 reported by Gukovskaya *et al.* (4). For $ThyH^+$, our pK_1 of -3.6 is at complete odds with -1.9, reported by the same group (4).

However, since our bases are different from the amides used to establish the H_A scale, we have selected the excess acidity method (13) to calculate the pK_n values that are listed in Table 3 together with the slopes m^*. We observed a good agreement between the values obtained by nmr and uv so that we can confidently reject the previously quoted pK_1 for $ThyH^+$ (4). Furthermore, the lower acidity found for $UraH^+$ ($pK_1 = -2.4$) compared with that of $ThyH^+$ ($pK_1 = -3.0$) is in agreement with what is expected from a methyl group (Thy is 5-methyluracil) in a conjugated system and in a position α to a protonated carbonyl on C-4, and, as we shall see, the proton in $ThyH^+$ is on O=C-4. For $CytH_2^{2+}$, our pK_2 of -6.4 is approximate and based on H_A because of the paucity of data at high acidities. It is worth noting that the differences between the pK_2 and pK_1 values in Table 3 indicate for $CytH^+$ a much stronger stabilization than for $UraH^+$, $ThyH^+$, and $DapH^+$, so that there must be additional factors to the conjugation of the amino group on C-4 with the ring, on protonation, to account for the increased stability of $CytH^+$. On the other hand, values of -NH deprotonation pK_0 (not reported here) for Cyt, Ura, and Thy show that this time neutral Ura and Thy are much more stabilized than Cyt with respect to deprotonation and monoprotonation. A comparison of first protonation data in solution with theoretical protonation energies and experimental gas phase proton affinities will be made later in a comparison of a larger series of nucleic acid bases.

Our ^{13}C nmr data have an interesting consequence. Previous researchers have used, for structural determinations, ^1H and ^{13}C nmr data obtained on trifluoroacetic (TFA) solutions of Ura (3) and Dap (15) with the assumption that $UraH^+$ and $DapH^+$ respectively were the species present in TFA. On the basis of our data, we calculate for TFA solutions $Ura/UraH^+ = 20:1$ and $DapH^+/DapH_2^{2+} = 3:1$. It is clear that when working with polyfunctional bases such as pyrimidines, dissolving the bases in one acid solvent and attributing to a single species the observed chemical shifts may be misleading.

Protonation sites

The values of pK_1 and pK_2 given for Cyt in Table 3 suggest that the first protonation of Cyt is likely to be on N-1 while its second protonation (and also both protonations of Ura and Thy) takes place on the exocyclic C=O. However, the ^{13}C data in Table 5 and particularly the direction and magnitude of the shifts on protonation give additional information on the protonation sites. First, for Dap, where there is only nitrogen protonation, we note that the first protonation expected on N-1 for this 4-aminopyrimidine (15) is indeed accompanied by an upfield

TABLE 5. ^{13}C shift values[a] (ppm) of neutral and protonated cytosine, uracil, thymine, and related bases

Base	C-2	C-3	C-4	C-5	C-6		
Cyt[b]	158.12		167.90	93.75	143.96		
$CytH^+$[b]	149.14		161.41	94.00	148.00		
$CytH^+$	150.19		161.03	95.80	147.60		
$CytH_2^{2+}$	155.4		158.3	105.4	145.2		
Ura	154.1		168.6	102.3	144.2		
$UraH^+$	150.3		171.6	97.3	153.9		
$UraH_2^{2+}$[c]	154.3		171.6	105.6	155.0		
						$CH_3(5)$	
Thy	154.04		168.71	111.93	140.66	12.52	
$ThyH^+$	150.86		169.60	109.72	150.57	11.96	
$ThyH_2^{2+}$[c]	154.3		169.6	117.8	151.0	12.0	
						$CH_3(2)$	$CH_3(6)$
Dap	167.08		164.31	102.18	165.55	24.59	23.06
$DapH^+$	163.58		165.70	102.99	156.29	21.75	18.91
$DapH_2^{2+}$	164.24		156.80	108.31	159.28	19.64	20.07
Hypy	165.33	119.54	144.84	110.20	135.94		
$HypyH^+$	160.66	115.24	149.73	118.59	137.91		
						$CH_3(1)$	
$MeCytH^+$	150.31		160.59	95.04	151.55	37.87	
$MeCytH_2^{2+}$	154.36		157.45	104.30	150.67	40.71	

[a]Standard deviation usually better than 0.10 ppm.
[b]Spectra recorded in Me_2SO.
[c]Estimated from our data and pK_2 values (6).

shift of C-2 and C-6, which are adjacent to the protonation site N-1; this is in accordance with the α effect observed by Pugmire and Grant (16) on five- and six-membered heterocycles. We also note, however, that for the second protonation of Dap on N-3, while the adjacent C-4 also moves upfield, the adjacent C-2 has this time a small downfield shift. This must be related to the presence of the first proton on N-1. Then for Cyt, we observed an upfield shift of C-2 (−8.9 ppm) and C-4 (−6.5 ppm) in line with a first protonation on N-3. This N-3 protonation of Cyt parallels that of cytidine, the nucleoside derived from Cyt, where the corresponding ^{13}C shifts are −8.6 ppm (C-2) and −6.1 ppm (17). Furthermore, we can state that the first protonation of Cyt occurs exclusively at N-3 since our C-2 and C-4 protonation shifts are very close to the average N-3 methylation shifts (−8.5 ppm (C-2) and −6.7 ppm (C-4)) found for cytidine and deoxycytidine (12*a*). Concerning the second protonation of Cyt, obviously occurring on the carbonyl O=C-2, we observe not only the expected downfield shift of C-2 (+5.2 ppm), which is admittedly much smaller than the +30-ppm shifts reported for aliphatic ketones (18), but, as well, a larger ≈9.6-ppm downfield shift of C-5 emphasizing the importance of conjugation effects in the pyrimidine ring. The ^{13}C shifts for $MeCytH^+$ (Table 5) and the protonation shift for $MeCytH_2^{2+}$ are very close to those found for the corresponding Cyt cations (except for C-6 adjacent to the methyl group) and thus confirm the exclusive second protonation of the carbonyl O=C-2, so that there is no need to postulate the presence of a tautomeric monocation $^+HO{=}C\text{-}2$ (3).

Let us now turn to the assignment of the protonation site in both $UraH^+$ and closely related $ThyH^+$. It is generally agreed that the most stable monocation $UraH^+$ is that which is protonated at O-4 (3, 5, 19, 20). Our ^{13}C data for $UraH^+$, $UraH_2^{2+}$, $ThyH^+$, and $ThyH_2^{2+}$ in Table 5 support this assignment. To begin with, the first protonation at O-4 and the second one at O-2 are in line with the expected downfield protonation shifts of the affected carbonyl carbons, first C-4 for $UraH^+$ (+3.0 ppm) and for $ThyH^+$ (+0.9 ppm because of the α methyl group), then C-2 for $UraH_2^{2+}$ (+4.0 ppm) and $ThyH_2^{2+}$ (+3.2 ppm), which may be compared with C-2 for $CytH_2^{2+}$ (+5.2 ppm). The reverse order for the carbonyl protonation (O-2 then O-4) would not lead to downfield shifts. The large downfield shift of C-5 (+5.2 ppm) in the *para* position, observed with the unambiguous C=O protonation of $CytH^+$ at C-2, is also observed for the protonation at O-2 in $UraH_2^{2+}$ (+8.3 ppm) and $ThyH_2^{2+}$ (+8.1 ppm). While a downfield protonation shift of C-5 (+8.9 ppm) is also found for the O-2 protonation of tautomerized Hypy, originally taken as our model compound, the carbonyl C-2 of Hypy undergoes an unexpected upfield shift upon protonation, thus emphasizing the difficulties inherent in the choice of a model compound, Hypy apparently not being a good model for hydroxypyrimidines, possibly because of different conjugation effects.

Acknowledgements

The authors gratefully acknowledge the financial assistance of the Natural Sciences and Engineering Research Council of Canada and of the Ministère de l'Education du Québec. One of us (R.L.B.) wishes to thank Professor F. Terrier and Dr. J. C. Hallé for valuable discussions and Professor R. Schaal for his warm hospitality at Université Pierre et Marie Curie during a sabbatical leave when this manuscript was written.

1. R. L. BENOIT and M. FRECHETTE. Can. J. Chem. **63**, 3053 (1985), and references therein.
2. R. M. IZATT, J. J. CHRISTENSEN, and J. H. RYTTING. Chem. Rev. **71**, 339 (1971).
3. R. WAGNER and W. VON PHILIPSBORN. Helv. Chim. Acta, **53**, 299 (1970).

4. A. S. GUKOVSKAYA, B. I. SUKHARAKOV, T. M. PROKOPEVA, and V. L. ANTONOVSKI. Bull. Acad. Sci. USSR, **21**, 2614 (1972).
5. C. D. POULTER and G. D. FREDERICK. Tetrahedron Lett. **26**, 2171 (1975).
6. G. D. FREDERICK and D. POULTER. J. Am. Chem. Soc. **97**, 1797 (1975).
7. A. R. KATRITZKY and A. J. WARING. J. Chem. Soc. 1540 (1962).
8. C. J. POUCHERT. The Aldrich library of NMR spectra. 2nd ed. Vol. 1. Aldrich Chemical Co., Milwaukee. 1983. pp. 2 and 324.
9. R. J. ABRAHAM and P. LOFTUS. Proton and carbon-13 NMR spectroscopy. Heyden, London. 1980. pp. 14, 28–31, and 145.
10. C. D. JARDETZKY and O. JARDETZKY. J. Am. Chem. Soc. **82**, 222 (1960).
11. T. A. MODRO, W. F. REYNOLDS, and K. YATES. Can. J. Chem. **54**, 1439 (1976).
12. (*a*) C. CHANG, D. J. ASHWOTH, L. CHERN, J. DASILVA GOMES, C. LEE, P. W. MOU, and R. NARAYAN. Org. Magn. Reson. **22**, 671 (1984); (*b*) A. J. JONES, D. M. GRANT, M. W. WINKLEY, and R. K. ROBINS. J. Am. Chem. Soc. **92**, 4079 (1970).
13. R. A. COX and A. YATES. Can. J. Chem. **61**, 2225 (1983), and references therein; V. LUCCHINI, G. MODENA, G. SCORRANO, R. A. COX, and K. YATES. J. Am. Chem. Soc. **104**, 1958 (1982).
14. R. STEWART and M. R. GRANGER. Can. J. Chem. **39**, 2508 (1961).
15. J. RIAND, M. TH. CHENON, and N. LUMBROSO-BADER. J. Am. Chem. Soc. **99**, 6838 (1977).
16. R. J. PUGMIRE and D. M. GRANT. J. Am. Chem. Soc. (*a*) **90**, 697 (1968); (*b*) **90**, 4232 (1968).
17. L. KOZERSKI, H. SIERPUTOWSKA-GRACZ, W. KRZYZOSIAK, M. BRATEK-WIEWIOROWSKA, M. JASKOLSKI, and M. WIEWIOROWSKI. Nucleic Acids Res. **12**, 2205 (1984).
18. R. A. MCCLELLAND and W. F. REYNOLDS. Can. J. Chem. **54**, 718 (1976).
19. J. E. DEL BENE. J. Phys. Chem. **87**, 367 (1983).
20. S. MIERTUS and M. TREBATICKA. Collect. Czech. Chem. Commun. **48**, 3517 (1983).
21. A. TOTH and F. BILLES. Acta Chim. Acad. Sci. Hung. **56**, 229 (1968).
22. E. KLINSBERG. Heterocyclic compounds. Pyridines and derivatives. Part III. Interscience Publishers, New York. 1962.
23. C. G. SWAIN anbd J. F. BROWN. J. Am. Chem. Soc. **74**, 2538 (1952).

Electrostatic interactions as a factor in the determination of the HOMO in the liquid state

ENRIQUE SÁNCHEZ MARCOS AND JOAQUÍN MARAVER
Departamento de Química Física, Facultad de Química, Universidad de Sevilla, Tramontana s/n, Sevilla 41071, Spain

MANUEL F. RUÍZ-LÓPEZ
Laboratoire de Chimie Théorique, Université de Nancy I, Unité de Recherche associée au CNRS, No. 510, 54506 Vandoeuvre Les Nancy Cedex, France

AND

JUAN BERTRÁN
Departamento de Química Física, Facultad de Ciencias, Universidad Autónoma de Barcelona, Bellaterra, Barcelona, Spain

Received March 19, 1986

ENRIQUE SÁNCHEZ MARCOS, JOAQUÍN MARAVER, MANUEL F. RUÍZ-LÓPEZ, and JUAN BERTRÁN. Can. J. Chem. **64**, 2353 (1986).

An ellipsoidal cavity model has been used to study the energy changes in occupied molecular orbitals induced by solute–solvent electrostatic interactions. Some benzene derivatives have been selected as solutes. Calculations have been carried out at the CNDO and *ab initio* STO-4G levels. Important variations in the molecular orbital sequence, involving a change in the HOMO nature, have been observed. A perturbation analysis is employed to understand the orbital evolution from gas phase to solution.

ENRIQUE SÁNCHEZ MARCOS, JOAQUÍN MARAVER, MANUEL F. RUÍZ-LÓPEZ et JUAN BERTRÁN. Can. J. Chem. **64**, 2353 (1986).

On a utilisé un modèle à cavité ellipsoïdale pour étudier les changements énergétiques dans des orbitales moléculaires occupées, qui sont induits par des interactions électrostatiques soluté/solvant. On a choisi quelques dérivés benzéniques comme solutés. On a effectué des calculs aux niveaux CNDO et STO-4G *ab initio*. On a observé des variations importantes, impliquant un changement dans la nature de OM haute occupée, dans le cheminement des orbitales moléculaires. On a utilisé une analyse de perturbations pour comprendre l'évolution orbitale de la phase gazeuse à la solution.

[Traduit par la revue]

Introduction

The concept of frontier orbital (1) has been widely used in theoretical studies of chemical reactivity (2). The use of this static index can be theoretically justified by a perturbation treatment of intermolecular interactions (3, 4).

It has been rather general to apply Fukui's idea of frontier orbital from calculations where the molecules are isolated. However, chemical reactions of practical interest are usually performed in the liquid state.

The recent techniques of ICR (5), which permit the study of gas phase reactions, have shown the important variations that such processes can present when they are compared with the corresponding ones in the condensed phase. Therefore realistic values of the reactivity indexes are not easily derived in a scheme in which the solute–solvent interactions are neglected.

Two basic approaches are generally applied to these interactions. The first simulates the solvent by a limited number of solvent molecules which are placed around the solute, and is known as the supermolecule model (6). In the other approach, the solute is confined in a cavity surrounded by a dielectric continuum representing the solvent, which is characterized by a macroscopic quantity, i.e. the dielectric permittivity. Electrostatic interactions, which result from the polarization of the continuum in the presence of the solute charge distribution, can then be incorporated into the solute hamiltonian (7–11).

Several papers have been devoted to the study of the solvent effects on the frontier orbitals of a given molecule. Klopman (12) used the solvation model to predict the relative order or hard and soft Lewis acids and bases and nucleophilic or electrophilic reagents in a liquid. The influence of the solvent on electron affinities of cations has also been investigated (13). Other studies have considered systems including specific interactions (14–16) by using the supermolecule model. More recently, a cavity model, in which the electrostatic part of the solute–solvent interactions is computed by a multipole expansion of the electron distribution of the solute molecule, has been employed to analyze the role of these interactions in the frontier orbital energies of several small molecules, anions, and cations (17). This work was able to explain the changes in reactivity of various species when going from the gas phase into solution.

Apart from the crude representation of the solvent by a continuum, which has been discussed previously (18–20), the great limitation of the model employed by these authors is the use of a spherical cavity which makes it difficult to extend such calculations to molecules differing in spherical shape. This limitation can be overcome by the use of cavities fitting any molecular shape (7, 21). The application of such cavities is not very general owing to the fact that the electrostatic equations have to be integrated numerically. Constant coordinate cavities have been introduced because they allow analytic expressions for the electrostatic potential.

The use of a three-axes ellipsoidal cavity has recently been developed (22, 23). The equations derived allow us to write the perturbation hamiltonian in a form very similar to the expression obtained for the spherical cavity.

In this paper, the ellipsoidal cavity model has been employed in order to study the influence of the electrostatic solute–solvent interactions on a molecular orbital set of some molecules whose shape can not be fitted by a spherical cavity. The main aim of this work is to analyze the evolution of the HOMO on changing the medium. Given that strong solute–solvent interactions may be expected in some cases, a possible change in the nature of the HOMO should be envisaged. Therefore, we are interested in

analyzing the evolution of other occupied molecular orbitals. The molecules considered are some benzene derivatives. For such species the HOMO plays an important role in electrophilic substitution in which strong solvent effects have been emphasized.

Method of calculation

The method used to study the solvent effect is based on the spherical cavity model derived by Kirkwood, which has been adapted to quantum chemical calculations by Rivail and Rinaldi (8), and more recently extended to the use of three constant coordinate cavities (22, 23). This model has been widely used to evaluate solvation energies and solvent effects on molecular properties and has proved to be useful in the predictions of experimental values (24).

The Hartree–Fock equations for a solvated molecule are written

$$[1] \quad F_{\mu\nu} = F^0_{\mu\nu} + \sum_{l=0}^{\infty} \sum_{m=-l}^{+l} R_l^m \langle \mu | M_l^m | \nu \rangle$$

where M_l^m is a component of the spherical multipole moment of order l corresponding to the solute electron distribution and R_l^m is a component of the so-called reaction field. In the case of a spherical cavity these terms can be expressed in the simple form

$$[2] \quad R_l^m = f_l M_l^m$$

where f_l is the reaction field factor

$$[3] \quad f_l = \frac{(l+1)(\epsilon - 1)}{(l+1)\epsilon + l} \frac{1}{a^{2l+1}}$$

In the case of an ellipsoidal cavity the reaction field is written in a more involved form. Each component R_l^m is now expressed as a linear combination of spherical moments $M_{l'}^{m'}$ of the same parity and of the order $l' \leqslant l$, so that the reaction field factor adopts a tensorial form. Accordingly, one can write

$$[4] \quad R_l^m = \sum_{l'} \sum_{m'} F_{ll'}^{mm'} M_{l'}^{m'}$$

Detailed expressions for all these operators can be found in the original references (22, 23, 25).

The change in the solute molecular orbital levels where the solvent is considered is a consequence of two effects. First, the electrostatic interactions of the molecular orbital electron distribution with the reaction field, which modifies the initial eigenvalues, e_i^0, in the form

$$[5] \quad e_i = e_i^0 + \sum_{l,m} \langle R_l^m \rangle \sum_{\mu\nu} \langle \mu | M_l^m | \nu \rangle c_\mu^i c_\nu^j$$

Secondly, the polarization of the molecular wavefunction is a result of the non-homogeneous electric field. This effect can be taken into account by making a SCF calculation in which the total energy is minimized.

The results presented in this paper have been obtained by considering both electrostatic and polarization effects, i.e., SCF calculations where the total hamiltonian includes the solute – dielectric continuum interaction term. An attempt at interpretation of these results has been made by using the first-order perturbation theory which supplies a suitable picture to understand how the orbitals of isolated molecules are modified by the long-range solute–solvent electrostatic interactions.

The molecular geometries have been obtained by minimizing the total energy using the CNDO/2 method (26) and the wavefunctions have been evaluated by the CNDO/S technique (27). The calculations were performed by means of the GEOMO program (28), in which the electrostatic solute–solvent interaction, as described above, has been implemented. In the case of the benzoate anion, an additional *ab initio* calculation was made using a modified version (23) of the GAUSSIAN 76 program (29) including the method of cavity of Rivail and Rinaldi.

The volume of the cavities is taken as equal to the molecular volume of the pure liquid at room temperature. In the case of the anions the volume corresponding to their neutral molecule has been taken (17, 30).

Results

In a first step we will focus on the π MO's of the benzene derivatives (benzaldehyde, benzoic acid, nitrobenzene, benzoate anion, and phenolate anion). Table 1 shows the orbital energies in gas phase, $e(\epsilon = 1)$, for every occupied π orbital. In all cases the HOMO in the gas phase is the 1π orbital. From a second SCF calculation where the solute–solvent electrostatic interactions are taken into account (assuming $\epsilon = 78.0$), the MO's energies, $e(\epsilon = 78)$, have been obtained. The energy changes for the occupied π MO's, $\Delta e = e(\epsilon = 78) - e(\epsilon = 1)$ have also been included in Table 1. It is seen that these changes are very different for each orbital, even in the same molecule, and affect the Δe sign in some cases. Moreover, there are HOMO changes when the dielectric permittivity goes from 1 to 78.

We will begin analyzing the sign of Δe. A neutral solute must be chosen because in a charged solute the Born term is the main contribution leading to a global stabilization in all occupied MO's. Thus, Fig. 1 shows the scheme of the five occupied π MO's of nitrobenzene. This solute has been selected because its symmetry will simplify the discussion. 1π and 2π are the formerly degenerated orbitals of benzene, 3π is an oxygen lone pair orbital (non bonding, n), 4π is an orbital with nodal plane between the ring and the substituting group and 5π is the most stable bonding orbital. The dipolar interaction is the most important contribution to the stabilization energy of nitrobenzene given the strong dipole moment of this molecule. The molecular dipole moment, $\boldsymbol{\mu}_T$, and its associated reaction field term, $\boldsymbol{R}_1$, have the same direction as the C_2 molecular axis. The orbitals with high electron density in the oxygen atoms, 3π and 5π, give rise to orbital dipole moments parallel to $\boldsymbol{\mu}_T$, and so are stabilized when the dielectric permittivity goes from 1 to 78. On the contrary, the 1π, 2π, and 4π orbitals have the highest orbital coefficients associated with the ring atoms, giving rise to orbital dipole moments that go in the direction opposite to $\boldsymbol{\mu}_T$, thus their interactions with the reaction field are destabilizing.

Benzoic acid and benzaldehyde can be analyzed in the same way. Thus, we have predicted the sign of Δe for every studied π orbital of the neutral molecules considering only the dipolar interaction (Table 2). Comparing these results with those shown in Table 1, a good qualitative agreement is found except for the benzaldehyde 1π orbital. This case will be studied later.

A second fact deduced from Table 1 is the change in HOMO nature with the increase of the dielectric permittivity. Thus, at $\epsilon = 78$ the new HOMO is the 2π orbital for benzaldehyde and benzoic acid, and the 3π orbital for the benzoate anion. In the two former cases 2π was already the (HO-1)MO in gas phase, and therefore the crossing is only between π orbitals. However, in the crossing of the benzoate anion, σ orbitals are involved.

Figure 2 shows energy changes in the five higher occupied MO's of benzoate anion vs. dielectric permittivity. For charged solutes, the Born term, $l = 0$, is the main contribution to the

TABLE 1.[a] SCF results

Molecule		Energy 1π	2π	3π	4π	5π
Benzaldehyde	$e(\epsilon = 1)$	−0.3762	−0.3788	−0.5051	−0.5740	
	$e(\epsilon = 78)$	−0.3764	−0.3697	−0.5230	−0.5912	
	Δe	−0.0002	+0.0091	−0.0179	−0.0172	
Benzoic Acid	$e(\epsilon = 1)$	−0.3769	−0.3778	−0.4786	−0.5493	−0.6630
	$e(\epsilon = 78)$	−0.3664	−0.3657	−0.4833	−0.5316	−0.6414
	Δe	+0.0105	+0.0121	−0.0047	+0.0177	+0.0216
Nitrobenzene	$e(\epsilon = 1)$	−0.3935	−0.3983	−0.4358	−0.5559	−0.7187
	$e(\epsilon = 78)$	−0.3742	−0.3802	−0.4716	−0.5388	−0.7377
	Δe	+0.0193	+0.0181	−0.0358	+0.0171	−0.0190
Benzoate Anion	$e(\epsilon = 1)$	−0.2191	−0.2459	−0.2585	−0.3811	−0.4462
	$e(\epsilon = 78)$	−0.4709	−0.3736	−0.3732	−0.5319	−0.6345
	Δe	−0.2518	−0.1277	−0.1147	−0.1508	−0.1883
Phenolate Anion	$e(\epsilon = 1)$	−0.1524	−0.2297	−0.3040	−0.4107	
	$e(\epsilon = 78)$	−0.3200	−0.3744	−0.4745	−0.5754	
	Δe	−0.1676	−0.1447	−0.1705	−0.1647	

[a]Atomic units. Energies of the occupied π MO's for the isolated molecule, $e(\epsilon = 1)$, and the molecule introduced in a continuum of $\epsilon = 78$, $e(\epsilon = 78)$. Δe is the MO energy gap, $e(\epsilon = 78) - e(\epsilon = 1)$.

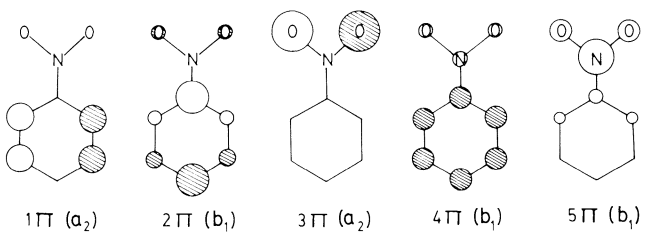

FIG. 1. Occupied π MO's of nitrobenzene.

TABLE 2. Estimates of Δe sign by comparing each orbital dipole moment with the total dipole moment (+ destabilizing effect, − stabilizing effect)

Molecule	Δe sign 1π	2π	3π	4π	5π
Benzaldehyde	+	+	−	−	
Benzoic acid	+	+	−	+	+
Nitrobenzene	+	+	−	+	−

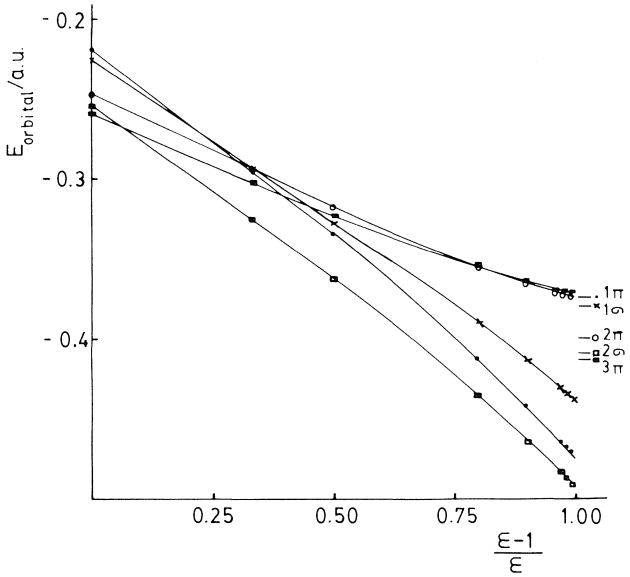

FIG. 2. Orbital energy evolution for the five higher occupied MO's of benzoate anion as a function of the dielectric permittivity. (The lines on the right hand represent the energy level that should have each MO if only the Born term was considered).

orbital energy change. This term affords a stabilizing and constant contribution for all occupied MO's, therefore the crossing between the MO's appearing in Fig. 2 have to be originated by the different kinds of interactions of each MO with the higher moments of the Reaction Field. Thus, 1π, 1σ, and 2σ are strongly stabilized (a larger extent than the Born contribution) while 2π and 3π are stabilized less than that corresponding to $l = 0$ term, i.e., the multipole terms give a destabilizing contribution to the MO energy. To explain these differential behaviors, in Fig. 3 the electron density of the benzoate anion MO's have been shown. Keeping in mind the constant contribution of the charge term, the relative energy changes can be explained by taking into account the dipole moments as done for neutral molecules, i.e., 2π and 3π have

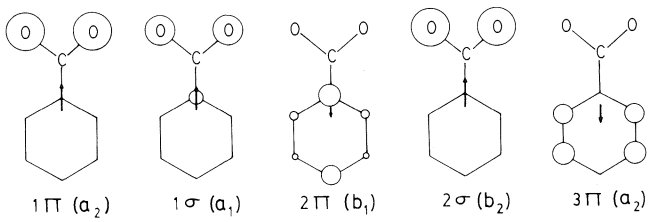

FIG. 3. Electron densities and orbital dipole moments of the five higher occupied MO's of benzoate anion.

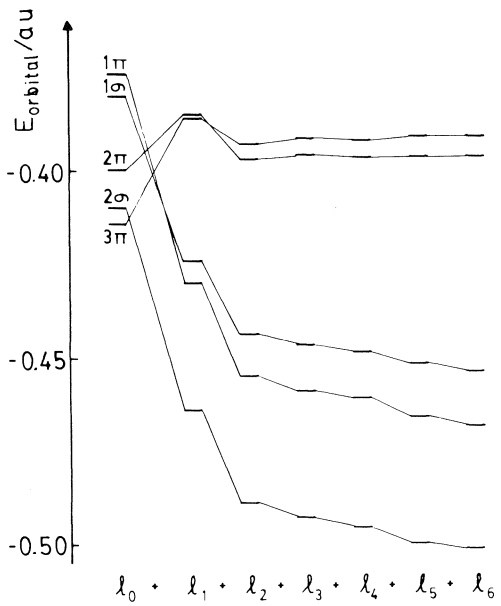

FIG. 4. Energy contribution, obtained by means of eq. [5], of each polar term to the five higher occupied MO's of benzoate anion.

TABLE 3.[a] Contributions of the first two polar moments to the 1π and 2π orbitals of benzaldehyde, obtained by means of the perturbational approach

	Contribution	
Polar moment	1π	2π
l_1	+0.0031	+0.0072
l_2	−0.0034	+0.0019

[a]Atomic units.

orbital dipole moments which point in the opposite direction from μ_T, while those of 1π, 1σ, and 2σ are parallel to μ_T.

A similar analysis may be applied to the phenolate anion. The 2π orbital, the one less stabilized due to the positive contribution to Δe of terms $l > 1$, corresponds to the benzoate anion 3π orbital, and the most stabilized one is 3π, an orbital with high electron density in the oxygen atom.

Nevertheless, the previous analysis does not allow the prediction of the orbital inversion but rather a qualitative idea of the energy gap between the different MO's. For this reason, to give a more quantitative estimate of the multipole moment effect, we have calculated the energy contribution of each multipolar term from eq. [5], in a perturbational way. A localized charge distribution in each atom has been taken. In Fig. 4 the energy vs. the l-polar term have been plotted for the MO's of the benzoate anion. A crossing appears for the dipolar term, l_1, but the order of orbitals does not match the sequence obtained by SCF calculations. To achieve this sequence the contribution of the quadrupolar term, l_2, must be taken into account. The terms higher than l_2 are small and do not alter the energy order.

A similar calculation has been carried out for benzaldehyde, and in Table 3 the contributions of the first two moments to the 1π and 2π orbitals are gathered. In this case the quadrupolar term cancels the dipolar one for the 1π orbital, changing our initial provisions. It must be pointed out that both contributions are nearly the total energy change shown in Table 1.

Finally, in order to test the charge distribution obtained by CNDO/S we have performed *ab initio* calculations of the benzoate anion using the STO-4G basis for $l = 1$ and $l = 78$. Table 4 shows the orbital energy variations obtained by means of CNDO/S and STO-4G, subtracting the constant contribution of the charge term.

Discussion

Solvation phenomenon is usually thought of as a unique effect, generally stabilizing, over the molecular system introduced in the condensed medium. In a cavity model the effect of solvation is envisaged as the interaction between the total charge distribution of the solute and the electrostatic potential generated by the reaction field of the polarized dielectric continuum within the cavity.

Given that the reaction field is generated by the charge distribution of the solute, it has the appropriate symmetry to lead to a global stabilizing interaction. Nevertheless, the charge distribution is not always the same in an orbital as in the whole molecule. Consequently, energy gaps of different sign may appear within the MO set. The estimate of Δe is not obvious in all cases. In a first approach the sign of the effect can be deduced taking into account the dipole moment, specially when this is the most important moment generated by the charge distribution, i.e. nitrobenzene. Thus, MO's with high contributions of electronegative atom orbitals, for instance the lone pair 3π orbital of nitrobenzene, show a strong stabilizing effect, since their dipole moment is parallel to the total dipole moment. On the other hand, MO's with high coefficients associated with the ring atom orbitals show a destabilizing effect because they have an orbital dipole moment whose direction is opposite to that of molecular dipole moment, i.e. the formerly degenerated π orbitals of benzene 1π, and 2π in nitrobenzene.

Nevertheless, this simple approach does not predict the solvation effect on the MO set when the solute does not have a strong dipole moment or when an orbital inversion takes place. In both cases a more thorough estimate of Δe using higher multipole moments must be carried out. As has been shown in the previous section, a perturbational analysis gives values of Δe near to the variational ones of Table 1. Calculations for the benzoate anion and benzaldehyde show that on considering the multipole expansion as far as the quadrupole moment, the results obtained agree quite well with those of SCF calculations. On introducing higher moments, small corrections to the final energy are obtained indicating the convergence of multipole expansion. Usually, good descriptions of solvation phenomena may be achieved with the main and the next two l-pole moments.

The small changes in the MO coefficient set observed when ϵ goes from 1 to 78 point out the minor role of polarization phenomena (31). It explains why our solvation energy estimates from perturbational calculations correlate quite well with the results obtained by SCF calculations. However, the behavior of the dipole expansion and its associated polarization phenomena are not general, due to the fact that a minimal basis set is used in all cases. This point will be dealt with below.

Changes in HOMO nature due to solvent effects may involve important alterations in chemical reactivity. For instance, Fig. 5 shows the shape of benzaldehyde HOMO in gas phase and condensed phase for $\epsilon = 78$. The orbital inversions found cause changes in the most suitable centers for electrophilic

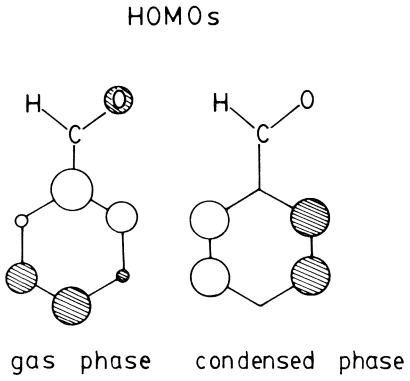

FIG. 5. HOMO's of benzaldehyde.

TABLE 4.[a] SCF results

MO	Orbital energy	
	CNDO/S	STO-4G
1π	−0.0968	−0.0638
1σ	−0.0541	−0.0510
2π	+0.0270	+0.0140
2σ	−0.0716	−0.0604
3π	+0.0403	+0.0326

[a]Atomic units. Orbital energy variations in benzoate anion are obtained by subtracting the Born term, $\Delta e' = \Delta e - I_0$.

substitution reactions if the conditions favor an orbital control. Nevertheless, a small energy gap between the HOMO donor level and the LUMO acceptor level is required for a frontier-controlled reaction. Therefore, in addition to the changes caused by the solvent in the MO set, the influence of solvation on the HOMO–LUMO gap must be kept in mind.

For the anions there is a loss of orbital control because the solvation strongly decreases all occupied orbital energies. However, reactions involving soft nucleophiles can allow a partial charge transfer which could make the HOMO play a more important role as the reaction progresses (1). This situation will be favored by the partial desolvation needed in reactant approximation, as Klopman has recently suggested (32).

For neutral molecules, there is a weaker influence of the solvent on the MO energies, since the strong stabilizing contribution of the Born term does not appear. Therefore, HOMO inversion may take place without a significant decrease in orbital control. On the other hand, the weak effect of the solvent prevents a great HOMO-(HO-1)MO energy gap. Nevertheless, following Fukui's principle of narrowing of inter-frontier level separation (1), the reaction progress will favor the increase of localized electron density over the interacting centers and it will increase the relative weight of HOMO within the MO set (33).

Analogous deductions were made from a solvation study of these molecules with the supermolecule model (34) using H_2O and HF as solvents. This similarity implies that specific and electrostatic solute–solvent interactions have common factors which must be linked to the properties of the solute more than to those of a particular solvent. Nevertheless, keeping in mind that hydrogen bonding itself is electrostatic to a large extent (31, 35), and that the solutes considered form strong hydrogen bonds in the supermolecule, one may deduce that the discrete study represents a limit of the specific interactions close to the interactions detailed by the continuum model.

For this explorative work we have chosen a semiempirical quantum chemical method because of its relatively low computational time. The CNDO method gave reasonable electron distribution (36) and afforded quite good answers to a number of problems in which the influence of the solvent on chemical and spectroscopy phenomena was under study (37). The *ab initio* calculations performed on the benzoate anion support this hypothesis, as shown in Table 4. The use of a minimal basis set probably underestimates the electronic effects derived from higher harmonics. However, in the cases studied these contributions do not imply large modifications in the effects, owing to the high values of the first terms of the multipole moment. Another problem is that the diffuse nature of the charge density of anions is rendered rather poorly by a minimal basis set. In any case, the picture given in this work may be a good starting point for more accurate calculations. The use of more complete basis sets is needed to supply a more correct representation of the electrostatic solute–solvent interactions. In order to get a deeper insight into the behavior of the multipole expansion and the role of the polarization phenomena, *ab initio* calculations using double-ζ and diffused basis sets are in progress.

Acknowledgments

We would like to thank Professor J. L. Rivail for his warm hospitality and helpful advice during the stay of E.S.M. at Laboratoire de Chimie Theorique in Nancy.

1. K. FUKUI. Top. Curr. Chem. **15**, 1 (1970); K. FUKUI, T. YONEZAWA, and K. SHINGU. J. Chem. Phys. **20**, 722 (1952); K. FUKUI. Angew. Chem. Int. Ed. **21**, 801 (1982).
2. I. FLEMING. Frontier orbitals and organic chemical reactions. 2nd ed. John Wiley and Sons, London. 1978.
3. G. KLOPMAN and R. F. HUDSON. Theor. Chim. Acta, **8**, 165 (1967).
4. L. SALEM. J. Am. Chem. Soc. **90**, 543 (1968); **90**, 553 (1968).
5. W. N. OLMSTEAD and J. I. BRAUMAN. J. Am. Chem. Soc. **97**, 6967 (1975); D. H. AUE and M. T. BOWERS. *In* Gas phase ion chemistry. Vol. II. *Edited by* M. T. Bowers. Academic Press, New York. 1979. Chapt. 9; K. TAKASHIMA and J. M. RIVEROS. J. Am. Chem. Soc. **100**, 6128 (1978).
6. A. PULLMAN and B. PULLMAN. Quart. Rev. Biophys. **7**, 505 (1975); P. SCHUSTER, W. JAKUBETZ, and W. MARIUS. Top. Curr. Chem. **60**, 1 (1975); A. PULLMAN. *In* "Quantum theory of chemical reactivity." Vol. II. *Edited by* R. Daudel, A. Pullman, L. Salem, and A. Veillard. Reidel Publishers, Dordrecht. 1980. pp. 1–24.
7. M. J. HURON and P. CLAVERIE. J. Phys. Chem. **76**, 2123 (1972); **78**, 1853 (1974).
8. J. L. RIVAIL and D. RINALDI. Chem. Phys. **18**, 233 (1976).
9. S. HILTON-MCGREERY, R. E. CHRISTOFFERSEN, and G. C. HALL. J. Am. Chem. Soc. **98**, 7191 (1976).
10. P. CLAVERIE, J. P. DAUDEY, J. LANGLET, B. PULLMAN, D. PIAZZOLA, and M. J. HURON. J. Phys. Chem. **82**, 405 (1978).
11. O. TAPIA and R. CONSTANCIEL. Theor. Chim. Acta, **48**, 75 (1978).
12. G. KLOPMAN. J. Am. Chem. Soc. **90**, 223 (1968).
13. C. DECORET, J. ROYER, and O. CHALVET. Tetrahedron, **31**, 973 (1975).
14. C. MINOT and N. T. ANH. Tetrahedron Lett. **45**, 3905 (1975).
15. V. IORERO, J. BERTRÁN, and J. I. FRNÁNDEZ-ALONSO. *In* Progress in theoretical organic. Vol. II. *Edited by* I. G. Csizmadia. Elsevier, Amsterdam. 1977. p. 310.

16. W. L. JORGENSEN. J. Am. Chem. Soc. **99**, 280 (1977).
17. J. BERTRÁN, A. OLIVA, D. RINALDI, and J. L. RIVAIL. Nouv. J. Chim. **4**, 209 (1980).
18. L. SALEM. Electrons in chemical reactions. John Wiley and Sons, New York. 1982. Chapt. 2.
19. O. TAPIA. *In* "Molecular interactions". *Edited by* H. R. Atajezade and W. J. Orville-Thomas. John Wiley and Sons, New York. 1982. Chapt. 2.
20. B. BLAIVE and J. METZGER. Nouv. J. Chim. **7**, 361 (1983); **7**, 365 (1983).
21. S. MIERTUS, E. SCROCO, and J. TOMASI. Chem. Phys. **55**, 117 (1981).
22. J. L. RIVAIL and B. TERRYN. J. Chim. Phys. Phys.-Chim. Biol. **79**, 1 (1982).
23. D. RINALDI, M. F. RUIZ-LÓPEZ, and J. L. RIVAIL. J. Chem. Phys. **78**, 834 (1983).
24. J. L. RIVAIL and D. RINALDI. *In* Intermolecular forces. *Edited by* B. Pullman. Reidel, Dordrecht. 1981. pp. 343–360; B. TERRYN, J. L. RIVAIL, and D. RINALDI. J. Chem. Res. M, 1815 (1985); J. L. RIVAIL. Stud.-Phys. Theor. Chem. **21**, 389 (1982).
25. D. RINALDI. Comput. Chem. **6**, 155 (1982).
26. J. A. POPLE and G. SEGAL. J. Chem. Phys. **43**, 136 (1965); **44**, 3289 (1966).
27. J. DEL BENE and H. H. JAFFÉ. J. Chem. Phys. **48**, 1807 (1968).
28. D. RINALDI. Comput. Chem. **1**, 108 (1976); QCPE No. 290.
29. C. M. COOK. QCPE No. 391.
30. J. L. RIVAIL, B. TERRYN, D. RINALDI, and M. F. RUÍZ-LÓPEZ. TEOCHEM, **21**, 387 (1985).
31. E. SÁNCHEZ MARCOS, B. TERRYN, and J. L. RIVAIL. J. Phys. Chem. **89**, 4695 (1985).
32. G. KLOPMAN. TEOCHEM, **12**, 121 (1983).
33. H. FUJIMOTO, N. KOGA, and I. HATAVE. J. Phys. Chem. **88**, 3539 (1984).
34. E. SÁNCHEZ MARCOS, J. MARAVER, and J. BERTRÁN. Nouv. J. Chim. **10**, 357 (1986).
35. C. A. COULSON and O. DANIELSSON. Ark. Fys. **8**, 239 (1954); **8**, 245 (1954).
36. H. MORIISHI, O. KIKUCHI, K. SUZUKI, and G. KLOPMAN. Theor. Chim. Acta, **64**, 319 (1984).
37. V. BELLAGAMBA, R. ERCOLI, and M. SIMONETTA. J. Chem. Soc. Perkin Trans. **2**, 185 (1985).

A quantum approach to the mechanism of electrochemical reductions

JUAN J. NOVOA

Departamento de Quimica Fisica, Facultad de Quimica, Universidad de Barcelona, Av. Diagonal 647, 08028-Barcelona, Spain

Received July 19, 1986

JUAN J. NOVOA. Can. J. Chem. **64**, 2359 (1986).

Using the Hartree–Fock method and, in some cases, the second order Moller–Plesset perturbational method, with 4-31G, 4-31 + G, and 4-31 + G* basis sets, a first approach to the study of the mechanism of electrochemical reduction from formaldehyde to ethanol is presented. The total energy and optimized geometry of each of the molecules involved are also given. A proton–electron–proton–electron type mechanism is proposed.

JUAN J. NOVOA. Can. J. Chem. **64**, 2359 (1986).

Faisant appel à la méthode de Hartree–Fock et, dans quelques cas, à la méthode des perturbations du second ordre de Moller–Plesset, avec des ensembles de base 4-31G, 4-31 + G et 4-31 + G*, on présente une première approche à l'étude du mécanisme de la réduction électrochimique du formaldéhyde en éthanol. On rapporte aussi l'énergie totale ainsi que la géométrie optimisée de chacune des molécules impliquées. On a trouvé un mécanisme du type proton–électron–proton–électron.

[Traduit par la revue]

Introduction

The mechanism in an electrochemical reduction is one of the unresolved problems in electrochemistry. This is due to the difficulties encountered in experimental detection and the identification of the intermediates. This is therefore an area where quantum chemistry can be of some use since it enables one to study all the postulated intermediates, even if they are not available experimentally.

One of the problems in the theoretical study of the electrochemical reductions is the large variety of global processes present and the competition, between them, as shown by the types of final products present: monomers, dimers, and organometallic compounds. The product ratios depend on the compound studied and the medium characteristics (pH, temperature, solvent, ...). Let us start by focussing our attention on only one reaction, for example, the reduction of a compound A to its associated monomers AH_2, following the reaction

[1] $A + 2H^+ + 2e^- \rightarrow AH_2$

The mechanism is known once we can establish the order of the addition of the two protons and the two electrons. The following square diagram presents all possible paths going from A to AH_2 for reaction [1]:

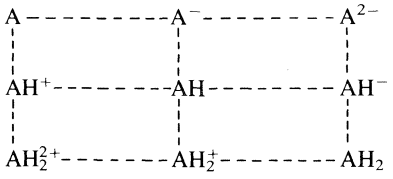

where horizontal lines represent an electroaddition, and vertical lines the addition of a proton. Once the total energy for all the systems is known, and the transition states between them are located, one can establish the most stable pathway. This can be done by means of any of the currently available quantum chemical methods (1). In this work, we present a first approach to the problem by studying the gas phase mechanism. In further studies we will focus our attention on the solvent effect of the proposed mechanism using the appropriate methodology (2).

Methodology

In this study we have used the analytical form of the Hartree–Fock method (3) (RHF for the closed-shell systems, and UHF for the open-shell ones) and the 4-31G, 4-31 + G, and 4-31 + G* basis sets, while the electron correlation is computed by means of second order Moller–Plesset method (MP2). Previous studies have shown that with the 4-31G* basis set at the HF level one obtains a mean error lower than 10 kcal/mol in the computed proton affinities of neutral and charged compounds (4), while the error is considerably higher for the electron affinities (5, 6), the only two types of reactions present. When anions are present, it has been established (7) that it is necessary to include diffuse orbitals in the basis set to obtain a proper description of the electronic distribution. For this reason, we have used the 4-31 + G and 4-31 + G* basis sets, constructed by adding a set of *s* and *p* diffuse functions (7) to the 4-31G and 4-31G* bases. For the computation of electron affinities, one also needs to include the electron correlation to achieve a high enough accuracy when anions are involved (8). We bear in mind at all times that accurate results are essential in mechanistic studies.

In our case, the application of the Hartree–Fock method is straightforward. We compute the optimum geometry for each molecule in the square diagram, thereby we will know the total energy for all the molecules and therefore their relative stability. Using these relative stability indicators, we may derive a mechanism for the reaction. One can go somewhat further by computing the potential energy curve for the energetically allowed additions to find the possible transition states. Assuming the Franck–Condon approach is correct, then barriers only exist in exothermic proton additions, which simplify our computational effort. Using the relative stability data and those relative to the barriers it is possible to define a path for reaction [1].

All these computations are done with the same basis set to minimize the influence of the truncation error in energy differences. Therefore, even if there are better computations for some of the molecules using more extended basis sets, they would not be useful for our studies because the basis set truncation error changes from basis to basis and can be quite important. In this work we use three different standard bases widely employed in the literature to study the effect of the quality of these basis sets.

Results and discussion

The total energy computed for each molecule present in the square diagram corresponding to formaldehyde in its optimum geometry, together with the final symmetry group to which they

TABLE 1. Total electronic energy for the optimum geometry (see text) computed with each basis in the given electronic state; the final symmetry is also shown

Molecule	State	Symmetry	Basis	Energy (au)
H_2CO	$^1A_1$	C_{2v}	4-31G	−113.692616
			4-31+G	−113.699167 (−113.920084)
			4-31+G*	−113.757091 (−114.060741)
H_2CO^-	$^2A_1$	C_s	4-31G	−113.619955
			4-31+G	−113.654635 (−113.880195)
			4-31+G*	−113.697718 (−114.014200)
H_2CO^{2-}	$^1A_1$	C_{2v}	4-31G	−112.974798[a]
			4-31+G	−113.418459 (−113.663087)[b]
			4-31+G*	−113.469919 (−113.798343)[b]
H_2COH^+	$^1A_1$	C_{2v}	4-31G	−113.981288
			4-31+G	−113.982912 (−114.189208)
			4-31+G*	−114.040642 (−114.327892)
H_2COH	^2A	C_1	4-31G	−114.245862
			4-31+G	−114.094330 (−114.289592)
			4-31+G*	−114.295616 (−114.586814)
H_2COH^-	^1A	C_1	4-31G	−114.158527
			4-31+G	−114.024762 (−114.258050)
			4-31+G*	−114.235395 (−114.566807)
H_3CO^+			Gives H_2COH^+	
H_3CO	$^2A'$	C_s	4-31G	−114.262847
			4-31+G	−114.267371 (−114.463302)
			4-31+G*	−114.307516 (−114.575469)
H_3CO^-	$^1A'$	C_s	4-31G	−114.218406
			4-31+G	−114.245692 (−114.245692)
			4-31+G*	−114.289651 (−114.621096)
$H_2COH_2^{2+}$	$^1A'$	C_{2v}	4-31G	−113.973801
			4-31+G	−113.976252 (−114.169718)
			4-31+G*	−114.013578 (−114.289808)
$H_2COH_2^+$	$^2A'$	C_s	4-31G	−114.545770
			4-31+G	−114.548880 (−114.740517)
			4-31+G*	−114.576775 (−114.856537)
H_2COH_2	$^1A'$	C_s	4-31G	−114.737537
			4-31+G	−114.658532 (−114.877073)
			4-31+G*	−114.783020 (−115.008664)
H_3COH^{2+}			Gives $H_2COH_2^{2+}$	
H_3COH^+	$^2A''$	C_s	4-31G	−114.528012
			4-31+G	−114.529820 (−114.708112)
			4-31+G*	−114.569269 (−114.830567)
H_3COH	$^1A'$	C_s	4-31G	−114.870980
			4-31+G	−114.879575 (−115.101649)
			4-31+G*	−114.925402 (−115.240286)

[a]This energy corresponds to the sum of the energies of CO plus two H^- into which the system dissociates.
[b]4-31+G basis set optimized geometry.

TABLE 2. Energetic differences (in kcal/mol) for the linked systems by the lines[a]

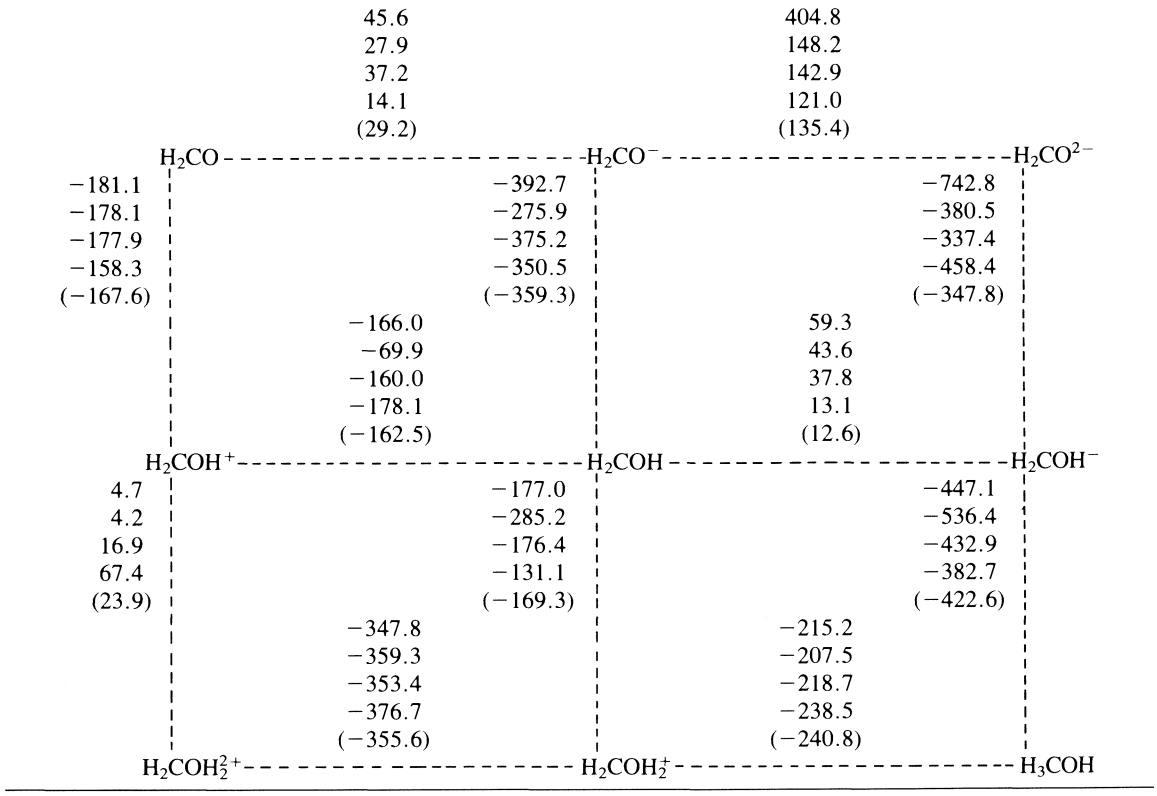

[a]The first value is the 4-31G result, the second one corresponds to the 4-31+G value, the third one is the 4-31+G* value, and the fourth is the MINDO/3 result. The values in parentheses are the MP2 values computed with the 4-31+G* basis set.

belong, and the associated electronic state, are given in Table 1 for all the basis sets employed. The values obtained in a previous computation (9) using the semiempirical MINDO/3 method (10) have also been included for comparison. From the results in Table 1 we have computed the energetic increment in each possible step of the reaction, following the normal procedure ($\Delta E = E_f - E_i$). Those results are included in Table 2 and, because the total energy of the isolated proton and electron are equal to zero, they also correspond to the relative stability of these systems.

With respect to the *ab initio* results, one must notice that the geometry optimization was only carried out with the 4-31G basis set. When the 4-31+G or 4-31+G* basis are used, we have used the 4-31G optimized geometry because previous experience has shown that there are only minor changes in the 4-31G geometry when reoptimized at the 4-31+G or 4-31+G* basis set level.

Even if geometry is not important in the reduction mechanism, it gives an idea of the route of transformations of the molecules. For this reason, we have included in Table 3 the values of the geometrical parameters together with a computer-generated tridimensional plot of the geometries, Fig. 1, which gives an overall idea of the transformations. All values are given in the usual units (Å for lengths, deg for angles). For comparison, the MINDO/3 values computed in ref. 9 are also given.

In all tables and in Fig. 1, we have used the following conventions for the names of the molecules: Each molecule is identified by its stoichiometry, but the hydrogen atoms are grouped near the atom to which they are bounded. This enables one to easily distinguish the various isomers of a molecule. Thus, H_2COH^+ is obtained by adding one proton to the oxygen atom in H_2CO while H_3CO^+ is the isomer with the proton on the carbon atom.

All computations have been done using the GAUSSIAN-80 set of programs (11).

Energy and geometry

The results included in Table 1 show, as expected, a decrease in total energy as with an increase in quality of the basis set. Computations with the 4-31G* basis set show that in all cases except for the dianion H_2CO^{2-}, the addition of a set of polarization functions seems to give better total energy than the inclusion of a set of *sp* diffuse functions. The same trend is observed when going from the 4-31+G to the 4-31+G* basis set. However, the inclusion of the diffuse set is very important to correctly describe the anions while it practically leaves the stability of the neutral systems unchanged in agreement with results from the literature (4, 6). All the total energies computed here are in good agreement with the values reported in the bibliography.

There are two remarkable facts about the results in Table 3. One is the good agreement of the experimental and *ab initio* results, in particular when the 4-31G basis is used. The other, is that MINDO/3 geometries are very similar to the *ab initio* ones and, therefore, the latter method describes remarkably well the type of geometrical changes the molecules undergo. This seems to be promising for this method to be used in the computation of the square diagrams of big molecules.

Results of Tables 1 and 3 show that the addition of an electron to a neutral molecule is always an endothermic process at the HF level with the basis set employed. However, the only reported

TABLE 3. Optimum geometry computed for the molecules present in Table 2[a]

Molecule	Basis	Parameters								
H_2CO		CO	CH1	H1CH2						
	4-31G	1.206	1.081	116.4						
	MINDO/3	1.181	1.123	126.6						
	Exp.	1.203	1.101	116.5						
H_2CO^-		CO	CH1	H1CH2	H1CO—H2					
	4-31G	1.315	1.105	120.2	144.2					
	MINDO/3	1.231	1.178	122.7	132.2					
H_2CO^{2-}		CO	CH1	H1CH2						
	4-31G	1.129	[a]							
	4-31+G	1.2486	1.082	121.9						
	MINDO/3	1.135	[a]							
H_2COH^+		CO	CH1	CH2	OH3	H1CO	H2CO	COH3		
	4-31G	1.246	1.071	1.075	0.967	116.1	122.0	124.7		
	MINDO/3	1.223	1.110	1.111	0.960	115.2	125.5	124.0		
H_2COH		CO	CH1	CH2	OH3	OCH1	OCH2	COH3	H1CO—H3	H1CO—H2
	4-31G	1.381	1.067	1.073	0.950	113.0	118.8	114.8	150.7	177.9
	MINDO/3	1.294	1.117	1.115	0.951	113.0	121.4	114.7	136.0	196.1
H_2COH^-		CO	CH1	CH2	OH3	OCH1	OCH2	COH3	H1CO—H3	H1CO—H2
	4-31G	1.565	1.115	1.115	0.959	101.5	101.5	104.6	127.1	105.7
	MINDO/3	1.317	1.185	1.185	0.978	114.1	114.1	125.7	305.1	108.3
$H_2COH_2^{2+}$		CO	CH1	OH3	OCH1	COH3				
	4-31G	1.326	1.088	1.002	117.2	123.2				
	MINDO/3	1.277	1.122	0.987	116.1	126.6				
$H_2COH_2^+$		CO	CH1	OH3	OCH1	COH3	H1CO—H2	H3OC—H4		
	4-31G	1.479	1.067	0.962	111.0	121.5	148.1	172.2		
	MINDO/3	1.335	1.107	0.962	114.3	122.7	141.2	208.1		
H_3COH		CO	CH4	CH2	OH3	OCH4	OCH2	COH3[b]	H4CO—H2	
	4-31G	1.430	1.076	1.083	0.951	106.2	111.6	113.2	118.6	
	MINDO/3	1.341	1.118	1.123	0.952	114.9	107.8	110.7	119.2	
	Exp.	1.427	1.096	1.096	0.956	106.6	109.0	105.9	122.0	

[a]All the distances in Å and angles in deg. The parameters are as follows: AB means the distance between atoms A and B; H1CH2 represent the angle formed by the bonds H1—C, and C—H2 (the hydrogens are numbered as in Fig. 1); H1CO—H4 is the dihedral angle between the atom H4 and the plane formed by the atoms H1, C, and O, looking from the atom bonded to H4 (see Fig. 1). Only the symmetry nonequivalent parameters are indicated. The MINDO/3 and experimental (ref. 10) values are also given for comparison.

[b]Only the geometry of the CO fragment is given. The two H^- fragments are at dissociation distance. The experimental CO distance is 1.128 Å.

[c]Corresponding to the staggered conformation (the most stable with a 4-31G base).

datum on these molecules is the electron affinity of the H_3CO molecule, whose experimental value is 36.7 kcal/mol. Previous studies in this field have shown that if one wants to reproduce the experimental electron affinity of the neutral compounds one needs, at least, to work with a 4-31+G basis set and the MP2 method (8). A computation at that level, using the optimized 4-31+G geometry, gives a total energy for the H_3CO molecule of −114.448669 au, while the same value for the H_3CO^- anion is −114.484130 au, that is, one obtains the correct stability between the systems and a value of 22.3 kcal/mol (experimental value of 41.3 kcal/mol), while at the 4-31+G* level, the same property takes the value of 29.13 kcal/mol. In any case, when compared to the Hartree–Fock results, we see that they are correct in sign, and the error is almost of chemical precision. Having these results in mind we have performed computations using the 4-31+G* basis for all the systems, at the MP2 level and with the 4-31G geometries. From these values, one can conclude that the addition of an electron to the neutral molecules H_2CO and H_2COH is endothermic, while the same process is exothermic for the cations, and endothermic for

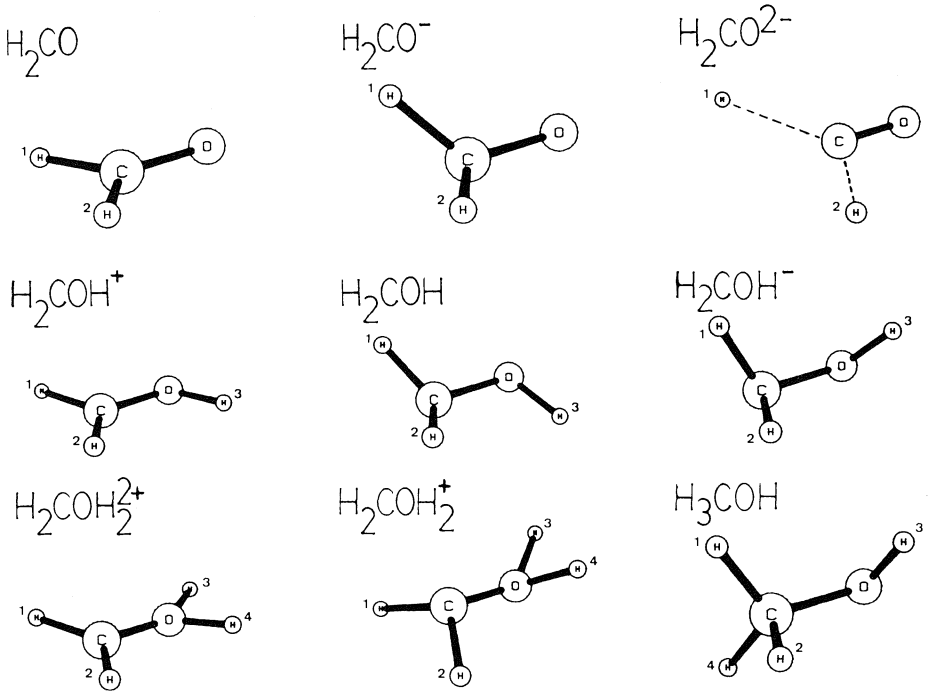

FIG. 1. Three dimensional plot of the optimized geometries of the molecules included in Table 2. The atoms are identified by their atomic symbol and the molecules to which they belong are indicated in the upper-left corner. Broken lines are used to represent non-bonds and solid ones for bonds.

H_2CO^-. At this point, one must notice that the MINDO/3 values reproduce remarkably well the MP2 values for the electronic affinity of all the systems, either neutral or not.

In relation to the proton addition process, the results computed here show that the protonation of formaldehyde is only possible on the oxygen atom and with a geometry which preserves the C=O double bond. After this step, a second protonation can happen on the formaldehyde molecule. Previous computations on both isomers (12), H_3COH^{2+} and $H_2COH_2^{2+}$, done under the constraint of C_{3v} symmetry on the methyl group of the first molecule, show that the most stable isomer is $H_2COH_2^{2+}$ because it preserves the double bond. A full optimization of both systems does not change the conclusion. The only new fact which appears is that H_3COH^{2+} is not stable and splits into $HCOH^+$ and H_2^+.

The addition of an electron to the planar and isoelectronic compounds H_2CO, H_2COH^+, and $H_2COH_2^{2+}$ breaks up their planarity. This is an endothermic process for the first compound, but an exothermic one in the last two cases. The exothermicity is proportional to the net charge of the system.

The addition of a second proton to the H_2COH molecule is possible on either the carbon or the oxygen. However, the $H_2COH_2^+$ isomer is 5 kcal/mol more stable than H_3COH^+ at the 4-31G* level, while in the other cases the stability is preserved. The addition of a new electron reverses the relative stability and the H_3COH isomer is about 100 kcal/mol more stable than H_2COH_2.

Energetics

From the results in Table 1, one can compute values in Table 2 as simple differences. Furthermore, we have also included for comparison the MINDO/3 results obtained from a previous study (9).

Let us take note that Table 2 do not include the H_3CO^+, H_3CO, and H_3CO^- molecules. H_3CO^+ does not exist as it transforms into H_2COH^+ without a barrier. Thus the H_3CO system can only be obtained through protonation of the H_2CO^- molecule. However, because the H_2CO^- molecule is energetically unstable, this path is not possible and H_3CO is never formed. Similarly, we can not obtain H_3CO^- as an intermediate in the reduction of H_2CO.

Before using results in Table 2 to establish a reduction mechanism, it is necessary to know the quality of these results, by comparing these with the experimental values for the two types of reaction described in this table: proton and electron additions. Electron additions have been dealt with above and we have concluded that MP2 computations done with a 4-31+G* basis describe the sign and value of the energy increment with almost chemical precision. The MP2 values obtained are included in parentheses, and can be used as reference for all the other results in the same table. For proton affinities, one can see that the experimental value for the proton affinity of formaldedyde in the gas phase (−177.2 kcal/mol) compares very well with the 4-31G* computed value of −180.7 kcal/mol, and with the 4-31+G and 4-31+G* values (−178.1 and 177.9 kcal/mol, respectively), while for the H_3CO^- system the theoretical value using a 4-31G* basis set gives a value of −411.1 kcal/mol while the experimental value is −384.6 kcal/mol. Both results lend confidence to the theoretical prediction of this property at the 4-31+G* level. We can conclude that the sign and the order of magnitude of the energetic variation involved in the reaction is correctly described by our best result. Therefore, we have the level of precision to establish the mechanism of reduction for our compound.

Electronic correlation exerts practically a uniform effect on the HF results of the cations and the neutral molecules (a lowering of about 0.2 au in the total energy) and a slightly higher results (a lowering of 0.3 au in the same property) for the anions. However, this correction does not affect the sign of the energy increments included in Table 2 and, therefore, for the reaction studied, the electron correlation does not affect the main facts of the reaction energetics.

Finally, we can compare the "best" results reported here with those computed with the other basis sets and with MINDO/3. In the first case, one can also see that the results from using 4-31G are very similar to those from using 4-31+G*, except when the dianion is also involved. In relation to the MINDO/3 results, the electron and proton affinities are very well matched for the compounds studied here. Thus, the MINDO/3 values computed for the proton affinity for H_2CO and H_3CO^- are −158.3, −322.7 kcal/mol, respectively (experimental values are −177.2, −384.6 kcal/mol) while the computed electron affinity of H_3CO is 45.2 kcal/mol (the experimental value is 36.7 kcal/mol). As to the relative stabilities shown in Table 2, one can see that the tendencies in the MINDO/3 results are exactly the same as those reported for 4-31+G* MP2.

Mechanism

Looking at Table 2, we can establish a mechanism for the reduction of formaldehyde to ethanol by successive addition of two protons and two electrons. This, as has already been indicated, can be done by, first, seeking the exothermic pathways and, then, studying their kinetic behaviours. Thus, the first step is the protonation of the initial compound on the oxygen atom (the only exothermic pathway). Since there is no activation barrier in this reaction, it is therefore kinetically allowed.

After the first protonation, the next step is an electroaddition, because the proton addition to the H_2COH^+ system to give $H_2COH_2^{2+}$ has a barrier and is endothermic (12). The third step can only be a new protonation for energetic reasons. Again, there is no barrier for this reaction. Finally, the fourth step is an electroaddition. This mechanism proton–electron–proton–electron is known experimentally as CECE because the proton addition is said to be the chemical step, while the electroaddition is the electrochemical one.

Conclusions and final comments

Previous results have shown that it is possible to elucidate the mechanism of electroreduction of a compound by using quantum chemical methods. Even if the experimental conditions are far from the isolated molecule, the chemical information behind the reported results are of interest. Thus, they show that the electroaddition of the formaldehyde is not energetically stable because the double bond is broken, an effect which is independent of the existence of a solvent, whose primary effect is to stabilize the charged systems. In any case, we are now starting a study to elucidate the effect of solvent in electrochemical reductions.

Acknowledgments

The author wishes to thank the Spanish Science and Education Department (CAICYT-657-81) for a grant which made possible the computations presented here.

1. P. Carsky and M. Urban. Ab initio calculations. Lecture notes in chemistry. Vol. 16. Springer Verlag, Berlin. 1980.
2. O. Tapia. Mol. Interact. **3**, 47 (1982).
3. C. C. J. Roothaan. Rev. Mod. Phys. **23**, 69 (1951).
4. W. A. Lathan, L. A. Curtiss, W. J. Hehre, J. B. Lisle, and J. A. Pople. Prog. Phys. Org. Chem. **11**, 175 (1974); J. A. Pople. Int. J. Mass Spectrom. Ion Phys. **19**, 89 (1976); F. Bernardi, N. D. Epiotis, W. Cherry, H. B. Schlegel, M. H. Whangbo, and S. Wolfe. J. Am. Chem. Soc. **98**, 469 (1976); W. J. Hehre. Modern theoretical chemistry. Vol. 4. *Edited by* H. F. Schaeffer. Plenum Press. 1977; L. Radom. Modern theoretical chemistry. Vol. 4. *Edited by* H. F. Schaeffer. Plenum Press. 1977; A. Pross, D. J. DeFrees, B. A. Levi, S. K. Pollack, L. Radom, and W. J. Hehre. J. Org. Chem. **46**, 1693 (1981); J. Chandrasekhar, J. G. Andrade, and P. von R. Schleyer. J. Am. Chem. Soc. **103**, 5609 (1981); A. M. de P. Nicholas, R. J. Boyd, and D. R. Arnold. Can. J. Chem. **60**, 3011 (1982); T. Clark, J. Chandrasekhar, G. W. Spitznagel, and P. von R. Schleyer. J. Comput. Chem. **4**, 294 (1983); K. E. Edgecombe and R. J. Boyd. Can. J. Chem. **61**, 45 (1983); **62**, 2887 (1984).
5. T. H. Dunning and P. J. Hay. Methods in electronic structure theory. Vol. 4. Plenum Press, New York. 1977.
6. G. W. Spitznagel, T. Clark, J. Chandrasekhar, and P. v. R. Schleyer. J. Comput. Chem. **3**, 363 (1982); T. Clark, J. Chandrasekhar, G. W. Spitznagel, and P. v. R. Schleyer. J. Comput. Chem. **4**, 294 (1983).
7. J. Chandrasekhar, J. G. Andrade, and P. von R. Schleyer. J. Am. Chem. Soc. **103**, 5609 (1981), and references therein.
8. J. J. Novoa and F. Mota. Chem. Phys. Lett. **119**, 135 (1985), **123**, 399 (1986); G. Frenking and W. Koch. J. Chem. Phys. In press.
9. E. Brillas, E. Duch, J. J. Novoa, and J. Virgili. An. Quim. **81**, 35 (1985).
10. R. C. Bingham, M. J. S. Dewar, and D. H. Lo. J. Am. Chem. Soc. **97**, 1294 (1975); M. J. S. Dewar and W. Thiel. J. Am. Chem. Soc. **99**, 4899 (1977).
11. J. S. Binkley, R. A. Whiteside, R. Krishnan, R. Seeger, D. J. DeFrees, H. B. Schlegel, S. Topiol, L. R. Kahn, and J. A. Pople. Program GAUSSIAN-80, Carnegie-Mellon University.
12. J. J. Novoa. J. Mol. Struct. **22**, 29 (1985).

Solvent effects on the rates and equilibria of the proton transfer reaction of 4-nitrophenylphenylcyanomethane to tetramethylguanidine

MAHMOOD HOJATTI[1] AND KENNETH T. LEFFEK
Department of Chemistry, Dalhousie University, Halifax, N.S., Canada B3H 4H6

Received April 30, 1986

MAHMOOD HOJATTI and KENNETH T. LEFFEK. Can. J. Chem. **64**, 2365 (1986).

The equilibrium constants and second-order rate constants, both at 25°C, have been determined for the proton transfer reaction from 4-nitrophenylphenylcyanomethane to tetramethylguanidine in a number of different solvents. While the equilibrium constants show a good correlation with the dielectric constant function $D - 1/2D + 1$, the rate constants are randomly scattered with respect to this parameter and also the solvent parameter E_T. The rate constants do show a general trend in relation to the solvent parameters AN and DN. These results are interpreted as support for the hypothesis that the transition state of the proton transfer occurs early along the reaction path.

MAHMOOD HOJATTI et KENNETH T. LEFFEK. Can. J. Chem. **64**, 2365 (1986).

Opérant dans un certain nombre de solvants, à 25°C, on a déterminé les constantes d'équilibre ainsi que les constantes de vitesse du deuxième ordre pour la réaction de transfert de proton du nitro-4 phényl phénylcyanométhane à la tétraméthylguanidine. Alors que les constantes d'équilibre présentent une bonne corrélation avec la fonction de constante diélectrique $D - 1/2D + 1$, les constantes de vitesse sont réparties au hasard par rapport à cette fonction ainsi que par rapport au paramètre E_T du solvant. Les constantes de vitesse présentent une corrélation générale par rapport aux paramètres AN et DN du solvant. On croit que ces résultats supportent l'hypothèse selon laquelle l'état de transition du transfert de proton se produirait tôt au cours de la réaction.

[Traduit par la revue]

Introduction

Previous investigations of the proton transfer reaction of 4-nitrophenylphenylcyanomethane and substituted derivatives with tetramethylguanidine (TMG) studied the activation parameters, deuterium isotope effects, and the Hammett correlation (1, 2). These studies led to the conclusion that the transition state for the reaction occurred early along the reaction coordinate with the negative charge development still concentrated on the central carbon atom of the methane.

In this paper the variation of the equilibrium constant K_e and the second-order rate constant k_f with the solvent are studied to further test this hypothesis. A variety of pure solvents were selected in order to test whether K_e and k_f were governed by specific or non-specific solvation effects.

Results and discussion

In each solvent studied the reaction of 4-nitrophenylphenylcyanomethane with TMG base gave a product with a single broad absorption peak, λ_{max} varying between 565 nm and 590 nm, depending on the solvent. The product has been shown by previous work (1, 2) to be the ion-pair of reaction [1]. The equilibrium constants, K_e, were determined for the reaction

[1] $$NO_2C_6H_4\underset{\displaystyle C_6H_5}{\underset{|}{C}}HCN + HN{=}C(N(CH_3)_2)_2 \underset{k_b}{\overset{k_f}{\rightleftharpoons}} NO_2C_6H_4\underset{\displaystyle C_6H_5}{\underset{|}{C}}\bar{C}N\ldots H_2\overset{+}{N}{=}C(N(CH_3)_2)_2$$

using the Hildebrand–Benesi method (3). The method yields eq. [2] for reaction of the type shown in [1] in which

[2] $$a/A = \frac{1}{K_e b \epsilon} + \frac{1}{\epsilon}$$

the product is an ion-pair. The initial concentrations of the acid and base are represented by a and b, respectively, A is the absorbance at equilibrium and ϵ is the molar extinction coefficient of the ion-pair product.

In each solvent, for a given concentration of the methane within the range of 1×10^{-5} M to 5×10^{-5} M, the absorbance was measured at λ_{max} for a series of different base concentrations. The results were fitted to eq. [2] by a linear least squares calculation. The correlation coefficients for 7 to 9 base concentrations were generally 0.999 or better. Values of K_e and ϵ were calculated from the slope, $1/K_e\epsilon$, and the intercept, $1/\epsilon$, for each solvent. The results are summarized in Table 1.

Caldin and Mateo (4) carried out an investigation of the variation of the equilibrium constant with solvent for the proton transfer reaction from 4-nitrophenylnitromethane to tetramethylguanidine and found only a general trend for the variation of log K_e with the standard dielectric constant functions D^{-1} and $D - 1/2D + 1$ (5), indicating that in that reaction non-electrostatic interactions are important. In contrast to this, the results in Table 1 show quite a good correlation with both D^{-1} and $D - 1/2D + 1$. The plot of log K_e vs. $D - 1/2D + 1$ is shown in Fig. 1. With the exception of the value of log K_e in methanol, the remaining seven points give a correlation coefficient of 0.987. A similar plot of log k_e vs. D^{-1} gives a correlation with a slightly better coefficient of 0.991, again with the methanol point badly off the line correlating the other seven solvents. Attempted correlations with the solvent parameters E_T (6, 7), AN (8, 9), and DN (9, 10) give very low correlation coefficients.

It is concluded that the solvation factors controlling the value of the equilibrium constant, K_e, for the reaction in [1] in the solvents studied are general electrostatic effects and involve only a small amount of specific solvation, except for the reaction in methanol solvent. Either the methanol is acidic enough to result in specific solvation of the carbanion ion-pair or there is an acid–base equilibrium between methanol and TMG yielding a methoxide ion which then acts as the proton-abstracting base from the carbon acid. The latter reaction would lead to the same product as [1], but at least one methanol molecule would be specifically solvated to the carbanion. Also, the observed

[1]Postdoctoral Fellow 1982–1984.

TABLE 1. Equilibrium constants for the reaction of 4-nitrophenylphenylcyanomethane with tetramethylguanidine at 25.0°C

Solvent	Dielectric constant D	λ_{max} (nm) of product	$10^{-3}\,\epsilon$	K_e (dm^3 mol^{-1}) ± std. dev.
1. Ethyl acetate	6.0	576	96	1.65±0.15
2. Tetrahydrofuran	7.6	580	31	37.0±1.3
3. 2-Butanol	16.6	582	35	1300±31
4. Ethanol	24.5	570	32	4300±50
5. Benzonitrile	25.2	590	40	2000*
6. Methanol	32.7	565	29	230±2
7. Acetonitrile	37.5	582	39	6000*
8. Propylene carbonate	65.1	584	336	18000±2400

*Reference 1.

TABLE 2. Second-order rate constants for the reaction of 4-nitrophenylphenylcyanomethane with tetramethylguanidine at 25.0°C

Solvent	E_T	DN	AN	$10^{-3}\,k_f$ (dm^3 mol^{-1} s^{-1}) ± std. dev.
2. Tetrahydrofuran	37.4	20.0	8.0	19.2
3. 2-Butanol	—	—	—	0.76±0.01
4. Ethanol	51.9	31.5	37.1	36.2±0.1
5. Benzonitrile	42.0	11.9	15.5	23.9±0.6*
6. Methanol	55.5	25.7	41.3	34.5±0.9
7. Acetonitrile	46.0	14.1	18.9	7.9±0.2*
8. Propylene carbonate	46.6	15.1	18.3	11.25±0.5

*Reference 1.

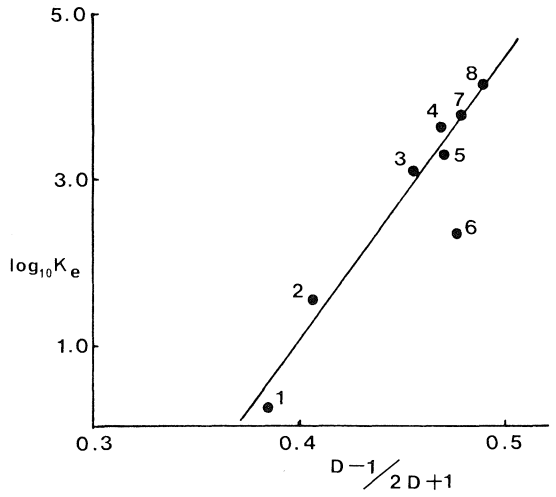

FIG. 1. Plot of $\log_{10} K_e$ vs. $D - 1/2D + 1$ for the proton transfer between 4-nitrophenylphenylcyanomethane and tetramethylguanidine.

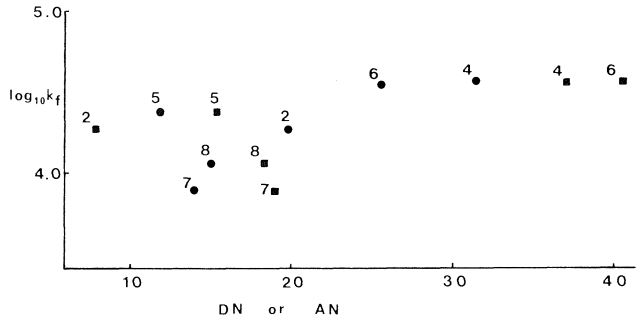

FIG. 2. Plot of $\log_{10} k_f$ vs. DN (●) and AN (■) for the proton transfer between 4-nitrophenylphenylcyanomethane and tetramethylguanidine.

equilibrium constant would be the product of K_e for reaction [1] and the equilibrium constant for the acid–base reaction between methanol and TMG.

The pseudo first-order rate constants, k_f, were determined for the proton transfer reaction using a large excess of base, as previously described (1). The results are shown in Table 2. The log k_f values show no correlation with the dielectric constant functions D^{-1} or $D - 1/2D + 1$ (correlation coefficient 0.04), nor with the solvent parameter E_T (6, 7) (correlation coefficient 0.4). There does exist a general trend, shown in Fig. 2, between log k_f and the electron acceptor parameter AN (8, 9) (correlation coefficient 0.60) and also between log k_f and the electron donor parameter DN (9, 10) (correlation coefficient 0.72) indicating that the transition state of the reaction may be stabilized by specific solvation of both the developing positive and negative charges.

The possibility of a contribution from proton tunnelling exists in the values of the rate constants, which is not the case for the equilibrium constants. Evidence for a significant contribution to k_f from proton tunnelling was found (1) for this reaction in acetonitrile and benzonitrile solvents, but it was not possible to make any quantitative estimate of its importance. However, it is unlikely that this effect would play a major role in determining the rate constant in comparison to specific solvation effects on the transition state.

The marked difference between the variation of the equilibrium constant with solvent and that of the second-order rate constant with solvent, clearly shows that the transition state of the reaction is not at all product-like. The fact that the

second-order rate constant does not correlate well with any solvent parameter probably means that the amount of charge development in the transition state varies from solvent to solvent, but is not extensive in any of the solvents studied. Thus, this study of solvent effects on the proton transfer from 4-nitrophenylphenylcyanomethane to TMG supports the hypothesis that the transition state occurs early on the reaction coordinate.

Experimental

The preparation and purification of the reactants have been described previously (2). The solvents were purified carefully by standard methods. Reagent grade ethyl acetate was purified by washing it with aqueous sodium carbonate (5%), then with a saturated solution of calcium chloride. After drying over anhydrous potassium carbonate, the solvent was fractionally distilled from P_2O_5.

Peroxide-free reagent grade tetrahydrofuran (THF) was dried over potassium hydroxide pellets and then refluxed over a mixture of sodium wire and benzophenone. The pure solvent was fractionally distilled from this mixture.

The alcohols were purified using the procedure of Lund and Bjerrum (11). Magnesium turnings (5 g) were added to the alcohol (60 mL) together with sublimed iodine (0.5 g) and the mixture was refluxed until the iodine colour had disappeared and all the magnesium was converted to the alkoxide. Additional alcohol (900 mL) was added, refluxed for 1 h, and then fractionally distilled. The purified alcohol was stored over 4A molecular sieves.

Reagent grade propylene carbonate was dried over 4A molecular sieves for 2 days. Potassium permanganate (10 g/kg) was added with constant stirring and the resultant MnO_2 was filtered off. The excess permanganate was destroyed by heating the solution to 120°C. The solvent was distilled at reduced pressure and passed through a column of alumina. It was then twice fractionally distilled at reduced pressure, each time taking the middle two-thirds fraction and storing it under an inert atmosphere.

Acetonitrile and benzonitrile were purified as previously described (1).

The equilibrium measurements were carried out using a Cary 219 spectrophotometer and the kinetic measurements were made with a Durrum-Gibson stopped-flow spectrophotometer as described previously (2).

Acknowledgment

The authors are grateful for financial support by the Natural Sciences and Engineering Research Council of Canada.

1. A. Jarczewski, P. Pruszynski, and K. T. Leffek. Can. J. Chem. **61**, 2029 (1983).
2. M. Hojatti and K. T. Leffek. Can. J. Chem. **62**, 2653 (1984).
3. H. A. Benesi and H. H. Hildebrand. J. Am. Chem. Soc. **71**, 1876 (1943).
4. E. Caldin and S. Mateo. J. Chem. Soc. Faraday Trans. I, **71**, 1876 (1975).
5. J. F. Kirkwood. J. Chem. Phys. **2**, 351 (1934).
6. K. Dimroth, C. Reichardt, T. Siepmann, and F. Bohlmann. Liebigs Ann. Chem. **661**, 1 (1963).
7. C. Reichardt. Angew. Chem. Int. Ed. **4**, 29 (1965).
8. U. Mayer, V. Gutmann, and W. Gerger. Monatsh. Chem. **106**, 1235 (1975).
9. V. Gutmann. Coord. Chem. Rev. **18**, 225 (1976).
10. V. Gutmann and E. Wychera. Inorg. Nucl. Chem. Lett. **2**, 257 (1966).
11. A. I. Vogel. Practical organic chemistry. Longmans, Green and Co. Ltd., London. 1954. p. 166.

Experimentally determined proton affinities of 4-methyl-3-penten-2-one, 2-propyl ethanoate, and 4-hydroxy-4-methyl-2-pentanone in the gas phase

AFAF KAMAR,[1] ALEXANDER BALDWIN YOUNG, AND RAYMOND EVANS MARCH[2]
Department of Chemistry, Trent University, Peterborough, Ont., Canada K9J 7B8

Received June 17, 1985[3]

AFAF KAMAR, ALEXANDER BALDWIN YOUNG, and RAYMOND EVANS MARCH. Can. J. Chem. **64**, 2368 (1986).

Proton affinities have been determined for 4-methyl-3-penten-2-one, 2-propyl ethanoate, and 4-hydroxy-4-methyl-2-pentanone in the gas phase at 333 K. A quadrupole ion store (QUISTOR) was employed to study mass spectrometrically the equilibrium between a species of known proton affinity and one of the above compounds; equilibrium between protonated species was monitored over an ion storage duration of 100 ms. The values of the proton affinities were found to be 870.5 ± 0.8 kJ mol^{-1} for 4-methyl-3-penten-2-one (mesityl oxide); 842.7 ± 0.6 kJ mol^{-1} for 2-propyl ethanoate; and 831.6 ± 0.8 kJ mol^{-1} for 4-hydroxy-4-methyl-2-pentanone (diacetone alcohol).

AFAF KAMAR, ALEXANDER BALDWIN YOUNG et RAYMOND EVANS MARCH. Can. J. Chem. **64**, 2368 (1986).

Opérant en phase gazeuse, à 333 K, on a déterminé les affinités protoniques de la méthyl-4 pentène-3 one-2, de l'éthanoate de propyle-2 et de l'hydroxy-4 méthyl-4 pentanone-2. On a utilisé un emmaganisage quadrupolaire d'ions (QUISTOR) pour étudier par spectrométrie de masse l'équilibre entre une espèce d'affinité protonique connue et chacun des composés mentionnés ci-dessus; on a enregistré les équilibres entre les espèces protonées à des périodes d'emmagasinage ionique de 100 ms. On a trouvé que les affinités protoniques sont les suivantes : pour la méthyl-4 pentène-3 one-2 (oxyde de mésityle), 870,5 ± 0,8 kJ mol^{-1}; pour l'éthanoate de propyle-2, 842,7 ± 0,6 kJ mol^{-1}, et pour l'hydroxy-4 méthyl-4 pentanone-2 (diacétone alcool), 831,6 ± 0,8 kJ mol^{-1}.

[Traduit par la revue]

Introduction

In the course of a study of the ion chemistry of 2-propanone and the infrared multiphoton dissociation of protonated dimers of 2-propanone, it was found necessary to investigate the ion chemistry and photochemistry of both diacetone alcohol and mesityl oxide (1). In order to compare the reactivities of isomeric ions within the above systems, a knowledge of the proton affinities of diacetone alcohol and mesityl oxide was necessary. However, the proton affinities were not available in the literature (2). With the quadrupole ion store (QUISTOR) in which gaseous ions can be stored for up to 200 ms we believe that thermal equilibria can be measured (3), hence the relative proton affinities for diacetone alcohol and mesityl oxide, along with that for isopropyl acetate were determined.

A knowledge of the gas phase basicities or proton affinities (PA) of molecules is crucial in the calculation of enthalpies of formation of protonated species and further, the calculation of enthalpies of reaction for subsequent reactions and particularly for unimolecular dissociation. In addition, the hierarchy of gas phase basicities permits the investigation of structural and electronic substituent effects in the absence of the complicating and often considerable role of solvent.

Experimental

The basic apparatus used in this study consisted of a QUISTOR mounted in place of the ion source of a quadrupole mass filter (Vacuum Generators QXK 400). Known mixtures of gases were admitted to the QUISTOR and ionized with a pulsed electron beam. The temporal variation of ionic products of subsequent ion molecule reactions was monitored over a period of 100 ms. The ratio of protonated ion intensities was plotted as a function of time to ensure that equilibrium was established; as revealed by a constant ratio over the final 20–60 ms.

Although the apparatus has been described in detail previously (1, 4), a brief description of the technique used in this work is presented here. The QUISTOR was composed of three electrodes as required for the generation of a three dimensional quadrupole field, and consisted of a hyperboloid of one sheet combined with a hyperboloid of two sheets forming the ring and end-cap electrodes, respectively. These electrodes were fabricated from stainless steel and polished to a mirror finish. The radius of the ring electrode, from which the physical size of the QUISTOR may be established (4), was 1 cm. The end-cap electrodes were perforated to permit the passage of electrons or ions through the electrodes. The three electrodes were arranged symmetrically with the ring electrode located between the end-cap electrodes and were separated by ruby sphere spacers which provided both electrical insulation and accurate spacing of the electrodes. The reactant inlet system was contained in a heated oven and consisted of a 6 L glass bulb with a side arm and septum holder. The total pressure with the glass bulb was measured with a pressure gauge (Matheson, Model 63-5601, pressure range 0–760 Torr) while the pressures of each of the reactants was calculated from a knowledge of the temperature of the oven the volume of the reactant inlet system and the volume of sample injected. The temperature of the oven was such that all reactants existed in the vapour phase. The reactants were admitted to the vacuum tank surrounding the QUISTOR and quadrupole mass filter assembly through a heated stainless steel line in which the rate of flow was controlled by a micrometer needle valve (Whitey). The total pressure within the vacuum tank was measured using a Penning gauge.

Once the reactant mixture of known composition was admitted to the vacuum tank, gaseous positive ions were formed within the QUISTOR by a short pulse of electrons, of 100 μs duration and 70 eV energy, controlled by a pulse generator (Hewlett-Packard). Reactions between primary ions produced by electron impact and reactant molecules were initiated with the onset of the electron pulse and continued concurrently with reactions of secondary and tertiary ions with reactant molecules for up to 100 ms. A scan delay generator was used to vary continuously the storage time over this range of 100 ms at a predetermined rate. The scan delay generator triggered both an extraction pulse and a detection pulse. Equilibrium with respect to proton transfer between each pair of reactants was judged to have been attained when the ratio of protonated ion intensities remained constant during the final 20–60 ms of storage.

Results and discussion

A general proton transfer reaction may be written

[1] $AH^+ + B \rightleftharpoons A + BH^+$

[1]Registered in the Ph.D. programme in Chemistry at Queen's University, Kingston, Ont., Canada K7L 3N6.

[2]Adjunct Professor, Department of Chemistry, Queen's University, Kingston, Ont., Canada K7L 3N6.

[3]Revision received July 31, 1986.

and the associated equilibrium constant, K_{eq} as

[2] $$K_{eq} = \frac{[A][BH^+]}{[B][AH^+]}$$

The ratio of the concentrations of A and B may be calculated from the known volumes of each injected into the bulb; the ratio of the concentrations of the protonated species AH^+ and BH^+ is determined mass spectrometrically from the respective ion intensities. The equilibrium constant may be expressed in terms of Gibbs' free energy, ΔG.

[3] $$\Delta G = -RT \ln K_{eq}$$

where R is the gas constant and T the absolute temperature.

[4] $$\Delta G = \Delta H - T\Delta S$$

The enthalpy change (ΔH) for reaction [1] is equal to the difference in proton affinity between molecule A and molecule B.

[5] $$\Delta H = PA(A) - PA(B) = \Delta PA$$

Thus in order to obtain ΔH or to obtain the proton affinity for either A or B when the proton affinity of either B or A is known, the $T\Delta S$ term or entropy contribution to ΔG must be evaluated. The ΔS term in eq. [4] may be subdivided into individual contributions due to translational, vibrational, and rotational entropies.

[6] $$\Delta S = \Delta S_{trans} + \Delta S_{vib} + \Delta S_{rot}$$

When the molecular masses of the species A and B in eq. [1] are approximately equal, the translational entropy contribution is insignificant; furthermore, vibrational changes due to the transfer of a proton from A to B may also be expected to be negligible when A and B are similar molecules. The contribution due to rotational symmetry changes may be calculated if structures are assumed for the gas phase protonated species. Save for the case of diisopropyl ether, ΔS_{rot} is assumed to be zero for the equilibria employed in these studies.

Diisopropyl ether has a rotational axis of symmetry about the oxygen atom which may be retained if a planar configuration with respect to the oxygen atom is adopted in the protonated ether. However, if the configuration adopted is pyramidal as is suggested in both protonated water and methanol (5), the axis of symmetry is lost in the protonated ether and a rotational entropy correction of $R \ln 2$ must be applied. Invocation of Occam's razor allows no rotational entropy contribution for the equilibrium between mesityl oxide and diisopropyl ether, i.e. $\Delta S^0_{rot\ sym} = 0$, hence for all the equilibria investigated

[7] $$\Delta G = PA(A) - PA(B) = \Delta PA$$

Since the proton affinity of one of the species in the equilibrium is known from the literature (2), the proton affinity of the other may be inferred from the calculated ΔPA.

Diacetone alcohol

The relatively low volatility of diacetone alcohol and its facile dehydration to mesityl oxide at temperatures in excess of 350 K posed some experimental problems. Furthermore, attempts to establish equilibrium with respect to proton transfer with compounds of proton affinity lower than that of diacetone alcohol resulted in the rapid dehydration of protonated diacetone alcohol to form protonated mesityl oxide. Equilibrium for proton transfer was established at 330 K for mixtures of diacetone alcohol with 2-butanone (of higher proton affinity), typically 1:6, in the reaction

[8] 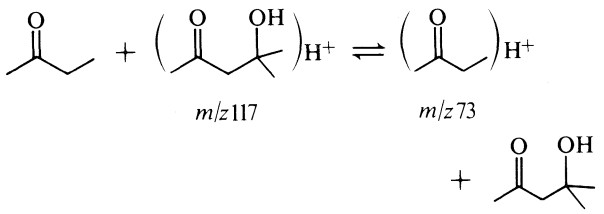

at 333 K and a total pressure of 8×10^{-5} Torr. An equilibrium constant of 4.9 ± 0.4 was obtained, from which it was determined that the proton affinity of diacetone alcohol was 4.4 kJ mol^{-1} (1.05 kcal mol^{-1}) less than that of 2-butanone which is reported (2) as 836.0 kJ mol^{-1} (199.8 kcal mol^{-1}).

Thus as shown in Fig. 1, the proton affinity of diacetone alcohol is 831.6 kJ mol^{-1} (198.8 kcal mol^{-1}) with an experimental uncertainty of ± 0.8 kJ mol^{-1} (± 0.2 kcal mol^{-1}).

There is no information on the proton affinities of hydroxy ketones in the literature (2) from which an estimate of the proton affinity of diacetone alcohol may be made. However, an additivity route may be followed wherein the proton affinity of the unsubstituted ketone 4-methyl-2-pentanone is estimated and the effect of substitution of a hydroxyl group for hydrogen at position 4 is determined. On the basis of proton affinities for 2-butanone, 836.0 kJ mol^{-1} (2), 3-pentanone, 842.6 kJ mol^{-1} (2), 3-methyl-2-butanone, 841.4 kJ mol^{-1} (2), and 3,3-dimethyl-2-butanone, 846.6 kJ mol^{-1} (2), the proton affinity of 4-methyl-2-pentanone is estimated to be 848.5 kJ mol^{-1} (202.8 kcal mol^{-1}). Based on this estimate, the substitution of a hydroxyl group for a hydrogen at position 4 would appear to lower the proton affinity by some 16.9 kJ mol^{-1} (4.0 kcal mol^{-1}); this effect is attributed to electron withdrawal by the hydroxy group and the formation of an intramolecular H-bond in the neutral species as depicted by structure **1**.

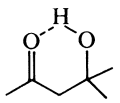

1

When a bridged structure is assumed also for the protonated species it is anticipated, as one of the referees has pointed out, that stabilization due to cyclization will be probably greater in the protonated species than for the neutral species. Thus the above argument for the lowering of the proton affinity of diacetone alcohol from that calculated by additivity rules to that observed experimentally would be invalidated. Enhanced stability due to cyclization of the protonated species should be manifested as enhanced proton affinity, yet the experimental findings indicate a lowered proton affinity. Thus we conclude that the formation of a bridged structure for the protonated species which is indicated by the ready infrared multiphoton dissociation of this species (1) does not explain, in itself, the lower than anticipated proton affinity of diacetone alcohol.

Mesityl oxide

The proton affinity of mesityl oxide was found to be close to that estimated from the addition (6.3 kJ mol^{-1}) of a methyl group to 3-penten-2-one (PA 864.8 kJ mol^{-1} (2)). Equilibria with respect to proton transfer between mesityl oxide and 2-propoxy-2-propane were readily established for each of several optimum mixtures (1:7.5) of the two compounds at a total pressure of 8×10^{-5} Torr. The equilibrium constant for the reaction

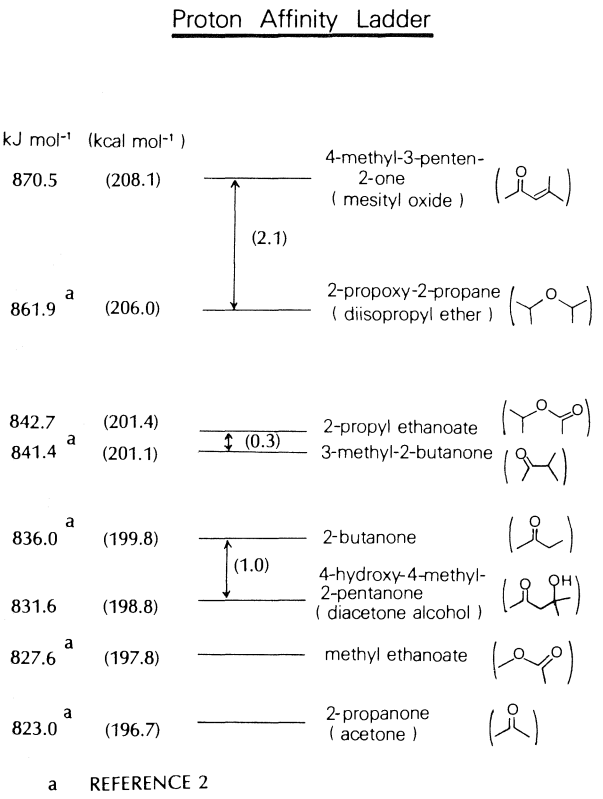

FIG. 1. Proton affinity ladder. Values for proton affinities are shown on the left hand side. Equilibria between pairs of compounds are shown by double-headed arrows with the value of ΔG for each equilibrium given in parentheses and in kcal mol^{-1}. Equilibria between each of 2-propanone and methyl ethanoate with diacetone alcohol could not be obtained as explained in the text.

[9] 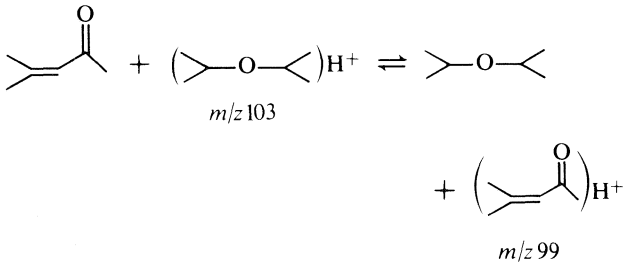

was determined to be 23 ± 2 at 333 K from which it was determined that the proton affinity of mesityl oxide exceeded that of 2-propoxy-2-propanone by 8.6 kJ mol^{-1}.

As the proton affinity of 2-propoxy-2-propanone is given (2) as 861.9 kJ mol^{-1} (206.0 kcal mol^{-1}), then the proton affinity of mesityl oxide is 870.5 kJ mol^{-1} (208.1 kcal mol^{-1}), as shown in Fig. 1 with an experimental uncertainty again of ±0.8 kJ mol^{-1}. The enhanced proton affinities of α,β unsaturated ketones with respect to aliphatic ketones we attribute to resonance stabilization of the protonated α,β unsaturated ketone.

[10] 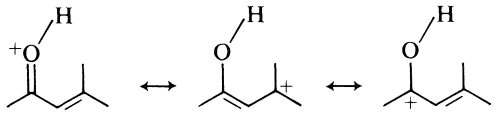

Isopropyl acetate

While the proton affinity of isopropyl acetate is not recorded in the literature, it was thought to be similar to that of the isomeric ester methyl 2-methyl propanoate which is given (2) as 843 kJ mol^{-1}. As the equilibrium is determined mass spectrometrically, a direct comparison between the two esters cannot be made without resorting to isotopic substitution.

Equilibrium between isopropyl acetate and 3-methyl-2-butanone, reaction [11], was readily established for several mixtures (1:1) at a total pressure of 8 × 10^{-5} Torr. Equilibrium was observed over a time period greater than that required to reach equilibrium.

[11] 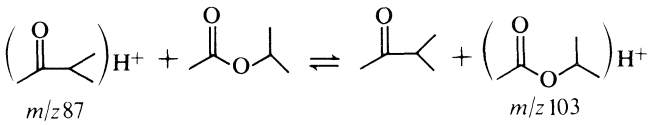

The equilibrium constant was found to be 1.6 ± 0.1 from which it was determined that the proton affinity of the former exceeded that of the latter by 1.3 kJ mol^{-1}. As the proton affinity of 3-methyl-2-butanone is given (2) as 841.4 kJ mol^{-1} (201.1 kcal mol^{-1}), then the proton affinity of isopropyl acetate is 842.7 kJ mol^{-1} (201.4 kcal mol^{-1}), as shown in Fig. 1, with an experimental uncertainty of ±0.6 kJ mol^{-1}.

1. A. KAMAR, A. B. YOUNG, and R. E. MARCH. Can. J. Chem. **64**, 1979 (1986).
2. S. G. LIAS, J. F. LIEBMAN, and R. D. LEVIN. J. Phys. Chem. Ref. Data **13**, 695 (1984).
3. M. A. ARMITAGE, M. J. HIGGINS, E. G. LEWARS, and R. E. MARCH. J. Am. Chem. Soc. **102**, 5064 (1980).
4. R. J. HUGHES, R. E. MARCH, and A. B. YOUNG. Can. J. Chem. **61**, 834 (1983).
5. R. H. NOBES and L. RADOM. Org. Mass Spectrom. **17**, 340 (1982).

Electrometric studies on molecular complexes. Part 1. Biamperometric study of some molecular complexes of iodine

RAM ADHAR SINGH
Department of Chemistry, Faculty of Science, Banaras Hindu University, Varanasi-221 005, India

Received January 13, 1986[1]

RAM ADHAR SINGH. Can. J. Chem. **64**, 2371 (1986).

A simple method for separate determination of thermodynamic parameters of molecular complexes in solution is reported. It is based on a polyiodide dissociation equilibrium in conjunction with the biamperometry. The equilibrium constants and the enthalpies determined by this method are in good agreement with the recent literature data, lending support for the applicability of the method. The advantages of the present technique over the other have been outlined.

RAM ADHAR SINGH. Can. J. Chem. **64**, 2371 (1986).

On décrit une méthode simple pour déterminer séparément les paramètres thermodynamiques de complexes moléculaires en solution. Cette méthode est basée sur un équilibre de dissociation d'un poly-iodure, de concert avec la biampérométrie. Les constantes d'équilibre ainsi que les enthalpies qui ont été déterminées par cette méthode sont en bon accord avec le données récentes de la littérature; ceci laisse croire que la méthode peut être appliquée. On met en relief les avantages de cette méthode par rapport aux autres techniques.

[Traduit par la revue]

Introduction

A molecular complex between an electron donor and an electron acceptor is an association somewhat stronger than Van der Waal's association, having definite stoichiometry in which the identities of the molecules are retained to a large extent (1). The existence of the molecular complexes has been recognized for a long time (2, 3), but the recent interest in this field arose after the discovery of new absorption bands in the electronic spectra of iodine in organic solvents by Benesi and Hildebrand (4). Mulliken proposed the valence bond theory of the molecular complex formation on the basis of charge transfer from the electron donor to the electron acceptor molecules (5, 6). Since then, this field has been an active area of research as is evident from a number of monographs (7–9) and reviews (10). However, there are a number of reports in the literature in which the experimental results do not conform to theoretical predictions (1, 11–14). These raised doubts on the reliability of experimental data obtained by electronic spectroscopy, particularly for weak molecular complexes (11). This conventional spectral method yields the equilibrium constant (K_c) and molar extinction coefficient (ϵ_λ) of the complex from the composite spectral data $K_c\epsilon_\lambda$, obtained from the slope of BH plots and ϵ_λ from the intercept (4). Since for weak molecular complexes, K_c is of the order of 1 $dm^3\ mol^{-1}$ whereas ϵ_λ is of the order of 10^4–$10^5\ dm^2\ mol^{-1}$, a slight error in the intercept (ϵ_λ values) would lead to a sizable error in K_c values. It has been suggested that if the K_c values can be determined separately and reliably, a more accurate value of ϵ_λ can be obtained from the composite spectral data, $K_c\epsilon_\lambda$ (11, 15). Recently we have explored the possibility of separate determination of K_c by common physical techniques, e.g., refractometry (16–18), surface tension measurement (19), spectral–solubility method (20), and the radiotracer solubility technique (21–23) for a range of molecular complexes and have found them as feasible and convenient alternative to the conventional electronic spectroscopy. No doubt, these techniques have distinct advantages, but they do offer some difficulties. For example, in the spectral solubility method, a prior knowledge of isosbestic point is needed for the separate determination of K_c (11, 20). In the radiotracer solubility method a radioactive constant activity source [$(CH_3)_4NI_5$*] is to be synthesized using radioactive molecular iodine prior to the addition of donors (21–24). To overcome these difficulties we turned our attention to the electrometric techniques which are known to yield reliable and quantitative determinations of iodine concentrations. The polyiodide-solubility equilibria offer a unique advantage. Once the equilibria in the solvent and donor solutions are established and the solutions have been removed from the constant activity source, they can be analysed by any technique which bears a quantitative relationship with the iodine concentration, at any temperature, in any medium, and in any chemical form (11, 20–23).

Motivated by this fact, we have initiated a study on the use of electrometric techniques for the direct determination of equilibrium constants and enthalpies of molecular complex formation in liquid solutions. The techniques like potentiometry, biamperometry, conductometry, etc., are well known for quantitative analysis (25–29) but they have been used only rarely in the study of molecular complexes.

Only a few reports have appeared in the literature on the use of the electrometric techniques in the study of molecular complexes (30–37). The polarography has been used to determine the formation constants for some aromatic molecular complexes with strong electron acceptors (30, 31). The conductometric titrations have been used to determine stoichiometries and the trend in the stabilities of some charge transfer complexes in solution (32–37). However, to the best of our knowledge, the above and other electrometric techniques have not been used for the determination of all thermodynamic parameters in the molecular complex formation equilibria. In this report, we have used the biamperometric titration method in conjunction with the constant activity method to evaluate the equilibrium constants, enthalpies, free energy, and entropy changes associated with the formation of molecular complexes in liquid solution. The acceptor chosen is molecular iodine which forms molecular complexes with electron donors ranging from some of the weakest to some of the strongest complexes known (1, 9). Also, a convenient constant activity source, namely, tetramethylammonium pentaiodide, $(CH_3)_4NI_5$, is available for this acceptor. The donors chosen are such that the recent data are available for comparison so that accuracy of the technique can be tested. The electron donors used in this study to form typically weak and moderate molecular complexes with iodine

[1]Revision received August 6, 1986.

are aromatic hydrocarbons, namely, benzene, mesitylene, hexamethylbenzene, biphenyl, naphthalene, and anthracene and aromatic amines, namely, diphenylamine, aniline, and *o*-toluidine. The biamperometric titration method will be discussed in detail in the next section.

Materials and methods

Carbon tetrachloride and benzene (BDH both of spectral grade) were dried over molecular sieve (A_4 size). Naphthalene and anthracene (both of BDH microanalytical reagent grade), hexamethylbenzene (Ega Chemie), biphenyl and diphenylamine (both of BDH AnalaR grade) were purified by fractional crystallization in suitable solvents. Mesitylene (Koch-light), aniline, and *o*-toluidine (both of E. Merck) were purified by fractional distillation at reduced pressure, after drying over KOH pellets. Tetramethylammonium iodide, $(CH_3)_4NI$, and tetramethylammonium pentaiodide, $(CH_3)_4NI_5$, were synthesized as reported in the literature (38). Sodium thiosulphate (AnalaR grade) and KIO_3 (AnalaR grade) were used without further purification. Deionized water was used for making aqueous solutions.

Constant activity method

This method is based on the dissociation equilibrium of tetramethylammonium pentaiodide $(CH_3)_4NI_5$ (11, 20–23) and is as follows:

$$[1]\quad (CH_3)_4NI_5(\text{solid}) \underset{\text{solvent}}{\overset{K_d}{\rightleftharpoons}} (CH_3)_4NI_3(\text{solid}) + I_2(\text{solvent})$$

where K_d is the dissociation constant of $(CH_3)_4NI_5$. At a fixed temperature and in a non-polar solvent, e.g., CCl_4, $(CH_3)_4NI_5$ and $(CH_3)_4NI_3$ are insoluble and remain as solids whereas the molecular iodine goes into the solvent. After the above equilibrium is reached a constant iodine concentration is obtained in CCl_4. The addition of donor, D, to the system (reaction [1]) results in the formation of the donor–iodine molecular complex. Assuming the stoichiometry of the complex as 1:1, donor–iodine equilibrium in CCl_4 solution can be written as follows:

$$[2]\quad D + I_2 \overset{K_c}{\rightleftharpoons} D.I_2$$

where K_c is the equilibrium constant. The above complex formation results in the loss of iodine obtained through reaction [1]. To compensate for this loss, some more $(CH_3)_4NI_5$ dissociates to maintain the same iodine concentration as in reaction [1]. The system now becomes,

$$[3]\quad (CH_3)_4NI_5(\text{solid}) + D(\text{solution}) \rightleftharpoons (CH_3)_4NI_3(\text{solid}) + (D.I_2 + I_2)(\text{solution})$$

The increase in iodine concentration in reaction [3] over to that in reaction [1] is equal to the concentration of the complex whereas the free iodine concentration in reaction [3] is the same as that in reaction [1].

It has been established experimentally that no other equilibria exist between polyiodides and donor–polyiodides (since the donor is in solution and polyiodides are solids and have I_5^- and I_3^- centers thus no interaction with electron donor is expected). In the experimental concentrations range, I_3^- species have also not been detected. The equilibrium constant, K_c, for eq. [2] can be written as

$$K_c = \frac{[DI_2]}{[D][I_2]} = \frac{(C_2 - C_1)}{(C_0 - (C_2 - C_1))C_1}$$

or

$$[4]\quad K_c = \frac{(C_2 - C_1)}{(C_0 + C_1 - C_2)C_1}$$

where C_0 is the initial donor concentration, C_1 is the concentration of iodine in solution after equilibrium [1] is reached, at a particular temperature, and in a particular solvent, and C_2 is the concentration of iodine in solution after the equilibrium [3] is reached, i.e. after adding the donor to the solvent–polyiodides system.

Thus with the help of the constant activity method, determination of K_c requires only a reliable estimation of iodine concentration in reactions [1] and [3]. We have made use of the biamperometry to determine the iodine concentrations in solutions.

Biamperometry

The biamperometric determination of the concentrations is performed by observing the changes in current as a function of titrant volume. A small emf (100–150 mV) is applied between two indicator electrodes (Pt–Pt or Pt–graphite) which are immersed in a well stirred solution. A reversible redox couple (6) must exist before or after the end point (24–29). In this particular case, we have iodine–iodide reversible couple and the titrant is aqueous sodium thiosulphate solution. One indicator electrode is platinum and the other is graphite. This electrode system has been found to be more sensitive than the Pt—Pt combination (39) and is used in all experiments in this study. Bradbury (40–41) and Kolthoff (42) have shown mathematically that the current in the equivalence point region is proportional to the concentration of iodine remaining in solution. Before the titrant is added, a large amount of iodine is present and a high current is observed. However as the titration proceeds, iodine reacts with sodium thiosulphate and iodide is formed, resulting in a decrease in iodine concentration and thus a decrease in current. The current is calibrated in this study against the deflection in a ballistic galvanometer, the torsion in its wire being proportional to the current passing through it. The deflection is spotted on a linear scale with the help of a small mirror, illuminated by light. The biamperometric titration method for estimating iodine concentrations requires very simple instrumentation and offers great sensitivity (10^{-5}–10^{-6} *M*). It is the best electrometric technique for determining the tracer concentration (26). The equivalence point is the intersection of two straight line portions in the galvanometer deflection vs. titrant volume plots and can be determined reliably.

Experimental

About 150 mg of $(CH_3)_4NI_5$ was placed in different stoppered vessels containing 50 mL CCl_4 in one and 50 mL of donor solutions of different concentrations in CCl_4 in others. These vessels were shaken in a thermostat maintained at a particular temperature for 2–3 days after which the dissociation equilibria of $(CH_3)_4NI_5$ were established as evident from a constant iodine concentration as a function of time. No I_3^- species in measurable amounts in any solutions were present as no electronic absorption bands at 363 and 290 nm, characteristics of I_3^- species, were detected (9, 11, 20). The iodine solutions in CCl_4 were then separated from $(CH_3)_4NI_5$ and $(CH_3)_4NI_3$ and iodine concentrations were determined using biamperometric titration method. Since iodine in CCl_4 could not be analysed with aqueous sodium thiosulphate due to phase separations, 10–20 mL methanol and some solid KI was added to facilitate the extraction of iodine from CCl_4 to the aqueous phase. An emf of 50–150 mV was applied between the electrodes. A 2 mL semimicroburette with 0.01 mL division graduation connected to a self-filling reservoir was used for adding the titrant.

The current is measured with the help of a ballistic galvanometer, the torsion being proportional to the current passing through it. Thus the greater the current, the higher the torsion in the wire of the ballistic galvanometer which is calibrated on a linear scale on which the mirror reflection from the galvanometer is spotted. The equivalence point was obtained by plotting galvanometer deflection against the titrant volume. At least three titrations were performed for each solution and the results were reproducible within the experimental error. It was found that the presence of donors in CCl_4 solution does not interfere with the quantitative estimations of iodine concentrations as the iodine concentrations obtained by this method are comparable to the results obtained using other methods (20–23). The equilibrium constants at different tmeperatures (25, 30, 35, 40°C) were calculated using eq. [4] and $-\Delta H^0$, $-\Delta G^0$, and ΔS^0 values for the complexes evaluated using suitable thermodynamic relations. The data were analysed by least squares on a ICL 1905 S computer.

Results and discussion

A representative set of biamperometric titration plots between the galvanometer deflection and titrant volume for the estima-

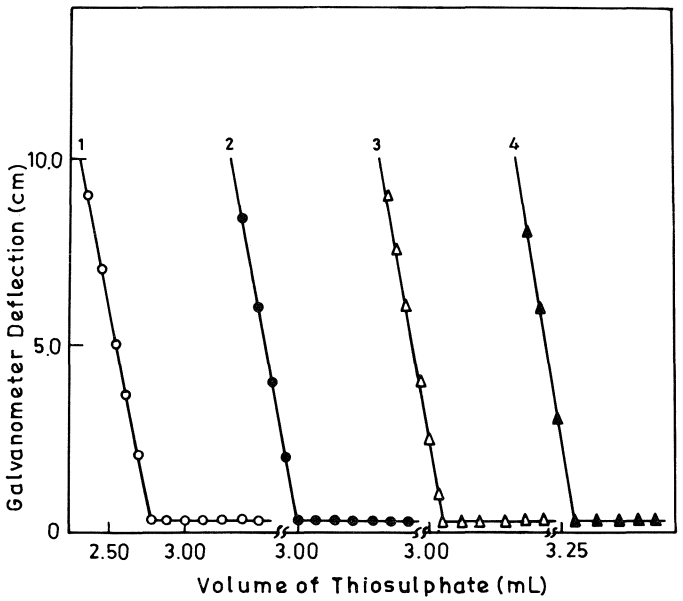

FIG. 1. Galvanometer deflection–titrant volume curves for biamperometric determination of iodine concentrations in solution using platinum–graphite electrode system for 10 mL iodine solutions after equilibration at 25°C. *1*, CCl_4; *2*, benzene (0.2 *M*); *3*, naphthalene (0.2 *M*); *4*, mesitylene (0.15 *M*). Concentration of sodium thiosulphate used = 3.25×10^{-3} *N*.

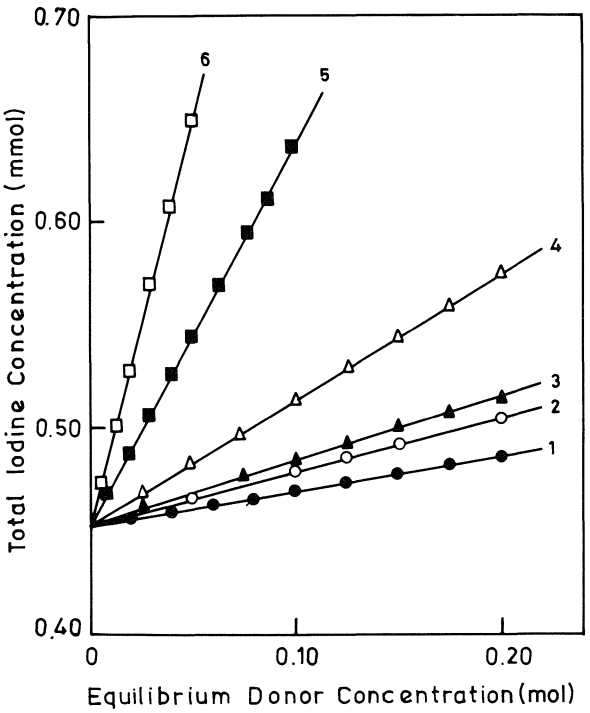

FIG. 2. Plot of total iodine concentration (mmol) against equilibrium donor concentration (mol) in CCl_4 at 25°C determined by biamperometry. *1*, Benzene; *2*, naphthalene; *3*, biphenyl; *4*, mesitylene; *5*, hexamethylbenzene; *6*, diphenylamine.

tion of iodine solutions in CCl_4 and donor solutions as indicated have been shown in Fig. 1. For all other iodine solutions, i.e., obtained for different donor concentrations and at different temperatures, similar titration plots have been obtained. It is evident from the slanted portion of the figure that a linear relationship exists between the galvanometer deflection and the concentration of iodine before the equivalence point. At and after the equivalence point, no redox couple (I_3^-/I^-) is present as all the iodine present has been consumed by thiosulphate, no deflection in the galvanometer is observed. This is evident from the horizontal linear portion in Fig. 1. The equivalence point is the intersection of the two linear portions (40–42).

The iodine concentrations determined by this method are in excellent agreement with those obtained by the spectral and the radiotracer techniques. The heat of dissociation of $(CH_3)_4NI_5$ obtained from the concentration of iodine in pure solvent at different temperatures using this method (34.1 kJ mol^{-1}) also agrees well with the available data (33.9 kJ mol^{-1} by the spectral solubility method (20) and 34.3 kJ mol^{-1} by the radiotracer solubility method (21).

The total iodine concentrations in different donor solutions in CCl_4 at 25°C as determined by biamperometry when plotted against the equilibrium donor concentrations vary linearly as shown in Fig. 2. The concentration of the different molecular complexes formed, determined from the increase in iodine concentrations for different donors concentrations in CCl_4 over that in the pure CCl_4 at 25°C is also found to vary linearly with the equilibrium donor concentrations. This indicates that predominantly 1:1 molecular complexes are formed in the experimental range of donor concentrations. This supports the assumption (reaction [2]) of 1:1 stoichiometries for all the complexes studied. The equilibrium constants for different complexes in CCl_4 at 25°C calculated using eq. [4] by least squares method are reported in Table 1. In the same table, we have also given the standard enthalpies ($-\Delta H^0$), free energy ($-\Delta G^0$), and entropy changes (ΔS^0) for different complexes.

Literature data are included in parentheses for comparison. It is evident that the results obtained by using this technique are in very good agreement with those obtained by spectral solubility and radiotracer solubility methods based on polyiodide dissociation equilibria. As reported earlier (9, 11, 22, 23), the values obtained by these methods are slightly higher than those obtianed by conventional spectral methods using Benesi–Hildebrand and related equations (10). This can be explained on the basis of the solubility method which includes both the specific (charge-transfer) and non-specific (solvent effects) interactions whereas the conventional spectral method is based on specific charge-transfer interactions only. The non-specific solvent effects include solvent caging, dispersion, and polarization effects (11, 20, 21). There is also the possibility of different conformational isomers of the complexes in solution. Thus with solubility equilibria, we observe the total effect of all the above parameters in addition to the specific charge transfer interactions, and hence a higher K_c value. In the case of aromatic amines the existence of mixed complexes of $n - \sigma$ as well as $\pi - \sigma$ in the same solution may also be responsible for higher K_c values. It may be mentioned here that it is quite difficult to determine the different contributions proposed above but when the molar extinction coefficients of these complexes are reevaluated using the composite $K_c\epsilon_\lambda$ value obtained from the slope of BH plots and K_c values obtained by the present method, the new ϵ_λ values vary in accordance with the Mulliken's theory, i.e. higher molar extinction coefficients for stronger complexes in a particular series (1). K_c and $-\Delta H^0$ values using the present technique also vary in the same order as predicted theoretically on the basis of the electron donating ability of different donors, viz. benzene < naphthalene < biphenyl < mesitylene < hexamethylbenzene < anthracene < diphenylamine < aniline < *o*-toluidine. The plot of $-\Delta H^0$ vs. ΔS^0 values for different complexes is nearly linear indicating

TABLE 1. Equilibrium constants and other thermodynamic parameters for the molecular complexes of iodine with some donors in CCl_4 solution determined by biamperometry

Donor	K_c (dm^3 mol^{-1}) (25°C)	$-\Delta H^0$ (kJ mol^{-1})	$-\Delta G^0$ (kJ mol^{-1}) (25°C)	$-\Delta S^0$ (J K^{-1})
Benzene	0.38±0.01 (0.40,[a] 0.36[b])	6.1±0.3 (6.3[a])	−1.04	24.0
Naphthalene	0.58±0.01 (0.62,[a] 0.54[c])	7.7±0.4 (7.1,[a] 8.0[c])	−0.58	27.8
Biphenyl	0.69±0.02 (0.51[c])	13.4±0.6 (14.8[c])	−0.40	46.3
Mesitylene	1.34±0.04 (0.89[d])	15.0±0.6	0.31	49.3
Hexamethylbenzene	3.20±0.05 (3.31,[a] 2.99[c])	17.8±0.8 (16.9,[a] 18.1[c])	1.25	55.5
Anthracene	6.25±0.051 (6.08[a])	18.6±0.8 (18.8[a])	1.96	55.8
Diphenylamine	8.20±0.10	21.3±0.8	2.25	63.9
Aniline	23.5±0.20 (21.6[c])	25.5±1.0	3.38	74.2
o-Toluidine	26.8±0.20 (25.0[c])	27.2±1.0	3.52	79.5

[a]Value from ref. 19.
[b]Value from ref. 11.
[c]Value from ref. 20.
[d]Value from ref. 43.

that sufficient charge-transfer contribution exists for the formation of these complexes.

Two systems, anthracene–iodine and diphenylamine–iodine, deserve special mention. These systems could not be studied by the spectral solubility method as their isosbestic points could not be located. Since the determination of isosbestic points is not needed in the present technique, these systems could be easily studied by the biamperometric technique and their K_c and $-\Delta H^0$ values have been determined. Thus this technique can be used successfully where other techniques have failed. Further study of alcohol–iodine, aliphatic amine–iodine, and some nitroamino–toluenes–iodine systems have indicated the general applicability of the present technique. These data are under publication elsewhere (44). The differential potentiometry has also successfully been used for separate determinations of equilibrium constants and enthalpies of the molecular complexes of iodine in liquid solution (45). This also supports the electrometric techniques as viable alternatives to conventional methods.

The results presented in this paper clearly show that the biamperometry solubility method is a convenient alternative to the conventional spectral method for the direct determination of equilibrium constants of molecular complexes in solution. It has some advantage over the spectral solubility method as the exact location of isosbestic points is not needed prior to establishing the solubility equilibria. In addition, the problem of overlapping spectral bands is avoided. The present method also has the advantage over the radiotracer solubility method as no labelled polyiodide source is needed. The biamperometry requires very simple instrumentation but offers great sensitivity. The method is relative and is best for electrometric determinations of low concentrations. The biamperometry–solubility is a useful combination which gives direct and reliable values of equilibrium constants and the other thermodynamic parameters for the molecular complexes in solutions.

Acknowledgements

The author is grateful to Professor S. M. Verma, Head, Department of Chemistry, Banaras Hindu University, Varanasi, for providing necessary facilities and for his interest in the work. Thanks are also due to Dr. Tej Bahadur Singh, Scientist(B), National Metallurgical Laboratory, Jamshedpur, for his help in some preliminary experiments. The publication cost assisted by CSIR (India) is thankfully acknowledged.

1. R. S. MULLIKEN and W. B. PERSON. Molecular complexes. Wiley Interscience, New York. 1969.
2. P. PFEIFFER. Organische molekulverbindungen. Ferdinand Enke, Stuttgart. 1927.
3. G. N. LEWIS. J. Franklin Inst. **226**, 293 (1938).
4. H. A. BENESI and J. H. HILDEBRAND. J. Am. Chem. Soc. **71**, 2703 (1949).
5. R. S. MULLIKEN. J. Am. Chem. Soc. **72**, 600 (1950).
6. R. S. MULLIKEN. J. Am. Chem. Soc. **74**, 811 (1952).
7. R. FOSTER. Organic charge transfer complexes. Academic Press, London. 1969.
8. R. FOSTER. Molecular complexes. Vols. I and II, Elek Science, London. 1973.
9. J. YARWOOD (*Editor*). Spectroscopy and structure of molecular complexes. Plenum Press, London. 1973.
10. C. N. R. RAO, S. N. BHAT, and P. C. DWIVEDI. Appl. Spectrosc. Rev. **5**, 1 (1971).
11. J. D. CHILDS, S. D. CHRISTIAN, and J. GRUDNES. J. Am. Chem. Soc. **94**, 5657 (1972).
12. P. H. EMSLIE, R. FOSTER, C. A. FYFE, and I. HORMAN. Tetrahedron, **21**, 2843 (1965).
13. W. B. PERSON. J. Am. Chem. Soc. **87**, 167 (1965).
14. R. L. SCOTT. J. Phys. Chem. **75**, 3843 (1971).
15. R. A. SINGH. Ph.D. Thesis, Banaras Hindu University, Varanasi. 1980.
16. R. A. SINGH and S. N. BHAT. Ind. J. Chem. **15A**, 1106 (1977).
17. R. A. SINGH and S. N. BHAT. J. Phys. Chem. **82**, 2322 (1978).

18. R. A. SINGH and S. N. BHAT. Bull. Chem. Soc. Jpn. **55**, 1624 (1982).
19. R. A. SINGH, S. P. MISHRA, and S. N. BHAT. Proc. Ind. Acad. Sci. **89**, 139 (1980).
20. R. A. SINGH and S. N. BHAT. Can. J. Chem. **59**, 1212 (1981).
21. S. P. MISHRA and R. A. SINGH. J. Chem. Soc. Faraday Trans. 1, **78**, 1767 (1982).
22. S. P. MISHRA, R. A. SINGH, and V. UPADHYAY. Proc. Int. Sym. Appl. Technol. Ion. Rad. Vol. 2, 913 (1982).
23. S. P. MISHRA, R. A. SINGH, and V. UPADHYAY. J. Radioanal. Nucl. Chem. Lett. **96**, 481 (1985).
24. S. P. MISHRA, R. A. SINGH, and V. UPADHAYA. Radiochim. Acta. In press.
25. D. R. BROWNING. Electrometric methods. McGraw Hill, New York. 1969.
26. J. BASSET, R. C. DENNEY, G. H. JEFFEREY, and J. MENDHAM. Vogel's textbook of quantitative inorganic analysis. 4th ed. ELBS Longman, London. 1978.
27. H. H. WILLARD, L. L. MERRITT, and J. A. DEAN. Instrumental methods of analysis. 5th ed. Von Nostrand, New York. 1974.
28. J. T. STOCK. Amperometric titrations. Interscience, New York. 1965.
29. J. T. STOCK. Anal. Chem. **46**, 1 (1974).
30. M. E. PEOVER. Trans. Faraday Soc. **60**, 417 (1964).
31. R. D. HOLM, W. R. CARPER, and J. A. BLANCHER. J. Phys. Chem. **71**, 3960 (1967).
32. F. GUTMAN and H. KEYZER. Electrochim. Acta, **11**, 555 (1966).
33. F. GUTMAN and H. KEYZER. Electrochim. Acta, **11**, 1163 (1966).
34. F. GUTMAN and H. KEYZER. Electrochim. Acta, **12**, 1255 (1967).
35. M. V. RAMANMURTHY and A. QAYUM. Ind. J. Chem. **12**, 1308 (1974).
36. M. V. RAMANMURTHY and A. QAYUM. Trans. SAEST, **11**, 503 (1976).
37. M. V. RAMANMURTHY and P. V. S. S. PRABHU. Electrochim. Acta, **27**, 481 (1982).
38. T. MOELLER (*Editor*). Inorganic syntheses. Vol. V. McGraw Hill, New York. 1957.
39. T. B. SINGH. Ph.D. Thesis. Banaras Hindu University, Varanasi. India. 1981.
40. J. H. BRADBURY. Trans. Faraday Soc. **49**, 304 (1953).
41. J. H. BRADBURY. Trans. Faraday Soc. **50**, 959 (1954).
42. I. M. KOLTHOFF. Anal. Chem. **26**, 1685 (1954).
43. B. B. BHOWMICK and S. P. CHATTOPADHYAY. Spectrochim. Acta, **37**A, 135 (1981).
44. R. A. SINGH. Part II. To be published.
45. R. A. SINGH. Part III. To be published.

X-ray and ^{1}H nmr analyses of 5-(*m*-benzyloxybenzyl)-1-[(1,3-dihydroxy-2-propoxy)methyl]uracil, an acyclonucleoside inhibitor of uridine phosphorylase[1]

GEORGE I. BIRNBAUM AND JEAN-ROBERT BRISSON
Division of Biological Sciences, National Research Council of Canada, Ottawa, Ont., Canada K1A 0R6

AND

SHI HSI CHU, ZHI HAO CHEN, AND ELIZABETH C. ROWE
Division of Biology and Medicine, Brown University, Providence, RI 02912, U.S.A.

Received April 21, 1986

GEORGE I. BIRNBAUM, JEAN-ROBERT BRISSON, SHI HSI CHU, ZHI HAO CHEN, and ELIZABETH C. ROWE. Can. J. Chem. **64**, 2376 (1986).

The title compound crystallizes in the triclinic space group $P\bar{1}$ and the cell dimensions are a = 16.890(3), b = 9.586(2), c = 6.316(1) Å, α = 91.09(1), β = 93.50(1), γ = 93.04(1)°. X-ray intensity data were measured on a diffractometer, and the crystal structure was determined by direct methods. Least-squares refinement, which included all hydrogen atoms, converged at R = 0.056 for 3454 observed reflections. Adjacent six-membered rings are approximately perpendicular to one another. The glycosidic torsion angle [C(6)—N(1)—C(1′)—O(4′)] is 96.2(2)°. In the acyclic moiety, both C—OH bonds are *gauche* with respect to C(4′)—O(4′). The *gauche* conformation is also dominant in solution, as determined by high-resolution ^{1}H nmr spectroscopy. Results of nuclear Overhauser experiments lead to conclusions about the flexibility of the molecule.

GEORGE I. BIRNBAUM, JEAN-ROBERT BRISSON, SHI HSI CHU, ZHI HAO CHEN et ELIZABETH C. ROWE. Can. J. Chem. **64**, 2376 (1986).

Le composé mentionné dans le titre cristallise dans le groupe d'espace $P\bar{1}$, avec a = 16,890(3), b = 9,586(2), c = 6,316(1) Å, α = 91,09(1), β = 93,50(1) et γ = 93,04(1)°. On a mesuré les données d'intensité des rayons-X à l'aide d'un diffractomètre et on a déterminé la structure cristalline par des méthodes directes. On a affiné la structure, incluant tous les atomes d'hydrogènes, par la méthode des moindres carrés jusqu'à une valeur de R = 0,056 pour 3454 réflexions observées. Les cycles à six chaînons qui sont adjacents sont pratiquement perpendiculaires l'un par rapport à l'autre. L'angle de torsion de la liaison glycosidique [C(6)—N(1)—C(1′)—O(4′)] est égal à 96,2(2)°. Dans la portion acyclique, les deux liaisons C—OH sont *gauche* par rapport à la liaison (C4′)—O(4′). D'après la rmn du ^{1}H à haute résolution, la conformation *gauche* prédomine aussi en solution. En se basant sur les résultats d'effets Overhauser nucléaires, on a tiré des conclusions relatives à la flexibilité de la molécule.
[Traduit par la revue]

Introduction

The title compound, also called 4′-hydroxymethyl-5-benzyloxybenzylacyclouridine, HM–BBAU (1), is a derivative of 5-benzyloxybenzylacyclouridine (BBAU) (2–4) and is one of the most potent inhibitors known to date for the enzyme uridine phosphorylase (UrdPase). It is a uridine analog of the antiviral agent known variously as 9-(1,3-dihydroxy-2-propoxymethyl)guanine or DHPG (5), 2′-nor-2′-deoxyguanosine or 2′NDG (6), or BIOLF-62 (7), and was originally synthesized to improve the water solubility characteristics of BBAU.

Uridine phosphorylase is one of two important mammalian phosphorylases in the salvage pathway of nucleic acid metabolism. As inhibition of this enzyme would be expected to affect adversely the growth and replication of cells, it is a target enzyme in the design of drugs for cancer chemotherapy (8). Inhibitors of uridine phosphorylase are potentially useful not only as inhibitors of pyrimidine salvage but also as potentiators of the action of antineoplastic drugs such as 5-fluoro-2′-deoxyuridine (FUdR, FdUrd) which are subject to phosphorolytic cleavage *in vivo* to less active and more toxic bases (4).

The "acyclo" side chain (beta-hydroxyethoxymethyl-) of acyclovir and of BBAU is an open chain corresponding to the C(1′)—O(4′)—C(5′)—O(5′) portion of the furanose ring of natural nucleosides. HM derivatives carry the resemblance one carbon atom further, containing both C(5′)—OH and C(3′)—OH groups in the side chain.

The crystal structure and conformation of acyclovir have been determined (9), with especial attention to the conformation of the side chain (two orientations in the three independent molecules) and its possible relevance to antiviral activity. The inhibitory activity of the BBAUs against UrdPase (no antiviral activity) may be mediated by other parts of the molecule as well. For these reasons, we considered it worthwhile to determine the detailed conformation of HM–BBAU (**1**) in the solid state and in solution.

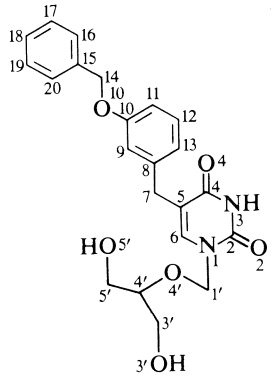

1

Experimental

HM–BBAU was prepared as previously described (1) and crystallized from ethanol. Precession photographs indicated the triclinic space group $P\bar{1}$. A prism measuring 0.15 × 0.25 × 0.50 mm was mounted on a CAD4 diffractometer; the crystal data are as follows:

$C_{22}H_{24}N_2O_6$ mw = 412.43
Triclinic, a = 16.890(3), b = 9.586(2), c = 6.316(1) Å, α = 91.09(1), β = 93.50(1), γ = 93.04(1)°, V = 1018.8 Å^3, ρ_c =

[1]NRCC No. 26398.

1.34 g cm^{-3}, $Z = 2$ (20°C, CuKα_1, $\lambda = 1.54056$ Å); $F(000) = 436$, μ(CuKα) = 7.7 cm^{-1}.

Unit cell dimensions were determined from a least-squares refinement of the angular settings of 25 high-order ($40 < \theta < 50°$) reflections. Intensities were measured with Ni-filtered CuKα radiation, using $\omega/2\theta$ scans with variable scan ranges and speeds. Three standard reflections were measured at regular intervals; their intensities decreased to 75% of the starting values during the data collection. Of the 4231 unique reflections with $\theta \leqq 76°$ there were 3458 (81.7%) with $I \geqq 3\sigma(I)$ which were considered observed. The intensities were corrected for crystal decay and for Lorentz and polarization factors; absorption corrections were unnecessary.

The structure was determined by direct methods with the aid of the computer program MULTAN 78 (10). Of the 64 starting sets subjected to tangent refinement, the solution with the highest combined figure of merit yielded an E map on which all 30 non-hydrogen atoms were located. The atomic parameters of these atoms were refined by block-diagonal least squares with anisotropic temperature parameters. All hydrogen atoms were found on difference Fourier maps and their parameters were refined with isotropic temperature factors. The scattering factors were taken from the "International tables for X-ray crystallography" (11). Throughout the refinement the function $\Sigma w(|F_o| - |F_c|)^2$ was minimized and a factor of 0.8 applied to all shifts. The following weighting scheme was used during the final stages: $w = w_1 \cdot w_2$, where $w_1 = 1$ for $|F_o| \leqq 5$, $w_1 = 5/|F_o|$ for $|F_o| > 5$; and $w_2 = \sin^2\theta/0.5$ for $\sin^2\theta < 0.5$, $w_2 = 1$ for $\sin^2\theta \geqq 0.5$. This scheme made the average values of $w(\Delta F^2)$ independent of $|F_o|$ and $\sin^2\theta$. After the final cycle the average parameter shift equalled 0.06σ and the largest 0.50σ. Four strong, low-order reflections suffered from secondary extinction effects and were given zero weights. The final conventional residual index R is 0.056 and the weighted index R_w is 0.079. A final difference Fourier map showed no significant features. The coordinates of non-hydrogen atoms are listed in Table 1. Anisotropic temperature parameters, hydrogen atom parameters, and a list of observed and calculated structure factors are available from the Depository of Unpublished Data.[2]

The proton nuclear magnetic resonance spectrum of HM–BBAU at 300 K was obtained on a Bruker AM-500 spectrometer. The sample (10 mg) was dissolved in 0.5 mL DMSO-d_6 with a drop of tetramethylsilane as the internal reference. The ^{1}H nmr spectrum was assigned by spin decoupling and two-dimensional homonuclear shift-correlated experiments. The nuclear Overhauser experiments were performed by irradiation of each separate line in a multiplet (12) followed by subtraction of one off-resonance control.

Results and discussion

Solid-state structure

A stereoscopic view of the molecule is shown in Fig. 1. The pyrimidine ring is almost planar, C(2) deviating most from coplanarity (by 0.007(2) Å); the two benzene rings are completely planar. The dihedral angle between the pyrimidine ring and the benzene ring attached to C(7) is 82.0° while the angle between the two benzene rings is 96.1°. The former orientation is necessary in order to avoid steric interactions between two six-membered rings joined by a single carbon atom. However, the relative orientation of the two benzene rings, joined by —O—CH_2—, is not only unnecessary but is, in fact, highly unusual. We will discuss this feature in more detail below.

Most bond lengths in the pyrimidine moiety (Fig. 2) are in good agreement with average values which we recently calculated for thymine residues (13). The only exception is the lengthening of the C(4)—C(5) bond by 0.011 Å, probably attributable to the bulky substitution at C(7). The agreement in bond angles is also very good, except at C(2) where N(1)—C(2)—N(3) is 1.5° larger while N(1)—C(2)—O(2) is 1.7° smaller than normal; these deviations amount to 3σ.

The glycosidic torsion angle is 96.2(2)° (Fig. 3). This is exactly the mean value for ten molecules of acyclonucleosides in which C(1′) is a secondary carbon atom (14). In this conformation there is minimal steric interaction between the aglycon and its acyclic side chain. The conformations about the C(3′)—C(4′) and C(4′)—C(5′) bonds (Fig. 3) are those favored by the *gauche* effect (15). In the former case the orientation of adjacent C—O bonds is *gauche*$^-$ while in the latter it is *gauche*$^+$. The C(1′)—O(4′) bond is significantly shorter than C(4′)—O(4′). This phenomenon is commonly observed in nucleosides as well as in acyclonucleosides (9, 16, 17).

The following three intermolecular hydrogen bonds are observed in the crystal:

O(3′)—H···O(5′)—H···O(2) N(3)—H···O(4)

The distances and angles are listed in Table 2. The corrected H···A distances were calculated after extending the covalent O—H and N—H bond lengths to their nominal values of 0.97 and 1.04 Å, respectively. As expected on the basis of the cooperativity effect (18), the O(5′)—H···O(2) bond is the strongest one.

The packing of the molecules in the crystal is shown in Fig. 4. As in the individual molecules, benzene rings in adjacent molecules are almost perpendicular to one another. Thus, H(12)

TABLE 1. Final atomic coordinates and thermal parameters[a]

Atom	x/a	y/b	z/c	U_{eq}
N(1)	8834(1)	6064(2)	−784(3)	460
C(2)	9487(1)	6384(2)	578(3)	466
O(2)	9995(1)	7270(2)	185(3)	622
N(3)	9537(1)	5613(2)	2380(3)	451
C(4)	8999(1)	4582(2)	2955(3)	428
O(4)	9110(1)	3967(2)	4630(2)	542
C(5)	8316(1)	4302(2)	1467(3)	423
C(6)	8271(1)	5046(2)	−306(3)	448
C(7)	7710(1)	3168(2)	1947(3)	457
C(8)	7156(1)	3536(2)	3641(3)	420
C(9)	6939(1)	2544(2)	5081(3)	452
C(10)	6390(1)	2804(2)	6574(3)	485
O(10)	6239(1)	1718(2)	7902(3)	625
C(11)	6048(2)	4080(3)	6659(4)	616
C(12)	6270(2)	5081(3)	5216(5)	701
C(13)	6817(2)	4827(2)	3731(4)	585
C(14)	5763(1)	1938(3)	9654(4)	625
C(15)	4885(1)	1822(2)	9107(4)	524
C(16)	4377(2)	2141(3)	10674(5)	696
C(17)	3564(2)	2003(4)	10292(6)	808
C(18)	3244(2)	1564(4)	8350(6)	808
C(19)	3736(2)	1247(3)	6756(5)	755
C(20)	4559(2)	1372(3)	7137(4)	611
C(1′)	8735(1)	6898(2)	−2697(3)	526
C(3′)	8618(3)	9699(4)	−5148(5)	891
O(3′)	8869(2)	8603(2)	−6426(3)	952
C(4′)	8797(2)	9409(3)	−2866(4)	589
O(4′)	8407(1)	8157(2)	−2124(3)	602
C(5′)	8527(2)	10589(3)	−1505(4)	615
O(5′)	8916(1)	10616(2)	521(3)	679

[a]All values were multiplied by 10^4. $U_{eq} = (1/3)\sum_i\sum_j U_{ij}a_i^*a_j^*\boldsymbol{a}_i\cdot\boldsymbol{a}_j$.

[2]These tables may be purchased from the Depository of Unpublished Data, CISTI, National Research Council of Canada, Ottawa, Ont., Canada K1S 0S2.

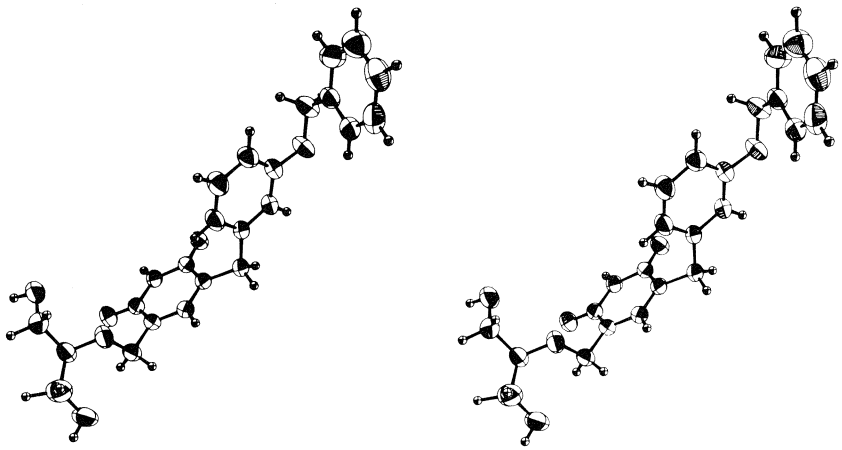

FIG. 1. Stereoscopic view of HM–BBAU; the thermal ellipsoids correspond to 50% probability.

TABLE 2. Distances and angles for hydrogen bonds

			Distances, Å			Angles, deg
D	*A*	*A* at	*D*···*A*	H···*A*	H···A_{corr}	*D*—H···*A*
O(3′)—H···O(5′)		$x, y, -1 + z$	2.755	1.98	1.85	156
O(5′)—H···O(2)		$2 - x, 2 - y, \bar{z}$	2.725	1.80	1.77	167
N(3)—H···O(4)		$2 - x, 1 - y, 1 - z$	2.881	1.99	1.85	170

and H(13) are pointed toward the π-electron cloud of the terminal benzene ring in a symmetry-related molecule, as indicated by fairly short H(12)···C(19) and H(13)···C(18) distances, 2.85 and 2.83 Å, respectively.

Solution conformation of the hydroxymethyl groups

The conformations about the C(4′)—C(3′) and C(4′)—C(5′) bonds are the same since the geminal protons of C(3′) and C(5′) have similar chemical shifts (Table 3) and coupling constants. In solution, the hydroxymethyl group is usually assumed to be in dynamic equilibrium between three staggered rotamers. The observed vicinal coupling constants are then an average of the coupling constants for each rotamer. Using the modified Karplus equation proposed by Haasnoot *et al.* (19), the coupling constants for each rotamer were obtained and from these the fractional populations of the three rotamers were estimated (Table 4). Since the assignment of the geminal protons can be reversed, there are two possible solutions. However, in the solid state both *gauche* rotamers are present, but not the *trans* rotamer (Fig. 3). Consequently, the first set of values in Table 4 is in better agreement with the X-ray results and with the *gauche* effect (15) and is therefore more likely (16).

Solution conformation about other bonds

The degree of flexibility of the molecule could be ascertained by observing that the protons of all the other CH_2 groups (i.e. at C(7), C(14), and C(1′)) appeared as single lines. If the molecule had been rigid or a CH_2 group slowly reorienting itself between different conformers, the individual protons in the CH_2 group would have different chemical shifts.

Nuclear Overhauser experiments presented in Table 5 also indicate that there is a high degree of internal motion in the molecule since both positive and negative nOe's were observed when irradiating different resonances. The sign of the nOe depends on the correlation times of the protons which experience an nOe, and as the degree of internal motion increases more positive nOe values should be observed (20). Thus, upon saturation of the H(1′) signal a negative enhancement was observed for H(6) while a positive enhancement was observed for H(4′), indicating that there is more internal motion between H(4′) and H(1′) than between H(6) and H(1′). Hence, there appears to be more rotation about the C(4′)—O(4′)—C(1′) linkage than about the N(1)—C(1′) bond. This interpretation of the nOe's is in agreement with the observed preference for a torsional angle of ~90° about the N(1)—C(1′) bond (see above). There is, nevertheless, sufficient flexibility about the glycosidic bond to allow a change from the *anti* to the *syn* conformation. This may be relevant to the interaction of HM–BBAU with UrdPase in view of the suggestion that the natural substrate, i.e. uridine, is in the *syn* conformation when bound to the enzyme (14). Upon saturation of the H(7) resonances a negative enhancement was observed for H(6) while positive values were detected for H(9) and H(13), again suggesting that the C(7)—C(8) bond is more flexible than C(5)—C(7). When the resonance of H(14) was irradiated, only positive enhancements were observed for H(9), H(11), H(16), and H(20), indicating a higher degree of internal motion about the C(10)—O(10)—C(14)—C(15) bonds.

Biological implications

In recent years it has been found (2, 21–23) that addition of the acyclo side chain to a series of uracils increases the inhibition of S-180 cytosol UrdPase by a factor of $10–10^2$ over that of the corresponding uracil. It was also found that a free terminal —OH group in the acyclo side chain was necessary for activity. Since substitution of the terminal —OH by a chloro or nitro group, or esterification, resulted in loss of the inhibitory capacity, and substitution by an amino group diminished but did not abolish it, it was concluded that hydrogen bonding in this region was important in binding the

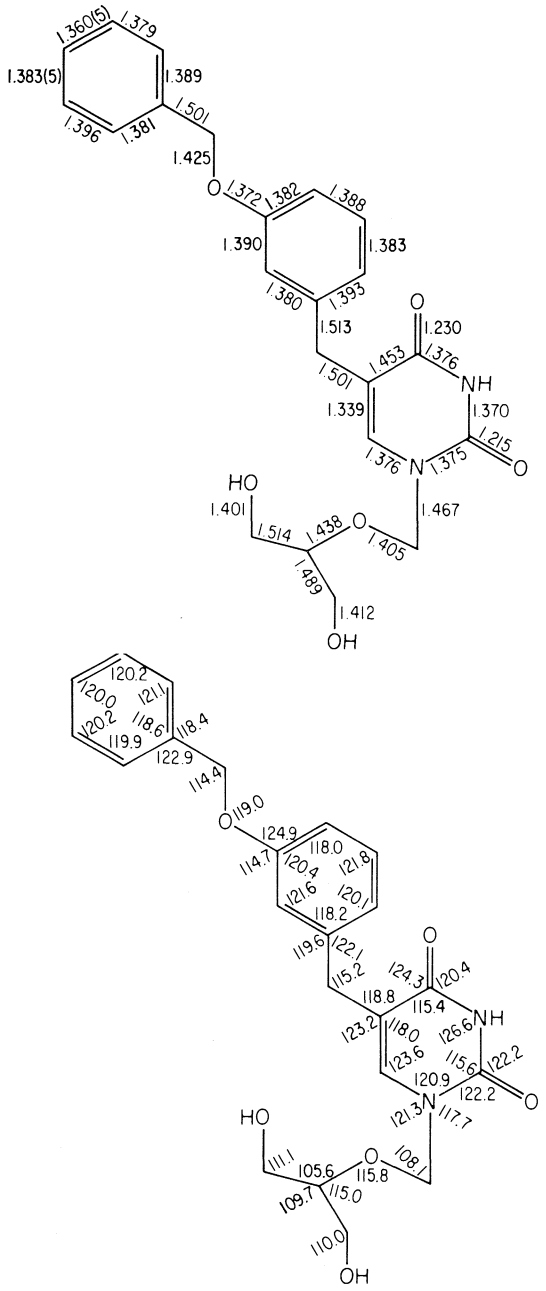

FIG. 2. (Top) Bond distances (in Å); unless otherwise indicated, their estimated standard deviations (esd's) are 0.003–0.004 Å. (Bottom) Bond angles (in deg); their esd's are 0.2–0.3°.

inhibitor to the enzyme (21). The participation of the —NH and 2-keto groups in hydrogen bonding also appears to be essential.

The early observation of increased binding of acyclothymidine over acyclouridine (21) and the comparative inhibitory activities of a series of uracil derivatives evaluated by Baker and Kelley (24) led to the speculation that a hydrophobic region exists adjacent to the active site of UrdPase and participates in the binding of effective inhibitors. In support of this conclusion, Niedzwicki *et al.* (2) have calculated from inhibition constants that the contributions of $\Delta G^{0\prime}$ brought about by substituting a benzyloxy group on the *meta* position of 5-benzyluracil and converting the uracil to an acyclouridine are very nearly additive. Both regions seem to be involved in the binding of the inhibitor to UrdPase.

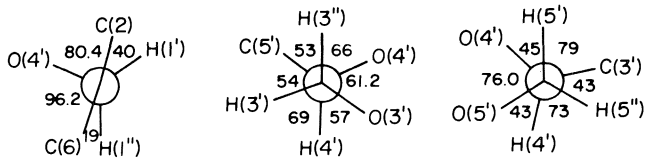

FIG. 3. Newman projections along N(1)—C(1′), C(3′)—C(4′), and C(4′)—C(5′). The esd's are 0.2–0.3° for torsion angles which do not involve hydrogen atoms and 2° for those which do.

TABLE 3. First order proton chemical shifts (in ppm) for HM–BBAU

H	δ (H)	H	δ (H)
H(6)	7.634	H(16), H(20)	7.441
H(7)	3.511	H(17), H(19)	7.383
H(9)	6.907	H(18)	7.320
H(11)	6.839	H(1′)	5.182
H(12)	7.182	H(3′)	3.458, 3.361
H(13)	6.827	H(4′)	3.553
H(14)	5.055	H(5′)	3.458, 3.361

TABLE 4. Population of rotamers (in %) for the hydroxymethyl groups in HM–BBAU

		Population		
$^3J(H,H_a)$	$^3J(H,H_b)$	*gauche*$^+$	*trans*	*gauche*$^-$
4.6	6.1	46	22	32
6.1	4.6	20	43	37

As mentioned above, the orientation of the two benzene rings in HM–BBAU is unusual. A survey of the recent Cambridge crystallographic database (25) revealed twelve molecules with an Ar—O—CH_2—Ar fragment. In all of the them the C(Ar)—O—CH_2—C(Ar) torsion angle corresponds to a *trans* orientation about the O—CH_2 bond, the average absolute value of that angle being 174(3)°. In HM–BBAU the torsion angle C(10)—O(10)—C(14)—C(15) has the abnormal value of 82.1(3)°. The orientation about the C(14)—C(15) bond is also somewhat unusual, the O(10)—C(14)—C(15)—C(20) torsion angle being only 5.6(2)°. In only three of the twelve molecules surveyed was the corresponding angle less than 11°, the other nine ranged from 24 to 82°. The small angle in HM–BBAU brings about a non-bonded interaction between O(10) and H(20) which is relieved by increasing the bond angle O(10)—C(14)—C(15) to 114.4(2)°. The solid-state conformation of the benzyloxybenzyl moiety may be significant in view of the suggestion that this hydrophobic portion of HM–BBAU fits into a binding site adjacent to the active site of UrdPase.

The near-perpendicular orientation of the two benzene rings in the HM–BBAU molecule and the "herringbone" packing of these rings in the crystal lattice, where H atoms at the edge of one molecule point toward C atoms on the face of the adjacent molecule (Fig. 4), are reminiscent of recent findings by Burley and Petsko (26). Their analysis of four biphenyl peptides or peptide analogs and 34 proteins revealed similar aromatic–aromatic interactions which, it was suggested, may contribute to the stabilization of protein structures. Similarly, the binding of HM–BBAU to UrdPase must be stabilized by an interaction

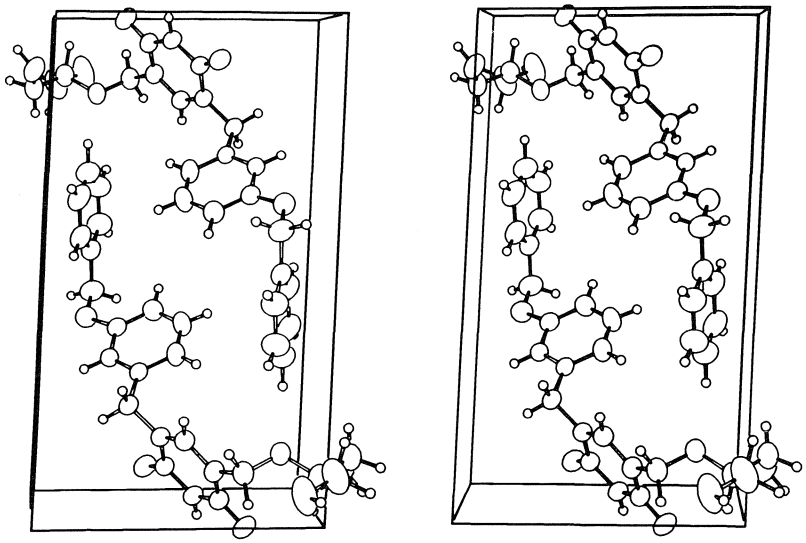

FIG. 4. Stereoscopic view of the molecular packing in the crystal. The directions of the axes are $x \uparrow$, $y \leftarrow$, $z \odot$.

TABLE 5. Intensity changes (in %) due to nuclear Overhauser effects[a]

Saturated signal	H(6)	H(7)	H(9)	H(11)	H(12)	H(13)	H(14)	H(16) H(20)	H(1′)	H(4′)
H(6)	[b]	−1	<−1	<−1	−2				−1	
H(7)	−1	[b]	+1			+2				
H(9)		<+1	[b]				+3	+1		
H(12)	<−1			−3	[b]	−3				
H(14)			+3	+4			[b]	+5		
H(1′)	−1								[b]	+2

[a]The estimated errors are ±20%.
[b]The area of the saturated peak was set to −100%.

between the benzene rings of the inhibitor with aromatic residues of the enzyme.

Acknowledgements

Apart from the MULTAN system (10), all crystallographic calculations were carried out with programs written by Ahmed *et al.* (27). Figures 1 and 4 were drawn with the ORTEP program of Johnson (28). This work was supported in part by United States Public Health Service Grants CA 13943, CA 20892 and CA 39427.

1. S. H. CHU, Z. H. CHEN, E. C. ROWE, F. N. M. NAGUIB, M. H. EL KOUNI, and M. Y. CHU. Nucleosides Nucleotides, **3**, 303 (1984).
2. J. G. NIEDZWICKI, S. H. CHU, M. H. EL KOUNI, E. C. ROWE, and S. CHA. Biochem. Pharmacol. **31**, 1857 (1982).
3. S. H. CHU, M. Y. CHU, F. N. M. NAGUIB, M. H. EL KOUNI, S. CHA, and P. CALABRESI. Proc. Am. Assoc. Cancer Res. **24**, 305 (1983).
4. M. Y. CHU, F. N. M. NAGUIB, M. H. ILTZSCH, M. H. EL KOUNI, S. H. CHU, S. CHA, and P. CALABRESI. Cancer Res. **44**, 1852 (1984).
5. J. C. MARTIN, C. A. DVORAK, D. F. SMEE, T. R. MATTHEWS, and J. P. H. VERHEYDEN. J. Med. Chem. **26**, 759 (1983).
6. W. T. ASHTON, J. D. KARKAS, A. K. FIELD, and R. L. TOLMAN. Biochem. Biophys. Res. Commun. **108**, 1716 (1982).
7. K. O. SMITH, K. S. GALLOWAY, W. L. KENNELL, K. K. OGILVIE, and B. K. RADATUS. Antimicrob. Agents Chemother. **22**, 55 (1982).,
8. H. J. SCHAEFFER. *In* Nucleosides, nucleotides, and their biological applications. *Edited by* J. L. Rideout, D. W. Henry, and L. M. Beacham III. Academic Press, New York. 1983. p. 1.
9. G. I. BIRNBAUM, M. CYGLER, and D. SHUGAR. Can. J. Chem. **62**, 2646 (1984).
10. P. MAIN, S. E. HULL, L. LESSINGER, G. GERMAIN, J. P. DECLERCQ, and M. M. WOOLFSON. MULTAN78, University of York, England, and University of Louvain, Belgium. 1978.
11. International tables for X-ray crystallography. Vol. IV. Kynoch Press, Birmingham. 1974.
12. M. KINNS and J. K. M. SANDERS. J. Magn. Reson. **56**, 518 (1984).
13. G. I. BIRNBAUM, K. L. SADANA, W. J. P. BLONSKI, and F. E. HRUSKA. J. Am. Chem. Soc. **108**, 1671 (1986).
14. G. I. BIRNBAUM and D. SHUGAR. *In* Topics in nucleic acid structure. Part 3. *Edited by* S. Neidle. Macmillan, London. In press.
15. S. WOLFE. Acc. Chem. Res. **5**, 102 (1972).
16. G. I. BIRNBAUM, R. STOLARSKI, Z. KAZIMIERCZUK, and D. SHUGAR. Can. J. Chem. **63**, 1215 (1985).
17. G. I. BIRNBAUM, E. DE CLERCQ, P. W. HATFIELD, and M. J. ROBINS. Heterocycles. In press.
18. G. A. JEFFREY and J. MITRA. Acta Crystallogr. Sect. B, **39**, 469 (1983).
19. C. A. G. HAASNOOT, F. A. A. M. DE LEEUW, and C. ALTONA. Tetrahedron, **36**, 2783 (1980).
20. J. H. NOGGLE and R. E. SCHIRMER. The nuclear Overhauser effect. Academic Press, New York. 1971.
21. J. G. NIEDZWICKI, M. H. EL KOUNI, S. H. CHU, and S. CHA. Biochem. Pharmacol. **32**, 399 (1983).

22. J. G. NIEDZWICKI, M. H. EL KOUNI, S. H. CHU, and S. CHA. Biochem. Pharmacol. **30**, 2097 (1981).
23. H. M. ABRAMS, L. HO, and S. H. CHU. J. Heterocycl. Chem. **18**, 947 (1981).
24. B. R. BAKER and J. L. KELLEY. J. Med. Chem. **13**, 461 (1970).
25. F. H. ALLEN, S. BELLARD, M. D. BRICE, B. A. CARTWRIGHT, A. DOUBLEDAY, H. HIGGS, T. HUMMELINK, B. G. HUMMELINK-PETERS, O. KENNARD, W. D. S. MOTHERWELL, J. R. RODGERS, and D. G. WATSON. Acta Crystallogr. Sect. B, **35**, 2331 (1979).
26. S. K. BURLEY and G. A. PETSKO. Science, **229**, 23 (1985).
27. F. R. AHMED, S. R. HALL, M. E. PIPPY, and C. P. HUBER. J. Appl. Crystallogr. **6**, 309 (1973).
28. C. K. JOHNSON. ORTEP II Report ORNL-5138, Oak Ridge National Laboratory, Oak Ridge, TN. 1976.

ipso Nitration. XXVII.[1] The crystal structure and stereochemistry of 3-bromo-6-methyl-6-nitrocyclohexa-2,4-dienyl acetate, 5-bromo-2-methyl-6-nitrocyclohexa-2,4-dienyl acetate, and 3-bromo-6-methyl-6-nitrocyclohexa-2,4-dienyl chloride

GORDON W. BUSHNELL, ALFRED FISCHER, GEORGE N. HENDERSON, AND SUMIT RAY MAHASAY
Department of Chemistry, University of Victoria, Victoria, B.C., Canada V8W 2Y2

Received January 9, 1986

GORDON W. BUSHNELL, ALFRED FISCHER, GEORGE N. HENDERSON, and SUMIT RAY MAHASAY. Can. J. Chem. **64**, 2382 (1986).

The adduct obtained on nitration of 4-bromotoluene in acetic anhydride is (*Z*)-3-bromo-6-methyl-6-nitrocyclohexa-2,4-dienyl acetate. Its stereoselective rearrangement product, obtained on thermolysis in the presence of *p*-cresol, is (*Z*)-5-bromo-2-methyl-6-nitrocyclohexa-2,4-dienyl acetate. Reaction with hydrogen chloride in ether is also stereospecific and gives (*Z*)-3-bromo-6-methyl-6-nitrocyclohexa-2,4-dienyl chloride. The crystal structures of these compounds are reported.

GORDON W. BUSHNELL, ALFRED FISCHER, GEORGE N. HENDERSON et SUMIT RAY MAHASAY. Can. J. Chem. **64**, 2382 (1986).

L'adduit obtenu par nitration du bromo-4 toluène dans l'anhydride acétique est l'acétate de bromo-3 méthyl-6 nitro-6 cyclohexadiène-2,4 yle-(*Z*). Son produit de transposition stéréosélective, obtenu par thermolyse en présence de *p*-crésol, est l'acétate de bromo-5 méthyl-2 nitro-6 cyclohexadiène-2,4 yle-(*Z*). Sa réaction avec le chlorure d'hydrogène dans l'éther est aussi stéréospécifique et elle conduit au chlorure de bromo-3 méthyl-6 nitro-6 cyclohexadiène-2,4 yle. On a déterminé les structures cristallines de ces composés.

[Traduit par la revue]

Nitration in acetic anhydride of aromatic compounds in which a substituted position is of a comparable or greater degree of activation than an unsubstituted position often leads to the formation of nitronium acetate adducts (1, 2) in which the nitro group is attached to the activated substituted (*ipso*) position. Most commonly the 1,4 adduct is formed, normally as a pair of diastereomers. However, a 1,2 adduct is obtained when *p*-*tert*-butyltoluene (3), 2-methyl-2-(2′-methylphenoxy)propanoic acid (4), 4-methoxy- or a 4-halotoluene (5) is the substrate. Only one diastereomer of the 1,2 adduct is obtained. The 1,2 adducts undergo a 1,5 thermal rearrangement of the nitro group (6). Both stereospecific and stereorandom rearrangement processes have been observed (6). In the case of the diene from 4-bromotoluene, 3-bromo-6-methyl-6-nitrocyclohexa-2,4-dienyl acetate (**1***a*), the stereorandom rearrangement is made stereospecific when *p*-cresol is added. The *p*-cresol is believed to suppress a radical rearrangement process (6, 7). Two stereochemical questions arise from these observations. (*i*) What is the stereochemistry (*syn* or *anti*) of the nitration addition reaction? (*ii*) What is the stereochemistry of the stereospecific rearrangement process, i.e., is the nitro group rearrangement suprafacial or antarafacial? In the present work we report the results of single crystal X-ray diffraction structure determinations on **1***a* and its stereospecific rearrangement product, **2***a*, a diastereomer of 5-bromo-2-methyl-6-nitrocyclohexa-2,4-dienyl acetate, which provide the answers to these questions. We have also determined the structure of the single diastereomer of 3-bromo-6-methyl-6-nitrocyclohexa-2,4-dienyl chloride, **3***a*, obtained on reaction of **1***a* with hydrogen chloride.

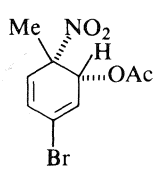

1*a*

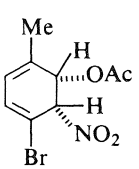

2*a*

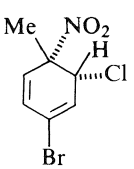

3*a*

[1]For part XXVI, see ref. 2.

Results and discussion

Diene **1***a* was formed in 64% yield as a single diastereomer on the nitration of 4-bromotoluene in acetic anhydride containing trifluoroacetic anhydride and was isolated by crystallization of the crude reaction product. Diene **1***a* isomerized and partially aromatized when a solution in chloroform was allowed to stand at ambient temperature. The isomerization was carried out on a preparative scale by heating a solution of **1***a* in benzene at 74°C for 1 h when a mixture of **2***a* (35%), its diastereomer **2***b* (35%), unreacted **1***a* (26%), and its diastereomer **1***b* (4%), together with a trace of 5-bromo-2-methylphenyl acetate was obtained. The diastereomers **2***a* and **2***b* were isolated from the reaction mixture by fractional crystallization. Diene **1***b* was obtained from the mother liquor by treatment with aqueous ammonia to selectively aromatize the rearranged dienes **2***a* and **2***b*, followed by chromatography. The secondary nitro group makes the elimination of acetic acid from the rearranged dienes extremely facile, whereas the tertiary nitrodienes are unreactive under the same conditions. Isomerization of diene **1***a* in the presence of *p*-cresol gave only one product diene, **2***a*. The dienyl chloride **3***a* was obtained in 82% isolated yield when hydrogen chloride was bubbled through a solution of **1***a* in ether at −78°C and the mixture then worked up.

The structures of **1***a*, **2***a*, and **3***a* were determined by X-ray crystallography (Table 1). Dienes **1***b* and **2***b* decomposed too rapidly on irradiation for structure elucidation. Table 2 contains fractional atomic coordinates and isotropic temperature parameters for **1***a*, **2***a*, and **3***a*. Table 3 contains bond lengths, which agree well with the literature values for similar bonds as compiled in the Chemical Society's special publications (8). Table 4 contains bond angles and shows sp^3 and sp^2 hybridised atoms subtending angles close to 109.5° and 120°, respectively. Tables deposited[2] contain anisotropic temperature parameters for **1***a* and **3***a* (Tables S1, S2), intermolecular distances (Tables S3, S4, S5), mean planes, torsion angles, and Newman

[2]Copies may be purchased from the Depository of Unpublished Data, CISTI, National Research Council of Canada, Ottawa, Ont., Canada K1A 0S2.

TABLE 1. Crystal data for **1***a*, **2***a*, and **3***a*

Crystal system	Orthorhombic	Monoclinic	Orthorhombic
Space group	*Pbca* (No. 61)	$P2_1/n$ (No. 14)	$Pca2_1$ (No. 29)
a (Å)	27.445(8)	7.386(3)	11.901(5)
b	9.683(3)	7.618(2)	6.758(2)
c	8.335(2)	19.498(6)	11.495(4)
β (deg)	—	92.91(4)	—
V (Å^3)	2215(1)	1095.7(6)	924.5(6)
Formula	$C_9H_{10}NO_4Br$	$C_9H_{10}NO_4Br$	$C_7H_7NO_2ClBr$
Mol. wt.	276.09	276.09	252.5
Z	8	4	4
D_{meas}(g cm^{-3})	—	1.67	1.78
D_{calcd}	1.656	1.674	1.814
Mounting axis	*c*	*a*	*a*
Standard reflections	18 00, 080, 006	060, 006, 400	200, 006, 020
Measured range (2θ)	0–40°	0–30°	0–50°
No. of steps (0.01° in 2θ, 0.25 s)	160	200	160
Background count (s)	40	50	40
Fraction of reflections with $F/\sigma(F) > 3$	0.82	0.93	0.89
μ(cm^{-1}) (λ = 0.71069 Å)	39.25	39.67	49.40
Crystal shape. Perpendicular distance, origin to faces: ±(100), ±(010), ±(001)	0.081, 0.300, 0.473 mm	0.231, 0.180, 0.162 mm	0.237, 0.080, 0.189 mm
Transmission	0.10–0.53	—	0.17–0.47
Convergence Δ/σ(max)	0.11	0.007	0.004
R	0.0763	0.1033	0.0551
R_w	0.0941	0.1029	0.0601
Difference map maximum (e Å^{-3})	0.83	1.17	0.58
No. of observations	1033	597	862
No. of parameters	136	61	108

projections (Tables S6, S7, S8), and structure factors (Tables S9, S10, S11). The intermolecular distances are all greater than 3.1 Å, demonstrating the molecular nature of the crystals. When the three structures are compared there are many similarities. The nitro groups plus the adjacent C atom are planar as are the acetate groups. The hexadienyl rings are non-planar, with the saturated atoms 0.24 Å (ave.) from the weighted least squares (w.l.s.) planes. Each saturated ring atom is on the opposite side of the plane relative to the nearest ethylene moiety, and the unsaturated ring carbon atoms are generally close to 0.10 Å from the w.l.s. plane. Birch, Hinde, and Radom attributed the non-planarity of the parent molecule, 1,3-cyclohexadiene, to angle strain at the saturated carbon atoms and steric interaction between eclipsed methylene hydrogen atoms outweighing the stabilizing effect of conjugation (9). Computed values for the C=C—C=C torsion angle in 1,3-cyclohexadiene range from 8 to 20°C (9–14) indicating a shallow minimum in the energy function (11). Experimentally obtained values are consistently close to 17.5° (15–18). Our experimental values for the substituted cyclohexadienes are lower, 9.9(13)°, 12(3)°, and 13.2(15)°, respectively.

The (*Z*) configuration of the *a* isomers is evident from the *cis* disposition of nitro and acetate in **1***a* and **2***a* and the *cis* arrangement of nitro and chlorine in **3***a* (Figs. 1–3). The structures of **1***b* and **2***b* follow from the fact that these are the diastereomers of the *a* isomers, as is indicated by the close similarity of the nmr spectra of **1***a* with those of **1***b* and of **2***a* with those of **2***b*. There are two possible conformations of each diastereomer and, in the cases of **1***a* and **3***a*, that in which the adjacent methyl and acetate or chlorine groups are (pseudo) *trans* diaxial and the nitro group and neighbouring hydrogen are therefore equatorial is preferred. This preference is reasonable in that the conformer with the smaller substituent (hydrogen) *gauche* to both methyl and nitro and the larger substituent (acetate or chlorine) *gauche* only to nitro, would exhibit less torsional strain than the other conformer in which the larger substituent is *gauche* to both neighbouring substituents. The preferred conformer of **2***a* is that which has axial nitro and equatorial acetate rather than vice versa. It is likely that this preference reflects a greater electronic repulsion between the neighbouring C—Br and C—NO_2 dipoles than that between the C—OAc and C—CH_3, the consequence being that the bromine and the nitro group are forced to be further apart (i.e. nitro axial) than the methyl and acetate or chlorine (acetate or chlorine equatorial). Interaction between the neighbouring dipoles at sp^2 and sp^3 carbons should be minimized when the substituent at the tetrahedral carbon is axial.

On nitration of 4-bromotoluene formation of the *cis* 1,2 adduct **1***a* is completely dominant, none of the *trans* diastereomer **1***b* being detected in the product mixture. Generally the formation of adducts is under kinetic control (19) as is evident in the present instance from the fact that in the thermal rearrangement, when equilibrium conditions are approached, both diastereomers **1***a* and **1***b* are present together. Thus we must look to the transition state to account for the stereoselectivity. Three possible explanations come to mind. Ridd has suggested that in acetic anhydride the nitronium ion is complexed with acetic acid and that it only becomes free in the encounter pair (20). If the reaction with the substrate occurs immediately after the nitronium ion is liberated, and the further reaction of the carbocation occurs before the solvation shell has had time to relax, then the acetic acid molecule which was

TABLE 2. Fractional atomic coordinates and temperature parameters

(*a*) **1***a*[a]

Atom	*x/a*	*y/b*	*z/c*	U_{eq}
Br	7954(4)	43634(10)	98615(11)	718(6)
O(1)	2147(2)	6522(7)	3824(8)	85(3)
O(2)	1877(3)	4794(8)	2473(8)	81(3)
O(3)	997(2)	5763(4)	4359(7)	50(2)
O(4)	355(2)	4590(7)	3430(7)	70(3)
N(1)	1933(3)	5412(8)	3731(10)	58(3)
C(1)	1197(3)	4474(7)	4969(9)	46(3)
C(2)	957(3)	4119(7)	6536(11)	54(3)
C(3)	1117(3)	4666(8)	7861(12)	57(3)
C(4)	1555(4)	5548(8)	7945(13)	63(4)
C(5)	1842(4)	5639(7)	6661(12)	58(4)
C(6)	1746(3)	4728(9)	5253(9)	48(3)
C(7)	2016(3)	3350(8)	5405(12)	69(4)
C(8)	563(3)	5674(10)	3586(10)	55(4)
C(9)	407(3)	7030(8)	2962(12)	74(4)

[a]Coordinates $\times 10^5$ for Br and $\times 10^4$ otherwise; temperature parameters $\times 10^4$ for Br and $\times 10^3$ otherwise.

(*b*) **2***a*[a]

Atom	*x/a*	*y/b*	*z/c*	U_{iso}
Br	−3659(4)	1735(4)	2124(1)	566(13)
O(1)	−2089(25)	3426(27)	432(10)	82(6)
O(2)	−1151(26)	5713(31)	953(10)	91(7)
O(3)	2463(19)	4116(20)	1152(7)	43(5)
O(4)	2601(23)	5121(24)	2222(9)	73(6)
N(1)	−1359(30)	4135(34)	904(12)	65(7)
C(1)	1452(28)	2598(29)	1388(11)	31(6)
C(2)	1614(30)	1124(31)	861(11)	41(7)
C(3)	425(31)	−188(32)	882(11)	45(7)
C(4)	−1173(30)	−35(32)	1336(11)	43(7)
C(5)	−1612(29)	1487(30)	1615(11)	38(7)
C(6)	−518(30)	3133(30)	1523(11)	39(7)
C(7)	3260(32)	1123(34)	419(12)	54(8)
C(8)	2986(35)	5306(36)	1646(14)	62(8)
C(9)	4178(36)	6713(37)	1352(14)	72(9)

[a]Coordinates $\times 10^4$; temperature parameters $\times 10^4$ for Br and $\times 10^3$ otherwise.

(*c*) **3***a*[a]

Atom	*x/a*	*y/b*	*z/c*	U_{eq}
Br	−233(1)	4655(1)	1715(0)	708(4)
Cl	2686(2)	3307(4)	4798(3)	654(8)
N(1)	1720(7)	−382(11)	5670(6)	46(3)
O(1)	1287(6)	201(11)	6555(5)	62(2)
O(2)	2558(7)	−1388(12)	5651(7)	70(3)
C(1)	2052(7)	1440(15)	3853(7)	46(3)
C(2)	1516(8)	2573(16)	2858(7)	51(3)
C(3)	440(8)	3059(13)	2941(7)	45(3)
C(4)	−268(8)	2558(15)	3933(9)	53(3)
C(5)	101(7)	1222(16)	4711(8)	49(3)
C(6)	1182(8)	198(12)	4500(7)	42(3)
C(7)	964(10)	−1711(15)	3822(10)	64(4)

[a]Coordinates $\times 10^4$. The Br atom *z* coordinate was fixed; temperature parameters $\times 10^4$ for Br and Cl, $\times 10^3$ otherwise; estimated standard deviations are given in parentheses; U_{eq} is the equivalent isotropic temperature parameter; $U_{eq} = (1/3)\Sigma_i\Sigma_j U_{ij} a_i^* a_j^* (\mathbf{a}_i \cdot \mathbf{a}_j)$; $T = \exp -(8\pi^2 U_{iso} \sin^2 \theta/\lambda^2)$.

TABLE 3. Interatomic distances (Å)[a]

Atoms	Distance	Atoms	Distance
	(*a*) **1***a*		
C(3)—Br	1.909(8)	C(6)—C(1)	1.543(12)
N(1)—O(1)	1.228(8)	C(3)—C(2)	1.302(12)
N(1)—O(2)	1.218(9)	C(4)—C(3)	1.475(13)
C(1)—O(3)	1.455(9)	C(5)—C(4)	1.332(13)
C(8)—O(3)	1.358(10)	C(6)—C(5)	1.492(11)
C(8)—O(4)	1.202(9)	C(7)—C(6)	1.532(12)
C(6)—N(1)	1.520(10)	C(9)—C(8)	1.476(11)
C(2)—C(1)	1.503(11)		
	(*b*) **2***a*		
C(5)—Br	1.86(2)	C(6)—C(5)	1.51(3)
N(1)—O(1)	1.17(2)	C(3)—C(4)	1.51(3)
N(1)—O(2)	1.22(3)	C(2)—C(3)	1.33(3)
C(1)—O(3)	1.46(2)	C(1)—C(2)	1.53(3)
C(8)—O(3)	1.36(3)	C(7)—C(2)	1.53(3)
C(8)—O(4)	1.18(3)	C(6)—C(1)	1.55(3)
C(6)—N(1)	1.53(3)	C(9)—C(8)	1.52(3)
C(4)—C(5)	1.33(3)		
	(*c*) **3***a*		
C(3)—Br	1.947(8)	C(1)—Cl	1.828(9)
O(1)—N(1)	1.207(10)	O(2)—N(1)	1.207(10)
C(6)—N(1)	1.540(11)	C(7)—C(6)	1.530(13)
C(3)—C(2)	1.325(13)	C(5)—C(4)	1.344(14)
C(1)—C(2)	1.517(12)	C(6)—C(5)	1.480(13)
C(4)—C(3)	1.457(13)	C(1)—C(6)	1.527(12)

[a]Estimated standard deviations are given in parentheses.

attached to the nitronium ion will be favourably placed to add to the 2-position in a *cis* manner. The second explanation proposes that the nitro group in the carbocation favours *cis* addition of the acetic acid molecule through hydrogen bonding of the latter to the nitro oxygen. This sets up the carbonyl group in a favourable position to add *cis* to the nitro group. The third explanation proposes that the carbocation is stabilized through carbon–carbon hyperconjugation involving the ring–methyl bond. This would result in the ring tending towards being planar with the carbon–nitrogen bond in the plane of the ring and the ring–methyl bond perpendicular to the ring. Approach of the acetic acid molecule would then be less hindered from the nitro face than from the methyl face.

Diene **2** is thermodynamically more stable than diene **1** (in the rearrangement reaction, **1** forms **2** to an extent of more than 50%) yet no diene **2** is obtained from the nitration reaction. Thus, even though some (8%) attack of nitronium ion occurs at the position *ortho* to the bromine, none of the resulting nitrocyclohexadienyl cation is trapped by acetate, all of it undergoing deprotonation to the 4-bromo-3-nitrotoluene. Likewise, none of the nitrocyclohexadienyl cation resulting from addition of nitronium ion *ortho* to methyl is trapped. Trapping of secondary nitrocyclohexadienyl cations is extremely rare (21, 22). The deprotonation reaction with its attendant gain in resonance energy is almost always greatly favoured over addition of a nucleophile. It is thus evident that the rearrangement cannot involve a cationic intermediate, rather stereorandom radical and stereospecific sigmatropic pathways are involved (4, 6, 7). This is of course also evident from the non-polar conditions under which the rearrangement is carried out. The addition of *p*-cresol suppresses the radical reaction and allows the observation of the sigmatropic process. Since (*Z*)-**1**

TABLE 4. Bond angles[a]

(*a*) **1***a*

C(4)—C(3)—Br	115.1(7)	C(2)—C(3)—Br	121.4(7)
C(5)—C(4)—C(3)	118.9(8)	C(3)—C(2)—C(1)	119.7(7)
C(6)—C(5)—C(4)	119.2(8)	C(6)—C(1)—C(2)	109.4(6)
C(5)—C(6)—C(1)	112.8(7)	O(2)—N(1)—O(1)	123.0(8)
C(5)—C(6)—N(1)	109.8(7)	C(1)—C(6)—N(1)	105.8(6)
C(6)—N(1)—O(1)	119.4(8)	C(6)—N(1)—O(2)	117.5(7)
C(6)—C(1)—O(3)	106.6(6)	C(2)—C(1)—O(3)	109.5(6)
C(8)—O(3)—C(1)	116.3(6)	C(4)—C(3)—C(2)	123.4(8)
C(7)—C(6)—N(1)	106.6(7)	O(4)—C(8)—O(3)	121.6(8)
C(7)—C(6)—C(1)	110.3(7)	C(9)—C(8)—O(3)	111.4(8)
C(7)—C(6)—C(5)	111.3(7)	C(9)—C(8)—O(4)	127.0(8)

(*b*) **2***a*

Atoms	Angle	Atoms	Angle
C(8)—O(3)—C(1)	116(2)	C(7)—C(2)—C(1)	118(2)
O(2)—N(1)—O(1)	125(3)	C(2)—C(1)—O(3)	108(2)
C(6)—N(1)—O(1)	123(2)	C(6)—C(1)—O(3)	110(2)
C(6)—N(1)—O(2)	113(2)	C(6)—C(1)—C(2)	115(2)
C(4)—C(5)—Br	122(2)	C(5)—C(6)—N(1)	108(2)
C(6)—C(5)—Br	116(2)	C(1)—C(6)—N(1)	110(2)
C(6)—C(5)—C(4)	122(2)	C(1)—C(6)—C(5)	108(2)
C(3)—C(4)—C(5)	121(2)	O(4)—C(8)—O(3)	121(2)
C(2)—C(3)—C(4)	120(2)	C(9)—C(8)—O(3)	111(2)
C(1)—C(2)—C(3)	117(2)	C(9)—C(8)—O(4)	128(3)
C(7)—C(2)—C(3)	124(2)		

(*c*) **3***a*

Atoms	Angle	Atoms	Angle
O(2)—N(1)—O(1)	123.5(8)	C(5)—C(6)—N(1)	109.7(7)
C(6)—N(1)—O(1)	118.4(7)	C(1)—C(6)—N(1)	106.4(7)
C(6)—N(1)—O(2)	118.1(7)	C(1)—C(6)—C(5)	114.3(7)
C(1)—C(2)—C(3)	118.5(8)	C(7)—C(6)—N(1)	107.5(7)
C(2)—C(3)—Br	118.8(7)	C(7)—C(6)—C(5)	109.3(8)
C(4)—C(3)—Br	117.2(7)	C(7)—C(6)—C(1)	109.3(8)
C(4)—C(3)—C(2)	123.8(8)	C(2)—C(1)—Cl	105.9(7)
C(5)—C(4)—C(3)	119.2(8)	C(6)—C(1)—Cl	111.7(6)
C(6)—C(5)—C(4)	119.2(8)	C(6)—C(1)—C(2)	111.1(7)

(*d*) Endocyclic torsion angles (deg)

Bonds	Torsion angle		
	1*a*	**2***a*	**3***a*
C(1)—C(2)—C(3)—C(4)	5.1(12)	10(3)	0.4(12)
C(2)—C(3)—C(4)—C(5)	9.9(13)	12(3)	13.2(15)
C(3)—C(4)—C(5)—C(6)	7.0(12)	2(3)	4.0(14)
C(4)—C(5)—C(6)—C(1)	35.6(11)	26(3)	32.1(12)
C(5)—C(6)—C(1)—C(2)	46.5(9)	46(2)	42.6(10)
C(6)—C(1)—C(2)—C(3)	32.7(10)	40(3)	27.7(12)

[a]Estimated standard deviations are given in parentheses.

gives (*Z*)-**2** this process is suprafacial as would be required if the new C—NO_2 bond is formed synchronously with the fission of the original C—NO_2 bond.

Reaction of acetate **1***a* with hydrogen chloride gives the dienyl chloride with retention of configuration. This reaction would be expected to involve a carbocation intermediate or, at least, an incipient carbocation intermediate. A S_Ni type mechanism with a six-membered cyclic transition state can be envisaged in which hydrogen chloride, hydrogen bonded to carbonyl oxygen, is situated with the chlorine conveniently located to displace the acetate function. Alternatively, the chlorine could displace the acetate in an S_Ni' reaction by adding to the 5-position through a cyclic transition state. Both mechanisms would lead to the same diastereomer although, in principle, they can be distinguished since, if a single enantiomer of the reactant were used, different enantiomers of the product would be formed from the two pathways. If C—O bond breaking runs slightly ahead of C—Cl bond formation both the incipient carbocation intermediate and a cyclic transition state, accounting for retention of configuration, can be accommodated.

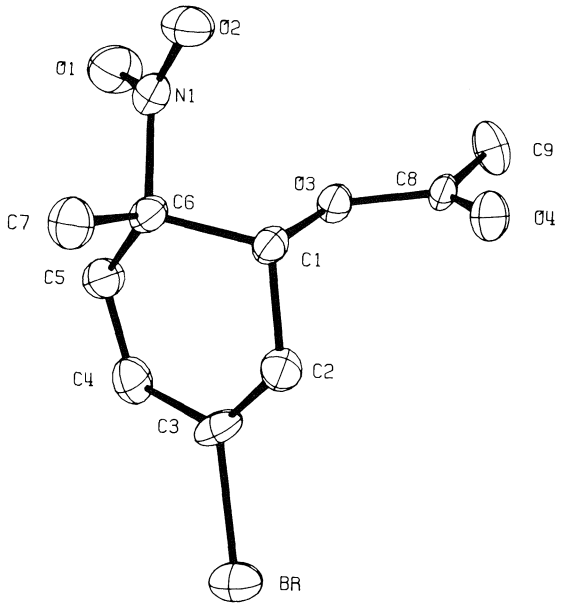

FIG. 1. An ORTEP drawing of the molecular structure of **1***a* showing the 25% probability ellipsoids.

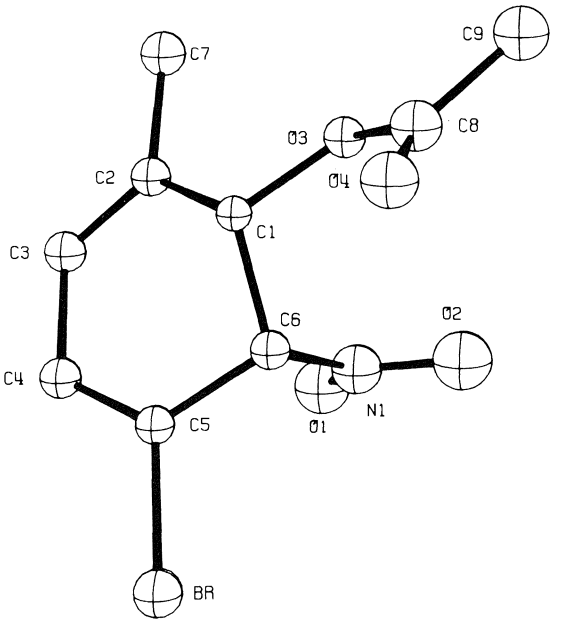

FIG. 2. An ORTEP drawing of the molecular structure of **2***a* showing the 25% probability spheres.

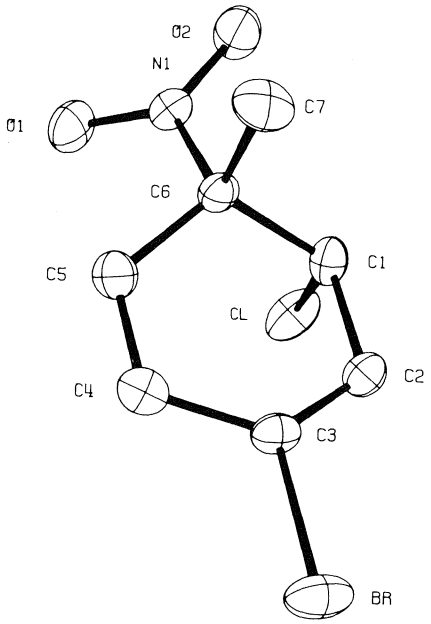

FIG. 3. An ORTEP drawing of the molecular structure of **3***a* showing the 25% probability ellipsoids.

Experimental

Melting points are uncorrected and were determined on a Buchi SMP-20 melting point apparatus. Infrared spectra calibrated with polystyrene were recorded on a Perkin Elmer 283 spectrometer. Observations were made on potassium bromide discs for solids and on thin films between sodium chloride plates for liquids. Proton nuclear magnetic resonance spectra were recorded on Perkin Elmer R-32 (90 MHz) or Bruker WM 250 (250 MHz) spectrometers. The nmr spectra of the nitration reaction mixture was recorded with the acetic anhydride peak at 2.15 ppm as the lock signal. The substitution reaction with hydrogen chloride was followed using the ether peak at 1.85 ppm as the lock signal. For all other solutions, tetramethylsilane (90 MHz) or the solvent deuterium signal (250 MHz) was used as the lock signal. Carbon-13 nuclear magnetic resonance spectra were recorded on the Bruker WM 250 (62.9 MHz) spectrometer using solutions in $CDCl_3$ with TMS as the internal standard. Ultraviolet spectra were recorded on a Beckman DU-8 spectrophotometer. Elemental analyses were carried out by Canadian Microanalytical Service Ltd., Vancouver, B.C.

4-Bromotoluene was from J. T. Baker, acetic anhydride was certified ACS from Fisher, trifluoroacetic anhydride was Aldrich gold label. Fuming nitric acid (Fisher, 300 cm^3) was purified by distilling from urea (10 g) and sulfuric acid (500 cm^3) at <35°C and was stored at −25°C.

Solvents for chromatography including pentane (reagent, Fisher), ether (Fisher), and petroleum ether (reagent, Fisher) were dried over sodium and distilled before use. Silica gel used for chromatography was 60–200 mesh, Davison Commercial grade H.

Nitration of 4-bromotoluene

A nitrating mixture was prepared by the careful addition of acetic anhydride (51.1 g, 0.5 mol) with stirring to freshly distilled nitric acid (12.6 g, 0.2 mol) at −78°C. After the completion of addition, the mixture was warmed to 0°C, stirred for 15 min at 0°C and cooled to −40°C. Trifluoroacetic anhydride (21.05 g, 0.1 mol) was then slowly added to the mixture at −40°C. A solution of 4-bromotoluene (17.1 g, 0.1 mol) in acetic anhydride (10.2 g, 0.1 mol) was added dropwise with stirring over 30 min to the nitrating mixture at −40°C. The reaction mixture was then stirred for an additional 90 min at −40°C and then cooled to −78°C and poured into ether (50 cm^3) at −78°C. Ammonium hydroxide (450 cm^3, 28%) was added in portions to the stirred mixture. After the addition was complete, stirring was continued for 1 h while the mixture warmed to room temperature. The ether layer was separated and the residue was washed with ether (300 cm^3). The combined ether solution was washed with cold water (4 × 300 cm^3) and then dried. Removal of ether on the rotovapor at 15°C yielded a reddish-brown oil (25.5 g). The ^1H nmr spectrum of the crude mixture gave the composition as (*Z*)-3-bromo-6-methyl-6-nitrocyclohexa-2,4-dienyl acetate (**1***a*) (64%), 4-bromo-3-nitrotoluene (8%) and 4-bromo-2-nitrotoluene (28%). Crystallization from ether–pentane mixture at −20°C afforded crude diene **1***a* (9 g) as pale yellow crystals which, after further recrystallization, had mp 48–49°C; ir (KBr): 1745 and 1230 ($OCOCH_3$), 1555 and 1365 (NO_2) cm^{-1}; uv (CH_2Cl_2): 266.4 nm (350 m^2 mol^{-1}); ^1H nmr (250 MHz, $CDCl_3$) δ: 1.77 (s, 3, CH_3), 1.98 (s, 3, $OCOCH_3$), 5.45 (dd, 1, H(1)), 6.13 (dd, 1, H(4)), 6.37 (ddd, 1, H(2)), 6.45 (ddd, 1, H(5)) ppm, J_{12} = 6.15, J_{15} = 1.76, J_{24} = 1.80, J_{25} = 0.55, J_{45} = 10.23 Hz; ^{13}C nmr ($CDCl_3$, 62.9 MHz) δ_c: 20.6 ($OCOCH_3$), 23.1 (CH_3), 70.4 (C(1)), 86.8 (C(6)), 122.0 (C(2)), 122.6 (C(3)), 127.8 (C(4)), 128.5 (C(5)), 169.0 ($OCOCH_3$) ppm. *Anal.* calcd. for $C_9H_{10}NO_4Br$: C 39.15, H 3.65, N 5.07; found: C 39.36, H 3.52, N 5.04.

*Isomerization of (Z)-3-bromo-6-methyl-6-nitrocyclohexa-2,4-dienyl acetate (**1**a)*

A solution of diene **1***a* (10 g, 36 mmol) in benzene (20 cm^3) was heated in a water bath at 74°C for 1 h. Removal of the benzene on the rotovapor at 25°C yielded a reddish-brown oil. The ^1H nmr spectrum of the oil indicated the presence of **1***a* (26%), its diastereomer **1***b* (4%), (*Z*)- and (*E*)-5-bromo-2-methyl-6-nitrocyclohexa-2,4-dienyl acetate (**2***a*) and (**2***b*) (70%), with traces of 4-bromo-3-nitrotoluene and 5-bromo-2-methylphenyl acetate. Fractional crystallization from 1:1 ether–pentane at −20°C gave diene **2***a* (2.56 g) in the first two crops. The third crop (0.96 g) contained a mixture of **2***a* and **2***b* (1:1). Further crystallization from 1:2 ether–pentane solution yielded a mixture of **2***b* and **2***a* (95:5) as the fourth crop (700 mg). Finally, from 1:3 ether – petroleum ether, diene **1***a* was obtained as the fifth crop (600 mg).

Recrystallization of the first crop (300 mg) from 1:1 ether – petroleum ether gave pure diene **2***a* as pale yellow crytals (240 mg), mp 93–95°C; ir (KBr): 1735 and 1230 ($OCOCH_3$), 1560 and 1370 (NO_2) cm^{-1}; uv (CH_2Cl_2): 279.75 nm (721 m^2 mol^{-1}); ^1H nmr (250 MHz, $CDCl_3$) δ: 1.82 (br dd, 3, CH_3), 2.17 (s, 3, $OCOCH_3$), 5.35 (d, 1, H(6)), 5.79 (ddq, 1, H(3)), 5.91 (ddq, 1, H(1)), 6.69 (d, 1, H(4)) ppm, J_{13} = 2.65, J_{16} = 8.70, $J_{1,2\text{-Me}}$ = 1.00, J_{34} = 6.25, $J_{3,2\text{-Me}}$ = 1.63 Hz; ^{13}C nmr (62.9 MHz, $CDCl_3$) δ_c: 18.0 (CH_3), 20.5 ($OCOCH_3$), 70.9 (C(1)), 87.5 (C(6)), 109.5 (C(5)), 119.5 (C(3)), 134.1 (C(4)), 135.1 (C(2)), 169.8 ($OCOCH_3$) ppm. *Anal.* calcd. for $C_9H_{10}NO_4Br$: C 39.15, H 3.65, N 5.07; found: C 39.08, H 3.67, N 5.07.

Recrystallization of the fourth crop (500 mg) from 1:1 ether – petroleum ether at −20°C gave pure diene **2***b* as pale yellow crystals (420 mg), mp 63–64°C; ir (KBr) 1745 and 1210 ($OCOCH_3$), 1558 and 1360 (NO_2) cm^{-1}; uv (CH_2Cl_2): 279.75 nm (820 m^2 mol^{-1}); ^1H nmr (250 MHz, $CDCl_3$) δ: 1.83 (d, 3, CH_3), 2.15 (s, 3, $OCOCH_3$), 5.24 (d, 1, H(6)), 5.86 (dq, 1, H(3)), 5.93 (d, 1, H(1)), 6.66 (d, 1, H(4)) ppm, J_{16} = 3.47, J_{34} = 6.32, $J_{3,2\text{-Me}}$ = 1.04 Hz; ^{13}C nmr (62.9 MHz, $CDCl_3$) δ_c: 19.9 (CH_3), 20.7 ($OCOCH_3$), 70.8 (C(1)), 90.1 (C(6)), 109.1 (C(5)), 122.4 (C(3)), 132.2 (C(4)), 132.5 (C(2)), 169.8 ($OCOCH_3$) ppm. *Anal.* calcd. for $C_9H_{10}NO_4Br$: C 39.15, H 3.65, N 5.07; found: C 39.3, H 3.54, N 5.18.

The ^1H nmr spectrum of the mother liquor at this stage showed the presence of dienes **2***a* and **2***b* (37%), **1***a* (37%), **1***b* (5%), 5-bromo-2-methylphenyl acetate and 4-bromo-3-nitrotoluene (21%). In order to isolate diene **1***b*, the dienes **2***a* and **2***b* were selectively aromatized. A solution of the reaction mixture (2 g) in ether (10 cm^3) was stirred in an ice bath with ammonium hydroxide (5 cm^3, 28%) for 15 min. The mixture was diluted with ether (80 cm^3), washed with cold brine (4 × 20 cm^3), and the solution dried over anhydrous magnesium sulfate. The ^1H nmr of the residual oil, obtained after removal of solvent at 15°C, revealed the presence of 4-bromo-3-nitrotoluene (37%), 5-bromo-2-methylphenyl acetate (21%), diene **1***a* (37%), and diene **1***b* (5%). The mixture (1.3 g) was separated by column chromatography on silica gel (180 g) using a mixture of ether –

petroleum ether as eluent at −40°C. Initial fractions eluted with 3% ether gave 4-bromo-3-nitrotoluene. Mixtures of phenyl acetate, bromonitrotoluene, and diene **1***a* were eluted next with 6% ether. Further elution with 10% ether gave mixtures containing diene **1***b* (95%) and 4-bromo-3-nitrotoluene (5%). Diene **1***b* did not crystallize from ether – petroleum ether and was characterized in solution. It had ^{1}H nmr (250 MHz, $CDCl_3$) δ: 1.74 (s, 3, CH_3), 2.13 (s, 3, $OCOCH_3$), 5.94 (m, 1, H(2)), 6.23 (m, 3, H(1), H(4) and H(5)) ppm; ^{13}C nmr (62.9 MHz, $CDCl_3$, −15°C) δ_c: 18.2 (CH_3), 19.6 ($OCOCH_3$), 70.8 (C(1)), 87.0 (C(6)), 117.1 (C(3)), 126.5 (C(2)), 127.2 (C(4)), 129.1 (C(5)), 169.5 ($OCOCH_3$).

In some small scale reactions, diene **1***a* was isomerized by heating a solution in $CDCl_3$ in an nmr tube in a thermostated water bath. *p*-Cresol was added to some reactions as an inhibitor. Reactions were followed by ^{1}H nmr at 90 MHz. Typical results were as follows: after 1 h at 60°C in the absence of inhibitor the composition was **1***a* (72%), **1***b* (trace), **2***a* (19%), **2***b* (9%); after 15 h in the presence of *p*-cresol (0.25 mol proportion) the composition was **1***a* (32%) and **2***a* (68%) and no **2***b* was detected at any prior stage.

*(Z)-3-Bromo-6-methyl-6-nitrocyclohexa-2,4-dienyl chloride (**3**a)*

Hydrogen chloride was bubbled through a solution of **1***a* (275 mg, 1 mmol) in ether (5 cm^3) at −78°C, for 15 min, and the mixture was then stirred for 45 min while the bath was allowed to warm to −40°C. The ^{1}H nmr spectrum of the mixture at this stage showed the presence of a new diene as the only product. The solution was diluted with ether (20 cm^3) at −78°C and neutralized by the addition of excess aqueous ammonia. The ether was separated and the aqueous layer extracted with ether. The combined ethereal extracts were dried ($MgSO_4$) and the ether removed on the rotavapor at 15°C to give chloride **3***a* (206 mg, 82% isolated yield). Crystallization from ether – petroleum ether at −20°C gave pale yellow crystals, mp 87°C; uv (CH_2Cl_2): 273 nm (351 m^2 mol^{-1}); ir: 1540 (NO_2), 740 (C—Cl) cm^{-1}; ^{1}H nmr (250 MHz, $CDCl_3$) δ: 1.81 (s, 3, CH_3), 4.89 (dd, 1, H(1)), 6.20 (dd, 1, H(4)), 6.36 (dd, 1, H(2)), 6.54 (dd, 1, H(5)) ppm, J_{12} = 6.47, J_{15} = 1.72, J_{24} = 1.81, J_{45} = 10.30 Hz; ^{13}C nmr (62.9 MHz, $CDCl_3$) δ_c: 24.2 (CH_3), 58.6 (C(1)), 89.1 (C(6)), 121.2 (C(3)), 124.2 (C(2)), 128.1 (C(4)), 129.1 (C(5)) ppm. *Anal.* calcd. for $C_7H_7NO_2ClBr$: C 33.29, H 2.79, N 5.55; found: C 33.39, H 2.67, N 5.51.

X-ray diffraction studies

Compounds **1***a*, **2***a*, and **3***a* were examined on Weissenberg and precession cameras to determine the symmetry and approximate cell dimensions, and subsequently transferred to a Picker 4-circle diffractometer automated with a PDP11/10 computer and using Zr filtered Mo radiation. The crystal data are given in Table 1. The symmetry positions for **2***a* were $x, y, z; -x, -y, -z; (\frac{1}{2}+x), (\frac{1}{2}-y), (\frac{1}{2}+z)$; and $(\frac{1}{2}-x), (\frac{1}{2}+y), (\frac{1}{2}-z)$. The cell dimensions were refined by least squares using pairs (19, 13, and 8, respectively) of 2θ measurements obtained by an automatic centering routine. The asymmetric unit was one molecule in each case. In measuring the intensities θ/2θ scans were used. Three standard reflections preceded each batch of 50 measurements and the sum of their intensities was used to correct for crystal decomposition. The class of compounds under study was soft and low melting. **1***a*, **2***a*, and **3***a* were selected as the best and most durable single crystals, but melting terminated the measurements on **2***a*. Lp corrections were done. Absorption corrections were applied by numerical integration for compounds **1***a* and **3***a* using Gaussian grids (4 × 10 × 12 for **1***a*, 12 × 8 × 8 for **3***a*). No reflections were omitted from the data sets.

Structure solution and refinement

SHELX (23), MULTAN (24), and ORTEP (25) and local programs were used. The structures were solved using direct methods and refined using electron-density maps and the method of least squares minimising $\Sigma w||F_o| - |F_c||^2$. The atomic scattering factors were those included in the SHELX program (23, 26). The weighting schemes employed were $w = 1/(\sigma^2(F) + 0.001F^2)$ for **1***a* and **3***a*, and unit weights for **2***a*. No special positions were occupied. For **3***a*, the *z* coordinate of the Br atom was fixed, since there was no reference point in the *z* direction provided by the symmetry elements. For compounds **1***a* and **3***a* anisotropic thermal parameters were used for all atoms, but for compound **2***a* isotropic temperature factors were employed. Hydrogen atoms were not found. Final difference maps were calculated as a further check and the maxima, given in Table 1, indicate no chemical mistakes.

Acknowledgements

We thank Mrs. Katherine A. Beveridge for technical assistance, the Natural Sciences and Engineering Research Council of Canada for financial support, and the University of Victoria for the award of a University of Victoria Fellowship (to S.R.M.).

1. D. J. Blackstock, A. Fischer, K. E. Richards, J. Vaughan, and G. J. Wright. Chem. Commun. 641 (1970).
2. A. Fischer, G. N. Henderson, and L. M. Iyer. Can. J. Chem. **63**, 2390 (1985).
3. A. Fischer and R. Roderer. Can. J. Chem. **54**, 3978 (1976).
4. G. S. Bapat. Ph.D. Dissertation, University of Victoria, Victoria, B.C. 1983.
5. A. Fischer, D. L. Fyles, and G. N. Henderson. J. Chem. Soc. Chem. Commun. 513 (1980).
6. G. S. Bapat, A. Fischer, G. N. Henderson, and S. Ray Mahasay. J. Chem. Soc. Chem. Commun. 119 (1983).
7. S. Ray Mahasay. Ph.D. Dissertation, University of Victoria, Victoria, B.C. 1984.
8. L. E. Sutton (*Editor*). Tables of interatomic distances and configurations in molecules and ions. The Chemical Society, London, 1958; Tables of interatomic distances in molecules and ions supplement 1956–1959. The Chemical Society, London. 1965.
9. A. J. Birch, A. L. Hinde, and L. Radom. J. Am. Chem. Soc. **103**, 284 (1983).
10. N. L. Allinger and J. C. Tai. J. Am. Chem. Soc. **99**, 4256 (1977).
11. A. Warshel and M. Karplus. J. Am. Chem. Soc. **94**, 5612 (1972).
12. G. Favini, F. Zuccarello, and G. Buemi. J. Mol. Struct. **3**, 385 (1963).
13. A. Komornicki and J. W. McIver. J. Am. Chem. Soc. **96**, 5798 (1974).
14. N. L. Allinger and J. T. Sprague. J. Am. Chem. Soc. **95**, 3893 (1973).
15. S. S. Butcher. J. Chem. Phys. **42**, 1830 (1965).
16. G. Dallinga and L. H. Toneman. J. Mol. Struct. **1**, 11 (1967).
17. M. Traetteberg. Acta Chem. Scand. **22**, 2305 (1968).
18. H. Oberhammer and S. Bauer. J. Am. Chem. Soc. **91**, 10 (1969).
19. A. Fischer and G. N. Henderson. Can. J. Chem. **59**, 2314 (1981).
20. J. H. Ridd. Adv. Phys. Org. Chem. **16**, 1 (1978).
21. G. G. Cross, A. Fischer, G. N. Henderson, and T. A. Smyth. Can. J. Chem. **62**, 1446 (1984).
22. R. G. Clewley. Ph.D. Dissertation, University of Victoria, Victoria, B.C., 1985.
23. G. M. Sheldrick. SHELX-76, a program for crystal structure determination. Anorganisch-Chemisches Institut der Universitat Gottingen. 1976.
24. P. Main. MULTAN-78, a system of computer programs for the automatic solution of crystal structures from X-ray diffraction data. Department of Physics, University of York, England, 1978.
25. C. K. Johnson. ORTEP: A Fortran thermal ellipsoid plot program for crystal structure illustrations. ORNL-3794, Revised. Oak Ridge National Laboratory, Oak Ridge, Tennessee. 1965.
26. D. T. Cromer and J. T. Waber. International tables for X-ray crystallography. Vol. 4. Kynoch Press, Birmingham, England. 1974. pp. 99 and 149.

Kinetic benzylidenation. Part I. The selective formation of five-membered ring benzylidene acetals from aldose diethyl dithioacetals

T. Bruce Grindley, Srihari Kusuma, and T. Stanley Cameron
Department of Chemistry, Dalhousie University, Halifax, N.S., Canada B3H 4J3

Received August 30, 1985[1]

T. Bruce Grindley, Srihari Kusuma, and T. Stanley Cameron. Can. J. Chem. **64**, 2388 (1986).

Reaction of D-arabinose diethyl dithioacetal with one equivalent of benzaldehyde dimethyl acetal in the presence of *p*-toluenesulfonic acid at −40°C gave a mixture of the two epimers of 5-*O*-methoxyphenylmethyl-D-arabinose diethyl dithioacetal initially. After 14 h at −20°C, the major products were *R*- and *S*-4,5-*O*-benzylidene-D-arabinose diethyl dithioacetal. The structure of the *S* isomer was determined by X-ray crystallography. The crystal was orthorhombic, with space group $P2_12_12_1$, cell dimensions $a = 5.179(4)$, $b = 12.469(3)$, $c = 27.150(4)$ Å, and $Z = 4$. The crystal structure was solved using the SHELX (76) system and refined to $R = 0.060$ for 714 reflections. The sugar chain was in a zigzag conformation, the 4,5-*O*-benzylidene ring in a $^{0-5}T_c$ conformation, and the plane of the phenyl ring was nearly perpendicular to the plane of the five-membered ring (88° angle). There were two short OH—S hydrogen bonds, one intramolecular and one intermolecular. Reaction of the diethyl dithioacetals of D-glucose, D-galactose, D-mannose, and D-ribose at −20°C as above also gave mixtures of the terminal five-membered ring *O*-benzylidene diastereomers.

T. Bruce Grindley, Srihari Kusuma et T. Stanley Cameron. Can. J. Chem. **64**, 2388 (1986).

La réaction du diéthyl dithioacétal du D-arabinose avec un équivalent du diméthyl acétal du benzaldéhyde, en présence d'acide *p*-toluènesulfonique, à −40°C, conduit initialement à un mélange des deux épimères du diéthyl dithioacétal du *O*-méthoxyphénylméthyl-5 D-arabinose. Après 14 h, à −20°C, les produits principaux sont les diéthyl dithioacétals des *O*-benzylidène-4(*R*) et 4(*S*), 5 D-arabinoses. En faisant appel à cristallographie par rayons-X, on a déterminé la structure de l'isomère *S*. Les cristaux sont orthorhombiques et appartiennent au groupe d'espace $P2_12_12_1$, avec $a = 5,179(4)$, $b = 12,469(3)$ et $c = 27,150(4)$ Å et $Z = 4$. On a résolu la structure cristalline en faisant appel au système SHELX (76) et on l'a affinée jusqu'à une valeur de $R = 0,060$ pour 714 réflexions. La chaîne de sucre existe dans une conformation en zigzag, le cycle *O*-benzylidène-4,5 existe dans une conformation $^{0-5}T_c$ et le plan du noyau phényle est pratiquement perpendiculaire au plan du cycle à cinq chaînons (angle = 88°). Il existe deux liaisons hydrogènes OH—S qui sont courtes, l'une est intramoléculaire alors que l'autre est intermoléculaire. Les réactions des diéthyl dithioacétals du D-glucose, du D-galactose, du D-mannose et du D-ribose, à −20°C, dans les conditions décrites plus haut, conduisent à des mélanges des *O*-benzylidènes à cinq chaînons diastéréoisomères en positions terminales.

[Traduit par la revue]

Introduction

Monosaccharide diethyl dithioacetals can be easily prepared and are potentially attractive synthons for chiral synthetic targets. Their acyclic structure allows the employment of protecting group strategies different from those adopted from pyranose and furanose sugars. Study of techniques for selective blocking of the various hydroxyl groups of these compounds has not been extensive. Cyclic acetals are convenient protecting groups and a particularly useful one is the benzylidene acetal. In the past few years, this "protecting group" has been shown to also be a versatile functional group that can be selectively transformed in a large number of ways.[2]

The preparation of *O*-benzylidene derivatives of acyclic carbohydrates has been studied to some extent. In most known cases, products have been obtained under conditions of thermodynamic control (5, 6). Typical reaction conditions involve benzaldehyde as the solvent and give products of multiple acetalation. The structures of the major products can be predicted on the basis of the Hann–Hudson rules (7) and compounds containing 2-phenyl-1,3-dioxane rings are normally obtained. For instance, dithioacetals of D-ribose, D-xylose, and D-lyxose formed 2,4:3,5-di-*O*-benzylidene acetals (8).

Kinetic acetalation has a number of advantages over thermodynamic acetalation (9, 10). Most notable is the ease with which partially acetalated products can be obtained. In addition, the products often have different structures than the thermodynamic products. For instance, kinetic isopropylidenation of unsubstituted hexoses gave 4,6-*O*-isopropylidene derivatives (9), quite different products than those obtained under thermodynamic control. The reaction of methyl hexopyranosides with one equivalent of α,α-dimethoxytoluene (benzaldehyde dimethyl acetal) in *N*,*N*-dimethylformamide containing a trace of acid at 60°C under reduced pressure was shown by Evans (11) to give better yields of the normal 4,6-*O*-benzylidene derivatives than the typical 50% or lower yields obtained under thermodynamic conditions.[3] A number of other workers have used this reagent to make benzylidene derivatives of pyranose and furanose sugars (12). Brecknell and Carman (14) obtained a mixture of the diastereomeric 5,6-*O*-benzylidene derivatives of D-glucose phenylosotriazole in unspecified yield by reaction with benzaldehyde in dimethyl sulfoxide containing a trace of concentrated sulfuric acid at room temperature for 4 h. In this publication, we describe the kinetic benzylidenation of aldose diethyl dithioacetals using benzaldehyde dimethyl acetal.

Results and discussion

*Benzylidenation of D-arabinose diethyl dithioacetal (**3**a)*

The reaction of **3***a* with benzaldehyde dimethyl acetal in dimethylformamide at −40°C in the presence of a trace of *p*-toluenesulfonic acid was slow. Thin-layer chromatography suggested that one product formed initially, followed by two others. The initial product was shown to be a mixture of the

[1]Revision received July 22, 1986.

[2]For a summary, see ref. 1. More recent methods are reported in refs. 2 and 3. The related *p*-methoxybenzylidene acetal can also be selectively transformed (4).

[3]Another efficient way of performing benzylidenations has recently appeared (13).

TABLE 1. ^{13}C Nuclear magnetic resonance data[a]

	^{13}C Nuclear magnetic resonance chemical shifts (ppm)											
								Phenyl carbons		SEt group		$^1J_{C,H}$
Compound	C-1	C-2	C-3	C-4	C-5	C-6	Acetal C	Quat. C	Other C	CH_2	CH_3	Acetal C
3*a*	55.1	71.9	70.9	71.6	64.1					24.4, 24.6	14.5, 14.5	
3*b*[b]	55.7	71.63	70.46	70.35	67.75		103.14	137.7	126.65, 128.29,	23.52,	14.46,	163
	55.7	71.59	70.46	70.26	67.39		103.18	137.7	128.67	23.56,	14.59	163
3*c*	55.5	70.9	70.7	76.4	68.3		103.6	138.0	126.4, 128.3, 129.1	23.6, 23.4	14.5, 14.5	168
3*d*	55.4	71.2	70.5	76.4	68.4		104.4	137.2	126.8, 128.3, 129.3	23.8, 25.1	14.5, 14.5	167
4*a*	54.7	76.9	71.7	73.8	63.3					25.3, 25.3	14.6, 14.8	
4*c*	54.8	77.0	71.3	74.5	66.9		104.0	138.0	126.4, 128.4, 129.2	24.9, 25.5	14.5, 14.8	167
4*d*	54.8	77.0	71.3	74.5	66.9		104.0	137.0	126.6, 128.4, 129.4	25.1, 25.7	14.5, 14.7	167
5*a*	54.5	75.5	69.3	73.3	71.5	63.7				24.6, 24.9	14.5, 14.5	
5*b*	55.3	75.3	68.7	73.9	70.9	67.6	103.2, 103.3	138.0	126.8, 128.3, 128.4, 128.7	24.0, 25.8	14.5, 14.6	165
5*c*	55.4	75.0	68.9	74.3	75.6	68.1	103.8	138.1	126.4, 128.3, 129.1	23.7, 25.9	14.5, 14.7	169
5*d*	55.5	75.0	68.3	74.8	75.9	68.3	104.1	137.5	126.6, 128.4, 129.3	23.6, 25.9	14.5, 14.7	166
6*a*	55.1	71.6	70.3	69.7	70.4	63.7				24.2, 24.3	14.4, 14.4	
6*c*	55.8	71.2	70.5	72.2	76.6	67.8	104.2	138.0	126.6, 129.3, 129.5	23.7, 25.5	14.5, 14.6	168
6*d*	55.8	71.2	70.4	72.0	77.0	67.5	104.0	137.1	126.5, 128.4, 129.2	23.7, 25.5	14.5, 14.6	168
7*a*	55.2	74.1	69.7	70.3	71.9	64.0				25.3, 24.4	14.7, 14.8	
7*c*	55.2	73.7	70.6	71.0	76.2	68.0	103.8	138.0	126.2, 128.4, 129.2	25.3, 25.7	14.6, 14.7	169
7*d*	55.2	73.8	70.7	71.2	76.8	68.0	104.3	137.1	126.7, 128.4, 129.5	25.1, 25.7	14.5, 14.7	168

[a]At 20 MHz.
[b]At 90.8 MHz.

two epimers of 5-*O*-methoxyphenylmethyl-D-arabinose diethyl dithioacetal (**3***b*), chiefly on the basis of spectral data (discussed below), and also because it rearranged on standing to a mixture of the other two products. Compound **3***b* was shown to contain a methoxyphenylmethyl group by means of its mass spectrum and also from the observation of signals assignable to a methoxyl group both in the ^1H and ^{13}C nmr spectra. The mass spectrum contained an M^+ peak, minor peaks corresponding to loss of CH_3OH and ·CHOMePh, as well as a major peak at m/z 121, corresponding to $CHOMePh^{+}$. The location of this group was assigned from the observation of downfield shifts of 3.3 and 3.7 ppm for the signals of C-5 in the ^{13}C nmr spectrum of the two isomers present in **3***b* in comparison to the shift in the starting material, **3***a* (see Table 1). No other signals were shifted significantly. Downfield shifts of similar magnitude were always observed for hydroxyl-bearing carbon atoms when the hydroxyl group became attached to a benzylidene acetal carbon (see later).

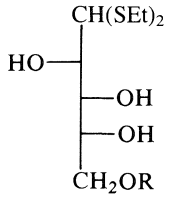

3*a* R = H
3*b* R = CHOMePh

Reaction under similar conditions at −20°C produced **3***b* initially, but after 14 h **3***b* had disappeared and the other two components from the previous reaction, **3***c* and **3***d*, were the sole products. These two components were separated by column chromatography. The component (**3***c*) that moved faster on tlc gave crystals suitable for X-ray crystallography.

The crystal structure was solved using the SHELX (76) package with a final R-factor of 6.0%. Tables 2 and 3 show atomic parameters and torsional angles. Figure 1 shows the crystal structure and Fig. 2 shows the crystal packing. In Fig. 1, hydrogen atoms are numbered in relation to the numbers of the carbon atoms to which they or, if hydroxyl hydrogens, their oxygen atoms, are attached. To avoid clutter, the minimum number of hydrogen atoms associated with a single carbon is

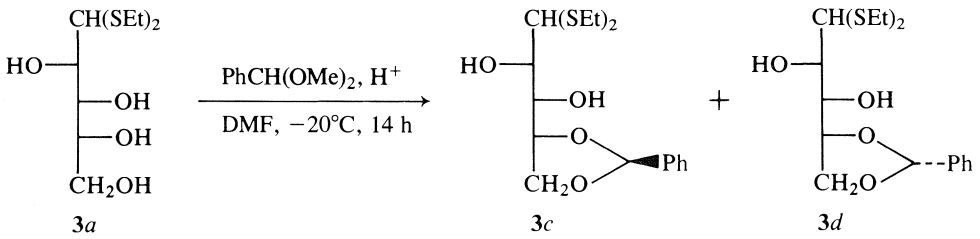

3a 3c 3d

TABLE 2. Atomic parameters for the non-hydrogen atoms of **3c**[a]

Name	X/a	Y/b	Z/c	Temperature factor[b]
S(1)	5484 (7)	10620 (3)	5357 (2)	570
S(2)	1261 (7)	9099 (3)	5679 (1)	580
C(12)	3798 (24)	9378 (9)	5247 (5)	410
C(1)	2079 (33)	11821 (13)	3132 (5)	570
C(2)	−30 (31)	11552 (12)	2848 (6)	580
C(3)	−1410 (33)	12318 (17)	2603 (6)	720
C(4)	−714 (42)	13356 (14)	2628 (7)	750
C(5)	1348 (39)	13651 (14)	2901 (7)	800
C(6)	2740 (33)	12896 (13)	3155 (6)	650
C(7)	3642 (35)	10985 (11)	3391 (5)	580
O(1)	4624 (20)	10206 (7)	3070 (3)	580
O(2)	2226 (19)	10412 (8)	3751 (3)	590
C(8)	5495 (28)	9379 (12)	3380 (5)	560
C(9)	3525 (29)	9424 (10)	3813 (5)	510
C(10)	4716 (24)	9359 (9)	4321 (5)	520
C(11)	2751 (22)	9260 (9)	4723 (5)	500
C(13)	2853 (30)	11600 (11)	5318 (5)	710
C(14)	3003 (55)	9065 (14)	6231 (6)	1320
C(15)	3136 (41)	12432 (12)	5697 (6)	880
C(16)	1346 (73)	8984 (24)	6679 (7)	1710
O(3)	6522 (15)	8507 (5)	4343 (3)	500
O(4)	1503 (15)	8247 (6)	4672 (3)	480

[a]Å × 10^4.
[b]Mod $(U)[(U_{11} \times U_{22} \times U_{33})^{1/3}]$, Å^2.

labelled. In the following discussion, carbohydrate numbering (see structures) indicated by a dash (e.g. C-1) will be used except in the discussion of the crystal structure where crystallographic numbering will be used (see Fig. 1). This numbering method is indicated by labels without dashes (e.g. C1).

The crystal structure demonstrated that compound **3c** was *S*-4,5-*O*-benzylidene-D-arabinose diethyl dithioacetal. The sugar chain was in the zigzag conformation, as expected for an arabinose derivative (15, 16). There was considerable thermal motion in the ethyl groups of the diethyl dithioacetal. Similar observations have been made for these groups in other diethyl dithioacetal derivatives (17).

This crystal structure determination is the first for a compound containing a five-membered benzylidene ring. The five-membered ring was in the $^{0-5}T_c$ conformation with O2 0.324(16) Å above the plane defined by O1, C8, and C9 and the acetal carbon, C7, 0.264(20) Å below the plane. The phenyl group adopted a quasi-equatorial orientation and was approximately perpendicular to the five-membered ring; a plane defined by O1, C7, and O2 had an angle of 88(3)° with a plane defined by the benzene ring (atoms C3, C4, C5, and C7 were used to define the plane). This orientation of the phenyl group resulted in short nonbonded distances between the acetal hydrogen and the nearly eclipsed aromatic *ortho* carbon, 2.42(10) Å, and its hydrogen, 2.35(14) Å.

The torsional angle that the phenyl ring makes with the 1,3-dioxane ring in 2-phenyl-1,3-dioxanes has attracted considerable interest (18–25). Two extreme conformations, termed parallel and perpendicular, are defined by the angle that the plane of the phenyl ring makes with the α-C—H bond. Compounds containing 2-phenyl-1,3-dioxane rings have adopted a wide range of conformations in the solid state (18–23). Results from calorimetric investigations were consistent either with free rotation about the acetal C to phenyl C bond or with a low barrier (<1.0 kcal mol^{-1}) (23, 24). Nuclear magnetic resonance results suggested that the parallel conformation is slightly favoured (0.4 ± 0.2 kcal mol^{-1}) (25) and recent molecular mechanics calculations supported the conclusion that this conformation is more stable (by about 1 kcal mol^{-1}) (23).

Application of the nmr method, the *J* technique, to a 2-phenyl-1,3-dioxolane derivative indicated that the parallel conformation was favoured to a greater extent (1.0 kcal mol^{-1}) for this ring size (25). In agreement with this result, compound **3c** was found here to adopt the same conformation.

Molecular mechanics calculations have now been performed on 2-phenyl-1,3-dioxolane using an MM2 program (26) modified to include improvements for alkylbenzenes (27) and the anomeric effect (28). The results were not consistent with the above conclusion. Initial calculations determined that the most stable ring conformation of 2-phenyl-1,3-dioxolane was the envelope conformation with the acetal C out of the plane and the phenyl group equatorial. Other conformations were examined by driving the various torsional angles internal to the 1,3-dioxolane ring. The barrier to rotation about the bond from the acetal C to the phenyl carbon was calculated by driving the *ortho*-C—C—C—αH torsional angle in 10° steps. The maximum for this latter process occurred at 40°, 0.1 kcal mol^{-1} above the 90° value and 0.3 kcal mol^{-1} above the 0° value. Allinger and Chung had calculated a 0 kcal mol^{-1} barrier for 2-phenyl-1,3-dioxane using the earlier MM1 force field (29). They ascribed the negligible barrier to a balance between *ortho*-hydrogen/ring oxygen repulsion in the perpendicular conformation and *ortho*-hydrogen/αH repulsion in the parallel conformation (29). Introduction of the anomeric effect in the recent calculation (23) shortened the C—O bonds and hence destabilized the perpendicular conformation. The smaller O—C—O bond angle in a 1,3-dioxolane ring should decrease the *ortho*-hydrogen/ring oxygen repulsion in the perpendicular conformation, which should cause the energy difference between the two extreme conformations to become smaller. The results of the calculations were in agreement with this expectation. The contradiction between the limited experimental results and those from the molecular mechanics calculations do not allow a firm conclusion to be drawn at this time.

There was only one OH—O hydrogen bond, a weak intramolecular bond between H102 and O4; the O4—O3 and O4—H102 distances were 2.767(11) Å and 2.53(8) Å, respectively, and the O4—H102—O3 angle was 99(6)°. However, there were two short OH—S hydrogen bonds. An intramole-

TABLE 3. Selected torsional angles for **3***c*

Atoms	Angle (deg)	Atoms	Angle (deg)
C(13)—S(1)—C(12)—S(2)	−59 (1)	C(3)—C(4)—C(5)—C(6)	0 (3)
C(13)—S(1)—C(12)—C(11)	68 (1)	C(4)—C(5)—C(6)—C(1)	1 (3)
C(12)—S(1)—C(13)—C(15)	140 (1)	C(1)—C(7)—O(1)—C(8)	−167 (1)
C(14)—S(2)—C(12)—S(1)	−60 (1)	C(1)—C(7)—O(2)—C(9)	157 (1)
C(14)—S(2)—C(12)—C(11)	171 (1)	O(2)—C(7)—O(1)—C(8)	−43 (1)
C(12)—S(2)—C(14)—C(16)	173 (2)	O(1)—C(7)—O(2)—C(9)	33 (1)
S(1)—C(12)—C(11)—C(10)	57 (1)	C(7)—O(1)—C(8)—C(9)	34 (1)
S(1)—C(12)—C(11)—O(4)	179 (1)	C(7)—O(2)—C(9)—C(8)	−11 (1)
S(2)—C(12)—C(11)—C(10)	−174 (1)	C(7)—O(2)—C(9)—C(10)	113 (1)
S(2)—C(12)—C(11)—O(4)	−52 (1)	O(1)—C(8)—C(9)—O(2)	−14 (1)
C(6)—C(1)—C(2)—C(3)	0 (2)	O(1)—C(8)—C(9)—C(10)	−135 (1)
C(2)—C(1)—C(6)—C(5)	−1 (2)	O(2)—C(9)—C(10)—C(11)	69 (1)
C(7)—C(1)—C(2)—C(3)	−178 (2)	O(2)—C(9)—C(10)—O(3)	−166 (1)
C(2)—C(1)—C(7)—O(1)	57 (2)	C(8)—C(9)—C(10)—C(11)	−173 (1)
C(2)—C(1)—C(7)—O(2)	−63 (2)	C(8)—C(9)—C(10)—O(3)	−48 (2)
C(7)—C(1)—C(6)—C(5)	177 (2)	C(9)—C(10)—C(11)—C(12)	−170 (1)
C(6)—C(1)—C(7)—O(1)	−121 (2)	C(9)—C(10)—C(11)—O(4)	67 (1)
C(6)—C(1)—C(7)—O(2)	119 (2)	O(3)—C(10)—C(11)—C(12)	65 (1)
C(1)—C(2)—C(3)—C(4)	1 (3)	O(3)—C(10)—C(11)—O(4)	−58 (1)
C(2)—C(3)—C(4)—C(5)	−1 (3)		

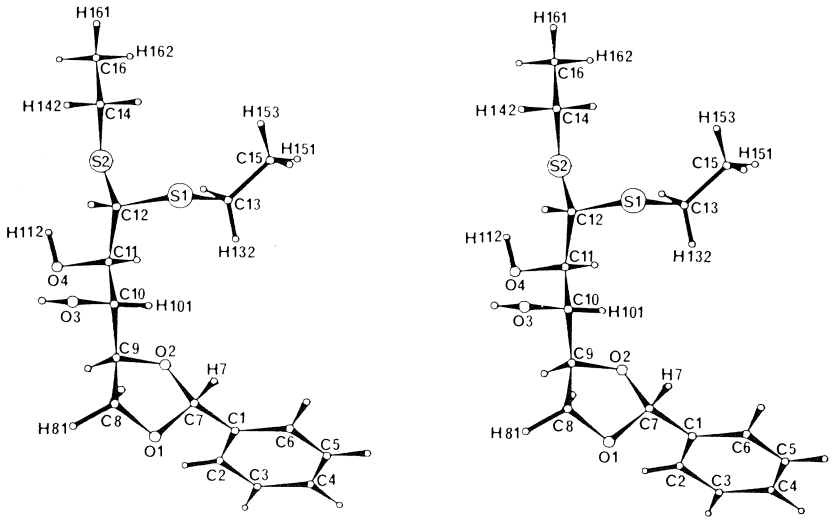

FIG. 1. Stereoview of **3***c* with the crystallographic atom numbering scheme.

cular bond was present between H112 and S2; the O4—S2 and H112—S2 distances were 2.934(9) and 2.26(10) Å, respectively, and the O4—H112—S2 angle was 130(8)°. The second hydrogen bond was intermolecular, between H102 on the adjacent molecule in the cell and the same sulfur atom S2; the O3—S2 and H102—S2 distances were 3.253(9) and 2.50(8) Å, respectively, and the S2—H102—O3 angle was 158(7)°. The O3—H102 bond distance was short, 0.80(8) Å. Because the O—H—S angle for this hydrogen bond was close to 180°, any increase in the O—H bond distance results in a decrease in the S—H distance of almost the same amount. Experimental evidence indicates OH—S hydrogen bonds have about the same strengths as OH—O hydrogen bonds (30) although theoretical studies suggest they are somewhat weaker (31). The S—H hydrogen bond distances observed here were considerably less than the sum of the van der Waals radii (3.05 Å) and are among the shortest known (30–32).

The structure of the slower moving component was unambiguously established as *R*-4,5-*O*-benzylidene-D-arabinose diethyl dithioacetal (**3***d*) from selective decoupling experiments in the ^{1}H nmr spectrum of its di-*O*-acetate derivative. The key experiment is shown in Fig. 3. It is known that signals of protons on secondary carbons bearing *O*-acetate groups are shifted downfield by ~1 ppm when compared to those of the hydroxy compounds (33). In the 361.08-MHz ^{1}H nmr spectrum of the diacetate, signals of two protons appear as doublets of doublets having chemical shifts greater than 5.0 ppm. Selective irradiation at the positions of either of these downfield signals reduces the other to a doublet, indicating that the signals arise from protons on adjacent carbons. Irradiation at 5.37 ppm, the position of one of these two quartets, reduces the doublet at 3.98 ppm to a singlet. Since only H-1 in these compounds can give rise to a doublet in its ^{1}H nmr spectrum, the two downfield signals are those of H-2 and H-3. Therefore the parent compound (**3***d*) has the 4,5-*O*-benzylidene structure. The assignment of the *R*-configuration in the 4,5-*O*-benzylidene ring of **3***d* followed from the previous assignment of the *S*-configuration to its epimer **3***c*.

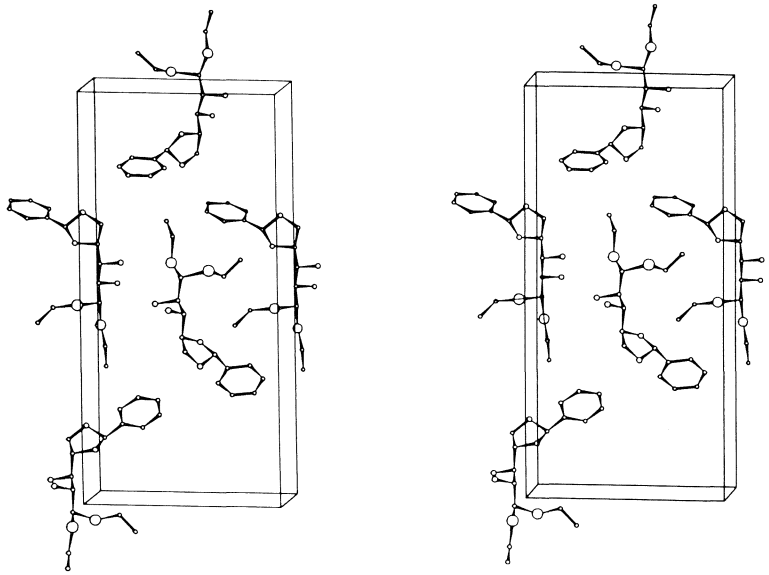

FIG. 2. Stereoview of the crystal packing of **3***c*.

Previous assignments of configuration in 2,4-disubstituted 1,3-dioxolanes have been based on unambiguous synthesis of *cis*-2,4-dimethyl-1,3-dioxolane (34, 35). Comparison of various physical properties including refractive index, thermodynamic stability, and chemical shift of the acetal proton for many *cis–trans* pairs indicated that the relationship of these properties for each pair was the same as in the unambiguously assigned dioxolanes, allowing further assignments to be made. The most useful technique is the last of the three above; the ^{1}H nmr signal from the acetal proton of the *trans* isomer is normally downfield of that of the *cis* isomer (36). For the D-aldose diethyl dithioacetal derivatives considered here, a 2-phenyl-1,3-dioxolane ring formed using the two terminal hydroxyl groups has the *S*-configuration at carbon-2 of the 1,3-dioxolane ring in the *trans* isomer. The definitive assignment of configuration made for compounds **3***c* and **3***d* allows an additional check of the reliability of the previous method of assignment. Compound **3***c*, the *trans* isomer, exhibited a more downfield shift of 5.93 ppm for the signal of the benzylidene acetal proton as compared to 5.78 ppm for this signal of **3***d*, in agreement with previous assignments (35, 36).

Other structural assignments

Assignment of structures of other compounds to be described later was made using the ^{1}H nmr chemical shift of the benzylidene acetal proton and also a number of ^{13}C nmr parameters. It has been shown that various ^{13}C nmr parameters may be used for ring-size determination of benzylidene acetals (37) and for configurational assignment in 2-phenyl-1,3-dioxolane rings fused to pyranose sugars (38). In chloroform-*d*, 2-phenyl-1,3-dioxolane derivatives have ^{1}H nmr chemical shifts for the proton on the benzylidene acetal carbon of 5.71–6.43 ppm, ^{13}C nmr chemical shifts for this carbon atom of 101.9–105.8 ppm, and $^1J_{C,H}$ values between these carbon and hydrogen atoms of 166.6–170.5 Hz (37). In contrast, the corresponding values for 2-phenyl-1,3-dioxane derivatives lie in the ranges 5.44–5.58 ppm, 100.6–101.4 ppm, and 159.7–161.8 Hz (37). The values of all of these parameters for the major products of the reaction of aldose diethyl dithioacetals fall in the ranges expected (37) for 2-phenyl-1,3-dioxolane derivatives (see Table 1 and Experimental).

In the ^{13}C nmr spectra of compounds **3***c* and **3***d*, signals of the primary carbon and of one secondary carbon were ~4 ppm downfield of those of the same carbons in the parent compound. Liptak *et al.* have noted that the signals of secondary carbons of pyranose sugars are shifted downfield by 4–8.6 ppm when the carbon becomes part of a 2-phenyl-1,3-dioxolane ring (39).

The ^{13}C nmr assignments of signals of carbons in aldose diethyl dithioacetals in dimethyl sulfoxide-d_6 had previously been made by Schnarr *et al.* (40). The ^{13}C chemical shifts obtained here for the same compounds in chloroform-d_6 containing a few drops of dimethyl sulfoxide-d_6 were ~0.5 ppm from the previous observations and all values recorded here were larger. Thus, the previous assignments were used (40). In all cases, the signal of the primary carbon in the ^{13}C nmr spectrum shifted downfield by 4 ± 1 ppm on formation of the *O*-benzylidene derivative. Thus, the major products of kinetic benzylidenations were terminal 2-phenyl-1,3-dioxolane derivatives.

It was also found that pairs of epimers were always produced. When these pairs could be separated, the compound with the larger R_f value always had the lower mp, the more downfield shift for the benzylidene acetal proton, the more upfield shift for the acetal carbon, and larger magnitude for the value of the coupling constant between the acetal carbon and proton, as also did **3***c* with respect to **3***d*. On this basis, the compound with the more downfield shift for the benzylidene acetal proton was assigned the *trans*- or *S*-configuration.

Reactions with the diethyl dithioacetal derivatives of D-*glucose,* D-*galactose,* D-*mannose, and* D-*ribose*

Reactions of the above compounds with 1.2 equivalents of benzaldehyde dimethyl acetal for 14 h at −20°C, under the same conditions as with D-arabinose diethyl dithioacetal, in all cases produced a mixture of the two epimeric *O*-benzylidene acetals having terminal 1,3-dioxolane rings as the major products in isolated yields ranging from 37 to 57%. The structures of these mono-*O*-benzylidene derivatives were assigned from the ^{1}H and ^{13}C nmr parameters as discussed above. In two cases (for D-glucose and D-mannose derivatives) the epimeric products could be separated by column chromatography. On one occasion, the reaction with D-glucose diethyl dithioacetal at −20°C for 15 h produced a mixture of the two epimeric 6-*O*-(methoxyphenylmethyl) derivatives in substantial amounts as well as

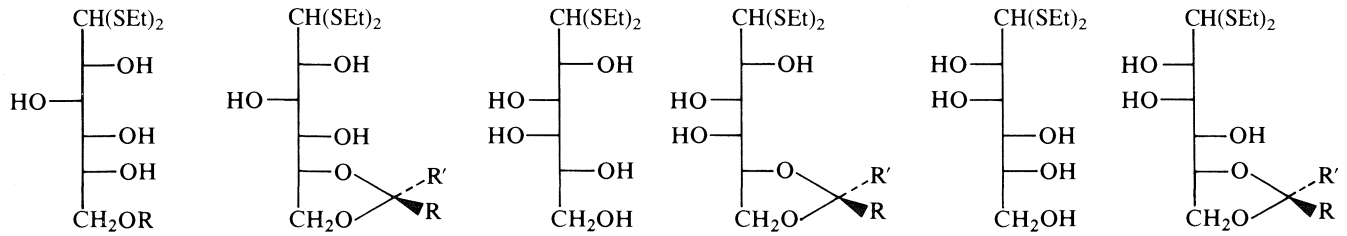

5*a* R = H
5*b* R = CHOMePh
5*c* R = Ph, R′ = H
5*d* R = H, R′ = Ph
6*a*
6*c* R = Ph, R′ = H
6*d* R = H, R′ = Ph
7*a*
7*c* R = Ph, R′ = H
7*d* R = H, R′ = Ph

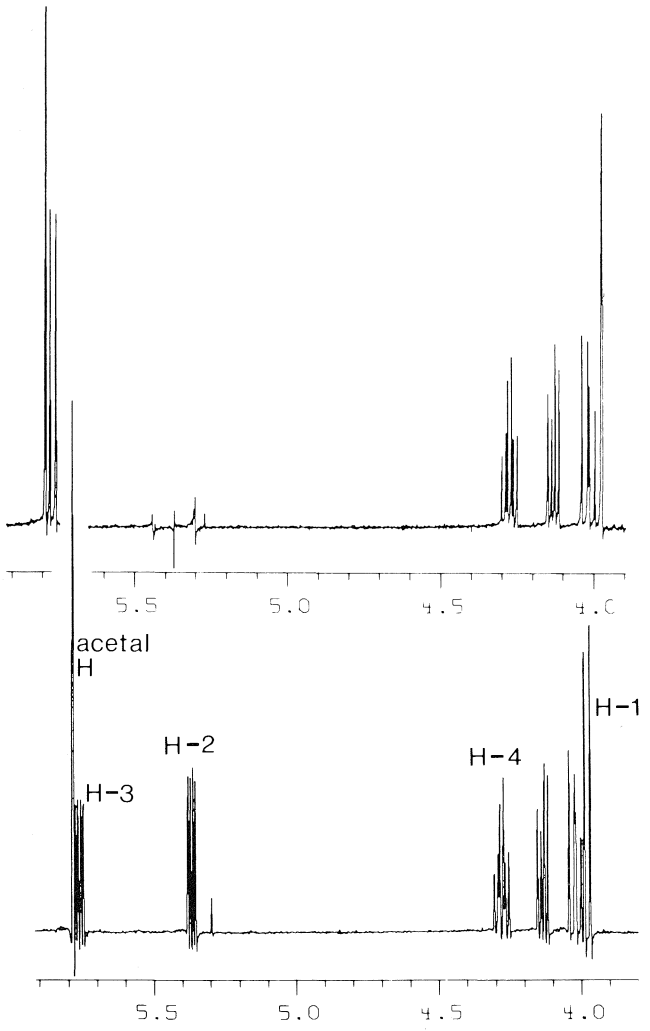

FIG. 3. Part of the 361.08 MHz ^{1}H nmr spectrum of **3***d* shown in the absence of decoupling (below), with decoupling at the signal of H-2 (above).

the normal products. For most of these reactions, the major products were accompanied by minor amounts (<4%) of materials that were not fully characterized but that were thought to be chiefly 2-phenyl-1,3-dioxane derivatives involving the terminal primary carbon, on the basis of their ^{1}H and ^{13}C nmr spectra.

The mass spectra of aldose diethyl dithioacetals have been investigated by DeJongh (41). The mass spectra of the present compounds showed most of the features observed (41), of which the most notable were prominent molecular ions, loss of thioethyl radical from the molecular ion (often supported by metastables), and base peaks at m/z 135 ($^+$CH(SEt)$_2$). The relative intensities of the peaks at m/z 149 and 179 were related, to some extent, to ring size. These ions probably arise from cleavage of the two or three terminal carbon atoms of the sugar chain along with the attached benzylidene acetal. In the compounds described in this paper, the peak at m/z 149 was normally more intense; the compounds in the following paper (42), which have a six-membered ring spanning the three terminal carbon atoms, gave rise to spectra with more intense peaks at m/z 179. However, there were enough exceptions (**4***c*, *d*) that these observations cannot be considered diagnostic of ring size.

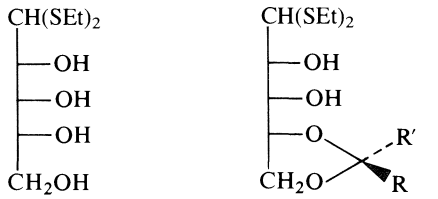

4*a*
4*c* R = Ph, R′ = H
4*d* R = H, R′ = Ph

The present results provide some information about the mechanism of this reaction. Isolation of the acyclic *O*-methoxyphenylmethyl acetal (**3***b*) from the reaction at −40°C indicates that the reaction at −20°C proceeds through this intermediate. This acyclic acetal rearranged to the five-membered ring acetals on standing in a chloroform-*d* solution as well as in the reaction medium at −20°C. The preference for attack by the primary alcohol is caused by steric factors. The five-membered ring diastereomers do not rearrange into one another or other products at −20°C. Thus, they are the kinetic products at this temperature. Presumably, they are preferred over the thermodynamically more stable six-membered rings because of the more favorable entropy of activation for their formation (10).

The rate constants for formation of the acyclic intermediates, e.g. **3***b*, were observed to be of the same order of magnitude as that for ring closure from this intermediate. In contrast, the rate constants for epimerization or rearrangement (42) are smaller by at least two orders of magnitude. Epimerization or rearrangement must take place through carbocation intermediates. Formation of the acyclic intermediate and its ring closure could occur via carbocation intermediates or via an S_N2 process. Both types of reactions would have an initial equilibrium protonation step, followed by the rate-determining step. The oxygen atom being protonated is in a methoxyl group for the faster reactions and is attached to a primary or secondary carbon for the slower ones. The latter type of oxygen atom is probably more basic (2). Thus, the difference in the rates of reaction must occur in the rate-determining step. This step is therefore different in mechanism for the faster reactions and involves an S_N2 process. The greater steric interactions present in an S_N2 transition state are more consistent with the great

discrimination between primary and secondary hydroxyl groups observed here.

Experimental

Melting points were determined with a Fischer–Johns melting point apparatus and are uncorrected. The ^1H and ^{13}C nmr spectra were recorded at 79.6 and 20 MHz, respectively, on Varian CFT-20 or FT-80 spectrometers in chloroform-*d* with tetramethylsilane as the internal standard, unless otherwise specified. Selective homonuclear decoupling was performed with a Wavetek Model 171 frequency synthesizer. The ^1H nmr spectra at 60 MHz and ^1H nmr spectra at 361.08 MHz or ^{13}C nmr spectra at 90.8 MHz were measured on Varian T-60 and Nicolet NT-360 NB spectrometers, respectively. The ^1H nmr spectra were analysed on a first-order basis. Mass spectra were obtained with a CEC 21-104 mass spectrometer with an inlet temperature of 150°C operating at a 70-eV ionizing voltage unless otherwise specified. The ir spectra were recorded on a Pye Unicam SP 1000 spectrophotometer. Optical rotations were determined on Perkin–Elmer 141 or Bellingham and Stanley polarimeters. Bath temperatures between −20°C and room temperature were controlled with a Haake FK bath while those at −20°C and below were controlled in a Neslab bath by a Neslab CC-100 cooler and an Exatrol 30 control unit. Thin-layer chromatography (tlc) was performed on 0.25 mm thick precoated (BDH EM reagents) silica gel 60F-254 glass plates cut to be approximately 7 cm long. Plates were developed by spraying with a 2% ceric sulfate solution in 1 *M* sulfuric acid and heating for a few minutes at 150°C. The term pet. ether refers to petroleum ether 30–60°C unless otherwise specified. Compositions of eluent systems used were as follows: A, pet. ether:ethyl acetate, 2:1; B, pet. ether:ethyl acetate, 2:3; C, pet. ether:ethyl acetate, 7:3; D, pet. ether:ethyl acetate, 3:1; E, benzene:methanol, 9:1; F, pet. ether:ethyl acetate, 1:1. Column chromatography was performed using silica gel 60 (70–230 mesh) (Merck). Anhydrous *p*-toluenesulfonic acid was obtained from the commercial monohydrate by heating 5 h at 56°C under vacuum (0.5 Torr; 1 Torr = 133.3 Pa) in a drying pistol in the presence of phosphorus pentoxide. *N,N*-Dimethylformamide was purified by distillation from calcium hydride. Microanalyses were performed by the Canadian Microanalytical Service, Ltd., Vancouver, B.C.

General method for benzylidenation under kinetic control

A solution of dried aldose diethyl dithioacetal (10 mmol) and anhydrous *p*-toluenesulfonic acid (**1**) (50 mg, 0.58 mmol) in dry *N,N*-dimethylformamide (DMF) (20 mL) was cooled to −20°C. α,α-Dimethoxytoluene (**2**) (12 mmol) was added and the reaction flask attached to a water aspirator. After 14 h at −20°C, when tlc indicated complete conversion of starting material, the solution was poured into a 5% sodium bicarbonate solution (50 mL) and the mixture was extracted with ether (3 × 30 mL). The combined extracts were washed with water (2 × 30 mL), dried over anhydrous magnesium sulfate, filtered, and concentrated on a rotary evaporator at 40°C. All recrystallizations of solid products were from dichloromethane/pet. ether 65–75°C, and all crystals were colorless.

*Benzylidenation of D-arabinose diethyl dithioacetal (**3**a) at −20°C*

Compound **3***a* (2.56 g, 10 mmol) in DMF (10 mL) was treated with compounds **1** (100 mg) and **2** (1.824 g, 12 mmol) as in the general method. The product, a pale yellow syrup, contained two components by tlc (solvent A), which were separated by column chromatography on silica gel (100 g) using solvent A as eluent.

The first fraction (0.936 g, 27%, R_f 0.44) crystallized and was recrystallized to give fine needles of *S*-4,5-*O*-benzylidene-D-arabinose diethyl dithioacetal (**3***c*), mp 71–72°C; $[\alpha]_D^{24}$ −31° (*c* 4.00, chloroform); ^1H nmr δ: 1.26, 1.28 (2t, 6H, 2 SCH_2CH_3, J = 7.3, 7.5 Hz), 2.50 (br s, exchanged with D_2O, OH-3), 2.67, 2.69 (2q, 4H, 2 SCH_2CH_3, J = 7.3, 7.5 Hz), 3.37 (d, 1H, exchanged with D_2O, OH-2, $J_{2,OH}$ = 2.6 Hz), 3.79 (dd after D_2O exchange, 1H, H-2, $J_{1,2}$ = 9.7 Hz, $J_{2,3}$ = 2.0 Hz), 4.05 (d, 1H, H-1, $J_{1,2}$ = 9.3 Hz), 4.12–4.36 (complex m, 5H), 5.93 (s, 1H, benzylidene H), 7.24–7.51 (m, 5H, Ph); *m/z*: 344 (19, M^+), 283 (2, M − ·SEt), 177 (19), 149 (5), 137 (14), 136 (11), 135 (100, $^+CH(SEt)_2$), 107 (16), 105 (23), 91 (13), 75 (13). *Anal.* calcd. for $C_{16}H_{24}O_4S_2$: C 55.78, H 7.02; found: C 55.62, H 7.16.

The second fraction (1.404 g, 41%, R_f 0.33) crystallized and was recrystallized to give very fine needles of *R*-4,5-*O*-benzylidene-D-arabinose diethyl dithioacetal (**3***d*), mp 87–88°C; $[\alpha]_D^{24}$ −60° (*c* 4.00, chloroform); ^1H nmr δ: 1.24 (t, 6H, 2 SCH_2CH_3, J = 7.4 Hz), 2.65, 2.68 (2q, 4H, 2 SCH_2CH_3, J = 7.6, 7.5 Hz), 2.90 (br s, 1H, exchanged with D_2O, OH-3), 3.34 (d, 1H, exchanged with D_2O, OH-2, $J_{2,OH}$ = 2.3 Hz), 3.78 (dd after D_2O exchange, 1H, H-2, $J_{1,2}$ = 9.3 Hz, $J_{2,3}$ = 1.8 Hz), 4.01 (d, 1H, H-1, $J_{1,2}$ = 9.3 Hz), 4.04–4.36 (complex m, 5H), 5.78 (s, 1H, benzylidene H), 7.25–7.53 (m, 5H, Ph); *m/z*: 344 (4, M^+), 283 (6, M − ·SEt), 177 (16), 149 (7), 135 (100, $^+CH(SEt)_2$), 107 (21), 105 (24), 91 (16), 77 (13), 75 (16); metastable: 232–235 (344–283). *Anal.* calcd. for $C_{16}H_{24}O_4S_2$: C 55.78, H 7.02; found: C 55.77, H 7.23.

*Benzylidenation of D-arabinose diethyl dithioacetal (**3**a) at −40°C*

Compounds **1** (50 mg), **2** (0.912 g, 6 mmol), and **3***a* (1.28 g, 5 mmol) were kept in DMF (10 mL) at −40°C for 100 h. The product, a pale yellow syrup, was separated by column chromatography, on silica gel (100 g) using solvent A as eluent, into 3 fractions, A (0.078 g, 5%, R_f 0.44), B (0.098 g, 6%, R_f 0.33), and C (0.306 g, 18%, R_f 0.20). Fractions A and B were shown to be identical to compounds **3***c* and **3***d*, respectively.

Fraction C, a solid, was recrystallized to give fine needles, a mixture of *R*- and *S*-5-*O*-(methoxyphenylmethyl)-D-arabinose diethyl dithioacetal (**3***b*), mp 71–73°C; $[\alpha]_D^{24}$ +4° (*c* 1.56, chloroform); ^1H nmr (60 MHz) δ: 1.28 (t, 6H, 2 SCH_2CH_3, J = 7.5 Hz), 2.70, 2.72 (2q, 4H, 2 SCH_2CH_3, J = 7.5 Hz), 2.95–3.22 (m, exchanged with D_2O, 3H, 3OH), 3.32 (s, 3H, OCH_3), 3.46 (br s, exchanged with D_2O, OH), 3.66–4.32 (complex m, 6H), 5.48 (s, 1H, benzylidene H), 7.28–7.60 (m, 5H, Ph); ^{13}C nmr δ: 50.0, 50.2 (2 OMe C); *m/z*: 376 (4.5%, M^+), 344 (11, M − CH_3OH), 283 (10, 344 − ·SEt), 256 (3), 255 (5, M − $CHPhOCH_3$), 209 (6, 344 − 135), 179 (10), 177 (29), 135 (100, $^+CH(SEt)_2$), 121 (50, $^+CHOMePh$), 107 (34), 105 (35), 91 (20), 77 (26), 75 (24).

A reaction, as above, but for 253 h, yielded **3***b* (6%), **3***c* (20%), and **3***d* (22%).

S-*2,3-Di*-O-*acetyl-4,5*-O-*benzylidene-D-arabinose diethyl dithioacetal*

Compound **3***c* (0.258 g, 0.75 mmol) in dry pyridine (1.184 g, 15 mmol) and acetic anhydride (3.06 g, 30 mmol) was stirred 14 h, then poured into ice-water (30 mL). The mixture was extracted with ether (3 × 30 mL), and the ether extracts were combined, washed with saturated cupric sulfate solutions (3 × 30 mL), saturated sodium bicarbonate solutions (3 × 30 mL), and water (3 × 30 mL), dried over anhydrous magnesium sulfate, filtered, and concentrated. The resulting pale yellow syrup (0.295 g, 89%) was homogeneous on tlc (R_f 0.75 in solvent A); ir (neat): 1745 cm^{-1} (C=O), no OH stretching band; ^1H nmr δ: 1.22 (t, 6H, 2 SCH_2CH_3, J = 7.3 Hz), 2.10 (s, 6H, $2COCH_3$), 2.67 (q, 4H, 2 SCH_2CH_3, J = 7.3 Hz), 3.92–4.23 (complex m, 4H), 5.43 (dd, 1H, H-3), 5.77 (m, 1H, H-2), 5.95 (s, 1H, benzylidene H), 7.29–7.47 (m, 5H, Ph); ^1H nmr (benzene-d_6) δ: 1.05, 1.09 (2t, 6H, 2 SCH_2CH_3, J = 7.4 Hz), 1.79, 1.85 (2s, 3 $COCH_3$), 2.52, 2.61 (2q, 4H, 2 SCH_2CH_3, J = 7.2 Hz), 3.94–4.29 (complex m, 4H), 5.68 (dd, 1H, H-3, $J_{3,4}$ = 7.0 Hz, $J_{2,3}$ = 3.5 Hz), 5.95 (s, 1H, benzylidene H), 6.04 (dd, 1H, H-2, $J_{1,2}$ = 6.6 Hz, $J_{2,3}$ = 3.5 Hz), 7.12–7.21 (complex m, 3H, 3 phenyl H), 7.41–7.55 (m, 2H, 2 phenyl H).

R-*2,3-Di*-O-*acetyl-4,5*-O-*benzylidene-D-arabinose diethyl dithioacetal*

Compound **3***d* (0.258 g, 0.75 mmol) was acetylated as in the previous reaction. The product (R_f 0.66 in solvent A) crystallized and was recrystallized twice to give feathery crystals of the title compound (0.26 g, 31%); mp 87–88°C; $[\alpha]_D^{24}$ +30° (*c* 3.04, chloroform); ^1H nmr (361.08 MHz) δ: 1.18, 1.19 (2t, 6H, 2 SCH_2CH_3, J = 7.29, 7.34 Hz), 2.08, 2.15 (2s, 6H, $2COCH_3$), 2.59 (q, 4H, 2 SCH_2CH_3, J = 7.36 Hz), 3.98 (d, 1H, H-1, $J_{1,2}$ = 7.0 Hz), 4.02 (dd, 1H, H-5, $J_{4,5}$ = 7.2 Hz, $J_{5,5'}$ = 8.3 Hz), 4.13 (dd, 1H, H-5′, $J_{4,5'}$ = 4.6 Hz, $J_{5,5'}$ = 8.5 Hz), 4.28 (dt, 1H, H-4, $J_{3,4}$ = 6.8 Hz, $J_{4,5'}$ = 4.6 Hz, $J_{4,5}$ = 6.8 Hz), 5.37 (dd, 1H, H-2, $J_{1,2}$ = 7.1 Hz, $J_{2,3}$ = 3.2 Hz), 5.76

(dd, 1H, H-3, $J_{2,3}$ = 3.1 Hz, $J_{3,4}$ = 6.8 Hz), 5.78 (s, 1H, benzylidene H), 7.27–7.37 (complex m, 3H, 3 phenyl H), 7.46–7.49 (m, 2H, 2 phenyl H).

Attempted rearrangements of R- *and* S-*4,5-*O*-benzylidene-*D*-arabinose diethyl dithioacetal (**3**d *and* **3**c, *respectively) at* −21°C

Compound **1** (10 mg) was added to a solution of compound **3***d* (126 mg) in dry DMF (2 mL) at −21°C. The solution was kept at −21°C for 14 h, then worked up in the normal fashion. The product was shown to be identical with starting material (**3***d*) by tlc and ^{1}H nmr.

Attempted rearrangement of **3***c* under the same conditions for 14 h also produced starting material only.

Benzylidenation of D*-ribose diethyl dithioacetal (**4**a)*

Compound **4***a* (1.28 g, 5 mmol) in dry DMF (7 mL) was treated with compounds **1** (50 mg) and **2** (0.912 g, 6 mmol) as in the general method but for 49 h. The product, a pale yellow syrup, was fractionated by column chromatography, on silica gel (100 g) using solvent A as eluent, into a major compound (0.982 g, 57%, R_f 0.50) and two very minor components (R_fs 0.20 and 0.17), which were not examined further. The major component was a mixture of *R*- and *S*-4,5-*O*-benzylidene-D-ribose diethyl dithioacetal (**4***c* and **4***d*), $[\alpha]_D^{24}$ +0.1 (*c* 4.52, chloroform); ^{1}H nmr δ: 1.24, 1.25 (2t, 6H, 2 SCH_2CH_3, *J* = 7.1, 7.5 Hz), 2.67, 2.70 (2q, 4H, 2 SCH_2CH_3, *J* = 7.4, 7.2 Hz), 3.00–4.26 (complex m, 8H), 5.79, 5.98 (2s, 1H, benzylidene H's from *R* and *S* isomers, intensity ratio δ 5.79:δ 5.98, 2:3), 7.26–7.46 (complex m, 5H, Ph); *m/z*: 344 (17, M^+), 283 (4, M − ·SEt), 256 (9), 221 (3), 209 (2), 179 (13), 177 (29), 159 (3), 149 (4), 135 (100, $^+CH(SEt)_2$), 133 (9), 117 (9), 107 (48), 105 (49), 104 (16), 103 (15), 77 (20), 75 (34), metastable: 232–235 (344–283).

Benzylidenation of D*-glucose diethyl dithioacetal (**5**a)*

Compound **5***a* (8.58 g, 30 mmol) in dry DMF (60 mL) was treated with compounds **1** (300 mg) and **2** (5.472 g, 36 mmol) as in the general method. The product, a pale yellow solid, was fractionated by column chromatography, on silica gel (300 g) using solvent B as eluent, into three fractions, A (1.80 g, 16%, R_f 0.66), B (3.89 g, 35%, R_f 0.60), and C (0.31 g, 3%, R_f 0.40 (not examined further)).

Fraction A crystallized and was recrystallized to give fine needles of *S*-5,6-*O*-benzylidene-D-glucose diethyl dithioacetal (**5***c*), mp 91–92°C; $[\alpha]_D^{24}$ +65° (*c* 4.00, chloroform); ^{1}H nmr δ: 1.25 (t, 6H, 2 SCH_2CH_3, *J* = 7.3 Hz), 2.66, 2.69 (2q, 2H, 2 SCH_2CH_3, *J* = 7.5 Hz), 3.20 (d, exchanged with D_2O, 1H, OH-2, $J_{2,OH}$ = 8.9 Hz), 3.61–4.36 (complex m, 9H), 5.92 (s, 1H, benzylidene H), 7.28–7.48 (complex m, 5H, Ph); *m/z*: 374 (38, M^+), 313 (2, M − ·SEt), 251 (1, 313 − HSEt), 239 (10), 209 (2), 207 (3), 177 (3), 149 (8), 135 (100, $^+CH(SEt)_2$), 107 (30), 105 (28), 103 (12), 91 (19), 77 (11), 75 (13), metastable: 260–264.

Fraction B crystallized and was recrystallized to give flakes of *R*-5,6-*O*-benzylidene-D-glucose diethyl dithioacetal (**5***d*), mp 108–109°C; $[\alpha]_D^{24}$ +28° (*c* 4.00, chloroform); ^{1}H nmr δ: 1.25 (t, 6H, 2 SCH_2CH_3, *J* = 7.3 Hz), 2.64, 2.69 (2q, 4H, 2 SCH_2CH_3, *J* = 7.5 Hz), 2.95 (d, exchanged with D_2O, 1H, OH, *J* = 8.8 Hz), 3.58–4.34 (complex m, 9H), 5.81 (s, 1H, benzylidene H), 7.32–7.47 (m, 5H, Ph); *m/z*: 374 (23, M^+), 313 (9, M − ·SEt), 251 (5, 313 − HSEt), 239 (44), 209 (8), 207 (11), 177 (7), 149 (25), 135 (100, $^+CH(SEt)_2$), 117 (13), 107 (83), 105 (75), 103 (44), 91 (57), 77 (36), 75 (41), metastable: 260–264. *Anal.* calcd. for $C_{17}H_{26}O_5S_2$: C 54.52, H 7.00; found: C 54.44, H 7.11.

In only one of several reactions performed as above on compound **5***a* (5.12 g, 20 mmol), poor yields of the normal products, **5***c* (0.98 g, 13%) and **5***d* (1.62 g, 25%), were obtained and another product, 6-*O*-(methoxyphenylmethyl)-D-glucose diethyl dithioacetal (**5***b*) (0.84 g, 11%, R_f 0.43 in solvent B), was also isolated. **5***b* was probably the same compound as fraction C above. Compound **5***b* was a syrup, $[\alpha]_D^{24}$ +25° (*c* 4.8, chloroform); ^{1}H nmr δ: 1.24 (t, 6H, 2 SCH_2CH_3, *J* = 7.5 Hz), 2.70, 2.72 (2q, 4H, 2 SCH_2CH_3, *J* = 7.5 Hz), 3.32 (s, 3H, OCH_3), 3.52–4.68 (complex m, 11H), 5.50 (s, 1H, benzylidene H), 7.34–7.62 (m, 5H, Ph); *m/z*: 406 (0.4, M^+), 374 (12, M − CH_3OH), 313 (3, 374 − ·SEt), 286 (4, M − $PhCOCH_3$), 239 (11, 374 − 135), 207 (5), 149 (8), 135 (100, $^+CH(SEt)_2$), 121 (49, $^+CHOMePh$).

Benzylidenation of D*-galactose diethyl dithioacetal (**6**a)*

Compounds **6***a* (8.58 g, 30 mmol), **1** (300 mg), and **2** (5.472 g, 36 mmol) were kept in DMF (80 mL) as in the general method. The pale yellow syrupy product was fractionated by column chromatography, on silica gel (300 g) using solvent D as eluent, into two components, A (4.15 g, 37% yield, R_f 0.66) and B (0.47 g, 4%, R_f 0.32).

Fraction A crystallized and was recrystallized to give colorless flakes, a mixture of *R*- and *S*-5,6-*O*-benzylidene-D-galactose diethyl dithioacetal (**6***c* and **6***d*), mp 106–107°C; $[\alpha]_D^{24}$ +66° (*c* 3.53, chloroform); ^{1}H nmr δ: 1.27 (t, 6H, 2 SCH_2CH_3, *J* = 7.4 Hz), 2.55–2.86 (m, 4H, 2 SCH_2CH_3), 3.41 (d, 1H, exchanged with D_2O, OH, *J* = 2.3 Hz), 3.92–4.37 (complex m, 9H), 5.82, 5.97 (2s, 1H, benzylidene H's, intensity ratio δ 5.82:δ 5.97, 2:3), 7.32–7.55 (m, 5H, Ph); *m/z*: 374 (4, M^+), 313 (3, M − ·SEt), 295 (2), 251 (8), 239 (10), 221 (7), 209 (3), 207 (8), 189 (5), 179 (4), 177 (13), 175 (3), 149 (11), 145 (6), 137 (14), 136 (13), 135 (100, $^+CH(SEt)_2$), 133 (7), 127 (4), 117 (5), 115 (3), 107 (32), 105 (17), 104 (7), 103 (11), 91 (17), 85 (6), 79 (7), 77 (11), 75 (13). *Anal.* calcd. for $C_{17}H_{26}O_5S_2$: C 54.52, H 7.00; found: C 54.49, H 6.91.

On tlc in solvent E, fraction A could be separated into two components (R_f's 0.37 and 0.40). Fraction B was a syrup, a mixture of two compounds from its ^{1}H nmr spectrum (60 MHz): δ 5.40 and 5.90 (2s in intensity ratio 4:1). It was not examined further.

Benzylidenation of D*-mannose diethyl dithioacetal (**7**a)*

Compounds **7***a* (2.002 g, 7 mmol), **1** (100 mg), and **2** (2.55 g, 16.8 mmol) were kept in DMF (15 mL) as in the general method. The pale yellow syrupy product was fractionated by column chromatography, on silica gel (115 g) using solvent F as eluent, into two components, A (1.02 g, 40%, R_f 0.50) and B (0.49 g, 19%, R_f 0.35).

Fraction A crystallized and was recrystallized to give needles of *S*-5,6-*O*-benzylidene-D-mannose diethyl dithioacetal (**7***c*); mp 76–77°C; $[\alpha]_D^{24}$ +13° (*c* 0.86, chloroform); ^{1}H nmr δ: 1.27 (t, 6H, 2 SCH_2CH_3, *J* = 7.3 Hz), 2.68, 2.72 (2q, 4H, 2 SCH_2CH_3, *J* = 7.4 Hz), 3.00–3.12 (br m, 2H, exchanged with D_2O, OH-3, and OH-4), 3.25 (d, 1H, exchanged with D_2O, OH-2, *J* = 3.3 Hz), 3.97–4.34 (m, 7H), 5.95 (s, 1H, benzylidene H), 7.25–7.41 (m, 4H, Ph); *m/z*: 374 (37, M^+), 313 (5, M − ·SEt), 295 (2), 251 (2, 313 − HSEt), 239 (13), 209 (3), 207 (9), 189 (5), 177 (7), 149 (10), 145 (6), 135 (100, $^+CH(SEt)_2$), 107 (35), 105 (37), 103 (17), 91 (20), 77 (14), 75 (18), metastable: 261–263. *Anal.* calcd. for $C_{17}H_{26}O_5S_2$: C 54.52, H 7.00; found: C 54.30, H 6.98.

Fraction B crystallized and was recrystallized to give fine needles of *R*-5,6-*O*-benzylidene-D-mannose diethyl dithioacetal (**7***d*); mp 85–86°C; $[\alpha]_D^{24}$ −3° (*c* 3.56, chloroform); ^{1}H nmr δ: 1.24, 1.26 (2t, 6H, 2 SCH_2CH_3, *J* = 7.4 Hz), 2.64, 2.69 (2q, 4H, 2 SCH_2CH_3, *J* = 7.5 Hz), 3.00–3.12 (br m, 2H, exchanged with D_2O, OH-3 and OH-4), 3.17 (d, 1H, exchanged with D_2O, *J* = 3.7 Hz), 3.94–4.33 (complex m, 7H), 5.78 (s, 1H, benzylidene H), 7.30–7.52 (m, 5H, Ph); *m/z*: 374 (6, M^+), 313 (3, M − ·SEt), 295 (2), 251 (2), 239 (12, *M* − 135), 207 (5), 189 (4), 179 (1), 177 (4), 149 (68), 137 (9), 136 (8), 135 (100, $^+CH(SEt)_2$), 133 (3), 127 (3), 117 (5), 115 (3), 107 (29), 105 (27), 104 (8), 103 (16), 91 (17), 79 (7), 77 (9), 75 (13), metastables: 263–261 (374–313), 277–280 (313–295).

X-ray crystallographic study of **3**c

Recrystallization of **3***c* twice more from dichloromethane/pet. ether 65–75° gave needles suitable for the crystallographic study.

Crystal data

$C_{16}H_{24}O_4S_2$ fw = 344.5

Crystal size (mm), 0.3 × 0.3 × 0.4, orthorhombic, space group $P2_12_12_1$ with *a* = 5.179(4) Å, *b* = 12.469(3) Å, *c* = 27.150(4) Å, *V* = 1753.3 Å^3, *Z* = 4, D_c = 1.305 g cm^{-3} (20 ± 2°C); MoKα radiation, λ = 0.70926 (graphite monochromator), μ(MoKα) = 2.70 cm^{-1}, *F*(000) = 736 e.

Structure determination

An Enraf–Nonius CAD-4 diffractometer was used to determine the unit-cell dimensions from 25 general reflections with 10 < θ < 14°C. 953 unique reflections were collected, of which 714 had $I > \sigma(I)$, 0 < 2θ < 46°. These were used in the structure solution and refinement.

The intensities were reduced by routine procedures described previously (43). Lorentz and polarization corrections were applied, but no absorption or extinction corrections. Scattering factors were taken from ref. 44 and were corrected for the real part of the anomalous dispersion effect. The structure was solved using the SHELX (76) system (45).

The non-hydrogen atoms were located from the E-map. Full-matrix least-squares refinement was performed using first isotropic, then anisotropic, temperature factors. The hydrogen atoms were located from a difference Fourier map, except for H161, H162, and H163, which were placed geometrically in chemically reasonable positions. Refinement was continued with anisotropic temperature factors on the non-hydrogen atoms and isotropic temperature factors on the hydrogens until $R = 0.60$, $R_w = 0.061$. The least-squares weights were calculated from $w^{-1} = \sigma^2|F_o| + 0.10414|F_o|^2$. In the final cycle, the maximum parameter shift (Δ/σ) was 0.01. The final atomic parameters for the non-hydrogens atoms are given in Table 2 and torsional angles in Table 3.[4]

Molecular mechanics calculations

Molecular mechanics calculations were performed using the MM2 program (1980 version), modified for use on a Perkin–Elmer computer (26). The program was modified locally to incorporate improvements in the force field for alkylbenzenes (27) and for the anomeric effect (28). Calculations were performed on a Perkin–Elmer 3230 computer.

Acknowledgements

T.B.G. and T.S.C. thank the Natural Sciences and Engineering Research Council of Canada for financial support. We thank Amarita Kumari and Wanda Tancreiter for technical assistance and the Atlantic Regional Laboratories of the National Research Council for use of their Perkin–Elmer 141 polarimeter and Varian FT-80 nmr spectrometer.

1. J. Gelas. Adv. Carbohydr. Chem. Biochem. **39**, 71 (1981).
2. P. J. Garegg, H. Huitberg, and S. Wallin. Carbohydr. Res. **108**, 97 (1982).
3. D. R. Williams, Y. Harigaya, J. L. Moore, and A. D'Sa. J. Am. Chem. Soc. **106**, 2641 (1984).
4. R. Johansson and B. Samuelsson. J. Chem. Soc. Perkin Trans. 1, 2371 (1984).
5. J. D. Wander and D. Horton. Adv. Carbohydr. Chem. **32**, 15 (1976).
6. D. M. Clode. Chem. Rev. **79**, 491 (1979).
7. R. M. Hann and C. S. Hudson. J. Am. Chem. Soc. **66**, 1909 (1944); **70**, 765 (1948); S. A. Barker and E. J. Bourne. Adv. Carbohydr. Chem. **7**, 137 (1952).
8. D. J. J. Potgietter and D. L. Macdonald. J. Org. Chem. **26**, 3934 (1961); H. Zinner, B. Richard, M. Blessman, and M. Schlutt. Carbohydr. Res. **2**, 197 (1966); H. Zinner and H. Banz. J. Prackt. Chem. **314**, 428 (1972).
9. J. Gelas and D. Horton. Heterocycles, **16**, 1587 (1981).
10. T. B. Grindley, J. C. P. Cote, and C. Wickramage. Carbohydr. Res. **140**, 215 (1985).
11. M. E. Evans. Carbohydr. Res. **21**, 473 (1972).
12. D. Horton and W. Weckerle. Carbohydr. Res. **44**, 227 (1975); P. Rollin and P. Sinay. C. R. Acad. Sci. Ser. C, **284**, 65 (1977); J. C. Florent and C. Monneret. Synthesis, 29 (1982); I. Grishkovets, A. E. Zemlyakvov, and V. Ya. Chirva. Khim. Prir. Soedin. 119 (1982); Chem. Abstr. **96**, 200035j (1982); A. Liptak, J. Imre, J. Harangi, P. Nanasi, and A. Neszmelyi. Tetrahedron, **38**, 3721 (1982).
13. D. H. Hall. Carbohydr. Res. **86**, 158 (1980).
14. D. J. Brecknell and R. M. Carman. Aust. J. Chem. **22**, 1669 (1969).
15. J. D. Wander and D. Horton. J. Org. Chem. **39**, 1859 (1974).
16. G. W. Schnarr, D. M. Vyas, and W. A. Szarek. J. Chem. Soc. Perkin Trans. 1, 496 (1979); S. J. Angyal and R. Lefur. Carbohydr. Res. **84**, 201 (1980).
17. A. Ducruix, D. Horton, C. Pascard, J. D. Wander, and T. Prange. J. Chem. Res. 5438 (1978); A. Ducruix and C. Pascard-Billy. Acta Crystallogr. Sect. B, **30**, 1056 (1974); T. J. McLennan, W. T. Robinson, G. S. Bethell, and R. J. Ferrier. Acta Crystallogr. Sect. B, **33**, 2888 (1977).
18. D. C. Rohrer, J.-C. Fischer, D. Horton, and W. Weckerle. Can. J. Chem. **56**, 2915 (1978).
19. A. J. Dekok and C. Romers. Recl. Trav. Chim. Pays-Bas, **89**, 313 (1966).
20. T. E. Conturo and G. A. Jeffrey. Carbohydr. Res. **104**, 33 (1982); E. Rossmanith, K. H. Klaska, H. Bunsch, and H. Paulsen. Acta Crystallogr. Sect. B, **34**, 3805 (1978).
21. P. Luger, B. Elevers, and H. Paulsen. Chem. Ber. **112**, 3855 (1979).
22. R. D. Guthrie, R. W. Irvine, B. E. Davison, K. Henrick, and J. Trotter. J. Chem. Soc. Perkin Trans. 2, 468 (1981); F. W. Nader. Tetrahedron Lett. 1207 (1975).
23. T. B. Grindley, S. Kusuma, T. S. Cameron, and A. Kumari. Carbohydr. Res. In press.
24. W. F. Bailey, H. Connon, E. L. Eliel, and K. B. Wiberg. J. Am. Chem. Soc. **100**, 2202 (1978).
25. T. Schaefer, W. Niemczura, and W. Danchura. Can. J. Chem. **57**, 355 (1979).
26. N. L. Allinger. J. Am. Chem. Soc. **99**, 8127 (1977); M. Froimowitz. QCPE, **2**, 448 (1982).
27. H.-D. Biekhaus. Chem. Ber. **116**, 86 (1983).
28. L. Norskov-Lauritsen and N. L. Allinger. J. Comput. Chem. **5**, 326 (1984).
29. N. L. Allinger and D. Y. Chung. J. Am. Chem. Soc. **98**, 6798 (1976).
30. I. V. Zuika and Y. A. Bankovskii. Usp. Khim. **42**, 39 (1973).
31. W. R. Snyder, H. D. Schreiber, and J. N. Spencer. Spectrochim. Acta Part A, **29**, 1225 (1973); O. Novaro, A. Les, M. Galvin, and G. del Conde. Theor. Chim. Acta, **64**, 65 (1983).
32. N. Satyamurthy, R. Swakumar, R. Ramalingam, K. D. Berlin, R. A. Loghry, and D. Van der Helm. J. Org. Chem. **45**, 349 (1980).
33. L. D. Hall. Adv. Carbohydr. Chem. **19**, 51 (1964).
34. D. J. Triggle and B. Belleau. Can. J. Chem. **40**, 1201 (1962); N. Baggett, J. M. Duxbury, A. B. Foster, and J. M. Weber. J. Chem. Soc. C, 208 (1965).
35. W. E. Willy, G. Binsch, and E. L. Eliel. J. Am. Chem. Soc. **92**, 5394 (1970).
36. N. Baggett, K. W. Buck, A. B. Foster, M. H. Randall, and J. M. Webber. J. Chem. Soc. 3394 (1965).
37. V. Gulasekharam and T. B. Grindley. Carbohydr. Res. **74**, 7 (1979).
38. A. Neszmelyi, A. Liptak, and P. Nanasi. Carbohydr. Res. **58**, C7 (1977).
39. A. Liptak, P. Fugedi, P. Nanasi, and A. Neszmelyi. Tetrahedron, **35**, 1111 (1979).
40. G. W. Schnarr, D. M. Vyas, and W. S. Szarek. J. Chem. Soc. Perkin Trans. 1, 496 (1979).
41. D. C. DeJongh. J. Org. Chem. **30**, 1563 (1965).
42. T. B. Grindley and S. Kusuma. Can. J. Chem. **64**, 0000 (1986).
43. T. S. Cameron and R. E. Cordes. Acta Crystallogr. Sect. B, **35**, 748 (1979).
44. International Tables for X-Ray Crystallography. Vol. IV. Kynoch Press, Birmingham, England. 1974.
45. G. Sheldrick. X-Ray system report. University Chemical Laboratory, Lensfield Road, Cambridge, England. 1976.

[4]Tables of observed and calculated structure factor amplitudes (Table 7), of bond distances and bond lengths (Table 4), of anisotropic temperature factors (Table 5), and of the atomic parameters for the hydrogen atoms (Table 6) may be purchased from the Depository of Unpublished Data, CISTI, National Research Council of Canada, Ottawa, Ont., Canada K1A 0S2.

Kinetic benzylidenation. Part II. Rearrangement of the kinetic products from benzylidenation of aldose diethyl dithioacetals

T. Bruce Grindley and Srihari Kusuma
Department of Chemistry, Dalhousie University, Halifax, N.S., Canada B3H 4J3

Received August 30, 1985[1]

T. Bruce Grindley and Srihari Kusuma. Can. J. Chem. **64**, 2397 (1986).

Terminal five-membered *O*-benzylidene derivatives of aldose diethyl dithioacetals can be rearranged at room temperature in *N*,*N*-dimethylformamide, often in high yields. Derivatives with the *arabino* configuration for their three terminal secondary hydroxyl groups, i.e. D-glucose, D-mannose, and D-arabinose derivatives, rearranged to structures containing terminal six-membered *O*-benzylidene rings. 4,5-*O*-Benzylidene-D-ribose diethyl dithioacetal rearranged chiefly to the 2,4 isomer, which was obtained by crystallization. Chromatography yielded some of the 3,5 isomer. 5,6-*O*-Benzylidene-D-galactose diethyl dithioacetal rearranged to a mixture of the two 4,5-*O*-benzylidene diastereomers, contrary to predictions based on the Hann–Hudson rules. A revised set of rules for acetal stability in *N*,*N*-dimethylformamide has been formulated. D-arabinose and D-ribose diethyl dithioacetal were shown to react with α,α-dimethoxytoluene under rearrangement conditions to give the products noted above in good yields.

T. Bruce Grindley et Srihari Kusuma. Can. J. Chem. **64**, 2397 (1986).

Dans le *N*,*N*-diméthylformamide, à la température ambiante, on peut provoquer une transposition, généralement avec de bons rendements, des dérivés *O*-benzylidènes à cinq chaînons de diéthyl dithioacétals d'aldoses situés en position terminale. Les dérivés possédant une configuration *arabino* pour leurs trois groupements hydroxyles secondaires en position terminale, par exemple, les dérivés du D-glucose, du D-mannose et du D-arabinose, se transposent en structures contenant des cycles *O*-benzylidènes à six chaînons situés en position terminale. Le diéthyl dithioacétal du *O*-benzylidène-4,5 D-ribose se transpose principalement en son isomère-2,4 qui est obtenu par cristallisation. Par chromatographie, on a aussi obtenu un peu de l'isomère-3,5. Le diéthyl dithioacétal du *O*-benzylidène-5,6 D-galactose se transpose en un mélange des deux *O*-benzylidènes-4,5 diastéréoisomères; ce résultat est contraire à celui prévu sur la base des règles de Hann–Hudson. On propose une nouvelle formulation décrivant la stabilité des acétals dans le *N*,*N*-diméthylformamide. On démontre que le diéthyl dithioacétal du D-arabinose et du D-ribose réagissent tous les deux avec l'α,α-diméthoxytoluène, dans les conditions de la transposition, pour conduire aux produits mentionnés ci-dessus, avec de bons rendements.

[Traduit par la revue]

Introduction

The preceding paper outlines a convenient method for the preparation of terminal monosubstituted five-membered ring *O*-benzylidene derivatives of aldose diethyl dithioacetals under kinetic conditions (1). These monosubstituted derivatives would be considerably more useful if they could be rearranged to other monosubstituted derivatives in a predictable fashion. The results herein demonstrate that such rearrangements can be achieved.

The stabilities of di- and tri-*O*-benzylidene derivatives of alditols and related acyclic carbohydrates have been studied extensively (2–4). However, monosubstituted derivatives have been considerably more difficult to prepare and hence few reports of their rearrangements have appeared.

Results

Structural assignments

Literature methods for structural assignments to compounds containing 2-phenyl-1,3-dioxolane rings have been discussed in the preceding paper (1). In addition, chemical shift changes on formation of five-membered *O*-benzylidene rings were outlined (1). Similar considerations are useful for determining the location and confirming the ring size of six-membered *O*-benzylidene acetals. Table 1 outlines a comparison of the chemical shifts of the carbons of some model diols with those of the same carbons in the derived 2-phenyl-1,3-dioxane compounds. The chemical shift of carbon-2 of a 1,3-propanediol was shifted upfield markedly (6–10 ppm) on formation of an *O*-benzylidene acetal, as had previously been noted for formation of *O*-methylene (5), *O*-isopropylidene (5), *O*-cyclohexylidene (5), and *O*-ethylidene acetals (6). Since this effect occurs only on formation of six-membered rings, it, along with other indicators (7), can confirm the presence of this ring size. Conway *et al.* had observed a marked upfield shift for the signal of carbon-5 in pyranose sugars on formation of 4,6-*O*-benzylidene derivatives (8). The signals of carbons-1 and -3 of a 1,3-propanediol are shifted downfield by approximately 4–

Table 1. ^{13}C Nuclear magnetic resonance chemical shifts for model compounds[a]

				
C-1	Diol	59.2	60.0	68.4
	Benzylidene derivative	67.0	66.7	72.6
	Difference[b]	7.8	6.7	4.2
C-2	Diol	34.9	40.8	46.6
	Benzylidene derivative	25.9	33.0	40.4
	Difference[b]	−9.0	−7.8	−6.2
C-3	Diol	59.2	66.3	68.4
	Benzylidene derivative	67.0	73.0	72.6
	Difference[b]	7.8	6.7	4.2

[a]In ppm. Values for diols from ref. 6, for benzylidene derivatives from ref. 7. For numbering purposes, all compounds are treated as substituted 1,3-propanediols.
[b]Value for benzylidene derivative − value for diol.

[1]Revision received July 22, 1986.

TABLE 2. ^{13}C Nuclear magnetic resonance data[a,b]

Compound	^{13}C Nuclear magnetic resonance chemical shifts (ppm)											$^{1}J_{C,H}$ (Hz) Acetal C
								Phenyl carbons		SEt group		
	C-1	C-2	C-3	C-4	C-5	C-6	Acetal C	Quat. C	Other C	CH_2	CH_3	
3*e*	54.6	70.0	80.2	61.7	71.3		101.1	137.5	126.2, 128.2, 129.0	24.1, 25.3	14.5, 14.5	160
3*e*–**3***a*	−0.5	−1.9	+9.3	−9.8	+7.2							
4*e*	53.8	76.7	79.1	65.9	70.5		100.8	137.5	126.0, 128.3, 129.0	25.9, 25.9	14.5, 14.5	160
4*e*–**4***a*	−1.0	−0.2	+7.4	−7.9	+7.3							
4*f*	51.9	85.5	64.4	80.9	62.6		100.7	137.7	126.3, 128.1, 128.8	25.1, 25.4	14.6, 24.6	160
4*f*–**4***a*	−3.2	+8.6	−7.3	+7.0	−0.7							
5*e*	54.7	73.5	69.9	82.8	61.6	71.2	101.1	137.4	126.2, 128.3, 129.1	24.8, 25.5	14.5, 14.5	161
5*e*–**5***a*	+0.2	−2.0	+0.5	+9.5	−9.9	+7.5						
6*g*	55.5	71.1	70.7	77.8	81.5	63.2	103.6	137.3	126.8, 128.5, 129.6	23.7, 25.4	14.1, 14.5	168
6*g*–**6***a*	+0.4	−0.5	+0.5	+8.3	+9.1	−0.5						
6*h*	55.4	71.5	71.0	78.5	80.7	62.9	103.8	137.6	126.8, 128.4, 129.4	23.9, 25.2	14.5, 14.5	167
6*h*–**6***a*	+0.3	−0.1	+0.8	+8.9	+10.3	−0.8						
7*e*	55.3	73.1	69.0	80.6	60.5	71.4	100.6	138.3	126.3, 127.9, 128.6	25.5, 25.5	14.8, 14.7	161
7*e*–**7***a*	+0.2	−1.0	−0.7	+10.3	−11.4	+7.4						

[a]At 20 MHz in chloroform-*d*.
[b]Data for **3***a*–**7***a* from ref. 1.

8 ppm on benzylidenation; the size of the effect decreases with increases in substitution.

This latter observation was applied extensively in the current study. Most products were 2-phenyl-1,3-dioxane derivatives with alkyl substituents only at position-4. The signal of the primary carbon in these products was assigned readily by off-resonance decoupling. A significant downfield shift (>6 ppm) for this signal in comparison with that of the same carbon in its precursor allowed the structure of the product monobenzylidene derivative to be assigned unambiguously.

Reactions

R-4,5-*O*-Benzylidene-D-arabinose diethyl dithioacetal (**3***d*)[2] rearranged slowly at room temperature in *N*,*N*-dimethylformamide containing 6% *p*-toluenesulfonic acid to *R*-3,5-*O*-benzylidene-D-arabinose diethyl dithioacetal (**3***e*). The rearrangement was complete after 100 h and the product was isolated in high yield (93%). Yields were lower at higher temperatures. The product was shown to contain a six-membered ring by the chemical shifts of the acetal C (101.1 ppm) (7) and the acetal proton (5.52 ppm) (7), the $^{1}J_{C,H}$ value of the acetal carbon (160 Hz) (7), and the upfield shift of a secondary carbon (C-4, −9.8 ppm). The location of the ring was apparent from the downfield shift obtained for the ^{13}C nmr signal for C-5 when its position in the spectrum of **3***e* was compared with its position in D-arabinose diethyl dithioacetal acetal (**3***a*) (shift +7.2 ppm). The same product (**3***e*) was obtained under the same conditions from the *S*-epimer of **3***d* (**3***c*)[2] slightly more slowly (140 h) and in slightly lower yield. **3***e* was also obtained in 76% yield directly from D-arabinose diethyl dithioacetal (**3***a*) by reaction

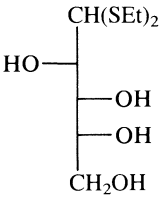

3*a*

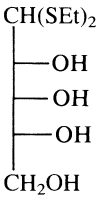

4*a*

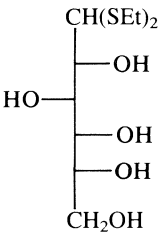

5*a*

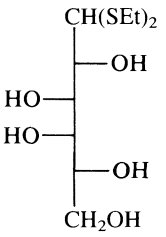

6*a*

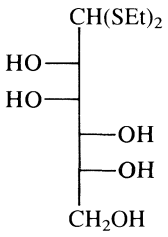

7*a*

with α,α-dimethoxytoluene under the conditions for the above rearrangements.

The rearrangement of a mixture of *R*- and *S*-4,5-*O*-benzylidene-D-ribose diethyl dithioacetal (**4***c*) was more complex. After 63 h, two components were evident, one of which had the same R_f as the starting material. The compound which moved much slower on tlc was *R*-2,4-*O*-benzylidene-D-ribose diethyl dithioacetal (**4***f*). This compound had previously been prepared indirectly by Zinner (9). An efficient method of preparation of the analogous derivative of the dipropyl dithioacetal has been developed (10). The faster moving component (obtained by preparative tlc) was a mixture of **4***c* and *R*-3,5-*O*-benzylidene-D-ribose diethyl dithioacetal (**4***e*) from which the latter compound was crystallized. The structure of this compound was assigned as for **3***e* (see Table 2). The ratio of **4***f* to **4***e* in the

[2]Numbering of compounds in this paper is based on that in Part I (1). The *a* series of compounds are the unsubstituted aldose diethyl dithioacetals while the *b* series do not appear in this publication.

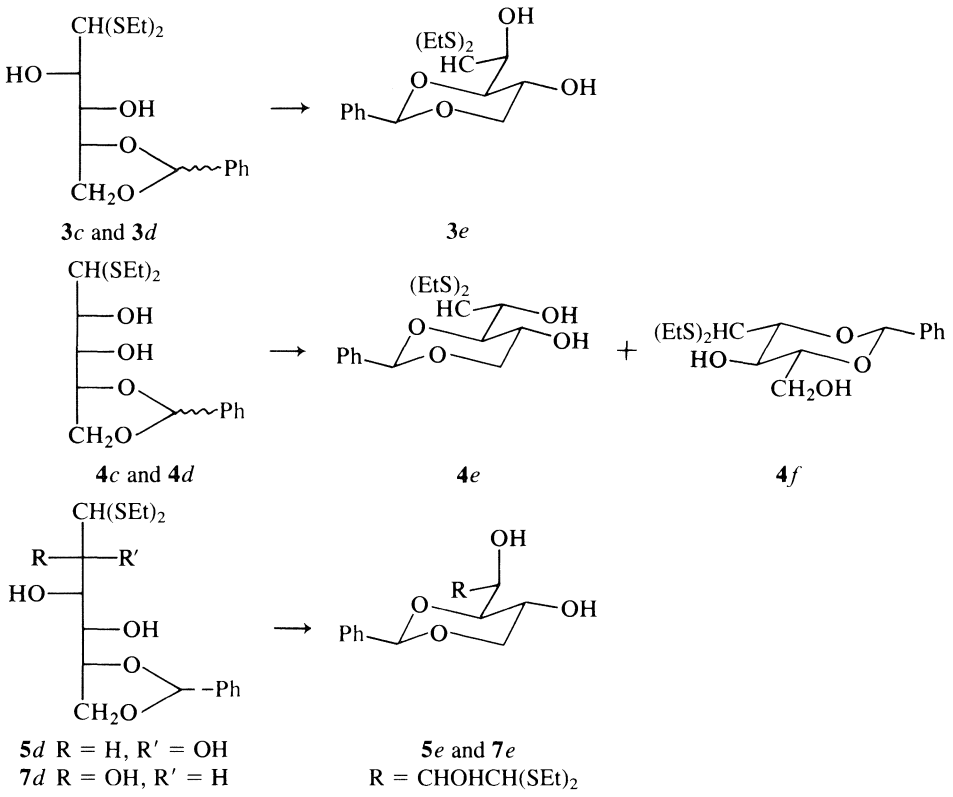

original product was 2:1. The product after 142 h of rearrangement contained only **4***f* and **4***e* in the ratio of 6:1 and **4***f* was isolated by recrystallization (61% yield). Reaction of D-ribose diethyl dithioacetal (**4***a*) with α,α-dimethoxytoluene under rearrangement conditions for 133 h gave a mixture of **4***f*, isolated by crystallization (64%), **4***e* (19%), and the known (9) 2,4:3,5-di-*O*-benzylidene-D-ribose diethyl dithioacetal (10%). Unidentified five-membered ring derivatives were present in trace amounts but were not isolated.

Rearrangements of the *R*-5,6-*O*-benzylidene derivatives of D-glucose (**5***d*) and D-mannose diethyl dithioacetal (**7***d*) for 100 and 40 h gave the *R*-4,6-*O*-benzylidene isomers **5***e* and **7***e* in 57 and 84% yields, respectively. The structures of both products could be assigned unambiguously as outlined above (see Table 2).

Rearrangement of a mixture of *R*- and *S*-5,6-*O*-benzylidene-D-galactose diethyl dithioacetal for 140 h gave two products, *R*- and *S*-4,5-*O*-benzylidene-D-galactose diethyl dithioacetal (**6***g* and **6***h*), which were separated by column chromatography. The location of the *O*-benzylidene ring was assigned by analysis of part of the ^{1}H nmr spectra of the triacetates of each of these compounds and confirmed by homonuclear decoupling experiments. The configurations at the acetal centers in the five-membered rings were not assigned. The crude product contained a lesser amount of a third compound (**6***e*), which was not isolated. **6***e* had an ^{1}H nmr signal for an acetal proton at 5.56 ppm, consistent only with a 2-phenyl-1,3-dioxane ring without axial substituents at positions-4 and -6 (7). Only one such *O*-benzylidene derivative can be obtained from D-galactose diethyl dithioacetal, *R*-4,6-*O*-benzylidene-D-galactose diethyl dithioacetal (**6***e*).

Rearrangement for a shorter period of time (70 h) yielded more of the first product (**6***g*) (47% vs. 17%). However, the second fraction was a mixture of two compounds, **6***h* and **6***e*, which were not separated.

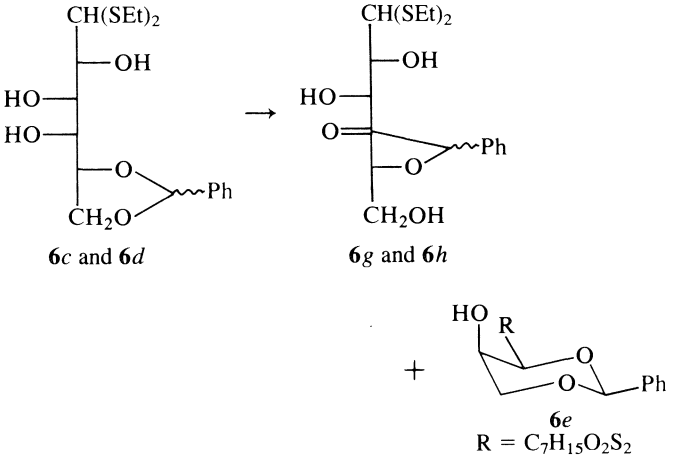

Discussion

If the rearrangement occurred via an intramolecular mechanism, the product distribution would be determined solely by product stability. The stability of benzylidene acetals derived from acyclic polyols has been extensively investigated (2–4). Stability orders for all acetals under the conditions of preparation (generally in the aldehyde in the presence of an acid catalyst) have been codified as the Hann–Hudson rules (4, 11). For the *O*-benzylidene acetals, the order (4) of decreasing stability is: 4,6-*cis*-disubstituted-2-phenyl-1,3-dioxane rings > 4-substituted-2-phenyl-1,3-dioxane rings > 4,5-*trans*-disubstituted-2-phenyl-1,3-dioxolane rings = 4-substituted-2-phenyl-1,3-dioxolane rings > 4,6-*trans*-disubstituted-2-phenyl-1,3-dioxane rings = 4,7-*trans*-disubstituted-2-phenyl-1,3-dioxepane rings.

Of the compounds rearranged, only the D-glucose and D-ribose derivatives could form the most stable type of *O*-benzylidene acetal, a 2,4-*O*-benzylidene derivative in each case. This

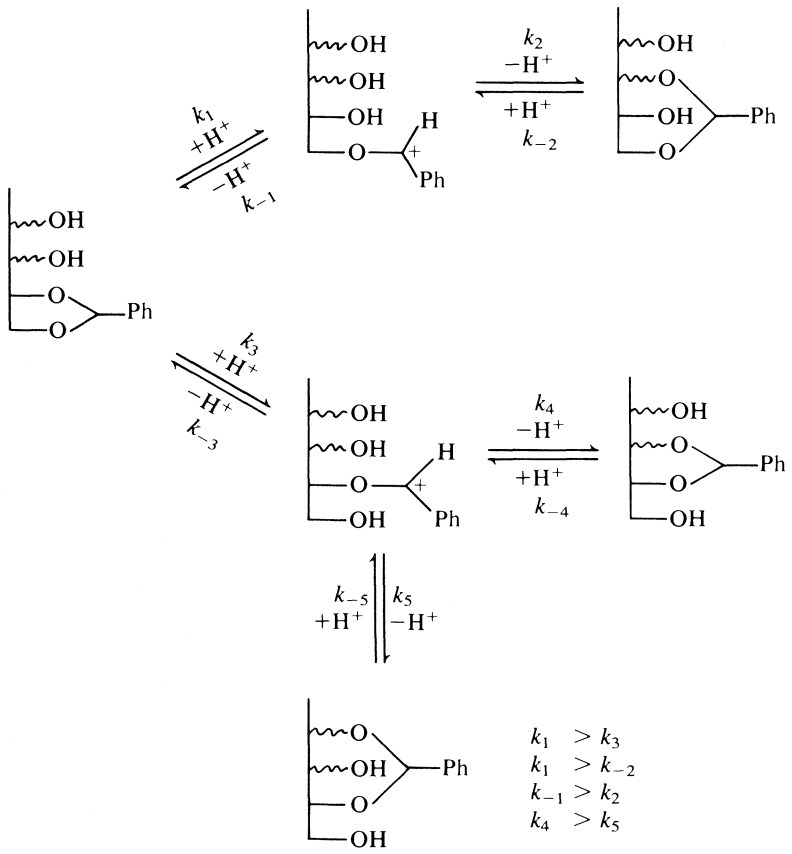

SCHEME 1. Mechanism pathways available for rearrangements of terminal *O*-benzylidene derivatives of aldose diethyl dithioacetals.

derivative was the major product from the D-ribose reactions but was predominant only after very long rearrangement times. It was not isolated from any D-glucose reactions although a compound with an ^{1}H nmr signal at 5.58 ppm was a major component in the crude product (not separated) from a rearrangement reaction performed over a long time (163 h). The 4,5-*O*-benzylidene isomers obtained in the galactose reaction were *trans*-4,5-disubstituted-2-phenyl-1,3-dioxolanes. The 2,3-*O*-benzylidene-D-galactose diethyl dithioacetal diastereomers not observed would also have 4,5-*trans* disubstitution in a 1,3-dioxolane ring and should have about the same stabilities as their 4,5 isomers. Thus, the major and perhaps sole route for these rearrangements was intramolecular.

An intramolecular rearrangement would proceed in stepwise fashion up the carbohydrate chain. A probable mechanism is illustrated in Scheme 1. The reaction of 4,6-*O*-benzylidene-hexopyranosides with hydrogen chloride and sodium cyanoborohydride to give 6-*O*-benzyl derivatives (12) indicated that the acetal C—O bond to a secondary oxygen is cleaved more rapidly than the bond to primary oxygens in the presence of Bronsted acids. Ring closure of the carbocation to form the five-membered ring of the starting material is faster (1) but the terminal six-membered ring product obtained as the final product in the arabinose, glucose, and mannose cases is more stable.

The rapid appearance of 2,4-*O*-benzylidene-D-ribose diethyl dithioacetal (**4***f*) (the major rearranged product after 13 h) suggests that it was obtained directly from starting material. Protonation of the primary oxygen, cleavage to give the carbocation, and ring closure is a possible route to **4***f*. Alternatively, 3,4-*O*-benzylidene-D-ribose diethyl dithioacetal, a relatively unstable *cis*-4,5-disubstituted-1,3-dioxolane derivative, could be an intermediate. Cleavage of 2-phenyl-1,3-dioxane rings would be expected to be slower on the principle of microscopic reversibility and has been observed to be slower in hydrogenolysis reactions (13). The very slow appearance of 2,4-*O*-benzylidene-D-glucose diethyl dithioacetal in the rearrangement of **5***d* supports this contention. The former compound could be obtained directly from the first rearranged product, the 4,6-*O*-benzylidene isomer.

The rearrangement of 5,6-*O*-benzylidene-D-galactose diethyl dithioacetal to *R*- and *S*-4,5-*O*-benzylidene-D-galactose diethyl dithioacetal in preference to the 4,6-*O*-benzylidene isomer (**6***e*) was a violation of the Hann–Hudson rules of acetal stability (4, 11), if the reaction was thermodynamically controlled. The slightly decreased amount of **6***e* present in the crude product after 140 h, as compared to the amount after 60 h, suggests that the three products were close to equilibrium. The Hann–Hudson rules were formulated on the basis of the products obtained from benzylidenation of alditols in benzaldehyde, sometimes containing water or ethanol. The stated preference for 4-substituted-2-phenyl-1,3-dioxanes over *trans*-4,5-disubstituted-2-phenyl-1,3-dioxolanes was originally based on the reactions of galactitol (14) and D-glycero-D-galactoheptitol (D-perseitol) (15). 1,3:4,6-Di-*O*-benzylidenegalactitol and 1,3:5,7-di-*O*-benzylidene-D-perseitol were obtained in 93 and 89% yields, respectively. However, in both cases, the product crystallized in the reaction mixture, which was allowed to stand overnight to continue crystallization. Thus, this particular part of the Hann–Hudson rules was based on the ability of the product to crystallize rather than on its stability in solution.

A number of publications that are related to this problem have

recently appeared. The most relevant was on the benzylidenation of 1-deoxy-D-galactitol in benzaldehyde (16). Separation of the product mixture by chromatography gave a 1:1 mixture of 2,3:4,5- and 2,3:4,6-di-*O*-benzylidene isomers (680 mg) plus a pure 2,3:4,5 isomer (160 mg). Thus, the ratio of products containing 4,5-*O*-benzylidene rings to their 4,6 isomers was about 3:2, contrary to the Hann–Hudson rules, and the individual 4,5 isomers were present to almost the same extent as the 4,6 isomers (assuming the two configurations in the 4,5 rings were equally populated).

The reaction of D-glucitol with benzaldehyde in aqueous *N,N*-dimethylformamide containing hydrochloric acid gave a mixture of the 2,3-*O*-benzylidene diastereomers, which rearranged slowly to the 2,4-*O*-benzylidene isomer. Although the reaction was followed by gas–liquid chromatography and ^{1}H nmr spectroscopy, no evidence for the presence of either the 1,3- or 4,6-*O*-benzylidene isomers was obtained at any reaction time (17). The results in the preceding paper (1) suggest that the initial products of this reaction are the 1,2- and 5,6-*O*-benzylidene derivatives, which rearrange to the 1,3- 4,6-, and 2,3-*O*-benzylidene isomers. However, benzylidenations with benzaldehyde are probably not as selective for primary hydroxyl groups as those with α,α-dimethoxytoluene.

A number of publications have reported alkylidenation of alditols (18–22). Although a consistent pattern of preference was not observed for all aldehydes and conditions, the results (18–22) suggest that 4-monosubstituted-2-alkyl-1,3-dioxane rings are favoured over *trans*-4,5-disubstituted-2-alkyl-1,3-dioxolane rings (19, 20) in contrast to the results for benzylidenation. The actual preferences must be small and hence are strongly dependent on reaction conditions. Where conditions can be characterized (present study, and refs. 16–20), it appears that solvents of greater polarity (present study) lead to more of the dioxolane ring containing products. This observation is not what would be expected on the basis of the polarity of the parent ring systems; the dipole moments of 1,3-dioxane (23), 2-phenyl-1,3-dioxane (24), 1,3-dioxolane (25), and 2-phenyl-1,3-dioxolane (24) are 2.13 (benzene), 2.05 (carbon tetrachloride), 1.47 (benzene), and 1.37 D (carbon tetrachloride), respectively. However, the stabilities of the acetalated products depend on the polarities of the whole molecules, which are difficult to predict.

Another factor that could be important is hydrogen bonding. The OH group on C-5 of 4,6-*O*-benzylidene-D-galactose diethyl dithioacetal has an axial orientation at the C-5 position of the 1,3-dioxane ring. The hydrogen bonding of an axial hydroxyl group at position-5 made *cis*-2-isopropyl-5-hydroxy-1,3-dioxane more stable than its *trans*-isomer (26), by amounts which decreased in more polar and hydrogen bond accepting solvents. The change in stability was 0.64 kcal mol^{-1} when the position of equilibrium in cyclohexane was compared with that in 1,2-dimethoxyethane. A similar change in stability for the two types of rings in benzaldehyde, as opposed to *N,N*-dimethylformamide, could explain the difference in the results obtained here as compared to those in ref. 16. The combination of these results indicates that in the absence of hydrogen bonding, 4,5-*trans*-disubstituted-2-phenyl-1,3-dioxolane rings are more stable than 4-substituted-2-phenyl-1,3-dioxane rings.

The above conclusion suggests that rearrangements of any mono-*O*-benzylidene-D-arabinose diethyl dithioacetal should lead eventually to a mixture in which the 2,3-*O*-benzylidene derivatives are prominent, and any mono-*O*-benzylidene-D-mannose diethyl dithioacetal should give 3,4-*O*-benzylidene derivatives. However, attempts to equilibrate 2,3- and 3,5-*O*-benzylidene-D-arabinose diethyl dithioacetal were unsuccessful. Loss of the *O*-benzylidene group occurred faster than equilibration, particularly for the latter compound.

In conclusion, the above results support a somewhat different order for benzylidene acetal stability in *N,N*-dimethylformamide than that presented in the Hann–Hudson rules (4). The order of decreasing stability is: 4,6-*cis*-disubstituted-2-phenyl-1,3-dioxane rings > 4,5-*trans*-disubstituted-2-phenyl-1,3-dioxane rings > 4-substituted-2-phenyl-1,3-dioxane rings > 4-substituted-2-phenyl-1,3-dioxolane rings > 4,5-*cis*-disubstituted-2-phenyl-1,3-dioxolane rings. No information was obtained about the relative stabilities of 1,3-dioxepane rings.

Experimental

For general methods, see Part I.

General method for the rearrangement of O-*benzylidene rings*

R-*3,5*-O-*Benzylidene*-D-*arabinose diethyl dithioacetal (***3***e) by the rearrangement of* R-*4,5*-O-*benzylidene*-D-*arabinose diethyl dithioacetal (***3***d)*

A solution of **3***d* (0.344 g, 1 mmol) and anhydrous *p*-toluenesulfonic acid (**2**) (10 mg, 0.058 mmol) in *N,N*-dimethylformamide (2 mL) was stirred for 100 h, when tlc (solvent A) indicated that all of the starting material had disappeared and a single product had been obtained (R_f 0.33). The solution was poured into an ice-cold sodium hydrogen carbonate solution (2%, 10 mL), which was extracted with ether (3 × 10 mL). The combined ether extracts were washed with water (2 × 10 mL), dried ($MgSO_4$), filtered, and concentrated under reduced pressure at 40°C. The crystalline product (0.320 g, 93%) was recrystallized from dichloromethane/pet. ether (65–75°C) to give colorless crystals of the title compound (**3***e*); $[\alpha]_D^{20}$ −66° (*c* 4.00, chloroform); mp 125–126°C; ^{1}H nmr δ: 1.26 (t, 6H, 2 SCH_2CH_3, *J* = 7.4 Hz), 2.70 (q, 4H, 2 SCH_2CH_3, *J* = 7.3 Hz), 3.14 (d, 1H, OH, *J* = 6.4 Hz), 3.57–4.55 (complex m, 7H), 5.52 (s, 1H, benzylidene H), 7.17–7.62 (m, 5H, Ph); *m/z*: 344 (19, M^+), 283 (6, M − ·SEt), 265 (1), 221 (4), 179 (16), 177 (12), 149 (5), 135 (100, $^+CH(SEt)_2$), 117 (5), 115 (3), 107 (30), 105 (21), 103 (7), 91 (11), 79 (11), 77 (13), 75 (9). *Anal.* calcd. for $C_{16}H_{24}O_4S_2$: C 55.78, H 7.02; found: C 55.85, H 6.88.

3e *by the rearrangement of* S-*4,5*-O-*benzylidene*-D-*arabinose diethyl dithioacetal (***3***c)*

Compound **3***c* (0.344 g, 1 mmol) was rearranged as in the general method, but for 140 h. The crystalline product (0.289 g, 81%) (R_f 0.33, solvent A) was recrystallized to give colorless crystals, mp 123–125°C, undepressed when mixed with the product from the rearrangement of **3***d*.

3e *from* D-*arabinose diethyl dithioacetal (***3***a)*

A solution of **3***a* (5.12 g, 20 mmol), α,α-dimethoxytoluene (3.648 g, 24 mmol), and anhydrous *p*-toluenesulfonic acid (**2**) (0.2 g, 1.16 mmol, 6%) in *N,N*-dimethylformamide (40 mL) was stirred 100 h, then worked up as in the general method for rearrangement reactions. The pale yellow crystalline product (5.213 g, 76%) (R_f 0.33, solvent A) was recrystallized to give colorless crystals, mp 123–125°C, undepressed when mixed with **3***e*.

R-*1,3*-O-*Benzylidene*-D-*ribose diethyl dithioacetal (***4***f)*

(a) By rearrangement

The mixture of *R*- and *S*-4,5-*O*-benzylidene-D-ribose diethyl dithioacetal (**4***c*) (1) (0.344 g, 1 mmol) was rearranged for 63 h as in the general procedure. The pale yellow crystalline product (0.28 g, 82%) contained two components (R_f's of 0.50 and 0.21, solvent A). The ratio of integrals of signals in the ^{1}H nmr spectrum of 5.58 and 5.49 ppm was 2:1.

Recrystallization gave the slower moving component, the title compound (**4***f*), as colorless needles (0.155 g, 45%). A second recrystallization from methanol/water gave needles, mp 121–122°C (lit. (9) mp 119–120°C); $[\alpha]_D^{22}$ −26.3° (*c* 1.68, chloroform) (lit. (9) α_D −22.4°); ^{1}H nmr (60 MHz) δ: 1.27 (t, 6H, 2 SCH_2CH_3, *J* = 7 Hz), 2.75 (q, 4H, 2 SCH_2CH_3, *J* = 7 Hz), 3.20 (br s, 1H, OH), 3.62–4.32 (complex m, 7H), 5.57 (s, 1H, benzylidene H), 7.15–7.46 (m, 5H,

Ph); *m/z*: 344 (23, M^+), 283 (5, M − ·SEt), 265 (3), 221 (6), 209 (7), 179 (4), 177 (23), 149 (3), 137 (9), 138 (8), 135 (100, $^+CH(SEt)_2$), 117 (9), 108 (4), 107 (45), 105 (12), 104 (5), 103 (11), 91 (5), 89 (6), 87 (8), 79 (13), 77 (12), 75 (34). *Anal.* calcd. for $C_{16}H_{24}O_4S_2$: C 55.79, H 7.03, S 18.61; found: C 55.69, H 6.96, S 18.55.

Preparative tlc (solvent F) on the mother liquor from the first recrystallization of **4***f* gave a crystalline product recrystallized from dichloromethane/pet. ether, then from methanol/water. The colorless needles of *R*-3,5-*O*-benzylidene-D-ribose diethyl dithioacetal (**4***e*) had mp 68–69.5°C; $[\alpha]_D^{22}$ −47.0° (*c* 3.57, chloroform); ^{1}H nmr (60 MHz) δ: 1.22 (t, 6H, 2 SCH_2CH_3, *J* = 7 Hz), 2.60, 2.70 (2q, 4H, 2 SCH_2CH_3, *J* = 7 Hz), 3.30 (br d, 1H, OH, *J* = 3 Hz), 3.50–4.55 (complex m, 7H), 5.49 (s, 1H, benzylidene H), 7.31–7.55 (m, 5H, Ph); *m/z*: 344 (17, M^+), 283 (4, M − ·SEt), 265 (1), 221 (3), 179 (23), 177 (16), 149 (2), 137 (9), 136 (8), 135 (100, $^+CH(SEt)_2$), 117 (4), 115 (3), 107 (37), 105 (10), 91 (6), 79 (14), 77 (10), 75 (10), metastable: 232–235 (344 → 283).

Rearrangement exactly as above, but for 142 h, gave **4***f* in 61% yield after recrystallization. The ^{1}H nmr spectrum of the crude product had signals for the benzylidene H of **4***f* and **4***e* with a peak height ratio of 6:1.

(b) Directly from D-*ribose diethyl dithioacetal (***4**a*)*

Compound **4***a* (8.04 g, 31.4 mmol), α,α-dimethoxytoluene (5.73 g, 35 mmol), and anhydrous *p*-toluenesulfonic acid (0.47 g) were stirred in anhydrous *N,N*-dimethylformamide (70 mL) for 133 h. Normal work-up gave a solid product, which on recrystallization from dichloromethane/hexane gave colorless needles of **4***f* (6.1 g). The mother liquor (4.72 g) was separated by column chromatography on silica gel (200 g) (solvent D). Three crystalline fractions A (1.40 g, 10%), B (2.10 g, 19%), and C (0.84 g) were obtained.

Fraction A was recrystallized from dichloromethane/hexanes to give colorless needles of 2,4:3,5-di-*O*-benzylidene-D-ribose diethyl dithioacetal, mp 125–126°C (lit. (9) mp 122–123°C); $[\alpha]_D^{22}$ −71.0° (*c* 1.68, chloroform (lit. (9) $[\alpha]_D$ −64.2°); ^{1}H nmr δ: 1.23 (t, 6H, SCH_2CH_3, *J* = 7.5 Hz), 2.76 (q, 4H, 2 SCH_2CH_3, *J* = 7.5 Hz), 3.72–4.50 (complex m, 6H), 5.67, 5.72 (2 s, 2H, benzylidene H), 7.17–7.63 (m, 10 H, Ph); ^{1}C nmr δ: 14.5, 14.6 (Me), 25.3 (SCH_2), 51.0 (C-1), 72.5 (C-5), 75.3, 72.5 (C-3, C-4), 83.7 (C-2), 101.6, 101.8 (acetal C, $^1J_{C,H}$ = 162.7, 162.4 Hz), 126.1, 128.2, 129.1 (Ph), 137.0, 137.2 (quaternary Ph).

Fraction B was shown to be **4***e* while Fraction C was **4***f*. The total yield of **4***f* was 6.94 g, 64%.

R-*4,6-*O*-Benzylidene-*D*-glucose diethyl dithioacetal (***5**e*)*

R-5,6-*O*-Benzylidene-D-glucose diethyl dithioacetal (**5***d*) (2.47 g, 6.6 mmol) was rearranged for 100 h with the same proportions of reagents as in the general method. The crude pale yellow syrupy product (2.213 g) contained one major and one minor component, which were separated by column chromatography on silica gel (solvent B).

Fraction A (1.40 g, 57%), a solid, was recrystallized to give colorless crystals of the title compound (**5***e*); mp 114–115°C; $[\alpha]_D^{20}$ −9° (*c* 2.09, chloroform); ^{1}H nmr (60 MHz) δ: 1.21 (t, 6H, 2 SCH_2CH_3, *J* = 7.5 Hz), 2.40–2.85 (m, 4H, 2 SCH_2CH_3), 3.45–4.53 (complex m, 10H), 5.40 (s, benzylidene H), 7.00–7.60 (m, 5H, Ph); *m/z*: 374 (0.3, M^+), 288 (1), 287 (2), 286 (11), 225 (1), 207 (3), 193 (2), 177 (3), 163 (6), 145 (3), 137 (11), 136 (26), 135 (100), 117 (4), 107 (24), 106 (6), 105 (35), 104 (10), 103 (11), 102 (10), 75 (7), 73 (13), 71 (8).

An intermediate fraction (0.24 g, 10%), had ^{1}H nmr signals at 5.90 (major), 5.80, 5.64 (minor), 5.52 (minor), and 5.40 (minor) ppm.

Fraction B (0.17 g, 7%, R_f), a pale yellow syrup, had ^{1}H nmr signals at 5.52 and 6.05 ppm and was not investigated further.

Rearrangement of **5**d *for 163 h*

Rearrangement of **5***d* (1.496 g) as previously, but for 163 h, gave a pale yellow syrup (1.104 g), a complex mixture on tlc; ^{1}H nmr δ: 6.04, 5.94, 5.58, and 5.44 with peak heights in the ratio 2:8:4:5, respectively.

R-*and* S-*4,5-*O*-benzylidene-*D*-galactose diethyl dithioacetal (***6**g and **6**h)*

A mixture of *R*- and *S*-5,6-*O*-benzylidene-D-galactose diethyl dithioacetal (**6***c* and **6***d*) (1) (1.870 g, 5 mmol) was rearranged as in the general procedure for 140 h. The colorless crystalline product (1.7 g, 91%) (partial ^{1}H nmr, δ: 5.54, 5.88, and 5.95 (3s, benzylidene H, intensity ratio 13:19:22, respectively)) was separated by column chromatography on silica gel (100 g) using solvent F as eluent.

Fraction A (0.032 g, 2%, R_f 0.60), the starting material, was followed by an overlapping fraction (0.034 g, 2%).

Fraction B (0.314 g, 17%, R_f 0.49), a solid, was recrystallized to give colorless crystals of 4,5-*O*-benzylidene-D-galactose diethyl dithioacetal (**6***g*); mp 106–107°C; $[\alpha]_D^{20}$ +5° (*c* 3.72, methanol), ^{1}H nmr (60 MHz) δ: 1.24 (t, 6H, 2 SCH_2CH_3, *J* = 7 Hz), 2.67, 2.70 (2q, 4H, 2 SCH_2CH_3, *J* = 7 Hz), 3.40 (br s, 1H, OH), 3.53–4.33 (complex m, 9H), 5.88 (s, 1H, benzylidene H), 7.06–7.50 (m, 5H, Ph); *m/z*: 374 (34, M^+), 313 (8, M − ·SEt), 312 (8), 279 (7), 256 (5), 251 (7), 207 (7), 206 (11), 179 (9), 177 (9), 167 (6), 150 (6), 149 (43), 137 (11), 136 (12), 135 (100, $^+CH(SEt)_2$), 107 (32), 105 (36), 91 (23), 79 (9), 77 (12).

Fraction C (0.675 g, 36%, R_f 0.36), a solid, was recrystallized to give colorless crystals of 4,5-*O*-benzylidene-D-galactose diethyl dithioacetal (**6***h*), mp 85–86°C; $[\alpha]_D^{20}$ +13° (*c* 3.08, methanol); ^{1}H nmr (60 MHz) δ: 1.21 (t, 6H, 2 SCH_2CH_3, *J* = 7 Hz), 2.62 (q, 4H, 2 SCH_2CH_3, *J* = 7 Hz), 3.45 (br d, 1H, OH, *J* = 3 Hz), 3.55–4.42 (complex m, 9H), 5.95 (s, 1H, benzylidene H), 7.12–7.62 (m, 5H, Ph); *m/z*: 374 (14, M^+), 327 (2), 326 (2), 313 (7), 312 (5), 295 (3), 279 (7), 251 (9), 239 (3), 221 (3), 207 (7), 206 (6), 189 (3), 179 (8), 177 (9), 149 (23), 145 (5), 137 (12), 136 (13), 135 (100, $^+CH(SEt)_2$), 133 (7), 122 (11), 107 (32), 106 (6), 105 (30), 104 (13), 103 (13), 91 (12), 85 (6), 79 (9), 77 (12), 75 (11), 73 (10).

Rearrangement of **6***c* (0.374 g, 1 mmol) as above, but for 70 h, gave a syrupy product with ^{1}H nmr signals at 5.94, 5.88, and 5.54 ppm with peak heights in the ratio 10:21:14. The mixture was separated by column chromatography into two fractions, A and B. Fraction A (0.218 g, 47%) was compound **6***g*. Fraction B (0.105 g, 23%) was a mixture of compound **6***h* and compound **6***e*; partial ^{1}H nmr, δ: 5.58, 5.95 (2s, benzylidene H).

*2,3,6-Tri-*O*-acetyl-4,5-*O*-benzylidene-*D*-galactose diethyl dithioacetal (***6**i)*

Compound **6***g* (0.28 g, 0.75 mmol), acetic anhydride (3.06 g, 30 mmol), and dry pyridine (1.184 g, 15 mmol) were stirred 14 h, then poured into ice-water (30 mL). The mixture was extracted with ether (3 × 30 mL) and the combined extracts were washed with saturated cupric sulfate solutions (3 × 3 mL), saturated sodium hydrogen carbonate solutions (3 × 30 mL), and water (3 × 30 mL), then dried ($MgSO_4$), filtered, and concentrated to a pale yellow syrup (0.309 g, 83%), homogeneous on tlc (R_f 0.42, solvent C); $[\alpha]_D^{24}$ +48° (*c* 1.415, chloroform); ir (neat): 1746 cm^{-1} (acetate CO), no OH stretch; ^{1}H nmr δ: 1.13–1.42 (m, 6H, 2 SCH_2CH_3), 2.06, 2.13, 2.15 (3s, 9H, 3 $COCH_3$), 2.67 (q, 4H, 2 CH_2CH_3, *J* = 7.3 Hz), 3.90–4.45 (complex m, 4H, H-4, H-5, H-6, H-6′), 4.12 (d, 1H, H-1, $J_{1,2}$ = 6.4 Hz), 5.44 (dd, 1H, H-2, $J_{1,2}$ = 6.5 Hz, $J_{2,3}$ = 3.8 Hz), 5.83 (dd, 1H, H-3, $J_{2,3}$ = 3.8 Hz, $J_{3,4}$ = 8.6 Hz), 5.98 (s, 1H, benzylidene H), 7.35–7.42 (m, 5H, Ph).

*2,3,6-Tri-*O*-acetyl-4,5-*O*-benzylidene-*D*-galactose diethyl dithioacetal (***6**j)*

Compound **6***h* (0.374 g, 1 mmol), dry pyridine (1.58 g, 20 mmol), and acetic anhydride (4.08 g, 40 mmol) were stirred 14 h, then worked up as for **6***h*. The pale yellow syrup (0.44 g, 88%), homogeneous on tlc (R_f 0.30, solvent C); $[\alpha]_D^{24}$ +71° (*c* 1.09, chloroform); ir (neat): 1750 cm^{-1} (acetate, CO), no OH stretch; ^{1}H nmr δ: 1.08–1.42 (m, 6H, 2 SCH_2CH_3), 2.11, 2.11, 2.13 (2s, 9H, 3 $COCH_3$), 2.58 (q, 4H, 2 SCH_2CH_3, *J* = 7.3 Hz), 3.42–4.78 (complex m, 4H, H-4, H-5, H-6, H-6′), 3.98 (d, 1H, H-1, $J_{1,2}$ = 6.6 Hz), 5.38 (dd, 1H, H-2, $J_{1,2}$ = 6.5 Hz, $J_{2,3}$ = 3.3 Hz), 5.75 (dd, 1H, H-3, $J_{2,3}$ = 3.4 Hz, $J_{3,4}$ = 7.6 Hz), 5.95 (s, 1H, benzylidene H), 7.28–7.51 (m, 5H, Ph).

R-*4,6-*O*-Benzylidene-*D*-mannose diethyl dithioacetal (***7**e)*

R-5,6-*O*-Benzylidene-D-mannose diethyl dithioacetal (**7***d*) (1) (1.015 g, 2.71 mmol) was rearranged for 40 h as in the general procedure. The pale yellow crystalline product (0.835 g, 84%), homogeneous on tlc (R_f 0.50, solvent F), was recrystallized to give fine

colorless needles of the the title compound (**7***e*), mp 175–176°C, $[\alpha]_D^{24}$ −1° (*c* 3.39, chloroform); ^{1}H nmr δ: 1.27 (t, 6H, 2 SCH_2CH_3, J = 7.3 Hz), 2.69, 2.75 (2q, 4H, 2 SCH_2CH_3, J = 7.4 Hz), 2.83 (br s, 1H, OH), 3.41–4.33 (complex m, 8H), 4.76 (br s, 1H, OH), 5.53 (s, 1H, benzylidene H), 7.20–7.50 (m, 5H, Ph); *m/z*: 374 (1, M^+), 327 (1), 313 (9), 295 (2), 251 (3), 239 (5), 209 (3), 207 (5), 189 (4), 179 (5), 177 (9), 149 (4), 145 (8), 137 (9), 136 (9), 135 (100, $^+CH(SEt)_2$), 107 (42), 105 (26), 104 (9), 103 (18), 91 (9), 85 (8), 79 (12), 77 (12), 75 (14), 73 (9). *Anal.* calcd. for $C_{17}H_{26}O_5S_2$: C 54.52, H 7.00, S 17.12; found: C 54.23, H 6.94, S 16.83.

*Rearrangement of 2,3-O-benzylidene-D-arabinose diethyl dithioacetal (**3**g)*

Compounds **3***g* (27) (180 mg) and **2** (20 mg) in *N,N*-dimethylformamide (2 mL) were kept 192 h, then worked up normally. The ^{1}H nmr spectrum of the product had signals at 6.09 and 5.51 ppm with integrals in the ratio 3.4:1. Signals having intensities approximately 1/10 that of the signal at 5.51 ppm were apparent at 5.78, 5.91, and 6.23 ppm.

Rearrangement exactly as above, but for 336 h, gave a product with ^{1}H nmr signals at 6.09 and 5.52 ppm having a ratio of integrals of 4.1:1.

To the product from immediately above (100 mg) in *N,N*-dimethylformamide (2 mL) was added **2** (150 mg). Aliquots removed after 120 and 264 h and worked up normally both had intensity ratios for ^{1}H nmr signals at 6.09 and 5.52 ppm of 3:2.

*Rearrangement of 3,5-O-benzylidene-D-arabinose diethyl dithioacetal (**3**e)*

Compounds **3***e* (30 mg) and **2** (10 mg) in *N,N*-dimethylformamide (1 mL) were kept 288 h, then worked up normally to give a syrup; partial ^{1}H nmr, δ: 6.09 and 5.52 (2s, intensity ratio 1:5).

A second rearrangement reaction identical to the above was kept 288 h, then more **2** (100 mg) was added and the reaction kept a further 288 h, and worked up to give a syrup (3 mg); partial ^{1}H nmr, δ: 5.55 (s, only benzylidene H signal visible).

Acknowledgements

We thank the Atlantic Regional Laboratories of the National Research Council for use of the Perkin–Elmer 141 polarimeter and the Natural Sciences and Engineering Research Council of Canada for continuing financial support. We are grateful to Dr. S. P. Rao for supplying a starting material.

1. T. B. Grindley, S. Kusuma, and T. S. Cameron. Can. J. Chem. **64**, 2388 (1986).
2. D. M. Clode. Chem. Rev. **79**, 491 (1979).
3. J. F. Stoddart. Stereochemistry of carbohydrates. Wiley–Interscience, New York. 1971. pp. 186–220.
4. S. A. Barker and E. J. Bourne. Adv. Carbohydr. Chem. **7**, 137 (1952).
5. T. B. Grindley, C. J. P. Cote, and C. Wickramage. Carbohydr. Res. **140**, 215 (1985).
6. T. B. Grindley and C. Wickramage. J. Carbohydr. Chem. **4**, 193 (1985).
7. T. B. Grindley and V. Gulasekharam. Carbohydr. Res. **74**, 7 (1979).
8. E. Conway, R. D. Guthrie, S. D. Gero, G. Lukacs, and A.-M. Sepulchre. J. Chem. Soc. Perkin Trans. 2, 542 (1974).
9. H. Zinner and E. Wittenburg. Chem. Ber. **94**, 1298 (1961).
10. D. J. J. Potgietter and D. L. Macdonald. J. Org. Chem. **26**, 3934 (1961).
11. R. M. Hann and C. S. Hudson. J. Am. Chem. Soc. **66**, 1909 (1944).
12. P. J. Garegg, H. Huitberg, and S. Wallin. Carbohydr. Res. **108**, 97 (1982).
13. U. E. Diner and R. K. Brown. Can. J. Chem. **45**, 1297 (1967).
14. W. T. Haskins, R. M. Hann, and C. S. Hudson. J. Am. Chem. Soc. **64**, 132 (1942); E. Fischer. Ber. **27**, 1524 (1884).
15. A. T. Ness, R. M. Hann, and C. S. Hudson. J. Am. Chem. Soc. **70**, 765 (1948).
16. P.-E. Jansson and B. Lindberg. Carbohydr. Res. **65**, 291 (1978).
17. T. G. Bonner, E. J. Bourne, P. J. V. Cleare, and D. Lewis. J. Chem. Soc. B, 827 (1968).
18. T. G. Bonner, E. J. Bourne, D. Lewis, and L. Yuceer. J. Chem. Soc. Perkin Trans. 1, 1323 (1975).
19. T. G. Bonner, E. J. Bourne, D. Lewis, and L. Yuceer. Carbohydr. Res. **33**, 1 (1974).
20. T. G. Bonner, D. Gibson, and D. Lewis. Carbohydr. Res. **78**, 243 (1980).
21. S. Yanai, M. Halmann, and D. Vofsi. Carbohydr. Res. **83**, 243 (1980).
22. S. Yanai. Carbohydr. Res. **113**, 336 (1983).
23. R. Walker and D. W. Davidson. Can. J. Chem. **37**, 492 (1959).
24. B. A. Arbusov, V. E. Kataev, S. G. Vul'fson, and A. N. Vereshchagin. Izv. Acad. Nauk SSSR, Ser. Khim. 323 (1976).
25. C. W. N. Cumper and A. I. Vogel. J. Chem. Soc. 3521 (1959).
26. E. L. Eliel and M. Kaloustain. J. Chem. Soc. Chem. Commun. 290 (1970).
27. C. F. Huebner, R. A. Pankratz, and K. P. Link. J. Am. Chem. Soc. **72**, 4811 (1950); H. Zinner and H. Banz. J. Prakt. Chem. **314**, 431 (1972).

Freeze-drying Fourier transform infrared attenuated total reflection spectroscopy of surface adsorbed layers. Water-assisted proton transfer in cytidine-5′-phosphoric acid

SIMONA BADILESCU AND CAMILLE SANDORFY
Département de Chimie, Université de Montréal, Montréal (Qué.), Canada H3C 3J7

Received May 8, 1986

SIMONA BADILESCU and CAMILLE SANDORFY. Can. J. Chem. **64**, 2404 (1986).

The zwitterionic structure of cytidine-5′-phosphoric acid (5′-CMP) in the acid form has been studied by means of freeze-drying ATR spectroscopy. Surface deuteration and protonation studies of the hydrated sample were accomplished and some band assignments are made. The dependence of the proton transfer process in the zwitterionic CMP(H) on relative humidity is evidenced. The ability of the water molecules adsorbed on the thallium bromide iodide crystal to act as proton donors and the enhancement of the degree of dissociation of the adsorbed water are demonstrated.

SIMONA BADILESCU et CAMILLE SANDORFY. Can. J. Chem. **64**, 2404 (1986).

Nous avons examiné la structure de l'acide-5′-cytidyl-phosphorique (5′-CMP) par spectroscopie infrarouge de réflexion totale atténuée, combinée avec la technique de la congélation suivie par sublimation ("freeze drying"). Des études de deutération et de protonation ont été accomplies sur le composé hydraté adsorbé sur une surface de KRS-5 (TlBrI). L'équilibre de protonation dans le CMP(H) zwitterionique dépend de l'humidité relative. On démontre que les molécules d'eau adsorbées sur la surface d'un cristal de bromure-iodure de thallium sont capables d'agir comme des donneurs de proton. L'augmentation du degré de dissociation de l'eau adsorbée est également mise en évidence.

Introduction

The site of protonation in some ^{15}N-labeled cytosine derivatives in water solution has been studied by high-resolution proton and nitrogen-15 nmr spectroscopy (1, 2). The results were compatible with protonation at the N(3) nitrogen of the cytosine. Strong delocalization of the unshared electron pair on the amino nitrogen to N(3) has been inferred.

X-ray investigations have shown (3–6) that the free acids of cytidine 5′- and 3′-monophosphates (CMP) occur as zwitterions in the solid state. The protonation results from the migration of one of the phosphate protons onto the N(1) of the cytosine. Significant differences in molecular dimensions (bond lengths and bond angles) between the protonated and unprotonated cytosine bases were observed. Protonation results in a distortion from coplanarity of the pyrimidine ring and in enlarged bond angles and bond distances at the site of protonation. A shortening of the exocyclic amino carbon–nitrogen bond has been also observed. The hydrogen atoms were located and the state of ionization of the phosphate has been established. The phosphate group in CMP is present as the monovalent anion $RHPO_4^-$ and the individual P—O bonds differ significantly from each other. Generally, the protonated P—O(H) distance is longer than the unprotonated P—O^- or the P=O distance. In the sodium salt of 5′-CMP the phosphate group is a double anion with two negative charges distributed between the three oxygen atoms. The P—O distances are all nearly equal (7).

X-ray studies have evidenced (5) a very specific association pattern of the molecules in the zwitterion form instead of the well-known base stacking association. The molecules are linked together through hydrogen bonds involving the amino hydrogen atoms, the hydrogen atoms of the protonated N(3) nitrogen and the phosphate groups forming an infinitely extended right handed spiral around the screw axis.

Important frequency shifts toward higher frequencies in comparison with the neutral form have been observed for the double bond stretching and "amino" scissoring bands (1800–1500 cm^{-1}) of the protonated cytosine and poly C (8–11). The observed shifts have been accounted for by increased π-electron "localization" in specific double bonds. Normal coordinate analysis of cytosine was performed (12) with a valence force field and the potential energy distribution among the internal coordinates was calculated. The complexity of this region and the high degree of coupling between different modes has been emphasized.

Infrared spectra of zwitterions involving phosphate groups have been particularly studied in model phospholipid head molecules (13). In these molecules, asymmetrical intramolecular hydrogen bonds with large proton polarizability have been evidenced. The absorbance of the infrared continuum which is characteristic of the easily polarisable hydrogen bonds with a double minimum potential well (14) has been investigated as a function of the degrees of deprotonation and protonation. The samples were deprotonated by addition of various amounts of sodium hydroxide to the solution of the zwitterion. At 100% deprotonation (Na^+ salt) all easily polarisable hydrogen bonds have disappeared.

The spectroscopic behaviour of some phospholipids with respect to hydration has been related to the polar head interaction of the terminal part of the molecule (15, 16). The perturbation of the intramolecular hydrogen bond between the PO_2^- and NH_3^+ groups by the insertion of water molecules between the two head groups has been assumed.

Freeze-drying FT-IR-ATR (FD-FT-ATR) spectroscopy has been proposed as a method for hydration studies of biologically important molecules in two previous papers (17, 18). We have studied the ATR spectrum of hydrated cytidine-5′-phosphoric acid as a function of relative humidity and have observed a strong dependence of the general spectral pattern on the degree of hydration. Surface deuteration experiments have evidenced the involvement of most parts of the molecule of 5′-CMP in surface hydration. We have observed a contribution of the water bending band to the intensity of some of the 5′-CMP bands in the solid state spectra (1800–1600 cm^{-1}). Our previous results have indicated that this effect is more important in the free acid spectra. The "hydration" behavior of the different vibrations in the CMP molecule seems to be different in the acid and in the

sodium salt forms. The zwitterion structure determines a very specific association pattern and the strong involvement of the phosphate groups in these associations has been evidenced.

A study of the zwitterion–water interaction by freeze-drying FT-IR-ATR spectroscopy will be presented in this paper.

Experimental

The spectra were recorded on a Nicolet 5DXB FT-IR spectrometer, with a resolution of 2 cm^{-1} equipped with a DTGS detector. Collection times for the spectra (100 co-added interferograms) were less than 2 min. The Model 300 ATR attachment (Barnes Analytical) with a parallelogram (25 × 10 × 3 mm) KRS-5 plate was used.

The ATR crystals have been hydrated (before the deposition of the sample) by keeping them for a day in an atmosphere of constant relative humidity (r.h.). Constant r.h. was maintained by a saturated solution of an appropriate salt contained in a flat dish. Humidities were chosen so that the controlling salts had a constant temperature coefficient between 20 and 27°C for their relative humidity (19).

The ATR spectrum of the adsorbed sample was recorded and the crystal was kept in the sealed container holding the appropriate saturated salt solution at a controlled temperature. The attainment of equilibrium between the water of the adsorbed layers and the r.h. of the ambient atmosphere was followed spectroscopically and was found to require several hours.

Cytidine-5′-phosphoric acid (5′-CMP, MW 323, from yeast) and cytidine-5′-monophosphate (disodium salt) were obtained from the Sigma Chemical Company, and used without further purification. A solution (250 μL) (0.1–0.2 mg mL^{-1} in deionized water) of the compound was deposited on the hydrated crystal surface and the freeze-drying procedure was accomplished. The stages of freeze-drying and the cleaning procedure of the crystal have been described elsewhere (17). The crystal with the adsorbed sample was kept again for several hours in a controlled r.h. atmosphere.

Surface deuteration experiments were performed. A layer of liquid deuterium oxide was deposited on the hydrated sample and freeze-dried. The frozen deuterium oxide was removed by sublimation. CMP molecules were deposited on the hydrated crystal surface by freeze-drying and then the crystal was kept for several hours in the corresponding r.h. atmosphere. After recording of the ATR spectrum, an aqueous solution of HCl (pH ≃ 2) was deposited and the freeze-drying procedure was performed again.

Hydration experiments were carried out at different mechanical states of the crystal surface. When the surface is pumped at 50°C for 4 h, water is removed from the microvoids of the surface. During the freeze-drying procedure, molecules are trapped into the microvoids and the control of the r.h. is no more possible.

Results and discussion

The structure and atom numbering of cytidine-5′-phosphoric acid, 5′-CMP(H), in the zwitterion form is given in Fig. 1. The ATR spectra of the 5′-CMP(H) show infrared continua extending over the entire range from 4000 to 1800 cm^{-1} and again below 1400 cm^{-1}. Such a continuum is characteristic of easily polarisable hydrogen bonds with a double minimum potential well (14, 20, 21). According to X-ray data (5) this type of hydrogen bond may be formed between the phosphate group and the protonated cytosine base nitrogen. For the cytidine-3′-phosphate molecule, Sundaralingam and Jensen (3) have found 2.783 Å between the purine(3) nitrogen and the phosphate oxygen atoms and the hydrogen–oxygen distance is 1.679 Å. This hydrogen bond is represented by the proton boundary structures P—OH^+...N and P—O^-...$^+$HN, the second being of greater weight. The ir continuum in this system may also be caused by the polarizable H-bonds formed by the excess and defect protons which occur due to protolytic splitting of the adsorbed molecules (14).

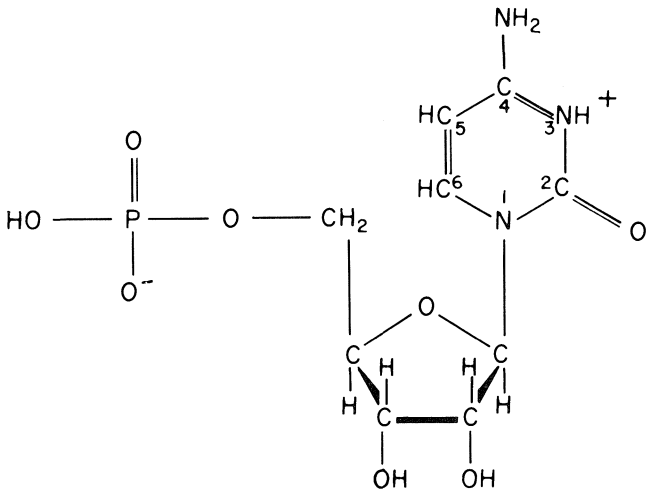

FIG. 1. Structure and numbering the 5′-CMP molecule.

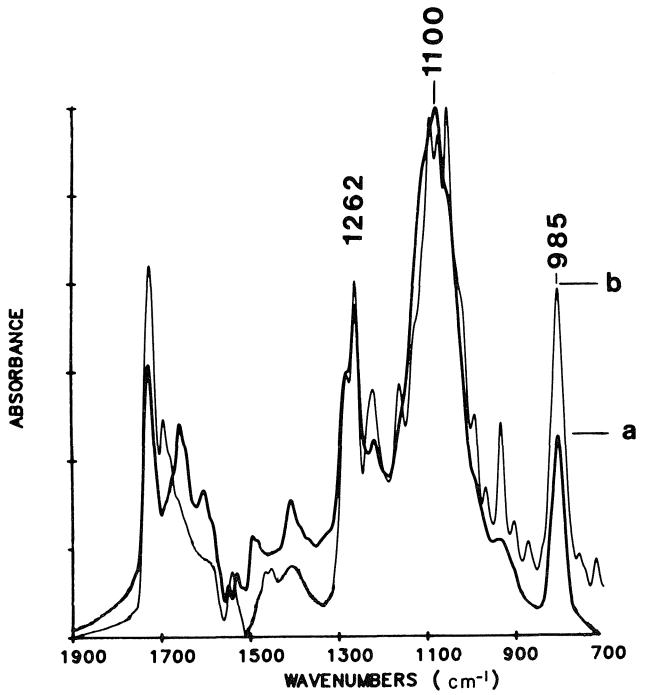

FIG. 2. ATR spectra of highly hydrated 5′-CMP(H) (1800–400 cm^{-1} region): (*a*) 66% r.h.; (*b*) 86% r.h.

In the spectrum corresponding to 66% r.h., the continuous absorption extends towards low wavenumbers and the absorbance of the continuum exceeds significantly the values corresponding to both 20% and 92% r.h. The strong absorption in the 4000–3600 cm^{-1} region has been assigned in a previous paper (17) to the stretching vibration of the water adsorbed on the thallium bromide iodide crystal surface. Figure 2 shows the 1900–700 cm^{-1} region in the 5′-CMP(H) spectra for two different r.h. values — 66% (*a*) and 86% (*b*). As r.h. is increased (Fig. 2*b*) the bands become sharper and better defined in the phosphate region. A strong dependence of the absorbance ratio A_{1280}/A_{1262} on the r.h. is observed. The absorption of the 1280 cm^{-1} band increases with increasing amounts of water in the 66–92% r.h. range. For the main 1100 cm^{-1} band, at lower r.h. values the bands are broad, many bands overlap, and the

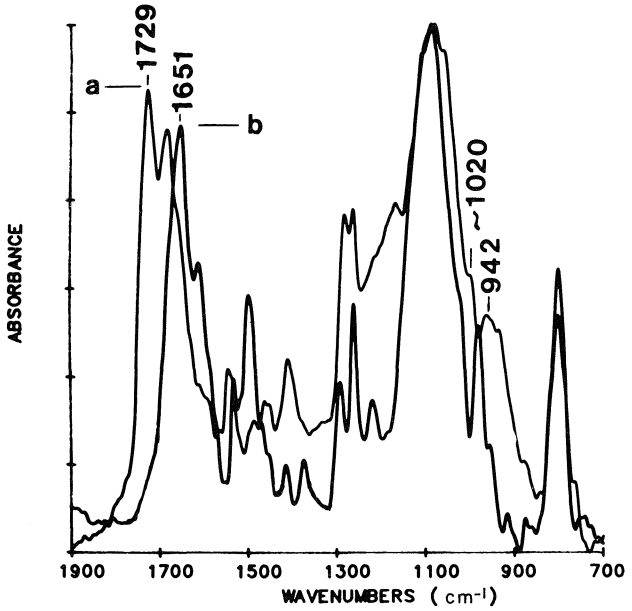

FIG. 3. ATR spectra of the hydrated 5′-CMP at 44% r.h.: (*a*) acid form; (*b*) sodium salt form.

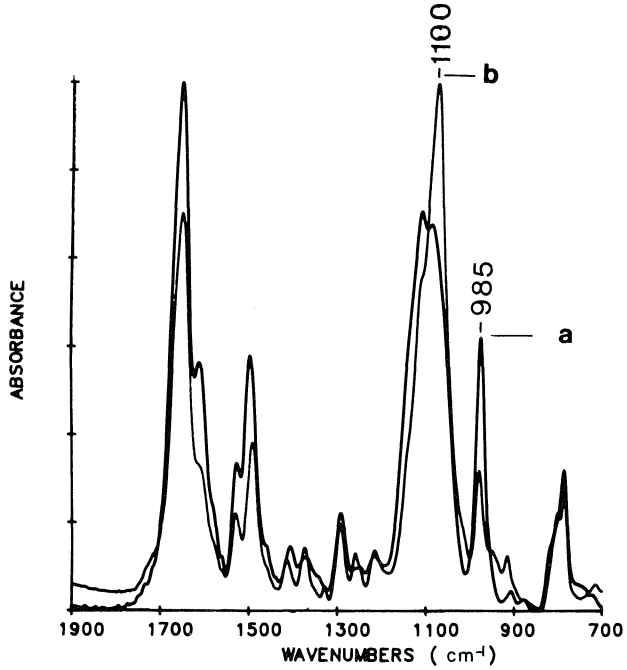

FIG. 4. ATR spectra of the hydrated 5′-CMP in sodium salt form at different r.h. values: (*a*) 20% r.h.; (*b*) 76% r.h.

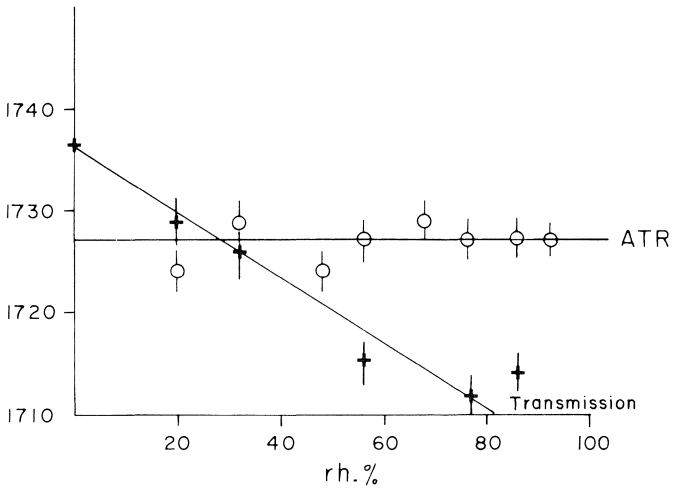

FIG. 5. Dependence of the frequency of the carbonyl band ($\nu_{C=O}$) on the r.h. values in transmission and ATR.

resolution of the spectral features is not possible. In a previous paper (19) the ATR spectra of 5′-CMP were given for six different r.h. values and some assignments of the bands were made. A thorough examination of the phosphate region in both zwitterion and ionic forms (Fig. 3) leads to a tentative assignment of the observed bands. In the sodium salt form (Fig. 4) the asymmetrical and symmetrical $\nu_{PO_3^{2-}}$ vibrations corresponding to the fully ionized phosphate group have been assigned to the bands near 1100 and 985 cm^{-1}, respectively. Figure 4 shows that the intensity of the asymmetrical phosphate band (1100 cm^{-1}) increases with increasing r.h. but no significant frequency displacements have been observed. As we have previously (17, 18) pointed out the phosphate group is the main hydration site in the mononucleotide molecule.

In the zwitterion structure in the solid state ionized and unionized phosphate groups occur simultaneously and both of them are influenced by the degree of hydration. Therefore, the complexity of the zwitterion spectrum (Fig. 3*a*) may be accounted for by a further lowering of the symmetry of the molecule with respect to the Na^+ salt form. In addition, adsorption effects due to the field of the ATR crystal lattice have been observed. At lower r.h. the broad absorption centered at 942 cm^{-1} can be assigned to hydrated ionic phosphate groups. The presence of water molecules affects the intramolecular hydrogen bond by insertion between the two groups. As Bertoluzza *et al.* (16) have recently pointed out in the case of some phospholipids an indirect perturbation of the intramolecular hydrogen bond by interaction of water molecules with the P—O^- group is also possible.

The shoulder at the lower frequency side of the broad band between 1050 and 1000 cm^{-1} can be assigned to unionized P—OH groups (22) hydrogen bonded to the adsorbed water (in the first layers of the surface). This absorption is markedly reduced in the Na^+ salt form (Fig. 3*b*) as well as in the highly hydrated acid form (Fig. 2). The band located at 1280 cm^{-1} may receive an important contribution from the external C—N vibration, but the strong coupling with C—C and ring C—N vibrations (10) does not allow a precise assignment. The other band in this region, the 1262 cm^{-1} band was assigned to the $\nu_{P=O}$ vibration (22, 23).

The important contribution of water to the absorption band of the CMP zwitterion structure has been demonstrated. The spectral pattern changes due to the surface deuteration of a highly hydrated sample. In the 1800–1600 cm^{-1} region, both the water bending (about 1650 cm^{-1}) and the 1680 cm^{-1} band (assigned previously (9, 10) to the scissoring vibration of the amino group) are removed by deuteration. The strong dependence of $\nu_{C=O}$ on the r.h.% values has been observed in the transmission measurements (Fig. 5). The decrease of the frequency with increasing r.h. can be accounted for by the presence of C=O..H—O—H hydrogen bonds in the hydrated molecule. The lack of this relationship in the surface hydration

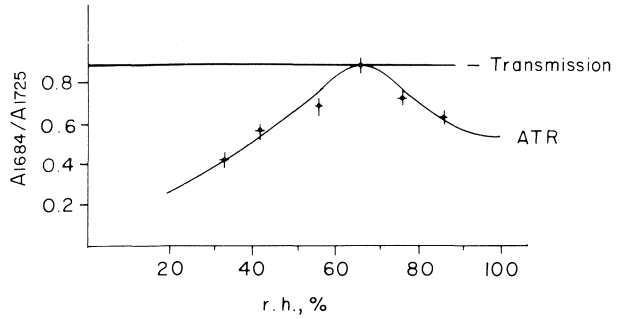

FIG. 6. Dependence of the protonation degree (A_{1684}/A_{1725}) on r.h. values.

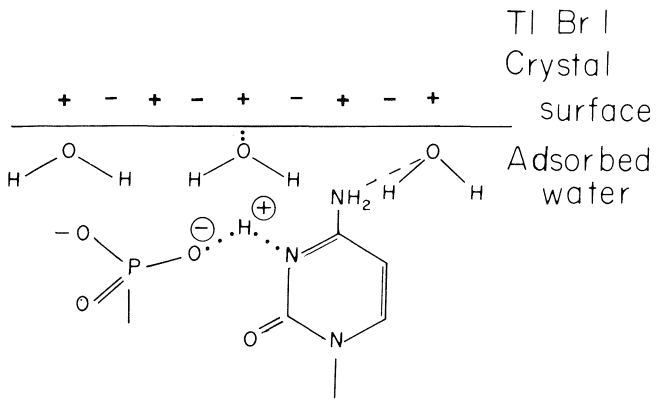

FIG. 7. Water-assisted proton transfer at the crystal surface.

(ATR measurements) seems to show that the carbonyl groups are less involved with hydrogen bonding with surface water.

Further protonation of CMP(H) results in an enhanced absorbance of the 1680 cm^{-1} band. This band belonging to the "amino" scissoring receives an important contribution from the protonated structure (–CO—NH^+). In addition, a weak absorption band near 2700 cm^{-1} has been observed. We have considered the A_{1680}/A_{1725} absorbance ratio as a measure of the degree of protonation. This ratio does not depend on the degree of hydration in the transmission measurements (Fig. 6). To the contrary, a strong dependence of this ratio on the r.h. has been found in the ATR spectra. The degree of protonation seems to be the highest when the r.h. value is approximately 66%. These results show the involvement of the surface adsorbed water molecules in the proton transfer processes (Fig. 7). The mechanism of this water-assisted proton transfer is not known. Zundel (14) pointed out that proton transfer equilibria are strongly shifted to the right when water molecules are added to the water-free solutions or to films of polymers. The ability of the adsorbed water to act by itself as a proton donor is evidenced by the following experiment. The crystal was pretreated under vacuum at 50°C and this has provoked a partial surface dehydration. In this way a network of very fine pores accessible to water was developed and the contact surface between the crystal and water strongly increased. Trapped CMP molecules in a crystal pretreated in this manner are strongly protonated by the adsorbed water molecules. In Fig. 8 the intensity of the 1684 cm^{-1} band is strongly increased. The general pattern of the spectrum corresponding to the trapped molecules is the same as that of molecules protonated by addition of HCl. These results show that the adsorbed water may act as a strong donor by releasing its proton.

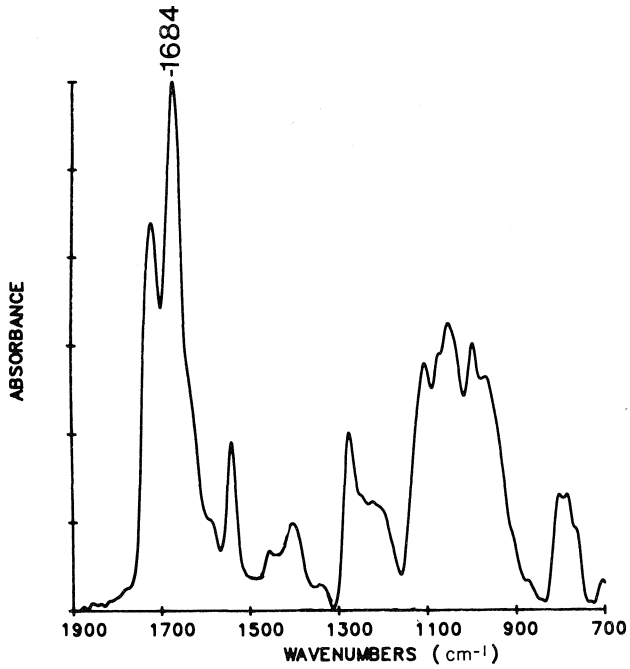

FIG. 8. Enhanced protonation in the "trapped" molecules.

The increased degree of dissociation of the adsorbed water was reported in many of the earlier works on the special properties of the water adsorbed on silica glass surfaces (24, 25). Because of the stronger ionic character of the thallium bromide iodide surface as compared to silica, one may also expect a high degree of dissociation for water adsorbed on this surface. In order to explain the increased surface electrical conductivity a strong enhancement of the water dissociation by surface electrical fields was assumed by Fripiat *et al.* (24). Recently Ibach (26) and Chabal *et al.* (27, 28) showed that water adsorption on Si (100) is dissociative. Hydride formation upon molecular chemisorption of water on annealed surfaces has been indicated. Moreover, the electronic structure of molecularly adsorbed water has been computed theoretically (29, 30) with a semiempirical approach and it was demonstrated that water is chemisorbed to silicon surfaces.

We have observed the occurrence of very narrow (microscopical) scratches on the surface when the crystal was submitted to a great number of freeze-drying procedures. Freezing of water in the voids involving volumetric expansion produces some mechanical destruction (frost action) (31–33). This mechanical inhomogeneity of the surface induces an energetic and structural inhomogeneity in the adsorbed water layers. Therefore, with low amounts of water (degassed crystal) the strongly adsorbed water can enhance proton transfer in the molecule. At higher r.h. values the depth of the adsorbed water layer becomes too thick and its properties are similar to those of bulk water. Our results show the importance of the mechanical state of the crystal in the FD-ATR measurements. Crystals having many microscopical channels adsorb water very strongly and the keeping of a constant r.h. level is quite difficult.

Conclusions

The freeze-drying ATR spectra of hydrated 5′-CMP in both acid and Na salt forms have been studied. Intramolecular hydrogen bonding with proton transfer resulting in an infrared

continuum has been found for zwitterionic 5′-CMP(H) on the hydrated crystal.

The dependence of the general spectral pattern of 5′-CMP(H) on the r.h. has been pointed out. Assignments for the bands in the phosphate region of the hydrated 5′-CMP(H) are proposed.

Surface deuteration of the semiprotonated 5′-CMP(H) showed the important contribution of the water bending vibration to the absorbance of the bands in the 1800–1600 cm^{-1} region. Deuteration and protonation studies on the hydrated samples were carried out in order to ascertain some assignments for the bands in this region. The 1684 cm^{-1} band has been assigned to a vibration having mainly NH^+ character.

The role of the adsorbed water in the proton transfer process has been underscored. The ability of the water molecules to act as proton donors has been accounted for by an increased degree of dissociation of the water adsorbed on the thallium bromide iodide crystal surface.

Acknowledgments

Financial assistance from the Natural Sciences and Engineering Research Council of Canada and from the Ministère de l'Éducation du Québec is gratefully acknowledged. The authors also thank Dr. N. J. Harrick for valuable discussions on the FD-ATR technique.

1. V. Markowski, G. R. Sullivan, and J. D. Roberts. J. Am. Chem. Soc. **99**, 714 (1977).
2. B. W. Roberts, J. B. Lambert, and J. D. Roberts. J. Am. Chem. Soc. **87**, 5439 (1965).
3. M. Sundaralingam and L. H. Jensen. J. Mol. Biol. **13**, 914 (1965).
4. M. Sundaralingam and L. H. Jensen. J. Mol. Biol. **13**, 930 (1965).
5. M. A. Viswamithra, B. Swaminatha Reddy, G. H.-Y. Lin, and M. Sundaralingam. J. Am. Chem. Soc. **93**, 4565 (1971).
6. M. Sundaralingam and P. Prusiner. Nucl. Acid Res. **5**, 4375 (1978).
7. J. Pandit, T. P. Seshadri, and M. A. Viswamitra. Acta Crystallogr. C**39**, 342 (1983).
8. T. Shimanouchi, M. Tsuboi, and Y. Kyogoku. Advances in chemical physics. Vol. VII. The structure and properties of biomolecules and biological systems. *Edited by* J. Duchesne. Wiley Interscience, New York. pp. 435–498.
9. M. Tsuboi, Y. Kyogoku, and T. Shimanouchi. Biochim. Biophys. Acta, **55**, 1 (1962).
10. R. C. Lord and G. J. Thomas, Jr. Spectrochim. Acta, **23**A, 2551 (1967).
11. G. Zundel, W. D. Lubos, and K. Kölkenbeck. Biophys. J. **12**, 1509 (1972).
12. H. Susi, J. S. Ard, and J. M. Purcell. Spectrochim. Acta, **29**A, 725 (1973).
13. G. Papakostidis and G. Zundel. Z. Naturforsch. **28**B, 323 (1973).
14. G. Zundel. *In* The hydrogen bonds. Recent developments in theory and experiments. Vol. II. *Edited by* P. Schuster, G. Zundel, and C. Sandorfy. 1976.
15. S. Bush, R. G. Adams, and I. W. Levin. Biochemistry, **19**, 4429 (1980).
16. A. Bertoluzza, S. Bonora, G. Fini, and M. A. Morelli. Can. J. Spectrosc. **29**, 93 (1984).
17. S. Badilescu and C. Sandorfy. Appl. Spectrosc. In press.
18. S. Badilescu and C. Sandorfy. Appl. Spectrosc. In press.
19. E. M. Bradbury, W. C. Price, and G. R. Wilkinson. J. Mol. Biol. **3**, 301 (1961).
20. D. Schiöberg, K. P. Hofmann, and G. Zundel. Z. Phys. Chem. Neue Folge, **90**, 181 (1974).
21. G. Zundel and J. Fritsch. J. Phys. Chem. **88**, 6295 (1984).
22. M. B. Abramson, W. T. Norton, and R. Katzman. J. Biol. Chem. **240**, 2389 (1965).
23. H. C. Nelson and J. F. Villa. J. Inorg. Nucl. Chem. **42**, 1669 (1980).
24. J. J. Fripiat, A. Jelli, G. Poncelet, and J. André.. J. Phys. Chem. **69**, 2185 (1965).
25. M. Prigogine and J. J. Fripiat. Bull. Soc. Chim. Fr. 4291 (1971).
26. H. Ibach, H. Wagner, and D. Bruchmann. Solid State Commun. **42**, 457 (1982).
27. Y. J. Chabal. Phys. Rev. B**29**, 3677 (1984).
28. Y. J. Chabal and S. B. Christman. Phys. Rev. B**29**, 6974 (1984).
29. S. Ciraci and H. Wagner. Phys. Rev. B**27**, 5180 (1983).
30. S. Ciraci, S. Erkoc, and S. Ellialoglu. Solid State Commun. **45**, 35 (1983).
31. G. G. Litvan. Can. J. Chem. **44**, 2617 (1966).
32. R. F. Feldman. Can. J. Chem. **48**, 287 (1970).
33. G. G. Litvan. J. Coll. Interface Sci. **38**, 75 (1972).

Comparison of oxygen and sulphur adsorption on the (0001) surface of zirconium

P. C. WONG AND K. A. R. MITCHELL

Department of Chemistry, University of British Columbia, 2036 Main Mall, Vancouver, B.C., Canada V6T 1Y6

Received June 27, 1986

P. C. WONG and K. A. R. MITCHELL. Can. J. Chem. **64**, 2409 (1986).

Low energy electron diffraction (LEED) and Auger electron spectroscopy (AES) have been used to compare the adsorption and coadsorption of O_2 and H_2S on the (0001) surface of zirconium where exposures are in the one to five Langmuir regime. The new observations made are as follows: (*i*) that sulphur forms a stable (3 × 3) surface structure after heating to 600°C; (*ii*) that the Zr(0001) surface with high O coverage adsorbs H_2S, whereas the surface with high S coverage does not adsorb oxygen in detectable amounts; and (*iii*) that for surfaces with adsorbed H_2S a sudden increase in the 150 eV to 92 eV Auger peak ratio occurs on heating to 530°C.

P. C. WONG et K. A. R. MITCHELL. Can. J. Chem. **64**, 2409 (1986).

On a utilisé la diffraction électronique à basse énergie (DEBE) et la spectroscopie électronique du Auger (SEA) pour comparer l'adsorption et la coadsorption du O_2 et du H_2S sur la surface (0001) du zirconium, où les expositions se situent dans le régime un à cinq de Langmuir. Les nouvelles observations qui ont pu être faites sont les suivantes : (*i*) après avoir été chauffé à 600°C, le soufre forme une structure de surface (3 × 3) stable; (*ii*) la surface (0001) du Zr très couverte par le O adsorbe le H_2S alors que la surface très couverte par le S n'adsorbe pas de quantités détectables d'oxygène et (*iii*) dans le cas des surfaces qui ont adsorbé du H_2S et qui ont été chauffées à 530°C, il se produit une augmentation rapide du rapport des pics à 150 eV et 92 eV du spectre électronique de Auger.

[Traduit par la revue]

1. Introduction

There is considerable technological interest in the surface chemistry of zirconium (1–3), although information is still very limited on the structural aspects of chemisorption at coverages of the order of a monolayer (formed by exposures of just a few Langmuir, where 1 L = 10^{-6} Torr s). Some studies have recently investigated the chemisorption of small molecules like H_2, O_2, N_2, CO, and NO on polycrystalline zirconium (4–7), and concluded that dissociative chemisorption occurs followed by diffusion into the bulk on heating at above 500 K (except hydrogen which desorbs at above 700 K). In addition, preliminary surface structural analyses with low-energy electron diffraction (LEED) for surface structures involving oxygen chemisorption provide support for the model of subsurface incorporation at low coverages (8, 9). In this model, O atoms occupy octahedral hole sites in zirconium, and therefore the structure relates to that of bulk ZrO rather than to that of the final oxidation product ZrO_2, which forms at higher oxygen exposures or higher temperatures (3, 10).

This present paper uses LEED and Auger electron spectroscopy (AES) to compare the adsorption and coadsorption of O_2 and H_2S on the Zr(0001) surface. It is believed that such studies can provide further insight into the surface structures formed by low-exposure chemisorption on zirconium.

2. Experimental

The apparatus and cleaning procedures used were as described previously from this laboratory for a LEED crystallographic analysis for the clean Zr(0001) surface (11). Adsorption studies were made on surfaces which showed sharp (1 × 1) LEED patterns, with hexagonal symmetry at normal incidence, and for which no contaminants were apparent with AES measured by a cylindrical mirror analyser. The experiments used high-purity oxygen or H_2S which were directed to the Zr(0001) surface via a nozzle. For various exposures of the adsorbing gas, the relative amounts of adsorbed species were assessed with appropriate Auger peak height ratios; specifically for oxygen

$$R_O = A_{510}/A_{92}$$

(i.e. the ratio of the Auger peak height for O at 510 eV to that of Zr at 92 eV), and for sulphur

$$R_S = A_{150}/A_{92}$$

(where A_{150} is the peak height for overlapping Zr and S Auger signals at 150 eV). For Zr it appears advantageous to use the Auger peak which involves emission from the N shell; this limits the influence of attenuation and shift/broadening effects which have been noted in the valence shell spectra (4, 12). After each adsorption experiment, the sample surface was cleaned by Ar^+ bombardment and re-ordered by heating to 600°C followed by immediate cooling (heating and cooling rates are approximately 1°C s^{-1}). The cleaned zirconium surface is characterized with $R_O = 0.0$ and $R_S = 1.4$.

3. Results and discussion

3.1. O_2 adsorption

Exposure of a clean, ordered Zr(0001) surface to oxygen at room temperature yields (1 × 1) LEED patterns with high background, although (2 × 2) patterns can be observed after heating at below 220°C. This is less than the temperature at which diffusion into the bulk occurs, and therefore we interpret the heating as providing just an ordering effect. The sharpest (2 × 2) pattern was obtained for an initial oxygen exposure (1.2 L) which gives R_O equal to 0.16; the associated surface structure appears sufficiently stable at room temperature and 10^{-10} Torr for the sharp LEED pattern to be maintained for at least 3 days. With larger initial exposures to oxygen the (2 × 2) pattern gives way to a (1 × 1) pattern, which is best established with an exposure of about 3.6 L and a surface coverage corresponding to $R_O = 0.23$. The LEED intensity-versus-energy curves for this structure have clear differences from those of the clean Zr(0001) surface; examples for (1,1) beams are included in Fig. 1.

3.2. H_2S adsorption

When a cleaned and ordered Zr(0001) surface was exposed to about 4.2 L of H_2S at room temperature, sulphur adsorption occurred ($R_S = 2.8$), but no extra LEED beams were detectable even after heating to 500°C. However, on heating to 530°C, R_S was found to increase to 3.1, an observation, which in conjunction with a report by Lin and Gilbert (7), appears to be associated with hydrogen desorption. Further, with a short heating to 600°C, a very sharp (3 × 3) LEED pattern was observed on cooling to room temperature, for which R_S remained at 3.1. Higher S coverages, as measured by R_S, can be

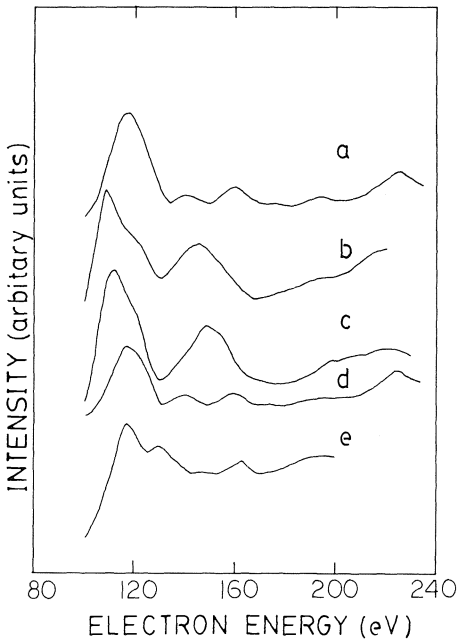

FIG. 1. Intensity versus energy curves measured for the (1,1) beam from (*a*) clean Zr(0001), (*b*) Zr(0001)—(2 × 2)—O with $R_O = 0.16$, (*c*) Zr(0001)—(1 × 1) with $R_O = 0.23$, (*d*) Zr(0001)—(3 × 3)—S with $R_S = 2.4$, (*e*) Zr(0001)—(3 × 3)—S with $R_S = 3.1$.

obtained by giving larger initial exposures to H_2S; however, following annealing at 600°C, the (3 × 3) LEED patterns show increasing disorder as R_S increases beyond 3.1. Intensity-versus-energy curves for the diffracted beams (e.g. Fig. 1) suggest that the moderate coverage (3 × 3) structures with R_S less than 3.1 correspond to mixed regions of clean surface and of (3 × 3) domains. The latter regions appear to be stable for long periods.

3.3. O_2 and H_2S coadsorption

A series of experiments for assessing structural aspects of the coadsorption of O_2 and H_2S on an initially clean Zr(0001) surface have been made, and the results are summarized in the following subsections.

3.3.1. O_2 on Zr(0001)—(3 × 3)—S with $R_S > 3.1$

No evidence could be found from AES or LEED for oxygen chemisorption occurring on (3 × 3) surfaces with R_S greater than 3.1 when exposed to oxygen at room temperature. The same statement holds for these surfaces when annealed following the procedures used above for the formation of the Zr(0001)—(2 × 2)—O and Zr(0001)—(1 × 1)—O surface structures.

3.3.2. O_2 on Zr(0001)—(3 × 3)—S with $R_S < 3.1$

When a partially S covered (3 × 3) structure was exposed to oxygen, and treated according to the conditions that give the (2 × 2)—O structure as in 3.1, the LEED pattern shows a superposition of the individual (2 × 2)—O and (3 × 3)—S patterns. This observation is consistent with the existence of separate (2 × 2)—O and (3 × 3)—S domains on the surface, with linear dimensions larger than the transfer width of the instrument used (~100 Å) (13). For an initial partially S covered surface with $R_S = 2.3$, values of R_S and R_O were found to be 2.1 and 0.13, respectively, after the preparation of the mixed surface. The decrease of R_S appears associated with the effect of oxygen on the Auger zirconium signal at 150 eV (12). On further heating to 600°C, the (3 × 3) part of the LEED pattern remains essentially unchanged and R_S returns to 2.3, while the (2 × 2) pattern disappears and R_O goes to zero as expected for oxygen diffusion into the bulk.

3.3.3. H_2S on Zr(0001)—(2 × 2)—O

When an oxygen surface which shows a (2 × 2) LEED pattern with $R_O = 0.16$ and $R_S = 1.3$ was exposed to about 3.5 L of H_2S at room temperature and annealed at 530°C, a diffuse (1 × 1) LEED pattern with high background was observed. However, with further heating at 600°C, a very sharp (3 × 3) LEED pattern was recovered on cooling to room temperature ($R_O = 0.0$, $R_S = 2.3$).

3.3.4. H_2S on Zr(0001)—(1 × 1)—O

The observation in 3.3.3 was found to extend even to a surface with the highest oxygen coverage considered here (viz. Zr(0001)—(1 × 1)—O with $R_O = 0.23$). After exposure to H_2S at room temperature, the LEED pattern becomes diffuse with high background ($R_S = 2.3$, $R_O = 0.26$), but after annealing at 600°C and cooling to room temperature a sharp Zr(0001)—(3 × 3)—S pattern results with $R_S = 2.9$ and $R_O = 0.0$.

3.3.5. Coadsorption without annealing

AES shows that the basic tendencies observed in 3.3.2 and 3.3.4 extend also to a Zr(0001) surface which is treated entirely at room temperature. Specifically it was found that oxygen does not significantly adsorb on a high S coverage Zr(0001) surface, whereas H_2S will adsorb on a high O coverage surface.

4. Concluding remarks

This work highlights the contrasting behaviours of oxygen and sulphur chemisorption on the Zr(0001) surface. Thus while the highest coverage oxygen surface is still able to adsorb H_2S, the highest coverage sulphur surface does not adsorb oxygen in detectable amounts. These observations are consistent with oxygen forming subsurface structures (8), whereas sulphur probably forms a coincidence-site (3 × 3) structure in which the overlayer involves either a sufficiently high density of S atoms to block O adsorption, or a protective combined layer of Zr and S, perhaps with a zirconium sulphide structure. Analyses of the surface geometries of these systems are in progress, but the general chemical observations reported here do appear to set some limits on the possible structural arrangements. Investigations are also underway to probe the origin of the increase in R_S at 530°C for surfaces which initially contain H_2S. Finally it is noted that this work provides no evidence for significant sulphur and oxygen combination processes, either when surfaces with coadsorbed S and O are heated, or when S-saturated surfaces are heated in oxygen.

Acknowledgements

We thank Dr. P. R. Norton for supplying the zirconium crystal used in these studies. We also gratefully acknowledge the support of this research provided by the Natural Sciences and Engineering Research Council of Canada.

1. G. L. MILLER. Zirconium. Butterworths, London. 1957.
2. J. H. SCHEML and H. S. ROSENBAUM (*Editors*). Zirconium in nuclear applications. American Society for Testing and Materials, Special Technical Publ. 551, Philadelphia. 1973.
3. R. L. TAPPING. J. Nucl. Mat. **107**, 151 (1982).
4. J. S. FOORD, P. J. GODDARD, and R. M. LAMBERT. Surface Sci. **94**, 339 (1980).

5. G. B. HOFLUND, D. F. COX, and R. E. GILBERT. J. Vac. Sci. Technol. A, **1**, 1837 (1983).
6. G. B. HOFLUND, D. A. ASBURY, D. F. COX, and R. E. GILBERT. Appl. Surface Sci. **22/23**, 252 (1985).
7. J. M. LIN and R. E. GILBERT. Appl. Surface Sci. **18**, 315 (1984).
8. K. C. HUI, R. H. MILNE, K. A. R. MITCHELL, W. T. MOORE, and M. Y. ZHOU. Solid State Commun. **56**, 83 (1985).
9. K. C. HUI. Ph.D. Thesis, University of British Columbia. 1986.
10. D. P. VALYUKHOV, M. A. GOLUBIN, D. M. GREBENSHCHIKOV, and V. I. SHESTOPALOVA. Soviet Phys. Solid State, **24**, 1594 (1982).
11. W. T. MOORE, P. R. WATSON, D. C. FROST, and K. A. R. MITCHELL. J. Phys. C, **12**, L887 (1979).
12. M. Y. ZHOU, R. H. MILNE, M. A. KAROLEWSKI, D. C. FROST, and K. A. R. MITCHELL. Surface Sci. **139**, L181 (1984).
13. G. COMSA. Surface Sci. **81**, 57 (1979).

Comparative sulphur cation chemistry in a hydrocarbon flame with H_2S, OCS, and SO_2 additives

NICHOLAS S. KARELLAS AND JOHN M. GOODINGS

Department of Chemistry and Centre for Research in Experimental Space Science, York University, 4700 Keele Street, Downsview, Ont., Canada M3J 1P3

Received May 13, 1986

NICHOLAS S. KARELLAS and JOHN M. GOODINGS. Can. J. Chem. **64**, 2412 (1986).

A fuel-rich, conical, premixed, methane–oxygen flame at atmospheric pressure was doped separately with 0.2 mol% of H_2S, OCS, and SO_2 to probe the chemistry of sulphur at its source during combustion. These three additives represent a broad range of fuel-sulphur contaminants since they occur early, intermediate, and late in the sulphur oxidation sequence. A wide variety of sulphurous cations, formed by chemical ionization reactions, is observed for each additive by sampling the flame into a mass spectrometer. The total ionization profile measured along the flame axis is enhanced in the reaction zone when a sulphur additive is present; the mechanism involves the formation of sulphurous negative ions which reduces the rates of cation loss by electron–ion recombination and ambipolar diffusion. Mass spectra measured in the mass range 10–110 u at fixed points on the flame axis are very similar for all three additives, and are not helpful in the identification of the additive. However, the general presence of sulphur is evident from large signals measured near the reaction zone at five principal mass numbers; namely, 45 u (CHS^+), 47 u (CH_3S^+), 58 u ($C_2H_2S^+$), 59 u ($C_2H_3S^+$), and 69 u (C_3HS^+) related to CS, thioformaldehyde, thioketene, and C_3S.

NICHOLAS S. KARELLAS et JOHN M. GOODINGS. Can. J. Chem. **64**, 2412 (1986).

Dans le but d'étudier la chimie du soufre à sa source au cours de sa combustion, on a dopé une flamme oxygène/méthane, prémélangée, conique, riche en carburant et opérant à la pression atmosphérique avec 0,2 mol% de l'un ou l'autre des composés suivants, soit le H_2S, le OCS ou le SO_2. Ces trois additifs correspondent à un évantail large de contaminants carburant/soufre, puisqu'ils se retrouvent tant au début, qu'à la fin ou au cours du stade intermédiaire de la suite des oxydations du soufre. Pour chacun des additifs et faisant appel à un échantillonage par spectrométrie de masse, on peut observer une grande variété de cations sulfureux, qui se forment par des réactions d'ionisations chimiques. Lorsqu'un additif de soufre est présent, le profil total d'ionisation, tel que mesuré en suivant le développement de l'axe de la flamme, subit une augmentation dans la zone de la réaction; le mécanisme implique une formation d'ions sulfureux négatifs qui réduit les taux de perte de cations par recombinaison électron/ion et par diffusion ambipolaire. Les spectres de masses, mesurés entre 10 et 100 u et à des points fixes de l'axe de la flamme, sont très semblables pour chacun des trois additifs et ne sont pas utiles pour l'identification de l'additif. Toutefois, la présence générale de soufre est évidente à partir de signaux très importants qui sont mesurés près de la zone réactionnelle, à cinq valeurs principales de masse, soit 45 u (CHS^+), 47 u (CH_3S^+), 58 u ($C_2H_2S^+$), 59 u ($C_2H_3S^+$) et 69 u (C_3HS^+) qui sont reliées respectivement au CS, au thioformaldéhyde, au thiocétène et au C_3S.

[Traduit par la revue]

Introduction

Combustion processes account for more than 90% of the energy consumed in the United States (1). Also, more than 90% of SO_x emissions result from combustion (1). A Canadian emissions inventory indicates that 80% of the total SO_2 emissions arise from a relatively few point sources concentrated in industrial sectors involving smelters, major utilities, and fossil fuel production plants (2). Our objective has been to learn as much as possible about the chemistry of sulphur in combustion by observations of sulphurous ions formed in a hydrocarbon flame doped with fuel-sulphur additives. By sampling the flame at atmospheric pressure into a mass spectrometer, it is possible to probe the sulphur chemistry at its source in and around the flame reaction zone.

Initially, studies of sulphurous anions were carried out in a premixed, fuel-rich, CH_4–O_2 flame doped with OCS (3), and with H_2S and SO_2 in addition for comparison purposes (4). The sulphur chemistry gives rise to a variety of species of high electron affinity leading to large sulphurous anion signals confined mainly to the flame reaction zone. The positive ion chemistry is more complex, but extends through the reaction zone into the burnt gas downstream. In a recent study of the same flame with OCS additive, more than 40 sulphurous cations were observed in the mass range below 110 u (5). The ion chemistry leading to the formation of these cations has been considered in detail involving reactions of primary sulphur ions with neutral hydrocarbon flame constituents (5).

The present study extends the observations of sulphurous cations in the same fuel-rich, CH_4–O_2 flame doped separately with 0.2 mol% of H_2S, OCS, and SO_2. These three additives were chosen to be early, intermediate, and late in the sulphur oxidation sequence. As such, they cover a broad range of possible fuel-sulphur contaminants. We hoped to establish mass-spectrometric fingerprints in different flame regions from which the nature of the sulphur contaminant could be identified. In fact, the three additives give very similar mass spectra, indicative of extensive pyrolysis of the fuel-sulphur early in the reaction zone. However, general fingerprints for sulphur compounds are evident at five principal mass numbers. Also, the sulphur additives enhance the observed total positive ion signals primarily in the flame reaction zone. The mechanism of the latter enhancement has been traced to the formation of sulphurous anions which affect the normal rates of cation loss by electron–ion recombination and ambipolar diffusion.

Experimental

All of the ion concentration measurements were performed on the same CH_4–O_2 flame of fuel-rich composition (equivalence ratio $\phi = 2.15$) whose ion chemistry we have studied extensively in the past (6, 7). It was of the laminar premixed type with a conical luminous reaction zone (height 5 mm, base diameter $\simeq$ 3 mm, thickness $\simeq$ 0.3 mm) to facilitate ionic sampling along the flame axis into the mass spectrometer. The flame has a burnt gas velocity of approximately 1 m s^{-1} and an adiabatic flame temperature of 2460 K, although the measured temperature of the equilibrium burnt gas was close to

2200 K. The flame was stabilized at atmospheric pressure on a simple, tubular, quartz burner (2.3 mm id) surrounded by a flowing argon shield to minimize the entrainment of atmospheric air. Provision was made to add separately 0.2 mol% of H_2S, OCS, or SO_2 to the premixed gas in exactly the same way as was done previously for the study with OCS (5). The additive could be introduced or removed without altering the flame. All gases were used straight from the cylinders without further purification ($CH_4 > 99.0\%$, $O_2 > 99.6\%$, $Ar > 99.9\%$, $H_2S > 97.5\%$, $OCS > 97.5\%$, $SO_2 > 99.90\%$). The burner was mounted on a motor-driven carriage with accurate alignment of the flame axis with the sampling orifice of the mass spectrometer. The calibrated burner drive provided spatial resolution of ± 0.02 mm along the flame axis (designated z) for measurements of ion concentration profiles.

The flame-ion mass spectrometer has been described previously in detail (6). The flame burned against a 60°, conical, chromium, sampling nozzle of orifice diameter ca. 0.1 mm mounted in a water-cooled flange of the type described by Hayhurst and Telford (8). The sampled ions pass through two stages of differential pumping into a quadrupole mass filter. The mass-analyzed ions are detected with a parallel-plate Faraday collector connected to a vibrating reed electrometer having a grid-leak resistance of 10^{10} ohms. The ion signal magnitudes in the figures are quoted in volts based on the detected ion current passing through 10^{10} ohms. The mass spectra shown below have been corrected for mass discrimination in the filter against ions of high m/e measured at high resolving power. The dynamic range of sensitivity of the apparatus is five orders of magnitude.

A method has been described (6) involving a relatively sharp minimum in the pressure profile of the sampled gas for locating a reproducible origin ($z = 0$) in the *flame* (not referred to the burner). It corresponds to the downstream edge of the luminous reaction zone on the flame axis. In this way, a family of ion profiles at different mass numbers m/e can be accurately overlaid on the distance scale z. It is also an important consideration when comparing mass spectra at fixed points on the flame axis (e.g. $z = -0.15$ mm upstream in the reaction zone, and $z = 0.2$ and 1.5 mm downstream) for the undoped flame with those measured in the presence of an additive. Small changes in position can alter the spectra considerably.

Results and discussion

Ion profiles

Figure 1 gives profiles of the total positive ion signal measured along the flame axis for the undoped flame and for the flame doped separately with 0.2 mol% of H_2S, OCS, and SO_2. These signals are obtained by removing the dc voltage from the rods of the quadrupole mass filter so that ions of every m/e are transmitted. Although the peak magnitude of all four profiles is constant within experimental error, the upstream ion signals in the reaction zone are enhanced. A shoulder is evident on the profiles, particularly that for SO_2 where the total ion signal is almost doubled. The effect is progressively smaller with OCS and H_2S although still clearly evident. One possible explanation is the occurrence of a new chemi-ionization reaction involving sulphur species such as

$$[1] \quad CH + S \rightarrow HCS^+ + e^- \qquad \Delta H^0 = +38$$

which is analogous to the usual fundamental chemi-ionization process normally associated with hydrocarbon flames (9)

$$[2] \quad CH + O \rightarrow HCO^+ + e^- \qquad \Delta H^0 = -5$$

(standard heats of reaction ΔH^0 are given in kcal mol^{-1} at 298 K). However, reaction [1] is unlikely because it is so endothermic. Also, it is difficult to explain the constant profile peak magnitude if a second chemi-ionization reaction is operative. In the previous OCS study (5), we stated that we did not have a satisfactory explanation of the enhanced total ion signal in the flame reaction zone. However, the correct explanation of the phenomenon is now forthcoming and has far-reaching consequences, particularly for the mass spectra observed with the SO_2 additive.

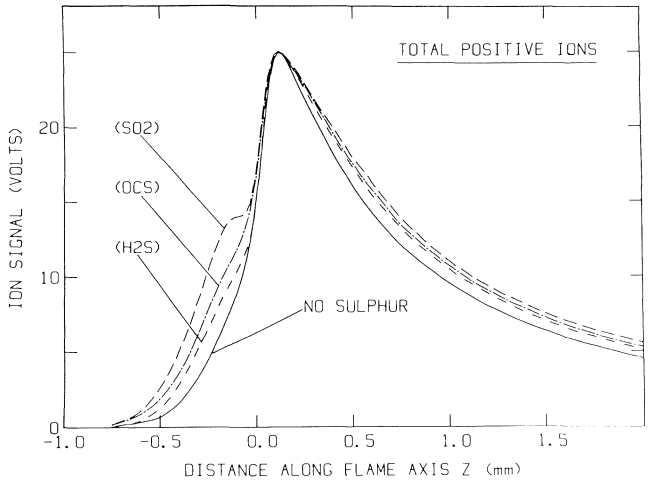

FIG. 1. Total positive ion profiles in the absence of sulphur (solid line) and with the flame doped with 0.2 mol% of H_2S, OCS, and SO_2. The reaction zone is located upstream of $z = 0$ (negative z).

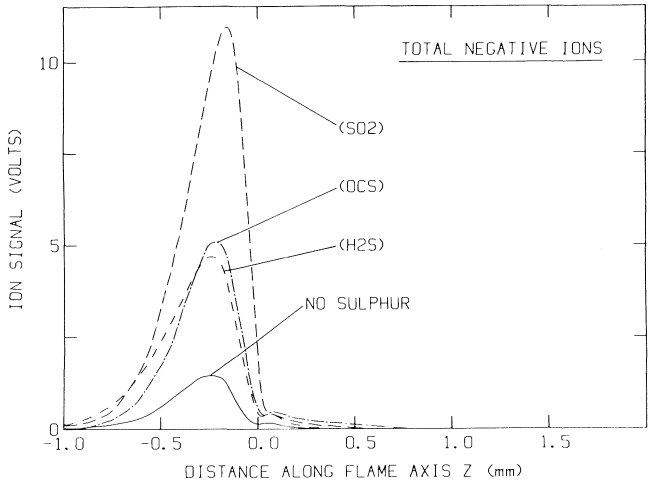

FIG. 2. Total negative ion profiles in the absence of sulphur (solid line) and with the flame doped with 0.2 mol% of H_2S, OCS, and SO_2. The reaction zone is located upstream of $z = 0$ (negative z).

At each point in the flame, the steady-state ion signal observed is governed mainly by the advection of ions (i.e. transport by the neutral flow) to and from that point. The *slope* on the total ion profile depends on the relative rates of ion production, essentially by reaction [2], and ion loss via recombination processes and ambipolar diffusion. Upstream in the reaction zone, the profiles with sulphur additives rise more steeply than the undoped flame profile. The steeper rise is indicative of either increased ion production or decreased loss. Decreased loss is the logical candidate for the following reason.

Figure 2 shows total negative ion profiles for the undoped flame and for the same three sulphur additives under the same flame conditions taken from an earlier study of sulphurous anions (4). The order of anion peak magnitudes is undoped $< H_2S < OCS < SO_2$. Since a flame is a quasi-neutral plasma, an increased negative ion concentration implies a decreased concentration of free electrons. Rate coefficients α for ion–ion recombination are, in general, about an order of magnitude

smaller than electron–ion recombination coefficients (10–12). Also, for a plasma at thermal equilibrium, it is easy to show that the ambipolar diffusion coefficient D_a for ion–ion diffusion can decrease by at most a factor of two compared with D_a for electron–ion diffusion (13). Thus, relatively fast electron–ion loss processes are replaced by slower ion–ion processes in the presence of sulphur additives, with a concomitant increase in the total positive ion signal. In the reaction zone, the rate of diffusion loss $-D_a d^2n/dz^2$ along the flame axis z involving the second derivative of the charge concentration n can be estimated from the upstream undoped profile given in Fig. 1. It amounts to 2×10^{13} ions cm^{-3} s^{-1} for $D_a = 2$ cm^2 s^{-1} at 1500 K and 1 atm (9, 14) and a peak ion concentration of 2×10^{10} cm^{-3} (15). Diffusion loss in a radial direction can be neglected because the radial concentration profile is flat near the flame axis in the reaction zone. The electron–ion recombination loss rate αn^2 has the same value for $\alpha = 2 \times 10^{-7}$ cm^3 s^{-1} (9, 14). When the negative ion concentration is increased by the addition of sulphur compounds, α decreases more than D_a and the change of the recombination rate is probably dominant. However, the approximate equivalence of diffusion loss and recombination loss in the reaction zone is a rather surprising result for a flame at atmospheric pressure. In contrast, near the peak of the positive ion profile "at pressures above about 30 mm Hg, ambipolar diffusion does not play an important role" (16). In any event, Fig. 1 shows that the upstream positive ion signal magnitudes follow the expected negative ion order given in Fig. 2: namely, undoped < H_2S < OCS < SO_2. It is not necessary to invoke a new chemi-ionization reaction for ion production involving sulphurous neutrals.

A bit further downstream in the reaction zone near $z = -0.2$ mm, the shoulders on the positive ion profiles in Fig. 1 are observed to occur near the negative ion profile peaks given in Fig. 2. At this point in the reaction zone, the flame temperature is rising rapidly and the negative ion signals decrease sharply due to thermal detachment processes which regenerate free electrons. The slower loss of cations by ion–ion processes is replaced by faster electron–ion processes; the slopes of the cation profiles decrease and bend over to form the shoulders observed in Fig. 1. The shoulders indicate an enhanced rate of ion loss by electron–ion processes, and the profiles for the doped flames "catch up" to the undoped flame profile. By the time the peak position of the total positive ion curves is reached all of the profile magnitudes are the same within experimental error. In general, the anion and the cation chemistry proceed independently in flames. This upstream phenomenon is a rare case where the anions and cations interact, albeit indirectly.

Downstream of the peak in Fig. 1, the profile magnitudes for the doped flames are slightly greater than the magnitude of the undoped flame profile. In this region, the negative ion concentration is too small to alter the cation signal significantly and a different explanation must be invoked. The outstanding difference between the undoped and the doped flames is that the latter all show a number of sulphurous cations whose profiles maximize just downstream of the total ion peak. The major sulphurous ion profiles are given in Fig. 3 for the flame doped with OCS, together with the H_3O^+ profiles for the doped and undoped flames. In decreasing order of signal magnitude these ions are assigned to 45 u (CHS^+), 47 u (CH_3S^+), 58 u ($C_2H_2S^+$), 69 u (C_3HS^+), and 59 u ($C_2H_3S^+$). That is, the large sulphurous cations at this point in the flame are protonated forms of CS, HCHS, CH_2CS, and C_3S except for ionized thioketene $C_2H_2S^+$. The latter is probably formed from protonated

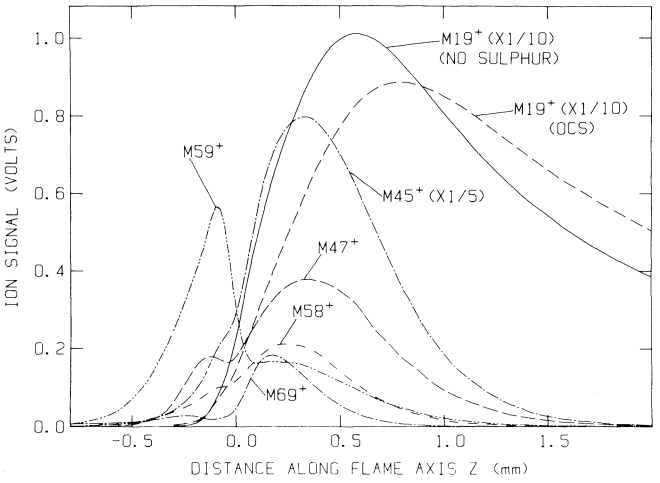

FIG. 3. Profiles of the five major sulphurous cations at 45 u (CHS^+), 47 u (CH_3S^+), 58 u ($C_2H_2S^+$), 59 u ($C_2H_3S^+$), and 69 u (C_3HS^+) for the flame doped with 0.2 mol% of OCS additive. The profile at 19 u (H_3O^+) is also shown with OCS present (dashed line) and absent (solid line). The reaction zone is located upstream of $z = 0$ (negative z).

thioketene $C_2H_3S^+$ by exothermic reactions such as (5)

[3] $C_2H_3S^+ + H\,(OH) \rightleftharpoons C_2H_2S^+ + H_2\,(H_2O)$

All of these sulphur species have high proton affinities (17). Their presence effectively *delays* the protonation of water to a region further downstream in the flame, as shown by the shift of the H_3O^+ profile in Fig. 3. The behaviour with H_2S and SO_2 additives is similar to that shown for OCS. The enhanced total ion signals downstream in Fig. 1 for the sulphur-doped flames indicate a lower rate of electron–ion recombination for the sulphurous cations. That is, a reduced ionic loss rate correlates with an enhanced total ion signal. The expected loss process for protonated cations is dissociative recombination of the type

[4] $XYH^+ + e^- \rightarrow XY + H$

involving the proton bond. It is tempting to hypothesize a correlation of a high proton affinity with a low electron–ion recombination coefficient, but available data are inadequate to substantiate such a claim.

Mass spectra

In our previous study with the OCS additive (5), it was shown that primary sulphur ions CH_xS^+ ($x = 1, 3, 5$) in the reaction zone undergo extensive ion–molecule reactions with CH_4/CH_3, C_2H_2, and OCS to form a considerable variety of secondary sulphurous cations. Just downstream of the reaction zone, the ion chemistry appears to be dominated by reactions of primary sulphur ions including H_xS^+ ($x = 0$–3) with C_2H_2 present as an intermediate. A few ions (H_xS^+, SO^+, S_2^+) persist throughout the burnt gas region in equilibrium with the natural flame ions HCO^+ and H_3O^+. As a general comment about the present study, much of the detailed ion chemistry observed with OCS appears to be operative with the H_2S and SO_2 additives as well. However, it was not the purpose of the present study to reiterate the sulphur ion chemistry in detail discussed previously for OCS (5). Rather, it was the intention to see if different additives provide distinctive sulphurous cation signals at various points in the flame which can be identified with a particular additive.

Mass spectra were scanned in the range 10–110 u in the undoped flame and in the flame doped separately with 0.2 mol% of H_2S, OCS, and SO_2. The spectra were measured at three

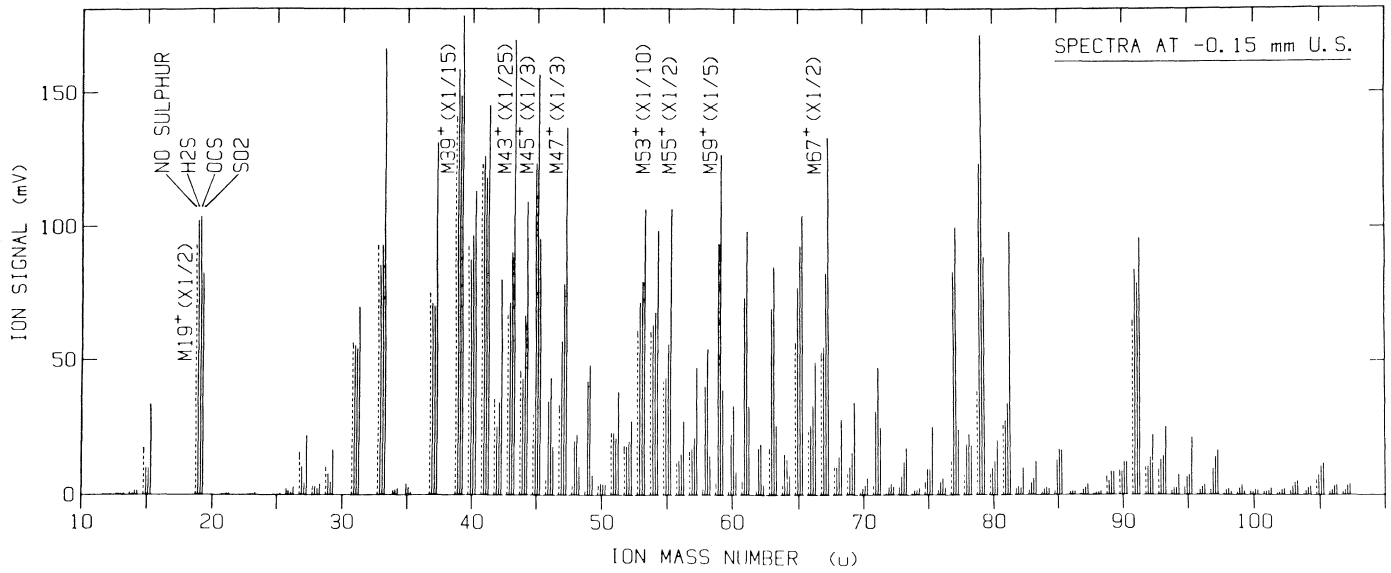

FIG. 4. Mass spectra measured at $z = -0.15$ mm upstream in the flame reaction zone. The spectra are presented in groups of four at each mass number corresponding (from left to right) to the undoped flame (dashed line) and the flame doped with 0.2 mol% of H_2S, OCS and SO_2 (solid lines).

fixed points on the flame axis: upstream in the reaction zone, near the peak of the total positive ion profile, and downstream in the burnt gas. Figure 4 refers to a point in the reaction zone at $z = -0.15$ mm upstream near the shoulder position on the total positive ion profiles. At each mass number, the spectra are presented in groups of four corresponding (from left to right) to the undoped flame (dashed) followed by the H_2S, OCS, and SO_2 additive signals. Essentially two types of behaviour are observed. Firstly, the presence of sulphurous cations is evident at those mass numbers where all three additives produce a substantial increase in signal magnitude compared with that of the undoped flame. Prominent examples occur at 45–49 u (CH_xS^+, x = 1–5), 58–61 u ($C_2H_xS^+$, x = 2–5), 71 u ($C_3H_3S^+$), 77–79 u ($CH_xS_2^+$, x = 1–3 and possibly also $(CH_3)_2SOH^+$ at 79 u), 85 u ($C_4H_5S^+$), and 97 u ($C_5H_5S^+$). Within many of these groups, the highest ion signal is observed with OCS, the next highest with H_2S, and the smallest with the SO_2 additive. As mentioned previously (5), OCS appears to be an effective donor of S atoms in ion–molecule reactions of the type

[5] $XY^+ + OCS \rightarrow XYS^+ + CO$

In general, most of the sulphurous cations involve the formation of a C—S bond. For a given ion, the relative signal magnitudes for the three additives correlate with the inverse order of their bond dissociation energies which is OC—S (71.6 kcal mol^{-1}) < HS—H (89.0) < OS—O (130.5). In the case of SO_2, both S—O bonds must ultimately be broken to form a $C_nH_xS^+$ ion but the initial formation of SO as a reactive intermediate is probably required for sulphurous cation formation.

The second type of behaviour is evident at mass numbers where the additives produce little change from the undoped flame signal (e.g. H_3O^+ at 19 u, $C_3H_3^+$ at 39 u, etc.). In a number of these cases, however, H_2S and OCS produce little change but SO_2 shows a substantial increase (e.g. protonated ions of formaldehyde CH_3O^+ at 31 u, methyl alcohol CH_5O^+ at 33 u, ketene $C_2H_3O^+$ at 43 u, and hydrated hydronium $H_5O_2^+$ at 37 u, etc.). The reason for the enhancement with SO_2 follows directly from the explanation already given for the upstream shoulders on the total ion profiles shown in Fig. 1. Negative ions are most readily formed with the electronegative SO_2 additive so that the loss rates of individual ions by electron–ion recombination and ambipolar diffusion are correspondingly decreased. In general, an increase in signal magnitude at a given mass number in the presence of a sulphur additive is not sufficient evidence for the production of a sulphurous cation, and caution must be exercised.

The prospects for the identification of a particular sulphur additive from the mass spectra are disappointing. This is exemplified in the present study involving the three additives H_2S, OCS, and SO_2 which occur early, intermediate, and late in the sulphur oxidation sequence. Distinguishable behaviour of different additives is most likely to be observable in the reaction zone before very much time for chemical reaction has elapsed. From these spectra it is evident that pyrolysis of the additive precedes the ion chemistry to a considerable degree such that all three additives show substantially the same sulphurous cation signals. Even the behaviour observed with SO_2 is not unique since any electronegative additive will show the same phenomenon. The high mobility of free electrons permits them to diffuse upstream against the flow to some degree where they attach to electronegative species to form negative ions; the process is aided by the lower upstream flame temperature.

The behaviour further downstream with the three additives is even more regular as equilibrium is approached. Figure 5 presents spectra at $z = 0.2$ mm, a point on the flame axis near the maximum of the total positive ion profiles. The same groups of four signals are given at each mass number for the updoped flame (dashed) and for the flame doped with H_2S, OCS, and SO_2. Series of sulphurous cations are evident at 34 and 35 u (H_2S^+ and H_3S^+, protonated HS and H_2S), 44–49 u (CH_xS^+, x = 0–5), 57–61 u ($C_2H_xS^+$, x = 1–5), 68–71 u ($C_3H_xS^+$, x = 0–3), 81–86 u ($C_4H_xS^+$, x = 1–6), and >92 u ($C_5H_xS^+$, $x > 0$) although the signal magnitudes are very small above 72 u.

Those ions which persist well downstream in the burnt gas are shown in Fig. 6 measured at $z = 1.5$ mm for the undoped and sulphur-doped flames. The usual signals are obtained for H_3O^+ (19 u) with its ^{18}O isotopic derivative (21 u) and first hydrate $H_5O_2^+$ (37 u). The presence of HCO^+ (29 u) is indicative of the

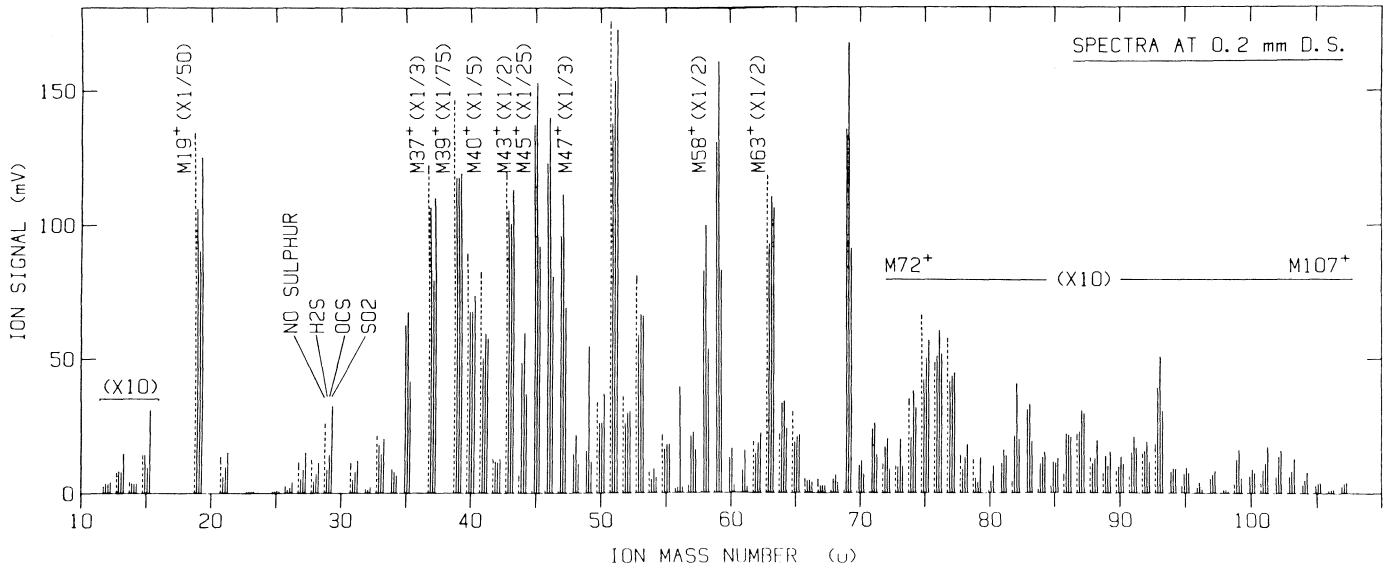

FIG. 5. Mass spectra measured at $z = 0.2$ mm, just downstream of the flame reaction zone. The spectra are presented in groups of four at each mass number corresponding (from left to right) to the undoped flame (dashed line) and the flame doped with 0.2 mol% of H_2S, OCS, and SO_2 (solid lines).

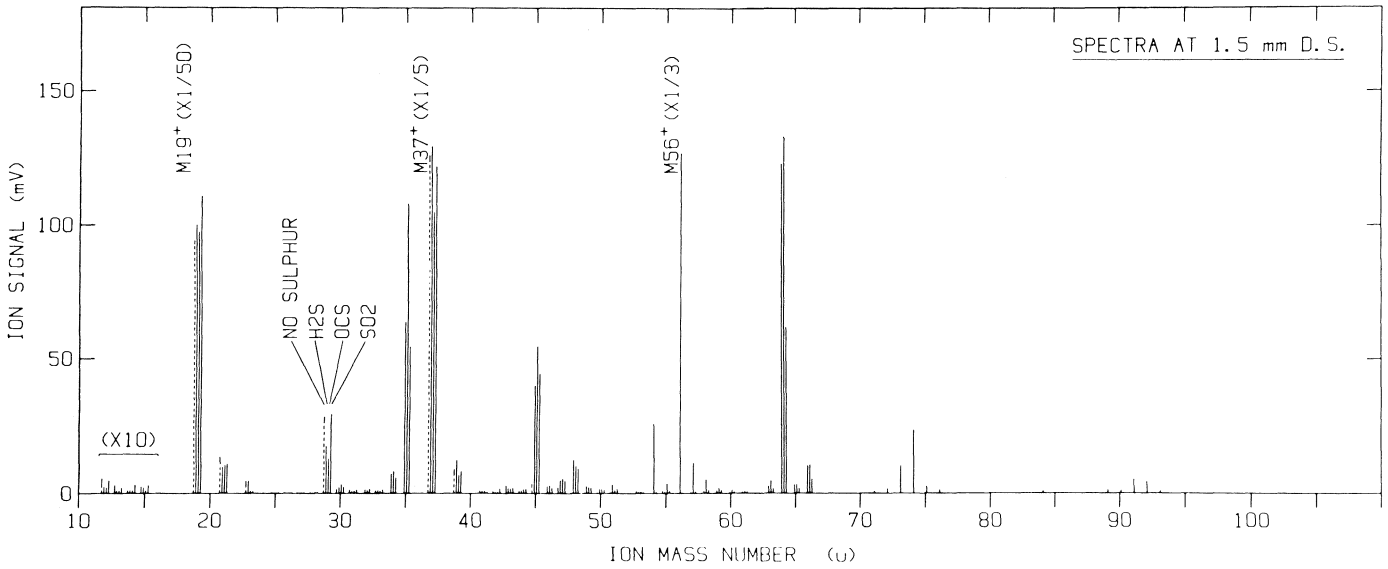

FIG. 6. Mass spectra measured at $z = 1.5$ mm downstream in the burnt gas. The spectra are presented in groups of four at each mass number corresponding (from left to right) to the undoped flame (dashed line) and the flame doped with 0.2 mol% of H_2S, OCS, and SO_2 (solid lines).

proton transfer equilibrium

[6] $HCO^+ + H_2O \rightleftharpoons H_3O^+ + CO$

where CO (mole fraction 0.30), not CO_2, is the major carbon-containing product in the burnt gas of this fuel-rich flame. The remnants of the very large $C_3H_3^+$ signal (39 u) are still observable, and a trace of Na^+ impurity (23 u) is observable too. The very curious groups of signals around 56, 74, and 91 u have been traced to $Fe(CO)_5$ present as an impurity in the lecture bottle of OCS. In addition to the major isotope ^{56}Fe (91.8% abundance), iron has the stable isotopes ^{54}Fe (5.8%), ^{57}Fe (2.1%), and ^{58}Fe (0.3%). The major isotope produces the ions Fe^+ (56 u), FeH^+ (57 u), $FeOH^+$ (possibly formed by protonation of FeO, 73 u), $Fe^+.H_2O$ (= protonated FeOH, 74 u), $FeOH^+.H_2O$ (= protonated $Fe(OH)_2$, 91 u), and $Fe^+.2H_2O$ (= the first hydrate of protonated FeOH, 92 u), with a hint of $FeCO^+$ (84 u). The same signals were reproduced by spraying an aqueous solution of $Fe(Cl)_3$ into the flame using an atomizer. A number of these iron ions, notably Fe^+ (56 u), are also evident in Fig. 5 for the OCS additive. The flame-ion chemistry of transition metals is the subject of ongoing research in our laboratory.

The persistent sulphurous cations in Fig. 6 include H_2S^+ (protonated HS, 34 u), H_3S^+ (protonated H_2S, 35 u) and the remnants of some of the CH_xS^+ ions ($x = 0$–5 at 44–49 u) whose profiles decrease to zero somewhat further downstream. Within this latter group, SO^+ (48 u) is evident for all three additives. Relatively large signals are obtained for S_2^+ (64 u) and its ^{34}S isotopic derivative (66 u, 4.2% natural abundance). The flame was doped separately with an equal concentration (0.2 mol%) of the three sulphur additives, although these sulphur compounds tend to "stick" in the tygon tubing connect-

ing the flow meter to the burner. Even allowing for some experimental variation in additive concentration, the sulphurous cation signals at a given mass number from the three additives are not constant. Evidently the sulphur species have not attained equilibrium 1.5 mm downstream of the reaction zone.

Conclusions

A fuel-rich, CH_4–O_2 flame was doped separately with 0.2 mol% of H_2S, OCS, and SO_2 chosen to be early, intermediate, and late in the oxidation sequence of fuel-sulphur. A number of conclusions can be drawn about the comparative behaviour of the three additives.

(*1*) A great variety of sulphurous cations is observed in the mass range 30–110 u, but the same cations are observed with all three additives.

(*2*) The total ionization profile is enhanced in the flame reaction zone when sulphur additives are present. The *magnitude* of the enhancement increases with increasing tendency of the additive to form negative ions.

(*3*) The *mechanism* of the enhancement involves a decreased rate of loss for positive ions when relatively fast cation–electron recombination and ambipolar diffusion are replaced by the corresponding cation–anion processes which have slower rates. The change of the recombination rate is probably the dominant effect.

(*4*) When a sulphur additive is present, the observation of an enhanced ion signal does not constitute *a priori* evidence for the formation of a sulphurous cation. The above mechanism is also applicable to non-sulphurous ions in the flame reaction zone, and caution must be exercised.

(*5*) This phenomenon is a rare case in flame-ion chemistry in which the positive ion chemistry and the negative ion chemistry interact, albeit indirectly.

(*6*) Just downstream of the reaction zone, the maximum total positive ion signal observed is the same whether or not a sulphur additive is present. This provides evidence that the sulphurous species are not involved in any new chemi-ionization reaction.

(*7*) Downstream throughout the burnt gas, the total ion signal is slightly enhanced when a sulphur additive is present. In general, sulphurous species have higher proton affinities than their oxygen analogues (17). The formation of a number of protonated sulphurous cations early in the burnt gas appears to delay the normal recombination of H_3O^+ ions to a region further downstream.

(*8*) Mass spectra of sulphurous cations scanned at fixed points in the flame are very similar for all three additives, even at an early stage in the flame reaction zone. Evidently appreciable pyrolysis of the sulphur additive precedes the ion chemistry.

(*9*) The mass spectra are not helpful in revealing the identity of the sulphur additive. The detailed sulphurous ion chemistry has already been discussed for the OCS additive (5). It is expected to be very similar for H_2S and SO_2, and also for other sulphur compounds present as fuel contaminants.

(*10*) For analytical or monitoring purposes, sulphurous cations are best observed just downstream of the flame reaction zone where the sulphur ion chemistry is fully developed. In order of increasing mass number or, coincidentally, decreasing signal size, the major ions occur at 45 u (CHS^+), 47 u (CH_3S^+), 58 u ($C_2H_2S^+$), 59 u ($C_2H_3S^+$), and 69 u (C_3HS^+). Most of the total sulphurous cation signal is encompassed by these five ionic species.

Acknowledgement

Support of this work by the Natural Sciences and Engineering Research Council of Canada under Grant No. A-1604 is acknowledged.

1. R. F. Sawyer. Ber. Bunsenges. Phys. Chem. **87**, 979 (1983).
2. E. C. Voldner, Y. Shah, and D. M. Whelpdale. Atm. Environ. **14**, 419 (1980).
3. J. M. Goodings, K. Elguindi, and D. K. Bohme. Can. J. Chem. **61**, 1703 (1983).
4. J. M. Goodings, D. K. Bohme, K. Elguindi, and A. Fox. Can. J. Chem. **64**, 689 (1986).
5. N. S. Karellas and J. M. Goodings. Can. J. Chem. **64**, 1733 (1986).
6. J. M. Goodings, D. K. Bohme, and C.-W. Ng. Combust. Flame, **36**, 27 (1979).
7. J. M. Goodings, D. K. Bohme, and C.-W. Ng. Combust. Flame, **36**, 45 (1979).
8. A. N. Hayhurst and N. R. Telford. Combust. Flame, **28**, 67 (1977).
9. H. F. Calcote. Eighth Symposium (International) on Combustion. Williams & Wilkins, Baltimore, MD. 1962. p. 184.
10. N. A. Burdett and A. N. Hayhurst. J. Chem. Soc. Faraday Trans. I, **74**, 63 (1978).
11. N. A. Burdett and A. N. Hayhurst. J. Chem. Soc. Faraday Trans. I, **72**, 245 (1976).
12. D. Smith and N. G. Adams. *In* Physics of ion–ion and electron–ion collisions. Vol. 83. *Edited by* F. Brouillard and J. W. McGowan. Plenum Publishing Corp., New York. 1983. p. 501.
13. E. W. McDaniel. Collision phenomena in ionized gases. John Wiley and Sons, Inc., New York, NY. 1964. p. 514.
14. S. C. Brown. Basic data of plasma physics, 1966. The M.I.T. Press, Cambridge, MA. 1967. pp. 128, 129 and 213–17.
15. J. M. Goodings and N. S. Karellas. Int. J. Mass Spectrom. Ion Processes, **62**, 199 (1984).
16. J. Lawton and F. J. Weinberg. Electrical aspects of combustion. Clarendon Press, Oxford. 1969. p. 222.
17. S. G. Lias, J. F. Liebman, and R. D. Levin. Evaluated gas phase basicities and proton affinities of molecules; heats of formation of protonated molecules. J. Phys. Chem. Ref. Data, **13**, 695 (1984).

Sulfoconjugation of dopamine. A critical examination of the reaction between dopamine and concentrated sulfuric acid

TIKAM JAIN,[1] CARL KAISER, DENNIS M. ACKERMAN,[2] DAVID L. LADD, KEI-LAI FONG, GERALD D. ROBERTS, DAVID B. STAIGER, LOUISA LAM DAVIS, AND R. LEE WEBB

Research and Development Division, Smith Kline & French Laboratories, Philadelphia, PA 19101, U.S.A.

AND

LLOYD M. JACKMAN

Department of Chemistry, The Pennsylvania State University, University Park, PA 16802, U.S.A.

Received March 3, 1986[3]

TIKAM JAIN, CARL KAISER, DENNIS M. ACKERMAN, DAVID L. LADD, KEI-LAI FONG, GERALD D. ROBERTS, DAVID B. STAIGER, LOUISA LAM DAVIS, R. LEE WEBB, and LLOYD M. JACKMAN. Can. J. Chem. **64**, 2418 (1986).

Dopamine, a physiologically important biogenic amine, is readily sulfoconjugated in vivo to give the 3- and 4-*O*-sulfates of pharmacologic importance. A major synthetic source of these esters has involved reaction of dopamine with sulfuric acid; however, the homogeneity of the products of this apparently straightforward reaction has been questioned. For this reason, in the present study this reaction was studied in considerable detail and our results establish that the concern about the authenticity and purity of dopamine-*O*-sulfates used for pharmacological studies is justified. In addition to the esters, difficultly separable dopamine-2, -5, and -6-sulfonic acids, plus several unidentified products, were obtained. A detailed account of the isolation and physicochemical characteristics of the identified products is presented. The dopamine-*O*-sulfates, whose structures have recently been established unequivocally by single crystal X-ray diffractometric analysis in this laboratory, were further characterized by means of mass (electron impact, field desorption, and fast atom bombardment) and ^{1}H and ^{13}C nuclear magnetic resonance spectroscopy. In addition, redox potentials for the isolated reaction products, as well as high performance liquid chromatography, thin-layer chromatography, and color reactions of the dopamine-*O*-sulfates, are reported. Thermolysis of the 3- and 4-*O*-sulfates yielded similar mixtures of products.

TIKAM JAIN, CARL KAISER, DENNIS M. ACKERMAN, DAVID L. LADD, KEI-LAI FONG, GERALD D. ROBERTS, DAVID B. STAIGER, LOUISA LAM DAVIS, R. LEE WEBB et LLOYD M. JACKMAN. Can. J. Chem. **64**, 2418 (1986).

La dopamine, une amine physiologiquement importante, est facilement sulfoconjuguée in vivo, donnant les sulfates-3-*O* et -4-*O* de dopamine qui ont une importance pharmacologique. Une source synthétique principale de ces esters est la réaction de la dopamine avec l'acide sulfurique; cependant, l'homogénéité de ces produits a été mise en doute. Pour cette raison, cette réaction a été étudiée en détail. En plus des esters, les acides sulfoniques de la dopamine et de plusieurs autres produits non identifiés ont été obtenus. Un compte rendu detaillé du procédé de séparation et des caractéristiques physico-chimiques des produits identifiés est présenté. Les sulfates-*O* de la dopamine, dont les structures ont été établiés sans ambiguïté au moyen de l'analyse par diffraction d'un monocristal par les rayons X, ont été caracterisés de plus au moyen de la spectrométrie de masse et de la résonance magnétique nucléaire ^{1}H et ^{13}C. Les résultats obtenus indiquent que ces doutes concernant l'authenticité et la pureté des sulfates de dopamine utilisés dans les études pharmacologiques étaient justifiés. En plus, les potentiels oxydo-réducteurs des produits isolés, la chromatographie en phase liquide, la chromatographie en couche mince et les analyses des couleurs de réaction des sulfates-*O* de dopamine sont aussi décrits dans ce rapport. La thermolyse des sulfates-3 et -4-*O* ont donnés des mélanges semblables.

Dopamine (**1**) is an important neurotransmitter and biosynthetic intermediate in the conversion of tyrosine to the biogenic amines norepinephrine (**2**) and epinephrine (**3**) (1). Both dopamine and its metabolites undergo extensive sulfoconjugation in humans and animals (2). High performance liquid chromatographic (hplc) analysis of human urine (3) indicates that the major metabolic products are the *O*-sulfates **4** and **5**. The possible physiological role of these conjugates has received considerable attention in recent years; however, their precise function is uncertain. They may simply represent metabolic products that are readily eliminated (4). Alternatively, they may act as protected forms of the biogenic amine, which serve as a reservoir that can be transported in the mammalian system to release dopamine via sulfatase catalyzed hydrolysis (5). Jenner and Rose (6) in 1973 first demonstrated the in vitro conversion of dopamine to its 4-*O*- (**4**) and 3-*O*-sulfates (**5**) by phenolsulfotransferase-containing rat liver preparations. These researchers also reported the preparation of **4** and **5** by treating dopamine with concentrated sulfuric acid (6). For the past ten years, dopamine-*O*-sulfates used for pharmacological studies have derived primarily from this procedure. Unfortunately, until recently the chemical characterization and homogeneity of these products had not been established unequivocally (7).

For this reason, as described in this paper, we undertook a critical examination of the reaction between dopamine and concentrated sulfuric acid under identical conditions (6), giving particular emphasis to spectral and physicochemical characterization of the products. Fractionation of the reaction products by Dowex (H^+ and $\bar{O}Ac$) column chromatography was accomplished as described in the literature (6). The course of fractionation was monitored by thin-layer chromatography (tlc) using ultraviolet light (uv), ninhydrin, and Gibbs' and Pauly's reagents for visualization. More importantly, unlike the literature procedure, selected chromatographic fractions were examined by FT (Fourier transform) ^{1}H nmr spectroscopy. This eventually led to the isolation of hitherto unknown nuclear sulfonated products together with the dopamine-*O*-sulfates; of special interest was the isolation of dopamine-2-sulfonic acid.

The initial fractions of the column chromatography (see Experimental) yielded two crystalline products. On the basis

[1]Author to whom correspondence may be addressed.

[2]Present address: Ayerst Laboratories Research, Inc., Princeton, NJ 08540-0340, U.S.A.

[3]Revision received August 22, 1986.

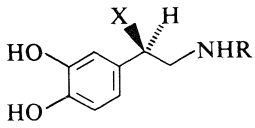

1 R = X = H
2 R = H; X = OH
3 R = CH_3; X = OH

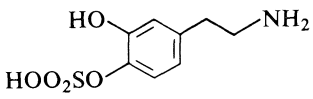

4

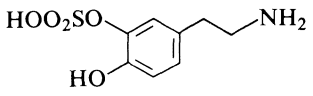

5

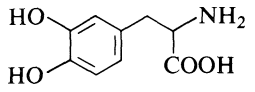

6

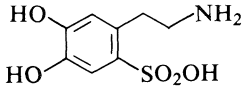

7

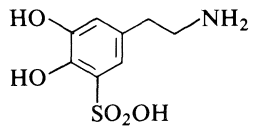

8

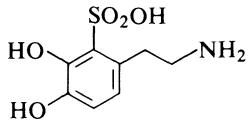

9

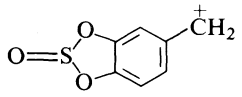

10

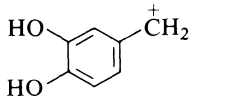

11

of FT ^{1}H nmr spectroscopy these substances were identified as dopamine-6- and -5-sulfonic acids (**7**, **8**), respectively.[4] Perhaps significantly, these products, which were not described in the original report (6), have tlc mobility profiles that are remarkably similar to those of dopamine-3-*O*-sulfate (**5**) and its 4-isomer (**4**). For this reason, ^{1}H nmr examination of the reaction product is a particularly important determinant of homogeneity.

Further elution of the Dowex (H^+) column with water yielded dopamine-4-*O*-sulfate, mp 265–267°C, whose ^{1}H nmr spectrum was consistent with the structure. Compared to dopamine, the aromatic proton on C-5 (δ 7.06, *ortho* coupled, J = 8.11 Hz) was deshielded by the 4-sulfate ester (Δδ 0.38 ppm). The mother liquors of the above crystalline crops were pooled and chromatographed over a Dowex ($\bar{O}Ac$) column. Elution of the column with 0.05 *M* HOAc yielded a further crystalline material. This was identified as dopamine-2-sulfonic acid (**9**) by ^{1}H and ^{13}C nmr spectroscopy.

Interestingly, **9** is slightly more mobile than dopamine and the tlc spot turns characteristically pink upon standing in air. Further elution of the column with 0.15 *M* HOAc yielded fractions that upon crystallization from water gave additional dopamine-4-*O*-sulfate, mp 257–258°C. The mother liquors of the crystalline crops were pooled and chromatographed over a Dowex ($\bar{O}Ac$) column to give dopamine-3-*O*-sulfate, mp 268–270°C (dec.).[5] Again compared to dopamine, the proton on C-2 (δ 7.07, *meta* coupled, J = 1.5 Hz) was deshielded by the 3-sulfate ester (Δδ 0.44 ppm).

Some of the physicochemical properties of **4** and **5**, whose structures have been unequivocally confirmed by single-crystal X-ray diffractometric analysis in this laboratory (12, 14), were also examined. The ^{13}C nmr spectra of dopamine sulfonic acids (Table 1) are diagnostic. Interestingly, the sulfonic acid group had a greater deshielding effect at C-6 (Δδ 21.74 ppm) than at C-2 (Δδ 12.74 ppm) and at C-5 (Δδ 11.79 ppm). Relatively, the sulfonic acid group in the form of the *O*-ester (Table 2) has very little effect on the carbon shift, e.g. Δδ 3.17 ppm for **4** and 5.56 ppm for **5**.

In aqueous solution dopamine-3-*O*-sulfate (**5**) failed to undergo appreciable hydrolysis upon standing at room temperature for eight hours. Conversely, under similar conditions or upon storage of an aqueous solution at 0–5°C for several days, **4** was partially hydrolyzed to dopamine in tlc detectable amounts. However, identical hydrolytic behavior of the two *O*-sulfates was observed during our cyclic voltametric measurements in phosphate buffer at pH 7.4, where a second peak at 0.24 and 0.28 volts appeared to originate from hydrolysis of dopamine-4-*O*- and -3-*O*-sulfates, respectively. The cyclic voltammograms of the sulfonic acids (Table 3) showed a characteristic oxidation at 0.40 V against a standard calomel electrode. This value is considerably lower than those observed for the *O*-methyl or *O*-sulfate derivatives. Thus this procedure offers a means to distinguish the sulfonic acid derivatives from the *O*-sulfates at relatively low concentrations. Thermolysis of dopamine-*O*-sulfates, like treatment of **1** with concentrated sulfuric acid, gave an array of products of which the dopamine sulfonic acids are the major identifiable products. Perhaps significantly, the overall ratios of identifiable products from both reactions are almost similar. This suggests that the dopamine sulfonic acids (**7**, **8**, and **9**) may be thermolytic products originating from dopamine-*O*-sulfates that may be the primary reaction products deriving from sulfation of **1**.

The mass spectra of dopamine-*O*-sulfates and sulfonic acids have been studied in some detail using electron impact, field desorption (FD), and fast atom bombardment (FAB) techniques. The FAB and FD mass spectra of dopamine-3-*O*-sulfate display relatively more intense peaks at m/e 153 than do those of dopamine-4-*O*-sulfate. This fragment, resulting from the expulsion of SO_3, seems a characteristic feature of dopamine-3-*O*-sulfate. The peak at m/e 169 represents the benzylic ion fragment containing a cyclic sulfate unit, i.e., **10**, which may also exist as the corresponding tropylium ion. The expulsion of SO_3 as well as of the $—CH_2NH_2$ unit of the ethylamine side chain to yield the benzylic ion fragment **11** seems a common feature among both dopamine sulfonic acids and dopamine-*O*-sulfates.

In summary, in our study possible contaminants in dopamine-*O*-sulfates prepared by the sulfation method have been identi-

[4]After our isolation of **7** and **8**, Osikowska *et al.* (8) employed preparative hplc to isolate a product, mp 272–275°C (dec.) from the sulfation of dopamine. This was identified as dopamine-6-sulfonic acid on the basis of ^{1}H nmr spectroscopy. The published ^{1}H nmr spectrum corresponds to that of our crystalline dopamine-6-sulfonic acid (**7**), mp 215–220°C; however, the reported mp corresponds more closely to that of our crystalline dopamine-5-sulfonic acid (**8**), mp 279–283°C. This inconsistency is unexplained.

[5]Melting points reported for both **4** and **5** vary considerably. Thus mp's of 257–259°C (9), 264–265°C (10), 278–280°C (11), 265–267°C (12), and 273–274°C (13) have been reported for **4** and mp's of 275–277°C (11), 254–256°C (10), and >250°C (9) are given for **5**. We have isolated various analytically pure crystalline crops with different degrees of hydration and melting point range. All these preparations displayed identical high-field nmr spectral features. Thus, for an unambiguous identification of dopamine-*O*-sulfate, one must rely on the proton nmr, not on the melting point, of the crystalline material.

TABLE 1. Chemical shifts (ppm) for sp^2 carbons in ^{13}C nmr spectra of dopamine sulfonic acids

Compound	Chemical shift (ppm) at indicated sp^2 carbon					
	C-1	C-2	C-3	C-4	C-5	C-6
Dopamine	126.0	116.3(d)	146.5	143.0	118.2(d)	115.4(d)
Dopamine-2-sulfonic acid	125.9	129.0(s)	144.9	143.1	120.6(d)	116.1(d)
Dopamine-5-sulfonic acid	129.2	119.1(d)	140.5	146.5	130.0(s)	118.9(d)
Dopamine-6-sulfonic acid	126.0	115.4(d)	146.4	142.9	118.2(d)	137.2(s)

TABLE 2. ^{13}C Nuclear magnetic resonance shifts with coupling constants of dopamine-*O*-sulfates

	Dopamine-3-*O*-sulfate (**5**)				Dopamine-4-*O*-sulfate (**4**)			
		H-2	H-5	H-6		H-2	H-5	H-6
	δ ^1H:	7.065	6.827	6.776	δ ^1H:	6.740	7.063	6.639
Carbon position	δ ^{13}C	J_{C-H2}	J_{C-H5}	J_{C-H6}	δ ^{13}C	J_{C-H2}	J_{C-H5}	J_{C-H6}
1	128.0	—	7.4	—	134.2	[a]	8.5	[a]
2	123.2	158.5	—	6.0	117.7[b]	156.3	0.0	6.4
3	140.9	4.4	6.7	—	149.3	2.0	0.0	6.9
4	148.0	4.4[c]	—	6.7[c]	139.8	6.9	4.2	10.1
5	117.3	—	159.3	—	123.3	0.0	159.7	1.7
6	125.0	8.2	8.2	161.5	119.8	8.1	0.0	158.2

[a]Unresolved splitting.
[b]Exhibits a partially resolved splitting of ca. 3.0 Hz from the hydroxylic proton.
[c]These two values can be interchanged.

TABLE 3. Redox potentials of catechols

	Oxidation (V)	Reduction (V)
Catechol	0.30	0.03
Dopamine (**1**)	0.30	0.06
Dopamine-6-sulfonic acid (**7**)	0.40	0.05
Dopamine-5-sulfonic acid (**8**)	0.40	0.05
Dopamine-4-*O*-sulfate (**4**)	0.24	0.03
	0.73	
Dopamine-3-*O*-sulfate (**5**)	0.28	—
	0.64	
4-*O*-Methyldopamine	0.60	—
3-*O*-Methyldopamine	0.54	—

fied and characterized. Thus, caution should be exercised in evaluating reported pharmacological data for dopamine-3- and -4-*O*-sulfates prepared by treatment of dopamine with concentrated sulfuric acid. This method is impracticable for the synthesis of dopamine-3-*O*-sulfate, unlike that of dopamine-4-*O*-sulfate, since it involves a tedious isolation procedure coupled with a low yield. The recently reported synthetic procedure (9) is clearly preferable for the preparation of the former.

Experimental

Melting points were obtained using a Thomas–Hoover Uni-Melt® capillary melting point apparatus and are uncorrected. Electron impact, field desorption (FD), and fast atom bombardment (FAB) mass spectra were recorded on Varian Mat CH-5 DF and VG ZAB 1-F mass spectrometers, respectively. FAB mass spectra were run in glycerol DMF matrix. The ^1H and ^{13}C nmr spectra were obtained in DMSO-d_6 with a Bruker IWP 200 spectrometer; for the sake of brevity and relevance only the aromatic region is reported. The data in Table 2 were generated using a Bruker WP 360 spectrometer. Unless otherwise specified, hplc was performed on a Waters HPLC using Partisil 5-ODS-3 RAC II columns (5.0 μm, 10 cm, id 4.60 mm) with mobile phase (0.025 *M* $ClCH_2COOH$ and 0.001 *M* EDTA adjusted to pH 2.8 by NaOH plus 0.004 *M* *n*-octylamine) at 0.7 mL/min with a Kratos SF 769 detector at 280 nm. The tlc plates (Analtech 20 × 20 cm, prescored) were developed in a *n*-BuOH–HOAc–H_2O (4:1:5, upper phase) system. The tlc spots were visualized by uv light, aerial oxidation, ninhydrin, and Gibbs' and Pauly's reagents. The tlc plates sprayed with Gibbs' reagent (1% ethanolic solution of 2,6-dichloroquinone-*p*-benzoquinone-4-chlorimine) were exposed to ammonia vapors. Freshly dissolved Pauly's reagent (diazotized sulfanilic acid, 1%, aqueous Na_2CO_3 solution, 10%) was used for spraying purposes.

Cyclic voltammetry experiments were performed using EG&G Princeton Applied Research equipment including a Model 175 universal programmer and Model 173/179 potentiostat/digital coulometer. A three-electrode system consisting of a glassy carbon working electrode, a platinum wire auxiliary electrode, and a saturated calomel electrode was used for all voltammetric studies. The cyclic voltammograms were recorded on a Houston Instrument Model 2000 X–Y recorder with a scan rate of 200 mV/s. All samples were prepared at a 5 m*M* concentration using 0.1 *M* phosphate buffer at pH 7.4 as the supporting electrolyte.

Reaction of dopamine and concentrated H_2SO_4

Dopamine hydrochloride (4.0 g; 21 mmol), after being dried at 100°C over P_2O_5 *in vacuo* for 6 days, was added with vigorous stirring in small portions to 11 mL of concentrated H_2SO_4 (206 mmol; d = 1.84) maintained at 0°C throughout the experiment. The addition took about 53 mins. Stirring was continued for an additional 7 min. The reaction mixture was then quickly poured with vigorous stirring into 100 mL of water – crushed ice mixture and the resulting solution was immediately applied to a column (30 × 5 cm) of Dowex 50W (X8, 200–400 mesh, H^+ form, 450 g).

Fractionation and isolation of products

The column was eluted with water and fractions were collected at the rate of 20 mL/10 min (total fractions = 150); each fraction was evaluated by tlc and color reactions of the spot, pooled according to the R_f values and color reactions. Fractions 1–20 contained highly polar and uv positive material and the solutions were highly acidic. These fractions were not pursued. The tail fractions (101–150) upon lyophilization gave a trace of white solid material, which was combined with the mother liquors for Dowex (ŌAc) column chromatography (*vide infra*).

*Dopamine-6-sulfonic acid (**7**)*

Fractions 21–35 upon standing at 0–5°C gave crystalline material as stout rectangular crystals of dopamine-6-sulfonic acid (500 mg; overall yield: 8.2%): mp 215–220°C (dec.); tlc: R_f 0.40, spot turns brown upon standing in air; hplc: retention time 2.76 min; ^{1}H nmr δ: 7.34, 6.62 (s, 1H each); ms (70 eV) *m/e* (% relative abundance (% RA)): molecular ion at 233 absent, 153 (10; $M^+ - SO_3$), 124 (71, **11** + H), 123 (26, **11**); FD *m/e* (% RA): 233 (60, M^+), 123 and 153 absent; FAB (+ mode) *m/e* (% RA): 234 (44, *M* + 1), 153, 123, 124; (− mode): 232 (33, *M* − 1), 152, 121. *Anal.* calcd. for $C_8H_{11}NO_5S \cdot 1\ H_2O$: C 38.24, H 5.18, N 5.58, S 12.75; found: C 38.05, H 5.06, N 5.52, S 12.26. An aqueous solution on standing at room temperature develops coloration.

*Dopamine-5-sulfonic acid (**8**)*

The pool containing fractions 36–60 was lyophilized and crystallized from water to give dopamine-5-sulfonic acid (200 mg; overall yield: 3.3%); mp 279–283°C (dec.); tlc: R_f 0.29, spot turns brown in air; hplc: retention time 3.87 min; ^{1}H nmr δ: 6.84 (d, 1H, *J* = 2 Hz), 6.63 (d, 1H, *J* = 2 Hz); ms (70 eV) *m/e* (% RA): no molecular ion at 233, 153 (29, $M^+ - SO_3$), 124 (100, **11** + H), 123 (59, **11**); FD *m/e* (% RA): 234 (>90, *M* + 1), 123 and 153 absent; FAB (+ mode) *m/e* (% RA): 234 (78, *M* + 1), 153, 123, dimeric fragments: 466, 467; (− mode) *m/e* (% RA): 232 (100, *M* − 1), 153, 123. *Anal.* calcd. for $C_8H_{11}NO_5S \cdot H_2O$: C 38.24, H 5.18, N 5.58, S 12.75; found: C 38.37, H 5.32, N 5.49, S 12.56. A clear aqueous solution upon standing at room temperature decomposes to give a colored solution.

*Dopamine-4-*O*-sulfate (**4**)*

Lyophilization of fractions 61–100 yielded a white powder that after three crystallizations from water gave dopamine-4-*O*-sulfate (300 mg; overall yield: 4.9%); mp 265–267°C; hplc: retention time 8.04 min; ^{1}H nmr δ: 7.06 (d, H-5, *J* = 8.1 Hz), 6.74 (d, H-2, *J* = 2.1 Hz), 6.63 (dd, H-6, *J* = 2.1 and 8.1 Hz); ^{13}C nmr: see Table 2; ms (70 eV) *m/e* (% RA): no molecular ion at 233, 169 (3, 10), 153 (2, $M^+ - SO_3$), 124 (19, **11** + H), 123 (8, **11**); FD *m/e* (% RA): 234 (27, *M* + 1), 154 (5), 153 (2, $M^+ - SO_3$), 124 (1), 123 (absent); FAB (+ mode) *m/e* (% RA): 234 (3, *M* + 1), 153 (1), 124 (0.3), 123 (0.7); (− mode): 232 (11, *M* − 1), 151 (6), 122, 121 (absent). *Anal.* calcd. for $C_8H_{11}NO_5S \cdot 0.5\ H_2O$: C 39.67, H 4.96, N 5.79, S 13.22; found: C 39.40, H 4.80, N 5.82, S 13.25.

*Dowex 1 (X8, ŌAc) column chromatography: dopamine-2-sulfonic acid (**9**)*

The mother liquors of the above crystalline crops containing some dopamine were combined and applied on a column of Dowex 1 (X8, 200–400 mesh, ŌAc form, 500 g) and eluted with water (2 L). Elution of the column with 0.05 *M* HOAc (200 mL) followed by lyophilization and crystallization from water yielded dopamine-2-sulfonic acid (**9**, 150 mg; overall yield: 3.1%); mp 260°C; tlc: R_f 0.58, spot turns pink in air; hplc: retention time 4.68 min: FT ^{1}H nmr δ: 6.57 (AB quartet, 2H, *J* = 8.0 Hz); ms (70 eV) *m/e* (% RA): molecular ion at 233 absent, 153 ($M^+ - SO_3$), 154 (M + 1 − SO_3), 123 (31, 11), 124 (87, **11** + H); FD *m/e* (% RA): 234 (*M* + 1), 233 (100, M^+), 154, 153; FAB *m/e* (% RA) (positive mode): 234 (85, *M* + 1), dimeric fragments: 466, 467. *Anal.* calcd. for $C_8H_{11}NO_5S \cdot 0.5\ H_2O$: C 39.67, H 4.96, N 5.79; found: C 39.82, H 4.84, N 5.34.

*Dopamine-3-*O*-sulfate (**5**)*

Elution of the above column with 0.15 *M* HOAc (500 mL) and 0.5 *M* HOAc (200 mL) gave 20-mL fractions, which were evaluated by tlc and Pauly's reagent. Fractions showing yellowish-pink color were pooled, lyophilized, and crystallized from water. The crystalline crops (mp 257–258°C) were identified as dopamine-4-*O*-sulfate by 360-MHz ^{1}H nmr spectroscopy. The mother liquors of the crystalline crop were chromatographed over Dowex 1 (X8, 200–400 mesh, ŌAc form, 100 mL) and eluted with 0.15 *M* HOAc (200 mL) and 0.5 *M* HOAc (75 mL). Fractions showing pink reactions with Pauly's reagent were pooled, lyophilized, and crystallized from water to give dopamine-3-*O*-sulfate (8 mg; overall yield: 0.13%); mp 268–270°C (dec.); hplc: retention time 7.53 min; 360-MHz ^{1}H nmr δ: 7.07 (d, 1H, *J* = 1.5 Hz), 6.86–6.76 (m, 2H); ^{13}C nmr: see Table 2; ms (70 eV) *m/e* (% RA): no molecular ion at 233, 169 (1, 10), 153 (50, $M^+ - SO_3$), 124 (100), 123 (74, **11**); FD *m/e* (% RA): 234 (12, *M* + 1), 154 (59), 153 (6), 124 (0.24), 123 (1); FAB (+ mode) *m/e* (% RA): 234 (34, *M* + 1), 154 (15), 153 (8), 124 (4), 123 (1.1); (− mode): 232 (100, *M* − 1), 153 (0.8), 152 (8), 123 (1), 122 (1). *Anal.* calcd. for $C_8H_{11}NO_5S$: C 41.20, H 4.75, N 6.01; found: C 40.98, H 4.76, N 5.96.

An aqueous solution of dopamine-3-*O*-sulfate standing at room temperature for 8 h did not show any decomposition to dopamine (by hplc and tlc), whereas dopamine-4-*O*-sulfate displayed some decomposition to dopamine (by tlc).

Redox potentials

Cyclic voltammetric measurements of dopamine, dopamine-*O*-methyl ethers, and dopamine sulfonation products were carried out in 0.1 *M* phosphate buffer at pH 7.4 using a glassy carbon paste electrode. The oxidation and reduction peaks are given in Table 3 with reference to a saturated calomel electrode.

*Thin-layer chromatography and color reactions of dopamine-*O*-sulfates*

Identical concentrations of the solutions of dopamine-*O*-sulfates were spotted on tlc plates (20 × 20 cm) and the plates were run in the same tank containing the upper phase of *n*-butanol – acetic acid and water (4:1:5). The plates were air dired and sprayed under identical conditions using dopamine (**1**) as a control. The results are given below:

	DA (**1**)	DA-4-*O*-sulfate (**4**)	DA-3-*O*-sulfate (**5**)
R_f	0.43	0.32	0.40
Aerial oxidation on plate	dark	light yellow	bright yellow
Ultraviolet light	++	+	++
Pauly's reagent	dark	yellow	pink
Ninhydrin	yellowish	brown	purplish brown
Gibbs' reagent	dark	blue	brown

Mixed spot analysis with authentic samples of dopamine-*O*-sulfates yielded identical results.

*Thermolysis of dopamine-*O*-sulfates*

A few crystals of dopamine-3-*O*-sulfate (mp 268–270°C) and dopamine-4-*O*-sulfate (mp 257–258°C) were allowed to melt in capillary tubes for less than a second. The capillary tubes containing the melt were immediately chilled and extracted with water. The tlc analysis of the extract revealed the presence of three sulfonic acids, proven by mixed spot analysis. The hplc analysis of the thermolysate of dopamine-3-*O*-sulfate revealed the presence of dopamine (20%), dopamine-6-sulfonic acid (21%), dopamine-5-sulfonic acid (38%), dopamine-2-sulfonic acid (7%), dopamine-3-*O*-sulfate (0.3%), dopamine-4-*O*-sulfate (7%), plus unidentified peaks with retention times 7.92 min (7%), 12.24 min (0.5%), and 18.93 min (2%). The hplc analysis of the thermolysate from dopamine-4-*O*-sulfate showed the presence of dopamine (19%), dopamine-6-sulfonic acid (19%), dopamine-5-sulfonic acid (20%), dopamine-2-sulfonic acid (3%), dopamine-3-*O*-sulfate (2%), and dopamine-4-*O*-sulfate (6%).

High performance liquid chromatographic analysis of dopamine-O-sulfates

The hplc analysis of **4** and **5** was demonstrated by using a sample of "dopamine-3-*O*-sulfate" prepared by the method of Jenner and Rose (6). Analysis of this sample using solvents A and B[6] in the ratio of 8:92 yielded a major peak with retention time of 5.79 min and a minor peak with retention time of 5.56 min, corresponding to dopamine-3-*O*- and -4-*O*-sulfates, respectively. The areas of two peaks were in the ratio of 6:1.

Acknowledgments

We are grateful to Drs. A. A. Manian and J. Stephen Kennedy of the NIMH for authentic synthetic samples of dopamine-*O*-sulfates and the samples prepared by the method of Jenner and Rose (6). The FD and 70-eV mass spectra reported herein were recorded by Walter Johnson.

1. C. KAISER and T. JAIN. *In* Highlights in receptor chemistry. *Edited by* C. Melchiorre and M. Giannella. Elsevier Biomedical Press, Amsterdam. 1984. p. 29.
2. J. A. ROTH and A. J. RIVETT. Biochem. Pharmacol. **31**, 3017 (1982).
3. M. A. ELCHISAK and J. H. CARLSON. Life Sci. **30**, 2325 (1982).
4. O. KUCHEL, T. N. BUU, and T. UNGER. *In* Advances in biosciences. *Edited by* J. L. Imbs and J. Schwartz. Pergamon, Oxford. 1979. p. 15.
5. A. A. BOVE, J. D. DEWEY, and G. M. TYEE. J. Lab. Clin. Med. **104**, 77 (1984).
6. W. N. JENNER and F. A. ROSE. Biochem. J. **135**, 109 (1973).
7. J. R. IDLE, B. A. OSIKOWSKA, P. S. SEVER, and F. J. SWINBOURNE. Proceedings of the British Pharmacological Society, 837P (1981).
8. B. A. OSIKOWSKA, J. R. IDLE, F. J. SWINBOURNE, and P. S. SEVER. Biochem. Pharmacol. **31**, 2279 (1982).
9. S. L. HARBESON, D. J. KERKMAN, and J. F. DEBERNARDIS. Org. Prep. Proced. Int. **15**, 143 (1983).
10. R. P. BODNARYK and P. C. J. BRUNET. Biochem. J. **138**, 463 (1974).
11. B. HEGEDÜS. Helv. Chem. Acta, **46**, 2604 (1963).
12. D. M. ACKERMAN, J. P. HIEBLE, H. M. SARAU, and T. JAIN. Arch. Int. Pharmacodyn. Ther. **267**, 241 (1984).
13. S. K. ARORA, B. S. CHO, and D. L. VENTON. Synthesis, 884 (1984).
14. D. S. EGGLESTON, D. F. CHODOSH, T. JAIN, C. KAISER, and D. M. ACKERMAN. Acta Crystallogr. Sect. C: Cryst. Struct. Commun. **41**, 76 (1985).

[6]Solvent A: acetonitrile; solvent B: 1 L of water containing sodium acetate (22 g), citric acid (21 g), sodium hydroxide (9.8 g), EDTA (0.67 g), heptanesulfonic acid (2.06 g), HOAc (15 mL); hplc columns: Whatman Partisil 5 ODS-3 (4.6 × 250 mm).

Mobility of thermal cations in low density alkane gases[1]

NORMAN GEE, M. ANTONIO FLORIANO, AND GORDON R. FREEMAN
Chemistry Department, University of Alberta, Edmonton, Alta., Canada T6G 2G2

Received June 27, 1986

NORMAN GEE, M. ANTONIO FLORIANO, and GORDON R. FREEMAN. Can. J. Chem. **64**, 2423 (1986).

Mobilities μ of thermal cations were measured in gases of six linear *n*-alkanes, ethane to *n*-decane, and in *i*-butane and *neo*-pentane, as functions of density n and temperature T. The low density limit was reached where $n\mu$ and the temperature coefficient at constant n, $(dn\mu/dT)_n$, were constant. At all temperatures the average momentum transfer cross sections σ_{ave} equalled (1.2 ± 0.4) times the cross sections expected from simple polarization. At high temperature σ_{ave} might be approaching a hard sphere limit.

NORMAN GEE, M. ANTONIO FLORIANO et GORDON R. FREEMAN. Can. J. Chem. **64**, 2423 (1986).

On a mesuré les mobilités, μ, des cations thermiques dans des gaz de six *n*-alcanes linéaires, de l'éthane au *n*-décane, ainsi que dans l'isobutane et le néo-pentane; on a mesuré ces mobilités en fonction de la densité, n, ainsi que de la température, T. On atteint la limite minimale de la densité lorsque $n\mu$ ainsi que le coefficient de température à valeur constante de n, $(dn\mu/dT)_n$, sont constants. A toutes les températures, les sections droites moyennes des moments de transfert, σ_{ave}, sont égales à 1,2 ± 0,4 fois les valeurs auquelles on pourrait s'attendre pour les sections droites en se basant sur une polarisation simple. A des températures élevées, il est possible que les valeurs de σ_{ave} approchent une limite de sphère dure.

[Traduit par la revue]

Introduction

We have previously reported mobility values μ for radiolytically generated cations in simple molecular fluids (1) and hydrocarbons (1–3) over wide ranges of conditions, from the normal liquid where μ is determined by the fluid viscosity η to moderately dense gases where the number density n determines μ. The transition between viscosity and density control occurred at $0.6 \lesssim \eta/\eta_c \lesssim 3$ (subscript c denotes critical fluid), corresponding to $0.5 \lesssim n/n_c \lesssim 1.9$. This transition zone is the dense gas – low density liquid region. Clustering effects were important, especially in the saturated gas. In hydrocarbon gases, clustering persisted down to the lowest n used and appeared as a density dependence of $n\mu$ and of $(dn\mu/dT)_n$, the temperature coefficient at constant n. In ethene and cyclopropane gases density independence of $n\mu$ and of $(dn\mu/dT)_n$ was reached at $n < 3 \times 10^{25}$ molecules/m^3 (4). The present work extends measurements of μ in alkanes to $n < 3 \times 10^{25}$.

Experimental

The suppliers of the hydrocarbons, the purification techniques, a diagram of a conductance cell, a listing of the voltage supplies, a description of temperature control and sources of density values are given in ref. 5. A sample current against time signal trace, a description of the signal amplifier and data collection system, and the method of checking that results at high temperature are free from effects of thermal decomposition of the hydrocarbons or outgassing of the cell are given in ref. 4.

To obtain the mobility we ionized the sample in the conductance cell with a 100 ns pulse of X rays from a van de Graaff accelerator. The pulse delivers $\sim 6 \times 10^{10}$ eV/g to the sample. The ion drift distance l in the conductance cells was measured directly with an inside micrometer to within ±0.001 cm; values for the five cells used ranged from 0.465 to 1.058 cm. The drift time t_d was measured from a current–time trace (see Fig. 1 of ref. 4), and $\mu = l^2/Vt_d$.

Results and discussion

A. Field independence

The mobility was measured typically at field strengths $0.4 \leq (E/n)(\text{Td}) \leq 5$, where Td = 10^{-21} V m^2/molecule; occasionally fields as low as 0.13 Td and as high as 50 Td were used. No field dependence was found. At each (n,T) more than 10 measurements (half using positive and half with negative applied voltage) were averaged to give μ with average deviation of 1–3%.

The density normalized mobilities $n\mu$ in the saturated vapors are in Fig. 1. The nonsaturated gases are used to study the effect of temperature on $n\mu$. The effect is more clearly shown by normalizing the different density sets to an average $n\mu$ at a given T (4). The present results (Fig. 2) were normalized at 294 ± 1 K to (10^{21} molecules/m V s): C_2H_6, 2.82; C_3H_8, 1.86; *n*-C_4H_{10}, 1.32; *i*-C_4H_{10}, 1.35; *n*-C_5H_{12}, 1.07; *neo*-C_5H_{12}, 1.23. The exceptions were $n\mu$ for *n*-C_8H_{18} which were normalized to 6.14×10^{20} molecules/m V s at 382 K and *n*-$C_{10}H_{22}$ which were not normalized. The average change in $n\mu$ on normalization was ±3% and the maximum change 8%.

Ion mobilities are often referenced to $n = 2.69 \times 10^{25}$ molecules/m^3 and symbolized as K_0. The present results (Figs. 1 and 2) can be expressed as K_0 using K_0 (cm^2/V s) = $n\mu$ (molecules/m V s)/2.69×10^{21}.

The observed mobilities are independent of applied field strength because the threshold for ion heating was not reached. Ion heating is appreciable when the ion drift velocity $v_d = \mu E$ approaches the speed of random thermal motion of the molecules, $v_{mol} = (3k_BT/M_{mol})^{1/2}$ where k_B is Boltzmann's constant and M_{mol} is the molecular mass (6, 7). This indicates that the threshold field for ion heating is

$$E_{thr} \approx v_{mol}/\mu \text{ (low field)}$$

or

$$[1] \quad (E/n)_{thr} \approx v_{mol}/n\mu \text{ (low field)}$$

Equation [1] gives $(E/n)_{thr} \approx 160$ Td in ethane at 293 K (2*b*).

In many cases ion heating is observed when v_d approaches the speed of sound c_0 in the gas (8, 9). This result is similar to [1], because $c_0 = (\gamma k_BT/M_{mol})^{1/2}$, where the heat capacity ratio γ (10) ranges from 1.66 in ethane to 1.15 in *n*-decane (11). Hence $c_0 \approx 0.7v_{mol}$, which would give $(E/n)_{thr} \approx 110$ Td in ethane at 293 K. Similar calculations indicated that the values of $(E/n)_{thr}$ at 300 K in the other alkanes are larger than 110 Td.

[1]Assisted financially by the Natural Sciences and Engineering Research Council of Canada.

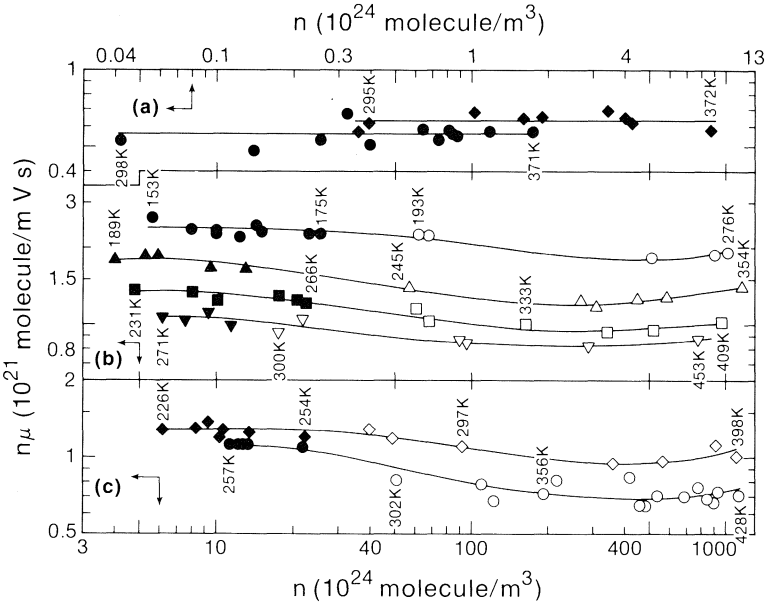

FIG. 1. Density dependence of $n\mu$ in saturated vapors: (*a*) *n*-octane, ◆; *n*-decane, ●; (*b*) ethane, ●, ○; propane, ▲, △; *n*-butane, ■, □; *n*-pentane, ▼, ▽. (*c*) *i*-butane, ◆, ◇; *neo*-pentane, ●, ○. Solid symbols are present work. Open symbols are refs. 2*b* and 3. The temperatures for some $n\mu$ accompany the symbol.

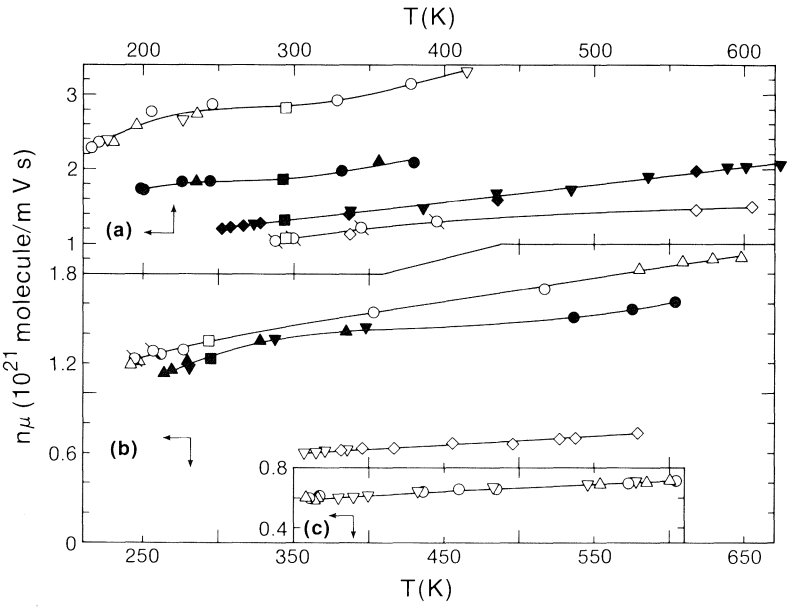

FIG. 2. Temperature dependence of present $n\mu$ values in nonsaturated gases at ($n/10^{25}$ molecules m^{-3}): (*a*) ethane, ○ (1.40); ▽ (1.50); △ (2.70); propane, ● (0.69), ▲ (1.38); *n*-butane, ◆ (1.10), ▼ (2.26); *n*-pentane, ◇ (0.59), ⬡ (1.13); (*b*) *i*-butane, △ (1.17), ⬡ (1.46), ○ (2.56); *neo*-pentane, ● (0.59), ▲ (1.37), ▼ (2.63); *n*-octane, ▽ (0.485), ◇ (0.99); (*c*) *n*-decane, △ (0.096), ○ (0.105), ▽ (0.228). □, ■: average of room temperature values, used to normalize the different density sets to remove random scatter produced by uncertainties in the gas densities and cell dimensions. The *n*-octane values had been normalized at 382 K by shifting one set up and the other down by 2.3%.

All of our measurements were taken at E/n less than $(E/n)_{thr}$, therefore the mobilities are those of thermal cations.

B. Low density limit

At constant T, low n and very low ion mole fraction the product $n\mu$ should be independent of n (6). Along the liquid–vapor coexistence curve n and T increase concomitantly; a 10-fold increase in n can occur for a 1.3-fold increase in T (Fig. 1). Since at constant n, the temperature coefficient $(dn\mu/dT)_n \geq 0$ (2*b*), then in saturated gases $dn\mu/dn \geq 0$ was expected. However, at $n > 2 \times 10^{25}$ molecules/m^3 we found that $n\mu$ in most hydrocarbon gases initially *decreased* before increasing at yet higher n (refs. 2*b*, 3 and Fig. 1).

At these densities $(dn\mu/dT)_n$ increased strongly with n. In terms of an Arrhenius model, the activation energy at constant n in C_2–C_4 alkanes increased from ~3 kJ/mol at $\sim 0.07 \times 10^{27}$ molecules/m^3 to ~13 kJ/mol at $\sim 1.4 \times 10^{27}$ and ~30 kJ/mol at $n_c = (3 \pm 1) \times 10^{27}$ molecules/m^3 (2*b*). Hence $dn\mu/dn < 0$ in the saturated gas was attributed to clustering of neutral molecules on the cations yielding lowered $n\mu$ values (1, 2*b*).

We chose therefore to consider the low density limit for cation behavior to be attained when $n\mu$ (T) and hence

TABLE 1. Average momentum transfer cross sections

Molecule	$\frac{\alpha^a}{4\pi\epsilon_0}$ (10^{-30} m^3)	T (K)	σ_{ave} (10^{-20} m^2) Expt[b]	σ_{ave} (10^{-20} m^2) Pol[c]	Expt/Pol	$\sigma_{mol}{}^d$ (10^{-20} m^2)
C_2H_6	4.45	160	310	224	1.4	61
		300	161	163	1.0	
		400	140	142	1.0	
C_3H_8	6.3	200	308	238	1.3	85
		300	230	194	1.2	
		380	179	177	1.0	
n-C_4H_{10}	8.1	250	347	241	1.4	109
		300	286	220	1.3	
		450	183	180	1.0	
		620	127	153	0.8	
i-C_4H_{10}	8.1	250	333	241	1.4	106
		300	277	220	1.2	
		475	181	175	1.0	
		650	133	149	0.9	
n-C_5H_{12}	10.0	300	316	232	1.4	117
		450	209	190	1.1	
		600	161	164	1.0	
neo-C_5H_{12}	10.0	265	319	247	1.3	
		300	269	232	1.2	
		450	192	190	1.0	
		600	150	164	0.9	
n-C_8H_{18}	15.4	360	409	262	1.6	172
		580	265	207	1.3	
n-$C_{10}H_{22}$	19.1	360	380	293	1.3	
		600	240	227	1.1	

[a]Reference 19.
[b]Equation [2] using $n\mu$ from Fig. 2 and $M_r = M_{mol}$.
[c]Equation [6].
[d]Bimolecular neutral–neutral cross section from Lennard–Jones diameter, ref. 20.

$(dn\mu/dT)_n$ becomes density independent. At such densities $n\mu$ in the saturated gas is also expected to be approximately constant over a fairly large range in n, as it would correspond to a small range in T (Fig. 1 and ref. 4). For cations in ethene and cyclopropane the low density limit was reached at $n < 3 \times 10^{25}$ molecules/m^3 (4). All the present measurements were near or at the low density limit (Figs. 1 and 2).

C. Average cross sections

The product $n\mu$ is related to the average ion–molecule momentum transfer cross section σ_{ave} by (12):

$$[2] \quad \sigma_{ave} = (3e/4M_r)/\langle v\rangle n\mu$$

where M_r is the ion–molecule reduced mass, e the protonic charge, v the relative velocity of the ions with respect to the molecules, and for a Maxwellian distribution,

$$[3] \quad \langle v\rangle = (8k_BT/\pi M_r)^{1/2}$$

The averaging in eq. [2] is equivalent to:

$$[4] \quad \sigma_{ave} = \langle v^3\sigma_m\rangle/\langle v^3\rangle$$

where σ_m is the momentum transfer cross section. Equation [2] is derivable from eq. [5-3-18] of ref. 6 in which $\overline{\Omega}^{(1,1)}$ is σ_{ave}. For N_4^+ in N_2, σ_m at low collision energy $\xi = M_r v^2/2$ was equal to that of the simple polarization potential σ_{pol}, and at high ξ it was close to the hard sphere value for N_2–N_2 collisions (13). This behavior is expected from the Langevin model (14, 15).

In the radiolysis of the present hydrocarbons, the initial monomer or dimer cations (16–18) might polymerize with product olefins, so M_r in eqs. [2] and [3] can vary from $0.5M_{mol}$ to M_{mol}. Using $n\mu$ from Fig. 2 and $M_r = M_{mol}$ gave lower limit values of σ_{ave} (Table 1). At a given temperature increasing the carbon skeleton length from ethane to n-octane increased σ_{ave}; on going from n-octane to n-decane σ_{ave} seemed to decrease ~9%. Comparison of n- and i-butane σ_{ave} at a given T revealed little isomeric structure effect, but σ_{ave} in neo-pentane was consistently less than in n-pentane at the same T. This is attributed to fragmentation of the neo-pentane ions to t-butyl ions. Our previous finding of a larger σ_{ave} in neo-pentane at 7.2×10^{25} molecules/m^3 than in n-pentane at 2.25×10^{25} (3) is due to the effect of density at $n > 3 \times 10^{25}$ (Fig. 1).

The σ_{ave} values can be compared with values of the average polarization $\sigma_{pol,ave}$. Substitution of σ_{pol} (15)

$$[5] \quad \sigma_{pol}/m^2 = 2.21\pi(\alpha e^2/32\pi^2\epsilon_0^2\xi)^{1/2}$$

where α (C m^2/V) is the polarizability of the molecule and ϵ_0 is the permittivity of vacuum, into eq. [4] gives

$$[6] \quad \sigma_{pol,ave}/m^2 = 0.0133(\alpha/4\pi\epsilon_0 T)^{1/2}$$

Values of $\alpha/4\pi\epsilon_0$, corresponding to polarizability in the non-SI units of volume, were taken from ref. 19 to calculate values of $\sigma_{pol,ave}$ listed in Table 1. At all temperatures the ratio of experimental to polarization average cross section expt/pol equalled 1.2 ± 0.4. This is much different from the case of electron scattering in these same gases where expt/pol ranged from 0.02 to 0.2 (5).

At high temperatures σ_{ave} might be expected to approach a hard sphere value σ_{hs} (14, 15). A lower limit to σ_{hs} is the neutral molecule – neutral molecule cross section $\sigma_{mol} = \pi d_{LJ}^2$, where d_{LJ} is the Lennard–Jones diameter (20); multimer formation would increase σ_{hs}, so $\sigma_{hs} > \sigma_{mol}$ would result. Values of σ_{mol} from ref. 20 are listed in Table 1. Above 600 K σ_{ave} approaches σ_{mol}. However, even in the butanes where $\sigma_{ave} < \sigma_{pol,ave}$ at $T > 620$ K, σ_{ave} is still about 20% larger than σ_{mol}. These results are consistent with either incomplete transition between polarization and hard sphere potential controlling the mobility, or with the cations being multimers.

Acknowledgement

We thank the staff of the Radiation Research Center for their assistance.

1. N. GEE, S. S.-S. HUANG, T. WADA, and G. R. FREEMAN. J. Chem. Phys. **77**, 1411 (1982).
2. N. GEE and G. R. FREEMAN. Can. J. Chem. (*a*) **58**, 1490 (1980); (*b*) **59**, 2988 (1981).
3. I. GYÖRGY, N. GEE, and G. R. FREEMAN. Can. J. Chem. **63**, 1105 (1985).
4. N. GEE, M. A. FLORIANO, and G. R. FREEMAN. Z. Naturforsch. **39***a*, 1225 (1984).
5. M. A. FLORIANO, N. GEE, and G. R. FREEMAN. J. Chem. Phys. **84**, 6799 (1986).
6. E. W. MCDANIEL and E. A. MASON. The mobility and diffusion of ions in gases. John Wiley and Sons, New York. 1973. Chapt. 1.
7. R. E. ROBSON and E. A. MASON. Phys. Rev. A, **25**, 2411 (1982).
8. S. S.-S. HUANG and G. R. FREEMAN. J. Chem. Phys. **68**, 1355 (1978).
9. B. V. PARANJAPE. Phys. Rev. A, **21**, 405 (1980).
10. E. HAUSMANN and E. P. SLACK. Physics. Van Nostrand, New York. 1944. p. 412.

11. R. C. WEAST (*Editor*). Handbook of chemistry and physics. 64th ed. CRC Press, Boca Raton, Florida. p. D-177.
12. N. GEE and G. R. FREEMAN. Can. J. Chem. **61**, 1644 (1983).
13. T. WADA, N. GEE, and G. R. FREEMAN. Can. J. Chem. **64**, 777 (1986).
14. P. LANGEVIN. Ann. chim. phys. **5**, 245 (1905).
15. E. W. MCDANIEL. Collision phenomena in ionized gases. J. Wiley and Sons, New York. 1964. Chapt. 9.
16. C. M. WODETZKI, P. A. MCCUSKER, and D. B. PETERSON. J. Phys. Chem. **69**, 1045 (1965).
17. R. E. REBBERT and P. AUSLOOS. J. Res. NBS, **76A**, 329 (1972).
18. S. LUCAS. Rad. Phys. Chem. **15**, 713 (1980).
19. H. STUART. *In* Landolt-Börnstein, Zahlenwerte und Funktionen, I. Band, 3. Teil, Sec. 14207. *Edited by* A. Eucken and K. H. Hellwege. Springer-Verlag, Berlin. 1951. pp. 512 and 513.
20. E. A. MASON. *In* Molecular theory of gases and liquids. *Edited by* J. O. Hirschfelder, C. F. Curtiss, and R. B. Bird. J. Wiley and Sons, New York. Corrected printing, 1964. pp. 1213, 1214.

Short synthesis of 1,3*Z*,6*Z*,9*Z*-tetraene hydrocarbons. Lepidopteran sex attractants[1]

JOCELYN G. MILLAR[2] AND EDWARD W. UNDERHILL

National Research Council, Plant Biotechnology Institute, 110 Gymnasium Road, Saskatoon, Sask., Canada S7N 0W9

Received May 13, 1986

JOCELYN G. MILLAR and EDWARD W. UNDERHILL. Can. J. Chem. **64**, 2427 (1986).

A short, convergent synthesis of 1,3*Z*,6*Z*,9*Z*-tetraene hydrocarbons was developed. A key step was the regioselective alkylation of 1,5-dibromo-2-pentyne. The method was used to synthesize tetraenes of chain lengths C_{18}–C_{20}, to be used in field trials as sex attractants and (or) inhibitors of the winter moth, *Operophtera brumata* L., and the Bruce spanworm *O. bruceata* H. (Lepidoptera: Geometridae).

JOCELYN G. MILLAR et EDWARD W. UNDERHILL. Can. J. Chem. **64**, 2427 (1986).

On a mis au point une courte synthèse convergente des hydrocarbures tétraéniques-1,3(*Z*),6(*Z*),9(*Z*). Une étape clé implique l'alcoylation régiosélective du dibromo-1,5 pentyne-2. On a utilisé la méthode pour synthétiser des tétraènes comportant de 18 à 20 atomes de carbone; on a utilisé ces hydrocarbures pour déterminer leurs propriétés comme attractant sexuel et (ou) inhibiteurs des espèces *Operophtera brumata* L. et *O. bruceata* H. (Lepidoptera; Geometridae).

[Traduit par la revue]

To date, two 1,3*Z*,6*Z*,9*Z*-tetraene hydrocarbons **1** (Scheme 1) have been reported as lepidopteran sex attractants. These are the nonadecatetraene **1***b*, which appears to be the sole component in the sex pheromone of the winter moth, *Operophtera brumata* L. (Lepidoptera: Geometridae) (1, 2), and the heneicosatetraene **1***d*, which is one of several components in the sex pheromone of *Utetheisa ornatrix* L. (Lepidoptera: Arctiidae) (3). As these homologous hydrocarbons were found in species from two different families, it is very likely that these compounds or their homologs are sex pheromone components for other lepidopteran species as well (4). As part of our work in screening potential sex attractants, we were interested in obtaining a series of these compounds for field testing. In particular, we wanted the tetraenes **1***a–c* to test as sex attractants and (or) inhibitors for two sympatric species, *O. brumata*, mentioned above, and the Bruce spanworm, *O. bruceata* H. Both species are morphologically very similar, and can only be differentiated by dissection. In addition, they both appear to use the nonadecatetraene **1***b* as a sex attractant (1). One species, *O. brumata*, is an economic pest of hardwoods and fruit trees (1), while the other is of lesser economic importance (5, 6). It would therefore be advantageous to develop sex attractant lures that were specific for each species.

To construct efficiently the series of homologous tetraenes, we required a common intermediate to which a chain of varying length could be appended. Of the five previously reported syntheses of tetraenes of this type, three routes (2, 7, 8) involved progressive extension of the carbon skeleton from the saturated end of the chain, which is not efficient for synthesis of a series of homologs. The other two routes (4, 9), one of which (9) appeared while our work was in progress, were amenable to synthesis of a homologous series. However, both routes made use of protecting groups, thus necessitating extra steps for the introduction and removal of these groups, and for the subsequent manipulation of the deprotected functionality. We felt that a considerably shorter synthesis that did not require protecting groups could be devised, by judicious choice of the sequence of steps and of regioselective reaction conditions.

This more direct approach has proven to be successful (Scheme 1). Thus, cuprous salt-catalyzed reaction of 3-butyn-1-ol **2** with aqueous formaldehyde gave diol **3** (55–62%) (10). The diol was converted to the dibromide **4** (89%) by treatment with carbon tetrabromide and triphenylphosphine (11). The diynes **6***a–c* required for the alkylation step were constructed by cuprous salt-catalyzed reaction of the Grignard reagent of the appropriate terminal alkyne **5** with propargyl bromide (12, 13). Cuprous iodide-catalyzed reaction of the Grignard reagents of the diynes **6** with dibromide **4** (12, 13) selectively gave the desired 1-bromo-3,6,9-alkatriynes **7**, contaminated with small amounts (6–12%) of isomeric impurities. The impurities were easily removed by recrystallization of the crude bromotriynes from pentane at 0°C (64–69%). The pure bromotriynes **7** were stereoselectively reduced with dicyclohexylborane to the bromotrienes **8** (59–65%) (14, 15). In our hands, this method of partial hydrogenation has proven to be completely stereospecific, with no trace of *trans* isomers detected by capillary gc/ms of the crude product. In contrast, we and others (16) have found that catalytic semihydrogenation of methylene-interrupted poly-ynes is frequently beset with problems such as catalyst poisoning with trace impurities, isomerization of the resulting *cis* double bonds, and over-reduction.

The syntheses were completed by base-induced elimination of HBr. Thus, heterogeneous mixtures of potassium *tert*-butoxide, bromotrienes **8**, and phase transfer catalyst (18-crown-6), stirred in hexane at −10 to 0°C (17), gave tetraenes **1** (58–65% isolated yields). Temperature control was critical in this reaction, as warming the mixture to room temperature gave reduced yields and some isomerization, while the reaction proceeded very slowly below −15°C.

This method thus represents a short and highly stereoselective route to 1,3*Z*,6*Z*,9*Z*-tetraene hydrocarbons.

Experimental

All reactions were carried out under N_2, in oven-dried glassware. THF was distilled from benzophenone ketyl under N_2 before use. Routine capillary gc runs were carried out with a Hewlett–Packard 5790 instrument, fitted with DB-5 column (30 m × 0.25 mm). Proton nmr spectra were recorded at 360 MHz on a Bruker AM-360-WB spectrometer. The ir spectra were recorded on a Perkin–Elmer 237B instrument. Electron impact (EI) mass spectra (70 eV unless otherwise stated) were recorded on a Finnigan 4000E gc–ms unit with an Incos 2300 data system, using an SP2100 capillary gc column. The ms data are reported in the form *m/z* (relative intensity). Accurate mass measurements were performed by the Mass Spectrometry Laboratory, Psychiatric Research Unit, University of Saskatchewan, with an

[1]Issued as NRC No. 26110.

[2]Author to whom correspondence may be addressed.

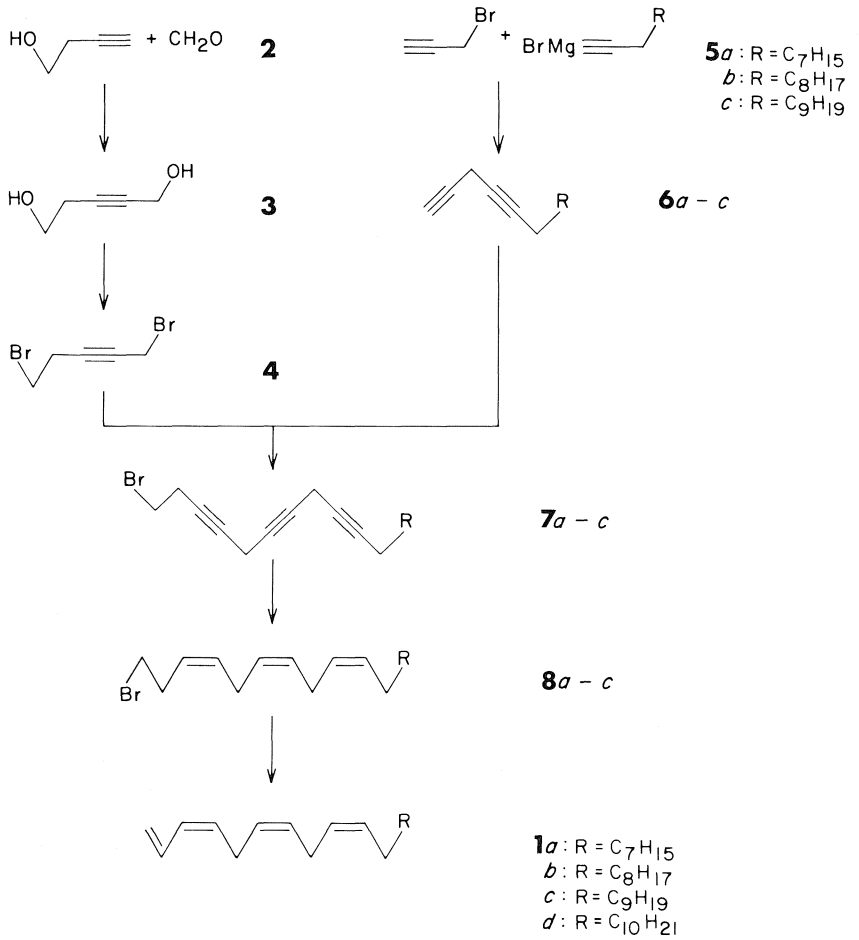

SCHEME 1

MS902S instrument with VG console update, using PTFBA internal standard.

Preparation of 2-pentyn-1,5-diol (3)

The preparation of **3** was a minor modification of that previously reported (8). Cuprous chloride (4.0 g, 40 mmol) was dissolved in 12% aqueous HCl (60 mL), and the solution was cooled in an ice bath. 40% Aqueous KOH (60 mL) was added dropwise over 1 h, giving a brown suspension. The mixture was filtered with suction, and the solid residue was washed well with water. The moist solid residue was added to a mixture of 3-butyn-1-ol **2** (13.0 g, 186 mmol), 37% aqueous formaldehyde (21.67 g, 267 mmol), water (4 mL), and $CaCO_3$ (0.2 g). The mixture was refluxed under N_2 for 3 days, cooled to room temperature, diluted with ethyl acetate (250 mL), and dried with anhydrous Na_2SO_4 (10 g). The mixture was filtered with suction through a plug (2.5 cm × 5 cm) of anhydrous Na_2SO_4, and the solids were rinsed thoroughly with ethyl acetate. The filtrate was concentrated and distilled, giving diol **3** as a viscous oil (10.23 g, 55%), bp 90–91°C (0.1 Torr (1 Torr = 133.3 Pa)) (lit. (10) bp 90–95°C (0.03 Torr)); ir (neat) λ_{max}: 3700–3000 (s), 2235 (w), 1100–990 (s) cm^{-1}; nmr (D_2O) δ: 4.09 (t, 2H, J = 2.1 Hz, H-1), 3.56 (t, 2H, J = 6.7 Hz, H-5), 2.35 (tt, 2H, J = 6.7, 2.1 Hz, H-4); ms: 100 (M^+, 0.03), 99 (0.24), 82 (20.6), 70 (7.5), 69 (8.5), 53 (20.8), 52 (100), 51 (18.9), 50 (12.5), 44 (13.9).

Preparation of 1,5-dibromo-2-pentyne (4)

A solution of diol **3** (2.0 g, 20 mmol) and carbon tetrabromide (14.94 g, 45 mmol) in dry CH_2Cl_2 (100 mL) was cooled to 0°C, and triphenylphosphine (11.79 g, 45 mmol) was added in portions over 20 min. The mixture was warmed to 20°C over 1 h. The CH_2Cl_2 was removed on a rotary evaporator, with no heating, and hexane (100 mL) was added to the residue. The mixture was cooled to 0°C and filtered. The solid residue was washed with ice-cold hexane (2 × 25 mL), and the filtrate was concentrated and distilled under vacuum. After a large forerun of bromoform and excess carbon tetrabromide, dibromide **4** was obtained as a pale yellow oil (4.01 g, 89%), bp 40–43°C (0.04 Torr); ir (neat) λ_{max}: 2240 cm^{-1} (w); nmr ($CDCl_3$) δ: 3.80 (t, 2H, J = 2.4 Hz, H-1), 3.33 (t, 2H, J = 7.2 Hz, H-5), 2.71 (tt, 2H, J = 7.2, 2.4 Hz, H-4); ms: 228 (3.5), 226 (6.8), 224 (3.5), 147 (55.1), 145 (56.7), 95 (2.8), 93 (3.5), 66 (50.4), 65 (100), 63 (11.7). *Exact Mass* calcd. for $C_5H_6{}^{79}Br_2$: 223.8836; found 223.9118.

Preparation of 1,4-diynes (6)

Ethyl magnesium bromide (approximately 65 mmol) was prepared from ethyl bromide (7.63 g, 70 mmol) and Mg turnings (1.58 g, 65 mmol) in THF (75 mL). 1-Decyne **5***a* (8.28 g, 60 mmol) was added dropwise, and the solution was heated at 40–45°C for 2 h. The solution was then cooled to < −10°C in an ice–salt bath, CuI (190 mg, 1 mmol) was added, and the mixture was stirred 20 min. Propargyl bromide (7.3 g, 61 mmol) was then added dropwise, maintaining the temperature < −10°C. The mixture was warmed to 20°C over 3 h, stirred overnight, quenched with aqueous NH_4Cl (100 mL), and extracted with hexane (3 × 100 mL). The combined organic extracts were dried (Na_2SO_4), concentrated, and distilled under vacuum, giving diyne **6***a* (7.85 g, 74%) as a colourless oil, bp 53°C (0.2 Torr), which yellowed rapidly upon exposure to air; ir (neat) λ_{max}: 3330 (m), 2960 (m), 2935 (s), 2860 (m), 2130 (w) cm^{-1}; nmr ($CDCl_3$) δ: 3.12 (dt, 2H, J = 2.7, 2.4 Hz, H-3), 2.13 (tt, 2H, J = 7.1, 2.4 Hz, H-6), 2.03 (t, 1H, J = 2.7 Hz, H-1), 1.46 (br quintet, 2H, J = 7.0 Hz, H-7), 1.4–1.1 (m, 10H, H-8 to H-12), 0.86 (t, 3H, J = 7 Hz, H-13); ms (25 eV): 176 (M^+, 0.1), 119 (20.4), 105 (35.7), 95 (29.5), 91 (100), 81 (46.7), 79 (32.6), 78 (27.0), 67 (40.2), 55 (44.8).

The known 1,4-tetradecadiyne **6***b* was similarly prepared in 75% yield, bp 65°C (0.15 Torr) (lit. (7) bp 125°C (25 Torr)). 1,4-Penta-

decadiyne **6***c* was prepared in 76% yield, bp 82°C (0.1 Torr). The ir and nmr spectra were analogous to those of **6***a*. Mass spectra (25 eV) were characterized by a base peak at m/z 91, diagnostic fragments at $M - 39$ (2–4%) and $M - 81$ (3–9%), and a series of ions at $M - C_nH_{2n+1}$. The molecular ion was very small or absent.

Capillary gc/ms showed that the diynes **6** were contaminated with small amounts of isomeric materials (≃5%). These isomeric impurities were carried through to the next step, where they were removed during the purification procedure. The diynes appeared to be stable for several months if stored at −25°C under N_2.

Preparation of 1-bromo-3,6,9-triynes (7)

Diyne **6***a* (1.85 g, 10.5 mmol) was added to a freshly prepared solution of ≃11.5 mmol of ethyl magnesium bromide (prepared from 280 mg Mg (11.5 mmol) and ethyl bromide (1.36 g, 12.5 mmol)) in THF (15 mL) at 20°C. The resulting solution was warmed at 40–45°C for 2 h, then cooled to 0°C, and CuI (95 mg, 0.5 mmol) was added. The mixture was stirred for 20 min, then cooled to < −15°C in an ice–salt bath, and a solution of dilbromide **4** (2.26 g, 10 mmol) in THF (5 mL) was added dropwise over 20 min. The mixture was warmed to 0°C over 2 h, stirred at 0°C for 8 h, and warmed to 20°C overnight. The mixture was poured into 5% aqueous NH_4Cl (50 mL), extracted with hexane (3 × 25 mL), backwashed with brine (1 × 25 mL), dried (Na_2SO_4), and filtered with suction through a plug (3 cm × 3 cm) of Na_2SO_4. The filtrate was concentrated under reduced pressure, and the residue was recrystallized from hexane at −25°C, giving **7***a* (2.21 g, 69%) as white plates, mp 26–27.5°C, which slowly yellowed after exposure to air and (or) light; ir (neat) λ_{max}: 2960 (m), 2930 (s), 2860 (m), 2215 (w) cm^{-1}; nmr ($CDCl_3$) δ: 3.39 (t, 2H, J = 7.4 Hz, H-1), 3.13 (m, 4H, H-5, H-8), 2.71 (tt, 2H, J = 7.4, 2.2 Hz, H-2), 2.13 (tt, 2H, J = 7.2, 2.2 Hz, H-11), 1.46 (m, 2H, H-12), 1.5–1.1 (m, 10H, H-13 to H-17), 0.86 (t, 3H, J = 6.7 Hz, H-18); ms (25 eV): 279, 277 ($M - 43$, 1.2), 155 (33.0), 143 (34.7), 137 (48.4), 129 (46.7), 128 (48.1), 95 (54.4), 91 (35.0), 82 (45.4), 81 (100), 67 (61.4). *Exact Mass* calcd. for $C_{18}H_{25}{}^{81}Br - C_3H_7$: 279.0572; found: 279.0493.

1-Bromo-3,6,9-nonadecatriyne **7***b* was similarly prepared in 81% crude yield. In this case the crude material was used directly in the next step; an analytical sample recrystallized from hexane at −10°C gave mp 30–32°C. 1-Bromo-3,6,9-eicosatriyne **7***c* was obtained in 64% yield after recrystallization from hexane, mp 35–37°C. The ir and nmr spectra of **7***b* and **7***c* were analogous to those of **7***a*. Mass spectra (25 eV) were characterized by a base peak at m/z 81, doublets of ions at (279, 277), (265, 263), etc., and diagnostic fragments at $M - C_8H_8Br$ (30–50%), $M - C_5H_6Br$ (9%), and m/z 211 (2–4%). The molecular ion was very small or absent.

The pure crystalline compounds gave a single peak on capillary gc, and appear to be stable when stored at −25°C under N_2.

Preparation of 1-bromo-3Z,6Z,9Z-trienes (8)

A suspension of dicyclohexylborane (21 mmol) was prepared by dropwise addition of cyclohexene (3.45 g, 42 mmol) to a solution of borane–dimethylsulfide complex (10 *M*, 2.1 mL, 21 mmol) in THF (25 mL), maintaining the temperature at 0–5°C. The resulting mixture was warmed to 20°C, stirred 2 h, then cooled to 0°C again, and bromotriyne **7***a* (1.61 g, 5.0 mmol) in THF (5 mL) was added. The mixture was warmed to 20°C over 2 h, and stirred an additional 2 h. Glacial acetic acid (8 mL) was then added dropwise and the resulting solution was stirred overnight. The solution was then cooled and made basic by slow addition of aqueous NaOH (5 *M*, 30 mL), followed by dropwise addition of 30% aqueous H_2O_2 (8 mL). The resulting mixture was diluted with water (100 mL) and extracted with pentane (3 × 50 mL). The combined organic extracts were dried (Na_2SO_4) and concentrated, and low-boiling by-products were removed by warming at 45°C under vacuum (0.1 Torr). The residue was purified by flash chromatography on silica gel (3.5 cm id × 20 cm), eluting with hexane, giving **8***a* (1.07 g, 65%) as a colourless oil, isomerically pure by capillary gc; ir (neat) λ_{max}: 3020 (m), 2960 (m), 2930 (s), 2860 (m), 1210 (m) cm^{-1}; ^1H nmr ($CDCl_3$) δ: 5.51 (dtt, 1H, J = 10.7, 6.3, 1.4 Hz, H-4), 5.42–5.32 (m, 4H, H-3, H-6, H-7, H-10), 5.31 (dtt, 1H, J = 10.6, 6.9, 1.3 Hz, H-9), 3.36 (t, 2H, J = 7.1 Hz, H-1), 2.80 (m, 4H, H-5, H-8), 2.64 (m, 2H, H-2), 2.04 (m, 2H, H-11), 1.5–1.1 (m, 12H, H-12 to H-17), 0.86 (t, 3H, J = 6.9 Hz, H-18); ms: 328, 326 (M^+, 0.6), 188 (29.3), 186 (30.6), 95 (19.3), 93 (33.8), 82 (20.0), 81 (27.9), 80 (55.7), 79 (100), 67 (41.5), 55 (15.6).

Exact Mass for **8***a* could not be measured due to interference from the internal standard. *Exact Mass* for a pure sample of **8***b*, calcd. for $C_{19}H_{33}{}^{81}Br$: 342.2745; found: 342.1914.

Known triene **8***b* (4, 9) was similarly prepared from crude triyne **7***b*, in 71% overall yield from **4**. The isolated material was contaminated with isomers (7%), and was used in the next step without further purification. Triene **8***c* was prepared in 59% yield from pure **7***c*. The ir and nmr spectra of **8***b* and **8***c* were analogous to those of **8***a*. Mass spectra were characterized by a base peak at m/z 79, a doublet at $M - C_4H_6$ (1%), a doublet at m/z 186 and 188 (15–20%), and doublets at (91, 93), (105, 107), etc. The molecular ions were small but discernable (1%).

Preparation of 1,3Z,6Z,9Z-tetraenes (1)

A solution of bromotriene **8***a* (0.50 g, 1.53 mmol) in hexane (15 mL) was cooled to −23°C (CCl_4/CO_2 slush) and potassium *tert*-butoxide (250 mg, 2.23 mmol) and 18-crown-6 (40 mg, 0.15 mmol) were added sequentially. The mixture was slowly warmed to 0°C, and stirred at 0°C for 3 h. The reaction was quenched by addition of powdered NH_4Cl (1 g) and stirring for 1 h at 0°C. The mixture was then poured into ice-water (25 mL), and the organic layer was separated, washed with brine, and passed through a short column of neutral alumina (2 cm id × 5 cm). The column was rinsed well with hexane, and the combined eluate was concentrated, giving tetraene **1***a* (215 mg, 58%), >98% pure by capillary gc (the only impurity detected was 1.4% unreacted starting material); ir (neat) λ_{max}: 3085 (w), 3020 (m), 2960 (m), 2930 (s), 2860 (m), 995 (m) cm^{-1}; nmr ($CDCl_3$) δ: 6.65 (dddd, 1H, J = 16.9, 10.8, 10.6, 1.1 Hz, H-2), 6.00 (br t, 1H, J = 10.8 Hz, H-3), 5.46–5.26 (m, 5H, H-4, H-6, H-7, H-9, H-10), 5.19 (br d, 1H, J = 16.9 Hz, H-1 *cis*), 5.10 (br d, 1H, J = 10.1 Hz, H-1 *trans*), 2.95 (t, 2H, J = 6.1 Hz, H-5), 2.80 (t, 2H, J = 6.1 Hz, H-8), 2.04 (br dt, 2H, J = 6.8, 6.7 Hz, H-11), 1.41–1.1 (m, 12H, H-12 to H-17), 0.86 (t, 3H, J = 6.6 Hz, H-18); ms (25 eV): 246 (M^+, 4.2), 192 (15.4), 119 (25.0), 106 (29.0), 105 (24.2), 93 (44.4), 92 (46.1), 91 (64.1), 80 (100), 79 (87.1), 78 (33.0), 67 (29.6). *Exact Mass* calcd. for $C_{18}H_{30}$: 246.2348; found: 246.2356.

Known tetraene **1***b* (2, 4, 7, 9) was prepared from the isomerically impure **8***b*. After purification by flash chromatography on $AgNO_3$-impregnated silica gel (10%), eluting with stepwise gradients of ether in pentane, chemically and isomerically pure tetraene **1***b* was obtained in 63% yield. All spectra were identical to literature data. Tetraene **1***c* was prepared in 65% yield as described for **1***a*. The ir and nmr spectra were completely in accord with those of **1***a* and **1***b*. Mass spectra of **1***b* and **1***c* were characterized by a base peak at m/z 80, diagnostic peaks at $M - 41$ (2–3%) and $M - 54$ (10–15%), and clusters of ions centered at m/z 80, 91, 106, 119, 133, 147, 161, and 175. The molecular ion was easily discernable (4–6%).

1. W. L. Roelofs, A. S. Hill, C. E. Linn, J. Meinwald, S. C. Jain, H. J. Herbert, and R. F. Smith. Science, **217**, 657 (1982).
2. S. C. Jain, W. L. Roelofs, and J. Meinwald. J. Org. Chem. **48**, 227 (1983).
3. W. E. Connor, T. Eisner, R. K. Vander Meer, A. Guerrero, D. Ghiringelli, and J. Meinwald. Behav. Ecol. Sociobiol. **7**, 55 (1980).
4. W. Huang, S. P. Pulaski, and J. Meinwald. J. Org. Chem. **48**, 2270 (1983).
5. C. E. Brown. Can. Entomol. **94**, 1103 (1962).
6. R. Martineau. Insects harmful to forest trees. Multiscience Publications Ltd., Montreal. 1984. pp. 158–160.
7. H. J. Bestmann, T. Brosche, K. H. Koschatsky, K. Michaelis, H. Platz, K. Roth, J. Suss, O. Vostrowsky, and W. Knauf. Tetrahedron Lett. **23**, 4077 (1982).
8. S. C. Jain, D. E. Dussourd, W. E. Connor, T. Eisner, A. Guerrero, and J. Meinwald. J. Org. Chem. **48**, 2266 (1983).

9. R. BAKER, M. J. O'MAHONY, and C. J. SWAIN. J. Chem. Res. **5**, 190 (1984).
10. O. HEUBERGER and L. N. OWEN. J. Chem. Soc. 910 (1952).
11. R. G. WEISS and E. I. SNYDER. J. Org. Chem. **36**, 403 (1971).
12. L. BRANDSMA. Preparative acetylenic chemistry. Elsevier Publishing Co., Amsterdam. 1971. p. 31.
13. J. M. OSBOND, P. G. PHILPOTT, and J. C. WICKENS. J. Chem. Soc. 2779 (1961).
14. H. C. BROWN, A. K. MANDAL, and S. U. KULKARNI. J. Org. Chem. **42**, 1392 (1977).
15. H. C. BROWN. Organic syntheses via boranes. John Wiley & Sons, Inc., New York. 1975. pp. 81, 98, 99.
16. E. N. MARVELL and T. LI. Synthesis, 457 (1973).
17. E. VON DEHMLOW and M. LISSEL. Synthesis, 272 (1979).

Cellules photoélectrochimiques de phtalocyanine d'hydroxyaluminium déposées par rotation

GÉRARD PERRIER ET LÊ H. DAO[1]

Institut National de la Recherche Scientifique (INRS–Énergie), C.P. 1020, Varennes (Qué.), Canada J0L 2P0

Reçu le 12 mai 1986

GÉRARD PERRIER et LÊ H. DAO. Can. J. Chem. **64**, 2431 (1986).

Des cellules photoélectrochimiques à base de phtalocyanine d'hydroxyaluminium (PcAlOH) ont été fabriquées par la méthode de déposition par rotation («spin-coating»). Le comportement spectral et électrique des cellules NESA/PcAlOH/BQ/HQ/Pt est étudié et comparé à celui de cellules où les films de PcAlOH sont produits par sublimation. À cause de la faible solubilité de PcAlOH dans les solvants organiques volatils, le DMSO utilisé pour la déposition par rotation semble rester piégé dans le film solide et diminue le rendement de la cellule photoélectrochimique. L'étude de l'influence de la contre-électrode sur l'efficacité des cellules a permis de montrer qu'une contre-électrode en vanadium conduisait à des valeurs plus élevées de J_{sc}, V_{oc} et η comparée à une contre-électrode en platine, mais présentait des phénomènes de corrosion.

GÉRARD PERRIER and LÊ H. DAO. Can. J. Chem. **64**, 2431 (1986).

The spin-coating technique was used to produce hydroxyaluminum phthalocyanine (PcAlOH) photoelectrochemical cells. The spectral and electrical behavior of NESA/PcAlOH/BQ/HQ/Pt cells is studied and comparisons are made with cells based upon sublimed PcAlOH films. Due to the weak solubility of PcAlOH in volatile organic solvents, the DMSO used in the spin-coating method seems to be trapped in the solid film, and leads to a decrease in the photoelectrochemical cell efficiency. Studies on the influence of the counter-electrode showed that a vanadium counter-electrode gave higher values of J_{sc}, V_{oc}, and η than a platinum one, but corrision phenomena were observed in that case.

1. Introduction

Une approche intéressante de la conversion de l'énergie lumineuse en énergie électrique consiste en l'utilisation de cellules solaires à base de semiconducteurs organiques. L'intérêt en est surtout économique, le coût du matériau semiconducteur étant peu élevé car les techniques de synthèse et de purification sont en général assez simples, de même que les méthodes de fabrication des films minces.

Les propriétés des semiconducteurs organiques ont été connues dès les années 1950 alors que leurs forces photo–électromotrices ont été mesurées sur des substrats inorganiques (1, 2). Des progrès remarquables ont été réalisés dans l'augmentation de l'efficacité de conversion des cellules photovoltaïques organiques, passant de 10^{-5}% au début des années 1970 à 1% actuellement (3). Les composés de type phtalocyanine ont reçu une attention particulière en tant que colorants pour la sensibilisation spectrale et la stabilisation de semiconducteurs inorganiques (4–9) et en tant que semiconducteurs formant des jonctions liquides avec des couples rédox (10–25).

On connait de nombreuses formes polymorphiques de phtalocyanines, en particulier les formes α, β et x (26). Ces formes correspondent à un empilement différent des molécules planaires; les formes α et x sont les plus conductrices (27–29). La présence de l'oxygène augmente grandement la conductivité des phtalocyanines (30) et intervient dans la formation d'états de surface accepteurs d'électrons (31).

La sublimation est la technique de déposition la plus fréquemment utilisée pour la fabrication de films de phtalocyanines (10–19), mais on retrouve aussi l'électrodéposition (20) et la déposition par monocouches (32, 33). Les phtalocyanines peuvent être aussi dispersées dans un polymère et le mélange obtenu peut être étalé en films minces à l'aide d'un couteau ou d'un rouleau (23, 24), ou déposé par rotation (27, 34) sur un support transparent.

Ce travail présente une nouvelle cellule photoélectrochimique à base de phtalocyanine d'hydroxyaluminium où le film mince de semiconducteur organique pur a été déposé par rotation («spin-coating»). Le comportement spectral et électrique de ces cellules est étudié et comparé à celui de cellules où le film mince de phtalocyanine d'hydroxyaluminium a été déposé par sublimation; la cellule est ensuite optimisée et un diagramme des niveaux d'énergie est élaboré.

2. Partie expérimentale

2.1 Matériaux

La phtalocyanine d'hydroxyaluminium (PcAlOH) a été préparée comme suit. La phtalocyanine de chloroaluminium a d'abord été synthétisée en chauffant de l'*o*-phtalonitrile et du chlorure d'aluminium dans de la quinoline; le produit purifié est ensuite chauffé à reflux dans une solution aqueuse d'ammoniaque (30%) en présence de pyridine (35) pour donner PcAlOH. Après des extractions répétées avec des solvants organiques, PcAlOH est dissoute dans l'acide sulfurique concentré et la solution obtenue est versée dans un mélange eau–glace. Le solide bleu foncé est filtré et lavé successivement avec l'eau, l'éthanol et l'acétone.

Les films organiques ont été déposés sur des supports conducteurs transparents de dimensions 25 mm × 50 mm constitués de lamelles de NESA (SnO_2 dopé, PPG Industries); ces lamelles ont été nettoyées par immersion successive dans une solution de détergent, dans l'eau du robinet et l'eau distillée, puis dans le méthanol. La méthode de déposition par rotation consiste en la déposition d'une goutte d'une suspension de PcAlOH dans du DMSO au centre du substrat en rotation; la force centrifuge permet ainsi l'étalement de la goutte sur le substrat. L'épaisseur des films (de 100 à 3000 Å) peut être variée en jouant sur la vitesse de rotation (de 1000 à 3500 r/min) ainsi que sa durée, et sur la concentration de PcAlOH dans le DMSO; le séchage est effectué à l'air libre pendant une dizaine de jours. La méthode de déposition par sublimation utilise le système décrit par Linkous *et al.* (13); la température de sublimation est de 520°C à des pressions typiques de 5×10^{-6} Torr (1 Torr = 133.3 Pa). L'épaisseur du film (de 100 à 5500 Å) peut être variée en jouant sur la durée de la sublimation (de 5 min à 1 h).

Les contacts électriques sont réalisés à l'aide d'un fil de cuivre collé sur la partie conductrice du substrat et recouvert d'une peinture à l'argent (G.C. Electronics). Une surface active variant de 1 à 4 cm^2 est définie en recouvrant l'électrode d'un vernis incolore limitant le contact avec la solution. L'épaisseur des films est déterminée à l'aide d'un

1. Auteur à qui adresser toute correspondance.

profilomètre de surface Sloan Dektak II, puis une courbe d'étalonnage absorbance maximale – épaisseur est tracée. Les spectres d'absorption visible ont été enregistrés avec un spectrophotomètre Hitachi 100-60.

2.2 Mesures photoélectrochimiques

La photoélectrode est plongée dans une solution aqueuse non-déoxygénée, agitée magnétiquement et contenant un sel (Na_2SO_4 0,1 *M*) et un couple rédox (benzoquinone/hydroquinone) dans une cellule électrochimique. La surface du semiconducteur organique est placée à 2 mm de la fenêtre transparente pour minimiser l'absorption de la lumière par la solution, et l'interface semiconducteur–électrolyte est éclairée directement. Une contre-électrode en platine (8 cm^2) sert d'électrode auxiliaire. Une source de lumière blanche (lampe au tungstène-halogène) de 650 W (Schoeffel) et un monochromateur Kratos (Schoeffel) fournissent la lumière monochromatique. L'intensité lumineuse est mesurée par un radiomètre United Detector Technologies 21A et le courant de court-circuit est mesuré par un électromètre Keithley 616. La variation des courants avec le potentiel appliqué fait intervenir un potentiostat PAR 362 et les courbes courant–tension (J–V) ainsi obtenues sont tracées à vitesse lente (2 mV/s). La cellule électrochimique comprend alors une troisième électrode, une électrode de référence au calomel saturé (ECS). Sauf indication contraire, l'intensité de lumière blanche sera $I = 10$ mW/cm^2 (fournie par la lampe ELH de 300 W d'un projecteur Kodak Ektagraphic AF2).

3. Résultats et discussion

3.1 Morphologie des films

Des photographies de la surface des films ont été prises au microscope électronique à balayage dans le cas d'un film d'épaisseur 700 Å déposé par rotation (figures 1*A* et 1*B*) et d'un film d'épaisseur 600 Å sublimé (fig. 1*C*). Les grossissements sont de 2 000 (*A*) et de 20 000 (*B* et *C*). Un film déposé par rotation présente de gros grains (de 1 à 4 μm) dépassant une structure plus fine mais néanmoins rugueuse (fig. 1*A*). La surface des films minces, obtenus à des vitesses de rotation plus élevées, présente des grains plus petits et moins nombreux que la surface des films plus épais où l'effet centrifuge a été moins grand. Dans le cas d'un agrandissement de 20 000 (fig. 1*B*), il n'apparait pas de fissure dans les films. Par contre, la surface des films sublimés présente une structure de «nouilles» qui ont une longueur dépassant 1 μm pour une section de 0,1 μm (fig. 1*C*). Cet aspect de la surface ne dépend pas de l'épaisseur des films et de grands espaces sont visibles entre les «nouilles». La morphologie des films sublimés est typique d'un taux de sublimation élevé (15–17), qui est ici d'environ 40 Å/min. De grands espaces sont visibles entre les solides, laissant supposer une certaine porosité du film aux couples rédox; ceci a d'ailleurs été confirmé par voltamétrie cyclique pour des films sublimés de PcAlOH sur du platine et avait été montré pour des morphologies semblables de films minces de InPc-Cl et GaPc-Cl (13, 17).

3.2 Paramètres de l'électrolyte

Comme les autres phtalocyanines et la plupart des semiconducteurs organiques, PcAlOH est un semiconducteur de type *p*, menant à l'observation de photocourants cathodiques en court-circuit. La variation du courant de court-circuit J_{sc} et de la tension en circuit ouvert V_{oc} pour une irradiation en lumière blanche avec le pH de la solution est montrée à la figure 2. Le couple rédox utilisé est le couple benzoquinone/hydroquinone (BQ/HQ) de concentration 10^{-2} *M* et la contre-électrode est en platine; l'épaisseur du film de PcAlOH est de 280 Å. Des valeurs maximales pour J_{sc} et V_{oc} sont atteintes pour un pH de 2,5.

Les phtalocyanines (H_2Pc, SnPc, MgPc) ne sont pas connues comme ayant leurs niveaux d'énergie reliés au pH (14); on pense qu'il en est de même pour PcAlOH et la variation de J_{sc} et V_{oc} avec le pH serait due à la variation du potentiel rédox du couple BQ/HQ. Cette variation change le recouvrement des niveaux d'énergie de la benzoquinone avec ceux du semiconducteur organique. Nous verrons plus loin que la variation du pH de la solution BQ/HQ induit un déplacement du potentiel de bande plate de la phtalocyanine. Le meilleur recouvrement est obtenu à pH 2,5 où le potentiel rédox du couple BQ/HQ est de 0,28 V/ECS dans les conditions optimales de concentration.

La figure 3 représente l'allure des variations de J_{sc} et V_{oc} avec la concentration du couple rédox (quinhydrone, fig. 3*A*). Le courant de court-circuit J_{sc} augmente quand la concentration augmente, puis tend à se stabiliser à partir de 4×10^{-3} *M*; ceci indique que les recombinaisons à l'intérieur du semiconducteur, plutôt que la réduction du couple rédox, sont un facteur limitatif du courant dans la phtalocyanine (23, 24). La tension en circuit ouvert V_{oc} diminue de façon monotone dans le domaine de concentration considéré.

En choisissant la concentration de l'oxydant (BQ) égale à 4×10^{-3} *M* et en faisant varier la concentration du réducteur (HQ), on obtient la figure 3*B* en reportant J_{sc} et V_{oc}. Le maximum de courant est atteint pour une concentration du réducteur égale à la moitié de celle de l'oxydant, suggérant que le transfert des électrons de l'hydroquinone sur le platine est plus rapide que celui de PcAlOH à la benzoquinone. La variation de V_{oc} avec la concentration d'hydroquinone est négligeable. Les paramètres de l'électrolyte ont ainsi été optimisés : $[BQ] = 2[HQ] = 4 \times 10^{-3}$ *M* à pH 2,5. Les valeurs de J_{sc} et V_{oc} décroissent lentement avec le temps à cause du brunissement de la solution jaune clair. Une solution fraîche restaure les valeurs initiales.

3.3 Spectres d'absorption et d'action

Les spectres d'absorption des films de PcAlOH déposés par rotation ne présentent qu'une seule bande à 640 nm (fig. 4*A*, épaisseur 250 Å). PcAlOH a été aussi électrodéposé à partir d'une suspension dans le butanol-1 et l'isooctane et ne présente aussi qu'une seule bande d'absorption. Par contre, les spectres d'absorption des films de PcAlOH produits par sublimation présentent, en plus de la bande principale située autour de $\lambda =$ 635 nm, un épaulement qui apparait lorsque l'épaisseur du film augmente et qui devient un pic d'absorption situé à $\lambda = 735$ nm pour les épaisseurs élevées (fig. 5*A*, où les spectres des films d'épaisseur 80 Å, 2800 Å et 4200 Å sont présentés sur une échelle arbitraire relative au spectre du film d'épaisseur 150 Å). Ces spectres ont une allure similaire à ceux des films sublimés de diverses phtalocyanines (H_2Pc, MgPc, FePc, CuPc, CoPc, ZnPc) décrits par Davidson (36), lesquels présentent en général deux bandes d'absorption dans le visible. Dans le cas de MgPc, les deux bandes ont une importance relative qui varie avec l'épaisseur, expliqué en termes de vibrations moléculaires variant avec l'environnement de la molécule. Ce phénomène se retrouve dans le cas de PcAlOH, comme le montrent les spectres d'absorption de la figure 5*A*, où l'intensité relative de l'absorbance à 735 nm passe de 13% (80 Å) à 80% (4200 Å).

Ceci peut être raisonnablement expliqué par le fait qu'il y ait deux formes d'aggrégation de PcAlOH. Ces deux formes pourraient bien être les formes α et β que l'on retrouve chez la plupart des phtalocyanines (26). La forme β est obtenue à partir de la forme α pour des températures du substrat plus élevées (environ 200°C) pour des films de H_2Pc (37). Dans notre cas, la forme α aurait sa contribution à 635 nm (38) et la forme β à

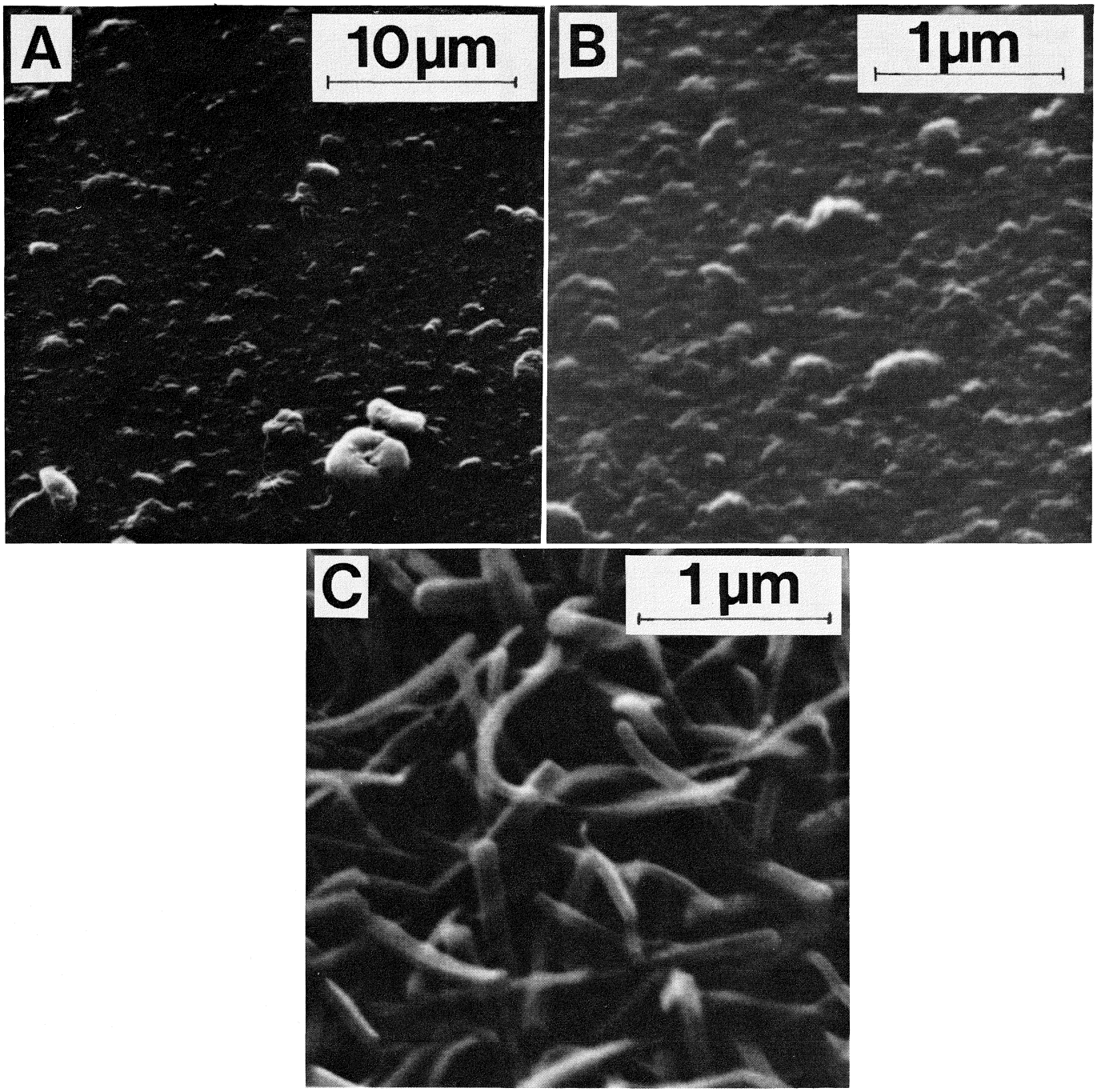

FIG. 1. Photographies obtenues au microscope électronique à balayage de la surface de films de PcAlOH : *A* : film d'épaisseur 700 Å déposé par rotation, grossissement 2 000; *B* : film d'épaisseur 700 Å deposé par rotation, grossissement 20 000; *C* : film d'épaisseur 600 Å sublimé, grossissement 20 000.

735 nm; celle-ci se trouve en plus grande quantité dans les films épais, obtenus pour des temps de sublimation plus longs, où le substrat a atteint des températures plus élevées.

Les spectres d'action des cellules à base de PcAlOH déposée par rotation et sublimée sont présentés aux figures 4*B* et 5*B* pour des épaisseurs de 250 Å et 150 Å, respectivement. Le courant mesuré doit être corrigé pour l'intensité de la lampe, ainsi que pour la réponse du détecteur et la variation du courant J_{sc} avec l'intensité lumineuse I (variée en modifiant la tension d'alimentation de la lampe). Cette variation prend la forme (29) :

$$[1] \quad J_{sc} = kI^{\gamma}$$

où k est une constante de proportionnalité et γ l'exposant de lumière de la cellule, dont la valeur se situe autour de 0,90 pour toutes les cellules. Les spectres d'action corrigés représentent alors le photocourant obtenu en court-circuit pour un flux constant de photons à chaque longueur d'onde; il est donné par la formule :

$$[2] \quad J_{\lambda_{corrig}} = J_{\lambda_{mesur}} \left(\frac{N_{max}}{N_{\lambda}}\right)^{\gamma}$$

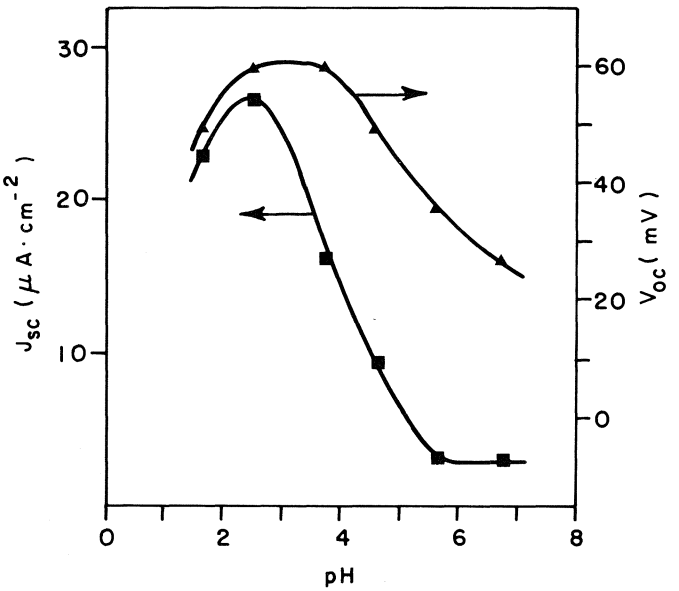

FIG. 2. Variation de J_{sc} et V_{oc} avec le pH de la solution ([BQ] = [HQ] = 10^{-2} M et I = 10 mW cm^{-2}).

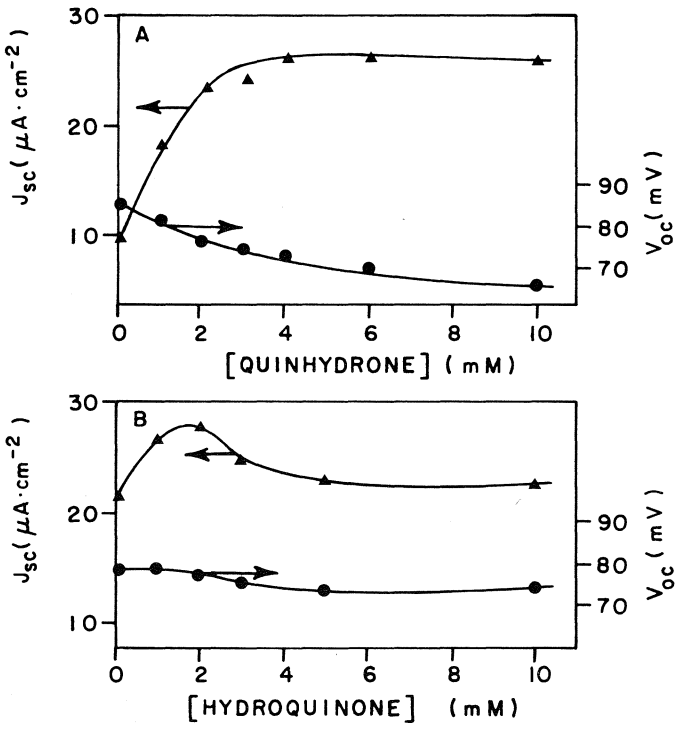

FIG. 3. *A* : Variation de J_{sc} et V_{oc} avec la concentration du couple rédox ([BQ] = [HQ]; pH 2,5; I = 10 mW cm^{-2}). *B* : Variation de J_{sc} et V_{oc} avec la concentration du réducteur ([BQ] = 4 × 10^{-3} M; pH 2,5; I = 10 mW cm^{-2}).

où N_{max} et N_λ sont le flux de photons incidents maximum et le flux de photons incidents pour la longueur d'onde considérée, respectivement. Le flux de photons maximum est ici de 8,3 × 10^{14} photons cm^{-2} s^{-1} pour une irradiation directe de l'interface. Les spectres d'action suivent l'allure des spectres d'absorption pour les deux types de films. Dans le cas d'un film sublimé, la forme α serait la plus photoactive; la contribution de la forme β au photocourant est assez faible et ne varie que très peu avec l'épaisseur du film de PcAlOH.

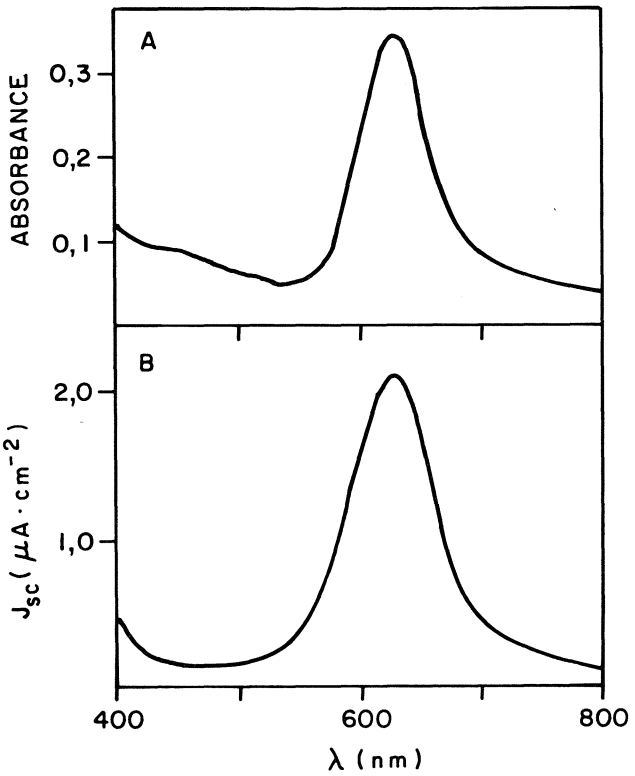

FIG. 4. *A* : Spectre d'absorption d'un film d'épaisseur 250 Å de PcAlOH déposé par rotation. *B* : Spectre d'action du même film.

On peut tirer le rendement quantique de la cellule à partir du spectre d'action à l'aide de l'éq. [3] (39) :

[3] $\phi(\%) = 100\, J_{sc} h\nu / qI$

qui peut aussi s'écrire :

[4] $\phi(\%) = 100\, J_{sc} / qN$

où $h\nu$ est l'énergie du photon, q la charge de l'électron et N le flux de photons incidents. Le rendement quantique est alors le rapport entre le nombre d'électrons collectés et le nombre de photons incidents et prend une valeur de 1,58% à 628 nm pour un film d'épaisseur 250 Å déposé par rotation et 0,93% à 618 nm pour un film sublimé d'épaisseur 150 Å. Cependant, la réponse spectrale d'un film sublimé couvre une part plus grande du spectre visible.

3.4 Courbes courant–tension

La figure 6*A* nous montre les caractéristiques *J–V* d'une cellule NESA/PcAlOH/BQ/HQ/Pt dans les conditions optimales d'électrolyte; la courbe 1 représente les caractéristiques du NESA dans le noir, les courbes 2 et 3 celles d'un film d'épaisseur 250 Å déposé par rotation, dans le noir (2) et sous illumination (3), et les courbes 4 et 5 celles d'un film sublimé d'épaisseur 150 Å dans le noir (4) et sous une même illumination (5). Les courbes *J–V* de PcAlOH dans le noir montrent des rectifications moyennes, les rapports de rectification étant, à 0,2 volts, de 5,8 pour le film déposé par rotation et de 2,2 pour le film sublimé. Lorsque les électrodes sont irradiées en lumière blanche, on note l'apparition de photocourants cathodiques dans la zone de polarisation inverse, indiquant que les électrons provenant du semiconducteur organique vont réduire la benzoquinone en solution.

Dans la région où la polarisation de l'électrode est directe, un

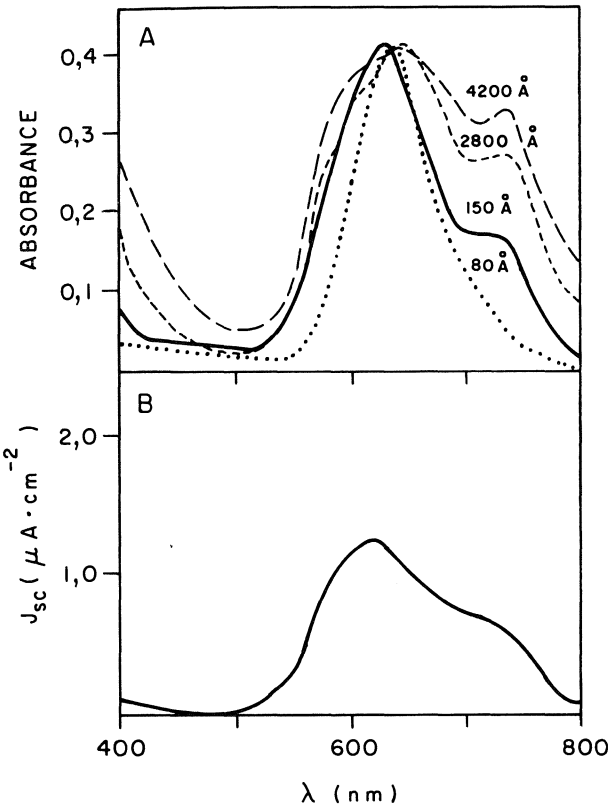

FIG. 5. *A* : Spectre d'absorption de films sublimés de PcAlOH pour différentes épaisseurs. *B* : Spectre d'action d'un film sublimé de PcAlOH d'épaisseur 150 Å.

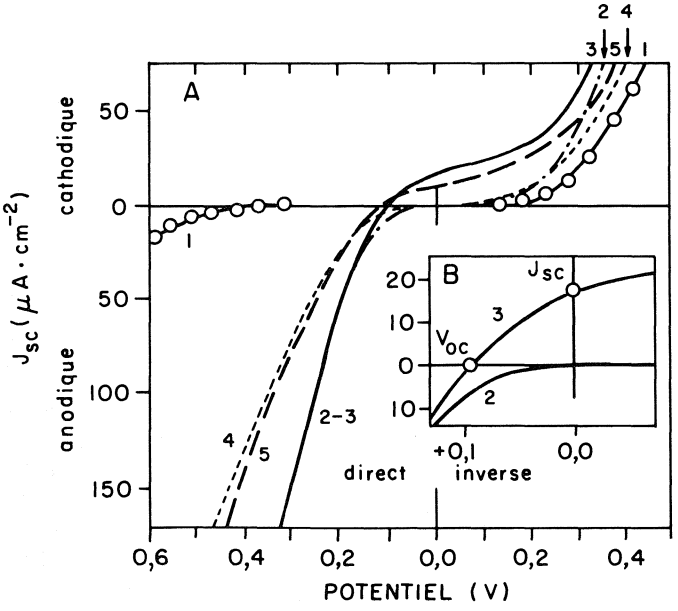

FIG. 6. *A* : Caractéristiques *J–V* (1) du NESA dans le noir; (2) d'un film d'épaisseur 250 Å de PcAlOH déposé par rotation, dans le noir et (3) sous illumination en lumière blanche de 10 mW cm^{-2}; (4) d'un film de PcAlOH sublimé d'épaisseur 150 Å, dans le noir et (5) sous même illumination. *B* : Détermination graphique de J_{sc} et V_{oc}.

photocourant anodique apparait pour le film sublimé, contrairement au film déposé par rotation, pour lequel il n'existe aucun photocourant. D'autre part, la pente des courbes *J–V* en polarisation directe dans le noir est assez différente; ces portions de courbes suivent l'équation suivante (20) :

TABLEAU 1. Courant d'échange à l'équilibre J_0, paramètre de la diode m et résistance en série R_s de la cellule NESA/PcAlOH/BQ/HQ/Pt selon la technique de déposition du film organique

Méthode de déposition	J_0 (μA/cm^2)	m	R_s (Ω)
Rotation	0,4	1,4	500
Sublimation	0,1	1,2	1220

$$[5] \quad J = J_0\left[\exp\left(\frac{q(V - JR_s)}{mkT}\right) - 1\right]$$

où J_0 est la densité de courant d'échange, m est un paramètre ajustable et R_s est la résistance en série de la cellule photoélectrochimique. Cette expression est similaire à celle qui décrit les caractéristiques *J–V* dans l'obscurité pour une barrière de Schottky à la jonction métal–semiconducteur (40).

Lorsque $V \geqslant 3kT/q$, le dernier terme entre parenthèses peut être négligé (20). Si $R_s = 0$, un graphique de ln *J* en fonction de *V* donne une droite avec J_0 comme ordonnée à l'origine; m est obtenu à partir de la valeur de la pente. Si $R_s \neq 0$, sa valeur peut être déterminée par la déviation de la courbe à la linéarité lorsque le potentiel appliqué est élevé. Les valeurs de J_0, m et R_s pour les deux types de films sont rapportées dans le tableau 1. On remarque principalement que le film déposé par rotation présente une résistance en série beaucoup plus faible que le film sublimé. Ce phénomène ainsi que l'absence de courant anodique dans le film déposé par rotation pourrait être dû à la présence de traces de solvant dans la masse du semiconducteur organique.

L'intersection de la courbe *J–V* sous illumination avec les axes des courants et tensions nous donne le courant en court-circuit J_{sc} et la tension en circuit ouvert V_{oc}, respectivement (fig. 6*B*). On peut ainsi calculer le facteur de remplissage *ff* défini comme suit :

$$[6] \quad ff = \frac{(J \cdot V)_{max}}{J_{sc} \cdot V_{oc}}$$

Cette valeur de *ff* varie peu d'une cellule à l'autre et se situe autour d'une valeur moyenne de 0,35. L'efficacité des cellules est alors donnée par :

$$[7] \quad \eta(\%) = 100\, J_{sc} V_{oc} ff / I$$

Les valeurs de J_{sc}, V_{oc}, *ff* et η sont présentées dans le tableau 2 pour les deux types de films. Des courants plus élevés et des tensions plus faibles sont produits lorsque le film de PcAlOH est déposé par rotation, conduisant à des valeurs très semblables de rendement de conversion qui se situent pour les deux types de films aux alentours de 5×10^{-3}%.

3.5 Photocourants et potentiels de bande plate

Les variations d'amplitude et de signe du photocourant en lumière blanche avec le potentiel appliqué sont tracées sur la figure 7 pour un film d'épaisseur 250 Å déposé par rotation à pH 2,5 (*a*) et pour un film sublimé d'épaisseur 230 Å à pH 2,5 (*b*), 4,5 (*c*) et 6,0 (*d*). Le couple rédox est BQ/HQ aux conditions optimales de concentration; les potentiels rédox dans les conditions de pH sont indiqués par de flèches.

Dans la gamme de potentiels utilisée, le photocourant atteint un maximum lorsque le potentiel est augmenté dans la direction cathodique. La décroissance du courant cathodique lorsque des tensions cathodiques élevées sont appliquées est due à la

TABLEAU 2. Courant de court-circuit J_{sc}, tension en circuit ouvert V_{oc}, facteur de remplissage ff et rendement de conversion η pour des films de PcAlOH déposés par rotation et par sublimation (I = 10 mW cm^{-2})

Méthode de déposition	J_{sc} (μA/cm^2)	V_{oc} (mV)	ff	η (10^{-3}%)
Rotation	17,5	96	0,34	5,7
Sublimation	11,8	118	0,36	5,0

TABLEAU 3. Potentiel de bandes plates V_{fb}, potentiel rédox E_{red}, tension maximale ΔV et tension en circuit-ouvert V_{oc} selon la méthode de déposition du film organique et le pH de la solution

Méthode de déposition	pH	V_{fb} (V)	E_{red} (V)	ΔV (V)	V_{oc} (V)
Rotation	2,5	0,43	0,29	0,14	0,10
Sublimation	2,5	0,46	0,29	0,17	0,12
	4,5	0,19	0,16	0,03	—
	6,0	0,10	0,12	−0,02	—

compétition entre les électrons produits dans le noir et les électrons photogénérés pour les espèces oxydées disponibles à l'interface (20). Cette compétition est visible sur la figure 6*A* où les valeurs des courants dans le noir réjoignent celles des courants sous illumination.

On observe des photocourants cathodique et anodique lorsque le film est déposé par sublimation, tandis qu'aucun courant anodique n'apparait pour un film déposé par rotation, comme l'indique la figure 6*A*.

Dans le modèle de bande du semiconducteur organique, en considérant que le contact PcAlOH/NESA est ohmique (24), le point où le photocourant passe de cathodique à anodique correspond au potentiel de bandes plates (V_{fb}) du pigment (10). Si un potentiel est appliqué du côté cathodique de V_{fb}, une région de charges d'espace est créée dans PcAlOH; les trous et les électrons photogénérés sont séparés par le champ électrique présent dans la région de charges d'espace, et les électrons sont injectés dans la solution. Du côté anodique de V_{fb}, PcAlOH se comporte comme une résistance variable pour le transfert des trous dans la solution. Lorsque PcAlOH est illuminée, sa résistance diminue à cause de l'augmentation de la densité en porteurs de charges. Les photocourants anodiques ne sont pas dus à une sensibilisation de SnO_2 car ils sont présents aussi lorsque le substrat est le platine. PcAlOH déposée sur du NESA n'est pas une simple couche résistive, mais sa présence modifie la disponibilité du rédox à l'interface comme le montre la figure 6*A* si on compare les courbes directes pour le NESA nu et recouvert de PcAlOH. Le tableau 3 rapporte les valeurs de V_{fb} mesurées sur la figure 7. Quand aucun photocourant anodique existe, on utilise une extrapolation des courbes pour déterminer V_{fb}. La différence ΔV est définie comme suit :

$$[8] \quad \Delta V = V_{fb} - E_{red}$$

et correspond à la tension maximale que peut fournir la cellule. Le potentiel de bande plate varie beaucoup avec le pH de la solution dans le cas du couple rédox BQ/HQ, alors qu'il a été trouvé indépendant du pH dans le cas du couple rédox I_3^-/I^-. Un comportement identique a été observé (20) pour un film de SAlPc. Il peut être expliqué en formulant l'hypothèse de la formation d'un faible complexe de transfert de charge entre PcAlOH et la benzoquinone à la surface du film. Un complexe de transfert de charge à l'état fondamental a déjà été observé

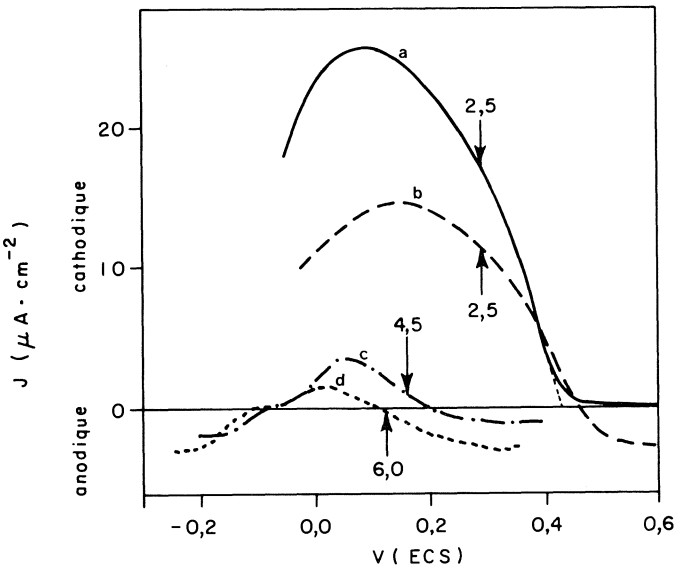

FIG. 7. Variation du photocourant avec le potentiel appliqué sur un film d'épaisseur 250 Å déposé par rotation à pH 2,5 (a) et pour un film sublimé d'épaisseur 230 Å à pH 2,5 (b), 4,5 (c) et 6,0 (d).

entre H_2Pc et le chloranil; il augmente la conductivité dans le noir et la photoconductivité du pigment (14, 41, 42). La benzoquinone est un accepteur plus faible que le chloranil, mais un complexe à l'état fondamental a été rapporté dans l'acétone entre BQ et des tétratolylporphines libres et de zinc (43), qui sont des molécules très proches de PcAlOH. La diminution de $E_{rédox}$ est de 0,059 V par unité de pH, et la présence de la benzoquinone sur l'électrode doit causer un déplacement du potentiel de bande plate si l'hydroquinone est aussi adsorbée sur la surface du semiconducteur. De pH 2,5 à pH 6,0, la diminution de $E_{rédox}$ doit être de 0,21 V (valeur mesurée : 0,17 V), et la variation de V_{fb} avec le pH est de 0,36 V dans le même sens. Cet effet est similaire au déplacement de V_{fb} avec le pH pour les oxydes semiconducteurs (44). Si BQ/HQ n'affectait pas le potentiel de bande plate de PcAlOH, on s'attendrait à une augmentation de la tension en circuit ouvert V_{oc} avec le pH, le potentiel rédox devenant de plus en plus cathodique. Ceci n'est pas observé expérimentalement.

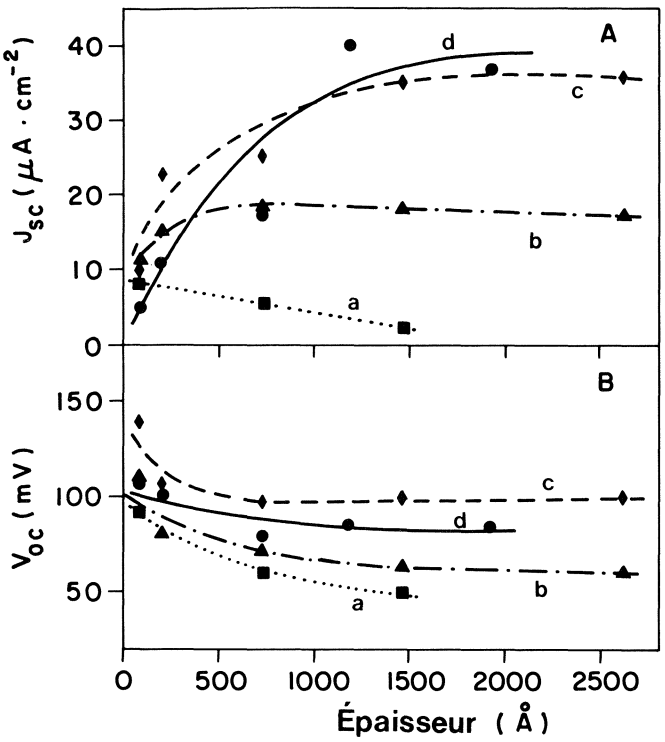

FIG. 8. Illumination en lumière blanche de I = 10 mW cm^{-2} : *A* : Variations de J_{sc} avec l'épaisseur du film de PcAlOH déposé par rotation. *B* : Variations de V_{oc} avec l'épaisseur du film de PcAlOH déposé par rotation. Courbes a : films fraîchement déposés; courbes b : laissés à l'air libre pendant 12 jours; courbes c : films laissés à l'air libre pendant 21 mois; courbes d : films plongés rapidement dans du DMSO.

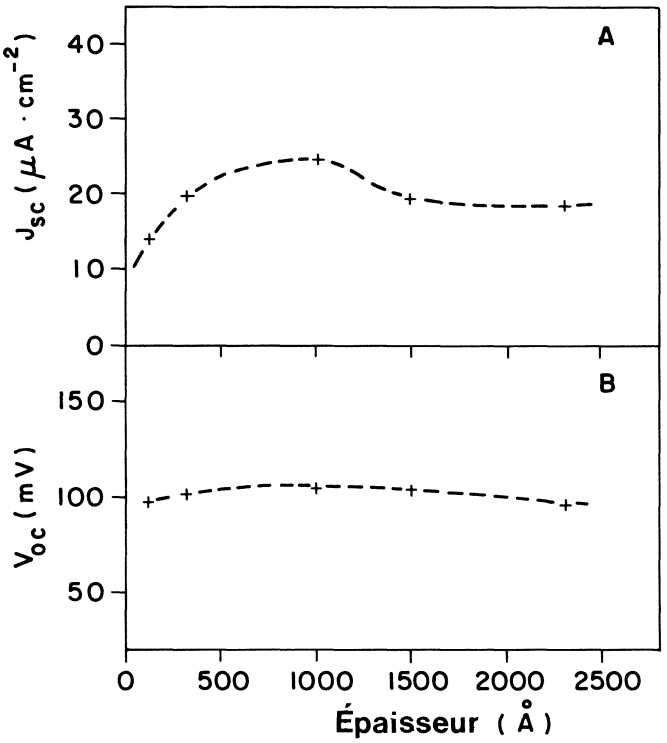

FIG. 9. Illumination en lumière blanche de I = 10 mW cm^{-2} : *A* : Variation de J_{sc} avec l'épaisseur du film sublimé de PcAlOH. *B* : Variation de V_{oc} avec l'épaisseur du film sublimé de PcAlOH.

La valeur de ΔV représente la tension maximale que peut fournir la cellule. Les valeurs de ΔV sont de 0,14 V pour un film déposé par rotation et 0,17 V pour un film sublimé, et des valeurs expérimentales respectives de 0,10 V et 0,12 V ont été atteintes.

3.6 Épaisseur des films

Les films de PcAlOH déposés par rotation ont été préparés en versant une goutte d'une suspension de PcAlOH dans du DMSO sur un support en rotation. Le DMSO est un solvant ayant un point d'ébullition relativement élevé (189°C) et il semble que sa présence ait un effet important sur la photoactivité du film semiconducteur. En effet, les films de différentes épaisseurs séchés à l'air libre pendant 12 jours donnent un courant de court-circuit plus important que les mêmes films fraîchement déposés (fig. 8*A*, courbes a et b). Cette évolution est continuelle et on observe une plus grande augmentation de J_{sc} (fig. 8*A*, courbe c) après avoir laissé les films à l'air libre pendant plusieurs mois. L'augmentation de J_{sc} est d'autant plus importante que le film est épais et contient plus de DMSO. L'allure de la courbe c (fig. 8*A*) est typique d'une absorption faible dans des films minces (jusqu'à 2600 Å) où la lumière pénètre tout le film de PcAlOH (14). Plonger rapidement ces films dans le DMSO fait chuter de nouveau le courant pour les films minces, mais ne semble pas affecter les films plus épais (fig. 8*A*, courbe d), probablement car le DMSO n'a pas eu le temps de diffuser suffisamment dans les films. Le même phénomène est observé pour la mesure de la tension en circuit ouvert V_{oc} et cette fois les variations sont indépendantes de l'épaisseur (fig. 8*B*, courbes a–d).

Les films préparés par sublimation présentent un maximum de courant de court-circuit pour une épaisseur de 1000 Å environ, tandis que la tension en circuit ouvert est pratiquement indépendante de l'épaisseur du film jusqu'à une épaisseur de 2500 Å (figures 9*A* et *B*).

Ainsi, le DMSO a une grande influence sur le comportement des cellules NESA/PcAlOH/BQ/HQ/Pt où le film de PcAlOH a été déposé par rotation. Sa présence dans les cellules fraîches limite le courant et la tension délivrés par la cellule, surtout pour les grandes épaisseurs. Cet effet disparait avec le temps et est réversible; plonger les lamelles dans le solvant diminue à nouveau le photocourant et la phototension. Il est probable que les molécules de DMSO agissent comme des sites de recombinaison pour les électrons et les trous formés par l'absorption de la lumière dans le corps du semiconducteur. Le point d'ébullition élevé du DMSO fait en sorte que son action dure longtemps, son taux d'évaporation dans l'air étant faible. Le fait de placer les lamelles fraîchement déposées dans une étuve à 160°C fait craqueler les films organiques. Le DMSO semble fortement piégé dans la structure du film car aucun changement n'est survenu après avoir placé une lamelle sous vide primaire (10^{-2} Torr) pendant une nuit.

Enfin, il est connu que l'oxygène s'adsorbe sur les phtalocyanines et a un effet important sur la photoconductivité de leurs films minces (30, 31, 45). Le DMSO pourrait altérer cet effet en occupant certains des sites préférentiels de l'oxygène.

3.7 Contre-électrode

Loutfy et McIntyre (23, 24) ont réalisé une étude systématique de différents métaux M utilisés dans des cellules NESA/x-H_2Pc/rédox/M. Il en résulte que les photocourants les plus élevés sont obtenus avec des contre-électrodes en aluminium et en indium, mais aucune remarque sur la stabilité de ces systèmes n'a été faite. Dans nos conditions d'électrolyte utilisées, certaines contre-électrodes donnent des courants très

TABLEAU 4. Variation du courant de court-circuit sous illumination (J_{sc}) et dans le noir (J_{noir}), du rapport $|J_{noir}|/J_{sc}$, de la tension en circuit ouvert sous illumination (V_{oc}) et dans le noir (V_{noir}), du rapport $|V_{noir}|/V_{oc}$ et de l'efficacité de conversion η en fonction de l'épaisseur du film de PcAlOH, de la puissance lumineuse incidente et de la nature de la contre-électrode (films déposés par rotation)

Épaisseur (Å)	Puissance lumineuse (mW cm^{-2})	Contre-électrode	J_{sc} (μA cm^{-2})	J_{noir} (μA cm^{-2})	$\lvert J_{noir}\rvert/J_{sc}$ (%)	V_{oc} (mV)	V_{noir} (mV)	$\lvert V_{noir}\rvert/V_{oc}$ (%)	η (%)
100	10	Au	7,8	−0,02	0,3	88,8	+0,4	0,5	0,002
100	10	Pt	13,8	−0,2	1,4	70,9	−19,0	26,8	0,003
250	10	Pt	21,8	−0,2	0,9	74,2	−11,2	15,1	0,006
250	10	Zr	41,8	+1,3	3,1	210,0	+103,0	49,0	0,030
600	85	Pt	32,0	−0,5	1,6	93,0	−14,7	15,8	0,001
600	85	Zr	117,2	+0,9	0,8	266,0	+136,0	51,1	0,012
600	85	V	175,2	+27,4	15,6	337,0	+216,0	64,1	0,024

faibles (Ta, Nb, Pb, Sn, Cu, Fe, Ti, Zn, Al) ou s'oxydent très rapidement (Sc). Les électrodes du tableau 4 (Pt, Au, Zr, V) ont une réponse stable (films de PcAlOH déposés par rotation). Le meilleure réponse est fournie par une contre-électrode en vanadium avec $J_{sc} = 175{,}2\ \mu A/cm^2$ et $V_{oc} = 337$ mV pour une puissance lumineuse de 85 mW/cm^2. Des valeurs élevées sont aussi obtenues avec le zirconium ($J_{sc} = 117{,}2\ \mu A/cm^2$ et $V_{oc} = 226$ mV). Il semble donc que le rendement de la cellule soit limité par le taux de réaction du réducteur à l'électrode métallique. Cependant, l'électrode de zirconium est soumise à une corrosion assez rapide (10 h) due à un mécanisme électrochimique catalysé par les photocourants, et on pense qu'il en est de même avec le vanadium; en effet, les courants et tensions dans le noir sont importants (15,6% et 64,1% des courants et tensions totaux), bien qu'aucune corrosion ne soit visible à la surface de l'électrode métallique. Les contre-électrodes en platine et en or sont par contre très inertes dans les conditions d'expérience et nous permettent d'éviter la corrosion, mais elles conduisent à des valeurs plus faibles.

3.8 Modèle de bandes

L'absorption de photons par l'électrode semiconductrice conduit, à travers un processus excitonique, à la création de paires électron–trous; ces derniers se séparent sous l'effet du champ électrique de la jonction. Les électrons (porteurs minoritaires) arrivent à l'interface semiconducteur–électrolyte et vont réduire une espèce oxydante en solution. Les trous se déplacent à travers le semiconducteur lui-même; ils recombinent ensuite au contact ohmique (NESA) avec les électrons venant du circuit extérieur qui sont fournis par la réaction d'oxydation du réducteur à la contre-électrode. Le transfert d'électrons du semiconducteur à l'espèce électroactive de l'électrolyte est possible théoriquement si la distribution d'énergie de l'espèce en solution recouvre la bande de conduction du semiconducteur de type *p*.

Ainsi, il est possible de tracer un diagramme montrant les niveaux d'énergie du semiconducteur et le potentiel rédox du couple en solution (fig. 10). Le niveau de Fermi, E_F, de la solution est représenté par le potentiel rédox du couple, mesuré dans les conditions expérimentales ($E_{red} = 0.29$ V/ECS pour BQ/HQ à pH 2,5) et les bandes d'énergie du semiconducteur sont celles trouvées par Lawrence *et al.* (46) pour SAlPc, soit $E_c = 3{,}90$ eV pour la bande de conduction et $E_g = 1{,}80$ eV pour le saut de bande interdite. Le potentiel de bandes plates, V_{fb}, correspondant au niveau de Fermi du semiconducteur sous illumination, est déterminé par l'intersection avec l'axe des

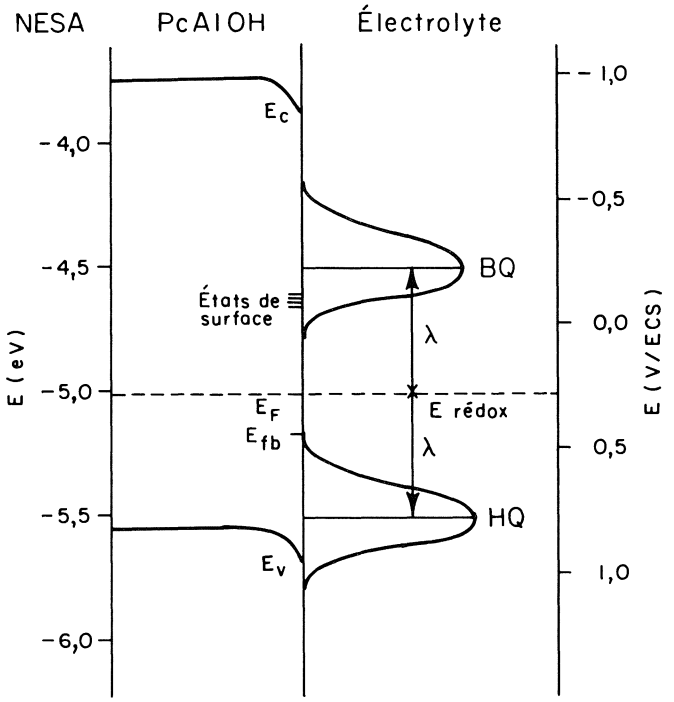

FIG. 10. Diagramme des bandes d'énergie de la cellule NESA/PcAlOH/BQ/HQ/Pt à pH 2,5.

tensions de la courbe photocourant–tension appliquée (photocourant = courant sous illumination − courant dans le noir). Quand aucun photocourant anodique n'est mesuré, on utilise une extrapolation de la courbe pour trouver V_{fb}. Dans le cas de la cellule formée d'un film de PcAlOH d'épaisseur 250 Å obtenu par rotation, la valeur de V_{fb} mesurée est de 0,43 V/ECS pour BQ/HQ. Après le contact avec l'électrolyte, les électrons passent de la solution au semiconducteur pour égaliser les niveaux de Fermi. Il en résulte une distribution de charges à l'intérieur du semiconducteur sur une profondeur *W*, ce qui crée un champ électrique conduisant à la séparation des paires électron–trou générées par la lumière. La vitesse de transfert des charges entre la phtalocyanine et l'oxydant en solution est la plus rapide quand l'énergie de l'état excité de la phtalocyanine (représenté par l'énergie de la bande de conduction) est proche de celle de l'accepteur d'électrons. D'après Gerisher (47), les fonctions de distribution des niveaux d'énergie du couple rédox BQ/HQ sont données par leur potentiel rédox et leur énergie de réorientation $\lambda = 0{,}5$ eV. Le recouvrement entre les niveaux

d'énergie de la benzoquinone et de la bande de conduction de la phtalocyanine n'est pas grand, mais de nombreuses données expérimentales (21, 23, 24) portent à croire qu'il existe chez les phtalocyanines des états de surface par l'intermédiaire desquels se fait l'échange de charges. Ces états de surfaces sont situés autour de $-0,1$ V/ECS et on observe alors un bon recouvrement d'énergie entre ces états de surface et la benzoquinone en solution, comme le représente la figure 10.

4. Conclusion

Des films minces de semiconducteurs organiques ont été préparés par déposition par rotation sur des substrats transparents. Les efficacités des cellules photoélectrochimiques ainsi obtenues sont du même ordre de grandeur que celles obtenues pour des films sublimés. Cependant, le solvant DMSO utilisé durant la déposition est difficile à éliminer et sa présence tend à diminuer l'efficacité des cellules photoélectrochimiques.

La formation d'un faible complexe de transfert de charge entre la benzoquinone et PcAlOH peut être à l'origine du déplacement du potentiel de bande plate avec le pH de la solution. L'emploi d'une contre-électrode en vanadium a permis d'atteindre des valeurs élevées pour le courant de court-circuit ($J_{sc} = 0,175$ mA/cm^2) et pour la tension en circuit ouvert ($V_{oc} = 0,337$ V) sous une irradiation de 85 mW/cm^2 en lumière blanche avec le couple rédox BQ/HQ. Le rendement de la cellule est alors de $2,4 \times 10^{-2}$%, mais des phénomènes de corrosion apparaissent à la contre-électrode. Une cellule stable NESA/PcAlOH/BQ/HQ/Pt possède une efficacité de conversion de 0,006% sous illumination de lumière blanche d'intensité 10 mW/cm^2. Ce rendement peut être amélioré en augmentant la photoconductivité et en élargissant le spectre d'absorption de la phtalocyanine d'hydroxyaluminium par un traitement chimique approprié (38, 48, 49).

Remerciements

Ce travail est supporté par des subventions du Conseil de recherches en sciences naturelles et en génie. Les auteurs tiennent à remercier Monsieur J. P. Ricbourg et l'INRS–Géoressources pour les expériences de microscopie électronique à balayage, ainsi que le professeur F. Rheault de l'INRS–Énergie pour son soutien constant.

1. H. Kallman et M. Silver (*Éditeurs*). Symposium on electrical conductivity in organic solids. Wiley Interscience, New York. 1961.
2. F. Gutman et L. E. Lyons. Organic semiconductors. Wiley Interscience, New York. 1967.
3. G. A. Chamberlain. Sol. Cells, **8**, 47 (1983).
4. C. D. Jaeger, F.-R. F. Fan et A. J. Bard. J. Am. Chem. Soc. **102**, 2592 (1980).
5. A. Giraudeau, F.-R. F. Fan et A. J. Bard. J. Am. Chem. Soc. **102**, 5137 (1980).
6. Y. Nakato, M. Shioji et H. Tsubomura. J. Phys. Chem. **85**, 1670 (1981).
7. T. M. Mezza, C. L. Linkous, V. R. Shepard, Jr., N. R. Armstrong, R. Nohr et M. Kenney. J. Electroanal. Chem. **124**, 311 (1981).
8. N. R. Armstrong et V. R. Shepard, Jr. J. Electroanal. Chem. **131**, 113 (1982).
9. P. Leempoel, M. Castro-Acuna, F.-R. F. Fan et A. J. Bard. J. Phys. Chem. **86**, 1396 (1982).
10. H. Tachikawa et L. R. Faulkner. J. Am. Chem. Soc. **100**, 4379 (1978).
11. N. Minami, T. Watanabe, A. Fujishima et K. Honda. Ber. Bunsenges. Phys. Chem. **83**, 476 (1979).
12. N. Minami. J. Chem. Soc. Faraday Trans. 2, **78**, 1871 (1982).
13. C. Linkous, T. Klofta et N. R. Armstrong. J. Electrochem. Soc. **130**, 1050 (1983).
14. P. Leempoel, F.-R. F. Fan et A. J. Bard. J. Phys. Chem. **87**, 2948 (1983).
15. P. C. Rieke, C. L. Linkous et N. R. Armstrong. J. Am. Chem. Soc. **88**, 1351 (1984).
16. P. C. Rieke et N. R. Armstrong. J. Am. Chem. Soc. **106**, 47 (1984).
17. T. J. Klofta, P. C. Rieke, C. A. Linkous, W. J. Buttner, A. Nanthakuma, T. D. Mewborn et N. R. Armstrong. J. Electrochem. Soc. **132**, 2134 (1985).
18. B. Marsan, G. Bélanger et D.-L. Piron. Can. J. Chem. **63**, 1580 (1985).
19. W. J. Buttner, P. C. Rieke et N. R. Armstrong. J. Am. Chem. Soc. **107**, 3738 (1985).
20. D. Bélanger, J. P. Dodelet, L. H. Dao et B. A. Lombos. J. Phys. Chem. **88**, 4288 (1984).
21. F.-R. F. Fan et L. R. Faulkner. J. Am. Chem. Soc. **101**, 4779 (1979).
22. H. T. Tien et J. Higgins. Chem. Phys. Lett. **93**, 276 (1982).
23. R. O. Loutfy et L. F. McIntyre. Sol. Energy Mater. **6**, 467 (1982).
24. R. O. Loutfy et L. F. McIntyre. Can. J. Chem. **61**, 72 (1983).
25. J. R. Harbour, B. Dietelbach et J. Duff. J. Phys. Chem. **87**, 5456 (1983).
26. J. Simon et J. J. André. Molecular semiconductors, Springer Verlag, Berlin. 1985.
27. R. O. Loutfy, C. K. Hsaio et R. Ho. Can. J. Phys. **61**, 1416 (1983).
28. A. M. Hor et R. O. Loutfy. Thin Solid Films, **106**, 291 (1983).
29. H. Meier. Organic semiconductors. Verlag Chemie, Weinheim. 1974.
30. G. H. Heilmeier et S. E. Harrison. Phys. Rev. **132**, 2010 (1963).
31. S. C. Dahlberg et M. E. Musser. J. Chem. Phys. **72**, 6706 (1980).
32. S. Baker, M. C. Petty, G. G. Roberts et M. V. Twigg. Thin Solid Films, **99**, 53 (1983).
33. G. J. Kowacs, P. S. Vincett et J. H. Sharp. Can. J. Phys. **63**, 346 (1985).
34. N. Minami, K. Sasaki et K. Tsuda. J. Appl. Phys. **54**, 6764 (1983).
35. J. P. Linsky, J. R. Paul, R. S. Nohr et M. E. Kenney. Inorg. Chem. **19**, 3131 (1980).
36. A. T. Davidson. J. Chem. Phys. **77**, 168 (1982).
37. M. S. Mindorff et D. E. Brodie. Can. J. Phys. **59**, 249 (1981).
38. L. H. Dao et G. Perrier. Chem. Lett. **8**, 1259 (1986).
39. J. P. Dodelet, H.-P. Pommier et M. Ringuet. J. Appl. Phys. **53**, 4270 (1982).
40. E. H. Rhoderick. Metal–semiconductor contacts. Calendon Press, Oxford. 1980.
41. D. R. Kearns, G. Tollin et M. Calvin. J. Chem. Phys. **32**, 1020 (1960).
42. S. C. Dahlberg et M. E. Musser. Surf. Sci. **90**, 1 (1979).
43. S. Yamada, T. Sato, K. Kano et T. Agawa. Photochem. Photobiol. **37**, 257 (1983).
44. K. L. Hardee et A. J. Bard. J. Electrochem. Soc. **122**, 739 (1975).
45. M. Martin, J. J. André et J. Simon. J. Appl. Phys. **54**, 2792 (1983).
46. M. F. Lawrence, J. P. Dodelet et L. H. Dao. J. Electrochem. Soc. **131**, 2977 (1984).
47. H. Gerischer. Top. Appl. Phys. **31**, 115 (1979).
48. G. Perrier et L. H. Dao. J. Electrochem. Soc. Soumis pour publication.
49. G. Perrier, L. H. Dao et K. Cole. J. Phys. Chem. Soumis pour publication.

The synthesis, X-ray structure, and substitution lability of chloro(2,3,7,8,12,13,17,18-octaethylporphinato)(triphenylphosphine)rhodium(III)

DAVID C. THACKRAY, SARA ARIEL, TAK W. LEUNG, KUSUM MENON, BRIAN R. JAMES,[1] AND JAMES TROTTER
Department of Chemistry, University of British Columbia, Vancouver, B.C., Canada V6T 1Y6

Received May 22, 1986

DAVID C. THACKRAY, SARA ARIEL, TAK W. LEUNG, KUSUM MENON, BRIAN R. JAMES, and JAMES TROTTER. Can. J. Chem. **64**, 2440 (1986).

The rhodium(III) octaethylporphyrin complex Rh(OEP)(PPh_3)Cl (**1**) has been synthesized via Rh(III) or Rh(I) precursors, and fully characterized both by spectroscopy and single crystal data. The crystals, available as a bis(chloroform) solvate are triclinic, $P\bar{1}$, $a = 13.478(5)$, $b = 14.300(5)$, $c = 15.346(4)$ Å, $\alpha = 102.33(2)$, $\beta = 102.89(2)$, $\gamma = 90.56(3)°$, $Z = 2$, $D_x = 1.384$ g cm^{-3}. The structure was determined from Mo diffractometer data and refined by least-squares methods to $R = 0.095$, $R_w = 0.068$ for 5189 reflections. The octahedrally coordinated rhodium atom is displaced by 0.077 Å from the mean plane of the four N atoms, towards the triphenylphosphine group. The average Rh – ring nitrogen distance is 2.024 Å, Rh—P is 2.306(3) Å and Rh—Cl, 2.442(2) Å. Solution equilibria studies on **1** describe formation of Rh(OEP)L_2^+ (L = PPh_3, P^nBu_3) via thermal reactions (including thermodynamic data for the PPh_3 system), and formation of Rh(OEP)Cl(L′) species (L′ = CO, THF, MeCN) via photochemical processes.

DAVID C. THACKRAY, SARA ARIEL, TAK W. LEUNG, KUSUM MENON, BRIAN R. JAMES et JAMES TROTTER. Can. J. Chem. **64**, 2440 (1986).

On a synthétisé le complexe d'octaéthylporphyrine rhodium(III), Rh(OEP)(PPh_3)Cl (**1**) à partir de précurseurs de Rh(III) ou de Rh(I) et on l'a complètement caractérisé tant par spectroscopie que par diffraction des rayons-X sur un cristal unique. Les cristaux, obtenus sous une forme solvatée par deux molécules de chloroforme, sont tricliniques et ils appartiennent au groupe d'espace $P\bar{1}$ avec $a = 13,478(5)$, $b = 14,300(5)$ et $c = 15,346(4)$ Å et $\alpha = 102,33(2)$, $\beta = 102,89(2)$ et $\gamma = 90,56(3)°$, $Z = 2$ et $D_x = 1,384$ g cm^{-3}. On a déterminé la structure à partir de données de diffraction au Mo et on a affiné la structure par la méthode des moindres carrés jusqu'à des valeurs de $R = 0,095$ et de $R_w = 0,068$ pour 5189 réflexions. L'atome de rhodium, de coordination octaédrique, est déplacé vers le groupe triphénylphosphine et il s'éloigne ainsi de 0,077 Å du plan moyen des quatre atomes de N. La distance moyenne Rh-azote du cycle est égale à 2,024 Å, celle de Rh—P à 2,306(3) Å et celle de Rh—Cl à 2,442(2) Å. Des études d'équilibres en solution (qui incluent des données thermodynamiques pour le système PPh_3), effectuées sur le composé **1**, décrivent la formation de Rh(OEP)L_2^+ (L = PPh_3, P^nBu_3) par le biais de réactions thermiques ainsi que la formation d'espèces Rh(OEP)Cl(L′) (L′ = CO, THF, MeCN) par le biais de processus photochimiques.

[Traduit par la revue]

Introduction

Of particular interest to us is the investigation and development of metalloporphyrin chemistry as it relates to catalysis involving small molecules such as O_2, CO, and H_2. While most of the focus has been on ruthenium porphyrin chemistry (1–8), we have renewed interest in our earlier work on rhodium porphyrins (9).

In this paper, we report the details of the preparation and characterization of Rh(OEP)(PPh_3)Cl,[2] **1**, including an X-ray structure and some solution chemistry. Solution data on the formation of the bisphosphine cations Rh(OEP)$(L)_2^+$, where L is PPh_3 or P^nBu_3, are also presented. The latter complexes are of interest because isoelectronic ruthenium porphyrin complexes containing tertiary phosphines as axial ligands have a key role in catalytic decarbonylation of aldehydes (3), and oxidation of phosphines and thioethers by molecular oxygen (6). Coordination of tertiary phosphines to a Rh(III) porphyrin superoxide complex at low temperature has been suggested from esr data (10), but to our knowledge **1** is the first reported isolated rhodium porphyrin complex containing a phosphine.

Experimental

Materials and methods

Elemental analyses were performed by P. Borda (University of British Columbia). Electronic spectra were recorded on a Cary 17D or a Perkin-Elmer 552A uv/vis spectrophotometer fitted with a Perkin-Elmer Model C550–0555 Thermoelectric single cell holder and a Model C570–0701 Digital Controller. Solution infrared spectra were obtained using a Nicolet 5DX FT-IR instrument. Nuclear magnetic resonance spectra were obtained on a Bruker WP-80 or a Varian XL-300 instrument in FT mode. Conductivity measurements were made at 25°C under anaerobic conditions using a Thomas Serfass conductivity bridge and a cell from Yellow Springs Instrument Co.

Spectral grade benzene, toluene, and THF from Fisher Scientific were freshly distilled from benzophenone ketyl, and were freeze–pump–thaw degassed prior to use. *N,N′*-Dimethylacetamide was vacuum-distilled from CaH_2. Samples for uv/vis experiments were handled anaerobically under vacuum or an argon atmosphere using tonometers (1 mm pathlength) described elsewhere (11). Deuterated solvents were from MDS Isotopes and were used without further purification. All other solvents used were either spectral or reagent grade and used as purchased. The phosphines were reagent grade from Strem Chemicals Inc.

Rhodium was obtained as $RhCl_3 \cdot 3H_2O$ (42.61% Rh) from Johnson, Matthey Ltd. H_2OEP was a gift from Dr. D. Dolphin (University of British Columbia). The $[Rh(COE)_2Cl)]_2$ dimer (12) and Rh(OEP)Cl·$2H_2O$ (13) were prepared by the literature methods.

Chloro(octaethylporphyrinato)(triphenylphosphine)rhodium(III) monohydrate

Method A: 82 mg (0.12 mmol) Rh(OEP)Cl·$2H_2O$ and 33 mg (0.12 mmol) PPh_3 were placed in a small Schlenk tube under argon. The solids were dissolved in 20 mL freshly dried benzene. After ~15 min the solution was filtered and the filtrate volume reduced *in vacuo* to ~3 mL. The product was precipitated by addition of freshly dried hexanes and collected on a frit, and washed 3 times with 2 mL portions of hexanes before drying *in vacuo*. Yield was 52 mg (50%) of a red purple powder. *Anal.* calcd. for $C_{54}H_{61}N_4RhClPO$: C 68.20,

[1]To whom correspondence should be addressed.

[2]Ligand abbreviations used: OEP = dianion of octaethylporphyrin; TPP = dianion of tetraphenylporphyrin; THF = tetrahydrofuran; DMA = *N,N′*-dimethylacetamide; NBD = norbornadiene; COE = cyclooctene; DMSO = dimethylsulphoxide; porp = general porphyrin dianion.

TABLE 1. Nuclear magnetic resonance spectral data at 30°C for Rh(III) octaethylporphyrin complexes[a]

Complex	^{1}H	*meso*-H	—CH_2—	CH_3	*o*-H	*m*-H	*p*-H	
Rh(OEP)(PPh_3)Cl[b,c]		9.56s	4.10m, 3.97m	1.91t	3.58	6.42	6.84	
Rh(OEP)(PPh_3)Cl[d]		10.00s	3.92m, 3.78m	1.85t	~3.9[e]	6.16	6.47	
Rh(OEP)(PPh_3)$_2^+$[f]		9.74s	3.96q	1.88t	3.45	6.38	6.85	
					—CH_2—	—CH_2—	—CH_2—	—CH_3
Rh(OEP)(P^nBu_3)$_2^+$[b,c]		10.31s	4.17q	1.92t	−3.51m	−1.93m	0.058m	0.18t
Rh(OEP)(CO)Cl[g]		10.36s	4.22m	2.00t				
Rh(OEP)(THF)Cl[g,h]		10.31s	4.20m	1.94t				
	$^{31}P\{^1H\}$							
Rh(OEP)(PPh_3)Cl	9.68(124);[i] 9.52(124);[j] 9.05(116)[k]							
Rh(OEP)(PPh_3)$_2^+$	−2.60(86);[j] −2.1(83)[l]							
Rh(OEP)(P^nBu_3)$_2^+$	3.82(81)[i]							

[a] ^{1}H nmr shifts, 300 MHz, relative to TMS; ^{31}P shifts (all doublets, J(Rh—P) Hz given in parentheses) relative to 85% H_3PO_4, downfield being positive. Proton integrations were consistent with the assignments.
[b] Phenyl and butyl protons all appear as multiplets.
[c] In CD_3CN; data very similar in CD_2Cl_2.
[d] In C_6D_6.
[e] Overlaps with —CH_2— proton shifts.
[f] In CD_2Cl_2.
[g] In THF-d_8.
[h] Formed *in situ* by dissolving Rh(OEP)Cl·$2H_2O$ in THF-d_8.
[i] In CD_3CN at 121.421 MHz.
[j] In CD_2Cl_2 at 121.421 MHz.
[k] In toluene at 32.21 MHz.
[l] In DMA at 32.21 MHz.

H 6.31, N 5.89, P 3.26, Cl 3.78; found: C 68.3, H 6.7, N 5.6, P 3.3, Cl 3.8.

Method B: 400 mg (0.56 mmol)of $[Rh(COE)_2Cl]_2$[3] were suspended in 100 mL of mesitylene together with 0.6 g (1.1 mmol) of H_2OEP. A stream of CO gas was passed through the mixture while refluxing for 6 h. To the resulting red solution, 0.3 g (1.1 mmol) of PPh_3 were added and the CO flow replaced by a N_2 flow. Refluxing was continued for 1 h. After cooling the solution to room temperature, the solvent was removed *in vacuo*. The crude product was purified by recrystallization from CH_2Cl_2/hexane. Typical yields were ~65%.

Crystals for X-ray crystallographic analysis were obtained with two solvate $CHCl_3$ molecules by slow evaporation of a solution of $RhOEP(PPh_3)Cl\cdot H_2O$ in $CHCl_3$/hexane. The solvated complexes were soluble in MeOH, EtOH, acetone, $MeNO_2$, THF, $CHCl_3$, DMA, DMSO, MeCN, C_6H_6, and toluene, slightly soluble in diethyl ether, and insoluble in alkanes. Dilute solutions were found generally to be light-sensitive; the MeCN solutions were non-conducting.

^{1}H and ^{31}P data are given in Table 1: uv/vis. λ_{max}/nm (log ϵ) in C_6H_6, [Rh] = (0.9–6.0) × 10^{-3} M, 25°C *in vacuo*: 608 (3.41), 563 (4.47), 533 (4.41), 422 (5.20), 351 (4.59); in Nujol mull: 617, 564, 535, 418, 350.

Solution equilibrium measurements

Equilibrium constants for replacement of chloride by PPh_3 in CH_2Cl_2 solution, reaction [1], were measured by a spectrophotometric

$$[1]\quad \underset{\mathbf{1}}{Rh(OEP)(PPh_3)Cl} + PPh_3 \overset{K}{\rightleftharpoons} \underset{\mathbf{2}}{Rh(OEP)(PPh_3)_2^+} + Cl^-$$

titration technique. Ambient light was excluded during sample manipulations by using dimmed room lighting and by covering all exposed surfaces with black plastic tape. Aliquots (μL) of 10^{-1} M PPh_3 in CH_2Cl_2 (or alternatively solid PPh_3) were added to dilute solutions (~5 × 10^{-4} M) of **1** in CH_2Cl_2. Formation of **2** within seconds was evidenced by a red shift of the Soret from 419 to 429 nm, and the α and β bands from 560 to 568 and 529 to 537 nm, respectively, with a concomitant decrease in the intensity of the α band relative to the β band (Fig. 1). Measurements were also performed on solutions containing various amounts of $[Ph_4As]Cl$, $[^nBu_4N]Cl$ or $[^nBu_4N][ClO_4]$ to examine the effect of ionic strength and $[Cl^-]$. No change from the initial spectrum of the complex was noted on addition of the chloride salts to solutions of **1**.

The value of K was found by using visible data (at 560 nm) obtained using different combinations of initial concentrations of **1** (C_0), and added Cl^- (Cl_0) and PPh_3 (P_0). By defining A and A_0 as the absorbances measured at 560 nm with and without added PPh_3, and ϵ_0 and ϵ_∞ as the extinction coefficients of **1** and **2**, eq. [2] may be derived (l = path length):

$$[2]\quad K_{obs} = \frac{\left\{C_0 - \left[\frac{A_0 - A}{(\epsilon_0 - \epsilon_\infty)l}\right]\right\}\left\{Cl_0 + C_0 - \left[\frac{A_0 - A}{(\epsilon_0 - \epsilon_\infty)l}\right]\right\}}{\left\{\frac{A_0 - A}{(\epsilon_0 - \epsilon_\infty)l}\right\}\left\{P_0 - C_0 - \left[\frac{A_0 - A}{(\epsilon_0 - \epsilon_\infty)l}\right]\right\}}$$

The ϵ_0 (23 350) and ϵ_∞ (6 500 M^{-1} cm^{-1}) values were available experimentally because the limiting spectra of **1** and **2** for the equilibrium could be measured under readily attainable conditions (high $[Cl^-]$ with no added phosphine, and high $[PPh_3]$ with no added Cl^-, respectively). Since ionic products are involved, the thermodynamic equilibrium constant (K) will be a function of the mean ionic activity coefficient ($\gamma_\pm$) and the experimental equilibrium constant (K_{obs}).

$$[3]\quad K = \gamma_\pm^2 \times \frac{[\mathbf{2}][Cl^-]}{[\mathbf{1}][PPh_3]} = \gamma_\pm^2 K_{obs}$$

where $\gamma_\pm$ is defined by the familiar Debye–Hückel limiting law

$$[4]\quad \log_{10}\gamma_\pm = Az_+z_-\mu^{1/2}$$

The value of K was determined from the intercept of $\log_{10} K_{obs}$ plotted vs. $\mu^{1/2}$ at a particular temperature. Figure 2 shows such a plot for the data at 25°C (Table 2), and, for the data at $\mu < 7 \times 10^{-4}$ M, the line drawn gives an intercept corresponding to $\log_{10} K = -1.75$ (K = 0.0174). The slope of the least squares line drawn (of slope $-2Az_+z_-$

[3] Similar results were obtained using $[Rh(NBD)Cl]_2$ or $Rh(py)_3Cl_3$ as starting materials.

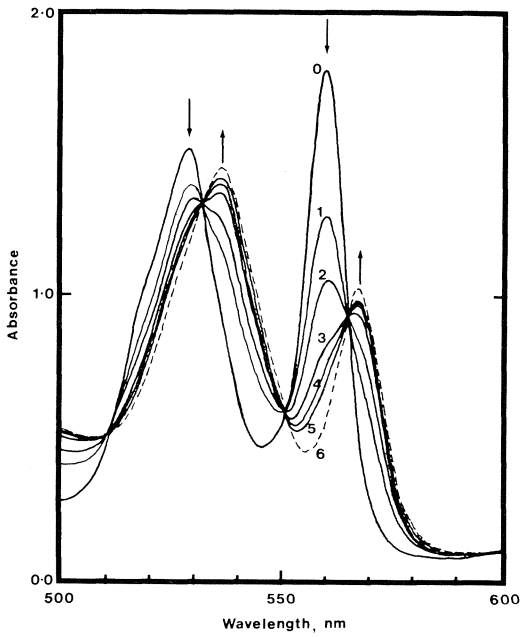

FIG. 1. Spectrophotometric titration of $Rh(OEP)(PPh_3)Cl$ with added PPh_3 in CH_2Cl_2 at 25°C, [Rh] = 8×10^{-4} *M*; curves *0–5* result added [PPh_3] of 0.0, 0.38, 1.09, 2.69, 5.01, and 7.18 $\times 10^{-2}$ *M*, respectively. *6* shows the spectrum of $Rh(OEP)(PPh_3)_2^+$ (formed at [PPh_3] ~ 5×10^{-2} *M* and $\mu \sim 0.02$ *M*).

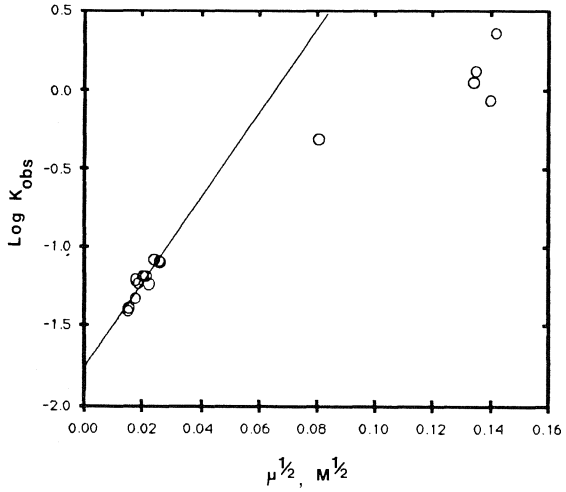

FIG. 2. Plot of $\log_{10} K_{obs}$ vs. (ionic strength)$^{1/2}$ for data of Table 2.

or +2*A* for this particular equilibrium) is 26.9. The calculated value for the slope using the standard expression for *A* (14)[4] is 26.7, showing remarkably good agreement.

Thermodynamic parameters for equilibrium [1] were obtained by repeating the equilibrium measurements (log K_{obs} vs. $\mu^{1/2}$) at four other temperatures over the range 10–30°C. Values of *K* (temp) are 0.0327 (10°C), 0.0262 (15°C), 0.0202 (20°C), and 0.0128 (30°C). The data give an excellent Van't Hoff plot from which values of ΔH^0 ($-7.8 \pm 0.5 \pm$ kcal mol^{-1}) and ΔS^0 (-34.8 ± 0.8 cal mol^{-1} K^{-1}) were estimated.

[4] $A = \dfrac{(2\pi N)^{1/2}}{2.303}\left(\dfrac{e^2}{10\epsilon kT}\right)^{3/2}$, where *N* = Avogadro's number, *e* = electronic charge, ϵ = dielectric constant (8.90 for CH_2Cl_2 at 25°C), *k* = the Boltzmann constant, *T* = absolute temperature.

TABLE 2. Variation of K_{obs} for reaction [1] in CH_2Cl_2 at 25°C[a]

$\mu \times 10^4$ *M*	$K_{obs} \times 10^2$	$\mu \times 10^4$ *M*	$K_{obs} \times 10^2$
2.16	3.91	5.94	8.53
2.26	4.06	6.49	8.28
2.97	4.77	6.74	8.13
3.11	6.29	64.8[b]	49.9
3.45	6.06	179[c]	114
4.05	6.65	182[d]	136
4.50	6.44	196[e]	86
4.88	5.83	203[f]	240

[a] Up to $\mu = 6.74 \times 10^{-4}$ *M*, the ionic strength results solely from the ions generated by reaction [1], i.e., no salt has been added. Initial [$Rh(OEP)(PPh_3)Cl$] between $(4.0–8.0) \times 10^{-4}$ *M*.
[b] Added 6.48×10^{-3} *M* $Ph_4AsCl \cdot H_2O$.
[c] Added 1.79×10^{-2} *M* $Ph_4AsCl \cdot H_2O$.
[d] Added 1.82×10^{-3} *M* $Ph_4AsCl \cdot H_2O$; addition of H_2O to 2×10^{-2} *M* had no measurable effect on the equilibrium reaction.
[e] Added 1.76×10^{-2} *M* $^nBu_4NClO_4$.
[f] Added 2.03×10^{-2} *M* $^nBu_4NCl$.

X-ray crystallographic analysis

A reddish-brown crystal of $Rh(OEP)(PPh_3)Cl \cdot 2CHCl_3$, with {100}, {010}, and {001} faces and of dimensions $0.35 \times 0.43 \times 0.20$ mm, was mounted on an Enraf-Nonius CAD4-F diffractometer in a general orientation. Unit cell parameters were refined by least squares treatment of sin θ values measured with Mo$K\alpha_1$ radiation for 25 reflections with $30 \leq 2\theta \leq 40°$. Crystal data (at 22°C) are:

$C_{56}H_{61}Cl_7N_4PRh$ fw 1172.18

Triclinic, $a = 13.478(5)$, $b = 14.300(5)$, $c = 15.346(4)$ Å, $\alpha = 102.33(2)$, $\beta = 102.89(2)$, $\gamma = 90.56(3)°$, $V = 2812(3)$ Å^3, $Z = 2$, $D_x = 1.384$ g cm^{-3}, Mo$K\alpha_1$ radiation, $\lambda = 0.70930$ Å, $\mu = 6.6$ cm^{-1}. Space group $P\bar{1}$, from structure analysis.

Intensities were measured for $\pm h$, $\pm k$, l reflections with $4 \leq 2\theta \leq 54°$, with graphite-monochromatized Mo$K\alpha$ radiation, ω–(5/3)θ scan at 0.7–10.1°min^{-1}, ω range $(1.00 + 0.35 \tan \theta)°$ (extended by 25% on both sides for background measurements), horizontal aperture $(2.0 + \tan \theta)$ mm, vertical aperture 4 mm, Lorentz polarization and absorption corrections (transmission factors from 0.787 to 0.887); three standard reflections (500, 530, 525) were monitored for orientation and intensity control (intensity decay during data collection of 35%, probably resulting from loss of chloroform, limited the accuracy of the data set). 9394 Independent reflections were measured, and 5189 with $F \geq 3\sigma(F)$ were used in the analysis; $\sigma^2(I) = S + 2B + [0.04(S - B)]^2$, *S* = scan count, *B* = background count.

The coordinates of the Rh and P atoms were determined from the Patterson function and those of the remaining non-hydrogen atoms from a subsequent difference Fourier map; the asymmetric unit contains one porphyrin–rhodium complex and two chloroform molecules. The structure was refined by block-diagonal least-squares methods, with minimization of $\Sigma w(F_o - F_c)^2$, $w = 1/\sigma^2(F)$; SHELX computer programs (15) were used, with scattering factors of ref. 16 and anisotropic thermal parameters. Hydrogen atoms were included at calculated positions but were not refined positionally, apart from adjustment of methyls as rigid groups. Isotropic temperature factors of the H atoms were refined. Refinement converged at $R = 0.095$, $R_w = 0.068$ for 5189 reflections and 721 variables refined in three blocks of 209, 270, and 242 variables, respectively. The error in an observation of unit weight was 2.02e, the mean and maximum shifts in the final cycles were 0.2 and 0.9σ, respectively, and the maximum fluctuations in a final difference map were ± 1.6 e Å^{-3}. The chloroform molecules and the outer atoms of the ethyl and phenyl groups exhibit large thermal motion, with rms displacements of up to 0.5 Å.

Final positional parameters for the non-hydrogen atoms are given in Table 3, with equivalent isotropic thermal parameters ($U_{eq} = 1/3 \times$ trace *U*). Anisotropic thermal parameters, bond lengths and angles, hydrogen parameters, and measured and calculated structure factors

TABLE 3. Atom coordinates ($\times 10^4$) and equivalent temperature factors ($Å^2 \times 10^3$)

Atom	x/a	y/b	z/c	U_{eq}[a]
Rh(1)	1933(1)	1853(1)	2262(1)	27
P(1)	3631(2)	1520(2)	2532(2)	33
Cl(1)	141(2)	2219(2)	1907(2)	42
Cl(2)	9448(3)	3751(3)	4668(3)	152
Cl(3)	8866(3)	1751(3)	4144(3)	127
Cl(4)	7736(3)	3015(3)	3218(4)	156
Cl(5)	8207(3)	4647(4)	1665(4)	167
Cl(6)	9935(3)	5133(3)	1085(3)	146
Cl(7)	10049(3)	5323(4)	2968(3)	174
N(1)	1833(5)	2060(5)	3558(5)	31
N(2)	2302(5)	3294(5)	2443(6)	37
N(3)	1924(5)	1668(5)	925(5)	29
N(4)	1451(5)	445(5)	2048(6)	32
C(1)	1520(6)	1401(7)	3986(7)	34
C(2)	1564(7)	1806(7)	4940(7)	42
C(3)	1891(7)	2746(7)	5092(7)	46
C(4)	2049(7)	2881(9)	4258(8)	50
C(5)	2360(8)	3767(8)	4068(9)	43
C(6)	2460(7)	3953(7)	3279(8)	35
C(7)	2691(8)	4889(7)	3111(8)	47
C(8)	2648(7)	4760(7)	2218(8)	45
C(9)	2396(7)	3732(7)	1787(8)	36
C(10)	2297(7)	3369(7)	886(8)	42
C(11)	2080(6)	2373(7)	453(7)	36
C(12)	1997(7)	1972(7)	−511(7)	38
C(13)	1743(6)	1009(7)	−628(6)	33
C(14)	1688(7)	865(7)	235(7)	34
C(15)	1364(7)	−44(7)	395(8)	38
C(16)	1270(7)	−197(7)	1218(7)	34
C(17)	929(6)	−1129(6)	1342(7)	30
C(18)	878(6)	−1007(6)	2240(8)	36
C(19)	1215(7)	8(7)	2657(7)	35
C(20)	1227(7)	430(8)	3555(8)	40
C(21)	1315(9)	1277(8)	5617(7)	60
C(22)	2182(11)	766(10)	6068(10)	90
C(23)	2093(9)	3499(8)	5988(7)	66
C(24)	3220(11)	3601(13)	6478(9)	105
C(25)	2957(9)	5787(6)	3864(8)	59
C(26)	4017(10)	5841(10)	4470(11)	96
C(27)	2739(9)	5545(7)	1688(8)	61
C(28)	3806(12)	5689(11)	1559(16)	121
C(29)	2113(8)	2527(7)	−1189(7)	55
C(30)	3229(10)	2748(12)	−1165(12)	98
C(31)	1588(8)	261(7)	−1510(7)	59
C(32)	2520(13)	−294(11)	−1585(10)	103
C(33)	649(7)	−2017(7)	594(7)	51
C(34)	1582(9)	−2550(9)	393(10)	82
C(35)	595(8)	−1715(7)	2720(7)	51
C(36)	1506(10)	−2089(10)	3304(10)	87
C(37)	4385(7)	2384(7)	2176(7)	39
C(38)	4690(8)	3246(8)	2786(8)	60
C(39)	5312(9)	3918(9)	2639(11)	79
C(40)	5611(10)	3758(10)	1844(12)	87
C(41)	5271(12)	2966(12)	1200(10)	122
C(42)	4684(11)	2232(11)	1382(9)	119
C(43)	4412(7)	1536(6)	3683(7)	36
C(44)	4047(8)	1458(7)	4409(7)	52
C(45)	4688(9)	1394(8)	5240(8)	67
C(46)	5724(9)	1407(8)	5318(9)	61
C(47)	6109(8)	1483(8)	4592(9)	69
C(48)	5472(8)	1548(7)	3772(8)	56
C(49)	3857(7)	312(6)	1953(7)	35
C(50)	3902(11)	−410(9)	2414(9)	101
C(51)	4077(13)	−1333(9)	2074(11)	116
C(52)	4286(9)	−1560(9)	1229(12)	85
C(53)	4189(13)	−881(10)	716(13)	139
C(54)	3945(11)	63(9)	1064(11)	115
C(55)	8950(9)	2807(8)	3726(9)	83
C(56)	9509(10)	4659(9)	1875(10)	92

[a] U_{eq} is one third the trace of the diagonalized temperature factor matrix.

(Tables 4–8, respectively) have been placed in the Depository of Unpublished Data.[5]

Discussion

The synthesis of Rh(OEP)(PPh_3)Cl, **1**, via addition of phosphine to Rh(OEP)Cl·$2H_2O$ (method A) is straightforward but the route to the precursor Rh(III) complex via $[RhCl(CO)_2]_2$ involves separation from other rhodium porphyrin products (13). The second method (B) described, via the readily synthesized $[Rh(COE)_2Cl]_2$ precursor, is somewhat more convenient, but **1** is obtained from what is undoubtedly a complex mixture of rhodium porphyrin species. The labile cyclooctene is likely to be readily displaced by the CO to form $[RhCl(CO)_2]_2$ and the synthesis then becomes akin to that described in method A. However, *in situ* monitoring by infrared in the carbonyl region reveals a myriad of bands that indicate the presence of several carbonylporphyrin complexes (see ref. 13), including what is probably Rh(OEP)(CO)Cl, 2085 cm^{-1}, from which **1** can be formed by treatment with PPh_3 (see below).

Structure description

The molecule of the porphyrin complex (Fig. 3) contains a central Rh(III) ion coordinated to the four N atoms, with a PPh_3 and Cl ligand completing distorted octahedral geometry at Rh. Rh is displaced from the mean plane of the four N atoms towards the phosphine ligand by 0.077 Å. The whole porphyrin nucleus shows deviations from exact planarity, with a maximum deviation of 0.098 Å and a root-mean-square deviation of 0.06 Å from a mean plane. The eight outer C atoms of the peripheral ethyl groups are displaced from the porphyrin plane by about 1.3 Å, all on the same side of the plane as the phosphine group. There are no obvious non-bonding interactions that force the Rh atom to lie out of the plane towards the phosphine, and it is not clear why all the ethyl groups point towards the phosphine, although the analogous situation exists in the structure of Ru(OEP)(PPh_3)Br (5). The variable orientations found for the ethyl groups within OEP structures have been discussed previously but not rationalized (17).

The Rh–N distances are 1.982–2.061(8) Å, the average distance of 2.024 Å being reasonably close to values observed in the few other Rh—porphyrins which have been studied (18–21). The Rh—P and Rh—Cl distances of 2.306(3) and 2.442(2) Å are also with the ranges usually observed. The P—C bond lengths are 1.828–1.839(10) Å, mean 1.834 Å. The angles at P show some large variations from the tetrahedral value, with Rh—P—C = 110.9, 113.5, 123.0(4)° and C—P—C = 99.0, 100.5, 108.3(4)°. These variations presumably result from steric interaction between the phenyl

[5] The structure factor table, anisotropic thermal parameters, hydrogen parameters, bond distances and angles may be purchased from the Depository of Unpublished Data, CISTI, National Research Council of Canada, Ottawa, Ont., Canada K1A 0S2.

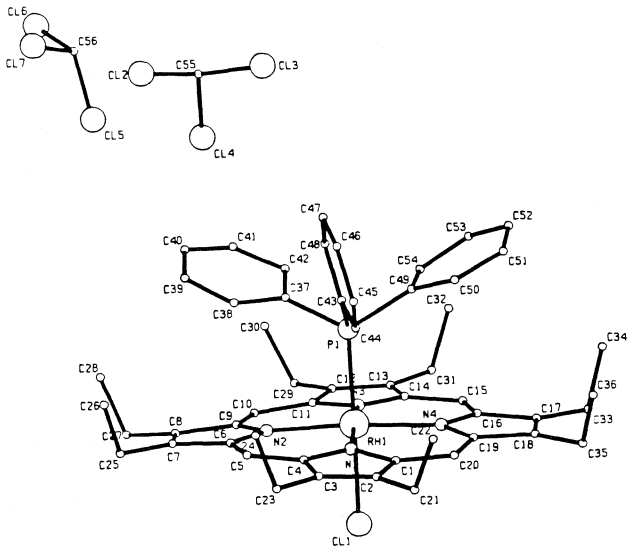

FIG. 3. Structure of the $Rh(OEP)(PPh_3)Cl \cdot 2CHCl_3$ complex.

rings and the porphyrin nucleus; the large Rh—P(1)—C(43) angle of 123.0(4)° involves the P—C bond which eclipses the Rh—N(1) bond. There are some variations in bond distances and angles within the porphyrin nucleus, but the lengths and angles are generally close to normal values (5).

Intermolecular distances correspond to normal van der Waals interactions. The two solvent chloroform molecules have normal dimensions, mean C—Cl = 1.73 Å.

Solution species

The non-ionic chlorotriphenylphosphine complex **1** remains 6-coordinate in solution. Beer's law was obeyed over the range $(0.9–8.0) \times 10^{-4}$ *M* in benzene solution, *in the dark*. The ^1H nmr spectrum of solutions at $10^{-3}–10^{-2}$ *M* (Table 1) is consistent with the presence of a diamagnetic metallo-octaethylporphyrin complex, that is substituted unsymmetrically with regard to the porphyrin plane, i.e., two different axial ligands are present (5–8). Within such complexes the methylene protons of the ethyl side-chains become anisochronous and appear as an ABX_3 multiplet (6, 22). In symmetrically substituted species, e.g. the bisphosphine complexes (see below), the $—CH_2—$ protons appear as a single quartet due to coupling with the adjacent $—CH_3$ group. There is no evidence for free phosphine in solutions of **1**, and the uv/vis spectrum is unaffected by addition of Cl^-. Coordination of a single PPh_3 is shown by integration of the *o*-, *m*-, and *p*-protons which are shifted upfield from their normal positions by the ring current of the porphyrin (7, 17). Further, the solid state uv/vis spectrum shows absorption maxima that correspond closely to those measured in solution.

Addition of PPh_3 or P^nBu_3 to the complex in polar solvents (MeCN, CH_2Cl_2, diethyl ether, DMA) resulted in formation of cationic bisphosphine complexes, reactions [1] and [5].

[5] $Rh(OEP)(PPh_3)Cl + 2P^nBu_3 \rightarrow Rh(OEP)(P^nBu_3)_2^+ + Cl^- + PPh_3$

The nmr spectroscopic evidence was cleanest for the reaction with P^nBu_3. Upon addition of two equivalents of phosphine to CD_3CN or CD_2Cl_2 solutions of **1**, the ^1H nmr spectrum of **1** was replaced by a new set of signals due to $Rh(OEP)(P^nBu_3)_2^+$ (Table 1). The methylene protons of the ethyl side chains appear as the expected quartet, while the upfield resonances due to coordinated P^nBu_3 were in a 2:1 equivalent ratio relative to the porphyrin. Reaction [5] was also monitored by $^{31}P\{^1H\}$ nmr, free PPh_3 being clearly observed. An excess of PPh_3 (to $\sim 10^{-1}$ *M*) was required for *in situ* formation of $Rh(OEP)(PPh_3)_2^+$, which was observable by ^1H and $^{31}P\{^1H\}$ nmr of CD_2Cl_2 solutions (Table 1). The conductance of a MeCN solution of **1** after addition of PPh_3 rose to a limiting value of 125 Ω^{-1} cm^2 mol^{-1}, consistent with formation of a 1:1 electrolyte (23, 24). Essentially identical nmr data in CD_2Cl_2 and CD_3CN argue against formation of the ion-pair $[Rh(OEP)(PPh_3)_2^+ \ldots Cl^-]$ in dichloromethane. Stronger binding of P^nBu_3 relative to triarylphosphines has been reported for the isoelectronic, d^6 Ru(II)OEP and Ru(II)TPP complexes (17) and was accounted for by the higher basicity of the trialkylphosphines (25).

Formation of mixed PPh_3/P^nBu_3 or $Rh(OEP)(P^nBu_3)Cl$ complexes was not evident by nmr. Also, the ionic bisphosphine complexes were not formed at all in toluene or benzene solution. The more polar CH_2Cl_2 ($\epsilon \approx 9$) or MeCN ($\epsilon \approx 36$) were required to promote equilibria [1] or [5].

Reactions [1] and [5] could also be monitored by uv/vis spectroscopy. Addition of phosphine resulted in a red shift of the Soret and visible bands (see Experimental section) with a marked diminution of the α band (Fig. 1). These findings are qualitatively consistent with coordination of an additional strong ligand (26). A corresponding reverse blue shift of the spectrum of $Ru(OEP)(P^nBu_3)(S)$ (S = DMSO or MeCN) compared with that of $Ru(OEP)(P^nBu_3)_2$ has been noted previously (17).

Equilibrium [1] was studied quantitatively using uv/vis spectroscopy, following qualitative observations on the inhibition of the forward reaction in the presence of added chloride. The same isosbestic points (Fig. 1) were observed during a spectrophotometric titration with PPh_3 at a given temperature, or during variation of temperature over the range 10–30°C at any chosen $[PPh_3]$. Indeed, the latter type of experiment allows for a rapid estimation of K_{obs} as a function of temperature using just a single solution; such values were in good agreement with those estimated from the more extensive data sets described in the Experimental.

The net rapid substitution reaction [1] almost certainly occurs via a dissociative process and a 5-coordinate intermediate, reactions [6], [7]. The overall *K* value ($= K_1K_2$) shows that a $[PPh_3]$ of ~ 0.2 *M* is required to convert 90% of **1** (initially at $\sim 5 \times 10^{-4}$ *M*) into **2** at 25°C.

[6] $\underset{\mathbf{1}}{Rh(OEP)(PPh_3)Cl} \overset{K_1}{\rightleftharpoons} \underset{\mathbf{3}}{Rh(OEP)(PPh_3)^+} + Cl^-$

[7] $\mathbf{3} + PPh_3 \overset{K_2}{\rightleftharpoons} \underset{\mathbf{2}}{Rh(OEP)(PPh_3)_2^+}$

The stoichiometric conversion with P^nBu_3 implies that the equilibrium constant for [5] is $>10^3$ at corresponding conditions. The large negative ΔS^0 value (-34.8 cal mol^{-1} K^{-1}) for reaction [1] is reasonable for transformation of neutral species into solvated charged ones. Chloride is expected to form a stronger bond than PPh_3 to Rh(III), and thus the overall exothermicity (-7.8 kcal mol^{-1}) of the forward reaction presumably results from contributions of the solvation enthalpies of the product ions.

Under dark (thermal) conditions (see below), CH_2Cl_2 solutions of **1** do not react with 1 atm CO ($\sim 5 \times 10^{-3}$ *M*), implying that CO at this concentration cannot compete for **3** with the back

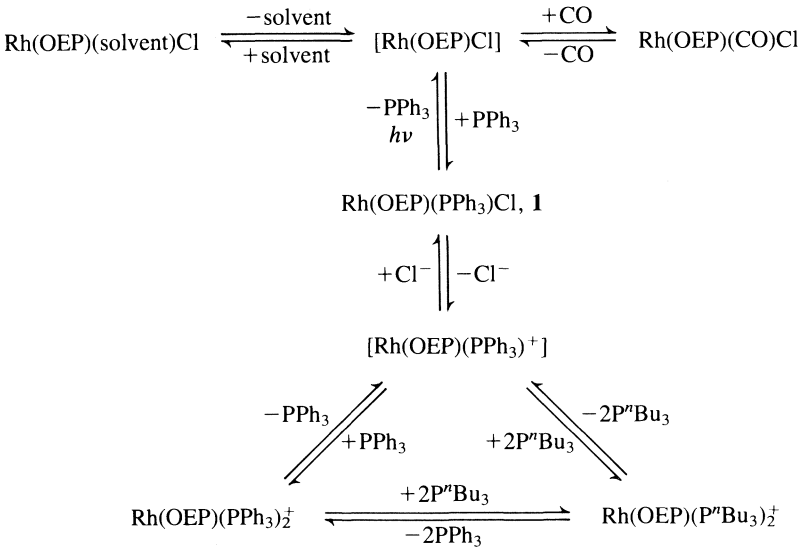

SCHEME 1. Reactivity scheme for solutions of Rh(OEP)(PPh$_3$)Cl.

TABLE 9. Visible spectral data (α and β) at 25°C for Rh(III) octaethylporphyrin complexes

Complex	α band ($\log_{10}\epsilon$), β band ($\log_{10}\epsilon$)
Rh(OEP)(PPh$_3$)Cl	564, 535;[a] 563(4.38), 533(4.32);[b] 562(4.34), 529(4.30);[c] 560(4.37), 529(4.28);[d] 560(4.35), 528(4.25)[e]
Rh(OEP)(PPh$_3$)$_2^+$	568(4.11), 537(4.27)[d]
Rh(OEP)(CO)Cl[f]	557, 526[b–d]
Rh(OEP)(THF)Cl[f]	549, 517[c]
Rh(OEP)(MeCN)Cl[f]	552, 521[e]

[a]Nujol.
[b]Benzene.
[c]THF.
[d]CH_2Cl_2.
[e]MeCN.
[f]Formed *in situ* from Rh(OEP)Cl·2H$_2$O.

reaction of equilibrium [6], even though the [Cl$^-$] must be very low since K_1 is immeasurably small. At an added [PPh$_3$] of about 5×10^{-3} *M*, reaction [1] with [**1**] ~ 5×10^{-4} *M* would generate ~35% of the bisphosphine cation. This implies that K_2 (reaction [7]) is much smaller for CO addition than for PPh$_3$ addition. Isoelectronic with **3**, the neutral, isolated Ru(OEP)(PPh$_3$) species reacts more readily with CO (3, 6, 17), presumably because the better π-acceptor properties of CO (vs. PPh$_3$) are more compatible with the lower oxidation state of Ru(II). The lack of reaction with CO also indicates negligible dissociation of PPh$_3$ under these conditions to form Rh(OEP)Cl, which is known to react with CO to form Rh(OEP)(CO)Cl (27, and see below), reactions [8] and [9]:

[8] Rh(OEP)(PPh$_3$)Cl ⇌ Rh(OEP)Cl + PPh$_3$

[9] Rh(OEP)Cl + CO ⇌ Rh(OEP)(CO)Cl

Complex **1** in benzene, THF, or MeCN, however, is photochromic in the presence of 1 atm CO, and reacts according to reactions [8] and [9]. Exposure to laboratory light or sunlight yields within minutes an *in situ* carbonyl (ν_{CO} = 2087 cm^{-1} in THF) with concomitant release of PPh$_3$, and the nmr data (Table 1) are consistent with the presence of Rh(OEP)(CO)Cl. Quantitative re-formation of **1** occurs in the dark over a few hours via intermediate Rh(OEP)(solvent)Cl species (as judged by comparison with the visible spectrum of Rh(OEP)Cl dissolved in the appropriate solvent). Solutions of **1** in THF or MeCN on exposure to light in the absence of CO also yield the Rh(OEP)(solvent)Cl species. Visible spectral data are given in Table 9.

The noted reversible carbonylation–decarbonylation reaction, in the daylight and dark, respectively (somewhat atypical in that the *decarbonylation* process is often photo-assisted), is of potential interest as a further model for solar energy storage in biological systems (28).

The ^{1}H and ^{31}P nmr data for all the species (Table 1) show shifts that are typical for diamagnetic, octahedral, metalloporphyrin complexes (2, 17, 29), and the magnitudes of the ^1J(RhP) coupling constants are appropriate for octahedral Rh(III) products (30).

The findings on reactivity can be summarized as shown in Scheme 1. Phosphine ligation of **1** is thermodynamically favoured relative to CO ligation. However, reactivity towards CO is enhanced in the presence of these ligands by "forcing" the system through unsaturated intermediates generated photochemically. These equilibria are of particular relevance to the reactions of M(porp)L$_2$ complexes (M = Fe, Ru; L = phosphine, MeCN, THF, etc.) with gas molecules such as CO and O$_2$, that also go via a dissociative mechanism (1, 3, 31–35).

[10] $$M(porp)(L)_2 \underset{+L}{\overset{-L}{\rightleftharpoons}} M(porp)L \underset{-gas}{\overset{+gas}{\rightleftharpoons}} M(porp)L(gas)(L)$$

Enhancement of the concentration of the 16-electron, 5-coordinate complexes is important in a catalytic context, such as decarbonylation of aldehydes which can proceed via the M(porp)(CO)L species (3, 33). In this regard, preliminary data indicate that phenylacetaldehyde can be used as a carbonyl source, instead of CO gas, to form Rh(OEP)(CO)Cl from Rh(OEP)(PPh$_3$)Cl, under conditions of laboratory lighting.

Concluding remarks

The synthesis, along with characterization by uv/vis, ^{1}H and ^{31}P{^{1}H} nmr spectroscopy and X-ray crystallography, of the complex Rh(OEP)(PPh$_3$)Cl, **1**, are presented. Additionally, spectroscopic evidence is presented for solution equilibria of **1**

involving formation of $Rh(OEP)L_2^+$ (L = PPh_3, P^nBu_3) via thermal reactions, and Rh(OEP)(Cl)(L′) (L′ = CO, THF, MeCN) via photochemical processes. Thermodynamic data have been estimated for formation of the bis(triphenylphosphine) species.

Acknowledgements

We thank the Natural Sciences and Engineering Research Council of Canada for financial support (in terms of operating grants to B.R.J. and J.T., and a summer undergraduate fellowship to K.M. (1983)), the University of British Columbia Computing Centre for assistance, and Johnson, Matthey Ltd. for the loan of rhodium.

1. (*a*) B. R. James, A. W. Addison, M. Cairns, D. Dolphin, N. P. Farrell, D. R. Paulson, and S. Walker. *In* Fundamental research in homogeneous catalysis. Vol. 3. *Edited by* M. Tsutsui. Plenum Press, New York. 1979. p. 751; (*b*) B. R. James. *In* Fundamental research in homogeneous catalysis. Vol. 5. *Edited by* A. E. Shilov. Gordon and Breach, New York. 1986. p. 309.
2. R. G. Ball, G. Domazetis, D. Dolphin, B. R. James, and J. Trotter. Inorg. Chem. **20**, 1556 (1981).
3. G. Domazetis, B. R. James, B. Tarpey, and D. Dolphin. Am. Chem. Soc. Symp. Ser. No. 152, 243 (1981).
4. M. Barley, J. Y. Becker, G. Domazetis, D. Dolphin, and B. R. James. Can. J. Chem. **61**, 2389 (1983).
5. B. R. James, D. Dolphin, T. W. Leung, F. W. B. Einstein, and A. C. Willis. Can. J. Chem. **62**, 1238 (1984) and references therein.
6. B. R. James, S. R. Mikkelsen, T. W. Leung, G. M. Williams, and R. Wong. Inorg. Chim. Acta, **85**, 209 (1984).
7. C. Sishta, M. Ke, B. R. James, and D. Dolphin. J. Chem. Soc. Chem. Commun. 787 (1986) and references therein.
8. M. J. Camenzind, B. R. James, and D. Dolphin. J. Chem. Soc. Chem. Commun. 1137 (1986).
9. (*a*) B. R. James and D. V. Stynes. J. Chem. Soc. Chem. Commun. 1261 (1972); (*b*) B. R. James and D. V. Stynes. J. Am. Chem. Soc. **94**, 6225 (1972).
10. B. B. Wayland and A. R. Newman. J. Am. Chem. Soc. **101**, 6472 (1979).
11. B. R. James, K. J. Reimer, and T. C. T. Wong. J. Am. Chem. Soc. **99**, 4815 (1977).
12. A. van der Ent and A. L. Onderderlinder. Inorg. Synth. **14**, 92 (1973).
13. H. Ogoshi, J. Setsune, T. Omura, and Z. Yoshida. J. Am. Chem. Soc. **97**, 6461 (1975).
14. G. W. Castellan. Physical chemistry. 2nd ed. Addison Wesley, Reading, MA. 1972. p. 375.
15. G. M. Sheldrick. SHELX (1976). Program for crystal structure determination. University of Cambridge.
16. International tables for X-ray crystallography. Vol. IV. Kynock Press, Birmingham, England. 1974. p. 99.
17. S. Ariel, D. Dolphin, G. Domazetis, B. R. James, T. W. Leung, S. J. Rettig, J. Trotter, and G. M. Williams. Can. J. Chem. **62**, 755 (1984).
18. L. K. Hanson, M. Gouterman, and J. C. Hanson. J. Am. Chem. Soc. **95**, 4822 (1973).
19. A. Takenaka, Y. Sasada, H. Ogoshi, T. Omura, and Z.-I. Yoshida. Acta Crystallogr. Sect. B, **31**, 1 (1975).
20. A. Takenaka, S. K. Syal, Y. Sasada, T. Omura, H. Ogoshi, and Z.-I. Yoshida. Acta Crystallogr. Sect. B, **32**, 62 (1976).
21. A. B. Abeysekera, R. Grigg, J. Trocha-Grimshaw, and T. J. King. J. Chem. Soc. Perkin Trans. 1, 2184 (1979).
22. C. A. Busby and D. Dolphin. J. Magn. Reson. **23**, 211 (1976).
23. J. T. Mague and J. P. Mitchener. Inorg. Chem. **8**, 119 (1969).
24. A. Davison, D. V. Howe, and E. T. Shawl. Inorg. Chem. **6**, 458 (1967).
25. T. Allman and R. G. Goel. Can. J. Chem. **60**, 716 (1982).
26. A. H. Corwin, A. B. Chivvis, R. W. Poor, D. G. Whitten, and E. W. Baker. J. Am. Chem. Soc. **90**, 6577 (1968).
27. I. A. Cohen and B. C. Chow. Inorg. Chem. **13**, 488 (1974).
28. D. V. Stynes. J. Am. Chem. Soc. **96**, 5942 (1974).
29. G. Domazetis, B. R. James, and D. Dolphin. Inorg. Chim. Acta, **54**, L47 (1981).
30. E. B. Boyar, D. S. Moore, S. D. Robinson, B. R. James, M. Preece, and I. Thorburn. J. Chem. Soc. Dalton Trans. 617 (1985) and references therein.
31. N. P. Farrell, D. Dolphin, and B. R. James. J. Am. Chem. Soc. **100**, 324 (1978).
32. B. R. James. *In* The porphyrins. Vol. V. *Edited by* D. Dolphin. Academic Press, New York. 1978. p. 205.
33. (*a*) S. G. Walker. M.Sc. Thesis, University of British Columbia. 1980; (*b*) B. Tarpey. M.Sc. Thesis, University of British Columbia. 1981; (*c*) R. Belani. M.Sc. Thesis, University of British Columbia. 1985.
34. J. Martinson, M. Miller, D. Trojan, and D. A. Sweigart. Inorg. Chem. **19**, 2162 (1980).
35. L. F. Barringer, D. P. Rillema, and J. H. Ham. J. Inorg. Biochem. **21**, 195 (1984).

The reactions of trichloromethylium with oxygen- and sulfur-containing compounds

JOHN ALFRED STONE AND NANCY JOAN MOOTE
Department of Chemistry, Queen's University, Kingston, Ont., Canada K7L 3N6

Received June 25, 1986

JOHN ALFRED STONE and NANCY JOAN MOOTE. Can. J. Chem. **64**, 2447 (1986).

The gas phase reactions of CCl_3^+ with acetone, diethyl ketone, dimethyl ether, diethyl ether, several cyclic ethers, sulfides, and disulfides have been examined using high pressure mass spectrometry. In many of the reactions a stabilized ion–molecule complex is observed which may or may not react further. With disulfides a second reaction channel is electron transfer, the observation of which shows that the 0–0 ionization energies of these compounds are lower than the ionization energy of CCl_3 (8.28 eV) and hence lower than the values obtained by photoelectron spectroscopy. Rate constants for the disappearance of CCl_3^+ in general show an increase in value with increase in reaction exothermicity. The lack of a measurable effect of pressure on rate constants is discussed for some association reactions which have reaction efficiencies well below unity.

JOHN ALFRED STONE et NANCY JOAN MOOTE. Can. J. Chem. **64**, 2447 (1986).

Utilisant la spectrométrie de masse à haute pression, on a étudié les réactions en phase gazeuse du CCl_3^+ avec l'acétone, la pentanone-3, le méthoxyméthane, l'éthoxyéthane et plusieurs éthers, sulfures et disulfures cycliques. Dans plusieurs de ces réactions, on a observé la formation de complexes ion/molécule qui peuvent éventuellement donner d'autres réactions. Avec les disulfures, les transferts d'électrons offrent une deuxième voie de réaction; leur observation démontre que les énergies d'ionisation 0–0 de ces composés sont plus basses que l'énergie d'ionisation du CCl_3 (8,28 eV) et donc plus basses que les valeurs obtenues par spectroscopie photoélectronique. Les vitesses de disparition du CCl_3^+ augmentent généralement avec une augmentation de l'exothermicité de la réaction. On discute du fait que, pour quelques réactions d'association qui ont des efficacités réactionnelles bien au-dessous de un, il n'y a pas d'effet mesurable de la pression sur les constantes de vitesse.
[Traduit par la revue]

Introduction

The mechanisms of the reactions of CCl_3^+ with carbonyl-containing compounds were examined by Ausloos and co-workers (1) using ion cyclotron resonance (icr) at pressures in the range 10^{-6}–10^{-5} Torr (1 Torr = 133 Pa) and ambient temperature. For aldehydes and ketones it was suggested that the preferential addition of CCl_3^+ to oxygen is immediately followed by a four-centre reaction leading to the formation a mono halogenated carbonium ion:

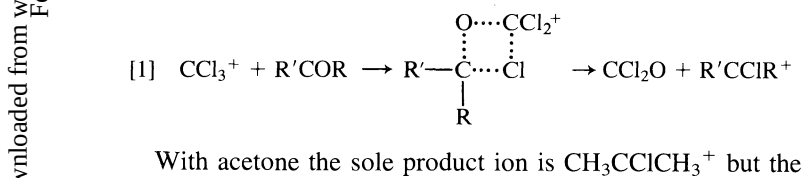

[1] $CCl_3^+ + R'COR \rightarrow R'—C(\cdots O\cdots CCl_2^+)\cdots Cl \; (R) \rightarrow CCl_2O + R'CClR^+$

With acetone the sole product ion is $CH_3CClCH_3^+$ but the more exothermic reaction of CCl_3^+ with diethylketone results in the further decomposition of 95% of the initially produced $C_2H_5CClC_2H_5^+$ by loss of HCl to give $C_5H_9^+$.

The measured rate constants for the reactions of CCl_3^+ and other halomethyl ions with carbonyl-containing compounds appeared to correlate well with reaction exothermicity. For example, the second order rate constants for the reactions of CCl_3^+ with CH_3COCH_3 and $C_2H_5COC_2H_5$ were respectively $< 3 \times 10^{-11}$ and 9×10^{-10} cm^3 molecule^{-1} s^{-1}. It was concluded that not only does reaction efficiency (defined as $k_{reaction}/k_{collision}$ where k is a specific rate constant) vary directly with exothermicity but that the results also indicate that the lifetime of the ion–molecule complex is probably an even more important factor; the shorter the complex lifetime, the lower the reaction efficiency. Such lifetimes are, however, not readily determined.

In earlier experiments with CCl_3^+ using high pressure mass spectrometry (HPMS) with ion source pressures in the range 2–5 Torr, we found that stable aromatic·CCl_3^+ adducts were observable (2) whereas previous studies at much lower ion source pressures ($\sim 10^{-4}$ Torr) had failed to detect such species (3, 4). Thus while collisional stabilization is not of importance at low pressures, it can be of significance at the higher pressures of our HPMS studies. The mean times between collisions of ions with neutrals at 4 Torr and 10^{-5} Torr are roughly 10^{-9} and 10^{-3} s, respectively, at 300 K. There is thus the possibility, using HPMS, of investigating whether Ausloos' claim that the very low reaction efficiency of CCl_3^+ with acetone (1) is due to a very short ion–molecule complex lifetime. If this complex can be observed using HPMS then its lifetime is at least 10^{-9} s.

The reactions of CCl_3^+ with another major class of oxygen bases, namely, the ethers have not been reported. We have examined such reactions using both linear and cyclic ethers and make comparisons with the results for carbonyl compounds. These ether results have also been compared with those obtained for thioethers.

Thiosulfonium ions of the type $(CH_3SSCH_3)R^+$ (R = H, alkyl) have been generated by displacement reactions in icr studies (5) and although they have been known and studied for some time in the condensed phase (6), their gas phase reactions have received little attention. We have therefore investigated the possibility of generating thiosulfonium ions by the addition of CCl_3^+ to RSSR under HPMS conditions. If this is possible then other thiosulfonium ions might be generated in a similar manner.

Experimental

The pulsed electron beam, high pressure ion source mass spectrometer has been described previously (7). Premixed samples of accurately known composition are flowed into the field free ion source from a heated reservoir via a heated leak valve. The source is operable in the pressure range 1–4 Torr, the ion beam being most intense at the higher pressures. Kinetic data are obtained by pulsing the electron beam, the temporal profiles of the different ion currents emerging from the ion source exit slit after the electron beam pulse being monitored with ion counting equipment and a multichannel analyser.

Methane (Matheson Ultra-high Purity) had a stated purity exceeding 99.99%; carbon tetrachloride (Fisher Spectrograde) was used as received; all other compounds were of the highest purities available. In no cases were ions attributable to impurities observed in any mass spectrum.

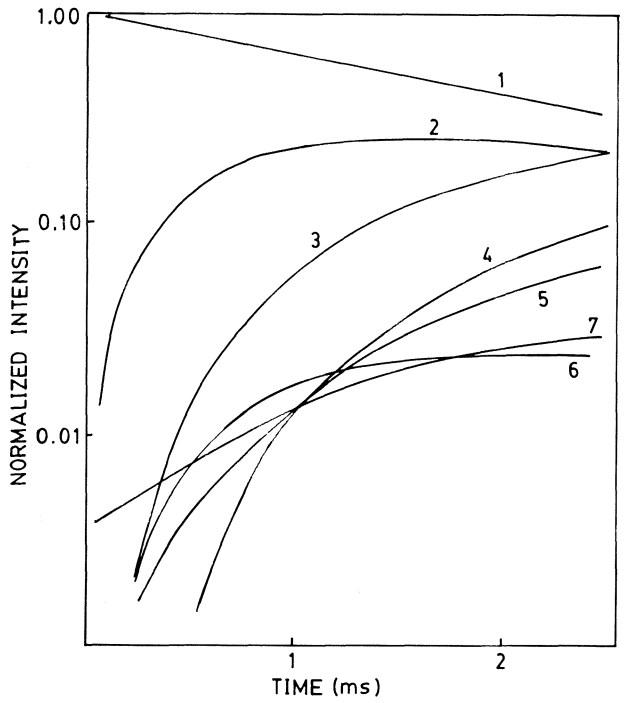

FIG. 1. Normalized ion intensities after a 85 μs pulse of ionizing electrons in a $CH_3COCH_3/CCl_4/CH_4$ (0.0011/0.46/99.5) mixture at 1.37 Torr and 300 K. To enhance clarity no experimental points are shown. The curves show the temporal profiles of *1*, CCl_3^+; *2*, $CH_3COCH_3 \cdot CCl_3^+$ (m/z 175); *3*, $C_4H_5OCl_2$ (m/z 139); *4*, $(CH_3COCH_3)_2H^+$ (m/z 117); *5*, $C_6H_{11}O^+$ (m/z 99); *6*, $C_7H_{11}O_2Cl_2^+$ (m/z 197); *7*, $CH_3COCH_3 \cdot H^+$ (m/z 59). The (m/z) value for the most abundant form of the ion is given but the graph shows the total normalized intensity for the ion.

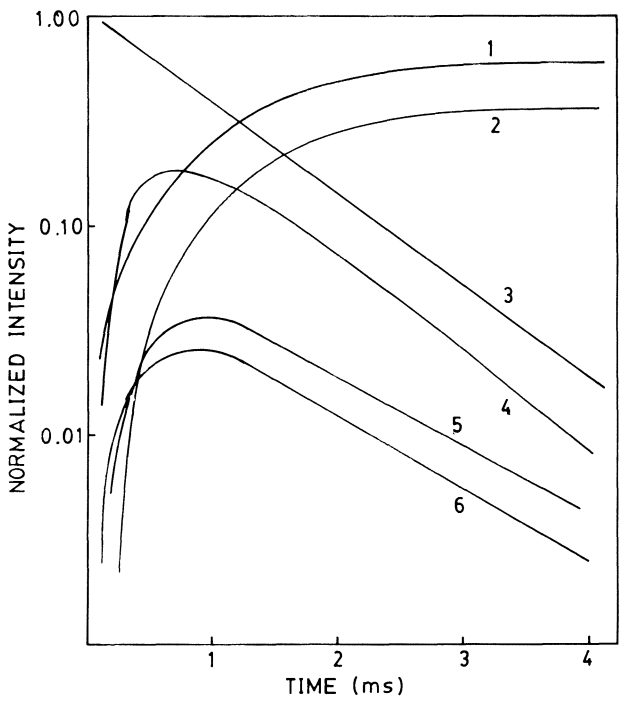

FIG. 2. Normalized ion intensities after a 50 μs pulse of ionizing electrons in a $C_2H_5COC_2H_5/CCl_4/CH_4$ (0.0059/0.32/99.7) mixture at 3.6 Torr and 455 K. The curves show the temporal profiles of *1*, $C_2H_5COC_2H_5 \cdot H^+$ (m/z 87); *2*, $(C_2H_5COC_2H_5)_2H^+$ (m/z 175); *3*, CCl_3^+; *4*, $C_2H_5COC_2H_5 \cdot CCl_3^+$ (m/z 203); *5*, $C_5H_9^+$ (m/z 69); *6*, $C_2H_5CClC_2H_5^+$ (m/z 105).

Results and discussion

CCl_3^+ is formed from CCl_4 by dissociative proton transfer from CH_5^+ and $C_2H_5^+$, the major reagent ions in methane (2).

[2] $CH_5^+(C_2H_5^+) + CCl_4 \rightarrow CH_4(C_2H_4) + HCl + CCl_3^+$

It is the only ion present at times greater than 100 μs after a pulse of ionizing electrons in a CH_4/CCl_4 (100/0.3) mixture at ion source pressures from 1–4 Torr and temperatures from 300–600 K. The CCl_3^+ ions formed then react with molecules of interest introduced into the gas mixture at very low concentrations (<0.01 mol%).

The plots of normalized ion currents as functions of time such as those in Figs. 1 to 4 can be interpreted to show the sequences of reactions following the interaction of CCl_3^+ with an added neutral. In addition, the linear decay with time of the logarithm of the normalized CCl_3^+ ion current allows the determination of the pseudo first order rate constant of the reaction of CCl_3^+ with the neutral. Knowing the concentration of the latter in the ion source the second order rate constant may be determined.

[3] $M + CCl_3^+ \rightarrow$ products

$$[4] \quad \frac{-d[CCl_3^+]}{dt} = k[M][CCl_3^+] = k'[CCl_3^+]$$

Taking the measured ion current i_t as being proportional to ion concentration in the ion source at time t and i_0 that at time zero, eq. [4] may be integrated to yield

$$[5] \quad \ln \frac{i_t}{i_0} = -k't$$

Values of k for the various neutrals studied under a variety of temperatures and pressures are given in Table 1. Also given are the efficiencies of reaction per ion–neutral collision, k/k_{ADO}, where k_{ADO} is the rate constant for collision calculated using the average-dipole orientation theory of Su and Bowers (8).

CCl_3^+ + acetone

This system was examined at pressures around 3.8 Torr at several temperatures and also at a pressure of 1.37 Torr at 302 K. The results for the latter experiment are shown in Fig. 1. The results for the other conditions do show some marked changes from those in Fig. 1 but these changes involve secondary reactions occurring at long ion residence times. The only primary reaction observed in all cases is the formation of the acetone·CCl_3^+ adduct

[6] $CCl_3^+ + CH_3COCH_3 \rightarrow$

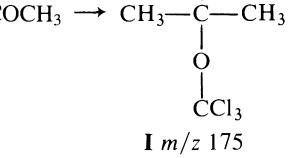

I m/z 175

The tertiary carbocation **I** reacts further with acetone via four different channels whose relative importances change markedly with change of temperature and to a much lesser extent with change of ion source pressure.

The structures shown for the products of reaction [7] are plausible but not proven. At 302 K channel [7b] is dominant (Fig. 1) but with increasing temperature the protonation reaction [7a] increases in importance. Above 462 K neither m/z 139 nor m/z 197 are observed, the only chlorine-containing ion being **I**, which is of course only present at short reaction times. m/z 59

[7a] $\mathbf{I} + CH_3COCH_3 \rightarrow (CH_3)_2COH^+ + C_4H_5OCl_3$

m/z 59

[7b] $\rightarrow CH_2{=}C(CH_3^+)O{-}CCl_2^+ + C_3H_7OCl$

m/z 139

[7c] $\rightarrow CH_3{-}C^+(CH_3){-}O{-}C(CH_3){=}CH_2 + HCl + COCl_2$

m/z 99

[7d] $\rightarrow CH_3{-}C(CH_2){-}O{-}C(CH_3)_2{-}O{-}CCl_2^+ + HCl$

m/z 197

reacts rapidly with neutral acetone to yield m/z 117 the proton-bound dimer $((CH_3)_2CO)_2H^+$.

It is noteworthy that the sole product ion observed using icr at pressures of $\sim 10^{-5}$ Torr, and ambient temperature $CH_3CClCH_3^+$ (1) formed in reaction [1], was not observed in this HPMS study. The reported reaction efficiency of 0.015 in the icr study is much less than the value of 0.5 for the association reaction observed in this study at 302 K (Table 1). There is the possibility that any $CH_3CClCH_3^+$ formed reacts immediately by chloride abstraction from the CCl_4, which is present in high concentration, to regenerate CCl_3^+ so that it itself is not observable. Such a reaction was not reported in the icr study.

CCl_3^+ + diethylketone

The adduct $(C_2H_5)_2COCCl_3^+$ is the only product at 298 K. It reacts rapidly by proton transfer yielding first $(C_2H_5)_2COH^+$ which is further solvated to $((C_2H_5)_2CO)_2H^+$. At 455 K two other initial products first appear, viz. $C_5H_9^+$ and $(C_2H_5)_2CCl^+$ in approximately equal but quite low yields (Fig. 2) whose relative values change little with pressure. In the icr study at $\sim$320 K the only two products were $C_5H_9^+$ (95%) and $(C_2H_5)_2CCl^+$. The present higher temperature, higher pressure results show that decomposition of the nascent diethyl ketone·CCl_3^+ complex is possible in a manner similar to that which occurs at low pressure but only if sufficient thermal energy is available. The total energy available in the CCl_3^+ adduct of diethyl ketone at any temperature before a stabilizing collision occurs is greater than that for the acetone·CCl_3^+ adduct under the same conditions because of the larger number of atoms present and because of the greater exothermicity of the adduct forming reaction. The latter is presumed to follow from the greater basicity of diethyl ketone. Although the four-centre intermediate illustrated by reaction [1] is possible for both

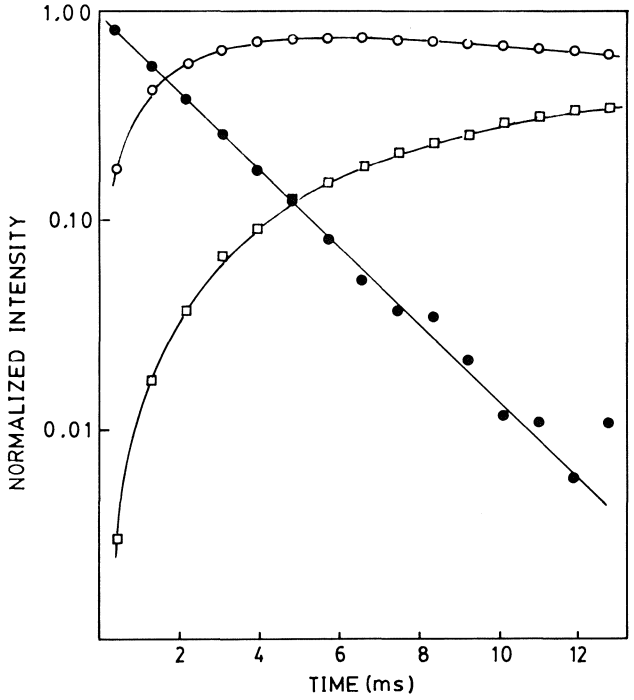

FIG. 3. Normalized ion intensities after a 100 μs pulse of ionizing electrons in a $(CH_3)_2O/CCl_4/CH_4$ (0.0031/0.44/99.6) mixture at 4.6 Torr and 360 K. ● CCl_3^+; ○ $(CH_3)_2OCCl_3^+$ (m/z 163); □ $(CH_3)_3O^+$ (m/z 61).

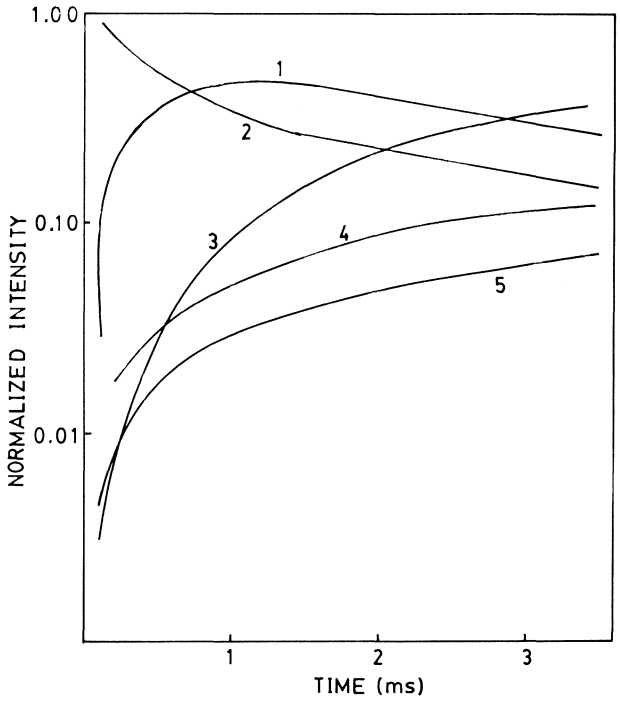

FIG. 4. Normalized ion intensities after a 60 μs pulse of ionizing electrons in a $(C_2H_5)_2O/CCl_4/CH_4$ (0.0058/0.32/99.6) mixture at 3.2 Torr and 464 K. The curves show the temporal profiles of *1*, $C_2H_5OCCl_2^+$ (m/z 127); *2*, CCl_3^+; *3*, $(C_2H_5)_3O^+$ (m/z 103); *4*, $(C_2H_5)_2O{\cdot}H^+$ (m/z 75); *5*, $C_4H_9O^+$ (m/z 73).

dimethyl and diethyl ketone, only the CCl_3^+ complex of the latter decomposes in such a manner under HPMS conditions.

The only reactions observed for $(C_2H_5)COCCl_3^+$, $(C_2H_5)_2CCl^+$, and $C_5H_9^+$ are proton transfer to the neutral ketone, again followed by further solvation to give the proton bound dimer.

TABLE 1. Rate constants and reaction efficiencies for the reaction M + CCl_3^+ → products

M	Temperature (K)	Pressure (Torr)	k (10^{10} cm^3 molecule^{-1} s^{-1})	k/k_{ADO}
Dimethylether	298	2.71	4.1	0.32
Dimethylether	298	3.0	3.8	0.30
Dimethylether	298	4.2	4.1	0.32
Dimethylether	298	4.9	3.5	0.27
Dimethylether	298	5.3	4.0	0.31
Dimethylether	345	2.3	1.8	0.14
Dimethylether	345	3.4	1.8	0.14
Dimethylether	345	4.1	2.0	0.16
Dimethylether	345	4.6	2.2	0.18
Dimethylether	345	5.4	2.2	0.18
Dimethylether	464	2.8–3.2	9 ± 2[a]	0.74
Acetone	302	1.2–3.7	10 ± 0.5	0.50
Acetone	396	3.7	2.2	0.13
Acetone	462	3.9	0.2	0.012
Diethylketone	455	3.6	2.2	0.14
Diethylketone	455	2.1	2.7	0.17
Furan	459	2.3–3.5	3.5 ± 0.5	0.34
2,5-Dihydrofuran	459	3.0	4.7	—
Tetrahydrofuran	459	3.0	5.4	0.43
2,5-Dimethyltetrahydrofuran	459	2.8	9.9	0.76
2-Methylfuran	459	2.9	9.1	0.80
2,3-Dihydropyran	459	3.4	8.7	0.71
Tetrahydrothiophene	460	3.1	9.0	0.66
Dimethylsulfide	450	3.7	3.5	0.27
Diethylsulfide	460	4.0	14	1.1
Diethyldisulfide	453	3–3.6	13 ± 1	1.0 (0.38)[b]
Di-*n*-propyldisulfide	300	2.2–3.1	14 ± 1	0.97 (0.73)[b]
Di-*n*-propyldisulfide	454	2.3–4.7	11 ± 2	0.75 (0.29)[b]
Di-*n*-propyldisulfide	570	3.4	14	1.0 (0.11)[b]

[a]Obtained using eq. [14].
[b]Efficiency for formation of $(C_3H_7S)_2CCl_3^+$ or $(C_2H_5S)_2CCl_3^+$.

CCl_3^+ + dimethyl ether

The adduct $(CH_3)_2OCCl_3^+$ is the sole initial product. Its yield decreases with increasing temperature until at temperatures above 530 K no reaction is observed. There is no evidence for an equilibrium between complex and reactants and the complex, an oxonium ion, reacts further with the neutral ether to yield the more stable trimethyloxonium ion (Fig. 3).

[8] $$CCl_3^+ + (CH_3)_2O \rightarrow (CH_3)_2OCCl_3^+$$

[9] $$(CH_3)_2OCCl_3^+ + (CH_3)_2O \rightarrow (CH_3)_3O^+ + CH_3OCCl_3$$

Reaction [9] is slow, $k = 2.5 \pm 1 \times 10^{-11}$ cm^3 molecule^{-1} s^{-1} at both 298 K and 360 K. It may be regarded as a bimolecular nucleophilic displacement, i.e., attack by the neutral ether on one of the methyl groups of $(CH_3)_2OCCl_3^+$. There are at least two possible explanations for this low reaction rate constant. The reaction is thermoneutral or more probably slightly endothermic since the stabilizing effect of a CCl_3 on a positively charged centre is a little greater than that for CH_3 (9). The lack of a significant temperature coefficient for the rate constant shows that the endothermicity cannot be large, and indeed if it were the reaction would not be observed. Another explanation might be that displacement occurs with high efficiency but attack occurs mainly at CCl_3 leading to no net change. However, it has long been known that the substitution of hydrogen by halogen on a carbon atom engenders a lowering of reaction rate for liquid phase S_N2 reaction at that carbon (10, 11), suggesting that attack will be mainly at CH_3.

CCl_3^+ + diethyl ether

Unlike dimethyl ether, diethyl ether produced no observable CCl_3^+ adduct. The reaction was studied only at 464 K when the sole product was $C_2H_5OCCl_2^+$ formed by loss of C_2H_5Cl or C_2H_4 + HCl from the initial collision complex.

[10] $$(C_2H_5)_2O + CCl_3^+ \rightarrow C_2H_5OCCl_2^+ + C_2H_5Cl(C_2H_4 + HCl)$$

Figure 4 shows that the disappearance of CCl_3^+ has two components, an initial rapid decay followed by a much slower decay. At long times the decay curves for CCl_3^+ and $C_2H_5OCCl_2^+$ have identical slopes, a behaviour that was found to be independent of both diethyl ether and carbon tetrachloride concentrations. This may be rationalized by invoking a reaction which regenerates CCl_3^+.

[11] $$C_2H_5OCCl_2^+ + CCl_4 \rightarrow C_2H_5OCCl_3 + CCl_3^+$$

$C_2H_5OCCl_2^+$ also disappears by a slow reaction with diethyl ether yielding mainly the triethyloxonium ion and a much smaller amount of the protonated ether.

[12a] $$C_2H_5OCCl_2^+ + (C_2H_5)_2O \rightarrow (C_2H_5)_3O^+ + COCl_2$$

[12b] $$\rightarrow (C_2H_5)_2OH^+ + C_3H_4Cl_2O$$

Because of the occurrence of reaction [11] it is impossible to obtain a satisfactory rate constant for reaction [10] using eq. [5]. A minimum value of 3×10^{-10} cm^3 molecule^{-1} s^{-1} is obtained from the initial slope of the decay curve. A better value is obtained by noting that reactions [10] and [11] are much faster than any other reactions involving CCl_3^+ and $C_2H_5OCCl_2^+$ and that in a given experiment the concentrations of both diethyl ether and carbon tetrachloride, which are much greater than those of the ions, remain constant. Reactions [10] and [11] may

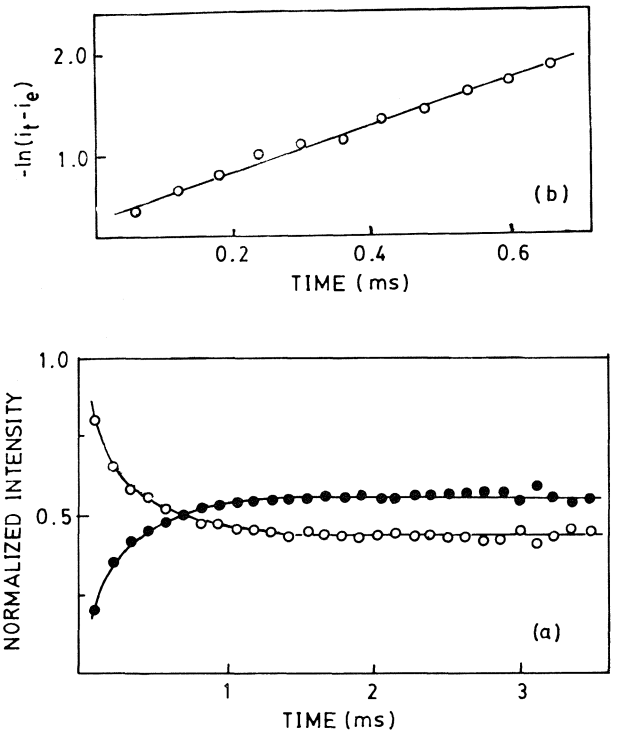

FIG. 5. (*a*) The temporal profiles of $C_2H_5OCCl_2^+$ (●) and CCl_3^+ (○). The data are from Fig. 4 and have been renormalized. (*b*) The kinetic plot for the data in (*a*) according to eq. [14].

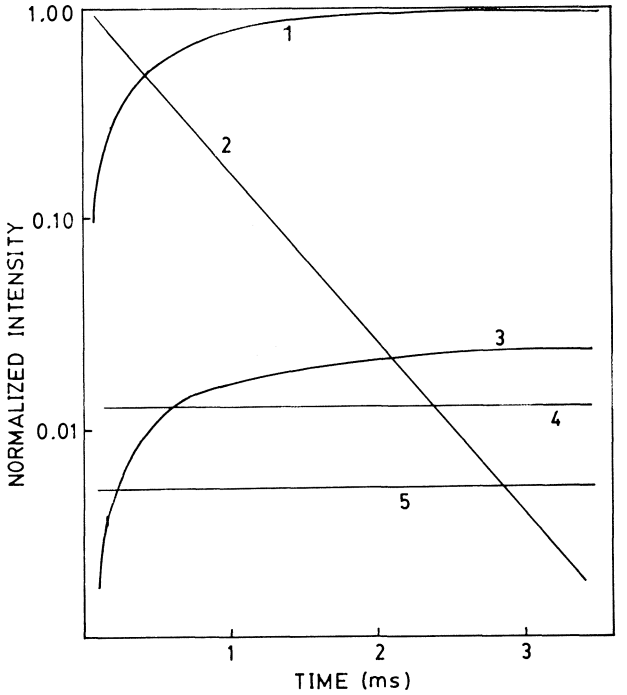

FIG. 6. Normalized ion intensities after a 60 μs pulse of ionizing electrons in a furan/CCl_4/CH_4 (0.0079/0.32/99.6) mixture at 3.5 Torr and 458 K. The curves show the temporal profiles of *1*, $C_4H_4O{\cdot}CCl_3^+$ (*m/z* 185); *2*, CCl_3^+; *3*, $C_4H_3OCCl_2^+$ (*m/z* 149); *4*, $C_4H_4OH^+$ (*m/z* 69); *5*, $C_4H_4OC_2H_5^+$ (*m/z* 97).

therefore be combined as a pair of opposing pseudo first order reactions

$$[13] \quad CCl_3^+ \underset{k_-}{\overset{k_+}{\rightleftharpoons}} C_2H_5OCCl_2^+$$

where $k_+ = k_{10}[(C_2H_5)_2O]$ and $k_- = k_{11}[CCl_4]$. The CCl_3^+ and $C_2H_5OCCl_2^+$ ion currents in Fig. 4 are renormalized in Fig. 5*a* in which the approach to equilibrium is given by (12)

$$[14] \quad \ln\frac{i_t - i_e}{i_0 - i_e} = -(k_+ + k_-)t$$

where i_0, i_t, and i_e are the renormalized ion currents for either ion at times zero, t, and after attainment of equilibrium. The approach to the equilibrium normalized ion current value is exponential for both ions in Fig. 5*a* as shown by the plot of $\ln(i_t - i_e)$ vs. t (Fig. 5*b*). The slope of this plot gives $(k_+ + k_-)$ and the ratio k_+/k_- is obtained from the ratio of renormalized equilibrium ion currents. The values of k_{10} and k_{11} are obtained from k_+ and k_- using appropriate diethyl ether and carbon tetrachloride concentrations. Four different experiments gave $k_{10} = (9 \pm 2) \times 10^{-10}$ cm^3 molecule^{-1} s^{-1} and $k_{11} = (2 \pm 1) \times 10^{-11}$ cm^3 molecule^{-1} s^{-1}, the error limits representing one standard deviation.

CCl_3^+ + cyclic ethers

The reactions of CCl_3^+ with a number of furans and 2,3-dihydropyran were briefly examined. The results of the rate constant measurements which are shown in Table 1 are generally for single measurements and are therefore to be taken only as indications of the magnitudes of the values, each result should, however, be within ±25% of the average value that would be obtained if multiple determinations had been performed.

Both furan and 2-methylfuran give the CCl_3^+ adduct as the major primary product. The only other product observed with both compounds is formed by loss of HCl from the adduct. As shown in Fig. 6 for furan, this ion has the same temporal profile as that of the adduct implying that it is formed competitively with the adduct and not by its further reaction. This lack of further reaction of the adducts shows that CCl_3^+ probably adds at oxygen and not at the double bond. Under HPMS conditions, addition to the double bond would lead to an ion which condenses with or transfers a proton to the neutral ether. No such reactions were observed, the very small constant yields of protonated furan and ethyl furan cation seen in Fig. 6 almost certainly arise from protonation by CH_5^+ and $C_2H_5^+$ and addition of $C_2H_5^+$ from the methane reagent gas. CCl_3^+ addition to furan is therefore different to protonation for which the preferred site is the α carbon (13) even though the most basic site is oxygen (14). Protonation probably occurs first at oxygen but subsequent transfer to an α carbon with concurrent geometry relaxation leads to a more stable structure. The oxonium ion is the preferred structure for the CCl_3^+ adduct because a CCl_3 group at the α carbon would have a destabilizing effect on the resulting carbocation.

When the heterocyclic ring is partially or fully hydrogenated the CCl_3^+ adduct is not observed at all (2,3-dihydrofuran, tetrahydropyran, 2,5-dimethyltetrahydrofuran) or its yield is very small (tetrahydrofuran). In all cases the spectra are very complex. Ions are observed which are formed by hydride transfer to CCl_3^+ and by loss of HCl, 2HCl, and $COCl_2$ from an initially formed adduct. For example, the reaction of CCl_3^+ with 2,3-dihydropyran (C_5H_8O) yields, in decreasing order of intensities, $C_5H_7Cl_2^+$, $C_5H_7O^+$, and $C_3H_3Cl_2^+$.

CCl_3^+ + sulfides and disulfides

The sulfur compounds are different to the oxygen compounds in their behaviour towards CCl_3^+ in that very stable adducts are invariably formed. For example, while tetrahydrofuran gives $C_4H_7^+$ and $C_3H_4OCl^+$ as major products, tetrahydrothiophene

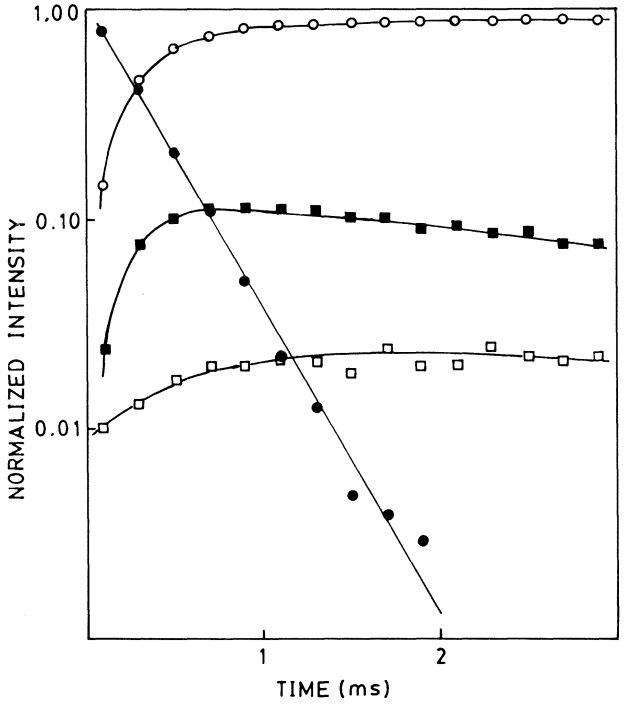

FIG. 7. Normalized ion intensities after a 60 μs ionizing pulse of electrons in a $(C_2H_5)_2S/CCl_4/CH_4$ (0.0050/0.46/99.5) mixture at 4.1 Torr and 460 K: ● CCl_3^+; ○ $(C_2H_5)_2SCCl_3^+$ (m/z 207); ■ $C_4H_9S^+$ (m/z 89); □ $(C_2H_5)_2SH^+$ (m/z 91).

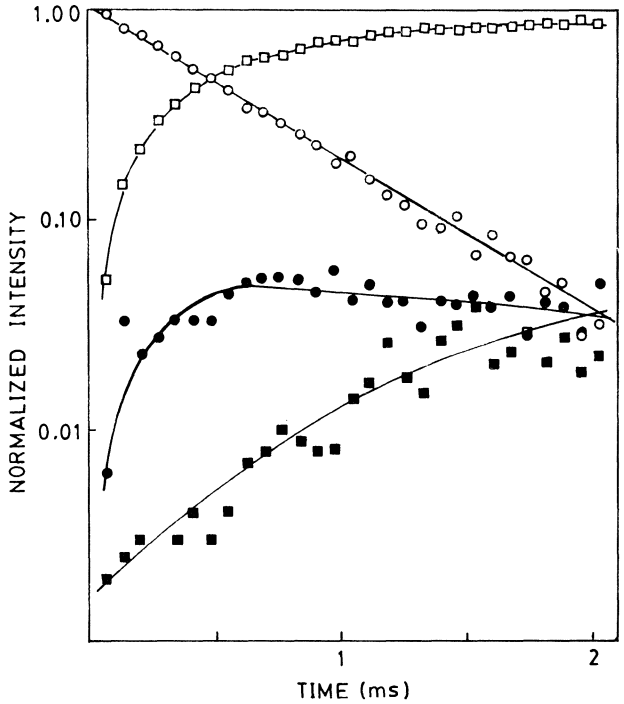

FIG. 8. Normalized ion intensities after a 60 μs ionizing pulse of electrons in a $(C_3H_7S)_2/CCl_4/CH_4$ (0.0025/0.51/99.5) mixture at 3.4 Torr and 570 K. ○ CCl_3^+; □ $(C_3H_7S)_2^+$ (m/z 150); ● $(C_3H_7S)_2CCl_3^+$ (m/z 267); ■ $(C_3H_7S)_3^+$ (m/z 225).

gives the adduct (90%) and $C_4H_7S^+$ formed by hydride transfer to CCl_3^+. Neither of these ions reacts further with neutral thiophene. Dimethyl sulfide (CH_3SCH_3) shows similar behaviour, the adduct comprises 92% of the products, the remainder being $CH_3SCH_2^+$ formed by hydride ion transfer. The latter ion reacts further by association with neutral sulfide to give $C_4H_{11}S_2^+$. There is no evidence for the formation of a trialkylsulfonium ion analogous to the trialkyloxonium ion observed with dimethyl ether (reaction [9]) even though such ions are much more stable than the analogous trialkyloxonium ions (15).

Both diethyl sulfide and di-*n*-propyl sulfide give the adduct as the major product, diethyl sulfide also yields 10% $C_2H_5SC_2H_4^+$ formed by hydride ion transfer. The analogous product for di-*n*-propyl sulfide is isobaric with $C^{35}Cl_3^+$ at m/z 117, but using the known isotopic pattern of chlorine to subtract the contribution from CCl_3^+ it is calculated that the yield of $C_3H_7SC_3H_6$ is much less than 10% of the total product ions. These results are to be contrasted with those for diethyl ether for which the sole product is $C_2H_5OCCl_2^+$. Also in contrast to the dimethyl ether adduct, these sulfide adducts, like that of dimethyl sulfide are unreactive and do not yield a trialkylsulfonium ion. Figure 7 shows that $C_2H_5SC_2H_4^+$ formed in the reaction of CCl_3^+ with diethyl sulfide reacts slowly, probably by proton transfer, to the neutral sulfide.

With the disulfides a new reaction channel opens up as electron transfer becomes competitive with adduct formation. For example, in the case of di-*n*-propyl disulfide the reactions are

[15a] $C_3H_7SSC_3H_7 + CCl_3^+ \rightarrow C_3H_7SSC_3H_7^+ + CCl_3$

[15b] $\rightarrow (C_3H_7S)_2CCl_3^+$

Temperature has a significant effect on the relative yields of the products, electron transfer being favoured at high temperature (Fig. 8) while adduct formation is favoured at low temperature (Fig. 9). At long ion residence times both products react further to give the dithiosulfonium ion $(C_3H_7S)_3^+$

[16] $(C_3H_7S)_2CCl_3^+ + (C_3H_7S)_2 \rightarrow (C_3H_7S)_3^+ + C_3H_7SCCl_3$

[17] $(C_3H_7S)_2^+ + (C_3H_7S)_2 \rightarrow (C_3H_7S)_3^+ + C_3H_7S$

The rate constants for reactions [16] and [17] were calculated from the linear slopes of the ion current curves at long reaction times for a temperature of 298 K (Fig. 8*b*); $k_{16} = 7 \times 10^{-10}$ cm^3 molecule^{-1} s^{-1} and $k_{17} = 2 \times 10^{-11}$ cm^{-3} molecule^{-1} s^{-1}. Values cannot be calculated at higher temperatures since the decay curves have a small slope and the precursor ion CCl_3^+ is still present in significant amounts.

One of the few studies of the ion chemistry of disulfide systems involved dimethylsulfide using ion cyclotron resonance (5). No rate constants were measured but the molecular ion, $(CH_3S)_2^+$ was found to react only very slowly with the disulfide, the reaction product being $(CH_3S)_3^+$. However, it was found that the thiosulfonium ion $(CH_3S)_2CH_3^+$, unlike $(C_3H_7S)_2CCl_3^+$ in this study, did not react further; a reaction analogous to 16 was calculated to be endothermic by about 3 kcal mol^{-1}. We have no estimate of the enthalpy change for reaction [15] but since it occurs with almost unit efficiency it must be exothermic by >4 kcal mol^{-1}.

Since most of the dithiosulfonium ion, $(CH_3H_7S)_3^+$, arises via reaction [16], as seen from the slopes of the decay curves in Fig. 8*b*, the branching ratio k_{15a}/k_{15b} may be obtained with small error from the ratio $\{[(C_3H_7S)_2CCl_3^+)] + [(C_3H_7S)_3^+]\}/[(C_3H_7S)]_2^+$. The ratio shows very little variation with pressure over the range 2–4 Torr but does tend to decrease by about 20% over the ion residence times. Table 2 shows that such variations are small compared with the dramatic effect of temperature.

Table 1 shows that the rate constant for the disappearance of

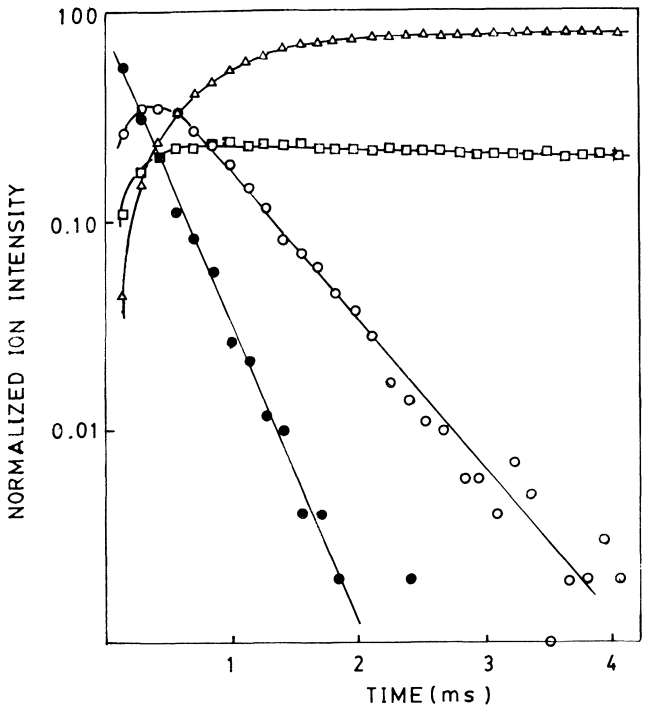

FIG. 9. Normalized ion intensities after a 60 μs pulse of ionizing electrons in a $(C_3H_7S)_2/CCl_4/CH_4$ (0.0025/0.51/99.5) mixture at 3.1 Torr and 298 K. ● CCl_3^+; □ $(C_3H_7S)_2^+$ (m/z 150); ○ $(C_3H_7S)_2CCl_3^+$ (m/z 267); △ $(C_3H_7S)_3^+$ (m/z 225).

CCl_3^+ in the presence of disulfide which is equal to (k_{15a} + k_{15b}) is essentially independent of temperature and is equal to the rate constant for collision. The factor of fifty change in the branching ratio which strongly favours electron transfer at high temperature probably reflects the decreased lifetime of the collision complex at high temperature. Since electron transfer is one of the accessible channels, the ionization energy of CCl_3 is greater than those of $(C_3H_7S)_2$ and $(C_2H_5S)_2$. Electron transfer can occur over a much greater distance than group or atom transfer and will occur upon first collision. Presumably with disulfides electron transfer to CCl_3^+ is always the first step in the ion–neutral encounter. This may or may not be followed by the formation of a stabilized complex. At high temperature the ion–molecule collision complex contains significant thermal energy as well as the ion–molecule interaction energy and consequently has a much shorter lifetime than at lower temperatures. The association reaction [15b] which may require third body stabilization is therefore discriminated against. At low temperature the association complex has a much reduced energy content, and hence a longer lifetime and a stabilized complex can be formed, i.e. [15b] is favoured over [15a].

The occurrence of the electron transfer reaction [15a] supports the contention that the reported ionization energies of alkyl disulfides do not correspond to a 0–0 transitions (16). For example, photoelectron spectroscopy yields ionization energies for diethyl- and di-*n*-propyl disulfides of 8.44 and 8.34 eV, respectively (17), well above the ionization energy of CCl_3^+ (8.28 eV (18)). Both CCl_3^+ and CCl_3 are planar, or almost planar, the lone electron in the radical being accommodated in a P_z orbital. There will be little geometry change on ionization of the radical and the reported ionization energy obtained using monochromatic electrons corresponds to the 0–0 transition. The neutral disulfides have a CSSC dihedral bond angle close to 90° (19) while calculations suggest an angle close to 180° for $CH_3SSCH_3^+$ (20). There are therefore very large geometry changes on ionization and photo electron spectroscopy ionization potential values will be larger than those for 0–0 transitions. Kinetic considerations suggest that the 0–0 ionization energy of CH_3SSCH_3 is 7.4 eV (16) which is consistent with the present results.

TABLE 2. The branching ratio (electron transfer/complex formation) for CCl_3^+ + RSSR

R	Temperature (K)	Branching ratio
C_3H_7	570	8.0
C_3H_7	454	1.6
C_3H_7	300	0.32
C_2H_5	453	1.6

Rate constants for the reactions of CCl_3^+

Under icr conditions (10^{-6}–10^{-5} Torr, 320 K) no stable adducts are observed when CCl_3^+ reacts with acetone, the only product being $CH_3CClCH_3^+$ (1). Under HPMS conditions (3–3.5 Torr, 300–460 K) the adduct $CH_3COCH_3CCl_3^+$ is the only product. The measured second order reaction rate constants are also very different at 300 K, viz. icr 3×10^{-11} cm^3 molecule^{-1} s^{-1} and HPMS 1×10^{-9} cm^3 molecule^{-1} s^{-1}. In addition, in the present study, the efficiency of reaction at 300 K is 0.5, a value independent of pressure. The efficiency of the reaction of CCl_3^+ with acetone was not measured as a function of pressure at other temperatures but the association reaction of CCl_3^+ with dimethyl ether was studied. Although the rate constant decreases when the temperature is raised from 298 to 345 K, the reaction efficiency is essentially independent of pressure at both temperatures. The above facts have several implications.

At 10^{-5} Torr the mean time between ion–molecule collisions is 10^{-3} s while at 3 Torr it is 5×10^{-9} s. Since the reaction efficiency is 0.5 for CCl_3^+ + acetone at high pressure and 300 K, based on the measured pseudo second order rate constant, 50% of the initially formed reaction complexes must have lifetimes of at least 10^{-8}–10^{-9} s. The lack of a pressure dependence of the rate constant over the range 1–4 Torr implies that the lifetimes of these collision complexes which are finally detected as stabilized species are somewhat longer. Since only ~50% of the initial collisions between CCl_3^+ and acetone and 30% of those between CCl_3^+ and dimethyl ether at 300 K lead to a stabilized complex then respectively 50% and 70% of the collision complexes have lifetimes much shorter than 10^{-8} s. There are three possible explanations for this behaviour. (*a*) There are two populations of initial collision complexes, those with lifetimes sufficiently long for stabilization to occur under HPMS but not icr conditions and those with much shorter lifetimes which decompose to reactants. This is equivalent to invoking a geometrical or steric factor in the initial collision which selects reactive versus non-reactive collisions. Such a factor would not be strongly temperature dependent, contrary to what is observed. (*b*) Secondly, it is possible that the first collision with a neutral molecule by a long-lived collision complex may be either stabilizing or dissociative. The general scheme would be

$$[18] \quad A^+ + B \underset{k_{-1}}{\overset{k_{+1}}{\rightleftharpoons}} AB^{+}*$$

$$[19a] \quad AB^{+}* + M \xrightarrow{k_2} AB^+ + M$$

$$[19b] \quad AB^{+}* \xrightarrow{k_3} A^+ + B + M$$

The branching ratio k_2/k_3 would be temperature dependent and would decrease as the total energy of AB^+* increases with increasing temperature as collisions of AB^+* with M become less efficient at stabilizing the complex. This energy includes both the thermal energy and the energy of the interaction of the ion and neutral molecule. (*c*) The third possibility is a radiative stabilization of a fraction of the initially formed association complexes in competition with back dissociation. Smith and Adams (21) favour such an explanation for their observation that above their experimental minimum pressure of 0.2 Torr the association reaction between CH_3^+ and H_2O has a constant, less than unit efficiency. An explanation for the absence of a pressure dependence on the efficiency is not given.

The problem encountered when trying to decide between (*b*) and (*c*) is the lack of data covering a sufficiently large but continuous pressure range. A phase space model for the association reaction $CH_3^+ + HCN \rightarrow CH_3 \cdot HCN^+$ in which both radiative and third body stabilization are considered shows a linear dependence of reaction efficiency on pressure only at very low pressure (22). At pressure above 0.2 Torr the model predicts that the observed second order rate constant changes only slowly with pressure and has values which are considerably less than the collision rate constant if the efficiency of the third body stabilization reaction is well below unity. Such a slow change of measured second order rate constant with pressure may not then be experimentally observable over a small range of pressure such as used in the present work. If radiative stabilization is a significant factor in the association reaction of CCl_3^+ with acetone, then $CH_3COCH_3CCl_3^+$ should be observed in icr experiments at very low pressures where the mean lifetime between collisions is larger than in HPMS. The fact that no such complexes were observed does not necessarily negate the argument in favour of radiative stabilization. As Adams and Smith (23) have pointed out, the presence of residual excitation energy from their method of formation in ions taking part in association reactions under icr conditions leads to results which may be far removed from those obtained when the ions are thermalized. In the icr study (1), CCl_3^+ was formed by electron impact dissociative ionization of CCl_4 in mixtures containing 5–10% CH_3COCH_3 in CCl_4. The ten to twenty thermalizing collisions of CCl_3^+ with CCl_4 prior to an encounter with acetone may not have been sufficient to eliminate all the excess energy of formation, although if Cl^- transfer occurs at a significant rate in CCl_3^+/CCl_4 collisions it is generally accepted that thermalization can be very efficient.

Adams and Smith (23) have recently discussed the kinetics of ion–molecule association reactions with special emphasis on the association of small species. Their conclusions regarding such relatively simple systems are similar to those stated above, in particular the difficulty in determining the role of radiative association and indeed in determining whether the measured effective rate constants for some quite simple association reactions (eg. $CH_3^+ + HCN \rightleftharpoons CH_3^+ \cdot HCN$) do exhibit pressure dependences in the pressure range 0.2–4 Torr, i.e., has or has not "saturation" occurred? The mechanisms of reactions involving more complex species such as those reported here will probably be even more difficult to decipher.

The reaction efficiencies shown in Table 1 are computed in terms of the experimental second order rate constants. As stated previously none of these rate constants shows a significant pressure dependence and so even nominally third order reactions may be discussed in terms of the efficiencies per initial ion–molecule collision. In general, the efficiency for the oxygen bases increases with increasing complexity of the neutral. For example, CCl_3^+ reacts with diethyl ketone in 16% of the encounters at 455 K while only 1.2% of the encounters with acetone lead to product. In both cases the major initial product is formation of $R_2CO \cdot CCl_3^+$ (R = CH_3, C_2H_5). Similarly, dimethyl ether has a lower reaction efficiency than diethyl ether at the same temperature. The reactions in this case are of course different in that dimethyl ether forms a stabilized complex whereas no stabilized complex is observed with diethyl ether.

The cyclic ethers show a rather limited range of reaction efficiencies. Furan, which mainly forms the adduct has the lowest efficiency while the efficiency increases as the degree of hydrogenation and the complexity of the ring increases. Since many of these results are from single experiments this can only be a generalization. The relatively high efficiency of tetrahydrothiophene compared with furan or tetrahydrofuran is consistent with the greater efficiencies of reaction of CCl_3^+ with the thioethers compared with the ethers. Although the disulfides react with essentially unit efficiency at all temperatures and pressure, the efficiency for chemical reaction other than electron transfer is little different from that of the sulfides, in both cases this is mainly an association reaction.

Conclusion

The reactions of CCl_3^+ with many of the compounds studied are very efficient even at the temperature of ~460 K used in most of the studies. This is in spite of the fact that for many of the compounds the primary product is a stabilized ion–neutral complex. As suggested by Ausloos and co-workers (1), reaction efficiency does appear to increase with increasing exothermicity of reaction, e.g. diethyl ketone > acetone and diethyl ether > dimethyl ether. For the ketones this implies that a greater number of ion–molecule complexes have sufficiently long lifetimes for stabilization to occur when the size of the neutral molecule increases, which is also in agreement with a suggestion of Ausloos and co-workers. In their icr work no stabilized complexes were observed and bimolecular chemical changes were studied. The present results show that such changes, provided that they are initiated by excited ions, will be preceded by long-lived ($>10^{-8}$ s) ion–molecule complexes.

The lack of a significant pressure dependence of the experimental second order rate constants for association reactions is not a unique observation but the explanation for it is still unclear. An examination of such reactions might profitably be carried out using a selected ion flow tube at pressures in the range 0.05 to 1 Torr.

Acknowledgement

The authors thank the Natural Sciences and Engineering Council of Canada for financial support.

1. P. Ausloos, S. G. Lias, and J. R. Eyler. Int. J. Mass Spectrom. Ion Phys. **18**, 261 (1975).
2. J. A. Stone, N. J. Moote, and A. C. M. Wojtyniak. Can. J. Chem. **63**, 2608 (1985).
3. L. P. Theard and W. H. Hamill. J. Am. Chem. Soc. **84**, 1134 (1962).
4. L. I. Virin, Yu.A. Safin, and R. V. Dzhagatspanyan. Khim. Vys. Energ. **2**, 16 (1968).
5. J. K. Kim, J. Bonicamp, and M. C. Caserio. J. Org. Chem. **46**, 4230 (1981).
6. G. K. Helmkamp, H. N. Cassey, B. A. Olsen, and D. J. Pettitt. J. Org. Chem. **30**, 933 (1965).

7. J. A. STONE and D. E. SPLINTER. Can. J. Chem. **59**, 1779 (1981).
8. T. SU and M. T. BOWERS. Int. J. Mass Spectrom. Ion. Phys. **12**, 347 (1973).
9. M. CHARTON. *In* Progress in physical organic chemistry. Vol. 13. *Edited by* R. W. Taft. Interscience, New York. 1981. p. 119.
10. J. HINE, C. H. THOMAS, and S. J. EHRENSON. J. Am. Chem. Soc. **77**, 3886 (1955).
11. A. STREITWIESER. Chem. Rev. **56**, 571 (1956).
12. J. W. MOORE and R. G. PEARSON. Kinetics and mechanism. 3rd ed. John Wiley and Sons, New York. 1981.
13. R. HOURIET, H. SCHWARZ, W. ZUMMACK, J. C. ANDRADE, and P. v. R. SCHLEYER. Nouv. J. Chim. **5**, 505 (1981).
14. M. T. NGUYEN, A. F. HEGARTY, T.-K. HA, and G. R. DE MARE. J. Chem. Soc. Perkin Trans. 2, 147 (1986).
15. G. A. OLAH, G. K. S. PRAKASH, and J. SOMMER. Superacids. John Wiley and Sons, New York. 1985. p. 191.
16. J. J. BUTLER, T. BAER, and S. A. EVANS. J. Am. Chem. Soc. **105**, 3451 (1983).
17. G. WAGNER and H. BOCK. Chem. Ber. **107**, 68 (1974).
18. F. P. LOSSING. Bull. Chem. Soc. Belges. **81**, 125 (1972).
19. R. J. BOYD, J. S. PERKYNS, and R. RAMANI. Can. J. Chem. **61**, 1082 (1983).
20. K. KIMURA and K. OSAFUNE. Bull. Chem. Soc. Jpn. **48**, 2421 (1975).
21. D. SMITH and N. G. ADAMS. Chem. Phys. Lett. **47**, 145 (1977).
22. L. M. BASS, P. R. KEMPER, V. G. ANICICH, and M. T. BOWERS. J. Am. Chem. Soc. **103**, 5283 (1984).
23. N. G. ADAMS and D. SMITH. *In* Swarms of ions and electrons in gases. *Edited by* W. Lindinger, T. D. Mark, and F. Howarka. Springer-Verlag, New York. 1984. p. 194.

A water soluble dimeric steroid with catalytic properties. Rate enhancements from hydrophobic binding

J. Peter Guthrie,[1] John Cossar, and Brian A. Dawson
Department of Chemistry, University of Western Ontario, London, Ont., Canada N6A 5B7

Received June 6, 1986

J. Peter Guthrie, John Cossar, and Brian A. Dawson. Can. J. Chem. **64**, 2456 (1986).

Dimeric steroids can be formed by reductive amination of terephthalaldehyde with 3-amino steroids using cyanoborohydride. An amino group in the 11β-position can be blocked using a formyl group, and this can be removed by acid hydrolysis after dimerization. Trifluoroacetyl is not a suitable blocking group; although it can be removed by acid hydrolysis from monomeric steroids, it was only removed from the dimer under forcing conditions which caused degradation. The dimeric steroid is a catalyst for the hydrolysis of arylpropionate esters with good leaving groups. Acylation is markedly accelerated by hydrophobic binding of the aryl group of the substrate to the steroids. Rate enhancements, relative to imidazole, of up to 5.5×10^2 were obtained, and analysis of the data shows that the potential rate enhancement is 1.1×10^5. The magnitude of the hydrophobic binding is consistent with what was seen with earlier catalysts. Aggregation, even at very low concentrations, was a problem with anionic substrates.

J. Peter Guthrie, John Cossar et Brian A. Dawson. Can. J. Chem. **64**, 2456 (1986).

On peut former des stéroïdes dimères par amination réductrice du téréphtalaldéhyde avec des amino-3 stéroïdes, sous l'influence du cyanoborohydrure. On peut bloquer un groupement amino-11β à l'aide d'un groupement formyle qui peut être enlevé par une hydrolyse acide, à la suite de la dimérisation. Le groupement trifluoroacétyle n'est pas approprié pour bloquer, même si on peut l'enlever des stéroïdes par hydrolyse acide; en effet, on ne peut l'enlever monomères qu'en utilisant des conditions fortes qui provoquent une dégradation. Le stéroïde dimère est un catalyseur pour l'hydrolyse des esters arylpropionates portant de bons groupement nucléofuges. L'acylation est fortement accélérée par une fixation hydrophobe du groupement aryle du substrat par les stéroïdes. On a observé des augmentations de vitesses, relatives à l'imidazole, allant jusqu'à $5{,}5 \times 10^2$ et une analyse des données démontre qu'il est possible d'obtenir des augmentations de vitesse de l'ordre de $1{,}1 \times 10^5$. L'amplitude de la fixation hydrophobe est en accord avec ce qui a été observé antérieurement avec d'autres catalyseurs. Même à de faibles concentrations, l'aggrégation est un problème avec les substrats anioniques.

[Traduit par la revue]

Introduction

We have reported studies of various catalytic molecules based on a steroid skeleton, which provided a hydrophobic binding surface (1–4). By linking two steroid moieties in a dimeric catalyst we were able to achieve larger rate enhancements (5), but encountered severe experimental difficulties as a result of the very low solubility of this catalyst. We now wish to report the preparation of a very soluble dimer, which should allow extensive studies of the hydrophobic interaction. We have confirmed the large rate enhancements previously reported for phenanthryl substrates. In the initial experiments we found that, despite the high solubility of the catalyst, there can be severe problems of aggregation when the substrate has the opposite charge.

Results

Preparation and proof of structure for model dimers

Our plan was to prepare steroid dimers by reductive amination of 3-β-aminosteroids using terephthalaldehyde and cyanoborohydride (6). We first examined two model systems to test the reaction conditions. We prepared the dimer derived from cyclohexylamine, as shown in Scheme 1. Initial experiments using methanol as solvent led to the desired compound but in impure form. Addition of molecular sieves improved the efficiency, but the presence of pulverized sieves at the end of the reaction was undesirable. Upon changing to methoxyethanol as solvent we found that the reductive amination gave quite pure material in 90% yield with no further attempts at optimization. We tried to titrate this material to obtain pK_a values for use with the dimeric steroid but were frustrated by the extreme insolubility of the neutral compound; even at 0.00065 *M* precipitation occurred at pH 9.85. The pH after addition of half an equivalent of OH^- can be taken as an approximation to the first pK_a; with a solution at 0.1 *M* ionic strength (KCl) this value was 9.0; with a somewhat more concentrated solution at 1.0 *M* ionic strength the value observed was about 10.0 (this required a short extrapolation past the point where precipitation occurred).

Then we prepared 3-β-amino-androstane-17-β-ol (7), **5**, and the dimer derived from it, as outlined in Scheme 1. The amine function was introduced stereospecifically by dissolving metal reduction of the oxime, **4** (7, 8). That the reduction occurred with the desired stereochemistry was shown by the broad signal in the spectrum of the dimer attributed to $\rangle CH\text{—}NH_2^+\text{—}$. The width at half height, $w_{1/2}$, was ca. 24 Hz; for $\rangle CH\text{—}OH$, which we assume is a reasonable model, an α-H has $w_{1/2}$ = 7 Hz, while a β-H has $w_{1/2}$ = 20 Hz (9). The monomeric amine was obtained as the hydrochloride, and was very insoluble, so that the signals from the methine protons were not readily visible; it was simpler to examine the dimer to establish the stereochemistry of the first reduction step. Dimerization proceeded smoothly; a yield of 54% was obtained with little effort at optimizing the conditions. The identity of the dimer, **5**, was established by its ^1H nmr spectrum and its exact mass.

Dimerization of 17-β-(4(5)-imidazolyl)-11-β-trifluoroacetamido-5α-androstan-3-β-amine

In order to prepare the desired dimer of 17-β-(4(5)-imidazolyl)-5α-androstane-3-β,11-β-diamine, **8**, was necessary to block the 11-β-amino group. Trial experiments at reductive amination of **6** using terephthalaldehyde had led to insoluble gelatinous precipitates.[2] This was interpreted as polymerization involving reaction at both the 3- and 11-amino groups. Since we had found that the trifluoroacetyl group resisted base hydrolysis

[1]Author to whom correspondence should be addressed.

[2]J. P. Guthrie, unpublished observations.

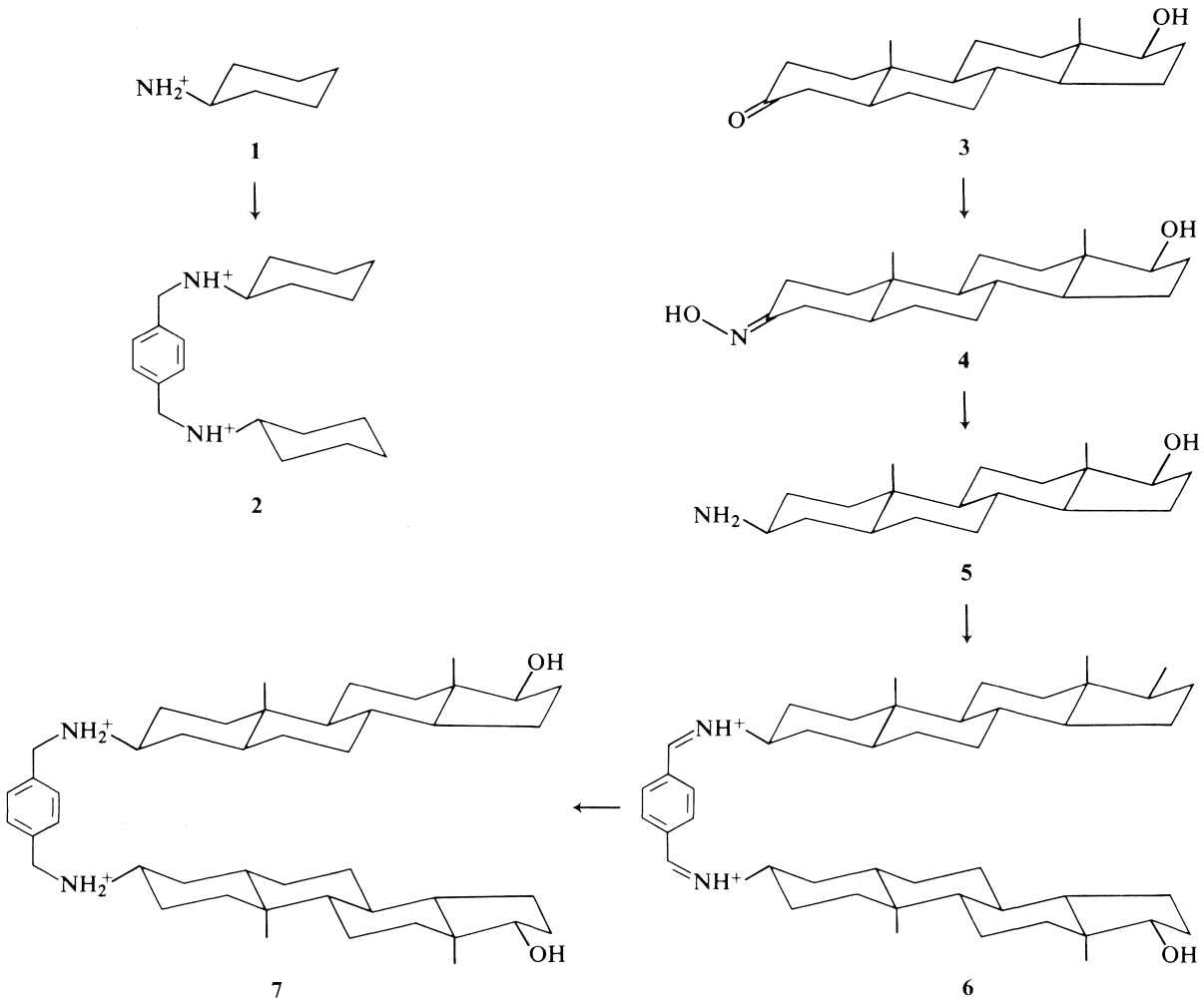

SCHEME 1

from an 11-β-amide, but could be hydrolyzed in acid (4), we initially tried this blocking group, as outlined in Scheme 2. Dimerization of 17-β-(4(5)-imidazolyl)-11-β-trifluoroacetamido-5α-androstan-3-β-amine, **10***a*, proceeded reasonably well, to give a material with an nmr spectrum consistent with structure **12***a*, but on attempting to hydrolyze the blocking groups we found that they did not come off under conditions which sufficed for the monomeric steroid (either refluxing 6 *N* HCl or refluxing 6 *N* CH_3SO_3H), and use of more vigorous conditions led to extensive degradation of the dimer.

Dimerization of 17-β-(4(5)-imidazolyl)-11-β-formamido-5α-androstan-3β-amine

We found that formyl was a suitable blocking group for the 11-β-amino function, since it could be put on readily, resisted alkaline hydrolysis (which hydrolyzed a 3-formamido group), and could be removed by acid hydrolysis. Conditions were found which gave the desired dimerization of **10***b*, and for **12***b* the blocking groups were removable by acid hydrolysis using 3 *N* HCl at 100°C for 6 h. The stereochemistry of **8** has been established (1), and this establishes the stereochemistry of **13**. The integration of the ^1H nmr proves that two steroids have been linked by one *p*-xylylene bridge. The ^{13}C nmr spectrum proves the symmetry of the molecule because we observe the correct number of peaks for two identical steroid residues linked by a *p*-xylylene bridge. Without further experiments a detailed assignment cannot be made with any confidence. The exact mass confirms the composition of **13**.

Kinetics of reactions with p*-nitrophenyl esters*

All of the kinetics data are found in Table 1. By working at low substrate concentrations it was possible to obtain rate constants for the reaction of **13** with **14***b*, **15***b*, and **16***b*. In the case of **16***b* it was necessary to use concentrations of less than 10^{-7} *M* to avoid precipitation and/or aggregation which led to spuriously low rates. We found that the use of tris buffers led to erratic and irreproducible behavior, which we have also observed in other reactions (10), but that borate buffer was well behaved. The second order rate constants obtained from plots of k_{obs} vs. [**13**] are found in Table 2.

Figures 1, 2, and 3 show the kinetics behavior of the phenyl-, naphthyl-, and phenanthrylpropionate substrates. In each case it should be noted that the inherent reactivity of the substrates, as shown by the rates of uncatalyzed hydrolysis, was trimethylammonionitrophenyl > carboxynitrophenyl > nitrophenyl, but the rate constants for **13** catalyzed reactions were in the order carboxynitrophenyl > trimethylammonionitrophenyl > nitrophenyl, except for the esters of 3-(3-phenanthryl)propionic acid. As we have observed in related studies (4), the electrostatic interactions of substrate and catalyst have a powerful influence on the observed reactivity patterns.

Kinetics of reactions with esters of 3-hydroxy-4-nitrobenzoic acid

These esters had been the best ester substrates for **8**, so we had expected that they would also be best for **13**. Although **14***a* and **15***a* were relatively straightforward to study, we had extra-

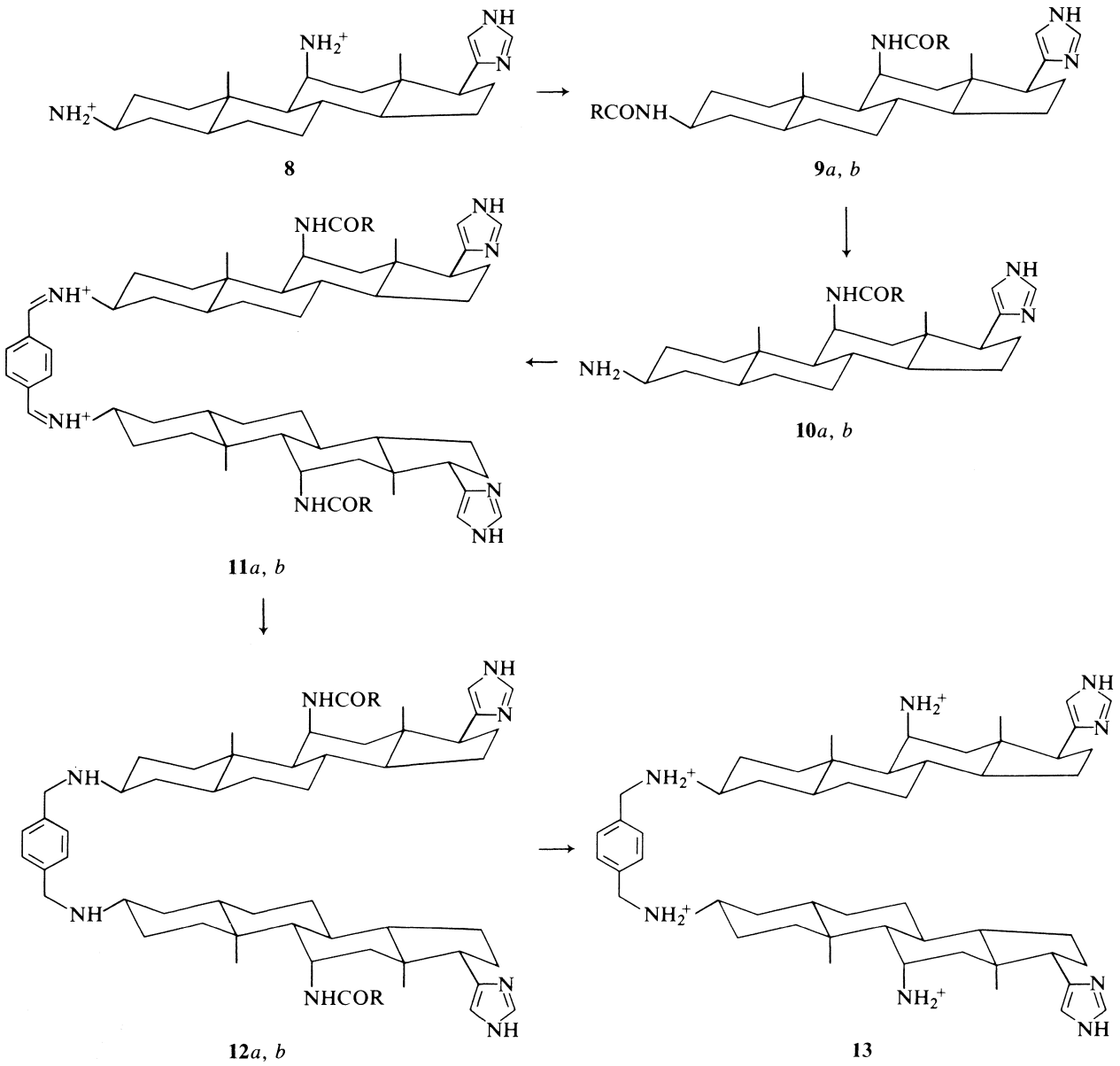

SCHEME 2

ordinary difficulty getting readily interpretable rate constants from the reaction of **13** and **16***a*. It was only possible to get simple behavior by using solutions where the reagent in excess was at a concentration less than 3×10^{-6} *M* with the other reagent at about a ten-fold lower concentration. Figure 3 illustrates the simple behavior shown at low concentrations, and the major and variable inhibitory effects seen at higher concentrations with either catalyst or substrate in excess. The second order rate constants are found in Table 2. In the case of **14***a* simple kinetic behavior was observed even at high concentrations of **13**; plots of k_{obs} vs. [**13**] showed distinct curvature, which could be analyzed in terms of preassociation. An Eadie–Hofstee (11, 12) plot was reasonably linear, see Fig. 4, and led to an apparent binding constant of $(6.3 \pm 1.4) \times 10^{-4}$ *M*. Although the behavior seen is qualitatively what would be expected for binding of substrate by catalyst, the linearity of the Eadie–Hofstee plot is imperfect, so that what was observed may be the result of some more complex aggregation process. In any case the binding constant determined from such an analysis need not refer to the productive mode of binding which leads directly to the catalytic transition state, but may refer to some form of non-productive binding which has the substrate improperly oriented relative to the catalytic groups. The phenomenon of non-productive binding is a well known complication in enzymology (13). For the other carboxynitrophenyl esters no signs of binding, or at least of simple binding behavior, were apparent.

Kinetics of reactions with 4-trimethylammonio-6-nitrophenyl esters

These substrates were, as anticipated, well behaved. The second order rate constants are found in Table 2. In the case of **16***c* we carried out experiments over a wide range of concentrations of **13** and observed apparent saturation kinetics. Figure 5 shows an Eadie–Hofstee plot for the data; although there is considerable scatter, it is clear that we have observed saturation kinetics, with an apparent binding constant of $(4.62 \pm 0.98) \times 10^{-5}$ *M*. At this point it would be rash to build much interpretation upon this number because of the possibilities for non-productive binding or aggregation. We have frequently

TABLE 1. Kinetics of ester reactions with **13**[a]

[Ester] $\times 10^6$	[Dimer] $\times 10^6$	a_1	a_2	$a_3 \times 10^4$	$a_4 \times 10^8$	
Carboxynitrophenyl esters[b]						
14*a*						
0.342	0.	0.0185(0.0001)	−0.0165(0.0001)	0.1785(0.0013)		
8.39	0.	0.3696(0.0001)	−0.3679(0.0001)	0.1669(0.0001)		
1.28	13.9	0.0436(0.0001)	−0.0429(0.0001)	2.591(0.0036)	1.78(0.064)	
0.428	5.81	0.0344(0.0001)	−0.0200(0.0001)	1.054(0.0087)		
3.77	40.6	0.1982(0.0001)	−0.1746(0.0002)	6.757(0.018)		
30.0	377.	0.2949(0.0002)	−0.2761(0.0003)	49.82(0.099)	348.(14)	c,d
82.9	1152.	0.5288(0.0002)	−0.1478(0.0005)	75.56(0.64)		d,e
$k = (0.167 \pm 0.016) \times 10^{-4} + (17.1 \pm 0.4)$[dimer][f]						
15*a*						
0.88	23.2	0.0461(0.0001)	−0.0388(0.0001)	13.24(0.07)	25.5(0.9)	
0.44	11.6	0.0255(0.0001)	−0.0195(0.0001)	8.335(0.03)		
0.21	5.81	0.0108(0.0001)	−0.0090(0.0001)	3.716(0.016)		
0.105	3.48	0.0086(0.0001)	−0.0055(0.0001)	2.946(0.045)		
1.73	34.8	0.0943(0.0002)	−0.0564(0.0003)	18.57(0.22)	95.5(4.7)	
0.176	5.81	0.0092(0.0001)	−0.0089(0.0001)	2.606(0.014)	2.80(0.05)	
0.176	3.48	0.0066(0.0001)	−0.0068(0.0001)	2.266(0.033)		
0.141	1.74	0.0079(0.0001)	−0.0054(0.0001)	1.241(0.024)		
0.352	0.	0.0207(0.0001)	−0.0229(0.0001)	0.5265(0.0072)		
0.345	0.	0.0123(0.0001)	−0.0126(0.0001)	0.3539(0.0069)	−0.693(0.073)	
$k = (0.389 \pm 0.153) \times 10^{-4} + (54.1 \pm 4.5)$[dimer][f]						
16*a*						
1.65	0.	0.0940(0.0004)	−0.0841(0.0004)	0.527(0.008)		
0.20	5.81	0.0095(0.0001)	−0.0059(0.0006)	25.60(0.49)	19.4(0.5)	d
0.20	2.90	0.0074(0.0001)	−0.0071(0.0001)	14.26(0.20)	8.89(0.73)	
0.136	1.74	0.0067(0.0001)	−0.0050(0.0001)	9.16(0.11)		
0.101	1.16	0.0003(0.0001)	−0.0288(0.0001)	7.558(0.124)		
1.0	0.116	0.0137(0.0001)	−0.0117(0.0001)	8.673(0.159)	121.(2)	
2.01	0.232	0.0366(0.0001)	−0.0159(0.0001)	15.36(0.24)	197.2(2)	g
0.060	0.581	0.0017(0.0001)	−0.0016(0.0001)	3.678(0.112)		
0.52	0.	0.0268(0.0001)	−0.0269(0.0001)	0.564(0.0062)		
1.16	0.	1.263(0.0019)	−0.809(0.0018)	0.171(0.0010)		d
0.10	11.6	0.0078(0.0001)	−0.0031(0.0001)	33.32(0.88)	14.3(1.0)	d
0.17	11.6	0.0198(0.0001)	−0.0038(0.0001)	20.36(0.92)		d
0.96	11.5	0.1152(0.0001)	−0.0415(0.0001)	15.17(0.10)		d
0.449	23.2	0.0279(0.0001)	−0.0160(0.0001)	27.54(0.16)		d
0.10	23.2	0.0069(0.0001)	−0.0042(0.0001)	24.68(0.57)		d
0.22	23.2	0.0138(0.0001)	−0.0074(0.0001)	35.80(0.31)		d
9.52	1.16	0.1355(0.0004)	−0.0377(0.0004)	31.62(0.78)	1002.(15)	d,g
9.9	0.116	0.0315(0.0002)	−0.0103(0.0001)	9.356(0.272)	485.(2)	d,h
9.9	0.348	0.0445(0.0005)	−0.0204(0.0005)	11.34(0.69)	443.(5)	d,h
$k = (0.552 \pm 0.055) \times 10^{-4} + (547 \pm 43)$[dimer][f]						
p-Nitrophenyl esters						
17*b*						
26.	290.	0.4534(0.0002)	−0.499(0.025)	2.640(0.119)		e,i
			0.082(0.025)	1.151(0.170)		
26.	0.	0.4316(0.0003)	−0.400(0.0003)	0.4091(0.0022)		e
14*b*						
1.18	0.	0.2010(0.0001)	−0.2007(0.0002)	0.5954(0.0014)		
0.944	5.79	0.1557(0.0001)	−0.1557(0.0001)	0.6305(0.0010)		
0.904	16.6	0.0862(0.0001)	−0.0811(0.0001)	0.7201(0.0013)		j
0.93	45.6	0.0338(0.0001)	−0.0311(0.0001)	1.165(0.00064)		c
0.946	111.	0.0126(0.0001)	−0.0118(0.0001)	2.165(0.0224)		e
1.04	322.	0.0201(0.0001)	−0.0196(0.0001)	4.368(0.020)		e
0.91	215.	0.0172(0.0001)	−0.0130(0.0001)	3.291(0.014)		e
$k = (0.559 \pm 0.019) \times 10^{-4} + (1.30 \pm 0.05)$[dimer][f]						

TABLE 1. (*continued*)

[Ester] $\times 10^6$	[Dimer] $\times 10^6$	a_1	a_2	$a_3 \times 10^4$	$a_4 \times 10^8$	
15*b*						
0.318	3.47	0.0578(0.0001)	−0.0404(0.0001)	0.8347(0.0037)		*k*
0.318	0.	0.0731(0.0001)	−0.0428(0.0001)	0.7800(0.0041)		*k*
0.317	11.6	0.0443(0.0001)	−0.0424(0.0001)	1.674(0.0075)		
0.394	23.0	0.0571(0.0001)	−0.0560(0.0001)	1.714(0.0069)		
0.0396	11.68	0.0063(0.0001)	−0.0056(0.0001)	1.676(0.022)		
0.513	63.2	0.0166(0.0001)	−0.0155(0.0001)	3.902(0.033)		*c*
1.18	215.	0.0172(0.0001)	−0.0157(0.0001)	11.35(0.149)	17.14(0.38)	*e*
0.516	310.	0.0106(0.0001)	−0.0101(0.0001)	20.41(0.19)	38.8(0.8)	*e*
0.557	101.	0.0629(0.0001)	−0.0172(0.0001)	5.318(0.040)		*c*
0.702	23.0	0.1155(0.0002)	−0.1144(0.0002)	1.947(0.011)		
0.632	176.	0.0088(0.0001)	−0.0072(0.0001)	10.73(0.10)	6.54(0.35)	*e*
0.704	11.5	0.0603(0.0001)	−0.0590(0.0001)	1.221(0.008)		*j*
0.347	0.	0.0554(0.0001)	−0.0565(0.0001)	0.9057(0.0066)		
0.497	93.5	0.0210(0.0001)	−0.0145(0.0001)	5.270(0.0671)		*c*
$k = (0.758 \pm 0.051) \times 10^{-4} + (4.90 \pm 0.38)$[dimer] *f*						
16*b*						
0.14	0.	0.0203(0.0001)	−0.0207(0.0001)	0.3000(0.0038)		
0.35	29.0	0.0813(0.0001)	−0.0553(0.0002)	9.269(0.050)		
0.35	29.0	0.1512(0.0001)	−0.0566(0.0002)	8.242(0.045)		
0.14	23.0	0.0390(0.0001)	−0.0286(0.0001)	1.199(0.098)		
0.70	11.6	0.0287(0.0001)	−0.0109(0.0001)	6.921(0.074)		
0.07	11.62	0.0417(0.0001)	−0.0103(0.0001)	4.940(0.050)		
0.0605	0.	0.0112(0.0001)	−0.0104(0.0001)	1.075(0.0079)		
0.0604	2.32	0.0134(0.0001)	−0.0091(0.0001)	1.819(0.021)	−0.122(0.037)	
0.0604	4.63	0.0096(0.0001)	−0.0095(0.0001)	3.440(0.032)		
0.0603	8.68	0.0132(0.0001)	−0.0099(0.0001)	4.334(0.0223)		
0.0751	17.3	0.0203(0.0001)	−0.0116(0.0001)	9.056(0.064)		
0.0747	34.4	0.0226(0.0001)	−0.0150(0.0001)	15.13(0.08)		
0.0743	48.0	0.0170(0.0001)	−0.0158(0.0001)	20.47(0.15)		
$k = (0.553 \pm 0.163) \times 10^{-4} + (42.9 \pm 2.2)$[dimer] *f*						
4-Trimethylammonio-2-nitrophenyl esters *l*						
14*c*						
10.1	0.	0.1697(0.0001)	−0.1344(0.0001)	1.456(0.003)		*m*
1.06	11.5	0.0512(0.0001)	−0.0506(0.0001)	2.250(0.004)	1.61(0.09)	
1.06	23.0	0.0517(0.0001)	−0.0501(0.0001)	2.905(0.007)		
1.05	45.6	0.0565(0.0001)	−0.0486(0.0001)	4.633(0.025)	2.12(0.15)	
5.69	92.4	0.0507(0.0001)	−0.0484(0.0001)	7.376(0.009)		*c*
9.87	172.	0.0455(0.0001)	−0.0422(0.0001)	12.34(0.040)		*e*
14.2	360.	0.0693(0.0001)	−0.0583(0.0001)	21.24(0.043)		*d*,*e*
$k = (1.48 \pm 0.02) \times 10^{-4} + (6.40 \pm 0.08)$[dimer] *f*						
15*c*						
6.78	174.	0.0329(0.0001)	−0.0281(0.0001)	49.57(0.19)	36.1(1.0)	*e*
1.44	18.5	0.0662(0.0005)	−0.0647(0.0001)	8.172(0.029)		
3.61	0.	0.1769(0.0004)	−0.1447(0.0003)	1.570(0.0054)	7.26(0.84)	
3.61	4.17	0.1942(0.0003)	−0.1511(0.0002)	2.451(0.0079)	5.67(0.68)	
9.62	111.	0.0970(0.0001)	−0.0823(0.0001)	30.89(0.095)	67.2(3.2)	*c*
5.29	65.6	0.2826(0.036)	−0.1706(0.0004)	20.42(0.12)	72.1(10.9)	
3.97	46.3	0.1951(0.0002)	−0.1639(0.0002)	16.24(0.051)	5.85(2.01)	
21.5	0.	1.042(0.0010)	−0.8513(0.0010)	1.449(0.0032)	81.4(1.98)	
14.1	0.	0.7122(0.0007)	−0.6851(0.0007)	1.462(0.0040)	14.0(0.60)	
2.82	34.4	0.1342(0.0001)	−0.1350(0.0002)	9.727(0.040)	4.733(0.39)	
$k = (1.47 \pm 0.07) \times 10^{-4} + (27.6 \pm 1.3)$[dimer] *f*						
16*c*						
7.24	310.	0.0446(0.0001)	−0.0122(0.0001)	548.6(5.3)	54.7(4.4)	*e*
16.1	0	0.9020(0.0005)	−0.6906(0.0002)	1.528(0.0013)		
0.766	12.1	0.0192(0.0001)	−0.0110(0.0001)	100.7(1.3)		*j*
3.94	46.4	0.2137(0.0001)	−0.1274(0.0002)	317.6(1.16)	5.43(0.55)	

TABLE 1. (*concluded*)

[Ester] $\times 10^6$	[Dimer] $\times 10^6$	a_1	a_2	$a_3 \times 10^4$	$a_4 \times 10^8$
3.99	0	0.1956(0.0001)	−0.1861(0.0001)	1.806(0.0015)	
1.98	23.3	0.1106(0.0001)	−0.0931(0.0004)	193.6(1.16)	
1.00	11.6	0.0491(0.0001)	−0.0427(0.0001)	103.4(0.73)	0.311(0.054)
0.475	5.83	0.0264(0.0001)	−0.0229(0.0001)	76.18(0.45)	0.408(0.0148)
3.94	46.4	0.2110(0.0001)	−0.1761(0.0004)	310.2(0.81)	8.40(0.169)
1.98	23.3	0.1070(0.0001)	−0.0901(0.0002)	220.9(1.06)	3.80(0.323)
1.00	11.6	0.0482(0.0001)	−0.0465(0.0002)	111.9(0.76)	
0.475	5.83	0.0226(0.0001)	−0.0229(0.0001)	49.32(0.60)	−0.348(0.066)

$k = (706 \pm 82)/(1 + (5.91 \pm 1.03) \times 10^{-5})/[\text{dimer}])^n$

[a]All reactions in aqueous solution at 25°C, ionic strength 0.1 (KCl), pH 8.00 maintained by 0.0928 *M* borate buffer. Substrates were added as acetonitrile solutions; the final solutions were 0.01–3.6% acetonitrile (v/v). Data were fitted to $y = a_1 + a_2 \exp(-a_3 t)$; if there was a drift in absorbance at long times the data were fitted to $y = a_1 + a_2 \exp(-a_3 t) + a_4 t$.
[b]Followed at 425 nm using 10 cm cells unless otherwise noted.
[c]2 cm cell.
[d]Omitted from the fit of k_{obs} vs. [reagent in excess].
[e]1 cm cell.
[f]Fitted by least squares; $k = a + b$[reagent in excess]; in most reactions the catalyst is in excess.
[g]This run was carried to completion and showed the pattern of an initial burst of phenoxide release followed by a long pseudo zero order phase of phenoxide production.
[h]Followed at 450 nm.
[i]Data fitted to $y = a_1 + a_2 \exp(-a_3 t) + a_4 \exp(-a_5 t)$; the absorbance time curve showed a small but definite decrease in absorbance at long times, constituting a second exponential phase. a_4 and a_5 are given in the second row for this experiment.
[j]5 cm cell.
[k]Followed at 402 nm.
[l]Followed at 400 nm using 10 cm cells unless otherwise noted.
[m]Followed at 350 nm.
[n]Fitted by least squares to $y = a_1/(1 + a_2/x)$.

encountered considerable scatter in kinetics when aggregation of the reagents influences the overall rate of reaction (10, 14).

The behavior for all of the substrates is shown in Fig. 6, which plots the observed second order rate constants for all nine substrates with **13**, as well as the two times the rate constants for the reactions of imidazole and **8** with the corresponding acetate esters as a function of π, the Hansch hydrophobicity parameter (15, 16) for the aryl group in the arylpropionic acids. The lines have no theoretical significance but simply join related points. For the overall rate constants the dependence upon the hydrophobicity of the aryl binding group is clearly non-linear, suggesting that the observed rate constants are not simple

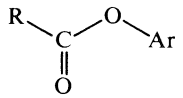

14, **15**, **16**, **17***a–c*

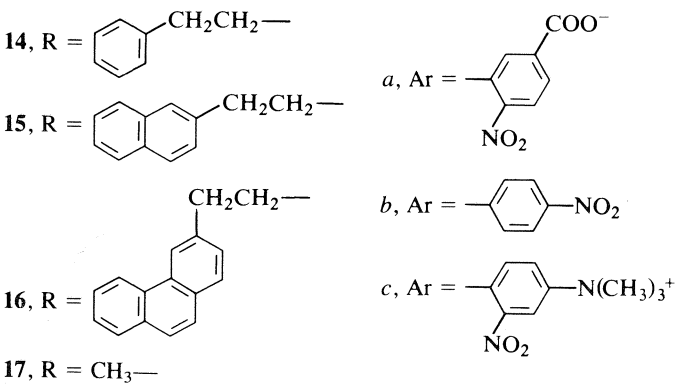

SCHEME 3

quantities. It should be noted that the rates of reaction of the smaller substrates are strongly affected by electrostatic interactions between catalyst and substrate, but that for **16***a–c* the reactivity order is the same as for imidazole as catalyst, i.e. the inherent reactivity of the substrates has reasserted itself.

Discussion

Analysis of hydrophobic effects

To analyze the effect of hydrophobic stabilization of the transition state upon the rates of reaction of **13** with the various substrates we must correct for all other modes of reaction than the one of special interest, namely, reaction with both steroid residues interacting with the aryl group in the arylpropionate substrate molecule. The imidazolyl groups are able to react by themselves without any hydrophobic interaction, and reaction could occur with only one steroid residue in contact with the substrate. We can achieve the desired correction by subtracting twice the rate constant for the reaction of **8** with a substrate from the observed rate constant for the reaction of **13** with the substrate. This can be done with the negatively charged substrates which have been thoroughly studied with various catalysts. As a measure of hydrophobicity we use the π (15, 16) value of the aryl binding group. The results of this analysis are seen in Fig. 7. It is clear that there is a linear dependence of $\log k_{corr}$ upon the hydrophobicity of the aryl group; if we extrapolate to $\pi = 0$, i.e. to the hypothetical rate of reaction of a priopionate ester reacting by the same transition state as the aryl propionates, it is possible to calculate the stabilization of the transition state for the observed reactions relative to this hypothetical reference state. For the phenanthryl substrate this rate enhancement amounts to a factor of 1.1×10^5-fold, or 6.9 kcal/mol in stabilization. As we have observed before (4, 5) only part of this potential rate enhancement is actually observed;

TABLE 2. Rate constants for reactions of substituted imidazoles with ester substrates

Catalyst	Second order rate constant (M^{-1} s^{-1}) for Imidazole	**8**	A[d]	B[e]	**13**	No catalyst
17*a*	0.898 ± 0.022[b]	5.07 ± 0.12[b]	0.823 ± 0.011[c]			1.2×10^{-5}[b]
14*a*	0.98[b]	7.5 ± 0.7[b]	1.37 ± 0.06[c]	7.38 ± 1.76[c]	17.1 ± 0.04	9.7×10^{-6}[b] $(1.67 \pm 0.02) \times 10^{-5}$
15*a*	0.955 ± 0.025[b]	10.2 ± 0.3[b]	2.04 ± 0.38[c]	115 ± 19[c]	54.1 ± 4.5	1.11×10^{-5}[b] $(3.9 \pm 1.5) \times 10^{-5}$
16*a*	1.00 ± 0.05[b]	18.0 ± 1.3[b]	5.42 ± 1.36[c]	337 ± 262[c]	547 ± 43	1.08×10^{-5}[b] $(5.5 \pm 0.4) \times 10^{-5}$
17*b*	0.453 ± 0.012[b]	0.425 ± 0.002[b]				1.4×10^{-5}[b]
14*b*					1.30 ± 0.05	$(5.59 \pm 0.19) \times 10^{-5}$
15*b*	0.403 ± 0.03[b]	0.763 ± 0.15[b]			4.90 ± 0.38	$(7.6 \pm 0.5) \times 10^{-5}$
16*b*					42.9 ± 2.2	$(5.5 \pm 1.6) \times 10^{-5}$
17*c*	4.03 ± 0.1[b]	1.68 ± 0.17[b]				7.8×10^{-5}[b]
14*c*					6.40 ± 0.08	$(1.48 \pm 0.02) \times 10^{-4}$
15*c*	5.27 ± 1.0[b]	3.9 ± 0.7[b]			27.6 ± 1.3	$(1.47 \pm 0.07) \times 10^{-4}$
16*c*					1194 ± 80	

[a]All in aqueous solution at 25°C, ionic strength 0.1 (KCl). In the present work the pH was maintained at 8.0 using 0.0928 *M* borate buffer.
[b]Reference 4; pH was maintained at 7.9 using 0.0097 *M* tris buffer.
[c]Reference 5; pH was maintained at 8.0 using 0.01 *M* tris buffer.
[d]17β-4(5)-Imidazolyl-11-keto-3β-amino-5α-androstane.
[e]α,α′-Bis-(17β-4(5)-imidazolyl-11-keto-5α-androstan-3β-amino)-*p*-xylene.

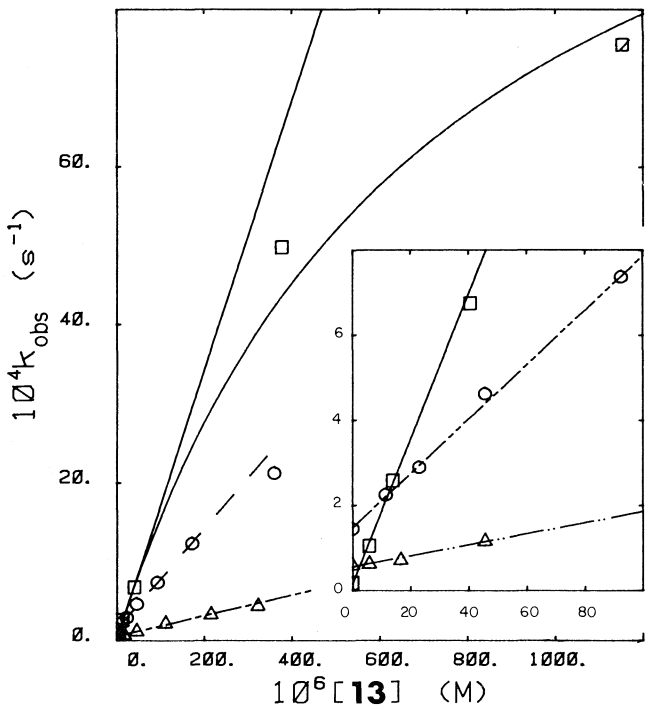

FIG. 1. Rates of reaction of esters of 3-phenylpropionic acid as a function of the concentration of **13**; (□) 5-carboxy-2-nitrophenyl esters; (○) 4-trimethylammonio-2-nitrophenyl esters; (△) 4-nitrophenyl esters. Inset: data for low concentrations of **13** only.

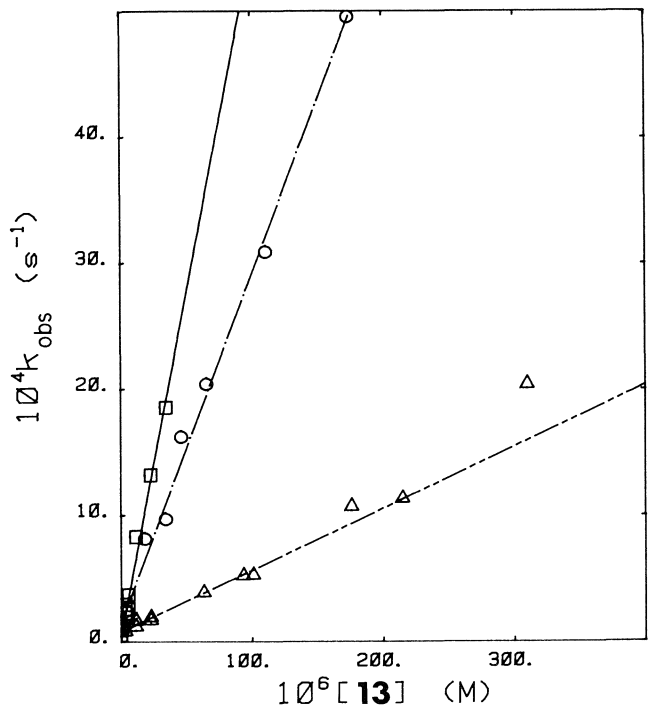

FIG. 2. Rates of reaction of esters of 3-(2-naphthyl)propionic acid as a function of the concentration of **13**: (□) 5-carboxy-2-nitrophenyl esters; (○) 4-trimethylammonio-2-nitrophenyl esters; (△) 4-nitrophenyl esters.

this is attributed to the crowding and torsional strain involved in achieving a transition state where the imidazole has attacked the ester carbonyl and simultaneously the aryl substituent is arranged parallel to the hydrophobic face of the steroid bearing the imidazole. Despite this unfavorable interaction we have now achieved an observable effect of 550-fold in rate. By using alternative substrates, less subject to steric interactions, we hope to obtain more of the potential rate enhancement. The next class of substrates to investigate will be ketones subject to general base catalyzed elimination reactions (3).

We wished to relate the observed stabilization energy to the surface area of the substrates removed from contact with solvent. A rough approximation to this surface area can be calculated by taking the area of the polygon whose vertices lie

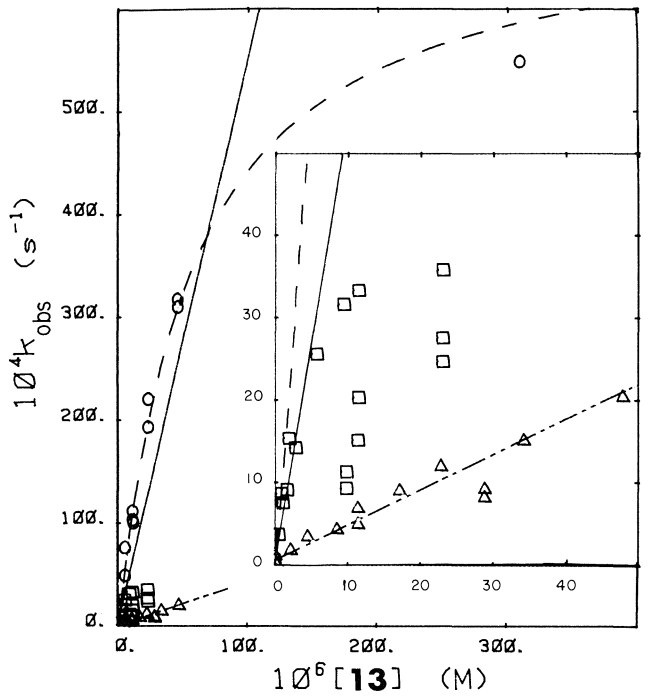

FIG. 3. Rates of reaction of esters of 3-(3-phenanthryl)propionic acid as a function of the concentration of **13**: (□) 5-carboxy-2-nitrophenyl esters; (○) 4-trimethylammonio-2-nitrophenyl esters; (△) 4-nitrophenyl esters.

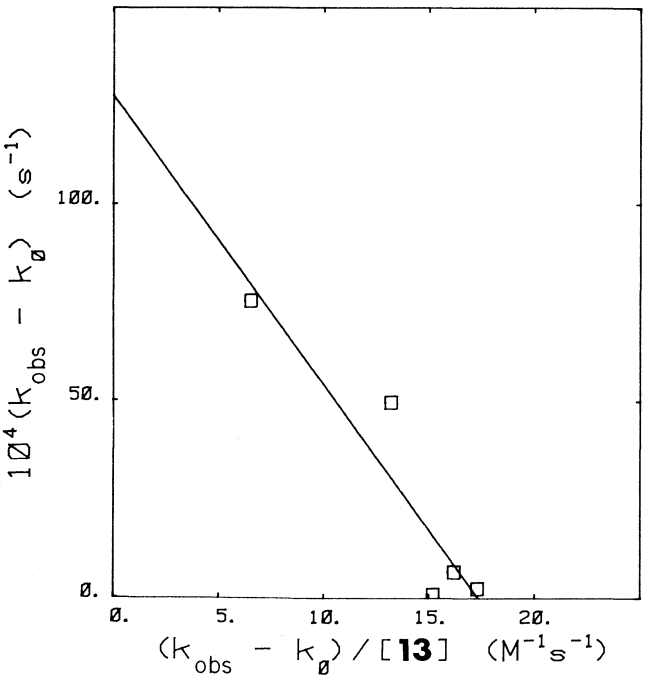

FIG. 4. Eadie–Hofstee plot of the data for the reaction of **14***a* with **13**. The line was fitted by least squares, and gives $k_{max} = (1.28 \pm 0.24) \times 10^{-2}\,s^{-1}$; $K_m = (7.36 \pm 1.67) \times 10^{-4}\,M$.

along the C—H bonds of the arene at the van der Waals radius of hydrogen. This gives a value of 144 Å^2 for the combined upper and lower surfaces of phenanthrene. When a phenanthryl group is bound by **13** both surfaces should be removed from contact with water, as well as some part of the edge surface which is near the bridging *p*-xylylene group. Since this interaction produces 5.4 kcal/mol of potential stabilization, we may calculate the strength of the hydrophobic interaction as 0.038 kcal/Å^2.

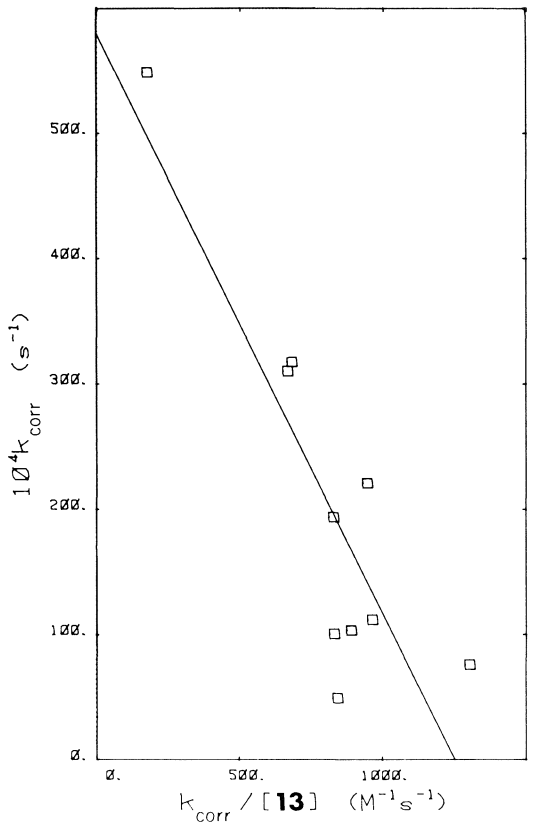

FIG. 5. Eadie–Hofstee plot of the data for the reaction of **16***a* with **13**. The line was fitted by least squares, and gives $k_{max} = (5.79 \pm 0.84) \times 10^{-2}\,s^{-1}$; $K_m = (4.62 \pm 0.98) \times 10^{-5}\,M$.

Figure 8 shows the absorbance vs. time curve for an experiment in which **16***a* was allowed to react with a catalytic amount of **13**, and the reaction was followed to completion. The pattern seen is of "burst" kinetics (17) with rapid acylation of the catalyst, followed by slower turnover kinetics, with hydrolysis of the acylimidazole intermediate regenerating catalyst which is promptly acylated again. The reaction, once the burst was over, was roughly zero order in substrate until the substrate was consumed. Observation of this behavior confirms that **13** is a catalyst, although the deacylation is in fact quite slow, since nothing in the design of **13** acts to facilitate it.

Our preliminary results with trimethylammonionitrophenyl esters suggest that the above calculation of the hydrophobic interaction energy may be too low. We were surprised to find that the rate constants for the reaction of the ester of 3-(3-phenanthryl)propionic acid with a cationic phenol were faster than for the corresponding ester of an anionic phenol. This contradicts our previous findings concerning the electrostatic effects on catalysis by **8** (4). However, the rate effect shows up consistently for all three cationic esters of arylpropionic acids. When we compare rates for each type of substrate relative to the rate constant for **8** plus the corresonding acetate, the relative rates for corresponding anionic and neutral esters are quite similar but those for the cationic esters are faster. The effect is less striking for the smaller aryl groups.

Two hypotheses spring to mind to expain these results: (*1*) That the anionic esters, although they have a stabilizing electrostatic interaction in the transition state for imidazole attack, obtain this stabilization at the price of less than optimal hydrophobic interactions. Thus an anionic ester with a large binding group is superior for **8**, where the total hydrophobic

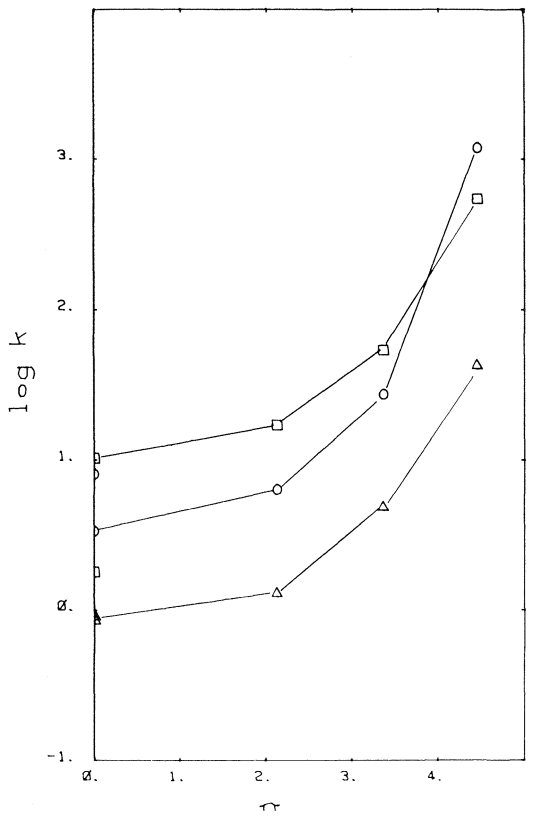

FIG. 6. log k_2 for various substrates as a function of the hydrophobicity parameter, π. The lines are arbitrary, serving only to join related points. The points at $\pi = 0$ are for imidazole (unfilled) and **8** (filled) as catalyst, and are twice the observed rate constant to allow for the two imidazolyl groups in **13**; (□) carboxynitrophenyl esters; (○) trimethylammonionitrophenyl esters; (△) nitrophenyl esters.

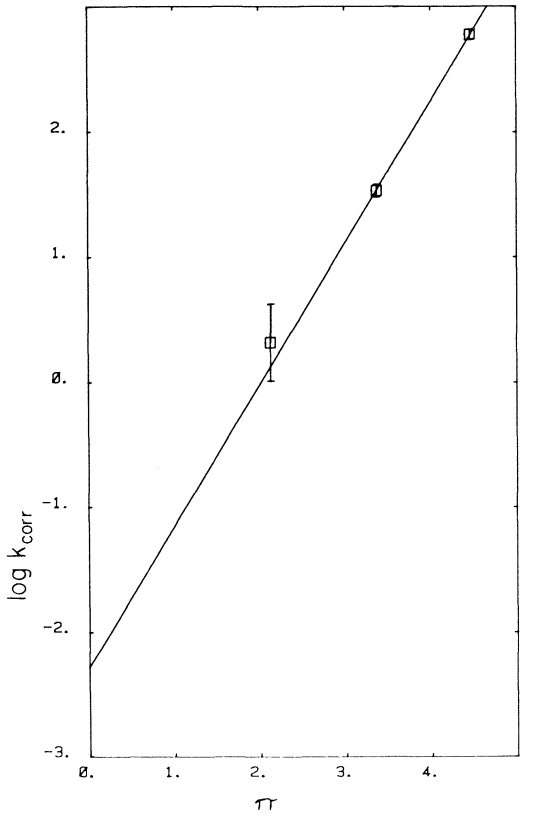

FIG. 7. log k_{corr} for **14***a*, **15***a*, and **16***a* as a function of the hydrophobicity parameter, π. The line was fitted by least squares: $\log k_{corr} = -2.28 \pm 0.14 + (1.13 \pm 0.04)\pi$.

stabilization available is modest, but not for **13** where much stronger hydrophobic stabilization is potentially available. (*2*) That the rates observed for **16***a* are subject to inhibition resulting from aggregation, even at the lowest concentration which we could use, and the true value is actually larger than for **16***c*.

To test these hypotheses will require further experiments and in particular an investigation of the effect of ionic strength on the behavior of these substrates. At 1 *M* ionic strength the importance of electrostatic stabilization should be much decreased, as should the severity of aggregation problems.

The first hypothesis is given some support by the imperfect parallelism between the rate constants for the reaction of carboxynitrophenyl esters with **13** and the 11-keto analog (5) as summarized in Table 2. Although the rate constants for **16***a* are the same within experimental error, the rate constant for **15***a* is greater for the 11-keto steroid, and that for **14***a* is greater for the 11-ammonio steroid. This could be the result of the sort of trade off between hydrophobic and electrostatic stabilization discussed above.

Aggregation

A distressing finding in these experiments was that even though the dimeric steroid with four positive charges was very soluble, there were still extreme difficulties with aggregation of substrates and/or catalyst plus substrate, leading to spuriously low reaction rates. For the *p*-nitrophenyl esters, which are of very low solubility in water, these results were not surprising, but the difficulties encountered with the hydroxynitrobenzoate esters, which had been relatively well behaved with **8**, constituted an unpleasant surprise. It is, however, not without precedent that hydrophobic anions and cations show precipitation at very low concentrations (18). We are forced to conclude that the use of anionic substrates with **13** is unlikely to be desirable. By contrast the cationic trimethylammonionitrophenyl esters were well behaved, despite the inherent rate inhibiting effect of repulsions between substrate and catalyst. These substrates are, however, very reactive and difficult to purify. Our finding of peculiar behavior, probably attributable to precipitation of anionic substrate by cationic catalyst at low concentrations suggests that in the design of enzyme models it would be more desirable to avoid the use of one charge type of solubilizing substituent, and use enzyme models with a small net charge.

Conclusions

The experiments reported above demonstrate that with a soluble, stereochemically defined catalyst, it is possible to achieve significant rate enhancements, of up to 5.5×10^2, resulting from hydrophobic stabilization of a transition state, and there is the potential for considerably larger effects, of 1.1×10^5. Two design principles for artificial enzymes emerge from our work: the hydrophobic binding energy for simple binding regions such as we have used amounts to 0.038 kcal/mol Å^2; hydrophobic artificial enzymes should not have high electrostatic charges.

Experimental

Methods

Compounds containing imidazole were visualized on tlc plates by spraying first with a freshly prepared 1:1 mixture of saturated

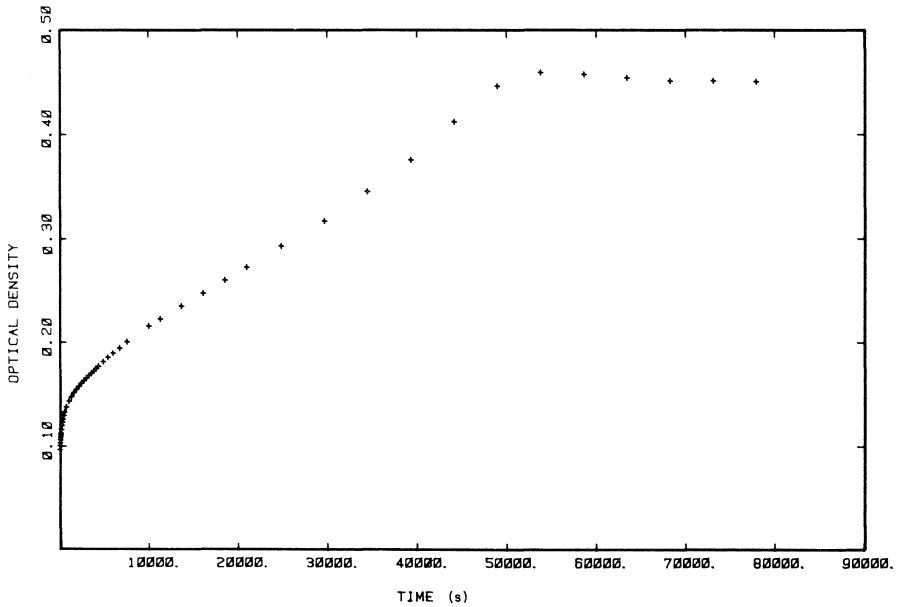

FIG. 8. Absorbance vs. time curve for the reaction of 9.52×10^{-6} *M* **16***a* with 1.16×10^{-6} *M* **13**. Acylation of the catalyst is followed by turnover, giving zero order kinetics.

methanolic sodium nitrite and 1% sulfanilic acid in 1 *M* HCl, and immediately afterwards spraying with 2 *M* methanolic KOH. Column chromatography was carried out using Glenco columns and mixing chambers, which allow the use of linear solvent gradients. Samples, dissolved in the minimum volume of solvent, were mixed with dry silica and evaporated. The dry residue was placed on top of the column and rinsed in with a little of the initial elution solvent. Elution was carried out under pressurization by nitrogen at 10–15 psi to give a flow rate of 2 mL/min. The water content of solvents was determined using a Photovolt Aquatest IV moisture analyzer. The presence of borohydride was tested for using aqueous triiodide–starch solution. A few drops of a solution containing active borohydride dispelled the color. Silica for column chromatography was Merck Silicagel 60 PF254. Thin layer chromatography was carried out using Analtech Uniplates with silica gel GF. Nuclear magnetic resonance spectra were recorded on Varian T60, EM360, XL200, or XL300 instruments. TMS, for organic solvents, and DSS (4,4-dimethyl-4-silapentanesulfonic acid), for D_2O were used as internal standards.

Materials

Sodium cyanoborohydride was purified as described by Borch *et al.* (6), and assayed by iodometric titration. A weighed amount of cyanoborohydride was washed (methanol) into a flask containing excess potassium iodide and a known volume of potassium iodate standard solution which had been acidified with excess acetic acid. Each hydride in cyanoborohydride reduced one molecule of iodine to two iodides. The remaining iodine was titrated using thiosulfate solution freshly standardized against potassium iodate. Terephthaldehyde was purified by sublimation in vacuum. Ethyl formate for use as a formylating agent was freshly distilled from sodium carbonate. 2-Methoxyethanol (Fisher Certified) was distilled; the fraction boiling at 123–124°C was used. A test for peroxides was negative; the water content was 500 μg/mL. The last 25% of the distillate had only 60 μg/mL of water. Dimethylformamide, DMF, was dried by storing it over CaH_2. Acetonitrile used as a solvent for stock solutions of substrates was purified by distillation.

α,α′-Biscyclohexylamino-p-*xylene*

Terephthaldehyde, 335 mg (2.5 mmol), was dissolved by heating in dry (60 μg/mL water) 2-methoxyethanol, 5.0 mL cyclohexylamine, 0.50 g (5.0 mmol), was added and the mixture refluxed gently for 30 min. On cooling to room temperature, the di-aldimine crystallized out. A few drops of the reaction mixture, reheated to dissolve the product, were used for a proton spectrum in $CDCl_3$: δ 7.75 (s) aromatic protons; 8.30 (s) aldimine CH; 0.5–1.7 cyclohexyl CH_2. The cyclohexyl CH—H was obscured by solvent absorptions from δ 3–5. A small portion of the di-imine was recrystallized from methanol, mp 128.5–129.5°C.

To the reaction mixture was added acetonitrile, 2 mL and more methoxyethanol, 4 mL, and it was warmed gently until the solids dissolved. $NaBH_3CN$, 200 mg (9.5 mequiv.), dissolved in methanol, 2 mL, was added after the mixture had cooled to ca. 50°C. Acetic acid, 1 drop, was added and bubbles slowly started to form. The mixture was cooled to room temperature. Acetic acid, 0.3 mL, in 3 mL acetonitrile, 3 mL, was added over a period of 5 min and the mixture stirred for another hour without heating. After evaporating about half the solvents, the mixture was left overnight. By morning it had partially solidified. Rewarming gently dissolved the solids; the ^{1}H-nmr ($CDCl_3$) showed that all of the aldimine signal at 8.3 had disappeared. There was no signal at ca. 10δ indicating the absence of aldehydes. The signal attributed to the aromatic protons had shifted to 7.5δ. After adding methanol, 20 mL, and water, 20 mL, the solution was homogeneous and the pH was 7.6. The solution was washed into a separatory funnel with 1 *M* HCl, 25 mL, and ether, 30 mL. The ether layer was discarded and the aqueous layer was basified with NaOH to pH 13, and extracted four times with ethyl acetate, 50 mL. The ethyl acetate extracts were dried (Na_2SO_4), evaporated, and dried at 70°C, 0.25 Torr. The residue, 664 mg of slightly yellow oily liquid (93% of expected weight), would not crystallize. ^{1}H-nmr ($CD_3OD/CDCl_3$) δ: 7.25 (s), 2H, aromatic protons; 4.7–4.8, 3H, overlapping Ar—CH_2 and N*H*; 2.2–2.8, 1H, cyclohexyl CH—N; 0.5–2.2, 10H, aliphatic CH_2. Exact mass: expected for $C_{20}H_{32}N_2$: 300.25654; found 300.25531.

The oily liquid diamine was treated with 2 *M* HCl in methanol, 3 mL, and the mixture allowed to cool in the freezer. Crystallization was complete after 2 h and the solid dihydrochloride was washed with cold ethanol, yielding 486 mg (55%) white non-hygroscopic fine crystals, mp 335 with partial decomposition and partial sublimation. ^{1}H-nmr (D_2O; DSS as internal reference) δ: 7.60 (s) 4H, aromatic C*H*; 4.30 (s), 4H, Ar—CH_2; 3.14 (br, $w_{1/2}$ = 26 Hz), 2H, cyclohexyl C*H*—N; 1.0–2.4, aliphatic CH_2.

5α-Androstan-17β-ol-3β-amine

5α-Androstan-17β-ol (stanolone, Sigma) was converted to the oxime by reaction with hydroxylamine hydrochloride in pyridine. The crude product had mp 203–209°C; lit. (7) mp 213–214°C. ^{1}H-nmr ($CDCl_3$) δ: 18-CH_3, 0.75 (s); 19-CH_3, 0.93 (s). The oxime was reduced to the amine by refluxing with sodium in propanol. The crude

product had mp 153–156°C; three recrystallizations from ether – petroleum ether gave material with mp 169–170°C; lit. (7) mp 170–171°C; (19) mp 167–169°C. ^{1}H-nmr ($CDCl_3$:CD_3OD) δ: 18-CH_3, 19-CH_3, 0.70 (s), 0.80 (s); (0.5 *M* DCl in D_2O:CD_3OD) δ: 18-CH_3, 0.87 (s); 19-CH_3, 1.01 (s). Exact mass: expected for $C_{19}H_{33}NO$ 291.25621; found 291.25573.

α,α′-Bis-(17β-hydroxy-5α-androstan-3β-amino)-p-*xylene*

5α-Androstan-17β-*ol*-3β-amine, 249 mg (0.854 mmol), and terephthalaldehyde, 54 mg (0.40 mmol), were each dissolved in 2-methoxyethanol, 1 mL, and washed together into a 100 mL flask with an extra 6 mL of the solvent. A precipitate formed almost immediately upon mixing. More solvent, 20 mL, was added and the mixture heated to a gentle reflux with stirring, but the precipitate did not completely dissolve. The mixture was cooled to 50°C and treated with $NaBH_3CN$, 200 mg, dissolved in methoxyethanol, 5 mL. After stirring 5 min, glacial acetic acid, 60 μL, was added and the mixture kept warm (60–70°C) for 2 h, during which time another seven portions of acetic acid, 60 μL, were added at intervals (ca. 0.5 mL acetic acid in all). Midway through the reaction, the mixture became homogeneous and the cloudiness disappeared, but a different kind of precipitate began to form almost immediately after the solution cleared. It dissolved when the temperature was raised to 100°C but came out of solution again on cooling to room temperature at the end of 2 h. The mixture was cooled in an ice-bath and the precipitate filtered, washed with cold methanol–water, and air-dried. The pH of the mother liquor was 4.6. The solid was most soluble in chloroform–methanol. Thin layer chromatography with 50:50 $CHCl_3$:1 *M* NH_3/MeOH gave one iodine-staining spot, rf = 0.9. The proton nmr spectrum showed two singlets at 0.87 and 0.73 ppm, assigned to the methyl groups, with the same separation as the signals from the methyl groups in 5α-androstan-17β-ol-3β-amine HCl. A singlet at 2.0 ppm suggests that the compound was the diacetate salt of the dimer desired, and the rest of the spectrum was consistent with that. A signal assigned to the benzylic methylene was apparent at 4.0 ppm. Aromatic protons appeared at 7.4 ppm. The yield of product as the diacetate (mw 805.2; mp 270–280) was 187 mg (0.232 mmol). Yield based on terephthalaldehyde 58%; based on steroid, 54%.

After dissolving in aqueous methanol, basifying, and extracting with ethyl acetate, 149 mg of the free base was recovered; mp 270–280 decomp.; yield, 54% based on aldehyde, 51% based on steroid. ^{1}H nmr ($CDCl_3$/CD_3OD): δ: CH_3 (s) 0.73, 0.83; CH—N (br.) 2.2–2.7; CH—O (br) 3–3.5; ArCH_2—N (s) 3.77; aromatic CH (s) 7.28. The compound was essentially pure by tlc (rf = 0.5 with 5% Et_2NH/20% EtOH/75% benzene, I_2 stain). Exact mass: expected for $C_{46}H_{72}N_2O_2$ 684.55936; found 684.55954.

α,α′-Bis-(17β-4(5)-imidazolyl-11β-trifluoracetamido-5α-androstan-3β-amino)-p-*xylene,* ***12****a*

17β-4(5)-Imidazolyl-3β,11β-diamino-5α-androstane trihydrochloride, **8**, 100 mg, was dissolved in trifluoroacetic acid, 2 mL, and cooled in an ice bath before addition of trifluoroacetic anhydride, 1 mL. Sodium carbonate, 400 mg, was then added and the mixture stirred, with cooling in ice, for 2 h. Then methanol, 2 mL, was added and the reaction mixture was basified using 30% aqueous ammonia, 10 mL, and extracted with ethyl acetate, 3 × 30 mL. The extracts were dried (Na_2SO_4) and evaporated. The crude 17β-4(5)-imidazolyl-3β,11β-bistrifluoracetamido-5α-androstane, **9***a*, was dissolved in 2 *N* methanolic KOH and left 3 h at room temperature. Aqueous HCl (2 *N*), 5 mL, and water, 10 mL, were then added and the solution extracted with ethyl acetate, 5 mL. The aqueous solution was then basified using 30% aqueous ammonia, 5 mL, and extracted with 1:9 methanol:chloroform, 4 × 40 mL. The organic layer was evaporated and then purified by preparative layer chromatography (silica) developing with 50:50 chloroform:1 *M* methanolic ammonia. The extract from the thick plate was freed of silica by extracting from aqueous ammonia using chloroform. The material so obtained was used for dimerization experiments. An amount of **10***a* corresponding by Pauly assay (25) to 167 mg (0.358 mmol) of **8**.3HCl was dissolved in 2-methoxyethanol, 5 mL, to form a nearly clear solution and combined with a solution of purified terephthalaldehyde, 19.9 mg (0.148 mmol), in the same solvent, 5 mL. The solution was heated gently and allowed to cool under a stream of nitrogen. No precipitate formed. Dry $NaBH_3CN$, 100 mg, was added and dissolved with stirring. Glacial acetic acid, 0.3 mL, was added in five portions, 60 μL, at 15 min intervals while the mixture was gently heated and stirred under a stream of nitrogen. The mixture was left at room temperature under a stream of nitrogen overnight and by morning, about 80% of the solvent had evaporated and a small amount of fine precipitate had settled. After adding water, 20 mL, a voluminous semi-solid separated; the pH was 4.35. The iodine test indicated that borohydride was still present.

The mixture was cautiously acidified with concentrated HCl, 8 mL, and made up to 75 mL with aqueous methanol. Most of the precipitate dissolved after stirring on a steam bath for 30 min. The solution was washed into a separatory funnel with water, 50 mL, methanol, 10 mL, and ether, 25 mL, and shaken. The ether layer yielded about 20 mg of white solid which was not Pauly positive; this was discarded. The aqueous layer was basified, 5 *M* NaOH, 40 mL, to give a pH of 12.5. A fluffy precipitate formed; the mixture was extracted with ethyl acetate, 3 × 75 mL. The first three extracts yielded 228.8 mg of slightly yellow glassy solid. Thin layer chromatography, 15% diisopropylamine:10% methanol:75% $CHCl_3$, visualized with Pauly spray, showed two red spots at rf = 0.7 and 0.55, an orange spot at rf = 0.4, and a red spot attributed to starting material at rf ca. 0.2. Column chromatography on 14 g of silica gel eluted with a gradient from $CHCl_3$ to 3% *i*-Pr_2NH, 15% MeOH, 82% $CHCl_3$ gave 53 mg of a fraction consisting mainly of what is believed to be 17β-4(5)-imidazolyl-3β-(4′-hydroxymethylphenylmethylamino)-11β-trifluoroacetamido-5α-androstane (^{1}H nmr ($CDCl_3$/CD_3OD) δ: 0.6 (s), 0.9 (s), CH_3; 4.6 (s) ArCH_2OH; 6.7 (s), 7.4 (s) imidazolyl CH; 7.3 (s) *p*-phenylene CH), and 58 mg of the desired dimeric compound (^{1}H-nmr ($CDCl_3$/CD_3OD) δ: 0.62 (s), 0.94 (s) CH_3; 2.60 (br, $w_{1/2}$ = 20 Hz) C3H—N; 3.83 (br, $w_{1/2}$ = 6 Hz) C11H—N; 4.57 (s) ArCH_2; 6.73 (s), 7.49 (s) imidazolyl CH; 7.32 *p*-phenylene CH), as well as 30 mg of starting material. There were small amounts of other unidentified byproducts.

Attempted hydrolysis by refluxing for 24 h in 6 *M* methanesulphonic acid, basifying with a large excess of 20% Na_2CO_3 and extracting with ethyl acetate gave mixtures showing that there had been extensive degradation.

17β-4(5)-Imidazolyl-11β-formamido-5α-androstane-3β-amine, ***10****b*

8.3HCl, 595 mg, dissolved in methanol, 10 mL, and triethylamine, 10 mL, was added to ethyl formate, 50 mL. A white precipitate formed. The mixture was refluxed under nitrogen for 7 days. The precipitate was nearly dissolved after day 3. The reaction solution was evaporated to near dryness then MeOH, 50 mL, was added and the mixture evaporated again. Then it was washed into a separatory funnel with MeOH, 20 mL, and water, 100 mL. K_2CO_3 (3 *M*), 20 mL, was added and the mixture extracted with EtOAc, 7 × 150 mL. Drying and evaporating to dryness yielded a caked glassy solid weighing 645 mg: 90.6% of expected. It had only one major Pauly positive spot (rf = 0.7 with 20% MeOH:3% Et_3N:77% $CHCl_3$). ^{1}H nmr ($CDCl_3$/CD_3OD) δ: 0.66 (s), 0.99 (s) CH_3; 2.62 (br, $w_{1/2}$ = 14 Hz) C17H—imidazolyl; 3.68 (br, $w_{1/2}$ = 22 Hz) C3H—N; 4.59 (br, $w_{1/2}$ = 8 Hz) C11H—N; 6.76 (v br), 7.52 (v br) imidazolyl CH; 7.93 (s), 7.97 (s) CHO—N. The crude formylation product, 645 mg, was dissolved in 0.6 *M* methanolic KOH, 50 mL, and left 7 days at room temperature under nitrogen. The base was neutralized with CO_2 gas, concentrated NH_3, 30 mL, added and the mixture washed into a 500 mL separatory funnel with water, 125 mL, and extracted with 7% MeOH:93% $CHCl_3$, 7 × 100 mL. Evaporation yielded 615 mg of residue, 102%. Column chromatography on silica, eluting with a gradient from $CHCl_3$ to 3% ET_3, 20% MeOH in $CHCl_3$. The major product recovered was 11β-formamido-17β-4(5)-imidazolyl-5α-androstan-3β-amine, 306 mg, 51%, (^{1}H-nmr (CD_3OD/$CDCl_3$) δ: 0.67 (s), 0.98 (s) CH_3; 7.83 (s) CHO—N; 7.5 (s) CHOO$^-$) with some byproducts running ahead and behind. The slower eluting material, 117 mg, was in part the corresponding diamine, which could be recycled.

Acid hydrolysis of 11β-formamido-17β-4(5)-imidazolyl-5α-androstan-3β-amine, ***10*** b

10*b*, 20 mg, was refluxed 18 h in 2 *M* methanolic HCl, 10 mL, washed into a separatory funnel with water, 10 mL, 20% Na_2CO_3, 30 mL, and 1 *M* KOH – saturated KCl, 10 mL. Extraction with ethyl acetate, 6 × 6 mL, yielded 16 mg, identified by ^{1}H nmr and tlc behaviour as 17β-4(5)-imidazolyl-5α-androstane-3β,11β-diamine. The imidazole protons could be seen at 6.6 and 7.4 but no formyl protons could be seen at 7.9. Thin layer chromatography gave one major spot at low rf which ran side-by-side with the 3,11-diamine and several minor spots with higher rf's.

*α,α′-Bis-(17β-4(5)-imidazolyl-11β-formamido-5α-androstan-3β-amino)-*p*-xylene,* ***12*** b

11β-Formamido-17β-4(5)-imidazolyl-5α-androstan-3β-amine, **8***b*, 242 mg (0.629 mmol), was dissolved in dry 2-methoxyethanol, 10 mL, and methanol, 4 mL. Terephthalaldehyde, 38.25 mg (0.285 mmol), was dissolved in 2-methoxyethanol, 5 mL. The two solutions were mixed to form a clear solution containing a calculated 10% excess of amine. Most of the methanol was evaporated by gentle heating under a stream of nitrogen. A white precipitate formed on cooling, $NaBH_3CN$, 340 mg, dissolved in MeOH, 3 mL, was added. (6.8 mequiv., a 6-fold excess). A solution of acetic acid, 0.5 mL, in MeOH, 10 mL, was added in 1 mL portions over a period of 2 h, at a temperature of ca. 30°C. Reaction continued overnight at room temperature under a slow stream of N_2. A positive iodine test confirmed that cyanoborohydride was still present. The solution was clear and colorless. Acetic acid, 5 mL, was added and produced no visible effect. The reaction mixture was washed into a beaker with methanol, 20 mL, and 2 *M* HCl, 5 mL, added. Hydrogen evolution stopped after about 1 h. The solution was extracted using ether. The ether extract was discarded. The pH of the aqueous phase was 1.6. Basifying with concentrated NH_3, 40 mL, brought the pH to 10.1 and caused precipitation of product. Extraction with 7% MeOH: 93% $CHCl_3$, 5 × 200 mL, drying with Na_2SO_4, and evaporating yielded 300 mg of white solid. Repeated column chromatography was necessary to separate the desired material from monomeric steroid. The second column was eluted with a gradient from 10% MeOH, 90% $CHCl_3$ to 20% MeOH:3% Et_3N:77% $CHCl_3$. This gave 118 mg of pure dimer and 75 mg mixed dimer and monomer. The third column was eluted using a gradient from 10% MeOH, 90% $CHCl_3$ to 30% MeOH:3% Et_3N:67% $CHCl_3$. This gave 57 mg of pure dimer, 7 mg of a mixture of dimer and monomer, and 9 mg of monomer. With 118 mg of pure dimer from the second column this gave 175 mg product (0.201 mmol, 71% based on terephthalaldehyde and 64% based on monomer. Exact mass: expected for $C_{54}H_{78}N_8O_2$, 870.62477; found 870.62066. The fragmentation pattern showed an ion with nearly equal intensity 15 amu lower, and no equal or greater intensity ions above 627 amu. The most prominent fragment above 400 amu is the one at 486 corresponding to a loss of one steroid skeleton without its attached benzyl carbon. There are almost as prominent fragments 14 amu lighter and 17 amu heavier than 486. The most prominent mass between 100 and 400 is 384 which is the mass of 11-formyl monomer.

Acid hydrolysis of ***12*** b

Chromatographically purified **12***b*, 100 mg, was dissolved in 1 *M* DCl in D_2O, 1 mL. After four cycles of addition of D_2O, 1 mL, and evaporation to dryness, the deliquescent crystalline solid was dissolved in D_2O, 0.4 mL. ^{1}H-nmr δ: 0.5 (s), 0.9 (s) CH_3; 4–4.5 (v br) ArCH_2 and C*H*—N; 7.3 (s), 1H, 7.9 (s), 1H, imidazolyl C*H*; 7.5 (s), 2H, aromatic C*H*; 8.5 (s), 1H, C*H*O—N. When 0.1 mL of 35% DCl/D_2O was added, the spectrum was hardly changed except that the exchange signal was increased and shifted from 5.0 to 5.5 ppm. It appears that the benzylic CH protons, expected to absorb at 4–5 ppm by comparison with the model compound dicyclohexylamino-*p*-xylene dihydrochloride do not give as sharp a signal as expected. The dimer was left in the ~2 *M* DCl solution to allow time for hydrolysis at room temperature, anticipating a slight change in spectrum. The growth of a new signal at 8.0 ppm at the expense of the *N*-formyl signal at 7.75 ppm permitted the reaction to be followed. It was slow at 25°C, but after 4 h at 85°C hydrolysis was 90% complete. ^{1}H-nmr δ: 0.9 (s), 1.1 (s) CH_3; 3.9 (br, $w_{1/2}$ = 8 Hz) C11*H*—N; 4.2 (br, $w_{1/2}$ = 6 Hz) ArCH_2; 7.2 (s), 8.4 (s) imidazolyl C*H*; 7.4 (s) *p*-phenylene C*H*. Heating for another half-hour at 95°C completed the reaction. ^{13}C-nmr spectrum: (D_2O with excess DCl) δ wrt TMS (formic acid used as internal standard): 133.63, 133.27, 132.60, 130.94, 116.24, 57.03, 56.66, 54.89, 48.66, 48.11, 46.97, 45.33, 42.16, 35.76, 35.16, 31.57, 31.24, 30.48, 27.19, 25.99, 24.32, 23.84, 15.07, 14.55.

*α,α′-Bis-(17β-4(5)-imidazolyl-11β-amino-5α-androstan-3β-amino)-*p*-xylene,* ***13***

12*b*, 459 mg (0.53 mmol) was dissolved in 3 *N* HCl and heated 6 h on a steam bath. Basification and extraction yielded 248 mg of material shown by tlc analysis to contain some Pauly positive impurities. This material was chromatographed on silica, 70 g, slurried in toluene, and packed in a 2.5 cm diameter column. Elution was carried out with a gradient from 20% methanol:1% aq. NH_3:79% toluene to 75% methanol:5% aq NH_3:20% toluene a pressure of 12 psi (N_2) to give a flow rate of 2 mL/min, yielding 126 mg of almost pure dimer (21% based on monomer). Exact mass: expected for $C_{52}H_{78}N_8$: 814.635; found 814.632. The fragmentation pattern showed a mass of 3/4 intensity 17 amu lower than 814.6 and no equal or greater intensity masses above 500 amu. The most prominent fragment heavier than 400 is the one at 458 corresponding to a loss of one steroid skeleton. There are fragments with half this intensity 17 amu heavier and 15, 16, and 17 lighter than 458. The most prominent mass between 200 and 400 amu is 356, which is the mass of the monomer.

13 which had been purified by column chromatography, 100 mg, was dissolved in methanol, 3 mL, and an excess of 1 *M* HCl was added, 0.8 mL. Ethyl ether, 20 mL was added to cause precipitation of the dimer hydrochloride. 200 MHz ^{1}H nmr (D_2O) δ: 0.72 (s), 3H, C18H_3; 1.00 (s), 3H, C19H_3; 2.90 (t, J = 9 Hz), 1H, C17*H*; 3.30 (br, $w_{1/2}$ = 20 Hz), 1H, C3*H*; 4.00 (br, $w_{1/2}$ = 12 Hz), 1H, C11*H*; 4.32 (s), 2H, Ar—CH_2—; 7.34 (d, J = 1.4 Hz), 1H, imidazole (C5′*H*; 7.57 (s), 2H, *p*-phenylene C*H*; 8.61 (d, J = 1.4 Hz), 1H, imidazole C2′*H*.

Substrates for kinetics

14*a*, **15***a*, **16***a*, **15***b*, **15***c*, and **17***b* were prepared and purified as previously described (4).

p-*Nitrophenyl hydrocinnamate,* ***14*** b

Hydrocinnamic acid, 900 mg (6 mmol) was dissolved in a mixture of CH_2Cl_2, 10 mL, $SOCl_2$, 3 mL, and DMF, 0.5 mL, and the mixture refluxed under N_2 for 6 h. It was evaporated to near dryness, redissolved in ethyl acetate, 10 mL, and added to a solution of sodium *p*-nitrophenoxide, 1 g, in pyridine, 30 mL, refluxed for 3 h, poured into a mixture of ice, 100 g, and 6 *M* HCl, 100 mL, extracted once with ethyl acetate, 75 mL, washed once with water, 25 mL, dried over Na_2SO_4, evaporated and purified by column chromatography on 60 g silica eluting with 10% ethyl acetate:90% hexanes as solvent. One recrystallization of the eluate from CCl_4 gave pure material, mp 97–97.5°C in 16% yield. 200 MHz ^{1}H-nmr ($CDCl_3$) δ: 2.94, 3.08 (distorted triplets of A_2B_2), 4H, —CH_2—CH_2—; 7.18 (d, J = 9.2 Hz), 7.2–7.4 (complex), 7H, nitrophenyl C2*H* and C6*H* overlapping *Ph*—CH_2—; 8.25 (d, J = 9.2 Hz), 2H, nitrophenyl C3*H* and C5*H*. Exact mass: expected for $C_{15}H_{13}NO_4$ 271.08444; found 271.08469.

p-*Nitrophenyl-3-(2-naphthyl)-propionate,* ***15*** b

This was prepared using the same procedure: mp 124.5–125°C (ether:petroleum ether) Lit. mp 126–128°C (95% ethanol) (4). 200 MHz ^{1}H-nmr ($CDCl_3$) δ: 3.00, 3.22 (distorted triplets of A_2B_2, J = 7.4), 4H, —CH_2—CH_2—; 7.13 (d, J = 9.2), 2H, nitrophenyl C2*H* and C6*H*; 7.3–7.8 (complex), 7H, naphthyl; 8.17 (d, J = 9.2 Hz), 2H, nitrophenyl C3*H* and C5*H*. Exact mass: expected for $C_{19}H_{15}NO_4$ 321.10009; found 321.10000.

p-*Nitrophenyl-3-(3-phenanthryl)-propionate,* ***16*** b

Phenanthrylpropionic acid, 176 mg, was heated to reflux with $SOCl_2$, 2 mL, DMF, 0.5 mL, CH_2Cl_2, 25 mL, for 2 h. The solvent and excess $SOCl_2$ were evaporated, CH_2Cl_2, 25 mL, added followed by a solution of sodium *p*-nitrophenoxide, 200 mg, in dry pyridine, 5 mL, with stirring at room temperature for 2 h. The mixture was

poured into a separatory funnel and partitioned between water and ethyl acetate. The organic layer was washed twice with 1 *M* HCl and once with saturated aqueous sodium chloride. After drying and evaporating, the last traces of pyridine were removed by heating to 100°C at 0.5 mm for 10 min. The red oil was chromatographed through a column of 85 g silica with 30% ethyl acetate:1% acetic acid:69% hexanes. A crystallization from 5 mL cold CCl_4 yielded 25 mg of light yellow solid, mp 108–110°C. 200 MHz ^{1}H-nmr ($CDCl_3$) δ: 2.94 (t, J = 7.4 Hz), 3.23 (t, J = 7.4 Hz), 4H, —C*H*$_2$—C*H*$_2$—; 6.99 (d, J = 9.2), 2H, nitrophenyl C2*H* and C6*H*; 7.4–8.6 (complex), 9H, phenanthryl; 8.02 (d, J = 9.2 Hz), 2H, nitrophenyl C3*H* and C5*H*. Exact mass: expected for $C_{23}H_{17}NO_4$, 371.11574; found 371.11535.

A condensation between 3-PPA and *p*-nitrophenyl using trifluoroacetic anhydride both as solvent and condensing agent all in one step gave a purer product, mp 111–112°C, after column chromatography and crystallization as above.

A stock solution of **16***b* was prepared using 5.23 mg in 5.0 mL, using 40% acetic acid:60% acetonitrile as the solvent. This solution was 0.00252 *M* in ester. This stock solution (300 μL) added to 75 mL 0.1 *M* aqueous KCl gave a cloudy mixture (1.0×10^{-5} *M* in ester) which, after stirring 2 days was clear and colorless with white solid floating on top. After filtering and adding solid NaOH to make it 1.0 *M* in hydroxide, the uv spectrum was measured. The absorbance at 400 nm was 0.0124 and that at 500 nm was 0.0036. The spectrum from 500 to 250 was an almost featureless rise with barely discernible lumps at 400 nm, 320 nm (A = 0.025), and 270 nm (A = 0.05). This puts an upper limit on the solubility of PNP–PPA, based on the known extinction coefficient of *p*-nitrophenoxide of 17500 ± 2500 (20), of 7×10^{-7} *M*.

4-Trimethylammonio-6-nitrophenyl-3-phenylpropionate iodide, ***14****c*

Prepared by the method used for **15***c* (2); mp 160–160.5°C. 200 MHz ^{1}H nmr (DMSO-d_6) δ: 3.02 (s), 4H, —C*H*$_2$—C*H*$_2$—; 3.83 (s), 9H, $N^+(CH_3)_3$; 7.30 (distorted s), 5H, C_6H_5—; 7.65 (d, J = 9.0 Hz), 1H, nitrophenyl C6—*H*; 8.58 (d of d, J = 9.0, 3.2), 1H, nitrophenyl C5—*H*; 8.81 (d, J = 3.2 Hz), 1H, nitrophenyl C3—*H*.

4-Trimethylammonio-6-nitrophenyl-3-(2-naphthyl)-propionate iodide, ***15****c* (2)

For this compound, mp 158–160°C. 200 MHz ^{1}H-nmr (DMSO-d_6) δ: 3.02 (distorted triplet — A_2B_2), 4H, —C*H*$_2$—C*H*$_2$—; 3.76 (s), ?H, $N^+(CH_3)_3$; 7.4–7.5 (complex), 3H and 7.8–7.9 (complex) 4H, naphthyl; 7.74 (d, J = 9.2 Hz), 1H, nitrophenyl C6—*H*; 8.54 (d of d, J = 9.4, 3.2), 1H, nitrophenyl C5—*H*; 8.80 (d, J = 3.0 Hz), 1H, nitrophenyl C3—*H*.

4-Trimethylammonio-6-nitrophenyl-3-(3-phenanthryl)propionate iodide, ***16****c*

3-(3-Phenanthryl)propionic acid, 515 mg (2.06 mmol), was dissolved in dry DMF, 3 mL, containing dry Et_3N, 0.30 mL (2.1 mmol). Ethyl chloroformate, 0.2 mL (2.1 mmol) was then added and the mixture stirred for 15 min. 4-Hydroxy-3-nitrophenyltrimethylammonium iodide (2, 21), 676.2 mg (2.087 mmol), dissolved in dry DMF, 4 mL, containing Et_3N, 0.3 mL (2.1 mmol), was added to the first solution and the mixture was stirred at room temperature for 1 h. The reaction mixture was then poured into ether, 100 mL, and the precipitate was filtered, washed with ether and petroleum ether, and then dried. The crude yield was 1.25 g. This material was dissolved in CH_2Cl_2, 150 mL, and methanol, 10 mL, and then poured into ether, 200 mL. The precipitate, 850 mg, had mp 130–133°C. The solid was dissolved in $CHCl_3$, 200 mL, and methanol, 3 mL, and poured into ether, 250 mL; after cooling in ice, 624 mg of solid, mp 133–134°C, was recovered. Recrystallization from methanol:acetic acid:benzene:ether 5:5:20:10 gave mp 135–136°C. Recrystallization from acetic acid:ethanol, with cooling to −10°C gave mp 137–138°C. 200 MHz ^{1}H-nmr spectrum (DMSO-d_6): δ: 3.27 (A_2B_2 pattern), 4H, Ar—C*H*2—C*H*2—CO; 3.76 (s), 9H, N—C*H*$_3$; 7.71 (d, J = 9.4 Hz), 1H, nitrophenyl C6—*H*; 7.5–8.8 (complex), 9H, phenanthryl H; 8.55 (d of d, J = 3.2, 9.2 Hz), 1H, nitrophenyl C5—*H*; 8.82 (d, J = 3.4 Hz), 1H, nitrophenyl C3—*H*. Peaks attributed to the trimethylammonionitrophenyl residue are assigned by comparison with a spectrum of the phenol. 200 MHz ^{1}H-nmr (DMSO-d_6) δ: 3.71 (s), 9H, $N^+(CH_3)_3$; 7.32 (d, J = 9.4 Hz), 1H, C6—*H*; 8.24 (d of d, J = 9.4, 3.2 Hz), 1H, C5—*H*; 8.49 (d, J = 3.4 Hz), 1H, C3—*H*.

Spectra in DMSO of all of these esters had signals corresponding to minor amounts of unesterified phenols, signals which grew in intensity after the DMSO solutions were kept at room temperature for a few hours, and which became major ones after heating. It was confirmed by taking a spectrum of the acetate that this compound, which had a reasonably sharp melting point, 155–158°C, lit: mp 152–155°C (21); mp 154–156.5°C (4), also appeared contaminated in DMSO. It seemed likely that solvolysis was occurring in DMSO.

Spectrophotometric analysis for trimethylammonionitrophenyl esters

Stock solutions of the phenol and the esters were made up in purified acetonitrile. The absorbance changes at 400 nm were determined for replicate injections, and the extinction coefficients determined. Compound, extinction coefficient (number of injections); 4-hydroxy-3-nitrophenyltrimethylammonium iodide, 4940 ± 20 (7); **14***c*, 4970 ± 20 (5); **15***c*, 4920 ± 40 (8); **16***c*, 4920 ± 50 (6). We conclude that these esters are pure within the limits of this assay, i.e. 1%.

Kinetics

Kinetics experiments were carried out as previously described (5). A stock solution of **13** was prepared from 6.00 mg **13**.6HCl in 2.0 mL water. Initial experiments were carried out using pH 8 tris buffer, as previously employed (5), but we encountered severe problems of non-reproducible rates, and spuriously fast reactions, which have been seen in other reactions (10). The kinetics reported in Table 1 were carried out using borate buffer, ionic strength 0.1, pH 8.00 (22); 0.0928 *M* $B(OH)_3$, 0.0072 *M* NaOH, and 0.0928 *M* KCl. Stock solutions of the esters were prepared in purified acetonitrile.

Data were fitted to theoretical equations by weighted least squares (5, 23, 24), using suitable computer programs. Kinetics data were fitted to $y = a_1 + a_2 \exp(-a_3 t)$, $y = a_1 + a_2 \exp(-a_3 t) + a_4 t$, or $y = a_1 + a_2 \exp(-a_3 t) + a_4 \exp(-a_5 t)$.

Acknowledgment

We thank the Natural Sciences and Engineering Research Council of Canada for financial support of this work.

1. J. P. Guthrie. Can. J. Chem. **50**, 3993 (1972).
2. J. P. Guthrie and Y. Ueda. Can. J. Chem. **51**, 3936 (1973).
3. J. P. Guthrie and S. O'Leary. Can. J. Chem. **53**, 2150 (1975).
4. J. P. Guthrie and Y. Ueda. Can. J. Chem. **54**, 2745 (1976).
5. J. P. Guthrie, P. A. Cullimore, R. S. McDonald, and S. O'Leary. Can. J. Chem. **60**, 747 (1982).
6. R. F. Borch, M. D. Bernstein, and H. D. Durst. J. Am. Chem. Soc. **93**, 2897 (1971).
7. A. Yagi, J. Liang, and D. K. Fukushima. J. Org. Chem. **32**, 713 (1967).
8. C. W. Shoppee, D. E. Evans, H. C. Richards, and G. H. R. Summers. J. Chem. Soc. 1649 (1956).
9. J. E. Bridgeman, P. C. Cherry, A. S. Clegg, J. M. Evans, E. R. H. Jones, A. Kasal, V. Kumar, G. D. Meakins, Y. Morisawa, E. E. Richards, and P. D. Woodgate. J. Chem. Soc. (C), 250 (1970).
10. J. P. Guthrie and S. O'Leary. Can. J. Chem. **59**, 2358 (1981).
11. G. S. Eadie. J. Biol. Chem. **146**, 85 (1942).
12. B. H. J. Hofstee. Nature, London, **184**, 1296 (1959).
13. A. Fersht. Enzyme structure and mechanism. Freeman, San Francisco. 1977. p. 95.
14. J. P. Guthrie. Can. J. Chem. **51**, 3494 (1973).
15. T. Fujita, J. Iwasa, and C. Hansch. J. Am. Chem. Soc. **86**, 5175 (1964).
16. M. S. Tute. Adv. Drug. Res. **6**, 1 (1971).
17. A. Fersht. Enzyme structure and mechanism. Freeman, San Francisco. 1977. p. 114.
18. R. L. Reeves. J. Am. Chem. Soc. **97**, 6019 (1975); H. W.

HOYER, A. MARMO, and M. ZOELLNER. J. Phys. Chem. **65**, 1804 (1961); G. I. MUKHAYER and S. S. DAVIS. J. Coll. Interface Sci. **66**, 110 (1978); F. M. MENGER, A. J. A. DEGREIFF, and D. A. JAEGER. J. Chem. Soc. Chem. Commun. 543 (1984).

19. M. M. JANOT, Q. KHUONG-HUU, and R. GOUTAREL. Bull. Soc. Chim. Fr. 1640 (1960).
20. M. J. KAMLET (*Editor*). Organic electronic spectral data. Vol. I. Interscience, New York. 1960; H. E. UNGENADE (*Editor*). Organic electronic spectral data. Vol. II. Interscience, New York. 1960.
21. T. C. BRUICE, J. KATZHENDLER, and L. FEDOR. J. Am. Chem. Soc. **90**, 1333 (1968).
22. C. LONG (*Editor*). Biochemists' handbook. E. and F. N. Spon Ltd., London. 1961.
23. W. E. DEMING. Statistical adjustment of data. Dover, New York. 1964.
24. P. R. BEVINGTON. Data reduction and error analysis for the physical sciences. McGraw-Hill, New York. 1969.
25. J. P. GREENSTEIN and M. WINITZ. Chemistry of the amino acids. Wiley, New York. 1961. p. 1979; H. PAULY. Z. Physiol. Chem. **42**, 508 (1904).

The pK_a values of simple aldehydes determined by kinetics of chlorination

J. Peter Guthrie[1] and John Cossar

Department of Chemistry, University of Western Ontario, London, Ont., Canada N6A 5B7

Received June 20, 1986

J. Peter Guthrie and John Cossar. Can. J. Chem. **64**, 2470 (1986).

From the kinetics of chlorination of acetaldehyde and isobutyraldehyde we have been able to determine the pK_a values of the free aldehydes (corrected for covalent hydration) as 16.9 ± 0.5 and 15.7 ± 0.5, respectively. These values are in reasonable accord with other work and show that our kinetic method for ketone pK_a's can be extended to aldehydes. For isobutyraldehyde the transition from rate-determining halogenation to rate-determining enolization occurs at [OCl^-] values around 10^{-3} *M* for hydroxide concentrations of 0.1 to 1. For acetaldehyde the transition would only occur at much higher [OCl^-].

J. Peter Guthrie et John Cossar. Can. J. Chem. **64**, 2470 (1986).

En se basant sur la cinétique de la chloration de l'acétaldéhyde et de l'isobutyraldéhyde, on a pu déterminer que les valeurs des pK_a des aldéhydes libres (corrigées pour l'hydratation covalente) sont respectivement 16,9 ± 0,5 et 15,7 ± 0,5. Ces valeurs sont en bon accord avec d'autres travaux et ces concordances démontrent que notre méthode cinétique pour déterminer des pK_a de cétones peut être étendue aux aldéhydes. Dans le cas de l'isobutyraldéhyde, la transition entre une halogénation qui détermine la vitesse de la réaction et une énolisation qui détermine la vitesse de la réaction se produit à des valeurs de [OCl^-] qui se situent autour de 10^{-3} *M* pour des concentrations d'ions hydroxydes allant de 0,1 à 1 *M*. Dans le cas de l'acétaldéhyde, la transition ne se produirait qu'à des valeurs beaucoup plus élevées de [OCl^-].

[Traduit par la revue]

Introduction

We have reported (1–3) a method for determining the pK_a of a simple ketone by analysis of the kinetics of alkaline

halogenation. The kinetics are normally carried out with the halogenating agent in excess, under pseudo-first order conditions, so that

$$v = k_{obs}[\text{ketone}]$$

$$k_{obs} = k_2[\text{halogen}]_{total}$$

$$k_2 = k_2^0 + k_2^-[OH^-]$$

The basis of the method is the evaluation of the term in the rate law which is first order in carbonyl compound and first order in halogenating agent, but zero order in base; this is expressed as k_2^0. Such terms were first detected by Bartlett (4, 5). We have shown (1, 2) that these terms represent diffusion-controlled reaction of the enolate with the hypohalous acid, i.e. the conjugate base of one reagent and the conjugate acid of the other. The other term in the rate law, k_2^-, represents reaction of the enolate ion with the hypohalite ion. The pK_a of the carbonyl compound is then easily calculated from:

$$[1] \quad \log k_2^0 = \log k_{diff} + pK_a^{HOX} - pK_a^K$$

where k_{diff} is the rate constant for a diffusion-controlled reaction, pK_a^{HOX} is the acid dissociation constant for the hypohalous acid, and pK_a^K is the acid dissociation constant for the keto tautomer of the carbonyl compound. We have examined the question of the best value to use for the rate constant of a diffusion-controlled process involving an unsymmetrical reagent such as a carbon–carbon double bond and proposed that the best value is log $k_{diff} = 9.2 \pm 0.5$ (2). A value of this magnitude, $k_{diff} = (2.8 \pm 0.2) \times 10^9\ M^{-1}\ s^{-1}$, has been reported recently for the reaction of bromine with acetophenone enol (6).

[1]Author to whom correspondence should be addressed.

Recently Kresge has reported a pK_a of 15.49 ± 0.04 for isobutyraldehyde (7), based on measurements of the rates of ketonization of the enolate and of base-catalyzed enolization. Kresge has also determined a pK_a of 16.73 ± 0.06 for acetaldehyde (8, 9).[2]

In addition to our work on acetone (1–3) we have been investigating a number of other ketones in work now nearing completion, and have examined the question of whether our method can be applied to simple aldehydes. We wish now to report a determination of the pK_a of acetaldehyde, and a less detailed examination of the behavior of isobutyraldehyde showing that our method is consistent with the results of Kresge and co-workers (7, 10).

Results

When the observed pseudo-first order rate constants for the chlorination of acetaldehyde with hypochlorite in excess are plotted vs. [OCl^-], good linear relations are obvious; see Fig. 1. For some of the sets of data the best straight lines appeared to have non-zero intercepts. When straight lines are fitted to the data by least squares it is found that the intercepts are small and show little sign of any simple dependence upon the hydroxide concentration. For some of the data sets it was noticed that the point at highest [OCl^-] falls below the line determined by the other points. This suggests that the first signs of curvature are being detected; the data do not, however, define a curve. The best data treatment appears to be the use of straight lines constrained to pass through the origin. As shown in Fig. 1, such lines give a reasonable description of the data, and correspond to the expected pattern.

The slopes of these plots constitute the apparent second order rate constants for the chlorination reaction; when they are plotted against [OH^-], as shown in Fig. 2, the trend is monotonic, but non-linear. It is, however, necessary to correct for both addition of water and ionization of the hydrate, as shown in Scheme 1. Good values for K_h (11) and K_h^- (12, 13)[3] are available and permit calculation of corrected rate constants

[2]We thank Professor Kresge for communicating this result prior to its publication.

[3]$K_h^- = K_a/K_w$; pK_a = 13.57 (12, 13).

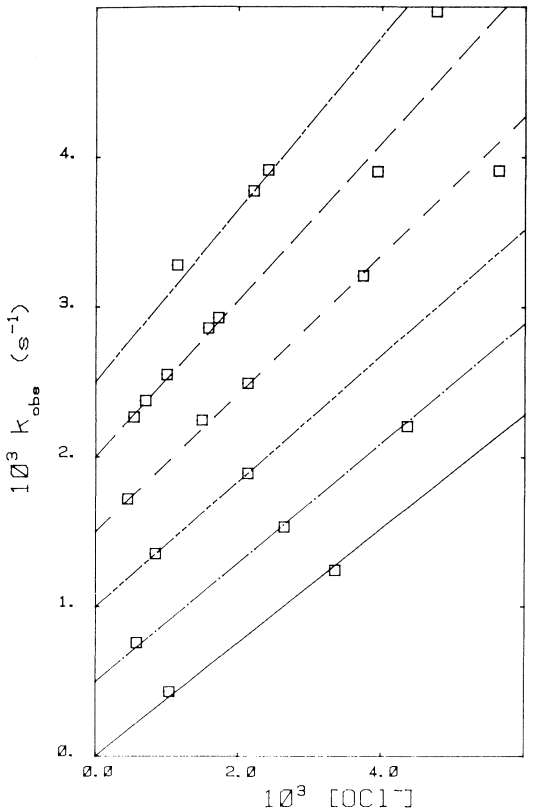

FIG. 1. Kinetics of chlorination of acetaldehyde at various hydroxide concentrations. Successive offsets of 0.5 in 10^3 k have been added to the rate constants so that the different data sets do not overlap: (—) $[OH^-] = 0.026$; (-·-·-) $[OH^-] = 0.054$; (-···-) $[OH^-] = 0.106$; (--) $[OH^-] = 0.243$; (––) $[OH^-] = 0.486$; (–––) $[OH^-] = 0.984$.

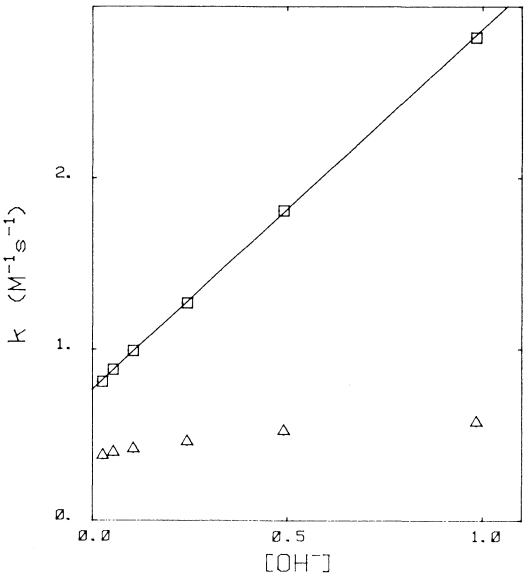

FIG. 2. Pseudo-second order rate constants for the chlorination of acetaldehyde: (△) k_{2app}, the slopes derived from Fig. 1; (□) k_{2corr}, the same values corrected for hydration and hydrate anion formation as described in the text.

corresponding to reaction of the free aldehyde. When these k_{corr} values are plotted against $[OH^-]$, as shown in Fig. 2, an excellent straight line results, with a slope of 2.10 ± 0.02 and an intercept of 0.769 ± 0.0022. This leads to a carbon pK_a for the aldehyde of 16.8 ± 0.5.

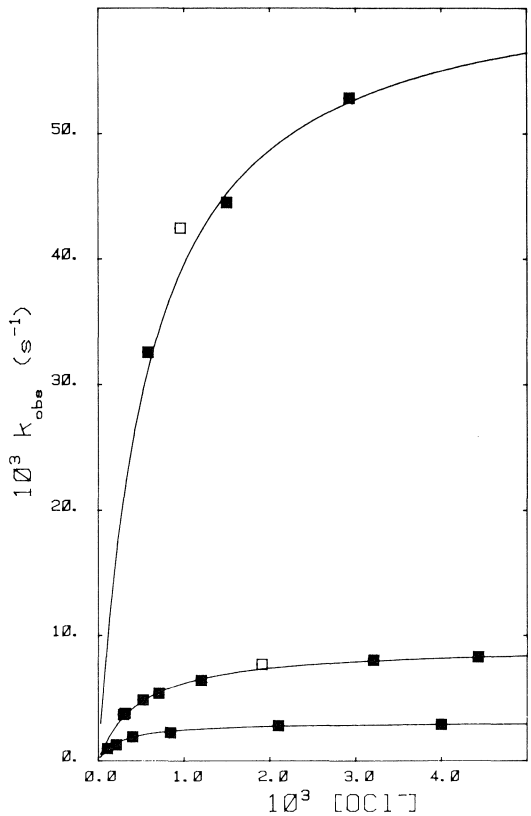

FIG. 3. Kinetics of chlorination of isobutyraldehyde at various hydroxide concentrations. The lines were determined by least squares fitting: (■) points included in the least squares fitting; (□) points omitted in the least squares fitting.

One process which might lead to non-zero intercepts for plots of k_{obs} vs. $[OCl^-]$ at fixed $[OH^-]$, corresponding to hypochlorite independent consumption of acetaldehyde, would be aldolization. However, the equilibrium constant for this process is only 400 M^{-1} (14) and it would not proceed to a significant extent at 10^{-4} M acetaldehyde.

When the observed pseudo-first order rate constants for the chlorination of isobutyraldehyde are plotted vs. $[OCl^-]$ at fixed $[OH^-]$ a non-linear dependence is obvious, see Fig. 3, with leveling off at high $[OCl^-]$. The data were fitted to eq. [2] by

$$[2] \quad k_{obs} = a_1/(1 + a_2/[OCl^-])$$

non-linear least squares. For each of two sets of data one point was clearly divergent from the line defined by the others; in the final calculations these two divergent points were omitted. The theoretical lines based on the least-squares parameters are shown in Fig. 3.

In analyzing the hydroxide and hypochlorite dependence of these kinetics we make use of the mechanism shown in Scheme 1. In terms of this mechanism, the observed rate constant is given by eq. [3]

$$[3] \quad k_{obs} = \{k_1[OH^-]/\{1 + K_h(1 + K_h^-[OH^-])\}\}/ \{1 + k_{-1}/\{k_2^0 K_w/K_a^{HOCl}[OH^-] + k_2^-\}[OCl^-]\}$$

K_h, the equilibrium constant for hydration of isobutyraldehyde, and K_h^-, the equilibrium constant for ionization of the hydrate, are available from the work of Hine *et al.* (15). The quantity $k_1[OH^-]$ can be extracted from the a_1 values using these equilibrium constants. At 0.034 M OH^- $k_1[OH^-]$ is 0.00500 ± 0.00008; at 0.106 M OH^- $k_1[OH^-]$ is 0.0153 ± 0.002; at

TABLE 1. Kinetics of chlorination of aldehydes[a]

[Aldehyde] × 10^3	[OH^-]	[OCl^-] × 10^3	A_1	A_2	$A_3 \times 10^3$	$-A_4 \times 10^6$
			(*a*) Acetaldehyde			
0.24	0.978	4.76	1.510	1.171	2.471(0.023)	0.492(0.169)
0.127	0.984	2.21	0.685	0.098	1.277(0.006)	
0.064	0.989	1.14	0.360	0.049	0.7803(0.0095)	0.667(0.018)
0.118	0.984	2.41	0.769	0.0866	1.416(0.0100)	0.271(0.025)
0.059	0.496	0.544	0.148	0.044	0.2678(0.0023)	0.096(0.003)
0.099	0.496	1.00	0.284	0.071	0.5507(0.0029)	0.091(0.009)
0.104	0.488	1.58	0.486	0.077	0.8610(0.0062)	0.223(0.045)
0.183	0.484	3.94	1.257	0.140	1.905(0.012)	0.583(0.036)
0.352	0.484	0.705	0.224	0.0293	0.3771(0.0044)	0.234(0.001)
0.085	0.497	1.72	0.544	0.0654	0.9300(0.0063)	0.171(0.021)
0.023	0.245	0.457	0.144	0.0214	0.2203(0.0032)	0.174(0.002)
0.0738	0.244	1.49	0.470	0.0585	0.7470(0.0045)	0.147(0.003)
0.107	0.244	2.13	0.672	0.0837	0.9943(0.0057)	0.214(0.006)
0.183	0.242	3.74	1.177	0.142	1.709(0.008)	0.212(0.018)
0.279	0.241	5.63	1.761	0.224	2.409(0.016)	0.433(0.073)
0.0444	0.1066	0.841	0.268	0.0370	0.3563(0.0030)	0.170(0.003)
0.103	0.1057	2.13	0.669	0.0849	0.8944(0.0025)	0.192(0.003)
0.0297	0.0539	0.580	0.181	0.0251	0.2608(0.0021)	0.153(0.002)
0.129	0.0541	2.64	0.812	0.1183	1.036(0.005)	0.239(0.003)
0.219	0.0535	4.36	1.351	0.188	1.708(0.008)	0.661(0.033)
0.0518	0.0241	1.036	0.317	0.0495	0.4330(0.0025)	0.387(0.004)
0.165	0.0276	3.35	1.037	0.145	1.245(0.0040)	0.673(0.011)
			(*b*) Isobutyraldehyde			
0.33	0.986	2.93	0.9308	0.0983	52.84(0.69)	11.66(0.65)
0.167	0.992	1.50	0.4708	0.0513	44.51(0.75)	2.43(0.49)
0.123	0.994	0.958	0.2973	0.0433	42.48(1.03)	3.50(0.75)
0.077	0.995	0.582	0.1810	0.0299	32.57(1.49)	1.65(1.21)
0.033	0.107	0.314	0.0995	0.0137	3.793(0.084)	1.02(0.06)
0.033	0.107	0.296	0.0933	0.0124	3.689(0.085)	0.556(0.049)
0.050	0.107	0.523	0.1689	0.0175	4.864(0.095)	0.731(0.053)
0.082	0.107	0.708	0.2096	0.0433	5.386(0.045)	1.02(0.07)
0.115	0.106	1.20	0.384	0.0402	6.446(0.054)	1.55(0.07)
0.164	0.106	1.91	0.6175	0.0563	7.699(0.064)	2.79(0.09)
0.328	0.105	3.21	1.013	0.1189	8.050(0.053)	7.51(0.20)
0.458	0.104	4.43	1.397	0.1671	8.302(0.056)	13.82(0.36)
0.0097	0.0342	0.108	0.3304	0.0515[b]	0.978(0.010)	3.53(0.02)
0.0194	0.0343	0.211	0.6639	0.0831[b]	1.280(0.014)	3.66(0.05)
0.0416	0.0344	0.401	1.261	0.1489[b]	1.922(0.009)	4.99(0.05)
0.0852	0.0346	0.841	1.329	0.1490[c]	2.262(0.017)	7.33(0.10)
0.199	0.0351	2.10	1.345	0.1353[d]	2.806(0.017)	7.30(0.08)
0.413	0.0347	4.00	2.539	0.2747[d]	2.908(0.056)	22.30(0.67)

[a]All in aqueous solution at 25°C, ionic strength = 1.0 *M* (KCl). Data were fitted to $y = A_1 + A_2 \exp(-A_3 t)$ or $y = A_1 + A_2 \exp(-A_3 t) + A_4 t$. Quantities in parentheses are estimated standard deviations of the parameters calculated by the least-squares program. The calculated standard deviations for A_1 and A_2 were ≤ 0.001 in all cases except the last entry in the table (where $A_1 = 2.439$) for which both were ca. 0.002. All reactions in cells with 1 cm path unless noted.

[b]10 cm path length.

[c]5 cm path length.

[d]2 cm path length.

0.992 *M* OH^- it is 0.140 ± 0.006. From these values k_1 = 0.145 ± 0.001 was calculated, which is in excellent agreement with Kresge's value of 0.142 ± 0.011 (10). The apparent second order rate constant, which would be obtained directly at very low [OCl^-], can be calculated as a_1/a_2. The values so obtained are 12.13 ± 0.85 ([OH^-] = 0.034); 19.1 ± 0.7 ([OH^-] = 0.106); and 106 ± 13.8 ([OH^-] = 0.992); see Fig. 4. Uncertainties in the apparent second order rate constants were calculated including the covariance between a_1 and a_2 (16). After correcting for hydration and hydrate anion formation we obtain 19.6 ± 1.4, 31.8 ± 1.1, and 235 ± 31, respectively. Least-squares fitting gives k_2 = (12.17 ± 2.43) + (190.7 ± 27.0)[OH^-]. From the intercept we calculate (2) a pK_a value of 15.67 ± 0.51. Kresge *et al.* reported 15.49 ± 0.04 (7).

Discussion

It is a striking observation that the kinetics of alkaline chlorination of acetaldehyde show almost no signs of a tendency to undergo a change in rate-determining step with increasing [OCl^-] in the range covered by our experiments, while for isobutyraldehyde the change in rate-determining step is quite apparent, and indeed becomes nearly complete at low [OH^-]. A major reason for the difference lies in the carbon acidities of the two carbonyl compounds, and in the fact that the rates of

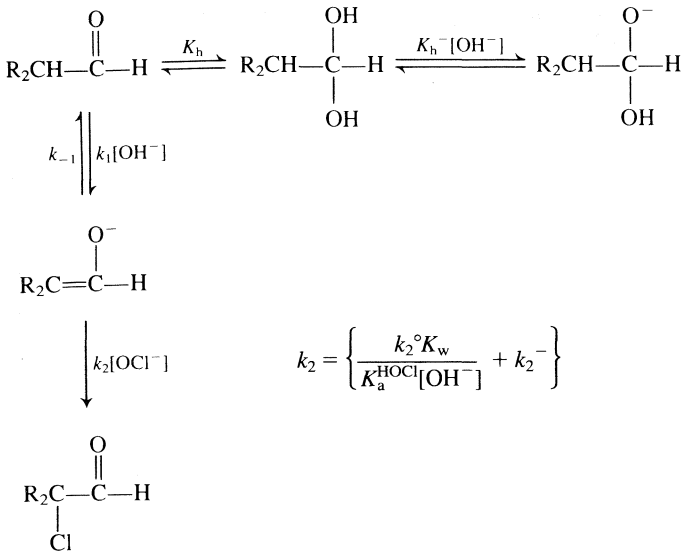

SCHEME 1

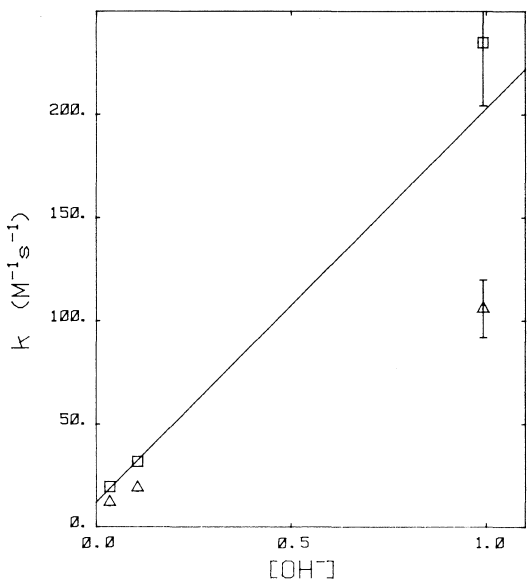

FIG. 4. Pseudo-second order rate constants for the chlorination of isobutyraldehyde: (△) k_{2app}, the values derived from the data in Fig. 1; (□) k_{2corr}, the same values corrected for hydration and hydrate anion formation as described in the text. The line is calculated by weighted least squares.

base-catalyzed proton abstraction are in the reverse order compared to acidity. The pK_a values are 16.8 and 15.7, and the rates of proton abstraction are 1.17 M^{-1} s^{-1} (9)[2] and 0.145 M^{-1} s^{-1} for acetaldehyde and isobutyraldehyde. As a consequence the rate of reprotonation of acetaldehyde enolate by water is about 100 times faster than for isobutyraldehyde enolate. Since partitioning between the two available paths determines which step is rate determining, a larger rate constant for reprotonation of the enolate will require a higher [OCl^-] to cause a change in rate-determining step, if the rates of halogenation of the enolates are the same. This is the case at low [OH^-], where diffusion-controlled reaction with HOCl dominates the kinetics of halogenation. At high [OH^-] the rate of halogenation is dominated by the contribution from reaction of OCl^- with the enolate. These rate constants are not expected to be the same, and are well below the diffusion-controlled limit. Surprisingly, however, it seems unavoidable to conclude that the relative rates of the reactions of the enolates with OCl^- are in the unexpected sense, with isobutyraldehyde being the more reactive. Thus the more hindered and the more stable enolate is the more reactive. The rate constants for the reactions of the enolates with OCl^- are 1.3×10^3 for acetaldehyde and 9.5×10^3 for isobutyraldehyde. A possible explanation for this unexpected order might be a transition state for the reaction of enolate with hypochlorite ion which resembles a charge transfer complex between the alkene and hypochlorite ion.

The change in absorbance for each reaction provides a measure of the stoichiometry. Although there is considerable scatter in the values for both aldehydes, it seems clear that for acetaldehyde the stoichiometry is greater than 2 but less than 3. There is no clear dependence of the observed stoichiometry upon the hypochlorite concentration. For isobutyraldehyde the observed values scatter about the expected value of 1. Observation of a stoichiometry less than 3 for acetaldehyde suggests that for this compound as for acetone (3) hydrolysis of the intermediate partially chlorinated aldehydes is a major side reaction.

Our method for the determination of pK_a values of simple carbonyl compounds has now been shown to work for aldehydes as well as ketones. The major disadvantage of the method is that it relies upon an imprecisely known value of the rate constant for a diffusion-controlled reaction. Although the uncertainties in this value will diminish as more absolute determinations become available, it will probably be found to vary for different compounds and/or reactions even though it is very insensitive to the chemical nature of the reaction occurring after diffusion. The major advantage of the method is that it uses standard, widely available, apparatus and inexpensive chemicals.

Experimental

Materials

Isobutyraldehyde, Aldrich 98%, was distilled at atmospheric pressure and the middle fraction boiling at 62–63°C was used for kinetics. A stock solution, 0.168 *M*, was prepared using glass-distilled water as solvent.

Acetaldehyde dimethyl acetal, Eastman, was distilled at atmospheric pressure and the middle fraction boiling at 63–64°C was used for kinetics. Weighed amounts of the acetal were hydrolyzed in 0.001 *M* HCl (4 h at room temperature), neutralized to pH 8 (pH meter) using 1 *M* NaOH, and then made to a known volume with water. Two stock solutions, 0.191 *M* and 0.0446 *M*, were used.

Solutions containing sodium hydroxide and sodium hypochlorite were made up and titrated as previously described (2, 3). The ionic strength was held at 1 *M* using KCl.

Methods

Kinetics procedures were as previously described (2, 3). Reactions were initiated by injecting small volumes of an aldehyde stock solution into alkaline hypochlorite solution; the volume change was always less than 1%.

Calculations. Data were fitted to theoretical equations by non-linear least squares (16, 17), using computer programs written for the purpose.

Acknowledgments

We thank the Natural Sciences and Engineering Research Council of Canada, and the Academic Development Fund of the University of Western Ontario for financial support of this work.

1. J. P. GUTHRIE, J. COSSAR, and A. KLYM. J. Am. Chem. Soc. **104**, 895 (1982).

2. J. P. GUTHRIE, J. COSSAR, and A. KLYM. J. Am. Chem. Soc. **106**, 1351 (1984).
3. J. P. GUTHRIE and J. COSSAR. Can. J. Chem. **64**, 1250 (1986).
4. P. D. BARTLETT. J. Am. Chem. Soc. **56**, 967 (1934).
5. P. D. BARTLETT and J. R. VINCENT. J. Am. Chem. Soc. **57**, 1596 (1935).
6. Y. CHIANG, A. J. KRESGE, and J. WIRZ. J. Am. Chem. Soc. **106**, 6392 (1984).
7. Y. CHIANG, A. J. KRESGE, and P. A. WALSH. J. Am. Chem. Soc. **108**, 6315 (1986).
8. A. J. KRESGE. Chemtech, 250 (1986).
9. Y. CHIANG, M. HOJATTI, J. R. KEEFFE, A. J. KRESGE, N. P. SCHEPP, and J. WIRZ. To be published.
10. Y. CHIANG, A. J. KRESGE, and P. A. WALSH. J. Am. Chem. Soc. **104**, 6122 (1982).
11. J. L. KURZ. J. Am. Chem. Soc. **89**, 3524 (1967).
12. J. HINE and G. F. KOSER. J. Org. Chem. **36**, 1348 (1971).
13. R. P. BELL. Adv. Phys. Org. Chem. **4**, 1 (1966).
14. J. P. GUTHRIE. Can. J. Chem. **52**, 2037 (1974).
15. J. HINE, J. G. HOUSTON, and J. H. JENSEN. J. Org. Chem. **30**, 1184 (1965).
16. P. R. BEVINGTON. Data reduction and error analysis for the physical sciences. McGraw-Hill, New York. 1969.
17. W. E. DEMING. Statistical adjustment of data. Dover, New York. 1964.

COMMUNICATION

Total syntheses of the sesquiterpenoids (±)-axamide-1, (±)-axisonitrile-1, and the corresponding C-10 epimers

EDWARD PIERS AND BIK WAH ANISSA YEUNG
Department of Chemistry, University of British Columbia, 2036 Main Mall, University Campus, Vancouver, B.C., Canada V6T 1Y6

Received July 7, 1986

EDWARD PIERS and BIK WAH ANISSA YEUNG. Can. J. Chem. **64**, 2475 (1986).

Total syntheses of (±)-axamide-1 (**1**), (±)-axisonitrile-1 (**2**), and the corresponding C-10 epimers **16** and **17** are described. The key steps of the synthetic sequence involve methylenecyclohexane annulation of 2-methyl-2-cyclopenten-1-one and $TiCl_4$-catalyzed conjugate addition of 3-methyl-1,1-bis(trimethylsiloxy)-1-butene to the bicyclic enone **8**.

EDWARD PIERS et BIK WAH ANISSA YEUNG. Can. J. Chem. **64**, 2475 (1986).

On décrit les synthèses totales des (±)-axamide-1 (**1**), (±)-axisonitrile-1 (**2**) et de leurs épimères en C-10, **16** et **17**. Les étapes clés de la synthèse impliquent l'annelation de la méthyl-2 cyclopentène-2 one-1 avec le méthylènecyclohexane et l'addition conjuguée, catalysée par le $TiCl_4$, du méthyl-3 bis(triméthylsiloxy)-1,1 butène-1 sur l'énone bicyclique **8**.

[Traduit par la revue]

The structurally unusual natural products (+)-axamide-1, (+)-axisonitrile-1, and (+)-axisothiocyanate-1, isolated from the marine sponge *Axinella cannabina*, have been shown to possess the constitution (1) and absolute stereochemistry (2)[1] depicted in structural formulas **1**–**3**, respectively. These substances, which belong to the relatively small group of axane-type sesquiterpenoids (carbon skeleton **4**), appear to be biogenetically related to the eudesmane family of terpenoids (carbon skeleton **5**). We report herein a total synthesis of (±)-**1**, (±)-**2**, and the corresponding C-10 epimers (**16** and **17**, respectively) via a route (see Scheme 1) in which our recently developed methylenecyclohexane annulation method (3) played a key role.

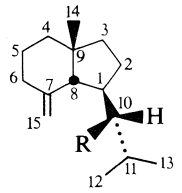

1 R = NH—CHO
2 R = $\overset{+}{N}\equiv\bar{C}$
3 R = N=C=S

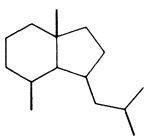

4

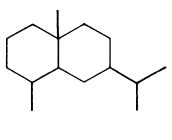

5

Conjugate addition of 2-(5-chloro-1-pentenyl)magnesium bromide (3) to 2-methyl-2-cyclopenten-1-one (**6**) and subsequent intramolecular alkylation of the resultant product provided (85%) the *cis*-fused bicyclic ketone **7**.[2] Conversion (4) of **7** into the corresponding α-bromo ketone, followed by dehydrobromination (5) of the latter substance, gave the enone **8** (77% from **7**). Interestingly, at least under the conditions employed for the formation of **8**, the exocyclic double bond showed no inclination to migrate into conjugation with the enone function.

It is evident from an examination of molecular models that conjugate addition to the enone system of **8** would occur preferentially from the convex (β) face of the molecule. In the event, treatment of **8** with 3-methyl-1,1-bis(trimethylsiloxy)-1-butene[3] in the presence of $TiCl_4$ gave, in 88% yield, a mixture of two keto acids **9** and **10**, in a ratio of about 3:2, respectively.[4] Separation of this mixture by a combination of fractional crystallization and column chromatography (silica gel) provided the pure substances **9** (44%, mp 172–173°C) and **10** (32%, mp 120–121°C). Removal of the keto function from **9** by Wolff–Kishner reduction gave the acid **11**[5] (90%, mp 120–121°C), which was converted via the acid chloride **12** into the acyl azide **13**. Curtius rearrangement of the latter substance, followed by treatment of the resultant isocyanate with 2-trimethylsilylethanol (7), afforded the crystalline carbamate **14** (mp 79.5–80.5°C, 89% from **11**). Reaction of **14** with tetra-*n*-butylammonium fluoride (7) provided (72%) the primary amine **15**, which, when treated with acetic formic anhydride (8) gave (±)-axamide-1 (**1**), a viscous oil, in 90% yield.

The ^{1}H nmr spectrum of (±)-**1** indicated that it consisted of a 3:2 mixture of rotamers associated with the amide linkage.

[1] In ref. 2*a*, the absolute configuration at C-10 of compounds **1**–**3** is depicted incorrectly.

[2] All compounds reported herein exhibited spectra in accord with structural assignments. New compounds gave satisfactory molecular mass determinations (high resolution mass spectrometry).

[3] This reagent was prepared (86%) by treatment of 3-methylbutanoic acid with $LiNPr^i_2$ (2.2 equiv.) in dry tetrahydrofuran (THF) – hexamethylphosphoramide, followed by trapping of the resultant dianion with Me_3SiCl (2.4 equiv.).

[4] Titanium tetrachloride-catalyzed addition of (*E*)-1-ethoxy-3-methyl-1-trimethylsiloxy-1-butene to the enone **8** (see ref. 6) provided (89%) a mixture of ethyl esters corresponding to **9** and **10** (ratio ≈ 45:55, respectively). Hydrolysis of this mixture with potassium hydroxide in refluxing ethanol was slow and caused (some) synthetically unproductive epimerization of the chiral center adjacent to the ester function. Acids **9** and **10** were produced in a ratio of about 1:2, respectively (82% yield).

[5] In the ^{1}H nmr spectrum of **11**, the angular (C-8) proton gives rise to a doublet (J = 10.5 Hz) at δ 1.86. In what appears to be the most stable conformation of **11**, the dihedral angle between the *trans*-related protons at C-8 and C-1 (axane numbering) is close to 180° and, thus, the observed coupling constant is consistent with the assigned stereochemistry. Similar observations were made for 10-*epi*-**11** (Wolff–Kishner reduction product of **10**).

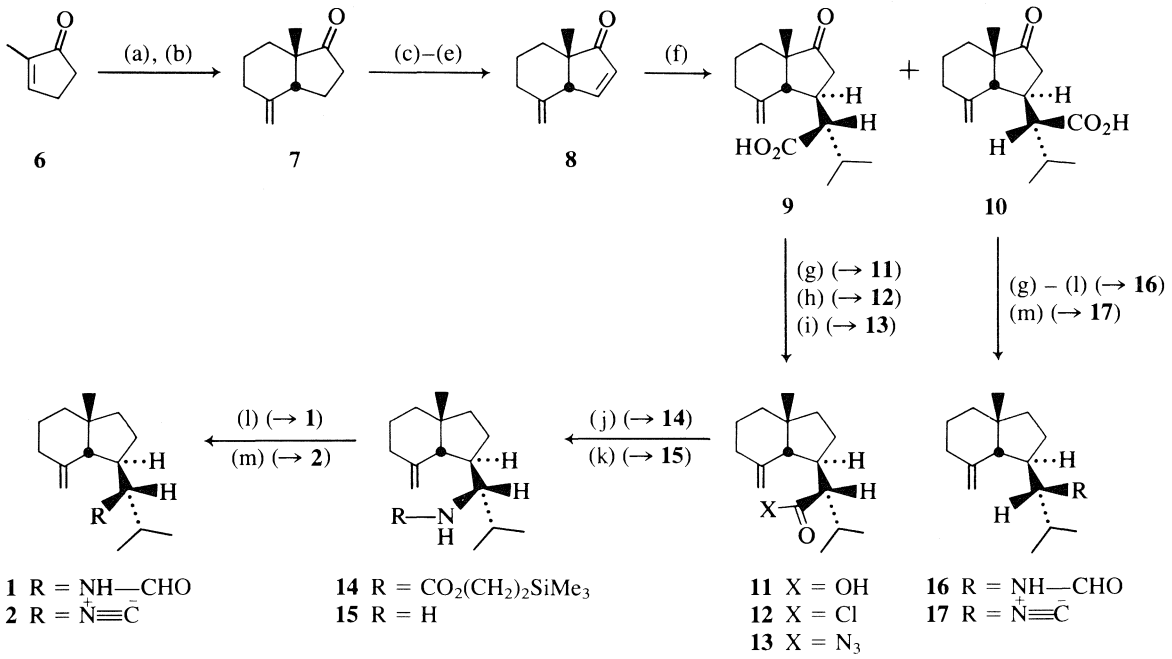

(a) 2-(5-Chloro-1-pentenyl)magnesium bromide (1.3 equiv.), $CuBr \cdot Me_2S$ (0.32 equiv.), $BF_3 \cdot Et_2O$ (1.3 equiv.), THF, −78°C, 3 h; NH_4Cl, H_2O; (b) KH, THF, room temperature, 2 h; (c) $LiNPr^i_2$, THF, −78°C; Me_3SiCl, −78°C to room temperature, 1.5 h; (d) *N*-bromosuccinimide, THF, 0°C, 15 min; (e) LiBr, Li_2CO_3, *N,N*-dimethylformamide, reflux, 3 h; (f) 3-methyl-1,1-bis(trimethylsiloxy)-1-butene, $TiCl_4$, CH_2Cl_2, −78°C, 2 h; H_2O; (g) $H_2N–NH_2$, diethylene glycol, 110°C, 3 h; 190°C, 30 min; cool, add KOH, then heat at 190°C, 6 h; H^+; (h) $(COCl)_2$, $PhCH_3$, room temperature; (i) NaN_3, acetone–H_2O, 0°C; (j) $PhCH_3$, 80°C, 2 h; $Me_3SiCH_2CH_2OH$, $PhCH_3$, 80°C, 20 h; (k) *n*-Bu_4NF, THF, 50°C, 35 min; (l) CH_3CO_2CHO, Et_2O, room temperature, 10 h; (m) *p*-toluenesulfonyl chloride, pyridine, room temperature, 3 h.

SCHEME 1

Comparison of the (limited) spectral data reported (1*b*) for natural (+)-axamide-1 with those exhibited by our synthetic material did not lead to an unambiguous conclusion regarding compound identity. However, dehydration (9) of (±)-**1** afforded (86%) (±)-axisonitrile-1 (**2**), which exhibited mp 45–46°C (recrystallization from petroleum ether); ir (CCl_4): 3070, 2136, 1645, 1390, 1376, 899 cm^{-1}; ^1H nmr ($CDCl_3$, 400 MHz) δ: 0.88, 1.03 (d, d, 3H each, J = 6.5, 6.5 Hz), 0.99 (s, 3H), 1.20–1.26 (m, 1H), 1.41–1.57 (m, 5H), 1.60–1.71 (m, 1H), 1.96–2.12 (m, 3H), 2.15–2.22, 2.18 (superimposed m, d (J = 10 Hz), respectively, 2H), 2.42–2.52 (m, 1H), 3.20–3.26 (m, 1H, $w_{1/2}$ = 17 Hz), 4.79–4.85 (m, 2H, $w_{1/2}$ = 5.5 Hz). The chromatographic behavior (glc, tlc) and the 400-MHz ^1H nmr spectrum of our synthetic (±)-**1** were found to be identical with those of an authentic sample of (+)-axisonitrile-1.[6]

Subjection of the keto acid **10** to a sequence of reactions very similar to that described above provided (±)-10-*epi*-axamide-1 (**16**) (47% from **10**), which, upon dehydration (9), gave (±)-10-*epi*-axisonitrile-1 (**17**) (87%). The latter substance exhibited mp 53–54°C; ^1H nmr (400 MHz, $CDCl_3$) δ: 0.92, 1.04 (d, d, 3H each, J = 6.5, 6.5 Hz), 1.00 (s, 3H), 1.22–1.30 (m, 1H), 1.39–1.59 (m, 4H), 1.60–1.75 (m, 2H), 1.75–1.92 (m, 2H), 1.93–2.03 (m, 1H), 2.05 (d, 1H, J = 11 Hz), 2.14 (br d, 1H, J = 14 Hz), 2.22–2.34 (m, 1H), 3.18–3.25 (m, 1H, $w_{1/2}$ = 15 Hz), 4.72 (t, 1H, J = 2 Hz), 4.80 (t, 1H, J = 2 Hz). The chromatographic behavior (glc) and ^1H nmr spectrum of (±)-**17** were clearly different from those of natural (+)-axisonitrile-1.[6]

[6]We are grateful to Professor D. Sica for a sample of (+)-axisonitrile-1 and for a copy of its ^1H nmr spectrum.

Acknowledgements

We are grateful to the Natural Sciences and Engineering Research Council of Canada, Merck Frosst Canada, Inc., and Merck and Co. Inc. for financial support.

1. (*a*) F. CAFIERI, E. FATTORUSSO, S. MAGNO, C. SANTACROCE, and D. SICA. Tetrahedron, **29**, 4259 (1973); (*b*) E. FATTORUSSO, S. MAGNO, L. MAYOL, C. SANTACROCE, and D. SICA. Tetrahedron, **31**, 269 (1975).
2. (*a*) M. ADINOLFI, L. DE NAPOLI, B. DI BLASIO, A. IENGO, C. PEDONE, and C. SANTACROCE. Tetrahedron Lett. 2815 (1977); (*b*) A. IENGO, C. SANTACROCE, and G. SODANO. Experientia, **35**, 10 (1979).
3. E. PIERS and B. W. A. YEUNG. J. Org. Chem. **49**, 4567 (1984).
4. L. BLANCO, P. AMICE, and J. M. CONIA. Synthesis, 194 (1976).
5. G. VIDARI, S. FERINNO, and P. A. GRIECO. J. Am. Chem. Soc. **106**, 3539 (1984).
6. K. SAIGO, M. OSAKI, and T. MUKAIYAMA. Chem. Lett. 163 (1976); C. H. HEATHCOCK, M. H. NORMAN, and D. E. UEHLING. J. Am. Chem. Soc. **107**, 2797 (1985).
7. T. L. CAPSON and C. D. POULTER. Tetrahedron Lett. **25**, 3515 (1984).
8. C. W. HUFFMAN. J. Org. Chem. **23**, 727 (1958).
9. W. R. HERTLER and E. J. COREY. J. Org. Chem. **23**, 1221 (1958).

K. R. Fountain, Pamela Heinze, Mark Sherwood, Dave Maddox, and Greg Gerhardt. Can. J. Chem. **58**, 1198 (1980). Acylation of aromatic substrates with ketenes. An example of vinyl oxocation reactivity.

Page 1201. In Table 6 (Substrate specificity for diphenylketene), the first entry under "Area ratio (mols/mol)" should read 189 instead of 18.9.

K. R. Fountain, Pamela Heinze, Dave Maddox, Greg Gerhardt and Paul John. Can. J. Chem. **58**, 1939 (1980). Acylation of aromatic substrates with ketene. II. Hammett–Brown studies on substituted aromatic compounds.

Page 1944. The last paragraph on the right hand column "The results for the 5:1 experiment were used to determine the toluene/benzene ratio as follows." should read "The results of the 5:1 experiment were used to calculate the partial rate factor for the methyl group as follows."

J. Peter Guthrie and John Cossar. Can. J. Chem. **64**, 1250 (1986). The chlorination of acetone: a complete kinetic analysis.

Page 1262. The expression for the stoichiometry of chlorination of acetone should be:

$$n_{\text{acetone}} = 1 + f_1(1 + f_2) + (1 - f_1) + [(1 - f_1) + f_1(1 - f_2)]f_3$$

Page 1264. Figure 7, which is calculated using this expression should be:

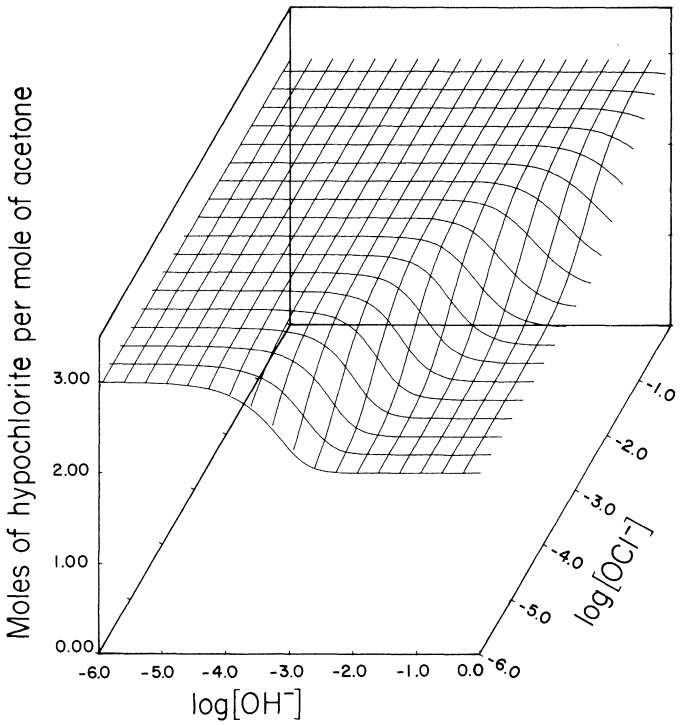

FIG. 7. Stoichiometry for chlorination of acetone in aqueous alkali. Number of moles of hypochlorite consumed per mole of acetone reacting, as a function of hydroxide and hypochlorite concentrations.